BULLETIN
OF THE AMERICAN PHYSICAL SOCIETY

Vol. 51, No. 1, Part 1, March 2006

# March Meeting 2006

## TABLE OF CONTENTS

BULLETIN
OF THE AMERICAN PHYSICAL SOCIETY

Vol. 51, No. 1, Part 2, March 2006
March Meeting 2006

# TABLE OF CONTENTS

BULLETIN
OF THE AMERICAN PHYSICAL SOCIETY

Vol. 51, No. 1, Part 1, March 2006

# March Meeting 2006

## TABLE OF CONTENTS

# APS MARCH MEETING 2006

March 13–17, 2006
Baltimore Convention Center
Baltimore, MD

## General Information

Welcome to the Annual March Meeting of the American Physical Society. All scientific sessions and some APS-sponsored sessions will be held at the Baltimore Convention Center (BCC). APS affiliated meetings and satellite meetings will be held at the Marriott Waterfront Hotel, headquarters hotel for the meeting. Consult the schedule of APS affiliated and satellite meetings, in this Bulletin for exact locations.

An outstanding scientific program has been planned by the March Meeting Program Committee. The five-day program consists of approximately 6,900 papers to be presented in invited, contributed, focus and poster sessions. A larger, enhanced exhibit show will complement the scientific program. Attendees are encouraged to visit with exhibitors who will be displaying the latest products, instruments and equipment, computer software, as well as science publications related to the research and application of physics.

## Participating APS Units

**Divisions:** Condensed Matter Physics (DCMP); Materials Physics (DMP); Polymer Physics (DPOLY); Chemical Physics (DCP); Biological Physics (DBP); Fluid Dynamics (DFD); Computational Physics (DCOMP); Atomic, Molecular and Optical Physics (DAMOP); Laser Science (DLS).

**Topical** Groups: Instrument and Measurement Science (GIMS); Magnetism and Its Applications (GMAG); Quantum Information, Concepts, and Computation (GQI); Shock Compression of Condensed Matter (SCCM); Statistical and Nonlinear Physics (GSNP).

**Forums:** Industrial and Applied Physics (FIAP); Physics and Society (FPS); History of Physics (FHP); International Physics (FIP); Education (FEd); Graduate Student Affairs (FGSA).

## Registration Location/Hour

Pratt Street Lobby
Baltimore Convention Center (BCC)

The APS Registration Desk will open and close at the following times.

| | |
|---|---|
| Sunday, March 12 | • 1:00pm –7:00pm |
| Monday, March 13 | • 7:00am – 5:00pm |
| Tuesday, March 14 | • 7:00am – 5:00pm |
| Wednesday, March 15 | • 7:00am – 4:00pm |
| Thursday, March 16 | • 7:30am – 3:00pm |
| Friday, March 17 | • 7:30am – 10:00am |

## Badge Monitoring

All attendees must register for the meeting. Attendees must wear their badges at all times. Security personnel will be checking for badges before allowing admission to the sessions. Attendees without badges will not be admitted to sessions or exhibits. If you have lost your badge, please go to the APS registration desk for a new one. We will give you one replacement badge free. After that replacement badges will be charged $10.00.

## Wireless Connection at the Convention Center

The Baltimore Convention Center has wireless internet connection available free of charge, sponsored by the American Physical Society.

## APS Job Fair

Whether you are looking for a job or recruiting, the American Physical Society Annual March Meeting Job Fair is the place to be! The Job Fair will provide job seekers and hiring managers with unsurpassed recruitment and networking opportunities. Last year, we assisted hundreds of job seekers and more than 50 employers.

*March 12 –16*
*Job Fair Schedule*

| | |
|---|---|
| *March 12* • | Employer/Job Seeker on-site pre-registration and check-in 1:00pm – 4:00pm |
| March 13 • | Job Fair hours of operation 10:00am – 5:00pm |
| March 14 • | Job Fair hours of operation 10:00am – 5:00pm |
| March 15 • | Job Fair hours of operation 10:00am – 4:00pm |
| March 16 • | Last day to view/search jobs and résumés online |

Join in with hundreds of individuals specializing in the following areas:

*Computational Physics*
*Insulators and Detectors*
*Polymeric and Organic Materials*
*Metals History and Physics*
*Statistical and Nonlinear Physics*
*Phase Transitions and Strongly Correlated Systems*
*Artificially Structured Materials*
*Surface, Interfaces and Thin Films*
*Physics and Society Magnetism*

*International Physics Instrumentation and Measurement*
*Quantum Information, Concepts and Computation*
*Education Chemical Physics*
*Biological Physics*
*Superconductivity*
*Fluids*
*Complex Structured Materials*
*Industrial and Applied Physics*

## Job Seekers utilize the Job Fair services to:

- Network with technical staff and human resource recruiters
- Post your résumé and search open positions
- Interview for positions

## Employers utilize the Job Fair services to:

- Showcase your company with a Recruitment Booth
- Advertise open positions
- Interview qualified job seekers
- Search résumés specific to this meeting

*For more information contact abrice@aip.org*

## APS Store

| | |
|---|---|
| Monday – Wednesday | • 9:30am – 5:00pm |
| Thursday | • 9:30am – 1:00pm |

Come browse our t-shirts, bumper stickers, and more.

## APS Exhibit Show/APS Lounge

*Exhibit Hall E*

| | |
|---|---|
| Monday, March 13 | • 10:00am – 5:00pm |
| Tuesday, March 14 | • 10:00am – 5:00pm |
| Wednesday, March 15 | • 10:00am – 4:00pm |

The annual exhibit show days are Monday through Wednesday. The exhibits are an important adjunct to the meeting, offering information on a wide variety of physics-related products and services. In addition, book and periodical publishers will be participating as exhibitors. The poster sessions, and food concessions will be located in the exhibit hall, as will the E-mail Pavilion. A wine and cheese reception will be held in the exhibit hall on Monday and Tuesday from 4:00pm – 5:00pm. Plan to stop by to visit the exhibits, view the posters and enjoy the refreshments. **NOTE:** *You must wear your badge to be admitted to the exhibit hall.*

## APS Membership Booth

The APS Membership Booth is located near APS Registration in the Pratt Street Lobby. Membership Department staff will be on hand to answer questions about APS Membership and journal subscriptions.

## E-mail Service

E-mail service will be available on Monday, Tuesday and Wednesday in the Exhibit Hall during exhibit hours only. E-mail will be available on Thursday and Friday in the Pratt Street Lobby. Email stations will be available for your use during the following hours:

| | |
|---|---|
| Monday, March 13 | • 10:00am – 5:00pm (exhibit hall) |
| Tuesday, March 14 | • 10:00am – 5:00pm (exhibit hall) |
| Wednesday, March 15 | • 10:00am – 4:00pm (exhibit hall) |
| Thursday, March 16 | • 7:00am – 6:00pm (Pratt Street Lobby) |
| Friday, March 17 | • 7:00am – 12:00noon (Pratt Street Lobby) |

Please be advised that e-mail access is provided as a service to attendees, and that we cannot provide unlimited access to e-mail stations, both in terms of the number of stations provided and the length of time that they are available.

## Speaker-Ready Room

*BCC/Room 330*

The speaker-ready room will be open as follows:

| | |
|---|---|
| Sunday, March 12 | • 1:00pm – 7:00pm |
| Monday, March 13 | • 7:00am – 5:00pm |
| Tuesday, March 14 | • 7:00am – 5:00pm |
| Wednesday, March 15 | • 7:00am – 5:00pm |
| Thursday, March 16 | • 7:00am – 5:00pm |
| Friday, March 17 | • 7:00am – 12:00noon |

## Press Room

*Press Room: BCC/Room 334*
*News Conference Room: BCC/Room 333*

| | |
|---|---|
| Monday through Thursday | • 8:00am – 5:00pm |
| Friday | • 8:00am – 12:00noon |

Phone: 410–649–6498
Fax: 410–649–6494

## Press Conference Room

*BCC/Room 333*

A schedule of news conferences can be obtained from the Press Room (Room 334).

## City Information Desk

The Baltimore Convention and Visitors Bureau will host an information desk in the BCC/Pratt Street Lobby:

| | |
|---|---|
| Sunday, March 12 | • 2:00pm – 6:00pm |
| Monday, March 13 | • 11:00am – 5:00pm |
| Tuesday, March 14 | • 11:00am – 5:00pm |

Stop by to inquire about restaurants in the city and sightseeing.

## Business Center

The Baltimore Convention Center business center is located off the Pratt Street Lobby across from Room 333. The business center offers a full range of services and is open Monday through Friday 8:30am – 4:30pm.

## Hotel List - March Meeting

- Marriott Waterfront Hotel (HQ)
  700 Aliceanna Street
  *Bussing provided to and from Convention Center*
- Sheraton Inner Harbor
  300 South Charles Street
  *Within walking distance*
- Days Inn
  100 Hopkins Place
  *Within walking distance*
- Renaissance Harborplace Hotel
  202 East Pratt Street
  *Within walking distance*
- Hyatt Regency Baltimore
  300 Light Street
  *Connected to Center*
- Holiday Inn
  301 West Lombard Street
  *Within walking distance*
- Wyndham Inner Harbor
  101 West Fayette Street
  *Within walking distance*

# PRE-MEETING PROGRAMS

**DPOLY Short Course – Baltimore Convention Center (BCC)**
Polymers in Existing and Emerging Patterning Technologies (no on-site registration – you must be pre-registered to attend this course)
**Room 304**
Saturday March 11 • 8:30am – 5:00pm
Sunday March 12 • 8:30am – 3:00pm

**Tutorials – Baltimore Convention Center (BCC)**
*(No on-site registration – you must be pre-registered to attend a tutorial)*
**Sunday, March 12**
**Baltimore Convention Center**
**Morning Tutorials #1–4**
*8:30am –12:30pm*
T1 Spintronics: What's New – Room 307
T2 Molecular Magnetics – Room 301
T3 Current Interpretations of Quantum Mechanics – Room 302
T4 Thermoelectric Energy Conversion – Room 303

**Afternoon Tutorials #5–8**
*1:30pm – 5:30pm*
T5 Solid State Implementations of Cavity QED – Room 301
T6 Spallation Neutron Sources – Room 302
T7 Forefront Methods and Limits of Lithography – Room 303
T8 Polymeric Templating – Room 305

**Professional Skills Development for Women Physicists**
**Sunday, March 12**
*8:00am – 5:00pm*
*Reception 5:00pm – 6:30pm*
Marriott Waterfront Hotel/Dover A (workshop)
Marriott Waterfront Hotel/Grand Salon I (reception)
This one-day workshop will offer training on persuasive negotiation and communication skills for tenure track and newly-tenured women physicists. Workshop will be led by professional facilitators using an interactive format that encourages highly personal learning. Lunch will be provided and a reception for participants will follow the workshop. Limited to 30 participants. Pre-registration required.

**Workshop on Opportunities in Biology for Physicists**
**Organized by APS Division of Biological Physics**
**Sunday, March 12**
*8:00am – 5:00pm*
Lunch break on your own.
BCC/Room 310
Biology is a rapidly changing field that has been making tremendous strides forward in recent years. Biology is changing from a descriptive to a quantitative and conceptually profound field. This workshop will showcase a sample of the rich opportunities in biology for physicists. It is aimed at physicists, especially graduate students and postdocs, who are curious about how a background in physics can provide a unique perspective of biological systems. We believe that physicists will make a substantial contribution to this revolution by working together with biologists.

**Invited speakers include:**
- William Bialek (Princeton)
- Steven Block (Stanford) (tentative)
- Robijn Bruinsma (UCLA)
- Hans Frauenfelder (Los Alamos)
- Klaus Lehnertz (Bonn)
- Yale Goldman (Penn)
- Boris Shraiman (Santa Barbara) (tentative)
- Charles Stevens (Salk Institute)
- Zuzanna Siwy (Irvine)
- Sunney Xie (Harvard)

Co-chairs of Organizing Committee:
Dean Astumian, DBP Vice Chair, astumian@maine.edu
Clare Yu, cyu@uci.edu

On-site registration is available but payable in cash only – no credit cards or checks.
Students: $50
Post Docs: $75
Regular Members: $100

**Special Workshop: Quantum Mechanics with Interactive Computer-based Tutorials**
Sponsored by the APS Forum on Education
**Sunday, March 12**
1:30pm – 5:30pm
BCC/Room 306
• No cost to attend the workshop - all are welcome.
Although quantum mechanics is one of the most widely taught topics on the college/university level in the physical sciences, the teaching of quantum mechanics has not changed significantly since the 1940s. This workshop will present recently developed computer-based curricular material that has shown to improve understanding of traditional quantum topics and that makes many heretofore inaccessible topics in quantum mechanics accessible to undergraduate and graduate students. Participants will receive a CD containing curricular material from the Quantum Interactive Learning Tutorials (QUILT) project as well as a collection of ready to run Java programs from the Open Source Physics (OSP) project. All programs are freely distributable under the GNU GPL license.
This workshop will benefit anyone teaching or planning to teach quantum mechanics as well as computational physicists wishing to adopt the OSP Java libraries for their own teaching and research. We will discuss the general pedagogical and technical issues in the design of interactive computer-based tutorials as well as how OSP programs can be adapted to your local situation. Additional information can be obtained at www.opensourcephysics.org

**Speakers:**
- Chandralekha Singh, University of Pittsburgh
- Wolfgang Christian, Davidson College
- Mario Belloni, Davidson College

**Career Workshop**
**Sunday, March 12**
*3:00pm – 7:00pm*
BCC/Room 308

Attendance is free. All are welcome.

# PRE-MEETING PROGRAMS

**NRC/NAS Town Meeting**
**Sunday, March 12**
*7:30pm – 9:30pm*
Marriott Waterfront Hotel, Grand Ballroom Salon V

**Condensed Matter and Materials Physics In the Next Decade**

M. A. Kastner, Chair, Solid State Sciences Committee of the National Research Council and Department of Physics, MIT

• The National Research Council (NRC) will soon appoint a committee to carry out a decadal study of condensed-matter and materials physics called CMMP2010. The study, which will result in an NRC report, is supported by the NSF and DOE. The committee will assess the current and future opportunities of our field. It will identify the most important fundamental scientific problems, as well as problems whose solutions are likely to help meet national or societal needs. It will also examine the current status and future needs for resources that will be necessary to solve these problems, such as small and large facilities, individual and multi-investigator research support, as well as university, national and industrial laboratories. After a brief introduction to the work done so far, under the auspices of the Solid State Sciences Committee, attendees will be invited to offer their views about issues to which the panel should pay special attention.

# APS MEETINGS / EVENTS

***(In chronological order)***

**Contact Congress**
**Mon-Thurs 9:00am–6:00pm**
Sponsored by DCMP and DMP
BCC/Pratt Street Lobby

Worried about the slashing of NSF, DOE and NASA funding? Concerned about the dearth of science literacy in our high-schoolers? Anxious about where the country's security is heading? YOU can have an impact on national science policy! Come write your representatives in Congress to let them know how you feel about science issues of interest to you. The most important letters that a Member of Congress receives are the ones from his or her constituents – you elect them, and you matter. The American Physical Society feels that it is incumbent on all of us to interact with the government, to offer technical assistance where we can, and to remind our Members of Congress that scientists have much to offer the country, in areas of basic science R&D funding, education, and energy policy. We have set up computers in the entrance area where you can send a letter to your Senators and Representatives - you can use our template or write your own letter on issues that matter to you. If the state of affairs in Washington, DC, interests you, we have another way for you to get involved: the APS "Physics and Government Network," a group of APS members who volunteer to contact their representatives in Congress a few times a year at critical junctures. PGNet signup fliers will be available at the registration desk and at the "Contact Congress" computers. Come help make science more visible in Congress!

**Awards Program**
**Monday, March 13**
*5:45pm – 6:30pm*
BCC/Room 309
Prizes and awards will be bestowed on individuals for outstanding contributions to physics. Please plan on attending the Awards Program and join us in honoring these individuals. See page 13 for a list of award and prize winners. The Awards Program will be followed by the Welcome Reception at 6:45pm.

**Welcome Reception**
**Monday, March 13**
*6:45pm – 8:00pm*
BCC/Ballroom II

All Attendees welcome.

### *Special Symposium:*

**Emerging Emergent Phenomena (Session F50)**
**Monday, March 13**
Sponsored by DCMP
*8:00pm – 10:00pm*
Marriott Waterfront Hotel, Grand Ballroom Salons V-VI

Session Chair: Leo Kadanoff, University of Chicago
*Speakers:*

- Edward Witten: Emergent Phenomena In Particle Physics
- Susan J. Lolle: Revisiting Mendel and the Paradox of Gene Restoration
- Albert Laszlo Barabas: Complex Networks: From the Internet to Biology
- Bernard Sadoulet: Condensed Matter Physics and the Nature of Dark Matter in the Universe

**Wine and Cheese Reception**
**Monday and Tuesday • 4:00pm – 5:00pm**
BCC/Exhibit Hall E

**APS Journal Editors Panel Discussion**
**Tuesday, March 14**
*2:30pm – 3:30pm*
BCC/Room 337
All are invited to a panel discussion with the Editors of the American Physical Society journals. The panel will include Editors from Physical Review Letters, Physical Review B, and Physical Review E. They will briefly discuss some current issues facing the journals such as how to express appreciation for good refereeing, possible inclusion of popular abstracts in PRL to make Letters accessible to physicists in all fields, the challenge posed by open access, etc. The Editors look forward to hearing opinions on these and other issues. They will also respond to questions and comments. The Panel Discussion will be followed by the Meet the Editors Reception.

**Meet the Journal Editors of AIP and APS**
**Tuesday, March 14**
*3:30pm – 5:30pm*
BCC/Camden Lobby

The Editors of the AIP and APS journals cordially invite you to join them for conversation and refreshments. Your questions, criticisms, compliments, and suggestions about the journals are welcome. We hope you will be able to join us.

**Journals of the American Institute of Physics:**
- Applied Physics Letters
- Chaos
- Journal of Applied Physics
- The Journal of Chemical Physics
- Journal of Mathematical Physics
- Physics of Fluids
- Physics of Plasmas
- Review of Scientific Instruments

**Journals of the American Physical Society:**
- Physical Review A
- Physical Review B
- Physical Review E
- Physical Review Focus
- Physical Review Letters
- Reviews of Modern Physics

# APS MEETINGS / EVENTS
***(In chronological order)***

### *Special Symposium:*

**Intelligent Design: Its Impact and Responses to It**
**Tuesday, March 14**
*7:30pm – 9:30pm*
Marriott Waterfront Hotel/Grand Ballroom Salon V

Session Chair: Robert Eisenstein
Speakers:

- Jeremy Gunn, ACLU - Dover, PA Case
- Marshall Berman - Action at the Local Level
- Cory Dean, New York Times - Media Coverage
- Francis Slakey, APS Office of Public Affairs - APS Activities

**Congressional Visits during March Meeting 2006**
**Congressional Visits Office –**
**BCC/East Pratt Show Office, Lower Level**

The APS Office of Public Affairs (OPA) is organizing Congressional visits during the 2006 APS March Meeting in Baltimore. The advantageous location of this year's Meeting provides an exciting opportunity to have attendees from as many districts and states as possible travel down to Washington, DC to educate Congress on the importance of science research funding. The visit days are scheduled for Wednesday, March 15th and Thursday March 16th.

Carrying the message to individual offices remains one of the best means of influencing a Member of Congress. The timing of these visits is excellent since Congress will have just started its considerations of the appropriations for the next fiscal year. In addition to influencing Congress, we hope that participants see first-hand the importance of informing their elected officials about what physicists do. While our members are getting more active in this regard and more APS meeting attendees write letters at the Contact Congress computers, there is much more to do.

OPA will assist the participants in all aspects of the congressional visits from scheduling to follow up. Leading up to the meeting, OPA will contact participants to inform them of the organizational logistics of the visits and provide a means of coordination of their meetings on the Hill with other participants in their state or district. During the March Meeting, briefings will be held in Baltimore in the evenings preceding the visits to outline a common message, offer advice on how to conduct an effective meeting, and cover the logistics of a congressional visit. We will also provide materials to be left with each office that will present useful talking points and have state specific information. Shuttle bus transportation to and from the Meeting and Washington, DC will be provided for participants.

We would like you and all APS members to view Congressional visits as part of developing a relationship with an office rather than a one-time event. We would hope that you would follow up with the Congressional office at opportune times, make visits to the home offices and perhaps invite staff or Members of Congress to visit their labs. You may also become resources for a Member's office.
For more information visit the Congressional Visits office as noted above.

**Session on Refereeing**
**Wednesday, March 15**
*9:30am – 11:00am*
BCC/Room 337

Editors from Physical Review Letters and the Physical Review will provide useful information and tips for referees. Following short presentations from the editors, there will be a moderated discussion where questions relevant to refereeing will be addressed. Refreshments will be served.

**Estate Planning Seminar**
**Wednesday, March 15**
*1:00pm – 2:00pm*
BCC/Room 301

### *Special Symposium:*

**Perspectives on our Energy Future**
**Wednesday, March 15**
*7:30pm – 9:00pm*
Marriott Waterfront Hotel/Grand Ballroom Salon V

Session Chair: George Crabtree, Argonne National Laboratory
Speakers:

- Steven E. Koonin, Chief Scientist, BP
- Patricia Dehmer, Office of Basic Energy Sciences, DOE

**Physics Sing-a-Long/Listen-a-Long**
**Wednesday, March 15**
9:00pm – 10:00pm
Grand Salon II, Marriott Waterfront Hotel

**Changing Dynamics of Industrial Research as a Consequence of Global Trends (Session V19)**
Sponsored by APS and AIP
**Thursday, March 16**
BCC/Room 316

Session Chair: Mark Bernius, The Dow Chemical Company
Speakers:

- **Alan Taub**: General Motors' R&D: Managing Innovation Globally
- **Hans Stork**: Not Only Texas is Flat …
- **Mark Durcan**: Micron R&D: Global Scope and Nano-Scale in N-Dimensions
- **Abel Weinrib**: Leap Ahead: Global R&D at Intel
- **Thomas Feist**: Sustaining Breakthrough Research in a Changing Global Environment

# APS EVENTS FOR SPECIAL GROUPS

***(In chronological order)***

**Companions Breakfast**
**Monday, March 13**
*8:00am – 9:30am*
Marriott Waterfront Hotel/Dover A

Companions of the attendees of the March Meeting are invited to a complimentary breakfast to meet other companions and learn about the city of Baltimore. Presentations will be made by a representative of the Baltimore Convention and Visitors Bureau. At the breakfast you will receive information about the sites and attractions in the city.

**SPS Undergraduates and Mentors Gathering**
**Monday, March 13**
*1:50pm – 2:20pm*
BCC/Room 345

Undergraduates and their mentors, as well as graduate school representatives, are especially invited to hear the student presentations and mingle with the presenters during this gathering. The event is sandwiched between two exciting undergraduate research sessions - B42 and D42 in room 345. Light refreshments will be available for those attending the talks.

**CSWP/FIAP Networking Breakfast for Women in Physics**
**Tuesday, March 14**
*7:30am – 9:30am*
Marriott Waterfront Hotel, Grand Ballroom Salon VII
$20 (pre-registration only)

The Committee on the Status of Women in Physics (CSWP) and the Forum on Industrial and Applied Physics (FIAP) will host a networking breakfast for women in physics. All are welcome, both men and women. Thanks to the generosity of FIAP, the breakfast is free for physics students who pre-register. Only a limited number of walk-ins can be accepted.

**High School Physics Teachers Day**
**Tuesday, March 14**
*8:00am – 2:30pm*
Marriott Waterfront Hotel, Grand Ballroom Salons II–III

In conjunction with the 2006 March Meeting, the APS Department of Education & Outreach is sponsoring a High School Physics Teachers' Day for teachers in the Baltimore region. For more information contact Ed Lee: lee@aps.org

*The day's program includes:*

- Hands-on workshops presenting innovative, class room-ready activities
- Research talks on cutting-edge physics
- A welcoming breakfast, and a chance to network with fellow teachers
- Lunch with a physicist

**Congressional Visits Meeting**
**Tuesday, March 14**
*5:00pm – 6:30pm*
BCC/Room 337

**DCMP/DMP/DCOMP Fellows & Awards Reception**
**Tuesday, March 14**
*5:30pm – 7:00pm*
Marriott Waterfront Hotel/Grand Salon VI

**FIP Reception**
**Tuesday, March 14**
*6:30pm – 8:00pm*
Marriott Waterfront Hotel/Dover C

**Students Lunch with the Experts**
**Wednesday, March 15**
*1:00pm – 2:30pm*
BCC/Ballroom II

Students can sign up on-site to enjoy a complimentary box-lunch while participating in an informal discussion with an expert on a topic of interest to them. Sign-up will take place beginning on Monday, March 13 at 1:00pm at the APS registration desk, and will be on a first-come, first-served basis. Attendance is limited to eight students per topic. See page 12 for list of topics and experts.

**Congressional Visits Meeting**
**Wednesday, March 15**
*5:00pm – 6:30pm*
BCC/Room 311

**Status of Funding Opportunities in NSF's Division of Materials Research**
**Wednesday, March 15**
*5:00pm – 7:00pm*
BCC/Room 338

**Student Reception**
**Wednesday, March 15**
*5:30pm – 6:30pm*
BCC/Ballroom II
Sponsored by the Forum on Graduate Student Affairs (FGSA)

All students are welcome. Plan to attend and socialize with your fellows and enjoy the refreshments. The Forum on Graduate Student Affairs (FGSA) will present a short program.

# APS EVENTS FOR SPECIAL GROUPS

***(In chronological order)***

## APS Unit Business Meetings

### SUNDAY, MARCH 12

**GSCCM Business Meeting**
*3:00pm – 4:00pm*
Falkland Room, Marriott Waterfront Hotel

### TUESDAY, MARCH 14
### 5:30pm – 6:30pm

**DPOLY Business Meeting**
BCC/Room 315

**FIAP Business Meeting**
BCC/Room 312

**FIP Business Meeting**
Marriott Waterfront Hotel, Galena

**DCP Business Meeting**
BCC/302

**GSNP Business Meeting**
BCC/Room 336

**GMAG Business Meeting**
BCC/Room 320

**GQI Business Meeting**
BCC/Room 343

**GIMS Business Meeting**
BCC/Room 301

### TUESDAY, MARCH 14
### 7:00pm–8:00pm

**DCMP Business Meeting**
Marriott Waterfront Hotel/Dover A

**DMP Business Meeting**
Marriott Waterfront Hotel/Dover B

### WEDNESDAY, MARCH 15

**FED Business Meeting and Reception**
*5:30pm – 7:00pm*
Marriott Waterfront Hotel/Grand Ballroom Salon III

**DCOMP Business Meeting**
*6:30pm – 730pm*
Marriott Waterfront Hotel, Dover C

# SATELLITE MEETINGS

***(ancillary events sponsored by non-APS groups)***

**Sunday, March 12**
**High Magnetic Field Laboratory Users Group**
*5:00pm – 9:00pm*
Marriott Waterfront Hotel/Grand Ballroom Salon X

**Sunday, March 12**
**Socialize with Science - Oxford Instruments**
*7:00pm – 9:00pm*
Marriott Waterfront Hotel/Grand Salons VIII–IX

**Monday, March 13**
**Discussions and Updates on the Nanoscale Ordered Materials Diffractometer at the Spallation Neutron Source (NOMAD)**
11:00am – 2:00pm
Marriott Waterfront Hotel/Dover C

**Tuesday, March 14**
**Research Corporation Reception**
*5:00pm – 7:00pm*
Marriott Waterfront Hotel/Grand Ballroom Salon I

**Tuesday, March 14**
**Alumni Reunions**
*6:00pm – 8:00pm*
Marriott Waterfront Hotel
- Cornell University, Grand Ballroom Salons IX–X
- University of Illinois, Grand Ballroom Salons II–III
- Michigan State University, Bristol
- IBM, Grand Salon VIII
- Brown University, Falkland
- State of Florida Universities, Harborside Ballrooms AB
- Sigma Pi Sigma, Essex B
- Brandeis Alumni Reunion, Essex C

**Tuesday, March 14**
**Chinese Academy of Sciences Reception**
*6:00pm–8:00pm*
Marriott Waterfront Hotel/Essex A

**Tuesday, March 14**
**American Chapter of the Indian Physics Association**
*7:30pm – 9:30pm*
Marriott Waterfront Hotel/Grand Ballroom Salon IV

**Wednesday, March 15**
**RSI Editorial Board Meeting**
*12:00noon – 2:00pm*
Marriott Waterfront Hotel/Grand Salon IX

**Wednesday, March 15**
**Status of Funding Opportunities in NSF's Division of Materials Research**
*5:00pm – 7:00pm*
BCC/Room 338

**Wednesday, March 15**
**MRFM Workshop**
**(Magnetic Resonance Force Microscopy)**
*6:30pm – 10:30pm*
Marriott Waterfront Hotel/Atlantic Room

# STUDENTS LUNCH WITH THE EXPERTS

**Wednesday, March 15**
*1:00pm – 2:30pm*
Ballroom II

Students can sign up on-site to enjoy a complimentary box-lunch while participating in an informal discussion with an expert on a topic of interest to them. Topics are listed below. Sign-up will take place beginning on Monday, March 13 at 1:00pm at the APS registration desk, and will be on a first-come, first-served basis. Attendance is limited to eight students per topic/expert. You must show your ticket and badge at the door, and sit at the table for which you have a ticket.

Lunch topics
sponsored by:

| | | | |
|---|---|---|---|
| **1.** | **DMP** | **Jaqueline Krim** | **Nanotribology: Applications and Implications of Friction at the Atomic Scale** |
| 2 | DMP | Lynn Boatner | Smart Nanocomposite Materials and How to Make Them |
| **3.** | **DFD** | **Ray Goldstein** | **Biological Physics** |
| 4. | DFD | Wolfgang Losert | Complex Fluids from Sand to Cells |
| **5.** | **DFD** | **Dave Weitz** | **Squishy Physics** |
| 6. | FPS | Francis Slakey | The Issue of Intelligent Design |
| **7.** | **GMAG** | **Jeff Childress** | **Research in Magnetic Recording - Industrial and Academic Perspectives** |
| 8. | GMAG | Jim Rhyne | Neutron Scattering Insights into Condensed Matter Systems |
| **9.** | **DCMP** | **Allen Goldman** | **Superconductivity** |
| 10. | DCMP | Art Ramirez | Frustrated Magnetism |
| **11.** | **DCMP** | **Gwyn P. Williams** | **Careers in the National Labs: Development of the Jefferson Lab FEL** |
| 12. | DCMP | David Awschalom | Spin Dynamics and Spin Coherence in Condensed Matter Systems (Spintronics) |
| **13.** | **DCMP** | **Julia Phillips** | **Sandia & Los Alamos Center for Integrated Nanotechnologies** |
| 14. | DCMP | Alan Dorsey | Supersolids |
| **15.** | **DCMP** | **Garnett Bryant** | **Quantum Nano-optics and Quantum Dots** |
| 16. | DCMP | Arthur F. Hebard | Magnetism in Reduced Dimensions: Ultra Thin Films and Thin-Film Interfaces |
| **17.** | **DCMP** | **Christopher Homes** | **Optical Spectroscopy of Superconductors** |
| 18. | DCMP | Richard Newrock | One Dimensional Conductance: Coulomb Drag and Luttinger Liquids |
| **19.** | **DCMP** | **Eric Shirley** | **Optical Properties of Materials: From Basic Theory to Industrial Impact** |
| 20. | DCMP | Lia Krusin-Elbaum | Can Disorder be Useful? |
| **21.** | **DCMP** | **David Reitze** | **Ultrafast Spectroscopy in High Magnetic Fields: Experiments at the NHMFL** |

# 2006 PRIZES AND AWARDS

**Award Session (Session E5)**
**Monday, March 13**
*5:45pm – 6:45pm*
*BCC/309*

## Biological Physics Prize

**Alfred G. Redfield**
*Brandeis University*

"For his seminal contributions to the theory and technical development of nuclear magnetic resonance spectroscopy, and for pioneering applications of this technique to the study of biological molecules."

## Lars Onsager Prize

**Rodney Baxter**
*Australian National University*

"For his original and groundbreaking contributions to the field of exactly solved models in statistical mechanics, which continue to inspire profound developments in statistical physics and related fields."


## Oliver E. Buckley Prize

**Noel A. Clark**
*University of Colorado*

**Robert Meyer**
*Brandeis University*

"For groundbreaking experimental and theoretical contributions to the fundamental science and applications of liquid crystals, particularly their ferroelectric and chiral properties."

## George E. Pake Prize

**Charles B. Duke**
*Xerox Innovation Group*

"For groundbreaking theoretical contributions to the understanding of tunneling in solids, and inelastic scattering of low-energy electrons in solids, and for his outstanding contributions to Xerox Corporate Research both as an intellectual leader and research manager."

## Frank Isakson Prize

**Roberto Merlin**
*University of Michigan*

"For original contributions to spontaneous Raman and ultrafast spectroscopy of fundamental excitations in solids."

## Earle K. Plyler Prize

**Mark Johnson**
*Yale University*

"For the applications of spectroscopic methods towards the understanding of solvation on the microscopic scale, especially the solvation of protons and hydroxide anions by water."


## James C. McGroddy Prize

**Hongjie Dai**
*Stanford University*

**Alex Zettl**
*University of California, Berkeley*

"For developing novel synthesis pathways for preparing carbon and boron nitride nanotubes and for pioneering applications of these for sensing, electronics and nanomechanics."

## Polymer Prize

**Ludwik Leibler**
*Ecole Superieure de Physique et Chimie Industrielles, Paris*

"For outstanding theoretical contributions to the fundamental understanding of self-assembly of diblock copolymers and gels, and wetting."

# 2006 PRIZES AND AWARDS

## Aneesur Rahman Prize

**David Vanderbilt**
*Rutgers University*

"For his conceptual breakthroughs in his development of the ultrasoft pseudopotential and the modern theory of polarization, and their impact on first-principles investigations of the properties of materials."


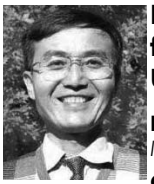

## Prize to a Faculty Member for Research in an Undergraduate Institution

**Rainer Grobe**
*Illinois State University*

**Q. Charles Su**
*Illinois State University*

"For their outstanding effort at creating a successful and renowned optical theory research program at Illinois State University, and for their exemplary involvement of undergraduates in this research."

## David Adler Lectureship Award

**James Chelikowsky**
*University of Texas*

"For his creative and outstanding research in computational materials physics and for his effectiveness in communicating research results through lectures and publications."


## LeRoy Apker Award

**Nathaniel Craig**
*Harvard University*

**Matthew Paoletti**
*Bucknell University*

"Tunable Nonlocal Spin Control in a Coupled Quantum Dot System."
"Experimental Studies of the Effects of Chaotic Mixing on an Advection-Reaction-Diffusion System."

## Edward A. Bouchet Award

**Angel Garcia**
*Rensselaer Polytechnic Institute*

"For his contributions to the understanding of the role of water in the dynamics and folding of proteins through computer simulations."

Photo not available

## John H. Dillon Medal

**Kenji Urayama**
*Kyoto University*

"For insightful experiments that probe the nature of polymer networks."

## Keithley Award

**Frances Hellman**
*University of California, Berkeley*

"In recognition of using emerging micromachining techniques to significantly extend the range of calorimetry into the realm of nano-scale science, by construction of Si based microcalorimeters capable of operating in extreme environments with unprecedented sensitivity and accuracy."

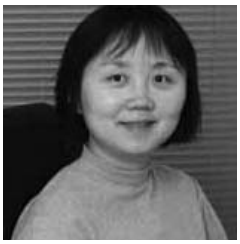

## Maria Goeppert-Mayer Award

**Hui Cao**
*Northwestern University*

"For her groundbreaking contributions to the experimental studies of coherent light generation and transport in disordered media, including her invention of microlasers based on disordered media."

Photo not available

## Nicholas Metropolis Award

**Joseph A. Barranco**
*University of California, Berkeley*

"For the development of computational techniques to handle 3D compact vortices in rotating shear flows, and for the application of these techniques to solve longstanding problems in the theory of planet and star formation."

**Additional Awards:**

**Marshak Lectureship Award: Zohra ben Lakhdar (Session D3)**

**Beller Lectureship Award: Pierre-Gilles de Gennes (Session Y29)**

Each year, the APS Committee on International Scientific Affairs (CISA) will award the APS Beller and Marshak Lectureships to bring distinguished foreign scientists to speak at the March and April meetings.

The Beller Lectureship was endowed by Esther Hoffman Beller for the purpose of bringing distinguished physicists from abroad as invited speakers at APS meetings. The Marshak Lectureship, endowed by Ruth Marshak, in honor of her late husband and former APS president, Robert Marshak, provides travel support for physicists from a developing country or Eastern Europe invited to speak at APS meetings.

# FOCUS SESSIONS

**DAMOP**
A43 - Focus Session: Strongly Interacting Fermi Gases and the BCS - BEC Crossover I
D43 - Focus Session: Vortices and Vortex Lattices in Fermi and Bose Superfluid Gases
H43 - Focus Session: Strongly Interacting Fermi Gases and the BCS - BEC Crossover II
U43 - Focus Session: Novel Phases in Low Dimensional Quantum Gases

**DAMOP/GQI**
W43 - Focus Session: Cold Atoms in Optical Lattices

**DBP**
G26 - Focus Session: Trapping of Nanoscale Biological Objects
G29 - Focus Session: Physical and Engineering Constraints on the Function of Biological Systems
H29 - Focus Session: Physical Aspects of Morphogenesis: Computational Approaches
N29 - Focus Session: Physical Models of Ion Channel Function
R26 - Focus Session: Counterion Dynamics in Charged Biopolymer Systems
R28 - Focus Session: Biological Networks: Structure, Dynamics and Function
W26 - Focus Session: Biological Photophysics
Y26 - Focus Session: Physics of Physiological Systems

**DBP/DCMP**
K26 - Focus Session: Single Molecule Biophysics I

**DBP/DCP**
P26 - Focus Session: Protein Dynamics in Folding and Function

**DBP/DFD**
N26 - Focus Session: DNA and Protein Analysis with Micro and Nano Fluidics

**DBP/DPOLY**
B26 - Focus Session: Single Molecule Biophysics: DNA & RNA
D26 - Focus Session: Dynamics of Nuclei Acid-Protein Interaction: Single Molecule
U29 - Focus Session: Nonequilibrium Fluctuation in Biomolecules and Artificial Nanodevices
Y29 - Focus Session: Noise and Fluctuation in Biological Systems

**DBP/GSNP**
B29 - Focus Session: Micro-Organism Motility
A39 - Focus Session: Magnesium Diboride and Related Compounds: Multi Gap Superconductivity
D15 - Atomic Tunneling, Films, Nanostructures
H39 - Focus Session: Josephson Junctions and Pairing State Symmetry

**DCMP/DCOMP**
*G39* - Focus Session: Superconductivity: Theory and Computation I

**DCMP/GSCCM**
R42 - Focus Session: Plasticity and Phase Transitions

**DCOMP**
D27 - Focus Session: Novel Computational Algorithms I
G27 - Focus Session: Novel Computational Algorithms II

**DCOMP/DFD**
V8 - Focus Session: Simulations Using Particles

**DCOMP/DCMP**
K39 - Focus Session: Superconductivity: Theory and Computation II
P39 - Focus Session: Superconductivity: Theory and Computation (Mainly First Principles)
V39 - Focus Session: Superconductivity: Theory and Computation III
Z39 - Focus Session: Superconductivity: Theory and Computations (Mostly Phonons)

**DCOMP/DMP**
B32 - Focus Session: Computational Nanoscience I
D32 - Focus Session: Computational Nanoscience II
G31 - Focus Session: Simulation of Complex Materials I
H31 - Focus Session: Simulation of Complex Materials II
H32 - Focus Session: Computational Nanoscience III
K31 - Focus Session: Simulation of Complex Materials III
K32 - Focus Session: Computational Nanoscience IV
R32 - Focus Session: Computational Nanoscience V

**DCOMP/GSCCM/DMP**
N42 - Focus Session: Simulations of Matter at Extreme Conditions I
U42 - Focus Session: Simulations of Matter at Extreme Conditions II
W42 - Focus Session: Simulations of Matter at Extreme Conditions III

**DCOMP/GQI**
P40 - Focus Session: Pathways to Practical Quantum Computing I
R40 - Focus Session: Pathways to Practical Quantum Computing II

**DCOMP/GQI/DAMOP**
U40 - Focus Session: Pathways to Practical Quantum Computing III

**DCP**
A10 - Focus Session: Physical Chemistry of Nanoscale Systems I
A11 - Focus Session: Promises and Challenges in Chemical Dynamics I
B10 - Focus Sessions: Physical Chemistry of Nanoscale System II
B11 - Focus Session: Promises and Challenges in Chemical Dynamics II
D10 - Focus Session: Physical Chemistry of Nanoscale System III
D11 - Focus Session: Promises and Challenges in Chemical Dynamics III
G10 - Focus Sessions: Physical Chemistry of Nanoscale System IV
G11 - Focus Session: Promises and Challenges in Chemical Dynamics IV
H10 - Focus Session: Frontiers in Computational Chemical Physics I
H11 - Focus Session: Chemical and Spectroscopic Applications of Nonlinear Optics I
K10 - Focus Session: Frontiers in Computational Chemical Physics II
K11 - Focus Session: Chemical and Spectroscopic Applications of Nonlinear Optics II

# FOCUS SESSIONS

N10 - Focus Session: Frontiers in Computational Chemical Physics III
N11 - Focus Session: Aerosols, Clusters, Droplets: Physics and Chemistry of Nanoobjects I
N13 - Focus Session: Ultrafast and Ultrahigh Field Chemistry I: Strong Field Phenomena
P10 - Focus Session: Frontiers in Computational Chemical Physics IV
P11 - Focus Session: Aerosols, Clusters, Droplets: Physics and Chemistry of Nanoobjects II
P13 - Focus Session: Ultrafast and Ultrahigh Field Chemistry II: Quantum Control
R10 - Focus Session: Surfaces and Interfaces in Electronic Materials I
R11 - Focus Session: Aerosols, Clusters, Droplets: Physics and Chemistry of Nanoobjects III
R13 - Focus Session: Ultrafast and Ultrahigh Field Chemistry III: Ultrafast Processes
U10 - Focus Session: Surfaces and Interfaces in Electronic Materials II
U11 - Focus Session: Aerosols, Clusters, Droplets: Physics and Chemistry of Nanoobjects IV
V10 - Focus Session: Surfaces and Interfaces in Electronic Materials III
V11 - Focus Session: Aerosols, Clusters, Droplets: Physics and Chemistry of Nanoobjects V
W10 - Focus Session: Surfaces and Interfaces in Electronic Materials IV
W11 - Focus Session: Aerosols, Clusters, Droplets: Physics and Chemistry of Nanoobjects VI

**DCP/DBP**

A13 - Focus Session: Spectroscopy of Biomolecules from Isolated Molecules to Cell Environoment I
B13 - Focus Session: Spectroscopy of Biomolecules from Isolated Molecules to Cell Environoment II
D13 - Focus Session: Spectroscopy of Biomolecules from Isolated Molecules to Cell Environoment III
G13 - Focus Session: Spectroscopy of Biomolecules from Isolated Molecules to Cell Environoment IV

**DFD**

H21 - Focus Session: Microfluidic Physics I

**DFD/DBP**

R21 - Focus Session: Biological Hydrodynamics I
U28 - Focus Session: Biological Hydrodynamics II

**DFD/GSNP**

P8 - Focus Session: Jets, Shocks & Splashes

**DMP**

A18 - Focus Session: Carbon Nanotubes: Synthesis and Growth I
A35 - Focus Session: Nanoscale Thermal, Thermoelectricity and Mass Transport: Measurement and Characterization
A46 - Focus Session: Wide Bandgap Semiconductors I
B18 - Focus Session: Carbon Nanotubes: Synthesis, Processing and Characterization
B35 - Focus Session: Nanoscale Thermal, Thermoelectricity and Mass Transport: Theory and Simulation
B46 - Focus Session: Wide Band Gap Semiconductors II
D18 - Focus Session: Carbon Nanotubes: Synthesis and Growth II
D35 - Focus Session: Thermal Transport and Thermoelectricity in Nanotubes and Graphene
D38 - Focus Session: Magnesium Diboride and Related Compounds: Properties of Doped and Irradiated MgB2
D46 - Focus Session: Wide Band Gap Semiconductors III
G18 - Focus Session: Carbon Nanotubes: Electronic and Optical Properties I
G37 - Focus Session: Nanoscale Materials Physics of Phase Transitions I
G38 - Focus Session: Magnesium Diboride and Related Compounds: Carbon Alloying of MgB2
G40 - Focus Session: Materials for Quamtum Computing I
H18 - Focus Session: Carbon Nanotubes: Electronic and Optical Properties II
H36 - Focus Session: Single Molecule Conductance
H37 - Focus Session: Nanoscale Materials Physics of Phase Transitions II
H40 - Focus Session: Materials for Quantum Computing II
H46 - Focus Session: Wide Band Gap Semiconductors IV
K40 - Focus Session: Materials for Quantum Computing III
K41 - Focus Session:Dielectric, Ferroelectric, and Piezoelectric Oxides II
N18 - Focus Session: Carbon Nanotubes: Transport I
N36 - Focus Session: Optical Properties of Nanostructures with S, Se, Te, and Ge
N37 - Focus Session: Nanoscale Fabrication, Assembly and Semiconductor Nanowires
N39 - Focus Session: Magnesium Diboride and Related Compounds: MgB2 Thin Films and Junctions
P18 - Focus Session: Carbon Nanotubes: Opto-Electronics
P36 - Focus Session: Plasmon Resonances in Nanostructures
P41 - Focus Session: Dielectric, Ferroelectric, and Piezoelectric Oxides III
R18 - Focus Session: Carbon Nanotubes: Transport II
R36 - Focus Session: Optical and X-ray Properties of Nanostructures
R37 - Focus Session: Nanoscale Conductance Theory I
R41 - Focus Session: Dielectric, Ferroelectric, and Piezoelectric Oxides IV
U18 - Focus Session: Carbon Nanotubes: Transport III
U36 - Focus Session: Optical Properties of Nano-Dots, Holes, and Wires
U37 - Focus Session: Nanowire and Nanodot Quantum Devices
V18 - Focus Session: Carbon Nanotubes: Transport IV
V36 - Focus Session: Optical Properties of Carbon Nanotubes and C60
V41 - Focus Session: Dielectric, Ferroelectric, and Piezoelectric Oxides V
W18 - Focus Session: Carbon Nanotubes: Electronic and Optical Properties IV
W36 - Focus Session: Optical Properties of Nanostructures of Si & GaAs
Y18 - Focus Session: Carbon Nanotubes: Adsorption and Gas Surface Interactions with Carbon Nanotubes
Y37 - Focus Session: Probing Novel Nanostructures
Z18 - Focus Session: Carbon Nanotubes: Double Wall Nanotubes, Sheets and Chains
Z37 - Focus Session: Nanoscale Conductance Theory III

**DMP/DCMP**

A12 - Focus Session: Steps, Growth, and Smoothing
D15 - Focus Session: Atomic Tunneling, Films, Nanostructures
K12 - Focus Session: Magnetic Thin Films and Narrow Gap

# FOCUS SESSIONS

Semiconductors
N12 - Focus Session: Alloy and Interface Composition
U12 - Focus Session: Electrochemical and Related Growth
V12 - Focus Session: Wetting and Hard-Soft Interfaces

**DMP/DCOMP**
A42 - Focus Session: Planetary Materials I
K42 - Focus Session: Planetary Materials II
P42 - Focus Session: Planetary Materials III

**DMP/DPOLY**
N32 - Focus Session: Carbon Nanotubes: Composites and Applications

**DMP/GMAG**
A20 - Focus Session: Complex Oxide Thin Films Surfaces and Interfaces I: Superlattice Fabrication and Properties
D20 - Focus Session: Multiferroics I: Improper Ferroelectrics
G20 - Focus Session: Complex Oxide Thin Films Surfaces and Interfaces II: Surfaces and Theory
G32 - Focus Session: Orbital/Charge Order in Complex Oxides
K20 - Focus Session: Multiferroics II - Hexagonal Systems
N20 - Focus Session: Complex Oxide Thin Films Surfaces and Interfacess III: New Materials, New Techniques, and Effects of Strain
P20 - Focus Session: Cobaltites, Nickelates and Vanadates
R20 - Focus Session: Multiferroics III: Perovskites
U20 - Focus Session: Metal-Insulator Transition and Electron Phonon Coupling in Perovskites
W20 - Focus Session: Multiferroics IV

**DMP/GSNP**
D33 - Focus Session: Friction, Fracture and Deformation I
H33 - Focus Session: Friction, Fracture and Deformation II
P33 - Focus Session: Friction, Fracture and Deformation III
R33 - Focus Session: Friction, Fracture and Deformation IV

**DPOLY**
A30 - Focus Session: Block Copolymer Dynamics
D25 - Focus Session: Particle Dynamics and Organization; Polymer Tethers and Interfacial Segregation
G28 - Focus Session: Microphysical Properties of Block Copolymer Aggregates I
H25 - Focus Session: Particle Dynamics and Organization
K18 - Focus Session: Dillon Medal Symposium
K28 - Focus Session: Microphysical Properties of Block Copolymer Aggregates II
U30 - Focus Session: Mechanical Properties: Deformation, Rupture and Failure
V30 - Focus Session: Mechanical Properties: Microscale Deformation and Failure
W24 - Focus Session: Lithography

**DPOLY/DBP**
W30 - Focus Session: Biopolymers at Interfaces
Y30 - Focus Session: Biopolymers I: Phase Transitions

**DPOLY/DMP**
A24 - Focus Session: Organic Interfaces
A25 - Focus Session: Organic Field Effect Transistors
G30 - Focus Session: Electronic Transport in Organic Films
H28 - Focus Session: Energetics and Transport in Conjugated Organics
N25 - Focus Session: Organic Photovoltaics

**FIAP**
A16 - Focus Session: Hydrogen Storage I
A17 - Focus Session: Structure and Properties of Nanoscale Oxide Films
B16 - Focus Session: Molecular-Scale Electronics I
B17 - Focus Session: Phase Transitions and Domains in Ferroelectric Nanostructures I
D16 - Focus Session: Negative Refractive Index I
D17 - Focus Session: Phase Transitions and Domains in Ferroelectric Nanostructures II
G17 - Focus Session: Emerging Research Devices and Materials for Microelectronics Industry I
H16 - Focus Session: Hydrogen Storage II
H17 - Focus Session: Emerging Research Devices and Materials for Microelectronics Industry II
K16 - Focus Session: Molecular-Scale Electronics II
K17 - Focus Session: Si, Ge and SiGe Nanostructures
N16 - Focus Session: Hydrogen Storage III
N17 - Focus Session: Semiconductors for THz and IR I
P16 - Focus Session: Molecular-Scale Electronics III
R17 - Focus Session: Semiconductors for THz and IR II

**GMAG/DMP**
A19 - Focus Session: Optical and Electrical Spin Generation in Semiconductors
B19 - Focus Session: Transition Metal Oxide Ferromagnetic Semiconductors
B20 - Focus Session: Phase Competition and Separation in Pervoskite Oxides
D19 - Focus Session: Semiconductor Spin Injection and Detection
D22 - Focus Session: Magnetic Nanopatterns
G19 - Focus Session: III-V Magnetic Semiconductors I
G22 - Focus Session: Magnetic Nanoparticles I
H19 - Focus Session: III-V Magnetic Semiconductors II
H22 - Focus Session: Nanoparticles and Nanocomposites
K19 - Focus Session: III-V Magnetic Semiconductors III
N22 - Focus Session: Magnetic Vortices and Exchange Biased Thin Films
P19 - Focus Session: Spin Interference and Spin Hall Effect
R19 - Focus Session: Spin Hall Effect and Spin Transport
R22 - Focus Session: Biomagnetism and Exchange Biased Thin Films
U19 - Focus Session: Semiconductor Spin Nanostructures for Quantum Computing
V20 - Focus Session: Semiconductor Spin Dynamics: Optics
W19 - Focus Session: Semiconductor Spin Transport: Noise/Theory
W22 - Focus Session: Magnetic Nanoparticles II
Y19 - Focus Session: Novel Ferromagnetic Semiconductors I
Y20 - Focus Session: Ruddlesden-popper Phase Manganites
Z19 - Focus Session: Spin Dynamics in Quantum Dots
Z20 - Focus Session: Novel Ferromagnetic Semiconductors II

**GMAG/DMP/DCOMP**
D23 - Focus Session: MAG.THY I / Spin Structures and Dynamics
G23 - Focus Session: MAG.THY II / Transport & General
N23 - Focus Session: MAG.THY III: Oxides and Phase Transitions
W23 - Focus Session: MAG.THY IV / ab initio Studies

# FOCUS SESSIONS

*Focus Sessions (cont'd)*

**GMAG/FIAP**
R23 - Focus Session: Theory and Simulation for Information Storage Applications
Y22 - Focus Session: Coupled Thin-Film Structures for Magnetic Recording
Z22 - Focus Session: FePt Nanoparticles for Information Storage

**GMAG/FIAP/DMP**
A22 - Focus Session: Current Driven Magnetization Dynamics I
B22 - Focus Session: Current Driven Magnetization Dynamics II
K22 - Focus Session: Magnetization Dynamics
P22 - Focus Session: Spin Transport in Metals
U22 - Focus Session: Magnetic Tunneling I
V22 - Focus Session: Magnetic Tunneling II

**GSCCM/DCMP**
H42 - Focus Session: Dynamic Compression

**GSNP**
A33 - Focus Session: Econophysics
H8 - Focus Session: Jamming in Glasses, Grains, and Gels I
K8 - Focus Session: Jamming in Glasses, Grains and Gels II
N33 - Focus Session: Instabilities & Turbulence in Complex Fluids
N35 - Focus Session: Organization of Complex Networks
V33 - Focus Session: Social Networks

**GSNP/DBP**
P7 - Focus Session: Physics of Transcriptional Regulatory Networks
U26 - Focus Session: Cytoskeletal Dynamics

**GSNP/DFD**
B8 - Focus Session: Granular Materials Near Jamming
W8 - Focus Session: Nonlinear Electrokinetics

**GQI/DCMP**
D40 - Focus Session: Foundations of Quantum Theory
V40 - Focus Session: Linear Optics Quantum Computation

# POSTER SESSIONS

**Poster Sessions**
*Exhibit Hall*
Poster sessions will be held Monday, Tuesday and Wednesday. Posters will be on display from 10:00am to 5:00pm on Monday and Tuesday and from 10:00am to 4:00pm on Wednesday. Authors should be in attendance at the times listed below. APS is not responsible for poster materials that are left in the exhbiti hall after the session is over. No A/V is allowed in poster sessions.

**C1: Poster Session 1**
**Monday, March 13**
Authors in attendance from 2:00pm – 5:00pm
(DPOLY Session from 11:15am – 2:15pm)

Posters 1-99: DPOLY Posters I
Posters 100-152: Biological Physics
Posters 153-184: Chemical Physics
Posters 185-215: Statistical and Nonlinear Physics
Posters 216-256: Artificially Structured Materials
Posters 257-270: Instrumentation and Measurements

**J1: Poster Session II**
**Tuesday, March 14**
Authors in attendance from 2:00pm – 5:00pm

- Posters 1-19: Metals
- Posters 20-48: Semiconductors
- Posters 49-65: Insulators and Dielectrics
- Posters 66-88: Superconductivity
- Posters 89-147: Magnetism Poster
- Posters 148-195: Complex Structured Materials
- Posters 196-245: Fluids and Soft Matter Poster
- Posters 246-259: Phase Transitions and Strongly Correlated Systems
- Posters 260-292: Surfaces, Interfaces and Thin Films

**Q1: Poster Session III**
**Wednesday, March 15**
Authors in attendance from 1:00pm – 4:00pm
(DPOLY Session from 11:15am – 2:15pm)

- Posters 1-97: DPOLY Posters II
- Posters 98-122: Applications
- Posters 123-144: General Theory
- Posters 145-154: General Physics
- Posters 155-157: Quantum Fluids and Solids
- Posters 158-173: Atomic, Molecular & Optical (AMO) Physics
- Posters 174-186: Physics Education
- Posters 187-199: Quantum Information, Concepts, and Computation
- Posters 200-333: Post-Deadline Posters

# PROGRAM FORMAT

**Program Time-Blocks**

Normally contributed and invited sessions at APS general meetings are three hours in length - three sessions per day at 8:00am, 11:15am, and 2:30pm. The time blocks are designated in alpha order beginning with time-block "A" on Monday at 8:00am, and ending with "Z" designating the 11:15 time-block on Friday.

**Session Codes**

The number following the alpha that designates the time-block represents the sequential numbering of the sessions within the time-block. Session A1 is one of several sessions taking place in parallel in the first time-block on Monday. The number following the decimal in the session code represents the sequence of the papers to be presented in that session. For *example:* B3.004 = Time-block B (Monday at 11:15am); Session 3 (of several) within that time-block; and the 4th paper to be presented in that session.

**Poster Codes**

The poster sessions will take place on Monday, Tuesday, and Wednesday in the Exhibit Hall. A breakdown of the topics presented in each category is listed on page 19.

- Monday poster sessions = Sessions C1
- Tuesday poster session = Sessions J1
- Wednesday poster sessions = Sessions Q1

Each poster presentation (board) within each poster session is numbered sequentially.

## GUIDELINES FOR SPEAKERS

**Oral Presentations**

Please arrive at least 15 minutes prior to the scheduled time of your talk. Contributed papers are allocated 12 minutes each - 10 minutes for presentation and 2 minutes for questions from the audience, unless otherwise specified. Invited papers are allocated 36 minutes - 30 minutes for presentation and 6 minutes for questions from the audience.

Note: Occasionally (and unfortunately) the chair for a session may not appear, in which case we ask that the first presenter serve as chair of the session.

**Poster Presentations**

If you are presenting a poster, please be sure to have your poster up prior to 10:00am on the day of your poster presentation to which you have been assigned, and taken down immediately at the end of the day. You must be on hand at the beginning of the poster session (see epitome for times). APS will not be responsible for posters left up after the end of each poster session. No A-V is allowed in the poster sessions. Posters will be on display between the hours of 10:00am to 5:00pm Monday, Tuesday; 10:00am to 4:00pm, Wednesday. Consult the Poster Session Schedule for exact times and a breakdown of poster topics.

## GUIDELINES FOR SESSION CHAIRS

- Prior to the session, check the Corrigenda distributed with the Bulletin, as well as the Program-Changes Board in the registration area to see if any papers in the session you are chairing have been withdrawn.
- Arrive at the meeting room about 15 minutes prior to the start of the session and familiarize yourself with the controls for lights, microphones, A-V equipment and the timer. Technicians will be on hand to assist. If you encounter problems, you should immediately alert the Meetings Manager and/or the A-V specialist.
- Start the session on time. Briefly introduce yourself, announce the first paper and author, and start the timer.
- Please adhere to the time schedule listed in the Bulletin, so that simultaneous sessions are as closely synchronized as possible. Many attendees move from session to session in order to hear specific papers.

Note: any time used by the speaker and/or technicians to set up laptops for LCD (Powerpoint) presentations is deducted from the time allocated for the talk.

- The allotted time for contributed papers is 12 minutes; for invited papers - 36 minutes. If you are chairing a session that includes both contributed and invited papers please be aware of the different times allocated for each and set the timer as follows:

*Contributed papers* - set timer for 8 minutes to give initial warning, then set the final bell to go off 2 minutes later. When this time is up, allow 2 additional minutes for questions relating to the paper, thank the speaker and promptly introduce the next paper and speaker.

Invited papers - set timer for 25 minutes for initial warning, and the final bell to ring 5 minutes later. Then set the timer for 6 additional minutes for questions from the audience.

Explain the timing system to the audience prior to the start of the session, and as often during the session as you think necessary.

- The By-Laws of the Society request that speakers be asked to stop when their allotted time is up in a courteous but firm manner. Keep in mind that the session must end on time, and that the last speaker has just as much right to an audience as does the first speaker.
- Should a speaker fail to appear, you must wait 12 minutes before going on to the next speaker. At the end of the session, call again for the regularly scheduled paper, if time allows.
- When two or more papers are submitted by an author, only one of these will be assigned a scheduled presentation time within that session. It is assumed that the first author listed in the abstract is the person who will present the paper at the meeting. A second abstract submitted by the same author is automatically assigned to a poster.
- If any problems arise that you are unable to handle relative to successfully chairing the session, please inform the A-V tech in the room, or go immediately to the APS registration desk to alert the APS staff.

**General A-V Policy**

In keeping with our legally binding contract with our A-V vendor, speakers are not permitted to bring their own projection equipment for use at the meeting.

**Standard A-V in all Sessions**

The standard A-V package consists of an LCD projector, overhead projector, screen, laser pointer and 2 lapel microphones – one for the chair and one for the speakers. Any additional A-V equipment must be rented by the speaker directly through APS's designated A-V provider located in Rooms 331-332. The speaker is responsible for the cost of renting any additional equipment.

# PROGRAM FORMAT

**Policy and Guidelines on Use of LCD Projectors**

The responsibility for a smooth, technically trouble-free presentation ultimately rests with the presenter. Speakers who plan to use LCDs must do the following:

• Bring your own laptop computer, power cord, and any proprietary cords required for your computer. Do not bring your own projector to the meeting. NOTE: APS is not responsible for the security of personal laptop computers.

• Visit the Speaker-Ready room located in Room 330 to run through the presentation to ensure a smooth and technically trouble-free talk. Testing your presentation in the Speaker-Ready room prior to your presentation is strongly recommended to minimize equipment compatibility difficulties. Remember that time used to set up equipment reduces the time you have to make your presentation.

• Bring a back-up vu-graph presentation in case there are set-up difficulties with the LCD equipment.

# PROGRAM FORMAT & UNIT ACRONYMS

**Divisions**

DAMOP ..... Division of Atomic, Molecular and Optical Physics
DAP ..... Division of Astrophysics
DBP ..... Division of Biological Physics
DCP..... Division of Chemical Physics
DCMP ..... Division of Condensed Matter Physics
DCOMP ..... Division of Computational Physics
DFD..... Division of Fluid Dynamics
DLS..... Division of Laser Science
DMP ..... Division of Materials Physics
DNP..... Division of Nuclear Physics
DPB ..... Division of the Physics of Beams
DPF..... Division of Particles and Fields
DPP..... Division of Plasma Physics
DPOLY ..... Division of Polymer Physics

**Topical Groups**

GFBS ..... Few Body Systems Topical Group
GFC.....Precision Measurement and Fundamental Constants Topical Group
GGR ..... Gravitation
GHP.....Topical Group on Hadronic Physics
GIMS .....Instrumentation and Measurement
GMAG .....Magnetism and Its Applications Topical Group
GPAP .....Topical Group on Plasma Astrophysics
GQI.....Quantum Information, Concepts and Computation
GR.....Gravitation Topical Group
GSNP.....Statistical and Non-linear
GSCCM .....Shock Compression of Condensed Matter

**Forums**

FEd .....Forum on Education in Physics
FGSA .....Forum on Graduate Student Affairs
FHP.....Forum on History of Physics
FIAP .....Forum on Industrial and Applied Physics
FIP .....Forum on International Physics
FPS .....Forum on Physics and Society

**Committees**

COM ..... Committee on Minorities
CSWP ..... Committee on the Status of Women in Physics

# MARCH EXHIBIT SHOW GUIDE 2006

The following is a list of exhibitors participating in the March Meeting 2006. For complete information on exhibiting companies and their booth numbers, consult the Pocket Epitome/Exhibitor Guide distributed at registration. Please take time during the meeting to visit the exhibits. You must wear your badge to be admitted to the exhibits.

**APS Exhibit Hours:**
Monday, March 13 • 10:00am–5:00pm
Tuesday, March 14 • 10:00am–5:00pm
Wednesday, March 15 • 10:00am–4:00pm

A&N Corporation
ADE Phase Shift
Advanced Research Systems, Inc.
AIP Education & Society of Physics Students
AJA International, Inc.
Ambios Technology
American Institute of Physics
American Magnetics Inc.
American Physical Society
Amuneal Manufacturing Corporation
Andeen-Hagerling, Inc.
Applied Surface Technologies
AR Worldwide
Asylum Research
ATOMISTIX
Attocube Systems AG
Blake Industries, Inc.
Bruker BioSpin Corporation, EPR Division
Cambridge Magnetic Refrigeration
Cambridge University Press
COMSOL, Inc.
Cryo Industries of America, Inc.
Cryogenic Control Systems, Inc.
Cryogenic Ltd.
Cryomagnetics, Inc.
Cryomech Inc.
DCA Instruments
Easylab Technologies
Elsevier
Gatan
GMW Associates
Hamamatsu Corporation
Hinds Instruments, Inc.
Horiba Jobin Yvon
ICEoxford®
IEE/Inspec
IOP Publishing
J.A. Woollam Co., Inc.
Janis Research Company, Inc.
Keithley Instruments
Kimball Physics, Inc.
KLA Tencor Corporation
Kurt J. Lesker Co.
Lake Shore Cryotronics, Inc.
Lay Tec GmbH
MacKichan Software
Mad City Labs, Inc.
Mantis Deposition
Material Research Society
MDC Vacuum Products/Insulator Seal
Molecular Imaging
NanoAndMore USA Corp.
Nanomagnetics Instruments
Nanonics Imaging Ltd.
National High Magnetic Field Laboratory
National Nanotechnology
Infrastructure Network
National Research Council of the National Academies
Nature Publishing Group
Neocera, Inc.
Nor-Cal Products, Inc.
NOVOControl
NRC Research Press
Ocean Optics, Inc.
Omicron Nanotechnology USA
Origin Lab Corporation
Oxford Applied Research
Oxford Instruments Superconductivity
Oxford University Press
Photonics Specta
Physics Today
PI (Physik Instrumente) LP
Princeton University Press
Quantum Design
Raith USA, Inc.
RHK Technology, Inc.
Rigaku Molecular Metrology
Royal Society of Chemistry
Scientific Cryomagnetics Ltd.
Scientific Instruments, Inc.
Signal Recovery
Smithsonian/NASA ADS
SPECS GmbH
SPECS Scientific Instruments, Inc.
Springer
Staib Instruments, Inc.
Stanford Research Systems
STAR Cyroelectronics
Stone Ridge Technology
Taylor & Francis Group LLC - CRC Press
Teachspin, Inc.
Tristan Technologies, Inc.
Varian Inc.
VAT, Inc.
Veeco Instruments
Vericold Technologies GmbH
VG Scienta
WebAssign
Wiley
Witec Instruments Corp.
Wolfram Research
World Scientific Publishing Company

# *Epitome of the March Meeting 2006*

**15:00 SUNDAY AFTERNOON**
**12 MARCH 2006**

1B GSCCM: **GSCCM Business Meeting**
Falkland, Marriott Waterfront Hotel

**19:30 SUNDAY EVENING**
**12 MARCH 2006**

1A **NAS Town Meeting**
Grand Ballroom Salon V, Marriott Waterfront Hotel

**8:00 MONDAY MORNING**
**13 MARCH 2006**

A1 DCMP: **Quantum Properties of Superconducting Nanowires**
*Sachdev, Tian, Rogachev, Khlebnikov, Arutyunov*
Ballroom IV, Baltimore Convention Center

A2 DCMP: **Magnetic-Ferroelectric Coupling in Multiferroics**
*Cheong, Vajk, Harris, Chu, Mostovoy*
Ballroom III, Baltimore Convention Center

A3 DCMP: **Bilayer 2D Systems: Interlayer Drag and Spontaneous Coherence**
*Pillarisetty, Das Sarma, Kivelson, Simon, Pellegrini*
Ballroom I, Baltimore Convention Center

A4 DPOLY: **Particle Self Assembly**
*Crocker, Starr, Hammond, Douglas, Walker*
308, Baltimore Convention Center

A5 DMP/ FIAP: **Advanced Materials for Energy Applications**
*Dresselhaus, Kanatzidis, Christensen, Mavrikakis, Schubert*
309, Baltimore Convention Center

A6 DCOMP: **Frontiers of Computational Materials**
*Asta, Johnson, Marzari, Hart, Kolmogorov*
310, Baltimore Convention Center

A7 DBP: **Bacterial Flagellar Dynamics, Polymorphism, and Conformational Spread**
*Powers, Stark, Darnton, Shaevitz*
307, Baltimore Convention Center

A8 DFD/ GSNP: **Pattern Formation and Nonlinear Dynamics**
314, Baltimore Convention Center

A9 DCMP: **Electronic Structure on Surfaces and in Reduced Dimensions**
301, Baltimore Convention Center

A10 DCP: **Focus Session: Physical Chemistry of Nanoscale Systems I**
*Nesbitt, Van Duyne*
302, Baltimore Convention Center

A11 DCP: **Focus Session: Promises and Challenges in Chemical Dynamics I**
*Shapiro, Lin*
303, Baltimore Convention Center

A12 DMP/ DCMP: **Focus Session: Steps, Growth, and Smoothing**
*Margetis*
304, Baltimore Convention Center

A13 DCP/ DBP: **Focus Session: Spectroscopy of Biomolecules from Isolated Molecules to Cell Environment I**
*Anfinrud, Spence*
305, Baltimore Convention Center

A15 DCMP: **Metals: 1D, 2D, 3D**
311, Baltimore Convention Center

A16 FIAP: **Focus Session: Hydrogen Storage I**
*Frederick Pinkerton*
312, Baltimore Convention Center

A17 FIAP: **Focus Session: Structure and Properties of Nanoscale Oxide Films**
*Pennycook, Freund*
313, Baltimore Convention Center

A18 DMP: **Focus Session: Carbon Nanotubes: Synthesis and Growth I**
*Hata*
315, Baltimore Convention Center

A19 GMAG/DMP: **Focus Session: Optical and Electrical Spin Generation in Semiconductors**
*Sipe*
316, Baltimore Convention Center

A20 DMP/GMAG: **Focus Session: Complex Oxide Thin Films Surfaces and Interfaces I: Superlattice Fabrication and Properties**
*Varela*
317, Baltimore Convention Center

A21 DFD: **Colloids I: Emulsions, Foams, and Suspensions**
318, Baltimore Convention Center

A22 GMAG/FIAP/DMP: **Focus Session: Current Driven Magnetization Dynamics I**
*Pufall*
319, Baltimore Convention Center

A23 GMAG: **Strongly Correlated Electrons I**
320, Baltimore Convention Center

A24 DPOLY: **Semi-Crystalline and Structured Polymers**
321, Baltimore Convention Center

A25 DPOLY/DMP: **Focus Session: Organic Field Effect Transistors**
*Marks*
322, Baltimore Convention Center

A26 DBP: **Biomolecular Computation**
323, Baltimore Convention Center

A28 DPOLY: **Polymer Blends**
325, Baltimore Convention Center

A29 DBP: **Experimental Techniques in Biophysics**
326, Baltimore Convention Center

A30 DPOLY: **Focus Session: Block Copolymer Dynamics**
*Morse*
327, Baltimore Convention Center

A31 DCMP: **Metallic Nanostructures**
328, Baltimore Convention Center

A32 DCMP: **Fullerenes**
329, Baltimore Convention Center

A33 GSNP: **Focus Session: Econophysics**
*Yakovenko*
336, Baltimore Convention Center

A35 DMP: **Focus Session: Nanoscale Thermal, Thermoelectric and Mass Transport: Measurement and Characterization**
*Fon*
338, Baltimore Convention Center

A36 DCMP: **Structural, Optical, and Electronic Properties of Nanostructures**
339, Baltimore Convention Center

A38 DCMP: **Superconductivity—Vortex Matter**
341, Baltimore Convention Center

A39 DMP: **Focus Session: Magnesium Diboride and Related Compounds: Multi Gap Superconductivity**
342, Baltimore Convention Center

A40 TGQI/DCMP: **Quantum Entanglement**
343, Baltimore Convention Center

A41 DCMP: **Quantum Fluids and Solids**
344, Baltimore Convention Center

A42 DMP/DCOMP: **Focus Session: Planetary Materials I**
*Gironcoli, Lin*
345, Baltimore Convention Center

A43 DAMOP: **Focus Session: Strongly Interacting Fermi Gases and the BCS-BEC Crossover I**
*Denschlag*
346, Baltimore Convention Center

A45 GMAG: **Cuprates and Nickelates**
348, Baltimore Convention Center

A46 DMP: **Focus Session: Wide Bandgap Semiconductors I**
*Wetzel*
349, Baltimore Convention Center

**11:15 MONDAY MORNING**
**13 MARCH 2006**

B1 DCMP: **DCMP/DCOMP Prize Session**
*Clark, Meyer, Merlin, Vanderbilt*
Ballroom IV, Baltimore Convention Center

B2 DCMP: **Solid Helium**
*Clark, Beamish, Dai, Reatto, Ceperley*
Ballroom III, Baltimore Convention Center

B3 GSNP: **Uncovering the Structure of Complex Networks**
*Newman, Guimera, Vicsek, Muñoz, Almaas*
Ballroom I, Baltimore Convention Center

B4 DMP/ FIAP: **Advances in ZnO Materials Physics and Applications**
*Van de Walle, Tsukazaki, Brillson, Hsu, Norton*
308, Baltimore Convention Center

B5 FPS: **Nuclear Proliferation & Nuclear Terrorism**
*Cirincione, Fetter, Park, Carter*
309, Baltimore Convention Center

B6 DCMP: **Spin-Based Quantum Computing**
*Hanson, Ghosh, Flatté, Finley, Burkard*
310, Baltimore Convention Center

B7 DBP/ DCMP: **Bionanotechnology: Application and Fundamental Aspects of Processes at Nano-scale**
*Eisenberg, Kosztin, Stein, Yu, Kohli*
307, Baltimore Convention Center

B8 GSNP/ DFD: **Focus Session: Granular Materials Near Jamming**
*Campbell, Daniels*
314, Baltimore Convention Center

B9 DCMP: **Phase Transitions, Dynamics, and Excitations**
301, Baltimore Convention Center

B10 DCP: **Focus Sessions: Physical Chemistry of Nanoscale System II**
*El-Sayed, Dexheimer*
302, Baltimore Convention Center

B11 DCP: **Focus Session: Promises and Challenges in Chemical Dynamics II**
*Jortner, Brus*
303, Baltimore Convention Center

B12 DCMP/ DMP: **Quantum Metal Films and Overlayer Structures**
304, Baltimore Convention Center

B13 DCP/ DBP: **Focus Session: Spectroscopy of Biomolecules from Isolated Molecules to Cell Environment II**
*de Vries, Jarrold, Jockusch*
305, Baltimore Convention Center

B15 DCMP: **Metals: Lattice, Low D, Phonons**
*Burin*
311, Baltimore Convention Center

B16 FIAP: **Focus Session: Molecular-Scale Electronics I**
*Champagne*
312, Baltimore Convention Center

B17 FIAP: **Focus Session: Phase Transitions and Domains in Ferroelectric Nanostructures I**
*Levanyuk*
313, Baltimore Convention Center

B18 DMP: **Focus Session: Carbon Nanotubes: Synthesis, Processing and Characterization**
*Arnold*
315, Baltimore Convention Center

B19 GMAG/ DMP: **Focus Session: Transition Metal Oxide Ferromagnetic Semiconductors**
*Ogale*
316, Baltimore Convention Center

B20 GMAG/ DMP: **Focus Session: Phase Competition and Separation in Pervoskite Oxides**
*Wu*
317, Baltimore Convention Center

B21 DFD: **Colloids II: Colloidal Crystals, Gels, and Glasses**
318, Baltimore Convention Center

B22 GMAG/ FIAP/ DMP: **Focus Session: Current Driven Magnetization Dynamics II**
*Beach*
319, Baltimore Convention Center

B23 GMAG: **Quantum Spin Chains I**
320, Baltimore Convention Center

B26 DBP/ DPOLY: **Focus Session: Single Molecule Biophysics: DNA & RNA**
*Nelson*
323, Baltimore Convention Center

B28 DBP: **Experimental Techniques in Biomaterials Science**
325, Baltimore Convention Center

B29 DBP/ GSNP: **Focus Session: Micro-Organism Motility**
*Bodenschatz*
326, Baltimore Convention Center

B31 DCMP: **Insulating Nanostructures**
328, Baltimore Convention Center

B32 DCOMP/ DMP: **Focus Session: Computational Nanoscience I**
*Roundy*
329, Baltimore Convention Center

B33 GSNP: **Financial Markets and Other Applications of Statistical Physics**
336, Baltimore Convention Center

B35 DMP: **Focus Session: Nanoscale Thermal, Thermoelectric and Mass Transport: Theory and Simulation**
*Heinze*
338, Baltimore Convention Center

B36 DCMP: **Electronic Properties of Nanowires**
339, Baltimore Convention Center

B37 DCMP: **High-Tc: STM and Pseudogap**
340, Baltimore Convention Center

B38 DCMP: **Superconducting Devices and Applications**
341, Baltimore Convention Center

B39 DCMP: **Superconductivity—Magnetic Properties**
342, Baltimore Convention Center

B40 TGQI/ DCMP: **Topics in Quantum Foundations**
343, Baltimore Convention Center

B42 **SPS Undergraduate Research I**
345, Baltimore Convention Center

B43 DAMOP: **BEC in Trapped Atomic Gases**
346, Baltimore Convention Center

B46 DMP: **Focus Session: Wide Band Gap Semiconductors II**
*Wright*
349, Baltimore Convention Center

**13:30 MONDAY AFTERNOON 13 MARCH 2006**

B34 **Session on Authoring**
337, Baltimore Convention Center

**14:00 MONDAY AFTERNOON 13 MARCH 2006**

C1 **Poster Session I**
Exhibit Hall 2:00pm–5:00pm (DPOLY session: 11:15am–2:15pm), Baltimore Convention Center

**14:30 MONDAY AFTERNOON 13 MARCH 2006**

D1 DCMP: **Fluctuation and Relaxation Near Jamming**
*Langer, Makse, Abate, Silbert, Losert*
Ballroom IV, Baltimore Convention Center

D2 DCMP: **Quantum Hall Effect in Graphene**
*Kim, Geim, Sharapov, De Heer*
Ballroom III, Baltimore Convention Center

D3 FIP: **Scientists from Developing Countries: Is There an Effective Way to Support Meaningful Research?**
*Kofane, Ben lakdar, de Brito Cruz, M'Passi-Mabiala*
Ballroom I, Baltimore Convention Center

D4 DPOLY/ DMP: **Organic Electronics**
*Friend, Martin, Loo, Chabinyc, Lin*
308, Baltimore Convention Center

D5 FIAP: **Catalysis and Complexity: Ken Hass Memorial**
*Schneider, Wolverton, Carlsson, Davis*
309, Baltimore Convention Center

D6 DCOMP: **Simulating Hydrogen Storage: From Current Challenges to Future Promises**
*Johnson, Tse, Zhao, Jena, Goddard*
310, Baltimore Convention Center

D7 GMAG: **New Results in Geometrically Frustrated Magnets**
*Mendels, Moessner, Gardner, Schiffer, Lunkenheimer*
307, Baltimore Convention Center

D8 DFD/ GSNP: **Patterns and Instabilities I**
314, Baltimore Convention Center

D9 DBP: **Methods in Nanobiotechnology**
*Roukes, Austin, Michl, Wiseman, Hla*
301, Baltimore Convention Center

D10 DCP: **Focus Session: Physical Chemistry of Nanoscale System III**
*Leone, Xie*
302, Baltimore Convention Center

D11 DCP: **Focus Session: Promises and Challenges in Chemical Dynamics III**
*Kawasaki*
303, Baltimore Convention Center

D12 DCMP/ DMP: **Morphological Evolution and Instabilities**
304, Baltimore Convention Center

D13 DCP/ DBP: **Focus Session: Spectroscopy of Biomolecules from Isolated Molecules to Cell Environment III**
*Baumgart, Ha*
305, Baltimore Convention Center

D15 DCMP: **Focus Session: Atomic Tunneling, Films, Nanostructures**
*Enss*
311, Baltimore Convention Center

D16 FIAP: **Focus Session: Negative Refractive Index I**
*Brueck*
312, Baltimore Convention Center

D17 FIAP: **Focus Session: Phase Transitions and Domains in Ferroelectric Nanostructures II**
*Gregg*
313, Baltimore Convention Center

D18 DMP: **Focus Session: Carbon Nanotubes: Synthesis and Growth II**
315, Baltimore Convention Center

D19 GMAG/ DMP: **Focus Session: Semiconductor Spin Injection and Detection**
*Crowell*
316, Baltimore Convention Center

D20 DMP/ GMAG: **Focus Session: Multiferroics I**
317, Baltimore Convention Center

D21 DFD: **Colloids III: Particles at Interfaces and in Confined Geometries**
318, Baltimore Convention Center

D22 GMAG/ DMP: **Focus Session: Magnetic Nanopatterns**
*Chien*
319, Baltimore Convention Center

D23 GMAG/ DMP/ DCOMP: **Focus Session: MAGTHY I/Spin Structures and Dynamics**
*Dobrovitski*
320, Baltimore Convention Center

D25 DPOLY: **Focus Session: Particle Dynamics and Organization; Polymer Tethers and Interfacial Segregation**
*Smith*
322, Baltimore Convention Center

D26 DBP/ DPOLY: **Focus Session: Dynamics of Nuclei Acid-Protein Interaction: Single Molecule**
*Wang, Wuite*
323, Baltimore Convention Center

D27 DCOMP: **Focus Session: Novel Computational Algorithms I**
*Hu, Aspuru-Guzik*
324, Baltimore Convention Center

D28 DPOLY: **Block Copolymer Thin Films**
325, Baltimore Convention Center

D29 DBP/ GSNP: **Molecular Machines and Motors**
*Flood, Goldman*
326, Baltimore Convention Center

D30 DPOLY: **Multiphase Polymer Materials**
327, Baltimore Convention Center

D31 DCMP: **Properties of Semiconducting Nanostructures**
328, Baltimore Convention Center

D32 DCOMP/DMP: **Focus Session: Computational Nanoscience II**
329, Baltimore Convention Center

D33 DMP/GSNP: **Focus Session: Friction, Fracture and Deformation I**
*Dickinson*
336, Baltimore Convention Center

D35 DMP: **Focus Session: Thermal Transport and Thermoelectricity in Nanotubes and Graphene**
*Shi*
338, Baltimore Convention Center

D38 DMP: **Focus Session: Superconductivity—Properties of Doped and Irradiated Magnesium Diboride and Related Compounds**
*Putti*
341, Baltimore Convention Center

D39 DCMP: **Spin Properties of Superconductors**
342, Baltimore Convention Center

D40 TGQI/DCMP: **Focus Session: Foundations of Quantum Theory**
*Hardy*
343, Baltimore Convention Center

D42 SPS: **SPS Undergraduate Research II**
345, Baltimore Convention Center

D43 DAMOP: **Focus Session: Vortices and Vortex Lattices in Fermi and Bose Superfluid Gases**
*Zwierlein*
346, Baltimore Convention Center

D45 GMAG: **Strongly Correlated Electrons on Triangular Lattices**
348, Baltimore Convention Center

D46 DMP: **Focus Session: Wide Band Gap Semiconductors III**
*Huang*
349, Baltimore Convention Center

## 17:45 MONDAY EVENING 13 MARCH 2006

E5 **APS Prizes and Awards Ceremony**
309, Baltimore Convention Center

## 18:45 MONDAY EVENING 13 MARCH 2006

E6 **Welcome Reception**
Ballroom II, Baltimore Convention Center

## 20:00 MONDAY EVENING 13 MARCH 2006

F50 DCMP: **Emerging Emergent Phenomena**
*Witten, Lolle, Barabási, Sadoulet*
Grand Salons V-VI, Marriott Waterfront Hotel

## 8:00 TUESDAY MORNING 14 MARCH 2006

G1 **Nobel Prize Symposium and Special Prize Session**
*Hänsch, Hall, Glauber, Su, Grobe*
Ballroom IV, Baltimore Convention Center

G2 DCMP: **Quantum Criticality in Cuprates**
*Chamon, Tallon, Shibauchi, Lake, Broun*
Ballroom III, Baltimore Convention Center

G3 DCMP: **Coupled Superconducting Qubits**
*Shnirman, Martinis, Schuster, Plantenberg, Morpurgo*
Ballroom I, Baltimore Convention Center

G4 DPOLY: **Polymer Physics Prize**
*Leibler, Möller, Fredrickson, Candau, Colby*
308, Baltimore Convention Center

G5 DMP/FIAP: **Advanced Materials for Solar Energy Utilization**
*Lewis, Kurtz, Yong, Moore, Carlson*
309, Baltimore Convention Center

G7 GSNP: **Shear-Induced Patterns in Complex Fluids and Granular Matter**
*van Saarloos, Reichmann, Register, Davidovitch, Jaeger*
307, Baltimore Convention Center

G8 DFD/ GSNP: **Patterns and Instabilities II**
314, Baltimore Convention Center

G10 DCP: **Focus Sessions: Physical Chemistry of Nanoscale System IV**
*Yang, Xia*
302, Baltimore Convention Center

G11 DCP: **Focus Session: Promises and Challenges in Chemical Dynamics IV**
*Shafer-Ray*
303, Baltimore Convention Center

G12 DCMP/ DMP: **Self-Assembled Nanostructures: Growth and Patterning**
304, Baltimore Convention Center

G13 DCP/ DBP: **Focus Session: Spectroscopy of Biomolecules from Isolated Molecules to Cell Environment IV**
*Zwier, Hochstrasser, Mons*
305, Baltimore Convention Center

G15 DCMP: **Mechanical Properties of Metals**
311, Baltimore Convention Center

G16 FIAP: **Focus Session: Negative Refractive Index II**
*Narimanov*
312, Baltimore Convention Center

G17 FIAP: **Focus Session: Emerging Research Devices and Materials for Microelectronics Industry I**
*Vogel*
313, Baltimore Convention Center

G18 DMP: **Focus Session: Carbon Nanotubes: Electronic and Optical Properties I**
*Spataru*
315, Baltimore Convention Center

G19 GMAG/ DMP: **Focus Session: III-V Magnetic Semiconductors I**
*Poggio*
316, Baltimore Convention Center

G20 DMP/ GMAG: **Focus Session: Complex Oxide Thin Films Surfaces and Interfaces II: Surfaces and Theory**
317, Baltimore Convention Center

G21 DFD: **Colloids IV: Polymeric and Colloid-Polymer Systems**
318, Baltimore Convention Center

G22 GMAG/ DMP: **Focus Session: Magnetic Nanoparticles I**
*Leslie-Pelecky*
319, Baltimore Convention Center

G23 GMAG/ DMP/ DCOMP: **Focus Session: MAGTHY II/ Transport & General**
*Yao*
320, Baltimore Convention Center

G24 DPOLY: **Polymer Nanomaterials I**
321, Baltimore Convention Center

G25 DPOLY: **Structure and Dynamics of Functional Macromolecules**
322, Baltimore Convention Center

G26 DBP: **Focus Session: Trapping of Nanoscale Biological Objects**
*Cohen, Gratton*
323, Baltimore Convention Center

G27 DCOMP: **Focus Session: Novel Computational Algorithms II**
*Bai, Baroni*
324, Baltimore Convention Center

G28 DPOLY: **Focus Session: Microphysical Properties of Block Copolymer Aggregates I**
*Discher*
325, Baltimore Convention Center

G29 DBP: **Focus Session: Physical and Engineering Constraints on the Function of Biological Systems**
*Lezon, Doyle*
326, Baltimore Convention Center

G30 DPOLY/ DMP: **Focus Session: Electronic Transport in Organic Films**
*De Feyter, Charra*
327, Baltimore Convention Center

G31 DCOMP/ DMP: **Focus Session: Simulation of Complex Materials I**
*Wagner*
328, Baltimore Convention Center

G32 DMP/ GMAG: **Focus Session: Orbital/Charge Order in Complex Oxides**
*Ye*
329, Baltimore Convention Center

G33 GSNP: **GSNP Student Award Session and Glasses**
336, Baltimore Convention Center

G34 DFD: **Glassy Dynamics and Jamming**
337, Baltimore Convention Center

G35 DCMP: **Nanoparticles, Nanotubes and Nanocrystals: Optical and Structural Properties**
338, Baltimore Convention Center

G37 DMP: **Focus Session: Nanoscale Materials Physics of Phase Transitions I**
*Dawber*
340, Baltimore Convention Center

G38 DMP: **Focus Session: Superconductivity—Carbon Alloying of Magnesium Diboride and Related Compounds**
*Wilke*
341, Baltimore Convention Center

G39 DCMP/ DCOMP: **Focus Session: Superconductivity: Theory and Computation I**
*Scalapino*
342, Baltimore Convention Center

G40 DMP: **Focus Session: Materials for Quantum Computing I**
343, Baltimore Convention Center

G41 DCMP: **Supersolid**
344, Baltimore Convention Center

G42 FEd: **Physics Education Research and Undergraduate Education**
345, Baltimore Convention Center

G44 DCMP: **Charge-Density Waves**
347, Baltimore Convention Center

G45 GMAG: **Phase Transitions in Ruthenates**
348, Baltimore Convention Center

G46 FIAP: **QHE, Including Graphene**
349, Baltimore Convention Center

## 11:15 TUESDAY MORNING 14 MARCH 2006

H1 GQI: **Quantum Information, Concepts and Computation**
*Blatt, Yamamoto, Raizen, Gisin, Whaley*
Ballroom IV, Baltimore Convention Center

H2 DCMP: **Spin Liquids in 2D Frustrated Quantum Magnets**
*Coldea, Alicea, Kanoda, Motrunich, Lee*
Ballroom III, Baltimore Convention Center

H3 DCMP: **Soft Interfaces**
*Quere, Zhang, Stebe, Hilgenfeldt, Gopal*
Ballroom I, Baltimore Convention Center

H4 DCMP: **Physics for Everyone and Depletion Forces In Vitro and Out of Equilibrium**
*Dahlberg, Falco, Schwartz, Snir, Lewis*
308, Baltimore Convention Center

H5 FEd/ FGSA/ FPS/ CSWP: **Forum: What Has Actually Changed in Physics Departments in the Situation for Women, Graduate Students and Other People?**
309, Baltimore Convention Center

H6 DCOMP: **The Response of Extended Systems to Electrical and Magnetic Fields: Novel, Theoretical, and Computational Methods**
*Thonhauser, MacDonald, Cai, Umari, Ghosez*
310, Baltimore Convention Center

H7 DBP: **Nanopore Biophysics**
*Kasianowicz, Dekker, Movileanu, Li, Aksimentiev*
307, Baltimore Convention Center

H8 GSNP: **Focus Session: Jamming in Glasses, Grains, and Gels I**
*Maloney*
314, Baltimore Convention Center

H10 DCP: **Focus Session: Frontiers in Computational Chemical Physics I**
*Lin, Angel*
302, Baltimore Convention Center

H11 DCP: **Focus Session: Chemical and Spectroscopic Applications of Nonlinear Optics I**
*Eisenthal, Shultz*
303, Baltimore Convention Center

H12 DCMP/ DMP: **Thin Film Growth and Interfaces**
304, Baltimore Convention Center

H13 DCP: **Colloid and Polymer Interfaces**
305, Baltimore Convention Center

H15 DCMP: **Metals: Electronic Structure, Fermiology, Transport**
311, Baltimore Convention Center

H16 FIAP: **Focus Session: Hydrogen Storage II**
*Ahn*
312, Baltimore Convention Center

H17 FIAP: **Focus Session: Emerging Research Devices and Materials for Microelectronics Industry II**
*Coufal*
313, Baltimore Convention Center

H18 DMP: **Focus Session: Carbon Nanotubes: Electronic and Optical Properties II**
*Lienau, Chang*
315, Baltimore Convention Center

H19 GMAG/ DMP: **Focus Session: III-V Magnetic Semiconductors II**
*Burch*
316, Baltimore Convention Center

H20 GMAG: **Frustration in 3D**
317, Baltimore Convention Center

H21 DFD: **Focus Session: Microfluidic Physics I**
*Paoletti*
318, Baltimore Convention Center

H22 GMAG/ DMP: **Focus Session: Nanoparticles and Nanocomposites**
*Wang*
319, Baltimore Convention Center

H23 GMAG/ DMP/ FIAP: **GMR and AMR**
320, Baltimore Convention Center

H24 DPOLY: **Polymers at Interfaces**
321, Baltimore Convention Center

H25 DPOLY: **Focus Session: Particle Dynamics and Organization**
322, Baltimore Convention Center

H27 DCOMP: **Computational Methods: Multiscale Modeling**
324, Baltimore Convention Center

H28 DPOLY/ DMP: **Focus Session: Energetics and Transport in Conjugated Organics**
*Silva*
325, Baltimore Convention Center

H29 DBP: **Focus Session: Physical Aspects of Morphogenesis: Computational Approaches**
*Brodland, Jiang*
326, Baltimore Convention Center

H30 DPOLY: **Padden Award Symposium**
327, Baltimore Convention Center

H31 DCOMP/ DMP: **Focus Session: Simulation of Complex Materials II**
*Ogitsu*
328, Baltimore Convention Center

H32 DCOMP/ DMP: **Focus Session: Computational Nanoscience III**
*Zhang*
329, Baltimore Convention Center

H33 DMP/ GSNP: **Focus Session: Friction, Fracture and Deformation II**
*Gnecco*
336, Baltimore Convention Center

H35 DCMP: **Electronic Properties of Quantum Wells and Superlattices**
338, Baltimore Convention Center

H36 DMP: **Focus Session: Single Molecule Conductance**
*Weber*
339, Baltimore Convention Center

H37 DMP: **Focus Session: Nanoscale Materials Physics of Phase Transitions II**
*Albrecht*
340, Baltimore Convention Center

H38 DCMP: **Superconductivity—Disordered Thin Films and Quantum Phenomena**
341, Baltimore Convention Center

H39 DCMP: **Focus Session: Superconductivity—Josephson Junctions and Pairing State Symmetry**
*Klemm*
342, Baltimore Convention Center

H40 DMP: **Focus Session: Materials for Quantum Computing II**
*Buhrman*
343, Baltimore Convention Center

H41 DMP: **Dielectric, Ferroelectric, and Piezoelectric Oxides I**
344, Baltimore Convention Center

H42 GSCCM/ DCMP: **Focus Session: Dynamic Compression**
*Hayes, Minich*
345, Baltimore Convention Center

H43 DAMOP: **Focus Session: Strongly Interacting Fermi Gases and the BCS-BEC Crossover II**
*Regal*
346, Baltimore Convention Center

H44 DCMP: **Quantum Phase Transitions**
347, Baltimore Convention Center

H45 DCMP: **Theoretical Methods in Strongly Correlated Electron Systems**
348, Baltimore Convention Center

H46 DMP: **Focus Session: Wide Band Gap Semiconductors IV**
*Qian*
349, Baltimore Convention Center

## 14:00 TUESDAY AFTERNOON 14 MARCH 2006

J1 **Poster Session II**
Exhibit Hall, 2:00pm–5:00pm, Baltimore Convention Center

## 14:30 TUESDAY AFTERNOON 14 MARCH 2006

K1 DAMOP: **Optical Frequency Clocks and Experimental Quantum Optics**
*Gill, Udem, Ye, Bergquist, Haroche*
Ballroom IV, Baltimore Convention Center

K2 DCMP: **Exotic Ordering in Spinels**
*Croft, Horibe, Khomskii, Sushkov, Radaelli*
Ballroom III, Baltimore Convention Center

K3 DCMP: **Electron Doped High Tc Superconductors**
*Dagan, Blumberg, Takahashi, Motoyama, Naito*
Ballroom I, Baltimore Convention Center

K4 DMP/ CSWP: **DMP/CSWP Prize Symposium**
*Chelikowsky, Cao, Dai, Zettl*
308, Baltimore Convention Center

K5 FIAP: **Microelectronics for Mid-Infrared through Terahertz**
*Gmachl, Prober, Shaner, Tredicucci, Schmidt*
309, Baltimore Convention Center

K6 COM: **Minorities in the Nanosciences**
*Mason, James, Noveron, Stokes*
310, Baltimore Convention Center

K7 DBP: **New Methods and Algorithms for Biomolecular Modeling**
*Darve, Sagui, Thorpe, Tuckerman, Yang*
307, Baltimore Convention Center

K8 GSNP: **Focus Session: Jamming in Glasses, Grains and Gels II**
*Blair*
314, Baltimore Convention Center

K10 DCP: **Focus Session: Frontiers in Computational Chemical Physics II**
*Reuter*
302, Baltimore Convention Center

K11 DCP: **Focus Session: Chemical and Spectroscopic Applications of Nonlinear Optics II**
*Shen, Simpson, Morita*
303, Baltimore Convention Center

K12 DMP/DCMP: **Focus Session: Magnetic Thin Films and Narrow Gap Semiconductors**
*Weitering*
304, Baltimore Convention Center

K13 DCP: **Atomic And Molecular Processes at Solid Surfaces**
305, Baltimore Convention Center

K16 FIAP: **Focus Session: Molecular-Scale Electronics II**
*Karna*
312, Baltimore Convention Center

K17 FIAP: **Focus Session: Si, Ge and SiGe Nanostructures**
*Ross, Kamins*
313, Baltimore Convention Center

K18 DPOLY: **Focus Session: Dillon Medal Symposium**
*Urayama*
315, Baltimore Convention Center

K19 GMAG/DMP: **Focus Session: III-V Magnetic Semiconductors III**
*van Schilfgaarde*
316, Baltimore Convention Center

K20 DMP/GMAG: **Focus Session: Multiferroics II—Hexagonal Systems**
*Fennie*
317, Baltimore Convention Center

K21 DFD: **Colloids V**
318, Baltimore Convention Center

K22 GMAG/FIAP/DMP: **Focus Session: Magnetization Dynamics**
*Rasing*
319, Baltimore Convention Center

K23 GMAG: **Quantum Magnets: BEC and 2D**
320, Baltimore Convention Center

K24 DPOLY: **Polymer Nanomaterials II**
321, Baltimore Convention Center

K25 DPOLY: **Polymer Electrolytes and Conduction**
322, Baltimore Convention Center

K26 DBP/DCMP: **Focus Session: Single Molecule Biophysics I**
*Chu*
323, Baltimore Convention Center

K27 DCOMP: **Density Functional Theory**
324, Baltimore Convention Center

K28 DPOLY: **Focus Session: Microphysical Properties of Block Copolymer Aggregates II**
*Santore*
325, Baltimore Convention Center

K29 DBP: **Proteins Structure and Function**
326, Baltimore Convention Center

K30 DMP: **Carbon Nanotubes: Applications and Novel Phenomena**
327, Baltimore Convention Center

K31 DCOMP/DMP: **Focus Session: Simulation of Complex Materials III**
*Blum*
328, Baltimore Convention Center

K32 DCOMP/DMP: **Focus Session: Computational Nanoscience IV**
329, Baltimore Convention Center

K33 GSNP: **Novel Moving Boundary Problems**
*Krug, Kessler, Ebert, Goldstein, Karma*
336, Baltimore Convention Center

K34 **Panel Discussion**
337, Baltimore Convention Center

K35 DCMP: **Electronic Properties and the Kondo Effect in Quantum Dots**
338, Baltimore Convention Center

K36 GMAG: **Magnetic Domains and Applied Magnetic Materials**
339, Baltimore Convention Center

K37 DCMP: **Superconductivity—Time Resolved Optical and Inelastic X-ray Scattering in Cuprates**
340, Baltimore Convention Center

K38 DCMP: **Superconductivity—Mesoscopics and Theory**
341, Baltimore Convention Center

K39 DCOMP/DCMP: **Focus Session: Superconductivity—Theory and Computation II**
*Fabrizio*
342, Baltimore Convention Center

K40 DMP: **Focus Session: Materials for Quantum Computing III**
*McDermott*
343, Baltimore Convention Center

K41 DMP: **Focus Session: Dielectric, Ferroelectric, and Piezoelectric Oxides II**
*Venturini*
344, Baltimore Convention Center

K42 DMP/DCOMP: **Focus Session: Planetary Materials II**
345, Baltimore Convention Center

K43 DAMOP: **Trapped Fermi Gases**
346, Baltimore Convention Center

K44 DCMP: **Transport in Disordered Electronic Systems**
347, Baltimore Convention Center

K45 DCMP: **Heavy Fermions: Experiment**
348, Baltimore Convention Center

K46 FIAP: **Spectroscopy of Semiconductors**
349, Baltimore Convention Center

**17:30 TUESDAY EVENING**
**14 MARCH 2006**

L9 GIMS: **GIMS Business Meeting**
301, Baltimore Convention Center

L10 DCP: **DCP Business Meeting**
302, Baltimore Convention Center

L16 FIAP: **FIAP Business Meeting**
312, Baltimore Convention Center

L18 DPOLY: **DPOLY Business Meeting**
315, Baltimore Convention Center

L23 GMAG: **GMAG Business Meeting**
320, Baltimore Convention Center

L29 DBP: **DBP Business Meeting**
326, Baltimore Convention Center

L33 GSNP: **GSNP Business Meeting**
336, Baltimore Convention Center

L40 TGQI: **TGQI Business Meeting**
343, Baltimore Convention Center

L48 FIP: **FIP Business Meeting**
Galena, Marriott Waterfront Hotel

**17:45 TUESDAY EVENING**
**14 MARCH 2006**

L7 DBP: **Flexible Molecular Recognition: The New Paradigm**
*Matthews, Kern, Taylor, Jennings, Wang*
307, Baltimore Convention Center

**19:00 TUESDAY EVENING**
**14 MARCH 2006**

L49 DCMP: **DCMP Business Meeting**
Dover A, Marriott Waterfront Hotel

L50 DMP: **DMP Business Meeting**
Dover B, Marriott Waterfront Hotel

**19:30 TUESDAY EVENING**
**14 MARCH 2006**

M50 FPS: **Intelligent Design: Its Impact and Responses to It**
*Gunn, Berman, Slakey, Dean*
Grand Salon V, Marriott Waterfront Hotel

**8:00 WEDNESDAY MORNING**
**15 MARCH 2006**

N1 DCMP: **Topological Phases and Quantum Computing**
*Kitaev, Hermele, Freedman, Stern, Fendley*
Ballroom IV, Baltimore Convention Center

N2 DCMP: **Nanoscale Crystals**
*Craig, Alivisatos, Drndic, Krauss*
Ballroom III, Baltimore Convention Center

N3 DCMP: **Insulating Cobaltates: Mottness on a Triangular Lattice**
*Gasparovic, Hasan, Zandbergen, Balicas, Imai*
Ballroom I, Baltimore Convention Center

N4 DPOLY/DMP: **Polymer Crystallization**
*Cheng, Hsiao, Ungar, Muthukumar, Granasy*
308, Baltimore Convention Center

N5 FIAP: **Pake and AIP Industrial Physics Prizes**
*Duke, Semerjian, Palffy-Muhoray, Lubell, Edelstein*
309, Baltimore Convention Center

N6 DAMOP: **Fermi Superfluid Gases: Non-equal Spin Polarization (FFLO State) and p-Wave pairing**
*Son, Yip, Hulet, Diener, de Melo*
310, Baltimore Convention Center

N7 DCOMP: **Recent Advances in the Computation of Optical and Transport Properties of Nanostructures**
*Weissker, Bester, Gebauer, Sanvito, Pecchia*
307, Baltimore Convention Center

N8 DFD: **Granular Flows**
314, Baltimore Convention Center

N10 DCP: **Focus Session: Frontiers in Computational Chemical Physics III**
*Cui*
302, Baltimore Convention Center

N11 DCP: **Focus Session: Aerosols, Clusters, Droplets: Physics and Chemistry of Nanoobjects I: Helium Nanodroplets I**
*Drabbels, Tiggesbäumker*
303, Baltimore Convention Center

N12 DMP/ DCMP: **Focus Session: Alloy and Interface Composition**
*Hannon*
304, Baltimore Convention Center

N13 DCP: **Focus Session: Ultrafast and Ultrahigh Field Chemistry I: Strong Field Phenomena**
*Jones, Yamanouchi*
305, Baltimore Convention Center

N16 FIAP: **Focus Session: Hydrogen Storage III**
*Yildirim*
312, Baltimore Convention Center

N17 FIAP: **Focus Session: Semiconductors for THz and IR I**
*Perera*
313, Baltimore Convention Center

N18 DMP: **Focus Session: Carbon Nanotubes: Transport I**
*Strunk*
315, Baltimore Convention Center

N19 GMAG/ DMP: **Semiconductor Spin Transport**
316, Baltimore Convention Center

N20 DMP/ GMAG: **Focus Session: Complex Oxide Thin Films Surfaces and Interfacess III: New Materials, New Techniques, and Effects of Strain**
317, Baltimore Convention Center

N21 DFD: **Microfluidic Physics II**
318, Baltimore Convention Center

N22 GMAG/ DMP: **Focus Session: Magnetic Vortices and Exchange Biased Thin Films**
*Roshchin*
319, Baltimore Convention Center

N23 GMAG/ DMP/ DCOMP: **Focus Session: MAGTHY III: Oxides and Phase Transitions**
*Schulthess*
320, Baltimore Convention Center

N24 DPOLY: **Structure and Dynamics in Polymer Thin Films**
321, Baltimore Convention Center

N25 DPOLY/ DMP: **Focus Session: Organic Photovoltaics**
*Inganäs*
322, Baltimore Convention Center

N26 DBP/ DFD: **Focus Session: DNA and Protein Analysis with Micro and Nano Fluidics**
*Riehn, Hansen*
323, Baltimore Convention Center

N27 DCOMP: **Electronic Structure I**
324, Baltimore Convention Center

N28 DPOLY: **Polymer Adsorption and Surface Modification**
325, Baltimore Convention Center

N29 DBP: **Focus Session: Physical Models of Ion Channel Function**
*Gillespie, Coalson*
326, Baltimore Convention Center

N30 DPOLY: **Block Copolymer Phase Behavior**
*327, Baltimore Convention Center*

N31 DCMP: **Carbon Nanotubes: Theory**
*328, Baltimore Convention Center*

N32 DMP/ DPOLY: **Focus Session: Carbon Nanotubes: Composites and Applications**
*Baughman*
329, Baltimore Convention Center

N33 GSNP: **Focus Session: Instabilities & Turbulence in Complex Fluids**
*Sureshkumar*
336, Baltimore Convention Center

N35 GSNP: **Focus Session: Organization of Complex Networks**
*Mendes*
338, Baltimore Convention Center

N36 DMP: **Focus Session: Optical Properties of Nanostructures with S, Se, Te, and Ge**
339, Baltimore Convention Center

N37 DMP: **Focus Session: Nanoscale Fabrication, Assembly and Semiconductor Nanowires**
*Misra*
340, Baltimore Convention Center

N38 DCMP: **Transport Properties of High-Tc Superconductors**
341, Baltimore Convention Center

N39 DMP: **Focus Session: Superconductivity—Thin Films and Junctions Magnesium Diboride and Related Compounds**
*Xi*
342, Baltimore Convention Center

N41 DCMP: **Insulating and Dielectric Oxides**
344, Baltimore Convention Center

N42 DCOMP/ GSCCM/ DMP: **Focus Session: Simulations of Matter at Extreme Conditions I**
*Johansson*
345, Baltimore Convention Center

N43 DAMOP: **Quantum Optics and Strong Field Physics**
346, Baltimore Convention Center

N44 DCMP: **Quantum Criticality and Nematic Ordering**
347, Baltimore Convention Center

N45 DCMP: **Exotic Phases in Strongly Correlated Systems**
348, Baltimore Convention Center

N46 FIAP: **Semiconductor Devices/ Semiconductors General**
349, Baltimore Convention Center

## 9:30 WEDNESDAY MORNING 15 MARCH 2006

N34 **Session on Referreeing**
337, Baltimore Convention Center

## 11:15 WEDNESDAY MORNING 15 MARCH 2006

P1 DCMP: **Electron Transport in Single Molecules**
*Tao, Yao, Flensberg, Wolkow, Bar-Joseph*
Ballroom IV, Baltimore Convention Center

P2 DCMP: **The Electronic Properties of Overdoped Cuprates: The Clean Gateway to High-Tc Superconductivity**
*Hussey, Damascelli, Slezak, Taillefer, van der Marel*
Ballroom III, Baltimore Convention Center

P3 FEd: **Physics Teacher Preparation at a Crisis: Innovative Programs Addressing a National Need**
*Heron, Marder, Stewart, Finkelstein, Hein*
Ballroom I, Baltimore Convention Center

P4 GIMS: **Keithley Award Session**
*Hellman, Jach, Fortune, Migliori*
308, Baltimore Convention Center

P5 DFD: **Shedding Light on the Enigma of the Transition to Turbulence in Pipes and other Shear Flows**
*Mullin, Henningson, Waleffe, Kerswell, Tumin, Eckhardt*
309, Baltimore Convention Center

P6 GMAG: **Quantum Spin Dynamics in Molecular Nanomagnets**
*Waldmann, Chudnovsky, Sessoli, Harmon, Park*
310, Baltimore Convention Center

P7 GSNP/DBP: **Focus Session: Physics of Transcriptional Regulatory Networks**
*You, Buchler, Li, Huang, Vazquez*
307, Baltimore Convention Center

P8 DFD/GSNP: **Focus Session: Jets, Shocks & Splashes**
*Xu, Lohse*
314, Baltimore Convention Center

P10 DCP: **Focus Session: Frontiers in Computational Chemical Physics IV**
*Martinez*
302, Baltimore Convention Center

P11 DCP: **Focus Session: Aerosols, Clusters, Droplets: Physics and Chemistry of Nanoobjects II: Helium Nanodroplets II, Aerosols, and Miscellaneous**
*Signorell*
303, Baltimore Convention Center

P12 DCMP/DMP: **Metal Islands and Clusters**
304, Baltimore Convention Center

P13 DCP: **Focus Session: Ultrafast and Ultrahigh Field Chemistry II: Quantum Control**
*Silberberg, Girard*
305, Baltimore Convention Center

P16 FIAP: **Focus Session: Molecular-Scale Electronics III**
*Janes*
312, Baltimore Convention Center

P18 DMP: **Focus Session: Carbon Nanotubes: Opto-Electronics**
*Chen*
315, Baltimore Convention Center

P19 GMAG/DMP: **Focus Session: Spin Interference and Spin Hall Effect**
*Sih*
316, Baltimore Convention Center

P20 DMP/GMAG: **Focus Session: Cobaltites, Nickelates and Vanadates**
317, Baltimore Convention Center

P21 DFD: **Microfluidic Physics III**
318, Baltimore Convention Center

P22 GMAG/FIAP/DMP: **Focus Session: Spin Transport in Metals**
*Garzon*
319, Baltimore Convention Center

P23 GMAG: **Quantum Spin Chains II**
320, Baltimore Convention Center

P26 DBP/DCP: **Focus Session: Protein Dynamics in Folding and Function**
*Mildvan, de Alba, Miller, Summers, Campbell, Hall, Pastor, Redfield*
323, Baltimore Convention Center

P27 DCOMP: **Electronic Structure II**
324, Baltimore Convention Center

P29 DBP: **Biomolecular Structure and Functions**
326, Baltimore Convention Center

P30 DPOLY/DMP: **Focus Session: Organic Interfaces**
*Rosei*
327, Baltimore Convention Center

P31 DCMP: **Nanotubes: Theory and Experiment**
328, Baltimore Convention Center

P32 GMAG: **Spin Glasses**
329, Baltimore Convention Center

P33 DMP/GSNP: **Focus Session: Friction, Fracture and Deformation III**
*Falk*
336, Baltimore Convention Center

P35 DCMP: **Nanostructure Fabrication, Quantum Point Contacts, and Single Electron Transistors**
338, Baltimore Convention Center

P36 DMP: **Focus Session: Plasmon Resonances in Nanostructures**
339, Baltimore Convention Center

P38 DCMP: **Superconductivity—Optical Spectroscopy of Cuprates**
341, Baltimore Convention Center

P39 DCOMP/DCMP: **Focus Session: Superconductivity—Theory and Computation (Mainly First Principles)**
*Mazin*
342, Baltimore Convention Center

P40 DCOMP/TGQI: **Focus Session: Pathways to Practical Quantum Computing I**
*DiVincenzo*
343, Baltimore Convention Center

P41 DMP: **Focus Session: Dielectric, Ferroelectric, and Piezoelectric Oxides III**
*Dierolf*
344, Baltimore Convention Center

P42 DMP/ DCOMP: **Focus Session: Planetary Materials III**
345, Baltimore Convention Center

P43 DAMOP: **Novel Phases in Quantum Gases**
346, Baltimore Convention Center

P44 DCMP: **Organic Conductors**
347, Baltimore Convention Center

P45 DCMP: **Structural and Ferroelectric Phase Transitions**
348, Baltimore Convention Center

P46 FIAP: **FQHE**
349, Baltimore Convention Center

## 13:00 WEDNESDAY AFTERNOON 15 MARCH 2006

Q1 **Poster Session III**
Exhibit Hall, 1:00pm–4:00pm (DPOLY session: 11:15am–2:15pm), Baltimore Convention Center

## 14:30 WEDNESDAY AFTERNOON 15 MARCH 2006

R1 DCMP DBP: **Cytoskeletal Dynamics and Mechanics**
*Svitkina, Julicher, Gopinathan, Gardel, Storm*
Ballroom IV, Baltimore Convention Center

R2 DCMP: **Fractional Quantum Hall Systems**
*Csathy, Gallais, Peterson, Kim, Schulze-Wischeler*
Ballroom III, Baltimore Convention Center

R3 DCMP: **Lateral Spin Transport**
*Ji, Bauer, Valenzuela, Otani*
Ballroom I, Baltimore Convention Center

R4 DPOLY: **Ionic, Dipolar and H-bonding Polymers**
*Breedveld, Dormidontova, Pochan, Cremer, Prabhu*
308, Baltimore Convention Center

R5 FGSA/ FIAP: **Paths from Academics to Employment**
*Czujko, Silbernagel, Seiler, Stanton, Garg*
309, Baltimore Convention Center

R6 CSWP: **U.S. Women in Physics: An International Perspective**
*Michelman-Ribeiro, Whitten, Horton, Ong, Hodari*
310, Baltimore Convention Center

R7 DBP/ FEd/ FPS: **The Experimental and Theoretical Foundations of Evolution**
*Keymer, Deem, Fisher, Lenski, Shapiro*
307, Baltimore Convention Center

R8 DFD: **Monolayers, Membranes & Microemulsions**
314, Baltimore Convention Center

R9 GIMS: **Imaging, Signal Detection and Processing**
301, Baltimore Convention Center

R10 DCP: **Focus Session: Surfaces and Interfaces in Electronic Materials I**
*Wieckowski, Switzer*
302, Baltimore Convention Center

R11 DCP: **Focus Session: Aerosols, Clusters, Droplets: Physics and Chemistry of Nanoobjects III: Molecular Clusters**
*Johnson*
303, Baltimore Convention Center

R12 DCMP/ DMP: **Dynamics at Silicon Surfaces**
304, Baltimore Convention Center

R13 DCP: **Focus Session: Ultrafast and Ultrahigh Field Chemistry III: Ultrafast Processes**
*Schafer, Villeneuve, Matsumoto*
305, Baltimore Convention Center

R16 FIAP: **Thermoelectrics**
312, Baltimore Convention Center

R17 FIAP: **Focus Session: Semiconductors for THz and IR II**
*Zhang*
313, Baltimore Convention Center

R18 DMP: **Focus Session: Carbon Nanotubes: Transport II**
*Roche*
315, Baltimore Convention Center

R19 GMAG/DMP: **Focus Session: Spin Hall Effect and Spin Transport**
*Engel*
316, Baltimore Convention Center

R20 DMP/GMAG: **Focus Session: Multiferroics III: Perovskites**
317, Baltimore Convention Center

R21 DFD/DBP: **Focus Session: Biological Hydrodynamics**
*Aranson*
318, Baltimore Convention Center

R22 GMAG/DMP: **Focus Session: Biomagnetism and Exchange Biased Thin Films**
*Hoffmann*
319, Baltimore Convention Center

R23 GMAG/FIAP: **Focus Session: Theory and Simulation for Information Storage Applications**
*Schrefl*
320, Baltimore Convention Center

R24 DPOLY: **Block Copolymer Applications**
321, Baltimore Convention Center

R25 DPOLY: **Adhesion and Viscoelasticity in Polymer Thin Films**
322, Baltimore Convention Center

R26 DBP/DPOLY: **Focus Session: Counterion Dynamics in Charged Biopolymer Systems**
*Wong, Netz*
323, Baltimore Convention Center

R27 DCOMP: **Many-Body/Strongly Correlated**
324, Baltimore Convention Center

R28 DBP: **Focus Session: Biological Networks: Structure, Dynamics and Function**
*El-Samad, Suel*
325, Baltimore Convention Center

R29 DBP: **Biomolecular Structure and Function**
326, Baltimore Convention Center

R30 DPOLY: **Polymer Nanocomposites**
327, Baltimore Convention Center

R31 DCMP: **Properties of Carbon Nanotubes**
328, Baltimore Convention Center

R32 DCOMP/DMP: **Focus Session: Computational Nanoscience V**
*Tangney*
329, Baltimore Convention Center

R33 DMP/GSNP: **Focus Session: Friction, Fracture and Deformation IV**
*Houston*
336, Baltimore Convention Center

R34 DFD: **Turbulence**
337, Baltimore Convention Center

R36 DMP: **Focus Session: Optical and X-ray Properties of Nanostructures**
*Vasiliev*
339, Baltimore Convention Center

R37 DMP: **Focus Session: Nanoscale Conductance Theory I**
*Baranger*
340, Baltimore Convention Center

R38 DCMP: **Superconductivity—Optical Spectroscopy of Cuprates: IR Hall Effect**
341, Baltimore Convention Center

R39 DCMP: **Superconductivity—Sodium Cobaltate**
342, Baltimore Convention Center

R40 DCOMP/TGQI: **Focus Session: Pathways to Practical Quantum Computing II**
*Laflamme*
343, Baltimore Convention Center

R41 DMP: **Focus Session: Dielectric, Ferroelectric, and Piezoelectric Oxides IV**
*Streiffer*
344, Baltimore Convention Center

R42 DCMP/GSCCM: **Focus Session: Plasticity and Phase Transitions**
*Robinson, Lorenz*
345, Baltimore Convention Center

R43 DAMOP: **One Dimensional Bose Gases**
346, Baltimore Convention Center

R44 DCMP: **Experimental Studies of 115 Materials**
347, Baltimore Convention Center

R45 DCMP: **Strong Correlation in Metals: Mott Transition**
348, Baltimore Convention Center

R46 FIAP: **Electronic and Optical Properties of Semiconductors: First Principals**
349, Baltimore Convention Center

**17:30 WEDNESDAY EVENING 15 MARCH 2006**

S48 FED: **FED Business Meeting & Reception**
Grand Ballroom Salon III, Marriott Waterfront Hotel

**17:45 WEDNESDAY EVENING 15 MARCH 2006**

T7 DBP: **Physics, Chemistry and Biology of the Hydrophobic Effect**
*Li, Widom, Chandler, Truskett*
307, Baltimore Convention Center

**18:30 WEDNESDAY EVENING 15 MARCH 2006**

S49 DCOMP: **DCOMP Business Meeting**
Dover C, Marriott Waterfront Hotel

**19:30 WEDNESDAY EVENING 15 MARCH 2006**

T50 **Perspectives on our Energy Future**
*Koonin, Dehmer*
Grand Salon V, Marriott Waterfront Hotel

**8:00 THURSDAY MORNING 16 MARCH 2006**

U1 DCMP: **Spin Liquids and Superconductivity near the Mott Transition**
*Lee, Schmalian, Tremblay, Mook, Bourges*
Ballroom IV, Baltimore Convention Center

U2 DCMP: **Quantum Magnets in High Magnetic Fields**
*Broholm, Grenier, Zheludev, Hagiwara, Essler*
Ballroom III, Baltimore Convention Center

U3 DCMP: **Nanomechanical Architecture of Strained Thin Films**
*Prinz, Liu, Schmidt, Blick*
Ballroom I, Baltimore Convention Center

U4 DPOLY: **Lithography**
*Willson, Dammel, Nealey, Jones, Hinsberg*
308, Baltimore Convention Center

U5 FHP: **Low Temperature Physics, A Historical Perspective**
*Wheeler, Donnelly, Meyer, Lee*
309, Baltimore Convention Center

U6 DCOMP: **Strong Electronic Correlation in Solids: Applications of the LDA+U method**
*Louie, Janotti, Lichtenstein, Kunes, Cococcioni*
310, Baltimore Convention Center

U7 FIAP: **Nanoscale Pattern Generation and Lithography**
*Hector, Smith, Baglin, Kim, Russell*
307, Baltimore Convention Center

U8 DFD: **Granular Materials**
314, Baltimore Convention Center

U9 GIMS: **Scanning Probe Microscopy**
301, Baltimore Convention Center

U10 DCP: **Focus Session: Surfaces and Interfaces in Electronic Materials II**
*Buriak, Wang*
302, Baltimore Convention Center

U11 DCP: **Focus Session: Aerosols, Clusters, Droplets: Physics and Chemistry of Nanoobjects IV: Metal Clusters I**
*Duncan, Woeste*
303, Baltimore Convention Center

U12 DMP/ DCMP: **Focus Session: Electrochemical and Related Growth**
*Wang*
304, Baltimore Convention Center

U16 FIAP: **Nanotechnology: Applications and Measurements**
312, Baltimore Convention Center

U17 DBP: **Physics and Imaging in Medicine**
*Amols, Soares, Baird, Gueye*
313, Baltimore Convention Center

U18 DMP: **Focus Session: Carbon Nanotubes: Transport III**
*Ferrari*
315, Baltimore Convention Center

U19 GMAG/ DMP: **Focus Session: Semiconductor Spin Nanostructures for Quantum Computing**
*Mizel*
316, Baltimore Convention Center

U20 DMP/ GMAG: **Focus Session: Metal-Insulator Transition and Electron Phonon Coupling in Perovskites**
*Alvarez*
317, Baltimore Convention Center

U21 DFD: **Liquid Crystals I**
318, Baltimore Convention Center

U22 GMAG/ FIAP/ DMP: **Focus Session: Magnetic Tunneling I**
*Yang*
319, Baltimore Convention Center

U23 GMAG: **Frustration in 2D**
320, Baltimore Convention Center

U24 DPOLY: **Liquid-Crystalline Polymers**
321, Baltimore Convention Center

U25 DPOLY/ DMP: **Focus Session: Oligoacene Semiconductors**
322, Baltimore Convention Center

U26 GSNP/ DBP/ DPOLY: **Focus Session: Cytoskeletal Dynamics**
*Danuser*
323, Baltimore Convention Center

U27 DCMP: **Computational Methods: Monte Carlo/Molecular Dynamics I**
324, Baltimore Convention Center

U28 DBP/ DFp: **Focus Session: Biological Hydrodynamics II**
*Groisman, Brenner*
325, Baltimore Convention Center

U29 DBP/ DPOLY: **Focus Session: Nonequilibrium Fluctuation in Biomolecules and Artificial Nanodevices**
*Astumian, Janko*
326, Baltimore Convention Center

U30 DPOLY: **Focus Session: Mechanical Properties: Deformation, Rupture and Failure**
*Marder*
327, Baltimore Convention Center

U31 DCMP: **Nanotubes, Experiment**
328, Baltimore Convention Center

U33 GSNP: **Dynamics and Systems Far From Equilibrium**
336, Baltimore Convention Center

U35 DCMP: **Nanowires**
338, Baltimore Convention Center

U36 DMP: **Focus Session: Optical Properties of Nano-Dots, Holes, and Wires**
339, Baltimore Convention Center

U37 DMP: **Focus Session: Nanowire and Nanodot Quantum Devices**
*Doh*
340, Baltimore Convention Center

U38 DCMP: **1-D Superconductors and Organics**
341, Baltimore Convention Center

U39 DCMP: **Superconducting Proximity Effect—S/N and S/F**
*Eschrig*
342, Baltimore Convention Center

U40 DCOMP/ TGQI/ DAMOP: **Focus Session: Pathways to Practical Quantum Computing III**
*Cirac*
343, Baltimore Convention Center

U41 DCMP: **Dielectrics: Response Properties**
344, Baltimore Convention Center

U42 DCOMP/ GSCCM/ DMP: **Focus Session: Simulations of Matter at Extreme Conditions II**
*Ashcroft*
345, Baltimore Convention Center

U43 DAMOP: **Focus Session: Novel Phases in Low Dimensional Quantum Gases**
*Porto, Ho*
346, Baltimore Convention Center

U44 DCMP: **Models of Strongly Correlated Electrons**
347, Baltimore Convention Center

U45 DCMP: **Structural, Surface and Other Phase Transitions**
348, Baltimore Convention Center

U46 FIAP: **Optical Properties of Semiconductors: Excitons and Phonons**
349, Baltimore Convention Center

**11:15 THURSDAY MORNING 16 MARCH 2006**

V1 DCMP: **Quantum Hall Edges**
*Grayson, Yang, Rezayi, Roddaro, Papa*
Ballroom IV, Baltimore Convention Center

V2 DCMP: **Excitons in Single-Walled Carbon Nanotubes**
*Lanzani, Sheng, Zhao, Mirlin, Reich*
Ballroom III, Baltimore Convention Center

V3 DCMP: **Nonequilibrium Nano-oscillators**
*Cleland, Chan, Dykman, Vijayaraghavan, Clerk*
Ballroom I, Baltimore Convention Center

V4 DAMOP: **Dynamics and Non-equilibrium Phenomena in Optical Lattices**
*Batrouni, Polkovnikov, Weiss, Rigol, Minguzzi*
308, Baltimore Convention Center

V5 DMP: **Surfaces and Interfaces of Correlated Oxides**
*Kawasaki, Ahn, Santamaria, Bozovic, Mannhart*
309, Baltimore Convention Center

V7 GSNP/DBP: **Noise in Biological Systems**
*Cluzel, Tu, Levine, Setayeshgar, Sourjik*
307, Baltimore Convention Center

V8 DCOMP/DFD: **Focus Session: Simulations Using Particles**
*Koplik, Cottet*
314, Baltimore Convention Center

V9 GIMS: **Magnetic Force Microscopies**
301, Baltimore Convention Center

V10 DCP: **Focus Session: Surfaces and Interfaces in Electronic Materials III**
*Uosaki, Wei*
302, Baltimore Convention Center

V11 DCP: **Focus Session: Aerosols, Clusters, Droplets: Physics and Chemistry of Nanoobjects V: Metal Clusters II**
*Schooss, Cheshnovsky*
303, Baltimore Convention Center

V12 DMP/DCMP: **Focus Session: Wetting and Hard-Soft Interfaces**
*Cicero*
304, Baltimore Convention Center

V16 FIAP: **Nanotechnology: Biological and Polymer**
312, Baltimore Convention Center

V17 DBP: **Medical Physics Panel Discussion**
313, Baltimore Convention Center

V18 DMP: **Focus Session: Carbon Nanotubes: Transport IV**
*Gruner*
315, Baltimore Convention Center

V19 APS/AIP: **The Changing Dynamics of Industrial Research as a Consequence of Global Trends**
*Taub, Stork, Durcan, Weinrib, Feist*
316, Baltimore Convention Center

V20 GMAG/DMP: **Focus Session: Semiconductor Spin Dynamics: Optics**
*Hall*
317, Baltimore Convention Center

V21 DFD: **Liquid Crystals II: Nano & Bio**
318, Baltimore Convention Center

V22 GMAG/FIAP/DMP: **Focus Session: Magnetic Tunneling II**
319, Baltimore Convention Center

V23 GMAG: **Spin Waves**
320, Baltimore Convention Center

V24 DPOLY: **Charged and Ion-Containing Polymers: Properties**
321, Baltimore Convention Center

V25 DPOLY: **Polymer Composites—Nanotubes and Nanoclays**
*Dhinojwala*
322, Baltimore Convention Center

V26 DBP: **Cellular Biomechanics**
323, Baltimore Convention Center

V27 DCOMP: **Computational Methods: Monte Carlo/Molecular Dynamics II**
324, Baltimore Convention Center

V28 DPOLY: **Rheology of Biopolymer Solutions**
325, Baltimore Convention Center

V29 DBP/ DCMP: **Nonlinear Phenomena & Pattern Formation in Biology**
326, Baltimore Convention Center

V30 DPOLY: **Focus Session: Mechanical Properties: Microscale Deformation and Failure**
*Sue*
327, Baltimore Convention Center

V31 DCMP: **Nanotubes: Transport**
328, Baltimore Convention Center

V33 GSNP: **Focus Session: Social Networks**
*Redner*
336, Baltimore Convention Center

V35 DCMP: **Photonic Crystals**
338, Baltimore Convention Center

V36 DMP: **Focus Session: Optical Properties of Carbon Nanotubes and C60**
*Ma*
339, Baltimore Convention Center

V38 DCMP: **Superconductivity—Thermodynamics and Structure**
341, Baltimore Convention Center

V39 DCOMP/ DCMP: **Focus Session: Superconductivity—Theory and Computation III**
342, Baltimore Convention Center

V40 TGQI/ DCMP: **Focus Session: Linear Optics Quantum Computation**
*Rudolph*
343, Baltimore Convention Center

V41 DMP: **Focus Session: Dielectric, Ferroelectric, and Piezoelectric Oxides V**
*Warusawithana*
344, Baltimore Convention Center

V42 FHP/ FEd: **History and Physics Outreach**
345, Baltimore Convention Center

V43 DAMOP: **Atomic/Molecular Structure and AMO Processes on Surfaces and in Condensed Matter**
346, Baltimore Convention Center

V44 DCMP: **Kondo Physics and Luttinger Liquids**
347, Baltimore Convention Center

V45 GMAG: **Spin Structure and Phase Transitions: Theory**
348, Baltimore Convention Center

V46 FIAP: **Defects and Impurities in Si/Ge**
349, Baltimore Convention Center

V47 FIAP: **Spectroscopy and Transport in 2D Semiconductors**
350, Baltimore Convention Center

## 14:30 THURSDAY AFTERNOON 16 MARCH 2006

W1 DCMP: **ARPES in High Tc Superconductors**
*Dessau, Valla, Chubukov, Cuk, Ino*
Ballroom IV, Baltimore Convention Center

W2 DCMP: **Imaging Charge and Spin and Semiconductors**
*Steele, Komiyama, LeRoy, Aidala, Hasegawa*
Ballroom III, Baltimore Convention Center

W3 DCMP: **Topological Aspects of Electron Transport in Solids**
*Nagaosa, Haldane, Kane, Bernevig*
Ballroom I, Baltimore Convention Center

W4 DPOLY: **Carbon Nanotube Dispersions**
*Hobbie, Pasquali, Poulin, Windle, Winey*
308, Baltimore Convention Center

W5 FHP: **A Century of Critical Phenomena**
*Sengers, Voronel, Ahlers, Fisher, Kadanoff*
309, Baltimore Convention Center

W6 FIAP: **New Applications of Silicon in Photonics and Biomedicine**
*Manalis, Jalali, Lipson, Murphy, Vlasov*
310, Baltimore Convention Center

W7 DBP/ DPOLY: **Physics of Cell Elasticity, Interactions and Tissue Formation**
*Riveline, Bruinsma, Janmey, Safran, Suresh*
307, Baltimore Convention Center

W8 GSNP/ DFD: **Focus Session: Nonlinear Electrokinetics**
*Rubinstein*
314, Baltimore Convention Center

W9 GIMS: **X-ray, Light, and Particle Scattering and Diffraction**
301, Baltimore Convention Center

W10 DCP: **Focus Session: Surfaces and Interfaces in Electronic Materials IV**
*Penner, Goesele*
302, Baltimore Convention Center

W11 DCP: **Focus Session: Aerosols, Clusters, Droplets: Physics and Chemistry of Nanoobjects V: Nanocatalysis, Supported Clusters I**
*Heiz, Moseler*
303, Baltimore Convention Center

W12 DCMP/ DMP: **Molecules on Surfaces**
304, Baltimore Convention Center

W16 FIAP: **Semiconductor Applications**
312, Baltimore Convention Center

W18 DMP: **Focus Session: Carbon Nanotubes: Electronic and Optical Properties III**
*Maruyama*
315, Baltimore Convention Center

W19 GMAG/ DMP: **Focus Session: Semiconductor Spin Transport: Noise/Theory**
316, Baltimore Convention Center

W20 DMP/ GMAG: **Focus Session: Multiferroics IV**
*Loidl*
317, Baltimore Convention Center

W21 DFD: **Liquid Crystals III**
318, Baltimore Convention Center

W22 GMAG/ DMP: **Focus Session: Magnetic Nanoparticles II**
*Dvorak*
319, Baltimore Convention Center

W23 GMAG/ DMP/ DCOMP: **Focus Session: MAGTHY IV/ab initio Studies**
*Stepanyuk*
320, Baltimore Convention Center

W24 DPOLY: **Focus Session: Lithography**
*Soles, Jonas*
321, Baltimore Convention Center

W25 DPOLY: **Gels and Networks**
322, Baltimore Convention Center

W26 DBP: **Focus Session: Biological Photophysics**
*Zhong, Venugopalan*
323, Baltimore Convention Center

W28 DPOLY/ DMP: **Focus Session: Ordered Optoelectronic Organics**
325, Baltimore Convention Center

W29 DBP: **Biological Networks and System Biology**
326, Baltimore Convention Center

W30 DPOLY/ DBP: **Focus Session: Biopolymers at Interfaces**
*Ober*
327, Baltimore Convention Center

W31 DCMP: **Nanotubes: Devices**
328, Baltimore Convention Center

W32 DCMP: **Glassy and Amorphous Systems**
329, Baltimore Convention Center

W33 DFD: **Nonequilibrium and Templated Assembly**
336, Baltimore Convention Center

W34 DFD: **Fluid Structure & Properties**
337, Baltimore Convention Center

W36 DMP: **Focus Session: Optical Properties of Nanostructures of Si & GaAs**
*Chou, Dal Negro*
339, Baltimore Convention Center

W37 DMP: **Nanoscale Conductance Theory II**
340, Baltimore Convention Center

W38 DCMP: **Flux Pinning and Critical Currents**
341, Baltimore Convention Center

W39 DCMP: **Superconductivity—Josephson Junctions and Qubits**
342, Baltimore Convention Center

W40 TGQI/ DAMOP: **Quantum Communication, Cryptography and Computation**
343, Baltimore Convention Center

W41 DCMP: **Cold Fusion**
344, Baltimore Convention Center

W42 DCOMP/ GSCCM/ DMP: **Focus Session: Simulations of Matter at Extreme Conditions III**
*Streitz*
345, Baltimore Convention Center

W43 DAMOP/ GQI: **Focus Session: Cold Atoms in Optical Lattices**
*Demler*
346, Baltimore Convention Center

W45 GMAG: **Spin Structure in Magnetic Materials**
*348, Baltimore Convention Center*

W46 FIAP: **Compound Semiconductor Defects and Dopants**
349, Baltimore Convention Center

W47 FIAP: **Quantum Transport in Semiconductors: Theory and Experiment**
350, Baltimore Convention Center

**8:00 FRIDAY MORNING 17 MARCH 2006**

Y1 DCMP/ DBP: **Engineering Biomolecules and Circuits by Rational Design and Genetic Selection**
*Hwa, Guet, Goulian, Liao, Noireaux*
Ballroom IV, Baltimore Convention Center

Y2 DCMP: **Electrostatic Levitation and High Energy X-rays**
*Rogers, Hyers, Goldman, Fadley, Lee*
Ballroom III, Baltimore Convention Center

Y4 GMAG: **High TMR MgO Tunneling and Spin Momentum Transfer Materials, Physics, and Devices**
*Parkin, Yuasa, Fuchs, Huai, Sun*
308, Baltimore Convention Center

Y5 FIAP: **New Functionalities in Glasses and Nanomaterials**
*Chakravorty, Gopalan, Jain, Kieffer, Mazur*
309, Baltimore Convention Center

Y6 DCOMP: **Is the Hubbard/t-J Model a High Temperature Superconductor?**
*Pryadko, Putikka, Troyer, Ogata*
310, Baltimore Convention Center

Y7 DCMP: **Challenges and Issues in Nanowire Nanodevices**
*Friedman, Hashizume, Cobden, Aono*
307, Baltimore Convention Center

Y8 DFD: **General Fluid Dynamics**
*Barranco*
314, Baltimore Convention Center

Y12 DCMP/ DMP: **Oxide Surface and Interfaces**
304, Baltimore Convention Center

Y16 FIAP: **Optics and Optoelectronics**
312, Baltimore Convention Center

Y18 DMP: **Focus Session: Carbon Nanotubes: Adsorption and Gas Surface Interactions with Carbon Nanotubes**
315, Baltimore Convention Center

Y19 GMAG/ DMP: **Focus Session: Novel Ferromagnetic Semiconductors I**
*Saito*
316, Baltimore Convention Center

Y20 GMAG/ DMP: **Focus Session: Ruddlesden-popper Phase Manganites**
*Hayward*
317, Baltimore Convention Center

Y22 GMAG/ FIAP: **Focus Session: Coupled Thin-Film Structures for Magnetic Recording**
*Thiele*
319, Baltimore Convention Center

Y23 GMAG: **Single Molecule Magnets**
320, Baltimore Convention Center

Y24 DPOLY: **Polymer Melts & Solutions: Structure & Solubility**
321, Baltimore Convention Center

Y25 DPOLY: **Charged and Ion-Containing Polymers: Computation**
322, Baltimore Convention Center

Y26 DBP: **Focus Session: Physics of Physiological Systems**
*Ben-Jacob*
323, Baltimore Convention Center

Y28 DPOLY/DMP: **Focus Session: Magnetic and Doping Effects in Cojugated Organics**
325, Baltimore Convention Center

Y29 DBP/DPOLY: **Focus Session: Noise and Fluctuation in Biological Systems**
*van Oudenaarden, de Gennes*
326, Baltimore Convention Center

Y30 DPOLY/DBP: **Focus Session: Biopolymers I: Phase Transitions**
*Garcia, Onuchic*
327, Baltimore Convention Center

Y31 DCMP: **Quasicrystals, Adsorption on Quasicrystals, Porous and Random Materials**
329, Baltimore Convention Center

Y33 GSNP: **Statistical Physics: Dynamics and Transitions**
336, Baltimore Convention Center

Y37 DMP: **Focus Session: Probing Novel Nanostructures**
*Fölsch*
340, Baltimore Convention Center

Y38 DCMP: **Superconductivity—Vortex Lattices and Pinning Center Arrays**
341, Baltimore Convention Center

Y39 DCMP: **Superconductivity—Materials and Processing**
342, Baltimore Convention Center

Y40 TGQI/DCMP: **Solid State Quantum Computing I**
343, Baltimore Convention Center

Y45 GMAG: **Magnetic Phase Transitions**
348, Baltimore Convention Center

Y46 FIAP: **Bilayers, Wigner Crystals**
349, Baltimore Convention Center

## 11:15 FRIDAY MORNING 17 MARCH 2006

Z1 DCMP: **Strong Interaction Effects in Small Conductors**
*Petta, Matveev, Steinberg, Fiete, LeHur*
Ballroom IV, Baltimore Convention Center

Z2 DCMP: **Resonant Inelastic X-ray Scattering in Complex Oxides**
*Kim, Hancock, Ishii, Ghiringhelli, Li*
Ballroom III, Baltimore Convention Center

Z4 DPOLY/DBP: **Biopolymers**
*Vogel, Sheetz, Perkins, Greer, Horkay*
308, Baltimore Convention Center

Z7 DBP: **Synchrony and Complexity in Brain Activity and Function**
*Towle, Nadkarni, Schiff, Lehnertz, Zochowski*
307, Baltimore Convention Center

Z18 DMP: **Focus Session: Carbon Nanotubes: Double Wall Nanotubes, Sheets and Chains**
*Kuzmany*
315, Baltimore Convention Center

Z19 GMAG/DMP: **Focus Session: Spin Dynamics in Quantum Dots**
*Abstreiter*
316, Baltimore Convention Center

Z20 GMAG/DMP: **Focus Session: Novel Ferromagnetic Semiconductors II**
317, Baltimore Convention Center

Z22 GMAG/FIAP: **Focus Session: FePt Nanoparticles for Information Storage**
*Weller*
319, Baltimore Convention Center

Z23 GMAG: **Strongly Correlated Electrons II**
320, Baltimore Convention Center

Z24 DPOLY: **Polymer Melts & Solutions: Rheology & Dynamics**
321, Baltimore Convention Center

Z25 DPOLY: **Molecular Dynamics: Theory and Simulation**
322, Baltimore Convention Center

Z26 DBP: **Radiation Therapy and Medical Imaging Techniques**
323, Baltimore Convention Center

Z28 DBP/ GSNP: **Methods of Statistical Physics, Population Dynamics and Epidemiology**
*Brockmann*
325, Baltimore Convention Center

Z31 DCMP: **Complexed Structured Materials, Glasses and Clathrates**
329, Baltimore Convention Center

Z33 GSNP: **Statistical and Nonlinear Physics**
336, Baltimore Convention Center

Z37 DMP: **Focus Session: Nanoscale Conductance Theory III**
340, Baltimore Convention Center

Z38 DCMP: **High Tc Cuprates: ARPES**
341, Baltimore Convention Center

Z39 DCOMP/ DCMP: **Focus Session: Superconductivity—Theory and Computations (Mostly Phonons)**
342, Baltimore Convention Center

Z40 TGQI/ DCMP: **Solid State Quantum Computing II**
343, Baltimore Convention Center

Z45 GMAG: **Mostly Spinels**
348, Baltimore Convention Center

Z46 FIAP: **2D Multi-Valley Systems: QHE Experiment**
349, Baltimore Convention Center

# MAIN TEXT

**SESSION 1B: GSCCM BUSINESS MEETING**
**Sunday Afternoon, 12 March 2006; Falkland, Marriott Waterfront Hotel at 15:00**

**SESSION 1A: NRC/NAS TOWN MEETING**
**Sunday Evening, 12 March 2006; Grand Ballroom Salon V, Marriott Waterfront Hotel at 19:30**

**SESSION A1: QUANTUM PROPERTIES OF SUPERCONDUCTING NANOWIRES**
**Monday Morning, 13 March 2006; Ballroom IV, Baltimore Convention Center at 8:00**
**Nina Markovic, Johns Hopkins University, presiding**



**8:00**
**A1 1 Universal conductance of nanowires near the superconductor-metal quantum transition.**
SUBIR SACHDEV, *Harvard University*

We consider wires near a zero temperature transition between superconducting and metallic states. The critical theory obeys hyperscaling, which leads to a universal frequency, temperature, and length dependence of the conductance; quantum and thermal phase slips are contained within this critical theory. Normal (NN), superconducting (SS) and mixed (SN) leads on the wire determine distinct universality classes. For the SN case, wires near the critical point have a universal d.c. conductance which is independent of the length of the wire at low temperatures.

**8:36**
**A1 2 Suppression of superconductivity in zinc nanowires by bulk superconductors.**
MINGLIANG TIAN, *Center For Nanoscale Science and Department of Physics, Penn State University, University Park, PA 16802*

When a superconducting nanowire of a few micrometers in length is connected to two macroscopic normal metal electrodes, a substantial fraction of the wire will become resistive due to the proximity effect. When such a wire is sandwiched between two macroscopic superconducting electrodes, the superconductivity of a nanowire is intuitively expected to become more robust through the coupling with its strong superconducting environment. This expectation is not fulfilled in our recent observation in a system consisting of zinc nanowires (ZNWs) between two bulk superconductors (Sn, In and Pb). We found evidence that the superconductivity of the ZNWs of 40 nm in diameter and 2 or 6 it $\mu$m in length is suppressed completely or partially when bulk Sn or In electrodes are superconducting. When bulk Sn or In electrodes are driven into the normal state by applying a magnetic field, the ZNWs switch back to their superconducting state. This anti-proximity effect is significantly weakened when both Sn or In leads were replaced by Pb or one of the two superconducting electrodes is replaced by a normal metal. The phenomenon is not seen in wires with diameters equal to and thicker than 70 nm. itThis work is in collaboration with N. Kumar, S. Y. Xu, J. G. Wang, J. Kurtz and M.H.W.Chan and supported by the Center for Nanoscale Science (Penn State MRSEC) funded by NSF under grant DMR-0213623.

**9:12**
**A1 3 Effects of a strong magnetic field on superconducting nanowires.**
ANDREY ROGACHEV, *Department of Physics, University of Illinois at Urbana-Champaign*

Effects of strong magnetic fields on superconducting Nb and MoGe nanowires with diameters 5-15 nm have been studied. We have found that the Langer-Ambegaokar-McCumber-Halperin (LAMH) theory of thermally activated phase slips is applicable in a wide range of magnetic fields and describes well the temperature dependence of the wire resistance, over 11 orders of magnitude. We do not observe any resistance in excess of the LAMH theory, even in wires, which are close to the critical point of the superconductor-insulator transition. This fact can be considered as an evidence of the absence of quantum phase slippage. In thicker wires the field dependence of the critical temperature agrees well with the theory of pair-breaking perturbations that takes into account both spin and orbital contributions. In the insulating-phase wires, the magnetic field has a little effect on electron transport, indicating that the superconductivity in the insulating-phase wires is completely suppressed and the Coulomb blockade is the dominant factor, which causes suppression of the charge transport. [1] A. Rogachev, A.T. Bollinger, and A. Bezryadin, Phys. Rev. Lett. 94, 017004 (2005).

**9:48**
**A1 4 Quantum phase slips with and without disorder.**
SERGEI KHLEBNIKOV, *Purdue University*

The rate of quantum phase slips (QPS) in one-dimensional superfluids and superconductors can be computed from first principles in two limiting cases. One [1] is the uniform (no-disorder) limit, appropriate for suitably prepared atomic gases. The other [2] is the limit when the core resistance of a QPS is effectively infinite, appropriate for a sufficiently long disordered superconducting wire. In the latter case, the calculation applies on the superconducting side of the superconductor-insulator transition, where the dilute instanton gas approximation can be used. It is essential to first compute the instanton rate for a given disorder configuration and then average over disorder, as opposed to working with instantons of a disorder-averaged effective theory. Curiously, in neither of the above cases the system is in the XY universality class: in the uniform limit, the QPS rate is suppressed exponentially at low temperatures, as a consequence

of the momentum conservation, while the second case (a relatively long disordered wire) maps onto dissipative quantum mechanics, with the dissipative coefficient controlled by the plasmon impedance *Z*. The role of a finite core resistance can be understood within the picture of effective resistors, representing different dissipative effects, connected in parallel. [1] S. Khlebnikov, Phys. Rev. Lett. **93**, 090403 (2004); Phys. Rev. A **71**, 013602 (2005). [2] S. Khlebnikov and L. P. Pryadko, Phys. Rev. Lett. **95**, 107007 (2005).

**10:24**
**A1 5 Size Dependent Breakdown of Superconductivity in Ultra-Narrow Nanowires.**
KONSTANTIN ARUTYUNOV, *NanoScience Center, Department of Physics, University of Jyväskylä, PB 35, 40014, Jyväskylä, Finland*

Below a certain temperature $T_c$ (typically cryogenic) some materials lose their electric resistance R entering a superconducting state. Following the general trend towards a large scale integration of greater number of electronic components it is desirable to use superconducting elements in order to minimize heat dissipation. It is expected that the basic property of a superconductor, i.e. dissipationless electric current, will be preserved at reduced scales required by modern nanoelectronics. Unfortunately, there are indications that for a certain critical size limit of the order of $\sim$ 10 nm below which a 'superconducting' nanowire is no longer a superconductor in a sense that it acquires a finite resistance even at temperatures close to absolute zero. We developed a method of non-destructive reduction of a nanostructure dimension(s) by low-energy $Ar^+$ ion sputtering. The method enables study of a purely size phenomena between the sputtering sessions: itsame sample with progressively reduced characteristic dimension. We were able to trace the evolution of the shape of superconducting transition R(T) an aluminum nanowire with original effective diameter $\sim$ 70 nm down $\sim$ 8 nm. Below $\sim$ 15 nm the initially abrupt R(T) dependence suddenly broadens. With further reduction of the wire cross section finite resistance is observed down to temperatures much below the initial superconducting transition. We associate the observed phenomena with the quantum phase slippage process: destruction of superconductivity in quasi-1D channels due to quantum fluctuations of the order parameter. The effect should have a universal validity setting a fundamental size limit for utilization of superconducting elements as building blocks of nanoelectronics circuits.



## SESSION A2: MAGNETIC-FERROELECTRIC COUPLING IN MULTIFERROICS
**Monday Morning, 13 March 2006; Ballroom III, Baltimore Convention Center at 8:00**
**Jeffrey Lynn, National Institute of Standards and Technology, presiding**

**8:00**
**A2 1 Multifunctional Multiferroics.**
SANG-WOOK CHEONG, *Rutgers Center for Emergent Materials*

Discovery of intriguing phenomena due to significant cross-coupling in multiferroics where magnetic order and ferroelectric structural distortion coexist has drawn enormous attention in materials science and condensed mater physics community for the last about two years, partially due to the possible realization of new multifunctional devices. I will overview the recent progress and discuss the key issues in understanding and optimizing the cross-coupling effects.

**8:36**
**A2 2 Magnetic Order and Spin Dynamics in Ferroelectric $HoMnO_3$ and $TbMnO_3$.**
OWEN VAJK, *National Institute of Standards and Technology*

Although there are many ferroelectric and magnetic materials, very few have simultaneous magnetic and ferroelectric order. Only a select few of these materials, known as multiferroics, exhibit significant coupling between the magnetic and ferroelectric properties, and the nature of these interactions is not well understood. We have performed neutron scattering studies of two multiferroics which exhibit significant magnetic-ferroelectric coupling, hexagonal $HoMnO_3$ [1] and perovskite $TbMnO_3$ [2]. In $HoMnO_3$, inelastic neutron scattering measurements of the $Mn^{3+}$ spin-wave spectrum and $Ho^{3+}$ crystal field excitations reveal a significant coupling between magnons and the crystal field levels which may contribute to the complex phase diagram and strong magnetic-ferroelectric coupling. In $TbMnO_3$, extensive neutron diffraction studies show that the magnetic transition from a spin density wave to an incommensurate spiral order phase breaks the inversion symmetry of the lattice and induces the onset of ferroelectric distortion. Our results should help lead to a fuller understanding of the interaction between magnetism and ferroelectricity in multiferroics.

[1] O.P. Vajk et al., Phys. Rev. Lett. 94, 087601 (2005) [2] M. Kenzelmann et al., Phys. Rev. Lett. 95, 087206 (2005)

**9:12**
**A2 3 Ferroelectricity in Incommensurate Magnets.**
A. BROOKS HARRIS, *University of Pennsylvania*

In several systems (e. g. $Ni_3V_2O_8$ and $TbMnO_3$) there occurs a phase transition in which a new incommensurate magnetic order parameter appears simultaneously with the development of a uniform spontaneous electric polarization, $P$. Here I review the Landau theory which gives a phenomenological explanation (independent of the microscopic details) of this phenomenon. The key point is that although the quadratic term in $P$ in the free energy is always stable (positive), a nonzero value of $P$ is induced by a trilinear coupling of the $\Sigma_{kmn}a_{kmn}P_kM_m(q)M_n(-q)$, where subscripts label Cartesian components and $M(q)$ is the $q$-Fourier component of the magnetization. Using representation theory to identify the symmetry of the magnetically ordered phases, I identify the symmetry of this term which is consistent with crystal symmetry. This analysis shows that in the highest temperature magnetically incommensurate phase a nonzero value of $P$ is not allowed (as observed) and also that in the lower temperature magnetically incomensurate phase a nonzero $P$ can only appear in the direction which is observed by experiment. This theory indicates that a microscopic model must involve a trilinear interaction between a phonon displacement and two spin operators. A microscopic analysis of phonon distortions of the spin Hamiltonian reproduces these symmetries, as expected and indicates which gradients of the most general anisotropic exchange tensor can possibly come into play. Inelastic neutron scattering data on a $Ni_3V_2O_8$ powder sample and a symmetry analysis of the phonon spectrum enables us to speculate as to which phonon modes are crucial for this phenomenon. See PRL **95**, 087205 and cond-mats: 0508617, 0508730, 0510386, and 0510807 whose coauthors I hereby acknowledge.



**9:48**
**A2 4 (H,T,P) Phase Diagrams in Multiferroics: $RMnO_3$, $RMn_2O_5$ (R = Rare Earth) and $Ni_3V_2O_8$.**
PAUL C.W. CHU, *University of Houston*

Recently, great interest has been generated in the class of materials known as multiferroics (MF), which exhibit the simultaneous occurrence of two or more of the following properties, namely, ferro(anti) magnetic, ferro(anti) electric, ferroelastic, ferroacoustic, and ferroplastic. A subset of MF, known as magnetoelectrics (ME), in which the magnetic and ferroelectric orders coexist, can display the ME-effect where their magnetic and dielectric properties can be affected by an electric and a magnetic field, respectively. The attention first generated in the 60's waned due to the smallness of the effect. However, the situation has drastically changed in recent years due to the observation of a giant ME-effect [1]. Complex diagrams have been induced by magnetic field in the hexagonal single-crystalline rare-earth manganites $RMnO_3$ [2] and the Kagome-staircase compound $Ni_3V_2O_8$ [3], as evidenced by anomalies in their dielectric constant, specific heat, magnetic susceptibility, and thermal expansion coefficients at the phase boundaries. Some of these anomalies occur simultaneously. In this talk, our results of the dielectric, magnetic, calorimetric, and dilatometric properties of $RMnO_3$ (R = Ho, Y, Dy, Er, Tm, and Tb), $HoMn_2O_5$ and $Ni_3V_2O_8$ at ambient pressure in different magnetic fields up to 7 T and some under high pressures up to 2 GPa will be presented. Analysis of the anomalies and examination of the pressure effects on the phase boundaries demonstrate the critical role of strong spin-phonon coupling in the ME-effect and the richness of physics in the study of ME phase diagrams. Possible avenues to further enhance the ME-effect will be discussed. [1] see for example N. Hur et al., PRL 93, 107207 (2004). [2] B. Lorenz et al., PRL 92, 087204 (2004); B. Lorenz et al., PRB 71, 014438 (2005); C. dela Cruz et al., PRB 71, 060407(R) (2005); F. Yen et al., PRB 71, 180407(R) (2005). [3] G. Lawes et al., cond-mat/0503385.

**10:24**
**A2 5 Ferroelectricity in frustrated magnets.***
MAXIM MOSTOVOY

The coupling between ferroelectricity and magnetism in multiferroics is a complex many-body phenomenon resulting from the interplay between charge, spin, and lattice degrees of freedom, and interesting both for its fundamental physics and possible technological applications. An exceptionally strong sensitivity of ferroelectric ordering to an applied magnetic field was recently found in a number of frustrated magnets with periodic non-collinear spin structures. In this talk I will present a phenomenological approach to ferroelectric magnets, which explains the relation between electric polarization and magnetic ordering, anomalies in dielectric constant at magnetic transitions, and sudden flops of electric polarization in magnetic field, observed in these materials. I will also discuss microscopic mechanisms that can give rise to ferroelectricity in magnetically ordered states and possible roads to high- temperature multiferroics.

*The financial support by the DFG (Merkator fellowship) and MSCplus program is gratefully acknowledged.

**SESSION A3: BILAYER 2D SYSTEMS: INTERLAYER DRAG AND SPONTANEOUS COHERENCE**
**Monday Morning, 13 March 2006; Ballroom I, Baltimore Convention Center at 8:00**
**Jim Eisenstein, CalTech, presiding**



**8:00**
**A3 1 Coulomb drag experiments in dilute p-GaAs double layer systems.***
RAVI PILLARISETTY,† *Princeton University*

Low density (or dilute) two-dimensional systems, which have large ratios of Coulomb interaction energy to kinetic energy ($r_s$ is roughly greater than 10), are found to exhibit some bizarre transport properties. These include an anomalous metallic temperature dependence and an apparent metal-insulator transition. Furthermore, the application of an in-plane magnetic field, which spin polarizes the 2D system, produces some very unique effects, including a giant magnetoresistance. These unusual transport properties have raised serious doubts regarding the applicability of Fermi liquid theory to the large $r_s$ regime. Despite intense efforts, no conclusive understanding of these transport anomalies currently exists. To gain new insights into the role the strong carrier interactions play in this regime, we have measured the Coulomb drag in low density p-GaAs 2D bilayers. The drag resistivity is directly proportional to the interlayer carrier-carrier scattering rate, and allows us to directly study the carrier interactions in this regime. Our findings are that as the density is lowered into the large $r_s$ regime, the drag resistivity develops a two to three orders of magnitude enhancement over that expected from simple Fermi liquid calculations. We also observe significant deviations from the expected $T^2$ dependence, which correlate with the anomalous metallic temperature dependence observed in the single layer resistivity. Furthermore, we find that both the single layer resistivity and drag resistivity exhibit the exact same qualitative in-plane magnetic field dependence, with both exhibiting similar features associated with spin polarization. These observations suggest that the origin of these transport anomalies, affects both the single layer resistance and drag resistance in exactly the same way, and is surprising since these are two extremely different transport properties. We conclude by discussing these experimental results in light of recent theoretical interpretations of our data.

*Work done in collaboration with H. Noh, E. Tutuc, E.P. De Poortere, D.C. Tsui, and M. Shayegan.
†Research conducted at Princeton University; Current Affiliation: Components Research, Intel Corporation.

**8:36**
**A3 2 Many-body effects in low-density strongly-interacting 2D structures: Fermi liquids or not?**
SANKAR DAS SARMA, *Condensed Matter Theory Center, University of Maryland*

I will discuss our many-body theoretic studies of low-density semiconductor-based 2D carrier systems, emphasizing remarkable qualitative and semi-quantitative agreement with recent experimental measurements. In particular, our Fermi liquid many-body theory quantitatively explains the experimentally measured density, temperature, disorder, and magnetic field dependence of bilayer drag, thermodynamic parameters (e.g. spin susceptibility, quasiparticle effective mass), and transport properties in both electron and hole-based low-density 2D semiconductor structures. Our work convincingly demonstrates that the 2D electron liquid remains a Fermi liquid down to fairly low densities, and speculative non-Fermi liquid considerations are unnecessary in order to understand the phenomenology of low-density 2D systems. This work is done in collaboration with Euyheon Hwang, and supported by ONR, LPS, and NSF.

**9:12**
**A3 3 Drag resistance of 2D electronic microemulsions.***
STEVEN KIVELSON, *Stanford University*

In two dimensional electron systems with Coulomb or dipolar interactions, a direct transition, whether first or second order, from a liquid to a crystalline state is forbidden. As a result, between these phases there must be other (microemulsion) phases which can be viewed as a meso-scale mixture of the liquid and crystalline phases. We investigate the transport properties of these new electronic phases and present arguments that they are responsible for the various transport anomalies that have been seen in experiments on the strongly correlated 2DEG in high mobility semiconductor devices with low electron densities. In particular, motivated by recent experiments of Pillarisetty et al, PRL 90, 226801 (2003), we present a theory of drag in electronic double layers at low electron concentration. We show that the drag effect in such systems is anomalously large, it has unusual temperature and magnetic field dependences associated with the Pomeranchuk effect, and does not vanish at zero temperature.

*In collaboration with B. Spivak.

**9:48**
**A3 4 Transition between Composite-Bosons and Composite-Fermions in $\nu = 1/2 + 1/2$ Quantum Hall Bilayers.***
STEVEN H. SIMON, *Lucent Technologies, Bell Labs*

There has been considerable recent interest in bilayer quantum Hall systems at filling fraction $\nu = 1/2 + 1/2$. At large spacing between the layers, the system is described as two independent $\nu = 1/2$ composite fermion fermi seas, with each electron being bound to two vortices of the wavefunction within the same layer. At small spacing between the two layers the system can be described as a composite boson condensate (also known as ''111 state'' or exciton condensate) where each electron is bound to one vortex of the wavefunction within the same layer and to one vortex of the wavefunction in the opposite layer. As the spacing between the layers is continuously decreased, intra-layer correlations must be replaced by inter-layer correlations, and the composite fermion sea must be replaced by the composite boson condensate. In this talk we will focus on the nature of this transition. For intermediate distances between the two layers, we propose a scenario where composite bosons and composite fermions coexist in two interpenetrating fluids[1]. In other words, we allow some electrons to bind to vortices within the same layer, and some to bind to vortices in the opposite layer. Trial wavefunctions describing these mixed composite-boson-composite-fermion states compare favorably with exact diagonalization results. A Chern-Simons transport theory is constructed that is compatible with experiment. More recent work[2] has shown that pairing interactions between the composite fermions occur. Once this pairing is treated properly we obtain almost perfect numerical agreement with exact diagonalizations. Possible implications for experiments are discussed. [1] S. H. Simon, E. H. Rezayi, and M. V. Milovanovic. Phys. Rev. Lett. 91, 046803 (2003) [2] G. Moller, E. H. Rezayi, and S. H. Simon, to be published.

*Work done in Collaboration with E. H. Rezayi, M. V. Milovanovic, and G. Moller

**10:24**
**A3 5 Spectroscopy of Emergent Phases of Electron Bilayers in the Quantum Hall Regime.***
VITTORIO PELLEGRINI, *NEST INFM-CNR Scuola Normale Superiore, Pisa (Italy)*

Electron bilayers in semiconductor heterostructures in the quantum Hall regime are contemporary realizations of highly correlated systems where bizarre quantum phases may appear. A mean field configuration occurs when a tunneling gap splits the single-particle levels in their symmetric and anti-symmetric combinations and the Landau level filling factor is 1. This configuration has full spin and pseudospin ferromagnetic order, where pseudospin is a quantum operator describing layer occupation. The presentation considers optics experiments that offer evidence of the breakdown of the pseudospin order of the mean-field paradigm based on measurements of low-lying spin excitations [1]. The suppression of the pseudospin order manifests a new quantum phase that can be interpreted as a highly correlated fluid of electron-hole excitonic pairs across the tunneling gap. Evidence of a phase transition to a non-quantum-Hall phase is found in measurements of elastically-scattered light (Rayleigh scattering) and of spectral lineshapes of spin-excitations [2]. The transition occurs when the pseudospin order fully collapses by application of an in-plane magnetic field component. [1] S. Luin, et al. Phys. Rev. Lett. **94**, 146804 (2005). [2] S. Luin, et al., to be submitted.

*Work done in collaboration with S. Luin, A. Pinczuk, B.S. Dennis, L.N. Pfeiffer, K.W. West.

## SESSION A4: PARTICLE SELF ASSEMBLY
**Monday Morning, 13 March 2006; 308, Baltimore Convention Center at 8:00**
**Maria Santore, University of Massachusetts, presiding**

**8:00**
**A4 1 DNA-Mediated Colloidal Crystallization, Interactions and Dynamics.**
JOHN CROCKER, *University of Pennsylvania*

DNA has emerged as a powerful and versatile tool for nanoscale self-assembly. Several researchers have assembled nanoparticles and colloids into a variety of structures using the sequence specific binding properties of DNA. Until recently, however, all of the reported structures were disordered, even in systems where ordered colloidal crystals might be expected. We detail the experimental approach and surface preparation that we used to form the first DNA-mediated colloidal crystals, using polystyrene microspheres. We also report the first direct measurements of such DNA-induced interactions between such micron-sized particles. The interactions measured with our optical tweezer method can be modeled in detail by well-known statistical physics and chemistry, boding well for their further application to directed self-assembly. The microspheres reversible adhesion dynamics have an unexpected power-law scaling, which we hypothesize is due to the non-exponential kinetics of DNA hybridization process itself.

**8:36**
**A4 2 Assembly and Gelation of Four-Armed DNA Dendrimers.***
FRANCIS STARR, *Wesleyan University*

The disordered-arrested state of matter is ubiquitous in existing materials like glasses, and is prevalent in many new materials, due to the uncommon mechanical, thermal and electrical properties. The ''bottom-up'' construction of new materials is one of the central aims of nanotechnology. DNA is potentially an optimal choice for the construction of three-dimensional supramolecular assemblies since it can self-assemble into long and fairly rigid helices, based simply on sequence complementarity. We numerically study a model designed to mimic the behavior of recently synthesized single-stranded DNA dendrimers. Complementarity of the base sequences of different strands results in the formation of strong cooperative intermolecular links with a valency controlled by the number of strands. We simulate the bulk behavior of a system containing many 4-armed DNA dendrimers and find that in an extremely narrow temperature range the system forms a large-scale, low-density network via a thermo-reversible gel transition. The sharpness of the crossover the gel state can be controlled by the length of the DNA strands, since longer strands will form cooperative bonds over a narrower temperature range. As a result, the percolation temperature of the network formed by the dendrimers can be made arbitrarily close to the gel transition by tuning the length of DNA strands. This is in contrast with recent model systems designed to understand thermo-reversible gelation. Given that gelation and percolation coincide in irreversible chemical gels, this system provides an excellent model material to bridge the understanding between reversible and chemical gels.

*This work in collaboration with Francesco Sciortino (U Roma I) and supported by NSF grant DMR-0427239

**9:12**
**A4 3 Directing Colloidal Particle Organization Using Soft Lithography and Polyelectrolyte Assembly.***
PAULA HAMMOND, *Massachusetts Institute of Technology*

The use of electrostatic interactions to guide colloidal assembly can be used to achieve an elegant level of control on the ordering of particles at surfaces. We have utilized a combination of self-assembled monolayers and electrostatic layer-by-layer assembled thin films as templates for the directed deposition of colloidal particles. In this work, it is also of interest to manipulate two or more colloid components on a surface using attractive and/or repulsive interactions. This work has since led to an investigation into other interactions that can be used to guide colloid assembly. By extending our understanding of interactions between polyelectrolytes and different forms of functional surfaces, we have been able to guide polyelectrolyte coated colloids to different surface regions based on hydrophobic or hydrogen bonding interactions as well as charge attraction. Recent success has been obtained in our group on the use of DNA acid/base pairs to direct the deposition of polyion functionalized colloids to specific regions of surfaces. In this work, the strong and highly specific hydrogen bonding interactions that take place between poly(phosphonic acids) is being pursued. New developments have included the formation of hydrogen bonded Janus particles – colloids that have been functionalized with a different polybase on either side of the particle. Finally, we have also begun to use a range of soft lithographic methods, combined with polyelectrolyte multilayer assembly on nanometer scale patterns to direct nanoparticles into patterned arrays. The interactions involved in this work, guiding principles, as well as the interplay between hard boundaries and surface chemistry in template surfaces, will be discussed, and potential applications and new collaborations will be addressed in display, microfluidic and biological applications.

*supported by the NSF funded Center for Materials Science and Engineering at MIT

**9:48**
**A4 4 Symmetry, Equivalence and Self-Assembly.**
JACK DOUGLAS, *Polymers Division, NIST*

Molecular self-assembly at equilibrium is central to the formation of many biological structures and the emulation of this process through the creation of synthetic counterparts offers great promise for nanofabrication. The central problems in this field are an understanding of how the symmetry of the interacting particles encodes the geometrical structure of the organized structure and the nature of the thermodynamic transitions involved. Our approach is inspired by the self-assembly of actin, tubulin and icosahedral structures of plant and animal viruses. We observe chain, membrane,'nanotube' and hollow icosahedron structures using 'equivalent' particles exhibiting an interplay between directional (dipolar and multi-polar) interactions and short-range (van der Waals) interactions. Specifically, a dipolar potential (continuous rotational symmetry) gives rise to chain formation, while potentials having discrete rotational symmetries (e.g., square quadrupole or triangular ring of dipoles) led to the self-organization of nanotube and icosahedral structures with some resemblance to tubulin and icosahedral viruses. The simulations are compared to theoretical models of molecular self-assembly, especially in the case of dipolar fluids where the corresponding analytic theory of equilibrium polymerization is well developed. These computations give insights into the design elements required for the development of synthetic systems exhibiting this type of organization.

**10:24**
**A4 5 Structured Nanocomposites: Organization of Particles Templated in Self-Assembled PEO-PPO-PEO Mesophases.**
LYNN WALKER, *Carnegie Mellon University*

The design of materials with tailored properties and function requires control over their structure in the nanometer scale. It is advantageous to many engineering applications that this is carried out using self-assembly processes that occur at reasonable concentrations ( $\sim 10^{20}$ particles/L) and short timescales (ns – $\mu$s). In this work, we have developed a novel approach using an ordered template to control the nanoscale structure of materials that would not otherwise order in solution. We use close-packed cubic and cylindrical mesophases of a thermoreversible block copolymer (PEO-PPO-PEO) to impart spatial order on dispersed nanoparticles. The thermoreversible nature of the template allows for the dispersion of particles synthesized outside the template. This feature extends the applicability of this templating method to many particle-polymer systems and also permits a systematic evaluation of the impact of design parameters on the structure and mechanical properties of the nanocomposites. The approach is extremely robust and we have successfully templated solutions of silica and gold inorganic nanoparticles as well as a series of proteins, which act as organic nanoparticles in our system. The influence of relative size (particle to template sites), relative concentration, temperature and shear are experimentally determined using small angle neutron scattering (SANS) and rheology. SANS with contrast variation is used to characterize the structure of the polymer mesophase and the templated particles in a nanocomposite independently. SANS experiments also demonstrate that shear can be used to align the nanocomposites into single-crystal macro-domains; the first demonstration of the formation of single-crystal nanoparticle superlattices. The outcome of this work serves as a basis for designing new soft nanocomposite materials.



## SESSION A5: ADVANCED MATERIALS FOR ENERGY APPLICATIONS
**Monday Morning, 13 March 2006; 309, Baltimore Convention Center at 8:00**
**George Crabtree, Argonne National Laboratory, presiding**

**8:00**
**A5 1 Overview of the Hydrogen Initiative.**
M. S. DRESSELHAUS, *Massachusetts Institute of Technology, Cambridge, MA*

One of the Grand Challenges of the 21st Century is to achieve a sustainable energy supply. The 20th Century has seen remarkable advances in Science and Technology, resulting in expectations for a higher standard of living. This has required large increases in global per capita energy consumption. Projections of per capita energy needs for the 21st Century indicate that new technologies for sustainable energy production, storage and use will need to be developed in the next 50 years. The so-called hydrogen economy is one such proposal that is presently being considered worldwide. In this talk the big picture of the Grand Energy Challenge will be presented. In this context requirements of a hydrogen economy will be broadly discussed in terms of hydrogen production, storage and utilization, with emphasis given to the large gap between present science and technology know-how and the requirements in efficiency and cost for a sustainable hydrogen economy. Opportunities for nanoscience and nanotechnology to narrow this gap will be discussed, and examples of recent progress will be presented.

**8:36**
**A5 2 Direct Energy Conversion: Chemistry, Physics, Materials Science and Thermoelectrics.***
MERCOURI KANATZIDIS, *Michigan State University*

Interest in all-solid-state thermal to electrical conversion has been steadily increasing in recent years and this has been coinciding with an increasing recognition of rising energy demands in the future. Thus there is now renewed awareness of the need to find new energy sources and make conservation efforts more efficient. In this context thermoelectric materials seem poised to have an impact. Research is needed to understand at the fundamental level the scientific issues that are crucial in designing and discovering new highly efficient thermoelectrics. The progress in the field of thermoelectrics has been significant both at the concept level and at the materials discovery level thanks to a convergence of chemistry, physics and materials science efforts. I will describe how each of these disciplines impact each other to produce synergies that propel advances in this area. I will present recent progress in novel nanostructured chalcogenide materials that stimulate new experimentation and hold considerable promise for higher efficiencies in heat to electricity conversion.

*Supported by ONR.

**9:12**
**A5 3 Novel Indirect Hydrogen Storage Materials.**
CLAUS HVIID CHRISTENSEN, *Technical University of Denmark*

Materialization of a hydrogen economy could provide a solution to significant global challenges. In particularly, the possibility of improving the efficiency and simultaneously minimizing the environmental impact of energy conversion processes, together with the opportunity to reduce the dependency of fossil fuels, are main drivers for the currently increasing research and development efforts. However, significant technological breakthroughs are necessary for making a hydrogen economy feasible. Particularly, it is necessary to develop appropriate hydrogen storage and transportation technologies. Recently, metal ammine salts were proposed as safe, reversible, high-density and low-cost hydrogen carriers. Here, we discuss how this development could provide a platform for using ammonia as a fuel for the hydrogen economy. We do that by comparing various possible hydrogen carriers with respect to energy and cost efficiency, infrastructure requirements, safety concerns and also environmental impact.

**9:48**
**A5 4 Near-surface alloys for improved catalysis.**
MANOS MAVRIKAKIS, *UW-Madison*

Periodic self-consistent Density Functional Theory (DFT-GGA) calculations have emerged as a valuable partner to experiment in explaining reactivity of transition metal surfaces. These methods provide detailed itatomic level mechanistic information on individual elementary reaction steps, in terms of reaction thermochemistry, reaction paths, and activation energy barriers. itTrends in reactivity derived from systematic investigations of specific steps on a number of different metal surfaces are reliable, when compared to experiment. In particular, we will attempt to demonstrate how first-principles methods can extend beyond the detailed mechanistic analysis of catalytic reactions to reach the ambitious goal of identifying promising catalysts for specific applications. Among others, we will discuss opportunities to design bimetallic catalysts for highly selective hydrogen transfer reactions, and for designing cheaper and more active oxygen reduction catalysts, the latter being most relevant to the cathode reaction of low temperature fuel cells.

**10:24**
**A5 5 Materials challenges for solid-state lighting.**
E. FRED SCHUBERT

The use of highly efficient semiconductor light-emitting diodes (LEDs) suitable for illumination applications will enable huge energy savings and have a very positive effect on the environment. This talk will discuss materials challenges in solid-state lighting, including a new class of materials, low-refractive-index materials, with refractive indices much lower than conventional materials. Arrays of $SiO_2$ nanorods are shown to have unprecedented low refractive indices ( $<$ 1.10) yet viable thin-film properties. Their use for omni-directional reflectors and the resulting improvement in LED light-extraction efficiency will be discussed. We will show that optimized phosphor distributions in white LED lamps, particularly remote-phosphor distributions, combined with diffuse reflectors, strongly enhance luminous efficiency. Finally, we will discuss materials issues that limit the efficiency of ultraviolet (UV) light emitters.

## SESSION A6: FRONTIERS OF COMPUTATIONAL MATERIALS
**Monday Morning, 13 March 2006; 310, Baltimore Convention Center at 8:00**
**Stefano Curtarolo, Duke University, presiding**

**8:00**
**A6 1 Multiscale Modeling of Solidification Microstructure: Atomic-Scale Simulations of Crystal-Melt Interfaces and Beyond.**
MARK ASTA, *Department of Chemical Engineering and Materials Science*

This abstract was not received electronically.

**8:36**
**A6 2 Reliable First-Principles Alloy Thermodynamics via Optimal, Truncated Cluster Expansions.***
DUANE JOHNSON, *Department of Materials Science and Engineering*

Cluster expansions (CE) are increasingly used to combine first- principles electronic-structure structural formation energies and Monte Carlo methods to predict phase stability in alloys, and search for new materials. As a basis-set expansion in terms of lattice geometrical clusters and effective cluster interactions, the CE is exact if infinite, but is

tractable only if truncated. We present an optimal truncation for CE basis sets that provides reliable thermodynamics and is easy to implement in mulitcomponent alloys, whereas former truncations were not well defined and sometimes led to unreliable results. We discuss predictive error estimation, error estimation of temperature prediction, Rayleigh- Ritz variation errors associated with basis set truncation for both concentration-dependent and independent version (similar to local compact support in finite-element methods), as well as a means for rapid assessment of transition temperatures without performing Monte Carlo. We exemplify all of the issues in various binary alloys. A Thermo Toolkit (TTK) that automates construction of the optimal, truncated CE, generation of linear-independent unit-cell structures, electronic-structure job submission for the required unit-cell, collection into database, and ultimately Monte Carlo construction of phase diagram is exemplified also.

*Acknowlegdments to Dr. Nikolai Zarkevich and Teck Tan Leong for developments of TTK and funding through the National Science Foundation ITR (DMR-03-25939), and DOE under grant DE-FG02-03ER46026, and the Metal-Hydride Center of Excellence at Sandia.



**9:12**
**A6 3 Realistic nanostructures from first-principles: fluxional handles to control the conductance of carbon nanotubes.***
NICOLA MARZARI, *Department of Materials Science and Engineering, Massachusetts Institute of Technology*

We have combined large-scale, $\Gamma$ − point electronic-structure calculations and the maximally-localized Wannier functions approach to calculate efficiently and with full first-principles accuracy the electronic structure and the quantum conductance of complex systems containing thousands of atoms. This approach is applied to study covalent functionalizations in metallic single-wall carbon nanotubes. We find that for most covalent ligands (from hydrogens to aryl moieties) the electronic structure around the Fermi energy is much less dependent on the chemical nature of the ligands than on the $sp^3$ functionalization pattern disrupting the conjugation network. These covalent functionalizations are more stable when paired with saturating hydrogens. Even when paired, they still act as strong scattering centers that degrade the conductance of the tubes already at low degrees of coverage. Instead, we find that cycloadditions of carbenes or nitrenes can preserve metallicity to an unusually high degree, whenever bond cleavage between two sidewall carbon atoms is induced. This process restores the original $sp^2$ hybridization for the sidewall carbons and preserves, even in the presence of significant distortions, the original ''transparency'' of the $\pi$ manifold. The chirality and curvature of the nanotube and the chemistry of the addends determine this bond cleavage and in turn the transport properties. Remarkably, a well-defined range of diameters can be found for which certain addends - such as dicyanocarbene - exhibit a bistable switchable state, where the opening or closing of the bond, and thus the opening and closing of the conduction channels, could be directed with chemical, electrochemical or optical means. This discovery opens the way to novel and promising routes to control and modulate nanotube conductance, with applications ranging from sensors to memories to opto- and nano-electronics.

*Support from NSF-NIRT DMR-0304019 and from MIT Institute for Soldier Nanotechnologies is gratefully acknowledged.

**9:48**
**A6 4 Evolutionary approach for determining first-principles model Hamiltonians.***
GUS L. W. HART, *Northern Arizona University*

The ability to perform accurate solid-state calculations based completely on first principles (for relatively small unit cells) has made it possible to develop model Hamiltonians that can be rapidly ''searched'' for optimal target properties—i.e., true materials-by-design. Recent applications include ferroelectric properties and band-gap engineering. The most difficult step in ''training'' such model Hamiltonians is making choices for the number and types of parameters in the model that insure the *predictive* power of the model. Based on an evolutionary approach, we have developed an algorithm[1] for selecting the types and number of terms in a Cluster Expansion model for a binary alloy. This approach removes much of the tedium of constructing the model and robustly finds the best possible set of parameters. The approach is general and can be applied to a wide variety of other models as well. I illustrate the success of the new approach first on systems where the best parameter set is known analytically, and second, as applied to several recent ''real-world'' examples, including (1) the role of long-period-superlattices in the Cu-Pd system, (2) predicting configuration-dependent bulk-moduli in transition- metal carbides and nitrides, (3) predicting optimal superlattice stacking/orientations to engineer desired band-gaps in MgO-ZnO wide gap alloys.

*Supported by NSF-0244183; DFG-MU 1648/2 1,2; and a Cottrell College Science Award (Research Corporation).

[1]Gus L. W. Hart, V. Blum, M. J. Walorski, and A. Zunger, Nature Materials **4** 391 (2005); V. Blum, Gus L. W. Hart, M. J. Walorski, and A. Zunger, Phys. Rev. B **72**, 165111 (2005).

**10:24**
**A6 5 Prediction of new crystal structure phases in metal borides.**
ALEKSEY KOLMOGOROV, *Duke University*

Identification of novel crystal structures is an important step for predicting new stable compounds in alloys, since most theoretical search algorithms are restricted to a given prototype library or a lattice type. Performing *ab initio* data mining [1] of intermetallic compounds we have discovered that even in such a well-studied class of systems as metal borides there are previously unknown phases comparable in energy to the existing ones [2]. We demonstrate that even though the new structures are relatively simple, their identification is not straightforward. We systematically investigate the stability and electronic properties of the new metal boride phases. Our calculations show that some phases exhibit electronic features similar to those in the famous $MgB_2$ and could be good superconductors. The new phases are likely to have random stacking faults, so they might not be detected with standard x-ray methods. Our results could thus be used as an important guide in the search for new superconducting metal borides. [1] S. Curtarolo *et al.*, Phys. Rev. Lett. **91**, 135503 (2003). [2] A.N. Kolmogorov *et al.*, submitted (2005).



## SESSION A7: BACTERIAL FLAGELLAR DYNAMICS, POLYMORPHISM, AND CONFORMATIONAL SPREAD
**Monday Morning, 13 March 2006; 307, Baltimore Convention Center at 8:00**
**Phil Nelson, University of Pennsylvania, presiding**

**8:00**
**A7 1 Theory of polymorphic transformations of flagella.**
THOMAS POWERS, *Brown University*

Bacterial flagellar filaments can abruptly change shape in response to mechanical load or changes in solution pH or ionic strength. These polymorphic transformations are an instance of a ubiquitous phenomenon, the spread of conformational change in large macromolecular assemblies. We propose a new theory for polymorphism, whose essential elements are two molecular switches, an elastic mismatch strain between the inner and outer cores of the filament, and cooperative interactions between neighborhing subunits on the same protofilament. We calculate the phase diagram for helical and straight states, and the response of a helical filament to an external moment.

**8:36**
**A7 2 Synchronization of rotating flagella by hydrodynamic interactions.**
HOLGER STARK, *Universität Konstanz, Fachbereich Physik, D-78457 Konstanz, Germany*

Rotating bacterical flagella form bundles, which means that their rotations have to be synchronized. The aim of our study [1] is to show that hydrodynamic interactions, i.e., interactions mediated by the flow field the helical flagella create, can be at the origin of such a synchronization. We consider two stiff helices that are modeled by rigidly connected beads, neglecting any elastic deformations in a first approach [1]. The helices are driven by constant and equal torques. They are fixed in space by anchoring their terminal beads in harmonic traps so that they can jiggle around. We observe that, for finite trap strength, hydrodynamic interactions, treated in the low-Reynolds-number regime, do indeed synchronize the helix rotations to a phase difference zero. The speed of phase synchronization decreases with increasing trap stiffness and becomes zero in infinitely stiff traps. So strictly parallel helices do not synchronize. This limit is consistent with recent work based on slender-body theory [2]. We furhermore show that phase synchronization is stable against fluctuations in the torques driving the helices. Our results clearly indicate that some kind of flexibility is essential to allow for phase synchronization. In reality, this flexibility might have its origin in the proximal hook connecting the flagellum to the rotatory motor or in elastic deformations of the rotating flagella. Indeed, when we extend our model by implementing the elasticity of a helical worm-like chain, synchronization occurs much faster even for relatively stiff helices.

[1] M. Reichert and H. Stark, Eur. Phys. J. E **17**, 493 (2005).

[2] M.J. Kim and T.R. Powers, Phys. Rev. E **69**, 061910 (2004).

**9:12**
**A7 3 Bacterial Flagellar Transformations.**
NICHOLAS DARNTON, *Rowland Institute at Harvard*

In many of the bacteria that swim by rotating helical flagella, the flagellum itself is not a simple, passive propeller. Flagella can adopt several helical shapes of varying pitch, radius and handedness in response to changing conditions such as temperature, pH, and load. In itEscherichia coli, in particular, at least 5 (out of 12 predicted) helical forms are observed

during normal swimming. Polymorphic changes commonly occur during tumbling, appear to aid in the reorientation of swimming direction, and are induced by torque- changing variations in motor speed. Measurements on individual, isolated flagellar filaments are revealing the forces required to cause polymorphic transformations. These data will be necessary for a quantitative understanding of the connections between motor reversal, polymorphic change, and tumbling behavior. Since the filament is a uniform polymer of flagellin protein, whose structure is known, it provides a simple, macroscopically visible model of highly cooperative conformational changes in a biological polymer.

**9:48**
**A7 4 Spiroplasma swim by a processive change in body helicity.**
JOSHUA SHAEVITZ, *University of California, Berkeley*

Microscopic organisms must rely on very different strategies than their macroscopic counterparts to swim through liquid. To date, the best understood method for prokaryotic swimming employs the rotation of flagella. I will present data that Spiroplasma, tiny helical bacteria that infect plants and insects, use a very different approach. By measuring cell kinematics during free swimming, we find that propulsion is generated by the propagation of kink pairs down the length of the cell body. A processive change in the helicity of the body creates these waves and enables directional movement. Unlike the motion of other helical swimmers such as Spirochetes, Spiroplasma swimming velocity increases with increasing viscosity. In addition, cell morphological parameters such as helical pitch and cell length influence swimming velocity.



**SESSION A8: PATTERN FORMATION AND NONLINEAR DYNAMICS**
**Monday Morning, 13 March 2006**
**314, Baltimore Convention Center at 8:00**
**P. Palffy-Muhoray, Kent State University, presiding**

**8:00**
**A8 1 The effects of initial seed size and transients on dendritic crystal growth** ANDREW DOUGHERTY, THOMAS NUNNALLY, *Dept. of Physics, Lafayette College* The transient behavior of growing dendritic crystals can be quite complex, as a growing tip interacts with a sidebranch structure set up under an earlier set of conditions. In this work, we report on two observations of transient growth of $NH_4Cl$ dendrites in aqueous solution. First, we study growth from initial nearly-spherical seeds. We have developed a technique to initiate growth from a well-characterized initial seed. We find that the approach to steady state is similar for both large and small seeds, in contrast to the simulation findings of Steinbach, Diepers, and Beckermann[1]. Second, we study the growth of a dendrite subject to rapid changes in temperature. We vary the dimensionless supersaturation $\Delta$ and monitor the tip speed $v$ and curvature $\rho$. During the transient, the tip shape is noticeably distorted from the steady-state shape, and there is considerable uncertainty in the determination of the curvature of that distorted shape. Nevertheless, it appears that the ''selection parameter'' $\sigma^* = 2d_0D/v\rho^2$ remains approximately constant throughout the transient. [1] I. Steinbach, H.-J. Diepers, and C. Beckermann, itJ. Cryst. Growth, **275**, 624-638 (2005).

**8:12**
**A8 2 Control of eutectic solidification microstructures through laser spot perturbations** SILVERE AKAMATSU, *CNRS* KYUYONG LEE, *Ames Laboratory* WOLFGANG LOSERT, *UMD* We report on a new experimental technique for controlling lamellar eutectic microstructures and testing their stability in directional solidification (solidification at fixed rate V in a uniaxial temperature gradient) in thin sample of a model transparent alloy. A eutectic binary alloy solidifies into a mixture of two crystal phases. In stationary regimes, periodic front patterns made of an alternate stacking of lamellae of the two solid phases are observed. We observe the solidification front in real time by optical microscopy. We use micromanipulation with laser spot arrays for perturbing the solidification front on a scale ranging from one to ten times the average value of the lamellar spacing (spatial period), i.e., typically 10 to 100 microns. These perturbations arise from local heating due to the absorption of the laser light by the liquid slightly ahead of the front. We use the laser spot perturbation technique as a tool for mapping out the large range of accessible lamellar spacings at given V and for creating desired patterns (smooth spatial modulation, tilt domains).

**8:24**
**A8 3 Pattern Formation in a NaCl Crystal undergoing Strain-enhanced Dissolution** ZVI KARCZ, DENIZ ERTAS, RICHARD POLIZZOTTI, *ExxonMobil Research and Engineering* EINAT AHARONOV, *Weizmann Institute of Science* CHRIS SCHOLZ, *Lamont Doherty Earth Observatory* Observations of an initially circular contact ( $\sim 300\mu$m in diameter) between the [100] face of a single-crystal NaCl shaped as a truncated cone and a flat silicate plate immersed in saturated solution indicate that the crystal deforms in two sequential stages under constant normal load. The first is characterized by contact area reduction and slow convergence rates, and the second by fluctuations in contact area and fast and fluctuating convergence rates. Fluctuations are on a timescale of $\sim$ 14 hours. The transition between the stages occurs at the maximum contact stress, which shortly precedes the maximum convergence rate. Confocal images indicate that the crystal dissolves coaxially during the first stage, producing a decreasing static contact. During the second stage, the contact shape is highly irregular, with channels and ridges forming inside the contact. These observations reflect a system evolving towards a non-equilibrium steady state, controlled by the interaction between strain-energy driven undercutting dissolution and plastic flow. Undercutting dissolution reduces the area of the contact, and preferentially removes regions with high dislocation density, while plastic flow increases the contact area by mobilizing dislocations that strain harden the crystal. The feedback between these two mechanisms drives the system towards a dynamic steady state.

**8:36**
**A8 4 Controlled Irradiative Formation of Penitentes** VANCE BERGERON, *Ecole Normale Superieure, Lyon* CHARLES BERGER, *Ecole Normale Superieure, Paris* M. D. BETTERTON, *University of Colorado* Spike-shaped structures are produced by light-driven ablation in very different contexts. Penitentes 1-4 m high are common on Andean glaciers, where their formation

changes glacier dynamics and hydrology. Laser ablation can produce cones 10-100 $\mu$m high with a variety of proposed applications in materials science. We report the first laboratory generation of centimeter-scale snow and ice penitentes. Systematically varying conditions allows identification of the essential parameters controlling the formation of ablation structures. We demonstrate that penitente initiation and coarsening requires cold temperatures, so that ablation leads to sublimation rather than melting. Once penitentes have formed, further growth of height can occur by melting. The penitentes intially appear as small structures (3 mm high) and grow by coarsening to 1-5 cm high. Our results are an important step towards understanding and controlling ablation morphologies.

**8:48**

**A8 5 Transient growth and controlled side branching of xenon dendrites** MARCO FELL, J. H. BILGRAM, *ETH Zurich, Switzerland* In our experiments we study the influence of transient growth conditions on the growth of xenon dendrites from undercooled melt. Here we report on the response of crystal growth on heating the melt. We start heating at a given temperature and steady-state growth. The dendrite tip reacts on this change by slowing down growth rate $v$ and increasing tip radius $R$. We observe that side branches emerge from an unstable surface. As we continue heating up to slightly above melting temperature, the tip radius continuously decreases to a new value. The reverse temperature change unveils a hysteretic behavior: As soon as we cool down the melt from a temperature tight above melting temperature, $v$ and $R$ both increase. The curvature of the tip becomes too small to be stable at the given undercooling and an instability leads to a new, thin tip growing out of the oversized sphere-like tip. The value $R^2v$ shows a sharp peak and then settles to a constant value in only about 20 seconds. The same instability also gives rise to side branches whose formation can be controlled by a repetitive application of the described mechanisms. Highly symmetric xenon crystals can be grown by this technique.

**9:00**

**A8 6 Late time growth dynamics in the Cahn-Hilliard equation*** TMOTHY S. SULLIVAN, *Department of Physics, Kenyon College* P. PALFFY-MUHORAY, *Liquid Crystal Institute, Kent State University* Numerical simulations were carried out in 2D of the scaled Cahn-Hilliard equation $[\partial\psi/\partial t = (1/2)\nabla^2(-\psi + \psi^3 - \nabla^2\psi)]$ starting from Gaussian distributed, random initial conditions on a 540x540 square grid. Simulations were run for a dimensionless time of 200,000, a factor of ten beyond previously reported results. The simulations also covered a broad range of values of the mean composition, including several at values that had not previously been reported. For each composition and for time intervals of no longer than 5000 in dimensionless time, the structure factor was calculated for sixty separate runs and averaged. The pair correlation function was then calculated from the average structure factor and its first zero crossing,$R_G(t)$, taken as a measure of the average domain size, was determined. An equation of the form $R_G(t) = at^b + c$ was then fit to our data over the dimensionless time range from 5000 to 200,000. In contrast to previous work, we find that the scaling exponent $b$ varies with mean coomposition and does not appear to be consistent with the Lifshitz-Slyozov result $b = 1/3$. The largest deviation occurs at a mean composition of 0.2, where $b = 0.244 \pm 0.003$. We discuss the possible effects of morphology on both the scaling law and the time it takes to reach the scaling regime.

*Work supported by Kenyon College, the Liquid Crystal Institute, and The Ohio Supercomputer Center

**9:12**

**A8 7 Domain Growth in 2D Hexagonal Patterns with Diffuse Interfaces** DANIEL A. VEGA, LEOPOLDO R. GÓMEZ, *Department of Physics - Universidad Nacional del Sur - CONICET. (8000) - Bahía Blanca - Argentina* RICARDO J. PIGNOL, *Department of Mathematics - Universidad Nacional del Sur. (8000) - Bahía Blanca - Argentina* The coarsening process in planar patterns has been extensively studied during the last two decades. Although progress has been made in this area, there are still many open questions concerning the basic mechanisms leading the system towards equilibrium. Some of these mechanisms (including curvature driven growth, grain rotation and defect annihilation) have mostly been addressed in systems displaying sharp interfaces. In this work we traced the dynamics of phase separation in hexagonal patterns with diffuse interfaces through the Cahn-Hilliard model. By studying orientational and translational order and densities of topological defects we were able to identify a mechanism of coarsening simultaneously involving curvature driven growth, front propagation and grain rotation. In this regime we found that different correlation lengths characterizing the hexagonal pattern increase logarithmically with time.

**9:24**

**A8 8 Oscillatory patterns near the instability threshold in extended systems with reflection symmetry** ALEXANDER NEPOMNYASHCHY, IRINA SMAGIN, *Technion, Haifa, Israel* VLADIMIR VOLPERT, ALEXANDER GOLOVIN, *Northwestern University* It is well known that the envelope function of a modulated traveling wave spontaneously generated by a short-wave instability is governed by a complex Ginzburg-Landau equation (CGLE). Various modulation phenomena, which include the nonlinear development of a modulational instability of periodic waves in the supercritical region, as well as the formation of stable modulated waves in the subcritical region, have been extensively studied in the framework of CGLE. The nonlinear interaction between two waves moving in the opposite directions is described by a system of two non-locally coupled CGLEs that has not been studied in detail yet. We use this system for studying several phenomena related to modulations of standing waves: (i) nonlinear development of a modulational instability; (ii) propagation of defects in standing-wave patterns; (iii) subcritical modulated waves. The results are applied to problems of transverse instabilities of fronts in combustion and explosive crystallization.

**9:36**

**A8 9 Effects of the Deep of Quench on the Mechanisms of Pattern Formation of Sphere Forming Block Copolymers** LEOPOLDO R. GÓMEZ, DANIEL A. VEGA, *Department of Physics - Universidad Nacional del Sur - CONICET. (8000) - Bahía Blanca - Argentina* ENRIQUE M. VALLÉS, *Plapiqui - Universidad Nacional del Sur - CONICET. (8000) - Bahía Blanca - Argentina* The disorder-order transition of a two dimensional sphere forming block copolymer is studied through the Cahn-Hilliard model at different deeps of quench. The process of microphase separation and kinetic of pattern formation are controlled by the spinodal and order-disorder temperatures. In the spinodal region the deep of quench strongly affect both, ordering times and

density of topological defects. As the spinodal temperature is approached, the density of disclination becomes very small and grains show a perfect orientational and translational order. In a narrow region of temperatures the system relax towards equilibrium via the nucleation and growth mechanism. In this region the critical grain size is approximately one lattice constant in the neighborhood of the spinodal line and diverges as the order-disorder temperature is approached.



**9:48**

**A8 10 Feedback Control of Pattern Formation** LIAM STANTON, ALEXANDER GOLOVIN, *Northwestern University* Global feedback control of spatially-regular patterns described by the Swift-Hohenberg (SH) equation is studied. Two cases are considered: (i) the effect of control on the competition between roll and hexagonal patterns; (ii) the suppression of sub-critical instability by feedback control. In case (i), it is shown that control can change the stability boundaries of hexagons and rolls. Particularly, for certain values of the control parameter, both hexagons and rolls are unstable, and one observes non-stationary patterns with defects. In case (ii), the feedback control suppresses the unbounded solutions of a sub-critical SH equation and leads to the formation of spatially-localized patterns.

**10:00**

**A8 11 Grain boundary stability in stripe configurations of non potential, pattern forming systems** JORGE VINALS, ZHIFENG HUANG, *McGill University* We describe numerical solutions of nonpotential models of pattern formation in non equilibrium systems to address the motion of grain boundaries separating large domains of stripe configurations. One of the models allows for mean flows. Wavenumber selection at the boundaries, boundary instability, and defect formation and motion at the boundary are described as a function of the distance to onset.

**10:12**

**A8 12 Mesoscale Theory of Grains and Cells: Crystal Plasticity and Coarsening*** SURACHATE LIMKUMNERD, JAMES SETHNA, *Laboratory of Atomic and Solid State Physics, Cornell University* Line-like topological defects inside metals are called dislocations. At high temperatures, polycrystalline grains form from the melt and coarsen with time: these dislocations can both climb and glide. At low temperatures under shear the dislocations (which allow only glide) form into cell structures. While both the microscopic laws of dislocation motion and the macroscopic laws of coarsening and plastic deformation are well studied, we have had no simple, continuum explanation for the evolution of dislocations into sharp walls. We present here a mesoscale theory of dislocation motion which provides a quantitative description of deformation and rotation, grounded in a microscopic order parameter field exhibiting the topologically conserved quantities. The topological current of the Nye dislocation density tensor is derived from a microscopic theory of glide driven by Peach-Koehler forces between dislocations using a simple closure approximation. The evolution law leads to singularity formation in finite time, both with and without dislocation climb. Implementation of finite difference simulations using the upwind scheme and the results in one and higher dimensions will be discussed.

*ITR/ASP ACI0085969 and DMR-0218475

**10:24**

**A8 13 Numerical Studies of annular electroconvection in the weakly nonlinear regime** PEICHUN TSAI, *Department of Physics, University of Toronto* ZAHIR A. DAYA, *Defence R&D Canada* STEPHEN W. MORRIS, *Department of Physics, University of Toronto* We study 2D electrically-driven convection in an annular geometry by direct numerical simulation. The simulation models a real experiment which consists of a weakly conducting, submicron thick liquid crystal film suspended between two concentric electrodes. The film is driven to convect by imposing a sufficiently large voltage $V$ across it. The flow is driven by a surface charge density inversion which is unstable to the electrical force. This instability is closely analogous to the mass density inversion which is unstable to the buoyancy force in conventional thermally-driven Rayleigh-Bénard convection. The important dimensionless parameters are a Rayleigh-like number $R$, proportional to $V^2$, a Prandtl-like number $P$, equal to the ratio of the charge and viscous relaxation times, and the radius ratio $\alpha$, characterizing the annular geometry. The simulation uses a pseudo-spectral method with Chebyshev polynomials in the radial direction and Fourier modes in the azimuthal direction. We deduce the coefficient $g$ of the leading cubic nonlinearity in the Landau amplitude equation from the computed amplitude of convection. We investigate the dependence of $g$ on $\alpha$ and $P$ and compare the results to experimental data and to linear and nonlinear theory.

**10:36**

**A8 14 Demodulation of Electroconvective patterns in Nematic Liquid Crystals*** GYANU ACHARYA, *Kent State University* JOSHUA LADD, *Colorado State University* J.T. GLEESON, *Kent State University* IULIANA OPREA, GERHARD DANGELMAYR, *Colorado State University* We present the results of pattern formation in electroconvection of liquid crystal 4-ethyl-2-fluoro-4'-[2-(trans-4-pentylclohexyl)-ethyl]biphenyl(I52) with planar alignment. The pattern was a function of three control parameters: applied ac voltage, driving frequency and electrical conductivity. Over certain range of conductivity, the initial transition (supercritical Hopf bifurcation) leads to right and left traveling zig and zag rolls.For the demodulation of images, Fourier transform (FT) of a time series of images were taken with the sampling rate greater than the Hopf frequency. To demodulate zig/zag rolls, the region around $\mathbf{k}_n$( the wave vector of a given mode) of interest at one quarter of the FT was taken setting all FTs zero. Taking the index of the maximum FT value at that region as the reference point, again this region was separated into four parts and redistributed at four corners. The absolute value of the inverse FT of the modified function gives the required envelope.

*supported by NSF-DMS0407418

**10:48**

**A8 15 Pattern Formation and Dynamics in Electroconvection of Nematic Liquid Crystals: a Theoretical and Experimental Study of the Weak Electrolyte Model*** IULIANA OPREA, *Colorado State University* J.T. GLEESON, *Kent State University* GERHARD DANGELMAYR, *Colorado State University* Ginzburg Landau formalism is used in the study of electrohydrodynamic convection in a planar layer of nematic liquid crystal based on the weak electrolyte model. Stable wave patterns predicted by weak electrolyte model near a Hopf bifurcation of the basic state are analyzed and bounds for the Eckhaus stability are obtained. The weak electrolyte model, that treats the conductivity as a dynamical variable, is tested by quantitative comparison of experimentally measured and theoretically calculations of specific pa-

rameters, such as the recombination rate and charge transport, for the nematic I52. The experimentally observed spatiotemporal chaos evolving at the onset is qualitatively compared with the spatiotemporal chaos obtained in the numerical simulations of the four globally coupled Ginzburg Landau equations describing the dynamics of the amplitudes of the bifurcated patterns.

*Supported by NSF DMS-0407418

**SESSION A9: ELECTRONIC STRUCTURE ON SURFACES AND IN REDUCED DIMENSIONS**
**Monday Morning, 13 March 2006**
**301, Baltimore Convention Center at 8:00**
**Hanno Weitering, University of Tennessee, presiding**

**8:00**
**A9 1 Single-electron tunneling force spectroscopy of electronic states in nonconducting surfaces*** EZRA BUSSMANN, NING ZHENG, CLAYTON C. WILLIAMS, *University of Utah* Typically, the scanning tunneling microscope (STM) cannot directly perform current-voltage spectroscopy on any electronic state with a lifetime greater than $\sim 10^{-6}$ seconds—the state cannot empty fast enough to supply the necessary $\sim 0.1$ pA ( $\sim 10^6$ e/s) imaging current. Recently, we reported a scanning probe technique that detects, by electrostatic force, single-electron tunneling events between a probe and states in a nonconducting surface. Here we determine the energy level of such a state by a single-electron tunneling spectroscopy, implemented by tuning the probe Fermi level with respect to the state by a dc voltage. A random telegraph signal (RTS), due to an electron tunneling back-and-forth between the probe and state, is observed when the Fermi level is near the state energy. We present spectroscopic data and extract the energy of a state in a thermal silicon dioxide film. The origin of the RTS is discussed. Additionally, we find evidence for energy relaxation and charge movement in these states. This new nanometer-scale approach provides the means to characterize electronic states in nonconducting surfaces, opening for exploration materials not accessible to the STM. [1] E. Bussmann, D. J. Kim & C.C. Williams, itAppl. Phys. Lett. **85**, 2538 (2004)

*This work supported by the Semiconductor Research Corporation.

**8:12**
**A9 2 High Resolution Studies of the Electronic Properties of Graphite and Graphene** SHUYUN ZHOU, *Department of Physics, University of California, Berkeley, CA 94720; Materials Sciences Division, Lawrence Berkeley National Laboratory, Berkeley, CA* GEY-HONG GWEON, DANIEL GARCIA, ELIZABETH ROLLINGS, *Department of Physics, University of California, Berkeley, CA 94720* CATALIN SPATARU, STEVEN LOUIE, DUNG-HAI LEE, ALESSANDRA LANZARA, *Department of Physics, University of California, Berkeley, CA 94720; Materials Sciences Division, Lawrence Berkeley National Laboratory, Berkeley, CA* We report a high-resolution angle-resolved photoemission spectroscopy (ARPES) study on the electronic properties of bulk graphite and atomically-thin graphene layers. Data as a function of both in-plane and out-of-plane momenta, binding energy and photon energy will be presented. We have observed for the first time using ARPES some very interesting electronic properties near the Fermi energy $E_F$, whichshows that inter layer coupling is an important ingredient in understanding the electronic properties of graphite. In addition, the unique electronic properties in atomically–thin graphene layers will be discussed and compared with those from the bulk graphite sample.

**8:24**
**A9 3 Positron Trapping and Annihilation at Reconstructed Ge(100)-(2x1) and Ge(111)-(2x8) Surfaces** ARNAB K. PAL, NAIL G. FAZLEEV, *University of Texas at Arlington* The results of experimental studies of Ge(100) and Ge(111) surfaces using high-resolution positron-annihilation-induced Auger electron spectroscopy are analyzed by performing calculations of the ''image-potential'' surface states and annihilation characteristics for positrons trapped at the reconstructed Ge(100)-(2x1) and Ge(111)-(2x8) surfaces. Estimates of positron binding energy, work function, and annihilation characteristics reveal their sensitivity to surface reconstruction of the topmost layers of clean Ge. These results are compared to the ones obtained for the reconstructed Si(100)-(2x1), Si(100)-p(2x2), and Si(111)-(7x7) surfaces. Comparison of theoretical positron annihilation probabilities computed for different reconstructed surfaces of Ge with experimental ones estimated from the measured Auger peak intensities permits identification of the atomic structure of the topmost layers of the reconstructed surfaces. The effects of adsorbates on the localization of positron surface state at the semiconductor surface and positron annihilation characteristics are discussed.

**8:36**
**A9 4 Probing electron correlation effects of Ni(111) with STM** KEES FLIPSE, *Eindhoven University of Technology* K. BRAUN, *Ohio University, Athens, USA* A. GRECHNEV, M. KATSNELSON, *Radboud University of Nijmegen, The Netherlands* K. RIEDER, *Free University of Berlin, Germany* The role of electron correlation effects in the electronic structure of Ni-metal has been attracting interest for a long time. Here we present an extensive scanning tunneling microscopy and spectroscopy investigation on Ni(111) at low temperature which shows a parabolic surface state with a surprisingly low effective mass compared to the noble metals like Au, Ag and Cu and a d-surface resonance showing an electron-electron interaction signature which can be understood by a many-body calculation of the electronic structure (DMFT). For the first time, a small energy shift and a significant broadening of the electron state due to electron-electron correlation effects are obtained in a STM experiment. This opens the possibility to study electron many-body effects of surface states in detail with a very high energy resolution on a clean and defect free part of the surface.

**8:48**
**A9 5 Low temperature scanning tunneling microscopy study on electronic standing waves and step motion on Au(111) surface** HUI WANG, JONGHEE LEE, DAN SULLIVAN, *Lab for Physical Sciences, Dept. of Physics, University of Maryland* MICHAEL DREYER, *Lab for Physical Sciences, Dept. of Electrical And Computer Engineering, University of Maryland* BARRY BARKER, *Lab for Physical Sciences, National Security Agency* We present a Low Temperature Scanning Tunneling Microscope investigation of step motion and electronic standing waves of Au(111) surface epitaxially grown on Mica. By performing Fourier Transform Scanning Tunneling Spectroscopy, we measured the parabolic surface state dispersion with an effective

mass of $0.25m_e$. This agrees well with the theory and the photoemission data. We also report the step motion of Au(111) surface at 4K. The speed of the motion is around 5 to 20nm/hr. Potential causes for this motion include tip-sample interaction and surface contamination. These and other possible causes will be discussed.

**9:00**

**A9 6 On the inhomogeneous structure and charge transfer of $C_{60}$ monolayer on Ag(001)** XIEQIU ZHANG, AIDI ZHAO, XUDONG XIAO, *Department of Physics and Institute of Nano Science and Technology, Hong Kong University of Science & Technology, Hong Kong, China* WEI HE, JINLONG YANG, *Heifei National Laboratory for Physical at Microscales, University of Science and Technology of China, Heifei, Anhui 230026, China* We have studied the morphological and electronic structure of $C_{60}$ ML/Ag(001) by STM/STS and first principles calculation. The bright-dim contrast of adsorbed $C_{60}$ molecules is identified as originating from geometric effects. Among the dim $C_{60}$ molecules, there consist of dim monomers (DM) and dim dimers (DD), which display distinguished STS. The dI/dV spectra give the energy locations of HOMO, LUMO and LUMO+1-derivated energy bands and the different STS spectra for B, DM, and DD $C_{60}$ molecules indicate that the charge transfer from the substrate is strongly inhomogeneous. The charge transfer has been estimated as $\sim$ 0, $\sim$ 1, $\sim$ 2 electrons/molecule for B, DM and DD from the shift of their corresponding LUMO+1 energy bands, respectively. The DFT calculations give the consistent spectra for B, DM and DD $C_{60}$ molecules with experimental STS data, but with smaller charge transfer.

**9:12**

**A9 7 Electronic Effects in the Length Distribution of Si(553)-Au Chains*** JASON CRAIN, MARK STILES, JOSEPH STROSCIO, DANIEL PIERCE, *Electron Physics Group, NIST* The electronic structure of nanostructures directly impacts their energetics. For example, the confinement of electronic states determines preferred sizes for clusters and thin films. In the present study we investigate the effects of the electronic structure on the self-assembly of Si(553)-Au atomic chains, which are broken into finite-size segments by defects [1,2]. Chains are first fabricated by depositing gold on stepped silicon surfaces [3]. Scanning tunneling microscopy measures the distribution of chain lengths and the correlation between defects separating chains. The distribution of chain lengths reveals incommensurate oscillations that are linked to the electronic scattering vectors at the Fermi surface of the surface states. The pairwise correlation function between defects shows long-range correlations that extend beyond nearest-neighbor defects, indicating coupling between chains. [1] J. N. Crain, A. Kirakosian, K. N. Altmann, C. Bromberger, S. C. Erwin, J. L. McChesney, J. L. Lin, and F. J. Himpsel, Phys. Rev. Lett., 90, 176805 (2003). [2] J. N. Crain and D. T. Pierce, Science, 307, 703 (2005). [3] J. N. Crain, J. L. McChesney, F. Zheng, M. C. Gallagher, P. C. Snijders, M. Bissen, C. Gundelach, S. C. Erwin, and F. J. Himpsel, Phys. Rev. B, 69, 125401 (2004).

*Supported in part by the Office of Naval Research.

**9:24**

**A9 8 An Electronic View of the Step-edge Schwoebel Barrier Problems** YINA MO, *Harvard University* ZHENYU ZHANG, *Oak Ridge National Lab, University of Tennessee* EFTHIMIOS KAXIRAS, *Harvard University* Using First-principle calculations, we studied the energetics of adatoms Co, Fe, Cu, and Zn on the stepped Cu(111) surfaces and that of adatoms Rh, Pd, and Ag on the stepped Pd(111) surfaces. We found that the behavior of the adatoms at the step edge of these substrates is governed by the electronic interactions instead of stain strain effects. The different energetics and kinetics of the different adatoms on the same substrates result from the difference in which these adatoms *see* the charge distributions from the identical substrates. We further clarified that atomic level studies of these cases are required because the bond counting rules are not univeral.

**9:36**

**A9 9 Electronic Structure of NiO (100) and CoO (100) Ultrathin Films on $Fe_3O_4$(100)*** HUI-QIONG WANG, VICTOR HENRICH, *Department of Applied Physics, Yale University, PO Box 208284, New Haven, CT 06520* The electronic structure of ultrathin epitaxial films of two insulating antiferromagnets, NiO and CoO, grown on the metallic ferrimagnet $Fe_3O_4$ is being investigated. NiO (100) and CoO (100) are grown monolayer by monolayer on $Fe_3O_4$ (100) using molecular beam expitaxy; the thin-film electronic properties are characterized by measuring ultraviolet photoelectron spectra (UPS) as a function of overlayer thickness. The evolution of the density-of-states in the O 2p/Fe 3d and O 2p/Ni 3d bands exhibits a shift in the position of the NiO valence band for ultrathin films relative to bulk-like thick films; that band shift is also observed for ultrathin CoO (100) films grown on $Fe_3O_4$ (100). Several possibilities for the origin of that shift will be discussed: one is modification of metal 3d - O 2p hybridization in the thin film; another is change of the on-site Coulomb interaction, U, due to polarization energy and substrate image potentials.

*This research was supported by U.S. Department of Energy Grant DE-FG02-00ER45844.

**9:48**

**A9 10 Modification of Surface States in Ultrathin Films via Hybridization with the Substrate – a Study of Ag on Ge** SHU-JUNG TANG, TOM MILLER, TAI-CHANG CHIANG, *University of Illinois at Urbana-Champaign* The Shockley surface state of Ag(111) develops unusual band dispersion relations for Ag films of decreasing thicknesses on Ge(111), as observed by angle-resolved photoemission. Its parabolic dispersion in the thick-film limit shifts toward higher binding energies and splits into multiple bands with dispersions that reflect the valence band structure of Ge including the heavy-hole, light-hole, and split-off bands. The results are explained in terms of a hybridization interaction between the Ag surface state and the Ge substrate states.

**10:00**

**A9 11 Surface electronic structure of H/Li(110) – an application of the semi-infinite method.*** YONAS ABRAHAM, N.A.W. HOLZWARTH, *Wake Forest University* We report the application of our new semi-infinite method to study the Li (110) surface. This method calculates continuum and bound electronic states in the vicinity of a surface of a semi-infinite crystal. It is designed for solving the Kohn-Sham equations in a pseudopotential formulation, including both local and separable non-local contributions. It is based on the Numerov integration algorithm and uses singular value decomposition to control the exponentially growing contributions. For Li (110), we see that H changes the interference patterns of the continuum states. In addition, we are able to locate the energies of H-induced surface states relative to the bulk band edges. Comparison with supercell calculations of the same system, reveal interesting differences.

*Supported by NSF Grant No. DMR-0427055.

**10:12**

**A9 12 Possible superconductivity in hetero-polar interfaces of CuCl/Si superlattices: (001) and (111)*** S. H. RHIM, R. SANIZ, A.J. FREEMAN, *Northwestern U,* J.J. YU, *Seoul Natl. U.* To investigate possible interfacial superconductivity[1] in CuCl/Si superlattices, we carried out first-principles calculations using the highly precise FLAPW[2] method. Two possible growth directions, (001) and (111), are compared through their band structures, density of states (DOS), charge densities and Fermi surfaces. While the (111) superlattice is always metallic, the (001) superlattice is metallic or insulating depending on the number of Si and CuCl layers. Both directions exhibit two dimensional (2D) character at the interfaces which is a result of charge transfer between CuCl and Si layers. For metallic superlattices, the 2D conduction bands at the interfaces, resemble the 2D Cu-O $dp\sigma$ bands of cuprate superconductors. To obtain $T_C$ based on conventional electron-phonon (e-p) interactions, we calculated the e-p coupling constant, $\lambda$, within the rigid muffin-tin approximation.[3] The results indicate that while e-p coupling is present in both directions, it gives $T_C = 0.41 \sim 1.69$ K, i.e. one order of magnitude lower than the previously reported high transition temperature[2]- which, if confirmed, would indicate a possible role for excitonic effects.

*DOE (DE-F602-88ER45372/A022))

[1]%Mattes, %Physica C **162**,554 (1989); Mattes and Foiles, Physica 135B, 139 (1985)
[2]Wimmer, Krakauer, Weinert, and Freeman, Phys.Rev.B, **24**, 864 (1981)
[3]Gaspari and Gyoffry, Phys. Rev. Lett. **28**, 801, (1972)

**10:24**

**A9 13 Measurement of Valley Splitting in a Si/SiGe 2DEG Point Contact** L.M. MCGUIRE, K.A. SLINKER, S. GOSWAMI, *University of Wisconsin-Madison* J.O. CHU, *IBM Research Division, T. J. Watson Research Center* M.A. ERIKSSON, *University of Wisconsin-Madison* We measure the valley splitting as a function of magnetic field in a Si/SiGe two-dimensional electron gas (2DEG) point contact defined by metal top-gates. Using a pair of point contacts on a quantum dot, and a two-point measurement technique, we apply a small ac bias to the source-drain and measure the differential current as we pinch off the channel by applying a negative voltage to the top-gate. As the voltage on the top-gate is varied in zero magnetic field, we observe the conventional steps at conductance values of multiples of $4e^2/h$. By applying a perpendicular magnetic field, we lift both the spin and valley degeneracies, and we see corresponding steps in conductance at every $e^2/h$. By fitting the conductance as a function of magnetic field, we can extract both the subband spacing and the valley splitting energy. Temperature dependence and source-drain spectroscopy plots are shown. At high magnetic fields, step-like features appear at non-integer conductance values in addition to the integer steps. Research made possible by ARDA, the NSA, and NSF.

**10:36**

**A9 14 Quantum effects in the conductivity of high-mobility Si MOSFETs at ultra-low temperatures.** NIKOLAI N. KLIMOV, *Rutgers University* ALEXANDER KUNTSEVICH, VLADIMIR M. PUDALOV, *Lebedev Physics Institute* HARRY KOJIMA, MICHAEL E. GERSHENSON, *Rutgers University* By thorough suppression of electromagnetic noise in our experimental set-up, we were able to cool the electrons in high-mobility Si MOSFETs down to 17mK. We have studied how the conductivity depends on the temperature and the in-plane magnetic field over the density range $n = (2 - 10) \cdot 10^{11} cm^{-2}$, with the focus on the crossover from ballistic transport ($T\tau \gg 1$, where $\tau$ is the momentum relaxation time) to diffusive transport ($T\tau \ll 1$). For our samples, this crossover was observed $T \sim 0.3K$. The quasi-linear dependence $\sigma(T)$ observed in the ballistic regime [1] is in a quantitative agreement with the theory of interaction corrections to the conductivity [2]. At lower temperatures, the interaction corrections are strongly affected by the inter-valley scattering. We have determined the inter-valley scattering rate by analyzing the weak-localization corrections and the dephasing time in the studied Si inversion layers. We will discuss how the interaction corrections in the diffusive regime are modified by the inter-valley scattering. [1] V.M.Pudalov, M.E.Gershenson, H.Kojima, G.Brunthaler, A.Prinz, G.Bauer, Phys.Rev.Lett. 91,126403 (2003) [2] G.Zala, B.N.Narozhny, and I.L.Aleiner, Phys. Rev.B 64, 214204 (2001); 65, 020201 (2002).



## SESSION A10: FOCUS SESSION: PHYSICAL CHEMISTRY OF NANOSCALE SYSTEMS I

**Monday Morning, 13 March 2006; 302, Baltimore Convention Center at 8:00**
**Tim Lian, Emory University; Ken Kuno, University of Notre Dame, presiding**

*Invited Papers*

**8:00**

**A10 1 Fluorescence Kinetics in Nanoscale Systems.** DAVID NESBITT, *JILA/NIST*

This abstract was not received electronically.

*Contributed Papers*

**8:36**

**A10 2 Magneto-optical spectroscopy of single CdSe nanocrystal quantum dots** H. HTOON, V. I. KLIMOV, *Chemistry Division, Los Alamos National Laboratory, New Mexico* M. FURIS, S. A. CROOKER, *National High Magnetic Field Laboratory, Los Alamos, New Mexico* Understanding the spin structure of excitons within nanocrystal quantum dots (NCs) is important on both fundamental grounds and also for technological spintronic applications. While single-NC photoluminescence (PL) studies have become routine, there are no reports of spin-resolved magneto-PL studies with single-NC sensitivity. To this end, we measure low temperature (4 K), polarization resolved, magneto-PL of individual CdSe NCs to 5 Tesla. We clearly observe an energy splitting between left- and right-circularly polarized PL peaks and a strong degree of circular polarization in a subset ( $< 10\%$) of the studied NCs. We attribute this effect to a Zeeman splitting of spin-up and spin-down excitons in those NCs having wurzite-c

axes aligned parallel to the applied magnetic field. Our data reveal that 5T Zeeman splittings vary widely from one NC to another, occasionally reaching values in excess of 2 meV. We compare the results from many single nanocrystals with magneto-PL measurements of NC ensembles.

**8:48**
**A10 3 Optical properties of current carrying molecular wires** MICHAEL GALPERIN, *Northwestern University* ABRAHAM NITZAN, *Tel Aviv University* We consider several fundamental optical phenomena involving single molecules in biased metal-molecule-metal junctions. The molecule is represented by its highest occupied and lowest unoccupied orbitals, and the analysis involves simultaneous consideration of three coupled fluxes: the electronic current through the molecule, energy flow between the molecule and electron-hole excitations in the leads, and the incident and/or emitted photon flux. Using a unified theoretical approach based on the non-equilibrium Green function method we derive expressions for an absorption lineshape (not an observable but a useful reference for considering yields of other optical processes) and for the current induced molecular emission in such junctions. We find that current driven molecular emission and resonant light induced electronic currents in single molecule junctions can be of observable magnitude under appropriate realizable conditions. In particular, light induced current should be observed in junctions involving molecular bridges that are characterized by strong charge transfer optical transitions. For observing current induced molecular emission we find that in addition to the familiar need to control the damping of molecular excitations into the metal substrate the phenomenon is also sensitive to the way in which the potential bias is distributed on the junction.

**9:00**
**A10 4 Observation of Synchronous Photoluminescence Intensity Fluctuations within Single CdSe Quantum Wires** JOHN GLENNON, RUI TANG, WILLIAM BUHRO, RICHARD LOOMIS, *Department of Chemistry and Center for Materials Innovation Washington Unviersity in St. Louis* The intensity of the photoluminescence (PL) within single colloidal CdSe quantum wires (QWs) is observed to synchronously fluctuate along the entire length of the wire in time. Statistical analysis of 'on' and 'off' events within the QWs indicates a power-law temporal dependence nearly identical to that seen in colloidal CdSe quantum dots (QDs). The low PL quantum yields (0.2-2%) of ensemble samples of CdSe QWs suspended in solution are placed in perspective by considering the large inhomogeneity observed in the PL intensities of different QWs. Estimates of the quantum yields for the 'on' events in CdSe QWs are similar to those of CdSe QDs. We also report on the observation of coordinated PL intensity fluctuations in multiple QWs that lie in contact with each other, a surprising entity dubbed a quantum network.

**9:12**
**A10 5 Plasmons in nearly touching metallic nanoparticles: singular response in the limit of touching dimers** ISABEL ROMERO, *Donostia Intl Physics Center, DIPC, Donostia, Spain* JAVIER AIZPURUA, *DIPC, Donostia, Spain* GARNETT W. BRYANT, *NIST, Gaithersburg, MD* F. JAVIER GARCIA DE ABAJO, *Unidad mixta CSIC-UPV/EHU and DIPC, Donostia, Spain* The response of gold nanoparticle dimers is studied near and beyond the limit where the particles are touching. As the particles approach each other, a dominant dipole feature is observed that is pushed into the infrared due interparticle coupling and that is associated with a large pileup of induced charge in the gap region. Lower-frequency, higher-order modes are observed in near touching dimers. After touching, singular behavior is observed through the emergence of infrared absorption peaks, accompanied by huge charge pileup at the nanoparticles junction region. These results explain recent experiments on metallic nanoparticle dimers and are relevant in the design of nanoparticle-based sensors and plasmon circuits.

**9:24**
**A10 6 Surface-Enhanced Raman Scattering Based on Novel Metal Nanostructures (Aggregates, Nanorods, and Nanoshells)** JIN ZHANG, ADAM SCHWARTZBERG, LEO SEBALLOS, TAMMY OSHIRO, *UC Santa Cruz* CHAD TALLEY, *Lawrence Livermore National Lab* REBECCA SUTPHEN, *University of South Florida* YIPING ZHAO, *University of Georgia Athens* Rational design and study of new surface enhanced Raman scattering (SERS) substrates is key to advancing chemical and biological sensing. The next generation of biological probes will ideally be single, small, SERS active nanostructures able to penetrate the inner workings of cells. To this end, we have developed various metal nanostructures based on aggregates, nanorods, and nanoshells with the goal to optimize their SERS activities. We have very recently demonstrated SERS from single, hollow nanostructures. Exceptional sample homogeneity leads to a nearly tenfold increase in signal consistency over standard silver substrates. At 30 nm in diameter, this is the smallest confirmed single SERS active particle ever reported, representing a major step in advancing sensing technology based on SERS. In the meantime, we have applied some of the substrates developed in detection of cancer biomarkers and have achieved high sensitivity and molecular selectivity. The results have shown that SERS is extremely promising for chemical and biological sensing and imaging applications. To control the structure of the nanomaterials and thereby their optical absorption as well as SERS properties is critical for these emerging technological applications.

***Invited Papers***

**9:36**
**A10 7 Nanoparticle Optics: New Materials, Concepts, and Characterization Methods.**
RICHARD VAN DUYNE, *Northwestern University Department of Chemistry*

Nanoparticle Optics is a materials driven subject. The unifying theme in this lecture will be the fabrication of size and shape-tunable, metal nanoparticles using nanosphere lithography (NSL), electron beam lithography (EBL), and chemical synthetic methods. Size and shape tunability leads to an exquisite degree of control over the magnitude and spatial extent of the surface electromagnetic fields that surround optically excited nanoparticles. In turn, this has enabled fundamental

new insights into the electromagnetic (EM) field enhancement mechanism underlying both localized surface plasmon resonance (LSPR) spectroscopy and surface enhanced Raman spectroscopy (SERS). This lecture will focus on three topics: (1) LSPR spectroscopy and its application to the development of nanoscale optical biosensors for the study fundamental biological recognition events; (2) Dark-field Rayleigh scattering spectroscopy is used to show that diffractively narrowed plasmon bands can be produced in columnar arrays of Ag nanoparticles, fabricated by EBL, that are spaced by approximately the single particle plasmon wavelength; and (3) the relationship between the LSPR spectrum of Ag nanoparticles and the wavelength-scanned excitation spectra for both surface-enhanced Raman spectroscopy (WS SERES) and second harmonic generation (WS SHGES) is discussed.

*Contributed Papers*

**10:12**

**A10 8 Dielectric confinement effects on the emission lineshipe of single semiconductor nanocrystals** DANIEL GOMEZ, JOEL VAN EMBDEN, PAUL MULVANEY, *The University of Melbourne* We have explored the influence of different matrices on the photoluminescence line shape of individual CdSe core shell nanocrystals (NCs) at room temperature using confocal microscopy / spectroscopy. The results obtained corroborate previous observations of a correlation between blinking events and spectral diffusion but in addition, we have found that the extent of spectral diffusion is almost independent of the dielectric environment of the NC, thus suggesting that ionization and charge reorganization events in the matrix are not responsible for the observed continuous spectral shifts. We also observed that the emission line width is correlated with the emission peak position and that the correlation coefficient between these two variables is a function of the dielectric constant of the matrix surrounding the NC. These results are analyzed in terms of dynamic rearrangements of charges trapped at the surface of the nanocrystal.

**10:24**

**A10 9 Semi-empirical Study of a Multi-associated Rotaxane** KI-HO LEE, KARL SOHLBERG, *Drexel University* Rotaxanes are prototype molecular devices based on two components; one or more ring molecules threaded by a dumbbell-shaped, shaft molecule. In a switchable rotaxane, the shaft has two or more sites strongly attracting the ring with different binding intensity, and translation of the ring between the sites may be induced by switching the relative binding intensity. For amine binding sites, for example, this switching may be accomplished by the protonation of the amine to form a cationic ammonium site. In this study, semi-empirical (AM1) electronic structure calculations have been carried out for a multi-ring, multi-shaft rotaxane. Each of three rings is threaded by a shaft and the three shafts are chemically bonded to each other, limiting the number of degrees of freedom in co-conformations of the entire complex. Each of the three shafts contains one bipyridinium site and one amine site. The latter can be switched to an ammonium site by protonation to induce translation of the associated shaft. We investigate concerted versus stepwise protonation of the amine sites.

**10:36**

**A10 10 Unoccupied electronic structure of and CO Chemisorption on ultrathin Ni films** HUA YAO, A.G DANESE, R.A BARTYNSKI, *Rutgers University* The Ni/Cu(100) system has drawn considerable of attention in recent years because of its importance in both fundamental research and technological applications. Whereas many ultrathin metal systems are dominated by quantum size effects (QSEs), for epitaxial Ni films on Cu(100) there is an intermingling of QSEs, electronic hybridization, and surface/interface effects, making it complicated and challenging to obtain a microscopic picture of this bimetal system. We have performed a series of inverse photoemission (IPE) studies of the unoccupied electronic structure of the Ni/Cu(100) and CO/Ni/Cu(100) systems as a function of Ni thickness. IPE spectra from Ni films exhibit very rich structures. A Phase Accumulation Model calculation suggests only one of the three main features is consistent with metallic quantum well (MQW) State in Ni film. CO adsorption strongly modifies the spectrum by dramatically suppressing one of the main features indicating that this feature is a Ni surface resonance. Furthermore, by comparing spectra from Ni/Cu(100) with results from Cu/Ni/Cu(100), we suggest the third feature is a state confined to the Ni/Cu interface. Since the electronic structure of these films changes as a function of film thickness, it provides a very interesting opportunity to investigate how different electronic state can modify the chemisorption properties of Ni/Cu(100). We have used temperature programmed desorption (TPD) to investigate the bonding between CO and Ni in Ni/Cu(100) system.

**10:48**

**A10 11 Are mechanochemistry and thermal chemistry equal?: probing by nanonewton forces.** MARTIN KONOPKA, IVAN STICH, *Slovak University of Technology* DOMINIK MARX, *Ruhr Universitaet Bochum* Chemical reactions can be triggered by different energies, the most common being the thermal energy. Despite the fact that mechanochemistry, where mechanical energy is used instead of the thermal energy was long known, its practical use and impact was limited. Recently advances in experimental techniques, such as atomic force microscopy, fully opened the intriguing possibility to use mechanical energy as a tool for chemical reactions driven by mechanical energy. We use technologically important systems, short−chain (ethyl) thiolated copper clusters and surfaces to investigate the differences between mechano andthermal chemistry. This is an important and opened question as mechanochemistry and thermal chemistry are rarely applied to the same system. Quantum mechanics simulations based on density functional theory indicate that the two chemical reactions are vastly different. While thermal chemistry affects selectively the thiolate-carbon bond, mechanochemistry leaves that bond intact and leads to metal-metal bond breaking processes and creation of unusual high- energy structures nonexistent in the nature.

**SESSION A11: FOCUS SESSION: PROMISES AND CHALLENGES IN CHEMICAL DYNAMICS I**
**Monday Morning, 13 March 2006; 303, Baltimore Convention Center at 8:00**
**Malcolm Bersohn, University of Toronto, presiding**



*Invited Papers*

**8:00**
**A11 1 Symmetry breaking and coherent control: the importance of the envelope.**
MOSHE SHAPIRO, *University of British Columbia*

I shall review the progress of the field of ''coherent control,'' according to which control of dynamical processes is achieved by using lasers to induce (destructive or constructive) interferences between different quantum pathways leading to the same final outcome. I shall then discuss symmetry breaking stimulated by external laser fields and the role played by the relative and the ''envelope'' phase. Applications to chiral purification and the control of photo-current directionality in semiconductors will be given.

*Contributed Papers*

**8:36**
**A11 2 Coherent Phase Control of the Ionization and Dissociation of Vinyl Chloride*** ROBERT J. GORDON, VISHAL J. BARGE, ZHAN HU, JOYCE WILLIG, *Department of Chemistry, University of Illinois at Chicago* Two-pathway quantum interference was used to control the photochemical reactions of vinyl chloride ($C_2H_3Cl$, VCl). A molecular beam of VCl was irradiated simultaneously with 532 and 177 nm laser light, produced from the second and sixth harmonics of a Nd:YAG laser. The relative phase of the visible and UV lasers was adjusted by passing them through a cell containing a variable pressure of hydrogen gas, and the parent and fragment ($C_2H_3$ and HCl) ions of VCl were detected with a time-of-flight mass spectrometer. The phase lags between different pairs of modulated ion signals depended on the location of the laser focus. This variation of the phase lags was produced by the axial spatial phase of the focused laser beam. A non-zero phase lag between the parent and fragment ions produced when the laser was focused in the center of the spectrometer slit is indicative of coherent control of the branching between ionization and dissociation.

*Support by the National Science Foundation is gratefully acknowledged.

**8:48**
**A11 3 Reaction Control through Coherent Excitation of a Superposition State: Resonant Multiphoton Dissociation-Ionization of Sulfur Dioxide** BING XUE, JUN HAN, HAI-LUNG DAI, *Department of Chemistry, University of Pennsylvania* Through coherent excitation of a pair of eigenlevels, an oscillation of 130 kcal/mole in energy excitation between electronic and vibrational motions on nano second time scale is created for the molecule sulfur dioxide. The reactivity of the molecule can be influenced depending on whether the molecule is vibrationally or electronically excited with this large amount of energy. The effect of excitation on reactivity is demonstrated in resonance enhanced multiphoton dissociation-ionization of sulfur dioxide as a function of time following the coherent excitation.

*Invited Papers*

**9:00**
**A11 4 Recent Developments in Radiationless Transitions.**
SHENG-HSIEN LIN, *IAMS*

This abstract was not received electronically.

*Contributed Papers*

**9:36**
**A11 5 Energy transfer of highly vibrationally excited azulene: crossed-beam study of collisions between azulene and krypton** CHI-KUNG NI, *Institute of Atomic and Molecular Sciences, Academia Sinica* The energy transfer dynamics between highly vibrationally excited azulene molecules and Kr atoms in a series of collision energies was studied using a crossed-beam apparatus along with time-sliced velocity map ion imaging techniques. The shapes of the collisional energy-transfer probability distribution functions were measured directly from the scattering results of highly vibrationally excited or ''hot'' azulene. At low enough collision energies an azulene-Kr complex was observed, resulting from small amounts of translational to vibrational/rotational (T-V/R) energy transfer. T-V/R energy transfer was found to be quite efficient. On the other hand, only a small fraction of vibrational energy is converted to translational energy (V-T). We find that substantial amounts of energy are transferred in the backward scattering direction due to supercollisions at high collision energies.

**9:48**
**A11 6 Systematic degeneracies as a guide to the vibrational dynamics of methanol** DAVID PERRY, *The University of Akron* The vibrational dynamics of the CH stretch and torsional vibrations of methanol are explored using a 4-dimensional effective Hamiltonian. The model parameters are constrained by a combination of low-resolution and high-resolution spectral data. At low excitation energies, the torsion-vibration states are at most 2-fold

degenerate as expected for the combination of the E-type torsional tunneling species with the A' and A'' (in Cs) CH stretch vibrations. At high torsional energies, we find a series of approximate 4-fold degeneracies characteristic of a degenerate E-type asymmetric CH stretch in combination with the decoupled degenerate free internal rotation. When a single CH bond is excited to a high level, torsional tunneling is quenched causing all such levels to be 3-fold degenerate. When both a local CH stretch and internal rotation are highly excited, we find systematic 6-fold degeneracies characterized by free internal rotation decoupled from three equivalent local CH stretches. The transition regions between these simple limiting behaviors are explored.

**10:00**
**A11 7 Vibrationally Enhanced Reactions of Highly Excited Pyridine-$d_5$ ($E_{vib}$=38,000 $cm^{-1}$) with Cl Radicals** AMY MULLIN, ZIMAN LI, QINGNAN LIU, *University of Maryland* High resolution transient IR probing of DCl reaction products at 4.9 $\mu$m is used to study the influence of large amounts of internal energy on D-atom abstraction reactions of pyridine-$d_5$ ($E_{vib}$=38,100 $cm^{-1}$) with Cl radicals. Vibrationally hot pyridine-$d_5$ molecules are prepared using 266 nm pulsed excitation and Cl radicals are generated by photodissociation of $Cl_2$ at 355 nm. Cl radicals undergo collisions with pyridine-$d_5$ with $E_{rel}$=2990 $cm^{-1}$ which is near $\Delta H_{rxn}$=3050 $cm^{-1}$. The D-atom abstraction rates are enhanced by a factor of 200-300 when the pyridine reactant is vibrationally excited. Energy measurements of the products show that the pyridinyl radical has lost only one quantum of the C-D stretch. We find that the reaction mechanism is direct with a linear transition state. The lack of energy equilibration among the reaction products highlights the local nature of the transition state and shows that most of the pyridine vibrational energy is not available to the reaction. The experimental results are compared to phase space theory calculations that predict a vibrational enhancement of $\sim 10^6$-$10^8$.



## SESSION A12: FOCUS SESSION: STEPS, GROWTH, AND SMOOTHING
**Monday Morning, 13 March 2006; 304, Baltimore Convention Center at 8:00**
**Mina Yoon, Oak Ridge National Laboratory, presiding**

*Invited Papers*

**8:00**
**A12 1 Crystal Surface Morphological Evolution: From Step Motion to A Continuum Theory.**
DIONISIOS MARGETIS, *Massachusetts Institute of Technology*

Modern technological advances rely on the synthesis of nanoscale surface features on crystalline materials. Despite 50 years of progress, the related evolution laws have evaded a complete theoretical description. In this talk I describe analytically the recent derivation and applications of a continuum theory in 2+1 dimensions for crystal surfaces evolving below the roughening temperature. First, microscopic laws are formulated for the motion of atomic steps, which compose crystal surfaces, by incorporating: (i) diffusion of point defects (adatoms) on each terrace between steps; (ii) atom attachment-detachment at step edges; (iii) step curvature and elastic step interactions; and (iv) material deposition from above. Second, macroscopic laws are derived from step models: The surface height satisfies a fourth-order, nonlinear PDE for the anisotropic effect of fluxes of adatoms via an appropriate tensor mobility. The continuum solutions become questionable near macroscopic, flat surface regions (''facets'') and step bunches. Third, particular solutions are invoked to plausibly unify experimental observations of decaying bi-directional profiles via an interplay of step kinetics and surface topography. Fourth, free-boundary problems are solved for the facet evolution of axisymmetric crystal shapes: The appropriate boundary conditions are nonlocal with time. The continuum predictions compare favorably with numerical simulations for individual steps. The formation of step bunches is studied via suitable continuum coordinates of step motion.

*Contributed Papers*

**8:36**
**A12 2 Mass Transport in Nano-scale Step Fluctuations*** FERENC SZALMA, T.L. EINSTEIN, M. DEGAWA, E.D. WILLIAMS, *U. of Maryland* D.B. DOUGHERTY, *U. of Pittsburgh* Extending earlier work,[1] we investigate the linear response of a 2D nano-scale system to small perturbations and determine its transport properties. We use a 2-parameter-based energy landscape to simulate a supersaturated lattice gas by a BKL kinetic MC algorithm. The 2D gas atoms condense into a small island surrounded by a dilute gas. Island-edge fluctuations are due to both the diffusion of island atoms along its edge and atom exchange with the surrounding rare gas. Their relative importance depends on the ratio of the two energy parameters. We focus on adatom diffusion on Pb(111) surfaces below the roughening temperature, with energy parameters taken from EAM calculations. We find that edge fluctuations are mainly due to diffusion along the island edge, and determine the temperature dependence of the associated hopping rate. The Arrhenius behavior of the rates yields an effective energy barrier which fits well in the series of similar barriers for Pt, Au, and Ag. After comparing with experiments involving spirals as well as islands on Pb, we assess our simple model.

*Work at UM supported by NSF MRSEC DMR 0520471 and partially by DOE-CMSN DEFG0205ER46227

[1]F. Szalma et al., Phys. Rev. B 71, 035422 (2005)

**8:48**
**A12 3 Persistence Properties of Interacting Steps: Qualitative Failure of Mean Field*** HAILU GEBREMARIAM, T. L. EINSTEIN, *U. of Maryland, College Park* CHANDAN DASGUPTA, *Indian Inst. of Science, Bangalore* In studying the persistence properties of fluctuating steps on a vicinal surface, we examine the effect of interactions between steps on the correlation function $C(t)$ of step excursions from their mean position. For times much

longer than the correlation time $\tau_c$, $C(t) \propto exp(-t/\tau_c)$. The standard way to include step repulsions ($\propto A/l^2$) simply is the mean field, Gruber-Mullins (GM) approximation, in which each step experiences a harmonic potential that narrows with increasing repulsion.[1] Monte Carlo simulations of a terrace-step-kink model show that $\tau_c$ then decreases with increasing $A$. Including the full repulsion between neighboring steps, we find the opposite trend: $\tau_c$ increases with $A$, due to in-phase meandering absent in GM.[2] However, the time constant $\tau_s$ associated with the exponential decay of the survival probability decreases with $A$. The ratio $\tau_s/\tau_c$ decreases slowly with $A$, from 0.38 at $A = 0$, thereby satisfying the theorem that this ratio be $< 1$.[2]. We also discuss the scaling properties of autocorrelation and survival, in particular the dependence on sampling time and on lateral system size.

*Work at UM supported by NSF MRSEC DMR 0520471.

[1]C. Dasgupta et al., Phys. Rev. B 69, 022101 (2004)
[2]Hailu Gebremariam, Ph.D thesis, and HG, CD, & TLE, to be published.

**9:00**

**A12 4 Debye Model of Steps on Vicinal Crystal Surfaces*** HOWARD L. RICHARDS, CLINT A. GREENE, *Texas A & M University-Commerce* The steps on a vicinal crystal surface can be mapped onto the world lines of spinless fermions, with the average direction of the steps (the $y$-direction) being mapped to time. If the interaction energy per unit length between neighboring steps is given by $V(L) = A/L^2$ (as is common), this resulting quantum system is integrable for only three values of $\tilde{A} \equiv \tilde{\beta}A/(k_BT)^2$. For other values of $\tilde{A}$, the Pairwise Einstein Model gives an excellent approximation for the Terrace Width Distribution (TWD, the histogram of $x_{i+1}(y) - x_i(y)$) but is severely limited in describing $g_x(\Delta y) \equiv \langle [x_i(y + \Delta y) - x_i(y)]^2 \rangle$, particularly for $\Delta y > \xi$, the correlation length. Here we show how the one- dimensional Debye model correctly gives $g_x(\Delta y)$ even for large $\Delta y$. The Pairwise Einstein Model also suggests a relationship between the compressibility of the steps and the tails of the TWD, a relationship we clarify using the Debye model.

*Supported by a TAMU-Commerce Mini Grant and a Cottrell College Science Award from Research Corporation.

**9:12**

**A12 5 Step Evolution Toward Equilibrium: Fokker-Planck Approach*** AJMI BEN HAMOUDA, ALBERTO PIMPINELLI, *LASMEA, U. Blaise Pascal Clermont-2, France* HAILU GEBREMARIAM, T. L. EINSTEIN, *U. of Maryland, College Park* We have derived a Fokker-Planck equation (FPE) that describes the relaxation of steps on vicinal surfaces toward the generalized Wigner surmise $P_\varrho(s) = as^\varrho \exp(-bs^2)$, arguably the best (both conceptually and quantitatively) description of the equilibrium terrace-width distribution (TWD) of steps on a vicinal surface.[1] Focusing on the variance of the terrace-width distribution, we consider several physically-relevant initial states: perfect cleavage (straight, uniformly spaced), step bunch, and equilibrated distributions at different temperatures (prior to quenching), as well as other models. We compare analytic results with Monte Carlo studies, Metropolis and kinetic. We discuss the crucial question of how to make connections between the FPE time scale in analytic results and the actual time scale in simulations of models and in measurements of physical systems.

*Work at UM supported by NSF MRSEC DMR 0520471.

[1]A. Pimpinelli, Hailu Gebremariam, & T.L. Einstein, Phys. Rev. Lett. 95, xxx (2005)

**9:24**

**A12 6 Ab-initio Evaluation of Extended Lattice Gas Interactions of Cu on Cu(111) and Cu(001)*** T. J. STASEVICH, T. L. EINSTEIN, *University of Maryland, College Park* S. STOLBOV, *Kansas State University* Lattice gas models connect macroscopic evolution to microscopic energies. The traditional empirical parameterization of these models can lead to incomplete descriptions that yield effective rather than actual energies. More recently, self-consistent computations from first principles of the relevant interaction energies can be used to diminish the risk of incompleteness. We have used such an approach to calculate a variety of lattice-gas interaction energies between Cu adatoms on Cu(001) and Cu(111). We find that pair interactions beyond first neighbors are negligible on Cu(111), whereas second neighbor interactions are significant on Cu(001). Besides pair-interactions, we find that trio-interactions can also be quite large. On Cu(111) these include two orientation dependent trios that account for the difference in the formation energies of A- and B-steps. When taken together, the calculated interaction energies are self-consistent and compare well with previous theory and experiment[1].

*Work supported by the NSF-MRSEC

[1]T. J. Stasevich et al., Phys. Rev. B 70, 245404 (2004); 71, 245414 (2005)

**9:36**

**A12 7 Surface Smoothening Mechanism of Plasma-Deposited Amorphous Silicon Thin Films** MAYUR VALIPA, *University of California, Santa Barbara* TAMAS BAKOS, *University of Massachusetts, Amherst* ERAY AYDIL, *University of Minnesota, Minneapolis* DIMITRIOS MAROUDAS, *University of Massachusetts, Amherst* An important concern in the plasma deposition of thin hydrogenated amorphous silicon (a-Si:H) films is to obtain smooth surfaces. Under conditions that lead to device-quality a-Si:H films, the dominant deposition precursor is the $SiH_3$ radical. In this presentation, we report results of molecular-dynamics simulations combined with first-principles density functional theory calculations to elucidate the smoothening mechanism of plasma deposited a-Si:H thin films. We show that $SiH_3$ may diffuse rapidly on the a-Si:H film surface via overcoordinated surface Si atoms and incorporate into the film preferentially in surface valleys, after H atom transfer and formation of two Si-Si backbonds, with activation barriers for incorporation dependent on the local surface morphology. Experimental data on smoothening and $SiH_3$ diffusion are accounted for.

**9:48**

**A12 8 On the Phase Shift of RHEED Intensity Oscillation during Homoepitaxy by MBE** B. SHIN, *DEAS, Harvard Univ.* J.P. LEONARD, *Dept. Mat. Sci. & Eng., Univ. of Pittsburgh* J.W. McCAMY, M.J. AZIZ, *DEAS, Harvard Univ.* Despite the widespread usage of RHEED over many years, there still remain fundamental questions unanswered with regard to the interpretation of RHEED measurements. One of these issues is the phase shift of the RHEED intensity oscillations upon changing the incidence angle of electron beams. Therefore, we have conducted a systematic investigation of the phase shift of the RHEED intensity oscillations during homoepitaxy of Ge(001) by MBE for a wide range of diffraction conditions. Our results show that for small incidence angles with a beam azimuth several degrees away from crystallo-

graphic symmetry directions, the phase stays the same; it starts to shift once the (004) Kikuchi line appears in the RHEED pattern. Moreover, under some conditions we observe the oscillations from only the Kikuchi feature and not from the specular spot, and the oscillatory behavior of the Kikuchi feature is almost out of phase with that of the specular spot. All these results convincingly demonstrate that the phase shift is caused by the interference of the specular spot by the Kikuchi features. The lesson that can be learned from our study is that in order to use the RHEED specular intensity oscillation to learn about surface morphology, one must be extremely careful that the RHEED measurements be conducted under conditions where the influence of the Kikuchi features is minimal.

**10:00**
**A12 9 Properties of steps at faceted crystal-melt interfaces from molecular dynamics simulations** DOREL BUTA, *Northwestern University* MARK ASTA, *University of California Davis* JEFFREY HOYT, *Sandia National Laboratories* The properties of steps at faceted solid-liquid interfaces are key elements to understanding the anisotropy of interfacial free energies and mobilities, which in turn control the morphology of crystals grown from the melt. We investigate the equilibrium and non-equilibrium dynamics of arrays of steps at vicinal interfaces of Si(111) with molecular dynamics simulations of the Stillinger-Weber model. Step mobilities determined from isothermal crystallization simulations are found to decrease as the density of steps increases. We relate the decrease in step mobility to an increase in the effective stiffness of the interacting steps, manifested by a reduction in the width of equilibrium step fluctuations as the average distance between steps decreases. The analysis of step fluctuations is also instrumental in determining the nature of step-step interactions.

**10:12**
**A12 10 Ensemble Approach to Vicinal Crystal Surfaces** RYAN P. JACOB, HOWARD L. RICHARDS, *Physics, Texas A & M University-Commerce* T.L. EINSTEIN, *Physics, University of Maryland* Recent studies of the Step Position Distribution (SPD) have made it clear that there exists a characteristic length $L_W$ (along the $y$-axis, parallel to the average step direction) at which the variance of the SPD is correctly predicted by the Pairwise Einstein Model. We extend this to the case when neighboring steps have different stiffnesses. A similar characteristic length along $y$ must be introduced to calculate average properties from an ensemble of Gruber-Mullins models, subject to the constraint that the variance of the Terrace Width Distribution (TWD) is as given by the Pairwise Einstein Model. We discuss the relationship between these length scales for a range of step interactions.

**10:24**
**A12 11 Growth and Atomic Structure of Periodically Striped Ag Films on a One-dimensional Surface Reconstruction** TAKASHI UCHIHASHI,* *Nanomaterial Laboratory, National Institute for Materials Science, 1-1, Namiki, Tsukuba, Ibaraki, 305-0044, Japan* CHIGUSA OHBUCHI, SHIGERU TSUKAMOTO, TOMONOBU NAKAYAMA, We report the growth behavior of Ag thin films formed on the Si (111)4x1-In reconstruction, which is composed of periodic indium atomic chain arrays on a silicon surface. We use a two- step growth method, i.e., low temperature ( 100K) deposition of a Ag film followed by annealing up to room temperature. Scanning tunneling microscope (STM) and low energy electron diffraction (LEED) measurements clarify that Ag films have stripe structures with a periodicity equal to that of the Si (111)4x1-In reconstruction (= 1.33 nm), thus demonstrating its viability of an atomic-scale geometrical template. The stripe structure persists up to the film thickness as large as 30 monolayers (ML), contrary to the expectation that strained films should relax rapidly. We attribute this stability to a coincidental matching of the transverse periodicity and the corrugation amplitude between the stripe structure and the substrate, which is realized by periodic insertion of stacking faults into the Ag fcc lattice.

*E-mail: UCHIHASHI.Takashi@nims.go.jp; also affiliated with Nanoscale Quantum Conductor Array Project, ICORP, Japan Science and Technology Agency, 4-1-8, Honcho, Kawaguchi, Saitama, 332-0012, Japan

**10:36**
**A12 12 Mound slope and shape selection during unstable multilayer growth: Exact continuum formulation from a step dynamics model** JIM EVANS, *Iowa State University* MAOZHI LI, *Iowa State University* Multilayer growth is unstable in the presence of a step-edge barrier which leads to the formation of mounds. Mound sides steepen at first, but then often attain a selected slope controlled by such processes as downward funneling. Atomistic modeling is very successful in describing such behavior [1], but continuum PDE formulations are often more efficient and instructive [2]. However, by analysis of a step-dynamics model for mound formation, we show that existing phenomenological PDEs fail to correctly predict mound slopes and shapes [3]. We coarse-grain the step-dynamics models to obtain a correct theory. [1] K.J. Caspersen et al. PRB 65 (2002) 194407; [2] M. Siegert, PRL 81 (1998) 5481; [3] M. Li and J.W. Evans, PRL in press.



## SESSION A13: FOCUS SESSION: SPECTROSCOPY OF BIOMOLECULES FROM ISOLATED MOLECULES TO CELL ENVIRONMENT I

**Monday Morning, 13 March 2006; 305, Baltimore Convention Center at 8:00**
**David Pratt, University of Pittsburgh, presiding**

***Invited Papers***

**8:00**
**A13 1 Watching proteins function with picosecond X-ray crystallography and molecular dynamics simulations.*** PHILIP ANFINRUD, *NIH*

Time-resolved electron density maps of myoglobin, a ligand-binding heme protein, have been stitched together into movies that unveil with $<$ 2-Å spatial resolution and 150-ps time-resolution the correlated protein motions that accom-

pany and/or mediate ligand migration within the hydrophobic interior of a protein. A joint analysis of all-atom molecular dynamics (MD) calculations and picosecond time-resolved X-ray structures provides single-molecule insights into mechanisms of protein function. Ensemble-averaged MD simulations of the L29F mutant of myoglobin following ligand dissociation reproduce the direction, amplitude, and timescales of crystallographically-determined structural changes. This close agreement with experiments at comparable resolution in space and time validates the individual MD trajectories, which identify and structurally characterize a conformational switch that directs dissociated ligands to one of two nearby protein cavities. This unique combination of simulation and experiment unveils functional protein motions and illustrates at an atomic level relationships among protein structure, dynamics, and function. In collaboration with Friedrich Schotte and Gerhard Hummer, NIH.

*This research was supported by the Intramural Research Program of the NIH, NIDDK.



***Contributed Papers***

**8:36**

**A13 2 Raman spectra of normal and cancerous mouse mammary gland tissue using near infrared excitation energy** VAMAN NAIK, *University of Michigan-Dearborn* G.K. SERHATKULU, H. DAI, N. SHUKLA, R. WEBER, J.S. THAKUR, D.C. FREEMAN, A.K. PANDYA, G.W. AUNER, R. NAIK, *Wayne State Univ.* R.F. MILLER, *Karmanos Cancer Research Inst., Detroit, MI* A. CAO, M.D. KLEIN, R. RABAH, *Children's Hospital of Michigan* Raman spectra of normal mammary gland tissues, malignant mammary gland tumors, and lymph nodes have been recorded using fresh tissue from mice. Tumors were induced in mice by subcutaneously injecting 4T1 BALB/c mammary tumor (a highly malignant) cell line. The Raman spectra were collected using the same tissues that were examined by histopathology for determining the cancerous/normal state of the tissue. Differences in various peak intensities, peak shifts and peak ratios were analyzed to determine the Raman spectral features that differentiate mammary gland tumors from non-tumorous tissue. Tissues that were confirmed by pathology as cancerous (tumors) show several distinctive features in the Raman spectra compared to the spectra of the normal tissues. For example, the cancerous tissues show Raman peaks at 621, 642, 1004, 1032, 1175 and 1208 $cm^{-1}$ that are assignable to amino acids containing aromatic side-chains such as phenylalanine, tryptophan and tyrosine. Further, the cancerous tissues show a greatly reduced level of phospholipids compared to the normal tissues. The Raman spectral regions that are sensitive to pathologic alteration in the tissue will be discussed.

**8:48**

**A13 3 Probing the $\beta$-hairpin local structure by FTIR, 2D IR and ab initio calculations*** JIANPING WANG, *Department of Chemistry, University of Pennsylvania, PA 19104* JIANXIN CHEN, ROBIN M. HOCHSTRASSER, Small peptides form vibrational exciton systems that can be examined by means of recently developed two-dimensional infrared (2D IR) correlation techniques. We used these methods to examine a 12-residue $\beta$-hairpin (trpzip2) and its two $^{13}C$-isotopomers in the 6-$\mu$m region. Different frequency shifts are seen when $^{13}C{=}^{16}O$ substitution is in the terminal or turn region of the hairpin. The difference is believed to be due to the localization of the amide-I modes, which is supported by molecular dynamics simulations. In addition, $^{13}C$-substitution perturbs the amide-I vibrational exciton band, providing a spectroscopic probe for peptide local conformation. Peptide global and local structural information were derived from the diagonal and the cross peaks of the 2D IR correlation spectra. The measured intermode vibration coupling constants were compared with those predicted by ab initio DFT computations and transition charge coupling calculations.

*This research was supported by grants from NIH (GM12592 and RR01348) and NSF to R.M.H.

**9:00**

**A13 4 Spectral Signatures of $3_{10}$- and $\alpha$-Helices Revealed by Two-Dimensional Infrared Spectroscopy*** NIEN-HUI GE, HIROAKI MAEKAWA, *Department of Chemistry, University of California at Irvine* CLAUDIO TONIOLO, *Department of Chemistry, University of Padova, Italy* QUIRINUS BROXTERMAN, *DSM Research, Life Sciences, Advanced Synthesis and Catalysis, The Netherlands* Femtosecond two-dimensional infrared (2D IR) spectroscopy is applied to the amide I modes of the homo-octapeptide *Z*-[L-($\alpha$Me)Val]$_8$-O*t*Bu in $CDCl_3$, TFE and HFIP solutions to acquire 2D spectral signatures that distinguish between $3_{10}$- and $\alpha$-helix structures. Suppression of diagonal peaks by controlling polarizations of IR pulses clearly reveals cross-peak patterns that are crucial for structural determination. A doublet feature is observed when the peptide forms a $3_{10}$-helix in $CDCl_3$ and TFE, and when it is at the initial stage of $3_{10}$- to $\alpha$-helix transition in HFIP. In contrast, the 2D IR spectrum shows a multiple peak pattern after the peptide has become an $\alpha$-helix in HFIP. This is the first report on the experimental 2D IR signature of a $3_{10}$-helical peptide. These results for a model octapeptide demonstrate the powerful capability of 2D IR spectroscopy to discriminate between different helical structures.

*Supported by ACS PRF and NSF

**9:12**

**A13 5 Terahertz Absorption and Circular Dichroism Spectroscopy of Solvated Biopolymers*** JING XU, *Physics, UCSB* KEVIN PLAXCO, *Chemistry and BioChemistry, UCSB* S. JAMES ALLEN, *Physics, UCSB* Biopolymers are expected to exhibit broad spectral features in the terahertz frequency range, corresponding to their functionally relevant, global and sub-global collective vibrational modes with $\sim$ picosecond timescale. Recent advances in terahertz technology have stimulated researchers to employ terahertz absorption spectroscopy to directly probe these postulated collective modes. However, these pioneering studies have been limited to dry and, at best, moist samples. Successful isolation of low frequency vibrational activities of solvated biopolymers in their natural water environment has remained elusive, due to the overwhelming attenuation of the terahertz radiation by water. Here we have developed a terahertz absorption and circular dichroism spectrometer suitable for studying biopolymers

in biologically relevant water solutions. We have precisely isolated, for the first time, the terahertz absorption of solvated prototypical proteins, Bovine Serum Albumin and Lysozyme, and made important direct comparison to the existing molecular dynamic simulations and normal mode calculations. We have also successfully demonstrated the magnetic circular dichroism in semiconductors, and placed upper bounds on the terahertz circular dichroism signatures of prototypical proteins in water solution.

*Supported by ARO, NASA.

*Invited Papers*

**9:24**
**A13 6 Intermediate couplings: NMR at the solids-liquids interface.**
MEGAN SPENCE, *University of Pittsburgh*

Anisotropic interactions like dipolar couplings and chemical shift anistropy have long offered solid-state NMR spectroscopists valuable structural information. Recently, solution-state NMR structural studies have begun to exploit residual dipolar couplings of biological molecules in weakly anistropic solutions. These residual couplings are about 0.1% of the coupling magnitudes observed in the solid state, allowing simple, high-resolution NMR spectra to be retained. Inthis work, we examine the membrane-associated opioid, leucine enkephalin (lenk), in which the ordering is ten times larger than that for residual dipolar coupling experiments, requiring a combination of solution-state and solid-state NMR techniques. We adapted conventional solid-state NMR techniques like adiabatic cross- polarization and REDOR for use with such a system, and measured small amide bond dipolar couplings in order to determine the orientation of the amide bonds (and therefore the peptide) with respect to the membrane surface. However, the couplings measured indicate large structural rearrangements on the surface and contradict the published structures obtained by NOESY constraints, a reminder that such methods are of limited use in the presence of large-scale dynamics.



*Contributed Papers*

**10:00**
**A13 7 Time correlation functions in Light Harvesting Complexes embedded in Glassy Hosts*** FELIPE CAYCEDO, FERNEY RODRIGUEZ, *Universidad de los Andes* Using a Monte Carlo Wave function approach we describe the dynamics and correlation functions of light harvesting complexes (LH2) embedded in glassy hosts interacting with a classical light field. Using a dipolar interaction, we investigate the general features of coherence and (anti) bunching on a multiple-molecular system subject to cw excitation light. Spectral difusion due to environmental perturbations, produces distinct features on the fluorescent intensity and statistical properties of light emitted by the chromophores. We demonstrate how it is possible to quantify the number of chromophores involved in emission through the second-order correlation function $g^{(2)}(\tau)$ at small $\tau$ values. By changing properly the incident field, it is possible modulate the bunching or antibunching features. Finally we compare $g^{(2)}(\tau)$ for different environment conditions.

*Banco de la Republica. Facultad de Ciencias.

**10:12**
**A13 8 Conformational Dynamics of the Receptor Protein Galactose/Glucose Binding Protein*** TROY MESSINA, DAVID TALAGA, *Rutgers, the State University of New Jersey, Department of Chemistry and Chemical Biology, Pistataway, NJ 08854* We have performed time-correlated single photon counting (TCSPC) anisotropy and Stokes Shift measurements on bulk solutions of galactose/glucose binding protein. Site-directed mutagenesis was used to provide a single cysteine amino acid near the sugar-binding center of the protein (glutamine 26 to cysteine – Q26C). The cysteine was covalently labeled with the environmentally-sensitive fluorophore acrylodan, and a long-lived ruthenium complex was covalently attached to the N-terminus to provide a fluorescent reference. The TCSPC data were analyzed using global convolute-and-compare fitting routines over the entire glucose titration and temperature range to provide minimal reduced chi-squared values and the highest time resolution possible. Using a standard ligand-binding model, the resulting distributions show that the closed (ligand-bound) conformation exists even at zero glucose concentration. At 20°C, the relative abundance of this conformation is as high as 40%. The temperature dependence of this conformational study will be discussed and related to the ligand-binding free energy surface.

*supported by NIH Ruth L. Kirschstein NRSA Post Doctoral Fellowship F32GM072328

**10:24**
**A13 9 Quantifying Energy, Entropy and Free-Energy in Protein Folding Funnels*** BERNARD GERSTMAN, PREM CHAPAGAIN, *Department of Physics, Florida International University* The folding of proteins is a self-organizing process in which a long chain heteropolymer in a disorganized configuration spontaneously changes its shape to a highly organized structure. Several different forces work together to organize the structure while random thermal motion tends to cause disorganization. In order for folding to occur in a biologically relevant time, the Levinthal Paradox shows that folding cannot occur by a process that samples all of configuration space by randomly jumping from one microstate to another. Instead, folding pathways allow the organizing forces to incrementally direct the chain to ever-shrinking regions of configuration space in a funneling process. In order to understand how these self-organizing forces direct folding, we have quantified the narrowing of the folding funnel for a model two helix bundle. We have calculated the dependence of entropy and free-energy as a function of average energy by determining the statistical mechanical canonical probability for the chain to occupy each possible configuration as a function of average energy.

*PC acknowledges the support of the Graduate School at FIU through a Dissertation Year Fellowship

**10:36**

**A13 10 Landscape model of protein-DNA search: coupling of folding and sliding.** MICHAEL SLUTSKY, MEHRAN KARDAR, LEONID MIRNY, *MIT* In search for its specific site on genomic DNA, a DNA-binding protein needs to sample $10^6$-$10^9$ other sites. Classical model of this process suggests that sliding along DNA provides an efficient mechanism for sampling sites. This model however disregards the sequence-specific energy of binding and flexibility of the protein. Recent NMR studies suggest that a protein searching for its site is partially unfolded, while folding on the cognate site. Can conformational flexibility of the protein-DNA complex help it to sample sites fast and then strongly bind its cognate site? Here we study how a protein finds its site on DNA by modeling protein sliding as diffusion in the sequence-specific free energy landscape. The landscape has two dimensions: one corresponds to motion along DNA, the other is a reaction coordinate of protein's conformational transition. Our simulations demonstrate that low-energy sites can trigger folding transition in the protein, making it fold preferentially on cognate-like sites. This mechanism provides kinetic pre-selection of sites, allowing a protein to search fast and strongly bind its cognate site. Importantly our study connects microscopic time of the conformational transition ($10^{-5}$-$10^{-3}$s) to the macroscopic time of promoter binding ($10^1$-$10^3$s). Comparison with recent experimental studies of LacI conformational dynamics suggests that coupling between protein flexibility and sequence-specific binding is necessary for rapid regulation of gene expression.

**10:48**

**A13 11 Modelling Ultra-fast folding proteins** KINGSHUK GHOSH, S. BANU OZKAN, KEN DILL, *Dept of Pharm. Chem, University of California, San Francisco* Ultrafast-folding proteins are interesting because of their complex temperature dependent rates (including negative activation barriers). We develop a simple mesoscopic model that represents protein folding as a funnel through multiple routes. We have compared the model to experiments on several ultra-fast folding proteins. The model predicts the observed temperature dependences of folding and unfolding relaxation. Our model allows us to calculate the number of routes a molecule takes as it folds. We show that number of folding routes correlates with the folding time and also with the relative contact order: faster folders have more folding routes. Our model suggests a hard speed limit of 50 ns, when every protein folds via its own private route, and this corresponds to the folding time of an alpha helix. The model also computes folding time distributions which will be of interest for single molecule experiments.

**SESSION A15: METALS: 1D, 2D, 3D**
**Monday Morning, 13 March 2006**
**311, Baltimore Convention Center at 8:00**
**Duane Johnson, University of Illinois, Urbana-Champaign, presiding**

**8:00**

**A15 1 Ultrasmall metal clusters and their interaction with a molecular matrix – the fullerene-Au model system** PETRA REINKE, HUI LIU, *University of Virginia* HELGE KROEGER, *Universitaet Goettingen* Metal clusters with less than 50 atoms, are of great interest in the development of true nanoscale electronics. The electronic structure is strongly size dependent and future applications rely on a narrow size distribution. Our goal was to investigate the possibility to use fullerene surfaces as templates in the formation of cluster arrays, to analyze the cluster-fullerene interface and the electronic structure of the components. This study was performed by using photoelectron spectroscopy, and scanning tunneling microscopy and spectroscopy (UHV-conditions). The Au-cluster size is controlled by the coverage and the fullerene lattice limits the cluster surface mobility, making them accessible to STM analysis. The fullerene matrix enhances the cluster stability and ripening occurs above 500 K. A comprehensive description of the Au-cluster-fullerene system has been achieved and includes the interface characteristics, local and global electronic structure, and the spatial distribution of Au-clusters with respect to the fullerene matrix. Our understanding is currently most advanced for the Au-$C_{60}$ and Si- $C_{60}$system, where in the latter, a preferential nucleation at the interstitial lattice sites of the $C_{60}$ was confirmed.

**8:12**

**A15 2 Simulation of tunneling I-V curves from gold nanocrystals** JIANFEI SHAO, PHILLIP FIRST, *Georgia Institute of Technology* Tunneling current versus voltage (I-V) spectra were simulated for model double junction systems where the central electrode has a discrete energy spectrum, chosen to approximately model gold nanocrystals in the diameter range of 1-3 nm. The interplay between Coulomb charging and the discrete energy states introduces interesting features in the I-V curves. Electron-hole excited configurations of the nanocrystal, with up to two e-h excitations, have been included in the calculations. As compared with the orthodox theory, features in the dI/dV spectra can be modified substantially as a consequence of the nanocrystal excited states, depending on the energy spacing between states relative to both the HOMO-LUMO gap and the charging energy.

**8:24**

**A15 3 Modeling of UV laser-induced patterning of ultrathin Co films on bulk SiO2: verification of short- and long-range ordering mechanisms** JUSTIN TRICE, *Department of Physics, Washington University in St. Louis, MO 63130* CHRISTOPHER FAVAZZA, *Department of Physics, Washington University in St. Louis, MO 63130* RAMKI KALYANARAMAN, *Department of Physics, Washington University in St. Louis, MO 63130* R. SURESHKUMAR, *Department of Chemical Engineering, Washington University in St. Louis, MO 63130* DEPARTMENT OF PHYSICS, WASHINGTON UNIVERSITY IN ST. LOUIS, MO 63130 TEAM, DEPARTMENT OF CHEMICAL ENGINEERING, WASHINGTON UNIVERSITY IN ST. LOUIS, MO 63130 COLLABORATION, Irradiating ultrathin Co films (1 to 10 nm) by a short-pulsed UV laser leads to pattern formation with both short- and long-range order (SRO, LRO). Single beam irradiation produces SRO, while two-beam interference irradiation produces a quasi-2D arrangement of nanoparticles with LRO and SRO. The pattern formation primarily occurs in the molten phase. An estimate of the thermal behavior of the film/substrate composite following a laser pulse is presented. The thermal behavior includes the lifetime of the liquid phase and the thermal gradient during interference heating. Based on this evidence, the SRO is attributed to spinodal dewetting of the film while surface tension gradients induced by the laser interference pattern appear to influence LRO [1]. [1] C.Favazza, J.Trice, H.Krishna, R.Sureshkumar, and R.Kalyanaraman, unpublished.

**8:36**

**A15 4 X-Ray Study of the Epitaxial Growth of Magnetron Sputtered Ni-Al Thin Films** WOLFGANG DONNER, *University of Houston* NOUREDDINE ANIBOU, *University of Houston* Epitaxial growth of metals on semiconductors is of significant interest for both fundamental and technological reasons. Nickel-rich NiAl alloys are model materials for high-temperature shape-memory alloys. The sputter deposition growth of NiAl thin films and the X-ray study of the different phases grown on those films are the main purpose of this work. NiAl films were grown on different substrates. The Ni63Al37/Si(001) system is investigated and showed a fiber textured growth along the [111] direction of the low temperature phase L1o. On the other hand, the system NiAl/Cu(001)/Si(001) with different compositions ranging from 36% to 50% Aluminium showed epitaxial BCC films with 2 different domains. The two domains grow in the [110] direction and are rotated 90 degrees with respect to each other. The FCC phase L12 (Ni3Al) was seen to grow first in sample Ni63Al37/Cu(001)/Si(001).

**8:48**

**A15 5 Two-dimensional magic Ag nanopucks on Pb quantum islands*** Y.P. CHIU, L.W. HUANG, *Institute of Physics, Academia Sinica, Taipei, Taiwan, ROC* C.M. WEI, *Institute of Physics, Academia Sinica, Taipei, Taiwan, ROC and Institute of Atomic and Molecular Sciences, Academia Sinica, Taipei106, Taiwan, ROC* C.S. CHANG, TIEN T. TSONG, *Institute of Physics, Academia Sinica, Taipei, Taiwan, ROC* Periodic patterns of electronic origin found on Pb quantum islands can be employed as the templates to grow self-organized nanopucks of various materials. Owing to a strong interaction existing between Ag and the template, nearly perfect two-dimensional arrays of Ag nanopucks can be grown from 70 K to 150K. Not only is the notable site-selected feature of Ag nanopucks observed on Pb islands but their size distribution also registers a remarkable abundance variation. Those nanopucks with significantly enhanced intensity are denoted as two dimensional magic Ag nanoclusters. Detailed calculations based on itab initio density functional theory have been made to illuminate how the size and shape effects related to electronic confinement influence the formation of two-dimensional metal nanostructures. Furthermore, when the Ag nanopuck grows to a certain size, the geometrical effect takes hold from the electronic effect as the major attribute, which drive the Ag nanopucks towards well defined hexagonal crystalline structures.

*This project is sponsored by National Science Council of Taiwan, ROC. (grand no. NSC94-2120-M-001-006).

**9:00**

**A15 6 Geometric and Electronic Structure of Self-Assembled Monolayers Grown on Noble Metal Substrates: Dodecanethiol on Au, Ag, Cu, and Pt** HEIKE GEISLER, LAUREN POWELL, *Dept. of Chemistry, Xavier Univ.* SHAWN HUSTON, TIM SWEENEY, DANIEL BORST, CARL VENTRICE, *Dept. of Physics, Univ. of New Orleans* The geometric and electronic structure of dodecanethiol ($C_{12}H_{25}SH$) SAMs on Au(111), Ag(111), Cu(111), and Pt(111)) substrates has been studied using angle-resolved ultra-violet photoelectron spectroscopy and low energy electron diffraction. The SAMs were grown both by vapor deposition in UHV and in solution. The electronic structure of the fully saturated SAM is similar on all of these substrates, with peaks observed at binding energies of 6.5, 10, 14, and 20 eV. The geometric structure of the molecular films at intermediate coverages is different for each substrate. Growth on Au proceeds through a well-ordered lying-down phase followed by a disordered phase and a well-ordered $\sqrt{3}$ standing-up phase at saturation. Initial growth on Pt(111) shows first a p(2x2)symmetry followed by a $\sqrt{3}$ symmetry, which indicates that the initial growth is via standing-up phases on Pt. This is followed by a disordered phase at saturation. Films on Ag show a great deal of disorder at all stages of growth.

**9:12**

**A15 7 Scanning tunneling microscopy study of the charge density wave in rare-earth tritellurides*** ALEKSANDRA TOMIC, CHRISTOS MALLIAKAS, HYUN-JEONG KIM, MERCOURI KANATZIDIS, SIMON BILLINGE, STUART TESSMER, *Michigan State University* A number of correlated electron oxides exhibit surprisingly intricate ordered density modulations which underlie their novel properties. These modulations arise from incommensurate charge density waves (IC-CDWs). We have applied scanning tunneling microscopy (STM) to study the nature of IC-CDWs in the rare- earth tritellurides – simple, cleavable, layered materials. In particular, for CeTe3 we have observed both the atomic lattice of surface Te atoms and the CDW modulations oriented at 45 degrees with respect to the Te net. Two-dimensional Fourier transforms of the STM images were obtained to search for discommensurations. These are essentially domain walls whose presence has been strongly suggested by atomic pair distribution function studies. We observe satellite peaks in addition to the principal CDW peaks. These represent strong evidence for the presence of discommensurations with a characteristic length scale of about 38 angstroms.

*Research supported by the National Science Foundation grant No DMR03-05461.

**9:24**

**A15 8 Electronic Structure of Ultra-thin Graphite** GEY-HONG GWEON, ELIZABETH ROLLINGS, SHUYUN ZHOU, *University of California, Berkeley* BONGJIN MUN, ALEXEI FEDOROV, *ALS, LBNL* P. N. FIRST, W.A. DE HEER, *School of Physics, Georgia Tech* ALESSANDRA LANZARA, *University of California, Berkeley* We report a high resolution angle resolved photoemission spectroscopy (ARPES) study on ultra-thin graphite samples, grown and characterized successfully in ultra-high-vacuum environment by a thermalization of SiC. We discuss similarities to and differences from the data obtained on bulk graphite. Notable differences include doping, electronic structure as a function of $k_z$ (momentum component perpendicular to graphene layer), line width, and substrate-induced features in ultra-thin graphite samples. We discuss the effects of grain boundaries, disorder, and symmetry breaking, as possible explanations of these differences.

**9:36**

**A15 9 Transverse Plasmon Wakes in the Electron Gas** ZACHARY LEVINE, *NIST* ERIC COCKAYNE, *NIST* Relativistic electrons have transverse electric fields comparable in magnitude to the longitudinal fields. We determine the relative effects of transverse and longitudinal fields of a moving point charge on the dielectric response of a uniform electron gas, using Lindhard's longitudinal and transverse dielectric functions and, separately, the Drude dielectric function. In the direction of motion, the transverse wake fields are approximately $-v^2/c^2$ times the longitudinal wake fields. The stopping power, as determined by applying

Poynting's theorem, is reduced. Perpendicular to the direction of motion, the transverse wake fields are small compared to the longitudinal fields. Electromagnetic fields of a moving point charge are given in Fourier space for the Lorentz, Hamiltonian, and Coulomb gauges.

**9:48**

**A15 10 Optical conductivity of MnN: a combined experimental and theoretical study.** WALTER R. L. LAMBRECHT, *Case Western Reserve University* S. GRANVILLE, B. J. RUCK, F. BUDDE, A. KOO, J. E. DOWNES, H. J. TRODAHL, *Victoria University of Wellington* A. BITTAR, N. STRICKLAND, G. V. M. WILLIAMS, *Industrial Research Limited, Lower Hutt, NZ* TIMOTHY LEARMONT, KEVIN E. SMITH, *Boston University* V. J. KENNEDY, A. MARKWITZ, *Inst. Geol. and Nuclear Sciences, Lower Hutt, NZ* A comparison between measured and calculated optical conductivity is presented for MnN films prepared by ion assisted deposition. X-ray diffraction and extended x-ray absorption fine structure show the films to be nanocrystalline but phase pure. X-ray emission spectroscopy of the N K-edge and X-ray absorption near edge spectroscopy of the N K- and Mn L-edges are used to probe the occupied and empty densities of states, which compare well with the N-2p and Mn-3d partial densities of states calculated using the linearized muffin-tin orbital method. The optical conductivity was measured by spectroscopic ellipsometry/reflectivity in the infared to UV range. The major differences between calculated and measured spectra can be understood on the basis of a limited electron mean-free-path in these nanocrystalline films, which relaxes the momentum conservation requirement. The calculated optical functions are analyzed in terms of their dominant band-to-band contributions including the polarization dependence. The temperature dependent conductivity shows a clear metallic behaviour and a weak Kondo-like low temperature anomaly.

**10:00**

**A15 11 Europium $L_{2,3}$ and iron $K$-edge x-ray magnetic circular dichroism investigation of ferromagnetic ordering in $EuFe_4Sb_{12}$*** VEMURU KRISHNAMURTHY, *Oak Ridge National Laboratory* JONATHAN LANG, DANIEL HASKEL, GEORGE SRAJER, *Advanced Photon Source, Argonne National Laboratory* LEE ROBERTSON, BRIAN SALES, DAVID MANDRUS, *Oak Ridge National Laboratory* The magnetic behavior of Eu and Fe in the filled skutterudite ferromagnet $EuFe_4Sb_{12}$ has been investigated using Eu $L_{2,3}$ edge and Fe $K$ edge x-ray magnetic circular dichroism (XMCD) spectroscopy. Eu $L_3$ edge x-ray absorption spectra (XAS) in $EuFe_4Sb_{12}$ clearly show that Eu is in a mixed valence state with about 15% non-magnetic $Eu^{3+}$ states at 5 K. By comparing the XMCD spectra measured at the Eu $L_{2,3}$ edges in the ferromagnetic state at 5 K in $EuFe_4Sb_{12}$ and in the clathrate $Eu_8Ga_{16}Ge_{30}$, in which the *4f* magnetic moment of Eu is known to be 7 $\mu_B$, and by accounting for the mixed valence of Eu in the XAS, we show that $Eu^{2+}$ has the free ion like magnetic moment of $\sim$ 7 $\mu_B$ in $EuFe_4Sb_{12}$. XMCD observed at the Fe $K$ edge in $EuFe_4Sb_{12}$ at 5 K indicates magnetic short range order and a small orbital magnetic moment for the *4p* states of Fe. The relative signs of XMCD at Eu $L_3$ edge and Fe $K$ edge indicate that the $5d$ spin moment of Eu and the $4p$ spin moment of Fe are ferromagnetically coupled in $EuFe_4Sb_{12}$.

*This work is supported by US Department of Energy

**10:12**

**A15 12 Modeling of LMM-MVV Auger-Auger Coincidence Spectra From Solids** R. SUNDARAMOORTHY, A.H. WEISS, *University of Texas at Arlington* S.L. HULBERT, *Brookhaven National Laboratory* R.A. BARTYNSKI, *Rutgers University* Atoms that are highly excited due to the presence of a hole in an inner shell often relax via an Auger transition. This auto-ionizing process results in a final state with two or more holes from an Auger cascade. We present results of the direct measurements of the second and third Auger decays in this sequence. We have measured the Mn MVV Auger spectra from a single-crystal sample of MnO in time coincidence with Auger electrons emitted from prior Mn LMM Auger decays and find these to be much wider than the MVV spectrum measured in time coincidence with M core photoelectron emission. We present a model which attributes the increased energy width of the MVV transitions that follow LMM decays to the rearrangement of ''not so innocent'' bystander hole(s) in the valence band. The energetics of the Auger cascade process are modeled mathematically in terms of correlation integral(s) and convolution integral(s) over the valence band density of states. Comparisons with recent Auger-Auger coincidence studies of Ag and Pd will be made. Acknowledgements: Welch Foundation, NSF DMR98-12628, NSF DMR98-01681, and DOE DE-AC02-98CH10886.

**10:24**

**A15 13 $EuB_6$ and the Low-Density Double Exchange Model*** VITOR M. PEREIRA, J.M.B. LOPES DOS SANTOS, *CFP and Departamento de Física, Faculdade de Ciências Universidade do Porto, 4169-007 Porto, Portugal* ANTONIO H. CASTO NETO, *Department of Physics, Boston University, 590 Commonwealth Avenue, Boston, Massachusetts 02215, USA* The low electronic density regime of the double exchange model is explored in the presence of electron-electron interactions. The single particle problem and its extension to low densities, when a Wigner crystal of magnetic polarons is generated due to unscreened Coulomb interactions, is studied. It is argued that the Wigner crystal is the natural alternative to phase separation when the Coulomb interaction is taken into account. We address the thermal and quantum stability of the crystalline phase towards a polaronic Fermi liquid and a homogeneous, metallic, ferromagnetic phase. These results are relevant in the context of the polaronic physics recentely observed in $EuB_6$, and provide an important consistency-check for the double-exchange description of these magnetic hexaborides. **References:** V. M. Pereira *et al.*, tt cond-mat/0505741; V. M. Pereira *et al.*, Phys. Rev. Lett. **93**, 147202 (2004).

*Acknowledgements: We acknowledge FCT and EU through grant SFRH/BD/4655/2001 and POCTI(QCA III), and the NSF grant DMR-0343790.

**10:36**

**A15 14 Magneto-optical evidence of double exchange in a percolating lattice** G. CAIMI, A. PERUCCHI, H.R. OTT, *ETH Zurich* V.M. PEREIRA, A.H. CASTRO NETO, *Dept. of Physics, Boston University* A.D. BIANCHI, *Hochfeldlabor Dresden* Z. FISK, *Dept. of Physics, UC Davis* L. DEGIORGI, *ETH Zurich* Substituting $Eu$ by $Ca$ in ferromagnetic $EuB_6$ leads to a percolation limited magnetic ordering. We present and discuss magneto-optical data of the $Eu_{1-x}Ca_xB_6$ series, based on measurements of the reflectivity $R(\omega)$ from the far infrared up to the ultraviolet, as a function of temperature and magnetic field. Via the Kramers-Kronig transformation of $R(\omega)$ we extract the complete absorption spectra of samples with different values of $x$. The change of

the spectral weight in the Drude component by increasing the magnetic field agrees with a scenario based on the double exchange model, and suggests a crossover from a ferromagnetic metal to a ferromagnetic Anderson insulator upon increasing *Ca*-content at low temperatures.

**10:48**
**A15 15 Constructing the effective spin model of $Mn_6R_6$ from ab initio calculations** SHUN TONOOKA, KOICHI KUSAKABE, *Osaka University* HIROKI NAKANO, *University of Hyogo* NAOSHI SUZUKI, *Osaka University* Determination of the effective spin model is an important issue for molecular magnetism. Generally, the effective spin model is determined so that the model reproduces the structure of the excitation spectrum. Only this strategy sometimes could not determine which model is the most suitable among several candidates. An example showing this difficulty is seen in $[Mn(hfac)_2NITPh]_6$ abbreviated as $Mn_6R_6$. Two different models are proposed for $Mn_6R_6$ by reproducing the magnetization process. One is the Heisenberg model with three-spin interactions. The other is the Heisenberg model with frustration. In this work, in order to examine the validity of each model, we calculate the spin density by the itab- initio calculation based on the unrestricted Hartree-Fock method and the density functional theory. We also calculate the spin density of the ground state in each model by numerical diagonalization. Each model shows the different spin density. The spin density of the ground state should give essential knowledge so as to constructing the effective spin model. We discuss the method to connect the effective spin model with the first principle calculation by calculating the spin density.



## SESSION A16: FOCUS SESSION: HYDROGEN STORAGE I
**Monday Morning, 13 March 2006; 312, Baltimore Convention Center at 8:00**
**Louis G. Hector, General Motors, presiding**

*Invited Papers*

**8:00**
**A16 1 Quaternary Li-B-N-H Hydrides: New Hydrogen-Rich Storage Materials.**
FREDERICK PINKERTON, *General Motors Research and Development Center*

We have synthesized light metal Li-B-N-H quaternary hydrides by ball milling mixtures of $LiNH_2$ and $LiBH_4$ for a series of compositions $(LiNH_2)_x(LiBH_4)_{1-x}$ (x = 0.33 to 0.8). We discovered a new quaternary hydride phase, referred to here as $\alpha$ Li-B-N-H, as the primary constituent for amide-rich (x > 0.6) compositions. Although previously tentatively identified as $Li_3BN_2H_8$, its true equilibrium composition is $Li_4BN_3H_{10}$ as determined by single crystal x-ray diffraction (XRD). $Li_4BN_3H_{10}$ has a body-centered cubic crystal structure, space group $I2_13$ (# 199) with a = 10.68 Å. In situ XRD data demonstrate that the $\alpha$-phase also forms without ball milling by reacting mixed $LiNH_2$ and $LiBH_4$ powders at temperatures above about 95$^o$C. The $\alpha$ phase melts at about 190[r]C and releases hydrogen from the liquid above 250[r]C, forming solid $Li_3BN_2$. Using mass spectrometry residual gas analysis (RGA) we observe that $NH_3$ is released concurrently, and the quantity of $NH_3$ released is strongly dependent on the composition x. Maximum hydrogen release, exceeding 10 wt%, with minimum $NH_3$ release (1-3 mole % of the evolved gas) occurs for compositions near $LiNH_2$:$LiBH_4$ = 2:1 (x = 0.667). Small additions of Ni, Pt, or Pd as powder or metal chloride reduce the dehydrogenation temperature by as much as 112[r]C, and also reduce the quantity of $NH_3$ released by about an order of magnitude. Differential scanning calorimetry shows an endothermic melting peak above 190[r]C, followed by substantial exothermic heat flow above 250[r]C associated with hydrogen release and solidification of $Li_3BN_2$. The exothermic hydrogen release suggests that the reverse reaction is not thermodynamically favored. This new quaternary compound and its derivatives nonetheless represent promising research candidates in the search for practical on-board hydrogen storage materials.

*Contributed Papers*

**8:36**
**A16 2 Composition dependence of hydrogen and ammonia release in the lithium-boron-nitrogen-hydrogen quaternary system** GREGORY P. MEISNER, MATTHEW L. SCULLIN, FREDERICK E. PINKERTON, MARTIN S. MEYER, MICHAEL P. BALOGH, *Materials and Processes Lab and Chemical and Environmental Sciences Lab, General Motors Research and Development Center* The new quaternary hydride in the lithium-boron-nitrogen-hydrogen (Li-B-N-H) quaternary phase diagram forms by the reaction of lithium amide ($LiNH_2$) and lithium borohydride ($LiBH_4$) near the approximate composition $LiB_{0.33}N_{0.67}H_{2.67}$. When heated, the quaternary hydride first melts and then releases greater than 10 wt% hydrogen and a small amount of ammonia (2-3 mole% of the generated gas). We studied hydrogen and ammonia release from the series of reactant mixtures $(LiNH_2)_x(LiBH_4)_{1-x}$ as a function of composition using volumetric, gravimetric, mass spectrometer, and itin situ x-ray diffraction measurements. We found that maximum hydrogen and minimum ammonia release do occur for x = 0.67. We observe that this composition corresponds to the ternary decomposition end product $Li_3BN_2$ rather than to the true single phase composition of the quaternary hydride as determined from our single crystal x-ray diffraction measurements.

**8:48**
**A16 3 First-principles Study on Li-N-H System for Hydrogen Storage** TAKAO TSUMURAYA, TATSUYA SHISHIDOU, TAMIO OGUCHI, *ADSM, Hiroshima University* Lithium amide ($LiNH_2$) and lithium imide ($Li_2NH$) have been noticed as one of the most promising candidates for hydrogen storage due to their high gravimetric densities of hydrogen. As regards the hydrogenating and dehydrogenating processes that involve these lithium

hydrides, there is an argument about whether ammonia gas is relevant and it still remains as a matter to be studied. Furthermore, the crystal structure of $Li_2NH$ is not fully determined yet because of the difficulty in identifying hydrogen positions. Recently, various transition-metal compounds have been examined with ball milling technique for exploring catalysis to promote reaction processes, and they found that some of the Ti compounds show good performance. Measurements of x-ray absorption spectroscopy (XAS) at Ti K edge are currently under way to have a clue for understanding the catalysis mechanism. To address these issues and to get fundamental insights from microscopic level, we performed first-principles calculations by using all-electron full-potential linear augmented plane wave (FLAPW) method. We will discuss structural stability, electronic structure of lithium hydrides $LiNH_2$ and $Li_2NH$ and the heat of formation in reaction processes. Structural optimization is carried out to evaluate total energies involved in reaction processes. XAS spectra and electronic structure of Ti compounds are also discussed.

**9:00**

**A16 4 First-principles study of structural properties of $Li_2NH$** AMRA PELES, *Georgia Institute of Technology, Atlanta, Georgia, USA* SUCHISMITA SANYAL, MAHESH CHANDRAN, *GE Global Research, John F Welch Technology Centre, Bangalore, 560066 INDIA* JOB RIJSSENBEEK, *GE Global Research, 1 Research Circle, Niskayuna, New York, 12309 USA* MEI-YIN CHOU, *Georgia Institute of Technology, Atlanta, Georgia, USA* Nitrogen containing hydrides have attracted much attention recently as viable candidates for hydrogen storage materials. One example is the amide and imide involved in the reversible chemical reaction

$$LiNH_2 + LiH \rightarrow Li_2NH + H_2 .$$

In an effort to understand the reaction mechanism, one needs to have the informations on the structural properties of these compounds. There is a disagreement in the existing literature regarding the crystal symmetry of $Li_2NH$. We present a summary of first-principles investigations of the structural properties of $Li_2NH$ in an attempt to identify the lowest energy structure. Calculations were performed within density functional theory framework employing plane waves and projector-augmented-wave potentials. Various crystal structures were obtained by minimazing the total energy and the forces. The stability and energetics of these structures will be discussed.

**9:12**

**A16 5 Theoretical Investigation of the Li amide/Li imide Hydrogen Storage Reaction** JAN HERBST, LOUIS HECTOR, JR., *GM R&D Center* Considerable recent interest has centered on the reaction $LiNH_2 + LiH \leftrightarrow Li_2NH + H_2$ as a mechanism for hydrogen storage. We have conducted density functional calculations of the electronic structure, vibrational properties, and enthalpy of formation for each component. The long established crystal structures for LiH and $LiNH_2$ (Li amide) were employed, while a newly determined orthorhombic structure for $Li_2NH$ (Li imide) was used. Our 298K results within the generalized gradient approximation for $\Delta H(LiNH_2)$ and $\Delta H(LiH)$, as well as for the overall heat of reaction, are in excellent accord with experiment, suggesting that the measured $\Delta H(Li_2NH)$ is inaccurate. Phonon densities of states calculated for the amide and imide compare very favorably with observed infrared and Raman spectra.

**9:24**

**A16 6 More insights into $LiNH_2$-(LiH, $MgH_2$) system from DFT studies** C. MOYSÉS ARAÚJO, RALPH H. SCHEICHER, *Condensed Matter Theory Group, Dept of Physics, Uppsala University, Sweden* PURU JENA, *Physics Dept, Virginia Commonwealth University, Richmond VA* RAJEEV AHUJA, *CMT Group, Uppsala; Applied Materials Physics, Dept of Materials Science and Engineering, Royal Institute of Technology, Stockholm, Sweden* First-principles calculations based on density functional theory have been carried out by us to understand the hydrogen desorption reactions for systems involving $LiNH_2$ mixed with either LiH or $MgH_2$. We first determined the crystalline structures and total energies of the reactants and possible products, which have been proposed from experiment. Our results for $LiNH_2$ and $Li_2NH$ show good agreement with experimental data. For the mixed compound $Li_2Mg(NH)_2$, we have performed geometry optimization by force minimization and in addition also using molecular dynamics and simulated annealing. The circumstance that the crystalline structure of this system has not yet been resolved-prevented us from comparing our results with experimental data. However, the calculated reaction enthalpy agrees very well with recent measurements [1]. Furthermore, we have also investigated all involved reactions in the gas phase by carrying out molecular calculations. This approach has allowed us to achieve a better understanding of the reaction mechanisms. We found that reaction energies for the molecular systems follow the same trend as for the bulk systems. [1] Weifang Luo, J. Alloys Comp. 381, 284 (2004).

**9:36**

**A16 7 In-situ Neutron Diffraction Studies of the Hydrogen storage material $Li_3N$*** ASHFIA HUQ, *IPNS, Argonne National Laboratory* JAMES W. RICHARDSON, *IPNS, Argonne National Laboratory* EVAN R. MAXEY, *IPNS, Argonne National Laboratory* DHANESH CHANDRA, *Metallurgical and Materials Engineering, University of Nevada, Reno* WEN-MING CHIEN, *Metallurgical and Materials Engineering, University of Nevada, Reno* The search for alternative fuel has spurred interest in complexes with high hydrogen absorption-desorption capacities. Among these compounds complex metal hydrides have received much attention. More recently it was proposed that simple metal nitrides such as Lithium Nitride ($Li_3N$), with its 9 wt % recyclable hydrogen uptake, could be good candidates for reversible hydrogen storage. In this presentation we present the results of detailed structural study of $Li_3N$ through the temperature range 20K to 673K using Neutron Powder Diffraction. Commercially purchased compound showed a coexistence of alpha and beta phases of $Li_3N$. We observed a steady decline of the beta phase above 473K and a very small fraction ( $\sim$ 3 wt %) was frozen in at 673K. This transformation ($\beta$ to $\alpha$) was not reversible on cooling. We will also present the findings of in-situ neutron diffraction measurements of hydrogen absorption and desorption of the title material.

*Research carried out at the Intense Pulsed Neutron Source at Argonne National Laboratory is funded by the U.S. Department of Energy under Contract W-31-109-ENG-38.

**9:48**

**A16 8 Characterization of Lithium Borohydride using Neutron Scattering Techniques** MICHAEL HARTMAN, JACK RUSH, TERRY UDOVIC, *National Institute of Standards and Technology* Lithium borohydride, $LiBH_4$, is a complex metal hydride that shows great promise as a hydrogen storage medium with a volumetric hydrogen density of 122 kg H/$m^3$ and a gravimetric hydrogen density of 18.5 wt. %. While numerous NMR, Raman,

and infrared investigations have been reported in the literature, neutron scattering investigations of $LiBH_4$ have been limited due to the large neutron absorption cross-section of naturally occurring lithium and boron. We have recently synthesized an isotopically-enriched lithium borohydride, containing $^7Li$ and $^{11}B$, which eliminates the large neutron absorption cross-section that arises from the presence of $^6Li$ and $^{10}B$. The results of powder neutron diffraction, inelastic neutron scattering, and quasi-elastic neutron scattering investigations on the $^7Li^{11}BH_4$ material are presented. These measurements provide a fundamental understanding of the behavior of hydrogen within lithium borohydride, and they provide a basis to understand changes concomitant with the introduction of catalytic or destabilizing compounds.

**10:00**
**A16 9 Structural transitions in NaBH4 under pressure*** RAVHI KUMAR, ANDREW CORNELIUS, *University of Nevada, Las Vegas* The structure of the technologically important hydrogen storage compound $NaBH_4$ has been investigated under pressures up to 30 GPa by itin situ angle dispersive high pressure x-ray diffraction using synchrotron x-rays and a diamond anvil cell. Our experimental results show pressure-induced structural transitions of $\alpha$-$NaBH_4$ (cubic – itFm3m) to $\beta$ – $NaBH_4$ (tetragonal – $P42_1c$) at 6.3 GPa and further to orthorhombic phase (itPnma) at 8.9 GPa. The high pressure orthorhombic phase is found to be stable up to 30 GPa. The cubic phase is completely recovered on releasing the pressure to the ambient.

*We acknowledge support from DoE Award No. DE-FG36-05GO08502.

**SESSION A17: FOCUS SESSION: STRUCTURE AND PROPERTIES OF NANOSCALE OXIDE FILMS**
**Monday Morning, 13 March 2006**
**313, Baltimore Convention Center at 8:00**
**Gennadi Bersuker, SEMATECH, presiding**

***Contributed Papers***

**8:00**
**A17 1 Crystallization and defect formation in $HfO_2$ films on silicon.** JACOB GAVARTIN, ALEXANDER SHLUGER, MARSHALL STONEHAM, *University College London* GENNADI BERSUKER, *SEMATECH* Hafnium dioxide currently is considered a dielectric of choice for novel MOSFET devices but it has an important drawback (as most high-k films on silicon) of low crystallization temperature. We use large scale plane wave density functional simulations of the $HfO_2/SiO_x/Si$ system to determine the properties of the amorphous hafnia films and the mechanisms of their crystallization and defects formation associated with it. We propose that the kinetics of interface formation stipulates some oxygen sub-stoichiometry in hafnia. The resulting 'amorphous' films are characterized by the sub-coordinated (by less than 7 oxygen) Hf ions and some shortened Hf-Hf distance ( $\sim$ 3 Å compared to $\sim$ 3.5 Å in the monoclinic $HfO_2$). Such structures may not have defect states (understood as localized states with energies in the band gap). However, they are characterized by the long band tails, whose origin will be discussed. Crystallization of such amorphous structures during thermal annealing results in the oxygen vacancy formation. We discuss the role of these vacancies in the trapping and de-trapping of carriers from the channel and the possibilities of control of their concentration.

**8:12**
**A17 2 Observation of Oxygen Bridging at the Si-$SiO_2$ Interface** PHILIP BATSON, *IBM Thomas J. Watson Research Center* Annular Dark Field (ADF) images of the Si-$SiO_2$ interface have been obtained using a 0.08 nm probe in an aberration corrected Scanning Transmission Electron Microscope (STEM). The 2 nm thick $SiO_2$ layer lies under an $HfO_2$ high dielectric constant structure, and contains isolated Hf atoms which are highly mobile under the beam. Assuming that Hf atoms occupy low energy sites within the oxide, they can substitute for Si atoms in tetrahedral coordination, or occupy incomplete octahedral pockets. In either case, they should provide a probe of the structure of the amorphous oxide. 0.3-0.6 nm from the crystalline Si, Hf atoms move mostly parallel to the interface, suggesting that quasi-planar structures may occur near the Si interface. Within 0.3 nm of the Si, tunnels run parallel to the [110] direction. Inside the tunnels, a single column of atoms is observed between two adjacent interface Si columns. ADF image simulations show that the observed scattering intensity for this column is consistent with oxygen, supporting the oxygen bridging model proposed by Tu and Tersoff (Phys Rev. Lett. **84** 4393 (2000)).

***Invited Papers***

**8:24**
**A17 3 Atomic-level imaging and properties of stray Hf atoms in Si-$SiO_2$-$HfO_2$ nanoscale structures.*** STEPHEN PENNYCOOK, *Oak Ridge National laboratory*

The aberration-corrected scanning transmission electron microscope (STEM) provides a new level of sensitivity for analyzing nanoscale oxide films. The sub-Ångstrom probe provides much improved resolution, but equally important, greatly increased sensitivity to individual atoms. Single Hf atoms are visible within the nanometer thick $SiO_2$ interlayer between a $HfO_2$ dielectric and the Si substrate. Furthermore, the depth of focus of the aberration-corrected STEM is greatly reduced, and Hf atoms can be located in depth to better than 1 nm precision. Strikingly, no Hf atoms are seen to be in contact with the Si substrate, and exhibit preferred distances from the interface. First-principles density-functional calculations find that the energy of single Hf atoms rises sharply if they approach closer than $\sim$ 0.3 nm, in agreement with

observations. The Hf atoms introduce localized states within the Si band gap, which are detected by electron energy loss spectroscopy. These states may mediate leakage currents. The effect of the stray Hf atoms on the electron mobility in the Si channel has been calculated using a novel first-principles approach and found to be consistent with measured mobility values. Work performed in collaboration with K. van Benthem, S. N. Rashkeev, M. H. Evans, and S. T. Pantelides.

*Research sponsored by the U.S. DOE under Contract # DE-AC05-00OR22725 with ORNL, NSF grant ECS-0524655, AFOSR grant FA9550-05-1-0306 and the Alexander-von-Humboldt Foundation in the framework of a Feodor-Lynen research scholarship.



*Contributed Papers*

**9:00**

**A17 4 Characterization of local electronic structure and dielectric properties at a HfO2/SiO2/Si gate dielectric interface.*** KLAUS VAN BENTHEM, *ORNL* SERGEY RASHKEEV, *ORNL* GENNADI BERSUKER, *International Sematech* SOKRATES PANTELIDES, *Vanderbilt University* STEPHEN PENNYCOOK, *ORNL* Electron Energy-Loss Spectroscopy (EELS) measurements were performed using an aberration-corrected Scanning Transmission Electron Microscope (STEM) to investigate local electronic structure across a HfO2/SiO2/Si gate dielectric interface with a lateral resolution of approximately 0.1 nm. The low energy-loss regime in EELS is dominated by intra-and interband transitions and plasmon excitations. Hence, by a Kramers-Kronig analysis of the low energy-loss regime the determination of the complex dielectric function becomes possible on a sub-nanometer length scale. As a consequence, local optical properties and the local interband transition strength can be discussed as a function of position across the gate dielectric. Single Hf atoms present within the SiO2 interlayer introduce localized states in the Si band gap and gradients in the local dielectric function. Microscopic measurements will be correlated with macroscopic device characteristics.

*K.v.B. acknowledges partial financial funding from the Alexander-von-Humboldt Foundation

**9:12**

**A17 5 Oxygen transport and interfacial layer engineering in high-k metal oxide gate stacks** LYUDMILA GONCHAROVA, MATEUS DALPONTE, ERIC GARFUNKEL, TORGNY GUSTAFSSON, *Rutgers University* GENNADI BERSUKER, BRENDAN FORAN, PAT LYSAGHT, *Sematech* Much recent work has been devoted to integrating metal oxide dielectrics into silicon based CMOS. High-$\kappa$ metal oxide stacks processing may lead to diffusion and reactions with negative impact on the electrical properties. We report here results from Medium Energy Ion Scattering (MEIS) on (i) the mechanism of oxygen transport and interfacial layer behavior in multilayer high-$\kappa$ gate stacks and (ii) the influence of crystallinity and grain boundaries on thin Hf oxide and silicate films using isotope tracing. Changes in oxide and silicate interface composition and thickness, phase mixing and crystallization within the film, and film decomposition will be discussed in terms of bulk and grain boundary diffusion. A functional device must include not just a dielectric, but a conducting gate as well. Our results show that the interfacial $SiO_2$ layer thickness is reduced by using a Ti overlayer with high solubility for oxygen. We also find that Si atoms initially present in the interfacial $SiO_2$ layer incorporate in the high-$\kappa$ layer. Oxygen is also being removed from the Hf oxide, leaving an oxygen depleted $HfO_x$ layer. The presence of grain boundaries in crystalline $HfO_2$ films suggests an additional path for Si diffusion through the high-$\kappa$ film in the presence of Ti gate.

*Invited Papers*

**9:24**

**A17 6 Defects on Magnesium Oxide Surfaces: An STM and ESR Study.** HANS-JOACHIM FREUND, *Fritz Haber Institute*

Thin MgO(100) films have been prepared on Ag(100) und Mo(100) substrates. Color centers are not present on these MgO surfaces but can be induced by electron bombardment. $F^+$ and $F^0$ centers may be identified with scanning tunnelling spectroscopy and found to be located not on terrace but rather on edge sites primarily. This is corroborated by electron spin resonance experiments. Methods are described to engineer surfaces with particular defects and thus its interaction with both, molecules and metal atoms, can be studied. Additional techniques such as Fourier-Transform Infrared Spectroscopy allow us to get closer insight into the influence of defects on the properties of adsorbed atoms and molecules.

*Contributed Papers*

**10:00**

**A17 7 Zintl Concepts for Interface Engineering** ALEX DEMKOV, *The University of Texas at Austin* Crystalline epitaxial oxides on semiconductors (COS) could very well extend the Complimentary Metal Oxide Semiconductor (CMOS) technology from Si to other semiconductors and thus give new lease on life to the paradigm responsible for the outstanding success of the semiconductor electronics. Another tantalizing possibility is the growth of functional oxide structures utilizing ferroelectricity, superconductivity, magnetism, and other such properties not normally accessible in conventional semiconductors in monolithic integration with Si. There also may be applications of COS at the end of the Si Roadmap. Two dimensional (2D) crystal growth of ionic oxides on covalent semiconductors and visa versa is essential for these approach to work. In this talk I will discuss how concepts developed by Edward Zintl more than seventy years ago can be used for interface engineering. I will use itab-initio density functional theory to demonstrate how the bonding character at the oxide/semiconductor interface is manipulated through charge transfer in the engineered intermetallic contact layer. This transition layer lowers the energy of the interface and results in 2D growth, and high quality epitaxial films.

**10:12**

**A17 8 One-dimensional $PtO_2$ oxide at Pt steps: formation and reaction with CO** J.G. WANG, W.X. LI, T.M. PEDERSEN, B. HAMMER, *University of Aarhus, Denmark* J. KLIKOVITS, M. SCHMID, *Technische Universität Wien, Austria* M. BORG, J. GUSTAFSON, A. MIKKELSEN, J. WEISSENRIEDER, E. LUNDGREN, J.N. ANDERSEN, *Lund University, Sweden* The structure and catalytic activity of a one-dimensional $PtO_2$ oxide, which forms along the steps on the Pt(332) surface, is studied using HRCLS and DFT [1]. Our investigations reveal a much higher CO-oxidation activity of the one-dimensional oxide as compared to the chemisorbed oxygen phase of Pt(111). The reason could be explained by DFT by the detection of a significantly lower barrier for the $CO_2$ formation using O from the oxide stripe, as compared to the O chemisorbed on the terrace. Finally, the one-dimensional oxide is predicted to be stable at conditions between chemisorbed oxygen and the bulk oxide, which at 500 K includes ambient oxygen pressures. This range is expected to be similar on other step structures of Pt. Hence the one-dimensional oxide could be of major importance for the catalytic activity of Pt nano particles, as used in industrial catalytic devices. [1] J. G. Wang et al., Phys. Rev. Lett. In Press. This work was financially supported by the Swedish Research Council, the Danish Research Council, Dansk Center for Scientific Computing, the EC contract No. NMP3-CT-2003-505670 (NANO2), and the Austrian Fonds zur Förorderung der Wissenschaftlichen Forschung.

**10:24**

**A17 9 Ultrathin $TiO_x$ films on Pt(111)** GAETANO GRANOZZI, FRANCESCO SEDONA, *Dept. of Chemical Sciences, University of Padova* KLAUS SCHIERBAUM, *Heinrich-Heine-Universität Düsseldorf* Ultrathin ordered titanium oxide films on Pt(111) surface were prepared by reactive evaporation of Ti in oxygen. By varying the Ti dose and the annealing conditions, several long-range ordered phases were obtained and characterized by means of LEED, XPS, UPS, photoelectron diffraction, STM and XAS. XPS and photoelectron diffraction data indicate that all the phases, except two, are one-monolayer thick and composed of a Ti-O bilayer with interfacial Ti. Atomically resolved STM images of all the prepared phases have been obtained. At a low Ti dose (0.4 MLE), an incommensurate itkagomé-like low density phase is observed where hexagons are sharing their vertices. At a higher Ti dose (0.8 MLE) two denser phases are found, both characterized by a zigzag motif, but with distinct rectangular unit cells. When the post-annealing of the 0.8 MLE deposit is carried out at high temperatures and oxygen partial pressures, an incommensurate non-wetting fully oxidized phase is found, whose symmetry and lattice dimensions are almost identical with those observed in the system $VO_x$/Pd(111). At higher coverage, two commensurate hexagonal phases are formed, which show wagon-wheel-like structures and have slightly different lattice dimensions. Competitively to the formation of ultrathin films, nanosized $TiO_2$ crystallites can grow on top of the surface. They predominate the entire morphology only for large initial Ti deposits.

**10:36**

**A17 10 Surface structure of alumina ultrathin film grown on Ni3Al (111) studied by nc-AFM** CLAUDE R. HENRY, CLEMENS BARTH, GUIDO HAMM, *CRMCN-CNRS, Campus Luminy, 13288 Marseille* CLUSTER GROUP TEAM, Alumina ultrathin films grown by high temperature oxidation of a Ni3Al (111) surface have the peculiarity to be nanostructured. Indeed, as shown previously by the group of C. Becker [1], they present two hexagonal structures with lattice parameters of 2.4 and 4.16 nm. However, no atomic resolved structure was evidenced by this STM study. In the present study we used the same preparation technique to grow the alumina film. The surface structure of the film was studied, in situ under UHV, by nc-AFM. By this technique we confirm the presence of the two structures and we clearly show that the larger one is the basic structure of the topmost layer of the film. The 2.4 nm structure is a sub-lattice of the 4.1 structure. These two structures provide two different local environments that could explain why metals condensed on this film form hexagonal lattice with a parameter of 2.4 or 4.1 nm. Atomic resolution has been obtained showing that the topmost surface is terminated by a distorded hexagonal lattice of atoms (most probably oxygen). The relationships betwen the atomic lattice and the two superstructures have been derived from the nc-AFM measurements. We will discuss on the possible origin of the complex structure of this films. [1] S. Degen et al. Surf. Sci. 576(2005)L57

**10:48**

**A17 11 Oxygen storage and release by Ceria: New insights into the mechanism based on STM** FRIEDRICH ESCH, *CNR-INFM Laboratorio TASC* STEFANO FABRIS, *SISSA and CNR-INFM DEMOCRITOS, Trieste* CRISTINA AFRICH, CECILIA BLASETTI, *University of Trieste and CNR-INFM Laboratorio TASC* PAOLO FORNASIERO, *University of Trieste and INSTM* RENZO ROSEI, GIOVANNI COMELLI, *University of Trieste and CNR-INFM Laboratorio TASC* In the attempt to understand the structure-dependent characteristics of ceria ($CeO_2$) surfaces with various morphologies (films, nanoparticles, single crystals), we focus on high-resolution scanning tunneling microscopy of a (111) single crystal surface. A new preparation procedure is described that generates one trilayer deep pits on the surface, exposing (001) and (110) steps that can systematically be studied. Pit shapes reflect the surface mobility of ceria and relative stability of the steps. Atomic oxygen exposure leads to the formation of ceria nanoparticles at step edges. Upon reduction, various oxygen vacancies can be distinguished on the (111) terraces and are assigned to single 1st layer vacancies, single 2nd layer vacancies, linear and other vacancy clusters (VCs) by comparison to density functional calculations [1]. It is shown that electron localization determines which VCs can be formed and which can not: VCs expose exclusively reduced $Ce^{3+}$ ions. In linear VCs, that dominate the strongly reduced surface, this occurs by including one single subsurface vacancy per VC. [1] F. Esch et al., Science 309 (2005) 752.

**SESSION A18: FOCUS SESSION: CARBON NANOTUBES: SYNTHESIS AND GROWTH I**
**Monday Morning, 13 March 2006; 315 Baltimore Convention Center at 8:00**
**Michael Arnold, Northwestern University, presiding**



*Invited Papers*

**8:00**
**A18 1 Super Growth Carbon Nanotubes.**
KENJI HATA, *AIST*

Water assisted CVD (denoted as Super Growth) results in a significant enhanced catalyst activity and enlonged lifetime of the catalysts to synthesize carbon nanotubes. The high efficient growth results in massive growth of vertically-aligned single-walled nanotubes forests with heights up to 2.5 millimeters and carbon purity over 99.98%. Super Growth simultaneously addresses many critical problems such as scalability, purity, and cost, and opens up innumerable opportunities ranging from fundamental research to real applications. This presentation will provide an overview of our recent development of the ''Super Growth'' CVD. First, the synthesis of highly efficient impurity free SNWT forest will be described. Second, the growth dynamics will be explored with our recent advance in CNT synthesis, as well as characterizing the physical and chemical properties of SWNT forests. Third, various new forms of carbon nanotube material such as DWNT forests, SWNT solids made by utilizing the super-growth technique will be demonstrated with emphasis on their applications such as super-capacitors. Lastly, challenges and future projects that are planed will be summarized.

*Contributed Papers*

**8:36**
**A18 2 Density functional study of cyclacene-based carbon nanotubular compounds.*** SHINYA OKANO, *Michigan State University* GLEN P. MILLER, *University of New Hampshire* DAVID TOMANEK, *Michigan State University* We use *ab initio* Density Functional calculations to investigate the interplay between structural and electronic properties of a new class of one-dimensional nanowires, related to carbon nanotubes. The cyclacene building blocks consist of phenyl rings, and can be viewed as the shortest segments of (n,0) zigzag nanotubes. In our study, we focus on cyclacenes with n=6-12 phenyl rings, and compare our results to infinitely large cyclacenes, corresponding to narrow graphene ribbons. The nanowires are formed by inter-connecting cyclacenes to a chain using biphenyl, tetrazine, or acetylene linkers. Depending on the nature and the orientation of the linkers, we find it possible to change the systems from narrow- to wide-gap semiconductors, and to modulate the band dispersion, suggesting the possibility of band gap engineering. We will also discuss the relevance of our results for a diameter- and chirality-selective synthesis of carbon nanotubes.

*Supported by NSF NIRT grant ECS-0506309 and NSF NSEC grant EEC-425826.

**8:48**
**A18 3 The mechanism for low temperature growth of vertically aligned boron nitride nanotubes*** JIESHENG WANG, *Michigan Tech University* MING XIE, *Michigan Tech University* YOKE KHIN YAP, *Michigan Tech University* Boron nitride nanotubes (BNNTs) are well recognized as the candidate that will complement the uses of carbon nanotubes (CNTs) in nanotechnology. However, high growth temperatures ( $>$ 1100 $^{o}$C), low production yield, and impurities have prevented effective synthesis and applications of boron nitride nanotubes (BNNTs) in the past ten years. For the first time, we have succeeded on the growth of pure BNNTs on substrates [1, 2]. This has been realized based on our experiences of growing CNTs and boron nitride (BN) phases (cubic phase BN, hexagonal phase BN). According to our hypothetical model, energetic growth species play an important role on controlling the phases of BN solids. We have experimentally verified that BNNTs can be grown by energetic growth species by a plasma-enhanced pulsed laser deposition (PEPLD) technique. These BNNTs can be grown vertically aligned into arrays of regular patterns at 600 $^{o}$C, and can be used for applications without purification. The growth mechanism of thee BNNTs will be discussed. [1]. Yap et al., Bull APS Vol 50, 1346-1347 (March 2005). [2]. Wang itet al., nano Letters (2005) ASAP, DOI: 10.1021/nl051859n.

*Y.K.Y acknowledges supports from Army Research Office (W911NF-04-1-0029), CNMS at ORNL, and NSF CAREER Award (0447555).

**9:00**
**A18 4 Selective Growth of Single Wall Carbon Nanotubes from Superparamagnetic Maghemite** RAMA BALASUBRAMANIAN, RICHARD GRANT, *Roanoke College* PAOLA BARBARA, *Georgetown University* The growth of carbon nanotubes in specific configurations and geometry is crucial to developing useful applications in nanoelectronics and smart coatings. We have shown that single wall carbon nanotubes (SWNT) of diameters less than 2 nanometers can be grown directly from catalyst particles comprising of maghemite ( $\gamma - Fe_2O_3$) on a Silicon substrate using the conventional chemical vapor deposition process. The sizes of SWNT were measured using Atomic Force Microscopy. The average tube diameter was measured to be 1.5$\pm$ 0.2 nm. Scanning Electron Microscopy measurements revealed that the catalyst oxide particles formed in clusters of 100 nm diameters. Transmission Mössbauer measurements at room temperature showed the presence of a magnetic sextet corresponding to maghemite with a particle size $>$ 100 nm and a superparamagnetic phase with particle size less than 20 nm. Our results also indicate that the superparamagnetic phase of maghemite with average particle size of about 5 nm plays a critical role in the formation of SWNT with specific tube dimensions. Experiments are currently underway to characterize the relaxation rates of the superparamagnetic phase of maghemite. The fundamental role of arrays of metal nano-catalysts and superparamagnetic nanoclusters

of maghemite in the selective growth of single wall carbon nanotubes will be presented.

**9:12**

**A18 5 Controlling the height of CVD-grown multi-wall nanotube arrays** MICHAEL STADERMANN, SARAH SHERLOCK, BRIAN DICK, HYUNG-GYU PARK, ALEXANDER ARTYUKHIN, WILLIAM PITZ, ALEXANDER NOY, OLGICA BAKAJIN, *Lawrence Livermore National Laboratory* Due to various difficulties, carbon nanotube arrays have seen only limited use in industrial applications to date. One of the difficulties is the reproducible growth of these arrays, let alone a good measure of control over the obtained height. In this work, we have preformed a parametric study of multi-wall carbon nanotube (MWNT) growth. The investigated parameters were gas flow rate, process pressure, and water content of the feed gas. We were able to identify a region in the parameter space that yields stable and highly reproducible growth of tall nanotubes arrays. As a result, we can controllably grow MWNT forests to any height between 1 $\mu$m and 1 mm by choosing the right combination of pressure, humidity, flow rate, and growth time. Additionally, we were able to perform kinetic studies of the carbon nanotube growth, and our results suggest that the precursor for nanotube growth is formed in the gas phase.

**9:24**

**A18 6 Real-Time Study of the Kinetics of Vertically Aligned Single Wall Carbon Nanotube Array Nucleation and Growth** GYULA ERES, *Oak Ridge National Laboratory* H. CUI, C. M. ROULEAU, A. A. PURETZKY, D. B. GEOHEGAN, A molecular beam of carbon containing molecules in conjunction with time resolved reflectivity was used to study the kinetics of nucleation and growth of vertically aligned single wall carbon nanotube arrays. The molecular beam environment decouples the source gas and the substrate temperature dependent variables and eliminates secondary gas phase reactions, to allow carbon nanotube growth by surface reactions only [1]. The incidence rate of the carbon containing species is the key variable that through the nucleation density determines all the important properties of the arrays including the type, the diameter, and the packing density of the nanotubes. The addition of trace amounts of impurities such as water and oxygen enhances the nucleation density but does not affect growth. This highly controlled reaction environment reveals that carbon nanotube growth is a complex multicomponent reaction in which not just C but also H and O play a critical role. The picture that emerges form this study is at odds with the conventionally accepted dissolution/precipitation model for carbon nanotube growth. Instead, we explain the observed results by a new mechanism that is based on carbon network formation and stabilization by stepwise addition of acetylene type species. [1] G. Eres itet al. J. Phys. Chem. B **109**, 16684 (2005).

**9:36**

**A18 7 Defect induced modification in thermal property of Regioreguler Poly(3-hexylthiophene) nanotube composites** ANANTA ADHIKARI, *College of Nanoscale Science and Engineering, State University of New York, Albany, NY-12203* CHANG RYU, *Department of Chemistry and Chemical Biology, Rensselaer Polytechnic Institute Troy, NY-12180* PULLICKEL AJAYAN, *Department of Material Science and Engineering, Rensselaer Polytechnic Institute Troy, NY-12180* HASSARAM BAKHRU, The interaction particularly, interfacial bonding between polymer and filler has remained a crucial phenomenon to be understood to optimize their uses in many practical applications. Up to now, most of the work is on the chemical fuctionalization for improving nanotube/matrix interaction. In this paper, we studied the effects of ion irradiation induced defects on thermal behaviors of Poly(3-hexylthiophene) nanotube composites using Thermogravimetry Analysis (TGA) and Differential Scanning Calorimetry (DSC). Where, the irradiation is used to introduce the defects in a control way on pristine nanotube before composite formation. Several interesting effects were observed; including thermal stability enhancement and defects induced enhanced interaction between nanotube and polymer, and substantial changes in spectroscopic behaviors of the composites due to irradiation.

**9:48**

**A18 8 Effect of graphitic order on the electron field emission of carbon nanotube films*** BENJAMIN ULMEN, *Michigan Tech University* VIJAYA KAYSTHA, *Michigan Tech University* YOKE KHIN YAP, *Michigan Tech University* Carbon Nanotubes (CNTs) are known to be excellent electron field emitters. However, the fundamental factors that contribute to the emission stability have not been well studied. Here, we found that stability of emission current from CNTs is related to their graphitic orders. We have tested various types of CNTs grown by thermal chemical vapor deposition (CVD) and plasma enhanced CVD (PECVD). Our samples were grown in a circular area of 0.385cm$^2$ on low resistance Si substrates. Field emission measurements were conducted in a planar diode configuration, with a pair of electrodes separated with a gap of 1000 $\pm$ 10 $\mu$m. The vacuum level during the measurement is $\sim$ 2.0 X $10^{-7}$ mbar. We found that the emission currents from PECVD grown CNTs degraded by as much as 70% within a period of 20 hours. In contrast, random CNTs grown by thermal CVD exhibit stable emission current for at least 20 hours. These CNTs also have relatively lower threshold electric field of field emission. Since all samples are tested in a same condition, the detected results are thus related to the structural order of the CNTs. Transmission electron microscopy and Raman spectroscopy confirmed that field emission stability is depends on the graphitic structures of these CNTs.

*Y.K.Y acknowledges supports from Army Research Office (W911NF-04-1-0029) and CNMS at ORNL,

**10:00**

**A18 9 Structure and Applications of Nanoporous Carbon*** MIKAEL WOOD, JACOB BURRESS, ROBERT SCHOTT, DEMETRIUS TAYLOR, PETER PFEIFER, *Physics Dept., University of Missouri, Columbia, MO 65211* Recently fractal networks of nanopores in activated carbon have been discovered (Pfeifer et al., Phys. Rev. Lett. 88, 115502 (2002)). We study the formation and properties of these networks with the goal of using them to store methane at low pressures (Alliance for Collaborative Research in Alternative Fuel Technology, http://allcraft.missouri.edu). Van der Waals forces in the nanopores force methane into a dense fluid (supercritical adsorption). We investigate the pore structure by nitrogen and methane adsorption isotherms, small-angle x-ray scattering (SAXS), and electron microscopy, and use the data to model the formation of the pore network using probabilistic cellular automata on a lattice. The calculated scattering from our simulated networks is in close agreement with experimental SAXS data. The models are designed to give us a deeper understanding of the growth of these networks and allow us to optimize their properties. Currently our best sample stores 0.11

g methane per $cm^3$ monolithic carbon at 25 $^oC$ and 34 atm (90% of industry target).

*Support: National Science Foundation (EEC-0438469), University of Missouri, Midwest Research Institute, U.S. Department of Education (GAANN), and U.S. Department of Energy (W-31-109-Eng-38)

**10:12**

**A18 10 Boron-doped SWNTs for Electromagnetic Interference Shielding** P. EKLUND, D. NAREHOOD, *Dept. of Physics, The Pennsylvania State University* N. DITROLIO, N. ANDREWS, *CarboLex, Inc., 500 Parkway Ave, Broomall, PA 19008* U.J. KIM, X.M. LIU, H.R. GUTIERREZ, *Dept. of Physics, The Pennsylvania State University* SWNTs have been proposed for electromagnetic interference shielding as an additive in polymers. However, 2/3 of the SWNTs are expected to be semiconducting and only 1/3 are metallic. B-doping of graphite is known to lead to strongly p-doped material. In SWNTs, doping is therefore expected to lead to degenerately-doped semiconducting tubes and then a shielding benefit can be derived from all tubes in the sample. We find that 1-2 at% B-doping is possible at 25-50 gr/hr production. The quality of the HCl-purified product has been investigated by Raman scattering (RS), optical adsorption, transmission electron microscopy and temperature programmed oxidation. RS spectra were found to exhibit sharp G,R bands and a very weak D-band component is also observed. We note that after B-doping the $2^{nd}$ order RS cross section is enhanced, as reported previously for pulsed laser produced B-doped SWNTs by Rao et al. All band positions are very close to that observed for undoped SWNTs, indicating a reasonably good molecular structure of the B-SWNTs and consistent with the small size of atomic boron (i.e., substitutional dopant). OA show that the interband absorption peaks associated with semiconducting and metallic tubes upshift by 20-50 meV, indicating p-doping.

**10:24**

**A18 11 Detachment and re-attachment of vertically aligned single-walled carbon nanotube films** YOICHI MURAKAMI, SHIGEO MARUYAMA, *The University of Tokyo* A hot-water assisted detachment method of CVD-grown vertically aligned single-walled carbon nanotube (VA-SWNT) films from substrates has been developed. In particular, we found that the VA-SWNT films is efficiently peeled off by submersing the substrate into heated ( $\geq$ 60 [r]C) distilled water, and the detached film floats on the water surface. Furthermore, the detached film is readily re-attached to arbitrary surfaces. SEM observation confirms that the aligned morphology is perfectly preserved even after the re-attachment to other substrates. Mechanism of the proposed hot-water assisted film detachment method is investigated and suggested.

**10:36**

**A18 12 Fabrication and characterization of nanopatterned ultrathin epitaxial graphite films.*** ZHIMIN SONG, XUEBIN LI, TIANBO LI, CLAIRE BERGER, PHILLIP FIRST, WALTER A. DE HEER, *Georgia Institute of Technology* High quality ultrathin graphite films, composed of less than 10 graphene layers, have been epitaxially grown on single crystal SiC substrate by thermal decomposition. Hall bar structures, top gate and side gated field transistor structures have been fabricated using electron beam lithography methods. Scanning Electron Microscopy (SEM), Atomic Force Microscopy (AFM) and Electrostatic Force Microscopy (EFM) have been used to characterize the structures. These results demonstrate that nanopattened epitaxial graphite (NPEG) is a promising quasi-two-dimensional electronic material.

*NSF,NIRT,INTEL

**10:48**

**A18 13 Structural modification of boron nitride nanotubes by plasma irradiation** TAKASHI IKUNO, GAVI BEGTRUP, SHAUL ALONI, ANDRAS KIS, DAVID OKAWA, ALEX ZETTL, *UC Berkeley, Lawrence Berkeley National Laboratory* Boron nitride (BN) and boron-carbon-nitride (B-C-N) nanotubes (NTs) are candidates for potential nanosized electronic and optical devices due to extraordinary physical and chemical properties. In terms of electronic property, in contrast to the insulating BNNTs with about 5.5 eV band gap, ternary B-C-N NTs has semiconducting property, the band gap of which is primarily determined by their chemical compositions. Although one of the methods to make B-C-N NTs is C doping to BNNTs, it is difficult to modify the structure and composition of BNNTs due to its chemical inertness and strong sp2 bond. In this study, we performed to modify the structure and composition of BNNTs by plasma irradiation for synthesizing B-C-N NTs. Hydrocarbon plasma was utilized for structural modification of BNNTs. The structural properties and the composition were characterized by high-resolution transmission electron microscopy and electron energy loss spectroscopy. After the plasma irradiation, outer several BN layers were modified to wavy structure from straight shape, and the defects were observed in almost BN layers, indicating destruction of crystal structure by collision of energetic particles in plasma and BNNTs. There are 5 – 30 at% of C in BNNTs and C atoms were inhomogeneously distributed in B-C-N NTs. The electron transport property of the modified B-C-N NTs will be reported in our presentation.

## SESSION A19: FOCUS SESSION: OPTICAL AND ELECTRICAL SPIN GENERATION IN SEMICONDUCTORS

**Monday Morning, 13 March 2006**
**316, Baltimore Convention Center at 8:00**
**David Awschalom, University of California, Santa Barbara, presiding**

***Contributed Papers***

**8:00**

**A19 1 Spatial Imaging and Mechanical Control of Spin Coherence in Strained GaAs Epilayers*** HADRIAN KNOTZ, VANESSA SIH, JASON STEPHENS, DAVID AWSCHALOM, *Center for Spintronics and Quantum Computation, University of California, Santa Barbara, CA 93106* Recent work has shown that electron spins in GaAs and related compounds respond to strain dramatically. In particular, the manipulation of the spin-orbit coupling in GaAs via strain may be used for the development of all-electrical spintronic devices. Here we have developed a mechanical vise to controllably and reproducibly tune the tensile strain in-situ over a typical range for strain engineered heterostructures, from 0.0 - 0.2%[1]. The effect of uniaxial tensile strain on spin

coherence and transport phenomena in n-type GaAs epilayers is probed using time-resolved Kerr rotation, photoluminescence, and optically-detected nuclear magnetic resonance spectroscopies. The bandgap, electron spin lifetime, electron g-factor, and nuclear quadrupole splitting are imaged over millimeter scale areas of the epilayers for continuously varying values of strain. Simple non-destructive techniques for characterizing strain dependent phenomena in semiconductor heterostructures will facilitate the development of strain engineered spintronic devices.

*This work was supported by DARPA/DMEA and the AFOSR.

[1]H. Knotz, A Holleitner, J. Stephens, R. C. Myers, and D. D. Awschalom, submitted (2005)

**8:12**
**A19 2 Generating spin currents mechanically in a semiconductor*** PRASHANT SHARMA, *Argonne National Laboratory* It is theoretically predicted that a traveling shear wave will create a spin current in certain direct-gap (for example III-V compound) semiconductors with contributions from both the valence bands and the conduction band (for *n*-doped semiconductors). We show that this spin-current is a property of the Fermi-Dirac sea, and is controlled by a geometric phase accumulated by the strain-induced Rashba parameters in a cycle.

*The author acknowledges support from the U.S. Dept. of Energy, under Contract No. W-31-109-ENG-38

**8:24**
**A19 3 Adiabatic quantum pumping of a desired ratio of spin current to charge current** SUNGJUN KIM, *Department of Physics, The Pennsylvania State University, University Park, PA* KUNAL DAS, *Department of Physics, Fordham University, Bronx, NY* ARI MIZEL, *Department of Physics, The Pennsylvania State University, University Park, PA* We present a prescription for generating pure spin current or spin selective current, based on adiabatic quantum pumping in a tight-binding model of a one dimensional conductor. A formula for the instantaneous pumped current is derived without introducing the scattering matrix. Our calculations indicate that some pumping cycles produce the maximum value 2 of pumped spin while others reverse the direction of current as a result of small alterations of the pumping cycle. We find pumping cycles which produce essentially any ratio of spin current to charge current.



***Invited Papers***

**8:36**
**A19 4 Theory of coherent optical generation of ballistic spin currents.**
JOHN SIPE, *Department of Physics and Institute for Optical Sciences, University of Toronto*

Ballistic spin polarized currents, and ballistic pure spin currents, can be directly injected in semiconductors by a variety of all-optical processes. No bias voltage is required. Carrier and spin distributions far from equilibrium can thus be produced in both doped and undoped semiconductors, and their evolution and the resulting transport studied. We review the calculations we have made of these processes, and highlight some of the experimental results of our colleagues.

***Contributed Papers***

**9:12**
**A19 5 Ballistic-diffusive crossover in spin propagation and precession** CHRIS WEBER, JOE ORENSTEIN, JASON STEPHENS, DAVID AWSCHALOM, *University of California, Berkeley* In the transient spin grating (TSG) technique, electron spins are optically oriented in a standing wave (''grating'') of spin polarization with wavevector $q$. TSG measures spin propagation through the time-dependence of the grating amplitude. We have shown[1] that for GaAs 2DEGs diffusive spin motion at low mobility $\mu$ crosses over at high $\mu$ to motion that is ballistic on length-scale of the grating—the mean free path exceeds $q^{-1}$. The ballistic regime is characterized by oscillations in the spin-grating amplitude with frequency $\omega \approx v_F q$. In this talk we present data from TSG and time-resolved Kerr rotation measurements on *n*-doped GaAs quantum wells. We explore the crossover between ballistic and diffusive behavior as a function of temperature and of disorder. We also explore a second, distinct crossover in the spin dynamics that occurs as $v_F q$ is tuned through the spin-orbit precession frequency, $\Omega_{SO} \approx 0.2$ THz. [1] C. P. Weber itet al. Nature **437** p. 1330 (2005).

**9:24**
**A19 6 Dissipation through spin Coulomb drag in electronic spin transport and optical excitations*** IRENE D'AMICO, *Department of Physics, University of York* CARSTEN A. ULLRICH, *Department of Physics and Astronomy, University of Missouri-Columbia* Spin Coulomb drag (SCD) constitutes an intrinsic source of dissipation for spin currents in metals and semiconductors. We discuss the power loss due to SCD in potential spintronics devices and analyze in detail the associated damping of collective spin-density excitations. It is found that SCD contributes substantially to the linewidth of intersubband spin plasmons in semiconductor quantum wells, which suggests the possibility of a purely optical quantitative measurement of the SCD effect in a parabolic well through inelastic light scattering.

*Work supported by DOE Grant No. DE-FG02-05ER46213, NSF Grant No. DMR-0553485, Research Corporation, and the Nuffield Foundation Grant NAL/01070/G.

**9:36**
**A19 7 Inhomogeneously-doped semiconductor junctions as a source of spontaneous spin polarization*** YUNONG QI, MICHAEL FLATTÉ, *University of Iowa* The dynamics of electric-field-driven packets of spin polarized carriers passing through an n+/n semiconductor junction have been studied. We find that spin packets that are initially very weakly spin polarized can have their polarization significantly amplified within the junction. The nonlinear spin transport and amplification is due to a spin-polarization dependent mobility originating from the Pauli exclusion principle that also gives rise to the spin Gunn effect. The spin polarization amplification we describe here is driven by the inhomogeneous doping density, and thus does not require the large applied electric field of the spin Gunn effect. Hence it may apply

to situations at low electric fields and low temperatures in which spontaneous spin polarization has been seen experimentally. We further believe that these studies provide a direct way to study the spin-polarization dependent mobility in semiconductors.

*Work supported by DARPA/ARO DAAD19-01-1-0490.

**9:48**

**A19 8 Enhancement and suppression of spin density polarization due to inhomogeneous electric fields*** DAN CSONTOS, SERGIO ULLOA, *Dept. of Physics and Astronomy, Ohio University, Athens, OH 45701* We report on a theoretical and computational study of the spin polarization propagation in charge and spin inhomogeneous semiconductor structures. We use a self-consistent, semiclassical approach based on the Boltzmann transport equation to calculate the spin density imbalance, $\delta n_s$, defined as $\delta n_s = n_\uparrow - n_\downarrow$, and the spin density polarization, $P_s$, defined as the ratio $P_s = \delta n_s / n$, where $n$ is the total charge density, in the presence of inhomogeneous electric fields. We find that the spin-polarized transport can be drastically enhanced or suppressed by inhomogeneous electric fields, such as those arising at semiconductor interfaces. Furthermore, we find that the spin density imbalance, $\delta n_s$, and spin density polarization, $P_s$, have diametrally opposite dependence on doping concentrations and charge inhomogeneous distributions. This is in contrast to the common assumption in the literature that these two quantities essentially have the same spin relaxation lengths.

*This work was supported by the Indiana 21st Century Research and Technology Fund.

**10:00**

**A19 9 Spin polarization amplification within nonmagnetic semiconductors at room temperature** SOON-WOOK JUNG, HYUN-WOO LEE, *Department of Physics, Pohang University of Science and Technology* We show theoretically that the spin polarization of current can be electrically controlled within nonmagnetic semiconductors by exploiting the fact the spin current, compared to the charge current, is weakly perturbed by electric driving forces. In particular, in a T-shaped current branching geometry made entirely of a nonmagnetic semiconductor, the spin polarization can be amplified to 100% by tuning current branching ratios properly. The proposed amplification scheme does not use ferromagnets or magnetic field, and does not require low temperature operation, providing an efficient way to generate a highly spin polarized current in nonmagnetic semiconductors at room temperature.

**10:12**

**A19 10 Spin currents in the presence of non-uniform fields.** ADNAN REBEI, *Seagate Technology* A two dimensional electron gas with spin-orbit coupling and in the presence of an in-plane electric field give rise to a spin Hall current independent of the Rashba coupling. We show that this universality of the strength of the spin current survives even in the presence of non-uniform electric and magnetic fields. Gradients in magnetic fields are shown to couple charge and spin transport and hence provide a better way to detect spin currents. Our calculation parallels that of the derivation of the Chern-Simons effective action in a relativistic electron gas and hence avoids the use of the Kubo formula. The spin conductivity is also discussed in terms of spin accumulation in a non-uniformly magnetized square loop.

**10:24**

**A19 11 Magneto-Oscillations of Current-Induced Spin Polarization in 2DEG** MAXIM VAVILOV, *Yale University* We consider a disordered two-dimensional electron gas with spin-orbit coupling placed in a perpendicular magnetic field and calculate the magnitude and direction of the current-induced spin polarization. We find that in strong magnetic fields the polarization becomes an oscillatory function of the magnetic field and that the amplitude of these oscillations is parametrically larger than the polarization at zero magnetic field. We show that the enhanced amplitude of the polarization is a consequence of strong electron-hole asymmetry in a quantizing magnetic field.

**10:36**

**A19 12 Spontaneous Spin Polarization in Quantum Wires*** A. D. KLIRONOMOS, J. S. MEYER,† K. A. MATVEEV,‡ *Materials Science Division, Argonne National Laboratory, Argonne IL, 60439, USA* A number of recent experiments report spin polarization in quantum wires in the absence of magnetic fields. These observations are in apparent contradiction with the Lieb-Mattis theorem, which forbids spontaneous spin polarization in one dimension. We show that sufficiently strong interactions between electrons induce deviations from the strictly one-dimensional geometry and indeed give rise to a ferromagnetic ground state in a certain range of electron densities. At higher densities, more complicated spin interactions lead to a possibly novel ground state.

*This work was supported by the U. S. Department of Energy, Office of Science, under Contract No. W-31-109-ENG-38.
†On leave from The Ohio State University, Columbus, OH 43210-1117.
‡On leave from Duke University, Durham, NC 27708-0305.

**10:48**

**A19 13 Spin-polarized current created by quantum point contacts with spin-orbit interaction** MIKIO ETO, *Faculty of Science and Technology, Keio University, Japan* We propose a new idea to create spin-polarized currents using quantum point contact (QPC) with spin-orbit interaction.[1] Neither magnetic fields nor magnetic materials are required. By numerical studies using Green function recursion method,[2] we show that (i) the conductance is quantized in units of $2e^2/h$ even in the presence of spin-orbit (SO) interaction, (ii) the current is spin-polarized in the transverse direction, and (iii) a spin polarization of more than 50% can be realized with SO interaction strength in InGaAs heterostructures. The spin polarization stems from the transition between subbands of different spins during the transport through QPC. The spin-polarization ratio is determined by the adiabaticity of the transition, which is evaluated by the Landau-Zener theory. Since the two-terminal devices with QPC are easy to fabricate on semiconductors, they may be utilized for the spin injection in the spintronics.

[1]M. Eto, T. Hayashi, and Y. Kurotani, J. Phys. Soc. Jpn. **74**, 1934 (2005).
[2]T. Ando, Phys. Rev. B **44**, 8017 (1991).

**SESSION A20: COMPLEX OXIDE THIN FILMS SURFACES AND INTERFACES I: SUPERLATTICE FABRICATION AND PROPERTIES**
**Monday Morning, 13 March 2006; 317, Baltimore Convention Center at 8:00**
**John Mitchell, Argonne National Laboratory, presiding**



***Invited Papers***

**8:00**
**A20 1 An atomic-scale view of the structure and electronic properties of manganite thin films and superlattices.***
MARIA VARELA, *Oak Ridge National Laboratory*

Epitaxial manganite ultrathin films and heterostructures constitute an ideal system to study the nature and effects of inhomogeneity and phase competition in these materials. The presence of interfaces and epitaxial strain may cause new phenomena to arise, and a comprehensive study of the relations between structural, chemical and electronic properties at the atomic scale is needed. The combination of scanning transmission electron microscopy and energy loss spectroscopy represents a very powerful tool to analyze locally such relations. Unlike diffraction techniques, STEM-EELS allows clear separation of electronic valence from structural relaxations. Several examples will be presented, including the study of charge ordering in $Bi_{0.37}Ca_{0.63}MnO_3$. We find atomically-resolved striping of the Mn $L_{2,3}$ spectra that correlate with two distinct formal charge states (+3/+4). Theoretical results obtained by first-principles density-functional calculations reproduce the structural relaxation that leads to the striping with minimal charge transfer. In contrast, charge transfer may occur across $YBa_2Cu_3O_{7-x}/La_{0.67}Ca_{0.33}MnO_3$interfaces, where extensive charge transfer processes drastically affect the ferromagnetic/superconducting properties. Epitaxial strain can also play a determining role in ultrathin LCMO films, inducing a nanoscale modulation in the Mn+3/Mn+4 ratio which evidences the existence of nanoclusters with different electronic densities.

*Collaborators: W. Luo, J. Tao, S. Pantelides, S. Pennycook, H. Christen, H.N. Lee, D. Mandrus, V. Pena, Z. Sefrioui, J. Santamaria. Research sponsored by the LDRD Program of ORNL, managed by UT-Batelle LLC, for the US DOE under Contract DE-AC05-00OR22725.

***Contributed Papers***

**8:36**
**A20 2 Doping without Disorder: Digital Synthesis of Manganite Superlattices*** ANAND BHATTACHARYA, *Argonne National Laboratory* XIAOFANG ZHAI, MAITRI WARUSAWITHANA, *University of Illinois at Urbana Champaign* JERALD KAVICH, *University of Illinois, Chicago and Argonne National Laboratory* JOHN FREELAND, *Argonne National Laboratory* JIM ECKSTEIN, *University of illinois at Urbana Champaign* SAM BADER, *Argonne National Laboratory* We have synthesized digital superlattices of $(LaMnO_3)_m(SrMnO_3)_n$ using ozone-assisted oxide MBE. This technique of itdigital synthesis allows the realization of superlattices with the same overall stoichiometry as random alloys of composition $La_{m/m+n}Sr_{n/m+n}MnO_3$, without introducing the random *A*-site disorder associated with bulk synthesis. In these digital superlattices, the 'doping' or charge transfer occurs at well ordered coherent interfaces, whose electronic and magnetic properties may be studied by local probes, scattering techniques, and transport and magnetization studies. We shall present our results on a series of samples synthesized for various values of *m* and *n*, exploring both metallic and insulating phases of the nominal phase diagram for the bulk counterpart. The results will be discussed in the context of the interfacial states that arise in structures obtained with digital synthesis.

*work supported in part by DOE contract # W-31-109-ENG-38

**8:48**
**A20 3 Electronic Interfacial Effects in Epitaxial Heterostructures based on $LaMnO_3$.** HANS M. CHRISTEN, M. VARELA, H.N. LEE, D.H. KIM, M.F. CHISHOLM, C. CANTONI, L. PETIT, T.C. SCHULTHESS, D.H. LOWNDES, *Oak Ridge National Laboratory, Oak Ridge, TN, USA* Studies of chemically abrupt interfaces provide an ideal platform to study the effects of discontinuities and asymmetries of the electronic configuration on the transport and magnetic properties of complex oxides. In addition, the behavior of complex materials near interfaces plays the most crucial role not only in devices and nanostructures but also in complex structures in the form of composites and superlattices, including artificial multiferroics. Interfaces in the $ABO_3$ perovskite system are particularly attractive because structurally similar oxides with fundamentally different physical properties can be integrated epitaxially. To explore the electronic effects at interfaces and to probe the physical properties that result from local electronic changes, we have synthesized structures containing $LaMnO_3$ and insulating perovskites using pulsed laser deposition. The local electron energy loss spectroscopy (EELS) capability of a scanning transmission electron microscope (STEM) is used to probe the electronic configuration in the $LaMnO_3$ films as a function of the distance from the interfaces. The results are compared to macroscopic measurements and theoretical predictions. Research sponsored by the U.S. Department of Energy under contract DE-AC05-00OR22725 with the Oak Ridge National Laboratory, managed by UT-Battelle, LLC.

**9:00**
**A20 4 Phase Separation in Ferromagnetic/Charge-ordered Superlattices** T. ZAC WARD, *University of Tennessee* JIANXING MA, *University of Tennessee* DANE GILLASPIE, *Unversity of Tennessee* HONG-YING ZHAI, *ORNL* E. WARD PLUMMER, *University of Tennessee* JIAN SHEN, *ORNL* The coexistence of ferromagnetic metal (FFM) and charge-ordered insulator (COI) observed in manganites, such as $La_{5/8-y}Pr_yCa_{3/8}MnO_3$, has been an intensive focus in the study of transition metal oxides (TMO).

Theories related to structural nanoscale disorder of charge carrier dopants and self-organization caused by an intrinsic elastic energy landscape have been proposed. To understand the subtle balance and competition between the different electronic phases, we have grown $La_{5/8}Ca_{3/8}MnO_3/Pr_{5/8}Ca_{3/8}MnO_3$ superlattices with different stacking periods in order to control the chemical ordering of La/Pr ions and thus the elastic energy landscape. The magnetic and transport properties of FM/CO superlattices as well as La/Pr disordered $La_{5/16}Pr_{5/16}Ca_{3/8}MnO_3$ will be presented and the driving mechanism of FM/CO phase separation will be discussed. Research sponsored by the U. S. Department of Energy under contract DE-AC05-00OR22725 with the Oak Ridge National Laboratory, managed by UT-Battelle, LLC

**9:12**

**A20 5 New metallic interface state in oxide artificial superlattices investigated by optical spectroscopy** SUNG SEOK A. SEO, WOO SEOK CHOI, KYUNGWAN KIM, *School of Physics and Research Center for Oxide Electronics, Seoul National University, Seoul 151-747, Korea* HO NYUNG LEE, *Condensed Matter Sciences Division, Oak Ridge National Laboratory, Oak Ridge, TN 37831* LI YU, CHRISTIAN BERNHARD, *Department of Physics, University of Fribourg, Fribourg, CH-1700, Switzerland* TAE WON NOH, *School of Physics and Research Center for Oxide Electronics, Seoul National University, Seoul 151-747, Korea* Interfaces between the artificial structures of oxides have been attracting a lot of attention because of their novel physical properties, which are usually not obtained in single-phase bulk materials. As a model system to understand the interfaces between the Mott insulators and the band insulators, high quality artificial superlattices of $SrTiO_3$ / $LaTiO_3$ were epitaxially grown by pulsed laser deposition equipped with reflection high energy electron diffraction. Mid infrared-visible optical transmittance and reflectance spectra were measured to show highly conducting interface, providing clear evidences for electronic reconstruction at the interface. Moreover, temperature-dependent infrared ellipsometry results showed that the interface state was different from conventional metal, indicating a new two dimensional metallic state.

**9:24**

**A20 6 Understanding the atomic structure of epitaxial $SrTiO_3$-GaAs (001) hetero-interfaces.** ROBERT KLIE, YIMEI ZHU, *Center for Functional Nanomaterials, Brookhaven National Laboratory, Upton NY 11021* YONG LIANG, *Motorola Labs, Tempe, AZ 85284* ERIC ALTMAN, *Department of Chemical Engineering, Yale University, New Haven, CT 06520* WERONIKA WALKOSZ, JUAN-CARLOS IDROBO, SERDAR OGUT, *Department of Physics, University of Illinois at Chicago, Chicago IL 60607* The combination of high-resolution Z-contrast imaging, electron energy-loss spectroscopy (EELS), and density functional theory (DFT) calculations was used to study the interfacial structure of ultra-thin $SrTiO_3$ films on GaAs(001). Z-contrast imaging suggests an atomically sharp hetero-interface with $SrTiO_3$ [110] in registry with As-terminated GaAs [100] with no visible reconstruction of either surface. Our initial DFT-calculations reveal that such a stoichiometric interface would have states in the band gap, while X-ray photoelectron spectroscopy (XPS) shows a clean band gap and a valence band offset more than twice of the calculated offset. Therefore, we will use atomic-column resolved EELS and further DFT-calculations to explore the role of oxygen vacancies at the interface in compensating for the As dangling bonds and search for the low-energy semi-conducting $SrTiO_3$/GaAs-system.

**9:36**

**A20 7 Magnetic properties of $La_{2/3}Sr_{1/3}MnO_3/Pr_{2/3}Ca_{1/3}MnO_3$ superlattices** DARIO NIEBIESKIKWIAT, *Department of Physics, University of Illinois at Urbana-Champaign, Urbana, IL 61801* LUIS HUESO, *Department of Materials Science, University of Cambridge, Cambridge CB2 3QZ, UK* MYRON SALAMON, *Department of Physics, University of Illinois at Urbana-Champaign, Urbana, IL 61801* NEIL MATHUR, *Department of Materials Science, University of Cambridge, Cambridge CB2 3QZ, UK* We present a magnetization study of ferromagnetic/antiferromagnetic (FM/AFM) manganite superlattices, grown by pulsed laser deposition on $SrTiO_3$ substrates. The FM layers are 15-nm-thick $La_{2/3}Sr_{1/3}MnO_3$ (LSMO) sheets and the AFM layers were made of $Pr_{2/3}Ca_{1/3}MnO_3$ (PCMO), with variable thickness $t_A$ between 0 and 7.6 nm. Although all our multilayers exhibit a PM-FM transition of the LSMO layers at $T_C \sim 340$K, only for $t_A = 0$ do we observe a FM moment $M_0$ close to the expected saturation for the 1/3 doping. As soon as the AFM layers are added ($t_A = 0.8$nm) $M_0$ decreases, related to the introduction of the FM/AFM interfaces. The lack of exchange bias would indicate that the reduction of the FM moment is due to the appearance of a magnetically dead layer in the LSMO close to the interface with the AFM volume. Upon a further increase of $t_A$, the FM moment increases again and develops a peak at $t_A \sim 3.5$ nm. We explain this behavior in terms of the accommodation of nanometric FM droplets in the PCMO layers.

**9:48**

**A20 8 Strong interaction of ultra thin cuprate superconductor and ferromagnetic manganites** XIAOFANG ZHAI, JAMES ECKSTEIN, *University of Illinois, Urbana* We have made bi-layer films with thick manganite layers on top of thin layers of the cuprate superconductor $Bi_2Sr_2CaCu_2O_{7+\delta}$ (BSCCO). The samples were grown using ozone assisted atomic layer by layer molecular beam epitaxy. For samples in which the manganite is the ferromagnet $La_{2/3}Sr_{1/3}MnO_3$(LSMO), the normal and superconducting properties of the BSCCO can be strongly affected by the LSMO when the BSCCO layer is sufficiently thin. In particular, samples with ten molecular layers of BSCCO were largely unaffected by the LSMO. On the other hand, when the number of BSCCO molecular layers was reduced to 5 and then to 4, the normal state above 80K became much more resistive and the superconducting Tc was reduced. However, a sample with four molecular layers of BSCCO capped with insulating and presumably antiferromagnetic SrMnO3 showed no effect of the manganite of BSCCO transport. This indicates that the reduced conductivity of the 4-layer sample capped with LSMO is due to the interaction of mobile carriers from the two systems at the interface. This interaction extends about 4 unit cells into the BSCCO.

**10:00**

**A20 9 Oscillatory behavior of the magnetoresistance of F/S/F trilayers** NORBERT M. NEMES, *Instituto de Ciencia de Materiales de Madrid (ICMM-CSIC). 28049 Cantoblanco. Madrid* M. GARCIA-HERNANDEZ, *ICMM* V. PEÑA, Z. SEFRIOUI, J. GARCIA-BARRIOCANAL, C. VISANI, D. ARIAS, C. LEON, *UCM* J. SANTAMARIA, *GFMC, Departamento de Física Aplicada III, Universidad Complutense de Madrid, 28040 Madrid, Spain* S.G.E. TE VELTHUIS, *ANL* A. HOFFMANN, *Materials Science Division, Argonne National Laboratory, Argonne, Illinois 60439* We have measured magnetoresistance of trilayers made of highly spin polarized $La_{0.7}Ca_{0.3}MnO_3$ ferromagnets and high-$T_c$ superconducting $YBa_2Cu_3O_{7-\delta}$ with the current in plane

(CIP) geometry. Large magnetoresistance peaks occur for antiferromagnetic (AF) alignment of the manganite layers, much resembling the GMR in metallic superlattices, and probably resulting of enhanced interface scattering in the AF configuration. We show RKKY-type oscillations in the intensity of the giant magnetoresistance (GMR) peak as a function of the thickness of the superconductor, perhaps originating in oscillatory magnetic coupling. The magnetoresistance vanishes for thickness of the superconductor in excess of 30 nm suggesting that this length could be an upper limit for the spin diffusion length.

**SESSION A21: COLLOIDS I: EMULSIONS, FOAMS, AND SUSPENSIONS**
**Monday Morning, 13 March 2006**
**318, Baltimore Convention Center at 8:00**
**P. Chaikin, New York University, presiding**

**8:00**
**A21 1 Bubble size distribution in a steady-state column of aqueous foam.** KLEBERT FEITOSA, DOUGLAS J. DURIAN, *University of Pennsylvania* We report on measurements of the distribution of bubble sizes in a vertical column of aqueous foam. The sample is generated and maintained in steady-state by continuous bubbling of gas ([**mathtt**]$CO_2$) in a surfactant solution ([**mathtt**]$H_2$[**mathtt**]$O$ + AOS + NaCl) at the bottom of a tall Lucite cylinder. The constant flow of gas produces nearly identical bubbles that accumulate at the liquid/foam interface and subsequently move up with constant velocity. The distribution of bubble sizes depends on height, being monodisperse near the bottom, turning bidisperse at some intermediate height, and then becoming polydisperse further up in the column. This behavior is exclusively due to coarsening and drainage, since film-rupture and convection are not observed. The development of a bidisperse distribution cannot be explained by mean-field theories of coarsening, in which bubbles of a given size grow or shrink at a rate that depends only on their size in comparison with a mean size.

**8:12**
**A21 2 Rheology of Foams Bubble by Bubble** STEPHAN KOEHLER, *Physics, Emory University* We present rheological measurements of single bubbles, and collections of bubbles to investigate cooperative effects between the bubbles that comprise a foam. For small numbers of monodisperse bubbles we measure the elastic behavior and yield stresses, and make comparisons with polydisperse foams composed of many bubbles. We also present a technique for measuring an ageless foam, where the bubble size and liquid volume fraction remain constant, outside of a microgravity environment.

**8:24**
**A21 3 Pattern formation in flowing foams.** SOMA SANYAL, JAMES GLAZIER, *Indiana University* We report on a new fingering morphology which an expanding air bubble generates in a foam flowing due to an applied pressure across a Hele-Shaw cell. Previous studies have only looked at patterning when the background is stationary. Our simulations using the Glazier & Grainer's Cellular Potts model show that the transition between the different morphologies depend on the rate of bubble flow into the foam. Since the rate of bubble in-flow is related to the shear strain rate, this agrees with previous experiments which have shown fingering morphologies in foams depend on the shear strain rate. The new mushroom morphology occurs for a high rate of bubble inflow corresponding to a very low shear strain rate. It is associated with a highly non-uniform velocity profile of the bubbles in the foam. These new morphologies should be easy to observe experimentally.

**8:36**
**A21 4 Rigidity percolation in foamy sands** SYLVIE COHEN-ADDAD, REINHARD HOHLER, MARCEL KRZAN, MARIJO MARINIC, *Universite de Marne-la-Vallee* BENJAMIN HERZHAFT, *Institut Francais du Petrole* When subjected to a small shear stress, an aqueous foam behaves as a linear viscoelastic materials, whereas large applied shear stress triggers bubble rearrangement which causes the foam to flow as a viscous liquid. The elastic behavior arises from the surface tension of the gas-liquid interfaces. We study experimentally how the shear modulus and the yield stress of foam are modified if non colloidal solid particles of controlled size are dispersed in the sample. We show that even small amounts of non colloidal particles added to a foam can enhance the viscoelastic shear modulus by more than an order of magnitude. The yield stress is also increased, but to a smaller extent. The scaling of the elasticity enhancement with solid fraction qualitatively agrees with that predicted by an effective medium rigidity percolation model in the superelastic limit. To gain insight about the interactions between solid particles that are involved in the rigidity percolation, we study the dependence of the percolation threshold with particle to bubble size ratio.

**8:48**
**A21 5 Diffusive liquid transport in poroelastic materials : the case of foams in microgravity** ARNAUD SAINT-JALMES, SEBASTIEN MARZE, HERNAN RITACCO, DOMINIQUE LANGEVIN, *Laboratoire de Physique des Solides, Universite Paris-Sud, Orsay* On Earth, the liquid inside an aqueous foam irreversibly flows due to coupled gravitational and capillary effects. In microgravity, one can study liquid transport with only capillarity as a driving force. Here, we report results of capillary imbibition experiments performed in parabolic flights in which we follow how and where some liquid locally injected into a foam spreads with time. Different setup geometries, imbibition modes and bubble surface mobilities are studied. New behaviors, not observed on ground, with high liquid fractions are found. Comparisons with theoretical models are presented, allowing us to find their limits of validity as the liquid fraction is increased. These experiments also give us some insights on the convective instability occurring on ground, and allow us to discuss the analogy with diffusive liquid transport and swelling in other poroelastic materials, like plants and tissues.

**9:00**
**A21 6 Structure and dynamics of foam-like emulsions** VINOTHAN MANOHARAN, *Dept of Physics and Division of Engineering and Applied Sciences, Harvard University* JOHN C. CROCKER, *Chemical and Biomolecular Engineering, University of Pennsylvania* We report the results of real-space, microscopic experiments on model concentrated emulsions ($\phi > 0.65$) in which the continuous and dispersed phases are both index- and density-matched. Like foams, these systems coarsen and age due to diffusion of fluid from small to large droplets, but unlike foams,

they are transparent and do not drain during the course of an experiment. Thus we are able to probe their internal structure and dynamics at volume fractions ranging from 0.65 to 0.90. Measurements of the mean-squared displacement of small tracer particles embedded in the emulsion reveal that the system exhibits non-thermal stress fluctuations with Lorentzian power spectral density. We relate these fluctuations to intermittent droplet rearrangements, presumably driven by coarsening, that we observe directly through confocal microscopy.

**9:12**

**A21 7 Mean Field Theory of Foam Aging** OLIVIA HALT, *University of Pennsylvania* RANDALL KAMIEN, *University of Pennsylvania* We describe our work on the geometrical properties of a random foam as a function of the number of faces, based on Isotropic Plateau Polyhedra [1,2]. Analytic values of specific area, the stretching moment, and curvature can be obtained for these geometrical constructs. The expression for curvature is a ratio of the volume to the area of the foam cell. Focusing on this quantity will allow a better description of the coarsening of a foam. Conclusions from this mean field study will be discussed. [1] Glicksman M., itPhil. Mag., **85** (2005) 3. [2] Hilgenfeldt S., Kraynik A., Reinelt D., and Sullivan J. itEurophys. Lett. **67** (2004) 484.

**9:24**

**A21 8 Emulsions Plugging Agent for Sealing Leaky Gas Wells** KHALIL ZEIDANI, MARCEL POLIKAR, *University of Alberta* This study was undertaken to investigate the physics of emulsion flow in porous media. The objective of experiments were to study the applicability of oil-in-water emulsion as a plugging agent in the vicinity of the well bore for thousands of Canadian gas wells that are continuously leaking gas to surface. The motion of oil droplets and the capture mechanisms were investigated through visualized experiments. Well-characterized emulsions were injected into a micro model resembling a two parallel plate model packed with glass beads. Effects of emulsion properties and wettability of the medium were studied on a plugging mechanism. The results demonstrate the reduction in permeability mainly due to droplets size exclusion compared to the pore constrictions. Also, smaller droplets may lodge and coalesce in pores crevices thereby accelerating the blockage process. Moreover, more viscous emulsions are more effective compared with the less viscous ones due to combined effects of capillary and viscous forces. The deposition of droplets was adjusted through utilizing different preflush solutions. Criteria were set for enhancing emulsion penetration depth thereby defining the extent of the blocked region. In conclusion, this work characterizes the physics of emulsion flow in porous media and demonstrates its application as a novel sealant in near well bore region. The novelty, which constitutes a step-change in technology, is a method that emplaces an emulsion at a desired location in underground media.

**9:36**

**A21 9 Wigner Crystals from Charge Stabilized Water in Oil Emulsions** MIRJAM E. LEUNISSEN, ALFONS VAN BLAADEREN, *University of Utrecht* ANDREW D. HOLLINGSWORTH, MATT SULLIVAN, *Princeton Unviersity* PAUL CHAIKIN, *New York University* SOFT CONDENSED MATTER GROUP COLLABORATION, PRINCETON INSTITUTE FOR THE SCIENCE AND TECHNOLOGY OF MATERIALS COLLABORATION, A drop of water shaken or sonicated in a CHB-Decalin oil mixture produces a stable emulsion of 1-100 micron scale water droplets. The interdroplet correlations indicate strong electrostatic repulsion. When the preparation is by sonication the particle size is smaller and more uniform and the water droplets arrange in a BCC structure characteristic of a Wigner Crystal. The lattice constants are up to 20 microns. We suggest that the water droplets deionize the organic solvent due to water's high dielectric constant and hydration energy. This decreases the electrostatic screening. A slight preference of the water hydration energy for different ionic species will lead to slightly larger droplet uptake of one charge over the other and will result in the droplets being charged. The amount of charging can be controlled by changing pH. Experiments with oil-water and colloids will also be discussed.

**9:48**

**A21 10 Microrheological Study of the Time Dependent Gelation of Single Wall Carbon Nanotube Suspensions** D.T.N. CHEN, L.A. HOUGH, M.F. ISLAM, A.G. YODH, *Dept. of Physics & Astronomy, University of Pennsylvania* Single wall carbon nanotubes (SWNTs) dispersed in water using an anionic surfactant, sodium dodecylbenzene sulfonate (NaDDBS) form reversible gels because of the bonding between the individual nanotubes (L.A. Hough, M.F. Islam, P.A. Janmey and A. G. Yodh Phys. Rev. Lett. **93**, 168102 (2004)). We study the time dependence of this reversible gelation using particle tracking microrheology. We empirically collapse the mean square displacement onto a single master curve that extends over several decades in time using a time-cure superposition. The frequency scaling exhibited by the viscoelastic moduli obtained from the master curve is remarkably similar to that of semiflexible polymer networks. By comparing the results from a range of initial SWNT concentrations below and above the rigidity percolation threshold, we gain insight into the evolution of structure during gelation. This work has been partially supported by the NSF through Grants DMR 05-20020 (MRSEC) and DMR-0505048, and by NASA grant NAG8-2172.

**10:00**

**A21 11 Yielding and flow of soft particle dispersions: the role of elasto-hydrodynamic interactions.** MICHEL CLOITRE, *Matiere Molle et Chimie (UMR ESPCI-CNRS 7167), ESPCI, 10 rue Vauquelin, Paris, France* JYOTI SETH, ROGER BONNECAZE, *Department of Chemical Engineering and Texas Materials Institute, The University of Texas at Austin, Austin, Texas 78172, USA* Concentrated dispersions of soft particles such as emulsions, colloidal pastes and granular suspensions exhibit many fascinating phenomena such as yielding, shear thinning, aging and memory, slip and fracture. Elucidating the physical parameters controlling these properties and the mechanisms at work is a formidable challenge. Recently we have found that various soft particle pastes share in common universal flow properties that can be characterized with very simple constitutive equations involving the solvent viscosity, the bulk elasticity and geometrical factors. We shall describe a generic flow model based on internal slip and non-contact elasto-hydrodynamic forces between squeezed particles[1] that quantitatively accounts for the measured properties. This approach offers new routes to predict the bulk non-linear rheology of pastes. [1]S.P. Meeker, R.T. Bonnecaze, M. Cloitre, itPhys. Rev. Lett. **92**, n[r] 198302 (2004).

**10:12**

**A21 12 Mixture Stress in a Non-Uniform Suspension*** QUAN ZHANG, ANDREA PROSPERETTI,[†] *Johns Hopkins University* In nature, most suspensions are non-uniform and the particles are subjected to external forces, such as gravity. The external force induces relative motions between the particles and the fluid, which

introduce a new degree of freedom. We investigate the ensemble averaged stress system in a non-uniform suspension of equal spheres with external forces. It is found that, as a consequence of the spatial non-uniformity of the particle distribution and the relative motion between the two phases, new terms arise in the symmetric part of the bulk stress. In addition, an anti-symmetric contribution is found even in the absence of external torques. All the new terms in the stress tensor depend on the particle volume fraction and the gradient of the relative velocity but, for a given volume fraction, are independent of the particle size. To determine the new transport coefficients for small volume fractions, the renormalization method is extended to the non-uniform situation. For finite volume fractions, numerical simulations of several prototypical physical problems are carried out, from which the new transport coefficients are calculated. The numerical results agree well with the dilute limit calculations.

*Supported by NASA and NSF
†University of Twente and Burgerscentrum

**10:24**

**A21 13 Brownian Motion of an ellipsoid*** YILONG HAN, *Department of Physics and Astronomy; University of Pennsylvania* AHMED ALSAYED, MAURIZIO NOBILI, *CNRS-University Montpellier II, France* JIAN ZHANG, TOM LUBENSKY, ARJUN YODH, We report direct digital-video-microscopy measurements of the Brownian motion of isolated anisotropic (ellipsoidal) particles in water under quasi-2D confinement. The probability density function (PDF) of displacements in the lab-frame is found to be nonGaussian. This effect originates from the anisotropy of the hydrodynamic drag coefficient. The transition from anisotropic to isotropic diffusion and the correlations between translational and rotational motions are also measured. The observations are confirmed numerically and understood theoretically via a Langevin formalism. We also observed the ratio of diffusion coefficients, $D_a/D_b$, along long and short axes, respectively, could be larger than 2, the theoretical upper limit in three dimension.

*ACKNOWLEDGE GRANTS: DMR05-20020

**10:36**

**A21 14 Sound propagation in nanofluids** X. XIE, R. ANNAMALAI, R. SOORYAKUMAR, D. STROUD, V. SUBRAMANIAM, J. HEREMANS, *The Ohio State University* The thermal properties of nanofluids, i.e. liquids containing nanoparticles of sizes in the 3 to 100 nm range, have recently been shown to exhibit an unexpectedly large enhancement in thermal conductivity. While this enhancement has been observed for metallic nanoparticles and carbon nanotubes, the physical origin of the enhancement remains to be understood. The propagation of acoustic waves through a nanoparticle-laden colloidal fluid system offers many advantages towards understanding its thermal properties. We report on results of Brillouin scattering which probes the frequency range of $\sim$ 1 – 100 GHz to study sound propagation in such complex fluids which possess structures on length scales larger than the molecules that comprise the host fluid. Thus compared to simple liquids, nanofluids possess additional relaxation mechanisms that can be observed in the frequency dispersion of the sound propagation. We present light scattering results from nanofluids comprised of a suspension of relatively long (1 - 2 $\mu$m) 20 nm diameter single-walled carbon nanotube bundles dispersed in N,N dimethylformamide.

**10:48**

**A21 15 Electrokinetic Phenomena of Colloidal Suspensions** JIAN LIU, *Department of Physics and Texas Center for Superconductivity, University of Houston, 202 Houston Science Center, Houston, Texas 77204-5002* JASON SHULMAN, *Department of Physics and Texas Center for Superconductivity, University of Houston, 202 Houston Science Center, Houston, Texas 77204-5002* YUYI XUE, *Department of Physics and Texas Center for Superconductivity, University of Houston, 202 Houston Science Center, Houston, Texas 77204-5002* FENG CHEN, *Department of Physics and Texas Center for Superconductivity, University of Houston, 202 Houston Science Center, Houston, Texas 77204-5002* CHING-WU CHU*, *Department of Physics and Texas Center for Superconductivity, University of Houston, 202 Houston Science Center, Houston, Texas 77204-5002* We investigate the colloidal particle motion of colloid suspension in which giant electrorheological effect has been found. The colloids consist of urea coated $Ba_{0.8}Rb_{0.4}TiO(C_2O_4)_2$ particles suspended in silicon oil. In the experiment, a cell with cross-aligned top and bottom stripe-electrodes is used. The electric potential, the field and the field gradient, therefore, possess different space distribution. Significant difference of colloids motions and equilibrium particle distributions are observed under ac, dc and ac+dc fields. The result suggests dipole may not be the only factor for colloid aggregation (meso-structure), and hence, its electrorheological effect. *also at Hong Kong University of Science and Technology and Lawrence Berkeley National Laboratory



## SESSION A22: FOCUS SESSION: CURRENT DRIVEN MAGNETIZATION DYNAMICS I

**Monday Morning, 13 March 2006**
**319, Baltimore Convention Center at 8:00**
**Andrew Kent, New York University, presiding**

***Contributed Papers***

**8:00**

**A22 1 Spin-Transfer Effect in Nanopillar Spin Valves With A Thick Polarizing Layer** VLAD PRIBIAG, G.D. FUCHS, P.M. BRAGANCA, N.C. EMLEY, O. OZATAY, J. SANKEY, D.C. RALPH, R.A. BUHRMAN, *Cornell University* I. KRIVOROTOV, *U.C. Irvine* Current-induced magnetization switching has been the object of intensive study, motivated in part by possible applications for non-volatile magnetic storage. To date, the majority of studies have focused on structures where the moments of the magnetic layers lie in plane. Recently, however, it has been predicted that significantly faster switching times, as well as lower switching currents could be achieved in a device where the magnetization of the polarizing layer is perpendicular to the plane of the free layer [1, 2]. To study this effect we have fabricated Py 60nm / Cu 40nm / Py 5nm nanopillar spin valves patterned as 80 nm by 150 nm ellipses. The magnetization of the thick polarizing layer can be readily coerced to high out-of-plane angles by applying a weak field perpendicular to plane, while the much thinner free layer is only weakly affected. Here we present a phase diagram for our devices, obtained through DC and microwave-

frequency measurements as function of current and applied out-of-plane field. We will discuss the results in the context of switching with an out-of-plane polarizer. [1] A. D. Kent et al., Appl. Phys. Lett. 84, 3897 (2004). [2] K. J. Lee et al., Appl. Phys. Lett. 86, 022505 (2005).

**8:12**
**A22 2 Spin-transfer-induced magnetization reversal in bilayer magnetic nanopillars at high fields: dependence on free layer thickness*** WENYU CHEN, ANDREW D. KENT, *Department of Physics, New York University* M.J. ROOKS, N. RUIZ, JONATHAN Z. SUN, *IBM T. J. Watson Research Center* Spin transfer in asymmetric Co/Cu/Co bilayer magnetic nanopillar junctions has been studied as a function of free (thin) Co layer thickness from 1.8 to 5.3 nm. In particular, the critical current for magnetization reversal in large magnetic fields applied perpendicular to junction surface has been measured. Junctions with submicron lateral size were fabricated using a nano-stencil process. Junctions resistances scale with lateral area and their in-plane magnetoresistance was found to be independent of free layer thickness. The critical current decreases linearly with decreasing free layer thickness and extrapolates to a finite critical current in the limit of zero thickness. This can be understood as either a decrease in efficiency of the spin-transfer torque and/or an interfacial contribution to the damping of the free magnetic layer.

*The research is supported by NSF-DMR-0405620.

**8:24**
**A22 3 Linewidths for spin-transfer-driven precession in magnetic nanopillars as a function of the direction of applied magnetic field** KIRAN V. THADANI, J.C. SANKEY, I.N. KRIVOROTOV, O. OZATAY, P.M. BRAGANCA, R.A. BUHRMAN, D.C. RALPH, *Cornell University* In a magnetic multilayer spin valve, the spin-transfer torque from a spin-polarized DC current can drive the free-layer magnetic moment into steady-state precessional modes [1, 2]. We report measurements of how the linewidths of these modes depend on the angle and magnitude of an applied magnetic field, for devices in the nanopillar configuration with elliptical cross sections. We find that the field direction studied most commonly, in-plane along the magnetic easy axis of the ellipse, generally gives the largest linewidths, corresponding to the least coherent precession. As the field is rotated either in plane or out of plane, the linewidths can change dramatically, decreasing by a factor of 50 or more in some devices. We will discuss the temperature dependence of the linewidths for the field directions that give the minimum linewidths, and we will compare both the field-angle dependence and the temperature dependence to theoretical models. [1] S. I. Kiselev et al., Nature 425, 380 (2003). [2] J. C. Sankey et al., cond-mat/0505733.

***Invited Papers***

**8:36**
**A22 4 Phase Locking of Spin-Transfer Oscillators.**
MATTHEW PUFALL, *NIST, Boulder, CO*

DC current flowing through a nanometer-scale lithographic contact made to a continuous spin-valve multilayer induces stable magnetic precession of the free layer at GHz frequencies. The resonance frequency of the spin-transfer oscillator (STO) is a function of both the applied current and external magnetic field, and the resonance has linewidths on the order of MHz. To study the properties of this resonance, and to determine the suitability of STOs for communications applications, we measured the response of these oscillators to variations in the magnetic field, electric current, and spin-wave environments. We studied phase locking effects induced by injecting ac currents, and by applying ac magnetic fields near the precession frequency of the device. In addition, we have fabricated two nanocontact devices in close proximity on the same magnetic film, and looked at the interactions between the two devices. In each case, when the impressed ac signal is sufficiently close to the STO frequency, the device will phase lock. For ac currents and fields, the device locks to the external signal via injection locking, a general property of nonlinear oscillators, taking on the frequency and phase characteristics of the source. For interacting nanocontacts, the devices modify each other's resonances, and lock together at frequency slightly different from the individual resonances. I will review these phase locking results, and discuss the variations of the locking with the excited mode of the oscillator. I will also present results on mutual locking of STOs, discuss the relative roles of dipolar fields and spin-wave interactions in the locking mechanism, and comment on the possible uses of phase controlled, coherent STOs.

***Contributed Papers***

**9:12**
**A22 5 Probing wavenumbers of current-induced excitations in point-contact experiements** MAXIM TSOI, *The University of Texas at Austin* ZHEN WEI, *The University of Texas at Austin* The magnetic state of a ferromagnet can be altered by an electrical current. For instance, the current was shown to induce spin waves, precession, and reversal of magnetization in magnetic nanostructures. Today a variety of experimental techniques provide a vast amount of data on such current-induced excitations. A typical experiment usually exploits dc resistance measurements to detect the excitations. In addition, high-frequency techniques can provide valuable information on frequencies of the current-induced spin waves. Probing wavenumbers of the excitations, however, represents an experimental challenge. Point contacts were instrumental both for our original observation of current-induced excitations and in providing the first data on frequencies of the current-induced spin waves. In the present work we demonstrate that point-contact technique can also provide valuable information on the wavenumber of spin waves induced by the current. By varying the size of point contacts we have been able to control the size of the excitation volume and therefore the wavelength of current-induced spin waves. This leads to a technique with in situ sensitivity to wavenumbers of current-induced excitations. The detailed size-dependent measurements of the current-induced excitations display an interesting relation between current and voltage thresholds for such excitations.

**9:24**

**A22 6 Influence of Electrode Structure on Switching Characteristics in Nanopillar Spin Valves** P. M. BRAGANCA, O. OZATAY, A. G. F. GARCIA, J. C. SANKEY, N. C. EMLEY, D. C. RALPH, R. A. BUHRMAN, *Cornell University* We examine the effect spin scattering within the electrodes of a spin-valve nanopillar has on spin torque and damping within the structure. Devices were fabricated with the free layer adjacent to either the top or bottom electrode and with Au or Pt top electrodes. Macrospin simulations, when compared to pulsed current switching experiments, indicate that gold electrode samples of either free layer orientation have similar switching parameters, while devices with the free layer adjacent to a top platinum electrode exhibit lower spin torque and larger damping than Au capped devices, in agreement with spin accumulation [1, 2] and spin pumping [3] models. However, by placing the free layer opposite a platinum cap, the largest values for spin torque and damping were achieved, which was an unexpected result. In addition, we will discuss how placement of the free layer close to the bottom electrode induces effects such as fixed layer switching and microwave excitations in zero effective field, which are not seen in the opposite configuration. [1] J. Manschot, A. Brataas, G. E. W. Bauer, Appl. Phys. Lett. **85**, 3250 (2004). [2] A. A. Kovalev, A. Brataas, G. E. W. Bauer, Phys. Rev. B **66**, 224424 (2002). [3] Y. Tserkovnyak, A. Brataas, G. E. W. Bauer, Phys. Rev. B. **67**, 140404 (2003).

**9:36**

**A22 7 X-Ray Imaging of Spin Transfer Induced Magnetization Reversal** YVES ACREMANN, *Stanford Synchrotron Radiation Laboratory* J.P. STRACHAN, V. CHEMBROLU, *Department of Applied Physics, Stanford University* S.D. ANDREWS, *Department of Materials Science and Engineering, Stanford University* T. TYLISZCZAK, *Advanced Light Source* J.A. KATINE, M.J. CAREY, *Hitachi Global Storage Technologies San Jose Research Center* B.M. CLEMENS, *Department of Materials Science and Engineering, Stanford University* H.C. SIEGMANN, J. STÖHR, *Stanford Synchrotron Radiation Laboratory* Magnetization switching by spin injection has been observed in giant magnetoresistance measurements, giving an insight into the temporal evolution of the magnetization. So far, however, the nanoscale magnetization distribution during the switching process has remained hidden. Here we report, for the first time, imaging the magnetic switching process using advanced pump-probe x-ray microscopy. We observe that the switching process is initiated and determined by the lateral motion of a magnetic vortex driven by the spin current. Motion pictures with 200 picosecond time resolution show that the switching process is based on the motion of a magnetic vortex, leading to C-like patterns which may decay later into a uniform magnetic state. Our measurements show the fundamental role played by the curled Oersted field which necessarily accompanies the spin injection current.

**9:48**

**A22 8 Effects of current on the magnetization states of Permalloy nanodisks** SERGEI URAZHDIN, *West Virginia University* CHIA-LING CHIEN, *Johns Hopkins University* KONSTANTIN GUSLIENKO, *Argonne National Laboratory* We will describe expreimental evidence and theoretical model demonstrating that both the vortex and the single domain magnetic configurations of Ni80Fe20 circular nanodiscs can be achieved by the application of magnetic field or current flowing perpendicular to the disc plane. The magnetic configurations of Ni80Fe20/Cu/Ni80Fe20 trilayers have been determined by the response to a small current via the giant magnetoresistance. In addition, we report detection of the vortex state in a single magnetic layer, by exploiting a magnetoresitance arising from the suppression of spin-accumulation in the vortex state. Our analysis shows that this magnetoresistance effect becomes increasingly significant in small nanostructures.

**10:00**

**A22 9 Spin-mixing effects on magnetic switching, probed by thermoelectric measurements*** JEAN-PHILIPE ANSERMET, LAURENT GRAVIER, MOHAMED ABID, SANTIAGO SERRANO-GUISAN, *IPN, EFPL, Station 3, CH-1015 Lausanne, Switzerland* Current-Induced Magnetization switching has been observed in single nanowires of Co, Ni, Co-Cu and Ni-Cu multilayers. A novel thermoelectric measurement under high DC current is presented. It features a field dependence stronger than GMR. Its dependence on field orientation shows that it provides information complementary to GMR or magneto-thermoelectric power measurements. It is argued with a simple model that this measurement depends strongly on the difference of spin mixing rates of spin conversions going from ''up'' to ''down'' and conversely. Thus, this novel transport measurement provides information on electron-magnon collisions in magnetic nanostructures. The field dependence of this signal is about 10 times larger than the magnetoresistance of the same sample, be it AMR or GMR. In multilayers, the field dependence is shown to decay away when the thickness of the layers is larger than the spin-diffusion length.

*Swiss National Science Foundation grant 200020-100271

**10:12**

**A22 10 Universal spin pumping with rf magnetic fields** S. M. WATTS, C. H. VAN DER WAL, B. J. VAN WEES, MATERIALS SCIENCE CENTER, UNIVERSITY OF GRONINGEN, PHYSICS OF NANODEVICES TEAM, A new method for generating spin accumulation in metals or semiconductors is by application of an rf magnetic field [1], similar to the spin battery effect induced by a ferromagnet in resonance [2]. A dc spin accumulation is produced that is in general a small fraction of $\hbar\omega$, where $\omega$ is the rotation frequency of the rf field. When a resonant dc magnetic field is also applied the spin accumulation can be enhanced towards the universal value $\hbar\omega$. In addition, spin diffusion into an adjacent region without fields can dramatically enhance spin accumulation at the interface. We discuss the application of this method to produce spin accumulation in semiconductor or metal spin electronic devices without the necessity of either ferromagnetic electrodes or charge currents. [1] S. M. Watts *et al.*, submitted to PRL [2] A. Brataas *et al.*, Phys. Rev. **B** 66 (2002).

**10:24**

**A22 11 Spin Transfer in Magnetic Nano Devices with Perpendicular Anisotropy** JIAN-PING WANG, HAO MENG, *Electrical Engineering, University of Minnesota* Spin transfer predicted by Slonczewski and Berger has attracted a great deal of attention in recent years. Experimental findings have proved spin transfer in current-perpendicular-to-plane (CPP) spin-valves (SV) and magnetic tunnel junctions (MTJs) with in-plane magnetization configuration. MRAM cells with perpendicular magnetic anisotropy may support high recording density than that using shape anisotropy with in plane magnetization configuration. However, there is no report on spin transfer in any magnetic nano device with perpendicular anisotropy. In this work, perpendicular magnetized

spin transfer nano-devices with sub-200 nm dimensions: Si/$SiO_2$/bottom electrode/$[CoFe2.5Å/Pt15 Å]_m$/CoFe5 Å /Cu30 Å /$[CoFe4.5 Å /Pt23 Å]_n$/Top electrode, has been fabricated and tested. Two $[CoFe/Pt]_n$ multilayers with different coercivities are used as the free layer and fixed layer in nano-devices. CPP magnetoresistive (MR) loop tested under perpendicular magnetic field shows the GMR is around 0.47%. The switching field for the free layer is around 200 Oe. Current induced magnetization switching was realized with a positive switching current 48 mA and a negative switching current -62 mA, respectively. Furthermore, field dependence of the switching current will also be demonstrated.



**SESSION A23: STRONGLY CORRELATED ELECTRONS I**
**Monday Morning, 13 March 2006**
**320, Baltimore Convention Center at 8:00**
**Chris Stock, John Hopkins University, presiding**

**8:00**
**A23 1 High magnetic field thermal-expansion and magnetostriction of $URu_2Si_2$** VICTOR CORREA, TIMOTHY MURPHY, ERIC PALM, STANLEY TOZER, *National High Magnetic Field Laboratory, Florida State University* PETER SHARMA, NEIL HARRISON, MARCELO JAIME, *National High Magnetic Field Laboratory, Los Alamos National Laboratory* GEORGE SCHMIEDESHOFF, *Occidental College* JOHN MYDOSH, *II Physikalisches Institut, Universität zu Köln* We present high magnetic field (up to 45 T) thermal-expansion and magnetostriction results on $URu_2Si_2$ single crystals. The volume change associated with the transition to the ''hidden'' order phase becomes increasingly discontinous as the magnetic field is raised above 30 T. This confirms recent thermal conductivity and specific heat experiments indicating a strong coupling between the ''hidden'' order parameter and the lattice which suggest some sort of charge ordered state. Several other transitions are observed at higher fields, many of them showing hysteresis, while a change in the sign of the magnetostriction coefficient is observed at the metamagnetic transition ($B_M \sim$ 38 T).

**8:12**
**A23 2 Phonon Thermal Transport of $URu_2Si_2$: Broken Translational Symmetry and Strong-Coupling of the ''Hidden Order'' to the Lattice** PETER SHARMA, *National High Magnetic Field Laboratory-LANL* N. HARRISON, M. JAIME, *NHMFL-LANL* Y.S. OH, K.H. KIM, *Seoul Nat'l University* C.D. BATISTA, *LANL* H. AMITSUKA, *Hokkaido University* J.A. MYDOSH, *Max Planck Institute, Dresden* A dramatic increase in the total thermal conductivity ($k$) is observed in the Hidden Order (HO) state of single crystal $URu_2Si_2$. Through measurements of the thermal Hall conductivity, we explicitly show that the electronic contribution to $k$ is extremely small, so that this large increase in $k$ is dominated by phonon conduction. An itinerant BCS/mean-field model describes this behavior well: the increase in $k$ is associated with the opening of a large energy gap at the Fermi Surface, thereby decreasing electron-phonon scattering. Our analysis implies that the ''Hidden Order'' parameter is strongly coupled to the lattice, suggestive of a broken symmetry involving charge degrees of freedom.

**8:24**
**A23 3 On Heavy Fermion Superconductivity and Quantum Criticality in the 115 series** KENNETH BURCH, *University of California, San Diego* We have performed a detailed analysis of the optical properties of the 1-1-5 series (CeTIn5 where T=Co,Ir,Rh), revealing the hybridization gap ($\Delta$) as key to understanding their rich phase diagram. Surprisingly we find that $\Delta$ for only one of the four bands crossing the Fermi surface determines the properties of the system. Furthermore, these carriers are the lightest and produce the smallest $\Delta$. Additionally we discuss connections between this $\Delta$, the superconducting transition temperature and the symmetry of the superconducting gap. This study demonstrates an experimental link between superconductivity and the parameter governing the magnetic Quantum Critical Point.

**8:36**
**A23 4 Quantum Criticality in $CeMIn_{5-x}Sn_x$ (M = Rh, Co)** FILIP RONNING, ED BAUER, *Los Alamos National Laboratory* C. CAPAN, *Louisiana State University* Y. TOKIWA, J.D. THOMPSON, J.L. SARRAO, R. MOVSHOVICH, *Los Alamos National Laboratory* Non-Fermi liquid behavior, as characterized by a T-linear resistivity and a T log(T) behavior in specific heat, is observed in zero field in the heavy fermion system $CeCoIn_5$. The application of magnetic field has revealed a field tuned quantum critical point surprisingly coincident with the superconducting $H_{c2}$. We present data that shows the application of pressure reduces the critical field $H_{QCP}$ more rapidly than $H_{c2}$ is suppressed. We also investigate doping studies which show an anisotropically field tuned QCP in $CeRhIn_{5-x}Sn_x$ at x=1.0, the critical doping where antiferromagnetism is suppressed, while results on $CeCoIn_{5-x}Sn_x$ maintains that the quantum critical field and the superconducting upper critical field are intimately connected. We attempt to reconcile whether all the critical behavior in the $CeMIn_5$ family can have a common origin.

**8:48**
**A23 5 Superconducting properties of $Ce_2CoIn_8$** N. HUR, T. PARK, E. D. BAUER, J. D. THOMPSON, J. L. SARRAO, *Los Alamos National Laboratory, Material Science Technology Division, MST-10, Los Alamos, NM 87545* The new family of Ce-based heavy-fermion compounds with the general formula $Ce_nTIn_{3n+2}$ (T=transition metal) have attracted sparked interest in recent years owing to their various interesting phenomena, such as pressure induced superconductivity, quantum criticality, and non-Fermi liquid behaviors. However, among n=2 compounds, $Ce_2CoIn_8$ has not been studied sufficiently mainly because of the difficulty in the synthesis of crystals of decent size. Herein, we report the successful reproduction of $Ce_2CoIn_8$ single crystals and present their magnetic, thermal and transport properties. Observed anomalies in resistivity and their magnetic field dependence will be explained within the context of a filamentary superconductivity. The nature and possible origin of the resistivity transition is discussed in comparison with that in $CeIrIn_5$.

**9:00**
**A23 6 Point Contact Spectroscopy Study of the Heavy Fermion Superconductor $Pr(Os_{1-x}Ru_x)_4Sb_{12}$*** C. S. TUREL, J. Y. T. WEI, *University of Toronto* N. A. FREDERICK, W. M. YUHASZ, S. K. KIM, J. PAGLIONE, M. B. MAPLE, *University of California at San Diego* The recent discovery of superconductivity in the heavy fermion material $Pr(Os_{1-x}Ru_x)_4Sb_{12}$ has generated widespread interest. In particular, there is evidence for the existence of two competing superconducting order parameters, at least

one of which is believed to have nodes. We have performed point-contact spectroscopy measurements on single crystals of $Pr(Os_{1-x}Ru_x)_4Sb_{12}$, using Pt-Ir tips in a dilution refrigerator with a pulsed technique to minimize Joule heating. We present differential conductance spectra down to 100 mK, along with the magnetic field evolution. We discuss the implications of our data in relation to recently proposed pairing symmetries.

*Acknowledgements: NSERC, CFI/OIT and Canadian Institute for Advanced Research.

**9:12**

**A23 7 de Haas van Alphen perspective on the origin of heavy fermions in $UPt_3$** PATRICK ROURKE, *University of Toronto* ALIX McCOLLAM, *University of Toronto* GREG McMULLAN, *MRC-LMB, Cambridge* MIKE NORMAN, *Argonne National Laboratory* STEPHEN JULIAN, *University of Toronto* ANDREW HUXLEY, *DRFMC-CEA, Grenoble* Precise de Haas van Alphen (dHvA) oscillation measurements on the heavy fermion superconductor $UPt_3$ are available as a function of magnetic field angle. It was recently proposed that the heavy quasiparticles in this material arise from the localization of two of the three 5f electrons of the U ions [Zwicknagl et al., PRB 65, 081103R (2002)]. The predicted Fermi surface topology however differs from traditional band-structure calculations. We will focus on the experimentally observed angle dependence of the hole-like $\delta$-orbit, as this appears difficult to reconcile with the Fermi surface of Zwicknagl et al.

**9:24**

**A23 8 NMR measurement of spin-spin relaxation ($T_2$) of $URu_2Si_2$** TOD CALDWELL, *Los Alamos National Laboratory* NICHOLAS CURRO, *Los Alamos National Laboratory* We report detailed temperature dependences of the 29Si spin-spin relaxation rate T2 in the heavy fermion superconductor $URu_2Si_2$ as a function of field and temperature. All experimental work was carried out on an aligned powder sample. Both Carr-Purcell-Meiboom-Gill (CPMG) and Hahn-Echo pulse sequence techniques were employed to examine differences in spin-spin relaxation. We find unusual enhancements of the relaxation rate near the hidden order transition, and will discuss our results in the context of various theoretical scenarios.

**9:36**

**A23 9 Indications of a Field Dependent Vortex Core Size in $CeCoIn_5$** L. DEBEER-SCHMITT, M. R. ESKILDSEN, *Department of Physics, University of Notre Dame, Notre Dame, IN 46556 USA* C. D. DEWHURST, *Institut Laue-Langevin, 6 Rue Jules Horowitz, F-38042 Grenoble, France* B. W. HOOGENBOOM, *University of Basel, Klingelbergstasse 70, CH-4056 Basel, Switzerland* C. PETROVIC, *Department of Physics, Brookhaven National Laboratory, Upton, NY 11973 USA* Using Small-Angle Neutron Scattering, we have imaged the flux- line lattice (FLL) in the *d*-wave, heavy fermion superconductor $CeCoIn_5$. At low fields, a hexagonal FLL is observed which undergoes a first order transition to a rhombic (distorted square) symmetry as the field is increased above 0.55 T. As the field is increased futher, the FLL approaches a square symmetry. Measurements of the FLL reflectivity yields a constant form factor independent of the applied magnetic field, in stark contrast to the exponential decrease usually observed. The field-independent form factor may indicate a field dependent vortex core size, $\xi \propto H^{-1/2}$, in qualitative agreement with recent theoretical predictions for ultra-clean, high-$\kappa$ superconductors [V.G. Kogan and N.V. Zhelezina, PRB **71**, 134505 (2005)].

**9:48**

**A23 10 Quantum Criticality in Itinerant Antiferromagnet $Cr_{0.965}V_{0.035}$** D.A. SOKOLOV, G. STRYCKER, M.C. ARONSON, M.C. BENNETT, *The University of Michigan* S.E. NAGLER, M. LUMSDEN, *HFIR, ORNL* We report results of triple-axis neutron scattering experiments, in which we studied the development of the magnetic fluctuations in the quantum critical itinerant antiferromagnet $Cr_{0.965}V_{0.035}$. Unexpectedly, we found temperature dependent elastic scattering at the incommensurate wavevector q $*=(001\pm\ \delta)2\ \pi$/a, which corresponds to the spin density wavevector in pure Cr and no elastic scattering at the commensurate wavevector $q=(001)2\ \pi$/a. We propose an electronic phase separation scenario to account for the observed elastic scattering. Temperature independent inelastic scattering was observed at the commensurate wavevector q. This scattering showed a linear increase with energy transfer $E_t$, saturating at $E_t=18$ meV, which we interpret as a characteristic energy scale expected for the Fermi liquid. The wave vector dependence of the scattering at q* is Lorentzian, with an intensity which decreases with increasing energy transfer, and is temperature independent below 100 K. The Lorentzian linewidth approaches the spectrometer resolution at the lowest temperatures and energy transfers. These observations suggest that the susceptibility underlying the incommensurate scattering is maximized, and is perhaps critical, for $q=q^*$, $E\rightarrow 0$, and $T \rightarrow 0$, as has been observed near other antiferromagnetic quantum critical points. Work at the University of Michigan supported by the National Science Foundation.

**10:00**

**A23 11 Attractive electron-electron interaction induced by the Bloch band topological field** JUNREN SHI, *Institute of Physics, Chinese Academy of Sciences* QIAN NIU, *University of Texas at Austin* We demonstrate a new possibility for the occurrence of the attractive electron-electron interaction in ferromagnetic metals. Unlike that of the conventional origin via the boson-exchange (spin fluctuation), this attractive interaction is induced by the Bloch band topological field, which transforms the Coulomb repulsion to a direct attractive interaction between electrons, resulting in unconventional superconductivity with the isotropic $p-$wave pairing. Our study highlights the fundamental effects of the Bloch band topological field, which presents in a large class of crystalline materials. It also provides a plausible alternative theory for the recently discovered ferromagnetic superconductors $UGe_2$ and $ZrZn_2$.

**10:12**

**A23 12 Theory of the helical spin crystal. A candidate for the partially ordered state of MnSi** BENEDIKT BINZ, ASHVIN VISHWANATH, *UC Berkeley* VIVEK AJI, *UC Riverside* MnSi is an itinerant magnet which at low temperatures develops a helical spin density wave. Under pressure it undergoes a transition into an unusual partially ordered state whose nature is debated. Here we propose that the helical spin crystal (the magnetic analog of a solid) is a useful starting point to understand partial order in MnSi. We consider helical spin crystals with BCC structure (composed of superpositions of six different helical spin-density waves) and determine conditions under which they may be energetically fa-

vored. We introduce a Landau theory to study the properties of these states, in particular the effect of crystal anisotropy, magnetic field and disorder. These results compare favorably with existing data on MnSi from neutron scattering and magnetic susceptibility measurements. Future experiments to test this scenario are also proposed.

**10:24**

**A23 13 Anomalous quasiparticle transport in the superconducting state of $CeCoIn_5$** YUICHI KASAHARA, *Department of Physics, Kyoto Univ.* YASUYUKI NAKAJIMA, *ISSP Univ. of Tokyo* KOICHI IZAWA, *CEA-Grenoble, ISSP Univ. of Tokyo* KAMRAN BEHNIA, *Laboratoire de Physique Quantique (CNRS) ESPCI, ISSP Univ. of Tokyo* YUJI MATSUDA, *Kyoto Univ., ISSP Univ. of Tokyo* HIROAKI SHISHIDO, RIKIO SETTAI, YOSHICHIKA ONUKI, *Osaka Univ.* To investigate the quasiparticle dynamics in the superconducting state of quasi-two dimensional heavy fermion superconductor $CeCoIn_5$, the thermal Hall conductivity $\kappa_{xy}$ is measured. In zero magnetic field, thermal Hall angle shows up a steep increase below $T_c$, indicating that the quasiparticle mean free path is strongly enhanced. In spite of the presence of a periodic vortex lattice, this enhancement is easily suppressed by a very weak magnetic field. We found that the density states of the delocalized quasiparticles $N_{\mathrm{del}}$, which is obtained from $\kappa_{xx}$ and $\kappa_{xy}$, exhibits a $\sqrt{H}$- dependence, indicating a Volovik effect. Moreover, $\kappa_{xy}$ reveals the scaling relation with respect to $T/\sqrt{H}$, which is expected for *d*-wave symmetry. These results provide a further support for *d*-wave superconducting symmetry in $CeCoIn_5$. We also argue that a small Fermi energy, a short coherence length, and a long quasiparticle mean free path all indicate $CeCoIn_5$ is in the superclean regime. These results highlight that $CeCoIn_5$ is unique among superconductors.

## SESSION A24: SEMI-CRYSTALLINE AND STRUCTURED POLYMERS

**Monday Morning, 13 March 2006**
**321, Baltimore Convention Center at 8:00**
**N. Sanjeeva Murthy, University of Vermont, presiding**

**8:00**

**A24 1 Crystalline Structure, Morphology and Gas Transport in Semicrystalline Syndiotactic Polystyrene** BRIAN OLSON, JUSTIN BRANDT, SERGEI NAZARENKO, *School of Polymers and High Performance Materials, University of Southern Mississippi* Crystalline syndiotactic polystyrene (s-PS) continues to amuse the researchers by showing very unusual properties. This work mainly explored the remarkable free volume properties of the crystalline structure of this polymer, and also very unusual gas transport behavior. It was possible by varying the temperature of the melt and crystallization conditions to prepare a series of semicrystalline samples with different crystallinities (0-50%) containing either pure $\alpha$-form, pure $\beta$-form and pure $\gamma$-form. Solid-state structure and the morphology of all prepared systems were examined by an assortment of techniques: DSC, density, WAXS, SAXS, and AFM. The structure was also probed by passing through small gas molecules, and by means of positron lifetime spectroscopy (PALS).

**8:12**

**A24 2 Large Strain Requirements for Shear Induced Crystallization of Isotactic Polypropylene*** H. HENNING WINTER, AADIL ELMOUMNI, DEEPAK ARORA, *University of Massachusetts Amherst* Strain effects on the crystallization of a series of isotactic polypropylenes (*i*PP), with various molecular weights, were studied using rheology, light transmission, birefringence, differential scanning calorimetry, and wide-angle X-ray diffraction. Transmitted light intensity measurements demonstrate that the effect of pre-shear on crystallization rate keeps increasing up to very larger strain levels, much beyond strains that are required to reach steady shear flow (at given itWe). Crystal orientation sets in at a total strain of about it$\gamma_0 = 600$ or higher. WAXD and DSC analyses corroborated the light transmission results. The samples were pre-sheared and then crystallized at constant temperature. Total shear strains it$\gamma_0$=200 to 1000 were applied to the *i*PP samples at the beginning of a crystallization experiment, after the samples had reached the crystallization temperature of 145$^o$C (undercooled state). A constant Weissenberg number itWe=1 (itWe, defined as the product of shear rate and a relaxation time) was maintained throughout the study. itWe=1 corresponds to the onset of shear thinning in steady shear. Deborah number values were low, itDe$< <$1, indicating that steady shear flow had been reached in all pre-shearing runs.

*Supported by PRF

**8:24**

**A24 3 Real-time, Depth-Resolved Structure Development of Flow-Induced ''Skin-Core'' Morphologies in Polypropylene.** LUCIA FERNANDEZ-BALLESTER, DEREK THURMAN, *California Institute of Technology* IGORS SICS, LIXIA RONG, *Brookhaven National Lab* JULIE KORNFIELD, *California Institute of Technology* We present a new method to isolate the signal arising from a given depth at each time point during flow-induced crystallization of isotactic polypropylene using real time rheo-optical and rheo-WAXD measurement based on the linear stress-depth relationship in a pressure-driven flow through a rectangular slit. Using thoughtfully selected sets of shearing conditions (constant ts with varied $\sigma$w), data analysis of the suite of experiments allows us to examine the incremental contribution to the real-time data from one shear stress to another (with all other conditions fixed) and to attribute the difference to a small spatial region of the sample. This ''depth sectioning'' technique has enabled us to confirm several existing results and uncovers several new keys to understanding how anisotropic crystalline is induced by flow. Threads first form near the channel wall where stress is highest and grow in length with prolonged flow. After sufficient time, thread length per unit volume saturates. The propagation of threads varies in a nonlinear manner with stress. Prior to saturation, thread propagation is linear with shearing time, providing promising conditions for measuring the thread propagation velocity.

**8:36**

**A24 4 Crystallization in Precision Polyolefins** RUFINA ALAMO, ANINDYA GHOSAL, *FAMU-FSU College of Engineering, Tallahassee Fl* EMINE BOZ, KENNETH WAGENER, *University of Florida, Chemistry Department, Gainesville, Fl* RIQIANG FU, *NHMFL, Tallahassee, Fl* ALAMO, GHOSAL, FU COLLABORATION, WAGENER, BOZ COLLABORATION, Understanding the crystallization behavior of highly branched polyolefins can be accomplished with model polymers with well defined microstructures. Models for branched polyethylenes with

precisely placed O, F, Cl or Br on each and every 19 carbons have been synthesized via acyclic diene metathesis (ADMET) polymerization followed by hydrogenation. Compared to broad WAXS and DSC melting peaks of systems with a random distribution of the substituent, similar properties of precisely substituted polyolefins are very sharp, typical of the behavior of homopolymers. A uniform partitioning of the substituent between crystalline and non-crystalline regions, observed by NMR, relatively thick lamellar crystallites (240 A) and WAXS angular shifts, parallel the homopolymer-like crystallization behavior. In this series, orthorhombic isomorphic structures are maintained in O and F substituted polymers or up to a van der Waals radius of about 1.6 A, while accommodation of bulkier atoms in the lattice promotes the formation of a new triclinic form. A linear correlation between melting points and vdw radius in the halogen series is indicative to the degree to which each substitution perturbs the symmetry of the neighboring carbons in the lattice.

**8:48**

**A24 5 Transitions of Polymers with Precise Oligomethylene Sequences.*** BERNHARD WUNDERLICH, WULIN QIU, *University of Tennessee, Knoxville, and ORNL, Oak Ridge* Polyethylene, PE, with precise branches has been analyzed by TMDSC and X-ray diffraction. The branches were methyl, dimethyl, and ethyl groups. Furthermore, atactic poly(octadecyl acrylate) and poly(4,4'-phthaloimidobenzoyl-doeicosyleneoxycarbonyl) were studied. All are compared to LLDPE, of similar branch concentration and linear PE. Compared to LLDPE the precisely structured polymers show much sharper melting. Compared to HDPE lower melting temperatures and heats of fusion were observed, and all have non-orthorhombic structures. In contrast to paraffins of equal length which melt fully reversibly at a similar temperature, the precisely designed polymers melt largely irreversibly with only small amounts of reversing melting which is least for the best-grown crystals. These results have important implications for the description of melting of copolymers. Initial literature: W. Qiu, J. Sworen, M. Pyda, E. Nowak-Pyda, A. Habenschuss, K. B. Wagener, B. Wunderlich, itMacromolecules, **39** (2006).

*Supported by NSF, Polymers Program, DMR-0312233, and the Div. of Mat. Sci., BES, DOE at ORNL, managed by UT-Battelle, LLC, for the U.S. Department of Energy, DOE-AC05-00OR22725.

**9:00**

**A24 6 Ellipsometry as a Probe of Crystallisation Kinetics in Thin Diblock Copolymer Films** JESSICA L. CARVALHO, MICHAEL V. MASSA, KARI DALNOKI-VERESS, *Physics and Astronomy, McMaster University* We present our recent results on the use of ellipsometry to probe the crystallisation kinetics of thin films of a diblock-copolymer. Ellipsometry uses the ellipticity induced upon reflection of light from a film covered substrate to allow calculation of the refractive index and thickness of the film. By studying the temperature dependence of these quantities one can measure phase transitions including the crystallisation kinetics. The samples used are thin films of a polybutadiene-b-poly(ethylene oxide) diblock. The PB-b-PEO diblock has block molecular weight of 26,000 and 6,800 respectively and micro phase-separates into PEO minority spheres in a PB matrix. The study presented is very similar to what is typically performed by DSC, except that the ellipsometer also provides the expansion and contraction of the film (i.e. expansion coefficients, contraction upon crystallisation). We will discuss the results which can be obtained with this approach.

**9:12**

**A24 7 Growth mechanism changes in pseudo-dewetted monolayer poly(ethylene oxide) crystallization** DUN-SHEN ZHU, ER-QIANG CHEN, AN-CHANG SHI, STEPHEN CHENG, PEKING UNIVERSITY, CHINA COLLABORATION, MCMASTER UNIVERSITY, CANADA COLLABORATION, UNIVERSITY OF AKRON, USA COLLABORATION, Crystal growth mechanism changes have been observed in pseudo-dewetted monolayers of low molecular weight (LMW) (PEO) on freshly cleaved hydrophilic mica surfaces [HPEO(4250) which have -OH groups at both ends and MHPEO(4700) which has one -OH and one -$OCH_3$ as end groups]. X-ray scattering reflectivity measurements show a wetted monolayer of molten PEO with a thickness of $\sim$ 4.5 nm on the mica surface. Non-adsorbed PEO droplets sit on top of the wetted monolayer. A two-step process for PEO single crystal growth under isothermal conditions was identified utilizing in-situ atomic force microscopy at different crystallization temperatures ($T_x$). In the first step, the crystal grows within the droplet which supplies the molten PEO that participates in the crystal formation. In this second-step, the wetted monolayer at the growth front is depleted by about 1.5 - 2.5 nm. The growing crystal lateral sizes obey a power law of $t^{\alpha}$ ($t$: time). At a high $T_x$ of 63 [r]C for MHPEO(4700), the growth behavior obeys itr $\propto$ t ($\alpha = 1$). While in the case of HPEO(4250), its growth behavior follows itr $\propto$ $t^{0.5}$ ($\alpha = 0.5$) in the whole $T_x$ range. With decreasing $T_x$, the growth of MHPEO(4700) falls into a scaling law of itr $\propto$ $t^{\alpha}$ ($0.5 < \alpha < 1$).

**9:24**

**A24 8 Guiding the orientation of polymer crystals by nanoimprint lithography** ZHIJUN HU, JEAN-FRANÇOIS GOHY, VINCENT BAYOT, ALAIN JONAS, *Universite catholique de Louvain* CERMIN TEAM, Polymer crystallization is notoriously difficult to control at a local scale. Here, we report on a fast and easy method to guide the orientation of crystals of semicrystalline polymers at the nanometer scale by using nanoimprint lithography (1). Whenever a silicon mold bearing topographical nano-features (typical lateral size 50-250 nm; typical height 100 nm) is pressed against a molten film of a crystallizable polymer (poly(vinylidene fluoride was used here), the molten polymer is forced to flow into the cavities of the mold. The isolation of polymer in separate nano-cavities, which strongly decreases the importance of nucleation by impurities, the confinement of the polymer in nano-sized cavities, the probable partial orientation of chains near the vertical walls of the mold due to polymer flow, and interfacial effects, lead to a fine control over crystallographic orientation, crystal size and shape. This is shown for a series of geometries, from simple straight lines to more complex shapes such as concentric circles and small squares. References (1) Zhijun Hu et al., Nano Letters 2005, 5, 1738.

**9:36**

**A24 9 An Atomic Force Microscopy study of the thin film crystallization behavior of blends of poly-(L-lactide) and poly-(D-lactide).** YURY YURYEV, PAULA WOOD-ADAMS, *Concordia University* JOSEE BRISSON, *Universite Laval* MARIE-CLAUDE HEUZEY, CHARLES DUBOIS, *Ecole Politechnique* POLYLACTIDE RESEARCH COLLABORATION, Blends of poly-(L-lactide) and poly-(D-lactide) form a triclinic stereocomplex during racemic crystallization while the pure optical isomers crystallize in a pseudo-orthorhombic crystalline form. The triclinic stereocomplex has a high melting point of 503 K compared to 453 K for the other crystalline form. Atomic Force Microscopy (AFM)

allows one to image a polymer surface with nanoscale resolution and is best suited for the studies of crystalline morphology in thin polymer films. Individual spherulitic morphology, its growth rate and its dependence on temperature and blend composition were studied using tapping mode AFM. 500-600 nm thick polylactide films were produced by solution casting. Excess nucleation sites were eliminated by melting for a short time. It is found that spherulites protrude from the surface of the film after annealing. The crystallization rate is slower when both optical isomers are present.

**9:48**

**A24 10 Spectroscopic Analysis of Unusual Poly (lactic acid) Structures.** KAORU AOU, GUOLIN WU, SHUHUI KANG, SHAW LING HSU, *Polymer Sci. and Engn., Univ. of Massachusetts Amherst* Poly (lactic acid) (PLA) is a biomass-derived polymer with a broad range of applications. We previously unambiguously determined the chain conformation of PLA to be a 10/3 helix based on a combination of experimental and normal coordinate analyses, in the process assigning band splittings to the intrahelical interactions. Here, we investigate the nature of intermolecular interactions within the PLA crystals as well as their molecular orientation. In PLA, specific intermolecular interactions such as dipolar coupling strongly influence the spectral features. Crystal field splitting bands in the PLA crystal vibrational spectra were identified. They indicated the strength and proximity of interacting carbonyls and C-H groups and are thus relevant to PLA crystal packing. Results of the studies were used to understand the origins of unusual thermal stability of the PLA stereocomplex with a melting point higher than the $\alpha$-crystal by at least 50 $^{o}$C. The knowledge was also applied to characterization of orientation development in PLA tubes during different stages of sequential biaxial deformation.

**10:00**

**A24 11 Poly(L-lactic acid) Crystals: From 2D to 3D** SUOLONG NI, ROBERT E. MAJOR, ALAN R. ESKER, *Department of Chemistry (0212), Virginia Tech, Blacksburg, VA 24061* The crystallization behavior of poly(L-lactic acid) (PLLA) is studied in Langmuir and Langmuir-Blodgett (LB) films. PLLA Langmuir films exhibit a first-order liquid expanded to condensed (LE/LC) phase transition. Temperature dependent isotherm studies reveal an experimentally accessible critical temperature (Tc) for the LE/LC phase transition. Below Tc, the LE/LC phase transition induces the ordering of PLLA single chain helices, giving rise to two dimensional (2D) smectic liquid crystalline-like lamella in the condensed phase. The nucleation and growth of three dimensional (3D) crystals from 2D helices can be achieved through isobaric experiments. Above Tc, PLLA Lamgmuir monolayers collapse directly from the isotropic LE phase to form 3D single crystals. Annealing studies of the LB-films with 2D lamellar patterns via in-situ atomic force microscopy track the time and temperature dependence growth of 3D crystals. Our system provides a model system for studying crystallization kinetics in ultra-thin films.

**10:12**

**A24 12 Amylose Crystallization From Concentrated Aqueous Solution: Role of Degree of Polymerization** JOHN CREEK, JAMES RUNT, GREGORY ZIEGLER, *The Pennsylvania State University* In earlier research, we demonstrated that amylose forms a spherulitic morphology when crystallized from concentrated amylose - water solutions, over a wide degree of crystallization conditions. The process has been described as depending on a competition between crystallization and liquid-liquid phase separation processes. In the present study acid degradation and enzymatic debranching are utilized to create a number of amylose fractions differing in degree of polymerization, ranging from DPs of 20 to 920. It was determined (using DSC and x-ray diffraction) that the shorter the chain length, the higher the final degree of crystallinity. Atomic force microscopy is used to investigate the microstructure of amylose lamella within the spherulites.

**10:24**

**A24 13 Diffusion-limited growth of poly (caprolactone) in poly (tert-butyl acrylate) matrices at the air/water interface** BING-BING LI, ALAN R. ESKER, *Department of Chemistry (0212), Virginia Tech, Blacksburg, VA 24061* Surface pressure induced crystallization of poly (caprolactone) (PCL) in poly (tert-butyl acrylate) (PtBA) matrices at the air/water interface has been monitored in real time by Brewster angle microscopy (BAM). Diffusion-limited morphologies of PCL crystals grown in PCL/PtBA mixed monolayers were observed during the compression process. The lateral forces applied on the mixed monolayer during compression assist the diffusion of PCL molecules from the surrounding monolayer to the crystal growth fronts, where the amorphous PtBA components are excluded. Surface pressure-area per monomer isotherm studies suggest that the nucleation and growth of PCL occurs at about 11 mN/m. The lamellar thickness of PCL dendrites determined by atomic force microscopy is about 7-8 nm. With decreasing surface concentration during expansion of the mixed films, PCL chains slowly detach from the crystalline domains and diffuse into the monolayer. These findings provide an interesting model system for future studies of crystallization in confined geometries.

**10:36**

**A24 14 Crystallization and orientation studies in SWNTs based nanocomposites** TIRTHA CHATTERJEE, *University of Houston* RAMANAN KRISHNAMOORTI, *University of Houston* VIKTOR HADJIEV, *University of Houston* Single walled carbon nanotubes (SWNTs) based polymer nanocomposites are attractive for their improved mechanical, electrical and thermal properties. We have obtained well-dispersed SWNTs samples in two semi-crystalline polymers poly($\varepsilon$-caprolactone) and poly(ethylene oxide) respectively. Initial crystallization studies show tubes acts as a nucleating agent for PCL where as it hinders nucleation of PEO crystals. Both polymer composites are studied for aligned SWNTs samples. Raman spectroscopy studies show SWNTs are aligned along the draw direction. The crystallization studies of the aligned nanocomposites are performed using synchrotron small angle x-ray scattering (SAXS). Our studies reveal that for an aligned tube direction polymer crystals arrange themselves in a particular orientation. For PCL the lamellar normal is parallel to the tube axis where as for PEO it is perpendicular to the draw direction. As SWNTs act as a nucleating agent for PCL, chains grow parallel to the draw direction. For PEO, SWNTs act as barriers and polymer lamellae grow parallel to the SWNTs axis. This observation is interesting because oriented tubes can be used as a template to orient polymer crystals.

**SESSION A25: FOCUS SESSION: ORGANIC FIELD EFFECT TRANSISTORS**
**Monday Morning, 13 March 2006; 322, Baltimore Convention Center at 8:00**
**David Martin, University of Michigan, presiding**



*Invited Papers*

**8:00**
**A25 1 Organic Semiconductors and Nanodielectrics for Flexible, Low Voltage Thin-Film Transistors.**
TOBIN MARKS, *Northwestern University*

Molecular materials scientists are skilled at designing and constructing individual molecules with the goal of imbuing them with predetermined chemical and physical properties. However, the subsequent task of rationally assembling them into organized, functional supramolecular architectures with precise, nanometer-level control of bulk opt-electronic properties presents another level of challenge. In this lecture, synthetic and computational approaches to addressing such problems are described in which the ultimate goal is the fabrication of flexible electronic circuits employing unconventional materials classes and unconventional fabrication techniques. The issues here concern not only the rational design, realization, and understanding of high-mobility p- and n-type organic semiconductors, but also robust enabling nanoscopic gate dielectrics having ultra-high capacitance, low leakage, and high breakdown fields. In the former area, routes to and properties of, new high-mobility heterocyclic materials are described. These materials are then used to fabricate high-performance organic thin film transistors and CMOS circuits. In the latter topic, the design, synthesis, and characterization of new high-k nanoscopic gate dielectrics are described. It is then shown how these dielectrics can be employed to significantly enhance the performance of thin-film transistors and other devices fabricated from a wide variety of both organic as well as inorganic semiconductors.

*Contributed Papers*

**8:36**
**A25 2 Complex Organic Semiconductor Devices Utilizing Threshold Voltage Shifting and Carrier Sign Reversal** HOWARD KATZ, CHENG HUANG, JAMES WEST, *Johns Hopkins University* We consider a range of materials and mechanisms that lead to nonvolatile switching in field-effect transistors made from organic semiconductors (OFETs). Charging of gate dielectrics, secondary dielectrics, and/or the semiconductor/dielectric interface can greatly shift the threshold voltage in these OFETs. The dielectrics can consist of nonpolar electrets or ferroelectric polymers. In the particular case of $SiO_2$ electret coated with a hydrophobic surface layer, the shift is permanent on the timescale of years and is in quantitative agreement with measured surface charge. The semiconductor perfluoro copper phthalocyanine is shifted from electron- to hole-carrying by application of sufficient field from a corona apparatus. Inverter circuits were built from pairs of OFETs based on a single semiconductor, differing only in the quantity of stored gate charge.

**8:48**
**A25 3 Improving the electrical characteristics of a solution-processable, anthradithiophene organic semiconductor by solvent vapor annealing** KIMBERLY DICKEY, *University of Texas at Austin* JOHN ANTHONY, *University of Kentucky* YUEH LIN LOO, *University of Texas at Austin* The development of organic semiconductors is driven by the promise of low-cost device applications. To fully realize cost-effective organic electronics, solution-processable materials need to be developed. While several solution-processable materials have been demonstrated, these materials often suffer from significantly reduced carrier mobilities due to defects and grain boundaries introduced during the deposition process. We have been studying triethylsilyl anthradithiophene (TES ADT), a solution-processable, p-type organic semiconductor. Transistors fabricated with spun-cast TES ADT exhibit low carrier mobilities ($0.002 cm^2$/V-s). Subjecting the fabricated transistors to dichloroethane solvent vapor annealing, however, yields average carrier mobilities of $0.2 cm^2$/V-s. Additionally, the current hysteresis observed during device operation is eliminated with this annealing. This dramatic improvement in transistor performance is solvent choice dependent, and can be directly correlated with morphological transformations in the thin film.

**9:00**
**A25 4 Dielectric relaxation in semiconducting regioregular poly(3-hexylthiophene)*** TATIANA PSUREK, JAN OBRZUT, *Polymers Division, National Institute of Standards and Technology* Regioregular effect transistor applications. While, the electrical mobility properties of P3HT have been examined the dielectricpoly (3−hexylthiophene) (P3HT) is a material typically used as an organic semiconductor in thin film field−relaxation processes have not been systematically studied. We investigated the dielectric response of P3HT films in the temperature range of 240 K to 315 K and at frequencies up to 12 GHz. In the low frequency range P3HT shows a semi−conducting character and the overall dielectric response is dominated by dc−conductivity with $E_a$=17 kJ/mol. The apparent semi−conducting character cease at certain frequency above which, the material becomes a dielectric. At room temperature the semi−conducting to dielectric transition takes place at about 5 kHz. In the range of 10 kHz to 12 GHz the dielectric dispersion is insignificant and the dielectric constant is about 4. The dielectric relaxation process, with $\tau = 3*10^{-5}$s and $E_a$ = 24 kJ/mol, can be attributed to local molecular motion of thiophene rings.

*Official contribution of NIST; not subject to copyright in the United States.

**9:12**

**A25 5 All Electronic Time of Flight Mobility Measurements in Pentacene Organic Field Effect Transistors** LAWRENCE DUNN, *University of Texas at Austin and Institute of Materials Research and Engineering, Singapore* DEBARSHI BASU, LIANG WANG, ANANTH DODABALAPUR, *University of Texas at Austin* One of the most important figures of merit for an organic semiconductor is its mobility, which is the proportionality constant relating the velocity of charge carriers to the electric field in the material. We present an all-electronic time of flight method for measuring the in-plane mobility of charge carriers using a voltage pulse (rise time $<$ 60 ns) applied to the source of an OFET at temperatures between 300 K and 77 K. The transit time mobilities extracted at all temperatures are compared with the DC mobilities extracted from the OFET transfer characteristics. We observe significantly higher transit time mobilities at higher temperatures that merge with the DC mobilities at lower temperatures. This is noteworthy because the transit time technique measures the mobility of the fastest carriers, which at higher temperatures seems to be uninfluenced by the interaction of charge carriers with deep traps, and also before the bias stress effect influences transport. By comparing the DC and transit time mobilities at varying temperatures we may gain an understanding of the time scale of the charge carriers' interaction with traps in the semiconducting material.

**9:24**

**A25 6 Infrared Imaging of Charge Injection Landscape in Organic Field-Effect Transistors** ZHIQIANG LI, *UCSD* GUANGMING WANG, *UCSB* NA SAI, *UCSD* DANIEL MOSES, *UCSB* MICHAEL MARTIN, *Lawrence Berkeley National Laboratory* MASSIMILIANO DI VENTRA, *UCSD* ALAN HEEGER, *UCSB* DIMITRI BASOV, *UCSD* UCSD COLLABORATION, UCSB COLLABORATION, LAWRENCE BERKELEY NATIONAL LABORATORY COLLABORATION, We report on infrared (IR) spectro-microscopy study of charge injection phenomena in organic field-effect transistors (OFET) based on regioregular poly(3-hexylthiophene) (P3HT). An analysis of the oscillator strength of the spectroscopic signatures of charge injection allowed us to quantify the density of the injected carriers and examine its evolution with applied voltages. Using IR microscopy, the uniformity of the field- induced charge layer in OFETs with high dielectric constant insulator $TiO_2$ as well as $SiO_2$ as gate dielectrics was explored. These data uncover the critical role of the gate insulator in defining the relevant charge injection length scales. This work demonstrates the unique potential of IR spectroscopy for the investigation of the electronic excitations in nanometer-thick accumulation layers in OFET devices.

**9:36**

**A25 7 Oligothiphene nanostructure evolution in transition from monolayer to multilayers.** GEETHA DHOLAKIA, M. MEYYAPPAN, *NASA Ames Research Center, Moffett Field, CA 94035* ANTONIO FACCHETTI, TOBIN MARKS, *Department of Chemistry, Northwestern University, Evanston, IL 60208.* Organic electronics offers tremendous potential in applications requiring structural flexibility and large area coverage, with the added advantage of low fabrication cost. While the mobilities of organic field effect transistors (OFETs) have recently increased to the level needed for practical applications, differences in the orientation of interchain stacking, as well as defects in the film interfaces and the presence of grain boundaries act as scattering centers and charge traps, hence degrade their performance. Here we present tunneling spectroscopic results and STM studies at the nanoscale analyzing the evolution in morphology and grain connectivity of fluoroalkyl-functionalized DFH-4T (a, w-diperfluorohexyl-4T) oligothiophene films on Au(111) substrates, as the thickness is varied from one monolayer to many multilayers. Monolayer thick DFH-4T films exhibit a featureless morphology except for a number of pits similar to those in self-assembled thiol monolayers, while multilayer films have a drastically different terraced morphology consisting of overlapping platelets. This study provides important information on the nature of the interface between organic semiconductors and the source\drain electrodes in OFET devices.

**9:48**

**A25 8 Charge injection and band alignment in organic field effect transistors.** BEHRANG HAMADANI, *Department of Physics and Astronomy, Rice University* HUANJUN DING, *Department of Physics and Astronomy, University of Rochester* JACOB CISZEK, *Department of Chemistry, Rice University* YONGLI GAO, *Department of Physics and Astronomy, University of Rochester* JAMES TOUR, *Department of Chemistry, Rice University* DOUGLAS NATELSON, *Department of Physics and Astronomy, Rice University* GAO LABORATORY COLLABORATION, TOUR LABORATORY COLLABORATION, We have studied metal/organic semiconductor charge injection in poly(3-hexylthiophene) (P3HT) field effect transistors with Pt and Au electrodes as well as Au electrodes modified by self-assembled monolayers (SAMs) as a function of annealing in vacuum. At low impurity dopant densities, Au/P3HT contact resistances show nonohmic behavior, whereas Pt/P3HT contacts remain ohmic. Ultraviolet photoemission spectroscopy (UPS) reveals that metal/P3HT band alignment shifts dramatically as samples are dedoped, leading to an increased injection barrier for holes. We also present the results of a preliminary study in which we modified the Au surface with electron poor (rich) SAMs, resulting in an effective increase (reduction) of the workfunction of Au and drastically changing the nature of charge injection at the contacts. Our results indicate that understanding the band alignment at the metal/polymer interface is an important step towards understanding the nature of charge injection in these devices.

**10:00**

**A25 9 Structural Determination of Interfaces in Organic Semiconductors using Coherent Bragg Rod Analysis** BRANDON CHAPMAN, RONALD PINDAK, *Brookhaven National Lab* YIZHAK YACOBY, *Hebrew University* JULIE CROSS, *Argonne National Lab* EDWARD STERN, *University of Washington* CHRISTIAN KLOC, *Bell Labs* The low charge carrier mobilities long associated with organic semiconductors have increased by several orders of magnitude in recent years. Charge mobilities in field-effect transistors (FETs) using single-crystals of rubrene (5,6,11,12-tetra-phenyl-tetracene) have been reported with values in the range from 5 to 30 cm2/Vs. However, little information is known about the integrity of interfaces formed by electrical contacts in organic FETs, which can play a significant role in determining device performance. We are using a novel approach called Coherent Bragg Rod Analysis (COBRA) to determine the atomic structure of interfaces in organic FETs. COBRA uses the measured x-ray diffraction intensities along the substrate defined Bragg (crystal truncation) rods to investigate the electron density near the surface, interface and throughout the thin-film. The COBRA method is uniquely suited for probing buried interfaces formed by electrical contact materials on molecular crystals. Here,

we present preliminary measurements of Bragg rods from the free surface of rubrene single-crystals and we discuss progress toward measuring a complete set of inequivalent Bragg rods from rubrene that will provide a model-independent determination of the surface structure.

**10:12**

**A25 10 Transfer Printing of Pentacene Thin-Film Transistors onto Flexible Substrates** DANIEL HINES, *University of Maryland* VINCE BALLAROTTO, *Laboratory for Physical Sciences* ELLEN WILLIAMS, *University of Maryland* Transfer printing methods were optimized to fabricate high quality organic thin-film transistors (TFT) on flexible substrates. Flexible TFT devices fabricated from a 50 nm thick pentacene (Pn) semiconductor layer, a 600 nm thick polymer dielectric layer and Au electrodes on a polyethylene terephthalate (PET) substrate constitute a model system. A set of TFT devices with length L = 1 $\mu$m to 45 $\mu$m and width W = 100 $\mu$m were fabricated with both poly(methyl methacrylate) (PMMA) and poly(4-vinylphenol) (PVP) as the dielectric material. Output and transfer IV characteristics of these devices were measured as a function of L. The data sets were analyzed to determine both contact resistance and mobility. The Pn/PMMA/PET device set exhibited a contact resistance of 2 M$\Omega$ and a mobility of 0.237 $cm^2$/Vs while the Pn/PVP/PET device set exhibited a contact resistance of 0.5 M$\Omega$ and a mobility of 0.2 $cm^2$/Vs. A detailed comparison of these transfer printed device sets will be presented. *Work supported by the Laboratory for Physical Sciences, College Park, MD and ARDA.

**10:24**

**A25 11 Optical Probe of the Density of Defect States in Organic Thin-Film Transistors** MIHAELA BREBAN, DANILO ROMERO, *University of Maryland* VINCENT BALLAROTTO, *Laboratory for Physical Sciences* ELLEN WILLIAMS, *Univerity of Maryland* We investigate the role of defect states associated with different gate dielectric materials on charge transport in organic thin film transistors. Using a modulation technique we measure the magnitude and the phase of the photocurrent[1] in pentacene thin film transistors as a function of the modulation frequency. The photocurrent generation process is modeled as exciton dissociation due to interaction with localized traps. A time domain analyses of this multi-step process allows us to extract the density of defect states. We use this technique to compare the physical mechanism underlying performances of pentacene devices fabricated with different dielectric materials. *Supported by the Laboratory for Physical Science [1] M. Breban, et al. ''Photocurrent probe of field-dependent mobility in organic thin-film transistors'' Appl. Phys. Letts. 87, 203503 (2005)

**10:36**

**A25 12 Architecture Effects for Transfer-Printed Carbon Nanotube Mat Transistors*** VINOD SANGWAN, *University of Maryland, College Park (MD)* DAN HINES, VINCENT BALLAROTTO, GOKHAN ESEN, MICHAEL FUHRER, ELLEN WILLIAMS, UNIVERSITY OF MARYLAND, COLLEGE PARK (MD) TEAM, LABORATORY FOR PHYSICAL SCIENCES, (MD) COLLABORATION, Transfer printing methods have been developed to assemble both top gate – top source/drain and bottom gate – bottom source/drain carbon nanotube (CNT) thin-film transistors (TFT) onto flexible substrates. The devices consist of CNT mats as the semiconductor layer, a poly(methyl methacrylate) dielectric layer and gold electrodes on a polyethylene terephthalate substrate. As a function of gate voltage ($V_G$), the top gate – top source/drain devices exhibit ambipolar behavior with no hysteresis*. This is in contrast to bottom gate – top source/drain CNT mat TFTs with a $SiO_2$ dielectric layer which show only p-type characteristics and a large hysteresis. Fabrication and characterization of both CNT TFT architectures fabricated on flexible substrates via transfer printing will be presented and discussed. * D. R. Hines et al., Appl. Phys. Lett. 86, 163101 (2005).

*Work supported by the Laboratory for Physical Sciences, College Park, MD and ARDA

**10:48**

**A25 13 ESR Study of Electric-Field Controlled Conductance of Fully-doped Polymers in a Transistor Structure*** FANG-CHI HSU, ARTHUR J. EPSTEIN, *Department of Physics, The Ohio State University* It was recently reported that use of doped ''metallic'' polymer as the active channel in a field effect transistor structure results in unexpected ''normally on'' transistor-like behavior. Epstein itet al. proposed [1] that ion motion is involved in the conductance modulation of the ''metallic'' polymer. We study here the role of ion migration in the ''metallic'' polymer (poly(3,4-ethylenedioxythiophene) doped with poly(styrenesulfonic acid) (PEDOT:PSS)) based transistors by employing ESR spectroscopy. We found that approximately 18% reduction of localized polaron concentration in PEDOT:PSS caused by ions insertion results in $10^3$ times decrease in the polymer conductance. The $N(E_F)$ determined from the Pauli susceptibility remains essentially unchanged after ions are inserted into the active channel. This indicates that the major conductance suppression in PEDOT:PSS occurs in the disordered regions. We proposed that the inserted ions modulate the charge carrier hopping distance in the disordered regions of the PEDOT:PSS resulting in a conductor-nonconductor transition. [1]A. J. Epstein itet al., Curr. Appl. Phys. **2**, 339 (2002).

*Authors thank Dr. Vladimir N. Prigodin for invaluable discussion.Supported in part by AFOSR Grant No. F49620-03-1-0175.



## SESSION A26: BIOMOLECULAR COMPUTATION

**Monday Morning, 13 March 2006**
**323, Baltimore Convention Center at 8:00**
**Thomas Darden, National Institute of Health, presiding**

**8:00**

**A26 1 Quantum Mechanical Study of C-Terminal Cleavage Reaction in Inteins*** PHILIP SHEMELLA, SAROJ NAYAK, BRIAN PEREIRA, SHEKHAR GARDE, GEORGES BELFORT, *Rensselaer Polytechnic Institute - Troy, NY* PATRICK VAN ROEY, VICKY DERBYSHIRE, MARLENE BELFORT, *Wadsworth Center - Albany, NY* Although inteins undergo autocatalytic cleaving and splicing reactions via a relatively well accepted reaction scheme, the mechanism that induces these reactions is not well understood. The reactions can be prevented or speeded up through mutations of various critical amino acids proximal to the active site or through changes in the solution pH and/or temperature. We are interested in obtaining an atomic level understanding of the C-terminal cleavage reaction using quantum mechanical reaction simulation techniques. The reaction is based on the highly conserved catalytic module of histidine-asparagine-cysteine. Ex-

perimentally, intein C-terminal cleavage occurs more readily at low pH and high temperature. Working closely with experimentalists, we use a combination of gas phase and implicit solvent techniques with density functional theory to compare energy barriers for various proposed mechanisms. The mechanism with the lowest energy barrier is consistent with experimental results and is based on the protonation of the peptide amide by a hydronium ion and the subsequent cyclization of the asparagine amino acid, resulting in cleavage of the peptide bond.

*Supported by NSF CTS03-04055-NIRT



**8:12**

**A26 2 Evolutionary Strategies for Protein Folding** SRINIVASA MURTHY GOPAL, WOLFGANG WENZEL, *INT, Forschungszentrum Karlsruhe* The free energy approach for predicting the protein tertiary structure describes the native state of a protein as the global minimum of an appropriate free-energy forcefield. The low-energy region of the free-energy landscape of a protein is extremely rugged. Efficient optimization methods must therefore speed up the search for the global optimum by avoiding high energy transition states, adapt large scale moves or accept unphysical intermediates. Here we investigate an evolutionary strategies(ES) for optimizing a protein conformation in our all-atom free-energy force field([1],[2]). A set of random conformations is evolved using an ES to get a diverse population containing low energy structure. The ES is shown to balance energy improvement and yet maintain diversity in structures. The ES is implemented as a master-client model for distributed computing. Starting from random structures and by using this optimization technique, we were able to fold a 20 amino-acid helical protein and 16 amino-acid beta hairpin[3]. We compare ES to basin hopping method. [1]T. Herges and W. Wenzel,Biophys.J. **87**,3100(2004) [2] A. Verma and W. Wenzel *Stabilization and folding of beta-sheet and alpha-helical proteins in an all-atom free energy model*(submitted)(2005) [3] S. M. Gopal and W. Wenzel *Evolutionary Strategies for Protein Folding* (in preparation)

**8:24**

**A26 3 Towards predictive molecular dynamics simulations of DNA: electrostatics and solution/crystal environments** VOLODYMR BABIN, JASON BAUCOM, *North Carolina State University* THOMAS DARDEN, *National Institute of Environmental Health Sciences* CELESTE SAGUI, *North Carolina State University* We have investigated to what extend molecular dynamics (MD) simulatons can reproduce DNA sequence-specific features, given different electrostatic descriptions and different cell environments. For this purpose, we have carried out multiple unrestrained MD simulations of the duplex d(CCAACGTTGG)2. With respect to the electrostatic descriptions, two different force fields were studied: a traditional description based on atomic point charges and a polarizable force field. With respect to the cell environment, the difference between crystal and solution environments is emphasized, as well as the structural importance of divalent ions. By imposing the correct experimental unit cell environment, an initial configuration with two ideal B-DNA duplexes in the unit cell is shown to converge to the crystallographic structure. To the best of our knowledge, this provides the first example of a multiple nanosecond MD trajectory that shows and ideal structure converging to an experimental one, with a significant decay of the RMSD.

**8:36**

**A26 4 Coarse-grained model of chaperonin-mediated protein folding** GEORGE STAN, *National Institutes of Health* D. THIRUMALAI, GEORGE LORIMER, *University of Maryland* BERNARD BROOKS, *National Institutes of Health* Chaperonins are biological nanomachines that employ a spectacular mechanism for simulated annealing. During the chaperonin cycle, concerted, large scale, rigid body conformational changes, ultimately driven by ATP hydrolysis, result in a dramatically expanded chaperonin cavity serving as folding chamber. Chaperonins repeatedly bind misfolded proteins, randomly disrupt their structure, and release them in less folded states, allowing these substrate proteins multiple opportunities to find pathways leading to the native state. What is the fate of the non-native protein during the chaperonin cycle? We addressed this question using coarse-grained molecular dynamics simulations. We find that the fundamental annealing function of the GroEL chaperonin consists of forced unfolding and refolding of the substrate protein. The annealing action is related to the change in the nature of the interaction between the substrate protein and the GroEL particle from predominantly hydrophobic to largely hydrophilic. To identify the proteins most likely to be natural substrates for GroEL we use a bioinformatic approach. Our hypothesis is that natural substrates contain patterns of residues similar to the co-chaperonin GroES.

**8:48**

**A26 5 Using Molecular Dynamics simulations in the analysis of Electron Spin Resonance spectra** DENIZ SEZER, *Physics Dept., Cornell Univ.* BENOIT ROUX, *IMPS, IBD, CIS, Univ. of Chicago* ESR spectra from spin labeled sites in proteins are sensitive both to the conformations of the spin label at the labeled site and to its flexibility and rate of transition between multiple conformations. Even though measures of spin label mobility can be extracted directly from the spectrum, deducing the wealth of factors that affect the spectral line shape is impossible in most of the cases. Often, one has to model the motion of the spin label and calculate spectra for different values of the parameters of the model. From the work where this approach has been followed it appears that anisotropic Brownian diffusion in a restricting potential constitutes a good description of the spin label motion. This hydrodynamic depiction correlates poorly with the molecular structure of the spin label and its linker. To address this limitation, we combine MD simulations with stochastic models in the simulation of ESR spectra. This allows us to treat the structure and the fast dynamics of the spin label and its environment in atomistic detail, while handling the slower motional modes to which the spectrum is susceptible phenomenologically. We analyse the MD trajectories with the Redfield formalism, appropriate in the fast motional regime. The exchange between the populated rotamers of the spin label and the overall tumbling of the macromolecule, occurring on a longer time scale, are accounted for using stochastic dynamics.

**9:00**

**A26 6 Locating structural energy minimum of biological molecules in explicit solvent** ERIC DYKEMAN, OTTO SANKEY, *Arizona State University* Biological molecules in waters often adopt several structural conformers. These structures correspond to the various local energy minima on the solute-solvent potential energy hyper-surface. Methods capable of predicting the various conformations that a molecule can adopt in solution have involved, (naming a few), annealing and replica exchange molecular dynamics simulations. However, implementation of these methods

with systems containing explicit solvent still requires large amounts of computation time due to the requirement of a small time step. The recent development of the activation relaxation technique (ART) of Mousseau et al. provides an alternative that may reduce computational costs. Instead of following a Newtonian trajectory, ART locates local energy minima through a series of activations to energy saddles followed by relaxation to a local energy minimum. Here we discuss extensions of the method to explicit solvent models. This development and extension of the technique offers insight into how water affects the potential energy surface of molecules in solution.

**9:12**

**A26 7 Predicting 3D structures of transient protein-protein complexes** PETRAS KUNDROTAS, EMIL ALEXOV, *Dept. of Physics & Astronomy, Clemson University, Clemson, South Carolina* Predicting transient protein-protein complexes is a major task of the post genomic era since the ultimate goal is to understand how proteins interact in the living cell. Apparently experimental methods as X-ray and NMR cannot be used at such large scale and therefore numerical methods for predicting protein-protein complexes should be applied. In this presentation we propose homology based approach to predict 3D structure of protein complexes. The underlying presumption is that if two proteins are homologous to other two proteins that form a complex then they will form a complex, 3D structure of which should be similar to the 3D structure of the existing complex. In order to test our method we have created a database of template complexes. The methodology of database creation will be presented and discussed. Due to very limited number of protein-protein complexes in the Protein Data Bank we expanded our database by including proteins containing loosely connected domains. A jack-knife test was performed and the quality of the models was evaluated against existing protein-protein complexes. It is shown that including interfacial information and residue pairing restrains in the sequence alignment improves the results.

**9:24**

**A26 8 Charge transfers from Na atom in (H2O)n clusters and in water solution** TAKESHI NOZUE, JUNICHI HOSHINO, KAZUO TSUMURAYA, *Meiji University* The charge state of sodium ions in water is an essential issue in both biophysical and physicochemical areas. Although the nominal charge state of sodium is +1 in water solution, the true charge is less than unity and will depend on the environments. We clarify the true charges states with ab initio density functional methods. There have been several methods to evaluate the charges that belong to each atom in molecules: Bader analysis divides up into regions where the dividing surfaces are at a minimum in the density. [1] The Bader charge analysis [2] has difficulty of finding all the critical points around the atom. Henkelman et al. have proposed a modified partition scheme. [3] We use a modified version of the Henkelman's scheme to integrate the core charge densities separately. The method gives the charge transfer from Na to H2O to be 0.167e and that to (H2O)2 to be 0.522e. The original Bader charge scheme gives 0.156e and 0.596e respectively. We present the transfers surrounded by a large number of water molecules and those in water solution in periodic system. [1]R.F.W.Bader, Atoms in Molecules: A Quantum Theory, Clarendon:Oxford. 1990. [2]C.F-.Guerra, et al., J.Comp.Chem. 25, 189(2003). [3]G.Henkelman, et al., Comp. Mat. Sci. in press.

**9:36**

**A26 9 Coarse-graining protein energetics in sequence variables** FEI ZHOU, GEVORG GRIGORYAN, AMY KEATING, *Departments of Biology, MIT* GERBRAND CEDER, *Departments of Materials Science and Engineering, MIT* DANE MORGAN, *Department of Materials Science and Engineering, University of Wisconsin - Madison* We show that cluster expansions (CE), previously used to model solid-state materials with binary or ternary configurational disorder can be extended to the protein design problem. We present a generalized CE framework, in which properties such as energy can be unambiguously expanded in the amino-acid sequence space. The CE coarse grains over non-sequence degrees of freedom (e.g., side-chain conformations) and thereby simplifies the problem of designing proteins, or predicting the compatibility of a sequence with a given structure, by many orders of magnitude. The CE is physically transparent, and can be evaluated through linear regression on the energies of training sequences. [PRL 95, 148103 (2005)]. We show, as example, that good prediction accuracy is obtained with up to pairwise interactions for a coiled-coil backbone, and that triplet and/or quadruplet interactions are important in the energetics of the more globular zinc-finger and WW domain backbones. In the coiled-coil system, where experimental data is available, the calculated pair interaction parameters compare favorably with measured coupling energies. The clear advantage of a CE driven optimization over a direct one is demonstrated by searching for low-energy sequences on the zinc-finger backbone. Other possible applications of our approach are also discussed.

**9:48**

**A26 10 MAME Water Model: hydrogen bonding, electrostatic, polarization and van der Waals interactions in water.** EUGENE TSIPER, Hydrogen bonding is key to many unusual properties of water and its role in biological systems. I will describe an elegant water model derived using the minimal atomic multipole expansion (MAME). The minimal set for water consists of three multipoles that are chosen to satisfy experimental molecular dipole and both components of the molecular quadrupole. Two atomic polarizabilities, $\alpha_O = 1.4146\ \mathrm{A}^3$ and $\alpha_\mathrm{H} = 0.0836\ \mathrm{A}^3$, reproduce all three components of the polarizability tensor due to a relation between the latter, which follows from the model and is indeed satisfied experimentally. The model thus based on the known monomer properties reproduces hydrogen bonding in the dimer and compares favorably to the best available water-water interaction potentials. I will also discuss the meaning of distributed polarizabilities for computing dispersion (van der Waals) interactions. The atomic polarizabilities in water yield reasonable dispersion energy of 1.4 kcal/mol, which is otherwise underestimated when water molecules are treated as polarizable points. [E.V. Tsiper, Phys. Rev. Lett. 94, 013204, 2005]

**10:00**

**A26 11 Accurate computation and interpretation of spin-dependent properties in metalloproteins*** JORGE RODRIGUEZ, *Department of Physics, Purdue University* Nature uses the properties of open-shell transition metal ions to carry out a variety of functions associated with vital life processes. Mononuclear and binuclear iron centers, in particular, are intriguing structural motifs present in many heme and non-heme proteins. Hemerythrin and methane monooxigenase, for example, are members of the latter class whose diiron active sites display magnetic ordering. We have developed a computational protocol based on spin density functional theory (SDFT) to accurately predict

physico-chemical parameters of metal sites in proteins and bioinorganic complexes which traditionally had only been determined from experiment. We have used this new methodology to perform a comprehensive study of the electronic structure and magnetic properties of heme and non-heme iron proteins and related model compounds. We have been able to predict with a high degree of accuracy spectroscopic (Mössbauer, EPR, UV-vis, Raman) and magnetization parameters of iron proteins and, at the same time, gained unprecedented microscopic understanding of their physicochemical properties. Our results have allowed us to establish important correlations between the electronic structure, geometry, spectroscopic data, and biochemical function of heme and nonheme iron proteins.

*Supported by NSF grant CHE-0349189 (JHR)

**10:12**

**A26 12 Computational studies of a redox-driven proton pump: Cytochrome c oxidase and biological energy transduction*** ALEXEI A. STUCHEBRUKHOV, *UC Davis* Cytochrome c oxidase (CcO) is a redox-driven proton pump, an energy converting molecular machine, which reduces atmospheric oxygen to water and couples the oxygen reduction reaction to the creation of a membrane proton gradient. The proton gradient subsequently drives the synthesis of ATP. The structure of the enzyme has been solved; however, the molecular mechanism of proton pumping is still poorly understood. The correlated electron and proton transport plays a crucial role in the function of the enzyme. Our computer simulations – combined ab initio and classical, MD and MC-indicate a possible mechanism of CcO. We find that one of the His ligands of the catalytic site, and certain chains of water molecules inside of the enzyme play a crucial role. In this presentation, computational and experimental studies directed toward understandingthe mechanism of cytochrome c oxidase will be discussed. D.M. Popovic and A.A. Stuchebrukhov, Proton pumping mechanism and catalytic cycle of cytochrome c oxidase: Coulomb pump model with kinetic gating, FEBS Lett. 2004.

*NSF Che-0137652, NIH GM4052

**10:24**

**A26 13 Ab Initio QM/MM Study of the Ester-hydrolysis Reaction Mechanism in Haloalkane Dehalogenase** YIMING ZHANG, *Departent of Physics and Astronomy, Rensselaer Polytechnic Institute* YU ZHOU, *Departent of Physics and Astronomy, Rensselaer Polytechnic Institute* SAROJ NAYAK, *Departent of Physics and Astronomy, Rensselaer Polytechnic Institute* ANGEL GARCIA, *Departent of Physics and Astronomy, Rensselaer Polytechnic Institute* CENTER FOR BIOTECHNOLOGY AND INTERDISCIPLINARY STUDIES COLLABORATION, DEPARTMENT OF PHYSICS COLLABORATION, Ab Initio QM/MM calculations are used to investigate the ester-hydrolysis step of dichloroethane hydrolysis catalyzed by haloalkane dehalogenase. Amino acids around the active site (which includes ASP124, HIS289, ASP260, TRP125, TRP175), dichoroethane and water are treated by QM at a level of HF/6-31G(d,p). The remainder of the protein and solvent are treated classically. Two scenarios of hydrolysis mechanism for the alkyl-enzyme intermediate have been considered. In one, the HIS289-catalyzed water oxygen could be incorporated in the carboxylate group of ASP124, leading the cleavage of one of the original carbonyl bonds on ASP124. In the other, the ASP124 and HIS289 as general base, activate water as the nucleophilic agent, which attacks the alkyl carbon in substrate. The reaction paths and potential energy profiles are compared for both mechanisms.

**10:36**

**A26 14 Combining biophysical and bioinformatical approaches for predicting residue's contacts.** EMIL ALEXOV, AMBER ALLARDICE, PETRAS KUNDROTAS, *Clemson University* One of the most important task of the post genomics era is to utilize the enormous sequence information delivered from the genomes and to predict 3D structure of proteins. The quality of the predicted structure depends on many factors including the improvement made in ab initio, threading and homology modeling methods. Here we combine the method of correlated mutations with biophysical restrains in order to predict residue's contacts from amino acids sequence alone. The parameters of the protocol were optimized against a set of 21 proteins with known high resolution 3D structures. The effects of the degree of residue conservation, sequence similarity among the sequences within the multiple sequence alignment and conservation coefficient of two amino acids positions were studied. It was shown that the prediction accuracy of the method of correlated mutations alone is pure, on average only 10% of the contacts are predicted correctly. However, adding biophysical filters greatly improves the accuracy of the predictions. Thus, implying pairing rules for charged, polar and hydrophobic residues significantly reduces the total number of the predictions, e.g. reduces the coverage, however, most of the rejected predictions are false positives. As result, the relative rate of the correct predictions increases.

## SESSION A28: POLYMER BLENDS
**Monday Morning, 13 March 2006**
**325, Baltimore Convention Center at 8:00**
**Kalman Migler, National Institute of Standards and Technology, presiding**

**8:00**

**A28 1 Component Terminal Dynamics in PEO / PMMA Blends** TIMOTHY LODGE, ILAN ZERONI, SAHBAN OZAIR, *University of Minnesota* FRED COLLABORATION, As our understanding of the linear viscoelasticity of linear homopolymers improves, miscible blends of linear homopolymers constitute model systems at the next level of complexity. PEO / PMMA miscible blends are remarkable in that the disparity between the component glass transitions and monomeric friction factors is immense. We are exploring this system further by obtaining component terminal dynamics for linear PEO/PMMA miscible blends of various compositions using two different methods: forced Rayleigh scattering, providing tracer diffusivity of a labeled component, and tracer rheology, examining the relaxation of a few long chains in lower molecular weight blend matrices of varying composition. Results obtained by the two methods agree well. Furthermore, results show that the mobility of PMMA is strongly affected by the presence of PEO, its monomeric friction factor dropping precipitously upon addition of small amounts of PEO. The mobil-

ity of PEO, on the other hand, is not as greatly affected by the presence of PMMA, although still much more than indicated by published measurements on PEO segmental dynamics. These results will be discussed in the context of current models.

**8:12**

**A28 2 A molecular dynamics simulation study of the segmental relaxations in model polymer blends** DMITRY BEDROV, *University of Utah* Molecular dynamics simulations of model miscible polymer blends consisting of chemically realistic 1,4-polybutadiene (CR-PBD) (slow component) and PBD chains with reduced dihedral barriers (LB-PBD) (fast component) have been performed in order to study the influence of blending on segmental relaxation processes. We find that blending with a slow (high glass transition temperature, or $T_g$) component significantly increases the separation between the $\alpha$- and $\beta$-relaxations of the fast (low $T_g$) component, which may be unresolvable or nearly unresolvable in the pure melt. Detailed analysis of the dielectric response of the blend allows us to conclude that the high-frequency loss observed in numerous dielectric spectroscopy studies of miscible polymer blends that is apparently uninfluenced by blending can be due to the intrinsic $\beta$-relaxation of the fast component and not due to concentration fluctuations and/or structural heterogeneities within the blend. In other words, instead of assuming that some fraction of the fast component is not affected upon blending due to presence of the pure melt-like local environments. We further investigate the segmental relaxations by examining torsional autocorrelation functions, dipole moment autocorrelation function, and dielectric response for each component and for the blend as a function of temperature and concentration.

**8:24**

**A28 3 Dielectric Spectroscopy of Miscible Polymer Blends** WENJUAN LIU, RALPH H. COLBY, *Materials Science and Engineering Department, Penn State University* JANE E. G. LIPSON, *Department of Chemistry, Dartmouth College* Segmental dynamics are studied in two miscible polymer blends; both involve polystyrene, which has sufficiently small polarizability to be ignored in dielectric spectroscopy. One blend is with poly (vinyl methyl ether) where the low-$T_g$ component is seen in dielectric response and the other blend is with tetra-methyl BPA- polycarbonate where the high-$T_g$ component dominates the dielectric response. Both blends have reasonably disparate glass transitions, and both are weakly interacting. The glass transition temperature ($T_g$), linear viscoelasticity and dielectric spectroscopy of the pure components and blends, respectively, are measured by differential scanning calorimetry, Rheometric Scientific ARES$^{TM}$ Rheometer and Novocontrol Broadband Dielectric Spectrometer in the frequency range of $10^{-2} \sim 10^{6}$ Hz. We compare the experimental results with a prediction for the relaxation spectrum obtained using a simple lattice model, wherein we generate a distribution of environments around a given segment in the blend which leads to a prediction for that component's dielectric relaxation spectrum. We show that it is possible to model the dielectric relaxation spectrum by considering concentration fluctuations at the scale of the Kuhn length (the shortest Rouse mode), which we take to be both composition and temperature independent.

**8:36**

**A28 4 Assessment of the Flory diluent theory to evaluate its applicability in the determination of the amorphous-amorphous interaction energy*** RUSHIKESH MATKAR, THEIN KYU, *University of Akron* In the derivation of the Flory diluent theory, Flory has removed two of three assumptions inherent in Prigogine's model to determine the solubility of solids using regular solution theory, but the third assumption that solvent is completely immiscible in the crystal. An analytical expression for the calculation of the liquidus line is a consequence of the third assumption. Various researchers have also applied this theory to determine $\chi_{FH}$ representing the amorphous-amorphous interaction energy. We contest this methodology in light of the reported discrepancies in the determination of $\chi_{FH}$ in comparison with other test methods. We have removed the third assumption and established the thermodynamics of binary crystalline mixtures by the incorporation of crystal-solvent interaction effects. We identify the source of the discrepancies in this framework and recommend that all literature regarding the present topic should be treated with circumspect.

*NSF-DMR 05-14942

**8:48**

**A28 5 Designing Balanced Surfactants for Organizing Immiscible Polymers** MEGAN RUEGG, BENEDICT REYNOLDS, NITASH BALSARA, *University of California, Berkeley* MIN LIN, DAVID LOHSE, *ExxonMobil Research and Engineering* The phase behavior of A/B/A-C polymer blends with attractive and repulsive interactions was analyzed with scattering experiments and mean field theories. Transitions between lamellar phases, microemulsions, homogeneous phases and macrophase separated states are easily accessed in A/B/A-C blends simply by adjusting the temperature. The domain spacing was predicted utilizing the Random Phase Approximation (RPA) and Self-Consistent Field Theory (SCFT) in the homogeneous and organized states, respectively, with no adjustable parameters. The only inputs into the calculations were the binary Flory-Huggins interaction parameters (chi) and statistical segment lengths. The domain spacing determined from theory was often within 5 percent of the experimental values. Furthermore, in this particular A/B/A-C system, in which the chi parameter between the immiscble A and B homopolymers is 2.0-2.6 in our accessible temperature range, a blend was found to form an organized phase with only 3 percent of the diblock copolymer in the blend. This is the lowest amount of polymeric surfactant to form an organized phase to our knowledge. The transition temperature from single-phase systems to a macrophase separated state determined from theory was in good agreement with experimental values.

**9:00**

**A28 6 The Effect of Copolymer Composition on the Dynamics of Random Copolymers in a Homopolymer Matrix.** SUDESH KAMATH, MARK DADMUN, *University of Tennessee* Copolymers can be used as interfacial modifiers in phase separated polymer blends and selective surface segregation. Important parameters in both processes include the amount of copolymer that migrates to the surface and the rate of this segregation, both of which are altered by changing the copolymer composition. The dynamics of random copolymers in a homopolymer matrix are studied using Neutron Reflectivity (NR), Quasi-Elastic Neutron Scattering (QENS) and Lattice Monte Carlo simulations. We have carried out NR and QENS measurements on blends containing 10% Poly(S-ran-MMA) random copolymers with 3 different copolymer compositions dispersed in a PMMA matrix. We have also carried out lattice Monte-Carlo simulations on blends of A-B random copolymers containing 33%, 50% and 66% A in a matrix of

a homopolymer melt containing only A monomers using the bond-fluctuation model for polymer melts. Our results indicate that the copolymer composition has a significant impact on the dynamics of the copolymer. Our simulation results also indicate that copolymer composition has a significant impact on the conformation of the copolymer in the homopolymer melt, which in turn has an impact on the system dynamics.

**9:12**

**A28 7 Dynamics of Ternary Mixtures with Photosensitive Chemical Reactions: Designing Three Dimensional Hierarchically Ordered Composites** OLGA KUKSENOK, RUI D.M. TRAVASSO, ANNA C. BALAZS, *University of Pittsburgh* Using coarse-grained computer modeling, we show that photo-induced chemical reactions can be exploited to create long-range order in binary and ternary mixtures. In the binary case, a photosensitive AB blend is illuminated by a spatially uniform light and therefore undergoes both a reversible chemical reaction and phase separation. The late-time morphology resembles the lamellar morphology of diblock copolymers, with lamellae oriented isotropically within the sample. Rastering a secondary, higher intensity light over the sample locally increases the reaction rate and introduces long-range ordering along the rastering direction (i.e., effectively ''combing'' the lamellar domains). We also illustrate an application of our combing technique as a replicative process, which transfers an image on the substrate through the sample. In the ternary case, we add a non-reactive component C, which is immiscible with both A and B. We show that C migrates to regions that are illuminated by the secondary, higher intensity light. Using a stationary secondary light source allows us to effectively write a three-dimensional pattern of C onto the AB sample. Rastering over the ternary system with an additional light source leads to hierarchically ordered patterns of A, B and C.

**9:24**

**A28 8 Shear-Induced Crystallization and Rheology Behavior of Isotactic Polypropylene and Poly (ethylene-co-octene) Blend** XIA DONG, KUN MENG, CHARLES C. HAN, *PPCL, Joint Lab. of Polymer Science and Materials, Institute of Chemistry, Chinese Academy of Sciences, Beijing 100080, China* YONGYAN PANG, DUJIN WANG, *KLEP, Joint Lab. of Polymer Science and Materials, Institute of Chemistry, Chinese Academy of Sciences, Beijing 100080, China* Shear-induced crystallization of isotactic polypropylene (iPP) and poly (ethylene-co-octene) (PEOc) blend was studied by means of in-situ optical microscopy with a shear hot stage. Shear promoted the orientation of the polymer chains in shear direction, which results in cylindrite crystals. The cylindrites were observed when the shear rate is necessarily higher than $10s^{-1}$after liquid-liquid phase separation (LLPS) at 170° for 420min. The cylindrites appear and grow across the phase regions and have some defects after decomposition. The cylindrites growth rates remain unchanged with shear at any given temperature, while the nucleation density increases dramatically after LLPS when shear rate is more than $10s^{-1}$. The Blends viscosity and modulus depending on shear frequency was increased with the PEOc contents.

**9:36**

**A28 9 Eutectic Modeling of Blend Crystallization from the Homogeneous Melt** SUDHAKAR BALIJEPALLI, *Dow Chemical Company* JEROLD SCHULTZ, *University of Delaware* The morphology and kinetics of binary polymer blends crystallizing from the homogeneous melt is similar to that of eutectic crystallization in small-molecule or metal systems. While analyses of the small molecule case exist, extension to the polymer blend case requires accounting for (a) large deviation from equilibrium and (b) growth velocity dependence on temperature and composition. Such analytical modeling has been performed, assuming low Peclet numbers. The model and results are presented here and compared with the crystallization of a blend of high and low molecular weight fractions of poly(ethylene oxide). The analysis shows a sharply peaked relationship between growth arm periodicity and velocity of growth. An assumption that the operating condition is the maximum growth velocity appears to hold. A satisfactory correlation between analysis and experiment is found.

**9:48**

**A28 10 Interplay Between Two Phase Transitions: Crystallization and Liquid-Liquid Phase Separation in a Polyolefin Blend** CHARLES C. HAN, XIAOHUA ZHANG, *PPCL, Joint Lab. of Polymer Science and Materials, Institute of Chemistry, Chinese Academy of Sciences, Beijing 100080, China* The correlation between liquid-liquid phase separation (LLPS) and crystallization at several compositions in statistical copolymer blends of poly (ethylene-co-hexene) (PEH) and poly (ethylene-co-butene) (PEB) has been examined by optical microscopy (OM), atomic force microscopy (AFM) and differential scanning calorimetry (DSC). The overwhelming change in the crystallization kinetics due to the density fluctuation caused by the spontaneous spinodal LLPS is observed. This coupling mechanism suggests a new mechanism in the nucleation-crystallization process. All evidences are pointing to a cross-over mechanism from the spinodal fluctuations (of liquid-liquid phase separation) to the nucleation and than crystallization. The detailed experimental evidences and a suggested physical model will be presented.

**10:00**

**A28 11 Rheological modeling relating mesoscopic morphology for polymer blends** YUANZE XU, *Dept. Macromol.Sci., Fudan University, Shanghai 200433, China* WEI YU, *Department of Polymer Science and Engineering, Shanghai Jiao Tong University, Shanghai 200240, P.R. China* CHARLES C. HAN, *PPCL, Joint Lab. of Polymer Science and Materials, Institute of Chemistry, Chinese Academy of Science, Beijing 100080, China* The key issue to model polyblends rheologically is to solve the problem of dynamic coupling between interfacial morphology and viscoelastic flow. This work will outline our approaches. The framework of irreversible thermodynamics was employed and the conformation of both polymer chains are introduced. By comparing with the ellipsoidal model, the constitutive equation of dilute immiscible viscoelastic blends is established. To construct the model of concentrated blends, the hydrodynamic interaction of drops was treated. The theoretical predictions were proved by measured rheological material functions and the drop dynamics in a four-roll mill rheometer. Even greater challenge exists in the formulation of multi-scale rheological model of immiscible blends with complex morphology evolution, including drop break-up and collapse. Experiments show how the interfacial processes are interfered by non-linear viscoelasticity of polymers.

**10:12**

**A28 12 Design of Co-Continuous Nanostructured Polymer Blends by Solid-State Shear Pulverization.** YING TAO, JUNGKI KIM, JOHN M. TORKELSON, *Northwestern University, Evanston, IL 60208* Achievement of co-continuous nanostructured polymer blends is of interest as such materials may have enhanced properties (e.g., toughness, stress at break, and creep

resistance) in comparison to conventional blends with a micron-scale dispersed phase in a matrix phase. Leibler and co-workers (Nature Materials 1, 54 (2002)) recently produced co-continuous nanostructured blends via reactive melt blending in which irregular graft copolymers were made in situ. Here we demonstrate that achievement of such blends is possible in the solid state by use of solid-state shear pulverization (SSSP). During SSSP, polymers are mixed by exposure to high shear and compressive forces in the absence of melt processing. The morphology of the blended SSSP output is obtained by forming a consolidated sample using a cold platen press and then analyzing by scanning electron microscopy. In the case of polystyrene (PS)/poly(methyl methacrylate) (PMMA) blends, the PMMA phase can be etched with acetic acid, revealing the presence of a 3-D, nanostructured ( $\sim$ 100 nm length-scale), irregular morphology. Studies are underway to determine whether such a blend nanostructure can be maintained during subsequent, limited melt processing into a final product via addition of block copolymers or gradient copolymers to the blend during SSSP. Studies are also underway with other blend systems.

**10:24**

**A28 13 Polymer blends containing Linear Telechelic Supramolecular Polymers** MITCHELL ANTHAMATTEN, *University of Rochester, Dept. of Chemical Engineering* MICHELLE WRUE, *University of Rochester, Dept. of Chemical Engineering* We are studying a new class of polymer blends: linear polymers blended with end-to-end associating supramolecular polymers (unimers). Since the degree of unimer association depends on concentration and temperature, we expect unusual phase behavior that differs greatly from traditional blends of two linear polymers. Low molecular weight polybutadiene unimers that bear strong hydrogen-bonding, ureidopyrimidinone end groups were synthesized. These polymers were systematically blended with monodisperse polystyrene polymers, and the resulting blends were studied using a combination of optical microscopy and light scattering techniques. Results are compared to predictions made using a simple lattice association model. Inputs include the lengths of the unimers and polymers, the free energy of forming supramolecular bonds, and a Flory-Huggins interaction parameter.

**10:36**

**A28 14 Rheology of blends of dense star-like polystyrene soft nanospheres** AJAY KULKARNI, R.M. KANNAN, *Wayne State University* Highly branched polymeric materials exhibit significantly different rheological behavior compared to linear polymers, suggesting that controlled branch density can have technological benefits. We have synthesized a dense star polystyrene molecule, ($PS_{nano}$) with 50 arms, $M_a$= 5,000 g/mol. Using rheo-optics and triple-detection GPC, we have shown that these materials act as soft nanospheres, with a size of $\sim$ 8 nm. We are studying the effect of the nanospheres on the blending behavior of miscible polystyrene/ poly (vinyl methyl ether) (PS/PVME) blends with the help of dynamic stress-optical measurements. In $PS_{nano}$/PVME blends, at higher $PS_{nano}$wt. fractions, the interparticle distance between $PS_{nano}$ is smaller than radius of gyration of PVME. Therefore we expect to see the conformational changes in PVME chains induced by $PS_{nano}$ and compare it with linear PS (L−PS)/ PVME blends. However the rheo−optics data suggests that the relaxation dynamics of PVME is not significantly altered by $PS_{nano}$ whereas for L−PS/PVME blends the relaxation dynamics of PVME is slowed down by L−PS. DSC results show a single transition suggesting miscibility. Our results suggest that, the segments of PS near the periphery of $PS_{nano}$ may be miscible, but the segments at the core would be immiscible, resulting in a molecularly dispersed blend, rather than a segmentaly miscible L−PS/ PVME blend.

**10:48**

**A28 15 Reactive extrusion: A computational approach.** MANORANJAN PRUSTY, PATRICK ANDERSON, HAN GOOSSENS, HAN MEIJER, *Technical Univeristy Eindhoven* Reactive extrusion is attractive for various reasons. One of them is the flexibility of extruders for processing of polymers, but also the choice of the scale of the operation that can be adjusted to the needs for research and development or commercial production. We model reactive extrusion using a diffuse interface modeling (DIM) approach. The problem is studied by dividing it into four small/sub problems. First, the structure growth in case of homopolymer blends was studied with the effect of hydrodynamics. The logarithmic structure factor was found to scale as 1/3 with time for higher capillary numbers and 2/3 for lower capillary numbers. Second, the growth of structure for the block copolymer was studied for the symmetric blocks, for which only micro phase separation was observed. Then, the structure growth for the mixture of block copolymers and homo-polymers was studied and both micro and macro phase separation can be observed. The final step including the reaction kinetics of the formation of block copolymers from the homo-polymer is studied. Results are mainly presented showing morphology development and growth rates as a function of time.



## SESSION A29: EXPERIMENTAL TECHNIQUES IN BIOPHYSICS

**Monday Morning, 13 March 2006**
**326, Baltimore Convention Center at 8:00**
**J. P. Landry, University of California, Davis, presiding**

**8:00**

**A29 1 The healing mechanism for excited molecules near metallic surfaces** B. BARBIELLINI, *Northeastern U.* P.M. PLATZMAN, *Bell Labs* Radiation damage prevents the ability to obtain images from individual molecules. We suggest that this problem can be avoided for organic molecules by placing them in close proximity with a metallic surface. The molecules will then quickly dissipate any electronic excitation via their coupling to the metal surface. They may therefore be observed for a number of elastic scattering events that is sufficient to determine their structure.[1] B. Barbiellni and P. M. Platzman, cond-mat/0506403

**8:12**

**A29 2 Pulse-shaping and Fourier Transform Techniques in Multiphoton Microscopy** JENNIFER OGILVIE,*DELPHINE DÉBARRE, EMMANUEL BEAUREPAIRE, ANTIGONI ALEXANDROU, MANUEL JOFFRE, *Laboratoire d'Optique et Biosciences, Ecole Polytechnique* Multiphoton microscopy is an important tool that is increasingly used in biological research. The ease with which broadband femtosecond pulses can be created and manipulated has opened up new directions for enhancing multiphoton microscopy. In particular, pulse-shaping techniques can

tailor broadband light to selectively excite fluorescent species.[1] Here we demonstrate the use of pulse-shaped excitation to enhance multiphoton fluorescence imaging of live drosophila embryos. Other promising multiphoton techniques include coherent anti-Stokes Raman scattering (CARS) microscopy, which offers endogenous contrast based on the inherent vibrations of different chemical species.[2] Most implementations of CARS microscopy image single vibrational modes, providing limited ability to simultaneously follow multiple chemical species. An alternate time-domain Fourier transform-based method can produce spectrally resolved CARS images over the considerable bandwidth of a broadband laser source, This approach provides straightforward removal of the nonresonant background from CARS images while offering a compact, single-laser approach. [1] V. V. Lozovoy et al. J. Chem. Phys, (2003) 118, 3187. [2] A. Zumbusch et al. Phys. Rev. Lett. (1999) 82 4142.

*current address: Department of Physics/Biophysics Research Division, University of Michigan

**8:24**

**A29 3 Templated biomineralization on self assembled protein fibers** S. PALMACCIO, *Sachem High School NY* K. SUBBURAMAN, N. PERNODET, *Stony Brook Univ Stony Brook NY* S.-Y. KWAK, E. DIMASI, *BNL, Upton, NY* S. GE, *Stony Brook Univ Stony Brook NY* N.L. YANG, *CUNY, Staten Island, NY* M. RAFAILOVICH, *Stony Brook Univ Stony Brook NY* We have previously shown that fibrillogenesis of extracellular matrix (ECM) proteins like Fibronectin and Elastin can be induced when adsorbed on charged polymer surfaces. These self assembled fiber networks reach sizes of dimensions similar to natural ECM. Here we present a study of biomineralization on these protein fibers, achieved using $CaCO_3$ through Kitano & Flow cell methods. The mechanical properties were measured usingShear Modulation Force Microscopy (SMFM) as part of early stage mineralization studies. Results indicated increase in modulus with exposure time on fibers, with no increase off the fibers. Control studies with other Ca salts showed no change in fiber modulus, differentiating mineralization from salt adsorption. Late Stage Mineralization studied using ToF SIMS showed preferential Ca adsorption on the fibers. Optical Microscopy also showed preferential crystal formation on fibers. TEM was used to identity the crystal structure and orientation. Effect of proteins on crystal orientation and mineralization of natural ECM from osteoblasts are under study. Supported by USDOE Contract No. DE−AC02−98CH10886, NSF−MRSEC & BNL−SBU Seed Grant.

**8:36**

**A29 4 Advances in energy filtered electron tomography for quantitative 3-D phosphorus imaging of cell nuclei** MARIA A. ARONOVA, GUOFENG ZHANG, RICHARD D. LEAPMAN, *NIH* Electron tomography (ET) is an established and valuable tool for determining three-dimensional subcellular structure at a macromolecular scale. Contrast in conventional tomograms is generated through high-angle elastic scattering of the incident electrons by heavy atoms in stained plastic sections or through phase differences of elastic scattering in frozen hydrated specimens. Energy filtered transmission electron microscopy (EFTEM) has undergone recent developments to provide an improved capability for quantitative mapping of elemental distributions. We have developed a new approach where specific chemical elements in biological systems can be imaged in three dimensions. This method of collecting electron tomograms with inelastically scattered electrons combines ET and EFTEM. We have applied this technique to analyze unstained sections of rapidly frozen, freeze-substituted and embedded cells. Using intrinsic phosphorus as a label for nucleic acid, we have investigated the distribution of DNA in nuclei of itDrosophila larvae. We show that quantitative analysis of the three-dimensional phosphorus distribution has the potential to provide new information about the DNA packing density of chromatin.

**8:48**

**A29 5 Adaptive wave-front correction for multi-photon microscopy using coherence-gated wave-front sensing** MARKUS RUECKEL, WINFRIED DENK, *Max-Planck Institute for Medical Research, Germany* The contrast and the resolution of a multiphoton microscope highly depend on the shape of the focus which can be distorted by refractive index inhomogeneities within the specimen. Coherence-gated wave-front sensing (CGWS) allows reliable adaptive wave-front correction of these distortions (M. Feierabend, M. Ruckel, and W. Denk, Optics Letters, 2004, 29(19)). We developed a model for CGWS for which we evaluated in detail, using Monte-Carlo simulations, how the measured wave-fronts depend on the density of scatterers, the position and length of the coherence gate, and on the polarization of the light used. Predictions from this model were confirmed experimentally. Further we report on early results from an exploration of how much the two-photon excitation efficiency improves when applying corrections as predicted by CGWS. Experiments and numerical simulations show for a wave-front with a RMS distortion of $\lambda/5$ that the excitation efficiency was about 60% of that for a diffraction-limited focus. This was done for both astigmatism and coma.

**9:00**

**A29 6 Label-free optical detection of protein binding on small-molecule ligand microarrays*** Y. S. SUN, J. P. LANDRY, X. D. ZHU, *Dept. of Physics, Univ. of California at Davis* T. BAO, K. S. LAM, *Dept. of Internal Medicine, Univ. of California at Davis Medical Center* Biomolecular microarrays are becoming indispensable tools in proteomic research and biomarker discovery processes. The need for label-free microarray detection methods that are complementary to fluorescence-based methods is also increasing. We have developed oblique-incidence reflectivity difference (OI-RD) microscopes for detecting protein-protein and protein-small molecule reactions in microarray format through changes in density, thickness, and conformation of surface-bound proteins on solid supports. This can be done without extrinsic labeling molecules (e.g. organic fluorophores or quantum dots), which are costly and potentially intrusive. Of particular interest to one of our current investigations are microarrays of small molecules that may be used for high-throughput screening for protein ligands. With OI-RD microscopes, we have detected antibody-antigen capture and streptavidin-biotin binding reactions in microarray format using mixtures of proteins as well as pure proteins in prescribed sequences. In the streptavidin-biotin binding reaction, we used BSA molecules as the scaffold to anchor biotin molecules on the solid support. We will report these recent experimental results and the analysis.

*This work was supported by a UC-BREP GREAT Fellowship and the NSF Center for Biophotonics Science and Technology.

**9:12**

**A29 7 Dynamic Dimensional Analysis of itIn-Vivo Microorganisms Using Polarized Light Scattering** WILLEM VAN DE MERWE, *Indiana Wesleyan University* JOZSEF CZEGE, *USUHS* We have successfully determined average lengths and diameters of randomly-oriented rod-shaped bacteria in-vivo by evaluating the Mueller matrix ratio $< S_{34} > / < S_{11} >$ together with Coulter counter measurements of cell volumes (references 1 and 2.) We showed that our technique allows one to follow real-time dimensional changes taking place at a rate of about 14 nm/min. We expect to extend this method to synchronized cultures and will attempt to measure changes in the ratio for partially aligned bacterial cells. We will give a rationale for our expectation that this will provide additional information for example about growth characteristics of the bacteria. We used the coupled dipole model to compare theoretical predictions and experimental observations. Specifically, by refining our dimensional analysis we expect soon to be able to study the dynamic of bacterial cell division real-time as well as obtain additional identifying signatures of importance to medicine, biotechnology and detection. 1) Applied Optics 43 (2004) 5295-5302 2) Biophysical J. 69 (1995) 1170-1177

**9:24**

**A29 8 Fast Cooling and Vitrification of Aqueous Solutions for Cryopreservation*** MATT WARKENTIN, *Laboratory of Applied and Solid State Physics, Physics Department, Cornell University* NAJI HUSSEINI, VIATCHESLAV BEREJNOV, *Laboratory of Applied and Solid State Physics, Physics Department, Cornell University* ROBERT THORNE, *Laboratory of Applied and Solid State Physics, Physics Department, Cornell University* In many applications, a small volume of aqueous solution must be cooled at a rate sufficient to produce amorphous solid water. Two prominent examples include flash-freezing of protein crystals for X-ray data collection and freezing of cells (i.e. spermatozoa) for cryopreservation. The cooling rate required to vitrify pure water ( $\sim 10^6$ K/s) is unattainable for volumes that might contain cells or protein crystals, but the required rate can be reduced by adding cryoprotectants. We report the first measurements of the critical concentration required to produce a vitrified sample as a function of the sample's volume, the cryogen into which the sample is plunged, and the temperature of the cryogen, for a wide range of cryoprotectants. These experiments have broad practical consequences for cryopreservation, and provide insight into the physics of glass formation in aqueous systems.

*This work is supported by a grant from the NIH

**9:36**

**A29 9 Active and Passive Microscopic Viscoelastic Response in Poly(Ethylene) Oxide Solutions** OLGA LATINOVIC, H. DANIEL OU-YANG, It has been proposed that one can determine the viscoelastic response function from the thermal fluctuations of colloidal tracer particles. Despite attempts to validate the approach, there has not been a direct comparison between the viscoelastic response obtained by thermally driven particles, and independent microscopic measurements which do not depend on thermal fluctuations. This paper reports a study that compares the two approaches. In the passive measurements, the Brownian motion of a probe particle was used to obtain the viscoelastic modulus of poly (ethylene) oxide solutions using the fluctuation-dissipation theorem and the generalized Stokes-Einstein relation. In the active measurements, the same probe particle is set into forced oscillations by oscillating optical tweezers and the viscoelastic moduli of the solution are obtained from the in-phase and out-of-phase components of the particle's motion.

**9:48**

**A29 10 Specifically Detect Vascular Endothelia Growth Factor (VEGF) with Micro Cantilever Resonator*** JIANHUA GU, DEBIN LI, DAVID LEDERMAN, *Dept of Physics, West Virginia University* JAROD KABULSKI, PETER GANNETT, *Basic Pharmaceutical Sciences, West Virginia University* DANIEL FLYNN, *Mary Babb Randolph Cancer Center, West Virginia University* VEGF is an important protein marker for lung cancer. Current state of the art detection strategies use enzyme linked immunosorbent assays (ELISA), where only nanogram levels can be detected in serum. We have developed a sensing method to rapidly detect VEGF based on the micro cantilever resonator technique, which has advantages over the standard ELISA method. We have covalently linked a polyclonal anti-VEGF antibody to a silicon cantilever surface. The shift of cantilever resonant frequency due to specific VEGF binding with this antibody allows us to detect the presence of VEGF in solution at detection levels of approximately one picogram or even smaller. Efforts were made to reduce non-specific adsorption on cantilever either by covering non-specific sites on the cantilever with proteins (such as bovine serum albumin (BSA)), or by self-assembly of a protein resistant monolayer on the cantilever surface. We also used different protein samples (like VEGF-C or MMP-9) to confirm the specific detection of VEGF.

*Supported by the West Virginia University WVNano Initiative.

**10:00**

**A29 11 Serial Crystallography: imaging single proteins at a synchrotron*** DAVID SHAPIRO, *Center for Biophotonics Science and Tech.* JOHN SPENCE, R. BRUCE DOAK, DMITRI STARODUB, UWE WEIERSTAL, *Arizona State University* HENRY CHAPMAN, STEFANO MARCHESINI, *Lawrence Livermore Nat. Lab.* MALCOLM HOWELLS, *Lawrence Berkeley Nat. Lab.* A new method is proposed for the imaging of uncrystallized proteins at third generation x-ray sources. The method, serial crystallography, uses the diffraction pattern produced by a beam of hydrated proteins as they sequentially traverse a continuous x-ray beam after having been aligned by an intense laser field. Each particle is exposed to the x-ray beam so briefly that radiation damage is not a concern. The diffraction pattern is integrated as many identically aligned particles cross the beam and then the laser polarization is rotated to allow collection of other particle orientations. The diffraction pattern can then be phased by an iterative algorithm and the protein structure recovered with a Fourier transform. We are currently constructing a serial crystallography apparatus to be installed on beamline 9.0.1 of the Advanced Light Source at Lawrence Berkeley National Lab that will be operational by May, 2006. Preliminary experiments will use a 5 Watt CW IR laser to align particles of Tobacco Mosaic Virus and their soft x-ray diffraction patterns will be collected. We present the design of the serial crystallography apparatus and the current status of this project.

*Supported by NSF funding SGER DBI-0429814 and CBST

**10:12**
**A29 12 Structural investigations of human hairs by spectrally resolved ellipsometry** BENJAMIN SCHULZ, D. CHAN, M. RUEBHAUSEN, *Institute of Applied Physics, Jungiusstrasse 11, D-20355 Hamburg, Germany* S. WESSEL, R. WEPF, *Beierdorf AG, Hamburg, Germany* Human hair is a biological layered system composed of two major layers, the cortex and the cuticle. We show spectrally resolved ellipsometry measurements of the ellipsometric parameters $\Psi$ and $\Delta$ of single human hairs. The spectra reflect the layered nature of hair and the optical anisotropy of the hairs structure. In addition, measurements on strands of human hair show a high reproducibility of the ellipsometric parameters for different hair fiber bundles from the same person. Based on the measurements, we develop a model of the dielectric function of hair that explains the spectra. This model includes the dielectric properties of the cuticle and cortex as well as their associated layer thicknesses. In addition, surface roughness effects modelled by a roughness layer with an complex refractive index given by an effective medium approach can have a significant effect on the measurements. We derive values for the parameters of the cuticle surface roughness layer of the thickness $d_{ACu} = 273 - 360$nm and the air inclusion $f_A = 0.6 - 5.7\%$. [1] accepted for publication in J. Biomed Opt., 2005

**10:24**
**A29 13 Evanescent Wave Excitation and Raman Spectroscopy of Bacteriorhodopsin on Gallium Nitride Waveguide Structures** ALFONS SCHULTE, SONYA ORTIZ, ALFRED KELLER, APRIL POPE, YU GUO, HEIDI HOCKEL, ERIC JOHNSON, *University of Central Florida* Composite structures of protein-semiconductor layers have potential for molecular electronics and sensor applications. We investigate gallium nitride waveguide structures created by UV lithographic techniques as substrates for photoactive bacteriorhodopsin films. The waveguides were characterized through electron and optical interference microscopy. The top biomolecular layer is optically accessible through the evanescent field of a mode propagating in the gallium nitride waveguide. A 488 nm or 514 nm beam from an Argon ion laser was coupled into the waveguide and the evanescent field was employed to initiate the photocycle and excite Raman scattering in the bacteriorhodopsin film. Under stationary conditions the Raman spectrum in the fingerprint region shows the presence of the light-adapted state and the M intermediate. This suggests that the protein is in its native state and that optical switching of bacteriorhodopsin can be achieved and probed by evanescent wave excitation.

**10:36**
**A29 14 Probing Protein Structural Dynamics Using Microfluidic Diffusional Mixer Based FT-MIR Micro-Spectroscopy** PETER GALAJDA, ROBERT AUSTIN, *Princeton University* JARMILA GURJARRO, JESUS VEGA, CYRUS ARIAN, AIHUA XIE, *Oklahoma State University* AUSTIN TEAM, XIE TEAM, Time-resolved Fourier transform Infrared (FTIR) spectroscopy is a powerful technique to ''see'' proteins in action. Such a technique has been mostly applied to study photoreceptor proteins since their biological functions can be conveniently triggered in synchronization using short laser pulses. However, only a few proteins in nature are photo-active. In order to study a broad range of chemically activated proteins, we have developed a microfluidic diffusional mixing device, based on computational modeling of microfluidic flow and advection diffusion, microlithographic fabrication, and time-resolved FTIR micro-spectroscopy. This technique can be applied to probe functionally important structural dynamics of proteins that are chemically activated, thus opening up a broader application of time-resolved FTIR spectroscopic techniques. We will report such applications including experimental studies on GTPase system in biological signal transduction.

**10:48**
**A29 15 Modeling Electric Fields of Peripheral Nerve Block Needles.*** JAMES CH. DAVIS, NORMAN E. ANDERSON, MARK W. MEISEL, *Dept. of Physics, Univ. of Florida* JASON G. RAMIREZ, F. KAYSER ENNEKING, *Dept. Anesthesiology, Univ. of Florida* Peripheral nerve blocks present an alternative to general anesthesia in certain surgical procedures and a means of acute pain relief through continuous blockades. They have been shown to decrease the incidence of postoperative nausea and vomiting, reduce oral narcotic side effects, and improve sleep quality. Injecting needles, which carry small stimulating currents, are often used to aid in locating the target nerve bundle. With this technique, muscle responses indicate needle proximity to the corresponding nerve bundle. Failure rates in first injection attempts prompted our study of electric field distributions. Finite difference methods were used to solve for the electric fields generated by two widely used needles. Geometric differences in the needles effect variations in their electric field and current distributions. Further investigations may suggest needle modifications that result in a reduction of initial probing failures.

*This work was supported in part by the NSF through DMR-0305371 and by the University of Florida through the University Scholars and the Alumni Fellows Programs.

## SESSION A30: FOCUS SESSION: BLOCK COPOLYMER DYNAMICS
**Monday Morning, 13 March 2006; 327, Baltimore Convention Center at 8:00**
**Nitash Balsara, University of California, Berkeley, presiding**

***Invited Papers***

**8:00**
**A30 1 A Renormalized Theory of Composition Fluctuations in Polymer Mixtures.**
DAVID MORSE, *University of Minnesota*

Attempts to calculate corrections to Flory-Huggins theory using field theoretic methods have been plagued by an unwanted sensititivity to very short wavelength fluctuations, or to the value of an arbitrary cutoff length. This reflects the fact that the total free energy of a polymer mixture is dominated by effects of local fluid structure. Z.-G. Wang [1] has shown how the cutoff-dependence of a one-loop approximation for the free energy of a binary blend can be absorbed into

an expression for the experimentally observed $\chi$ parameter, yielding a cutoff-independent renormalized theory of the contributions of mesoscopic fluctuations. We apply an analogous renormalization procedure to one-loop calculations of intramolecular and collective correlation functions at arbitrary wavenumbers in both homopolymer blends and copolymer melts, in which the dependence on local fluid structure is absorbed into the values of $\chi$ and of statistical segment lengths. We discuss predictions for homopolymer blends and diblock copolymer melts, and relationships to earlier work. [1] Z.-G. Wang, J. Chem. Phys. 117, 481 (2002).

*Contributed Papers*

**8:36**

**A30 2 An efficient pseudo-spectral algorithm for the RPA response of ordered phases of block copolymer melts** AMIT RANJAN, DAVID MORSE, *Department of Chemical Engineering and Materials Science, University of Minnesota* We present a pseudo-spectral algorithm for calculating the linear response of monomer concentration field in ordered phases of block copolymer melts to small perturbations of the monomer chemical potential fields. The method is both considerably simpler and more efficient than the fully spectral perturbation theory presented by Laradji, Shi and coworkers.[1] The method will be used to re-examine the stability of the gyroid phase in diblock copolymer melts. [1] Laradji *et al.*, *Macromolecules*, **30**, 3242 (1997).

**8:48**

**A30 3 Random isotropic structures and possible glass transitions in diblock copolymer melts** CHENGZHONG ZHANG, ZHEN-GANG WANG, *Chemical Engineering, Caltech* We study the microstructural glass transition in diblock-copolymer melts using a thermodynamic replica approach. Our approach performs an expansion in terms of the natural smallness parameter – the inverse of the scaled degree of polymerization $\bar{N}$, which allows us to systematically study the approach to mean-field behavior as the degree of polymerization increases. We find that in the limit of infinite chain length, both the onset of glassiness and the vitrification transition (Kauzmann temperature) collapse to the mean-field spinodal, suggesting that the spinodal can be regarded as the mean-field signature for glass transitions in this class of microphase-separating system. We also study the order-disorder transitions (ODT) within the same theoretical framework; in particular, we include the leading-order fluctuation corrections due to the cubic interaction in the coarse-grained Hamiltonian, which has been ignored in previous studies on the ODT in block copolymers. We find that the cubic term stabilizes both the ordered (body-centered-cubic) phase and the glassy state relative to the disordered phase. In melts of symmetric copolymers the glass transition always occurs after the order-disorder transition (below the ODT temperature), but for asymmetric copolymers, it is possible for the glass transition to precede the ordering transition.

**9:00**

**A30 4 Dynamics of PEO-PMMA diblock copolymers.** JAVIER SACRISTAN, CHUNXIA CHEN, JANNA MARANAS, *Department of Chemical Engineering, The Pennsylvania State University, University Park, Pennsylvania 16802* The structure and dynamics of a poly(ethylene oxide)–poly(methyl methacrylate) diblock copolymer (PEO-PMMA) are studied by molecular dynamics simulation using a united atom model, with emphasis on the junction point effect. These results are compared to those from a homopolymer blend. The intermolecular pair distribution function reveals that the internal packing of unlike segments is enhanced in the copolymer with respect to the blend. Thus the effective concentration of both PEO and PMMA decay towards the bulk faster as a function of local volume size in the copolymer than in the blend. The mean square displacement (MSD) illustrates differing mobilities of PEO and PMMA in both systems. In the copolymer, their mobilities are separated by less than in the blend. The junction point accelerates motion of PMMA up to a distance of 5A. In contrast, on both systems PEO mobility reach the average value close to the junction point. In spite of the different PMMA effective concentration on both systems copolymer and blend its dynamics are not affected by changes in local packing. In contrast PEO dynamics are strongly influenced by the differences on its effective concentration.

**9:12**

**A30 5 Kinetics of Transition between HEX and Lamellar Phases in a triblock copolymer solution in a selective solvent.** YONGSHENG LIU, RAMA BANSIL, *Boston University* MILOS STEINHART, *Institute of Macromoleculear Chemistry, Academy of Sciences of the Czech Republic* Synchrotron based time-resolved small angle x-ray scattering (SAXS), was used to study the kinetics of ordering transition (OOT) between cylindrical micelles in HEX phase and lamellar (LAM) phase in a 0.4 (w/v) solution of a triblock of polystyrene (PS) and poly(ethylene-itco-butylene) (PEB), SEBS (PS-PEB-PS) copolymer in Dibutyl Phthalate (DBP), a selective solvent for the PS block. From a temperature ramp experiment the OOT was identified at about 137C and an ODT above 160 C. Several temperature jump experiments from HEX to LAM and the reverse were performed over the temperature range of 110-155C. Detailed analysis of the time evolution of the intensities of the Bragg peaks to follow the kinetics of the transition between HEX and LAM phases will be presented. A model to explain the transition mechanism will be discussed. This research was supported by NSF-DMR.

**9:24**

**A30 6 Kinetics of HEX-BCC Transition of Cylinders to Spheres: Comparison of Time-resolved SAXS data with a Model of Coupled Anisotropic Fluctuations*** RAMA BANSIL, MINGHAI LI, *Boston University* MILOS STEINHART, *Institute of Macromolecular Chemistry, Czech Academy of Sciences* The kinetics of the transition of HEX cylinders to BCC spheres was studied by coupling anisotropic fluctuations on cylinders, similar to the pearling instability, according to which the amplitude of a transverse wave along the length of the cylinder grows causing the cylinder to break up into spheroidal droplets. We find that the sphere BCC phase arises with phase shifts of 0, **it4$\pi$/3** and **it8$\pi$/3** for the sinusoidal waves on 3 neighboring cylinders on the HEX lattice, which correspond to the minimum of overlap volume of rippled cylinders and wavelength it$\lambda$ related to the nearest neighbor distance of the rippled cylinders by $d = 2\sqrt{2}\lambda/3$. The azimuthally averaged scattering function from an un-oriented system of cylinders, as well as the 2-dimensional scattering from an oriented system was calculated with varying amplitude of the fluc-

tuation. The results are in excellent agreement with time-resolved SAXS measurements of the kinetics of this transition in a Styrene (S)-ethylene-co-butylene (EB)-Styrene (S)) triblock copolymer in mineral oil, a selective solvent for the EB block.

*Supported by NSF-DMR

**9:36**

**A30 7 Modeling of twist grain boundaries in block copolymers: structure, stability, and motion** XUSHENG ZHANG, ZHI-FENG HUANG, JORGE VINALS, *McGill University* Twist grain boundaries, which are widely observed in block copolymer samples of lamellar phase, have been investigated through both direct numerical solution and multiscale analysis of a coarse-grained mesoscopic model equation. We show that the twist boundary profile can be well described by two sets of appropriate amplitude equations characterizing the slow evolution of lamellae. Stability of the grain boundary configuration has been examined, and our results show that the boundary width, albeit varying with twist angle, is of order $\epsilon^{-1/4}$, with $\epsilon$ the measure of the distance from the order-disorder threshold. We also study the motion of twist grain boundaries subjected to slow transversal modulations of lamellae, and obtain both analytically and numerically the traveling velocity of the boundary as well as its dependence on modulation wave number.

**9:48**

**A30 8 Removal of non-equilibrium microdomain defects in block copolymer thin film simulations** AUGUST BOSSE, *University of California, Santa Barbara* SCOTT SIDES, *Tech-X Corporation* KIRILL KATSOV, CARLOS GARCIA-CERVERA, GLENN FREDRICKSON, *University of California, Santa Barbara* In recent years, there has been increased interest in using microphase-separated block copolymer thin films as sub-optical lithographic masks in next generation semiconductor and magnetic media fabrication. However, if such techniques are to evolve into a useful and commercially feasible lithographic tool, one must have control over, or at least an understanding of the in-plane ordering of the block copolymer microdomains. In the context of self-consistent field theory (SCFT), we introduce new simulation techniques intended to efficiently remove non-equilibrium microdomain defects in 2D block copolymer simulations, and thus allow further study of equilibrium defect populations associated with 2D systems (cf., KTHNY theory) and/or defects induced by confinement. The first technique, which we call *spectral amplitude filtering*, is used in parallel with a saddle point relaxation algorithm. Spectral amplitude filtering zeros out all Fourier components with amplitude below some fraction of the maximum amplitude. This encourages symmetries associated with the dominant Fourier modes to rapidly set in. The other technique is a variation on a force-biased, Fourier-accelerated Monte Carlo algorithm, which is shown to be efficient in controlled removal of non-equilibrium microdomain defects.

**10:00**

**A30 9 Mixed Lamellae in Symmetric Diblock Copolymer Thin Films** DONG MENG, QIANG WANG, *Colorado State University* For symmetric diblock copolymers confined between two flat and homogeneous surfaces, three morphologies (parallel, perpendicular, and mixed lamellae) have been obtained in experiments. While the effects of surface preference (for one of the two blocks) and film thickness on the thin-film morphology are well understood, less studied is the influence of a hard (impenetrable) surface on the copolymer chain conformations, referred to as the ''hard-surface effect.'' It is this effect that favors the perpendicular lamellae between two neutral surfaces over parallel lamellae, at all film thicknesses. It also leads to the formation of mixed lamellae between asymmetric surfaces. Here we use the self-consistent field (SCF) theory in continuum to study the morphology of mixed lamellae. The SCF equations are solved in real space with high accuracy. Results under different boundary conditions (zero-density vs. non-flux) are compared to examine their effects on the copolymer chain conformations near the surface. We also study in detail the chain conformations at the T-junction in the mixed lamellae. Conditions under which the mixed lamellae are a stable phase (over parallel and perpendicular lamellae) are determined, and compared with experiments and Monte Carlo simulations.

**10:12**

**A30 10 Correlated defect dynamics in block copolymer melts*** ROBERT MAGERLE, *Technische Universitaet Chemnitz* LARISA TSARKOVA, ARMIN KNOLL, *Universitaet Bayreuth* With in-situ scanning force microscopy we image the ordering of cylindrical microdomains in a thin film of a diblock copolymer melt. Tracking the evolution of individual defects reveals their annihilation pathways via interfacial undulations and formation of transient phases, such as spheres and lamella. Repetitive transitions between distinct defect configurations suggest a cooperative movement of chain clusters. The microdomain dynamics is correlated on a length scale of several domain spacings. Characteristic times of structural relaxations range from $\sim$ 1 to $\sim$ 100 min.

*Supported by Deutsche Forschungsgemeinschaft (SFB 481)

**10:24**

**A30 11 Dislocation Density and Orientational Order of Spherical Microdomains in Shear-Aligned Block Copolymer Thin Films** ANDREW MARENCIC, MINGSHAW WU, RICHARD REGISTER, *Princeton University* PAUL CHAIKIN, *New York University* Studies of annealed monolayers of cylindrical diblock copolymers (striped patterns) showed that the disclination density dictated the orientational correlation length. Here we test the role of dislocations in the orientational order of shear aligned hexagonal patterns. Shearing block copolymer thin films using a viscous fluid overlayer creates long-range orientational order of the microdomains, extending over a centimeter or more, by eliminating grain boundaries. However, some isolated dislocations remain that perturb the both translational and local orientational order of the hexagonal lattice formed by the spherical microdomains in these thin films. Atomic force microscopy was used to image the lattice, and image analysis software was written to determine dislocation density and alignment quality using an orientational order parameter. In such shear- aligned films, a linear relationship between the density of isolated dislocations and the orientational order parameter was found.

**SESSION A31: METALLIC NANOSTRUCTURES**
**Monday Morning, 13 March 2006**
**328, Baltimore Convention Center at 8:00**
**Michael Haftel, Naval Research Laboratory, presiding**

**8:00**

**A31 1 Gold Nanorod/Single-Wall Carbon Nanotube Heterojunctions Formed Directly on Surfaces** ROMANEH JALILIAN, *University of Louisville, Department of Physics* ANETA MIESZAWSKA, FRANCIS ZAMBORINI., *University of Louisville, Department of Chemistry* GAMINI SUMANASEKERA, *University of Louisville, Department of Physics* In this presentation we describe work on the formation of heterojunctions between single-wall carbon nanotubes (SWNTs) and one-dimensional (1D) gold nanorods (AuNRs) assembled directly on surfaces. The chemical procedure is a simple benchtop method using commercially available reagents. Au NRs are grown directly and selectively on surface-attached SWCNTs by depositing hexanethiolate-terminated Au monolayer protected clusters (MPCs) on the SWCNTs and growing Au MPCs into NRs by seed-mediated growth, involving reduction of $AuCL_4^-$ onto Au MPCs in the presence of cetyltrimethylammonium bromide (CTAB). UV-vis, AFM, and SEM show highly selective growth of Au on SWCNTs only. Different combinations of junctions are possible, including AuNRs connecting two CNTs or two AuNRs attached to one CNT. We also show that Au nanostructures enhance Raman scattering of SWNTs. Several NRs and CNTs integrated into a connected assembly were studied. Electrical measurements with contacts on the AuNRs of these heterostructures will be presented. Finally carbon-supported metal structures with unique size and shape may be useful in electrocatalysis or electrochemical sensing applications.

**8:12**

**A31 2 Formation of Silver Nanostructures (nanowires, nanoshells, and nanorods) on MgZnO hexagonal and Cubic Alloys** SHIVA HULLAVARAD, TA KUN CHEN, R. VISPUTE, T. VENKATESAN, *University of Maryland* With potential applications in many fields from fundamental science to engineering technology, multi-dimensional (MD) metal nanostructures such as nanowires, nanoshells, and nanotubes have been very popular topics of research. They have been used to experimentally probe the effects of quantum confinement on electronic, magnetic, and other related properties, and they could be used as active components or interconnects in fabricating electronic, photonic, and sensing devices. Silver nanowires are particularly interesting to explore because bulk silver exhibits the highest electrical and thermal conductivities among all metals. Other modern applications of silver nanowires have also been discovered in many fields including catalysis, electronics, photonics, and photography. In this study, we present the formation of silver nanowires, shells and rods by the thermal reduction of an aqueous silver nitrate solution on the surface of Magnesium Zinc Oxide ($Mg_xZn_{1-x}O$) multiphase alloy thin films. In this context, the formation of silver nanostructures on MgZnO alloy films is technologically important as it would lead in to the potential area of nano metallic contacts to emerging oxide electronic materials.

**8:24**

**A31 3 Oxygen clamps in gold nanowires.** ANTÔNIO J. R. DA SILVA, FREDERICO D. NOVAES, EDWIN HOBI JR., A. FAZZIO, *Instituto de Física, Universidade de São Paulo* EDISON Z. DA SILVA, *Instituto de Física ''Gleb Wataghin,'' UNICAMP* We investigate how the insertion of an oxygen atom in an atomically thin gold nanowire can affect its rupture. We find, using itab initio total energy density functional theory calculations, that O atoms when inserted in gold nanowires form not only stable but also very strong bonds, in such a way that they can extract atoms from a stable tip, serving in this way as a clamp that could be used to pull a string of gold atoms (see Novaes et al., Phys. Rev. Lett. 2006). In all calculations we have used a GGA-PBE approximation and norm-conserving pseudopotentials. All calculations were performed using the SIESTA code, and we employ a DZP basis function. We observe that the presence of O atoms increases the stability of a local configuration composed of the O atom and its two nearest neighbors at each side (an Au-Au-O-Au-Au structure). This indicates that in an oxygen reach atmosphere it may be possible to pull a longer string of gold atoms (an effect as predicted here has been observed by W. H. A. Thijssen et al., cond-mat/0509376). Finally, local vibrational modes will be investigated.

**8:36**

**A31 4 Phase transitions in escape processes of metal nanowires*** JÉRÔME BÜRKI, *University of Arizona* CHARLES STAFFORD, *University of Arizona* DANIEL STEIN, *New York University* Thermally induced conductance jumps of metal nanowires are modeled using stochastic Ginzburg-Landau field theories. The activation rate displays nontrivial dependence on nanowire length, and undergoes first- or second-order-like transitions, with a critical length proportional to the wire radius. Several experimental manifestations of the predicted phase transition are identified, including the temperature- and radius-dependence of peak heights in conductance histograms, and the length dependence of I-V characteristics of gold nanowires.

*This work was supported by NSF Grant Nos. 0312028 and 0351964.

**8:48**

**A31 5 Stability of metal nanowires with multipolar cross sections** CHARLES STAFFORD, *University of Arizona* HAKAN TÜRECI, *Yale University* JÉRÔME BÜRKI, *University of Arizona* DANIEL URBAN, *Albert-Ludwigs University, Freiburg, Germany* HERMANN GRABERT, *Albert-Ludwigs University, Freiburg, Germany* DOUGLAS STONE, *Yale University* A linear stability analysis of metal nanowires with arbitrary cross sections is performed within the nanoscale free-electron model, focusing on quadrupolar, hexapolar, and octopolar deformations. Families of stable wires with similar cross sections and various dimensions are found, which are stabilized semiclassically in the vicinity of bifurcations of important classical periodic electron orbits. For large deformations, quadrupolar cross sections are found to be most favorable. The predicted highly-deformed stable structures are compared to experimental data for Aluminum nanowires.

**9:00**

**A31 6 Mechanical testing of slanted and isolated copper nanorods using Atomic Force Microscope*** C. GAIRE, D.-X. YE, T.-M. LU, G.-C. WANG, *Dept. of Physics, Rensselaer Polytechnic Inst, Troy, NY 12180* C. R. PICU, *Dept. of Mechanical, Aerospace and Nuclear Engg, Rensselaer Polytechnic Inst, Troy, NY,*

*12180* Recently, the study of mechanical properties of sub-micron and nano-scale specimen has drawn a renewed attention. With the atomic force microscope (AFM) it is possible to probe the mechanics of these structures. Here we report one such test to find the force constant, Young's modulus and yield stress of a new type of nanostructures - polycrystalline Cu slanted nanorods of approximately rectangular cross section, fixed at one end to the substrate. These were grown by oblique angle physical vapor deposition. An AFM was used to image, locate the rod and apply force to get deflection at its free end as a function of applied force. Samples with different dimensions and rise angles were tested in bending using this technique. The method employed by our group for fabrication as well as the mechanical testing will be discussed and a comparison of the mechanical properties of the bulk and nanoscale specimen will be made based on our results. *Supported by NSF grant No. CMS-0324490.

**9:12**

**A31 7 Electron Transport through curved and rolled Two Dimensional Electron Gas** NAKUL SHAJI, *Univeristy of Wisconsin-Madison* HUA QIN, LEVENTE KLIEN, MARK ERIKSSON, ROBERT BLICK, CHRISTOPHER DENEKE, *Max-Plank-Institut für Festkörperforschung* OLIVER SCHMIDT, We report on topology dependent electron transport in tubular shaped two-dimensional electron gases. These micron-sized tubes are realized in a strained InGaAs quantum well. This is the first step towards investigating geometric potentials in low dimensional quantum systems. We investigate magneto-resistance of the tubular systems in a perpendicularly applied magnetic field. At low magnetic field, an increased zero field magneto resistance followed by a negative magneto resistance is observed. We ascribe this effect to an increase in electron scattering along the curved regions due to newly formed dangling bonds. At high magnetic fields we observe a linear increase in resistance of the curved region as compared to planar regions.

**9:24**

**A31 8 Intensity-Intensity correlations of waves propagating in disordered quasi-one-dimensional geometries** GABRIEL CWILICH, *Department of Physics, Yeshiva University* LUIS S. FROUFE-PEREZ, JUAN JOSE SAENZ, *Departamento de Fisica de la Materia Condensada, Universidad Autonoma de Madrid* Spatial intensity correlations between waves transmitted through random media are analyzed within the framework of the random matrix theory of transport. Assuming that the statistical distribution of transfer matrices is isotropic, we found that the spatial correlation function of the normalized intensity can be expressed as the sum of three terms, with distinctive spatial dependences. This result coincides with the one obtained in the diffusive regime from perturbative calculations, (Patrick Sebbah et al in Phys. Rev. Lett. 88, 123901,(2002)) but holds all the way from quasi-ballistic transport to localization. Only the specific value of the prefactors depends on the transport regime. Their values obtained from the Monte Carlo solution of the Dorokhov, Mello, Pereyra, and Kumar (DMPK) scaling equation are in full agreement with microscopic numerical calculations of bulk disordered wires. The experimental and numerical results are recovered in the large-N (number of propagating channels)limit in Random Matrix theory. While correlations are positive in the diffusive regime, we predict a transition to negative correlations as the length of the system decreases.

**9:36**

**A31 9 Manipulation of nanowires in suspension by ac electric fields** D.L. FAN, F.Q. ZHU, R.C. CAMMARATA, C.L. CHIEN, *Johns Hopkins University* While highly desirable for nanoscale devices, manipulation of nanoentities in suspension has been a formidable problem because of the extremely low Reynolds number at the level of $10^{-5}$. In this work, we show that nanowires a few m in length can be efficiently manipulated by ac electric fields applied to strategically designed microelectrodes. The nanowires, both magnetic and non-magnetic, can be driven to align, to chain, to accelerate in directions parallel or perpendicular to the nanowires orientation. The nanowires can also be patterned into desired structures with high efficiency. This versatile method of manipulation has also been applied to other small elongated entities such as carbon nanotubes.

**9:48**

**A31 10 On the Formation of Monatomic Metal Wires** A. HASMY,* *NIST Center for Theoretical and Computational Nanosciences, Gaithersburg,MD* R. HERNANDEZ, *Escuela de Quimica, UCV, Caracas, Venezuela* L.C. RINCON, *Dpto. de Quimica, ULA, Merida, Venezuela* V. MUJICA, *Escuela de Quimica, UCV, Caracas, Venezuela* R.J. MAGYAR, C. GONZALEZ, *NIST Center for Theoretical and Computational Nanosciences, Gaithersburg,MD* The formation of monatomic metal wires under stress has been observed with HRTEM. It has been revealed that gold chains can be obtained if the stress is applied on the (111) and (100) orientations, while not on the (110) orientation. Other experiments have evidenced that some metals are unable to exhibit this monatomic wire formation. Theoretical efforts addressed to determine what are the geometrical and chemical conditions for such monatomic chain formations is still lacking in the literature. We have implemented Tight-Binding Molecular Dynamics simulations for the formation of metallic wires under stress, making special attention to the dynamics at the end of the contact breakage. Different geometrical orientations and chemical elements were considered. In order to determine the evolution of the electronic structure the simulations were complemented with ab initio calculations of the atomic configurations. The study allows us to give some insights about the required conditions for the formation of such monatomic metal wires.

*Also: INEST Group, PMUSA, Richmond, VA

**10:00**

**A31 11 Quantum confinement between self-organized Pt nanowires on Ge(001)** NURI ONCEL, ARIE VAN HOUSELT, JEROEN HUIJBEN, WOUTER J. VAN BEEK, ANN SOFIE HALLBÄCK, HAROLD J.W. ZANDVLIET, BENE POELSEMA, *University of Twente, MESA + Institute for Nanotechnology, Solid State Physics Group* Annealing of Pt covered Ge(001) surface leads to formation of one atom thick, hundreds of nanometers long, literally defect free chains of Pt atoms, hereafter named as Pt nanowires. By using scanning tunneling spectroscopy (STS) we have discovered one dimensional (1D) electronic states, confined between these Pt nanowires. The nanowires are separated by either 1.6 or 2.4 nm. The Pt atoms create a potential barrier for the surface state electrons on modified Ge-terraces located just below the Fermi level. The peak positions obtained from I-V spectroscopy experiments are in good agreement with the eigenvalues of a quantum mechanical particle in box problem. The spatial mapping of the differential conductivity of the 1D states reveals that the states are confined in the troughs between the nanowires.

As an additional proof, we performed careful analysis of the regions, where either the nanowires or the underlying substrate have defects. This analysis clearly shows that the confined states around the defect sites fade away, i.e. the electron states ''leak'' out of the trough via the defects.

**10:12**

**A31 12 Hall of Mirrors Scattering from Impurities in Quantum Waveguides** J. Y. VAISHNAV, *Harvard University Department of Physics* A. ITSARA, *Harvard College* E. J. HELLER, *Harvard University Department of Physics and Harvard University Department of Chemistry and Chemical Biology* We develop a scattering theory to examine how a point impurity affects transport through multimode quantum wires. While some of our new results apply specifically to hard-walled wires, others are more general; for example, an effective optical theorem which we derive for two- dimensional waveguides. Using the method of images, we examine the hard-walled guide, explicitly showing the effect of each reflection from the impurity on the wire's conductance. We express the effective cross section of a confined s-wave scatterer entirely in terms of the empty waveguide's Green's function, suggesting a way in which to use semiclassical methods to understand transport properties of smooth wires. In addition to predicting some new phenomena, our approach provides a simple physical picture for previously observed effects such as conductance dips and confinement-induced resonances. We discuss generalizations of this work to include higher partial waves, as well as the case of two interacting particles confined in other geometries, such as nanotubes and tori.

**10:24**

**A31 13 A fine-scale nanostructure in $\gamma$-alumina*** GIANLUCA PAGLIA, EMIL BOZIN, SIMON BILLINGE, *Department of Physics and Astronomy, Michigan State University, Biomedical Physical Sciences, East Lansing, MI, 48824-2320* Despite the preeminent industrial importance of $\gamma$-alumina in catalysis, details of the structure remain unresolved due to its 15-30$\sim$ nm domain nanocrystalline nature. Diffraction patterns are broad and single crystals are not available making accurate structural solution difficult using conventional crystallographic methods. We have applied a local structural technique, the atomic pair distribution function (PDF) analysis of powder diffraction, to obtain a quantitative structure. This is a total scattering technique that incorporates both Bragg and diffuse scattering information in the PDF, allowing all diffracted intensities from the XRD pattern to be equally considered. Surprisingly, we find a previously unknown fine-scale nanostructure with a domain size $\sim$ 1 nm. Within these nanodomains the oxygen sublattice is modified from the average structure and retains aspects of the boehmite precursor. This results in a novel and unexpected view of the $\gamma$-alumina structure since earlier controversies about it centered on the arrangement of Al ions among different cation sites, whereas the oxygen sublattice arrangement was not usually questioned.

*The work at MSU was funded under National Science Foundation (NSF) grant no. CHE-0211029. X-ray data were collected at beamline 6IDD of the Advanced Photon Source at Argonne National Laboratry.

**10:36**

**A31 14 Conversion of CDW $TaS_3$ to superconducting $TaS_2$ nanowires** YEW SAN HOR, TAO WU, JOHN F. MITCHELL, *Materials Science Division, Argonne National Laboratory, Argonne, Illinois 60439* PETER L. LEE, *Advanced Photon Source, Argonne National Laboratory, Argonne, Illinois 60439* The synthesis of nanowires has attracted considerable interest for their potential applications in many areas of advanced nanotechnologies. Recently we have developed a simple method to fabricate nanowires of a transition metal dichalcogenide through a nondestructive reduction from one-dimensional (1D) trichalcogenide nanostructures.[1] In this report, we present results on synthesis and characterization of $TaS_2$ nanowires. Our approach includes the synthesis of 1D charge-density-wave (CDW) $TaS_3$ nanostructure precursors followed by the nondestructive and controlled adjustment of the S composition. The nanowires, as identified with scanning electron microscopy, have a rectanglelike cross section with widths of 20 to 700 nm and lengths of up to a few millimeters. $TaS_3$ nanowires show the canonical CDW behaviors. However, the converted $TaS_2$ nanowires show superconducting behavior with Tc $\sim$ 4 K, which is different from the bulk property. [1] Appl. Phys. Lett. 87, 142506 (2005).



**SESSION A32: FULLERENES**
**Monday Morning, 13 March 2006**
**329, Baltimore Convention Center at 8:00**
**Tunna Baruah, University of Texas, El Paso, presiding**

**8:00**

**A32 1 The measuring the conductance of carbon fullerene and onion.** MAKOTO YOSHIDA, YOSHIHIKO KURUI, YOSHIFUMI OSHIMA, KUNIO TAKAYANAGI, *Tokyo Institute of Technology Department of Physics* TOKYO INSTITUTE OF TECHNOLOGY DEPARTMENT OF PHYSICS TEAM, In this study, we simultaneously observed the conductance and the structure of carbon nano-materials (C60 and carbon onion) using transmission electron microscopy(TEM). This TEM is combined with scanning tunneling microscope (STM) system. C60 and carbon onion was fabricated and sandwiched between two gold electrodes of STM. As a results, the C60 and carbon onion show a metallic conductance (the same order magnitude of $2e^2/h$) at the low bias. These values are near to results of previous theoretical reports. Further more, we obtained the conductance variation which is strongly affected by the connection between the C60 and metal electrodes.

**8:12**

**A32 2 On the zero-bias anomaly in K-doped $C_{60}$ on Ag(100)** NOAH BRAY-ALI, AMY KHOO, *Department of Physics, UC Berkeley* JEFFREY NEATON, STEVEN LOUIE, *Department of Physics, UC Berkeley and the Molecular Foundry, Lawrence Berkeley National Laboratory* RYAN YAMACHIKA, ANDRE WACHOWIAK, MICHAEL CROMMIE, JOEL MOORE, *Department of Physics, UC Berkeley and the Materials Science Division, Lawrence Berkeley National Laboratory* The fullerene molecule $C_{60}$ is known to undergo a strong Jahn-Teller distortion when electrons are added. Recent STM/STS experiments indicate that a single $C_{60}$ molecule on a Ag(100) surface can be control-

lably doped with charge-donating potassium atoms; [1] moreover, the experiments suggest that the molecular electronic structure can be tuned so that a single electronic orbital lies near the Fermi level. Starting from a Hamiltonian with parameters inferred from companion density functional theory (DFT) calculations of $K_xC_{60}$ on Ag(100), we use Wilson's numerical renormalization group to compute the spectrum near the Fermi level of a doped $C_{60}$ molecule coupled to a metallic continuum. The result compares favorably with spectroscopic measurements of the zero-bias anomaly and, together with the DFT calculations, explains the electronic structure of this system over a range of dopings. [1] R. Yamachika, M. Grobis, A. Wachowiak, and M.F. Crommie, *Science* **304**, 281-284 (2004).

**8:24**

**A32 3 Ab initio modeling of STM elastic and inelastic tunneling spectra of tetramantane on Au(111) surface.** EMMANOUIL KIOUPAKIS,*R. YAMACHIKA, Y. WANG, X.H. LU, *Department of Physics, University of California at Berkeley* M.F. CROMMIE, STEVEN G. LOUIE, *Department of Physics, University of California at Berkeley and Materials Sciences Division, Lawrence Berkeley National Laboratory* The recent discovery of the higher diamondoids in crude oil has stimulated interest in their study and several potential technological applications of these molecules have already been proposed. In studying the electronic properties of molecular or nanoscale structures on surfaces, the scanning tunneling microscope is usually the probe of choice. Currently, scanning tunneling microscopy experiments of isolated tetramantane molecules on a (111) gold surface are being carried out. We have performed ab initio pseudopotential density functional theory calculations of the electronic properties of tetramantane and provide a comparison of the elastic and inelastic tunneling spectra between our simulation and the ongoing experiment. This work was supported by the NSF Grant Nos. DMR04-39768 and EEC-0425914 and U.S. DOE Contract No. DE-AC03-76SF00098.

*Fellow of the Onassis Foundation

**8:36**

**A32 4 Anomalous electric conductivity in C60-Ag co-deposited films at low temperature** GENKI YOSHIKAWA, *IMR, Tohoku University; The University of Tokyo* YUKI TSURUMA, SUSUMU IKEDA, KOICHIRO SAIKI, *The University of Tokyo* The C60-Ag interface has attracted interest recently. In addition to charge transfer from Ag to C60 or metallization of C60, temperature dependent gap was observed at the Fermi level of the C60 monolayer on Ag, suggesting the possibility of interfacial superconductivity. In order to clarify the effect of this interfacial electronic state on the transport properties, we measured the electric conductivity of the C60-Ag complex films. To increase the interface area, Ag and C60 were co-deposited on the insulating substrate, such as mica, maintained at 23 K, suppressing the aggregation of Ag atoms. The electric conductivity of the C60-Ag co-deposited films was measured in-situ in a temperature range of 23-300 K. Two peaks were observed in the conductivity curve around 50 K and 85 K. They disappeared once the film was annealed up to room temperature. This phenomenon was observed when the Ag/C60 ratio is approximately 1 to 6 while we studied in the range of 0.5-20. We confirmed that these peaks were not caused by the influence of Joule heating or residual gases. The observed anomalous electric conductivity strongly suggests the formation of peculiar structure and electronic states in the films at low temperature.

**8:48**

**A32 5 Novel orientational ordering in a K-doped $C_{60}$ monolayer** RYAN YAMACHIKA, YAYU WANG, ANDRE WACHOWIAK, MICHAEL GROBIS, DUNG-HAI LEE, AMY KHOO, STEVEN LOUIE, MICHAEL CROMMIE, *Department of Physics, University of California, Berkeley, Materials Sciences Division, Lawrence Berkeley National Laboratory, Berkeley, CA* Orientational ordering, which originates from broken rotational symmetry, is a central feature of a broad range of materials including liquid crystals, quantum magnets, and some biological systems. By doping $C_{60}$ monolayers with alkali impurities, the symmetry of $C_{60}$ molecules can be broken, opening up the possibility for unique two-dimensional molecular orientational ordering. Here we present a scanning tunneling microscopy/spectroscopy study of $K_xC_{60}$ monolayers on Au(111), $x \geqslant 4$. We find novel orientational orderings in the $C_{60}$ monolayers at different doping levels, which coincide with strong variations in the monolayer local density of states. This demonstrates the importance of the interplay between Coulomb repulsion, electron-phonon coupling, electronic quadrupolar interactions, and direct orbital overlap in determining the behavior of fullerene nanostructures.

**9:00**

**A32 6 Study of Trapping Sites for Beryllium Atom in $C_{60}$-Fullerene and Electron Capture for $^7$Be Nucleus.** LEE CHOW, ARCHANA DUBEY, *University of Central Florida, Orlando* GARY S. COLLINS, *Washington State University, Pullman* R.H. SCHEICHER, *Michigan Technological University. Houghton* R.H. PINK, DIP N. MAHATO, T.P. DAS,* *State University of New York at Albany* First-Principles Hartree-Fock studies of Be atom in $C_{60}$-fullerene are being carried out for the trapping sites and electron densities at the $^7$Be nucleus for these sites, the latter expected to be helpful for understanding the significantly higher electron capture rate for $^7$Be as compared to a number of other materials experimentally studied including graphite [1]. Possible trapping sites including those found from Hartree-Fock investigations [2] on muonium (H atom) and additional ones above and below the surface perpendicular to C-C bond centers are being investigated. Results will be presented and discussed. [1] T. Ohtsuki et al, Phys. Rev. Lett. 93, 112501-1 (2004) and references therein. [2] O. Donzelli, T. Briere and T.P. Das, Sol. St. Comm. 90, 663(1994); Indian J. Phys. 67(Spec. Issue), 35(1993).

*Also UCF Orlando

**9:12**

**A32 7 Novel Silicon-Carbon Nanostructures: A DFT Study on the Stability of $Si_{60}C_{2n}$ (n= 3, 10, 12) Clusters.*** A. SRINIVASAN, *University of Texas at Arlington* M.N. HUDA, *University of Texas at Austin* A.K. RAY, *University of Texas at Arlington* In this work, we extend our previous work on $Si_{60}C_{2n}$ (n=1, 2) clusters by the addition of six, twenty and twenty-four carbon atoms on the surfaces of the $Si_{60}$ cages by substitution and inside the cage at various symmetry orientations [1]. The theoretical formalism used is the generalized gradient approximation to density functional theory and full geometry and spin optimizations have been performed using the Gaussian 03 software. For the silicon atom, the Hay-Wadt pseudo-potential with the associated basis set is used for the core and the valence electrons, respectively. For the carbon atom, the Dunning/Huzinaga double zeta basis set is employed. Different electronic properties of these nanostructures will be discussed in detail. The binding energy per atom for these nanostructures increases with the number of carbon atoms, with

the structures having carbon atoms on the surface being more stable. The stability of the nanostructures depends on the orientation of the carbon atoms, as well as on the natures of Si-C and C-C bondings. [1] A. Srinivasan, M. N. Huda and A. K. Ray, Phys. Rev. A, in press; A. Srinivasan and A. K. Ray, J. Nanosci. and Nanotech., in press.

*Work supported, in part, by the Welch Foundation, Houston, Texas (Grant Nos. Y-1525 and F-0934).

**9:24**

**A32 8 What is the Goundstate Structure of Intermediate-sized Carbon Clusters?** M. YU, I. CHAUDHURI, C.S. JAYANTHI, S.Y. WU, *Univ. of Louisville* Recent study on the equilibrium structures of quantum dots of tetravalent semiconductors such as Si clusters revealed that the ground state structures of these clusters with diameters d$<$ 5 nm are icosahedrons comprising of tetrahedral building blocks rather than corresponding bulk-truncated clusters[1]. Among tetravalent semiconductors, carbon is the only element whose atoms could form sp, or $sp^2$ or $sp^3$ bonding configurations, leading to compact, fullerene, and bucky-diamond clusters[2]. It is then natural to raise the question as to what is the ground-state structure for the carbon cluster $C_n$ for a given $n \geqslant 20$? We have recently initiated a preliminary study on the relative stability of carbon clusters $C_n$ with $n$up to 700, using a molecular dynamics scheme based on a self-consistent and environment-dependent Hamiltonian developed at the U. of Louisville in the framework of the linear combination of atomic orbitals[3]. Our preliminary result indicates that in the range of $n$ studied, the carbon fullerene clusters are still the most stable clusters, in contrast to the icosahedral cluster being the ground state structure for a series of discrete $n$ values for the other tetravalent clusters. We will also discuss the other electronic properties of intermediate-sized carbon clusters. This work was supported by the U.S. DOE (DE-FG02-00ER4582). [1] Y. Zhao, itet al**it.,** Phys. Rev. Lett. **93**, 015502 (2004). [2] J. Y. Raty, itet al.**it,** Phys. Rev. Lett. **90**, 037401 (2003). [3] S.Y. Wu, itet. al., itHandbook of Materials Modeling Vo.**l,** p.2935 (2005).

**9:36**

**A32 9 Electronic structure and electron-phonon coupling in carbon diamondoids studied by scanning tunneling microscopy** YAYU WANG, X.H. LU, R. YAMACHIKA, A. WACHOWIAK, E.S. KIOUPAKIS, S.G. LOUIE, M.F. CROMMIE, *Department of Physics, University of California at Berkeley, Materials Sciences Division, Lawrence Berkeley National Laboratory, Berkeley, CA* J.E. DAHL, S.G. LIU, R.M.K. CARLSON, *MolecularDiamond Technologies, ChevronTexaco Technology Ventures, CA* Diamondoids are hydrocarbon molecules with diamond-like cage structures. Their structural complexity and chemical bond tunability make them ideal building blocks for creating novel nanostructures. We have used cryogenic scanning tunneling spectroscopy to examine the electronic structure of individual diamondoid molecules on the Au(111) surface. We observed variations in the filled and empty state local density of states for individual 121-tetramer diamondoid molecule. Despite a large HOMO-LUMO gap ($\Delta >$ 5eV) around the Fermi energy, there exists a strong interaction between the tunneling electrons and the diamondoid C-H stretch mode, as revealed by inelastic tunneling spectroscopy (IETS). We further show that the strength of the electron-phonon coupling has a distinct spatial distribution with the dominant inelastic channel localized to a specific region of the diamondoid molecule.

**9:48**

**A32 10 NMR Probes of the Molecular Orientational Dynamics of the Endohedral Fullerene $Sc_3N@C_{80}$.** JOE MARTINDALE, KRZYSZTOF GORNY, CHARLES PENNINGTON, *Department of Physics, The Ohio State University* PAGE PHILLIPS, STEVEN STEVENSON, *Department of Chemistry and Biochemistry, University of Southern Mississippi* We report NMR lineshapes and spin-lattice relaxation times for both $^{13}C$ and $^{45}Sc$ in the endohedral fullerene $Sc_3N@C_{80}$. The data show rapid reorientation of the molecule with an activated temperature dependence for the motion over the observed temperature range (50 – 350 K). The ratchet to rotator transition found in $C_{60}$ is not observed in $Sc_3N@C_{80}$. The measurements strongly suggest the motion of the encapsulated $Sc_3N$ derives from the reorientational dynamics of the $C_{80}$ cage, however without the $Sc_3N$ being fixed to the cage in the motional narrowing regime.

**10:00**

**A32 11 Towards Implementation of a Solid State Quantum Computer Based on Endohedral Fullerenes** D.V. PELEKHOV, *The Ohio State University* P. BANERJEE, *The Ohio State University* I.H. LEE, *The Ohio State University* K.C. FONG, *The Ohio State University* YU. OBUKHOV, *The Ohio State University* J. MARTINDALE, *The Ohio State University* P. C. HAMMEL, *The Ohio State University* J.P. PHILLIPS, *University of Southern Mississippi* S. STEVENSON, *University of Southern Mississippi* We report on progress investigating the feasibility of fabricating a Solid State Quantum Computer based on endohedral fullerenes (fullerenes containing species with unpaired electron spins). The results of experiments on endohedral fullerene systems using Magnetic Resonance Force Microscopy, conventional Electron Spin Resonance and Scanning Tunneling Microscopy will be presented.

**10:12**

**A32 12 Quasi Small-World Nanomaterials: Quantum Studies*** M.A. NOVOTNY, JEREMY YANCEY, STEVEN GWALTNEY, SERKAN CALISKAN, *Mississippi State U.* We present results for two studies of quasi-small-world nanomaterials [1,2]. These are materials that would have the connectivity governed by small-world (SW) networks. Hence these materials should have both their critical behavior and transport properties governed by mean-field fixed points, not finite-dimensional fixed points. One study utilizes density-functional-theory to obtain reasonable carbon-based molecules that should have the SW property. In particular, several candidates for quasi- SW nanomaterials (or molecules) based solely on carbon will be presented. Trends in the energy per atom of various types of SW nanomaterials and numbers of carbon atoms will be presented. The transmission coefficient and conductivity for related quantum models of SW nanomaterials connected to metal leads will also be presented. [1] M.A. Novotny, et al, J. Appl. Phys, vol. 97, p.10E510 (2005). [2] M.A. Novotny and S.W. Wheeler, Brazilian J. Phys., vol. 34, p. 395 (2004).

*Supported by the NSF.

**10:24**

**A32 13 Dynamics of Bulk vs. Nanoscale $WS_2$: Local Strain and Charging Effects*** J. L. MUSFELDT, S. BROWN, R. D. LUTTRELL, J. CAO, *University of Tennessee, Knoxville* R. ROSENTSVEIG, R. TENNE, *Weizmann Institute of Science, Israel* We measured the infrared vibrational properties of bulk and nanoparticle $WS_2$ in order to investigate the structure- property relations in these novel materials. In addition to the symmetry-

breaking effects of local strain, nanoparticle curvature modifies the local charging environment of the bulk material. Performing a charge analysis on the *xy*-polarized $E_{1u}$ vibrational mode, we find an approximate 1.5:1 intralayer charge difference between the layered 2H material and inorganic fullerene-like (IF) nanoparticles. This effective charge difference may impact the solid-state lubrication properties of nanoscale metal dichalcogenides.

*This work is supported by U.S. Department of Energy.



**10:36**

**A32 14 Collective excitations in concentric metallic nanoshells** SHYAMALENDU BOSE, EDWARD ZALE, *Drexel University* Invention of nanoshells made of a silica core coated with an ultrathin metallic layer [1] has opened a floodgate of many applications in medical and other fields. Most of these applications are triggered by the fact that the nanoshells have unusual electronic and optical properties which can be controlled by controlling the inner and outer radii of the nanoshell. Employing a classical hydrodynamic model, we have obtained a general expression for the resonant frequencies (plasmons) of the electrons for N concentric nanoshells. Results obtained using this theory will be compared with previous calculations for two concentric nanoshells [2] and possible applications of the new results will be discussed. 1. S.J. Oldenburg, et al., Chem. Phys. Letts. **288**, 243 (1998). 2. E. Prodan, et al., Science **302**, 419 (2003).

**10:48**

**A32 15 A $^{13}$C NMR Spectroscopic Investigation of Carbon Nanohorns** HIDETO IMAI, PANAKKATTU BABU, ERIC OLDFIELD, ANDRZEJ WIECKOWSKI, DAISUKE KASUYA, TAKESHI AZAMI, YUICHI SHIMAKAWA, MASAKO YUDASAKA, YOSHIMI KUBO, SUMIO IIJIMA, UNIVERSITY OF ILLINOIS AT URBANA-CHAMPAIGN TEAM, FUNDAMENTAL AND ENVIRONMENTAL RESEARCH LABORATORIES, NEC CORPORATION, JAPAN TEAM, SORST, JAPAN SCIENCE AND TECHNOLOGY AGENCY, C/O NEC TEAM, MEIJO UNIVERSITY, NAGOYA, JAPAN TEAM, $^{13}$C NMR spectroscopic investigation of carbon nanohorn aggregates (CNH) shows that they consist of two components, characterized by different chemical shifts and spin-lattice relaxation ($T_1$) behavior. The first component with a chemical shift of 124 ppm and faster $T_1$ is assigned to the nanotube-like horns on the particles' surface. The second component with a chemical shift of 116 ppm and much slower $T_1$ is assigned to the graphite-like part of the CNH. Integrated peak area measurements indicate a 1:2 ratio of nanohorns to the graphite-like substrate. The lack of a Knight shift and the absence of a clear Korringa relaxation for either component of $T_1$ ruled out any metallic behavior and indicate a relaxation behavior characteristic of semiconducting materials with paramagnetic centers arising from structural defects. We also observed an anomalous change in $T_1$ in the nanohorn domains near 17 K, suggesting the development of an antiferromagnetic correlation between localized electron spins.

## SESSION A33: FOCUS SESSION: ECONOPHYSICS

**Monday Morning, 13 March 2006; 336, Baltimore Convention Center at 8:00**
**Mark Newman, University of Michigan, presiding**

***Invited Papers***

**8:00**

**A33 1 Statistical Mechanics of Money, Income, and Wealth.**
VICTOR YAKOVENKO, *Department of Physics, University of Maryland*

In Ref. [1], we proposed an analogy between the exponential Boltzmann-Gibbs distribution of energy in physics and the equilibrium probability distribution of money in a closed economic system. Analogously to energy, money is locally conserved in interactions between economic agents, so the thermal Boltzmann-Gibbs distribution function is expected for money. Since then, many researchers followed and expanded this idea [2]. Much work was done on the analysis of empirical data, mostly on income, for which a lot of tax and census data is available. We demonstrated [3] that income distribution in the USA has a well-defined two-class structure. The majority of population (97-99%) belongs to the lower class characterized by the exponential Boltzmann-Gibbs (''thermal'') distribution. The upper class (1-3% of population) has a Pareto power-law (''superthermal'') distribution, whose parameters change in time with the rise and fall of stock market. We proposed a concept of equilibrium inequality in a society, based on the principle of maximal entropy, and quantitatively demonstrated that it applies to the majority of population. Income distribution in other countries shows similar patterns. For more references, see http://www2.physics.umd.edu/~ yakovenk/econophysics.html. References: [1] A. A. Dragulescu and V. M. Yakovenko, ''Statistical mechanics of money,'' Eur. Phys. J. B **17**, 723 (2000). [2] ''Econophysics of Wealth Distributions,'' edited by A. Chatterjee, S. Yarlagadda, and B. K. Chakrabarti, Springer, 2005. [3] A. C. Silva and V. M. Yakovenko, ''Temporal evolution of the 'thermal' and 'superthermal' income classes in the USA during 1983-2001,'' Europhys. Lett. **69**, 304 (2005).

*Contributed Papers*

**8:36**
**A33 2 A study of personal income distributions in Australia and Italy** ANAND BANERJEE, VICTOR YAKOVENKO, *Department of Physics, University of Maryland* The study of income distribution has a long history. A century ago, the Italian physicist and economist Pareto proposed that income distribution obeys a universal power law, valid for all time and countries. Subsequent studies proved that only the top 1-3% of the population follow a power law. For USA, the rest 97-99% of the population follow the exponential distribution [1]. We present the results of a similar study for Australia and Italy. [1] A. C. Silva and V. M. Yakovenko, Europhys. Lett.**69**, 304 (2005).

**8:48**
**A33 3 An out-of-equilibrium price model for Gamma-Pareto distributions of wealth and income** NICOLA SCAFETTA, *Duke University* SERGIO PICOZZI, BRUCE J. WEST, The distribution of wealth/income among the members of a society is herein assumed to result from two fundamental mechanisms, trade and investment. An empirical distribution of wealth/income shows an abrupt change between the low-medium range, that may be fitted by a non-monotonic function with an exponential-like tail such as a Gamma distribution, and the high wealth range, that is well fitted by a Pareto or inverse power-law function. We demonstrate that an appropriate trade-investment model, depending on three adjustable parameters associated with the total wealth of a society, a social differentiation among agents, which causes the prices to be out-of-equilibrium, and economic volatility referred to as investment can successfully reproduce the distribution of empirical wealth/income data in the low, medium and high ranges.

**9:00**
**A33 4 Boltzmann–Gibbs distribution of fortune and broken time reversible symmetry in econodynamics** PING AO, *University of Washington* Within the framework of stochastic differential equations it is demonstrated that the existence of Boltzmann–Gibbs type distribution in economy is independent of the time reversal symmetry in econodynamics. Both power law and exponential distributions can be accommodated naturally. The demonstration is based on a mathematical structure discovered during a study in gene regulatory network dynamics. Further possible analogy between equilibrium economy and thermodynamics is explored, suggesting that statistical physics methods can indeed play an important role in the study of complex systems. Ref: 1. P. Ao, **Commun. Nonlinear Sci. Num. Sim. (online September 8, 2005)** Arxiv: physics/0506103

**9:12**
**A33 5 The Inequality Process as a Wealth Maximizing Process** JOHN ANGLE, *Inequality Process Inst., P.O. Box 429, Cabin John, MD 20818-0429* The Inequality Process (IP) is a particle system scattering a positive quantity, wealth. The IP is abstracted from social theory which sets tests for it. It is a jump process in which wealth exchange is driven by a discrete 0,1 uniform random variable. The losing particle, $i$, gives up a fixed proportion of its wealth, $\omega_i$. IP win/loss asymmetry is clearer than in more recent generalizations of the ideal gas model, some isomorphic to the IP up to its stochastic driver. The IP's asymmetry acts like Maxwell's Demon transferring wealth from particles with larger $\omega_i$ to smaller $\omega_i$, those more productive of wealth. While the stationary distribution of the IP is not a gamma pdf, a gamma pdf approximation to it is found from the IP's solution. This gamma pdf model is tightly constrained, expressed in terms of IP parameters, and fits both the IP's stationary distribution and empirical distributions. Annualizing the IP's wealth allows it to model the distribution of wage income conditioned on education in the U.S. 1961-2001. Smaller $\omega_i$ fit the distribution of the more educated, as hypothesized. The IP is also confirmed by the dynamics of individual wage incomes and wealth distributions over techno-cultural evolution. The smaller the harmonic mean of the $\omega_i$'s, the more active the IP's Demon, the less noise and the more $\omega_i$ signal there is in wealth, the ''cooler'' the process. The process models the emergence of skill as a society's primary form of wealth and the reduction in competition that accompanies it. To appear in Physica A.

**9:24**
**A33 6 Econo-Thermodynamics: The Nature of Economic Interactions** JUERGEN MIMKES, *Physics Department, Paderborn University, Germany* Physicists often model economic interactions like collisions of atoms in gases: by interaction one agent gains, the other loses. This leads to a Boltzmann distribution of capital, which has been observed in wealth distributions of different countries. However, economists object: no economic agent will attend a market in which he gets robbed! This conflict may be resolved by writing basic laws of economics into terms of calculus. In these terms the daily struggle for survival of all economic systems turns out to be a Carnot cycle that is driven by energy: heat pumps and economic production depend on oil, GNP and oil consumption run parallel for all countries. Motors and markets are based on the same laws of calculus (macro-economics) and statistics (micro-economics). Economic interactions mean exploiting a third party (nature) and are indeed close to robbing! A baker sells bread to his customers, but the flour comes from nature. Banks sells loans to investors, but the money comes from savers. Econo-thermodynamics is a thrilling new interdisciplinary field.

**9:36**
**A33 7 Correlation between the Gini index and the observed prosperity** IGOR MAZIN, *Georgetown University* It has been well established by computer simulations that a free, unregulated market economy (in the simplest model of a yard sale economy) is unstable and collapses to a singular wealth distribution. It is now a common procedure in computer simulations to stabilize a model by favoring the poorer partner in each transaction, or by redistributing the wealth in the society in favor of the poorer part of the population. Such measures stabilize the economy and create a stationary state with a Gini index $G < 1$. This suggests that there is some optimal range of the Gini index which is indicative of a healthy and dynamic economy. To verify this assumption, I plotted the PPP (parity purchasing power) for all countries in the world against their Gini indices, and found that they all (with only 2 outliers) fall into one of two groups: ''wealthy'' countries with PPP$>$ \$10,000/year, and the rest. The former are characterized by $G = 0.29 \pm 0.07$, and the latter by a uniform distribution of all

possible $G$s. This means that an enforced wealth redistribution is not a moral act of social consciousness, but a necessary precondition for a sustainable economy. The existence of an optimal $G$ is illustrated through a simple model of a yard sale economy with taxation.

**9:48**

**A33 8 Reflection on econophysics by a statistician** SAMUEL KOTZ, *Department of Engineering, George Washington University, DC* Some comments on econophysics from a statistician steeped in income distributions and power law. The pioneering work T. Lux and J. Angle will be discussed, and its connection with the classical approach to income distributions and inequalities will be analized. Special attention will be devoted to tracing the changes in the income inequalities in Russian Federation during the transiton period 1992–2004.

**10:00**

**A33 9 Proposal of a New SI Base Unit for Value. An Hedonic Estimation of the Physical Purchasing Power (PhPP) of Money.** STEIVAN DEFILLA, *Technology, Environment and Energy Policy Division, SECO, Berne* Hitherto, the purchasing power of money, i.e. its transaction value, has been measured in terms of inflation index numbers and consumer baskets. Consumer baskets are variable phenomena and their use as measurement units for value confuses the measuring with the measurand. We propose an invariant numeraire, or value unit, based on the market value of a Planck energy (1956 MJ). Planck units form a natural system of units independent of any civilization. The hedonic estimation of the PhPP of a currency differentiates energy by product as well as by thermodynamic quality (exergy). Following SI rules, we propose to name the value unit walras (Wal) in honour of the economist Leon Walras (1834 - 1910). One Wal can also be interpreted as the minimum cost of physiological life of a reference person during one year. The study uses official disaggregated Swiss Producer and Consumer Price Index data and estimates the PhPP of the Swiss franc in 2003.

**10:12**

**A33 10 Wealth per capita in inhomogeneous wealth distributions model of self-organized hierarchies** MARCELO CASTILLO-MUSSOT, GERARDO NAUMIS, LUIS PEREZ, GERARDO VAZQUEZ-FONSECA, *Instituto de Fisica, UNAM, Mexico* A simple model explained the emergence of social hierarchies through fighting and randomness, and a phase transition between an egalitarian and an hierarchical society was found when the past fights are not forgotten fast enough [1]. Here we include in the model inhomogeneous wealth (water, food, oil, etc.) in the 2D lattice. Agents move randomly except when a preferred rich rich site is nearby. A strong dependence of the global inequality on the distribution of wealth is found, specially in the case when the density of the agents is small. Therefore, the overall phase diagram for the first-order transition between egalitarian and hierarchical societies does change much by inclusion of preferred sites. For low densities of agents with a poor distribution of wealth, it is found that the wealth per capita does not reach its maximum value due to lack of global information of the agents. [1] A. O. Sousa and D. Stauffer, Int. J. Mod. Phys. C, **11**, 1063 (2000).

**10:24**

**A33 11 A Statistical Approach to Project Cost Estimation: Modeling the Stochastic Component of the Projected Cost** DORU VELEA, ANATOLEY ZHELEZNYAK, *Planning Systems Inc., VA* Based on the assumption that there is always a stochastic component in project cost data, we developed a statistical methodology for the analysis of the project cost fluctuations. We considered as examples two different AF projects: a relatively short term project in the framework of the Earned Value Model, and a long-term project in the framework of the traditional accounting. For both data sets we extracted the stochastic component of the project cost fluctuations and found the appropriate statistical description. We calculated the variance on different time scales and established the presence of two statistical regimes: uncorrelated with linear time dependence of variance, and correlated where variance saturates as a function of time. We applied the Ornstein-Uhlenbeck stochastic model and calculated the time scaled parameter of the so-called return force, which characterizes the time period it typically takes for the project cost to return to the estimated value. We predicted the project cost for the near term future and defined the respective cost margins. We formulated criteria for the identification of the potential cost overruns.

**10:36**

**A33 12 Statistical Anomalies of the Project Cost and Stock Market Fluctuations** ANATOLEY ZHELEZNYAK, DORU VELEA, *Planning Systems Inc., VA* Based on the analysis of fluctuations of both project cost and stock market data, we identified some conditions when the statistics significantly depart from conventional distributions such as Heston and Ornstein-Uhlenbeck. Considering the Probability Distribution Functions (PDF) for subsets of fluctuations with the initial conditions corresponding to the extreme fluctuations, we found that the bell-shaped PDFs are gradually distorted and approach the form that is better approximated by the uniform distribution, once the magnitude of initial fluctuations is increased. Similar statistical anomalies were found from analysis of the stock market time series intra-day data. Considering the PDFs for different volumes, we found the similar distortion of the statistical regimes when the large volume transactions occur on the short time intervals, which potentially could be used as a viable tool for identifications of the extreme fluctuations. We believe that the fluctuations could be divided into two classes: the first class covering the majority of fluctuations that obeys the conventional statistical models, and the second class of the fluctuations having the entirely different statistical behavior and possibly belonging to non-Markov processes.

**SESSION A35: FOCUS SESSION: NANOSCALE THERMAL, THERMOELECTRIC AND MASS TRANSPORT: MEASUREMENT AND CHARACTERIZATION**
**Monday Morning, 13 March 2006; 338, Baltimore Convention Center at 8:00**
**Heiner Linke, University of Oregon, presiding**



*Invited Papers*

**8:00**
**A35 1 Nanoscale, phonon-coupled calorimetry with sub-attojoule/kelvin resolution.**
WARREN FON, *Caltech*

We have developed a nanofabricated calorimeter for ultrasensitive heat capacity measurements upon externally-affixed (phonon-coupled) samples at low temperatures. For a 5s measurement at 2K, we demonstrate unprecedented resolution of C of 0.5 aJ/K (approximately 36,000 kB). This sensitivity enables, for example, possible applications such as heat capacity measurements upon zeptomole-scale samples and upon adsorbates at extremely minute coverage. We describe the configuration and operation of these devices, and demonstrate their operation by measuring an adsorbed He4 film with maximum resolution of approximately 3 x 10e-5 monolayers upon the minute device surface area, A approximately 1.2 x 10e-9 m2.

*Contributed Papers*

**8:36**
**A35 2 Thermal relaxation below 1 K by phonons and photons in metallic nanostructures** ILARI MAASILTA, JENNI KARVONEN, PANU KOPPINEN, LASSE TASKINEN, *University of Jyvaskyla, Finland* We present experimental results on thermal energy flow (dissipation) from different metallic nanostructures below 1K, concentrating on the two possible channels: relaxation by phonon or by photon emission. We show how phonon emission can be suppressed either by lowering the dimensionality of the phonon gas (2D membranes), or by introducing impurities into the metal. As an example, we discuss Aluminum doped with Manganese, a material with significant technological importance for ultrasensitive detectors and solid-state coolers. We also discuss relaxation by photon emission in the near field, which becomes siginificant for distances in the sub-micron lengthscale at the sub-Kelvin temperature range. Theoretical understanding for most of the results obtained is still lacking.

**8:48**
**A35 3 Profiling the Seebeck Coefficient of III-V Superlattice Structures with nanometer resolution using Scanning Thermoelectric Microscopy (SThEM)** JIANLONG LI, ALEXANDER KHAJETOORIANS, HO-KI LYEO,*COLIN FOLTA, *The Univ. of Texas at Austin, Dept. of Mech. Engr.* ALI SHAKOURI, *Univ. of California Santa Cruz, Dept. of Elect. Engr., Quantum Electronics Group* LI SHI, *The Univ. of Texas at Austin, Dept. of Mech. Engr.* CHIH-KANG SHIH, *The Univ. of Texas at Austin, Dept. of Physics* Recent theoretical efforts demonstrate that quantum well structures such as superlattices, nanowires, and quantum dots are good candidates for high itZT materials. The ability to probe the thermoelectric properties of these materials on the nanometer scale requires the ability to resolve thermoelectric parameters with high spatial resolution. Recently, Scanning Thermoelectric Microscopy (SThEM) has demonstrated the ability to resolve the Seebeck coefficient and the carrier profile of GaAs $p-n$ junctions with unprecedented spatial resolution (H.K. Lyeo et al itScience v.303 p816 (2004)). By applying this new technique, this work focuses on direct measurement of local thermoelectric power of GaAs/AlAs and GaAs/InGaAs superlattice structures using ultra high vacuum SThEM. We observed that the thermoelectric power in the superlattice region is greatly enhanced. Moreover, oscillations of Seebeck coefficient within the superlattice regions, with a periodicity commensurating with the superlattice structure, are also observed.

*Now at Korea Research Institute of Standards and Science

**9:00**
**A35 4 A modified high-resolution TEM for thermoelectric properties measurements of nanowires and nanotubes** C. DAMES, C. T. HARRIS, *Mechanical Engineering, MIT* S. CHEN, J. Y. HUANG, Z. F. REN, *Physics, Boston College* M. S. DRESSELHAUS, *Physics and EECS, MIT* G. CHEN, *Mechanical Engineering, MIT* Nanowires are interesting candidates for thermoelectric applications because of their potentially low thermal conductivity and high Seebeck coefficient. However, measurements at the single-wire level are challenging and tend to lack detailed information about the atomic-level structure of the sample and contacts. We are modifying a high-resolution transmission electron microscope (HRTEM) with integrated scanning tunneling microscope (STM) for in-situ measurements of thermoelectric properties. A slender Wollaston wire is used to make electrical and thermal contact to the free end of a single nanowire or nanotube. The electrical conductance of the sample can be measured with the usual STM mode of operation. The Seebeck coefficient of the sample can be extracted from the transient voltage response to a step change in the joule heating of the Wollaston wire. These measurements are combined with detailed HRTEM observations.

**9:12**
**A35 5 Bi nanobelts, nanocubes and their thermoelectric properties** WENZHONG WANG, SHUO CHEN, JIANYU HUANG, ZHIFENG REN, *Boston College* T. HARRIS, GANG CHEN, M. DRESSELHAUS, *Massachusetts Institute of Technology* Highly crystallized Bi nanobelts and monodispersed nanocubes have been synthesized via a low-temperature organic solution approach, in which sodium bismuthate was reduced by ethylene glycol in the presence of poly(vinylpyrrolidone) (PVP). By changing some experimental conditions, Bi nanobelts and nanocubes have been prepared successfully. The as-prepared Bi nanobelts are single crystal with high crystallinity. The width of the nanobelts is in the range

of 50-500 nanometers and the length is up to of several tens of micrometers. The as-synthesized Bi nanocubes are highly crystallized and monodispersed with edge length of 50-60 nm. The electrical, thermal, and Seebeck properties of the as-grown nanobelts were studied by a TEM-STM probe inside a high resolution TEM. The same studies were also carried out on bulk samples made by hot-press using the nanocubes.

**9:24**

**A35 6 Bismuth Nanobelts for Enhanced Thermoelectric Performance*** XU ZHAO, MING TANG, GANG CHEN, M. S. DRESSELHAUS, *Massachusetts Institute of Technology, Cambridge, MA* ZHIFENG REN, *Boston College, Chestnut Hill, MA* Bismuth is a semimetal with high promise for thermoelectric applications if it could be made into a semiconductor by a combination of size reduction (based on quantum confinement considerations) and antimony addition. The recent experimental preparation of bismuth Nanobelts has motivated calculation of the phase diagram for the bismuth-antimony system in the regime of nanobelt cross sectional area and antimony concentration where semiconducting behavior is expected. Both direct and indirect bandgap regions are considered and regimes where the highest valence band is at the T-point, the L-point and the H-point are identified. The dependence of the semiconductor-semimetal transition on sample geometry, crystal orientation and temperature will be considered to guide in the preparation of a sample set for use in exploration of this materials system for thermoelectric applications.

*The authors gratefully acknowledge support from the NSF NIRT program CTS-0506830.

**9:36**

**A35 7 Facet-edge fluctuations on finite volume crystallites*** MASASHI DEGAWA, WILLIAM CULLEN, ELLEN WILLIAMS, *Univ. of MD phys dept. MRSEC* Technological demands of the fabrication of nano-structures provide renewed motivation for understanding the atomistic properties that control the morphology changes of nano-structures and nano-crystallites. Using the continuum step model of the thermodynamic correlation function of step fluctuation has proven to be very powerful in such studies. For straight isolated steps on fcc(111) metal surfaces, the principal mass transport mechanism is often found to be periphery diffusion, with time correlations $\sim t^{1/4}$. However with decreasing structure size, issues of finite size and shape effects become non-negligible. When considering facet-edge fluctuations, the normal assumptions of ''straight'' and ''isolated'' do not apply. ''Straight'' is changed to ''curved'' due to finite size, which results in a KPZ term in the equation of motion. ''Isolated'' is changed to ''restricted'' where the amplitude of fluctuation is restricted due to mass conservation, which alters the scaling property of the noise term. Such considerations result in a different universality class of dynamic scaling giving $\alpha=1/3$, $\beta=1/11$ and $z=11/3$. Here we present results of facet-edge fluctuation measurements on Pb crystallites using scanning tunneling microscopy. Results of the temporal correlation function show an exponent different from 1/4, of $0.15\pm 0.02$ at early times, closer to 2/11 predicted for facet-edge fluctuations. *Supported by the UMD NSF-MRSEC, with originating support from DOE-NNI.

**9:48**

**A35 8 Pb-based Nanomaterials for Thermoelectric Application** BED POUDEL, DEZHI WANG, LILI CHEN, WENZHONG WANG, YI MA, ZHIFENG REN, *Boston College* QING HAO, HOHYUN LEE, GANG CHEN, *Department of Mechanical Engineering, MIT* MILDRED S. DRESSELHAUS, *Department of Physics and Department of Electrical Engineering, MIT* PbTe, PbSe, PbSeTe, and PbSnTe nanocrystals having sizes in the range of $\sim$ 5-50 nm have been synthesized using a simple hydrothermal method. As-prepared nanopowder was processed using $P^2C$ device, and samples with almost 100 percent density and small grain sizes were achieved. The thermoelectric properties of such samples have been investigated. Lower values of thermal conductivity were obtained from the samples prepared from nanomaterials. For further enhancement of the thermoelectric properties, the nanocrystals were doped with different elements, for example Ag, Cu, Eu, Bi, Sb, etc., and their thermoelectric properties have been studied.

**10:00**

**A35 9 Nanoscale clusters in the thermoelectric $AgPb_mSbTe_{m+2}$ and $Ag_nSn_mSb_nTe_{m+2n}$ materials*** HE LIN, EMIL BOZIN, KHANG HOANG, S.D. MAHANTI, SIMON BILLINGE, *Department of Physics and Astronomy, Michigan State University* ERIC QUAREZ, JOHN ANDROULA, MERCOURI KANATZIDIS, *Department of Chemistry, Michigan State University* The local structure of the $AgPb_mSbTe_{m+2}$ series of high performance thermoelectric materials has been studied using the atomic pair distribution function (PDF) method. The dimensionless thermoelectric figure of merit, $ZT$, of the $m \sim 18$ composition material was found to reach 1.7 at 700 kelvin, compared to the highest observed $ZT$ of only 0.84 for PbTe at 648 kelvin in n-doped material. This is asurprisingly large enhancement in $ZT$ for the addition of just 10%per formula-unit of silver and antimony ions. It is clearly of the greatest importance to trace the origin of the $ZT$ enhancement. Three candidate-models were attempted for thestructure of this class of materials using either a one-phase or a two-phase modeling procedure. Combining modeling the PDF with HRTEM data we show that $AgPb_mSbTe_{m+2}$ contains nanoscale inclusions with composition close to $AgPb_3SbTe_5$ randomly embedded in a PbTe matrix. We extended the local structural PDF study to $Ag_nSn_mSb_nTe_{m+2n}$, preliminary results of which suggest the presence of nanoscale inclusions in this system as well.

*NSF NIRT grant DMR-0304391

**10:12**

**A35 10 Thermal conductivity of nanoparticle suspensions** DAVID CAHILL, SHAWN PUTNAM, *University of Illinois* We present our experimental study on the thermal conductivity of nanofluids loaded with small volume fractions of $C_{60}$-$C_{70}$ fullerenes and alkanethiolate-protected Au nanoparticles. We use an optical beam deflection technique that measures the thermal diffusivity of fluid mixtures and suspensions of nanoparticles with a precision of better than 1%. Our approach is tested using the thermal conductivity of ethanol-water mixtures; in nearly pure ethanol, the increase in thermal conductivity with water concentration is a factor of two larger than predicted by effective medium theory. The solutions of the $C_{60}$-$C_{70}$ fullerenes and the alkanethiolate-protected Au nanoparticles were measured to maximum volume fractions of 0.6% and 0.35 vol%, respectively. We do not observe anomalous enhancements of the thermal conductivity that have been reported in previous studies of nanofluids; the largest increase in thermal conductivity we have observed is 1.3

± 0.8% for 4 nm diameter Au particles suspended in ethanol. However, within the context of effective medium theory, these findings are expected: effective medium theory predicts that the largest possible increase in the thermal conductivity of a fluid loaded by a volume fraction $\phi \ll 1$ of spherical particles will be $3\phi\Lambda_0$, where $\Lambda_0$ is the thermal conductivity of the carrier fluid.

**10:24**
**A35 11 Thermal Conductance of metal-metal interfaces** BRYAN GUNDRUM, DAVID CAHILL, ROBERT AVERBACK, *University of Illinois* The first quantitative measurement of a metal-metal interface thermal conductance has been carried out using time-domain transient reflectivity in the temperature rage 78 $<$ T $<$ 278 K. The thermal conductance, at room temperature, for the as deposited Al-Cu interface was measured to be 4 GW $m^{-2}$ $K^{-1}$. This is an order of magnitude larger than the largest phonon-mediated interface transport measured to date. It is shown that an extension of the diffusive mismatch model to electrons reproduces the magnitude and temperature dependence accurately. The chemical abruptness of the Al-Cu interface is systematically varied by ion-beam mixing using 1 MeV Kr ions. These results combined with the interface form of the Wiedemann-Franz law could provide a powerful tool for investigating the thermal and electrical transport across metal interfaces.

**10:36**
**A35 12 Thermal conductance of hydrophilic and hydrophobic interfaces** ZHENBIN GE, PAUL BRAUN, DAVID CAHILL, *University of Illinois at Urbana-Champaign* Interfaces between water and hydrophilic or hydrophobic surfaces are of great importance for many biological and engineering systems. Using time-domain thermoreflectance, we have measured the transport of thermally-excited vibrational energy across planar interfaces between water and solids that have been chemically functionalized using self-assembled monolayer. The thermal conductance per unit area of the interface G for hydrophobic Al or Au surface in water is determined to be 37 to 55 MW $m^{-2}$ $K^{-1}$. G for hydrophilic Al or Au surface in water is 150 to 300 MW $m^{-2}$ $K^{-1}$. Our new work on thermal transport complements the extensive research literature on momentum transport at aqueous interfaces: the Kapitza length—i.e., the thermal conductivity of water divided by the thermal conductance per unit area of the interface—is analogous to the ''slip-length'' for water flowing tangentially past a solid surface. We find that the Kapitza length at hydrophobic interfaces (11-16 nm) is a factor of 3-8 larger than the Kapitza length at hydrophilic interfaces (2-4 nm); a change of terminal group from methyl to hydroxyl increases the Kapitza length by approximately 10 nm.

**10:48**
**A35 13 Interfacial thermal transport at Liquid-Liquid and Biomolecular Interfaces** PAWEL KEBLINSKI, NATALIA SHENOGINA, HARSHIT PATEL, SHEKHAR GARDE, *Rensselaer Polytechnic Institute* Systems with nanoscopic features contain a high density of interfaces. Thermal transport in such systems can be governed by the resistance to heat transfer of the interface. Although soft interfaces, such as those between immiscible liquids or between a biomolecule and solvent, are ubiquitous, few studies of thermal transport at such interfaces have been reported. Here we characterize the interfacial conductance, i.e., the inverse of the interfacial resistance, of soft interfaces as a function of molecular architecture, chemistry, and the strength of cross-interfacial intermolecular interactions through detailed molecular dynamics simulations. The conductance of various interfaces studied here, for example, water-organic liquid, water-surfactant, surfactant-organic liquid, is relatively high (in the range of 65-370 MW/m2/ K) compared to that for solid-liquid interfaces ( 10 MW/m2/ K). Interestingly, the dependence of interfacial conductance on the chemistry and molecular architecture cannot be explained solely in terms of either bulk property mismatch or the strength of intermolecular attraction between the two phases. We will also discuss vibrational mode dependent thermal coupling at biomolecule-water interfaces.



**SESSION A36: STRUCTURAL, OPTICAL, AND ELECTRONIC PROPERTIES OF NANOSTRUCTURES**
**Monday Morning, 13 March 2006**
**339, Baltimore Convention Center at 8:00**
**Stefan Badescu, Naval Research Laboratory, presiding**

**8:00**
**A36 1 3-D Structure of Semiconductor Nanomaterials** ILKE ARSLAN, *University of Cambridge* NIGEL BROWNING, *University of California-Davis* TIMOTHY YATES, JENNA TONG, PAUL MIDGLEY, *University of Cambridge* In recent years, nanotechnology has become a key component in the field of materials physics, placing a more rigorous demand on characterization of nanomaterials, ultimately in three dimensions. This has led to the development of electron tomography for inorganic materials using Z-contrast imaging in the scanning transmission electron microscope (STEM). Here we present high resolution 3-D reconstructions of quantum dots and tetrapods. The results from Sn quantum dots in a Si matrix illustrate the ability to identify the size, shape and distribution of embedded dots in a layer in three dimensions, as well as identifying their formation mechanism. Dual axis tomography is demonstrated for the first time for inorganic materials on semiconducting nanorods in the shape of tetrpaods made of CdTe. These results indicate approximately 1nm resolution in all three dimensions using single axis tomography.

**8:12**
**A36 2 Propagation of coherence in X-ray Optics for Nanocrystallography** MENGNING LIANG, IAN ROBINSON, *University of Illinois at Urbana-Champaign* Coherent X-ray Diffraction is a powerful tool for studying the internal structure of nanostructures to angstrom precision in three dimensions. A coherent diffraction pattern is a single 2D slice through the 3D Fourier Transform of an object. These diffraction images can be inverted with iterative phasing algorithms to obtain an image of a projection of the physical object. The success and accuracy of the inversion depends strongly on the quality of the initial diffraction pattern and thus on the coherence properties of the incoming X-ray beam. Coherence of synchrotron radiation depends on machine parameters but also on the optics in the beam path. Focusing optics, which are necessary to provide sufficient flux onto the sample, distort the wavefront and can especially alter the coherence of the beam. For a finite object, fringes will result from the interference

of opposite sides or facets and the visibility of these fringes is a quantitative measure of the coherence quality. We present a study of the effect of optical elements in altering the coherence of an x-ray beam by using the coherent diffraction images from gold nanoparticles.

**8:24**

**A36 3 X-ray Studies of Ultrathin Wires and Tubes in Nanoscale Confinement** JONATHAN M. LOGAN, OLEG G. SHPYRKO, ERIC D. ISAACS, *Center for Nanoscale Materials, Argonne National Laboratory, Argonne, IL and JFI/Physics Department, University of Chicago, Chicago, IL* RAFAEL JARAMILLO, YEJUN FENG, *JFI/Physics Department, University of Chicago, Chicago, IL* JEFFREY W. ELAM, *Energy Systems Division, Argonne National Laboratory, Argonne, IL* DAVID J. COOKSON, *Australian Synchrotron Research Program, Argonne, IL* MICHAEL J. PELLIN, *Materials Science Division, Argonne National Laboratory, Argonne, IL* Nanoporous Anodized Aluminum Oxide (AAO) membranes are composed of self-assembled, densely packed, co-aligned cylindrical pores. The pore diameter of these membranes can be controllably reduced to as little as $\approx$ 1 nm through Atomic Layer Deposition (ALD) process. AAO pores have been used as templates for formation of metallic nanotubes and nanowires through ALD or thermal vapor deposition. These embedded structures have been characterized by small- and wide-angle x-ray scattering (SAXS, WAXS). The penetrating ability of x rays provides a non- destructive structural characterization technique for materials confined within AAO matrix, on both atomic (WAXS) and nanometer (SAXS) length scales.

**8:36**

**A36 4 Three-dimensional Structure of Nanoparticles from High-energy X-ray Diffraction and Atomic Pair Distribution Function Analysis** VALERI PETKOV, *Dept. Physics, Central Michigan University* Knowledge of the atomic-scale structure is an important prerequisite to understand and predict the properties of materials. In the case of crystals it is obtained from the positions and intensities of the Bragg peaks in the diffraction patterns. However, materials constructed at the nanoscale lack the translational symmetry and long-range order of perfect crystals. The diffraction patterns of such materials show only a few Bragg peaks, if any, and a pronounced diffuse component. This poses a real challenge to the usual techniques for structure characterization. The challenge can be met by employing the so-called atomic Pair Distribution Function (PDF) technique and high energy x-ray diffraction. This non-traditional experimental approach takes into account both Bragg and diffuse scattering and yields the atomic structure in terms of a small set of parameters such as a unit cell and atomic coordinates. The basics of the technique will be introduced and its potential demonstrated with results from recent structural studies gold, $ZrO_2$ and GaN nanoparticles.

**8:48**

**A36 5 Anomalous scattering and PDF analysis of HgSe nanoclusters in zeolites using synchrotron X-ray radiation*** M. CASTRO-COLIN, M. ABEYKOON, S.C. MOSS, W. DONNER, E. ANOKHINA, A.J. JACOBSON, *U. of Houston* HgSe, has been grown inside LTL and Nd-Y zeolites (tubular and spherical nanosized pores, respectively). A first sharp diffraction peak appears in an X-ray diffraction profile, that we associate with the clustering of HgSe constrained to the zeolite pore diameter. Charge imbalance within the zeolite pores, combined with the guest material properties, affects the cluster-cluster correlation (clusters in separate pores), either in a filled-unfilled-like fashion or through a relative local orientational order. Such correlations are expressed through a broad diffuse modulation, absent in the pure host, upon which the more obvious, Bragg peaks are imposed. This effect might be seen via pair-distribution function (PDF) analysis. Anomalous scattering experiments carried out both below the Se K-edge and the Hg L-edge, as well as off-edge for each zeolite, aided in calculating average crystallographic parameters of HgSe. These results and the PDF analyses promise to reveal an understanding of the structural configuration and cluster allocation mechanisms. A potential technological application of this system should arise, due to the transparency of these zeolites and ease of interaction of visible light with species contained within the pores.* M.C-C. now at U.T. El Paso

*DOE/BES DE-FG02-04ER46160

**9:00**

**A36 6 Amorphous-Ge Nanocluster Formation During Ion Implantation** I.D. SHARP, *Materials Science and Engineering, University of California, Berkeley and Materials Sciences Division, Lawrence Berkeley National Laboratory, CA 94720* D.O. YI, *Applied Science and Technology, University of California, Berkeley and Materials Sciences Division, Lawrence Berkeley National Laboratory, CA 94720* C.W. YUAN, Q. XU, C.Y. LIAO, *Materials Science and Engineering, University of California, Berkeley and Materials Sciences Division, Lawrence Berkeley National Laboratory, CA 94720* J.W. AGER III, *Materials Sciences Division, Lawrence Berkeley National Laboratory, CA 94720* DARYL CHRZAN, E.E. HALLER, *Materials Science and Engineering, University of California, Berkeley and Materials Sciences Division, Lawrence Berkeley National Laboratory, CA 94720* Ge nanocrystals formed by ion implantation followed by thermal annealing have an average diameter of 5.1 nm with a distribution full width at half maximum (FWHM) of 3.4 nm. This contrasts with Kinetic Monte Carlo (KMC) and rate equation predictions which give a much narrower distribution. Here, we show that the difference between theory and experiment is the result of amorphous nanocluster formation during room temperature implantation. Therefore, thermal annealing to form nanocrystals is predominantly a crystallization process rather than a conventional nucleation, growth, and coarsening process during thermal annealing. This work is supported in part by U.S. Department of Energy under contract No. DE-AC02-05CH11231 and in part by U.S. NSF Grant No. DMR-0109844.

**9:12**

**A36 7 A Computational Investigation of the Structure and Optical Properties of Nanoconfined Semiconducting Polymers** M.L. DRUMMOND, B.G. SUMPTER, *Oak Ridge National Laboratory* M.D. BARNES, *University of Massachusetts, Amherst* W.A. SHELTON, JR., R.J. HARRISON, *Oak Ridge National Laboratory* The promise of semiconducting organic polymers lies in their incredible flexibility, both through varied structure types and via chemical modifications of the polymer backbone. One type of structure we have recently explored, both experimentally and theoretically, arises from the use of ink-jet printing methods to produce nanoconfined particles with arbitrary size and composition. We have found substantial evidence indicating the production of highly ordered, rod-shaped, pi-stacked folded chain structures for single molecule PPV-based systems. Results show that chain organization, which is greatly influenced by the solvent, is crucial in determining the photophysical properties. Recent multiscale calculations, including molecular dynamics, molecular mechanics,

and both ground-state and excited-state ab initio calculations, have been used to elucidate the role of the substituents in controlling the structure of the nanoconfined polymer, as well as the resultant effect on the optical properties. Through this work, a structure-property relationship is developed that will prove to be of great utility to experimentalists and polymer theorists alike.

**9:24**

**A36 8 Single-particle energy levels and interparticle Coulomb interactions in CdSe quantum dots measured by Scanning Tunneling Spectroscopy** LUCIAN JDIRA, *Institute for Molecules and Materials, Radboud University Nijmegen, The Netherlands* PETER LILJEROTH, *Debye Institute, Utrecht University, The Netherlans* ERIC STOFFELS, *Institute for Molecules and Materials, Radboud University Nijmegen, The Netherlands* DANIEL VANMAEKELBERGH, *Debye Institute, Utrecht University, The Netherlans* SYLVIA SPELLER, *Institute for Molecules and Materials, Radboud University Nijmegen, The Netherlands* Semiconductor quantum dots (QDs) provide the opportunity to study the evolution of electronic properties in a size range intermediate between molecular and solid state regime. We report a detailed size evolution analysis of the electronic structure of colloidal CdSe QDs of different sizes, by employing Scanning Tunneling Spectroscopy to individual dots. Tuning the tunnelling-in versus tunnelling-out rates allows one to show the electron occupation in the dot. The energy level structure and electron-hole Coulomb attraction in the dot are obtained by a combination of shell-tunneling spectroscopy and optical spectroscopy. The results are in agreement with tight-binding calculations. The electron-electron interactions are investigated by shell-filling spectroscopy. The tunneling spectra in this regime are analyzed by solving the master equation for electron and hole occupancy of the QD.

**9:36**

**A36 9 Optical Phonons and Multiphonon Raman Scattering in Spherical PbSe Quantum Dots*** SERGEI KLIMIN, VLADIMIR FOMIN, JOZEF DEVREESE, *TFVS, Departement Fysica, Universiteit Antwerpen, B-2610 Antwerpen, Belgium* YUL HYUN, FRANK WISE, *Department of Applied Physics, Cornell University, Ithaca, New York 14853, USA* The experimentally observed multi-phonon resonant Raman scattering spectra in spherical PbSe quantum dots are interpreted using our non-adiabatic approach [1]. The optical phonons in quantum dots are treated within the multimode dielectric continuum model, taking into account both the electrostatic and mechanical boundary conditions for the relative ionic displacement. Our multimode dielectric continuum model, which includes, as a substantial ingredient, the realistic dispersion of optical phonons, adequately describes the optical-phonon spectra of spherical PbSe quantum dots. The non-adiabaticity leads to a substantial enhancement of the relative intensities of multiphonon peaks with respect to the intensity of the one-phonon peak. The peak positions and intensities of the calculated Raman scattering spectra for spherical PbSe quantum dots are in good agreement with recent experimental results on the Raman scattering in oleic-acid-capped colloidal PbSe nanocrystals. [1] E. P. Pokatilov, S. N. Klimin, V. M. Fomin, J. T. Devreese, and F. W. Wise, Phys. Rev. B **65**, 075316 (2002).

*This work was supported by the GOA BOF UA 2000, IUAP, FWO-V projects G.0274.01N, G.0435.03 and the WOG WO.035.04N (Belgium) and by the US National Science Foundation.

**9:48**

**A36 10 Power dependent spectral diffusion in single CdSe quantum dots** Y. SHEN, L. PANG, K. TETZ, Y. FAINMAN, *Department of Electrical and Computer Engineering, University of California, San Diego* M. GRISWOLD, SEN YANG, L.V. BUTOV, L.J. SHAM, *Department of Physics, University of California, San Diego* Optical emission from a single CdSe quantum dot was investigated. We studied spectral diffusion effects which were observed earlier[1].We found that the spectral diffusion characteristic frequency increases with the pump power. In addition, increasing laser pump power causes occurrence of additional emission lines. The measured correlations show that the lines correspond to multiparticle complexes. The physics describing these effects is analyzed. [1]S. A. Empedocles, D. J. Norris, and M. G. Bawendi, Phys. Rev. Lett. 77, 3873 (1996).

**10:00**

**A36 11 Experimental and numerical confirmation of composite diffracted evasnescent-wave (CDEW) model for enhanced transmission of subwavelength apertures** HENRI J. LEZEC, *Caltech, Pasadena CA, and CNRS, Paris, France* TINEKE THIO, *Arinna LLC* When a subwavelength aperture in an opaque film is surrounded by periodic surface corrugations, its optical transmission can be enhanced or suppressed with respect to that of an identical aperture without surface corrugations. We have proposed a model in which the subwavelength surface structure scatters the incident light into evanescent waves: The total, or composite, diffracted evanescent waves (CDEWs) travel along the surface and their interference with the light directly falling on the aperture leads to the transmission modulation. The CDEW model is valid for metallic as well as non-metallic surfaces, and thus differs qualitatively from the surface plasmon model, which requires a metallic surface. We show that the optical transmission of an embedded periodic array of dots, where the surface is absent altogether, is related to the transmission of hole arrays by Babinets principle, underscoring the importance of diffraction. Furthermore, numerical calculations on small- area corrugations verify the functional form of the CDEWs.

**10:12**

**A36 12 Transport Properties of Gold Nanoparticle Arrays at Low Temperatures** T. TRAN, *University of Chicago* I. BELOBORODOV, X.M. LIN, V. VINOKUR, *Argonne National Laboratory* P. JIANG, W. KANG, H. JAEGER, *University of Chicago* We investigated the effects of elastic and inelastic cotunneling on the electronic transport properties of Au monolayers and multilayers. Highly-ordered monolayers of dodecanethiol-ligated Au particles (6nm in diameter)[1] were assembled onto $Si_3N_4$ substrates with prefabricated electrodes. Multilayers were created by adding layers to the original monolayers[2]. Current-voltage (IV) measurements were performed with 50fA resolution down to 30mK. TEM images were taken posterior to all measurements. We found that transition from inelastic to elastic cotunneling occurred at T$\sim$ 5K. In the inelastic cotunneling regime, the IV curves were found to be nonlinear for $k_BT < eV/N < E_C$ and linear when $k_BT > eV/N$ where N is the number of grains across the electrode gap. In the elastic regime below 5K, the IV curves were found to be linear for $eV/N < (E_C\ \delta)^{1/2}$where $\delta$ is the level spacing and $E_C$ is the charging energy. As a consequence of cotunneling, Efros-

Shklovskii variable-range-hopping-like conduction (VRH) was observed near zero bias. Above T~ 80-100K, transition from VRH to nearest-neighbor hopping took place. X.M. Lin, itet.al., J. Nanoparticle Res. **2** 157 (2000). T.B. Tran, itet.al., Phys. Rev. Lett. **95** 076806 (2005),

**10:24**

**A36 13 Observation of Optical Signature of the Aharonov-Bohm Phase in Type-II Quantum Dots** IGOR KUSKOVSKY, W. MACDONALD, *Queens College, NY* M.C. TAMARGO, *City College, NY* A.O. GOVOROV, *Ohio U., Athens* X. WEI, *NHMFL* M. TADIC, F.M. PEETERS, *University of Antwerp* Recent theoretical studies[1,2] on the optical response of type-II excitons in the magnetic field have shown that the excitons will acquire the Aharonov-Bohm (AB) phase as the electrical dipole, formed due to carrier separation, interacts with the field, resulting in the field dependent exciton energy and the emission intensity. Experimentally, the former has been reported[3]; however, the behavior of the intensity is still not fully understood. We present results of magneto-photoluminescence studies on type-II ZnTe/ZnSe quantum dots (QDs) formed in Zn-Se-Te multilayer systems[4]; this ensures that electron move within the $x - y$ plane. The observed strong oscillations in the intensity is explained in terms of the AB effect[1,2,5] due to the electron motion around a stack of QDs, when the hole is strongly localized in one them. This is in qualitative agreement with the theoretical predictions[2]. 1. Kalameitsev, itet al., JETP Lett. **68**, 669 (1998); Govorov, itet al., PRB **R66**, 081309 (2002); Janssens, itet al., PRB **67**, 235325 (2003). 2. Janssens, itet al., PRB **69**, 235320 (2004). 3. Ribeiro, itet al., PRL **92**, 126402 (2004). 4. Gu, itet al., PRB **71** 045340 (2005). 5. Dias da Silva, itet al., PRB **70**, 155318 (2004).

**10:36**

**A36 14 Observation of the Aharonov-Bohm Effect in Self-Assembled InGaAs/GaAs Nano-Volcanoes*** N.A.J.M. KLEEMANS, P. OFFERMANS, J.H. WOLTER, P.M. KOENRAAD, *Department of Semiconductor Physics, TU Eindhoven, The Netherlands* I.M.A. BOMINAAR-SILKENS, U. ZEITLER, P.C.M. CHRISTIANEN, J.C. MAAN, *High Field Magnet Laboratory, IMM, Radboud University Nijmegen, The Netherlands* D. GRANADOS, J.M. GARCÍA, *Instituto de Microelectrónica de Madrid, CSIC, Spain* V.M. FOMIN, V.N. GLADILIN, J.T. DEVREESE, *TFVS, Universiteit Antwerpen, Belgium* According to our X-STM data, self-assembled InGaAs/GaAs nano-volcanoes are characterized by an asymmetric rim and a depression rather than an opening at the center. We show that these asymmetric singly connected structures still can effectively manifest the electronic properties, like the Aharonov-Bohm (AB) oscillations, peculiar to the doubly connected geometry of ideal rings. AB oscillations in the persistent current are observed in low temperature magnetization measurements using torsion magnetometry in magnetic fields up to 15 T. The experimental results are in excellent agreement with theoretical predictions for strained nano-volcanoes.

*The work has been supported by the GOA BOF UA 2000, IUAP, FWO-V project G.0435.03, the WOG WO.035.04N (Belgium), MEC NANOSELF project (Spain) and the EC SANDiE Network of Excellence.

**10:48**

**A36 15 Mesoscopic conductance fluctuations in a coupled quantum dot system** KAZUTAKA TAKAHASHI, *RIKEN, Japan* TOMOSUKE AONO, *Ben-Gurion University of the Negev, Israel* We study electron transport properties of an Aharonov-Bohm ring containing two quantum dots. One of the dots has well-separated resonant levels and the other dot is chaotic and is treated by random matrix theory. We develop a statistical theory of the conductance through the dot using the supersymmetry method and the numerical calculation, and find that the conductance is significantly affected by mesoscopic fluctuations. The Breit-Wigner resonant peak of the conductance is changed to an antiresonance by increasing the ratio of the level broadening to mean level spacing of the random dot. The asymmetric Fano form turns into a symmetric one and the resonance peak can be controlled by magnetic flux. We also find that the conductance distribution shows rich behavior depending on the fluctuations of the chaotic dot and the position of the resonance peaks.

## SESSION A38: SUPERCONDUCTIVITY-VORTEX MATTER

**Monday Morning, 13 March 2006**
**341, Baltimore Convention Center at 8:00**
**Wai Kwok, Argonne National Laboratory, presiding**

**8:00**

**A38 1 Josephson-vortex states in $Bi_2Sr_2CaCu_2O_{8+y}$** KAZUTO HIRATA, *National Institute for Materials Science* SHUUICHI OOI, TAKASHI MOCHIKU, Josephson-vortex (JV) states have been studied by measuring the flow resistance in $Bi_2Sr_2CaCu_2O_{8+y}$ (Bi-2212) as a function of the parallel magnetic field with the current along the *c*-axis. From the periodic oscillations, we can assign the three-dimensionally long-range-ordered state (3DLOS) of JVs (PRL**89**, 247002(2002), Physica **C412-414**, 454(2004)). The lower and upper boundaries of 3DLOS were determined from the magnetic field of beginning and stopping in the oscillations, respectively. From the flow resistance and the $I - V$ characteristics measurements crossing the upper boundary, we suggest that the JVs are in ordered state in itin-plane, but have less ordering along the *c*-axis. This JV state may correspond to the 2D-quasi-long-range ordered state, proposed by Hu&Tachiki (PRB**70**, 064506(2004)).

**8:12**

**A38 2 Vortex phase diagram of nearly stoichiometric $Bi_2Sr_2CaCu_2O_{8+\delta}$ single crystal*** NORIKO CHIKUMOTO, *Superconductivity Research Laboratory, ISTEC* There have been a large number of reports on the vortex phase diagram of Bi2212. However, the Bi2212 crystals used for these studies mostly have Bi-rich composition, with typically Bi : Sr = 2.1 : 1.9. Recently, Eisaki *et al.* [1] reported that $T_c$ in Bi2212 single crystal is largely depressed by the cation disorder at the Sr-site, typically the substitution of Sr-site by $Bi^{3+}$. In the present study, we found that the Bi-Sr substitution also depress the vortex pinning. We have successfully grown Bi2212 single crystals with Bi : Sr ratio very close to 2:2. It showed very high critical current density, $2 times 10^6$

A/cm$^2$, at 20K, and reduced reversible region ($J_c = 0$ region) in the magnetic phase diagram. We also show the dependence of the irreversibility field on the cation nonstoichiometry. The author thanks K. Furusawa, H. Eisaki and Y. Nakayama for growing Bi2212 single crystals.

*This work was partially supported by the New Energy and Industrial Technology Department Organization (NEDO).

**8:24**

**A38 3 Melting of vortex solid phase in irradiated $Bi_2Sr_2CaCu_2O_{8+\delta}$ single crystals in tilted magnetic fields** JOVAN MIRKOVIC, *Inst of Materials Science, Univ of Tsukuba, 305-8573 Tsukuba, Japan, and Faculty of Sciences, Univ. of Montenegro, Podgorica, Serbia and Montenegro* SERGEY SAVEL'EV, *Frontier Research System, The Institute of Physical and Chemical Research (RIKEN), Wako-shi, Saitama, 351-0198, Japan* HIROKAZU SATO, TAKASHI YAMAMOTO, ITSUHIRO KAKEYA, *Institute of Materials Science, University of Tsukuba, 305-8573 Tsukuba, Japan* FRANCO NORI, *Frontier Research System, The Institute of Physical and Chemical Research (RIKEN), Wako-shi, Saitama, 351-0198, Japan* KAZUO KADOWAKI, *Institute of Materials Science, University of Tsukuba, 305-8573 Tsukuba, Japan* The boundary between the vortex-solid and the vortex-liquid in $H_c - H_{ab}$ phase plane for irradiated $Bi_2Sr_2CaCu_2O_{8+\delta}$single crystals is studied by measuring the local ac-magnetic permeability by using the miniature coils in tilted magnetic fields. It was found that the *c*-axis magnetic field component at the phase transition decreases linearly when increasing the in-plane magnetic field at high temperatures even in a wider angular range than in pristine samples. At lower temperatures, this linear decrease transforms to a concave (hyperbolic-like) curve that differs even stronger from the usual elliptical phase boundary derived from Ginzburg-Landau theory. A theoretical approach to this challenging problem is discussed.

**8:36**

**A38 4 Field dependence of the lock-in transition of Josephson vortex in $Bi_2Sr_2CaCu_2O_{8+\delta}$ mesoscopic crystals** ITSUHIRO KAKEYA, YUIMARU KUBO, MASASHI KOHRI, TAKASHI YAMAMOTO, KAZUO KADOWAKI, *University of Tsukuba, Tsukuba, Ibaraki 305-8573 Japan* We have investigated vortex states in magnetic fields close to the *ab*-plane of $Bi_2Sr_2CaCu_2O_{8+\delta}$ (Bi2212) by means of the *c*-axis resistivity $\rho_c$ in Bi2212 mesoscopic crystals fabricated by the FIB technique. When magnetic field $H \leqslant$ 1T was tilted from the *ab*-plane at $T$ = 60 K, a sharp drop in $\rho_c$ was observed at an angle $\theta_{th}$ ($\theta$ = 0 for $\mathbf{H} \| ab$-plane) depending on the field (typically $\theta_{th}$=0.5 deg. for $H$ = 1T). $\rho_c$ below $\theta_{th}$ does not depend on angle and is almost proportional to $H$, suggesting $\rho_c$ being Josephson vortex (JV) flow resistivity. Above $\theta_{th}$, it is considered that the JV flow is strongly impeded by pancake vortices (PVs), which attract with JVs and do not flow by the *c*-axis current, resulting in $\rho_c \approx 0$. Moreover, the penetration field of PVs $H\sin\theta_{th}$ decreases with increasing $H$. This is considered to be yielded by decrease of the line energy of pancake stacks due to the formation of the crossing lattice (CL). Therefore, the drop in $\rho_c$ corresponds to the transition from the lock-in (LI) state to the CL state. At high magnetic fields, the decrease in $\rho_c$ is broadened and has a shoulder structure. These results suggest that other vortex states between the LI and CL states emerge with increasing magnetic field and have intermediate JV viscosity. The expected vortex structures will be argued.

**8:48**

**A38 5 Vortex phase diagram from $^{17}$O NMR study in single crystal BSCCO*** BO CHEN, WILLIAM HALPERIN, *Northwestern University* One of the most fascinating aspects of high temperature superconductors is the extreme anisotropy and the effect this has on the properties of vortices. At sufficiently high magnetic field it is expected that vortices are two dimensional and the melting transition temperature tends to a constant value, independent of field. For the most anisotropic materials such as $Bi_2Sr_2Ca_1Cu_2O_{8+\delta}$ such fields are attainable allowing almost complete decoupling of the two dimensional vortex pancakes from each other along the direction of the anisotropy axis. In our work the vortex melting phase diagram for single crystals of $Bi_2Sr_2Ca_1Cu_2O_{8+\delta}$ have been determined from $^{17}$O NMR up to 22 Tesla and can be related to results at low field for the more strongly coupled three dimensional case that has been extensively studied by transport and magnetization methods. Additionally, an abrupt change in vortex structure, seemingly an order−disorder transition, was found between 5 and 8 Tesla, below 10 K.

*In collaboration with V.F. Mitrovic, Brown University; A.P. Reyes, P. Kuhns, W.G. Moulton, National High Magnetic Field Laboratory, Tallahassee, FL; Prasenjit Guptasarma, David Hinks, Argonne National Laboratory; and P. Sengupta, Northwestern University.

**9:00**

**A38 6 Anomalous angular dependence of the *c*-axis resistivity in $Bi_2Sr_2CaCu_2O_{8+x}$ mesas*** TAKASHI TACHIKI, *MSD, Argonne Nat. Lab. and Dept. of E & E Eng., Nat. Defense Academy, Japan* L. OZYUZER, *MSD, Argonne Nat. Lab. and Dept. of Phys., Izmir Inst. of Technol., Turkey* C. KURTER, *MSD, Argonne Nat. Lab. and Illinois Inst. of Technol.* U. WELP, A. KOSHELEV, D. HINKS, K. GRAY, W. KWOK, *MSD, Argonne Nat. Lab.* K. KADOWAKI, *Institute of Mat. Sci., Univ. of Tsukuba, Japan* We study flux-flow properties of Josephson vortices in highly anisotropic high-$T_c$ superconductors. The flux-flow resistance in pristine and $HgBr_2$-intercalated $Bi_2Sr_2CaCu_2O_{8+x}$ (BSCCO) single crystals was measured as a function of the angle between the itab-plane and an applied magnetic field. These samples have a mesa structure with the in-plane area of 200 $\mu$m x 20 $\mu$m and consist of 50 – 70 intrinsic junctions. For both pristine and intercalated BSCCO, a sharp resistance peak was observed within a threshold angle of a few degrees. However, while the angle decreases with increasing field for the pristine BSCCO, the intercalated BSCCO shows the opposite field dependence. We interpret this peak and its field dependence as an interplay between two effects: initial penetration of pancake vortices and extra damping of Josephson-vortex lattice induced by pancake vortices.

*This work was supported by the U.S. Department of Energy under grant no. W-31-109-ENG-38

**9:12**

**A38 7 Thermal depinning and transverse-field tilting transitions in a planar vortex array pinned by a columnar defect*** LEO RADZIHOVSKY, *University of Colorado at Boulder* I will discuss results on a thermal and a transverse magnetic field response of a vortex line array confined to a plane with a dilute concentration of columnar pins. As a function of temperature, for a magnetic field aligned with defects this system exhibits a one-dimensional analog of a roughening transition, with a low-temperature ''smooth'' phase corresponding to a vortex array pinned by the defects, and a high-temperature ''rough'' phase in

which at long scales thermal fluctuations effectively average away pinning by the defects. In the low-T pinned phase, the vortex lattice tilt response to a transverse magnetic field proceeds via a soliton proliferation ''transition,'' governed by an integrable sine-Hilbert equation. Combining the aforementioned roughenning transitition with this commensurate-incommensurate transition, I map out the transverse-field—temperature phase diagram for this system.

*supported by the NSF DMR-0321848

**9:24**

**A38 8 RF-induced flux lattice annealing (RIFLA) in the electron-doped superconductor $Pr_{1.85}Ce_{0.15}CuO_{4-y}$.*** W.G. CLARK, GUOQING WU, S.E. BROWN, *UCLA Physics and Astronomy* R.L. GREENE, *U. of Maryland Physics* H. BALCI, *UIUC Physics* A strained flux lattice (FL) in a superconductor (SC) can be annealed to a lower free energy by the RF-field used to generate an NMR spin-echo signal [W.G. Clark et al., J. Phys. IV Proceedings **9**, Pr10-49-52 (1999)]. Here, this effect is reported for the SC phase of $Pr_{1.85}Ce_{0.15}CuO_{4-y}$. The distorted FL is prepared by rotating the sample through a small angle in a magnetic field well below the transition temperature, which leaves the FL pinned in a non-equilibrium configuration. Then, the first spin echo has almost no amplitude. Subsequent echoes have a progressively larger amplitude until a final, steady value is reached. The interpretation is that shaking of the distorted vortex lattice by the RF pulses progressively anneals it to a lower free energy configuration. The corresponding change in the local field between the de-phasing and re-phasing pulse for each echo then reduces the height of the echo.

*The work done at UCLA was supported by NSF Grants DMR-0334869 (WGC) and DMR-0203806 (SEB).

**9:36**

**A38 9 Ground state of interlayer Josephson vortex systems: General description based on energy landscape** YOSHIHIKO NONOMURA, XIAO HU, *Computational Materials Science Center, National Institute for Materials Science, Tsukuba, Ibaraki 305-0047, Japan* Although Josephson vortex systems have been intensively studied, their phase diagrams have not been established yet even in the ground state. In the present study, we draw the full energy landscape with respect to magnetic field and the displacement from aligned vortex lattices by neglecting the spatial variation in the amplitude of superconductivity order parameter and in the gauge field in the Lawrence-Doniach model. We find that the ground state changes continuously from the aligned lattice to sheared lattices, and then to rotated lattices as the magnetic field decreases, and that rotated lattices are characterized by multi-valley structures of the energy landscape. Owing to effects of the underlying layer structures, the rotated vortex lattices realized at the valleys of the energy landscape are distorted from the rigid ones expected from the picture based on the London model, and this distortion becomes weak as the magnetic field decreases. We would like to thank Dr. A. E. Koshelev for sending his article prior to publication.

**9:48**

**A38 10 Vortex dynamics investigated using low temperature scanning tunneling microscope: collective motion and collective pinning of vortices in $NbSe_2$** JONGHEE LEE, WANG HUI, DAN SULLIVAN, *Department of Physics, University of Maryland, College Park, MD 20740* MICHAEL DREYER, *Department of Electrical & Computer Engineering, University of Maryland, College Park, MD 20740* BARRY I. BARKER, *Laboratory for Physical Sciences, National Security Agency, College Park, MD 20740* PAVEL SHUK, MARK HIGGINS, EVA Y. ANDREI, *Department of Physics, Rutgers University, Piscataway, NJ 08854* We report the observation of the collective motion and the collective pinning of vortices of $NbSe_2$ under various magnetic fields and from $\sim$ 6 K to $\sim$ 2 K using scanning tunneling microscopy (STM). Scanning Tunneling Spectroscopic maps were taken continuously, providing ''movies'' of the vortex motion. Based on the analysis of this data, the speed of the collective motion of vortices was $\sim$ 1 pm/s. The vortices showed clear signs of weak collective flux pinning. We will quantify the collective transport behavior of vortices based on our STM measurements and compare with the pertinent theories as well as related measurements done by other groups.

**10:00**

**A38 11 Observation of the Signatures of Glassy Vortex Dynamics in $2H$-$NbSe_2$*** XU DU, GUOHONG LI, EVA Y. ANDREI, MARK J. HIGGINS, *Department of Physics and Astronomy, Rutgers University* PAVEL SHUK, MARTHA GREENBLATT, *Department of Chemistry, Rutgers University* Using time resolved transport measurements, we observed clear evidence of glassy dynamics in the current driven vortex system in clean, weak pinning $2H$-$NbSe_2$single crystals prepared by field cooling through the superconducting transition. Simple aging was observed by means of scaling over the waiting times between two consecutive current pulses. A memory function was defined to describe how the previous pulse is ''memorized'' when the system is probed by a second pulse. The complex behavior of the driven vortex system in the glassy state is well characterized by a simple picture of the time evolution of the glassy states in configuration space. Preliminary results on direct imaging of the current driven vortices using Hall probe microscopy will be discussed.

*Work supported by NSF-DMR-0102692 and by DOE-DE-FG02-99ER45742

**10:12**

**A38 12 Thermodynamic Measurements at the Bragg Glass Transition in Nb*** N. D. DANIILIDIS, I. K. DIMITROV, V. MITROVIC, C. ELBAUM, X. S. LING, *Brown University* We report measurements of mixed-state entropy changes and specific-heat on a Nb single crystal, in which previous neutron scattering studies showed that an order-disorder transition of the vortex lattice occurs at the peak effect (PE). Preliminary measurements of (dS/dH) as a function of field applied in the [111] direction reveal a sharp peak at the PE. This corresponds to a discontinuity in the entropy of the vortex system of order $\Delta s = 2.7\ k_B$ per vortex per (111) Nb plane at 5.16 K. The entropy discontinuity is found to decrease and finally disappear as the multicritical[1] point is approached on increasing temperature. The behavior of S(H,T) in the vicinity of the PE shows hysteresis on increasing and decreasing field due to nonequilibrium magnetization effects. In specific heat measurements there is no sign of latent heat at the PE, indicating that the latent heat is very small in this system. [1] S. R. Park itet al. PRL **91** 167003 (2003).

*This work was supported by the National Science Foundation under Grant No. DMR-0406626.

**10:24**

**A38 13 Vortex chains decoration in anisotropic spin-triplet superconductor $Sr_2RuO_4$*** KLAUS HASSELBACH, *CRTBT-CNRS* VOICU DOLOCAN, *CRTBT-CNRS* YING LIU, *Pennsylvania State University* PASCAL LEJAY, *CRTBT-CNRS* DOMINIQUE MAILLY, *LPN-CNRS* CRTBT-CNRS TEAM, PENNSYLVANIA STATE UNIVERSITY TEAM, LPN-CNRS TEAM, We study flux structures in single crystals of the anisotropic spin triplet superconductor $Sr_2RuO_4$ by scanning microSQUID microscopy[1]. The appearance of vortex chains is noted as the applied field is tilted towards the inplane direction of the 3D superconductor. The vortex chains are easily turned in the ab plane by rotation of the inplane component of the applied magnetic field. The decoration of vortex chains by crossing vortices is observed: two vortices orientations appear, one along the layers and the other closely perpendicular to the layers. The findings are discussed in view of the Lawrence-Doniach and Ginzburg Landau models of anisotropic superconductors. Ref. 1 V.O. Dolocan PRL Vol 95 (2005) 97004

*CNRS/NSF INT 03-40779

**SESSION A39: FOCUS SESSION: MAGNESIUM DIBORIDE AND RELATED COMPOUNDS: MULTI GAP SUPERCONDUCTIVITY**
**Monday Morning, 13 March 2006**
**342, Baltimore Convention Center at 8:00**
**Lance Cooley, Brookhaven National Laboratory, presiding**

**8:00**

**A39 1 Current-induced phase textures and pairbreaking in multilayered structures and two-gap superconductors.** ALEX GUREVICH, *University of Wisconsin, Madison, WI* VALERII VINOKUR, *Argonne National Laboratory, Argonne, IL* We predict an inhomogeneous state in current-carrying multilayers or superconductors with multicomponent order parameters. Using the GL theory, we show that the current I flowing along a weakly coupled bilayer (with two different superconducting layers) can result in a two-stage pairbreaking process: 1. Current-induced interlayer decoupling due to a transition from the phase-locked state at $I < I_b$ to a periodic chain of interlayer $2\pi$ phase slips for $I > I_b$. This phase texture re-distributes currents between the layers, the period of the texture L(I) decreases as I increases similar to the period of the vortex lattice L(H) in a long Josephson junction. 2. The global pairbreaking at the depairing current $I_d >> I_b$. The same current-induced band decoupling and interband phase textures occur in two-gap superconductors with two weakly coupled s-wave order parameters, such as $MgB_2$.Using the Usadel equations we derive an equation for the interband phase difference valid for all temperatures. This equation shows that at small currents $I < I_b$, the $\pi$ and $\sigma$ bands are phase-locked, while for $I > I_b$, the band decoupling transition occurs as an equilibrium interband phase slip structure forms along the direction of current flow. These interband phase textures can manifest themselves in dc transport, vortex properties and nonlinear rf impedance.

**8:12**

**A39 2 Theory of superconducting fluctuations in magnesium diboride** ANDREI VARLAMOV, *Coherentia-INFM-CNR, via del Politecnico, 1, 00133 Rome, Italy* ALEXEI KOSHELEV, VALERII VINOKUR, *Argonne National Laboratory* A theory of fluctuations in two-band superconductor $MgB_2$ is developed. Since the standard Ginzburg-Landau (GL) approach fails in description of its properties, we generalize it basing on the microscopic theory of a two-band superconductor. Calculating the microscopic fluctuation propagator, we build up the nonlocal two-band GL functional and the corresponding time-dependent GL equations. This allows us to calculate the main fluctuation observables. Temperature dependencies of the fluctuation specific heat, magnetic susceptibility, and in-plane conductivity are determined by the same function which interpolates between two regimes: the standard GL regime very close to $T_c$, where superconductivity is described by the unique order parameter for both bands, and the regime of dominating $\sigma$-band which is settled at temperatures slightly further away from $T_c$. This work was supported by the U.S. DOE, Office of Science, under contract # W-31-109-ENG-38. A.A.V. acknowledges the support of the FIRB project of the Italian Ministry of Science and Education.

**8:24**

**A39 3 Multi-Gap Superconductivity in $MgB_2$: Magneto-Raman Spectroscopy** A. MIALITSIN, B.S. DENNIS, G. BLUMBERG, *Bell Labs, Lucent Technologies* N. D. ZHIGADLO, J. KARPINSKI, *ETH, Zurich* We report polarization-resolved Raman scattering measurements on $MgB_2$ single crystals as a function of excitation, temperature and magnetic field with special attention paid to the superconductivity induced electronic collective modes and phonon renormalization. In addition to the two previously reported SC features: a fundamental gap below 32 and a SC coherence peak at 109 $cm^{-1}$ - we observe a continuum onset shoulder at 48 and a collective mode at 78 $cm^{-1}$ in the $A_{1g}$ channel. Because $MgB_2$ optical conductivity exhibits inter-band excitation in the visible range resonant Raman coupling allows us to turn on and off SC features induced by different coupling mechanisms as we scan the Raman excitation energy. Since the absorption at 2.6 eV originates from distinctive inter-band transitions we are able to selectively determine inter-band coupling constant. Finally we demonstrate how the frequency and the line width of the Raman active $E_{2g}$ phonon evolve with temperature and magnetic field. Tracking this evolution across the SC phase transition illustrates the self energy effect as the electronic spectra renormalize along with the blue-shift of the $E_{2g}$ phonon.

**8:36**

**A39 4 Feshbach shape resonance in a superlattice of superconducting layers: the case of aluminum doped magnesium diboride*** A. BIANCONI, M. FILIPPI, M. FRATINI, V. PALMISANO, L. SIMONELLI, N. L. SAINI, *Dept. of Physics, University of Rome ''La Sapienza'' P.le. A. Moro 2, 00185 Roma, Italy* E. LIAROKAPIS, *Department of Applied Mathematics and Physics, National Technical University of Athens, GR-157 80 Athens, Greece* We have synthesized highly pure cristalline magnesium diboride samples where Mg is substituted by Al. We show that by electron doping magnesium diboride it is possible to tune the chemical potential to the Feshbach shape resonance in a superlattice of metallic layers. In this multiband superconductor in the clean limit, showing two gap superconductivity, the interband exchange like pairing term shows a Feshbach shape resonance in the proximity of the 2D to 3D Lifshitz electronic topological transition

(2D/3D ETT). This is shown that the Feshbach resonance is the key term controlling the increase of the critical temperature in the low temperature range to 40K. The variation of the electron phonon interaction is probed by micro-Raman. The 2D/3D ETT is shown by micro Raman and a lattice anomaly. The control of the nanoscale phase separation tuning the chemical potential in the proximity of the ETT is discussed. The Feshbach resonance inthe interband pairing is indicated by the suppression of the isotope coefficient in the critical temperature as a function of aluminum substitution.

*This work is supported by EU strep project COMEPHS

**8:48**

**A39 5 Ground electronic state of $MgB_2$: Intrinsic nonadiabatic state at broken translation symmetry.** PAVOL BANACKY, *Comenius University* Study of the band structure of $MgB_2$has shown that electron coupling to $E_{2g}$ phonon mode induces not only $\sigma$-bands splitting at $\Gamma$ point but also fluctuation of the top of one of $\sigma$ band at the Fermi level, resulting in dramatic decrease of the Fermi energy. As a consequence, the original adiabatic state ($\omega/E_F < 1$) corresponding to the equilibrium nuclear geometry has been changed to the intrinsic nonadiabatic state ($\omega/E_F > > 1$) at distorted geometry, already at the displacement which is smaller than the rms. displacement of B-B atoms corresponding to zero-point energy of the $E_{2g}$ phonon mode. At these circumstances, not only Migdal theorem but also Born-Oppenheimer approximation has been broken, and standard treatment of EP interactions, including calculation of nonadiabatic corrections to adiabatic ground state by means of perturbation theory, can not be applied. Study of the electron-nuclear Hamiltonian by means of the quasiparticle unitary transformation (Q,P–dependent) which treats electrons and nuclei on the same footing, has revealed that EP interactions in the intrinsic nonadiabatic state stabilize the fermionic ground state of $MgB_2$ at broken translation symmetry and corresponding wave function is dependent not only on nuclear coordinates, but it is strongly modulated mainly by nuclear momenta. From the results follow that in this case, instead of Cooper pairs formation, condensation process is represented rather by real-space, T-dependent formation of mobile bipolarons.

**9:00**

**A39 6 Elucidating strong coupling between $E_{2g}$ phonon mode and electrons in $MgB_2$*** RICHARD PEREZ, YONG-JIHN KIM, OSWALD UWAKEH, *University of Puerto Rico - Mayaguez* ERIC HELLSTROM, *University of Wisconsin - Madison* Although the isotope effect and the Testardi correlation provide definite proof of the phonon mechanism in $MgB_2$, the detailed electron-phonon coupling is not clear yet. For instance, point contact and tunneling spectroscopy experiments show only qualitative information on the (strong) coupling between the $E_{2g}$ phonon mode and the electrons that was predicted by theory. Raman scattering and inelastic x-ray scattering demonstrate the anomalously damped and broad $E_{2g}$ phonon mode due to strong electron-phonon coupling. We follow the change of the anomalously broadened linewidth of the$E_{2g}$mode as the system becomes disordered by impurity substitution and/or ball milling. We expect that the broadening due to the electron-phonon coupling will decrease significantly when $T_c$ is reduced to zero due to weak localization. We combine Raman scattering and resistance ratio data to clarify the importance of the coupling between the $E_{2g}$ phonon mode and the electrons in $MgB_2$.

*This work is based on work supported by the National Science Foundation under grant No. 0351449

**9:12**

**A39 7 Electron phonon coupling and phonon renormalization in covalent metals** PEIHONG ZHANG, *SUNY - Buffalo* STEVEN G. LOUIE, MARVIN L. COHEN, *UC Berkeley* Electron-phonon (el-ph) coupling contributes to the finite lifetime of both electrons and phonons, renormalizes their energy, and is responsible for conventional superconductivity. Therefore, phonon renormalization relates directly to the el-ph coupling in metals and is a convenient indication of the coupling strength. In this talk, we will discuss phonon renormalization effects in materials with strong el-ph coupling using a recently developed formalism [1]. We will focus on covalent metals such as $MgB_2$ and related systems and heavily doped covalent semiconductors. [1] P. Zhang, S. G. Louie, and M. L. Cohen, PRL **94**, 225502 (2005).

**9:24**

**A39 8 Hole-doped diamond: a 3D version of MgB2?** JENS KORTUS, *Leipziger Str. 23, D-09596 Freiberg (Germany)* LILIA BOERI, OLE KROGH ANDERSEN, *Max-Planck Institut fuer FestKoerperForschung, Heisenbergstrasse 1, D-70569 Stuttgart, Germany* The discovery of superconductivity in heavily-boron doped diamond in 2004 has caused great excitement both in the fields of superconductors and of semiconductors. In this contribution we show, via first-principles and analytical calculations, that the observed superconductivity can be explained with an electron-phonon mechanism very similar to the one which is causing superconductivity in MgB2: holes at the top of the zone-centered, degenerate $\sigma$ bands couple strongly to the optical bond-stretching modes. We discuss similarities and differences between the two materials, the doping dependence of the critical temperature and the possibility to observe superconductivity in the other group-IV semiconductors.

**9:36**

**A39 9 Studying the electronic structure in pure and electron doped $MgB_2$*** Y. ZHU, R.F. KLIE, L. WU, J.C. ZHENG, *Center for Functional Nanomaterials* L.D. COOLEY, *Dept. Cond. Matt. Phys. & Mat.Sci., Brookhaven National Lab* We use high-energy electrons to reveal electronic structure information to understand the effects of electron doping in $MgB_2$ superconductors. Angle-resolved electron energy-loss spectroscopy was used to investigate the difference in the excited states, while image-coupled quantitative electron diffraction was used to map the valence electron distribution, in pure and Al-doped $MgB_2$. The results were compared with density functional theory calculations. We found significant changes in the B K-edge fine structure as a function of electron doping concentration, suggesting the corresponding $\sigma$ and $\pi$ bands are being filled simultaneously. The filling of the $\sigma$-band states near the Fermi level reduces the critical temperature $T_c$ of highly doped $MgB_2$ to a level comparable to that of other $\pi$-band superconductors such as intercalated graphite. Valence electron maps reveal that electron doping causes considerable charge transfer and accumulation in charge density between both Al-B and B-B bonds. This results in a shortened c-axis of the unit cell and higher phonon frequency, which eventually quenches su-

perconductivity altogether. The relationship between charge transfer and inter-band scattering are also examined.

*Work supported by the U.S. Department of Energy under contract DE-AC02-98CH10886

**9:48**

**A39 10 $MgB_2$; Al and C doping, $\sigma$-band filling and anisotropy reduction** SABINA RUIZ-CHAVARRIA, PABLO DE LA MORA, *Depto. de Fis., Fac. de Ciencias, UNAM, Mexico* GUSTAVO TAVIZON, *Depto. de Fis. y Quim. Teorica, Fac. de Quimica, UNAM, Mexico* Al and C-$MgB_2$ doping adds an electron to the system for each atom. This extra electron fills up the $\sigma$-bands thus diminishing the number of $\sigma$-carriers; this has been the usual explanation for the $T_c$ reduction. Nevertheless in this work we show that there is also a large reduction of anisotropy in the electrical conductivity due to the $\sigma$-carriers which should also have an effect on the $T_c$ reduction. Al and C doping produce a different $T_c$ pattern; this difference can be largely explained by the relative shift between the $\sigma$-bands and $\pi$-bands. After adjusting to this shift there is a small but visible difference, at low doping $T_c$ in the Al compounds drops faster than in the C compounds, this can be directly related to the faster loss of conductivity anisotropy in the Al compounds.

**10:00**

**A39 11 Electrons and phonons in the hexagonal layered superconducting alloy $CaAl_{2-x}Si_x$** GIOVANNI B. BACHELET, *INFM and Dipartimento di Fisica, Università ''La Sapienza,'' I-00185 Roma, Italy* LILIA BOERI, *Max-Planck-Institut für Festkörperforschung, D-70569 Stuttgart, Germany* MATTEO GIANTOMASSI, *UPCPM, Université Catholique de Louvain, B-1348 Louvain-la-Neuve, Belgium* We report a first-principles study of structural, electronic and vibrational properties of the superconducting $C_{32}$ phase of the ternary alloy $CaAl_{2-x}Si_x$, both in the experimental range of stability, $0.6 \leqslant x \leqslant 1.2$, and outside, in the limits of high Al and high Si concentration. We find that the dependence of the electronic bands on composition is well described by a rigid-band model, which breaks down outside the experimental range of stability. This breakdown, in the limit of high Al concentration, is connected to vibrational instabilities, and results in important differences between $CaAl_2$ and $MgB_2$. Unlike $MgB_2$, the interlayer band and the out-of-plane phonons play a major role on the stability and superconductivity of CaAlSi and related $C_{32}$ intermetallics.

**10:12**

**A39 12 Direct observation of superconducting gap anisotropy in $YNi_2B_2C$ : Angle-resolved photoemission spectroscopy** TERUHISA BABA, *Institute for Solid State Physics., Univ. of Tokyo* TAKAYOSHI YOKOYA, *Okayama University* SHUNSHUKE TSUDA, SHIK SHIN, TADATAKA WATANABE, *Institute for Solid State Physics., Univ. of Tokyo* MINORU NOHARA, HIDEAKI TAKAGI, *Dept. of Advanced Materials Science., Univ. of Tokyo* TAMIO OGUCHI, *Dept, of Quantum Matter., Hiroshima University* In a borocarbide superconductor $YNi_2B_2C$($T_c$=15K), various experimental results have shown the existence of a gap anisotropy with node. More recently even the direction and type of node have been reported. However, the type of the nodal structure (point or line) seems to be controversial. Also, the position of the node on Fermi surfaces, which is essential for determining the origin of the large anisotropy, has not been clarified, yet. Therefore, we have performed low-temperature ultrahigh-resolution angle-resolved photoemission spectroscopy (ARPES) to clarify the origin of the large anisotropy. We successfully observed experimental valence band dispersions, Fermi surfaces, and momentum-dependent superconducting gap of $YNi_2B_2C$ (001). Superconducting gaps have shown large anisotropy. From these results, we discuss possible orgins of the large anisotropy in $YNi_2B_2C$.

**SESSION A40: QUANTUM ENTANGLEMENT**
**Monday Morning, 13 March 2006**
**343, Baltimore Convention Center at 8:00**
**Christopher Fuchs, Bell Labs & Lucent Technologies, presiding**



**8:00**

**A40 1 A set of entanglement monotones for characterising experimental data** PETER LOVE, *D-Wave Systems Inc* ALEC MAASSEN VAN DEN BRINK, *D-Wave Systems Inc* MOHAMMED AMIN, *D-Wave Systems Inc* ANATOLY SMIRNOV, *D-Wave Systems Inc* MIROSLAV GRAJCAR, *Institute for Physical High Technology, P.O. Box 100239, D-07702 Jena, Germany* EVGENI IL'ICHEV, *Institute for Physical High Technology, P.O. Box 100239, D-07702 Jena, Germany* ANDREI IZMALKOV, *Institute for Physical High Technology, P.O. Box 100239, D-07702 Jena, Germany* ALEX ZAGOSKIN, *University of British Columbia* We define a set of elementary entanglement monotones and give a single measure of entanglement in terms of these monotones which is zero except on globally entangled states. We compute this measure for the ground state of a four qubit superconducting experimental system, and thus confirmed the presence of genuine four-qubit entanglement in the ground state.

**8:12**

**A40 2 Dynamic learning of an experimental entanglement witness for an n-qubit system*** KATHLEEN WALSH, ELIZABETH BEHRMAN, *Department of Physics, Wichita State University* JAMES STECK, *Department of Aerospace Engineering, Wichita State University* STEVEN SKINNER, *Department of Electrical and Computer Engineering, Wichita State University* We extend our previous work on dynamic learning of an entanglement witness for a two-qubit system to n qubits, and show detailed comparisons for the two- and three-qubit systems to published entanglement measures. Our method can also be used for quNits, and can handle a small amount of noise and decoherence.

*Supported by NSF, ECS 0201995

**8:24**

**A40 3 Dynamics and scaling of multi-partite entanglement** FLORIAN MINTERT, *Harvard University* We derive reliable estimates which allow for an efficient evaluation of a specific entanglement measure, concurrence, for further implementation in the monitoring of the time evolution of multipartite entanglement under incoherent environment coupling. This allows us to define a life time of entanglement for different realistic experimental scenarios, and investigate its scaling behaviour with increasing system size.

**8:36**

**A40 4 The entanglement entropy and the Berry phase in solid states*** SHINSEI RYU, *KITP, UCSB* YASUHIRO HATSUGAI, *Dept. of Appl. Phys., Univ. of Tokyo* The entanglement entropy (von-Neumann entropy) has been used to characterize the quantum entanglement of many-body ground states in strongly correlated systems. In this talk, we try to establish a connection between the lower bound of the von-Neumann entropy and the Berry phase defined for quantum ground states. As an example, a family of 1D Hamiltonians with two bands separated by a finite gap is investigated. We argue that when the Berry phase (Zak's phase) of the occupied band is equal to $\pm\ \pi \times$ (odd integer) and when the ground state respects a discrete unitary particle-hole symmetry (chiral symmetry), the entanglement entropy in the thermodynamic limit is at least larger than ln2 (per boundary), i.e., the entanglement entropy that corresponds to a maximally entangled pair of two spins. We also discuss it is related to vanishing of the expectation value of a certain non-local operator which creates a kink in 1D systems.

*Supported in part by NSF under Grant No. PHY99-0 7949

**8:48**

**A40 5 Multiparticle interference, GHZ entanglement, and full counting statistics** HEUNG-SUN SIM, *Department of Physics, Korea Advanced Institute of Science and Technology, Daejeon 305-701, Korea* EUGENE V. SUKHORUKOV, *Department of Theoretical Physics, University of Geneva, CH-1211 Geneva 4, Switzerland* We study [1] quantum coherent transport in a generalized *N*-particle Hanbury Brown-Twiss setup enclosing magnetic flux, where electrons are injected from *N* independent sources and collected in *N* distant detectors, and show that the *N*-th order cumulant of current cross correlations exhibits flux-dependent periodic Aharonov-Bohm (AB) oscillations, while there is no such oscillation in all the lower-order cumulants. The origin of the multiparticle interference is the orbital Greenberger-Horne-Zeilinger entanglement of *N* identical particles. For sufficiently strong AB oscillations the generalized *N*-particle Bell inequalities may be violated, proving the *N*-particle quantum nonlocality. [1] H.-S. Sim and E. V. Sukhorukov, condmat/0508399.

**9:00**

**A40 6 Correlations in a multi-qubit state** D.L. ZHOU, *School of Physics, Georgia Institute of Technology, Atlanta, Georgia 30332, USA* B. ZENG, *Department of Physics, Massachusetts Institute of Technology, MA 02139, USA* Z. XU, *Center for Advanced Study, Tsinghua University, Beijing 100084, China* L. YOU, *School of Physics, Georgia Institute of Technology, Atlanta, Georgia 30332, USA* For an arbitrary partition of a multi-qubit system, we define a correlation measure, which is directly based on a series of multi-qubit correlation functions, to characterize the total correlation among different parts. As an instructive application of our correlation measures, we investigate the entanglement of graph states.

**9:12**

**A40 7 Entanglement of overlapping systems and the breakdown of the tensor product** MATTHEW LEIFER, *Perimeter Institute for Theoretical Physics* Recent work on entanglement in the presence of superselection rules has shown that entanglement ought to be defined operationally, i.e. with respect to sets of local operations actually available to Alice and Bob rather than with respect to an arbitrary tensor product factorization of the state space. Usually Alice and Bob's local operations are assumed to commute, which is an appropriate assumption when their systems are well separated. In this talk I address the question of how far the usual formalism can be maintained if the local operations do not commute. This might be an appropriate description of the spin entanglement between two particles with overlapping spatial wavefunctions, since local operations might then have an effect on both spins. In this situation, the appropriate notion of entanglement is no longer associated to a tensor product factorization of the state space, but it can be approximated by one provided the overlap of the two systems is small and/or the preparable states are sufficiently mixed. In this talk I will present a simple model of the breakdown of the tensor product for two qubits, characterize the states that need to be prepared to observe the effect and discuss how the observed entanglement is related to the entanglement with respect to the usual tensor product factorization.

**9:24**

**A40 8 Modelling Pauli measurements on arbitrary stabilizer states via local hidden variables assisted by classical communication** MATTHEW ELLIOTT, BRYAN EASTIN, CARLTON CAVES, *University of New Mexico* JONATHAN BARRETT, *Perimeter Institute* STEFANO PIRONIO, *California Institute of Technology* In this talk I present communication-assisted local-hidden-variable models for measurements of products of Pauli matrices on stabilizer states. Models are analyzed with respect to restrictions imposed and their efficacy in predicting overall measurement outcomes as well as outcomes of correlated subsets of measurements. In particular, I present a model in which the quantum mechanical results of Pauli product measurements can be predicted by a local-hidden-variable table supplemented by an efficient amount of classical communication and computation.

**9:36**

**A40 9 Quantum Chaos, Localization, and Entanglement in Disordered Heisenberg Models** WINTON BROWN, *Dartmouth College* DAVID STARLING, *SUNY Fredonia* LEA SANTOS, LORENZA VIOLA, *Dartmouth College* We explore the relation between quantum chaos, localization, and entanglement in a two-dimensional disordered Heisenberg spin-1/2 system. Apart from the recent interest in such systems as models for proposed quantum computing architectures, they exhibit interesting transition regions from integrability to chaos and from higher to lower degree of symmetry. Complementing the standard eigenvalue-based analysis for identifying the cross-over into chaos, we suggest looking at the relative delocalization of eigenvectors related to different disorder realizations as a basis-independent indicator of chaoticity. We investigate the behavior of several measures of bipartite and multipartite entanglement – including concurrence; von Neumann entropy; and, using the framework of generalized entanglement, a family of local purities. Our results indicate that bipartite entanglement decreases in the chaotic region, whereas the opposite holds for multipartite entanglement. Connections are established with predictions from random matrix theory.

**9:48**

**A40 10 Entanglement Scaling at Quantum Phase Transitions in Correlated Electron Systems** DANIEL LARSSON, *Philipps-Universität Marburg, Germany* HENRIK JOHANNESSON, *Göteborg University, Sweden* We have carried out an analytic study of the entanglement scaling properties in the one-dimensional Hubbard model. We present exact scaling formulas for the local (''single-site'') entanglement $\mathcal{E}$ at a quantum phase

transition driven by a magnetic field or a chemical potential. The leading divergences of $d\mathcal{E}/dh$ and $d\mathcal{E}/d\mu$ are shown to be directly related to those of the zero-temperature spin and charge susceptibilities. Logarithmic corrections signal a change in the number of local states accessible to the system as it undergoes the transition. We show that the results for the leading divergences are generic, and follow from the scaling hypothesis that any local observable exhibits a singularity at a quantum phase transition. Illustrations from other strongly correlated electron systems are given, including the long-range Hubbard model in one dimension.

**10:00**

**A40 11 Coherent Interaction of Spins Induced by Thermal Bosonic Environment.** DENIS TOLKUNOV, DMITRY SOLENOV, VLADIMIR PRIVMAN, *Clarkson University* We obtain the indirect exchange interaction between two two-state systems, e.g., spins, in a formulation that also incorporates the quantum noise that they experience, due to an environment of bosonic modes, for instance, phonons. We predict that for low enough temperatures the interaction is coherent over time scales sufficient to create entanglement, dominated by the zero-point quantum fluctuations of the environment. We utilize a perturbative approach to obtain a quantum evolution equation for the two-spin dynamics. The induced interaction is calculated exactly. We identify the time scales for which the spins develop and sustain entanglement for various spatial separations.

**10:12**

**A40 12 Entanglement entropy of random quantum critical points with general spin** JOEL MOORE, *UC Berkeley* GIL REFAEL, *California Institute of Technology* The bipartite entanglement at 1D critical points of a subsystem of $N$ sites with the remainder is known to diverge as log$N$, with a coefficient that is related to the central charge for conformally invariant critical points. It was recently shown that for a class of spin-half random critical points, there is also a logarithmic divergence with a coefficient that is universal and corresponds to an irrational ''effective central charge.'' This talk discusses generalizations of this result to higher-spin chains, including the permutation-symmetric critical points found by Damle and Huse, using a combination of analytic and numerical real-space renormalization group methods. Higher-spin chains show numerous complications relative to the spin-half case, such as the introduction of ferromagnetic bonds; their study provides a stringent test of the conjectured $c$-theorem for central charges defined via entanglement entropy.

**10:24**

**A40 13 Local Entanglement and Quantum Phase Transition in Spin Models*** SHI-JIAN GU, *Department of Physics and Institute of Theoretical Physics, The Chinese University of Hong Kong, Hong Kong, China* GUANG-SHAN TIAN, *School of Physics, Peking University, Beijing 100871, China* HAI-QING LIN, *Department of Physics and Institute of Theoretical Physics, The Chinese University of Hong Kong, Hong Kong, China* In this work, we study quantum phase transitions in both the one- and two-dimensional XXZ models with either spin $S=1/2$ or $S=1$ by a local entanglement We show that the behavior of $E_v$ is dictated by the low-lying spin excitation spectra of these systems. Therefore, the anomalies of $E_v$ determine their critical points. It reminds us the well-known fact in optics: The three-dimensional image of one subject can be recovered from a small piece of holograph, which records interference pattern of the reflected light beams from it. Similarly, we find that the local entanglement, which is rooted in the quantum superposition principle, provides us with a deep insight into the long-range spin correlations in these quantum spin systems. **References:** [1] S. Sachdev, itQuantum Phase Transitions (Cambridge University Press, Cambridge, 2000). [2] Shi-Jian Gu, Guang-Shan Tian, and Hai-Qing Lin quant-ph/0509070

*This work is supported by RGC Projects CUHK 401703 and 401504 and by CNSF grant No. 90403003.

**10:36**

**A40 14 Quantum Entanglement in a Spin Ladder with Ring Exchange*** JUN-LIANG SONG, SHI-JIAN GU, HAI-QING LIN, *Institute of Theoretical Physics and Physics Department, The Chinese University of Hong Kong, Hong Kong, China* In this paper we've studied entanglement properties of a spin ladder with ring exchange. Several entanglement properties, e.g. pair concurrence and block-block entanglement were obtained by exact diagonalization method. The relationship between the global phase diagram and ground-state quantum entanglement was investigated. It was shown that block-block entanglement of different block size and configurations manifests richer information of the system. It was also found that the block-block entanglement reaches its maximum or minimum at some QPT points which is also the high symmetry point. The temperature dependence of the entanglement properties is also investigated and it is shown that entanglement is suppressed by the temperature fluctuations and vanishes at some threshold temperatures.

*This work is supported by RGC Projects CUHK 401703 and 401504.

**10:48**

**A40 15 Entanglement and dissipation in a quantum-dot array.** LESVIA DEBORA CONTRERAS-PULIDO, *Centro de Investigacion Cientifica y de Educacion Superior de Ensenada (CICESE)* FERNANDO ROJAS, *Centro de Ciencias de la Materia Condensada-UNAM* RAMON AGUADO, *Condensed Matter Theory, ICMM, CSIC* Primarily motivated by quantum information theory, charge in quantum dots (QD) seems to be a promising candidate for implementation of qubits and entangled states [1]. We explore theoretically the dynamical formation of entangled states, including dissipative effects, of two parallel double QD uncoupled between them but strongly coupled to the same phonon thermal bath. The QD array is modeled with an extended Hubbard type Hamiltonian and dissipation is taken into account by using a polaron transformation to obtain the reduced density matrix of the system [2]. We find that it is possible to obtain entangled electronic states through a strong electron-phonon interaction, characterized by: Wootters' concurrence, charge distribution and probabilities for each Bell state as a function of relevant parameters (hopping, temperature, electron-phonon amplitude). The work is supported by DGAPA project IN114403 and CONACyT project 43673-F [1] Hichri et al., Phys.E 24,234 (2004) [2] Aguado and Brandes, Phys.Rev.Lett.92, 206601 (2004).

**SESSION A41: QUANTUM FLUIDS AND SOLIDS**
**Monday Morning, 13 March 2006**
**344, Baltimore Convention Center at 8:00**
**Haruo Kojima, Rutgers University, presiding**

**8:00**

**A41 1 Specific heat of liquid He-4 near the superfluid transition and confined in cylindrical channels*** TAHAR AOUAROUN, GUENTER AHLERS, *UCSB* We present new measurements of the specific heat near the lambda transition of liquid He-4 at saturated vapor pressure and confined in microchannel plates containing cylindrical holes. We investigated two channels diameters: 1$\mu$m and 2$\mu$m. Our results for the scaling function near the specific-heat maximum are in reasonably good agreement with previous measurements on channels with a 1 $\mu$m $\times$ 1 $\mu$m square cross section[1] and on cylindrical channels with a 0.26$\mu$m diameter[2]. They also are consistent with the scaling function derived from Monte Carlo calculations.[3] However, they suggest a size- dependent systematic departure from a unique scaling function that is consistent with earlier measurements[3] on cylindrical channels of 8$\mu$m diameter.

*Work supported by NASA Grant NAG 3 2872

[1]M.O. Kimbal, K.P. Mooney, and F.M. Gasparini, Phys. Rev. Lett. **92**, 115301 (2004)
[2]J.A. Lipa, M. Coleman, and D.A. Stricker, J. Low Temp. Phys. **124**, 443 (2001)
[3]N. Schultka and E. Manousakis, J. Low Temp. Phys. **111**, 783 (1998)

**8:12**

**A41 2 Deformation and damage in silica aerogels during fluid filling*** TOBIAS HERMAN, JOHN BEAMISH, *University of Alberta* Interfaces are present throughout any porous medium during fluid adsorption below the liquid-vapor critical point. Surface tension in these curved liquid-vapor interfaces produces the pressure difference between the two phases which is responsible for capillary condensation. The surface tension also exerts a force on the solid, although it is usually much smaller than the elastic moduli of the porous medium. Aerogels, however, have extremely small elastic moduli so surface tension induced deformation can be significant and even destructive. We present measurements of the dilation and compression of two silica aerogels (densities 110 and 51 kg/m$^3$) during adsorption and desorption of low surface tension fluids (helium and neon). The denser aerogel changed its length by up to 2% during adsorption of helium, still within its elastic regime; the lighter aerogel shrank by even larger amounts and appeared to sustain permanent damage.

*Supported by a grant from NSERC Canada

**8:24**

**A41 3 Cryogenic Pulsed Laser Deposition of Lithium for $^4$He Absorption Experiments** E. VAN CLEVE, P. TABOREK, J.E. RUTLEDGE, *University of California, Irvine* We are developing techniques to prepare films of alkali metals on cryogenic surfaces by laser ablation. The alkali metals are known to provide weak adsorption potentials for $^4$He which results in nontrivial wetting and superfluid onset phenomena. Film preparation technique strongly affects some $^4$He wetting properties as has been seen in contact angle measurements of $^4$He on Cs surfaces. Of particular interest are Li surfaces which at low temperatures are predicted (1) to be superfluid with less than monolayer total $^4$He coverage. We have grown Li films on using 532 nm light from an Nd-YAG laser on to room temperature quartz crystal microbalances (QCM). We will present measurements of film growth rate as a function of the laser fluence. Preliminary $^4$He isotherm measurements on Li films laser ablated onto 4K QCMs will be compared with adsorption isotherms on the heavier alkali metal surfaces. (1) Massimo Boninsegni and Milton W. Cole, J. Low Temp. Phys. 113, 393 (1998).

**8:36**

**A41 4 Acoustic crystallization*** SEBASTIEN BALIBAR, RYOSUKE ISHIGURO, FREDERIC CAUPIN,[†] *ENS-Paris* By focusing high intensity acoustic waves in the middle of a liquid, it is possible to pressurize it far beyond its solid-liquid equilibrium pressure. This is because, in the absence of walls or defects, the nucleation of crystals needs to be ''homogeneous,'' and that the threshold pressure for this phenomenon is usually very high. In a classical liquid, the viscosity increases with pressure so that the dynamics blocks as the pressure is increased and a transition to a glassy state occurs. However, we did not expect this to occur in a superfluid, and we looked for acoustic crystallization in liquid helium. We have found evidence that an acoustic wave travelling in superfluid helium can indeed crystallize this liquid on its path. We relate this phenomenon to the existence of an instability where Landau's ''rotons'' become soft modes. We discuss further developments of this experiment in relation with the existence of superfluidity in a very dense liquid.

*RI acknowledges support from the JSPS
[†]associated with CNRS and Universities Paris 6 and 7

**8:48**

**A41 5 Bose-Einstein Condensation and atomic kinetic energies in liquid $^3$He-$^4$He mixtures*** SOULEYMANE DIALLO, *University of Delaware* JONATHAN PEARCE, *Institut Laue Langevin* RICHARD AZUAH, *NIST Center for Neutron Research* HENRY GLYDE, *University of Delaware* We present neutron scattering measurements of the momentum distribution of liquid $^3$He-$^4$He mixtures. The experiments were performed at wavevectors $Q$, 26 $\leqslant$ $Q \leqslant$ 29 Å$^{-1}$, on the MARI time-of-flight spectrometer at the ISIS pulsed spallation neutron source. Mixtures with $^3$He concentrations $x$ between 0 and 20% were investigated both in the superfluid and normal phases. From the data, we extract, to new accuracy, the Bose-Einstein condensate fraction $n_0$ and the momentum distributions of $^3$He and $^4$He atoms. We find an increase in $n_0$ above the pure $^4$He value; from 7.25$\pm$ 0.75% ($x$ = 0%) to 11.2 $\pm$ 1.85% at $x$ = 15%, in agreement with theoretical calculations but in disagreement with the only other measurement. The $^4$He kinetic energy, \kef, is found to be largely independent of $x$. The $^3$He momentum distribution $n(\mathbf{k})$ is not well fitted with a Fermi step function alone. A high momentum tail in $n(\mathbf{k})$ is needed to get a good fit - a tail that is consistent with calculated tails in $n(\mathbf{k})$. The $^3$He atomic kinetic energy, $K_3$, is determined almost entirely by this tail. It is therefore not a well determined single property for comparing theory and experiment. This finding resolves a long-standing discrepancy on $K_3$ between theory and experiment.

*Work supported by BES DOE, DE-FG02-03ER46038 and ISIS

**9:00**

**A41 6 Bose-Einstein Condensation in liquid $^4$He films*** JONATHAN PEARCE, *Institut Laue Langevin* SOULEYMANE DIALLO, *University of Delaware* RICHARD AZUAH, *NIST Center for Neutron Research* TOM ARNOLD, *ISIS Pulsed Neutron Facility* JOHN LARESE, *University of Tennessee* HENRY GLYDE, *University of Delaware* Neutron scattering measurements of Bose-Einstein condensation in liquid $^4$He fils will be presented. The measurements were carried out on the MARI time-of-flight spectrometer at the CCLRC ISIS Facility, Rutherford Appleton Laboratory, UK. The goal is to determine whether the condensate fraction, $n_0$, is enhanced above the bulk liquid value at a liquid $^4$He surface. It is also to determine $n_0$ in 2D thin films and, by varying the film thickness, observe a 2D to 3D cross-over. Data for films on a flat MgO substrate [1] and on carbon-black will be presented. The data shows, that $n_0$ is indeed significantly enhanced at a film - vapor surface suggesting a lower liquid density there [2]. [1] J.V. Pearce *et al.*, *J. Phys. Condens. Matter* **16**, 4391 (2004) [2] E.W. Drager and D.M. Ceperley, *Phys. Rev. Lett.* **89**, 15301 (2002)

*Work supported by BES DOE, DE-FG02-03ER46038 and ISIS.

**9:12**

**A41 7 Bilayer Thermometers for Third Sound Detection*** J.D. CUMMINGS, R.B. HALLOCK, *Univ. of Mass. Amherst* We present results from an experiment to develop bilayer metallic films of aluminum and gold as superconducting transition edge thermometers for the detection of third sound waves. Generally, traditional transition edge thermometers operate in a temperature range that is dictated by the choice of superconductor, e.g. $\sim$ 1.5K for aluminum and $\sim$ 0.8K for zinc, which is tunable over a modest range by application of a magnetic field or bias current. Bilayers offer the option of selecting the optimal transition temperature for an experiment to be done by adjusting the ratio of normal metal (Au) thickness to the superconductor (Al) thickness. This allows a detector to be designed to operate at any temperature below the transition temperature for the pure superconducting film. We will present transition edge data for such thermometers and document their utility for third sound detection.

*Supported by the NSF and UMass Research Trust Funds

**9:24**

**A41 8 Anomalous Coupling Between Superfluid Vortices and Curvature** ARI TURNER, VINCENZO VITELLI, DAVID NELSON, *Harvard University* Vortices in a thin film of superfluid helium on a curved surface are predicted to have a long range interaction with the curvature of the surface. Vortices are trapped by features of the surface with appropriate Gaussian curvature. The energetics will be compared and the dynamics contrasted with those of particles experiencing a two dimensional Coulomb force.

**9:36**

**A41 9 SQUID NMR Studies of Two-Dimensional $^3$He Films on HOPG ZYX Graphite** JINSHAN ZHANG, LEI GUO, YULIANG DU, C.M. GOULD, H.M. BOZLER, *Dept. of Physics & Astronomy, Univ. of Southern California, Los Angeles, CA 90089* SQUID NMR experiments on the second layer of $^3$He films on Grafoil substrates in the low field limit found ferromagnetic ordering for coverages over 20 atoms/nm$^2$. The appearance of ordering in a two-dimensional magnetic film can be caused by weak anisotropy and/or dipolar interactions, or could be a manifestation of finite size effects. By replacing Grafoil with Highly Oriented Pyrolytic Graphite (HOPG) ZYX grade, we increased the substrate structural coherence length by a factor of 10 in order to study the importance of finite size effects through a magnetization measurement on 2-D $^3$He films. Our recent experiments found the ferromagnetic ordering temperature to be the same or higher on ZYX than on Grafoil at coverages over 20 atoms/nm$^2$, showing no evidence for an increased suppression of the ordering due to the increasing coherence length. We also saw evidence for bound spin waves in the ordered layer. Studies in the coverage range 20-24 atoms/nm$^2$ are complicated by the possibility of coexistence of two phases. Recently we extended our measurements to higher coverages where the situation is less complicated and a single incommensurate solid phase is formed unambiguously. We report on these studies which continue to support the picture of a 2-D magnetically ordered solid. *Supported by NSF through grant DMR-0307382

**9:48**

**A41 10 Ultrasonic Spectroscopy in Liquid $^3$He in 98% Porosity Aerogel by Direct Propagation*** H.C. CHOI, N. MASUHARA, J.-H. PARK, M.W. MEISEL, Y. LEE, *Dept. of Physics, University of Florida, P.O. Box 118440, Gainesville, FL 32611, USA* N. MULDERS, *Department of Physics and Astronomy, University of Delaware, Newark, DE 19716, USA* Systematic investigations on the effect of static disorder on itp-wave superfluid $^3$He have been made possible by utilizing its unique structure of high porosity silica aerogel. For the past 10 years, a burst of experimental effort revealed that three distinct superfluid phases exist in the P-H-T phase diagram of the $^3$He/98% aerogel system. These three phases are conveniently named the A-, B-, and $A_1$-phases as in the bulk, although only spin structures of the superfluid phases have been identified. In particular, the verdict on the so called A-phase is by no means conclusive. As has been the case in the bulk, for a clear identification of the order parameter structure, both spin and orbital components need to be examined. We report our preliminary results of sound propagation in an attempt to directly investigate the orbital structure of the superfluid phases in 98% aerogel using a pulsed ultrasound spectroscopic technique. Preliminary data for the transmission and the surface impedance will be presented.

*This work was partially supported by an Alfred P. Sloan Research Fellowship (YL), NSF grants DMR-0239483 (YL) and DMR-0305371 (MWM).

**10:00**

**A41 11 Transverse acoustic spectroscopy of Superfluid $^3$He in compressed aerogel.*** P. BHUPATHI, H. C. CHOI, J. JHAVERI, B. H. MOON, Y. LEE, *University of Florida, Gainesville, FL 32611-8440.* In light of the recent developments on the A-B transition in superfluid $^3$He in aerogel and the effect of anisotropic scattering[2], we have designed an experiment to perform transverse acoustic impedance measurements on compressed aerogel. We investigate the effect of global anisotropy on the phase transition, generated by introducing uniaxial compression of 5 % on the aerogel. We report our preliminary results together with the measurements on the uncompressed aerogel.

*This work is partially supported by an Alfred P. Sloan Research Fellowship(YL) and NSF grants DMR-0239483. [2] C. L. Vincente *etal.*, Phys. Rev. B 72, 094519 (2005).

**10:12**

**A41 12 Spin Relaxation Phenomenon in Superfluid $^3$He $A_1$*** H. KOJIMA, *Rutgers University* S. KOBAYASHI, A. YAMAGUCHI, H. ISHIMOTO, *Institute for Solid State Physics* The spin relaxation phenomenon in superfluid $^3$He $A_1$ phase is studied using a newly constructed magnetic fountain pressure cell in which two reservoirs are connected via a superleak channels of height 20 $\mu$m. Experiments are carried out to explore the relaxation mechanism of the induced fountain pressure under externally applied magnetic field gradient along the superleak. The relaxation of fountain pressure reflects that of spin density. The observed relaxation time $\tau$ varies from less than 1 s near $T_{c2}$ to about 80 s near $T_{c1}$. The maximum relaxation time may be limited by the normal fluid flow in the channels. Near $T_{c2}$, the observed relaxation rate may be described by a power law dependence on reduced temperature as $1/\tau \propto [(T - T_{c2})/(T_{c1} - T_{c2})]^{-\beta}$, where $\beta \approx 1.5$ and has little dependence on the static magnetic field(up to 8 tesla) and liquid pressure(10 - 29 bars). To our knowledge, there is no theory which predicts such increase in relaxation rate over a relatively large temperature range near $T_{c2}$. A preliminary interpretation is given in terms of intrinsic spin relaxation arising from small but increasing presence of minority spin pair condensate in $A_1$ phase as $T_{c2}$ is approached.

*supported in part by NSF.

**10:24**

**A41 13 Measurements of Longitudinal and Transverse NMR Frequencies in Superfluid $^3$He using dc SQUID Detectors*** YULIANG DU, H.M. BOZLER, C.M. GOULD, *University of Southern California* The most important tools in the initial identification of the order parameters of the superfluid phases of $^3$He in bulk were longitudinal and transverse NMR because the detailed comparison of these frequencies and their magnetic field dependences strongly differentiated between alternative models. In contrast, for superfluid $^3$He confined within aerogel, longitudinal resonance has not been measured to date, having only been inferred from transverse measurements and the simple sum of squares relation known to hold for the axial state in bulk. This relationship has not been confirmed for the aerogel-confined phase, and there are theoretical suggestions that it may not be valid. We have begun an experiment to directly compare longitudinal and transverse resonance frequencies in aerogel-confined superfluid $^3$He using some of the same dc SQUID NMR techniques we have developed over the last 20 years in our lab. In initial experiments to prove the technique, we are making optimal use of the broadband nature of the dc SQUID detector and have measured the superfluid's longitudinal response to a sudden field step.

*Supported by the National Science Foundation through grant DMR0307382.

## SESSION A42: FOCUS SESSION: PLANETARY MATERIALS I

**Monday Morning, 13 March 2006; 345, Baltimore Convention Center at 8:00**
**Renata Wentzcovitch, University of Minnesota, presiding**

***Invited Papers***

**8:00**

**A42 1 Electronic structure and phase transition in iron bearing minerals.**
STEFANO DE GIRONCOLI, *SISSA and DEMOCRITOS – Trieste*

First-principles calculations are playing an important role in the development of our understanding of Earth interior. A proper treatment of iron bearing minerals is fundamental in this respect. Unfortunately standard DFT approaches such as the local density (LDA) or generalized gradient (GGA) approximations fail in describing even qualitative features of even simple iron minerals, such as the insulating nature and magnetic structure of many oxides. DFT+U approximation has demonstrated to improve significantly the physical description of transition metal and rare earth compounds. In order to make DFT+U a really ''ab-initio'' approach, an internally consistent determination of the involved U parameter is however needed. In alternative computationally more demanding, but supposedly more accurate, approaches such as PBE0 or B3LYP Hartree-Fock-DFT hybrid functionals can be explored. I'll report on my recent research on these subjects, focussing on iron oxide, magnisium-wustite high-spin-low-spin phase transition, and ematite.

***Contributed Papers***

**8:36**

**A42 2 High-to-low spin transition in iron in Magnesiowüstite: elastic properties*** CESAR R.S. DA SILVA, *Minnesota Supercomputing Institute, University of Minnesota* TAKU TSUCHIYA, *Geodynamics Research Center, Ehime University, Japan* RENATA M. WENTZCOVITCH, *Department of Chemical Engineering and Materials Science, Minnesota Supercomputing Institute, University of Minnesota* STEFANO DE GIRONCOLI, *SISSA and DEMOCRITOS National Simulation Center, Trieste, Italy* The high-to-low spin transition in iron in Magnesiowüstite (Mw), $Mg_{(1-x)}Fe_x,O$, is accompanied by considerable volume reduction. This changes the elastic properties of Mw across this transition. Using an LDA+U method with consistently calculated Hubbard U, we investigate the elastic signature of this transition. We find temperature sensitive changes in elasticity across this transition. In Earth's lower mantle, this transition should occur continuously and leave behind an unnoticeable sign.

*Research supported by NSF/EAR 0230319, NSF/ITR 0428774, VLab, NSF/ITR 0325218, ITAMIT, Ehime University Project Fund DE: 3620 Mineral and crystal chemistry (1042)

**8:48**

**A42 3 Spin state of ferrous iron in perovskite** RYAN REQUIST, *Stony Brook University* KOICHIRO UMEMOTO, *University of Minnesota* RENATA WENTZCOVITCH, *University of Minnesota* Diamond anvil cell experiments at pressures up to 145 GPa have shown evidence for a high spin to low spin transition in iron in magnesium silicate perovskite ($MgSiO_3$.) The spin transi-

tion will influence the optical absorption spectrum and elastic properties of this mineral. We present density functional calculations of (Mg,Fe)$SiO_3$ with ferrous iron substituting for magnesium at a concentration of 12.5%. The calculations use the local density approximation with Hubbard term (LDA+U) and supercells containing up to 160 atoms. We describe the pressure dependence of the iron spin state. Research supported by NSF/EAR 0230319, NSF/ITR 0428774 and 0426757, VLab, NSF/ITR 0325218, ITAMIT.

**9:00**

**A42 4 Ab Initio Study of Thermodynamics of Fe and Spin Transitions in the Lower Mantle** DANE MORGAN, AMELIA BERTA, *University of Wisconsin - Madison* KRISTIN PERSSON, GERBRAND CEDER, *Massachusetts Institute of Technology* Recent experiments have demonstrated spin transitions in Fe in both the rocksalt ferropericlase (Mg,Fe)O and perovskite (Mg,Fe)$SiO_3$ phases at lower mantle pressures. The spin transitions have potentially profound implications for the materials properties of the lower mantle. However, the coupling of thermodynamic temperature effects and the spin transition is still poorly understood. In this talk we present an ab initio based thermodynamic model for Fe spin transitions in lower mantle phases. We build a free energy model which includes configurational, vibrational, magnetic, and electronic contributions. The resulting free energy expressions are used to construct a phase diagram for the lower mantle ferropericlase which includes the impact of Fe spin transitions.



***Invited Papers***

**9:12**

**A42 5 Effects of the Spin Transition of Iron in Magnesiowüstite-(Mg,Fe)O: Applications to the Earth's Lower Mantle.***

JUNG-FU LIN, *Lawrence Livermore National Laboratory*

Magnesiowüstite [(Mg,Fe)O] is the second most abundant mineral in the Earth's lower mantle. Here I will discuss the spin states of iron in magnesiowüstite and the isolated effects of the electronic transitions on the elastic, thermodynamic, magnetic, and vibrational properties of magnesiowüstite under high pressures and high temperatures. Pressure-induced electronic spin transitions of iron from high-spin to low-spin states have been recently observed to occur in magnesiowüstite under high pressures using high-pressure X-ray emission spectroscopy and synchrotron Mössbauer spectroscopy. Based on the synchrotron Mössbauer studies of $(Mg_{0.75},Fe_{0.25})O$, the simultaneous disappearance of the quadrupole splitting and the drop of the isomer shift at above 62 GPa are consistent with a high-spin to low-spin electronic transition of iron in the sample between 62 and 70 GPa. Addition of FeO in MgO stabilizes the high-spin state to higher pressures and the high-spin to low-spin transition of iron in magnesiowüstite results in an abnormal compressional behaviour between the high-spin and the low-spin states[1]. Moreover, there are also significant changes in particular physical properties of magnesiowüstite such as force constant across the electronic spin transition. Here I have combined results from a variety of high-pressure techniques to understand the effects of the electronic transition on the physical properties of magnesiowüstite and to explore possible geophysical consequences of the transition in the Earth's lower mantle. [1]J. F. Lin, V. V. Struzhkin, S. D. Jacobsen, M. Hu, P. Chow, J. Kung, H. Liu, H. K. Mao, and R. J. Hemley, Spin transition of iron in magnesiowüstite in Earth's lower mantle, itNature, 436, 377-380, 2005.

*This work was performed under the auspices of the U.S. DOE by UC and LLNL under Contract W-7405-Eng-48.

***Contributed Papers***

**9:48**

**A42 6 Electronic Spin State and Elasticity of (Mg, Fe)(Si, Al)O3-perovskite at high pressure** LI LI, DONALD WEIDNER, *Stony Brook University* JOHN BRODHOLT, STEPHEN STACKHOUSE, MARIA ALFREDSSON, DAVID PRICE, *Universtiy College London* We investigate the effect of pressure on the electronic spin state of ferric iron in Al-bearing $MgSiO_3$-perovskite using first-principle computations (Density Functional Theory with the Generalized Gradient Approximation). We also calculate the single crystal elastic moduli ($c_{ij}$) for (Mg, $Fe^{3+}$)(Si, Al)$O_3$ perovskite to understand the effect of chemical variations and spin state transitions of the $Fe^{3+}$ ions on these properties. Ferric iron (6.25 mol%) and Al (6.25 mol%) substitute for Mg and Si respectively. Our results show that spin state transition from high spin (HS) to low spin (LS) occurs on the $Fe^{3+}$ ions at high pressure, while there is no stability field for the intermediate spin state. Fe $^{3+}$ alone can be responsible for the spin state transition. The models witness a transition pressure ranging from 97-126 GPa. Differential stress can change the pressure for the spin collapse. These results are one explanation to the reported experimental observations that the spin transition occurs over a wide pressure range. We find that ferric iron lowers the elastic moduli relative to the Al charge-coupled substitution. The spin state of the iron for this composition has a relatively small effect ( $<$ 0.5% variation) on both bulk modulus and shear modulus. Replace this text with your abstract body.

**10:00**

**A42 7 Theory of magnesium silicates with bearing Fe and Al in the lower mantle and the Earth's D'' layer*** FEIWU ZHANG,[†] ARTEM OGANOV,[‡] *ETH Zurich* Although iron and aluminum incorporation into Earth's mantle minerals are expected to have important effects, little is known about Fe valence and spin state in such major phases as $MgSiO_3$ perovskite (itPv, main mineral of the lower mantle) and post-perovskite (itPPv, main mineral of the Earth's D'' layer). Here, we perform itab initio simulations, indicating that $Fe^{2+} \rightarrow Fe(metal) + Fe^{3+}$ in itPv& itPPv. A new detailed microscopic picture of $MgSiO_3$ itPv& itPPv is presented, including the complexity of Fe-Al incorporation, the spin transitions in $Fe^{3+}$ and lack of such in $Fe^{2+}$, and the effects of $Fe^{2+}$,

$Fe^{3+}$, $Al^{3+}$ on the stability of itPPv. These theory results explain and reconcile the recent diverse experimental results on the iron-spin transition in $MgSiO_3$ and provide basis for future geodynamical and petrological studies of the mantle and the D'' layer.

*Acknowledge access to supercomputers at CSCS (Manno) and the HP Superdome of ETH Zurich. Funding by ETH Zurich

†http://olivine.ethz.ch/ feiwu

‡http://olivine.ethz.ch/ artem



**10:12**

**A42 8 High Pressure studies on nanoparticles of gamma $Fe_2O_3$** ARUN BOMMANNAVAR, MADDURY SOMAYAZULU, *HPCAT, Advanced Photon Source, Chicago* VAMAN NAIK, *University of Michigan-Dearborn* RATNA NAIK, *Wayne State University* Compressibility of the gamma phase of $Fe_2O_3$ (Maghemite) nano-particles was studied using angle dispersive x-ray diffraction on the micro-diffraction beamline at HPCAT of the Advanced Photon Source. Nano-particles of three different sizes (3 and10 and 20 nm) were studied up to 31 GPa using a diamond anvil cell equipped with c-BN seats. Two samples were synthesized by treating sulfonated divinyl benzene polystyrene resin matrix with aqueous solutions of (1) FeCl2,(2) $FeCl_3$. The particle size of $\gamma$-$Fe_2O_3$ prepared using FeCl3 was $\sim$ 3 nm and with FeCl2 was $\sim$ 10 nm. The 20 nm particle size sample was bought commercially. The bulk modulii for 10 nm and 20 nm samples were 212 (5) and 207 (5) GPa which are close to the bulk value of 203 (10) GPa, whereas 3.4 nm sample shows a higher value of 240 (5) GPa. Transition pressure ($P_{tr}$) at which maghemite transforms to hematite varies with particle size and was estimated to be 10 (2) GPa, 17 (2) GPa and 27 (2) GPa for 3 nm, 10 nm and 20 nm particle size samples, respectively.

**10:24**

**A42 9 Composition Dependence of Pressure-Induced Spin Transitions in the (Mg,Fe)SiO3 Perovskite and (Mg,Fe)O Rocksalt System** AMELIA BERTA, *University of Wisconsin-Madison* KRISTIN PERSSON, *Massachusetts Institute of Technology* GERBRAND CEDER, *Massachusetts Institute of Technology* DANE MORGAN, *University of Wisconsin-Madison* Recent experimental results suggest that Fe undergoes a high-spin to low-spin transition in both the rocksalt and perovskite phases at lower mantle pressures. These spin transitions may have a profound impact on the properties of lower mantle phases. In this work the critical spin-transition pressures for Fe in perovskite $(Mg,Fe)SiO_3$ and rocksalt (Mg,Fe)O are calculated using itab initio methods. We focus in particular on the alloy nature of the material, studying the spin-transition pressure for varying concentrations of Fe. The results show that as the concentration of Fe increases, the transition pressure decreases in the perovskite. This is directly opposite the trend observed for spin transition pressures found in rocksalt (Mg,Fe)O. The difference in trends in spin-transition pressure is explained by the difference in physics between the two structures.

## SESSION A43: FOCUS SESSION: STRONGLY INTERACTING FERMI GASES AND THE BCS-BEC CROSSOVER I

**Monday Morning, 13 March 2006**
**346, Baltimore Convention Center at 8:00**
**C. Chin, University of Chicago, presiding**

***Contributed Papers***

**8:00**

**A43 1 A Two-Channel R-Matrix Analysis of Magnetic Field Induced Feshbach Resonances** PAUL JULIENNE, *National Institute of Standards and Technoloy* NICOLAI NYGAARD, *Aarhus University* BARRY SCHNEIDER, *National Science Foundation* A two channel model of magnetic field induced Feshbach resonances in ultra-low atom-atom collisions is presented. The model uses realistic potentials and is parametrized using available theoretical and experimental data to reproduce the known low-energy scattering properties of the colliding atoms. The coupled equations are solved using the R-Matrix method, expanding the wavefunction in a Finite Element Discrete Variable basis. This basis enables us to capture both the short-range behavior of the molecular vibrational states as well as the long-range scattering states. Results will be presented showing the behavior of the wavefunctions and T- matrices as a function of the external magnetic field for selected alkali atom pairs.

**8:12**

**A43 2 Many-body Feshbach Hamiltonians in the two-body limit.** NICOLAI NYGAARD, *University of Aarhus* JAMES E. WILLIAMS, PAUL S. JULIENNE, *NIST* We discuss how the many-body theory of a gas with interactions controlled by a Feshbach resonance can be constructed in a manner, which incorporates the correct two-body physics. This entails the introduction of an energy dependent renormalized coupling constant for atom-molecule conversion that embodies the low energy scattering properties of the entrance channel potential. We demonstrate that with this model the binding energies of the dressed Feshbach molecules may be faithfully reproduced.

**8:24**

**A43 3 Properties of the BCS-BEC condensate in the BEC regime** JESPER LEVINSEN, VICTOR GURARIE, *University of Colorado at Boulder* We study a gas of fermions undergoing a wide resonance s-wave BCS-BEC crossover, in the BEC regime at zero temperature. We calculate the chemical potential and the speed of sound of this Bose-condensed gas, as well as the condensate depletion, in the low density approximation. We discuss how higher order terms in the low density expansion can be constructed. We demonstrate that the standard BCS-BEC gap equation is invalid in the BEC regime and is inconsistent with the results obtained here. The low density approximation we employ breaks down in the intermediate BCS-BEC crossover region. Hence our theory is unable to predict how the chemical potential and the speed of sound evolve once the interactions are tuned towards the BCS regime. As a part of our theory, we derive the well known result for the bosonic scattering length diagrammatically and check that there are no bound states of two bosons.

*Invited Papers*

**8:36**
**A43 4 Studying the BEC-BCS crossover with an ultracold gas of $^6$Li atoms.**
JOHANNES HECKER DENSCHLAG, *Institut fuer Experimentalphysik, Universitaet Innsbruck, Austria*

Collective oscillations are a good tool to investigate the properties of an ultracold Fermi gas in the BEC-BCS crossover. We will present new and improved measurements on these collective excitations. Our results help to determine the equation of state of the strongly interacting Fermi gases.

*Contributed Papers*

**9:12**
**A43 5 Radio frequency spectroscopy and the pairing gap in trapped Fermi gases*** YAN HE, QIJIN CHEN, KATHRYN LEVIN, *University of Chicago* We present a theoretical interpretation of radio-frequency (RF) pairing gap experiments in trapped atomic Fermi gases, over the entire range of the BCS-BEC crossover, for temperatures above and below $T_c$. Our calculated RF excitation spectra, as well as the density profiles on which they are based, are in semi-quantitative agreement with experiment. We provide a detailed analysis of the physical origin of the two different peak features seen in RF spectra, one associated with nearly free atoms at the edge of the trap, and the other with (quasi-)bound fermion pairs. Reference: Phys Rev. A 72, 011602(R) (2005).

*NSF-MRSEC Grant No. DMR-0213745

**9:24**
**A43 6 Dynamical projection of atoms to Feshbach molecules at strong coupling.** ROMAN BARANKOV, *UIUC* LEONID LEVITOV, *MIT* An interesting method of atomic state projection to the Feshbach molecules using the magnetic field sweep through the resonance was employed in the recent experiments [1]. The sweep could be made very fast compared to typical fermion time scales, such as the collision frequency or inverse Fermi bandwidth, making the process a ''snapshot probe'' with regard to the collective fermion processes. On a single particle level, broad Feshbach resonances studied in Ref.[1], exhibit strong atom-molecule coupling in a relatively wide detuning range. In this sense, the sweep speed [1] corresponds to essentially adiabatic atom/molecule conversion, slow on the scale of the resonance width. We develop a theory [2] that describes molecules at a sweep fast compared to the elastic collisions, when only the quantum-mechanical processes involving two atoms transition into a molecule are relevant. Our approach accounts for resonance dissociation/association in the presence of time-dependent detuning as well as for fermion pairing correlations in the initial state. An exact solution is found, predicting a 1/3 power law dependence on the inverse sweep rate for molecule production efficiency at fast sweep. The predicted production efficiency agrees with experimental observations for both condensed and incoherent molecules away from saturation. [1] C. A. Regal, *et al.*, Phys. Rev. Lett. **92**, 040403 (2004); M. W. Zwierlein, *et al.*, Phys. Rev. Lett. **92**, 120403 (2004) [2] R. A. Barankov and L. S. Levitov, cond-mat/0506323

**9:36**
**A43 7 Dressed Feshbach molecules in the BEC-BCS crossover** MATHIJS ROMANS, HENK STOOF, *Utrecht University* There has been a lot of interest in Feshbach resonances and the BEC-BCS crossover that is associated with it. We present work that describes the crossover in terms of dressed molecules, and gives a theory to calculate the internal structure of the paired state. We integrate out the fermions exactly, and take into account the fluctuations of the molecular field to determine the probability $Z$ for dressed molecules to be in the closed channel state. Our approach includes the relevant two-body physics completely. Also the density of condensed and noncondensed dressed molecules can be determined for the entire BEC-BCS crossover. We compare our results to experiment.

**9:48**
**A43 8 Two-fluid hydrodynamic modes in a trapped Fermi superfluid gas*** EDWARD TAYLOR, ALLAN GRIFFIN, *University of Toronto* In the collisional region at finite temperatures, the collective modes of superfluids are described by the Landau two-fluid hydrodynamic equations. This region can now be probed over the entire BCS-BEC crossover in trapped Fermi superfluids with a Feshbach resonance. We have recently developed a variational formulation of the two-fluid hydrodynamic equations that greatly simplifies calculations of the collective modes in trapped superfluid gases. The frequencies are given in terms of effective spring constants involving spatial integrals over position-dependent equilibrium thermodynamic functions. We present results based on this theory using the LDA and thermodyanmic functions for a uniform gas in the BCS-BEC crossover region, with pair fluctuations included using the Nozières and Schmitt-Rink approximation. The temperature dependent out-of-phase hydrodynamic modes (the analogue of second sound) are of particular interest.

*Work supported by NSERC

**10:00**
**A43 9 Sound in a strongly-interacting Fermi gas*** BASON CLANCY, LE LUO, J. KINAST, J. JOSEPH, A. TURLAPOV, J.E. THOMAS, *Duke* Sound propagation in an optically-trapped gas of strongly interacting fermionic $^6$Li atoms is studied. The atoms are prepared as a 50/50 mixture of the two lowest-energy internal states. Strong interactions are achieved by applying a magnetic field in the vicinity of a broad (834 G) s-wave Feshbach resonance. A sound wave is excited by locally applying a pulse of a repulsive blue-light potential. We measure the propagation of the excitation along the axial direction of the cigar-shaped cloud.

*Supported by ARO, NSF, NASA, and DOE

**10:12**
**A43 10 Potential-energy (BCS) to kinetic-energy (BEC)-driven pairing in the attractive Hubbard model*** BUMSOO KYUNG, *University of Sherbrooke* ANTOINE GEORGES, *Centre de Physique Théorique, École Polytechnique* ANDRE-MARIE TREMBLAY, *University of Sherbrooke* UNIVERSITY OF SHERBROOKE COLLABORATION, CENTRE DE PHYSIQUE THÉORIQUE, ÉCOLE POLYTECHNIQUE COLLABORATION, The BCS-BEC crossover within the two-dimensional attractive Hubbard model is studied by using the Cellular Dynamical Mean-Field Theory both in the normal and superconducting

ground states. Short-range spatial correlations incorporated in this theory remove the normal-state quasiparticle peak and the first-order transition found in the Dynamical Mean-Field Theory, rendering the normal state crossover smooth. For $U$ smaller than the bandwidth, pairing is driven by the potential energy, while in the opposite case it is driven by the kinetic energy, resembling a recent optical conductivity experiment in cuprates. Phase coherence leads to the appearance of a collective Bogoliubov mode in the density-density correlation function and to the sharpening of the spectral function.

*The present work was supported by NSERC (Canada), FQRNT (Québec), CFI (Canada), CIAR, and the Tier I Canada Research Chair Program (A.-M.S.T.), and AC-Nanosciences ''Gaz Quantiques'' (Project Nr.201) (A.G.)



**10:24**

**A43 11 Many-body Effects near s- and p-wave Feshbach resonance in BEC-BCS Problem: A Tractable Crossing-symmetric Approach*** KHANDKER QUADER, RENYUAN LIAO, *Department of Physics, Kent State University* In the fermion BEC-BCS crossover problem. many-body effects may influence properties, such as scattering parameters, nature of pairing, etc. close to a Feshbach resonance. We study effects such as these using a tractable diagrammatic crossing-symmetric approach. Our method allows us to include quantum fluctuations, such as, density, current, spin, spin-current, and higher-order fluctuations in a self-consistent fashion. The underlying fermionic interaction is reflected in the ''driving'' term. Taking the ''driving'' term to be finite-range, and of arbitrary strength, we perform calculations on the BEC and BCS sides. These are related to the 2-body singlet and triplet scattering parameters, and can be connected with experimental s and p-wave Feshbach resonances. We include the l=0 density and spin fluctuations, as well as the l=1 current and spin-current fluctuatiuons. We obtain renormalized scattering amplitudes, pairing amplitudes and nature of pairing, etc. on the BEC and BCS side. We compare our results with experiment, and with other theory calculations.

*Supported in part by Institute for Complex Adaptive Matter (ICAM)

**10:36**

**A43 12 Critical Rotating Frequency for Superfluid Fermionic Gases across Feshbach Resonance** HUI ZHAI, *Department of Physics, the Ohio State University* TIN-LUN HO, *Department of Physics, the Ohio State University* Vortex lattices have been observed recently in the rotating Fermionic quantum gases near Feshbach resonance. However, a much faster rotation may destroy the superfluid pairing amplitude and reveal the normal state. In this talk, we present the phase diagram for different interaction strength and rotating frequency. We discover that at resonance, pairing is so robust that it can not be destroyed by rotation. In the BCS side close to resonance, we find that the critical frequency as a function of interaction strength shows a series of plateaus as a consequence of quantized Landau levels. In a fast rotating harmonic trap, the superfluid core with vortices is surrounded by a normal cloud, and the area of the superfluid regime gradually shrinks as the increase of the rotating frequency.

**SESSION A45: CUPRATES AND NICKELATES**
**Monday Morning, 13 March 2006**
**348, Baltimore Convention Center at 8:00**
**John Tranquada, Brookhaven National Laboratory, presiding**

**8:00**

**A45 1 Optical evidence for a magnetically driven structural transition in the spin web $Cu_3TeO_6$** L. DEGIORGI, G. CAIMI, *ETH Zurich* H. BERGER, L. FORRO', *EPF Lausanne* $Cu_3TeO_6$ is a modest frustrated $S = 1/2$ spin system, which undergoes an anti-ferromagnetic transition at $T_N \sim 61$ $K$. The anti-ferromagnetic spin alignment in $Cu_3TeO_6$ below $T_N$ is supposed to induce a magneto-elastic strain of the lattice. The complete absorption spectrum of $Cu_3TeO_6$ is obtained through Kramers-Kronig transformation of the optical reflectivity, measured from the far-infrared up to the ultraviolet spectral range as a function of temperature ($T$). Below $T^* \sim 50$ $K$, we find a new mode at 208 $cm^{-1}$. The spectral weight associated to this additional mode increases as $\propto (T^* - T)^{1/2}$ with decreasing $T$ below $T^*$. The implication of the optical findings will be discussed in relation to the magnetic phase transition at $T_N$.

**8:12**

**A45 2 Transport Anisotropy due to Spiral Spin Order in Underdoped Cuprates** VALERI KOTOV, *Boston University* OLEG SUSHKOV, *University of New South Wales* I will discuss the in-plane transport anisotropy in the spin-glass phase of $La_{2-x}Sr_xCuO_4$ within a theoretical scenario where the physics is purely spin driven (no charge order is present), and a spiral spin density wave is formed in the ground state. Such an approach is well justified for the extended t–J model at low doping. In the low-temperature, variable-range hopping regime, the calculated anisotropy of 50–80 percent (depending on temperature) is in excellent agreement with experiment [1], demonstrating that charge ordering tendencies are not necessary to explain the observed transport anisotropy. This work is part of a series in which we show that the spiral approach provides a consistent description of the low-doping region. [1] V.N. Kotov and O.P. Sushkov, Phys. Rev. B 72, 184519 (2005).

**8:24**

**A45 3 High Energy Spin Dynamics in the electron-doped high-$T_c$ cuprate $Pr_{.88}LaCe_{.12}CuO_4$ ($T_c$=21K)*** STEPHEN WILSON, SHILIANG LI, *University of Tennessee* PENGCHENG DAI, *University of Tennessee/Oak Ridge National Laboratory* HYUNGJE WOO, *University of Tennessee* CHRIS FROST, *ISIS Rutherford Appleton Laboratory* HERB MOOK, *Oak Ridge National Laboratory* YOICHI ANDO, SEIKI KOMIYA, *CRIEPI, Japan* We use high-resolution inelastic neutron scattering to study the low-temperature magnetic excitations of electron-doped superconducting $Pr_{0.88}LaCe_{0.12}CuO_{4-\delta}$ ($T_c$=21 K) over a wide energy range (4 meV$<$ hbar $\omega <$ 260 meV). The effect of electron-doping and superconductivity is to cause a wave vector broadening in the low-energy ( $<$ 50 meV) commensurate spin fluctuations at ($\pi$, $\pi$) and to suppress the intensity of spin-wave-like excitations at high energies ( $>$ 80 meV). This leads to a substantial redistribution in the spectrum of the local dynamical spin susceptibility $\chi''(\omega)$, and reveals a new energy scale considerably

smaller than that of the hole-doped materials [1]. [1] Stephen D. Wilson et. al., PRL submitted (2005).

*This work is supported by the U. S. NSF DMR-0453804 and DOE Nos. DE-FG02-05ER46202 and

**8:36**

**A45 4 Magnetic and transport properties of lightly doped $La_{2-x}Sr_xCuO_4$** V. JURICIC, M.B. SILVA NETO, C. MORAIS SMITH, *Inst. for Theoretical Physics, Univ. of Utrecht, The Netherlands* L. BENFATTO, *Dept. of Physics, Univ. of Rome ''La Sapienza,'' Italy* A.O. CALDEIRA, *Inst. of Physics, Univ. of Campinas, Brazil* We address the problem of the static magnetic correlations in $La_2CuO_4$ [1] and lightly doped $La_{2-x}Sr_xCuO_4$ within the framework of a dipolar frustration model for a canted antiferromagnet [2]. We show that the Dzyaloshinskii-Moriya and XY anisotropies are responsible for robustness of the Neel state for $x < 2\%$ while, for higher doping, the antiferromagnetic ground state is unstable towards a helicoidal magnetic phase. The helicoidal spin structure gives rise to incommensurate peaks in elastic neutron scattering, and is consistent with recent Raman and magnetic susceptibility experiments in $La_{2-x}Sr_xCuO_4$. We propose that the dissipative dynamics of topological defects in a spiral state is responsible for the transport properties in the spin-glass phase of cuprates [3]. The calculated damping matrix is related to the in-plane resistivity, which exhibits an anisotropy and linear temperature dependence in agreement with experimental data. References: [1] M. B. Silva Neto, L. Benfatto, V. Juricic, and C. Morais Smith, cond-mat/0502588. [2] V. Juricic, M. B. Silva Neto, and C. Morais Smith, cond-mat/0510312. [3] V. Juricic, L. Benfatto, A. O. Caldeira, and C. Morais Smith, Phys. Rev. Lett. 92, 137202 (2004).

**8:48**

**A45 5 High binding energy band structure of Bi-2212 as measured by ARPES** K. MCELROY, J. GRAF, *MSD, Lawrence Berkeley National Laboratory, California* G.-H. GWEON, S.Y. ZHOU, *Department of Physics, UC Berkeley, California* S. SAHRAKORPI, M. LINDROOS, R.S. MARKIEWICZ, A. BANSIL, *Physics Department, Northeastern University, Boston MA* H. EISAKI, *AIST, Tsukuba, Japan* T. SASAGAWA, H. TAKAGI, *Department of Advanced Materials Science, U of Tokyo, Japan* S. UCHIDA, *Department of Physics, U of Tokyo, Tokyo, Japan* A. LANZARA, *Department of Physics, UC Berkeley, California* The study of the electronic structure of high temperature superconductors by angle resolved photoemission spectroscopy (ARPES) has so far focused on the states near the Fermi level, believed to be fundamental for most of the properties of cuprates. However, it is well known that in doped Mott insulators the low and high energy physics are strongly coupled one to the other. Therefore, to gain insight on the real physics of cuprates a full characterization of the electronic band structure up to energies of the order of the lower Hubbard band and beyond is needed. Here we report a detailed, doping dependent study of the band structure of Bi2212 superconductors at energies of the order of 1-2 eV. The experimental results are interpreted in terms of local density approximation (LDA) based computations, where the presence of the ''spaghetti'' of Cu-O and O-bands is predicted. Comparison between computed and measured bands provides insight into many-body renormalization effects.

**9:00**

**A45 6 Unidirectional Order and 3D Stacking of Stripes in Orthorhombic $Pr_{1.67}Sr_{0.33}NiO_4$ and $Nd_{1.67}Sr_{0.33}NiO_4$.** MARKUS HÜCKER, JOHN M. TRANQUADA, GEN D. GU, *Brookhaven National Laboratory* MARTIN V. ZIMMERMANN, *HASYLAB at DESY, Hamburg, Germany* BERND K. BÜCHNER, *IFW Leibniz-Institute, Dresden, Germany* The crystal structure and charge stripe order in $Pr_{1.67}Sr_{0.33}NiO_4$ and $Nd_{1.67}Sr_{0.33}NiO_4$ was studied by means of single crystal x-ray diffraction in zero and high electric fields. In contrast to tetragonal $La_{1.67}Sr_{0.33}NiO_4$, these crystals are orthorhombic at room temperature. We find that the distortion of the $NiO_2$ planes associated with the orthorhombic strain dictates the direction of the charge stripes. The critical temperature for charge stripe order is the same as in $La_{1.67}Sr_{0.33}NiO_4$ ($T_{CO} \sim 245$ K), i.e., it does not depend on the crystal symmetry. A second structural transition observed only in $Nd_{1.67}Sr_{0.33}NiO_4$ at temperatures $T \sim 100$ K has no noticeable influence on the stripe order. In crystals with a hole content very close to 1/3 we observe a tripling of the charge stripe unit cell along the c-axis for temperatures $T < 225$ K, which indicates a strong tendency towards a well defined three dimensional order. A high electric field applied to $Nd_{1.67}Sr_{0.33}NiO_4$ had no noticeable impact on the charge stripe order, i.e., a sliding of stripes was not observed. *The work at Brookhaven was supported by the Office of Science, U.S. Department of Energy under Contract No. DE-AC02-98CH10886.*

**9:12**

**A45 7 The ground state of the quasi-one-dimensional cuprate $PrBa_2Cu_4O_8$: field-induced dimensional crossovers and disorder-induced one-dimensionality** ALESSANDRO NARDUZZO, ARAZ ENAYATI-RAD, *University of Bristol* SHIGERU HORII, *University of Tokyo* FEDOR BALAKIREV, *Los Alamos National Laboratory* NIGEL HUSSEY, *University of Bristol* $PrBa_2Cu_4O_8$, the non-superconducting analogue of the high-$T_c$ cuprate $YBa_2Cu_4O_8$, is an extremely anisotropic quasi-one-dimensional (Q1D) metal ($t_b^2 : t_a^2 : t_c^2 \sim$ 4000: 2: 1). The in-chain ($b$-axis) charge dynamics were investigated as a function of temperature and applied magnetic field for several samples of different disorder content. Measurements in magnetic fields up to 65 T confirm the correspondence between dimensional crossovers due to magnetic field carrier confinement and temperature-induced decoherence, opening the possibility of accessing the Tomonaga-Luttinger liquid state in this material. A metal-insulator transition is observed with increasing disorder concentration for samples with nominal mean free path of $\sim 100b$. The onset of this remarkable localisation phenomenon reveals a striking correlation between the scattering rate and the interchain hopping rate(s), suggesting a disorder-induced crossover to a one-dimensional (1D) ground state. $b$-axis magnetoresistance measurements were performed in order to identify the nature and properties of the Q1D metallic and disorder-induced 1D insulating states.

**9:24**

**A45 8 Lattice fermion models with spontaneous orbital currents in strong-interaction limit*** CHRISTOPHER L. HENLEY, *Cornell University* A suggestion that the cuprate pseudogap state has a hidden order, in the form of staggered currents [1], led to toy spinfull fermion models on ladders and bilayers which exhibit such a symmetry breaking [2]. This invites the question, which features of the model are conducive to such phases? Taking (for maximal simplicity) spinless fermions, with large or infinite repulsion, I find a ground state with spontaneous-current order in two models: each consists of rings of sites, coupled by weak hopping to form a ladder or a $d = 2$ lattice. So far, all my examples require lattices modulated with alternately strong and weak hopping. I also argue that spontaneous currents depend on the presence of Berry-

like phases as one takes the system around loops in the abstract graph of all configurations coupled by hops: it would follow that spontaneous currents are impossible in lattice boson models. [1] S. Chakravarty et al, Phys. Rev. B 63, 094503 (2001). [2] M. Tsuchiizu and A. Furusaki, %%% spontaneous currents Phys. Rev. B 66, 245106 (2002); U. Schollwöck et al, Phys. Rev. Lett. 90, 186401 (2003); S. Capponi, C. Wu, and S.-C. Zhang, Phys. Rev. B 70, 220505 (2004).

*Supported by NSF grant DMR-0240953

**9:36**

**A45 9 A proposal for giant spin-orbital resonance in AFM/SDW conductors.** REVAZ RAMAZASHVILI, *LPTMS, Bât. 100, Université Paris-Sud, 91405 Orsay cedex, France* SERGUEI BRAZOVSKII, *LPTMS, Bât. 100, Université Paris-Sud, 91405 Orsay cedex, France* Essential dependence of the electron *g*-factor on the quasiparticle momentum is a fundamental property of antiferromagnetic conductors (AFM), which so far has been largely overlooked. It leads to an anomalously strong spin-orbit interaction, of which a giant combined spin-orbital resonance may be a striking manifestation. We advance a theory of this combined resonance (excitation of electron spin transitions by AC *electric* field) in a weakly doped antiferromagnetic insulator. The combined resonance intensity exceeds that of the electron spin resonance (ESR) by orders of magnitude. We study transitions in the continuous spectrum, as well as in a quantizing magnetic field, and calculate the resonance lineshape, and the angular dependence of the resonance intensity. Our predictions may be relevant for various magnetically ordered conductors, including electron- and hole-doped cuprates, and organic metals with a spin density wave (SDW).

**9:48**

**A45 10 Dual vortex theory of doped antiferromagnets** SUBIR SACHDEV, *Harvard University* LEON BALENTS, *University of California, Santa Barbara* We present a general framework for describing the quantum phases obtained by doping paramagnetic Mott insulators on the square lattice. The undoped insulators are efficiently characterized by the projective transformations of various fields under the square lattice space group (the PSG). We show that the PSG also imposes powerful constraints on the doped system, and enables derivation of an effective action for the vortex and Bogoliubov quasiparticle excitations of superconducting states. This action also describes transitions to supersolid or insulating states at nonzero doping. For the case of a valence bond solid (VBS) insulator, we show that the doped system has the same PSG as that of elementary bosons with density equal to the density of electron pairs. We also obtain the action for a d-wave superconductor obtained by doping a ''staggered-flux'' spin liquid state.

**10:00**

**A45 11 Strong coupling theory of phonons in the Hubbard Model** SHILADITYA CHAKRABORTY, *Univ. of Illinois, Urbana-Champaign* TUDOR STANESCU, *Univ. of Illinois, Urbana-Champaign* PHILIP PHILLIPS, *Univ. of Illinois, Urbana-Champaign* The role of phonons in strongly correlated electronic systems including the high Tc cuprates has not been completely well understood. Recent experimental results, notably those of Lanzara et. al reveal the existence of a kink in the quasiparticle dispersion data for various classes of cuprate superconductors including BiSCO, LSCO and NCCO at an energy scale of around 50 meV to 70 meV using ARPES techniques. Direct comparison of ARPES and neutron scattering data has also been done for LSCO. One of the possible explanations for this kink is believed to be coupling of electrons with phonon modes of the above energy scale. We obtain the electron spectral function as a function of electron- phonon coupling strength using Cluster Dynamic Mean Field Theory (CDMFT on the 2-D Hubbard Model with phonons and compare it with the experimental data.

**10:12**

**A45 12 Spin Correlations and Magnetic Susceptibilities of Lightly Doped Antiferromagnets** I.R. PIMENTEL, F. CARVALHO DIAS, *University of Lisbon, Portugal* We calculate the spin correlation function and the magnetic longitudinal and transverse susceptibilities of a two-dimensional antiferromagnet doped with a small concentration of holes, in the t-J model. We find that the motion of holes generates spin fluctuations which add to the quantum fluctuations, the spin correlations decaying with the inverse of the spin distance, while increasing with doping as the critical hole concentration, where the long-range order disappears, is approached. Moreover, the longitudinal susceptibility becomes finite in the presence of doping, due to the strong damping effects induced by the hole motion, while the transverse susceptibility is renormalized by softening effects. Both the longitudinal and the transverse susceptibilities increase with doping, the former more significantly than the latter. Our results imply that doping destroys the long-range order while local antiferromagnetic spin correlations persist. This is consistent with experiments on the doped copper oxide superconductors.

**10:24**

**A45 13 Unconventional antiferromagnetism in the presence of Dzyaloshinskii-Moriya interactions: the case of $La_2CuO_4$** LARA BENFATTO, *CNR-INFM and University of Rome ''La Sapienza,'' Italy* MARCELLO SILVA NETO, *University of Utrecht, The Netherlands* Between the several anomalous properties of cuprates superconductors, the attention has been put recently on the magnetic properties of the undoped compounds, which display antiferromagnetism. In particular, $La_2CuO_4$ has been extensively investigated, and several unusal magnetic properties have been observed, as for example the temperature dependence of the uniform magnetic susceptibility and the magnetic-field dependence of the magnon gaps. Using a long-wavelength non-linear sigma model approach, we study effect of Dzyaloshinskii-Moriya interactions in the quantum Heisenberg antiferromagnet. With this technique one can easily recognize that the Dzyaloshinskii-Moriya interaction mediates an anomalous coupling between the uniform magnetic field and the antiferromagnetic order parameter. We can then provide a simple and clear explanation for all the recently reported anomalies, and we demonstrate explicitly why $La_2CuO_4$ can not be classified as an ordinary easy-axis antiferromagnet.

**10:36**

**A45 14 $^{63,65}$Cu NMR Spectrum and Spin Lattice Relaxation in the Two-dimensional Antiferromagnet $Pr_2CuO_{4-y}$*** G. GAIDOS, W.G. CLARK, *UCLA Physics and Astronomy* R.L. GREENE, B. LIANG, *U. of Maryland Physics* The $^{63,65}$Cu NMR spectra and spin lattice relaxation rate ($1/T_1$) are reported for a single crystal of the two-dimensional antiferromagnet $Pr_2CuO_{4-y}$ as a function of the applied magnetic field ($\mathbf{itB}_0$) over the temperature ($T$) range 3 - 20 K. When $\mathbf{itB}_0 = 0$, the NMR spectrum has six lines, which correspond to the quadrupolar spectrum (central transition and two satellites) of both Cu isotopes in an antiferromagnetic (AF) internal field of 9.626 T. This value is 0.75 T

less than that of the related compound $Nd_2CuO_{4-y}$ [1]. The spectra as a function of $\mathbf{itB}_0$ are consistent with the noncollinear structure of the AF ordered $Cu^{2+}$ spins seen in neutron diffraction studies [2]. The values of $1/T_1$ over the range $5\ K \leqslant T \leqslant 20\ K$ follow the power law $1/T_1 \propto T^2$, which may indicate $1/T_1$ is dominated by two-dimensional AF spin waves [3]. [1] Y. Yosinari itet al., J. Phys. Soc. Jpn. **59**, 36 (1990). [2] I. Sumarlin itet al., Phys Rev B, **51**, 5824 (1995). [3] S. Chakravarty itet al., Phys Rev B **43**, 2796 (1991).

*Work at UCLA supported by NSF Grant DMR-0334869.

**10:48**
**A45 15 Spectroscopy of stripe order in $La_{1.8}Sr_{0.2}NiO_4$ using resonant soft x-ray diffraction** J. SCHLAPPA, C. SCHUESSLER-LANGEHEINE, Z. HU, C. F. CHANG, M. BENOMAR, H. OTT, O. FRIEDT, M. BRADEN, L.H. TJENG, *II. Physikalisches Institut, Universitaet zu Koeln, Germany* A. TANAKA, *ADSM, Hiroshima University, Japan* E. SCHIERLE, E. WESCHKE, G. KAINDL, *Institut fuer Experimentalphysik, Freie Universitaet Berlin, Germany* G.A. SAWATZKY, *Department of Physics and Astronomy, UBC, Canada* H.-J. LIN, C.T. CHEN, *NSRRC, Hsinchu, Taiwan* We studied the electronic structure and temperature dependence of the stripe phase in Sr-doped $La_2NiO_4$ using resonant diffraction at the Ni $L_{2,3}$ and La $M_{4,5}$ edge in combination with a realistic microscopic theory. Making use of the very high sensitivity of the method to ordered modulations of the electronic state, we found the doped holes to be mainly located on the oxygen ligands in the $NiO_2$ planes, each centered around one Ni ion. The Ni ions in the hole-rich stripes are essentially in a high-spin $d^8$ state and the hole spin is coupled antiparallel to the Ni spin in close analogy to the Zhang-Rice singlet state in cuprates. Such an understanding of the charge-ordered phase could not be obtained before, neither by conventional x-ray or neutron diffraction techniques, nor by x-ray absorption spectroscopy.



## SESSION A46: FOCUS SESSION: WIDE BANDGAP SEMICONDUCTORS I
**Monday Morning, 13 March 2006; 349, Baltimore Convention Center at 8:00**
**Mary Ellen Zvanut, University of Alabama, presiding**

***Invited Papers***

**8:00**
**A46 1 Efficiency in Piezoelectric GaInN/GaN Green Light Emitting Diodes.**
CHRISTIAN WETZEL, *Rensselaer Polytechnic Institute*

The color of green is most closely related to human's perception of light, while red and blue have more of a signal character. Wide bandgap GaInN/GaN heterostruture devices successfully expanded the wavelength range of light emitting diodes (LEDs) from the red to blue and the UV. Performance in the green (500 – 570 nm), however, substantially lags behind requirements for energy efficient solid state white lighting. In particular, it is a significant challenge to extent the wavelength range from the blue back to the lower emission energies of green. Problems to incorporate high fractions of In and large biaxial strain are compounded by strong polarization properties of the material system. From detailed bandstructure spectroscopy we reveal that and how the piezoelectric properties play the pivotal role in the light emission properties. On these premises, polarization optimized green LED dies have been developed with superior performance at 525 nm and the deep green to 560 nm. In an ongoing process, device performance and efficiencies are analyzed and compared to a large set of sample data and provide relevant optimization feedback.

***Contributed Papers***

**8:36**
**A46 2 Growth and Characterization of III-Nitride LEDs on Vicinal Sapphire Substrates** N. KHAN, J. LI, J. Y. LIN, AND H. X. JIANG, *Department of Physics, Kansas State University, Manhattan, KS 66506-2601* GaN and related III-N alloys have great potential applications in optoelectronic devices such as light emitting diodes (LEDs), laser diodes (LDs) and high power electronic devices such as transistors. For improved performance and greater versatility of these devices, it is essential to improve the quality of materials and devices. It has been reported that growth on vicinal or misaligned substrates compared to flat ones, lead to smoother and higher crystalline quality thin films. Improved brightness and quantum efficiency, and a reduction of the forward current at which maximum quantum efficiency occurs are among the improved optical properties resulting from the use of misaligned substrates and a thick base layer. We report on the characteristics of InGaN based blue/green LEDs grown by metal organic chemical vapor deposition (MOCVD) on specially fabricated dome shaped sapphire substrates. These dome shaped substrates provide varying degrees of off-cut within a single wafer. Surface morphologies, crystalline qualities and emission properties across the entire wafer surface have been mapped by various techniques, including optical and atomic force microscopy (AFM), x-ray diffraction and electroluminescence and photoluminescence spectroscopy. The results are compared with those of blue/green LEDs grown on conventional on-axis substrates.

**8:48**
**A46 3 Improvement of AlGaN-based deep-ultraviolet light emitting diodes performance with a nano-textured/roughened sapphire substrate** MUHAMMAD KHIZAR, YASIN RAJA, *Department of Physics & Optical Sciences, University of North Carolina at Charlotte, NC 28223* Performance improvement of the fabricated AlGaN-based deep-ultraviolet light emitting diode (DUV LEDs) on sapphire with nano-textured/roughned substrate is reported. The output optical powers as well as the current-voltage characteristics of the processed devices with and without textured/roughened substrate are compared. Lapping/polishing

and dry-etching techniques were employed for nano-texturing/ roughening of the substrate. Magnetron dry etching was performed using a mixed $CF_2Cl_2$/Ar feed gases followed by an inductively coupled plasma (ICP) etching in $BCl_3/Cl_2$ plasma chemistry. An etching rate of $\sim$ 145 nm/min for the sapphire was easily obtained. The result show that the optical emission power of the fabricated devices with textured/roughened sapphire substrate is higher as compared to similar un-textured/roughened devices. Based on the analysis, it is concluded that a textured/roughened substrate surface with an RMS $\sim$ 15 – 25 nm shows improved light extraction efficiency, which is the result of the reduced internal reflection of the light caused by the nano-textured/roughened surface profile thereby causing deviation for critical angle.

**9:00**

**A46 4 Growth and Optical Properties of Al rich AlN/AlGaN Quantum Wells** T.M. AL TAHTAMOUNI, N. NEPAL, M.L. NAKARMI, J.Y. LIN, AND H.X. JIANG, *Department of Physics, Kansas State University, Manhattan, Kansas 66506-2601* Al rich AlGaN alloys are promising materials for the applications in the optoelectronic devices such as deep ultraviolet (UV) emitters and detectors in the spectral range down to 200 nm. AlGaN based UV emitters ($\lambda < 340$nm) has applications in bio-chemical agent detection and medical research/ health care. To realize deep UV emission ($\lambda <$ 280 nm) Al rich AlGaN based quantum wells (QWs) are required. We report here the growth of $AlN/Al_xGa_{1-x}N$QWs ($x>0.65$) on AlN/sapphire templates by metalorganic chemical vapor deposition (MOCVD). Deep UV photoluminescence (PL) was employed to study the optical properties of the QWs. Well width (Al composition) dependence was studied by varying the QW thickness (Al composition) with fixed $x\sim 0.65$ (well width at 3 nm). Optical properties of these QWs such as the effects of alloy fluctuation, temperature, strain and piezoelectric field, carrier and exciton localizations on the quantum efficiency have been studied. Carrier and exciton dynamics were probed. Implications of our findings on the applications of Al rich AlN/AlGaN QWs for UV emitters and detectors will also be discussed.

**9:12**

**A46 5 Optical properties of Er doped III-nitride epilayers and quantum wells synthesized by MOCVD** C. UGOLINI, M.L. NAKARMI, N. NEPAL, J.Y. LIN, AND H.X. JIANG, *Department of Physics, Kansas State University, Manhattan, KS 66506* The wide bandgap semiconductor, GaN, is an excellent host for Er since the thermal quenching of radiative intra-4f it$Er^{3+}$ transitions is very low in Er implanted or Er doped GaN, and the solubility of Er in GaN is high. Due to these properties and the characteristic transition of 1.54 $\mu$m of $Er^{3+}$, Er doped GaN structures are promising for Er related emitters operating in the infrared region. In recent studies, Er doped III-Nitride epilayers were obtained by ion implantation or molecular beam epitaxy (MBE). But, in-situ Er doping of III-Nitride epilayers has not been achieved by metalorganic chemical vapor deposition (MOCVD), mostly due to the low vapor pressure and lack of suitable, metalorganic Er sources. However, due to the large output and high-crystalline quality of MOCVD grown III-nitride epilayers, use of this process to grow Er doped III-nitride epilayers would be very useful for commercial applications. We report on the synthesis of Er doped III-nitride epilayers and quantum wells (QW) grown by MOCVD, and their optical properties. Optical properties in the visible and infrared region for epilayers and QW's of different Er concentrations and growth conditions are discussed. The mechanisms of optical transitions involving different intra-4f $Er^{3+}$ energy levels are also discussed. Lastly, potential applications of Er doped III-nitride structures in the communication wavelength will be presented.

**9:24**

**A46 6 Structural and optical properties of GaN films grown on GaAs substrates by molecular beam epitaxy** O. MAKSIMOV, V. HEYDEMANN, *Electro-Optics Center, Pennsylvania State University* P. FISHER, H. DU, M. SKOWRONSKI, *Dept. of Mat. Sci. and Eng., Carnegie Mellon University* Y. GONG, I. KUSKOVSKY, *Dept. of Physics, Queens College of NY* ELECTRO-OPTICS CENTER TEAM, CARNEGIE MELLON UNIVERSITY TEAM, QUEENS COLLEGE OF NY TEAM, GaN emerged during the past decade as a wide band gap semiconductor with promising material properties for the development of short-wavelength optoelectronic, high frequency and high power electronic devices. Most GaN research has been focused on the growth of high quality GaN epitaxial layer on A12O3 and SiC substrates. The MBE growth of GaN on GaAs substrates is much less studied, although it provides several advantages, such as a closer thermal expansion coefficient matching and a possibility to stabilize cubic $\beta$-GaN. In this work we report on MBE growth of GaN films on the (100) GaAs substrates. Contrary to previous literature accounts, we do not employ an As beam, neither during oxide desorption nor during GaN nucleation and growth. We determine that direct growth on thermally desorbed GaAs results in a polycrystalline film that contains inclusions of both $\alpha$ and $\beta$ GaN. Low-temperature nitridation followed by annealing improves structural properties resulting in the growth of $\alpha$-GaN with 0002 orientation.

**9:36**

**A46 7 Characterization of stress in thin-film wurtzite GaN grown on c-plane sapphire by molecular beam epitaxy.** FRANCISCO PARADA, MICHAEL MARCINIAK, *Air Force Institute of Technology* LAVERN STARMAN, JASON FOLEY, *Air Force Research Laboratory* YUNG KEE YEO, *Air Force Institute of Technology* The stress distribution in wurtzite gallium nitride (GaN) grown on c-plane sapphire substrates by molecular beam epitaxy is characterized. Micro ($\mu$)-Raman spectroscopy is particularly useful for stress characterization because of its ability to measure the spectral shifts in Raman peaks in a material, and correlate those shifts with stress and strain. The phonon deformation potential is determined by applying pressure to the material using a four-point strain fixture while simultaneously monitoring the applied pressure using a strain gauge and recording the Raman spectrum. The deformation potentials are then used to determine stress distribution; the spectral positions of the $E_2$ Raman mode ($\nu$ = 569 cm-1) in GaN and $A_{1g}$ Raman mode ($\nu = 418$ cm$^{-1}$) in sapphire are recorded at each spatial position in a raster map. The $\mu$-Raman spectroscopy is performed using a Renishaw InVia Raman spectrometer with argon ion ($\lambda = 514.5$ nm, $h\nu = 2.41$ eV) and helium-neon ($\lambda = 633$ nm, $h\nu = 1.96$ eV) excitation sources, and the data is collected across the samples with 5- to 10-$\mu$m spatial resolution. Inherent stress and evidence of significant damage in the GaN layer due to MEMS processing will be discussed.

**9:48**

**A46 8 The Influence of Phonons and Phonon Decay on the Optical Properties of GaN** D. Y. SONG, M. BASAVARAJ, S. A. NIKISHIN, M. HOLTZ, *Texas Tech University, Lubbock, Texas 79409* V. SOUKHOVEEV, A. USIKOV, V. DMITRIEV, *TDI, Inc., 12214 Plum Orchard Dr., Silver Spring, MD 20904* The temperature dependences of vibrational and optical properties of high-quality GaN are studied using Raman and photoluminescence (PL) spectroscopies in the range 20 to 325 K. The Raman-active $A_1$(LO) phonon has temperature dependence described well by combined two- and three-phonon decay. The temperature dependences of $E_2^2$phonon are almost entirely dominated by the thermal expansion, and the contribution of three-phonon decay process is very small throughout interested temperature range. The shallow neutral donor-bound exciton ($D^0$,X) and two free excitons ($X_A$ and $X_B$) are observed at low temperatrue PL spectra. Also seen are two $A_1$(LO) phonon sidebands (PSBs), originating from the $X_B$ free exciton, with the characteristic asymmetry attributed to interactions between discrete and continuum states. Analysis of the band-edge excitons reveals that energy gap shrinkage and exciton linewidths are completely described based on electron-phonon interactions with phonon properties consistent with the Raman analysis. First and second PSBs have temperature dependence associated with the $A_1$(LO) phonon. The shift, broadening, and asymmetry of the PSBs are explained by Segall-Mahan theory adding the decay mechanism of $A_1$(LO) phonon and the exciton broadening from electron-phonon interactions. Work at Texas Tech University supported by National Science Foundation grant ECS-0323640.

**10:00**

**A46 9 Bandedge transitions in GaN and AlN at elevated temperatures** N. NEPAL, M. L. NAKARMI, J. LI, J. Y. LIN, AND H. X. JIANG, *Department of Physics, Kansas State University, Manhattan, KS 66506* GaN and AlN are recognized as promising materials for high power high temperature optoelectronic and electronic devices. For device realization, understanding fundamental properties of these materials at elevated temperature is very important. Probing the optical properties such as the temperature dependence of the bandedge transitions reveals important information pertaining to the fundamental band structures, exciton and carrier recombination and activation processes. Deep-ultraviolet photoluminescence (PL) spectroscopy has been employed to study the bandedge transitions in metalorganic chemical vapor deposition grown GaN and AlN epilayers up to 800 K. The temperature dependence of the PL emission intensity revealed two different activation processes in both GaN and AlN epilayers. The first process occurring below $T_t$ = 325 K ($T_t$ = 500 K) for GaN (AlN) is due to the activation of free excitons to free carriers. Whereas the second activation process occurring above $T_t$ with an activation energy of 0.29 eV (0.3 eV) for GaN (AlN) is believed to be associated with the existence of a satellite valley ($\Gamma_3$) at about 0.3 eV above the conduction band minimum, $\Gamma_1$. Consequence of this satellite valley in the conduction band on the high temperature and high power device applications of GaN and AlN will be discussed.

**10:12**

**A46 10 Hot carrier dynamics in bulk GaN under short laser pulse excitation** S. RUDIN, *U.S. Army Research Laboratory* E. BELLOTTI, *Boston University* G. A. GARRETT, M. WRABACK, *U.S. Army Research Laboratory* In this work, we apply the semiconductor Bloch equation formalism to the study of the electron-hole dynamics in bulk GaN under short laser pulses excitation. Both coherent and non-coherent processes contribute to the dynamics on short time scales. The numerical solution of the equations of motion for the electron-hole plasma and the polarization is obtained by using a generalized Monte Carlo algorithm. This includes a direct solution of the coherent process and a stochastic description of the dephasing mechanisms. Screened carrier-carrier interaction and carrier-phonon interaction are considered in the dephasing processes. The model also includes the description of the interaction of the ultra-short laser pulse with the semiconductor media. The non-parabolic two-band analytical approximation was used in this work. The interaction of LO-phonons with electrons in GaN is much stronger than in GaAs, and the LO-phonon-electron scattering rate in GaN is almost one order higher than that in GaAs. The computed time dependent carrier densities were used to obtain time dependent luminescence at different probe wave-lengths for different excitation powers. The results were compared with the experimental results obtained by the subpicosecond time-resolved spectroscopy of UV luminescence.

**10:24**

**A46 11 Nonequilibrium carrier dynamics in AlGaN/GaN surface quantum wells monitored by time-resolved photoluminescence spectroscopy** Y. D. GLINKA,*J. V. FOREMAN,†W. DAVENPORT, H. O. EVERITT,‡ *U.S. Army Aviation and Missile RDEC, Redstone Arsenal, AL* X. ZHANG, I. P. WELLNIUS, J. F. MUTH, *Electrical and Computer Engineering, North Carolina State Univ., Raleigh, NC* J. ROBERTS, P. RAJAGOPAL, J. COOK, E. PINER, K. LINTHICUM, *Nitronex Corporation, Raleigh, NC* The photoluminescence (PL) from a GaN surface quantum well of an AlGaN/GaN heterostructure has been studied by using a wide range of ultrafast ( $\sim$ 200 fs) laser excitations and temperatures (4.2 – 300 K) for quantum wells of varying widths. We observe a broad ( $\sim$ 100 meV) PL band whose peak shifts linearly from 3.5 to 3.8 eV with decreasing GaN quantum well thickness from 2.9 to 1.5 nm. The spectral shift of the band is accompanied by the corresponding temporal shift in the range $<$ 30 ps. The dynamics of nonequilibrium electrons in the GaN layer confined by the AlGaN barrier and the vacuum level is discussed, with particular emphasis on carrier interactions with both acoustic and optical phonons.

*Nano and Micro Devices Center, University of Alabama in Huntsville, Huntsville, AL
†Dept. of Physics, Duke University, Durham, NC
‡Dept. of Physics, Duke University, Durham, NC

**10:36**

**A46 12 Time Resolved Photoluminescence Measurements in hexagonal $Mg_xZn_{1-x}O$ (x=0.13) alloys** SHIVA HULLAVARAD, R. VISPUTE, S. DHAR, *University of Maryland* HENRY EVERITT, JOHN FOREMAN, *Duke University* I. TAKEUCHI, *University of Maryland* In this work we present results on the optical characterization of Pulsed Laser Deposited epitaxially grown thin films of $Mg_xZn_{1-x}O$ on sapphire. The crystalline quality and composition of the alloys are characterized by X-Ray Diffraction and Rutherford Back Scattering (RBS) – ion channeling techniques respectively. The composition of the films is found to have strong dependence on the growth parameters. The

photo generated carrier decay times are analyzed by time-resolved photoluminescence (TRPL) measurements. Since most optical and electrical devices are operated at room temperature, understanding the fundamental excess carrier recombination dynamics at 300 K is required to evaluate the relevant radiative and non-radiative recombination mechanisms and thus to improve the performance of devices. We have observed from initial PL measurements evidence of varying amounts of non-radiative relaxation processes competing with radiative PL in the MgZnO samples. More importantly, we have observed a decay time of 125 ps for films from TR-PL measurements. The efficiency of the radiative recombination, and therefore the material quality, is strongly related to the decay time of the particular transition. The correlation of the results obtained from RBS and PL-TRPL measurements will be presented.

**10:48**
**A46 13 Optical and magnetic properties of $Zn_{1-x}Co_xO$ and $ZnCo_2O_4$ thin films.** K. SAMANTA, P. BHATTACHARYA, R.S. KATIYAR, *University of Puerto Rico, PR* W. IWAMOTO, R.R. URBANO, C.P. PAGLIUSO, C. RETTORI, *Instituto de Fisica Unicamp, Campinos, Brazil* UPR TEAM, CAMPINO BRAZIL TEAM, The transition metal doped wide bandgap ZnO are considered possible candidates for room temperature ferromagnetic semiconductor for spintronic devices. Thin films of Co substituted ZnO and $ZnCo_2O_4$ were deposited using pulsed laser deposition on c-axis (0001) oriented $Al_2O_3$ substrates. The XRD results showed all the films were highly (002) oriented with a less intense peak of (311) for $ZnCo_2O_4$ thin film. Micro-Raman spectra of ceramic targets showed the modes related to wurtzite ZnO and spinel $ZnCo_2O_4$ structure. In thin films of $Zn_{1-x}Co_xO$ no such modes related to $ZnCo_2O_4$ were detected. The intensity of $E_1(LO)$ and multiphonon peaks at 540 and 584 $cm^{-1}$, respectively, increased with increase in the Co substitution. The optical absorption of the films showed that the band gap decreased with the increase of Co concentrations at room temperature along with the sub-bandgap absorption due to $d - d$ transitions of $Co^{2+}$. Similar sub-bandgap $d - d$ transition was also observed in absorption spectra $ZnCo_2O_4$ thin film.

**SESSION B1: DCMP/DCOMP PRIZE SESSION**
**Monday Morning, 13 March 2006; Ballroom IV, Baltimore Convention Center at 11:15**
**Susan Coppersmith, University of Wisconsin, presiding**

**11:15**
**B1 1 Liquid Crystal Phases of Molecular Bananas: Polarity and Chirality as Broken Symmetries.***
NOEL CLARK, *University of Colorado*

The study of the interplay of chirality and polarity has been a particularly rich theme of soft matter science since Meyer's seminal discovery that tilted smectics of chiral molecules are macroscopically polar. This event, and the subsequent realization of polar domains and high-speed electro-optic switching in chiral smectics, engaged the liquid crystal community in a worldwide pursuit of novel smectics for applications, featured by the synthesis of more than 50,000 new liquid crystal compounds, and by a consequent broad diversification of the palette of liquid crystal phases and possibilities for supermolecular ordering. A current important activity in this scenario is the study of polar order in synthetically achiral molecules, for example, in molecular bananas, which, as their shape suggests, might be expected to organize in a polar way. Indeed they do, but beyond this, almost everything learned about them has been surprising, including their persistent tendency to exhibit chirality as a spontaneously broken symmetry. I will discuss some of these new phases and phenomena, including the discovery of fluid conglomerates (Pasteur's experiment in a fluid), triclinic fluid order, chiral twist grain boundary phases of achiral molecules, chirality flipping and field-induced deracemization, ferroelectric and antiferroelectric phases with supermolecular- scale polarization modulation, and chiral thermotropic sponge phases.

*Work in collaboration with the Boulder Liquid Crystal Group, supported by NSF MRSEC Grant DMR 0213918.

**11:51**
**B1 2 Curvature, chirality, and polar symmetry in liquid crystals.**
ROBERT MEYER, *Brandeis University*

Charles Frank taught us the relationship between curvature and polarity in liquid crystals. He showed that polar ordering of dipolar molecules, with the polar axis parallel to the nematic director, would lead to spontaneous splay deformation of the otherwise uniaxial nematic state. Likewise, he showed that molecular chirality leads to spontaneous twisting of the director field, resulting in the helicoidal textures of chiral nematics. Augmenting Frank's insight on polarity induced splay with the realization that bend induces polarization perpendicular to the director, led to the concept of curvature induced polarization of liquid crystals, or flexoelectricity. The concepts of chirality induced twist and bend induced polarization became intimately combined in the case of chiral smectic C liquid crystals. The chirality induced twisting of the molecular tilt direction from layer to layer in the smectic produces a helical state incorporating both spontaneous twist and bend, and therefore inducing polarization in the smectic layers, normal to the molecular tilt direction. Thus, Frank's original insights led eventually to the discovery of ferroelectric liquid crystals. In fact, spontaneous polarization and helical order are independent consequences of molecular chirality in tilted smectics. The fundamental combination of

monoclinic local symmetry in the smectic C phase with molecular chirality leads directly to spontaneous polarization, with no requirement of helical twisting. This realization leads to generalizations of ferroelectricity to include anti-ferroelectric and ferri-electric smectics, among the fascinating array of polar liquid crystal phases. The consequences of these concepts in fundamental science, materials development, and applications will be reviewed.

**12:27**
**B1 3 Generating Coherent Phonons and Spin Excitations with Ultrafast Light Pulses.***
ROBERTO MERLIN, *FOCUS Center and Department of Physics, University of Michigan, Ann Arbor, MI 48109-1040*

Recent work on the generation of coherent low-lying excitations by ultrafast laser pulses will be reviewed, emphasizing the microscopic mechanisms of light-matter interaction. The topics covered include long-lived phonons in ZnO [C. Aku-Leh, J. Zhao, R. Merlin, J. Menéndez and M. Cardona, itPhys. Rev.B **71**, 205211 (2005)], squeezed magnons [J. Zhao, A. V. Bragas, D. J. Lockwood and R. Merlin, itPhys. Rev. Lett. **93**, 107203 (2004)], spin- and charge-density fluctuations [J. M. Bao et al., itPhys. Rev. Lett. **92**, 236601 (2004)] and cyclotron resonance [J. K. Wahlstrand, D. M. Wang, P. Jacobs, J. M. Bao, R. Merlin, K. W. West and L. N. Pfeiffer, AIP Conference Proceedings **772** (2005), p. 1313] in GaAs quantum wells. In addition, unpublished results on surface -avoiding phonons in GaAs-AlAs superlattices [M. Trigo et al., itunpublished] and magnons in ferromagnetic $Ga_{1-x}Mn_xAs$ [D. M. Wang et al., itunpublished] will be discussed. It will also be shown that frequencies can be measured using pump-probe techniques with a precision comparable to that of Brillouin scattering. It is now widely accepted that stimulated Raman scattering (SRS) is (often but not always) the mechanism responsible for the coherent coupling. Results will be presented showing that SRS is described by two separate tensors, one of which accounts for the excitation-induced modulation of the susceptibility, and the other one for the dependence of the amplitude of the oscillation on the light intensity [T. E. Stevens, J. Kuhl and R. Merlin, itPhys. Rev. B **65**, 144304 (2002)]. These tensors have the same real component, associated with itimpulsive coherent generation, but different imaginary parts. If the imaginary term dominates, that is, for strongly absorbing substances, the mechanism for two-band processes becomes itdisplacive in nature, as in the DECP (displacive excitation of coherent phonons) model. It will be argued that DECP is not a separate mechanism, but a particular case of SRS. In the final part of the talk, an attempt will be made to identify emerging areas of research on coherent excitations and coherent control, relevant to condensed matter systems, that could benefit from ultrafast electron and x-ray diffraction studies.

*Supported by NSF and AFOSR.

**13:03**
**B1 4 Berry Phases and Curvatures in Electronic-Structure Theory.**
DAVID VANDERBILT, *Rutgers University*

In the last fifteen years, Berry phases have been found to play an increasingly important role in electronic-structure theory. I will briefly review some of the important developments in which Berry phases have been involved, starting with the modern theory of polarization[1] and the closely related theory of Wannier functions and their Wannier centers.[2] Next, I will discuss the theory of insulators in finite electric fields,[3] in which the field is taken to couple linearly to the Berry-phase polarization. I will then conclude by discussing the role of Berry phases and Berry curvatures in systems in which time-reversal symmetry has been broken, and in particular, the theory of orbital magnetization[4] and the anomalous Hall effect in ferromagnets.

[1] R.D. King-Smith and D. Vanderbilt, Phys. Rev. B **47**, 1651 (1993).
[2] Nicola Marzari and D. Vanderbilt, Phys. Rev. B **56**, 12847 (1997).
[3] I. Souza, J. Íñiguez, and D. Vanderbilt, Phys. Rev. Lett. **89**, 117602 (2002).
[4] T. Thonhauser, D. Ceresoli, D. Vanderbilt, and R. Resta, Phys. Rev. Lett. **95**, 137205 (2005).

**SESSION B2: SOLID HELIUM**
**Monday Morning, 13 March 2006; Ballroom III, Baltimore Convention Center at 11:15**
**Michael Ma, University of Cincinnati, presiding**

**11:15**
**B2 1 Observation of superfluidity in solid helium and solid hydrogen.**
ANTHONY CLARK, *Penn State University*

A torsional oscillator technique is used to search for non-classical rotational inertia of solid helium[1] and solid hydrogen. Several important experimental details already observed will be reviewed for both systems. Some of these include the

transition temperature, supersolid fraction, and dependencies on oscillation speed and impurities. Comparisons will be made in order to demonstrate the similarities and/or differences between helium and hydrogen. With further work currently underway, we will also report on recent experimental progress. This work is done in collaboration with Eunseong Kim, Xi Lin and Moses Chan and is supported by the NSF under grant 0207071. [1] E. Kim and M. H. W. Chan, Nature **427**, 225 (2004); Science **305**, 1941(2004); J. Low Temp. Phys. **138**, 859 (2005).

**11:51**
**B2 2 Pressure-driven Flow of Solid Helium.***
JOHN BEAMISH, *University of Alberta*

Recent torsional oscillator measurements by Moses Chan's Penn State group showed evidence of ''non-classical rotational inertia'' for solid helium at temperatures below 200 mK. This discovery followed decades of theoretical speculation and experimental searches for ''supersolidity'' in helium. The experiments generated a great deal of interest but the origin and properties of such a state are still unclear. It would be very interesting to know whether supersolids share any of the other unusual properties of superfluids: persistent currents, second sound and quantized vortices. We have studied the response of solid helium to pressure changes in order to look for unusual flow properties that might be associated with supersolidity. The measurements involved both helium confined in the nanometer pores of Vycor glass and bulk solid helium, at temperatures as low as 30 mK. Pressure changes were generated with piezoelectrically driven diaphragm and flow was monitored with sensitive capacitive techniques. Near melting, solid helium flows very easily but we did not see any evidence of superflow at low temperatures. If helium does become a supersolid at low temperatures then its response to pressure gradients must be very different from that of liquid helium.

*This research was supported by a grant from NSERC Canada.



**12:27**
**B2 3 Theory for supersolid 4He: Vacancy condensation facilitated by a low-energy bound state.**
XI DAI, *Department of Physics, University of Hong Kong*

Although both vacancies and interstitials have relatively high activation energies in the normal solid, we propose that a lower energy bound state of a vacancy and an interstitial may facilitate vacancy condensation to give supersolidity in 4He. We use a phenomenological two-band boson lattice model to demonstrate this new mechanism and discuss the possible relevance to the recently observed superfluidlike, nonclassical rotational inertial experiments of Kim and Chan in solid 4He. Some of our results may also be applicable to trapped bosons in optical lattices.

**13:03**
**B2 4 Off diagonal long range order in solid 4He.**
LUCIANO REATTO, *Dipartimento di Fisica, Universita' di Milano*

The presence both of long range order (LRO) and of off diagonal long range order (ODLRO) in solid 4He is discussed on the basis of an accurate variational theory (shadow wave function, SWF) and of an exact projection method (shadow path integral ground state, SPIGS). If the solid is incommensurate (e.g. solid with a vacancy: number of atoms different from number of equilibrium sites) both SWF and SPIGS give ODLRO and close to melting density there is a BEC of about 0.3 He atoms per vacancy. For a commensurate solid (number of atoms equal to number of sites) SWF gives ODLRO with a condensate of about one part per thousand. Preliminary evidence indicates that also SPIGS gives a finite BEC. The key process is the spontaneous formation of unbound vacancy-interstitial pairs. These results support the presence of supersolidity in bulk solid 4He. As a final point we address the question if the exact ground state of bulk solid 4He is commensurate or incommensurate and conclude that there is not yet a definite answer to this question from microscopic theory.

**13:39**
**B2 5 Path Integral Simulations of Solid $^4$He.***
DAVID CEPERLEY, *University of Illinois Urbana-Champaign*

Kim and Chan have found indications that solid $^4$He is a supersolid by measuring the period of a torsional oscillator. To understand the state of solid $^4$He at low temperature, we [1] have calculated tunnelling frequencies for ring exchanges in bulk solid helium with Path Integral Monte Carlo by finding the free energy of a path that begins with the atoms in one configuration and ends with a permutation of those positions. The exchange frequencies are found to be described by a lattice model which does not show superfluid behavior. However, simulations [2] of $^4$He absorbed in Vycor find that $^4$He forms a layered structure with the first layer solid-like and highly localized, the second layer disordered with some atoms delocalized and possibly superfluid. This persistent liquid layer mechanism can only be relevant for bulk $^4$He in a very disordered crystal. New calculations [3] of the single particle density matrix, (the fourier transform of the momentum distribution) to measure ODLRA will also be discussed. [1] D. M. Ceperley and B. Bernu, Phys. Rev. Letts. 93, 155303(2004). [2] S. A. Khairallah and D. M. Ceperley, Phys. Rev. Letts. 95, 185301 (2005). [3] B. Clark and D. M. Ceperley, unpublished.

*supported by NASA, fundamental physics

**SESSION B3: UNCOVERING THE STRUCTURE OF COMPLEX NETWORKS**
**Monday Morning, 13 March 2006; Ballroom I, Baltimore Convention Center at 11:15**
**Albert-Laszlo Barabasi, University of Notre Dame, presiding**

**11:15**
**B3 1 Modularity and community structure in networks.**
MARK NEWMAN, *University of Michigan*

Many systems of scientific interest can be represented as networks—sets of nodes joined in pairs by lines or edges. Examples include metabolic and other biochemical networks, neural networks, food webs, the Internet and the worldwide web, and social networks. The physics community has made substantial contributions to the study of networked systems in the last decade, drawing particularly on ideas from statistical physics, field theory, and data analysis. One issue that has received considerable attention is the detection and characterization of ''modules'' or ''communities'' within networks—densely connected groups of nodes, with only sparser connections between groups. The ability to find and quantify such communities has proved to be of significant practical worth in the study of biochemical, technological, and social networks, among others, and there has been a lot of activity directed at the development of community-finding methods and algorithms to make these kinds of studies possible. This talk will describe some of the work in this area, focusing in particular on several powerful methods developed recently that appear to outperform previous ones by a substantial margin. A number of example applications will be shown demonstrating the utility of community structure detection in the analysis of real-world network data.

**11:51**
**B3 2 Modular structure of flat and hierarchial networks.**
ROGER GUIMERA, *Northwastern Univ.*

This abstract was not received electronically.

**12:27**
**B3 3 Uncovering the overlapping modules of complex networks.***
TAMAS VICSEK, *Eotvos University*

Many complex systems in nature and society can be described in terms of networks capturing the intricate web of connections among the units they are made of. A fundamental question of great current interest is how to interpret the global organisation of such networks as the coexistence of their structural sub-units (called modules, communities, clusters, etc) associated with more highly interconnected parts. Identifying these unknown building blocks (e.g., functionally related proteins, industrial sectors, groups of people) is crucial to the understanding of the structural and functional properties of networks. The existing deterministic methods used for large data sets find separated modules, while most of the actual networks are made of highly overlapping cohesive groups of nodes. Here we introduce an approach to analyse the main statistical features of the interwoven sets of overlapping communities making a much needed step towards the uncovering of the modular structure of complex systems. After defining a set of new characteristic quantities for their statistics, we apply an efficient technique to explore overlapping communities on a large scale. We find that overlaps are indeed very significant, and the distributions we introduce reveal novel universal features of networks. Our studies of collaboration, word association, and protein interaction graphs demonstrate that the web of modules has highly non-trivial correlations and specific scaling properties.

*This work was carried out in collaboration with G. Palla, I. Derenyi and I. Farkas and supported by OTKA No: T09764.

**13:03**
**B3 4 Spectral methods and Network Communities.***
MIGUEL A. MUÑOZ, *Universidad de Granada (Spain)*

Spectral methods provide us with a powerful tool-box to explore the topology of networks. In this presentation we will review an application of spectral techniques to the analysis of communities in complex networks. Communities are network sub-groups formed by highly interconnected nodes, which are sparsely connected to the rest of the network. They appear ubiquitously in natural and artificial nets, and are believed to play a key role as functional units, and detecting them has become a crucial problem in complex-system analyses.The efficient and relatively fast algorithm we will present here exploits spectral properties of some matrices encoding the network topology (as the Laplacian matrix), combined with standard hierarchical-clustering techniques, and the use of the ''modularity parameter'' allowing to quantify the goodness of any possible community subdivision. The algorithm performance, will be compared with that of other existing methods, as applied to different well-known examples of artificial and real networks. Our results are in all the

tested cases, at least as good as the best ones obtained with any other methods, and faster in most of the cases than methods providing similar-quality results. This converts the algorithm in a valuable computational tool for detecting and analyzing communities and modular structures in complex networks.The connection of these results with the problem of determining the optimal network topology to achieve synchronization within the net and to optimize other dynamical processes will also be put forward.

*In collaboration with L. Donetti. COSIN-project-IST2001-33555.

**13:39**
**B3 5 Changes in metabolic modules under environmental variations.**
EIVIND ALMAAS, *Lawrence Livermore National Laboratory*



During the last few years, network approaches have shown great promise as a tool to both analyze and provide understanding of complex systems as disparate as the world-wide web and cellular metabolism. Much effort has been focused on characterizing topological properties of such systems. However, in order to develop detailed descriptions of complex networks, we need to look beyond their topology and incorporate dynamical aspects. The cellular metabolism, where nodes correspond to metabolites and links indicate chemical reactions, is an excellent model system where theoretical predictions can be compared with experimental results. I will present recent insights into the principles governing the modular utilization of the cellular metabolism [1,2,3]. We find that, while most metabolic reactions have small fluxes, the metabolism's activity is dominated by an interconnected sub-network of reactions with very high fluxes [1]. For the bacteria *H. pylori* and *E. coli* and the yeast *S. cerevisiae*, the metabolism responds to changes in growth conditions by reorganizing the rates of select reactions predominantly within this high-flux backbone. Furthermore, these networks are organized around the metabolic core – a set of reactions that are always in use [2]. Strikingly, the activity of the metabolic core reactions is highly synchronized, and the core reactions are significantly more essential and evolutionary conserved than the non-core ones. [1] E. Almaas, B. Kovacs, T. Vicsek, Z.N. Oltvai and A.-L. Barabasi. Nature 427, 839 (2004). [2] E. Almaas, Z.N. Oltvai and A.-L. Barabasi. PLoS Comput. Biol. In press (2005). 10.1371/journal.pcbi.0010068.eor [3] P.J. Macdonald, E. Almaas and A.-L. Barabasi. Europhys. Lett. 72, 308 (2005).

## SESSION B4: ADVANCES IN ZNO MATERIALS PHYSICS AND APPLICATIONS
**Monday Morning, 13 March 2006; 308, Baltimore Convention Center at 11:15**
**Tom Myers, West Virginia University, presiding**

**11:15**
**B4 1 Theory of defects and doping in ZnO.***
CHRIS G. VAN DE WALLE, *University of California, Santa Barbara*

In spite of rapid progress in materials quality, zinc oxide still suffers from serious problems in controlling its conductivity. We are addressing these issues by performing first-principles calculations based on density-functional theory (DFT) in the local density approximation (LDA). In addition, we have developed an approach (based on LDA+U) for overcoming the DFT band-gap problem, allowing us to more accurately compare and predict defect levels. Native point defects are still frequently invoked as sources of n-type conductivity, but our results do not support this hypothesis. Oxygen vacancies are deep donors; our configuration coordinate diagrams for this defect provide a detailed interpretation of the recent ODEPR results of Vlasenko and Watkins [1]. Zinc interstitials are shallow donors, but their formation energy is high and they diffuse very rapidly, with a migration barrier as low as 0.6 eV, making it very unlikely that they would be stable. For the zinc antisite, we find an unexpected low-symmetry configuration. While still high in energy, this defect may play a role under non-equilibrium conditions such as irradiation. We suggest that unintentional incorporation of impurities (such as hydrogen) is a more likely explanation for n-type background doping. However, native defects play a crucial role as compensating centers in p-type material, and we will discuss ways of overcoming this problem. Among the native defects that act as acceptors, zinc vacancies have the lowest formation energy; they introduce deep levels likely responsible for green luminescence. Our calculated migration barriers for the point defects are in good agreement with experimental data where available, and provide insight in the processes that take place during growth, irradiation, or annealing.

[1] L. S. Vlasenko and G. D. Watkins, Phys. Rev. B 71, 125210 (2005).

*Work performed in collaboration with Anderson Janotti, and supported in part by the Palo Alto Research Center and by AFOSR.

**11:51**
**B4 2 Key Materials Aspects for Valence Control of ZnO.**
ATSUSHI TSUKAZAKI, *Institute for Materials Research, Tohoku University*

ZnO has significant advantages for light emitting diodes (LEDs) and lasers from the following reasons; 1) exciton binding energy in ZnO is 60 meV and can be enhanced over 100 meV in superlattices, 2) it is possible to tune the bandgap from 3 eV to 4.5 eV in $Zn_{1-x}Cd_xO$ and $Mg_xZn_{1-x}O$ alloy films having quite small lattice mismatch, and 3) large and high-quality single-crystal wafers are commercially available. In order to harvest these advantages in real devices, reliable technique for fabricating p-type ZnO has to be properly established. Recently we have reported on the improvements of undoped ZnO film quality with inserting a ZnO self-buffer layer onto lattice matched $ScAlMgO_4$ substrate [1]. In view of point defect formation during the epitaxy, we have carefully optimized the growth conditions. We selected nitrogen as an acceptor, because the ionic radius is close to that of oxygen. Here we propose a repeated temperature modulation (RTM) technique for efficient nitrogen doping into ZnO with keeping high crystallinity [2]. By carefully optimizing the conditions, p-type ZnO with a hole concentration of $10^{16}$ - $10^{17}$ $cm^{-3}$ can be reproducibly fabricated. We also demonstrated blue electroluminescence from p-i-n homojunction LED [3]. The details of thin film growth, characteristics of p-type ZnO and device performance will be presented. [1] A. Tsukazaki et al. itNature Mater. **4**, 42 (2005). [2] A. Tsukazaki et al. itAppl. Phys. Lett.**83**, 2784 (2003). [3]A. Tsukazaki et al. itJpn. J. Appl. Phys.Lett.44, L643 (2005).

**12:27**
**B4 3 Localized States and Charge Transfer at ZnO Surfaces and Interfaces.***
LEONARD BRILLSON, *The Ohio State University*

With the advent of techniques to probe semiconductor electronic properties in the near-interface region on a nanometer scale, it is now possible to understand and control the mechanisms playing a role in localized state formation and charge transfer at ZnO interfaces. While world-wide research activity into this major new semiconductor has increased dramatically, the ability to control ZnO interfaces has been a major challenge to their opto- and microelectronic applications. Nanoscale depth-resolved cathodoluminescence and x-ray photoemission spectroscopies reveal the segregation of point defects and the donor character of hydrogen in the near-surface region. A conversion from ohmic to rectifying behavior is observed for gold contacts on atomically ordered polar ZnO surfaces following remote oxygen plasma treatment. This transition is accompanied by reduction of the well-known ''green'' deep level emission, suppression of the hydrogen donor-bound exciton photoluminescence and a large increase in n-type band bending. These results demonstrate that the contact type conversion involves more than one mechanism, specifically, removal of the adsorbate-induced accumulation layer plus lowered tunneling due to reduction of near-surface donor density and defect-assisted hopping transport. Schottky barriers for a wide array of metals on ZnO reveal that the strength of interface reaction plays a dominant role in forming near-interface defects and the resultant Schottky barriers. Similar correlations for other compound semiconductors indicate that the impact of near-interface native defects on Schottky barriers is more general in nature. [1] H.L. Mosbacker, Y.M. Strzhemechny, B.D. White, P.E. Smith, D.C. Look, D.C. Reynolds, C.W. Litton, and L.J. Brillson, ''Role of Near-Surface States in Ohmic-Schottky Conversion of Au Contacts to ZnO,'' Appl. Phys. Lett. 87, 012102 (2005). [2] Y.M. Strzhemechny, H.L. Mosbacker, D.C. Look, D.C. Reynolds, C.W. Litton, N.Y.Garces, NC. Giles, L.E. Halliburton, S. Niki, and L.J. Brillson, ''Remote Hydrogen Plasma Doping of Single Crystal ZnO,'' Appl. Phys. Lett. 84, 2545 (2004).

*Supported by the National Science Foundation and the Office of Science, Department of Energy.

**13:03**
**B4 4 Growth, Assembly, and Characterization of ZnO Nanostructures on Ag Films.***
JULIA W. P. HSU, *Sandia National Laboratories*

In the past decade, significant advances have been made in the synthesis of ZnO nanostructures. The next step in making these nanomaterials useful is to assemble them on surfaces in a controlled and desired fashion. In this talk, I will discuss the growth of complex ZnO nanostructures via a solution method in which organic templates are used to control assembly of these nanostructures on substrate surfaces. The low temperature aqueous growth method used in this work is an environmentally benign process, which is compatible with organic templates and modifiers, can be used to grow large areas uniformly, and has potential for inexpensive manufacturing. To control the assembly of these solution grown nanostructures, we modify the substrate surfaces with patterned self-assembled monolayers, which in turn determines the final spatial organization of the ZnO nanorods. This is a bottom-up approach in which materials are deposited only where they are needed. Using this approach, we have achieved excellent control in spatial placement, selectivity, crystal orientation, and nucleation density. In addition, complex, hierarchical structures have been synthesized by controlling solution chemistry and growth conditions. Due to lack of inversion symmetry in hexagonal crystal, ZnO is a piezoelectric material with Zn (0001) polar and O $(000\bar{1})$ polar surfaces exhibiting drastically different physical and chemical properties. Hence, it is important to determine the orientation of the ZnO nanorods on surfaces. Using piezoelectric force microscopy (PFM) and a well-characterized ZnO single crystal reference, we have measured the amplitude and phase of

piezoelectric responses of over 100 individual ZnO rods. The phase of the PFM signal is 180[r] from the applied electric field, indicating that the nanorods are [0001] oriented. This result contradicts what would have been expected based on an examination of rod morphology. Also, the PFM amplitude of the nanorods was found to be significantly larger than that of the ZnO single crystal. The origin behind this observation and the variation among different nanorods will be discussed.

*In collaboration with D. Scrymgeour, Z. R. Tian, N. C. Simmons, C. M. Matzke, J. A. Voigt, and J. Liu.

**13:39**
**B4 5 Charge- and Spin-Based Devices in ZnO Thin Films and Nanostructures.**
DAVID NORTON, *Univeristy of Florida*

ZnO is a wide bandgap semiconductor of potential for device concepts based on charge and/or electron spin. As a direct bandgap material with emission in the ultraviolet, ZnO is being actively pursued in the areas of ultraviolet light emitting diodes and laser diodes. The critical issue in developing such optoelectronic devices is p-type doping. As a dilute magnetic semiconductor, numerous experimental reports indicate ferromagnetism in transition metal doped ZnO. However, the mechanism for this magnetic behavior continues to be a topic of debate. In addition, numerous techniques have been utilized to synthesize ZnO nanoscale structures, many of which appear to be useful for sensors and nanoelectronics. In this talk, pertinent issues for spin and charge-based ZnO devices will be discussed. The focus will be on p-type doping, pn junction formation, magnetic doping, and nanowire-based sensor development. This work is supported by the National Science Foundation (DMR-029086), the Department of Energy (DE-FC26-04NT42271), and the Air Force Office of Scientific Research (030967).



## SESSION B5: NUCLEAR PROLIFERATION & NUCLEAR TERRORISM
**Monday Morning, 13 March 2006; 309, Baltimore Convention Center at 11:15**
**David Hafemeister, California Polytechnic State University, presiding**

**11:15**
JOSEPH CIRINCIONE, *Carnegie Endowment for International Peace*

This abstract was not received electronically.

**11:51**
**B5 2 National Academy of Sciences Study on Monitoring Nuclear Weapons and Materials.**
STEVE FETTER, *University of Maryland*

This abstract was not received electronically.

**12:27**
**B5 3 Advances in Nuclear Monitoring Technologies.**
BRENT PARK, *Los Alamos National Laboratory*

Homeland security requires low-cost, large-area detectors for locating and identifying weapons-usable nuclear materials and monitors for radiological isotopes that are more robust than current systems. Recent advances in electronics materials and nanotechnology, specifically organic semiconductors and inorganic quantum dots, offer potential improvements. We provide an overview of the physical processes involved in radiation detection using these new materials in the design of new device structures. Examples include recent efforts on quantum dots, as well as more traditional radiation-detecting materials such as CdZnTe and high-pressure xenon. Detector improvements demand not only new materials but also enhanced data-analysis tools that reduce false alarms and thus increase the quality of decisions. Additional computing power on hand-held platforms should enable the application of advanced algorithms to radiation-detection problems in the field, reducing the need to transmit data and thus delay analysis.

**13:03**
**B5 4 Monitoring Illicit Nuclear Materials.**
MIKE CARTER, *Department of Homeland Security*

This abstract was not received electronically.

**SESSION B6: SPIN-BASED QUANTUM COMPUTING**
**Monday Morning, 13 March 2006; 310, Baltimore Convention Center at 11:15**
**David DiVincenzo, T.J. Watson Research Center, presiding**



**11:15**
**B6 1 Spin Readout and Hyperfine Interaction in Few-Electron Quantum Dots.**
RONALD HANSON, *Kavli Institute of Nanoscience Delft*

This talk presents recent experimental progress toward using few-electron quantum dots as spin qubits. First, we have developed a new spin readout technique that is based on the difference in tunnel rate between different spin states[1]. Unlike earlier techniques, it is robust against background charge fluctuations and high-frequency noise, and presently achieves single-shot fidelities up to 90%. Using this readout technique, we have measured the two-electron spin relaxation time as a function of magnetic field strength and orientation, and studied the back-action of the charge detector. Second, we have investigated the effect of nuclear spins on the electron spin state[2]. Transport measurements on a double quantum dot in the spin blockade regime reveal that the delocalized two-electron singlet and triplet states are mixed by an inhomogeneous hyperfine field of about 1 mT. We demonstrate that this mixing can be controlled by changing either the external magnetic field or the interdot tunnel coupling. The transitions between triplet and singlet states in turn lead to current-induced dynamical nuclear polarization. In certain regimes, marked current bistabilities appear as a function of both field and time.

[1]R. Hanson, L.H. Willems van Beveren, I.T. Vink, J.M. Elzerman, W.J.M. Naber, F.H.L. Koppens, L.P. Kouwenhoven, and L.M.K. Vandersypen, Phys. Rev. Lett. 94, 196802 (2005).
[2]F.H.L. Koppens, J.A. Folk, J.M. Elzerman, R. Hanson, L.H. Willems van Beveren, I.T. Vink, H.P. Tranitz, W. Wegscheider, L.P. Kouwenhoven, and L.M.K. Vandersypen, Science 309, 1346 (2005).

**11:51**
**B6 2 Enhancement of Spin Coherence Using Q-factor Engineering in Semiconductor Microdisk Lasers.***
SAYANTANI GHOSH,† *Center for Spintronics and Quantum Computation, University of California, Santa Barbara, CA 93106, USA*

Semiconductor microcavities offer unique means of controlling light-matter interactions in confined geometries, resulting in a wide range of applications in optical communications and inspiring proposals for quantum information processing and computational schemes. Studies of spin dynamics in microcavities have revealed novel effects such as polarization beats, stimulated spin scattering, and giant Faraday rotation. Here, we study the electron spin dynamics in optically-pumped GaAs microdisk lasers with quantum wells (QWs) and interface-fluctuation quantum dots (QDs) in the active region. Using all-optical time-resolved measurement techniques, we examine how the electron spin dynamics are modified by the stimulated emission in the disks, and observe a surprising enhancement of the spin coherence time when the optical excitation is in resonance with a high quality ($Q \sim 5000$) lasing mode[1]. This resonant enhancement, contrary to expectations from the observed trend in the carrier recombination time, is then manipulated by altering the cavity design and dimensions. In analogy to devices based on excitonic coherence, this ability to engineer coherent interactions between electron spins and photons may provide novel pathways towards spin dependent quantum optoelectronics.

*This work was supported by DARPA/QUIST and NSF.
†In collaboration with F. M. Mendoza, R. C. Myers, W. H. Wang, X. Li, N. Samarth, A. C. Gossard, and D. D. Awschalom.

[1]S. Ghosh, W. H. Wang, F. M. Mendoza, R. C. Myers, X. Li, N. Samarth, A. C. Gossard, and D. D. Awschalom, Nature Materials, accepted for publication (2005). (cond-mat/0509500).

**12:27**
**B6 3 Teleportation of electronic many-qubit states via single photons.**
MICHAEL FLATTÉ, *The University of Iowa*

I will describe a proposed a teleportation scheme[1] that relies only on single-photon measurements and Faraday rotation, for teleportation of many-qubit entangled states stored in the electron spins of a quantum dot system. The interaction between a photon and the two electron spins, via Faraday rotation in microcavities, establishes Greenberger-Horne-Zeilinger entanglement in the spin-photon-spin system. The appropriate single-qubit measurements, and the communication of two classical bits, produce teleportation. This scheme provides the essential link between spintronic and photonic quantum information devices by permitting quantum information to be exchanged between them. Work supported by DARPA/ARO DAAD19-01-1- 0490. [1] M. N. Leuenberger, M. E. Flatté, and D. D. Awschalom, Phys. Rev. Lett. 94, 107401 (2005).

**13:03**
**B6 4 Optically probing charge and spin states in quantum dots and molecules.**
JONATHAN FINLEY, *Walter Schottky Institut*

In this talk I will discuss recent experiments in which we electrically manipulate coupled excitonic states (neutral and negatively charged single excitons) in individual QD-molecules using static electric fields. The samples investigated consist of a single pair of vertically stacked, self assembled InGaAs QD-molecules embedded in an n-type GaAs Schottky photodiode. This device geometry enables us to control the coherent coupling between excitonic states in the upper and lower dots by tuning the electric field oriented along the axis of the QD-molecule by applying a bias voltage between the n-contact and the Schottky-gate. New information is obtained on the spin structure of negatively charged trions in coupled quantum dot nanostructures. At low excitation power densities, field dependent luminescence reveals a clear anticrossing of spatially direct (e,h in the same dot) and indirect (e,h in different dots) neutral excitons, with coupling energies in the range $2E_{ee}$=1.2-3.2meV. Our experimental findings are shown to be in very good accord with realistic calculations of the single exciton spectrum, confirming that the tunnel coupling is mediated by hybridization of the electron component of the exciton wavefunction over the two dots. In contrast, the spectrum and controlled hybridization of itnegatively charged excitons is shown to be much richer due to the complex spectrum of three particle states ($X^-$=2e+1h) that can exist in a QD-molecule. For example, the spin structure of the spatially localized and dissociated $X^-$ states is found to play a major role in the spectrum of controlled hybridization with distinct triplet and single states evolving very differently as the coupling is tuned. The demonstration of tunable coupling and manipulation of spin and exchange couplings in negatively charged systems may constitute an important step towards the development of optically gateable QD-molecules for applications in quantum information science.

**13:39**
**B6 5 Production and Detection of Spin-Entangled Electrons in Mesoscopic Conductors.**
GUIDO BURKARD, *University of Basel, Switzerland*

Electron spins are an extremely versatile form of quantum bits. When localized in quantum dots, they can form a register for quantum computation. Moreover, being attached to a charge in a mesoscopic conductor allows the electron spin to play the role of a mobile carrier of quantum information similarly to photons in optical quantum communication. Since entanglement is a basic resource in quantum communication, the production and detection of spin-entangled Einstein-Podolsky-Rosen (EPR) pairs of electrons are of great interest. Besides the practical importance, it is of fundamental interest to test quantum non-locality for electrons. I review the theoretical schemes for the entanglement production in superconductor-normal junctions [1] and other systems. The electron spin entanglement can be detected and quantified from measurements of the fluctuations (shot noise) of the charge current after the electrons have passed through an electronic beam splitter [2,3]. This two-particle interference effect is related to the Hanbury-Brown and Twiss experiment and leads to a doubling of the shot noise $S_I = \langle \delta I \, \delta I \rangle_{\omega=0}$ for spin-entangled states, allowing their differentiation from unentangled pairs. I report on the role of spin-orbit coupling (Rashba and Dresselhaus) in a complete characterization of the spin entanglement [4]. Finally, I address the effects of a discrete level spectrum in the mesoscopic leads and of backscattering and decoherence. [1] P. Recher, E. V. Sukhorukov, D. Loss, Phys. Rev. B **63**, 165314 (2001) [2] G. Burkard, D. Loss, E. V. Sukhorukov, Phys. Rev. B **61**, R16303 (2000) [3] G. Burkard and D. Loss, Phys. Rev. Lett.**91**, 087903 (2003) [4] J. C. Egues, G. Burkard, D. Saraga, J. Schliemann, D. Loss, cond-mat/0509038, to appear in Phys.Rev.B (2005).

## SESSION B7: BIONANOTECHNOLOGY: APPLICATION AND FUNDAMENTAL ASPECTS OF PROCESSES AT NANO-SCALE

**Monday Morning, 13 March 2006; 307, Baltimore Convention Center at 11:15**
**Zuzanna S. Siwy, University of California, Irvine, presiding**

**11:15**
**B7 1 Ion Channels as Nanodevices.**
ROBERT EISENBERG,* *Molecular Biophysics: Rush University*

Ion channels are proteins surrounding a hole that allow substances to cross biological membranes. The concentration or current of these substances controls an enormous range of biological function: ion channels are nearly as important in biology as transistors in computers. Ion channels have a stable structure (on biological time scales $> 0.1\mu$sec) once open and so current through them can be analyzed by 'physics as usual'. The permanent charge on the wall of the channel is large and the volume is tiny, so the number density of ions in the channel is very large, $>$ 10 M. Physical properties of channels can be understood from the balance between electrical and van der Waals forces of charge crowded into a tiny space. Many biological properties of channels can be understood in the engineering tradition of devices: channels follow reasonably robust 'device equations' determined by their specific structural design and general physical environment. Channel research seeks to understand these device equations in **itjust** enough detail to control them. Channels—like most

engineering devices—function away from equilibrium, so spatially non-uniform boundary conditions and non-equilibrium statistical mechanics must be used in their description. Atomic scale simulations pose certain problems since trace concentrations of ions ( $< \mu$M) often control biological function and ions flow on time scales very much slower than the time steps of simulations. Atomic scale simulations of microM activities requires enormous numbers of water molecules ( $> 10^{11}$); direct simulation of ionic current involves many billions ( $> 10^{11}$) of time steps, suggesting that analysis must be multiscale if it is to be useful. This should come as no surprise, since the function of ion channels is inherently multiscale: ion channels act as nanovalves, nanodevices that allow details of atomic structure to control macroscopic flows and biological function.

*Chicago IL.

**11:51**
**B7 2 Fluctuation driven active molecular transport in passive channel proteins.**
IOAN KOSZTIN, *University of Missouri - Columbia*

Living cells interact with their extracellular environment through the cell membrane, which acts as a protective permeability barrier for preserving the internal integrity of the cell. However, cell metabolism requires controlled molecular transport across the cell membrane, a function that is fulfilled by a wide variety of transmembrane proteins, acting as either passive or active transporters. In this talk it is argued that, contrary to the general belief, in active cell membranes passive and spatially asymmetric channel proteins can act as active transporters by consuming energy from nonequilibrium fluctuations fueled by cell metabolism. This assertion is demonstrated in the case of the E. coli aquaglyceroporin GlpF channel protein, whose high resolution crystal structure is manifestly asymmetric. By calculating the glycerol flux through GlpF within the framework of a stochastic model, it is found that, as a result of channel asymmetry, glycerol uptake driven by a concentration gradient is enhanced significantly in the presence of non-equilibrium fluctuations. Furthermore, the enhancement caused by a ratchet-like mechanism is larger for the outward, i.e., from the cytoplasm to the periplasm, flux than for the inward one, suggesting that the same non-equilibrium fluctuations also play an important role in protecting the interior of the cell against poisoning by excess uptake of glycerol. Preliminary data on water and sugar transport through aquaporin and maltoporin channels, respectively, are indicative of the universality of the proposed nonequilibrium-fluctuation-driven active transport mechanism. This work was supported by grants from the Univ. of Missouri Research Board, the Institute for Theoretical Sciences and the Department of Energy (DOE Contract W-7405-ENG-36), and the National Science Foundation (FIBR-0526854).

**12:27**
**B7 3 Pressure-driven DNA polymer transport in microfluidic and nanofluidic channels.**
DEREK STEIN, *Delft University of Technology*

The transport of DNA and proteins within micro- and nanofluidic channels is of central importance to ''lab-on-a-chip'' bioanalysis technology. As fluidic devices shrink, a new regime is encountered where critical device dimensions approach the molecular scale, and the behavior of polymers often departs significantly from the bulk. Here, we present a study of the pressure-driven transport of individual DNA molecules in 175 nm – 3.8 $\mu$m high silica channels. Two distinct transport regimes were observed: The pressure-driven mobility of DNA increased with molecular length in channels higher than a few times the molecular radius of gyration, whereas DNA mobility was practically independent of molecular length in thin channels. In addition, both the Taylor dispersion and the self-diffusion of DNA molecules were observed to decrease significantly in confined channels, each obeying a power-law scaling relationship. These unusual transport properties are shown to be rooted in the statistical nature of DNA polymer coils. Our results show that simple fluidic channels can be engineered to achieve either hydrodynamic DNA length separation or uniform transport with minimal dispersion using pressure-driven flows.

**13:03**
**B7 4 The Transportation System Inside a Living Cell.***
CLARE YU,† *University of California, Irvine*

A living cell has an infrastructure much like that of a city. We will describe the transportation system that consists of roads (filaments) and molecular motors (proteins) that haul cargo along these roads. This transportation system is essential for such diverse processes as neuronal function and mitochondrial transport. While there have been studies of how motors function at the single molecule level, and studies of the structure of filamentary networks, studies of how the motors effectively use the networks for transportation have been lacking. We will give an example showing that pigment cells regulate transport by controlling how often pigment granules switch from one filament to another, rather than by altering individual motor activity at the single molecule level, or by relying on structural changes in the network.

*This work was supported by NIGMS grant GM-64624-01 to SPG, grants from NIGMS GM-62290-01 and NCRR RR13186 to V.I.Rodionov, and a grant from DOE DE-FG03-00ER45843 to C. C. Yu.
†Collaborators: J. Snider, F. Lin, S. P. Gross (University of California, Irvine), N. Zahedi and V. Rodionov (Center for Biomedical Imaging Technology, Farmington, CT and Randall Centre for Molecular Mechanisms of Cell Function, King's College London.

**13:39**
**B7 5 Bio-functionalized Nanotube Membranes For DNA Separation.**
PUNIT KOHLI, *Southern Illinois University*

The studies of translocation and transport of ions, biopolymers, and other genetics materials is very important in medical and scientific communities. The transport of biopolymers such as RNA, DNA, and polypeptides across membrane occurs in many biological systems. Examples include the transport of RNA molecules and transcription factors through nuclear pores, injection of DNA from a virus head into the host cell, and the uptake of oligonucleotides by specific membrane proteins. Another example is the transport of ions through protein ion channels across cell membranes, which converts the concentration of transported analytes through a channel into change in channel conductance. Nature's highly selective biosensor are based on molecular-recognition of one species of interest in the presence of others. In this presentation, I will discuss the fabrication of a new DNA biosensor. I will also talk about the transport behavior of DNA molecules through nanotubes. These sensors based on monodisperse ensemble of gold nanotubes. Single stranded oligonucleotides were immobilized onto the inner walls of nanotubes. These bio/nano-membranes selectively transport complementary DNA across the membrane with selectivity greater than 5 was observed. With these membranes, single nucleotide polymorphism detection is also demonstrated.



## SESSION B8: FOCUS SESSION: GRANULAR MATERIALS NEAR JAMMING
**Monday Morning, 13 March 2006; 314, Baltimore Convention Center at 11:15**
**Bob Behringer, Duke University, presiding**

***Invited Papers***

**11:15**
**B8 1 Elastic Granular Flows.**
CHARLES CAMPBELL, *University of Southern California*

There is no fundamental understanding of the mechanics of granular solids. Partially this is because granular flows have historically been divided into two very distinct flow regimes, (1) the slow, quasistatic regime, in which the bulk friction coefficient is taken to be a material constant, and (2) the fast, rapid-flow regime, where the particles interact collisionally. But slow hopper flow simulations indicate that the bulk friction coefficient is not a constant. Rapidly moving large scale landslide simulations never entered the collisional regime and operate in a separate intermediate flow regime. In other words, most realistic granular flows are not described by either the quasistatic or rapid flow models and it is high time that the field look beyond those early models. This talk will discuss computer simulation studies that draw out the entire flowmap of shearing granular materials, spanning the quasistatic, rapid and the intermediate regimes. The key was to include the elastic properties of the solid material in the set of rheological parameters; in effect, this puts solid properties back into the rheology of granular solids. The solid properties were previously unnecessary in the plasticity and kinetic theory formalisms that respectively form the foundations of the quasistatic and rapid-flow theories. Granular flows can now be divided into two broad categories, the Elastic Regimes, in which the particles are locked in force chains and interact elastically over long duration contact with their neighbors and the Inertial regimes, where the particles have broken free of the force chains. The Elastic regimes can be further subdivided into the Elastic-Quasistatic regime (the old quasistatic regime) and the Elastic-Inertial regime. The Elastic-Inertial regime is the ''new'' regime observed in the landslide simulations, in which the inertially induced stresses are significant compared to the elastically induced stresses. The Inertial regime can also be sub-divided into an Inertial-Non-Collisional where the stresses scale inertially, but the particles interact in clusters through long duration contacts, and the Inertial-Collisional (or the old rapid-flow) regime. Finally, the simulations show that Stress-Controlled flows are rheologically different from Controlled-Volume flows. Physically, there is a range of dense concentrations ($0.5 < \nu < 0.6$) in which it is possible, but not necessary to form force chains and demonstrate elastic behavior. (In other words it is possible for the material to exhibit two different states at the same concentration.) By forcing the material to support an applied loads across force chains, Stress-Controlled flows may behave elastically through this range of concentrations while, at the same shear rates rate Controlled-Volume flows, fixed at the average concentration of the Stress-Controlled flow, behave inertially.

***Contributed Papers***

**11:51**
**B8 2 Force distributions and stress fluctuations in a triangular lattice of rigid bars*** BRIAN TIGHE, JOSHUA SOCOLAR, *Physics Dept., Duke University, Durham, NC* We study the uniformly weighted ensemble of force balanced configurations on a triangular network of nontensile contact forces as a model of force distribution on a hyperstatic granular material. For periodic boundary conditions corresponding to isotropic compressive stress, the probability distribution for single-contact forces, $P(f)$, decays faster than exponentially, and a field closely related to the lattice version of the Airy stress function is found to have fluctuations characterized by a structure factor $S(q) \sim 1/q^4$. The super-exponential decay of $P(f)$ persists in lattices diluted to the rigidity percolation threshold. On the other hand, for anisotropic imposed

stresses, a broader tail emerges, becoming a pure exponential in the limit of infinite lattice size and infinitely strong anisotropy.

*Supported by NSF Grants No. DMR-0137119 and DMS-0244492.

**12:03**

**B8 3 Measurement of Forces inside Three-Dimensional, Frictionless, Disordered Matter** JING ZHOU, ANTHONY DINSMORE, *University of Massachusetts at Amherst* We directly measured individual forces inside the concentrated piles of frictionless droplets. We report on the distribution of contact forces normalized by the droplet mean, in addition to the distribution of forces normalized by sample mean, as well as the distribution of contact angles. We compare these results to existing models and to a new, numerical calculation that treats the droplets as independent particles and derive the contact-force probability distribution that arises self-consistently from balancing forces. The force chain architecture was visualized, and quantified with a new definition based on long-range correlations. The obtained chain persistence length helps to establish a connection between microscopic force network and the modulus of meso- or macroscopic piles. This work is supported by NSF (DMR-0305395).

**12:15**

**B8 4 Effects of Particle Size Dispersity on the Response to Compressive Strains*** MEENAKSHI DUTT, *University of Cambridge* BRUNO HANCOCK, *Pfizer Inc., Groton, Connecticut, USA* CRAIG BENTHAM, *Pfizer Ltd., Sandwich, Kent, USA* JAMES ELLIOTT, *University of Cambridge* Particle packings found in nature and industry are rarely comprised of single components, in terms of particle size. These packings are generated under a variety of circumstances which influence its response to an external load or strain. We explore both the effect of packing history prior to application of compressive strain, and the variation in the response with the size distribution of the component particles. We generate the packings by allowing the particles to settle under gravity for a fixed interval of time, or until a cut-off packing fraction is attained, followed by application of a compressive strain for a fixed interval of time. We repeat these studies using numerical experiments for samples of discrete size (200 microns, 195-225 microns, 170-260 microns, 150-295 microns) and random (100-300 microns, 100-400 microns, 100-500 microns) size distributions. We find the number of particles with fewer than 4 contacts to increase with size dispersity of the sample after the particles settle under gravity. In addition, the fraction of plastic contacts decreases with increasing variation in particle size during the compression. We also present correlations between the populations of low and high force bearing contacts, particle size and the yield state of the contacts.

*Special Acknowledgements to Pfizer for funding

**12:27**

**B8 5 Measurements of the Yield Stress in Repulsive Athermal Systems** NING XU, COREY O'HERN, *Yale University* We performed molecular dynamics of dry frictionless granular media to gain a deeper understanding of the yield shear stress in these materials. The measurements were obtained by shearing the systems in both the constant shear force and constant shear velocity ensembles. At fixed shear force, we identified the yield shear stress as the shear stress $\Sigma_{yf}$ required to maintain steady flow in an initially unsheared static state. At fixed shear velocity, we identified the yield shear stress as the average shear stress $\Sigma_{yv}$ in the limit of zero shear velocity. At finite system size, $\Sigma_{yf} > \Sigma_{yv}$, which implies that there is a shear rate discontinuity when the system begins flowing in the constant shear force ensemble. However, the difference between the two measures of the yield shear stress decreases with increasing system size; $\Sigma_{yf}$ and $\Sigma_{yv}$ become identical in the infinite system size limit. Thus, the jump discontinuity in the shear rate at the unjamming threshold is a finite-size effect in frictionless granular systems.

**12:39**

**B8 6 Experiment test of a Janssen formula in a dense granular column*** KEVIN FACTO, *University of Massachusetts-Amherst* TOM SCHICKER, *University of Massachusetts-Amherst* NARAYANAN MENON, *University of Massachusetts-Amherst* The stresses inside a tall column of either static or flowing granular material saturate with depth, because the weight of the material is borne by friction with the walls. In the static case, the height dependence of the stress is traditionally described by the Janssen formulation, in which the shear stress at the wall is assumed to be proportional to the normal stress. We report measurements of all three components of force at the wall of a dense, gravity-driven flow of glass beads. We find that the depth dependence of the stress in this slow flow is well-described by a Janssen-like formula. We are also able for the first time to directly test the Janssen assumption, and find that the fluctuations in the shear and normal forces at the wall are highly correlated. The measured friction angle is independent of flow rates for the slow flows we have examined, and is surprisingly close to the ensemble average of the friction angle measured when the flow is stopped.

*We acknowledge support from NSF-DMR 0303596

**12:51**

**B8 7 Impact of Particle Elasticity on Granular Force Networks** JOHN WAMBAUGH, *Duke University* ANNIE THEBPRASITH, *Mount Holyoke College* ROBERT HARTLEY, *Duke University* ROBERT BEHRINGER, *Duke University* We investigate the distribution of force within vertically-confined granular assemblies using photoelastic techniques that allow determination of both geometric configuration and force upon each particle. By binning multiple realizations with depth, we are able to compare our results with the simple, continuum model of Janssen. Recent experimental studies of the force at the boundaries of such assemblies have largely confirmed Janssen's prediction that mean force saturates exponentially with depth due to frictional contacts at the boundaries. [Ovarlez, Fond and Clement, PRE 67, 060302 (2003)] We have observed deviations from these predictions in our system, which we quantify in terms of the structure of the network that distributes forces. We examine the role of internal elasticity of the particles in causing these deviations. This research is supported by NSF grants DMR-0137119 and DMS-204677 and NASA grant NNC04GB08G.

*Invited Papers*

**13:03**
**B8 8 Freezing and Melting in Granular Materials.**
KAREN DANIELS, *Dept. of Physics, North Carolina State University*

From bowls of nuts to eroding soil, granular materials are all around us. In spite of the fact that granular materials are dissipative and athermal, statistical mechanics allows considerable insight into their behavior. I will present experiments on particles which are vibrated from below and sheared from above within an annular channel. The vibrations have the remarkable effect of crystallizing the material, rather than melting it as temperature would an ordinary material. This freezing/melting transition is hysteretic, with the critical line corresponding to equal kinetic energies for vibration and shear. We characterize the transition between these two states, and observe features reminiscent of both a jamming transition and critical phenomena. Another remarkable property is the increase of pressure with volume over a continuum of partially and/or intermittently melted states, in contrast to standard thermodynamic behavior.



*Contributed Papers*

**13:39**
**B8 9 Plastic Failure Events in 2D Sheared Granular Systems*** TRUSH MAJMUDAR, ROBERT BEHRINGER, *Physics Department, Duke University* We present experimental measurements of plastic failure events in a two dimensional granular system consisting of polymer photoelastic disks, placed horizontally, and confined within a rectangular biaxial cell. The bi-refringence of these disks allows us to determine the normal and tangential components of contact forces. We image the system at various deformation states and measure the stress changes and displacements of the disks during one complete shear cycle. The stress changes are found by computing the stress tensor of each disk and the displacements are measured by particle tracking. We obtain bulk stress-strain curves by spatial averaging and find that the system exhibits regions of reversible deformation interrupted by irreversible plastic failure events. We also obtain the behavior of shear modulus of the system. The spatial distribution of reversible and plastic deformations found by studying the displacements of the disks show that in two corners, the disks move uniformly but in a central band aligned along a principal strain direction, we observe multiple vortices. Reversing the direction of shear causes maximum plastic deformation which results in disruption of the vortex structure. We compare our results to the shear transformation zone (STZ) theory.

*Funding: NSF DMR - 0137119, NSF DMS - 204677, NASA - NNC04GB08G

**13:51**
**B8 10 Statistical Properties of Granular Solid to Liquid Transition in Small Systems under Shear** MARTIN MELHUS, IGOR ARANSON, *Argonne National Laboratory* DMITRY VOLFSON, LEV TSIMRING, *University of California, San Diego* The fluidization transition of a dense granular assembly under shear is studied numerically using soft particle molecular dynamics simulations in two dimensions using a previously verified predictor-corrector algorithm. We focus on small systems in a thin Couette cell, examining the bistable region while increasing shear, with varied amounts of random noise, and determine the statistics of shear required for fluidization. We find an approximately linearbetween noise and fluidization shear threshold over the transition regime, and that the variance in the threshold decreases as the system size increases.

**14:03**
**B8 11 Granular shear flow with imposed vibrations** BRIAN UTTER, *James Madison University* ERIC HOPPMANN, *James Madison University* We present results on a 2D photoelastic shearing experiment in which we impose force fluctuations by vibrating the shearing surface. The experiment consists of a dense assembly of 2D photoelastic grains between two belts moving in opposite directions, such that the central region approximates planar shear. The granular medium lies horizontally between the belts such that gravity does not compact the grains. One of the shearing surfaces is vibrated at a known frequency and amplitude during shear. We measure properties of the particle flow and characterize the force network by placing the photoelastic grains between crossed polarizers. We find that as vibration amplitude is increased, the number and magnitude of these force chains decreases drastically. The vibration also leads to increased slip at the shearing surface and decreased particle flow at both shearing surfaces.

**SESSION B9: PHASE TRANSITIONS, DYNAMICS, AND EXCITATIONS**
**Monday Morning, 13 March 2006**
**301, Baltimore Convention Center at 11:15**
**Alberto Pimpinelli, Universit, presiding**

**11:15**
**B9 1 Competing periodicities in fractionally filled quasi-1D bands** P.C. SNIJDERS, *Kavli Institute of Nanoscience* S. ROGGE, *Kavli Institute of Nanoscience, Delft, The Netherlands* H.H. WEITERING, *University of Tennessee, Knoxville, and Oak Ridge National Laboratory, USA* We present a variable temperature Scanning Tunneling Microscopy and Spectroscopy (STM and STS) study of the Si(553)-Au atomic chain reconstruction. This quasi one-dimensional (1D) system undergoes at least two charge density wave (CDW) transitions at low temperature, which can be attributed to electronic instabilities in the fractionally-filled 1D bands of the high-symmetry phase. Upon cooling, Si(553)-Au first undergoes a single-band Peierls distortion, resulting in period doubling along the imaged chains. This Peierls state is ultimately overcome by a competing tripleperiod CDW, which in turn is accompanied by a $\times$ 2 periodicity in between the chains. These locked-in periodicities indicate small charge transfer between the nearly half-filled and quarter-filled 1D bands. The mobility of atomic scale dislocations in the $\times$ 3 CDW state indicates the pos-

sibility of manipulating phase solitons carrying a (spin,charge) of (1/2,± e/3) or (0,± 2e/3).

**11:27**

**B9 2 Order-disorder phase transitions: a DFT - (Wang-Landau) MC study** MIRA TODOROVA, *School of Physics, The University of Sydney, Australia* MIKAEL BORG, *University of Toronto, Toronto, Canada* CATHERINE STAMPFL, *School of Physics, The University of Sydney, Australia* MATTHIAS SCHEFFLER, *Fritz-Haber-Insitut der Max-Planck Gesellschaft, Berlin, Germany* Using a hybrid statistical mechanics method comprising the use of a Lattice-gas Hamiltonian (LGH) determined from ensity-functional theory and subsequent Monte Carlo (MC) calculations, we obtain a phase diagram for Na-Al surface alloys from first-principles and compare it to experimental results [1]. A safe approach towards parametrizing a LGH from the self-consistent evaluation of the electronic structure starts with an analytic form for the long-range pair-interactions. This expression is corrected in the short and medium range using DFT derived data, also including nearsighted many-body terms. An ensuing cross-validation is of utmost importance to ensure that the corrections (to the long-range part) are assessed with an optimum accuracy. The thus extracted LGH is used to perform MC calculations, also using the new Wang-Landau MC algorithm [2], which allows us to reliably determine the transition temperature. [1] M. Borg *et al.*, Chem. Phys.Chem. **6**, 1923 (2005). [2] F. Wang and D.P. Landau, Phys. Rev. Lett. **86**, 2050 (2001).

**11:39**

**B9 3 Bose Einstein condensation of magnons in mesoscopic ferromagnets.** L.H. BENNETT, E. DELLA TORRE, *George Washington University* R.E. WATSON, *Brookhaven National Laboratory* Bulk magnetic materials are comprised of magnetic domains. As the size of the sample is reduced, it forms a single domain state. Further reduction of particle size yields a superparamagnetic state. There is an apparent phase transition[1] between the single domain state and the superparamagnetic state at some critical size in the single-domain mesoscopic region. We had found[2,3] a Bose-Einstein condensation in a number of mesoscopic ferromagnets (30 - 60 nm diam). We hypothesize that the superparamagnetic-to-single domain ferromagnetic transition involves the same type of Bose-Einstein condensation.

[1]J.J. Becker, ''Precipitation and magnetic annealing in a Cu-Co alloy,'' Trans Met SocAIME, **212** 138-144 (1958).
[2]E. Della Torre, L.H. Bennett, and R.E. Watson, ''Extension of the Bloch $T^{3/2}$ law to magnetic nanostructures: Bose-Einstein condensation,'' Phys. Rev. Lett. **94,** 147210 (2005).
[3]S. Rao, E. Della Torre, L. H. Bennett, H. M. Seyoum, and R.E. Watson, ''Temperature variation of the fluctuation field in Co/Pt,'' J. Appl. Phys. **97**, 10N113 (2005).

**11:51**

**B9 4 Bose-Einstein Condensation of Ni spin degrees of freedom observed from susceptibility measurements at high magnetic field in $NiCl_2$-4SC$(NH_2)_2$** CATALIN MARTIN, KENNETH PURCELL, TIMOTHY MURPHY, ERIC PALM, STAN TOZER, *National High Magnetic Field Laboratory, FSU, Tallahassee, FL* VIVIEN ZAPF, ALEX LACERDA, *National High Magnetic Field, Los Alamos, NM* ARMANDO PADUAN-FILHO, *Instituto de Fisica, Universidade de Sao Paulo, Sao Paulo, Brazil* NHMFL, FSU, TALLAHASSEE, FL TEAM, LANL, LOS ALAMOS, NM TEAM, INSTITUTO DE FISICA, UNIVERSIDADE DE SAO PAULO, SAO PAULO, BRAZIL TEAM, The organic compound $NiCl_2$-4SC$(NH_2)_2$ is a new candidate for Bose-Einstein condensation (BEC) of spins system. Involving a technique based on a self-resonant LC-oscillator, we measured the change in magnetic susceptibility of $NiCl_2$- 4SC$(NH_2)_2$ in magnetic field up to 18 Tesla, and temperatures down to 60 mK. We have found the existence of two phase boundaries. One appears at $H_{c1} \sim 2$ T, where the gap between the $S_z = 0$ ground state and the $S_z = -1$ excited state is overcome by the Zeeman effect and the spin condensation starts. The other boundary is at $H_{c2} \sim 12$ T, where the system saturates. Our results on temperature and angular dependence of critical fields will be discussed in connection with previous experimental reports and theoretical predictions for BEC.

**12:03**

**B9 5 Spin Density Wave Suppression in Thin Films of Cr.** DANIEL QUEEN, ZOE BOEKELHEIDE, DAVID COOKE, FRANCES HELLMAN, *University of California, Berkeley* The magnetic and electronic properties of thin films of Cr are critical to their use in GMR multilayers and are not the same as bulk Cr. For example, itinerant spin density waves have been shown to be suppressed in thin films of Cr. This suppression has been attributed to disorder in the microstructure of the films. For bulk Cr the electronic contribution to the heat capacity $\gamma = 3.5$ J/mol $\cdot$ $K^2$ for nonmagnetic Cr and $\gamma = 1.4$ J/mol $\cdot$ $K^2$ for magnetic Cr. Recent heat capacity measurements on Cr thin films have found $\gamma = 3.2$ J/mol $\cdot$ $K^2$ in agreement with the nonmagnetic bulk value. These Cr films also have a reduced $\theta_D$ with respect to the bulk and indicate a softening of phonon modes as seen in nanocrystalline materials. We present magnetization and heat capacity results for Cr thin films.

**12:15**

**B9 6 Phase transitions in metal-oxide particulate-surface interactions: insights through ab initio study** DANIEL FREEDMAN, TOMAS ARIAS, *Cornell University* We present results for *ab initio* molecular dynamics calculations of collisions between metal-oxide particulates and metal-oxide surfaces. Detailed examinations of the resulting trajectories suggest particulate internal kinetic energy as a key parameter in obtaining smooth laminar deposition of thin films. Based on *ab initio* calculations and more extensive supporting classical molecular dynamics modelling, we propose a phase-diagram which maps both translational and internal kinetic energy to modes of crystal growth.

**12:27**

**B9 7 Optical Measurements of Grain Boundary Melting** ERIK THOMSON, *Yale University* JOHN WETTLAUFER, *Yale University* LARRY WILEN, *Ohio University* Bulk properties of polycrystalline solids are strongly influenced by effects of grain boundary melting. While numerical simulations and theory support the idea of disorder along grain boundaries, direct experimental access to the interface of two crystals in thermodynamic equilibrium remains difficult. Polycrystalline ice, however, possesses unique properties which lend it to experimental probing. In addition to its transparency and birefringency the melting temperature of ice, which is relatively close to ambient temperatures, make it an ideal solid within which to experimentally explore grain boundary melting. Here using light scattering by a 4mW Helium-Neon laser we

directly explore the boundary in an ice bicrystal, prepared within a thin ice growth cell. Reflected light intensity is measured as a function of the thermodynamic variables, temperature and impurity concentration. C-axis orientation of individual crystals can be determined by systematically measuring the difference between incident and transmitted polarized beams. Assuming the index of refraction for bulk water, for any melted layer, we anticipate a greater than 10% change in reflected signal strength for a 15 angstrom melt layer. Experimental results are compared with a recent theoretical study of impurity driven grain boundary melting.



**12:39**

**B9 8 Photoelectron Emission Microscopy at the Manganese L-edge of Thin $La_{1-x}$ $Sr_x$ Mn $O_3$ Films through the Phase Transition** M.A. DELEON, T. TYSON, *New Jersey Institute of Technology, Applied Physics* C. DUBOURDIEU, *Laboratoire des Máteriaux et du Génie Physique UMR CNRS 5628, INPG, 38402 St.Martin d'Héres, France* A. SCHOLL, A. DORAN, *ALS* Surface magnetization of $La_{1-x}$ $Sr_x$ Mn $O_3$ films has been observed directly by x-ray photoelectron emission microscopy (XPEEM) at the manganese L-edge. Two sets of films of similar thickness range have been grown via metal-organic chemical vapor deposition (MOCVD) on $LaAlO_3$ and $SrTiO_3$ substrates. The data provides direct observation of magnetic domain melting and growth through the transition temperature. A comparison of domain geometry between the two sets of films will be presented. The effect of the coupling of the strain (tensile vs. compressive) with the magnetization will be discussed. This research is supported by NSF DMR-0209243 and DMR-0512196.

**12:51**

**B9 9 Thermodynamic Investigation of n-Hexane and Cyclohexane on MgO (100) Surfaces*** PETER N. YARON, JOHN Z. LARESE, *Univ. of Tennessee, Knoxville* Thermodynamic properties of thin films of n-hexane and cyclohexane adsorbed on MgO (100) surfaces were investigated and compared using high-resolution volumetric isotherm techniques. A series of high-resolution adsorption isotherm measurements were recorded for n-hexane and cyclohexane between 197K to 255K and 230K to 280K respectively using an automated volumetric isotherm apparatus. Adsorption data was used to determine thermodynamic quantities e.g. the two-dimensional isothermal compressibility and isosteric heats of adsorption and to identify regions where phase transitions might occur. Evidence is found for the presence of two layering transitions in both systems.

*Office of Basic Energy Sciences US-DOE DE-AC05-00OR22725

**13:03**

**B9 10 Complex Conductance Measurements of Ultra-thin MoGe films near the Superconductor-Insulator Transition** LUKAS URBAN, MICHAEL CALLAHAN, *University of Illinois at Urbana-Champaign* ALI YAZDANI, *Princeton University* The application of a magnetic field drives a two-dimensional superconductor through an unexpected conducting state into an insulating state. While this transition has been studied using electrical transport techniques, we present a different way to study the magnetic field-tuned transition. Using a two coil mutual inductance probe inside a top-loading dilution refrigerator, we measure the complex conductance of $Mo_{43}Ge_{57}$ thin films as we vary the temperature or apply a magnetic field. From the complex conductance we determine the superconducting electron density around this field-tuned transition. This work was supported by NSF grants DMR-98-75565 and DMR-03-1529632, U.S. Department of Energy grant DEFG-02-91ER4539 through the Frederick Seitz Materials Research Laboratory and Office of Naval Research grant N000140110071.

**13:15**

**B9 11 Crystallization behaviors of *n*-nonadecane in confined space: observation of metastable phase induced by surface freezing** DUJIN WANG, BAOQUAN XIE, *KLEP, Joint Lab. of Polymer Science and Materials, Institute of Chemistry, CAS, Beijing 100080, China* HAIFENG SHI, XIA DONG, YING ZHAO, CHARLES C. HAN, DUANFU XU, *PPCL, Joint Lab. of Polymer Science and Materials, Institute of Chemistry, Chinese Academy of Sciences, Beijing 100080, China.* Crystallization and phase transition behaviors of *n*-nonadecane in microcapsules was studied with the combination of differential scanning calorimetry (DSC) and synchrotron radiation X-ray diffraction (XRD). As evident from the DSC measurement, a surface freezing monolayer, which is formed in the microcapsules before the bulk crystallization, induces a novel metastable rotator phase ($R_{II}$), which has not been reported anywhere else. We argue that the existence of the surface freezing monolayer decreases the nucleating potential barrier of $R_{II}$ phase and turns the transient $R_{II}$ phase to a 'long-lived' metastable phase.

**13:27**

**B9 12 Ordering and Dynamics of $CN^-$/Cu(001) Surfaces*** ERKAN CIFTLIKLI, IAN SHUTTLEWORTH, ALEXEI ERMAKOV, JANE HINCH, *Department of Chemistry and Chemical Biology, Rutgers University, NJ 08854.* $C_2N_2$ adsorption on Cu(001) is largely dissociative, yielding adsorbed $CN^-$ species. Exposure dependent angular-resolved Helium Atom Scattering (HAS) measurements show the initial development of a diffuse backscattered intensity, followed by the onset of c(10x6) superstructure domain growth only in a limited exposure temperature range. Diffraction from an ordered phase is not observed for exposures above 323K, nor below 223K. Yet, even at optimal deposition temperatures, a diffuse scattering contribution remains at saturation and persists beyond 473K. Energy and angular resolved measurements show that the diffuse He intensity is strongly inelastic, and multiphonon-like; i.e. not showing features with resolvable discrete energies. The surface temperature and momentum exchange dependencies of this intensity will elaborate the nature of the dynamics of $CN^-$ on Cu(001) surfaces. The $CN^-$ coverage dependence of the inelastic intensity also illustrates the influence of intermolecular interactions in $CN^-$ motion.

*NSF, Rutgers LSM

**13:39**

**B9 13 Theoretical treatment of non-vibrationally-relaxed electron transfer in organic solar cells** KUO KAN LIANG, *Division of Mechanics, Research Center for Applied Sciences, Academia Sinica, Taiwan* CHIH-KAI LIN, *Institute of Atomic and Molecular Sciences, Academia Sinica, Taiwan* HUAN-CHENG CHANG, *Institute of Atomic and Molecular Sciences, Academia Sinica, Taiwan* MICHITOSHI HAYASHI, *Center for Condensed Matter Sciences, National Taiwan University, Taiwan* SHENG HSIEN LIN, *Institute of Atomic and Molecular Sciences, Academia Sinica, Taiwan* In this work we shall show how to calculate the single vibronic- level electron transfer rate constant, which will be compared with the thermal averaged one. To apply the theoretical

results to the dye- sensitized nano-crystalline semiconductor (Grätzel type) solar cells, we use a simple model to describe how we model the final state of the eletron- transfer process (oxidized dye and reduced semiconductor). Numerical calculations of the single-level electron transfer rate constants and the simulation of the quantum beat in the photo-excited state and the product state will be performed to demonstrate the theoretical results.

**13:51**
**B9 14 Investigating chemicurrent production from hyperthermal-energy ion impacts** S.A. MOODY, M.P. RAY, C.E. SOSOLIK, *Department of Physics and Astronomy, Clemson University* The production of chemicurrents by thermal-energy molecular beam scattering from thin-film Schottky diode surfaces has generated considerable interest in the field of gas-surface physics. These experiments promise to give insight into energy transfer processes at surfaces. However, few experiments have investigated chemicurrent production at higher impact energies. We propose experiments to study beam impact events on Schottky diode/thin film surfaces using hyperthermal ion beams, with the added capability of studying the mechanism of charge transfer. These experiments will utilize our lab's highly versatile beamline. The beamline is ideal for exploring chemicurrent phenomena at higher energies because of the capability it gives us to producewell-characterized ion beams at hyperthermal- and low-energies with a wide variety of gas and solid-state sources. This talk will focus on optimization of our beamline for this experiment. Specific attention will be given to the addition of a new load lock/sample transfer system and the electronic interfacing required for simultaneous scattering/chemicurrent data acquisition. Preliminary results from hyperthermal impact events on thin film Schottky diodes are also presented.



## SESSION B10: FOCUS SESSIONS: PHYSICAL CHEMISTRY OF NANOSCALE SYSTEM II

**Monday Morning, 13 March 2006; 302, Baltimore Convention Center at 11:15**
**Haw Yang, University of California, Berkeley; Clemens Burda, Case Western Reserve University, presiding**

*Invited Papers*

**11:15**
**B10 1 Potential Application of the Enhanced Absorption and the Enhanced Scattering Processes of Plasmonic (Gold and Silver) Nanoparticles of Different Shapes.**
MOSTAFA EL-SAYED, *Georgia Institute of Technology*

The crossections of absorption and scattering of plasmonic nanoparticles are orders of magnitude larger than those of molecular dyes. Their strong scattering properties make them much better contrast agents in biological and medical applications than fluorescent dyes. Their strong absorption makes them useful in photothermal therapy and in changing their shape or their location in assembled arrays. These applications will be illustrated.

*Contributed Papers*

**11:51**
**B10 2 Studying Photoluminescence Dynamics of Single Quantum Dots Photon by Photon*** HAW YANG, KAI ZHANG, AIHUA FU, PAUL ALIVISATOS, *UC Berkeley* CARL HAYDEN, *Sandia National Laboratory* Colloidal semiconductor nanocrystals, or quantum dots (QDs), have been the focus of much research effort in the past decade. The development of these colloidal dots has allowed the concepts of quantum confinement and dimensional control of electronic and optical properties to find entirely new areas of application, for instance in fluorescent labeling of biological specimens. At the single-particle level, however, colloidal QDs exhibit surprisingly complicated time-dependent behavior in their photoluminescence (PL) characteristics. The PL dynamics of the biologically compatible CdSe/ZnS/streptavidin quantum dots were studied using time-resolved single-molecule spectroscopy. Statistical tests of the photon-counting data suggested that the simple ''on/off'' discrete state model is inconsistent with experimental results. Instead, a continuous emission state distribution model was found to be more appropriate. Autocorrelation analysis of lifetime and intensity fluctuations showed a nonlinear correlation between them. These results were consistent with the model that charged quantum dots were also emissive, and that time-dependent charge migration gave rise to the observed photo-luminescence dynamics.

*Work supported by the US Department of Energy

**12:03**
**B10 3 Photothermal properties of gold nanocages studied by time-resolved spectroscopy** MIN HU, JINGYI CHEN, YOUNAN XIA, XINGDE LI, *University of Washington, Seattle* HRISTINA PETROVA, GREGORY HARTLAND, *University of Notre Dame* MANUEL MARQUEZ, *INEST Group, Research Center, Philip Morris USA Inc.* Gold nanocages of different sizes synthesized via galvanic replacement reaction have been studied by ultrafast time-resolved spectroscopy. The vibrational phonon modes were excited and the periods of these modes increase with the size of the gold nanocages. For a specific size of nanocage, experiments with different excitation powers of the pump laser were performed (from 2 $\mu$J to 20 $\mu$J), we found that the period of the vibrational mode increased with the laser intensity. This was compared to experiments on spherical gold nanoparticles, which allow us to roughly estimate the temperature of the nanocages when the electrons and the phonons reach the equilibrium. The temperature of the nanocages can increase up to 1000 K, near the melting point of the bulk metal, while the particles maintain their integrity. This makes the nanocages potentially useful for photothermal therapy applications. The heat dissipation rate for the nanocages was also studied in these experiments, and was found to have the similar trend as spherical nanoparticles, i.e., larger particles stay hot for longer times than smaller particles.

**12:15**
**B10 4 Photoluminescence and Dynamics Measurements of Individual CdSe Quantum Wires** JOHN GLENNON, RUI TANG, WILLIAM BUHRO, RICHARD LOOMIS, *Department of Chemistry and Center for Materials Innovation Washington University*

*in St. Louis* The photoluminescence (PL) spectroscopy of highly monodispersed colloidal CdSe quantum wires (QWs) are investigated in the single nanocrystal environment using confocal fluorescence microscopy and are compared to similar studies preformed on three dimensionally confined CdSe quantum dots (QDs). The PL intensity of the QWs is observed to increase and then to decrease at room temperature ambient conditions with continued irradiation at moderate to high laser powers ( $>$ 10 kW*cm$^{-2}$) at much slower rates than similar processes in QDs. The energy of the peak intensity of the PL is monitored throughout the experiments and does not shift for the QWs. This is in contrast to the blue-shift observed for QDs as the PL intensity decays. For the QWs, it is shown that the change in PL intensity is localized to the diffraction limit irradiation spot and is not delocalized along the length of the QW. Differences in exposed crystalline facets and surface coverage between QWs and QDs are explored in context of the experimental observations. These phenomena are studied under different atmospheres and surface environments in order to elucidate the optical properties of these quantum-confined semiconductors.

**12:27**
**B10 5 Photo-Induced Single Molecule Electron Transfer at the Molecule-Nanoparticle Interface*** TIANQUAN LIAN, WANHEE GOH, JIANCHANG GUO, XI LIU, *Dept. of Chemistry, Emory Univ.* MICHAEL AHRENS, EMILIE SCHIERLOH, MICHAEL WASIELEWSKI, *Dept. of Chemistry, Northwestern Univ.* Single molecule fluorescence spectroscopy was used to study photoinduced electron transfer (ET) dynamics across single donor-bridge-acceptor junctions consisting of perylene-3,4:9,10-bis(dicarboximide) (PDI), n-phenylene bridge with COOH anchoring group, and antimony doped Tin Oxide(ATO) nanoparticles. Photo-excitation of PDI initiates electron transfer from its excited state into ATO nanoparticles. Electron transfer was confirmed and ensemble average rate was measured by transient infrared absorption spectroscopy, in which injected electrons in ATO were directly monitored. Single molecule fluorescence from donor molecule was confirmed by the observed blinking behavior, fluorescence spectrum, and excitation polarization dependence. Single molecule fluorescence lifetime was measured by time-correlated single photon counting, from which forward electron transfer rate from adsorbate excited state to nanoparticle was determined. The dependence of these single molecule ET rates and their fluctuation on the length of phenylene bridge and the nature of semiconductors are being investigated.

*We acknowledge the financial support of the donor of the Petroleum Reseach Fund and the national science fundation (to T. L.) and the department of energy (to M. W.)

***Invited Papers***

**12:39**
**B10 6 Dynamics of photoexcitations in quasi-one-dimensional systems.***
SUSAN DEXHEIMER, *Washington State University*

Low dimensional materials, and in particular, quasi-one-dimensional systems have attracted considerable interest owing to their unusual electronic properties. In many of these systems, strong electron-phonon couplings can lead to the formation of nonlinear excitations such as self-trapped excitons and polarons, in which electronic excitations become localized as a result of their interaction with the lattice. I will present the results of femtosecond time-resolved experiments in which we have studied the dynamics of the formation and evolution of localized excitations in quasi-one-dimensional molecular solids. This work has been carried out on mixed-valence halide-bridged transition metal linear chain (or MX) complexes, a class of materials that serve as model systems for the physics of low-dimensional materials. In these complexes, the relative strengths of the electron-electron and electron-phonon interactions, the fundamental physical parameters that determine the properties of the excitations, can be systematically tuned by chemical substitutions in the chain structure. Using femtosecond vibrationally impulsive excitation techniques, we have studied the coupled electronic and vibrational dynamics associated with excitonic self-trapping in a series of quasi-one-dimensional structures, and using time-resolved THz techniques, we have studied the dynamics of the formation and subsequent evolution of polarons.

*This work is supported by the National Science Foundation.

***Contributed Papers***

**13:15**
**B10 7 Dynamics of the heat transfer at the interface of diamond {111} nanosurfaces.** OLEG A. MAZYAR, *Texas Tech University* Energy transfer across the interface between a small, hot model diamond {111} nanosurface and a much larger identical, cold nanosurface was studied by a classical molecular dynamics method. Kinetics of this energy transfer was found to be exponential with a rate constant increasing linearly with the increase of the normal load applied to the hot nanosurface. The rate constant of the heat transfer depends on the thickness of the small, hot nanosurface, both chemical and isotopic composition of the interface, but does not demonstrate significant changes with the increase of the nanosurfaces' contact area or the increase of the initial temperature difference between the nanosurfaces.

**13:27**
**B10 8 The Static and Dynamic Wetting of Si Nanorod Arrays*** JIANGUO FAN, YIPING ZHAO, The wettability of a solid state surface is affected by both the surface roughness and the surface chemical composition. Here, we report a systematic investigation on the static and dynamic wetting of vertically aligned Si nanorod arrays with different heights (aspect ratio) fabricated by the glancing angle deposition technique. For as-deposited hydrophilic films, there was a contact angle transition from a rough surface to a hemi-wicking porous surface at normal film thickness $d$ = 500

nm; while for the HF treated hydrophobic films, a transition from partial composite to composite surface was observed at the same film thickness. The observed results can be reasonably interpreted within framework of the classic Young's theory. We have also observed that for the hydrophilic nanorod arrays, the spreading of the water droplet causes the bundling of Si nanorods, and generates intriguing percolation patterns that change with the spreading diameter. The dynamic spreading process of a water droplet on the same surface has been recorded by a fast CCD camera, and scaling laws of the contact line, the precursor rim, and the spreading speed have been observed. Models based on capillary force, mechanical bending, as well as flow in a groove, have been proposed to qualitatively explain all the phenomena observed.

*work supported by NSF

**13:39**
**B10 9 Inorganic Nanotubes, Nanofluidic Transistors and DNA Translocation** PEIDONG YANG, *University of California* Inorganic nanotubes, representing a new class of nanostructures, have been attracting considerable attention during the past few years. Single crystalline semiconductor GaN nanotubes can be synthesized by nanowire templated epitaxial casting method. Partial conversion of existing nanowires leads to the synthesis of silica nanotubes after etching off remaining cores. Silica nanotubes can be integrated into metal-oxide-solution field effect transistors (MOSitolFETs) which exhibit rapid field effect modulation of ionic conductance. Surface functionalization can change inherent carrier concentration as well channel polarity to fabricate p-type, n-type and ambipolar transistors. These nanofluidic devices were further demonstrated to be useful in single molecule sensing. Single DNA molecules can be electrically detected either by charge effect or geometry effect. These nanofluidic FETs have potential implications in sub-femtoliter analytical technology and large-scale nanofluidic integration.

**13:51**
**B10 10 Monitoring Gold Nanorod Synthesis based on their Localized Surface Plasmon Resonance*** AMNEET GULATI, *Department of Physics and Astronomy, Rice University* HONG-WEI LIAO, *Department of Chemistry, Rice University* JASON HAFNER, *Department of Physics and Astronomy, and Chemistry, Rice University* The extinction spectra of structurally anisotropic gold nanoparticles exhibit surface plasmon resonances that may be tuned through the visible and near-infrared portions of the electromagnetic spectrum by controlling their geometry. Gold nanorods, whose longitudinal extinction peak is proportional to their aspect ratio, are synthesized by reduction of gold chloride onto gold seed nanoparticles. While growth anisotropy is known to be induced by a surfactant (cetyltrimethylammonium bromide), the detailed growth mechanism is poorly understood. Here, we study the growth kinetics of nanorods by continually monitoring their extinction spectra during synthesis. The spectra are analyzed by Rayleigh-Gans theory to determine the instantaneous length and diameter of the growing nanorods. This data yields microscopic growth rates which provide insight into the mechanism of nanorod synthesis.

*This work is supported by the Robert A. Welch Foundation.

**14:03**
**B10 11 Desorption and Dissociation of Water Induced by Photoexcitation of Silver Nanoparticles** DINKO CHAKAROV, *Department of Applied Physics, Chalmers University of Technology* HANS FREDRIKSSON, The photodesorption and photodissociation of water from silver nanoparticles grown in situ on graphite has been studied by HREELS, TPD and PID. We discuss the factors which influence dissociative versus associative desorption pathways when the system is irradiated with cw and ns pulsed UV light. The observations are attributed to increased optical absorption and hot electron production at the Ag clusters and their vicinity due to particle plasmon excitations.



## SESSION B11: FOCUS SESSION: PROMISES AND CHALLENGES IN CHEMICAL DYNAMICS II
**Monday Morning, 13 March 2006; 303, Baltimore Convention Center at 11:15**
**Jim Valentini, Columbia University, presiding**

*Invited Papers*

**11:15**
**B11 1 Adventures in Cluster Dynamics.**
JOSHUA JORTNER

We report on the exploration of new scientific territories of energetics, response, dynamics and function of large, finite atomic and molecular systems. Studies of ultrafast (attosecond to femtosecond) electron and nuclear dynamics of clusters in ultraintense laser fields (peak intensity $10^{15}$–$10^{20}$Wcm$^{-2}$) led to the advent of table-top nuclear fusion driven by cluster Coulomb explosion. The eighty years' quest for nuclear fusion driven by chemical reactions was achieved by ''hot–cold'' fusion in the chemical physics laboratory. Moving from femtosecond nuclear dynamics in the energy domain of nuclear physics (1keV–1MeV) towards ultralow energies and ultraslow millisecond dynamics in ultracold (T = 100 $\mu$K–1nK) finite systems, we address the bridging between the nuclear dynamics of clusters and of finite, ultracold atomic clouds. References [1] I. Last, Y. Levy, J. Jortner. PNAS 99, 9107 (2002). [2] I. Last, J. Jortner. Phys. Rev. Letts. 87, 033401-1 (2001); Phys. Rev. A 64, 063201-1 (2001); J. Chem. Phys. 120, 1336 (2004); 120, 1348 (2004); 121, 3030 (2004); 121, 8329 (2004); Phys. Rev. A 71, 063204-1 (2005). [3] J. Jortner, M. Rosenblit, Adv. Chem. Phys. 132, 247 (2005).

*Contributed Papers*

**11:51**
**B11 2 Isomer morphology and vibrational mode dependence of the coupling between an excess electron and small water networks.** MARK JOHNSON, *Yale University* Negatively charged water clusters are presently the subject of intense study because of their promise to unravel the surprisingly complex dynamics of the hydrated electron. We focus on the use of vibrational spectroscopy to establish the morphologies and local binding motifs of the water networks that bind an electron. Here we will discuss the rearrangement pathways of the H-bond network in the elementary act of free electron accommodation, where we use argon-mediated population modulation to isolate the geometries of the neutral cluster precursors. We then obtain isomer-selective vibrational spectra of the anions that produced, where we correlate the local binding motifs with the overall electron binding energies. Finally, in the small cluster limit, we reveal how different intramolecular vibrational motions interact with the diffuse electron cloud by analysis of the resulting ''Fano'' lineshapes when vibrations are embedded in the electron continuum. These interactions vary by over an order of magnitude for various ''free OH'' bands. The implications of these observations on the extrapolation to bulk behavior will be considered in light of the trends displayed by the cluster properties up n=30 or so.

**12:03**
**B11 3 Vibrational energy at interfaces** DANA DLOTT, *University of Illinois* New advances in ultrafast vibrational spectroscopy now permit the real-time observation of vibrational energy at interfaces. Using a liquid suspension of reverse micelles, consisting of a nanodroplet of water separated from an organic solvent by a monolayer of surfactant, we pumped vibrational energy into either the water or surfactant layer using an ultrashort IR laser pulse. Incoherent anti-Stokes Raman probe techniques were used to watch the vibrational energy move across this surfactant monolayer. The results were quite different that what would be expected if we were watching heat flow. The specific pathways of vibrational energy are invoked to explain these results.

**12:15**
**B11 4 Atomic Beam Scattering as a Probe of the Glass Transition of Polymer Thin Films** MIRIAM FREEDMAN, AARON ROSENBAUM, STEVEN SIBENER, *The James Franck Institute and Department of Chemistry, University of Chicago* We have investigated the thin film dynamics of poly(methyl methacrylate) (PMMA) using inelastic helium atom scattering. The glass transition in the surface region of a polymer film is thought to be at a lower temperature than the bulk, but it is unclear whether this reduction is due to the film surface or the near-surface layer. Because helium atom scattering is a surface sensitive, nonperturbative technique with which we can directly probe the surface dynamics, we hope to be able to clarify this debate. We obtain broad time of flight spectra, which are well fit by a semi-classical scattering model. From these fits, we note deviations near the bulk glass transition that could be due to changes in surface presentation or dynamics. At low beam energies and sample temperatures, we observe elastic scattering from which we calculate Debye-Waller factors that are similar to other organic thin films. This study has shown that helium atom scattering provides a unique means of exploring the glass transition of polymer thin films.

*Invited Papers*

**12:27**
**B11 5 Optical Spectroscopy and Photophysics of Single Wall Carbon Nanotubes.**
LOUIS BRUS, *Columbia University*

We explore the fundamental nature and dynamics of excited electronic states in SWNT. Psec luminescence and photobleaching dynamics of SWNTs in micellar solution show that non-radiative Auger recombination is extremely fast. At low pH, nanotube surface endoperoxides protonate and introduce holes that quench the luminescence. At higher concentration these holes also bleach the band gap optical absorption. Near infrared two photon luminescence excitation spectra quantitatively reveal the importance of excitons. In order to characterize excited states in both metallic and semiconducting SWNTs at the single-tube level, we detect white-light Rayleigh scattering from individual tubes suspended over an open slit in a substrate. Diagnostic spectra with high signal to noise are obtained in just a few minutes.

*Contributed Papers*

**13:03**
**B11 6 First hyperpolarizability ($\beta$) of bare and polymer protected copper nanoparticles** PUSPENDU DAS, MANABENDRA CHANDRA, *Indian Institute of Science* We have prepared bare as well as polyvinyl pyrrollidone (PVP) capped Cu nanoparticles (NPs) of $<$ 10 nm size by laser ablation and measured their first hyperpolarizabilities ($\beta$ values) using the hyper-Rayleigh scattering technique in solution. The $\beta$ values for the bare and capped NPs are 414 ( $\pm$ 19) x $10^{-30}$ and 808 ( $\pm$ 12) x $10^{-30}$ esu/atom$^{1/2}$, respectively. The bare NPs are stable in isopropanol for weeks but are short-lived compared to the capped particles. Our results of capped NPs having a $\beta$ value twice as high compared to the bare NPs of the same size show that surface capping is necessary for enhancing $\beta$ in noble metal NPs. In addition to the bulk and surface quadrupolar contributions which exist in bare NPs, dipolar contribution to $\beta$ becomes important for the capped NPs due to the destruction of centro-symmetry at the surface, leading to a significant increment in $\beta$. Experiments with smaller size NPs show that $\beta$ goes down with size. The bulkquadrupolar polarization which decreases with particle size, perhaps, rationalizes the size dependence of $\beta$.

**13:15**
**B11 7 RRKM Theory at the Gas-Surface Interface: Hydrogen Dissociation Dynamics on Cu(111)** HEATHER ABBOTT, IAN HARRISON, *Chemistry Department, University of Virginia* A simple picture of the hydrogen dissociation/associative desorption dynamics on Cu(111) emerges from a two-parameter, full dimen-

sionality microcanonical unimolecular rate theory (MURT) model of the gas-surface reactivity. Vibrational frequencies for the reactive transition state were taken from 6D density functional theory calculations [Hammer, itet al. Phys. Rev. Lett. **73**, 1400 (1994)]. The MURT's parameters were fixed by simulation of experiment as: a $H_2$ dissociation threshold energy of $E_0 = 79$ kJ/mol and $s = 1$ surface atoms that actively exchange energy within the reactive transition state. Remarkably, MURT quantitatively predicts much of the dynamical behavior observed. The divergence of the statistical theoretical predictions from the experimental results at low rotational quantum numbers, $J \leqslant 5$, points towards the importance of dynamical steering at low J. The surface degrees of freedom are calculated to provide $\sim$ 30% of the energy required to surmount $E_0$ under thermal equilibrium conditions. Explicit treatment of the surface (i.e., $T_s > 0\ K$) is a novel aspect of the MURT theoretical approach.

**13:27**

**B11 8 An STM and Theoretical Study of the Interaction of hexabenzocorone on a Ru(0001) Surface** KWANG TAEG RIM, LI LIU, *Department of Chemistry and Columbia Center for Integrated Science and Engineering, Columbia University* CHAOCHIN SU, *Department of Molecular Science and Engineering, National Taipei University of Technology* SHENGXIONG XIAO, MICHAEL STEIGERWALD, *Department of Chemistry and Columbia Center for Integrated Science and Engineering, Columbia University* MARK HYBERTSEN, *Department of Applied Physics and Applied Mathematics and Columbia Center for Integrated Science and Engineering, Columbia University* COLIN NUCKOLLS, GEORGE FLYNN, *Department of Chemistry and Columbia Center for Integrated Science and Engineering, Columbia University* The interaction of hexabenzocorone (hbc) with a metal surface has been investigated using Scanning Tunneling Microscopy (STM) and Scanning Tunneling Spectroscopy (STS) in ultrahigh vacuum. The images obtained at room temperature, after hbc molecules were vacuum deposited at 325$^o$C onto a pristine ruthenium (0001) surface, exhibit surface bound molecules with off-centered bonding sites. I(V) curves over hbc molecules show high tunneling current at positive bias voltages. After annealing of the hbc-bonded Ru sample surface at 600$^o$C for 15min, hbc molecules appear to aggregate laterally and to bond symmetrically to the surface. The possibility of growing carbon nanotubes on the hbc-Ru precursor surface upon dosing with $C_2H_2$ will also be discussed along with a theoretical model for bonding and growth of nanotubes.

**13:39**

**B11 9 Single-molecule vibrational spectroscopy of water molecules using an LT-STM** CHIKAKO MATSUMOTO, *Gakushuin Univ., RIKEN* YOUSOO KIM, *RIKEN* KENTA MOTOBAYASHI, *Univ. of Tokyo* MAKI KAWAI, *Univ. of Tokyo, RIKEN* Single-molecule vibrational spectroscopy has attracted considerable attention as a powerful tool for nanoscale chemistry. The adsorption of water molecules on metal surfaces plays an important role in understanding many phenomena in nature, such as heterogeneous catalysis and corrosion, etc. The structure of water at low coverage has been investigated on a variety of transition-metal surfaces with various techniques. But the microscopic understanding of the adsorption feature of single water molecules is still unclear. We report molecular scale study of adsorption behaviors of water molecules on Pt (111) surface at 4.7 K by use of single-molecule vibrational spectroscopy with the scanning tunneling microscopy (STM). The Pt (111) surface was dosed with a small amount of water molecules ( $<$ 0.01 ML) at the temperature less than 20 K. A water monomer appears as a single protrusion in the STM images. A dimer was formed by manipulating monomers with an STM tip. The shape of a water dimer looks like 'cherry blossom', which can be explained by one of the water molecules rotating around the other**.** Inelastic electron tunneling spectroscopy using the STM was utilized to determine vibrational modes of individual water dimers.

**13:51**

**B11 10 A Novel Vibrational Spectroscopic Study of a Single Molecule using an STM – Measurement and Selection rules of Action spectroscopy** YOUSOO KIM, *RIKEN* YASUYUKI SAINO, *Tohoku Univ.* TOSHIRO OKAWA, *Gakushuin Univ.* TADAHIRO KOMEDA, *Tohoku Univ.* HIDEMI SHIGEKAWA, *Univ. of Tsukuba* MAKI KAWAI, *Univ. of Tokyo, RIKEN* The excitation of molecular vibration by means of the inelastically tunneled electrons from the tip of a scanning tunneling microscope (STM) can lead to various dynamical processes at surfaces. In addition, inelastic electron tunneling spectroscopy with the STM (STM-IETS) is now applicable to the vibrational spectroscopy of the individual molecules. The vibrational spectrum of a single molecule provides useful information not only for the chemical identification of the molecule but also for investigating how molecular vibration can couple with the relevant dynamical processes. Inelastically tunneled electrons from the STM were used to induce vibrationally mediated motions of a single itcis-2-butene molecule among four equivalent orientations on Pd(110) at 4.7 K. Action spectrum obtained from the motions clearly detects more vibrational modes than STM-IETS. We demonstrate the usefulness of the action spectroscopy as a novel single molecule vibrational spectroscopic method. We also discuss its selection rules in terms of the resonance tunneling.



**SESSION B12: QUANTUM METAL FILMS AND OVERLAYER STRUCTURES**
**Monday Morning, 13 March 2006**
**304, Baltimore Convention Center at 11:15**
**Zhenyu Zhang, Oak Ridge Natinoal Laboratory, presiding**

**11:15**

**B12 1 Growth of Pb nanowires on the Si(111)-In (4x1) a combined STM and SPALEED study*** MYRON HUPALO, MICHAEL YAKES, MICHAEL TRINGIDES, *Ames Laboratory-Iowa State University* Due to the combined effect of QSE and the anisotropic strain potential of the substrate, Pb deposited on Si(111)–In (4x1) at 180K grows in nanowires of uniform 4-layer height and controllable uniform width of $5w_0$ (where $w_0 = 1.33$nm is the width of the reconstruction unit cell along [1_1_2] direction). SPA-LEED studies confirm this selected 4-layer height (from Intensity vs $K_z$ variation) which is unusually stable because it is unchanged even after annealing to room temperature. The same selected 4-layer height is observed on a different interface Si(111)-In $\sqrt{31}$x$\sqrt{31}$ which independently confirms the unusual 4-layer stability. Differences in the observed corrugation on the tops of the nanowires due to the Moiré pattern at the metal/

semiconductor interface confirm the strain anisotropy on the reconstructed substrate. Further Pb deposition on top of the nanowires results in the completion of the Pb layer with unusually atomically flat film interfaces over mesoscopic distances.

*Ames Laboratory is operated by the U.S. Department of Energy by Iowa State University under Contract No. W-7405-Eng-82.

**11:27**

**B12 2 Novel Phase Separation for Pb/Ge(111)** SHIRLEY CHIANG, YU SATO, *University of California Davis* NORMAN BARTELT, *Sandia National Laboratories Livermore* Using low energy electron microscopy (LEEM), we have elucidated the phase diagram for the growth of Pb on Ge(111). As Pb is deposited on Ge, the Pb atoms substitute into the top layer, causing released Ge atoms to form into c(2x8) adatom islands, with the size and density of these Ge islands controllable by the substrate temperature. During the reversible $\beta$ (dense ($\sqrt{3}$x$\sqrt{3}$)R30[r]) to (1x1) phase transition, we discovered a novel phase separation mechanism. Above the 1.33ML saturation coverage of the $\beta$ phase, a sharp first order phase transition is observed near 295C. For Pb coverage just $<$ 1.33ML, the phase transition is no longer sharp, with $\beta$ and (1x1) phases coexisting and the transformation occurring from 232C to 181C. Reducing coverage by $\sim$ 0.01ML causes a dramatic change, with small domains of the new phase appearing and disappearing, due to fluctuations between the two phases. Additional domains appear and fluctuate until the whole surface is completely transformed. We attribute the fluctuating domains to thermal fluctuations of the density of Pb atoms within a domain. By comparing LEEM images of the $\beta$ and (1x1) phases during the phase transition between [$\alpha$+(1x1)] and ($\alpha$ + $\beta$), the Pb coverage of the (1x1) phase at the eutectic point was determined to be $\sim$ 1.29 ML.

**11:39**

**B12 3 Hard superconductivity of a soft metal in the quantum regime*** M.M. OZER, J.R. THOMPSON, H.H. WEITERING, *Physics, Univ. Tennessee, Knoxville, TN, 37996 & ORNL, Oak Ridge, TN, 37831* Superconductivity is a collective quantum phenomenon that is inevitably suppressed in reduced dimensionality. Questions of how thin superconducting wires or films can be before losing their superconducting properties have important technological ramifications and go to the heart of understanding formation, coherence, and robustness of the superconducting state in quantum confined geometries. Here, we exploit quantum confinement of itinerant electrons in a soft metal (Pb), to stabilize atomically-flat superconductors with lateral dimensions of mm and vertical dimensions of only a few atomic layers. They show no indication of defect- or fluctuation- driven suppression of superconductivity and support macroscopic super-currents of up to $\sim$ 10% of the depairing current density. The hardness of the critical state can be attributed to the presence of intrinsic vortex traps that are stabilized by quantum confinement. The study presents a conceptually appealing picture of a model nano-scale superconductor with calculable critical state properties, suggesting the possibility of achieving and exploiting superconductivity in the ultimate low-dimensional limit.

*This work is funded by NSF grant DMR-0244570. ORNL is managed by UT-Battelle, LLC, for US DOE under Contract DEAC05-00OR22725.

**11:51**

**B12 4 Modification of the Quantum Electronic Stability of Thin Films by Interfactants** T. MILLER, D. A. RICCI, M. H. UPTON, T.-C. CHIANG, *Univ. of Illinois at Urbana-Champaign* Electronic states are quantized in thin films, resulting in a modulation of physical properties with film thickness. The thermal stabilities of films differing in thickness by even a single monolayer can be dramatically different due to this quantization. The spectrum of allowed energy states depends on the film thickness, but it is also dependent on the phase shift of the wavefunctions reflected from the film-substrate interface. This phase shift in turn can be adjusted by changing the interface using interfactant atoms. This implies that the physical properties of thin films, including the thermal stability, could be controlled by interfacial engineering. We have grown atomically-uniform thin films of Pb on Si(111). Their thermal stabilities show bilayer oscillations with thickness due to the quantization of electronic states. The stabilities are strongly modified by the introduction of Au, In, or Pb at the film/substrate interface. For example, with In as an interfactant, films an odd number of monolayers thick are more stable than ones with an even number of layers, whereas for the other materials this pattern is reversed.

**12:03**

**B12 5 Novel Coarsening Behavior of Pb nanocrystals on Si(111)*** P. F. MICELI, C. A. JEFFREY, *Dept. of Physics and Astronomy, University of Missouri-Columbia* R. FENG, E. H. CONRAD, *School of Physics, Georgia Institute of Technology* M. HUPALO, M. C. TRINGIDES, *Ames Lab, Iowa State University* C. KIM, *Dept. of Physics and Research Inst. of Basic Sciences, Kyunghee University, Korea* P. J. RYAN, *MUCAT, Advanced Photon Source, Argonne National Lab* We show that Pb nanocrystals grown on Si(111)7x7 exhibit novel coarsening behavior that cannot be described by the classical Gibbs-Thomson effect. This system is known for quantum size effects (QSE) that lead to preferred island heights which depend on the coverage and temperature. Using complementary surface x-ray diffuse scattering and STM, we find an unexpected and unusual flux rate dependence, a lack of scaling of the island densities, and island decay times that are orders of magnitude faster than expected from the classical analysis. For example, a highly mono-disperse island height distribution is observed if the islands are grown at high rather than low flux rates. These results have important implications for understanding the controlled growth and self-organization of nanostructures.

*The MUCAT beamline is supported through the Ames Lab by the US-DOE. Research funding is supported by NSF, PRF (PFM, CAJ), Ames Lab (MCT, MH), Canim Scientific (EHC), NSERC-Canada (CAJ), Ministry of Science & Tech.-Korea (CK).

**12:15**

**B12 6 The formation of a sharp metal-semiconductor interface for the growth of Quantum Size Effect islands*** C.A. JEFFREY, P.F. MICELI, *Dept. of Physics and Astronomy, University of Missouri-Columbia* E.H. CONRAD, R. FENG, *School of Physics, Georgia Institute of Technology* C. KIM, *Dept. of Physics and Research Inst. of Basic Sciences, Kyunghee University, Korea* P.J. RYAN, *MUCAT, Advanced Photon Source, Argonne National Lab* In order to form Quantum Size Effect (QSE) metal islands on semiconductors, a smooth island-substrate interface is necessary to set up the electron standing waves that lead to the new quantum confined states. How this occurs for the Pb-Si(111)7x7 system is a mystery because of the large lattice mismatch and the highly cor-

rugated 7x7 reconstruction. To understand how QSE islands develop in this system we have performed structural Surface X-ray scattering measurements on the initial formation of Pb islands grown on Si(111). We show how a smooth Pb-semiconductor interface develops through a series of structural arrangements. Once a vertically disordered Pb monolayer is completed, second layer atoms nucleate fcc clusters. These clusters undergo a displacive transition lifting them above the Si adatoms. This allow the Pb islands to ''float'' above the Si substrate so that the first island layer is smooth, thus setting up the proper boundary condition for QSE.

*$\mu$CAT is supported through Ames Lab by the US-DOE. Research is supported by NSF, PRF (PM, CJ), DOE (MT, MH), Canim Scientific (EC), NSERC-Canada (CJ), Ministry of Sci. & Tech.-Korea (CK).

**12:27**

**B12 7 The Pb corrugation on Si(111) Pb $\alpha - \sqrt{3}x\sqrt{3}$ as a probe of the island crystallography*** MICHAEL YAKES, MYRON HUPALO, JIZHOU CHEN, MICHAEL TRINGIDES, *Ames Laboratory-Iowa State University* Although the corrugation on top of the uniform height Pb islands has been studied by STS, quantitative information about the island morphology is still missing. With this complementary study based on SPA-LEED and STM we use the dependence of the corrugation on coverage to deduce the detailed island crystallographic structure. The two types of bilayer islands which have been identified from their opposing contrasts in STM are analyzed with diffraction and extended STM images to deduce their relative population. Islands with one type of FCC faulted stacking (i.e. ACB) are replaced with coverage by the islands with opposite stacking (i.e. ABC). Since the island shapes are triangular (due to inequivalent type of A- and B- steps) the population reversal is also confirmed from changes in the island orientation with coverage. In addition, a change in the rotation of the Pb overlayer relative to the Si substrate (measured from the location of the Pb(10)) is used to explain the changing intensity ''hexagon-like'' to ''star-like'' distribution of the SPA-LEED pattern near the (00) spot. This rotation explains quantitatively the changing corrugation period. As the coverage increases the preferred Pb orientation changes from $0^o$ to $5.6^o$ rotated with respect to the [110] substrate direction.

*Ames Laboratory is operated by the U.S. Department of Energy by Iowa State University under Contract No. W-7405-Eng-82.

**12:39**

**B12 8 Restructuring Due to Quantum Size Effects During Annealing in Ultrathin Films of Ag/Si(111)*** K.R. KIMBERLIN, D.C. LUDOIS, S.M. BINZ, K.R. ROOS, J. LOZANO, P.W. WANG, J.H. CRAIG, JR., *Bradley University* Ultrathin films of silver have been epitaxially grown itin situ at low temperature and studied with scanning tunneling microscopy (STM) and reflection high energy electron diffraction (RHEED). Restructuring occurs during annealing to 300 K producing flat-topped islands two atomic layers in height in accordance with previous work.[1] Further annealing produces a diverse distribution of heights and sizes of flat topped, vertical-sided islands. At higher coverage, a smooth films anneal to dentritic structures of a single height. A RHEED transmission pattern is formed after annealing the films and crystal orientation is determined. Finally, annealing above 550K produces typical 3D island ''wedding cake'' structures atop the $\sqrt{3} \times \sqrt{3}$ wetting layer on Si(111). These results will be discussed in an ''electronic growth'' model where Quantum Size Effects are thought to stabilize particular island heights, producing this unusual flat island growth.

*This work is supported by NSF grants 0203097, 0215899, 0511811, and selected grants from Bradley Univ.

[1]Gavioli, et. al., Phys. Rev. Lett., **82**(1) 1999, p. 129-132.

**12:51**

**B12 9 Kelvin Force Microscopy of $1 \times 1$ and $\sqrt{3} \times \sqrt{3}$ phases of Pb/Si(111)*** E. D. WILLIAMS, W. G. CULLEN, MASA ISHIGAMI, *Department of Physics, University of Maryland, College Park, Maryland 20742* Using non-contact atomic force microscopy, we have determined the contact potential difference (CPD) of $1 \times 1$ and $\sqrt{3} \times \sqrt{3}$ phases in the Pb/Si(111) system. Furthermore, we have tracked the barrier formation layer-by-layer by observing multilayer structures. We will discuss the origin of the observed CPD contrast between different phases and thicknesses of the Pb films in light of recent theoretical calculations. In addition, we will present the effect of the reduced dimensionality to the observed electrostatic potential variation at boundaries between different phases.

*Materials Research Science and Engineering Center at University of Maryland, College Park

**13:03**

**B12 10 Fluctuations of Pb/Si(111) Domain Boundaries*** WILLIAM CULLEN, *Department of Physics and MRSEC, University of Maryland* DANIEL DOUGHERTY,[†] *Department of Chemistry, University of Pittsburgh* MASA ISHIGAMI, *Department of Physics and MRSEC, University of Maryland* ELLEN WILLIAMS, *Department of Physics and MRSEC, University of Maryland* We have used variable-temperature scanning tunneling microscopy to study fluctuations of a 1D interface — the boundary between two coexisting surface phases. We have prepared Pb/Si(111) surfaces that consist of high-density $(1 \times 1)$-Pb domains coexisting with a lower-density $\sqrt{3} \times \sqrt{3} - R30°$-Pb phase. The domain boundaries between these phases fluctuate at moderate temperatures, allowing direct observation with STM. Measurement of the temporal correlation function for the fluctuating boundary between 525 K and 625 K allows determination of the mass transport mechanisms below and above the onset of thermal desorption of the $(1 \times 1)$ phase. In the desorption regime, our measured dynamical exponent of 1/2 provides microscopic confirmation that fluctuations of the $(1 \times 1)$ boundaries occur via exchange of mass with a 2D adatom gas on the $\sqrt{3} \times \sqrt{3}$ phase, consistent with the zeroth-order desorption kinetics inferred from macroscopic measurements.

*Supported by UMD-NSF-MRSEC
[†]Present Address

**13:15**

**B12 11 Influence of Band Structure and Pb/Si Interfacial Property on Transmission Resonance of Thin Pb Films by Scanning Tunneling Spectroscopy** S.M. LU, M.C. YANG, C.L. JIANG, H.T. SHIH, W.B. SU, C.S. CHANG, TIEN T. TSONG, *Institute of Physics, Academia Sinica, Taipei, Taiwan, Republic of China* The transmission spectrum of a metal film for free electrons at low energy may reveal resonance, which is the quantum size effect above the vacuum level. We use scanning tunneling spectroscopy to observe the transmission resonance for Pb films grown on incommensurate Pb/Si(111) and Si(111)7x7 surfaces. Our observations demonstrate that Pb band structure and Pb/Si interfaces

significantly affect the signal of the transmission in the tunneling spectra. First, the transmission resonance is not detectable in the range of 5~ 6 eV above Fermi level, which can be attributed to that Pb band structure along the (111) direction in this energy range is flat. Secondly, the signal of the transmission resonance acquired on Pb films/incommensurate Pb/Si(111) is more obvious than that acquired on Pb films/Si(111)7x7. This difference can be attributed to that the Pb/Si interface for the former is adiabatic but is non-adiabatic for the latter.

**13:27**

**B12 12 Thin Film Fractal Morphology and the Enhancement of Superconducting Critical Parameters** J. KRIM, M. HIGHLAND, *North Carolina State University* In superconducting films, it is known that the use of artificial defects can enhance a films' superconducting critical parameters. In particular, it has recently been reported that regular arrays of sub-micron sized holes produced by means of lithographic techniques can substantially increase the critical temperature for all fields. [1] We report here our observations that careful control of Pb film deposition conditions can result in film texture that has naturally occurring ''holes'' and enhanced critical parameters reminiscent of the artificially structured films. We characterize the texture of these films via their fractal dimension, and find that it is a useful approach for characterizing a films superconducting critical parameters. This work was funded by NSF and AFOSR. [1] A.V. Silhanek et al., PRB **72**, 014507 (2005)

**13:39**

**B12 13 Binding site H3 to T4 occupation switching and the Pb/Si(111) ''Devil's Staircase'' phase diagram*** V. YEH, M. YAKES, M. HUPALO, M.C. TRINGIDES, *Ames Laboratory-Iowa State University* Z. CHVOJ, *Czech Academy of Science* With SPA-LEED and STM it has been observed that there is a switching occupation from only H3 sites to H3 and T4 sites within the unit cell of the DS (''Devil's Staircase'') (n,m) linear phases at the (1,1) phase or theta=1.25ML. This is observed from the doubling of the linear phase period and the ''flipping'' of the triangle diffraction pattern. The transition temperature from linear to HIC shows a minimum at ~ 120K for the (1,1) phase and follows a U-shaped curved in the whole DS range 6/5ML< theta< 4/3. This unusual dependence (instead of the monotonic decrease of the transition temperature expected for repulsive interactions) indicates the presence of other interactions in the system which can originate from the binding site switching. A statistical mechanical model that includes these two interactions is analyzed and accounts semi-quantitatively for the U-shaped curve and the phase diagram topology. However, a complete treatment should also include the comparison with the free energy of the HIC phases since the linear phases transform to these phases at higher temperatures. The binding site H3 to T4 switching is also relevant to theoretical predictions for the ordered phases in Ba(3x2) grown on stepped Si(111) due to the presence of similar long range interactions.

*Ames Laboratory is operated by the U.S. Department of Energy by Iowa State University under Contract No. W-7405-Eng-82.

**13:51**

**B12 14 Quantum Size Effects in $\delta$ – Pu (111) and (110) Films*** HAORAN GONG, ASOK KUMAR RAY, *Department of Physics, the University of Texas at Arlington, Arlington, TX 76019* First-principles full-potential linearized-augmented-plane-wave (FP-LAPW) calculations have been carried out for $\delta$-Pu (111) and (110) films up to seven layers. The layers have been studied at the non-spin-polarized-no-spin-orbit coupling (NSP-NSO), non-spin-polarized-spin-orbit coupling (NSP-SO), spin-polarized-no-spin-orbit coupling (SP-NSO), spin-polarized-spin-orbit coupling (SP-SO), anti-ferromagnetic-no-spin-orbit coupling (AFM-NSO), and anti-ferromagnetic-spin-orbit-coupling (AFM-SO) levels of theory. The ground state of both $\delta$-Pu (111) and (110) films is found to be at the AFM-SO level of theory and the surface energy is found to rapidly converge. The semi-infinite surface energy for $\delta$-Pu (111) and (110) films is predicted to be 1.18 and 1.42 J/m$^2$, while the magnetic moments show an oscillating behavior, gradually approaching the bulk value of zero with increase in the number of layers. Work functions indicate a strong quantum size effect up to and including five layers for the (111) surface and seven layers for the (110) surface, respectively. The work functions of $\delta$-Pu (111) and (110) films at the ground state are predicted be 3.41 and 2.99eV, respectively. *This work is supported by the Chemical Sciences, Geosciences, and Biosciences Division, Office of Basic Energy Sciences, Office of Science, Department of Energy (Grant DE-FG02-03ER15409) and the Welch Foundation, Houston, Texas (Grant Y-1525).

**14:03**

**B12 15 Novel Atomic Rearrangement in the Pb Monolayer on Si(111) surfaces Induced by Atomic Hydrogen Adsorption.** CHUNG-KAI FANG, *Institute of Physics, Academia Sinica, Taiwan, R.O.C. and Department of Materials Science and Engineering, National Tsing Hua University,Taiwan, R.O.C* ING-SHOUH HWANG, SHIH-HSIN CHANG, *Institute of Physics, Academia Sinica, Taiwan, R.O.C.* LIH-JUANN CHEN, *Department of Materials Science and Engineering, National Tsing Hua University, Taiwan, R.O.C.* TIEN-TZOU TSONG, *Institute of Physics, Academia Sinica, Taiwan, R.O.C.* Using a scanning tunneling microscopy, we have observed interesting hydrogen-adsorption induced atomic rearrangements on Pb/Si(111) system at room temperature. A hexagonal ring-like pattern with decaying intensity is formed around the hydrogen-induced point defect. Moreover, interference-like patterns can be seen in the region among the H-induced point defects. The detailed pattern depends on the relative position of defects. With certain relative positions, a new superstructure of hexagonal cells can be seen. The phase boundaries are found to either enhance or suppress the formation of the hexagonal ring-like pattern. We believe that the intricate interplay between atomic displacement and electronic structure causes the formation of the patterns. [Ref] : I. S. Hwang, S. H. Chang, C. K. Fang, L. J. Chen, and T. T. Tsong, Phys. Rev. Lett. 94, 045505 (2005)

**SESSION B13: FOCUS SESSION: SPECTROSCOPY OF BIOMOLECULES FROM ISOLATED MOLECULES TO CELL ENVIRONMENT II**
**Monday Morning, 13 March 2006; 305, Baltimore Convention Center at 11:15**
**Philip Anfinrud, National Institutes of Health, presiding**



*Invited Papers*

**11:15**
**B13 1 Structure and Interactions of Isolated Biomolecular Building Blocks.**
MATTANJAH DE VRIES, *UCSB*

We investigate biomolecular building blocks and their clusters with each other and with water on a single molecular level. The motivation is the need to distinguish between intrinsic molecular properties and those that result from the biological environment. This is achieved by a combination of laser desorption and jet cooling, applied to aromatic amino acids, small peptides containing those, nucleobases and nucleosides. This approach is coupled with a number of laser spectroscopic techniques, including resonant multi-photon ionization, spectral hole burning and infra-red ion-dip spectroscopy. We will discuss examples illustrating how information can be obtained on spatial structure of individual biomolecules, including peptide conformations and details of DNA base-pairing.

**11:51**
**B13 2**
MARTIN JARROLD, *Indiana University*

This abstract was not received electronically.

*Contributed Papers*

**12:27**
**B13 3 Folding an infinitely long polypeptide into a helical conformation** JOEL IRETA, MATTHIAS SCHEFFLER, *Fritz-Haber Institut der Max-Planck-Gesellschaft, Berlin, Germany* The potential-energy surface and harmonic vibrational analysis of an infinitely long polypeptide are studied using density- functional theory in the Perdew, Burke, and Ernzerhof approximation to the exchange-correlation functional. We find that the $\pi$-helix, $\alpha$-helix, and $3_{10}$-helix are stable respect to the fully extended structure (FES) at 0 K, both in right- and left-handed conformations. Accounting for the temperature effects it is found that the left-handed helices are energetically degenerated respect to FES and the right-handed helices slightly more stable than FES, at room temperature. The minimum-energy pathway along the potential- energy surface shows that the barrier to fold a FES into a left- handed helix is at least three times larger than the barrier to fold it into a right-handed helix. This suggests that the very low occurrence of left-handed helices in protein structures is due to both thermodynamic and kinetic effects.

**12:39**
**B13 4 The Effect of Terminal Truncation on the Folding Dynamics of Coiled-coil GCN4-p1** MICHELLE BUNAGAN, LIDIA CRISTIAN, WILLIAM DEGRADO, FENG GAI, *University of Pennsylvania* Structural perturbation by terminal truncation has been used extensively in protein folding studies because it yields valuable information that could be used to dissect the folding mechanism of the protein of interest. Herein, we studied the folding dynamics of a truncated variant of a cross-linked GCN4-p1 coiled-coil using the technique of laser-induced temperature-jump (T-jump) in conjunction with infrared spectroscopy. While the full-length GCN4-p1 exhibits first-order kinetics in stopped-flow CD and fluorescence folding experiments, a recent T-jump study has shown that one or two folding intermediates may exist at the native side of the major folding barrier. However, the current truncated variant of GCN4-p1 not only shows first order folding kinetics, but also exhibits ultrafast folding behaviors, suggesting that there are no detectable intermediates populated on its folding pathway. Therefore, these results have interesting implications for the understanding of the folding mechanism of coiled-coil structures.

**12:51**
**B13 5 Fast Events in Protein Folding following Ultrarapid Mixing** LISA LAPIDUS, KIMBERLY COOPER, EMILY TUBMANN, *Michigan State U.* DAVID HERTZOG, *Stanford U. & LLNL* JUAN SANTIAGO, *Stanford U.* OLGICA BAKAJIN, *LLNL* A continuous flow microfluidic mixer fabricated out of fused silica was used to study microsecond time scales of protein folding by monitoring natural tryptophan fluorescence. This mixer uses hydrodynamic focusing and diffusion to lower the concentration of the initial denaturant, inducing the protein to fold. The mixing time can be as fast as 8 $\mu$s and allows access to times that are inaccessible in conventional mixers. Using a confocal microscope we observe the UV fluorescence spectrum from naturally occurring tryptophans in 3 well-studied proteins, cytochrome c, apomyoglobin and lysozyme, as a function of time after rapid mixing. Single value decomposition of the time dependent spectra reveal two separate processes: 1) a spectral shift which occurs within the mixing time and 2) a fluorescence decay occurring between 100 and 300 microseconds. We attribute the first process to hydrophobic collapse and the second process the formation of the first tertiary contacts. While the slower rate obviously depends on the details of the folding trajectory of each protein, we note that all three measured rates anti-correlate well with the fraction of secondary structure formed. This work demonstrates that hydrophobic collapse is much faster than had been estimated with slower mixing methods and is in good agreement with measured rates of intramolecular diffusion in unstructured peptides.

**13:03**

**B13 6 Fast diffusive folding dynamics of Tryptophan Zipper peptides*** STEPHEN HAGEN, *Physics Dept., University of Florida, Gainesville FL 32611* Simple synthetic peptides that fold into elemental structures like $\alpha$-helices and $\beta$-hairpins serve as useful model systems for experimental and computational studies of protein folding dynamics. The folding of the Tryptophan Zippers, for example, represents an interesting case of nearly barrierless folding. These short (12-16 residue) peptides designed by Cochran et al. (2001) fold into stable, well-defined $\beta$-hairpins on time scales of just a few microseconds. Our laser temperature-jump fluorescence spectroscopy shows that the ''TrpZip'' molecules encounter little internal friction and almost no enthalpic barrier as they proceed from the unfolded to the folded state: Favorable solvent conditions reduce the entropic barrier as well, until the folding dynamics become complex and diffusive, and different experimental probes see the system as folding on rather different time scales. We will present experimental signatures of these complex dynamics, discuss the role of internal polymer friction in TrpZip folding, and briefly consider suitable approaches for modeling the free energy surface that controls such a folding reaction.

*supported by National Science Foundation, MCB-0347124

***Invited Papers***

**13:15**

**B13 7 Sugars in the gas phase.**

REBECCA JOCKUSCH, *University of Toronto*

The functional importance of carbohydrates in biological processes, particularly those involving specific molecular recognition is immense. Characterizing the three-dimensional structures of carbohydrates and glycoconjugates and their interactions with other molecules, particularly the ubiquitous solvent, water, are key starting points on the road towards the understanding of these processes. A new strategy, combining electronic and vibrational spectroscopy of mass-selected carbohydrate molecules and their hydrated complexes, conducted under molecular beam conditions, with ab initio computation is being exploited to characterize carbohydrate conformations and hydrated structures, the hydrogen-bonded networks they support (or which support them) and the specificity of their interactions with other molecules. The spectral features of monosaccharide residues can be used to refine the assignment of larger, oligosaccharide structures - a supplementary 'building-block' approach to the study of complex structures based upon an 'alphabet' of established IR spectral signatures of different conformations of the monosaccharide units - when their spectroscopic patterns are retained. When their patterns are altered the changes may be understood by analyzing the modification of the hydrogen-bonded networks, eg., the retention (or disruption) of the secondary structural motifs generated by intra-residue hydrogen-bonding. Feedback from the increasing body of experimental data will also help to inform and guide future theoretical conformational searches.

***Contributed Papers***

**13:51**

**B13 8 2D IR measurements of the coupling in transmembrane helix dimers*** CHONG FANG, *Department of Chemistry, University of Pennsylvania* LIDIA CRISTIAN, ALESSANDRO SENES, WILLIAM DEGRADO, *Department of Biochemistry & Biophysics, University of Pennsylvania* ROBIN HOCHSTRASSER, *Department of Chemistry, University of Pennsylvania* Ultrafast 2D IR photon echo spectroscopy has been adapted to the study of transmembrane helix dimers. Residues Gly-79 on each of the two helical strands of Glycophorin A (GpA) dimers in sodium dodecyl sulfate (SDS) micelles were isotopically selected. The 2D IR spectra reveal the tertiary interaction between the helices. The waiting time dependence of the echo informs on the conformational dynamics of different regions of the GpA dimer. Both the $^{13}C$ and $^{13}C{=}^{18}O$ labeled homodimers showed elongated diagonal peaks in the 2D IR correlation spectra. The cross peaks in the heterodimer spectrum indicated an off-diagonal anharmonicity of $\sim$ 3.8 $cm^{-1}$. This anharmonicity is caused by through-space interactions between amide units on different strands. The angle between the two Gly-79 amide-I transition dipoles was estimated to be $\sim$ 35[r] from the polarization of the 2D IR signal in the cross-peak region. The method also identifies residues that are exposed to water.

*This research was supported by NSF-CHE, NIH-GM and by an NIH Resource Grant all to RMH.

**14:03**

**B13 9 Solvent and Peptide Conformational Fluctuations Revealed with Two-Dimensional Infrared Spectroscopy** ZIAD GANIM, ANDREI TOKMAKOFF, *Department of Chemistry, Massachusetts Institute of Technology* Two-dimensional nonlinear infrared spectroscopy (2D-IR) is emerging as a new biophysical tool that offers the sensitivity to protein secondary structure and fast time resolution of linear Fourier transform infrared spectroscopy (FT-IR), but with the added ability to separate overlapping contributions and reveal vibrational couplings. Amide I nonlinear spectroscopy has been used to probe the thermal stability of proteins and peptides and reveal a detailed picture of how the beta-sheet of ubiquitin unfolds from nanoseconds to milliseconds. We show that the standard techniques that are sufficient in calculating FT-IR spectra from a static structure fail to reproduce observed 2D-IR lineshapes. By combining DFT parameterized semi-empirical models and structure trajectories from molecular dynamics simulations, we obtain good agreement with experimental FT-IR and 2D-IR spectra of trpzip2, a model beta-hairpin. We then demonstrate how hydrogen bonding, conformational variation, and their fluctuations are each manifested in 2D-IR spectra.

This methodology provides a means of calculating FT-IR and 2D-IR spectra directly from any atomistic molecular dynamics simulation - allowing richer data analysis and a means of validating mechanistic predictions from simulations.

**SESSION B15: METALS: LATTICE, LOW D, PHONONS**
**Monday Morning, 13 March 2006**
**311, Baltimore Convention Center at 11:15**
**Larry Boyer, Naval Research Laboratory, presiding**

*Contributed Papers*

**11:15**
**B15 1 Anomalous equilibrium volume change of magnetic Fe-Al crystals** MARTIN FRIÁK, JÖRG NEUGEBAUER, *Max-Planck Institute for Iron Research, Max-Planck-Strasse 1, 40237 Düsseldorf, Germany* Iron aluminides represent a very promising class of intermetallic materials with great potential for substituting stainless steels at elevated and high temperatures. Experiments observed an anomalous equilibrium volume behaviour as a function of concentration in Fe-rich compounds [1]. This effect has been tentatively assigned to be due to an order-disorder transition. We have studied the role of magnetism in Fe-Al crystals employing density functional theory (DFT) within the generalized gradient approximation (GGA). The excess energies, equilibrium lattice parameters and magnetic states have been determined for a dense set of different iron concentrations and a large variety of atomic configurations. Both external and internal relaxations were allowed. The spin-polarized calculations for *ordered* ferromagnetic Fe-rich compounds nicely reproduce the anomalous volume behaviour, i.e. the effect is *not* related to an order-disorder transition. Analyzing different magnetic states we identified the change in magnetism to be the driving force. In fact, performing the same calculations but switching off magnetism removed the anomalous volume dependence and showed a clear linear dependence. Based on these results the importance of order-disorder transition in Fe-Al systems is revisited. [1] R. A. Buckley and S. Kaviani, Mat. Sci. Eng. A258, 173 (1998).

**11:27**
**B15 2 Internal stress generation during electrochemically deposited Volmer-Weber thin films.** TIANZHI LUO, ROBERT CAMMARATA, *Johns Hopkins University* The real-time itin situ stress generation during electrochemical deposition of metallic thin films deposited by an island (Volmer-Weber) growth process will be presented. The stresses were measured using a sensitive substrate curvature system optimized for use in an electrochemical cell. Films were deposited on crystalline and amorphous substrates. In many cases, the films displayed an early stage compressive stress, followed by a large tensile jump, and finally ending with a compressive stress at large thickness. Also, interruption of growth led to significant relaxation of the stress. These behaviors were qualitatively similar to those found for evaporated films, and suggest that similar stress generation mechanisms operate for both types of depositions. In other systems, the stress generation behavior was much different, generally displaying a small compressive stress throughout. Correlation of the stress behaviors with microstructural evolution will be presented, and possible mechanisms for the generation of the stresses will be discussed.

**11:39**
**B15 3 Anomalous Magnetic Particle Distribution in Annealed Granular CuCo Thin Films** JIAN-QING WANG, NAM H. KIM, JARDON PECK, A SQUID magnetometer was used to measure ZFC and FC c-T data to study the microstructure of annealed granular Cu80Co20 thin films. The films of thicknesses ranging from 40 nm to 1 mm with 20% vol. Co were magnetron sputtered at base pressure $<$ 1.5 10- 7 torr. The annealing was done at various temperatures up to 400°C in a tube furnace with a reducing gas flow. As-deposits showed the standard single-peak c-T curve with an average size of 3.0 nm in dia. for the Co nanoparticles as calculated by Curie-Weiss analysis. Langevin fitting to magnetization at elevated temperature of 300 K also provided the same particle size. As annealing temperature increased, the first peak occurring around 40K decreased in height while the second, occurring around 300 K, grew. These anomalous features, observed over a wide range of thickness (40-200 nm), appeared to result from microstructural evolution, namely an increase in large particle population at the expense of smaller particles. It is likely that the film contains a mixture of small particles and larger particles that are induced by annealing, which gives rise to the double peak structure.

**11:51**
**B15 4 Metal Diffusion in Granular Bismuth Thin Films** JOHN SADLEIR, *NASA GSFC & UIUC Physics Dept* Bismuth's exotic electro-thermal properties makes it attractive for many device applications. Despite such incentives, fabrication of high quality bismuth films has proven difficult, and measured properties of such films are highly variable in the literature. Implementing a bismuth deposition process in device fabrication presents additional challengesparticularly at interfaces due to the inherent granularity and surface roughness of its films, its low melting point, and its tendency to diffuse and form undesired intermetallic phases. We report on the properties of the granular bismuth films grown at NASA Goddard and studies of solid state diffusion of Au and Cu in these films.

**12:03**
**B15 5 Temperature effect on structure of copper phthalocyanine thin films** KEDAR MANANDHAR, KENNETH PARK, *Baylor University* ZHEN SONG, TANHONG CAI, JAN HRBEK, *Brookhaven National Laboratory* In situ deposited heteroepitaxial thin films of copper phthalocyanine (CuPc) on Ag(111) surfaces have been investigated by scanning tunneling microscopy. The molecules lay flat on the substrate forming a well ordered closed pack square lattice. A lattice vector of ordered film makes $4^0 \pm 0.5^0$with [0-11] direction of Ag (111) lattice. The lattice vectors of the overlayer have been measured 14Åx14Å corresponding to the surface molecular density of 5.10 x $10^{13}$molecules/cm$^2$. The close packed square lattice remains highly ordered when annealed up to $500^0$K. However further annealing of film to $\sim$ $700^0$K desorbs 75 % of molecules leaving submonolayers coverage of molecules. The remaining molecules aggregate to form dendrite like form, which appears to result from dimerization and polymerization. Molecular orientation in well ordered film, structural change of molecules in dendrite like form, and further discussion of temperature effects on CuPc thin films will be presented.

**12:15**

**B15 6 Lattice defects and electronic properties of graphene** FRANCISCO GUINEA, *Instituto de Ciencia de Materiales de Madrid. CSIC* NUNO M.R. PERES, *Universidade do Minho. Portugal* ANTONIO H. CASTRO NETO, We analyze the electronic properties of graphene. Extended lattice defects, and deviations from electron-hole symmetry, lead to self doping, and to a finite Fermi surface. Point lattice defects give rise to a finite inverse elastic lifetime at low energies, and to a universal value of the dc conductivity at low frequencies or temperatures. Transport properties at optical frequencies are also investigated.

**12:27**

**B15 7 Electron-phonon coupling at the Be(0001) Surface*** TIMUR KIM, *University of Aarhus, Denmark* PHILIP HOFMANN, *University of Aarhus, Denmark* TEYU CHIEN, *University of Tennessee, Knoxville TN 37996* HONG LIU, *University of Tennessee, Knoxville TN 37996* WARD PLUMMER, *University of Tennessee, Knoxville TN 37996* The temperature dependent angle-resolved photoemission spectrum (ARPES) of the surface state centered at $\Gamma$ point of Be(0001) surface along the $\Gamma$-K and the $\Gamma$-M directions have been measured as a function of binding energy and momentum. The surface state centered at $\Gamma$ point is highly symmetric in reciprocal space. The temperature dependent ARPES data along these two directions were analyzed by means of energy distribution curves (EDCs) and momentum distribution curves (MDCs) with the help of the spectral function. From the analysis, the information yields the magnitude of the imaginary part of the self energy as a function of E and **k**. Attempts to extract the electron-phonon coupling constant from this data are so dependent upon the model for the phonons and the bare band structure that it is impossible to extract any useful information. But the E and **k** dependence of the imaginary part of the self-energy can be compared directly to first-principles calculations.

*Work supported jointly by NSF and DOE NSF -DMR-0451163.

**12:39**

**B15 8 Wannier-Stark Ladders in Torsional Waves** GUILLERMO MONSIVAIS, *Instituto de fisica, UNAM* RAFAEL MÉNDEZ-SÁNCHEZ, ALFREDO DIAZ-DE-ANDA, JORGE FLORES,* *Centro de Ciencias Físicas, UNAM* LUIS GUTIÉRREZ, ALEJANDRO MORALES, *Centro de Ciencias Físicas UNAM* We study the normal modes of torsional waves in an elastic rod consisting of a set of *n*circular cylinders of varying length determined by a parameter $\gamma$. We present experimental, theoretical, and numerical results. It is shown that some analogies to the Wannier-Stark ladders, originally introduced by Wannier (1960), are exhibited by this classical system. The ladders consist of a series of equidistant energy levels for the electrons in a crystal in the presence of a static external electric field, the nearest-neighbor spacing being proportional to the intensity of the external field. For the case of torsional waves in the rod, we have observed a similar behavior: the vibrations of the rod show resonances of equidistant frequencies, the nearest neighbor spacing being proportional to $\gamma$, associated with the geometry of the rod. One should point out, however, that the analogy is not perfect. References: Wannier G. H. (1960) Wave Functions and Effective Hamiltonian for Bloch Electrons in an Electric Field, Phys. Rev. **117**, 432-439; Wannier G. H.

*Permanent Address: Instituto de Fisica, UNAM

**12:51**

**B15 9 Resonant frequency shifts of Al micro-resonator by electric currents and nonlinear oscillation** SEONG SOO KIM, JUNG HO KIM, KOOKRIN CHAR, *School of Physics, Seoul National University, Seoul, Republic of Korea* Mechanical microbridge resonators are fabricated from polycrystallin aluminum thin film using micromachining processes. A movement of the microbridge smaller than a nm can be measured by optical method. The microstructures are self-oscillating or can be actuated by an external electrostatic field, and oscillations with quality factors up to 2400 in vacuum were measured. The observed resonant frequencies reveal the important role of the internal stress in thin metal film. A substantial resonance frequency shift induced by electric current was observed, which we attribute to thermal expansion caused by Joule heating. Nonlinear oscillation was observed readily due to the large length to thickness aspect ratio ( $\sim$ 1000). Amplitude-dependent resonant frequency shifts show qualitative changes of the resonator response. We will try to correlate the motions of grain boundaries and/or dislocations with the resonator response.

**13:03**

**B15 10 Collective Excitations in a Molten Early transition Metal** AYMAN SAID, *Argonne National Laboratory, USA* HARALD SINN, *Argonne National Laboratory, USA* AHMET ALATAS, *Argonne National Laboratory, USA* CLEMENT BURNS, *Western Michigan University* DAVID PRICE, *Oak Ridge National Laboratory, USA* MARRY SABOUNGI, *CNRS, France* WALTER SCHIRMACHER, *Technische Universitat Munchen, Germany* We report inelastic x-ray scattering measurements of the atomic collective excitations of an early transition metal, namely liquid titanium at T=2023K. The data show well defined sound excitations with a low damping constant comparable to the damping observed in liquid alkaline metals. The data agree very well with the predictions of mode-coupling theory.

**13:15**

**B15 11 Modified Debye spectra in disordered solids** J.C. LASHLEY, D.J. SAFARIK, M.F. HUNDLEY, R.B. SCHWARZ, *Los Alamos National Laboratory* A. PLANES, *Univeresitat de Barcelona* Low-energy modes, as manifested by an excess phonon heat capacity, are ubiquitous in glasses and is often thought to be a signature of a glassy or disordered state. However, this feature is also observed in negative thermal expansion crystals, thermoelectrics, and shape-memory alloys. We compare the peaks in metallic glasses and shape-memory alloys as a function of disorder and crystallinity.

*Invited Papers*

**13:27**
**B15 12 Effect of nuclear quadrupole interactions on the dynamics of two-level systems in glasses.**
ALEXANDER BURIN, *Tulane University*

We consider the effect of the internal nuclear quadrupole interaction on quantum tunneling of complex multi-atomic two-level systems. Two distinct regimes of strong and weak interactions are found. They depend on the relationship between the characteristic energy of the internal interaction $\lambda_*$, which is directly proportional to the number of tunneling atoms per tunneling system, and a bare tunneling coupling strength $\Delta_0$. When $\Delta_0 > \lambda_*$, the internal interaction is negligible and tunneling remains coherent, being defined by the strength of $\Delta_0$. When $\Delta_0 < \lambda_*$, coherent tunneling breaks down and the effective tunneling amplitude decreases by an exponentially small overlap factor $\eta^* \ll 1$ between the internal ground states of the left and right well, affecting thermal and kinetic properties of tunneling systems.The theory is applied to interpret the anomalous behavior of the resonant dielectric susceptibility in amorphous solids for $T \leqslant 5mK$ in terms of the nuclear quadrupole interaction. This interaction breaks coherent tunneling for $T \leqslant 5mK$, where the characteristic tunneling amplitude becomes comparable with the interaction strength. We suggest clarifying experiments using external magnetic fields to test the theories predictions and to shed some light on the internal structure of tunneling systems in amorphous solids.



## SESSION B16: FOCUS SESSION: MOLECULAR-SCALE ELECTRONICS I
**Monday Morning, 13 March 2006; 312, Baltimore Convention Center at 11:15**
**Udo Pernisz, Dow Corning Corporation, Midland MI, presiding**

*Invited Papers*

**11:15**
**B16 1 Mechanically-Adjustable and Electrically-Gated Single-Molecule Transistors.***
ALEXANDRE CHAMPAGNE,[†] *Cornell University*

We describe the fabrication and characterization of single-molecule transistors whose properties can be tuned in two independent ways to achieve systematic measurements of electron transport. The spacing between the source and drain electrodes can be adjusted with better than 1 pm stability using the mechanical breakjunction technique – the electrodes are freely suspended above a flexible substrate, and their spacing can be varied by bending the substrate. In the same devices, we are also able to apply a gate voltage to the molecule. This is done by employing lithographic techniques to suspend the breakjunction only 40 nm above the substrate surface and using the substrate as an electrostatic back gate. With the independent in-situ variations provided by these two experimental ''knobs,'' we are able to achieve a more detailed characterization of electron transport through the molecule than is possible with either technique separately. To demonstrate the device capabilities, we have studied transport through single $C_{60}$ molecules at low temperature. We observe Coulomb blockaded transport and can resolve discrete energy levels of the molecule. We are able to mechanically tune the spacing between the electrodes (over a range of 5 Å) to modulate the lead-molecule coupling, and we can electrostatically tune the energy levels on the molecule by up to 160 meV using the gate electrode. We will also present data of Kondo transport in single $[Co(tpy\text{-}SH)_2]^{2+}$ molecules. We are able to vary the strength of the Kondo resonance in these devices by changing the spacing between the source and drain electrodes.

*This work was conducted with J. J. Parks, A. N. Pasupathy, and D. C. Ralph.
[†]Current address: Physics Dept., California Institute of Technology

*Contributed Papers*

**11:51**
**B16 2 Spontaneous oscillation of current in fullerene molecular junctions** CHAO-CHENG KAUN, RYAN JORN, TAMAR SEIDEMAN, *Department of Chemistry, Northwestern University* We study the correlated phenomena of resonant conduction and current-driven dynamics in Au–$C_{60}$–Au molecular junctions from first principles. A significant resonant component of the transmission gives rise to vibrations of the $C_{60}$ center of mass between the electrodes [C.-C. Kaun and T. Seideman, PRL 94, 226801 (2005)]. An interesting interplay between conductance channels of different symmetries and different degrees of spatial localization results in strong dependence of the transmission on the location of the fullerene within the junction. The distance-dependence, in turn, leads to oscillating current in the THz regime. Rotation of the $C_{60}$ about its axis likewise markedly modifies the transmission characteristics.

**12:03**
**B16 3 Nano-electromechanical structures for single molecule transport studies and position sensing** SHAWN TANNER, CHARLES ROGERS, *Department of Physics, University of Colorado, Boulder, CO 80309* We have developed a process for making sub-micron cantilevers, clamped beams, and more complicated electro-mechanical structures that carry integrated electrical leads.

Such objects are useful as test structures for measuring the electrical properties of molecular sized objects, as high frequency electromechanical components for radio frequency and microwave applications, and as sensor components for studying fluctuations in small systems. Our process uses two realigned electron beam lithography steps, a thin-film angled deposition system, and differential removal of sacrificial aluminum layers to produce freely suspended sub-micron electro-mechanical components. We have produced cantilevers and beams on a variety of substrates (silica, silicon, and polyimide) and have produced insulating, conductive, and multilayer electro-mechanical structures. The process allows the use of essentially any material that can be deposited from a thermal or electron-beam deposition source. We have constructed mechanically adjustable gold-vacuum-gold contacts and have demonstrated vacuum tunneling. The behavior of these contacts indicates a gold work function in excess of 4 eV, consistent with clean gold surfaces.

**12:15**

**B16 4 Gold Nanogap Junctions Fabricated by Temperature-Controlled Electromigration** G. ESEN, M.S. FUHRER, *Department of Physics and Center for Superconductivity Research, University of Maryland, College Park,MD* Electromigration of gold nanowires of different cross-sectional areas are studied using a feedback-controlled electromigration algorithm. We have observed a linear correlation between the cross sectional area of the gold nanowire and the power dissipated in the junction during electromigration, indicating that the feedback mechanism primarily controls the junction temperature. We also show that the role of external feedback circuit is to prevent thermal runaway; minimization of series resistance allows control of electromigration with a simple voltage ramp. We also discuss the I-V characteristics of the junctions after they are formed.

**12:27**

**B16 5 Electron transport through OPE-based molecules in junctions formed by electromigration** XUEQING LIU, WEI CHEN, ZHONGKUI TAN, KONSTANTIN K. LIKHAREV, JAMES LUKENS, *Department of Physics and Astronomy, Stony Brook University* ANDREAS MAYR, *Department of Chemistry, Stony Brook University* We have studied the self-assembly and electron transport properties of (i) simple oligo(phenylene ethynylene) (OPE) chains (2.2 nm) and (ii) OPE based molecules with a naphthalene diimide acceptor group (4.5 nm). Both are capped with terminal isocyanide groups. The molecules are self-assembled on gold wires with a cross-section $\sim 20\times 100$ nm$^2$. The junctions are formed by electromigration and the transport measurements are carried out at 4.2 K. For simple OPE chains, more than 40% of the junctions have shown non-linear I-V curves with resistance R in the range from M$\Omega$ to G$\Omega$, due to trapping of single or multiple molecules. In $\sim$ 10% of the junctions (R $\sim$ a few G$\Omega$), we observe I-V curves with discrete current steps due to electron transport through one or a few molecules. The histogram of the step voltages shows grouping at certain levels. These levels are in a semi-quantitative agreement with our calculations based on the general theory of single-electron transport. For long OPE molecules with acceptor groups, the yield is low ( $<$ 15%), and the data show Coulomb blockade with threshold voltages from 30 to 200meV. Currently we are working on different support nanostructures that will promise higher yield. This work is supported by AFOSR and NSF.

**12:39**

**B16 6 Electronic Quantum Interference in Molecular Devices** FENG MIAO, *Physics Department, University of California, Riverside, CA 92507* DOUGLAS OHLBERG, R. STANLEY WILLIAMS, *HP Labs, 1501 Page Mill Rd., Palo Alto, CA 94304* C.N. LAU, *Physics Department, University of California, Riverside, CA 92507* Understanding the mechanisms for electrical transport and conductance switching in molecular devices is necessary for developing molecular electronics. Here we use pressure-modulated conductance microscopy to characterize Pt/stearic acid monolayer/metal molecular heterostructures. We use either titanium or chromium as the top electrodes. By using atomic force microscope (AFM) to apply a localized force to the junction while monitoring device conductance, we observe nanoscale conductance peaks in response to applied pressure, indicating nanoscale conductance channels through the devices. Additionally, for devices with conductance of $\sim$ 1 to 2 conductance quantum, we also observe conductance dips and oscillations under localized pressure. The results are consistent with quantum interference of electrons between partially transmitting electrodes.

**12:51**

**B16 7 Molecular conductance measurements through printed Au nano-dots.** WEIRONG JIANG, *Rutgers University* NIKOLAI ZHITENEV, *Bell Laboratories, Lucent Technologies* ZHENAN BAO, *Standford University* DAVID ABUSCH-MAGDER, *Bell Laboratories, Lucent Technologies* DON TENNANT, *Bell Laboratories, Lucent Technologies* ERIC GARFUNKEL, *Rutgers University* Gold pads with $\sim$ 100 nm diameter are imprinted on self-assembled monolayers of alkane dithiols of different lengths using nano-transfer technique. The fabrication technique ensures formation of chemical bonds at both ends of molecules while minimizes defect creations compared to other metallization methods. The pads are contacted by conductive atomic force microscope (CAFM) to study electron transport through the SAM as a function of contact force. We found that atomic scale topography at the metal-molecules interface is essential to describe the conductance-stress relationship. In as-fabricated devices, only small percentage of molecules (below 1%) is wired to both contacts. A finite force (1-10 nN) deforms devices resulting in two competing effects: (a) contacting larger number of molecules leading; (b) deforming interfacial bonds and/or tilting the molecules. The estimated conductance of molecules is significantly smaller than in previous CAFM experiments and calculations.

**13:03**

**B16 8 Single-Molecule STM Studies on Atomically-Flat Nanoparticles*** D.H. DAHAYANAKA, D.W. KELLE, D.J. WASIELEWSKI, E.S. DAY, D.R. WHITE, L.A. BUMM, *Center for Semiconductor Physics in Nanostructures, Homer L. Dodge Department of Physics and Astronomy, University of Oklahoma, Norman, OK 73019, USA* C.M. WAITE, J.L. MOORE, R.L. HALTERMAN, *Department of Chemistry and Biochemistry, University of Oklahoma, Norman, OK 73019, USA* The scanning tunneling microscope (STM) has been broadly applied to measure electronic characteristics of individual molecules supported in an inert monolayer matrix, which is typically grown on gold thin films on mica or bulk single crystal substrates. Although these substrates are excellent for electronic measurements, they have serious disadvantages for optical measurements because they are not optically transparent and the metal surface can quench the molecular excited state. We demonstrate that single molecule electronic measurements can also be performed using atomically-flat

gold nanoparticles (FGNPs) supported on indium tin oxide coated glass as a replacement for the typical gold substrate. These substrates are optically transparent and each of the FGNP ''nanosubstrates'' is an optically resonant photonic antenna, thus they have the added advantage that optical measurements can be performed.

*This work has been supported by NSF CAREER grant No. CHE-0239803 and NSF MRSEC No. DMR-0080054.

**13:15**

**B16 9 Theory of Molecular Conformational Switching** SHASHI KARNA, *US Army Research Laboratory* We have investigated stability and current switching as a function of conformational change in tolane molecule by ab initio Hartree-Fock and density functional theory approaches. The planar conformation of the molecule in which the two benzene rings are coplanar is calculated to be more stable than a twisted conformation. The current ($I$) with respect to the applied external potential ($V$) increases from minimum to maximum as the two $\pi$-rings become planar, suggesting the ''ON'' and ''OFF'' mechanism of the molecular switch at planar and perpendicular conformations, respectively.

**13:27**

**B16 10 Comparison of Transport and Switching Characteristics of Ti/Molecule/Pt and Cr/Molecule/Pt Devices** MICHAEL TABER, FENG MIAO, *Department of Physics, University of California at Riverside, Riverside, CA 92521* DOUGLAS OHLBERG, R. STANLEY WILLIAMS, *Hewlett-Packard Labs, 1501 Page Mill Rd, Palo Alto, California 94304* C.N. LAU, *Department of Physics, University of California at Riverside, Riverside,CA 92521* Molecular devices that consist of a monolayer of stearic acid molecules sandwiched between Pt and Ti electrodes can be switched ''on'' and ''off'' reversibly. To gain insight into the switching and mechanism, we fabricated and measured similar molecular junctions by replacing Ti with chromium as the top electrode. These devices can be switched ''off'' controllably, but not ''on.'' The conductances of both types of devices display similar dependence on temperature. Latest data will be discussed in terms of various theoretical models.

**13:39**

**B16 11 Controlling Negative Differential Resistance in Molecular Electronic Devices by Means of Designer Transition Metal Interfaces*** HUGH DALGLEISH, GEORGE KIRCZENOW, *Department of Physics, Simon Fraser University, Burnaby, BC, Canada, V5A 1S6* Observations of negative differential resistance (NDR) have been reported for a number of molecular junctions with potential for device applications and have helped fuel the promise of viable molecular nano-electronic technologies. Here we present predictions of non-linear transport phenomena in molecular junctions where single organic molecules bridge transition metal nanocontacts. We predict the transmission to be mediated by interface states that appear within the HOMO-LUMO gap due to hybridization between thiol-terminated ends of the molecules and the d-orbitals of the transition metal. Our calculations reveal resonant enhancement and reduction in the interface state transmission under the application of moderate bias that result in NDR in molecular junctions with Pd nanocontacts. We show that this NDR can be tailored by suitably choosing the nanocontact materials: If a Rh electrode is substituted for one Pd contact we predict the NDR of the molecular junction to be strongly enhanced.

*Supported by NSERC and CIAR

## SESSION B17: FOCUS SESSION: PHASE TRANSITIONS AND DOMAINS IN FERROELECTRIC NANOSTRUCTURES I

**Monday Morning, 13 March 2006**
**313, Baltimore Convention Center at 11:15**
**Alex Bratkovsky, Hewlett-Packard, presiding**

***Contributed Papers***

**11:15**

**B17 1 Ferroelectric phase transitions in $BaTiO_3/SrTiO_3$ superlattices studied by ultraviolet Raman spectroscopy** DMITRI A. TENNE, X.X. XI, *Dept. of Phys., Pennsylvania State Univ.* A. SOUKIASSIAN, W. TIAN, Y.L. LI, L.Q. CHEN, D.G. SCHLOM, *Dept. of Mater. Sci. & Engin., Pennsylvania State Univ.* A. BRUCHHAUSEN, A. FAINSTEIN, *Centro Atomico Bariloche, Argentina* X.Q. PAN, *Dept. of Mater. Sci. & Engin., Univ. of Michigan* A. CANTARERO, *Univ. of Valencia, Spain* R.S. KATIYAR, *Dept. of Phys., Univ. of Puerto Rico, San Juan, PR* Ferroelectric $(BaTiO_3)_m/(SrTiO_3)_n$ superlattices (SLs) grown by molecular beam epitaxy on $SrTiO_3$ substrates have been investigated by ultraviolet (UV) Raman spectroscopy. Using the UV excitation allowed us to overcome the problem of overwhelming substrate contributions in Raman spectra and made possible the observation of phonons in SLs having the ferroelectric $BaTiO_3$ layers as thin as 2 unit cells. The ferroelectric-paraelectric phase transitions have been observed. Depending on the thickness of the $BaTiO_3$ layers and strain, the phase transition temperature varies by hundreds of degrees from $\sim$ 140 K to 630 K, which is over 200 degrees higher than in bulk $BaTiO_3$. Below $T_c$, the SLs likely remain in the single (tetragonal) ferroelectric phase down to 7 K, i.e. the low-temperature phases characteristic for bulk $BaTiO_3$, are suppressed by strain. The experimental data are in good agreement with the results of the thermodynamic calculations of polarization in SLs as a function of temperature. This work was supported by DOE, NSF, and ONR.

**11:27**

**B17 2 Interlayer Coupling and Dielectric Anomaly in Ferroelectric Bilayers and Multilayer Heterostructures** S. PAMIR ALPAY, SHAN ZHONG, *University of Connecticut* ALEXANDER L. ROYTBURD, *University of Maryland* JOSEPH V. MANTESE, *Delphi Research Laboratories* Ferroelectric multilayers and superlattices have gained interest for dynamic random access memory (DRAM) applications and as active elements in tunable microwave devices in the telecommunications industry. There have been a number of experimental studies that show that these materials have many peculiar properties that cannot be described by a simple series connection of the individual layers that make up the heterostructures. A thermodynamic analysis is presented to demonstrate that ferroelectric multilayers interact through internal elastic, electrical, and electromechanical fields and the ''strength'' of the coupling can be quantitatively described using Landau theory of phase transformations, theory of elasticity, and principles of electrostatics. The thermodynamic modeling indicates that the electrostatic coupling between the layers leads to the suppression of ferroelectricity at a critical paraelectric layer thickness for ferroelectric-paraelectric bilayers. This bilayer is expected to have a gigantic dielectric response similar to the dielectric anomaly near Curie-Weiss temperature in homogeneous ferroelectrics at this critical thickness.

*Invited Papers*

**11:39**
**B17 3 Phase Transitions and Domain Structures in Nanoferroelectrics.**
ARKADI LEVANYUK

A review of the Landau-type theory of size effects in ferroelectric phase transitions will be presented. An aspect of this theory, a question about the ''critical thickness'' of ferroelectric thin films will be the main emphasis. This question can be reduced to that of the size dependence of temperature of ferroelectric phase transition by taking into account two possibilities for such a transition: formation of (i) single- or (ii) multi-domain ferroelectric state. In a defect-free sample, two factors would define which of these possibilities is realized: the depolarizing field and the specific features of the sample surface reflected in the boundary conditions for the Landau-type equations in addition to the conventional electrodynamics boundary conditions. The possibility of the transition into the single domain state strongly depends on a character of electrodes and the additional boundary conditions, while it is much less important for the multi-domain case. In realistic conditions, the transition would proceed into the multi-domain state, especially in near cubic ferroelectrics, e.g. films of cubic perovskites with an elastic mismatch between the film and a substrate. Importantly, the shift of a transition temperature with respect to a bulk is relatively small in this case. The message is that, while studying the question about the ''critical thickness,'' multi-domain states rather than single domain ones should be considered first of all, contrary to the approach in some recent papers where only monodomain state was studied. In particular, there is no definite indication of ultimate ''critical thickness'' for a multi domain ferroelectric state in nearly cubic samples. Along with ultra thin films the ferroelectric nanopowders are also intensively studied now. Here the size effects are more complicated because of long-range interaction between the particles. The problems which the theory faces here are briefly commented upon. It is worth mentioning that several important results in the theory of the size effects have been obtained long ago but, unfortunately, seem not to be well known by the ferroelectrics community. They will be exposed together with more recent results obtained in collaboration with A.Bratkovsky at Hewlett-Packard Laboratories, Palo Alto.

*Contributed Papers*

**12:15**
**B17 4 Ferrolectric nanodots and nanowires under different electrical and mechanical boundary conditions*** INNA PONOMAREVA, IVAN NAUMOV, LAURENT BELLAICHE, *University of Arkansas* Intense effort has been recently made in synthesizing, characterizing and/or simulating ferroelectric nanostructures (FENs), because of their technological and fundamental promise. Among the different possible classes of FENs, thin films are, by far, the ones that have been the most investigated. However what is crucially missing nowadays is to gain a deep knowledge of 0D-like and 1D-like FEN and understand how their properties depend on mechanical and electrical boundary conditions. We report results on ferroelectric nanodots and infinite wires of $Pb(Zr_{0.4}Ti_{0.6})O_3$ alloy under different boundary conditions investigated via Monte-Carlo simulations using an atomistic first-principle-based effective Hamiltonian[1]. It was found that these nanosystems all exhibit a spontaneous polarization that points along a non-periodic direction, for situations close to short circuit electrical boundary conditions and independently of the epitaxial strain. On the other hand, unusual dipole patterns arise in these systems when they experience a large-enough depolarizing field. The dependency of these patterns on the nanostructure's dimensionality is revealed and explained. [1] L. Bellaiche *et al*, Phys. Rev. Lett. **8**, 5427 (2000).

*This work is supported by NSF grants DMR-0404335 and DMR-9983678, by ONR grants N 00014-01-1-0365, N 00014-04-1-0413, N 00014-01-1-0600 and DOE grant DE-FG02-05ER46188.

**12:27**
**B17 5 Self-assembled Nanoscale Domain Structures in Ferroelectrics: Formation and Evolution*** VLADIMIR SHUR, *Ural State University, Ekaterinburg* FERROELECTRIC LABORATORY TEAM, The formation and propagation of self-assembled nanodomain structures have been experimentally studied in lithium niobate single crystals. It has been shown that the ''discrete switching'' through appearance of the quasi-regular patterns consisting of individual nanodomains is a result of decay of highly non-equilibrium domain state. We have demonstrated that the necessary and sufficient condition for such abnormal domain behavior is ineffective screening of depolarization fields, which is characterized by the ratio between bulk screening and switching rates. We have systematically studied this effect in three different experimental situations: (1) ''super-fast'' switching in external electric field, (2) spontaneous backswitching, (3) intensive pulse irradiation by UV laser. The obtained nanoscale structures were classified and explained within unified approach. The main laws of formation of oriented short arrays and growth of strictly oriented ''super-long'' nanoscale domain ''rays'' accompanied by discrete turning and branching have been revealed. The geometry of the domain patterns obtained by computer simulation demonstrates one to one coincidence with experimental images.

*The research was made possible in part by Grants 03-51-6562 of INTAS and 04-02-16770 of RFBR.

**12:39**
**B17 6 Potential distribution and domain structure of metal-ferroelectric-semiconductor-metal heterostructures** RENE MEYER, *Stanford University* PAUL McINTYRE, *Stanford University* Recently, we proposed a novel resistive non-volatile memory concept based on the ferroelectric effect. The resistance switching originates from the unscreened polarization charge at the ferroelectric/semiconductor interface, which affects the distribution of the inner electric potential. A depletion or enrichment of mobile charge carriers leads to a reduced or increased conductivity of the near-interface region. The depolarizing field, however, which is inherently present in the ferroelectric in the case of imperfect screening, causes the formation of 180 deg. domains. The resulting alternation of positive and negative polarization charges at the ferroelectric/semiconductor interface could deteriorate the

performance of the proposed resistance switch. In this contribution, the domain pattern is studied numerically for a metal-ferroelectric-semiconductor-metal structure. A 2-dimensional finite differences method is used to calculate the inner electric field, the potential distribution and the electrostatic energy under short circuit conditions and for external electric fields. Based on empirical data, the domain size is estimated as a function of the screening efficiency of the electrodes and the applied field. Results of the 2-dimensional model are compared to a 1-dimensional approach, where a voltage dependence of the macroscopic polarization is approximated by an effective polarization.

**12:51**

**B17 7 Fabrication and Electrical Measurements of $CoFe_2O_4$ Nanopillars in a $BiFeO_3$ matrix*** SCOTT RUTHERFORD,[†] *University of Wisconsin - Madison* RASMI DAS,[‡] *University of Wisconsin - Madison* XIANGLIN KE,[§] *University of Wisconsin - Madison* DMITRY RUZMETOV, *Northwestern University* DONG-MIN KIM,[‖] *University of Wisconsin - Madison* SEUNG HYUB BAEK, *University of Wisconsin - Madison* MARK RZCHOWSKI, *University of Wisconsin - Madison* CHANG-BEOM EOM, *University of Wisconsin - Madison* CHANG-BEOM EOM COLLABORATION, MARK RZCHOWSKI COLLABORATION, NORTHWESTERN UNIVERSITY COLLABORATION, Coupling between ferromagnetic and ferroelectric ordering has recently stimulated many scientific and technological interests. This ''coupling,'' would provide an additional degree of freedom in the design of micro and nano-electronic devices such as actuators, transducers, or memories. Unfortunately, the clamping effect of the substrate negates any such magnetoelectric coupling through elastic interactions which evident in a multilayer structures. Therefore our focus is directed towads the design of a novel vertically aligned oxide nano-structures, which will allow us to switch the magnetic domains by applying the electric field and vice versa. These nano-structures will also be used as model system to understand the physics of order parameter coupling in ferroelctric and ferromagnetic systems. We have fabricated ferromagnetic nanopillar arrays of $CoFe_2O_4$ (CFO), surrounded by a ferroelectric $BiFeO_3$ (BFO) and $BaTiO_3$ matrix. $90^0$ off-axis sputtering is used to deposit $SrRuO_3$ (SRO), followed by CFO on single surface $TiO_2$-terminated $SrTiO_3$ (001) substrates. SRO provides a good lattice match and electrode capabilities for the subsequent deposition of CFO. E-beam patterning defines pillar dimensions and spacing, while ion milling etches down to the SRO layer. The pillar dimensions range between 100 nm and 500 nm in diameter and are spaced 0.5 to 1 $\mu$m apart. Atomic force microscopy and scanning electron microscopy measurements confirm the structure of the pillars following the pattering and etching steps. The BFO ferroelectric matrix is then deposited by on-axis sputtering. Fabrication of these pillars along with piezo force micrcroscopy and magnetic force microscopy was used to understand the microstructure and domain switching. The detailed scanning probe measurements of domain switching in these novel oxide nanostructures will be discussed.

*Fabrication and Electrical Measurements of CoFe2O4 Nanopillars in a BiFeO3 matrix

[†]Materials Science Department
[‡]Materials Science Department
[§]Physics Department
[‖]Materials Science Department

**13:03**

**B17 8 Structure and electronic properties of GeTe nanoparticles from ab initio calculations.*** GREGORY HAMMAD, *ENS, Strasbourg, France* PHILIPPE GHOSEZ, JEAN-YVES RATY, *University of Liege, Belgium* We use density functional theory to study the structure of small Ge-Te nanoparticles close to stoichiometry with various geometries. We particularly investigate the geometrical distortion of the rocksalt structure that gives rise to the ferroelectric effect in bulk GeTe. We observe that similar distortions appear in nanoparticles down to very small sizes (Ge15Te16). The electronic structure and the HOMO-LUMO states localization are shown to be in most cases related to the surface termination. Using linear response calculation (ABINIT code) we compute effective charges and compare these to the bulk value. We finally discuss the effect of the various factors (aspect ratio, facets, surface termination, stoichiometry) on the possibility that small (a few nm in size) Ge-Te nanoparticles could be ferroelectric.

*JYR acknowledges support by the FNRS, the FAME network of excellence and the NOMADE Region Wallonne contract.



## SESSION B18: FOCUS SESSION: CARBON NANOTUBES: SYNTHESIS, PROCESSING AND CHARACTERIZATION

**Monday Morning, 13 March 2006; 315, Baltimore Convention Center at 11:15**
**David Luzzi, University of Pennsylvania, presiding**

***Invited Papers***

**11:15**

**B18 1 Density gradient ultracentrifugation of single-walled nanotubes.**
MICHAEL ARNOLD, *Northwestern Univeristy*

We demonstrate the bulk separation and enrichment of single-walled carbon nanotubes (SWNTs) by diameter via density gradient ultracentrifugation.(1) Means for sorting SWNTs by their physical and electronic structures are essential for future electronic and optical applications where semiconducting SWNTs mono-disperse in diameter are necessary. The separation is driven by subtle variations in the buoyant density of these nanomaterials with small changes in their physical structure. After centrifugation in a density gradient, focused bands of various colors consisting of isolated SWNTs are clearly visualized by eye. By fractionating the centrifuge tube and characterizing the absorbance and photoluminescence spectra of the sorted SWNTs, it is apparent that SWNTs of decreasing diameter are increasingly more buoyant. This

scalable and non-destructive separation strategy uses centrifugation equipment already utilized in the solution-based processing of carbon nanotubes, and simultaneously separates isolated and aggregated SWNTs, which sediment to larger buoyant densities due the reduced solvation and surface-to-volume ratios of these larger structures. Along these lines, the removal of aggregates and spurious materials is evidenced by significantly lower background absorbencies in optical absorbance spectra. For the case of isolated SWNTs, we propose a geometric-based hydration model to describe the unexpected trend of increasing density with increasing diameter. The effectiveness of this technique is best demonstrated for SWNTs that are small in diameter. For example, in the small diameter regime, it is possible to sort the (6,5) and (7,5) tubes, which differ in diameter by only 0.7 Å. (1) M. S. Arnold et al. Nano Lett. 5 (2005) 713-718.

***Contributed Papers***



**11:51**

**B18 2 Determination of Diameter, Helicity, and Handedness of Carbon Nanotubes by Electron Diffraction** ZEJIAN LIU, LU-CHANG QIN, *University of North Carolina at Chapel Hill* We report a systematic procedure to determine the diameter, helicity and handedness of multiwalled carbon nanotubes by using nanobeam electron diffraction technique. Diameter and helicity of a nanotube can be measured directly from the scattering intensity distribution on the non-equatorial layer lines in its electron diffraction pattern, while the handedness information need be derived from several diffraction patterns of different orientations when if there exist concentric shells of the same helicities in the nanotube. Two selected examples of metallic triple-walled carbon nanotubes are presented to illustrate the detailed structure determination.

**12:03**

**B18 3 Diameter Recognition of Single Walled Carbon Nanotubes by Water-Soluble Proteins** KOJI MATSUURA, TAKESHI SAITO, TOSHIYA OKAZAKI, SATOSHI OHSHIMA, KOHEI MIZUNO, DON FUTABA, KENJI HATA, MOTOO YUMURA, SUMIO IIJIMA, *Res Ctr Adv Carbon Mat, Natl Inst of Adv Indust Sci and Technol (AIST)* The hybrid of proteins and single walled carbon nanotubes (SWCNT) is a promising advanced material that possesses both functions of associated proteins and SWCNTs. Using SWCNTs of varying diameter, synthesized by two distinct methods, Direct-Injection-Pyrolytic-Synthesis [1] (0.8- 1.2 nm) and super-growth chemical vapor deposition [2] (mean diameter of 3 nm), we observed diameter-selective dispersion for two differing proteins which is driven by the sizes of the hydrophobic pockets in the proteins. Hybrid solutions of both lysozyme (LYS) and bovine serum albumin (BSA) dispersed the smaller diameter SWCNTs as observed by absorbance and photoluminescence spectroscopy. The larger diameter SWCNTs were dispersed in the BSA solution, while not dispersed by LYS. A decrease in the mean molar ellipticity observed by far-UV circular dichroism spectroscopy following the removal of unadsorbed proteins suggests a loss in $\alpha$-helical contents of the proteins. These results, in addition to the difference in size of BSA and LYS (10 and 4 nm, respectively), indicate the hydrophobic pockets corresponding to the protein morphology can recognize the SWCNT diameters. [1] Saito et al. J. Phys. Chem. B (2005) 109, 10647. [2] Hata et al. Science (2004) 306, 1362.

**12:15**

**B18 4 Structure determination of a nine-wall carbon nanotube by nanobeam electron diffraction.** QI ZHANG, ZEJIAN LIU, *Department of Physics and Astronomy, the University of North Carolina at Chapel Hill* LU-CHANG QIN, *Department of Physics and Astronomy, Curriculum in Applied and Materials Sciences, the University of North Carolina at Chapel Hill* XINLUO ZHAO, YOSHINORI ANDO, *Meiji University, Japan* Multiwalled carbon nanotubes are composed of a series of coaxial single walled carbon nanotuebs. While great progress has been made in determining the atomic structure of single-walled carbon nanotubes, few direct measurements of the atomic structure of multiwalled carbon nanotubes have been available. Meanwhile, it is still a challenging task to determine the atomic structure of nanotubes with large diameter. In this work, the atomic structure of a nine-walled carbon nanotube was determined by nanobeam electron diffraction with the assignment of the chiral indices of each and every individual shell. The chiral indices of the innermost tubule has chiral indices [5,5], corresponding to the $C_{60}$ molecule. The diameters are from 0.678 nm to 6.445 nm with inter-shell spacings between the neighboring tubules in the range of 0.309 nm to 0.408 nm, the helical angles from $11.51^o$ to $30^o$, in which eight tubes are falling in the high helicity from $15^o$ to $30^o$.

**12:27**

**B18 5 Quantitative Characterization of Defect Densities in Single-Walled Carbon Nanotubes** YUWEI FAN, BRETT GOLDSMITH, PHILIP COLLINS, *Department of Physics and Astronomy, University of California Irvine, Irvine, CA 92697-4576* The prevailing conception of carbon nanotubes and particularly single-walled carbon nanotubes (SWNTs) continues to be one of perfectly crystalline wires. We have demonstrated a selective electrochemical method which labels point defects and makes them easily visible for quantitative analysis. High-quality SWNTs are confirmed to contain one defect per 4 um on average, with a distribution weighted towards areas of SWNT curvature. While this defect density compares favorably to high quality, silicon single crystals, the presence of a single defect can have tremendous electronic effects in one-dimensional conductors like SWNTs. We demonstrate a one-to-one correspondence between chemically-active point defects and sites of local electronic sensitivity in SWNT circuits, confirming the expectation that individual defects may be critical to understanding and controlling variability, noise, and chemical sensitivity in SWNT electronic devices. By varying the SWNT synthesis technique, we further show that the defect spacing can be varied over orders of magnitude. The ability to detect and analyze point defects, especially at very low concentrations, indicates promise of this technique for quantitative process analysis, especially in nanoelectronics development. This work is partly supported by NSF grant DMR-0239842.

**12:39**

**B18 6 Shape Engineerable Single Walled Carbon Nanotube Solid as a Flexible Conducting Mesoporous Material** DON N. FUTABA, KENJI HATA, TATSUKI HIRAOKA, TAKEO YAMADA, KOHEI MIZUNO, YUHEI HAYAMIZU, TATSUNORI NAMAI, YOZO KAKUDATE, OSAMU TANAIKE, HIROAKI HATORI, KOJI MIYAKE, SHINYA SASAKI, MOTOO YUMURA, SUMIO IIJIMA, *National Institute of Advanced Industrial Science and Technology (AIST)* We present a new form of carbon nanotubes (CNT) material where CNTs are aligned and packed densely in a bulk solid. This single-walled carbon nano-

tube (SWNT) solid is fabricated from liquid-induced collapse of the sparse as-grown SWNT forest synthesized by super-growth CVD [1], which results in a 20x increase in mass density and a 70x increase in the Vickers hardness while retaining alignment and high surface area. As such, SWNT solid is an ideal form of CNTs for material and energy storage. The high surface area and well-defined microscopic structure imply that SWNT solid can be regarded as a conductive and flexible mesoporous material. In addition, we can engineer shapes suitable to the application. These unique characters make SWNT solid as a valuable material for supercapacitor electrodes and flexible heaters. Furthermore, we show how partial shrinking of the as-grown material creates a ithandle for robust mechanical and electrical connection to demonstrate exceptional tribological character and wear rate. The SWNT solid promises to open new frontiers in within the carbon nanotube field. [1] K. Hata itet al, Science, **306**, 1241 (2004).

**12:51**

**B18 7 Filtration Patterning of Single Walled Carbon Nanotube Films** DAVID A. DALY, ZHUANGCHUN WU, ANDREW G. RINZLER, *Dept. of Physics, University of Florida, Gainesville, FL* Carbon nanotubes are increasingly being explored for applications exploiting the bulk electrical conductivity of aggregate nanotubes in the form of fibers and films. Attractive in this regard are electrical conductivities orders of magnitude greater than those of conducting polymers, while retaining many of the useful features of polymers, e.g. flexibility, transparency (in thin films) and alternative device fabrication strategies. Here we describe a novel, non-lithographic patterning technique that should also be applicable to other nano-materials. The technique is based on our method for forming thin, pure nanotube films on the surface of a filtration membrane followed by transfer of the film to the desired substrate.[1] To generate patterned films we block the pores of the filtration membrane in the inverse of the ultimately desired film pattern, prior to film formation on the surface of the membrane. The nanotubes only accumulate in the membrane regions that are not occluded, resulting in the desired pattern. Blocking of the membrane pores is accomplished with use of a commercial printer. Implementation and limitations of the technique will be discussed. 1. Z. Wu, Z. Chen, X. Du, J. M. Logan, J. Sippel, M. Nikolou, K. Kamaras, J. R. Reynolds, D. B. Tanner, A. F. Hebard, A. G. Rinzler, Science 305, 1273 (2004).

**13:03**

**B18 8 The Order in Vertically Aligned Carbon Nanotube Arrays** HOWARD WANG, ZHIYONG XU, *Department of Materials Science and Engineering, Michigan Technological University, Houghton, MI 49931* GYULA ERES, *Condensed Matter Sciences Division, Oak Ridge National Laboratory, Oak Ridge, TN 37831* Vertically aligned carbon nanotube (CNT) arrays can exploit the remarkable properties of individual nanotubes in macroscopic applications. Here we report the first measurements of the degree of alignment order in as-grown vertically aligned CNT arrays using small angle neutron scattering. The scattering patterns reveal continuously varying alignment order along the growth and two distinctly different morphologies of CNTs. The observations are discussed in the light of growth mechanisms.

**13:15**

**B18 9 Physical properties of self-assembled monolayers of carbon nanotubes** V.A. SAMUILOV, *Dept. of Materials Sci., SUNYSB and Dept. of Physics, State Univ. of Belarus* J. GALIBERT, *Laboratoire National des Champs Magnetiques Pulses, France* V. KSENEVICH, N.A. POKLONSKI, *Dept. of Physics, State Univ. of Belarus* L. FORRO, *Ecole Polytechnique Federale de Lausanne, Switzerland* J. KOO, K. YOON, M. RAFAILOVICH, J. SOKOLOV, *Dept. of Materials Science, SUNYSB* The controlled method of self-assembly of functionalized carbon nanotubes into 2-D layers with highly regular structure and unique electronic properties has been developed. We use the Langmuir-Blodgett (LB) technique and newly developed inverted LB techniques. The alignment carbon nanotubes in the self-assembled 2-D layers was also introduced. The methods we propose, could be used for covering large surfaces with dense, molecularly ordered ultra-thin films of nanotubes of controlled thickness and orientation. The electrical, thermal conductivity and magneto-transport properties of the monolayers (arrays) of multi-wall and single-wall carbon nanotubes in the temperature range 1.8-300K and in magnetic fields up to 35 T have been tested.

**13:27**

**B18 10 Linear Dichroic Cell Based on Magnetic Alignment of Carbon Nanotubes** Y. J. LEE, J. SHAVER, S. ZARIC, J. KONO, *Rice University, Houston, TX 77005* Single-walled carbon nanotubes align with a magnetic field due to their anisotropic magnetic properties. A simple yet sensitive setup utilizing a balance detector has been constructed to study the alignment of micelle-suspended single-walled carbon nanotubes. We present alignment data in response to static and dynamic magnetic fields. The results of our ensemble measurements show that the amount of signal change depends on the strength and frequency of the applied magnetic field, thus allowing us to determine the minimum field required to align single-walled carbon nanotubes. This data can then be analyzed to characterize the physical parameters of the carbon nanotubes and to determine information about the time scale of the alignment process and local environment.

**13:39**

**B18 11 The Conformation of Polymers Dispersing Single-Walled Carbon Nanotubes in Water.** YAEL DROR, YACHIN COHEN, *Technion, Israel* WIM PYCKHOUT-HINTZEN, *Fz. Juelich, Germany* Amphiphilic polymers have been used to disperse single-walled carbon nanotubes (SWCNT) in water. The polymer conformation around the nanotube surface is important for understanding the nature of the interactions leading to successful dispersions. Two extreme cases are ''tight wrapping'' of the polymer around the nanotube and ''loose adsorption'' of solvated polymer coils on the nanotube surface. We studied aqueous dispersions of SWCNTs with an alternating copolymer of styrene and sodium maleate (PSSty) by small-angle neutron scattering (SANS) and cryo transmission electrons microscopy (cryo-TEM). Dispersion of long, isolated nanotubes and thin bundles was revealed by cryo-TEM. The SANS patterns (at different solvent contrasts) were evaluated by a modification of Pedersen's ''cylindrical block copolymer micelle'' model, depicting the nanotube-polymer complex as composed of a thin core, the radius of which is about 20 A thus containing about 3-4 nanotubes, surrounded by a thick corona of water-swollen polymer coils with a radius of gyration of 150-170 A. Long-term stabilization is achieved by the steric barrier provided by the adsorbed polymer coils reinforced by electrostatic repulsion due to charged groups distributed along the polymer.

**13:51**

**B18 12 High performance field emission in hybrid carbon nanotube-PDMS composite** CATERINA SOLDANO, *Department of Physics, Applied Physics and Astronomy, Rensselaer Polytechnic Institute, Troy, New York* SWASTIK KAR, *Department of Materials Science and Engineering, Rensselaer Polytechnic Institute, Troy, New York* YUNG J. JUNG, *Northeastern University, Boston MA* SAROJ K. NAYAK, *Department of Physics, Applied Physics and Astronomy, Rensselaer Polytechnic Institute, Troy, New York* OMKARAM NALAMASU, PULICKEL M. AJAYAN, *Department of Materials Science and Engineering, Rensselaer Polytechnic Institute, Troy, New York* We present a novel method of fabricating flexible carbon nanotube polymer composites by embedding aligned multi-walled carbon nanotube (MWNT) architectures into a polydimethylsiloxane (PDMS) polymer matrix. These structures are easily transferable, electromechanically robust and extremely flexible, and therefore suitable for applications as multifunctional flexible electronic devices. A combination of controlled placement of aligned multi-walled nanotubes on pre-patterned locations and an effective suppression of mutual screening gives these devices impressive field emission properties. With large field emission factors ($\beta \sim 10^4$) and low (sub 1V/$\mu$m) turn-on fields, these composites can easily operate at high current densities ( $>$ 1mA/cm$^2$) at relatively low voltages making them also suitable for applications in electrically and mechanically stable flexible sensors and display devices.

**14:03**

**B18 13 Thermal Oxidation Profiling of Single-Walled Carbon Nanotubes** BRIAN LANDI, CORY CRESS, CHRIS EVANS, RYNE RAFFAELLE, *NanoPower Research Labs, R.I.T.* A method of thermal oxidation profiling (TOP) to monitor the properties of single-walled carbon nanotube (SWNT)-containing samples has been developed. In the present analysis, the thermal decomposition of raw and acid-refluxed SWNT samples is evaluated by a systematic series of oxidative thermal treatments with subsequent calculation of the SWNT mass retention using a verified purity assessment technique. The TOP results indicate that there are no discernable regions of a raw soot TGA curve that can be ascribed to SWNT combustion independent of impurity influence. In contrast, the acid-refluxed SWNT sample shows that chemical oxidation of the metal can enable optimization of SWNT retention during thermal purification. The established understanding allows for purification efficiencies (the highest purity at the maximum retention) of 75% w/w to be achieved in laser-produced SWNTs, without modification to the diameter distribution.

## SESSION B19: FOCUS SESSION: TRANSITION METAL OXIDE FERROMAGNETIC SEMICONDUCTORS

**Monday Morning, 13 March 2006; 316, Baltimore Convention Center at 11:15**
**Stephan von Molnar, Penn State University, presiding**

***Invited Papers***

**11:15**

**B19 1 Oxide Ferromagnetic Semiconductors.***
SATISHCHANDRA OGALE, *University of Maryland, College Park*

The field of oxide ferromagnetic semiconductors has witnessed tremendous interest and activity over the past few years, especially in the context of realization of intrinsic oxide based diluted magnetic semiconductors (O-DMS). In this talk I will review the important developments in this field, highlighting apparent successes, concerns and questions. Research results obtained by various groups on a number of systems such as transition element (especially Co, Mn, Cr) doped TiO2, ZnO, La1-xSrxTiO3, HfO2 will be discussed including some related device efforts involving spin transport and field induced modulation of magnetization. Some cases of undoped or dual doped oxide films will also be addressed. In the light of the potentially serious possibility of extrinsic effects in most systems the significance of the choice and implementation of an appropriate characterization scheme will also be highlighted. Collaborators: T. Venkatesan, Nigel Browning, Y. V. Idzerda, R. Ramesh, D. K. Kundaliya, S. X. Zhang, L. F. Fu, S. Dhar, A. Lussier, S. R. Shinde, Y. Zhao, M. S. R. Rao, T. Zhao.

*Work Supported under DARPA SpinS program and NSF-MRSEC grant DMR 00-80008.

***Contributed Papers***

**11:51**

**B19 2 Model for vacancy-induced ferromagnetism in ''d0'' magnetic oxides** TIMOTHY ZIMAN, *Institut Laue Langevin and CNRS, Grenoble* GEORGES BOUZERAR, *Labo. Louis Neel, CNRS Grenoble* J. Coey has coined the term ''d0'' ferromagnetism to describe exciting but puzzling effects seen in HfO2, ZrO2 and other oxides. He has also postulated a connection to the occurrence of cation or anion vacancies, which, recent theories indicate, may reasonably lead to the formation of local moments. What has lacked has been a theory which explains why, and at what temperatures, one could expect ferromagnetism. Here we present a simple model for vacancy-based ferromagnetism which permits quantitative estimates of the Curie temperature. The model is based on a random Hubbard model for anions with potentials that represents the occurrence of cation vacancies. By an extension of techniques successfully used to model ferromagnetism in host substituted III-V diluted magnetic semiconductors, we calculate the Curie temperature and dynamical magnetic correlations as a function of the effective strength of the vacancy potential and doping properties, the density of vacancies, as well as the correlation and bandwidth of the host. For physically reasonable parameters this explains large Curie temperatures for rather small concentrations of vacancies.

**12:03**

**B19 3 Anisotropic magnetic properties of Co-doped $SnO_2$ thin films*** JUN ZHANG, RALPH SKOMSKI, *Dept. of Physics and Astronomy and Center for Materials Research and Analysis, Univ.*

*of Nebraska-Lincoln* YONGFENG LU, *Dept. of Electrical Engr. and Center for Materials Research and Analysis, Univ. of Nebraska-Lincoln* DAVID SELLMYER, *Dept. of Physics and Astronomy and Center for Materials Research and Analysis, Univ. of Nebraska-Lincoln* There is strong interest in oxide magnetic semiconductors, which show not only room-temperature ferromagnetism (FM), but also other interesting magnetic properties. Large magnetic moments and anisotropic FM have been observed in Co-doped $SnO_2$ [1] and Co-doped ZnO [2], respectively. Here we report the preparation and magnetic properties of Co-doped $SnO_2$ ($Sn_{1-x}Co_xO_2$, x=0.05) thin films. $Sn_{1-x}Co_xO_2$ thin films were grown on different substrates by pulsed-laser deposition and characterized by X-ray diffraction and SQUID magnetometry, and their magnetic properties depend on the substrates on which the films are grown. Interestingly, the films grown on R-plane-cut $Al_2O_3$ show strongly anisotropic magnetic properties, with [101] being the easy axis. The anisotropy also depends on the substrate on which the films are grown. The results will be discussed in terms of spin-orbit coupling and crystalline defects. [1]. S. B. Ogale, et al., Phys. Rev. Lett. 91, 077205 (2003). [2]. M. Venkatesan, et al., Phys. Rev. Lett. 93, 77206 (2004).

*This research is supported by NSF-MRSEC, W. M. Keck Foundation, NRI and CMRA.

**12:15**

**B19 4 Defect compensation determined magnetism in wide gap dilute magnetic semiconductors (DMS)** LIN-HUI YE, A.J. FREEMAN, DEPARTMENT OF PHYSICS & ASTRONOMY, NORTHWESTERN UNIVERSITY TEAM, Ferromagnetism (FM) in wide gap DMS is thought to be closely related to intrinsic defects; the F-center Bound Magnetic Polaron (FC/BMP) model proposes that it is mediated by shallow donor defects. Our first principles FLAPW calculations show that Cr:$TiO_2$ is a charge transfer insulator with strong defect compensation - which explains the insulating behavior and the Cr chemical valence. We predict different magnetic phases can form at different compensation levels, consistent with the $p-d$ hopping interaction model[1]. FM only exists with uncompensated $Cr^{4+}$, which explains the high $T_c$ FM initially reported[2]. Fully-compensated $Cr^{3+}$ is predicted NOT to be FM which has been verified recently[3]. Due to insufficient hybridization between dopant and impurity states, the FC/BMP mechanism does not apply, and oxygen vacancies destroy the FM instead of mediating it. Our theory extended to Mn:GaN is found to work equally well; it provides a new understanding of the correlation between defects and magnetism. This may explain why magnetism in wide gap DMS seems to be extremely sensitive to fabrication processes. Supported by NSF through the NU MRC.

[1]Mahadevan, Zunger, Sarma, Phys.Rev.Lett. **93**, 177201 (2004)
[2]T.Droubay *et al.* J.Appl.Phys. **97**, 046103 (2005)
[3]T.C.Kaspar *et al.*, Phys.Rev.Lett. **95**, 217203 (2005)

**12:27**

**B19 5 Room temperature ferromagnetism in highly-resistive Ni-doped $TiO_2$ films prepared by sol-gel method** DONGHO KIM, JONGHO CHO, YOUNGGULL JOH, *Yeungnam University* KEEJOO LEE, *Choongnam National University* We investigated the magnetic and transport properties of Ni-doped $TiO_2$ films grown by a sol-gel method with Ni concentrations from 1% to 8%. All the samples exhibited ferromagnetism at room temperature identified by optical magnetic circular dichroism (MCD)along with SQUID measurement. For the samples with low Ni concentrations, both results argee each other, however, MCD results of 8% Ni-doped sample showed a noticeable difference in the temperature dependence of the coercive field and the saturation magnetization from the SQUID results. The Hall effect study showed that the carriers are electrons with densities lower than $10^{18} cm^3$ at room temperature, but no anomalous Hall effect has been observed due to the high resistivity of our samples. The observation of ferromagnetism in highly-resistive Ni-doped $TiO_2$ films questions the carrier-mediated exchange interaction as an origin of ferromagnetism in this material.

**12:39**

**B19 6 Niobium doping effects on the ferromagnetism and microstructure of anatase Co: $TiO_2$ films*** SHIXIONG ZHANG, SATISH OGALE, SANKAR DHAR, DARSHAN KUNDALIYA, WEGDAN RAMADAN, JOSHUA HIGGINS, RICHARD GREENE, THIRUMALAI VENKATESAN, *Center for Superconductivity Research, Department of Physics, University of Maryland, College Park, MD 20742-4111.* LIANFENG FU, NIGEL BROWNING, *Lawrence Berkeley National Laboratory, NCEM, 1 Cyclotron Road, MS 72-150, Berkeley, CA 94720* Niobium doping is shown to have a significant effect on the ferromagnetism and microstructure of dilutely cobalt-doped anatase $TiO_2$ films. Epitaxial films of anatase $TiO_2$ with 3% Co, with and without 1% niobium doping were grown by pulsed-laser deposition at 875 $^0$C at different oxygen pressures. For growth at $10^{-5}$Torr Niobium doping suppresses ferromagnetism, while it enhances the same in films grown at $10^{-4}$Torr. The results of High-resolution Z-contrast Scanning Transmission Electron Microscopy and Electron Energy Loss Spectroscopy study reveal uniform surface enrichment of cobalt in the form of $Ti_{1-x-y}Co_xNb_yO_{2-\delta}$g phase, without cobaltmetal clusters. The transport and Hall effect results will also be presented and discussed.

*Work Supported under DARPA SpinS program

**12:51**

**B19 7 Correlation between ferromagnetism and film structure in Co-doped ZnO films** SEBASTIAAN VAN DIJKEN, *Trinity College Dublin* R. BAUERSCHMIDT, *Trinity College Dublin* V. KARTHIK, *Trinity College Dublin* J.M.D. COEY, *Trinity College Dublin* An experimental study on reactively sputtered ZnO films with a fixed Co doping concentration of 6 percent is presented. The magnetic moment of these films is largest (about 0.7 Bohr magneton per Co) for deposition temperatures between 650 K and 800 K. The evolution of the magnetic moment with temperature correlates with an increase of the lattice parameter perpendicular to the film plane. For films on C-plane (0001) and R-cut (1-102) sapphire substrates the maximum elongation amounts to 2.5 percent and 1.3 percent, respectively. Annealing the films at 720 K for 6 hours in vacuum results in a relaxation of the lattice parameters towards the bulk values. In addition, the Co-doped films become electrically conducting during the annealing procedure. Both effects, however, do not drastically alter the magnetic moment of the Co-doped films: For films on C-plane sapphire the moment remains practically unchanged, while the magnetic moment increases only slightly for films on R-cut sapphire. These results and their implications for the understanding of ferromagnetism in Co-doped ZnO will be discussed.

**13:03**

**B19 8 Room Temperature Ferromagnetism in Transition Metal Doped CVD-Grown ZnO Films and Nanostructures*** D.H. HILL, R. GATEAU, R.A. BARTYNSKI, P. WU, Y. LU, L. WIELUNSKI, V. POLTAVETS, M. GREENBLATT, *Rutgers University* D.A. ARENA, *NSLS* J. DVORAK, *Montana State University* S. CALVIN, *Sarah Lawrence College* We have characterized the chemical, compositional, and magnetic properties of Mn- and Fe-ion implanted epitaxial ZnO films and single crystal nanostructures grown by MOCVD as candidate room temperature diluted magnetic semiconductors. X-ray absorption spectroscopy (SXAS) shows that Mn-implanted films contain $Mn^{2+}$ ions which convert to a mixture of $Mn^{3+}$ and $Mn^{4+}$ upon annealing. Fe-implanted films contain a mixture of $Fe^{2+}$ and $Fe^{3+}$ which converts to a higher concentration of $Fe^{3+}$ upon annealing. XAS and preliminary analysis of EXAFS data indicate that the TM ions are substitutional for Zn. SQUID magnetometry shows that as-implanted films are ferromagnetic at 5K and the annealed films are ferromagnetic at room temperature. X-ray diffraction shows that the annealed films remain epitaxial with excellent long range order. Rutherford backscattering spectrometry indicates a substantial recovery of local order upon annealing as well. The properties of in-situ Fe-doped MOCVD-grown ZnO epitaxial films and nanostructures will also be discussed.

*NSF-ECS-0224166

**13:15**

**B19 9 Defect activated room temperature ferromagnetism in Co:ZnO films - micro-Raman studies** P. KHAREL, C. SUDAKAR, G. LAWES, R. NAIK, *Wayne State University, Detroit* R. SURYANARAYANAN, *LPCES,Université Paris-Sud, France* V.M. NAIK, *University of Michigan-Dearborn* Intense research for room temperature (RT) ferromagnetism (FM) in semiconductors doped with both magnetic and non-magnetic dopants is ongoing because of their potential applications in spin- & photo-electronics. We success fully employ a simple nonvacuum based spin−coating technique to prepare $Zn_{1-x}Co_xO$ films (0.5 to $1_{\mu}$m) on $Al_2O_3$ (001) substrate using precursor solutions of Zn and Co−ethylhexanoate. The films were annealed in air at 700 $^0$C/1h followed by annealing at 550 $^0$C/1h at $10^{-5}$–$10^{-6}$ Torr. X−ray and Raman spectrum indicate no change of wurtzite structure and no cluster formation due to the incorporation of Co in ZnO. Magnetic measurements reveal lack of RTFM in air annealed films, whereas on vacuum annealing films acquire FM ordering. Raman spectra gives a direct evidence on the influence of defect activated FM. The observed FM varies non−monotonically with cobalt concentration. Finally, the effect of annealing, role of oxygen defects, and concentration of $Co^{2+}$ ion on the magnetization properties will be discussed.

**13:27**

**B19 10 Annealing Temperature Dependence of the Magnetic Moment Observed in ZnO Nanotips Implanted with Mn** JEREMY RALEY,* *Air Force Institute of Technology* JEAN WEI, *Air Force Research Laboratory* YUNG KEE YEO, ROBERT HENGEHOLD, MICHAEL MARCINIAK, *Air Force Institute of Technology* PAN WU, YICHENG LU, *Rutgers, The State University of New Jersey* Magnetic properties of Mn ion-implanted ZnO nanotips grown on quartz substrates have been investigated as a function of anneal temperature. This work tracks the strength of the coercive ($H_C$) and remanent ($B_R$) fields of these samples as a function of anneal temperature over a range of 675 to 800 $^o$C for a period of 10 or 20 min in flowing $O_2$. The results show that the magnetic properties are highly dependent on anneal temperature. It has been found that 750 $^o$C is the optimal anneal temperature for producing the greatest values of $H_C$ and $B_R$, and a noticeable drop is observed when this annealing temperature is exceeded. This observation is true for magnetic moment measurements at both 5 and 300 K. The presence of an optimal temperature above which $H_C$ and $B_R$ decrease seems to indicate that post annealing causes magnetic activation and ordering in this material. These observations would not be expected if the ferromagnetic effects observed in this material were due purely to clusters, precipitates, or secondary phase formation.

*Current address: Air Force Research Laboratory, Sensors Directorate, WPAFB, OH

**13:39**

**B19 11 Characterization of Mn and Fe diffusion into ZnO Films and single crystals for diluted magnetic semiconductor applications.*** R. GATEAU, D.H. HILL, R.A. BARTYNSKI, P. WU, Y. LU, *Rutgers University* There is growing interesting in the use of transition metal (TM) doped ZnO films as a diluted magnetic semiconductor for room temperature spintronics applications. Various methods of doping have been investigated including ion implantation and co-deposition during the growth process. In essentially all approaches, doping either accompanies, or is followed by, an annealing step intended to achieve a uniform distribution of the TM dopant, and/or encourage substitution of TM ions for Zn in the Wurtzite lattice. We have studied the diffusion of Mn and Fe into epitaxial and highly-oriented ZnO films, and into ZnO single crystals. The epitaxial films were grown on r-sapphire, exposing the (11-20) surface, while the highly oriented films were grown on a-sapphire exposing the (0001) surface of ZnO. The single crystal substrates were cut to the (0001) and (1100) orientations. Metallic films of $\sim$ 20nm thickness were deposited onto the ZnO substrates, which were subsequently annealed to 700C for between 10 and 40 minutes. We find that the diffusion rate for Mn is approximately an order of magnitude larger than for Fe under the same annealing conditions. Differences in diffusion rates associated with crystallographic orientation and film morphology will be discussed.

*Supported by NSF-ECS-02224166

**13:51**

**B19 12 Magnetic Properties of Co-doped HfO2** Y.S. CHANG, W.C. LEE, M.L. HUANG, Z.K. YANG, M. HONG, *Dept. of Materials science and Engineering, National Tsing Hua University, Taiwan* S.F. LEE, *Inst. of Phys., Academia Sinica, Nankang, Taiwan* L. GONCHAROVA, T. GUSTAFSSON, *Physics Dept., Rutgers Univ., Piscataway, NJ, USA* M.C. HANG, Y.L. SOO, J. KWO, *Dept. of Physics, National Tsing Hua Univ., Taiwan* Dilutely doped Co in $HfO_2$ films were recently reported to show strong enhancement of Co magnetic moments. We have systematically studied the structural, chemical, and magnetic properties of $HfO_2$ epitaxial films $\sim$ 1000Å thick grown on YSZ with Co doping concentrations of 1, 2, 4, and 20 atomic percent. The crystal structures of these samples are predominantly monoclinic, and the XPS Co spectra also indicate the co-existence of cobalt metals and cobalt oxides. Tendency to form Co metal clusters in high doping concentrations was also observed by EXAFS. M-H loops at 10K and 300K by SQUID magnetometer were clearly seen for samples with Co doping of 4% and higher. But no evidence for

strong moment enhancement was found. However, our magnetic measurement do showed the unusual decay of magnetic moment with time, which was also seen in Co-doped $SnO_2$ films.

**14:03**

**B19 13 Local Environment Surrounding Co in MBE-grown $HfO_2$:Co Thin Films Probed by EXAFS and XMCD*** Y.L. SOO, S.C. WENG, W.H. SUN, S.L. CHANG, W.C. LEE, Y.S. CHANG, M. HONG, J. KWO, *National Tsing Hua University* Z.S. YANG, H.-J. LIN, D.G. LIU, J.F. LEE, C.T. CHEN, *NSRRC* Y.H. KAO, J.M. ABLETT, C-. C. KAO, *NSLS* Local structures in MBE-grown $HfO_2$:Co films with different Co concentration has been investigated using the EXAFS technique. The average local environment surrounding Co exhibited by our EXAFS data consists of two major near shells attributed to O and Co neighboring atoms at distances of 2.04 Å and 2.49 Å from the central Co atom, respectively. As the Co concentration increases, the average coordination number of the Co shell systematically increases while that of the O shell decreases. Our experimental results indicate that while chemically bonded with O at a most-likely interstitial location, Co impurity atoms may also form Co clusters even at a relatively low concentration of $\sim$ 1%. The progressive formation of Co clusters is also consistent with our XMCD results that demonstrate increasing magnetic moment with increasing Co concentration.

*This research is supported by NSC in Taiwan and NSF in the US.



**SESSION B20: FOCUS SESSION: PHASE COMPETITION AND SEPARATION IN PERVOSKITE OXIDES**
**Monday Morning, 13 March 2006; 317, Baltimore Convention Center at 11:15**
**Chris Leighton, University of Minnesota, presiding**

***Invited Papers***

**11:15**

**B20 1 Phase Competition and Magnetotransport Phenomena in Manganite Films and Mesoscopic Structures.** TOM WU, *Materials Science Division and Center for Nanoscale Materials, Argonne National Laboratory*

The importance of competition between ferromagnetic metallic (FMM) and charge-ordered insulating (COI) phases in the physics of bulk manganites has been established through a wide variety of techniques. One exotic consequence of this phase competition is step-like features in magnetotransport observed in bulk and single-crystals of $Pr_{0.65}(Ca_ySr_{1-y})_{0.35}MnO_3$ (PCSMO) with $0.7 \leqslant y \leqslant 0.8$. The length-scale of the phase coexistence is $\sim$ 1 micron, motivating a study of structures with dimensions similar to this natural length scale where phenomenology distinct from that of bulk counterparts is expected. Toward that end, we have synthesized films and laterally confined mesoscopic bridges of PCSMO and studied their magnetotransport properties. In particular, we observed: (1) itIntrinsic ultrasharp magnetization steps below 5 K in both bulk and film samples and their dependence on the itextrinsic measurement protocols; (2) Spontaneous jumps of resistance during both the ramping of magnetic field and the relaxation after the field cycle; (3) I-V curves exhibiting negative differential resistance (NDR) in certain ranges of temperature and magnetic field. All of these phenomena can be explained in the context of interconversion between the COI phase and the FMM phase. As expected, this interconversion can be triggered by external magnetic field, as found in the case of the magnetization and resistance steps. Alternatively, in the mesoscopic structures with dimensions similar to the size of the competing FMM and COI domains, a local Joule heating-induced annihilation of conducting filaments causes the anomalous NDR.

***Contributed Papers***

**11:51**

**B20 2 Mapping nanometer-sized phase separation in La1-xCaxMnO3** JING TAO, M. VARELA, S.J. PENNYCOOK, *Oak Ridge National Lab* D. NIEBIESKIKWIAT, M.B. SALAMON, J.M. ZUO, *University of Illinois at Urbana-Champaign* W.D. LUO, S.T. PANTELIDES, *Vanderbilt University* It is well known that three phases dominate over a wide doping range in La1-xCaxMnO3: the paramagnetic (PM) phase is favored for all x at high temperatures, while at low temperatures, the ferromagnetic (FM) phase is favored for x less than 0.5, and the charge ordered (CO) phase for x greater than 0.5. The transitions between these phases are not simple in this system and the mechanism is still not fully understood [1-2]. Here we report direct observation of the formation and melting of CO droplets in the PM-FM regime (x less than 0.5) using in-situ electron microscopy. The distributions of the CO droplets are directly mapped in real space and show maximum density near the PM-FM transition temperature. This behavior contrasts strongly with the behavior in the PM-CO (x greater than 0.5) regime, where the CO clusters are found to nucleate as nanophase domains and percolate on cooling through the transition temperature [3]. We attribute the nanoscale phase separation observed in this system to the competition between electron mobility and localization. Free energies of the competing phases will be estimated using density-functional calculations to understand the nature of the observed phase separation phenomena. [1]. G.C. Milward, M.J. Calderon and P.B. Littlewood, Nature 433, 607 (2004) [2]. J.M. Zuo and J. Tao, PRB 63, 060407 (2001) [3]. J. Tao and J.M. Zuo, PRB 69, 180404 (2004)

**12:03**

**B20 3 Implications of a dimeron magnetic pair model for CMR manganites.*** FRANK BRIDGES, LISA DOWNWARD, *UC Santa Cruz* Recently, based on extensive EXAFS data, we have proposed a magnetic pair model for clusters that exist above the ferromagnetic transition temperature, Tc [1]. The magnetic clusters must contain equal numbers of hole and electron Mn sites and have a reduced distortion compared to the remaining Jahn-Teller distorted electron sites. The smallest such unit (one electron and one hole site) we call a dimeron - it is an electron delocalized over two Mn sites. Here we consider why such a model might be stable, possible configurations of the local distortions for the site pair, and the implications for filamentary clusters throughout the sample when it is only partially magnetized. We also address

electrical transport via hopping dimerons and include the coulomb interactions between dimerons and the Ca(+2) dopants, which provides a quenched-in disorder. Several open questions such as the possible interactions between dimerons will also be discussed. [1] L. Downward et. al., Phys Rev Lett. 95, 106401 (2005).

*Supported by NSF grant DMR0301971.

**12:15**

**B20 4 Microscopic Ferromagnetic and Antiferromagnetic Clusters in $Pr0.7Ca_{0.3}MnO_3$** HAO SHA, JIANDI ZHANG, *Florida Intl. Univ.* FENG YE, JAIME FERNANDEZ-BACA, *ORNL* PENGCHENG DAI, *Univ. of Tenn. and ORNL* Y. TOMIOKA, *CERC, Japan* Y. TOKURA, *Univ. of Tokyo and CERC, Japan* ''Colossal'' magnetorestive manganite $Pr_{0.7}Ca_{0.3}MnO_3$ (PCMO30) is an ideal system to test the microscopic phase separation scenario because it has an inhomogeneous low-temperature insulating metastable state where ferromagnetic (FM), antiferromagnetic (AF), and charge/orbital (CO-OO) phases coexist. On cooling from room temperature, a CO-OO state occurs below $T_{CO-OO} \sim 200$ K, followed by AF ordering below $T_N \sim 140$ K. Below $T_C \sim 110$ K, the magnetic structure develops a FM component coexisting with AF ordering. We have used neutron scattering to study FM, AF and CO-OO phase transitions in a single-crystal PCMO30. The diffuse scattering of FM component demonstrates the presence of short-range ferromagnetic clusters both above and below $T_C$, while no diffuse component in the CO-OO scattering peaks has been observed near $T_{CO-OO}$. Interestingly, the short-range AF correlations associated with $Mn^{4+}$ sites but not with $Mn^{3+}$ sites are observed for both above and below $T_N$, indicating that the local AFM clustering is directly associated with doped holes in this system. The work was supported by NSF-DMR0453804, NSF-DMR0346826, DE-FG02-05ER46202, and DOE DE-FG02-04ER46125. ORNL is managed by UT-Battelle, LLC, for the U.S. DOE under contract DE-AC05-00OR22725.

**12:27**

**B20 5 Phase separation in magnetic spinels induced by Jahn-Teller distortions** SUNMOG YEO, CHENGLIN ZHANG, *Rutgers Center for Emergent Materials and Department of Physics & Astronomy, Rutgers University, Piscataway, New Jersey 08854* YOICHI HORIBE, *Dept. of Physics, Osaka Prefecture Univ.1-1 Gakuen-cho, Sakai, Osaka 599-8531, Japan* SABYA GUHA, SANG-WOOK CHEONG, *Rutgers Center for Emergent Materials and Department of Physics & Astronomy, Rutgers University, Piscataway, New Jersey 08854* We found a strong tendency of chemical/structural phase separation in spinels with Jahn-Teller ions, and this phase separation and the associated microstructure are sensitive on how specimens are cooled down from high temperatures. From our comprehensive study of magnetic and structural properties of magnetic spinels with Jahn-Teller ions with various cooling rates, we have found close relationship between bulk magnetic properties and microstructure.

**12:39**

**B20 6 Photoinduced phase-coexistence in $Bi_{0.4}Ca_{0.6}MnO_3$ thin films.** VERA SMOLYANINOVA, R. KENNEDY, E. TALANOVA, L. ALDACO, R.M. KOLAGANI, M. OVERBY, *Towson University* Doped manganites exhibit a wide variety of physical phenomena due to complex interplay of electronic, magnetic, orbital, and structural degrees of freedom. One of the most intriguing properties of manganites is coexistence of several distinct electronic phases. A photoinduced insulator to conductor transition in charge-ordered (CO) manganites is especially interesting from the point of view of creating photonic devices [1]. We have observed a photoinduced sub-micron phase coexistence of CO insulating phase and conducting phase via optical contrast in Near-field Scanning Optical Microscope images. Such phase coexistence is possible because of the presence of two local energy minima corresponding to CO insulating and charge-disordered conducting phases in the energy landscape [2]. To better understand the physics of phase coexistence in manganites we studied the dynamics of photoinduced conductivity changes. The temperature dependence of this process will be presented. The energy barrier separating the CO insulating and conducting states will be discussed. This work is supported by NSF grants DMR-0348939, DMR-04221141. [1] V. N. Smolyaninova at al., APL 86, 071922 (2005). [2] K. H. Ahn at el., Nature 428, 401 (2004).

**12:51**

**B20 7 Electron-correlation induced phase separation in $Li_xFePO_4$** GERBRAND CEDER, *Department of Materials Science and Engineering, Massachusetts Institute of Technology* FEI ZHOU, *Department of Physics, Massachusetts Institute of Technology* $Li_xFePO_4$ is a promising rechargeable Li-ion battery cathode material. The $Li_xFePO_4$ system is known experimentally to phase separate into $FePO_4$ end $LiFePO_4$ up to $\sim$ 400 K, and form solid solutions above $\sim$ 600 K. Phase separation in this system is surprising as one would expect $Li^+$ ions to repel each other and form ordered compounds at compositions between those of the end members $FePO_4$ and $LiFePO_4$. This is exactly what is found in the local density or generalized gradient approximations to DFT, though it is in stark disagreement with experiments. The fact that the LDA+U method corrects this qualitative error points at the role of electron correlation in inducing phase separation in this material. We have thoroughly studied the LixFeO4 phase diagram with LDA+U. We found that the charge ordering of $Fe^{2+}/Fe^{3+}$ on the iron sub-lattice, induced by *d* electron localization, couples delicately with Li/vacancy ordering on the lithium sub-lattice. Although the repulsion within each sub-lattice favors compound formation, the Li-$e^-$ attraction favors phase separation. It is the balance of interactions within and between the two sub-lattices that gives rise to the unexpected phase behavior of $Li_xFePO_4$. Possible relevance of this novel phase transition mechanism to other alkali metal-intercalated materials will be discussed.

**13:03**

**B20 8 The electric field effect on the electronic soft matter in the manganite $(L_{1-y}Pr_y)_{0.67}Ca_{0.33}MnO_3$ ($y=0.4$, 0.5 and 0.6)** TARA DHAKAL, JACOB TOSADO, SUNGHEE YUN, AMLAN BISWAS, *Department of Physics, University of Florida* Hole-doped manganites are known for their colossal magnetoresistive (CMR) property and insulator to metal phase transition near their curie temperatures. For certain compositions of manganites a coexistence of a charge ordered insulating (COI) and ferromagnetic metallic (FMM) phases has been observed. Changing the temperature, magnetic field or strain modifies the spatial arrangement and relative proportions of these two phases, in this mixed phase state. This property suggests the existence of electronic soft matter in manganites. We have studied the properties of the electronic soft matter in one such material $(La_{1-y}Pr_y)_{0.67}Ca_{0.33}MnO_3$ (LPCMO, $y=0.4$, 0.5 and 0.6). We have grown thin films of LPCMO using pulsed laser deposition. To understand the dynamics of the local phase, we have experimentally mapped the temperature-magnetic field ($T-H$) phase dia-

gram of this material. The phase diagram shows 4 distinct regions, namely the COI state, the fluid phase separated state (FPS), the static phase separated state (SPS), and the FMM state. We have measured the effect of an electric field on this phase diagram and observed that the electric field can significantly modify the FPS state. We will explain the reason behind the electronic soft matter like behavior in the FPS state and the origin of the electric field effect in manganites.

**13:15**

**B20 9 High Temperature EXAFS Studies of $La_{1-x}Ca_xMnO_3$: New Evidence for Magnetic Dimers** L. DOWNWARD, F. BRIDGES, T.A. O'BRIEN, *Univ of California Santa Cruz* J.J. NEUMEIER, *Montana State University* We present Extended X-ray Absorption Fine Structure (EXAFS) data on the CMR perovskite manganites $La_{1-x}Ca_xMnO_3$ ($0.2 < x < 0.5$) to high-temperature (300-600 K) We have recently reported[1] changes in the Mn-O distortion (measured as a broadening, $\sigma$ of the Mn-O pair distribution function) as a function of magnetic field, temperature and Ca-concentration, $x$. Extensive data indicate that there is a universal relationship between changes in the local distortion ($\Delta\sigma^2$) and the sample magnetization. These data suggest that small magnetic clusters containing equal numbers of electron and hole sites must exist just above $T_c$. These clusters have little Jahn-Teller distortion and must form at some higher temperature; the smallest such unit would be an electron/hole site pair, which we call a dimeron. The new high temperature data presented here shows another significant step in the Mn-O distortion near 450 K, which we associate with the dimeron formation temperature, T*. This second step occurs at the same temperature for which other authors have observed a break in the inverse magnetic susceptibility. [1] L. Downward *et al.*, Phys Rev Lett **95**, 106401 (2005).

**13:27**

**B20 10 Origin of the non-thermal photoresponse in thin films of two-phase manganites*** ANTHONY DAVIDSON III, MASON OVERBY,[†] RAJEH MUNDLE, GRACE YONG, DAVID COX, ELENA TALANOVA, VERA SMOLYANINOVA, DAVID SCHAEFER, RAJESWARI M. KOLAGANI,[‡] *Towson University* TOWSON UNIVERSITY TEAM, Our studies of light-induced resistance changes (photoresponse) in thin films the colossal magnetoresistive manganite material $(La,Pr)_{0.67}Ca_{0.33}MnO_3$experiments have revealed a non-thermal component of the light-induced resistance change.This non-thermal component is also observed in thin films of oxygen deficient $La_{0.67}Ca_{0.33}MnO_3$.The common feature of both these material systems is the co-existence of metallic and insulating phases. Our results indicate that this component may be associated with the light-induced resistance decrease in the insulating regions through an electronic mechanism. Previous studies have shown insulator-metal transitions induced by magnetic fields as well as electric fields in these materials. We will present our studies of the correlation of the observed non-thermal photoresponse with magnetoresistance as well as current-voltage characteristics.

*Support from Research Corporation Grant # 443158, NSF MRI # 523176 and Towson University /FCSM Undergraduate Research Grants are acknowledged

[†]Currently at Physics Dept, Purdue University

[‡]Formerly M. Rajeswari

**13:39**

**B20 11 Charge Separation and Pre-percolation Regime in Manganites** ZSOLT MARTON, *University of Pennsylvania* TAKESHI EGAMI, *University of Tennessee/Oak Ridge National Laboratory* RINAT MAMIN, *Zavoisky Physical-Technical Institute of RAS, Kazan 420029, Russia* ZAVOISKY PHYSICAL-TECHNICAL INSTITUTE OF RAS COLLABORATION, Complex manganites have been intensively studied in the last decade since they are model objects for investigations of the collosal magnetoresistance. Temperature dependence of $La_{0.875}Sr_{0.125}MnO_3$ single crystals' dielectric and magnetic properties are investigated in the wide range of temperature and external magnetic field. In order to clarify the nature of the charge, spin and orbital ordering as well as the nanoscale inhomogeneity dynamics, we studied their low-frequency capacitances. It is found that giant dielectric permittivity arises in this manganite. The origin of this enormous dielectric response is believed to be connected with the fact that in the pre-percolation regime of charge separation there are very thin regions of insulator phase with large net surface embedded in metallic matrix. The features of the temperature and field dependence of these dielectric properties are explained by the nanoscale dynamic inhomogeneties appearing due to charge and spin ordering.

**13:51**

**B20 12 Magnetic Phase Diagram of $(NaMn_3)Mn_4O_{12}$** A. PRODI, F. BOLZONI, F. LICCI, E. GILIOLI, *IMEM-CNR* M. MAREZIO, *CRETA-CNRS* M. AFFRONTE, *U. Modena e Reggio Emilia* A. GAUZZI, *U. PM Curie* The double pervoskite $(NaMn_3)Mn_4O_{12}$ represents a model system to explore ordering phenomena usually sought after in half-doped manganites thanks to its unique crystal structure characterized by the absence of quenched disorder. We present here magnetization, transport and specific heat measurements performed under magnetic field aimed at characterizing the two distinct paramagnetic and two antiferromagnetic phases observed in $(NaMn_3)Mn_4O_{12}$ upon cooling. In particular, we investigated the change of paramagnetic regime associated with the structural phase transition at 176 K, the stability of the resulting charge ordered state as well as the peculiar magnetic response of the CE spin structure which orders below 125 K. Analysis of the corresponding specific heat anomalies confirms the nature of the transitions while at low temperatures specific heat data evidences a large Sommerfeld coefficient, unexpected for the insulating state, and reveals the presence of extra entropy with origin in nonmagnetic excitations.

**14:03**

**B20 13 Magnetic ordering of rare-earth compounds: first-principles studies** CHUN-GANG DUAN, *University of Nebraska Lincoln* R. F. SABIRIANOV, L LIU, W.N. MEI, *UNO* P.A. DOWBEN, *UNL* E.Y. TSYMBAL, *UNL* We report a systematic theoretical study on the magnetic ordering in heavy rare-earth compounds with face-centered cubic structure. Based on first-principles total energy calculations of Gd monopnictides, we deduced the exchange interaction parameters of these systems from fitting the total energies of different magnetic configurations to those computed from the Heisenberg model. Then we demonstrated the formation of different magnetic structures in these compounds by using the Monte Carlo simulations. The so obtained Curie (Néel) temperatures agreed well with experiments. Detailed analysis on the trend of exchange parameters changing with anion sizes and distances between neighboring magnetic sites clearly

demonstrate the co- existence of RKKY type metallic exchange interactions and anti- ferromagnetic superexchange interactions. We then propose a Bethe-Slater type curve which can qualitatively explain the behaviors of the exchange parameters in Gd monopnictides.

**SESSION B21: COLLOIDS II: COLLOIDAL CRYSTALS, GELS, AND GLASSES**
**Monday Morning, 13 March 2006**
**318, Baltimore Convention Center at 11:15**
**Maria Kilfoil, McGill University, presiding**



**11:15**
**B21 1 Phase diagram and direct mechanical measurements of colloidal gels** NA WANG, MARIA KILFOIL, We study the phase diagram of colloidal aggregates according to different salt concentration and particle volume fraction, in the absence of gravity. This phase diagram then helps us to locate the region to form strong colloidal gels, whose mechanical properties are studied with time-sharing optical tweezers.

**11:27**
**B21 2 Real Time Observations of Decaying Colloidal Clusters** MARCO POLIN, SANG-HYUK LEE, *Department of Physics and Center for Soft Matter Research, New York University* WILLEM KEGEL, *van 't Hoff Laboratories for Physical and Colloid Chemistry, Debye Research Institute Utrecht University* ANDREW HOLLINGSWORTH, DAVID GRIER, *Department of Physics and Center for Soft Matter Research, New York University* We have studied model colloidal dispersions characterized by long-range electrostatic repulsions and short-range entropically driven attractions. Through a combination of holographic optical trapping and precision digital video microscopy we can create nonequilibrium cluster configurations and track their decay fluctuations. These measurements reveal density and shape fluctuations that accompany the decay of the clusters. Such processes may cast additional light on decay of large atomic nuclei.

**11:39**
**B21 3 Length scale dependent relaxation in colloidal gels** EMANUELA DEL GADO, *Dipartimento di Scienze Fisiche, Universita' degli Studi di Napoli ''Federico II''* WALTER KOB, *Laboratoire des Cooloides, Verres et Nanomateriaux, Universite Montpellier II* Although gels are ubiquitous in fundamental science, technological applications and also in our daily life, their structural and dynamical properties are not well understood. In contrast to other systems that show a slow relaxation, such as glass-forming liquids, the structure of gels is given by an open network that is thought to be responsible for the unusual dynamical properties of these systems. We present the results of a recent study based on a simple model that does indeed have the characteristics of (colloidal) gel-forming systems at a finite temperature. By means of molecular dynamics computer simulations, we investigate the gel formation from the equilibrium sol phase. In particular we show that the strong length scale dependence of the dynamics in gel forming systems is tightly related to the formation of the gel structure and is therefore a general feature. This study allows for the first time to investigate on a microscopic level the relaxation processes in the incipient gel and to understand why they must strongly depend on the length scale investigated. In our model the mesh-size of the incipient gel network corresponds to a crossover length between dramatically different relaxation processes, from stretched to compressed exponentials. Moreover our results link the super-exponential relaxation at low temperature to the motion of pieces of the incipient gel structure.

**11:51**
**B21 4 Crossover from Intermittent to Continuum Dynamics for Locally Driven Colloids** CHARLES REICHHARDT, CYNTHIA J. OLSON REICHHARDT, *Theoretical Division and Center for Nonlinear Studies, Los Alamos National Laboratory* We simulate a colloid with charge $q_d$ driven through a disordered assembly of interacting colloids with charge $q$ and show that, for $q_d \approx q$, the velocity-force relation is nonlinear and the velocity fluctuations of the driven particle are highly intermittent with a $1/f$ characteristic. When $q_d \gg q$, the average velocity drops, the velocity force relation becomes linear, and the velocity fluctuations are Gaussian. We discuss the results in terms of a crossover from strongly intermittent heterogeneous dynamics to continuum dynamics. We also make several predictions for the transient response in the different regimes.

**12:03**
**B21 5 Evolving Bulk Properties of Collapsing Colloidal Gels** STEPHEN KAMP, MARIA KILFOIL, *McGill University* We present a study of the time evolution of the elastic properties of colloidal depletion gels. Silica colloids were suspended in NaCMC solutions and homogenized. Both the colloid volume fraction and the interaction strength (polymer concentration) were varied. The time evolution of the elastic properties of the suspensions was studied with a bulk rheometer in a double-wall Couette cell throughout the gel lifetime. The early lifetime is characterized by an elastic shear modulus that increases logarithmically with time, following which the gels experience catastrophic failure and the elastic modulus drops dramatically. As the gel collapses, various complex behaviors are seen, including a temporary stabilization against collapse, and reformation of a new gel with its own elastic properties which then follows its own trajectory to collapse. Time-lapsed images were taken of identical samples in a separate transparent cell of identical dimensions and the gel height was used to calibrate the measured shear modulus values. The visual cell also allows us to see the sample-spanning collective rearrangement involved in the collapse.

**12:15**
**B21 6 Experimental characterization of the interface of a colloidal suspension.** JESSICA HERNANDEZ-GUZMAN, ERIC R. WEEKS, We investigate experimentally the interface between liquids and solids by using a suspension of colloids as our model. Their size and slow motion makes colloidal suspensions experimentally accessible using 3D high speed confocal microscopy. We track the position of the particles over time, and characterize the spatial structure using bond order parameters as has been done by previous workers. We additionally measure the mobility of each particle. We study the thickness of the interface both in terms of the static structure (which changes from liquid-like disorder to crystal-like order across the interface) and the mobility of the particles with respect to distance from the interface. We find a transition region with a thickness of a few particle diameters.

**12:27**

**B21 7 Freezing and Melting of Colloidal Crystals with Short-Range Attractive Potential** J.R. SAVAGE, D.W. BLAIR, R.A. GUYER, A.D. DINSMORE, We study the kinetics of melting and freezing of colloidal crystals formed by a short-range attractive potential. We use aqueous suspensions of micron-sized latex spheres mixed with surfactant micelles, which create a depletion attraction among the spheres. Single- and multi-layer crystals appear on the glass surface. Upon uniformly heating or cooling, the micelles grow or shrink. Upon heating, the depletion attraction weakens by up to 0.7 kT, and the crystals melt. Optical microscopy is used to track the motions of hundreds of colloidal spheres for up to 8 hours, until crystals have melted. We initially observe a steady decrease in the size of the crystallites. When the size reaches approximately 20-30, however, crystallites rapidly shrink. Once the crystals have melted, we then supercool them and monitor the nucleation and growth of crystallites. The kinetics of individual bond-breaking events and the evolution of the crystalline order parameter in both melting and freezing will be presented. This work is supported by the NSF-DMR 0305395.

**12:39**

**B21 8 Melting of Temperature-Sensitive 3D Colloidal Crystals** AHMED ALSAYED, YILONG HAN, ARJUN YODH, *University of Pennsylvania* We employ thermally responsive monodisperse microgel colloidal spheres to study the melting mechanisms of colloidal crystals [1]. The particle diameter decreases with increasing temperature and leads to volume fraction changes that drive phase-transitions. We will describe observations of a variety of phenomena. Premelting, the localized loss of crystalline order near defects (e.g. grain boundaries) at volume fractions above the bulk melting transition, is directly observed by video microscopy, and is characterized by monitoring the first peak position of the particle pair correlation function. We find the position of the first peak shifts toward smaller particle separations at the onset of premelting. After Delaunay triangulation, mean square rotational and translational fluctuations of bonds were measured close to and away from defects. The behavior of all such quantities exhibits increased disorder near the defects. By locally heating the material within a crystal domain, we also studied the superheating and melting of a perfect 3D crystal. Finally, the introduction of weak attractions between spheres reveals free-floating 3D crystal 'blobs' which can be made to melt and recrystallize by tuning the temperature. [1] A. M. Alsayed, M. F. Islam, J. Zhang, P. J. Collings, A. G. Yodh, Science **309**, 1207 (2005). This work was supported by grants from NSF (DMR-0505048 and MRSEC DMR05-20020) and NASA (NAG8-2172).

**12:51**

**B21 9 Evolution of Particle-Scale Dynamics in Suspensions of Weakly Attractive Colloids Undergoing Structural Arrest** H. GUO, D. LIANG, *Johns Hopkins U.* S. RAMAKRISHNAN, C.F. ZUKOSKI, *UIUC* J.L. HARDEN, *U. of Ottawa* R.L. LEHENY, *Johns Hopkins U.* Suspensions of colloids with weak, short-range attractions can undergo an ergodic to nonergodic transition (ENT) as the strength of the attraction or the particle concentration increases. At low densities the transition corresponds to gelation, while at high densities it is identified as an attractive glass transition. We employ x-ray photon correlation spectroscopy (XPCS) to investigate the slowing dynamics associated the ENT in suspensions of nanometer-scale silica colloids coated with octadecyl-hydrocarbon-chains at wavevectors corresponding to interparticle length scales. At high temperatures the chains form a solvated brush that stabilizes the colloids. At low temperature, the brush collapses leading to a short-range attraction between colloids. Following a quench in temperature, the intermediate scattering function displays two features, a plateau value and a terminal relaxation time, that increase with time since the quench. A comparison between suspensions with concentrations of $\phi = 0.20$ and 0.43 shows qualitative differences in their temporal evolution, indicating a crossover from gelation-like to glass- like dynamical arrest. Further, a comparison with rheometry indicates how the slowing particle-scale dynamics correlates with the growth of the system's elastic modulus.

**13:03**

**B21 10 Microstructure and micromechanics of hard spheres with short-range attraction** MYUNG HAN LEE, ERIC M. FURST, *University of Delaware* We study the microscopic mechanical response of colloidal gels, such as yielding, compression and rearrangement, by manipulating single probe particles within the network. For this work, we use fluorescent polymethylmethacrylate (PMMA) dispersed in mixtures of decalin and cyclohexylbromide, with a refractive index and density close to that of PMMA. The strength of attraction is controlled by the concentration of a non-adsorbing polymer, polystyrene, which induces a depletion attraction between particles. In the presence of sufficiently strong attractive forces, particles form a colloidal gel. Confocal microscopy is used to observe the structural evolution in real time. This enables us to investigate the role of the local structure and particle interactions in the elasticity of the network. Specifically, we identify local elastic and plastic deformations in gels, which depend on the probe oscillation amplitude and strength of attractive interactions.

**13:15**

**B21 11 Deformation of Colloidal Glasses** PETER SCHALL, *WZI, University of Amsterdam* ITAI COHEN, *Physics Department, Cornell University* FRANS SPAEPEN, DAVID WEITZ, *DEAS, Harvard University* Amorphous colloidal suspensions are known to be powerful models for studying dynamical processes in glasses. Since the particles can be observed optically in real time, colloidal systems offer the unique opportunity of studying important mechanisms at the single particle level. We use confocal microscopy to investigate structural rearrangements in colloidal glasses under applied shear. Our setup allows us to track the motion of the individual particles in three dimensions while the suspension is sheared. We use the particle positions determined by confocal microscopy to calculate the local strain tensor and to identify regions of non-affine deformation. We observe ''shear zones'' that are accompanied by a complex strain field around them. Using the single particle data, we elucidate the particle rearrangements in the shear zones, and we investigate correlations between the location of these shear events and regions of high free volume.

**13:27**

**B21 12 Rotational perturbations of colloidal suspensions near the colloidal glass transition.** PIOTR HABDAS, *Dept. of Physics, Saint Joseph's University* ERIC R. WEEKS, *Dept. of Physics, Emory University* By increasing the concentration of small solid particles in a liquid (colloidal suspension) a colloidal glass transition is approached. This is due to the fact that the system becomes increasingly crowded and when it reaches the glass transition it becomes essentially jammed. Therefore, a colloidal suspension is a model system that exhibits a glass transition. There are a few

ways of locally perturbing a colloidal suspension. For example, one of the colloidal particles can be dragged through the colloidal suspension or a dimer made out of two small particles can be rotated. To perform the latter, we mix a small number of paramagnetic beads with dense PMMA particles. Some of the beads form dimers which can be put into rotation by rotating an external permanent magnet. Using confocal microscopy we study response of the system to such local perturbation. In particular, we investigate average spatial range of these perturbations and how it varies with the rotational rate and sample concentration.



**13:39**

**B21 13 Microscopy studies of the re-entrant glass transition.** ANDRZEJ LATKA, NORA GRANETO, PIOTR HABDAS, *Dept. of Physics, Saint Joseph's University* Colloidal suspensions are a model system for studying the glass transition. At the volume fraction $\phi_g \approx 0.58$ a glass transition occurs and a hard sphere colloidal glass is formed. The formation of hard sphere glass is attributed to the ''caging'' effect, in which the particles form cages around each other that restrict their movement. Introducing an attractive depletion force between the particles surprisingly causes the hard sphere glass to melt and the system becomes a liquid. Interestingly, by further increasing the attractive force an attractive glass is formed. Our system is a suspension of nearly hard-sphere colloidal particles and nonadsorbing linear polymer which induces a depletion attraction between the particles. We study the dynamics of the colloidal particles using microscopy techniques. In particular, our research is focused on the transition into the attractive glass phase.

**13:51**

**B21 14 Scaling of non-linear viscoelastic transitions in soft colloidal glasses** MATTHEW HELGESON, NORMAN WAGNER, *Center for Mol. and Eng. Thermodynamics, Dept. of Chemical Engineering, Univ. of Delaware, Newark, DE 19711* DIMITRIS VLASSOPOULOS, *FORTH, Inst. of Electronic Structure and Laser, Gr-71110, Heraklion, Crete, Greece* Soft colloidal particles undergo a transition to a glass-like state at sufficient concentration, due to kinetic trapping, similar to the glass transition in hard sphere systems. In this work we explore the use of rheological measurements as a tool to probe the mechanisms that lead to structure formation and breakage under shear in the glassy state for a monodisperse solution of multi-arm star polymers in an athermal solvent. Maxima in the loss moduli are observed with increasing strain amplitude at the onset of shear melting. We show that the transition to non-linear viscoelastic behavior and the onset of flow follow a systematic, rate-dependent trend. Specifically the critical strain increases with frequency. We discuss this trend in terms of phenomenological understanding of the kinetic trapping of soft colloids in the glassy state, leading to characterization of the softness of the colloidal glass as well as mechanisms of shear melting.

## SESSION B22: FOCUS SESSION: CURRENT DRIVEN MAGNETIZATION DYNAMICS II

**Monday Morning, 13 March 2006**
**319, Baltimore Convention Center at 11:15**
**Mark Stiles, National Institute of Standards and Technology, presiding**

***Contributed Papers***

**11:15**

**B22 1 Reduction of the FMR damping in the nonlinear regime.** OLIVIER KLEIN, GREGOIRE DE LOUBENS, VLADIMIR V. NALETOV,* *CEA Saclay, Service de Physique de l'Etat Condense* It is well known in magnetic resonance, that the Gilbert damping coefficient cannot be extracted directly from the linewidth measurements. The later quantity only yields an upper bound value of the coupling to the lattice. In contrast simultaneous measurement of the microwave susceptibility and the longitudinal component of the magnetization gives directly the ratio between energy stored over the energy absorbed in the sample. This quantity is proportional to the spin-lattice relaxation rate of the excited system. We have recently measured the power dependence of this ratio in the nonlinear regime of YIG samples. Surprisingly, we find that the energy damping coefficient decreases dramatically above the Suhl's thresold while the linewidth increases.

*also at: Physics Department, Kazan State University.

**11:27**

**B22 2 The Periodic Table of Damping in Doped Permalloy Thin Films** JAMES RANTSCHLER, *NIST* DEEPTHI PULUGURTHA, *GWU* LAWRENCE MATTHEW CONNORS, *Rice Univ.* ANDREW CHEN, AUDI CASTILLO, ALEXANDER SHAPIRO, WILLIAM EGELHOFF, JR., ROBERT McMICHAEL, BRIAN MARANVILLE, *NIST* In a survey of thin film Permalloy doped with transition metals, we have constructed a periodic table of damping. We have co-sputtered 25 nm Permalloy films with twenty-one different dopants (Ti, V, Cr, Mn, Co, Cu, Zr, Nb, Mo, Ru, Rh, Pd, Ag, Hf, Ta, W, Re, Os, Ir, Pt, and Au) with at least ten cocnetrations. We measured damping with ferromagnetic resonance spectroscopy (FMR) and concentration with energy dispersive x-ray spectroscopy. Out-of-plane rotation FMR experiments were used to separate the extrinsic linewidth contributions produced by inhomogeneities in the sample from the intrinsic damping of the material. In all samples, doping increased damping, but the effect varied considerably. Trends in the periodic table include larger damping for the heavier elements and larger damping when the d shells are half-full. When using the dimensionless damping parameter of the Landau-Lifshitz-Gilbert equation to describe magnetization dynamics, undoped Permalloy is generally found to have a damping parameter of 0.008. In this study doping increased the damping parameter in all cases; the weakest effects were as little as 0.0001 per atomic percent of copper or silver, while the largest effect was measured to be 0.006 per atomic percent of osmium.

**11:39**

**B22 3 Enhanced Magnetic Damping in Spin-Transfer Excitation** E. M. RYAN, P. M. BRAGANCA, J. C. READ, N. C. EMLEY, G. D. FUCHS, J. C. SANKEY, D. C. RALPH, R. A. BUHRMAN, *Cornell University* While magnetic damping is understood to play a fundamental role in spin-torque phenomena, little experimental work has been done to study the effect of varying the damping parameter $\alpha$. Recently, light terbium (Tb) doping in thin films of permalloy (Py) has been shown to increase $\alpha$ by several orders of magnitude [1]. To directly study the effect of increased $\alpha$ on spin-transfer systems, we have fabricated 0.008 $um^2$ Py/Cu/Py nanopillar spin valves with Tb-doping between 0 and 2% in the free layer. We find that the critical currents for reversibly switching the free layer (proportional to $\alpha$) are several times larger on average in the 2% Tb samples than in pure Py samples. This substantial increase is still considerably less than the increase in $\alpha$ observed in the bulk film measurements of similar composition samples, suggesting that processes other than intrinsic spin-orbital coupling can dominate $\alpha$ in spin-transfer nanopillars, in agreement with simulation and pulsed measurements [2]. We compare this effect across a range of temperatures, and also discuss how the Tb doping affects the processional dynamics. These results suggest one approach for controllably reducing the negative impact of spin torque effects on nanoscale spin valve and tunnel junction read head sensors. [1] W. Bailey, P. Kabos, F. Mancoff, and S. E. Russek, IEEE Trans. Magn. 37, 1749 (2001). [2] P. M. Braganca, et al. Appl. Phys. Lett. 87, 112507 (2005).



***Invited Papers***

**11:51**

**B22 4 Field and Current-Driven Domain Wall Motion in Permalloy Nanowires.***
GEOFFREY BEACH, *The University of Texas at Austin*

Ferromagnetic nanowires provide a well-defined conduit for domain walls, which may be manipulated and used in a variety of information storage and processing schemes. A domain wall may be displaced by a magnetic field or by an electric current traversing the wall via spin-momentum transfer. Many experiments have focused on the depinning of a domain wall by a current, but few have addressed the subsequent propagation of a depinned wall, whether driven by current [1], field [2,3], or both. Using high-bandwidth scanning Kerr polarimetry, we have studied time-resolved motion of field and current-driven domain walls in Permalloy nanowires. Domain dynamics models predict that above a threshold field, uniform wall translation gives way to turbulent wall motion, a dynamic internal wall structure, and a substantial drop in wall mobility. We have observed this transition at an unexpectedly low field [3], suggesting that in many experiments, wall motion is far more complex than the smooth translation typically assumed. The interaction of a dc current with a propagating domain wall is likewise more complex than existing spin-torque models predict. We find a nonlinear response of the wall velocity to a dc current, with velocity enhancements approaching 40 m/s at a current density of $\sim 6\times 10^{11}$ A/$m^2$. The response may be represented by a field-independent linear term, consistent with theory, and a field-dependent nonlinear term that overtakes the linear term at moderate currents. This latter term may arise from the interaction of the current with a vortex in the wall. [1] A. Yamaguchi, et al., Phys. Rev. Lett. **92**, 077205 (2004) [2] T. Ono, et al., Science **284**, 468 (1999); D. Atkinson, et al., Nature Mater. **2**, 85 (2003). [3] G. S. D. Beach, et al., Nature Mater. **4**, 741 (2005).

*Supported by NSF-DMR-0404252 and the R. A. Welch Foundation.

***Contributed Papers***

**12:27**

**B22 5 Direct observation of current driven domain wall distortions, transitions, and propagation in ferromagnetic wires.** W. CASEY UHLIG, JOHN UNGURIS, *National Institute of Standards and Technology, Gaithersburg, MD 20899-8412* Spin transfer torque induced domain wall distortions, transitions between vortex and transverse wall states, and defect-to-defect hopping of domain walls were all observed while flowing current through narrow ferromagnetic wires. Domain walls in 100 nm, 300 nm, and 1 um wide stripes fabricated from 12 nm and 24 nm thick NiFe films were directly imaged using scanning electron microscopy with polarization analysis (SEMPA). SEMPA images revealed that small current densities initially distort the domain walls which are fixed at random pinning defects along the wires. If the current density is increased above $5x10^{11}$ A/$m^2$, the wall is usually swept from the wire, but at smaller currents, the domain wall simply jumps a short distance to the next pinning site before stopping. For vortex type domain walls, the vortex core moves towards the stripe edge, perpendicular to the wall propagation direction. If the core reaches the edge, it is annihilated, thereby converting the vortex into a transverse wall. The direction of the vortex core motion and thus the chirality of the resulting transverse wall are dependent on the applied current direction. The observed domain wall distortions, transitions, and interactions with defects are all expected to play a significant role in spin torque driven magneto-electronics. Work supported in part by the Office of Naval Research.

**12:39**

**B22 6 Spin Transfer Torque for Continuously Variable Magnetization** JIANG XIAO, ANDREW ZANGWILL, *School of Physics, Georgia Institute of Technology* MARK STILES, *National Institute of Standards and Technology* We report quantum and semi-classical calculations of spin current and spin-transfer torque in a free-electron Stoner model for systems where the magnetization varies continuously in one dimension. Analytic results are obtained for an infinite spin spiral and numerical results are obtained for realistic domain wall profiles. The adiabatic limit describes conduction electron spins that follow the sum of the exchange field and an effective field produced by the gradient of the magnetization in the wall. Non-adiabatic effects arise for short domain walls but their magnitude decreases exponentially as the wall width increases. Our results cast doubt on the existence of a non-adiabatic contribution to the spin-transfer torque.

**12:51**

**B22 7 Nonlinear regimes of current-induced domain wall motion** YA. B. BAZALIY, M. HAYASHI, B. A. JONES, S. S. P. PARKIN, *IBM Almaden Research Center* A. JOURA, *Department of Physics, Georgetown University* We study theoretically the current-induced motion of a magnetic domain wall in a nanowire in the presence of external magnetic field and pinning potential. The wall is assumed to be rigid and is described by the one-dimensional model equations [1,2]. Both ''adiabatic'' and ''non-adiabatic'' spin-transfer terms are taken into account. The current-induced motion differs significantly below and above the Walker breakdown, i.e., in the regimes when the deflection angle is close to a particular value vs. when it makes the full circles. We find two novel phenomena. The first one is the existence of a stable auto-generation regime for a wall trapped in a shallow pinning center. The second is the ''reversed motion window'' regime in the situation when current and magnetic field push the domain wall in opposite directions. Both regimes are qualitatively different from the domain wall resonance regime studied in Ref. [1,3], or zero field current induced motion [1,2]. Reversal of the domain wall velocity by a relatively small current above the Walker breakdown was recently achieved in Ref. [4]. 1. Gen Tatara and H. Kohno, Phys. Rev. Lett. **92**, 086601 (2004). 2. A. Thiaville *et al.*, Europhys. Lett., **69**, 990 (2005). 3. E. Saitoh *et al.*, Nature, **432**, 203 (2004). 4. M. Hayashi *et al.*, submitted (2005).

**13:03**

**B22 8 Interactions between domain walls and spin currents** M. KLAUI, M. LAUFENBERG, D. BACKES, W. BUHRER, U. RUDIGER, *Fachbereich Physik, University of Konstanz, Germany* L. VILA, C. VOUILLE, G. FAINI, *LPN - CNRS, Maroussis, France* A promising novel approach for switching magnetic nanostructures is current-induced domain wall propagation (CIDP), where due to a spin torque effect, electrons transfer angular momentum to a head-to-head domain wall and thereby push it in the direction of the electron flow without any externally applied fields. This effect has been observed with a variety of techniques including MFM [1] and spin polarized scanning electron microscopy [2] to directly observe current-induced domain wall propagation in ferromagnetic nanostructures and magnetoresistance measurements to systematically probe the critical current densities as a function of the geometry [3]. The observed wall velocities and critical current densities, where wall motion sets in at room temperature, do not agree well with theoretical 0K calculations [4]. We have therefore measured the critical current densities as a function of the sample temperature. We find that the spin torque effect becomes more efficient at low temperatures, which could account for some of the observed discrepancies between the 300K experiment and the 0K simulation. [1] A. Yamaguchi et al., Phys. Rev. Lett. 92, 77205 (2004); [2] M. Klaui et al., PRL 95, 26601 (2005); [3] M. Klaui et al., PRL 94, 106601 (2005); [4] A. Thiaville et al., EPL 69, 990 (2005); G. Tatara et al., APL 86, 252509 (2005);

**13:15**

**B22 9 Current-Driven Resonance of Single Domain Wall in Permalloy Nanowires** SEOK-HWAN CHUNG, FRANK Y. FRADIN, AXEL HOFFMANN, *Materials Science Division and Center for Nanoscale Materials, Argonne National Laboratory* The manipulation of magnetic domain structures with electrical transport current is of fundamental interest for understanding the magneto-transport properties of spintronic devices. We measured current driven domain wall resonance by using a well-defined single domain wall in half-circle nanowires with 35 $\mu$m radius. Nanowires of 40 nm-thick and 250 nm-wide Permalloy with contact pads were fabricated by multi-step electron beam lithography and subsequent lift-off processes. A single ittransverse magnetic domain wall can be effectively introduced and pinned in the center of the nanowire, due to the strong shape anisotropy, by applying external field perpendicular to the center of the wire. This was confirmed with magneto-transport measurement, magnetic force microscopy and micromagnetic simulation. We observed single domain wall resonance by measuring the reflected power as a function of driving frequency and applied pinning field. From these measurements, we can obtain the domain wall inertia (Döring mass), which is $4\times\ 10^{-8}$g/cm$^2$ in our sample. The critical current density for the wall motion is $\sim\ 1\times\ 10^7$A/cm$^2$. We attribute the mechanism of the current driven wall motion in our sample to the spin and momentum transfer from *s* electrons in the conduction band to the local *d* electrons in the domain wall. * Supported by DOE, BES under contract W-31-109-ENG-38.

**13:27**

**B22 10 Spin accumulation and resistance due to a moving domain wall** J. IEDA, S. TAKAHASHI, *CREST, Japan Science and Technology Agency; Institute for Materials Research, Tohoku University* S. E. BARNES, *Physics Department, University of Miami* S. MAEKAWA, *CREST, Japan Science and Technology Agency; Institute for Materials Research, Tohoku University* The resistance of magnetic nanowires containing a moving domain wall (DW) is studied. The excess resistance due to the DW has been shown in a number of transport experiments [1]. Theoretically, the DW resistance is investigated along with the concepts of the spin dependent scattering with spin mistracking and the spin accumulation, where the DW is assumed static just producing the exchange field to conduction electrons. For a moving DW, however, the angular momentum transfer effect [2] should be incorporated to those mechanisms. In this presentation, we discuss this effect along with the spin accumulation mechanism. The frequency dependence of the spin accumulation is also presented. [1] J. F. Gregg et al., PRL77, 1580 (1996); U. Ebels et al., PRL84, 983 (2000); E. Saitoh et al., Nature432, 203 (2004). [2] S. E. Barnes and S. Maekawa, PRL95, 107204 (2005); cond-mat/0410021.

**13:39**

**B22 11 Theory of Antiferromagnetic Metal Spintronics** REMBERT DUINE, *The University of Texas at Austin* ALVARO NUNEZ, PAUL HANEY, ALLAN MACDONALD, *The University of Texas at Austin* Spintronics in ferromagnetic metals is built on a complementary set of phenomena in which magnetic configurations influence transport coefficients and transport currents alter magnetic configurations. In this talk I will argue that nanostructure circuits containing antiferromagnetic elements have large potential for applications, partly because the critical current for inducing magnetization dynamics may be smaller than for ferromagnets. This occurs in part because spin torques that lead to current-induced switching act through the entire volume of an antiferromagnet. I will explain how this follows from the special symmetry properties of antiferromagnets.

**13:51**
**B22 12 Towards ab-initio calculations for antiferromagnetic metal spintronic devices.** PAUL HANEY, DEREK WALDRON, ALVARO NUNEZ, REMBERT DUINE, HONG GUO, DEREK WALDRON, In conventional spintronics, the electron's spin degree of freedom is exploited to construct systems which exhibit behavior of practical importance and fundamental scientific interest. The prototypical system is a heterostructure which consists of alternating layers of ferromagnetic and paramagnetic materials. Such a system is used to study GMR and spin transfer torque, the two most important phenomena in spintronics today. In GMR, the relative orientation of magnetic layers affects the current flowing through a heterostructure, while in spin transfer the current flowing through the structure effects the orientation of the magnetic layers. It is of interest to consider what type of effects occur in structures containing antiferromagnetic materials. To this end, realistic calculations of GMR and spin transfer in antiferromagnetic heterostructures are presented. The calculations are carried out using ab-initio NEGF methods, using the LSDA extended to non-collinear magnetic configurations. Preliminary results of a Cr-Au-Cr structure are presented as an example of an experimentally realizable antiferromagnetic system.

**14:03**
**B22 13 Nonequilibrium Green's function calculations for antiferromagnetic metal spintronic nanocircuits** ALVARO NUNEZ, REMBERT DUINE, PAUL HANEY, ALLAN MACDONALD, *The University of Texas at Austin* In this talk I will present results of nonequilibrium Green's function calculations on toy-model heterostructures containing antiferromagnetic elements that are intended to illustrate some generic aspects of their spintronic properties. Using this formalism we calculate the nonequilibrium spin density of the electrons which, in a microscopic picture of spin transfer, gives rise to spin transfer torques. The main result is that, unlike the case of ferromagnets to ferromagnets, the spin transfer acts throughout the entire antiferromagnet, making current a very effective way to induce collective magnetization dynamics. Preliminary results on the influence of disorder and surface roughness will be presented.

**SESSION B23: QUANTUM SPIN CHAINS I**
**Monday Morning, 13 March 2006**
**320, Baltimore Convention Center at 11:15**
**Christopher Landee, Clark University, presiding**

**11:15**
**B23 1 Calculated And Experimental Exchange Interactions In A Strong-rail Spin Ladder** CHRISTOPHER LANDEE, A. SHAPIRO, M. M. TURNBULL, *Clark University, Worcester, MA 01610* J. NOVOA, J. RIBAS, *Departament de Quimica Fisica, Universitat de Barcelona, Barcelona, Spain.* Low-dimensional magnetic lattices with moderate exchange interactions can be conveniently formed by combining organic cations with tetrahalocuprates. In these compounds, the ultimate structure is ultimately determined by size, shape and hydrogen-bonding capacity of the cation with the magnetic interactions occurring through halide-halide contacts. A variety of these compounds have been studied [1] and techniques have been developed for calculating the magnetic exchange interactions from first principles [2,3]. We report on the synthesis, structure and magnetic properties of (2,3-dimethylpyridinium)$_2$CuBr$_4$, which is the second spin ladder to be found with a stronger rail interactions ($J_{rung}/k_B$ = 9 K, $J_{rail}/k_B$ = 17 K). Comparison will be made between the exchange constants calculated from first principles and those obtained from experimental data. 1. C. P. Landee itet al, itPhys. Rev. B **63** 100402 (2001). 2. M. Deumal itet al, itPolyhedron **22** 2235-2239 ( 2003). 3. M. Deumal itet al, itEuro. J. Inorg. Chem. **2005**, 4697-4706.

**11:27**
**B23 2 Novel Raman resonance in ladder spin systems** ALEXANDER DONKOV, ANDREY CHUBUKOV, *UW-Madison* We consider Raman intensity in spin $S$ two-leg- spin-ladder, with the goal to understand recent experiments[1,2]. We argue that the Raman intensity has a pseudo-resonance peak whose width is very small at large $S$. The pseudo-resonance originates from the existence of a local minimum in the magnon excitation spectrum, and is located slightly below twice the magnon energy at the minimum. The physics behind the peak is surprisingly similar to that in the excitonic scenario for the neutron and Raman resonances in a $d-$ wave superconductor. We also consider mid-infrared X-ray scattering in 2D systems and compare the results with recent measurements [3]. [1] A. Gozar et al, Phys. Rev. Lett. **87**, 197202 (2001). [2] S. Sugai and M. Suzuki, Phys stat sol (b) **215**, 653 (1999). [3] J. P. Hill, G Blumberg et al, [unpublished]

**11:39**
**B23 3 Theory of spin gaps in the dimerized quarter-filled two-leg rectangular ladder*** YONGGUO YAN, SUMIT MAZUMDAR, *University of Arizona* Despite the extensive work on even-leg spin-ladders and 1/2- filled band electron-ladders[1] , little is known currently about commensurate non-1/2-filled band electron ladders. We report density-matrix renormalization group calculations of spin gaps in the 1/4-filled band correlated two-leg rectangular ladder with dimerization along the legs of the ladder. In contrast to the uniform ladder, spin gaps in the dimerized ladder can be significant. Very large spin gaps, as are found experimentally in quarter-filled band organic charge-transfer solids with coupled pairs of quasi-one-dimensional stacks[2], however, occur within the model only for large leg dimerization and electron hopping along the rungs that are nearly equal to the hopping along the legs.

*Supported by NSF-DMR-0406604

[1]E. Dagotto and T.M. Rice, Science **271**, 618 (1996).
[2]E. Ribera et al., Chem. Eur. J. 5, 2025 (1999).

**11:51**
**B23 4 Magnetic and electrical properties of the double chain-type compounds $NaRh_2O_4$ and $NaMn_2O_4$** K. YAMAURA, *NIMS (Japan)* Q. HUANG, *NIST* M. MOLDOVAN, D.P. YOUNG, *Louisiana SU* E. TAKAYAMA-MUROMACHI, *NIMS (Japan)* Both compounds share the same structure basis in which the 6- fold coordinated transition metal, $RhO_6/MnO_6$, forms a double chain-type unit by sharing the octahedra edges ($CaFe_2O_4$-type structure, not spinel-like). We were interested in the compounds because those magnetic and electrical properties might reflect nature of the correlated $4d/3d$ electrons on the anisotropic basis. The compounds were recently synthesized for the

first time. The structure, magnetic and electrical properties were investigated by neutron diffraction, magnetic susceptibility, and electrical transport measurements of those high-quality polycrystalline samples. The data indicate $NaRh_2O_4$ is metallic down to 1.8 K and the magnetic susceptibility shows a broad cusp around $\sim$ 100 K. $NaMn_2O_4$ is highly electrically insulating with and without presence of a magnetic field. The manganese oxide goes into an anti-ferromagnetically ordered state at low temperatures through two-steps process at $\sim$ 40 K and $\sim$ 10 K. We will give a detailed report about the properties of the two new compounds.

**12:03**

**B23 5 Spinless Fermionic ladders in a magnetic field** SAM CARR, BORIS NAROZHNY, ALEXANDER NERSESYAN, *The Abdus Salam ICTP, Trieste, Italy* We study a system of interacting spinless fermions hopping on a two-leg ladder subject to an external magnetic field perpendicular to the ladder. At 1/2-filling, we find a series of quantum phase transitions as a function of the magnetic field: these are either $U(1)$ Gaussian phase transitions between two phases with distinct types of long-range order or Berezinskii-Kosterlitz-Thouless transitions between ordered and gapless phases. At 1/4-filling, we also find long-range order: a bond density wave or a staggered flux phase, each supporting excitations with fractional charge.

**12:15**

**B23 6 Magnetic Susceptibility and Heat Capacity of Single Crystal $CaV_2O_4$ Containing $S = 1$ $J_1$-$J_2$ Antiferromagnetic Spin Chains*** A. NIAZI, D. C. JOHNSTON, S. BUD'KO, D. L. SCHLAGEL, T. A. LOGRASSO, *Ames Lab., Iowa State U., Ames, IA 50011, USA* A. HONECKER, *TU Braunschweig, Inst. Theor. Phys., 38106 Braunschweig, Germany* The compound $CaV_2O_4$ has an orthorhombic *Pnam* structure and contains spin $S = 1$ zig-zag ($J_1$-$J_2$) chains running along the crystallographic *b*-axis. Structural considerations suggest that $J_1 \approx J_2$, which would result in competing frustrating antiferromagnetic (AF) interactions in this low-dimensional system. Previous studies on powders have suggested collinear spin models, a gapless chiral phase, or spin freezing below 20 K@. We have grown single crystals of $CaV_2O_4$ for the first time and carried out magnetization and heat capacity measurements down to 1.8 K@. We observe long-range AF ordering at $T_N = 54$ K with the easy axis being the *c*-axis, as reflected by anisotropic susceptibility $\chi$ below $T_N$. The magnetic specific heat $C_p^{mag}(T)$ up to 100 K, obtained after subtracting the lattice contribution of nonmagnetic isostructural $CaSc_2O_4$, shows a clear signature of long-range magnetic order at $T_N$. However, the molar entropy attains only $\approx$ 1/4 of its maximum value 2Rln(3) by 100 K, indicating strong short range order above $T_N$ and large values $J_1, J_2 > 100$ K@. This is consistent with our estimates $J_1 \approx J_2 \sim$ 150–300 K obtained by comparison of our $\chi(T)$ data with exact diagonalization calculations of $\chi(T)$.

*Supported by the USDOE under Contract No. W-7405-ENG-82.

**12:27**

**B23 7 Profiles of magnons and spinons in a spin ladder** DAVID CLARKE, OLEG TCHERNYSHYOV, *Department of Physics and Astronomy, Johns Hopkins University* JEAN-BAPTISTE FOUET, *Institut Romand de Recherche Numérique en Physique des Matériaux* FRÉDÉRIC MILA, *Institute of Theoretical Physics, École Polytechnique Fédérale de Lausanne* We have studied quantum phase transitions between magnetization plateaux and gapless incommensurate states in a frustrated spin ladder placed in a magnetic field[1]. The transitions are triggered by a condensation of magnons (spinons) at the edge of an integer (half-integer) magnetization plateau. In this talk we will describe magnetization patterns formed in a finite ladder just off a magnetization plateau, i.e. at low concentrations of magnons or spinons. In these regimes the magnons and spinons behave as noninteracting fermions carrying spins $S^z = \pm 1$ and $\pm$ 1/2, respectively. The spinons also act as domain walls, thus causing a dramatically different magnetization pattern from that of the magnons. The analytical results obtained agree well with numerical data.

F. Mila, Eur. Phys. J. B **6**, 201 (1998).

**12:39**

**B23 8 Ferromagnetic-antiferromagnetic alternating exchange spin-dynamics in the low-dimensional quantum magnet $DMACuCl_3$** MATTHEW STONE, *Oak Ridge National Laboratory* WEI TIAN, *University of Tennessee* MARK LUMSDEN, GARRETT GRANROTH, DAVID MANDRUS, *Oak Ridge National Laboratory* JAE-HO CHUNG, *National Institute for Science and Tecnology* STEPHEN NAGLER, *Oak Ridge National Laboratory* The spin magnet dimethylammonium trichlorocuprate, $DMACuCl_3$, has been considered both an alternating ferromagnetic-antiferromagnetic chain along the crystalline a-axis as well as a collection of isolated ferromagnetic and antiferromagnetic spin pairs. However, no spectroscopic probes have been applied until now to determine the underlying nature of the spin dynamics. We present results of single crystal inelastic neutron scattering measurements which clearly indicate that the magnetic excitations in $DMACuCl_3$propagate along the crystalline b-axis, not the proposed a-axis. A single magnetic excitation is observed with a gap of 0.98 meV and a bandwidth of approximately 0.67 meV. The quasi-one-dimensional excitation spectrum is dominated by a strongly coupled ferromagnetic spin-pair or dimer with weaker antiferromagnetic interdimer interactions. In light of this classification, we make comparisons to previously measured specific heat and magnetization measurements. We also place a limit on inter-dimer interactions perpendicular to the chain axis and propose a potential multi-chain model for $DMACuCl_3$.

**12:51**

**B23 9 Copper Phenazine Dichloride, a S=1/2 Heisenberg Antiferromagnetic Chain** R. T. SCHNEIDER, C. P. LANDEE, M. M. TURNBULL, *Clark University, Worcester, MA 01610* F. F. AWWADI, *Department of Chemistry, Washington State University, Pullman, WA 99164* Low-dimensional antiferromagnets provide good testing grounds for predictions of cooperative quantum behavior. S=1/2 copper ions bridged by organic ligands such as pyrazine form antiferromagnetic chains with exchange strengths weak enough to be overcome by available magnetic fields. [1] Phenazine (Phz) ($C_{12}H_8N_2$) is similar to pyrazine in its ability to form magnetic chains but has a different electronic structure resulting in different exchange strengths. We report on the synthesis, crystal structure, magnetic susceptibility, and high field magnetization of $Cu(Phz)Cl_2$. Its behavior can be described as that of a Heisenberg antiferromagnetic chain with an exchange constant $|J|/k_B = 33$ K. The exchange strengths of chains with pyrazine, quinoxaline, and phenazine will be compared. [1] M. B. Stone et al, Physical Review Letters **91**, 037205 (2003).

**13:03**

**B23 10 Real-Space Treatment of Spin-Peierls Transitions: Gap Equation of the S = 1/2 Heisenberg Antiferromagnetic Chain** ZOLTAN SOOS, SHARON BEWICK, *Princeton University* The spin-Peierls transition at $T_{SP}$ of s = 1/2 Heisenberg AF

chains with linear spin-phonon (sp-ph) coupling is modeled by exact solution up to 18 spins. Spin correlations alter the gap relation between $T_{SP}$ and the singlet-triplet gap, $E_{ST}$, from the free-fermion or mean-field (mf) result by 30%. Direct solution accounts for the spin-Peierls transition, magnetic susceptibility and magnetization of the prototypical $TTF^+$ (tetrathiafulvalene) spin chain in TTFCu(BDT). Strong sp-ph coupling is required for size convergence. Exact analysis of finite chains conserves total spin, while mf or bosonization approximations for spinless fermions in infinite chains only conserve the z component and have axial rather than spherical symmetry in spin space.

**13:15**

**B23 11 Phonon spectra in Spin-Peierls transitions** FRANZ MICHEL, *TU Graz, Austria* HANS GERD EVERTZ, *TU Graz, Austria* We present phonon and spin spectra from precise Quantum Monte Carlo simulations of Spin-Peierls systems, in one and two dimensions with acoustical and with optical phonons. We introduce a new technique which allows the direct integration of phonons for a given spin configuration. Together with cluster simulations for spins and a mapping from SSE to continuous time this allows efficient simulations of large systems at finite temperature and close to T=0.

**13:27**

**B23 12 Spin excitations in $S = 1/2$ AFM chains with alternating *g*-tensor and the Dzyaloshinskii-Moriya interaction.** S.A. ZVYAGIN, J. WOSNITZA, *Dresden High Magnetic Field Laboratory (HLD), Forschungszentrum Rossendorf, 01314 Dresden, Germany* A.K. KOLEZHUK, *Physics Dept., Harvard University, Cambridge, MA 02138* J. KRZYSTEK, *National High Magnetic Field Laboratory, Tallahassee, FL 32310* R. FEYERHERM, *Hahn-Meitner-Institute (HMI), 14109 Berlin, Germany* The magnetic excitation spectrum of copper pyrimidine dinitrate (Cu-PM), an $S = 1/2$ antiferromagnetic chain system with alternating *g*-tensor and the Dzyaloshinskii-Moriya interaction, is probed using ESR spectroscopy in magnetic fields up to 25 T. The field-induced gap is measured *directly*. Signatures of a soliton and three breather branches are identified, and their frequency-field dependences are described in frame of the quantum field sine-Gordon model. Furthermore, the ESR linewidth and shift behavior in Cu-PM in the *perturbativespinon* regime is studied as function of temperature and field. Excellent quantitative agreement between theoretical predictions (Phys. Rev. Lett. 82, 5136 (1999)) and experiment is obtained. The results are published in: S.A. Zvyagin *etal.*, Phys. Rev. Lett. 93, 027201 (2004); *ibid.* 95, 012707 (2005).

**13:39**

**B23 13 Dzyaloshinskii-Moriya interaction in $LiCu_2O_2$*** LASZLO MIHALY, *Stony Brook University* HELMUTH BERGER, *EPFL, Lasuanne* LASZLO FORRO, *EPFL, Lausanne* The far-infrared optical spectrum of the spin 1/2 helimagnet $LiCu_2O_2$ was investigated in magnetic fields up to 14Tesla. In the paramagnetic state a spin resonance line was observed corresponding to a *g*-factor of about 2. The resonance broadens and practically disappears around the phase transition temperature of T=25K, but it is recovered at lower temperatures at a new position. The 2.5K field dependence of the spin susceptibility and resonance frequency is characteristic of a magnetically ordered system, where the Dzyaloshinskii-Moriya interaction causes a finite gap of 1.5meV in the spin wave spectrum at q=0.

*Use of the National Synchrotron Light Source, Brookhaven National Laboratory, was supported by the U.S. Department of Energy, Office of Science, Office of Basic Energy Sciences, under Contract No. DE-AC02-98CH10886.

**13:51**

**B23 14 Meron and Haldane-Shastry spin chain states in quantum dots** MILICA MILOVANOVIC, ALEKSANDRA PETKOVIC, *Institute of Physics, Belgrade* We study solutions of the Coulomb interaction problem, in the lowest Landau level approximation, of a quantum dot with N = 4 and N = 6 electrons, without Zeeman term, and above the maximum density or filling factor one state. By making maps of spin correlations of the solutions we are able to connect excitations of the dot with states of the (one-dimensional) Haldane-Shastry spin chain. We also argue that the solutions of the problem without Zeeman term can be described as meron quasiparticle excitations analogous to vortex excitations in the completely polarized state. As a result we will describe how these meron excitations and states of the dot can be connected with spinon states of the Haldane-Shastry chain. This connection will enable us to associate orbital spin currents to quantum dot states.



## SESSION B26: FOCUS SESSION: SINGLE MOLECULE BIOPHYSICS: DNA & RNA
**Monday Morning, 13 March 2006; 323, Baltimore Convention Center at 11:15**
**Ching-Hwa Kiang, Rice University, presiding**

***Invited Papers***

**11:15**

**B26 1 Dynamics of molecular motors with finite processivity on heterogeneous tracks.**
DAVID NELSON, *Lyman Laboratory of Physics, Harvard University, Cambridge, Massachusetts 02138, USA*

The dynamics of molecular motors which occasionally detach from a heterogeneous track like DNA or RNA is considered.[1] Motivated by recent single-molecule experiments, we study a simple model for a motor moving along a disordered track using chemical energy while an external force opposes its motion. The motors also have finite processivity, i.e., they can leave the track with a position-dependent rate. We show that the response of the system to disorder in the hopping-off rate depends on the value of the external force. For most values of the external force, strong disorder

causes the motors which survive for long times on the track to be localized at preferred positions. However, near the stall force, localization occurs for any amount of disorder. To obtain these results, we study the complex eigenvalue spectrum of the time evolution operator. Existence of localized states near the top of the band implies a stretched exponential contribution to the decay of the survival probability. A similar spectral analysis also provides a very efficient method for studying the dynamics of motors with infinite processivity. 1. Y. Kafri D. K. Lubensky and D. R. Nelson, Phys. Rev. E 71, 041906 (2005).

*Contributed Papers*



**11:51**

**B26 2 DNA electrophoresis in Pluronic F127*** SEUNGYONG YOU, DAVID VAN WINKLE, *Center for Materials Research and Technology and Physics Department, Florida State University* Electrophoresis involves the separation of bio-molecules in a sieving medium by applying an electric field. DNA molecule fragments are separated in conventional gels and a several models have been successfully applied for understanding the separations. Recently, a pluronic gel was found to be an effective sieving medium for electrophoresis. However, the mobility of DNA in this gel cannot be described by the conventional theories. One reason is that Pluronic F127 is not a crosslinked gel, but a lattice of polymer micelles. The migration of single DNA molecules stained with various dye molecules was studied in slab gel electrophoresis by real-time fluorescence microscopy. Results for a variety of sizes will be presented.

*Research Corporation, Martech

**12:03**

**B26 3 Model for passage time of polymer trough a pore (weak external forces limit)** STANISLAV KOTSEV, ANATOLY KOLOMEISKY, *Rice University* Polymer translocation through a pore is an important problem in biophysics. Recent experiments measure the dynamics of the process with a single-molecule precision. In these experiments a single-stranded RNA or DNA molecule is driven trough a narrow pore by an external electric field. In our work we concentrate on theoretical modeling of polymer translocation when external forces are weak. In this regime the entropic forces are dominating. Then for long polymers the passage time scales with the number of monomers as $N^{\alpha}$. However, the exact value of $\alpha$ is still a matter of discussion. We are proposing a simple phenomenological model which can be solved exactly. Our results are in a good agreement with off-lattice $3D$ Monte Carlo simulations.

**12:15**

**B26 4 Driven DNA translocation through thin and long nanopores*** ANIKET BHATTACHARYA, WILLIAM H. MORRISON, *University of Central Florida* We utilize Brownian dynamics simulation to study polymer translocation through a nanopore driven by an electric field using a coarse-grained bead-spring model for the translocating DNA. We study mean translocation time $\langle \tau \rangle$ as a function of the chain length N, the width $w$ of the pore, and external bias F. Unlike many previous studies, we critically examine the scaling of $\langle \tau \rangle$ as a function of the ratio $N/w$ and F. For a thin pore, our preliminary results indicate that the mean translocation time $\langle \tau \rangle \sim N^{2\nu}$, where $\nu$ is the Flory exponent, although the slope shows a weak but non-negligible dependence on the external bias F for the chain lengths considered so far. Our simulation results are consistent with experiments done in solid-state nanopore*,+. *Work done in collaboration with Heath Morrison, Prof. Kurt Binder and Prof. Andrey Milchev. + A. J. Storm, C. Storm, J. Chen, H. Zandbergen, J-F Joanny, C. Dekker, Nano Letters, **5**, 1193 (2005).

*Partially supported by NSF

**12:27**

**B26 5 Conformational Analysis of Single DNA Molecules Undergoing Entropically Induced Motion in Nanochannels.** JOHN MANNION, CHRISTIAN RECCIUS, JOSHUA CROSS, HAROLD CRAIGHEAD, *Cornell University* We have used the interface between a nanochannel and a microchannel as a tool for applying controlled forces on a DNA molecule. A molecule with a radius of gyration larger than a nanochannel width, that straddles such an interface, is subject to an essentially constant entropic force which can be balanced against other forces such as the electrophoretic force from an applied electric field. By controlling the applied field, we can position the molecule as desired and observe the conformation of the molecule as it stretches, relaxes and recoils from the nanochannel. We quantify and present models for the molecular motion in response to the entropic, electrophoretic and frictional forces acting on it. By determining the magnitude of the drag coefficients for DNA molecules in the nanostructure, we are able to estimate the confinement induced recoil force. Finally, we demonstrate that we can use a controlled applied field and the electrophoretic interfacial forces to unfold molecules, which can then be manipulated and positioned in their simple extended morphology.

**12:39**

**B26 6 The Physics of Nanoconfined DNA** WALTER REISNER, *Department of Physics, Princeton University* KEITH MORTON, *Electrical Engineering, Princeton University* ROBERT RIEHN, YANG MEI WANG, *Department of Physics, Princeton University* STEPHEN CHOU, *Electrical Engineering, Princeton University* JONAS TEGENFELDT, *Department of Physics, Lund University* ROBERT AUSTIN, *Department of Physics, Princeton University* Top-down approaches to nanotechnology have the potential to revolutionize biology by making possible the construction of chip-based devices that can not only detect and separate single DNA molecules by size but also–it is hoped in the future–actually sequence at the single molecule level. While a number of top-down approaches have been proposed, all these approaches have in common the confinement of DNA to nanometer scales, typically 5-200nm. Nanoconfinement effects the equilibrium conformation of the DNA. Here we present measurements of the static and dynamic properties of single DNA molecules confined in nanochannels using fluorescence microscopy techniques. In particular, we investigate the dynamics of DNA in novel structures, including structures with defects (bulges and constrictions) and channels that funnel in depth and width. We also discuss observations of possible topological structures on the confined DNA (knots or loops observed on the extended molecules).

**12:51**

**B26 7 DNA entropic elasticity for short molecules** JINYU LI, *University of Colorado* PHILIP C. NELSON, *University of Pennsylvania* M. D. BETTERTON, *University of Colorado* Single-molecule experiments in which force is applied to DNA or RNA molecules have enabled important discoveries of nucleic acid properties and nucleic acid-enzyme interactions. These experiments rely on a model of the polymer force-extension behavior to calibrate the experiments; typically the experiments use the worm-like chain (WLC) theory for double-stranded DNA and RNA. This theory agrees well with experiments for long molecules. Recent single-molecule experiments have used shorter molecules, with contour lengths in the range of 1-10 persistence lengths. Most WLC theory calculations to date have assumed infinite molecule lengths, and do not agree well with experiments on shorter chains. Key physical effects that become important when shorter molecules are used include (i) boundary conditions which constrain the allowed fluctuations at the ends of the molecule and (ii) rotational fluctuations of the bead to which the polymer is attached, which change the apparent extension of the molecule. We describe the finite worm-like chain (FWLC) theory, which takes into account these effects. We show the FWLC predictions diverge from the classic WLC solution for molecules with contour lengths a few times the persistence length. Thus the FWLC will allow more accurate experimental calibration for relatively short molecules, facilitating future discoveries in single-molecule force microscopy.

**13:03**

**B26 8 Single Molecule Visualization of DNA in Wicking Flows** CHAD DELONG, DAVID HOAGLAND, *University of Massachusetts - Amherst* An understanding of polymers in flow through micro- and nano-structured materials is critical to the success of bioseparations (proteins, DNA, etc.). An open, nanofluidic system has been developed to drive flow through a packed bed of colloidal particles using capillary forces (wicking), allowing the study of polymer dynamics in the absence of the electric field is typically used to drive micro- and nano-fluidic flows. This is especially important when dealing with charged molecules whose confirmation can be affected by the electric field or those insoluble in water. Single molecule imaging is performed in this system on fluorescently labeled DNA using an optical microscope equipped with a fluorescent light source, image intensifier, and CCD camera. Chain elongation in the flow depends sharply on flow rate, with fully relaxed configurations observed below a critical flow rate. At high flow rates, flow induced degradation can be seen. Molecular entanglements with the separation matrix cause molecular weight separation because longer molecules elongate in the flow and become entangled, leading to a longer retention time.

**13:15**

**B26 9 Abundance of pseudoknots in the RNA world*** DANIEL AALBERTS, EVAN MILLER, *Williams College* The pseudoknot fold is often seen in auto-catalytic RNA and in viruses. A recent polymer physics model and statistical-mechanical theory predicts relative probabilities of different pseudoknot folds consonant with a database of known folds. Now we extend that theory for a preliminary estimate of the abundance of pseudoknot folds in RNA sequences, finding approximately 1 per 40,000 nucleotides. This theoretical probability density compares favorably to what we infer from structure databases and has implications for genome organization, RNA folding algorithms, and the RNA World.

*supported by NIH grant GM068485

**13:27**

**B26 10 DNA sequencing via transverse electronic transport** JOHAN LAGERQVIST, *University of California - San Diego* MICHAEL ZWOLAK, *California Institute of Technology* MASSIMILIANO DI VENTRA, *University of California - San Diego* Recently, it was theoretically shown that transverse current measurements could be used to distinguish the different bases of single stranded DNA. [1] If electrodes are embedded in a device, e.g., a nanopore, which allows translocation of ss-DNA, the strand can be sequenced by continuous measurement of the current in the direction perpendicular to the DNA backbone. [1] However, variations of the electronic signatures of each base in a real device due to structural fluctuations, counter-ions, water and other sources of noise will be important obstacles to overcome in order to make this theoretical proposal a reality. In order to explore these effects we have coupled molecular dynamics simulations with transport calculations to obtain the real time transverse current of ss-DNA translocating into a nanopore. We find that distributions of currents for each base are indeed different even in the presence of all the sources of noise discussed above. These results support even more the original proposal [1] that fast DNA sequencing could be done using transverse current measurements. Work supported by the National Humane Genome Research Institute. [1] M. Zwolak and M. Di Ventra, ''Electronic Signature of DNA Nucleotides via Transverse Transport,'' Nano Lett. 5, 421 (2005).

**13:39**

**B26 11 Polymer effects in forced passage of DNA and macromolecules through nanopores** FRANCISCO SOLIS, *Integrated Natural Sciences* The forced passage of DNA, RNA and other linear molecules through nanopores has been proposed as a method to investigate the properties of these molecules and, in particular, as a sequencing method. This talk will discuss the polymer effects that arise when a macromolecule is pulled with constant velocity and with adjustable force through a pore. For homogeneous, strongly stretched molecules, the passage rate is proportional but slower than the pulling velocity. In addition, if the molecule contains a set of inhomogeneities that act as well defined obstacles, each of these will exhibit a waiting time for passage, and a relaxation period to return to the steady passage rate. These waiting and relaxation times increase with the length of the segment of already processed molecule.

**13:51**

**B26 12 Mapping the phase diagram of DNA force-induced melting in the presence of DNA intercalators** IOANA VLADESCU, MICAH McCAULEY, *Department of Physics, Northeastern University* MEGAN NUNEZ, *Department of Chemistry, Mount Holyoke College* IOULIA ROUZINA, *Department of Biochemistry Molecular Biology and Biophysics, University of Minnesota* MARK WILLIAMS, *Department of Physics, Northeastern University* The interactions between single DNA molecules and different non-covalent binding agents - the classical intercalator ethidium and compounds from the family of ruthenium complexes - are investigated using an optical tweezers instrument and their effects on the structure and mechanical stability of DNA molecules are quantitatively analyzed using a model of force-induced melting. When a single DNA molecule is stretched beyond its normal contour length, a melting phase transition is observed. Drug binding increases the dsDNA contour length, decreases the DNA elongation upon melting, and increases the DNA melting force. At concentrations of intercalator above critical, no force induced melting of dsDNA is possible. The DNA stretching

curves map out a phase diagram for DNA melting in the presence of intercalator, and define its critical point in the force-extension-drug concentration space. Our results allow for the complete thermodynamic characterization of the interaction of these intercalators with DNA.

**14:03**

**B26 13 DNA and RNA unzipping using nanopore force spectroscopy** AMIT MELLER, JEROME MATHE, MENI WANUNU, *Harvard University* BARAK AKABAYOV, IRIT SAGI, *Weizmann Institute for Science* DNA and RNA molecules can be electrophoreticaly threaded through nanoscale pores, such as the $\sim$ 1.5 nm alpha-Hemolysin. Information about their translocation dynamics is obtained by probing the ionic current flowing through the pore during their passage. We experimentally study the translocation process of unstructured and structured DNA molecules through a single nanopore. We find that the translocation process depends on DNA properties, such as its sequence and its direction of entry. With intense electrical field structured DNA and RNA can be unzipped in a controlled way, and the unzipping kinetics can be directly quantified. We study the unzipping kinetics of DNA and RNA molecules under a wide range of voltage gradients. We find that the unzipping kinetics is characterized by two limiting regimes: the strong field limit in which the system is unzipped in an irreversible process, and the weak field regime, in which it is in quasi equilibrium. Interestingly the unzipping kinetics of RNA molecules is very different from their DNA analogues. A theoretical model that accounts for our experimental results will be discussed.

**SESSION B28: EXPERIMENTAL TECHNIQUES IN BIOMATERIALS SCIENCE**
**Monday Morning, 13 March 2006**
**325, Baltimore Convention Center at 11:15**
**Kevin Hewitt, Dalhousie University, presiding**

**11:15**

**B28 1 Dual-beam Oscillating Optical Tweezers-Based 3-D Confocal Microrheometer** JING WANG, CHUAN PU, H. DANIEL OU-YANG, Optical tweezers are widely used in the studies of complex fluids and biological cells and tissues. Confocal microscopy visualizes detailed structures of sample specimen with high resolution in 3-D. In this report, we present the setup, calibration and application of a new powerful microrheometer that integrates a novel high temporal and spatial resolution dual-beam oscillating optical tweezers cytorheometer (DOOTC) with spinning disk confocal microscopy. The DOOTC uses the less photodamaging 1064nm laser, and detects the forced oscillatory particle motions by a lock-in amplifier. It can operate at single oscillating beam mode or the orthogonally polarized dual-beam mode to get large deflected forward scattering signals at both high and low frequencies. The system is demonstrated to identify granular structures trapped by optical tweezers with confidence, and at the same time measure dynamic mechanical modulus in the frequency range of 0.1-3000Hz at up to 10 data point per second and with sub-nanometer spatial resolution, while monitoring the sample structure and its transformation itin situ.

**11:27**

**B28 2 Integrated Fiber-optic Dipping-probe Microfluorometer** ROBERT W. GAMMON, *IPST, Univ. of Maryland* VILDANA HODZIC, CHRISTOPHER C. DAVIS, *Department of Electrical and Computer Engineering, Univ. of Maryland* An integrated fiber-optic device has been built that is with multimode fiber and found to exhibit exceptional performance as a dipping probe microfluorometer. This was discovered in the course of testing its performance using the device with simple, cleaved fibers. Thus the fiber both excites and collects fluorescence from the fluid along the axis direction in solutions of dye. The novel feature is that the light is restricted to coming from a region very near the end of the cleaved fiber. It then lends itself to testing very small volumes of sample fluid for fluorescence. Since the probe is a 200 micron diameter multimode fiber is can easily fit into small capillaries and also be stuck into small drops of sample fluid, i.e. drops sitting in microwell in multi-well test plates. Because the device uses an avalanche photodiode, the sensetivity is high and has a large dynamic range (4 to 6 orders of magnitude). The combination of small diameter, flexible fibers with high effeciency of exciting and collecting of fluorescence, and a sensitive detector makes this device unique. There is nothing on the commercial market or literature like it. Most devices that are called fiber-optic fluormeters use stiff fibers of diameter about 1 mm or larger (rods, really). They ususally excite through one of more fibers and collect through nearby fibers. The collection efficiency is low and the net diameters are far too large to allow use with microliter samples.

**11:39**

**B28 3 Characterization of RNase Immobilization at Surfaces by NEXAFS** XIAOSONG LIU, *Department of Physics, UW-Madison (DOP)* CHANG-HYUN JANG, *Department of Chemical and Biological Engineering, UW-Madison (DOCBE)* FAN ZHENG, *DOP* ASTRID JURGENSEN, *CSRF* NICHOLAS L. ABBOTT, *DOCBE* F.J. HIMPSEL, *DOP* Immobilization of proteins at surfaces plays an increasingly-important role for applications in biosensors and biochips, bioelectronics, bio-compatible implants, and biomimetic devices. In this study, Ribonuclease A (RNase A) is immobilized on silver surfaces in oriented and random form via self-assembled monolayers (SAMs) of alkanethiols as described previously.[1] The immobilization process is characterized step by step using chemically-selective near edge x-ray absorption fine structure spectroscopy (NEXAFS) at the C, N, and S K-edges. Oriented protein layers exhibit a small, but distinct polarization dependence of the N1s to $\pi^*$ orbital that is delocalized over O=C-NH, which is not seen for random orientation. They also have higher coverage. Oxidation and partial desorption of the alkanethiol SAMs are found to be predominant causes of imperfect immobilization. The results show how NEXAFS is able to provide feedback for optimizing the immobilization of proteins. [1] Luk, Y.-Y.; Tingey, M. L.; Dickson, K. A.; Raines, R. T.; Abbott, N. L. itJournal of the American Chemical Society **2004,** 126, (29), 9024.

**11:51**

**B28 4 Surface-enhanced Raman scattering of a hydrophilic ligand (tiopronin) adsorbed on gold nanoparticles.*** JOEL ST.AUBIN, *Dalhousie University* KEVIN HEWITT, *Dalhousie University* Surface enhancement of the Raman signal derived from tiopronin coated gold nanoparticles was observed. The gold nanoparticles were synthesized to mean diameters of 40 nm and 130 nm. Enhancement greater than 360 times was measured for the 40 nm gold nanoparticles and greater than 500 times for the 130 nm particles. New phonon modes appear that are possibly due to elec-

tric field gradient effects. Experiments to partially substitute tiopronin with a small fraction of hydrophobic thiols are underway. Surface-enhanced Raman scattering studies of these mixed (hydrophobic/hydrophilic) ligands will be reported.

*Natural Sciences and Engineering Research Council of Canada

**12:03**

**B28 5 Employing Grating Couplers in Biosensors** AMAL KASRY, WOLFGANG KNOLL, *Max Planck Institute for Polymer Research* Grating couplers have become very important tool in developing optical biosensors. In this work, surface plasmon polaritons excited by a dye molecule on the surface of a grating were studied. These polaritons can couple out to bulk radiation by scattering from the grating, and the emitted light comes off in certain well-defined directions. We focused here in studying how the coupling between the emitted light of a chromophore at the surface of a metallic grating and the scattered surface plasmons depends on the chromophore-metal separation. This was done using a protein layer-by-layer system as a spacer between the metal and the dye. The results show that the back coupling efficiency is maximum at distance about 30-50 nm, which is also the optimum distance for the fluorescence intensity. These results agree with the results determined on a planar metallic surface, and the behavior of the fluorescence was proved to be the same in different media (air or liquid). It was also proved that the back coupling could still be seen at the high distance reached here (106 nm), where the surface plasmon can scatter till this high distance.

**12:15**

**B28 6 15nm diameter upconversion nanophosphors as biolabels.** SHUANG FANG LIM, ROBERT RIEHN, CHIH-KUAN TUNG, ROBERT H. AUSTIN, *Department of Physics, Princeton University* NORA KHANARIAN, *University of Pennsylvania* WILLIAM S. RYU, DAVID TANK, *Lewis-Sigler Institute for Integrative Genomics, Princeton University* We have synthesized 15 nm diameter yttrium oxide based nanophosphors that are capable of visible to infrared upconversion. We show that these phosphors can be used for dual-mode imaging of biological systems by observing visible emission under both infrared excitation, and electron excitation in a scanning electron microscope. We have investigated the optical properties, confirmed the 2-photon nature of the upconversion process, and verified that similar narrow band emission spectra are obtained under electron and infrared excitation. We will also report on progress in surface functionalization for targeted bio-labeling. We demonstrate that biocompatibility is sufficient for in-vivo imaging in the nematode worm C. Elegans, and locate phosphors with high spatial resolution using energy dispersive X-ray imaging in scanning electron microscope.

**12:27**

**B28 7 Thermal Stability, and Curvature Dependence of Bovine Serum Albumin on Gold Nanoparticles Using Localized Surface Plasmon Resonance** JONATHAN TEICHROEB, *University of Waterloo* JAMES FORREST, *University of Waterloo* VALENTINA NGAI, Gold nanoparticles exhibit Surface Plasmon Resonance (SPR), whose absorption peak is strongly dependent on the index of refraction, and coating thickness of the near surface region. A macromolecule bound to the nanoparticle will typically undergo a shift in index of refraction as its conformation changes, leading to a shift in the peak wavelength. Nanospheres can be made with a large variety of diameters, and present a novel method of looking at curvature dependencies of stability. In this study, Bovine Serum Albumin (BSA) was conjugated to Au nanospheres. Using a visible absorption spectrometer, the peak wavelength vs. temperature for eight diameters from 5nm to 60nm, was collected. Diameters above 20nm exhibited a continual increase in peak wavelength with temperature. Theoretical calculations indicate that this is a thickening of the protein layer. Below 20nm, peak wavelength shifts indicated a thinning of the BSA layer, and possible a decrease in index of refraction, followed by thickening at higher temperatures. Additionally, the study indicates that the peak shifts are highly time dependent, and a kinetic study has been performed at several temperatures.



**12:39**

**B28 8 High Q RF Resonant Cavity for Detecting Biological Tissue Nonlinearities** VILDANA HODZIC, *Department of Electrical and Computer Engineering, Univ. of Maryland* ROBERT W. GAMMON, *IPST, Univ. of Maryland* QUIRINO BALZANO, CHRISTOPHER C. DAVIS, *Department of Electrical and Computer Engineering, Univ. of Maryland* To investigate whether biological cells exhibit nonlinearity in the radiofrequency (RF) region, a high quality factor resonant cavity has been built. The cavity is fitted with two loop antennas, one transmitting at 880-890 MHz and a second one receiving at 1760-1790 MHz. The antenna operating at the low frequency (LF) band actively excites the $TE_{111}$ cavity mode; the high frequency antenna must receive the energy of the $TE_{113}$ mode at twice the frequency of the LF antenna. The cavity and the two antennas have been built. The Q of the cavity is over 6000 for both the frequencies of operation. Experiments to detect nonlinear RF frequency conversion by biological tissue can be performed using this high quality factor device.

**12:51**

**B28 9 Micromachined piconewton force sensor for biophysics investigations*** STEVEN KOCH, GAYLE THAYER, ALEX CORWIN, GEORGE BACHAND, MAARTEN DE BOER, *Sandia National Laboratories* We describe a polysilicon surface-micromachined force sensor that is able to measure forces as small a few pN in both air and water. The simple device consists of compliant springs with force constants as low as 0.3 mN/m and Moire patterns for nanometer-scale optical displacement measurement. First, we measured the force field produced by an electromagnet on individual 2.8 micron magnetic beads glued to the force sensor. Forces matched predictions from finite element magnetic modeling and provided a calibration for future biophysical applications of the magnet. By repeating with several different beads, we measured a 9 percent standard deviation in saturation magnetization. We also demonstrated that the force sensor was fully functional when immersed in aqueous buffer and when performing the kinesin inverted motility assay on the sensor surfaces. These results show the force sensors can be useful for calibrating magnetic forces on magnetic beads and also for direct measurement of biophysical forces on-chip.

*Sandia is a multiprogram laboratory operated by Sandia Corporation, a Lockheed Martin Company, for the United States Department of Energy's National Nuclear Security Administration under Contract DE-AC04-94AL85000

**SESSION B29: FOCUS SESSION: MICRO-ORGANISM MOTILITY**
**Monday Morning, 13 March 2006**
**326, Baltimore Convention Center at 11:15**
**Udo Erdman, Humboldt University, presiding**

*Contributed Papers*



**11:15**
**B29 1 Direct measurement of the propulsion efficiency of bacterium Escherichia Coli** SUDDHASHIL CHATTOPADHYAY, RADU MOLDOVAN, *Department of Physics and Astronomy, University of Pittsburgh, Pittsburgh, PA 15260* CHUCK YEUNG, *School of Science, Pennsylvania State University at Erie, The Behrend College, Erie, PA 16563* XIAO-LUN WU, *Department of Physics and Astronomy, University of Pittsburgh, Pittsburgh, PA 15260* Swimming of flagellated bacterium in an aqueous medium is studied in vivo with the aid of optical tweezers and an imposed external flow. By trapping the bacterium perpendicular to the optical axis, the beating frequency of the flagellum $\omega$and the counter rotation of the cell body $\Omega$ can be measured simultaneously. Measurements of the trapping force $F$ and the two rotation speeds, $\omega$ and $\Omega$, enable us to determine all the elements of the propulsion matrix for individual cells as well as their statistics in a population. Further we obtain the propulsion efficiency, defined as the ratio of the input rotational power provided by the motors to the output propulsive power, to be $\sim 0.2\%$. Significant heterogeneities are observed among the bacteria despite their starting from a single colony.

**11:27**
**B29 2 Modeling the motion of microscale synthetic swimmers** ALEXANDER ALEXEEV, VICTOR YASHIN, ROLF VERBERG, ANNA BALAZS, *Chemical Engineering Department, University of Pittsburgh, Pittsburgh, PA* By direct numerical simulations, we study the motility of synthetic micro-swimmers in a quiescent fluid. The micro-swimmers examined here are composed of an elastic polymeric material and comprise one or more wiggling tails, which propel the swimmer through its low-Reynolds number environment. The tails are driven to move by a reactive gel, which constitutes part of the swimmer's body. The gel undergoes a periodic swelling and deswelling due to a reaction or an external stimulus. To model the interaction of this micro-swimmer with the surrounding fluid, we adopt our recently developed LBM/LSM approach, which integrates the lattice Boltzmann model (LBM) for fluid dynamics with the lattice spring model (LSM) for the micromechanics of an elastic solid. Using this model, we investigate different aspects of the swimmer's propulsion. In particular, we determine how the properties of the swimmer and the oscillatory gel affect the swimmer's velocity and efficiency. Our goal is to design autonomous micro-swimmers that can be guided along a particular direction in order to perform a specified task.

**11:39**
**B29 3 Detecting the gravitational sensitivity of itParamecium caudatum using magnetic forces*** KARINE GUEVORKIAN, JAMES M VALLES JR., *Brown University* Under normal conditions, itParamecium cells regulate their swimming speed in response to the pN level mechanical force of gravity. This regulation, known as gravikinesis, is more pronounced when the external force is increased by methods such as centrifugation. Here we present a novel technique that simulates gravity fields using the interactions between strong inhomogeneous magnetic fields and cells. We are able to achieve variable gravities spanning from 10 $\times$ $g$ to -8$\times$ $g$; where $g$ is earth's gravity. Our experiments show that the swimming speed regulation of itParamecium caudatum to magnetically simulated gravity is a true physiological response. In addition, they reveal a maximum propulsion force for paramecia. This advance establishes a general technique for applying continuously variable forces to cells or cell populations suitable for exploring their force transduction mechanisms.

*Supported by NASA OBPR under NAG3-2882. Experiments performed at National High Magnetic Field Laboratory.

**11:51**
**B29 4 Precise adaptation in chemotaxis through ''assistance neighborhoods''*** ROBERT ENDRES, NED WINGREEN, *Princeton University* The chemotaxis network in Escherichia coli is remarkable for its sensitivity to small relative changes in the concentrations of multiple chemical signals over a broad range of ambient concentrations. Key to this sensitivity is an adaptation system that relies on methylation and demethylation/deamidation of specific modification sites of the chemoreceptors by the enzymes CheR and CheB, respectively. These enzymes can access 5-7 receptors once tethered to a particular receptor. Based on these ''assistance neighborhoods,'' we present a model for precise adaptation of mixed clusters of two-state chemoreceptors. In agreement with experiment the response of adapted cells to addition/removal of attractant scales with the free-energy change at fixed ligand affinity. Our model further predicts two possible limits of precise adaptation: either the response to further addition of attractant stops through saturation of the receptors, or receptors fully methylate before they saturate and therefore stop adapting.

*We thank for financial support from HFSP.

**12:03**
**B29 5 Cellular individuality in the gradient sensing response of itDictyostelium** AZADEH SAMADANI, JEROME METTETAL, ALEXANDER VAN OUDENAARDEN, *MIT* It is generally assumed that single cells in an isogenic population exhibit the same behavior. However, it is becoming increasingly clear that even in a genetically identical population, gene expression levels can vary significantly from cell-to-cell. As a result of this variation, a physiological response such as gradient sensing might also display a significant variability from cell-to-cell. Although it is known that most cell populations are heterogeneous, the response of a typical cell or the average response of a population is often reported. However, quantitative information of cellular variability may contain important information on the intracellular signaling events. Here we explore the chemotactic response in single itDictyostelium cells in response to repeated spatio-temporal pulses of chemoattractant. We find that the response of a single cell is reproducible from pulse-to-pulse. In contrast, a large variability in the chemotactic response is observed from cell-to-cell even when different cells in the population are exposed to the same pulse. We propose a simple model, which allows for the broken symmetry of the chemotactic response and reproduces the cellular variability within the population fairly well.

**12:15**
**B29 6 How does Dicty find its way?** ERIN RERICHA, *University of Maryland College Park* CAROLE PARENT, *National Institute of Health* WOLFGANG LOSERT, *University of Maryland at College Park* As a cell chemotaxes, moves towards a chemical signal, it transduces external chemical signals into mechanical motion. Efficient chemotaxis is crucial for many biological processes from wound healing to the spread of cancer. We present our experimental investigations on itDictyostelium discodeum a model organism for chemotaxis. We expose cells to three types of external signals: a shallow background gradient of the signaling molecule cyclic-AMP a localized signal composed of cyclic-AMP attached to beads and a mechanical stimulus caused by pushing beads against the exterior of the cell. For each stimulus we ask: what is the stability of the gradient sensing pathway and how does it influence the mechanical response. We find that the cell speed increases with increasing concentration of cyclic-AMP. In addition, Dictyostelium cells relay the signal by releasing internally manufactured cyclic-AMP out of the back of the cell. A collection of cells moves in streams, where cells follow closely behind one another. We find that the cells moving in a stream move slower towards a source of attractant than cells that are chemically treated such that they do not stream.



***Invited Papers***

**12:27**
**B29 7 Dictyostelium discoideum chemotaxis: threshold for directed motion.**
EBERHARD BODENSCHATZ, *Cornell University (LFPN) and Max Planck Institute for Dynamics and Self-Organization (Goettingen)*

The chemotactic response of Dictyostelium discoideum cells to stationary, linear gradients of cyclic adenosine 3′, 5′-monophosphate (cAMP) was studied using microfluidic devices. In shallow gradients of less than $10^{-3}$ nM/$\mu$m, the cells showed no directional response and exhibited a constant basal motility. In steeper gradients, cells moved up the gradient on average. The chemotactic speed and the motility increased with increasing steepness up to a plateau at around $10^{-1}$ nM/$\mu$m. In very steep gradients, above 10 nM/$\mu$m, the cells lost directionality and the motility returned to the sub-threshold level. In the regime of optimal response the difference in receptor occupancy at the front and back of the cell is estimated to be only about 100 molecules. The work is supported by the Biocomplexity Program of the NSF and the Max Planck Society.

***Contributed Papers***

**13:03**
**B29 8 Impact of Helicobacter Pylori on Mucus Rheology*** JONATHAN CELLI, *Boston University* SARAH KEATES, *Beth Israel Deaconess Medical Center* CIARAN KELLY, *Beth Israel Deaconess Medical Center* BRADLEY TURNER, *Beth Israel Deconess Medical Center* RAMA BANSIL, *Boston University Department of Physics* SHYAMSUNDER ERRAMILLI, *Boston University Department of Physics* It is well known that the viscoelastic properties of gastric mucin are crucial to the protection of the lining of the stomach against its own acidic secretions and other agents. Helicobacter Pylori, a rod shaped, gram-negative bacteria that dwells in the mucus layer of approximately 50% of the world's population is a class I carcinogen and is associated with gastric ulcers and severe gastritis. The structural damage to the mucus layer caused by H. Pylori is an important aspect of infection with this bacteria. We are examining the impact of H. Pylori on mucin and mucus rheology quantitatively using a combination of dynamic light scattering and multiple particle tracking experiments. Video microscopy data will also be presented on the motility of this bacteria in mucin at different pH and in other viscoelastic gels.

*We gratefully acknowledge support from the NSF, the NSF GK12 program, and the DOD.

**13:15**
**B29 9 The effect of viscosity on the contraction of the stalk of itVorticella Convallaria*** DEEPENDRA KANTHA, DAVID VAN WINKLE, *Center for Materials Research and Technology and Department of Physics, Florida State University* The contraction of the stalk of itVorticella Convallaria behaves as one of the most powerful single cell biological engines.Contractions in three different viscous mediums were recorded by a PhantomV5 camera (Vision Research) on a bright field microscope with 20X objective. The contractions were recorded as cines (image sequences) with the image resolution of 256 pixels X 128 pixels at 7000 pictures per second. The maximum variation in maximum velocity of one organism was 5.2 cm/s and the minimum variation for a different organism was 0.4 cm/s for the same viscous medium. It occurred at 2-3ms after the start of contraction. The force of contraction and the force constant were calculated as a function of the time to see the effect of viscosity on the contraction of the stalk. This experiment needs further investigation to see the net effect of viscosity on the contraction of the stalk.

*Research Corporation

**13:27**
**B29 10 Optimal Foraging Strategy: Angle Matters*** UDO ERDMANN, SEBASTIAN GÖLLER, IGOR M. SOKOLOV, LUTZ SCHIMANSKY-GEIER, *Insitut für Physik, Humboldt-Universität zu Berlin* We report a theory to describe the motion of zooplankton. In contrast to move just randomly like a classical Brownian particle, zooplankters like Daphnia or Copepods pick their turning angle from a distribution which is far from being Gaussian or equally distributed. This leads to different behavior in the motion compared to normal diffusion. The question which can be asked here is: Is there an evolutionary reason to forage for food in the aforementioned manner? The talk is planned to give an answer into that direction.

*supprted by the Collaborative Research Center ''Complex Nonlinear Processes of the German Science Foundation (DFG-Sfb555)

**13:39**

**B29 11 Nonlinear electromagnetic responses of active molecular motors in live cells and organelles** DHARMAKIRTHI NAWARATHNA, JEFFREY GARDNER, GUSTAVO CARDENAS, DAVID WARMFLASH, JOHN MILLER, WILLIAM WIDGER, *University of Houston* JAMES CLAYCOMB, *Houston Baptist University* The response of biological cells to an oscillatory electric field contains both linear and nonlinear (eg. induced harmonic) components. At low frequencies (about 10Hz), harmonic generation by budding yeast cells is observed. These induced harmonics are sensitive to sodium metavanadate, an inhibitor, and glucose, a substrate, respectively, of P-type ATPase membrane pumps. At higher frequencies, two peaks, around 3kHz and 12kHz, are observed in the frequency-dependent harmonic responses. These are sensitive to potassium cyanide, a respiratory inhibitor that blocks cytochrome c oxidase, an enzyme of the mitochondrial respiratory chain. We have also measured the response of uncoupled mitochondria extracted from bovine heart cells, for which a second harmonic sensitive to pericidin A and carboxin is detected at applied frequencies of 3-4kHz. Finally, in coupled mouse mitochondria, an ADP sensitive peak (12-15kHz) is observed, likely due to the F0 domain of ATP synthase, which acts as a molecular turbine.

**13:51**

**B29 12 Mechanism of formin-associated actin filament elongation** DIMITRIOS VAVYLONIS, *Columbia University, Yale University* DAVID R. KOVAR, *University of Chicago* BEN O'SHAUGHNESSY, *Columbia University* THOMAS D. POLLARD, *Yale University* Formins control the kinetics of actin filament polymerization by remaining processively attached at the growing filament end. The FH2 formin domain associates with the barbed end while FH1 interacts with profilin and is thought to mediate profilin-actin polymerization. We combined TIR microscopy (Kovar et al., Cell, in press) with theoretical modeling to study the dependence of the rate of formin-associated actin filament elongation on profilin and actin concentrations. We assume a transfer mechanism of profilin-actin from FH1 to the barbed end, gated by FH2 as described by the gating parameter p measuring the accessibility of the barbed end. The model explains the main experimental trends and rationalizes (i) how filaments associated with formin mDia1 elongate more rapidly than formin-free filaments due to the the large number of profilin binding sites and p 1, and (ii) how filaments associated with formins with $p<1$ elongate slowly in the absence of profilin but more rapidly in the presence of profilin. High profilin concentrations suppress elongation and in the model this is attributed largely to the saturation of FH1 by profilin. Consistent with our ADP-actin experiments, the proposed mechanism does not require ATP hydrolysis though we cannot exclude the possibility that formin translocation accelerates ATP hydrolysis for ATP-actin.

**14:03**

**B29 13 Spreading of neutrophils: from activation to migration** HELIM ARANDA-ESPINOZA, *Department of Chemical and Biomolecular Engineering, University of Maryland* KHEYA SENGUPTA, *Forschungzentrum Julich, Germany* LEE SMITH, *Department of Chemical and Biomolecular Engineering* PAUL JANMEY, *Institute for Medicine and Engineering* DANIEL HAMMER, *Department of Bioengineering, University of Pennsylvania* Reflection Interference Contrast Microscopy was used to study the dynamics of neutrophil spreading. The images were analyzed to identify simultaneously the changes in the overall cell adhesion and the zones of close contact with the substrate. We show that for neutrophils, cell spreading is anisotropic and directional from the very initial stage. The curve describing the spreading area of the cell as a function of time can be fitted piecewise as power laws. Different spreading regimes are identified and related to the adhesion state and/or dynamical state of the cell. All cells follow a slow spreading, fast spreading and finally area saturation. After saturation the adhesion area of the cell fluctuates as the neutrophil migrates. Close contacts occur at opposite sides of the cell where the uropod and lamellipodium develop. The apparition of close contacts seems to indicate a change in adhesion regime.

## SESSION B31: INSULATING NANOSTRUCTURES

**Monday Morning, 13 March 2006**
**328, Baltimore Convention Center at 11:15**
**Babak Nikoobakht, National Institute of Standards and Technology, presiding**

**11:15**

**B31 1 Structural and electronic properties of aluminate nanotubes** KEE JOO CHANG, YONG-JU KANG, *Department of Physics, Korea Advanced Institute of Science and Technology* Recently, lithium containing aluminate nanotubes have been synthesized by the surfactant templating method. However, their structural and electronic properties have not been clearly understood yet. In this work, using first-principles theoretical calculations, we present a stable tubular structure in the form of $AlO_2$, which is energetically stable with fewer strain energies, compared with $MoS_2$ nanotubes with similar diameters. All the $AlO_2$ nanotubes are metallic with pseudogaps, independent of chilality. For small diameter zigzag tubes, more electron conduction occurs through the outer O shell with longer Al-O bonds, while the whole tube wall contributes to electron conduction for large diameter tubes or armchair tubes, which have similar inner and outer Al-O bond lengths. We find that an AlO tubular form can be stabilized by hole doping.

**11:27**

**B31 2 Formation of SiOx nanoflowers during the VLS growth of silicon nanowires** JOONHO BAE, REBECCA THOMPSON-FLAGG, MICHAEL MARDER, *Physics Department, University of Texas* JOHN EKERDT, *Department of Chemical Engineering, University of Texas* CHIH-KANG KEN SHIH, *Physics Department, University of Texas* We report the formation of SiOx nanoflowers at the tip of the VLS grown silicon nanowires. The morphology and complexity of the flowers can be reproducibly controlled by varying the growth conditions. Structural and compositional analysis of the nanoflowers formed at different stages (from open geometry to close geometry) using TEM and SEM with energy dispersive spectroscopy reveal that the flower results from selective oxidation of silicon at the interface between nanowire and the gold catalyst. There is no detectable oxidation in the wire region. The underlying mechanism and the intriguing pattern formation will be discussed.

**11:39**

**B31 3 Ferromagnetism of MnO and Mn3O4 nanowires** MYUNG-HWA JUNG, *Quantum Materials Research Team, Korea Basic Science Institute, Daejeon 305-333, Korea* JEUNGHEE PARK, *Department of Chemistry, Korea University, Jochiwon 339-700, Korea* KOREA BASIC SCIENCE INSTITUTE COLLABORATION, KOREA UNIVERSITY COLLABORATION, The MnO and Mn3O4 nanowires were grown by thermal evaporation of MnCl2 under the Ar flow. The diameter is in the range 50-100 nm and the length is about 20 ?m. The MnO and Mn3O4 nanowires consist of single-crystalline cubic MnO and tetragonal Mn3O4 crystals, respectively, grown uniformly with the [100] direction. The XPS data suggest that the majority of nanowires could be MnO nanowires. The temperature-dependent FC and ZFC magnetization curves with H=0.1-30 kOe, and the hysteresis curves measured at 5-300 K provide an evidence for the ferromagnetism with TC = 12 K and 43 K, for the MnO and Mn3O4 nanowires, respectively. The hysteresis curves at low temperatures were resolved well by two ferromagnetic components based on Brillouin function form, confirming the ferromagnetism of both MnO and Mn3O4 nanowires. We conclude that the single- crystalline MnO and Mn3O4 nanowires could be excellent ferromagnetic nanomaterials.

**11:51**

**B31 4 Metal-insulator transition in vanadium oxide nanowires** JIANG WEI, ZENGHUI WANG, YUJIE XIONG, YOUNAN XIA, DAVID COBDEN, The oxides of vanadium are strongly correlated electronic materials. In the form of nanostructures, the correlations and the phenomena associated with them should be modified. For instance, in sufficiently thin nanowires the metal-insulator transition, which is first-order in the bulk, should become a crossover. We report on our synthesis of vanadium oxide nanowires and preliminary measurements of their transport properties. The nanowires as grown by vapor phase deposition on $SiO_2$ appear to be mainly $V_2O_5$, a semiconductor, and their conductance shows no features as a function of temperature. After annealing in hydrogen, hysteresis is seen in the conductance within a limited temperature range above room temperature, consistent with partial reduction to $VO_2$ which undergoes a metal-insulator transition in the bulk at $67^o$ C. After further annealing, the conductance increases by two orders of magnitude and the hysteresis disappears, consistent with further reduction of the nanowires to $V_2O_3$ which is a correlated metal at room temperature.

**12:03**

**B31 5 Magnetoresistive Core-Shell Nanowires** BO LEI, CHAO LI, CHONGWU ZHOU, *University of Southern California* Magnetoresistive La0.67Sr0.33MnO3 nanowires have been synthesized and studied using pulsed laser deposition with MgO nanowires working as the template. Transport studies on these novel nanowires revealed a remarkable metal-insulator transition at 325 k, accompanied by room-temperature colossal magnetoresistance 10 percent under 1 T magnetic field. Furthermore, shape-induced magnetoresistance was observed for magnetic fields applied parallel or perpendicular to the nanowire. In addition, polycrystalline La0.67Sr0.33MnO3 have been obtained by tuning the synthesis condition, leading to a low-field magnetoresistance up to 16 percent at 0.06 T.

**12:15**

**B31 6 Table Salt's New Application in High Throughput Growth of Zinc Oxide Nanowires from Zinc Powder** JIAN YANG, *Boston College* WENZHONG WANG, *Boston College* YI MA, *Boston College* D.Z. WANG, *Boston College* ZHIFENG REN, *Boston College* Table salt was found to be very helpful in producing single crystal zinc oxide (ZnO) nanowires in grams quantity with a conversion efficiency of about 60-80%. The growth process involves heating the mixture of zinc powder and table salt at about 600-700C in flowing gases of oxygen and argon. A conversion efficiency of only 5-10% was achieved when salt was not used. The salt was completely removed by a few times water rinse. The as-grown ZnO nanowires are about 40 – 100 nm in diameter and 5 – 10 micrometer in length, and are grown on either zinc oxide particles or on the surfaces of the table salt crystals. Transmission electron microscope studies showed that these ZnO nanowires are highly crystallized single crystals. Photoluminescence spectra of the as-grown and salt-free ZnO nanowires using excitation of 325 nm showed that the ZnO nanowires have a very strong emission in the visible frequency without any emission from the band edge, meaning that surface states dominate the emission. The important role of the salt plays in the high conversion efficiency is discussed.

**12:27**

**B31 7 Growth of Ultra-long Horizontally Grown Zno NWs, their Photoluminescence and Electrical Properties** BABAK NIKOOBAKHT, MICHAEL BEVERSLUIS, MARK VAUDIN, STEPHAN STRANICK, *National Institute of Standards and Technology* In this presentation a technique for growth of very long horizontal ZnO NWs on $(11\bar{2}0)$ sapphire surface is discussed, which is a modification to our previously published work (**Appl. Phys. Lett. 2004, 85(15), 3244**). This technique provides the in situ alignment, predictable positioning, large scale assembly, diameter control, and production of quantum wires. A crystallographic model explaining the unique growth direction of $[11\bar{}00]$ is proposed, which is supported by electron-back scattering diffraction results. Two photon photoluminescence microscopy of oriented NWs with diameter about 5 nm as well as electrical characterization of individual NWs are discussed.

**12:39**

**B31 8 $W_3O$ Nanowires as Gas Sensors** SHARVIL DESAI, *University of Louisville, Department of Physics* BISWAPRIYA DEB, *University of Louisville, Department of Chemical Engineering* GAMINI SUMANASEKERA,* *University of Louisville, Department of Physics* MAHENDRA SUNKARA, *University of Louisville, Department of Chemical Engineering* $N_2O$ interaction on thin films of $W_3O$ nanowires and nanoparticles at different temperatures and concentrations was investigated. $W_3O$ nanowire and nanoparticle films were synthesized on quartz substrates by Hot Filament Chemical Vapor Deposition. DC resistance measurements in the Van der Pauw geometrical methods were conducted on the films. It was observed that the $W_3O$ nanowire thin film as a gas sensor resulted in an improved sensitivity as compared to the $W_3O$ nanoparticle thin film. Impedance Spectroscopy measurements (1mHz - 100kHz) were also performed in both films to understand the underlying mechanism for these different responses. Measurements on single $W_3O$ nanowire will also be presented.

*Primary Reference

**12:51**

**B31 9 Semiconducting Oxide Nanobelt Field Effect Transistors: Characteristics and Applications** YI CHENG, P. XIONG, *MARTECH/Physics Department, Florida State University* LENWOOD FIELDS, J.P. ZHENG, *Department of Electrical and Computer Engineering, FAMU/FSU College of Engineering* R. YANG, Z.L. WANG, *School of Materials Science and Engineering, Georgia Institute of Technology* Single-crystalline ZnO and $SnO_2$nanobelts with thickness of 10 -150 nm were synthesized by thermal evaporation of oxide powders without any catalyst. Field-effect transistors have been fabricated based on these oxide nanobelts, using a doped-Si/$SiO_2$ substrate. Multi-terminal electrical contacts to individual nanobelts were defined by photolithography, which enabled us to correlate the FET characteristics with the behavior of the contacts. FETs with nonohmic high-resistance contacts showed enhancement mode Schottky barrier FET behavior. In contrast, in devices with low-resistance ohmic contacts, characteristics of an n-channel depletion-mode FET were observed, with ON/OFF ratio as high as $10^3$ (ZnO) and $10^5$ ($SnO_2$), and well-defined linear and saturation regimes. Electrical measurements also revealed high transconductance and field-effect mobility for these nanobelt FETs. Effects of surface oxygen adsorption and desorption have been studied by monitoring the transport properties of $SnO_2$ nanobelt FET in different gas flow. Importantly, the FET characteristics of the $SnO_2$ device showed significant modification by a 2% hydrogen gas flow at room temperature. *This work is supported by NSF NIRT grant ECS-0210332.

**13:03**

**B31 10 Electromechanical Properties of GaN Nanowires** CHANG-YONG NAM, PAPOT JAROENAPIBAL, DOUGLAS THAM, DAVID E. LUZZI, JOHN E. FISCHER, *Dept. of Materials Science and Engr., University of Pennsylvania* STEPHANE EVOY, *Dept. of Electrical and Computer Engr., University of Alberta* GaN, an important wide and direct bandgap semiconductor for optoelectronic devices, also possesses excellent thermal stability, chemical inertness, and a high piezoelectric constant, making it suitable for high temperature chemical sensors and transducers. While one-dimensional GaN nanowires have attracted extensive research recently for nano-scale optoelectronic devices, their high aspect ratio, straightness and smooth surfaces suggest potential in nanoelectromechanical system (NEMS) applications such as high sensitivity mass sensing. In spite of such importance, electromechanical properties of GaN nanowires have not been accessed so far. Here, we investigate Young's modulus $E$ and resonance quality $Q$ of GaN nanowires by itin-situ detection of electromechanical resonances in a transmission electron microscope. For the largest nanowire diameter observed (84 nm), $E$ is close to the theoretical value of bulk GaN ( $\sim$ 300 GPa) and gradually decreases for smaller diameters. Also we find $Q$ generally higher than that of conventionally micromachined nano-scale Si resonators despite the larger surface-to-volume ratio, implying significant advantage of GaN nanowires in NEMS applications. Most nanowires display two closely-spaced resonances, which we attribute to low-symmetry triangular cross-sections.

**13:15**

**B31 11 Electronic and Transport Characteristics of Two-Phase Coaxial Gallium Nitride Nanowires** V.M. AYRES, B.W. JACOBS, M.A. CRIMP, *Michigan State University, East Lansing, MI 48824* R.E. STALLCUP, A. HARTMAN, *Zyvex Corporation, Richardson, TX, 75081* M.A. TUPTA, *Keithley Instruments, Cleveland, OH 44139* J.B. HALPERN, M.Q. HE, *Howard University, Washington, DC 20059* We will present results of investigations of electronic and transport characteristics of two-phase coaxial gallium nitride nanowires. The$\sim$ 50-100 nm gallium nitride nanowires grown in a direct reaction of metal gallium vapor with flowing ammonia at 850-900[r]C without a catalyst have a two phase coaxial zinc-blende/wurtzite structure, shown by high resolution TEM and nanodiffraction experiments. The electronic characteristics were investigated by STM. The transport characteristics were investigated in 2-point and 4-point probe configurations using a Keithley-Zyvex KZ100 Nanoprobing System, in which specially sharpened $\sim$ 30 nm radius tungsten nanoprobes were coupled to an ultra low noise semiconductor characterization system. The transport experiments were performed under direct SEM observation. Results indicating coaxial transport with different transport characteristics will be presented.

**13:27**

**B31 12 In-situ STM-TEM Studies of Individual GaN Nanowires** MITRA TAHERI, *Materials Science and Technology (Code 6360), Naval Research Laboratory, Washington, D.C. 20375* BLAKE SIMPKINS, *Surface Chemistry (Code 6170), Naval Research Laboratory, Washington, D.C. 20375* PEHR PEHRSSON, *Surface Chemistry (Code 6170), Naval Research Laboratory, Washington, D.C. 20375* RHONDA STROUD, *Materials Science and Technology (Code 6360), Naval Research Laboratory, Washington, D.C. 20375* The electronic and structural properties of individual GaN nanowires were studied using a scanning tunneling microscopy (STM) stage that operates inside a high-resolution transmission electron microscope (TEM) allowing simultaneous evaluation of electrical, compositional, and structural properties with nm-scale resolution. The GaN nanowires were prepared by atmospheric CVD on $SiO_2$/Si substrates. Catalyst metal deposition consisted of electron-beam lithography patterned Ni dots, enabling diameter- and position-controlled nanowire growth for device-compatible processing. A focused ion beam- scanning electron microscope with an in situ micromanipulator was used to extract single GaN nanowires from the substrate and attach them to copper TEM supports. Analysis of I-V characteristics of individual wires, and any correlation with microstructure, such as wire dimensions, growth habit and defect concentration will be presented.

**13:39**

**B31 13 Spatially Resolved Luminescence from CdSe Nanowires** YONG-JOO DOH, KRISTIN N. MAHER, LIAN OUYANG, *Department of Chemistry and Chemical Biology, Harvard University* JIWOONG PARK, *The Rowland Institute at Harvard* HONGKUN PARK, *Department of Chemistry and Chemical Biology, and Department of Physics, Harvard University* We report photoluminescence (PL) and electroluminescence (EL) from devices incorporating single cadmium selenide (CdSe) nanowires. Electrical measurements and spatially resolved optical measurements are carried out simultaneously at room temperature, and under constant uniform illumination ($\lambda$ = 480 nm). At low bias voltages ($V$), photoluminescence is observed along the length of the wire, with a spectral peak at 706 nm. Once $V$ exceeds $\pm$ 1V, the PL intensity begins to decrease, and above $V = \pm 2.5$V localized emission can be seen at one of the contacts (at the positively biased electrode). The EL spectrum shows a peak that is broadened and blue-shifted in comparison to the PL. A mechanism for the observed light emission will be discussed.

**13:51**

**B31 14 Compositional and magnetic ordering in $Mo_6S_{9-x}I_x$ nanowires*** TENG YANG, SHINYA OKANO, DAVID TOMANEK, *Michigan State University* We investigate the effect of atomic ordering and geometry on the relative stability and electronic as well as magnetic structure of $Mo_6S_{9-x}I_x$ nanowires using *ab initio* Spin Density Functional calculations. The skeleton of these unusually stable nanowires consists of Mo octahedra, which are decorated with S and I atoms and connected by sulfur bridges. These sulfur bridges turn out to be bi-stable, providing the nanowires with the unusual capability to stretch by 20% at no energy cost. Depending on the degree the nanowires have been stretched, they may reversibly acquire or lose their magnetic moment. The ordering of the decorating atoms, observed in these nanowires, reflects our finding that the total energy depends sensitively on the atomic arrangement at a given stoichiometry.

*Supported by NSF NIRT grant ECS-0506309 and NSF NSEC grant EEC-425826

**14:03**

**B31 15 Dielectric properties and band gap determination of individual nanostructures via valence electron energy loss spectroscopy** SHAUL ALONI, *Molecular Foundry, MSD, LBNL, Berkeley, Caifornia 94720 and Dept. of Physics, UC Berkeley, California, 94720* DAVID OKAWA, *Dept. of Physics, UC Berkeley, California, 94720* MICHAEL JOHNSON, *Materials Sciences Division, LBNL, Berkeley, Caifornia 94720* MICHAEL ROUSSEAS, *Dept. of Physics, UC Berkeley, California, 94720* ALEX ZETTL, *Dept. of Physics, UC Berkeley, California, 94720 and Molecular Foundry, MSD, LBNL, Berkeley, Caifornia 94720* Recent developments in electron energy loss spectroscopy allow us to measure the dielectric properties near the band gap of the material with resolution better then 0.2 eV. The energy loss spectra in the 0-50 eV range carries information about the dielectric properties of the nanostructures providing information about the plasmon excitations and allows accurate bandgap determination of individual nanostructures.



## SESSION B32: FOCUS SESSION: COMPUTATIONAL NANOSCIENCE I

**Monday Morning, 13 March 2006; 329, Baltimore Convention Center at 11:15**
**Andrew Canning, Lawrence Berkeley National Laboratory, presiding**

*Invited Papers*

**11:15**

**B32 1 Losses due to phonon-phonon interactions in nanotube oscillators: From classical potentials through one-dimensional elasticity and many-body perturbation theory.**
DAVID ROUNDY, *Cornell University*

Phonon-phonon losses are an intrinsic loss mechanism and it is therefore important to calculate their magnitude as an upper bound on the quality factor of any nano-oscillator. We will present an approach to handling the problem of phonon-phonon interactions in nanotube oscillators which uses an empirical interatomic potential to compute the input parameters for a fully quantum-mechanical green function-based method. This approach allows us to compute losses at temperatures comparable to or below the Debye temperature ( $>$ 500K), allowing comparison with experimental results.

*Contributed Papers*

**11:51**

**B32 2 Scalable Linear Electronic Structure Method for Free Standing Clusters** KAB SEOK KANG, JAMES DAVENPORT, DAVID KEYES, JAMES GLIMM, *Brookhaven National Laboratory* We have developed a Scalable Linear Augmented Slater Type Orbital (LASTO) method for electronic-structure calculations on free standing clusters. As with other linear methods we solve the Schrodinger equation using a mixed basis set consisting of numerical functions inside atom centered spheres matched onto tail functions outside. The tail functions are Slater type orbitals which are localized, exponentially decaying functions. To solve the Poisson equation between spheres, we use a finite difference method replacing the rapidly varying charge density inside the spheres with a smoothed density with the same multipole moments. We use multigrid techniques on the mesh which are well-known scalable solvers. This yields the Coulomb potential on the spheres which in turn defines the potential inside via a Dirichlet problem. To solve the linear eigen-problem, we use SCALAPACK, a well-developed package to solve large eigen-problems with dense matrices. We have tested the method on finite clusters of palladium and palladium hydride. Supported by the US Department of Energy under contract DEA02-98CH10886.

**12:03**

**B32 3 ONETEP: linear-scaling density-functional theory with plane waves** PETER HAYNES, *Cavendish Laboratory, University of Cambridge, UK* CHRIS-KRITON SKYLARIS, *Physical and Theoretical Chemistry Laboratory, University of Oxford, UK* ARASH MOSTOFI, *Department of Materials Science and Engineering, Massachusetts Institute of Technology* MIKE PAYNE, *Cavendish Laboratory, University of Cambridge, UK* Plane waves are a popular choice of basis set for first-principles quantum-mechanical simulations based on density-functional theory because the implementation is straightforward and the completeness can be controlled systematically with a single parameter. The resulting simulations require a computational effort which scales as the cube of the system-size, which makes the cost of large-scale calculations prohibitive. Extended basis functions would appear to be an inappropriate choice for expanding the localized orbitals of linear-scaling methods or for embedding the calculation within a larger model. In spite of these apparent difficulties, the ONETEP linear-scaling method can achieve the same accuracy as traditional plane-wave calculations and overcomes the apparent difficulties mentioned above. An outline of the ONETEP method will be presented, focusing on its distinctive features and primarily the ability to optimize the localized orbitals in each particular environment. These optimized orbitals are known as non-orthogonal

generalized Wannier functions within ONETEP, and justification for this term will be presented, in addition to results that demonstrate the scaling and accuracy of the method.

**12:15**

**B32 4 Acceleration of the Convergence in *ab initio* Atomic Relaxations*** ZHENGJI ZHAO, LIN-WANG WANG, JUAN MEZA, *LBNL* Atomic relaxations is often required to accurately describe the properties of nanosystems. In *ab initio* calculations, a common practice is to use a standard search algorithm, such as BFGS (Broyden-Fletcher-Goldfarb-Shanno) or CG (conjugate gradient) method, which starts the atomic relaxations without any knowledge of the Hessian matrix of the system. For example, the initial Hessian in BFGS method is often set to identity, and there is no preconditioning to CG method. One way to accelerate the convergence of the atomic relaxations is to estimate an approximate Hessian matrix of the system and then use it as the initial Hessian in BFGS method or a preconditioner in CG method. Previous attempts to obtain the approximated Hessian were focused on the use of classical force field models which rely on the existence of good parameters. Here, we present an alternative method to estimate the Hessian matrix of a nanosystem. First, we decompose the system into motifs which consist of a few atoms, then calculate the Hessian matrix elements on different motif types from *ab initio* calculations for small prototype systems. Then we generate the Hessian Matrix of the whole system by putting together these motif Hessians. We have applied our motif-based Hessian matrix in *ab initio* atomic relaxations in several bulk (with/without impurity) and quantum dot systems, and have found a speed up factor of 2 to 4 depending on the system size.

*Supported by U. S. Department of Energy under Contract No. DE-AC02-05CH11231.

**12:27**

**B32 5 Electric field polarization calculations using charge patching method*** LIN-WANG WANG, *Lawrence Berkeley National Lab, Berkeley CA 94720* XAVIER CARTOIXA SOLER, *Universidad Autonoma de Barcelona, Barcelona, SPAIN* Charge patching method has been used to calculate the electronic structures of thousand atom nanosystems with ab initio accuracy. Within the charge patching method, the ab initio charge density of a nanostructure is patched together using charge motifs which are calculated from small prototype systems. However, the current charge patching method can only be used for systems without long range electric field. In this talk, we will present results which include the polarizations of charge motifs. These polarization motifs accurately describe the charge responses of a nanosystem under external electric fields, and the results agree well with direct ab initio calculations, including part of the local field effects. This motif polarization method enables us to calculate nanosystems such as charged impurities, quantum dots with permanent dipole moments, or charged quantum dots. It also makes it possible to calculate the charge density of a nanosystem selfconsistently when combined with the folded spectrum method in solving a few band edge electronic states.

*This work was supported by U.S. Department of Energy under Contract No. DE-AC02-05CH11231 and used the resources of the National Energy Research Scientific Computing Center.

**12:39**

**B32 6 A divide and conquer method for Bader decomposition** JUN-ICHI HOSHINO, KAZUO TSUMURAYA, *Meiji University* The ionicity of atoms in crystals or molecules is a measure of the bonding states among the atoms. There have been several methods to evaluate the electron charges that belong to each atom. Bader analysis is a direct method and divides up into atomic regions where the dividing surfaces are at a minimum in the charge density. [1] The algorithm, however, has computational difficulties to find the critical points for complex circumstance of atoms. A Henkelmans algorithm [2] is free of the points, assign each point on a regular grid to one of the regions by following a steepest ascent (SA) method contrary to the Baders steepest descent (SD) algorithm. We have found the SA method separates the regions more precisely than the SD method, although they are reverse relation. The SA method however requires much memory capacity for all-electron densities which are oscillating in the core regions. We implement a divide and conquer method to calculate the core region separately from the other region, assess the proposed method, and compare it with the Henkelmans decomposition.

R.Bader, Atoms in Molecules:A Quantum Theory, Oxford,1990. G.Henkelman,et al., Comp.Mater.Sci.(in press)

**12:51**

**B32 7 Direct enumeration of alloy configurations for semiconductor electronic structure properties*** SIRICHOK JUNGTHAWAN, SUKIT LIMPIJUMNONG, *National Renewable Energy Laboratory, U.S.A. and Suranaree University of Technology, Thailand* PETER A. GRAF, KWISEON KIM, WESLEY B. JONES, *National Renewable Energy Laboratory, Golden, CO 80401* GUS L. W. HART, *Department of Physics and Astronomy, Northern Arizona University, Flagstaff, AZ 86011-6010* We present an approach to directly enumerating the electronic structure of all possible zincblende-based alloy configurations whose unit cell contains up to a specified number of atoms. This method allows us to map the space of bandgaps and effective masses versus alloy composition and atomic configuration. We demonstrate for GaInP alloys that a large range of bandgaps and masses are available for a given composition. By decomposing the space of possible atomic configurations into categories based on superlattice structure, we can identify trends in bandgap extrema. For example, bandgap maxima typically occur in [0 h k] superlattices where h is not equal to k, and minima typically occur in [1 1 1] superlattices. We focus on dilute alloys where the minority composition is below 10 percent. The empirical pseudo potential method (EPM) and folded spectrum method are used to solve the single particle Schrödinger equation. The results from the EPM are compared with first- principle calculations.

*supported by US DOE-SC-ASCR-MICS.

**13:03**

**B32 8 Surface passivation optimization using DIRECT*** KWISEON KIM, PETER A. GRAF, WESLEY B. JONES, *National Renewable Energy Laboratory, Golden, CO 80401* LIN-WANG WANG, *Lawrence Berkeley National Laboratory, Berkeley, CA, 94720* The calculation of the electronic structure of a nanostructure must take into account surface effects. In experiments, the dangling bonds at the surface of a semiconductor nanostructure are passivated by other semiconductors or by organic ligands. In either case, photoluminescence measurements reveal that the emission comes from bulk-like, dot-interior states. These observations suggest that an approach to passivating a simulated nanostructure would be to attach pseudo-atoms to each dangling

bond. Here we present an automated methodology for generating surface passivating pseudo potentials for bulk empirical pseudo potentials. Our method is based on the global optimization method DIRECT. We apply it to two materials, CdSe and InP. Incorporated into a larger computational nanoscience infrastructure, our work represents a much needed improvement in the usability of the empirical pseudo potential method.

*supported by US DOE-SC-ASCR-MICS.

**13:15**

**B32 9 Non-linear dynamics of the electron wave packet propagating through the resonant tunneling structure under the presence of the electron-photon and inter-electron interactions** MASAKAZU MURAGUCHI, KYOZABURO TAKEDA, *Waseda University* We solved the TD Schrodinger equation numerically in the framework of the TD Hartree-Fock (HF) approach both in the real space and time, and studied the TD phenomena of an electron wave packet propagating through the time-modulated resonant tunneling structure (TMRTS). We suppose that a single electron Gaussian wave packet is injected into the TMRTS by varying its group velocity. For the inter-electron interaction in the TMRTS, we combine Poisson's equation with TD-HF equation. We found that the TD features of the wave function confined in the TMRTS (e.g., lifetime) strongly depend on the choice of the resonant states as well as the frequency and strength of the applied electric field. Furthermore, TD non-linear processes based on the multi-photon interaction are recognized. For extracting characteristics of these TD phenomena, we expanded the resulting wave function in terms of the RTS resonant sates at each time-step. This projection approach enables us not only to estimate the lifetime precisely but also provides a guiding principle to control the wave packet artificially.

**13:27**

**B32 10 Multi-Scale Modeling of Carbon Nanotube/Carbon Fiber/Epoxy Lamina** S.J.V. FRANKLAND, *National Institute of Aerospace* J.C. RIDDICK, *Army Research Laboratory* T.S. GATES, *NASA Langley Research Center* A carbon fiber/epoxy lamina in which the carbon fibers are coated with single-walled carbon nanotubes is modeled with a multi-scale method. The multi-scale model is designed to predict the effect of the carbon nanotubes on the constitutive properties of the lamina. Within the model both the nanotube volume fraction and nanotube distribution are varied. The multi-scale analysis links results from molecular dynamics and equivalent-continuum techniques with micromechanics and strength of materials models. The multi-scale method will be used in a parametric study to examine the relative effect of nanotube concentration, orientation, and distribution on the constitutive properties of the lamina.

**13:39**

**B32 11 Tight binding models derived from k-dot-p theory** C. E. PRYOR, *Dept. of Physics and Astronomy, University of Iowa* M.-E. PISTOL, *Dept. of Physics, Lund University, Sweden* Calculations of the electronic properties of semiconductor nanostructures rely on one of three different methods: tight-binding, pseudopotentials, or k-dot-p theory. The first two are well suited to modeling small scale structures, however their parameters must be fitted to bulk properties, which can be a complicated procedure, especially for tight-binding. In contrast, k-dot-p theory is best at describing large nanostructures in which the placement of individual atoms is not important, and the parameters of k-dot-p theory are directly related to experimentally determined quantities. To bridge the gap between atomistic and large scale models, we will present a method for constructing tight-binding models directly from k-dot-p theory by considering a real-space representation of k-dot-p theory with finite differences on a grid which matches the desired crystal lattice. Conversely, given a tight-binding model it is also possible to construct an equivalent k-dot-p theory in the long wavelength limit

**13:51**

**B32 12 Mobility of Lithium and Hydrogen Ions in Nanotubes in Terms of Fokker-Plank Equation** ANDREW KINCHEN, YURIY MALOZOVSKY, *Southeastern Louisiana University* We present the theory of mobility of Li and H ions in metallic nanotubes. We derived the mobility of ions in terms of the kinetic Fokker-Plank equation with the consideration of both the motion of an ion in the cylindrical periodic potential of a nanotube and interaction of an ion with lattice vibrations of the tubule. We argue that there is an optimum diameter of the tubule below which the mobility of ions is significantly reduced.



## SESSION B33: FINANCIAL MARKETS AND OTHER APPLICATIONS OF STATISTICAL PHYSICS

**Monday Morning, 13 March 2006**
**336, Baltimore Convention Center at 11:15**
**Victor Yakovenko, University of Maryland, presiding**

**11:15**

**B33 1 What physicists should learn about finance (if they want to)** ANATOLY SCHMIDT, *EBS Dealing Resources, Parsippany, NJ* There has been growing interest among physicists to Econophysics, i.e. analysis and modeling of financial and economic processes using the concepts of theoretical Physics. There has been also perception that the financial industry is a viable alternative for those physicists who are not able or are not willing to pursue career in their major field. However in our times, the Wall Street expects from applicants for quantitative positions not only the knowledge of the stochastic calculus and the methods of time series analysis but also of such concepts as option pricing, portfolio management, and risk measurement. Here I describe a synthetic course based on my book ''Quantitative Finance for Physicists'' (Elsevier, 2004) that outlines both worlds: Econophysics and Mathematical Finance. This course may be offered as elective for senior undergraduate or graduate Physics majors.

**11:27**

**B33 2 Relation between bid-ask spread and volatility in financial markets** JEAN-PHILIPPE BOUCHAUD, *Service de Physique de l'Etat Condense, CEA-Saclay, France* J. KOCKELKOREN, M. POTTERS, M. WYART, We establish empirically a linear relation between the bid-ask spread and the volatility per trade in stock markets. We give a theoretical argument explaining this relation and why it should hold on all electronic markets.

**11:39**

**B33 3 An equation of state for the financial markets: connecting order flow to price formation.** AUSTIN GERIG, *University of Illinois at Urbana-Champaign* SZABOLCS MIKE, *Budapest University of Technology and Economics* J. DOYNE FARMER, *Santa Fe Institute* Many of the peculiarities of price formation in the financial marketplace can be understood as the result of a few regularities in the placement and removal of trading orders. Based on a large data set from the London Stock Exchange we show that the distribution of prices where people place orders to buy or sell follows a surprisingly simple functional form that depends on the current best prices. In addition, whether or not an order is to buy or sell is described by a long-memory process, and the cancellation of orders can be described by a few simple rules. When these results are combined, simply by following the rules of the continuous double auction, the resulting simulation model produces good predictions for the distribution of price changes and transaction costs without any adjustment of parameters. We use the model to empirically derive equations of state relating order flow and the statistical properties of prices. In contrast to previous conjectures, our results demonstrate that these distributions are not universal, but rather depend on parameters of individual markets. They also show that factors other than supply and demand play an important role in price formation.

**11:51**

**B33 4 An empirical analysis of waiting times for price changes and orders in a financial market** NAOYA SAZUKA, *Sony Corporation* We discuss an empirical analysis of waiting time distribution for price changes and orders in a financial market and its Weibull approximation. It is widely assumed that trades in financial markets occur independently and the waiting time distribution is exponential. However, recent empirical results [Raberto et al 2002, Scalas et al 2005 etc] of high frequency financial data show that the distribution is non-exponential. Therefore, in order to understand market behavior quantitatively and systematically, it is important to check the validity of the exponential distribution hypothesis and which non-exponential distribution is appropriate. In this talk, we analyze the waiting times of Sony bank USD/JPY rate and orders. We show that the waiting time distribution for not only price changes, but also orders, is non-exponential by using non-double auction market data. We also measure exactly how much better the Weibull distribution is as an approximation by using the Weibull paper and divergence measurements. Moreover, the estimated value of the shape parameter in Weibull distribution is similar in both price changes and orders waiting time distributions.

**12:03**

**B33 5 Dynamics of the return distribution in the Korean financial market** JAE-SUK YANG, SEUNGBYUNG CHAE, WOO-SUNG JUNG,*HIE-TAE MOON, *Korea Advanced Institute of Science and Technology* In this paper, we studied the dynamics of the log-return distribution of the Korean Composition Stock Price Index (KOSPI) from 1992 to 2004. Based on the microscopic spin model, we found that while the index during the late 1990s showed a power-law distribution, the distribution in the early 2000s was exponential. This change in distribution shape was caused by the duration and velocity, among other parameters, of the information that flowed into the market.

*Present address: Boston University

**12:15**

**B33 6 Grouping in the stock markets of Japan and Korea** WOO-SUNG JUNG,*OKYU KWON, *Korea Advanced Institute of Science and Technology* TAISEI KAIZOJI, *International Christian University* SEUNGBYUNG CHAE, *Korea Advanced Institute of Science and Technology* WOONG LEE, *Yonsei University* HIE-TAE MOON, *Korea Advanced Institute of Science and Technology* We investigated the temporally evolving network structures of the Japanese and Korean stock markets through the minimum spanning trees composed of listed stocks. We tested the validity of conventional grouping by industrial categories, and found a common trend of decrease for Japan and Korea. This phenomenon supports the increasing external effects on the markets due to the globalization of both countries. At last the Korean market are grouped with the MSCI Korea Index, a good reference for foreigners' trading, in the early 2000s. In the Japanese market, this tendency is strengthened more and more by burst of the bubble in 1990's.

*Present address: Boston University

**12:27**

**B33 7 Dynamical Structures of High-Frequency Financial Data** KYUNGSIK KIM, *Department of Physics, Pukyong National University, Pusan 608-737, Korea* SEONG-MIN YOON, *Division of Economics, Pukyong National University, Pusan 608-737, Korea* SOO YONG KIM, *Department of Physics, Korea Advanced Institute of Science and Technology, Daejeon 305-701, Korea* YUP KIM, *Department of Physics, Kyung Hee University, Seoul 130-701, Korea* We study the dynamical behavior for high-frequency data of the Korean stock price index (KOSPI) using the movement of returns in Korean financial markets. It is shown that the dynamical behavior for a binarized series of our models is not completely random. The conditional probability are numerically estimated from a return series of tick data in the KOSPI. Non-trivial probability structures can be constituted from binary time series of the autoregressive (AR), logit, and probit models for which the Akaike Information Criterion (IC) value shows a minimum value at the 15th-order. From our result, the value of correct match ratio for the AR model is found to relatively have slightly larger than calculated findings of other models.

**12:39**

**B33 8 Systematic Analysis of Group Identification in Stock Markets** DONG-HEE KIM, HAWOONG JEONG, *Department of Physics, KAIST* We propose improved methods to identify stock groups using the correlation matrix of stock price changes. By filtering out the marketwide effect and the random noise, we construct the correlation matrix of stock groups in which nontrivial high correlations between stocks are found. Using the filtered correlation matrix, we successfully identify the multiple stock groups without any extra knowledge of the stocks by the optimization of the matrix representation and the percolation approach to the correlation-based network of stocks. These methods drastically reduce the ambiguities while finding stock groups using the eigenvectors of the correlation matrix.

**12:51**

**B33 9 Virtual Volatility, an Elementary New Concept with Surprising Stock Market Consequences** RICHARD PRANGE, A. CHRISTIAN SILVA, *University of Maryland* Textbook investors start by predicting the future price distribution, PDF, of a candidate stock (or portfolio) at horizon T, e.g. a year hence. A (log)normal PDF with center (=drift =expected return) $\mu$T and

width (=volatility) $\sigma\sqrt{T}$ is often assumed on Central Limit Theorem grounds, i.e. by a random walk of daily (log)price increments $\Delta s$. The standard deviation, stdev, of historical (itex post) $\Delta s$ 's is usually a fair predictor of the coming year's (itex ante) stdev($\Delta s$) $= \sigma_{daily}$, but the historical mean E($\Delta s$)it at bestroughly limits the true, to be predicted, drift by $\mu_{true}T \sim \mu_{hist}T \pm \sigma_{hist}\sqrt{T}$. Textbooks take a PDF with $\sigma \sim \sigma_{daily}$ and $\mu$ as somehow known, as if accurate predictions of $\mu$ were possible. It is elementary and presumably new to argue that an average of PDF's over a range of $\mu$ values should be taken, e.g. an average over forecasts by different analysts. We estimate that this leads to a PDF with a 'virtual' volatility $\sigma \sim 1.3\sigma_{daily.}$ It is indeed clear that uncertainty in the value of the expected gain parameter increases the risk of investment in that security by most measures, e. g. Sharpe's ratio $\mu T/\sigma\sqrt{T}$ will be 30% smaller because of this effect. It is significant and surprising that there are investments whichit benefit from this 30% virtual increase in the volatility

**13:03**
**B33 10 Volatility, Persistence, and Survival in Financial Markets** MAGDALENA CONSTANTIN, SANKAR DAS SARMA, *Condensed Matter Theory Center, University of Maryland, College Park* We study the temporal fluctuations in time-dependent stock prices (both individual and composite) as a stochastic phenomenon using general techniques and methods of nonequilibrium statistical mechanics. In particular, we analyze stock price fluctuations as a non-Markovian stochastic process using the first-passage statistical concepts of persistence and survival. We report the results of empirical measurements of the normalized $q$-order correlation functions $f_q(t)$, survival probability $S(t)$, and persistence probability $P(t)$ for several stock market dynamical sets. We analyze both minute-to-minute and higher frequency stock market recordings. We find that the fluctuating stock price is multifractal and the choice of the sampling time has no effect on the qualitative multifractal behavior displayed by the $1/q$-dependence of the generalized Hurst exponent $H_q$. The probability $S(t)$ of the stock price remaining above the average up to time $t$ is very sensitive to the total measurement time $t_m$ and the sampling time. The probability $P(t)$ of the stock not returning to the initial value within an interval $t$ has a universal power-law behavior, $P(t) \sim t^{-\theta}$, with a persistence exponent $\theta$ close to 0.5 that agrees with the prediction $\theta = 1 - H_2$. The empirical financial stocks also present an interesting feature found in turbulent fluids, the extended self-similarity. This work is partially supported by the NSF and U.S. ONR.

**13:15 alves**
**B33 11 Comparing Extremal and Hysteretic Optimization on the Satisfiability Problem*** BRUNO GONÇALVES, *Emory University* STEFAN BOETTCHER, *Emory University* We apply physically inspired optimization methods to the classical combinatorial Satisfiablity problem. Treating the usual boolean variables as Ising spins and each clause as a p-spin interaction we can use the pre-existing physical intuition about spin glasses and magnetic systems to find the optimal solution for this problem (the ground state energy). We compare the performance of Extremal Optimization[1] ($\tau EO$) and Hysteretic Optimization[2] ($HO$) and determine the parameter values that provide the best results. Comparisons with previously published results on well known benchmarks[3] are also made.

*This work has been supported by grant 0312510 from the Division of Materials Research at the National Science Foundation.

[1]PRL 23:5211, 2001
[2]PRL 89:150201, 2002
[3]DIMACS 35:393, 1997

**13:27**
**B33 12 What is the most interesting team sport?** FEDERICO VAZQUEZ, *Boston University* ELI BEN-NAIM, *Los Alamos National Laboratory* SIDNEY REDNER, *Boston University* What is the most interesting team sport? We answer this question via an extensive statistical survey of game scores, consisting of more than 1/4 million games in over a century. We propose the likelihood of upsets as a measure of competitiveness. We demonstrate the utility of this measure via a comparative analysis of several popular team sports including soccer, baseball, hockey, basketball, and football. We also develop a mathematical model, in which the stronger team is favored to win a game. This model allows to us conveniently estimate the likelihood of upsets from the more easily-accessible standings data.

**13:39**
**B33 13 Diagnosis of weaknesses in modern error correction codes: a physics approach*** MIKHAIL STEPANOV, MICHAEL CHERTKOV, *Los Alamos National Laboratory* VLADIMIR CHERNYAK, *Wayne State University* BANE VASIC, *University of Arizona* One of the main obstacles to the wider use of the modern error-correction codes is that, due to the complex behavior of their decoding algorithms, no systematic method which would allow characterization of the bit-error-rate (BER) is known. This is especially true at the weak noise where many systems operate and where coding performance is difficult to estimate because of the diminishingly small number of errors. We show how the instanton method of physics allows one to solve the problem of BER analysis in the weak noise range by recasting it as a computationally tractable minimization problem. The material is based on Phys. Rev. Lett. 95 (22) 228701 (2005).

*The work is supported by DOE LDRD program at LANL, NSF Grant No. CCR-0208597 and No. ITR-0325979, and start-up grant at WSU.

**SESSION B34: SESSION ON AUTHORING**
**Monday Afternoon, 13 March 2006; 337, Baltimore Convention Center at 13:30**

**13:30**
**B34 1 Session on Authoring**

**SESSION B35: FOCUS SESSION: NANOSCALE THERMAL, THERMOELECTRIC AND MASS TRANSPORT: THEORY AND SIMULATION**
**Monday Morning, 13 March 2006; 338, Baltimore Convention Center at 11:15**
**Joel E. Moore, University of California, Berkeley, presiding**



***Invited Papers***

**11:15**
**B35 1 Electromigration Forces on Ions in Carbon Nanotubes.**
STEFAN HEINZE, *Institute of Applied Physics, University of Hamburg, Jungiusstrasse 11, 20355 Hamburg*

Due to their unique structural, electronic, and optical properties carbon nanotubes (CNs) are promising candidates for future nanoelectronic devices. Recently, field-effect transistors (FETs) from single-wall CNs have been a research focus. In particular, ballistic transport has been demonstrated [1] and key transport parameters compare well with state-of-the-art silicon FETs. In many cases improved CN-FET performance has been achieved by the use of dopants such as alkali metal atoms (see e.g. [2]). However, during transistor operation a current-induced, *electromigration*, force will be exerted on the alkali metal ions. Due to the low diffusion barriers the alkali ions may move along the CN which can influence the FET characteristics. On the other hand, electromigration forces can be used to intentionally transport atoms along a CN [3]. Here, we present self-consistent non-equilibrium Greens function calculations to treat a ballistic CN-FET within a tight-binding approximation. We use a cylindrically symmetric device and calculate the current-induced forces on ions located either inside or outside of the CN. We observe that the forces are especially large in the turn-on regime of the transistor, and much smaller in the off- and on-states. The electromigration forces are mainly due to momentum transfer from the charge carriers, i.e. due to the ''wind'' forces. The sign of the ''effective valence'' $Z^*$ is independent of the actual charge sign, but can be reversed with gate voltage, providing a dramatic illustration of the quantum character of the wind force. [1] A. Javey, J. Guo, Q. Wang *et al.*, Nature **424**, 654 (2003). [2] M. Radosavljević, J. Appenzeller, and Ph. Avouris, Appl. Phys. Lett. **84**, 3693 (2004). [3] B. C. Regan, S. Aloni, R. O. Ritchie, U. Dahmen, and A. Zettl, Nature **428**, 924 (2004).

***Contributed Papers***

**11:51**
**B35 2 Molecular Dynamics Simulations of the Thermal Conductivities of Group IV Bulk Materials and Nanowires** JOHN REED, ANDREW WILLIAMSON, *Lawrence Livermore National Laboratory* GIULIA GALLI, *University of California, Davis* We present the results of equilibrium molecular dynamics simulations of the thermal conductivities of bulk C, Si, Ge, and SiC using the Green-Kubo formalism. We use an empirical interatomic potential developed by Tersoff [1] and investigate the effects of modifications to this potential suggested by Porter et al [2]. We also investigate the effects of choosing a symmetric versus nonsymmetric definition of the local heat. A generalization of this approach to study the dependence of the thermal conductivity of SiGe nanowires on their size and composition will also be presented. [1] J. Tersoff, PRB 39 (8), 5566-5568 [2] L. Porter, J. Li, S. Yip, J. Nuc. Matl. 246 (1997) 53-59 This work was performed under the auspices of the U.S. Dept. of Energy at the University of California/Lawrence Livermore National Laboratory under contract no. W-7405-Eng-48.

**12:03**
**B35 3 The Nanocomposite Approach to Enhanced Thermoelectric Performance** G. CHEN, R. YANG, H. LEE, Q. HAO, M. TANG, M. S. DRESSELHAUS, *MIT, Cambridge, MA* D. WANG, Z. REN, *BC, Chestnut Hill, MA* J. P. FLEURIAL, P. GOGNA, *JPL, Pasadena, CA* Model calculations and experimental results confirm that a nanocomposite approach leads to an enhancement in the thermoelectric performance of a bulk nanocomposite sample based on Si-Ge relative to its 3D alloy counterpart, though the predictions are quite general and should be applicable to a variety of nanocomposite systems. Modeling and experimental results here are reported for nanocomposites of Si-Ge made of Si and Ge nanoparticles (typically the particles are 20 nm or less in size prepared from the liquid phase or by ball milling or other techniques) and consolidated by hot press in an inert argon atmosphere to theoretical density. Most important is the large decrease in the thermal conductivity, well below that of the alloy of the same composition, both at room temperature and up to 1000K. Although the electrical conductivity decreases somewhat, the selective filtering of the high energy electron carriers enhances the Seebeck coefficient much more than the decrease in electrical conductivity, resulting in a gain in the power factor as well over a large temperature range. Emphasis is given to physical phenomena associated with nanostructures that serve to enhance the thermoelectric performances generally, and can be used for other Nanocomposite systems. The authors acknowledge support from NASA under the Radio Isotope Power Conversion program.

**12:15**
**B35 4 Theory of the thermoelectric properties of semiconductor-matrix nanocomposites** NATALIO MINGO, *NASA-Ames Center for Nanotechnology* DAVID BROIDO, *Boston College* We theoretically investigate the thermoelectric properties of a nanocomposite nanowire array where the matrix material is a semiconductor. We take InSb to be the nanocomposite matrix that surrounds an array of cylindrical holes, and we calculate the density-optimized power factor, P, and the lattice thermal conductivity, k, employing a relaxation time approach and including band nonparabolicity. For fixed aspect ratio of wire diameter to cylindrical-hole period, we obtain universal curves for P. For small period, we find that P is enhanced above the bulk value with the magnitude of this enhancement increasing with the aspect ratio. For k, we model the phonon scattering by a frequency-dependent relaxation time [1] and use a boundary-scattering ge-

ometry introduced by Prasher [2]. For fixed aspect ratio and small periods we find reductions in k of around 50%. Our results for P and k suggest that choosing a thermoelectric material as the matrix of a nanowire composite can contribute to enhance the composites ZT. [1] N. Mingo and D. A. Broido, Phys. Rev. Lett. 93, 246106 (2004). [2] R. Prasher, submitted.

**12:27**

**B35 5 Molecular dynamics simulation of shock-induced chemical, mechanical and thermal processes in Ni/Al nanolaminates** SHIJIN ZHAO, TIMOTHY GERMANN, ALEJANDRO STRACHAN, *Los Alamos National Laboratory* Nanostructured metastable intermolecular composites (MICs) are a new class of energetic materials with a wide range of applications. MICs can be made to react to form a more stable compound while releasing a large amount of energy and exhibit several unique properties, for example, extremely fast propagation of the chemical reactions when the initial components are intermixed at the nanometer scales. The fundamental molecular-level mechanisms that govern the unique properties of these materials are to a large extent unknown. We employ molecular dynamics to characterize the chemical and mechanical response of MICs induced by shock loading. We use detailed analysis methods to characterize the atomic level processes responsible for the initiation and propagation of the chemical reactions. Our simulations are designed to characterize the role of composition and nanostructure on the initiation and subsequent ultra-fast propagation of chemical reactions in nanostructured MICs as well as their mechanical and thermal properties.

**12:39**

**B35 6 Vibrations and thermal conductivity in inorganic and polymeric glasses.** SERGEI SHENOGIN, ARUN BODAPATI, PAWEL KEBLINSKI, *Rensselaer Polytechnic Institute* The mechanism of thermal transport in amorphous materials was studied by means of vibrational mode analysis and classical nonequilibrium molecular dynamics (MD) simulations. We studied four different model systems of (a) Lennard-Jones glass, (b) bead-spring model of an amorphous polymer, (c) amorphous silicon with Stillinger-Weber potential; and (d) all-atom model of glassy polystyrene with PCFF-type force field. For all structures we evaluated thermal conductivity from the harmonic theory of disordered solids [P.B.Allen, and J.L.Feldman, Phys.Rev.B 48, 12581 (1993)] and from direct MD simulations. We found that for all models but polystyrene, the harmonic theory accurately predicts thermal conductivity. By contrast, in the case of polystyrene, only $\sim$ 1/2 of thermal conductivity can be explained within the harmonic approximation. Consequently, a major part of the transport has to be attributed to anharmonic coupling between vibrational modes. The reasons for the failure of harmonic theory of disordered solids to model amorphous glassy polymers will be discussed.

**12:51**

**B35 7 Anomalous thermal transport in the low-conductivity phase of granular metals** VIKRAM TRIPATHI, *University of Cambridge, U.K.* YEN LEE LOH, *Purdue University, U.S.A.* We study the thermal conductivity of a nonmagnetic, nonsuperconducting granular metal in the low-conductivity phase using the Kubo formula approach, and compare it with the electrical conductivity. We find that the physical mechanisms and the temperature dependences of the two are very different. In a regular granular array, electrical transport, which takes place through the intergrain hopping of quasiparticles, obeys an Arrhenius law due to Coulomb blockade of quasiparticle hopping. Certain many-particle processes such as particle-hole cotunneling do not suffer Coulomb blockade due to their charge-neutrality and show a much slower power-law decrease with temperature; however, because of their charge-neutrality, these processes make no qualitative difference to the electrical conductivity. Cotunneling of particle-hole pairs does transport heat, and therefore, the thermal conductivity decreases only algebraically with temperature. This picture is reminiscent of excess thermal transport in disordered semiconductors due to low-energy excitons.

**13:03**

**B35 8 Molecular heat pump** DVIRA SEGAL, *Department of Chemical Physics Weizmann Institute of Science Rehovot 76100 Israel* ABRAHAM NITZAN COLLABORATION, A heat pump is a device that transfers heat from a low to a high temperature reservoir by applying an external work that modulates the system's parameters. In this work we discuss a novel molecular machine of this kind. The system consists of a molecular element connecting two thermal reservoirs that are characterized by different spectral properties. The pumping action is achieved by applying an external force that periodically modulates molecular levels. This modulation affects periodic oscillations of the internal temperature of the molecule and the strength of its coupling to each reservoir resulting in a net heat flow in the desired direction. The heat flow is examined in the slow and fast modulation limits and for different modulation waveforms, thus making it possible to optimize the device performance.

**13:15**

**B35 9 Transport and Noise in Mesoscopic Conductors Coupled to Quantized Electro-Magnetic Fields.** A.D. STONE, M.G. VAVILOV, *Yale University* Previous analyses of the effects of electro-magnetic (EM) fields on transport through mesoscopic systems have employed a classical treatment of the fields. To describe experiments on circuit electrodynamics [A. Wallraff et al., Nature 431, 162 (2004)] this treatment is no longer applicable. In this talk we discuss how the current and current noise through mesoscopic conductors are modified by the presence of such non-classical EM fields. For example when the EM field corresponds to a thermal state with temperature different from the electron temperature typically a steady-state current will flow through the system at zero bias due to the lack of detailed balance. The magnitude and direction of this current can be used to measure the temperature of the EM field. More generally, this current and its noise will allow measurement of non-classical properties of the EM field coupled to the system.

**13:27**

**B35 10 Elastomeric Network/Air Structures for Mechanically Tunable Hypersonic Phononic Crystals** TARAS GORISHNYY, JI-HYUN JANG, CHAITANYA K. ULLAL, EDWIN L. THOMAS, *Massachusetts Institute of Technology* Hypersonic phononic crystals allow control over high frequency phonons, which is crucial for a whole range of applications from acousto-optics to thermal management and high resolution nondestructive evaluation techniques. The ability to fabricate phononic crystals with a band diagram that can be modified reversibly and repeatedly opens an interesting possibility to create tunable acoustic devices. In this talk we will describe the use of submicron elastomeric PDMS (poly(dimethylsiloxane))/air network structures as tunable phononic crystals operating in hypersonic frequency re-

gime. The structures were fabricated from interference lithography templates, which were infiltrated with PDMS precursor and then after crosslinking the photoresist template was removed in water-based basic solution. Brillouin light scattering was used to monitor the modification of the phononic band diagram of these elastomeric structures as a function of the direction and degree of reversible mechanical deformation. The influence of symmetry and anisotropic sound velocities on the features of the phononic band diagram will be discussed.



**SESSION B36: ELECTRONIC PROPERTIES OF NANOWIRES**
**Monday Morning, 13 March 2006**
**339, Baltimore Convention Center at 11:15**
**Allan Bracker, Naval Research Laboratory, presiding**

**11:15**
**B36 1 1D-1D Tunneling in Vertically Coupled Quantum Wires** E. BIELEJEC, S. K. LYO, J. A. SEAMONS, J. L. RENO, M. P. LILLY, *Sandia National Laboratories* We report tunneling measurements between two vertically coupled quantum wires in a GaAs/AlGaAs double quantum well structure with a 7.5 nm barrier. Split gates above and below the electron bilayer define each quantum wire and allow separately controlled 1D densities. Separate contacts are achieved with additional depletion gates. Parallel conductance as a function of split gate voltages provides a map of the 1D subband occupation; tunneling measurements can be made with any combination of subbands occupied in each wire. The full tunneling spectroscopy is measured using both a voltage between the wires and parallel magnetic field to explore the energy and momentum dependence of the tunneling. We observe a number of features, such as resonance peaks at high parallel magnetic fields, that can be explained within the framework of non- interacting 1D systems. These resonance features change in a systematic way as the number of occupied subbands changes. Other characteristics of the data such as very broad tunnel resonances as a function of the interwire voltage may require many-body interactions for a complete description of the tunneling physics. Sandia is a multiprogram laboratory operated by Sandia Corporation, a Lockheed Martin Company, for the United States Department of Energy under contract DE-AC04- 94AL85000.

**11:27**
**B36 2 Tunable double quantum dots in InAs nanowires defined by local gate electrodes.** CARINA FASTH, ANDREAS FUHRER, LARS SAMUELSON, *Lund University* We present low-temperature transport measurements on quantum dots induced in homogeneous InAs quantum wires 50 nm in diameter. Quantum dots are induced by electrical depletion of the wire using local gate electrodes with down to 30 nm electrode spacing. This scheme has permitted the realization of fully gate-defined multiple quantum dots along the nanowire [1]. Tunability in double quantum dots is a prerequisite for the system to be operated as a quantum gate. We demonstrate control over the lead tunnel barrier transparencies and, in the case of double quantum dots, the interdot coupling. Using the local gate electrodes also as plunger gates we measure double dot honeycomb stability diagrams which show the transition from a single large dot to two weakly coupled dots at 4.2K. The induced quantum dots can be tuned into the few-electron regime which is shown from Coulomb blockade measurements. We extract values of orbital energy-level spacings, capacitances and capacitive and tunnel interdot coupling for this system. [1] C. Fasth et al., NanoLett 5, 1487 (2005).

**11:39**
**B36 3 Orbital and Spin Effects in Single- and Double-Quantum Dots Defined in InAs/InP Nanowire Heterostructures.** ANDREAS FUHRER, LINUS FROBERG, LARS SAMUELSSON, *The Nanometer Structure Consortium, Lund Universtity, Lund, Sweden* Heterostructures in semiconducting nanowires are highly promising in terms of their potential for novel physics and device applications. We present measurements on single (double) quantum dots fabricated using InP double (triple) barrier heterostructures in InAs nanowires. Transport spectroscopy measurements on single dots show that we can design few-electron quantum dots in nanowires where the well defined geometry leads to shell structure effects. We also show that the Zeeman splitting of the first few electrons can be engineered to any desired effective g-factor between $|g^*|=2.5$ and values close to the bulk value of InAs $|g^*|=13$ [1]. In extension of this, transport spectroscopy in the few- electron regime of double quantum dots consisting of two InAs islands in series have been performed. These double dots are tuned using a single homogenous backgate, which together with a source-drain bias allows us to controllably empty both dots down to the last electron. Again we observe a shell-structure which can be linked to the geometric cross-section of the wire and an orbital blockade effect is observed depending on the character of the wavefunctions in each dot. [1] M. Björk et al., cond-mat/0507433, 2005

**11:51**
**B36 4 Ultra-dense nanowire arrays*** EZEKIEL JOHNSTON-HALPERIN, J.E. GREEN, D.W. WANG, E. DEIONNO, J.W. CHOI, Y. LUO, A. BOUKAI, Y. BUNIMOVICH, B.A. SHERIFF, J.R. HEATH, *Division of Chemistry and Chemical Engineering, The California Institute of Technology, Pasadena, CA* The development of the superlattice nanowire pattern transfer (SNAP) technique has allowed for the fabrication of highly ordered arrays of hundreds of nanowires (both metallic and semiconducting) at pitches down to 16 nm and aspect ratios up to $10^6$. Applications of these nanowire arrays range from bridging length scales via binary-tree demultiplexing [1], to the development of ultra-dense arrays of molecular switch tunnel junctions ( $\sim$ 1 TBit/in$^2$), to the integration of complementary logic arrays within a crossbar architecture. In addition, at the narrowest pitches the periodicity of the SNAP array is only a few tens of atoms, allowing access to length scales compatible with coherent electronic transport and opening the door to fundamental studies. These topics will be discussed within the context of the flexibility of the SNAP fabrication technique and its wide applicability to a number of both basic and applied challenges in nanoscience/nanotechnology. [1] Science, 310, 465 (2005).

*Funding provided by DARPA.

**12:03**

**B36 5 Ag nanowires on Cu(110) and Ni(110): atomic structure and electronic dimensionality*** RICHARD KURTZ, PHILLIP SPRUNGER, WEICHANG ZHAO, YAROSLAV LOSOVYI, *Louisiana State University* Epitaxial Ag nanowires have been found to self-assemble on Cu(110) or on Ni(110) at Ag coverages exceeding 1.2 ML. The atomic and electronic structure of these nanowires have been characterized by scanning tunneling microscopy (STM) and angle-resolved photoemission spectroscopy (ARPES). STM shows that the Ag(110)-oriented nanowires that are straight and parallel to the [110] direction with a uniform width (height) ranging between 10-30 nm (2-3 nm) depending on coverage. The nanowires have a triangular cross-section and expose two sides of facets that slope at an angle of approx 25 deg with respect to the surface. Overall length-to-width aspect ratios up to 20:1 have been observed. The substrate-wire lattice mismatch induces an anisotropy in the nanowire with a strained lattice match in the [001] (across-wire) direction and an incommensurate periodicity, essentially decoupled from the substrate, in the [110] (along-wire) direction. Angle-resolved photoemission data reveals Ag d-band dispersion in the vertical (or (110)) and the lateral [110] (or along-wire) direction, but absence of dispersion in the lateral [001] (or across-wire) direction because of the limited dimension of the nanowire width. This anisotropic electronic dimensionality correlates with the structural asymmetry.

*Funding through NSF-0504654 & LA BoR

**12:15**

**B36 6 Electronic structure of self-assembled Si nanowires on Ag(110) surfaces** TAISUKE OHTA, *Fritz Haber Institute/LBNL* ELI ROTENBERG, *Lawrence Berkeley National Laboratory* KARSTEN HORN, *Fritz Haber Institute* Much attention has recently been paid to the physics of one- dimensional (1-D) systems, since exotic properties are predicted from basic theoretical consideration. However, it is not easy to realize such one-dimensional systems experimentally. Recently, Leandri et al.[1] have reported the growth of self-assembled 1D linear structures of silicon on Ag(110), perfectly aligned along [-110] direction and 16Å wide. We have investigated the electronic structure of such self-assembled Si nanowires using angle resolved photoemission spectroscopy. The Si 2p core level line shows two narrow components in agreement with earlier work [1]. Silicon-induced features in the valence band region are observed, most clearly within the band gap of the Ag s-p states. The silicon-induced band exhibits a sizeable dispersion only in the direction along the linear structure, i.e. the [- 110] azimuth of the Ag(110) substrate. Details of the experimentally observed bands will be presented and related to the atomic structure within the 1D structure and its arrangement on the silver substrate. T.O. acknowledges financial support from Max Planck Society. Experiments were performed at the Advanced Light Source, Lawrence Berkeley National Laboratory operated by the U.S. DOE under Contract No. DE-AC03-76SF00098. [1] C. Leandri et al., Self-aligned silicon quantum wires on Ag (110), Surface Science 574 (2005) L9L15

**12:27**

**B36 7 One-dimensional Pt induced chains on Si(337)** JESSICA MCCHESNEY, *Montana State University* A. BOSTWICK, E. ROTENBERG, *Advanced Light Source* GERALD LAPEYRE, *Montana State University* The use of high index Si surfaces as templates for the formation of adsorbate induced one-dimensional chain structures have attracted considerable interest. These systems have been used as a test bed in which to study low-dimension physics and components of nanoelectronics. In addition to the Ag and Au induced chains reported to form on the Si(337) surface, Pt also produces one-dimensional chains. Angle-resolved photoemission spectroscopy was used to investigate the electronic structure of these new Pt chains. The valence band mapping confirms the one-dimensional nature of these chains as seen in LEED. Supported by ONR and DOE.

**12:39**

**B36 8 The Coulomb blockade regime in disordered AlAs cleaved-edge overgrown quantum wires** JOEL MOSER, *Walter Schottky Institut, TU Muenchen, Am Coulombwall 3, D-85748 Garching, Germany* DIETER SCHUH, *Walter Schottky Institut, TU Muenchen, Am Coulombwall 3, D-85748 Garching, Germany* MAX BICHLER, *Walter Schottky Institut, TU Muenchen, Am Coulombwall 3, D-85748 Garching, Germany* MATTHEW GRAYSON, *Walter Schottky Institut, TU Muenchen, Am Coulombwall 3, D-85748 Garching, Germany* STEFANO RODDARO, *Scoula Normale Superiore, Via della Faggiola 17/19, I-56126 Pisa, Italy* VITTORIO PELLEGRINI, *Scoula Normale Superiore, Via della Faggiola 17/19, I-56126 Pisa, Italy* We present transport measurements on AlAs quantum wires in the pinch-off regime, where the wire breaks up into zero-dimensional islands of electrons and Coulomb blockade sets in. Conductance resonances as a function of gate bias vanish at low temperature T, and a gap bounded by two peaks opens up in the differential conductance as a function of source-drain dc bias V. We propose two interpretations for these results: (i) low T, low V transport is limited by incoherent tunneling through 2 asymmetric quantum dots in series; (ii) at pinchoff the wire carries a collective mode that is pinned by disorder, but can be depinned by a finite threshold bias V.

**12:51**

**B36 9 The transition from a one-dimensional to a quasi-one-dimensional state in interacting quantum wires*** JULIA S. MEYER, *The Ohio State University* KONSTANTIN A. MATVEEV, *Argonne National Laboratory* ANATOLY I. LARKIN, *W.I. Fine Theoretical Physics Institute, University of Minnesota* Upon increasing the density of electrons in a quantum wire, the system undergoes a transition from a one-dimensional to a itquasi-one-dimensional state. In the absence of interactions between electrons, this corresponds to filling up the second subband of transverse quantization. On the other hand, strongly interacting one-dimensional electrons form a Wigner crystal, and the transition corresponds to it splitting into two chains (zig-zag crystal). While the two subbands in the non-interacting case represent two gapless electron modes, in the Wigner crystal the two chains are locked, i.e., the relative motion is gapped, and only one gapless mode remains. We study the evolution of the system as the interaction strength changes. In particular, we establish that only one gapless mode exists near the transition at any interaction strength.

*This work was supported by the U.S. DOE, Office of Science, under Contract No. W-31-109-ENG-38.

**13:03**

**B36 10 Exciton Energy Transfer between Asymmetric Quantum Wires** S.K. LYO, *Sandia National Laboratories, U. S. A.* K.F. KARLSSON, H. WEMAN, K. LEIFER, A. RUDRA, E. KAPON, *Ecole Polytechnique Federale de Lausanne (EPFL), Switzerland* We present theoretical result and data for the Stokes exciton transfer rate from a narrow quantum wire (n-QWR) to a parallel wide QWR (w-QWR) separated by a wide barrier and also to an array of parallel w-QWRs. The transfer rate is calculated as

a function of the distance $d$ between n-QWR and w-QWR and also the array. The dependence of the rate on the temperature and the localization radius is studied for free and localized excitons, respectively. Both the resonant and non-resonant rates are considered. We find that, for energy transfer between two QWRs, the Förster dipole-dipole transfer dominates the transfer rate at short and intermediate distances. The photon-exchange transfer prevails only at an extremely long distance where the rate is negligibly small. This behavior is in contrast with the two-dimensional quantum wells, where the photon-exchange mechanism is dominant except at a very short distance. However, the photon-exchange transfer rate continues to increase as the array size grows to a macroscopic scale due to its slow range dependence while the dipolar rate saturates quickly with the array size. The prediction of the theory is consistent with the data from V-groove $GaAs/Al_xGa_{1-x}As$ double QWRs. Supported by the US DOE (SKL), Swedish Foundation for Strategic Research, Swedish Research Council, and Ericsson's Research Foundation.



**13:15**

**B36 11 Spin excitation velocities in multi-channel quantum wires** EUGENE PIVOVAROV, MICHAEL FOGLER, *UC San Diego* We investigate how an external magnetic field affects the interaction corrections to the velocities of spin collective modes in quantum wires. We show that both many-body and single- particle effects are important. The former generate logarithmic field dependence that can alter the Hartree-Fock results by up to a factor of two. On a single-particle level, the field modifies the subband wavefunctions and therefore the effective interaction strength. This theory is applied to quantum wires fabricated by the recently introduced cleaved edge overgrowth technique and the results are compared with experiments [Auslaender *et al.* Science **308**, 88 (2005)].

**13:27**

**B36 12 Junctions of Three Quantum Wires of spin-1/2 Electron System** CHANG-YU HOU, *Department of physics, Boston University* CLAUDIO CHAMON, *Department of physics, Boston University* MASAKI OSHIKAWA, *Department of Physics, Tokyo Institute of Technology* IAN AFFLECK, *Dept. of Phys. and Astro., University of British Columbia* We study a junction of three interacting quantum wires which are joined by a ring enclosing a magnetic flux. The wires are modeled as single channel spin-1/2 Tomonaga-Luttinger Liquids (TLL). We study the problem by identifying the boundary conditions corresponding to the low energy fixed points through both Delay Evaluation Boundary Condition and Boundary Conformal Field Theory method. We obtain a rich phase diagram as the function of the TLL interacting parameter, $g_c$ and $g_s$, including a chiral regime in which the asymmetric current flow is highly sensitive to the sign of the flux and a phase in which electron pair tunneling dominates.

**13:39**

**B36 13 Effect of electron-electron interaction on linear and nonlinear optical phenomena in quantum dot systems in interlevel resonance region** VICTOR BONDARENKO, *WSU* MIROSLAW ZALUZNY,* *IF UMCS* YANG ZHAO, *WSU* We theoretically investigate linear and nonlinear optical phenomena in quantum dot (QD) systems caused by interlevel transitions. Effect of electron-electron (e-e) interaction in the systems on the optical phenomena is in the focus of the work. The e-e interaction is taken into account by employing the self-consistent field approach in the quasistatic limit. We show that presence of metal surface, and especially another resonant system, can dramatically enhance the effect of the e-e interaction on the optical phenomena. We discuss the conditions for the intrinsic optical bistability in QD systems caused by the e-e interaction. The obtained results can find applications for design, fabrication, and exploiting nanooptoelectronics devices, in part, all-optical components like QD-based optical switches and optical transistors.

*Poland

**SESSION B37: HIGH-TC: STM AND PSEUDOGAP**
**Monday Morning, 13 March 2006**
**340, Baltimore Convention Center at 11:15**
**J. Y. T. Wei, University of Toronto, presiding**

**11:15**

**B37 1 Signatures of strong correlations in the tunneling spectra of superconducting doped Mott insulators** TIAGO C. RIBEIRO, *University of California, Berkeley* XIAO-GANG WEN, *Massachusetts Institute of Technology* We compare the tunneling spectra from BCS mean-field theory and from a mean-field theory of superconducting doped Mott insulators to address the signatures of strong correlations in tunneling experiments, namely the bias sign asymmetry, the generic lack of evidence for the Van Hove singularity and, in some cases, the absence of coherence peaks. We also establish the connection between tunneling spectroscopy and ARPES observations in the cuprate superconductors. Thus, we provide a consistent description of these two experimental techniques which probe the single electron microscopic physics of the cuprates.

**11:27**

**B37 2 Controlling hole concentration in superconducting $YBa_2Cu_3O_{7-\delta}$ thin films for spectroscopic studies*** MATTHEW BRINKLEY, WAN KYU PARK, XIAOFANG ZHAI, JAMES ECKSTEIN, LAURA GREENE, *University of Illinois at Urbana-Champaign* UNIVERSITY OF ILLINOIS AT URBANA-CHAMPAIGN COLLABORATION, One of the remaining controversial issues in the high-$T_c$ cuprate superconductors is whether the $d$-wave order parameter is robust over the whole doping range. As an essential first step to address this, we optimize a growth procedure for high-quality sputter-deposited $YBa_2Cu_3O_{7-\delta}$ thin films with various hole concentrations by controlling the oxygen content (and by cation doping in the future). Two different approaches have been attempted successfully: annealing in an oxygen-controlled environment and ozonization. We have developed an itin-situ annealing procedure employing two-step post-deposition anneals in vacuum and $O_2$. The oxygen content is estimated from high-resolution x-ray diffraction data. This procedure produces high-quality thin films, optimally doped (e.g., $7\text{-}\delta \approx 6.88$, $T_{c,on}=91.8$ K, and $\Delta T_c < 0.9$ K) and underdoped (e.g., $7\text{-}\delta \approx 6.43$, $T_{c,on}=55.1$ K, and $\Delta T_c < 2.9$ K). Preliminary ozonization experiments show that varying the oxygen content in a controlled manner is feasible, especially in the overdoped regime. We will present detailed transport measurements, materials characterizations, and some initial conductance spectra from planar tunneling and Andreev reflection spectroscopies. *Supported by the U.S. DoE Award No. DEFG02-91ER45439 through the FSMRL and the CMM at UIUC.

**11:39**

**B37 3 Point-contact spectroscopy of the electron-doped cuprate superconductor $Pr_{2-x}Ce_xCuO_4$ in magnetic fields up to 32 tesla*** SUNGHEE YUN, TARA DHAKAL, JACOB TOSADO, AMLAN BISWAS, *Department of Physics, University of Florida, Gainesville, FL* BING LIANG, RICHARD GREENE, *Center for Superconductivity Research, University of Maryland, College Park, MD* Tunneling spectra of the normal state of electron-doped cuprates at low temperatures and in magnetic fields higher than the upper critical field ($H_{c2}$) have shown evidence of a pseudogap. However, to understand if the origin of this pseudogap is the same as the pseudogap observed in hole-doped cuprates and to determine the theoretical model it supports, it is necessary to study the effect of high magnetic fields on this pseudogap. Point contact spectroscopy (PCS) was carried out on junctions between electron doped cuprate $Pr_{2-x}Ce_xCuO_4$ (PCCO, $0.13 < x < 0.17$) single crystals and normal metal (Pt-Rh). To probe the normal state at low temperatures ($T \sim 1.5$ K), the superconductivity was suppressed by applying high magnetic fields (up to 32 T). These experiments showed that the normal state gap is present for all the dopings, including the overdoped one. These results at high magnetic fields can be interpreted as a combined effect of precursor superconductivity and the presence of disorder in these materials.

*Supported by the In House Research Program of the NHMFL, Tallahassee

**11:51**

**B37 4 Density of state correlations in pseudogap systems** MARIANNA MALTSEVA, *Rutgers University* PIERS COLEMAN, *Rutgers University* Developments in the scanning tunneling microscopy and spectroscopy (STM/STS), make it possible to probe the detailed position and energy- dependent density of states in electronically inhomogenious media [1,2]. Theoretical analysis to date has focused on the spatial autocorrelations of the density of states as a probe of the quasiparticle spectrum. In this work we discuss how correlations between the density of states above and below the Fermi energy can be used to discern the underlying nature of the pseudogap order. We can divide the density of states fluctuations into components that are symmetric and antisymmetric about the Fermi energy. Density waves produce a signal in the antisymmetric channel whereas superconductors produce a signal in the symmetric channel. Moreover, a careful analysis of the momentum dependence can be used to discern between off-diagonal and diagonal disorder [3]. We will present our theory of these topics. [1] H. C. Fu, J. C. Davis, and D.-H. Lee, cond-mat/0403001. [2] J.-X. Zhu, K. McElroy, J. Lee, T. P. Devereaux, Qimiao Si, J.C. Davis, and A.V. Balatsky, cond-mat/0507621. [3] T.S. Nunner, B.M. Andersen, A. Melikyan, and P.J. Hirschfeld, Phys. Rev. Lett. 95, 177003 (2005).

**12:03**

**B37 5 Observation of the pseudogap features in overdoped Bi2Sr2CaCu2O8+d by breakjunction tunneling spectroscopy*** Y. XUAN, H. J. TAO, Z. Z. LI, B. R. ZHAO, Z. X. ZHAO, *National Laboratory for Superconductivity, Institute of Physics and Center for Condensed Mater Physics, Chinese Academy of Sciences, China* C.T. LIN, *Max-Planck-Institut für Festkörperforschung, 70569 Stuttgart, Germany* Tunneling measurements of Bi2Sr2CaCu2O8+d single crystals with different oxygen doping have been carried out by using break-junction technique to study the pseudogap in the overdoped regime. The normal-state pseudogap has been observed clearly in the three overdoped crystals with Tc = 90 K, 82 K, and 72 K, respectively. Furthermore, direct measurements on the pseudogap opening temperature T*, by tracing the disappearance of the tunneling conductance peak, reveal that the relationship of T* versus hole concentration is linear and its extrapolation just crosses the end of the superconducting phase boundary.

*This work was Supported by a grant for State Key Program for Basic Research of China, and the National Center for Research and Development on Superconductivity.

**12:15**

**B37 6 Gap Inhomogeneity-Induced Electronic States in Superconducting $Bi_2Sr_2CaCu_2O_{8+\delta}$** ALAN FANG, *Stanford University* LUCA CAPRIOTTI, *Credit Suisse First Boston, Ltd. (Europe)* DOUG SCALAPINO, *University of California, Santa Barbara* STEVE KIVELSON, *Stanford University* NOBU KANEKO, *National Institute of Advanced Industrial Science and Technology (Japan)* MARTIN GREVEN, AHARON KAPITULNIK, *Stanford University* We use STM to measure nearly optimally doped $Bi_2Sr_2CaCu_2O_{8+\delta}$ in zero field. Focusing on the superconducting gap, we find patches of what appear to be two different phases in a background of some average gap, one with a relatively small gap and sharp large coherence peaks and one characterized by a large gap with broad weak coherence peaks. We compare these spectra with calculations of the local density of states for a simple phenomenological model in which a $2\xi_0 \times 2\xi_0$ patch with an enhanced or supressed d-wave gap amplitude is embedded in a region with a uniform average d-wave gap.

**12:27**

**B37 7 Electronic modulations in the pseudogap state of $Bi_2Sr_2CaCu_2O_{8+d}$ and $Ca_{2-x}Na_xCuO_2Cl_2$*** ABHAY PASUPATHY, AAKASH PUSHP, KENJIRO GOMES, *Princeton University* SHIMPEI ONO, *CRIEPI* YASUSHI ABE, *AIST* YOICHI ANDO, *CRIEPI* HIROSHI EISAKI, *AIST* KYUNG HEE KIM, HYE KYONG LEE, SUNG-IK LEE, *POSTECH* ALI YAZDANI, *Princeton University* The nature of the local modulations of the density of states (DOS) found in the pseudogap regime of the cuprates is still a mystery. Using variable-temperature scanning tunneling spectroscopy we observe non-dispersive spatial DOS modulations in the pseudogap state of $Bi_2Sr_2CaCu_2O_{8+d}$ (1) and $Ca_{2-x}Na_xCuO_2Cl_2$ (2). We will compare the nature of modulations found in these materials to various models such as those arising from interference effects due to impurity scattering or from local electronic organization. We will also discuss the spatial variation of the pseudogap in $Bi_2Sr_2CaCu_2O_{8+d}$ and $Ca_{2-x}Na_xCuO_2Cl_2$. (1) Vershinin et al., Science 303, 1995 (2004) (2) Hanaguri et al., Nature 430, 1001 (2004).

*This work was supported by NSF, DOE and ONR

**12:39**

**B37 8 Influence of vortex quantum fluctuations on the electronic spectra of superconductors** LORENZ BARTOSCH, *Harvard University* SUBIR SACHDEV, *Harvard University* We compute the influence of the zero point motion of vortices on the electronic quasiparticle spectra of two-dimensional *s*- and *d*-wave superconductors. In the core region the zero point motion of the vortices leads to a shift of spectral weight away from the Fermi level and thereby reduces the zero bias conductance peak. We discuss the relationship of our results to STM measurements on the cuprates and the observed 7 meV LDOS peaks near the core of vortices.

**12:51**

**B37 9 Local effects of impurities on the Pseudogap State of Bi-2212*** KENJIRO GOMES, *Princeton University* AAKASH PUSHP, *Princeton University* ABHAY PASUPATHY, *Princeton University* SHIMPEI ONO, *CRIEPI* YASUSHI ABE, *AIST* YOICHI ANDO, *CRIEPI* HIROSHI EISAKI, *AIST* ALI YAZDANI, *Princeton University* Some of the most surprising properties of the cuprates are found in the pseudogap state, above the superconducting transition temperature Tc on underdoped samples. Modifications of the local density of states (LDOS) due to the presence of atomic impurities can unveil clues about the nature of the pseudogap. Using atomically resolved scanning tunneling spectroscopy we map the LDOS near Zn and Ni impurities in Bi-2212 above Tc. We find modifications of the pseudogap LDOS near both Ni and Zn sites. We will report on the spatial dependence of these variations and how they relate to the underlying pseudogap state.

*This work was supported by NSF, DOE and ONR

**13:03**

**B37 10 Scanning Tunneling Spectroscopy Studies of Current-Carrying Superconductors*** J. NGAI, P. MORALES, J. Y. T. WEI, *Department of Physics, University of Toronto* Understanding how a superconducting order parameter evolves in the current-carrying state is of fundamental physical importance. In this talk we present novel applications of scanning tunneling spectroscopy (STS) on current-carrying superconductors, with the current either directly applied [D. Zhang et al., Phys. Rev. B 70, 172508 (2004)] or induced by a magnetic field [G. Deutscher, Rev. Mod. Phys. 77, 109 (2005)]. We will discuss STS measurements on YBa2Cu3O7 thin-film strips under directly-applied current, showing suppression of the d- wave Andreev states [J. Ngai et al. Phys. Rev. B 72, 054513 (2005)]. We will also discuss more recent STS experiments on high-Tc and other superconductors, performed under magnetic field-induced currents.

*This work was supported by NSERC, CFI/OIT, CIAR,Walter C. Sumner Foundation

**13:15**

**B37 11 High Precision Spectroscopic Imaging of Single Layer Cuprate: $Bi_2Sr_{1.6}La_{0.4}CuO_{6+x}$** A.M. WANG, J. LEE, J. SLEZAK, *LASSP, Dept. of Physics, Cornell University* K. FUJITA, *Dept. of Adv. Mater. Sci., University of Tokyo* H. EISAKI, *AIST, Japan* S. UCHIDA, *Dept. of Physics, University of Tokyo* J.C. DAVIS, *LASSP, Dept. of Physics, Cornell University* We present high spatial resolution scanning tunneling spectroscopy (STS) study of single layer cuprate $Bi_2Sr_{1.6}La_{0.4}CuO_{6+x}$. The sample is optimally doped, with $T_c = 34$K. We focus on two main points: (1) Quasiparticle interference pattern obtained by Fourier transform of high resolution local density of states (LDOS) map, (2) LDOS map shows even stronger nanoscale electronic disorder than double layer cuprate $Bi_2Sr_2CaCu_2O_{8+x}$ of similar doping. Inside the primary energy gap, at very low energies, small LDOS peaks emerge and exhibit short range modulations in their heights. Scattering by La substitution on Sr sites may be key to these new phenomena.

**13:27**

**B37 12 Atomic-resolution tunneling asymmetry mapping in $Ca_{2-x}Na_xCuO_2Cl_2$: charge distribution, crystal distortion and superconducting electronic structure properties of glassy electronic nanodomains** Y. KOHSAKA, C. TAYLOR, *LASSP, Cornell University* C. LUPIEN, *Universite de Sherbrooke* T. HANAGURI, H. TAKAGI, *RIKEN* M. AZUMA, M. TAKANO, *Kyoto Univerisity* J. C. DAVIS, *LASSP, Cornell University* We report spectroscopic imaging on the electronic state in a lightly-doped high-$T_c$ superconductor $Ca_{2-x}Na_xCuO_2Cl_2$. Conductance maps at $|E| < 100$ mV show $4a_0$ correlation 'checkerboard' patterns ($a_0$: in-plane lattice constant) [1]. At higher energies, the electronic state shows strong hole-electron asymmetry changing with the doping levels. The asymmetry integrated up to 600 mV changes at atomic scale and exhibits spatial patterns with $4a_0$ correlation, consistent with spatial modulation of hole density [2]. At intermediate energies, the asymmetry structures locally break rotational symmetry of background lattice, forming uni-directional and glassy nano-domains with $4a_0$ correlation. In-plane oxygen atoms appear electronically inequivalent, implying oxygen orbitals are key for physics in this energy range. We also discuss atomic motions and relationship of superconductivity to the glassy electronic nano-domains. [1] T. Hanaguri *et al.*, Nature 430, 1001 (2004). [2] M. Randeria *et al.*, PRL 95, 137001 (2005).

**13:39**

**B37 13 Low energy spectroscopic mapping study on $(Ca,Na)_2CuO_2Cl_2$** T. HANAGURI, *RIKEN (Inst. Phys. and Chem. Research)* Y. KOHSAKA, J. C. DAVIS, *LASSP, Cornell University* I. YAMADA, M. AZUMA, M. TAKANO, *Inst. Chem. Research, Kyoto University* K. OHISHI, *Japan Atomic Energy Agency* H. TAKAGI, *RIKEN (Inst. Phys. and Chem. Research) / University of Tokyo* Spatial variations of the low energy ( $<$ 50 meV) local density of states (LDOS) spectra of $(Ca,Na)_2CuO_2Cl_2$ ($T_c \sim$ 25 K) have been studied using scanning tunneling microscopy/spectroscopy (STM/STS) in the temperature range between 0.4 K and 20 K. Previous STM/STS studies revealed the checkerboard-like glassy electronic order which is associated with a V-shaped pseudogap $\sim$ 150 mV. [1] We have found another small gap ( $\sim$ 10 mV) with LDOS peaks at the gap edges. The gap-edge peak is spatially inhomogeneous and tends to disappear at elevated temperatures, suggesting that the small gap is related to superconductivity. [1] T. Hanaguri *et al.*, Nature **430**, 1001 (2004).

**13:51**

**B37 14 Many-Impurity Effects in Fourier Transform Scanning Tunneling Spectroscopy** WILLIAM ATKINSON, *Trent University* Fourier transform scanning tunneling spectroscopy (FTSTS) is a useful technique for extracting details of the momentum-resolved electronic band structure from inhomogeneities in the local density of states due to disorder-related quasiparticle scattering. To a large extent, current understanding of FTSTS is based on models of Friedel oscillations near isolated impurities. Here, a framework for understanding many-impurity effects is developed based on a systematic treatment of the variance $\Delta\rho^2(\mathbf{q},\omega)$ of the Fourier transformed local density of states $\rho(\mathbf{q},\omega)$. One important consequence of this work is a demonstration that the poor signal-to-noise ratio inherent in $\rho(\mathbf{q},\omega)$ due to randomness in impurity positions can be eliminated by configuration averaging $\Delta\rho^2(\mathbf{q},\omega)$. Furthermore, we develop a diagrammatic perturbation theory for $\Delta\rho^2(\mathbf{q},\omega)$ and show that an important bulk quantity, the mean-free-path, can be extracted from FTSTS experiments.

**14:03**

**B37 15 Atomic-resolution Inelastic Electron Tunneling Spectroscopy studies of doping dependence of electron-boson interaction in Bi-2212** JINHO LEE, *Cornell University* K. MCELROY, *Lawrence Berkeley Laboratory* J. SLEZAK, *Cornell University* K. FUJITA, *University of Tokyo, Japan* J.-X. ZHU, *Los Alamos National Laboratory* A.V. BALATSKY, *Los Alamos National Laboratory* S. UCHIDA, *University of Tokyo, Japan* H. EISAKI, *University of Tokyo, Japan* J.C. DAVIS, *Cornell University* Inelastic Electron Tunneling Spectroscopy(IETS) has been one of the most powerful tool to probe collective modes in the solids. We use the recently developed itSTM-based Atomic-resolution Inelastic Electron Tunneling Spectroscopy(IETS) technique to study the doping dependence of the electron-boson interactions(EBI) in Bi-2212 high-Tc cuprates. According to our results, the distribution of the bosonic mode energy($\Omega$) does not change as doping level changes, while the gap distribution changes greatly. Also $\Omega$-maps show nano-scale disorder. We will discuss the possible origin of this doping independent EBI.

**SESSION B38: SUPERCONDUCTING DEVICES AND APPIICATIONS**
**Monday Morning, 13 March 2006**
**341, Baltimore Convention Center at 11:15**
**Michael Bleiweiss, Naval Academy Prep School, presiding**

**11:15**

**B38 1 Transition-edge sensors based on superconducting nanowires.** MATTHEW BELL, ANDREI SERGEEV, *University at Buffalo* GREGORY GOLTSMAN, *Moscow State Pedagogical University* JONATHAN BIRD, ALEKSANDR VEREVKIN, *University at Buffalo* We present our experimental study of superconducting NbN nanowire-based sensor. The responsivity of the sensor is strongly affected by the superconducting transition width of the nanostructure, which, in turn, is determined by the phase slip centers (PCSs) dynamics. The fluctuations and noise properties of the sensor are also discussed, as well as the devices' behavior at high magnetic fields. The ultimate performance of the sensor and prospects of the devices will be discussed, as well.

**11:27**

**B38 2 Frequency Noise in Superconducting Thin-Film Resonators** SHWETANK KUMAR, *Caltech* PETER DAY, HENRY LEDUC, BENJAMIN MAZIN, *JPL* MEGAN ECKART, JIANSONG GAO, *Caltech* JONAS ZMUIDZINAS, *Caltech* We present the results of low temperature (120 – 1200 mK) noise measurements performed on thin-film superconducting niobium resonators fabricated on a silicon substrate. The devices studied use coplanar waveguide (CPW) transmission lines and have resonance frequencies of around 4 GHz and quality factors in the range of Q $\sim$ $10^4$ to $10^6$. These resonators are similar to those used to make novel photon detectors and read out charge qubits. These resonators show excess frequency noise which varies as approximately $f^{-1/2}$. This excess noise limits the sensitivity of our photon detectors and likely effects the qubit performance as well. Two level systems (TLS) in amorphous thin-film dielectrics and oxide tunnel barriers have been shown to cause dissipation and decoherence in phase qubits. We suggest that noise in our resonators is also caused by TLS most likely near the surfaces of the substrate and metal films. To test this idea, we have measured the frequency shift, the quality factor and the frequency noise as a function of the device temperature and the microwave readout power. The frequency shift data agrees well with existing weak field TLS theory. We also find that the frequency noise decreases with increasing readout power and temperature and that decreased noise at higher powers is not due to simply device heating.

**11:39**

**B38 3 Measurement of environmental impedance at plasma frequency of Josephson junctions with microwave induced escapes** BO MAO, SIYUAN HAN, *Department of Physics and Astronomy, University of Kansas* Impedance of electromagnetic environment of a Josephson junction is critical to its dynamics. We show that microwave induced escape rate of Josephson junctions as a function of microwave frequency and power provides an excellent quantitative measurement of the environmental impedance at plasma frequency of the junction. It is shown that in strong microwave fields the effect of anharmonicity of the junction's potential well must be taken into account. Direct comparison of experimental result with numerical simulation allows one to extract environmental impedance at junction's plasma frequency.

**11:51**

**B38 4 Probing superconducting samples using a two-superconducting-nanowire device** DAVID PEKKER, *University of Illinois at Urbana-Chanmpaign* ALEXEY BEZRYADIN, DAVID S. HOPKINS, PAUL M. GOLDBART, An NQUID (nanowire SQUID) is a device featuring two thin-film superconducting leads connected by a pair of parallel narrow superconducting wires [1,2]. Thermal fluctuations of the order parameter in the superconducting wires endow the device with a nonzero lead-to-lead resistance ($R$). For short wires, $R$ also depends on the phase profile of the order parameter in the leads. Here, we consider the situation in which one of the leads carries a supercurrent perpendicular to the wires (a cross-current). We show that $R$ is a periodic function of this cross-current. Minima of $R$ occur whenever the phase-gain between the wire attachment-points along the lead carrying the cross-current is an integer multiple of $2\pi$. NQUID devices such as these may be useful for probing superconducting order in the leads or determining current-phase relations in various settings. The results of experiments on devices carrying cross-currents will be presented in a companion talk by Hopkins et al. [1] Hopkins et al., Science 308, 1762 (2005). [2] Pekker et al., Phys. Rev. B 72, 104517 (2005).

**12:03**

**B38 5 Measurement of superconducting phase gradients using a DNA-templated nanowire interference device** DAVID S. HOPKINS, DAVID PEKKER, PAUL M. GOLDBART, ALEXEY BEZRYADIN, *University of Illinois at Urbana-Champaign* We have fabricated an NQUID (i.e., a Nanowire SQUID) [1,2] in which two thin ( $\sim$ 15 nm) superconducting nanowires templated by DNA molecules are used to directly measure phase gradients of the Ginzburg-Landau order parameter along a superconducting strip of width $\sim$ 1 $\mu$m. A supercurrent flowing along the strip creates a phase difference between the contact-points of the nanowires. This causes the resistance of the two-wire device to oscillate as a function of the current flowing along the strip with a period equal to the amount of current required to create a $2\pi$ phase difference between the contact-points of the wires. We find that the period increases with decreasing

temperature, due to the increase in superfluid density in the film. Using this device we are able to study the process of superconductivity suppression in the thin film strip caused by a high bias-current and/or a magnetic field. A theory of the operation of such NQUIDs will be presented in a companion talk by Pekker et al. [1] Hopkins et al., Science 308, 1762 (2005). [2] Pekker et al., Phys. Rev. B 72, 104517 (2005).

**12:15**

**B38 6 Impedance matching using superconducting planar spiral inductors** UTKU KEMIKTARAK, *Physics Department, Boston University* KEITH SCHWAB, *Laboratory for Physical Sciences* KAMIL L. EKINCI, *Department of Aerospace and Mechanical Engineering, Boston University* We discuss the use of superconducting Nb inductors for impedance matching. The micro-fabricated inductors we used in our experiments had submicron line-widths with 50 to 200 turns. We first characterized these inductors by measuring their inductances, quality factors and self resonance frequencies. Then we compared these results with existing models. With the measured parameters, we showed that these inductors could be used for matching impedances on the order of megaohms to 50 $\Omega$.

**12:27**

**B38 7 Microstrip SQUID amplifiers with cooling fins*** DARIN KINION, *LLNL* JOHN CLARKE, *UC Berkeley and LBNL* Amplifiers based on dc SQUIDs (superconducting quantum interference devices) with integrated input coils configured as a microstrip resonator operate at frequencies between 50 MHz and 2 GHz, and in principle are capable of reaching the Standard Quantum Limit (SQL) for linear amplifiers. The SQUIDs are fabricated with Nb-AlOx-Nb tunnel junctions with Pd shunt resistors to eliminate hysteresis. In practice, Johnson noise in the shunt resistors often limits the noise temperature before the SQL is reached. To reduce this noise contribution we have attached large area cooling fins to the shunts to minimize hot- electron effects when the amplifier is operated at miilikelvin temperatures. Previous measurements were performed at frequencies corresponding to peak gain, but theory predicts that the lowest noise temperature should be attained at a slightly lower frequency. We have measured the noise temperature of a number of devices as a function of frequency and bath temperature. We compare our results to the predicted frequency dependence of the noise temperature and to the predicted value of the SQL.

*This work was supported by DOE.

**12:39**

**B38 8 RF Amplifiers Based on DC SQUID for 3-4 GHz Band*** G.V. PROKOPENKO, K.D. OSBORN, *National Inst. of Standards and Tech. - Boulder* S.V. SHITOV, *Inst. of Radio Engineering and Electronics, Moscow, Russia. Natl. Astronomical Observatory of Japan, Mitaka, Japan.* M. MAEZAWA, *Natl. Inst. of Advanced Industrial Science and Technology, Tsukuba.* A.J. SIROIS, K. CICAK, R.W. SIMMONDS, *National Inst. of Standards and Tech. - Boulder* DC SQUID based RF Amplifiers (SRFAs) are known to dissipate very little power and can be integrated on-chip with existing micro-fabricated circuits for low-noise, low temperature measurements. The SRFA chip has 4 independent channels, which amplify at different signal frequencies and have integrated output filters, which prevent the leakage of high frequency resonances associated with the Josephson frequency. A compact two-layer input signal coil is integrated with the washer of the SQUID (L=20 pH) and planar capacitors for tuned frequency and impedance matching. The input reflected power is further reduced using proven balanced configuration on the SQUID. The shunt resistors are made from a multilayer film Ti(2 nm)/Pd(55 nm)/Ti(2 nm), which allow the SRFA to operate down to 0.4 K. Low-noise SRFAs have been tested with an operating frequency range of 3-4 GHz.

*This work was supported by ARDA through Grant No. MOD717304

**12:51**

**B38 9 SQUID-detected magnetic resonance imaging in zero static magnetic field** N. KELSO, S-K. LEE, L. BOUCHARD, V. DEMAS, A. PINES, J. CLARKE, *UC Berkeley and LBNL* Conventional magnetic resonance imaging (MRI) is performed in a static homogenous magnetic field $B_0$ in the presence of applied field gradients that generate a magnetic field change $\Delta B << B_0$ across the sample. In this case, the concomitant gradients can be ignored and the applied gradients are unidirectional. When $\Delta B \sim B_0$, this approximation breaks down and the concomitant gradients distort the image. In the limit $B_0 \rightarrow 0$ these distortions can be eliminated by means of a pulse sequence consisting of a train of short, spatially uniform magnetic field pulses. Between the pulses, the spins evolve in a pure gradient field (with zero spatial average). The effect of the pulse train is to average out the concomitant terms to leave an effectively unidirectional gradient field (Meriles itet al., itPNAS 102, 1840 (2005)). We acquire magnetic signals with a superconducting gradiometer coupled to the input loop of a low-transition temperature superconducting quantum interference device. Using this pulse sequence we have acquired undistorted two-dimensional images of methanol phantoms in a residual static field $< 1\ \mu$T. Supported by USDOE.

**13:03**

**B38 10 Fast Non-Destructive Evaluation of Superconducting Magnet Wires using a Flow-Through SQUID Microscope*** JOHN MATTHEWS, FREDERICK WELLSTOOD, *University of Maryland* HAROLD WEINSTOCK, *Air Force Office of Scientific Research* We have developed a cryocooled high-Tc SQUID microscope for fast non-destructive evaluation (NDE) of long wires, designed for detecting defects in superconducting magnet wire. A feedthrough mechanism pulls the wire at speeds of up to 20 cm/s through a thin mylar tube that separates the room temperature wire from the SQUID. We present results on test wires where we detect defects down to about 0.3 mm diameter. We discuss how we extract information from the data, such as defect size and location, and also outline a method for fast automated detection of defects in long wires.

*Supported by the Center for Superconductivity Research, and Air Force Office of Scientific Research

**13:15**

**B38 11 Low-field SQUID MRI: To tune or not to tune?** MICHAEL HATRIDGE, WHITTIER MYERS, MICHAEL MÖßLE, NATHAN KELSO, JOHN CLARKE, *UC Berkeley / LBNL* BEN INGLIS, *UC Berkeley* ANDREAS TRABESINGER, *110 Stapleton Hall Rd., London N4, UK* Our magnetic resonance imaging (MRI) system detects protons precessing at 5.6 kHz in a 132-$\mu$T field using a superconducting quantum interference device (SQUID) coupled to an untuned superconducting second-order gradiometer with 65-mm diameter coils. The magnetic flux noise of the SQUID corresponds to a magnetic field noise of 0.4 fT $Hz^{-1/2}$. We consider whether the use of a tuned input circuit could

reduce the noise. The high intrinsic quality factor of the superconducting circuit must be damped to obtain the bandwidth required for MRI. The simplest approach is to insert a resistor in series with the gradiometer. However, the associated Nyquist noise causes this configuration to underperform the untuned version at frequencies below 100 kHz. In a more sophisticated approach Seton and coworkers damped the input circuit by coupling the SQUID output to the pickup coil. In principle, such feedback damping enables the tuned detector to achieve a field noise of 0.05 fT $Hz^{-1/2}$ at 5.6 kHz. The relative merits of these approaches over a wide frequency range are discussed. Work supported by USDOE.

**13:27**

**B38 12 SQUID-detected microtesla MRI: a new modality for tumor detection?** MICHAEL MÖßLE, SARAH BUSCH, MICHAEL HATRIDGE, WHITTIER MYERS, ALEXANDER PINES, JOHN CLARKE, *UC Berkeley and LBNL* LARS SCHMITT, JEFF SIMKO, *UC San Francisco* We are investigating the use of low-field magnetic resonance imaging with enhanced longitudinal-relaxation-time ($T_1$)-weighted contrast to detect tumors. Our technique involves prepolarizing the sample in a magnetic field up to 0.3 T and detecting the nuclear magnetic resonance (NMR) signal at microtesla fields using a superconducting quantum interference device. This technique enables us to obtain $T_1$ dispersion curves and $T_1$-weighted contrast images in fields from 1.4 $\mu$T to 0.3 T. We have shown that for materials such as agarose gel the $T_1$-weighted contrast is greatly enhanced in microtesla fields. To investigate the use of this enhancement for tumor imaging we measured the $T_1$ relaxation times of healthy and cancerous tissue specimens, maintained at 4[r]C, shortly after their surgical removal. To minimize artifacts we measured normal and cancerous tissues simultaneously and separated their NMR signals by applying a magnetic field gradient. We present $T_1$ dispersion curves for several sets of samples, and discuss the applicability of this technique to itin vivo imaging. Work supported by USDOE.

**SESSION B39: SUPERCONDUCTIVITY-MAGNETIC PROPERTIES**
**Monday Morning, 13 March 2006**
**342, Baltimore Convention Center at 11:15**
**Daniel Agterberg, University of Wisconsin, presiding**

**11:15**

**B39 1 Low temperature penetration depth measurements as a probe of anisotropic superconductivity in $NbSe_2$** ANTONY CARRINGTON, *University of Bristol, U.K.* JON FLETCHER, *University of Bristol, U.K.* PIERRE RODIERE, *CRTBT, Grenoble, France* Measurements of the field dependent thermal conductivity [1] and angle resolved photoemission spectroscopy (ARPES) [2] have provided evidence for strong gap anisotropy in $NbSe_2$ ($T_c \simeq 7.2$ K). A key result of the ARPES study was that one of the sheets of Fermi surface has a much smaller energy gap than the others. Here we investigate the gap structure of $NbSe_2$ using measurements of the temperature dependence of the magnetic penetration depth in single crystal samples at temperature down to less than 0.1 K. Although there is evidence for moderate gap anisotropy (around a factor two) we do not find any evidence for the energy gap being as small as suggested by the ARPES measurements on any sheet of Fermi surface. We will compare these $\lambda(T)$ measurements to specific heat measurements on the same samples. [1] Boaknin *et al.*, Phys. Rev. Lett. **90**, 117003 (2003) [2] Yokoya *et al.* Science **294**, 2518 (2001).

**11:27**

**B39 2 Phase-sensitive measurements of harmonic response in high-Tc superconducting thin films by means of local microwave microscopy** DRAGOS MIRCEA, STEVEN ANLAGE, *Center for Superconductivity Research, Department of Physics, University of Maryland* The microscopic origins of Meissner-state nonlinearities in superconductors are still not clear. Traditionally, microwave nonlinear measurements of superconducting thin films employ a spectrum analyzer to measure the power carried by the harmonic signals ($P_{2f}$and $P_{3f}$). Such measurements have provided strong evidence for the Nonlinear Meissner Effect (NLME) at the critical temperature $T_c$ in cuprates [PRB 71, 014507 (2005)]. Investigations of the NLME in underdoped $YBa_2Cu_3O_{7-\delta}$ (YBCO) thin films have revealed the existence of an additional nonlinear mechanism that onsets at $T_c$ and leads to the persistence of $P_{3f}$ above $T_c$, a feature which has not been observed in optimally-doped samples. A possible nonlinear source active at and slightly above $T_c$ is the current-dependent normal conductivity, as proposed earlier by Mishonov and co-workers [PRB 65, 064519 (2002)]. The measurements performed with a spectrum analyzer do not provide phase information about the harmonic signals and therefore the nature of the nonlinear source (inductive vs. resistive) remains undetermined. However, nonlinear phase-sensitive measurements can be carried out with a network analyzer in the frequency offset mode and such data are instrumental in disentangling the effects of different types of nonlinear mechanisms. Work supported by NSF-GOALI, grant no. DMR-0201261

**11:39**

**B39 3 Doping Dependence of the Magnetic Penetration Depth and Coherence Length in $YBa_2Cu_3O_y$** JEFF SONIER, FERGAL CALLAGHAN, *Simon Fraser University* JESS BREWER, WALTER HARDY, DOUG BONN, RUIXING LIANG, *University of British Columbia* While linear scaling of $T_c$ with superfluid density has been inferred from early muon depolarization rate ($\sigma$) measurements on high-temperature superconductors, this interpretation of $\mu$SR data assumes an invalid relation between $\sigma$ and the in-plane magnetic penetration depth $\lambda_{ab}$. From detailed measurements and analysis of the $\mu$SR line shapes in $YBa_2Cu_3O_y$ single crystals, we have accurately determined the doping dependence of $\lambda_{ab}$ and the superconducting coherence length $\xi_{ab}$. We find that $T_c$ exhibits a sublinear dependence on $1/\lambda_{ab}^2$, and that $\xi_{ab}$ increases with decreasing hole doping. In addition, the $\mu$SR line shapes for $y = 6.50$ are found to be consistent with $y = 0$ antiferromagnetism in and around the vortex cores, compatible with static stripes. We find that the antiferromagnetic order occurs only where superconductivity is suppressed, indicating that the ordering of copper spins competes with high-temperature superconductivity.

**11:51**

**B39 4 A magnetic analog of the isotope effect in cuprates** RINAT OFER, GALINA BAZALITSKY, AMIT KANIGEL, AMIT KEREN, ASSA AUERBACH, *Technion - Israel Institute of Technology* JAMES LORD, *Rutherford Appleton Laboratory, UK* ALEX AMATO, *Paul Scherrer Institute, Switzerland* Since the discovery of superconductivity in the cuprates, it has been speculated that their pairing mechanism is due to magnetic inter-

actions. However, this was never proven. Such a proof would require an experiment similar to the isotope effect in metallic superconductors, namely, a measurement of $T_c$ versus the in-plane super-exchange J, with no other structural changes. We have done this experiment using the $(Ca_xLa_{1-x})(Ba_{1.75-x}La_{0.25+x})Cu_3O_y$ system with its 4 different families having different $T_c^{max}$. For each family, we measured the Néel Temperature $T_N$, the anisotropies of the magnetic interactions, the spin glass temperature $T_g$ of underdoped samples, and, of course, $T_c$ from under to overdoped compounds. These properties were determined using the zero field muon spin resonance ($\mu$SR) technique, where one injects polarized muons into the sample and measures the time evolution of their spin polarization. Our measurements allow us to demonstrate that $T_c^{max} J_f^{-1}$ =const where f is a family index, and to prove experimentally that pairing in the cuprates stems from magnetic interactions.

**12:03**

**B39 5 Magnetization curves in underdoped cuprates measured at low T in fields up to 45 Tesla** LU LI, *Physics Department, Princeton University* YAYU WANG,* *Physics Department, Princeton University* MIKE NAUGHTON, *Boston College* S. ONO, *Central Research Inst., Electric Power Industry, Tokyo* YOICHI ANDO, *Central Research Inst.,Electric Power Industry, Tokyo* NAI PHUAN ONG, *Physics Department, Princeton University* Torque magnetometry is capable of resolving the weak diamagnetic which extends to temperatures $T \gg T_c$ in hole-doped cuprate crystals. Recently, we reported[1] that the magnetization $M$ above $T_c$ scales accurately as the Nernst signal $e_N$ and remains robust to fields of 33 T. The results strongly support the scenario in which thermally created vortices destroy long-range phase coherence at $T_c$. We have extended these studies to explore the fluctuation magnetization to 45 T in underdoped LSCO and Bi 2201 in a series of samples doped near the critical value $x_c \sim 0.055$. We investigate the loss of phase coherence as we decrease $x$ below $x_c$ keeping $T$ as low as 0.5 K. We use the $M$-$H$ curves to explore how singular phase fluctuations occur as superfluidity is destroyed when $x$ approaches the insulating Mott limit at low $T$. *Supported by NSF grant (DMR 0213706). 1. Yayu Wang et al., Phys. Rev. Lett., **95**, xxx *in press*, cond-mat/0503190; Lu Li $\eta$l, Eurpophys. Lett. **72**, 451-457 (2005).

*Current Address:University of California, Berkekey

**12:15**

**B39 6 Superconductivity and Glassiness in Strongly Underdoped $Y_{1-x}Pr_xBa_2Cu_3O_{7-\delta}$*** C. C. ALMASAN, V. SANDU, P. GYAWALI, *Kent State University* B. J. TAYLOR, M. B. MAPLE, *University of California at San Diego* We performed magnetic investigations on single crystals of $Y_{0.47}Pr_{0.53}Ba_2Cu_3O_{7-\delta}$ ($T_c$ = 7.0 K) at temperatures $4 < T < 80$ K. Magnetization $M$ vs field $H$ data measured at $T > 6.3$ K exhibit an evolution from a hysteretic loop ty pical for superconducting mixed state at low $H$ to one typical for a spin glass state at high $H$. The latter opens as a separate loop above the irreversible field and expands on the account of the superconducting loop with which overlaps at $T < T_c$. This second loop survives up to temperatures higher than 40 K and shows positive magnetization. The $M$ vs $T$ dependence displays also a hysteresis above $T_c$ for fields between 10 and 60 mT with a maximum width at about 30 mT. Magnetic susceptibility $\chi$ vs $T$ data follow a Curie dependence $\chi(H,T) = C(H)/[T + \theta(H)]$ at low fields with field-dependent $C$ and $\theta$, as for an antiferromagnetic glass. These findings are consistent with the previously reported intrinsic inhomogeneity of the underdoped cuprates, where superconducting and antiferromagnetic nano-droplets coexist over a large $T$ range, while the latter droplets persist up to $T >> T_c$.

*This research was supported by the National Science Foundation under the Grant No DMR 0406471 at KSU and the US Department of Energy under the Grant No DE-FG03-86ER-45230 at UCSD

**12:27**

**B39 7 FFLO surface bound state** SHI-HSIN LIN, PAWEL REDLINSKI, BOLDIZSAR JANKO, *University of Notre Dame* DANIEL AGTERBERG, *University of Wisconsin - Milwaukee* Here we study the inhomogeneous superconducting phase of heavy fermion superconductor CeCoIn5. Specifically, we propose a possible existence of FFLO surface bound states. We anticipate that the node of FFLO superconducting state would coincide with the surface to lower the energy. The order parameter vanishes at the interface and increases towards the bulk. This is similar to the case in vortex core of type II superconductor in that the normal region is confined by superconducting wall, except that one side now is vacuum. We thus anticipate bound states to exists at the surface, just as the Caroli-de Gennes-Matricon states exist in the vortex core. We will perform a self-consistent calculation using Bogoliubov-de Gennes equation to obtain the bound surface state spectrum, which can be directly compared to scanning tunnelling microscope (STM) measurements.

**12:39**

**B39 8 Current driven FFLO state in unconventional superconductors** MATTHEW SONG, HYEONJIN DOH, HAE-YOUNG KEE, *Dept. of Physics, Univ. of Toronto, Canada* The typical Fulde-Farell-Larkin-Ovchinnikov (FFLO) state is known as the superconducting state with periodic spatial variation of order parameter which becomes stable under a Zeeman magnetic field. Here, we suggest that a kind of FFLO state, Cooper pair with a finite center of mass momentum, can be induced without a magnetic field. We investigate the FFLO state in $d$-wave superconductivity with an external current. In this case, the direction of the induced center of mass momentum of FFLO state is orthogonal to the direction of the external current. We discuss the detail conditions of the gap function for the current driven FFLO state.

**12:51**

**B39 9 Formation of non-unitary state near the upper-critical field of $Sr_2RuO_4$** MASAFUMI UDAGAWA, YOUICHI YANASE, MASAO OGATA, *Dept. of Physics, School of Science, Univ. of Tokyo* We have studied the superconducting state of $Sr_2RuO_4$ under a magnetic field parallel to the superconducting plane. On the basis of quasiclassical analysis, we show that non-unitary $k_y(\hat{\mathbf{z}} - i\alpha\hat{\mathbf{y}})$ state is stabilized right at $H_{c2}$ as a result of the competition between spin-orbit interaction and Zeeman energy. As a magnetic field is lowered, this state changes to unitary $k_y\hat{\mathbf{z}}$ state. On the basis of this crossover, we address the origin of the observed double peaks of specific heat and the disappearance of the double peaks at low fields. We have also investigated the position of the phase transition line proposed by Agterberg in terms of the quasiclassical theory, and determined the magnetic field-temperature phase diagram of $Sr_2RuO_4$.

**13:03**

**B39 10 Conductance characteristics between a normal metal and a two-dimensional Fulde-Ferrell-Larkin-Ovchinnikov superconductor** QINGHONG CUI, *Physics Department, Florida State University* CHIA-REN HU, *Physics Department, Texas A&M University* J.Y.T. WEI, *Physics Department, University of Toronto* KUN YANG, *Physics Department, Florida State University* The Fulde-Ferrell-Larkin-Ovchinnikov (FFLO) state has received renewed interest recently due to the experimental indication of its presence in $CeCoIn_5$. In this work we explore the possibility of detecting the phase structure of the order parameter directly using conductance spectroscopy through microconstrictions, which probes the phase sensitive surface Andreev bound states of *d*-wave superconductors. We employ the Blonder-Tinkham-Klapwijk formalism to calculate the conductance characteristics between a normal metal and a 2-dimensional *s*- or *d*-wave superconductor in the Fulde-Ferrell state, for all barrier parameter $z$ from the point contact limit ($z=0$) to the tunneling limit ($z \gg 1$). We find that the zero-bias conductance peak due to these surface Andreev bound states observed in the uniform *d*-wave superconductor is split and shifted in the Fulde-Ferrell state. This work was supported by NSF grant No. DMR-0225698, NSERC, CFI/OIT, MMO/OCE and CIAR. Reference: cond-mat/0510717.

**13:15**

**B39 11 A novel homogeneous superconducting state to compete with the inhomogeneous FFLO states in conductors with exchange or Zeeman split Fermi surfaces** CHIA-REN HU, *Texas A&M University* The Fulde-Ferrell-Larkin-Ovchinikov (FFLO) states have been proposed as the states to replace the usual BCS state when the Fermi surfaces of spin-up and down electrons are sufficiently different due to exchange or Zeeman splitting. The FF state has a space-varying phase and the LO state has an oscillating order-parameter magnitude. Thus both are inhomogeneous states. Here I propose a novel homogeneous state to compete with the FFLO state: Instead of forming Cooper pairing of one spin-up electron of momentum $\mathbf{k}$ and one spin-down electron on momentum $-\mathbf{k}$, this new state involves a generalized Cooper pair which is actually a triplet: One spin-up electron of momentum $(1+\delta)\mathbf{k}$, one spin-down electron of momentum $-(1-\delta)\mathbf{k}$, AND one boson of momentum $-2\delta\mathbf{k}$, which can be a phonon, or a magnon, etc. (This state might also form in Fermion-Boson atomic mixtures, and in quark-gluon plasma.) The value of $\delta$ is such that $(1+\delta)k_F$ is the spin-up Fermi momentum, and $(1-\delta)k_F$ is the spin-down Fermi momentum. Since the boson involved does not have a fixed momentum $\mathbf{q}$, this state is not a density wave state of any sort coexisting with superconductivity. A mean field theory of this state will be presented.

**13:27**

**B39 12 The Fulde-Ferrell-Larkin-Ovchinnikov state in two-dimensional *s*-wave and *d*-wave superconductors*** QIAN WANG, HONGYI CHEN, *Texas Center for Superconductivity, University of Houston, Houston, Texas 77204* CHIA-REN HU, *Department of Physics, Texas A&M University, College Station, Texas 77843* CHIN-SEN TING, *Texas Center for Superconductivity, University of Houston, Houston, Texas 77204* We study the Fulde-Ferrel-Larkin-Ovchinnikov (FFLO) states for two-dimensional superconductors under a strong magnetic field at low temperature. Using a tight-binding model, the spatial variation of the superconducting order parameter is self-consistently determined by solving Bogliubov-de-Gennes equations iteratively. We then calculate the magnetization and the LDOS of the FFLO state. When the magnetic field is parallel to the superconducting plane, our results show that for 2D s-SC (d-SC), 1D stripe (2D lattice) solutions are more energetically favorable. At certain symmetric sites, we find that the features in the local density of states can be ascribed to two types of bound states. We also investigate the effect of impurities on the FFLO state and the vortex structure when the FFLO state is subjected to an orbital magnetic field.

*This work was supported by a grant from the Robert A. Welch Foundation under NO. E-1146 and by the Texas Center for Superconductivity at the University of Houston through the State of Texas.

**13:39**

**B39 13 Quantum fluctuations in LOFF superconductors*** KIRILL SAMOKHIN, MAXIM MAR'ENKO, *Department of Physics, Brock University* We study the order parameter fluctuations near the phase transition into the Larkin-Ovchinnikov-Fulde-Ferrell superconducting state at zero temperature. In contrast to the usual normal metal-to-uniform superconductor transition, the fluctuation corrections are dominated by the modes with the wave vectors away from the origin. We find that the superconducting fluctuations lead to a divergent spin susceptibility and a breakdown of theFermi-liquid behavior at the quantum critical point in the clean limit.

*supported by NSERC

**13:51**

**B39 14 Helical phases in broken parity superconductors*** RAMINDER KAUR, *University of Wisconsin-Milwaukee* DANIEL AGTERBERG, *University of Wisconsin-Milwaukee* KAORI TANAKA, *University of Saskatchewan* PAOLO FRIGERI, *ETH, Zurich* MANFRED SIGRIST, *ETH, Zurich* The recently discovered broken inversion superconductors, $CePt_3Si$, $Li_2Pt_3B$, and $Li_2Pd_3B$, have provided a unique opportunity to study the role of broken parity in the superconducting state. In these superconductors, a magnetic field leads to a novel inhomogeneous superconducting state, a helical phase. Although the origin of the helical phase is quite different from another well known inhomogeneous superconducting phase, Fulde-Ferrell-Larkin-Ovchinnikov (FFLO) state, the consequences of both phases are similar, for example; a relative enhancement of transition temperature as a function of magnetic field over that of a uniform state. FFLO states are quite unstable and hard to observe experimentally as that exist only in the low temperature and high field regime. Until now, the FFLO state has only been identified in $CeCoIn_5$ as an unusual magnetic field enhanced superconducting state near a quantum critical point. We argue that the helical phases is more stable than the FFLO state and will exist in all broken parity superconductors. We present results on the microscopic quasiparticle structure and the stability of the helical phase in broken inversion superconductors.

*DMR-0381665 National Science Foundation

**14:03**

**B39 15 Superconductivity in $PrRu_4As_{12}$ single crystals** W. M. YUHASZ, P. -C. HO, T. A. SAYLES, T. YANAGISAWA, N. A. FREDERICK, M. B. MAPLE, *University of California San Diego* Single crystals of the filled skutterudite compound $PrRu_4As_{12}$ were characterized by magnetization, specific heat, and electrical resistivity measurements. These measurements reveal the occur-

rence of superconductivity below $\sim$ 2.4 K. The magnetic susceptibility exhibits behavior consistent with a $Pr^{3+}$ ninefold degenerate $J = 4$ Hund's rule ground state multiplet split in a tetrahedral crystalline electric field with either a nonmagnetic singlet or doublet ground state. Fits to the specific heat data indicate an electronic contribution to the specific heat $\gamma$ of $\sim$ 70 mJ/mol $K^2$ and a Debye temperature $\Theta_D$ of $\sim$ 344 K. The value of $\Delta C/\gamma T_c \approx 1.53$ for $PrRu_4As_{12}$ is close to the weak-coupling BCS value of 1.43. Electrical resistivity measurements in field were used to determine $H_{c2}$ as a function of temperature from which the zero temperature value of the orbital critical field $^*H_{c2}(0)$ was calculated and used to estimate the coherence length $\xi_0$ of $PrRu_4As_{12}$. In contrast to $PrRu_4As_{12}$, the compound $PrOs_4As_{12}$ displays two phase transitions at 2.2 K and 2.3 K in zero field, one of which is antiferromagnetic and the nature of the other is yet to be determined. $PrOs_4As_{12}$ also displays heavy fermion behavior with an enhanced electronic specific heat coefficient $\gamma$ on the order of 200 mJ/mol $K^2$ and a $\Theta_D$ of only 260 K. This research was supported by the U.S. DOE (No. DE-FG02-04ER46105) and NSF (No. DMR 0335173).

**SESSION B40: TOPICS IN QUANTUM FOUNDATIONS**
**Monday Morning, 13 March 2006**
**343, Baltimore Convention Center at 11:15**
**Terry Rudolph, Imperial College London, presiding**

**11:15**
**B40 1 Bell's inequalities: derivation, violation, and implications** LOUIS SICA, *Naval Research Laboratory (Retired)* Cross-correlations among jointly present data sets satisfy the Bell inequality as a fact of mathematics. Violation of Bell's inequalities by data correlations obtained in independent trials of quantum mechanical correlation experiments shows that a wide-sense spatially stationary (in angle) process cannot account for the Bell cosine correlation. Since the correlations usually measured are cosinusoidal, at least one variable pair of those constrained by a Bell's inequality must have a correlation function different from the usual cosine in order to satisfy the inequality. When nonlocal information is used to construct correlations among real and counterfactual measurements, the correlation functions obtained are not all of the simple cosine form, and the set of correlations satisfies the Bell inequalities. Thus, the resulting correlations are not based on a wide-sense stationary process. The same conclusion holds for properly correlated experimental data. These considerations may be extended to the domain of well-known inequalities in probabilities that follow from the correlational inequalities upon assuming a simple symmetry condition. Such results imply that a proof of nonlocality based on Bell's inequality violation must use different reasoning from that used historically.

**11:27**
**B40 2 Correlated observables in field theoretic terms: single- and multi-particle systems** IAN DURHAM, *Saint Anselm College* In recent years correlations between two degrees of freedom for a single particle have been experimentally demonstrated and further experiments have been suggested. This has presented a more direct test of non-contextuality. The results indicate that quantum mechanical entanglement is a more complex process than non-local theories generally suggest. The nature of both the single-particle and multi-particle entanglement processes suggest that perhaps a field theoretic solution is tenable where measurements actually transform the entire field.

**11:39**
**B40 3 Differences between the Measurement Process and Schrödinger Evolution** STEINER MICHAEL, *NRL* An overview of the Measurement Problem is given and an argument is presented that reduces the measurement problem to a 2-qubit problem of entanglement. In current experiments, the measurement problem has not been a limitation on what can be predicted. If the problem were to continue to not be a limitation for all future experiments of interest, then the problem may be interesting from a philosophical perspective, but is not limiting in terms of physical predictions. However, the author will show examples to illustrate why this is not the case. Certain experiments would be incorrectly predicted if the measurement process were replaced by Schrödinger evolution. Hence understanding the reason for measurement is of primary interest. A new direction toward developing a comprehensive theory will be proposed.

**11:51**
**B40 4 Inference of Schrödinger Equation from Classical-Mechanics Solution*** JX ZHENG-JOHANSSON, *IOFPR, SWE* P-I JOHANSSON, *Uppsala Univ, SWE* We set up the classical wave equation for a particle formed of an oscillatory massless charge, traveling at velocity $v$ in a potential $V(X)$ in a one-d box along $X$ axis, and its electromagnetic waves $\{\varphi_p^j\}$ (as virtual or ''hidden'' processes) as: $[c^2 - V/m]\partial^2\psi/\partial X^2 = \partial^2\psi/\partial T^2$ (1). Where $\psi = \Sigma\varphi_p^j$; $p =$ *incident* or *reflected*, $j = \dagger$ or $\ddagger$ for $\angle[c,v] = 0$ or $\pi$, $c$ velocity of light, $M = m\sqrt{1-(v/c)^2} = h\Omega/2\pi c^2$ the particle's rest mass, $\Omega/2\pi$ wave frequency for $v = 0$, and $h$ Planck constant. For $V =$ const, Eq (1) has the plane wave solutions: $\{\varphi_p^j = C_1 e^{i(K^jX-\Omega^jT)}\}$; $K^j(j = \dagger\ddagger) = K/1 \mp v/c$ is a Doppler-displaced wavevector; $\Omega^j = K^jc$. From $\Sigma\varphi_p^j$, we get a standing beat, or de Broglie phase wave for the particle total motion: $\psi = 4C_1\cos(KX)e^{i(\Omega+\Omega_d/2)T}\Psi$. Where $\Psi = C\sin(K_dX)e^{-i\Omega_d/2T}$ describes the particle motion, and $K_d = \sqrt{(K^\dagger-K)(K-K^\ddagger)} = (v/c)K$ the de Broglie wavevector; $\Omega_d = vK_d$. For $V$ varying, we get similarly a $\psi$ and $\Psi$ from sums of partial plane waves from all of infinitesimal $(X_i, X_i + \Delta X)$. We can in turn subtract (1) by itself but with $v = 0$, getting an equation for $\Psi$: $[ - \hbar^2/2M\ \partial^2/\partial X^2 + V(X)]\Psi = i\hbar\,\partial\Psi/\partial T$, which is equivalent to the Schrödinger equation. (The so represented QM invites not the so-called EPR paradox.)

*JXZJ & P-IJ, *Unification of Classical, Quantum and Relativistic Mechanics and the Four Forces*, Nova Science, NY, 2005; *Quantum Theory and Symmetries IV*, ed VK Dobrev, Heron Press, 2006.

**12:03**
**B40 5 Aton, Relativity, and Quantum Mechanics** ALFRED PHILLIPS, JR., *Source Institute* In the mechanics of the Aton, we have shown that the Davisson-Germer experiments and other crystal based experiments can be modeled without recourse to particle-wave notions. We have also shown that the energy levels of the hydrogen atom and the helium atom can be calculated accurately

with Atonic Mechanics, subject to the limits of three-body effects in the latter atom. Using the Aton concept, we now provide a way to unify Einstein's Relativity with what we commonly refer to as quantum mechanics. We note that entanglement is an intrinsic part of the mechanics of the Aton.

**12:15**
**B40 6 Vortex Theory and Photon Acceleration Effect** KONSTANTIN GRIDNEV, RUSSELL MOON, VICTOR VASILIEV, Using the principles of the Vortex Theory, it was theorized that when a photon encounters an electromagnetic field, both the velocity and the frequency of the photon will change. To prove this idea an experiment was devised using a laser interferometer and electromagnets. The electromagnets were arranged so that when the beam splitter divided the initial beam of laser light into two secondary beams; one of the two secondary beams passed back and forth between the magnets. With the DC current to the electromagnets turned off, the two beams formed an interference pattern on the target screen. When the current to the electromagnets was suddenly turned on, the pattern fluctuated wildly until the two beams again reached a quiescent state creating a stable pattern on the screen; when the current to the electromagnets was suddenly turned off, again the pattern fluctuated wildly until it reached a quiescent state forming the initial stable pattern on the screen. It was determined that this new effect was a phenomenon created by the changing frequency of the laser light whose velocity is increasing as it passes between the expanding electromagnetic field of the magnets. Because it is a new phenomenon in science revealing that the speed of light is not a constant but indeed can be varied.

**12:27**
**B40 7 The classical – quantum border at $10^{11}$ Hz and Cosmic Microwave Background** SIMON BERKOVICH, *George Washington University* Findings of non-trivial anisotropy of CMB challenge current cosmology. Notably, this has been predicted by our model of the Universe – a cellular automaton with a rule of distributed fault-tolerant synchronization (http://arxiv.org/abs/astro-ph/0509743). This model yields spectrum of elementary 'quasi-particles' and fast operational background: 'action-at-the-distance' for gravitation, underlying mechanism for Bohm-Hilley's interpretation of quantum phenomena and holographic reference waves for biological information. Matter creation is accompanied with 'shock wave' and synchronization-desynchronization undulations of $10^{-11}$ sec that form CMB. Its structurization is due to eccentric observation, the $2.72^0$K 'temperature' of black body spectrum is indicative of $10^{11}$frequency. Quantum strangeness stems from multiplexing of synchronized and desynchronized stages resulting in sophisticated behavior at the former and loose motion at the latter. The relative stage durations are determined by placing in the Universe, and propagation front may impact large molecules depending on their orientation. Quantum and Life mysteries being interrelated, both can be affected by the border frequency. Millimeter waves cause biological effects neither by heating nor direct action, but as a trigger. Mesoscopic quantum phenomena, like, e.g. superconductivity, can be destroyed by $10^{11}$ Hz. Thus, there is a possibility for a $10^{11}$ Hz threshold in disrupting quantum entanglement through the suggested multiplexed machinery.

**SESSION B42: SPS UNDERGRADUATE RESEARCH I**
**Monday Morning, 13 March 2006**
**345, Baltimore Convention Center at 11:15**
**Gary White, Society of Physics Students, presiding**

**11:15**
**B42 1 Interferometric studies of a piano soundboard** SARAH ZIETLOW, THOMAS MOORE, *Department of Physics, Rollins College, Winter Park, Fl 32789* Electronic speckle pattern interferometry has been used to study the deflection shapes of a piano soundboard. During the experiments the soundboard remained attached to the piano, providing, to our knowledge, the first optical examination of soundboard movement itin situ. The lowest modes have been studied in detail, and the interferograms have been compared to predictions of a simple model that assumes the soundboard is well approximated by an isotropic plate clamped at the edges. Analysis indicates that this model is insufficient to explain the deflection shapes associated with the resonances of the soundboard. It is shown that a finite element model results in more accurate predictions of the mode shapes, and provides insight into the parameters that are important in determining the final sound of the instrument.

**11:27**
**B42 2 Acoustical study of the Nigerian slit log gong.** JACOB SKUBAL, ZACH HACKETT, THOMAS MOORE, *Department of Physics, Rollins College, Winter Park, FL 32789* The acoustically important resonances of a Nigerian slit gong consist of two significant mechanical resonances and a Helmholtz acoustical resonance. Beating in the acoustical signal from the struck gong suggests that energy is cyclically transferred between the acoustical and mechanical resonators, as is known to happen in similar idiophones. However, we have determined that in the slit log gong there is no significant two-way exchange of energy. Rather, the beating occurs as a result of interference between the frequencies associated with the mechanical and acoustic resonances. The relationship between these resonances has an impact on the tuning and sound quality of the gong.

**11:39**
**B42 3 Visualizing the sound field of an acoustic fire extinguisher*** DMITRIY PLAKS, ELIZABETH NELSON, NESHA HYATT, ZADE COLEY, GARY HUNTER, PATRICIA SAPONARI, JAMES ESPINOSA, *University of West Georgia* Our objective is to study the effects of acoustics on flames for the purpose of encouraging new research that will provide a different approach to reducing and extinguishing a combustion reaction. Through experiment, we have already demonstrated that it is possible to extinguish fire with sound. Our apparatus uses 12'' subwoofer speakers in order to generate the necessary acoustic field. By placing dry ice at the bottom of the apparatus, this field becomes visible. We give visual data of how various sound patterns affect the flame and combustion reaction and provide qualitative explanations of the physical phenomena responsible for the effects.

*Funded by: Physics Dept - UWG, Honors College - UWG, Georgia Space Grant Consortium, Siemens, PCB Piezotronics, FLIR Systems.

**11:51**

**B42 4 Construction and Investigation of three HTSC diamagnetic devices** JOHN JONES, ADAM REED, AZIZA DANG, TAHA FEROZPURI, POOYA AZAR, DANIEL GORDON, STEVEN HENDRICKSON, *Northern Virginia Community College* NVCC physics students plan to build and investigate the operation of three devices based on the interaction of permanent magnets and high termpature superconductors. Those devices are: A magnetic flywheel; A Meissner Effect Heat Engine: a wheel rimmed with superconductors which spontaneously spins in the presence of a magnetic field; A superconducting pendulum: Another thermodynamic engine—the pendulum transitions between superconducting and insulating states, gaining kinetic energy each time.

**12:03**

**B42 5 Construction of an apparatus to characterize the early evolution of ultracold neutral plasma*** LUCAS WILLIS, *Rowan University* MICHAEL LIM, *Rowan University* A magneto-optical trap was constructed for the purpose of charting early atomic recombination rates in an ultracold neutral plasma, which is created by photo-ionizing laser cooled rubidium atoms. Planned experiments will focus primarily on the first 100 nanoseconds of plasma evolution, during which a ramped electric field will be applied to Rydberg atoms that recombine from the plasma components. The ramped field will ionize loosely-bound states, liberating electrons at times that are correlated with binding energy. An electron beam comprised of a series of electrostatic lenses enables the transport of these electrons from the MOT region to a multichannel plate electron detector (MCP). We devised a system to raster the beam across the MCP to prevent detector saturation and the loss of signal due to electron multiplier recovery times. We will also discuss other apparatus features that allow flexible electric and magnetic field configurations.

*Work supported in part by Research Corporation

**12:15**

**B42 6 Mode shapes of the American five-string banjo** LAURIE STEPHEY, ISAAC CODREY, THOMAS MOORE, *Rollins College Department of Physics, Winter Park, FL 32789* Experimental studies of the mode shapes of the American five string banjo have revealed the importance of properly tuning the membrane that comprises the head of the instrument. Electronic speckle pattern interferometry has been used to visualize the deflection shapes of the banjo head at several frequencies. Although the off-center placement of the bridge results in asymmetric forces on the head, the mode shapes of a properly tuned banjo head appear symmetric. The implication is that the preferred sound results only when asymmetric pressure is applied to the rim of the membrane to compensates for the off-center placement of the bridge.

**12:27**

**B42 7 Electrical Characterization of Organic Conducting Polymers** LINDSAY WINDSOR, *Cornell University* As Moore's Law drives the silicon semiconductor industry to its limits, organic conducting polymers have been explored on a small scale as a possible solution to the breakdown of silicon. Here, the electrical properties of two organic polymers were measured using nanopore and micron-sized devices. In this electrical characterization, polypyrrole was found to exhibit hopping conduction, and both polypyrrole and polyaniline yield nonlinear I-V curves and degradation after sweeps of high voltage. Consequently, these organic polymers and possibly others may have only limited applications in the future semiconductor industry.

**12:51**

**B42 8 Contact Potential Difference Measurements of Self Assembled Monolayers** BRIDGER ANDERSON, *Society of Physics Students, NIST* In this work, the metal work function and its evolution with systematic chemical changes were studied using an Atomic Force Microscope. A technique, Scanning Kelvin Probe Microscopy, was used to measure the metal work function of various surface dipoles. This metal-molecule interface is also known as a Helmholtz double layer. We expect that this work will lead to a fundamental way of understanding and rationalizing the electrical characteristics of select metal-molecule-metal systems.

**13:15**

**B42 9 Nonlinear Optical Properties of CdSe Quantum Dots** CHARLES ANDERSON, SEAN BENTLEY, JOHN DOOHER, *Adelphi University* Detailed research into the nonlinear optical properties of several quantum dot samples is conducted. Data from the research is being used to investigate applications for the quantum dots. Possible applications may include quantum encryption for more secure forms of communication, lithography techniques for improved capabilities of writing computer chips, and the generation of entangled photons through the use of a four-wave mixing process. Other applications may also include more efficient and cheaper photovoltaic cells. Evident Technologies has provided several different samples of quantum dots, each with distinct nonlinear properties. Using z-scan techniques, absorptive and refractive information are extracted for each of the samples. The absorptive natures are observed by scanning the dot sample through varying intensities and measuring their transmission values with an open aperture. Comparing these values with the same process, but utilizing a closed aperture, allows extraction of values of $n_2$, the nonlinear refractive index.

**13:27**

**B42 10 Bond Angles in the Crystalline Silicon/Silicon Nitride Interface** ROBERT H. LEONARD, MARTINA E. BACHLECHNER, *West Virginia University, Physics Dept.* Silicon nitride deposited on a silicon substrate has major applications in both dielectric layers in microelectronics and as antireflection and passivation coatings in photovoltaic applications. Molecular dynamic simulations are performed to investigate the influence of temperature and rate of externally applied strain on the structural and mechanical properties of the silicon/silicon nitride interface. Bond-angles between various atom types in the system are used to find and understand more about the mechanisms leading to the failure of the crystal. Ideally in crystalline silicon nitride, bond angles of 109.5[r] occur when a silicon atom is at the vertex and 120[r] angles occur when a nitrogen atom is at the vertex. The comparison of the calculated angles to the ideal values give information on the mechanisms of failure in silicon/silicon nitride system.

**SESSION B43: BEC IN TRAPPED ATOMIC GASES**
**Monday Morning, 13 March 2006**
**346, Baltimore Convention Center at 11:15**
**Henry Glyde, University of Delaware, presiding**

**11:15**
**B43 1 Superfluidity without Symmetry-Breaking: The Time-Dependent Hartree-Fock Approximation** H.A. FERTIG, CHANG-HUA ZHANG, *Indiana University* We develop a time-dependent Hartree-Fock approximation that is appropriate for Bose-condensed systems. In order to explicitly capture the exchange energy for interactions between the condensate and single-particle excitations, we work with an ensemble with a fixed condensate particle number, so that there is no breaking of gauge symmetry in our approach. Defining a ''depletion Green's function'' allows the construction of condensate and depletion particle densities from eigenstates of a single time-dependent Hamiltonian, guaranteeing that our approach is a conserving approximation. We show that its application to the infinite uniform system produces the expected superfluid mode, and discuss the structure of the density response function.

**11:27**
**B43 2 Number-of-Particle Fluctuations and Stability of Bose-Condensed Systems** CHANG-HUA ZHANG, *Physics Department, Indiana University* In this paper we show that a normal total number-of-particle fluctuation can be obtained consistently from the static thermodynamic relation and dynamic compressibility sum rule. In models using the broken $U(1)$ gauge symmetry, in order to keep the consistency between statics and dynamics, it is important to identify the equilibrium state of the system with which the density response function is calculated, so that the condensate particle number $N_0$, the number of thermal depletion particles $\tilde{N}$, and the number of non-condensate particles $N_{nc}$ can be unambiguously defined. We also show that the chemical potential determined from the Hugenholtz-Pines theorem should be consistent with that determined from the equilibrium equation of state. The $N^{4/3}$ anomalous fluctuation of the number of non- condensate particles is an intrinsic feature of the broken $U(1)$ gauge symmetry. However, this anomalous fluctuation does not imply the instability of the system. Using the random phase approximation, which preserves the $U(1)$ gauge symmetry, such an anomalous fluctuation of the number of non-condensate particles is completely absent.

**11:39 ttl**
**B43 3 Measuring Correlations by Single Atom Detection in Quantum Degenerate Gases** ANTON ÖTTL, STEPHAN RITTER, TOBIAS DONNER, THOMAS BOURDEL, MICHAEL KÖHL, TILMAN ESSLINGER, *Institute for Quantum Electronics, ETH Zurich, Switzerland* We observe single atoms by means of cavity QED detection in a quantum degenerate gas. Starting from a magnetically trapped $^{87}$Rb BEC of 5 million atoms we coherently output couple a continuous atom laser by means of a local radio-frequency induced spin-flip into a magnetically untrapped hyperfine state. These atoms propagate freely downward due to gravity and enter the detector which is placed 36 mm below the BEC. Our single atom detector consists of an ultra-high finesse ($\mathcal{F} = 3 \cdot 10^5$) optical cavity in the strong coupling limit of cavity QED. We record the transmission of a weak resonant probe laser through the cavity with a single photon counter and detect single atom transits by their significant reduction of transmission. We measured the second order correlation function of an atom laser beam in a Hanbury Brown & Twiss type experiment. Analyzing the correlations in the arrival time of individual atoms reveals the second order coherence of the atom laser. The high quantum efficiency and fast response time of our single atom detector enables us to extract the full counting statistic of atomic beams. We verified a poissonian distribution for the atom laser whereas a pseudo-thermal atomic beam showed a bunching behavior corresponding to a Bose-Einstein statistical distribution function.

**11:51**
**B43 4 Casimir-like drag force in a slow-moving superfluid** DAVID ROBERTS, YVES POMEAU, *Ecole Normale Superieure* It is widely accepted that a superfluid flow exhibits a critical velocity below which there is no dissipation. However, the often-neglected zero-temperature quantum fluctuations have implications for the existence of this critical velocity. The drag force on an object created by the scattering of these quantum fluctuations in a three-dimensional, weakly interacting Bose-Einstein condensate is discussed. A non-zero force at low velocities is found to exist for two specific experimentally realizable examples, which suggests that the effective critical velocity in these systems is zero.

**12:03**
**B43 5 Berry Phase Effect on Semiclassical Dynamics of Bogoliubov Quasiparticles*** CHUANWEI ZHANG, *Department of Physics & Center for Nonlinear Dynamics, The University of Texas at Austin* ARTEM DUDAREV, *Max-Planck-Institut für Physik Komplexer Systeme, Dresden, Germany* QIAN NIU, *Department of Physics, The University of Texas at Austin* We develop a semiclassical theory for Bogoliubov quasiparticles in a superfluid by following the center of mass motion of a quasiparticle wavepacket. Berry phase arises when the underlying condensate moves, invalidating the usual canonical relation between the mechanical momentum and position variables. The equations of motion become non-canonical, and the quantization rule and the density of states are also modified. We study quasiparticles in a condensate with a vortex to show explicitly the Berry phase effects and their experimental observation.

*This work is supported by the NSF and the R.A. Welch foundation.

**12:15**
**B43 6 Collective modes of a spherical shell condensate** COURTNEY LANNERT, *Wellesley College, Wellesley, Massachusetts 02481* TZU-CHIEH WEI, SMITHA VISHVESHWARA, *University of Illinois at Urbana-Champaign, Urbana, Illinois 61801* Dilute ultracold bosonic atoms in three-dimensional optical lattices with a harmonic confining potential are expected to exhibit inhomogeneous phases – in particular phases containing superfluid regions confined to a spherical shell. It may also be possible to confine superfluids in this geometry using a special trap designed for this purpose. We explore the low-energy collective modes of a superfluid confined to a thin spherical shell analytically. In particular, in the limit of strong interactions we find two breathing modes with frequencies distinct from the spherical condensate breathing mode.

**12:27**

**B43 7 Expansion of spherical shell condensates** SMITHA VISHVESHWARA, TZU-CHIEH WEI, *University of Illinois at Urbana-Champaign, Urbana, Illinois 61801* COURTNEY LANNERT, *Wellesley College, Wellesley, Massachusetts 02481* Bose-condensed atoms in traps of novel geometries can show dramatic features in time-of-flight measurements that are absent in conventional spherical trap settings. The specific case of a trap creating a spherical condensate shell is presented. The dynamics of such a shell can yield a significant accumulation of mass at the center upon release of the trapping potential. Morever, the expanded cloud can undergo self- interference and exhibit the associated interference fringes. These features are substantiated by numerical simulations and studied for a range of interaction strength between constituent atoms.

**12:39**

**B43 8 Bose-Einstein condensation and superfluidity in finite sized systems.** ALI SHAMS, *Department of Physics and Astronomy, University of Delaware, Newark, Delaware 19716* HENRY GLYDE, *Department of Physics and Astronomy, University of Delaware, Newark, Delaware 19716* We present results on the relationship between the superfluid fraction and the condensate fraction in finite sized systems of hard-core bosons. The systems are investigated using path integral Monte Carlo methods over a wide range of densities. While it is well known that in strongly interacting bose systems like liquid helium the condensate fraction is much smaller than the superfluid fraction, our results indicate that for finite sized systems and weak interaction, condensate fraction can actually exceed superfluid fraction. This is especially the case as we get closer to the superfluid transition temperature. Condensation in an interacting system can be suppressed both through increased correlation effects and decreased exchange effects. Our investigation also sheds light on the relative importance of these two depletion mechanisms.

**12:51**

**B43 9 Bose Einstein Condensation in a Box Trap: A Monte Carlo Study** CHONGSHAN ZHANG, KWANGSIK NHO, D. P. LANDAU, *Center for Simulational Physics, University of Georgia, Athens, GA 30602* Using the path-integral Monte Carlo method, we have investigated Bose-Einstein condensates in an optical box trap which has been produced very recently[1]. We have used the same geometry as the experiment, and approximated the trapping potential with Gaussian functions at the boundary in order to mimic such a trap. The two-body interaction was described by a hard-sphere potential whose radius equals the *s*-wave scattering length. We have studied the temperture dependence of the equilibrium properties such as the total energy, the total density profiles, and the superfluid fraction. In addition, we have calculated the equilibrium properties as a function of the strength of the two-body interaction. We will compare our simulation results with those for harmonic and hard wall traps. *Research supported by NASA

[1]T. P. Meyrath, F. Schreck, J. L. Hanssen, C.-S. Chuu, and M. G. Raizen, Phys. Rev. A **71**, 041604 (2005)

**13:03**

**B43 10 Transistor like behavior of a Bose Einstein condensate in triple well potential** JAMES STICKNEY, *Department of Physics, Worcester Polytechnic Institute* DANA ANDERSON, *Department of Physics and JILA, University of Colorado and National Institute of Standards and Technology* ALEX ZOZULYA, *Department of Physics, Worcester Polytechnic Institure* The availability of cold atom-based analogs of building blocks of electronic circuits, especially with the ability to integrate them into larger devices, may be extremely valuable in applications. We demonstrate that a device based on a BEC in a triple well potential can show behavior similar to a field effect transistor. The left well is coupled only to the middle and is equivalent to the source in a transistor, the middle is coupled to both the left and right wells and is the equivalent of a gate, and the right well is the drain. The potential is designed so that the chemical potential of the atoms in the empty middle well is sufficiently smaller than in the left or right wells to block tunneling. A small number of atoms placed in the middle well switches the device and enables strong tunneling from the left to the right. This tunneling, controlled by the middle well, is due the atom-atom interactions which increase the chemical potential in the middle well and remove the energy mismatch. We show that the number of atoms tunneling into the right well can be much larger than the number of controlling atoms in the middle well. The three well structure demonstrates both absolute and differential gain. Estimates of the switching time and parameters for the potential are presented.

**13:15**

**B43 11 Phase ordering kinetics of a spinor condensate** SUBROTO MUKERJEE, CENKE XU, JOEL MOORE, *Department of Physics, University of California, Berkeley* Bose-Einstein condensates of atoms with nonzero total spin show order parameters and gapless excitations that are distinct from both ordinary magnetic states and superfluid helium. In light of recent experiments on the development of magnetic order in this system, we construct a model dynamics (in the spirit of dynamical critical phenomena) that is consistent with the equilibrium physics of the system and reproduces all the relevant gapless modes of the magnetized condensate.Although the parameters in this time-dependent Ginzburg-Landau are fixed by quantities that are in principle measurable, there are several parameter-independent predictions that can be directly compared to existing experiments: we focus in this talk on the phase-ordering kinetics of magnetic and superfluid order in 2D condensates in an axial field, for comparison with the experiments of Higbie *et. al*(cond-mat/0502517).

**13:27**

**B43 12 The three-body recombination of a condensed Bose gas near a Feshbach resonance*** LAN YIN, *School of Physics, Peking University* We study the three-body recombination rate of a homogeneous dilute Bose gas with a Feshbach resonance at zero temperature. The ground state and excitations of this system are obtained. The three-body recombination in the ground state is due to the break-up of an atom pair in the quantum depletion and the formation of a molecule by an atom from the broken pair and an atom from the condensate. The rate of this process is in good agreement with the sodium experiment in a wide range of magnetic fields. The three-body recombination at finite temperatures is also discussed.

*Phys. Rev. A 72, 043607 (2005)

**13:39**

**B43 13 The Vortex Phase Qubit: Generating Arbitrary, Counter-Rotating, Coherent Superpositions in Bose-Einstein Condensates via Optical Angular Momentum Beams** KISHOR KAPALE, *Jet Propulsion Laboratory, California Institute of Technology* JONATHAN DOWLING, *Department of Physics and Astronomy, Louisiana State University* We propose a scheme for generation of arbitrary coherent superposition of vortex states in Bose-Einstein condensates (BEC) using the orbital angular momentum (OAM) states of light. We devise a scheme to generate coherent superpositions of two counter-rotating OAM states of light using known experimental techniques. We show that a specially designed Raman scheme allows transfer of the optical vortex superposition state onto an initially non-rotating BEC. This creates an arbitrary and coherent superposition of a vortex and anti-vortex pair in the BEC. The ideas presented here could be extended to generate entangled vortex states, design memories for the OAM states of light, and perform other quantum information tasks.



## SESSION B46: FOCUS SESSION: WIDE BAND GAP SEMICONDUCTORS II

**Monday Morning, 13 March 2006; 349, Baltimore Convention Center at 11:15**
**Paul Klein, Naval Research Laboratory, presiding**

***Invited Papers***

**11:15**

**B46 1 Interaction of the N vacancy with H and Mg acceptors in *p*-type GaN.***
A.F. WRIGHT,† *Sandia National Laboratories*

Results from recent experimental studies suggest that the N vacancy ($V_N$) may compensate Mg acceptors in GaN in addition to the compensation arising from H introduced during growth. To investigate this possibility further, density-functional-theory calculations were performed to determine the interactions of $V_N$ with H, Mg, and the MgH center in GaN, and modeling was performed to determine the state populations at elevated temperatures. The results indicate that $V_N$H and Mg$V_N$H complexes with H inside the vacancy are highly stable in *p*-type GaN and act to compensate or passivate Mg acceptors. Furthermore, barriers for formation of these complexes were investigated and the results indicate that they can readily form at temperatures $>$ 400[r] C, which is well below temperatures typically used for GaN growth. Overall, the results indicate that the $V_N$ compensation behavior suggested by experiments arises not from isolated $V_N$, but rather from $V_N$H and Mg$V_N$H complexes with H located inside the vacancy.

*Supported by the Office of Basic Energy Sciences, US DOE. Sandia is a multiprogram laboratory operated by Sandia Corporation, a Lockheed Martin Company, for the US DOE under Contract DE-AC04-94AL85000.
†With S. M. Myers, S. K. Estreicher, and M. Sanati.

***Contributed Papers***

**11:51**

**B46 2 First Principles Green's Function Calculations of the Electronic and Optical Properties of Point Defects in GaN** SOHRAB ISMAIL-BEIGI, *Yale University* Despite the successful use of GaN in light-emitting and laser diodes, its materials properties are not well understood or controlled: typical samples have high densities of point and extended defects. A wealth of experimental information exists on these defects, but disentangling the contributions of individual defects from aggregated measured signals requires theoretical input. To date, first principles studies of these defects have used density functional theory (DFT) to study their formation energies, charge states, and structures. However, DFT provides poor predictions of electronic excitations and thus optical and luminescence properties, whereas many experiments probe these very properties. We apply state-of-the-art first principles Green's functions methods (based on the *GW* approximation and the Bethe-Salpeter Equation) to GaN point defects. These methods have proven accurate enough to provide direct comparisons to experiments for a variety of materials. We report mainly on the properties of the gallium and nitrogen vacancies, $V_{Ga}$ and $V_N$, native defects with favorable formation energies in typical GaN samples.

**12:03**

**B46 3 Electron paramagnetic resonance of a donor in aluminum nitride crystals.** SEAN EVANS, *West Virginia University* NANCY GILES, LARRY HALLIBURTON, GLEN SLACK, *Crystal IS* SANDRA SCHUJMAN, LEO SCHOWALTER, Electron paramagnetic resonance (EPR) and electron-nuclear double resonance (ENDOR) have been used to characterize a dominant donor in single crystals of aluminum nitride (AlN). A broad EPR signal, with g (parallel) = 2.002 and g (perpendicular) = 2.006, is observed in the as-grown crystals. Exposure to x-rays (i.e., ionizing radiation) increases the concentration of this center by a factor of five to ten (depending on sample), thus indicating that most of these centers are initially present in the crystals in a nonparamagnetic charge state. ENDOR identifies a strong hyperfine interaction with one aluminum neighbor along the c axis (described by A (parallel) = 111.30 MHz, A (perpendicular) = 54.19 MHz, and P = 0.289 MHz) and weaker equivalent hyperfine interactions with three additional aluminum neighbors in the basal plane. These aluminum interactions indicate that the responsible center is a deep donor at a nitrogen site. The observed paramagnetic defect is either a neutral oxygen substituting for nitrogen or a neutral nitrogen vacancy. This work was supported at West Virginia University by the National Science Foundation (Grant DMR-0508140). One of the authors (SME) received support from the WV EPSCoR STEM fellowship program.

**12:15**

**B46 4 Comparison of point defects in 4H SI SiC grown by halide chemical vapor deposition and physical vapor transport*** M.E. ZVANUT, *University of Alabama at Birmingham* H.J. CHUNG, ALEXANDER POLYAKOV, *Carnegie Mellon University* Semi-insulating (SI) SiC may be produced by chemical vapor deposition using halides (HCVD) or physical vapor transport (PVT). Our electron paramagnetic resonance (EPR) studies address the point defects detected in PVT and HCVD 4H SI SiC substrates. EPR measurements are made 'in equilibrium' prior to illumination and after exposure to light. All samples reported here have resistivity of $10^{10}$ ohm-cm and activation energy greater than 0.8 eV. PVT samples exhibit the positively charged carbon vacancy ($V_c^+$) before illumination, which may be quenched by 1.5 eV light and revived at energies greater than 1.9 eV. The 'equilibrium' EPR measurement of the HCVD samples reveals an intrinsic defect which can be quenched by bandgap illumination. The amount of this unidentified defect is estimated to be an order of magnitude greater than that of $V_c^+$ typically observed in PVT substrates.

*The UAB work is supported by NSF

**12:27**

**B46 5 Observation of a three-site defect in SI 4H-SiC** N.Y. GARCES, W.E. CARLOS, E.R. GLASER, *Naval Research Laboratory, Washington, DC 20375* M.A. FANTON, *Electro-Optics Center, Freeport, PA 16229* High temperature anneals were used to study the evolution of native defects in semi-insulating 4H-SiC grown by PVT or HTCVD methods. The samples were annealed in an argon atmosphere for 30 min at temperatures from 1400$^o$C to 2100$^o$C. Using electron paramagnetic resonance (EPR), we observe a defect that is tentatively identified as $V_C$-$C_{Si}$-$V_C$. This spin S=1 defect is characterized by $g_{||}$=2.0029; $g_{\perp}$=2.0038, a fine structure splitting D$\sim$ 96G, and several hyperfine interactions with the low abundant Si (A$\sim$ 5.5G) and C (A$\sim$ 30G) neighboring nuclei. This center is diamagnetic in the ground state but can be excited into a paramagnetic triplet state by sub-bandgap light. The EPR intensity of this center increases significantly with annealing. This defect could result during annealing by the movement of an adjoining C atom onto the $V_{Si}$ site of the divacancy ($V_C$–$V_{Si}$) whose intensity decreases. This may be the simplest of a family of more complex defects that play a role in the SI character. A search for optical signatures associated with this defect from 0.7-3.2 eV PL studies will also be discussed.

**12:39**

**B46 6 Defects Controlling the Minority Carrier Lifetime in n$^-$ 4H-SiC epitaxial layers.*** P.B. KLEIN, B.V. SHANABROOK, *Naval Research Laboratory* S.W. HUH, A.Y. POLYAKOV, M. SKOWRONSKI, *Carnegie Mellon University* J.J. SUMAKERIS, M.J. O'LOUGHLIN, *Cree Inc.* The relationship between the minority carrier lifetime (MCL) and the concentration of deep trapping centers in n$^-$ 4H-SiC was investigated by low-injection time-resolved photoluminescence (TRPL) and by deep level transient spectroscopy (DLTS) and minority carrier transient spectroscopy (MCTS). Layers of varying layer thicknesses were studied in order to enable the separation of bulk lifetimes from surface recombination effects. A linear dependence of the inverse bulk MCL on the concentration of the Z1/Z2 defect, and the lack of significant correlation of the MCL on the concentration of any other traps, suggests that the Z1/Z2 defect controls the MCL. The results of DLTS measurements in 4H-SiC p-i-n diodes under forward bias reinforce the idea that Z1/Z2 alone is the lifetime killer in this material.

*Work supprted in part by DARPA and ONR.

**12:51**

**B46 7 Transition metal doped SiC: defect levels and magnetism*** M.S. MIAO, WALTER R.L. LAMBRECHT, *Case Western Reserve University* The properties of transition metal substitutions and interstitials in 3C and 4H SiC are studied by first principles supercell calculations. The defect levels change slightly for different polytypes or for different layers in 4H SiC. The calculated defect levels are generally in good agreements with DLTS results. Ti in 4H SiC has two acceptor levels close to the conduction band minimum, corresponding to cubic and hexagonal layers.V, Cr and Mn are amphoteric and have both donor and acceptor levels in the gap. We found Mn has deep trap levels which may be useful to achieve semi-insulating SiC, as is also well-known to be the case for V. The Cr and Mn acceptor levels are deep in the gap. They are unlikely to induce holes at the valence band maximum. Therefore the well-known hole-mediated ferromagnetic mechanism does not apply to Cr and Mn doped SiC. However, our calculations showed ferromagnetic coupling for Cr or Mn doped at neighboring sites. The ferromagnetic coupling is very strong but localized for Cr:SiC. However, it is relatively weak but long range for Mn:SiC. Such features are determined by the nature of the impurity bands. The highest occupied defect state of Cr:SiC is antibonding *e* which is localized whereas the state of Mn:SiC is *t*2 which is delocalized and strongly couples with the surrounding C dangling bonds.

*This work is supported by the Office of Naval Research. The calculations are run on Ohio Superconputer Center.

**13:03**

**B46 8 Heat Capacity of ZnO: Isotope Effects** MANUEL CARDONA, *Max-Planck-Institut für Festkörperforschung* JORGE SERRANO, *European Synchrotron Radiation Facility* REINHARD K. KREMER, GISELA SIEGLE, *Max-Planck-Institut für Festkörperforschung* ALDO H. ROMERO, *CINVESTAV, Departamento de Materiales, Unidad Querétaro* RUDOLF LAUCK, *Max-Planck-Institut für Festkörperforschung* We have measured the heat capacity of zinc oxide for several single crystals with different isotopic composition in the 5 – 350 K temperature range. In order to analyze the dependence of the heat capacity on the isotope mass of the oxygen and zinc atoms, we have performed first-principles calculations within the harmonic approximation. The Zn mass affects mainly the acoustic phonons, thus leading to isotopic effects on the heat capacity mostly at low temperatures, whereas the O mass affects mainly the optic phonons, which become thermally active at higher temperatures. This behavior is reproduced quantitatively by the calculations, and is also in agreement with theoretical predictions reported for wurtzite GaN, an isostructural semiconductor. The possibility of using these data to obtain the density of phonon states projected on the corresponding atoms will be discussed.

**13:15**

**B46 9 Unambiguous identification of an OH-Li center in ZnO: Experiment** G.A. SHI, M. STAVOLA, W.B. FOWLER, *Lehigh University* Theory has found that isolated H is always a donor in ZnO [1] and has led to a number of studies of the properties of H in this promising wide bandgap semiconductor. Of interest here is an OH vibrational line at 3577.3 $cm^{-1}$ that is dominant in ZnO grown by the hydrothermal method [2,3]. We show that the two naturally abundant isotopes of Li [$^6$Li (7.5%) and $^7$Li (92.5%)] cause the D-stretching counterpart of the 3577.3 $cm^{-1}$ IR line to be split into two components that can be separately resolved, even though the 3577.3 $cm^{-1}$ line itself shows no Li-related splitting. This unexpected result establishes unambiguously that the 3577.3 $cm^{-1}$ IR line is due to an OH-Li complex. Overtone and oxygen isotope data for the OH-Li center provide an unusually complete picture of the vibrational properties of this defect. Because isotope splittings for elements heavier than Li will be more difficult to detect, this OH-Li center may be considered a model system for H trapped by impurities in ZnO. [1] C. G. Van de Walle, Phys. Rev. Lett. **85**, 1012 (2000). [2] L. E. Halliburton itet al., J. Appl. Phys. **96**, 7168 (2004). [3] E. V. Lavrov itet al., Phys. Rev. B **71**, 035205 (2005).

**13:27**

**B46 10 Unambiguous identification of an OH-Li center in ZnO: Theory*** W.B. FOWLER, G.A. SHI, M. STAVOLA, *Lehigh University* Three structures[1] have been suggested for the OH-Li complex in ZnO whose Li isotope shift has been observed by Shi, Stavola, and Fowler: (a), an O-H-second neighbor Li; (b), Li-O-H; and (c), O-H-Li (a bond-centered hydrogen), with all three atoms along the c-axis. Wardleit et al. [2] have theoretically investigated the energies of two of these structures. They found (c) to be the ground state and (b) to be 0.5 eV higher in energy. We have used[3] CRYSTAL2003 to evaluate the structural and vibrational properties of this defect. We also find the ground state to be bond centered, with structure (b) higher in energy by 0.5 eV and structure (a) higher by 0.7 eV. We have then moved the O, H, and Li atoms by hand along the c-axis to obtain harmonic force constants and anharmonic constants and have used the harmonic force constants to predict the Li-related isotope shifts. Li-related isotope shifts for OD are predicted to be only 0.3 % and 25% of the experimental value, respectively, for structures (b) and (a). Structure (c), the bond-centered structure, is favored both by its stability and by a predicted Li-related isotope shift for OD of 76% of the experimental value. 1. L. E. Halliburton itet al., J. Appl. Phys. **96**, 7168 (2004). 2. M. G. Wardle itet al., Phys. Rev. B **71**, 155205 (2005). 3. V. R. Saunders itet al., itCrystal2003 User's Manual, University of Torino, Torino, 2003.

*Research supported by NSF Grant DMR 0403641.

**13:39**

**B46 11 Vibrational properties of a Li − OH complex in ZnO*** K. R. MARTIN, *Lehigh University, University of Pittsburgh at Johnstown* P. M. BLANEY, G. A. SHI, M. STAVOLA, W. B. FOWLER, *Lehigh University* Considerable interest has developed on the potential use of II-VI oxides as electronic and optical materials. In several cases alkali atoms have been suggested as dopants. We report on the theoretical and experimental investigation of infrared and vibrational properties of a Li-OH complex in ZnO. Earlier infrared experiments[1] revealed a broad OH-like band centered at 3577.3 $cm^{-1}$ (12K), with full width at half maximum ranging from 0.4 $cm^{-1}$ (12K) to 41.3 $cm^{-1}$ (300K) and a corresponding shift in peak position of - 29 $cm^{-1}$, suggesting a significant coupling of the OH stretch with other modes. We have performed similar experiments on the OD version of this defect and have theoretically investigated[2,3] the coupling of these stretch modes to other modes. The lack of a significant isotope dependence of the resulting parameters suggests that the defect couples to the host rather than the large-amplitude motion of the H or D itself. 1. L. E. Halliburton et al., J. Appl. Phys. **96**, 7168 (2004). 2. B. N. J. Persson and R. Ryberg, Phys. Rev. B **32**, 3586 (1985). [3] M. Budde et al., Phys. Rev. B **63**, 195203 (2001).

*Research supported by NSF Grant DMR 0403641 and the REU program.



**13:51**

**B46 12 Oxygen vacancies and titanium interstitials in rutile and anatase*** JOHN JAFFE, MICHAEL HENDERSON, *Pacific Northwest National Laboratory* Native point defects in reduced $TiO_2$, namely the oxygen vacancy and Ti interstitial, were investigated computationally for both the rutile and anatase structures. The generalized gradient approximation to density functional theory was used along with a plane-wave expansion and ultrasoft pseudopotentials. Defect formation energies were calculated after geometry relaxation from O vacancies created in the bulk rutile and anatase lattices, from the experimental Ti interstitial position in rutile, and from several trial initial geometries for the Ti interstitial in anatase. Contrary to traditional assumptions but consistent with much recent evidence, the Ti interstitial was found to be predominant over the O vacancy in rutile under most conditions. Donor ionization energies in rutile were consistent with experiment. Surprisingly, the calculations also indicate a dominant role for the Ti interstitial in anatase (lower formation energy than the O vacancy, though not by as much as in rutile, and much shallower ionization levels.) We evaluate these findings against experimental data on pure n-type $TiO_2$, and discuss possible implications for transition metal cation doping as well as anion doping of $TiO_2$.

*Supported by US Department of Energy, Basic Energy Sciences

**14:03**

**B46 13 Electron Distributions in Pure $TiO_2$ in Anatase Phase and with Hydrogen Impurities*** S. BYAHUT, *Tribhuvan University, Kirtipur, Kathmandu, Nepal* SUDHA SRINIVAS, *Central Michigan University, Mount Pleasant* LEE CHOW, *University of Central Florida, Orlando* R.H. SCHEICHER, *Michigan Technological University, Houghton* JUNHO JEONG, R.H. PINK, T.P. DAS**, *State University of New York at Albany* The electronic structures of pure $TiO_2$ in anatase phase and with hydrogen impurity have been investigated by the Hartree-Fock Cluster Procedure. They are used to study the associated $^{47}$Ti and $^{17}$O nuclear quadrupole coupling constants $e^2qQ$ and asymmetry parameters $\eta$. For pure $TiO_2$ in the anatase phase, comparison will be made with theoretical and experimental $e^2qQ$ in the rutile phase, the value of $\eta$ for $^{47}$Ti vanishing in the anatase phase due to local axial symmetry. *Supported by US-Nepal Research Program, UGC Nepal, and Senior Fulbright Post-Doctoral Fellowship (S.B.) **Also at UCF, Orlando

**SESSION C1: POSTER SESSION I**
**Monday Afternoon, 13 March 2006**
**Exhibit Hall, 2:00pm–5:00pm (DPOLY session: 11:15am–2:15pm), Baltimore Convention Center at 14:00**



## C1 1 DPOLY POSTER SESSION I

**C1 2 A Multi-Sample Melt Micro-Rheometer** KALMAN MIGLER, *NIST* ANTHONY BUR, We have developed a multi-sample melt micro-rheometer (M3R) based on pressure driven channel flow and designed for simultaneous measurement of multiple polymer melts. The required sample size is less than 100 mg. The driving force for the rheometer is pressurized gas from a nitrogen tank that forces polymer melt into a slit. The melt flow is monitored using a video camera that views the flow front through a sapphire window. The device contains no moving parts and no gaskets or O-rings. Measurements of polyethylene and polycarbonate are presented.

**C1 3 Collection of an electrospinning jet** TAO HAN, DARRELL RENEKER, Electrospinning [1, 2] of polymer nanofibers involves an electrically driven bending instability of the elongating jet. If the jet is collected on a stationary surface immediately before or after the bending instability occurs, the jet buckles as it stops. Bending and buckling are distinct phenomena. The determination of the behavior of the jet path in the vicinity of the onset of the first bending instability is important for the orderly collection of the nanofiber. Precise adjustment of the fluid flow, the electrical current, and the shape of the region from which the jet issued, produced a very stable jet which was observed with a high frame rate, short exposure time camera. The fluid jet and the resulting nanofibers were collected on a solid, electrically conducting substrate which was moved laterally, and simultaneously, away from the tip. This collected material preserved a record of the straight segment and the bending and buckling instabilities with a minimum of overlapping. The occurrence of a second bending instability was sometimes observed in the dry fiber. 1. Doshi, J.; Reneker, D.H., itJournal of Electrostatics; **35**, 151, **1995** 2. Reneker, D.H. ;Yarin,A.L.Fong, H.; Koombhongse, S., it Journal of Applied Physics, **87**, 4531, **2000**

**C1 4 Electrospun Nanofiber Yarn** SPHURTI DOIPHODE, DARRELL RENEKER, *The Maurice Morton Institute of Polymer Science, The University of Akron* Electrospinning creates an electrically charged jet of polymer solution or melt, which elongates dries and solidifies to give very long fibers with nanometer-scale diameters [1]. The yarn manufacturing method [2,3] involves collecting the electrically charged fibers between two parallel and electrically grounded collector surfaces separated by a distance commensurate with the diameter of the loops formed by the electrically driven bending instability [1]. One of the collector surfaces is rotated around its axis at an appropriate rate to twist the fibers into a nanofiber yarn. The yarn was extended, for example by translating the other collector away from the rotating collector. Properties such as yarn diameter, fiber count, and twist per unit length were controlled by changing the rotation rate of the disk. It appears that yarns of nanofibers can be produced from all polymer solutions that can be electrospun. References: [1] Reneker, D.H.; Yarin, A.L.; Fong, H. Koombhongse, S. itJ. App. Phys. 87, 2000, 4531. [2] Dalton, P. D.; Klee, D.; Möller, M. itPolymer 46(3), 2005, 611. [3] Dzenis, Y. itPrivate communication.

**C1 5 Branching in electrospinning of nanofibers** A. L. YARIN, *University of Illinois, Chicago* W. KATAPHINAN, D. H. RENEKER, *reneker@uakron.edu* Z. ZHONG, *The Maurice Morton Institute of Polymer Science, The University of Akron* . A sequence of secondary jet branches sometimes emanates from the electrically charged primary fluid jet during electrospinning experiments. This process was observed during the electrospinning of solutions of polycaprolactone dissolved in acetone [1]. Branching occurred both in the straight segment of the jet and after the onset of the bending instability. Jets with larger diameters, associated with higher voltages, tend to have more branches. Stereographic, stopped motion images of the path of the jet showed that the branches grow in all azimuthal directions around the jet with a smaller component of their growth along the direction of the applied electric field. An electrohydrodynamical model of the branching process showed that the surface of a conducting fluid jet can acquire complicated static equilibrium undulations which become unstable and are capable of transforming into branches. 1. Yarin, A. L.; Kataphinan, W.; Reneker, D. H. itJ. App. Phys., 98, 2005, 064501.

**C1 6 Developments of Novel Polymer Electrolyte Fuel Cell Membranes*** TOMOMI IRITA, *Polymer Science & Engr. Dept. UMass* MASAHIRO KONDO, HIROKAZU AOYAMA, *Fundamental Research Dept., Chemical Div. Daikin Industries, Ltd Osaka* THOMAS RUSSELL, *Polymer Science & Engr. Dept. UMass* Perfluorinated polymer electrolyte membranes (PEM), such as Nafion, are considered to be the most promising candidate for the development of the next generation fuel cell technology. The key technological challenges facing PEMs are their performance, durability and cost. In this research, the polymer electrolyte emulsions (PEE) were obtained by a simple hydrolysis reaction of the precursor polymer emulsion. PEMs are obtained by solvent casting the PEE. The PEE obtained here has a very low viscosity even at high solution concentrations. Using high concentration emulsions greatly reduces the amount of the waste, which makes this technology superior to the conventional ones. Casting conditions were optimized to enhance the mechanical properties, e.g. the tensile strength and viscoelastic properties, of the membrane. The PEMs obtained possessed better ionic conductivity than Nafion while their mechanical properties are comparable. Finally, the cost evaluation for this process was conducted and it was shown that the contribution to the cost reduction becomes bigger. (This research was sponsored by New Energy and Industrial Technology Development Organization, Japan)

*This research was sponsored by NEDO (New Energy and Industrial Technology Development Organization), Japan

**C1 7 Abstract Withdrawn**

**C1 8 Non-halogen Flame retardant High Impact Polystyrene Composites** MIRIAM RAFAILOVICH, MAYU SI, JONATHAN SOKOLOV, *Dept. of Materials Science and Engr., Stony Brook Univ.* JOSHIA OTAIGBE, *School of Polymers and High Performance Materials, Univ. of Southern Miss.* VLADIMIR E. YUDIN, *Head of Polymer Composites Lab, Inst. of Macromolecular Compounds, Russian Academy of Sciences* In recent years, driven by the health issues and the incurred banning policy of bromine compounds, it is a great demand to find an alternate to replace brominated compounds in polymer flame retardant industry. High impact polystyrene (HIPS), a popular materials widely used for electrical appliances and electronic instruments, attracts extensive attention for its dominant flame retardant agent, decabromodiphenyl ether. Here we propose a novel idea to prepare non-halogen HIPS self-extinguishing composites based on the combination of phosphorus compounds and clay. The combustion behavior was thoroughly investigated by UL 94 V-0, LOI, and cone calorimeter measurements. The addition of Cloisite 20A dramatically decreases the value of LOI and the resulted HIPS composites could not pass UL 94 V-0. On the other hand, the introduction of thermal stable clay significantly increases the value of LOI and the corresponding HIPS composites can successfully self-extinguish. These results strongly demonstrate that the thermal stability of clay is the key factor to determine the final flame retardant performance. The synergy between the clay and phosphorus compounds is further studied.

**C1 9 An ''Alternating-Curvature'' Model for the Nanometer-scale Structure of the Nafion Ionomer, Based on Backbone Properties Detected by NMR** KLAUS SCHMIDT-ROHR, Q. CHEN, *Ames Laboratory and Department of Chemistry, Iowa State University, Ames, IA* The perfluorinated ionomer, Nafion, which consists of a $(-CF_2-)_n$ backbone and charged side branches, is useful as a proton exchange membrane in $H_2/O_2$ fuel cells. A modified model of the nanometer-scale structure of hydrated Nafion will be presented. It features hydrated ionic clusters familiar from some previous models, but is based most prominently on pronounced backbone rigidity between branch points and limited orientational correlation of local chain axes. These features have been revealed by solid-state NMR measurements, which take advantage of fast rotations of the backbones around their local axes. The resulting alternating curvature of the backbones towards the hydrated clusters also better satisfies the requirement of dense space filling in solids. Simulations based on this ''alternating curvature'' model reproduce orientational correlation data from NMR, as well as scattering features such as the ionomer peak and the $I(q) \sim 1/q$ power law at small q values, which can be attributed to modulated cylinders resulting from the chain stiffness. The shortcomings of previous models, including Gierke's cluster model and more recent lamellar or bundle models, in matching all requirements imposed by the experimental data will be discussed.

**C1 10 Dynamics of Sulfonated Polystyrene Copolymers and Ionomers using Broadband Dielectric Spectroscopy** PORNPEN ATORNGITJAWAT, JAMES RUNT, *The Pennsylvania State University* The dynamics of sulfonated polystyrene (SPS) copolymers in acid and neutralized forms were investigated using broadband dielectric relaxation spectroscopy. SPS copolymers were synthesized by sulfonation of a monodisperse polystyrene to 1 and 7 mol %. Neutralization was achieved by exchanging the protons of the acid functionality with Na, Cs and Zn cations. Multiple relaxation processes were observed above the glass transition temperature of the neutralized and unneutralized materials. For the unneutralized copolymers, a 'chemical relaxation' was observed at temperatures above the segmental process, arising from the presence of hydrogen bonding. For the ionomers, a Maxwell-Wagner-Sillars process was observed due to the presence of ionic clusters. The 'chemical relaxation' followed Arrhenius behavior and its relaxation strength decreased significantly with increasing temperature. The relaxation times of the MWS process of all ionomers followed a VFT form. A local relaxation in the glassy state was observed for unneutalized copolymers and ionomers neutralized with monovalent cations, while it was suppressed for ionomers neutralized with divalent cations.

**C1 11 Molecular Dynamics Simulations of Polyelectrolyte Adsorption at Oppositely Charged Surfaces** JAN-MICHAEL CARRILLO, ANDREY DOBRYNIN, *University of Connecticut* We have performed molecular dynamics simulations of polyelectrolyte adsorption at oppositely charged surface from dilute polyelectrolyte solutions. In our simulations polyelectrolytes are modeled by chains of charged Lennard-Jones particles with explicit counterions. We have studied the effects of surface charge density, surface charge distribution, solvent quality for the polymer backbone, strength of the electrostatic and short-range interactions on the polymer surface coverage and thickness of the adsorbed layer. We have observed surface undercharging by adsorbing polyelectrolyte in most systems except for systems with low surface charge densities. This undercharging is due to partial screening of the surface charge by surface counterions however this effect is negligible at low surface charge densities. Surface overcharging was also observed for the so-called ''salt-free'' systems in which only counterions necessary for neutralization of the charge difference between surface charge and polyelectrolytes were kept in the system. Hydrophobic polyelectrolytes cover higher percentage of the adsorbing surface forming a thinner polymeric layer in comparison with those observed in the systems with hydrophilic polyelectrolytes. However, the polymer surface coverage is close for both these systems.

**C1 12 Molecular Dynamics Simulations of Polyelectrolyte-Polyampholyte Complexes. Effect of Solvent Quality and Salt Concentration.** JUNHWAN JEON, ANDREY DOBRYNIN, *Polymer Program, Institute of Materials Science, Department of Physics, University of Connecticut* Using molecular dynamics simulations we have studied complexation in polyelectrolyte-polyampholyte mixtures in poor solvent conditions for the polyelectrolyte backbone. In a poor solvent a polyelectrolyte form a necklace-like structure. Upon forming a complex with both random and diblock polyampholytes a polyelectrolyte chain changes its necklace conformation by forming one huge bead. The collapse of the polyelectrolyte chain occurs due to neutralization of the polyelectrolyte charge by polyampholytes. In the case of the random polyampholyte the more positively charged sections of the chain adsorb on the surface of the globular bead while more negatively charged chain sections form loops surrounding the collapsed core of the aggregate. In the case of diblock polyampholyte the positively charged block and a part of the negatively charged block wraps around the collapsed polyelectrolyte with a substan-

tial section of the negatively charged block sticking out from the collapsed center of the aggregate. These structures appear as a result of optimization of the net electrostatic energy of the complex and short-range attractive interactions between monomers of the polyelectrolyte chain.

**C1 13 Surface Treatment for Improved Mobility in Poly(3-hexylthiophene) Thin-Film Transistors*** ADRIAN SOUTHARD, MICHAEL FUHRER, *Department of Physics and Center for Superconductivity Research, University of Maryland* Thin films of poly(3-hexylthiophene), an organic semiconductor, were spin-coated from chloroform onto a self-assembled monolayer of octyltrichlorosilane (2 nm thick) and yielded an order of magnitude higher field-effect mobility than similar films deposited directly onto the $SiO_2$/Si substrate. Mobility was measured using the polymer as the conducting channel of a field-effect transistor with Au top contacts as the source and drain electrodes and the doped silicon as a gate. The higher mobility is presumed to be due to the increased order of the semiconducting layer. Evidence for this ordering and the effect of other self-assembled monolayers will be discussed along with the effect of various contact geometries. This work was supported by the Laboratory for Physical Sciences.

*Support from Laboratory of Physical sciences in College Park, MD

**C1 14 Age old antipodes united: stable *and* low-work-function surfaces are generic** M.A. UIJTTEWAAL, G.A. DE WIJS, R.A. DE GROOT, *Radboud University Nijmegen/Electronic Structure of Materials* Both a low work function and a stable surface are crucial for the application of cathodes in *e.g.* microwave ovens, organic photoconductors and displays as CRTs and OLEDs. Until recently they were considered antipodes. In previous work[1] we showed a stable low-work-function surface to be realised for the compound $BaAl_4$ and even predicted that stable, low-work-function surfaces would be generic for metals with polar surfaces. Now, *ab initio* calculations confirm the prediction for the compounds $CaAl_4$, $BaAuIn_3$ and $LaB_6$. [1] M.A. Uijttewaal, G.A. de Wijs, R.A. de Groot, R. Coehoorn, V. van Elsbergen, and C. H. L. Weijtens, *Chem. Mater.* **17**, 3879 (2005)

**C1 15 Effects of Local Dielectric Property on the Chain Conformation Distribution of Poly (vinylidene fluoride-hexafluoropropylene) Copolymers.** GUOLIN WU, SURIYAKALA RAMALINGAM, SHAW LING HSU, *Polymer Science & Engineering, Univ of Massachusetts* Poly(vinylidene fluoride) (PVdF) is a well known polymer possessing various polymorphic structures. Local dielectric property is known to affect the relative amount of polymorphic phases. The copolymer of PVdF and hexafluoropropylene units is especially fascinating. In this copolymer, changes in structure need to consider both localized dielectric property and steric effects of the comonomer units. The copolymer structure possesses smaller remnant polarization and fewer polar crystalline states in comparison to the homopolymer. Solution NMR studies reveal that the relative population of various rotational isomeric states has been changed in comparison to the homopolymer. This change in single chain structure obviously propagates into the condensed state yielding polar structure, that is, $\beta$ and $\gamma$ phases. NMR, Raman spectroscopy, wide-angle X-ray diffraction, and calorimetric methods were utilized in these studies. The steric effects of the comonomer units driving away from the $\beta$ phase have also been established.

**C1 16 The Effects of Surface Interactions and Confinement on the Melting Point of Semi-crystalline Polymer Thin Films** YANTIAN WANG, MIRIAM RAFAILOVICH, JONATHAN SOKOLOV, DILIP GERSAPPE, *State University of New York at Stony Brook, NY 11794-2275* ASHISH BAKSHI, *Manhasset High School, Manhasset, NY 11030* RAJESH ATLURI, *Herricks High School, New Hyde Park, NY 11040* TOHRU ARAKI, YING ZOU, HARALD ADE, *North Carolina State Univeristy, Raleigh, NC27695* DAVID LEWIS KILCOYNE, *Advanced Light Source, LBNL, Berkeley, CA94720* GAD MAROM, *The Hebrew University of Jerusalem, Jerusalem 91904, Israel* ARNOLD LUSTIGER, *ExxonMobil Research and Engineering Company, Annandale, NJ 08801* A decrease in melting temperature for semi-crystalline polyethylene thin films in the vicinity of a substrate was observed. The depression in the melting point increases with increasing surface interaction. The biggest $T_m$ depression is 38°C. We propose a model where the depression is attributed to the attractive force between the substrate and the polymer chains which competes with the ordering force among the polymer chains. In order to determine the universality of the effect, experiments were conducted on other polymers, i.e. polycaprolactone and poly(ethylene oxide) where similar results were obtained. The effects of confinement were then studied by crystallizing the films on patterned surfaces where the dimensionality of the patterns was continuously varied for nanometer to micron scale.

**C1 17 Oriented Lamellar Structure and Pore Formation Mechanism in CSX-Processed Porous High-Density Polyethylene** SHUJUN CHEN, SAMUEL P. GIDO, *Dept. of Polymer Sci. and Eng., Univ. of Massachusetts, Amherst, MA 01003* SOUVIK NANDI, H. HENNING WINTER, *Dept. of Chem. Eng., Univ. of Massachusetts, Amherst, MA 01003* Characterization of pore structure and pore wall crystal structure was performed on porous high-density polyethylene (HDPE) using SEM, TEM, and electron diffraction. The porous HDPE material was obtained through crystallization from swollen crosslinked polyethylene gels (CSX process) in supercritical propane. SEM showed an open pore structure of micron-sized pores, large void fraction and surface area, as well as thin yet rigid pore walls, making this material a good candidate for a variety of applications. TEM revealed oriented lamellar structure in the pore walls which was much different from structures found in typical bulk HDPE as well as that of the crosslinked HDPE before CSX processing. Electron diffraction results confirmed the presence of oriented lamellar stacking. Based on this oriented lamellar structure, possible mechanisms for crystallization and pore formation in the CSX process are suggested.

**C1 18 Melting Point Measurement of Polycaprolactone Thin Films*** CLIVE LI, *SUNY at Stony Brook* VICTOR WANG, *Great Neck South High School* JONATHAN SOKOLOV, *SUNY at Stony Brook* MIRIAM RAFAILOVICH, *SUNY at Stony Brook* GARCIA TEAM, GREAT NECK SOUTH HIGH SCHOOL COLLABORATION, We investigated the melting point of Polycaprolactone (PCL) thin films as a function of film thickness by using three different techniques, namely, Shear Modulation Force Microscopy (SMFM) technique, Atomic Force Microscopy (AFM) topographic technique, and optical birefringence technique which consisted of laser, polarizers, photoelasitc modulator (PEM), and a lock- in amplifier. The optical and the AFM topography results show PCL to behave similarly for film thicknesses of 215.8 and 37.0 nm, both melting around 331 - 335 K. However, the SMFM

show an approximate 8 K decrease in melting point, suggesting that the polymer may get softer at this lower temperature before it changes in structure for 37.0 nm PCL films. Possible explanations for the differences are discussed.

*This work is supported by the NSF

**C1 19 Effects of Residual Crystallinity on the Crystallization Behavior of Random Polypropylene-Polyethylene Copolymer** SAMUEL AMANUEL, *Materials Science and Engineering* XIAOFENG CHEN, *Chemical and Biological Engineering* RAHMI OZISIK, SANFORD S. STERNSTEIN, *Materials Science and Engineering, Rensselaer Polytechnic Institute* Differential scanning calorimeter measurements revealed that blends of isotactic polypropylene and random polypropylene- polyethylene copolymer have two separate melting peaks, with a peak at 45 $^{o}$C attributed to the copolymer and another peak at 160 $^{o}$C attributed to the homopolymer. Annealing at temperatures below and above the melting of the homopolymer, 145 $^{o}$C and 200 $^{o}$C, resulted in changes of the melting temperature and melting enthalpy of the copolymer. This suggests that the crystallization behavior of the copolymer has been influenced by the residual crystallinity of the homopolymer. Furthermore, this crystalline memory has significant influence on the aging process of the blend. For instance, dynamic measurements, at room temperature, revealed that samples annealed at 120 $^{o}$C have lower shear storage modulus compared to those that were annealed at 200 $^{o}$C. Although physical aging increases the storage modulus in both cases, the rate at which it changes is also dependent on the presence of residual crystallinity.

**C1 20 Disk, Cylinders, Stack-of-Disks, and Vesicles Morphologies from Amphiphilic Block Copolymer Solution-State Assemblies** ZHIBIN LI, ZHIYUN CHEN, HONGGANG CUI, KELLY HALES, KAI QI, KAREN WOOLEY, *Washington University in Saint Louis* DARRIN POCHAN, *University of Delaware* Disk formation has been examined through self-assembly of poly(acrylic acid)-*b*-poly(methyl acrylate)-*b*-polystyrene (PAA-*b*-PMA-*b*-PS) amphiphilic triblock copolymer with polyelectrolyte PAA as corona block and organic diamines as counterions in water/THF solvent mixtures. It was found that by using the same triblock copolymer but varying the type and amount of diamines, disk or cylindrical micelles could be selectively formed and intermediate structures between discs and cylinders were observed. Under certain solution conditions, disks were prefer to stacking together to form stack-of-disks, and stack-of-disks could also transfer to organized rods by increasing the counterion concentration. Discs within the stacks could be uniform in size, and organized rods had the same geometry while they changed from stack-of-disks. It was interesting to see the long range (microns) interactions between discs or organized-rods. By using diblock (PAA-*b*-PS) copolymer analogues, vesicles were obtained with the presence of diamine counterions. The stability of disc vs. vesicle will also be discussed, and the experimental results will be used to compare with the theoretical predictions. The system was investigated by means of transmission electron microscopy, cryogenic transmission electron microscopy, DLS and SANS.

**C1 21 Nanoporous Membrane with Ultrahigh Selectivity and Flux Suitable for Filtration of Viruses*** JIN KON KIM, *Department of Chemical Engineering, Pohang University of Science and Technology* SEUNG YUN YANG, *Department of Environmental Science and Engineering, Pohang University of Science and Technology* IN CHEOL RYU, SUNG KEY JANG, *Department of Life Sciences, Pohang University of Science and Technology* THOMAS P. RUSSELL, *Polymer Science and Engineering Dept., Univ. of Massachusetts at Amherst* We introduce a new double layered nanoporous membrane suitable for virus filtration. One layer is an 80 nm thick film having cylindrical pores with diameters of 15 nm and a narrow pore size distribution. This layer is prepared by using a thin film of the mixture of a block copolymer and a homopolymer, and mainly acts to separate viruses. The support layer is a conventional micro-filtration membrane with a broad pore size distribution. This asymmetric membrane showed very high selectivity and flux for the separation of human rhinovirus type 14 which has a diameter of $\sim$ 30 nm and is a major pathogen of the common cold in humans.

*This work was supported by the Creative Research Initiative Program (KOSEF).

**C1 22 Effect of Selective Solvent on the Morphological Phase Behavior of PS-b-PEO** PRACHUR BHARGAVA, XIAOLIANG ZHENG, YINGFENG TU, STEPHEN Z.D. CHENG, MAURICE MORTON INSTITUTE OF POLYMER SCIENCE, THE UNIVERSITY OF AKRON TEAM, Amphiphilic block copolymers with glassy cores can be self -assembled in solution to form various nanoscale morphologies by using a two solvent process. In the first step the block copolymer is dissolved in a common solvent and then a selective solvent for one of the blocks is added to induce micellization. We have used this method to obtain nanoscale morphologies for PS-b-PEO. We have used DMF as the common solvent and have investigated two selective solvents for PEO, water and acetonitrile. The morphologies obtained by using both these selective solvents are similar. Spheres, rods/worm and vesicles can be obtained by varying only the solvent composition in both the systems. However a 'worm network' can be obtained only by using water as a selective solvent. Also in case of water all the morphologies can be obtained in a very narrow range of water content while in case of acetonitrile the morphologies can be obtained only in a broad range of acetonitrile content. The difference in the behavior with water and acetonitrile can be attributed to their solubility parameters which affects the polymer solvent interaction parameter $\chi$.

**C1 23 Effect of Annealing Temperature on the Surface Composition of Block Copolymers with Semifluorinated Side Chains** K.E. SOHN, A. HEXEMER, *UCSB* S. KRISHNAN, M. PAIK, C.K. OBER, *Cornell* E.J. KRAMER, *UCSB* D. FISCHER, *NIST* The effect of the annealing temperature on the surface composition and orientation of semifluorinated side chains in styrene-isoprene based block copolymers has been studied using NEXAFS spectroscopy, angle resolved XPS, and AFM. Annealing brings the fluorogroups to the surface due to their lower surface energy, resulting in a decrease in styrene content at the surface. NEXAFS experiments on samples annealed in high vacuum and slowly cooled show orientation of the $CF_2$ helix of fluorinated side chains as characterized by a helix orientational order parameter, $S_{helix}$, (relative to the surface normal) that is increased by annealing at the optimum temperatuer. NEXAFS measurements during heating in-situ heating reveal how the orientation progresses at the annealing temperature.

**C1 24 Polystyrene Freeze Dried from Dilute Solution:Ê Tg Depression and Residual Solvent*** WEI ZHENG, SINDEE SIMON, *Texas Tech University* The calorimetric glass transition temperature, Tg, was measured for both linear and cyclic polystyrenes freeze-dried from dilute solution in benzene for concentrations of 0.10%, 0.05% and 0.02% polymer by weight. Upon freeze-drying, Tg was found to be depressed by 4 to 15 K depending on the sample, solvent concentration, and freezing conditions. Annealing under vacuum (0.05 torr) at moderate temperatures, 40 to 140° C, resulted in the shifts of Tg back to its bulk value and was accompanied by a decrease in sample weight. The observed weight loss is presumably due to residual solvent. The amount of solvent present in the original freeze-dried samples was determined from the weight loss observed after annealing under vacuum (0.05 torr) for one hour at 100° C and one hour at 140° C. The calorimetric glass temperature was measured as a function of the fraction of the residual solvent. A linear correlation was found between the Tg depression and the residual solvent concentration, in agreement with data in the literature. In addition, the structure of the freeze-dried polystyrene was examined using Fourier transform infrared spectroscopy. Results show that the recovery of Tg is not due to the structure change during annealing. We conclude that the residual solvent has a significant effect on the Tg depression observed for polymers freeze-dried from dilute solution; no depression or even a slight increase in Tg was observed in the absence of residual solvent.

*Funding from NSF DMR 0304640 is gratefully acknowledged.

**C1 25 Enthalpy Recovery of Polymeric Glasses: Is the Theoretical Limiting Liquid Line Reached?** QINGXIU LI, SINDEE SIMON, *Texas Tech University* Glasses are inherently non-equilibrium materials, and consequently, their properties evolve toward equilibrium in a process known as structural recovery or physical aging. Recently, several authors have suggested that the equilibrium liquid line is not reached even when properties have ceased to evolve. In this work, we present measurements of the enthalpy recovery of polystyrene (PS) at temperatures ranging from the vicinity of glass transition temperature to 10[r]C below Tg (90[r]C), for aging times up to 200 days. The results are analyzed in the context of the TNM model of structural recovery. In addition, we analyze data in the literature to determine whether enthalpy recovery ceases prior to the material reaching the equilibrium liquid line obtained by extrapolation of the liquid line above Tg. The results suggest that, in fact, the liquid enthalpy line is reached at temperatures below Tg when equilibrium is reached, i.e., when properties cease to evolve.

**C1 26 Universal Aspects of Macromolecules in Polymer Blends, Solutions, and Supercritical Mixtures*** YURI MELNICHENKO, *Oak Ridge National Laboratory* GEORGE WIGNALL, *Oak Ridge National Laboratory* DIETMAR SCHWAHN, *Kernforschungsanlage, Julich* ?We demonstrate that macromolecules in miscible polymer blends may behave as poor, theta and good polymeric solvents for each other. We construct a conceptual phase diagram, indicating the range of validity of the random phase approximation, outside of which molecules contract or expand beyond their unperturbed dimensions, contrary to common assumptions. Similarly, the concentration fluctuation correlation length collapses onto a master curve for polymeric, liquid and supercritical solvents, indicating that macromolecules behave uni-versally in these media over a wide range of thermodynamic variables.

*This work was supported by the Division of Materials Sciences, under Contract No. DE-AC05-00OR22725 with the Oak Ridge National Laboratory, managed by UT-Battelle, LLC.

**C1 27 Associative polymers bridging between layers of multilamellar vesicles.** SEO CHOI, *University of Massachusetts Amherst* SURITA BHATIA, *University of Massachusetts Amherst* Multilamellar vesicles can be found in a variety of pharmaceutical formulations, personal care products, and home care products. Hydrophobically modified associative polymers are often used to stabilize the vesicles or to control the rheological properties of these formulations. The hydrophobic groups are expected to insert themselves into the vesicle bilayers. Recent experimental work shows that hydrophobically modified polymers may from bridges between vesicles or may bridge between layers of a single vesicle. The latter configuration forces an interlayer spacing roughly equal to the radius of gyration of the backbone between associative groups. We have performed simple mean-field calculations on ideal telechelic associative polymers between concentric spherical surfaces. We find that the free energy per chain has an attractive minimum when the layer spacing is approximately $N^{1/2}l$, which is consistent with experimental results. The depth of the minimum depends on both chain length and curvature, and as expected when the curvature becomes small, the result for telechelic chains between flat surfaces is recovered.

**C1 28 Synthesis and characterization of thermoreversible hydrogels from associating polymers** JUN JIANG, CHUNHUA LI, *State University of New York at Stony Brook* MICHAEL RUBINSTEIN, *University of North Carolina at Chapel Hill* RALPH COLBY, *Pennsylvania State University* DANIEL COHN, *Hebrew University of Jersualem* MIRIAM RAFAILOVICH, JONATHAN SOKOLOV, *State University of New York at Stony Brook* STATE UNIVERSITY OF NEW YORK AT STONY BROOK TEAM, UNIVERSITY OF NORTH CAROLINA AT CHAPEL HILL COLLABORATION, PENNSYLVANIA STATE UNIVERSITY COLLABORATION, HEBREW UNIVERSITY OF JERSUALEM COLLABORATION, Multiblock copolymers of poly(ethylene oxide)$_{99}$-poly(propylene oxide)$_{69}$-poly(ethylene oxide)$_{99}$ were synthesized by coupling with hexamethylene diisocyanate (HDI). The rheological, morphological and structural properties of the gel were characterized as a function of temperature, composition and block number. Mixtures of multiblock and single block copolymers were also studied. Using neutron scattering we found that a large degree of alignment could be induced in the single block gel, but no order could be found in the multi-block or homopolymer multiblock mixture. The yield strain in samples with 3.2 of multiblocks was nearly an order of magnitude higher than the single bock gel. This was interpreted in terms of an ordered layered state of micelles being formed by steady shear. A model based on the competition between forming non-interacting micelles and forming bridges will be presented.

**C1 29 Design, Synthesis, and Evaluation of Non-Porous, Hydrophilic Membranes** SADIE WHITE, *University of Pennsylvania Department of Materials Science and Engineering* MICHAEL FRYD, *University of Pennsylvania Department of Chemistry* BRADFORD WAYLAND, *University of Pennsylvania Department of Chemistry* RUSSELL COMPOSTO, *University of Pennsylvania Department of Materials Science and Engineering* KAREN WINEY, *University of Pennsylvania Department of Materials Science and Engineering* The use of membranes in biological sciences, electrochemistry, and separation technologies is widely expanding. In this investigation, the water flux and filtra-

tion capacities of polyacrylamide-based hydrogel membranes were studied under gravity- and forced filtration processes. The crosslinked membranes were prepared via room-temperature aqueous free radical polymerization, initiated with ammonium persulfate. The crosslinker hydrophilicity and concentration (between 0.5 and 10 mole percent), as well as the membrane thickness, were varied to determine the dependence of gel swelling and water flux on these factors. Suspensions of narrowly-dispersed pigment particles (with a diameter of approximately 200 nanometers) were analyzed with light scattering before and after filtration to determine how effectively the membranes remove particulate matter in this size range. Ongoing work will broaden the investigation to include similar water throughput and filtration studies on crosslinked poly(acrylic acid) membranes.

**C1 30 Small angle neutron scattering study to determine the structure of high strength hydrogels.*** TAIKI TOMINAGA,† *Graduate School of Science, Hokkaido University, Japan* VIJAY R. TIRUMALA, ERIC K. LIN, WEN-LI WU, *Polymers Division, National Institute of Standards and Technology* JIAN PING GONG, HIDEMITSU FURUKAWA, YOSHIHITO OSADA, *Graduate School of Science, Hokkaido University* Hydrogels are swollen polymer networks containing more than 90% water. Most hydrogels, however, are mechanically too weak to be used as load bearing devices. Gong itet al. have overcome this problem by synthesizing hydrogels with a double network (DN) structure. Modifying the polyelectrolyte network structure by polymerization of high molecular weight uncharged polymer itin situ, resulted in orders of magnitude increase in their load bearing ability. Despite 90% water, these tough gels exhibit a fracture stress of 170 kg/cm$^2$, similar to that of articular cartilage found in the bone-joints of human body. In this work, we determined the structure of DN-gels using small angle neutron scattering. Structural origins for high toughness found in DN-gels were then examined by comparing the structure of DN-gels with that of pure polyelectrolyte network and polyacrylamide solution.

*NIST Center for Neutron Research, U. S. Department of Commerce facilities are acknowledged.
†Currently at: Polymers Division, NIST USA

**C1 31 Quantitative analysis of interfacial reaction and interfacial thickness by FTIR and Ellipsometry.** MANORANJAN PRUSTY, HAN GOOSSENS, GERT DE WIT, PIET LEMSTRA, *Technical University Eindhoven* MATRIN VAN DUIN, *DSM Research, Geleen* We have studied the development of interface and also interfacial reaction in Polyethylene-co-methacrylic-acid (PE-co-MA) and Styreneacrylonitrile-oxazoline (SAN-Oxaz) bilayer film. The interfacial reaction was studied in-line at different temperatures for the bilayer sample. A decrease in oxazoline and increase in amide and ester was observed. The intensity of amide I was found to have a plateau at higher time indicating that the reaction is diffusion limited. The growth of interface was also studied with the ellipsometer. The retardation, $\Delta$ and reflection ratio, tan$\psi$ data were recorded for the bilayer sample at three angles of incidence (60[r], 70[r] and 80[r]) and at different temperatures. These data were fitted according to a 4-layer model. The time variations of interfacial thickness in SAN-Oxaz/PE-co-MA bilayer was found to increase with time and finally go to a plateau at higher temperatures.

**C1 32 Confinement Effects on the Phase Separation of Polymer Dispersed Liquid Crystals** JIANFENG XIA, JUN WANG, ZHIQUN LIN, *Department of Materials Science and Engineering, Iowa State University, Ames, IA 50011600* FENG QIU, YULIANG YANG, *Department of Macromolecular Science, Fudan University, Shanghai 200433, China* The phase separation kinetics of polymer dispersed liquid crystals (PDLC) confined between two parallel, smooth walls are numerically studied for the first time. The time evolution of two order parameters (i.e., composition order parameter, it$\phi$ and orientational order parameter, $Q$) are calculated by solving coupled time-dependent Ginzburg–Landau (TDGL) model C equations. The external confinement is found to accelerate the ordering of LC. The results presented in the study may provide insights into the experiments on the control of LC domain morphology under nanoscopic confinement.

**C1 33 Crystallization of Ethylene Vinyl Acetate (EVA) and Polyethylene (PE) /deuterated Polystyrene (dPS) Blends in Supercritical Carbon Dioxide (scCO$_2$)** CHRISTOPHER PYNN, *Hals Hollow Hills High School West, NY* PAYVAND AHDOUT, *Rosyln High School, NY* JOHN JEROME, YANTIAN WANG, VLADIMIR ZAITSEV, JOHNATHAN SOKLOV, MIRIAM RAFAILOVICH, *Dept. of Mat. Sci. and Engr,, State Univ. of New York at Stony Brook* STEVEN SCHWARZ, *Dept. of Physics, CUNY Queens College* Thin films of EVA or PE and dPS were spun cast onto Si wafers and crystallized in supercritical carbon dioxide at pressures and temperatures corresponding to the density fluctuation ridge[1] or thermally annealed using standard protocols. The morphology composition and melting points of the films were studied using scanning force microscopy and imaging time-of-flight secondary ion mass spectrometry as function of film thickness and homopolymer concentration. The results showed that exposure to scCO$_2$ produced highly crystalline films. Furthermore, in contrast to the thermally annealed films, the homopolymer was fully incorporated into the crystalline phase. The surface morphology of the films after crystallization showed either island or hole structure, depending on the relation between the film thickness and the lamellar height. Supported in part by the NSF-MRSEC program and by a grant from the SRC-NYS consortium. Reference: [1]Koga T., Seo Y.S., Shin K., Zhang Y., Rafailovich M., Sokolov J., B. Chu, Satija, S.K. Macromolecules. Vol. 36. 2003: 5236-5243.

**C1 34 Phase structures of block copolymers blended with small molecules** KISHORE TENNETI, *Drexel University* XIAOFANG CHEN, *Peking University* CHRISTOPHER LI, *Drexel University* XINHUA WAN, QI-FENG ZHOU, *Peking University* IGORS SICS, BENJAMIN HSIAO, *University of Stony Brook* DREXEL UNIVERSITY TEAM, PEKING UNIVERSITY COLLABORATION, UNIVERSITY OF STONY BROOK COLLABORATION, We report our observations on the influence of blending small molecules on the phase structures of a block copolymer (BCP) system. Poly(styrene-b-4vinyl pyridine) (PS-b-P4VP) BCP was blended with 4-(3,4,5-tris(alkyloxy)benzoyloxy)phenyl 4- hydroxyphenyl isophthalate (BCLCn where n = 6-16) small molecule in different weight ratios. The terminal hydroxyl group of the BCLC is expected to form hydrogen bonding with the P4VP and thus alter the phase structure of the BCP. Thermal analysis, X-ray analysis and transmission electron microscopy were conducted and it was observed

that BCLCs with n = 6 and 8 did not have any influence on the BCP morphology and those with n = 14 and 16 have phase separated. There was a substantial decrease in the d-spacing of BCPs blended with BCLCs with n = 10 and 12 and a bilayer structure was evident.

**C1 35 Structure and Nanomechanical Properties of Well-aligned Electrospun PS/MWCNT Composite Nanofibers** YUAN JI, SHOUREN GE, JASEUNG KOO, BINGQUAN LI, *Department of Materials Science, SUNY at Stony Brook* BATYA HERZBERG, TOBY KLEIN, *SKA High School for Girls* JONATHAN SOKOLOV, MIRIAM RAFAILOVICH, *Department of Materials Science, SUNY at Stony Brook* SKA HIGH SCHOOL FOR GIRLS COLLABORATION, Carboxyl-functionalized multi-wall carbon nanotubes (MWCNT) were incorporated into polystyrene/DMF solutions and electrospun to form PS/MWCNT composite nanofibers. The nanofibers were spun onto a high speed rotator where they became well aligned. Scanning electron microscopy (SEM) and transmission electron microscopy (TEM) were used to investigate the surface morphology and interior structure of the electrospun nanofibers. A three-point bending test, using atomic force microscopy (AFM), was utilized to measure the Young's moduli of the nanofibers as a function of fiber diameter and MWCNT concentration. Shear modulation force microscopy (SMFM) was employed to measure the surface glass transition temperature of the composite nanofiber. The existence of MWCNT enhanced the Young's moduli of fibers and increased the glass transition temperature by nearly 10 degrees. Supported by NSF-MRSEC.

**C1 36 Spherical nanoparticle ordering in block copolymer systems** JOHN PAPALIA, MARY GALVIN, *University of Delaware* In recent years, nanoparticles and self-assembled systems have both been areas of extensive research. Our work combines the unique properties of both fields into a single system by investigating the ordering of nanoparticles in block copolymers (BCPs). Balazs et al. put forth an expansive set of theories which predict the behavior of hard nanoparticle inclusions in BCP systems. These composites combine the natural drive of the BCPs to self-assemble with the physical properties of the particles, yielding complex systems. Our goal is to methodically investigate the theories via model experimental systems. Silica nanoparticles ( $<$ 25nm have been incorporated into the styrene phase of a polystyrene-b-poly(ethylene-co-propylene) BCP. Parameters such as particle size, surfactant coverage, and particle volume fraction are varied in a controlled fashion with their effects on particle ordering studied. Results show surfactant use is almost mandatory to provide the particles with the energetic advantage needed to integrate them into the BCPs. Integrated particles show definitive ordering within discrete BCP domains. Our current and future systems seek to further investigate these results and trends. The combination of these result sets, along with experimentation related to domain size, will aid the design of multi-size particle systems potentially suited for improved photonic devices or nanoscale waveguides.

**C1 37 Dependence of Tg Upon Fiber Orientation in Epoxy-Matrix Composites** KRISTY VISCONTI, PATRICK BURTON, JOHN D. McCOY, *New Mexico Institute of Mining and Technology* SANDIA NATIONAL LABORATORIES COLLABORATION, Epoxy-matrix glass-fiber reinforced composites were tested using a Rheometrics RMS to investigate the dynamic complex shear modulus. The samples were constructed from woven prepreg tape with all layers layed-up at a single weave orientation. Rectangular samples were cut at various angles relative to the fiber direction. The material was found to be rheologically simple. Consequently, a single master curve was constructed for each sample orientation. From this master curve the corresponding shift factors were extracted and plotted against temperature. The WLF equation was used to estimate the glass transition temperature, Tg. An apparent shift in the glass transition temperature was observed as the orientation of the fiber weave relative to the torsional axis was varied.

**C1 38 One Dimensional Nanocomposites** NIKHIL SHARMA, DARRIN POCHAN, *Univ of Delaware, Dept of Materials Science & Engineering* Tailoring the structure of hybrid materials at the nano-scale in order to enhance their properties could produce advanced materials with remarkable attributes and poses significant research challenges. One- dimensional nanoparticle assemblies are an interesting class of materials that may provide an insight into the fundamentals of quantum mechanics of nanomaterials and have potential applications as sensors, in drug-delivery, and in the conduction of novel signals such as phonons and spin states. Experimental work with electrospinning of polyethylene oxide fibers with inorganic particles (silica and iron) is underway that utilizes a coaxial capillary electrospinning apparatus for the formation of one- dimensional assemblies of nanoparticles. The effect of change in solution concentrations and relative flow rates in internal and external channels of the coaxial electrospinning apparatus on the inter-particle distance are being investigated.

**C1 39 Structure, Morphology and Properties of Carbon Nanotube Containing Polymeric Materials** LINGYU LI, STEVE KODJIE, CHRISTOPHER LI, Carbon nanotubes (CNTs) are considered an ideal reinforcing fillers in polymer nanocomposites because of their high aspect ratio, nanosize diameter, very low density and excellent physical properties (such as extremely high mechanical strength, high electrical and thermal conductivity), However, in order to achieve homogeneous dispersion of CNTs without damaging their extraordinary properties, non-covalent functionalization is an essential step. Our study of functionalization of CNTs via controlled polymer crystallization method has resulted in the formation of ''nano hybrid shish-kebab'' (NHSK), which is CNT periodically decorated with polymer lamellar crystals. By tuning the experimental parameters such as concentration of polymer and crystallization temperature, hybrid polymer spherulite with CNT inside was achieved. This can be considered as CNT reinforced composite with ideally controlled CNT dispersion. Both Nylon 6, 6 and PE were used as the matrix materials. Excellent dispersion of CNTs in polymer matrix was achieved and the nanocomposites showed improved thermal stability.

**C1 40 Organic Photonic Crystal Lasers from Holographic Polymer Dispersed liquid Crystals (H-PDLCs)** TIMOTHY BUNNING, RACHEL JAKUBIAK, DEAN BROWN, RICHARD VAIA, *Air Force Research Laboratory* PAMELA LLOYD, *UES* VINCENT TONDIGLIA, LALGUDI NATARAJAN, RICHARD SUTHERLAND, *Science Applications International Corp.* Holographic polymerization of liquid crystal containing photopolymerizable resins enables one-step, rapid formation of multi-phase structures that exhibit partial photonic band gaps. These holographic polymer dispersed liquid crystals (H-PDLCs) provide a versatile platform for diffractive optical elements because the structures are not limited by multi-phase equilibrium but are con-

trolled by the interference of multiple lasers at discrete angles. Incorporation of laser dyes into H-PDLCs form 1-D and 2-D optically pumped distributed feedback lasers. Linewidths as narrow as 1.8 nm are observed with laser thresholds below 1 mJ/cm$^2$ in 2-D columnar structures compared to 9 nm and 25 mJ/cm$^2$ exhibited by 1-D H-PDLC Bragg stack lasers. In the 2-D lattices the energy of the laser action can be tuned within the gain spectrum of the lasing medium by an applied electric field.

**C1 41 Single-layer white-light polymeric luminescent film by plasma polymerization for light emitting diodes** CHUN-CHIH CHANG, YI-HSING CHANG, YING-CHU CHEN, ARNOLD CHANG-MOU YANG, *Department of Materials Science and Engineering, National Tsing Hua University, Hsinchu, Taiwan* KUO-CHU HWANG, *Department of Chemistry, National Tsing Hua University, Hsinchu, Taiwan* Efficient white polymeric light-emitting diodes (PLED) were fabricated with a single active layer consisted of three-dimentional crosslinking $\pi$-conjugated system by plasma polymerization from conjugated monomers. As indicated by the FTIR, XPS UV-vis and PL spectra, the plasma polymer chains were constructed by various chromophores including naphthalene, phenyl, polyene and alkyl groups. Upon optical excitation, the light emission was characterized with a broad peak (FMHW $\sim$ 100 nm) located at 430 nm. In a PLED device, however, the energy transfer by Foster processes (FRET) between multiple host-guest pairs give rise to white emission located in CIE coordinates of (0.3439, 0.3369). This result illustrated the feasibility of large area contour coating of single-layer white-light luminescent polymers for LEDs by simple plasma polymerization methods. This work is supported by National Science Council of Taiwan.

**C1 42 Evaporation induced hierarchical structure formation using diblock copolymers** SUCK WON HONG, JUN XU, ZHIQUN LIN, *Material Science and Engineering Department, Iowa State University, Ames, IA 50011* We present a study of the formation of the hierarchically ordered structures produced from the combination of two self-assembling processes on different length scales, i.e., the dynamic self-assembly via irreversible solvent evaporation in restricted geometries at the microscopic scale and the spontaneous self-assembly of diblock copolymer (e.g., PS-b-PMMA) at the nanoscale. This approach utilizes concurrent self-assemblies as a means to organize unique nanomaterials into spatially ordered structures.

**C1 43 A Unique Two-Stage Dewetting of Ultrathin Films of Entangled Chains Solution-Cast on a Deformable Surface** TONY MING-HSUN YANG, S.Y. HOU, ARNOLD CHANG-MOU YANG, *Department of Materials Science and Engineering, National Tsing Hua University, Hsinchu, Taiwan* F.C. CHANG, C.F. WANG, *Department of Applied Chemistry, National Chiao Tung University, Hsinchu, Taiwan* Stability of polystyrene (PS) thin films ($200\text{ki} \leqslant M_w \leqslant 2M, 20nm \leqslant h \leqslant 80nm$) on a deformable surface of low energy at 170 °C was investigated. A unique two-stage dewetting process was discovered and the magnitude of total forces driving the dewetting was determined from the strong substrate interaction. The film dewet by first nucleating small holes which grew rapidly but subsequently ran into a complete rest. Additional annealing of more than 4.5 hours, however, induced a second stage dewetting initiated from the intact region. The newly initiated holes were characterized with fingers growth that broke down into tiny droplets concurrent to holes expansion. The dewetting force was estimated to be around 0.036 N/m and decrease with aging time. Substrate interactions appeared to have a significant effect of increasing surface energy, hampering the rate of dewetting. This work is supported by Air Force (AFOSR-04-4074) and National Science Council of Taiwan.

**C1 44 Investigation of atomic force microscopic image resolution of organic molecules** MASANORI HARADA, MASARU TSUKADA, *Waseda University* NARUO SASAKI, *Seikei University* We simulated atomic force microscopic images of organic molecules using MM3 force field. Especially we investigated how higher the resolution of images can change using single atom tip compared with realistic tip model. This investigation was motivated by the fact that the resolution of the AFM images of organic molecules is not as good as the images of inorganic surfaces. The difference of the image resolutions can be seen for different element atom, which means using different van der Waals parameter. We also investigated the relation between resolution and mobility of molecules.

**C1 45 Surface Plasmon Resonance Studies of Hydroxypropyl Xylan Self-Assembly on Cellulose** DANIEL A. DRAZENOVICH, ABDULAZIZ KAYA, ALAN R. ESKER, *Virginia Tech Department of Chemistry (0212) Blacksburg, VA 24061* WOLFGANG G. GLASSER, *Virginia Tech Department of Wood Science and Forest Products (0323) Blacksburg, VA 24061* Wood is a multiphase material consisting of cellulose crystals embedded within a non-crystalline hetereopolysaccharide (hemicellulose) and lignin rich phase. The hierarchial arrangement of these three chief components in wood produces excellent properties like resistance to fracture and toughness. Through the study of self-assembly of hemicellulose onto a model cellulose surface, further insight into the interactions between hemicelluloses and cellulose can be gained. In our study, we used xylans with different degrees of substitution of hydroxypropyl groups. Surface plasmon resonance measurements (SPR) probe the self-assembly behavior of hydroxypropyl xylans (HPX) onto a cellulose coated gold surface. In addition, tensiometry provides the critical aggregation concentration (CAC) of different HPX samples. CAC results can be correlated to adsorption observed by SPR. Increasing the degree of hydroxypropyl substitution decreases the CAC and increases adsorption onto cellulose surfaces.

**C1 46 Microfluidic interfacial tensiometry** JAI PATHAK, *NIST* STEVEN HUDSON, *NIST* JOAO CABRAL, *Imperial College, London* A microfluidic instrument to measure interfacial tension of multicomponent immiscible liquids is reported. The instrument measures deformation and retraction dynamics of drops under extensional flow, and is accurate within a few percent. Binary and ternary mixtures have been examined. Surfactant transport phenomena and the effects of viscosity ratio and bounded flow have also been explored.

**C1 47 The Effect of Humidity on the Ordering of Block Copolymer Thin Films** JOONA BANG, BUMJOON J. KIM, *UCSB* THOMAS P. RUSSELL, *UMass* EDWARD J. KRAMER, CRAIG J. HAWKER, *UCSB* Solvent cast diblock/triblock copolymer films of poly(styrene-*b*-ethylene oxide) (PS-PEO) and poly(styrene-*b*-methyl methacrylate-*b*-ethylene oxide) (PS-PMMA-PEO), with cylindrical microdomains of PEO or PMMA-PEO, have a high degree of long-range lateral order after solvent

annealing. Relative humidity of the vapor during the solvent annealing has been shown to play an important role in achieving this order yet the origin of the humidity effect is has been the subject of debate. This work focuses on understanding the role of humidity on the ordering of block copolymer thin films. We find that PS-PMMA-PEO triblock copolymers that show a lamellar morphology in bulk develop a hexagonal array of PMMA-PEO domains on the film surface after solvent annealing in a humid environment. To study the effect of humidity further, hydrophilic nanoparticles, such as PEO-coated gold nanoparticles and PEO-star polymers, were incorporated into nonhydrophilic block copolymers, i.e., poly(styrene-*b*-methyl methacrylate) (PS-PMMA) diblock copolymers that exhibit PMMA cylinders. By controlling the relative humidity and the volume fraction of hydrophilic nanoparticles, it was found that lateral ordering of these PS-PMMA diblock copolymers can also be achieved. The thin film morphologies were investigated in detail using AFM, GISAXS, and TEM.

**C1 48 Surface Modification Using Photo-Crosslinkable Random Copolymers** JOONWON BAE, *UMass* JOONA BANG, *UCSB* PETER LOWENHIELM, *UCSB* CHRISTIAN SPIESS-BERGER, *UCSB* THOMAS P. RUSSELL, *UMass* CRAIG J. HAWKER, *UCSB* We recently reported that poly(styrene-*r*-methyl methacrylate) (PS-*r*-PMMA) random copolymers containing benzocyclobutene (BCB) group can be used to modify the surface effectively by thermal crosslinking. It was demonstrated that this method is simple, rapid, and robust, and can be applied to various surfaces. However, it requires the large amount of heat for processing, and the BCB monomer itself involves a hard chemistry. An alternative way that can replace BCB with easier chemistry and lower cost, if possible, is highly desirable. We introduce the new functional group, azide group, which can be crosslinked simply by UV irradiation, for this purpose. PS-*r*-PMMA random copolymers, containing various amounts of azide groups, were synthesized via controlled living-radical polymerization. It was demonstrated that even after 1 minute of the UV irradiation can crosslink the materials effectively, so that they can be used as crosslinked random copolymer mat to control the surface energy. However, it was observed that the longer irradiation time causes the damages on the surface due to the other side reactions. Depending on the UV intensity, the UV irradiation time, and the amount of azide group, the effective processing window that leads to the crosslinking without any surface damages was optimized.

**C1 49 Mean-field Description of Spinodal Growth of Surface Waves on Rupturing Films*** YONG JIAN WANG, OPHELIA K.C. TSUI, *Department of Physics and Institute of Nano Science and Technology, Hong Kong University of Science and Technology* We examine the extent to which the mean-field theory is applicable to the description of the experimentally observed growth of surface waves on a rupturing polystyrene film coated on an oxide-covered silicon that is known to be spinodal unstable. We find that good agreement between theory and experiment is obtainable if corrections due to non-linear effects and stochastic thermal fluctuations are considered.

*We acknowledge financial support of the Research Grant Council of Hong Kong through the projects HKUST6070/02P and 603604.

**C1 50 The Interface between Two Incompatible Polymers in Density Fluctuating Supercritical Carbon Dioxide*** J.S. KOO, T. KOGA, M. RAFAILOVICH, J. SOKOLOV, *SUNY at Stony Brook* The X-ray reflectivity was used to investigate an effect of $CO_2$ sorption on interface between two immiscible polymers, polystyrene (PS) and poly(methylmethacrylate) (PMMA). Thin films of PS and PMMA were spun cast onto Si wafers and the interfacial width was measured as a function of the film thickness of both PS and PMMA layers. The samples were then exposed $CO_2$ gas at pressures and temperature corresponding to the density fluctuation ridge (1). The relative dilation of the two layers and the change in the interfacial width was then determined. The results showed that the dilation was nearly independent of the PMMA film thickness, and maximal at thickness less than 3Rg of the PS layers. The interfacial width in all cases was almost twice as large after exposure. These results will be interpreted in terms of the interfacial reduction induced by the $CO_2$ and capillary wave theory. (1) Koga, T. itet al. Phys. Rev. Lett. **2002**, 89, 125506 ; Koga, T. itet al. Macromolecules **2003**, 36, 5236.

*Work supported in part by the NSF-MRSEC and the SRC-NYS consortium.

**C1 51 Trisilanolphenyl-POSS as an Adhesion Promoter** SARAH HUFFER, *Department of Chemistry (0212), Virginia Tech Blacksburg, VA 24061* UFUK KARABIYIK, ALAN ESKER, *Department of Chemistry (0212), Virginia Tech Blacksburg, VA 24061* Polyhedral oligomeric silsesquioxanes (POSS) have been an innovative research area for over twenty years. Potential aerospace applications include space-survivable coatings and ablative insulation. Recent studies showed that trisilanol-POSS derivatives form monolayers at the air/water interface. The purpose of this study was to improve adhesion between ceramics and metals and metals and polymers by preparing multilayer films at various pH values and metal ion concentrations using trisilanolphenyl-POSS (TPP). Multilayer systems were created by spincoating polystyrene, using the Langmuir-Blodgett technique for TPP, and physical vapor deposition of aluminum oxide. The resulting films were characterized for quality and stability using atomic force microscopy, optical microscopy, X-ray photoelectric spectroscopy, and dewetting experiments. Initial experiments demonstrated that TPP-aluminum ion complexes facilitated smooth aluminum oxide film formation on silicon wafers while TPP alone yielded a blistered aluminum oxide surface.

**C1 52 Interface Behavior in Diblock Copolymer Brushes** GOKCE UGUR, BULENT AKGUN, WILLIAM J. BRITTAIN, MARK D. FOSTER, *Maurice Morton Institute of Polymer Science,The University of Akron, Akron, OH 44325* XUEFA LI, DONG RYEOL LEE, JIN WANG, *Experimental Facilities Division, Argonne National Laboratory, Argonne, IL 60439* A polymer brush is an assembly of polymer chains with one end tethered to a surface or an interface with a tethering density high enough that the polymer chains are forced to stretch away from the substrate. This stretching of polymer chains along the direction normal to surface is different from the typical behavior of flexible chains. The study of surface and interface properties of polymer brushes is important for their use in nano-scale applications. We investigated the surface and interface structure of polystyrene-b-polymethylacrylate (PS-*b*-PMA) diblock copolymer brushes that have been synthesized using atom transfer radical polymerization (ATRP). Grazing incidence small angle X-ray scattering (GISAXS) was used to probe the structure of the surface as well as the buried interfaces of

the brushes. It showed that there are lateral correlations inside the brush and that the spacing of these structures is on the order of the top layer thickness of the brush. Analysis of the GISAXS data provides information for values of the in-plane scattering vector that are larger than those accessible using a conventional transverse scan.

**C1 53 Exciton Emission in PTCDA Thin Films under Uniaxial Pressure** A. DESILVA, V.R. GANGILENKA, H.P. WAGNER, *Department of Physics, University of Cincinnati, Cincinnati, Ohio 45221-0011, USA* R.E. TALLMAN, B.A. WEINSTEIN, *Department of Physics, SUNY at Buffalo, NY 14260-1500, USA* R. SCHOLZ, *Institut für Physik, Technische Universität Chemnitz, 09107 Chemnitz, Germany* We study the strain dependent photoluminescence (PL) of a 90 nm thick polycrystalline PTCDA film on Si(001) between 20 and 300 K. Uniaxial pressure up to 1 kbar is applied along the molecular stacking direction using a home made pressure cell. With increasing pressure we find a quenching of the total PL intensity which is mainly attributed to the creation of defects. At low temperature the charge transfer exciton emission (CT2) gains intensity relative to the Frenkel exciton emission. Furthermore the CT2 transition reveals a shift to lower energies by approximately 5 meV. At room temperature the PL is dominated by the excimer transition which shows a redshift of 5 meV at highest uniaxial pressure. The increase of the CT2 transition at low temperature and the redshift of the emission bands are attributed to an increased exciton trapping probability and enhanced binding energy with reduced distance between stacked molecules.

**C1 54 Evidence for Capillary Contributions to Gecko Adhesion from Single Spatula Nanomechanical Measurements** GERRIT HUBER, STANISLAV GORB, EDUARD ARZT, *Max Planck Institute for Metals Research, Heisenbergstrasse 3, D-70569 Stuttgart, Germany* RALPH SPOLENAK, *ETH Zurich, Laboratory for Nanometallurgy, Department of Materials, CH-8093 Zurich, Switzerland* KLAUS MECKE, *Erlangen University, Dept. of Theoretical Physics, D-91058 Erlangen, Germany* HUBERT MANTZ, KARIN JACOBS, *Saarland University, Dept. of Experimental Physics, D-66041 Saarbruecken, Germany* The hairy attachment system on a geckos toes, consisting of one billion spatulae in the case of Gekko gecko allows it to adhere to nearly all surface topographies. The mechanistic basis for gecko adhesion has been intensely investigated, but the lowest hierarchical level, that of the spatula, has become experimentally accessible only recently. This study details measurements of the adhesion force exerted by a single gecko spatula for various atmospheric conditions and surface chemistries. Through judicious choice and modification of substrates, the short- and long-range adhesive forces are separated. In contrast to previous work, our measurements clearly show that humidity contributes significantly to gecko adhesion on a nanoscopic level. These findings are crucial for the development of artificial biomimetic attachment systems.

**C1 55 The Influence of Stereoerrors on the Crystallization of Isotactic Polypropylene*** XIAOFENG CHEN, SANAT K. KUMAR, *Chemical and Biological Engineering* RAHMI OZISIK, *Materials Science and Engineering, Rensselaer Polytechnic Institute* Crystallization behavior of four isotactic polypropylenes (iPP) with stereoerrors was studied by Monte Carlo simulation. All systems were equilibrated above the melting temperature ($T_m$) and then cooled systematically to temperatures below the $T_m$. The conformations of the iPP chains were analyzed to characterize the crystallinity development in each system. The probability of helix formation, the average length of helices, and the fraction of repeat units involved in helical structures all increased as temperature decreased. As expected, the stereoregular iPP had the longest helical structures and the highest overall crystallinity compared to the other systems with stereoerrors. The overall crystallinity decreased with increasing number of stereoerrors. The influence of stereoerrors on the ability of iPP repeat units participation in helical structures was also investigated. The results showed that the stereoerrors can exist in helices but they strongly influence the ability of their neighbors to exist in helices.

*This material is based upon work supported by the National Science Foundation under Grant 0310596.

**C1 56 Investigation of the Structure and Dynamics of Polyethylene Nanocomposites*** PETER J. DIONNE, *Mechanical, Aerospace and Nuclear Engineering* RAHMI OZISIK, *Materials Science and Engineering* CATALIN R. PICU, *Mechanical, Aerospace and Nuclear Engineering, Rensselaer Polytechnic Institute* The structure and dynamics of linear, monodisperse polyethylene (PE) melts ($C_{160}H_{322}$ and $C_{440}H_{882}$) containing homogenously distributed spherical nanoparticles were investigated. The PE chains were simulated using a coarse grained model and a Monte Carlo algorithm. Two variables were considered: (i) the wall-to-wall distance between particles (itd), and (ii) the interaction energy between monomers and particles. The various chain structures changed greatly with itd while the monomer-particle interaction had little effect. The average size, shape, and orientation of PE chains did not differ significantly from those of a neat melt. Bridge segments were more stretched relative to segments in the neat melt and the stretch increased with increasing itd. However, the number of bridge segments decreased markedly with increasing itd. Chain dynamics was monitored by computing the Rouse relaxation modes and the mean-square displacement of the center of mass. The dynamics were slowed by both geometric effects (confinement by fillers) and energetic effects (monomer-particle energetic interaction).

*This material is based upon work supported in part by Procter & Gamble and by the National Science Foundation under Grant 0310596.

**C1 57 Extensions of an analytical coarse-grained description for polymer liquids: thermodynamic determinations and an intermediate length-scale description** EDWARD SAMBRISKI, MARINA GUENZA, *Department of Chemistry, Institute of Theoretical Science, University of Oregon, Eugene, Oregon 97403* We extend our previous analytical coarse-graining (CG) procedure[1], which maps polymer liquids onto a system of interacting soft-colloidal particles. First, we present an optimized representation of the effective pair potential, $v_{cc}(r)$ [initially determined via the hypernetted-chain closure], by carrying out an interative predictor-corrector (PC) scheme. Then, we compare the thermodynamics obtained through the virial and compressibility routes, for which we observe an improvement in their consistency when using the PC result. Finally, we present an intermediate length-scale CG treatment for polymers by performing an analytical remapping of the chain onto ''blobs'' (monomer aggregates). The derived expression for the blob-blob total correlation function,

$h_{bb}(r)$, is seen to be in agreement with data from united-atom molecular dynamics simulations.

[1]G. Yatsenko, E. J. Sambriski, and M. G. Guenza, J. Chem. Phys., **106,** 054907:1-12 (2005); G. Yatsenko, E. J. Sambriski, M. A. Nemirovskaya, and M. Guenza, Phys. Rev. Lett., **93,** 257803:1-4 (2004).



**C1 58 A Novel Approach for Understanding the Effect of Nano-Fillers on the Conformational Properties of a Polymer Matrix: Dimensions go up or down?** FATIH M. ERGUNEY, WAYNE L. MATTICE, *The University of Akron* MC simulations of a polymer matrix composed of linear POE chains and nano-fillers were performed on a 2nnd lattice to reveal the change in the $< s^2 >$ of matrix chains perturbed by nano fillers. Nano-fillers are obtained by the collapse of a desired number of linear chains by increasing the contribution of the attractive core of discretized intramolecular LJ potential. The resulting change in $< s^2 >_{matrix}$ is case sensitive in such a way that it might either go up or down depending on the size of both species. It tends to increase in the presence of nano-fillers when both kinds are represented by a small number of beads. There's a peak point observed in this case after which the dimensions start to decrease as the filler fraction is further increased. The contraction of chains is also of concern provided that chains have a larger number of beads. On the contrary, there's no peak point observed in such a case, but a plateau region is acquired at high filler fraction. Magnitude of the change depends on several parameters like mobility and compactness of fillers.

**C1 59 Density functional and molecular dynamics study of conducting polymers** Y. DAI, E. BLAISTEN-BAROJAS, *School of Computational Sciences, George Mason University, Fairfax, VA 22030* Polypyrrole belongs to the important class of conducting polymers and is a good candidate for photonic devices and chemical sensors. In this work we performed electronic structure calculations of pyrrole oligomers containing 6 to18 rings at the density functional (DFT) level and searched for the charge distribution in the oxidized and neutral phases. The description of bipolaron given in terms of charge localization over domains along the pure polymer chain by semiempirical methods could only be confirmed by DFT studies in the oxidized phase when dopants are present. A model potential for polypyrrole was developed based on the first principles calculations of the structure and charge distribution. Several finite temperature and dynamical properties were studied with molecular dynamics.

**C1 60 Structure and Spectra in Mutated Green Fluorescent Protein: A Combined Molecular Dynamics and QM/MM Study** SOUMYA PATNAIK, STEVEN TROHALAKI, RUTH PACHTER, *Air Force Research Laboratory* Recently, several Green Fluorescent Protein (GFP) mutants have been developed with red-shifted absorptions. The molecular structures of two such mutants with S65G and S65T mutations have been studied with an aim towards understanding the shift in their absorption spectra. A combined approach of molecular dynamics (MD) and Quantum Mechanics/Molecular Mechanics (QM/MM) has been used. Time dependent density functional theory (TDDFT) based absorption spectra calculations were found to be of excellent agreement with experimental data. These calculations were carried out on chromophore structures derived from QM/MM and MD studies, thus taking into account, both the effects of thermal fluctuations and the protein and solvent environment. In addition to providing information regarding the variation of the geometrical parameters due to temperature effects, the MD simulations also identify residues around the chromophore which are associated with conformational change on mutation. By using QM/MM to systematically analyze significant structural features that were identified by MD simulations, a detailed understanding of the energetics of the optimized chromophore conformations was achieved.

**C1 61 Biodegradable Epoxy Networks Cured with Polypeptides** SHIGEO NAKAMURA, *Ajinomoto Co., Inc.* EDWARD J. KRAMER, *University of California, Santa Barbara* Epoxy resins are used widely for adhesives as well as coatings. However, once cured they are usually highly cross-linked and are not biodegradable. To obtain potentially biodegradable polypeptides that can cure with epoxy resins and achieve as good properties as the conventional phenol novolac hardeners, poly(succinimide-co-tyrosine) was synthesized by thermal polycondensation of L-aspartic acid and L-tyrosine with phosphoric acid under reduced pressure. The tyrosine/succinimide ratio in the polypeptide was always lower than the tyrosine/(aspartic acid) feed ratio and was influenced by the synthesis conditions. Poly(succinimide-tyrosine-phenylalanine) was also synthesized from L-aspartic acid, L- tyrosine and L-phenylalanine. The thermal and mechanical properties of epoxy resins cured with these polypeptides are comparable to those of similar resins cured with conventional hardeners. In addition, enzymatic degradability tests showed that Chymotrypsin or Subtilisin A could cleave cured films in an alkaline borate buffer.

**C1 62 A novel Generalized Langevin approach to bridge different timescales of relaxation in Protein Dynamics** ESTHER CABALLERO MANRIQUE, *Department of Chemistry, University of Oregon* JENELLE BRAY, *Department of Chemistry, California Institute of Technology* MARINA GUENZA, *Department of Chemistry, University of Oregon* The derivation of a Generalized Langevin Equation (GLE) for the long-time dynamics of biological systems presents several challenges as hydrogen bonding, secondary and tertiary structure, Coulombic interactions, and hydrophobic effects come into play. Here we propose a novel GLE approach where the internal friction is explicitly included in the protein dynamics, allowing the distinction between hydrophobic and hydrophilic effects. The protein is described as a linear chain of beads (centered at the alpha carbons) that are connected by harmonic springs. Input for our theory is short time (ns) molecular dynamics simulations of a single protein (or complex) in solution, in this case the bacterial signal transduction protein CheY. Effective inter-bead potentials and local friction coefficients are obtained from the simulations. A comparison of the bond autocorrelation function predicted from the theory and calculated directly from the simulation affords the test of the theory in the short timescales (ns). In the long timescales (ms), the theory is tested against experimental NMR $T_1$ relaxation values. Our results show a remarkable agreement in both cases, indicating that our GLE correctly bridges from the short- to the long-time scale of protein dynamics.

**C1 63 Quantitative prediction for two-dimensional bacterial genomic displays** JEAN-FRANCOIS MERCIER, CHRISTINE KINGSBURRY, *University of Ottawa* BÉNÉDICTE LAFAY, *CNRS-IRD* GARY W. SLATER, *University of Ottawa* Two-dimensional bacterial genomic display (2DBGD) is a simple technique that allows one to directly compare complete genomes of

closely related bacteria. It consists of two phases. First, polyacrylamide gel electrophoresis (PAGE) is used to separate the DNA fragments resulting from the restriction of the genome by appropriate enzymes according to their size. Then, temperature gradient gel electrophoresis (TGGE) is used in the second dimension to separate the fragments according to their sequence composition. After these two steps, the whole bacterial genome is displayed as clouds of spots on a two-dimensional surface. 2DBGD has been successfully used to distinguish between strains of bacterial species. Unfortunately, this empirical technique remains highly qualitative. We have developed a model to predict the location of DNA spots, as a function of the DNA sequence, the gel electrophoresis and TGGE conditions and the nature of the restriction enzymes used. This model can be used to easily optimize the procedure for the type of bacteria being analyzed.

**C1 64 Osmotic Pressure induced by Poly(ethylene glycol) at High Salt Concentrations** SUNGKYUN SOHN, HELMUT STREY, SAM GIDO, *Polymer Sci. & Eng., Univ. of Massachusetts Amherst* The osmotic pressure method is one of the most effective tools that can be used in controlling self-assembly of polymers in solution, especially of water-soluble biopolymers. This study investigated if there is a noticeable synergistic osmotic pressure increase between co-existing polymeric osmolyte and salt when extremely highly concentrated salt molecules are present both at sample subphase and stressing subphase. PEG 8,000 and LiBr were chosen as osmolyte and salt, respectively, since this model system can be directly applied to the case of silk protein self-assembly, where hydrogen bonding plays a major role. In addition to the conventional methods for measuring osmotic pressure, such as membrane osmometry, vapor pressure osmometry, and ultracentrifuge, an 'equilibration method' that measures osmotic pressure relative to a reference with known osmotic pressure, was introduced. PEG 400 solution was chosen as the reference for this method. Osmotic pressure of aqueous LiBr solution up to 2.75M was measured and it was found that the synergistic effect was insignificant up to this salt concentration. Solution parameters and Arrhenius kinetics based on time-temperature relationship during the equilibration process were derived as well.

**C1 65 The Effect of Polymer-Clay Nano-Composites on Human Dermal Fibroblasts** LOURDES COLLAZO, HILANA LEWKOWITZ-SHPUNTOFF, MARY CATHERINE WEN, MIRIAM RAFAILOVICH, *Stony Brook University* The effect of polymer-clay nano-composites on the proliferation of Human Dermal Fibroblasts (HDF) as a function of clay content was investigated. Polybutadiene with different clay concentrations were spun cast on glass substrates. HDF cells were cultured on these substrates and growth curves were generated for a period of 2 weeks. The results show that the optimal growth occurred on Polybutadiene films with nano-composites that consisted of 90% polymer and 10% clay. The relative modulus of these polymer-clay nano-composites films were measured by Scanning Modulus Force Microscopy (SMFM) 1 and showed a linear increase with clay concentration, indicating that the nano-composites became harder with increased clay concentration.Confocal microscopy revealed that the morphology of the F-Actin fibrils is a function of the matrix modulus. In addition more focal adhesion points were found on the harder substrates. This adaptation of normal fibroblasts will be compared to cancer fibroblasts as well as protein distribution by western blotting. Reference: Shouren Ge et al. PRL (2000) 85(11) 2340-2343

**C1 66 Receptor/Ligand Interactions at an Oil/Water Interface** DANIEL CARVAJAL, *Northwestern University* CHI-YANG CHAO, *Northwestern University* KENNETH SHULL, *Northwestern University* The strength of the interaction between biotin and avidin has sparked major research interests as the system serves as a vehicle for both targeted drug delivery and the simulation of surface recognition processes. Interfacial tension measurements (IFT) using R-PEO-biotin[1] were used to obtain dynamic information on the avidin-biotin interaction. Real time IFT data was gathered from the liquid-liquid interface by monitoring the shape of the drop via a drop shape analysis (DSA) instrument. A drop, containing dissolved R-PEO-biotin block copolymers in an ''oil like'' phase, was formed in an immiscible embedding ''water like'' phase. The block copolymers were specially designed to segregate to the liquid-liquid interface and cover the drop surface. By adding avidin to the surrounding water phase, changes in the drop shape provided dynamic data on the avidin-biotin interaction, as avidin binds to biotin only at the drop surface. This is the first study to show that DSA can be applied to the dynamic study of the interaction between avidin and biotin. [1]Biotin-functionalized block copolymers with a hydrophobic aliphatic block and a hydrophilic PEO block

**C1 67 Theoretical Comparative Study of the Structure, Dynamics and Electronic Properties of Five Ally Molecules: Allicin, Methyl Propyl Disulfide (MPD), Allyl Methyl Sulfide (AMS), S-allyl cysteine (SAC) and S-allyl mercaptocysteine (SAMC)*** EMINE DENIZ CALISIR, SAKIR ERKOC, *Department of Physics, Middle East Technical University, 06531 Ankara, Turkey* HANDAN YILDIRIM, ABDELKADER KARA, TALAT S. RAHMAN, *Department of Physics, Kansas State University, Manhattan, USA* MAHMUT SELVI, FIGEN ERKOC, *Department of Biology Education, Gazi University, 06500 Ankara, Turkey* The structural, dynamics and electronic properties of five allyl molecules have been investigated theoretically by performing semi-empirical molecular orbital (AM1 and PM3), ab-initio (RHF) and density functional theory calculations. The geometry of the molecules have been optimized, the vibrational spectra and the electronic properties of the molecules have been calculated in their ground states in gas phase. For each molecule, we found that the optimized geometries resulting from calculations based on the three levels of accuracy, to be very similar. However, we found that an accurate description of the vibrational properties of these molecules necessitates calculations at the ab-initio level. The electronic structures of these molecules were performed at the DFTlevel, resulting in an accurate description of the HOMO-LUMO gap and the local charges.

*Work supported in part by NSF under grant No: INT_0244191

**C1 68 Spheres-to-vesicles morphological transition in polymer micelles** ZHIJUN HU, ALAIN JONAS, JEAN-FRANÇOIS GOHY, CERMIN COLLABORATION, Self-assembly of block copolymers in solution and the resultant nano-objects such as spheres, rods, and vesicles, have been the focus of much interest during the last 20 years. The ability to tune the micellar morphology and trigger the morphological transitions still remains a central challenge in this field. Here we present the possibility to control the micellar morphologies in poly(styrene)-itblock-poly(4-vinylpyridine)/surfactant complexes by dilution, which is believed to be due to the changes of order in the insoluble blocks. These complexes, that form spherical micelles at a concentration of 1 g/L, rearrange into vesicles when the solutions are diluted, as

confirmed by combined dynamic light scattering, atomic force microscopy and transmission electron microscopy investigations. This morphological transition can be further used as a tool to encapsulate molecules of interest in the interior of block copolymer vesicles.

**C1 69 Osmotic Pressure Measurements of the Order Disorder Transition in Acrylic Triblock Copolymer Gels** RAFAEL E. BRAS, *Northwestern University* KENNETH R. SHULL, *Northwestern University* Semi-dilute solutions of PMMA-PnBA-PMMA triblock co-polymers in alcohols are excellent binder materials for a novel ceramics processing method, thermo-reversible gel casting. Processing methods based on this technology offer a low cost alternative to traditional slip and gel casting techniques. The rapid transition of these gels from freely flowing liquids to elastic solids has been attributed to the aggregation of the PMMA endblocks to form small spherical domains. We have recently begun to examine the order disorder transition of the PMMA endblocks with vapor pressure osmometry. This technique measures osmotic pressure by monitoring the equilibrium temperature of a solution droplet relative to the temperature of a pure solvent droplet. Measurements of solutions consisting of 15 vol % acrylic triblock copolymer in butanol show a significant drop in osmotic pressure between 80 and 85 [r]C. This result indicates that the relaxation times of the ordered gels can be quite low, so that the order-disorder transition of the triblock copolymer occurs at temperatures higher than the rheologically determined gelation temperature of about 65 [r]C.

**C1 70 Scaling of Avrami Kinetics of Growing Anisotropic Grains** SAMUEL GIDO, ASHOUTOSH PANDAY, *University of Massachusetts, Amherst MA 01003* The kinetics of phase transformations proceeding by nucleation and growth are commonly modeled with the Avrami equation. In its most general form, the Avrami equation is expressed as $V(t) = 1- \exp[-V_e(t)]$, where $V(t)$ and $V_e(t)$ denote actual volume transformed and itextended volume respectively, as a function of time t. The extended volume, $V_e(t)$ is the imaginary volume of all the grains if they did not stop at impingement and grew into one another. We report an observation about the growth of anisotropic grains obtained through simulations. We have found that for both simultaneous and continuous nucleation of elliptical grains, of aspect ratio L, the extended volume is reduced by a factor of $L^{1/2}$ in random orientation as compared to unidirectional orientation. In other words, $V_e(t)_{,\ random} = [\ V_e(t)_{,\ unidirectional}] \ / \ L^{1/2}$.

**C1 71 Block Copolymer Nanotemplates for Biomolecular Arrays** JUNG HYUN PARK, YALE E. GOLDMAN, RUSSELL J. COMPOSTO, *NBIC, University of Pennsylvania* The controlled positioning of biomolecules on surfaces is important for applications such as high-throughput proteomic arrays as well as fundamental biological research. However, the development of biomolecule arrays requires well-ordered nanosize platforms. The perpendicular lamellar structure of diblock copolymer films deposited on silicon substrates is a good candidate as a nanotemplate because of their spatial dimensions and orientation. Using scanning probe microscopy, a nearly symmetric poly(styrene-b-methyl methacrylate) P(S-b-MMA) diblock copolymer spin coated on silicon and annealed at 175[r]C for 2 days exhibits a perpendicular lamellar morphology with a periodicity of 70nm. To further constrain biomolecules or proteins, topographical variations were etched into the film by exposure to UV radiation for varying times. This exposure was found to preferentially etch the MMA phase resulting in ''trenches'' of MMA stripes separated by hills of PS. Studies are underway to investigate the controlled attachment of biomolecules on both the perpendicular lamellar morphology and the same morphology with trenches.

**C1 72 X-ray Photon Correlation Spectroscopy Studies of Dynamics in a Polymer Bicontinuous Microemulsion** KRISTIN BRINKER, WESLEY BURGHARDT, *Northwestern University* SIMON MOCHRIE, *Yale University* Polymer bicontinuous microemulsions are ternary blends of otherwise immiscible homopolymers that are compatibilized with their corresponding diblock copolymer, leading to an equilibrium spongy interconnected morphology with domain sizes typically on the order of 10 - 100 nm. Recent research has demonstrated that the dynamics of this interconnected structure leads to rich and complicated linear and nonlinear viscoelastic behavior. Direct probing of the equilibrium dynamics of order parameter fluctuations within bicontinuous microemulsion phases has been achieved using dynamic light scattering; however, the range of accessible scattering vector in light scattering is poorly matched to the intrinsic length scale of the microemulsion morphology. Here we report experiments using small-angle X-ray Photon Correlation Spectroscopy, performed using facilties at Sector 8 of the Advanced Photon Source, to make direct measurements of the dynamic structure factor in a polystyrene- polyisoprene microemulsion sample in the vicinity of the Teubner-Strey scattering peak associated with the dominant length scale of the bicontinuous phase.

**C1 73 Morphology of Fluorinated and Sulfonated diblock Copolymers** TOMONORI HOSODA, SAM GIDO, *Polymer Sci. & Eng., Univ. of Massachusetts Amherst* TIANZI HUANG, JIMMY MAYS, *Univ. of Tennessee Knoxville* We have studied the microphase separation of Fluorinated and Sulfonated diblock Copolymers. The polymer was synthesized by post-polymerization fluorination and sulfonation of PI-b-PS diblocks. THF containing different weight fraction of water was used as solvents for the diblock copolymers to solution casting films. From the dry THF, we obtained a coexistence morphology of well-ordered lamella and cylinders. As the water content in the solvent was increased, the morphology changed from well-ordered to disordered. In addition, it was to be found that thermal annealing at 120C of the well ordered samples caused the morphology become disordered. The progressive disordering of the structure upon annealing was directly observed with TEM and SAXS. The results are very different the usual behavior or uncharged diblock copolymers in which annealing generally results in improvements in long range order. The disordering upon annealing may be the result of ion cluster formation which interferes with the normal block copolymer morphology.

**C1 74 Stereocomplex Formation in Incompatible Racemic Chiral Polylactide Block Copolymers** LU SUN, LEI ZHU, *Polymer Program, Institute of Material Science and Department of Chemical Engineering, University of Connecticut, Storrs, CT 06269-3136* Stereocomplexes in incompatible racemic chiral polylactide (PLA) block copolymers have not been widely studied. In this work, we synthesized PLLA and PDLA containing block copolymers by ring opening polymerization of L- and D-lactides from hydroxyl-terminated hydrophilic [poly(ethylene oxide)

(PEO)] and hydrophobic [poly(ethylene-itco-1,2-butylene) (PEB)] oligomers, respectively. Two samples PEO-*b*-PLLA (2,000-5,400) and PEB-*b*-PDLA (4,200-5,400) were chosen. The stereocomplexes were cast from equal molar blends of above two block copolymers in chloroform solution, followed by two different thermal treatments before stereocomplex formation; The blend was either heated to 250 [r]C and quickly quench to 160 [r]C or heated to 250 [r]C for 15 min and quench to 160 [r]C for stereocomplex crystal growth. Before the formation of stereocomplexes, lamellar and cylindrical morphologies were observed in blends for the first and second thermal treatments, respectively, as evidenced by small-angle X-ray scattering (SAXS). After complete crystal growth, the 100% stereocomplexes was confirmed by differential scanning calorimetry and wide-angle X-ray diffraction (WAXD). The morphologies of stereocomplexes grown from these two pre-existing microphases (lamellar vs. cylindrical) were studied by time-resolved SAXS and transmission electron microscopy (TEM).

**C1 75 Effect of local point group symmetry on self-assembly in thin films of block copolymers on topographically patterned substrates.*** ION BITA, *Department of Materials Science and Engineering, Massachusetts Institute of Technology* JOEL KANG, *Department of Electrical Engineering and Computer Science, Massachusetts Institute of Technology* KARL BERGGREN, *Department of Electrical Engineering and Computer Science, Massachusetts Institute of Technology* EDWIN THOMAS, *Department of Materials Science and Engineering, Massachusetts Institute of Technology* We have investigated the self-assembly of a diblock copolymer with spherical morphology on novel topographically patterned substrates. Poly(styrene)-b-poly(ferrocenyldimethylsilane), PS-*b*-PFS, was spin casted to form thin films with a PFS monolayer of spheres morphology. Topographically patterned silicon substrates were fabricated by both electron-beam and interference lithographies. To vary the local point group symmetry, a number of topographical patterns were designed and fabricated. Quasiperiodic arrays of posts allows access to multiple types of local symmetries with the average distance between posts an order of magnitude or more larger than the BCP period. Results for controlling long-range correlations of the BCP morphology and local 4-, 6-, 8-, and 12-fold rotational symmetries will be presented.

*Acknowledge support from NSF DMR 02-13282, NSF DMR-0308133.

**C1 76 Spectroscopy of the Primary Photoexcitation and the Origin of the Photocurrent in Rubrene Single Crystals** HIKMAT NAJAFOV, IVAN BIAGGIO, *Lehigh University* VITALY PODZOROV, MATT CALHOUN, MICHAEL GERSHENSON, *Rutgers University* By studying and correlating the photoexcitation spectra of several observables connected with excitons and charge transport we are able to gain new insights into the nature of the primary photoexcitation in organic molecular crystals. By simultaneously measuring the excitation spectra of the transient luminescence and of the transient photoconductivity after picosecond pulsed excitation in rubrene single crystals we show that free excitons are photoexcited starting at photon energies larger than 2.0 eV. We observed a competition between photoexcitation of free excitons and photoexcitation into vibronic excited states that subsequently decay into free carriers, while self-trapped molecular excitons are instead formed predominantly through the free exciton. At photon energies smaller than 2.25 eV free charge carriers are only created through a long-lived intermediate state with a lifetime of up to 0.1 ms and no free carriers appear during the exciton lifetime.

**C1 77 Exciton Dissociation by a Static Electric Field Followed by Nano-scale Charge Transport in PPV Polymer** HIKMAT NAJAFOV, *Lehigh University* IVAN BIAGGIO, *Lehigh University* TA-KO CHUANG, *Lehigh University* MILTIADIS K. HATALIS, *Lehigh University* The nature of the photoinduced generation of charge carriers in conjugated polymers is still the subject of an intense discussion. We investigate the main question of weather photoexcitation results in localized excitons or directly leads to mobile charge carriers by simultaneously studying the electric field dependence of the photoluminescence and the photoinduced charge-transport in a phenyl-substituted PPV derivative. We show that charge-carriers are created indirectly through field-induced ionization of excitons, and by quantitatively estimating the amount of carriers created by ionization of the exciton we identify a free-carrier mobility larger than $\sim 3.0\times 10^{-6}\mathrm{cm}^2\mathrm{V}^{-1}\mathrm{s}^{-1}$ that is valid for transport over a few nm during an apparent free-carrier lifetime of $\sim$ 50 ns. The time-dynamics of the photoluminescence and its temperature-quenching behavior indicate the presence of two species of excitons, which can be interpreted as intra-chain and inter-chain excitons.

**C1 78 Temperature Dependent Electroluminescence of $Alq_3$ Based OLEDs** AJITH DESILVA, H. P. WAGNER, *Deptartmet of Physics, University of Cincinnati, OH 45221* R. A. JONES, W. LI, A. STEKL, *Deptartment of ECECS, University of Cincinnati, Cincinnati OH 45221* The temperature dependent I-V characteristics and electroluminescence (EL) of an ITO/PEDOT/NPD/$Alq_3$/LiF–Al OLED is investigated. The I-V measurements reveal a trap charge limited current behavior with characteristic trap energy of 53 meV. The EL of the device is compared with the photoluminescence (PL) of a 50 nm thick $Alq_3$ film on Si (001) in the range from 10 to 320 K. The EL efficiency of the device shows similar temperature dependence as the PL intensity obtained from the $Alq_3$ film. The OLED brightness saturates at 10,000 cd/m$^2$ (T = 300 K; V = 15 V). For a constant forward bias (8 V) the maximum EL efficiency of the device is 2.2 cd/A obtained at 180 K. The maximum PL efficiency of the $Alq_3$ film is observed at the same temperature (180 K). Furthermore, both the EL and PL spectra reveal a maximum redshift at 180 K which is tentatively attributed to the formation of self-trapped excitons within the $Alq_3$ layer.

**C1 79 Multiplicative luminescence enhancement induced by chain relaxation in ultrathin films of a conjugated polymer (MEH-PPV)** CHIH-WEI YANG, JUO-HUEI JOU, ARNOLD CHANG-MOU YANG, *Department of Materials Science and Engineering, National Tsing Hua University, Hsinchu, Taiwan* A surprising multiplication of light-emitting efficiency was observed in dewetting process of the conjugated luminescent polymer of poly (2-methoxy- 5-(2'-ethyl-hexyloxy)-1,4-phenylene vinylene] (MEH-PPV). The luminescent efficiency increased with the dewetting process and became about six-fold when the polymer film ruptured into tiny droplets. This enhancement appeared to be related to the carrier transport mechanisms and the motions of polymer chains. The effects of inter-molecular energy transport and

molecular deformation of polymer chains were studied by examining the emission behavior in liquid and solid solutions. It was found that the molecular movements during stretching in the glassy state were quite different from that in the dewetting process. The latter was dominated by disengagement of intermolecular entanglements while the former was strongly influenced by trapping mechanisms of chain entanglements due to rapid local molecular strains. This work is supported by National Science Council of Taiwan.

**C1 80 How Fast Should Polymer/Drug Nanocrystal Dispersions Be Frozen?** JONGHWI LEE, *Chung-Ang University, Dept. of Chemical Engineering and Materials Science, Seoul, Korea* CHUL HO PARK, *Chung-Ang University* Recent advances in nanoparticle technologies have significantly enhanced the oral and parenteral delivery of poorly water-soluble active pharmaceutical ingredients (APIs). However, reports have been limited on the various drying procedures to convert a liquid nanocrystal dispersions into solid dosage forms. The solid dosage form should consist of nanocrystals that can readily reconstitute into their original size upon dissolution in water. Herein, the freeze drying process of nanocrystal dispersions was examined at varying freezing rates (speed of freezing interface). As freezing rate decreases, more particle-particle aggregation developed. A critical freezing rate, below which the dried nanocrystals cannot be re-dispersed, was identified based on the plot of the particle size of reconstituted nanocrystals versus freezing rate. Freeze drying at a freezing rate near the critical value produces dry powders of bimodal particle size distribution after re-dispersion. In addition, API concentration was found to significantly affect the critical freezing rate and therefore the re-dispersibility of dry powders. The concept of critical freezing rate is critical for the development of solid dosage forms of liquid nanocrystal dispersions. [1] J. Lee, Drug nano- and microparticles processed into solid dosage forms: physical properties, J. Pharm. Sci., 92(10) (2003) 2057-2068.

**C1 81 Equilibrium interactions and phase behavior of nanoparticles in solutions of adsorbing polymers** MEGHA SURVE, VICTOR PRYAMITSYN, VENKAT GANESAN, *University of Texas at Austin* We present the polymer mediated pair-interaction potentials, phase and percolation behavior of nanoparticles in presence of adsorbing polymers. We propose a ''saturable'' adsorption model to capture the effect of the finite surface saturation capacity for adsorption, and use polymer self-consistent field theory in combination with a McMillan-Mayer framework to compute the pair interaction potentials. Our results demonstrate novel size effects that distinguish the adsorption characteristics of nanoparticles from that of larger particles. Specifically, we predict that the nanoparticle regime is characterized by a significant adsorbance of polymers, distributed predominantly in the form of tails. We also demonstrate that an interplay between the surface saturation, polymer-to-particle size ratios and the polymer concentrations governs the overall effective interactions between nanoparticles in presence of adsorbing polymer. Our results show that the percolation threshold for smaller particles are significantly smaller (and overall correspond only to a few volume percent) compared to that of the larger particles. Further, with a decrease in the size of the particles, we also predict a considerable increase in the miscibility of the polymer-particle mixtures. The importance of surface saturation considerations is highlighted by comparing our results with the previous approaches.

**C1 82 How do colloidal particles rotate? New Materials and New Physics** LIANG HONG, *Materials Science and Engineering Department, University of Illinois at Urbana-Champaign* STEPHEN ANTHONY, *Department of Chemistry, University of Illinois at Urbana-Champaign* HUILIN TU, *Materials Science and Engineering Department, University of Illinois at Urbana-Champaign* STEVE GRANICK, *Materials Science and Engineering Department, Department of Chemistry, Physics and Chemical Engineering University of Illinois at Urbana-Champaign* Surface modification of colloidal particles to a Janus (asymmetric) chemical composition affords an opportunity to measure the rotational dynamics of colloidal particles in suspension as well as at interfaces. Using a metal deposition technique, we make particles half-covered by metal, and generate geometrically symmetric but chemically and fluorescently asymmetric materials. The rotational dynamics of single colloidal particles as well as rod-like structures have been measured utilizing imaging and tracking techniques. Increasing the concentration of polyelectrolytes in the solution results in the retardation of the rotational diffusion of single colloidal particles. This decrease, however, is not proportional to the viscosity of the solution. Moreover, we formed a metal-welded rod-like tetramer with this approach; for the first time, the rotational dynamics along the long-axis is measured. Research in progress includes chemical modification of the metal surface to form new colloid based materials and Brownian dynamics studies of these new materials.

**C1 83 The Prospects of Nanorods as Blending Agents in Immiscible Binary Polymer Blends** MICHAEL J. A. HORE, MOHAMED LARADJI, *Dept. of Physics, The University of Memphis* Systematic, large scale dissipative particle dynamics computer simulations performed in three dimensions indicate that the dynamics of phase separation of polymer blends containing rigid nanorods can be substantially slower than that of a pure binary blend, and that the dynamics depend greatly on the aspect ratio, i.e length/diameter, of the nanoparticles. When compared with spherical nanoparticles, it is also found that nanorods with the same volume fraction, or same surface area, are more effective in slowing down the dynamics of the blend – an indication that the anisotropy of the nanoparticles plays an important role in the phase separation kinetics. For a given volume fraction of rods, the domain growth exponent decreases (and growth may become non-algebraic) as the aspect ratio of the rods is increased. Growth is also slowed as the volume fraction of the nanorods is increased for a given aspect ratio. Additionally, it is found that the effect of lengthwise polydisperse rods is similar to that of monodisperse rods with a length equal to the mean length of the polydisperse rods. In cases with high aspect ratio rods or high volume fractions of rods, systems often proceed to micro-phase separated states – results not seen for nanospheres. The upshot of these results is that nanorods may potentially be used as effective emulsifiers of immiscible binary polymer blends. The thermodynamic stability of these micro-phase separated states will be discussed.

**C1 84 Adhesion and Release Mechanisms for Nanoimprint Lithography** DOUGLAS HOLMES, *University of Massachusetts, Amherst* JOHN WHANG, EDWIN CHAN, *University of Massachusetts, Amherst* ALFRED CROSBY, *University of Massachusetts, Amherst* Nanoimprint lithography is a leading candidate for fabricating next generation devices with features smaller than 50nm. A fundamental challenge with this emerging technology is the generation of defects during the release of the template

from the cured polymer pattern. This release process is dependent not only on the surface energetics of the template and the cured polymer, but also on the local mechanical properties of both materials – similar to the propagation of a crack at an interface. Here we present results on the investigation of adhesion and release properties of several polydimethylsiloxane-based polymer templates using UV-based imprint lithography techniques. We demonstrate that the framework of fracture mechanics and the theory of Johnson, Kendall, and Roberts (JKR) allows the separation of bulk and interfacial contributions to the overall release process. This decoupling of material properties guides the future development of both templates and imprintable resists for the success of nanoimprint lithography.

**C1 85 Nanotransfer printing for patterning conductive copper features** KIMBERLY DICKEY, YANGMING SUN, YUEH LIN LOO, *University of Texas at Austin* The drive for low-cost electronics creates a need for new techniques to directly and inexpensively pattern copper features in the 1-100$\mu$m range. We have developed a solventless, additive approach for printing permanent, conductive copper features at ambient conditions. Our technique is analogous to previously established nanotransfer printing (nTP) procedures for patterning gold with one marked difference. When copper is deposited onto a poly(dimethylsiloxane), PDMS, stamp, residual oligomers from the stamp penetrate between copper grains. This penetration disrupts the conductive pathway between copper grains; the printed copper patterns are electrically insulating as a consequence. This phenomenon is not observed with nanotransfer printing of gold features. A simple modification to the patterning procedure – leaching the PDMS stamps in boiling toluene for 2-3 days to remove uncrosslinked oligomers – results in printed copper patterns that are electrically conductive, with an average resistivity of 31$\mu$ohms-cm.

**C1 86 Surface grafting of carbon nanotubes with conjugated polybenzoxazole polymer** CHIH-WEI LIN, JEN-YOU LIN, ARNOLD CHANG-MOU YANG, *Department of Materials Science and Engineering, National Tsing Hua University, Hsinchu, Taiwan* CHEN-CHI M. MA, *Department of Chemical Engineering, National Tsing Hua University, Hsinchu, Taiwan* Surface-grafted carbon nanotubes impart extraordinary mechanical reinforcement to the polymer nanocomposites but considerably reduce the superior electrical conductivity of the neat carbon nanotubes. The conjugated polymer of polybenzoxaole (PBO) for grafting carbon nanotube therefore is very interesting as it may warrant reinforcement of both electrical and mechanical performances. The PBO-grafted carbon nanotubes was obtained from graft polymerization on nanotubes of polyhydroxyamide (PHA), the precursor of PBO, via condensation of 2,2'-bis(3-amino-4- hydroxyphenyl)-hexafluropropane ($BisPF_6$) and isophthaloyl chloride (IC) at low temperatures. The microstructure of the hybrid nanocomposites was investigated by FTIR, SEM, and TEM. The PBO/MWNT nanocomposites demonstrated excellence electronic (resistivity 0.374 $\Omega$-cm) and thermal (decomposition temperature 590 °C) properties. This work is supported by Air Force (AFOSR-04-4074) and National Science Council of Taiwan.

**C1 87 Modification of Nanocomposite POSS-PMMA Surfaces by Exposure to Reactive Oxygen.** REBEKAH ESMAILI, JACOB FORSTATER, BRIAN H. AUGUSTINE, WM. CHRISTOPHER HUGHES, *James Madison University* Thin films of the nanocomposite copolymer polymethylmethacrylate-polyhedral oligomeric silsequixane (PMMA-POSS) have been deposited onto glass and polymeric substrates and modified by exposure to reactive oxygen. The source of the oxygen was either a remote capacitively coupled plasma or UV-generated ozone. A change from hydrophobic to hydrophilic was observed after exposure to oxygen for time periods greater than 20 seconds. This change was quantified by measuring water contact angles on the surface which varied from greater than 90[r] before plasma exposure to less than 10[r] afterwards. A model for this behavior in which the isobutyl groups around the POSS cage are selectively removed by the oxygen plasma leaving a SiOx-rich surface is proposed. Time-of-flight secondary ion mass spectroscopy (ToF-SIMS) data were performed to test this model and show that the number of isobutyl groups on the surface does decrease with exposure time. Ongoing experiments involving the effect of oxygen exposure on the electro-osmotic flow in microfluidic structures which incorporate these films will be discussed.

**C1 88 Polypeptide-Based Silicate Layered Nanocomposite: Effect of Poly(L-lysine) Secondary Conformation on Physical Properties of the Hybrid** ROHAN HULE, *Dept of Mat. Sci. and Engg. and Del. Biotech Inst., Univ of Delaware, Newark, DE 19716* JEFFREY THOMPSON, *Dept of Mat. and Chem., UCSB, CA, 93106* TIMOTHY DEMING, *Dept of Bioengg., UCLA, CA 90095* DARRIN POCHAN, *Dept of Mat. Sci. and Engg. and Del. Biotech Inst., Univ of Delaware, Newark, DE 19716* The formation of nanocomposites from poly(L-lysine) (PLL) as the matrix and reinforced by $Na^+$- MMT clay is discussed. By varying solution conditions such as pH, temperature and concentration in the presence of MMT, the secondary conformation of PLL was controllably altered into $\alpha$-helical, $\beta$-sheet and random coil. Investigations were made into the PLL secondary conformation using FTIR, XRD and Circular Dichroism (CD). CD and FTIR revealed a strong propensity to fold into $\beta$-sheet when cast as films, irrespective of the initial secondary structure in solution. Two principles were observed for nanocomposite behavior: better mechanical properties at high molecular weight and controllable secondary structure at low molecular weight. Local morphology, observed using TEM and XRD confirmed the coexistence of intercalated and exfoliated MMT platelets over a wide range of compositions. Nanocomposite material properties relative to the secondary conformation of the matrix revealed significant enhancement in composite elastic modulus over neat polypeptides, with values comparable to traditional engineering polymers.

**C1 89 Oriented Mesoporous Inorganic Thin Films Using Laterally Confined Swellable Block Copolymer Templates.** SE GYU JANG, *UCSB* EDWARD J. KRAMER, *UCSB* SEUNG-MAN YANG, *KAIST* KAIST (SNL) COLLABORATION, UCSB (KRAMER) COLLABORATION, The control of grain orientation and long-range ordering of mesoporous inorganic materials produced by a sol-gel reaction of an inorganic precursor in self-assembling amphiphilic template systems have been limited due to the restrictions both on the time-scale and conditions for processing imposed by network formation of the inorganic component. Our goal is to form ordered mesoporous inorganic thin films by starting with a crosslinkable block copolymer template with long range order. A cylindrical poly(styrene-2-vinylpyridine) (PS-P2VP) diblock copolymer with Mn = 32.7 kg/mol and $f_{PS} = 0.21$ was spin-cast onto a set of 30 nm high and 2000 nm wide SiOx channels on Si substrates produced by optical lithography. An ordered PS-P2VP monolayer[1] is achieved via slow cooling after heating above its bulk order-disorder transition temperature (212

C), measured by small angle X-ray scattering. Hybrid inorganic/organic structures are fabricated by incorporation of inorganic precursor into the chemical cross-linked P2VP matrix.[2] Cylindrical pores within the inorganic matrix are then obtained by removal of the organic component using UV-ozone treatment. [1]M.R.Hammond, E. Cochran, G.H. Fredrickson, E.J. Kramer Macromolecules **38** 6575 (2005). [2]R.C. Hayward, B.F. Chmelka, E.J. Kramer Macromolecules **38** 7768 (2005).

**C1 90 Chemical composition effects on the crazing of PS-PMMA block copolymers** WON KIM, *Rensselaer Polytechnic Institute, Department of Chemistry and Chemical Biology* JUN-WON HAN, *Rensselaer Polytechnic Institute, Department of Chemical and Biological Engineering* HOICHANG YANG, *Rensselaer Polytechnic Institute, Rensselaer Nanotechnology Center* CHANG RYU, *Rensselaer Polytechnic Institute, Department of Chemistry and Chemical Biology* Using a large scale separation technique adopting interaction chromatography, we have fractionated as-synthesized PS-PMMA block copolymers in terms of the average chemical composition difference, while maintaining the same average molecular weight. Copper grid technique with optical, atomic force and transmission electron microscopy has been employed for the fracture study to reveal how the composition-dependent morphology affect the crazing of the glassy-glassy block copolymers, while maintaining the same level of Chi*N. In addition, we study how the thermal annealing affects the median strains for crazing and catastrophic failure.

**C1 91 Impact of Nanotube Addition on Stress Recovery of Thermoplastic Elastomer Nanocomposites.** DANIEL POWERS, MAX ALEXANDER, RICHARD VAIA, *Air Force Research Laboratories* MICHAEL ARLEN, *University of Akron* HILMAR KOERNER, *University of Dayton Research Institute* Recent extension of polymer nanocomposite concepts to shape memory polymers has demonstrated potential to substantially improve recovery stress and provide novel triggering options, while still maintaining large deformations. One such example is multi wall carbon nanotubes (MWCNT)s in thermoplastic polyurethane (PU), where the MWCNTs increase modulus and modify strain induced crystallization leading to improved strain set and recovery force relative to unfilled PU as well as conventionally-filled PU. The impact of MWCNT alignment on the stress recovery rate depends on MWCNT concentration and the procedure used to 'set' the deformation. Differences in response time upon shape recovery are observed whether the nanocomposites are 'set' above the melting point of soft segment crystallites or at room temperature (RT). A detailed dynamic mechanical analysis protocol reveals that recovery rate and shape fixity are increasing as a function of MWCNT volume fraction and that RT processed nanocomposites show overall superior results. Recovery times can be described with a modification of the Kohlrausch-Williams-Watt equation, indicating a contribution from elasticity of the carbon nanotubes or chain scission of the matrix PU.

**C1 92 Long DNA Molecules at Liquid-Solid Interfaces** VLADIMIR SAMUILOV, B. LI, J. SOKOLOV, M. RAFAILOVICH, *Dept. of Materials Science, SUNYSB, Stony Brook* B. CHU, *Dept. of Materials Science, Dept. of Chemistry, SUNY at Stony Brook* The electrophoresis of long DNA molecules was studied using a newly developed method of electrophoresis on flat surfaces [1] in the regime of strong electrostatic interaction. The mobility of lambda- DNA molecules on this surface was found to scale as the square root of the persistent length with the ionic strength at high buffer. This experimental result indicates that at high buffer concentration the separation mechanism of solid-liquid interface electrophoresis is expected to be due to surface friction rather than biased reptation [2-4]. At low buffer concentrations the DNA chains are stretched.The electric double layer is responsible for a velocity profile of the electroosmotic flow. The net electrophoretic mobility of longer DNA, being trapped closer to the surface as found to be higher then for the shorter ones in the electric field. [1]. N. Pernodet, V. Samuilov, K. Shin, et al. Physical Review Letters, 85 (2000) 5651-5654. [2] Y.-S. Seo, V.A. Samuilov, J. Sokolov, et al. Electrophoresis, 23 (2002) 2618-2625. [3] Y.-S. Seo, H. Luo, V. A. Samuilov, et al. DNA Electrophoresis on nanopatterned surfaces, Nano Letters, 4, 2004, 659-664.

**C1 93 Closed-Loop Phase Behavior: Is it Universal Phenomenon for Block Copolymers with Lower Critical Transition Temperature?*** JIN KON KIM, CHAOXU LI, DONG HYUN LEE, *Department of Chemical Engineering, Pohang University of Science and Technology* A closed-loop phase behaviour was found for Polystyrene-block- poly(n-pentyl methacrylate) (PS-PnPMA) copolymer having a weak interaction between two segments. On the other hand, PS-block- poly(n-butyl methacrylate) (PS-PnBMA) exhibited only lower disordered-to-ordered transition (LDOT). Then, a question might be raised: Is it possible that PS-PnBMA has the closed-loop phase behaviour, although the upper ordered-to-disordered transition (UODT) could not be detected in the experimentally accessible temperature. In this study, we clearly demonstrate that PS-PnBMA exhibits the closed-loop phase behaviour, where both LODT and UODT were measured at experimentally accessible temperatures (100 ~ 280°C) by using special solvents.

*This work was supported by the Creative Research Initiative Program (KOSEF).

**C1 94 Acoustic modes and elastic properties of polymeric nanostructures*** RYAN D. HARTSCHUH, A. KISLIUK, A.P. SOKOLOV, *University of Akron* V. NOVIKOV, *U of A and IA&E, Russian Academy of Sciences* P.R. HEYLIGER, *Colorado State University* C.M. FLANNERY, W.L. JOHNSON, *NIST, Boulder* C.L. SOLES, W.-L. WU, *NIST, Gaithersburg* Very few experimental techniques exist to quantify the mechanical properties of nanoscale photoresist structures. This inadequacy is going to become increasingly important as the rigidity of such structures is expected to change as the feature sizes approach the characteristic dimensions of the macromolecules and size-dependent material properties begin to compromise device fabrication and performance. Phonon spectra of polymeric linear nanostructures have been characterized using Brillouin light scattering. In addition to phonon modes similar to those present in uniform thin films, the phonon spectra of the nanolines reveal a new mode with a lower frequency that depends on the width of the nanolines. Classic wave theory and finite element analysis were combined to identify this new mode as a flexural vibration of the nanolines. Analysis of the phonon spectra gave estimates of elastic constants in the nanostructures and indicated that there is no significant deviation from bulk mechanical properties and no mechanical anisotropy in structures as small as 88 nm.

*This material is based upon work supported under a National Science Foundation Graduate Research Fellowship

**C1 95 Polymeric Micro/Nanostructures Fabricated through a Novel Method with Optical Microscopy** CHAO-MIN CHENG, BIN LI, PHILIP LEDUC, *Department of Mechanical Engineering, Carnegie Mellon University* We present a technique for building three-dimensional structures using optical methods with photocuring chemistry. This method merges an optics-based approach with chemical restructuring through the transition of materials from distinct phases. By activating a photocurable material in combination with controlling the intensity distributions that are inherent in optical patterns, in-situ fabrication of three-dimensional polymeric microstructures is demonstrated. Furthermore, polymeric nanostructures can be also obtained based on this method through combining this technique with Al2O3 nanopores. This experimentally simple approach combined with thermal control can create complex shapes including curved and asymmetric profiles. This method has potential applications in a variety of fields including optical technique, micro/nanoelectromechanical systems and microfluidics.

**C1 96 Nanoparticle arrays controlled by polymeric ligands** CHUN-KWEI WU, JEFFREY T. KOBERSTEIN, *Columbia University* Ligand chemistry on nanoparticles plays an important role in applying their unique properties to the real world. The original capping ligands on nanoparticles, i.e. oleic acid, limit their compatibility with some bulk materials of interest and can restrict some potential applications. We have successfully exchanged the original oleic acid ligands on $\gamma$-$Fe_2O_3$ nanoparticles with $\omega$-poly(dimethylsiloxane) (PDMS). A high grafting density of PDMS on iron oxide nanoparticles has been achieved by this ''grafting to'' method. $Fe_2O_3$ nanoparticles with PDMS ligands self-assemble with hexagonal packing when deposited on substrates. The interparticle spacing can be controlled by varying the molecular weight of the PDMS. The PDMS-modified $Fe_2O_3$ nanoparticles are totally compatible with bulk PDMS allowing nanocomposites to be formed. The PDMS components in resultant thin films can subsequently be converted to silicon oxide by room temperature UV/ozone treatment to fabricate $Fe_2O_3$-silica composite thin films. The use of such nanocomposite films in gas separation and catalyst membranes is being studied.

**C1 97 Crosslinked nanoparticle assemblies at liquid-liquid interfaces** RAVISUBHASH TANGIRALA, HABIB SKAFF,*YAO LIN,†THOMAS RUSSELL, TODD EMRICK, *University of Massachusetts, Amherst, MA* The assembly of nanoparticles at the interface of immiscible fluids holds promise for the preparation of new materials that benefit from both the physical properties of the nanoparticles and the chemistry associated with the ligands. The weak confinement of nanoparticles to the liquid-liquid interface enables the formation of particle-based assemblies that possess unique features relative to assemblies of micron-scale particles. Crosslinking of nanoparticles at a liquid-liquid interface lends greater stability to the interfacial assembly, leading to ultrathin nanoparticle-based capsules which possess mechanical integrity even after removal of the interface. Norbornene-functionalized CdSe/ZnS core/shell quantum dots are used in this study to afford facile capsule visualization by fluorescence confocal microscopy, as well as ease of crosslinking in mild conditions by means of ring-opening metathesis polymerization (ROMP) using a unique amphiphilic ruthenium benzylidene metathesis catalyst. The crosslinked capsules display a size-selective encapsulation capability, dictated by the interstitial spaces between the nanoparticles. The porosity of the capsules can be further tuned by the addition of small amounts of uncrosslinkable nanoparticles prior to crosslinking.

*Currently at Intezyne Technologies
†Currently at Argonne National Laboratories

**C1 98 Gold nanoparticle self-assembly and gold patterning using thin film polymer blend templates.** RANJAN D. DESHMUKH, RUSSELL J. COMPOSTO, *Materials Science and Engineering, University of Pennsylvania* In this study we have used thin films of polymer blend of Poly(methyl methacryalate), PMMA, and Poly(styrene-ran-acrylonitrile), SAN, as templates for patterning gold as well as gold nanoparticles on silicon substrate. PMMA/SAN phase separate above lower critical solution temperature, LCST, and form cylindrical and bi-continuous morphologies in 50/50 and 70/30 blend compositions. Selectively etching out PMMA phase by UV and acetic acid treatment results in a template, which is used for patterning. Gold is sputtered on these templates followed by removal of SAN in a solvent, leaving gold patterns on the substrate. Unique cylindrical island-like and bi-continuous patterns were observed by AFM. We also selectively patterned the etched region (PMMA) with a self-assembled monolayer, SAM, of 3-aminopropyl-triethoxysilane, APTES, followed by SAN removal and coating the exposed region with 3-mercaptopropyl-trimethoxysilane, MPTMS. Further, deposition of colloidal citrate-stabilized gold nanoparticles resulted in the selective deposition of gold nanoparticles on APTES (island-like and bi-continuous patterns), because of the charge-charge interactions between nanoparticles and SAM.

**C1 99 Organometallic Polymer-Derived Catalyst Dispersion Effects on SWNT Growth** SARAH LASTELLA, PULICKEL M. AJAYAN, CHANG Y. RYU, *Rensselaer Polytechnic Institute* DAVID RIDER, IAN MANNERS, *University of Toronto* Catalyst formation kinetics of a ferrocene-containing homopolymer, polyferrocenylethylmethylsilane or PFEMS, is investigated as it relates to the catalysis of single walled carbon nanotubes (SWNTs) and is compared with that of the corresponding diblock copolymer, poly(styrene-b-ferrocenylethylmethylsilane) or PS-b-PFEMS. The polystyrene blocks in the PS-b-PFEMS form a matrix to uniformly disperse discrete nanoscale iron domains that enhance the uniformity of nanotube diameters compared to the homopolymer. PFEMS homopolymer contains 23 percent iron by weight, while PS-b-PFEMS with a 25 vol percent PFEMS is only 6 percent iron, respectively. It is concluded that iron present in a block copolymer film is two times more active than a PFEMS film, and in turn, leaves a lower iron density on the substrate surface relative to its nanotube yield.

## C1 100 BIOLOGICAL PHYSICS POSTER SESSION

**C1 101 Elastic and osmotic properties of articular cartilage** DAVID LIN, EMILIOS DIMITRIADIS, IREN HORKAYNE-SZAKALY, FERENC HORKAY, *National Institutes of Health (NIH)* The pathophysiology of osteoarthritis involves cellular and biochemical processes linked to mechanical stress. A better understanding of the mechanism of these processes and how they cause

changes in the composition, macro- and micro-structure, and mechanical properties of cartilage is necessary for developing effective preventative and treatment strategies. In this study, elastic and osmotic swelling properties of tissue-engineered cartilage were explored using atomic force microscopy (AFM) and a tissue osmometer. AFM was also used to image the surface of the specimens while chemical composition was determined by biochemical analysis. Estimation of the Young's moduli of the tissue from AFM force-indentation data was performed using an optimization approach to fit appropriate models to the data. Force-indentation data were acquired both with sharp, pyramidal and with microspherical probes. The procedure has been validated by making measurements on model gel systems of known elastic properties. This approach is presented as a robust method of optimally extracting Young's moduli of soft, crosslinked materials from AFM data. Gross inhomogeneities at different scales in the cartilage tissue are manifested in the high degree of variance in local Young's moduli values obtained from both AFM and osmotic swelling data. These findings suggest that the mechanical properties of cartilage are affected by the local macromolecular composition.

**C1 102 The Influence of Environment Geometry on Injury Outcome: II. Lumbosacral Spine** SAAMI J. SHAIBANI, *Independent Modeling, Algorithms & Analytical Studies (IMAAS)* It is widely agreed that the type of motor vehicle in which an occupant is situated can sometimes make a noticeable difference in injury potential even when the insult suffered is the same. A simple example might be the same occupant being in a sports car as opposed to a minivan, but such anecdotal experience does not usually help to distinguish the effect of particular features within the same category of vehicle. Other research has addressed the role of environment geometry in neck injury,[1] and this paper adopts the same methodology for the low back. The heights, lengths and angles of the seat cushion and seat back (including head rest) are all examined as descriptors of passenger compartment geometry, and any changes caused by these are determined. Useful results are feasible with the large patient population available even if clear patterns in these are not always present. As in earlier work, there is still the option of finding individual outcomes on a case-by-case basis. [1] The influence of environment geometry on injury outcome: I. Cervical spine, Bull Am Phys Soc, in press (2006).

**C1 103 Analysis of a 2D simulation model of biofilms with autonomous cells** ANAND BHANDAR, YERGOU TATEK, GARY SLATER, *University of Ottawa* Biofilms are substances consisting of a large number of microorganisms that grow on surfaces in contact with liquids. They can be found growing in water pipes, on surgical instruments or on tooth surfaces. Mathematical models have been used for the last three decades in order to improve our understanding of their growth and behavior. We have designed and implemented a new Monte Carlo model based on the life of autonomous cells and investigated the static and dynamic characteristics of the resulting bacterial populations. Each cell is modeled as an autonomous agent whose behavior is controlled by thermodynamic parameters, mechanical properties, physiological rules and environmental conditions. In the 2D version studied, a cell is represented by a closed chain of self-avoiding beads linked together using the bond fluctuation algorithm. The cell is controlled both by the rigidity of its membrane and a pressure difference. The model is complemented by key features such as the processes of cell division, growth and death, attractive interactions between the cell and the surface, and the explicit presence of nutrient diffusion. Tuning model parameters leads to the growth and maturation of various types of biofilms. Typical colonies incorporating these and other important characteristics of biofilms such as the exopolymeric substance (EPS), metabolism and waste production, cell motility and chemotaxy, and cell mutation will be presented.

**C1 104 A physiologically-based spatiotemporal model of fMRI hemodynamic responses.** JACKIE HUBER, *School of Physics, University of Sydney, Australia* PETER DRYSDALE, PETER ROBINSON, *School of Physics, University of Sydney, Australia; Brain Dynamics Center, Westmead Hospital, Australia* A 3D cerebrovascular model is developed to describe the spatiotemporal Blood Oxygen Level Dependent (BOLD) functional MRI (fMRI) response. Modelling spatial effects is particularly important as technology improves, shrinking image voxels and thereby increasing voxel interdependence. Specifically, poroelastic theory, originally developed in geophysics, is used to model the brain tissue and vasculature as a porous continuum. The model yields equations describing conservation of mass, momentum, and deoxyhemoglobin, plus the effect of neuronal activity on blood flow. The equations reproduce existing, non-spatial, hemodynamic models in the relevant limit. Imposition of continuity of flow between adjacent points enables potential investigation of spatial phenomena such as 'blood steal' which has been proposed to account for negative BOLD signals abutting sites of positive BOLD responses. This model will enable future study of spatiotemporal relationships between stimuli and experimental fMRI BOLD responses.

**C1 105 BOLD Responses to Stimuli: Dependence on Frequency, Stimulus form, Amplitude, and Repetition Rate.** PETER ROBINSON, PETER DRYSDALE, *School of Physics, University of Sydney, Australia; Brain Dynamics Center, Westmead Hospital, Australia* HELENA VAN DER MERWE, ELIZABETH KYRIAKOU, MICHELLE RIGOZZI, BILJANA GERMANOSKA, *School of Physics, University of Sydney, Australia* CHRISTOPHER RENNIE, *School of Physics, University of Sydney, Australia; Brain Dynamics Center, Westmead Hospital, Australia* A quantitative theory is developed for the relationship between stimulus and the resulting Blood Oxygen Level Dependent (BOLD) functional MRI signal in the brain. The relationship of stimuli to neuronal activity during evoked responses is inferred from recent physiology-based modeling of evoked response potentials (ERPs). A hemodynamic model is then used to calculate the BOLD response to neuronal activity. The predicted response is analyzed vs. form, frequency, and amplitude of stimulus. The BOLD frequency response is very nearly linear in the parameter ranges of interest, with the form of a low-pass filter with a weak resonance at 0.07 Hz. For short stimuli, the response is closely proportional to the time-integrated stimulus-evoked activity, rather than the peak amplitude, as often assumed. There can thus be widely differing proportionalities between BOLD and peak activity, a likely reason for the weak expected correlation between ERPs and BOLD.

**C1 106 Measurement of the Mechanical Properties of Intact Collagen Fibrils** H. MERCEDES, A. HEIM, W.G. MATTHEWS, *Department of Physics, University of South Florida* T. KOOB, *Shriners Hospital for Children* Motivated by the genetic disorder Ehlers-Danlos syndrome (EDS), in which proper collagen synthesis is interrupted, we are investigating the structural and mechani-

cal properties of collagen fibrils. The fibrous glycoprotein collagen is the most abundant protein found in the human body and plays a key role in the extracellular matrix of the connective tissue, the properties of which are altered in EDS. We have selected as our model system the collagen fibrils of the sea cucumber dermis, a naturally mutable tissue. This system allows us to work with native fibrils which have their proteoglycan complement intact, something that is not possible with reconstituted mammalian collagen fibrils. Using atomic force microscopy, we measure, as a function of the concentration of divalent cations, the fibril diameter, its response to force loading, and the changes in its rigidity. Through these experiments, we will shed light on the mechanisms which control the properties of the sea cucumber dermis and hope to help explain the altered connective tissue extracellular matrix properties associated with EDS.

**C1 107 Design and use of an artificial capillary in the study of metastatic cell adhesion** ADAM RAFI, ANTONIO PERAMO, REBECCA BOREN, AUGUST HEIM, WILLIAM G. MATTHEWS, *Department of Physics, University of South Florida* To improve the quality of life of patients with cancer, treatments will need to both minimize existing tumors and reduce the metastasis of cancer cells. The effectiveness of potential treatments on existing tumors can be directly probed, but anti-metastasis treatments are difficult to quantify. Therefore, a detailed understanding of the metastatic process is required for drug design. Details of the metastatic deposition of tumor cells in the circulatory system are not well understood. We are investigating the binding of tumor cells to an artificial endothelium. The model system allows for control over molecular composition at the interface, presenting the proteoglycans (PGs) found in the glycocalyx to tumor cells under shear flow conditions. Whether rolling or static adhesion is preferred, as well as what mechanical properties of the interaction between the cells and the PGs are important is to be determined. The outcomes of these experiments will help guide the search for pharmaceuticals that can disrupt the metastatic process at the endothelial adhesion step.

**C1 108 Study of Native Type I Collagen Fibrils** AUGUST HEIM, *University of South Florida* Presented in this work is direct imaging and force microscopy of native, intact type I collagen fibrils extracted from the sea cucumber itCucumaria frondosa dermis with affiliated proteoglycan molecules. The prototypical collagen fibril structure is well conserved through higher mammalian species and presents a model for study of the mechanical properties of the primary individual components of the dermis and skeletal ligature. Common practice is to use reconstituted fibrils which lack the precise conformal structure and affiliated proteoglycans. We have performed force microscopy to probe the mechanical properties of native fibrils and extract the elastic modulus under natural conditions. This knowledge is combined transmission and atomic force imaging, in conjunction with applied computation models, to demonstrate an inherent semitubular structure of these fibrils.

**C1 109 Conformational analysis of tripeptides: a molecular dynamics study of rigid and non-rigid tripeptides** JOHN SHIBATA, MARK MOCHEL, *The University of the South* Molecular dynamics simulations have been performed on different tripeptides classified as structurally rigid and non-rigid (1). The simulations were run using the OPLS-AA force field (2) with and without explicit solvent. Two modeling programs, Tinker (3) and Macromodel (4), were used to simulate the dynamics. The accessible conformations were analyzed using Ramachandran plots of the dihedral angles. The results of this study are compared to the rigidity classification scheme (1), and differences in the results using explicit solvent and a continuum solvent model are noted. (1) Anishetty, S., Pennathur, G., Anishetty, R. BMC Structural Biology **2**:9 (2002). Available from http://www.biomedcentral.com/1472-6807/2/9. (2) Jorgensen, W. L., Maxwell, D. S., Tirado-Rives, J. J. Am. Chem. Soc. **118**, 11225 (1996). (3) Dudek, M. J., Ramnarayan, K., Ponder, J. W. J. Comput. Chem. **19**, 548 (1996). Available from http://dasher.wustl.edu/tinker. (4) Mohamadi, F., Richards, N. G. J., Guida, W. C., Liskamp, R., Lipton, M., Caufield, C., Chang, G., Hendrickson, T., Still, W. C. J. Comput. Chem. **11**, 440 (1990).

**C1 110 Examination of the Interface Formed from Protein Interactions in Gels** PERUMAL RAMASAMY, *Dept. Of Materials Science and Engineering, SUNY Stony Brook* LISA M. MILLER, *National Synchrotron Light Source, Brookhaven National Laboratory* M. RAAFAT EL-MAGHRABI, *Department Of Physiology And Biophysics, SUNY Stony Brook* MIRIAM RAFAILOVICH, *Dept Of Materials Science and Engineering, SUNY Stonybrook* Understanding the interaction of proteins with one another in confined environments serves as an important step for developing faster protein separation methods. To understand proteinprotein interaction of oppositely charged proteins, fluorescently-labeled Albumin and poly-L-Lysine were subjected to electrophoresis in Agarose gels, in which the cationic albumin and the anionic poly-lysine were allowed to migrate towards each other and interact. Confocal microscopy was used to image the fluorescently-tagged proteins in the gel. The secondary structure of the proteins was studied using FTIR microspectroscopic imaging. Results showed that sharp interfaces were formed where the proteins met. Protein-protein interactions were observed through fluorescence quenching. The migration of the interface in the gel was found to be dependent upon the relative concentration of the proteins. The structure of the proteins at the interface, the fluorescent intensity modifications, and the mobility of the interface for different pore sizes are currently under investigation.

**C1 111 Simple Model for Phase Diagram of Lysozyme as a Function of Salt Type and Salt Concentration** NATHANIEL WENTZEL, JAMES D. GUNTON, *Lehigh University* The liquid-liquid phase separation curves for lysozyme are known to depend on the salt type and salt concentration. For the case of monovalent cations, the cloud point temperature typically increases with increasing salt concentration, for fixed lysozyme concentration. For the case of divalent cations, however, a maximum in the cloud point temperature is observed that has been interpreted as being due to ion binding to the protein surface and subsequent water structuring. In this paper we use a simple square well model due to Grigsby et al (Biophys. Chem. 91, 231 (2001)), whose well depth depends on salt type and salt concentration, to determine the phase diagram for both monovalent and divalent cations. The phase diagrams are calculated using standard Monte Carlo simulations and compared with known experimental results.

**C1 112 Computationally Efficient Method of Simulating Creation of Electropores** JOHN NEU, *University of California, Berkeley* WANDA KRASSOWSKA, *Duke University* Electroporation, in which electric pulses create transient pores in the cell membrane, is an important technique for drug and DNA delivery.

Electroporation kinetics is described by an advection-diffusion boundary value problem. This problem must be solved numerically with very small time and space steps, in order to resolve very fast processes occurring during pore creation. This study derives a reduced description of the pore creation transient. This description consists of a single integrodifferential equation for the transmembrane voltage V(t) and collateral formulas for computing the number of pores and the distribution of their radii from V(t). For pulse strengths corresponding to those used in drug and DNA delivery, relative differences in predictions of the reduced versus original problem are: voltage V(t), below 1%; number of pores, below 10%; pore radii, below 6%. Computational efficiency increases with the number of pores and thus with the pulse strength. For the strongest pulses, the run time of the reduced problem was below 1% of the original one. Such time savings can bridge the gap between problems that can be simulated on today's computers and problems that are of practical importance.

**C1 113 Hydrophobic Mismatch and Phase Transition in a Membrane Composed by a Mixture of Linear and Bola Phospholipids** GABRIEL LONGO, IGAL SZLEIFER, *Department of Chemistry, Purdue University* Archeobacteria are microorganisms that can survive and proliferate in extreme habitats, such as high salt concentration environments, anaerobic conditions, and high or low temperatures. A membrane composed of bolaform phospholipids is what gives these unique survival qualities to the bacteria. The nature and composition of this membrane has not yet been elucidated. In this work, a membrane composed by a mixture of linear and bola phospholipids is studied using a molecular theory. The effect of changing the fraction of bolaform phospholipids, as well as the length of the hydrocarbon chain of the linear lipid are studied. A phase separation in the mixture between a thin bola rich membrane and a thick linear rich membrane is found. The thin membrane is mainly composed by ''spanning'' bola molecules whose polar heads are in opposed hydrophilic regions of the membrane. The phase separation is only present when the hydrocarbon chains of both molecular species have comparable sizes. The driving force for the phase separation is the size matching between the hydrophobic chains of the linear phospholipid and the spanning bola lipid.

**C1 114 Renormalized Elasiticity of Lipid Membranes with Adsorbed Polymers** JOEL D. REVALEE, *Physics Department, University of Memphis* MOHAMED LARADJI, *Physics Dept., University of Memphis* Renormalized elastic moduli of self-assembled lipid membranes, with anchored polymers that interact attractively with the membrane, are determined by means of large scale dissipative particle dynamics simulations. We show that the effective surface tension and the bending modulus of the membrane behave non-monotonically with the molecular weight or/and polymer coverage. At low molecular weight or grafting densities, the surface tension increases, while the bending modulus decreases, with increasing molecular weight or grafting density of the polymer chains. However, at high molecular weight or grafting densities, when the polymers are in the brush regime, we found that the surface tension decreases while the bending modulus increases with increasing grafting density or molecular weight of the polymers. We will also present results on the pearling instability of the lipid membrane due to grafted polymers.

**C1 115 On the Registry of Lipid Domains in Multicomponent Lipid Membranes** CLAYTON H. DAVIS, *Physics Department, University of Memphis* MOHAMED LARADJI, *Physics Dept., University of Memphis* Recent experiments on multicomponent lipid vesicles, composed of a saturated lipid, unsaturated lipid and cholesterol, have shown that the liquid-ordered domains in the two leaflets of the bilayer are in strong registry [1,2]. In order to understand the reasons behind this domain registry, we propose a simple lattice model, where the two leaflets are represented by two spin-half Ising surfaces, where the up and down spins represent the saturated and unsaturated lipids, respectively. Since lipid flip-flops are very rare events, spins in the two Ising lattices are only allowed to diffuse within each leaflet through spin-exchange Kawasaki dynamics. In addition each lattice point can also be occupied by a cholesterol particle which is allowed to both diffuse within each lattice and flip-flop between the two lattices. We found that registration can occur even for small concentrations of cholesterol. We will discuss the effects of cholesterol saturation and intra-layer and inter-layer lipid-cholesterol interaction on domains registration. [1] S.L. Veatch and S.L. Keller, Phys. Rev. Lett. 89, 268101 (2002) [2] T. Beaumgart, S.T. Hess, and W.W. Webb, Nature 425 (2003)

**C1 116 Cubic Phase Formation in Peptide/Lipid Systems*** BRANDON SCUFFINS, BETH CUNNINGHAM, *Bucknell University* DAVID WOLFE, *Lycoming College* Previous studies have shown that the phenomena of spontaneous membrane self-assembly can be used to incorporate membrane peptides into lipid bilayers. Once a peptide is incorporated in these peptide/lipid systems they may then be crystallized through the process of itin meso crystallization. In this study, we used x-ray diffraction and $^{31}$P NMR to show that a system of dioloeoylphosphatidylethanolamine (DOPE), monoolein (MO), and DOPE with polyethylene glycol covalently attached to the headgroup (PEG-lipid) can create a system with a higher concentration of peptide incorporated into the cubic phase then previously reported. We have observed that DOPE:MO:PEG-lipid at a molar ratio of 97.5:100:2.5 naturally forms the Im3m cubic phase at room temperature. Furthermore, we found that the DOPE:MO:PEG-lipid system can incorporate a concentration of up to 25 mole % peptide at room temperature. Preliminary results indicate that the lipid/peptide system requires a stable cubic phase for peptide crystallization to occur.

*We acknowledge support from NSF grant PHY-0097424

**C1 117 Conformational Change in Fibrinogen on Langmuir Blodgett Clay Monolayer*** J.S. KOO, T. KOGA, M. RAFAILOVICH, J. SOKOLOV, *SUNY at Stony Brook* We have studied the adsorption of the plasma protein, fibrinogen, on two different clay monolayers. Surface pressure-molecular area ($\pi - A$) isotherm measurements, atomic force microscopy (AFM), X-ray reflectivity and grazing incident X-ray diffraction (GID) were used to characterized formation of organo-clay and sodium clay monolayers. These clays serve as model hydrophobic and hydrophilic surfaces, respectively. The overall conformational structure of fibrinogen is dramatically different on organo-clay and sodium clay surfaces. On the sodium clay surface, individual fibrinogen molecules appear globular in shape whereas, on orgnoclay, the trinodular structure is most commonly observed. Time dependent studies were also conducted. The results show that uniform multilayer formation occurred only on the hydrophobic surfaces. Fibrillar fibrinogen structures are observed over their uniform bilayers. Non-uniform adsorption occurred on the hydrophilic surfaces.

*Work supported by the NSF-MRSEC.

**C1 118 pH-dependent conformational changes of diphtheria toxin adsorbed to lipid monolayers by neutron and X-ray reflection** MICHAEL KENT, *Sandia National Labs* HYUN YIM, *Sandia National Labs* SUSHIL SATIJA, *National Institute of Standards and Technology* IVAN KUZMENKO, *Argonne National Labs* Several important bacterial toxins, such as diphtheria, tetanus, and botulinum, invade cells through a process of high affinity binding, internalization via endosome formation, and subsequent membrane penetration of the catalytic domain activated by a pH drop in the endosome. These toxins are composed of three domains: a binding domain, a translocation domain, and an enzyme. The translocation process is not well understood with regard to the detailed conformational changes that occur at each step, To address this, we performed neutron reflectivity measurements for diphtheria toxin bound to lipid monolayers as a function of pH. While the final membrane inserted conformation will not be reproduced with the present monolayer system, important insights can still be gained into several intermediate stages. In particular, we show that no adsorption occurs at pH = 7.6, but strong adsorption occurs over at a pH range from 6.5 to 6.0. Following binding, at least two stages of conformational change occur, as the thickness increases from pH 6.3 to 5.3 and then decreases from pH 5.3 to 4.5. In addition, the dimension of the adsorbed layer substantially exceeds that of the largest dimension in the crystal structure of monomeric diphtheria, suggesting that the toxin may be present as multimers.

**C1 119 Topology based theory of helix-coil transition** KINGSHUK GHOSH, *Dept of Pharm Chem, UCSF 2240* KEN DILL, *Dept of Pharm. Chem, University of California, San Francisco* We revisit the problem of helix-coil transition. We propose a new theory based on topology, significantly different from Zimm-Bragg theory. Our model predicts the cooperativity and is in excellent agreement with available experimental data. The model can be extended to study the thermodynamics of other structures as well. It also provides a framework to understand the kinetics of formation for different structures.

**C1 120 An Inside Look at Traube's Rule: A Molecular Dynamics Study** ALLISON DICKEY, ROLAND FALLER, *UC Davis* According to Traube's Rule [1], the alcohol concentration required to maintain the interfacial tension ($\gamma$) of a bilayer is reduced by a factor of three for each additional $CH_2$ group that is added to the alkyl chain of the alcohol. Recent experimental work confirmed that Traubes Rule applies to 1-stearoyl, 2-oleoyl phosphatidylcholine (SOPC) lipid bilayers that are exposed to alcohol solutions of methanol, ethanol, propanol, and butanol [2]. To examine the molecular mechanisms leading to Traubes Rule, we use molecular dynamics simulations to study the interactions between a dipalmitoylphsphatidylcholine (DPPC) bilayer and ethanol, propanol, and butanol solutions. We first examine how the bilayer structure variation depends on alcohol chain length via the area per lipid headgroup, lipid chain disorder, and electron distribution functions. We also study the alcohol dynamics within the bilayer by monitoring the time length, number, and location of hydrogen bonds. Lipid mean squared displacements are also calculated to determine the extent to which lipid mobility is affected by alcohols. [1] I. Traube Liebigs Annalen (1891) [2] H. Ly, M. Longo Biophys J (2004)

**C1 121 Optimum pH for protein-protein complexes.** PETRAS KUNDROTAS, EMIL ALEXOV, *Dept. of Physics & Astronomy, Clemson University, Clemson, South Carolina* The structure and function of proteins are influenced by external parameters such as pH of the environment. The pH at which proteins are most stable is the optimum pH of stability and the pH at which the binding affinity of protein-protein complexes is maximal is called optimum pH of the complexes. Therefore it is plausible to suggest that two proteins forming a complex in a particular environment should have their optimum pH's correlated as well as they should be correlated with the optimum pH of the complex. In order to test this hypothesis, we have calculated the pH dependencies of electrostatic folding free energy and total net charge for a set of 60 protein complexes previously used for protein-protein docking benchmark. The calculations have been performed for the entire complex and for each individual molecule separately. It was shown that there exists a clear correlation between optimum pH of the complex and optimum pH's of its components. In addition, the correlations between the net charges of the individual molecules and between the charges of the interfaces were also studied. The above findings could be used as additional criteria in evaluating models of protein-protein complexes.

**C1 122 Excited state of peptide nanorings** TETSUO YAMADA, HIROSHI MIYAZAKI, HAJIME OKAMOTO, KYOZABURO TAKEDA, *Waseda University* Peptide nanorings (PNRs) has a closed ring form composed of alternating D- and L-$\alpha$-amino acid residues. Much interest has been attracted owing to their function as a selective ion receptor. Here, based on itab initio molecular orbital theory, the excited as well as the ground state structures have been theoretically studied and discussed how the photoexcitation changes the ion-capturing ability with regarding on the two ring skeletons of Extended (E)- and Bound (B)-type PNR geometries. Because the HOMO-LUMO transition is optically allowed, we took into account this single excitation via the unrestricted Hartree-Fock (UHF/6-31G**) calculations. Our results reveal that the HOMO-LUMO single electron transition expands the bore of E-type PNR while narrows that of B-type one. This itad hoc treatment, however, causes an overestimation, because the electronic states both near the HOMO and LUMO are itpseudo-degenerated. An inclusion of other configurations due to the single electron excitation (CIS) relaxes the above geometrical changes predicted by the UHF HOMO-LUMO single excitation. Thus, the ring molecular geometry in the first optical excitation is rather indistinguishable compared with that in the ground state.

**C1 123 Free energy versus potential energy landscapes of drug-like molecules*** YONAS ABRAHAM, *Wake Forest University* REBECCA HARRIS, PHILIP S. HAMMOND, JEFFREY D. SCHMITT, *Targacept Inc* To gain information about molecular shape tendencies, the life science community has traditionally focused primarily on conformational search methodologies that explore the Potential Energy Surface (PES). The output of these methods is a collation of so-called minimum energy conformers. In our effort to gain more insight into molecular shape and overall behavior, we have used both PES conformational search techniques and *ab initio* molecular dynamics to study a set of neuronal nicotinic receptor (NNR) ligands that possess a non-trivial structure-affinity relationship. This latter method, properly executed, provides the free energy landscape. In this poster we show the sometimes dramatic difference in predicted behavior between these two methods. Significantly, conformers predicted to be

highly populated in one method are disallowed in the other method. This work constitutes our first exploration into the use of an *ab initio* derived free energy landscape to better understand small molecules of biological interest.

*ATP Project, Grant 70NANB3H3065

**C1 124 Surface Charge Method Calculation of Biomolecular Electrostatic Force with Application to a Model System*** TIMOTHY DOERR, YI-KUO YU, *National Center for Biotechnology Information, NLM, NIH* Due to the presence of ions, a high dielectric constant solvent (water with $\varepsilon = 80$), and significant charges and polarizabilities associated with many biomolecules, electrostatic forces play a crucial role in biomolecular interactions. It is particularly important to adequately account for the effects of the solvent. The surface charge method presented here has been applied to a system of an arbitrary number of charged dielectric spheres embedded in an infinite dielectric medium (the solvent). The surface charge method allows calculation (to any accuracy desired) of the energy and the various forces using only matrix inversion. The energy and forces are relatively insensitive to the value chosen for the dielectric constant inside the spheres. For the special case of two isolated charged dielectric spheres in an infinite medium, the results are not obvious: The repulsive force for like-charged spheres is strengthened (compared to point charges in the solvent medium) at short distances, while the attractive force for oppositely-charged spheres is to a lesser degree weakened at short distances. In the limit that the charges associated with a biomolecule are point-like, the excess repulsion and suppressed attraction found here might play a role in minimizing the effect of energetic traps.

*This work was supported by the Intramural Research Program of the National Library of Medicine at National Institutes of Health/ DHHS.

**C1 125 Gamma Oscillations and Visual Binding** PETER A. ROBINSON, JONG WON KIM, *School of Physics, University of Sydney, Australia. Brain Dynamics Center, Westmead Hospital and University of Sydney, Australia* At the root of visual perception is the mechanism the brain uses to analyze features in a scene and bind related ones together. Experiments show this process is linked to oscillations of brain activity in the 30-100 Hz gamma band. Oscillations at different sites have correlation functions (CFs) that often peak at zero lag, implying simultaneous firing, even when conduction delays are large. CFs are strongest between cells stimulated by related features. Gamma oscillations are studied here by modeling mm-scale patchy interconnections in the visual cortex. Resulting predictions for gamma responses to stimuli account for numerous experimental findings, including why oscillations and zero-lag synchrony are associated, observed connections with feature preferences, the shape of the zero-lag peak, and variations of CFs with attention. Gamma waves are found to obey the Schroedinger equation, opening the possibility of cortical analogs of quantum phenomena. Gamma instabilities are tied to observations of gamma activity linked to seizures and hallucinations.

**C1 126 Experimental Study of the Dynamics of Foraging Ants** J. I. WALKER,*R. P. FETZNER, G. W. BAXTER, *Penn State Erie, The Behrend College* We study the search paths of foraging ants in order to describe their behavior mathematically. Ants have become popular as simple agents in models of artificial life. Here, the ant is presented the problem of finding food when no food cues are present. In this experiment, individual ants (Formicinae lasius flavus) are allowed to forage on a two-dimensional textured surface in the absence of a food source. The position of the ant as a function of time is determined with a high resolution digital camera. The scaling properties of the resulting foraging paths compare favorably with those of certain types of random walk.

*Supported by a Penn State Behrend Undergraduate Summer Research Grant

**C1 127 Coarse-grained dynamics of alignment in animal group models** SUNG JOON MOON, SIMON LEVIN, YANNIS KEVREKIDIS, Coordinated motion in animal groups, such as bird flocks and fish schools, and their models gives rise to remarkable coherent structures. Using equation-free computational tools we explore the coarse-grained dynamics of a model for the orientational movement decision in animal groups, consisting of a small number of informed ''leaders'' and a large number of uninformed, nonidentical ''followers.'' The direction in which each group member is headed is characterized by a phase angle of a limit-cycle oscillator, whose dynamics are nonlinearly coupled with those of all the other group members. We identify a small number of proper coarse-grained variables (using uncertainty quantification methods) that describe the collective dynamics, and perform coarse projective integration and equation-free bifurcation analysis of the coarse-grained model behavior in these variables.

**C1 128 Assigning p-values to complex biological systems** NATALIE ARKUS, MICHAEL BRENNER, *Harvard University* Models of complex biological systems with many free parameters do not describe a unique data set, nor is a data set uniquely described by one of them. Their conclusions may therefore not reveal an underlying biological phenomenon, but rather be model or parameter specific. We propose a method of assigning p-values to these models and their conclusions. As an example, we consider feedback and open loop models of the e. coli heat shock response system. We determine to what degree properties associated with the feedback loops are a result of the loops themselves or of the model and its specific parameter regime.

**C1 129 Applications of non-equilibrium thermodynamics to signaling and metabolic pathways** DAWEI HU, ENSHENG LIU, JIAN-MIN YUAN, *Drexel University* Signaling transduction pathways play important roles in regulating cell functions, such as growth, differentiation, and apoptosis. Metabolic pathways, on the other hand, generate many metabolites utilized by human body. Abnormal regulations of the enzymes and metabolites associated with these pathways may be related to diseases. In view of their importance, we are interested in applying non-equilibrium thermodynamics to investigate the properties and dynamic behaviors of these two types of pathways. The systems of concentration are the MAPK, coupled MAPK-PI3K, and insulin metabolic pathways. In the case of signaling pathways we study the properties of thermodynamic variables, such as the affinities and fluxes of individual reaction steps, as affected by the perturbations of rate constants, protein-protein interactions, and cross talks. In the case of metabolic pathways, we study the system dynamics, the stability of steady states, and the flux-affinity relations as functions of constant inputs and outputs as well as the parameters of feedback loops. Our goals are to shed light on the design principles of the biological pathways and to rank the most vulnerable nodes of these pathways.

**C1 130 Discovering Fuzzy Motifs in Yeast Genome through a generalized REDUCE algorithm** XING ZHENG, CAIYI LANG, WEIQUN PENG, CHEN ZENG, *George Washington University* Chromatin immunoprecipitation followed by cDNA microarray hybridization (ChIP-on-Chip) has become a popular procedure for studying genome-wide protein-DNA interactions and transcription regulation. We present here a fuzzy REDUCE computational method on the genes subgroup significantly associated with each of 203 DNA-binding transcriptional regulators, based on the model in which upstream motifs contribute additively to the logRatio of chip fluorescent intensities between the enriched sample and the control sample. Statistically significant motifs are deduced from the analysis of publicly available ChIP data for Saccharomyces cerevisiae and compared to the motifs obtained using other approaches. Interactions and formations of multi-transcription activation complex are discussed.

**C1 131 Recovery of Elasticity of Aged Human Epithelial Cells itIn-Vitro** IGOR SOKOLOV, SWAMINATHAN IYER, *Dept. of Physics, Clarkson University* CRAIG WOODWORTH, *Dept. of Biology, Clarkson University* We recently found a considerable increase in rigidity of human epithelial cells during ageing itin-vitro. This is important because the loss in elasticity of epithelial tissues with ageing contributes to many human diseases. We also found that cultured cells had three distinct regions of rigidity, and that the increase in rigidity correlated with an increase in density of cytoskeletal fibres. However, it was not clear which type of fibre was important. Atomic Force Microscopy (AFM) and imunofluorescence microscopy were used in this study to characterize aging human epithelial cells in vitro, both before and after treatment with cytochalasin B. We found that the fibres associated with increased rigidity were mostly F-actin microfilaments. Furthermore, using cytochalasin B, a chemical that inhibits polymerization of F-actin, we restored the rigidity of old cells to the young level in all three areas of rigidity simultaneously. In conclusion, these results clarify how the cell mechanics changes during aging itin vitro, and they may be relevant for treatment of age-related loss of elasticity in epithelial tissues. The trials of this new treatment are in progress.

**C1 132 The Effect of Polybutadiene Polymer on Cell Aging In Vitro.*** YING LIU, LOURDES COLLAZO, MIRIAM RAFAILOVICH, JONATHAN SOKOLOV, *Dept. Mat. Sci. & Eng., SUNY Stony Brook, NY 11794* Cell experimentation often undergoes several weeks of culturing. The most common problem that scientists face is the variability of cell behavior due to subculturing. Most cells have a limited lifespan in vitro, changing their cell characteristic after just a few passages. Here we focus on the changes in cell function with passage. We used human CRF31 dermal fibroblasts initially cultured from lower passages (P11) to higher passages (P20) at a density of 5000/cm2. We first generated a series of cell growth curves for the different passages. We observed that as cell passage number increased, cell proliferation decreased significantly. Western Blot analysis indicated that the composition of the extracellular matrix proteins changed with increasing passage. The effect of these changes on migration and actin production will be presented.

*Supported by NSF-MRSEC program

**C1 133 Regulation of an Actin Spring** BARNEY TAM, *Dept. of Physics, MIT* JENNIFER SHIN, *Dept. of Mechanical Engineering, KAIST* RICARDO BRAU, *Div. Biol. Eng., MIT* MATTHEW LANG, *Div. Biol. Eng. & Dept. of Mech. Eng., MIT* L. MAHADEVAN, *DEAS & Dept. of Systems Biol., Harvard* PAUL MATSUDAIRA, *Whitehead Institute, Dept. of Biol., & Div. of Biol. Eng., MIT* To produce motion, cells rely on the conversion of potential energy into mechanical work. One such example is the dramatic process involving the acrosome reaction of itLimulus sperm, whereby a 60 $\mu$m-long bundle of actin filaments straightens from a coiled conformation to extend out of the cell in five seconds. This cellular engine and the motion it produces represent a third type of actin-based motility fundamentally different from polymerization or myosin-driven processes. The motive force for this extension originates from stored elastic energy in the overtwisted, pre-formed coil—much like a compressed mechanical spring. When the actin bundle untwists, this energy is converted to mechanical work powering the extension. We report on experiments probing the regulation of this actin spring by extracellular calcium. We find that extracellular calcium needs to be present for the spring to activate, and that calcium regulates the velocity of the extension.

**C1 134 Radiation Hazard from Galactic Cosmic Rays** ASHRAF FARAHAT, *Department of Physics and Technology, Edinboro University of Pennsylvania* Space radiation is a major hazard to astronauts in long-duration human space explosion. Astronauts are exposed to an enormous amount of radiation during their missions away from the Earth in outer space. Deep space is a rich environment of protons, gamma rays and cosmic rays. A healthy 40 years old man staying on Earth away from large doses of radiation stands a 20% chance of dying from cancer. If the same person travels into a 3- year Mars mission, the added risk should increase by 19%. This indicates that there is 39% chance of having cancer after he comes back to Earth. Female astronaut chances to get cancer is even almost double the above percentage. The greatest threat to astronauts en route to the red planet is galactic cosmic rays (GCR). GCRs penetrate through the skin of spaceships and people like tiny firearm bullets, breaking the strands of DNA molecules, damaging genes, and killing cells. Understanding the nature of the GCRs, their effect on biological cells, and their interactions with different shielding materials is the key point to shield against them in long space missions. In this paper we will present a model to evaluate the biological effects of GCRs and suggestion different ways to shield against them.

**C1 135 A Comparative Study of Different Monte Carlo Modeling Techniques for Proton Dose in Biological Materials*** DAN FRY, WILFRED SEWCHAND, JOHN O'CONNELL, *Walter Reed Army Medical Center, Radiation Oncology, Washington, DC 20307* We have performed a comparison of the Monte Carlo simulation tools SRIM, PTRAN, and GEANT 4.7.0. The comparative parameters were chosen according to the degree of flexibility, ability to handle complex simulation geometries and physical processes modeled. Proton depth-doses in water have been compared with experimental measurements at 72 MeV, 110 MeV 158.5 MeV and 250 MeV. At the lowest incident proton energy all tools are in agreement with measurement. With increasing energy, SRIM underestimates the entrance and plateau dose. PTRAN and GEANT consistently predict the measured depth-dose over all energies simulated. Comparison was also done by simulating the depth-dose distribution in aluminum, tissue equiva-

lent plastic (A-150) and graphite. The entrance ($D_0$) and peak doses ($D_m$), and the FWHM $\sigma_{50}$ were simulated with both SRIM and GEANT at incident proton energies of 70 MeV, 100 MeV, 150 MeV, 200 MeV and 250 MeV. Comparison was made with the extended PTRAN-X code results of Palmans *et al.* (Phys. Med. Biol., 42, 1175, 1997). Neither SRIM nor GEANT are in agreement with PTRAN-X. Differences range from a few to over 100%.

*This work was supported by the US Army Medical Research and Materiel Command under Contract Agreement No. DAMD 17-W81XWH-04-2-0022. Opinions and conclusions are those of the authors.

**C1 136 Mössbauer Spectroscopy on Compounds of Biomedical Interests** F. OLIVER, *Morgan State University* N. EWING, E. HOFFMAN, A. KINYUA, F. OLADEINDE, A. MURDOCK, *Morgan State University* MORGAN STATE UNIVERSITY COLLABORATION, MORGAN STATE UNIVERSITY TEAM, MORGAN STATE UNIVERSITY TEAM, MORGAN STATE UNIVERSITY TEAM, MORGAN STATE UNIVERSITY TEAM, Mössbauer spectroscopy (nuclear gamma resonance spectroscopy)[1] has been used in our laboratory for many biomedical applications. This presentation will demonstrate uses of Mössbauer spectroscopy to obtain qualitative and quantitative information about the electronic and magnetic properties of various systems. Information is obtained related to the electronic spin, electric quadrupole interaction, and magnetic hyperfine interactions. This technique has a very broad spectrum of applications, most of them in solid state physics and chemistry. Experiments may be done using transmission or backscattering geometry. For the past fifteen years we have successfully applied this technique to investigate materials of biomedical interest. Materials investigated include porphyrins containing europium[2], plants, over the counter medicines, hemoglobin, and ion implanted implant materials. Results of these experiments and other possible applications will be reported. 1. Leopold May, An Introduction to Mössbauer Spectroscopy, Plenum Press Z(1971). 2. Oliver, et al., Inorganica Chimica Acta, Vol. 186, 119 (1991). * Partially supported by NIH, ** Partially supported by NSF-SEM program.

**C1 137 Chlorophyll-a self-assembly: A low temperature STM investigation** VIOLETA IANCU, SAW-WAI HLA, *Quantitative Biology Institute, and Department of Physics and Astronomy, Ohio University, Athens, Ohio, 45701, USA* We investigate self-assembly of chlorophyll-a molecules on a Au(111) surface by using a low temperature scanning tunneling microscope (LT-STM) at 4.6 K. Chlorophyll-a is a vital resource for the sustenance of life on Earth and responsible for the green color in plant leaves. Chlorophyll-a forms hexagonal close-packed structures that grow epitaxially on Au(111). The STM images show the detailed structure of the self-assembled molecular (SAM) layer where the molecules are positioned in pairs with the heads facing each other. Within a single row along the long-molecular axis direction, the molecules are assembled in an alternating head-tail-tail-head arrangement. The tunneling spectroscopy of single chlorophyll-a molecules inside this SAM layer reveals that their lowest unoccupied molecular orbital (LUMO) is located at 2.8eV above the Au(111) Fermi level. This investigation provides detailed structural and electronic properties of self-assembled chlorophyll-a and may be useful for the development of bio-molecular electronic devices. This work is supported by a US-DOE grant, DE-FG02-02ER46012 and Ohio University Nanobio Technology Initiative program BNNT

**C1 138 A statistical model for bacterial speciation triggered by lateral gene transfer** SUNJEET SIDHU, WEQUIN PENG, *Physics Department at The George Washington University* The process of bacterial speciation has been a major unresolved issue in the study of bacterial evolution. It has been proposed that lateral gene transfer and homologous recombination play critical and complementary roles in speciation.[1] We introduce a statistical model, of a population, for the evolution under lateral gene transfer and local homologous recombination. We examine the evolutionary dynamics and its dependence on various evolutionary operators.

[1]J. G. Lawrence, Theor. Popul. Biol. **61**, 449(2002).

**C1 139 Three Laws in Darwinian Evolutionary Theory** PING AO, *University of Washington* Recent works to formulate laws in Darwinian evolutionary dynamics will be discussed. Specifically, three laws which form a consistent mathematical framework for the evolutionary dynamics in biology will be spelt out. The second law is most quantitative and is explicitly expressed in the unique form of a stochastic differential equation. Salient features of Darwinian evolutionary dynamics are captured by this law: the probabilistic nature of evolution, ascendancy, and the adaptive landscape. Four dynamical elements are introduced in this formulation: the ascendant matrix, the transverse matrix, the Wright evolutionary potential, and the stochastic drive. The first law may be regarded as a special case of the second law. It gives the reference point to discuss the evolutionary dynamics. The third law describes the relationship between the focused level of description to its lower and higher ones, and defines the dichotomy of deterministic and stochastic drives. It is an acknowledgement of the hierarchical structure in biology. A new interpretation of Fisher's fundamental theorem of natural selection is provided in terms of the F-Theorem. Ref. P. Ao, Physics of Life Reviews 2 (2005) 117-156.

**C1 140 Impact of Stability on Random and Small-World Brain Networks*** RICHARD GRAY, PETER ROBINSON, CANDY FUNG, *School of Physics, University of Sydney* The dynamics and stability of networks of brain components are studied to determine the role stability plays in constraining the network structure of the brain. The linear stability of a brain network is determined from a physiologically based continuum model of the brain's electrical activity. If instabilities correspond to neurological disorders such as seizures, stability is an important constraint on network structure and, hence, brain physiology and anatomy. Results for random brain networks and small-world networks are presented, showing that stability sharply constrains random network structure to satisfy $npg < 1$, where $n$ is the number of components, $p$ the probability of connection, and $g$ the connection gain. In contrast, small-world networks have a stability boundary independent of $n$ with a connectivity similar to experimentally determined cortical networks. Implications of these results to brain structure and its evolution are made, along with comparisons with cortical connection networks.

*School of Physics, The University of Sydney, Australia; Brain Dynamics Center, Westmead Millennium Institute, Westmead, Australia.

**C1 141 Large-scale simulation of the primary visual cortex*** JIM WIELAARD, PAUL SAJDA, *Columbia University, New York* We have developed a large-scale computational model of a 4x4 $mm^2$ patch of a primary visual cortex (V1) input layer. The model is constructed from basic established anatomical and physi-

ological data. Based on numerical simulations with this model we are able to suggest neural mechanisms for a wide variety of classical response properties of V1, as well as for a number of extra-classical receptive field phenomena. The nature of our model is such that we are able to address stationary as well as dynamical behaviour of V1, both on the single cell level and on a population level of up to about $10^5$ cells.

*This work was supported by grants from ONR (MURI program, N00014-01-1-0625) and NGA (HM1582-05-C-0008).

**C1 142 Comparative Genomic Study of Plant Putative Glutamate Receptors** YOSHIHISA ISHIZUKA, *The George Washington University, Department of Physics* MIMMIE HUANG, *The George Washington University, Department of Computer Science* SHERI CHURCH, *The George Washington University, Department of Biological Sciences* FRANK TURANO, *The George Washington University, Department of Biological Sciences* WEIQUN PENG, *The George Washington University, Department of Physics* Glutamate receptors are ion channels that were first discovered in vertebrates and found to play a vital role in the mediation of signal transmission in the central nervous system. Recently, sequence homologs of these receptors were found in Arabidopsis, which was a surprise, as plants do not have a true nervous system. These putative glutamate receptors (GLRs) have been shown to play a critical physiological role in the regulation of carbon and nitrogen metabolism in Arabidopsis. However, their functions at the molecular and biochemical levels are not known. The newly completed genome of a second plant, rice, presents an opportunity to investigate the functions of the GLRs via a comparative genomic approach. Using phylogenetic and bioinformatics analysis, we identify the important residues, functional specificity, and potentially interacting sites and domains.

**C1 143 Modeling phototaxis in complex networks** OLGA KUKSENOK, ANNA C. BALAZS, *University of Pittsburgh* Phototaxis is the movement of organisms towards or away from light. It is one of the most important photo-biological processes, which in turn are responsible for light reception and the use of photons as a source of information. We briefly review current models of phototaxis of biological organisms and we develop a simple, minimal model for synthetic microscale units that can undergo phototactic motion. We then use this model to simulate the collective motion of such photosensitive artificial objects within a complex network, which is illuminated in a non-uniform manner by an external light.

**C1 144 Energy Flow Analysis of Photoactive Yellow Protein** TAKAKAZU ISHIKURA, KAZUTOMO KAWAGUCHI, HIROSHI WATANABE, *Nagoya Univ* TAKAHISA YAMATO, *Nagoya Univ / CREST, JST* The signal transduction of photosensory receptors is intimately related to the energy relaxation associated with the relevant functional motion. To understand this energy conversion process, it is useful to analyse the energy flux vector field in a polypeptide chain matrix. Recently, we developed a new formalism for energy flux, $J_{AB}$, between two different sites A and B in a protein. Flexibility is one of the attractive points of this method, namely, sites A/B can be consisted of an atom or any groups of atoms. In addition, huge computation resource is not required for this method. Since this method is based on the linear response theory, the energy flux, $J_{AB}$, can be obtained from a classical molecular dynamics simulation trajectory. We can define energy conductivity between the sites A and B in terms of the time-correlation function of $J_{AB}$. This quantity corresponds to the transport coefficient of heat and potential energy, representing the strength of the direct energetic coupling between the two sites. We applied this method to a photosensory receptor, photoactive yellow protein (PYP). We calculated the energy conductivity between the chromophore and the surrounding amino acid residues, Tyr42, Glu46, Thr50, Arg52, and Tyr98. As a result, we observed the values of energy conductivity decreased in this order. We will discuss the possibility of finding energy transfer pathway in PYP with this method.

**C1 145 IRMPD Spectroscopic Analysis of Peptides and Oligosaccharides Using FTICR With Mid-Infrared Free-Electron Laser*** KAZUHIKO FUKUI, KATSUTOSHI TAKAHASHI, *National Institute of Advanced Industrial Science and Technology (AIST)* The fragmentation in gas-phase peptides and oligosaccharides has been investigated by using electrospray ionization (ESI) Fourier-Transform Ion Cyclotron Resonance (FTICR) mass spectrometry (MS) with a laser cleavage infrared multiphoton dissociation (IRMPD) technique. In order to cleave the ionized sample introduced in the FTICR cell, an infrared free electron laser (FEL) is used for the technique of IRMPD as a tunable infrared light source. The gas-phase infrared spectra of protonated peptides (Angiotensin II, Substance P) and sodiated ologosaccharide (Sialyl Lewis X) are obtained in the range from 5.7 $\mu$m to 9.5 $\mu$m. The results of the IRMPD spectra of the peptides show that the peaks for the photoproducts are observed as y/b type fragment ions in the IR range from 5.7 $\mu$m to 7.5 $\mu$m, corresponding to the cleavage of backbone in the parent amino acid sequence, while the spectra of the oligosaccharide have the peaks for the B/Y type in the range from 7.1 $\mu$m to 9.3 $\mu$m.

*This work was supported by the New Energy and Industrial Technology Development Organization (NEDO) as a part of the Research and Development Projects of Industrial Science and Technology Frontier Program in Japan.

**C1 146 Divergence of protein structure in solvent from that in X-ray quality crystals: probing the local environment of Chl *a* in the cytochrome $b_6f$ complexes by ultrafast spectroscopy** SERGEI SAVIKHIN, NARANBAATAR DASHDORJ, HANYOUP KIM, JOHN SCHAIBLEY, *Department of Physics, Purdue University* HUAMIN ZHANG, JIUSHENG YAN, EIKI YAMASHITA, WILLIAM CRAMER, *Department of Biological Sciences, Purdue University* The cytochrome $b_6f$ complex in oxygenic photosynthesis mediates electron transfer between the reaction centers of photosystems I and II, and coupled proton translocation across the membrane. High-resolution X-ray crystallographic structures of the $b_6f$ complex show a single chlorophyll $a$(Chl $a$) molecule as an intrinsic component of the complex. Using ultrafast optical spectroscopy, we have shown that the excited state lifetime of the Chl $a$ in dissolved complex is unusually short ( $\sim$ 200 ps) and attributed the observed quenching to the electron transfer exchange with a nearby amino acid. Similar optical time resolved experiments performed on single crystals of the $b_6f$ complex reveal significant changes in the lifetime of the excited state and suggest structural dissimilarities between the complexes within crystals and in solvents. The extent of the structural variations is discussed and modeled using molecular dynamic simulation methods (NSF MCB-0516939, NIH GM-38323).

**C1 147 Raman study of CaDNA films as a function of water content and excess $CaCl_2$ concentration: Stability of the B conformation.** MEGAN SCHWENKER, *University of Toledo* ROBERT MARLOWE, *University of Tennessee at Chattanooga* SCOTT LEE, *University of Toledo* ALLAN RUPPRECHT, *University of Stockholm* Highly oriented, wet-spun films of CaDNA expand in the direction perpendicular to the helical axis as the hydration of the film is increased. CaDNA films with a high $CaCl_2$ content show an unexpected shrinkage at a relative humidity of about 93%. We have performed Raman experiments on CaDNA films as a function of both water content and excess $CaCl_2$ concentration in order to determine if this unexpected shrinkage might be related to a conformational transition of the DNA molecules. We find that the DNA molecules remain in the B conformation for all salt contents down to a relative humidity of 59%.

**C1 148 High pressure mid-infrared study of deoxyadenosine** SCOTT LEE, IAN LAWSON, *University of Toledo* LAUREN LETTRESS, ANTHONY ANDERSON, *University of Waterloo* Crystalline deoxyadenosine has been studied via infrared spectroscopy at room temperatures up to about 10 GPa of pressure. Samples, typically 250 microns in diameter and roughly 25 microns in thickness, were loaded into a piston-cylinder type diamond anvil cell supplied by Diacell Ltd. and fitted with type IIa diamonds. To avoid saturation of strongly absorbing modes, the deoxyadenosine sample was diluted with KBr powder, which also served as an isotropic pressure-transmitting medium. A number of changes in the infrared spectra are noted near 2 GPa, suggesting a phase transition.

**C1 149 Multivariate statistical analysis of Raman spectra to distinguish normal, tumor, lymph nodes and mastitis in mouse mammary tissues** H. DAI, J.S. THAKUR, G.K. SERHATKULU, A.K. PANDYA, G. W. AUNER, R. NAIK, D. C. FREEMAN, *Wayne State University* V.M. NAIK, *University of Michigan-Dearborn* A. CAO, M.D. KLEIN, R. RABAH, *Childrens Hospital of Michigan, Detroit, MI* Raman spectra ( $>$ 680) of normal mammary gland, malignant mammary gland tumors, and lymph node tissues from mice injected with 4T1 tumor cells have been recorded using 785 nm excitation laser. The state of the tissues was confirmed by standard pathological tests. The multivariate statistical analysis methods (principle component analysis and discriminant functional analysis) have been used to categorize the Raman spectra. The statistical algorithms based on the Raman spectral peak heights, clearly separated tissues into six distinct classes, including mastitis, which is clearly separated from normal and tumor. This study suggests that the Raman spectroscopy can possibly perform a real-time analysis of the human mammary tissues for the detection of cancer.

**C1 150 Influence of Temperature and Hydration on Protein dynamics** J.H. ROH, *University of Akron, USA* J.E. CURTIS, *NIST, USA* S. AZZAM, *Kent State University, USA* V.N. NOVIKOV, *Russian Academy of Sciences, Russia* I. PERAL, Z. CHOWDHURI, V. GARCIA-SAKAI, *NIST, USA* R.B. GREGORY, *Kent State University, USA* A.P. SOKOLOV, *University of Akron, USA* Protein dynamics and function are strongly influenced by temperature and hydration. Dynamic transition is believed to be closely related to onset of protein function since protein function activates at dynamic transition temperature, $T_d$. However, understanding of correlation between protein dynamics and function and of microscopic mechanism of the dynamics activated above $T_d$ is sill a subject of discussion. We used neutron and light scattering measurements to study temperature and hydration dependence of protein-lysozyme dynamics in the frequency range from 100 MHz to 1 THz. Our detailed analyses of protein dynamics provide i) two onsets of anharmonicity: methyl group rotation that activates regardless of hydration at 100 K and slow relaxation process that appears only in wet proteins at 200 K, ii) slow relaxation process is the mode that activates dynamic transition and enzymatic activity, and iii) temperature dependence of slow relaxation process exhibits Arrhenius-like behavior at $T > T_d$.

**C1 151 A new Monte Carlo approach for exact calculation of polymer translocation time through a channel** MICHEL G. GAUTHIER, GARY W. SLATER, *Univerity of Ottawa* Molecular Dynamics simulations are useful to study the impact of hydrodynamic interactions on the translocation process, but this technique requires large computer resources (both time and memory) which limit the size of the systems that we can study. We propose a new Monte Carlo algorithm that integrates various effects such entropic forces, external force fields frictional effects, and polymer-channel interactions. Our novel approach allows us to study the polymer as a single Brownian particle diffusing on a one-dimensional lattice in a non-constant force field. The calculation technique we suggest gives us the exact value of the translocation time via the resolution of a simple system of linear equations. This Monte Carlo approach can be used to obtain scaling laws of polymer translocation through a channel much faster than by using fluctuating-bond simulation models.

**C1 152 Kinetics of Protein Adsorption at liquid/solid interfaces** MARKUS BELLION, LUDGER SANTEN, *FR 7.1 Theoretische Physik, Universität des Saarlandes, 66041 Saarbrücken* ARMIN NAGEL, HUBERT MANTZ, ANTHONY QUINN, KARIN JACOBS, *FR 7.2 Experimentalphysik, Universität des Saarlandes, 66041 Saarbrücken* Protein adsorption processes are of crucial importance in many biomedical processes. From a physical point of view these processes raise a number of challenging questions, e.g.: How does the surface influence the conformation of proteins at the surface? What are the characteristics of the protein film at the liquid/solid interface? In this work we investigate the adsorption kinetics of salivary proteins on different kinds of surfaces in a liquid environment. The adsorbed protein layers are analyzed by means of ellipsometry, plasmon resonance, and SPM. It turns out that the adsorbed amount of proteins is sensitive to the long ranged interactions of the solid surface. The experimental data are compared to extensive Monte Carlo simulation of a colloidal protein model. The Monte Carlo results strongly suggest that induced conformal changes lead to the experimentally observed three step kinetics of amylase.

## C1 153 CHEMICAL PHYSICS POSTER SESSION

**C1 154 Thermally activated escape rate for a Brownian particle in a tilted periodic potential for all values of the dissipation: classical and quantum regimes** WILLIAM COFFEY, *Dept. of Electronic and Electrical Engr., Trinity College* YURI

KALMYKOV, *MEPS, Université de Perpignan, France* SERGEY TITOV, *Inst. of Radio Engr. and Electronics of the Russian Academy of Sciences, Russia* B. MULLIGAN, *Dept. of Electronic and Electrical Engr., Trinity College* The translational Brownian motion of a particle in a tilted periodic potential is considered. The classical and semiclassical escape rates of a particle out of the well are estimated both numerically and analytically. In order to accomplish this, the continued-fraction method of solving classical Fokker–Planck equations is adapted to treat quantum master equations of the Caldeira–Leggett type using the phase-space (Wigner) representation of the quantum density matrix as suggested by Garcia-Palacios [J. Phys. A: Math. Gen. **37,** 10735 (2004)]. The numerical escape rates are compared with those obtained in the context of the Kramers theory of the escape rate of a Brownian particle from a potential well as extended by Mel'nikov [Physica A **130**, 606 (1985); Phys. Rep. **209**, 1 (1991).] and Rips and Pollak [Phys. Rev. A **41**, 5366 (1990)] for all values of the dissipation including the very low damping, very high damping, and turnover regimes. It is shown that in the low temperature limit, the universal expressions for the escape rate provide a good estimate of escape rates both in classical and quantum regimes.

**C1 155 Nonequilibrium phase transition of a model of diffusion, aggregation and fragmentation on complex networks** YUP KIM, SUNGMIN LEE, SUNGCHUL KWON, *Department of Physics, Kyung Hee University* We investigate condensation phase transitions of symmetric conserved-mass aggregation (SCA) model on random networks (RNs) and scale-free networks (SFNs) of degree distribution $P(k) \sim k^{-\gamma}$. In SCA model, masses diffuse with unite rate, and unit mass chips off from mass with rate $\omega$. The dynamics conserves total mass density $\rho$. In the steady state, on RNs and SFNs of $\gamma > 3$ for $\omega \neq \infty$, we numerically show that SCA model undergoes the same type condensation transitions as those in regular lattice. However the critical line $\rho_c(\omega)$ depends on network structures. On SFNs of $\gamma \leqslant 3$, the fluid phase of exponential mass distribution completely disappears and no phase transitions occurs. Instead, the condensation with exponentially decaying background mass distribution always takes place for any non- zero density. For the existence of the condensed phase for $\gamma \leqslant 3$ at the zero density limit, we investigate one lamb-lion problem on RNs and SFNs. We numerically show that a lamb survives indefinitely with finite survival probability on RNs and SFNs of $\gamma > 3$, and dies out exponentially on SFNs of $\gamma \leqslant 3$. The finite life time of a lamb on SFNs of $\gamma \leqslant 3$ ensures the existence of the condensation at the zero density limit on SFNs of $\gamma \leqslant 3$. At $\omega = \infty$, we numerically confirm that complete condensation takes place for any $\rho > 0$ on RNs.

**C1 156 Adsorption on an Equilateral Triangular Terrace Three Atomic Sites in Width: Application to Chemisorption of CO on Pt(112).*** ALAIN PHARES, *Villanova University* DAVID GRUMBINE, JR., *St. Vincent College* FRANCIS WUNDERLICH, *Villanova University* The study of monomer adsorption on equilateral triangular terraces three atomic sites in width is presented. Adsorbate-substrate interactions at the terrace edges differ from those at bulk sites. Adsorbate-adsorbate interactions up to second neighbors are included. Phase diagrams for all possible interactions whether attractive or repulsive are obtained at low temperature. The effect of increasing temperature is also investigated. Results of the model are applied to chemisorption of CO on Pt(112).

*This research is supported in part by grant number PHY910014P from the Pittsburgh Supercomputing Center, supported by several federal agencies, the Commonwealth of Pennsylvania and private industry.

**C1 157 Single Walled Carbon Nanotubes as Macroscopic Surfactant Molecules** ERIK K. HOBBIE, BARRY J. BAUER, *NIST* Single-walled carbon nanotubes (SWNTs) are made hydrophyllic through coating and wrapping with short segments of single-stranded DNA (ssDNA) containing alternating guanine (G) and thymine (T) units. Small-angle neutron scattering (SANS) measurements on dilute to semi-dilute aqueous suspensions of these colloidal SWNTs raise interesting questions about the degree of nanotube dispersion, with power-law exponents suggestive of weak attractive interactions. The SWNT-ssDNA complexes also act as nanoparticle surfactant, stabilizing the interface between water and toluene, for example. We exploit this to make hydrophillic cross-linked polymer particles coated and stabilized by the ssDNA-SWNT complex. Near-infrared fluorescence microscopy demonstrates the band-gap fluorescence of these SWNT-coated particles, suggesting potential routes to novel platforms and applications. Light scattering and optical microscopy from index-matched suspensions of the SWNT-coated colloids are compared with similar measurements on colloids made with conventional surfactants.

**C1 158 Rotational Energy Exchange in Molecule-Surface Collisions*** HAILEMARIAM AMBAYE, JOSEPH MANSON, *Clemson University* A theoretical approach that combines classical mechanics for treating translational and rotational degrees of freedom and quantum mechanics for describing the excitation of internal molecular modes is applied to the scattering of diatomic molecules from metal surfaces. Calculations are carried out for determining the extent of energy transfer to the rotational degrees of freedom of the projectile molecule. For the case of observed spectra of intensity versus final rotational energy, quantitative agreement with available experimental data for the scattering of NO and $N_2$ from close packed metal surfaces is obtained. It is shown that such measurements can be used to determine the average rotational energy of the incident molecular beam. Measurements of the exchange of energy between translational and rotational degrees of freedom upon collision are also well described by calculations for these same systems.

*Work supported by the NSF and DOE

**C1 159 Understandings of Formation of N-Ntrosoamine in Smoke.*** YI-LEI ZHAO,[†] CARLOS GONZALEZ,[‡] *NIST* MANUEL MARQUEZ,[§] *PMUSA Research Center, 4201 Commerce Rd., Richmond, VA 23234* INEST TEAM,[‖] CTCN TEAM, Formation of N-nitrosoamine compounds is highly concerned in combustion and past-combustion. In chemical laboratory, nitrosylation of amine toward N-nitrosoamine generally requires nitrosonium donor and acidic condition. Recently, an unexpected reaction was observed to be relevant to nitrogen dioxide, a common component of past-combustion gas; an alternative non-ionic pathway must lead to the rapid nitrosylation. Here, we proposed a radical mechanism, by which amino-radical is formed by H-abstraction of nitrogen dioxide, followed by radical scavenging with nitric oxide.

Relatively low activation energy of 10-11 kcal/mol (ca., CBS-QB3) of the radical mechanism rationalized the feasibility of N-nitrosoamine formation in colloids after combustion of biomaterials. Acid-catalyzed nitrosylation in aqueous solution was also computed.

*INEST program - PMUSA
†INEST fellow
‡NIST Center for Theoretical and Computational Nanosciences
§INEST group
‖INEST = Interdisciplinary Network of Emerging Science and Technology



**C1 160 Classical nucleation theory based method for computing the crystal-melt interfacial free energy** XIAN-MING BAI, MO LI, *School of Materials Science and Engineering, Georgia Institute of Technology* The crystal-melt interfacial free energy is a fundamental thermodynamic parameter governing phase transformations. It is very weak and extremely difficult to obtain experimentally. Here we present a simple approach, which is based on classical nucleation theory, for calculating the solid-liquid interfacial free energy. Using molecular-dynamics simulations, we construct spherical crystal nuclei embedded in the supercooled liquids to create an ideal model of homogeneous nucleation. The interfacial free energy is extracted by fitting the relation between the critical nucleus size and the reciprocal of the critical undercooling temperature. The orientationally averaged interfacial free energy is found to be 0.301 with errors of 0.002 (in standard LJ unit). The temperature dependence of interfacial free energy is also obtained in this work. We find that the interfacial free energy increases slightly with increasing temperature. The positive temperature coefficient of interfacial free energy is in good agreement with Spaepen's analysis [Solid State Phys. **47**, FS181, (1994)] and Turnbull's empirical estimation [J. Appl. Phys. **21**, 1022 (1950)].

**C1 161 Polarization Model for the Hydration Forces.** OSCAR CALVO, MARIAN MANCIU, *Physics Department, University of Texas at El Paso* ELI RUCKENSTEIN, *Chemical and Biological Engineering, State University of New York at Buffalo* The interactions between hydrophilic surfaces in water cannot be always explained on the basis of the traditional DLVO theory, and an additional repulsion, the ''hydration force'' is sometimes required to accommodate the experimental data. While this force is in general associated with the organization of water in the vicinity of the surface, different models for the hydration were typically required to explain different experiments. We will show that the polarization model for the double layer/ hydration, which account for the correlations between neighboring dipoles, is consistent with a number of experiments, such as (i) the repulsion almost independent of the electrolyte concentration between neutral lipid bilayers, with a short decay length ( $\sim$ 2Å), (ii) the repulsion between weakly charged mica surfaces, with a longer decay length ( $\sim$ 10 Å), exhibiting not only a dependence on the ionic strength, but also strong ion specific effects. (iii) the repulsion between silica surfaces. It is shown that, for a particular structuring of water in the vicinity of a flat surface (in ice-like layers)., the polarization model leads to an oscillatory behavior of the polarization and a non-local dependence on the local electric field, as suggested by Molecular Dynamics simulations.

**C1 162 A particle-based simulation technique for fluid flow: applications to binary mixtures, microemulsions and colloids** ERKAN TUZEL, *School of Physics and Astronomy, University of Minnesota* THOMAS IHLE, GUOAI PAN, DANIEL KROLL, *Department of Physics, North Dakota State University* Particle-based simulation techniques provide an attractive alternative to traditional methods for the coarse-grained modeling of a fluctuating solvent. A particularly appealing algorithm was introduced by Malevanets and Kapral[1]. The algorithm has been successfully applied to study the behavior of polymer solutions, colloids and vesicles in shear flow. We present generalizations of this algorithm to fluids with non-ideal equations of state and binary mixtures with a miscibility gap[2]. We show the thermodynamic consistency of the model by measuring the pressure and density fluctuations and compare with analytical results. Results for the demixing of a binary mixture are presented such as the phase diagram and measurements of interface fluctuations and the surface tension of a droplet as well as the coarsening of domains during spinodal decomposition. Preliminary results for the lowering of the surface tension in microemulsions and the onset of emulsification are presented. Furthermore, colloids are included in the solvent and results for colloidal suspensions driven by external forces will be shown. [1] A. Malevanets, R. Kapral, J. Chem. Phys. 110, 8605 (1999). [2] T. Ihle, E. Tuzel, D. M. Kroll, cond-mat/0509631.

**C1 163 Thermodynamic Investigation of Ar, $CH_4$, and $D_2O$ Adsorption on ZnO surfaces** SAMI CHANAA, M. FARINELLI, A. FREITAG, M. ROSS, *University of Tennessee* JOHN Z. LARESE, *Oak Ridge National Laboratory, University of Tennessee* ZnO nanoparticles of different shape and exposed crystal face have raised considerable interest in the recent past, because their potential use for electronic and photonic devices, etc. Understanding the relationship between the macroscopic particle shape and the surface morphology, structure and polarity will play a crucial role in developing technologically useful devices. Using a recently developed synthetic method we have been able to produce large quantities of high quality pure and doped ZnO nanomaterial with shapes including plates, nanowires and tetrapods as observed by TEM. High resolution adsorption is otherms were used to investigate the interaction of the nanoparticle surfaces with different probe molecules. The shape of the resulting adsorption isotherms varies as the distribution of nanoparticle shapes and surfaces used as substrate is changed. Results of thermodynamic investigation of argon and methane adsorption below the respective triple points show the formation of 3 distinct adsobate layers before the onset of bulk adsorbate formation. $D_2O$ isotherms show weak evidence of different mono and multi layer capacities depending on previous exposure of the nanoparticle surface to UV radiation.

**C1 164 The non-dominance of counterions in the spherical electrical double layer: an integral equation and simulational study** ENRIQUE GONZÁLEZ-TOVAR, IVÁN GUERRERO-GARCíA, MARTíN CHÁVEZ-PÁEZ, *Instituto de Física, Universidad Autónoma de San Luis Potosí, México.* The ionic cloud around a charged colloid (or electrode) immersed in an electrolyte is known as the electrical double layer (EDL). An important amount of theoretical and simulational work in this topic has been done in the frame of the restricted primitive model (RPM) of an electrolyte, in which the ionic size correlations are taken into account considering equal-sized ions. Ionic size asymmetry, on the other hand, has been explored to much less extent. One possible explanation to this can be found in the common belief that coun-

terions dominate the EDL, i.e., that away from the zero-charge point the properties of the EDL are essentially equal for size-symmetric and size-asymmetric electrolytes if the counterions are the same in both cases. Recent developments, however, clearly show that size asymmetry can induce dramatic effects on the structure and properties of EDLs. In the present work we report Monte Carlo simulations and theroretical results that exhibit that the counterions not always rule the properties of the EDL, e.g. the ionic size asymmetry enhances the phenomenon of charge reversal (i.e., the overcompensation of the bare charge of the macroion) and the screening due to the electrolyte. Additionally, we find that the predictions of the HNC/HNC and HNC/MSA integral equations are in good agreement with simulations in a wide range of conditions.

**C1 165 Optical detection of sub-micron and nanoscale particles in liquids** SUBECHHYA PRADHAN, MATTHEW McGRATH, TOBIAS HERTEL, *Vanderbilt University* We discuss a scheme for detection of submicron and nanoscale particles using light scattering in combination with lock-in filtering for increased sensitivity and signal-to-noise ratio. In this experiment, suspended submicron and nanoscale particles flow downstream a microfluidic cell until they enter the detection volume where particles are subjected to forced oscillatory motion perpendicular to the flow direction. Scattered light can then be detected in the forward direction by a position sensitive detector or in backscattering geometry using an interferometric confocal setup. The signal to noise ratio is improved over previous experiments making use of low pass filtering by lock-in amplification. We explore the potential of this technique for nanoparticle detection in liquid environment and present preliminary results on the detection of low and high index spherical particles such as polystyrene beads or colloidal gold as well as of high aspect ratio particles such as carbon nanotubes and tobacco mosaic virus.

**C1 166 Coexistence curve of a near-critical, eight-arm star polystyrene in methylcyclohexane** MARK WELLONS, MARK LIGHTFOOT, D.T. JACOBS, *Physics Department, The College of Wooster, Wooster OH 44691* The coexistence curve of eight-arm star polystyrene in methylcyclohexane has been measured and used to determine the coexistence curve amplitude B. An automated measurement of the minimum deviated angle in each phase provides the refractive index and thus the composition in each phase. By exploring temperatures from a few milliKelvins to two Kelvin below the critical temperature, the shape of the coexistence curve is determined and compared to a simple power law of amplitude B and exponent $\beta$. The exponent should be independent of molecular weight while the amplitude should vary as a power-law in molecular weight. We report the results of one molecular weight (228,000) and compare them to published values for a smaller molecular weight (74,000) and to the results for a linear polystyrene in the same solvent. We acknowledge the support from the donors of the American Chemical Society Petroleum Research Fund.

**C1 167 Investigation of Gas Phase Gold Oxide Cations Towards the Oxidation of CO** NELLY MOORE, GRANT JOHNSON, A. WELFORD CASTLEMAN, JR., *Pennsylvannia State University* Studies are underway in our laboratory aimed at providing information to aid in the design of more efficient and selective catalysts. Gas phase metal oxide cluster studies are becoming a valuable complementary technique to surface methods for elucidating the mechanistic details and active sites of catalytic systems. It is our present goal to uncover possible species responsible for the increased activity and selectivity of gold oxide catalysts utilizing gas phase studies. To gain insight into the bonding properties and structures of gold oxide clusters, collision induced dissociation experiments were undertaken. In addition, reactivity studies of gold oxide clusters with CO provided information into different reaction pathways based on size, stoichiometry, and charge state. Reactions of gold oxide cations with CO were explored and compared to anionic cluster reactions previously conducted in our laboratory. These studies have provided evidence of various reaction mechanisms including oxidation, replacement, and association which will be presented.

**C1 168 Stern-Gerlach molecular beam deflection studies of magnetic sandwich clusters*** MARK KNICKELBEIN, *Argonne National Laboratory* KEN MIYAJIMA, ATSUSHI NAKAJIMA, *Keio University* Stern-Gerlach studies of transition metal-benzene $[M_n(bz)_m]$ and lanthanide-cyclooctatetarene $[Ln_n(COT)_m]$ sandwich clusters and related sandwich compounds have identified several systems that are ferromagnetically ordered. Such ordered organometallic systems are promising candidates as building blocks for spintronic and information storage applications: their quasi-one-dimensional molecular structures introduce the spatial anisotropy required for magnetic bistability. Magnetic moment measurements of representative magnetically ordered $M_n(bz)_m$ (M=Sc and V) and $Ln_n(COT)_m$ (Ln=Eu, Tb, Ho) systems will be presented.

*This work is supported by the US Department of Energy, Office of Basic Energy Sciences, Division of Chemical Sciences, under Contract W-31-109-ENG-38 and by the CREST program of the Japan Science and Technology Agency (JST).

**C1 169 Reactivity of Size-Selected Gas-Phase Transition Metal Sulfide Clusters with CO and $NH_3$*** JAMES LIGHTSTONE, MELISSA PATTERSON, *Stony Brook University* MICHAEL WHITE, *Brookhaven National Lab* Our current focus has been the production of early transition metal sulfide and carbide clusters for reactivity studies in both the gas-phase and deposited on well defined surfaces. The transition metal sulfides are particularly interesting due to their catalytic properties and their ability to form fullerene-like nanostructures that reflect the S-M-S layered structure of the bulk material. Gas-phase $M_xS_y^+$ clusters (M=Mo, Nb, Ta, W) were produced in a cluster deposition apparatus by reactive sputtering via a magnetron cluster source. Mass spectroscopy results show that Mo, Ta, and W preferentially produce clusters of similar stoichiometry (x/y = 2/6, 3/7, 4/6, 5/7, and 6/8) while all the metals are found to form the ''magic'' cluster, $M_4S_6^+$ . Several prominent $M_xS_y^+$ clusters in the mass spectra were size-selected and reacted with CO and $NH_3$ in a hexapole collision cell. In general, CO adsorbs sequentially on exposed metal sites, while the results for $NH_3$ appear to suggest the formation of solvation shells. These results and how they may relate to cluster structure and reactivity will be discussed. In addition, we will discuss current progress towards deposition of these nanomaterials on well-defined substrates.

*This work was supported by the U.S. Department of Energy, Office of Basic Energy Sciences, Division of Chemical Sciences under contract No. DE-AC02–98CH10886

**C1 170 Simulations of vapor water clusters at vapor-liquid equilibrium*** KIM BOLTON, *School of Engineering, University College of Boras, SE-501 90, Boras, Sweden; Physics Department, Goteborg University, SE-412 96, Goteborg, Sweden* PETER AHLSTROM, ERIK JOHANSSON, *School of Engineering, University College of Boras, SE-501 90, Boras, Sweden* ARNE ROSEN, *Physics Department, Goteborg University, SE-412 96, Goteborg, Sweden* Clustering of water molecules is important, for example, in the nucleation of water drops and in the penetration of water into hydrophobic polymers where water trees can be formed. Monte Carlo methods have been used to study the clustering of water under vapour-liquid equilibrium conditions between 300 and 600 K. The number of clusters, as well as the cluster size, increases with increasing temperature. In addition, due to entropic effects, the percentage of clusters that have linear (or open) topologies increases with temperature and dominate over the minimum-energy cyclic topologies at the temperatures studied here.

*Project funded by the Swedish National School in Materials Science

**C1 171 An Atom in a Golden Ring: M@$Au_6$(M = Ti, V, Cr)** KIRAN BOGGAVARAPU, *Virginia Commonwealth University* XI LI, LI-FENG CUI, LAI-SHENG WANG, *Washington State University* The electronic structure and magnetic properties in a series of transition metal doped Au clusters, $MAu_6^-$ (M = Ti, V, Cr), are investigated experimentally using photoelectron spectroscopy (PES) and density functional calculations. PES features due to the impurity atoms and the $Au_6$ host are clearly observed. It is found that all the $MAu_6^-$ and $MAu_6$ clusters possess a planar structure, in which the transition metal atom is located in the center of an $Au_6$ ring and carries large magnetic moments (2, 3, and 4 $\mu_b$ for $MAu_6$, M = Ti, V, and Cr, respectively).

**C1 172 Abstract Withdrawn**

**C1 173 Small Metallized Carbon Clusters.** A. PATRICK, P. WILLIAMS, E. BLAISTEN-BAROJAS, *School of Computational Sciences, George Mason University, Fairfax, Virginia 22030* Studies of carbon clusters with 1-4 Ca atoms metallized with Li and Be were performed within the density functional theory approach (DFT). Structures of the ground state and first 3 or 4 excited states where systematically calculated for $C_mLi_n$ and $C_mBe_n$ with $n$, $m$=1, 2, 3, and 4. Several of these clusters have ground states of high multiplicity, which make them interesting for magnetic applications. Overall, most stable structures are either linear or planar in the ground state for the smaller clusters, whereas larger clusters acquire 3D structures. Charge transfer in these compounds is notorious, showing no indication of covalent bonding. Calculations were done with DFT the gradient corrections and large basis sets, and compared for several excited states with CASSCF calculations.

**C1 174 Size-Evolution of the Structural and Energy Characteristics of Magnesium Clusters*** PAULO H. ACIOLI,[†] JULIUS JELLINEK, *Chemistry Division, Argonne National Laboratory, Argonne, IL 60439* The most fascinating and important from the applied point of view attribute of the cluster phase of matter is the unique and often unexpected variation of properties with the cluster size. The structural forms, electronic properties, nature and strength of bonding, and other physical characteristics all change as the clusters grow. The rate of change in different properties is, however, nonuniform and element/material dependent. The goal of this study is to investigate and characterize qualitatively and quantitatively the size evolution of the structural and energy characteristics of magnesium clusters. These include the transition from a tetrahedral- to pentagonal- to capped trigonal prism-based motif as the energetically most preferred one. The analysis will include also the higher energy isomers of the clusters and will address the issue of the transition to the bulk lattice.

*This work was supported by the Office of Basic Energy Sciences, Division of Chemical Sciences, Geosciences, and Biosciences, U. S. Department of Energy under Contract No. W-31-109-Eng-38.

[†]Present Address: Department of Physics, Northeastern Illinois University, Chicago, IL, 60625

**C1 175 Catalytic water formation on free platinum and palladium clusters** MATS ANDERSSON, ARNE ROSEN, *Göteborg University* A pulsed beam of neutral metal clusters is generated with a laser vaporization source. The cluster beam passes through two reaction cells, in which the clusters make from less than one up to a few collisions with the reactive molecules. The clusters are detected with laser ionization and time-of-flight mass spectrometry. By measuring the abundance of pure clusters and reaction products as a function of reaction cell pressure, the reaction probability in a cluster-molecule collision can be determined. Platinum clusters with more than 6 atoms form stable reaction products with both oxygen and hydrogen. When the clusters first react with oxygen and then with hydrogen we measure a decreasing number of oxygen atoms adsorbed on the clusters as the number of cluster-hydrogen collisions is increased. The interpretation for this is that water molecules form on the clusters and desorb. The efficiency of the reaction is high on all cluster sizes measured (7-30 atoms), with only a weak size dependence. The water formation reaction also proceeds on palladium clusters in the same size range.

**C1 176 Size, charge, and isomer specific vibrational spectroscopy of isolated metal clusters in the far infrared** ANDRE FIELICKE, GERT VON HELDEN, GERARD MEIJER, *Fritz-Haber-Institut der MPG, Berlin, Germany* CHRISTIAN RATSCH, *Dep. of Mathematics, UCLA* We report on the vibrational spectra of neutral and charged metal clusters in the far infrared. These spectra are obtained via far infrared resonance enhanced multiple photon dissociation (FIR-MPD) of the complexes of metal clusters with rare gas atoms. The experiments make use of the Free Electron Laser for Infrared eXperiments (FELIX) in Nieuwegein, The Netherlands, as an intense and widely tunable far-infrared radiation source. The measured FIR-MPD spectra of the complexes represent the infrared absorption spectra of the bare metal clusters. These spectra are unique for each cluster size and are true fingerprints of the cluster's structure. This FIR-MPD technique has been applied to cationic vanadium clusters and cationic and neutral niobium clusters containing 3 to more than 20 atoms. For smaller sized clusters ($n < 15$), theoretical infrared spectra have been calculated using density functional theory and a comparison with the experimental spectra allows for the structure determination.

**C1 177 Multiphoton control of an electrocyclic ring-opening** ELIZABETH CARROLL, *FOCUS Center, Department of Physics, and Department of Chemistry, University of Michigan, Ann*

*Arbor* BRETT PEARSON, *Department of Physics, SUNY Stony Brook, Stony Brook, NY* JAMES WHITE, ANDREI FLOREAN, PHILIP BUCKSBAUM, ROSEANNE SENSION, *FOCUS Center, Department of Physics, and Department of Chemistry, University of Michigan, Ann Arbor, MI* We have investigated optical control over the photoisomerization of 1,3-cyclohexadiene to 1,3,5-cis-hexatriene via multiphoton excitation. Sub-80fs pulses at 800nm were shaped with an acousto-optic modulator. A closed-loop genetic algorithm (GA) searched for optimal excitation pulses while the effectiveness of each pulse was evaluated using differential absorption of a time-delayed, broadband, ultraviolet probe pulse. Reaction products were subsequently identified in an ultraviolet spectrophotometer. The GA identified pulses that increased the formation of hexatriene by a factor of two over the transform-limited pulse. Detailed analysis of the pulses in the GA search set has identified negative quadratic spectral phase and cubic phase as important control parameters. Multiphoton control mechanisms will be discussed.

**C1 178 Ultrafast Proton Transfer Driven by a Femtosecond Strong-Field Laser Pulse** ALEXEI MARKEVITCH, *Temple University, Department of Chemistry* DMITRI ROMANOV, *Temple University,Department of Physics* STANLEY SMITH, *Wayne State University, Department of Chemistry* ROBERT LEVIS, *Temple University, Department of Chemistry* TEMPLE UNIVERSITY COLLABORATION, WAYNE STATE UNIVERSITY COLLABORATION, Kinetic energy distributions of protons ejected from a polyatomic molecule, anthraquinone, subjected to 60 fs, 800 nm laser pulses of intensity between 0.2 and 4.0x10[1]4 W/cm[2], reveal field-driven restructuring of the molecule (intramolecular proton migration) prior to its Coulomb explosion. Model calculations demonstrate that proton migrates into a field-dressed metastable potential energy minimum. Isomerization mediated by strong field is an important novel phenomenon in coupling of polyatomic molecules with intense laser pulses.

**C1 179 Synthesis of anatase $TiO_2$ nanocrystals by low temperature sol-gel method modified with a hydrophobic ionic liquid** YEN-HUI LIU, CHIH-WEI LIN, ARNOLD CHANG-MOU YANG, *Department of Materials Science and Engineering, National Tsing Hua University, Hsinchu, Taiwan* MIN-CHAO CHANG, HSIN SHAO, *Center for Environmental, Safety and Health Technology Development, ITRI, Hsinchu, Taiwan* CHIH-JEN LIN, LI-JIAUN LIN, *Materials Research Laboratories, ITRI, Hsinchu, Taiwan* Anatase $TiO_2$ nanocrystals of uniform sizes were synthesized via low temperature sol-gel reaction of titanium tetraisopropoxide (TIP) with water in the presence of small amount of hydrophobic ionic liquid (IL) molecules. It was found that the IL molecules did not actively participate in precursor hydrolysis and $TiO_2$ nucleation. However, the IL molecules strongly screened the abundant remaining hydroxylic bonds on the surfaces of the primordial $TiO_2$ particles, giving rise to low temperature transition to anatase phase at 100 °C and impeded inter-particle sintering. The former was believably induced by self-organization of the IL molecules that adsorbed on the hydroxylic bonds. This IL-modified sol-gel reaction resulted in uniform sized ( $\sim$ 10 nm) anatase $TiO_2$ nanocrystalline particles, useful for high efficiency photo-catalytic applications.

**C1 180 Semi-Classical Quantization of a [2] Rotaxane** KARL SOHLBERG, ARI SILVER, *Chem. Dept., Drexel University* Rotaxanes show tantalizing potential for functional nanosystems. A [2]rotaxane is a molecular complex consisting a long dumbbell-shaped chain molecule, (called the shaft) which threads a ring molecule, typically a crown-ether or cyclodextrin. The chain component is terminated on each end by a bulky substituent to prevent unthreading of the ring. The components are therefore chemically independent but mechanically interlocked. When such complexes are synthesized with two inter-component binding stations, bistability results, hinting at potential for switching or data storage applications. We have investigated the quantum-mechanical eigenstates associated with the shuttling motion between these co-conformations. The state density is very high because nanosystems exist at the transition/interface between molecular systems, which are dominated by quantum phenomena, and macroscopic systems where matter is essentially continuous and classical physics provides the best description. We show that state density is ithighest where quantum mechanical tunneling is most important.

**C1 181 Single molecule fluorescence investigates the heterogeneity of liquid crystal matrix.** YU-TSU CHUANG, JUI-HUNG HSU, *National Sun Yat-sen University* Liquid crystals are attracted for their existence of unique meso-phase between solid state and liquid state. We perform the single-molecule (SM) fluorescence investigation on the thermotropic liquid crystal matrix. Using the nm size fluorescent quantum dots as a probe, it allows us to investigate the local structural and dynamic heterogeneity in the liquid crystal matrix. Controlling the temperature allows us to probe how the local behaviors differ at different meso-phases. Fluorescence correlation spectroscopy (FCS) as well as the intensity time trace analysis indicate the much more heterogeneity in the liquid crystal phase than the other phases.

**C1 182 Synthesis and Characterization of Rectangular Palladium Nanoparticles.*** YUAN SUN, *Dept. Mat. Sci. & Eng., SUNY at Stony Brook* LIHUA ZHANG, ELI SUTTER, YIMEI ZHU, *Center for Functional Nanomaterials, Brookhaven National Laboratory* MIRIAM RAFAILOVICH, JONATHAN SOKOLOV, *Dept. Mat. Sci. & Eng., SUNY at Stony Brook* The optical, magnetic and catalytic and electronic properties of nanoparticles are affected not only by their size, but also by their shape. We have used a mild reducing agent, ascorbic acid, in the presence of sodium citrate and a surfactant, cetyltrimethylammonium bromide, at ambient conditions to prepare colloidal rectangular palladium nanoparticles, including nanocubes and nanorods. Our procedure requires no seed-mediated growth or nanoporous template so that it is more practical for large-scale synthesis. Upon changing the concentration of sodium citrate from $0.2 \times 10^{-3}$ M to $1.0 \times 10^{-3}$ M, TEM measurements indicate that the average size of the nanocubes decreases slightly from $31.8 \pm 3.2$ nm to $29.4 \pm 4.2$ nm and the aspect ratio of the nanorods increases from $2.48 \pm 1.42$ to $3.94 \pm 2.50$. HRTEM images and diffraction patterns indicate that the particles are highly crystalline and have strong (100) faceting. Being exposed to air for $\sim$ 100 days, the particles are oxidized to form 2$\sim$ 4 nm-thick amorphous shells.

*Supported by NSF-MRSEC. The CNF-BNL is supported by the U.S. DOE under DE-AC02-98CH10886.

**C1 183 Nucleation, composition and morphology of ALD $HfO_2$ films** JUSTIN C. HACKLEY, THEODOSIA GOUGOUSI, *University of Maryland Baltimore County* A hot wall Atomic Layer Deposition flow reactor equipped with a Quartz Crystal Microbalance (QCM) has been used in the development of a

$HfO_2$ process from tetrakis-ethylmethylamino hafnium (TEMAH) and $H_2O$ precursors. We have studied the nucleation, composition and morphology of $HfO_2$ films deposited on H- terminated Si, native oxide and SC1 chemical oxide. Ellipsometry and QCM measurements confirm linear growth of the films ( $\sim$ 1.2Å/cycle at 250[r]C). Similar incubation periods ( $\sim$ 10 cycles) are found for depositions on the H-terminated Si and native oxide starting surfaces in agreement with recently published results.[1] AFM measurements show rms roughness of the as deposited films below 4% of the total film thickness. FTIR measurements show some OH and carbonate content in the films that are corroborated by XPS measurements. Rapid Thermal Anneal of the films in Ar (500 to 900[r]C, 2 min) results in the destabilization of the $HfO_2/SiO_2$ interface, increased rms roughness and crystallization of the film. FTIR and XPS analysis of the films annealed at 900[r]C in Ar confirm removal of the OH and carbonate species from the films. Finally, we present QCM measurements for the nucleation of $HfO_2$ films on Si and H-terminated surfaces.

[1]M.-T. Ho, Y. Wang, R. T. Brewer, L. S. Wielunski, Y. J. Chabal, N. Moumen, and M. Boleslawski, APL 87, 133103 2005

**C1 184 Ranked solutions to a class of combinatorial optimizations - with applications in mass spectrometry based peptide sequencing*** TIMOTHY DOERR, GELIO ALVES, YI-KUO YU, *NCBI/NLM/NIH* Typical combinatorial optimizations are NP-hard; however, for a particular class of cost functions the corresponding combinatorial optimizations can be solved in polynomial time. This suggests a way to efficiently find approximate solutions —find a transformation that makes the cost function as similar as possible to that of the solvable class. After keeping many high-ranking solutions using the approximate cost function, one may then re-assess these solutions with the full cost function to find the best approximate solution. Under this approach, it is important to be able to assess the quality of the solutions obtained, *e.g.*, by finding the true ranking of $k$th best approximate solution when all possible solutions are considered exhaustively. To tackle this statistical issue, we provide a systematic method starting with a scaling function generated from the fininte number of high- ranking solutions followed by a *convergent* iterative mapping. This method, useful in a variant of the directed paths in random media problem proposed here, can also provide a statistical significance assessment for one of the most important *proteomic* tasks—peptide sequencing using tandem mass spectrometry data.

*This work was supported by the Intramural Research Program of the NLM at NIH/DHHS.

## C1 185 STATISTICAL AND NONLINEAR PHYSICS POSTER SESSION

**C1 186 Loschmidt echo decay in hard-disk billiards*** ARSENI GOUSSEV, KLAUS RICHTER, *Institute for Theoretical Physics, University of Regensburg* The Loschmidt echo (LE) quantifies the sensitivity of quantum dynamics to perturbations of system's Hamiltonian. In a chaotic system it is known to exhibit exponential time decay, for a certain range of perturbation strengths, with the decay rate given by the mean Lyapunov exponent of the counterpart classical system. This phenomenon makes the LE an attractive tool for quantifying *Quantum Chaos*. To date, all existing theories for the LE strongly rely on averaging over different realizations of the Hamiltonian and/or averaging over an ensemble of initial states. Thus, a theory for the LE in pure individual chaotic systems is needed. We attempt to fill in this gap by addressing the LE in pure open quantum hard-disk billiards. We find that in such systems the LE time decay is intimately connected to Lyapunov exponents as well as to quantities characterizing escape of classical trajectories from the system's chaotic repellor. Our theoretical findings are supported by results of numerical simulations.

*Supported by the Alexander von Humboldt Foundation

**C1 187 Random Walk Model with Waiting Times Depending on the Preceding Jump Length** VASILY ZABURDAEV, *Max Planck Institute for Dynamics and Self-Organization* In the present work the generalized continuous time random walk model with a coupled transition kernel is considered. The coupling occurs through the dependence of the waiting time probability distribution on the preceding jump length. The method, which involves the details of the microscopic distribution over the waiting times and arrival distances at a given point, is suggested for its description. In the particular case of coupling, when a waiting time is a simple function of a preceding jump length, a close analogy to the problem of a random walk with finite velocity is demonstrated. With its help an analytical solution for the generalized random walk model, including both effects (finite velocity and jump dependent waiting times) simultaneously, is found. Considered examples indicate a possibility to apply the developed approach to the biological problems where the random walk together with the recovery processes and the finite velocity are present, such as e.g. the foraging movements of animals or the motion of zooplankton.

**C1 188 Diameter of Random Cluster Models** D. W. BLAIR, J. MACHTA, *University of Massachusetts at Amherst* The diameter of critical clusters of the $q$-state Potts model in the random cluster representation is measured in numerical simulations. The diameter of a graph is the maximum over all pairs of connected sites of the minimum path length between the sites. Although the diameter of Fortuin-Kasteleyn clusters is not a thermodynamic quantity, it is expected to display power law critical behavior since the size of the largest cluster diverges at the critical point. The Swendsen-Wang algorithm is used for both for equilibrating the spin model and for identifying clusters. An efficient algorithm is employed to measure the diameter. The exponent characterizing the divergence of the diameter is obtained for $q = 1, 2, 3$ and 4. The relation to other critical exponents is discussed. This work is supported by NSF (DMR-0242402).

**C1 189 Empirical and model study on Travel-entering China*** XUE-FANG HAN, QI-JUAN CHEN, HUI CHANG, DA-REN HE, *Yangzhou University, China* We have done an empirical investigation on the travel-entering China from abroad to 31 regions of Chinese Mainland in recent ten years, including the development of the traveler's number, the traveler's number distribution for the traveler's home regions, the traveler's number distribution for the traveler's destination regions in Chinese mainland, and so on. We also suggest a dynamic model for simulating the competition between the 31 regions in the traveling market by considering two main influence factors, the attracting factor of the travel

destinations and the distance between the destination and the home regions of the travelers. The simulation results show a good agreement with the empirical data. We expect the model could suggest some advice and thoughts to the travel-entering management departments in China and may be also for other countries.

*supported by Chinese National Natural Science Foundation, No. 70371071

**C1 190 An empirical and model study on automobile market in Taiwan*** JI-YING TANG, RONG QIU, YUEPING ZHOU, DA-REN HE, *Yangzhou University, China* We have done an empirical investigation on automobile market in Taiwan including the development of the possession rate of the companies in the market from 1979 to 2003, the development of the largest possession rate, and so on. A dynamic model for describing the competition between the companies is suggested based on the empirical study. In the model each company is given a long-term competition factor (such as technology, capital and scale) and a short-term competition factor (such as management, service and advertisement). Then the companies play games in order to obtain more possession rate in the market under certain rules. Numerical simulation based on the model display a competition developing process, which qualitatively and quantitatively agree with our empirical investigation results.

*supported by Chinese National Natural Science Foundation, No. 70371071

**C1 191 Stochastic Synchronization in Lattices of Model Neurons** ANDY MUELLER, KLAUS LEHNERTZ, *Helmholtz-Institute for Radiation and Nuclear Physics and Dept. of Epileptology, University of Bonn* It has been shown recently that a wide class of uncoupled limit-cycle oscillators can be fully synchronized by a common weak additive white noise. We study the influence of noise on the dynamics of mutually uncoupled lattices that are composed of periodically spiking model neurons with an increasing complexity. In order to approximate characteristics of noise found in empirical data we use an Ornstein Uhlenbeck process (OUP) as the driving force. Varying the correlation time and the intensity of the OUP we study the time to full synchronization (ST) and the largest Lyapunov exponent (LLE) of the systems. For all investigated correlation times LLE is negative indicating the convergence of the trajectories of the systems. For a constant noise intensity we observe that both ST and LLE exhibit a minimum for a particular correlation time of the OUP. We discuss the possible relationship between the correlation time of the OUP and the time scales of the investigated systems.

**C1 192 Score Statistics of Global Sequence Alignment and a Modified Directed Polymer Problem*** MIHAELA SARDIU, *Stowers Institute* GELIO ALVES, YI-KUO YU, *NCBI/NLM/NIH* Sequence alignment is one of the most important bioinformatics tools for modern molecular biology. Using a variant of the directed path in random media model, we investigate the score statistics of global sequence alignment taking into account the compositional bias of the sequences compared. To accommodate the compositional bias, we introduce an extra parameter $p$ indicating the probability for positive matching scores to occur. When $p$ is large, the highest scoring point within a global alignment tends to be close to the end of both sequences, in which case we say the system percolates. By applying finite-size scaling theory on percolating probability functions of various sizes (sequence lengths), the critical $p$ at infinite size is obtained. For alignment of length $t$, the score fluctuation $\sim \chi t^{1/3}$ is confirmed via scaling of the alignment score. Using the Kolmogorov-Smirnov statistics test, we show that $\chi$ follows the Tracy-Widom distributions: Gaussian Orthogonal Ensemble for $p$ slightly larger than $p_c$ and Gaussian Unitary Ensemble for larger $p$. The possibility of characterizing score statistics for modest system size (sequence lengths), via proper reparametrization of alignment scores, is illustrated.

*This work was supported by the Intramural Research Program of the NLM at the NIH/DHHS

**C1 193 Nonequilibrium phase transition on a randomly diluted lattice** MAN YOUNG LEE, THOMAS VOJTA, *Department of Physics, University of Missouri-Rolla* We show that the interplay between geometric criticality and dynamical fluctuations leads to a novel universality class of the contact process on a randomly diluted lattice. The nonequilibrium phase transition across the percolation threshold of the lattice is characterized by unconventional activated (exponential) dynamical scaling and strong Griffiths effects. We calculate the critical behavior in two and three space dimensions, and we also relate our results to the recently found infinite-randomness fixed point in the disordered one-dimensional contact process.

**C1 194 Numerical Studies of the Edwards-Wilkinson interface equation: the influence of short-range time-correlated noise** MIKA SAUKKONEN, TEEMU LAURILA, TAPIO ALANISSILA, *Helsinki University of Technology* COMP TEAM, We study the properties of the Edwards-Wilkinson equation with finite temporal correlations of duration $t_d$. Two limiting cases can be calculated analytically, namely, the thermal white noise limit, where $t_d \to 0$, and the purely columnar limit, when $t_d \to \infty$. The surface growth exponents are $\beta = 1/4$ for the thermal white noise case and $\beta = 3/4$ for the columnar noise case. Correspondingly, the rougness exponents are $\chi = 1/2$ and $\chi = 3/2$. We study the crossover scaling of the surface width and the dynamical structure factor between these two limits by introducing a scaling ansatz and numerically verifying it. Furthermore, we present results from a comparison between the time correlated case and the case with quenched noise, which has the same effective correlation length. The scaling behavior in these two cases is similar exept close to the pinning transition for the quenched noise case.

**C1 195 A study of SOC models by the use of joint distributions** ESPEN JETTESTUEN, ANDERS MALTHE-SORENSSEN, JENS FEDER, *Centre for Physics of Geological Processes, University of Oslo* A precise characterization of scaling behavior is important for the further development of self-organized criticality. This has been achieved for models that display finite size scaling, but is lacking for systems that have more complicated scaling form. We propose that scaling of structures in joint probability densities can be used to identify the underlying structure in systems that show multi-scaling behavior. Here, we will study two simple models by the use of joint probability distributions. One is the BTW model that have multi-scaling behavior and the other is a randomized version of the Olami-Feder-Christensen earthquake model which has a simple finite size scaling form. We will also relate the scaling of the joint probability density to other well-known measures.

**C1 196 Glassy dynamics in interface growth: aging, fluctuation disipation and thermal avalanches** JOSE J. RAMASCO, *Emory University* JUAN M. LOPEZ, MIGUEL A. RODRIGUEZ, *Inst. de Fisica de Catabria (Spain)* In this work we study the KPZ interface growth equation subjected to both quenched and anealed disorder. We find that the interface dynamics shows a glassy behavior in the regime of low temperatures and low external force, a regime commonly known as creep in the superconductor literature. We also describe how the temperature affects to the avalanches in the front development.

**C1 197 Delayed Feedback and Chaos on the Driven Diode-Terminated Transmission Line** VASSILI DEMERGIS, STEVEN ANLAGE, *Dept of Physics, Univ of Maryland, College Park* EDWARD OTT, THOMAS ANTONSEN, *Institute for Research in Electronics and Applied Physics, Univ of Maryland, College Park* ALEXANDER GLASSER, MARSHAL MILLER, A simple model of a distributed, non-linear circuit that produces chaos at GHz frequencies is introduced and tested experimentally. The model circuit is a driven, diode-terminated transmission line with the transmission line impedance mismatched to that of the source. This model is motivated by the need to understand the mechanisms for RF upset in computer circuits. Experimental tests of the model were performed with driving frequencies of 10 MHz to 1.2 GHz, driving powers of -30 to +50 dBm, and delay times from 3 to 20 ns. Diode reverse recovery times (/tau/) ranged from 4 to 100 ns. Experimentally, it was found that chaotic behavior was strongly dependent on the reactance of the system as seen by the driving source, and influenced by an applied DC voltage-bias across the diode. In the experiments that showed period-doubling and / or chaos, the /tau/ was on the order of both the driving period and the delay time of the circuits. Comparisons between theory and experiment are in general agreement.Work supported by the DOD MURI AFOSR Grant F496200110374 and DURIP Grants FA95500410295, FA95500510240.

**C1 198 Geometrically induced nonlinear dynamics in one-dimensional lattices** MERLE D. HAMILTON, O.F. DE ALCANTARA BONFIM, *University of Portland* We present a lattice model consisting of a single one-dimensional chain, where the masses are interconnected by linear springs and allowed to move in a horizontal direction only, as in a monorail. In the transverse direction each mass is also attached to two other linear springs, one on each side of the mass. The ends of these springs are kept at fixed positions. The nonlinearity in the model arises from the geometric constraints imposed on the motion of the masses, as well as from the configuration of the springs, where in the transverse direction the springs are either in the extended or compressed state depending on the position of the masses. Under these conditions we show that solitary waves are present in the system. In the long wavelength limit an analytic solution for these nonlinear waves is found. Numerical integrations of the equations of motion in the full system are also performed to analyze the conditions for the existence and stability of the nonlinear waves.

**C1 199 Stochastic qualifyers of brain dynamics** JENS PRUSSEIT, *Helmholtz Institute for Radiation and Nuclear Physics, University of Bonn* KLAUS LEHNERTZ, *Department of Epileptology, University of Bonn* Despite the fact that both linear and nonlinear analyses of EEG time series have provided valuable insights into the complex spatio-temporal dynamics of physiological and patho-physiological brain functions, these processes are far from being fully understood. We here investigate the applicability of a previously proposed analysis method to characterize EEG time series from epilepsy patients using concepts from the theory of Markov-processes. To estimate the coefficients of a corresponding Fokker-Planck equation we adopt the method of Siegert et al (Phys. Lett. A **243**, 275 (1998)) to the problem at hand. To check the validity of our approach we reconstruct the driving noise force via the associated Langevin equation and show that the noise is approximately delta-correlated and Gaussian. We then integrate our model to compare the stationary probability distribution function (PDF) as well as the conditional PDFs on different time scales with the PDFs derived from the EEG data. Applying the analysis method to long-lasting multichannel EEG recordings we discuss the possible relevance for diagnostic purposes.

**C1 200 Berry curvature contributions to the density fluctuation spectrum of Bloch electrons** M. J. RAVE, W. C. KERR, *Wake Forest University* Recent work has shown that the equations of motion (EOM) for semiclassical Bloch electrons must be modified in the presence of a non-zero Berry curvature [1]. These corrections to the EOM have implications for many physical quantities: effective mass, electron orbits in a magnetic field, de Haas-van Alphen oscillations, etc. In addition the Boltzmann transport equation is also modified with possible ramifications for calculations of transport phenomena. We investigate these issues for a gas of spinless Bloch electrons in an external electric field. We find modifications to the traditional dispersion relation for density fluctuations; in particular we find a shift in the plasma frequency and an anisotropic sound velocity. [1] M.-C. Chang and Q. Niu, Phys. Rev. B 53, 7010 (1996)

**C1 201 Correlation functions and anisotropy in the XY model with a magnetic field*** WEI ZHANG*, H.A. FERTIG, *Department of Physics, Indiana University* Recent studies have demonstrated that the classical XY model with a magnetic field has three phases: a linearly confined vortex-antivortex phase, a logarithmically (Log) confined phase, and a free vortex phase. We calculate correlation functions in this model by making use of duality transformations and numerical simulations. In all three phases, the order parameter is nonzero and $< \cos(\theta(r_1))\cos(\theta(r_2)) > \rightarrow$ const., for $|\mathbf{r}| = |\mathbf{r}_1 - \mathbf{r}_2| \rightarrow \infty$, indicating true long range order, when the ordering field favors $\theta = 0$. A renormalization group analysis suggests that the Log phase may be distinquished from the other two in the correlation function $C(r) = < \sin(\theta(\mathbf{r}_1))\sin(\theta(\mathbf{r}_2)) >$, which is short-ranged with a correlation length that depends on the direction of $\mathbf{r}_1 - \mathbf{r}_2$ with respect to the lattice axes. However, it is shown that a directional anisotropy also enters all the phases through a prefactor. Our numerical simulations support the existence of these anisotropies, but the the anisotropy in the prefactor is generically relatively strong while the correlation length anisotropy is rather weak, making it difficult to distinquish the different phases from these correlation functions. *Present address: Department of Physics and Astronomy, Ohio University

*This work was supported by NSF Grant No. DMR-0454699

**C1 202 Emergent Structures in Dissipative Wave-Particle Systems*** DAVIT SIVIL, ALFRED HUBLER, *Center for Complex Systems Research, Department of Physics, University of Illi-*

*nois at Urbana-Champaign* We study the motion of a particle with mass m on a vibrated string of length L. We assume there is no friction force between the particle and the string. The string is sinusoidally forced at both ends. We find that the particle has attractors located at $x=L/2 - n\pi c/2\omega$, where $\omega$ is the frequency of the waves on the string, and $n \in \mathbf{Z}$. We also study the same system with friction and multiple driving frequencies. We also compared our results with numerical simulations

*The research is supported by the National Science Foundation Grant No. NSF PHY 01-40179, NSF DMS03-25939. ITR, and NSF DGE 03-38215.

**C1 203 Scaling in a cellular automaton model of earthquake faults with long-range stress transfer** JUNCHAO XIA, *Clark University* HARVEY GOULD, *Clark Unversity* M. ANGHEL, WILLIAM KLEIN, *Boston University* JOHN RUNDLE, *U. C., Davis* We present simulation data indicating that the scaling of earthquake events in models of faults with long-range stress transfer is composed of at least three distinct regions, corresponding to earthquakes with different underlying physical mechanisms. We discuss the interpretation of these events as fluctuations in the vicinity of a spinodal critical point. In addition to the scaling events, there are larger ''breakout'' events that do not scale. The nature of the stress density profile before an event is investigated and a possible way of predicting breakout events is discussed.

**C1 204 Time-Evolution of the Wigner Function in Phase-Space using Finite Differences** SHUBHABRATA RATH, TOMAS MATERDEY, *University of Massachusetts Boston* Phase-space density holes are vortex-like nonlinear structures that have been observed in the magnetosphere. To study the time evolution of these structures we evolve the Wigner function in time by solving the quantum Vlasov equation using finite-differences.

**C1 205 The Structural Database*** NIKOLAI ZARKEVICH, D.D. JOHNSON, *Department of Materials Science and Engineering, University of Illinois at Urbana-Champaign.* A Structural Database can be used as a universal tool for global accumulation and integration of structural and energy data from different methods, people, and places. It allows data mining and data validation by direct comparison of structural data from different sources. Being combined with multi-scale methods (e.g., ThermoToolkit), it can significantly reduce the cost of materials design. We exemplify these and other benefits of the Structural Database, and demonstrate its working prototype, available at http://data.mse.uiuc.edu. This database is a product of multi-disciplinary research involving Physics, Computer Science, and Materials Science and Engineering.

*Development is supported in part by the U.S. Department of Energy through grant DE-FC36-05GO15064.

**C1 206 Interacting Cracks in an Environmentally Assisted Fracture** ARTEM LEVANDOVSKY, ANNA BALAZS, *University of Pittsburgh* We perform the study of environmentally assisted fracture within the framework of a lattice model. Formation of an ensemble of environmentally assisted microcracks, their coalescence and formation of crack ''avalanches'' lead to a very rich dynamical picture. Under specific condition crack healing can occur due to cohesive forces, which hold material together and tend to pull atoms together even if they are separated by a crack over several lattice units. We investigate the dynamical interplay between crack formation, arrest, healing and re-cracking. The goal here is to provide an understanding of the conditions leading to the phenomena of crack healing that happens along with the crack formation. We study the morphology of crack patterns with the intentions to establish a way to enhance the healing property of a material sample.

**C1 207 Structure and Nonlinear dynamical response of Pinned Lattice systems: Application of the Phase Field Crystal Model to Pinned Lattices** MIKKO KARTTUNEN, CRISTIAN ACHIM, *Helsinki University of Technology* KEN ELDER, *Oakland University* TAPIO ALA-NISSILA, *Laboratory of Physics, Helsinki University of Technology* ENZO GRANATO, *Instituto Nacional de Pesquisas Espaciais, Sao Jose dos Campos, SP Brazil* S.C YING, *Department of Physics, Brown University* We present analytic and numerical results for the structure and dynamics of a lattice system in 2D in the presence of a pinning potential. We employ a new approach via the Phase Field Crystal (PFC) model which describes phenomena on atomic length and diffusive time scales. It can be used for modeling elastic and plastic deformation, free surfaces and multiple crystal orientations in non-equilibrium processes, and enables access to time scales much longer than conventional atomic methods. The competition between the length scales associated with the intrinsic ordering and the pinning potential leads to commensurate-incommensurate transitions. The dynamical response of the system in the presence of a driving force has also been studied via the time dependent Landau Ginzberg equation. Dynamically induced phases, mobility thresholds and hysteresis behavior have been observed. We will discuss the application of this model to physical problems such as the I-V characteristics of 2-D vortex lattices and sliding friction in interfaces with boundary lubricants.

**C1 208 Piconewton force measurement with a scanning tunneling microscope** KAI-FELIX BRAUN, APARANA DESHPANDE, SAW HLA, *Ohio University* The magnitude of force required to move a single atom across a crystal surface has been measured for the first time. During atomic manipulation experiments with a scanning tunneling microscope the tip heigth curve is recorded. Analysis of shape and period has yielded detailed knowledge about atomic movement while it is shown here that the amplitude of the manipulation curve is a measure of the interaction force between the microscopes tip and the manipulated atom on the surface. This interaction force has been measured for single Ag atoms on a Ag(111) substrate as a function of distance and amounts to several hundred piconewton.

**C1 209 Theory of the Effects of Multiscale Surface Roughness and Stiffness on Static Friction*** JEFFREY SOKOLOFF, *Northeastern University* It is shown on the basis of simple scaling arguments that an interface between two three dimensional elastic solids, consisting of completely flat disordered surfaces, which interact with interatomic hard core interactions, will be in a weak pinning regime, and hence exhibit negligibly small static friction. It is argued, however, that the presence of roughness on multiple length scales can lead to much larger friction (i.e., static friction coefficients not too much smaller than 1), as is characteristic of most solid surfaces. This approach suggests a possible way of understanding why coatings of materials with high elastic constants are often excellent lubricants.

*Work supported by DOE

**C1 210 Electrospinning frozen in time*** MATIJA CRNE, *Georgia Institute of Technology* JUNG OK PARK, *Georgia institute of Technology* MOHAN SRINIVASARAO, *Georgia Institute of Technology* Electrospinning is known to produce microfibers with small diameter and/or high surface area. Often times, the high surface area of these fibers is associated with their surface structures, consisting of nanometer-sized holes, droplets, or microcups, whose formation depends on the spinning condition and the type of the solutions used. A mixture of isotactic and syndiotactic PMMA in dimethyl formamide was used in our study to produce helical microfibers by electrospinning at elevated temperatures. Rapid cooling during electrospinning allows for fast physical gelation to take place and trap helical microstructures arising from instabilities due to electrostatic, capillary and viscous forces. The formation of these helices was considered in terms of stability theory for electrically forced jets.

*The authors would like to acknowledge the National Science Foundation (DMI-0423619) for supporting this research.

**C1 211 Response to disturbance*** WEN-XIU WANG, DAN SHEN, YU-MEI JIANG, YING-MEI WANG, DA-REN HE, *Yangzhou University, China* PEI-PEI ZHANG, *Jiangsu University, China* YUE HE, *Wuxi No.1 Middle School, China* We suggest a new concept named response to disturbance for describing a character of dynamic systems. In relatively simple systems the evolution usually tends to a final state, which may be an equilibrium state, a periodic oscillating state, a quasi-periodic state, or a chaotic state. A disturbance, which always exists in practical systems, sometimes vanishes gradually and indicates the final state is stable, while it sometimes grows up very quickly and indicates the final state is unstable. However, in a relatively complex system disturbance may cause emergence of (may be a very large number of) new structures and very long evolution processes. So, we are trying to suggest a parameter with suitable function form so that the different responses to disturbance in different type of systems can be quantitatively distinguished. We hope that the parameter can be useful for understanding complexity of the practical systems. The details will be presented elsewhere.

*supported by Chinese National Natural Science Foundation, No. 70371071

**C1 212 A model study on dyad act-degree distribution in some collaboration networks*** YUE-PING ZHOU, HUI CHANG, DA-REN HE, *Yangzhou University, China* We (and cooperators) have suggested extending the conception collaboration network to some non-social networks, which have structures as sets of completed graphs [1]. A dyad is composed of two nodes, which are connected by one edge. In social network studies dyad often is considered as the basic units in networks. It should be more important in the extended collaboration networks. We suggest emphasizing the importance of dyad in organizing a network and studying the evolution of the extended collaboration networks by a dyad-act organizing model. The analytic and numeric studies of the model lead to a conclusion that most of the collaboration networks should show a dyad act-degree distribution (how many acts a dyad belongs to) between a power law and an exponential function, which can be described by a shifted power law. We have done an empirical study on dyad act-degree distribution in some collaboration networks. The results show good agreement with this conclusion. The details will be published elsewhere. [1] P-P Zhang, K. Chen et al., to appear on Physica A.

*Supported by Chinese National Natural Science Foundation, No. 70371071.

**C1 213 Empirical study on dyad act-degree distribution in some collaboration networks*** HUI CHANG, *Yangzhou University* PEI-PEI ZHANG, *Jiangsu University* YUE HE, *Wuxi No.1 Middle School* DA-REN HE, *Yangzhou University, China* We (and cooperators) suggest studying the evolution of the extended collaboration networks by a dyad-act organizing model. The analytic and numeric studies of the model lead to a conclusion that most of the collaboration networks should show a dyad act-degree distribution (how many acts a dyad belongs to) between a power law and an exponential function, which can be described by a shifted power law. We have done an empirical study on dyad act-degree distribution in some collaboration networks. They are: the train networks in China, the bus network of Beijing, and traditional Chinese medical prescription formulation network. The results show good agreement with this conclusion. We also discuss what dyad act-degree implies in these networks and what are the possible applications of the study. The details will be published elsewhere.

*Supported by Chinese National Natural Science Foundation, No. 70371071.

**C1 214 Empirical study on assortativity in some collaboration networks*** BEI-BEI SU, HUI CHANG, DA-REN HE, *Yangzhou University, China* We (and cooperators) have suggested extending the conception collaboration network to some non-social networks, which have structures as sets of completed graphs [1]. In this view of point, we may divide practical networks into four groups: a) social collaboration networks, b) social non-collaboration networks, c) non-social collaboration networks, and d) non-social non-collaboration networks. We have done an empirical study on assortativity in some practical networks, which belong to the four groups. The results show that all the networks of a) and b) groups show positive assortativity, all the networks of d) group show negative assortativity. This is in agreement with the conclusion obtained by Newman [2]. However, for some of the networks belonging to group c), we obtained positive assortativity, but obtained negative one for other networks belonging to the same group. The details will be published elsewhere. Now we are trying to find the difference in the structure properties of these networks, which may be responsible for different sign of assortativity. [1] P-P Zhang, K. Chen et al., to appear on Physica A. [2] M. E. J. Newman, PRE 67, 026126 (2003).

*supported by Chinese National Natural Science Foundation, No. 70371071

**C1 215 Dynamical Stochastic Processes of Returns in Financial Markets** KYUNGSIK KIM, *Department of Physics, Pukyong National University, Pusan 608-737, Korea* SOO YONG KIM, *Department of Physics, Korea Advanced Institute of Science and Technology, Daejeon 305-701, Korea* GYUCHANG LIM, *Department of Physics, Korea Advanced Institute of Science and Technology, Daejeon 305-701, Korea* JUNYUAN ZHOU, *Department of Physics, Korea Advanced Institute of Science and Technology, Daejeon 305-701, Korea* SEUNG-MIN YOON, *Division of Economics, Pukyong National University, Pusan 608-*

*737, Korea* We show how the evolution of probability distribution functions of the returns from the tick data of the Korean treasury bond futures (KTB) and the S&P 500 stock index can be described by means of the Fokker-Planck equation. We derive the Fokker-Planck equation from the estimated Kramers-Moyal coefficients estimated directly from the empirical data. By analyzing the statistics of the returns, we present the quantitative deterministic and random influences on both financial time series, for which we can give a simple physical interpretation. Finally, we remark that the diffusion coefficient should be significantly considered to make a portfolio.

## C1 216 ARTIFICIALLY STRUCTURED MATERIALS POSTER SESSION

**C1 217 Diffusion and binding of CO on Pt nanowires** NURI ONCEL, WOUTER J. VAN BEEK, JEROEN HUIJBEN, HAROLD J.W. ZANDVLIET, BENE POELSEMA, *Solid State Physics, MESA + Research Institute for Nanotechnology, University of Twente* Room temperature scanning tunneling microscopy (STM) has been used to study the diffusion and binding of CO molecules on Pt nanowires. The perfectly straight Pt nanowires (with a cross-section of only one atom) are grown on Ge(001) surfaces. CO molecules bind on a bridge position of the Pt dimers and they are mobile at room temperature. The interaction between adsorbed CO molecules is strongly repulsive, which leads to low saturation coverage and ''restricted'' 1D Brownian motion along the nanowires.

**C1 218 Phononic crystals for the mode conversion of elastic waves.*** BETSABE MANZANARES-MARTINEZ, *División de Ciencias e Ingeniería, Unidad Regional Sur de la Universidad de Sonora* FELIPE RAMOS-MENDIETA, *Departamento de Investigación en Física de la Universidad de Sonora* We have studied theoretically the transmission of elastic waves in an Epoxy/Sn superlattice with Si and Epoxy as media of incidence and transmission, respectively. We found that this is a good system for conversion of the elastic mode polarization. Within some ranges of frequencies the incident longitudinal waves are converted to transverse waves with efficiency of 85%. In order to understand this effect the polarization states of the sagittal bands need be considered. The modes of sagittal bands can be mainly transverse or mainly longitudinal. We found that as higher the density of transverse modes, higher the conversion. The effect depends strongly on the sound velocity of the medium of incidence - high velocity as possible is required. For calculations we also include absorption effects.

*This work was supported by SESIC México, Grant Promep-2004 REDES, and by CONACyT México, Grant SEP-2004-C01-47636.

**C1 219 X-ray Studies of Ultrathin Wires and Tubes in Nanoscale Confinement.** JONATHAN M. LOGAN, OLEG G. SHPYRKO, ERIC D. ISAACS, *Center for Nanoscale Materials, Argonne National Laboratory, Argonne, IL and JFI/Physics Department, University of Chicago, Chicago, IL* RAFAEL JARAMILLO, YEJUN FENG, *JFI/Physics Department, University of Chicago, Chicago, IL* JEFFREY W. ELAM, *Energy Systems Division, Argonne National Laboratory, Argonne, IL* DAVID J. COOKSON, *Australian Synchrotron Research Program, Argonne, IL* MICHAEL J. PELLIN, *Materials Science Division, Argonne National Laboratory, Argonne, IL* Nanoporous Anodized Aluminum Oxide (AAO) membranes are composed of self-assembled, densely packed, co-aligned cylindrical pores. The pore diameter of these membranes can be controllably reduced to as little as $\approx$ 1 nm through Atomic Layer Deposition (ALD) process. AAO pores have been used as templates for formation of metallic nanotubes and nanowires through ALD or thermal vapor deposition. These embedded structures have been characterized by small- and wide-angle x-ray scattering (SAXS, WAXS). The penetrating ability of x rays provides a non- destructive structural characterization technique for materials confined within AAO matrix, on both atomic (WAXS) and nanometer (SAXS) length scales.

**C1 220 Electric Field Effects on Motion of a Charged Particle Through a Saddle Potential in a Magnetic Field** V. FESSATIDIS, *Fordham University* K. SABEEH, *Quaid-i-Azam University, Pakistan* N.J.M. HORING, *Stevens Institute of Technology* M.L. GLASSER, *Clarkson University* Electron transmission through a quantum point contact (QPC) in the presence of both electric and magnetic fields is examined. The QPC is modeled as a saddle potential. The first part of the paper is devoted to deriving the relevant Green's function including the effects of arbitrarily time dependent electric and constant magnetic fields. The derivation is carried out using Schwinger's operator equation of motion approach. In the second part of the paper we apply it to determine transmission of the electron guiding center through the QPC in constant electric and magnetic fields.

**C1 221 Hofstadter's butterfly with Rashba spin-orbit coupling*** SUKEY SOSA Y SILVA SALGADO, FERNANDO ROJAS, *Centro de Ciencias de la Materia Condensada, UNAM* We study the energy spectrum of an electron in a two-dimensional periodic lattice in a perpendicular magnetic field in the tight-binding approximation including the Rashba spin-orbit coupling. We have investigated how the fractal spectrum known as Hofstadters butterfly is modified if one includes the spin-orbit coupling. We find a set of decoupled Harper-like equations for each spinor by restricting the Rashba coupling along one direction. We solve the set of equations and evaluate the energy spectrum for each spinor. In order to characterize the energy spectrum we calculate its fractal dimension, in particular, we analyze the capacity and the correlation dimension of each spin-subbands buttlerfly as a function of the spin-orbit coupling parameter and magnetic field.

*Support by DGAPA project IN114403 and CONACyT project 43673-F

**C1 222 Ground state energy of an electron in a GaAs pillbox immersed in a GaAlAs substrate** GERARDO JORGE VAZQUEZ-FONSECA, MARCELO DEL CASTILLO-MUSSOT, *Instituto de Fisica, UNAM* SANDRA MILENA RAMOS-ARTEAGA, NELSON PORRAS-MONTENEGRO, *Universidad del Valle, Colombia* In this work we have studied the ground state energy behavior for a GaAs pillbox immersed in a system of GaAlAs as a function the thickness of the barrier potential when the length of the pillbox is fixed, as function the length of the pillbox when the thickness of the barriers remained

constant, and as a function of the pillbox position in the host of GaAlAs. Also, we studied the behavior of the energy of the ground state in this system for different Al concentrations. It is important to stress that for small lengths of the pillbox the energy of the ground state as function de relative position to the barrier potential presents a similar behavior as the binding energy of a hydrogenic impurity in quantum wells, quantum wires and quantum dots. We also found that there are critical values of the pillbox length for which there are no bound states.

**C1 223 Photoconductivity for an Array of Nanowires and Dots*** PAULA FEKETE, GODFREY GUMBS, *Hunter College, CUNY* We present a model calculation for the photoconductivity of a two-dimensional electron gas in an ambient perpendicular magnetic field. An electrostatic modulation which produces quantum wires or dots is also applied. The system is then subjected to a weak radiation field. The Landau eigenstates in the periodically modulated system are first obtained numerically and then used in the Kubo formula to obtain the conductivity. We analyze the frequency-dependent transport coefficients for their dependence on frequency and strength of modulation. The calculation is restricted to the low-frequency regime where the system is assumed to be in or close to equilibrium.

*Mailing Address: Department of Physics and Astronomy, Hunter College of the City University of New York, 695 Park Avenue New York, NY 10021

**C1 224 Dissipation Stabilized Superconductivity in Quantum Wires** HENRY FU, *University of California, Berkeley* ALEXANDER SEIDEL, *Lawrence Berkeley National Laboratory* JOHN CLARKE, DUNG-HAI LEE, *University of California, Berkeley* We present a theory of a superconducting wire dissipatively coupled to an environment. We show that due to the finite extent of the wire, in the absence of dissipation quantum phase slips always destroy superconductivity, even at zero temperature. Dissipation stabilizes the superconducting phase. We apply this theory to understand the ''anti-proximity effect'' recently seen by Tian et. al. [Phys. Rev. Lett. 95, 076802 (2005)] in Zinc nanowires.

**C1 225 Readout of single spins via Fano resonances in quantum point contacts** LEV MOUROKH, *Stevens Institute of Technology* ANATOLY SMIRNOV, VADIM PULLER, JONATHAN BIRD, We examine the feasibility of performing single-spin readout in a small quantum dot (SQD), using a quantum point contact (QPC) that is coupled to it by a larger dot with a quasi-continuous spectrum. When the Fermi energy in the QPC is approximately equal to one of the discrete levels of the SQD, a Fano resonance is observed in its conductance. We propose a procedure that uses such Fano peaks to determine the spin projection of a single electron in the SQD, in the presence of an external magnetic field that causes Zeeman splitting of its levels. We also show that this structure can exhibit Rabi oscillations when subject to microwave irradiation.

**C1 226 Fabrication of 3D-Ordered Nanoporous Gold for Chemical Sensors** DAVID HUNG, NEEPA SHAH, ZHU LIU, *Department of Materials Science and Engineering, Johns Hopkins University* YAOWU HAO, *Materials Science and Engineering Program, University of Texas at Arlington* PETER SEARSON, *Department of Materials Science and Engineering, Johns Hopkins University* 3D ordered nanoporous materials provide high surface-to-volume ratio and controlled nano-scale periodic architecture, making them attractive for applications such as energy storage, catalysis, separations, chemical sensing, and tissue engineering. 3D-ordered nanoporous gold structures were fabricated by electrodeposition of gold into colloidal crystal templates formed by self-assembly. The structures are replicas of the colloidal crystal and have pore sizes and feature sizes that are dependent on the particle size. When the dimensions of a conductor are sufficiently small the resistance is dominated by surface scattering. A prototype chemical sensor was created exploiting this architecture. Molecules with sulfhydryl groups adsorb strongly to gold surfaces and can be monitored by the change in resistance. A resistance change of approximately 2 percent was achieved and a chemical sensor based on surface scattering has been demonstrated.

**C1 227 Electronic and Magnetic Properties of Novel III-V-(M) Superlattices** J. RUFINUS, *Widener University* We present the results of computational works on the electronic and magnetic properties of ''novel'' III-V-(M) (where M is transition metals) superlattice. The calculations were performed using ABINIT and Gaussian 03 codes. The objective of this work is to determine the possibility of ferromagnetism in this type of superlattice.

**C1 228 Intersubband magnetophonon resonance in InAs/AlSb quantum cascade structures.** GEORGY FEDOROV, *National High Magnetic Field Laboratory* AARON WADE, *National High Magnetic Field Laboratory* DMITRY SMIRNOV, *National High Magnetic Field Laboratory* ROLAND TESSIER, *CEM2, University of Montpellier II* ALEXEI BARANOV, *CEM2, University of Montpellier II* Application of an external magnetic field offers a sensitive experimental tool to study and control basic processes which determine the performance of quantum cascade lasers – quantum confinement and intersubband relaxation. A strong magnetic field applied parallel to the confinement direction resonantly modulates the lifetime of the upper state of the laser transition, which is controlled by electron-optical phonon scattering. This effect of the intersubband magnetophonon resonance (ISMPR) allows for the investigation of the electronic structure and electron scattering mechanisms. We report on the observation of ISMPR in quantum cascade lasers based on InAs/AlSb heterostructures. Our experiments have been done under a magnetic field up to 33 T. We observe pronounced quantum oscillations in both the magnetoresistance and the intensity of the intersubband laser emission. Analysis of the obtained data is provided.

**C1 229 Development of Low-Temperature Scanning Capacitance Microscopy for Measurement of Single Quantum Dots*** GUANGLEI CHENG, *Department of Physics and Astronomy, University of Pittsburgh* JEREMY LEVY, *Department of Physics and Astronomy, University of Pittsburgh* GILBERTO MEDEIROS-RIBEIRO, *Laboratorio Nacional de Luz Sincrotron* COSMQC COLLABORATION,† Self-assembled single quantum dots are widely considered to be leading candidates for spin-based quantum bits. The characterization of such systems requires local information about both charge and spin degrees of freedom as a function of temperature and magnetic field. We describe an extension of a working low-temperature AFM/optical microscope to enable scanning capacitance measurements of quantum dots. Our system relies on the sensitivity of a microwave resonator to perturbations from the scanning probe (similar to RCA's CED technology), using a quartz tuning fork with an etched tungsten tip. The expected sensitivity of the instrument ($10^{-21}$ F) is much be-

low the capacitance of a single self-assembled quantum dot ($10^{-18}$ F). To measure the capacitance, we first use the AFM to locate a single quantum dot, and then collect local C-V information using the measured frequency shift of the resonator.

*This work was supported by the DARPA QuIST program (DAAD-19-01-1-0650).

†Center for Oxide Semiconductor Materials for Quantum Computation

**C1 230 Abstract Withdrawn**

**C1 231 Wigner Function for an Impurity in a Parabolic Quantum Dot** GARY SNYDER, *University of Massachusetts Boston* PRAVEEN NITTALA, *University Massachusetts Boston* TOMAS MATERDEY, *University of Massachusetts Boston* High sensitivity of quantum dots with impurities can be linked with phase space high sensitivity to initial conditions. We present the Wigner function for an impurity in a parabolic quantum dot obtained from a variational wavefunction.

**C1 232 Optical and phonon spectra of wurtzite ZnO quantum dots and nanocrystals** VLADIMIR A. FONOBEROV, KHAN A. ALIM, ALEXANDER A. BALANDIN, *Nano-Device Laboratory (http://ndl.ee.ucr.edu), Dept. of Electrical Engineering, University of California, Riverside, CA 92521* ZnO nanostructures have recently attracted attention due to the proposed optoelectronic and spintronic applications. Envisioned applications require accurate knowledge of exciton states and optical phonons. We report results of the investigation of wurtzite ZnO nanostructures with diameters from 2 nm to 20 nm (quantum dots to nanocrystals). The calculated size dependence of the exciton states and UV photoluminescence spectra of ZnO nanostructures is in agreement with the experimental data [1]. In addition, both interface and confined polar optical phonon modes in ZnO quantum dots and nanocrystals have been calculated and identified in the resonant and non-resonant Raman spectra [2]. It was found that the phonon confinement resulted in phonon frequency shifts of few $cm^{-1}$ in the non-resonant Raman spectra. We also show that UV laser excitation in resonant-Raman spectroscopy leads to large red shifts of phonon peaks (up to 14 $cm^{-1}$) due to heating. The authors acknowledge the support of MARCO and its Functional Engineered Nano Architectonics (FENA) Focus Center. [1] V.A. Fonoberov and A.A. Balandin, Appl. Phys. Lett. 85, 5971 (2004); [2] V.A. Fonoberov and A.A. Balandin, Phys. Rev. B 70, 233205 (2004); K.A. Alim, V.A. Fonoberov, and A.A. Balandin, Appl. Phys. Lett. 86, 053103 (2004).

**C1 233 A Study Of CdSe/ZnS Core-Shell Quantum Dots For Use in Luminescent Solar Concentrators** MEREDITH HYLDAHL, SHELDON BAILEY, PAUL FONTECCHIO, BRUCE WITTMERSHAUS, *Pennsylvania State University, Erie* A Luminescent Solar Concentrator (LSC) is a translucent plate that uses embedded fluorescent materials to absorb sunlight. The fluorescence that is produced is then transferred to the edges of the plate via total internal reflection where it is absorbed by photovoltaic cells. We compare a LSC made of CdSe/ZnS core-shell quantum dots (QD) (Evident Technologies) embedded in a transparent epoxy to a LSC made with the fluorescent organic dye Lumogen Red (BASF) cast in a thin polymer film. Fluorescence and absorption spectra and edge light output measurements are reported in this study. The Lumogen Red LSC outperforms the QD LSC suggesting a lower fluorescence quantum yield for the QDs. QDs are also easily oxidized, whereas the Lumogen Red dye is relatively more stable in the presence of oxygen. The merits of QDs as a fluorescent material for a LSC are discussed in terms of light output, photostability, and cost.

**C1 234 Effects of magnetic and electric fields on the excitonic properties of quantum rings** ZDENKA BARTICEVIC, MONICA PACHECO, *Universidad Santa María* JORGE SIMONIN, CESAR PROETTO, *Centro Atómico Bariloche and Instituto Balseiro,C.P. 8400, San Carlos de Bariloche, Argentina* We have studied the effects of an external electric field on the excitonic and optical spectra of a semiconductor quantum ring threaded by a magnetic flux. We have make a detailed analysis of the ground-state properties of radially polarized excitons and its dependence with magnetic fields applied perpendicular to the ring plane and electric fields parallel to the ring plane. In the absence of the electric field, the total angular momentum of the polarized exciton remains a good quantum number, even in the interacting regime, as a consequence of the Coulomb interaction only depends on the relative coordinate and the azimuthal rotational symmetry of the structured rings. The electric field breaks the azimuthal symmetry and mixes the eigenfunctions with differents angular momentum. For the extended regimen we have found that the electric field destroys the oscillations of the ground-state energy as a function of the magnetic field. The low-lying energy levels are almost independent of the magnetic field up to a region in energy where periodic Aharonov-Bohm-type oscillations appear.

**C1 235 Strong Blue Photoemission from Au/ZnO Nanocomposite Material** AKIRA UEDA, *Fisk University* ESOSA EJOMO, ROBERTO AGA, WARREN COLLINS, RICHARD MU, Several layers of Au (5 nm) and ZnO (20 nm) were alternatively deposited on Si and $SiO_2$ substrates with an electron beam evaporator. With post-annealing of the samples in air, the samples were characterized with XRD, RBS, SEM, AFM, and PL. The samples annealed at higher temperatures ($> 700^oC$) exhibit the growth of ZnO nanocrystals in the system. Along with these observations, the samples annealed at higher temperatures emit strong blue photons due to an electric field.

**C1 236 Faraday rotation in one-dimensional magnetic photonic crystals in electric field** I.L. LYUBCHANSKII, N.N. DADOENKOVA, M.I. LYUBCHANSKII, E.A. SHAPOVALOV, A.E. ZABOLOTIN, *Donetsk Physical and Technical Institute of the National Academy of Sciences of Ukraine, Donetsk, Ukraine* Y.P. LEE, *q-Psi and Department of Physics, Hanyang University, Seoul, Korea* TH. RASING, *IMM, Radboud University Nijmegen, Nijmegen, The Netherlands* In the last few years, magnetic photonic crystals (MPCs) or magnetic photonic bandgap materials, are the objects of intensive investigations because of promising application in photonics [1]. A large enhancement of the Faraday rotation (FR) in one-dimensional (1D) MPC was reported [2,3]. In this report, the influence of external electric field on the FR in 1D MPC with magnetic and non-magnetic defect layers is theoretically studied. For the theoretical description of FR we introduce electrical polarization, which depends on magnetization and external electric field. Numerical calculations of the dependence of FR on the strength and the direction of electric field is done for the 1D MPC based on yttrium-iron garnet. [1] I. L. Lyubchanskii, N. N. Dadoenkova, M. I. Lyubchanskii, and Th. Rasing, J. Phys. D: Appl. Phys. 36, R277 (2003). [2] M. Inoue and T. Fujii, J. Appl. Phys. 81, 5659 (1997). [3] M. Steel, M. Levy, and R. M. Osgood, J. Lightwave Technol. 18, 1298 (2000).

**C1 237 Optical and magneto-optical properties of 1-D dielectric and magnetic photonic crystals.** M.D. HUANG, Y.H. LU, P.J. KIM, S.Y. PARK, Y.P. LEE, *Quantum Photonic Science Research Center and Department of Physics, Hanyang University, Seoul, 133-791 Korea* The optical properties of one-dimensional (1-D) photonic crystals (PCs) and magnetic PCs (MPCs), composed of dielectric $TiO_2$ and $Al_2O_3$ as well as magnetic Bi:YIG layers deposited on a glass substrate, are investigated in this work. The structure of dielectric 1-D PCs was optimized and a narrow omni – photonic bandgap (PBG) is found away from the designed wavelength. When a Bi:YIG layer with an optical thickness of quarter wavelength is inserted, no defect mode is found within the PBG despite the structural defect. However, when the thickness becomes half wavelength, a defect mode can be obtained at the designed wavelength, revealing the localization of light. More magnetic defect layers induce correspondingly more defect modes within the PBG. Large Faraday rotation angles, indicating strong magneto-optical (MO) effects, are obtained at the defect modes in the MPCs. A considerable amount of coupled light, whose polarization is perpendicular to that of incident light, confirms the enhanced MO effects at the defect modes.

**C1 238 Band gap of a 3D dyed polystyrene photonic crystal from optical absorption.** NA YOUNG HA, *University of Pennsylvania* JEONG WEON WU, *Ewha Womans University* Three-dimensional (3D) photonic crystals (PCs), fabricated from colloidal spheres doped with organic dye and whose optical absorption overlaps with the photonic band gap (PBG), have been studied to determine the relation between the PBG widening and the increased contrast in refractive indices. In this work, we report on the identification of the role of the optical absorption of the dye in determining the PBG shape of a 3D dyed PC, which is fabricated from colloidal dyed-polystyrene spheres consisting of an inner core and an outer shell. In analyzing the optical reflection spectra of 3D dyed PCs, an analytical electromagnetic wave scattering theory was rigorously employed, with the dispersive and absorptive optical responses of the composite dyes fully taken into account. It was subsequently found that the characteristic PBG shape of the 3D dyed PC, when measured in the reflection spectra, results from two superimposed contributions with distinct origins, i.e., a Bragg reflection and a high reflection associated with the strong dye absorption.

**C1 239 Faraday effect of 1-D magnetic photonic crystals for normal and parallel incidence to the periodic direction** Y. H. LU, M. D. HUANG, S. Y. PARK, P. J. KIM, Y. P. LEE, *q-Psi and Dept. of Physics, Hanyang Univ., Seoul 133-791, Korea* J. Y. RHEE, *BK21 Physics Research Division and Institute of Basic Science, Sungkyunkwan Univ., Suwon 440-746, Korea* We calculated the Faraday rotation of one-dimensional (1-D) magnetic photonic crystals (MPCs), which are based on the dielectric $Ti_2O_3$ and $Al_2O_3$, and the magnetic Bi:YIG, by employing 4 x 4 transfer-matrix method for the general case that the linearly polarized incident beam is parallel to their periodic direction, as mostly studied for the 1-D MPCs. Furthermore, even for a special case of normal incidence, the calculation of Faraday rotation was also carried out for such discontinuous thin films with a 1-D array structure and the existence of rotation was proved, which had been scarcely studied yet. The magneto-optical Faraday effects obtained for these two cases are compared and discussed in detail.

**C1 240 Modeling and fabrication of photonic bandgap waveguiding structures*** M.Y. TEKESTE, *Physics Department, Miami University, Oxford, OH* P.R. RICE, *Physics Department, Miami University, Oxford, OH* J.M. YARRISON-RICE, *Physics Department, Miami University, Oxford, OH* Novel photonic devices based on the idea of photonic bandgap (PBG) crystals are poised to make contributions in modern optoelectronic and telecommunication applications. These nanophotonic devices have the ability to guide light with very low loss even around tight corners. Several PBG waveguide structures are modeled using using the finite difference time domain technique in EMlab software. The resulting electric field distributions allow us to study single line defect waveguiding and a wavelength demultiplexer structure for single mode propagation, the depth of light leakage into the lattice, and transmission coefficients. These models inform the experimental fabrication process where a 2D triangular lattice is etched into the silicon nitride on silicon dioxide planar wafer which has been patterned via e-beam lithography. SEM micrographs record the various fabrication steps. Optical characterization of the structures will include bulk transmission measurements, as well as near field scanning microscopy.

*We gratefully acknowledge computer support of OAST, Miami University

**C1 241 Fano Resonance in Photonic Crystals and Quantum Mechanics** SOLOMON DUKI, FRANCESC FERRER, H. MATHUR, *Case Western Reserve University* We study the resonant transmission through a photonic crystal channel dope device. The frequency dependence of the resonant transmission is shown to have an asymmetric Fano line shape. In contrast to previous work[1] we find the symmetric Lorentzian line shape results only under special conditions of high device symmetry. We also study quantum systems in which the resonant scattering cross section has an asymmetric Fano line shape as a function of energy. Surprisingly the associated long-lived quasi-bound state under goes simple exponential decay, just as it would in the symmetric Lorentzian case.

**C1 242 Raman Spectroscopy from Optical Trapped Nano Coated Microsphere Complexes** EMANUELA ENE, CHUCK BLACKLEDGE, JAMES WICKSTED, *Oklahoma State University* The Raman measurements from optically trapped gold nanowires and from nanoparticles coated on microspheres, under various visible laser excitation wavelengths, are being studied. Changes in the Raman spectra for the trapped coated microspheres when they were positioned at different distances from an immersed photonic crystal (PC) are being investigated. We are also developing a method which has the potential of detecting certain molecules present in biological environments.

**C1 243 Abstract Withdrawn**

**C1 244 Inelastic cotunneling current and shot noise of an interacting quantum dot with ferromagnetic correlations** BING DONG, *Shanghai Jiaotong University, China* NORMAN J. M. HORING, *Stevens Institute of Technology* V. FESSATIDIS, *Fordham University* We explore inelastic cotunneling through a strongly Coulomb-blockaded quantum dot attached to two ferromagnetic leads in the weak coupling limit using a Langevin equation approach.[1] We first develop a Bloch-type equation to describe the cotunneling-induced spin relaxation dynamics, and then derive explicit analytical expressions for the local magnetization, current,

and its fluctuations. On this basis, we predict a novel zero-bias anomaly of the differential conductance in the absence of a magnetic field for the anti-parallel configuration, and asymmetric peak splitting in a magnetic field, which are ascribed to rapid spin-reversal due to underlying spin-flip cotunneling.[2] [1] B. Dong, N. J. M. Horing, and H. L. Cui, Phys. Rev. B **72**, 165326 (2005). [2] B. Dong, X. L. Lei, and N. J. M. Horing, cond-mat/0509098.

**C1 245 Electron transport properties in InAs ballistic devices** MASATOSHI KOYAMA, MASATAKA INOUE, MASASHI FURUKAWA, HIROSHI TAKAHASHI, TOSHIHIKO MAEMOTO, SHIGEHIKO SASA, *New Materials Research Center, Osaka Institute of Technology* A ballistic rectifier is one of the applications using ballistic electron transport properties, and has been fabricated by using high quality compound semiconductor heterostructures. We have observed a rectification for the first time in InAs triangular anti-dot structures at 77K and room temperature [1]. InAs/AlGaSb heterostructures provide relatively long mean free path for ballistic electron transport because of its high carrier density ($1.0 * 10^{12}$ $cm^{-2}$ at 77K) and high electron mobility (200,000 $cm^2$/Vs at 77K). In the present report, we will focus on nonlinear electron transport properties in InAs asymmetric anti-dot structures as well as ballistic rectification effects at higher temperatures. In addition, the observed magnetotransport properties in the InAs ballistic rectifiers will be also presented at the conference. [1] M. Koyama et al., presented at the $14^{th}$ Int. Conf. on Nonequilibrium Carrier Dynamics in Semiconductors, 2005.

**C1 246 Electrode fabrication and attachment of organometallic molecules for conductivity measurements*** S. RAJAGOPAL, *Physics Department, Miami University, Oxford, OH* N. SMITH,† *Physics Department, Miami University, Oxford, OH* J.M. YARRISON-RICE, *Physics Department, Miami University, Oxford, OH* C. URIG, T. SCOTT, S. ZOU, H. ZHOU, *Department of Chemistry and Biochemistry, Miami University, Oxford, OH* The primary goal of this research is to understand the bonding and electronic structure within this class of compounds and the influence of a gated electric field on their conductivity. We report an approach for connecting a single molecule containing di-metal units to electrodes with nanometer gaps. We have succesfully fabricated pairs of terminal electrodes with intial gaps of $\sim$ 75 nm which we then close using electrodepostion and re-open with electromigration to nanometer gaps. The results of the time resolved voltage curve during the electrodepostion process show that most of electrodes have a very short closing time. We have also fabricated lateral three terminal devices for studying the influence of a gated third electrode. The present results show that a gap to gate distance of less than 50nm is acheivable. Our next step is to deposit molecules on the thin gap, and to measure the electrical conductivity when a single molecule bridges the gap and conducts current.

*We gratefully acknowledge NSF through the NER - award #0403669.

†Now at: ECECS, University of Cincinnati, Cincinnati, OH

**C1 247 Correlating Internal Chemical and Physical Structure with Electrical Data for Nanoscale Molecular-Electronic Devices** JASON J. BLACKSTOCK, *Quantum Science Research, HP Labs* WILLIAM F. STICKLE, *HP Labs Corvallis* CARRIE L. DONLEY, DUNCAN R. STEWART, R. STANLEY WILLIAMS, *Quantum Science Research, HP Labs* The critical limitation for most nanoscale molecular-electronic devices is the lack of physical/chemical characterization accompanying electrical data. Present most device geometries and fabrication processes are incompatible with conventional photon and electron spectroscopies and scanning probe microscopies – critical layers and interfaces are frequently inaccessibly buried inside the as-built device structures. We present the fabrication of a new stencil-based nanopore device geometry, along with techniques for studying the in-situ characterization of the as-build internal properties of these devices. These methods were developed in combination to allow the cleaving of completed device stacks at internal inorganic/organic interfaces in a UHV environment. This cleaving process exposes the uncontaminated and unaltered internal nanoscale chemical and physical structure in UHV for examination with a range of conventional tools. We specifically present on XPS, IR and STM data from several metal/organic-monolayer/metal device stacks of interest, and conclude by correlating temperature-dependant and IETS electrical data on nanoscale devices with the physical/chemical characterization.

**C1 248 Thermoelectric Properties of a Nanocontact** KEIVAN ESFARJANI, MONA ZEBARJADI, *Department of Physics, Sharif University of Technology, Tehran, Iran* Thermoelectric properties of a nanocontact made of two capped single wall carbon nanotubes (SWCNT) are calculated within the tight-binding approximation and by using Green's function method. It is found that doped semiconducting nanotubes can have high Seebeck coefficients. This in turn leads to very high figures of merit(ZT) for p-doped tubes which turn out to have also a large electrical to thermal conductivity ratio. Transport in the nanocontact device is dominated by quantum interference effects, and thus it can be tuned by doping (charge transfer and/or impurity potential) or application of a (nano-)gate voltage, or a magnetic field. Another reason for high ZT in this device is the absence of phonon transport as there is barely a contact between the two sides.

**C1 249 Microscopic Investigations of Phonon Thermal Conductivity in SiGe Superlattices with Rough Interfaces** SHANGFEN REN, *Illinois State University* WEI CHENG, *Illinois State University and Beijing Normal University* GANG CHEN, *Massachusetts Institute of Technology* Phonon thermal conductivity in semiconductor superlattices (SLs) has attracted a great research attention in recent years due to the potential applications of SLs in thermoelectric devices and other applications [1]. By using a microscopic model developed to investigate phonon properties in semiconductor nanostructures [2], we have calculated thermal conductivities of SiGe SLs with rough interfaces in both the growth and in-plane directions. The results are compared with SLs with perfect smooth interfaces as well as bulk random alloys. Our results show that thermal conductivities of SLs with rough interfaces are much lower than SLs with the same thickness but smooth interfaces in both directions. In the in-plane direction, the thermal conductivities of SLs with rough interfaces are about the same as random alloy but lower than random alloy in the growth direction. Our results indicate that the interface roughness is a true mechanism of thermal conductivity reduction in SLs. References: [1] Partially Coherent Phonon Heat Conduction in Superlattices, B. Yang and G. Chen, Phys. Rev. B 67, 195311 (2003). [2] A Microscopic Investigation of Phonon Modes in SiGe Alloy Nanocrystals, S. F. Ren, W. Cheng, and P. Y. Yu, Phys. Rev. B 69, 235327 (2004).

**C1 250 Semiconductor Nanocomposites for Direct Energy Conversion Applications** JEFF URBAN, *IBM/MSU* DMITRI TALAPIN, ELENA SHEVCHENKO, CHRIS MURRAY, *IBM* MERCOURI KANATZIDIS, *MSU* Novel materials for thermoelectric and photovoltaic applications may be rationally designed by assembling quantum dots with distinct thermal, optical, and electronic characteristics into nanocomposite superlattices and glassy thin films. Here we present the synthesis and initial thermoelectric characterization of semiconductor nanocomposites composed of lead chalcogenide (PbX = PbS, PbSe, PbTe) nanocrystals. Monodisperse nanocrystals of all PbX materials varying in size from $\sim$ 4-10nm are synthesized, and their structural, optical, and electronic properties are presented. Well-ordered nanocomposites composed of two different types of PbX nanocrystals are synthesized and their basic thermoelectric characteristics are studied. The strategy of using nanocrystal composites for thermoelectric applications will, in principle, provide an opportunity to independently tune the desired electronic and phonon scattering characteristics of these materials.

**C1 251 Crossover in Thermal Transport Mechanism in Nanocrystalline Silicon** ARUN BODAPATI, PAWEL KEBLINSKI, *Rensselaer Polytechnic Institute* PATRICK SCHELLING, *University of Central Florida* SIMON PHILLPOT, *University of Florida* Using vibrational mode analysis of model structures we demonstrate that lattice vibrations in small grain ( $<$ 3 nm) structurally inhomogeneous nanocrystalline silicon are almost identical to those of homogeneous amorphous structures. In particular, the majority of the vibrations are delocalized and unpolarized. As a consequence the principal thermal conductivity mechanism in such nanocrystalline materials is essentially the same as in the amorphous material. With increasing grain size the ability of vibrations to ''homogenize'' over the nanocrystalline structure is gradually lost and the phonon spectra and polarization become progressively more like that of a crystalline material; this is reflected in a crossover in the mechanism of thermal transport. Interestingly, a few of the vibrational modes are localized either on the grain boundary and the grain interiors.

**C1 252 Switching Light through Arrays of Sub-wavelength Holes in Vanadium Dioxide*** E. U. DONEV, J. Y. SUH, R. LOPEZ, R. F. HAGLUND, L. C. FELDMAN, *Vanderbilt University, Nashville, Tennessee, USA* Transmission of near- and far-field light through periodic arrays of sub-wavelength holes is a subject of intense interest. We present the first studies on perforated vanadium dioxide ($VO_2$) thin films that can modulate the transmission of near-infrared light by virtue of their semiconductor-to-metal transition. Modulation arises because of the marked difference in dielectric contrast between the holes and the surrounding material in the two phases of $VO_2$. In perforated structures consisting of a silver (or gold) layer atop a $VO_2$ layer, the modulation effect constitutes a novel kind of dynamical control of the enhanced optical transmission through sub-wavelength holes in opaque metal films. Surprisingly, such double-layer structures exhibit a reversal in the optical switching of $VO_2$, as the near-infrared transmission during the metallic phase exceeds its semiconducting-phase counterpart—opposite of the transmission behavior of plain $VO_2$ films. We explain this by accounting for the loss of transmitted intensity due to leaky evanescent waves inside the holes and scattering at the entrance and exit apertures.

*Supported by the U. S. Department of Energy (DE-FG02-01ER45916) and by the NSF (DMR-0210785 and DMR-9871234).

**C1 253 Integrated Semiconductor-Ferroelectric Nanostructures*** S. S. NONNENMANN, R. S. JOSEPH, L. CAO, J. E. SPANIER, *Department of Materials Science and Engineering and the A. J. Drexel Nanotechnology Institute, Drexel University, Philadelphia PA* The integration of semiconductor and ferroelectric nanostructured materials provides new opportunities for investigating ferroelectric stability in nanostructures and for the design of multifunctional nanoscale devices. We present progress in the development of new synthetic strategies for the preparation of nanostructures consisting of semiconducting and ferroelectric components. We report on characterizations of the structural, electronic and functional properties of these hybrid nanostructures and devices via electron microscopy, Raman scattering spectroscopy, scanning probe microscopy, and electronic transport measurements.

*Work supported by ARO under W911NF-04-1-0308.

**C1 254 Magnetic resonance study of nanoparticles systems** NATALIA NOGINOVA, FENG CHEN, TRACEE HARRIS, *NSU* EMMANUEL GIANNELIS, ATHANASIOS BOURLINOS, *Cornell University* VADIM ATSARKIN, *IRE, Moscow* Magnetic nanoparticles of gamma-$Fe_2O_3$ coated by organic molecules and suspended in liquid and solid matrices, as well as non-diluted magnetic fluid have been studied by ESR in the dependence on temperature and relative concentration. The ESR spectrum demonstrates an interesting double feature shape, with narrow peak at g=2 growing in intensity with increase in temperature. Angular dependence of the ESR signal in field cooled samples unambigously points to the dominating uniaxial magnetic anisotropy of the nanoparticles, suggesting a strong surface effect. The interpretation based on the FMR equations with account made for thermal fluctuations of the magnetic moment is compared with ''paramagnetic'' model suggesting a discrete energy spectrum of the lowest high-spin multiplet. Consideration of the superparamagnetic nanoparticles as intermediate between paramagnetic and ferromagnetic entities allows us to explain most of the obtained experimental results and estimate parameters of the magnetization, particle interactions and magnetization dynamics.

**C1 255 Interface effects in modulation-doped manganite superlattices** MARIA E. GOMEZ, G. CAMPILLO, P. PRIETO, *Excellence Center for Novel Materials. Universidad del Valle, A.A. 25360 Cali, Colombia* A. HOFFMANN, *Argonne National Laboratory, Materials Science Division, Argonne, Illinois 60439* A. BERGER, *Hitachi Global Storage Technologies, San Jose Research Center, San Jose, CA* J. GUIMPEL, N. HABERKORN, A. CONDO, *Centro Atómico de Bariloche Instituto Balseiro 8400 Bariloche, Argentina* Epitaxial superlattices of antiferromagnetic $La_{1/3}Ca_{2/3}MnO_3$ and ferromagnetic $La_{2/3}Ca_{1/3}MnO_3$ were grown using a high-pressure sputtering technique. Structural analysis was performed by simulation of X-ray diffraction data using the SUPREX program and Transmission Electron Microscopy. Both techniques confirmed interfacial roughness in the range of one unit cell. Magnetization measurements showed that magnetization

depth profile is incommensurate with the doping profile, such that the ferromagnetic order extends into the antiferromagnetically doped region beyond the chemical doping interface. Thermal demagnetization in the low temperature range obtained from the temperature dependence of the saturation magnetization shows an $\alpha=5/2$ power law dependence, independent of the ferromagnetic layer thickness. The $T^{5/2}$term is associated with long-wave length spin waves, and corresponds to the anharmonic second-order expansion of the magnetization. This work was supported by COLCIENCIAS contract 043-2005, and U.S. DOE-BES under contract W-31-109-ENG-38.

**C1 256 Isolated hollow nano-spheres of Co on the surface** TOSHIFUMI TERUI, TAKASHI NAGASE, HIROYUKI HASEGAWA, SHINRO MASHIKO, *National Institute of Information and Communications Technology* YASUHARU KODUKA, YE QUAN-LIN, HIROFUMI YOSHIKAWA, MOTOTAKA ONISHI, KUNIO AWAGA, *Department of Chemistry, Nagoya University* In magnetic materials of sub-micron and the nano-meter size, peculiar magnetic structures and characteristics are expected. The hollow sphere of Co is an interesting material in such nano magnetic materials because of the unique structure. The diameter and the thickness of shell of the hollow sphere of Co can be accurately controlled between 100-500nm and 40nm respectively. It is necessary to examine the physical properties about isolated hollow sphere of Co to apply this material as nano-spin material. Therefore, we combined the top down and the bottom up technique to isolate the sample on the surface. For example, the nanogap electrode and patterns were fabricated by EB lithography and FIB, and manipulation and the conduction measurement were performed by SEM with probe.

## C1 257 INSTRUMENTATION AND MEASUREMENTS POSTER SESSION

**C1 258 Low-Cost Cavity Ring-Down System For Measurement Of High Reflectivity Semiconductor Mirrors** DANIEL TREMBLAY, SUSAN LEHMAN, *The College of Wooster* A cavity ring-down system consisting of a half-symmetric optical resonator with a swept cavity design has been constructed from off-the-shelf components in order to investigate ultra-high reflectivity distributed Bragg reflectors (DBRs). Cavity ring-down is a sensitive technique often used for spectroscopy that measures the buildup and decay of laser light within a high finesse optical cavity. Once light is resonant in the cavity, the resonance is interrupted so that the light within the cavity decays. From this measured decay time, the amount of light lost per pass to mirror losses or absorptive and scattering losses is determined. As a measurement of time rather than absolute intensity, cavity ring-down has the advantage of not requiring calibration since it is unaffected by drifts in laser intensity or detector sensitivity. This low-cost ring-down system was designed with one planar mirror and one concave mirror to allow simple conversion to DBR measurement. The concave mirror is mounted on a piezoelectric modulator to enable rapid sweeping of the cavity length, eliminating the need for an acousto-optic modulator to shutter the light off, but increasing the analysis complexity due to Doppler shifting of the light by the moving mirror. A cw-laser tunable over 30 nm is used to probe the cavity and DBR system.

**C1 259 Potentiometric Sensing of the Organic Molecules*** YANTIAN WANG, *State University of New York at Stony Brook* VIJAY JAIN, *Herricks High School* HARRIMAN LEE, *The Wheatley School* KALLE LEVON, *Polytechnic University* MIRIAM RAFAILOVICH, JONATHAN SOKOLOV, *State University of New York at Stony Brook* A prototype detector was constructed for the detection of complex biomolecules, such as viruses and complete chromosomes. The technology is based on Ref. [1], where the technique was demonstrated for small molecules. A monolayer of 11-mercapto-1-undocanol (thiol) is coabsorbed with the organic molecules on a gold plated electrode. The thiolated molecules self assemble into a highly organized crystalline film chemically anchored to the surface. The biomolecules which are not attached and can then be removed by washing in water, leaving behind templated regions, or cavities in the monolayer with specific size and shape. The electrochemical response between the modified electrode and the Ag/AgCl reference electrode was measured by the potentiometer. When the electrode was exposed to the solution containing the template molecules, in a concentration as low as $10^{-6}M$, a sharp potential response was observed, while very slight response was observed when exposed to other kind of molecules. This was attributed to the selective absorption of the molecules onto the electrode. Reference: [1]. Zhou Y., Yu B., Shiu E., Levon K., itAnal. Chem. 2004, 76, 2689.

*Supported by the NYS Center for Maritime and Port Security

**C1 260 Magnetic Domain Wall Motion as a Basis for a New Type of Sensor.** SEONG-JAE LEE, YEVGEN MELIKHOV, *Center for NDE, Iowa State University, Ames, Iowa 50011, USA* CHOON-MAHN PARK, *Dept. of Physics, Seonam University,Namwon 590-711, Korea* HANS HAUSER, *Institute of Sesnor and Actuator Systems, Vienna Univ. of Technology, A-1040 Vienna, Austria* DAVID JILES, *Wolfson Centre for Magnetics, Cardiff University, Cardiff CF24 3AA, United Kingdom* It has been found that the periodic motion of a magnetic domain wall under the action of a magnetic field can be used as a basis for linear and angular displacement sensor. The domain wall between two opposite domains is created by the field from two opposite permanent magnets and the periodic motion is excited by an external ac current. When the up-domain covers both the incident and reflected laser beam paths, the Faraday rotation reaches a positive maximum and when the down-domain covers both beams, the Faraday rotation reaches a negative maximum. If when the domain wall is between the incident and reflected laser beams, the Faraday rotation cancels and a reference or nominal ''zero'' rotation occurs. The sensor system consists of a laser, magneto-optic film, magnets, and a detector. By observation of the pattern of detected light intensity as a result of periodic movements of magnetic domain wall, we can extract information about linear or angular displacement a surface with resolution down to 3 $\mu$m or 0.01 deg, respectively.

**C1 261 The challenge of characterizing an inefficient antenna field for health protection purposes** MARJORIE LUNDQUIST, *The Bioelectromagnetic Hygiene Institute* Growing evidence that the electromagnetic field around electrical wires is harmful to human health prompted a 1990s National Academy of Sciences study of power-frequency (50-60 Hz) fields; results for power-frequency fields were negative but data suggested that fields from *transients* may be hazardous.[1] Transients represent high frequencies that can reach into the radiofrequency (RF) range. What in-

strument can be used to measure an RF field around electric wires carrying RF current? Such an RF field is that of an *inefficient antenna*, which lacks the pure far-field region characteristic of an *efficient antenna field* for which standard RF measuring instruments are calibrated, making it impossible to obtain a properly calibrated measurement with such instruments. The *magnetic induction current* d**B**/d*t* is explored as an alternative way to characterize the *inefficient antenna RF field* sheathing electric wires carrying RF due to *poor power quality* ( *e.g.*, switching transients) or to utility use of *power line carrier* [2] or of FCC-approved *broadband on power lines*. [1]National Research Council, **Possible Health Effects of Exposure to Residential Electric and Magnetic Fields**, Washington, DC: National Academy Press, 1997. [2]M. Vignati & L. Giuliani, Environ. Health Perspect. **105** (Suppl 6):1565-1568(1997).

**C1 262 Current Status of LANSCE Single Crystal Diffractometer - SCD** ALICE I. ACATRINEI, LUKE L. DAEMEN, MONIKA A. HARTL, *Los Alamos National Laboratory, LANSCE-12, MS H805, Los Alamos, NM 87545* JACOB URQUIDI,* *New Mexico State University, Department of Physics, MSC 3D, Las Cruces, NM 88003* The Single Crystal Diffractometer (SCD) at LANSCE, Los Alamos National Laboratory, represents a powerful tool for many crystallographic and magnetic structure determinations. The instrument is located at the Lujan Neutron Scattering Center and utilizes the time-of-flight (TOF) Laue technique for neutron scattering data collection. This technique, combined with a 25 cm × 25 cm multi-wire 3He position-sensitive detector and the possibility of two axis of rotation for sample orientation yield to an 80% sphere of coverage in reciprocal space. The redesign and status of the Single Crystal Diffractometer at LANSCE are reported. We give an overview of the instrument characteristics and of the of calibration and data evaluation activities (higher intensity, lower background, better profile shape, improved resolution).

*Los Alamos National Laboratory, LANSCE-12, MS H805, Los Alamos, NM 87545

**C1 263 Effects of asphericity in charge distribution on electron scattering amplitude.*** JIN-CHENG ZHENG, LIJUN WU, YIMEI ZHU, *Brookhaven National Laboratory, Upton, NY 11973* The sensitivity of atomic scattering factors to valence-charge distributions has been compared quantitatively for x-ray and electron diffraction. It is found that electron diffraction provides information about valence charge densities via the low-order structure factors, which are relatively insensitive to thermal vibrations, but sensitive to the charge distribution that characterizes the chemical bonding properties in materials. The effects of asphericity in charge distribution on electron scattering amplitude have been examined using both analytical and numerical methods. We show that the aspheric effects are dominated in low-order scattering region, where the electron scattering factor of Bragg reflections can be measured very precisely by quantitative electron diffraction, and therefore enables us to quantitatively determine the spherical and aspherical orbital ordering. The applications of quantitative electron diffraction in strongly correlated materials are discussed.

*This work was supported by DOE under Contract No. DE-AC02-98CH10886

**C1 264 Analytical form for the tip-sample interaction in liquid for Atomic Force Microscopy** FREDY ZYPMAN, *Yeshiva University* Knowledge of the functional form of force-separation curves in Atomic Force Microscopy (AFM) is necessary to develop reconstruction algorithms to predict the morphology and chemical activity of the sample under study. In vacuum, the tip and the sample can be modeled as a collection of atoms. The tip-sample force can thus be evaluated from the appropriate atom-atom forces. These elemental forces have been modeled via Morse, 6-12 pair potentials, and more detailed quantum approaches with non pair-wise forces. Nevertheless, a large section of the AFM community is interested in tip-sample interactions in the presence of fluids. The production of theoretical expressions for colloidal interactions relevant to AFM has been hampered by the fact that analytical solutions to the Poisson-Boltzmann equation (PBE) are restricted, thus far, to planar geometries. Numerical solutions for other geometries do exist, but they are computationally expensive. We present a simple theoretical expression for the interaction forces between the Atomic Force Microscope tip, and a sample immersed in an electrolytic solution. Our result is based on the Surface Element Integration of the Dejarguin-Landau-Verwey-Overbeek interaction between flat surfaces. We apply our results to the Van der Walls and to the electrostatic double layer cases. Finally, we use our expression to show how it simplifies the analysis of extant experimental data. Acknowledgment. Work supported by Research Corporation through grant CC5786.

**C1 265 3D ESR-MRI with A Sub-Micrometer Resolution Using Magnetic Resonance Force Microscopy** SHIGENORI TSUJI, YOHSUKE YOSHINARI, *JEOL Ltd. and CREST-JST, Japan* KOSUKE INOMATA, *Kyoto Univ. and CREST-JST, Japan* We will present our progress of ESR Magnetic Resonance Force Microscopy (MRFM). In order to improve our previously achieved resolution (2∼ 3 micrometer), we used an electropolished magnetic tip made of a sintered Nd2Fe14B permanent magnet, which generated a larger magnetic field gradient (8000 T/m) in the very vicinity of the magnetic tip. To avoid a collision between a sample glued on a cantilever and the magnetic tip placed on a 3D stage, the tip-sample direction was set parallel to the cantilever long axis. Magnetic resonance force signals were induced by a cyclic saturation technique. In this setup, the observed signals had an anti-symmetrical phase with respect to a plane that contains a specimen and is perpendicular to the vibrational direction of the cantilever. MRFM image was then reconstructed from the force map through FT deconvolution. At present, our MRFM can produce 3D ESR-MRI with a sub-micrometer spatial resolution.

**C1 266 Optical properties of the tips for apertureless near-field microscopy*** DISHA MEHTANI, N. LEE, R. D. HARTSCHUH, A. KISLIUK, M. D. FOSTER, A. P. SOKOLOV, I. TSUKERMAN, *The University of Akron* Apertureless near-field optical microscopy is based on the enhanced optical signal in the vicinity of a metal or metal-coated tip via surface plasmon generation in the metal. Resonant excitation of the plasmons is crucial for maximizing enhancement under the tip. However, it remains a challenge to measure the optical properties of the nanoscale apex of a tip with a radius much smaller than the wavelength of light. We have developed a system to measure optical properties of tips based on the principle of total internal reflection microscopy. Optical resonance spectra of silver- and gold-coated tungsten and silicon nitride tips exhibit a dependence on the metal deposited. We also measured the wavelength dependence of tip-enhanced

Raman signal. The enhancement of the Raman signal for silicon with gold-coated silicon nitride tips was found to be ~ 3 times stronger for a wavelength of 647 nm than for 514.5 nm. The former is closer to the plasmon resonance observed for this tip at ~ 680 nm. Additional examples correlating enhancement with resonance excitation will be presented.

*This research was supported by an NSF-MRI grant (DMR-0215966) and Air Force Research Laboratory

**C1 267 High contrast nano-Raman spectroscopy with optimized polarization** NAM-HEUI LEE, RYAN HARTSCHUH, DISHA MEHTANI, ALEXANDER KISLIUK, MARK FOSTER, ALEXEI SOKOLOV, *Department of Polymer Science, The University of Akron, Akron, OH 44325, USA* JOHN MAGUIRE, *Materials and Manufacturing Directorate/MLBP, Wright-Patterson AFB, OH 45433, USA* For nanoscale characterization of chemical composition, structure, stresses and conformational states, tip-enhanced Raman spectroscopy (TERS) is an attractive tool. A TERS spectrometer based on side illumination geometry that shows reproducible enhancement of the order of $10^3$-$10^4$, for a variety of molecular, polymeric and semi-conducting materials using silver- and gold-coated silicon nitride tips, will be presented. The radius of the spot from which the Raman signal comes is estimated to be 20nm for CdS thin films. For thick samples, such as a silicon wafer, polarization was optimized to achieve high contrast between the near- and far-field Raman signals. Additionally, systematic studies to estimate the localization volume of the detected near-field Raman signal with the optimized polarization are being performed. Raman imaging with sub-wavelength lateral resolution will be demonstrated on several nano-structures.

**C1 268 UHV LT-STM system with Sample and Tip Exchange** MICHAEL DREYER, *Lab for Physical Sciences, Dept. of Electrical and Computer Engineering, University of Maryland* JONGHEE LEE, HUI WANG, DAN SULLIVAN, *Lab for Physical Sciences, Dept. of Physics, University of Maryland* BARRY BARKER, *Lab for Physical Sciences, National Security Agency* We developed and built a low temperature scanning tunneling microscope system with ultra high vacuum sample and tip preparation capabilities. The STM is mounted inside an UHV can which is submerged in a He bath cryostat. The cryostat is equipped with two superconducting magnets allowing a maximum in plane field of 2 T and a maximum out of plane field of 9 T. The two fields can be combined to a 1 T vector field. The vacuum can is connected to an UHV system at room temperature consisting of two chambers: One dedicated to transferring samples and tips to the STM, and the other chamber used for tip/sample preparation. It is equipped with two electron beam evaporators, an argon ion sputter gun as well as sample heaters. The whole system is supported by an optical table to decouple the STM from building vibrations. The system was successfully used to study standing electron waves on gold (111) as well as vortices on NbSe2. Details of the microscope, sample and tip handling system, as well as the UHV system will be presented.

**C1 269 Modification of Tips for Use With Tip-Enhanced Raman Spectroscopy (TERS)** SCOTT HAMILTON, NAM-HEUI LEE, DISHA MEHTANI, RYAN HARTSCHUH, ALEXEI SOKOLOV, MARK FOSTER, *Maurice Morton Institute of Polymer Science, University of Akron* In tip-enhanced Raman spectroscopy (TERS) the Raman signal is enhanced only in the vicinity of a probe tip that can be positioned near the surface of a sample. TERS tips were made by vapor-depositing gold onto AFM tips. These tips create plasmon resonances in the focal spot of the incident laser beam. Variation in the enhancement provided by the tips with the morphology of the metal surface was studied. Enhancement was found to be a function of film thickness and roughness. Deposition of metal nanoparticles on the tip surface was also studied as an alternative method of modification. Optical properties of various nanoparticles are being determined experimentally, allowing comparison with theoretical calculations.

**C1 270 Digitally Controlled Quad Sine Wave Generator.** MOHAMMED Z. TAHAR, *SUNY College at Brockport* Square, triangular, and sine and cosine waves of same frequency are generated with single digital command, using off the shelf components. This method does not synthesize the waves using the continuous digital control of the out put(s), as for arbitrary wave functions. The frequency ranges from below one to thousands of Hz, with the use of one capacitor. Also, the method lends itself to the use of embedded microcontrollers for frequency and independent amplitude control through the use of multiplying digital to analog converters. Because of the omnipresence of microcontrollers, the method is an inexpensive computer controlled frequency quad sine wave generation. With the addition of an analog-to-digital converter, one can use such a generator for systems studies in control and measurements.



## SESSION D1: FLUCTUATION AND RELAXATION NEAR JAMMING
**Monday Afternoon, 13 March 2006; Ballroom IV, Baltimore Convention Center at 14:30**
**Sharon Glotzer, University of Michigan, presiding**

**14:30**
**D1 1 Dynamic model of super-Arrhenius relaxation rates in glassy materials.***
J. S. LANGER, *University of California, Santa Barbara*

The principal theme of this talk is that anomalously slow, super- Arrhenius relaxation processes in glassy materials may be activated by chains of atomic displacements. The entropy of critically long excitation chains can enable them to grow without bound, thus stabilizing thermal fluctuations in the local density or atomic coordination of the material. I argue that the intrinsic atomic-scale disorder in a glass plays an essential role in determining the activation rate for such chains, and show that the resulting rate formula is essentially the same as the Vogel-Fulcher law. A key feature of this theory is that

the spatial extent of critically long excitation chains diverges at the Vogel-Fulcher temperature. I speculate that this diverging length scale implies that ergodicity is partially broken in the super-Arrhenius region above that temperature, and point out how this partially broken ergodicity may explain the vanishing entropy at that point and other observed relations between dynamics and thermodynamics of the glass transition.

*Research supported by U.S. Department of Energy Grant No. DE-FG03-99ER45762.

**15:06**
**D1 2 Experimental studies of jamming in colloids, grains and emulsions.**
HERNAN MAKSE



We review experimental progress towards the development of a statistical mechanics description of jamming in colloids, granular matter and emulsions. The approach is to consider the application of equilibrium concepts such as temperature, entropy and thermalization to this variety of jammed systems. We first present a study of the correlation and response functions to external fields in an aging colloidal glass. Our analysis reveals that even though the system is aging far from equilibrium, it behaves as if it were equilibrated at a constant temperature, independent of its age. This temperature is larger than the bath, and can be rationalized by the cage dynamics of the system and also in terms of theoretical descriptions of mean field models of spin-glasses. A scaling theory is shown to describe the global and local fluctuations of the observables. We then investigate the effective temperature of jammed granular matter. The measurement of the effective temperature is realized in the laboratory by slowly shearing a closely-packed ensemble of spherical beads confined by an external pressure in a Couette geometry. All the probe particles, independent of their characteristic features and the shear rate, equilibrate at the same temperature, given by the packing density of the system. This suggests that the temperature reveals the ''thermalization'' of the jammed system. Finally, jammed emulsions are investigated under the confocal microscope. Owing to a new technique to identify the contact network in a 3D assembly of droplets, we reveal new signatures of jamming from micromechanics to statistical mechanics.

**15:42**
**D1 3 Onset of jamming for gas-fluidized grains.***
ADAM ABATE, *University of Pennsylvania, Department of Physics*

Upon approach to jamming, whether for molecular liquids or colloidal particles or grains of sand, the microscopic dynamics can develop dramatic long-ranged correlations while the microscopic structure remains relatively unchanged. Experimentally, it has been difficult to study such phenomena in full detail due to the range of temporal and spatial scales involved. Here we introduce a new model system that is both easier to image and to manipulate at the microscale: a bidisperse system of steel beads rolling stochastically due to a nearly-levitating upflow of air. At fixed air flow, we demonstrate that this system exhibits all the hallmarks of a jamming transition as spheres are added and the area fraction increases toward close-packing. In terms of structure, the pair correlation function and the Voronoi cell shape distribution functions exhibit peak splitting. In terms of dynamics, the mean-squared displacement develops a plateau separating the short-time ballistic from the long-time diffusive motions; in this plateau the displacement distribution is non-Gaussian, due to spatial heterogeneities. While this phenomenology is familiar, one feature observed previously only in simulation is the presence of string-like swirls of rearranging grains. We highlight these by movies of an appropriately time-averaged velocity field. We hope to connect such dynamics both to a microscopic measure of effective temperature and to the macroscopic viscosity of the system.

*This work was done in collaboration with D.J. Durian.

**16:18**
**D1 4 Force heterogeneity and stress propagation inside 3D granular materials.**
LEONARDO SILBERT

The effect of increasing structural disorder on the (re)distribution of contact stresses inside three dimensional particle assemblies is systematically studied using computer simulations of granular packings. Starting from a face-centred cubic array, where all contact forces are identical, particles are removed at random and the system is then allowed to relax into a new mechanically stable state. Various measures are used to quantify the amount of disorder, including distributions of the coordination number, three-particle contact angle, and normal contact forces. Upon applying a localised, perturbative force within the central region of the packings, the resulting stress response is mapped inside the different particle assemblies, covering several orders of magnitude in the particle friction coefficient. There is a clear change in the propagative response between frictionless and highly-frictional packings, with an intermediate, crossover regime for packings with lower values of the friction coefficient.

**16:54**
**D1 5 Transitions from jammed to flowing granular matter.***
WOLFGANG LOSERT, *University of Maryland*

In static and slowly flowing granular materials forces are transmitted through a network of direct particle contacts. We experimentally examine how the contact networks fails and rearranges as granular matter starts to flow. Through surface measurements and 3D imaging of particle motion and forces we deduce how a granular contact network breaks and re-forms under shear forcing and point forcing. At small forcing, in the jammed state, we observe that low probability ''jumps,'' in which a grain moves significantly more relative to the others, play a significant role in the relaxation of the jammed state [1]. Under larger local forcing, the jammed state fails and grains rearrange locally. The characteristics of this rearrangement sensitively depend on the number density of particles and direction of forces that had been applied to jam the material (history dependence). If the direction of principal stress is changed (e.g. by changing the shear stress direction), the contact network breaks everywhere. The material is transiently weaker, more compact, and exhibits linear strain until a new contact network forms cooperatively[2]. [1] WL and M. Toiya with P. Ribiere, P. Richard, R. Delannay and D. Bideau to appear in Phys Rev. Lett. (2005). [2] M. Toiya, J. Stambaugh, and WL, Phys Rev Lett. 83, 088001-1 (2004).

*With M. Toiya. Supported by NASA Grant NAG-32736 and NSF Grant CTS0457431.



**SESSION D2: QUANTUM HALL EFFECT IN GRAPHENE**
**Monday Afternoon, 13 March 2006; Ballroom III, Baltimore Convention Center at 14:30**
**Gene Mele, University of Pennsylvania, presiding**

**14:30**
**D2 1 Experimental Observation of Quantum Hall Effect and Berry's Phase in Graphene.**
PHILIP KIM, *Department of Physics, Columbia University*

When electrons are confined in two-dimensional (2D) materials, quantum mechanically enhanced transport phenomena, as exemplified by the quantum Hall effects (QHE), can be observed. Graphene, an isolated single atomic layer of graphite, is an ideal realization of such a 2D system. Its behavior is, however, expected to differ dramatically from the well-studied case of quantum wells in conventional semiconductor interfaces. This difference arises from the unique electronic properties of graphene, which exhibits electron-hole degeneracy and vanishing carrier mass near the point of charge neutrality. In this talk I will present an experimental investigation of magneto transport in a high mobility single layer of graphene. Adjusting the chemical potential using the electric field effect, we discovered an unusual half integer QHE for both electron and hole carriers in graphene, which originates from the quantum mechanical phase associated with the topologically unique graphene Fermi surface. The existence of a non-zero Berry's phase in magneto-oscillations will be discussed in the connection to Dirac Fermion description in graphitic systems. In addition, I will discuss our recent results in transport measurement in strong quantum limit and spin transport in graphene samples.

**15:06**
**D2 2 QED in Graphene.***
ANDRE GEIM, *University of Manchester*

Electronic properties of materials are commonly described by quasiparticles that behave as non-relativistic electrons with a finite mass and obey the Schrödinger equation. I will describe our experimental studies of graphene (a free-standing single layer of carbon atoms) in which electron transport is essentially governed by Dirac's (relativistic) equation and charge carriers mimic relativistic particles with zero rest mass and an effective ''speed of light'' of $\approx 10^6$m/s. We have found a variety of unusual quantum phenomena characteristic of two-dimensional Dirac fermions. In particular, we have observed that a) the integer quantum Hall effect in graphene is anomalous in that it occurs at half-integer filling factors; b) graphene's conductivity never falls below a minimum value corresponding to the conductance quantum, even when carrier concentrations tend to zero; c) the cyclotron mass of massless carriers in graphene is described by Einstein's equation $E=mc^2$; and d) Shubnikov-de Haas oscillations in graphene exhibit a phase shift of $\pi$ due to Berry's phase. I will also explain another, third type of the integer quantum Hall effect that happens in bilayer graphene and accompanied by Berry's phase of $2\pi$.

*In collaboration with K. Novoselov.

**15:42**
**D2 3 Dirac fermions as a cause of unusual Quantum Hall Effect in Graphene.***
SERGEI SHARAPOV, *McMaster University*

The graphite films with a single atomic layer of carbon (graphene) have the low-energy ''relativistic-like'' quasiparticle excitations which can be described by two-dimensional Dirac equation. It is demonstrated that due to the Dirac-like character of carriers the quantization of the Hall conductivity is unusual: it occurs at half-integer filling factors. In addition, the phases and amplitudes of the de Haas - van Alphen and Shubnikov de Haas quantum magnetic oscillations in graphene differ drastically from the patterns observed in a more conventional materials with a parabolic dispersion.

*In collaboration with V.P. Gusynin.



**16:18**
**D2 4 Electronic coherence and confinement in patterned epitaxial graphene.**
WALT DE HEER, *Georgia Institute of Technology*

I will present very recent results from our studies of ultrathin graphite films that are epitaxially grown on single crystal silicon carbide. The quasi-two dimensional films consisting of a few to a few dozen graphene layers are patterned ($\geqslant 0.1\mu$m) using standard e-beam lithography methods. Relatively high mobilities ($\mu$ up to 10,000 $cm^2$/Vs) are deduced from transport measurements. Patterned structures reveal a variety of mesoscopic effects (i.e. universal conductance fluctuations and anomalous Shubnikov de Haas oscillations) from which coherence lengths of the order, or greater than $1\mu$m at cryogenic temperatures are deduced. Evidence for size dependent resistivities even at room temperature is observed. Changes the magnetoresistive properties at about 2K provide evidence for an unusual, first order phase transition. The properties of this new patternable quasi-2D material are promising for sub-micron electronics applications.

## SESSION D3: SCIENTISTS FROM DEVELOPING COUNTRIES: IS THERE AN EFFECTIVE WAY TO SUPPORT MEANINGFUL RESEARCH?

**Monday Afternoon, 13 March 2006; Ballroom I, Baltimore Convention Center at 14:30**
**Katepalli Sreenivasan, The Abdus Salam International Centre for Theoretical Physics, presiding**

**14:30**
TIMOLEON CREPIN KOFANE, *University of Yaounde*

This abstract was not received electronically.

**15:06**
**D3 2 Scientists in Developing Countries: Is there an effective way to support meaningful research?**
ZOHRA BEN LAKDAR, *Faculty of Sciences, Tunis, Tunisia*

Nations in the developing countries are in front of barriers for progress, but without progress how can they exist and take place in the society of 21 eme century, knowledge society or new technology society? Research in science suppose competivness in a specific area of science and at the same time exchange of ideas between researchers. Researchers shoud be good scientists, be in a scientific environment, have financial support and have possibility to direct their research. Competivness has never been as hard as in knowledge society! About 90% of human knowledge is produced during the last 50 years! African countries get independance in 1950-60.! At their independance they are in mean age and yet in the civilization of new technology! They never know industrial revolution. Thanks to pioneers scientits, in some developing countries, who begin from nothing, found solutions to built laboratories and conduct research activities.These solutions among which are principally -cooperation with laboratories from developed countries—regular training of researchers and —good vision for choice of research subjet- offer an example of an effective way to support meaningful research.

**15:42**
**D3 3**
CARLOS HENRIQUE DE BRITO CRUZ, *Director, Cientfico Fapesp*

This abstract was not received electronically.

**16:18**
**D3 4 Physics at Universities in Congo and Central Africa: Problems, Needs, hopes and solutions.**
BERNARD M'PASSI-MABIALA, *Université Marien NGouabi (Brazzaville)*

We present Teaching and Research Activities in Science, and that of Physics in particular, at Universities in Congo and in Central Africa. Although the number of Physics Students is increasing and that the Progress in Physics in a reality today also in some developing countries, problems that could promote this science remain in this geographic area of the world and are listed. Needs and hopes have to be exposed and Solutions are proposed to the international scientific community.



## SESSION D4: ORGANIC ELECTRONICS
**Monday Afternoon, 13 March 2006; 308, Baltimore Convention Center at 14:30**
**Chang Yeol Ryu, Rensselaer Polytechnic Institute, presiding**

**14:30**
**D4 1 Excited states at polymer semiconductor heterojunctions.**
RICHARD FRIEND, *University of Cambridge*

Excitons in bulk organic semiconductors are generally strongly bound due to the weakly-screened electrostatic electron-hole interaction, but can be de-stabilized at heterojunctions between semiconductors with substantial band-edge offsets. The charge-transfer states that then forms at the heterojunction (exciplexes) can still show radiative emission (with strongly increased radiative lifetimes and large red-shifts), and still require an external field to enable long-range charge separation as required in a photovoltaic diode. The effect of DC field on this process of charge separation, will be discussed, as measured by the suppression of exciplex luminescence and photocurrent. The strength of interchain interactions can be increased under pressure, and measurements of absorption and time-resolved luminescence under hydrostatic pressure will be reported. These reveal the changing character of the exciplex at the heterojunction.

**15:06**
**D4 2 Defects and Deformation in Organic Molecular Semiconductors.***
DAVID MARTIN,† *The University of Michigan*

We have been investigating microstructural defects in crystalline organic molecular semiconductors such as pentacene and soluble pentacene derivatives. We have examined the structure of grain boundaries, dislocations, and vacancies in these materials by polarized optical microscopy, X-ray diffraction, transmission electron microscopy, electron diffraction, low voltage electron microscopy, and low dose high resolution electron microscopy. We have quantified the nature and extent of local relaxations that occur near these structural defects. We have also studied the micromechanisms of plasticity using nanoindentation and scratching. Our microstructural studies provide detailed information about the defect-mediated mechanisms of plastic flow. We have also examined pentacene derivatives that can be processed from solution, and have found information about solid-state phase transformations that result in internal cracking within the organic semiconductor crystals. We have also examined the relationship between the type and density of these defects and the macroscopic properties in devices such as thin-film transistors.

*National Science Foundation.
†with Jihua Chen, Lawrence Drummy, and John Anthony.

**15:42**
**D4 3 Solution-Processable Organic Semiconductors and Conductors: Viable Materials for Functional Thin-Film Transistors.***
YUEH-LIN LOO, *University of Texas at Austin*

Large-area displays based on organic materials promise low-cost fabrication, lightweight construction, mechanical flexibility and durability. To truly realize the low-cost aspects of organic electronics, however, conventional high-vacuum deposition technologies will have to be replaced by solution processing methodologies. This need has in turn driven the development of solution-processable organic semiconductors and conductors. We have focused on fabricating thin-film transistors with triethynylsilyl antradithiophene (TES ADT), a solution-processable p-type organic semiconductor. Subjecting the as-cast thin films of TES ADT to short solvent vapor annealing dramatically increases the device characteristics: we observe three orders of magnitude increase in carrier mobility and current on/off ratio, and a decrease in current hysteresis and threshold voltage. The improvement in the electrical characteristics can be directly correlated with

morphological transformations during solvent vapor annealing. Our efforts in solution-processable organic conductors focus on water-dispersible polyaniline (PANI). We have fabricated bottom-contact thin-film transistors with PANI electrodes, which function as effectively as gold electrodes, when on-characteristics are concerned. Examination of the linear source-drain voltage regime suggests that PANI devices exhibit markedly less contact resistance than gold devices.

*In collaboration with Kimberly Dickey, Kwangseok Lee, Joungeun Yoo, University of Texas at Austin; and John Anthony, University of Kentucky.

**16:18**
**D4 4 Structural Effects on the Performance of Polymeric Thin Film Transistors.**
MICHAEL CHABINYC, *PARC*



Semiconducting polymers are currently being researched for use in thin-film transistors (TFTs) in large-area electronic devices such as displays. Most high performance semiconducting polymers form semicrystalline thin films, but the details of the connection between their structure and the field-effect mobility of charge carriers in these materials in TFTs are poorly understood. We have used a variety of techniques to reveal the connection between the microstructure of semiconducting polymers and their electrical performance. We have used synchrotron x-ray scattering to determine the molecular ordering in thin films of several high-performance poly(thiophene)-based semiconducting polymers including poly[5,5'-bis(3-dodecyl-2-thienyl)-2,2'-bithiophene], known as PQT-12, and poly(2,5-bis(3-alkylthiophen-2-yl)thieno[3,2-*b*]thiophene). These materials show evidence of thermotropic liquid crystalline phases that can be used to improve the ordering in the films. We have used a delamination technique to transfer these films between substrates without substantially perturbing their structure to help disaggregate the contributions of film structure and of interfacial structure to device characteristics. Using films of constant morphology, we have found that chemically modified dielectrics can have a strong influence on the threshold voltage of TFTs, but have little impact on mobility. These results suggest that the field-effect mobility is mainly controlled by the structure of the first few molecular layers of the semiconducting films at the interface with the gate dielectric.

**16:54**
**D4 5 NEXAFS measurements of the development of interfacial order in organic semiconductor thin films.**
ERIC K. LIN, *National Institute of Standards and Technology*

Interest in organic semiconductors has increased because of their potential use in new electronics applications such as radio frequency identification tags, biosensors, or photovoltaics. The development of solution processable organic semiconductors has made it possible to take advantage of low-cost processing methods such as spin coating, dip coating, or ink-jet printing onto flexible substrates. However, the performance of these materials in devices is difficult to control and new processing methods can deliver unexpected results. These deviations are often due to variability in film microstructure that leads to variability in carrier transport properties. The microstructure is sensitive to processing variables because they influence the dynamic assembly process of the material as it dries from a solution to a solid thin film that is crystalline or semicrystalline. To quantify structural changes, we employ synchrotron-based near-edge X-ray absorption fine structure (NEXAFS) spectroscopy, which measures the soft X-ray excitation of 1s electrons to unfilled molecular orbitals. For a polymer semiconductor, regioregular poly(3-hexylthiophene) (P3HT), we show that variations in the spin-coating process may be a source of differences in the P3HT microstructure because of changes in complex balance of inertial forces and solvent evaporation during the solidification of the film from solution. The morphology of semicrystalline polymers such as P3HT is affected by the rate of solidification; slower solvent removal rates result in materials closer to their equilibrium structure. For thermally convertible, oligomeric organic semiconductors, we show that the formation of interfacial order of the molecules is affected by the oligomer length.

## SESSION D5: CATALYSIS AND COMPLEXITY: KEN HASS MEMORIAL
**Monday Afternoon, 13 March 2006; 309, Baltimore Convention Center at 14:30**
**Willes Weber, APS, presiding**

**14:30**
**D5 1 Environmental Catalysis from First Principles.**
WILLIAM SCHNEIDER, *University of Notre Dame*

Innovation in environmental catalysis—catalysis related to sustainable production and consumption of energy and materials—is one of the most pressing societal needs of the day. Fuel cells, fuel reforming, hydrogen generation, emissions control, and many other processes all rely on effective catalysts to facilitate the transformation of chemicals into more desirable forms. Historically these heterogeneous catalysts, most often consisting of active transition metal

particles dispersed on a high surface area support, have advanced in a largely evolutionary fashion. Today, the increasing demands for more capable catalysts have dovetailed with a revolution in experimental and computational techniques available for preparing and studying these materials at the nanoscale to create the potential for unprecedented advances in catalyst research and discovery. Three central questions have emerged in nanoscale environmental catalysis: First, how does the structure and catalytic function of transition metal catalysts evolve as particles decrease in size from the micro to the nanoscale? Second, how do these particles interact and communicate with supports, and what are the effects on structure and catalytic function? Third, how does the particle/support system respond to realistic and dynamic reaction environments? Density functional theory (DFT) simulations provide a means to interrogate these questions independently and have proved a powerful complement to experiment in the investigation and development of nanocatalysis. In this talk we will review recent progress in studying these questions using DFT methods, with a particular emphasis on the connection between oxidation environment, catalyst composition, and activity for CO and NO oxidation with Pt and Ru catalysts.



**15:06**
**D5 2 Density functional calculations in the automotive industry: Catalyst supports and hydrogen storage materials.**
CHRISTOPHER WOLVERTON, *Ford Motor Company*

In my talk, I will describe some uses of density functional theory (DFT) calculations in the research laboratory at Ford, and particularly highlight work that was inspired by, or performed in collaboration with Ken Hass. I begin with a discussion of past work on $\gamma$-$Al_2O_3$ catalyst support materials, but also discuss the current main focus of our group's activities: hydrogen storage materials. Catalyst Supports: In current three-way automotive catalysts, precious metals are often supported by the phase of aluminum oxide known as $\gamma$-$Al_2O_3$. Despite the ubiquitous nature of this oxide in current automobile catalysts, and a considerable amount of effort expended to understand this material, many questions about the phase stability and even crystal structure of $\gamma$-$Al_2O_3$ remain. DFT calculations have made significant progress in unraveling these unanswered questions, allowing one to construct realistic models of the supported catalysts materials. Hydrogen Storage Materials: One of the major bottlenecks to the widespread use of hydrogen-fueled vehicles is the ability to store sufficient energy on-board to enable vehicle attributes acceptable to customers. I will give a general introduction to the topic of hydrogen storage, and a broad survey of the various classes of hydrogen storage technologies, and point out some pros and cons associated with each class. Currently known technologies have insufficient usable energy densities, and I will describe how DFT calculations are aiding the search for improved high density storage materials.

**15:42**
**D5 3 From Condensed Matter Theory to Complex Biological Structures.**
ANDERS CARLSSON, *Washington University*

Condensed matter theory has given us many successful examples of the combination of analytic theory and numerical modeling in treating microscale and nanoscale physical phenomena. The methods of condensed-matter theory are increasingly being applied to biological problems. We will describe recent work modeling the growth of actin networks in biological cells. Actin, an abundant intracellular protein, polymerizes into semiflexible filaments which are important for many processes, including cell motion and shape changes. The growth of the filaments is regulated by intracellular proteins that can, for example, cap the growing ends of filaments, cause new branches to grow on existing filaments, or sever filaments. These activities generate a dynamic actin filament network at the cell edge. The filaments' growth can generate forces large enough to move the cell and change its shape. The talk will describe Brownian-dynamics simulations of the growth of single filaments against an obstacle, and stochastic-growth modeling of the growth of the actin network. The single-filament growth simulations show that even filaments attached to an obstacle can grow and push it forward, at rates comparable to free-filament growth rates. This result is consistent with experimental observations of filament-obstacle attachments. The network-growth simulations use a minimal stochastic growth model including capping, branching, and severing. Simulation studies of this model yield a network structure quite similar to that seen by electron microscopy. Surprisingly, the growth velocity of the network is almost independent of the opposing force. Analytic theory shows that this effect is due to the autocatalytic nature of the branching route to filament generation. Studies of the polymerization dynamics of this model reveal a ''branching explosion'' in which large clusters of branched filaments form at short times, but the filaments are nearly unbranched at long times.

**16:18**
**D5 4 The Physics of Traffic.**
L. CRAIG DAVIS

Congestion in freeway traffic is an example of self-organization in the language of complexity theory. Nonequilibrium, first-order phase transitions from free flow cause complex spatiotemporal patterns. Two distinct phases of congestion are observed in empirical traffic data–wide moving jams and synchronous flow. Wide moving jams are characterized by stopped or slowly moving vehicles within the jammed region, which widens and moves upstream at 15-20 km/h. Above a critical density of vehicles, a sudden decrease in the velocity of a lead vehicle can initiate a transition from metastable

states to this phase. Human behaviors, especially delayed reactions, are implicated in the formation of jams. The synchronous flow phase results from a bottleneck such as an on-ramp. Thus, in contrast to a jam, the downstream front is pinned at a fixed location. The name of the phase comes from the equilibration (or synchronization) of speed and flow rate across all lanes caused by frequent vehicle lane changes. Synchronous flow occurs when the mainline flow and the rate of merging from an on-ramp are sufficiently large. Large-scale simulations using car-following models reproduce the physical phenomena occurring in traffic and suggest methods to improve flow and mediate congestion.



**SESSION D6: SIMULATING HYDROGEN STORAGE: FROM CURRENT CHALLENGES TO FUTURE PROMISES**
**Monday Afternoon, 13 March 2006; 310, Baltimore Convention Center at 14:30**
**Shengbai Zhang, National Renewable Energy Laboratory, presiding**

**14:30**
**D6 1 Computational Study of Metal Hydride Destabilization.**
KARL JOHNSON, *University of Pittsburgh*

The safe and efficient on-board storage of hydrogen in fuel cell vehicles is one of the major road-blocks for utilization of hydrogen in transportation. This talk will illustrate the use quantum molecular modeling techniques for investigating atomic- level details of hydrogen storage in new materials. Metal hydrides of period 2 and 3 materials have high volumetric and gravimetric hydrogen storage capacities. However, these materials typically have very high heats of reaction, meaning that high temperatures are required to dissociate the hydrides. Likewise, hydrogenation reactions evolve very large quantities of energy, making thermal management during refueling a impractical. Recent experimental work has focused on chemical destabilization of metal hydrides as a means of decreasing the heats of reaction. We have carried out quantum mechanical calculations, using the electronic density functional theory (DFT) formalism, for various metal hydride systems. The heats of reaction for over 300 different reactions have been computed. We have compared our calculations with experimental and tabulated data where available and find reasonable agreement. Our calculations demonstrate the utility of DFT for screening reactions and for identifying promising materials for further computational and experimental studies. We have also studied the hydration of $Mg_2Si$, a destabilized hydride of MgH2. Experiments have failed to hydrogenate this material in the laboratory under high pressures of $H_2$. We examine adsorption of H2 and dissociation on the $Mg_2Si(110)$ surface to see if kinetic limitations are responsible for the failure to observe hydrogenation of this material.

**15:06**
**D6 2 The potential of hydrogen storage in hydrate and graphitic systems.**
JOHN TSE, *University of Saskatchewan*

Many methods have been proposed for efficient storage of molecular hydrogen for fuel cell applications. Recently, it was found that molecular hydrogen can be stored in large quantity approaching the U.S. Department of Energy goals of 6.5% mass ratio in ice clathrate under high pressure and low temperature [1]. Attempts were made to increase the stability of the clathrate. Unfortunately, so far the modified hydrates failed to meet the elusive goal [2,3]. To understand the thermodynamic stability and storage capacity, hydrogen occupancy in clathrate hydrate was examined with a statistical mechanical model in conjunction with first−principles quantumchemistry calculations [4]. The theoretical approach is extended to graphitic systems [5]. It is shown that insufficiently accurate carbon–$H_2$ interaction potentials, together with the neglectand incomplete treatment of the quantum effects in previous theoretical investigations led to incorrect conclusions for the absorption capacity. A proper account of the contribution of quantum effects to the free energy and the equilibrium constantfor hydrogen adsorption suggest that the U.S. Department of Energy specification can be approached in a graphite−based physisorptionsystem. [1] W.L. Mao, H.-K. Mao, A.F. Goncharov, V.V. Struzhkin, Q Guo, Q., *et al. Science* 297, 2247–2249 (2002) [2] H.Lee, J. Lee, D.Y. Kim, J. Park, Y. Seo, H. Zeng, I.L. Moudrakovski, C.I. Ratcliffe, J.A. Ripmeester, *Nature* 434, 743–746, (2005) [3] L.J. Florusse, C.J. Peters, J. Schoonman, K.C. Hester, C.A. Koh, S.F. Dec, K.N. Marsh, E.D. Sloan, *Science*, 306, 469–471 (2004) [4] S. Patchkovskii, J.S. Tse, *Proc. Nat. Acad. Sci.*, 100, 14645–14650 (2003) [5] S. Patchkovskii, J.S. Tse, S.N. Yurchenko, L. Zhechkov, T. Heine, G. Seifert, *Proc. Nat. Acad. Sci.*, 102, 10439–10444 (2005).

**15:42**
**D6 3 Theory of Hydrogen Storage: A New Strategy within Organometallic Chemistry.**
YUFENG ZHAO, *National Renewable Energy Laboratory*

As one of the most vigorous fields in modern chemistry, organometallic chemistry has made vast contributions to a broad variety of technological fields including catalysis, light emitters, molecular devices, liquid crystals, and even superconductivity. Here we show that organometallic chemistry in nanoscale could be the frontier in hydrogen storage. Our study

is based on the notion that the 3d transition metal (TM) atoms are superb absorbers for H storage, as their empty d orbital can bind dihydrogen ligands (elongated but non-dissociated $H_2$) with high capacity at nearly ideal binding energy for reversible hydrogen storage. By embedding the TM atoms into a carbon-based nanostructures, high H capacity can be maintained. This presentation contains four parts. First, by comparing the conventional hydrogen storage media, e.g., metal hydrides and carbon-based materials, the general principles for designing hydrogen storage materials are outlined. Second, organometallic buckyballs are studied to demonstrate the novel strategy. The amount of $H_2$ adsorbed on a Sc-coated fullerene, $C_{48}B_{12}$ $[ScH]_{12}$, could approach 9 wt%, with binding energies of 30-40 kJ/mol. Third, the method is applied to the transition-metal carbide nanoparticles that have been synthesized experimentally. The similar non-dissociative $H_2$ binding is revealed in our calculation, thereby demonstrating the resilience of the overall mechanism. Moreover, a novel self-catalysis process is identified. In the fourth part, transition-metal functionalization of highly porous carbon-based materials is discussed heuristically to foresee macroscopic media for hydrogen storage. Finally follows the summary and discussion of the remaining challenges to practical hydrogen storage. Work in collaboration with A. C. Dillon, Y.-H. Kim, M. Heben & S. B. Zhang and supported by the U.S. DOE/EERE under contract No. DE-AC36-99GO10337.

**16:18**
**D6 4 Materials for Hydrogen Storage: From Nanostructures to Complex Hydrides.**
PURU JENA, *Virginia Commonwealth University*

The limited supply of fossil fuels, its adverse effect on the environment, and growing worldwide demand for energy has necessitated the search for new and clean sources of energy. The possibility of using hydrogen to meet this growing energy need has rekindled interest in the study of safe, efficient, and economical storage of hydrogen. This talk will discuss the issues and challenges in storing hydrogen in light complex hydrides and discuss the role of nanostructuring and catalysts that can improve the thermodynamics and kinetics of hydrogen. In particular, we will discuss how studies of clusters can help elucidate the fundamental mechanisms for hydrogen storage and how these can be applied in Boron Nitride and Carbon nanocages and how metallization of these nanostructures is necessary to store hydrogen with large gravimetric density. We will also discuss the properties of complex light metal hydrides such as alanates and magnesium hydrides that can store up to 18 wt % hydrogen, although the temperature where hydrogen desorbs is rather high. Using first principles calculations, we will provide a fundamental understanding of the electronic structure and stability of these systems and how it is affected due to catalysts. It is hoped that the understanding gained here can be useful in designing better catalysts as well as hosts for hydrogen storage.

**16:54**
**D6 5 First Principles predictions of Hydrogen Storage Materials.***
WILLIAM GODDARD, *Caltech*

A grand challenge in materials technology is the development of materials capable of reversible storage of $H_2$ at ambient temperatures and pressures capable of mass densities greater than 6% by weight. We report here the results of first principles calculations on several classes of materials including: Carbon-alkali based systems, Metal oxide framework systems, Metal alloy systems. These simulations indicate that the DOE goals for 2010 are achievable in materials that could be manufactured today.

*In collaboration with Weiqiao Deng, Caltech.

**SESSION D7: NEW RESULTS IN GEOMETRICALLY FRUSTRATED MAGNETS**
**Monday Afternoon, 13 March 2006; 307, Baltimore Convention Center at 14:30**
**Arthur Ramirez, Lucent Technologies, presiding**

**14:30**
**D7 1 Spin liquids and spin dynamics in kagome antiferromagnets.**
PHILIPPE MENDELS, *Universite Paris-Sud*

Among all the corner sharing highly frustrated magnets, only a few experimental systems are good candidates for a low-T fluctuating state, ie fulfilling the important conditions of the pure Heisenberg lattice with nn couplings. The combination of the weakness of the single-ion anisotropy and of a direct overlap antiferromagnetic exchange are certainly the major advantages of the chromate S=3/2 kagome bilayer $Ba_2Sn_2ZnGa_{10-7p}Cr_{7p}O_{22}$- BSZCGO(p)- and the long studied $SrCr_{9p}Ga_{12-9p}O_{19}$ - SCGO(p). Beyond the absence of ordering well below the Curie-Weiss temperature, the unusual large value of the specific heat unveils a high density of low lying excitations and its field independence suggests that the excited states are mostly singlets. Moreover, their ground state is found essentially fluctuating although an intrinsic spin

glass (SG) signature is observed in susceptibility measurements. Through a review of our past years work, I'll illustrate all the potential of local studies (NMR and $\mu$SR) to reveal some key aspects of the physics of these compounds: susceptibility, fluctuations, impact of dilution defects which generate an extended response of the spin-lattice ... as well as the puzzling spin-glass state. More recently we also investigated new series of compounds, among them volborthite and delafossites which feature S=1/2 spins on a corner sharing antiferromagnetic lattice. I'll introduce these compounds and shortly discuss their relation to ideal Hamiltonians and novel features. D. Bono et al.Phys. Rev. Lett. 93, 187201 (2004), 92, 217202 (2004) ; Cond-mat/0503496. F. Bert et al. Phys. Rev. Lett., 95, 087203 (2005). L. Limot, et al., Phys. Rev. B, 65, 132403 (2002). P. Mendels et al. Phys. Rev. Lett., 85, 3496 (2000).

**15:06**
**D7 2 Frustrated dipolar interactions – why spin ice obeys the ice rules.**
RODERICH MOESSNER, *CNRS and ENS Paris*



The low temperature entropy of the the spin ice compounds, such as $Ho_2Ti_2O_7$ and $Dy_2Ti_2O_7$, is well described by the nearest-neighbor antiferromagnetic Ising model on the pyrochlore lattice, i.e. by the ''ice rules.'' This is surprising since the dominant coupling between the spins is their long ranged dipole interaction. We show that this phenomenon can be understood rather elegantly: one can construct a model dipole interaction, by adding terms of shorter range, which yields *precisely* the same ground states, and hence $T = 0$ entropy, as the nearest neighbor interaction. A treatment of the small difference between the model and true dipole interactions reproduces the numerical work by Gingras et al in detail. We are also led to a more general concept of projective equivalence between interactions.

S. V. Isakov, R. Moessner, S. L. Sondhi, Phys. Rev. Lett. **95**, 217201 (2005).

**15:42**
**D7 3 Neutron studies of 3D Highly Frustrated Magnetism.**
JASON GARDNER, *BNL/NIST*

Because of their low propensity to order antiferromagnetic materials based on a pyrochlore lattice appear to be excellent systems for studying exotic ground states. It has also been shown that ferromagnetically coupled spins can be frustrated on such a lattice, if there is considerable local Ising anisotropy. I will review several neutron scattering studies on pyrochlore compounds done in the past couple of years, focusing on the study of spin dynamics. Evidence for large, dynamical spins at low temperatures in several antiferromagnets and a crossover from classical to quantum regime in the spin ices will be discussed. If time permits I will discuss new areas of neutron research in frustrated magnetism. [1] Magnetic Systems with Competing Interactions, edited by H.T. Diep (World Scientific, Singapore, 1994), Can. J. Phys. **79**, (2001) and Frustrated Spin Systems, ed H T Diep (World Scientific, Singapore, 2004). [2] S. T. Bramwell and M. P. Gingras, Science, **294**, 1495, (2001).

**16:18**
**D7 4 Natural and Artificial Spin Ice.***
PETER SCHIFFER, *Pennsylvania State University*

Geometrical frustration among spins in magnetic materials can lead to exotic low temperature states including ''spin ice,'' in which the local moments mimic the frustration of hydrogen ion positions in frozen water. We have performed extensive studies of spin ice materials and related compounds, and recently have begun study of an itartificial geometrically frustrated magnet which shares many of the properties of the spin ice materials. This artificial frustrated system is based on an array of lithographically fabricated single-domain ferromagnetic islands. The islands are arranged such that the dipolar interactions between them are analogous to those in spin ice. Images of the magnetic moments of individual elements in this correlated system allow us to study the local accommodation of frustration. We see both ice-like short range correlations and an absence of long range correlations, behavior which is very similar to the low temperature state of spin ice. These results demonstrate that artificial frustrated magnets can provide a rich new arena in which to study the physics of frustration. References: J. Snyder et al. (PRL 2003, and PRB 2004); R. F. Wangit et al. (Nature, in press). This research was supported by the Army Research Office and the National Science Foundation.

*In collaboration with R. F. Wang, C. Nisoli, R. S. Freitas, J. Li, W. McConville, B. J. Cooley, M. S. Lund, P. Lammert, N. Samarth, C. Leighton, V. H. Crespi, B. Ueland, J. Snyder, G. Lau, and R. Cava.

**16:54**
**D7 5 Colossal magnetocapacitive effects in geometrically frustrated chalcogenide spinels.**
PETER LUNKENHEIMER, *Center for Electronic Correlations and Magnetism, University of Augsburg, Germany*

It is well known that the spinel structure is susceptible to the occurrence of geometrical frustration, which in the past was invoked to explain a number of unusual observations concerning the magnetic and orbital degrees of freedom in these materials. We demonstrate that several chalcogenide spinels also exhibit very unusual dielectric behavior, especially an extremely strong coupling of magnetic and dielectric properties and the simultaneous occurrence of magnetic and polar

order. Especially, in $CdCr_2S_4$ a colossal magnetocapacitive effect is observed, which shows up as a sharp upturn of the dielectric constant it$\varepsilon$' when the sample becomes ferromagnetic and as a variation of it$\varepsilon$' up to a factor of 30 when the sample is subjected to external magnetic fields. As revealed by linear and non-linear dielectric measurements, this material shows the typical signatures of relaxor ferroelectrics, i.e. a strong increase of the static dielectric constant with decreasing temperature and considerable frequency dispersion of the complex permittivity. While in most relaxor ferroelectrics the freezing of polar moments is driven by frustrated interactions related to substitutional disorder, in the present pure system geometrical frustration seems a plausible mechanism to explain the relaxor behavior. However, one may also speculate on completely different mechanisms of ferroelectric polarization, e.g., the ordering of electronic degrees of freedom. The concomitant occurrence of polar and magnetic order makes $CdCr_2S_4$ another example of the rare species of multiferroic materials. In contrast to other members of this group of materials, it has sizable ordering temperatures and moments. A detailed investigation of the relaxational dynamics in this material provides clear evidence that the observed magnetocapacitive effect stems from an enormous acceleration of the relaxation dynamics induced by the development of magnetic order. In addition, recent results reveal even larger magnetocapacitive effects in In-doped $CdCr_2S_4$. In addition to $CdCr_2S_4$, we found similar effects also in ferromagnetic $CdCr_2Se_4$ and, most astonishing, in $HgCr_2S_4$, which exhibits a complex type of antiferromagnetic magnetic order at low temperatures. In the latter system, the magnetocapacitive effect, exemplified by the relative increase of it$\varepsilon$' in a field of 5 T, reaches values up to $8\times 10^5$ %.



**SESSION D8: PATTERNS AND INSTABILITIES I**
**Monday Afternoon, 13 March 2006**
**314, Baltimore Convention Center at 14:30**
**Brian Hunt, University of Maryland, presiding**

**14:30**
**D8 1 Nonlinear Analysis of the Self-assembly of Nanostructures** SHAOWEN HU, *University of Houston* GIRISH NATHAN, GEMUNU GUNARATNE, DONALD KOURI, We investigate properties of a model of nanoscale pattern formation on a uniform substrate. The coefficients of the Ginzburg-Landau equations are concentration dependent. We find that, above the threshold, there are two branches of solutions corresponding to the up and down hexagonal structures; their appearance is related to the initial concentration of the system. The stability of such structures is confirmed by the analysis of the phase dynamics. When system is away from the threshold, the theory predicts a competition of stripe and hexagonal structures. The predicted stability domain of the stripe structures is consistent with numerical simulations. This provides a framework to understand the guided self-assembly technology, e.g., by the photolithography, at a coarse scale. The possible interaction of a large scale mode with the pattern mode is also discussed.

**14:42**
**D8 2 Shear band instability in the presence of convection*** SEBASTIEN AUMAITRE, J.P. GOLLUB, *Haverford College* One of the main features of the atmospheric motion of giant gas planets, like Jupiter and Saturn, is their remarkably stable shear band structure. The stability and internal structure of this flow, and the consequences for the internal heat transport, are not fully understood. Here we present a flexible device to study in a laboratory experiment the stability of a shear band flow in the presence of convective heat transport. The shear band flow is generated in layer of conductive fluid by spatially periodic Lorentz forces resulting from an electric current passing through the fluid in the presence of a network of magnets placed under the cell. Moreover, a convective flow is created by an imposed temperature gradient across the fluid layer. By changing the current through the fluid, and the temperature difference across the layer, we are able to adjust independently the velocity fields resulting from the shear and thermal forcing. Heat transport, flow patterns, and velocity fields are monitored. Initial results on the threshold for the instability of the shear band flow, and the resulting flow patterns, will be presented.

*Supported by NSF-DMR -0405187.

**14:54**
**D8 3 Surfactant-enhanced thermocapillary flow in two-dimensional slots.** RAM HANUMANTHU, KATHLEEN STEBE, *Department of Chemical & Biomolecular Engineering; Johns Hopkins University; Baltimore, MD 21218* An insoluble surfactant at an aqueous-gas interface can assume a variety of surface states including gaseous (G), liquid expanded (LE), and liquid condensed (LC) states. The surface pressure-surface area isotherm for such monolayers is well established; however, their thermocapillary behavior has received less attention. Recently, Nguyen & Stebe reported surfactant-enhanced Marangoni-Benard flows in evaporating aqueous drops, created by the strong dependence of surface tension on temperature in LE-LC co-existence. In this work, flow in a two-dimensional slot in the presence of insoluble surfactant is modeled. The time-dependent, incompressible Navier-Stokes equations, coupled with energy conservation and surface convection-diffusion equations are solved using Galerkin's method of weighted residuals on a finite element mesh. The model is verified against the results of Sen & Davis for steady thermocapillary flows in two-dimensional slots; and of Homsy & Meiburg for surfactant effects in a linear limit. Finally, both steady-state and dynamic flow patterns are presented that evolve when a constitutive equation that captures the full, non-linear, concentration- and temperature-dependent phase-change behavior is used. Predicted flow patterns are compared qualitatively to the experimental observations.

**15:06**
**D8 4 Weakly nonlinear dynamics of the longwave Marangoni instability in a binary-mixture layer in the presence of the Soret effect.*** ALEXANDER ORON, *Mechanical Engineering* ALLA PODOLNY, *Mathematics* ALEXANDER A. NEPOMNYASHCHY, *Mathematics* TECHNION-ISRAEL INSTITUTE OF TECHNOLOGY TEAM, We consider a system consisting of a layer of an incompressible binary liquid with a deformable free surface. We investigate the long-wave Marangoni instability in the case of small Lewis and Galileo numbers for finite capillary and Biot numbers in the case of a specified heat flux at the solid

substrate. The Soret effect is taken into account. Both long-wave monotonic and oscillatory modes of instability are found in various parameter domains of the Biot and Soret numbers. We have derived a set of strongly nonlinear evolution equations describing the spatio-temporal dynamics of the layer in three dimensions in the case of the oscillatory instability. The weakly nonlinear analysis based on these equations demonstrates the presence of several kinds of stable supercritical standing and travelling waves.

*The research is partially supported by the Israel Science Foundation, Grant 31/03-15.3

**15:18**

**D8 5 Convection onset in a supercritical pure fluid** HORST MEYER, *Duke University* The convection onset of a pure supercritical fluid -$^3$He - in a Rayleigh-Bénard cell has been investigated along the critical isochore by measuring the temperature drop $\Delta T(t)$ across the fluid layer as a function of time $t$ after starting the heat current $q$. The measurements showed after the initial sharp rise in $\Delta T(t)$ a first maximum at the time $t_p$, which indicates that the convection has developed and that plumes have reached the upper plate. It was found empirically that $t_p$, scaled by the thermal diffusion relaxation time $\tau_D$, could be expressed as $t_p/\tau_D = F([Ra - Ra_c])$, where $Ra_c$ is the critical Rayleigh number[1]. A model is proposed which reproduces this observed scaled representation. It uses the instability criterion of the bottom (hot) boundary fluid layer and the calculated Nusselt and Ra numbers for the steady-state convection. The perturbations leading to the convection development, after the fluid instability point has been reached, are unknown. Therefore $t_p/\tau_D$ is determined within a constant multiplicative factor, the only fit parameter of this model. There is then good agreement over more than four orders of magnitude of $[Ra - Ra_c]$ between the calculations and the experiments. The fit parameter is a phenomenological measure for the effectiveness of the perturbations, and will be discussed. 1. A. Furukawa et al. Phys. Rev. E 68, 056309 (2003), Fig.5a.

**15:30**

**D8 6 The Resolution of the Domain Chaos Puzzle for Rotated Rayleigh-Bénard Convection*** NATHAN BECKER, GUENTER AHLERS, *UC Santa Barbara* Due to the Küppers-Lortz instability, Rayleigh-Bénard convection-patterns exhibit spatio-temporal chaos at the onset of convection when the sample rotates fast enough about a vertical axis. Previous work showed that the scaling of the correlation length $\xi$ determined from the experimental chaotic patterns disagreed with the prediction from a Ginzburg-Landau weakly-nonlinear model.[1] Commonly the power spectrum of the pattern images (the structure factor) is used to extract $\xi$ from the half-width of its peak. Past experiments and simulations used standard Fourier techniques to calculate the power spectrum. On the basis of simulations using the Swift-Hohenberg equation, we show that those results are influenced strongly by the finite image-size available from experiment. The disagreement between experiment and theory was resolved by using the maximum-entropy method to calculate the power spectra. The maximum-entropy method is not as sensitive to the finite image-size effect. When applied to new experimental images, it yielded results for $\xi$ that were in agreement with the theory.

*Work supported by NSF Grant DMR02-43336

[1]Y.-C. Hu, R. Ecke, and G. Ahlers, Phys. Rev. Lett. **74**, 5040 (1995).

**15:42**

**D8 7 Revealing the buidling blocks of chaos: Deviations from extensivity** DAVID A. EGOLF, *Dept of Physics; Georgetown University* MATTHEW P. FISHMAN, *Dept of Physics; Georgetown University & Medical College of Wisconsin* Researchers have made relatively little progress in developing a predictive theory of far-from-equilibrium, spatially-extended chaotic systems. Even descriptions of the fundamental degrees of freedom and the nature of their interactions — central elements of statistical mechanics — are lacking. Using high- precision studies of the fractal dimension as a function of system length for the complex Ginzburg-Landau equation, we have uncovered deviations from extensivity on a length scale consistent with the chaotic length scale, indicating that this spatiotemporal chaotic system is composed of weakly-interacting building blocks, each containing about two degrees of freedom. Our results also suggest an explanation of some of the 'windows of periodicity' found in spatiotemporal systems of moderate size.

**15:54**

**D8 8 Estimating the State of Large Spatio-Temporally Chaotic Systems: Application to a Rayleigh-Benard Convection Experiment** MATTHEW CORNICK, EDWARD OTT, BRIAN HUNT, *University of Maryland* Data Assimilation (DA) refers to the estimation of a dynamical system's state from the combined knowledge of past observations (possibly incomplete and noisy) and knowledge of an approximate model for the systems time evolution. Here we consider DA for spatio-temporally chaotic systems, and, in particular, we study the Local Ensemble Kalman Filter DA technique. We have applied this technique to Rayleigh-Benard convection undergoing spiral defect chaos. Using a system model (Boussinesq equations) and time series of noisy shadowgraphs we obtain estimates of the temperature and velocity field everywhere in a convection cell. This technique provides us with an indirect measurement of quantities previously inaccessible such as mean flow. We also demonstrate the utility of this method for forming initial conditions and producing 'forecasts' from the model.

**16:06**

**D8 9 Competition between left and right spiral vortices and their combinations with different or equal amplitudes** MANFRED LÜCKE, ALEXANDER PINTER, CHRISTIAN HOFFMANN, *University Saarbrücken* Stability, bifurcation properties, and the spatiotemporal behavior of different nonlinear combination structures of spiral vortices in the counter rotating Taylor-Couette system are investigated by full numerical simulations and by coupled amplitude equation approximations. Stable cross-spiral structures with continuously varying content of left and right spiral modes are found. Their solution provides a stability transferring connection between the initially stable, axially counter propagating wave states of pure spirals and the axially standing waves of so-called ribbons that become stable slightly further away from onset of vortex flow.

**16:18**

**D8 10 An Accurate Mode Selection Mechanism for Magnetic Fluids** DAVID JACKSON, *Dickinson College* JOSÉ MIRANDA, *Universidade Federal de Pernambuco* When a ferrofluid is trapped in a Hele-Shaw cell and subjected to a perpendicular magnetic field a fingering instability results in the droplet evolving into a complex branched structure. This fingering instability depends on the magnetic field ramp rate but it also depends critically on the

initial state of the droplet. Small perturbations in the initial droplet can have a large influence on the resulting final pattern. By simultaneously applying a stabilizing azimuthal magnetic field, we gain more control over the mode selection mechanism. In fact, a linear stability analysis predicts that any mode can be selected by appropriately adjusting the strengths of the applied fields. We present the results of numerical simulations that demonstrate that this mode-selection mechanism is quite robust and ''overpowers'' any initial perturbations on the droplet. This provides a predicable way to obtain patterns with any number of fingers whatsoever.

**16:30**

**D8 11 Controlling Interfacial Instabilities in Hele-Shaw Cells: Theory** SHUWANG LI, JOHN LOWENGRUB, *University of Californa at Irvine* JAKE FONTANA, PETER PALFFY-MUHORAY, *Liquid Crystal Institute, KSU* The growth of crystals in an undercooled melt and interface evolution in Hele-Shaw cells are governed by similar underlying mathematics. Hele-Shaw experiments can therefore give valuable insights into crystal growth. In the context of crystal growth, Li, Lowengrub and co-workers have demonstrated (e.g. see J. Crystal Growth, Physica D) that by varying the temperature conditions in the far-field in a prescribed way without feedback, interface instabilities (e.g. Mullins-Sekerka) can be suppressed and crystals may be grown with desired symmetries. Interestingly, at long times nonlinear stabilization is observed and leads to the existence of universal crystal shapes that depend only on the far-field temperature conditions. Here, this work is adapted to interface evolution in Hele-Shaw cells where the control parameter is the injection pressure. Namely, we consider the displacement of oil by air and we demonstrate that by varying the injection pressure in a prescribed, time-dependent way (without feedback) that the Saffman-Taylor instability can be suppressed and controlled such that bubbles of desired symmetries can form. This is in agreement with recent experimental predictions (presented separately in this session). We further predict the existence of universal bubble shapes that depend only on the injection pressure; the experimental confirmation of such universal shapes is the subject of ongoing studies.

**16:42**

**D8 12 Controlling Interfacial Instabilities in Hele-Shaw Cells: Experiments** JAKE FONTANA, *Liquid Crystal Institute, KSU* PETER PALFFY-MUHORAY, *Liquid Crystal Institute, KSU* SHUWANG LI, *University of California at Arvine* JOHN LOWENGRUB, *University of California at Arvine* LIQUID CRYSTAL INSTITUTE TEAM, UNIVERSITY OF CALIFORNIA AT ARVINE TEAM, The growth of crystals in an undercooled melt and interface evolution in Hele-Shaw cells are governed by similar underlying mathematics. Hele-Shaw experiments can therefore give valuable insights into crystal growth. We have constructed radial Hele-Shaw cells where oil between parallel glass plates could be displaced by air whose injection pressure is a function of time. Here we describe our experimental apparatus and present results for the interface evolution for different driving schemes. We have found that, in agreement with recent theoretical predictions (presented separately in this session), we can prevent the onset of the Saffman-Taylor instability, or we can select and grow a particular unstable mode and drive the interface towards a corresponding universal shape. Varying the injection pressure during growth thus allows control over interfacial instabilities.

**16:54**

**D8 13 Liquid manipulation via morphological transitions*** RALF SEEMANN, MARTIN BRINKMANN, EVGENY GUREVICH, STEPHAN HERMINGHAUS, *MPI for Dynamics and Self-Organization, D-37073 Goettingen* JEAN-CHRISTOPHE BARET, MICHEL DECRE, *Philips Research Laboratories, NL-5656AA Eindhoven* Liquid deposited on rectangular grooves, has a variety of possible liquid morphologies determined by the contact angle, $\theta$, and the exact channel geometry. In our experiments, electrowetting is used to tune $\theta$ reversibly from 100 to 50 °, leading to a reversible transition between a drop-like morphology at large $\theta$ and extended liquid filaments for small $\theta$. The transition is capillarity-driven but the behavior of the liquid above the transition is influenced by the electrical properties of the liquid. The static length of the liquid filament is a function of the applied Voltage and is in perfect agreement with a simple transmission-line model. Emphasis is put on the dynamic aspects of the filling and the draining behavior that follow a modified Washburn law. In case of thin and elastic ridges separating two grooves the cross talk of the liquid morphologies with the elastic substrate has an ordering effect on the position of the droplets.

*This work was partly funded by the German Science Foundation under grant number SE1118 within the priority program Nano- and Microfluidics SPP 1164.

**17:06**

**D8 14 Diffusion-induced spontaneous pattern formation on gelation surfaces** HIROAKI KATSURAGI, *University of Pennsylvania, Kyushu University* Polymer gels make various kinds of surface patterns, which are typical non-equilibrium phenomena, under the volume phase transition. Mechanical instabilities due to swelling or shrinking of polymer gels play an essential role in such pattern formations. However, there is no report on diffusion-induced spontaneous pattern formation in polymer gels. Here we report the diffusion-induced (not caused by the mechanical instability) macroscopic pattern formation on gelation surfaces. We experimented on two-dimensional poly-acrylamide gelation that is governed by free radical polymerization. Gel slabs were made on Petri-dishes with free upper surface boundary condition. Then, random and straight stripe patterns (surface deformations) were observed, depending on gelation conditions. We consider a reaction-diffusion dynamics to describe this pattern formation. Acrylamide is considered as an activator and oxygen works as an inhibitor in the gelation reaction-diffusion system. We found the scaling relation between the characteristic wavelength and the gelation time. This scaling is consistent with the reaction-diffusion dynamics.

**17:18**

**D8 15 Using Capillary Flows to Pattern Lines*** SAURABH VYAWAHARE, KATE CRAIG, AXEL SCHERER, *California Institute of Technology, Pasadena CA 91125* One can appreciate how capillary forces cause unexpected patterns and shapes by looking at a soap bubble. Pattern formation by surface tension is seen in ring patterns of coffee stains, fingering patterns in Hele-Shaw cells, ordering of two dimensional micro-sphere crystals, combing of DNA and skeleton formation in marine creatures called radiolarians. Though comman, problems involving the understanding and control of the self-assembly mechanism need to be resolved before using capillary forces as a practical lithographic tool. Here, we report capillary flows create line patterns in evaporating liquids between closely spaced parallel plates. The widths of these lines range from a few microns to a few nanometers. Delib-

erate patterning of such lines requires pinning of the contact line and the presence of foaming surfactants. The position and type of line can be controlled with artificial pinning points and varying solutes respectively, and large-scale photolithography can be used to guide and control the definition of nanostructures. We provide ''proof of principle'' demonstrations of this method's application by creating lines of colloidal quantum dots and micro-spheres. This represents the first step in using capillary phenomena to create controlled, self–assembling, one-dimensional wire-like structures

*Support from the DARPA Optofluidics center is acknowledged

**SESSION D9: METHODS IN NANOBIOTECHNOLOGY**
**Monday Afternoon, 13 March 2006; 301, Baltimore Convention Center at 14:30**
**Ido Braslavsky, Ohio University, presiding**



**14:30**
**D9 1 Nanomechanical Devices for Single Molecule Biophysics.**
MICHAEL ROUKES, *Caltech*

This abstract was not received electronically.

**15:06**
**D9 2 Single Molecule Dynamics of Polymers Confined in Nanochannels.***
ROBERT AUSTIN, *Princeton University*

I will review our work on the conformational dynamics of polymers, in particular genomic length DNA molecules, in nanochannels whose diameter is less than the persistence length of the polymer. I will discuss how these dynamics give some insight into how nanochannels can be used for the next generation of single molecule mapping/sequencing techniques.

*Supported by the NSF funded NBTC of Cornell University, NIH, DARA and US Genomics.

**15:42**
**D9 3 Surface-Mounted Artificial Dipolar Molecular Rotors.***
JOSEF MICHL, *University of Colorado*

We describe the synthesis, surface mounting, characterization, and operation of artificial molecular rotors of 1 - 3 nm size, attached to surfaces through one post (azimuthal rotors, axle normal to surface) or two posts (altitudinal rotors, axle parallel to surface). Rotor response to driving fields (electric and mechanical) has been simulated by molecular dynamics.

*In collaboration with Thomas Magnera, Dominik Horinek, Jaroslav Vacek, Xudong Chen, Deborah Casher, Mary Mulcahy, and Douglas Caskey, University of Colorado.

**16:18**
**D9 4 Mapping Protein Transport in Living Cells with Quantum Dots and Spatio-Temporal Image Correlation Spectroscopy.**
PAUL WISEMAN, *McGill University*

We will present recent advances in image correlation methods and recent use of this technique in combination with luminescent quantum dots for measurements of protein transport in living cells. The talk will focus on the development of image correlation spectroscopy (ICS) as an imaging extension of fluorescence correlation spectroscopy (FCS). The ICS technique is ideally suited to measure transport and clustering of fluorescently tagged proteins in cellular membranes where transport is slow and static proteins abound. The image correlation methods are based on the measurement of fluorescence intensity fluctuations as a function of space and time collected as image time series using a laser scanning microscope (either confocal or two-photon). Spatial and temporal variants of the basic ICS method will be introduced and the power of these approaches to measure both aggregation and transport of cell surface proteins will be demonstrated. The use of luminescent quantum dots as labels for image correlation studies will be discussed including the effects of quantum dot blinking on the fluctuation based image correlation measurements. We will discuss appropriate models and image correlation analysis approaches for dealing with the quantum dot blinking including a new reciprocal space image correlation technique. Finally we will present experimental results from image correlation experiments using quantum dots for mapping protein transport fluid flows in living migrating cells.

**16:54**
**D9 5 STM Manipulation of Nanoscale Biomolecules.**
SAW-WAI HLA, *Ohio University*

The fascinating advances in single molecule manipulations with the scanning-tunneling-microscope (STM)-tip allow scientists to fabricate artificial atomic scale structures, to study local quantum phenomena or to investigate and control properties of molecules at an atomic limit. The STM manipulation is facilitated by a precise control of tip-molecule interactions, or tunneling electrons, or the electric field between the tip and sample. By combining STM manipulation with imaging and tunneling spectroscopy, powerful experimental schemes can be developed, which opens novel routes to investigate or induce molecular conformation changes with atomic level control. In this talk, various cutting-edge STM manipulation techniques relevant to the biological systems will be introduced and our recent results on manipulation of nanoscale biological molecules including chlorophyll-a, $\beta$-carotene and amyloid $\beta$/A4 precursor protein on a Au(111) substrate will be presented.



## SESSION D10: FOCUS SESSION: PHYSICAL CHEMISTRY OF NANOSCALE SYSTEM III
**Monday Afternoon, 13 March 2006; 302, Baltimore Convention Center at 14:30**
**Yiping Zhao, University of Georgia, presiding**

***Invited Papers***

**14:30**
**D10 1 Chemical Imaging and Lasing of Nanoparticle Systems.**
STEPHEN LEONE, *University of California, Berkeley*

Scanned probe microscopy techniques are developed to investigate nanoscale materials and time-domain processes in nanostructured devices. These include apertureless near field microscopy probing of islanded semiconductor films, confocal microscopy ultrafast pump-probe experiments to interrogate stimulated emission processes in ZnO tetrapod species, and single pulse CARS microscopy using phase-shaped ultra-broad-band pulses for rapid spatial and spectral analysis of soft condensed matter. Apertureless near field microscopy studies of InN islands have revealed contrast mechanisms due to the real and imaginary parts of the index of refraction, providing measurements of nanometer size Ga metal islands and InGaN and InN islands on GaN. Pickup of gold nanoparticles permits tip enhancements with resolution of the electric field phase in the images. Ultrafast laser, differential gain experiments on ZnO stimulated emission in nanowires and tetrapods are performed to measure the timescales and ratios of the electron-hole plasma and exciton mechanisms during lasing in nanostructured materials. Two novel types of measurements are addressed, stimulated emission dumping and upconversion probing methods. A single pulse CARS microscopy instrument using an ultrafast laser and phase control with interferometric detection produces complete Raman spectra while spatially scanning. Polymer domains have been analyzed with vibrational spectral sensitivity. The merger of optical techniques with scanned probe methods to investigate nanoscale features is considered in relation to the scientific requirements for measurements and the results for each system.

***Contributed Papers***

**15:06**
**D10 2 Spectroscopic Near-Field Imaging of Flat Gold Nanoparticles*** L.A. BUMM, D.H. DAHANAYAKA, D.W. KELLE, D.J. WASIELEWSKI, E.S. DAY, D.R. WHITE, *Center for Semiconductor Physics in Nanostructures, Homer L. Dodge Department of Physics and Astronomy, University of Oklahoma, Norman, OK 73019, USA* B.S. PRALL, M. ACHERMANN, V.I. KLIMOV, *Chemistry Division, C-PCS, Los Alamos National Laboratory, Los Alamos, NM 87545, USA* Using a white-light near-field scanning optical microscope (NSOM) we demonstrate near-field imaging and local plasmon spectroscopy of flat gold nanoparticles (FGNPs). These nanoparticles are atomically-flat single crystal plates with well defined shapes ranging from equilateral triangles to regular hexagons, which include intermediate truncated triangle shapes. NSOM images reveal the FGNP plasmon mode structure and its dependence on FGNP size and shape. Moreover, spatially resolved spectroscopy shows position dependent coupling to different plasmon modes.

*This work has been supported by the Center for Intergrated Nanotechnologies (CINT) Jump Start Program, NSF CAREER grant No. CHE-0239803, and NSF MRSEC No. DMR-0080054.

**15:18**
**D10 3 Characterization of Palladium and Gold Nanoparticles Using X-ray Reflectivity, EXAFS and Electron Microscopy.*** YUAN SUN, *Dept. Mat. Sci. & Engr., SUNY at Stony Brook* ANATOLY FRENKEL, *Dept Phys, Yeshiva Univ., New York, NY* REBECCA ISSEROFF, CHERYL SHONBRUN, MICHELLE FORMAN, *Stella K Abraham High School, Hewlett, NY* KWAN-WOO SHIN, *Dept Mat Sci & Engr, K-JIST, Korea* TADANORI KOGA, HENRY WHITE, MIRIAM RAFAILOVICH, JONATHAN SOKOLOV, *Dept. Mat. Sci. & Engr., SUNY at Stony Brook* We compared the characteristics of thiolate Pd and Au nanoparticles synthesized by 1-phase and 2-phase methods. HRTEM showed that the 1-phase Pd particles had an ordered core

surrounded by a disordered shell structure while the 2-phase Pd particles appeared to be crystalline throughout; and multiple twinning existed in both the 1-phase and 2-phase Au particles. EXAFS measurements revealed that Pd particles contained large amount of disordered Pd-S compounds while the 1-phase Au particles have a larger fraction of amorphous or defective structures and higher grafting density of thiol chains than the 2-phase Au particles. Lattice expansion was found in the Pd particles, compared with lattice contraction in the Au particles. Only the 2-phase Pd and Au particles spread at the air/water interface and formed Langmuir films, which were deposited onto solid substrates and examined by x-ray reflectivity and EXAFS.

*Supported by NSF-MRSEC.



*Invited Papers*

**15:30**
**D10 4 ''CARS microscopy - Seeing the invisibles.''**
SUNNEY XIE, *Harvard University*

This abstract was not received electronically.

*Contributed Papers*

**16:06**
**D10 5 Probe single cyanine dye molecules' photo isomerization.** ZIH-HAO CHEN, CHANG-YEH LEE, CHAO-KUEI LEE, YU-TSU CHUANG, JUI-HUNG HSU, *National Sun Yat-sen University* Cyanine dyes are interested in the photosensitization, nonlinear optics, and their photophysical and photochemical behaviors. In particular, cyanine molecules, like DiI, plays an important role in single molecule fluorescence investigations. The high photo-stability, good QE, and low inter-system crossing rates, make it an good example for the single molecule investigations. We present the single molecule fluorescence investigation on the DiI molecules. In the investigation, we observe some (but not all) molecules exhibits reversible and quasi-stepwise polarization change. The decay dynamics is also changed correspondingly. Clear on-off blinking behaviors indicate the change in polarization from a single molecule, rather than the background noise, and we speculate it as the photo isomerization of the dye molecule. More detail analysis indicates some isomerization occurred at the singlet excited states, and it takes longer timescale ( $>$ ms) than expected.

**16:18**
**D10 6 Conductive probe AFM investigation on monolayer films of colloidal CdSe quantum dots** ITARU KAMIYA, *Toyota Technological Institute* ICHIRO TANAKA, *Wakayama University* RISA WADA, *Wakayama University* MASAYO ARIMOTO, *Wakayama University* KAZUYUKI UNO, *Wakayama University* TOMOHIRO HAYASHI, *Tokyo Institute of Technology* MASAHIKO HARA, *Tokyo Institute of Technology* The opto/electronic properties of single quantum dots (QDs) have attracted much attention due to their potential for applications to various future devices. We have been employing conductive probe AFM for measuring quantized energy levels of single QDs prepared by colloidal synthesis [1]. In contrast to measurements on QDs prepared by MBE [2], a difficulty we suffered was interaction between the probe and the colloidal QDs. We have shown that the use of conductive CNT tips can prevent such problems [3]. Here, we show that the use of monolayer films of close-packed colloidal QDs allows us to perform stable conduction measurements even with standard probes. Thin films of 1-2nm of Ti followed by 20nm of Pt were sputtered on Si(001) substrates, whereon monolayer CdSe QD films were prepared by horizontal adsorption. The nearly close-packed QDs are stably attached to the substrate, enabling us to perform local conduction measurement using AFM without tip-QD interaction. We report the film formation, and the conduction features due to the single QDs. [1] I.Tanaka, itet al., Surf.Sci. **532-535**, 801 (2003). [2] I.Tanaka, itet al., Appl.Phys-.Lett. **74**, 844 (1999). [3] I.Tanaka, itet al., Jpn.J.Appl.Phys. **44**, L249 (2005).

**16:30**
**D10 7 Ballistic Electron Emission Spectroscopy Studies of Gold Nanocrystals** SAMEH DARDONA, JIANFEI SHAO, RYAN PRICE, ROBERT WHETTEN, PHILLIP FIRST, *School of Physics, Georgia Institute of Technology* We report experimental measurements of ballistic electron emission spectroscopy (BEES) on single gold nanocrystals. Nanocrystals with core diameters from 1 nm to 3 nm were chemically attached to a 10-nm thick gold film that was vapor-deposited on a silicon substrate. Low temperature (77 K) scanning tunneling microscopy and spectroscopy were used to image and identify nanocrystals prior to BEES measurements. A comparison of BEES spectra acquired by tunneling through a nanocrystal with those acquired by tunneling directly to the gold film, shows attenuation of the BEES signal by a factor of typically 4-10. From a simple rate equation, electron relaxation times in these gold nanocrystals are estimated to be of order 10 picoseconds.

**16:42**
**D10 8 Neutron diffraction and thermodynamics of deuterium adsorption in amorphous carbon materials with a uniform pore network.** LILLIAN FRAZIER, *University of Tennessee* TOM ARNOLD, *ORNL CSD* THOMAS HANSEN, MIGUEL GONZALEZ, *ILL* DAVID MARTIN Y MARREO, *ISIS* SHENG DAI, ZUOJAIN LI, DAVID BEACH, *ORNL CSD* JOHN Z. LARESE, *University of Tennessee/ ORNL CSD* A coordinated thermodynamic and neutron diffraction investigation of the sorption properties of D2 within an amorphous carbon material with a uniform, close-packed network of open pores has been undertaken. The volumetric adsorption studies are used to determine the gas capacity, the heat of adsorption and as a guide to the neutron diffraction experiments. By combining the results of the thermodynamic measurements with the findings in the structural measurements a precise description of structure of the adsorbed phase as a function of gas filling is possible. Because the pores in these carbon materials are unequivocally open these findings have a direct impact on the interpretation of earlier adsorption and diffraction experiments involving carbon nanotubes.

**16:54**
**D10 9 Adsorption properties of amorphous carbon materials with a uniform pore network.** RICHARD E. COOK, LILLIAN FRAZIER, SAMI CHANAA, ANDREA E. FREITAG, *University of Tennessee* SHENG DAI, ZUOJIANG LI, DAVID BEACH, *ORNL CSD* JOHN Z. LARESE, *Univ of Tennessee / ORNL CSD* There has been increasing interest in various forms of high surface area carbon materials, such as buckyballs, nanotubes, and carbon black, because of their potential applications as support for catalysts, electrode materials in fuel cells, gas storage devices and as a component of nano-composites. The underlying mechanism for most of these applications involves adsorption and transport of molecules on the carbon surface. Understanding the details of the interaction potential for different adsorbate molecules with these carbon materials is an important step for tailor-making application-specific materials. The adsorption properties of a carbon material with a uniform, close packed pore distribution of approximately 2.5nm were examined using high resolution adsorption isotherms with different adsorbates. By varying the size of the adsorbate molecule we hope to learn about the potential energy surface offered by these materials and gain a keen insight into the role played by the relative surface curvature on the adsorption properties. Volumetric adsorption isotherms of H2, D2, Ar, N2, H2O, CH4, and Xe were recorded and the results will be presented. Thermodynamic properties derived from these adsorption isotherms will also be discussed.

**17:06**
**D10 10 Sonoelectrochemical Approach Towards Nanostructures** CLEMENS BURDA, XIAOFENG QIU, *Case Western Reserve University* We will report on the sonoelectrochemical synthesis of nanostructured semiconductor materials. The talk will focus on the control of the nanostructure size, shape, and composition using sonolectrochemistry as a versatile synthesis tool. The synthesis of targeted nanostructures requires thorough control of the redox chemistry during the growth process. The composition of the product can be controlled by changing the initial metal-ligand concentration. Futhermore, the properties of the novel materials will be discussed. Powder X-ray diffraction of the products confirmed the compositional change in the nanomaterials. Control of the involved sonoelectrochemistry also allows for the formation of highly monodispersed 1-D Nanorods. Qiu, Xiaofeng; Lou, Yongbing; Samia, Anna C. S.; Devadoss, Anando; Burgess, James D.; Dayal, Smita; Burda, Clemens. **PbTe nanorods by sonoelectrochemistry.** Angewandte Chemie, International Edition (2005), 44(36), 5855-5857. Qiu, Xiaofeng; Burda, Clemens; Fu, Ruiling; Pu, Lin; Chen, Hongyuan; Zhu, Junjie. **Heterostructured Bi2Se3 Nanowires with Periodic Phase Boundaries.** Journal of the American Chemical Society (2004), 126(50), 16276-16277.

**17:18**
**D10 11 Optical properties of single solution based semiconductor nanowires** MASARU KUNO, VLADIMIR PROTASENKO, *University of Notre Dame* The optical properties of solution based nanowires are studied using single molecule microscopy. Particular emphasis is placed on CdSe nanowires with diameters at or below 10 nm and lengths exceeding 1-10 microns. For comparison the bulk exciton Bohr radius is 5.6 nm. These wires therefore exhibit confinement effects as seen by blueshifts, both in the ensemble linear absorption and band edge emission. No deep trap emission is seen. Furthermore, branched nanowires with tripod, v-shape and y-shape morphologies can be made using the same solution based chemistry. In all cases, unusual intrawire spectral heterogeneity is observed in both the spectral position and linewidth. Fluorescence intermittency within the wire is also observed and has been shown to exhibit power law on-time and off-time probability densities. Possible explanations for this intrawire heterogeneity include dielectric contrast effects as well as more intrinsic causes due to zincblende/wurtzite phase admixtures present in the wires. However, such explanations do not explain any of the observed fluorescence dynamics. Complicating these (and other) possible explanations are recent experiments we have conducted, which show that external electric fields can modulate both the spatial position and intensity of the nanowire emission.



## SESSION D11: FOCUS SESSION: PROMISES AND CHALLENGES IN CHEMICAL DYNAMICS III
**Monday Afternoon, 13 March 2006; 303, Baltimore Convention Center at 14:30**
**Laurie Butler, University of Chicago, presiding**

***Invited Papers***

**14:30**
**D11 1 Photodissociation of water ice and adsorbed molecules.**
MASAHIRO KAWASAKI, *Department of Molecular Engineering, Kyoto University*

The TOF spectra of photofragment hydrogen atoms from the photodissociation of amorphous ice at 193 nm have been measured. The spectra consist of both a fast and a slow components characterized by translational temperatures of 2300 and 120 K, respectively. The photoabsorption of a branched cluster, $(H_2O)_{6+1}$ that is a $(H_2O)_6$ cyclic cluster attached by a water molecule with the hydrogen bond, is expected to appear at around 200 nm. The source of the hydrogen atoms is attributed to the photodissociation of the ice surface molecules that are attached by the $(H_2O)_6$ water structure with the hydrogen bond. Atmospheric implications are estimated for the photodissociation of the ice particles at 190-230 nm in the region between 80 and 85 km altitude. The photodissociation of ice has also performed at 157 nm. Since the bulk ice absorbs vacuum UV light, hydrogen atoms are produced from both the surface and bulk photodissociation processes. A difference in the UV photodissociation dynamics of chlorine and tricholorofluorocarbon has been observed when those molecules were adsorbed on water ice surfaces. In the photodissociation of $Cl_2$ at 300 to 414 nm, the branching ratios of the formation of $Cl(^2P_{1/2})$ with respect to $Cl(^2P_{3/2})$ are different from those reported in the gas phase photodissociation.

However, in the photodissociation of $CFCl_3$ at 193 nm, the ratio is in good agreement with that reported in the gas phase photodissociation. These results are mostly attributable to the difference in the interaction of the adsorbed molecule with surface water molecules of ice. The kinetic energy distributions of the photofragment chlorine atoms reflect the interaction between the adsorbed molecules and the surface water molecules. The photofragment spectroscopy developed by late Prof. Richard Besohn has been used in this work.



***Contributed Papers***

**15:06**

**D11 2 Photodissociation dynamics of ethyl ethynyl ether: A ketenyl radical precursor** MARIA KRISCH, JOHANNA MILLER, LAURIE BUTLER, *University of Chicago* HONGMEI SU, RICHARD BERSOHN,* *Columbia University* JINIAN SHU, *Lawrence Berkeley National Laboratory* We investigate the photodissociation dynamics of ethyl ethynyl ether at 193.3 nm with crossed laser-molecular beam photofragment translational spectroscopy and laser-induced fluorescence. We establish ethyl ethynyl ether as the first clean precursor to the ketenyl radical, a key species in combustion reactions. One major bond fission channel was observed for the system, cleavage along the HCCO-$C_2H_5$ bond, leading to ground state $C_2H_5$ (ethyl) radicals and HCCO (ketenyl) radical products in two distinct electronic states. We observed neither cleavage of the other C-O bond nor molecular elimination to form $C_2H_4$ + $CH_2CO$ (ketene). Ketenyl radicals formed in the higher recoil kinetic energy channel could be either $\tilde{X}(^2A'')$ or $\tilde{A}(^2A')$ state ketenyl radical. We assign the lower recoil kinetic energy channel to the spin forbidden $\tilde{a}(^4A'')$ state of the ketenyl radical, reached through intersystem crossing. Laser-induced fluorescence from the ketenyl radical peaks after a 20 $\mu$s delay, indicating that it is formed with a significant amount of internal energy and subsequently relaxes to the lowest vibrational level of the ground electronic state, a result consistent with the product assignment.

*Deceased

**15:18**

**D11 3 Multiphoton Photodissociation of Several Halocarbons.** BOB QUANDT, *Department of Chemistry Illinois State University* The 2 x 193 nm photodissociations of $CHCl_3$, $CFCl_3$, $CF_3CCl_3$, $CCl_4$, $CH_3$-$CCl_3$ and $CH_3CH_2$-$CCl_3$have been examined using dispersed fluorescence. It was found that the initial photodissociation of $CHCl_3$ forms large amounts of $CH(A^2\Delta)$ while the photodissociation of $CCl_4$ forms lesser but still significant amounts of $CX(A^2\Delta)$ The photodissociations of $CH_3$-$CCl_3$ and $CH_3CH_2$-$CCl_3$ produce $CH_3$-C and $CH_3CH_2$-C presumably in the $A^2\Delta$ state. The exact photoproducts of the fluorinated species are currently unknown. Fluorescence rise time measurements show that the $CH(A^2\Delta)$ and $CCl(A^2\Delta)$ photoproducts quickly react to form $C_2(d^3\Pi_g)$. However, formation of $C_2(d^3\Pi_g)$ is attenuated when the primary photoproducts are $CF_3C$, $CH_3$-C and $CH_3CH_2$-C and disappears completely when it is CF. In addition, the atomic and molecular halogen photoproduct channels were investigated using ab initio calculations. Intrinsic Reaction Coordinate calculations were performed at the MP2 level of theory using the LANL2DZ basis set in order to characterize the dissociation pathways for all of species investigation. The results of the calculations show the presence of three transition states and an ion-pair isomer intermediate for all molecules. The broken symmetry structure of the transition states for the formation of molecular bromine is in agreement with the first step of the addition mechanism proposed by Cain and co-workers for $CX_2+Y_2$ reactions.

**15:30**

**D11 4 Thick and thin slices of photoproducts: correlated state distributions in ketene dissociation*** GREGORY HALL, *Brookhaven National Laboratory* ANATOLY KOMISSAROV, *JPL* MIKE MINITTI, *Stony Brook University* ARTHUR SUITS, *Wayne State University* We have revisited the correlated product distribution of $CH_2$ + CO in the photodissociation of ketene at an energy 2350 $cm^{-1}$ above the barrierless singlet dissociation threshold. Using time-sliced ion imaging, we find the speed distribution of state-selected CO fragments to be quite different from previous measurements. For each CO rotational state observed, the deviations of the coincident $CH_2$ distribution from a statistical Phase Space Theory can be accurately described with a single parameter in the spirit of a linear surprisal. The distributions are consistent with calculations of exit channel rotational dynamics starting at a variational transition state.

*Work performed under DOE Contracts DE-AC02-98CH10886 at Brookhaven National Laboratory and DE-FG-02-04ER15593 at Wayne State University.

**15:42**

**D11 5 State-resolved reactive scattering by slice imaging: A new view of the Cl+ethane reaction** ARTHUR SUITS, WEN LI, CUNSHUN HUANG, *Wayne State University* The reactions of chlorine atoms with alkanes have been the subject of intense scrutiny as model systems for the detailed investigation of polyatomic reaction dynamics. Interest in these systems has accelerated in recent years as new experimental methods have provided the means of gaining insight into the reaction with quantum state specificity. In this presentation, we will show state-resolved crossed beam scattering results for the reaction Cl + $C_2H_6 \rightarrow$ HCl + $C_2H_5$, obtained using DC slice imaging. The HCl (v=0, J) images, recorded at a range of well-defined collision energies, show strongly coupled angular and translational energy distributions revealing features of the reaction not seen in previous studies. The overall distribution is mainly forward-sideways scattered with respect to the Cl beam, with a translational energy distribution peaking near the collision energy. However, there is a substantial backscattered contribution that is very different. It shows a sharp peak near the energetic limit, but extending to much lower energy, implying substantial internal excitation in the ethyl radical co-product. These results provide new insight into the reaction, and they are considered in terms of alternative models of the dynamics. This work represents the first genuine crossed-beam study in which a product other than the methyl radical was detected with quantum state specificity, showing the promise of the approach generally for high resolution state-resolved reactive scattering.

**15:54**

**D11 6 Propargyl Radical: ab initio Anharmonic Modes and the Polarized Infrared Absorption Spectra of Matrix-Isolated HCCCH2** BARNEY ELLISON, *University of Colorado* XU ZHANG, *University of Colorado* EVAN JOCHNOWITZ, *University of Colorado* MARK NIMLOS,* *University of Colorado* JOHN STANTON, *University of Texas* MYCHEL VARNER, *University of Texas* Propargyl Radical: ab initio Anharmonic Modes and the Polarized Infrared Absorption Spectra of Matrix-Isolated HCCCH2 The propargyl radical has twelve fundamental vibrational modes, Gamma(vib)(HCCCH2) = 5a1 + 3b1 + 4b2, and nine have been detected in a cryogenic matrix. Ab initio coupled-cluster anharmonic force field calculations were used to help guide the assignments. The experimental HCCCH2 matrix frequencies (cm-1) and polarizations are: a1 modes - 3308.5 +/- 0.5, 3028.3 +/- 0.6, 1935.4 +/- 0.4, 1440.4 +/- 0.5, 1061.6 +/- 0.8; b1 modes - 686.6 +/- 0.4, 483.6 +/- 0.5; b2 modes - 1016.7 +/- 0.4, 620 +/- 2. We recommend a complete set of gas-phase vibrational frequencies for the propargyl radical, HCCCH2 X 2B1.

*also at National Renewal Energy Laboratory

**16:06**

**D11 7 H-atom elimination of *n*-propyl and itiso-propyl radicals: a photodissociation study*** JINGSONG ZHANG, WEIDONG ZHOU, YAN YUAN, *University of California, Department of Chemistry* The H-atom elimination channels in the UV photodissociation of jet-cooled *n*-propyl and itiso-propyl radicals are studied in the region of 237 nm using the high-*n* Rydberg-atom time-of-flight technique. Upon excitation to the 3*p* state by the UV photolysis radiation, *n*-propyl radical and itiso-propyl radical dissociate into the H atom and propene products. The product center-of-mass translational energy release of both *n*-propyl and itiso-propyl radicals have bimodal distributions. The H-atom product angular distribution in *n*-propyl is anisotropic (with it$\beta \sim 0.5$), and that in itiso-propyl is isotropic. The overall average translational energy release is $\langle E_T \rangle \sim 0.27 E_{avail}$ for *n*-propyl and $\langle E_T \rangle \sim 0.21 E_{avail}$ for itiso-propyl. The bimodal translational energy distributions indicate two dissociation pathways: (i) a unimolecular dissociation pathway from the ground-state propyl after internal conversion from the 3*p* state, and (ii) a repulsive pathway directly connected with the excited state of the propyl radical. Isotope labeling has also been carried out. The possible photodissociation mechanisms will be discussed.

*Acknowledgement: National Science Foundation and Sloan Foundation

**16:18**

**D11 8 Photoinitiated decomposition of hydorxyalkyl radicals: Rydberg-valence interactions** HANNA REISLER, JIE WEI, BORIS KARPICHEV, LAURA EDWARDS, *University of Southern California* The photoinitiated dynamics of hydroxyalkyl radicals is investigated on the ground and excited surfaces. Overtone excitation of four quanta of OH stretch vibration of the hydroxymethyl radical gives rise to O-H bond fission via tunneling, without prior isomerization to the methoxy radical. Excitation of hydroxyethyl radicals to the lowest *s* and *p* Rydberg excited states accesses dissociative states lying as low as 2.5 eV above the ground state. These states undergo conical intersections with each other and the ground state, which are much more efficient than comparable interactions in the hydroxymethyl radical, and display increased opportunities for accessing crossing seams. Both O-H and C-H bond fission channels are observed. Dissociation mechanisms involving direct and indirect bond fission, isomerization and nonadiabatic interactions will be discussed. Research supported by DOE.

**16:30**

**D11 9 Determining the Products and Mechanism of the $C_2Cl_3+O_2$ Reaction by Time-Resolved FTIR Emission Spectroscopy** HONGMEI SU, TIANCHENG XIANG, SHAOLEI ZHAO, CONGYUN SHI, The reaction products and mechanism of the $C_2Cl_3$ radical with $O_2$ have been studied by time-resolved FTIR emission spectroscopy. The chlorinated vinyl radical, $C_2Cl_3$, was generated by 248 nm photolysis of a $C_2Cl_4$ precursor. Vibrationally excited CO, $CO_2$ and ClCO products were observed. The time evolution of the emission intensity shows that $CO_2$ and ClCO are primary reaction products. In contrast, CO emission does not decay until itms time scale indicating that CO products are due to secondary reactions, most likely, the further dissociation of ClCO. Two primary reaction channels are identified: $C_2Cl_3 + O_2 \diamond CO_2 + CCl_3 \diamond ClCO + COCl_2$ When reacting with $O_2$, the observed products and channels of the chlorinated vinyl radical, $C_2Cl_3$, turned out to be very similar to its counterpart, vinyl radical $C_2H_3$. Morokuma's DFT study[1] of the reaction $C_2H_3+O_2$ shows that the main reaction path proceeds through a three-membered CCO ring adduct. The question is, does $C_2Cl_3$ go through the same reaction path as $C_2H_3$? Does the substitution of H atom by heavier Cl atom make any difference in regard to the reaction mechanism? Further investigation combining itab initio calculation is under way. [1] A.M.Mabel, E.W.G.Diau, M.C.Lin, and K.Morokuma, J.Am.Chem.Soc. 118, 9759 (1996)

**16:42**

**D11 10 Experimental and Theoretical Investigation of the Electronic Spectroscopy of $H_2CN$** PAUL J. DAGDIGIAN, *Johns Hopkins University* ALEXEY TESLJA,* *Columbia University* MICHAEL BANCK, WOLFGANG EISFELD, *Technische Universität M|"unchen* The electronic spectrum of $H_2CN$, recorded through cavity ring-down spectroscopy, is reported. The radical was prepared by 193 nm photolysis of monomeric formaldoxime vapor. Two diffuse features are observed in the 34800-35800 $cm^{-1}$ spectral range, along with the $A - X$ (1,0) band of the OH co-fragment. These are assigned as vibronic transitions to the ground and $2b_1$ (umbrella mode) levels of the second excited, $^2A_1$ state from the ground $^2B_2$ state. Experimental and simulated rotational profiles of these bands agree extremely well with each other for an assumed type-B electric-dipole allowed $^2A_1 \leftarrow {}^2B_2$ transition appropriate to this transition. A theoretical investigation of the dissociation pathways for electronically excited $H_2CN$ is also presented. The upper states of the observed bands cannot dissociated directly, but higher $b_1$ levels are above the excited-state dissociation limit.

*formerly at Johns Hopkins University

**16:54**

**D11 11 Ab initio analysis of the BCN, NBC and CNB fragments formation** ROBERT JARA, VLADIMIR MAKAROV, GERARDO MORELL, BRAD WEINER, The Laser Ablation technique applied to the synthesis of nano-structured materials produce unique compositions, with correspondingly unique physical and chemical properties. In order to do smart utilization of this method, fundamental understanding of the precursor formation and incorporation mechanisms for the growth of different materi-

als is crucial. Particularly important is to know what fragments are formed during the ablation process, in order to understand its dynamic evolution and eventual incorporation in the synthesized material. In connection to the synthesis of Boron Carbonitride, we have focused our attention on the dynamic evolution of the primary reactions upon BCN ablation using the itab initio method (Gaussian-98 software pack). The results (including the formation energy, direct and inverse rate constants, etc.) were estimated by considering the elementary reactions as bimolecular reactions: reactions between atoms, and atoms with diatomic molecules. The temperature dependence of the dissociation rate constant of three-atomic fragments by different channels was also analyzed using the RRKM theory. It was found that BCN and NBC are the most thermodynamically stable fragments. This theoretical analysis helps understand the strong tendency for BCN to grow stoichiometrically under a variety of experimental conditions.

**17:06**

**D11 12 Variable (itT$_g$ , itT$_s$) Measurements of Alkane Dissociative Sticking Coefficients** LETICIA VALADEZ, KRISTY DEWITT, HEATHER ABBOTT, KURT KOLASINSKI, IAN HARRISION, *Dept. of Chemistry, University of Virginia* Dissociative sticking coefficients $S(T_g, T_s)$ for $CH_4$ and $C_2H_6$ on Pt(111) have been measured as a function of gas temperature ($T_g$) and surface temperature ($T_s$) using an effusive molecular beam. Microcanonical unimolecular rate theory (MURT) was employed to extract transition state characteristics [e.g., $E_0(CH_4) = 52.5 \pm 3.5$ kJ/mol$^{-1}$ and $E_0(C_2H_6) = 26.5 \pm 3$ kJ/mol$^{-1}$]. MURT allows our $S(T_g, T_s)$ values to be directly compared to other supersonic molecular beam and thermal equilibrium sticking measurements. The $S(T_g, T_s)$ depend strongly on $T_s$, however, only for $CH_4$ is a strong $T_g$ dependence observed. The fairly weak $T_g$ dependence for $C_2H_6$ suggests that vibrational mode specific behavior and/or molecular rotations play stronger roles in the dissociative chemisorption of $C_2H_6$ than they do for $CH_4$. Interestingly, thermal $S(T_g = T_s)$ predictions based on MURT modeling of our $CH_4$/Pt(111) data are three orders of magnitude ithigher than recent thermal equilibrium measurements on supported Pt nanocrystallite catalysts [J. M. Wei, E. Iglesia, J. Phys. Chem. B **108**, 4094 (2004)].

**SESSION D12: MORPHOLOGICAL EVOLUTION AND INSTABILITIES**
**Monday Afternoon, 13 March 2006**
**304, Baltimore Convention Center at 14:30**
**Ted Einstein, University of Maryland, presiding**

**14:30**

**D12 1 Langevin Equation for the Morphological Evolution of Strained Epitaxial Films*** DIMITRI VVEDENSKY, *Imperial College London* CHRISTOPH HASELWANDTER, *Imperial College London* A stochastic partial differential equation for the morphological evolution of strained epitaxial films is derived from an atomistic master equation. The transition rules in this master equation are based on previous kinetic Monte Carlo (KMC) simulations of a model that incorporates the effects of strain through local environment-dependent energy barriers to adatom detachment from step edges. The morphological consequences of these rules are seen in the transition from layer-by-layer growth to the appearance of three-dimensional islands with increasing strain. The regularization of the exact Langevin description of these rules yields a continuum equation whose lowest-order terms provide a coarse-grained theory of this model. The coefficients in this equation are expressed in terms of the parameters of the original lattice model, so a direct comparison between the morphologies produced by KMC simulations and this Langevin equation are meaningful. Comparisons with previous approaches are made to provide an atomistic interpretation of a similar equation derived by Golovin *et al.* based on classical elasticity.

*Supported by ESF-SONS Programme and EPSRC

**14:42**

**D12 2 Crystal Surfaces out of Equilibrium: Instabilities, Multiscaling and Non-locality** ALBERTO PIMPINELLI, *LASMEA, U. Blaise Pascal Clermont-2, France, & U. of Maryland* FLORIN NITA, *U. of Genoa, Italy* We have recently proposed a novel scenario for the step meandering instability on vicinal surfaces, in which the instability is ascribed to unhindered diffusion of atoms along the step edges.[1] Then, in a rather counterintuitive way, step meandering appears due to the very mechanism - step edge diffusion - which may be expected to oppose it. We discuss the detailed comparison of the scaling properties of unstable surfaces driven by different atomistic mechanisms. We have discovered an unsuspected richness of behaviors: anomalous scaling, multiaffinity, ... We discuss a number of continuum equations that share several features with the simulations. Implications for experiments are also discussed.

[1]F. Nita and A. Pimpinelli, Phys. Rev. Lett. 95, 106104 (2005)

**14:54**

**D12 3 Criticality of morphological instability of a strained film growing on a patterned substrate*** HANGYAO WANG, FENG LIU, *University of Utah* We show that the morphological instability of a strained film on a patterned substrate is fundamentally different from that on a flat substrate. It exhibits a film thickness ($t$) dependent critical wavelength, which takes a simple form as $\lambda_c = \lambda_0/2 + \pi t$ for a very thin film, where $\lambda_0$ is the critical wavelength on a flat substrate. It also defines three distinct regimes of growth stability depending on the wavelength of substrate undulation ($\lambda_s$): for $\lambda_s \leqslant \lambda_0/2$, growth is stable; for $\lambda_s \geqslant \lambda_0$, growth is unstable; in between, growth is unstable below a critical film thickness $t_c$, and stable above it.

*This work is supported by DOE

**15:06**

**D12 4 First-principles Investigation of the Stability of Surface Gold Oxides on Au(111)** HONGQING SHI, CATHERINE STAMPFL, *The University of Sydney* In contrast to the long held view that gold is catalytically inert and as such uninteresting, it is now well known that Au is significantly more active than Pt in the catalytic oxidation of CO under basic environments. Au can also promote many other reactions in the form of nanoparticles on metal oxide and activated carbon supports [1].This has simulated huge efforts in an attempt to understand the mechanisms responsible for the high activity, including investigations into the nature of oxygen on gold surfaces[2]. In the present work we have investigated the relative stability of oxygen adsorbed on and under the Au (111) surface, as well as thin surface oxides. We identify structures in which the binding of atomic oxygen is stronger than

that at under−coordinated surface Au atoms (e.g. at steps). To determine the stability of the structures for different pressure and temperature conditions, we use the approach of *ab initio* thermodynamics [3], which indicates that these structures should be stable under certain catalytic conditions.[1] Haruta, Catal. J. New. Mater. Electro. Sys. **7**, 163 (2004). [2] R. Meyer, *et al.*, Gold Bull. **37**, 72 (2004), and references therein. [3] K. Reuter, C. Stampfl and M. Scheffler, in Handbook of Materials Modeling, Volume 1, Fundamental Models and Methods, Sidney Yip (Ed) 2005, 149–194; K. Reuter and M.Scheffler, Phys. Rev. B **65**, 035406 (2002).

**15:18**

**D12 5 Modeling Nanoscale Dynamics for Film Growth** ALEXANDRA TEN BOSCH, *CNRS, Lab. Phys. Mat. Cond., Parc Valrose, 06108 Nice, France* Small scale particle motion controls the onset of a phase transition. A general method is developed which links atomic and mesoscopic dynamics in a nanoscale description reminiscent of the classical theory of fluid flow. Derived from a Fokker Planck equation for the non-equilibrium particle distribution, the dynamic equation includes inertia terms essential for high frequency fluctuations. Film nucleation and growth are modeled by the spatially inhomogeneous evolution of the instantaneous density profile which measures the average number of particles at a given time and position. The method is used to show how an alteration in the equilibrium distribution of particles at the boundary between parent and product phases induces transient film growth and/or damped vibrations at the surface. To illustrate, condensation of a simple fluid on a surface is considered.

**15:30**

**D12 6 Interface Roughening Dynamics of Spreading Droplets** HAIM TAITELBAUM, AVRAHAM BE'ER, INBAL HECHT, AVIAD FRYDMAN, *Department of Physics, Bar-Ilan University, Ramat-Gan 52900, Israel* YOSSI LEREAH, *Faculty of Engineering, Tel-Aviv University, Tel-Aviv 69978, Israel* We review our recent experimental data of interface roughening dynamics of spreading mercury droplets on thin films (silver or gold), obtained using optical microscopy and other techniques (AFM, SEM). We discuss the various results obtained for the roughness and growth exponents associated with the interface dynamics, and their universality classes. We analyze the temporal width fluctuations, obtained for single interfaces, and show that these fluctuations contain information on the lateral correlation length of these interfaces. We show how to extract this length from experimental data, and demonstrate the validity of this method in a wide range of growing interfaces (droplet spreading experiments as well as water imbibition on paper). References: 1. A. Be'er, Y. Lereah and H. Taitelbaum, Physica A, 285, 156 (2000). 2. A. Be'er, Y. Lereah, I. Hecht and H. Taitelbaum, Physica A, 302, 297 (2001). 3. A. Be'er, Y. Lereah, A. Frydman and H. Taitelbaum, Physica A, 314, 325 (2002). 4. A. Be'er and Y. Lereah, J. of Microscopy, 208, 148 (2002). 5. I. Hecht and H. Taitelbaum, Phys. Rev. E, 70, 046307 (2004). 6. A. Be'er, I. Hecht and H. Taitelbaum, Phys. Rev. E, 72, 031606 (2005). 7. I. Hecht, A. Be'er and H. Taitelbaum, Fluctuation and Noise Letters, 5, L319 (2005).

**15:42**

**D12 7 Evolution of the morphology and composition of metal germanosilicide thin films** MATHIEU BOUVILLE, DONGZHI CHI, *Institute of Materials Research and Engineering, Singapore* DAVID J. SROLOVITZ, *Princeton University* Metal germanosilicide thin films, formed from the reaction of metals on silicon-germanium substrates, are attractive for use in advanced metal-oxide-semiconductor field-effect transistors (MOSFETs). However, metal germanosilicide films are less stable than silicides films at elevated temperatures, easily agglomerating into isolated islands following severe grain boundary grooving. The resultant germanosilicide islands are noticeably different from both silicides and germanides. Agglomerated germanosilicide films consist of small, regular islands with faceted interfaces, whereas agglomerated silicides form irregular islands and uniformly curved island/substrate interfaces. Experimental observations show that the germanium composition is inhomogeneous both in the film and in the substrate. We use phase-field simulations to study the interplay between morphology, composition inhomogeneities, and strain during grain boundary grooving and agglomeration of polycrystalline metal germanosilicide films on silicon-germanium alloy substrates. By simulating the evolution of germanosilicide films on compressive and relaxed substrates, we demonstrate the important role played by misfit stress on agglomeration morphologies.

**15:54**

**D12 8 Effects of shadowing in oblique incidence epitaxial growth*** J.G. AMAR, Y. SHIM, V. BOROVIKOV, *University of Toledo* The results of kinetic Monte Carlo simulations of a simplified model of oblique incidence epitaxial growth on a metal fcc(100) surface are presented. Results for the effects of shadowing on the mound morphology, surface roughness, and nanoscale pattern formation as a function of the angle of incidence $\theta$ relative to the surface normal as well as the azimuthal angle $\phi$ relative to the high-symmetry direction are presented. In good agreement with experiment, we find that shadowing has little effect for deposition angles up to approximately $55^o$. However, for higher angles there is a significant effect. In particular, the formation of ripples perpendicular to the incident beam is found at $\theta \simeq 78^o$ while at even higher angles the formation of ripples parallel to the incident beam is observed. The coarsening behavior of the resulting ripple structures is also studied. Results are also presented for azimuthal angles away from the high-symmetry directions.

*Supported by the Petroleum Research Fund

**16:06**

**D12 9 Multiscale simulations of oblique-incidence Cu/Cu(100) epitaxial growth*** V. BOROVIKOV, Y. SHIM, J.G. AMAR, *University of Toledo* We present an improved method for multiscale simulations of homoepitaxial growth of metal thin films in which the effects of oblique incidence on the deposition process may be accurately taken into account. Our method combines a kinetic Monte Carlo (KMC) simulation for the thermal surface diffusion with a small scale molecular-dynamics simulation of every deposition event, in order to account correctly for both shadowing as well as the detailed atom-surface interaction of depositing atoms. To speed-up the simulations, that are very time consuming computationally, we have utilized a parallel algorithm that involves simultaneous depositions in different areas of the surface along with parallel kinetic Monte Carlo. Simulation results for the growth of Cu/Cu(100) at 160 and 200 K are presented and compared with both ordinary KMC simulations and experiments. Results will be presented for the case of both normal incidence as well as oblique angle incidence.

*Supported by the Petroleum Research Fund and NSF DMR-0219328

**16:18**

**D12 10 Evolution of Roughness and Wavelength Selection during Fluorocarbon Plasma Etching of Nanoporous Silica*** TAESOON KWON, HUNG-CHIH KAN, XUEFENG HUA, GOTTLIEB OEHRLEIN, RAY PHANEUF, *University of Maryland* Nanoporous silica is a technologically appealing candidate as a low-k dielectric material for high speed nano device applications. A crucial issue during plasma pattern transferring processes is the stability of the plasma/NPS interface. Induced surface/interface roughness may ultimately limit the minimum feature sizes attainable in devices using this material. Our results show a monotonic increase with porosity in the roughening rate, and pronounced disagreement with the predictions of simple models based upon self-affine behavior. In addition we find direct evidence for spontaneous pattern formation during etching.

*Work supported by the Laboratory for Physical Sciences and an NSF-MRSEC, DMR #00-80008.

**16:30**

**D12 11 Wavelength Tunability of Ion-bombardment Induced Surface Ripples on Sapphire** HUA ZHOU, LAN ZHOU, YIPING WANG, RANDALL L. HEADRICK, *Department of Physics, University of Vermont* AHMET S. OZCAN, YI-YI WANG, GOZDE OZAYDIN, KARL F. LUDWIG JR., *Department of Physics, Boston University* DAVID P. SIDDONS, *National Synchrotron Light Source, Brookhaven National Laboratory* Energetic particle bombardment on surfaces is known to produce well ordered 2-D (ripples or wires) and 1-D (dots) structures at submicron/nanoscale by a self-organization process. Recently, significant experimental and theoretical effort has been expended to develop methods to produce self-organized nanostructures on diverse substrates from semiconductors to metals. These studies have shown potential in tailoring surface morphology in order to exploit novel physical properties, and contributed much to reveal the mechanisms of the instability-driven self-organization process. In this work, a study of ripple formation on sapphire surfaces by ion sputtering is presented. Surface characterization by in-situ synchrotron grazing incidence small angle x-ray scattering (GISAXS) and ex-situ atomic force microscopy (AFM) for the wavelength, shape and amplitude of sapphire ripples is performed. The wavelength can be varied over two orders of magnitude by changing the ion incidence angle. The linear Bradley-Harper (B-H) theory with ion induced viscous flow (IVF) relaxation fits the general trends of the data. However, anomalous smoothing not predicted by current models is observed near normal incidence.

**16:42**

**D12 12 Atomistic calculations of mass redistribution and surface morphology evolution due to medium energy ion bombardment** HARLEY JOHNSON, *University of Illinois at Urbana-Champaign* NAGARAJAN KALYANASUNDARAM, *University of Illinois at Urbana-Champaign* BENJAMIN DAVIDOVITCH, *Harvard University* MICHAEL BRENNER, *Harvard University* MIKE AZIZ, *Harvard University* JONATHAN FREUND, *University of Illinois at Urbana-Champaign* Nanoscale mass redistribution mechanisms and dynamics near a surface due to ion bombardment are studied using molecular dynamics (MD). In addition to sputter erosion, as described by the well-known Bradley-Harper theory, ion assisted surface mass redistribution is identified as an important contributor to surface morphology changes. MD simulations yield a response function based on the change in surface height at any point on the surface due to impact at an arbitrary point on the surface. We derive a linear continuum equation for surface morphology evolution using the new response function and relate the results to pattern formation. We conclude that consideration of both sputtering and mass redistribution could explain the experimentally observed limits on the slopes of ripples formed in this process.

**16:54**

**D12 13 Measurement and modeling of temperature-dependent step bunching on Si(111)** BRIAN GIBBONS, JONATHAN PELZ, *The Ohio State University* Direct Current (DC) induced step bunching on Si(111) is a long-standing puzzle, with the required DC direction for bunching (relative to the ''step-down'' vicinal surface direction) reversing multiple times with increasing temperature. It was recently proposed [1,2] that this could be explained if step attachment is itfaster (slower) than terrace diffusion in Temperature Regime II (Regimes I and III). We have numerically simulated a similar model and directly compared with measurements of how the step bunching depends on the initial terrace width $l_0$ in all three regimes [3]. Using realistic parameter values for terrace diffusion and step attachment, this model can account for the bunching behavior in all three temperature regimes, provided there indeed exist modest (0.2 – 0.4 eV) temperature-dependent variations in the relative activation barriers for attachment and diffusion, and/or modest changes in the respective activation attempt rates. Work supported by NSF. [1] N. Suga itet al., itJpn. J. Appl. Phys. **39**, 4412 (2000). [2] T. Zhao itet al., itPhy. Rev. B **71**, 155326 (2005). [3] B.J. Gibbons itet al., submitted to Surf. Sci; Surf. Sci. Lett. **575**, L51-56 (2005).

**17:06**

**D12 14 Oxygen-induced faceting of NiAl(111)** E. LOGINOVA, W. CHEN, N. M. JISRAWI, *Department of Physics and Astronomy, Rutgers University* F. COSANDEY, *Materials Science and Engineering, Rutgers University* T. E. MADEY, *Department of Physics and Astronomy, Rutgers University* Our research is focused on the adsorption of oxygen and oxygen-induced faceting of NiAl(111), as studied by means of LEED, AES, SEM, AFM and high-resolution soft XPS (HRSXPS, using synchrotron radiation at NSLS). The atomically rough NiAl(111) surface remains planar at room temperature when exposed to oxygen. However, the surface changes its morphology and becomes faceted upon annealing at 1100K and higher; nucleation and growth of facets are studied. The adsorption and reaction of oxygen are characterized by HRSXPS measurements of Al 2p and Ni 3p core levels for the faceted and planar surfaces. The data indicate that a well-ordered thin aluminum oxide film can be formed on the faceted NiAl surface. After extensive annealing in oxygen, symmetric oxide features of micrometers in length are observed on the surface. We investigate the stoichiometry of these features by X-Ray mapping and propose a model for their formation. Our work is motivated by the possibility that alumina thin-film-covered NiAl facets might be used as templates for growth of metallic nanostructures with controlled size and spacing. The $Al_2O_3$/NiAl(111) system is a good model for studying catalytic reactions over $Al_2O_3$-supported metal catalysts.

**17:18**

**D12 15 Faceting of Re (11$\bar{2}$1) induced by oxygen** HAO WANG, WENHUA CHEN, THEODORE E. MADEY, *Department of Physics and Astronomy and Laboratory for Surface Modification, Rutgers University, Piscataway, NJ 08854* The oxygen-induced nanoscale faceting of Re (11$\bar{2}$1) has been studied by low energy electron diffraction (LEED) and Auger electron spectros-

copy (AES); the results are compared with recent STM and LEED studies of O-induced faceting of Re(12$\bar{3}$1). The evolution of surface morphology depends on oxygen exposures and deposition temperatures. Re(11$\bar{2}$1) remains planar after oxygen deposition at 300K. Annealing O-covered Re(11$\bar{2}$1) between 800K-1200K leads to the formation of (01$\bar{1}$0) and (10$\bar{1}$0) facets that coexist with the (11$\bar{2}$1) surface. Under oxidation conditions, i.e. dosing a large amount of oxygen at high temperatures (900-1000K), the (11$\bar{2}$1) surface is completely covered by 4-sided nanoscale pyramidal structures whose facets are identified as (01$\bar{1}$0), (10$\bar{1}$0), (01$\bar{1}$1) and (10$\bar{1}$1). The fact that the (11$\bar{2}$1) surface becomes completely faceted only after oxidation is consistent with our previous data for O-induced faceting of Re(12$\bar{3}$1), where one facet has the (11$\bar{2}$1) orientation and is unstable against oxidation. The faceted O/Re surfaces may be potential templates to grow nanostructures with narrow size distribution, and may also be substrates to study structural sensitivity in catalytic reactions.



**SESSION D13: FOCUS SESSION: SPECTROSCOPY OF BIOMOLECULES FROM ISOLATED MOLECULES TO CELL ENVIRONMENT III**
**Monday Afternoon, 13 March 2006; 305, Baltimore Convention Center at 14:30**
**Megan Spence, University of Pittsburgh, presiding**

***Invited Papers***

**14:30**
**D13 1 Imaging of protein partitioning in plasma membranes with coexisting fluid phases.**
TOBIAS BAUMGART, *University of Pennsylvania*

The membrane raft hypothesis postulates the existence of lipid bilayer membrane heterogeneities, or domains, important for cellular membrane functioning, including lateral sorting, signaling and trafficking. The itin vivo characterization of lipid membrane heterogeneities thus far has been challenging. Lipid membrane rafts have been suggested to be enriched in lipids that confer fluid ordered phase like character to these compositional heterogeneities. Lipid model membranes, on the other hand, allow fluorescence imaging of lipid domain coexistence, but so far micron-size coexisting fluid phases have been demonstrated only in simple, including ternary, lipid mixtures. We found that giant itplasma membrane itvesicles (PMVs) obtained from cultured rat basophilic leukemia cells can phase segregate into optically resolvable micron-size phases that are identified as both being fluid. We examined the partitioning of fluorescent lipid analogs and hydrophobic membrane markers and found them to be similar to the partitioning behavior in model membrane systems that show coexisting fluid ordered and fluid disordered phases. Significant temperature dependence of the tendency of PMVs to phase separate was found and analyzed. An advantage of these PMVs is that they contain, at least a large subfraction, of proteins associated with native plasma membranes. We are therefore able to study the partitioning of membrane proteins redistributing between coexisting fluid membrane phases. Trans-membrane proteins, outer leaflet associated peripheral and cytosolic peripheral membrane proteins were examined for their fluid phase partitioning. We suggest our method as a new approach for studying aspects of biological membrane heterogeneity.

***Contributed Papers***

**15:06**
**D13 2 Spectroscopic Characterization of ssDNA Brushes** D. Y. PETROVYKH, *University of Maryland, College Park, MD and Naval Research Laboratory, Washington, DC* A. OPDAHL, H. KIMURA-SUDA, M. J. TARLOV, *NIST, Gaithersburg, MD* L. J. WHITMAN, *Naval Research Laboratory, Washington, DC* We use X-ray photoelectron (XPS) and Fourier transform infrared (FTIR) spectroscopies to quantitatively characterize the structure and conformation of single-stranded DNA (ssDNA) brushes on gold surfaces. Self-assembly of these brushes exploits an intrinsic affinity between blocks of adenine nucleotides and gold surfaces. Using brushes of model block oligonucleotides, d(Tm-An), with systematically varied lengths of the thymine and adenine blocks [d(T) and d(A)], we demonstrate that this immobilization strategy enables independent and deterministic control of the grafting density (lateral spacing) and brush conformation. Quantitative analysis of XPS and IR spectroscopic signatures of the model d(Tm-An) brushes confirms that the d(T) blocks extend away from the surface in a brush-like conformation, at lateral spacing 2-3 times larger (grafting density 5-10 times lower) than in analogous films immobilized via standard thiol linkers. The conventional S-Au attachment strategy requires near-saturation grafting densities to adopt this upright conformation, therefore ssDNA immobilization via d(A) blocks offers a unique pathway to achieve a brush-like conformation at low grafting density.

**15:18**
**D13 3 Detection of $\beta$ − Amyloid Peptide Dimer in Solution by Fluorescence Resonance Energy Transfer** JUN HAN, *Department of Chemistry, University of Pennsylvania, Philadelphia, PA 19104* ERWEN MEI, *Regional Laser and Biotechnology Laboratory, University of Pennsylvania, Philadelphia, PA 19104* MEI-PING KUNG, HANK KUNG, *Department of Radiology, University of Pennsylvania, Philadelphia, PA 19104* HAI-LUNG DAI, *Department of Chemistry, University of Pennsylvania, Philadelphia, PA 19104* Studies have suggested that there is a connection between ß-amyloid-derived diffusible ligands (ADDLs), small oligomers formed from clustering of peptides with 39-42 amino acid units, and pathogenicity of Alzheimer's disease. It is believed that the soluble ADDL oligomers eventually coagulate and precipitate into fibrils that cause neurotoxicity. Although there have been studies characterizing the fibrils structure and the large coagulate

formation kinetics, little experimental information exists for the oligomers in the solution phase. We report here the use of fluorescence resonance energy transfer detected through a confocal microscope under single molecule conditions for the detection of the $\beta$-amyloid (1-40) peptide dimer in solution. The structure of the dimer is characterized in terms of the distance of the two N-terminals.

**15:30**
**D13 4 Nanolaser Spectroscopy of Genetically Engineered Yeast: New Tool for a Better Brew?** PAUL L. GOURLEY, JUDY K. HENDRICKS, *Sandia National Laboratories* ROBERT K. NAVIAUX, MICHAEL P. YAFFE, *UC San Diego* A basic function of the cell membrane is to selectively uptake ions or molecules from its environment to concentrate them into the interior. This concentration difference results in an osmostic pressure difference across the membrane. Ultimately, this pressure and its fluctuation from cell to cell will be limited by the availability and fluctuations of the solute concentrations in solution, the extent of inter-cell communication, and the state of respiring intracellular mitochondria that fuel the process. To measure these fluctuations, we have employed a high-speed nanolaser technique that samples the osmotic pressure in individual yeast cells and isolated mitochondria. We analyzed 2 yeast cell strains, normal bakers yeast and a genetically-altered version, that differ only by the presence of mitochondrial DNA. The absence of mitochondrial DNA results in the complete loss of all the mtDNA-encoded proteins and RNAs, and loss of the pigmented, heme-containing cytochromes. These cells have mitochondria, but the mitochondria lack most normal respiratory chain complexes. The frequency distributions in the nanolaser spectra produced by wild-type and modified cells and mitochondria show a striking shift from Gaussian to Poissonian distributions, revealing a powerful novel method for studying statistical physics of yeast.

**15:42**
**D13 5 The Influence of Environment on the Reactivity, Dynamics and Spectroscopy of B12 Coenzymes.*** ROSEANNE SENSION, *University of Michigan* D. AHMASI HARRIS, ELIZABETH CARROLL, ANDREW STICKRATH, Adenosylcobalamin (AdoCbl) dependent enzymes catalyze a variety of chemically difficult reactions that proceed by mechanisms involving organic radicals. In these enzymes radicals are initially generated by homolysis of the cobalt-carbon bond to produce an adenosyl radical and a cob(II)alamin radical. This radical pair may also be generated by optical excitation of the AdoCbl cofactor with visible light. In the work presented here, time-resolved spectroscopic measurements spanning the time range from 10 fs to 10 ns are used to investigate the energetics and dynamics of AdoCbl and other cobalamins as a function of environment. These studies probe the influence of environment on the energy of the low-lying charge transfer states of the cobalamin and on the barriers for dissociation and for recombination of the geminate radical pair. When the AdoCbl coenzyme is bound to the enzyme glutamate mutase, the protein environment is found to stabilize the charge transfer state of AdoCbl relative to observations in water and ethylene glycol. However, the intrinsic rate constant for recombination is only slightly smaller than the rate constant measured in free solution, suggesting the protein does not greatly perturb the ground state stability of the cobalt-carbon bond.

*This work is supported by the NSF

***Invited Papers***

**15:54**
**D13 6 Single molecule views of Nature's nano-machines.**
TAEKJIP HA, *University of Illinois at Urbana-Champaign*

We are interested in the perturbational analysis of biological molecules to better understand their mechanisms. Our redout is the fluorescence signal from individual biomolecules, mainly in the form of single molecule fluorescence resonance energy transfer (FRET). We are pioneering approaches to perturb and control biomolecular conformations using external force (combination of single molecule FRET and optical trap) or other biological motifs (DNA hybridization, G-quadruplex, aptamers). In this talk, I will present out latest results on mapping the conformational energy landscape of the Holliday junction through simultaneous fluorescence and force measurements. In addition, a new nanomechanical device called single molecule nano-metronome will be discussed with an outlook toward controlling protein conformations using nucleic acids motifs.

***Contributed Papers***

**16:30**
**D13 7 Time-Resolved Protein Superstructure Disassembly at the Single Particle Level** JASON PUCHALLA, KELLY KRANTZ, JULIE VIEHWEG, HAYS RYE, *Princeton University, Dept. of Mol. Biology* PETER GALAJDA, ROBERT AUSTIN, *Princeton University, Dept. of Physics* Many proteins are able to spontaneously self-organize itin vivo into large, complex structures. These superstructures are often disassembled through the action of key enzymes to fulfill a specific biological role. Yet, the mechanisms of disassembly of such complex structures are poorly understood. We demonstrate the ability to monitor the kinetics of the enzyme assisted disassembly of fluorescently labeled clathrin-coated vesicles in a micro-fluidic flow cell using photon burst and correlation spectroscopy.

**16:42**
**D13 8 Study of DNA uptake locations in single itE. coli cells** C. SHAN XU, L. MEADOW ANDERSON, *Department of Chemistry, University of California at Berkeley* HAW YANG, *Department of Chemistry, University of California, Physical Biosciences Division, Lawrence Berkeley National Laboratory* Artificial gene transfer of bacteria, such as itE. coli, has become the main stream technique in genetic engineering and molecular cell biology studies. In spite of the great improvements in transformation effi-

ciency, some fundamental questions remained to be answered. For instance, what are the DNA uptake channels and how do they form and function under external stimuli? Furthermore, where are these channels located on the cell membrane? Here we report a study aimed at DNA uptake locations in the two widely used gene transformation techniques: electroporation and heat shock. A direct visualization of the settling location of single DNA molecules inside individual itE. coli cells was obtained by fluorescence imaging and spectroscopy. Electroporation and heat shock exhibit two distinct characteristics of DNA uptake locations. A preferential distribution toward cell poles during electroporation is consistent with earlier experiments and previously proposed models. However, the result from heat shock is unanticipated in which the majority of DNA enters the cell near the center. Such observation suggests that uptake channels form preferentially where newly-synthesized membrane is located under cation and low temperature treatment

**16:54**
**D13 9 Real-Time, Nonlinear Optical Probe of Molecular Transport across Living itEscherichia coli Cell Membranes** JIA ZENG, HEATHER ECKENRODE, HAI-LUNG DAI, *Department of Chemistry, University of Pennsylvania, Philadelphia, PA 19104-6323* We will demonstrate for the first time that a nonlinear optical technique- Second Harmonic Generation- can be used to monitor, with real time resolution, the transport of a molecule across the membranes of a living cell. The transport of the hydrophobic ionic dye molecule malachite green (MG) through both membranes of the gram-negative bacteria itEscherichia coli, the outer membrane and the cytoplasmic membrane, has been studied. A kinetic model, assuming that the MG molecules penetrate the bacteria outer membrane through classic porin channels while transport across the cytoplasmic membrane is by diffusion through the phospholipid bilayer, is proposed to account for experimental observations. Analysis of the SHG data enables quantitative determination of the transport rate constants and the adsorption equilibrium constants for the itEscherichia coli cells living in different environments.

**17:06**
**D13 10 Photon-by-Photon Determination of Emission Bursts from Diffusing Single Chromophores** KAI ZHANG, HAW YANG, *University of California at Berkeley* Diffusing-type single molecule experiment is expected to provide rich information such as protein conformational distribution, DNA sequencing, ultrasensitive detection, to name a few. However, its application is greatly limited by the difficulty of extracting the useful information out of the noisy data because of the embedded Poissonian noise. Conventional analysis of such trajectories involves further smoothing the data followed by artificially setting a threshold to distinguish the signal, risking the chance of ignoring the fast transition events along the trajectory. Here we report a statistically robust algorithm, which operates on the trajectory photon by photon, based on the well established sequential test model. A demonstration experiment with the gold nanoparticle diffusing throuth the detection volume shows that our algorithm indeed retrieves more information, relieving the incertitude of artificial placement of bin width and threshold.

**17:18**
**D13 11 Quantum cooperative process in living cells** ROBERT FINKEL, *St. John's University* A model of a quantum cooperative process has accurately accounted for various quantitative observations.[1] That investigation considered chemical oscillations to be generated by generic quantum oscillators producing discrete quanta with well-defined energy and wavelength. The current work extends the theory by postulating that these oscillations arise from repetitive electron transfers in membranes. We find this produces a limit cycle completely consistent with the hypothetical generic oscillators, accurately reproduces the results of microwave irradiation experiments on yeast, and addresses limits for the smallest possible cell sizes. Questions of coherence in cells and implications for molecular information transfers are briefly considered. [1]R.W. Finkel, itJ. Theor. Biol. in press.



## SESSION D15: FOCUS SESSION: ATOMIC TUNNELING, FILMS, NANOSTRUCTURES
**Monday Afternoon, 13 March 2006; 311, Baltimore Convention Center at 14:30**
**Daniel Finkenstadt, Naval Research Laboratory, presiding**

***Invited Papers***

**14:30**
**D15 1 Dephasing of Atomic Tunneling by Nuclear Quadrupoles.**
CHRISTIAN ENSS, *Universität Heidelberg*

A few years ago strong magnetic field effects have been observed in low-temperature dielectric susceptibility measurements and in coherent polarization echo experiments on certain glasses and disordered crystals. The low-temperature dielectric properties of such materials are dominated by atomic tunneling systems. It has been suggested that the surprising magnetic field dependence is caused by tunneling particles with nuclear quadrupole moment. For such systems there exists a coupling of the tunneling motion with the nuclear quadrupole moments experiencing the electric field gradients in the localized states. This coupling gives rise to a quadrupole splitting of the energy levels of the tunneling systems. The applied magnetic field then leads to an additional Zeeman splitting of the nuclear levels. We review the results of polarization echo experiments in magnetic fields and discuss the role of the nuclear spins in such experiments.

*Contributed Papers*

**15:06**

**D15 2 Electronic Structures of Quasiperiodically Modulated Thin Ag films** D. EOM, J. SHI, Q. NIU, C.-K. SHIH, *The University of Texas at Austin* When electrons move in crystalline solids, the coherent scattering with the periodic potential enables them to sneak by all ions uninhibited, forming Bloch electrons with their own E vs. k dispersion relationship. This ''Bloch description'' underlies the electronic structures of all crystalline solids. In quasicrystals, however, such a description encounters conceptual difficulties since the Bloch theorem no longer applies. While theoretical investigations showed exotic characteristics such as the Cantor-set energy spectrum early experiments did not reveal such exotic properties. Recent attempt to measure E vs. k relation in a quasicrytal using angle-resolved photoemission revealed free-electron like states. Nevertheless, critical questions remain as how electronic states in a quasiperiodic solid differ from those in a periodic solid. By using low-tempeature scanning tunneling spectroscopy (STS) to probe a quasiperiodically modulated Ag metallic thin film, and by using Fourier analysis, we unravel the influences of individual Fourier components of the scattering potential (periodic vs. quasiperiodic) on the electronic structures.

**15:18**

**D15 3 Theoretical study of the morphology of stretched gold nanowires** FRANCESCA TAVAZZA, ANNE CHAKA, LYLE LEVINE, *National Institute of Standard and Technology* Gold nanowires (NW) have been proposed for a variety of applications, including as intrinsic force standards in the nanoregime. To determine if they are effectively suitable for such an usage, we analyzed the dependence of the evolving NW morphology on different strain rates and directions, using semi-static, density functional (DFT) calculations. The NW under examination are very thin, initially fcc and have the wire axis along the (110) crystallographic orientation. The uniqueness of the necking pathway and the corresponding pre- failure structure are analyzed. The structure evolution and the ultimate length of the NWs are shown to be extremely sensitive to the tensile direction, and possibly on the strain rate as well, indicating that the corresponding energy surface is complex and that any experimental quantitative evaluation of the forces necessary to break the NW should keep parameters such as stretching direction and strain rate under careful control.

**15:30**

**D15 4 Optical Properties of Silver Nanowires** ARIC SANDERS, MARK REED, *Yale University* We report on the propagation of light through silver nanowires mediated by plasmons. Light is observed to couple through crossed nanowires and around soft bends. Farfield Emission is observed from multiple bends in the nanowire. Propagation lengths of several microns are observed through structures less than 100nm in diameter. Light is coupled into silver nanowire fibers with a focused laser beam at both 830nm and 532nm.

**15:42**

**D15 5 Computer Simulation of Copper Nanowires*** EDISON Z. DA SILVA, E.P. AMORIM, *Instituto de Física ''Gleb Wataghin,'' UNICAMP,CP 6165, 13083-970, Campinas - SP, Brazil* A.J.R. DA SILVA, A. FAZZIO, *Instituto de Física, USP, CP 66381, 05315-970, São Paulo - SP, Brazil* Any device to operate, no matter how large or small, needs metallic contacts. The trend towards nano-miniaturization, with the development of nanodevices, will require the understanding of the behavior of metals at the nanoscale, especially gold and copper. Gold has received a lot of attention, while copper, also an important metal has not been studied as much. Recently the dynamical evolution of copper nanowires was observed with high resolution transmission electron microscopy (HRTEM) experiments [1]. We have performed tight binding molecular dynamics (TB-MD) simulations of copper nanowires under stress along some directions until their rupture. The TB-MD calculations have been show to be an excellent tool to study gold nanowires [2]. We present the time evolution of the structures, the formation of defects and the forces sustained by the nanowires. We discuss the possibility of the formation of short linear atomic chains before the breaking. Our results are in good agreement with experimental results. [1] J. C. Gonzalez, et al., Phys. Rev. Lett. **93**, 126103-1 (2004). [2] E. Z. da Silva, A. J. R. da Silva and A. Fazzio, Phys. Rev. Lett. **87**, 256102 (2001).

*Work supported by CNPq and FAPESP. E. P. M. A. supported by CAPES. CENAPAD-SP is acknowledged for computer time

**15:54**

**D15 6 Measurement of Temperature-Dependent Conductivity and Seebeck Coefficient of Self-assembled Gold Nanoparticle Wires** J.W. SUN, J.B. HUTCHISON, J.A. HOFFMANN, M.E. REEVES, *Department of Physics, The George Washington University* We are exploring the electrical and thermoelectrical properties of wires composed of 12nm diameter gold nanoparticles. The wires are deposited on glass substrates via evaporation-driven vertical colloidal deposition (VCD). We then measure the temperature-dependence of the resistance and thermopower (Seebeck coefficient) between 30 and 120K. We will discuss these measurements in the context of the constituent nanoparticle size and the preparation of the deposited wire; we also make comparisons to similar measurements of bulk gold and gold-iron alloys.

**16:06**

**D15 7 Electrical Detection of Surface Plasmon Resonance in Individual Gold Nanowires** CHRISTOPHER LAFRATTA, *Univeristy of Maryland College Park* DANIEL LIM, JULIET ZNOVENA, *University of Maryland College Park* LINJIE LI, *University of Maryland College Park* JOHN FOURKAS, *University of Maryland College Park* Plasmon absorption in individual gold nanowires has been detected electrically. Gold nanowires, electrochemically synthesized in polycarbonate templates with diameters of 40 nm and lengths of 5 $\mu$m, are connected under an optical microscope using multiphoton absorption polymerization (MAP). MAP uses a prepolymer acrylic based resin and a focused ultrafast laser to stereolithographically pattern with sub-micron resolution. For this experiment, nonconducting acrylate leads are made by MAP to connect to a single gold nanowire. These polymer leads can then be made conductive by surface modification followed by electroless copper enhancement. In this way the resistance of a single nanowire can be measured in a four-probe scheme. The gold rod can then be optically excited near its plasmon absorption peak. The excitation is quickly converted to heat, which is observed as an increase in resistance. This electrically detected plasmon absorption has been found to be linearly dependent on light intensity and is also sensitive to the direction of the polarization with respect to the rod. This non-optical plasmon detection is of basic interest but may be applicable for intrabeam polarization detection or electrical detection of biomolecules.

**16:18**

**D15 8 The Metal-Insulator Transition in Metal Transition Granular Films** N.E. MASSA, *Lanais EFO-CEQUINOR, U.N.L.P., C. C. 962, (1900) La Plata, Argentina* J.C. DENARDIN, *Depto de Fisica, USACH, Santiago, Chile* L. SOCOLOSKY, M. KNOBEL, *Inst de Fisica, UNICAMP, 13083-970, Campinas-SP, Brazil* X.X. ZHANG, *Inst. of Nanoscience and Technology, UST, Hong Kong, China* We study with infrared reflectivity the concentration and temperature dependence of the regime change from metallic to insulating in granular films made of transition metals embedded in $SO_2$. The $TM_x(SO_2)_{1-x}$ (TM=Fe, Ni, Co), ($0.25 \leqslant x \leqslant 0.85$) systems yield spectra typical of conducting oxides where hopping carriers undergo electron-phonon interactions with localization enhanced by nanoparticles and substrate roughness. The distinct Drude component, extending beyond 1.3 eV in the metallic state, undergoes a dramatic change in intensity due to the progressive reduction of carriers critical paths as the transition temperature is reached in the glassy matrix. At the intermediate conducting state for $x \sim 0.55$, about the percolation threshold, a well defined reflectivity edge and band, considered fingerprint for small polarons, emerges in addition to the vibrational bands. A very good agreement is found between the measured optical conductivity and current small polaron models. This, in addition to underlying the importance of polarization effects, provides grounds toward a quantitative microscopic description of transport properties. It also adds toward an understanding of a non-magnetic factor in the magnetoresistance and extraordinary Hall coefficient enhancements.

**16:30**

**D15 9 Jahn-Teller distortion mediated phase separation in spinel thin films** S. PARK, N. LEE, S. GUHA, S-W. CHEONG, *Department of Physics and Astronomy, Rutgers University, Piscataway, NJ 08854, USA* Self-assembled nano-structures have been acquired in various forms, giving significant impacts both on industrial and academic realms. Recently, nano-structures in spinel oxides have been observed in bulk materials by harnessing the Jahn- Teller distortions. Realization of magnetic nano-stuructures could give a breakthrough in the magnetic recording industry. We have grown chemically phase separated spinel films utilizing pulsed laser deposition method, and the inter- relationship between structural and magnetic properties will be discussed.

**16:42**

**D15 10 Synthesis and properties of multiferroic Bi(Fe,Cr)$O_3$ thin films** S. FUJINO, M. MURAKAMI, S.-H. LIM, C. LONG, L. SALAMANCA-RIBA, *Univ. of MD* H. SUGAYA, *Tokyo Inst. of Technology* T. HASEGAWA, *Univ. of Tokyo* S. LOFLAND, *Rowan Univ.* M. WUTTIG, I. TAKEUCHI, *Univ. of MD* Bi based magnetic oxide systems, including $BiFeO_3$ and $BiCrO_3$, have spontaneous magnetization and display charge polarization. Bi(Fe,Cr)$O_3$ system has been predicted to be a new candidate of multiferroic materials. In this study, we will present systematic investigation of multiferroic properties of Bi(Fe,Cr)$O_3$ thin films. The films are fabricated by pulsed laser deposition under various deposition conditions. We have succeeded in synthesizing single phase epitaxial $BiCrO_3$ films on $LaAlO_3$ (001), $SrTiO_3$ (001) and $NdGaO_3$ (110) substrates. It shows weak ferromagnetic behavior with the Curie temperature at 120 K. Pseudo-binary epitaxial thin film composition spreads of $BiFe_{1-x}Cr_xO_3$ have been fabricated using the combinatorial pulsed laser deposition technique in order to investigate their changing multiferroic properties as a function of composition. Their magnetic and dielectric properties mapped using low temperature scanning SQUID microscopy and microwave microscopy will be discussed. This work was supported by ONR N000140110761, ONR N000140410085, NSF DMR 0094265 (CAREER), NSF DMR 0231291, MRSEC DMR-00-0520471, and W. M. Keck Foundation.

**16:54**

**D15 11 Domains in Multiferroic Films** JULIA SLUTSKER, *NIST* A. ARTEMEV, *Carleton University* ALEXANDER ROYTBURD, *University of Maryland* The theory and modeling of equilibrium self-assembling nanostructures based on concept of elastic domains in multiphase epitaxial films successfully explained the morpholgies of $CoFe_2O_4$-$PbTiO_3$ films grown on differently oriented substrates. It is shown that it is possible to design the different nanostructure architectures: cobalt ferrite rods in lead titanate matrix and vise versa as well as differently oriented laminar structures. The elastic interactions between the phases determine the mutual change of order parameters: magnetization and polarization, that allow one to estimate the magneto-electric coupling through the study of constrained polarization and magnetization.

**17:06**

**D15 12 Schottky-Barrier height at Si(001)/PtSi(010) and Si(111)/$ErSi_2$(001) interface** M.K NIRANJAN, S. ZOLLNER, L. KLEINMAN, A.A DEMKOV, According to the Si roadmap (ITRS) one of the most pressing concerns of CMOS technology beyond the 65 nm node is the contact resistances in source/drain regions between the doped silicon and silicide. For the 45 nm node it is expected to amount to one-fourth of the total parasitic resistance. This contribution will clearly only rise as the scaling continues. Thus the roadmap calls for a new contact technology by the 45 nm node. A monosilicide would have an additional advantage in lower Si consumption. The transition from $CoSi_2$ to NiSi is a step in that direction. Physically, the contact resistance comes from a relatively high Schottky-barrier between Si and silicide. For both $CoSi_2$ and NiSi the barrier is about 0.5 eV. Thus, it is desirable to identify new metals or alloys that will have lower Schottky barrier to n- and p- type Si for use in NMOS and PMOS, respectively. In deep submicron regime, PtSi, $ErSi_2$ and NiSi have been shown to be prospective candidates for replacing conventional silicides. We have studied the electronic structure of bulk PtSi and $ErSi_2$ within the framework of density functional theory. We then calculate work functions and surface energies for different surface orientations and come up with plausible interface structures with Si. Our calculated valance band Schottky-barrier height of 0.26 eV at Si(001)/PtSi(010) is in excellent agreement with the experiments. We have, also, calculated the valance band Schottky-barrier height of 0.29 eV at Si(111)/$ErSi_2$(001) interface.

**17:18**

**D15 13 Magnetic Resonance Force Microscopy investigations of a continuous ferromagnetic thin film** J. KIM, *The Ohio State University* T. MEWES, *University of Alabama* F. YANG, *The Ohio State University* P. WIGEN, *The Ohio State University* YU. OBUKHOV, *The Ohio State University* D. PELEKHOV, *The Ohio State University* P. C. HAMMEL, *The Ohio State University* The ferromagnetic resonance of a 50nm thick Permalloy film has been investigated using a magnetic resonance force microscope operated at UHV and 4K. A low boron doped silicon cantilever with a hardmagnetic SmCo tip attached to its end was used to detect the locally excited ferromagnetic resonance in the film. The high coercivity of the tip magnet enables the measurement of FMRFM spectra with the tip magnetization aligned either parallel

or antiparallel to the external magnetic field, while saturating the Permalloy film perpendicular to the film plane. The variation of the spectra as a function of the tip-film separation reveals a bulk resonance and the excitation of spin waves originating where the magnetic resonance condition is locally met. This local resonance may be used to characterize the dynamic properties of ferromagnetic thin film samples with high spatial resolution.



**SESSION D16: FOCUS SESSION: NEGATIVE REFRACTIVE INDEX I**
**Monday Afternoon, 13 March 2006**
**312, Baltimore Convention Center at 14:30**
**Vladimir M Shalaev, Purdue University, presiding**

***Contributed Papers***

**14:30**
**D16 1 Single Superconducting Split-Ring Resonator Electrodynamics** MICHAEL C. RICCI, STEVEN M. ANLAGE, *University of Maryland, College Park* In order to create compact metamaterial devices in the microwave frequency range, current designs must be scaled down to smaller dimensions. However, at such scales, normal metal losses dominate, and desirable device properties (*e.g.* negative index of refraction) are lost. We investigate the properties of superconducting Nb metamaterials that do not suffer from these limitations. The experiments are performed in an all-Nb waveguide, with Nb wires and Nb thin film split-ring resonators (SRRs). Transmission experiments performed in vacuum show a narrow, deep notch for a single Nb SRR (quality factor $\sim$ 50,000), and no notch for a Cu resonator of similar dimensions. Adding SRRs increases the notch bandwidth, but decreases the insertion loss of individual resonators. In addition, placing a single superconducting SRR into an array of superconducting wires produces a single negative-index passband 40 dB above the noise floor, with a quality factor of $\sim$ 22,000. Models based on the permeability of individual SRRs and the effective dielectric response of a wire array are used to fit the data. This work is supported by the NSF through Grant No. NSF/ECS-0322844, and the DI Outreach Program.

***Invited Papers***

**14:42**
**D16 2 Experiments on the Goos-Hänchen shift with negative and positive index of refraction materials** NATHAN ORLOFF, MICHAEL RICCI, *Univ. of Maryland, College Park* COLLIN ANDERSON, *Yale University* CHRISTIAN LONG, SUDEEP DUTTA, STEVEN ANLAGE, *Univ. of Maryland, College Park* The negative Goos-Hänchen shift occurs when a beam of radiation having a finite transverse extent undergoes total internal reflection at a positive to negative index of refraction interface, hence the reflected beam experiences a negative lateral shift. This phenomenon has been predicted for materials with a negative index of refraction. We investigate a composite wire and split-ring resonator medium between 8-12 GHz, based on that first implemented by [1]. In addition, we present an experiment to investigate the Goos-Hänchen shift and show preliminary results on transmission, refraction, and total internal reflection. Work supported by NSF/ECS-0322844. [1] R. Shelby, D. R. Smith and S. Schultz, Science, 292, 77 (2001)

**14:54**
**D16 3 Optical properties of Ag nanoparticle arrays: Tuning the plasmon resonance*** J.R. SIMPSON, H.D. DREW, S.H. GUO, R. PHANEUF, *Department of Physics, University of Maryland, College Park, MD 20742 and Laboratory for Physical Sciences, College Park, MD 20740* Potential applications in the optical spectral range of meta-materials displaying negative permittivity and negative permeability has driven recent interest in nanostructured materials. Electromagnetic radiation incident on metallic nanoparticles induces a collective electronic excitation, or plasmon, which results in a detectable optical resonance. We report polarization-dependent transmission measurements of Ag nanoparticle arrays in the near-infrared to visible frequency range. E-beam lithography patterns arrays of nanoparticles from Ag deposited on transparent ITO-glass substrates. The array grid spacing is several hundred nanometers and the nanoparticle thickness and width are approximately 75 nm. We vary the length to provide an in-plane aspect ratio (length to width) from 1 : 1 to 4 : 1. The resonance shifts to lower (higher) energy with increasing aspect ratio for polarizations parallel to the long (short) axis. This work demonstrates the ability to tune optical resonance energies and widths in nanostructured materials with quality factors $Q$ exceeding 10. Additionally, we discuss the effects of radiation damping, carrier scattering, and inhomogeneous broadening on the resonance widths.

*This work supported, in part, by the Laboratory for Physical Sciences.

**15:06**
**D16 4 Large-Area Infrared Metamaterials using Interferometric Lithography.***
STEVEN BRUECK, *University of New Mexico*

Large area (several $cm^2$) mid- and near-infrared metamaterial samples including analogs to split ring resonators and negative index materials have been fabricated using interferometric lithography and standard integrated circuit fabrication techniques. The split ring resonators are vertical structures with the smallest dimensions defined by deposition rather than by lithography. The negative index material is a Au-$Al_2O_3$-Au stack structure perforated with a 2D hole pattern. Both the amplitude and phase of the transmission and reflectivity are measured with phase-mask, zero-path-length difference, interferometric techniques and the refractive index is deduced by inverting these measurements. A rigorous coupled wave

analysis (RCWA) is in excellent agreement with the measurement. Improvements in the original structure to provide a lower loss and an improved transmission for the structure are presented. Prospects for continued reduction in the loss and an improved figure of merit, [$|\mathrm{Re}(n)|/\mathrm{Im}(n)$], are discussed. Interferometric lithography provides an inexpensive, facile, large-area technology for the fabrication of visible/infrared metamaterials with a 2D array patterning capability extending to as small as 30-nm features.

*Partial support from DARPA, AFOSR and ARO.

***Contributed Papers***

**15:42**

**D16 5 Zero-n band-gap in 1D periodically layered photonic superlattices*** NICOLAE PANOIU, RICHARD OSGOOD, *Columbia University* SHUANG ZHANG, STEVEN BRUECK, *University of New Mexico* COLUMBIA UNIVERSITY TEAM, UNIVERSITY OF NEW MEXICO TEAM, We demonstrate that photonic superlattices consisting of a periodic distribution of alternating layers of materials with positive and negative index of refraction present a photonic band-gap at a frequency at which the spatial average of the index of refraction is zero (these stop bands are called zero-n band-gaps). We prove that these results can be generalized to two cases, namely i) a superlattice of alternating layers, one layer made of a homogeneous material with positive index of refraction and the other layer consisting of a photonic crystal, with negative index of refraction and ii) a superlattice consisting of alternating photonic crystal slabs, which, have positive and negative index of refraction. We demonstrate that, in both cases, the central frequency of the zero-n band-gap corresponds to the frequency at which the spatial average of the refractive index, taken over the unit supercell, is zero. We also show that, unlike the Bragg gaps, these zero-n band-gaps are invariant to the geometrical scaling of the superlattice or the direction of wave propagation in the superlattice.

*UNM DARPA Optocenter and AFOSR-STTR.

**15:54**

**D16 6 Negative Refraction in One-Dimensional Photonic Crystal*** PLARENTA VODO, *Northeastern University* WENTAO LU, *Northeastern University* PATANJALI PARIMI, *Northeastern University* SRINIVAS SRIDHAR, *Northeastern University* We demonstrate experimentally negative refraction of plane waves by a one-dimensional Photonic crystal (PhC) prism at microwave frequencies. The prism was fabricated from a microwave alumina PhC acting as a left-handed metamaterial. Focusing of plane waves from a one-dimensional PhC plano-concave lens is predicted theoretically and realized experimentally. The focal point is observed to move with the radius of curvature of the lens. The measured values of refractive index are in complete agreement with those determined from band structure calculations.

*Work supported by NSF and Hanscom Air Force Lab

**16:06**

**D16 7 Determination of Refractive Indices of Photonic Crystals: Theory and Experiments*** WENTAO LU, SRINIVAS SRIDHAR, *Northeastern University* We develop a method to calculate the refractive indices of photonic crystal based on plane wave expansion. The appearance of surface waves and subwavelength imaging is explained within this frame. Numerical simulations of 1D and 2D crystals are performed to support our theory. Comparisons are presented with experimental results on microwave photonic crystals.

*Work supported by NSF and Hanscom Air Force Lab.

**16:18**

**D16 8 Free space microwave focusing by a negative-index gradient lens** TOM DRISCOLL, PATRICK RYE, DIMITRI BASOV, SIA NEMAT-NASSER, *University California, San Diego* TONY STARR, *Sensormetrix, inc.* DAVID SCHURIG, DAVID SMITH, *Duke University* The complexity of left-handed metamaterials has advanced rapidly to the point where direct applications are now viable. We present a radial gradient-index lens with an index-of-refraction ranging from -2.67(edge) to -0.97(center). Experimentally, we find the lens can produce field intensities at the focus that are greater than that of the incident plane wave. These results are obtained at 10.3 GHz and are in excellent agreement with full-wave simulations. We also discuss the design and construction of this lens - which involved an advanced fabrication technique using conventional printed circuit board technology. This technique offers significant design, mechanical, and cost advantages over other microwave lens constructions.

**16:30**

**D16 9 Dynamical Electric and Magnetic Metamaterial Response at Terahertz Frequencies** WILLIE PADILLA, ANTOINETTE TAYLOR, *Los Alamos National Laboratory* CLARK HIGHSTRETE, MARK LEE, *Sandia National Laboratories* RICHARD AVERITT, *Los Alamos National Laboratory* Utilizing terahertz time domain spectroscopy, we have characterized the electromagnetic response of a planar array of split ring resonators (SRRs) fabricated upon a high resistivity GaAs substrate. The measured frequency dependent magnetic and electric resonances are in excellent agreement with theory and simulation. For two polarizations the SRRs yield negative electric response ($\epsilon < 0$). We demonstrate, for the first time, dynamical control of the electrical response of the SRRs through photoexcitation of free carriers in the substrate. An excited carrier density of $\sim 4 \times 10^{16}\mathrm{cm}^{-3}$ is sufficient to short the gap of the SRRs thereby turning off the electric resonance demonstrating the potential of such structures as terahertz switches. Due to the universality of metamaterial response over many decades of frequency, these results have implications for other regions of the electromagnetic spectrum.

**16:42**

**D16 10 Nanofabricated materials with negative refractive indices at optical wavelengths** WENSHAN CAI, *School of Electrical and Computer Engineering, Purdue University, W. Lafayette, IN 47907* UDAY CHETTIAR, HSIAO-KUAN YUAN, VLADIMIR DRACHEV, ALEXANDER KILDISHEV, ANDREY SARYCHEV, VLADIMIR SHALAEV, The efforts to construct media exhibiting negative refraction have been extended to the optical range. In this work we present examples of structures with negative refraction at optical frequencies, including paired

nanorods arrays and coupled metal strips. The negative refractive indices in such nanofabricated metamaterials result from plasmon resonances for both the electric and magnetic components of light at overlapping wavelength ranges. Simulations and experimental verification of the negative indices are demonstrated. The agreement between simulations and experimental data is excellent, confirming the validity of the proposed structures as negative index materials. Optimization of the parameters of the nanostructure is also discussed.

**16:54**

**D16 11 Negative static dielectric constant in a nano-colloid** JASON SHULMAN, STEPHEN TSUI, FENG CHEN, YUYI XUE, C. W. CHU,* *TcSUH/University of Houston* We have investigated the dielectric properties of assemblies of urea-coated $Ba_{0.8}Rb_{0.4}TiO(C_2O_4)_2$ nanoparticles. The effective dielectric constant, $\varepsilon$', is negative below a certain bias dependent frequency. $\varepsilon$' follows a plasma-like dispersion with an extremely low plasma frequency and damping rate. This dielectric response is linear with bias fields larger than 2.5 kV/mm. Additionally, after a step increase of the electric field, the transient current changes sign and is opposite to the applied field. These two properties rule out electrochemical effects as well as carrier trapping/de-trapping as the source of the negative dielectric constant. More importantly, this latter feature verifies that the static dielectric function, $\varepsilon$'(k, $\omega$=0), is negative. Furthermore, measurements on cold pressed (solid) pellets of the nanoparticles demonstrate that the effect is not due to rearrangement or large scale motion of the particles. In fact, the data suggests that the negative static $\varepsilon$' is correlated to the interfacial conductivity of the nanoparticles.

*Also at: Lawrence Berkeley National Laboratory and Hong Kong University of Science and Technology

**17:06**

**D16 12 Scaling Behavior of Dielectric Switching in Nano-assemblies*** FENG CHEN, JASON SHULMAN, STEPHEN TSUI, YUYI XUE, C. W. CHU,† *Texas Center for Superconductivity, University of Houston, Houston, TX 77204-5002* Recently, we have reported a field-induced sign-switch of dielectric constant ($\varepsilon$') for urea-coated $Ba_{0.8}Rb_{0.4}Ti_O(C_2O_4)_2$ nano-particles (U-BRTOCO) in silicone oil and demonstrated that the observed negative $\varepsilon$' is an intrinsic property of the nanoparticle assemblies A systematic study has been subsequently carried out on the switching of $\varepsilon$' under a bias field for U-BRTOCO and other nano-particle assemblies under different conditions. The switching frequency ($\omega_c$) is found to be closely related to the zero-frequency electrical conductivity ($\sigma$(0)) of the assemblies. Such a scaling behavior for different nano-assemblies under various conditions gives us strong insight of the origin of the negative $\varepsilon$'. The possible models such as plasma and 2D electron-gas (2DEG) are compared.

*We thank Prof. W. J. Wen for supplying U-BRTOCO samples.
†Also at: Lawrence Berkeley National Laboratory, Hong Kong University of Science and Technology

**17:18**

**D16 13 Magnetic resonances in nano-scale metamaterials*** ZHAO HAO, ALEX LIDDLE, MICHAEL MARTIN, *Lawrence Berkeley National Laboratory* We have designed, fabricated, and optically measured several different kinds of nano-scale metamaterials. We make use e-beam nano-lithography technology at LBNL's Center for X-Ray Optics for fabricating these structures on extremely thin SiN substrates so that they are close to free-standing. Optical properties were measured as a function of incidence angle and polarization. We directly observe a strong magnetic resonance consistent with a negative magnetic permeability in our samples at mid- and near-IR optical frequencies. We will discuss the results in comparison with detailed simulations, and will discuss the electric dipole or quadrupole resonances observed in the samples. Finally, we will report on our progress towards constructing a fully negative index of refraction meta-material.

*This work was supported by the Director, Office of Science, of the U.S. Department of Energy under Contract No. DE-AC02-05CH11231.

## SESSION D17: FOCUS SESSION: PHASE TRANSITIONS AND DOMAINS IN FERROELECTRIC NANOSTRUCTURES II

**Monday Afternoon, 13 March 2006**
**313, Baltimore Convention Center at 14:30**
**Alex Demkov, The University of Texas, presiding**

***Contributed Papers***

**14:30**

**D17 1 High Spatial and Temporal Resolution Optical Probes of Ferroelectric Thin Films*** HONGZHOU MA, JEREMY LEVY, *Department of Physics and Astronomy, University of Pittsburgh* MIKE D. BIEGALSKI, DARRELL G. SCHLOM, SUSAN TROLIER-MCKINSTRY, *Department of Materials Science and Engineering, the Pennsylvania State University* WON-JEONG KIM, JAMES S. HORWITZ, *Naval Research Laboratory* Optical probes can provide unique insight into the local ferroelectric properties of thin films. We will describe two techniques that provide sensitive measures of domain structure and dynamics with high spatial and/or temporal resolution: (1) confocal scanning optical microscopy (CSOM), which measures in-plane domain structure of ferroelectric films, and (2) GHz apertureless near-field scanning optical microscopy (GHz-ANSOM) which probes ferroelectric domain dynamics with high spatial resolution ( $<$ 50 nm) and temporal resolution ( $\sim$ ps). The electro-optic effect, measured using CSOM on strained $SrTiO_3$ films, shows clear hysteresis at room temperature, indicating the existence of ferroelectric domains below the diffraction limit. The microwave dynamics of such nanoscale domains can be revealed using GHz-ANSOM.

*This work was supported by NSF DMR-0333192, DMR-0507146 and DMR-0103354

**14:42**

**D17 2 Domains and Hysteresis Loops in Ferroelectric Thin Films with Metallic and Semiconductor Electrodes** A.M. BRATKOVSKY, *Hewlett-Packard Labs, Palo Alto, California 94304* A.P. LEVANYUK, *UA Madrid, Spain* Detailed thermodynamic description of the ferroelectric (FE) thin films with metallic and semiconductor electrodes is presented. We show that imperfect screening by the electrodes results in uncompensated depolarizing field and leads to a tilt of the hysteresis loops, as observed experimentally. We solve for the domain instability analytically

and find a simple criterion for stability of homogeneously polarized state in thin films with realistic metallic electrodes. In most cases the film breaks into domains, and they can exist in near cubic (perovskite) ferroelectrics down to ''atomic'' thicknesses (one unit cell thick). Domain structures under bias voltage are investigated. In the case of semiconductor electrodes the screening is poor at small values of polarization $P$ and highly nonlinear at larger $P$ close to a spontaneous polarization in the bulk. This formally allows for the ''Batra-like'' jumpwise transition at lowering temperature, which is not observed since it is preempted by domain instability. Additional boundary conditions [1] modify the above behavior, but mainly for a homogeneous state. The unusual phase behavior in cases of symmetric and asymmetric boundary conditions is discussed together with available experimental data. [1] A. M. Bratkovsky and A. P. Levanyuk, Phys. Rev. Lett. **94**, 107601 (2005) and to be published.

*Invited Papers*

**14:54**
**D17 3 Domain Structures in Nano-Toroids and Ultra-Thin Single Crystals.***
MARTY GREGG, *Queen's University Belfast*

Rationalisation of the formation of domain structures, in ferroics of limited dimensions, has been a topic of interest since the 1940's [1], with early work, specifically in ferroelectrics, in the 1950's [2]. Experimental studies at that time primarily involved domain investigations using optical microscopy, on samples down to the order of hundreds of microns. More modern studies, extending domain research into the thin and ultrathin film regime [3], suggest that our understanding of certain aspects of domain behaviour remain relatively unchanged, despite the intervening decades. This might imply that reduction of scales into the nanometre range will not reveal anything new or interesting in ferroelectric domain research. In this talk, we hope to illustrate that this is not the case. We describe results from two recent research programmes on the characterisation of ferroelectric domain structures in single crystal $BaTiO_3$ (BTO) using Scanning Transmission Electron Microscopy. In both studies sample preparation was performed using a Focused Ion Beam Microscope (FIB). In the first study, the domain periodicity has been measured as a function of thickness of parallel-walled BTO slabs from several hundred nanometres down to $\sim$ 50nm. Early work [2] suggested that the domain width should vary as the square root of slab thickness, and this is consistent with our data. However, we find, in plotting data from several works on different ferroelectric materials, with differing surface boundary conditions, across six decades in thickness, that all data lie on the it same parent function, with the itsame constants of proportionality. This is totally unexpected, as the proportionality constants should be material and surface boundary state dependent. We suspect that this reveals fundamental aspects in the physics of ferroelectric domain formation that will be discussed. The second study was motivated by modelling done in 1994 by Gorbatsevich and Kopaev [4] and more recently by Fu and Bellaiche [5] and Naumov, Bellaiche and Fu [6]. Here, the influence of depolarization fields at ferroelectric surfaces were found to create polarization vortex structures when the ferroelectrics were sufficiently small. In toroidal shapes, Gorbatsevich and Kopaev even envisioned ordering of the vortices to produce nanoscale ferroelectric 'solenoids'. We have used the FIB to make toroidal structures and have characterized their domain morphologies. At the time of writing, only conventional domain behaviour has been observed down to scales of the order of $\sim$ 100nm. However, results on smaller scales to be performed over the next few months will be described, as well as the novel imaging techniques we intend to use to probe for the ferroelectric vortices. [1] C. Kittel, Physical Review, **70**, 965 (1946) [2] T. Mitsui and J. Furuichi, Physical Review, **90**, 193 (1953) [3] S. K. Streiffer et al. Phys. Rev Lett. **89**, 067601 (2002) [4] A. A. Gorbatsevich & Yu V. Kopaev, Ferroelectrics **161**, 321 (1994) [5] I. Naumov et al. Nature **432**, 737 (2004) [6] H. Fu and L. Bellaiche, Physical Review Letters, **91**, 257601 (2003).

*Authors acknowledge the EPSRC and NanotecNI for finacial support.

*Contributed Papers*

**15:30**
**D17 4 Three perimeter effects in ferroelectric nanostructures**
ANDREAS RUEDIGER, FRANK PETER, RAINER WASER, *Center of Nanoelectronic Systems for Information Technology, Research Center Juelich, Germany* HYSTERETIC OXIDES TEAM, As the lateral size of ferroelectric nanoislands is now well below 50 nm, the question of size effects becomes increasingly relevant. Three independent techniques provided data of pronounced ferroelectric features along the perimeter: impedance spectroscopy [1], piezoelectric force microscopy [2] and pyroelectric current sensing [3]. However, as we can show, all three observations are related to the measurement technique that interferes with the lateral confinement and still there is no direct evidence of a lateral size effect in ferroelectric nanostructures. We discuss some scenarios of further downscaling and possible consequences. [1]M.Dawber, D.J. Jung, J.F. Scott, Perimeter effect in very small ferroelectrics,Appl. Phys. Lett. 82, 436 (2003) [2 ]F. Peter, A. Ruediger, R. Dittmann, R. Waser, K. Szot, B. Reichenberg, K. Prume, Analysis of shape effects on the piezoresponse in ferroelectric nanograins with and without adsorbates, Applied Physics Letters, 87, 082901 (2005) [3] B.W. Peterson, S. Ducharme, V.M. Fridkin, Mapping surface Polarization in thin films of the ferroelectric polymer P(VDF-TrFE),Ferroelectrics, 304, 51 (2004)

**15:42**
**D17 5 Static Field Anisotropies in Composition-Graded Ferroics** J.V. MANTESE, A.L. MICHELI, N.W. SCHUBRING, *Delphi Research Laboratories* R.W. HAYES, G. SRINIVASAN, *Oakland University* S.P. ALPAY, *University of Connecticut* Compositionally graded ferroelectrics and ferrites are formed as the dielectric and inductive analogues of semiconductor junction devices. The internal, or ''built-in,'' ferroic fields are intrinsic to the

structures and are determined from ferroelectric hysteresis and ferromagnetic resonance microscopy. The dynamic response of the ferroelectric and magnetic analysis graded ferroic devices (GFD's) is determined from quasi-static analysis in terms of the spatially dependent order parameters, the polarization and magnetization, respectively; yielding values for the internal ferroic fields consistent with experimental observations. Our results are extended to the general class of ferroic and other ''smart'' materials via a spatially dependent free energy potential.



**15:54**

**D17 6 Geometry Conditions Affecting Piezoresponse Force Microscopy** FRANK PETER, BERND REICHENBERG, ANDREAS RÜDIGER, KRZYSZTOF SZOT, RAINER WASER, Piezoresponse force microscopy provides valuable insight into the inverse lateral and vertical piezoelectric effect on the nanoscale. When examining ferroelectric grains as opposed to continuous thin films, the measured response is substantially influenced by the topography. Furthermore, a lateral piezoresponse exists in axially symmetric samples. An analysis of the piezoelectric tensor of the material and the radially symmetric electric field applied by the cantilever shows that the lateral as well as the vertical piezoresponse depends on more than one piezoelectric coefficient. This results in an increase of the unexpected lateral response near the perimeter of a grain. Due to the geometry of the cantilever this enhancement is only visible on certain sides of a grain. As a result of a mechanical crosstalk, a part of the lateral signal at the cantilever can be observed in the vertical response.

**16:06**

**D17 7 Calculations of anomalies in properties of relaxor ferroelectric films** MAYA GLINCHUK, EVGENIY ELISEEV, *Institute for Problems of Materials Science, NAS, Kiev, Ukraine* For the first time, we have calculated the properties of thin relaxor ferroelectric films in a framework of random field theory allowing for a misfit strain between the film and a substrate via surface piezoelectric effect, that causes a built-in electric field in the strained films. We demonstrate that this misfit-induced electric field, as well as the random electric fields created by randomly distributed electric dipoles and charged defects, lead to a smearing of ferroelectric phase transition, namely, they wash out a dielectric susceptibility maximum and a spontaneous polarization temperature dependence. As an example, a dependence of an order parameter and the dielectric susceptibility on the film thickness, temperature, and random fields distribution function was obtained. For the first time, we have shown that a frequency dispersion of susceptibility temperature maximum in relaxor thin films obeys modified Vogel-Fulcher law. In the proposed modified Vogel-Fulcher law the freezing temperature and activation energy depend on the film thickness, namely, freezing temperature decreases and activation energy increases with film thickness decrease. The obtained results quantitatively agree with the available experimental data for $PbMg_{1/3}Nb_{2/3}O_3$ relaxor thin films.

**16:18**

**D17 8 Charge pumping and ferroelectricity in the disordered one-dimensional system** CHYH-HONG CHERN, SHIGEKI ONODA, *Spin Superstructure Project, ERATO, and Department of Applied Physics, University of Tokyo, 7-3-1, Hongo, Tokyo 113-8656, Japan* SHUICHI MURAKAMI, NAOTO NAGAOSA, *CREST and Department of Applied Physics, University of Tokyo, 7-3-1, Hongo, Tokyo 113-8656, Japan* We consider the adiabatic charge pumping in the isolated disorder system in one dimension. Different from the Thouless charge pumping, the system has no gap even though all the states are localized, i.e., Anderson Localization. The charge pumping can be done by making a loop adiabatically in the 2- dimensional parameter space $\vec{Q} = (Q_1, Q_2)$ of the Hamiltonian. It is because there are many $\delta$-function- like fluxes distributing over the parameter space with random strength, in sharp contrast to the single $\delta$-function in the pure case. This provides a new and more efficient way of charge pumping. On the other hand, we also consider the situation when system is connected with leads, in which the weakly disordered ferroelectrics will be formulated in the Landauer-Buttiker formalism. In this case, the ''vortex'' structure emerges in the parameter space, which is the origin of the charge transfer for one lead to the other. The vortex core corresponds to the perfect transmittance which can be explained as a resonance tunneling. The time required for the adiabatic charge transfer is also estimated.

**SESSION D18: FOCUS SESSION: CARBON NANOTUBES: SYNTHESIS AND GROWTH II**
**Monday Afternoon, 13 March 2006**
**315, Baltimore Convention Center at 14:30**
**Robert Hauge, Rice University, presiding**

**14:30**

**D18 1 Growth of Single-Walled Carbon Nanotubes with Size-Controlled Catalysts** YAQIONG XU, *Department of Electrical & Computer Engineering and Carbon Nanotechnology Laboratory, Rice University* KUNAL SHAH, *Department of Chemistry and Carbon Nanotechnology Laboratory, Rice University* BEHRANG HAMADANI, *Department of Physics, Rice University* RICHARD SMALLEY,*ROBERT HAUGE, *Department of Chemistry and Carbon Nanotechnology Laboratory, Rice University* A single-walled carbon nanotube (SWNT) growth system has been developed with chlorine-containing gas to control the size of catalysts during growth. The role of catalyst size has been studied with respect its effects on SWNT growth, such as random surface growth, organized vertical growth and SWNT seeds re-growth. The effect of catalyst size on SWNT etching will also be reported.

*Passed way Oct. 28, 2005

**14:42**

**D18 2 Seeded Growth of Single-Walled Carbon Nanotubes from Open-ended SWNT Substrates*** MYUNG JONG KIM, ERIK HAROZ, HONGWEI SHAN, NOLAN NICHILAS, CARTER KITTRELL, *CNL, Rice University* ROBERT WHEELER, TIA BENSON-TOLLE, *Air Force Research Laboratory* YEONWOONG JUNG, DAVID LUZZI, *Dept. of Materials Science and Engineering, University of Pennsylvania* T.J. WAINERDI, *CNL, Rice University and CNI* HOWARD SCHMIDT, ROBERT HAUGE, RICHARD SMALLEY, *CNL, Rice University* We prepared nanoscopically flat open-ended SWNT substrates from SWNT spun fibers by using the focused ion beam cutting technique followed by various etching and clean-

ing schemes or alternatively from vertically aligned SWNT film by flipping over. Deposited catalyst was docked to the open ends of SWNTs, and carbon feedstocks were catalyzed into continued single-walled carbon nanotube growth resembling 1D molecular epitaxy in both the cold wall furnace and the hot wall furnace setups. The data obtained from Raman spectroscopy indicates that the (n, m) structure of the newly grown SWNT was cloned from that of the pre-existing SWNT substrate. Such results lead us to believe that this method will provide us with a means of chirality-controlled SWNTs growth on a macroscopic scale using a fairy general and scalable setup in the future.

*This work is supported by DOE and NASA.

**14:54**

**D18 3 Position-Controlled, Rapid Growth of Single-walled Carbon Nanotubes*** D. STYERS-BARNETT, Z. LIU, C. M. ROULEAU, H. CUI, D. B. GEOHEGAN, *Oak Ridge National Lab, Oak Ridge, Tennessee 37831-6031* A. A. PURETZKY, *Department of Materials Science and Engineering, University of Tennessee, Knoxville* 'Fast-heating' chemical vapor deposition (CVD) is a proven approach for the growth of long individual single-walled carbon nanotubes (SWCNTs). However, obtaining insights into how fast a carbon nanotube can grow is still of scientific and technical importance. Here, we describe a new CVD technique to synthesize SWCNTs using laser irradiation as the heat source. By adjusting the laser conditions, the heating time can be precisely controlled. Additionally, using a laser provides localization of the thermal energy, allowing position controlled growth. Temperature profiles of the substrate, measured by fast, in situ optical pyrometry, show controlled heating to CVD temperatures in a few seconds. Growth rate, yield, and diameter distribution of SWCNTs vary dramatically depending on catalysts, feedstock gases, and heating profile parameters, indicating this laser-CVD technique may provide local control over growth conditions and may pave a way for investigating the growth mechanism of 'fast-heating' carbon nanotubes.

*Research on Functional Nanomaterials at ORNL is supported by the U. S. Department of Energy, Division of Materials Science, Basic Energy Sciences.

**15:06**

**D18 4 Effect of Catalyst Particle Size on CVD Growth of Single-Walled Carbon Nanotubes.** A. HARUTYUNYAN, *Honda Research Institute* E. MORA, J-W. YOO, *Department of Physics The Ohio State University* T. TOKUNE, *Honda Research Institute* A.J. EPSTEIN, *Department of Physics The Ohio State University* HONDA RESEARCH INSTITUTE COLLABORATION, THE OHIO STATE UNIVERSITY COLLABORATION, A series of Fe catalysts with different mean diameter supported on alumina with different molar ratios were studied before and after SWNTs growth by using magnetic and Raman measurements to follow changes on catalyst particle size and its relationship with diameter of grown tubes. After the growth, based on blocking temperature values and Langevin function analysis, it was determined that for all catalysts, an increase and redistribution of particle size occurred. This is explained in terms of particle agglomeration, due to carbon-induced liquefaction accompanied with an increase in catalyst mobility. The free path of supported Fe particles was estimated to be $>$ 2.1nm. For big particles no correlation between catalyst size and nanotube diameter was observed. Analysis of the intensity of Breit-Wigner-Fano line contribution in the Raman G-band revealed that big catalyst particles are more selective to tubes chiralities, and more favorable to the growth of particular metallic tubes.

**15:18**

**D18 5 New empirical potentials between iron nanoparticles and oxide substrates*** AIQIN JIANG, NEHA AWASTHI, ALEKSEY KOLMOGOROV, *Duke University* KIM BOLTON, *Goteborg University, Sweden* ELENA MORA, *Ohio State University* TOSHIO TOKUNE, AVETIK HARUTYUNYAN, *Honda Research Institute, USA* STEFANO CURTAROLO, *Duke University* Interaction of iron catalyst nanoparticles with a substrate may influence nucleation and growth mechanism of carbon nantobutes (CNT) by shifting the melting temperature of the supported iron particles. To account for this effect we have used ab initio calculations to develop empirical potentials between iron nanoparticles and oxide substrates. Simulations have been performed on $Fe/Al_2O_3$ system with $Al_2O_3$ substrate fully relaxed. We have demonstrated that the surface rearrangement effects are significant but can be naturally incorporated into a simple Morse potential, which describes the total nanoparticle-substrate binding. The influence of different substrate surface terminations and positions of Fe layers on the strength of binding are discussed. Potentials for Fe and other oxide substrates are also being evaluated.

*Research sponsored by Honda Research Institute

**15:30**

**D18 6 Phase diagrams for Fe-C nanoparticles: A Molecular Dynamics Study*** NEHA AWASTHI, AIQIN JIANG, ALEKSEY KOLMOGOROV, *Duke University (USA)* FENG DING, *Rice University (USA)* KIM BOLTON, *Goteborg University (Sweden)* ELENA MORA, *Ohio State University (USA)* TOSHIO TOKUNE, AVETIK HARUTYUNYAN, *Honda Research Institute (USA)* STEFANO CURTAROLO, *Duke University (USA)* Fe nanoparticles are widely used as catalysts for carbon nanotube growth. In order to better understand the melting and phase transition properties of these nanoparticles, molecular dynamics (MD) simulations are performed to determine the melting point of Fe-C nanoparticles ( $\sim$ 1- 4 nm size) as a function of size and carbon concentration. The temperature dependence of the total energy and the Lindemann index characterize the melting of nanoparticles. For free (unsupported) Fe-C clusters, it is observed that the eutectic point (in the phase diagram) shifts with nanoparticle size. We have investigated how the presence of a substrate affects the melting process of the Fe-C nanoparticles.

*Research sponsored by Honda Researc Institute

**15:42**

**D18 7 Carbon Nanotube Growth Under Applied Pressure: Mechanical Energy Output and Control of Film Structure** A.J. HART, A. SLOCUM, *Dept. of Mechanical Engr., MIT* We measure the force which can be exerted by a film of vertically-aligned carbon nanotubes (CNTs) as it grows by thermal CVD. The thickness of the film measured after a growth duration of 15 minutes decreases in an approximately linear fashion with the logarithm of pressure which is applied by placing a tungsten weight on the substrate prior to growth. With increasing pressure, the internal structure of the film changes from well-aligned, to less-aligned with bending and possible single-mode buckling of the CNTs, to predominately collapsed in an ''accordion'' pattern having a spa-

tial wavelength of 0.1-1 $\mu$m. While the mechanical energy exerted is significantly less than major energetic steps in the growth reaction, a growing CNT film can lift tens of thousands of times its own weight. The equivalent volumetric energy density of $2.4\times 10^4$ J/m$^3$ is comparable to muscle. We utilize this principle to fabricate CNT structures which grow to conform to the shape of an etched silicon template, which is clamped against the growth substrate. This technique surpasses traditional methods using two-dimensional catalyst patterns, as it enables fabrication of CNT structures having arbitrarily sloped surfaces, and does not require catalyst patterning. CNT films and structures having controlled density and conformation, such as fabricated by changing the pressure applied during growth, will be useful for applications including electrochemical energy storage and fluid filtration, and as scaffolds for biological materials.

**15:54**

**D18 8 Laser Irradiation Pretreatment Effects on Catalyst-Coated Silicon and Subsequent CVD Nanotube Growth*** C.M. ROULEAU, G. ERES, H. CUI, D.B. GEOHEGAN, *Condensed Matter Sciences Div., Oak Ridge National Laboratory* I.N. IVANOV, A.A. PURETZKY, *Dept. of Mat. Sci. and Engr., Univ. of Tennessee* Developing methods for directed growth of nanotube arrays is important for many nanotube-based applications. Although we are currently growing mm-lengths of vertically-aligned nanotube arrays (VANTAs) from e-beam evaporated catalyst films, further enhancement of length, rate, and density are desired. One promising approach is catalyst modification using laser irradiation. Results are presented on the effects of pulsed KrF laser irradiation prior to chemical vapor deposition of VANTAs. Under typical conditions, a single laser shot was directed at a catalyst coated Si wafer to produce a well-defined laser affected zone. Fluences that ranged from 0.5 to 1.5 J/cm$^2$ were employed. In-situ videography was used to study VANTA growth rate in, and adjacent to, the laser affected zone. Atomic force microscopy was used to characterize catalyst surfaces prior to, and following, laser irradiation. The results show that the growth rates for VANTAs within the affected region improved remarkably. The efficacy of this technique in producing changes in VANTA length are shown.

*This research was sponsored by Oak Ridge National Laboratory, managed by UT-Battelle, LLC, for the U.S. Department of Energy, Office of Basic Energy Sciences

**16:06**

**D18 9 Large-Scale 'Surface-Programmed Assembly' of Carbon Nanotube-Based Biosensors*** DONG JOON LEE, BYUNG YANG LEE, JIWOON IM, MINBAEK LEE, SEUNGHUN HONG, *School of Physics, Seoul National University, Seoul, Korea* The unique electrical properties of single-wall carbon nanotubes (swCNT) have generated a huge amount of research on nanoelectronic devices and nanosensors. However, a lack of mass-production method of such devices has been holding back their practical applications. Herein, we present a method to assemble a large scale array of swCNT-based biosensors. In this method, self-assembled monolayer patterns direct the 'selective assembly' and 'alignment' of swCNTs onto substrates in the swCNT solution without relying on any externals forces. Using this method combined with microfabrication, we successfully demonstrated the fabrication of 256 x 256 swCNT-junction array on transparent glass substrates. Furthermore, by immobilizing glucose oxidase or L-glutamate oxidase on the CNT junctions, we fabricated swCNT-based biosensors for real-time detection of glucose or L-glutamate, respectively.

*supported by MCIE.

**16:18**

**D18 10 A biomimetic functionalization approach to integration of carbon nanoutbes into biological systems** XING CHEN, UN CHONG TAM, CAROLYN BERTOZZI, ALEX ZETTL, *Departments of Chemistry and Physics, University of California, Berkeley and Materials Sciences Division, Lawrence Berkeley National Laboratory* Due to their remarkable structural, electrical, and mechanical properties, carbon nanotubes (CNTs) have potential applications in biology ranging from imaging and tissue engineering. To realize these applications, however, new strategies for controlling the interaction between CNTs and biological systems such as proteins and cells are required. Here we describe a biomimetic approach to functionalize CNTs and therefore render them biocompatibility in order to facilitate their integration into biological systems. CNTs were coated with synthetic gycopolymers that mimic cell surface mucin gycoproteins. The functionalized CNTs were soluble in water, resisted non-specific protein binding and bound specifically to biomolecules. The coated CNTs could then be integrated onto mammalian cell surface by virtue of glycan-receptor interactions. Furthermore, the functionalized CNTs are non-toxic to cells. This strategy offers new opportunities for development of biosensor to probe biological processes. References: 1. X. Chen, G. S. Lee, A. Zettl, C. R. Bertozzi, Angewandte Chemie-International Edition **43**, 6111 (2004). 2. X. Chen, U. C. Tam, J. L. Czlapanski, G. S. Lee, D. Rabuka, A. Zettl, C. R. Bertozzi, submitted.

**16:30**

**D18 11 Temperature stability of ferritin as a catalyst for Carbon nanotube growth** RICHARD VANFLEET, MARK ESTY, ROBERT DAVIS, *Brigham Young University* In Carbon nanotubes grown with thermal CVD the distribution of tube diameters is dependant upon the growth catalyst. Use of biologically derived catalysts particles have been explored with the hope of narrower diameter distributions resulting from the tight distribution of catalyst particle diameters. Ferritin is the iron storage system in biological systems and consists of a protein shell with an iron hydroxide core. Previous use of catalyst particles generated from ferritin has not consistently resulted in narrow nanotube size distributions. To explore this inconsistency we have studied the particle distribution and temperature stability of surface deposited ferritin on various substrates by TEM. The effects of common substrates (Carbon, $SiO_2$ and $Si_3N_4$) on particle densities will be reported. We removed the protein shell with either a low temperature oxygen plasma or a high temperature anneal. With plasma removal of the protein shell the initial particle size and spacing distribution can be maintained at temperatures up to 600 C.

**16:42**

**D18 12 The Effect of Atomic Hydrogen on the Growth of Single-Walled Carbon Nanotubes** ROBERT HAUGE, *Department of Chemistry and Carbon Nanotechnology Laboratory, Rice University* YA-QIONG XU, *Department of Electrical and Computer Engineering and Carbon Nanotechnology Laboratory, Rice University* KUNAL SHAH, *Department of Chemistry and Carbon Nanotechnology Laboratory, Rice Univeristy* MYUNG KIM, *Department of Physics and Carbon Nanotechnology Laboratory,*

*Rice University* RICHARD SMALLEY,* *Department of Chemistry and Carbon Nanotechnology Laboratory, Rice University* The role of atomic hydrogen generated in situ with a hot filament has been studied with respect its effects on single-walled carbon nanotube (SWNT) etching and growth. SWNT growth has been studied for both random new surface growth and organized new vertical growth of SWNTs. Its effects on continued growth of SWNT seeds will also be reported. Comparisons will be made to previous studies of SWNT growth in the presence of atomic hydrogen.

*(passed away, Oct. 28th, 2005)

**16:54**

**D18 13 Ultra-high-yield growth of vertical single-walled carbon nanotubes** GUANGYU ZHANG, DAVID MANN, LI ZHANG, *Stanford University* ALI JAVEY, YIMING LI, ERHAN YENILMEZ, QIAN WANG, HONGJIE DAI, *Stanford University* JAMES MCVITTIE COLLABORATION, YOSHIO NISHI COLLABORATION, JAMES GIBBONS COLLABORATION, An oxygen-assisted hydrocarbon chemical vapor deposition method is developed to afford large-scale, highly reproducible, ultra-high-yield growth of vertical single-walled carbon nanotubes. It is revealed that reactive hydrogen species, inevitable in hydrocarbon-based growth, are damaging to the formation of sp2-like SWNTs in a diameter-dependent manner. The addition of oxygen scavenges H species and provides a powerful control over the C/H ratio to favor SWNT growth. The revelation of the roles played by hydrogen and oxygen leads to a unified and universal optimum-growth condition for SWNTs. Further, a versatile method is developed to form V-SWNT films on any substrate, lifting a major substrate-type limitation for aligned SWNTs.

**17:06**

**D18 14 Synthesis of Single Wall Carbon Nanotubes and Carbon Nanohorns by High Power Laser Vaporization** D. B. GEOHEGAN, A. A. PURETZKY, D. STYERS-BARNETT, C. M. ROULEAU, B. ZHAO, H. HU, H. CUI, I. N. IVANOV, P. F. BRITT, *Oak Ridge National Laboratory, Oak Ridge, TN and Dep. of Mater. Sci. and Eng., Univ. of Tennessee* In this study we present the results of high volume, high yield synthesis of single wall carbon nanotubes (SWNTs) based on a high power industrial Nd:YAG (600 W av. power) laser vaporization of a composite C/Co/Ni target at elevated temperatures. The high power laser also allows us to synthesize single wall carbon nanohorns (SWNHs) as well as metal nanoparticle (e.g., Pt, Pd) decorated SWNHs. Efficiencies and similarities between the conditions for SWNH synthesis are compared with those for SWNTs. itEx situ characterizations are compared with itin situ diagnostics (fast laser plume photography and target pyrometry) to correlate the synthesis conditions with the resulting products and gain insight into their formation processes. Research on Functional Nanomaterials at the Center for Nanophase Materials Sciences is supported by the U. S. Dep. of Energy, Div. of Materials Science, Basic Energy Sciences. The SWNH part of this research is supported by DOE Center of Excellence on Carbon-based Hydrogen Storage Materials.

**17:18**

**D18 15 In situ Optical Monitoring and Modeling of Vertically-Aligned Carbon Nanotube Array Growth During Chemical Vapor Deposition*** A. A. PURETZKY, D. B. GEOHEGAN, H. CUI, G. ERES, I. N. IVANOV, *Condensed Matter Sciences Division, Oak Ridge National Laboratory, and Dep. of Mat. Sci. and Eng., Univ. of Tennessee* A detailed experimental study of vertically aligned carbon nanotube array (VANTAs) growth by chemical vapor deposition (CVD) based on time-resolved reflectivity and direct remote microscope imaging as a diagnostic to measure and control the length of VANTAs in situ was performed. The VANTA growth was investigated between 500 [r]C and 900 [r]C on Si substrates with different evaporated multilayer catalysts and different feedstock gases. Nanotube lengths were controlled by rapid evacuation of the chamber. A kinetic model was developed to explain the observed growth kinetics, to discuss the main processes responsible for the growth of VANTAs, and to predict optimal growth conditions for single-wall carbon nanotube (SWNT) arrays. High quality VANTAs containing SWNTs were synthesized and characterized using Raman Spectroscopy.

*This research was sponsored by the U.S. Department of Energy under contract DE-AC05-00OR22725 with the Oak Ridge National Laboratory, managed by UT-Battelle.



## SESSION D19: FOCUS SESSION: SEMICONDUCTOR SPIN INJECTION AND DETECTION

**Monday Afternoon, 13 March 2006**
**316, Baltimore Convention Center at 14:30**
**Berry Jonker, Naval Research Laboratoy, presiding**

***Contributed Papers***

**14:30**

**D19 1 Onsager relations and the detection of current-induced spins by Ferromagnetic contacts** INANC ADAGIDELI, *University of British Columbia* The recent prediction of intrinsic spin Hall currents raised many questions about methods of detection. We focus on the theoretical issues related to the detection of spin currents and accumulations via ferromagnetic contacts. Along the way, based on Onsager-like relations for the conductance, we show the unfeasibility of detecting spin current from a non-magnetic conductor in a two probe geometry within linear response. It is nevertheless possible to detect spin current in a four probe geometry, in which the spin current flowing into the ferromagnet leads to a potential difference between the Hall contacts. We calculate the Hall conductivity and compare this effect to the Anomalous Hall effect. Work done in collaboration with G.E.W. Bauer and B.I. Halperin

**14:42**

**D19 2 Low temperature annealing and spin injection in Fe/AlGaAs Spin-LEDs** A.T. HANBICKI, G. KIOSEOGLOU, R. GOSWAMI, T.J. ZEGA, C.H. LI, R.M. STROUD, G. SPANOS, B.T. JONKER, *Naval Research Laboratory* With the Fe/AlGaAs/GaAs spin-LED system, it is now routine to obtain electron spin polarizations of up to 32% in the GaAs quantum well. Because the nature of the interface between a magnetic contact and a semiconductor is expected to influence the spin-injection efficiency we have undertaken an annealing study to isolate the role of the Fe/AlGaAs interface on the overall spin injection efficiency. Optimized annealing can improve the measured spin polarization, therefore multiple pieces of a single sample can be annealed to generate a systematic dataset. Enhancement in polarization is seen with anneals as low as 175°C, and the maximum increase in po-

larization occurs for anneals above 200°C. Upon annealing, there is a net gain in measured spin polarizations of 8 to 10 percentage points independent of the starting value. Details on changes in parameters affected by annealing such as the magnetization, polarization, I-V characteristics, and interface structure will be presented. The role of the interface on changes in these parameters will be discussed. This work was supported by the DARPA SpinS program and ONR.

**14:54**

**D19 3 Spin Injection from Fe and FeGa into side-emitting GaAs spin LEDs** G. KIOSEOGLOU, O.M.J VAN 'T ERVE, A.T. HANBICKI, C.H. LI, B.T. JONKER, *Naval Research Laboratory, Washington DC* Most of the spin LEDs used as spin detectors are of the surface type. In this type of LEDs, using Fe as spin polarized source, electron spin polarizations up to 40 % have been reported. Since Fe has its magnetization easy axis in the substrate plane, a large magnetic field B (2.5 tesla) along the surface normal is required to saturate the magnetization. A side-emission geometry, on the other hand, enables magnetic switching fields of $\sim$ 100 Oe, a much more practical range for applications. We present a study of electrical spin injection from Fe and FeGa into side-emitting GaAs spin LEDs in which the applied magnetic field is parallel to electroluminescence emitted from the cleaved side. Several samples with different quantum well (QW) widths were investigated. The optical polarization for the 100Å QW spin LED is zero, as expected due to hole spin orientation. For wider QWs, the confinement energy diminishes and the magnetic field rather than the confinement defines the quantization axis. An optical circular polarization P = 6 % is measured for the 1000 Å QW LED which corresponds to an electron spin polarization of 12 %. The non-volatile character of the side-emitting spin LED will be also discussed using FeGa as a spin injector. This work was supported by DARPA and ONR.

**15:06**

**D19 4 Atomic structure of the interface between Fe and AlGaAs and its impact on spin transport** THOMAS ZEGA, AUBREY HANBICKI, STEVEN ERWIN, IGOR ZUTIC,* GEORGE KIOSEOGLOU, CONNIE LI, BEREND JONKER, RHONDA STROUD, *Materials Science and Technology Division, Naval Research Laboratory, Washington, D.C. 20375* We combined density-functional theory (DFT) with experimental- and simulated- transmission-electron-microscope (TEM) imaging to determine the atomic structure of the interface between Fe and AlGaAs in light-emitting diodes (LEDs) used to investigate the transport of spin-polarized electrons. We show that a 44% increase in the spin-injection efficiency occurs after a low-temperature anneal, which produces an interface consisting of a single atomic plane of alternating Fe and As atoms. Our results provide the structural information required to develop accurate models of charge transport and spin injection at complex interfaces between dissimilar materials.

*Present address: Dept. of Physics, State University of New York at Buffalo

**15:18**

**D19 5 Resonant X-Ray Emission investigation of Fe/GaAs Spin Devices** JESSICA MCCHESNEY, *Montana State Universit and ALS* C. ADELMANN, *University of Minnesota* PER-ANDERS GLANS, K.E. SMITH, *Boston University* The ability to produced spin polarized electrons has important consequences to electronics, as we know it. One such spintronics system is Fe on GaAs. Fluorescence measurements, using synchrotron radiation, were used to probe the electronic structure of the Fe at the interface of a working device structure. These ferromagnetic-semiconductor heterostructures were grown via molecular beam epitaxity. Absorption spectroscopy (NEXAFS) and energy-resolved fluorescence (RIXS) both on and off resonance were done on the Fe L-edge. Subtle differences between samples with differing degrees of spin polarization were observed. These differences are discussed in terms of bonding at the interface. Supported by ONR and DOE.

**15:30 m**

**D19 6 Molecular Beam Epitaxy of $Fe_3Ga/Ga_{1-x}Al_xAs$ Heterostructures: Growth, Properties and Spin Transport** C. J. PALMSTRØM, C. ADELMANN, X. LOU, S. K. SRIVASTAVA, P. A. CROWELL, *University of Minnesota* Single crystal $Fe_3Ga$ thin films have been grown on $Ga_{1-x}Al_xAs$ (001) by molecular beam epitaxy. The films are found to be pseudomorphic on $Ga_{1-x}Al_xAs$ and grow in a tetragonally-distorted Heusler-like $D0_3$ crystal structure. The $Fe_3Ga$ films are ferromagnetic above room temperature with a saturation magnetization of 1200 emu/cm$^3$. They exhibit a perpendicular magnetic anisotropy due to the strain-induced tetragonal distortion. Rutherford backscattering spectrometry finds no interfacial reactions of $Fe_3Ga/GaAs$ heterostructures, suggesting that $Fe_3Ga$ is thermally stable on GaAs. Spin injection from $Fe_3Ga$ into GaAs has been assessed by using $Fe_3Ga/Ga_{1-x}Al_xAs$ spin light-emitting diode (LED) structures. A steady-state spin polarization of 20% is obtained at 2K. The bias dependence of spin injection is found to be very similar to that of $Fe/Ga_{1-x}Al_xAs$ spin LEDs [1]. This work was supported in part by ONR and NSF-MRSEC. [1] C. Adelmann itet al., Phys. Rev. B **71**, 121301 (2005).

***Invited Papers***

**15:42**

**D19 7 Imaging Spin Injection and Accumulation in Lateral Ferromagnet/Semiconductor Devices.***
PAUL A. CROWELL, *University of Minnesota*

We have directly imaged electrical spin injection and accumulation in the GaAs channel of a lateral spin transport device.† The ferromagnetic source and drain tunnel-barrier contacts at each end of the channel are epitaxial Fe Schottky barriers separated by a distance of 300 $\mu$m, which is much longer than the spin diffusion length. Emission of majority-spin electrons from the Fe source contact is observed using scanning Kerr microscopy. A majority spin polarization in the channel is also detected near the drain electrode, and we show that this accumulation is due to a spin current flowing away from the drain, against the unpolarized incident electron current. This result implies that the transmission of electrons through the forward-biased Schottky barrier is spin-sensitive. This is confirmed by demonstrating that the electrical

conductance of the device can be modulated by controlling the spin orientation of optically injected electrons flowing through the drain. These experiments are conducted in a geometry sensitive only to spin precession and allow for detailed modeling of spin transport in the channel. We show how this approach can be used to detect the spin accumulation at the drain electrode using purely electrical means. †S. A. Crooker *et al.*, Science **309**, 2191 (2005).

*In collaboration with S. A. Crooker, M. Furis, X. Lou, C. Adelmann, D. L. Smith, and C. J. Palmstrøm. This work was supported by the DARPA SPINS program, ONR, the NSF MRSEC program under DMR 02-12032, and the Los Alamos LDRD program.

***Contributed Papers***

**16:18**

**D19 8 Electrical Detection of Spin Accumulation at a Ferromagnet-Semiconductor Interface** X. LOU, C. ADELMANN, *University of Minnesota* M. FURIS, S.A. CROOKER, *Los Alamos National Laboratory* C.J. PALMSTRØM, P.A. CROWELL, *University of Minnesota* We report a direct electrical transport measurement of spin accumulation in epitaxial Fe/GaAs heterostructures. This result is obtained in lateral transport devices consisting of two Fe Schottky tunnel barriers at the opposite ends of a lightly *n*- doped GaAs channel. Polarized spin accumulates near the forward- biased GaAs/Fe Schottky interface, resulting in an additional voltage that is observed between the channel and the ferromagnetic drain contact. We establish that the spin accumulation, which can also be observed with Kerr microscopy, occurs when unpolarized electrons are incident on the interface. The voltage due to the electron spin accumulation is suppressed in a small transverse magnetic field as a result of precession. The width of the voltage peak is determined by a combination of spin diffusion and relaxation and can be modeled accurately using parameters determined from transport and optical experiments. These results demonstrate that Fe/GaAs Schottky barriers can be used as electrical spin detectors as well as injectors. This work was supported by DARPA, ONR, NSF- MRSEC, and LANL.

**16:30**

**D19 9 Scanning Kerr Rotation Microscopy of Lateral Spin Transport Devices** M. FURIS, D.L. SMITH, S.A. CROOKER, *Los Alamos National Laboratory, New Mexico* X. LOU, C. ADELMANN, C.J. PALMSTRØM, P.A. CROWELL, *University of Minnesota, Minneapolis* Scanning Kerr-rotation microscopy is employed to image electrical spin injection and accumulation in the GaAs channel of lateral spin transport devices having ferromagnetic Fe/GaAs Schottky barrier source and drain contacts [1]. Because electrically-injected spins are initially oriented in the $xy$ sample plane ($S_0 \| \hat{x}$), we measure the Kerr rotation ($\theta_K \propto S_z$) as a function of small in- plane magnetic field ($B_y$). We specifically investigate how these ''Hanle curves'' vary across a series of devices with systematically increasing electron density $n_e$ in the n-type GaAs channel ($2 \times 10^{16}\ \mathrm{cm}^{-3} < n_e < 3 \times 10^{17}\ \mathrm{cm}^{-3}$). The width of the Hanle curves near the source contact increases with $n_e$, reflecting the decreasing electron spin lifetime. The amplitude of the Hanle curves (a measure of the spin polarization) decays on a lengthscale related to the $n_e$-dependent spin diffusion constant, lifetime, and mobility. [1] S.A. Crooker, M. Furis, X. Lou, C. Adelmann, D.L. Smith, C.J. Palmstrøm, P.A. Crowell, Science **309**, 2191 (2005).

**16:42**

**D19 10 Complete non-equilibrium spin polarization of electrons in degenerate semiconductors** A. G. PETUKHOV, *Physics Department, South Dakota School of Mines and Technology, Rapid City, SD* V. V. OSIPOV, V. N. SMELYANSKIY, *NASA Ames Research Center, Moffett Field, CA* We show that spin polarization of electrons in nonmagnetic degenerate semiconductors near specially tailored forward- biased ferromagnet-semiconductor junctions can achieve 100%. This effect is realized even at moderate spin polarization of the interfacial contact resistance. Our conclusions are based on detailed analysis of non-linear spin diffusion equation with realistic boundary conditions. The effect of complete spin extraction occurs at relatively strong electric fields and arises from a reduction of spin penetration length due to the drift of electrons from a semiconductor towards the spin- selective tunnel junction. We further demonstrate that non- equilibrium electrons in thin nonmagnetic semiconductor layers can be almost fully spin polarized by means of simultaneous electrical spin injection and extraction. The complete spin polarization is achieved if the thin layer is placed between two ferromagnetic metal contacts with moderate spin injection coefficients and antiparallel magnetizations. The sign of the spin polarization is determined by the direction of the current. Applications of this effect in spintronics and quantum information processing are discussed.

**16:54**

**D19 11 Ballistic spin injection spectroscopy of a (Ga,Mn)As spin Esaki diode** MAKOTO KOHDA, *Laboratory for Nanoelectronics and Spintronics, RIEC, Tohoku Univ. Japan* TOMOHIRO KITA, *Semiconductor Spintronics Project, ERATO, JST, and Laboratory for Nanoelectronics and Spintronics, RIEC, Tohoku Univ., Japan* YUZO OHNO, *Laboratory for Nanoelectronics and Spintronics, RIEC, Tohoku Univ., and CREST, JST, Japan* FUMIHIRO MATSUKURA, HIDEO OHNO, *Laboratory for Nanoelectronics and Spintronics, RIEC, Tohoku Univ. and Semiconductor Spintronics Project, ERATO, JST, Japan* A p-type ferromagnetic semiconductor (Ga,Mn)As is one of the promising materials for spin injector by interband tunneling [1]. In this work, we investigated injection of spin-polarized electrons in a (Ga,Mn)As/n$^+$-GaAs Esaki diode (ED) by using a three-terminal device integrating a (Ga,Mn)As ED and a light emitting diode (LED), which allows us to apply bias voltages to the ED and LED independently. Electroluminescence polarization ($P_{\mathrm{EL}}$) from the LED was measured under the Faraday configuration as a function of bias voltages. The maximum $P_{\mathrm{EL}}$ of 32.4% was observed when the valence electrons near the Fermi energy of (Ga,Mn)As are ballistically injected into the LED. The experimental results proved high spin polarization of valence electrons ( $>$ 85%) for 100 meV below the Fermi energy of (Ga,Mn)As. [1] M. Kohda et al., Jpn. J. Appl. Phys. Part2 **40**, L1274 (2001); E. Johnston-Halperin et al., Phys. Rev. B **64**, 041306(R) (2002); P. Van Dorpe et al., Appl. Phys. Lett. **84**, 3495 (2004).

**17:06**

**D19 12 Electrical Spin Injection into Two Dimensional Electron Gas.*** JONGHWA EOM, *Department of Physics, Sejong University, Korea* HYUN CHEOL KOO, DONGHWA JUNG, HYUNJUNG YI, JOONYEON CHANG, JAE BEOM KO, SUKHEE HAN, *Nano Device Research Center, Korea Institute of Science and Technology, Korea* While electrical spin injection has been observed in a variety of metal films, the signal of the electrical spin injection into semiconductors has been hardly observed. We have overcome the difficulties of spin injection by developing a well-controlled interface treatment between the ferromagnetic films and the InAs semiconductor surface. We have found the evidence of electrical spin injection and accumulation in permalloy(Py)/InAs 2DEG/permalloy(Py) lateral devices. Ferromagnetic metal electrodes with different aspect ratio being separated by various separations were fabricated on top of the InAs 2DEG channels. Our multi-terminal geometry allows us to measure non-local spin valve effect as well as local spin valve effect. In the non-local spin valve measurement, we were able to completely isolate the spin valve signal from other spurious effects and observed clear spin accumulation signals. Based on the spin accumulation signal depending on the channel length, we have evaluated the spin relaxation length in the InAs based 2DEG.

*This work was supported by the KIST Vision 21 program, the SRC program of MOST/KOSEF, and the Korea Research Foundation Grant (KRF-2003-015-C00224)

**17:18**

**D19 13 Fabrication of GaAs spin injection devices** Y. JUNG, *Physics department, Oho State University* O. KWON, V. P. BHALLAMUDI, *Physics department, Oho State University* R. YU, *Physics department, Oho State University* D. V. PELEKHOV, *Physics department, Oho State University* S. A. RINGEL, *Electrical and Computer Engineering, Oho State University* P. R. BERGER, *Electrical and Computer Engineering, Oho State University* P. C. HAMMEL, *Physics department, Oho State University* We report on the progress towards fabrication of a ferromaget-GaInP(or AlGaAs)-GaAs devices. The devices are designed for use in future experiments to electrically detect, and spatially map spin accumulation in GaAs using a high sensitivity magnetic force microscope. The device consists of n-GaAs channel capped with a 3-5nm thick highly doped GaInP or AlGaAs layer. Both the GaAs channel and GaInP( or AlGaAs) layers are MBE grown. The ferromagnetic injector and detector are deposited ex-situ over the GaInP (or AlGaAs) barrier layer. We will discuss the electrical characteristics and transport behavior of the devices.

**SESSION D20: FOCUS SESSION: MULTIFERROICS I**
**Monday Afternoon, 13 March 2006**
**317, Baltimore Convention Center at 14:30**
**Nicola Spaldin, University of California, Santa Barbara, presiding**

**14:30**

**D20 1 Local Structure of the Multiferroic System $RMn_2O_5$*** TREVOR TYSON, QING QIAN, *NJIT* ALEXANDER IGNATOV, *Case Western University* SOONYONG PARK, SANG-WOOK CHEONG, *Rutgers University* In order to understand the origin of the coupled magnetic and ferroelectric properties observed in the system $RMn_2O_5$, detailed temperature dependent local structure measurements on powders and single crystals have been performed. The local structure about the rare earth (R) and the Mn sites have been examined. Comparisons with optical measurements and with various models of the temperature dependence of the pair correlations functions are made.

*Supported by NSF DMR-0512196.

**14:42**

**D20 2 Ferroelectricity induced by acentric spin-density waves in YMn2O5** GRAEME R. BLAKE, *ISIS Facility, Rutherford Appleton Laboratory* LAURENT C. CHAPON, *ISIS Facility, Rutherford Appleton Laboratory, UK* PAOLO G. RADAELLI, *ISIS Facility, Rutherford Appleton Laboratory, UK* S. PARK, *Rutgers University, USA* S-W. CHEONG, *Rutgers University, USA* The commensurate and incommensurate magnetic structures of the magnetoelectric system $YMn_2O_5$, as determined from neutron diffraction, were found to be spin-density waves lacking a global center of symmetry. We propose a model, based on a simple magneto-elastic coupling to the lattice, which enables us to predict the polarization based entirely on the observed magnetic structure. Our data accurately reproduce the temperature-dependence of the spontaneous polarization, in particular its sign reversal at the commensurate-incommensurate transition.

**14:54**

**D20 3 X-ray and neutron scattering studies of the magnetoelectric $DyMn_2O_5$** V. KIRYUKHIN, A. BORISSOV, S-W. CHEONG, *Rutgers University* W. RATCLIFF II, S.-H. LEE, *NIST* Magnetic phase diagram of magnetoelectric $DyMn_2O_5$ is established using neutron and magnetic x-ray scattering. The magnetic origin of the complex dielectric anomalies in this material is revealed. New diffraction peaks arising due to structural distortion at low temperatures are found and analyzed in the framework of the existing models of the ferroelectric state. Effects of an applied electric field on the magnetic structure are discussed.

**15:06**

**D20 4 Structural anomalies at the magnetic and ferroelectric transitions in $RMn_2O_5$*** B. LORENZ, C.R. DELA CRUZ, F. YEN, Y.Y. SUN, C.W. CHU,† *Dept. of Physics, University of Houston* S. PARK, S-W. CHEONG, *Dept. of Physics and Astronomy and RCEM, Rutgers University* Multiferroic $RMn_2O_5$ (R =rare earth, Y), have attracted significant attention because of their magneto-electric properties giving rise to complex phase diagrams and novel phenomena such as magnetic control of ferroelectric polarization and giant magneto-dielectric effects. In understanding their ferroelectricity and magneto-electric properties the magneto-elastic lattice distortions at the phase transitions are assumed to play a key role. Such distortions are difficult to detect by x-ray or neutron scattering experiments due to the limited resolution. Employing high-precision capacitance dilatometry, we show the existence of distinct, anisotropic lattice anomalies in $RMn_2O_5$ (R=Ho, Tb, Dy) at all magnetic and ferroelectric phase transitions as function of temperature and magnetic fields. These data provide unambiguous evidence for strong magneto-elastic coupling in multiferroic $RMn_2O_5$.

*Supported by NSF, DoE, and the State of Texas through TCSUH.

†Also at LBNL, Berkeley and HKUST, Hong Kong

**15:18**

**D20 5 The Pressure Effect on the Ferroelectricity in Multiferroic $R$Mn$_2$O$_5$ ($R$=Tb, Dy, Ho)** CLARINA DELA CRUZ, BERND LORENZ, CHING-WU CHU, *Dept. of Physics and TCSUH, University of Houston* SOON YONG PARK, SANG-WOOK CHEONG, *Dept. of Physics and Astronomy and RCEM, Rutgers University* MARIN GOSPODINOV, *Inst. of Solid State Physics, Bulgarian Academy of Sciences* The effect of isotropic pressure (**P**) up to 1.7 GPa on the magnetic and ferroelectric phase diagram of $R$Mn$_2$O$_5$ ($R$=Tb, Dy, Ho) is investigated. Distinctive anomalies of the *b*-axis dielectric constant identifying the critical temperatures for the various magnetic and ferroelectric transitions are monitored as a function of **P** and the temperature-pressure phase diagram of multiferroic $R$Mn$_2$O$_5$ was constructed. The magnetic and ferroelectric orders are stabilized under pressure and their respective onset temperatures increase with **P**. Most notably, the step-like change of the dielectric constant at lower temperatures ($T_{C2}$) that is associated with a drop in the ferroelectric polarization is suddenly quenched upon passing a critical pressure. These results suggest that above the critical pressure the ferroelectric polarization is restored below $T_{C2}$ and the ferroelectric phase in RMn$_2$O$_5$ is stabilized and extends to the lowest temperatures. *also at LBNL, Berkeley and HKUST, Hong Kong

**15:30**

**D20 6 High Magnetic Field Investigations of Multiferroic RMn2O5 (R=Tb, Dy, Bi, and Y)** KEE HOON KIM, S. Y. HAAM, J. W. KIM, Y. S. OH, *Seoul National University* N. HUR, S. PARK, S.-W. CHEONG, *Rutgers University* P. A. SHARMA, N. HARRISON, A. MIGLIORI, *NHMFL, Los Alamos National Laboratory* We have systematically investigated electric/magnetic phase diagram of a series of multiferroic crystals RMn2O5 (R =Tb, Dy, Bi, and Y) from dielectric constant, electric polarization, and magnetization measurements under intense magnetic fields up to 45 tesla by use of various static and pulsed magnets. Comparative studies of the phase diagram reveal several unprecedented findings: (1) phase evolution of the incommensurate antiferromagnetic Mn d spin ordering and related magneto-dielectric effects up to 33 T, (2) a new high field phase coupled to an incommensurate Mn d spin ordering appearing around 20 T, (3) phase evolution coupled to rare earth f-spin ordering and resultant polarization changes, and (4) significant modification of phase boundaries due to strong d-f spin interaction. Based on the determined electric/magnetic phase diagram, we also discuss how dielectric constant and polarization can be dependent on the commensurate and incommensurate magnetic phases under magnetic field to result in the observed large magneto-dielectric effects.

**15:42**

**D20 7 Phonon anisotropy in $ZnCr_2O_4$ from first principles** CRAIG J. FENNIE, *RutgersUniversity* KARIN M. RABE, The geometrically frustrated spinel $ZnCr_2O_4$ undergoes a cubic-to-tetragonal structural transition simultaneously as it enters a Neel state at $T_c$=12.5K. A recent experiment[1] using infrared spectroscopy measured a large splitting of an optical phonon frequency at $T_c$; it was argued that this splitting was due to a direct spin-phonon coupling. Here, we describe a first-principles study of the zone-center optical phonons in metrically cubic $ZnCr_2O_4$, with the LSDA+U as implemented in VASP. For selected collinear magnetically ordered structures, the influence of magnetic order on the phonon frequencies is identified, confirming the recent experimental results. The origin of this large phonon anisotropy will be discussed.

[1]A.B. Sushkov et al., Phys. Rev. Letters 94 (2005) 137202.

**15:54**

**D20 8 IR phonons induced by the helical magnetic order in multiferroic $TbMn_2O_5$*** ROLANDO VALDES AGUILAR, A. SUSHKOV, H.D. DREW, *University of Maryland. College Park, MD 20742* S.W. CHEONG, *Rutgers University. Piscataway, NJ 08854* The interplay between magnetic order and the lattice in multiferroic crystals has produced such interesting phenomena as polarization reversal and change of dielectric properties with magnetic fields[1]. Ferroelectricity in the multiferroic materials $REMn_2O_5$ (RE = rare earth) is thought to originate from a helical antiferromagnetic order. In order to study this possiblity we have made an infrared study of $TbMn_2O_5$. We find that several IR phonons show correlations with the distinct magnetic and dielectric phase transitions. Of special interest is the phonon spectrum for light polarization along the b axis where a mode at $\sim$ 706 $cm^{-1}$ exists only in the commensurate magnetic phase with **k** = (1/2,0,1/4) in the temperature range of 24-33 K. Possible scenarios for this phonon are: (1) the appearance of zone-folded modes; (2) the activation of previously silent modes due to the reduction of crystal symmetry. These scenarios are discussed in terms of the spin-lattice coupling in this class of materials.

*Work supported by NSF-MRSEC under grant DMR-0520471

[1]Hur, N et al. Nature **429** (2004) 392.

**16:06**

**D20 9 Microwave dielectric constant measurements of multiferroic $TbMn_2O_5$*** SAMUEL LOFLAND, *Rowan University* A SUSHKOV, *University of Maryland* H.D. DREW, *University of Maryland* S.W. CHEONG, *Rutgers University* We have measured the temperature dependence of the dielectric constant of $TbMn_2O_5$ by a cavity perturbation technique at frequencies between 2 and 13 GHz. There are three anomalous features seen in the quasistatic dielectric constant as a function of termperature below the onset of magnetic ordering ( $\sim$ 38 K); however at microwave frequencies, the enhancement in the dielectric constant is significantly reduced. In fact, by 13 GHz, the anomalies have nearly disappeared. Each anomaly has its own characteristic relaxation frequency, with the ones at higher and lower temperature being in the GHz range and the intermediate one being in the MHz. We discuss these results in terms of magnetoelectric domains.

*This work was supported in part by NSF Grant DMR-0520471.

**16:18**

**D20 10 Phonon coupling to the Tb spin in multiferroic TbMn2O5*** YOUNG-NOH YOON, A.B. SUSHKOV, R. VALDES AGUILAR, H.D. DREW, *MRSEC, University of Maryland* N. HUR, S.W. CHEONG, *Rutgers University* TbMn2O5 is a representative of a group of multiferroic materials where ferroelectricity is induced by spiral magnetic ordering at low temperatures. These materials demonstrate several weak structural and magnetic transitions reflecting complex interplay between magnetic order and the lattice. Phonons serve as a probe of lattice changes and, via spin- phonon coupling, of magnetic ordering. We measured the reflectivity spectra in a- and b-polarizations of an orthorhombic single crystal. The Tb-dominating phonons are ac-

tive in both polarizations but only b-polarization shows a magnetic shift below 24 K where Tb moments start to order. We made lattice dynamics calculations using popular GULP program to understand why a particular infrared phonon is strongly coupled to spin ordering.

*This work supported in part by NSF-MRSEC Grant DMR-0520471.



**16:30**

**D20 11 Temperature depending studies of multiferroic $TbMnO_3$ by spectral ellipsometry and Raman scattering** ILKA MAHNS, *Institute of Applied Physics, University of Hamburg, Germany* M. BASTJAN, R. RAUER, G. NEUBER, B. SCHULZ, S. MUELLER, A. RUSYDI, M. RUEBHAUSEN, *e 11, D-20355 Hamburg, Germany* D. N. ARGYRIOU, *Hahn-Meitner Institute, Germany* M. KIM, H. BARATH, S.L. COOPER, *Dept. of Physics and Frederick Seitz Materials Research Laboratory, University of Illinois at Urbana-Champaign* $TbMnO_3$ has been studied in order to understand the orbital, structural, and magnetic structure as a function of temperature by Raman scattering and spectral ellipsometry. We present optical spectra, in which anomalies can be observed above and below the Néel temperature of 41 K. Below $T_N$, $TbMnO_3$ develops a complex magnetic structural phase. Another characteristic temperature of this material is $T_F = 28$ K. Below this temperature, $TbMnO_3$ develops a multiferroic state. From the ellipsometry data, we find a rearrangement of the spectral weight at 41 K. Raman scattering with an excitation energy of 1.91 eV shows Jahn-Teller mode changes below $T_N$. Below $T_F$ we also detected a new ferroelectric mode at 128 $cm^{-1}$. In the ellipsometry data as well as in the Raman spectra we identify another critical temperature at $T^* \sim 150$ K. From our observations we can conclude that there is a strong coupling between the electronic and lattice degrees of freedom, which influence both the formation of the multiferroic state and the Jahn-Teller-distortions.

**16:42**

**D20 12 Investigation of coupling between antiferromagnetic and ferroelectric orders in $TbMnO_3$ using magnetic field dependent Raman scattering** HARINI BARATH, MINJUNG KIM, S.L. COOPER, *Dept. of Physics and Frederick Seitz Materials Research Laboratory, University of Illinois at Urbana-Champaign, Urbana, Illinois 61801* I. MAHNS, M. RUEBHAUSEN, *Institut fur Angewandte Physik, Univeristat Hamburg, Jungiusstrasse 11, D-20355 Hamburg, Germany* D.N. ARGYRIOU, *Hahn-Meitner Institut, Glienicker Str. 100, D-15109 Berlin, Germany* $TbMnO_3$ is an antiferromagnetic insulator with a distorted orthorhombic perovskite structure and a Néel temperature at $T_N = 41$K. $TbMnO_3$ is of particular interest because it is one of the few materials that exhibits not just a co-existence, but a strong coupling between antiferromagnetic and ferroelectric order, as evidenced by a para- to ferro- electric transition below T = 28K. In this talk, we discuss magnetic field dependent Raman scattering measurements of $TbMnO_3$ – both for magnetic fields oriented along various crystallographic directions and as a function of temperature through the ferroelectric and Néel transitions - the goal of which is to investigate the magnetic-ferroelectric coupling mechanism in this interesting material.

**16:54**

**D20 13 Dielectric properties of $TbMnO_3$ and $La(Sr,Ca)_{0.3}MnO_3$ – evidence for spectral weight changes up to 20 eV.** S. MÜLLER, M. RUBHAUSEN, R. RAUER, A. RUSYDI, M. BASTJAN, G. NEUBER, S. DASTJANI-FAHARANI, B. SCHULZ, S. SINGER, A. LICHTENSTEIN, *Universität Hamburg* D. ARGYRIOU, *Hahn-Meitner Institut, Berlin* K. DÖRR, *IFW, Dresden* In order to analyze changes in the kinetic energy that occur at the transition into the magnetic state we have performed ellipsometry measurements (0.5-5.5 eV) and reflectance measurements (4 – 20 eV) covering in total a spectral range between 05 and 20 eV. First, we evaluate thermal difference reflectance spectra and find changes at the transition into the magnetic state for both undoped TbMnO3 and doped La(SrCa)MnO3 exceeding energies up to 20 eV. We find distinct changes at the magnetic transitions for energies around 2 eV, 4 eV, 8 eV, 12 eV, and 18 eV. We attribute the first two transitions to Mn d-d high-spin and Op-Mnd charge transfer transitions. The transition at 18 eV is most likely connected to the O2s to O2p transition, whereas the origin of the transitions at 8 and 12 eV remain to be discussed.

**17:06**

**D20 14 The role of lattice distortions in magnetoelectrics** TURAB LOOKMAN, AVADH SAXENA, *Los Alamos National Lab* The orthorhombic magnetoelectrics, such as RMnO3, R=Tb,Dy,Gd, exhibit lattice modulations as measured by diffraction. Symmetry analysis predicts a shuffle based transition associated with the magnetoelectric state. We include coupling of the shuffle modes to polarization and incoommensurate magnetization within a Landau free energy framework. We explore the possible role of strain in recently observed pressure effects in some of the materials. In addition, using strain we model the orthorhombic to monoclinic structural transition in certain doped materials. We attempt to connect the free energy coefficients to avaliable structural and thermodynamic data.

**17:18**

**D20 15 Field induced linear magneto-elastic coupling in multiferroic $TbMnO_3$** NADIR ALIOUANE, DIMITRI ARGYRIOU, *Hahn-Meitner-Institut, Glienicker Str. 100, Berlin D-14109* J. STREMPFER, I. ZEGKINOGLOU, *Max-Planck-Institut fur Festkorperforschung,Heisenbergstrasse 1, 70569 Stuttgart, Germany* M. V. ZIMMERMAN, *HASYLAB at Deutsches Elektronen-Synchrotron DESY, Notkestr. 85, 22603 Hamburg, Germany* We have used in-field neutron and X-ray single crystal diffraction to measure the incommensurability $\delta$ of the crystal and magnetic structure of multiferroic $TbMnO_3$. We show that the flop in the electric polarization at the critical field $H_C$, for field $H$ along the $a-$ and $b-$ axis coincides with a 1st order transition to a commensurate phase with propagation vector $\kappa = (0,\frac{1}{4},0)$. In-field X-ray diffraction measurements show that the quadratic magneto-elastic coupling breaks down with applied field as shown by the observation of the 1st harmonic lattice reflections above and below $H_C$. This indicates that magnetic field induces a linear magneto-elastic coupling. We argue that the commensurate phase can be described by an ordering of Mn-O-Mn bond angles.

**SESSION D21: COLLOIDS III: PARTICLES AT INTERFACES AND IN CONFINED GEOMETRIES**
**Monday Afternoon, 13 March 2006**
**318, Baltimore Convention Center at 14:30**
**Charles Reichhardt, Los Alamos National Laboratory, presiding**

**14:30**
**D21 1 Phase behavior of standing disks in 2D** KUN ZHAO, *Princeton University* CHRISTOPHER HARRISON, *Schlumberger-Doll Research Center* MATTHEW SULLIVAN, *Princeton University* THOMAS MASON, *University of California- Los Angeles* DAVID HUSE, WILLIAM RUSSEL, *Princeton University* PAUL CHAIKIN, *New York University* We use photolithography to fabricate plate-like colloidal PMMA disks (diameter$\sim$ 5.3micron, thickness$\sim$ 0.8micron). Using an electric field normal to the cover slip, we can get a monolayer of disks standing on their edges. The system resembles a 2D set of colloidal rectangles. We study the phase behavior of this system and find that there is K-T transition from isotropic to nematic (quasi-smectic). Between these two phases, we find a regime where tetratic correlations are longer range than nematic. By studying the disclinations and domain walls, we suggest that the tetratic phase is driven by the nearby nematic and exists on a length scale larger than the nematic domain wall spacing but smaller than the inter-disclination distance.

**14:42**
**D21 2 Attraction between charged silica spheres at a water-air interface*** PENGER TONG, WEI CHEN, *Department of Physics, Hong Kong University of Science & Technology* SUSHENG TAN, WARREN T. FORD, *Department of Chemistry, Oklahoma State University* Charged colloidal particles at aqueous interfaces are found to experience attractive interactions but the origin of such attraction is not well understood. Here we report an experimental study of attractive interactions between micron- sized charged silica spheres at a water-air interface. Atomic force microscopy is used to examine the charge distribution of the silica surface. Digital video microscopy is used to measure the equilibrium pair potential between the interfacial silica spheres over varying salt concentrations in the aqueous phase. It is found that the measured interaction potential U (r) has an energy barrier with height $\sim 0.15k_BT$ at large particle separation r. For smaller separations, U(r) has an attractive well of order $0.3k_BT$. At even smaller separations, the usual Coulomb repulsion dominates. The experimental observation can be explained in terms of a balance between the screened Coulomb repulsion and unscreened dipole interactions.

*Work supported in part by the Research Grants Council of Hong Kong SAR under Grant No.

**14:54**
**D21 3 Like-charge attraction originated from intrinsic charge inhomogeneity** YI ZHOU, ZHOUSHEN HUANG, TAI KAI NG, *Department of Physics, Hong Kong University of Science and Technology, Clear Water Bay, Kowloon, HongKong* We study attractions between charged colloidal spheres in a solution and at a water-air interface. Both intrinsic inhomogeneous charge distribution and induced charge fluctuations may result in like-charge attraction. The intrinsic inhomogeneous charge distribution comes from the inhomogeneous surfaces of colloidal spheres, characterized by the number of patchy domains, while charge fluctuations occur in a homogenous background of charges. As the number of patchy domains increases, it will change from the intrinsic charge inhomogeneity to the induced charge fluctuation case. This crossover is studied theoretically and the results are compared with the recent experiments on polystyrene and silicon particles. A simple mechanism is presented to explain the enhancement of the attraction between two charged colloidal particles when they are suspended near a wall.

**15:06**
**D21 4 Attraction between charged colloidal spheres at oil-water interface** CHUAN ZENG, HUGO BISSIG, ANTHONY DINSMORE, *Department of Physics, University of Massachusetts Amherst* The behavior of micron-sized, charged-stabilized colloidal spheres confined at oil-water interface was studied using microscopy. Aggregates of colloidal particles were observed, suggesting an attractive capillary force arising from electrostatic stress on the interface. We report measurements of a long-range attraction between carboxyl-modified polystyrene spheres (radius $\sim$ 1 micron) at the interface between 1,1,1-trifluoroheptan-2-ol and water using image analysis and particle tracking. The interaction between two isolated spheres was measured and compared to recent theoretical models. We also measured the interaction of single particles with large clusters as well as the interactions between clusters. We found acceleration due to the capillary attraction and a complex angular dependence owing to the anisotropy of the meniscus around a cluster. We acknowledge support from NASA through the Fluid Physics program (NRA 02-OBPR-03-C).

**15:18**
**D21 5 The elasticity of nanoparticle networks on liquid droplets** YOUNG-HSYANG CHEN, HSUAN-YI CHEN, *Department of Physics, National Central University, Taiwan* ALEX LEVINE, *Department of Chemistry and Biochemistry, University of California, Los Angeles, California* Inspired by recent experiments on the formation of linked nanoparticle networks [A.D. Dinsmore et al Science, **298**, 1006, (2002)] on the surface of oil-in-water droplets, we study the modification of the droplet surface elasticity due to the formation of a percolating network of linked nanoparticles. What coverage of nanoparticles is required to modify the elasticity of the droplet? Using Brownian dynamics simulations to model the DLCA (diffusion limited cluster aggregation) of nanoparticles on the surface we construct these networks and monitor the appearance of an elastic contribution due to the nanoparticles at a critical nanoparticle area density. This transition is a type of rigidity percolation on a compact surface.

**15:30**
**D21 6 Crystalline Particle Packings on Spheres*** YAPING JING, *Iowa State University* ALEX TRAVESSET, *Iowa State University and Ames lab* The problem of packing particles on spheres appears in several soft condensed matter systems such as the building of PMMA cages (Pickering emulsions or colloidosomes), the micropatterning of colloidal particles relevant for photonic crystals or the geometric strucures of Clathrin cages responsible for the vesicular transport of cargo in cells, just to name a few. In this talk we show how the structural and mechanical properties of spherical crystals can be described analytically from continuum elastic models and discuss how the results are extended to describe other geometries as well.

*funded by NSF-DMR-0426597

**15:42**

**D21 7 A 3d View of Spherical Crystals and Grain Boundary Scars** MARK BOWICK, *Syracuse University* THOMAS EINERT, PETER LIPOWSKY, JORG SCHILLING, ANDREAS BAUSCH, *Technical University of Munich* We present an experimental system suitable for producing spherical crystals and for observing the distribution of lattice defects (disclinations and dislocations) on a significant fraction (50%) of the sphere. The introduction of fluorescently labeled particles enables us to determine the location and orientation of grain boundary scars. We find that the total number of scars and the number of excess dislocations per scar agree with theoretical predictions and that the geometrical centers of the scars are roughly positioned at the vertices of an icosahedron.

**15:54**

**D21 8 Formation of nanoparticle-coated liquid metal droplets and measurement of their electronic properties.*** KAN DU, C. KNUTSON, RUI HONG, M. TUOMINEN, T. EMRICK, T. RUSSELL, A. DINSMORE, *University of Massachusetts Amherst* We form stable droplets of molten metal, investigate their stability, and demonstrate their potential for forming electronic devices. Droplets of liquid Ga, 0.1-100 microns in diameter, were stabilized by surfactants and by insulating, conducting, and semiconducting nanoparticles. We investigate electronic transport through the nanoparticle-coated droplets. Here we use silica, gold and CdSe nanoparticles which spontaneously form a layer on the droplets. A few droplets form junctions between two platinum wires; we apply a bias voltage to the wires and measure the current before and after evaporation of the solvent. Improved understanding of the electrical characteristics may allow inexpensive assembly of a large number of devices with controlled size, symmetry and function. We acknowledge support from the Center for UMass/Industry Research on Polymers (CUMIRP).

*Center for UMass/Industry Research on Polymers (CUMIRP)

**16:06**

**D21 9 Controlled Three-Dimensional Assembly of Colloidal Particles Using Optical Trapping** C.R. KNUTSON, J. PLEWA, *Arryx, Inc.* Optical trapping has become a widespread and valuable tool to assist researchers in the positioning of colloidal particles in solution. However, unless an additional potential acts on the particle, it freely diffuses from this position once the trap is removed. Previous researchers have used colloidal particles suspended in a gelatin to provide mechanical stability once the trap has been removed. We demonstrate that the van der Waals potential combined with Holographic Optical Trapping (HOT) can be used to build three-dimensional structures consisting of dozens of colloidal spheres. Particles are first positioned using HOT. An electrolyte solution is then flowed into the sample cell which screens the Coulomb repulsion and allows the van der Waals potential to affix the particles in place. We demonstrate that this technique can be used to build controlled three-dimensional structures formed on a substrate and in solution. Furthermore, many of these structures can be removed from solution without the aid of critical point drying or polymer fixation. This technique might provide a new route towards the assembly of photonic crystals and biotechnology devices.

**16:18**

**D21 10 MR Colloid Self-Assembly in Confined Geometries** PATRICK DOYLE, RAMIN HAGHGOOIE, *MIT* The characteristic length scales found in microfluidic devices have been shrinking drastically over the past several years. As a result it is becoming increasingly important to study the effects of this tight confinement. We have used the Brownian Dynamics simulation technique to study the self-assembly of magnetorheological (MR) colloids under confinement. To compliment these simulations, we have used particle tracking to study micron-sized colloids assembling in fluidic channels. For quasi-two dimensional systems, we report a seemingly contradictory response of the system to confinement between parallel hard walls. In contrast to previous circular geometries, we see re-entrant melting with respect to changing channel width and not with respect to field strength. As the channel height is increased (in the range of a few particle diameters), we observe oscillations in the mean cluster spacing with respect to gap height. These oscillations and the transition to the large gap scaling regime will be discussed.

**16:30**

**D21 11 Confocal Microscopy of Hard Sphere Crystal Growth** MATTHEW SULLIVAN, *Princeton University / Schlumberger-Doll Research* KUN ZHAO, ANDREW HOLLINGSWORTH, P.M. CHAIKIN, *Princeton University / New York University* WILLIAM B. RUSSEL, *Princeton University* Classical crystal growth is determined by the competition between chemical potential differences and surface tension. We use confocal microscopy to measure three dimensional crystal growth in a density matched suspension of PMMA-PHSA colloidal particles. The crystal is nucleated from a surface template that forces growth of face-centered-cubic crystals. The growing crystal surface is rough on the scale of several particle diameters, but the average growth rate is well described by the classical Wilson-Frenkel growth law. The local growth rate does depend on the roughness of the surface, however, and this growth rate variation provides a measure of interfacial surface tension.

**16:42**

**D21 12 Simulated Crystallite Melting Kinetics in Two Dimensions** D. W. BLAIR, J. R. SAVAGE, A. D. DINSMORE, J. MACHTA, R. A. GUYER, *University of Massachusetts at Amherst* A. J. LEVINE, *University of California, Los Angeles* We report on results of numerical simulations of the melting of two-dimensional crystallites. Recent experiments in colloidal systems demonstrate that colloidal crystallites undergo a two-stage melting process. Initially large crystallites melt at a constant rate until reaching a critical size at which there is a dramatic increase in the melting rate. Throughout the initial melting stage the crystallite interior maintains bond orientational order; this order is abruptly lost at the critical size. Using Brownian dynamics simulations of particles interacting via a variety of short-range central potentials, we find that in two dimensions small crystallites generically melt in two-stages characterized by a sudden increase in melting rate that coincides with an abrupt loss of bond orientational order. The critical size, particle number $\mathcal{O}(20)$, is in agreement with experimental data and appears insensitive to details of the short-range interparticle potential. We discuss a possible mechanism for this change in melting dynamics at a critical crystallite size. This work is supported in part by NSF (DMR-0242402) and NASA (NAG8-1659).

**16:54**

**D21 13 Influence of hydrodynamic coupling on pair-diffusion in a quasi-one-dimensional colloid system*** BINHUA LIN, XINLIANG XU, STUART RICE, *University of Chicago* HAIM DIAMANT, *Tel Aviv University* The effect of hydrodynamic interaction on the separation dependence of the center of mass and relative pair diffusion coefficients of colloid particles in a quasi-one-dimensional system, including the influence of proximate walls, has been calculated using the method of reflections. There is excellent agreement between the theoretical predictions and the experimental data. We show that the separation dependence of the relative pair diffusion coefficient has oscillatory structure on the scale length of the correlation length in the system, and we directly relate that oscillatory structure to the pair correlation function of the system.

*This research was supported by grants from the NSF (CHE-0241133, CTS-021774).

**17:06**

**D21 14 Short-time dynamics of a Brownian particle** BRANIMIR LUKIC, *Ecole Polytechnique Federale de Lausanne (EPFL), Switzerland* SYLVIA JENEY, ZELJKO SVIBEN, *EPFL Lausanne* CHRISTIAN TISCHER, *EMBL Heidelberg, Germany* ERNST-LUDWIG FLORIN, *Center for Nonlinear Dynamics, University of Texas, Austin* ANDRZEJ J. KULIK, LASZLO FORRO, *EPFL Lausanne* We record the thermal position fluctuations of a *single* micron- sized sphere immersed in a fluid by optical trapping interferometry with nanometer spatial and microsecond temporal resolution. On the shortest time scales investigated, the sphere's inertia has a small, but measurable, effect. We find, in accord with the theory of Brownian motion including hydrodynamic memory effects, that the transition from ballistic to diffusive motion is delayed to significantly longer times than predicted by the standard Langevin equation. This delay is a consequence of the inertia of the fluid. When the particle is confined by a harmonic potential with a depth on the order of $k_BT$, we find that these inertial effects determine the particle's motion at the similar time scale as the potential. Surprisingly, we don't observe the free diffusive behavior in such confined system.

**17:18**

**D21 15 Transport of nanoparticles in a temperature gradient** SHAWN PUTNAM, DAVID CAHILL, Thermodiffusion, mass transport in a temperature gradient, is commonly characterized by either the thermodiffusion coefficient $D_T$ or the Soret coefficient $S_T$; e.g., at low particle concentration $c$, the particle flux of a colloidal suspension subjected to a temperature gradient $\nabla T$ is $\mathbf{J} = -cD_T\nabla T - D_c\nabla c$, where $D_c$ is the diffusion coefficient and the Soret coefficient is $S_T = D_T/D_c$. We present our measured $D_T$ data for aqueous suspensions of charged polystyrene spheres, alumina nanoparticles, and globular proteins of lysozyme. Special emphasis is given to our published work on charged polystyrene spheres with different surface functionalities. For example, in solutions with large concentrations of monovalent salts, $\gtrsim$ 100 mM, $D_T$ for 26 nm spheres with carboxyl functionality can be varied within the range $-0.9 \times 10^{-7}$ cm$^2$ s$^{-1}$ K$^{-1}$ $< D_T <$ $1.5 \times 10^{-7}$ cm$^2$ s$^{-1}$ K$^{-1}$ by changing the ionic species in solution; in this case $D_T$ is the product of the electrophoretic mobility $\mu_E$ and the Seebeck coefficient of the electrolyte $S_e = (Q_C^* - Q_A^*)/2eT$, $D_T = -S_e\mu_E$, where $Q_C^*$ and $Q_A^*$ are the single ion heats of transport of the cationic and anionic species respectively. On the contrary, in low ionic strength solutions of LiCl, $\lesssim$ 5 mM, $D_T$ for the 26nm carboxyl spheres is negative, independent of particle concentration, and independent of the Debye length; $D_T = -0.73 \pm 0.05 \times 10^{-7}$ cm$^2$ s$^{-1}$ K$^{-1}$. The temperature dependence of $D_T$ is also discussed with results from our current work with polystyrene spheres, alumina nanoparticles, and protein solutions of lysozyme.

**SESSION D22: FOCUS SESSION: MAGNETIC NANOPATTERNS**
**Monday Afternoon, 13 March 2006**
**319, Baltimore Convention Center at 14:30**
**Laura Lewis, Brookhaven National Laboratory, presiding**



***Contributed Papers***

**14:30**

**D22 1 Magnetization reversal process and domain wall resistance in a water drop shape ring** D.C. CHEN, *Department of Material Science and Engineering, National Chiao Tung University* D.P. CHIANG, *Ming Hsin University of Science and Technology* Y.D. YAO, *Institute of Physics, Academia Sinica* Patterned permalloy (Ni80-Fe20) materials have been fabricated by e-beam lithography in the shape of water drop ring. A tip is intentionally added into ring as geometrical defects to interrupt the continuity of magnetization reversal process, in order to create domain wall. Image from Magnetic force microscopy (MFM) with real- time external field confirmed this domain structure. As a result of magneto- resistance (MR) measurement, the ratio of MR is about $0.137 \sim 0.233\%$ and $0.23 \sim 0.71\%$ at sweeping angles of samples and sweeping external field, respectively. The ratio of the change in the electric resistance which is measured by I-V curve is just about the value of domain wall MR ratio which is measured by sweeping angles and external field. In summary, we have successfully demonstrated that the domain wall motion along the direction of perimeter in a ferromagnetic ring at its onion state; and the critical field to form onion state is near 200 Oe and the lowest field which can still drag the domain wall is between 100 and 50 Oe.

**14:42**

**D22 2 Arrays of Ultrasmall Nanoscopic Ferromagnetic Rings*** DEEPAK SINGH, *Dept. of Physics, UMASS* HONGQI XIANG, *Dept. of Polymer science and Engineering, UMASS* ROBERT KROTKOV, *Dept. of Physics, UMASS* TING XU, *Dept. of Polymer Science and Engineering, UMASS* QIJUN XIAO, *Dept. of Physics, UMASS* THOMAS RUSSELL, *Dept. of Polymer Science and Engineering, UMASS* MARK TUOMINEN, *Dept. of Physics, UMASS* There has been a considerable amount of recent interest in the magnetic properties of ultrasmall ferromagnetic rings. This is largely motivated by the unique stability of the vortex state of magnetization and its relevance in future data storage elements. In this work, we discuss experimental research on ultra small cobalt nano rings. We fabricate arrays of ultra small rings using a technique involving self-assembled diblock copolymer templates, glancing angle evaporation and ion beam etching. The nanoscopic rings have an outer diameter of 13 nm and inner diameter of 5 nm. The magnetization properties of these arrays are measured in both parallel and perpendicular field orientations in SQUID magnetometer. We compare these measurements to analytical calculations

for different magnetic configurations that take into account the competition between exchange energy, Zeeman energy and magnetostatic energy. Based on analytical calculation and magnetic measurement we find that for such ultrasmall ring structures vortex states are the dominant remanent magnetic states.

*This work is supported by NSF grant DMR-0306951.

**14:54**

**D22 3 Reversal mechanism of patterned ferromagnetic elements*** YIMEI ZHU, J.W. LAU, V.V. VOLKOV, *Brookhaven National Lab* CFN TEAM, Understanding of magnetization reversal dynamics in patterned ferromagnetic elements, or building blocks, is crucial to the development of modern magnetic storage media and spintronic devices. Using state-of-the-art, field-emission transmission electron microscope (TEM) equipped with a custom-made objective lens (the only one of its kind in the world) that allows high-resolution magnetic imaging and electron holography, we study the reversal mechanism and hysteresis behavior of patterned rings, squares, and ellipses with different aspect ratios of Permalloy and Co thin-films. By quantitative analysis of the local magnetization, we measure magnetic properties and shape effect of individual elements, and compare experimental observations with theoretical calculations. We explain why a parent state of the elements, isolated or in an array environment, can result in different low-energy ground states, depending on the switching rate, and how the energy barrier to the vortex nucleation can be measured. New results using a magnetic force microscope built into a TEM stage to locally induce magnetic field gradient and to change magnetic polarization of the elements to study element-element interaction and magnetic reversal will be also reported.

*Work supported by U.S. DOE, under contract No. DE-AC02-98CH10886.

***Invited Papers***

**15:06**

**D22 4 Magnetic nanorings and manipulation of nanowires.**
C.L. CHIEN, *Johns Hopkins University*

The properties of nanoscale entities, such as nanorings and nanowires, and the response of such entities to external fields are dictated by their geometrical shapes and sizes, which can be manipulated by fabrication. We have developed a method for fabricating a large number of nanorings ($10^{10}$) of different sizes in the range of 100 nm and ring cross sections. During magnetic reversal, both the vortex state and the rotating onion state appear with different proportions, which depend on the ring diameter, ring cross section, and the profile of the ring cross section. In the case of nanowires in suspension, the large aspect ratio of the nanowires can be exploited for manipulation despite extremely small Reynolds numbers of $10^{-5}$. Using AC electric field applied to microelectrodes, both magnetic and non-magnetic nanowires can be efficiently assembled into desired patterns. We also demonstrate rotation of nanowires with precisely controlled rotation speed and chirality, as well as an electrically driven nanowire micromotor a few [**micron**] in size. In collaboration with F. Q. Zhu, D. L. Fan, O. Tchernyshyov, R. C. Cammarata (Johns Hopkins University) and X. C. Zhu and J. G. Zhu (Carnegie-Mellon University).

***Contributed Papers***

**15:42**

**D22 5 Bistability and controllable magnetic switching of 100-nm asymmetric ferromagnetic nanorings** F.Q. ZHU, GIA-WEI CHERN, OLEG TCHERNYSHYOV, C.L. CHIEN, *Johns Hopkins University* Nanorings can acquire the vortex state with flux closure and zero stray field. We have developed a method for fabricating a large number of nanorings over a macroscopic area. However, for 100-nm nanorings, the nanorings can acquire both the rotating onion state and the vortex state during magnetic reversal with comparable probability. In this work, we report the fabrication and properties of asymmetric nanorings, whose thickness and width vary along the circumference. In contrast to symmetric nanorings, the percentage of vortex formation in asymmetric nanorings can be controlled by the direction of the magnetic field. When the field is along the asymmetry axis, nearly every nanoring can acquire the vortex state. The introduction of asymmetry in the nanorings allows full vortex formation without losing the virtue of small dimension, high stability and high areal density. We have also developed a theoretical model to calculate the dependence of domain wall energy on the local width and thickness of the nanorings to account for the enhancement of vortex state in asymmetric nanorings.

**15:54**

**D22 6 Self-Assembled Cobalt Nanodots along $Al_2O_3$ (0001) step edges*** JORGE ESPINOSA, DAVID LEDERMAN, *Dept of Physics, West Virginia University* Ultrathin films of Co with thicknesses of 0.80 monolayers (ML) and 0.20 ML were grown on Al $_2O_3$ (0001) via molecular beam epitaxy at room temperature. itIn situ non-contact atomic force microscopy images obtained after annealing the 0.80 ML film in-situ at 400 °C revealed the formation of nano-dots distributed randomly on the sapphire surface with an average diameter of approximately 18 nm and a height of 0.4 nm. The annealing of the 0.20 ML film showed the formation of nanodots with diameters of 16 nm for the film annealed at 500 °C and 28 nm for an annealing temperature of 500 °C. In general, the nanodots increase their sizes with the annealing temperature and they move towards the top of the sapphire step edges, indicating a certain degree of self organization.

*This work was supported by the National Science Foundation (CIAM grant # 0502825).

**16:06**

**D22 7 Interaction effects in heterostructures of nanoscale magnetic particles and magnetic thin films** JENS MUELLER, STEPHAN VON MOLNAR, *Florida State University* YUZO OHNO, HIDEO OHNO, *Tohoku University, Sendai, Japan* Elongated magnetic nanoparticles attract continuing attention because of potential technological applications. STM assisted CVD is an

advantageous fabrication technique for exact positioning of individual Fe particles (diameter 5 – 20 nm) on different substrate materials. A first step towards an application of these small and local magnetic flux sources to intentionally influence and investigate other materials is to study structures of magnetic particles grown onto an underlying magnetic film. This enhances interaction effects between adjacent particles. Also, the particles alter the magnetic domain structure of the thin film making the transport properties of the latter sensitive to the magnetization state of the particles grown on top leading to a distinct switching effect in the magnetoresistance that persists up to room temperature. The interaction effects in such magnetic particles/thin-film heterostructures are further investigated in a device with a single magnetic nanoparticle and an underlying film of the concentrated magnetic semiconductor EuS. The magnetic interaction of this system can be tuned by sweeping the temperature through $T_C$ of EuS. We discuss the heterostructure's magnetization behavior in terms of different magnetic interaction strengths.

**16:18**

**D22 8 Perpendicular Anisotropy in Cobalt-nanodots on Rutile TiO2(110)*** N. WIDJAJA, *University of Tennessee* JIANDI ZHANG, *Florida International University* C.G. ZHOU, *ORNL* MINGHU PAN, *University of Tennessee and ORNL* E.W. PLUMMER, *University of Tennessee* J. SHEN, *ORNL* We report the structural and magnetic properties of self-assembled Co-nanodots on rutile $TiO_2$(110) substrates. Co-dots with different coverage density were prepared inside a UHV chamber (base pressure $< 1x10^{-10}$ Torr) by thermally evaporating Co-source on the well ordered rutile $TiO_2$(110) surface. The size of the Co-dots can be tuned by changing the coverage density and the dose rate of Co independently. The in-situ STM imaging indicates that the size of the Co-dots ranges from 0.5 nm to 1 nm. The magnetization of the systems was measured ex-situ using a Quantum Design SQUID magnetometer after they were capped with NaCl. The magnetization as a function of field measured at various temperatures for $2 < T < 250$K reveals significant perpendicular anisotropy. The origin of the anisotropy is explained in terms of the competition between magnetocrystalline anisotropy and shape anisotropy of the nanodots.

*The work was supported by NSF-DMR0346826 and ORAU faculty summer research program. ORNL is managed by UT-Battelle, LLC, for the U.S. Dept. of Energy under contract DE-AC05-00OR22725.

**16:30**

**D22 9 Geometrical frustration in a regular lattice of nanoscale ferromagnetic islands: artificial spin ice** R.F. WANG, C. NISOLI, R.S. FREITAS, J. LI, W. McCONVILLE, B.J. COOLEY, N. SAMARTH, V.H. CRESPI, P. SCHIFFER, *Department of Physics and Materials Research Institute, Pennsylvania State University, University Park, PA 16802 USA* M.S. LUND, C. LEIGHTON, *Department of Chemical Engineering and Materials Science, University of Minnesota, Minneapolis MN 55455 USA* We studied frustration in lithographically defined lattices of permalloy islands with lattice geometry designed so that the dipolar interactions are analogous to those of the spin ice materials. These islands are approximately 80 nm by 220 nm laterally and 25 nm in thickness, and the array lattice constant ranges from 320 nm to 880 nm. Our MFM measurements demonstrated that the single domain magnetic moment of individual islands had short range correlations but no long range correlations. The correlations showed behavior consistent with the ice rules for this system, which decreased with increased spacing between the islands. Research was supported by the Army Research Office. Reference: R. F. Wang et al. (Nature, in press).

**16:42**

**D22 10 ''Live'' Surface Ferromagnetism in Fe Dot Multilayers on Cu(111)*** MARIA TORIJA, *Univ. of Tenn. Knoxville/ Oak Ridge National Laboratory* AN PING LI, CHARLES GUAN, *Oak Ridge National Laboratory* WARD PLUMMER, JIAN SHEN, *Univ. of Tenn. Knoxville/ Oak Ridge National Laboratory* We investigate the crossover behavior from two-dimensional (2D) to three dimensional (3D) in multilayers of magnetic nanodots grown by stacking 2D Fe nanodot assemblies on Cu(111) single crystal substrate with a Cu spacing layer. Using in-situ magneto-optical Kerr effect, we have observed a striking ferromagnetic to spin-glass phase transition with increasing number of Fe dot layers. The topmost layer of the Fe dots survives the phase transition and remains ferromagnetic. This unusual surface ferromagnetism is likely caused by a stronger surface state-mediated intralayer dot coupling which is stronger than the interlayer dot coupling, as confirmed by the fact that the critical temperature of the surface ferromagnetism is considerably higher than that of the bulk spin glass phase in the system.

*Supported by ORNL, managed by UT-Batelle, LLC for the U.S. Departament of Energy (Contract No. DE-AC05-00OR227525) and by the U.S. National Science Foundation (Contract DMR 0105232)

**16:54**

**D22 11 Fabrication and magnetism of sub-100 nm exchange-biased magnetic dot arrays and porous networks.*** CHANG-PENG LI, IGOR V. ROSHCHIN, ZHI-PAN LI, IVAN K. SCHULLER, *Physics Dept., UCSD, La Jolla, CA, USA* Studies of exchange bias (EB) at nanoscale, when the structure size is comparable to magnetic domain sizes, can offer new insights for the mechanism of EB. For these studies, sub-100 nm ferromagnetic (Ni)-antiferromagnetic ($FeF_2$) dots and porous network bilayers are fabricated using self-assembled porous alumina masks. The size and periodicity of the nanopatterns are controlled by anodization conditions and pore widening time. Magnetization of the field cooled dots and networks is measured at 10 K by SQUID magnetometry and magneto-optical Kerr effect (MOKE), respectively. For the dots, the EB field is found to decrease as the dot diameter decreases. For example, with Ni/$FeF_2$ dot diameter decreasing from 98 nm to 52 nm, the EB field decreases from 640 Oe to 240 Oe. For networks with the constant pore periodicity, an increase in pore diameter from 50 nm to 70 nm results in a decrease of EB field from 150 Oe to 90 Oe. The results suggest that the EB decreases as the magnetic structure size decreases, regardless of its actual shape.

*Work is supported by AFOSR.

**17:06**

**D22 12 Domain walls resistance study in magnetic thin films by means of thickness modulation*** WEI-LI LEE, *Department of Physics and Astronomy, Johns Hopkins Univ.* F.Q. ZHU, V. THAMPY, C.L. CHIEN, The manner with which the magnetic domain wall (DW) affects the transport properties of a ferromagnet remains an interesting but difficult topic. Experimental extraction of magnetoresistance (MR) of DWs is challenging because of other dominating contributions especially the anisotropic magnetoresistance (AMR). We have explored one way to extract DW resistance by creating structures with built-in thickness modula-

tion (THM). By capitalizing on the thickness dependence of coercivity, the domain size and hence the number of DWs can be controlled through the period of THM. In a previous work, we used lithography to pattern a 50 nm thick Co film, 5$\mu$m in width and 60$\mu$m in length. We then used a focused ion beam to create grooves transverse to its length with depth $\sim$ 8 nm and period $\sim$ 500 nm. Magnetic force microscopy reveals an induced magnetic anisotropy along the groove direction. By applying magnetic field along various directions and taking in account the AMR contributions, we have deduced that the DW resistance in Co is positive with a value of $\sim$ 29.3 m$\Omega$ corresponding to $\sim$ 0.14% MR. In the present work, the structure is prepared in different way and geometry so that current parallel to walls and current perpendicular to walls DW resistance can be both obtained from the experiment. The latest results and comparison with theoretical models will be discussed.

*Work supported by NSF Grant No. DMR05-20491.

**17:18**

**D22 13 Ferromagnetic Nanocrystals of Antiferromagnetic FeGe** C.G. ZENG, MARIA VARELA, PAUL KENT, MARKUS EISENBACH, GEORGE MALCOLM STOCKS, MARIA TORIJA, JIAN SHEN, HANNO WEITERING, Epitaxial nanocrystals of FeGe have been stabilized on Ge(111). The nanocrystals assume a quasi one-dimensional shape as they grow exclusively along the $< 11^{-}0 >$ direction of the Ge(111) substrate, culminating in the monoclinic modification of FeGe. The uni-directional growth results from a close match between the Ge-atom spacing along $< 1\bar{1}0 >$ Ge and monoclinic b-axis of FeGe. Whereas monoclinic FeGe is antiferromagnetic in the bulk, the nanocrystals are surpisingly strong ferromagnets below $\sim$ 200 K with an average magnetic moment of 0.8 $\mu_B$ per Fe atom. Density functional calculations demonstrate that volume ferromagnetism is stabilized predominantly by compressive strain normal to the growth direction of the nanocrystals.



## SESSION D23: FOCUS SESSION: MAG.THY I / SPIN STRUCTURES AND DYNAMICS

**Monday Afternoon, 13 March 2006; 320, Baltimore Convention Center at 14:30**
**Dale Koelling, Department of Energy, presiding**

*Invited Papers*

**14:30**

**D23 1 Decoherence in Quantum Spin Systems.**
VIATCHESLAV V. DOBROVITSKI, *Ames Laboratory and Iowa State University, Ames IA 50011*

Understanding decoherence of quantum spin systems strongly coupled to a bath of environmental spins (spin bath) is important for many areas of physics, such as spintronics, quantum computing, nuclear and electronic magnetic resonance. Decoherence is a complex non-equilibrium many-body phenomenon, and for many interesting situations, exact numerical simulations are needed. We have developed highly efficient and accurate numerical techniques of solving the time-dependent Schrödinger equation for quantum many-spin systems. We used these techniques to directly model the evolution of the central spin system and its environment. I will demonstrate usefulness of this approach for several experimentally and theoretically important cases, where the many-body correlations between the system and the bath are particularly important. I will present, among others, our studies of the NMR spin echo of Si:dopant systems, and our investigation of decoherence by a spin bath in the regime of quantum chaos. Moreover, I will present our results on decoherence of an electron spin by a bath of nuclear spins in a quantum dot, which has been recently studied in experiments, and discuss novel numerical approaches based on techniques borrowed from quantum optics. This work was supported by US DOE, and NSA, ARDA and ARO.

*Contributed Papers*

**15:06**

**D23 2 Analysis of Density Matrix Off Diagonal Correlations for NMR Spin Echoes in Dipolar Solids** JOHN CHALLIS, VADIM OGANEYSAN, *Yale University* The experiments done by Barrett et al.* have established that repeated pi pulses can slow longitudinal relaxation in a dipolar solid. This result clearly lies outside any independent spin approximation, and so off diagonal terms in the density matrix cannot be neglected. We have calculated the size and correlations of these terms as a first step in diagnosing the mechanism behind the slow decay. *Dementyev et al. Phys. Rev. B 68, 153302 (2003)

**15:18**

**D23 3 Forces on spins in a field gradient: apparent spin relaxation** YULIN CHANG, MARK CONRADI, *Washington University* A magnetic field gradient exerts opposite forces on spin magnetic moments oriented up and down. The result is to partially segregate spins by orientation, with more spins-up at one end of the sample and more spins-down at the other. This apparent relaxation, involving only sorting and no flipping of spins, may be dominant in systems of high diffusivity and long $T_1$. The sorting mechanism competes with a well-known distinct, true $T_1$ mechanism driven by diffusion through field gradients. The results of our calculations and numerical solutions of the Bloch-Torrey equations, modified to include the force term, will be presented in detail.

**15:30**

**D23 4 Finite temperature modeling of magnetization processes in exchange-coupled films** R. H. KODAMA, *Univ. of Illinois at Chicago* A. E. BERKOWITZ, *Univ. of California, San Diego* Recent experimental studies by Berkowitz, et al. [PRB **72**, 134428 (2005)] have explored the effect of setting the exchange anisotropy of ferromagnetic / antiferromagnetic bilayers (FM/AFM) such as Co / (Ni,Co)O by deposition in a magnetic field at temperatures well below the $T_N$ or blocking temperature of the AFM

material. Two remarkable effects inspired this theoretical study: (1) the magnitude and direction of unidirectional anisotropy is modified by changing the applied magnetic field during deposition of the FM overlayer, and (2) there is a ''latent period'' after deposition is complete, during which the unidirectional anisotropy is modified by changing the field. We set out to determine if these effects could be understood using orthodox models of exchange anisotropy (invoking uncompensated interfacial moments on an ensemble of AFM grains) carried to an unprecedented level of detail. Finite interactions between FM- FM, AFM-AFM, and FM-AFM grains allow modeling of domain processes in both FM and AFM films. Finite temperature is included in a novel way, using a detailed analysis of the spin system's energy surface to determine sets of activation barriers and final states for low-energy collective modes. Results indicate that some of the observed effects can indeed be simulated in this way, although some of the experimental results are more consistent with a slow, interfacial redox reaction that changes the magnetic state of the interface.

**15:42**

**D23 5 First Principles Approach to the Magnetic Structure of Realistic Models of Nanoparticles*** G. MALCOLM STOCKS, AURELIAN RUSANU, DON NICHOLSON, MARKUS EISENBACH, *Oak Ridge National Laboratory* YANG WANG, *Pittsburgh Supercomputer Center* SAM FAULKNER, *Florida Atlantic University* Magnetic nanostructures are of great interest because of their potential applications in a wide range of technologies - data storage, magneto-electronics, permanent magnets, smart drug delivery, etc. Unfortunately magnetic nanostructures present substantial theoretical challenges due to the need to treat the electronic interactions quantum mechanically whilst dealing with a, still, large number of atoms – e.g., a 5nm cube of Fe contains $\sim$ 12,000 atoms, 4,000 of which are in the surface and subsurface layers. Here, we discuss a new implementation of the itab initio order-N Locally Self-consistent Multiple Scattering (LSMS) method that is capable of treating tens of thousands of atoms. We will present scaling data that show the performance of the code both in the real space mode of the original method and in the k-space mode based on screened structure constants and sparse matrix solvers. Illustrative results will be shown for a BCC Fe-nanoparticle embedded in a stoichiometric B2-FeAl binary alloy, a magnetic nanostructure model containing 16,000 atoms.

*The research of GMS, DMCN, ME, and AR is sponsored by DOE-OS, BES-DMEP under contract number DE-AC05-00OR22725 with UT-Battelle LLC.

**15:54**

**D23 6 Electronic and Magnetic Structure of Fe Nanoparticle Embedded in FeAl*** YANG WANG, *Pittsburgh Supercomputing Center* G. MALCOLM STOCKS, AURELIAN RUSANU, DON M.C. NICHOLSON, MARKUS EISENBACH, *Oak Ridge National Laboratory* J.S. FAULKNER, *Florida Atlantic University* Magnetic nanostructures are of great scientific interest because of their potential applications in a wide range of technologies - data storage, magneto-electronics, permanent magnets, smart drug delivery, etc. Unfortunately magnetic nanostructures present substantial theoretical challenges due to the need to treat the electronic interactions quantum mechanically whilst dealing with a, still, large number of atoms. In this presentation, we discuss our recent studies of magnetic nanoparticles using the Locally Self-consistent Multiple Scattering (LSMS) method, an order-N itab initio method capable of treating tens of thousands of atoms. In particular, we show results for a Fe nanoparticle embedded in a stoichiometric B2-FeAl binary alloy. The Fe nanoparticle, has the shape of a BCC Wigner-Seitz cell, contains 4,409 Fe atoms, and measures about 5 nm across the diagonal corners. Including the surrounding matrix the calculation involves 16,000 atoms. We show results for the moment and charge distribution within nanoparticle, on the facets, and in the FeAl matrix.

*The research of GMS, DMCN, ME, and AR is sponsored by DOE-OS, BES-DMEP under contract number DE-AC05-00OR22725 with UT-Battelle LLC. Calculations were performed at PSC, NERSC and ORNL-CCS.

**16:06**

**D23 7 Density functional calculations of the magnetic structure of FePt nano-particles** P.R.C. KENT, *University of Tennessee, TN* D.M.C. NICHOLSON, *Metals and Ceramics Division, Oak Ridge National Laboratory* M. EISENBACH, *Metals and Ceramics Division, Oak Ridge National Laboratory* T.C. SCHULTHESS, *Computer Science and Mathematics Division, Oak Ridge National Laboratory* The spin moment distribution in magnetic nano-particles is both scientifically interesting and technologically relevant. Here, we discuss the magnetic structure of FePt nano-particles, as determined by projector-augmented wave (PAW) and locally self-consistent multiple scattering (LSMS) local density calculations on nano-particles up to 3nm in size. The magnetic structure changes as a function of nano-particle size, composition, and chemical order, encompassing both ferromagnetic and anti-ferromagnetic tendencies. This behavior will be described and related to charge redistribution, structural relaxation, and local coordination. This work was enabled by computational resources of the Center for Computational Sciences at Oak Ridge National Laboratory and is supported by the Division of Scientific User Facilities and the Division of Materials Science and Engineering, U. S. Department of Energy.

**16:18**

**D23 8 Spin dynamics of a magnetic anti-vortex** HAO WANG, C.E. CAMPBELL, *University of Minnesota* We report the study of the spin dynamics of a magnetic anti-vortex in a submicron, asteroid shaped permalloy particle using micromagnetic simulations. A gyrotropic mode was found when a shifted anti-vortex core spirals back to the center of the asteroid. Azimuthal spin wave modes with in-plane wave vectors around the center have been excited using an in-plane pulsed field. The simultaneously excited gyrotropic mode causes a splitting of degenerate azimuthal modes. Radial spin wave modes with in-plane wave vectors along radial directions of the asteroid were excited by an out-of-plane pulsed field, which is created by a current surrounding the asteroid. The size dependence of dynamic modes has been systematically studied. The frequency of the gyrotropic mode increases with the thickness of the asteroid, but decreases with its size. The frequencies of both azimuthal and radial spin wave modes decrease with the thickness of the asteroid, and also decrease with the size of the asteroid, as may be expected by simple physical arguments.

**16:30**

**D23 9 Conductance and spin-flip of molecular magnets in a time-dependent magnetic field.*** ANH NGO, SERGIO E. ULLOA, *Ohio University* The properties of single molecular magnets and clusters with high spin, such as the Mn- or Fe-acetates, have been under intense study in recent years. The signature of magnetization tunneling on the conductance of films obtained by scanning tunneling microscopy (STM) has been recently studied theoretically [1]. We present here the effects of finite bias voltage and

temperature on the STM conductance using a model for tunneling among different magnetic states. The system consists of a single molecule magnet between two conducting leads (the substrate and the STM tip). Because of the spin-phonon interaction and finite bias voltage, a time-dependent magnetic field produces tunneling to different magnetic states even away from the fully resonant condition. We use an approximation to reduce the original $(2s + 1)$-level dynamical problem to a four-level sequence for the $s$-spin system. The differential conductance exhibits stepwise behavior with increasing longitudinal field that deviates substantially for increasing bias voltage and finite temperature. Analysis of the conductance vs. field and bias yields information on the spin-flip mechanisms. [1] G.-H. Kim and T.-S. Kim, Phys. Rev. Lett. 92, 137203 (2004).

*Supported by NSF-NIRT

**16:42**

**D23 10 Spin Anisotropy Effects in Dimer Single Molecule Magnets*** DMITRI EFREMOV, *Technische Universitaet Dresden, Germany* RICHARD KLEMM, *Kansas State University* We present a model of equal spin $s_1$ dimer single molecule magnets. The spins within each dimer interact via the Heisenberg and the most general set of four quadratic anisotropic spin interactions with respective strengths $J$ and $\{J_j\}$, and with the magnetic induction **B**. For antiferromagnetic Heisenberg couplings ($J < 0$) and weak anisotropy interactions ($|J_j/J| \ll 1$), the low temperature $T$ magnetization $\boldsymbol{M}(\boldsymbol{B})$ exhibits $2s_1$ steps, the height and midpoint slope of the $s$th step differing from their isotropic limits by corrections of $\mathcal{O}(J_j/J)^2$, but the position occurring at the energy level-crossing magnetic induction $B^{\rm lc}_{s,s_1}(\theta,\phi)$, where $\theta,\phi$ define the direction of $\boldsymbol{B}$. We solve the model exactly for $s_1 = 1/2$, 1, and 5/2. For weakly anisotropic dimers, the Hartree approximation yields analytic formulas for $\boldsymbol{M}(\boldsymbol{B})$ and $C_V(\boldsymbol{B})$ at arbitrary $s_1$ that accurately fit the exact solutions at sufficiently low $T$ or large $B$. Low-$T$ formulas for the inelastic neutron scattering $S(\boldsymbol{q},\omega)$ and the EPR $\chi(\omega)$ in an extended Hartree approximation are given. Our results are discussed with regard to existing experiments on $s_1 = 5/2$ $Fe_2$ dimers, suggesting further experiments on single crystals of these and some $s_1 = 9/2$ $[Mn_4]_2$ dimers are warranted.

*Supported by the Netherlands Foundation for the Fundamental Research of Matter and by the NSF under contract NER-0304665

**16:54**

**D23 11 A Mean Field Theory for Superspin Glasses** DEREK WALTON, Concentrated assemblies of magnetc nanopartcles have been shown to exhibit spin glass phenomena, particularly rejuvenation. It is clear that these effects are dependent on interactions among the nanoparticles. I will describe a classic mean field theory for the local magnetic field resulting from the interactions, and show how it can account for superspin glass phenomena.

## SESSION D25: FOCUS SESSION: PARTICLE DYNAMICS AND ORGANIZATION; POLYMER TETHERS AND INTERFACIAL SEGREGATION

**Monday Afternoon, 13 March 2006; 322, Baltimore Convention Center at 14:30**
**Francis Starr; Wesleyan University, presiding**

***Invited Papers***

**14:30**

**D25 1 Multiscale Simulation Studies of the Self-Association of Poly(ethylene oxide)-Tethered Fullerenes.** GRANT SMITH, *University of Utah*

I will discuss our multiscale molecular simulation studies of the aggregation of PEO-tethered C-60 fullerenes in water. Our simulations reveal that adjustment of the attachment pattern and molecular weight of the PEO ligands provides exquisite control of the morphology of the self-associating nanostructures formed through a balance of strong fullerene-fullerene attraction, moderately attractive fullerene-PEO interactions and repulsive steric interactions between the PEO ligands. I will also discuss results of our investigations of the influence of external fields (electrical and shear) on the morphology of the self-assembled fullerene nanostructures in bulk aqueous solution as well as results of simulation studies of the self-association of PEO-tethered fullerenes at air-water interfaces.

***Contributed Papers***

**15:06**

**D25 2 Polymer Models of Interphase Chromosomes*** JOSHUA MARTIN, JANÉ KONDEV, *Martin A. Fisher School of Physics* DEBRA BRESSEN, JAMES HABER, *Rosenstiel Center & Dept. of Bio., Brandeis Univ., Waltham MA 02454* Experiments during interphase, the growth phase of the cell cycle in eukaryotic cells, have shown that parts of chromosomes are tethered to the nuclear periphery[1]. Using a simple polymer model of interphase chromosomes that includes tethering, we compute the probability distribution for the distance between two marked points on the chromosome. These calculations are inspired by recent experiments with two or more fluorescent markers placed along the chromosome[2]. We demonstrate how experiments of this kind, in conjunction with simpe polymer models, can be used to systematically dissect the spatial organization of interphase chromosomes in the nucleus of living cells. This comparison of theory with experiments has lead to the conclusion that the structure of chromosome III in yeast is consistent with a 10nm-fiber model of chromatin. [1]Wallace F. Marshall. Current Biology, 12, 2002. [2] Kerstin Bystricky, Patrick Heun, Lutz Gehlen, Jörg Langowski and Susan M. Gasser. PNAS, 101(47) 2004

*This work is supported by NSF DMR-0403997. JK is a Cotrell Scholar of the Research Corporation.

**15:18**

**D25 3 Dynamics of Adsorption-Desorption of Linear Polymer Chains to Spherical Nanoparticles: A Monte Carlo Investigation*** PETER J. DIONNE, CATALIN R. PICU, *Mechanical, Aerospace and Nuclear Engineering* RAHMI OZISIK, *Materials Science and Engineering, Rensselaer Polytechnic Institute* Dynamics of attachment/detachment processes of chains to/from spherical fillers in a polymer nanocomposite is investigated by means of numerical simulations using a chemistry-specific model for the polymer. The effects of chain length, chain-to-filler distance, filler radius, and polymer-particle interaction energy on the attachment/detachment processes are studied. It is found that the time a chain is in contact with a filler scales with the number of attached beads as expected from Rouse behavior. A deviation from Rouse behavior is observed at long attachment times where a plateau value in the number of attached beads is observed. This deviation was found to depend on the relative size of the chain and adsorption volume but was not related to entanglement effects. Changing the polymer-particle interaction energy from repulsive to attractive slows down the detachment process. An average characteristic detachment time was calculated as a function of polymer-particle interaction energy that follows an Arrhenius equation, where the activation energy is proportional to the polymer-particle interaction energy.

*This material is based upon work supported in part by Procter & Gamble and by the National Science Foundation under Grant 0310596.

**15:30**

**D25 4 Manipulating assembly of nanoparticles by polymer tethers** ZHENLI ZHANG, MARK HORSCH, CHRISTOPHER IACOVELLA, SHARON GLOTZER, A major challenge in nanoscience and nanotechnology is the ability to control and guide the self-assembly of nano building blocks into target structures in a predictable way. In this talk, we use molecular simulation to show how polymer tethers can be used to manipulate the assembly of nanoparticles into various one-dimensional, two-dimensional, and three-dimensional structures. We present results on the self-assembly of polymer-tethered nanospheres, nanorods, and more exotic shapes, and present temperature versus concentration phase diagrams for the nanosphere and nanorod systems. For polymer-tethered nanorods we predict tetragonally perforated lamellar and honeycomb phases, which have been observed experimentally but have not been predicted by any previous theory. We also predict a new phase—a racemic mixture of hexagonally ordered chiral cylinders that self-assemble from these achiral building blocks. For the system of polymer-tethered nanospheres we predict that in contrast to flexible amphiphiles, the nanospheres are locally ordered and there is an increase in the local ordering with an increase in concentration or relative nanoparticle diameter. [1] Zhang, Mark A. Horsch, Monica H. Lamm, and Sharon C. Glotzer, itNano Lett., 3(10), 1341-1346, 2003. [2] Mark A. Horsch, Zhenli Zhang and Sharon C. Glotzer, itPhys. Rev. Lett., 95(5), 056106, 2005. [3] Christopher R. Iacovella, Mark A. Horsch, Zhenli Zhang and Sharon C. Glotzer, itLangmuir, 21(21), 9488, 2005.

**15:42**

**D25 5 Phase behavior and clustering of nanoparticles with approximate polymer interactions** ANDREW RAHEDI, FRANCIS STARR, *Wesleyan University* In nanoparticle polymer composite (NPC) materials, the clustering or dispersion of the nanoparticles strongly influences the material properties. The purpose of this study is to better understand the factors that influence nanoparticle clustering as a step towards developing more efficient simulation approaches. To understand the clustering of nanoparticles in an NPC, we simulate both pure nanoparticles and nanoparticles with approximate polymer interactions and compare our results with simulations that include explicit polymer interactions. We find that pure nanoparticles without polymeric interactions undergo ordinary phase separation. Thus the previously observed lack of nanoparticle phase separation in an NPC is due to interactions with the polymer matrix; this interaction includes short-range attractions due to monomer interactions and long-range repulsions due to the excluded volume of the chains. We approximate this interaction by including a Yukawa potential as a weak long-ranged repulsion acting between nanoparticles. Since the simulation of an NPC is computationally expensive due to the polymer-polymer interactions, this approach improves the efficiency of our simulations and enables us to study the thermodynamic properties over a much broader range of conditions.

**15:54**

**D25 6 Stable Bicontinuous Polymer Blend Films by Jamming Nanoparticles at the Interface** RUSSELL J. COMPOSTO, HYUN-JOONG CHUNG, *MSE and LRSM, U. of Pennsylvania* KOHJI OHNO, TAKESHI FUKUDA, *ICR, Kyoto U.* Polymer blends containing nanoparticles (NP) are attractive functional material for optoelectronic devices, chemical sensors, and nanoreactors. Because structure governs performances of these devices, a self-regulating, stable structure is highly desirable for many applications. Adding surface-modified silica NP to dPMMA:SAN (50:50) films (550 nm), we demonstrate that directed interfacial segregation of NP stabilize either three dimensional (3D) interpenetrating or 2D discrete structures at high and low volume fractions of NP, respectively. A simple interfacial energy argument provides a general guideline for predicting whether the NP are directed into one phase or to the interface between phases. If NP partition into one phase, the structural evolution slows down, but phase coarsening continues resulting in a roughened film [Europhys. Lett. (2004) **68**, 219]. However, if NP are driven to the interface between phases, phase coarsening ceases when NP jamming occurs at the interface. The final morphology and domain size can be predicted from the volume fraction of NP, film thickness, and NP size [Nano Lett. (2005) **5**, 1878]. These studies show that wetting and domain coarsening in polymer blend films can be controlled by the judicial addition of surface modified NP.

**16:06**

**D25 7 Directed self-assembly of nanoscale building blocks through coded bonding potentials** JASON J. BENKOSKI, RONALD L. JONES, JACK F. DOUGLAS, ALAMGIR KARIM, *National Institute of Standards and Technology* Herein we investigate the competition among the forces that drive the assembly of nanoscale building blocks, the results of which lay the groundwork for complex, hierarchichal topologies like those seen in Nature. We observed the self assembly of various nanoscale building blocks at the interface between water and a photocrosslinkable oil (dodecanediol dimethacrylate, DMA). While both liquids have a low viscosity at room temperature, DMA can be flash cured with UV light in the presence of a photoinitiator to produce a solid in less than 1 s. Such crosslinking allows one to obtain a ''snapshot'' of the self-assembly process for particles that segregate to the oil/water interface. Among the particles investigated were 400 nm

PMMA latex spheres, 10 nm quantum dots, multi-walled carbon nanotubes, and colloidosomes. Micrographs of each experiment were then captured using either an atomic force microscope (AFM) or light optical microscope (LOM). The agglomerates formed by this process were typically either globular or fractal-like in appearance. By comparing with theory and simulation, we argue that the geometry of the aggregates is coded directly in the particles through the symmetry of the bonding potentials.

**16:18**

**D25 8 Selective trapping nanoparticles on an adaptive, topographic surface** SHU YANG, YING ZHANG, SHUHUI QIN, *Materials Sci. and Eng., Univ. of Pennsylvania* JOHN A. TAYLOR, JOANNA AIZENBERG, *Bell Labs, Lucent Technologies* Control of interfacial properties, such as wettability, adhesion, and friction, is of great importance for both fundamental science and practical applications. One of the major challenges is how to spatially control the molecular recognition in different regions of surface and interface. Here, we report selective trapping and repelling of particles at different locations of a topographic substrate. It is achieved by tuning surface from highly hydrophobic to superhydrophilic within a narrow temperature window ( $= sim 10°C$). A thin layer ( $\sim$ 10 nm) of thermoresponsive polymer brushes from poly(N-isopropylacrylamide) (PNIPA) were ''grafted from'' the tips or everywhere on the micropost arrays (1 micron in diameter, 10 micron tall and 1 micron pitch), using surface- initiated atom transfer radical polymerization (ATRP). PNIPA has a lower critical solution temperature (LCST) of 32°C in water and becomes increasingly hydrophobic when heated from room temperature to 40°C. Above 40°C, the surface is highly hydrophobic (contact angle of 120-135 degree) on the microposts, which repels the hydrophilic silica particles. At room temperature, the surface becomes superhydrophilic (contact angle $<$ 10 degrees). The silica particles are found selectively trapped either on the tips, the bottom, or homogeneously along the microposts, depending on the particle size (900 nm vs. 90 nm), type of brushes (single vs. binary brushes), and the grafting location of PNIPA.

**16:30**

**D25 9 Wetting of polymer thin films with nanoparticles** IGAL SZLEIFER, *Purdue University* We theoretically study the ability of nanoparticles to induce wetting of polymer thin films on flat solid surfaces. Our studies show that there is an entropically driven attraction between the nanoparticles and the surface. The strength and range of the attraction depends upon the polymer melt molecular weight and the nanoparticles size. When the nanoparticles are mixed with the polymer melt and the film is put in contact with the surface, a very large number of nanoparticles adsorb on the surface, lowering the surface tension and enabling the wetting of the surface by the polymer melt. If the surface is modified with a grafted polymer layer of the same type as the polymer melt, nanoparticle adsorption on the surface is reduced for intermediate tethered polymers surface coverage. For high grafted surface coverage we predict a large adsorption of nanoparticle on the tip of the brush. As a result we find that nanoparticle induces wetting of polymer thin films on bare surfaces and on surfaces with grafted polymers at high surface coverage. These are the two regimes where experiments have shown that polymer thin films do not wet the surfaces. The predictions of the theory will be put in the context of available experimental observations.

**16:42**

**D25 10 The Effects of Supercritical $CO_2$ and Nanoparticles on Metallization of Polymer Thin Films*** B. KUGLER, *Jericho High School* F. SHAIKH, *Half Hollow Hills West* J. ROSENGARD, *Half Hollow Hills East* R. HOLZER, *Rambam Mestiva* J. JEROME, T. KOGA, M. RAFAILOVICH, J. SOKOLOV, *Stony Brook Univerisity* Thin films of Poly (methyl methacrylate), Polystyrene (PS), and Ethylene Vinyl Acetate (EVA) were metallized by vapor deposition of chromium (Cr). The surface morphology was analyzed using atomic force microscopy and correlated to the interfacial width between the polymer and metallized layers. The results showed that in all cases exposure of the substrates to supercritical $CO_2$ resulted in doubling the interfacial width between the metal and polymer. This was in turn manifested by a reduction of the RMS roughness and surface contact angles. Metallization of films containing nanoparticles was also performed. The results showed that the addition of POSS-PMMA particles dramatically reduced the RMS roughness for PMMA and EVA while increasing it for PS. Addition of Au nanoparticles decreased the roughness for EVA and PS. X-ray reflectivity indicated that the Au nanoparticles segregated to the surface thereby providing a wetting layer for the Cr. A model to explain these effects based or preferential surface segregation of nanoparticles for films exposed to supercritical fluids will be represented.

*This work was supported by NSF (the Garcia MRSEC) and by the SRC-NY CAIST funding (2005-KC-1292-012).

**16:54**

**D25 11 Optimal Confinement for Internal Polymer Binding** NAM-KYUNG LEE, *Department of Physics/Sejong University* CAMERON ABRAMS, *Department of Chemical and Biological Engineering/Drexel University* ALBERT JOHNER, *Institut Charles Sadron* Internal binding between specific groups dilute along a polymer chain plays a paramount role in many technological and biological systems. Against common intuition, we show that the interplay between excluded volume correlations and hydrodynamic interactions can produce an optimal confinement where the binding is fastest. Similarly there is an optimal osmotic pressure for the binding rate of a chain immersed in a solution of (non-binding) spectator chains. When internal binding leads to higher order vertices as in self-assembly, confinement can set the same kinetic rate for the formation of several low order vertices.

**SESSION D26: FOCUS SESSION: DYNAMICS OF NUCLEI ACID-PROTEIN INTERACTION: SINGLE MOLECULE**
**Monday Afternoon, 13 March 2006; 323, Baltimore Convention Center at 14:30**
**Mark C. Williams, Northeastern University, presiding**



*Invited Papers*

**14:30**
**D26 1 Probing Nucleosome Remodeling by Unzipping Single DNA Molecules.**
MICHELLE WANG, *Cornell University*

At the core of eukaryotic chromatin is the nucleosome, which consists of 147 bp of DNA wrapped 1.65 turns around an octamer of histone proteins. Even this lowest level of genomic compaction presents a strong barrier to DNA-binding cellular factors that are required for essential processes such as transcription, DNA replication, recombination and repair. Chromatin remodeling enzymes use the energy of ATP hydrolysis to regulate accessibility of the genetic code by altering chromatin structure. While remodeling enzymes have been the subject of extensive research in recent years, their precise mechanism remains unclear. In order to probe the structure of individual nucleosomes and their remodeling, we assembled a histone octamer onto a DNA segment containing a strong nucleosome positioning sequence. As the DNA double helix was unzipped through the nucleosome using a feedback-enhanced optical trap, the presence of the nucleosome was detected as a series of dramatic increases in the tension in the DNA, followed by sudden tension reductions. Analysis of the unzipping force throughout the disruption accurately revealed the spatial location and fine structure of the nucleosome to near base pair precision. Using this approach, we investigate how remodeling enzymes may alter the location and structure of a nucleosome.

*Contributed Papers*

**15:06**
**D26 2 Binding Study of T7 Gene 2.5 Protein to Single- and Double−Stranded DNA from Single Molecule Stretching**
LEILA SHOKRI, *Department of Physics, Northeastern University* BORIANA MARINTCHEVA, *Department of Biological Chemistry and Molecular Pharmacology, Harvard Medical School* CHARLES C. RICHARDSON, *Department of Biological Chemistry and Molecular Pharmacology, Harvard Medical School* MARK C. WILLIAMS, *Department of Physics, Northeastern University* Bacteriophage T7 gene 2.5 protein binds preferentially to single-stranded DNA. This property is essential for its role in DNA replication, recombination, and repair. We present the first quantitative study of the thermodynamics and kinetics of equilibrium and non-equilibrium DNA helix destabilization in the presence of gp2.5 and a deletion mutant lacking 26 C-terminal amino acids that binds with higher affinity to ssDNA (gp2.5-delta26C). Our measured force-extension curves of lambda-DNA in the presence of these proteins suggest strong cooperative binding. By measuring the DNA melting force as a function of time and pulling rate, we obtained binding site size and the association constants of these proteins to ssDNA and dsDNA, over a range of salt and protein concentrations. The results are used to characterize the electrostatic interactions that determine the DNA-protein binding in each case.

**15:18**
**D26 3 Dynamics of Protein-DNA Interactions probed with Laser Temperature-Jump and Time-Resolved FRET Measurements.** SERGUEI KUZNETSOV, *UIC* PAULA VIVAS, *UIC* SAWAKO SUGIMURA, *Yale* DONALD CROTHERS, *Yale* ANJUM ANSARI, *UIC* In many protein-DNA complexes, the DNA is often bent or sharply kinked. In order to elucidate the energetics of the binding mechanism it is necessary to study the dynamics of the binding and bending of DNA. Previous kinetics measurements failed to resolve DNA bending on the millisecond time-scales of stopped-flow techniques. Here we report measurements on the binding of IHF, an architectural protein from itE. coli, to its native H' substrate end-labeled with FRET pair to monitor the DNA bending. Stopped-flow measurements show relaxation kinetics that become concentration independent at high IHF concentrations, suggesting that under these conditions, the DNA bending becomes rate-limiting. To test this interpretation, we use a laser temperature-jump to perturb the IHF-H' complex, and to probe the dynamics with submillisecond time-resolution. These measurements support a sequential model for DNA binding and bending to IHF. The time-scales for DNA bending, when in complex with the protein, are not inconsistent with thermal fluctuations that can spontaneously bend DNA.

**15:30**
**D26 4 Inferring the itin vivo looping properties of DNA.** JOSE VILAR, *Memorial Sloan-Kettering Cancer Center* LEONOR SAIZ, *Memorial Sloan-Kettering Cancer Center* MIGUEL RUBI, *University of Barcelona* The free energy of looping DNA by proteins and protein complexes determines to what extent distal DNA sites can affect each other [1]. We inferred its itin vivo value through a combined computational-experimental approach for different lengths of the loop [2] and found that, in addition to the intrinsic periodicity of the DNA double helix, the free energy has an oscillatory component with about half the helical period. Moreover, the oscillations have such an amplitude that the effects of regulatory molecules become strongly dependent on their precise DNA positioning and yet easily tunable by their cooperative interactions. These unexpected results can confer to the physical properties of DNA a more prominent role at shaping the properties of gene regulation than previously thought. [1] J.M.G. Vilar and L. Saiz, Current Opinion in Genetics & Development, 15, 136-144 (2005). [2] L. Saiz, J.M. Rubi, and J.M.G. Vilar, Proc. Natl. Acad. Sci. USA, 102, 17642-17645 (2005).

*Invited Papers*

**15:42**
**D26 5 DNA kept under tension reveals mechanochemical properties of protein reaction pathways.**
GIJS WUITE, *Vrije Universiteit Amsterdam*

The genetic information of an organism is encoded in the base pair sequence of its DNA. Many specialized proteins are involved in handling DNA, preserving and processing the vast amounts of information on the DNA. In order to do this swiftly and correctly these proteins have to move quickly and accurately along and/or around the DNA. Using model systems such as restriction enzymes and abundant bacterial gene regulators such as H-NS we try to understand the physics (forces, energies, mechanochemistry) behind such DNA processing. We are currently performing single molecule experiments on (non-)specific protein-DNA interactions in general and the organization of the bacterial nucleoid in particular. The experiments aim to elucidate the induced-fit reaction, substrate binding and DNA hydrolysis. Moreover, we are studying the relation between DNA configuration and association rates. The results of these model systems are generalized and though to be applicable to many DNA-protein interactions.



*Contributed Papers*

**16:18**
**D26 6 A Model for Folding and Aggregation in RNA Secondary Structures*** VISHWESHA GUTTAL, RALF BUNDSCHUH, *The Ohio State University* We study the statistical mechanics of RNA secondary structures designed to have an attraction between two different types of structures as a model system for heteropolymer aggregation. The competition between the branching entropy of the secondary structure and the energy gained by pairing drives the RNA to undergo a '*temperature independent*' second order phase transition from a molten to an *aggregated phase*. The aggregated phase thus obtained has a macroscopically large number of contacts between different RNAs. The partition function scaling exponent for this phase is $\theta \approx 1/2$ and the crossover exponent of the phase transition is $\nu \approx 5/3$. The relevance of these calculations to the aggregation of biological molecules is discussed.

*RB is supported by the NSF through grant no. DMR-0404615.

**16:30**
**D26 7 Mechanism of gene-regulating proteins diffusion along DNA: hopping vs. sliding** YAN MEI WANG, *Physics Department, Princeton University* EDWARD COX, *Molecular Biology Department, Princeton University* ROBERT AUSTIN, *Physics Department, Princeton University* It has been a long controversy as whether non-energy-driven proteins diffuse along DNA in the form of hopping or sliding. In the hopping model, the protein jumps on and off DNA frequently while diffusing, switching between 1D and 3D diffusions, and in the sliding model the protein diffuses along DNA basepair by basepair, staying in continuous contact with the DNA. We have investigated the diffusion mechanisms of LacI repressor protein along nonspecific sequences of DNA using single molecule imaging measurements. By studying the standard deviation (SD) of the diffusing LacIs point spread functions, we observed that the SD values in both the longitudinal and transverse directions to DNA elongation to be significantly higher than what can be accounted for by the sliding model. We will show that the large SD values agree with the hopping model.

**16:42**
**D26 8 Protein jamming on DNA** ZEBA WUNDERLICH, *Harvard* MICHAEL SLUTSKY, MEHRAN KARDAR, LEONID MIRNY, *MIT* The mechanisms by which DNA-binding proteins find their sites on DNA have been the subject of intensive research in biophysics. Most theoretical models consider proteins searching naked DNA for their binding sites. In the cell, however, myriads of proteins and protein complexes (*e.g.* nucleosomes) are constantly binding DNA. What is the effect of DNA-bound proteins and nucleosomes on the rate of protein-DNA association and dissociation? Here we study how a protein finds its site on DNA, and how long it stays on its site, considering DNA that is bound by other proteins. The process of association and dissociation is modeled by rounds of 3D diffusion and 1D sliding. We assume that proteins bound to DNA act as reflecting boundaries and obstruct sliding of other proteins. We demonstrate that if the density of proteins on the DNA is above a critical level, a protein's mobility on DNA is significantly reduced, leading to jamming. We find that proteins bound to DNA in the proximity of the specific site can (i) significantly increase the time it takes for the protein to find its site, and (ii) simultaneously increase the time a protein spends on its site. The increase in the residence time of a protein on its site can have important biological implications. Our results are consistent with recent experiments on p53 and the organization of nucleosomes in yeast promoters. The structures of eukaryotic enhancers also suggest that jamming may play a role in the assembly of protein complexes on DNA.

**16:54**
**D26 9 Single-molecule Study of Nucleocapsid Protein Chaperoned DNA Hairpin Structural Dynamics** YINING ZENG, *Department of Chemistry and Biochemistry, University of Texas at Austin* GONZALO COSA, *Department of Chemistry, McGill University* HSIAO-WEI LIU, CHRISTY LANDES, DMITRII MAKAROV, PAUL BARBARA, *Department of Chemistry and Biochemistry, University of Texas at Austin* KARIN MUSIER-FORSYTH, *Department of Chemistry, University of Minnesota* In HIV-1 reverse transcription, the nucleocapsid protein, NC, induces secondary structure fluctuations in the transactivation response (TAR) region of DNA and RNA hairpins. Time resolved single-molecule fluorescence resonance energy transfer was used to study NC chaperoned secondary fluctuations of DNA hairpins. The experiments reveal that the NC induced secondary fluctuations are limited to the terminal stems, and the mechanism for the fluctuations is complex. The dynamic processes occur over a wide time range, i.e. $\sim$ 5 to $>$ 250 milliseconds and involve long-lived inter-

mediates. The dynamic role of DNA loop regions and NC binding/dissociation events are discussed.

**17:06**
**D26 10 Mechanism of Nucleic Acid Chaperone Function of Retroviral Nuceleocapsid (NC) Proteins** IOULIA ROUZINA, MY-NUONG VO, KRISTEN STEWART, KARIN MUSIER-FORSYTH, MARGARETA CRUCEANU, MARK WILLIAMS, *Northeastern University* U OF M TEAM, NORTHEASTERN TEAM, Recent studies have highlighted two main activities of HIV-1 NC protein contributing to its function as a universal nucleic acid chaperone. Firstly, it is the ability of NC to weakly destabilize all nucleic acid,(NA), secondary structures, thus resolving the kinetic traps for NA refolding, while leaving the annealed state stable. Secondly, it is the ability of NC to aggregate NA, facilitating the nucleation step of bi-molecular annealing by increasing the local NA concentration. In this work we use single molecule DNA stretching and gel-based annealing assays to characterize these two chaperone activities of NC by using various HIV-1 NC mutants and several other retroviral NC proteins. Our results suggest that two NC functions are associated with its zinc fingers and cationic residues, respectively. NC proteins from other retroviruses have similar activities, although expressed to a different degree. Thus, NA aggregating ability improves, and NA duplex destabilizing activity decreases in the sequence: MLV NC, HIV NC, RSV NC. In contrast, HTLV NC protein works very differently from other NC proteins, and similarly to typical single stranded NA binding proteins. These features of retroviral NCs co-evolved with the structure of their genomes.

**17:18**
**D26 11 Fis protein induced λF-DNA bending observed by single-pair fluorescence resonance energy transfer** FU CHI-CHENG, *Institute of Atomic and Molecular Science, Academia Sinica,Taipei, Taiwan* FANN WUNSHAIN, *Institute of Atomic and Molecular Science, Academia Sinica,Taipei, Taiwan* YUAN HANNA S., *Institute of Molecular Biology, Academia Sinica,Taipei, Taiwan* Fis, a site-specific DNA binding protein, regulates many biological processes including recombination, transcription, and replication in E.coli. Fis induced DNA bending plays an important role in regulating these functions and bending angle range from ~ 50[r] to 95 [r] dependent on the DNA sequence. For instance, the average bending angle of λF-DNA (26 bp, 8.8nm long, contained λF binding site on the center) measured by gel mobility shift assays was ~ 94 [r]. But the traditional method cannot provide information about the dynamics and the angle distribution. In this study, λF-DNA was labeled with donor (Alexa Fluor 546) and acceptor (Alexa Fluor 647) dyes on its two 5' ends and the donor-acceptor distances were measured using single-pair fluorescence resonance energy transfer (sp-FRET) with and without the present of Fis protein. Combing with structure information of Fis-DNA complex, the sp-FRET results are used to estimate the protein induced DNA bending angle distribution and dynamics.



## SESSION D27: FOCUS SESSION: NOVEL COMPUTATIONAL ALGORITHMS I
**Monday Afternoon, 13 March 2006; 324, Baltimore Convention Center at 14:30**
**Francois Gygi, University of California, Davis, presiding**

***Invited Papers***

**14:30**
**D27 1 Linear scaling techniques for the solution of the time-dependent Schrödinger equation.***
SUXING HU, *Los Alamos National Laboratory*

An efficient, accurate solution of the time-dependent linear/nonlinear Schrödinger equation (TDSE) is required for a wide variety of problems in physics and chemistry. These include the dynamics of atoms and molecules in intense/ultrashort external fields, time-dependent approaches to atomic collisions, the dynamics of ultracold media such as Bose-Einstein Condensates and plasmas, and the behavior of materials under extreme conditions. Various techniques have been developed for this purpose. We shall describe a new approach in which the Finite Element Discrete Variable Representation (FEDVR) is combined with the Real-Space Product (RSP) algorithm to generate a highly effective procedure (RSP-FEDVR) for solving the TDSE on supercomputers. Emphasis will be placed on the complete formalism and the implementation of parallelization within the Message-Passing-Interface (MPI) scheme on large, distributed-memory supercomputer clusters. Its superior performance will be illustrated by a number of three-/four-dimensional problems, in comparison to the conventional finite-difference (FD) methods.

*In collaboration with Barry I. Schneider (NSF) and Lee A. Collins (LANL).

***Contributed Papers***

**15:06**
**D27 2 Solution of the Time-Dependent Schroedinger Equation using a Real Space Product Finite Element Discrete Variable Representation (RSPFEDVR)** BARRY SCHNEIDER, *National Science Foundation* LEE COLLINS, SUXING HU, *Los Alamos National Laboratory* A novel approach to the solution of the time-dependent Schroedinger equation using a RSPFEDVR method is described. The method is applied in both a second and fourth order version. In this talk we describe the essential features of the approach and compare the method as to its accuracy and efficiency in a number of model problems. The method may be transparently and efficiently parallelized using MPI as a consequence of the structure of the RSPFEDVR propagator which leads to a minimal number of communications at each step in the propagtion.

**15:18**
**D27 3 A Nonlinear Finite Difference Scheme for the Time-Dependent Schrodinger Equation*** RONALD MICKENS, In general, the time-dependent Schrodinger equation (TDSE) cannot be explicitly solved for an arbitrary boundary and/or initial value

problem. One resolution of this difficulty is to construct discrete models of this equation and use them to calculate numerical solutions. We consider the case of the TDSE, in one space dimension, and demonstrate that a nonlinear finite difference scheme can be formulated. We study its various limiting forms and compare their mathematical properties with those of the corresponding ordinary and partial differential equations. A formal solution is presented for the fully discrete TDSE. We discuss the basis of this nonlinear discretization within the framework of the nonstandard finite difference methodology created by Mickens [1] and the work of Bhattacharya [2]. [1] R. E. Mickens, Nonstandard Finite Difference Models of Differential Equations (World Scientific, Singapore, 1994). [2] M. C. Bhattacharya, Applied Mathematical Modeling 10 (1986), 68-70.

*Research supported in part by a DOE grant.



**15:30**

**D27 4 Efficient Boundary Integral Method for Quantum Billiards** HARALD G.L. SCHWEFEL, *Max Planck Research Group, Optics, Photonics & Information, Erlangen, Germany* HAKAN E. TÜRECI, *Center for Theoretical Physics, Sloane Physics Laboratory, Yale University, New Haven, CT* A. DOUGLAS STONE, *Department of Applied Physics, Yale University, New Haven, CT* Calculating highly excited eigenvalues of the Laplace equation and their corresponding eigenfunctions are of great current interest in many areas. We present an efficient algorithm based on a novel Fredholm formulation of the Laplace eigenvalue problem, in the spirit of the scattering quantization method proposed by the authors in the context of the basis function expansion technique.[1] We also point out the connection to the scaling eigenfunctions[2] and show how this method can be generalized to dielectric cavities.

[1]H. E. Tureci, H. G. L. Schwefel, Ph. Jacquod, and A. Douglas Stone. Modes of wave-chaotic dielectric resonators. *Progress In Optics*, 47, 2005.

[2]A. H. Barnett. Quasi-orthogonality on the boundary for Euclidean Laplace eigenfunctions. *submitted, Comm. Pure Appl. Math.*, 2004

***Invited Papers***

**15:42**

**D27 5 Quantum Computation for Quantum Chemistry.** ALAN ASPURU-GUZIK, *UC Berkeley*

The calculation time for the energy of atoms and molecules scales exponentially with system size on a classical computer, but polynomially using quantum algorithms. We demonstrate that such algorithms can be applied to problems of chemical interest using modest numbers of quantum bits. Calculations of the $H_2O$ and LiH molecular ground-state energies have been carried out on a quantum computer simulator using a recursive phase estimation algorithm. The recursive algorithm reduces the number of quantum bits required for the read-out register from approximately twenty to four. Mappings of the molecular wave function to the quantum bits are described. An adiabatic method for the preparation of a good approximate ground-state wave function is described and demonstrated for stretched $H_2$. The number of quantum bits required scales linearly with the number of basis functions used and the number of gates required grows polynomially with the number of quantum bits.

***Contributed Papers***

**16:18**

**D27 6 The ''Inverse Band Structure ( IBS) Approach'' for designer nanostructures and designer impurities in semiconductors.** ALEX ZUNGER, S. DUDIY, *NREL* While in standard computational physics and chemistry one first defines the molecular or crystalline structure and then computes the ensuing electronic structure and properties, we adopt a reverse approach in which we search for the atomic configuration having a prescribed target property. Using either Simulated Annealing or Genetic Algorithms as search strategies we determine the configuration of groups of Nitrogen atoms having either the deepest or the shallowest level in the GaP gap, or the highest/lowest oscillator-strength for optical absorption. Similar approaches are used to determine the extremal band gaps of alloys and the configuration of Mn atoms in GaAs having the highest Curie temperature. This approach allows one to scan a large number of configurations of e.g, alloys in search of the optimal one with a desired property.If the property is readily calculable, the IBS search is done on-the-fly. If its difficult to calculate ( e.g, Tc of ferromagnets), we first do a cluster expansion,then IBS search. Work supported by DOE-SC-BES-DMS under NREL contract AC3699GO10377.

**16:30**

**D27 7 A Real-Space Genetic Algorithm for Crystal Structure Determination** LUKE ABRAHAM, MATT PROBERT, *University of York* There has been much interest in using genetic algorithms for determining the ground-state structure of clusters [1] and nanowires [2], and more recently silicon surfaces [3]. We present a real-space encoded genetic algorithm which is suitable not only for surface structure calculations, but also for bulk crystal structure determination. This algorithm makes use of a novel crossover technique in the generation of offspring. The method is also suitable as a polymorph search, and is flexible enough that population members can have different supercells. We will present results from a variety of empirical and *ab initio* systems, where all calculations have been performed using the CASTEP [4] code.
[1]D. M. Deaven and K. M. Ho,*Phys. Rev. Lett.*,**75** (1995) 288-291 [2]B. Wang *et al*, *Phys. Rev. Lett.*, **86** (2001) 2046-2049 [3]F. C. Chuang *et al*, *Surf. Sci.*, **573** (2004) L375-L381 [4]M. D. Segall *et al*, *J. Phys.: Cond. Matt.*, **14** (2002) 2717-2743

**16:42**

**D27 8 Traveling the configurational space of binary alloys*** G. TRIMARCHI, S. V. BARABASH, A. ZUNGER, *National Renewable Energy Lab., Golden CO 80401* Binary $A_{1-x}B_x$ alloys can exist in any of the $2^N$ possible configurations on a periodic lattice of $N$ sites. In many areas of the alloy theory one needs to

search all lattice configuration. Such a problem arises, for example, when the $T = 0$ ground state configurations are sought, or in problems of materials design, where it is desirable to scan all the configurations to find the configuration $\sigma^*$ that has specific property. This task is complicated by (i) the huge computational demand for large $N$ and (ii) by the possibility that the $P(\sigma)$ is sensitive to the cell shape. In this talk we present a new computational approach for defining and searching the configurational space, that is based on (i) the exhaustive *enumeration* of the ''Inequivalent Cell Shapes,'' and, for a given cell shape on (ii) the *sampling* of the related ''Same-Shape-Structures'' via a Genetic Algorithm. We apply this procedure to few ground state problems in semiconductor and metal alloys: For $(AC)_x(BC)_{1-x}$ tetrahedral semiconductor alloys we predict the lattice configurations of minimum bond-bending and bond-stretching strain both in free-floating bulk and under the epitaxial strain. We show that the chalcopyrite structure remains a ground state even under epitaxy. For Au-Pd alloy modelled with the mixed basis cluster expansion Hamiltonian, we determine the ground state structures and compare the convex hull to the one found previously by the direct enumeration approach.

*Funded by DOE-SC-BES-DMS

**16:54**

**D27 9 Simulating Charged Systems with the Geometric Cluster Algorithm** STEPHEN BARR, ERIK LUIJTEN, *University of Illinois at Urbana-Champaign* The recently introduced generalized geometric cluster algorithm (GCA) for colloidal suspensions [J. Liu and E. Luijten, Phys. Rev. Lett.**92**, 035504 (2004)] is extended to systems with electrostatic interactions. The Ewald summation is used to determine the pair potentials. However, the resulting pair potentials cannot be used directly in the GCA because the long range nature of the electrostatic potential causes all particles to be included in a cluster. In our new method, the cluster size is therefore controlled by using only the real-space part of the potential during cluster construction, then accepting or rejecting the cluster move based on the part of the internal energy that is computed in Fourier space. Although the resulting algorithm is, in contrast with the original approach, no longer rejection-free, it is possible to perform collective nonlocal moves while maintaining a significant acceptance ratio. The method is particularly beneficial for systems containing components with large size asymmetries, such as suspensions of charged colloids in the presence of salt.

**17:06**

**D27 10 Multi-physics/scale simulations using particles** PETROS KOUMOUTSAKOS, *ETH Zurich* Particle simulations of continuum and discrete phenomena can be formulated by following the motion of interacting particles that carry the physical properties of the systems that is being approximated (continuum) or modeled (discrete) by the particles. We identify the common computational characteristics of particle methods and emphasize their key properties that enable the formulation of a novel, systematic framework for multiscale simulations, that can be applicable to the simulation of diverse physical problems. We present novel multiresolution particle methods for continuum (fluid/solid) simulations, using adaptive mesh refinement and wavelets, by relaxing the grid-free character of particle methods and discuss the coupling of scales in continuum-atomistic flow simulations.

**17:18**

**D27 11 Algorithmic Refinements for Multicanonical System Measurements** DAVID YEVICK, TAO LU, DEREK DUMAS, MICHAEL REIMER, WITOLD BARDYSZEWSKI, BRETT HAMILTON, *University of Waterloo* We have adapted, to our knowledge for the first time, multicanonical sampling and its Wang-Landau extension to the analysis of the statistics of communication systems, and by extension, arbitrary stochastic physical systems.[D. Yevick, ''A First Course in Computational Physics and Object Oriented Programming with C++'', Cambridge University Press, Ch. 22 and references] Subsequently, we applied the technique experimentally with and without a novel biasing procedure for the intermediate pdf distributions that significantly enhances the statistics in selected regions of system variables. [T. Lu, D. Yevick et. al.**,** IEEE Photon. Technol. Lett, **17**, 1420 (2005) and to be published]. Here we additionally discuss procedures that (1) bias the statistical samples by raising the estimated pdf to a power (2) combine intermediate results in a manner identical to that employed in importance sampling (3) incorporate non-uniform Markov chain displacements and (4) interpolate the histogram and pdf values during iterations. These significantly impact experiments with a restricted number of samples.[D. Yevick et. al., submitted to J. Opt. Soc. Am. A]



**SESSION D28: BLOCK COPOLYMER THIN FILMS**
**Monday Afternoon, 13 March 2006**
**325, Baltimore Convention Center at 14:30**
**Travis Bailey, Colorado State University, presiding**

**14:30**

**D28 1 Tuning Surface Interactions to Control Thin Film Block Copolymer Orientation** ALAMGIR KARIM, RONALD JONES, DUANGRUT JULTHONGPIPUT, MICHAEL FASOLKA, ERIC AMIS, *Polymers Division, NIST* SUSHIL SATIJA, *Center for Neutron Research, NIST* SUSHIL SATIJA COLLABORATION, We tune polymer-substrate surface interactions in order to control the orientation and ordering of diblock copolymers of polystyrene – polymethylmethacrylate (PS-b-PMMA) ultrathin films. To this end we utilize UV to alter the surface energy of a SAM coated substrate and anneal spin coated thin films of high molecular weight (approx. 50kDa) PS-b-PMMA. We have previously utilized a combinatorial approach of substrate surface energy vs. diblock film thickness to map out the distribution of surface topography measured by optical microscopy (such as island and hole formation regions), and observed a switch in symmetry of topography with surface energy variation across a ''neutral'' region. In the present work, we report results pertaining to the neutral surface energy substrate conditions. We utilize AFM, neutron reflection, SEM and TEM to characterize the morphology of ordered structures on the controlled surface energy substrates. The advantage of the present work is the relative ease of surface energy control with UV and the tunability of surface energy to potentially match neutral boundary conditions for a broad set of block copolymers with different chemical blocks components.

**14:42**

**D28 2 Internal and Interface Structure in Diblock Copolymer Brushes** MARK D. FOSTER, BULENT AKGUN, GOKCE UGUR, WILLIAM J. BRITTAIN, *Maurice Morton Institute of Polymer Science, The University of Akron, Akron, OH 44325* XUEFA LI, DONG RYEOL LEE, JIN WANG, *Experimental Facilities Division, Argonne National Laboratory, Argonne, IL 60439* Internal and surface structure of polystyrene-*b*-polyacrylate diblock copolymer brushes have been studied using grazing-incidence small-angle X-ray scattering (GISAXS) and atomic force microscopy (AFM). Polystyrene-*b*-polyacrylate or polyacrylate-*b*-polystyrene brushes were synthesized using atom transfer radical polymerization. Poly (methylacrylate) or poly (*n*-butyl acrylate) is used as the acrylate block. Each as-deposited diblock brush show an internal lateral structure with a spacing comparable to the thickness of the top layer of the brush on the order of 10 nm. After a brush is treated with a selective solvent which is a good or theta solvent for the bottom block and poor solvent for the top block, Bragg rods appear in GISAXS pattern. The lateral spacing corresponding to the Bragg rods is on the order of the total thicknesses of the brushes. This lateral correlation is also detected by the power spectral density analysis of the AFM measurements of the samples' surfaces using tapping mode imaging. The Bragg rods disappear upon heating to 80 [r]C and this behavior does not depend on which polyacrylate block was used.

**14:54**

**D28 3 Internal Morphology of Diblock Copolymer Brushes Determined by Neutron Reflectivity.** BULENT AKGUN, WILLIAM J. BRITTAIN, MARK D. FOSTER, *Maurice Morton Institute of Polymer Science, The University of Akron, Akron, OH 44325* CHARLES F. MAJKRZAK, *National Institute of Standards and Technology, Gaithersburg, Maryland 20899* Although diblock copolymer brushes (BCB) have been extensively studied in recent years, their internal structure is still unknown. To elucidate the interface width and internal structure of BCBs, neutron reflectivity (NR) has been used. BCBs of deuterated polystyrene (dPS) and poly(methyl acrylate) (PMA) with dPS adjacent to the surface (d-PS-*b*-PMA) or with PMA adjacent to the surface (PMA-*b*-dPS) and having different thicknesses were synthesized using atom transfer radical polymerization. In ultrathin BCBs a gradient in composition perpendicular to the surface extends essentially through the entire thickness of the brush. The interface width, defined as the full-width at half-maximum of a Gaussian function needed to represent the broadening of the step interface profile, is found to be smaller for PMA-*b*-dPS than for dPS-*b*-PMA brushes. The interface width for a film spun from untethered chains of dPS-b-PMA has been measured and the results compared with those for the BCBs. BCBs have been measured in both good solvent and poor solvent vapors with NR and the concentration profiles and extent of swelling determined.

**15:06**

**D28 4 Resonant X-Ray Scattering in Block Copolymer Thin Films** JUSTIN VIRGILI, *University of California, Berkeley* JEFFREY KORTRIGHT, *Lawrence Berkeley National Laboratory* NITASH BALSARA, RACHEL SEGALMAN, *University of California, Berkeley* Resonant x-ray scattering in a transmission geometry is reported in block copolymer films for the first time. By tuning soft x-rays to the carbon $\pi^*$-$\pi^*$ bonds in a poly(styrene-b-isoprene) (PS-PI) diblock copolymer thin film, the scattering intensity is enhanced, thereby overcoming the small scattering volume inherent to a thin film geometry. This technique provides an alternative polymer thin film characterization technique to GISAXS that shares the same benefit of averaging over large sample areas (100's $\mu$m x 100's $\mu$m). The characterization of large sample areas is not readily accessible via real-space characterization techniques, such as TEM and AFM, and is of growing importance to applications such as optoelectronic devices. We will demonstrate the use of the resonant x-ray scattering technique in thin films of PS-PI and will demonstrate the effects block copolymer composition and film thickness on the observed scattering profiles. We will also compare our results from resonant x-ray scattering to TEM and AFM data.

**15:18**

**D28 5 The development of order in ultra-thin PS-PMMA diblock copolymer films.** WARD LOPES, HAI QIAN, GENE MAZENKO, HEINRICH JAEGER, *James Franck Institute, The University of Chicago* Knowledge of how two dimensional systems order is important for techniques like hierarchical self-assembly or diblock copolymer lithography. The applicability of these techniques can be limited by the defects which influence the late stage of ordering. Further, one would like to know whether or not the qualitative features of ordering depend only on the symmetry of the system. We address these concerns by studying the growth of order in weakly-segregated, cylindrical-phase, PS-PMMA diblock copolymer films. Our samples have smectic (striped) symmetry and form a single layer of half-cylinders with more than $10^5$ repeat spacings. We have found qualitative differences between our results and results reported on strongly segregated cylindrical-phase diblock copolymer films(1). We find, for example, that the number of dislocations and disclinations are approximately equal and that grain boundaries persist for long times. We are using time lapse atomic force microscopy to track disclination dipole, tripole, and quadrupole annihilations and will report on the relative frequency of each. We will compare our results with numerical simulations of the Swift-Hohenberg Model. (1) Harrison et. al. Science, **290**, 1558 (2000); Harrison et. al. Phys. Rev. E, **66**, 11706 (2002).

**15:30**

**D28 6 Thickness Dependent Packing Symmetries of Spherical-Domain Block Copolymer Multilayers** G.E. STEIN, E. COCHRAN, G.H. FREDRICKSON, E.J. KRAMER, *UCSB* X. LI, J. WANG, *ANL* The packing of spherical block copolymer domains confined to a thin film is investigated with grazing-incidence small angle x-ray scattering. Whereas the equilibrium structure of a monolayer is hexagonal (HEX), and that of the bulk is body-centered cubic (BCC), we find a remarkably complex transition from 2D to 3D packing as a function of film thickness. Films 1-3 layers of spheres thick have close-packed hexagonal symmetry. At four layers the hexagonal symmetry breaks to form an orthorhombic phase, characterized by a second-to-first nearest-neighbor distance ratio $a_1/a_2 = 1.08$ with an angle $\phi = 57°$ between $\vec{a}_1$ and $\vec{a}_2$. As the number of layers is increased from 4 to 23, $a_1/a_2$ increases monotonically to 1.17, and $\phi$ decreases monotonically to 54.2°, a structure similar to the stacking of BCC (110) planes. From measurements above and below the polymer critical angle, we determine that all phases are uniform throughout the depth of the film. These results are interpreted in the context of a Landau-type theory, using SCFT calculations to demonstrate the competition between the packing preferred in the bulk with that at the interfaces.

**15:42**

**D28 7 Effect of chain architecture and surface energies on the microdomain orientation in block copolymer films** V. KHANNA, E. J. KRAMER, E. W. COCHRAN, G. H. FREDRICKSON, *UCSB* X. LI, J. WANG, *Argonne National Lab* S. F. HAHN, *Dow Chemical Company* We investigate the effect of surface energy and chain architecture on the orientation of microdomains in relatively thick films ( 600nm) of lamellar and cylindrical block copolymers of poly(vinylcyclohexane)(C) and poly(ethylene)(E). The E block has 26 ethyl branches per 1000 backbone carbon atoms. Melt surface energies of the C and E blocks are 22.3 and 20.9 $mJ/m^2$, respectively. GISAXS, SFM and cross sectional TEM show that cylindrical and lamellar CEC triblock copolymers orient their microdomains normal to the surface through the film thickness. However, a lamellar CE diblock prefers a parallel orientation of the sheets with an E surface. Moreover, a cylindrical CEBC triblock copolymer where the EB block has 125 ethyl branches per 1000 backbone carbon atoms leads to EB cylinders that always orient parallel to the surface. In this case the lower surface energy EB block dominates the surface. Self-consistent field theory calculations allow us to interpret the experimental results in terms of the entropic cost of forming a wetting layer comprised entirely of looping blocks. Thus in triblock copolymers, parallel orientations are only stabilized when the surface energy of the midblock is low enough to compensate for this conformational penalty, which is absent in diblock copolymers.

**15:54**

**D28 8 Symmetry Breaking In Block Copolymer Thin Films** ERIC COCHRAN, *Iowa State University* KIRILL KATSOV, GILA STEIN, ED KRAMER, GLENN FREDRICKSON, *University of California, Santa Barbara* Recent experiments by Stein and Kramer show that thin films of poly(styrene-b-vinylpyridine) diblock copolymer undergo a discontinuous transformation from hexagonally-close packed spheres to a Fmmm orthorhombic packing as the thickness of the film is increased; beyond the hcp-Fmmm transition, the unit cell deforms to asymptotically approach bcc symmetry, which is preferred in the bulk system. We use a Landau-type theory to construct various scenarios of symmetry-breaking in this system. High resolution SCFT calculations show the nature of the competition between the preferred packing in the bulk and that at the interface. We conclude that character of the transition from thin-film to bulk behavior may be either continuous or discontinuous, depending on the bulk properties of the block copolymer and the surface energy.

**16:06**

**D28 9 Ion Complexation in Salt Containing Block Copolymer Thin Films** MATTHEW MISNER, *University of Massachusetts* SEUNG HYUN KIM, *Inha University* LING YANG, *University of Massachusetts* THOMAS RUSSELL, *University of Massachusetts* Ion complexation within cylinder-forming PS-b-PEO thin films was investigated, where added salts bound the PEO block as the minor component. Small amounts of added salts, on the order a few ions per chain, show large effects on the ordering and orientation of the copolymer films during solvent annealing, a process where we have shown a large degree of long-range lateral order can be obtained. The orientation of the cylindrical microdomains was found to strongly depend on salt concentration and the nature of the counter ion. Furthermore, with the addition of relatively large amounts of salts, we observed that the copolymer microdomains remained ordered at a high degree of swelling and an extremely large amount of lateral spatial correlations of the cylindrical microdomains was found in the swollen state, as observed by grazing incidence small angle scattering. By using gold or cobalt salts, well-organized patterns of nanoparticles were generated in the copolymer microdomains after the reduction of the corresponding salts.

**16:18**

**D28 10 Homopolymer Penetration on Crosslinked Copolymer Mat** DU YEOL RYU, *Yonsei University* JIA-YU WANG, *UMASS-Amherst* ERIC DROCKENMULLER, *UCSB* KRISTOPHER LAVERY, *UMASS-Amherst* CRAIG HAWKER, *UCSB* THOMAS RUSSELL, *UMASS-Amherst* UMASS-AMHERST COLLABORATION, UCSB COLLABORATION, Ultra-thin films of benzocyclobutene (BCB)-functionalized random copolymers of styrene and methyl methacrylate were thermally-crosslinked on a substrate, but applicable to other systems, with a controlled thickness. Contact angles measured in nano scale describe that over the critical minimum thickness ( 5.5nm) interfacial interaction of crosslinked random copolymer is well balanced. Neutron Reflectivity has been used to investigate in terms of the penetration of the polymer into crosslinked random copolymer P(S-r-BCB-r-MMA). Thus, to evaluate the critical minimum thickness which is at least required to control over the microdomain orientation of the PS- PMMA block copolymer systematically, deuterated PMMA was spin coated on crosslinked random copolymer controlled with various thickness from 1 to 10 nm. The neutron scattering length densities (SLD) of crosslinked random copolymer are increased with decreasing thickness, which means that the SLD contribution of d-PMMA to BCB layer is getting bigger because thin BCB layer is not enough to cover the SiOx.

**16:30**

**D28 11 Enhanced order in thinfilms of Pluronic (A-B-A) and Brij (A-B) block copolymers blended with poly(acrylic acid)*** VIJAY R. TIRUMALA, BRYAN D. VOGT, HAE-JEONG LEE, ERIC K. LIN, *Polymers Div., NIST* JAMES J. WATKINS, *Polymer Science & Engr. Dept., UMass-Amherst* Pluronic ($PEO_m$-$PPO_n$-$PEO_m$) and Brij ($PEO_m$-$PE_n$) based block copolymer films have recently been used as sacrificial templates for the fabrication of mesoporous low-*k* thinfilms. We have found that the addition of a low molecular weight third component homopolymer exhibiting strong interactions with one of the blocks enhances the local and long-range order of both Pluronic and Brij templates in the melt. In this work, small-angle neutron scattering and x-ray reflectivity were used to investigate the microstructure of block copolymer/poly(acrylic acid) blend templates. In templates where PEO serves as a majority phase, both scattering and reflectivity measurements show that addition of PAA decreases the interfacial width and strengthens domain segregation. In templates with PEO as the minority phase, addition of PAA can induce an order-order transition. Tuning the microphase morphology of block copolymer thinfilms using a low-molecular weight homopolymer additive has many implications for methods that use block copolymer melts as sacrificial templates.

*Financial support from NSF (CTS- 0304159) and Neutron research facilities provided by the NIST Center for Neutron Research, U.S. Department of Commerce are acknowledged.

**16:42**

**D28 12 Ordering transition of block copolymer films under compressed CO2** ABRAHAM ARCEO, PETER F. GREEN, *University of Michigan* It is well-known that a bulk, symmetric, A-b-B diblock copolymer forms a lamellar morphology, with period L, below an order- disorder transition temperature (TODT), for XN $<$ 10.5; X is the Flory-Huggins interaction parameter and N is the degree of polymerization of the copolymer. The ordering temperatures of poly(styrene-b-methyl methacrylate) (PS-b-PMMA) thin film diblock copolymers of thickness ca. 2L, supported by SiOx/Si substrates, in vacuum environments, are shown to increase beyond the bulk, having unusually large shifts of the transition temperature with small changes of XN. We find that in compressed $CO_2$ environments, these films are ordered at temperatures where the films are disordered in vacuum (or air) environments. This latter observation is of particular significance because small molecule diluents, including compressed $CO_2$, are known to decrease the TODT of the bulk (enhanced miscibility). We will discuss these results in light of the thin film compressibility and preferential sorption of the individual blocks at the experimental conditions.

**16:54**

**D28 13 Self-Organization of PS-b-PFOMA Block Copolymer Aggregates in Thin Films** YUAN LI,*LUCIANA MELI,†KEITH JOHNSTON, *Graduate Program of Materials Science and Engineering, Department of Chemical Engineering, The University of Texas at Austin* KWON LIM, *Division of Image and Information Engineering, Pukyong National University, Korea* PETER GREEN, *Department of Materials Science and Engineering, The University of Michigan* SFM, STEM and XPS were employed to study the morphologies of polystyrene-b-poly(1,1',2,2'-tetrahydroperflurooctyl methacrylate) (PS-b-PFOMA) films. The copolymer was dissolved in the co-solvent mixture of Freon 113 and toluene. Upon spin-casting on Si/SiOx substrate, PS-b-PFOMA was found to self-organize into spherical aggregates, where the cores of the spheres were composed primarily of PFOMA and the matrix was composed by PS. However, exposing the films to supercritical $CO_2$ led to a reversed morphology, where spheres of PS were embedded in the matrix of PFOMA. In addition, the degree of ordering was improved in sc-$CO_2$ and the domain size was tuned by adjusting sc-$CO_2$ density. The results were discussed based on the effects of sc-$CO_2$ on the interfacial tension and the relative PS-PFOMA interactions.

*Graduate Program of Materials Science and Engineering
†Department of Chemical Engineering

**17:06**

**D28 14 Scaling of Domain Spacing of Block Copolymers Dilated by High-Pressure Carbon Dioxide** TIMOTHY FRANCIS, BRYAN VOGT, XIAOHUI WANG, JAMES WATKINS, DEPARTMENT OF CHEMICAL ENGINEERING, UNIVERSITY OF MASSACHUSETTS COLLABORATION, POLYMERS DIVISION, NATIONAL INSTITUTE OF STANDARDS AND TECHNOLOGY COLLABORATION, POLYMER SCIENCE AND ENGINEERING DEPARTMENT, UNIVERSITY OF MASSACHUSETTS COLLABORATION, The dependence of the interdomain spacing on the sorbed solvent volume fraction of microphase separated poly(styrene-*b*-dimethyl siloxane) in the high concentration limit was probed using high-pressure carbon dioxide as the diluent. Domain spacing was measured using itin situ small angle neutron scattering, both isothermally and at constant polymer volume fraction. The results indicate that high-pressure $CO_2$ behaves similarly to a selective liquid solvent and that d-spacing is strongly influenced by solvent selectivity, which is a function of temperature for this system. The data also show that the d-spacing as a function of solvent volume fraction cannot be described by the traditional power law scaling that does not account for solvent selectivity, but collapse to a line when scaled by a swelling asymmetry factor. Data measured at constant polymer volume fraction are in good agreement with previously reported findings, and show that the interdomain spacing exhibits power law scaling with the temperature dependent interaction parameter.

**17:18**

**D28 15 Amphiphilic Block Copolymers in Condensed Carbon Dioxide** WILLIAM EDMONDS, *Department of Chemical Engineering and Materials Science, University of Minnesota* TIMOTHY LODGE, MARC HILLMYER, *University of Minnesota* Condensed carbon dioxide represents a promising ''green'' solvent alternative on the basis of its abundance and modest critical conditions. Amphiphilic block copolymers offer the potential of enhancing the versatility and usefulness of this solvent through the formation of micelles. Our goal is to understand and define the parameters that control aggregate shape and dimensions in solution; these parameters include copolymer volume fraction and solvent density. We will present dynamic light scattering and solubility data for a series of polybutadiene-*b*-poly(hexafluoropropylene oxide) and polylactide-*b*-poly(hexafluoropropylene oxide) copolymers. At modest pressures ( $<$ 500 bar), these materials are readily soluble. In addition, initial measurements suggest the formation of non-spherical micelles in solution.

## SESSION D29: MOLECULAR MACHINES AND MOTORS

**Monday Afternoon, 13 March 2006**
**326, Baltimore Convention Center at 14:30**
**Dean Astumian, University of Maine, presiding**

***Contributed Papers***

**14:30**

**D29 1 Processivity of helicase-induced DNA strand separation** M. D. BETTERTON, *University of Colorado* F. JULICHER, *Max Planck Institute for the Physics of Complex Systems* Helicases are molecular motors which unwind double-stranded nucleic acids (dsNA) in cells. Many helicases move with directional bias on single-stranded nucleic acids (ssNA), and couple their directional translocation to strand separation. A simple model of the coupling between translocation and unwinding uses an interaction potential between the helicase and the ss-ds junction which can capture both 'passive' and 'active' mechanisms of NA unwinding. A passive helicase relies on fluctuations which open the dsNA base pairs to advance while its presence on the strand inhibits NA closing. An active helicase directly destabilizes dsNA base pairs where it is bound, thus accelerating the opening rate. Here, we take into account the effects of helicase detachment from the NA strand corresponding to a limited processivity. The average helicase attachment time then depends on the form of the interaction potential.

For a passive helicase the mean attachment time does not change between ss translocation and ds unwinding, while for an active helicase in general a decrease in attachment time occurs during unwinding as compared to ss translocation.

**14:42**
**D29 2 A nanojet: propulsion of a molecular machine by an asymmetric distribution of reaction−products*** TANNIEMOLA LIVERPOOL, *University of Leeds, U.K.* RAMIN GOLESTANIAN, *University of Sheffield, U.K.* ARMAND AJDARI, *ESPCI, Paris, France* A simple model for the reaction-driven propulsion of a small device is proposed as a model for (part of) a molecular machine in aqueous media. Motion of the device is driven by an asymmetric distribution of reaction products. We calculate the propulsive velocity of the device as well as the scale of the velocity fluctuations. We also consider the effects of hydrodynamic flow as well as a number of different scenarios for the kinetics of the reaction.

*Funding from the Royal Society

**14:54**
**D29 3 Twirling of Actin by Myosins II and V** JOHN F. BEAUSANG, *Phyiscs Dept.* HARRY W. SHROEDER, *Biochemistry and Mol. Biophysics* JAMES A. GILMOUR, *Dept of Bioengineering* YALE E. GOLDMAN,* *Pennsylvania Muscle Institute* A polarized total internal reflectance fluorescence microscope was used to measure the 3D orientation of single rhodamine molecules with 40 ms time resolution (Forkey et al., itNature 422:399, 2003). We modified this setup by adding excitation polarizations at $\pm$ 45° relative to the optical axis of the microscope, thus enabling us to uniquely monitor 1/4 of the probe's angular phase space (previously 1/8). Phase shifts in the optics were compensated with an adjustable waveplate. Using actin filaments sparsely labeled with tetramethylrhodamine at Cys-374, the increased range of discernable angles was used to determine the handedness of filament rotation about its axis in a gliding filament assay. During translocation by Myosin II or V, approximately half of the observed actin filaments exhibit a 'twirling' helical path of rotation around the filament axis. Myosin II and V consistently induce a left-handed twirling motion (opposite to the long-pitch helix of actin) with pitch of 1.0 $\pm$ 0.2 $\mu$m for myosin II and 1.5 $\pm$ 0.1 $\mu$mfor myosin V. Several factors may be the cause of this twirling including: the direction of the force vector between actin and myosin, the distribution of myosin binding sites on actin, and cooperation between myosins translocating an individual actin filament. Supported by NIH grant AR26846 and NSF grant DMR04-25780.

*University of Pennsylvania



***Invited Papers***

**15:06**
**D29 4 Synthetic Motors and Nanomachines.**
AMAR FLOOD, *Department of Chemistry, Indiana University*

A bistable and palindromically-constituted [3]rotaxane incorporating two mechanically-mobile rings interlocked around a linear dumbbell component, has been designed to operate like the sarcomeres of skeletal muscle. Contraction and extension occurs when the inter-ring distance of the two rings switch, ideally, between 4.2 and 1.4 nm upon redox stimulation either chemically or electrochemically in the solution phase. When the mobile rings of these artificial molecular muscles are bound onto the tops of gold-coated, micron-scale cantilever beams, their controllable nanometer motions have a chance to be amplified along the long axis of each cantilever. It turns out that $\sim$ 6 billion of the self-assembled [3]rotaxanes can bend the cantilevers in a bistable manner concomitant with the cycled addition of redox agents. The extent of bending is commensurate with 10's of pN of force per [3]rotaxane. Recent studies on a set of ''single-shot'' control [2]rotaxanes have provided additional evidence for the origins of the force generation as it arises from a molecule-based electrostatic repulsion energy of about 10 kcal/mol at 300 K. These findings will be presented in terms of the underlying thermodynamics and kinetics that have been utilized extensively to direct the design and synthesis of artificial molecular machines and which may also serve as a guide for the rational design of unidirectional molecular motors.

***Contributed Papers***

**15:42**
**D29 5 Track Switching and Crossing by Microtubule Motors.** JENNIFER ROSS, KAREN WALLACE, HENRY SHUMAN, ERIKA HOLZBAUR, YALE GOLDMAN, *Pennsylvania Muscle Institute, University of Pennsylvania* Cytoskeletal filaments in cells form a network of crossing tracks for motor proteins carrying vesicular and protein cargoes. The ability to pass through, switch, or dissociate at such intersections is relevant to the motor's ability to effectively navigate in the cell and deliver goods to the appropriate location. We have formed an itin vitro system of crossed microtubules to study the outcome of kinesin motors and dynein-dynactin complexes when they encounter an intersection. Micro-tubules were flowed into the sample chamber from two orthogonal directions and aligned with the flow direction when they attached to glass cover slips via biotin-streptavidin. The first flow direction defined the microtubules closest to the glass surface. Using total internal reflection fluorescence (TIRF) microscopy, we visualized single GFP-kinesin motors and dynein-dynactin-GFP complexes during processive motility at 1 mM ATP. Both dynein and kinesin can switch microtubules, pass by an intersection, or dissociate. Using optical trapping, we placed 1 $\mu$m polymer beads decorated with multiple motors to simulate a large cargo encountering an intersection at 1 mM ATP. Beads are more likely to pause at the intersection at high motor number and can pass and switch as the motor concentration is titrated down. The differences between kinesin and dynein could inform of the ability of these motors to navigate the cell, both separately and in coordination. Supported by NIH grant AR51174.

**15:54**

**D29 6 Collective dynamics of molecular motors pulling on fluid membranes*** JAUME CASADEMUNT, *Universitat de Barcelona* OTGER CAMPAS, *Universitat de Barcelona / Institut Curie* YARIV KAFRI, *Institut Curie / Technion, Haifa* KONSTANTIN B. ZELDOVICH, *Harvard University* JEAN-FRANCOIS JOANNY, *Institut Curie* The collective dynamics of $N$ weakly coupled processive molecular motors when an external force is exerted on the first one, are considered theoretically. We show, using a discrete lattice model, that the velocity-force curves strongly depend on the effective dynamic interactions between motors and differ significantly from the mean field prediction. They become essentially independent of $N$ when this number is large enough. For strongly biased motors such as kinesin, this may occur for $N$ as small as 5. The study of a two-state model shows that the existence of internal states can induce effective interactions. Several analytical predictions are discussed and checked numerically both for the discrete lattice model and the two-state model with Langevin dynamics. Typically, motors cooperate constructively so that the collective stall force and the mean velocity are larger than the mean field expectations. The implications on the interpretation of previous experiments on membrane tubes pulled by collective motors and possible design of new experiments are discussed.

*Supported by PHYNECS European Network

**16:06**

**D29 7 Entropic pulling: how Hsp70 chaperones translocate proteins through membrane pores** PAOLO DE LOS RIOS, *Ecole Polytechnique Federale de Lausanne - EPFL* ANAT BENZVI, *Northwestern University* OLGA SLUTSKY, ABDUSSALAM AZEM, *Tel Aviv University* PIERRE GOLOUBINOFF, *University of Lausanne* Hsp70s are highly conserved ATPase molecular chaperones mediating the translocation of proteins across membranes and the active unfolding and disassembly of stress-induced protein aggregates. Here, we introduce a mechanism named itentropic pulling, based on entropy loss due to excluded volume effects, by which Hsp70 molecules can convert the energy of ATP hydrolysis into a force capable to drive the translocation of polypeptides into mitochondria. Entropic pulling represents a possible solution to the long-standing debate between the itpower-stroke and the itBrownian ratchet models for Hsp70-mediated protein translocation across membranes. Moreover, in a very different context devoid of membrane and components of the import pore, the same physical principles apply to the forceful unfolding, solubilization and assisted native refolding of stable protein aggregates by individual Hsp70 molecules, thus providing a unifying mechanism for the different Hsp70 functions.

***Invited Papers***

**16:18**

**D29 8 Biological motors: Conventional and Unconventional Myosins.***
YALE E. GOLDMAN, *University of Pennsylvania*

Molecular motors are smart, soft machines that regulate their dynamics and energy consumption for efficient tuning to their cell-biological role and mechanics of their cargo. The efficiency is derived partly from harnessing the chaotic thermal fluctuations nano-scale machines experience, rather than struggle against them. Reciprocal coupling between the enzymatic chemistry, structural changes, and mechanical steps is expected from the thermodynamics of an energy-transducing nano-machine. Strong evidence for this bidirectional coupling exists for muscle (conventional) myosin and unconventional myosins. The structural dynamics of myosin leading to translocation along actin are detectable by Optical Trap Mechanical Nanometry (OTNM), Single-Molecule Fluorescence Polarization Microscopy (SMFPM), Fluorescence Imaging at One Nanometer Accuracy (FIONA) and various combinations of these methods. We are in an Acronym Rich Environment (ARE). Progress and puzzles make this a lively research area.

*Supported by NIH grants AR26846 and AR51174, and NSF grant DMR04-25780.

***Contributed Papers***

**16:54**

**D29 9 A single polymer Brownian motor** MATTHEW DOWNTON, *Simon Fraser University* MARTIN ZUCKERMANN, *Simon Fraser University* ERIN CRAIG, *University of Oregon* MICHAEL PLISCHKE, *Simon Fraser University* HEINER LINKE, *University of Oregon* We study a polymer chain in a flashing ratchet potential to determine how the mechanism of this Brownian motor system is affected by the presence of internal degrees of freedom. Each monomer is acted upon by a 1D asymmetric, piecewise linear potential of spatial period $L$ comparable to the radius of gyration of the polymer. We characterize the average motor velocity as a function of $L$, $T_{\mathrm{off}}$, and $N$ to determine optimal parameter ranges, and we evaluate motor performance in terms of finite dispersion, Peclet number, rectification efficiency, stall-force, and transportation of a load against a viscous drag. We find that the polymer motor performs qualitatively better than a single particle in a flashing ratchet: with increasing $N$, the polymer loses velocity much more slowly than expected in the absence of internal degrees of freedom, and the motor stall force increases linearly with $N$. To understand these cooperative aspects of motor operation, we analyze relevant Rouse modes. The experimental feasibility is analyzed and the parameters of the model are scaled to those of $\lambda$-DNA. Finally, in the context of experimental realization, we present initial modeling results for a 2D flashing ratchet constructed using an electrode array.

**17:06**

**D29 10 Imaging and Manipulation of Nanocars by STM** A.J. OSGOOD, Y. SHIRAI, Y. ZHAO, J.M. TOUR, K.F. KELLY, *Rice University* The nanocar molecule - four fullerene wheels connected by rotating alkyne axles to a central chassis - is the first molecule designed and fabricated specifically for nanoscale manipulation. We have investigated the imaging and manipulation of the nanocar molecule on Au(111) by variable-temperature STM.

From the observed movement of the nanocars, we can show that their motion is due to rolling, not sliding, across the gold surface. Additionally, we have begun to explore the conditions for nanoscale rolling in a number of other molecules built from our set of ''molecular tinker toys'' with an eye towards remote manipulation and increased system complexity.

**17:18**

**D29 11 Physical mechanism of the nuclear pore transport.** A. ZILMAN, S. DI TALIA, M. MAGNASCO, M. ROUT, B. CHAIT, *Rockefeller University* Functioning of eukaryotic cells depends on precise regulation of the transport of proteins in and out of the nucleus. All the transport in an out of the nucleus proceeds through the nuclear pore complex (NPC). NPC is an efficient transport device, which transports proteins between the nucleus and the cytoplasm in milliseconds time. NPC is highly selective, only allowing efficient passage of the molecules bound to the transporter proteins. Although, one GTP is used per transported cargo, the process of translocation through the pore is passive and does not involve active energy consumption. The key component in the NPC function is the attractive interaction between the transporter proteins, and the flexible filaments, lining the internal surface of the pore. We model the transport through the NPC as diffusion in an effective potential due to attachments to the flexible filaments. Using analytical theory and computer simulations, we explain known functional features of the NPC, in terms of its basic physical properties.

## SESSION D30: MULTIPHASE POLYMER MATERIALS
**Monday Afternoon, 13 March 2006**
**327, Baltimore Convention Center at 14:30**
**Ali Dhinojwala, University of Akron, presiding**

**14:30**

**D30 1 Phonon Propagation in Dry and Wet Polystyrene Opals** GEORGE FYTAS, *Max Planck Institute for Polymer Research, P. O. Box 3148, 55128 Mainz, Germany and FO.R.T.H P.O.Box 1527 71110 Heraklion,Greece* WEI CHENG, JIAN JUN WANG, ULRICH JONAS, *Max Planck Institute for Polymer Research, P. O. Box 3148, 55128 Mainz, Germany* The phononic properties of fabricated soft opals consisting of closely packed spherical submicrometer polystyrene particles were investigated by Brillouin light scattering in the GHz frequency range. In air, the numerous modes found in the dry opal are theoretically identified as the particle eigenmodes using the two elastic constants for the bulk polystyrene. The line shape of the low-frequency modes can be utilized as an index of the particle size polydispersity and a sensitive probe for monitoring the latex film formation. Unlike for the dry opal, the study of the propagation of acoustic waves in the infiltrated (by silicon oil) opal for wave vector $k_{||}$ parallel to the fcc (111) planes of the slab has revealed two modes: an effective medium mode with linear dispersion over the examined $k_{||}$ range and a second mode the dispersion of which depends on the direction of $k_{||}$ relatively to the symmetry lines of the Brillouin zone. The experimental dispersion will be compared with phononic band structure calculations.

**14:42**

**D30 2 Kinetics of phase separation in a dilute short-ranged square-well system: a molecular dynamics study** HONGJUN LIU, *Department of Chemical and Biological Engineering, Rensselaer Polytechnic Institute, Troy, NY 12180* SHEKHAR GARDE, SANAT KUMAR, We report on a molecular simulation study of the phase separation in a dilute short-ranged square-well system. The phase diagram of model displays solid-fluid equilibrium, with a metastable fluid-fluid separation. Equilibrium fluid configuration are quenched along the isochore at a sequence of temperatures and followed during the time evolution. We present the clear evidence of the metastable fluid-fluid separation, of the homogeneous crystallization and of the kinetically arrested gel. We also discuss the relevance of our simulation to the ''crystallization slot.''

**14:54**

**D30 3 Styrene-Hydroxystyrene Gradient and Block Copolymers: Comparisions of Behavior as Compatibilizers of Immiscible, Crystallizable Polymer Blends and in the Neat and Solution States.** JUNGKI KIM, JOHN M. TORKELSON, *Northwestern University, Evanston, IL 60208* Styrene-hydroxystyrene (S-SOH) gradient and block copolymers are made by semi-batch nitroxide-mediated controlled radical polymerization of styrene and acetoxystyrene followed by hydrolysis of the acetoxystyrene repeat units to SOH. These copolymers are investigated as compatibilizers for polystyrene (PS)/polycaprolactone (PCL) blends made by melt mixing; the hydroxyl groups on the SOH units undergo attractive hydrogen-bonding interactions with the ester groups on PCL. Gradient copolymers of a wide composition range are effective compatibilizers of PS/PCL blends, with the dispersed phase (PCL) domain size being a function of gradient copolymer composition. Block copolymers are also effective compatibilizers, resulting in very small dispersed-phase domain sizes ( $\sim$ 200 nm average diameter). In addition, block copolymer addition has major effects on the crystallizability of the PCL domains; in contrast, only small effects on PCL crystallizability are observed upon addition of gradient copolymer to the blend. The different effects of block and graft copolymers are likely due to greater hydrogen bonding of the PCL with the block copolymer, which impedes crystallization. The properties of the block and gradient copolymers in the neat state and their micellization in solvent and in homopolymer will also be discussed.

**15:06**

**D30 4 An off-lattice Wang-Landau simulation of the coil-globule and solid-liquid transitions of flexible homopolymers.** DREW PARSONS, DAVID WILLIAMS, *Australian National University* The temperature-independent Wang-Landau Monte Carlo approach is implemented for an off-lattice model of flexible homopolymers and applied to the study of the coil-globule and solidification transitions. Transition temperatures are calculated and the thermodynamic limit of the two transitions is compared. We address the issue of obtaining crystal structure in the low energy solid globules, and raise the question of whether a glass-like state rather than crystalline is a correct description of the solid state.

**15:18**

**D30 5 Exploring the Effects of Deuteration on Polymer Blends** MICHAEL TAMBASCO, JANE LIPSON, *Dartmouth College* JULIA HIGGINS, *Imperial College* Deuterium labeling is a requirement of neutron scattering experiments, but the extent to which the H-D switch affects the thermodynamic properties of the

mixture under investigation has not been widely examined. In order to explore this, we apply a simple lattice theory to the analysis of a fairly complete set of experimental data on blends of polystyrene(PS)/polybutadiene(PB), in which all permutations of PS, dPS, PB, and dPB are of interest. Available data include cloud point curves, neutron scattering intensities, and pressure-volume-temperature surfaces. In this talk we discuss what we have learned regarding the consequences of deuterium substitution on the properties of this blend, and draw some broader conclusions.

**15:30**

**D30 6 Coarse-Grained Simulations of PEO/PMMA Blends** PRAVEEN DEPA, CHUNXIA CHEN, JANNA MARANAS, *Pennsylvania State University* Coarse-graining involves mapping successive atoms along a polymer chain to larger coarse-grained beads, which are then simulated using conventional molecular dynamics techniques. The interaction between the coarse-grained [CG] beads is parameterized so as to reproduce static properties observed in the underlying atomistic simulations. We extend this methodology to blends by developing CG models for poly(ethylene oxide) [PEO], poly(methylmethacrylate) (PMMA) and PEO/PMMA blends. In the case of PEO, six united atoms were mapped to a CG bead with the center at every other oxygen atom and for PMMA, each monomer was replaced with two CG beads, one centered along the main chain and the other centered at the ester-oxygen on the side group. The CG models reproduce static properties for both components. Dynamic properties evolve correctly if rescaled by a constant factor, specific to each component. The CG model is then used to simulate larger system for longer times such that whole chain dynamics can be accessed and compared to local dynamics.

**15:42**

**D30 7 Relationship between Fluctuation and Stress Relaxation in a Block Copolymer Melt** AMISH PATEL, NITASH BALSARA, *Department of Chemical Engineering, University of California, Berkeley* SURESH NARAYANAN, ALEC SANDY, *Argonne National Laboratory* SIMON MOCHRIE, *Department of Physics, Yale University* BRUCE GARETZ, *Othmer Department of Chemical & Biological Sciences & Engineering, Polytechnic University* HIROSHI WATANABE, *Institute for Chemical Research, Kyoto University* The relationship between microscopic fluctuation relaxation and macroscopic stress relaxation was explored in a disordered block copolymer melt containing disordered micelles. Experiments conducted near the order-to-disorder transition, show that the fluctuation relaxation time, measured by X-ray photon correlation spectroscopy is larger than the terminal stress relaxation time, measured by rheology, by factors as large as 100. These observations are in qualitative agreement with predictions of the Fredrickson-Larson theory. The lack of quantitative agreement suggests the need for a comprehensive theory that predicts stress relaxation in systems with complex free energy landscapes, such as those containing micelles and disordered fluctuations.

**15:54**

**D30 8 Self-consistent field theoretic calculations of stress in diblock** PANAGIOTIS MANIADIS, KIM O. RASMUSSEN, TURAB LOOKMAN, EDWARD M. KOBER, *Theoretical Division, Los Alamos National Laboratory* The elastic properties of diblock copolymers are studied using self-consistent field theoretical calculations. Our starting point is the approach of Fredrickson (J. Chem. Phys. 117, 6810, 2002) in which microscopic expressions of the elastic energy and stress of polymer chains are self-consistently incorporated into the free energy expression for a homopolymer. We extend this theory to phase separating diblock copolymers and calculate numerically the complete stress tensor in the presence of external strain. Our numerical method can be easily generalized to multi-block copolymers, and our method can be used to study the elastic properties of phase separating polymer materials in general.

**16:06**

**D30 9 Coarse-Grained Modeling of the Mechanical Properties of Entangled Polymer Systems** BRIAN PASQUINI, FERNANDO ESCOBEDO, YONG L. JOO, *Cornell University* The complexity of entangled polymer interactions is a promising area for simulation studies to build upon polymer physics theories; however, it is necessary to use a coarse-grained approach to simulate the dynamic response of large polymer systems. Such studies have been done by treating the entanglement interactions as a set of entanglement points, which serve as the ends for the coarse-grained simulation unit. One method from literature (Smith and Termonia) formulates the free energy of an entanglement network based exclusively on neighboring entanglement points and uses temporary bonds which break as the simulation progresses. Another method (Terzis, Theodorou and Stroeks) treats the coarse-grained units as delocalized polymer density clouds, and formulates an expression for the free energy based on local polymer density. The first method has been extended to three dimensions for direct comparison to the second in tensile strain experiments. These models also show promise to understanding microstructure effects on mechanical properties in materials such as spider silk.

**16:18**

**D30 10 Flame Retardant Homopolymer and Polymer Blend Composites** MIRIAM RAFAILOVICH, MAYU SI, JONATHAN SOKOLOV, *Department of Materials Science and Engineering, Stony Brook University, Stony Brook, NY 11794* TOHRU ARAKI, HARALD ADE, *Department of Physics, University of North Carolina* DANIEL HEFTER, *DRS High School, Woodmere, NY* ARYEH SOKOLOV, *Queens College, Flushing, NY* We investigated the flame retardant performance of homopolymer, EVA, PMMA, PP, and PS, and polymer blends, PS/PMMA, PC/SAN, with organoclay and conventional flame retardant agents such as decabromodiphenyl ether (DB) and phosphorus compounds. These materials were characterized by TEM, STXM, LOI and UL 94 V-0. TEM and STXM photographs show that the addition of organoclays into polymer blends drastically slows down the phase separation and accelerates the decompose of bromine compounds during the combustion. Further, UL 94 V-0 results indicate that PS/PMMA blend with DB can not achieve self-extinguishing in the absence of clay. The amounts of flame retardants and clay used were varied to try to achieve the optimal formula to pass UL 94 V-0. The synergism of clay and flame retardant agents were completely studied by various measurements, time dependence burning (TEM, Ion Chromatography), GC-MS, and cone calorimeter.

**16:30**

**D30 11 Ellipsometry studies of nanofilled polymer thin films.** UFUK KARABIYIK, ALAN ESKER, *Department of Chemistry (0212), Virginia Tech Blacksburg, VA 24061* Thermal properties of polymer thin films and polymer/nanofiller blends are crucial and expected to be different from their corresponding bulk properties because of the large surface area/volume ratio and the greater fractional free volume in confined geometries. Langmuir-

Blodgett thin films of trisilanolphenyl-POSS (TPP) and poly(t-butyl acrylate) (PtBA) blends were prepared by Y-type deposition. The films have been characterized by x-ray reflectivity and ellipsometry. Ellipsometry is able to measure thermally induced structural changes and can be used to monitor surface glass transition temperatures as well as layer deformation in multilayer thin films. The results show that TPP depresses the glass transition temperature(Tg) of PtBA LB-films like a plasticizer at low TPP concentrations less than 3 wt. percent TPP and that Tg increases for TPP concentrations greater than 3 wt. percent. A speculative mechanism for this cross-over is an increase in TPP aggregation that pins PtBA chains leading to lower chain mobility at higher wt. percent TPP.

**16:42**

**D30 12 Charge dissipation measurement on the surface of polymeric materials using modified surface potential electric force microscopy** MICHAEL REAGAN, SERGEI LYUKSYUTOV, IVAN DOLOG, ROBERT MALLIK, *The University of Akron, OH* SHANE JUHL, RICHARD VAIA, MICHAEL DURSTOCK, JOHN FERGUSON, *AF Research Laboratory, WPAFB OH* The AFMEN technique when combined with surface potential electric force microscopy (SP-EFM) reveals the pattern of electric charge build-up and dissipation in polymeric and organic materials. This information can be used to develop an adequate description of nanoconductivity in these materials. The description includes effects due to local electric field variations and charge transport mechanisms. Charge evolution was estimated by measuring electric currents using AFM. In addition to the SP-EFM and AFM work outlined above, we also use Inelastic Electron Tunneling Spectroscopy (IETS) to characterize the electronic and vibrational properties of polymer and composite materials. IETS has been used in the past by one of the authors to investigate ultra-thin (roughly 1 nm) polymer films, including PMMA. The films were deposited either by spin coating from or by plasma polymerization. This work is being extended to study the adsorption of spin-coated PMMA on photovoltaic materials such as CdS. Temperature dependent current-voltage and conductance voltage data obtained from tunnel diodes containing CdS/PMMA heterolayers can be used to determine the conduction mechanisms in these layers.

**16:54**

**D30 13 Preparation and Characterization of a Superparamagnetic Polymer Nanocomposite** N. BRENNER, R. ISSEROFF, *Lawrence High School, Cedarhurst, NY* M. RAFAILOVICH, G. RUDOMEN, R. GAMBINO, S.S. LIANG, D. SUNIL, M. SI, L. COLLAZO, N. PERNODET, X. FANG, $Fe(CO)_5$ decomposition produced ferro- and superparamagnetic polymer nanocomposites. $Fe(CO)_5$ and Cloisite 20A clay were combined in a closed vial for 12 hours, then opened to air for 2 hours. Mössbauer analysis indicated formation of $Fe_2O_3$ on clay; mass analysis indicated 12% Fe in clay. A Brabender mixed $Fe_2O_3$/clays with PMMA and EVA at ratios by mass of 9:4:36 and 1:1:4 respectively ($Fe(CO)_5$:clay:polymer). TEM displayed $Fe_2O_3$ nanoparticles, $3.3 \pm 0.8$ nm in diameter, adsorbed on exfoliated clay platelet surfaces in polymer matrices. VSM data indicated superparamagnetism with moments of 510.3 emu/$g_{(Fe2O3)}$ (PMMA) and 8.46 emu/$g_{(Fe2O3)}$ (EVA). DMA showed 37% decreased dynamic modulus (EVA) and 11% (PMMA) due to $Fe_2O_3$. TGA indicated PMMA stability to $400^oC$ (9.3% mass residual) and EVA to $435^oC$ (11% mass residual). Cell adhesion tests showed $Fe_2O_3$/clay enhanced proliferation, promising applications in bone implants.

**17:06**

**D30 14 Molecular Simulation of the intercrystalline region in isotactic polypropylene** VIKRAM KUPPA, GREGORY C. RUTLEDGE, *Massachusetts Institute of Technology* Monte Carlo (MC) computer simulations are used to study the crystal-amorphous interlamellar phase in semi-crystalline isotactic polypropylene. This represents the first such study of the detailed atomic level structure of the interlamellar phase for a polymer with side groups. The polymer is modeled using a united atom force-field model. Replica exchange in energy space is required in addition to local conformation and topology altering MC moves to achieve effective sampling of phase space. The simulations reveal the temperature dependence of structural features such as mass and energy density profiles as well as population distributions of tails, loops and bridges associated with the fold surface. These results for polypropylene are compared and contrasted with previous results for the prototypical linear polymer, polyethylene, in order to study the effect of architectural complexity on structure and properties of semi-crystalline polymers

**17:18**

**D30 15 Phase Transition Behavior of Isotactic Polypropylene Crystallized from a Homogeneous Melt*** XIAOFENG CHEN, SANAT K. KUMAR, *Chemical and Biological Engineering* RAHMI OZISIK, *Materials Science and Engineering, Rensselaer Polytechnic Institute* The equilibrium melting behavior of helical structures in isotactic polypropylene (iPP) was studied by a Monte Carlo simulation. It was found that the melting of iPP helical structure was an exponential process at high temperatures ($T > 470$ K), whereas it becomes highly stretched at low temperatures ($T < 400$ K). An estimate of the melting temperature was obtained from a novel application of the second moment of the waiting time distribution for helix melting as described by Odagaki (T. Odagaki, itPhys. Rev. Lett. **1995**, 75, 3701). The calculated melting temperature was approximately 455 K, which is in surprisingly good agreement with experimental values. A second transition temperature was also observed at a lower temperature ($T \sim 390$ K), which we can not explain by equilibrium considerations. We suggest that at this temperature, once a helix forms, it does not melt within the time scale studied.

*This material is based upon work supported by the National Science Foundation under Grant 0310596.

**SESSION D31: PROPERTIES OF SEMICONDUCTING NANOSTRUCTURES**
**Monday Afternoon, 13 March 2006**
**328, Baltimore Convention Center at 14:30**
**Steve Erwin, Navel Research Laboratory, presiding**

**14:30**

**D31 1 Enhanced Raman Scattering from Individual Semiconductor Nanocones and Nanowires*** LINYOU CAO, BAHRAM NABET, JONATHAN SPANIER, *Drexel University* DREXEL UNIVERSITY TEAM, We report strong enhancement ( $\sim 10^3$) of the spontaneous Raman scattering from individual silicon nanowires and nanocones as compared with bulk Si. The observed en-

hancement is diameter ($d$), excitation-wavelength ($\lambda_{laser}$), and incident polarization state-dependent, and is explained in terms of a resonant behavior involving incident electromagnetic radiation and the structural dielectric cross-section. The variation of the Raman enhancement with $d$, $\lambda_{laser}$ and polarization is shown to be in good agreement with model calculations of scattering from an infinite dielectric cylinder.

*Work supported by Commonwealth of PA, ARO and NSF.

**14:42**

**D31 2 Magic structures of H-passivated ⟨110⟩ silicon nanowires** TZU-LIANG CHAN, *Ames Laboratory and Physics Department, Iowa State University* CRISTIAN V. CIOBANU, *Division of Engineering, Colorado School of Mines* FENG-CHUAN CHUANG, NING LU, CAI-ZHUANG WANG, KAI-MING HO, *US. DOE Ames Laboratory and Physics Department, Iowa State University* We report a genetic algorithm approach combined with ab initio calculations to determine the structure of hydrogenated ⟨110⟩ Si nanowires. As the number of atoms per length increases, we find that the cross section of the nanowire evolves from chains of six-atom rings, to fused pairs of such chains, to hexagons bounded by {001} and {111} facets. Our calculations predict that hexagonal wires become stable starting at about 1.2 nm diameter, which is consistent with recent experimental reports of nanowires with diameters of about 3 nm.

**14:54**

**D31 3 Field Emission of Silicon Nanowires** BAOQUING ZENG, *Boston College, MA* GUANGYONG XIONG, *Boston College, MA* SHUO CHEN, *Boston College, MA* SUNG-HO JO, *Boston College, MA* WENZHONG WANG, *Boston College, MA* DEZHI WANG, *Boston College, MA* ZHIFENG REN, *Boston College, MA* Field emission of silicon nanowires (SiNWs), which were grown by chemical vapor deposition method with Au catalyst at a temperature of 480 C from silane, has been investigated. To obtain a current density of 1 mA/cm2, an electric field of 5.5 V/um is needed with a turn-on electric field of 2.9 V/um for a current density of 0.01 mA/cm2, which are the best ever reported values. The NWs were studied by scanning electron microscopy (SEM) and transmission electron microcopy (TEM). SEM showed that the length of the wires is about 100 um with diameters of around 100 nm. High-resolution TEM showed that the nanowires have high crystallinity. The low growth temperature makes the process applicable to glass substrates that are used as the backing of large area flat panel displays.

**15:06**

**D31 4 Growth of Pure and Long Silicon Nanowires on Table Salt Support** GUANGYONG XIONG, SHUO CHEN, BAOQIN ZENG, WENZHONG WANG, DEZHI WANG, ZHIFENG REN, *Boston College* REN'S GROUP TEAM, Table salt was found to be a very good support for the growth of silicon (Si) nanowires in large quantity by a simple thermal decomposition of diluted silane gas in argon and hydrogen gases at less than $500^{o}$C. Hydrogen gold tetrachloride was uniformly mixed into the salt and decomposed into gold nanoparticles at the growth temperature and acted as the catalyst particles to start the growth of Si nanowires. The scanning electron microscope images showed that the as-grown Si nanowires are about 50-100 nm in diameter and up to 200 micrometers long. X-ray diffraction patterns showed that the salt was completely removed by water rinse. The transmission electron microscope studies showed that these Si nanowires are highly crystallized single crystals with an amorphous silicon layer of less than a few nanometers.

**15:18**

**D31 5 Fabrication of single-crystal Si nanowires by ultrahigh vacuum magnetron sputtering.** J. W. KNEPPER, X. W. ZHAO, F. Y. YANG, *The Ohio State University* Semiconductor nanowires have attracted great interests due to the intriguing fundamental science and technological application they provide. Many semiconductor materials have been made into single crystal nanowires with superior crystal quality and high mobility. Among them, silicon is particularly interesting because silicon is the foundation of modern electronic technology. A majority of the nanowire synthesis used laser-assisted catalyst growth or chemical vapor deposition. Here we reported a different approach to the fabrication of semiconductor nanowires using ultrahigh vacuum magnetron sputtering. Using thin Au layers as catalyst via vopor-liquid-solid mechanism, single crystal Si nanowires have been grown on Si substrates at a temperature of $\sim$ 700[r]C. Electron microscopy revealed that most Si nanowires grew epitaxially on Si(111) surfaces. Si nanowires are perpendicular to the Si(111) surface with a Si/Au alloy sphere on the top of the nanowires. The growth of Si nanowires on Si wafers with other orientations and amorphous silicon oxide layers was also observed, but with much less probability. The diameter of the Si nanowires is about 200 nm using Au layers as catalyst. The nanowire diameter can be controlled to smaller size by patterning the Au layers into small dots to reduce the catalyst size. Si nanowires fabricated by ultrahigh vacuum sputter at a base pressure of 10-10 torr are high purity and can be easily doped to desirable carrier concentration.

**15:30**

**D31 6 Structures of Si and Ge nanowires in the sub-nanometer range** HELIO CHACHAM, RICARDO KAGIMURA, RICARDO W. NUNES, *Departamento de fisica, Universidade Federal de Minas Gerais, Brazil* We report [1] *ab initio* and tight-binding calculations of several structures of pristine Si and Ge nanowires with diameters D between 0.5 and 5.0 nm. For nanowires with D $<$ 2 nm, the calculations are performed in the framework of Kohn-Sham density functional theory, within the generalized-gradient approximation. Total-energy differences are converged to within 10 meV/atom. For nanowires with D $>$ 2 nm, an order-N density-matrix tight-binding methodology (DMTB) is employed. We consider nanowires based on the diamond structure, high-density bulk structures, and fullerene-like structures. Our calculations indicate a transition from $sp^3$ geometries to structures based on denser bulk phases and fullerene-like structures, for diameters smaller than $\sim$ 1.2 nm. We show that a continuum model is able to reproduce quantitatively this transition. According to the model, the transition originates from the larger surface energy density of the $sp^3$ wires as compared to those of the denser wires. We also find that diamond-structure nanowires are unstable for diameters smaller than 1 nm, undergoing considerable structural transformations towards amorphous-like wires. For diameters between 0.8 nm and 1 nm, filled-fullerene wires are the most stable. For even smaller diameters ( $\sim$ 0.5nm), we find that a simple hexagonal structure is particularly stable for both Si and Ge. [1] R. Kagimura, R. W. Nunes, and H. Chacham, Phys. Rev. Lett. 95, 115502 (2005)

**15:42**

**D31 7 Physics and Applications of Ge/Si Core/Shell Nanowires** JIE XIANG, WEI LU, YONGJIE HU, YUE WU, HAO YAN, CHARLES LIEBER, *Department of Chemistry and Division of Engineering and Applied Sciences, Harvard University* We recently reported hole-gas formation and ballistic transport through 1D modes in band-structure engineered Ge/Si core/shell nanowire heterostructures at cryogenic temperatures, opening up a new platform to study low-dimensional transport phenomena and applications such as high performance room temperature field effect transistors. In this talk we report studies of single Ge/Si nanowire field effect transistors employing high-k dielectrics with top gate geometry. The clean hole-gas system and enhanced gate coupling from the high-k dielectric allow clear identification of discrete 1D subbands, as well as the observation of superconductivity proximity effect with superconducting contacts. Room temperature FET characteristics exhibit the best performance achieved in nanowire FETs, and the calculated intrinsic delay as a function of gate length for these nanowire FETs shows a clear scaling advantage over planar Si MOSFETs. Studies investigating the effect of novel gate structures to control ambipolar behavior and threshold voltage will also be discussed.

**15:54**

**D31 8 What are new when Si nanowires get small: magic numbers and square shape*** RUQIAN WU, *Department of physics and astronomy, UCI, CA* Through systematic density functional studies, we found the existence of ''magic numbers'' for Si nanowires grown along the $< 100 >$ axis. Strikingly, Si nanowires prefer the sharp square cross-section with corner atoms when the diameter is smaller than 1.7 nm. This is promoted by two facts: (1) the presence of the corner atoms permits formation of benign reconstruction pattern to maximally saturate the dangling bonds; and (2) the corner atoms develop pairs and strongly interact with each other across nanowires.

*Work was supported by the DOE (grant No: DE-FG02-04ER15611) and ICTS, Chinese Academy of Science.

**16:06**

**D31 9 Effect of surface roughness, defects and phonon scattering on electron current through silicon nanowires*** ALEXEI SVIZHENKO, PAUL LEU, KYEONGJAE CHO, *Department of Mechanical Engineering, Stanford University, Stanford, CA, 94305* Silicon nanowires (SiNW) can become an important building block of nanoscale devices and circuits. Many experimental groups have fabricated SiNWs and measured their current-voltage characteristics. While electron current was found to be very high by some measurements, it is also highly sensitive to chemical modification of NW surfaces. It is therefore important to understand the detailed mechanisms of electron transport in the presence of external factors (e.g., surface roughness, surface defects, dopants, or phonon scattering) and estimate the current carrying capacity of SiNW. In this talk we will discuss our theoretical calculations of current-voltage characteristics of SiNW based on non-equilibrium Greens function (NEGF) equations using an $sp^3d^5s^*$ tight-binding Hamiltonian. We will focus on the effect of surface roughness, random defects and inelastic electron-phonon scattering on electron transport.

*This work was supported by Intel Corporation

**16:18**

**D31 10 Scanning Probe Microscopy of Semiconducting Nanowires*** A.C. BLESZYNSKI, R.M. WESTERVELT, *Dept. of Physics, Harvard University* F.A. ZWANENBURG, L.P. KOUWENHOVEN, *Kavli Institute of Nanoscience, Delft University of Technology* A.L. ROEST, E.P.A.M BAKKERS, *Philips Research Laboratories* We have used a liquid-He cooled scanning probe microscope (SPM) with a conducting tip to image electrical conduction through InAs nanowires. The charged SPM tip is scanned above the nanowire and the resulting change in nanowire conductance is recorded to form the image. These conductance images are used to study the behavior of electrons in the nanowire on a local scale. For example, the images reveal barriers to conduction at the contacts as well as sections of the wire that act as quantum dots. At 4K the wires exhibit Coulomb blockade oscillations in conductance versus backgate voltage that are indicative of multiple quantum dots in series. The images reveal the location of the quantum dots along the wire and the tip voltage can tune their charge state. The nanowires, grown catalytically from small gold particles, have diameters between 50 and 100 nm. Ti/Al source and drain contacts with a spacing of 1 to 2 $\mu$m were defined using e-beam lithography.

*This work was supported at Harvard and at Delft, by the NSEC grant NSF PHY-01-17795.

**16:30**

**D31 11 Tunable supercurrent through semiconductor nanowires** JORDEN VAN DAM, *Delft University of Technology* YONG-JOO DOH, *Delft University of Technology* AARNOUD ROEST, *Philips Research* ERIK BAKKERS, *Philips Research* SILVANO DE FRANCESCHI, *TASC-INFM, Trieste, Italy* LEO KOUWENHOVEN, *Delft University of Technology* We have developed a high-yield approach to the fabrication of nanoscale superconductor-semiconductor hybrid devices [1]. The devices are assembled from InAs semiconductor nanowires with diameters ranging from 30-130 nm, individually contacted by aluminum-based superconductor electrodes. Below 1 Kelvin, the high transparency of the contacts enables proximity-induced superconductivity. A supercurrent flows though the nanowire that can be tuned by a global gate acting on the electron density. Furthermore, we have used top-gates in order to make tunable barriers in InAs nanowires. By creating two closely spaced barriers in an InAs nanowire, we can define a Quantum Dot (QD) with tunable coupling. This enables us to study a tunable QD connected to superconducting leads. In these devices the supercurrent can be controlled by only a small change in gate voltage. If the QD is tuned at a charge degeneracy point, a supercurrent can flow through the QD. However, away from charge degeneracy the supercurrent is blocked due to coulomb blockade. [1] Y.-J. Doh, J.A. van Dam, et al., Science 309, 272 (2005)

**16:42**

**D31 12 Bandstructure Effects in Unstructured AlGaAs Nanowires** NEERAV KHARCHE, CLEMENS HEITZINGER, GERHARD KLIMECK, *Purdue University* MATHIEU LUISIER, *ETH Zurich, Switzerland* TIMOTHY BOYKIN, *Univ. Alabama in Huntsville* Atomic scale alloy disorders can have profound effects on the bandstructure and charge transport through nanowires. With decreasing diameters down to nanometer scales, alloy disorder can no longer be treated in an average manner using the virtual crystal approximation (VCA). Our zone unfolding algorithm along with supercell calculations can be used to treat alloy disorders even to atomic scales. We calculate bandstructures and transmission coef-

ficients of AlGaAs random alloy nanowires with diameters ranging from 2nm to 6nm. Using the nanoelectronic modeling tool (NEMO3D), eigenstates of the alloy nanowire supercell are calculated with the 20-band sp3d5s* spin model. Small cell bandstructures are then projected out of the supercell eigenstates. Transmission coefficients are calculated with an atomistic NEGF simulation of the alloy wire embedded between two ideal reservoirs. These projected bandstructures and transmission coefficients both show reduced bandgaps and noisy behavior and provide significant insight into the physics of charge transport.

**16:54**

**D31 13 Ground states of a novel AlAs quantum wire** TRINANJAN DATTA, ERICA W. CARLSON, *Department of Physics, Purdue University* Using abelian bosonization and renormalization group, we analyze the ground states of a recently fabricated novel AlAs quantum wire [Moser et al, Appl. Phys. Lett. (2005)]. There are two degenerate lowest energy bands, separated by half an umklapp vector. This bandstructure arrangement leads to four Fermi points and umklapp-induced pair processes, independent of filling. The ground states are different from those of a conventional quantum wire, where acquiring four Fermi points requires occupying two successive bands, leading to a CDW instability via density reorganization. Such an instability is forbidden in the AlAs wire, which may help stabilize other exotic gapped ground states.

**17:06**

**D31 14 Electrical Detection of Oscillations in Micro- and Nano-Cantilevers** GAYATRI KESKAR, JAY GAILLARD, RASVAN CIOCAN, MALCOLM SKOVE, APPARAO RAO, *Clemson University* Electrical Detection of Oscillations in Micro- and Nano- Cantilevers We described a fully electrical actuation and detection method for measuring mechanical oscillations in ambient conditions for two systems: Si-based micro- and multi-walled carbon nanotube (MWNT) based nano-cantilevers. In our studies, a cantilever is either a silicon microstructure shaped like a diving board, or a cantilevered MWNT. The cantilever is placed parallel to and within 1-10 $\mu$m from a counter electrode and is forced into resonance by applying an ac voltage ($V_{ac}$) with a dc offset ($V_{dc}$) on the counter electrode under ambient conditions. We measure the magnitude and phase of the electrical signal due to the charge induced on the cantilever. The signal showing the resonance frequency of the cantilever is best measured at harmonics of $V_{ac}$. A model describing the response of our electrical actuation and detection of resonance oscillations will be presented.

**17:18**

**D31 15 Position-dependent deflection (PPD) of a nanobeam: a new method to determine the Young's modulus of nanoscale matter** N. DUARTE, *Dept. of Electrical Engr., The Pennsylvania State University* QIHUA XIONG, *Dept. of Physics, The Pennsylvania State University* TADIGADAPA SRINIVAS, *Dept. of Electrical Engr., The Pennsylvania State University* PETER EKLUND, *Dept. of Physics, The Pennsylvania State University* In this approach, a nanowire beam is fixed at two ends and an AFM is used to apply a force F(x) where x locates the position along the beam and the beam deflection $\delta z(x)$ is measured simultaneously. This situation is realized by placing a nanobeam over a trench fabricated on a Silicon substrate via photolithography followed by metal evaporation, lift-off and $XeF_2$ etching. The AFM tip force-distance curve is first obtained from experiments on the rigid substrate. The slope of the AFM force-distance obtained when the tip contacts the beam is then measured and the Young's modulus Y is obtained from the change in slope using the Euler-Bernoulli (E-B) equation. The beam dimensions are also required: the beam height and length via AFM and the beam width and length by SEM. We believe this method can be used in any other nano-beam systems to measure the Young's modulus. Results for rectangular ZnS beams ( $\sim$ 100nm x 100 nm x 5$\mu$m long) will be presented that demonstrate the potential for this method. Values for Y lower than reported for the bulk are obtained (i.e. Y(nano) $\sim$ 70% Y(bulk)). This work was supported, in part, by NSF-NIRT DMR-0304178

**SESSION D32: FOCUSED SESSION: COMPUTATIONAL NANOSCIENCE II**
**Monday Afternoon, 13 March 2006**
**329, Baltimore Convention Center at 14:30**
**Joshua Schrier, Lawrence Berkeley National Laboratory, presiding**

**14:30**

**D32 1 The effect of polytype on energy gap in SiC nano-clusters** XIHONG PENG, AZAR ALIZADEH, NITIN BHATE, LARRY ROWLAND, *GE Global Research, Niskayuna, NY 12309* SAROJ NAYAK, SANAT KUMAR, *Departments of Physics and Chemical Engineering, Rensselaer Polytechnic Institute, Troy, NY 12810* The size dependence of energy gap is perhaps the most remarkable aspect of quantum confinements in low dimensional systems. Numerous models have been proposed to describe the quantum confined electronic states in Si, CdSe, etc, providing a precise description of the bandgap as a function of nano-crystal dimensions. Recently, ab-initio studies of energy gap in cubic SiC nanoparticles as a function of both size and surface composition have been reported. SiC is a remarkable semiconductor with over 200 different crystal structures (polytypes) due to different stacking orders. The always-indirect band gap of bulk SiC varies substantially among the different polytypes (2.4 eV for 3C-SiC to 3.3 eV for 2H-SiC). We have investigated the effect of polytypism on the size-dependency of energy gap in SiC nano-clusters using ab-initio calculations. For clusters smaller than 1 nm, all SiC polytypes show identical energy gap-size dependencies. For SiC nanoparticles larger than 1 nm, the effect of crystal structure becomes apparent approaching the bulk values.

**14:42**

**D32 2 Structural and electronic properties of InP nanowires: role of surface dangling bonds on nanowire facets** TORU AKIYAMA, KOHJI NAKAMURA, TOMONORI ITO, *Department of Physics Engineering, Mie University* InP nanowires are one of intriguing targets in the sources and detectors in fiber optic communications and high-speed electronic applications. In spite of this technological importance, however, understanding of atomic structures and electronic properties of InP nanowires still remain unclear. Here, we present first principles pseudopotential calculations that clarify structural stability and electronic properties of InP nanowires vertically grown on InP(111) substrates. Our calculations with diameter less than 23 Å demonstrate that the nanowires with zinc blende structure are less favorable than those with wurtzite structure, in which the surface dangling bonds on nanowire facets are found to be crucial to determine the stability. An analysis of the nanowire cohesive energy based on the number

of the dangling bonds predicts that the nanowires are bistable forming both wurtzite and zinc blende structures at large diameter around 120 Å, which leads to the exhibition of polytypes being consistent with experiments. In addition, the calculated Kohn-Sham energy bands for stable wurtzite nanowires show that the surface dangling bond states determine the band character and the gap energy for the nanowires with diameter less than 9 Å while the gap energy of nanowires with diameter larger than 14 Å is dependent on only the nanowire size.

**14:54**

**D32 3 Atomistic Simulations of Long-Range Strain and Close-Range Electronic Structure in Self-Assembled Quantum Dot Systems.** GERHARD KLIMECK, *Network for Computational Nanotechnology, Purdue University, W. Lafayette, IN 47907* SHAIKH AHMED, MAREK KORKUSINISKI, SEUNGWON LEE, FAISAL SAIED, *Network for Computational Nanotechnology, Purdue University, W. Lafayette, IN 47907* The electronic structure in self-assembled quantum dots depends on the detailed quantum dot configuration inside the embedding matrix and the nearest neighbor quantum dots through electronic and strain interactions. However, realistic determination of strain requires a large computational domain. To tackle this problem for an embedded InAs quantum dot NEMO-3D uses the atomistic VFF Keating model containing up to 64 million atoms. Interatomic distance changes obtained are used to influence the sp3d5s* tight-binding electronic Hamiltonian with 21 million atoms. Targeted eigenstates with correct symmetry are found reliably even in such large systems. Our investigations show a dramatic dependence of the dot states on the size of the strain domain and the boundary conditions. NEMO-3D is also used to study the electronic states in coupled quantum dots in stacks of 2 and 7 dots. There is an interesting interplay between strain induced and size induced state distributions.

**15:06**

**D32 4 Numerical modeling InAs/GaAs quantum ring capacitance spectroscopy using non-parabolic approximation.** IGOR FILIKHIN, VLADIMIR SUSLOV, BRANISLAV VLAHOVIC, *North Carolina Central University* Direct observation for discrete energy spectra of InAs/GaAs quantum dots (QD) and rings (QR) is possible by capacitance-voltage (CV) end far infrared (FIR) spectroscopy [1]. Existing theoretical explanations of experimental data are limited by the parabolic potential model [1,2] and infinite confinement, which they are using. In present work a single subband model for InAs/GaAs QD(QR) is used. The finite confinement band-gap potential is estimated by the band gap difference of InAs quantum object and GaAs substrate [3]. The non-parabolic approximation is defined by electron effective mass dependence on the confinement energy according to the Kane formula. The 3D confined energy problem is solved numerically by the finite element method. Obtained results for single electron levels are in good agreement with the CV spectroscopy. The calculations also reproduce experimental value for the energy-gate-voltage conversion coefficient equal to 7. Our estimation for the magnitude of the electron effective mass agrees with experimental data. The results are compared with the parabolic potential model calculations. [1] A. Lorke, et al., PRL **84** 2223 (2000). [2] A. Emperador, et al., PR B. **62** 4573 (2000). [3] I. Filikhin et al., Modelling Simul. Mater. Sci. Eng. **12** 1121 (2004).

**15:18**

**D32 5 A charge patching method calculation of a quantum dot/quantum well nanosystem.*** JOSHUA SCHRIER, LIN-WANG WANG, *Computational Research Division, Lawrence Berkeley National Laboratory* First principles density functional calculations typically involve finding self-consistent solution to the Kohn-Sham equations, scaling with the cube of system size. To study large systems, such as semiconductor nanocrystals, an approximate ab initio potential may be constructed by patching together local charge motifs determined from self-consistent calculations on small prototype systems, and the eigenvalues determined using the folded spectrum method for a few band-edge states. In this talk, I will discuss the recent applications of this method to CdS/CdSe/CdS colloidal quantum dot quantum wells. Results on the effect of core, well, and shell thicknesses on the wavefunction and optical properties will be discussed. We find the conduction band wavefunction to be significantly less confined to the CdSe quantum well layer than predicted by k.p theory, and discuss the implications of this result on the theoretical interpretation of recent time-resolved Faraday rotation experiments. We will also briefly discuss the extensions of this approach to the explicit treatment of surface ligand effects and transition-metal doped nanocrystals.

*This work was supported by U.S. Department of Energy under Contract No. DE-AC02-05CH11231 and used the resources of the National Energy Research Scientific Computing Center.

**15:30**

**D32 6 Discrete size series of CdSe quantum dots: A combined computational and experimental investigation** MIN YU, GAYANATH FERNANDO, RONGFU LI, FOTIOS PAPADIMITRAKOPOULOS, NING SHI, RAMAMURTHY RAMPRASAD, Ab initio computational studies were performed for CdSe nanocrystals over a wide range of sizes in conjunction with recent experimental work. Substantial relaxations and coordination of surface atoms were found to play a crucial role in determining the nanocrystal stability and optical properties. While optimally (three-fold ) coordinated surface atoms resulted in stable closed-shell structures with large optical gaps, sub-optimal coordination gave rise to lower stability and negligible optical gaps. These computations are in qualitative agreement with recent chemical etching experiments suggesting that closed shell nanocrystals contribute strongly to photoluminescence quantum yield while clusters with non-optimal surface coordination do not.

**15:42**

**D32 7 Excitonic absorption of million-atom (In,Ga)As/GaAs self-assembled quantum dots*** GUSTAVO A. NARVAEZ, ALEX ZUNGER, *National Renewable Energy Laboratory, Golden, Colorado 80401* We calculate the optical absorption spectra of (In,Ga)As/GaAs self-assembled quantum dots by adopting an atomistic pseudopotential approach to calculate the single-particle electron and hole confined states of the dot followed by a calculation of the neutral exciton $X^0$ states $|\Psi^{(\nu)}(X^0)\rangle$ based on the configuration-interaction approach. We predict three types of *allowed* transitions that would be naively expected to be forbidden. (i) Transitions involving low-lying electron and hole states that are forbidden in simple effective mass models (e.g. $1S$-$2S$, $1S$-$1P$) become allowed by virtue of single-particle band-mixing. (ii) Transitions involving a deep hole state, with a mixture of heavy-hole and light-hole character, and an electron in the lowest state are found to have oscillator strengths that are comparable in magnitude to those of the expected allowed transitions. Thus,

simple models based on single-band envelope functions cannot predict these transitions. (iii) Transitions whose intensity is large due to many-body borrowing of oscillator strength from allowed transitions. The transitions in (i) and (ii) appear, respectively, as low-energy and high-energy satellites of the allowed *P-P* transitions, as observed in PLE.

*Supported by DOE-SC-BES-DMS under NREL Contract DE-AC36-99GO10337.



**15:54**

**D32 8 Optimized Configuration Interaction Method for Electronic Excitations in Nanostructures*** CLAUDIA TROPAREVSKY, *Oak Ridge National Laboratory and National Renewable Energy Laboratory* ALBERTO FRANCESCHETTI, *National Renewable Energy Laboratory* The Configuration Interaction (CI) method has been widely used to calculate electronic excitations in semiconductor nanostructures. The main drawbacks of this method are its slow convergence with the number of configurations and the difficulty to select a-priori the most relevant configurations. Here we report a new approach for the selection of the CI basis set: For a given number $N_C$ of configurations, we use heuristic search methods to find the set of $N_C$ configurations that minimizes the excited-state energy of the nanostructure. We demonstrate this method for single excitons and biexcitons in CdSe quantum dots. We show that the best configurations not only are different from what one would expect based on the single-particle energy ladder, but also, they often do not correspond to the configurations that have the largest contribution to the full CI wave function. We also show that a few (less than 100) optimized configurations provide excitation energies with accuracy comparable to much larger (10,000 or more) non-optimized configuration basis sets.

*This work was supported by the U.S. DOE LAB03-17 initiative.

**16:06**

**D32 9 Molecular models for nanoporous amorphous carbons via a novel monte carlo algorithm** AMIT KUMAR, RAUL LOBO, NORMAN WAGNER, *Center for Mol. & Eng. Thermodynamics, Dept. of Chem. Eng. Univ. of Delaware, Newark, DE 19711* Nanoporous carbons (NPCs) are interesting amorphous phases of carbon that can exhibit very favorable gas permeation selectivity, which is an area of research. However, computational studies of such amorphous, nonequilibrium phases are hindered by the lack of a robust method to generate candidate molecular structures that validate against the known properties of such materials. A new monte carlo algorithm has been developed to create structural models for amorphous carbons. The simulation method mimics the experimental preparation of nanoporous carbons (NPC) by pyrolysis from polyfurfuryl alcohol as a guideline. The resulting molecular structures exhibits properties that compare favorably to those observed experimentally for real NPCs. These atomistic NPC models are approaching a realistic representation of NPCs used for gas separations and as such, are being used to study the diffusion of small gas molecules in these materials. Comparisons are made to other methods in the literature and possible improvements are discussed.

**16:18**

**D32 10 Solvophobic Solvation Forces between Nanoparticles: Size, Shape, and Solvent Effects** YONG QIN, KRISTEN A. FICHTHORN, *The Pennsylvania State University* The hydrophobic effect is an important phenomenon that can play a central role in biological and colloidal systems. Although hydrophobic hydration has been extensively studied, this is just a specialized case of the more general phenomenon of ''solvophobic solvation,'' which can occur in a wide variety of applications involving solutes in non-aqueous solutions, including colloid and polymer suspensions and assemblies. We report results from molecular-dynamics simulations of solvophobic nanoparticles immersed in n-decane liquid. Analogous to aqueous systems, we observe dewetting in the inter-particle region and attractive solvation forces when the particle separation becomes smaller than a critical value. We show that the critical separation can be affected by particle size and shape, and, in contrast to predictions by theories of hydrophobic hydration; it can be larger for small particles than for large ones. The complex size and shape dependence of solvophobic inter-particle forces allows new prospects for creating selective nonaqueous colloidal assemblies.

**16:30**

**D32 11 The Formation of Haeckelite Structures Induced by Vacancy Defects in Graphene Layers of Carbon Nanotube** GUN-DO LEE, *Seoul National University* C.Z. WANG, *Iowa State University* EUIJOON YOON, NONG-MOON HWANG, *Seoul National University* K.M. HO, *Iowa State University* SEOUL NATIONAL UNIVERSITY COLLABORATION, IOWA STATE UNIVERSITY COLLABORATION, The formation of haeckelite structures induced by vacancy defects in graphene layers of carbon nanotube are investigated by tight-binding molecular dynamics (TBMD) simulations and by first principles total energy calculations. It is observed in the TBMD simulations that two single vacancies coalesce into a 5-8-5 double vacancy at the temperature of 3,000 K, and it is further reconstructed into a new defect structure, the 555-777 defect, by the Stone-Wales type transformation at higher temperatures. First principles calculations confirm that the 555-777 defect is energetically much more stable than two separated single vacancies, and the energy of the 555-777 defect is also slightly lower than that of the 5-8-5 double vacancy. In TBMD simulation, it is also found that the four single vacancies reconstruct into two collective 555-777 defects which is the unit for the hexagonal haeckelite structure proposed by Terrones et al. [Phys. Rev. Lett. **84**, 1716 (2000)]

**16:42**

**D32 12 Viscoelastic Properties of Model Polymer Nanocomposites** JAMES THOMIN, SUCHIRA SEN, PAWEL KEBLINSKI, SANAT KUMAR, *Rensselaer Polytechnic Institute* The study of the dynamics of polymers in the presence of nano-scale particles is not only of fundamental interest but is also key to developing the tools necessary to engineer polymer nanocomposite materials. In this work, we investigate the effect of nanoscopic filler particles on the viscoelastic behavior of a model polymer melt. Molecular Dynamics simulations of bead-spring polymer systems containing roughly spherical nano-filler particles were performed. Equilibrium and non-equilibrium methods were used to determine the stress relaxation and shear-dependent viscosity of both the neat melt and filled systems. We will discuss the results of these simulations, as well as an interesting correlation between certain structural quantities and the observed mechanical reinforcement.

**SESSION D33: FOCUS SESSION: FRICTION, FRACTURE AND DEFORMATION I**
**Monday Afternoon, 13 March 2006; 336, Baltimore Convention Center at 14:30**
**H.G.E. Henstchel, Emory University, presiding**



*Invited Papers*

**14:30**
**D33 1 Tribochemical studies at the nanometer scale: synergisms of mechanical and chemical forces.***
J. THOMAS DICKINSON, *Washington State University*

The manipulation of matter on small size scales dominates a number of potential applications in nanoscience and nanotechnology. The forces and potentials available to break and reestablish bonds between ions, atoms, and molecules becomes greatly expanded when we consider combining stimuli. Our efforts on combining (mechanical + chemical) or (mechanical + radiative) stimulation aims at understanding the resulting synergisms in, for example, dissolution and/or deposition of material. We show that we can measure the kinetics of chemical mechanical wear (e.g., polishing) with a single asperity (the tip of an Atomic Force Microscope) on substrates of single crystals, amorphous materials such as silicate glasses,polymers, crystalline silicon, and on polycrystalline oxides, nitrides, and carbides in controlled chemical media. We find that although the mechanics are relatively straight forward to model, the itdependence on the applied normal force, the applied stress, the solution composition, the solution temperature, the duration time of the wear experiment, and the relative velocity of the AFM tip and substrate can be complex. With care, we have been able to properly measure and model the tribochemical wear on model systems. We present these studies and include new results on technologically interesting materials such as single crystal Si(100). We also present results on the use of an AFM tip to localize layer-by-layer growth of single crystals of inorganic carbonates, sulfates, and phosphates in saturated aqueous solutions.

*Supported by NSF Surface Engineering and Material Design Program.

*Contributed Papers*

**15:06**
**D33 2 Elucidation of the Atomic-Scale mechanisms of Friction in Model SAMs and DLC films*** JUDITH HARRISON, PAUL MIKULSKI, GUANGTU GAO, KEVIN VAN WORKUM, J. DAVID SCHALL, GINGER CHATEAUNEUF, *US Naval Academy* The development of micron-sized devices for terrestrial and space applications has prompted the need for protection of the surfaces of these devices. Amorphous carbon films, diamondlike carbon, and SAMs are all possible candidates for the passivation and lubrication of these devices. The fundamental problem associated with controlling friction is a lack of understanding of the underlying atomic-scale processes that govern it. Over the past several years, we have performed extensive molecular dynamics simulations aimed at understanding the atomic-scale mechanisms of friction. We have examined the contact forces present at the interface of a tip and SAMs during sliding. Compression- and shear-induced polymerization have also been modeled in SAMs. In addition, we have done simulations that analyzed the tribological properties of amorphous carbon films with various compositions and of diamondlike carbon films. Some of our recent results will be discussed.

*Work supported by AFOSR and ONR.

**15:18**
**D33 3 Relating structure and friction: Energy dissipation during the lateral manipulation of antimony nanoparticles** U.D. SCHWARZ, *Dept. of Mechanical Engineering, Yale University* C. RITTER, *Institute of Chemistry, Humboldt University Berlin* M. HEYDE, *Fritz-Haber Institute of the Max-Planck-Society, Berlin* K. RADEMANN, *Institute of Chemistry, Humboldt University Berlin* Despite its daily-life importance, the fundamentals of friction are still insufficiently understood. In particular, the interplay between friction, ''true'' contact area, and crystalline structure at the interface is an issue of current debate. Recently, a new technique had been introduced that allows determining the threshold energy dissipated during the lateral displacement of small nanoparticles on suitable substrates as a function of the particle-substrate contact area [Ritter et al., PRB **71**, 085405 (2005)]. Here, we present results of an extensive study of antimony nanoparticles 1000 $nm^2$ to 100000 $nm^2$ in size moved in air on graphite substrates. Complementary studies by electron microscopy reveal the internal structure of the islands, showing a transition from amorphous to crystalline of the island's cores at about 10000-15000 $nm^2$ size, while the surface layers are composed of amorphous antimony oxide in all cases. However, despite the similarities of the amorphous surface layer, islands with crystalline core show significantly higher energy dissipation during motion than the ones with amorphous core. Possible reasons for this effect are discussed.

**15:30**
**D33 4 Relationship between friction and quasicrystallinity; friction anisotropy in a decagonal Al-Ni-Co quasicrystal surface** JEONG YOUNG PARK, D. F. OGLETREE, M. SALMERON, *Lawrence Berkeley National Lab. University of California, Berkeley* R. A. RIBEIRO, P. C. CANFIELD, *Ames Laboratory, Dept. of Physics & Astronomy, Iowa State Univ* C. J. JENKS, P. A. THIEL, *Ames Laboratory, Dept. of Chemistry, Iowa State Univ* We investigated the nanoscale tribological properties of a decagonal quasicrystal using a combination of atomic force microscopy (AFM) and scanning tunneling microscopy (STM) in ultrahigh vacuum. This combination permitted a variety of in situ measurements, including atomic- scale structure, friction and adhesion force, tip-sample current, and topography. We found that thiol-passivated tips can be used for reproducible studies of the tip-quasicrystal contact while non-passivated probes adhere irreversibly to the clean quasicrystalline surface causing permanent

modifications. The most remarkable results were obtained on the 2-fold surface of the Al-Ni-Co decagonal quasicrystal where atoms are arranged periodically along the 10-fold axis and aperiodically in the perpendicular direction. Strong friction anisotropy was observed on this surface, with high friction along the periodic direction, and low friction in the aperiodic direction. These results reveal a strong connection between interface atomic structure and the mechanisms by which energy is dissipated, which likely include electronic or phononic contributions, or both.

**15:42**

**D33 5 New Phenomena in High Temperature Nanofriction on Nonmelting Surfaces: NaCl(100)** TATYANA ZYKOVA-TIMAN, DAVIDE CERESOLI, *SISSA, INFM, Democritos, via Beirut 2-4, 34014 Trieste, Italy* ERIO TOSATTI, *SISSA, INFM, Democritos, ICTP, P.O. Box 586, I-34014 Trieste, Italy* High temperature nanofriction is a difficult and so far unexplored area wwhere we made an initial attack by means of simulation. Alkali halide (100) surfaces were chosen as they would not automatically liquefy under a sliding tip, even at temperatures very close to the melting point. We conducted sliding friction molecular dynamics simulations of hard tips on NaCl(100),both in the heavy ploughing, wear-dominated regime, and in the light grazing, wearless regime. Ploughing friction shows for increasing temperature a strong frictional drop near the melting point. Here the tip can be characterized as ''skating'' over the hot solid, its apex surrounded by a local liquid halo, which moves along with the tip as it ploughs on. At the opposite extreme, we find that grazing friction of a lightly pressed flat-ended tip behaves just the other way around. Starting with an initially very weak low temperature frictional force, there is a surge of friction just near the melting point, where the surface is still solid, but not too far from a vibrational instability. This frictional rise can be envisaged as an analog of the celebrated ''peak effect'' found close to Hc2 in the mixed state critical current of type II superconductors.

**15:54**

**D33 6 Nanotribological studies of Temperature Rise in a Sliding Adsorbed Film** MATTHEW WALKER, *North Carolina State University* CHERNO JAY, *North Carolina State University* JACQUELINE KRIM, *North Carolina State University* Theoretical predictions of friction-induced temperature increases at sliding interfaces in general show a wide variation, with little opportunity for experimental verification. In order to explore temperature rise in a particularly simple geometry, we have recorded isotherms of sliding Kr layers adsorbed on graphene (a one-atom thick layer of graphite) and compared them to those recorded in the past in static conditions[ J.A. Venables, itIntroduction to surface and Thin Film Processes. Cambridge University Press, Cambridge, (2000) p. 116]. We synthesize graphene on a Ni(111), which has a lattice spacing stretched approximately 2% beyond that of graphite. The Ni(111) was prepared as an electrode on the surface of a quartz crystal microbalance (QCM) so that friction measurements in sliding conditions could be recorded [J. Krim and A. Widom, Phys. Rev. B, **38**, 12184 (1988)]. Superposition of the isotherms recorded for this system were superimposed on the static volumetric phase diagrams to infer a temperature increase of approximately 15K above the temperature at which the experiments were performed. Work funded by the NSF.

**16:06**

**D33 7 The Temperature Dependence of Macroscopic Sliding Friction*** J.C. BURTON, P. TABOREK, J.E. RUTLEDGE, *University of California, Irvine* We present measurements of the static and kinetic coefficients of friction of gold-plated copper on gold-plated copper and sapphire on sapphire as a function of temperature from 10K to 400K. The measurements were done by sliding a block down a controllable incline plane and using high-speed video to extract the acceleration. The large size of our optical cryostat allowed linear motion of 7.5 cm over which to measure the acceleration. Surfaces were baked under high vacuum at 400K, and data was taken as they cooled. Preliminary results indicate that the coefficient of friction for gold plated copper surfaces change by 10 percent from room temperature to 10K.

*This work has been supported by AFOSR MURI grant # FA9550-04-1-0381.

**16:18**

**D33 8 Measurements of Coefficients of Kinetic Friction Using a Driven Harmonic Oscillator*** M. G. AGGLETON, P. TABOREK, J. E. RUTLEDGE, *University of California, Irvine* We have developed a method of measuring the kinetic coefficient of friction of various materials. Instead of the standard pin-on-disc tribometer, we have developed a driven harmonic oscillator at frequencies around 50Hz to measure friction at the millimeter to centimeter scale. The system is driven by a magnetic field and measured by a linear variable differential transducer (LVDT). Contact between a plate attached to the oscillator and a sphere provides damping due to friction. We will present results for various material combinations, as well as perform a comparison between these results and those of other researchers using a variety of techniques. This apparatus was designed with the intention of being vacuum and low temperature compatible in order to explore the temperature dependence of friction in the cryogenic regime.

*This work has been supported by AFOSR MURI grant # FA9550-04-1-0381.

**16:30**

**D33 9 Free-standing micro locomotive structures driven by the thermal modulation** ONEJAE SUL, MICHAEL FALVO, LLOYD CAROLL, TIMOTHY O'BRIEN, RICHARD SUPERFINE, RUSSELL TAYLOR, JR., SEAN WASHBURN, *Univ. of North Carolina at Chapel Hill* NANO SCIENCE RESEARCH GROUP (DEPT. OF PHYSICS AND ASTRONOMY, DEPT. OF COMP. SCI.) TEAM, As the sizes of Microelectromechanical(MEMS) devices and also the sizes of their contact to environment shrink down to micrometers, the role of contact becomes more critical in understanding and applying it for realization of mobile devices. Since the dominating forces between objects under micro regime are attractive forces such as van der Walls and capillary force, any motion will be mainly influenced by the surface forces rather than inertia. The greatest barrier to actuation is to overcome such forces while achieving net motion. This necessitates smallest contact area. Our research pushed the limits of the contact area to nanometers for minimized friction against the substrate, thus small friction requires lesser thrust and enables faster actuation. We made the inch-worm style bimorph thin film devices standing on the graphite and they are non-umbilical by design. We will first discuss the estimation of thrust, friction of a device on the graphite. We will then discuss the walking mechanism of coordi-

nating three contact tips upon repeated heating and cooling thermal cycles. Additionally we will present predictions and measurements on various properties of our devices such as deflection depending on temperature, time constant of heat/cooling, and contact sliding speeds.

**16:42**
**D33 10 Superconductivity Dependent Friction in Superheated He Films** M. HIGHLAND, J. KRIM, *North Carolina State University* We report a quartz crystal microbalance (QCM) study of sliding friction levels in $N_2$, $H_2O$ and superheated He films adsorbed on Pb(111) above and below its superconducting transition temperature. Our findings establish firmly that superconductivity dependent friction is present in a wide range, if not all, of adsorbed film systems that remain unpinned at 7K, and that on and off cycling of an externally applied magnetic field may impact friction. Changes in friction at the superconducting transition are observed to be greater for $H_2O$ and $N_2$ than for the He films, consistent with a recent theory that attributed differences in electronic friction levels to the polarity of the adsorbate [L.W. Bruch, Phys. Rev. B. **61**, 16201 (2000)]. This work was supported by NSF and AFOSR.

**16:54**
**D33 11 Friction between Polymer Brushes*** JEFFREY SOKOLOFF, *Northeastern University* A polymer brush consists of a surface with a fairly concentrated coating of polymer chains, each one of which has one of its ends tightly bound to the surface. They serve as extremely effective lubricant, producing friction coefficients as low as 0.001 or less! Polymer brushes are a promising way to reduce friction to extremely low values. They have the disadvantage, however, that they must be immersed in a liquid solvent in order to function as a lubricant. The presence of a solvent is believed to result in osmotic pressure which partially supports the load. The density profile of a polymer brush (i.e., the density of monomers as a function of distance from the surface to which the polymers are attached) is well established. What is not understood is how the interaction of polymer brush coated surfaces in contact with each other is able to account for the details of the observed low friction. For example, molecular dynamics studies generally do not predict static friction, whereas surface force apparatus measurements due to Tadmor, et. al., find that there is static friction. This is the topic of the present presentation.

*Work partially supported by DOE



## SESSION D35: FOCUS SESSION: THERMAL TRANSPORT AND THERMOELECTRICITY IN NANOTUBES AND GRAPHENE

**Monday Afternoon, 13 March 2006; 338, Baltimore Convention Center at 14:30**
**B.C. Regan, University of California, Los Angeles, presiding**

***Invited Papers***

**14:30**
**D35 1 Thermal and thermoelectric properties of individual single-walled carbon nanotubes, Bi-based and III-V nanowires.***
LI SHI, *University of Texas at Austin*

Electronic and thermoelectric materials can be nanostructured to confine electrons and phonons in one or more dimensions so as to engineer the transport and interaction of charge and heat. Various classical and quantum size confinement effects on the thermal and thermoelectric properties have been suggested by theoretical calculations, but have not been experimentally verified due to the difficulty in nanoscale thermal transport measurements. We have developed MEMS (microelectromechanical systems) sensor devices for measuring the thermal and thermoelectric properties of individual one-dimensional nanostructures. Using the sensor devices, we have observed record-high thermal conductivity and ballistic phonon transport in single-walled carbon nanotubes, suppressed thermal conductivity in semiconductor nanowires, and enhanced thermoelectric figure of merit in bismuth telluride nanowires. These findings suggest an escalating self-heating problem in nanoelectronic devices and also novel uses of nanomaterials for thermal management and for efficient thermoelectric energy conversion.

*This work is supported by NSF Thermal Systems Program, ONR (Program manager: Dr. Mihal E. Gross), and NASA/Eloret Corporation.

***Contributed Papers***

**15:06**
**D35 2 Ballistic Phonon Thermal Transport and Thermal Properties of Carbon Nanotubes** HSIN-YING CHIU, VIKRAM DESHPANDE, HENK POSTMA, *California Institute of Technology* CHUN NING LAU, *University of California, Riverside* CSILLA MIKÓ, LÁSZLÓ FORRÓ, *IPMC/SB, EPFL, CH-1015 Lausanne-EPFL, Switzerland* MARC BOCKRATH, *California Institute of Technology* We report electrical transport experiments, using the phenomenon of electrical breakdown to perform thermometry, that probe the thermal properties of individual multiwalled carbon nanotubes. Our results show that nanotubes can readily conduct heat by ballistic phonon propagation. We determine the thermal conductance quantum, the ultimate limit to thermal conductance for a single phonon channel, and find good agreement with theoretical calculations. Moreover, our results suggest a breakdown mechanism of thermally activated C-C bond breaking coupled with the electrical stress of carrying $10^12$ A/m$^2$. We also demonstrate a current-driven self-heating technique to improve the conductance of nanotube devices dramatically. The results of our ongoing experiments will be reported.

**15:18**

**D35 3 Aspects of the Thermal Conductivity of Nanotubes** CHIH-WEI CHANG, ADAM FENNIMORE, ANDERI AFANASIEV, DAVID OKAWA, TAKASHI IKUNO, HENRY GARCIA, ALEX ZETTL, *Physics department, University of California at Berkeley and Materials Science Division, Lawrence Berkeley National Laboratory* DEYU LI, *Department of Mechanical Engineering, Vanderbilt University, Tennessee* ARUN MAJUMDAR, *Department of Mechanical Engineering, University of California at Berkeley* We have measured the thermal conductivity of individual multiwalled carbon and boron nitride nanotubes using a microfabricated suspended device. The structure of the measured nanotubes also has been characterized by using a transmission electron microscope. We have found that the thermal conductivity of an isotopically pure BN nanotube is comparable to that of a carbon nanotube with the same diameter. The temperature dependence, the effect of deformation, and localized defects on the nanotubes' thermal transport will also be presented.

**15:30**

**D35 4 Phonon Dynamics in Carbon Nanotubes** ARUN BODAPATI, PAWEL KEBLINSKI, *Rensselaer Polytechnic Institute* PATRICK SCHELLING, *University of Central Florida* Using vibrational mode analysis of pristine and defected carbon nanotubes we will demonstrate that defects cause a change in the spatial extension and polarization of phonons leading to a consequent loss of their ballistic nature. Furthermore, to gain a more detailed understanding of thermal energy flow in defected carbon nanotubes we use molecular dynamics simulation to investigate scattering of of well-defined phonon wave-packets either by structural defects or by other phonons. The dependence of scattering of longitudinal and transverse acoustic phonons on their wavelengths will be also discussed.

**15:42**

**D35 5 Heat transport and thermal management in single walled carbon nanotubes** HAREEM MAUNE, *California Institute of Technology* MARC BOCKRATH, *California Institute of Technology* Results from our investigation of thermal transport in CVD grown Single-Walled Carbon nanotubes (SWNT) on different substrates will be reported. Chiu et al. recently showed that multi-walled carbon nanotube devices cool by ballistic phonon heat transport. To harness the remarkable thermal properties of nanotubes for thermal management, it is of interest to understand how heat energy is transported into or out of nanotubes. In this work, we investigate the breakdown power for SWNT nanotube devices using different substrate materials to determine the effect of substrate thermal conductivity on nanotube breakdown. We compare our results with those obtained with the Si/ SiO2 substrate. Our results indicate higher power dissipation on a sapphire substrate for few micron SWNTs but lower than expected dissipation for the longer length scales. We will discuss the mechanism of power dissipation and thermal transport in our devices in light of our results.

**15:54**

**D35 6 Interfacial Thermal Transport Between Single Wall Carbon Nanotubes*** JENNIFER LUKES, HONGLIANG ZHONG, *University of Pennsylvania* Due to their superior thermal conductivity, single wall carbon nanotubes have elicited great interest as potential thermal management materials, for example as fillers in polymer composites and as thermal interface materials. Recent measurements on carbon nanotube composites have revealed lower-than-expected conductivities, and thermal interfacial resistance between the nanotubes and the surrounding medium has been implicated as a key factor limiting heat flow. However, one factor that has been little-considered is the role of interfacial thermal resistance between individual nanotubes. In these composites, the nanotubes form an interconnected network and for this reason interfacial resistance at the contact points between the nanotubes is also expected to have a significant effect on thermal energy transport. Our recent modeling results indicate that a four order of magnitude reduction in nanotube-nanotube interfacial resistance is obtained as the nanotubes are brought into intimate contact. These results will be discussed in this presentation.

*This work was supported by the Office of Naval Research

**16:06**

**D35 7 Graphene-based polymer nanocomposites: a new class of materials*** DMITRIY DIKIN, SASHA STANKOVICH, GEOFFREY DOMMETT, KEVIN KOHLHAAS, ERIC ZIMNEY, RICHARD PINER, XINQI CHEN, SONBINH NGUYEN, RODNEY RUOFF, *Northwestern University* We have developed an approach that yields a new class of materials: the graphene-based materials. I present our 'bottom up' approach to achieving highly dispersed chemically modified graphene (CMG) sheets in polymer composites. A host of novel studies of both individual CMG sheets as well as of the CMG sheet-based nancomposites, is thus now possible. An overview is given of the level of dispersion of the CMG sheets and their morphology in the composites, and of the composite thermal/electrical conductivity and thermomechanical properties. I also discuss our deposition of individual sheets and studies of them.

*We gratefully acknowledge the NASA University Research, Engineering and Technology Institute on Bio Inspired Materials (BIMat) under award No. NCC-1-02037.

**16:18**

**D35 8 Morphology and electrical characterization of polymer nanocomposite based on chemically modified graphene sheets*** DMITRIY DIKIN, SASHA STANKOVICH, KEVIN KOHLHAAS, GEOFFREY DOMMETT, ERIC ZIMNEY, RODNEY RUOFF, *Department of Mechanical Engineering* OLEKSANDR CHERNYASHEVSKYY, *Department of Physics and Astronomy* SONBINH NGUYEN, *Department of Chemistry, Northwestern University* Graphite particles may be oxidized yielding graphene (one atom thick graphite layer) oxide sheets. Furthermore surface modification allows controllable engineering of their properties including recovery of the electrical conduction and homogeneous dispersion in different polymers. Formation of percolative network for electrical transport at very low threshold in the dielectric polymer matrix will be discussed in relation to the composite samples morphology, chemical modification of graphene sheets, and their topological states. DC and AC electrical measurements in combi-

nation with scanning electron microscopy (surface and sub-surface imaging) were used for composites characterization.

*We gratefully acknowledge the NASA University Research, Engineering and Technology Institute on Bio Inspired Materials (BIMat) under award No. NCC-1-02037.

**16:30**

**D35 9 Transmission Electron Microscopy of a Graphene-based Polymer Nanocomposite** KEVIN KOHLHAAS, DMITRIY DIKIN, SASHA STANKOVICH, RODNEY RUOFF, *Department of Mechanical Engineering, Northwestern University, Evanston, IL 60208* ERIC STACH, *School of Materials Engineering, Purdue University, West Lafayette, IN 47906* A Polystyrene/CMG (chemically modified graphene) composite has been made by a solution-based processing technique followed by hot pressing or injection molding to form continuous specimens. Microtomed samples were prepared for study by transmission (TEM) and scanning (SEM) electron microscopy. The electron diffraction patterns and the resulting d-spacings, as well as high-resolution bright field TEM images, suggest that the platelets are individual graphene sheets randomly dispersed in the polymer matrix. Scanning electron microscopy observation indicates that the sheets are in a wrinkled conformation; this wrinkling has also been observed in TEM, in the form of 10 nm domains exhibiting lattice fringes of varying orientations. We gratefully acknowledge the NASA University Research, Engineering and Technology Institute on Bio Inspired Materials (BIMat; No. NCC-1-02037) and the National Science Foundation (No. DMR-0526959).

**16:42**

**D35 10 Electrical Properties of a Graphene-based Polymer Nanocomposite.** GEOFFREY DOMMETT, DMITRIY DIKIN, ERIC ZIMNEY, SASHA STANKOVICH, RODNEY RUOFF, *Northwestern University* A polymer/CMG (chemically modified graphene) composite has been prepared by a solution-based processing technique followed by hot pressing or injection molding to prepare continuous sample specimens. The electrical properties of these composites have been measured by 2- and 4-probe techniques, as a function of temperature and concentration to investigate the mechanisms by which electrical transport occurs in a composite with single graphene sheet filler material, and the percolation threshold at which conduction occurs. We gratefully acknowledge the itNASA University Research, Engineering and Technology Institute on Bio Inspired Materials (BIMat) under award No. NCC-1-02037.

**16:54**

**D35 11 Correction Factors for 4-probe Electrical Transport Measurements with Finite Size Electrodes: Analytical and Finite Element Analysis*** E.J. ZIMNEY, G. DOMMETT, D.A. DIKIN, R.S. RUOFF, *Department of Mechanical Engineering, Northwestern University, Evanston, IL 60208* In most real specimens the current density is non-uniform through the thickness between the sense (potential) probes. Non-uniformities in the current density can result from many effects including the geometry of the specimen, the finite size of the electrodes, anisotropic behavior of the material, etc. Thus great care must be taken in extracting the correct bulk resistivity from the measured resistance. We have developed a method, based on finite element analysis, to accurately determine the bulk in-plane resistivity from collinear 4-probe resistance measurements on isotropic and anisotropic materials. The effect of boundary conditions on the measured resistivity is explored. Our finite element approach can be universally applied to 4-probe measurements on complex specimen geometries with arbitrary electrode arrangements.

*We gratefully acknowledge the NASA University Research, Engineering and Technology Institute on Bio Inspired Materials (BIMat; No. NCC-1-02037) and the National Science Foundation (No. CMS-0304506).

**17:06**

**D35 12 Development of optical approaches for identifying individual graphene-based sheets on surfaces*** INHWA JUNG, RICHARD PINER, DMITRIY DIKIN, SASHA STANKOVICH, RODNEY S. RUOFF, *Department of Mechanical Engineering* MARTINA HAUSNER, *Department of Civil and Environmental Engineering, Northwestern University, Evanston, IL 60208* We are developing a light microscope-based method for identifying thin graphene-based sheets on silicon wafers with a thin dielectric layer (SiO2 or Si3N4). Different thicknesses of this dielectric layer have been tested. Optics, and experiments with these thin dielectric layers, enabled us to optimize the thickness that yields the best contrast; SiO2 is useful for discerning multiple stacked sheets and Si3N4 for identifying individual sheets. Both multiple or single wavelength sources can be used effectively. By comparing the optical images with data obtained by AFM and SEM, it has been possible to prove that our method can detect the presence of individual graphene- based sheets.

*We gratefully acknowledge the NASA University Research, Engineering and Technology Institute on Bio Inspired Materials (BIMat; No. NCC-1-02037) and the Naval Research Laboratory (No. N00173-04-2-C003).

**17:18**

**D35 13 Possibilities for graphene for field emission: Modeling studies using the boundary element method*** SUPINDA WATCHAROTONE, RODNEY S. RUOFF, *Department of Mechanical Engineering, Northwestern University, Evanston, IL 60208* FRANK H. READ, *Department of Physics and Astronomy, University of Manchester, Manchester, UK* Field emission from a graphene sheet has been modeled with the boundary element method. A modeled flat thin sheet is used. The local electric field and hence the field enhancement factor have been obtained, and the relative magnitude of the field enhancement factors at the corners and the edges has been established. A comparison with field emission from carbon nanotubes will be presented.

*We gratefully acknowledge the NASA University Research, Engineering and Technology Institute on Bio Inspired Materials (BIMat; No. NCC-1-02037) and the National Science Foundation (No. 1421-M3/ CMS-0304506).

**SESSION D38: FOCUS SESSION: SUPERCONDUCTIVITY—PROPERTIES OF DOPED AND IRRADIATED MAGNESIUM DIBORIDE AND RELATED COMPOUNDS**
**Monday Afternoon, 13 March 2006; 341, Baltimore Convention Center at 14:30**
**David Larbalestier, University of Wisconsin, presiding**



*Invited Papers*

**14:30**
**D38 1 Scattering in $MgB_2$ produced by substitutions and damage.**
MARINA PUTTI, *University of Genova, CNR-INFM-LAMIA*

The two-gap nature of superconductivity is a unique feature of $MgB_2$that stimulates many theoretical and experimental investigations. From the beginning it was pointed out that the peculiar role of disorder in a two-gap superconductor In fact, inter-band scattering by non-magnetic impurities is expected to suppresses the critical temperature $T_c$ down to 20 K, where an equivalent one-gap BCS system stabilizes. The verification of these predictions has motivated several efforts to introduce defects in $MgB_2$ by substitutions (Al in sites of Mg and C in sites of B) and by irradiation. Substitutions modify electronic structure so that superconductivity can be influenced. To overcome this problem we studied two different kind of samples: co-doped $Mg_{1-x}(AlLi)_xB_2$ in which the disorder induced by the Mg substitution is accompanied by a rather complete charge compensation, and neutron irradiated $Mg^{11}B_2$. In both the sample series remarkable changes in the band structure are not expected. The superconducting properties of $Mg_{1-x}(AlLi)_xB_2$are compared with those of $Mg_{1-x}Al_xB_2$. All the properties scale systematically as a function of the Al content rather than electron doping. This suggests that the lattice deformations induced by Al, namely point-like defects and lattice compression, are very effective in tuning the superconducting properties. Similar conclusion can be drawn by the study of neutron irradiated samples. By increasing the neutron fluence, $T_c$ monotonously decreases down to 9 K, the resistivity raises by two order of magnitude and the cell volume increases (1.7%). Our results demonstrate that the critical temperature is suppressed by the disorder well down the value of 20 K. On the other hand, the two-gap feature evident in the temperature range above 21 K, disappears when $T_c$ is lowered down to 11 and 8.7 K a single-gap superconductivity is established.

*Contributed Papers*

**15:06**
**D38 2 Effects of helium ion damage on the two-band superconductivity in $MgB_2$ thin films** L.H. GREENE, W.K. PARK, X. LU, *U. of Illinois at Urbana-Champaign* B. MOECKLY, *Superconductor Technologies, Inc.* R. SINGH, N. NEWMAN, J.M. ROWELL, *Arizona State U.* While the two-band superconductivity in $MgB_2$ has been well established, it remains controversial whether disorder in the Mg and B planes causes enhanced inter-band scattering, band filling or both. To address this, we have performed electronic transport and point-contact spectroscopy measurements on helium-ion irradiated $MgB_2$ thin films. Two sets of samples are prepared using: a) 1 MeV $He^+$ ions with uniform doses ranging from $1x10^{15}$ to $1x10^{17}$ ions/cm$^2$; b) 2 MeV alpha particles with gradient doses. The resistivity ($T_c$) is observed to increase (decrease) monotonically with increasing dose. The conductance spectra are taken from point-contact junctions between $MgB_2$ thin films and Au tips. The $T_c$ is determined by the onset of enhanced conductance at zero bias. Our preliminary results show that the two gaps tend to merge into one gap with increasing ion damage. Detailed results including $T_c$ vs. energy gap will be presented and discussed in terms of the electronic structure change caused by ion-induced point defects. WKP acknowledges Pavel Krasnochtchekov and Robert Averback for ion irradiation experiments at UIUC. This work is supported by the DoE DEFG02-91ER45439, through the FSMRL and the Center for Microanalysis of Materials at UIUC.

**15:18**
**D38 3 Effect of ion irradiation and annealing on scattering processes in MgB2** RAGHURAM GANDIKOTA, RAKESH SINGH, JIHOON KIM, BARRY WILKENS, NATHAN NEWMAN, JOHN ROWELL, *Arizona State University* ALEXEJ POGREBNYAKOV, XIAOXING XI, JOAN REDWING, SHENGYONG XU, QI LI, *Pennsylvania State University* BRIAN MOECKLY, *Superconductor Technologies Inc.* The effect of point defects introduced by ion irradiation on Tc, resistivity, and Hc2 of MgB2 films was studied. We will show that ion induced disorder in films with different as-made disorder, followed by annealing, offers advantages in the study of Hc2 of MgB2 films. Films, from three deposition processes, were damaged by 2 MeV alpha particles, followed by annealing after Tc was reduced to $<$ 10K. Damage increases Hc2 (0) in clean films, resulting in maxima ( $\sim$ 34T) near Tcs of 33K, for fields parallel to the film. For Tcs from $\sim$ 25K to below 10K, Hc2(0) decreases almost linearly with Tc. Annealing the films, after Tc has been reduced below 10K, reproduces the resistivity value but not the Hc2(0), for a given Tc. These results suggest that Tc is reduced by smearing of the density of states, and that the measured resistivity and Hc2 are determined by scattering in pi and sigma bands respectively.

**15:30**
**D38 4 Magnetic and non-magnetic substitutions in $MgB_2$ single crystals: influence on superconducting properties and structure** JANUSZ KARPINSKI, NIKOLAI D ZHIGADLO, KRZYSZTOF ROGACKI, BERTRAM BATLOGG, GETZ SCHUCK, *Laboratory for Solid State Physics ETH Zurich* ROMAN PUZNIAK, ANDRZEJ WISNIEWSKI, *Institute of Physics PAS Warsaw* RENATO GONNELLI, *Politecnico di Torino* Pure and substituted single crystals of $MgB_2$have been grown at high pressure (30 kbar) using the cubic anvil technique. The crystals

have very low residual resistivity $\rho_o(40\ \mathrm{K}) \approx 0.5$ and a sharp transition $\Delta T_c \approx 0.2$ K. Magnetic (Mn, Fe) and non-magnetic (Al, C) ions have been substituted to study their effect on superconductivity and on the impurity scattering in and between the $\sigma$ and $\pi$ bands. Single-phase $Mg_{1-x}Al_xB_2$ and $MgB_{2-x}C_x$ crystals were grown for x=0-0.3. Al and C cause a similar moderate decrease of $T_c$. Magnetic ions, such as $Fe^{3+}$ and $Mn^{2+}$ suppress $T_c$ very effectively, due to magnetic pair breaking. Superconductivity is completely suppressed for by 2% Mn. Fe substitution decreases $T_c$ less rapidly than Mn but much faster than Al and C. Carbon substitution increases the $H_{c2}$ twice, while Al, Fe and Mn substitutions decrease this field. $H_{c2}$ anisotropy decreases with all substitutions, but the temperature dependence of the anisotropy is different, due to different scattering rates in the $\pi$ and $\sigma$ bands. For Mn and Al, $\pi$ and $\sigma$ energy gaps exist up to the highest substitution level, while for C substitution, merging of these gaps is observed indicating interband scattering.

**15:42**

**D38 5 Evolution of two-gap superconductivity of $MgB_2$ by Al substitution** MIN-SEOK PARK, HEON-JUNG KIM, HYE-GYONG LEE, *National Creative Research Initiative Center for Superconductivity & Department of Physics, Pohang University of Science and Technology* MYUNG-HWA JUNG, YOUNGHUN JO, *Quantum Material Laboratory, Korea Basic Science Institute, DaeJeon 305-333, Republic of Korea* SUNG-IK LEE, *National Creative Research Initiative Center for Superconductivity & Department of Physics, Pohang University of Science and Technology* MIN-SEOK PARK, HEON-JUNG KIM, HYE-GYONG LEE, AND SUNG-IK LEE TEAM, MYUNG-HWA JUNG, YOUNGHUN JO, AND SUNG-IK LEE COLLABORATION, The temperature dependence of the upper critical fields ($H_{c2}(T)$) of the two-gap superconductors $Mg_{1-x}Al_xB_2$ not only for low doping level ($x < 0.1$) but also for high doping level ($0.1 \leq x \leq 0.3$) was obtained by resistivity measurements. The $H_{c2}(T)$ values were analyzed, within the dirty-limit two-gap model, using the calculated electron-phonon coupling constants and Coulomb pseudo potentials. As the Al contents increased, both $T_c$ and $H_{c2}(0)$ decreased, which was the direct manifestation of the increasing number of electrons. At the same time, the three-dimensional $\pi$ bands became much dirtier when Al was doped. In contrast, the intraband scattering of the two-dimensional $\sigma$ bands was relatively unaffected by the Al doping. These behaviors could be understood when the characters of both bands were considered. In all the samples that we investigated, the $\sigma$ bands were dirtier than the $\pi$ bands.

**15:54**

**D38 6 Thermal Expansion measurements on single crystals of the superconductor $MgB_2$*** JOHN J. NEUMEIER, R. BOLLINGER, C. A. M. DOS SANTOS, *Montana State University* N. D. ZHIGADLO, JANUSZ KARPINSKI, *Laboratory for Solid State Physics ETH Zürich* Thermal expansion measurements have been conducted along the a and c axes on single crystals of the superconductor $MgB_2$. The samples are platelets with typical thicknesses of 0.1 mm. The a axis lies in the plane of the platelets, this axis is typically 0.5 mm long. The measurements were conducted using a capacitive thermal expansion cell constructed entirely of fused silica; it is capable of detecting 0.1 Å changes in length. The results reveal that the linear thermal expansion $\Delta L/L = 21\text{x}10^{-4}$ and $5.2\text{x}10^{-4}$ along the c and a axes, respectively, in the temperature range $5\ \mathrm{K} < T < 300$ K. At the superconducting transition temperature $T_c$, jumps in the thermal expansion coefficient $\alpha$ are observed to be positive along both axes. Regions where $\alpha < 0$ are observed along both axes. The results are in general agreement with recently published data [1] on polycrystalline $MgB_2$. [1] J. J. Neumeier, T. Tomita, M. Debassai, J. S. Schilling, P. W. Barnes, D. G. Hinks, and J. D. Jorgensen, Phys. Rev. B. Rapid Commun. December 2005.

*This material is based upon work supported by the NSF through grant DMR 0504769.

**16:06**

**D38 7 Measurements of elastic constants for single crystals of magnesium diboride** KENNETH PESTKA, J.D. MAYNARD, XIAXING XI, QI LI, *Penn State Univeristy* Important information concerning the nature of the high temperature BCS superconductor magnesium diboride, $MgB_2$, may be obtained from measurements of elastic constants with single crystal samples. As derivatives of the free energy with respect to atomic displacements, the elastic constants are a sensitive probe of the lattice environment in which all solid state phenomena occur. We have used the technique of resonant ultrasound spectroscopy (RUS) for very small samples in order to measure good quality single crystals. The samples were grown epitaxially on silicon carbide substrates using physical vapor deposition; samples were a few hundred microns wide and 600 to 750 nm thick.

**16:18**

**D38 8 Nanoscale spatial non-homogeneity of 3D $\Delta_\pi$ in $Mg_{1-x}AlB_2$ single crystals** F. BOBBA, F. GIUBILEO, A. SCARFATO, A. M. CUCOLO, *CNR-INFM SUPERMAT Lab. And Physics Dept., University of Salerno, Via S. Allende, 84081 Baronissi (SA), Italy* D. RODITCHEV, *Institut des Nanosciences de Paris, Université Paris 6 et 7, CNRS (UMR 75 88), 75015 Paris, France* N. ZHIGADLO, S. KAZAKOV, J. KARPINSKI, *Solid State Physics Laboratory, ETH Zurich, CH-8093 Zurich, Switzerland* We have performed local I(V) and dI/dV(V) measurements on high quality $Mg_{1-x}Al_xB_2$ single crystals with different Al dopings by means of Scanning Tunneling Spectroscopy (STS). Both temperature and magnetic field dependences of the conductance spectra have been studied both in S-I-N and in S-I-S configurations. The measured spectra revealed only one gap at low temperatures as expected for pure c-axis tunneling. In the case of x=0.1, the measured superconducting gap $\Delta_{\pi g}$ appeared highly non-homogeneous in its spatial distribution on nanometer scale, with an amplitude varying between 1.5 meV and 2.3 meV. In pure $MgB_2$ the evolution of the zero bias conductance (ZBC) in magnetic field clearly showed two different regimes with a fast rise up to 1 T, followed by a slower refilling of states for higher fields. This effect results smoothed in doped single crystals. Consistently with the more recent theories, in comparison with the undoped material, we have found that for x=0.1 the $\Delta_\pi$ gap value and the $H_{c2}$ critical field increase of about 15% and 30%, respectively.

**16:30**

**D38 9 Superconductivity in $Y_2C_3$** SATOSHI AKUTAGAWA, JUN AKIMITSU, *Aoyama-Gakuin University* The discovery of superconductivity in $MgB_2$ revived the enthusiasm of non-oxides materials and initiated a search for novel superconductivity in intermetallic compounds including light elements, B and C. As a part of these researches, we have reported a relatively high-$T_c$ superconductivity in $Y_2C_3$ at 18 K whose $T_c$ could be changed

from 10 K to 18 K by synthesis conditions, although this material with a maximum $T_c$ of 11.5 K has already been investigated by Krupka *et al.*. The crystal structure of $Y_2C_3$ is a body-cente red cubic ($Pu_2C_3$-type) s tructure. In this structure, Y atoms are aligned along the $< 111 >$ direction and C atoms form dimers. We synthesized a high-purity sample of the medium-$T_c$ phase ($T_c$ = 13.9 K) in $Y_2C_3$ and examined its physical properties in detail. From a specific heat measurement, the superconducting gap is estimated to be 4.50, indicating that the superconductivity in $Y_2C_3$ can be described by an *s*-wave strong coupling regime. From specific heat in various magnetic fields, the upper critical field $H_{c2}(0)$ is estimated to be 24.7 T.



**16:42**

**D38 10 Li-Vacancy Ordering in LiBC Phase** EBRU GUNGOR, ENGIN OZDAS, *Advanced Materials Research Group, Physics Department, Hacettepe University, Beytepe, Ankara 06800, Turkey* The discovery of a phonon mediated superconductivity in $MgB_2$ with a $T_c$ of 40 K has accelarated the scientific interest in similar layered compounds and the electronic band structure calculations showed that the high-Tc superconductivity is possible for the hole-doped layered lithium borocarbide, $Li_xBC$ [1,2]. However, the superconducting features for Li off-stoichiometric borocarbide compounds have not been observed in any experimental studies, because of the difficulties in the sample preparation. In this work, the effects of synthesis conditions on the structure of $Li_xBC$ samples with the different Li-stoichiometries and the phase stability were investigated. The structural studies showed that the intercalation process has a staging behaviour as Li intercalated graphite and a novel Li vacancy ordered structure for off-stoichiometric $Li_xBC$ phases. [1] Rosner H.et al., PRL 88, 12 (2002) [2] Dewhurst et al., PRB 68, 020504(R) (2003)

**16:54**

**D38 11 Anomalous Magnetoresistance Effects in $(CrO_2)_{1-x}$ : $(MgB_2)_x$ powders** RAGHAVA PANGULURI, B. NADGORNY, *Department of Physics, Wayne State University, Detroit, MI 48201* It is known that the electrical conduction mechanism in compressed powders and polycrystalline $CrO_2$ films is due to the intergranular tunneling. Here, we focus on the percolation effects in the $CrO_2$ powders intermixed with a superconductor, $MgB_2$. A mixture of $(CrO_2)_{1-x}$ : $(MgB_2)_x$ powders with $0 \leq x \leq 1$ were cold-pressed to form circular disks. The electrical resistance measured by a four probe technique, as expected showed a lower resistance for the mixture when compared to the pure pressed $CrO_2$. The observed hysteresis extrinsic magnetoresistance (MR) showed peaks corresponding to the coercive fields of $CrO_2$ which can be associated with the alignment of magnetization of adjacent $CrO_2$ particles. Interestingly, the MR changed signs at around the superconducting transition temperature of $MgB_2$ ( $\sim$ 40K) and also the slope of MR at high magnetic fields changed from positive to negative. We will discuss a possible origin of the observed effects, which we believe are related to the ferromagnet/superconductor interaction.

**SESSION D39: SPIN PROPERTIES OF SUPERCONDUCTORS**
**Monday Afternoon, 13 March 2006**
**342, Baltimore Convention Center at 14:30**
**Jeff Lynn, National Institute of Standards and Technology, presiding**

**14:30**

**D39 1 Electron-phonon coupling associated with charge-stripe order in cuprate superconductors*** JOHN TRANQUADA, *Brookhaven National Lab* D. REZNIK, L. PINTSCHOVIUS, *Forschungszentrum Karlsruhe* M. ITO, S. IIKUBO, M. SATO, *Nagoya Univ.* M. FUJITA, K. YAMADA, *IMR, Tohoku Univ.* G. D. GU, *Brookhaven National Lab* We have used inelastic neutron scattering to study the Cu-O bond-stretching phonon in $La_{1.875}Ba_{0.125}CuO_4$ and $La_{1.48}Nd_{0.4}Sr_{0.12}CuO_4$, two cuprate compounds that exhibit charge-stripe order. This is the phonon mode that one expects to be most sensitive to spatial inhomogeneity in the electronic structure of the $CuO_2$ planes. Besides the cosine-like downward dispersion of the mode from zone center to zone boundary, we observe a dip in the dispersion and a very large energy width ( $>$ 10 meV) at $\mathbf{q} = \mathbf{a}^*/4$. The dip and width gradually become smaller with increasing temperature. These evidences of a strong electron-phonon coupling (the dispersion dip and large energy width) have not been predicted by any conventional calculations. The nature of the connection with charge-stripe order will be discussed.

*Work at Brookhaven is supported by DOE under Contract No. DE-AC02-98CH10886.

**14:42**

**D39 2 Magnetic Neutron Scattering Study of $Nd_{1.85}Ce_{0.15}Cu_{1-y}Ni_yO_4$ Single Crystals** INNA VISHIK, *Stanford University* GUICHUAN YU, *Stanford University* EUGENE MOTOYAMA, *Stanford University* OWEN VAJK, *National Institute of Standards and Technology* MARTIN GREVEN, *Stanford University* In order to arrive at a deeper understanding of the interplay between superconductivity and magnetism in the high-temperature superconductors, it is of interest to study the effects of impurity-doping on the copper site. A large body of work along these lines exists for hole-doped materials, yet relatively little is known about the effects of such impurities on the prototypical electron-doped material $(Nd,Ce)_2CuO_4$. In previous work, paramagnetic dopants (Ni, Fe) were shown to lower $T_c$ much more abruptly than non-magnetic ones (Zn). We grew large single crystals of $Nd_{1.85}Ce_{0.15}Cu_{1-y}Ni_yO_4$ using the traveling-solvent floating-zone technique and characterized our samples using SQUID magnetometry and DC transport measurements. Here we report on neutron scattering results for the spin correlations as a function of nickel concentration and temperature for superconducting ($y < 0.01$) and non-superconducing ($y > 0.01$) compositions.

**14:54**

**D39 3 Scattering Studies of the High $T_c$ Superconductor $La_{2-x}Ba_xCuO_4$** Y. ZHAO, S. R. DUNSIGER, B. D. GAULIN,* H. A. DABKOWSKA, *Dept. of Physics and Astronomy, McMaster University, Hamilton, Ontario, Canada.* Z. YAMANI, W. J. L. BUYERS, *Canadian Neutron Beam Centre, NRC, Chalk River Laboratories, Chalk River, Ontario, Canada* The interplay between superconductivity, magnetism and crystal structure is a central issue in the study of the high $T_c$ cuprates. The first to be

discovered, the Bednorz-Müller materials have been much less extensively studied due to the difficulty of growing large single crystals. Using floating zone image furnace techniques, we have recently successfully grown $La_{2-x}Ba_xCuO_4$ (x$\sim$ 0.095 and 0.08) single crystals on the underdoped side of the well known 1/8 anomaly. X-ray studies show a sequence of crystal structures with temperature, while incommensurate elastic peaks associated with the low temperature tetragonal phase are observed using neutron diffraction. This signature of static spin stripe order persists into the superconducting state. We discuss the relationship between the low temperature spin and lattice degrees of freedom, as well as their sensitivity to doping level.

*Canadian Institute for Advanced Research

**15:06**

**D39 4 Electronic inhomogeneities in superconducting $YBa_2Cu_3O_{6+x}$** FERENC STERCEL, *Dept. of Materials Science and Engr., University of Pennsylvania* JAE-HO CHUNG, *NIST* TAKESHI EGAMI, *Dept. of Physics and Astronomy and Department of Materials Science and Engineering, University of Tennessee-Knoxville* MASATOSHI ARAI, TETSUYA YOKOO, HYUNGJE WOO, *Dept. of Physics and Astronomy, University of Tennessee-Knoxville* MOHANA YETHIRAJ, HERB A. MOOK, *ORNL* CHRIS D. FROST, *Rutherford Appleton Laboratory, UK* FATIH DOGAN, *Dept. of Materials Science and Engr., University of Missouri-Rolla* There has been an increasing amount of experimental evidence for the presence of local electronic inhomogeneities in superconducting cuprates. Inelastic pulsed neutron scattering measurements on $YBa_2Cu_3O_{6+x}$single crystals with different oxygen concentrations show that the zone boundary softening of the in-plane LO Cu-O bond stretching mode is the same for all doping levels. In addition, the spectral weight of the softened mode increases with increasing doping. This indicates that there is a microscopic electronic phase separation in superconducting $YBa_2Cu_3O_{6+x}$. Furthermore, triple axis inelastic neutron scattering measurements on the underdoped $YBa_2Cu_3O_{6.6}$ performed at different temperatures revealed that a new local mode appears at 65 meV at higher temperatures (200 K and above). It might indicate the presence of polarons.

**15:18**

**D39 5 Spin Excitations of overdoped $La_{2-x}Sr_xCuO_4$** S. WAKIMOTO, *JAEA* R.J. BIRGENEAU, *UC Berkeley* C.D. FROST, *RAL* A. KAGEDAN, H.K. KIM, *U of Toronto* I. SWAINSON, *CRL* J.M. TRANQUADA, *BNL* K. YAMADA, *IMR* H. ZHANG, *U of Toronto* Spin excitations of LSCO in the overdoped regime have been studied by neutron scattering. Incommensurate excitations around 6 meV which are clearly observed in the $x = 0.25$ sample decrease with $T_c$ as doping increases, and finally, become unobservable at $x = 0.30$ coincidentally with the disappearance of bulk superconductivity. High-energy measurements performed at the MAPS spectrometer show remarkably weakened magnetic excitations of the overdoped samples also in the high energy region. These observations are apparently consistent with a microscopic phase separation of the overdoped samples into the superconducting and Fermi liquid phases based on muSR results. in contrast, magnetization measurements of overdoped LSCO with and without Zn impurities have revealed that the superconductivity vanishes in the overdoped regime as a result of a competition between the superconductivity and paramagnetism which is induced even in the Zn-free overdoped LSCO.

**15:30**

**D39 6 Search for Magnetic Order in Superconducting $RuSr_2Eu_{1.2}Ce_{0.8}Cu_2O_{10}$** J. W. LYNN, Y. CHEN, *NIST Center for Neutron Research, Gaithersburg, MD 20899-8562 and U. Maryland* S.K. GOH, G.V.M. WILLIAMS, *MacDiarmid Institute for Advanced Materials, Industrial Research, POB 31310, Lower Hutt, New Zealand* Neutron diffraction, polarized neutron transmission, and small angle neutron scattering have been used to investigate the nature of the magnetic order in the titled compound. The sample was made with the Eu-153 (98.8%) isotope to reduce the high neutron absorption for this element. At low T a single magnetic peak is clearly observed. A sharp spin reorientation transition (SRT) is observed around 35 K, close to the superconducting transition temperature (Tc 40K). Between the SRT and the Neel temperature of 59 K, additional magnetic reflections are observed. However, none of these can be simply indexed on the chemical unit cell, either as commensurate peaks or simple incommensurate magnetism, and the paucity of reflections at low T compels the conclusion that these arise from an impurity phase. X-ray and neutron diffraction both show that the sample does not appear to contain significant impurity phases. However, the impurity peaks exhibit strong preferred orientation, while the primary phase does not. We have been unable to observe any magnetic order that can be identified with the ruthenate-cuprate system. Additional field-dependent results will be discussed.

**15:42**

**D39 7 High-Energy Excitations near the boundary to antiferromagnetism-YBCO6.35** C. STOCK, *Physics Department, Johns Hopkins University* R.A. COWLEY, *Oxford Physics, Oxford University* W.J.L. BUYERS, *National Research Council, Chalk River* C.L. BROHOLM, *Physics Department, Johns Hopkins University* R. COLDEA, *Oxford Physics, Oxford University* C.D. FROST, *Appleton Rutherford Laboratories* R.J. BIRGENEAU, *Physics Department, University of California Berkeley* R. LIANG, D. BONN, W.N. HARDY, *Physics Department, University of British Columbia* The high-energy magnetic excitations in the cuprate superconductors have attracted considerable interest recently. We investigate magnetic excitations over the entire energy range in the heavily underdoped YBCO6.35 superconductor with a Tc=18 K. The spin response below 25 meV energy transfers is broad and has been discussed previously. The magnetic response above 25 meV is very similar to the parent insulators with similar spectral weight and spin-wave velocity. The excitations near the zone boundaries are however, much broader in energy than for the parent insulator. The onset of damping coincides approximately with the gap determined from transport measurements. This indicates that a new decay channel for spin waves becomes available above the pseudo-gap.

**15:54**

**D39 8 Spin susceptibility of underdoped cuprates: the case of Ortho-II $YBa_2Cu_3O_{6.5}$** ELENA BASCONES, *Instituto de Ciencia de Materiales de Madrid (CSIC) and Theoretische Physik, ETH-Zurich* T. MAURICE RICE, *Theoretische Physik, ETH-Zurich* Recent inelastic neutron scattering measurements found that the spin susceptibility of detwinned and highly ordered ortho-II $YBa_2Cu_3O_{6.5}$ exhibits, in both the normal and superconducting states, one-dimensional incommensurate modulations at low energies which were interpreted as a signature of dynamic stripes. We propose an alternative model based on quasiparticle

transitions between the arcs of a truncated Fermi surface. Such transitions are resonantly enhanced by scattering to the triplet spin resonance. We show that the anisotropy in the experimental spin response is consistent with this model if the gap at the saddle points is anisotropic.

**16:06**

**D39 9 Effect of Charge Inhomogeneity on the Diagonal Incommensurate Spin Correlations in $La_{2-x}Sr_xCuO_4$** MASAAKI MATSUDA, *Japan Atomic Energy Agency* MASAKI FUJITA, KAZUYOSHI YAMADA, *IMR, Tohoku Univ.* Neutron-scattering experiments are performed on Zn and Ni doped $La_{1.95}Sr_{0.05}CuO_4$ to study the impurity effect on the diagonal incommensurate spin correlations. Zn doping reduces the incommensurability and enhances the correlation length just slightly. On the other hand, Ni doping quickly destroys the incommensurability and restores N'eel ordering, indicating a strong effect on hole localization. This suggests that Ni and hole form a strongly bound state with the Zhang-Rice character, in which effective valence and spin number are trivalent and 1/2, respectively. Although it is expected that doped Ni with effective spin 1/2 does not disturb the magnetic interactions so much, the magnetic correlations are disordered considerably. This suggests that the charge inhomogeneity, caused by the random distribution of effectively trivalent Ni, disturbs the stripe formation and the magnetic correlations become disordered. This result supports the diagonal stripe state and probably rules out the spiral state, caused by the magnetic frustration, in lightly-doped $La_{2-x}Sr_xCuO_4$.

**16:18**

**D39 10 Magnetic Excitations of Stripes Near a Quantum Critical Point and Checkerboards** DAVID K. CAMPBELL, DAOXIN YAO, *Depts. of Physics and Electrical and Computer Engineering, Boston University* ERICA W. CARLSON, *Dept. of Physics, Purdue University* Competing tendencies in electronic systems with strong correlations can lead to spontaneous nanoscale structure, pattern formation, and even long-range spatial order. There has been continued interest in various charge and spin spatial order, including ''stripe'' and ''checkerboard'' phases. We explore the magnetic excitations of stripe and checkerboard phases within a semiclassical spin wave approximation. We show that simple checkerboard patterns are incompatible with recent neutron scattering experiments, while stripes near a quantum critical point (i.e. with weak coupling across the domain walls) exhibit much of the behavior seen in recent neutron scattering experiments on high temperature superconductors. At low energies, the spin wave cones of weakly coupled stripes have weight strongly peaked on the inner branches. As energy is increased, a saddlepoint produces a resonance peak, followed by a square-shaped continuum rotated 45 degrees from the low energy peak direction. We discuss the connection to recent high energy neutron scattering data on the cuprates, as well as the relation to quantum spin fluctations.

**16:30**

**D39 11 Effect of spin-orbit scattering on the observed time-reversal violating phase in the Pseudogap phase of the Cuprates** VIVEK AJI, CHANDRA VARMA, *UC Riverside* Fauque et al. [1] have recently reported observing the predicted symmetry breaking [2] in the Pseudogap region in the phase-diagram of the Cuprates, which had also been earlier inferred from dichroism in ARPES. Following Wu et al. [3], we study the effects of spin-orbit scattering inthe observed symmetry breaking. We study the following issues: spin-current, accompanying orbital currents, symmetry of any accompanying spin-order, and the effect of an external magnetic-field on the ordered state. 1. Fauque et al., arXiv.org/cond-mat/0509210; 2. M.E. Simon and C.M.Varma, Phys.Rev. Lett. 89, 247003 (2002) 3.Wu et al., arXiv.org/cond-mat/0505544

**16:42**

**D39 12 $^{17}O$ and $^{139}La$ NMR in a single crystal $La_{2-x}Ba_xCuO_4$, $x = 1/8$*** BEN-LI YOUNG, N. J. CURRO, *Condensed Matter and Thermal Physics, Los Alamos National Laboratory, Los Alamos, New Mexico 87545, USA* J. HAASE, H.-J. GRAFE, B. BÜCHNER, *Leibniz Institute for Solid State and Materials Research Dresden, P.O. Box 270116, Dresden 01171, Germany* M. HÜCKER, G. D. GU, *Physics Department, Brookhaven National Laboratory, Upton, New York 11973-5000, USA* We have performed $^{17}O$ and $^{139}La$ nuclear magnetic resonance (NMR) in a single crystal of $La_{2-x}Ba_xCuO_4$ with $x = 1/8$, in order to investigate how the static spin and charge structures, as revealed by neutron scattering, influence the NMR spectrum. We measured the NMR intensity of the $^{17}O$ and $^{139}La$ nuclei, as well as the $^{17}O$ nuclear quadrupole resonance frequency ($\nu_Q$) at several different temperatures. We will discuss possible correlation between the $^{17}O$ signal intensity and $\nu_Q$ as a function of temperature due to the stripe phase.

*Supported by I2CAM Junior Scientist travel program.

**16:54**

**D39 13 NMR studies of $Pr_{2-x}Ce_xCuO_{4-y}$ ($x = 0.15$ and 0.17) at high magnetic field** GUOQING WU, S.E. BROWN, W.G. CLARK, *UCLA Physics and Astronomy* R.L. GREENE, *Univ. Maryland* H. BALCI, *UIUC Physics* P. KUHNS, A.P. REYES, W.G. MOULTON, *NHMFL* Recent charge and thermal transport measurements on the electron- doped high-$T_c$ superconductor $Pr_{2-x}Ce_xCuO_{4-y}$ (PCCO) show unusual behavior in the superconducting dome at the doping level going from $x = 0.15$ (optimally doped) to 0.17 (overdoped), such as quantum phase transition and electron paring symmetry changes, suggesting a possible connection between the superconductivity and other competing phases like antiferromagnetism. We report the $^{63,65}Cu$-NMR spectrum in PCCO single crystals with $x = 0.17$ in a high magnetic field $B_0$, and contrast their properties with those of $x = 0.15$. The temperature dependence of the $^{63,65}Cu$-NMR Knight shift is dominated by the negative isotropic hyperfine coupling to the field-induced $Pr^{3+}$ ion moment, and changes little between $x = 0.15$ and 0.17. The $^{63,65}Cu$-NMR linewidths are propotional to the applied magnetic field $B_0$, but affected by the doping, indicating the existence of other sources besides the $Pr^{3+}$ ion moment that contributes to the static local field distribution at the Cu nuclei. The work at UCLA is supported at UCLA by NSF Grants DMR-0334869 (WGC) and 0203806 (SEB).

**17:06**

**D39 14 Impurity effect on nuclear magnetic relaxation due to orbital hyperfine interaction** A. KNIGAVKO, B. MITROVIC, K. V. SAMOKHIN, *Physics Department, Brock University, St. Catharines, Canada* We show that the nuclear magnetic relaxation rate $1/T_1$ due to the coupling of nuclear spin to the orbital moment of itinerant electrons is sensitive to impurity scattering in both normal and superconducting states. In the clean case $1/T_1$ diverges because of the contribution from distant currents, while in the dirty case its magnitude is controlled by the parameter $k_F l$, where $l$ is the electron mean free path. In the superconducting state temperature dependence of $1/T_1$ becomes significant.

**17:18**
**D39 15 On electron-hole symmetry and phase separation in some electron doped cuprates** LEV GOR'KOV, *NHMFL, Florida State University* GREGORY TEITEL'BAUM, *Zavoiskii Institute, Kazan',Russia* Analyzing the experimental NMR data for electron-doped cuprates, we concluded that the Coulomb effects caused by doping lead to dynamical spatial phase separation that contributes to the nuclear spin relaxation. Remarkable, the ''infinite-layer'' $Sr_{0.9}La_{0.1}CuO_4$ reveals unexpected electron-hole symmetry. Its $^{63}$Cu nuclear spin relaxation rate is the sum of a constant and the temperature dependent components, moreover, the latter turns out to be identical to the $1/63T_1(T)$-behavior in the stoichiometric $YBa_2Cu_4O_8$. Connection to fluctuation of a magnetic sub-phase is discussed.

**SESSION D40: FOCUS SESSION: FOUNDATIONS OF QUANTUM THEORY**
**Monday Afternoon, 13 March 2006; 343, Baltimore Convention Center at 14:30**
**Daniel Greenberger, City College of the City University of New York, presiding**



***Invited Papers***

**14:30**
**D40 1 From Quantum Foundations to Quantum Gravity.**
LUCIEN HARDY, *Perimeter Institute*

Quantum theory is a probabilistic theory with fixed causal structure. General relativity is a deterministic theory with dynamic causal structure. It seems likely then that a theory of quantum gravity will be a probabilistic theory with dynamic causal structure. Work in the foundations of quantum theory provides insight into how to build a framework for such theories. In this way we can hope that insights coming from quantum foundations can guide us in constructing a theory of quantum gravity.

***Contributed Papers***

**15:06**
**D40 2 Quantum Mechanics in Terms of Symmetric Measurements** CHRISTOPHER FUCHS, *Bell Labs, Lucent Technologies* In the neo-Bayesian view of quantum mechanics that Appleby, Caves, Pitowsky, Schack, the author, and others are developing, quantum states are taken to be compendia of partial beliefs about potential measurement outcomes, rather than objective properties of quantum systems. Different observers may validly have different quantum states for a single system, and the ultimate origin of each individual state assignment is taken to be unanalyzable within physical theory—its origin, instead, comes from prior probability assignments at stages of physical investigation or laboratory practice previous to quantum theory. The objective content of quantum mechanics thus resides somewhere else than in the quantum state, and various ideas for where that ''somewhere else'' is are presently under debate. What is overwhelmingly agreed upon in this effort is only the opening statement. Still, quantum states are not Bayesian probability assignments themselves, and different representations of the theory (in terms of state vectors or Wigner functions or C*-algebras, etc.) can take one further from or closer to a Bayesian point of view. It is thus worthwhile thinking about which representation might be the most propitious for the point of view and might quell some of the remaining debate. In this talk, I will present several results regarding a representation of quantum mechanics in terms of symmetric bases of positive-semidefinite operators. I also argue why this is probably the most natural representation for a Bayesian-style quantum mechanics.

**15:18**
**D40 3 Influence-free states on compound quantum systems** HOWARD BARNUM, *Los Alamos National Laboratory* CHRISTOPHER FUCHS, *Bell Laboratories, Lucent Technologies* JOSEPH RENES, *Institüt für Theoretische Physik, Universität Erlangen* ALEXANDER WILCE, *Dept. of Mathematical Sciences, Susquehanna University* Probability states for bipartite local measurements and correlations between local measurements are considered, in general and when the local systems behave quantum-mechanically. We review the facts that in general allowing local measurements conditional on classically communicated results from the other site imposes no-signalling in the direction opposite communication, and that in the locally quantum case, two-way no-signalling restricts states to be in the dual of the cone of unentangled states, isomorphic to that of positive maps. We show that in the ''decomposable'' subcone, generated by quantum states and their partial transposes, the extremal quantum states and extremal partial transposes remain extremal. And we show that decomposable states do not violate Cirelson inequalities. We show that locally-quantum no-signalling states must be combined in a thoroughoing no-signalling fashion. Thus Alice and Bob cannot consistently accumulate a sequence of independent states of this nature (as they might a supply of shared Bell states to use in entanglement distillation) while having available the full panoply of quantum observables and operations at their respective sites. The relation of no-signalling to the ''closest-to-Bayesian'' conditional quantum dynamics of C. Fuchs will also be touched on.

**15:30**
**D40 4 Liouville mechanics with an epistemic restriction and Bohr's response to EPR** TERRY RUDOLPH, *Imperial College* STEPHEN BARTLETT, *University of Sydney* ROBERT SPEKKENS, *Perimeter Institute* We introduce a toy theory that reproduces a wide variety of qualitative features of quantum theory for degrees of freedom that are continuous. Specifically, we consider classical mechanics supplemented by a constraint on the amount of information an observer may have about the motional state (i.e. point in phase space) of a collection of classical particles – Liouville mechanics with an epistemic restriction (This may well be how Heisenberg initially understood the Uncertainty Principle). We develop the formalism of the theory by deriving the consequences of this ''classical uncertainty principle'' on state preparations, measurements, and dynamics. The result is a theory of hidden variables, although it is not a hidden variable model of quantum theory because of its locality and noncontextuality. Despite admitting a simple classical interpretation, the theory also

exhibits the operational features of Bohr's notion of complementarity. Indeed, it includes all of the features of quantum mechanics to which Bohr appeals in his response to EPR. This theory demonstrates, therefore, that Bohr's arguments fail as a defense of the completeness of quantum mechanics.

**15:42**

**D40 5 Negativity and contextuality are equivalent notions of nonclassicality** ROBERT SPEKKENS, *Perimeter Institute for Theoretical Physics* An important problem in the foundations of quantum theory is the identification of the precise manner in which quantum theories differ from their classical counterparts. Two notions of nonclassicality that have been investigated intensively are: (1) negativity, that is, the necessity of negative values in real-valued representations of quantum states such as the Wigner representation, and (2) contextuality, that is, the impossibility of a hidden variable model of quantum theory wherein the representation of measurements is noncontextual (also known as the Bell-Kochen-Specker theorem). We shall argue for a particular way of generalizing and making precise both of these notions. With the refined versions of each in hand, it becomes apparent that they are in fact one and the same notion of nonclassicality. It follows that any proof of contextuality is also a proof of negativity and vice-versa.

**15:54**

**D40 6 Epistemic Excess Baggage of Hidden Variable Theories** NICHOLAS HARRIGAN, TERRY RUDOLPH, *Imperial College London* In Quantum Mechanics (QM) preparations of a system are represented by density operators acting on the associated Hilbert space. An ontological ('hidden' variable) model however, views preparations as being described by probability distributions (known as epistemic states) over a set of 'hidden' variables. We investigate restrictions on the efficiency of any such model of QM through studying its preparation contextuality, a property that one can prove to be possessed by ontological models. This property implies the existence of cases wherein more than one distinct epistemic state must be associated with a single density operator in order to correctly reproduce QM predictions. Traditional proofs of preparation contextuality have exhibited scenarios in which it can only be seen that an ontological model must associate more than one epistemic state with some density operator, the exact number being uncertain. We investigate the existence of upper or lower bounds on the number of distinct epistemic states that an ontological model must associate with density operators in order to reproduce QM statistics. The bounds obtained are yet another clue as to how one might quantify the non-classical nature of QM. We provide some speculation on how these results may shed light on the difficulty of simulating quantum mechanical systems on a classical computer.

**16:06**

**D40 7 Pushing the Experimental Limits of Bell Inequalities** JOSEPH ALTEPETER, EVAN JEFFREY, PAUL KWIAT, *University of Illinois at Urbana-Champaign* Using pairs of polarization-entangled photons, we report measurements of Bell's inequalities near the limits of physically allowable violations. As there are several methods by which one can judge the significance of a violation, we report the largest violation to date measured in both standard deviations (2417-sigma) and absolute size (2.826 +/- 0.005). These extremely precise and extremely non-classical results were obtained by carefully characterizing each experimental loss and inefficiency. Unfortunately, accounting for these losses and inefficiencies in the system requires auxiliary assumptions, assumptions which strictly fail to exclude local hidden variable models, and therefore also fail to rigorously test local realism. We therefore additionally report on progress towards a ''loophole-free'' test of Bell's inequality, whereby these experiemental losses and inefficiencies are virtually eliminated, and along with them, the need for auxiliary assumptions about the nature of the systems being measured.

**16:18**

**D40 8 Can Two-photon Correlation of Chaotic Light Be Considered as Correlation of Intensity Fluctuations?*** GIULIANO SCARCELLI, VINCENZO BERARDI, YANHUA SHIH, *University of Maryland, Baltimore County* Unlike first-order correlation, which is considered as a coherent effect of the electromagnetic field, the second-order correlation of radiation is considered as the classical statistical correlation of intensity fluctuations. The first second-order correlation experiment was demonstrated by Hanbury Brown and Twiss (HBT) stimulating a debate about the classical or quantum nature of the phenomenon. Although quantum models of HBT experiment have been attempted, the classical statistical interpretation has been widely accepted. The concept of intensity fluctuation has even been extended to quantum models: ''photon bunching'' is a phenomenological extension to quantum theory of the statistical correlation on photon number fluctuations. We argue that two-photon correlation phenomena, including HBT, have to be understood as a two-photon coherent effect: quantum interference between two-photon probability amplitudes. To do so, we present a ''ghost'' imaging experiment of chaotic light to show that the classical understanding in terms of intensity fluctuations does not give a correct interpretation for the observation. From a practical point of view, this experiment shows the possibility of having high contrast lensless two- photon imaging with chaotic light, suggesting imaging applications for radiations for which no effective lens is available.

*This research was supported in part by ARO and by NASA-CASPR.

**16:30**

**D40 9 Predictability sieve, pointer states, and the classicality of quantum trajectories** DIEGO DALVIT, *Los Alamos National Laboratory* JACEK DZIARMAGA, *Jagelonian University* WOJCIECH ZUREK, *Los Alamos National Laboratory* We study various measures of classicality of the states of open quantum systems subject to decoherence. Classical states are expected to be stable in spite of decoherence, and are thought to leave conspicuous imprints on the environment. Here these expected features of environment-induced superselection (einselection) are quantified using four different criteria: predictability sieve (which selects states that produce least entropy), purification time (which looks for states that are the easiest to find out from the imprint they leave on the environment), efficiency threshold (which finds states that can be deduced from measurements on a smallest fraction of the environment), and purity loss time (that looks for states for which it takes the longest to lose a set fraction of their initial purity). We show that when pointer states – the most predictable states of an open quantum system selected by the predictability sieve – are well defined, all four criteria agree that they are indeed the most classical states. We illustrate this with two examples: an underdamped harmonic oscillator, for which coherent states are unanimously chosen by all criteria, and a free particle undergoing quan-

tum Brownian motion, for which most criteria select almost identical Gaussian states (although, in this case, predictability sieve does not select well defined pointer states.) Reference: D.A.R. Dalvit, J. Dziarmaga, and W.H. Zurek, Phys. Rev. A 72, 062101 (2005).

**16:42**
**D40 10 Decoherence from Spin Environments** FERNANDO CUCCHIETTI, *Los Alamos National Laboratory* JUAN PABLO PAZ, *Universidad de Buenos Aires* WOJCIECH ZUREK, *Los Alamos National Laboratory* We examine two exactly solvable models of decoherence – a central spin-system, (i) with and (ii) without a self–Hamiltonian, interacting with a collection of environment spins. In the absence of a self–Hamiltonian we show that in this model (introduced some time ago to illustrate environment–induced superselection) generic assumptions about the coupling strengths can lead to a universal (Gaussian) suppression of coherence between pointer states. On the other hand, we show that when the dynamics of the central spin is dominant a different regime emerges, which is characterized by a non–Gaussian decay and a dramatically different set of pointer states. We explore the regimes of validity of the Gaussian–decay and discuss its relation to the spectral features of the environment and to the Loschmidt echo (or fidelity).

**16:54**
**D40 11 The Afshar Experiment and Complementarity** RUTH KASTNER, *University of Maryland, College Park* A modified version of Young's experiment by Shahriar Afshar demonstrates that, prior to what appears to be a ''which-way'' measurement, an interference pattern exists. Afshar has claimed that this result constitutes a violation of the Principle of Complementarity. This paper discusses the implications of this experiment and considers how Cramer's Transactional Interpretation easily accomodates the result. It is also shown that the Afshar experiment is isomorphic in key respects to a spin one-half particle prepared as ''spin up along x'' and post- selected in a specific state of spin along z. The terminology ''which way'' or ''which-slit'' is critiqued; it is argued that this usage by both Afshar and his critics is misleading and has contributed to confusion surrounding the interpretation of the experiment. Nevertheless, it is concluded that Bohr would have had no more problem accounting for the Afshar result than he would in accounting for the aforementioned pre- and post- selection spin experiment, in which the particle's preparation state is confirmed by a nondestructive measurement prior to post-selection. In addition, some new inferences about the interpretation of delayed choice experiments are drawn from the analysis.

**17:06**
**D40 12 Robust Weak Measurements** JEFF TOLLAKSEN, *George Mason University* YAKIR AHARONOV, *George Mason University, University of S. Carolina, and Tel Aviv University* We introduce a new type of weak measurement which yields a quantum average of weak values that is robust, outside the range of eigenvalues, extends the valid regime for weak measurements, and for which the probability of obtaining the pre- and post-selected ensemble is not exponentially rare. This result extends the applicability of weak values, shifts the statistical interpretation previously attributed to weak values and suggests that the weak value is a property of every pre- and post-selected ensemble. We then apply this new weak measurement to Hardy's paradox. Usually the paradox is dismissed on grounds of counterfactuality, i.e., because the paradoxical effects appear only when one considers results of experiments which do not actually take place. We suggest a new set of measurements in connection with Hardy's scheme, and show that when they are actually performed, they yield strange and surprising outcomes. More generally, we claim that counterfactual paradoxes point to a deeper structure inherent to quantum mechanics characterized by weak values (Aharonov Y, Botero A, Popescu S, Reznik B, Tollaksen J, Physics Letters A, 301 (3-4): 130-138, 2002).

**17:18**
**D40 13 Quantum of Information** CASLAV BRUKNER, ANTON ZEILINGER, *Institute of Experimental Physics, University of Vienna, Boltzmanngasse 5, 1090 Vienna, Austria* The violation of local realism is today a well established experimental fact. From it follows that either locality or realism or both cannot provide a foundational basis of Nature. Relaxing the locality condition would essentially not change the epistemological structure of classical physics but only extend its limits. Abandonment of reality, however, would require a radical revision of the conceptual background of all our theories so far. Is a novel conceptual basis of quantum theory feasible, in which the impossibility of defining external reality independent and prior to observation naturally emerges? We suggest the finiteness of information content of a quantum system as providing such basis. Any realistic theory that could arrive at an accurate prediction of a particular event would require the system to carry information as to which specific result will be observed for all possible future measurements. Because the system cannot carry more information than is in principle available, there must exist measurements for which individual events contain an element of irreducible randomness. Quantum entanglement arises from the possibility that information in a composite system resides more in the correlations than in properties of individuals. In the talk we will report on recent efforts towards providing derivations of the elements of the Hilbert space structure from the quantization of information.



**SESSION D42: SPS UNDERGRADUATE RESEARCH II**
**Monday Afternoon, 13 March 2006**
**345, Baltimore Convention Center at 14:30**
**Gary White, Society of Physics Students, presiding**

**14:30**
**D42 1 A mathematical model for late term cancer chemotherapy** ZAC IZARD, SARAH HIRSCHBECK, CHRISTIAN VOLK, MITRA SHOJANIA FEIZABADI, *Canisius College* A mathematical model for cancer treated with the ''on-off'' type where the drug is either active or inactive and when the chemotherapeutic treatment only affects the cycling cells is presented. This model is considered for late term chemotherapy when the total population of cells doesn't show a significant change. The size of the cycling cells as a function of time has been investigated.

**14:42**

**D42 2 Real Time Observation of DNA Nanotube Assembly*** LISA VAL VERDE, FYGENSON GROUP TEAM, DNA nanotubes are of interest for applications ranging from nanofabrication to biophysical studies. The DNA Nanotubes used in this research are self-assembling structures composed of DNA double-crossover tiles. These tiles are simply two connected helices composed of five single stranded DNA oligomers. Each tile exposes four sticky ends responsible for the linkage between neighboring tiles. This linkage creates the nanotube lattice, with intrinsic curvature. The curvature orients each tile with a $60^o$ angle from the previous one so that six tiles make up the circumference of a nanotube. Nanotube stability depends on conditions such as ionic strength and temperature. A PCR machine is used to anneal the strands into nanotubes. A duplicated annealing process was constructed under a light microscope. PVP (polyvinyl prolidone) coated glass both confined the DNA nanotubes to a 2-3 $\mu$m focal plane and prevented them from sticking to the sample surface. By the time the tubes were long enough to track ( $\geqslant$ 3 $\mu$m), they continued to lengthen primarily via end-to-end joining with some reaching lengths greater than 100 $\mu$m. These observations helped define more efficient annealing protocols that resulted in tubes with fewer imperfections.

*Fygenson Group, CAMP

**14:54**

**D42 3 Laser Assisted Cancer Immunotherapy: Mapping of the Necrosis Zone*** MEGAN FITZMAURICE, PRADIP BANDYOPADHYAY, *Hendrix College* The primary goal of this project is to assess the degree of thermal damage in malignant tumors using Laser Assisted Cancer Immunotherapy (LACI). In our laboratory, superficial tumors were grown in Balb/c mice by injection (s.c.) of the highly aggressive metastatic mammary cell line CRL-2539. When the tumors reached 5-7 mm in diameter, Indocyanine Green, a light absorbing dye, and Glycated Chitosan, the immunoadjuvant, were injected into the tumors. Following injection, the tumors were irradiated interstitially with an infrared Diode laser (1-15 W) operating at 805nm. Following the laser therapy, at a particular temperature, the tumors were excised at various time intervals ranging from immediately after treatment to 120 hours later. Using a Hematoxylin and Eosin stain, each slide was examined under the light microscope to map out the thermal damage induced by the diode laser and the dye-immunoadjuvant combination. The goal of this experiment is to quantify and map the thermal damage for $55^o$C, $65^o$C and $75^o$C, and to determine the temperature range that evokes maximum immune response.

*This work is supported by a grant fromThe National Institutes of Health

**15:06**

**D42 4 Interstitial Laser Irradiation of Solid Tumors in Laser Assisted Cancer Immunotherapy** LINDSAY EVANS, *Hendrix College* PRADIP BANDYOPADHYAY, *Hendrix College* Laser Assisted Cancer Immunotherapy (LACI) is an experimental therapeutic approach in cancer treatment. Current experiments in our laboratory begin with growing superficial tumors 5 to 7 mm in diameter in BALB/C mice using the CRL-2539 cell line. Tumor sizes were measured with a vernier caliper prior to injection of light absorbing dye (Indocyanine Green, ICG) and immunoadjuvant (Glycated Chitosan, GC). These measurements were continued during the post-therapy period. After injection with the ICG and GC, the mice underwent interstitial irradiation of the tumor with a diode laser operating at 804 nm. Microthermocouples were inserted into the tumor and the laser power was varied in order to monitor the temperature and keep it within in the desired range. Tumors were irradiated at $55^o$C, $65^o$C, and $75^o$C to find out at which temperature the maximum amount of tumor necrosis and strong immune response could be elicited. The growth of the tumors after the LACI treatment will be plotted to show the affect of the therapy at different temperatures. The data suggest that the growth rate of the tumors is slowed down considerably using this approach. * This work is supported by a grant from The National Institutes of Health.

**15:18**

**D42 5 Laser Assisted Cancer Immunotherapy: Surface Irradiation** JOSHUA WILSON, *Hendrix College* HSIN-WEI CHEN, *Hendrix College* PRADIP BANDYOPADHYAY, *Hendrix College* Experiments in our laboratory incorporate a non-invasive approach to treat superficial tumors in animal models. Based on the concept of Laser Assisted Cancer Immunotherapy, surface irradiation provides good information to compare to invasive alternatives. The procedure involves injecting an immunoadjuvant (Glycated Chitosan) as well as a light absorbing dye (Indocyanine Green) directly into the tumor (5 to 7 mm in diameter). The temperature of the tumor is raised using an infrared diode laser operating at 804 nm, with a silica fiber tip placed a set distance away from the surface of the tumor. We monitor the surface temperature using non-invasive (infrared detector probe) as well as the internal temperature of the tumor using invasive (micro thermocouples) methods. This study aims at the success of the surface irradiation mode to treat solid tumors. * This work is supported by a grant from The National Institute of Health.

**15:30**

**D42 6 The Computer Generation of Holographic Optical Tweezers** MICHAEL DECEGLIE, RODD PRIBIK, JEREMY LYON, KERRY BROWNE, *Dickinson College* Due to their ability to apply forces on a small scale, optical tweezers are useful for a variety of biological and physical applications. The utility of optical tweezers can be extended by producing multiple traps with different characteristics from a single beam. One method for achieving this is to manipulate the phase of a trapping laser's wave front with a computer generated kinoform displayed on a spatial light modulator. We compare the performance of two algorithms for kinoform calculation, a Gerchberg-Saxton algorithm and a direct search algorithm, and discuss how they address problems inherent to computer generated holographic optical tweezing.

**15:42**

**D42 7 Growth and Evaporation of Optically Trapped Liquid Droplets Viewed with a Two Axis Microscope** SCOTT DEWOLF, LOWELL I. McCANN, *Physics Dept., University of Wisconsin-River Falls* Water droplets in air can be trapped in a single-beam optical trap (optical tweezers) for extended periods of time. The trap used in this work is a unique two axis microscope system that allows the trapped object to be viewed from the top and the side simultaneously. Both views are imaged onto a single digital camera with temporal resolution of better than 5ms. We will report on the behavior of water droplets as they grow and evaporate while in the trap. We will discuss changes in the size and shape of the droplets over time, the onset of instabilities during the evaporation process, and how the trapping laser power affects the droplet. This research was supported by an award from Research Corporation.

**15:54**

**D42 8 Leidenfrost Ratchets** MICHAEL TAORMINA, *University of Oregon* BENJAMIN ALEMAN, *University of California, Berkeley* HEINER LINKE, *University of Oregon* Properties such as asymmetry and disequilibrium can be exploited in order to obtain useful work from a physical system. Our group is investigating one particularly interesting manifestation of the ''ratchet'' effect. We find that film-boiling (leidenfrost) drops of liquid placed on an asymmetrically-structured surface experience acceleration significant enough for transport to occur even against small inclines. We believe that a viscous drag force is the mechanism for this net flow of fluid, which is supported by a thin layer of vapor. Because heat is the primary input of energy into the system, this effect could prove useful in cooling applications where a classical ''pump'' may not be ideal.

**16:06**

**D42 9 The effect of M ( M=Ti, V) and A (A=Al, Ge) on thermal transport and heat capacity of nanolayered ternary carbides $M_2AC$*** A.P. BRYAN, *Rowan University* S.E. LOFLAND, *Rowan University* J.D. HETTINGER, *Rowan University* P. FINKEL, *Rowan University* M.W. BARSOUM, *Drexel University* A. GANGULY, *Drexel University* S. GUPTA, *Drexel University* We report an investigation of the specific heat and the thermal transport of a subset of the so-called MAX-phase family of materials: $V_2GeC$, $V_2AlC$, $Ti_2GeC$ and $Ti_2AlC$. The thermal transport results are analyzed to investigate the impact of the A-group and M-element on the phonon contribution to the thermal transport. The heat capacity results are investigated to determine the impact of the same elements on the density of electronic states and the Debye temperature. We find that M-element has a more significant impact on the electronic density of states and the thermopower. The Seebeck coefficient is significantly larger in the V-containing carbides (it is nearly zero in the $Ti_2AC$ compounds), although the sign is dependent on the A-group element. The A-group element has an expected impact on the Debye temperature due to the change in atomic masses, but the phonon contribution to the thermal conductivity is largest in the $V_2AC$ compounds

*This work was supported by NSF Grant DMR 0503711

**16:18**

**D42 10 Electron Spin Resonance of $VO_2$ thin films** K.C. MAYNES, P.H. BUNTON, D.B. BAKER, KENNETH HARTMAN, *William Jewell College* R.F. HAGLUND, JR., R. LOPEZ, A. HABALICA, *Vanderbilt University* The metal-insulator transition present in chromium doped $VO_2$ nanoscale film has been observed by electron spin resonance (ESR) spectroscopy. $VO_2$ is a highly correlated electron system with numerous practical applications pertaining to this transition, including ultra-fast optical switching and smart windows. We use $Cr^{3+}$ transition metal ions with concentration of order one percent as a probe in a 140 nm film to detect this transition. The film exhibited a four-fold decrease in chromium intensity as temperature increased through the transition temperature ( $\sim$ 67° C). ESR signal intensities were also used to characterize the hysteretic behavior of this particular transition; these results are in agreement with hysteresis observed through optical means. A discussion of how changes in ESR relaxation times affect signal intensities, as monitored through the transition, will be presented.

**16:30**

**D42 11 EPR Study of Amorphous $V_2O_5$From 125K − 370K** KENNETH HARTMAN, D.B. BAKER, K.C. MAYNES, P.H. BUNTON, *William Jewell College* S. FULLER, *Coe College* Previous EPR spectra for $V_2O_5$ at low temperatures ( $\sim$ 120K) reveal well-resolved resonances in which transitions are attributed to anisotropic hyperfine interactions. In contrast, recent results from our laboratory show EPR spectra with broad resonances that exist from 125K-370K with no apparent appearance of hyperfine interactions. EPR spin counting also indicates a high concentration ( $\sim 10^{20}$ spins/cm$^3$) of paramagnetic centers which suggests that the line widths are limited by spin-spin relaxation of the electron spin system. Current data reveal that EPR signal intensities increase more rapidly than (Temperature)$^{-1}$. In particular, a factor of $\sim$ 10 increase is seen when the temperature is decreased by a factor of 2. Possibilities for enhanced signal intensities include the presence of superparamagnetism or spin glass behavior. Current investigations are concerned with evaluations of a variety of EPR parameters over a temperature range from 125-370K.

**16:42**

**D42 12 Mean-Field Study of Magnetic Resonance for Spin-1 Condensates** ANDREW ROBERTSON, HONG LING, DAVID GROCHOWSKI, *Rowan University, Glassboro NJ* A spin-1 alkali atom has three hyperfine spin levels $|f=1,m=-1,0,+1>$ . An optical dipole trap is capable of simultaneously trapping and condensing all the hyperfine states, forming the so-called spinor Bose-Einstein condensate (BEC), where the spin degrees of freedom are virtually free. The spin-1 BEC is amenable to manipulation by magnetic field. Magnetic resonance theory is developed for a spin-1 BEC subject to both a rotating transverse magnetic field and a longitudinal magnetic field. The focus of the theory is the magnetization, which will be analyzed both analytically and numerically. Magnetization is used to probe the nonlinear two-body collisions, which strongly affect the properties of the spin-1 BEC. It is shown that while collisions modulate the population dynamics, it is the quadratic Zeeman interaction that couples the population dynamics due to collisions to the magnetization.

**16:54**

**D42 13 Width of a Ferrofluid Finger: Hysteresis and Multiple Energy Minima** NARELLE HILLIER, DAVID JACKSON,* *Dickinson College* The theoretical finger width dependence of a ferrofluid on the magnetic field in a Hele-Shaw geometry is investigated. A model of the finger enables the energy to be computed and then minimized to determine the finger width. Calculations predict a hysteresis effect as the applied magnetic field is varied. This results from the existence of two local energy minima for a range of magnetic bond numbers. Hence, for a given magnetic bond number, the stable ferrofluid configuration can be either a circle or a finger, depending on the whether the applied field is increasing or decreasing. A comparison with experimental results will be presented.

*To whom correspondence should be addressed

**17:06**

**D42 14 Design of Low Temperature AC Susceptibility Measurement Scheme for Molecular Magnets** SIMCHA KORENBLIT, BYOUNG MOON, YOONSEOK LEE, *University of Florida* REZA SULTAN, *Canterbury High School* AC susceptibility is one of the most important physical properties in many materials such as magnetic materials and superconductors. Al-

though there are many commercial AC susceptibility measurement systems which cover a broad range of temperatures, it is still a daunting task to extend their measurement range into the low millikelvins. We are currently developing a low temperature AC susceptometer for the mK range. As a part of this effort, we have developed a versatile low-cost computer controlled coil-winder to make various types of coils. We have designed primary and secondary coils and wound them using the machine, and performed characterization of the AC susceptometer. In this presentation, I will explain the basics of magnetic susceptibility, its measurement, design considerations for building an AC magnetic susceptometer, and discuss the details of an actual apparatus designed and realized by the authors.



**SESSION D43: FOCUS SESSION: VORTICES AND VORTEX LATTICES IN FERMI AND BOSE SUPERFLUID GASES**
**Monday Afternoon, 13 March 2006**
**346, Baltimore Convention Center at 14:30**
**D. Feder, University of Calgary, presiding**

***Contributed Papers***

**14:30**
**D43 1 Hardcore Bosons in a Rotating Lattice*** RAJIV BHAT, *JILA, NIST and CU-Boulder* LINCOLN CARR, *Colorado School of Mines* MURRAY HOLLAND, *JILA, NIST and CU-Boulder* Two of the most important themes in the developing area of quantum fluids and ultracold gases include the role of strong interactions and highly correlated effects. We study a novel and interesting problem combining these two key areas by looking at the experimentally relevant area of ultracold atoms in rotating optical lattices. This merges the effects of strong interactions generated by the lattice with the intriguing quantum effects present in the analogy of the quantum Hall effect at high rotation rate. Hardcore bosons in a 2D rotating square lattice are investigated via a modified Bose-Hubbard Hamiltonian. Our results show quantization of circulation and potential phase transitions between circulation values in which the symmetry of the ground state changes structure abruptly as a function of rotation.

*Support of DoE and NSF acknowledged.

**14:42**
**D43 2 Vortex lattice melting in a stack of Bose Einstein Condensates** MICHIEL SNOEK, HENK STOOF, *Utrecht University* The observation of fractional Quantum Hall liquids in rapidly rotating ultracold Bose gases is a long desired goal. Until now the experimentally accessible ratio of the numbers of particles to the number of vortices is far too high to melt the vortex lattice and to observe these states. This can be solved by means of an one-dimensional optical lattice, which divides the condensate in a stack of two-dimensional condensates in which the number of particles is strongly reduced and the quantum fluctuations are enhanced. We study the melting of a vortex lattice in such a configuration by calculating the quantum fluctuations around the classical Abricosov lattice for realistic numbers of particles and vortices. We find that the fluctuations are inhomogeneous and the lattice melts from outward to inward. Coupling neigbouring pancakes by tunneling reduces the anharmonicity as well as the size of the fluctuations and brings in the 3D regime.

**14:54**
**D43 3 Virial theorems and vortex states in confined Bose-Einstein condensates*** STAVROS KOMINEAS, NIGEL COOPER, *University of Cambridge* NIKOS PAPANICOLAOU, *University of Crete* We derive a class of virial theorems which provide stringent tests of both analytical and numerical calculations of vortex states in a confined Bose-Einstein condensate. In the special case of harmonic confinement we arrive at the surprising conclusion that the linear moments of the particle density, as well as the linear momentum, must vanish even in the presence of off-center vortices which lack axial or reflection symmetry. The effect of anharmonic confinement is also discussed. Two types of non-axisymmetric vortices have been observed to precess around the center of the condensate and they are refered to as the S-vortex and the U-vortex. We study numerically (Gross-Pitaevskii equation) and theoretically a single vortex in spherical and elongated condensates as a function of the interaction strength. For a given angular momentum the S-vortex has smaller precession frequency and a higher energy than the U-vortex in a rotating elongated condensate. We show that the S-vortex is related to the solitonic vortex and also to the dark soliton which are nonlinear excitations in the nonrotating system. In the dilute limit a lowest Landau level calculation provides an analytic description of these vortex modes. (Phys. Rev. A 72, 053609 (2005), Phys. Rev. A 72, 053624 (2005))

*Support from EPSRC is acknowledged

***Invited Papers***

**15:06**
**D43 4 Observation of High-Temperature Superfluidity in a Gas of Fermionic Atoms.**
MARTIN ZWIERLEIN, *MIT*

Ultracold quantum degenerate Fermi gases provide a remarkable opportunity to study strongly interacting fermions. In contrast to other Fermi systems, such as superconductors, neutron stars or the quark-gluon plasma of the early Universe, these gases have low densities and their interactions can be precisely controlled over an enormous range. A major goal has been the realization of superfluidity in a gas of fermions. Our observation of vortex lattices in a strongly interacting rotating Fermi gas provide definitive evidence for superfluidity. By varying the binding energy between fermion pairs, we have studied the crossover from a Bose–Einstein condensate of molecules to a Bardeen-Cooper-Schrieffer superfluid of loosely bound pairs. The crossover is associated with a new form of superfluidity. The observed transition temperatures normalized for the density of the gas by far exceed the highest transition temperatures achieved in high-Tc superconductors. Recently, we have extended those studies to interacting Fermi gases with imbalanced spin populations and observed a quantum phase transition at a critical imbalance, which is the Pauli limit of superfluidity.

*Contributed Papers*

**15:42**
**D43 5 Vortex lattice formation in Bose-condensed gases in rotating potentials** TETSURO NIKUNI, *Tokyo University of Science* TOSHIHIRO SATO, *University of Tokyo* TOMOHIKO ISHIYAMA, *Tokyo University of Science* We study vortex lattice formation in trapped Bose-condensed gases in various types of rotating potentials by solving the time-dependent Gross-Pitaevskii equation. We discuss the detailed characteristics of the formation dynamics and the structure of vortex lattices depending on the geometry of rotating potentials.

**15:54**
**D43 6 Vortex Structure and Dynamics in Fermi Superfluid Gas*** MASAHIKO MACHIDA, *CCSE, Japan Atomic Energy Agency* TOMIO KOYAMA, *IMR, Tohoku Univ.* YOJI OHASHI, *Institute of Physics, Univ. of Tsukuba* In order to study a universal structure of the quantized vortex in Fermi superfluid Gas, we numerically calculate the generalized Bogoliubov de Gennes equation derived from the fermion-boson model and clarify how the vortex structure changes through the BCS-BEC crossover. In the numerical calculations, we concentrate on a singly quantized vortex and compare the structure for both the narrow and the broad Feshbach resonance. Numerical calculation results reveal that in the BEC regime the matter density depression at the vortex core is complete while in the BCS regime the depression at the vortex core is relatively obscure. This feature is qualitatively common for both the narrow and broad Feshbach resonances, while in profiles of the molecular boson condensate the narrow and broad cases differ. In the broad case, the profile of the molecular boson condensate is quite similar to that of the fermionic superfluid gap. In addition, we show quasi-particle spectra from BCS to BEC for both Feshbach resonance cases. The number of the low-lying quasi-particle excitations localized inside the vortex core drastically decreases as one goes to the BEC regime. This result indicates that an origin of the vortex dissipation alters between BCS and BEC.

*JST(CREST)

**16:06**
**D43 7 Critical Current, Vortices and Fermionic Bound States in the BEC to BCS Crossover** RAJDEEP SENSARMA, MOHIT RANDERIA, TIN LUN HO, *Physics Department, The Ohio State University* We have analyzed a single vortex at $T = 0$ in a 3D superfluid atomic Fermi gas across a Feshbach resonance[1] using a fully self-consistent Bogoliubov-deGennes approach. From the current flow around a vortex we conclude that unitarity ($a_s = \infty$) is the most robust superfluid state in the entire BCS-BEC crossover, with the highest critical velocity $v_c$ of about $0.1v_F$. On either side of unitarity, $v_c$ decreases. It is determined by pair breaking on the BCS side and by collective excitations in the BEC regime. In the BCS limit, the order parameter near the vortex core shows a variation on both the scale of $k_F^{-1}$ and of the coherence length $\xi$, while away from the BCS limit only a variation on the scale of $\xi$ is seen. The density in the core rises quadratically with radial distance and is progressively depleted as one moves from BCS to BEC. The number of fermionic bound states in the core decreases as we move from the BCS to BEC regime. Remarkably, a bound state branch persists even on the BEC side reflecting the composite nature of bosonic molecules. [1] R. Sensarma, M. Randeria and T.L. Ho, cond-mat/0510761

**16:18**
**D43 8 Ground state description of a single vortex in an atomic Fermi gas: From BCS to Bose-Einstein condensation*** CHIH-CHUN CHIEN, *University of Chicago* YAN HE, *University of Chicago* QIJIN CHEN, *University of Chicago* K. LEVIN, *University of Chicago* We use a Bogoliubov-de Gennes (BdG) formulation to describe a single vortex in a neutral fermionic gas. It is presumed that the attractive pairing interaction can be arbitrarily tuned to exhibit a crossover from BCS to Bose-Einstein condensation. Our starting point is the BCS-Leggett mean field ground state for which a BdG approach is microscopically justified. At strong coupling, we demonstrate that this approach is analytically equivalent to the Gross-Pitaevskii description of vortices in true bosonic systems. We analyze the sizable density depletion found for the unitary regime and relate it to the presence of unoccupied (positive energy) quasi-bound states at the core center. Reference: arXiv:cond-mat/0510647

*NSF-MRSEC Grant No. DMR-0213745

**16:30**
**D43 9 Fermionic Paired Superfluids at High Rotation Rate*** MARTIN Y. VEILLETTE, DANIEL E. SHEEHY, VICTOR GURARIE, LEO RADZIHOVSKY, *University of Colorado* I will describe our recent work on rotating resonantly-paired superfluids, mapping out the Feshbach resonance detuning, temperature and rotational frequency phase diagram. I will compare our predictions with the recent experiments on degenerate atomic $^6$Li gases across a Feshbach resonance [Zwierlein et al. Nature **435**, 1047 (2005)] and will make proposals for future experiments in such systems.

*Supported by the NSF through Grant No. DMR-0331848 and DMR-0449521

**16:42**
**D43 10 Visualization and characterization of superfluid vortices in liquid helium*** DANIEL LATHROP, GREGORY BEWLEY, *University of Maryland* KATEPALLI SREENIVASAN, *International Center for Theoretical Physics* In superfluid helium 4, quantum vortices have been studied indirectly for nearly fifty years. We have discovered that micron sized solid hydrogen particles suspended within superfluid helium are attracted to and trapped by the vortex filaments and thereby make it possible to see individual vortex lines. The ability to produce the fine solid hydrogen particles is key to this new technique. We compare the line density in a steadily rotating superfluid with the Feynman prediction. Oscillating modes of the vortex array are also observed and characterized. Our observations also include periodic particle spacing on lines at low particle density, as well as complex vortex branching and networks. Our visualization technique makes it possible to observe the dynamics and geometry of vortices both in superfluid turbulence and in quench conditions passing through the phase transition.

*This research was funded by the National Science Foundation and the Center for Superconductivity Research at the University of Maryland

**16:54**

**D43 11 Nucleation and growth of vortices in a rotating BEC*** OLEG VOROV, *Drake University* PIET VAN ISACKER, *GANIL* MAHIR HUSSEIN, *Universidade de Sao Paulo* KLAUS BARTSCHAT, *Drake University* An analytic solution of the Gross-Pitaevskii equation [1] for a rotating Bose-Einstein condensate of trapped atoms describes the onset of vorticity when the rotational speed is increased, starting with the entry of the first vortex [2] and followed by the formation of growing symmetric Wigner molecules. It explains the staircase of angular momentum jumps and the behavior of the bosonic occupancies observed in numerical studies. The universalities of this behavior [3] and its similarity to the mesoscopic superconductors are discussed. [1] O.K. Vorov, P. Van Isacker, M.S. Hussein, and K. Bartschat, Phys. Rev. Lett. 95, 230406 (2005). [2] O.K. Vorov, P. Van Isacker, and M.S. Hussein,, Phys. Rev. Lett., 90, 200402 (2003). [3] O.K. Vorov, P. Van Isacker, and M.S. Hussein, and K. Bartschat, subm. To Nature (London).

*Supported by NSF

**SESSION D45: STRONGLY CORRELATED ELECTRONS ON TRIANGULAR LATTICES**
**Monday Afternoon, 13 March 2006**
**348, Baltimore Convention Center at 14:30**
**Cedomir Petrovic, Brookhaven National Laboratory, presiding**

**14:30**

**D45 1 Charge Localization and near zero in-plane thermal expansion in layered $Na_xCoO_2$, $x \sim \frac{1}{2}$** DIMITRI ARGYRIOU, C. MILNE, O. PROKHNENKO, *Hahn-Meitner-Institut, Glienicker Str. 100, Berlin D-14109, Germany* L.C. CHAPON, P.G. RADAELLI, *ISIS Facility, Rutherford Appleton Laboratory-CCLRC,U.K.* We have used neutron powder diffraction and X-ray single crystal diffraction to investigate the lattice response to charge localization and magnetic ordering in samples with stochiometry close to $Na_{0.5}CoO_2$ over the temperature range of 2 to 600K. Our measurements show there presence of two crystallographical distinguishable Co sites but with essentially identical bond valences. This indicates only a marginal charge disproportionation between $Co^3$ and $Co^4$. Our measurements show Na-ordering achieved by de-intercalation imposes a constraint on the charge and spin-state degrees of freedom that acts as to reduce the in-plane thermal expansion to near zero values between 2 to 300K. At higher temperatures we find a phase non-reversable transition to a phase with a $3a \times [**space**]3b \times [**space**]c$ cell, wtr to the orthorhombic P*nmm* low temperature phase. This phase does not exhibit any of the anomalies observed at 52 and 87K in the magnetic susceptibility of the as made phase.

**14:42**

**D45 2 Spin Glass Statics and Dynamics in the Disordered Stacked Quantum Ferromagnet LiNiO2** J.P. CLANCY, B.D. GAULIN, S.R. DUNSIGER, S. HARAVIFARD, *Department of Physics and Astronomy, McMaster University* J.R.D. COPLEY, Y. QIU, *National Institute of Standards and Technology* We have performed time-of-flight neutron scattering measurements on polycrystalline LiNiO2 using the Disk Chopper Spectrometer at the NIST Center for Neutron Research. Similar measurements performed on its sister compound, NaNiO2, show a simple magnetic structure below Tn$\sim$ 22K consisting of ferromagnetic sheets of s=1/2 moments stacked in an antiferromagnetic (AF) fashion [1]. Our measurements on LiNiO2 illustrate the absence of magnetic order down to 1.7K. Further they provide direct evidence for a spin glass transition at 9K through a narrowing of the inelastic magnetic scattering on approaching Tg from above, along with a concomitant increase in the elastic magnetic scattering, indicative of frozen disordered moments. The inelastic magnetic scattering in LiNiO2 resembles that in NaNiO2 above Tn, suggesting that the low Q spin response is due to short-lived spin wave modes below the lowest Q AF ordering wavevector. This reinforces the picture that the simple stacked ferromagnetic ordered state displayed by NaNiO2 is precluded by mixing between the Li and Ni sublattices, which occurs in LiNiO2 at the 1-3% level. [1] M.J. Lewis et al., PRB 72, 014408 (2005).

**14:54**

**D45 3 Coexistence of f-wave superconductivity, charge order, and spin antiferromagnetism around nonmagnetic impurities in $Na_{0.33}CoO_2 \cdot 1.3H_2O$*** JIN AN, HAI-QING LIN, *Chinese University of Hong Kong* CHANG-DE GONG, *Nanjing University* To check whether charge dynamics is responsible for the superconductivity in $Na_xCoO_2 \cdot yH_2O$, we investigate local electronic and magnetic structure around a nonmagnetic impurities embedded in this material at $x = 0.33$ in the vicinity of charge instability, by using a phenomenological model within the slave-boson framework including competitions among a $\sqrt{3} \times \sqrt{3}$ charge order, antiferromagnetism and f-wave superconductivity. Around the repulsive impurities, it is found that both local charge and spin orders are induced. Furthermore, the f-wave pairing order parameter is decreased on one sublattice but increased on another honeycomb sublattice. If the charge dynamics is responsible for the superconductivity, the predicted local electronic and magnetic structure could be observed by the STM and spatial resolved NMR experiments.

*Work partially supported by the RGC Project CUHK 401703

**15:06**

**D45 4 Thermoelectric properties of $Na_{0.68}CoO_2$ on a 2D triangular lattice** MICHAEL R. PETERSON, JAN O. HAERTER, B. SRIRAM SHASTRY, *University of California Santa Cruz* $Na_xCoO_2$ at $x = 0.68$ is a material with important and interesting thermopower. Using a new formalism for computing thermal response functions, via the response to dynamical temperature gradients, in the high frequency limit a nearly frequency independent term is identified for the thermopower $S^*$, the Lorentz ratio $L^*$, and the dimensionless figure of merit $Z^*T$. We calculate, via exact diagonalization for small systems, $S^*$, $L^*$, and $Z^*T$, at all temperatures for the *t-J* model on a 2D triangular lattice exploring the model parameters relevant to the experiments by I. Terasaki *et al, (PRB* **56**, R12685 (1997)) and Y. Wang *et al, (Nature* **423**, 425 (2003)). Our objective is to understand the (large) magnitude of the thermopower, and its remarkable sensitivity to a magnetic field. We also consider the hypothetical and interesting case of the opposite sign of hopping $t \rightarrow -t$.

**15:18**

**D45 5 Jahn-Teller distortion and magnetic ordering in layered nickelates** MICHELLE JOHANNES, IGOR MAZIN, NOAM BERNSTEIN, *Naval Research Laboratory* One of the long-standing challenges in the theory of layered nickelates is that $NaNiO_2$ is antiferromagnetic and has a strong Jahn-Teller induced orbital ordering, while $LiNiO_2$ has none. A variety of hypothesis have been proposed to explain this mystery: a difference in Li/Na ionic radii, differences in the underlying electronic structure, the zero-point motion of Li ions, etc. One of the most viable propositions is that the difference is due to the presence of $Na2^+$ ions (1% or more) on the Li sites. It remains unclear whether the magnetic interaction of $Na2^+$ with the in-plane $Na3^+$ is strong enough to cancel the Li-assisted antiferromagnetic superexchange even for 1% of $Na2^+$, and what effect it has on orbital ordering. We provide quantitative arguments, based on first principles calculations and atomistic simulations, that spin and orbital orderings are unrelated, and that both are destroyed (the latter in a rather unusual way) by $Na2^+$ impurities, but for entirely separate reasons.

**15:30**

**D45 6 Pronounced increase of the thermopower in $Na_xCoO_2$ in the large-$x$ regime ($x \geq 0.75$)** MINHYEA LEE, *Physics Department, Princeton Univerisity* LILIANA VICIU, *Chemistry Department, Princeton Univerisity* LU LI, YAYU WANG, *Physics Department, Princeton Univerisity* M. L. FOO, S. WATAUCHI, R. A. PASCAL JR., R. J. CAVA, *Chemistry, Princeton Univerisity* N. P. ONG, *Physics, Princeton Univerisity* We report for the first time the systematic transport study on high doped $Na_xCoO_2$ over series of samples which lie ($0.75 \leqslant x \leqslant 1$). We discovered two distinctive regions of phase diagram exist in high Na doping level: one is characterized by largely enhanced thermopower (200 – 300 $\mu$V/K at $\sim$ 130K) yet highly metallic resistivity in $0.75 \lesssim x \lesssim 0.88$ (region I). The other (region II) is emerged in $0.89 \lesssim x \lesssim 0.97$, in which the electronic phase is mixed with the region I phase and $x = 1$ of non-conducting end compound and the mixture seems to occur mainly along the layer. We will discuss the newly revised phase diagram of the high Na part and speculate on a relation to the characteristics of Na layer.

**15:42**

**D45 7 Single-particle excitation-spectra in the Hubbard model on a kagomé lattice** WATARU KOSHIBAE, NEJAT BULUT, KENJI TSUTSUI, SADAMICHI MAEKAWA, *Institute for Materials Research, Tohoku University, Sendai 980-8577, Japan* The effects of frustration in spin systems have been studied for many years. Recently, the transport properties of the layered cobalt oxide $Na_xCoO_2$ and of related oxides have generated new interest in the frustrated systems. In the cobalt oxides, the Co ions form a triangular lattice. The hopping matrix element of electrons in the cobalt 3*d* orbitals is not isotropic, and we have shown [PRL**91**, 257003] that the triangular $CoO_2$ lattice consists of four coupled kagomé sublattices. For this reason, here, we examine the single-particle excitation spectrum of the Hubbard model on the kagomé lattice, and study the motion of a carrier in this frustrated system. We use the quantum Monte Carlo and the exact-diagonalization methods. The dispersion relation of the tight-binding model on the kagomé lattice has a flat dispersion at the top or the bottom of the energy band depending on the sign of hopping-matrix element $t$. This causes a two-fold degeneracy at the $\Gamma$ point where the flat piece of the dispersion is located. However, in the interacting system, we find that the lowest- lying states have a two-fold degeneracy at the $\Gamma$ point independent of the sign of $t$, when the Coulomb repulsion is sufficiently strong. In this talk, we will discuss these numerical results on the electronic structure of the Hubbard model on the kagomé lattice.

**15:54**

**D45 8 Squaring the Triangle: Insulating Ground State of $Na_{0.5}CoO_2$*** TING-PONG CHOY, DIMITRIOS GALANAKIS, PHILIP PHILLIPS, *University of Illinois* We demonstrate that at a filling of $n = 1.5$, an hexatic insulating state obtains in the extended Hubbard model on a triangular lattice. Composed of two tetragonal sublattices with fillings of $n = 1$ and $n = 2$, the insulating state is charge ordered and possesses an antiferromagnetic superlattice with dimension $a \times \sqrt{3}$. Two distinct energy scales arise in our model, a charge gap for the insulator and the effective exchange interaction in the antiferromagnet. Our model is capable of explaining the sign change of the Hall-coefficient as a function of temperature as well as the persistence of antiferromagnetism above the insulating state.

*Partial funding from DMR-0305864

**16:06**

**D45 9 Itinerant correlated electrons on 2D and 3D triangular lattices** M. BRUEHWILER, *ETH Zuerich, Switzerland* S. M. KAZAKOV, J. KARPINSKI, B. BATLOGG, In insulating frustrated systems, where localized magnetic moments sit on the vortices of e.g. triangles or tetrahedra, competing interactions lead to a wealth of novel states of fundamental interest. Ground states of infinite degeneracy are a typical signature of such frustrated systems. While for local moments the intimate connection between spin and the lattice leads to the observed frustration effects, it is an open question to what degree itineracy modifies these features and how charge, spin, and lattice degrees of freedom are affected. In this context, the superconductivity recently discovered in 2D triangular $Na_xCoO_2 - yH_2O$ and 3D triangular $AOs_2O_6$ ($A$ = K, Rb, Cs) is of considerable interest. In order to shed light onto the above mentioned questions associated to these materials, we have performed thermodynamic and transport measurements on both the parent compound of the hydrated superconductor, $Na_xCoO_2$, and the pyrochlores $KOs_2O_6$ ($T_c = 9.5$ K) and $RbOs_2O_6$ ($T_c = 6.4$ K). We have mapped out parts of the phase diagram as a function of band filling of $Na_xCoO_2$ (varying Na content $x$) and find peculiar low-energy excitations below about 10 K. In the 3D system, we also find a significant mass enhancement by factors up to about 8 compared to band structure calculations, part of which can be attributed to electron-phonon interaction ($\lambda_{ep} = 1$ to 1.5).

**16:18**

**D45 10 Hall constant on the Icosahedral t-J model** JAN HAERTER, MICHAEL PETERSON, SRIRAM SHASTRY, *University of California at Santa Cruz* We investigate the Hall constant $R_H$ in the zero field limit through the exact diagonalization technique on small clusters within the triangular lattice t-J model. As a model system we study the icosahedron, a 12-site Platonic solid consisting solely of five fold coordinated triangles. We compare results with toroidal geometries up to 12 sites. While the high-temperature behavior of the high-frequency $R_H^*$ is quite well understood analytically, our objective is to explain the complete

T-dependence of $R_H$ in $Na_{.68}CoO_2$ as observed in experiments (Ong et al), especially in the low-T regime. Furthermore, we investigate $R_H$ as function of frequency by explicit evaluation of Kubo formulae. We compare results with existing studies of $R_H$ on square lattices.

**16:30**

**D45 11 Ground-state valency and spin configuration of the nickelates.** LEON PETIT, GEORGE M. STOCKS, TAKESHI EGAMI, *Oak Ridge National Laboratory* ZDZISLAWA SZOTEK, WALTER M. TEMMERMAN, *Daresbury Laboratory* The ab initio self-interaction-corrected local-spin-density approximation is used to study the electronic structure of both stoichiometric and non-stoichiometric nickelates. From total energy considerations it emerges that, in their ground-state, both $LiNiO_2$, and $NaNiO_2$ are insulators, with the Ni ion in the $Ni^{3+}$ low spin state ($t_{2g}^6 e_g^1$) configuration. We find that the substitution of Li/Na atoms by divalent impurities, drives an equivalent number of Ni ions in the $NiO_2$ layers from the JT-active trivalent low-spin state to the divalent JT-inactive state. We propose that an experimental study on $Mg_xNa_{1-x}NiO_2$ might clarify the role of $Ni^{2+}$ impurities with respect to the vanishing of long range orbital ordering in $Li_{1-x}Ni_{1+x}O_2$. (Work sponsored by the Laboratory Directed Research and Development Program (LDRD) program of ORNL (LP, GMS, TE), and by the DOE-OS through the Offices of Basic Energy Sciences (BES), Division of Materials Sciences and Engineering (LP, GMS, TE). Oak Ridge National Laboratory is managed by UT-Battelle, LLC, for the Department of Energy under Contract No. DE-AC05-00OR22725.)

**16:42**

**D45 12 Phase Diagram of the $Li_2O$-$V_2O_3$-$V_2O_5$ System at 700 °C: Correlations with Magnetic Defect Concentration in Heavy Fermion $LiV_2O_4$*** S. DAS, X. ZONG, X. MA, A. NIAZI, D.C. JOHNSTON, *Ames Lab. and Dept. Phys. Astron., Iowa State U., Ames, IA 50011* Polycrystalline samples of $LiV_2O_4$ have been synthesized with magnetic defect concentrations $n$ ranging from 0.01 mol% to 0.77 mol% and average spins $S$ from 3/2 to 4. (1) Low-temperature $T$ magnetic susceptibility $\chi$ and magnetization $M$ versus applied magnetic field $H$ isotherms were measured to determine these $n$ and $S$ values. Here we report the phase diagram of the $Li_2O$-$V_2O_3$-$V_2O_5$ ternary system at 700 °C for compositions in equilibrium with $LiV_2O_4$. This study provided a clarification of the synthesis conditions under which low and high magnetic defect concentrations can be obtained in $LiV_2O_4$. The samples were prepared using conventional solid state reaction of appropriate amounts of $Li_2CO_3$,$V_2O_3$ and $V_2O_5$. $M(H)$ isotherms and $\chi(T)$ data were obtained on many of these samples. We confirmed that the $LiV_2O_4$ phase can be obtained containing low (0.01 mol%) to high ( $\geq$ 0.5 mol%) magnetic defect concentrations and with consistently high defect $S$ values around 3 to 4. The highest $n$ values were obtained for $LiV_2O_4$ samples in equilibrium with $V_2O_3$ and the lowest values for $LiV_2O_4$ samples in equilibrium with $V_3O_5$, consistent with the results in Ref. (1). (1) S. Kondo et al., PRL **78**, 3721 (1997); PRB **59**, 2609 (1999).

*Supported by the USDOE under Contract No. W-7405-Eng-82

**16:54**

**D45 13 $^7$Li NMR Study of Magnetic Defects in Heavy Fermion $LiV_2O_4$*** X. ZONG, D.C. JOHNSTON, F. BORSA, S. DAS, J. SCHMALIAN, *Ames Lab. and Dept. Phys. Astron., Iowa State U., Ames, IA 50011* A small concentration ($n \approx 0.7$ mol%) of magnetic defects within the normal spinel structure of heavy fermion $LiV_2O_4$ was recently found to have a strong effect on the $^7$Li NMR at low temperatures $T < 4.2$ K@.(1) The $^7$Li nuclear magnetization relaxation versus time after saturation, $M(t)$, changed from a pure exponential in a pure sample with $n = 0.01$ mol% to a stretched exponential for $n = 0.7$ mol%. Here we present a systematic study of the variations of the $^7$Li NMR versus $n$ for additional $n$ values from 0.05 to 0.8 mol%. Non-exponential $M(t)$ recovery was consistently obtained for samples with $n \geq 0.2$ mol% and the nuclear spin lattice relaxation rate versus temperature evolved monotonically with increasing $n$, consistent with the interpretation in Ref. (1). In addition, we obtained relaxation data for much shorter times than studied in Ref. (1), which indicate a previously unknown initial $M(t) \propto \sqrt{t}$ dependence for all samples with $n \geq 0.5$ mol%, for times $t < 20$ ms. At present, there exists no microscopic theory for the influence of magnetic defects on our $^7$Li NMR results. Phenomenological models that may help to understand the data will be discussed. (1). D. C. Johnston et al., Phys. Rev. Lett. **95**, 176408 (2005).

*Supported by USDOE under Contract No. W-7405-ENG-82.

**17:06**

**D45 14 Magnetic Excitations in the Orbitally Degenerate Triangular Lattice $LiVO_2$ Studied by Inelastic Neutron Scattering** W. TIAN, *The University Of Tennessee, Oak Ridge National Laboratory* M.B. STONE, D.G. MANDRUS, B.C. SALES, R. JIN, *Oak Ridge National Laboratory* D.T. ADROJA, T. PERRING, *ISIS Facility, Rutherford Appleton Laboratory* S.E. NAGLER, *Oak Ridge National Laboratory* Inelastic neutron scattering experiments were performed to study a two dimensional triangular lattice material $LiVO_2$ (S=1, $V^{3+}$ ions) with orbital ordering involving threefold degenerate $t_{2g}$ orbitals. At $T_t \approx 500$ K, $LiVO_2$ undergoes a first order phase transition, accompanied by a large reduction in the magnetic susceptibility in the low temperature phase. It has been proposed that this phase transition is associated with the formation of trimers of $V^{3+}$ ions yielding a spin-singlet ground state. We report inelastic neutron scattering measurements on powder and single crystal samples of $LiVO_2$ carried out using the HET and MAPS spectrometers at ISIS. At low temperature, several magnetic excitations with energy transfers as large as several hundred meV were observed. We propose that the observed multiple magnetic excitations arise from the orbital ordering. Model calculations for trimers including an orbital-ordering term showing qualitatively similar spectra suggesting that localized orbiton excitations have been observed in $LiVO_2$.

**17:18**

**D45 15 Strong Electron correlation in the Cobaltates: a CD-MFT study** DIMITRIOS GALANAKIS, TUDOR STANESCU, PHILIP PHILLIPS, *Univ. of Illinois, Urbana-Champaign* The cobaltates $Na_xCoO_2$ with $0 < x < 1$ are highly anisotropic materials that consist of two dimensional $CoO_2$ layers separated by insulating layers of $Na^+$ ions. The structure is a triangular net of edge-sharing oxygen octahedra with the $Co$ ions occupying the center and having a valence determined by the sodium concentra-

tion. The experimental evidence suggests a strongly correlated physics similar to that of the cuprates. The main difference comes from the geometrical frustration of the triangular lattice. Their phase diagram consists of a paramagnetic metal for $x < 0.5$, a Curie-Weiss metal for $x > 0.5$ and a singular insulating state at $x = 0.5$. The properties of these phases are studied within the planar one-band Hubbard model in the framework of Cluster Dynamical Mean Field Theory (CDMFT) on a triangular lattice. The spectral function, magnetic susceptibility are obtained as a function of filling and temperature.

**SESSION D46: FOCUS SESSION: WIDE BAND GAP SEMICONDUCTORS III**
**Monday Afternoon, 13 March 2006; 349, Baltimore Convention Center at 14:30**
**Robert Nemanich, North Carolina State University, presiding**



*Invited Papers*

**14:30**
**D46 1 Step-Controlled Strain Relaxation in the Vicinal Surface Epitaxy of Nitrides.**
XIANRONG HUANG, *SUNY Stony Brook*

This abstract was not received electronically.

*Contributed Papers*

**15:06**
**D46 2 Observation of Standing Waves at Steps on the GaN(0001) Pseudo (1x1) Surface by Scanning Tunneling Spectroscopy at Room Temperature** MIKE HARLAND, LIAN LI, *University of Wisconsin, Milwaukee* Standing waves formed at steps of the GaN(0001) pseudo (1x1) surface are observed with scanning tunneling spectroscopy (STS) at room temperature. The oscillatory behavior of the itdI/itdV calculated for free electrons scattered by atomic steps agrees well with that measured by STS, and thus establishes that the surface state of the GaN(0001) pseudo (1x1) has a nearly free-electron like energy dispersion.

**15:18**
**D46 3 Novel low temperature surface reconstructions of GaN(000$\bar{1}$): A LT-STM investigations** KENDAL CLARK, DANDA P. ACHARYA, MUHAMMAD B. HAIDER, ARTHUR R. SMITH, SAW-WAI HLA, *Ohio University* The nitrogen polar gallium-rich GaN (000$\bar{1}$) samples are grown on sapphire (0001) substrates at sample temperature of 650 $^0$ C using r.f. N-plasma molecular beam epitaxy. During the growth, the surface is monitored by using reflection high energy electron diffraction and 3x3 and 6x6 reconstructed surface patterns have been observed. The freshly grown samples are then transferred to a low-temperature scanning tunneling microscope (LT-STM) system in an ultra-high-vacuum environment. Then the sample temperature is lowered to 75 K and 4.6 K for the STM investigations. The STM images reveal four novel low temperature reconstructions on this surface. We will also present voltage dependent STM images and tunneling spectroscopy data acquired on these structures. This work is financially supported by a NSF-NIRT grant no. DMR-0304314. (NIRT collaboration).

**15:30**
**D46 4 Dopant Adsorption and Incorporation at Irradiated GaN Surfaces*** QIANG SUN, *Princeton University* ANNABELLA SELLONI, *Princeton University* THOMAS MYERS, *West Virginia University* W. ALAN DOOLITTLE, *Georgia Institute of Engineering* Mg and O are two of the common dopants in GaN, but, in spite of extensive investigation, the atomic scale understanding of their adsorption and incorporation is still incomplete. In particular, high-energy electron irradiation, such as occurring during RHEED, has been reported to have an important effect on the incorporation of these impurities, but no study has addressed the detailed mechanisms of this effect yet. Here we use DFT calculations to study the adsorption and incorporation of Mg and O at the Ga- and N-polar GaN surfaces under various Ga, Mg and O coverage conditions as well as in presence of light or electron beam-induced electronic excitation. We find that the adsorption and incorporation of the two impurities have opposite surface polarity dependence: substitutional Mg prefers to incorporate at the GaN(0001) surface, while O prefers to adsorb and incorporate at the N-polar surface. In addition, our results indicate that in presence of light irradiation the tendency of Mg to surface-segregate is reduced. The O adsorption energy on the N-polar surface is also significantly reduced, consistent with the experimental observation of a much smaller concentration of oxygen in the irradiated samples.

*Work was funded under the AFOSR MURI Grant F49620-03-1-0330, monitored by Dr. D. Silversmith.

**15:42**
**D46 5 Imaging surface states of GaN(000$\bar{1}$) at low temperatures*** DANDA P. ACHARYA, KENDAL CLARK, MUHAMMAD B. HAIDER, ARTHUR R. SMITH, NANCY SANDLER, SAW-WAI HLA, *Ohio University* It is known that the surface layer of nitrogen polar gallium-rich GaN (000$\bar{1}$) is semi-metallic in contrast to the bulk GaN. Such semi-metallic behavior is predicted to be contributed by surface state bands [1]. Here, we are able to image two of the surface states associated with the GaN (000$\bar{1}$) surface for the first time at liquid helium temperatures using a low-temperature scanning tunneling microscope (LT-STM). The samples, GaN(000$\bar{1}$), are grown on sapphire (0001) substrates at sample temperature of 650 $^0$ C using r.f. N-plasma molecular beam epitaxy. The freshly grown samples are then transferred to LT-STM system in an ultrahigh vacuum environment for direct investigations. The voltage dependent STM images clearly reveal novel surface features associated with these structures, which are further confirmed by tunneling spectroscopy measurements. This work is financially supported by a NSF-NIRT grant, DMR-0304314. (NIRT collaboration). [1] J. Vac. Sci. Technol. B 16(4), 2241 (1998)

*Imaging surface states of GaN(000 -1) at low temperatures

**15:54**

**D46 6 Surface and interface studies of GaN growth on $ZrB_2$(0001)/Si(111)** YUKIKO YAMADA-TAKAMURA, Z. T. WANG, Y. FUJIKAWA, Q. K. XUE, T. SAKURAI, *IMR, Tohoku University* J. TOLLE, P.-L. LIU, A. V. G. CHIZMESHYA, J. KOUVETAKIS, I. S. T. TSONG, *Arizona State University* $ZrB_2$ is a conductive, reflective, and lattice-matched buffer layer for GaN growth on Si. This study demonstrates the inherent suitability of $ZrB_2$ as an ideal buffer layer for growing inversion domain-free GaN films on Si using an UHV MBE-SPM system. Single crystal $ZrB_2$ films had been grown on Si(111) by the thermal decomposition of single molecular precursor $Zr(BH_4)_4$. Annealing the film at 800$^o$C in UHV was enough to remove the surface oxides and recover the atomically smooth surface. The GaN grown on the oxide-free $ZrB_2$ by plasma-assisted MBE was found to be consistently N-polar independent of the growth conditions. The films were insulating and N-polarity was demonstrated by combined itin situ RHEED and non-contact AFM study. Various interface structures were proposed and as a result of first principles calculations, a single interface structure leading to N-polar GaN growth was found most stable for the wide range of growth conditions. Ref. Y. Yamada-Takamura itet al., Phys. Rev. Lett. itin press.

**16:06**

**D46 7 Electronic characterization of in-grown 8H inclusions in 4H-SiC using Ballistic Electron Emission Microscopy (BEEM)** K. -B. PARK, W. CAI, J. P. PELZ, *The Ohio State University* M. S. MIAO, W. R. L. LAMBRECHT, *Case Western Reserve University* X. ZHANG, M. SKOWRONSKI, *Carnegie Melon University* M. A. CAPANO, *Purdue University* Planar ''8H'' Stacking-fault inclusions (SFIs) formed during epilayer growth on an 8$^o$ miscut n-type 4H-SiC substrate were characterized using nm-resolution BEEM and first-principles electronic structure calculations. Enhanced BEEM current and a $\sim$ 0.39 eV lower local Schottky Barrier were observed along lines where these inclined SFIs intersect a thin Pt film, indicating that 8H SFIs are electron quantum wells (QWs), as observed for two types of cubic SFIs in 4H-SiC [1,2]. The measured $\sim$ 0.39 eV QW depth is close to our calculated value of $\sim$ 0.43 eV. We also observed the BEEM current amplitude and threshold voltage to be quite asymmetric with respect to the intersection lines of the SFIs with the Pt film. We will discuss on-going modeling to see if these asymmetries can be explained respectively by electron reflection from the inclined subsurface SFIs, and by the difference in spontaneous polarization between 8H- and 4H-SiC. Work supported by ONR. [1] Ding itet al., Phys. Rev. B **69**, 041305(R) (2004). [2] Park itet al., Appl. Phys. Lett. **87**, 232103 (2005).

**16:18**

**D46 8 Polarity effects on the electronic states of N- and Al-polar aluminum nitride surfaces** JI-SOO PARK, YINGJIE TANG, ROBERT DAVIS, ROBERT NEMANICH, *North Carolina State University* N- and Al-polar (0001) wurtzite AlN films were grown on C- and Si-polar 6H-SiC substrates, respectively. The polarity was confirmed by KOH chemical etching and atomic force microscopy (AFM) imaging. The surfaces were cleaned in situ by annealing to $\sim$ 1100$^o$C in a flux of ammonia, and X–ray photoemission spectroscopy (XPS) and UV photoemission spectroscopy (UPS) were employed to measure the electronic states at the surfaces. The results indicated a similar electron affinity for both surfaces which appears to approach a value of zero. Furthermore, it was determined that the Fermi energy (Ec-Ef) was 2.4 eV below the conduction band for N-face AlN and 3.0 eV for Al-face AlN. The 0.6eV difference in the Fermi energy indicates a difference in band bending near the surface which is discussed in terms of the built-in field induced by the polarization bound surface charges.

**16:30**

**D46 9 The Negative Electron Affinity Effect on the Thermionic Emission from Nitrogen Doped Diamond** YINGJIE TANG, FRANZ KOECK, ROBERT NEMANICH, *North Carolina State University* NORTH CAROLINA STATE UNIVERSITY TEAM, The thermionic emission properties of microwave CVD nitrogen doped diamond films with a negative electron affinity (NEA) were investigated with thermionic emission spectroscopy (TES) and UV photoelectron emission spectroscopy (UPS). At a temperature of 230$^o$C thermionic electron emission was observed with a current density $\sim$ 1nA/cm$^2$ and a minimum kinetic energy of 1.6eV relative to the Fermi level. Both the thermionic and photoemission spectra display the same sharp cutoff edge corresponding to the conduction band minimum (CBM) which is detected because of the NEA properties of films. With increasing temperature, electron emission is observed below the CBM which is attributed to tunneling phenomena from nitrogen related states and sp2 bonded defects. The emission extends to $\sim$ 1.3eV below the conduction band which would be consistent with prior measurements of the negative electron affinity of diamond surfaces. The effect of the NEA on space charge and defect related electron emission is also discussed.

**16:42**

**D46 10 Study of Thermally Induced Damage and its Recovery in ZnO Single Crystals by Elastic Resonant Ion Channeling** S. DHAR, D. PUGEL, S.S. HULLAVARAD, R.D. VISPUTE, S.B. OGALE, T. VENKATESAN, *Center for Superconductivity Research, Department of Physics, University of Maryland, College Park, MD 20742* ZnO is widely considered as the next generation wide-band gap material for optoelectronic device applications due to its excellent material properties. Although in recent years various studies on ZnO crystal have been made, very little is known about its response after thermal treatments. In this work, we studied the influence of thermal annealing on ZnO (0001) bulk single crystal in the temperature range of 30-1000 $^o$C by elastic resonant ion channeling and Rutherford backscattering (RBS) techniques using a 3.05 MeV He beam. After an isochronal1 h anneal, RBS-Ion channeling analysis showed the evolution of disorder in the Zn sub-lattice of the crystal with increasing annealing temperature. The maximum disorder was observed at 200 $^o$C above which it decreased. The induced disorder in the Zn sub-lattice at lower temperature ( $<$ 400 $^o$C) can almost be recovered by further annealing above 800 $^o$C. Elastic resonant ion channeling analysis, which monitors the oxygen in the near-surface region clearly revealed the evolution of thermally induced disorder in the oxygen sub-lattice with increasing temperature. In contrast to the disorder recovery of Zn sub-lattice, the disorder in oxygen sub-lattice did not recover completely. Possible mechanism on the disorder and its recovery will be discussed.

**16:54**
**D46 11 Band offset measurements on Metal/$Hf_{1-x}Si_xO_2$/Si stacks** ERIC BERSCH, *Rutgers University* SYLVIE RANGAN, *Rutgers University* ROBERT A. BARTYNSKI, *Rutgers University* ERIC GARFUNKEL, *Rutgers University* The study of high-k gate dielectric stacks with metal gate electrodes is motivated by the need to reduce the size of MOSFET devices. Controlling the band offsets between the metal/high-k/Si layers of devices is critical to reducing the leakage current through the dielectric. In order to understand the band alignment at the interfaces we have measured, for each layer of the stack, the conduction band edge (CBE) using inverse photoemission, and the core levels binding energies and valence band edge (VBE) using photoemission. For the high dielectric constant alloys $Hf_{1-x}Si_xO_2$ (x=0, $\sim$ 0.5, 1), the gap increases with x, and we will discuss the effect of x on the CBO and VBO between the silicon and the dielectric. Upon metallization with Ru or Al, Ru does not affect the position of the CBE and VBE of the dielectric, while Al induces a strong shift ( $\sim$ 0.5 eV toward higher binding energy) of the band edges. These results will be compared to other techniques, particularly internal photoemission.



## SESSION E5: APS PRIZES AND AWARD CEREMONY
**Monday Evening, 13 March 2006; 309, Baltimore Convention Center at 17:45**

## SESSION E6: WELCOME RECEPTION
**Monday Evening, 13 March 2006; Ballroom II, Baltimore Convention Center at 18:45**

## SESSION F50: EMERGING EMERGENT PHENOMENA
**Monday Evening, 13 March 2006; Grand Salons V-VI, Marriott Waterfront Hotel at 20:00**

**20:00**
**F50 1 Emergent Phenomena In Particle Physics.**
EDWARD WITTEN, *Institute for Advanced Study*

I will give a brief survey of the extent to which the notion of emergent phenomena is important in different areas of particle physics.

**20:36**
**F50 2 Revisiting Mendel and the Paradox of Gene Restoration.**
SUSAN J. LOLLE, *Purdue University*

According to the laws of classical Mendelian genetics, genetic information contained in the nuclear genome is stably inherited and is transmitted from one generation to the next in a predictable manner. Several exceptions to the principle of stable inheritance are known by all represent specialized cases where the mechanisms have been relatively well defined. We have recently demonstrated that *Arabidopsis* plants can inherit specific DNA sequence information that was not present in the chromosomal genome of their parents. This process appears to occur throughout the nuclear genome. Based on our findings we propose that this process represents a completely novel and hitherto unknown mechanism for the maintenance and inheritance of DNA sequence information.

**21:12**
**F50 3 Statistical Mechanics of Complex Networks: From the Internet to Biology.**
ALBERT-LÁSZLÓ BARABÁSI, *University of Notre Dame*

Networks with complex topology describe systems as diverse as the cell, the World Wide Web or the society. In the past few years we have learned that their evolution is driven by self-organizing processes that are governed by simple but generic scaling laws, leading to the emergence of a vibrant interdisciplinary field that uses the tools of statistical physics to explain the origin and the dynamics of real networks. One of the most surprising finding is that despite their apparent differences, cells and complex man-made networks, such as the Internet or the World Wide Web, and many communi-

cation networks share the same large-scale topology, each having a scale-free structure. I will show that the robustness against failures and attacks, with implications on drug design, the Internet's ability to survive attacks and failures, and our ability to understand the functional role of genes.
For further information and papers, see http://www.nd.edu/~networks

**21:48**
**F50 4 Condensed Matter Physics and the Nature of Dark Matter in the Universe.**
BERNARD SADOULET, *University of California, Berkeley*

The nature of dark matter, which may be 6 times more abundant that ordinary matter in the universe and make up a quarter of the energy density, remains a profound mystery. A leading hypothesis is that dark matter is made of Weakly Interactive Massive Particles (WIMPs), which may result from supersymmetry or additional spatial dimensions. If these WIMPs exist, we should be able to observe their elastic scattering on suitable targets, provided that we can recognize the nuclear recoils they are expected to produce among a background of electron recoils. Expected event rates are small (a few events /kg per year) and the energy deposition should be of the order of 15 keV. I will explain how we are trying to harness condensed matter physics at low temperature (physics of charge carriers, athermal phonons, quasiparticles in superconductors) to detect such events. Such efforts are currently led by our Cryogenic Dark Matter Search (CDMS II) experiment, which is currently ten times more sensitive than any other WIMP search in the world and we hope to obtain another factor ten in the coming two years. This effort is squarely at the intersection of condensed matter, low temperature physics, cosmology and particle physics and provide a good testimony of the Unity of Physics. CDMS II is supported by the National Science Foundation and the Department of Energy.

**SESSION G1: NOBEL PRIZE SYMPOSIUM AND SPECIAL PRIZE SESSION**
**Tuesday Morning, 14 March 2006; Ballroom IV, Baltimore Convention Center at 8:00**
**John Hopfield, Princeton University, APS President, and Charles Clark, National Institute of Standards and Technology, presiding**

**8:00**
**G1 1 The Heartbeat of Light.**
THEODOR W. HÄNSCH, *Max-Planc Institut für Quantenoptik and Sektion Physik, Ludwig-Maximilians-Universität München*

For three decades, precision spectroscopy of the simple hydrogen atom has motivated advances in laser spectroscopy and optical frequency metrology. Recently, femtosecond laser optical frequency comb synthesizers have arrived as revolutionary tools for ultraprecise optical spectroscopy. A new absolute frequency measurement of the hydrogen 1S-2S two-photon resonance sets upper limits for possible slow variations of the time structure constant $\alpha$. Frequency comb techniques are also making it possible to control the electric field of ultrafast laser pulses, opening intriguing opportunities in attosecond physics.

**8:36**
**G1 2 Defining and Measuring Optical Frequencies.**
JOHN L. HALL, *JILA, NIST and University of Colorado, Boulder*

This abstract was not received electronically.

**9:12**
**G1 3 One Hundred Years of Light Quanta.**
ROY J. GLAUBER, *Harvard University*

This abstract was not received electronically.

**9:48**
**G1 4 Laser Scattering in Turbid Media.**
Q. CHARLES SU, *Intense Laser Physics Theory Unit, Illinois State University, Normal, IL 61790-4560*

Light scattering in random media is an interesting research area from a fundamental and practical point of view. On the theoretical side, the precise relationship between the Maxwell, Boltzmann and diffusion descriptions are presently not very well understood. We have examined the validity of these approaches based on numerical solution techniques. On the practical side, an improved understanding of this interaction has the potential to lead to new medical imaging devices based on lasers. We will report on our first experimental data and discuss how they can be modeled by Monte-Carlo simulations. Major portions of this research involved several undergraduate students who performed computer simulations and laboratory measurements. This work has been supported by funds from NSF and Research Corporation. S. Menon, Q. Su, and R. Grobe, Phys. Rev. Lett. 94, 153904 (2005). S. Menon, Q. Su, and R. Grobe, Opt. Lett. 30, 1542–1544 (2005).

**10:24**
**G1 5 Computational Quantum Field Theory.**
RAINER GROBE, *Intense Laser Physics Theory Unit, Illinois State University, Normal, IL 61790-4560*

I will give an overview on recent attempts to solve the time-dependent Dirac equation for the electron-positron field operator. These numerical simulations permit a first temporally and spatially resolved insight into the mechanisms of how an electron-positron pair can be created from vacuum in a very strong force field. This approach has helped to illuminate a wide range of controversial questions. Some of these questions arise for complicated physical situations such as how an electron scatters off a supercritical potential barrier (Klein paradox). This requires the application of quantum field theory to study the combined effect of the pair-production due to the supercriticality of the potential together with the scattering at the barrier involving the Pauli-principle. Other phenomena include the Schrödinger's Zitterbewegung and the localization problem for a relativistic particle. This work has been supported by the NSF and Research Corporation. P. Krekora, K. Cooley, Q. Su, and R. Grobe, Phys. Rev. Lett. 95, 070403 (2005). P. Krekora, Q. Su, and R. Grobe, Phys. Rev. Lett. 93, 043004 (2004). P. Krekora, Q. Su, and R. Grobe, Phys. Rev. Lett. 92, 040406 (2004).

**SESSION G2: QUANTUM CRITICALITY IN CUPRATES**
**Tuesday Morning, 14 March 2006; Ballroom III, Baltimore Convention Center at 8:00**
**Lia Krusin-Elbaum, IBM, presiding**

**8:00**
**G2 1 Breakdown of One-Paramater Scaling in Quantum Critical Scenarios for the High-Temperature Copper-oxide Superconductors.***
CLAUDIO CHAMON, *Boston University*

We show that if the excitations which become gapless at a quantum critical point also carry the electrical current, then a resistivity linear in temperature, as is observed in the copper-oxide high-temperature superconductors, obtains only if the dynamical exponent, z, satisfies the unphysical constraint, $z<0$. At fault here is the universal scaling hypothesis that, at a continuous phase transition, the only relevant length scale is the correlation length. Consequently, either the electrical current in the normal state of the cuprates is carried by degrees of freedom which do not undergo a quantum phase transition, or quantum critical scenarios must forgo this basic scaling hypothesis and demand that more than a single correlation length scale is necessary to model transport in the cuprates. In collaboration with Philip Phillips, Univ. of Illinois at Urbana-Champaign.

*Phys. Rev. Lett. vol. 95, 107002 (2005). Support by DMR-0305482 and DMR-0305864.

**8:36**
**G2 2 Evidence for a generic quantum transition in high-Tc cuprates.**
JEFFERY TALLON, *MacDiarmid Institute, Industrial Research Ltd and Victoria University, PO Bx 31310, Lower Hutt*

The progressive evolution of physical properties with doping in the high-Tc cuprates remains a puzzle, as does the origins of superconducting pairing. This talk will focus on a broad range of physical properties that all signal the presence of a generic quantum transition near optimal doping in these materials which helps explain this unusual evolution in properties. The data includes specific heat, NMR, transport, muon spin relaxation, inelastic neutron scattering, frequency dependent IR conductivity and magnetic properties. In spite of the weight of evidence, however, some key elements appear to be missing. Reasons for this will be surveyed.

**9:12**
**G2 3 Pseudogap scaling and quantum critical end point in electron- and hole-doped cuprates.**
TAKASADA SHIBAUCHI, *Department of Physics, Kyoto University*

In spite of a large number of experiments on the anomalous pseudogap in cuprate superconductors, the real phase diagram of the pseudogap has not yet been established. We employ the interlayer tunneling transport to precisely detect the field dependence of low-energy density of states (DOS) in hole-doped $Bi_2Sr_2CaCu_2O_{8+y}$ and electron-doped $Sm_{2-x}Ce_xCuO_{4-\delta}$ crystals under high fields up to 60 T [1-4]. From a systematic analysis of negative interlayer magnetoresistance, we found a strong doping dependence of the pseudogap closing field whose Zeeman energy scales with the pseudogap energy scale, indicating a preeminent role of spin-singlet correlations in forming the pseudogap in cuprates. The results suggest no quantum critical point up to very overdoped side of the phase diagram. [1] T. Shibauchi *et al.*, Phys. Rev. Lett. **86**, 5763 (2001). [2] T. Shibauchi *et al.*, Phys. Rev. B **67**, 064514 (2003). [3] L. Krusin-Elbaum, T. Shibauchi, and C. H. Mielke, Phys. Rev. Lett. **92**, 097005 (2004). [4] T. Kawakami *et al.*, Phys. Rev. Lett. **95**, 017001 (2005).

**9:48**
**G2 4 Field-induced magnetism in a high-temperature superconductor.**
BELLA LAKE, *Hahn-Meitner Institut, Berlin*

Many physical properties of the high-temperature (high-$T_c$) superconductors are two-dimensional phenomena derived from their square planar $CuO_2$ building blocks. This is especially true of the magnetism from the copper ions electronically connected to each other via the *p*-orbitals of intervening oxygen atoms. As mobile charge carriers enter these $CuO_2$ layers, the antiferromagnetism of the parent insulators, where each copper spin is antiparallel to its nearest neighbours, evolves into a fluctuating state where the spins show tendencies towards magnetic order of a longer periodicity. For certain charge carrier densities, the quantum fluctuations are sufficiently suppressed to yield static long-period order and external magnetic fields also induce such order. Here we show, using neutron scattering measurements, that in contrast to the chemically-controlled order in superconducting $La_{2-x}Sr_xCuO_4$, the field-induced order is actually three-dimensional, implying significant magnetic linkage between the $CuO_2$ planes. The results are important because they reveal the presence of three-dimensional magnetic couplings which survive into the superconducting state, and coexist with the crucial inter-layer couplings responsible for the three-dimensional superconductivity.

**10:24**
**G2 5 Superfluid density in strongly underdoped $YBa_2Cu_3O_{6.333}$.**
DAVID BROUN, *Simon Fraser University*

Current research in high temperature superconductivity focuses on the underdoped cuprates, in the region of the phase diagram where *d*-wave superconductivity gives way to antiferromagnetism. Important clues for connecting these two states can be found in the evolution of the superfluid density $\rho_s$ with doping. $\rho_s$ is the most fundamental property of a superconductor, measuring its ability to resist perturbations to the phase of the superfluid wavefunction. In addition, the temperature dependence of $\rho_s$ provides a direct probe of the electrical current carried by the quasiparticle excitations. Here we report measurements of $\rho_s$ in ultra-high purity $YBa_2Cu_3O_{6.333}$, over a range of dopings near the boundary of the superconducting phase. We have succeeded in producing samples with sharp superconducting transitions and have harnessed the process of CuO-chain ordering to fulfill a long-held ambition in strongly correlated electron materials — continuous tunability of the carrier density in a *single sample*, with *no* change in cation disorder. We now have preliminary evidence for the production of so-called Ortho III′ oxygen order, in which every full CuO chain is separated by two empty chains. The superfluid density measurements are surprising and challenge current theoretical understanding of the underdoped cuprates. $\rho_s$ becomes anomalously small, but there is no vortex unbinding transition. The slope of $\rho_s(T)$ indicates that the current carried by the quasiparticles shrinks smoothly towards zero on approach to the Mott insulator. In addition, the correlation between $T_c$ and $\rho_s$ is sublinear, in disagreement with long-established phenomenology. In the same experiments, microwave spectroscopy of the quasiparticle conductivity has also been used to probe the evolution of the quasiparticle relaxation dynamics on the approach to the superconducting quantum critical point.

## SESSION G3: COUPLED SUPERCONDUCTING QUBITS
**Tuesday Morning, 14 March 2006; Ballroom I, Baltimore Convention Center at 8:00**
**Steven Girvin, Yale University, presiding**



**8:00**
**G3 1 Coupled superconducting qubits: A theoretical overview.**
ALEXANDER SHNIRMAN, *University of Karlsruhe, Germany*

In recent years we have witnessed great progress in quantum state engineering with superconducting qubits. Most experiments have been done with single qubits whereas several groups have reported multi-qubit manipulations. Having controllable coupling between the qubits is absolutely necessary for efficient quantum state engineering. I will overview various coupling schemes suggested in the literature. Among them are capacitive, inductive, nanomechanical, and cavity couplings. Special attention will be paid to the questions of accuracy to which the coupling can be switched off and of speed at which it can be manipulated.

**8:36**
**G3 2 High-Fidelity Measurements of Josephson Phase Qubits.**
JOHN MARTINIS, *UC Santa Barbara*

The Josephson junction is an ideal solid-state system for building electrical ''atoms'' that can function as quantum bits for a quantum computer. Recent advances in the materials and design of phase qubits have dramatically improved their coherence, with energy relaxation times as long as 500 ns and, in a separate device, measurement fidelities as high as 90%. Combined with advances in microwave electronics, full characterization of single and coupled qubit gates are now possible using quantum tomographic techniques. I will report on several ongoing experiments in our group: measurement of the evolution of a quantum state from incomplete measurement, violation of Bell's inequality in a coupled qubit, and the implementation and characterization of a CNOT gate.

**9:12**
**G3 3 Qubits in Cavities for Quantum Optics and Computing.***
DAVID SCHUSTER, *Departments of Applied Physics and Physics, Yale University*

I will describe a platform for quantum computation and quantum optics using superconducting circuits as both the linear and non-linear elements. One dimensional transmission line cavities realize well-defined microwave linear photon modes, while Cooper-pair boxes act as artificial atoms for use as qubits and strongly non-linear elements [1]. We have observed the coherent interaction between a qubit and a single photon, a feat previously only achievable in atomic systems [2]. Using such a coupling a high quality factor cavity can act as an entanglement bus where real or virtual photons mediate interactions between distant qubits [3]. The qubit-photon coupling is exploited to realize a quantum non-demolition measurement of the qubit state [4] and should also allow for direct measurement of the photon number state of the cavity

[5]. Using this measurement technique we have shown > 90% visibility and long coherence times ($T_1 \sim 7$us $T_2^* >$ 500ns) [6]. Off-resonant microwave irradiation is used to adjust qubit-cavity and qubit-qubit detunings for decoherence free control of interaction strengths. Pulsed two photon sideband transitions are shown to mediate off-resonant cavity-qubit interactions, as required to implement non-local two qubit gates. Such techniques could also be used to generate non-classical states of light. We will also discuss initial measurements on two qubits. [1] A. Wallraff et al. Nature (London) 431, 162 (2004) [2] A. Blais et al. Phys. Rev. A 69, 062320 (2004) [3] A. Blais et al. Phys. Rev. A submitted [4] D. I. Schuster et al. Phys. Rev. Lett. 94, 123602 (2005) [5] J. Gambetta et al. Phys. Rev. A submitted [6] A. Wallraff et al. Phys. Rev. Lett. 95 060501 (2005).

*In collaboration with A. Wallraff, A. Blais, J. Gambetta, L. Frunzio, J. Schreier, A. Houck, B. Johnson, J. Majer, M. H. Devoret, S. M. Girvin, R. J. Schoelkopf.

**9:48**
**G3 4 Spectroscopy of two coupled superconducting flux qubits.**
JELLE PLANTENBERG, *Kavli Institute of Nanoscience Delft*

We present measurements on a system of two flux or persistent current qubits, which are coupled by a shared Josephson junction. Spectroscopy measurements reveal the four energy levels in great detail, also showing transitions involving two photons. Remarkably good agreement was found when fitting to a simple model Hamiltonian of two magnetically coupled spins. From the fit the qubit persistent currents and energy gaps as well as the qubit-qubit coupling strength and asymmetry were derived. Coherent Rabi oscillations were induced between energy states of the coupled system, from which relaxation and dephasing times could be extracted. Conditional spectroscopy was performed by manipulating one qubit coherently and measuring the excitation spectrum of the second.

**10:24**
**G3 5 Non-local Andreev Reflection as a Source of Entangled Electrons.***
ALBERTO MORPURGO, *Kavli Institute of Nanoscience, Delft*

Cooper pairs in conventional superconductors form a robust reservoir of spin-entangled singlet ''particles.'' This has led to many theoretical proposals for the realization of ''entangler'' devices –i.e. devices capable of sourcing currents carried by entangled pairs into nanoelectronic circuits- that are of fundamental interest in the field of quantum information. These proposals rely on the possibility to ''split'' Cooper pairs by injecting the two constituent electrons into two spatially separated normal metal leads attached to a superconductors. It has been shown theoretically that such a Cooper-pair ''splitting'' process is equivalent to the process of non-local Andreev reflection, in which an electron (hole) injected from a metallic electrode connected to a superconductor is transmitted into a hole (electron) into a second, spatially separated electrode. In this talk I will discuss recent experiments[1] performed in Delft that demonstrate the occurrence of non-local Andreev reflection as a quantum mechanically phase coherent process. [1] S. Russo et al., Phys. Rev. Lett. **95**, 027002 (2005),

*Work done in collaboration with S.Russo, M.Kroug, and T.M. Klapwijk.



**SESSION G4: POLYMER PHYSICS PRIZE**
**Tuesday Morning, 14 March 2006; 308, Baltimore Convention Center at 8:00**
**Murugappan Muthukumar, University of Massachusetts, presiding**

**8:00**
**G4 1 On nanostructured dispersions and toughness of semi-crystalline polymers.***
LUDWIK LEIBLER, *Matière Molle et Chimie (UMR 7167 CNRS/ESPCI), Ecole Supérieure de Physique et Chimie Industrielles, 75005 Paris*

In the past 50 years, great research efforts have been devoted to increase toughness of plastics. Today, impact strength of millions of tons of plastics used in all sorts of applications relies upon dispersing rubber particles in semi-crystalline polymers (polyolefins, polyamides or polyesters). Yet, the underlying mechanisms controlling such toughening are controversial. Based on a large body of literature and some simple observations, we propose a theory of toughening that explains the existence of an often evoked critical distance between rubber particles which controls the brittle-to-tough transition and predicts how it depends on size and concentration of particles. Our model predicts the brittle-to- tough transition temperature and emphasizes the role of crystal organization and orientation of matrix. Adding rubber particles induces a substantial loss in stiffness. We report how to obtain super-tough polymers and avoid such softening by using

nanostructured dispersions of block- copolymers. We show that block copolymers having a three-dimensional co-continuous structure are particularly attractive as they disperse in a polymer matrix very differently from a lamellar one. In particular, droplet coalescence is much less pronounced for the co-continuous structure. Our observations arise interesting general questions about break-up and coalescence of structured fluid droplets. With Laurent Corté.

*Supported by CNRS, ESPCI and Arkema.

**8:36**
**G4 2 Function in block copolymer assembly.**
MARTIN MÖLLER, *Institute of Macromolecular and Technical Chemistry, RWTH Aachen University, DWI e.V.D-52056 Aachen, Germany*

Spontaneous mesophase and colloidal organization of linear blockcopolymers in bulk and in thin films yields a wealth of well defined metastable and equilibrium structures with intriguing perspectives of new materials functionalities. Besides length, composition, and the type and number of the constituent blocks, branching and chemical transformation provides a further parameter for controlling the molecular conformation and structure. Here we will report on thermal and photo induced single molecule collapse and micellar assembly switching.for comb, palmtree blockcoplymers, as well as for amphiphilic polymer complexes as a means to introduce novel and responsive functionalities, such as motility and hydrophilic/hydrophobic switching.

**9:12**
**G4 3 Field-Theoretic Polymer Simulations: At the Frontier.**
GLENN FREDRICKSON, *University of California, Santa Barbara*

I will review our recent work on the development of a theoretical framework and numerical strategies for conducting computer simulations of polymer field theory models. We invoke Hubbard-Stratonovich and related auxiliary field transforms to convert ''particle-based'' models of polymeric fluids into statistical field theories. This transformation has the effect of replacing polymer-polymer interactions with polymer-field interactions, and renders the action complex. We have developed efficient numerical techniques for computing saddle point field configurations (mean-field or SCFT solutions), as well as for sampling field fluctuations near or away from saddle points (''field-theoretic simulations''). This talk will focus on a number of contemporary topics including: high resolution and variable cell shape SCFT, geometrically complex domains, hybrid particle-field simulations, and strategies for avoiding the sign problem. Examples of applications to polymer alloys, block copolymers, and copolymer nanocomposites will be presented.

**9:48**
**G4 4 Structural an Dynamical Properties of Some Equilibrium Polymers.**
JEAN SAUVEUR CANDAU, *Universite Louis Pasteur*

The most detailed studies on equilibrium polymers have been performed on surfactant wormlike micellar solutions. Recently the formation of reversible supramolecular polymers through H bond mediated self assembly of two homofitopic heterocomplementary monomers were reported. In apolar solvents, highly viscoelastic solutions were observed at concentrations as low as 2 mM, thus indicating a network-like structure. We have studied a supramolecular polymeric system formed through a sextuple hydrogen bonding of a Janus-type wedge and a corresponding receptor. Small Angle Neutron Scattering experiments showed that the monomers self assemble into long unidimensionnal aggregates whose local structure is independent of temperature and concentration. From the values of the cross section and the mass per unit length of the fibers it can be inferred that these fibers contain several monomolecular wires. The concentration and temperature dependences of the average polymer length were found to be similar to those of worm-like micelles. Non linear rheological experiments showed a shear-banding instability as in micellar systems. However the concentration dependence of the terminal time of the stress relaxation suggests the formation of additional transient crosslinks in the supramolecular polymeric systems resulting in a slowing down of the relaxation as in associating polymers.

**10:24**
**G4 5 A Lattice Model for Segmental Dynamics of Miscible Polymer Blends.***
RALPH H. COLBY, *Materials Science and Engineering, Pennsylvania State University*

Thermally-driven concentration fluctuations make local regions (at the scale of monomers) have a wide range of local compositions for weakly interacting miscible blends of long chain polymers. These fluctuations remain important hundreds of degrees from the critical temperature because the entropy (and hence free energy) of mixing is small in polymer mixtures. The connected nature of the chain biases the local composition distribution, making the range of effective compositions surrounding a given monomer extend from the self-composition to environments very rich in that type of monomer. These two polymer physics issues make blends of polymers vastly more interesting than mixtures of small molecules. Time-temperature superposition can fail and motions can persist far below the glass transition temperature of the blend; both of these results are enhanced as the glass transition contrast between the two components increases. A simple lattice model is used to describe the segmental dynamics of miscible polymer blends. Concentration fluctuations

and chain connectivity effects are calculated at the scale of the Kuhn length, by considering a central monomer to be surrounded, out to the second shell of monomers, by 24 lattice sites. Including the central monomer, fraction 5/25 = 0.2 of the lattice sites are part of the central monomer's chain (the self-composition) and the other 20 sites are occupied stochastically, while preserving connectivity of all chains. The resulting concentration distributions are mapped onto segmental relaxation time distributions for each blend component using the composition dependence of the glass transition and dynamic scaling. The predicted distributions are compared with experimental dielectric data on miscible polymer blends using three methods: (1) A Debye (single exponential) relaxation of each composition predicts dielectric loss peaks for each blend component which are too narrow because the lattice model ignores density fluctuations. (2) The empirical Havriliak-Negami distribution can be fit to the dielectric loss of each pure component and then assigned to each composition in that component's distribution in the blend. (3) The pure component data can be modeled with a Gaussian distribution of density fluctuations with times related to free volume using the Doolittle equation, and subsequently this distribution is assigned to each composition in that component's blend distribution. The relative merits of these three approaches will be discussed in detail.

*With Jane E. G. Lipson, Dartmouth College.

**SESSION G5: ADVANCED MATERIALS FOR SOLAR ENERGY UTILIZATION**
**Tuesday Morning, 14 March 2006; 309, Baltimore Convention Center at 8:00**
**Julia Hsu, Sandia National Laboratories, presiding**



**8:00**
**G5 1 Scientific Challenges in Sustainable Energy Technology.**
NATHAN LEWIS, *California Institute of Technology*

This presentation will describe and evaluate the challenges, both technical, political, and economic, involved with widespread adoption of renewable energy technologies. First, we estimate the available fossil fuel resources and reserves based on data from the World Energy Assessment and World Energy Council. In conjunction with the current and projected global primary power production rates, we then estimate the remaining years of supply of oil, gas, and coal for use in primary power production. We then compare the price per unit of energy of these sources to those of renewable energy technologies (wind, solar thermal, solar electric, biomass, hydroelectric, and geothermal) to evaluate the degree to which supply/demand forces stimulate a transition to renewable energy technologies in the next 20-50 years. Secondly, we evaluate the greenhouse gas buildup limitations on carbon-based power consumption as an unpriced externality to fossil-fuel consumption, considering global population growth, increased global gross domestic product, and increased energy efficiency per unit of globally averaged GDP, as produced by the Intergovernmental Panel on Climate Change (IPCC). A greenhouse gas constraint on total carbon emissions, in conjunction with global population growth, is projected to drive the demand for carbon-free power well beyond that produced by conventional supply/demand pricing tradeoffs, at potentially daunting levels relative to current renewable energy demand levels. Thirdly, we evaluate the level and timescale of R&D investment that is needed to produce the required quantity of carbon-free power by the 2050 timeframe, to support the expected global energy demand for carbon-free power. Fourth, we evaluate the energy potential of various renewable energy resources to ascertain which resources are adequately available globally to support the projected global carbon-free energy demand requirements. Fifth, we evaluate the challenges to the chemical sciences to enable the cost-effective production of carbon-free power on the needed scale by the 2050 timeframe. Finally, we discuss the effects of a change in primary power technology on the energy supply infrastructure and discuss the impact of such a change on the modes of energy consumption by the energy consumer and additional demands on the chemical sciences to support such a transition in energy supply.

**8:36**
**G5 2 High-Efficiency, Multijunction Solar Cells for Large-Scale Solar Electricity Generation.**
SARAH KURTZ, *National Renewable Energy Laborator*

A solar cell with an infinite number of materials (matched to the solar spectrum) has a theoretical efficiency limit of 68%. If sunlight is concentrated, this limit increases to about 87%. These theoretical limits are calculated using basic physics and are independent of the details of the materials. In practice, the challenge of achieving high efficiency depends on identifying materials that can effectively use the solar spectrum. Impressive progress has been made with the current efficiency record being 39%. Today's solar market is also showing impressive progress, but is still hindered by high prices. One strategy for reducing cost is to use lenses or mirrors to focus the light on small solar cells. In this case, the system cost is dominated by the cost of the relatively inexpensive optics. The value of the optics increases with the efficiency of the solar cell. Thus, a concentrator system made with 35%- 40%-efficient solar cells is expected to deliver 50% more power at a similar cost when compare with a system using 25%-efficient cells. Today's markets are showing

an opportunity for large concentrator systems that didn't exist 5-10 years ago. Efficiencies may soon pass 40% and ultimately may reach 50%, providing a pathway to improved performance and decreased cost. Many companies are currently investigating this technology for large-scale electricity generation. The presentation will cover the basic physics and more practical considerations to achieving high efficiency as well as describing the current status of the concentrator industry. This work has been authored by an employee of the Midwest Research Institute under Contract No. DE-AC36-99GO10337 with the U.S. Department of Energy. 

**9:12**
**G5 3 Nanowire Based Solar Cells**
PEI-DONG YONG, *UC Berkeley*

This abstract was not received electronically.

**9:48**
**G5 4 Bio-inspired constructs for solar energy conversion.**
THOMAS MOORE, *Arizona State University*

Solar energy input to the biosphere is about $10^{24}$ joules/year. This makes human needs of even a projected $10^{21}$ joules/year a deceptively achievable goal. One key to global-scale use of solar energy is the synthesis of energy-rich fuel materials such as hydrogen and reduced carbon compounds. The latter have the almost inestimable advantage that the energy infrastructure for distribution and use is in place. The photosynthetic and respiratory enzymes provide paradigms for all of the important energy converting processes humans would need to achieve sustainable energy production and use. These include water oxidation, $O_2$ reduction and oxidation of energy dense organics at room temperature. These processes are carried out by biological catalysts at near thermodynamic efficiency without the use of precious metals. Copper, manganese, iron and nickel are typically used at their active sites. Energy rich organics such as ethanol and larger reduced-carbon compounds offer energy densities comparable to that of fossil fuels yet technology has not produced a low temperature catalyst for breaking carbon-carbon bonds. Biology offers myriad examples of such catalysts. Electroreductive synthesis of organics from $CO_2$ is also templated by Nature's catalysts. The challenge is clear: we must understand the structures and chemical reactivity of these catalytic sites and co-opt their essential features for human use. A number of parameters are involved and will be discussed. Even considering an artificial catalysts comprising only the atoms necessary for catalysis, the footprint is relatively large and, since biological turnover rates are often low, achieving current flows adequate for human needs in industry and transportation is problematic. A detailed understanding of efficiently coupling electromotive force to the active sites of redox enzymes will be one key to designing efficient hybrid catalytic devices. A model system for solar-driven reforming of biomass to $H_2$ will be presented.

**10:24**
**G5 5 The Status and Outlook for the Photovoltaics Industry.**
DAVID CARLSON, *BP Solar*

The first silicon solar cell was made at Bell Labs in 1954, and over the following decades, shipments of photovoltaic (PV) modules increased at a rate of about 18% annually. In the last several years, the annual growth rate has increased to $\sim$ 35% due largely to government-supported programs in Japan and Germany. Silicon technology has dominated the PV industry since its inception, and in 2005 about 65% of all solar cells were made from polycrystalline (or multicrystalline) silicon, 24% from monocrystalline silicon and $\sim$ 4% from ribbon silicon. While conversion efficiencies as high as 24.7% have been obtained in the laboratory for silicon solar cells, the best efficiencies for commercial PV modules are in the range of 17 18% (the efficiency limit for a silicon solar cell is $\sim$ 29%). A number of companies are commercializing solar cells based on other materials such as amorphous silicon, microcrystalline silicon, cadmium telluride, copper-indium-gallium-diselenide (CIGS), gallium arsenide (and related compounds) and dye- sensitized titanium oxide. Thin film CIGS solar cells have been fabricated with conversion efficiencies as high as 19.5% while efficiencies as high as 39% have been demonstrated for a GaInP/Ga(In)As/Ge triple-junction cell operating at a concentration of 236 suns. Thin film solar cells are being used in consumer products and in some building-integrated applications, while PV concentrator systems are being tested in grid-connected arrays located in high solar insolation areas. Nonetheless, crystalline silicon PV technology is likely to dominate the terrestrial market for at least the next decade with module efficiencies $>$ 20% and module prices of $<$ \$1/Wp expected by 2020, which in turn should allow significant penetration of the utility grid market. However, crystalline silicon solar cells may be challenged in the next decade or two by new low-cost, high performance devices based on organic materials and nanotechnology.

**SESSION G7: SHEAR-INDUCED PATTERNS IN COMPLEX FLUIDS AND GRANULAR MATTER**
**Tuesday Morning, 14 March 2006; 307, Baltimore Convention Center at 8:00**
**David Weitz, Harvard University, presiding**

**8:00**
**G7 1 Subcritical shear-induced instabilities and turbulence of visco-elastic fluids.**
WIM VAN SAARLOOS, *Leiden University*

While instabilities in normal Newtonian fluids are usually due to inertial effects, most visco-elastic instabilities are noninertial, i.e. happen at small Reynolds numbers. In polymeric fluids the viscoelastic instabilities and turbulence are due to shear-induced anisotropic elastic forces: when the so-called Weissenberg number is larger than about 1, a polymer fluid is very non-Newtonian: in this regime the fluid is anisotropic and elastic, and relaxation effects are important. After reviewing some recent experiments, I will discuss the recent progress on understanding the viscoelastic instabilities in parallel shear flows (planar Couette and Poiseuille flow). Contrary to common belief that such flows are absolutely stable in the small Reynolds number limit, our recent nonlinear amplitude analysis predicts that the transitions are subcritical. The critical Weissenberg number our analysis predicts is close to the values where in practice such flows are found to exhibit instabilities. The scenario suggested by these results shows strong resemblance to the transition to (weak) turbulence scenario in Newtonian shear flows. [1] A. N. Morozov and W. van Saarloos, *Subcritical finite-amplitude solutions in plane Couette flow of visco-elastic fluids*, Phys. Rev. Lett. **95**, 024501 (2005).

**8:36**
**G7 2 Shear thickening, thinning and jamming in colloidal suspensions.**
DAVID REICHMANN, *Columbia University*

A microscopic theory for shear thinning behavior in glassy colloidal suspensions is presented. This theory is tested against extensive computer simulation. The theory is extended to study non-linear viscoelastic properties, and is shown to be in remarkable agreement with the measured strain sweep dependence of the loss modulus in colloidal gels. Lastly, we present numerical simulations to address shear thinning and possible shear thickening behavior of dense colloidal suspensions with short-ranged depletion-induced attractions.

**9:12**
**G7 3 Shear Alignment of Hexagonal and Striped Patterns in Block Copolymer Thin Films.***
RICHARD REGISTER, *Princeton University*

Diblock copolymers spontaneously self-assemble into nanodomain structures: simple repeating patterns with a periodicity (typically 20-100 nm) set by the polymer molecular weight and a symmetry controlled by the relative lengths of the two blocks. Similar patterns are obtained when block copolymers are deposited onto substrates, as films with thicknesses accommodating only a few or even only one layer of nanodomains: cylindrical nanodomains form a striped pattern when viewed from above, while spheres form a hexagonal pattern. In the absence of any applied field, however, these patterns exist as a polygrain structure, with a grain size which is typically microns at most. Recently, we have developed methods to shear these thin films, producing samples free from grain boundaries and with orientational order extending over centimeters. But while excellent orientational order can be achieved by shearing, translational order is still limited to the micron scale due to isolated dislocations which remain in the sheared films (though at a markedly reduced density compared with unsheared films). Shear can be applied either with an elastomeric pad, or with a viscous fluid; in the latter case, the patterns can be induced to follow the shape of fluid flow channels of arbitrary shape and millimeter-scale width. For the striped patterns, shear alignment is effective on films containing either a single layer or multiple layers of nanodomains, but for the hexagonal pattern, two or more layers are required due to the mechanical isotropy of a two-dimensional hexagonal lattice. A threshold stress is required to achieve the limiting quality of alignment, a stress which decreases as the block copolymer's order-disorder transition temperature is approached. A simple model appears to capture the principal features of the stress, time, and temperature dependence of the alignment quality.

*With Dan Angelescu, Mingshaw Wu, Vincent Pelletier, Judith Waller, Andrew Marencic, Douglas Adamson, and Paul Chaikin, supported by the NSF MRSEC Program through the Princeton Center for Complex Materials (DMR-0213706).

**9:48**
**G7 4 Shear banding in complex fluids: Hints from colloidal crystals.***
BENNY DAVIDOVITCH, *Harvard University*

When sheared out of equilibrium, a variety of complex fluids exhibit an unusual behavior, where bands of high and low shear rates are spontaneously formed. This phenomenon is typically attributed to a nonlinear material rheology. In this talk I will describe a similar phenomenon observed in oscillatory shear experiment on dense colloidal crystal, where the

data reflect a linear, rather than nonlinear material rheology. This observation suggests an alternative mechanism for shear banding, as a coexistence under nonequilibrium conditions between two linearly responding phases of a complex fluid. Some consequences will be discussed, such as the singular role played by near-wall pure solvent layers, and possible nonequilibrium mechanisms for selection of the observed band width.

*Collaboration with: Itai Cohen, Michael P. Brenner, and David A. Weitz.

**10:24**
**G7 5 Force fluctuations and shear banding near the jamming transition in granular materials.**
HEINRICH JAEGER, *The University of Chicago*

What are the structural changes which turn an un-jammed system that flows like a liquid into a jammed, solid-like configuration or vice versa? For granular just as for molecular systems it turns out that these changes are so subtle that so far there still has been no clean way of identifying the transition based on direct measurements of the grains' or molecules' spatial arrangements. However, in macroscopic granular systems it is possible to measure also the forces between contacting grains. At high packing densities near jamming, where nearly all particles touch neighbors, contact force measurements pick up directly and sensitively what matters most, namely changes in relative grain position. They thus can act as magnifier for even minute structural rearrangements. This talk will discuss experiments [1] able to detect a structural signature of the jamming transition by analyzing changes in the shape of the distribution of contact forces. The second part of the talk will be devoted to discussing new experimental geometries in which shear bands, usually localized to within about 10 grain diameters at the onset of shear, can become much wider. This allows for detailed studies of the shear rate profile and the associated velocity fluctuations. I will compare data we recently obtained from direct imaging by video, magnetic resonance imaging of the interior, and molecular dynamics simulations [2]. [1] E. I. Corwin, H. M. Jaeger, S. R. Nagel, Structural signature of jamming in granular media, Nature 435, 1075 (2005). [2] X. Cheng, J. B. Lechman, A. F. Barbero, G. S. Grest, H. M. Jaeger, G. S. Karczmar, M. E. Möbius, and S. R. Nagel, Three-dimensional shear in granular flow, cond-mat/0507469.

**SESSION G8: PATTERNS AND INSTABILITIES II**
**Tuesday Morning, 14 March 2006**
**314, Baltimore Convention Center at 8:00**
**A. Prosperetti, Johns Hopkins University, presiding**

**8:00**
**G8 1 Dynamics of Swarms** NICHOLAS MECHOLSKY, EDWARD OTT, TOM ANTONSEN, *University of Maryland Deptartment of Physics* The collective behavior of animal groups (swarms, herds, flocks, etc.) provides a fascinating instance of a self-organizing system. In this poster we consider continuum model descriptions of animal groups with particular emphasis on dynamics and relaxation of the collective behavior of such groups. Topics considered will include equilibrium swarms, waves on swarms, relaxation to equilibrium, excitation of waves by obstacles and predators, and stability.

**8:12**
**G8 2 Drying Mediated Pattern Formation in a Capillary-Held Polymer Solution*** ZHIQUN LIN, JUN XU, SUCK WON HONG, JIANFENG XIA, *Materials Science and Engineering Department, Iowa State University, Ames, IA 50011* We demonstrated that concentric ring patterns of high regularity could form spontaneously, simply by allowing a droplet to evaporate in a consecutive ''stick-slip'' motion in a confined geometry. The process resembled neatly stacked rows of driftwood abandoned by receding tides. The use of solutions with different concentrations and different solvents effectively mediated the evaporative loss of the solvent and the deposition time of the solute, thereby affecting the center-to-center distance between adjacent rings and the height of the ring. A theoretical calculation based on the mass conservation of the solution has, for the first time, been performed to reveal the nature of the formation of gradient ring patterns in a confined geometry. The studies demonstrate that dynamic self-assembly in a confined geometry may offer a new approach to produce gradient features, as well as a simple, versatile, generalizable approach to produce yet more complex patterns. This natural, pattern-forming process could find use in the fields such as nanotechnology and optoelectronics.

*Acknowledgement: ISU startup, ISU University Research Grant, and ACS-PRF

**8:24**
**G8 3 A network model of channel competition in fracture dissolution*** TONY LADD, *University of Florida* PIOTR SZYMCZAK, *Warsaw University* During dissolution in porous or fractured rock, a positive feedback between fluid transport and chemical reactions at the mineral surfaces may lead to the formation of pronounced, wormhole-like channels. As the dissolution proceeds the channels interact, competing for the available flow, and eventually the growth of the shorter ones ceases. Thus the number of channels decreases with time while the characteristic distance between them increases, which leads to a scale-invariant, power-law distribution of channel lengths. A simple resistor network model of the evolution of dissolving channels is constructed and its properties studied. The results are compared with pore-scale simulations of fracture dissolution using a microscopic, three-dimensional numerical model. Despite its simplicity, the resistor model is found to retain the essential features of the nonlinear interaction between the channels.

*This work was supported by the US Department of Energy, Chemical Sciences, Geosciences and Biosciences Division, Office of Basic Energy Sciences (DE-FG02-98ER14853), and by the Polish Committee of Scientific Research (P03B 08127, 2004-2005)

**8:36**

**G8 4 Fractal growth of liquid crystals as a hysteresis phenomenon** HO-KEI CHAN, INGO DIERKING, *School of Physics and Astronomy, University of Manchester, Manchester (U. K.)* Fractal percolation growth of liquid crystal phases within a supercooled isotropic liquid medium has been observed in recent years. Notable examples include the B2 phase of 'banana' mesogens [1] and the smectic C phase of a calamitic hydrogen-bonding liquid crystal [2]. Here we present a dynamical model that describes such fractal growth as well as the spherical growth conventionally observed for nematics and cholesterics. The essential idea is that the supercooled medium does not fully respond to the temperature quench immediately (hysteresis). Its fraction of space available for the phase transition only relaxes from 0 to 1 at some finite rate. Depending on the coupling between the relaxation and growth rates, the liquid crystal phase either grows as a percolation cluster of fractal dimension $D \approx 1.89$ or approaches a spherical shape of Euclidean dimension $D \rightarrow 2$. The crossover behaviour from relatively slow to fast relaxation is thoroughly investigated. Possible causes of the hysteresis for fractal growth will be discussed. [1] I. Dierking, Liq. Cryst. Today **12(1)**, (2003), 1 [2] I. Dierking, Chan H. K., Culfaz F., McQuire S., Phys. Rev. E **70**, (2004), 051701.

**8:48**

**G8 5 Patterns in type-I superconductors and their dynamics** RINKE J. WIJNGAARDEN, MARIELA MENGHINI, *Department of Physics and Astronomy, Faculty of Sciences, Free University, De Boelelaan 1081, 1081 HV Amsterdam, The Netherlands* We report on patterns and their dynamics as observed in magneto- optical experiments on type-I superconductors. We observe: (1) A stripe-spot transition that is hysteretic, leading to two modes of stripe formation: slow continuous growth and avalanche growth. (2) A wiggling instability, similar to that in ferrimagnetic garnet films. (3) A zigzag instability when a pattern of parallel lines is rotated through a sample with low pinning. (4) Breaking and reconnection of stripes as such a pattern is rotated in a sample with strong pinning. (5) Random telegraph behavior close to the depinning of such pattern in the presence of a constant driving force. The observed patterns consist of superconducting and normal domains of macroscopic size in thin lamina of type-I superconductors and are observed by an advanced magneto-optical technique. The patterns are manipulated by changing the applied magnetic field vector or by applying an electrical transport current.

**9:00**

**G8 6 Scaling in activated escape of underdamped systems** IRA SCHWARTZ, *Naval Research Laboratory* MARK DYKMAN, MICHAEL SHAPIRO, *Michigan State University* Noise-induced escape from potentials is ubiquitous in many areas of physics. Here, noise-induced escape from a metastable state of a dynamical system is studied close to a saddle-node bifurcation point, but in a region where the system remains underdamped. We find the activation energy of escape scales as a power of the distance to the bifurcation point. Moreover, we find two types of scaling and the corresponding critical exponents.

**9:12**

**G8 7 The Analysis of Spatiotemporal Chaos in Very Large Data Sets Generated by Electroconvective Experiments with Nematic Liquid crystals*** JOSHUA LADD, *Colorado State University* GYANU ACHARYA, *Kent State University* J.T. GLEESON, *Kent State University* Spatiotemporal chaos (STC) has been empirically observed in electrohydrodynamic convection in a planar layer of the nematic liquid crystal I52. The observed spatiotemporal dynamics is due to the interaction of two families of counter propagating waves that loose stability at onset. Thus it is possible to describe the patterns through a system of Ginzburg –Landau equations that governs the evolution of the envelopes of these waves (Denin et al, Science 1996). In this work we extract the envelopes from spatiotemporal data generated by electroconvective experiments done at Kent State University using a demodulation procedure. Once obtained it is possible to separate spatial and temporal components of the dynamics by employing the singular value decomposition. This is done in order to study the chaotic nature of the pattern. Comparison is made with numerical STC obtained from computer simulations of the Ginzburg-Landau system derived from the weak electrolyte model (itDangelmayr & Oprea, 2002) of electroconvection.

*Supported by NSF-DMS 0407418

**9:24**

**G8 8 Pattern formation in liquids under unipolar space charge injection*** FRANCISCO VEGA REYES, *Departamento de Fisica, Universidad de Extremadura, E-06071 Badajoz, Spain* FRANCISCO J. GARCIA, *Departmento de Fisica Aplicada I, EUITA, Universidad de Sevilla, Spain* We study experimentally the hydrodynamic stability of thin liquid layers subjected to corona discharge in the air. We obtain clear direct images and movies of the observed hydrodynamic instabilities and patterns. After this we apply an image processing method that allows us to quantify the liquid interface deformation. We use a variety of liquids whose properties may differ in orders of magnitude. Particularly, we use series of liquids with different electric conductivity or viscosity while keeping constant the rest of the properties. In this way, we can track quantitatively the instabilities as a function of only one of these properties. This, together with our image processing method, allows us to study and classify the different instabilities. The peculiar properties of the electric field in the liquid interface when there is a space charge injection have not been studied until very recently. Results show clearly the influence (and relevancy) that the properties of this electric field have in the formation (or not) of the different patterns observed when the liquid properties are varied.

*This work was supported by the Spanish Ministry of Education and Science under research project BFM-2003-01739.

**9:36**

**G8 9 Path stability of a rising bubble*** BINZE YANG, ANDREA PROSPERETTI, *Johns Hopkins University* A millimeter-size gas bubble rises in a zigzag or spiral path in still water. A linear analysis of this process is presented assuming that the bubble has a fixed ellipsoidal shape of varying aspect ratio. The results exhibit a strong similarity to the stability features of the flow past a solid sphere. By focusing on the $m = 1$ azimuthal mode, it is found that a double-threaded wake responsible for the deviation from the vertical path develops when the aspect ratio is sufficiently large. The stability analysis of ''frozen'' states before steady conditions are achieved shows that the amount of vorticity

accumulated at the rear of the bubble plays an essential role for the instability. It is also shown that, in the common parameter ranges of interest, the instability is very sensitive to the deformation of the bubble, but relatively insensitive to the Reynolds number.

*Supported by NASA

**9:48**

**G8 10 Flame Propagation with Hydrodynamic and Body-Force Instabilities** KUO-LONG PAN, *Department of Mechanical Engineering, National Taiwan University* The hydrodynamic (Darrieus-Landau) instability is an intrinsic mechanism that wrinkles the flame surface. In the nonlinear stage, propagation of flame wrinkles can evolve to a quasi-stable state characterized by a solitary wave or chaotic form with corrugated front. The underlying structures, i.e. incessant merging of near wrinkles and creation of new cells, have been studied numerically. It reveals the significance of asymmetric perturbation in breaking the symmetry. The effect of gravity was also investigated. It was found that, while wrinkled flames can be stabilized by negative gravity of moderate magnitude, the wrinkles at short wavelength, it$\lambda$, remains intact if the magnitude is small while those at long it$\lambda$ are suppressed. As such, compared to the zero-gravity state, diminishing multiplicity of cellular scales and subsequently decreasing interactions among the multi-scale wrinkles mollify the chaotic complication. When slight positive gravity is introduced, the unsteady evolution is suppressed. The somehow stabilizing effect, while in contrast to the destabilization at linear stage, is due to the coupling of D-L instability and Rayleigh-Taylor instability that prevents excitation of secondary D-L instability. If the magnitude is strong enough, however, the ordered pattern degenerates and highly irregular flame surface is formed without specific cell structure. This is a typical appearance of R-T instability caused by buoyancy.

**10:00**

**G8 11 Numerical Simulation of Conductivity Gradient-Induced Electrokinetic Flow Instabilities** STEPHEN BRADFORD, *UC Santa Barbara* CARL MEINHART, *UC Santa Barbara* JON POSNER COLLABORATION, JUAN SANTIAGO COLLABORATION, This research is focused on the electrokinetic flow instabilities observed in long, thin microchannels with conductivity gradients orthogonal to the streamwise direction and applied potential. This situation often occurs in field amplified sample stacking (FASS) and isoelectric focusing, where control of the instabilities is imperative. Alternatively, the inherently chaotic flow patterns can be leveraged to fabricate an efficient micromixer under specific conditions. These instabilities arise from fluid body forces generated by the action of applied electric fields on electrolyte concentration-based conductivity gradients. A model is developed to describe the phenomena in general and applied specifically to thin microchannels with the conductivity gradient perpendicular to the applied field (both DC and AC). A higher-order, depth averaged correlation is proposed to account for the out of plane effects. Numerical simulations performed using COMSOL 3.2 are compared to 2-D and 3-D simulations as well as experimental data for multiple geometries with good agreement.

**10:12**

**G8 12 Particle production in non-dissipative shock-waves** ALEXANDER ABANOV, *Stony Brook University* FABIO FRANCHINI, We study non-dissipative shock-waves in the effective hydrodynamics of some correlated one-dimensional integrable systems. The semiclassical dynamics of these systems is governed by integrable non-linear classical equations such as the Benjamin-Ono and the KdV equations. The development of non- dissipative shock-waves from a large disturbance of the fluid is described by Gurevich-Pitaevsky theory. The theory describes how the instability of a large disturbance of the fluid is resolved by producing oscillations which develop into a train of solitons at large times. We establish the connection between this classical picture and the production of quasi-particles in the underlying quantum system. The semiclassical (background) configuration can then be thought of as an effective metric in which these excitations move. This approach is done in the spirit of the original proposal of Unruh, who suggested to model the Hawking radiation from black holes by an emission of thermal sound waves from the sonic horizon in transsonic fluid flow.

**10:24**

**G8 13 Torsional Motion of Rotating Particles with Graded Couplings** H.W. TSANG, J.J. XIAO, K.W. YU, *The Chinese University of Hong Kong* Localization of excitations occurs in many physical systems. There are two common types of localization. The first type is a consequence of interference of coherent vibrational waves due to diffusive scattering like Anderson localization in lattice vibration. The other type of localization is due to confinement by impurities like defect modes. Graded systems occur in a variety of physical system. It is of great interest to analyze the localization of excitations in graded system [1]. In this work, we consider a system of rotating particles with graded torsional couplings. The steady-state solutions are solved directly from the dynamic equations. Energy is localized in the region of stronger couplings at high frequencies. A dynamic stimulation based on forced rotors is performed both for the graded linear and graded non-linear coupling potential subjected to a sinusoidal driving torque. In the small amplitude region, the results of non-linear potential are similar to those of the linear ones. The major difference is that the rotational amplitude is larger for the non-linear potential. Energy transfer may thus be more effective in the non-linear case. In the large amplitude region, chaos may occur and contribute to the localization. [1] J. J. Xiao, K. Yakubo, and K. W. Yu, Harmonic vibrational excitations in graded elastic networks: transition from phonons to gradons, unpublished.

**10:36**

**G8 14 Numerical simulations of inertial migration in a square duct: An investigation of multiple equilibrium positions*** BYOUNGJIN CHUN, *University of Florida* TONY LADD, In Poiseuille flow, a neutrally-buoyant particle migrates to a position that is determined by the balance of forces generated by the gradient of the shear rate and interactions of the flow field with the container walls. In a cylindrical flow, uniformly distributed particles migrate to form a stable ring located at approximately 0.6 times the cylinder radius. However, recent experiments show two interesting new observations. First the suspended particles tend to align near the walls to make linear chains of more or less equally-spaced particles, and second, at high Reynolds numbers (Re 1000), an additional inner ring of particles is formed. The inner ring is only

formed when the particle are large, of the order of 1:10 the cylinder diameter. We have used numerical simulations based on the lattice-Boltzmann method to investigate inertial migration of neutrally buoyant particles in a square duct over a range of Reynolds numbers from 100 to 1000. Our results show trains of particles being formed along the axis of the flow, near the planar equilibrium positions of single particles. At Reynolds number greater than 750, particles appear near the center of the duct as well. We will present a new mechanism to interpret and understand these results, which was discovered by examining the migration of single particles and rigid dumbbells.

*This work was supported by the National Aeronautics and Space Administration, NAG NNCO4GA89G.

**SESSION G10: FOCUS SESSIONS: PHYSICAL CHEMISTRY OF NANOSCALE SYSTEM IV**
**Tuesday Morning, 14 March 2006; 302, Baltimore Convention Center at 8:00**
**Jin Zhang, University of California, Santa Cruz, presiding**

*Invited Papers*

**8:00**
**G10 1 Nanowire-based solar cell.**
PEIDONG YANG, *University of California*

Excitonic solar cells – including organic, hybrid organic-inorganic and dye-sensitised cells (DSCs) – are promising devices for inexpensive, large-scale solar energy conversion. The DSC is currently the most efficient and stable excitonic photocell. Central to this device is a thick nanoparticle film that provides a large surface area for the adsorption of light-harvesting molecules. However, nanoparticle DSCs rely on trap-limited diffusion for electron transport, a slow mechanism that can limit device efficiency, especially at longer wavelengths. Here we introduce a new version of the dye-sensitised cell in which the traditional nanoparticle film is replaced by a dense array of oriented, crystalline ZnO nanowires. The nanowire anode is synthesized via mild aqueous chemistry and features a surface area up to one-fifth as large as a nanoparticle cell. The direct electrical pathways provided by the nanowires ensure the rapid collection of carriers generated throughout the device, and a full Sun efficiency of 2.5% is demonstrated, limited primarily by the surface area of the nanowire array.

*Contributed Papers*

**8:36**
**G10 2 Structural and Conductance Change in Hydridosilsesquioxane Based Silicon Oxide Clusters Induced by an Electric Field** SAROJ NAYAK, PHILIP SHEMELLA, *Rensselaer Polytechnic Institute - Department of Physics, Applied Physics & Astronomy* Interesting results arise from the addition of a hydrogen atom to a hydridosilsesquioxane (HSQ) $Si_8O_{12}H_8$ cluster, and have been studied with density functional theory techniques. Three stable minima have been found (open, cluster, center), and energy barriers between each have been computed. Each state has different values in the HOMO-LUMO[1] energy gap, which is usually a metric for conductance. Simulating the electronic interaction with an applied electric field, we model the reactions and compute the energy barriers with and without an applied electric field. Asymmetric states with strong dipole moments will have the most energetic effects in an applied field, based on the electric field-dipole energy relation, $U = -\mathbf{p}\bullet\mathbf{E}$. We propose that the field forces the open structure to become energetically unstable, resulting in an overall loss in structures found in the open configuration and loss of the highly conducting properties. We have also modeled the critical energies points in implicit solvent, with results similar to gas phase calculations.

[1]Highest Occupied Molecular Orbital, Lowest Unoccupied Molecular Orbital

**8:48**
**G10 3 Designing Self-assembled Nanostructures: Metal-Organic Coordination Networks at Surfaces** STEVEN TAIT, NIAN LIN, SEBASTIAN STEPANOW, KLAUS KERN, *Max Planck Institute for Solid State Research* Networks consisting of organic molecules and isolated metal atoms have been demonstrated to self-assemble at surfaces. The components of the networks are designed to assemble in a desired pattern, forming periodic arrays of isolated metal atoms (or dimers) separated by organic molecule ligands. This 'bottom-up' formation of a nanometer-scale structure opens a wide range of questions related to the properties of the components of the networks: metal atom nodes, molecule ligands, and nanopores within the networks. Our group explores these properties, including the magnetic and catalytic properties of the isolated metal atoms and adsorptive properties of the nanopores within the networks. Some properties can be 'tuned' by rational design of the organic molecule size, structure, and functionality. The ability to tailor the size and functionality of nanometer-scale arrays produced by self assembly represents a fantastic opportunity for molecular recognition, heterogeneous catalysis, and other fields. We present here recent results from our group, including the use of ligands containg pyridyl groups and recent adsorption measurements on the networks.

**9:00**
**G10 4 Physical Chemistry of $TiO_2$ functionalized with oxo-manganese catalysts** SABAS G. ABUABARA, CLYDE W. CADY, JIM M. SCHLEICHER, JASON BAXTER, GARY W. BRUDVIG, ROBERT H. CRABTREE, CHARLES A. SCHMUTTENMAER, VICTOR S. BATISTA, *Department of Chemistry, Yale University, P.O.Box 208107, New Haven, Connecticut*

*06520-8107, U.S.A.* We describe the development and application of dye-sensitized semiconductors to heterogeneous photocatalysis. itAb initio-DFT electronic structure calculations and molecular dynamics simulations combined with quantum dynamics propagation of transient electronic excitations indicate that a surface complex consisting of a catalytic Mn oxo complex adsorbed onto a $TiO_2$ substrate via a catechol-substituted terpyridine ligand can be activated by photoinduced subpicosecond interfacial electron transfer. Experimental realization of the Mn oxo surface complex, achieved by a novel sequential synthesis technique, is briefly described and computational results supporting the spectroscopic characterization of the nanoscale assembly are presented. Studying the photocatalytic reaction dynamics of these uniquely functionalized semiconductor materials offers the prospect of gaining unprecedented control over a wide range of contrathermodynamic reactions. Furthermore, such biomimetic materials capable of splitting water or fixating $CO_2$ could provide viable solutions to problems ranging from current energy concerns to reducing atmospheric greenhouse gases.

***Invited Papers***

**9:12**
**G10 5 Silver and Gold Nanostructures: Engineering their Optical Properties for Biomedical Applications.**
YOUNAN XIA, *University of Washington*

We have focused on shape-controlled synthesis of silver and gold nanostructures. While the synthetic methodology mainly involves solution-phase redox chemistry, we have been working diligently to understand the complex physics behind the simple chemistry – that is, the nucleation and growth mechanisms leading to the formation of nanostructures with a specific shape. Polyol synthesis of silver nanostructures provides a good example to illustrate this concept. We discovered that the shape of silver nanostructures were dictated by both the crystallinity and shape of nanocrystallite seeds, which were, in turn, controlled by factors such as reduction rate, oxidative etching, and surface capping. We also exploited the galvanic replacement reaction between silver and chloroauric acid to transform silver nanocubes into gold nanocages with controlled void size, wall thickness, and wall porosity. We were able to engineer the optical properties of resulting gold nanocages with optical resonance peaks ranging from the blue (400 nm) to the near infrared (1200 nm) simply by controlling the molar ratio of silver to chloroauric acid. Thanks to their exceptionally large scattering and absorption coefficients in the transparent window for soft tissues, this novel class of gold nanostructures has great potential emerging as both a contrast agent for optical imaging in early-stage tumor detection, and a therapeutic agent for photothermal cancer treatment.

***Contributed Papers***

**9:48**
**G10 6 Aligned Silver Nanorod Array as SERS Substrates for Viral Sensing*** YIPING ZHAO, *Department of Physics and Astronomy* SARATCHANDRA SHANMUKH, *Department of Chemistry* STEPHEN B. CHANEY, *Department of Physics and Astronomy* LES JONES, *Department of Infectious Diseases* RICHARD A. DLUHY, *Department of Chemistry* RALPH A. TRIPP, *Department of Infectious Diseases, The University of Georgia* The aligned silver nanorod array substrates prepared by the oblique angle deposition method are capable of providing extremely high enhancement factors ( $\sim 10^9$) at near-infrared wavelengths (785 nm) for a standard reporter molecule 1,2 trans-(bis)pyridyl-ethene (BPE). The enhancement factor depends strongly on the length of the Ag nanorods, the substrate coating, as well as the polarization of the excitation laser beam. With the current optimum structure, we demonstrate that the detection limit for BPE can be lower than 0.1 fM. The applicability of this substrate to the detection of bioagents has been investigated by looking several viruses, such as Adenovirus, HIV, Rhinovirus and Respiratory Syncytial Virus (RSV), at low quantities ( $\sim$ 0.5uL). Different viruses have different fingerprint Raman spectrum. The detection of virus presented in infected cells has also been demonstrated.

*Work supported by NSF and NIH

**10:00**
**G10 7 Colloidal Platinum Nanoparticles: Synthesis, Structure and Properties.*** DANIEL KATZ, *Hebrew Academy of the Five Towns and Rockaway, Cedarhurst, NY* VIKAS MURALI, *Staples High School, Westport, CT* REBECCA ISSEROFF, *Stella K Abraham High School, Hewlett, NY* YUAN SUN, *Dept. Mat. Sci. & Eng., SUNY at Stony Brook* YIMEI ZHU, *Brookhaven National Laboratory, Upton, NY* VLADIMIR SAMUILOV, NADINE PERNODET, MIRIAM RAFAILOVICH, JONATHAN SOKOLOV, *Dept. Mat. Sci. & Eng., SUNY at Stony Brook* Interest in nanoparticles has risen in recent years as unique properties are being obtained from otherwise ordinary materials by reducing their sizes to molecular dimensions. We synthesized colloidal platinum nanoparticles with sizes of 1$\sim$ 8 nm through four novel chemical methods and investigated their properties. These particles had an electrical resistivity of 1$\sim$ 4 $\Omega \cdot$ m and also exhibited a ferromagnetic moment. When the particles were exposed to hydrogen we measured a 15% increase in their mass, indicating a high level of hydrogen absorption. The lattice constant was measured using HRTEM and was found to be the same as bulk Pt, even after $H_2$ exposure, indicating no lattice distortion occurred. When dermal fibroblasts were exposed to the particles, the particles disrupted cellular actin, structure, and function. Practical applications include the use of Pt particles in semiconductor chips, hydrogen storage in fuel cells and particle chemotherapy targeted against cancer cells.

*Supported by NSF-MRSEC.

**10:12**
**G10 8 Self organized growth of regular arrays of Pd-Au bimetallic nanoclusters on nanostructured alumina films** CLAUDE R. HENRY, *CRMCN-CNrs, Campus Luminy, 13288 Marseille* GUIDO HAMM, *CRMCN-CNRS* CONRAD BECKER, *IPTC, University of Bonn* Pd-Au clusters (1-4 nm)were grown under UHV on nanostructured alumina films in a two-step process. The alumina films, prepared by high temperature oxidation of a Ni3Al (111) surface, present an hexagonal array of defects, separated by 4.1 nm, which is a template for the growth of the bimetallic clusters. Pd and Au atoms are condensed sequentially on the alumina film, under UHV. The maximum density of metal clusters is fixed by the density of defects. The mean size of the clusters is controlled by the total amount of the deposited metals, while their composition is controlled by the ratio of the deposited amounts of the two metals. The nucleation and growth of the bimetallic clusters are followed in situ by STM. These arrays of bimetallic clusters are used as model catalysts for CO oxidation studied by molecular beam methods. The regular spatial organisation of the clusters allows the study and the correction of the reverse spillover effect of the CO during the reaction.

**10:24**
**G10 9 Reduction of nickel upon annealing of nickel zinc ferrite nanoparticles** S. CALVIN, *Sarah Lawrence College* S.A. MORRISON, M.D. SHULTZ, E.E. CARPENTER, *Virginia Commonwealth University* R. SWAMINATHAN, M.E. McHENRY, *Carnegie Mellon University* Nickel zinc ferrite (NZFO) nanoparticles were synthesized by two methods: radio-frequency plasma torch and reverse micellar syntheses. Upon annealing, x-ray absorption spectra of both sets of samples provided definitive evidence of a progressive reduction of nickel to an fcc metallic form. X-ray diffraction, however, does not show clear peaks corresponding to fcc nickel, suggesting the metallic crystallites are very small. In the case of the plasma torch samples, annealing under air for one hour at 900[r]C is sufficient to reduce nearly all of the nickel metal. Testing is still underway for the reverse micellar samples, but in at least one case approximately 80% nickel reduction was achieved by annealing under nitrogen for one hour at 500[r]C. To elucidate the mechanism of this reduction, a comparative study of annealing under air, nitrogen, and argon is underway, as well as thermogravimetric analysis.

**10:36**
**G10 10 Insulator − polaron conductor − metal transitions in a complex oxide $12CaO \cdot 7Al_2O_3$.** P. SUSHKO, A. SHLUGER, A. STONEHAM, *Department of Physics and Astronomy, University College London, UK* K. HAYASHI, S. MATSUISHI, M. HIRANO, H. HOSONO, *Frontier Collaborative Research Center, P.O. Box S2-13, Tokyo Institute of Technology, Japan* Recent experiments have demonstrated that a complex nano-porous oxide $12CaO \cdot 7Al_2O_3$ (C12A7) built of positively charged subnanometer cages can be converted from a transparent insulator to a transparent conductor by $H_2$ doping followed by UV-light irradiation with 4–4.5 eV photons [1]. This irradiation induces optical absorption bands with maxima at 0.4 eV and 2.8 eV and high concentrations of unpaired electrons. We use ab initio calculations to reveal the mechanism of photo-induced insulator–conductor transition and the role of H atoms in this process and to elucidate the transport properties of the electrons in this system as a function of electron concentration. Our theoretical modeling suggests that at concentration below $10^{20}$ cm$^{-3}$ electrons are responsible for the polaron type electrical conductivity with the activation energy close to 0.1 eV as well as for the optical absorption at 0.4 eV and 2.8 eV [2]. We demonstrate that, as the electron concentration exceeds $10^{20}$ cm$^{-3}$, the character of electronic conductivity changes from polaron type to metallic. [1] K. Hayashi et al., Nature **419**, 462 (2002). [2] P.V. Sushko, et al., Phys. Rev. Lett. **91**, 126401 (2003); P.V. Sushko et al., Appl. Phys. Lett. **86**, 092101 (2005).

**10:48**
**G10 11 Electronic control inside a molecule : towards single molecule devices** MATHIEU LASTAPIS, YURIE FUKUMA, JOHN BOLAND, *CRANN, Trinity College, Dublin* The chimerical single molecule engineering has been proven to be accessible through the use of scanning tunnelling microscopy (STM) [1]. In this field, one particularly attractive area is the study of single molecules adsorbed on semiconductor surfaces. It has been recently demonstrated that a spatial fine control of the molecular dynamics is possible through the use of tunnelling current [2]. In order to improve the electronic control of a single molecule, we are currently investigating a promising system: CaF2 on Si(111). This system has been extensively studied as a model system to deposit insulator on silicon. Here we are using this system to electronically decouple the molecule from the substrate. I will present LT STM experiments on atomically thick CaF islands on Si(111). The measured electronic properties of these islands demonstrate their potential as ideal templates to study single molecules. Finally I will present some preliminary results on N-HBC [3] adsorbed on a CaF island. [1] G. Binnig and H. Rohrer, ''In touch with atoms,'' Rev. Mod. Phys. 71, S324-S330 (1999) [2] M. Lastapis et al, Science, 308, 1000 (2005) [3] S.Draper et al, JACS, 126, 8694 (2004).



**SESSION G11: FOCUS SESSION: PROMISES AND CHALLENGES IN CHEMICAL DYNAMICS IV**
**Tuesday Morning, 14 March 2006**
**303, Baltimore Convention Center at 8:00**
**Sunita Satyapal, Department of Energy, presiding**

***Contributed Papers***

**8:00**
**G11 1 Phase and curvature** CURT WITTIG, *University of Southern California* It is known that geometric phases play important roles in atomic and molecular science, from the Aharonov-Bohm effect including flux quantization to the Born-Oppenheimer approximation and its conical intersections. When judged from a geometrical perspective, these and related phenomena can be assigned the common parentage of quantum holonomy on curved surfaces. Moreover, this perspective can be extended to larger arenas. For example, adiabatic transport of a state in phase space is nonzero if and only if $[x, p]$ is nonzero. This yields a curvature that is equal to $\hbar^{-1}$. This talk will explore additional aspects of geometric phase: (i) the origin of the curvature in parameter space imposed by $\hbar$, and therefore by the existence of quantum mechanics; and (ii) the relationship of the curvature to matrix elements, *e.g.*, between which kinds of states.

*Invited Papers*

**8:12**
**G11 2 A zero magnetic moment molecular probe of the electron's electric dipole moment.**
NEIL SHAFER-RAY, *Homer L Dodge Department of Physics and Astronomy, The University of Oklahoma*

The stationary states of a molecule in a pure electric field are degenerate in the sign of the projection of total angular momentum on the field axis. A lifting of this $\pm$ $M_F$ degeneracy would be an indication of CP (time reversal) symmetry violation. For heavy paramagnetic molecules, this CP violation would be attributed to an electron electric dipole moment (e-EDM) and could at once separate Supersymmetric models from the Standard Model and explain why we are made of matter instead of antimatter. A major obstacle to observing CP violation in this way is that the background magnetic-field induced splitting of the $\pm$ $M_F$ degeneracy normally dwarfs any possible electric-field induced splitting. Here we report how the physics of $^2\Pi_{1/2}$ PbF can be exploited to gain extraordinary sensitivity to the e-EDM while reducing the magnetic g factor to less than $10^{-7}$. The construction of a radical beam source of PbF, sensitive resonance enhanced multi-photon ionization (REMPI) detection of PbF, and progress toward measurement of the e-EDM are reported.

*Contributed Papers*

**8:48**
**G11 3 Ion Imaging Studies of Ultra-Cold Molecule Production**
DAVID W. CHANDLER, *Combustion Research Facility, Sandia National Laboratories* We report the cooling of molecules in a single collision between an atom and a molecule in a crossed molecular beam apparatus. In particular we will show data on cooling NO by collision with Ar and NH3 in collisiosn with Ne. We have produced in significant numbers ( $\sim 10^8$ molecules $cm^{-3}$ per quantum state) translationally cold NO($^2\Pi_{1/2}$,v′=0,j′=7.5) molecules in a specific quantum state with an upper-limit laboratory-frame rms velocity of 14.8$\pm$ 1.1 m/s, corresponding to a temperature of 406$\pm$ 28 mK. The translational cooling results from the kinematic collapse of the velocity distribution of the NO molecules after collision. We present experimental evidence to show that increasing the collision energy by a factor of $\sim$ 2.6 does not change the velocity spread of the cold NO molecules. Similarly, the energy condition for producing the cold NO does not depend on the energy of the Ar beam. However, the energy of the Ar beam does shift the scattering angle at which the cold molecules appear. We will highlight new studies on utilizing these cold molecules for collisional studies. This work was done in collaboration with Professor James Valentini of Columbia University.

**9:00**
**G11 4 Supersonic Molecular Beam Optical Stark Spectroscopy of MnH.*** JAMIE GENGLER, TONGMEI MA, JEREMY HARRISON, TIMOTHY STEIMLE, *Arizona State University* The large moment of inertia, large magnetic moment, and possible large permanent electric dipole moment of manganese monohydride, MnH, makes it a prime candidate for ultra-cold molecule production via Stark deceleration and magnetic trapping[1,2]. Here we report the first molecular beam production of MnH and the analysis of the Stark effect in the (0,0) $A^7\Pi - X^7\Sigma^+$ band. The sample was prepared by laser ablation of solid Mn in an $H_2$ supersonic expansion. The low rotational temperature ( $<$ 50 K) and near natural linewidth resolution ( $\sim$ 50 MHz) facilitated analysis of the $^{55}$Mn (I=5/2) and $^1$H (I=1/2) hyperfine structure. A comparison of the derived field-free parameters with those obtained from sub- Doppler optical[3] and Doppler limited infrared[4] measurements will be made. Progress on the analysis of the Stark effect will be given.

*Funding: NSF-Experimental Physical Chemistry (CHE-0317130)

[1]J.R. Bochinski, E.R. Hudson, H.J. Lewandowski, and J. Ye, itPhys. Rev. A **70**, 043410 (2004).
[2]S.Y.T. van de Meerakker, R.T. Jongma, H.L. Bethlem, and G. Meijer, itPhys. Rev. A **64**, 041401(R) (2001).
[3]T.D. Varberg, J.A. Gray, R.W. Field, and A.J. Merer, itJ. Mol. Spec. **156**, 296-318 (1992).
[4]I.E. Gordon, D.R.T. Appadoo, A. Shayesteh, K.A. Walker, and P.F. Bernath, itJ. Mol. Spec., **229**, 145-149 (2005).

**9:12**
**G11 5 Rotation of a generalized Eckart frame in atom-diatomic molecule scattering*** FLORENCE J. LIN, *University of Southern California* A cyclic change in the shape of an atom-diatomic molecule complex can lead to net rotation of not only the complex, but also the rotating axes of a generalized Eckart frame of the complex. Large-amplitude, ''internal'' motions of an atom-diatomic molecule van der Waals complex can lead to overall rotation of the complex in the center-of-mass frame. When the total angular momentum is conserved, the net angle of overall rotation is the sum of a dynamic phase plus a geometric phase. The classical geometric phase is describable in terms of molecular rotational constants. The scattering angle of the atom in a nonreactive ''slightly sticky collision'' between an atom and a diatomic molecule in molecular beams depends on an analogous ''internal'' motion. Thus, the scattering angle of the atom is also given by the sum of a dynamic phase plus a geometric phase.

*Supported by the WiSE Program, Office of the Provost, University of Southern California

**9:24**
**G11 6 Two- and three-state conical intersections in complex systems** SPIRIDOULA MATSIKA, *Temple University* KURT KISTLER, ZONGRONG XU, AKIHIKO YOSHIKAWA, Nonadiabatic processes play an important role on the excited state dynamics of chemical systems. Conical intersections (actual potential energy surface crossings) of two states have been established to facilitate nonadiabatic processes of molecules and radicals in the gas phase. More recently three-state conical intersections have made their appearance and may also play a key role in nonadiabatic processes. Here we present studies where the importance of

conical intersections is being investigated in photoinitiated processes of biologically relevant systems, and particularly the nucleobases and their analogs. Large scale ab initio multireference configuration interaction methods (MRCI) are being used. Our results show the presence of many seams of two- or three-state conical intersections that can complicate the potential energy surfaces and dynamics of these systems. Solvent effects on conical intersections are first being investigated using clusters of water with the system. A mixed quantum mechanical/ classical mechanical (QM/MM) approach where the solute is described with the MRCI method will also be presented as a means to study the effect of the solvent on excited states.

**9:36**

**G11 7 Saturation transfer studies on doorway states for $CH_2$ intersystem crossing*** YANGSOO KIM, ANATOLY KOMISSAROV, GREGORY HALL, TREVOR SEARS, *Department of Chemistry, Brookhaven National Laboratory, Upton, NY 11973-5000* Double-resonance transient photobleaching kinetics of singlet and mixed singlet-triplet eigenstates of $CH_2$ to characterize the closely related processes of rotational energy transfer and collision induced intersystem crossing in methylene will be reported. Qualitative features of the state-to-state rotational energy transfer matrix are revealed. Selective bleaching of individual eigenstates of mixed state (doorway) pairs shows very efficient collisional interconversion within the mixed-state pair.

*Work performed under DOE Contracts DE-AC02-98CH10886 at Brookhaven National Laboratory

**9:48**

**G11 8 Spectroscopic Identification of Multiple Conformers of $o,p$-$H_2 \cdots ICl$ and $o,p$-$H_2 \cdots I_2$ Complexes** JOSHUA DARR, RICHARD LOOMIS, *Department of Chemistry Washington University in St. Louis* Laser-induced fluorescence and action spectroscopy experiments have identified ro-vibronic transitions associated with multiple conformers of the $o,p$-$H_2 \cdots ICl(X,v=0)$ and $o,p$-$H_2 \cdots I_2(X,v=0)$ complexes. For each complex, the conformers with the hydrogen molecule localized at the end of the dihalogen, with a $C_{2v}$ symmetry, are more stable than the conformers with the hydrogen molecule localized in the T-shaped well, which lies orthogonally about the dihalogen bond axis. Furthermore, the conformers containing $o$-$H_2(j=1)$ and $p$-$D_2(j=1)$ are found to be more strongly bound than those containing $p$-$H_2(j=0)$ and $o$-$D_2(j=0)$. The role of multi-pole electrostatic interactions is elucidated by comparing the binding energies of the $H_2 \cdots ICl(X,v=0)$ and $H_2 \cdots I_2(X,v=0)$ complexes with $C_{2v}$ symmetries. The relative populations of the $C_{2v}$ and T-shaped conformers can be altered by changing the properties of the supersonic expansion used to stabilize the complexes. The relative populations of the $o$-$H_2 \cdots ICl(X,v=0)$ and $p$-$H_2 \cdots ICl(X,v=0)$ conformers can also be manipulated, with a population ratio of 3:1 approached by decreasing the hydrogen concentration in helium.

**10:00**

**G11 9 Double Resonance Spectroscopy of the $B''\bar{B}^1\Sigma_u^+$ state of $H_2$ above the double well barrier.*** ROBERT EKEY, AARON MARKS, ELIZABETH MCCORMACK, *Bryn Mawr College, Bryn Mawr, PA 19010* Double resonance spectroscopy via the $EF^1\Sigma_g^+, v'_{EF} = 6, J'$ state has been used to probe the rovibrational the itungerade double-well $B''\bar{B}^1\Sigma_u^+$ state of $H_2$. Many transitions to levels of the outer-well and the combined inner and outer-well above the barrier have been observed for the first time by detecting both molecular and atomic ion production as a function of energy by using a time of flight mass spectrometer. While significant perturbations are observed in the energy region above the double-well barrier, assignments to states with dominant inner and outer-well characteristics can still be made. Distinct dynamical behaviors of the levels below, at and above the barrier have also been observed.

*This work was supported by a grant from the National Science Foundation (PHY-0140296).

**10:12**

**G11 10 The Department of Energy's Hydrogen Storage Activities: Challenges and Needs in Chemistry and Chemical Dynamics** SUNITA SATYAPAL, GRACE ORDAZ, JOHN PETROVIC,*CAROLE READ, GEORGE THOMAS,† *Department of Energy* Hydrogen storage is a key area of research funded by the Department of Energy. Hydrogen, the simplest diatomic molecule known, has the highest energy content of all known fuels by mass, but the practical storage of sufficient hydrogen on-board a vehicle is a significant technological challenge. Hydrogen can be stored via various mechanisms within materials such as metal hydrides (e.g. $LiBH_4$, $AlH_3$) chemical hydrides (e.g. organic liquids), and nanostructured sorbents (e.g. carbon nanotubes, clathrates). Examples of mechanisms include physisorption, chemisorption, dissociative adsorption or combinations of the above. In addition to weight and volume, the kinetics of hydrogen charging and discharging as well as durability must be addressed. A fundamental understanding of hydrogen storage to help optimize materials is critical. The technical requirements for hydrogen storage, as well as some of the promises and challenges will be presented, with a focus on what chemical dynamics and chemistry can offer in solving the challenge of hydrogen storage for transportation applications.

*Los Alamos National Laboratory, retired (on assignment to DOE)
†Sandia National Laboratory, retired (on assignment to DOE)

**SESSION G12: SELF-ASSEMBLED NANOSTRUCTURES: GROWTH AND PATTERNING**
**Tuesday Morning, 14 March 2006**
**304, Baltimore Convention Center at 8:00**
**Christian Ratsch, University of California, Los Angeles, presiding**

**8:00**

**G12 1 A Level-Set Method for Epitaxial Growth and Self-Organization of Quantum Dots** CHRISTIAN RATSCH, YOUNG-JU LEE, XIAOBIN NIU, RUSSEL CAFLISCH, *UCLA* We have developed an island dynamics model that employs the level-set technique to describe epitaxial growth. One virtue of this method is that the typical simulation timestep can be chosen much larger than in an atomistic simulation, even when several microscopic processes with vastly different rates are relevant. This makes it feasible to solve the elastic equations and obtain the entire strain field at every timestep of the simulation. The strain field modifies the potential energy surface, and different limits will

be discussed. We will present simulation results where we self-consistently modify the strain dependent microscopic rates for surface diffusion and detachment of adatoms from island edges. Our results for the island size distributions indicate that such strain dependent kinetic rates lead to the regularization of island sizes, and ultimately the formation and self-organization of quantum dots.

**8:12**

**G12 2 Multiscale Theory of Fluctuating Interfaces: From Self-Affine to Unstable Growth*** CHRISTOPH HASELWANDTER, *Imperial College, London* DIMITRI VVEDENSKY, *Imperial College, London* We describe a framework for the multiscale analysis of atomistic surface processes which we apply to the Wolf-Villain model for epitaxial growth. Coarse-graining is accomplished by calculating the renormalization-group trajectories from initial conditions determined by the regularized atomistic theory. All of the intermediate scaling regimes known from computer simulations are obtained, but we also find that the asymptotic behavior of two-dimensional substrates is determined by a hitherto unknown fixed point. This provides an explanation of recent experiments on Ge(001) with the intriguing conclusion that the relaxation mechanism responsible for ordered structures early in the growth process produces an instability at longer times that leads to epitaxial breakdown.

*Supported by ESF-SONS Programme and EPSRC

**8:24**

**G12 3 The Structure and Evolution of Ge Nanoscale Structures on Si(111) − Observations and Theory** SANWU WANG, *Vanderbilt University* H.F. MA, Z.H. QIN, D.X. SHI, Y.L. WANG, H.M. GUO, H.-J. GAO, S.T. PANTELIDES, *Vanderbilt University and Oak Ridge National Laboratory* We report scanning tunneling microscopy (STM) observations and first-principles calculations for the evolution of self-organized Ge nanostructures formed on Si(111)-7 $\times$ 7 for Ge coverages up to 0.5 ML and operating temperatures from room temperature to 300°C. STM measurements show that, depending on coverage and temperature, Ge atoms form various structures ranging from single-atom correlated patterns, 2-D ordered nanoscale domains, and 3-D disordered and ordered nanoclusters. First-principles theory focuses on the single-atom patterns and 2-D ordered nanostructures. We show that Ge atoms replace the Si adatoms in the initial adsorption stage. We also show that annealing of the Ge/Si(111) surface results in a partial transformation of (7 $\times$ 7) reconstructed unit cells to unreconstructed Si(111) configurations on which the Ge adatoms reside at the $T_4$ sites and form a $(\sqrt{3} \times \sqrt{3})R30°$ reconstruction.

**8:36**

**G12 4 Evolution of Si nanostructures on the Ge(001) surface** YASUNORI FUJIKAWA, TOSHIO SAKURAI, *Institute for Materials Research, Tohoku University* Growth of compressively strained thin films has been studied extensively for the applications in quantum devices composed of 2D quantum well and/or 1D quantum dots. Recent progress in the strain-controlled Si and SiGe high-speed devices brings increasing interest in the growth control of the oppositely strained thin films and nanostructures. In this work, we report on the morphology evolution of the Si layer formed on the Ge(001) substrate to investigate the effect of tensile strain in the growth of Si. Initially the Si layer forms a wetting layer characterized by the formation of missing dimer rows with spacing of 3-4 rows. The direction of the defect row is 90-degree rotated from the case of the Ge wetting layer on Si(001), being explained by the anisotropic strain of the dimer-row structure. Successive growth of Si results in the formation of Si islands, whose surface is composed of four {113} facets with a small (001) terrace on top. Its differences from the Ge dome structure on Si(001) composed of {113} facets and {105} facets on top can be understood by considering the tensile strain of the {105} facets [1]. [1] Y. Fujikawa et al., Phys. Rev. Lett. **88**, 176101 (2002).

**8:48**

**G12 5 Atomic structure and strain of Ge wetting layer on silicon** HAO CHEN, BOQUAN LI, *University of Illinois at Urbana-Champaign* JIANGUO ZHENG, *Northwestern University* JIAN-MIN ZUO, *University of Illinois at Urbana-Champaign* The atomic structure of Ge wetting layer grown on Si(001) surfaces by chemical vapor deposition at several substrate temperatures under UHV was characterized by low energy electron diffraction and cross sectional high-resolution scanning transmission microscopy. The Ge film is atomically flat with sharp interface with silicon. The surface lattice constant changes with Ge coverage. At high Ge coverage on stepped Si surface, surface relaxation is observed near step edges. The ability to modify Si surface lattice with Ge has many applications.

**9:00**

**G12 6 Quantitative Correlation of Local Stress Field and Surface Morphology in Undulated Si1-xGex/Si(100) Thin Films*** CHI-CHIN WU,† ROBERT HULL, *University of Virginia* We have performed in-situ transmission electron microscope measurements of misfit dislocation propagation velocities to quantitatively characterize the stress field variations for undulated epitaxial Si1-xGex/Si(100) thin films. For a strained Si0.7Ge0.3 film with a 30 nm mean thickness and annealed at $\sim$ 480°C, the dislocation velocity varies from 50 to 200 nm/s as the threading arm of a propagating dislocation line traverses a period of the surface morphology. Using detailed correlations we have previously developed between misfit dislocation velocities and local driving stresses, we can translate this velocity range into an effective stress on the dislocation that varies from $\sim$ 0.3 to 1.2 GPa. These results show great promise for correlating local stresses with morphology in these materials.

*This work is funded by NSF-DMR (Grant# 0075116) and NSF-MRSEC at UVa ''The Center for Nanoscopic Materials Design''
†Corresponding author

**9:12**

**G12 7 Surface Mobility Difference between Si and Ge and its Effect on Growth of SiGe Alloy Films and Islands** LI HUANG, *Fudan University, China* GUANGHONG LU, *University of Utah* XINGAO GONG, *Fudan University, China* FENG LIU, *University of Utah* Based on first-principles calculations of surface diffusion barriers, we show that on a compressive Ge(001) surface, the diffusivity of Ge is $10^2 - 10^3$ times higher than that of Si in the temperature range of 300 to 900 K; while on a tensile surface, the two diffusivities are comparable. Consequently, growth of a compressive SiGe film is rather different from that of a tensile film. The diffusion disparity between Si and Ge is also greatly enhanced on the strained Ge islands compared to that on the Ge wetting layer on Si(001), explaining the experimental observation of Si enrichment in the wetting layer relative to that in the islands.

**9:24**

**G12 8 Modeling the Self-Assembly of Quantum Dots in Thin Solid Films** MARGO LEVINE, *Northwestern University* ALEXANDER GOLOVIN, STEPHEN DAVIS, PETER VOORHEES, The self-assembly of quantum dots in a thin solid film caused by epitaxial stress and wetting interactions with the substrate is studied. It is shown that wetting interactions change the instability spectrum from long wave to short wave which can lead to spatially regular arrays of quantum dots. A nonlocal, nonlinear evolution equation for the film shape is derived, and the stability of dot arrays with different symmetries is studied. Regions in the parameter space are determined where spatially regular surface structures can be observed in experiments.

**9:36**

**G12 9 Island Alignment on Patterned Substrates** DEMITRIS KOURIS, *University of Wyoming* ROBERT KUKTA, *SUNY Stonybrook* A recent approach to fabricating self-assembled epitaxial nanostructures involves the use of topographically patterned substrates to control the formation of material deposits during growth. This article investigates the energetic and kinetic mechanisms that guide the positioning of strained epitaxial islands in these systems. A continuum-level model is used wherein the free energy of system consists of surface energy and strain energy. The substrate shape is represented by small amplitude sinusoidal features. An energetic phase diagram is calculated to determine which sites are most favorable—peaks, valleys, or side walls—depending on factors as substrate shape, lattice mismatch, surface energy, and the amount of material deposited. The kinetic evolution through the processes of deposition and surface diffusion is then simulated. It is found that the resulting morphology depends largely on the rate of deposition relative to surface mobility. Relatively slow deposition rates produce configurations of minimum free energy while higher deposition rates give rise to novel metastable states. Mechanisms by which various configurations arise are discussed in detail. Results are found to be in excellent agreement with published experiments.

**9:48**

**G12 10 Utilizing Growth Kinetics to Self-Assemble Complex SiGe Nanostructures** JENNIFER GRAY, ROBERT HULL, *University of Virginia* JERROLD FLORO, *Sandia National Laboratories* Heteroepitaxial growth of $Si_xGe_{1-x}$ on Si (001) substrates under conditions of reduced adatom mobility results in limited formation of stress-relieving islands occurring only at energetically favorable sites. These favorable sites are at the edges of shallow pyramidal pits that form at random locations on the film surface under these conditions. However, by using a focused ion beam (FIB) to pattern the substrate before growth, it is possible to controllably create pits at predefined locations. This results in the formation of four self-assembled islands at the edges of each pit. In order to obtain uniform, well ordered islands, the FIB milling parameters and Si buffer thickness must be tailored to produce pits in the strained film with dimensions equal to or smaller than the compositionally-dependent natural length scale of the islands. The ability to produce islands at specific locations is important for applications such as quantum computing where quantum dots must be arranged into logic structures. Exploiting this constraint on islanding that occurs under kinetically limited growth may therefore provide a new route to hierarchical assembly of nanostructures when combined with substrate patterning techniques.

**10:00**

**G12 11 Shape and Composition Map of a Prepyramid Quantum Dot** BRIAN SPENCER, *SUNY Buffalo* We present a theory for the shape, size, and nonuniform composition profile of a small prepyramid island in an alloy epitaxial film when surface diffusion is much faster than deposition and bulk diffusion. The predicted composition profile has segregation of the larger misfit component to the island peak, with segregation enhanced by misfit strain and solute strain but retarded by alloy solution thermodynamics. Vertical composition gradients through the center of the island due to this mechanism are on the order of 2%/nm for $Ge_XSi_{1-X}$/Si and 10 - 15%/nm for $In_XGaAs_{1-X}$/GaAs [PRL 95, 206101 (2005)].

**10:12**

**G12 12 Temperature and Flux Dependence of Unstable Growth Mode on Patterned GaAs(001)*** TABASSOM TADAYYON-ESLAMI, HUNG-CHIH KAN, *University of Maryland* SUBRAMANIAM KANAKARAJU, CHRIS RICHARDSON, *Laboratory for Physical Sciences* RAY PHANEUF, *University of Maryland* We report on the temperature and flux dependence of the growth mode of GaAs(001) during molecular beam epitaxy (MBE). Our previous results [1] for growth on patterned GaAs(001) surfaces showed that growth under typical conditions produces a transient instability. Lowering the temperature beneath $\sim$ 530 $^o$C at a growth rate of $\sim$ 0.3 nm/s produces a qualitative change in the way that the corrugations evolve. This temperature is close to that of a preroughening transition in the absence of growth [2], however on increasing the As2 flux the onset temperature for preroughening moves itup, while the onset temperature of the growth mode change moves itdown. We correlate the change in growth mode with a change in the surface reconstruction. [1] H. C. Kan, S. Shah, Tadayyon-Eslami, and R. J. Phaneuf, Phys. Rev. Lett, **92**, 146101, (2004). [2] V. P. Labella et al. Phys. Rev. Lett. **84**, 4152, (2003).

*Work supported by the Laboratory for Physical Sciences and an NSF-MRSEC, DMR #00-80008.

**10:24**

**G12 13 Self-organized Evolution on Patterned GaAs(001) Surfaces during Homo-Epitaxial Growth*** HUNG-CHIH KAN, *Dept. of Physics, Univ. of MD, College Park, and Lab. for Physical Sciences* ERIN FLANAGAN, *Dept. of Materials Science and Engr., Univ. of MD., College Park* TABASSOM TADAYYON-ESLAMI, *Dept. of Materials Science and Engr., Univ. of MD, College Park, and Lab. for Physical Sciences* SUBRAMANIAM KANAKARAJU, CHRIS RICHARDSON, *Lab. for Physical Sciences* RAYMOND PHANEUF, *Dept. of Materials Science and Engr., Univ. of MD, College Park, and Lab. for Physical Sciences* We report on experimental characterization of morphological evolution of patterned GaAs(001) surfaces during homo-epitaxial growth. We lithographically patterned our GaAs(001) substrates with arrays of cylindrical pillars whose size and spacing are systematically varied. The growth of GaAs layers on the patterned substrate were performed in a MBE chamber at a substrate temperature of 580 [r]C. The growth rate is $\sim$ 2.7 Å/s. After each growth step, the surface topography is characterized with atomic force microscopy (AFM). AFM profiles along [-110] show that flat-topped pillars evolve into concave downward parabola whose curvature is nearly independent of the initial pillar diameter. We

also perform both physically based and phenomenological numerical calculations to simulate the growth and compare the results with our experimental observations.

*This work is supported by the Laboratory for Physical Sciences and an NSF-MRSEC Grant No. DMR-0080008.

**10:36**
**G12 14 Real-Time Studies of Ga Droplet Formation for the Directed Seeding of Semiconductor Nanopillars*** W. YE, B.L. CARDOZO, X. WENG, J.F. MANSFIELD, R.S. GOLDMAN, *University of Michigan* The directed self-assembly of low-dimensional semiconductor structures has been achieved using a variety of approaches to producing topographical patterns. However, an approach for producing highly ordered arrangements of nanostructures with well-controlled shapes and size distributions has yet to be developed. Therefore, we are exploring the seeded-assembly of semiconductor nanocrystal and nanopillars on substrates topographically patterned using a focused-ion-beam (FIB). For nanopillar formation, we have seeded ordered arrays of holes with controlled concentrations of Ga droplets using FIB implantation. These holes have nearly uniform sizes and shapes. By controlling the ion beam energy, current, and size, hole arrays with various sizes, depths, and periodicities may be produced. Interestingly, after scanning the ion beam over the patterned area, Ga atoms diffuse to the holes and agglomerate, leading to the formation of ordered arrays of nearly uniform sized Ga dots. We will discuss the mechanisms of Ga droplet formation and present real-time studies of Ga droplet dynamics and their interaction with various gases. We will also discuss the use of these ordered arrays of Ga dots as catalysts for vapor-liquid-solid growth of semiconductor nanopillars.

*This work is supported in part by the National Geospatial Intelligence Agency and the National Science Foundation

**10:48**
**G12 15 Real-Time UV-FEL PEEM of Silicide Nanostructure Coarsening Dynamics on Si(100)** MATTHEW ZEMAN, *North Carolina State University* WOOCHUL YANG, *Dongguk University* ROBERT NEMANICH, *North Carolina State University* The coarsening dynamics of nanoscale silicide ($TiSi_2$, $ZrSi_2$, $HfSi_2$) islands on Si(100) are observed in ultra high vacuum using tunable ultra-violet free electron laser (UV-FEL) excitation for photo electron emission microscopy (PEEM). The UV-FEL PEEM is employed for real-time, in situ observation of the nanostructure dynamics and evolution during continuous annealing at high temperatures (1200°C). In situ movies will be presented which detail the coarsening processes where the silicide nanostructures grow via Ostwald ripening and attractive migration and coalescence (AMC). AMC is a coarsening process where nearby islands are observed to migrate attractively towards each other and subsequently coalesce. This process has been attributed to the growth-decay flow of the island edges driven by a non-uniform chemical potential around the islands. This non-uniform chemical potential is predicted to result in an island shape distortion due to the local flux of adatoms from/onto the inner- facing edges of the coalescing islands. This non-uniform chemical potential is observed as an increase in the island radius along the migration direction as well as a decrease in the radius of curvature of the inner facing (growing) edges of the coalescing islands.



## SESSION G13: FOCUS SESSION: SPECTROSCOPY OF BIOMOLECULES FROM ISOLATED MOLECULES TO CELL ENVIRONMENT IV

**Tuesday Morning, 14 March 2006; 305, Baltimore Convention Center at 8:00**
**Tobias Baumgart, University of Pennsylvania, presiding**

***Invited Papers***

**8:00**
**G13 1 Laser spectroscopy probes of biomolecular conformation: Valley-to-valley searches for molecular-scale mountain passes.***
TIMOTHY ZWIER, *Purdue University*

This talk will describe recent studies of the spectroscopy and conformational isomerization dynamics of isolated gas-phase biomolecules with several flexible coordinates. These studies employ conformation-specific excitation and detection, taking advantage of the unique infrared and ultraviolet signatures of the individual conformations when cooled in a supersonic expansion. The examples given will include recent studies of the bichromophore 3-(4-hydroxyphenyl)-N-benzyl-propionamide (HNBPA) and of the 'double-chain' molecule O-(acetamidoethyl)-*N*-acetyltyramine (OANAT). In collaboration with Jasper Clarkson, Esteban Baquero, Virgil Shubert, Tracy LeGreve and William James, Dept. of Chemistry, Purdue University.

*Supported by NSF CHE0242818.

**8:36**
**G13 2 Ultrafast dynamic exchange of hydrogen bonds.**
ROBIN HOCHSTRASSER

Measurements of H-bond dynamics in solutions aim to obtain energetics and equilibrium dynamics of making and breaking these bonds. Two dimensional IR with fs pulses can follow both the vibrational kinetics associated with H-bonds and the dynamic effects of exchange on vibrational coherence. The principles are analogous to those from 2D-NMR chemical exchange but the 2D IR measures dynamics on the fs to ps time scales and exchange is coupled to ultrafast

spectral diffusion. Therefore distinctive types of reactions can be accessed by 2D IR. Results will be presented for CN vibrators in liquid methanol and carbonyl and NH groups of peptides in water and methanol. In all examples the solute modes act as probes of the dynamics of the surrounding liquid structures. As a consequence the exchange coupling between different vibrators that results in energy transport along the chains of peptides is also seen. This research was supported by NSF-CHE, NIH-GM and by an NIH Resource Grant all to RMH.

*Contributed Papers*

**9:12**

**G13 3 PS Dynamics and Dephasing Times of Internal Amino Acids in Proteins*** ROBERT AUSTIN, *Princeton University* AIHUA XIE, *Oklahoma State University* BRITTA REDLICH, *FOM Institute for Plasma Physics* LEX VAN DER MEER, *FOM Institute for Plasma Physics* We present results on very narrow linewidth (2 $cm^{-1}$), high peak flux (1 $\mu$J in a 50 $\mu$ spot) pump/probe and photon echo experiments on the amide I band of proteins. Using the continuous tuning capability of the FELIX FEL we scan across the amide I band with these narrow, high intensity pulses searching for signs of energy trapping in the inner core of a protein, and seach for correlations between trapped states and long dephasing times of the trapped states.

*Supported by AFOSR and FOM, Netherlands

**9:24**

**G13 4 Probing the conformation of DNA by time-resolved fluorescence*** ANITA JONES, ROBERT NEELY, ELEANOR BONNIST, DAVID DRYDEN, *University of Edinburgh* DALIA DAUJOTYTE, SAULIUS GRAZULIS, SAULIUS KLIMASAUSKAS, *Institute of Biotechnology, Vilnius* THOMAS LENZ, ELMAR WEINHOLD, *University of Aachen* The fluorescent adenine analogue, 2-aminopurine (AP), is a widely used probe of DNA structure and dynamics. We have investigated the time-resolved fluorescence of AP-labelled duplexes in single crystals, in solution and in frozen matrices, to elucidate the influence of interbase interaction and base dynamics on the photophysics of AP. DNA undergoes conformational change in response to interaction with agents such as enzymes and drugs. Base flipping, induced by DNA methyltransferase enzymes, is a remarkable example of conformational distortion; the target nucleotide is rotated around the phosphate backbone, out of the duplex and into the enzyme active site. We will report the first time-resolved fluorescence measurements of single crystals of AP-labelled DNA duplexes complexed with methyltransferase enzymes (M.HhaI and M.TaqI). Correlation of these results with studies on the analogous solution-phase systems shows that the fluorescence response of AP is a definitive indicator of the base flipping mechanism. Moreover, the AP decay parameters provide detailed information on the nature of the interaction between enzyme and duplex.

*We acknowledge support from the SHEFC, the EPSRC, the Royal Society, the Lithuanian Science and Study Foundation.

**9:36**

**G13 5 Conformational Structure Determination of Biomolecules in the Gas Phase using Broadband Fourier Transform Microwave Spectroscopy** BROOKS PATE, *University of Virginia* GORDON BROWN, BRIAN DIAN, KEVIN DOUGLASS, DAVID PRATT, *University of Pittsburgh* LEONARDO ALVAREZ, We have recently developed a true broadband Fourier transform microwave (FTMW) spectrometer that obtains the rotational spectrum in the 7.5 – 18.5 GHz range with 50 kHz resolution for each individual valve pulse in a molecular beam spectrometer. The ability to observe an 11 GHz broad rotational spectrum for each valve pulse is particularly useful for experiments where the molecular beam source conditions require optimization and in cases where the biological sample decomposes over a time scale of a few minutes. The high resolution of the measurement makes it possible to unravel the conformational complexity of gas phase biomolecules. Conformational assignments of the pure rotational spectrum of p-methoxyphenethylamine (MPEA) will be presented to illustrate the capabilities of the spectrometer. The spectrometer can also be employed in laser-FTMW double-resonance experiments where the conformational assignments in the pure rotational spectrum are used to automatically assign absorption features in either vibrational or electronic spectra.

*Invited Papers*

**9:48**

**G13 6 Probing secondary structures of peptide chains using gas phase laser spectroscopy.**
MICHEL MONS, *Lab. Francis Perrin, CEA/CNRS, Saclay, 91191 Gif-sur-Yvette, France*

A bottom-up approach involving conformer-specific IR studies of short peptide sequences enables us to map the intramolecular interactions that shape the peptide backbone, in particular those H-bonds that are responsible for stability and formation of secondary structures in proteins, like turns or helices. The combination of laser-desorption of solid samples coupled to the efficient cooling in a supersonic expansion makes it possible to isolate in the gas phase the lowest conformations of the energy landscape of small flexible biomolecules. The low temperature achieved enables spectroscopists to record UV spectra in which the contribution of each conformer populated can be distinguished and the corresponding conformation identified using IR/UV double resonance spectroscopy. Data collected are directly comparable to the best quantum chemistry calculations on these species and therefore constitute a severe test for the theoretical methods used. It will be shown how investigation of sequences with an increasing number of building blocks permits to deduce the robust structural trends of a peptide backbone: i) local conformational preference of the backbone in one-residue chains, ii) in capped dipeptides, the competition between a succession of local conformational preferences and

overall folded structures, in which a different type of H-bonding scheme, involving distant H-bonding sites along the backbone, takes place: in particular beta-turns, the secondary structure responsible for chain reversals, and finally iii) evidence for the spontaneous helical folding (short 3-10 helix) of three-residue chains will be presented, illustrating the relative weakness of the H-bonding in these molecular assemblies.

*Contributed Papers*

**10:24**
**G13 7 Permanent Electric Dipole Moments of Four Tryptamine Conformers in the Gas Phase. A New Diagnostic of Structure and Dynamics.*** DAVID PRATT, TRI V. NGUYEN, *University of Pittsburgh* Rotationally resolved electronic spectroscopy in the gas phase, in the absence and presence of an applied electric field, has been used to determine the charge distribution of a cross section of the energy landscape of tryptamine (TRA). We report the magnitude and direction of the permanent electric dipole moments of the four TRA conformers GPyout, GPyup, GPhup and Antiup in their $S_0$ and $S_1$ electronic states. Each dipole moment is unique, providing a powerful new tool for conformational analysis of biomolecules in the gas phase. A comparison of the results for the different conformers of TRA reveals that the position and orientation of the ethylamine side chain plays a major role in determining both the permanent and induced electric dipole moments of the different species in both electronic states

*This work has been supported by NSF.

**10:36**
**G13 8 Thermodynamics of Membrane Proteins: Kinetics** DIPTI SHARMA, ATIN MANDEL, JOSE ARGUELLO, GERMANO IANNACCHIONE, *Worcester Polytechnic Institute* An AC-Calorimetric study of membrane proteins was performed at various scan rates in order to probe the energetics and dynamics of the unfolding mechanism. Two thermophilic (Archaeoglobus Fulgidus: AfCopA and AfCopA+ATP) and one mesophilic (E. Coli: EcCopA) membrane proteins were studied at scan rates of 5 and 30 K/hr. Clear signatures of the protein unfolding were found whose character was dependent on the presence of ligands and scan rate. The slower scan rate data reveal a much broader temperature range of unfolding with evidence of a two stage unfolding process. Comparison between the two scan rates indicates that the kinetics of the first unfolding process is complex while the second primary feature represents the stability limit of that particular protein.

**10:48**
**G13 9 Conformational Isomerism in 1-Heptanal** JONATHAN M. FISHER, LI-HONG XU, *University of New Brunswick* R.D. SUEMRAN, *National Institute of Standards and Technology* BROOKS PATE, KEVIN DOUGLASS, *University of Virginia* The rotational spectrum of 1-heptanal has been recorded over the 10 GHz to 22 GHz region using a pulsed-molecular-beam, Fourier transform microwave spectrometer. The spectrum has been analyzed using the jb95 spectral analysis program. The spectra of thirteen conformational isomers have been identified and assigned in the rich soup of observed transitions. Transitions of these isomers have relative intensities that are well above the intensity level of the onset of $^{13}C$ isotopomers, which are a factor of 100 down in intensity. In addition to the above 13 isomers, two additional spectra were identified and assigned that belong to dimers that consist of 1-heptanal and one water molecule. In order to map the observed spectra to conformational geometries, high-level itab initio calculations have been carried out. All fifteen observed conformers have been associated with itab initio determined structure configurations. In general, the agreement in rotational constants and dipole intensity pattern between the itab initio results and the experimentally observed spectra is quite good.

## SESSION G15: MECHANICAL PROPERTIES OF METALS
**Tuesday Morning, 14 March 2006**
**311, Baltimore Convention Center at 8:00**
**Michael J. Mehl, Naval Research Laboratory, presiding**

**8:00**
**G15 1 Thermodynamic and transport properties of beryllium-copper alloys for less than 10 wt.% Cu.** JASON COOLEY, *Los Alamos National Laboratory* JASON LASHLEY, *Los Alamos National Laboratory* W. LARRY HULTS, *Los Alamos National Laboratory* TIM TUCKER, *Los Alamos National Laboratory* We have investigated the heat capacity and electrical conductivity of various beryllium-copper alloys in the composition range of 0 to 10 wt.% Cu.

**8:12**
**G15 2 Elastic properties of monoclinic $Gd_5(Si_2Ge_2)$** O. SVITELSKIY, A. SUSLOV, T.A. LOGRASSO, D.L. SCHLAGEL, V.K. PECHARSKY, K.A. GSCHNEIDNER, JR., *Ames Laboratory, Iowa State University, IA50011* $Gd_5(Si_2Ge_2)$ is an alloy characterized by a giant magnetocaloric effect ($\Delta T/\Delta B \sim 8K/2T$) and a colossal strain (up to 10,000ppm) that exist due to a magnetic- martensitic phase transition occurring close to the room temperature. Because of these unique properties, $Gd_5(Si_2Ge_2)$ has a potential for energy efficient environmentally friendly refrigeration and actuation uses. We show the results of the first-ever ultrasonic study of a single crystal of this alloy. Sound speeds measured in a number of different geometries allowed us to determine the full elastic constant tensor for this material in the monoclinic phase. The anisotropy of elasticity of the crystal is demonstrated by the polar plots of the speed of sound, Young's modulus and linear compressibility in all three main crystallographic planes. The pure modes directions are determined. The bulk modulus is estimated at $2.58 \times 10^{11} dynes/cm^2$ and the Debye temperature at 250 K. Work in Ames is supported by the US DOE. Work in NHMFL is supported by the In-House Research Program, NSF and State of Florida.

**8:24**
**G15 3 Explanation of the discrepancy between the theoretical and experimental yield stresses in bcc metals** ROMAN GROGER, VACLAV VITEK, *University of Pennsylvania, Department of Materials Science and Engineering* We propose a mesoscopic model that is capable to explain the factor of 2 to 3 discrepancy between experimentally measured low-temperature

yield stresses of bcc metals and those typically determined by atomistic simulations of an isolated screw dislocation. The model suggests that the reason for this discrepancy is that in reality the glide of the screw dislocations is cooperative, as commonly observed at low and intermediate temperatures. In this case the stress needed to move the most highly stressed screw dislocation in an array of dislocations and simultaneously operate a dislocation source is estimated to be about a factor of 2 to 3 lower than the Peierls stress of an individual screw dislocation. Since the above-mentioned discrepancy has been encountered not only in bcc metals but also, for example, for the prism slip in hexagonal crystals, the proposed model is likely to hold more generally.

**8:36**

**G15 4 Optical Investigation of the Effects of Substrate Orientation on Oxidation of Single Crystal beta-nickel aluminum (NiAl)** SERIF URAN, *Pittsburg State University* MARCOS H. GRIMSDITCH, *Argonne National Laboratory* BOYD W. VEAL, *Argonne National Laboratory* PAUL, A. PAULIKAS, *Argonne National Laboratory* Nondestructive optical techniques have been used to study the oxidation of low-index crystal faces of single-crystal beta-nickel aluminum (NiAl) as a function of temperature. Using these techniques, residual stress, phase composition, and thickness of the scales were determined at various temperatures. The oxidation of the three low-index surfaces, (001), (110) and (111) exhibit discernible differences. Consistently lower stress values are observed on (001) surfaces. Fluorescence and Raman results indicate a higher concentration of theta-aluminum oxide (Al2O3) on (001) faces and lower concentrations on (111) faces at all temperatures between 800 and 1200 Celsius degrees. Although the residual stresses are higher on (110) faces, these are the only surfaces which maintain adherence up to 1450 Celsius degrees. All surfaces exhibit a stress anomaly between 1200 and 1250 Celsius degrees.

**8:48**

**G15 5 Short-Range Order Effects on the Thermodynamic Properties of the $Ni_3Al$ Alloy*** ALEX ANTONELLI, BERNARDO MEIRELLES, *Universidade Estadual de Campinas* CAETANO MIRANDA, *Massachussetts Institute of Technology* The reasons for the substantial changes induced by disorder in the thermodynamic properties of the $Ni_3Al$ alloy still remain controversial. While several computational studies have found a significant increase in both vibrational entropy and volume as the alloy becomes disordered, there is also evidence that these properties remain unchanged upon disordering. In this work, we present a computational study of the excess vibrational entropy and excess volume of the disordered $Ni_3Al$ alloy, in which, we focused on the interplay between short-range order and long-range order effects on these properties. Using the Simulated Annealing optimization technique, we obtained several structures that exhibit no long-range order, but have different degrees of short-range order. Excess vibrational entropies were computed using an empirical potential, while excess volumes were obtained using both: an empirical potential and itab initio techniques. Our calculations indicate that, both excess vibrational entropy and excess volume are substantially reduced in alloys that have no long-range order but have some degree of local order. Both methodologies used to model the alloy give rise to similar results for the excess volume, indicating that the short-range effects are not an artifact of how the system is modelled.

*Support from FAPESP, CNPq, and FAEP-UNICAMP

**9:00**

**G15 6 Molecular Dynamics Study of Self-Interstitial Atoms in BCC Metals: Crystallization in Mo and ferromagnetic Fe** DANIEL FINKENSTADT, DIMITRIOS PAPACONSTANTOPOULOS, MICHAEL MEHL, *Naval Research Laboratory* Among point defects, the self-interstitial atom (SIA) is less well investigated than its relative, the atomic vacancy. Experimentally, the SIA is important for understanding of embrittlement in irradiated materials, however there are other processes in which the SIA may also be important, namely, the solidification and crystallization, at the atomic scale, of matter from the amorphous state. Amorphous structure may be treated within the context of density functional theory as a network of SIA and vacancies. We will present tight-binding molecular dynamics (TBMD) studies of interactions between SIA, vacancies, surfaces and interfaces, within bcc-based metals, with focus on Mo and ferromagnetic Fe. We will show, via TBMD simulation, that structural transformation and mass transfer are facilitated and made rapid by the presence of a SIA. Results are compared, as a benchmark, to previous plane-wave pseudopotential results for SIA formation energies.

**9:12**

**G15 7 Atomic displacements in binary alloys** YEVGENIY PUZYREV, *Oak Ridge National Laboratory* J.S. FAULKNER, *Florida Atlantic University* G. E. ICE, C.J. SPARKS, *Oak Ridge National Laboratory* Molecular dynamics calculations are used to model the thermal and static displacements in copper and copper-gold alloys. Adjusted embedded atom potentials that give very accurate atomic sizes for the pure metals are used. The agreement with experiments supports the argument that this is a reliable approach for predicting displacements, and will be useful in interpreting experimental data on atomic displacements in metals and alloys. The positions of the atoms in a binary alloy at temperature $T$ at all times $t$,$\mathbf{R}_i(t)$, can be found using molecular dynamics (MD)[1] if the forces on the atoms are known. It is still necessary to use supercells, but they can contain thousands of atoms. The set of $\mathbf{R}_i(t)$ contains all the information about both static and thermal displacements. Of course, MD is a classical theory, and the only quantum mechanical effects appear in the construction of the forces.

[1]D. C. Rapaport, itThe Art of Molecular Dynamics Simulation, **2**nd edition (Cambridge University Press, Cambridge, U. K., 2004)

**9:24**

**G15 8 First-Principles Predictions of Ordered Structures in Fe-Ni Alloys*** S. V. BARABASH, V. BLUM,[†]A. ZUNGER, *NREL* The observed ordered fcc Fe-Ni compounds are $L1_2$ $FeNi_3$ and (possibly metastable) $L1_0$ FeNi. Little is known about ordering tendencies in Fe-rich fcc alloys (stable at high $T$ at all compositions), despite the immense technological importance of such materials. We studied the $T = 0$ and finite-$T$ ordering in fcc Fe-Ni alloys, employing the mixed-basis cluster expansion approach built on *ab initio* input formation enthalpies. We address explicitly the fact that Fe-Ni alloys may occur in either of three distinct ferromagnetic phases: high-spin (HS) fcc, low-spin (LS) fcc, and bcc phases. We distinguish between fcc- and bcc- based structures by analyzing the coordination of the nearest neighbors, and between HS and LS fcc phases by analyzing the total magnetic moment and performing series of fixed-moment calculations. We cluster expand the properties of HS ferromagnetic fcc alloys, providing a special attention to the unstable HS fcc Fe end- point. We further compare the stability of our studied HS fcc compound

structures with alternative LS fcc and with bcc compound structures. For Fe-rich alloys, we find that due to instability of HS fcc Fe with respect to tetragonal deformations, the alloys have an exceptionally strong tendency to form (100) superlattices. For Ni-rich alloys, we predict new unsuspected ordered Fe-Ni compounds.

*Suported by DOE-SC-BES-DMS under NREL Contract DE-AC36-99GO10337

†Presently at FHI-MPG, Germany

**9:36**

**G15 9 Interplay between diffusive and displacive transformations: A Phase-Field approach** RAJEEV AHLUWALIA, MATHIEU BOUVILLE, *Institute of Materials Research and Engineering, IMRE* The phase-field method has been extensively used to study martensitic (displacive) transformations. However they have been studied ''in isolation.'' We study the competition between the diffusionless martensitic transformation and a diffusive phase transition which involves phase separation. Phase separation occurs if diffusivity is high enough whereas martensite will form only if little diffusion can occur. A complete description of martensite-forming materials should incorporate both difuusive as well as diffusionless modes of structural change. We use phase-field simulations to study the interplay between these diffusive and displacive phase transformations at different temperatures. TTT (temperature-time-transformation) diagrams can thus be obtained. We study the role of the temperature-dependence of diffusivity on the microstructure and TTT diagrams, by strengthening or weakening this dependence keeping other parameters unchanged.

**9:48**

**G15 10 Lattice Dynamics of Hydrogenated Austenitic Steels** SERGEY DANILKIN, *ANSTO* ANSTO TEAM, We investigated hydrogen vibrations in of Fe-18Cr-10Ni and Fe-25Cr-20Ni austenitic steels doped in H gas atmosphere at pressures up to 7 GPa with maximum H content about H/Me=0.9. In case of less stable Fe-18Cr-10Ni alloy formation of the martensite phase was observed after hydrogen treatment [1]. Inelastic neutron scattering measurements were performed with spectrometers FANS at NIST and TOSCA at ISIS. Experiments show broad H peak in energy spectrum of scattered neutrons at frequencies above the metal band modes. Vibrational energy of H atoms in studied steels decreases from 132 meV at H/Me=0.0033 to 111 meV at H/Me=0.9 due to lattice dilatation [2]. The energy dependence of H modes on interatomic distance is compared with experimental data on other Me-H systems. The broadening of the H modes at H contents from 0.003 to 0.4 - where the single broad peak is observed - is most probably connected with the Me-H force constant disorder. At higher H contents - where H-peak has the two-component structure - the H-H interaction becomes important resulting in the dispersion of the optical phonon branches. [1]. M. Hoelzel, S.A. Danilkin, H. Ehrenberg, et al., Mat. Sci. Eng., 2004, v. A384, p. 255. [2]. M. Hoelzel, V. Rajevac, S.A. Danilkin, et al., J of Phys. – Cond. Mat., 2005, v. 17 (23), p. 3537.

**10:00**

**G15 11 Ab initio calculations of MAX phases $M_2TlC$ (M = Ti, Zr, Hf), and $M_2GaN$ (M = Ti, V, Cr)** SANJAY KHARE, SUNIL PATIL, JACOB WARNER, *Department of Physics, University of Toledo, Toledo, OH 43606* MAX phases have been a subject of interest recently [cf. M. W. Barsoum Prog. Solid St. Chem. 28, 201 (2000).] because of their useful mechanical, electrical and thermal properties. Here we have studied two groups of $M_2AX$ : (i) M = Ti, V, Cr, A = Ga and X = N and (ii) M = Ti, Zr, Hf, A = Tl and X = C. We calculated the lattice parameters, bulk modulus B and local electronic density of states (LDOS) of these phases using first-principles total energy calculations. Our computed lattice structural parameters match the experimental values within 5% for all six materials. Values for B were computed to be (i) 158, 170, and 180 GPa and (ii) 125, 120, and 131 GPa for the first and second group respectively. These values suggest that $Ti_2TlC$, $Zr_2TlC$ and $Hf_2TlC$ maybe the softest of all the MAX phases explored so far. The total density of states shows that all six materials are conducting. The major features in LDOS are i) the hybridization of the M d orbitals with X p orbitals and (ii) M d orbitals with A p orbitals.

**10:12**

**G15 12 Thermal transport and heat capacity of $Ti_3AlCN$ and $Ti_2AlC_{0.5}N_{0.5}$*** T. H. SCABAROZI, M. BARSOUM, A. GANGULY, S. GUPTA, *Department of Materials Engineering, Drexel University* S.E. LOFLAND, J.D. HETTINGER, P. FINKEL, *Department of Physics and Astronomy, Rowan University* We report an investigation of the specific heat and the thermal transport of a subset of the so-called MAX-phase family of materials $Ti_3AlCN$ and $Ti_2AlC_{0.5}N_{0.5}$ .The thermal transport results are analyzed to investigate the impact of mixing C and N on the X-sites. The heat capacity results are investigated to determine if this mixing influences the density of electronic states. We find that these mixtures have larger thermal conductivities than $Ti_3AlC_2$, $Ti_2AlN$ or $Ti_2AlC$ ($Ti_3AlN_2$ has not yet been synthesized). This increase has been attributed to an increase in the phonon thermal conductivity due to solid solution hardening. An increased elastic modulus is consistent with this result and the fact that the Debye temperature increases in the mixture and is in excess of 700K.

*This work was supported by NSF grant DMR 0503711.

**10:24**

**G15 13 Electrical and structural properties of Tantalum nitride thinfilms near metal-insulator transition** LEI YU, RAKESH SINGH, JOHN ROWELL, NATHAN NEWMAN, *Dept. of Chemical and Material Engr., Arizona State Univ.* LIN GU, *Dept. of Physics, Arizona State Univ.* The resistivity of thin-film $Ta_xN$ can be tuned through the metal-insulator (MI) transition by adjusting the nitrogen partial pressure during the reactive sputtering process. Recent study show that NbTiN/$Ta_xN$/NbTiN structures with $Ta_xN$ tuned in this range can produce Josephson junctions with a high IcRn product and other device parameters required for the next generation of superconductive RSFQ circuits. Despite the practical possibilities, very little is known about transport over the small length scales associated with transversing the barrier. To address this issue, we focus on the transport and structural properties horizontally through NbTiN/$Ta_xN$/NbTiN structures and transversely across single $Ta_xN$ films for a wide range of $Ta_xN$ thicknesses. When TaxN films are deposited onto oxidized Si wafers, the resistivity (measured in the direction perpendicular to film growth) increases as films become thinner (from 500 nm to 20 nm). Surprisingly, the converse is found for NbTiN/$Ta_xN$/NbTiN structures. The conductivity of TaxN near the MI transition has temperature dependence of $\sigma(T) = \sigma(0) + AT^n$, common in disordered metallic systems. Our analysis of transport has allowed us to discern the role of percolation transport and the change in material parameter as a function of film thickness.

**10:36**
**G15 14 Alpha-plutonium's low-temperature elastic constants*** J. B. BETTS, A. MIGLIORI, H. LEDBETTER, D. DOOLEY, D.A. MILLER, *Los Alamos National Laboratory* Using resonant-ultrasound spectroscopy, we measured alpha-plutonium's polycrystal elastic constants between 18 and 344 K. All elastic constants – bulk, shear, extension, longitudinal moduli and Poisson ratio – behave smoothly during cooling, indicating no significant phase transition: electronic, magnetic, or structural. Both principal elastic constants (bulk and shear) increase about 30% upon cooling from 300 to 0 K, a large change among metals, which we attribute to 5*f*-electron delocalization. From the low-temperature elastic constants, we computed that the Debye temperature equals 205 K, exceeding significantly most previous estimates. From the bulk-modulus/temperature slope itdB/itdT, we computed that the Gruneisen parameter equals 5.1, intermediate among previous estimates using other approaches. Alpha-plutonium shows an unusually high shear-modulus/bulk-modulus ratio $G/B$, thus a low Poisson ratio: 0.18. Within 0.5%, the Poisson ratio shows temperature invariance; its small negative slope being opposite expectation. Again, we attribute this exceptional behavior to 5*f*-electron localization.

*This work was supported by the National Nuclear Security Administration, The State Of Florida, and the National Science Foundation

## SESSION G16: FOCUS SESSION: NEGATIVE REFRACTIVE INDEX II
**Tuesday Morning, 14 March 2006; 312, Baltimore Convention Center at 8:00**
**Gennady Shvets, University of Texas, presiding**

***Invited Papers***

**8:00**
**G16 1 Light in Strongly Anisotropic Media: Towards Negative Index Materials at Optical Frequencies.** EVGENII NARIMANOV, *Princeton University*

This abstract was not received electronically.

***Contributed Papers***

**8:36**
**G16 2 Mid-infrared transmission and reflection measurements of degenerately doped quantum wells*** A. J. HOFFMAN, L. ALEKSEYEV, E. E. NARIMANOV, C. GMACHL, *Princeton University* D. L. SIVCO, *Lucent Technologies* Degenerately doped quantum wells are proposed as a non-magnetic left-handed material in the mid-infrared wavelength range. Such anomalous wave propagation is predicted for waveguides with highly anisotropic dielectric constants. [V. A. Podolskiy, et al. Phys.Rev. B **71**, 201101 (2005)] Three samples consisting of 85 Å AlGaAs/InGaAs quantum wells and barriers were prepared. Doping densities of $1.7\text{x}10^{19}$ $cm^{-3}$ and $1.1\text{x}10^{19}$ $cm^{-3}$ were used for the degenerately doped samples and compared to a control sample doped $2\text{x}10^{17}$ $cm^{-3}$. Reflectance and transmittance as a function of incident angle, wavelength, and polarization were measured. Strong resonances were observed at 10.9 $\mu$m and 13.2 $\mu$m, respectively, for the two highly doped samples over a wide range of experimental incident angles (35[r] – 75[r]) for the relative reflectance of transverse magnetic to transverse electric polarization. No such resonances were observed for the low-doped sample or a highly doped bulk InGaAs sample.

*This work is partly supported by PRISM, Princeton University.

**8:48**
**G16 3 Imaging with negative-refraction planar waveguides** ROBYN WANGBERG, *Oregon State University* EVGENII NARIMANOV, *Princeton University* VIKTOR PODOLSKIY, *Oregon State University* We study the electromagnetic properties of planar waveguides with non-magnetic strongly anisotropic dielectric cores. We develop an analytical description of the mode propagation in these systems and show that their index of refraction can be either positive or negative depending on the configuration. We further demonstrate that it is possible to combine planar waveguide structures to build a planar lens. We study the far-field resolution limit of such a lens and show that it is feasible to achieve resolution better than the free-space diffraction limit. The coupling to and from planar waveguide systems is also explored.

**9:00**
**G16 4 Super-Lensing and Sub-Wavelength Antennas in Mid-IR Using Silicon Carbide*** GENNADY SHVETS, DMITRIY KOROBKIN, YAROSLAV A. URZHUMOV, CHRISTIAN ZORMAN, *The University of Texas at Austin* Extraordinary properties of SiC in mid-infrared (negative dielectric permittivity and small losses) make it an ideal building block for making negative index meta-materials in that important part of the electromagnetic spectrum. We report on a series of experiments demonstrating that thin films of SiC can be used as a ''perfect'' near-field lens. We have theoretically designed and experimentally implemented a super-lens ion mid-IR using SiC. We also report excitation of electrostatic resonances of two structures based on a submicron film of crystalline silicon carbide: (a) nano-holes drilled in the free-standing SiC membrane, and (b) metallic nano-posts evaporated on the SiC membrane. Applications of nano-hole resonances to excitation of magnetic moments in nano-structured SiC and development of negative index materials will be discussed, as will be the prospects of using nano-structured SiC films for laser processing of materials on a nanoscale.

*This work is supported by the DARPA Contract No. HR0011-05-C-0068 and the ARO MURI W911NF-04-01-0203

**9:12**

**G16 5 Surface Enhanced Raman Scattering from Vertical Arrays of Silver Nanowires** G. CHEN, *Department of Physics, The Pennsylvania State University, University Park, PA 16802 USA* J. HABIB, *Illuminex Corporation* T. RUSSIN, H.G. GUITIERREZ, PETER EKLUND, *Department of Physics, The Pennsylvania State University, University Park, PA 16802* We present results of optical studies of surface plasmons and surface enhanced Raman scattering (SERS) from vertical arrays of Ag nanowires. Arrays based on Ag wires with mean diameters d=100 nm have been studied. The wires were grown electrochemically in the pores of anodic aluminum oxide (AAO). To test the SERS activity of these vertical Ag nanowires arrays, we have carried out experiments to detect pyridine on the surface of the nanowires. The SERS enhancement factor is found to be in the order of $10^6$ compared to the Raman signal from bulk liquid. We also studied the surface plasmons of these nanowire arrays in transmission with the incident photon wavevector approximately parallel to the wire axis. Calculations of the plasmon resonances have been made and are found in reasonable agreement with the data.

**9:24**

**G16 6 Modeling Surface Plasmon Enhanced Contact Lithography** MATTHEW ARNOLD, RICHARD BLAIKIE, *MacDiarmid Institute for Advanced Materials and Nanotechnology, Electrical and Computer Engineering, University of Canterbury, New Zealand* Surface Plasmon Enhanced Contact Lithography (SPECL) is a technique for improving sub-wavelength image quality by placing a noble metal beneath the imaging layer in the near-field of a mask. Previous computational [1,2] and experimental[3] studies suggest that that SPECL can improve process latitude compared to pure contact techniques, but future investigations will benefit from a better understanding of the underlying mechanism. We present some numerical simulations, and interpret the results in terms of balanced interference of the ''sources'' consisting of the mask at the top and coupled plasmons at the bottom. Reflected evanescent fields are amplified by a factor that increases with the lateral propagation constant, and hence the usual ''phase'' decay is partially compensated. The observation of an optimal coupling distance is consistent with the inverse relationship between coupling distance and plasmon amplitude compared to the mask fields. Finally we present some data relevant to future experimental exploration. [1] R.J. Blaikie, and S. J. McNab, Assoc. of Asia Pacific Physical Societies Bull. **11**(3), 15 (2002). [2] D.B. Shao, and S.C. Chen, Opt. Express **13**, 6964 (2005). [3] D.B. Shao, and S.C. Chen, Appl. Phys. Lett. **86**, 253107 (2005).

**9:36**

**G16 7 A model for the influence of granularity in a negative refractive index metamaterial lens*** KEVIN WEBB, JIA-HAN LI, *Purdue University* An important goal in building a negative refractive index metamaterial lens at optical frequencies is the achievement of sub-wavelength image resolution. In assigning an effective medium negative refractive index, the electric and magnetic dipoles (which give rise to negative permittivity and permeability) need to be dense relative to the wavelength, i.e., operation near the center of the first Brillouin zone is a prerequisite. Sub-wavelength imaging requires good performance for a significant portion of the evanescent plane wave spectrum. We use a model comprised of discrete regions with negative permittivity and permeability, calculate the effective medium parameters, and show the impact of granularity level (scatterer density) on the performance of a discrete lens, using the slab lens as a reference. We thus arrive at a measure of metamaterial density required to achieve significant improvement over traditional lensing approaches.

*Supported in part by DOE and NSF.

**9:48**

**G16 8 Circuit elements at optical frequencies: A synthesis of first principles electronic structure and circuit theories** C. TANG, R. RAMPRASAD, *Department of Materials Science and Engineering, University of Connecticut* We present a new first principles based method to determine the equivalent circuit representations of nanostructured physical systems at optical frequencies. This method involves the determination of the frequency dependent effective permittivity of two constructs: an ordered composite system consisting of physical nano-elements using density functional theory, and an ordered arrangement of impedances using transmission line theory. Matching the calculated effective permittivity functions of these two constructs has enabled a mapping of the physical nano-system to its equivalent circuit. Specifically, we will show that silicon nanowires and carbon nanotubes can be represented as a series combination of inductance, capacitance and resistance. Once this mapping has been reasonably accomplished for a variety of physical systems, the nano-elements can be combined suitably to result in equivalent circuit topologies appropriate for optical and nanoelectronic devices, including left-handed (or negative refractive index) materials.

**10:00**

**G16 9 1-D, 2-D and 3-D Negative-Refraction Metamaterials at Optical Frequencies: Optical Nano-Transmission-Line and Circuit Theory** NADER ENGHETA, *University of Pennsylvania* ANDREA ALU, *University of Pennsylvania* In recent years metamaterials have offered new possibilities for overcoming some of the intrinsic limitations in wave propagation. Their realization at microwave frequencies has followed two different paths; one consisting of embedding resonant inclusions in a host dielectric, and the other following a transmission-line approach, i.e., building 1-D, 2-D, or 3-D cascades of circuit elements, respectively, as linear, planar or bulk right- or left-handed metamaterials. The latter is known to provide larger bandwidth and better robustness to ohmic losses. Extending these concepts to optical frequencies is a challenging task, due to changes in material response to electromagnetic waves at these frequencies. However, recently we have studied theoretically how it may be possible to have circuit nano-elements at these frequencies by properly exploiting plasmonic resonances. Here we present our theoretical work on translating the circuit concepts of right- and left-handed metamaterials into optical frequencies by applying the analogy between nanoparticles and nanocircuit elements in transmission lines. We discuss how it is possible to synthesize optical negative-refraction metamaterials by properly cascading plasmonic and non-plasmonic elements in 1-D, 2-D and 3-D geometries.

**10:12**

**G16 10 Three and four wave mixing in negative refractive index materials.*** ILDAR GABITOV, *University of Arizona* ANDREI MAIMISTOV, *Moscow Engineering Physics Institute* Nonlinear mixing of waves with different frequencies in materials with negative refractive index represents a new mechanism in nonlinear

optics. We will consider spatio-directional effects for parametric amplification in negative refractive index materials (NRI) with quadratic nonlinearity. We will also investigate photon echo in NRI materials with lambda configuration active dopants.

*Arizona Proposition 301, NSF Grant DMS-0509589

**10:24**

**G16 11 Numerical Calculations of the Magnetic Susceptibility of Split Gold Nanorings** JEREMY NEAL, BAHMAN TAHERI, PETER PALFFY-MUHORAY, *Liquid Crystal Institute, KSU* Metamaterials consisting of split ring resonators have shown negative permeabilities at microwave frequencies. A key challenge is the realization of such a negative index material in the visible spectrum. We consider here the magnetic susceptibility of cut gold nanorings as function of frequency. We have carried out numerical calculations of the polarizability of such particles using the Discrete Dipole Approximation of Draine and Flatau. We present our results for the magnetic susceptibility of different nanoparticle geometries, and compare our results with theoretical estimates. Since the susceptibilities are strongly anisotropic, liquid crystal-like orientationally ordered assemblies of such nanostructures may be useful in realizing bulk optical NIM materials.

**10:36**

**G16 12 Consequences of Spatial Antisymmetry on Light.*** ANGELO MASCARENHAS, BRIAN FLUEGEL, *NREL* When light traverses an interface across which the permittivity, $\varepsilon$, and permeability, $\mu$, change sign, it undergoes negative refraction and the medium with negative values of $\varepsilon$ and $\mu$ must be interpreted as having a negative refractive index $n = -\sqrt{\varepsilon\mu}$. In the past few years this has been experimentally demonstrated by several groups. We have analyzed light propagating in lattices comprised of 2-D tilings in which alternating tiles are made up of media with refractive index whose values alternate in sign acoss tile boundaries. Using both numerical ray tracing and wave equation expansion, we show that when the tiling belongs to certain antisymmetric plane groups, every light ray is exactly bound into a closed, lossless path. The extension to antisymmetric 3-D space groups is also discussed. The study provides unique insights into the consequences of spatial antisymmetry on light.

*We acknowledge the support of the DOE/SC/BES/DMS

**10:48**

**G16 13 Measured polarization rotation loss in negative index metamaterials*** JOHN DEROV, BEVERLY TURCHINETZ, EVERETT CRISMAN, DRAYTON HANNA, ALVIN DREHMAN, *U. S. Air Force Research Lab* The loss mechanisms in left-handed or negative refractive index metamaterial are still not well understood, even for the most common volumetric form using split ring resonators and posts at microwave frequencies. Loss due to polarization rotation, which can only be determined in free space experiments, is both a significant and neglected mechanism. We have measured rotation angles as large as 25 degrees after transmission through negative index media. Polarization rotation is observed as a radiative loss since it reduces the co-polarized power transmitted through the medium. The apparent loss can be reduced by optimizing the receiver polarization. We have measured metamaterial shaped as wedge prisms and rectangular blocks, thereby including and excluding refraction effects. Wedge prisms necessarily include refraction effects. The rectangular blocks can exclude or include refraction by changing the incident angle from normal to oblique. We have investigated whether the polarization type of the transmitted wave is linear or elliptical by using circularly polarized receiver antennas. The results of these measurements will be presented and discussed.

*This work was supported in part by AFOSR/NE.



## SESSION G17: FOCUS SESSION: EMERGING RESEARCH DEVICES AND MATERIALS FOR MICROELECTRONICS INDUSTRY I

**Tuesday Morning, 14 March 2006**
**313, Baltimore Convention Center at 8:00**
**Mike C. Garner, Intel Corporation, presiding**

***Contributed Papers***

**8:00**

**G17 1 The scanned-probe microscope as nano-metrology tool*** YING XU, K. MOLONI, M.G. LAGALLY, *nPoint, Inc., Madison WI 53714 www.npoint.com* Metrology is an essential requirement in the microelectronics industry. As features in computing and memory devices (and also in the flat-panel, hard disc, and CD/DVD industries) reach farther into the nanoscale, their metrology becomes increasingly difficult. Scanned–probe microscopes (SPMs) offer potential solutions. SPMs can produce images with resolution down to the atomic level. However, because of inherent nonlinearities, conventional SPMs possess poor metrology capabilities. Nanometrology requires closed-loop scanning, high throughput, and long-term stability, with subnanometer lateral and vertical resolution and extreme scan flatness over 100s of $\mu$m. We have developed metrology scanners suited for high-precision scanning and positioning applications. They have ultralow out-of-plane motion error ( $<$ 1 nm over 100 $\mu$m scan area). A DSP-based controller enhances the scanner performance. Advanced control algorithms improve dynamic characteristics of the system significantly by reducing phase lag and settling time. The motion control system routinely achieves sub-nanometer resolution and accuracy with high working bandwidth and long-term stability. Using the performance of these metrology scanners we propose a vision of a complete SPM-based CD metrology tool that will enable nanometrology of future generations of electronic devices.

*Partial Support: DARPA

**8:12**

**G17 2 Optical metrology of sub-wavelength critical dimensions of lines on Si wafers** B.M. BARNES, R. ATTOTA, T.A. GERMER, JAY JUN, E. MARX, H. PATRICK, M.T. STOCKER, R.M. SILVER, *NIST, Gaithersburg, MD* As semiconductor manufacturing progresses toward the 65 nm technology node, nondestructive characterization is required for the repeatable fabrication of devices. Optical metrology offers an advantageous solution in both cost and throughput, as the use of visible or uv light is less expensive to implement than scanning probe techniques and will offer greater flexibility as a parallel measurement process. The major impediment to using optics in the critical dimension (CD) metrology of features within the sub- wavelength regime is often thought to be the diffraction limit. However, comparisons of data to theoretical modeling can yield quantitative linewidth values.

Simulations indicate that sensitivity to changes in CD below 20 nm is accessible by using structured illumination, for example reducing the illumination numerical aperture (INA). To increase the rigor of this analysis, we have imaged single, isolated lines of Si on Si with it$\lambda = 546$ nm light with an INA$=0.11$. Although the lines measured in this case range in width nominally from 200 nm to 950 nm, the engineered illumination demonstrated here is directly applicable to the extensibility of optical metrology to technologically relevant dimensions. We also demonstrate that CD sensitivity can be enhanced further by collecting images as a function of focus position, mining additional linewidth information contained in the three-dimensional interference field above the sample.

**8:24**
**G17 3 Measurement of Thicknesses of High-$\kappa$ Gate-Dielectric Films on Silicon by Angle-Resolved XPS** CEDRIC POWELL, *NIST, Gaithersburg* WERNER SMEKAL, WOLFGANG WERNER, *Technical University of Vienna* We report on the use of a new NIST database for the Simulation of Electron Spectra for Surface Analysis (SESSA) in measuring thicknesses of candidate high-$\kappa$ gate-dielectric materials ($HfO_2$, $HfSiO_4$, $ZrO_2$, and $ZrSiO_4$) on silicon by angle-resolved XPS. For conventional measurements of film thicknesses, effective attenuation lengths (EALs) have been computed for these materials from SESSA as a function of film thickness and photoelectron emission angle (i.e., to simulate the effects of tilting the sample). These EALs are believed to be more accurate than similar EALs obtained from the transport approximation because realistic cross sections are used for both elastic and inelastic scattering in the film and substrate materials. We also present ''calibration curves'' showing calculated ratios of selected photoelectron intensities from thin films of $HfO_2$ on Si with an intermediate $SiO_2$ layer. These ratios provide a simple and convenient means of determining the thicknesses of $SiO_2$ and $HfO_2$ films for particular measurement conditions.

**8:36**
**G17 4 Terahertz Spectroscopy as a non contact estimation technique of defect states in high dielectric constant materials** AMARTYA SENGUPTA, APARAJITA BANDYOPADHYAY, *New Jersey Institute of Technology* HAKAN ALTAN, *City College of New York* JOHN FEDERICI, HAIM GREBEL, *New Jersey Institute of Technology* A large number of gate dielectric materials have been examined during the past few years to replace Silicon dioxide in the MOSFET industry to reduce gate leakage currents for microfabrication of devices. Among them, Hafnium based materials have become a very promising candidate. In the reported work, the effect of Hafnium dioxide films on p-type silicon substrates has been investigated and compared with conventional dielectric material, Silicon dioxide, using CW visible pump/THz probe spectroscopy. Drude analysis of the experimentally obtained differential transmission spectra evaluates the electric permittivity of the interfacial layer and the calculated defect density is found to be higher for $HfO_2$than for $SiO_2$which agrees with Hall measurements. Additional measurements on Silicon Nitride deposition and photoresist coated p+ Silicon on p-type silicon wafers without any oxide gave an interfacial defect density 50 times higher than that of $SiO_2$/p+ interface. Results indicate that the mobility of the layer underneath Hafnium is less than that of Silicon. Hence the present study emphasizes the advantage of THz spectroscopy as a non-contact tool for semiconductor metrological applications.

**8:48**
**G17 5 3D-Imaging of Non-spherical Silicon Nanoparticles Embedded in Silicon Oxide by Plasmon Tomography** AYCAN YURTSEVER, *School of Applied and Engineering Physics, Cornell University, Ithaca, NY 14850* MATTHEW WEYLAND, DAVID A. MULLER, We apply plasmon tomography to construct three-dimensional images of silicon nanoparticles in a silicon dioxide matrix, a materials system of interest for optical and storage devices, and at a level of detail and resolution not possible by conventional microscopies. We find that silicon particles with complex morphologies and high surface to volume ratios are dominant rather than the commonly assumed near-spherical structures. These results would affect quantum-confined excitons and interface density of states and, thus, the optical properties of this material. Our findings might explain some of the puzzles related with this material, including the broad photoluminescence band.



***Invited Papers***

**9:00**
**G17 6 Metrology for new microelectronic materials.**
ERIC VOGEL, *NIST*

Traditional scaling of the CMOS Field-Effect-Transistor (FET) has been the basis of the semiconductor industry for 30 years. The 15 year horizon of the International Technology Roadmap for Semiconductors (ITRS) is reaching a point which ''challenges the most optimistic projections for the continued scaling of CMOS (for example, MOSFET channel lengths of roughly 9 nm).'' As silicon CMOS technology approaches its limits, new device structures and computational paradigms will be required to replace and augment standard CMOS devices for ULSI circuits. These possible emerging technologies span the realm from transistors made from silicon nanowires to heteroepitaxial layers for spin transistors to devices made from nanoscale molecules. One theme that pervades these seemingly disparate emerging technologies is that the electronic properties of these nanodevices are extremely susceptible to small perturbations in structural and material properties such as dimension, structure, roughness, and defects. The extreme sensitivity of the electronic properties of these devices to their nanoscale physical properties defines a significant need for precise metrology. This talk will provide an overview of emerging devices and materials, and, through example, an overview of the characterization needs for these technologies.

*Contributed Papers*

**9:36**

**G17 7 Internal dielectric interface: $SiO_2$- $HfO_2$** ONISE SHARIA, ALEX DEMKOV, GENADI BERSUKER, BYOUNG HUN LEE, Hafnia is the leading candidate to replace silica as the gate dielectric in CMOS technology. Typically, hafnia films are deposited by atomic layer deposition (ALD) on the oxidized surface of a silicon wafer. The oxide could be native or thermally grown. Therefore, the high-k dielectric film is not in direct contact with Si, but rather with silicon dioxide. We investigate theoretically the atomic structure of the $SiO_2$-$HfO_2$ interface, its energretics, and thermodynamic stability with respect to oxygen exchange across the interface. We have examined the electronic properties of the interface including the band discontinuity using density functional theory. To model the interface we build a supercell structure by connecting $\beta$-crystobalite (crystalline silica polymorph) and cubic hafnia. This model, while being obviously rather simplistic allows for systematic study of the dielectric thickness effects, and consistent placement of defects with respect to the interface. The striking atomic feature of the calculated interface structure is three-fold coordinated interfacial oxygen atoms connected to one Si and two Hf neighbors. The Si-O and Hf-O bond lengths are 1.62 and 2.1 Å, respectively. The energy of the interface is estimated to be in the range of 900-4000 erg/cm$^2$ depending on the oxygen chemical potential. The structure has no states in the gap, and the estimated valence band offset agrees well with the MIGS theory. We discuss the effect of vacancies on the band alignment, and possible implications of our results to Si-$SiO_2$-$HfO_2$-Metal stacks.

**9:48**

**G17 8 Nanometer-resolution measurement and modeling of lateral variations of the effective work function at metal-bilayer /oxide interfaces** W. CAI, K. -B. PARK, J. P. PELZ, *Dept. of Physics, The Ohio State University* Future CMOS technology will require metal gates with a ''tunable'' effective work function (EWF) to precisely adjust the transistor turn-on voltage. It was shown using itmacroscopic $C - V$ measurements that this could be done by adjusting the thickness of a very thin low-EWF metal covered by a high-EWF metal film (or vice-versa) on a $SiO_2$ film [1,2]. We are using nm-resolution Ballistic Electron Emission Microscopy (BEEM) and Internal Photemission (Int-PE) to investigate whether a 5-nm Pt/1.4-nm Al/$SiO_2$ gate stack has a itlaterally inhomogeneous energy barrier at the metal/$SiO_2$ interface, produced by nm-sized pinholes in the thin Al film. Initial measurements of the average BEEM threshold voltage vs. applied oxide bias do in fact suggest an inhomogeneous energy barrier at the interface. Further BEEM and Int-PE measurements and finite-element electrostatic simulations are on-going, and will be discussed. Work supported by the Semiconductor Research Corp. [1] Gao et al., Mat. Res. Soc. Symp. Proc. 765, D1.4.1-6 (2003). [2] I.S. Jeon et al., IEDM-04, 303 (2004).

**10:00**

**G17 9 Is the oxygen vacancy the dominating charge trap in hafnia based MOSFETs?** JACOB GAVARTIN, DAVID MUNOZ-RAMO, ALEXANDER SHLUGER, MARSHALL STONEHAM, *University College London, U.K.* GENNADI BERSUKER, *SEMATECH, TX, U.S.A.* One of the factors affecting performance of high-k based MOSFETS is the instability of the threshold voltage, $V_T$, attributed to a high concentration of the carrier traps in the dielectric stack. Bulk oxygen vacancies in $HfO_2$ had been suggested as dominating electric traps, although this has not been unambiguously proved. We present ab initio calculations of the vacancies and divacancies in the monoclinic $HfO_2$ with the charge states $+2,+1,0,-1,-2$. Recent electrical I-V measurements probing $V_T$ relaxation under pulsed electrical stress [1] infer that: 1. The charge trapping under the applied stress is significantly faster than de-trapping following stress release suggesting significance of lattice relaxation upon trapping. 2. The kinetics of this $V_T$ relaxation is multiexponential with dominating activation energies in the range and 0.25-0.45 eV. We juxtapose the experimental data with the energetic parameters obtained from the calculations and consider whether the charge trapping and de-trapping by the variously charged vacancy levels accounts for all available experimental trends. [1] R. Choi, S.C. Song, C.D. Young, G. Bersuker, B.H. Lee, Appl. Phys. Lett. 87, 122901 (2005).

**10:12**

**G17 10 Resistive Switching of Individual Dislocations in Insulating Perovskites – A Potential Route Towards Nanoscale Non-Volatile Memories.** KRZYSTOF SZOT, WOLFGANG SPEIER, GUSTAV BIHLMAYER, RAINER WASER, *CNI & IFF, FZ Juelich* Electrically controlled resistive switching effects have been reported for a broad variety of binary and multinary oxides in recent years. In particular, titanates, zirconates, and manganites have been in the focus of the studies. In many cases, the mechanism of the switching and the geometrical extension of the phenomenon (filaments vs. bulk) are still under discussion. In this work, we present evidence for a redox-based switching mechanism and we indicate a potential route towards highly scalable non-volatile memories based on this switching effect. The challenge our work is to utilize resistive switching mechanism with the aim to construct itactive electronic elements on a real nanoscale level, here by reversibly switching the electrical properties of individual dislocations by electrical stimuli. We demonstrate that standard undoped $SrTiO_3$ single crystals, utilized as a model system, exhibit a switching behavior along filaments based on dislocations, mediated by oxygen transport. For this, we employed a three-step procedure: the crystals were, at first, annealed at elevated temperatures under reducing conditions, then exposed to 200mbar $O_2$ pressure at room temperature, and finally subjected to an electric field under ultrahigh vacuum (electroformation). This treatment induced in a metal-insulator ($SrTiO_3$)-metal (MIM) system a transition to metallic state. A hysteretic behavior appears after dynamical polarization of the MIM structure at the maximum electroforming currents. The shape of the I/V curve has the typical signature for bi-stable switching known for these types of perovskites. The positive temperature dependence of the resistance of the low- (LRS) and the high-resistance (HRS) state clearly identifies both states to be metallic in character. The inhomogeneity of the electrical transport becomes directly evident from a simple optical inspection and the conductivity maps as measured by LC-AFM of a planar structure. One can trace the formation of the filaments,

emerging from the cathode and propagating towards the anode during the electroformation process. These filaments are well-oriented along the $< 100 >$ -axis of the crystal and show a discrete and granular substructure on the nano-scale. The similarity in lateral distribution of exit points (spots) of conducting nano-filaments with respect to the distribution of etch pits suggests that the electrical transport along dislocations determines the micro- and meso-scopic electrical transport phenomena. Our results suggest that a dedicated contact arrangement is required to handle the filamentary conduction in a practical way by using macroscopic electrodes. At the same time, it emphasizes the need to control the relevant processes on the level of individual dislocations. With LC-AFM it is possible to specifically address single dislocations crossing the surface with adequate spatial resolution and use the conducting cantilever as the nano-electrode through galvanic point contact. We succeeded to initiate the local electroformation process for a single dislocation by applying a dc bias to the tip of the cantilever. Such nano-prepared dislocations reveal bi-stable switching behavior between a linear and a non-linear $I/V$-characteristics. The dynamic range of the electrical resistance covers at least 3 to 4 orders of magnitude at read-out voltages of 0.1 V. In order to develop a microscopic model for the filament, we performed first-principles calculations of extended, linear defects in $SrTiO_3$. Our analyse of electronic structure for extended defects with TiO enrichment establish that already subtle changes in O-content are sufficient to modulate the electronic properties and provide the necessary self-doping capability with a reversible transition between non-metallic and metallic behaviour. We propose a model for the resistive switching in $SrTiO_3$ based on the modulation of the electrical properties through electrical stimuli in a small segment of an orthogonal network of dislocations. Switching in our case corresponds then to an electrochemical ''closing'' or ''opening'' of the single dislocation in the uppermost portion of the network. Our results show that the switching behaviour in single-crystalline $SrTiO_3$ is an inherent property of the material and can be easily activated by external stimuli. Due to the availability of dislocation densities up to $10^{12}$ $cm^{-2}$ in single crystals and thin film, one can even envisage to approach the Tbit regime, as long as the dislocations can be successfully arranged into registered superstructures. In summary, evidence is given that the electrical conductance of individual dislocations in a prototype perovskite, $SrTiO_3$, can be switched between a low and a high conducting state by the application of an electrical field. We demonstrate on the basis of itab initio calculations and measurements with a scanning probe microscope SPM that the modulation of the electrical properties is related to the induced change in oxygen stoichiometry and the self-doping capability with a local insulator-metal transition along the core of the dislocations. A model is presented based on a three-dimensional network of such a filamentary structure to analyze the bi-stable resistive switching in the macroscopic metal-insulator-metal (MIM) structure. Our results show that electrically addressing individual dislocations in single crystals as well as epitaxial thin films provides a dynamic range for switching between low and high conducting states which covers several orders of magnitude in resistance and can be of technological interest for the application in Tbit non-volatile memory devices.

**10:24**

**G17 11 Electrical characteristic of metal-oxide-semiconductor with $NiSi_2$ nanocrystals embedded in oxide layer** JENN-KAI TSAI, IKAI LO, M.H. GAU, Y.L. CHEN, P.H. YEH, T.C. CHANG, PHYSICSDEPARTMENT, CENTER FOR NANO-SCIENCE & NANOTECHNOLOGY, NATIONAL SUN YAT-SEN UNIVERSITY, KAO TEAM, DEPARTMENT OF MATERIALS SCIENCE AND ENGINEERING, NATIONAL TSING HUA UNIVERSITY, HSINCHU, TAIWAN, REP COLLABORATION, The nano-structured electronic devices have received more attention recently. Metal-oxide-semiconductor structure with $NiSi_2$ nanocrystals embedded in the oxide layer, $HfO_2/SiO_2$, has been fabricated. Comparing with conventional ones, it could be operated under lower voltage and faster program/erase speed and has better endurance and retention. We have measured the temperature-dependent tunneling V-I curve on these $HfO_2/SiO_2$ nano-structured devices for the temperature from 1.2K to 300K. The results show an abnormal electrical characteristic. The tunneling V-I characteristics appear a new threshold voltage in the low temperature region, from 30K to 100K, while applied a negative voltage. The abnormal threshold voltage disappears when the temperature higher than 150K or lower than 30K. We attribute the new threshold voltage to the discrete quantum states of $NiSi_2$ nanocrystals in the oxide layer.

**10:36**

**G17 12 Photoemission Studies of Nitrided Hafnium Silicates for High-$\kappa$ Dielectrics** ANOOP MATHEW, KORHAN DEMIRKAN, *University of Delaware* CHANG-GONG WANG, GLEN WILK, *ASM America Inc.* ROBERT OPILA, *University of Delaware* Nitrided hafnium silicates are strong candidate materials for replacing the $SiO_2$ gate dielectric in transistors for low standby power applications. Integrating these materials with the silicon substrate of the channel or metal gates open up a variety of interfacial issues. Photoelectron spectroscopy with its sensitivity to local chemical bonding is an invaluable tool for investigating these interfaces. Hafnium silicates were deposited using Atomic Layer Chemical Vapor Deposition and subsequently nitrided. A maximum entropy based algorithm was used to non-destructively reconstruct concentration profiles as a function of depth from angle resolved photoemission data and a good correlation was obtained from depth profile data obtained using Medium Energy Ion Scattering. Nitrogen is seen to diffuse towards the gate stack/silicon interface at higher temperatures. Trends in the nitrogen and oxygen profiles suggest replacement of the oxygen with the nitrogen during nitridation. These films were rapid thermally annealed to study their phase stability, and shifts in the photoelectron spectra reveal behavior that is not entirely consistent with what would be expected with previously reported phase segregation of these films into pure $HfO_2$ and $SiO_2$. Interfacial charge associated with these systems is reflected in the photoemission spectra, and this complements observations from other techniques.

**SESSION G18: FOCUS SESSION: CARBON NANOTUBES: ELECTRONIC AND OPTICAL PROPERTIES I**
**Tuesday Morning, 14 March 2006; 315, Baltimore Convention Center at 8:00**
**Tobias Hertel, Vanderbilt University, presiding**



*Invited Papers*

**8:00**
**G18 1 Excitons in the optical properties of nanotubes.***
CATALIN SPATARU,† *UC Berkeley and LBNL, Berkeley, CA 94704*

We present *ab initio* calculation of self-energy and electron-hole interaction (excitonic) effects on the optical spectra of single-walled carbon and BN nanotubes. We employed a many-electron Green's function approach that determines both the quasiparticle and optical excitations from first principles. We found important many-electron effects that explain many of the puzzling experimental findings in the optical spectrum of these quasi-one dimensional systems, and the calculated spectra are in excellent quantitative agreement with measurements. In carbon nanotubes, excitons can bind by as much as one eV in semiconducting nanotubes[a)]. We discovered that bound excitons also exist in metallic carbon nanotubes with binding energy of many tens of meVs[a)]. Excitonic effects are shown to be even more inportant in BN nanotubes than in carbon nanotubes. Unlike the carbon nanotubes, theory predicts that excitons in some BN nanotubes are comprised of coherent superposition of transitions from several different subband pairs[b)]. We have also calculated the radiative lifetime of excitons in semiconducting carbon nanotubes. Assuming a thermal occupation of bright and dark exciton bands, we find an effective radiative lifetime of the order of 10 ns at room temperature, in good accord with recent experiments[c)]. **a)** C.D. Spataru, S. Ismail-Beigi, L.X. Benedict and S.G. Louie, Phys. Rev. Lett. **92**, 077402 (2004). **b)** C.-H. Park, C.D. Spataru and S.G. Louie, to be published. **c)** C.D. Spataru, S. Ismail-Beigi, R.B. Capaz and S.G. Louie, in press Phys. Rev. Lett.

*This work was supported by the NSF under Grant No. DMR04-39768, and the U.S. DOE under Contract No. DE-AC03-76SF00098. Computational resources have been provided by NERSC and NPACI.
†This work has been done in collaboration with Cheol-Hwan Park, Sohrab Ismail-Beigi, Lorin X. Benedict, Rodrigo B. Capaz and Steven G. Louie.

*Contributed Papers*

**8:36**
**G18 2 Exciton radiative lifetime in carbon nanotubes** VASILI PEREBEINOS, JERRY TERSOFF, PHAEDON AVOURIS, *IBM - Watson Research Center* The optical properties of carbon nanotubes are dominated by excitons, and the exciton radiative lifetime determines the optical efficiency. We calculate the exciton radiative lifetime as a function of tube diameter and chirality, finding an unusual nonmonotonic temperature dependence [1]. This reflects the crucial role of exciton bands that are optically inactive, due to spin or parity, below the optically active exciton. We determine the scaling with diameter of the singlet-triplet and parity forbidden exciton splittings. We also calculate the exciton dispersion, finding a non-parabolic behavior of the optically active band. Excitons that thermalize into low-energy optically inactive bands cannot contribute to light emission, unless they are thermally excited into the active band, resulting in reduced emission yield at low temperature. However, in real systems there is typically some symmetry breaking, which mixes optically allowed and forbidden bands; and as a result, some emission is still possible from the nominally forbidden bands. This may account for the multiple emission peaks and complex temperature dependence seen in some experiments. [1] NanoLett. 5 DOI: nl051828s (2005).

**8:48**
**G18 3 Magnetic brightening of ''dark'' excitons in carbon nanotubes** S. ZARIC, J. KONO, *Dept. of Elec. & Comp. Engineering, Rice Univ.* X. WEI, *NHMFL, Florida State Univ.* R. H. HAUGE, R. E. SMALLEY, *Chemistry Dept., Rice Univ.* We have measured polarized-excitation photoluminescence (PL) on micelle-suspended single-walled carbon nanotubes (SWNTs) in aqueous solution in external magnetic fields ($B$) up to 45 T at room temperature. Each PL peak, corresponding to a specific chirality, splits into two in a $B$ and the amount of splitting increases with $B$. The magnetic field dependence of the relative intensities of the two peaks reveals that the lower-energy peak increases in intensity (or ''brightens'') with increasing $B$. These results can be understood in terms of ''magnetic brightening'' of an excitonic state that is ''dark'' at 0 T. Namely, recent calculations taking into account intervalley Coulomb mixing in semiconducting SWNTs predict the existence of a dark excitonic state at an energy $\Delta_X$ below the lowest optically active (bright) excitonic state. On the other hand, magnetic flux it$\phi$ threading a nanotube removes the intervalley degeneracy which is seen in absorption measurements as peak splittings by an amount $\Delta_{AB}$ proportional to it $\phi$ (when it$\phi/\phi_0 \leqslant$ 1/6, it$\phi_0$: magnetic flux quantum). While two equally-bright excitonic peaks are predicted and observed at high fields ($\Delta_{AB} > > \Delta_X$), [1] magnetic brightening is expected at lower fields ($\Delta_{AB} \sim \Delta_X$), which is consistent with our observations. [1] S. Zaric et al, Phys. Rev. Lett., to appear (see also cond-mat/0509429)

**9:00**
**G18 4 Diameter and chirality dependence of exciton properties in carbon nanotubes** RODRIGO CAPAZ, *Instituto de Fisica, UFRJ, Brazil* CATALIN SPATARU, *U. C. Berkeley* SOHRAB ISMAIL-BEIGI, *Yale University* STEVEN LOUIE, *U. C. Berkeley* We calculate the binding energies and sizes of excitons in carbon nanotubes using a symmetry-based, effective-mass, variational method. This approach provides exciton binding energies in good agreement with available first-principles results and its simplicity allows calculations for a variety of diameters ($d$) and

chiralities. The exciton binding energies present an overall decrease with $1/d$, with strong chirality dependence and family behavior. The exciton sizes scale with $d$, also showing family behavior. We also address the important issue of bright-dark exciton splittings, which are found to decrease as $1/d^2$. Dependence of these properties on the dielectric screening will also be addressed, in the light of recent experimental measurements. This work was supported in part by the NSF under Grant No. DMR04-39768, and the U.S. DOE under Contract No. DE-AC03- 76SF00098.

**9:12**

**G18 5 Nearly quantitative fitting of exciton energies and exciton binding energies of semiconducting single-walled carbon nanotubes (S-SWCNTs) within a $\pi$-electron model*** ZHENDONG WANG, *University of Arizona* SUMIT MAZUMDAR, *University of Arizona* We use to Pariser-Parr-Pople $\pi$-electron Hamiltonian, which has been widely used to understand the excitonic energy spectra of $\pi$-conjugated polymers, to determine the energy spectra of S-SWCNTs. For the Coulomb interaction parameters, we use the screened Ohno parameters that were successfully used before for the quantitative fitting of the excitonic energy spectrum of poly-(paraphenylenevinylene)[1]. In order to take into account of the curvature effects, we use a $\pi$-electron nearest neighbor hopping integral that is substantially smaller than the standard 2.4 eV. With these modified parameters we are able to fit the lowest two exciton energies of a very large number of S-SWCNTs. We make detailed comparisons between the calculated and experimental[2]. We also obtain a binding energy of $\sim$ 0.4 eV for the lowest exciton of S-SWCNTs with diameters $\sim$ 0.8 nm, in agreement with experiments.

*Supported by NSF-DMR 0406604

[1]M. Chandross and S. Mazumdar, Phys. Rev. B **55**, 1497 (1997)
[2]R.B. Weisman and S.M. Bachilo, Nano Lett. **3**, 1235 (2003)

**9:24**

**G18 6 Determination of the exciton binding energy in single-walled carbon nanotubes** TODD KRAUSS, ZHENJIA WANG, HERMENEGILDO PEDROSA, LEWIS ROTHBERG, *University of Rochester* The optical properties of single-walled carbon nanotubes (SWNTs) are intrinsically important for potential applications in photonics and also provide insight into their structural and electrical properties. Absorption and emission of semiconducting SWNTs are dominated by excitonic effects, but a determination of central features such as exciton binding energies remains elusive. We will present measurements of the exciton binding energy in SWNTs using resonance Raman scattering of isolated SWNTs under an electrochemical bias. The Raman intensity under an applied voltage is sensitive to state filling and enables a determination of the (electronic) gap between the second Van Hove singularities in densities of states for electrons and holes in specific semiconducting SWNTs. On the other hand, Raman scattering preferentially selects sets of SWNTs whose excitonic transitions (optical gap) are resonant with the incident and scattered photon energies. Simultaneous measurement of the electronic gap and exciton resonance allows us to infer binding energies for the exciton of 0.49 and 0.62 eV for tubes with structural (n,m) indices (10, 3) and (7, 5), respectively. Analogous Raman and electrochemical studies in metallic SWNTs imply the absence of a sharp excitonic feature.

**9:36**

**G18 7 Nanotube exciton spectrum: Triangular quantum well model.** SLAVA V. ROTKIN, *Lehigh University, Physics Department, 16 Memorial Dr E, Bethlehem, PA 18015, e-mail: rotkin@lehigh.edu* ALEXEY G. PETROV, *Ioffe Institute, St.Petersburg, Russia* The analytical solution for the problem of NT-exciton is found using the approximation for the **screened** Coulomb potential between the electron and hole. We derive the screening via calculating a self-consistent dielectric function with **both spatial and time dispersion** taken into account, $\varepsilon(\vec{q},\omega)$, which characterizes the response to the $\vec{q}$ component of the Coulomb potential at the frequency $\omega$. The latter corresponds to the energy of the exciton and is to be sought. We calculated the RPA dielectric function of the SWNT in the orthogonal tight-binding approach. Then, the inverse Fourier transform of the screened Coulomb potential gives the shape of the potential well for the electron-hole pair (direct Coulomb interaction term). We show that this screened potential can be approximated by a triangular quantum well, which model allows ananlytical solutions for the exciton wavefunction and the binding energy. The exchange term is short-ranged and can be added as the delta-function barrier in the middle of the well. The exciton binding energy is calculated to be a universal function of $E_g$, the one-particle band gap, $R$, the NT radius and $\lambda$, the electric length in the triangular quantum well potential. The effective Bohr radius is also a universal function of $R$ and $\lambda$. The analytical expression for the oscillator strength of the optical transition is presented.

**9:48**

**G18 8 Theory of electroabsorption in semiconducting single-walled carbon nanotubes*** HONGBO ZHAO, SUMIT MAZUMDAR, *University of Arizona* Eletroabsorption (EA) is a standard nonlinear optical technique to probe the excitonic characteristics of semiconductors.[1] In the context of single-walled carbon nanotubes (SWCNTs) the advantage of EA is that it can directly probe the excitons associated with higher bands, which lie in the continuum region of the lowest band, and cannot be probed by other nonlinear optical techniques like photoinduced absorption or two-photon absorption. Although currently it is still difficult to carry out EA experiments, because it requires separation of semiconducting SWCNTs from metallic ones, theoretical calculations can provide a benchmark results for future study. We have calculated EA for several S-SWCNTs with both zigzag and chiral tubes.[2] For the lowest exciton we find the usual Stark shift, the emergence of absorption due to two-photon states and continuum band. We also find unusual and interesting behavior of the higher energy excitons from second band.

*Supported by NSF-DMR-0406604.

[1]L. Sebastian and G. Weiser, Phys. Rev. Lett. **46**, 1156 (1981); D. Guo *et al.*, Phys. Rev. B **48**, 1433 (1993).
[2]J. W. Kennedy, Z. V. Vardeny, S. Collins, R. H. Baughman, H. Zhao, and S. Mazumdar, cond-mat/0505071.

**10:00**

**G18 9 Interactions between individual carbon nanotubes studied by Rayleigh scattering spectroscopy** TONY HEINZ, *Columbia University* FENG WANG, MATTHEW SFEIR, LIMIN HUANG, X.M. HENRY HUANG, YANG WU, JAEHEE KIM, JAMES HONE, STEPHEN O'BRIEN, LOUIS BRUS, Single-walled carbon nanotubes (SWNTs), with diameters of nanometers and lengths up to millimeters, represent highly one-dimensional (1D) systems. Because all the carbon atoms of a SWNT lie on its

surface, the physical properties of SWNTs depend sensitively on local environment.[1] In particular, the electronic properties of SWNTs are altered by inter-tube coupling whenever nanotube bundles are formed. We examine such inter-tube interactions experimentally at the single nanotube level. This is achieved by applying Rayleigh scattering spectroscopy [2] to probe the optical transitions of individual SWNTs in their isolated and bundled forms. Upon bundling, the transition energies of SWNTs are observed to undergo red shifts of tens of meVs, without any significant line broadening. These inter-tube coupling effects can be understood as arising from the mutual dielectric screening of SWNTs in a bundle. 1. Kong, J., et al., Science, **287,** 622 (2000). 2. Sfeir, M.Y., et al., Science, **306,** 1540 (2004).

**10:12**

**G18 10 Exciton dynamics in DNA suspended SWNT agglomerates: From delocalized to one-dimensionally confined excited states** JARED J. CROCHET, *Vanderbilt University* MICHAEL ARNOLD, *Northwestern University* MARK HERSAM, *Northwestern University* ZIPENG ZHU, *Vanderbilt University* TOBIAS HERTEL, *Vanderbilt University* Exciton dynamics in chirality enriched, DNA suspended single-wall carbon nanotube agglomerates are studied using linear absorption, spectrofluorimetry, and ultrafast pump-probe spectroscopies. Suspended SWNT ropes with controlled diameter are isolated using isopycnic density gradient fractionation. Photoluminescence quantum yields are found to decrease with increasing rope diameter concomitantly to a broadening and redshift of exciton transitions. Spectrally resolved optical transients reveal that excited state dynamics are characterized by an increase of $E_{11}$ subband exciton decay rates as the rope size increases. These findings are discussed in terms of the roles of intertube coupling and exciton delocalization.

**10:24**

**G18 11 Raman characterization of electronic transition energies of metallic single-wall carbon nanotubes** HYUNGBIN SON, *Department of Electrical Engineering and Computer Science, MIT, Cambridge, MA* ALFONSO REINA CECCO, *Department of Materials Science And Engineering, MIT, Cambridge, MA* JING KONG, *Department of Electrical Engineering and Computer Science, MIT, Cambridge, MA* MILDRED DRESSELHAUS, *Department of Electrical Engineering and Computer Science and Department of Physics, MIT, Cambridge, MA* Theoretical studies using extended tight-binding model are shown to reproduce the optical transition energies of single-wall carbon nanotubes (SWNTs) obtained by experimental studies. However, some of the optical transitions for metallic SWNTs predicted by theory are not reported in previous experimental studies. We present that Raman characterization on a large number of individual SWNTs reveals these missing optical transitions. The intensity variations of different optical transitions are attributed to electron-phonon matrix elements.

**10:36**

**G18 12 Inelastic X-ray Scattering Studies of Plasmons in Carbon Nanotubes** M. H. UPTON, *Brookhaven National Laboratory* D. CASA, T. GOG, *Argonne National Laboratory* J. MISEWICH, J. P. HILL, *Brookhaven National Laboratory* D LOWNDES, G. ERES, *Oak Ridge National Laboratory* We report preliminary inelastic x-ray scattering measurements of the plasmon dispersions in oriented multi- and single- walled carbon nanotubes (M- and S-WCNT) and compare them to the plasmon dispersion in graphite. Two plasmon bands are observed dispersing along the nanotubes' axes: the $\pi$ and $\pi + \sigma$ plasmon bands. The $\pi + \sigma$ plasmon band exhibits an apparent systematic variation in energy. Specifically, it has a lower energy in MWCNT than in graphite, and a still lower energy in SWCNT. The energy of the $\pi + \sigma$ plasmon band is determined by the plasma frequency of the material, which is proportional to the square root of the electron density. We postulate that the energy shift is a result of a surface effect – the electron wave function extends past the surface, lowering the average electron density in the bulk. The higher surface-to-volume ratio of the mostly SW sample would then lower the plasmon frequency with respect to the MWCNT sample and graphite. Thus, the systematic variation in plasmon frequency may be explained by a lowering of the net electron density by the surfaces in S- and M-WCNT. Work performed at BNL and the Advanced Photon Source was supported by the US DOE under contracts No. DE-AC02-98CH10886 and No. W-31-109-Eng-38 respectively.

**10:48**

**G18 13 Atomic Entanglement in Carbon Nanotubes.*** IGOR BONDAREV, BRANISLAV VLAHOVIC, *North Carolina Central University* The development of materials that may host quantum coherent states is a critical research problem for the nearest future. Recent progress in the growth of centimeter-long small-diameter single-walled carbon nanotubes (CNs) [1] and successful experiments on the encapsulation of single atoms into CNs [2], stimulate the study of dynamical quantum processes in atomically doped CN systems. We have recently shown [3] that atomic states may be strongly coupled to vacuum surface photonic modes in the CN, thus forming quasi-1D cavity polaritons similar to those observed for quantum dots in semiconductor nanocavities [4], which were recently suggested to be a possible way to produce the excitonic qubit entanglement [5]. Here, we show that, being strongly coupled to the (resonator-like) cylindrical nanotube environment, the two atomic quasi-1D polaritons can be easily entangled as well, thus challenging a novel alternative approach towards quantum information transfer over centimeter-long distances. [1] L.X. Zheng et al, Proc. Nanotech 2005 (May 8-12, 2005, Anaheim, CA, USA), vol.3, p.126. [2] G.-H. Jeong et al, Phys. Rev. B 68, 075410 (2003). [3] I.V. Bondarev and Ph. Lambin, in: Trends in Nanotubes Reasearch (Nova Science, NY, 2005); Phys. Rev. B 70, 035407 (2004); Phys. Rev. B 72, 035451 (2005). [4] T. Yoshie et al, Nature 432, 200 (2004). [5] S. Hughes, Phys. Rev. Lett. 94, 227402 (2005).

*Supported by DoD and NASA (gr.No DAAD19-01-1-0795, NAG3-804)

**SESSION G19: FOCUS SESSION: III-V MAGNETIC SEMICONDUCTORS I**
**Tuesday Morning, 14 March 2006**
**316, Baltimore Convention Center at 8:00**
**Mark van Schilfgaarde, Arizona State University, presiding**

***Contributed Papers***

**8:00**

**G19 1 Prospects for high temperature ferromagnetism in (Ga,Mn)As semiconductors** JAIRO SINOVA, *Texas A&M University* T. JUNGWIRTH, J. MASEK, N.A. GONCHARUK, *Institute of Physics ASCR, Czech Republic* K.Y. WANG, K.W. EDMONDS, A.W. RUSHFORTH, R.P. CAMPION, L.X. ZHAO,

C.T. FOXON, B.L. GALLAGHER, *U. of Nottingham* A.H. MACDONALD, *U. of Texas* M. POLINI, *NEST-INFM, Pisa* M. SAWICKI, *Polish Academy of Science* J. KOENIG, *Ruhr-Universitat* We report on a comprehensive combined experimental and theoretical study of Courie temperature trends in (Ga,Mn)As ferromagnetic semiconductors. Broad agreement between theoretical expectations and measured data allows us to conclude that $T_c$ in high-quality metallic samples increases linearly with the number of uncompensated local moments on $Mn_{Ga}$ acceptors, with no sign of saturation. Room temperature ferromagnetism is expected for a 10% concentration of $Mn_{Ga}$. Based on the analysis of magnetotransport and magnetization data we find no fundamental obstacle to substitutional $Mn_{Ga}$ doping in high-quality materials beyond our current maximum level of 6.8%, although this achievement will require further advances in growth control. Modest charge compensation does not limit the maximum $T_c$ possible in ferromagnetic semiconductors based on (Ga,Mn)As. Ref: Jungwirth et al. Phys. Rev. B 72, 165204 (2005).

**8:12**
**G19 2 Spin and Charge Relaxations in Magnetic and Nonmagnetic Narrow-gap Semiconductors** K. NONTAPOT, A. GIFFORD, T. MERRITT, G. A. KHODAPARAST, *Department of Physics, Virginia Tech.* S. J. CHUNG, N. GOEL, M. B. SANTOS, *Department of Physics and Astronomy, University of Oklahoma* T. WOJTOWICZ, X. LIU, J. K. FURDYNA, *Department of Physics, University of Notre Dame* In light of the growing interest in spin-related phenomena and devices, there is now renewed interest in the science and engineering of narrow gap semiconductors. Narrow gap semiconductors offer several scientifically unique features such as a small effective mass, a large g-factor, a high intrinsic mobility, and large spin-orbit coupling effects. We will discuss our recent time resolved studies on InSb quantum wells with symmetric and asymmetric confinement potentials and InMnSb ferromagnetic structures with different Mn contents. We have measured the carrier and spin dynamics by degenerate and non-degenerate pump-probe and Kerr effect spectroscopy at different temperatures and laser intensities in these unique structures with strong spin-orbit interaction. Supported by NSF-DMR-0507866, Jeffress-J748, NSF-DMR02-45227, NSF Grant No. DMR-0510056 and DMR-0520550

**8:24**
**G19 3 Spin Waves in GaMnAs/GaAs Superlattices** D. M. WANG, R. MERLIN, *University of Michigan* Y. J. CHO, X. LIU, J. K. FURDYNA, *University of Notre Dame* We report on the spin-wave behavior of GaMnAs/GaAs superlattices as a function of the thickness of the nonmagnetic layer. Spin-wave frequencies were determined from time-domain magnetic Kerr measurements using a standard pump-probe setup. We studied two superlattices grown by molecular beam epitaxy on GaAs (001) substrates and, for comparison purposes, a single 120-nm-thick $Ga_{0.955}Mn_{0.045}As$ layer. The superlattices consist of 6 repetitions of 20-nm-thick $Ga_{0.955}Mn_{0.045}As$ layers separated by either $d = 3$ or 6 nm of GaAs. For magnetic fields $H < 0.22$ T, applied along the magnetic easy axis [100], the thin film and the superlattices exhibit a nearly $d$-independent mode of frequency it$\nu \cong 5 + 33$itH (GHz), whereas the sample with $d = 6$ nm shows a second oscillation at it $\nu \cong 7 + 33$itH (GHz), which we assign to a higher-order confined spin-wave. The existence of this mode is tentatively ascribed to a reduction in the coupling between neighboring magnetic layers.



***Invited Papers***

**8:36**
**G19 4 Measurement of the *s-d* exchange coupling in GaMnAs quantum wells.***
MARTINO POGGIO,† *Center for Spintronics and Quantum Computation, University of California, Santa Barbara, CA 93106*

The discovery of ferromagnetism in zinc-blende III-V Mn-based compounds and the realization that this collective magnetic behavior is mediated by delocalized or weakly localized holes has given a technological impetus for developing a clear picture of the carrier-shell exchange couplings. Surprising results regarding the magnitude and sign of the exchange between *s*-like conduction band electrons and electrons localized in the *d*-shell of the $Mn^{2+}$ impurities point to deficiencies in the current theory which has successfully described experimentsin II-VI DMS within a higher regime of doping[1]. Measurements of coherent electron spin dynamics in $Ga_{1-x}Mn_xAs/Al_{0.4}Ga_{0.6}As$ quantum wells with $0.003\% < x < 0.2\%$ show an antiferromagnetic (negative) *s-d* exchange coupling, $N_0\alpha$. The magnitude of $N_0\alpha$ varies as a function of width of the quantum well, which is consistent with a large and negative contribution due to kinetic exchange. MBE growth conditions are optimized in order to produce GaMnAs with low defect densities in which coherent spin dynamics can be observed optically, while at the same time incorporating enough Mn to make the *s-d* coupling observable. Polarization-resolved photoluminescence and reflectance measurements reveal the effects of *p-d* exchange between carriers in the valance band and spins localized on Mn sites. Light Mn doping is also seen to maximize the carrier electron spin lifetime, indicating the importance of the Dyakonov-Perel decoherence mechanism in these structures.

*Work supported by AFOSR, DARPA and ONR.
†In collaboration with R. C. Myers, N. P. Stern, A. C. Gossard, and D. D. Awschalom.

[1]R. C. Myers, M. Poggio, N. P. Stern, A. C. Gossard, and D. D. Awschalom, Phys. Rev. Lett. **95**, 017204 (2005); M. Poggio, R. C. Myers, N. P. Stern. A. C. Gossard, and D. D. Awschalom, cond-mat/0503521.

*Contributed Papers*

**9:12**

**G19 5 Confinement engineering of s-d exchange interactions in GaMnAs quantum wells*** N.P. STERN, R.C. MYERS, M. POGGIO, A.C. GOSSARD, D.D. AWSCHALOM, *Center for Spintronics and Quantum Computation, University of California, Santa Barbara, CA 93106* Recent measurements of coherent electron spin dynamics have observed antiferromagnetic *s-d* exchange coupling between conduction band electrons and electrons localized on $Mn^{2+}$ impurities in GaMnAs quantum wells[1]. Here we discuss systematic measurements of the *s-d* exchange interaction in $Ga_{1-x}Mn_xAs/Al_yGa_{1-y}As$ quantum wells with different confinement potentials using time- resolved Kerr rotation spectroscopy. Extending previous investigations of the well width dependence of the *s-d* exchange, $N_0\alpha$, we find that the magnitude of the exchange parameter, $N_0\alpha$, varies as a function of both well width and well depth ($y$). Both phenomena reduce to a general dependence on confinement energy, which is well-fit to a model taking into account the effect of kinetic exchange and band mixing on the exchange parameters.

*Work supported by DARPA, ONR, NSF, and the Fannie and John Hertz Foundation.

[1]R. C. Myers, M. Poggio, N. P. Stern, A. C. Gossard, and D. D. Awschalom, Phys. Rev. Lett. **95**, 017204 (2005).

**9:24**

**G19 6 Controlled placement of Mn acceptors in GaAs (110) surfaces: Crystal orientation and spacing dependences for interactions between Mn acceptors*** DALE KITCHEN, ANTHONY RICHARDELLA, ALI YAZDANI, *Princeton University* We report a controlled incorporation process substituting single Mn atoms into acceptor sites in GaAs (110) surfaces using a low temperature scanning tunneling microscope (STM). The incorporation process brings a Ga atom to the surface as an adsorbate loosely bound to the Mn that has replaced it in the lattice. Displacement of a Ga atom away from the substituted Mn via STM manipulation isolates the Mn atom in the surface layer acceptor configuration. In this acceptor configuration Mn atoms give rise to strong in-gap energy levels, with unusual and detailed spatial structure of highly anisotropic character. Modifications to this in-gap resonance level and its structure occur under controlled placement of two closely spaced Mn acceptors, revealing a striking dependence upon crystal orientation and spacing. For certain pair orientations, strong bonding/antibonding-like interactions split the in-gap level of the single Mn state, while the in-gap levels of other pairs of comparable spacing but different orientation are degenerate with the isolated Mn state.

*This work was supported under the ARO MURI DAAD19-01-1-0541.

**9:36**

**G19 7 Magnetic and Chemical Depth Profiles of an Exchange-Biased MnO/GaMnAs Bilayer** BRIAN KIRBY, *Los Alamos National Laboratory* JULIE BORCHERS, *National Institute of Standards and Technology* JIM RHYNE, MICHAEL FITZSIMMONS, *Los Alamos National Laboratory* XINYU LIU, JACEK FURDYNA, *University of Notre Dame* There is a great deal of interest in development of high Curie temperature (Tc) ferromagnetic (FM) semiconductors for use in spintronic applications. GaMnAs may be a candidate for such applications, as it shows true long range FM order among Mn at Ga sites, and has a relatively high Tc (up to 173 K). For many device applications, the ability to pin the magnetization of a FM semiconductor to a preferred direction is highly desirable. This can be achieved by exchange coupling a GaMnAs layer to an adjacent antiferromagnetic (AFM) layer in order to produce an exchange-bias in the FM layer. We report on polarized neutron reflectivity and x-ray reflectivity studies of a GaMnAs film exchange biased by an AFM MnO overlayer. Using the depth sensitivity of these reflectivity techniques, we have chemically and magnetically characterized the MnO/GaMnAs interface, and have investigated the magnetization reversal process by comparing the magnetic depth profile at the coercive field to the profile at magnetic saturation.

**9:48**

**G19 8 Asymmetric Planar Hall Effect in (Ga,Mn)As/MnO Exchange-Biased Structures** ZHIGUO GE, W. L. LIM, S. SHEN, Y. Y. ZHOU, X. LIU, J. K. FURDYNA, M. DOBROWOLSKA, *Department of Physics, University of Notre Dame, Notre Dame, IN 46556* We report the observation of asymmetric Planar Hall Effect (PHE) in a series of exchange-biased (EB) (Ga,Mn)As/MnO ferromagnetic (FM)/antiferromagnetic (AFM) bilayer structures after field cooling. The process of magnetization reversal was systematically studied by PHE measurements by varying the direction of the in-plane applied magnetic field. The analysis of experiment results based on the Stoner-Wohlfarth model (including domain nucleation and expansion in the FM layer) revealed that two magnetization reversal mechanisms are present in these EB systems due to the exchange coupling between MnO and (Ga,Mn)As: the magnetization reversal undergoes either a full circle or a half circle, depending on the direction of the applied field relative to the cooling field. Our model is confirmed by the close agreement between experimental data and theoretical predictions for the angular dependence of the exchange bias and of the coercive field. Supported by NSF Grant DMR02-45227.

**10:00**

**G19 9 Non-collinear giant magnetoresistance in (Ga,Mn)As/p-GaAs/(Ga,Mn)As trilayers** GANG XIANG, MENG ZHU, BEN LI SHEU, PETER SCHIFFER, NITIN SAMARTH, *Physics Dept., Penn State University, University Park PA 16802* Giant magnetoresistance (GMR) due to spin-dependent scattering has been extensively studied in ferromagnetic metal multilayers. However, the effect has eluded observation in ferromagnetic semiconductor multilayers where other sources of magnetoresistance (MR) are usually dominant. Here, we report the possible observation of GMR in (Ga,Mn)As/p-GaAs/(Ga,Mn)As trilayers. Samples are designed such that the (Ga,Mn)As layers have distinct coercive fields and the p-GaAs spacer layer has a conductivity comparable to the (Ga,Mn)As layers. We measure longitudinal and transverse MR using Hall bars oriented along different crystalline directions and observe signatures consistent with GMR when the relative magnetization orientation in the two (Ga,Mn)As layers switches between collinear and non-collinear arrangements. Our measurements show that these signatures are distinct from other known sources of MR and further suggest that the observed GMR is associated with spin-dependent scattering at interfaces. Supported by DARPA, ONR and NSF.

**10:12**

**G19 10 Magnetic anisotropy of (Ga,Mn)As formed by Mn ion implantation and pulsed-laser melting** Y. J. CHO, Z. GE, Y. Y. ZHOU, X. LIU, M. DOBROWOLSKA, J. K. FURDYNA, *Department of Physics, University of Notre Dame, Notre Dame, IN 46556* M. A. SCARPULLA, O. D. DUBON, *Lawrence Berkeley National Laboratory, Berkeley, CA 94720* We report on the magnetic anisotropy of (Ga,Mn)As formed by Mn ion implantation followed by pulsed-laser melting. Three specimens with different Mn doses have been systematically studied by SQUID magnetometry, magnetotransport and ferromagnetic resonance. The sample corresponding to the lowest Mn dose does not show any measurable magnetic anisotropy. With increasing Mn doses, however, complex magnetic anisotropy behavior clearly emerges. In particular, the high-Mn-dose samples show unambiguous in-plane uniaxial and cubic anisotropy, similar to that observed in (Ga,Mn)As layers grown by LT-MBE. As these samples were produced by a different processing method, this result lends credence to the hypothesis that the in-plane cubic symmetry breaking is intrinsic to the dilute (Ga,Mn)As phase. Furthermore, in contrast to LT-MBE grown (Ga,Mn)As, these specimens show small perpendicular uniaxial anisotropy, which can be interpreted by a small built-in compressive strain due to the absence of Mn interstitials characteristic of these specimens. Finally, we also observe that a super-paramagnetic phase with distinct perpendicular magnetic anisotropy exists in these specimens. An investigation into the origin of this second magnetic phase is in progress.

**10:24**

**G19 11 Gating in ferromagnetic semiconductor*** F. ALTOMARE, A. M. CHANG, *Department of Physics, Duke University, Durham, NC 27708* Y. J. CHO, X. LIU, J. K. FURDYNA, *Department of Physics, University of Notre Dame, Notre Dame, IN 46556* Ferromagnetic semiconductors have the potential of revolutionizing the way current electronic devices work: more so, because they are compatible with current fabrication lines and can easily be integrated with today technology. Particular interest lies in III-V Diluted Magnetic Semiconductor (DMS), where the ferromagnetism is hole-mediated and the Curie temperature can therefore be tuned by changing the concentration of free carriers[1]. In these systems, most of the effort is currently applied toward the fabrication of devices working at room-temperature: this implies high carrier density accompanied by low mobility and short mean free path. We will report our results in exploring devices with low hole concentration and Curie temperature ( $\sim$ 4 K) and we will discuss the effect of local gating[2] in light of possible applications to the fabrication of ferromagnetic quantum dots.

*Research supported in part by NSF DMR-02105191

[1]T. Dietl et al., Phys. Rev. B **63**, 195205 (2001)
[2]H. Ohno et al., Nature **408**, 944 (2000)

**10:36**

**G19 12 Trapping and manipulating magnetic domain walls in patterned (Ga,Mn)As devices** K. F. EID, GANG XIANG, O. MAKSIMOV, A. BALK, N. SAMARTH, *Physics Department and Materials Research Institute, Penn State University, University Park PA 16802.* We report magnetoresistance measurements that probe the trapping and manipulation of magnetic domain walls (DWs) in multi-element (Ga,Mn)As devices that include both vertically patterned (step-etched) microstructures [Yamanouchi et al, Nature 428, 539 (2004)] and laterally-patterned nanostructures. We exploit post-fabrication annealing to yield devices in which different elements have distinct switching fields, thus allowing us to establish stable antiparallel magnetization states separated by single DWs. We then use current pulses to manipulate DWs in these devices, and observe current-induced DW motion in some sample geometries. We describe ongoing efforts to map out the variation of electrically-driven DW motion with factors such as current amplitude, sample temperature and sample geometry. Supported by DARPA/ONR.

**10:48**

**G19 13 2D patterned ferromagnetic semiconductors for planar spintronics** ROUIN FARSHCHI, IAN SHARP, MIKE SCARPULLA, EUGENE HALLER, OSCAR DUBON, *Univ. of California, Berkeley, CA 94720, Berkeley Lab, Berkeley, CA 94720* JEFFREY BEEMAN, *Berkeley Lab, Berkeley, CA 94720* SOONJOO SEO, PAUL EVANS, *Univ. of Wisconsin, Madison, WI 53706* Fabrication of III-Mn-V ferromagnetic semiconductors by way of Mn ion implantation followed by pulsed laser melting (II-PLM) allows for the unique possibility of lateral patterning using optical and e-beam lithography. We have performed II-PLM on resist patterned substrates to create isolated ferromagnetically active $Ga_{1-x}Mn_xAs$ regions embedded in a GaAs substrate. We have prepared a uniform $Ga_{1-x}Mn_xAs$ film as well as a sample patterned with an array of $Mn^+$-implanted 100$\mu$m x 100$\mu$m squares that covers the equivalent of one-quarter the sample. The saturation magnetization of the patterned sample reflects this one-quarter implant area, and both samples display a $T_C$ of $\sim$ 100 K suggesting a similar maximum Mn concentration. The electrical and magnetic properties of this and other lateral structures consisting of sub-micron spaced active regions will be presented. This work was supported by the U.S. Department of Energy under contract No. DE-AC02-05CH11231.



**SESSION G20: FOCUS SESSION: COMPLEX OXIDE THIN FILMS SURFACES AND INTERFACES II: SURFACES AND THEORY**
**Tuesday Morning, 14 March 2006**
**317, Baltimore Convention Center at 8:00**
**Maria Varela, Oak Ridge National Laboratory, presiding**

**8:00**

**G20 1 Loss of Ferromagnetism at the Surface of in-situ cleaved $La_{1.28}Sr_{1.72}Mn_2O_7$** JOHN W. FREELAND, *Advanced Photon Source, Argonne National Laboratory* KEN GRAY, JOHN F. MITCHELL, *Materials Science Division, Argonne National Laboratory* JERALD KAVICH, RICHARD KODAMA, *Dept. of Physics, University of Illinois, Chicago* Instability of surface magnetism in the manganites is currently an area not well understood. In our previous work using exploring loss of ferromagnetic (FM) order at the surfaces of layered manganites, we found clear evidence for an intrinsic insulating non-FM surface layer atop adjacent ferromagnetic subsurface layers. [1] The presence of a non-FM surface layer of one bilayer thickness was observed by x-ray resonant magnetic scattering (XRMS), and point contact tunneling results showed this layer to be insulating. Although that study involved samples cleaved in air, our surface-sensitive spectroscopy indicated they were not chemically degraded. Here we present the XRMS results from samples cleaved under UHV con-

ditions at 75 K. The XRMS shows the same interference effect due to the loss of FM order in the surface layer, thus supporting our earlier claim that the magnetic instability is not related to the preparation conditions. This research was supported by the U.S. Department of Energy, Office of Science, under Contract No. W-31-109-Eng-38. [1] J.W. Freeland, K.E. Gray, L. Ozyuzer, P. Berghuis, Elvira Badica, J. Kavich, H. Zheng and J.F. Mitchell, Nature Materials 4, 62 (2005)

**8:12**

**G20 2 Surface Structural Phases of $Ca_{2-x}Sr_xRuO_4$*** R.G. MOORE, V.B. NASCIMENTO, *Univ of TN, Knoxville, TN 37996* JIANDI ZHANG, *Florida Intl Univ, Miami, FL 33199* ISMAIL NLS, R. JIN, D. MANDRUS, E.W. PLUMMER, *Oak Ridge Natl Lab, Oak Ridge, TN 37831 and Univ of TN, Knoxville, TN 37996* Surface structural phases of $Ca_{2-x}Sr_xRuO_4$ (CSRO) are investigated using Low Energy Electron Diffraction (LEED-IV). The surface structure and phases are compared to the bulk phases in this layered material. Normally at a crystal surface the reduced atomic coordination enhances electron-electron correlations, if there is not a reconstruction, and stabilizes the Mott-insulating phase resulting in higher MIT temperatures than in the bulk. Surprisingly, $Ca_{1.9}Sr_{0.1}RuO_4$ exhibits an unusual surface MIT 20K lower than the bulk. The properties of CSRO are extremely sensitive to the $RuO_6$ octahedral orientation. LEED-IV shows no symmetry change associated with the MIT, but small distortions of the $RuO_6$ octahedral that drive the surface MIT. In addition, the tetragonal-to-orthorhombic surface phase transition near the Quantum Critical Point at $x=0.5$ is investigated and contrasted with the bulk phase transition.

*Work supported jointly by NSF and DOE (DMS) NSF -DMR-0451163, NSF DMR-0346826, U.S. DOE DE-FG02-04ER46125 and by U.S. DOE under Contract No. DE-AC05-00OR22725 with UT-Battelle.

**8:24**

**G20 3 LEED study of TMOs surfaces** V.B. NASCIMENTO, R.G. MOORE, *The Univ of Tennesse, Knoxville, TN 37996* J. RUNDGREN, *Theory of Materials, Phys Dept, Royal Inst of Tech, SE-10691, Stockholm, Sweden* JIANDI ZHANG, LEI CAI, *Florida International Univ., Miami, FL 33199* R. JIN, D. G. MANDRUS, E.W. PLUMMER, *Oak Ridge National Lab, Oak Ridge, TN 37831* In contrast with the case of metals and semiconductors, the final theory-experiment agreement obtained for LEED $I-V$ data for TMOs is generally not very satisfactory. One reason is that the calculations of the phase shifts for metal oxides is not a straightforward procedure due to the charge transfer. In this work we address this issue of phase shift generation for TMOs by determining the structure of the (001) surface of $Ca_{1.5}Sr_{0.5}RuO_4$, a prototype layered TMS system. The adoption of an optimized muffin-tin potential approach, as proposed by Rundgren, has enabled reaching an acceptable final theory-experiment agreement. Our results indicate that the determination of an energy dependent inner potential plays a key role in the final agreement. *Work supported jointly by NSF and DOE (DMS) NSF -DMR-0451163, NSF DMR-0346826 and by U.S. DOE under DE-FG02-04ER46125 and DE-AC05-00OR22725.

**8:36**

**G20 4 Orbital ordering at the surface of the layered manganite $La_{0.5}Sr_{1.5}MnO_4$*** Y. WAKABAYASHI, *Photon Factory, High energy accelerator research organization, Japan and Brookhaven National Lab.* S. GRENIER, M.H. UPTON, J.P. HILL, C.S. NELSON, *Brookhaven National Laboratory* J.F. MITCHELL, *Argonne National Laboratory* J-W. KIM, P.J. RYAN, *Argonne National Laboratory and Ames Laboratory, Iowa State Univ.* A.I. GOLDMAN, *Ames Laboratory, Iowa State Univ.* Surface x-ray diffraction measurements were made on a (001) cleaved surface of the orbitally ordered layered manganite, $La_{0.5}Sr_{1.5}MnO_4$ at X22C and X21 at the NSLS and at 6ID at the APS. The termination of crystal by a surface gives rise to rods of scattered intensity normal to that surface; so-called crystal truncation rods. The intensity distribution along such rods is sensitive to details of the surface order. In principle, similar rods should arise from the surface termination of orbital order. We have successfully observed such orbital truncation rods for the first time. We find that the intensity distribution of the orbital rod has a slightly steeper $L$ dependence than that for the allowed Bragg rods, indicating that the surface roughness of the orbital ordering is larger than the crystallographic roughness. As the transition temperature is approached, this orbital roughness is seen to increase.

*Work supported by Yamada Science Foundation, Support for long-term visit, and US DOE, Basic Energy Sciences at Brookhaven under contract No. DE-AC02-98CH10886 and at Argonne under contract No. W-31-109-Eng-38.

**8:48**

**G20 5 Surface Modification of CMR Perovskite Manganite Thin Films using Atomic Force Microscopy** DAVID SCHAEFER, RAJESWARI KOLAGANI, CAMERON BOLLING, JOHN SUNDERLAND, ANTHONY DAVIDSON III, *Towson University* TYLER BRADLEY, *Towson High School* BONNIE LUDKA, *James Madison University* TOWSON UNIVERSITY TEAM, TOWSON HIGH SCHOOL TEAM, JAMES MADSION UNIVERSITY TEAM, Nanolithography using the atomic force microscope (AFM) is emerging as a promising tool for nanotechnology. We report our results of AFM- induced nanoscale surface modifications in thin films of the CMR manganite material $La_{0.7}Ba_{0.3}MnO_3$. CMR manganite materials have been demonstrated to be useful for a variety of technological applications including magnetic sensors and bolometric infrared detectors. AFM induced surface modifications would enable the realization of such sensors in nanotechnology applications. We have obtained reproducible patterns on these films in the form of nanoscale dots and lines induced by the AFM tip. We have studied these feature dimensions as a function of tip bias voltage, exposure time and humidity. We find that the feature heights are considerably larger on manganite thin film surfaces than those induced on silicon surface under similar conditions. Additionally, the speed of reproducible writing is also found to be significantly higher on the manganite films.

**9:00**

**G20 6 Time-dependent Surface Electronic Structure of $EuB_6$*** J.D. DENLINGER, *Lawrence Berkeley National Lab* F. WANG, J.W. ALLEN, *U. of Michigan* HAN-OH LEE, Z. FISK, B. DELLEY, *Paul Scherrer Institut* R. MONNIER, *ETH-Zürich* J. LOBO-CHECA, T. OKUDA, J. OSTERWALDER, *U. of Zürich* The surface electronic structure of UHV-cleaved divalent hexaboride $EuB_6$ is investigated using angle-resolved photoemission and the time-dependence of the Eu 4d-character X-point electron pocket, B-p band structure and Eu 4f states are characterized. Surface-slab LDA calculations allow identification in the data of a distinct surface-related band residing in the bulk-projected band gap along X-M and energy-shifted surface-atom Eu 4f states re-

sulting from an electric dipole at the highly ionic surface. The X-point electron pocket size is observed to initially increase in size and then recede to zero occupation. Similarly the Eu 4f surface component initially increases in binding energy and then reverses direction and loses intensity. This behavior is explained in terms clustering of mobile surface Eu atoms on the freshly cleaved surface, followed by adsorption of residual gases.

*Supported by the U.S. NSF at U. Mich. (DMR-03-02825) and by the U.S. DOE at the Advanced Light Source (DE-AC03-76SF00098)

**9:12**

**G20 7 Formation and stability of surface oxides and oxide surfaces of the O/Cu system: First-principles investigations** ALOYSIUS SOON, MIRA TODOROVA, *School of Physics, the University of Sydney, Australia* BERNARD DELLEY, *Paul-Scherrer-Institut (PSI)* CATHERINE STAMPFL, *School of Physics, the University of Sydney, Australia* Copper-based catalysts are important for several industrial reactions, e.g., the low-temperature water-gas-shift reaction and for methanol oxidation reactions. Despite this, very little is presently known about the surface structure, about the atomic and molecular processes involved and the associated reaction pathways. As a first step towards a microscopic understanding, we use density-functional theory to investigate chemisorption of oxygen on Cu(111), and the stability of surface oxides and oxide surfaces. Surface oxide structures are found to be energetically favoured over chemisorbed oxygen even at coverages as low as $\frac{1}{16}$ ML. Taking into account the pressure and temperature through the framework of itab initio thermodynamics [1,2] however, shows that for the conditions relevant to technical catalysis, bulk oxide structures are the appropriate ones to consider. Our results are compared to the behavior of other O/transition-metal systems. [1] K. Reuter, C. Stampfl and M. Scheffler, in Handbook of Materials Modeling, Volume 1, Fundamental Models and Methods, Sidney Yip (Ed). [2] C. Stampfl, Catal. Today 105, 17 (2005).

**9:24**

**G20 8 Thermal transport in strongly correlated multilayered nanostructures*** JAMES FREERICKS, *Department of Physics, Georgetown University* VELJKO ZLATIC, *Institute of Physics, Zagreb, Croatia* The formalism for thermal transport in strongly correlated multilayered nanostructures is developed. We employ inhomogeneous dynamical mean-field theory and the Kubo formula to derive relevant thermal transport coefficients, which take the form of matrices with respect to the planar indices. We show how to define the local versions of the current and heat current operators so that heat-current correlation functions can be easily evaluated via the Jonson-Mahan theorem. Thermal transport in nanostructures is complicated by the fact that the thermal current need not be conserved through the device, and a given experimental set-up determines both how the thermal current can change through the device and how the steady-state temperature profile can be determined. Formulae to analyze classic experiments such as the Peltier and Seebeck effects, the thermal conductivity, and for running a thermoelectric cooler or power generator are also discussed.

*Supported by the National Science Foundation under grant number DMR-0210717

**9:36**

**G20 9 Ab Initio Study of Multiferroicity in La(Al,Fe,Cr)$O_3$** ALISON HATT, *Physics Department, UC Santa Barbara* NICOLA SPALDIN, *Materials Department, UC Santa Barbara* We present the results of ab initio density functional calculations of perovskite-structure La(Al,Fe,Cr)$O_3$. Our calculations reveal two structurally distorted ground states of opposite polarization. Motivated by the growth of three-layer superlattices with enhanced polarization, we investigate the ferroelectricity and magnetic ordering of the La(Al,Fe,Cr)$O_3$ system with the goal of finding emergent multiferroicity due to interfacial strain and inversion symmetry breaking. Finally, we investigate constrained tetragonal $LaAlO_3$ to determine its role in the ferroelectric properties of the supercell.

**9:48**

**G20 10 Density-Functional Study of the Two-Dimensional Electron Gas at the Perovskite Titanate Interface*** RANJIT NANDA, ZORAN POPOVIC, SUNITA THULASI, SASHI SATPATHY, *University of Missouri* Oxide superlattices and microstructures hold the promise for creating a new class of devices with unprecedented functionalities. Density-functional studies[1] of the recently fabricated, lattice-matched perovskite titanates[2] $(SrTiO_3)_n/(LaTiO_3)_m$ reveal a classic wedge-shaped potential well for the monolayer structure, originating from the Coulomb potential of a charged La sheet. The potential in turn confines the electrons in the Airy-function-localized states. This resulting two-dimensional electron gas may be described in terms of the simplified jellium model[3] and it describes reasonably well the observed charge modulation of the Ti atoms near the interface. Concerning magnetism, it is suppressed for the monolayer $LaTiO_3$ structure, while in structures with a thicker $LaTiO_3$ part, bulk antiferromagnetism is recovered, with a narrow transition region separating the magnetic $LaTiO_3$ and the non-magnetic $SrTiO_3$. 1. Z. S. Popovic and S. Satpathy, Phys. Rev. Lett. 94, 176805 (2005) 2. A. Ohtomo et al., Nature 419, 378 (2002) 3. S. Thulasi and S. Satpathy, Phys. Rev. B (2006)

*Supported by DOE

**10:00**

**G20 11 Lattice relaxation, electronic screening, and spin and orbital phase diagram of $LaTiO_3/SrTiO_3$ superlattices** SATOSHI OKAMOTO, ANDREW MILLIS, *Department of Physics, Columbia University* NICOLA SPALDIN, *Materials Department, University of California, Santa Barbara* The effect of lattice relaxation on the electronic charge density, band structure, and phase diagram in oxide heterostructure, $LaTiO_3/SrTiO_3$ superlattices, the structure grown and measured by Ohtomo *et al.*[1], is investigated using density functional theory LDA and LDA+$U$ (VASP implementation). We observe substantial ferroelectric-like distortion of $TiO_6$ octahedra at the nearest-to-La region which screens the electrostatic force originating from $La^{3+}$ ion reducing the charge density in the La-rich region. We determine the changes in the low energy electronic Hamiltonian caused by the lattice relaxation and investigate the consequences for the ground state phase diagram using the Hartree-Fock approximation. Finally, we present a detailed comparison with previous calculations which neglected the lattice effect. [2] Support from DOE ER 46169. [1] Ohtomo et al., Nature **419**, 378 (2002). [2] Okamoto and Millis, Nature (London) **428**, 630 (2004), and Phys. Rev. B **70**, 195120 (2004).

**10:12**
**G20 12 Total energy calculations for magnetic $La_{2/3}S_{1/3}rMnO_3/SrRuO_3$ bilayers** YONGBIN LEE, BENJAMIN CAES, BRUCE HARMON, *Ames Laboratory US DOE* . Recently positive exchange bias was reported for ferromagnetic $La_{2/3}Sr_{1/3}MnO_3/SrRuO_3$ (LSMO/SRO) bilayers which indicated anti-ferromagnetic exchange interaction across the interface [1]. To address the physical origin of this anti-ferromagnetic exchange interaction, we have performed first principles calculations with both ferro, and anti-ferromagnetic interface structures. We have found that the anti-ferromagnetic interface is preferred to ferromagnetic case energetically. The calculations indicate the interfacial O 2p orbitals and their interaction with Mn, Ru spin polarized 3d orbitals are critical for this anti-ferromagnetic interface preference. In this talk, we will discuss the total energy calculations with various magnetic structures near the interface. [1] X. Ke et al. Appl. Phys. Lett. **84**, 5458 (2004)

**10:24**
**G20 13 Electronic and magnetic properties of Mn/Si superlattices*** C.Y. FONG, MEI QIAN, KAI LIU, *Department of Physics, UC Davis* We recently predicted a monolayer of Mn doped in 31 layers of Si, a Mn/Si digital ferromagnetic heterostructure, is a half metal. [1] In order to explore the possibility of realizing large magnetoresistance effect, we extend our studies to superlattices composed of periodically embedded monolayers of Mn in Si. By using a first-principles algorithm, we determine whether a superlattice can exhibit half metallic behavior. We then investigate the dependence of the half metallic properties on the thickness of the Si spacer. The energetics of the ferromagnetic and antiferromagnetic phases will be compared for each half metal. For the minimum Si spacer, the band structure near the Fermi energy of the superlattice showing half metallic properties will be given. We also analyze the character of the states at the Fermi energy as well as the associated Fermi surface. [1] M. C. Qian, et al. to appear in Phys. Rev. Lett.; cond- mat/0508269.

*Supported in part by NSF grant: ESC-6225007 and the Sloan Foundation

**10:36**
**G20 14 Electrostatic Interface Tuning in Correlated Superconducting Heterostructures*** NATALIA PAVLENKO, THILO KOPP, *Institute of Physics, Center for Electronic Correlations and Magnetism, University of Augsburg* EP VI TEAM, In high-temperature superconducting oxide films, transverse electric fields have been used to switch between superconducting and insulating states by electrostatically tuning the free carrier density. We analyze d-wave pairing within a microscopic model for heterogeneous multilayer systems and show that a coupling to electric dipoles and phonons at the interface of cuprate film and dielectric gate localizes the injected charge and leads to a superconductor-insulator transition [1]. We find that in the correlated oxide films, the strong interface polaron effect is inherently related to the stabilization of interface charge ordering and inhomogeneous states. The formation of such states results in a dramatic modification of the doping dependent phase diagram close to and above the optimal doping which is expected to shed light on recent electric field-effect experiments with HTSC cuprates. [1] N. Pavlenko and T. Kopp, Phys. Rev. B, in print (2005).

*This work has been supported through the DFG SFB-484, BMBF 13N6918A, and DAAD D/03/36760.

**10:48**
**G20 15 Quartet formation at (100)/(110) interfaces of d-wave superconductors*** ARNO KAMPF, *University of Augsburg* ARMANDO ALIGIA, *Centro Atomico Bariloche* JOCHEN MANNHART, *University of Augsburg* Across a faceted (100)/(110) interface between two $d_{x^2-y^2}$-superconductors the structure of the superconducting order parameter leads to an alternating sign of the local Josephson coupling. Describing the Cooper pair motion along and across the interface by a one-dimensional boson lattice model, we show that a small attractive interaction between the bosons strongly enhances their binding at the interface. As a consequence we propose that electrons tunnel in quartets across an interface with a staggered sequence of 0- and $\pi$-junction contacts. We connect this finding to the recently observed $h/4e$ oscillations in bicrystalline (100)/(110) SQUIDs of cuprate superconductors.

*Work supported by the DFG through SFB 484

## SESSION G21: COLLOIDS IV: POLYMERIC AND COLLOID-POLYMER SYSTEMS
**Tuesday Morning, 14 March 2006**
**318, Baltimore Convention Center at 8:00**
**Cynthia Olson Reichhardt, Los Alamos National Laboratory, presiding**

**8:00**
**G21 1 Self Assembly of Temperature-Sensitive Capsules using PNIPAm Microspheres*** D. B. LAWRENCE, *University of Massachusetts Amherst Physics* T. CAI, Z. B. HU, *University of North Texas* M. MARQUEZ, *INEST Group, Phillip Morris USA* A. D. DINSMORE, *University of Massachusetts Amherst Physics* We present a method for self assembly of novel semi-permeable capsules (colloidosomes) exhibiting temperature-dependent size and surface properties. These hollow micro-capsules are composed of micron-sized PNIPAm-co-acrylic acid particles that exhibit a reversible size transition at $32^oC$. The PNIPAm particles self-assemble at the spherical interface between 2-Octanol and water droplets. Electrostatic cross-linking with the di-block copolymer Poly(butadiene-b-N-methyl 4-vinyl pyridinium iodide) locks the particles in place, forming a rigid, elastic membrane that remains after the 2-Octanol/Water interface is removed. Such self-assembled capsules retain the temperature sensitivity of the PNIPAm particles from which they are constructed, and exhibit reversible size transitions. Controlled variation of the permeability and potential applications in controlled release will be discussed.

*We acknowledge support from the Kraft Foods, Inc. NanoteK consortium.

**8:12**
**G21 2 Femtonewton Measurements of Polymer-Mediated Colloidal Interaction** SVEN BEHRENS, *BASF* HELMUT AUWETER, *BASF* The stability of colloidal dispersions hinges on the repulsive interaction between the particle surfaces. This interaction can be modified by adsorbed polymer and further tuned by the response of the adsorbate layer to changes in the surrounding solution.Total internal reflection microscopy has been used in this study to investigate the effect of charged and neutral polymer

adsorbates on the interaction of a colloidal particle with a flat substrate. The results were correlated with light scattering studies of the employed polymers in solution and of polymer-coated particles; they reveal a subtle interplay of steric, electrostatic, and van der Waals forces.

**8:24**

**G21 3 Phase Behavior of Charged Colloid-Polymer Mixtures: A Simulation Study*** BEN LU, ALAN R. DENTON, *Department of Physics, North Dakota State University* We present a Monte Carlo simulation study of mixtures of charged colloids and nonadsorbing polymers. The multicomponent mixture of colloidal macroions, microions (counterions and salt ions), polymers, and solvent is modeled as an effective two-component mixture of pseudomacroions and neutral polymers. The pseudomacroions are assumed to interact via effective electrostatic interactions[1] (screened-Coulomb pair potential and one-body volume energy) and the polymers are treated as effective spheres that have hard interactions with the colloids but are mutually ideal. Previous studies have identified the volume energy as the driving force for phase separation of deionized colloidal suspensions[2] and polymer depletion-induced attraction as the origin of colloid-polymer demixing. Here we apply the Gibbs ensemble Monte Carlo method to the effective binary mixture to examine the combined influences of electrostatic and depletion-induced interactions on phase behavior.

*Support from the National Science Foundation (grant DMR-0204020) is gratefully acknowledged.

[1]A. R. Denton, *Phys. Rev.* E **62**, 3855 (2000).
[2]R. van Roij, M. Dijkstra, and J.-P. Hansen, *Phys. Rev.* E **59**, 2010 (1999); P. B. Warren, *J. Chem. Phys.* **112**, 4683 (2000).

**8:36**

**G21 4 Demixing of Charged Colloid-Polymer Mixtures: Variational Theory[1]** SHRIKANT SHENOY, ALAN R. DENTON, *Dept. of Physics, North Dakota State University* We investigate thermodynamic phase behavior of mixtures of charged colloids and neutral nonadsorbing polymers using a variational method for the free energy. The mixture of macroions, microions, and solvent is first mapped onto an effective one-component system of pseudomacroions that interact via effective electrostatic interactions. The polymers are modeled as effective spheres that have hard interactions with the colloids but are mutually ideal. The charged colloid-polymer mixture is then mapped onto an Asakura-Oosawa model with effective colloid and polymer diameters[2]. The free energy is approximated by combining thermodynamic perturbation theory for the colloids with free-volume theory for the polymers and minimizing with respect to the effective colloid diameter. Phase diagrams are computed by a coexistence analysis that ensures equality of pressures and of chemical potentials of all species in the two phases. The resultant phase behavior depends sensitively on colloid charge, polymer-to-colloid size ratio, and composition. Electrostatic repulsion between colloids is found to stabilize the mixture against polymer depletion-induced demixing, consistent with previous predictions[3] and experimental observations. [1]Support from the National Science Foundation (grant DMR-0204020) is gratefully acknowledged. [2]A. R. Denton and M. Schmidt, *J. Chem. Phys.* **122**, 2449111 (2005).

**8:48**

**G21 5 Preparation of PHSA-PMMA stabilizer for model hard sphere systems** ANDREW HOLLINGSWORTH, *New York University* WILLIAM RUSSEL, *Princeton University* CARLOS VAN KATS, ALFONS VAN BLAADEREN, *Utrecht University* Sterically-stabilized colloidal particles are an excellent model hard-sphere system used by many groups. One of the original stabilizers used for such systems was developed and patented by ICI more than 30 years ago. It consists of a 'comb-like' stabilizer of a poly(12-hydroxystearic acid) which is soluble in aliphatic hydrocarbons. These pendant PHSA chains are grafted to an insoluble poly(methyl methacrylate) backbone that strongly adsorbs to polymer particles and thus provides a means of anchoring stabilizer to particle surfaces. Unfortunately, the PHSA-g-PMMA stabilizer is not commercially available. Furthermore, the three-step procedure (Antl, et al. 1986) is generally regarded by non-chemists as technique intensive and time-consuming. We have systematically studied the PHSA-PMMA stabilizer synthesis with the goal of taking the mystery out of the protocol and making the entire synthesis reproducible. Several important details, not published in the literature, will be discussed, along with the analytical results from mass spectroscopy, proton NMR, acid titration and gel permeation chromatography, all of which were used to characterize the polymer and its precursors.

**9:00**

**G21 6 Self-assembly of Asphaltenes: Enthalpy, Entropy of Depletion and Dynamics at Crossover I-experimental** NATALIA LISITZA, DENISE FREED, PABITRA SEN, YI-QIAO SONG, *Schlumberger-Doll Research* The continuous rise of global demand for energy and the difficulty of significantly increasing production have driven the petroleum industry to develop much more difficult oil reservoirs, such as deep-water fields. Asphaltenes, naturally-occurring large aromatic molecules in crude oils, are known to be the ''cholesterol'' of petroleum because they self-associate to form solid aggregates and eventually clog the production pipes and the rocks. An extraordinary amount of work using many analytical techniques has been applied to elucidate the properties of asphaltenes. However, many fundamental issues, such as the molecular architecture and the aggregation mechanisms, are still in debate. Here we use NMR to detect asphaltene aggregation in toluene solutions and to obtain both the enthalpy and entropy of this process. We observe an abrupt drop of the asphaltene diffusion constant which is indicative of a molecular conformation (shape) change. This change is intimately related to or possibly a prerequisite of the aggregation. The entropy of aggregation was found to be positive due to the excluded volume effect for the solvent. This is reminiscent of the depletion entropy force, which is considered to be the driving force for the aggregation of much large artificial nanoparticles.

**9:12**

**G21 7 Self-assembly of Asphaltenes: Enthalpy, Entropy of Depletion and Dynamics at Crossover II - theoretical** DENISE FREED, NATALIA LISITZA, PABITRA SEN, YI-QIAO SONG, *Schlumberger-Doll Research* NMR spin-relaxation is directly sensitive to molecular dynamics and is therefore an excellent tool for studying the formation of nano-aggregates. When aggregates form, the molecular rotations are slowed down, and the spin-relaxation rate is enhanced, which reduces the NMR signal. This gives rises to a remarkable kink in the NMR signal intensity at the Critical Nano-Aggregate Concentration (CNAC). In this talk, we use Debye's two-state model for micelle formation to describe

asphaltene aggregation. We use the temperature dependence of the CNAC to determinate the enthalpy and entropy of aggregation. The enthalpy is negative, as expected, and indicates that the aggregate formation is energetically favorable due to $\pi$-stacking interactions. On the other hand, we find that the entropy is positive, which is quite a surprise. We propose that this increase comes from the depletion entropy of the solvent. As asphaltene molecules aggregate, the free volume available for the solvent molecules increases, giving rise to a depletion effect. An estimate of the depletion entropy from the sizes of asphaltene and toluene (solvent) is very close to the measured entropy gain. We will also discuss the applicability of Debye's two-state model to aggregate formation in asphaltene solutions.

**9:24**

**G21 8 Molecular Diffusivities of Asphaltene Monomers by Fluorescent Correlation Spectroscopy** BALLARD ANDREWS, *Schlumberger-Doll Research* RODRIGO GUERRA, *Harvard University* PABITRA SEN, *Schlumberger-Doll Research* OLIVER MULLINS, *Schlumberger-Doll Research* Many analytical techniques have been applied to elucidate the properties of asphaltenes due to their extraordinary importance in the petroleum industry. However, many fundamental issues such as the molecular size are still in debate. Using Fluorescence Correlation Spectroscopy (FCS) we measure the translational diffusion coefficient of asphaltene molecules in toluene at extremely low dilutions. To avoid focal volume artifacts common in FCS we use a scaling procedure to determine asphaltene diffusivities relative to known molecules such as porphyrins, perylene and quantum dots. We estimate a diffusion coefficient for the asphaltene molecules of 0.3, $10^{-5}$ $cm^2$/sec at room temperature. This value agrees with recent estimates from NMR studied at 10-100 fold higher concentrations. The Stokes-Einstein equation implies that the unaggregated hydrodynamic diameter of asphaltene monomers is 15-25 Å.

**9:36**

**G21 9 Novel emulsions stabilized by pH and temperature sensitive microgels** TO NGAI, *The Chinese University of Hong Kong* HELMUT AUWETER, *BASF* SVEN BEHRENS, *BASF* Poly(N-isopropylacrylamide-co-methacrylic acid) (PNIPAM-MAA) microgel particles in aqueous solution exhibit a volume phase transition that can be induced by changes of either pH or temperature. In the swollen state, these microgels self-assemble at an octanol-water interface and can be used to stabilize surfactant-free oil-in-water emulsions. This stabilizing efficiency is retained even in the collapsed state, provided that the microgels are fully charged. At very low charge (low pH), on the other hand, the microgels migrate completely into the oil phase, and the emulsion breaks. In an intermediate regime of practical interest the emulsion stability can be tuned by small adjustments of pH or temperature. Because of this unprecedented stability control, we believe that such stimulus-responsive charged microgels have a great potential for applications in the field of cosmetic or pharmaceutical formulations. Conceptually they belong to a new class of emulsifiers combining properties of both classical surfactants and solid particles.

**9:48**

**G21 10 Internal Dynamics of Double Emulsion Creams and Polymer-Dispersed Complex Droplets** HU GANG, *Hong Kong Baptist University* The availability of monodisperse double emulsions allows for detailed study of their stability and rheological properties. Practical use of double emulsions concerns the structure and structural evolution of the complex droplets. The usually achievable size of the complex droplets ranges from a micrometer to tens of micrometers. To obtain a homogeneous system, a double emulsion has to be in the form of cream or gel to avoid macroscopic phase separation. However, immobilizing the double emulsion drops does not cease the full dynamics since the internal smaller droplets are also subject to thermal agitation. The ability to track the evolution of the internal encapsulated phase is essential to the understanding of the kinetic stability of a new formulation. Conventional light scattering encounters significant difficulties to probe the structure of concentrated emulsions while diffusing-wave spectroscopy (DWS) shows a unique advantage. We prepare monodisperse W/O/W double emulsions and apply DWS to study the structure of double emulsion creams and gels. We also test the sensitivity of DWS when the amount of encapsulated phase is varied by induced coalescence or osmotic gradient.

**10:00**

**G21 11 Quasi-two-dimensional equilibrium and non-equilibrium thermodynamics of thin liquid films stabilized by colloidal particles*** JERZY BLAWZDZIEWICZ, *Yale University* ELIGIUSZ WAJNRYB, *IPPT, Warsaw, Poland* Due to the presence of oscillatory structural forces, static and dynamic properties of thin liquid films stabilized by colloidal particles, micelles, or macromolecules differ from the properties of particle-free films. During drainage process, particle-stabilized films often form a stepwise structure with coexisting regions (phases) of uniform but different thickness. We describe film phase equilibria using a quasi-two dimensional thermodynamic formalism. The key quantity in our approach is the film tension. We show that the particle contribution to this quantity results from the anisotropy of the particle osmotic-pressure tensor in the film. The quasi-2d description is also developed for non-equilibrium film states. We show that the motion of particle-stabilized films is analogous to the dynamics of a two-dimensional compressible fluid - the film thickness plays the role of mass density per unit area and film tension the role of pressure. In the linear-response regime, the film dynamics is characterized by the shear and extension viscosity coefficients. There are also two independent kinetic coefficients relating the particle flux to the gradients of the normal osmotic pressure and particle chemical potential. For a film stabilized by a suspension of hard spheres we have calculated these coefficients using a multipolar-expansion methods combined with a flow reflection technique.

*Supported by NASA grant NAG3-2704 and NSF grant CTS-0348175

**10:12**

**G21 12 Dynamics, Rectification, and Fractionation for Colloids on Flashing Substrates** ANDRAS LIBAL, *University of Notre Dame* CHARLES REICHHARDT, *Los Alamos National Laboratory* BOLDIZSAR JANKO, *University of Notre Dame* CYNTHIA OLSON REICHHARDT, *Los Alamos National Laboratory* We show that a rich variety of dynamic phases can be realized for mono- and bidisperse mixtures of interacting colloids under the influence of a symmetric flashing periodic substrate. These type of substrates have been attracting growing interest due to recent experimental breakthroughs that allow the creation of dynamic periodic arrays using optical and holographic techniques. With the addition of dc or ac drives, these system show phase locking, jamming, and new types of ratchet effects. We studied these effects in detail. The ratchet effect can be used for charge

separation of a bidisperse system. In this system, in some regimes we find that the addition of a non-rathceting species increases the velocity of the ratcheting particles. We show that these effects occur due to the collective interactions of colloids.

**10:24**
**G21 13 Formation of Extended Optical Traps by Shape-Phase Modulation - Measuring Inter-Colloidal Interactions in Tailored Potential Landscapes** YOHAI ROICHMAN, DAVID G. GRIER, *Soft Matter Research Center, Physics dept., New York* We describe methods for projecting holographic optical traps whose potential energy wells are extended along specified curves, typically a straight line, and whose intensity profiles also can be tailored. This class of optical traps is useful for manipulating elongated nano-items, creating anisotropic potential energy landscapes, and in particular for investigating the interactions and dynamics of micro-particles in reduced dimensionality. This new class of extended optical traps is created by modulating the shape and the phase of a complex hologram, projected by a phase-only diffractive optical element. We demonstrate rapid characterization of extended traps' potential wells through digital video microscopy of trapped colloidal spheres, and use arrays of calibrated traps for efficient measurement and screening of colloidal interactions.

**10:36**
**G21 14 Holographically Assembled Photonic Quasicrystals** YAEL ROICHMAN, DAVID G. GRIER, *New York University* Recently, the photonic band structure of a centimeter-scale three-dimensional icosahedral quasicrystal was measured in the microwave region and shown to feature prominent photonic band gaps at the effective Brillouin zone boundary. We demonstrate that similar two- and three-dimensional quasicrystalline photonic structures can be assembled from micrometer-scale colloidal particles through dynamic holographic optical trapping. The resulting colloidal heterostructures feature lengthscales appropriate for photonic bandgap applications at visible wavelengths, and can include specifically engineered defects such as vacancies, active centers and waveguides.

**10:48**
**G21 15 The Intermediate Scattering Function in Fluorescence Correlation Spectroscopy** RODRIGO GUERRA, *Harvard* BALLARD ANDREWS, PABITRA SEN, *Schlumberger-Doll Research* We formulate the autocorrelation function for Fluorescence Correlation Spectroscopy (FCS) $G_D(\tau)$ in reciprocal space in terms of the of the Intermediate Scattering Function ISF($\vec{k}$,$t$) and the fourier transform of the Optical Response Function ORF($\vec{k}$). In this way we may extend the use of FCS to processes that have been studied using NMR, DLS, and neutron scattering. This formalism is useful for the complicated propagators involved in confined systems and in the study of diffusion in cells: where diffusion is either restricted or permeation through membrane is important. Calculations in k-space produce approximate expressions for the ORF using cumulant expansions that are accurate for small wavevectors. This provides descriptions for longer timescales better suited for studying time-dependent diffusion $ISF([** overrightarrow **] k,t) \rightarrow exp[ - tD(t)k^2]$ and provides a natural separation of contributions from system dynamics and from optical artifacts and aberrations. We will show an explicit derivation of a semi-analytical fit function for free diffusion based on standard electromagnetic analysis of a confocal optical apparatus. This fit function is then used to analyze a representative data set and has no free fit parameters other than the diffusion constant.

## SESSION G22: FOCUS SESSION: MAGNETIC NANOPARTICLES I
**Tuesday Morning, 14 March 2006**
**319, Baltimore Convention Center at 8:00**
**Hariharan Srikanth, University of South Florida, presiding**

***Contributed Papers***

**8:00**
**G22 1 Monte Carlo study of transverse susceptibility in ordered arrays of magnetic nanoparticles*** DIMITRIS KECHRAKOS, KALLIOPI TROHIDOU, *Institute of Materials Science, NCSR Demokritos, 15310 Athens, GR* We present Monte Carlo simulations of the field-dependent reversible transverse susceptibility (RTS) for a hexagonal array of dipolar interacting magnetic nanoparticles with random anisotropy. The thermal evolution of the RTS curves exhibits three distinct temperatures that indicate the merge of the coercive to the anisotropy peak ($T_{sw}$), the crossover from double-peak to single-peak behavior ($T_{cross}$) and the transition to the superparamagnetic state ($T_b$), successively. Above $T_{cross}$ the array exhibits positive spin correlations attributed solely to dipolar interactions. With decreasing interparticle spacing, the anisotropy peak shifts to lower (or higher) values for in-plane (or off-plane) bias-field and the coercive peak merges to the anisotropy peak indicating a transition to collective reversal of the moments. Our results are in agreement with recent RTS measurements in self-assembled Fe nanoparticles.

*Work supported by EC contract No G4NMP4-CP-2004-013545 (NANOSPIN).

**8:12**
**G22 2 Railroading cells, microfluidic magnetic cell separation using ferromagnetic stripes** DAVID INGLIS, *Princeton Institute for the Science and Technology of Materials, Princeton University* ROBERT AUSTIN, *Princeton Universiy Dept. of Physics* JAMES STURM, *Princeton Institute for the Science and Technology of Materials, Princeton University* Magnetic cell separation has been demonstrated using recessed ferromagnetic stripes. Here we demonstrate precise control of the cell's positions using branched magnetic stripes in a microfluidic device. The technique allows magnetically separated cells to be delivered in precise locations to downstream cellular analysis components.

**8:24**
**G22 3 Directed self-assembly and detection of iron oxide nanoparticles on an InAs quantum well micro-Hall sensor** P. MANANDHAR, G. MIHAJLOVIC, W. SETYAWAN, S. VON MOLNAR, P. XIONG, *MARTECH & Dept of Phys, Florida State University* S. HONG, *Physics and NANO Systems Institute, Seoul National University* D. MAGANA, G. F. STROUSE, *Dept of Chem and Biochem, Florida State University* K. OHTANI, H. OHNO, *Laboratory for Nanoelectronics and Spintronics, Research Institute of Electrical Communication, Tohoku University* M. FIELD, G. J. SULLIVAN, *Rockwell Scientific Company LLC* Biosensors based on magnetic detection of superparamagnetic nanoparticles have potential in many bioanalysis and biomedical applications. An important step towards this goal is to assemble magnetic nanoparticles precisely on a sensing device and detect them. Here we demonstrate directed self-assembly of superparamagnetic iron oxide nanoparticles onto a micron or sub-micron sized semiconductor Hall sensor and their detection at room temperature using Hall magnetometry. Hall devices were fabricated from MBE grown InAs quantum well heterostructures using lithographical methods. Organic molecular templates were created on Au coated active Hall cross regions using dip pen nanolithography (DPN) with 16- mercaptohexadecanoic acid (MHA). Magnetic nanoparticles were then assembled specifically onto the MHA regions and characterized by detecting stray magnetic fields emanating from the nanoparticles in the presence of a magnetizing field by using phase sensitive Hall magnetometry. *This work has been supported by NSF NIRT grant ECS-0210332.

***Invited Papers***

**8:36**
**G22 4 Biomedical Applications of Magnetic Nanoparticles and Fluids.***
DIANDRA LESLIE-PELECKY, *University of Nebraska - Lincoln*

Nanomaterials play an increasingly important role in the research, diagnosis and treatment of numerous pathologies. Biomedical applications such as drug delivery, magnetic resonance imaging and hyperthermia require magnetic nanoparticles with a large saturation magnetization that are biocompatible, form stable suspensions in water-based fluids, and can be functionalized. We use chemical synthesis and inert-gas condensation into fluids to produce biocompatible magnetic nanoparticle fluids that allow magnetic targeting of drugs and simultaneous magnetic resonance imaging. We have developed a water-dispersible oleic-acid/Pluronic/iron-oxide nanoparticle formulation that can be loaded with high doses of water-insoluble anti-cancer drugs. An external magnetic field is used to attract the nanoparticles to the treatment region and MRI is used to verify their location. A primary limitation on magnetic targeting, however, is the low moment of iron-oxide nanoparticles. Inert-gas-condensation into fluids produces iron and cobalt nanoparticles from 5-45 nm in diameter. Coating or passivation of these materials is required to prevent oxidation; however, the interaction between surface atoms and surfactant or other functionalizing molecules can greatly diminish the magnetic moment. A study of surfactant interactions with iron nanoparticles shows that the physical barrier provided by a concentric shell of polymeric surfactant offers significantly more protection against oxidation than the radial barrier formed by most linear surfactants. The talk will conclude with a brief overview of the opportunities and challenges for condensed matter and materials physicists in biomagnetic materials. This work is done in collaboration with V. Labhasetwar and T. Jain at the University of Nebraska Medical Center, and Marco Morales, Nguyen Hai, Shannon Fritz, Kishore Sreenivasan and David Schmitter at the University of Nebraska – Lincoln.

*This work was supported by the National Science Foundation MRSEC program and the Nebraska Research Initiative.

***Contributed Papers***

**9:12**
**G22 5 Neutron diffraction studies of exchange-biased Co/CoO core-shell nanoparticles** SUE INDERHEES, GLENN STRYCKER, MEIGAN ARONSON, *University of Michigan* YIMING QIU, JULIE BORCHERS, *NIST* YADONG YIN, *Lawrence Berkeley National Lab* We present neutron diffraction data on exchange-biased Co/CoO core-shell nanoparticles. Surfactant-coated Co particles were prepared by thermal decomposition of $Co_2(CO)_8$, then oxidized to form core/shell particles with a polycrytalline CoO shell. Magnetization data display strong exchange bias below the 200K blocking temperature ($T_B$), well below the Neel temperature of bulk CoO (293 K). Neutron diffraction data show a broad peak at the (1/2 1/2 1/2) antiferromagnetic CoO ordering wave vector. The anti-ferromagnetic order parameter is constant below $T_B$, and decreases with increasing temperature above $T_B$. These results demonstrate that the diminished $T_B$ in small core/shell particles is not due to a reduction of $T_N$ of the antiferromagnetic shell.

**9:24**
**G22 6 Characterization of Epsilon-Co Nanoparticles with Thin Oxide Shells** KATHRYN KRYCKA, *State Univ. of New York, Stony Brook 11794* CHI-CHANG KAO, *National Synchrotron Light Source, BNL, New York 11973* SARA MAJETICH, MADHUR SACHAN, *Dept.of Physics, Carnegie Mellon University, Pittsburgh, Pennsylvania 15213* In order to fully understand the magnetism of nanosystems it is often necessary to characterize an unavoidable thin magnetic metal-oxide shell. This is particularly challenging when the system is comprised of self-assembled nanoparticles that can neither be treated as fully ordered nor randomly distributed, as was the case for our sample which coherently close packs in regions on the micron scale. X-ray powder diffraction was used to determine that the phase of the shell was cobalt monoxide while the core remained epsilon-Co. TEM showed that the particles were spherical with an average diameter of 7 nm [1], and using small angle x-ray diffraction the nearest neighbor distance was placed at 10.3 nm. Anomalous small angle

scattering taken at several energies about the Co k-edge was used to separate the contributions of the metallic cores, metal-oxide shells, and nanoparticle packing. From this experiment radial sizes were determined for both core and shell, the details of which will be presented. 1. ''Interaction effects within Langmuir Layers and three-dimensional arrays of epsilon-Co Nanoparticles'' (in press to J. Appl. Phys.)

**9:36**

**G22 7 Inelastic Neutron Scattering on Exchange-Biased Co/CoO Core-Shell Nanoparticles** GLENN STRYCKER, SUE INDERHEES, MEIGAN ARONSON, *University of Michigan* YIMING QIU, JULIE BORCHERS, *NIST* We report results of inelastic neutron scattering on exchange biased Co/CoO core-shell nanoparticles. Data were taken using time-of-flight techniques at the Disk Chopper Spectrometer (DCS) at the NIST Center for Neutron Research, which allows observation of the dynamics of magnetic spin reversal over a range of energies and length scales. Above the blocking temperature ($T_B$) the scattering is quasi-elastic, with an amplitude that peaks at the (1/2 1/2 1/2) antiferromagnetic CoO ordering wave vector. With decreasing temperature the quasi-elastic scattering narrows, consistent with the freezing of longitudinal moment fluctuations, and becomes resolution limited near $T_B$. Below $T_B$ we observe a spectrum of inelastic excitations arising from a log-normal distribution of energy barriers. We will discuss in detail the length scale and temperature dependences of these features. Work at the University of Michigan performed under the auspices of the Department of Energy.

**9:48**

**G22 8 Effect of dipolar interactions on the magnetization of a cubic array of nanomagnets*** MARISOL ALCANTARA ORTIGOZA, TALAT S. RAHMAN, RICHARD A. KLEMM, *Department of Physics, Kansas State University, Manhattan, KS 66506* We investigated the effect of intermolecular dipolar interactions on an ensemble of 100 3D-systems of $5 \times 5 \times 4$ nanomagnets, each with spin $S = 5$, arranged in a cubic lattice. We employed the Landau-Lifshitz-Gilbert equation to solve for the magnetization curves for several values of the damping constant, the induction sweep rate, the lattice constant, the temperature, and the magnetic anisotropy. The dependencies of the magnetic hysteresis curves on these parameters will be presented. We also reproduce and test a previously reported magnetization curve for a 2D-system [M. Kayali and W. Saslow, Phys. Rev. B **70**, 174404 (2004)]. Although in 3D systems, dipole-dipole interactions generally diminish the hysteresis, in two- dimensional systems, they strongly enhance it. For both square two- dimensional and rectangular three-dimensional lattices with $\boldsymbol{B}||(\hat{\boldsymbol{x}} + \hat{\boldsymbol{y}})$, dipole-dipole interactions can cause large jumps in the magnetization. New results including the low-temperature quantum effects appropriate for single molecule magnets will be presented.

*This work was supported in part by the NSF under Grant No. NER-0304665

**10:00**

**G22 9 Synthesis and Characterization of Magnetic Alloy Nanowire Arrays** M. PADI, S. TALAPATRA, *Rensselaer Nanotechnology Center and Department of MS&E, Rensselaer Polytechnic Institute, Troy NY.* X. TANG, *Department of Physics, Rensselaer Polytechnic Institute, Troy,NY 12180* T. KIM, R. VAJTAI, *Rensselaer Nanotechnology Center, Rensselaer Polytechnic Institute, Troy NY.* G.V.S. SASTRY, *Department of Metallugy, Banaras Hindu University, Varanasi, India* M. SHIMA, P. AJAYAN, *Rensselaer Nanotechnology Center and Department of MS&E, Rensselaer Polytechnic Institute, Troy NY.* We report the synthesis and characterization of ordered arrays of cobalt-nickel alloy nanowires electrodeposited into the pores of anodic alumina templates (AAO). Controlled diameters, lengths and compositions of these alloys were obtained by varying the pore sizes and electro-deposition conditions. The structural and magnetic properties of the samples were investigated using scanning electron microscopy (SEM), energy dispersive X-ray spectroscopy (EDS), transmission electron microscopy (TEM) and vibrating sample magnetometer (VSM). We also present the effect of the compositional ratio of cobalt and nickel on the magnetic properties of the nanowires.

**10:12**

**G22 10 CoPt Nanowires by Electrodeposition*** HAFSA KHURSHID, Y. HUANG, G.C. HADJIPANAYIS, *Department of Physics, University of Delaware, Newark, DE, 19716* CoPt nanoparticles with $L1_0$structure have been studied as a promising material for high density magnetic recording due to the high anisotropy value of the $L1_0$ phase ($K=2x10^7$ ergs/cc). In this study, we prepared CoPt nanowires (up to 200nm in diameter and 100 micrometer in length) embedded in anodized alumina templates by electrodeposition. The pH values have been varied from 3 to 6 by adding diluted NaOH into the deposition bath. The wires were then annealed in a high vacuum furnace at a temperature range between $650^o$C to 750°C in order to transform their structure from the disordered fcc phase to the ordered $L1_0$ phase. A higher pH value leads to a higher coercivity and smoother loop which can be attributed to a more uniform CoPt composition through out the wires. HRTEM data of as-made samples shows that the long wires consist of both tiny nanoparticles (1-2 nm) and elongated nanorods having a single crystal fcc structure. The microstructural data is consistent with the magnetic measurements, showing a slightly preferred orientation perpendicular to the long axis of the wires with $H_c = 5$ kOe and 5.5 kOe along and perpendicular to the direction of the wires, respectively.

*NSF and DEPSCoR

**10:24**

**G22 11 Ferromagnetism in colloidal Mn doped ZnO nanocrystals** GIL MARKOVICH, TAL MERON, EINAT TIROSH, GABRIEL SHEMER, *Tel Aviv University* Surfactant coated colloidal $Zn_{1-x}Mn_xO$ ($x=0.04\pm 0.03$) nanocrystals of average diameter of 5.5 nm were synthesized using high temperature hydrolysis of Zn(II) and Mn(II) alkoxides in a high boiling point solvent. The magnetic properties of the nanocrystals were measured both for isolated particles diluted in a hydrocarbon matrix and for a nanocrystal powder. Nanocrystals of manganese oxide and ZnO coated with manganese oxide were prepared for comparison to the $Zn_{1-x}Mn_xO$ nanocrystals. We find that the manganese ions primarily substitute zinc ions in the hexagonal ZnO lattice and part of them are ferromagnetically coupled up to room temperature even

in isolated non-interacting nanocrystals. The rest of the ions were magnetically disordered or uncoupled. Surprisingly, these small $Zn_{1-x}Mn_xO$ nanocrystals poses relatively large low-temperature magnetic coercivity and relatively high blocking temperature in the isolated form, which indicate large magnetic anisotropy. In the nanocrystal powder the coercive field decreased significantly. This study highlights the advantages of working with non-interacting single domain particles of these intriguing materials.

**10:36**

**G22 12 Superparamagnetic resonance in antiferromagnetic nanoparticles: systematic features in the temperature dependence*** PRASANTA DUTTA, MOHINDAR SEEHRA, *West Virginia University* Antiferromagnetic (AF) nanoparticles (NP) of dimensions $\approx$ 5 nm usually acquire significant magnetic moment even below $T_N$ due to uncompensated surface spins. This moment follows superparamagnetism (SPM) above the blocking temperature $T_B < T_N$. In this work, we will discuss some unique features in the temperature dependence of the electron magnetic resonance (EMR) spectra which have been reported in NP of ferrihydrite, NiO and $\gamma Fe_2O_3$ [1]. As T is lowered towards $T_B$ the resonance field $H_r$ decreases and the linewidth $\Delta H$ increases so that $\delta H_r \approx (\Delta H)^n$ with $n \approx 3$ is observed. This is in line with the variation expected from the demagnetizing fields of non-spherical particles [2]. From the temperature variation of the line intensity $I = (\Delta H)^2 h$ (h = peak-to-peak height), the location of $T_B$(m) and $T_B$(EMR) has been obtained [1]. For $T < T_B$(m), as $H_r$ approaches zero, the EMR line becomes highly asymmetrical, which is explained from the combined contributions of resonance at $+H_r$ and $-H_r$. [1]. Seehra et al, IEEE Trans. Magn; 37, 2207 (2001); Seehra et al, J. Appl. Phys. 97, 10J609 (2005); Dutta et al, Phys. Rev. B 70, 174428 (2004). [2]. Nagata & Ishihara, J. Magn. Magn. Mater. 104-107, 1571(1992).

*Supported by a grant from the U.S Department of Energy.

**10:48**

**G22 13 Competition between Thermoinduced Magnetization and Uncompensated Spins** GREGORY BROWN, MARKUS EISENBACH, G. M. STOCKS, *Oak Ridge National Lab* Thermoinduced magnetization (TiM) is the ferromagnetic response predicted for nanoparticles of normally antiferromagnetic materials. Unambiguous experimental observation of this phenomenon is complicated by the effects of the particle size-distribution within a sample and the uncompensated magnetic moments within a nanoparticle. Monte Carlo calculations of nanoparticles with odd numbers of spins have been employed to resolve the competition between TiM and uncompensated spins. The magnitude of the ferromagnetic response, $\langle |M|^2 \rangle$, is easily resolved into the two phenomena. Analysis for the response along the direction of crystalline anisotropy, $\langle M_z^2 \rangle$, is complicated by the temperature-dependent relaxation of individual spins away from the anisotropy axis. These results indicate that TiM may be confirmable in nanoparticles with uncompensated spins. However, quantitative estimates of the temperature- and anisotropy-dependence of TiM are significantly affected by uncompensated moments.



**SESSION G23: FOCUS SESSION: MAG.THY II / TRANSPORT & GENERAL**
**Tuesday Morning, 14 March 2006**
**320, Baltimore Convention Center at 8:00**
**Wei Cai, Standford University, presiding**

***Contributed Papers***

**8:00**

**G23 1 Efficient Ab-initio Calculation of the Anomalous Hall Conductivity of Fe by Wannier Interpolation** XINJIE WANG, DAVID VANDERBILT, *Rutgers University* JONATHAN YATES, IVO SOUZA, *LBNL and University of California, Berkeley* Recently, a first-principles calculation of the anomalous Hall conductivity (AHC) of Fe as a Brillouin-zone integral of the Berry curvature was carried out and found to be in reasonable agreement with experimental results.[1] However, these authors observed extraordinarily strong and rapid variations of the Berry curvature with wavevector $k$ in the vicinity of avoided crossings and near-degeneracies in reciprocal space. A conventional first-principles calculation thus requires an extremely dense k-point mesh and is quite time-consuming. Here, we present an efficient first-principles approach for computing the AHC based on Wannier interpolation. First, a conventional electronic-structure calculation is performed for Fe, with spin-orbit included, on a relatively coarse k-point mesh. Second, maximally-localized Wannier functions are constructed by a post-processing step,[2] thus transforming the full ab-initio problem into an effective tight- binding form. Finally, the needed quantities such as Berry potentials and curvatures are interpolated onto a fine k-point mesh and used to compute the AHC. Our approach gives good agreement with conventional, less efficient first-priciples calculations.

[1]Y. Yao *et al.*, Phys. Rev. Lett. **92**, 037204 (2004).
[2]I. Souza, N. Marzari, and D. Vanderbilt, Phys. Rev. B **65**, 035109 (2001).

**8:12**

**G23 2 Spin and charge currents and current rectification in Luttinger liquids*** B. BRAUNECKER, D. E. FELDMAN, J. B. MARSTON, *Brown University* Asymmetries in spin and charge transport properties are of great interest for spintronic and electronic applications. We show that externally-driven spin and charge currents in a Luttinger liquid model of a one-dimensional quantum wire are strongly modified by the presence of a localized magnetic or nonmagnetic scatterer. A diode effect appears at low voltages when this scatterer is spatially asymmetric, and a non-monotonous dependence of the current on the voltage is possible.[1]

*Supported in part by NSF DMR-0213818.

[1]D. E. Feldman, S. Scheidl, and V. M. Vinokur, *Phys. Rev. Lett.* **94**, 186809 (2005); B. Braunecker, D. E. Feldman, and J. B. Marston, *Phys. Rev. B* **72**, 125311 (2005)

**8:24**

**G23 3 Interplay of Rashba and itsp-d exchange couplings in magnetic 2DEGs*** FRANCISCO MIRELES, *CCMC-UNAM, Mexico.* HENRIQUE H. P. FREIRE, *IFSC, Universidade de Sao Paulo, Brazil* J. CARLOS EGUES, *IFSC, Universidade de Sao Paulo, Brazil* In diluted magnetic semiconductor (DMS) quantum wells the itsp-d exchange interaction between the itinerant conduction electrons in the well and the localized electrons in the *d*

orbitals of the Mn impurities gives rise to interesting spin-dependent physics [1]. Recently, the interplay of the Rashba spin-orbit and the itsp-d exchange interactions in Mn-based wells has been recognized via Shubnikov-de-Haas measurements [2]. While the Rashba spin-orbit has been extensively studied in non-magnetic 2DEGs, its role in DMS systems with a competing itsp-d exchange interaction has not yet been addressed theoretically. In this work we present a**it k.p** derivation of an effective Hamiltonian for a Mn-based quantum well with competing Rashba and itsp-d interactions, and show numerical results for the magnetoresistance $\rho_{xx}$ of typical magnetic 2DEGs using our effective Hamiltonian model. Our results shows interesting beating patterns of the $\rho_{xx}$ as a function of the temperature and carrier density which suggests a significant interplay between the spin-orbit and itsp-d exchange interactions, as a recent experiment observes [2]. [1] J. C. Egues, PRL **78**, 4578 (1998); H. J. P. Freire and J. C. Egues, cond-mat/0412491. [2] Y. S. Gui et al. EPL. **65**, 393 (2004).

*We acknowledge support from FAPESP/Brazil and CONACYT/Mexico through project No. 40521.

*Invited Papers*

**8:36**
**G23 4 Berry Phase and itAb initio Calculation of Anomalous & Spin Hall Effect.**
YUGUI YAO, *Institute of Physics, Chinese Academy of Sciences, China*

Berry phase in momentum space in spin-orbit coupled bands affects the charge and spin transport of electrons in real space, and produces fascinating new phenomena. Two examples are the anomalous Hall effect and the recently proposed intrinsic spin Hall effect. Avoiding the ambiguity introduced by model Hamiltonians, we evaluate the Berry curvature accurately for real materials by parameter-free itab initio methods. We have calculated the anomalous Hall conductivity for ferromagnetic crystals of Fe, Co, Ni, $Mn_5Ge_3$, and $CuCr_2Se_{4-x}Br_x$, and investigated the magnetization dependence and sign change, with results in quantitative agreement with experiments [1,2]. Using the itab initio technique, we have also evaluated the intrinsic spin Hall conductivity in non-magnetic semiconductors (GaAs, Si, Ge, AlAs) as well as metals (W and Cu) [3,4]. We have systematically studied how its sign and magnitude depend on strain, doping density, and frequency for the semiconductors, and found very large values for the metals. [1] Yugui Yao et al., Phys. Rev. Lett. 92, 037204 (2004). [2] Changgan Zeng, Yugui Yao, Qian Niu, and Hanno, H. Weitering, (Phys. Rev. Lett. in review). [3] Yugui Yao and Zhong Fang, Phys. Rev. Lett. 95, 156601 (2005). [4] Guangyu Guo, Yugui Yao, Qian Niu, Phys. Rev. Lett. 94, 226601 (2005).

*Contributed Papers*

**9:12**
**G23 5 Emerging Magnetism at Pt Nanocontacts and Nanowires** ERIO TOSATTI, *SISSA/ICTP/Democritos Trieste* ANDREA DAL CORSO, *SISSA/Democritos Trieste* ANNA DELIN, *KTH Stockholm* ALEXANDER SMOGUNOV, *SISSA/Democritos Trieste* RUBEN WEHT, *CNEA San Martin* Nanocontacts made of transition metals that are nonmagnetic in bulk may display a possible onset of Hund's rule local nanomagnetism. Zero-temperature DFT electronic structure calculations indicate that magnetism may occur in monatomic nanowires of 4d and 5d transition metals, generally favored by tensile stress, and sometimes also by spin-orbit coupling. [1] In the particular case of a Pt monatomic nanowire, resurgence of orbital magnetism is predicted to conspire with intra-atomic exchange to give rise to a spontaneous magnetization even at zero stress. Here we expect an extraordinarily large magnetic anisotropy, spin and orbital magnetization lying strictly parallel to the nanowire axis. A Pt nanowire-like contact should thus behave as an Ising nanomagnet. Since magnetic exchange splittings generally affect the number of conducting channels crossing the Fermi level, it is likely that the ballistic conductance through a nanowire-like contact [2] will be affected by the emerging nanomagnetism of Pt. [1] A. Delin and E. Tosatti, Phys. Rev. B 68, 144434 (2003); A. Delin, et al., Phys. Rev. Lett. 92, 057201 (2004). [2] A. Smogunov, A. dal Corso and E. Tosatti, Surface Science 507, 609 (2002); ibid. Surf. Sci. 532, 549 (2003); ibid. Surf. Sci. 566, 390 (2004); A. Smogunov et al., Phys. Rev. B 70, 045417 (2004); and to be published.

**9:24**
**G23 6 Atomic and electronic properties of $Ni/Al_2O_3/Ni$ magnetic tunnel junction** YOU LIN, *University of South Florida* IVAN OLEYNIK, *University of South Florida* Numerous experimental and theoretical investigations show that the spin-polarization of the tunneling current in magnetic tunnel junctions (MTJs) is not an intrinsic property of the ferromagnet alone, but depends on the electronic properties of the insulator and the ferromagnet-insulator interface. We report the results of first-principles density-functional studies of Ni_/$Al_2$_$O_3$_/Ni MTJs. The atomic structure has been studied for different interface terminations. The interfacial energetics was quantified based on the work of separation and the most stable interfacial structures have been identified. The electronic and magnetic properties have been thoroughly analyzed in the framework of local densities of states. The possibility of strongly-correlated electronic effects has also been considered by performing additional LDA+U calculations of interfacial electronic structure. We will discuss various factors that might contribute to spin polarization of the tunneling current in the MTJs.

**9:36**
**G23 7 Interface properties of nickel/organics/nickel magnetic tunnel junctions** WESLEY FABELLA, *University of South Florida* IVAN OLEYNIK, *University of South Florida* In recent years, substantial experimental efforts were directed towards developing a new class of spintronic devices based on organic polymers, oligomers and small molecules. In particular, recent experiments indicate efficient spin injection and spin transport in ferromagnet/organic systems. However, the electron and spin transport through metal-molecule-metal junctions depends crucially on the properties of ferromagnet/organics interfaces. We

performed first-principles density functional theory (DFT) calculations of nickel/organic-molecule/nickel magnetic tunnel junctions. Organic systems include both saturated alkane and unsaturated thiophene molecules. The choice of the system was made based on available experimental information. The atomic structures of metal/molecule interfaces were built and the geometries of molecule/metal interfaces were determined by optimizing the interfacial work of separation. We will discuss the electronic properties of molecule/electrode junctions including distribution of charge densities, local charges, local magnetic moments and local densities of states on individual atoms. The spin-dependent interfacial properties will be discussed in relation to spin-dependent transport in organics-based MTJs.

**9:48**
**G23 8 Nonequilibrium Transport in Quantum Impurity Models:(Bethe-Ansatz for open systems)** PANKAJ MEHTA, NATAN ANDREI, *Rutgers University* We develop an exact nonperturbative framework to compute steady-state properties of quantum-impurities subject to a finite bias. We show that the steady-state physics of these systems is captured by nonequilibrium scattering eigenstates which satisfy an appropriate Lippman-Schwinger equation. Introducing a generalization of the equilibrium Bethe-Ansatz - the Nonequilibrium Bethe-Ansatz (NEBA), we explicitly construct the scattering eigenstates for the Interacting Resonance Level model and derive exact, nonperturbative results for the steady-state properties of the system.

**10:00**
**G23 9 Ab initio investigation of domain walls in ferromagnetic films and wires*** HEIKE C. HERPER, PETER ENTEL, *Theoretical Physics, University of Duisburg-Essen, Lotharstrasse 1, D-47048 Duisburg* Domain walls can be viewed as special type of interfaces. In case of relatively thin domain walls a magnetoresistance effect can be observed due to the domain wall, which has been addressed in a considerable number of experimental and theoretical studies. However, only few ab initio investigations have been done in this field. We have determined the influence of domain walls on the resistance in ferromagnetic Co and Ni layers employing the fully-relativistic, spin-polarized Screened Korringa-Kohn-Rostoker method (SKKR) and the Kubo-Greenwood formula. In order to investigate the magnetoresistance in thin wires we made use of a real-space SKKR and Kubo-Greenwood method. The magnetoresistance and the formation energy of the domain walls have been calculated depending on the thickness and the type of the domain wall. As expected the formation energy decreases with increasing number of FM layers. Throughout this paper all domain walls are assumed to be oriented in the plane of layers. In order to avoid contributions from the anisotropic magnetoresistance the current flows perpendicular to the domain walls, i.e. parallel to the surface normal. The results support the predictions from Zhang and Levy concerning the width dependence of the domain wall resistance.

*This work is supported by the SFB 491

**10:12**
**G23 10 Orbital magnetic susceptibility in an integrable system** M.X. LOU, J.M.A.S.P. WICKRAMASINGHE, R.A. SEROTA, *University of Cincinnati* We investigate, analytically and numerically, the orbital magnetism of free electron gas in a rectangular box, which is a model classically integrable system. We find that both the average orbital susceptibility and its fluctuations are determined by the two-level van Vleck susceptibility that involves the last occupied (Fermi) level and the first unoccupied level. This is in line with previous results for disordered (classically chaotic) systems. The mesoscopic fluctuations, however, are much larger in integrable systems. We find that, in units of $\mu_B^2/\Delta$, where $\Delta$ is the mean level spacing, the average orbital susceptibility is $\langle|\hat{L}_{if}|^2\rangle\langle(\varepsilon_f - \varepsilon_i)^{-1}\rangle$, where $\langle|\hat{L}_{if}|^2\rangle \sim \sqrt{N}$, $L$ is the orbital angular momentum, $N$ is the number of electrons in the box, and $\varepsilon_f - \varepsilon_i$ is the level spacing (in units of $\Delta$) between the last occupied level and the first unoccupied level. $\langle\varepsilon_f - \varepsilon_i)^{-1}\rangle$ is principally divergent and hence determined by the relevant cut-off.

**SESSION G24: POLYMER NANOMATERIALS I**
**Tuesday Morning, 14 March 2006**
**321, Baltimore Convention Center at 8:00**
**Kookheon Char, Seoul National University, presiding**

**8:00**
**G24 1 Coffee Break**

**8:36**
**G24 2 Marker Motion Measurements of Nanoparticles in Polymer Matrices** ALETA HAGMAN, *Northwestern University & Argonne National Laboratory* KENNETH R. SHULL, *Northwestern University* JIN WANG, XUEFA LI, DONG RYEOL LEE, SURESH NARAYANAN, *Argonne National Laboratory* Marker motion can be used to infer the ordering kinetics and nanoparticle dynamics in model polymer/metal nanocomposite thin films. In current experiments, the thermally evaporated gold particles (few nanometers in diameter) act as a marker layer between two polymer layers with different mobilities. The disparity in the mobility causes a marker movement towards the layer with the higher mobility. X-ray standing waves (XSWs), generated by total external reflection above a mirror surface, are used to monitor the time evolution of the gold nanoparticle distribution as the nanocomposite ultrathin films are heated above the polymer glass transition temperatures. Diffusion coefficients are obtained from the time-dependence of the nanoparticle distribution evolution. Polymer/gold interactions has shown to be system dependent, with pol(tert-butyl acrylate) (PtBa) showing weak interactions while poly(2-vinyl pyridine) (PVP) shows strong interactions as expected. Free surface effects relating to mobility will also be discussed.

**8:48**
**G24 3 Effect of Areal Density of Polymer Chains on Gold Nanoparticles on Nanoparticle Location in a Block Copolymer Template** B.J. KIM, J. BANG, C.J. HAWKER, E.J. KRAMER, *UCSB* It is well established that one block of a copolymer can interact preferentially with an inorganic substrate to produce wetting and domain orientation. We take advantage of this preferential interaction to control the location of 2.5 nm diameter Au nanoparticles coated with short thiol-terminated polystyrene ($M_n$=3.4 kg/mol) chains (PS-SH) in a symmetric poly(styrene-*b*-2 vinylpyridine) (PS-b-P2VP) diblock copolymer ($M_n$=196 kg/mol) by changing the areal density $\Sigma$ of the PS-SH on the Au. If $\Sigma \geq$ 1.6 chains/nm$^2$, the preferential interaction between the P2VP of the PS-b-P2VP and the Au surface is screened and the Au localizes in the center of the PS domains. If $\Sigma \leq$ 1.4 chains/nm$^2$, the Au

particles are localized at the PS-P2VP interface. Au nanoparticles coated with thiol terminated P2VP ($M_n$=3 kg/mol) localize in the center of the P2VP domain of the PS-P2VP over the entire range of $\Sigma$, demonstrating the localization of the PS coated Au nanoparticles at the interface at low values of $\Sigma$ is due to the unscreened Au-P2VP interaction.

**9:00**

**G24 4 Nanocomposite Microdomain Inversion in Au Nanoparticle/ PS-b-PFOMA Block Copolymer Films** LUCIANA MELI, YUAN LI, KEITH P JOHNSTON, *The University of Texas at Austin* PETER F GREEN, *The University of Michigan, Ann Arbor* We report that Au nanocrystals sequestered within the microdomains of self-assembled aggregates of polystyrene-b-poly(1,1',2,2'-tetrahydroperflurooctyl methacrylate) (PS-b-PFOMA) thin films are capable of following the structure-guiding matrix in a morphological transition from spherical PFOMA aggregates in a PS matrix to the inverse morphology upon supercritical CO2 (scCO2) sorption. Furthermore, the domain size of the aggregates can be finely tuned by adjusting the scCO2 density. By pretreating the particles surface with a host of ligands with different chemical affinities for the constituent blocks, we observe that the Au/diblock co-assembly process is dependent not only on the ligand size and ligand- matrix compatibility, but also on the interaction of the ligands with the interfaces that confine the film.

**9:12**

**G24 5 Dielectrophoretic alignment of montmorillonite nanoplatelet suspensions in an organic matrix** EVANGELOS MANIAS, *Materials Science and Engineering, Penn State University* GEORGIOS POLIZOS, *Penn State University* HILMAR KOERNER, RICHARD VAIA, *Air Force Research Lab/MLBP* High orientational alignment of pseudo-two-dimensional inorganic platelets in an organic matrix is achieved by external AC electric fields ( $\sim$ 0.5V/$\mu$m, rms). Namely, montmorillonite aluminosilicate platelets are organically modified by alkyl-ammonium surfactants and dispersed in an uncrosslinked epoxy. Orientation is quantified through wide angle 2D X-Ray diffraction under an AC electric field ( $\sim$ 0.05-4V/$\mu$m), following the reorientation of inorganic stacks (tactoids), resulting in Hermans orientation factors of 0.7–0.9 even at moderate field strengths. The degree of orientation dependence on the electric field frequency and strength is presented. The electrophoretic motion of the cationic surfactants as a possible mechanism to produce alignment is delineated via broadband ($10^{-2}$-$10^{7}$ Hz) dielectric relaxation spectroscopy, and dipole moment theoretical analyses. The cationic electrophoretic motion does not have any major contribution for the platelet alignment, suggesting that the primary cause is due to induced dipoles (image charges) on the dielectric inorganic platelets.

**9:24**

**G24 6 Surface morphology in dewetting polystyrene/ polyhedral oligomeric silsesquioxane (POSS) thin-film bilayers** RITUPARNA PAUL, MICHAEL C. SWIFT, JOHN R. HOTTLE, ALAN R. ESKER, *Macromolecules & Interfaces Institute, Department of Chemistry (0212), Virginia Tech, Blacksburg, VA 24061* Polymer/polymer and polymer/nanoparticle bilayers on solid substrates are common in technological applications. Dewetting or the spontaneous formation of holes in polymer films above their glass transition temperature, poses a serious problem in the nanofabrication of polymeric multilayers. This study utilizes bilayer films of polystyrene (PS) and trisilanolphenyl- POSS (TPP) as a model to investigate the morphological evolution of polymer/nanoparticle bilayers upon annealing. X-ray photoelectron spectroscopy, and optical and atomic force microscopies have been used to study dewetting as a function of annealing time and temperature. Upon annealing the PS/TPP bilayers at 200 C, the upper TPP layer undergoes instantaneous cracking and these cracks serve as nucleation sites for dewetting of the TPP and PS layers for annealing times up to 90 minutes. For annealing times longer than 90 minutes, the dewetting of TPP and PS layers is complete resulting in the formation of TPP encapsulated PS droplets.

**9:36**

**G24 7 Block Copolymer Nanocomposites for RF Magnetodielectric Applications** TA-I YANG, PETER KOFINAS, *Department of Chemical and Biomolecular Engineering, University of Maryland, College Park, MD* The aim of this research is to develop novel block copolymer nanocomposites for radio frequency applications. Block copolymers (BCP) act as templates to enhance the ordering of nanoparticles within the polymer matrix and tailor the desired electromagnetic properties such as permeability ($\mu$) and permittivity ($\varepsilon$). We incorporated iron and strontium or titanium organometallic precursors into three different polymer matrices (styrene-*b*-isoprene-*b*-styrene (SIS), styrene-b-(ethylene-ran-butylene)-b-styrene (SEBS), and sulfonated styrene-b-(ethylene-ran-butylene)-b-styrene (S-SEBS)) and then formed mixed metal oxide nanoparticles within the BCP. Preliminary experimental results demonstrated we can obtain $\mu = \varepsilon$ near 2.7 with low loss tangent (tan $\delta < 0.01$) through the 1 M to 1G Hz frequency range by utilizing SIS or SEBS with templated $Fe_20_3$/SrO nanoparticles. For the S-SEBS copolymer composites, most mixed metal oxide nanoparticles were successfully templated into BCP self-assembled patterns confirmed by TEM, and the loss tangent could be significantly reduced by heat treatment.

**9:48**

**G24 8 Effect of confinement on the polymer segmental motion and on ion mobility in PEO/layered-silicate nanocomposites***
SPIROS H. ANASTASIADIS,[†] KIRIAKI CHRISSOPOULOU, ATHANASIOS AFRATIS, *Foundation for Research and Technology - Hellas, Heraklion Crete, Greece* M.M. ELMAHDY, GEORGE FLOUDAS, *University of Ioannina, Ioannina, Greece* BERNHARD FRICK, *Institut Laue-Langevin, Grenoble, France* The effect of confinement on the local, the segmental and the ionic processes of poly(ethylene oxide)/montmorillonite (PEO/MMT) intercalates are investigated. X-ray diffraction, DSC and polarizing optical microscopy data show that the intercalated PEO chains remain amorphous and it is only the excess PEO chains outside the galleries that crystallize. This is also verified by the behavior of the elastic intensity of quasi-elastic neutron scattering (QENS) experiments on the same hybrids. Dielectric relaxation spectroscopy reveals that confinement results in an acceleration of the PEO segmental dynamics that display an Arrhenius temperature dependence with very low activation energy, whereas the local beta-process remains unaffected. Likewise, ionic mobility is enhanced in the nanohybrids suggesting that ion mobility is assisted by the faster PEO segmental motion.

*Sponsored by NATO's Scientific Affairs Division (Science for Peace) and by the European Union (NMP3-CT-2005-506621)

[†]Also at Aristotle University of Thessaloniki, Thessaloniki, Greece

**10:00**

**G24 9 Photovoltaic Responses of Solar Cells Based on Lead Selenide Quantum Dots and Conducting Polymers** XIAOMEI JIANG, SERGEY LEE, ANVAR ZAKHIDOV, *University of Texas at Dallas, Richardson, TX, 75083* RICHARD D. SCHALLER, J.M. PIETRYGA, VICTOR KLIMOV, *Chemistry Division, Los Alamos National Laboratory, Los Alamos, NM, 87545* We report on hybrid solar cells based on nanocomposites of conjugated polymers (polythiophene and polyphenylvinylene derivatives) and IR-sensitive PbSe QDs that have a size-tunable energy gap between 0.3 and 1 eV. Thin film cells show very good diode characteristics and sizable photovoltaic response. The good performance of our devices in both photovoltaic and photodiode regimes indicates quite efficient charge separation between the polymer and QD components. To elucidate the mechanism for charge separation in these composite structures, we analyze conduction and valence-band energy offsets derived from cyclic voltammetry measurements. We find the significant increase of photocurrent due to more efficient charge separation when the surface of the quantum dots was treated with pyridine to remove the surface ligand. The analysis of a spectrally resolved photocurrent measurements reveals some evidence of carrier multiplication-enhanced photocurrent in our devices. Specifically, we observe indications of a rapid increase in the photocurrent at spectral energies in correlation with the size-dependent energy gap of the QD component. The onset of this increase correlates with what is expected for the onset of carrier multiplication in PbSe QDs.

**10:12**

**G24 10 Electric Field Effect on Wannier- Frenkel Hybrid Exciton in a Quantum Dot Coated by an Organic Shell** QUE HUONG NGUYEN, *Physics Department, Marshall University, One John Marshall Dr., WV 25701* JOSEPH L. BIRMAN, *Physics Department, City College, CUNY, Convent Ave. & 138 Street, NY 10031* The effect of external electric field on the Wannier Mott-Frenkel hybrid excitons in the configuration of a spherical semiconductor quantum dot coated by an organic shell has been studied. The electric field reduces the exciton binding energy and shifted the resonance region where the Wannier and Frenkel exciton are strongly mixed. The quadratic Stark dependence of the hybrid exciton energy on the electric field was found for the confined Stark effect for the hybrid exciton. Upon the application of field the coupling term between the two kinds of excitons increases. An important result is the possibility of tuning the Wannier-Frenkel exciton resonance by applied electric field

**10:24**

**G24 11 Transport measurements in semiconductor nanocrystals capped with electroactive ligands** CLAUDIA QUERNER, *University of Pennsylvania, USA* PETER REISS, *CEA Grenoble, France* MICHAEL D. FISCHBEIN, *University of Pennsylvania* PATRICE RANNOU, *CEA Grenoble* JOEL BLEUSE, *CEA Grenoble* ADAM PRON, *CEA Grenoble* MARIJA DRNDIC, *University of Pennsylvania* Organic-inorganic hybrid materials based on semiconductor nanocrystals and $\pi$-conjugated oligomers or polymers have seen an increasing interest over the past years mainly because of their possible applications in optoelectronic devices, such as solar cells. We report here the preparation of organic-inorganic hybrids by chemical grafting of tetraaniline onto the surface of semiconductor nanocrystals, such as CdSe and PbSe. We proved by spectroscopic and spectroelectrochemical studies that the grafting reaction does not influence in a significant way the electroactivity of both systems nor does it modify the doping mechanism of the grafted ligands. By cyclic voltammetry we were able to estimate the position of the energy levels in the hybrid, which are aligned such that a charge separation can occur at the organic-inorganic interface after photo-excitation. Highly efficient photoluminescence quenching confirmed such a process. Finally, we studied photoconductivity in these materials.

**10:36**

**G24 12 Photooxidation of sugar and alcohol on $TiO_2$ surfaces: A first-pirnciples study** MAO-HUA DU, JUN FENG, SHENG-BAI ZHANG, *National Renewable Energy Laboratory* First-principles studies are carried out on $TiO_2$/sugar (alcohol) interfaces under UV illumination. A rapid charge separation takes place at the interfaces through a two-step process: (1) trapping of photo-generated carriers at the gap levels induced by the chemisorbed molecules, and (2) upon the carrier trapping, a structural transformation of the adsorbed molecules, which in turn eliminates the gap levels. The second-step here is necessary to avoid carrier recombination, and hence results in an irreversible charge separation. Such a charge transfer across the semiconductor/molecule interface leads to various oxidation and reduction processes with structural reconfigurations (bond- forming and breaking) of the surface molecules. These results reveal the underlying microscopic mechanism of photo-catalytic reactions on the $TiO_2$ surfaces. The mechanism for the observed self-assembly of TiO2/cyclodextrin wires under UV illumination will also be discussed. This work was supported by the U. S. Department of Energy, BES and EERE, under Contract No. DE-AC39-98-GO10337.

**10:48**

**G24 13 Directly Patterned Mesoporous Carbon and Metal-Doped Carbon Films Prepared using Block Copolymer Templates in Supercritical CO2** GAURAV BHATNAGAR, JAMES WATKINS, *University of Massachusetts - Amherst* Porous carbon and metal-doped porous carbon films have wide applications in separations, sensors, catalysis and magnetic storage applications. Conventionally prepared carbon films have micropores in the size range of 2 nm. Recent techniques for the synthesize of mesoporous carbon with 10-50 nm pores using sacrificial silica templates have limitations with respect to pore connectivity and the preparation of patterned and metal-doped carbon films. Here we report supercritical fluid-assisted infusion and phase selective reaction within pre-organized block copolymer and block copolymer/homopolymer templates to synthesize mesoporous carbon and metal doped carbon films. Well-defined mesoporous carbon films patterned at the device level with good mechanical properties and metal doped carbon films by pre-infusion of block copolymer templates with metal precursors in supercritical carbon dioxide were synthesized. Platinum doped carbon films for applications in fuel cells having good electrochemical response were produced. The preparation of cobalt containing carbon films with potential use in magnetic storage applications demonstrates the general applicability of supercritical infusion technique to produce metal cluster containing films.

**SESSION G25: STRUCTURE AND DYNAMICS OF FUNCTIONAL MACROMOLECULES**
**Tuesday Morning, 14 March 2006**
**322, Baltimore Convention Center at 8:00**
**Xinyan Cui, University of Pittsburgh, presiding**

**8:00**
**G25 1 Coffee Break**

**8:36**
**G25 2 Structural Transitions of F-Actin:Espin Bundles** KIRSTIN PURDY, *University of Illinois at Urbana Champaign* JAMES BARTLES, *Northwestern University* GERARD WONG, *University of Illinois at Urbana Champaign* Espin is an actin bundling protein involved in the formation of the parallel bundles of filamentous actin in hair cell stereocilia. Mutations in espin are implicated in deafness phenotypes in mice and humans. We present measurements of the F-actin structures induced by wild type and by mutated espin obtained via small angle x-ray scattering and fluorescence microscopy. We found that wild type espin induced a paracrystalline hexagonal array of twisted F-actin, whereas the mutated espin only condensed the F-actin into a nematic-like phase. The possibility of coexisting nematic and bundled actin in mixtures containing both mutant and wild type espins was also investigated.

**8:48**
**G25 3 Nonequilibrium Self-Assembly of Linear Fibers** CHENGHANG ZONG, TING LU, TONGYE SHEN, PETER WOLYNES, *University of California, San Diego* From physical viewpoint, a dynamic bio-fiber represents an interesting one-dimensional nonequilibrium system. We construct a minimal dynamic model for this type of fibers. Our model incorporates features such as realistic dynamics rules and site resolution. The steady state solutions are obtained with the nonequilibrium variational principle. The projection of steady state distributions produces an effective potential for the pure dynamic system. We demonstrate how dynamic behaviors such as catastrophe, rescue, and dynamic instability can be analyzed under the effective reaction coordinate.

**9:00**
**G25 4 Energetics and Dynamics of Constrained Actin Filament Bundling** LE YANG, *Phys. Dept., Washington University* DAVID SEPT, *Dept. of Biomedical Engineering, Washington University* ANDERS CARLSSON, *Phys. Dept., Washington University* The formation of filopodia-like bundles from a dendritic actin network has been observed to occur in vitro as a result of branching induced by Arp2/3 complex. We study both the energetics and dynamics of actin filament bundling in such a network in order to evaluate their relative importance in bundle formation processes. Our model considers two semiflexible actin filaments fixed at one end and free at the other, described using a normal-mode approximation. This model is studied by both Brownian dynamics and Monte Carlo energetics methods. In the dynamic simulations, we evaluate the time required for the filaments to interact and bind, and examine the dependence of this bundling time on the filament length, the distance between the filament bases, and the crosslinking energy. For most of the cases we have studied, the energetics and dynamics simulations give similar results for critical distance. Over a broad range of conditions, we find that the times required for bundling from a network are compatible with experimental observations.

**9:12**
**G25 5 Evolution of growth modes for polyelectrolyte bundles** G.H. LAI, OLENA V. ZRIBI, *University of Illinois at Urbana-Champaign, Dept. of Physics* GOLESTANIAN RAMIN, *University of Sheffield, Dept. of Physics* GERARD C.L. WONG, *University of Illinois at Urbana-Champaign, Dept. of Physics, Dept. of Materials Science and Engineering, Dept. of Bioengineering* F-actin is a prototypical 'hard rod' polyelectrolyte, with a charge density of $\sim$ 1e/2.5Å and a persistence length of $\sim$ 5-10 $\mu$m. In the presence of multivalent ions, F-actin can condense into close-packed bundles. In this work, we use fluorescence microscopy to study the detailed growth mode of such bundles, and show how it evolves as a function of salt concentration. Preliminary results indicate that at sufficiently high salt concentrations, the bundle width is relatively insensitive to salt concentration. Moreover, the growth mode of the system changes as a function of salt concentration, varying from lateral growth (which increases the bundle width) to longitudinal growth (which increases the bundle length).

**9:24**
**G25 6 Nanoscopic tubulin rings*** HACENE BOUKARI, *NIH* DAN SACKETT, *NIH* PETER SCHUCK, *NIH* SUSAN KRUEGER, *NIST* RALPH NOSSAL, *NIH* We describe results of analysis of fluorescence correlation spectroscopy, small-angle neutron scattering, and sedimentation measurements of nanoscopic polymer rings formed following interactions of tubulin (100 kDa) and a small peptide, cryptophycin (340 Da). Tubulin is a ubiquitous dimeric protein found in eukaryotic cells, and is the building block of microtubules, which are dynamical biopolymers involved in many critical cell functions. The peptide, which is a marine natural product, inhibits the formation of microtubules and, instead, induces the formation of the rings. Under the studied conditions these rings appear rigid, have circular geometry ( $\sim$ 25 nm dia.), are monodisperse in size (8 tubulin dimers/ring), and are stable even with tubulin concentration as low as 1 nM. Remarkably, no intermediate oligomers (partial rings or others) are observed. Further, structural and hydrodynamic modeling confirms the number (8) of tubulin dimers per ring and shows that the tubulin monomers are not spherical, consistent with their known crystallographic structure. *H. Boukari, R. Nossal, D. Sackett, and P. Schuck, PRL 93, 98106 (2004).

**9:36**
**G25 7 Deformation of DNA and Polymer Labels during End-Labelled Free-Solution Electrophoresis.** GARY W. SLATER, LAURETTE C. McCORMICK, *University of Ottawa* Recent advancements to DNA sequencing by End Labelled Free Solution Electrophoresis (ELFSE) show the promise of this novel technique which overcomes the need for a gel by using a label (or drag-tag) to render the free solution mobility of the DNA size-dependent. It is the attachment of an uncharged drag-tag molecule of a set size to all the various lengths of DNA in the sample that selectively slows down smaller DNA chains which have less force to pull the drag-tag than larger DNA. Taking advantage of the modified hydrodynamic properties of tagged DNA, ELFSE has been used to successfully sequence up to about 100 bases of DNA in the absence of a gel or other sieving. So far, only globally random coil

conformations have been associated with ELFSE, i.e. the DNA and the label together form a single, undeformed hydrodynamic unit. However, next generation labels combined with high field strengths may allow for deformation of the DNA and/or a polymer label. We present here the necessary conditions for stretching, and some of the subsequent effects on separation, highlighting possible improvements to ELFSE performance via stretching of DNA and/or the polymer label.

**9:48**
**G25 8 Ferroelectric-specific peptides as building blocks for bio-inorganic devices** BRIAN REISS, GUO-REN BAI, ORLANDO AUCIELLO, LENIDAS OCOLA, MILLICENT FIRESTONE, *Argonne National Laboratory* Combinatorial phage display methods have been used to identify a circularly constrained heptapeptide sequence, ISLLHST, that strongly associates with a perovskite ferroelectric, lead zirconium titanate, $Pb(Zr_xTi_{1-x})O_3$ (PZT). The affinity and selectively of binding to polycrystalline MOCVD deposited PZT thin films supported on $Si/SiO_2/Pt$ substrates were determined by titering and immunofluorescence microscopy, and the peptide was shown to selectively bind PZT in the presence of Pt, Si, Au, and several different photoresists. Ferroelectric properties were determined by measurement of the $P - E$ hysteresis loop on unmodified and phage bound PZT thin films, and no change in the coercive field, $E_c$, or the saturation polarization, $P_s$ was observed after contacting the PZT with aqueous buffer or phage binding. This work represents an important first step towards rendering perovskite ferroelectrics compatible with biological molecules. Work is currently underway to study how conformational and positional control of tethered biomolecules can be controlled by the surface charge and/or polarization state of PZT as well as integration into several proto-type device architectures.

**10:00**
**G25 9 Bio-based Polymer Foam from Soyoil** LAETITIA M. BONNAILLIE, RICHARD P. WOOL, *Dept Chemical Engineering, University of Delaware* The growing bio-based polymeric foam industry is presently lead by plant oil-based polyols for polyurethanes and starch foams. We developed a new resilient, thermosetting foam system with a bio-based content higher than 80%. The acrylated epoxidized soybean oil and its fatty acid monomers is foamed with pressurized carbon dioxide and cured with free-radical initiators. The foam structure and pore dynamics are highly dependent on the temperature, viscosity and extent of reaction. Low-temperature cure hinds the destructive pore coalescence and the application of a controlled vacuum results in foams with lower densities $\sim$ 0.1 g/cc, but larger cells. We analyze the physics of foam formation and stability, as well as the structure and mechanical properties of the cured foam using rigidity percolation theory. The parameters studied include temperature, vacuum applied, and cross-link density. Additives bring additional improvements: nucleating agents and surfactants help produce foams with a high concentration of small cells and low bulk density. Hard and soft thermosetting foams with a bio content superior to 80% are successfully produced and tested. Potential applications include foam-core composites for hurricane-resistant housing, structural reinforcement for windmill blades, and tissue scaffolds.

**10:12**
**G25 10 Calculation of the Vibrational Continuum in Helical Polymers from First Principles: Application to Single-walled Carbon Nanotubes** HADLEY LAWLER, CARTER WHITE, *Naval Research Laboratory* JOHN MINTMIRE, *Oklahoma State University* A first-principles method for calculation of the full vibrational continuum in helical polymers is presented, with application to chiral single-walled carbon nanotubes. The dynamical matrix is calculated within a helical symmetry, utilizing a cylindrical basis for nuclear displacements. Sum rules within a helical symmetry, helical speeds of sound and helical flexure modes are addressed.

**10:24**
**G25 11 Optimizing the Geometry of Patterned Polymer Separation Media** DAVID HOAGLAND, *Univ. of Massachusetts Amherst* HELMUT STREY, *Stony Brook Univ.* A quantitative understanding of polymer transport in patterned polymer separation media would guide the design of media with optimized pattern geometries. For example, one might desire to know what confinement geometry best separates linear polymers by molecular weight as a driving field is applied to a polymer mixture. By asserting that transport is controlled by steric interactions with a periodic pore structure, and that the driving field is low enough for a linearity in the relationship between transport rate and field magnitude, we have derived a simple, general expression for polymer mobility as a function of parameters characterizing polymer and pattern. Our expression can be used to derive optimized separation geometries that can be produced by micro- or nano-lithography methods. Analysis will be discussed for several pattern geometries that exert periodic constriction on migrating polymers. Financial support: UMass MRSEC



## SESSION G26: FOCUS SESSION: TRAPPING OF NANOSCALE BIOLOGICAL OBJECTS
**Tuesday Morning, 14 March 2006; 323, Baltimore Convention Center at 8:00**
**W. E. Moerner, Stanford University, presiding**

***Invited Papers***

**8:00**
**G26 1 The Anti-Brownian Electrokinetic Trap (ABEL trap).***
ADAM COHEN, *Stanford University*

The Anti-Brownian Electrokinetic Trap (ABEL trap) provides a means to trap and manipulate individual nanoscale objects in solution. The ABEL trap works by monitoring the Brownian motion of a single fluorescent particle of interest, and then applying a feedback electric field to the solution so that the resulting electrokinetic drift exactly cancels this Brownian motion. The ABEL trap can trap objects far smaller than can be trapped by laser tweezers. I will describe

experiments on individual trapped molecules of fluorescently labeled λ-DNA. Due to its non-perturbative nature, the ABEL trap allows us to perform the first detailed studies of the conformation of individual DNA molecules in their equilibrium, unstretched state. We find that each molecule has a spectrum of conformational modes, and we experimentally determine the transition rates between modes. We compare the data to Rouse and Zimm models of polymer dynamics.

*This work was done in the lab of W. E. Moerner at Stanford University and was supported by a Hertz Foundation Fellowship.

***Contributed Papers***

**8:36**

**G26 2 The ac electrokinetic elongation mechanism of DNA.** CHRISTOPH WALTI, *University of Leeds* ANDRE GERMISHUIZEN, *University of Cambridge* PAUL TOSCH, *University of Leeds* CLEMENS KAMINSKI, *University of Cambridge* GILES DAVIES, *University of Leeds* The manipulation of molecules in a controlled manner is a crucial prerequisite for the emerging field of molecular nanotechnology. AC electrokinetics provide a powerful tool for both positioning and manipulation of molecules, as well as for inducing conformational changes in DNA. We performed three-dimensional imaging measurements of fluorescently labelled DNA strands tethered to gold microelectrodes and subjected to strong ac electric fields. The observed elongation patterns are compared with previously determined fluid flow patterns and with the electric field lines obtained from numerical simulations. We demonstrate that the major contribution to the elongation of the DNA molecules stems from the ac electrokinetic torque, supplemented by a small bias force provided by the electric-field-induced fluid flow. Further, we show that the observed restricted elongation owing to the geometry of the electrode results from a sign change in the bias force.

**8:48**

**G26 3 Tracking-FCS: Correlation Spectroscopy of Individual Particles** ANDREW BERGLUND, HIDEO MABUCHI, *California Institute of Technology* Recently developed methods for trapping and tracking fluorescent particles have already been exploited for monitoring free diffusion with high spatial accuracy. These achievements suggest the possibility of performing fluorescence correlation spectroscopy (FCS) on an individual molecule as it moves freely in solution. Such an approach may enable, for example, the investigation of heterogenous folding dynamics in protein molecules in their native environment. In this talk, we will discuss our own experimental and theoretical approach to this problem. We use a spatially modulated Gaussian excitation laser and lock-in detection in order to track fluorescent particles in two dimensions. We show that Ornstein-Uhlenbeck statistics are appropriate for describing the fluctuations of a tracked particle, and we apply a generalization of the familiar (free particle) FCS equations to the situation in which a tracked particle is observed for a long period of time. Based on the same statistical model, we calculate absolute limits on the accuracy with which a particle of a given brightness and diffusion coefficient can be tracked using similar methods. Our results establish a framework for interpreting fluorescence time series and determining the feasibility of near-term goals in single-particle tracking experiments.

**9:00**

**G26 4 Flexible polymers under spherical confinement** ANGELO CACCIUTO, ERIK LUIJTEN, *University of Illinois at Urbana-Champaign* We compute the free energy of confinement $\Delta F$ for a flexible self-avoiding polymer inside a spherical cavity. We find two different regimes depending on the degree of compression. For moderate confinement the free energy exhibits a power-law dependence on the diameter $D$ of the cavity. At larger packing fraction $\phi$, however, the excluded-volume interactions between monomers dominate and the scaling law breaks down. We demonstrate that in the low density regime $\beta\Delta F$ scales as $(R_G/D)^{3/(3\nu-1)}$, where $R_G$ is the radius of gyration of the unconstrained polymer. This behavior differs from what is observed for confinement inside an infinitely long cylinder or between parallel plates, $\beta\Delta F \sim (R_G/D)^{1/\nu}$. On the basis of our results we revisit the problem of the escape through a hole of a spherically confined polymer and provide a corrected scaling prediction for the average escape time.

**9:12**

**G26 5 Dynamic effects in alignment of biological macromolecules for diffraction experiments.*** D. STARODUB, U. WEIERSTALL, K. SCHMIDT, R. B. DOAK, P. FROMME, J. C. H. SPENCE, Molecular alignment by means of anisotropic polarizability interaction with a laser electric field is the crucial step in the recently proposed serial diffraction of non-crystallizable proteins, where protein damage is prevented by recording the x-ray diffraction pattern from an array of identically oriented proteins passing through the intersection of x-ray and laser beams. The proteins can be delivered using a periodically triggered Rayleigh beam of doped water droplets. The behavior of a small globular protein (lysozyme), a large protein complex (ribosome) and a rod-like virus (TMV) in a water droplet and a gas damping cell at various pressures is considered. Optimum conditions for alignment in terms of laser power, pressure in a damping cell and adiabatic field switch-on are discussed. The degree of molecular alignment depends on these conditions and has to be sufficient to obtain sub-nanometer resolution in the charge density maps recovered from diffraction patterns.

*Supported by NSF funding SGER DBI-0429814 and CBST

**9:24**

**G26 6 Directed Cell Assembly with Magnetic Nanowires** EDWARD J. FELTON, MARCIE JAFFEE, DANIEL H. REICH, *Department of Physics and Astronomy, Johns Hopkins University* CHRISTOPHER S. CHEN, *Department of Bioengineering, University of Pennsylvania* Control of the positioning and movement of mammalian cells in culture has a variety of important applications ranging from medical diagnostics to tissue engineering. We

have developed cell manipulation techniques that exploit the magnetic properties of high aspect ratio nanoparticles such as ferromagnetic nanowires. The large remanent magnetization of these nanoparticles permits delivery of cells bound to them to precise locations on biochips through the nanoparticles' interactions with the magnetic fields of micropatterned magnetic structures. Together with chemical functionalization of the surfaces to direct cell adhesion, a wide range of multicellular patterns can be achieved. These approaches have been used to produce directed assemblies of cells. Results of these experiments include localized heterotypic cell pairs and the extension of these techniques to cell localization in three dimensions.

*Invited Papers*

**9:36**
**G26 7 Tracking Protein-coated Particles in 3D.***
ENRICO GRATTON, *University of California at Irvine*

The utilization of 2-photon microscopy in the field of Cell Biology is of increasing importance because it allows imaging of living cells, including those systems where UV imaging is not possible due to photobleaching or photodamage limitations. We propose a novel approach using 2-photon excitation based on the use of a scanner to produce an effective ''intensity trap.'' As the particle moves in this trap (note that there is no force applied on the particle at the power level we are using for particle detection), the detection system continuously calculates the position of the particle in the trap. As the position of the particle is calculated with respect to the trap, the scanner position is moved to minimize the ''modulation'' of the light intensity in the trap. In practice, we set the scanner to perform an orbit around the particle in about 1 millisecond. The sampling rate is chosen such that many points (32 or 64) are acquired during the orbit. An FFT (Fast Fourier Transform) is performed on the points acquired during one orbit or after a series of orbits. The DC, AC and phase of the first harmonic of the FFT are calculated. The value of the modulation varies monotonically as the distance of the particle from the center of the orbit is increased so that for every value of the modulation we can estimate the value of the distance of the particle from the center of the orbit. The phase of the first harmonic gives the angular position of the particle with respect to the scanner zero phase which is known relative to the lab coordinates. The effective bandwidth of the tracking system depends on the maximum frequency for sinusoidal oscillation of the scanner, which is about 5 kHz for our galvano-scanner and on the number of photons needed for detecting the particle against the noise. Of course, there are other important considerations. First, if the motion of the particle is too fast such that after one orbit the particle moves too far from the new position calculated based on the previous orbit, tracking is lost since the feedback mechanism is too slow. Therefore, single molecules, which in water would move across the PSF in about 0.1 ms, cannot be tracked. We need at least a macromolecule the size of a large protein (100kD) or relatively high viscosity to increase the time a fluorescent particle can be observed in the PSF. The second consideration, perhaps the most important, is that the particle should not bleach during the length of the tracking. This is not a problem for particles made of many fluorophores, such as polystyrene fluorescent beads, which are also relatively large. Surprisingly, for relatively large particles such as viruses, photobleaching did not occur.

*In collaboration with Valeria Levim, Univeristy of Illinois at Urbana-Champaign.

*Contributed Papers*

**10:12**
**G26 8 A Device of Tracking a Single Nanometer-Sized Particle in 3D with Nanometer Resolution and Millisecond Response Time.** HU CANG, *Lawrence Berkeley National Lab.* C. SHAN XU, *University of California Berkeley* DANIEL MONTIEL, *University of California Berkeley* HAW YANG, *University of California Berkeley* We demonstrate a microscope system based on a confocal setup that can 'track' a moving particle in three dimensions (3D) and 'trap' it at a target position with nanometer spatial and millisecond time resolution. This is achieved by moving a 3D piezoelectric translation stage controlled by a feedback circuit to 'cancel' the displacement of the particle. By keeping the target particle inside the confocal volume, it is now possible to perform other spectroscopic experiments on the particle simultaneously for a long time while the particle is moving freely in solutions. Our device overcomes the difficulty of single molecule spectroscopy (SMS) experiment on free moving samples.

**10:24**
**G26 9 Nanoscale molecular traps*** CHIA-FU CHOU, QIHUO WEI, JIAN GU, FREDERIC ZENHAUSERN, *Arizona State University* NATHAN SWAMI, *University of Virginia* We have constructed nanoscale molecular traps using electrodeless, or insulator-based, dielectrophoresis [1,2]. The molecular traps consist an array of nanoscale dielectric constrictions defined using electron-beam lithography on nanofluidic passages. The device was then sealed using an extremely simple room-temperature sealing process with virtually no pressure applied. Upon the application of an external ac electric field, the field will be focused at the constrictions and high field gradient can be generated to trap molecules dynamically in aqueous solutions. We demonstrated the trapping of small protein molecules in an array of these nanoscale molecular traps down to 50 nm in size. [1] C.F. Chou, J.O. Tegenfeldt, O. Bakajin, S.S. Chan, E.C. Cox, N. Darnton, T.A.J. Duke, R.H. Austin (2002). ''Electrodeless Dielectrophoresis of Single and Double Stranded DNA,'' Biophys. J. **83**, 2170-2179. [2] C.F. Chou, F. Zenhausern (2003). ''Electrodeless Dielectrophoresis for

Micro Total Analysis Systems,'' IEEE Eng. Med. Biol., Nov./Dec., 62-67.

*C.F.C. and N.S.S. acknowledge the support from NSF BES Award No. 0403963 for this work.

**10:36**
**G26 10 Internal Structure, Fluctuations and Micromechanical Properties of Bovine Arterial Endothelial Cells: An Optical Tweezers Study*** CAROLYN PERRETTA, SHEENA FARRELL, OLGA LATINOVIC, H. DANIEL OU-YANG, The purpose of this study is to probe the micromechanical properties of cultured bovine arterial endothelial cells by using optical tweezers to trap endogenous granular structures in the cells. A novel application of oscillating optical tweezers and coherent detection of the forced oscillation of the trapped particle enables us to measure the viscoelastic properties in soft matter with a broad frequency range and with a high data sampling rate. This study was designed to determine the difference between the viscoelasticity of the cytoskeleton around granular structures in close vicinity of the nucleus and around the cell's edge. Time dependent measurements of the mechanical properties at a fixed oscillation frequency revealed pronounced fluctuation in living cells, indicating local dynamics of the cytoskeleton around the probed particle. Possible causes for the fluctuations will be discussed.

*This experiment was made possible by funding from the NSF-DMR 0421259 and the NSF-REU Site Program at Lehigh University.

**10:48**
**G26 11 Atomic force microscopy electrostatic nanolithography for proteins study in wiseana iridovirus and barley chromosomes** EWA ROWICKA, OLGA MAYEVSKA, SERGEI LYUKSYUTOV, *The University of Akron, OH* MEGUMI SASOU, SHIGERU SUGIYAMA, *National Food Research Institute, Japan* Manipulation of proteins and DNA at the nanoscale has been studied using atomic force microscopy electrostatic nanolithography (AFMEN) for two different biological objects: iridovirus wiseana, and stained barley chromosomes. Partially relaxed chromosomes were characterized using scanning near field optical/atomic force microscopy based on bent-type optical probe, which was used as a cantilever for constant force AFM mode. Virus capsids and chromosomes can be treated as polarized dielectrics in strong non-uniform electric field (up to $10^9$ $Vm^{-1}$) induced by biased AFM tip. It is suspected that an electric field inside a polar medium produces energy densities sufficient for either structural changes or reorganization of the protein structure. Recent results related to manipulation of proteins using AFMEN will be presented.



## SESSION G27: FOCUS SESSION: NOVEL COMPUTATIONAL ALGORITHMS II
**Tuesday Morning, 14 March 2006; 324, Baltimore Convention Center at 8:00**
**Barry Schneider, National Science Foundation, presiding**

***Invited Papers***

**8:00**
**G27 1 Optimization of Large Scale Matrix Computations for Multi-length Scale Structured Matrices.***
ZHAOJUN BAI,† *University of California, Davis*

Quantum monte carlo simulation of interacting electron systems is an increasingly powerful tool in investigating many of the most fundamental properties of materials, such as their magnetic and optical response, and conductivity. However, the simulations are currently limited to a few hundred particles. The primary bottleneck is the calculation of the inverse of a multi-length and highly structured matrix. In this talk, we will report our recent progress on this problem. We first present a semi-direct solver which is numerically stable and robust by a novel self-adapting block cyclic reduction technique depending on the parameters of the problem. The new solver is more than an order of magnitude faster than existing techniques. Then we will present robust preconditioning techniques in iterative solvers which can effectively precondition the matrices at much stronger coupling and lower temperatures than had hitherto been possible.

*Supported by NSF ITR grant DMR-0313390
†Joint work with Wenbin Chen, Richard Scalettar and Ichitaro Yamazaki

***Contributed Papers***

**8:36**
**G27 2 Equilibration of walkers and correlation of samples in QMC simulations** D. NISSENBAUM, B. BARBIELLINI, A. BANSIL, *Northeastern U.* When using the Metropolis algorithm from an unequilibrated starting point to obtain properly distributed samples for a Quantum Monte Carlo (QMC) calculation, and when analyzing the accuracy of the results after equilibration, one needs to properly handle two factors: the time taken for the walkers to equilibrate, and the presence of correlations in the sample points after the walkers have equilibrated. Inclusion of unequilibrated data gives a bias to the computed averages, while dealing appropriately with correlated data is essential in order to obtain accurate error bars. In this connection, we are developing reliable techniques to determine equilibration time and compute observable error bars. We present a careful study of several Li clusters, ranging from the Li dimer to a cluster containing 64 Li atoms, and focus particularly on scaling properties of the equilibration time with the size of the system. Work supported in part by the US-DOE.

**8:48**
**G27 3 Configuration Space Renormalization (CSR): a study of fractional quantization of charge in a dual-edge fractional quantum Hall system.** EUGENE TSIPER, *George Mason University and Naval Research Lab, Washington DC* A renormalization procedure is designed to find a subspace of high relevance in a many-body Hilbert space. Substantial reduction in the basis size can be achieved while approaching the exact diagonalization results. The idea is to search for a set of many-particle configurations that contribute the largest weight to the exact solution of the many-body Schrödinger equation, without actually computing the exact solution. We start with some suitable set of $K$ configurations and find the ground state of the Hamiltonian in the many-body subspace that they span. We then retain $K' < K$ configurations by discarding the ones which have little weight. We then re-expand our set with the new configurations that have large matrix elements with those retained. When repeated, the procedure converges after several iterations and yields some optimal set of configurations. The resulting truncation of the Hilbert space is essentially many-body, and cannot be achieved by truncating or rotating the single-particle basis. I will discuss an application of CSR to model resonant tunneling between the edges in the fractional quantum Hall regime, which has been used to experimentally observe fractional quantization of electric charge. Clusters large enough to contain two unconnected edges are modeled. The results suggest fractional quantization of the quasiparticle charge in units of $e/3$ and $e/5$ at fillings 1/3 and 2/5.

**9:00**
**G27 4 New eigensolvers and preconditioners for large scale nanoscience simulations*** ANDREW CANNING, OSNI MARQUES, LIN-WANG WANG, CHRISTOF VOEMEL, *CRD, Lawrence Berkeley National Laboratory* STANIMIRE TOMOV, JULIEN LANGOU, *University of Tennessee* First-principles materials science calculations typically involve a self-consistent solution of the Kohn-Sham equations. These types of methods typically scale with the cube of the system size and can only be used to study systems of up to a thousand atoms. To study larger systems we use semi-empirical potentials or approximated ab initio potentials such as those constructed using the charge patching method. Using these types of potentials does not require a self-consistent solution of our effective single particle equations and we can solve directly for the few states of interest around the gap. This leads to a method that is effectively O(N) if we consider the number of states we require to be fixed as the system size increases. The solution of our single particle equations now becomes an interior eigenvalue problem for a few states around a given energy rather than the self-consistent solution for the lowest n states where n is the number of bands. I will compare different methods (conjugate gradient, Jacobi-Davidson, Lanczos) for this problem with particular emphasis on solving large nanosystems on parallel computers. Work supported by the DOE under the Modeling and Simulation in Nanoscience Initiative.

*Work supported by the DOE under the Modeling and Simulation in Nanoscience Initiative



***Invited Papers***

**9:12**
**G27 5 Turbocharging time-dependent density-functional theory with Lanczos chains.**
STEFANO BARONI, *SISSA and Democritos National Simulation Center*

Using a super-operator formulation of linearized time-dependent density-functional theory, the dynamical polarizability of a system of interacting electrons is represented by a matrix continued- fraction whose coefficients can be obtained from the non-symmetric block- Lanczos method. The resulting algorithm, which is particularly convenient when large basis sets are used, allows for the calculation of the full spectrum of a system with a computational workload only a few times larger than needed for static polarizabilities within time-independent density-functional perturbation theory. The method is demonstrated with calculation of the spectrum of benzene and of fullerene, and prospects for its application to the large-scale calculation of optical spectra are discussed.

***Contributed Papers***

**9:48**
**G27 6 Large-Scale First-Principles Molecular Dynamics Simulations on the BlueGene/L Computer** FRANCOIS GYGI, *University of California Davis, Davis, CA 95616* ERIK W. DRAEGER, *Lawrence Livermore National Laboratory, Livermore, CA 94551* We present the results of large-scale First-Principles Molecular Dynamics (FPMD) simulations performed on the BlueGene/L computer, using up to 65,536 processors. Simulations involving 1000 molybdenum atoms were carried out using the Qbox code with non-local, norm-conserving pseudopotentials. A parallel efficiency of 85% can be attained when solving the same problem on partitions ranging from 512 nodes to 32,768 nodes. When using 65,536 processors, a floating point performance of 64 Tflops is reached. Optimization of the logical-to-physical mapping of tasks is essential in order to achieve this performance on the BlueGene/L torus architecture. We discuss the challenges encountered when implementing FPMD in the plane-wave, pseudopotential formalism on 10,000 processors and beyond. Part of this work was performed under the auspices of the U.S. Dept. of Energy at the University of California/Lawrence Livermore National Laboratory under contract no. W-7405-Eng-48.

**10:00**
**G27 7 Linear Scaling First-Principles Molecular Dynamics with Plane Waves accuracy*** JEAN-LUC FATTEBERT, *Lawrence Livermore National Laboratory, Livermore, CA 94551* FRANCOIS GYGI, *UC Davis, Davis, CA 95616* As an alternative to the Plane Waves (PW) approach for highly accurate and unbiased Density Functional Theory molecular dynamics simulations with pseudopotentials, we propose to use a real-space finite differences discretization and a localized orbitals representation of the electronic structure. As in the PW approach, the discretization error can be reduced systematically by decreasing the mesh spacing, while the truncation error due to orbitals localization constraints decreases exponentially with the size of the localization regions. Accurate atomic forces can be computed and allow microcanonical molecular dynamics simulations. Using a supercell

of 512 water molecules, we demonstrate an excellent energy conservation for localization regions large enough. We propose an explanation for the negative energy drift observed for smaller radii based on the presence of local minimas. Our implementation demonstrates an effective scaling complexity close to linear with the system size and a good parallel scaling with the number of processor.

*This work was performed under the auspices of the U.S. Department of Energy by University of California Lawrence Livermore National Laboratory under contract No. W-7405-Eng-48

**10:12**

**G27 8 Basis set limit and systematic errors in local-orbital based all-electron DFT** VOLKER BLUM, JÖRG BEHLER, RALF GEHRKE, KARSTEN REUTER, MATTHIAS SCHEFFLER, *Fritz-Haber-Institut, Faradayweg 4-6, 14195 Berlin, Germany* With the advent of efficient integration schemes,[1,2] numeric atom-centered orbitals (NAO's) are an attractive basis choice in practical density functional theory (DFT) calculations of nanostructured systems (surfaces, clusters, molecules). Though all-electron, the efficiency of practical implementations promises to be on par with the best plane-wave pseudopotential codes, while having a noticeably higher accuracy if required: Minimal-sized effective tight-binding like calculations and chemically accurate all-electron calculations are both possible within the same framework; non-periodic and periodic systems can be treated on equal footing; and the localized nature of the basis allows in principle for $O(N)$-like scaling. However, converging an observable with respect to the basis set is less straightforward than with competing systematic basis choices (e.g., plane waves). We here investigate the basis set limit of optimized NAO basis sets in all-electron calculations, using as examples small molecules and clusters ($N_2$, $Cu_2$, $Cu_4$, $Cu_{10}$). meV-level total energy convergence is possible using $\leqslant$ 50 basis functions per atom in all cases. We also find a clear correlation between the errors which arise from underconverged basis sets, and the system geometry (interatomic distance). [1] B. Delley, J. Chem. Phys. **92**, 508 (1990), [2] J.M. Soler *et al.*, J. Phys.: Condens. Matter **14**, 2745 (2002).

**10:24**

**G27 9 Iterative Optimized Effective Potential and Exact Exchange Calculations at Finite Temperature** N.A. MODINE, *Sandia National Laboratories* R.A. LIPPERT, *MIT Department of Mathematics* A.F. WRIGHT, R.P. MULLER, M.P. SEARS, A.E. MATTSSON, M.P. DESJARLAIS, *Sandia National Laboratories* We report the implementation of an iterative scheme for calculating the Optimized Effective Potential (OEP). Given an energy functional that depends explicitly on the Kohn-Sham wave functions, and therefore, implicitly on the local effective potential appearing in the Kohn-Sham equations, a gradient-based minimization is used to find the potential that minimizes the energy. Previous work has shown how to find the gradient of such an energy with respect to the effective potential in the zero-temperature limit. We discuss a density-matrix-based derivation of the gradient that generalizes the previous results to the finite temperature regime, and we describe important optimizations used in our implementation. We have applied our OEP approach to the Hartree-Fock energy expression to perform Exact Exchange (EXX) calculations. We report our EXX results for common semiconductors and ordered phases of hydrogen at zero and finite electronic temperatures. We also discuss issues involved in the implementation of forces within the OEP/EXX approach. Sandia is a multiprogram laboratory operated by Sandia Corporation, a Lockheed Martin Company, for the United States Department of Energys National Nuclear Security Administration under contract DE-AC04-94AL85000.

**10:36**

**G27 10 Towards an exact treatment of exchange and correlation in materials: Application to CO adsorption at transition-metal surfaces** MATTHIAS SCHEFFLER, QING MIAO HU, KARSTEN REUTER, *Fritz-Haber-Institut der Max-Planck-Gesellschaft, Faradayweg 4-6, D-14195 Berlin, Germany* We present an efficient scheme to correct the errors of density-functional theory (DFT) exchange-correlation (xc) functionals. The method locally corrects the xc interaction by analyzing clusters of the same local geometry as that of the calculations for the extended system. **The correction** is found to rapidly approach a universal dependence with cluster size, exhibiting a simple analytical behavior. As a consequence it is shown how high-quality cluster studies (e.g. using B3LYP, HF+MP2, or QMC) can be used to determine the DFT-LDA/GGA error for extended systems. The method is particularly efficient for defects in the bulk and at surfaces. — The approach is applied to CO adsorption at transition metals, where present xc functionals dramatically fail to predict the correct adsorption site.[1] The correct (experimentally confirmed) geometry is obtained by the correction scheme, and the origin of the LDA/GGA failure is discussed. [1] P.J. Feibelman, B. Hammer, J.K. Norskov, F. Wagner, M. Scheffler, R. Stumpf, R. Watwe, and J. Dumesic, The CO/Pt(111) puzzle. J. Phys. Chem. B 105, 4018 (2001).

**10:48**

**G27 11 Efficient Method for Electron-Phonon Coupling in Molecules and Nanoscale Systems** BEN POWELL, *University of Queensland, Brisbane, Queensland 4072, Australia* MARK PEDERSON, *Naval Research Laboratory* TUNNA BARUAH, *University of Texas El Paso* The coupling between electrons and phonons plays important roles in physics, chemistry and biology. However, the accurate calculation of the electron-phonon coupling constants is computationally expensive as it can involve solving the Schrödinger equation for $\mathcal{O}(3N)$ nuclear configurations, where $N$ is the number of nuclei. In analogy to the efficient field-induced extraction of IR and Raman spectra in molecules, [1] consideration of charge-induced changes in Hellman-Feynman forces as a function of electronic charge allows determination of all HOMO and LUMO electron-phonon coupling constants, including isotope dependencies, with only two SCF calculations *regardless of system size*. [2] The approach can also be used for electron-phonon interactions associated with other electronic states. The relation of this method to Janak's theorem [3] is discussed. This $\mathcal{O}(1)$ approach is numerically very stable and produces accurate results for electron-phonon coupling constants in tests on approximately 15-20 molecules ranging in size from $H_2$ to $C_{60}$. Adiabatic ionization potentials and relaxed Hubbard U parameters are presented as an example of the method. [1] D.V. Porezag and M.R. Pederson, Phys. Rev. B **54**, 7830 (1996). [2] B.J. Powell, M.R. Pederson and T. Baruah (submitted). [3] J.F. Janak, Phys. Rev. B **18**, 7165 (1978).

**SESSION G28: FOCUS SESSION: MICROPHYSICAL PROPERTIES OF BLOCK COPOLYMER AGGREGATES I**
**Tuesday Morning, 14 March 2006; 325, Baltimore Convention Center at 8:00**
**Erik Hobbie, National Institute of Standards and Technology, presiding**

*Invited Papers*

**8:00**
**G28 1 Coffee Break.**

**8:36**
**G28 2 Electric Field Manipulation of Charged Copolymer Worm Micelles.**
DENNIS DISCHER, *U. Pennsylvania*

This abstract was not received electronically.

*Contributed Papers*

**9:12**
**G28 3 Rheo-NMR measurements of shear alignment and banding in non-ionic wormlike micelles** LOUIS A. MADSEN, EDWARD T. SAMULSKI, *University of North Carolina - Department of Chemistry* RALPH H. COLBY, *Pennsylvania State University - Department of Materials Science and Engineering* BRADLEY S. DOUGLASS, PAUL T. CALLAGHAN, *Victoria University of Wellington - Department of Physics* Orientational order produces myriad nonlinear effects in complex fluids such as polymer solutions, liquid crystals, and anisotropic colloids. Wormlike micelles (WLMs) exhibit especially fascinating rheological properties since the component molecules order relative to the tube axis, which itself acts as a supramolecular polymer backbone. Equilibria between wormlike and spherical micelles may be controlled using temperature, concentration, or additives to modulate properties (e. g., viscosity) over several orders of magnitude. We have investigated a new class of WLMs composed of non-ionic triblock copolymers (PEO-PPO-PEO) mixed with alcohol additives to stabilize the core. We have employed in-situ rheo-NMR spectroscopy and microscopy in a Couette shear cell to observe the first shear-induced alignment and banding in a non-ionic block-copolymer system. Deuterium-labeled additives exhibit gap-dependent spectral splittings, assessing the molecular alignment versus shear rate. Proton NMR microscopy probes shear banding across the Couette cell gap with resolutions down to 20 microns.

**9:24**
**G28 4 Reversible morphological transitions of polystyrene-b-polyisoprene micelles*** ISAAC LARUE, SERGEI SHEIKO, MIREILLE ADAM, MICHAEL RUBINSTEIN, *University of North Carolina at Chapel Hill* MARINOS PITSIKALIS, NIKOS HADJICHRISTIDIS, *University of Athens* Morphological transitions of polymer micelles have long been sought after. Until now, the only way to change morphology was through the addition of a co-solvent or homopolymer. We have demonstrated for the first time that reversible morphological transitions can be caused solely through changes in temperature. Two polystyrene-b-polyisoprene samples with the same sized PS block of 20kDa were purposefully synthesized with PI blocks of 4 and 6kDa to be near the spherical-cylindrical and cylindrical-vesicle boundaries. It was found that only small changes in temperature are needed to cause the morphological change. The cylindrical sample adopted a spherical morphology after heating from 25-35°C and the vesicle sample became cylindrical upon heating from 25-40°C. While cylindrical and vesicle micelles were once again observed after cooling the samples back to 25°C, the fraction and size of the micelles were still increasing after several weeks.

*This research program is supported by the National Science Foundation (ECS 0103307 and DMR 0306787)

**9:36**
**G28 5 Growth of Nanostructured Bilayers and Vesicles by Self-assembly of ABC Mikto-arm Star Terpolymers** ZHIBO LI, MARC HILLMYER,*TIMOTHY LODGE,† *University of Minnesota, Chemistry Department* MULTICOMPARTMENT MICELLE TEAM, A new class of nanostructured vesicles and bilayers were observed from aqueous self-assembly of ABC mikto-arm star terpolymers with three mutually immiscible blocks. The micellar structures depend on the relative length of each block and can be tuned to form three classical types of micelles, i.e., sphere, cylinder, and vesicles, however with nanostructured multiple core compartments. The nanostructured vesicles grow by a three-stage process: (i) segmented wormlike micelles first self-assemble upon dissolution of terpolymers in water; (ii) then nanostructured bilayer sheets with apparently hexagonal ordered internal structures grow by consumption of already existing segmented worms, and subsequently (iii) large bilayer sheets curve and close off to form vesicles. The micellar structures at various stages were imaged by cryogenic transmission microscopy.

*Advisor & corresponding author
†Advisor & corresponding author

**9:48**
**G28 6 Self-Assembly of Block Copolymers in an Ionic Liquid** YIYONG HE, ZHIBO LI, TIMOTHY P. LODGE, *Department of Chemistry, and Department of Chemical Engineering and Materials Science, University of Minnesota, 55455* Amphiphilic diblock copolymers poly((1,2-butadiene)-*b*-ethylene oxide) (PB-PEO) were shown to aggregate and form well-defined micelles in an ionic liquid, 1-butyl-3-methyl imidazolium hexafluorophosphate ([BMIM][PF6]). The universal sequence of micellar structures (spherical micelle, wormlike micelle, and bilayered vesicle) were all resolved by varying the block copolymer composition. For the first time, the nanostructures of PB-PEO micelles formed in an ionic liquid were directly visualized by cryogenic transmission electron microscopy (cryo-TEM). The detailed micelle struc-

ture information was extracted from cryo-TEM and dynamic light scattering (DLS) measurements, and compared to their aqueous counterparts. The work demonstrates the feasibility of controlling micellar nanostructures of amphiphilic block copolymers in ionic liquids, and also provides important knowledge for further applications of copolymers for forming microemulsions and ion gels.

**10:00**

**G28 7 Controlling PS-b-PEO Morphologies by Solution Conditions** PRACHUR BHARGAVA, XIAOLIANG ZHENG, YINGFENG TU, STEPHEN Z.D. CHENG, MAURICE MORTON INSTITUTE OF POLYMER SCIENCE, THE UNIVERSITY OF AKRON TEAM, We have investigated the self-assembly behavior of amphiphilic diblock copolymer polystyrene-b-poly(ethylene oxide) (PS-b-PEO) in DMF/water and DMF/acetonitirile mixtures.The morphology of the block copolymer can be controlled in both these systems by varying copolymer concentration and solvent composition The morphologies were visualized directly by transmission electron microscopy. Increasing the water content in the DMF/water mixture or acetonitrile in the DMF/acetonitrile mixture changes the morphology from spheres to worm-like/rods and then to vesicles. Increasing the copolymer concentration shows a similar effect on the morphology. The block copolymer exhibits distinct phases of both exclusive and mixed morphologies. The morphological transitions were also captured by static light scattering and turbidity measurements. Although the trend in morphological changes is similar, there are remarkable differences in the morphological phase behavior of PS-b-PEO in the two solvent systems and thus the role of the 'selective solvent' in such systems is also evidenced.

**10:12**

**G28 8 Formation of Toroid Micelles: Mechanism and Size Control** HONGGANG CUI, KELLY HALES, ZHIBIN LI, DARRIN POCHAN, *Department of Materials Science and Engineering, University of Delaware, Newark, DE 19716* ZHIYUN CHEN, KAI QI, KAREN WOOLEY, *Department of Chemistry, Washington University in Saint Louis, Saint Louis, MO 63130* The toroid micelle morphology has been produced by the self assembly of poly(acrylic acid)-block-poly(methyl acrylate)-block-polystyrene triblock copolymer via interaction with organic diamines in mixed THF/H2O solution. The formation mechanism has been investigated from three aspects: (i) chain structure of organic counterions, including spacer length, chain hydrophobicity and the number of amine groups; (ii) molecular structure of triblock copolymer, including block length of polystyrene and chain architecture; (iii) variation of solution component, such as different ratios of THF to water and different ratios of amine groups to acid groups. It was found that toroids can be constructed either via a cylinder-toroid transition through elimination of high-energy, cylinder ends, or via a disc-toroid transition by disc perforation from the center. The prevalent mechanism depends on the chain length of polystyrene and the chain structure of diamines. Stability of the toroids was studied by varying the ratio of THF to water, and by applying a perturbation of either heat or sonication. Interestingly, the size of the toroids can be controlled by the amount of added diamines. The toroid morphology was characterized by means of cryo-TEM, SANS and light scattering.

**10:24**

**G28 9 Kinetics of chain exchange in diblock copolymer micelles** CHUN-CHUNG CHEN, ELENA E. DORMIDONTOVA, *Macromolecular Science and Engineering, Case Western Reserve University, Cleveland, Ohio 44106* Chain kinetic properties in the core of diblock copolymer micelles were studied using Monte Carlo simulations. In order to escape, a polymer chain first has to assume a compact conformation near the surface of the core. In our simulations, we studied the process of conformational changes of the core-forming block before it is ready to escape from a micelle. The radius of gyration or maximum distance of chain monomers from the core-corona interface were used as criteria to assess the compactness of the chain conformation and therefore its readiness to escape. When the chain exchange kinetics is limited mainly by the rate of conformational changes, the survival fraction of the original chains follows stretched exponential behavior. This is in contrast to theoretical predictions of a single activation process for unimer exchange in diblock copolymer micelles. In our simulations, we recover a single exponential behavior of the survival fraction only for the cases of very low escape probabilities. Increasing the width of the core-corona interface while maintaining the same aggregation number makes it easier for a chain to achieve a ready-to-escape conformation. This accentuates the stretched exponential behavior for the survival fraction which in turn shows a nearly logarithmic decay for a considerable portion of the overall time range.

**10:36**

**G28 10 Chain Exchange Kinetics in Diblock Copolymer Micelles: Comparison of Experimental and Simulation Results** ELENA DORMIDONTOVA, CHUN-CHUNG CHEN, *Department of Macromolecular Science and Engineering, Case Western Reserve University, Cleveland, Ohio 44106, USA* REIDAR LUND, LUTZ WILLNER, DIETER RICHTER, *Institut fuer Festkoerperforschung, Forschungszentrum Juelich, Germany* The exchange of chains between polymeric micelles in equilibrium has been studied experimentally using a novel Time Resolved Small Angle Neutron Scattering technique and modeled using Monte Carlo (MC) simulations. The experiments for PS-PB in alkanes and PEP-PEO micelles in DMF/water solutions revealed a logarithmic time dependence of the exchange kinetics. In the simulations, the time dependence of surviving chains ranges from a single exponential to stretched exponential behavior and is found to be strongly influenced by the chain conformation and escape criteria. In agreement with the experiments, a logarithmic time dependence was found in the MC simulations for an intermediate time range for micelles with a large number of escapable chains from micelle core and low probability of escaping or for micelles with a broader core-corona interface. The MC results suggest that dynamics of conformational rearrangements in a micelle core plays a decisive role in the micelle exchange kinetics.

**10:48**

**G28 11 Dynamics of Polystyrene-Polyisoprene (PS-PI) Micelles in Selective Solvents.** DVORA PERAHIA, *Chemistry Department Clemson University, Clemson SC 29634-0973* GANG CHENG, *Chemistry Department Clemson University, Clemson SC 29634-0973* We have recently shown that dissociation of isotropic-to-micelles phase transition of PS-PI micelles in decane

takes place gradually where the micelles dissociated into smaller ones and eventually into a unimolecular micelles where the polystyrene is surrounded by the polyisprene. In here we report the dynamics of the PS-PI block as studied by neutron spin echo experiments as the dissociation takes place. With increasing temperature the entire system becomes more dynamic as expected. However on the length scale of the size of the micelle, the diffusion is constrained up to temperatures where most of the micelles, have dissociated whereas on the segmental level the dynamics is characteristic of that of a free molecule. The dynamics with in the micelle and the nature of the dissociation transition will be discussed.

**SESSION G29: FOCUS SESSION: PHYSICAL AND ENGINEERING CONSTRAINTS ON THE FUNCTION OF BIOLOGICAL SYSTEMS**
**Tuesday Morning, 14 March 2006; 326, Baltimore Convention Center at 8:00**
**Partha Mitra, Cold Spring Harbor Laboratory, presiding**

*Invited Papers*

**8:00**
**G29 1 A Framework for Globular Proteins.***
TIMOTHY LEZON, *Pennsylvania State University*

Due to their remarkable chemical specificity and diversity, globular proteins play a crucial role in the network of molecular interactions of life. Over the past several decades, much experimental data has been accumulated on proteins, but the overarching principles that govern the general features of proteins remain largely unknown. Here, a novel framework for understanding many key attributes of globular proteins is presented. This framework suggests that the characteristics of globular proteins that make them well-suited for biological function are the emergent properties of a unique phase of matter. Implications of this picture include the provision of a fixed backdrop for molecular evolution and natural selection and design restrictions on molecular machinery. The work described here was carried out in collaboration with Jayanth Banavar and Amos Maritan.

*This research was supported in part by NSF IGERT grant DGE-9987589.

*Contributed Papers*

**8:36**
**G29 2 Chiral Heterorecognition of Organic Molecules and Inorganic Surfaces** THOMAS GREBER, RICHARD SCHILLINGER, JOACHIM WIDER, *Physik Institut der Universitat Zurich, Switzerland* ZELIKO SLJIVANCANIN, *IRRMA, Ecole Polytechnique Lausanne, Switzerland* BJORK HAMMER, *Department of Physics and Astronomy and iNANO, University of Aarhus, Denmark* Atomic kinks on surfaces are chiral and may thus be used to distinguish left-handed from right-handed molecules. Two distinct non-mirror-symmetric conformations of D- and L-cysteine were found after adsorption on Au(17 11 9)$^S$. This demonstrates chiral heterorecognition, i.e. enantioselectivity of *S*-kinks on vicinal Au(111). The structures as determined by angle scanned X-ray photoelectron diffraction (XPD) agree well with those from density functional theory (DFT) calculations. The calculations predict adsorption energies of $\approx$ 2 eV where D-cysteine binds 140 meV stronger than L-cysteine. The classical three point contact model for molecular recognition fails to explain these findings.

**8:48**
**G29 3 Nucleotide Mutation and Amino Acid Evolution** JOSE PARRA, BERNARD GERSTMAN, *Department of Physics, Florida International University* We have found a set of nucleotide coupling propensities (ncp) that best reproduces the currently observed probability distribution of amino acids found in protein data banks. These ncp represent the biochemical potentials that produce different probabilities for different mutations within a sequence of nucleotides. We have allowed these ncp to act on a random sequence of nucleotides whose codons initially produce a random arrangement of amino acid residues. Interestingly, though the mutating action of the ncp on the chain of nucleotides results in the correct evolution of the probability of appearance of each individual amino acid towards the present distribution, there is however no evolutionary trend in major global characteristics of the amino acid distribution. We present results that show that properties of amino acids that are considered important for protein structure do not evolve on average, such as: hydrophobic/hydrophilic, size, aromatic/non-aromatic, aliphatic/non-aliphatic, helical-preference/beta-strand.

**9:00**
**G29 4 Quantitative modeling and data analysis of SELEX experiments** MARKO DJORDJEVIC, *Mathematical Biosciences Inst., Ohio State Univ.* ANIRVAN M. SENGUPTA, *Dept. of Physics and BioMaPS Inst., Rutgers Univ.* SELEX (Systematic Evolution of Ligands by Exponential Enrichment) is an experimental procedure that allows extracting, from an initially random pool of DNA, those oligomers with high affinity for a given DNA-binding protein. We address what is a suitable experimental and computational procedure to infer parameters of transcription factor-DNA interaction from SELEX experiments. To answer this, we use a biophysical model of transcription factor-DNA interactions to quantitatively model SELEX. We show that a standard procedure is unsuitable for obtaining accurate interaction parameters. However, we theoretically show that a modified experiment in which chemical potential is fixed through different rounds of the experiment allows robust generation of an appropriate data set. Based on our quantitative model, we propose a novel bioinformatic method of data analysis for such modified experiment and

apply it to extract the interaction parameters for a mammalian transcription factor CTF/NFI. From a practical point of view, our method results in a significantly improved false positive/false negative trade-off, as compared to both the standard information theory based method and a widely used empirically formulated procedure. This work will appear in Physical Biology. This work was supported by NIH grant GM67794. Final parts of this work were supported by NSF under Agreement No. 0112050 and NSF grant MCB-0418891.

**9:12**
**G29 5 Low Temperature IPD AgO Bacterial Static / Bactericidal Coatings for Various Medical Applications** DANIEL STOREY, *Nexxion Corporation* NEXXION CORPORATION TEAM, Low temperature Ionic Plasma Deposition (IPD) has been successfully used to deposit silver and silver oxide large area ( $>$ 18,000 in2/hour) thin films on several types of wound care products, catheters, implantables, and surgical tools. The IPD process has been proven to be able to provide predictable infection control for short term bacterial-stasis implantable devices, to long term ( $>$ 60 day) bacterial toxicity. Silver and silver oxide has been deposited on substrates including PTFE, polypropylene, PVC, 440 stainless steel, Al2O3, and Ti6Al4V to name a few.

**9:24**
**G29 6 Energy Dependence of Cancer Cell Irradiation** RACHEL BLACK, *Hampton University* FOR CAMI COLLABORATION, A proof-of-principle experiment was done to investigate the energy damage of beta particles on cancer cells. This study is the first of its kind that spans into the MeV range. This research seeks to provide information on the possibility of monoenergetic Brachytherapy sources, reaction mechanisms of cancer cell death and cancer genome identification. It is expected that different cancer types will respond to different energies. Protein expressions from the irradiation of breast cancer cells were identified via a 2D diagram (pH versus mass) showing a strong energy dependence. Preliminary results will be presented and discussed.

**9:36**
**G29 7 Calibration Of A System For Energy Dependence Study Of Cancer Cell Irradiation** ARIANO MUNDEN, *Hampton University* FOR CAMI COLLABORATION, Calibration of individual electron energies and dose distribution exiting a dipole magnet perpendicular at the dispersive plane was performed using a collimated scintillating fiber based detector. The dipole was constructed from two 5.08x5.08x2.54 $cm^3$ permanent magnets separated by a distance of 2 cm and having a maximum filed of about 5 kG. A 1 cm diameter collimated electron beam exiting a $^{90}Sr/Y$ radioactive with a 25 $\mu$Ci activity and a 2.28 MeV maximum energy was placed at the entrance face of the magnet. Mapping of the magnetic field was done using a Hall probe with an accuracy of about 2 G. The electron detector consisted of blue shifted scintillating fibers with thicknesses of 1 mm. The setup provides an energy resolution of about 10%. This system will be used to study the differential response of cancer cell irradiation to selected energies. We will present results and discussed the results obtained from this work.



***Invited Papers***

**9:48**
**G29 8**
JOHN DOYLE, *California Institute of Technology*

This abstract was not received electronically.

***Contributed Papers***

**10:24**
**G29 9 Radiation Damage From Mono-energetic Electrons Up to 200 keV On Biological Systems** YURIY PRILEPSKIY, *Hampton University* FOR CAMI COLLABORATION, The electron gun of the CEBAF machine at Jefferson lab (Newport News, VA) is capable of delivering electrons with energies up to 200 keV with a resolution of about $10^{-5}$. This 1.5 GHz beam permits to generate cellular radiation damage within minutes. We have performed irradiation of cancer cells with different energies and different currents to investigate their biological responses. This study will permit to address the physical processes involved in the RBE and LET at a level that supersedes current data listed in the literature by orders of magnitude. We will discuss the experimental setup and results of the first stage of data collected with this novel system. This research is part of a global program to provide detailed information for the understanding of radiation based cancer treatments.

**10:36**
**G29 10 The cost of linearization** DANIELLE MOREL, WILLIAM B LEVY, *University of Virginia* Information processing in the brain is metabolically expensive and energy usage by the different components of the nervous system is not well understood. In a continuing effort to explore the costs and constraints of information processing at the single neuron level, dendritic processes are being studied. More specifically, the role of various ion channel conductances is explored in terms of integrating dendritic excitatory synaptic input. Biophysical simulations of dendritic behavior show that the complexity of voltage-dependent, non-linear dendritic conductances can produce simplicity in the form of linear synaptic integration. Over increasing levels of synaptic activity, it is shown that two types of voltage-dependent conductances produce linearization over a limited range. This range is determined by the parameters defining the ion channel and the 'passive' properties of the dendrite. A persistent sodium and a transient A-type potassium channel were considered at steady-state transmembrane potentials in the vicinity of and hyperpolarized to the threshold for action potential initiation. The persistent sodium is seen to amplify and linearize the synaptic input over a short range

of low synaptic activity. In contrast, the A-type potassium channel has a broader linearization range but tends to operate at higher levels of synaptic bombardment. Given equivalent 'passive' dendritic properties, the persistent sodium is found to be less costly than the A-type potassium in linearizing synaptic input.

**10:48**
**G29 11 Fast noniterative biexponential fluorescence lifetime imaging in the investigation of phagocyting neutrophyls**
RALUCA AURA NIESNER, *Technical University Braunschweig, Institute for Physical and Theoretical Chemistry; Society for Biotechnological Research (GBF) Braunschweig* The cofactors NADH and NADPH [NAD(P)H] belong to the principal endogenous indicators of the cellular metabolism. Since the metabolic activity of cells is given by the ratio between the concentrations of free and protein-bound NAD(P)H, the development of techniques which measure the modifications to this ratio is particularly significant. The biexponential fluorescence lifetime imaging (FLIM) is employed to discriminate between the free and the protein-bound NAD(P)H without any previous calibration. Thus a high-resolution map of the cellular metabolism, i.e. an image of the contribution of the protein-bound NAD(P)H to the cumulative NAD(P)H signal, is obtained. This method is applied in the investigation of neutrophyls phagocyting the spores of Aspergillus Fumigatus. Particularly the activation of the NADPH oxidase is studied. Since an important aspect in biological applications is to monitor the dynamics of the relevant processes, rapid techniques, e.g. fast biexponential FLIM, are needed. We implement for the first time in FLIM a noniterative method originally developed by Prony and verified it in biexponential time-domain FLIM experiments on homogenous mixtures and on different types of cells.

## SESSION G30: FOCUS SESSION: ELECTRONIC TRANSPORT IN ORGANIC FILMS
**Tuesday Morning, 14 March 2006; 327, Baltimore Convention Center at 8:00**
**Denis Fuchou, CNRS CEA-Saclay, presiding**



***Invited Papers***

**8:00**
**G30 1 Coffee Break.**

**8:36**
**G30 2 Scanning Tunneling Microscopy and Spectroscopy of Conjugated Oligomers at the Liquid-Solid Interface.**
STEVEN DE FEYTER, *Katholieke Universiteit Leuven*

Self-assembly - the spontaneous organization of molecules into stable, structurally well-defined aggregates - has been put forward as a possible paradigm for generating nanoscale templates under ambient conditions. A very convenient method for the formation of extended two-dimensional (2D) networks is physisorption at the liquid-solid interface. The preparation is relatively simple and scanning tunneling microscopy (STM) allows a detailed investigation of the structural aspects of the 2D patterns. A deep understanding and control of the spatial orientation and packing of pi-conjugated oligomers in self-assembled systems is indispensable for the development of future nanodevices. By means of STM, we have investigated the self-assembly of achiral and chiral pi-conjugated small organic molecules at the organic liquid-solid interface with submolecular resolution. In addition, by means of scanning tunneling spectroscopy (STS) we have investigated with molecular and submolecular resolution the electronic properties of isolated and stacked conjugated molecules at the liquid-solid interface. In the first part, we focus on the control of 2D molecular self-assembly of pi-conjugated systems driven by the molecular shape and/or by directional non-convalent interactions such as hydrogen bonding. Examples include alkylated molecules with a rhombus or triangle shaped pi-conjugated core, hydrogen bond forming p-phenylene vinylenes, and oligothiophenes. In the second part, we report on bias dependent imaging and STS experiments revealing information on the electronic properties of electron donor-acceptor-donor triads, and isolated and stacked oligothiophenes.

**9:12**
**G30 3 Directing molecular traffic by means of a nano-engineered surface.**
FABRICE CHARRA, *CEA Saclay*

The parallel manipulation of individual molecules is the ultimate goal of many current researches in nanosciences. A first route is the confinement of molecular motion until the continuum approximation breaks down and discrete-molecule effects appear, as observed in zeolite analogs or inside nanotubes. A bottom-up alternative consists in surface self-assemblies tailored at the molecular scale. Although most studies on nanostructured surfaces are still focused on their structure, the demonstrations of selective adsorptions inside single-molecule pores, the observation of rotating molecules inside an accidental bearing in a sub-monolayer film, or within self-assembled monolayers, represent pioneering first steps towards functional systems. In this context, we have demonstrated the sorting and routing of individual molecules

via surface diffusion inside bottom-up designed molecular sieves. We monitor the operation in-situ and in real time at the single-molecule scale through fast variable-temperature scanning-tunneling microscopy (STM). These studies unravel the mechanisms of molecular filtering. This permits to derive molecular-design guidelines for tuning cavity or channel selectivity. We discuss the opportunity to control optically and locally the molecular motion, using tip-induced field enhancements.

*Contributed Papers*

**9:48**

**G30 4 Determining the conductance of single molecular wire*** ALEXANDRE NDOBE, *University of Utah* VLADIMIR BURTMAN, *University of Utah* VALY VARDENY, *University of Utah* We have designed a method for determining the conductance of an isolated molecular wire from the I-V characteristic of molecular junctions. The molecular diodes were 1 $mm^2$ in area and consist of self-assembled monolayer (SAM) from a mixture of the molecular wires and non-conducting molecules that are used as spacers; coupled to two opposite gold electrodes. We studied the I-V characteristic dependence of the fabricated diodes on the ratio, *r* of wires/spacers. To obtain the number of molecular wires in the device we used multiple self-assemblies and titration techniques, as well as AFM of a small portion of the SAM surface. Our method was applied to a mixture of Me-BDT (methylbezenedithiol) molecules as wires and PT (pentathiol) molecules as spacers. For $10^{-8} < r < 10^{-3}$ we found that the device conductance is dominated by the molecular wires. From the current and obtained number of Me-BDT molecules in the device we determined the molecular conductance of Me-BDT to be 600 MΩ, in good agreement with a theoretical tunneling model.

*Supported in part by the NSF

**10:00**

**G30 5 Atomic-Scale Spectroscopy of Polydiacetylene Nanowires** RAJIV GIRIDHARAGOPAL, *Rice University* K. F. KELLY, *Rice University* In recent years, the appeal of organic electronic devices has spurred interest in conducting polymers, such as polydiacetylene. Polydiacetylene nanowires offer numerous possibilities for application in molecular electronics, and they are a model system for understanding conduction mechanisms in polymers. We have used scanning tunneling microscopy to investigate monolayer films of pentacosadiynoic acid formed on highly ordered pyrolytic graphite using the Langmuir-Blodgett and Langmuir-Schaeffer deposition techniques and subsequently polymerized to form polydiacetylene nanowires. By applying a novel method of microwave frequency mixing at the STM tip junction, we have obtained capacitance-voltage spectroscopic data to characterize the wires across a range of bias voltages, tunneling gap resistances, and microwave mixing frequencies.

**10:12**

**G30 6 Self-Organized Single-Crystal Polythiophene Microwires** KILWON CHO, *Pohang University of Science and Technology* DO HWAN KIM, *Pohang University of Science and Technology* Here we show a well-faceted, high-quality 1D single-crystal poly (3-hexylthiophene), P3HT microwire with unprecedented electrical characteristics such as a low resistance (0.5 MΩ), a channel current as high as 25 $\mu$A, and a well-resolved gate modulation via solution growth. We find that 1D single-crystal P3HT microwires are formed spontaneously through facile self-assembly of individual polymer chains, adopting preferential well-ordered inter-chain stacking along the wire axis. Our findings indicate that $\pi$-conjugated polymer single-crystals are capable of very efficient charge transport. This approach could lead to the development of chemical and biological sensors which are efficiently capable of electrical and /or optical monitoring. This work was supported by the National Research Laboratory Program, a grant (F0004022) from Information Display R&D Center under the 21st Century Frontier R&D Program, the BK21 Program, and the Pohang Acceleratory Laboratory for providing the synchrotron radiation source at the 4C2, 3C2, and 8C1 beam lines.

**10:24**

**G30 7 Bond resistances in molecular junctions** ANNA PAINELLI, *Universita' di Parma & INSTM UdR Parma* The description of molecular contacts is one of the hardest problems in modeling molecular junctions. In common approaches macroscopic leads ensure a finite potential drop and hence a driving force for the current. Recently, a different strategy is emerging where a steady-state DC current is forced in the molecule, by making resort to Lagrange multipliers, or by drawing a magnetic flux through the molecule. The strategy is promising, but two main problems remain to be solved: (1) the calculation of the potential drop needed to sustain the current, and (2) the definition of the potential profile along the molecule. Here the Joule law is used to evaluate the potential drop from the electrical power spent on the molecule, and continuity constraints for steady-state DC current are implemented to get information on the potential profile. Borrowing powerful concepts from the field of molecular spectroscopy, emphasis is put on the molecule, while clamping information about contacts in the molecular relaxation matrix. The molecule is described in a real-space approach, leading to a suggestive analogy between the molecule and an electrical circuit where resistances are associated with chemical bonds.

**10:36**

**G30 8 Transport Properties of SAM Molecular Diodes with Structural Tunability*** VLADIMIR BURTMAN, VALY Z. VARDENY, ALEX NDOBE, *University of Utah* A new molecular engineering approach is used to fabricate molecular junctions from self-assembled-monolayers (SAM) sandwiched between gold electrodes, with structural tunability based on two-component solid-state mixtures of molecular wires (1,4 methane benzenedithiol; Me-BDT, and molecular insulator spacers (1-pentanethiol; PT). The electrical transport of the fabricated SAM diodes was investigated at various temperatures versus the ratio r between the molecular wires and insulators. At $r < 10^{-3}$ the diodes are dominated by the isolated molecular wires dispersed in the dielectric spacer matrix; from the conductivity vs. r we determined the value for the Me-BDT molecular resistance to be $4x10^8$ Ohm. We also found that the activation energy in these devices is $\sim$ 50 meV at low bias and high temperatures; and injection barrier of $\sim$ 1.5 eV at intermediate bias and low temperatures. At $r > 10^{-3}$ Me-BDT aggregates are formed in the PT matrix resulting in additional in-plane order and substantive changes in the transport properties.

*This work was supported in part by the NSF NER 0507952, and DOE Grant No. ER 46109 at the University of Utah

**10:48**
**G30 9 Electron Hopping in Conducting Polymers in the Presence Of Mobile Ions*** VLADIMIR PRIGODIN, FANG HSU, JANE PARK, ARTHUR EPSTEIN, *Physics Department, The Ohio State University, Columbus, OH 43210-1106* We present the theoretical analysis for electrochemical transistors with the conductivity governed by the gate potential through bulk charging/discharging of the active channel. The predicted I(V) characteristics do not agree with the experimental dependencies for conducting polymer based transistors [1]. We suggest that the field effect in conducting polymers is related to their structural peculiarities. The large free volume within the polymer network enables ions to easily move into and out of the polymers. The main effect of ion insertion is breaking of the percolation network by removing critical hoping sites and, as a result, producing the conductor-nonconductor transition. The application of the present mechanism to the field effect in conducting polymers is discussed. [1] J. Liu, et al., **J. Appl. Phys. 92**, 6033-6038 (2002); A.J. Epstein, et al., **Current Applied Physics**, 2, 339-343 (2002); H. Okuzaki, et al., **Synth. Met. 137**, 947-948 (2003); F.C. Hsu, et al., to be published.

*This work is supported by AFOSR.



**SESSION G31: FOCUS SESSION: SIMULATION OF COMPLEX MATERIALS I**
**Tuesday Morning, 14 March 2006**
**328, Baltimore Convention Center at 8:00**
**Jeff Grossman, University of California, Berkeley, presiding**

***Contributed Papers***

**8:00**
**G31 1 Orbital-order-induced metal-insulator transition in manganites** SANJEEV KUMAR, ARNO KAMPF, *University of Augsburg (Germany)* PINAKI MAJUMDAR, *HRI, Allahabad (India)* We study a two-band double-exchange model with adiabatic Jahn-Teller phonons, weak antiferromagnetic superexchange and quenched disorder. This model for perovskite manganites is studied using a recently developed real space Monte-Carlo method (cond-mat/0406082). We present results for the optical conductivity and the density of states and provide a microscopic picture of the spin and orbital structures. The electron lattice coupling leads to orbital ordering at zero hole doping ($x = 0$), while the magnetism is controlled by the interplay of superexchange and double exchange interactions. We track the evolution upon hole doping of this orbital ordered insulator and locate the critical doping concentrations required for (i) the disappearance of orbital order and (ii) the emergence of the metallic behavior. We compare our results in detail with the experimental data on $La_{1-x}Ca_xMnO_3$ in the low $x$ regime.

**8:12**
**G31 2 Sequencing-Independent Delocalization in a DNA-Like Double Chain with Base Pairing*** RODRIGO CAETANO, *UNICAMP* PETER SCHULZ, *UNICAMP* The question of whether DNA is intrinsically conducting or not is still a challenger. Experiments on DNA conductivity are very controversial: Metallic, semiconducting, insulating and even superconductor behaviors have been reported. The theoretical studies of the electronics properties of DNA range from strictly one-dimensional tight-binding chains, up to ab initio calculations. Ab initio calculations give useful insight on environment influence but have to be limited to a reduced number of model DNA molecules. On the other hand strictly one-dimensional calculations deal with effectives sites instead of a base pair structure, underestimating the paring effects. Here, we focus in that intrinsic factor to show that double chains with base pairing with DNA-like correlation leads to delocalized states. We use a double-chain nearest-neighbor hopping tight-binding model to describe the system. The double chains are constituted by four different sites, representing the nucleotides (A, C, G and T). The sites in the first chain are randomly assigned, while the sites in the second chain obey the DNA pairing. The main consequence of the correlation is a localization-delocalization transition. The present result suggest the DNA is intrinsically a promising electronic material and the hidrance to DNA nanoelectronics is solely of technological nature.

*The authors acknowledge financial support from FAPESP, CNPq, UNICAMP and Ohio State University

**8:24**
**G31 3 Orientational Defects in Ice Ih: An Interpretation of Electrical Conductivity Measurements** MAURICE DE KONING, ALEX ANTONELLI, *Universidade Estadual de Campinas* ANTONIO J.R. DA SILVA, ADALBERTO FAZZIO, *Universidade de Sao Paulo* While the isolated water molecule is one of the simplest in Nature, the condensed phases of $H_2O$ reveal many complex features that still elude complete understanding. An example concerns the role of crystal defects in the peculiar electrical properties of proton-disordered hexagonal ice Ih. When an electric field is applied to an ice specimen, it becomes polarized by the thermally activated reorientation of the molecular dipoles through the motion of Bjerrum defects, which represent local disruptions of the hydrogen-bond network. While the conceptual picture of these Bjerrum defects is now well established, a quantitative understanding of their properties is still lacking, rendering a direct interpretation of experimental electrical conductivity data difficult. In this work we present a first-principles study of the structure and energetics of Bjerrum defects in ice Ih and compare the results to experimental electrical conductivity data. While the DFT result for the activation energy is in good agreement with experiment, we find that its two components have quite different values. Aside from providing new insight into the fundamental parameters of the microscopic electrical theory of ice, our results suggest the activity of traps in doped ice in the temperature regime typically assumed to be controlled by the free migration of L-type Bjerrum defects.

**8:36**
**G31 4 Scaling behavior of Film growth mechanism*** MINA YOON, LEE HO NYUNG, *Oak Ridge National Laboratory* ZHIGANG SUO, WEI HONG, *Harvard University* HANS M. CHRISTEN, DOUG LOWNDES, ZHENYU ZHANG, *Oak Ridge National Laboratory* Experimental evidence has accumulated that a strained film can grow stably on a vicinal surface. Linear perturbation analysis of the step-flow regime results in a dispersion relation which determines the persistence of the step-flow growth. The dispersion relation can also be used to probe the system parameters. Investigating the growth dynamics in the step-bunching regime, we found that there is a critical film thickness above which

step-bunching occurs. The critical thickness shows a scaling behavior depending on the terrace width and the deposition flux. Experiments show a qualitative agreement with the theory. Our results may open a way to grow films in a desired way.

*Supported by DOE.

**8:48**

**G31 5 One-dimensional Hartree-Fock calculations for electrons in a constriction** JIANG QIAN, BERTRAND HALPERIN, *Physics Department, Harvard University* WALTER HOFSTETTER, *Institut für Theoretische Physik A, RWTH Aachen* GERGELY ZARAND, *Institut für Theoreticshe Festkorperphysik, Universitat Karlsruhe* There are a number of puzzling experimental results associated with electron transport through a narrow constriction of finite length, such as the so-called 0.7 structure in the quantum point contact and the experiments on tunneling between two parallel quantum wires. To gain deeper insights into these experiments, it may be important to understand how a constriction region containing electrons at a very low-density is connected to higher density leads at each end. We have formulated Hartree-Fock methods applicable to one-dimensional models of such systems, in equilibrium or with a finite source-drain voltage. We will present results of the electron density profile and spin structures around the constriction for several models of interaction and constriction potentials. This work is supported in part by NSF grand DMR-02-33773 and PHY-01-17795.

**9:00**

**G31 6 Mixed Wannier-Bloch functions for electrons and phonons in extended disordered systems** ALFREDO PASQUARELLO, *Ecole Polytechnique Fédérale de Lausanne* FELICIANO GIUSTINO, *University of California at Berkeley* A major difficulty in the study of disordered systems arises from the inadequacy of the Bloch description of quasiparticle and collective excitations. The main alternative to the crystal momentum representation is provided by the Wannier picture. However, despite the success of the optimally localized Wannier functions in crystalline environments, their applicability to disordered systems is hindered by the lack of an explicit energy label, the latter being essential for interpreting spectroscopic data. We here introduce mixed Wannier-Bloch functions for studying electronic and vibrational spectra of extended disordered solids. These functions are designed to carry both spatial localization (Wannier character) and limited spectral broadening (Bloch character). Hence, they are best suited for associating specific spectral features to the underlying atomic-scale mechanisms. The new approach is demonstrated through applications to vitreous silica. The use of mixed Wannier-Bloch functions leads to a straightforward interpretation of the electronic spectrum of $v$-$SiO_2$ in terms of $s$ and $p$ atomic orbitals, and of the corresponding vibrational spectrum in terms of the molecular modes of the Si-O-Si bridge.



***Invited Papers***

**9:12**

**G31 7 Quantum Monte Carlo Calculations of Transition Metal Oxides.***

LUCAS WAGNER, *Center for High Performance Simulation, North Carolina State University*

Quantum Monte Carlo is a powerful computational tool to study correlated systems, allowing us to explicitly treat many-body interactions with favorable scaling in the number of particles. It has been regarded as a benchmark tool for first and second row condensed matter systems, although its accuracy has not been thoroughly investigated in strongly correlated transition metal oxides. QMC has also historically suffered from the mixed estimator error in operators that do not commute with the Hamiltonian and from stochastic uncertainty, which make small energy differences unattainable. Using the Reptation Monte Carlo algorithm of Moroni and Baroni (along with contributions from others), we have developed a QMC framework that makes these previously unavailable quantities computationally feasible for systems of hundreds of electrons in a controlled and consistent way, and apply this framework to transition metal oxides. We compare these results with traditional mean-field results like the LDA and with experiment where available, focusing in particular on the polarization and lattice constants in a few interesting ferroelectric materials. This work was performed in collaboration with Lubos Mitas and Jeffrey Grossman.

*NSF Graduate Research Fellow

***Contributed Papers***

**9:48**

**G31 8 First Principles Study of Formation Energies and Diffusion Mechanisms of Native Point Defects in Rutile $TiO_{2-x}$** HAKIM IDDIR, SERDAR OGUT, *University of Illinois at Chicago* NIGEL BROWNING, *University of California at Davis* We present results from first principles calculations for the formation energies and diffusion mechanisms of the oxygen vacancy ($V_O$), titanium interstitial ($Ti_I$) and titanium antisite ($Ti_O$) point defects in reduced rutile $TiO_{2-x}$. The calculations are performed in large supercells containing 240 to 270 atoms using the *ab initio* pseudopotential total energy method. As expected, the formation energy of $Ti_O$ is found to be significantly higher than $V_O$ and $Ti_I$, which have competitive formation energies as a function of the sample stoichiometry. The dominant charge states of $V_O$ and $Ti_I$ are found to be $(2+)$ and $(4+)$, respectively, for a wide range of the electron chemical potential. The calculated diffusion barriers for $Ti_I^{4+}$ are lower than those of $V_O^{2+}$, and do not present a significant anisotropy between the (100) open channels and the (110) direction. In fact, the barrier for the diffusion of $Ti_I^{4+}$ along the (100) open channels has an unexpectedly 0.1 eV higher barrier than along (110). The reasons for this observation and the implications of the present results are discussed in relation to bulk-defect assisted surface phenomena in rutile $TiO_2$.

**10:00**

**G31 9 Multifunctionality and Fluid Permeabilities of Triply Periodic Minimal Surfaces** YOUNGJEAN JUNG, *PRISM and Chemistry* SALVATORE TORQUATO, *PRISM, Chemistry, and PACM, Princeton University* It has recently been shown that triply periodic two-phase bicontinuous composites with interfaces that are the Schwartz P and D minimal surfaces are not only geometrically extremal but extremal for simultaneous transport of heat and electricity. The multifunctionality of such two-phase systems has been further established by demonstrating that they are also extremal when a competition is set up between the effective bulk modulus and electrical (or thermal) conductivity of the bicontinuous composite. We computed the fluid permeabilities of these and other triply periodic bicontinuous structures arranged on the sites of a simple cubic lattice at a porosity $\phi = 1/2$ [Y. Jung and S. Torquato, Phys. Rev. E **72**, 056319 (2005)]. We found that the Schwartz P porous medium has the largest fluid permeability among all of the six triply periodic porous media in consideration. The fluid permeabilities are shown to be inversely proportional to the corresponding specific surfaces for these structures. This leads to the conjecture that the maximal fluid permeability for a triply periodic porous medium with a simply connected pore space at a porosity $\phi = 1/2$ is achieved by the structure that globally minimizes the specific surface. We will also present specific single-length-scale, two-dimensional, isotropic multifunctional optimal microstructures at the phase volume fraction $\phi = 1/2$.

**10:12**

**G31 10 Ab Initio Structural Energetics of Bare $\beta - Si_3N_4$ Surfaces and the Interface with $Sm_2O_3$** JUAN CARLOS IDROBO, HAKIM IDDIR, SERDAR OGUT, *University of Illinois at Chicago* ALEXANDER ZIEGLER, NIGEL BROWNING, *University of California at Davis* R.O. RITCHIE, *University of California at Berkeley* Motivated by recent electron microscopy studies on the $Si_3N_4$/rare-earth oxide interfaces, the atomic and electronic structures of bare $\beta - Si_3N_4$ surfaces are investigated from first principles. The equilibrium shape of a $Si_3N_4$ crystal is found to have a hexagonal cross section and a faceted domelike base in agreement with experimental observations. The large atomic relaxations on the prismatic planes are driven by the tendency of Si to saturate its dangling bonds, giving rise to resonant-bond configurations or planar $sp^2$-type bonding. We predict three bare surfaces with lower energies than the open-ring $(10\bar{1}0)$ surface observed at the interface, which indicate that non- stoichiometry and the presence of the rare-earth oxide play crucial roles in determining the termination of $Si_3N_4$ matrix grains. We also present preliminary first principles results for the $Si_3N_4/Sm_2O_3$ interface and compare our findings to experimental observations.

**10:24**

**G31 11 Manipulation/Extraction of an Adatom from a Mound*** HANDAN YILDIRIM, ABDELKADER KARA, TALAT S. RAHMAN, *Physics Department Kansas State University* We present results of manipulation/extraction of Ag/Cu atoms from small Ag/Cu mounds on Ag(111)/Cu(111), rescpectively. Molecular dynamics (MD) and molecular static (MS) simulations were carried out using interaction potentials from the embedded atom method. Evaluation of the energy landscape in the absence of tip shows that for a Ag atom, lateral (sliding downwards) and vertical (climbing upwards) diffusion,the activation barrier is about 0.3 eV. We show that the presence of a Ag tip lowers the energy barrier for both lateral and vertical diffusion. We find that the optimum position of the tip to achieve extraction is when the tip is at the edge of the mound in front of the adatom, and at a height of 2.43 Å from the Ag adatom, for which the barriers for diffusion drop to 0.032 eV for lateral and 0.182 eV for vertical diffusion. In this case, the adatom is manipulated in the pulling mode. In the case of Cu, we found that the adatom manipulation/extraction is performed in the sliding/dragging mode.

*Work supported in part by DOE under grant No: BES DE-FGO3-97ER45650

**10:36**

**G31 12 Viscoelastic Stokes Flow*** M. GREGORY FOREST, *University of North Carolina at Chapel Hill* KE XU, *University of North Carolina at Chapel Hill* ISAAC KLAPPER, *Montana State University* We extend the formalism of Stokes flow from viscous to viscoelastic fluids, and then illustrate this correspondence with a variety of applications, including flow past a moving point source and flow around a driven oscillating sphere.

*Supported by the Air Force Office of Scientific Research and the NSF UNC Research Training Group Grant

## SESSION G32: FOCUS SESSION: ORBITAL/CHARGE ORDER IN COMPLEX OXIDES

**Tuesday Morning, 14 March 2006**
**329, Baltimore Convention Center at 8:00**
**Ray Osborn, Argonne National Laboratory, presiding**

***Contributed Papers***

**8:00**

**G32 1 Raman scattering studies of field- and temperature-dependent melting of charge order in $La_{1-x}Ca_xMnO_3$** MINJUNG KIM, HARINI BARATH, S.L. COOPER, *Dept. of Physics and Frederick Seitz Materials Research Laboratory, University of Illinois at Urbana-Champaign* M. RUEBHAUSEN, *Institut fur Angewandte Physik, Univeristat Hamburg, Jungiusstrasse 11, D-20355 Hamburg, Germany* S.W. CHEONG, *Dept. of Physics and Astronomy, Rutgers University, New Brunswick, NJ* The $La_{1-x}Ca_xMnO_3$ is one of the well-known perovskite manganites that display charge ordering behavior below a charge ordering temperature $T_{co}$ for $x \geq 0.5$. In particular, the strongest ordering is shown at commensurate doping x=0.5 with the transition temperature, $T_{CO}$=160K. We investigate the field-induced melting of charge ordering in this system using field-dependent Raman scattering at different temperatures. By monitoring the field- and doping-dependence of excitations specific to the charge-ordered state, we are able to sensitively monitor the breakdown of both long-range and local charge order, and to carefully examine the stability of the charge ordered state to both doping (x) and applied magnetic field.

**8:12**

**G32 2 Theoretical study of charge, spin, and orbital order in half-doped $La_{0.5}Ca_{0.5}MnO_3$.*** DMITRI VOLJA, WEIGUO YIN, WEI KU, *BNL* Deep microscopic insights into the half-doped $La_{0.5}Ca_{0.5}MnO_3$ are obtained with a novel construction of

many-body picture derived from LDA+U and Wannier state analysis. Experimentally observed zig-zag orbital order and CE-type magnetic structure is found to have only very weak charge disproportionation. The apparent contradiction between well-defined bridge (3+) and corner (4+) Mn sites and the weak charge disproportionation is resolved naturally with occupied Wannier states centered at 3+ sites extending to 4+ and O-sites (reflecting non-negligible charge-transfer nature of the system.) Contrary to current lore, electron-electron interaction is found crucial to the long-range order in ordering the orbital and the spin. Specific experimental means of verification (e.g.: measurement of pseudospin direction) are suggested.

*Work supported by U.S. D.O.E.

**8:24**

**G32 3 Charge versus orbital-occupancy ordering in manganites** WEIDONG LUO, MARIA VARELA, JING TAO, STEPHEN J. PENNYCOOK, SOKRATES T. PANTELIDES, *Vanderbilt University and Oak Ridge National Laboratory* It is generally assumed that density-functional theory (DFT) in the local-spin-density approximation (LSDA) or the generalized- gradient approximation (GGA) is not adequate to describe mixed- valence manganites. Here we report benchmark DFT/GGA calculations for the ground-state structural, electronic and magnetic properties for both undoped and doped $CaMnO_3$ and find the results to be in excellent agreement with available data, including new atomic-resolution Z-contrast imaging and electron-energy loss spectra. More specifically, we found that the DFT results predict two inequivalent Mn atoms in both 0.33 and 0.5 electron-doped $CaMnO_3$, in agreement with experimental evidence of $Mn^{+3}/Mn^{+4}$ oxidation state ordering. The inequivalent Mn atoms are marked by their distinctive orbital occupancies, dissimilar local Jahn-Teller distortion and different magnetic moments from DFT calculations. We also show that the spherically integrated charges associated with the two inequivalent Mn atoms are the same, and they are actually the same as in the Mn metal. This charge neutrality with different orbital occupancies is the result of self-consistency and atomic relaxations in the crystal. We conclude that DFT without additional correlations can account for the observed properties of oxidation-state ordering in this system. The impact of the results on other mixed-valence systems will be discussed.

**8:36**

**G32 4 Orbital and oxygen vacancy ordering in $La_{1-x}Sr_xMnO_{3-\delta}$ ($x \geq 0.8$, $\delta \geq 0.15$)** LEOPOLDO SUESCUN, *Materials Science Division, Argonne National Laboratory, Argonne, IL 60439 & Department of Physics, Northern Illinois University, DeKalb, IL 60115* BOGDAN DABROWSKI, *MSD, ANL, Argonne, IL 60439 & Dept. of Physics, NIU, DeKalb, IL 60115* JAMES MAIS, *Dept. of Physics, NIU, DeKalb, IL 60115* STANISLAW KOLESNIK, *Dept. of Physics, NIU, DeKalb, IL 60115* JAMES RICHARDSON, *Intense Pulsed Neutron Source Division, ANL, Argonne, IL 60439* JAMES JORGENSEN, *MSD, ANL, Argonne, IL 60439* We have developed synthesis method, obtained, and studied the highly Sr substituted LSM manganites. New oxygen and orbital ordered perovskite type phase $SrMnO_{2.6}$ (nominally $Sr_5Mn_5O_{13}$) was found tetragonal P4/m, a=8.61328(18) and c=3.80997(11) Å. Mn ion shows charge separation to $Mn^{3+}$ in a pyramidal and $Mn^{4+}$ in a regular octahedral coordination. Nonstoichiometry has been observed with oxygen compositions between $0.25 < \delta < 0.4$; upon oxidation a monoclinic distortion is observed. Analogous tetragonal and monoclinic phases have been found for $La_{1-x}Sr_xMnO_{3-\delta}$ ($0.3 < \delta < 0.5$) with x=0.05 and 0.2, respectively. In-situ neutron powder diffraction as well as susceptibility measurements show different magnetic arrangements below RT depending on x and $\delta$. This work was supported by the U.S. Department of Transportation and NSF-DMR-0302617.

**8:48**

**G32 5 A realistic approach to effective Hamiltonians for strongly correlated electron materials: Study of orbital ordering in $LaMnO_3$*** WEI-GUO YIN, DMITRI VOLJA, WEI KU, *Condensed Matter Physics & Materials Science Department, Brookhaven National Laboratory, Upton, NY 11973* We present a general scheme to the realistic derivation of many- body effective Hamiltonians, $H^{\text{eff}}$, for strongly correlated electron systems: Based on a novel Wannier state analysis of the LDA+$U$ electronic structure, relevant mechanisms can be clearly singled out and their strengths can be accurately determined by mapping $H^{\text{eff}}$ to the low-energy LDA+$U$ Hamiltonian within self-consistent Hartree-Fock mean-field theory [1]. Applying this scheme to $LaMnO_3$, the parent compound of colossal magnetoresistance manganites, we have quantified the relative importance of the effective electron-electron interaction ( $\sim$ 1.7 eV) and the Jahn-Teller splitting ( $\sim$ 0.9 eV) in ordering orbitals in $LaMnO_3$. We find that beyond the conventional Jahn-Teller picture, the electron-lattice (electron-electron) interaction alone is insufficient (sufficient) to stabilize the orbital ordering. Furthermore, our analysis indicates certain competition between different mechanisms, allowing direct experimental determination of their relative strengths. [1] W.-G. Yin, D. Volja, and W. Ku, cond-mat/0509075.

*Work supported U.S. DOE.

**9:00**

**G32 6 In-plane anisotropy of the electronic structure for the charge/orbital ordered state in half-doped Mn-oxide** Y.S. LEE, S. ONODA, Y. TOKUNAGA, J.P. HE, Y. KANEKO, *ERATO-SSS, Japan* T. ARIMA, *Tohoku University, Japan* N. NAGAOSA, Y. TOKURA, *Univeristy of Tokyo, Japan* We have investigated the in-plane anisotropy of the electronic response for the charge/orbital ordered phase in a half-doped Mn-oxide. Compared with the theoretical calculation the optical measurement with a single domain of $Eu_{1/2}Ca_{3/2}MnO_4$ reveals that the optical conductivity along the chain direction exhibits smaller optical gap and lower energy distribution of the spectral weight than along the stripe (interchain) direction. It is suggested that the electronic anisotropy reported here is attributed to the quasi-one-dimensional electron hopping which is subject to the zigzag chain-type $e_g$ orbital ordering.

**9:12**

**G32 7 Magnetic Excitations in the CE-type manganite $Pr_{0.5}Ca_{1.5}MnO_4$** J. A. FERNANDEZ-BACA, *ORNL and Univ. of Tennessee* FENG YE, *ORNL* SONGXUE CHI, *Univ. of Tennessee* PENGCHENG DAI, *Univ. of Tennessee and ORNL* J. W. LYNN, *NIST* R. MATHIEU, *Univ. of Tokyo* Y. TOKURA, *Univ. of Tokyo* Charge and orbital ordering (CO-OO) in doped manganites can control bulk and magnetic properties of the material. Canonical examples of the CO-OO compounds are 3D R(1-x)A(x)MnO3 and 2D R(1-x)A(1+x)MnO4 manganites near x=0.5. The magnetic ions in those systems are usually arranged in a checkerboard order, where spins of Mn3+ and Mn4+ form zigzap ferromagnetic chains coupling antiferromagnetically. Recent theoretical calculations and experimental observations suggest that the stabilization of CO-OO state in CE-type magnetic structure might be magnetic in origin. In this talk we will present our recent results on the study of the spin-wave excitations in the layered compound Pr0.5Ca1.5MnO4 with CE-type magnetic structure using inelastic neutron scattering. ORNL is managed by UT-Battelle, LLC, for the U.S. Dept. of Energy under contract DE-AC05-00OR22725. The work at UT was supported by the U.S. NSF DMR-0453804 and DOE DE-FG02-05ER46202.

**9:24**

**G32 8 How Cation-Covalency controls Electron Localization in t2g Perovskites** OLE KROGH ANDERSEN, ATSUSHI YAMASAKI, *Max-Planck Institute FKF, Stuttgart* EVA PAVARINI, *Forschungszentrum Juelich* In the series of perovskites, SrVO3-CaVO3-LaTiO3-YTiO3, the transition-metal d electron becomes increasingly localized and undergoes a Mott transition. By defining a low-energy Hubbard Hamiltonian in the basis of NMTO Wannier functions for the t2g LDA band and solving it in the single-site dynamical mean-field approximation, it was recently shown [1] that simultaneously with the Mott transition, the orbital fluctuations are strongly suppressed. Here, we explain the underlying chemical mechanisms [2]: Proceeding through the series, covalency between the empty large-cation-d states and the occupied oxygen-p states causes the oxygen octahedra to rotate and tilt. Moreover, since those oxygen-p orbitals which bond to the cations are the same as those which bond to the transition-metal t2g orbitals, the t2g Wannier functions exhibit residual covalency. This splits the t2g levels and reduces the width of the lowest subband. Cation covalency thus causes the electron to localize in LaTiO3 and YTiO3. [1] E. Pavarini, S. Biermann, A. Poteryaev, A.I. Lichtenstein, A. Georges, O.K. Andersen, Phys. Rev. Lett. 92 (2004) 176403. [2] E. Pavarini, A. Yamasaki, J. Nuss, O.K. Andersen, New Journal of Physics 7 (2005) 188.

**9:36**

**G32 9 Resonant soft x-ray diffraction from $Fe_3O_4$/MgO below the Verwey transition** C. SCHUESSLER-LANGEHEINE, J. SCHLAPPA, C. F. CHANG, H. OTT, Z. HU, L. H. TJENG, *II. Physikalisches Institut, Universitaet zu Koeln, Germany* E. SCHIERLE, E. WESCHKE, G. KAINDL, *Institut fuer Experimentalphysik, Freie Universitaet Berlin, Germany* A. TANAKA, *ADSM, Hiroshima University, Japan* The electronic structure of the low-temperature phase of magnetite ($Fe_3O_4$) has been studied for more than 60 years. In particular the question whether or to which extend the low-temperature phase is characterized by a charge order on the octahedral Fe-sites is controversially discussed. We studied this system using resonant soft x-ray diffraction at the Fe $L_{2,3}$ resonance, a technique particularly sensitive to spatial modulations of the electronic state. The resonance behaviour of the (001) peak, which is characteristic for the low temperature phase, is distinctly different from that of the also studied (001/2) diffraction peak; we assign the (001) peak to charge order with a modulation of about 16 percent of a unit charge, while the (001/2) peak is caused by a different order involving only $Fe^{2+}$ sites in octahedral environment.



***Invited Papers***

**9:48**

**G32 10 Electronically smectic-like phase in a nearly half-doped manganite.**
FENG YE, *Oak Ridge National Laboratory*

Charge/orbital ordering is one of the most important of phenomena in doped manganites [1-3]. In this talk, I am going to present our recent neutron scattering results on the charge/orbital ordering (CO-OO) and spin ordering in the nearly half-doped perovskite manganite $Pr_{0.55}(Ca_{0.8}Sr_{0.2})_{0.45}MnO_3$ (PCSMO) [4]. On cooling from room temperature, PCSMO first enters into a CO-OO state below $T_{CO}$ and then becomes a CE-type long-range ordered antiferromagnet below TN. At temperatures above TN but below $T_{CO}$ ($T_N < T < T_{CO}$), the spins in PCSMO form highly anisotropic smectic liquid-crystal-like texture with ferromagnetic (FM) quasi-long-range ordered one-dimensional zigzag chains weakly coupled antiferromagnetically. Such a magnetic smectic-like phase results directly from the spin-orbit interaction and demonstrates the presence of textured 'electronic soft' phases in doped Mott insulators [5,6]. This work was supported by the DOE No.DE-AC05-00OR22725 with UT/Battelle, LLC and U. S. NSF DMR-0139882. This work was performed under the US-Japan Cooperative Program on Neutron Scattering. [1] J. van den Brink et al., Phys. Rev. Lett. 83, 5118 (1999). [2] I. V. Solovyev and K. Terakura, Phys. Rev. Lett. 83, 2825 (1999). [3] I. V. Solovyev, Phys. Rev. Lett. 91, 177201 (2003). [4] F. Ye et al., Phys, Rev. B. (in press) [5] G. C. Milward et al., Nature 433, 607 (2005). [6] S. A. Kivelson et al., Nature 393, 550 (1998).

*Contributed Papers*

**10:24**
**G32 11 Spin moment over 10-300 K and the delocalization of magnetic electrons above the Verwey transition in magnetite** P. A. MONTANO, *U. of Illinois Chicago and USDOE* YINWAN LI, *U. of Illinois Chicago and Argonne National Laboratory* B. BARBIELLINI, *Northeastern U.* P. E. MIJNARENDS, *Northeastern U. and Delft University of Technology* S. KAPRZYK, *Northeastern U. and and AGH (Poland)* A. BANSIL, *Northeastern U.* In order to probe the magnetic ground state, we have carried out temperature dependent magnetic Compton scattering experiments on an oriented single crystal of magnetite ($Fe_3O_4$), together with the corresponding first-principles band theory computations to gain insight into the measurements. An accurate value of the magnetic moment $\mu_S$ associated with unpaired spins is obtained directly for the first time over the temperature range of 10-300K. $\mu_S$ is found to be non integer and to display an anomalous behavior with the direction of the external magnetic field near the Verwey transition. The anisotropy of the magnetic Compton profiles shows a dramatic jump through the Verwey temperature $T_v$ and indicates that magnetic electrons in the ground state of magnetite become delocalized above $T_v$. Work supported by the USDOE.

**10:36**
**G32 12 Dimensionality switching in electric conduction in FeS** TOMOHIRO TAKAYAMA, KOHSHI TAKENAKA, HIDENORI TAKAGI, *RIKEN(The Institute of Physical and Chemical Research), also at University of Tokyo and CREST-JST* Orbital degree of freedom plays an essential role in the properties of strongly correlated systems, and will be a key function in the next generation. The orbital state, namely, shape of electron cloud, can affect some macroscopic properties such as transport properties. We have indeed observed a dimensionality change in electric conduction in stoichiometric iron sulfide, FeS, as a consequence of change in orbital states. FeS crystallizes in a NiAs-based troilite structure and is an antiferromagnetic semiconductor below $T_N$ = 600 K. At $T_s \sim$ 400 K, spin-axis transition, the rotation of antiferromagnetically ordered spins of iron atoms, occurs; the spins are directed along *c*-axis at low temperatures, and they rotate and lie in *c*-plane at $T_s$. This transition involves a change in orbital states of $Fe^{2+}$ ions. The outermost electron of $Fe^{2+}$ ions spreads in basal-plane below $T_s$, while it elongates in *c*-direction above $T_s$. This change strongly couples onto the electric conduction and induces its dimensionality change from two-dimensional below Ts to three-dimensional above $T_s$. We will discuss this change in orbital states and its appearance in electric conduction.

**10:48**
**G32 13 First-order phase transition induced by disorder in a model for manganites** EDUARDO CASTRO, JOÃO SANTOS, *CFP and Departamento de Física, Faculdade de Ciências Universidade do Porto* The role of disorder in the physics of manganese oxides has been unveiled by a series of experiments in half-doped ordered and disordered manganites. For the ordered family a multicritical behaviour was found in the temperature vs bandwidth phase diagram, where a charge-order insulator (COI) competes with a ferromagnetic metal (FM). Chemical disorder induces a strong suppression of the transition to the COI state, effectively turning an insulator into a FM and enhancing the colossal magnetoresistive effect above the Curie temperature. Recently, a one orbital double-exchange model with cooperative phonons and quenched disorder was proposed to explain this metal-insulator transition induced by disorder. Treating the electronic degrees of freedom exactly, and the local spins and lattice distortions classically, in a variational mean-field approach, we have investigated the thermodynamic behaviour of the model in 2D systems larger by one order of magnitude than in previous works. Not only the suppression of the COI state by disorder was obtained, but we have also found that the second-order charge-order phase transition turns into first-order in the presence of intermediate disorder. This picture is consistent with experiments: first-order phase transitions are known to be present in half-doped disordered manganites which show the spectacular phenomena of the collapse of a charge-ordered state under a magnetic field.

## SESSION G33: GSNP STUDENT AWARD SESSION AND GLASSES
**Tuesday Morning, 14 March 2006**
**336, Baltimore Convention Center at 8:00**
**Narayanan Menon, University of Massachusetts, Amherst, presiding**



**8:00**
**G33 1 Rate of Entropy Extraction in Compressible Turbulence*** MAHESH BANDI, *Department of Physics and Astronomy, University of Pittsburgh* The rate of change of entropy is measured for a system of particles floating on the surface of a fluid maintained in a turbulent steady state. This rate of entropy $\dot{S}$ equals the time integral of the two point temporal velocity divergence correlation function with a negative prefactor. The measurements satisfactorily agree with the sum of Lyapunov exponents (Kolmogorov-Sinai entropy rate) measured from previous simulations, as expected of dynamical systems that are very chaotic (Sinai-Ruelle-Bowen statistics).

*This work is supported by the NSF (Grant No. DMR-0201805).

**8:12**
**G33 2 Toward Zero Surface Tension Limit: Granular Fingering Instability in a Radial Hele-Shaw Cell** XIANG CHENG, *The James Franck Institute and Department of Physics, The University of Chicago* Because of the absence of cohesive forces between grains, dry granular material can, in many respects, be thought of as a fluid with zero surface tension. In the zero surface-tension limit, viscous fingering is known to possess singular behavior. We have studied the viscous fingering instability in such a granular ''fluid.'' In our experiment, we use a conventional radial Hele-Shaw cell consisting of two parallel glass plates separated by a gap. Gas with controlled pressures is blown through a hole at the center of one glass plate and displaces the surrounding dry granular material. We have systematically studied the fingering pattern as a function of gas pressure, gap thickness, and grain size. Two stages are observed during pattern growth. In the first stage, we find fluid-like fingering. However, as opposed to normal fluids, the pattern is more ramified at low pressure. In the second stage, we find several new behaviors in the system such as merging and pinching off of fingers and the existence of satellite bubbles.

**8:24**

**G33 3 The effect of packing density on self-assembled monolayer friction: Investigation of frictional contrast between OTS phase-separated regions** ERIN FLATER, *University of Wisconsin - Madison* Motivated by the lack of fundamental understanding of friction, and that friction and wear are major limiting factors for surface micromachined devices, we use atomic force microscopy (AFM) to determine the nanoscale frictional properties of alkylsilane monolayers commonly used in these microscale devices to reduce adhesion and friction. Quantitative nanoscale single asperity measurements of friction and contact stiffness are performed using monolayer-terminated AFM tips on monolayer-terminated silicon. By comparing the two structural phases present in octadecyltrichrolosilane (OTS) monolayers, we observe that friction depends on the local molecular packing density. The liquid condensed phase shows measurably lower friction at low loads than the liquid expanded phase, demonstrating that lower friction is associated with higher molecular packing density. However, the phases exhibit the same frictional response at higher loads, suggesting that compressed forms of both phases are structurally and tribologically equivalent. We discuss these results in terms of stress-induced molecular conformational changes in the confined interface. We acknowledge our collaborators: W. Robert Ashurst at Auburn University, who provided the OTS samples, and Maarten P. de Boer and Alex D. Corwin at Sandia National Laboratories.

**8:36**

**G33 4 Universal Impedance, Admittance and Scattering Fluctuations in Quantum-chaotic Systems** SAMEER HEMMADY, *University of Maryland* We experimentally investigate fluctuations in the eigenvalues of the impedance, admittance and scattering matrices of wave chaotic systems using a microwave analog of a quantum chaotic infinite square well potential. We consider a 2-D, time-reversal symmetric chaotic microwave resonator driven by two non-ideally coupled ports. The system-specific coupling effects are removed using the measured radiation impedance matrix ($\overleftrightarrow{Z}_{Rad}$) [1] of the two ports. A normalized impedance matrix ($\overleftrightarrow{z}$) is thus obtained, and the Probability Density Function (PDF) of its eigenvalues is predicted to be universal depending only on the cavity loss. We observe remarkable agreement between the statistical properties of $\overleftrightarrow{z}$ and $\overleftrightarrow{y} = \overleftrightarrow{z}^{-1}$ for all degrees of loss, which is in accordance with [1,2] and Random Matrix Theory (RMT). We compare the joint PDF of the eigenphases of the normalized scattering matrix ($\overleftrightarrow{s}$) with that obtained from RMT for varying degrees of loss. We study the joint PDF of the eigenvalues of $\overleftrightarrow{s} \leftrightarrow \overleftrightarrow{s}^{\dagger}$ and find good agreement with [3]. [1] X. Zheng, et al., – Electromagnetics (in press); condmat/0408317; S. Hemmady, et al., Phys. Rev. Lett. **94**, 014102 (2005).[2] Y. V. Fyodorov, et al., – condmat/0507016.[3] P. W. Brouwer and C. W. J Beenakker – PRB **55**, 4695 (1997). Work supported by DOD MURI AFOSR Grant F496200110374, DURIP Grants FA95500410295 and FA95500510240.

**8:48**

**G33 5 Plastic Failure Events in 2D Sheared Granular Systems*** TRUSH MAJMUDAR, *Physics Department, Duke University* We present experimental measurements of plastic failure events in a two dimensional granular system consisting of polymer photoelastic disks, placed horizontally, and confined within a rectangular biaxial cell. The bi-refringence of these disks allows us to determine the normal and tangential components of contact forces. We image the system at various deformation states and measure the stress changes and displacements of the disks during one complete shear cycle. The stress changes are found by computing the stress tensor of each disk and the displacements are measured by particle tracking. We obtain bulk stress-strain curves by spatial averaging and find that the system exhibits regions of reversible deformation interrupted by irreversible plastic failure events. We also obtain the behavior of shear modulus of the system. The spatial distribution of reversible and plastic deformations found by studying the displacements of the disks show that in two corners, the disks move uniformly but in a central band aligned along a principal strain direction, we observe multiple vortices. Reversing the direction of shear causes maximum plastic deformation which results in disruption of the vortex structure. We compare our results to the shear transformation zone (STZ) theory.

*Funding: NSF DMR - 0137119, NSF DMS - 204677, NASA - NNC04GB08G

**9:00**

**G33 6 Locally fluctuating elasticity of vulcanized solids** XIAOMING MAO, PAUL GOLDBART, *University of Illinois at Urbana-Champaign* XIANGJUN XING, *Syracuse University* ANNETTE ZIPPELIUS, *Universitaet Goettingen* The elastic properties of vulcanized solids, such as rubbery polymeric media, are characterized not only by their small mean shear moduli but also by the random spatial fluctuations of their local elasticity. These fluctuations originate in the randomness locked in, e.g., to a polymer network during the cross-linking process. We examine these fluctuations in the local elasticity of random solids via vulcanization theory, i.e., the replica field theory that describes cross-linking- driven random solidification transitions and their emergent rigidity. To do this we identify the Goldstone excitations of the random solid state as local shear deformations, and interpret their effective free energy in terms of a phenomenological model of inhomogeneous, nonlocal rubber elasticity. Thus, we arrive at predictions for the statistical properties of the fluctuating elasticity of vulcanized solids.

**9:12**

**G33 7 Rheological Fluids under Perturbation: Reconstruction and Relaxation Processes*** ELSA MARIA DE LA CALLEJA,[†] *Universidad Autonoma de Puebla* JOSE LUIS CARRILLO,[‡] *Universidad Autonoma de Puebla* We study the evolution of the structure of electro rheological as well as magneto rheological fluids in the presence of perturbation fields. We have previously shown that the fibrous structure acquired by these dispersions in the presence of a static, electric or magnetic, field has multifractal characteristics [1]. If in addition to the static field a perpendicular pulsed field is applied, under certain conditions it is possible to rearrange the structure into an ordered one [2]. Based on the measured mass fractal dimension and the radial distribution of mass, we discuss these processes and other structural characteristics of the system approaching these phenomena as a glass transition. [1] J. L. Carrillo, F. Donado, and M. E. Mendoza: Fractal patterns, cluster dynamics, and elastic properties. Phys. Rev. E 68, 061509 (2003); J. L. Carrillo, M. E. Mendoza, and F. Donado: Fractal patterns and aggregation processes in rheological dispersions. J. Stat. Mech.

P06001 (2005). [2] J. L. Carrillo, E. M. De la Calleja, M. E. Mendoza, and F. Donado, Ferroelectrics (in press).

*Partial finantial support by CONACYT Mexico. Grant No. 44296

†regular member of the Sociedad Mexicana de Fisica

‡regular member of the Sociedad Mexicana de Fisica

**9:24**

**G33 8 Low temperature solution of the Sherrington-Kirkpatrick model** SERGEY PANKOV, *NHMFL, FSU, Tallahassee* We propose a simple scaling ansatz for the full replica symmetry breaking solution of the Sherrington-Kirkpatrick model in the low energy sector. This solution is argued to become exact in the limit $x \to 0$, $\beta x \to \infty$ of the Parisi replica symmetry breaking scheme parameter $x$. The distribution function $P(x,y)$ of the frozen fields $y$ has been known to develop a linear gap at zero temperature. We integrate the scaling equations to find an exact numerical value for the slope of the gap $\partial P(x,y)/\partial y|_{y\to 0} = 0.301046\ldots$ We also use the scaling solution to devise an inexpensive numerical procedure for computing finite timescale ($x = 1$) quantities. The entropy, the dynamical susceptibility at zero frequency and the local field distribution function are computed in the low temperature limit with high precision, barely achievable by other currently available methods.

**9:36**

**G33 9 Slowing dynamics of supercooled glycerol in the volume-temperature plane*** NARAYANAN MENON, K. WIN, *University of Massachusetts Amherst* We have measured[1] the dielectric susceptibility of supercooled glycerol from 0.01 Hz to 100 kHz at up to 900 MPa and close to the glass transition temperature. We find that the glass transition temperature and isobaric fragility increase with pressure. We separate the effects on the relaxation frequency of volume and temperature by studying the glass transition in the V-T plane. By introducing a generalized fragility we quantify these effects and show that V and T contribute almost equally to dynamic slowing-down. We exploit a connection between the generalized fragility and a recently discovered scaling exponent to show that these results are likely to hold for other fluids.

*We acknowledge support from NSF-DMR0305396

[1]K. Z. Win and N. Menon, cond-mat/0508648

**9:48**

**G33 10 Structure of solid metal ammonia systems*** XUE WANG, C. A. BURNS, D. HOOGERHEIDE, C. N. KODITUWAKKU, *Dept. of Physics, Western Michigan University, Kalamazoo MI 49008* Both crystalline and amorphous phases in metal ammonia solids have been studied using x-ray scattering. We have studied the structure of $Li(NH_3)_4$ over a temperature range of 10 K to 90 K and also studied the structure of quenched sodium-ammonia solutions at concentrations of 0, 3, 6, 9, 12, and 15 mole percent metal. We find a mixture of amorphous and crystalline phases in lithium-ammonia with at least two different crystalline phases. An amorphous phase is also found in certain of the quenched sodium-ammonia solutions.

*Work supported by DOE grant DE-FG02-99ER45772

**10:00**

**G33 11 Relaxation Width and Ionic Conductivity of Supercooled Glycerol at High Pressure*** KYAW ZIN WIN, NARAYANAN MENON, *University of Massachusetts Amherst* We have measured the dielectric susceptibility of supercooled glycerol from 0.01 Hz to 100 kHz at up to 900 MPa and close to the glass transition temperature. We find that, at a fixed relaxation frequency, the relaxation width increases with pressure. We also establish a relation between isobaric fragility and the width of glycerol and compare it to a correlation[1] between these quantities at 1 atmosphere for a variety of liquids. We find that volume has a much bigger effect than temperature on the changes in the width. We are also for the first time able to study the ionic conductivity as a function of temperature and pressure, and study the Nernst-Einstein relation between the conductivity and the relaxation frequency.

*We acknowledge support from NSF-DMR0305396

[1]R. Bohmer, K. L. Ngai, C. A. Angell, and D. J. Plazek, J. Chem. Phys. 99, 4201 (1993).

**10:12**

**G33 12 Calculation of the configurational entropy for a binary Lennard-Jones fluid below the mode-coupling temperature using a hybrid Monte Carlo method** ELIJAH FLENNER, GRZEGORZ SZAMEL, *Dept. of Chemistry, Colorado State University* We developed a novel, hybrid Monte Carlo algorithm that combines configurational bias particle swaps with parallel tempering. We use this new method to simulate a standard model of a glass forming binary mixture above and below the so-called mode-coupling temperature, $T_{MCT}$. We find that an itansatz that was used previously to extrapolate thermodynamic quantities to temperatures below $T_{MCT}$ breaks down in the vicinity of the mode-coupling temperature. Thus, previous estimates of the so-called Kauzmann temperature need to be reexamined. Also, we find that the Adam-Gibbs relations $D \propto \exp(-a/TS_c)$ and $\tau \propto \exp(b/TS_c)$, which connect the diffusion coefficient $D$ and the relaxation time $\tau$ with the configurational entropy $S_c$, are valid for all temperatures for which the configurational and vibrational contributions to the free energy decouple.

**10:24**

**G33 13 Enhanced Elasticity and Soft Glassy Rheology of a Smectic Liquid Crystal in a Random Porous Environment** DENNIS LIANG, RANJINI BANDYOPADHYAY, *Johns Hopkins U.* RALPH COLBY, *Pennsylvania State U.* JAMES HARDEN, *University of Ottawa* ROBERT LEHENY, *Johns Hopkins U.* We present rheometry studies of the frequency dependent shear modulus, $G^*(\omega) = G'(\omega) + iG''(\omega)$, of the smectic liquid crystal octylcyanobiphenyl (8CB) confined by a colloidal silica gel. When the 8CB is in the isotropic or nematic phase, the shear modulus is independent of temperature and dominated by the elasticity of the gel. With the onset of smectic order, $G'$ grows approximately linearly with decreasing temperature and reaches values that can exceed by more than 3 orders of magnitude the values for pure 8CB. The modulus in the smectic phase possesses a weak power-law dependence on frequency, $G^*(\omega) \sim \omega^\alpha$, with the exponent $\alpha$ approaching zero with increasing gel density. Within the soft glassy rheology model, such a decreasing exponent

indicates an approach to a glass transition, which we correlate with the increasing random field coupling between the gel and smectic. We further interpret the enhanced elasticity and weak power law dependence of $G^*(\omega)$ as the result of a dense population of defects in the disordered smectic.

**10:36**
**G33 14 Concept of a Bond in Metallic Glasses. Bond's Lifetime in a Supercooled Liquid. MD Modeling.** VALENTIN A. LEVASHOV, TAKESHI EGAMI, *University of Tennessee, Knoxville, TN 37996* RACHEL S. AGA, JAMES R. MORRIS, *Oak Ridge National Laboratory, Oak Ridge, TN 37831-6115* We have done constant volume MD simulations of a one component system of particles interacting via modified Johnson pair potential previously developed for iron. Negative curvature of the potential at the distances beyond potential minimum leads to the clear differentiation between the first and second nearest neighbors observed in the pair distribution function. Therefore a concept of a bond could be introduced. We studied the distribution of bond lifetimes in a liquid state. At high temperatures probability to find a long living bond is very small. As temperature decreases there appear bonds whose lifetime is very long. At the same time, the number of bonds whose lifetime is relatively small remains significant. This could be considered as an indication of the separation of the system into solid-like and liquid-like regions. Obtained bond lifetime distributions will be analyzed from this point of view of the presence in supercooled liquids different kinetic regimes at different temperatures.



**SESSION G34: GLASSY DYNAMICS AND JAMMING**
**Tuesday Morning, 14 March 2006**
**337, Baltimore Convention Center at 8:00**
**Eric Weeks, Emory University, presiding**

**8:00**
**G34 1 On the Lower Critical Dimension of the Edwards-Anderson Spin Glass*** STEFAN BOETTCHER, *Emory University, Physics Department* The Edwards-Anderson model of Spin Glasses is studied on dilute hyper-cubic lattices in dimensions $d = 2,3,\ldots,7$. Accurate predictions for the stiffness exponent $y_d$ are obtained that describes low-energy excitations. Continuing $y_d$ off the integers shows that its zero is located at $d = 5/2$ to within 0.1%, a prediction that is corroborated by other numerical and theoretical work. Related Publication: Phys. Rev. Lett. **95**, 197205 (2005). Related Webpage: http://www.physics.emory.edu/faculty/boettcher/.

*This work has been supported by grant 0312510 from the Division of Materials Research at the National Science Foundation and by the Emory University Research Council

**8:12**
**G34 2 Direct measurement of the distinct part of van Hove correlation function $G_d(r, t)$ in colloidal gels and glasses** YONGXIANG GAO, MARIA KILFOIL, Great effort has been put into understanding the mechanism and dynamics of glass formation, and progress has been made. It is now known that the cage effect causes the dynamical arrest, and thus the observed glass transition. This has been proven by direct observation by microscopy, by light scattering and rheology experiments of hard sphere systems near the glass transition, and by computer simulation. However, no real-space direct three dimensional measurements of large-length-scale dynamics have been done in glass samples. The distinct part of the van Hove correlation function $G_d(r, t)$ provides direct access to the dynamics in glassy systems at all length scales. We use confocal microscopy to measure this function in both colloidal gels and glasses. Since both glass and gel formation are kinetic and not thermodynamic phenomena, we may expect that they share similarities. By looking at their dynamics, we may gain more insights into the unified jamming picture of liquid-to-disordered-solid transition.

**8:24**
**G34 3 Fluctuations of Structure and Dynamics in an Aging Colloidal Glass*** GIANGUIDO C. CIANCI, ERIC R. WEEKS, *Department of Physics, Emory University, Atlanta, GA 30322 USA* When a liquid is quenched to form a glass it becomes trapped in a non-equilibrium state. The non-ergodicity of the system is most clearly highlighted by the dependence of the glass' properties on the time elapsed since the quench. This phenomenon is known as aging. Dense colloidal suspensions have been shown to be a good model for the glassy state. We use fast laser scanning confocal microscopy to image sterically stabilized, micron-sized, PMMA spheres in three dimensions and track their positions over time with sub-pixel accuracy. While aging is most commonly detected by measuring the evolution of variables (such as the mean squared displacement or the intermediate scattering function) averaged over the entire system and over time these quantities cannot yield information about the detailed, structural changes that occur during aging. Confocal microscopy, on the other hand, allows us to intimately study the aging process with minimal or no averaging. We study the statistics of the fluctuations of geometrical and dynamical quantities over time as the sample ages. In particular, we find that the aging process is heterogeneous in time and space and compare the fluctuations of the aging process to intermittent, record induced dynamics models.

*Funding: NASA (NAG3-2728)

**8:36**
**G34 4 Dynamic correlations and correlation length in the aging of a simple structural glass** AZITA PARSAEIAN, *Department of Physics and Astronomy, Ohio University* HORACIO CASTILLO, *Department of Physics and Astronomy, Ohio University* We present the results of a detailed molecular dynamics simulation of the spatial correlations of fluctuations in a simple binary Lennard-Jones glass former in the aging regime. We study the 4-point generalized density susceptibility $\chi_4(t,t_w)$ and the dynamic correlation length $\xi_4(t,t_w)$ associated with it, where $t_w$ is the waiting time. We find that these data are consistent with the scalings $\chi_4(t,t_w) = F(t_w)\chi_4^0(C(t,t_w))$ and $\xi_4(t,t_w) = G(t_w)\xi_4^0(C(t,t_w))$, where $C(t,t_w)$ is the incoherent part of the intermediate scattering function. We also find that $F(t_w)$ can be fit as a power of the waiting time, and $G(t_w)$ can be fit as a logarithm of the waiting time. These differing time dependencies, plus the dramatically different behavior of the scaling functions $\chi_4^0(C)$ and $\xi_4^0(C)$ for small $C$ lead to the conclusion that the time evolution of $\chi_4(t,t_w)$ *is not* controlled by its associated dynamic correlation length $\xi_4(t,t_w)$.

**8:48**

**G34 5 Dynamic fluctuations of elastic lines in three-dimensional random enviroments** SEBASTIAN BUSTINGORRY, *Centro Atomico Bariloche, Argentina* LETICIA CUGLIANDOLO, *LPTHE-Jussieu and LPT-ENS, Paris* DANIEL DOMINGUEZ, *Centro Atomico Bariloche, Argentina* Elastic lines embedded in three-dimensional random environments present a low temperature glassy regime, with aging characterized by multiplicative scaling. We studied the scaling properties of the distribution functions of different dynamical observables: the roughness, the mean-squared-displacement and its associated response function. Following the multiplicative scaling hypothesis, we numerically show that the distribution functions depend only on the mean scaled value of the variables, and not on the different time scales involved. These results could be extended to the scaling of distribution functions in critical-like systems.

**9:00**

**G34 6 Microstructure of a polymer glass overaged by application of instantaneous shear strains*** BELA JOOS, *University of Ottawa* MATTHEW L. WALLACE, *Université Louis Pasteur, Strasbourg* When applying a transient shear on jammed colloidal suspensions, Viassnoff and Lequeux (*Phys. Rev. Lett.* **89**, 065701 (2002)) observed both rejuvenation and overaging in the system, as the relaxation times are altered in a non- trivial way. Application of instantaneous, one-time shear deformations on a polymer glass by molecular dynamics simulations produces a similar behavior (M.L. Wallace and B. Joós, *Phys. Rev. Lett.*, in press). Two regimes are observed corresponding to elastic and plastic strains. Of particular interest are deformations in the plastic regime, above the yield strain ($\epsilon > 0.1$), where the characteristic relaxation times $\tau_{1/2}$ increase exponentially with $\epsilon$, after a long waiting time $t_w$ following the deformation. We are in the process of understanding the nature of this state of the glass. There is a slight increase in the average energy of the inherent structures $< e_{IS} >$, in particular in the inter-chain component. The bond orientational order parameter appears to increase especially in the elastic regime. The shear modulus decreases. And there are significant changes in the distribution of relaxation times. The average shifts to larger times, and the distribution broadens and resembles more a Gaussian. These properties suggest that, above the yield strain, the system becomes more homogeneous, and possibly less jammed.

*funded by NSERC (Canada)

**9:12**

**G34 7 Observed Effects of Confinement on Colloidal Glasses*** CAROLYN NUGENT, HETAL PATEL, JOE SALDANA, ERIC R. WEEKS, *Department of Physics, Emory University* We used a binary colloidal suspension to model glass molecules. By increasing the concentration of colloids, a glass transition is induced. Previous studies of colloidal suspensions show that as the glass transition is approached, colloids tend to move in groups of increasing size. In order to examine this phenomenon more closely, a colloidal suspension was confined between two parallel glass plates with a narrow gap of the order of a few colloid diameters in thickness. Confocal microscopy was used to observe the particles and follow their motion over time. We observed that motion in confined regions was much slower than motion in non-confined regions of the same sample. In addition, the motion perpendicular to the walls was slower than motion parallel to the walls. The arrangement of colloids into layers was also observed, which further influenced the motion.

*This project funded by NSF

**9:24**

**G34 8 The effective temperature and the universal scaling behavior of aging colloidal glass system** PING WANG, CHAOMING SONG, HERNAN MAKSE, *City College of New York, New York, NY 10031* Mostly due to the enormous practical importance of glassy systems there has been a vast literature describing different theoretical frameworks for glasses, yet without a common theory applicable to the diverse range of systems undergoing a glass transition. Here we present experimental results on a simple glassy system pointing to a unifying view of out-of-equilibrium systems. We investigate correlation and response functions to external fields to monitor the aging of a colloidal glass composed of highly concentrated hard spherical particles suspended in an refraction index matched fluid for visualization. Our analysis reveals that even though the system is aging far from equilibrium, it behaves as it is equilibrated at a constant temperature, independent of the age. This temperature is larger than the bath, and can be rationalized by the cage dynamics in the system. Global and local fluctuations in the observables are also studied showing a common scaling behavior with the age of the system. While these results can be interpreted within the framework of unifying formulations of aging, the observed scaling forms of the correlation functions do not conform to the theoretical predictions.

**9:36**

**G34 9 Aging of Johari-Goldstein Relaxation in Structural Glasses** HASAN YARDIMCI, ROBERT L. LEHENY, *Department of Physics and Astronomy, Johns Hopkins University* Using frequency-dependent dielectric susceptibility measurements we characterize the aging in two supercooled liquids, sorbitol and xylitol, below their calorimetric glass transition temperatures, $T_g$. In addition to the alpha relaxation that tracks the structural dynamics, the susceptibilities of both liquids possess a secondary Johari-Goldstein relaxation at higher frequencies. Following a quench below $T_g$, the susceptibility slowly approaches equilibrium behavior. For both liquids, features of the Johari-Goldstein relaxation display a dependence on the time since the quench, or aging time, that is very similar to the age dependence of the alpha peak. However, one can not assign a single fictive temperature to both the alpha and Johari-Goldstein relaxations. For example, the peak frequency of the Johari-Goldstein relaxation remains constant during aging for sorbitol while it increases with age for xylitol, inconsistent with a decreasing fictive temperature. This behavior contrasts with that of the high frequency tail of the alpha peak whose shape and position track the aging of the main part of the peak.

**9:48**

**G34 10 Glassy Dynamics in Suspensions of Non-Spherical Colloids** GALINA YATSENKO, KENNETH SCHWEIZER, *University of Illinois, Urbana, IL 61801* Glassy dynamics of isotropic fluids of hard symmetric dumbbells (diatomics), rods, cylinders and disks are studied using a simple form of mode coupling theory and its generalization to predict barriers and activated hopping transport. Orientational degrees of freedom dynamically enter in a pre-averaged manner, and structural correlations are quantified based on a center-of-mass version of the site-site Reference Interaction Site Model. A length-to-diameter (aspect) ratio serves as a principal parameter describing shape anisotropy. The ideal glass

transition volume fraction of dumbbells is predicted to be a non-monotonic function of aspect ratio. For continuous cylinders, ellipsoids and disks power law dependencies of glass transition volume fraction and localization length on aspect ratio are found in the highly anisotropic limit. The consequences of discotic liquid crystalline order for infinitely thin disks have also been studied. Multiple scaling behaviors with volume fraction and aspect ratio are predicted for the localization length, barrier height, elastic shear modulus and yield stress.

**10:00**

**G34 11 Microrheology of an aging colloidal glass** S. JABBARI-FAROUJI, *Univ. of Amsterdam* D. MIZUNO, M. ATAKHORRAMI, *Free Univ. of Amsterdam* E. EISER, *Univ. of Amsterdam* C. SCHMIDT, F. MACKINTOSH, *Free Univ. of Amsterdam* G. WEGDAM, D. BONN, *Univ. of Amsterdam* Laponite is a synthetic clay which after mixing with water, spontaneously evolves from an initially liquid and ergodic state to a non-ergodic glassy state that exhibits elastic behavior. We provide a direct experimental test of the Stokes-Einstein relation as a special case of the fluctuation-dissipation theorem (FDT) in this aging colloidal glass. The use of combined active and passive microrheology allows us to independently measure both the correlation and response functions in this non-equilibrium situation. Contrary to previous reports, we find no deviations from the FDT over several decades in frequency (1 Hz-10 kHz) and for all the observed aging times. Our measurements also demonstrate the applicability of fluctuation-based (passive) microrheology in a non-equilibrium glassy system. This method allows obtaining the viscoelastic properties over a very wide frequency range. Our striking observation is that there is a cross over in frequency behavior of complex shear modulus of system from single power law at early stages of aging to two power laws at later stages. This suggests the existence of two distinct viscoelastic contributions in the aging glass: (i) a high-frequency viscoelastic response in which the shear modulus increases rapidly with frequency; and (ii) a predominantly elastic (weakly frequency-dependent) response at lower frequencies, which becomes increasingly important as the system ages.

**10:12**

**G34 12 Activated Hopping and Dynamic Heterogeneity in Glassy Colloidal Suspensions** ERICA SALTZMAN, KENNETH SCHWEIZER, *University of Illinois at Urbana-Champaign* A microscopic statistical dynamical theory of barriers and activated transport in dense colloidal suspensions has been developed by combining and extending methods of mode coupling, density functional and particle hopping theories. Quasi-analytic results for the mean relaxation time and ensemble-averaged transport coefficients agree well with experiment. However, a full determination of the dynamics requires numerical integration of the nonlinear overdamped stochastic equation of motion, i.e. Brownian dynamics simulation. This enables calculation of average quantities including the mean-square displacement, incoherent dynamic scattering function and alpha relaxation time, as well as trajectory-based quantities such as displacement and relaxation time distributions. Dynamic heterogeneity effects are explored by studying various decoupling factors, the non-gaussian parameter, the bimodality of the displacement distribution and the non-Fickian wavevector dependence of the structural relaxation time. Comparisons to mode-coupling theory, simulation and experimental results are performed.

**10:24**

**G34 13 Dependence of relaxation time on effective temperature in driven glasses*** THOMAS HAXTON, *Physics Dept., Univ. of Pennsylvania* AJAY GOPINATHAN, *Physics Dept., Univ. of California, Santa Barbara* ANDREA LIU, *Physics Dept, Univ. of Pennsylvania* Relaxation times of a class of driven glassy systems are shown to depend on a well-defined effective temperature in much the same way that they depend on temperature in quiescent systems. Molecular dynamics simulations were run for two-dimensional systems of bi-disperse spheres interacting via soft repulsive pair potentials. At high density the systems undergo a glass transition as temperature is lowered. We study low-temperature systems driven by an imposed shear gradient in steady state at a fixed high density. Effective temperatures can be defined from fluctuation-dissipation relations by the long-time limit of the ratio of correlation to response. Throughout a range of bath temperatures and shear rates, relaxation times are found to depend only on the bath temperature $T$ and the effective temperature $T_{\text{eff}}$. In particular, the relaxation time of the driven system as a function of $T_{\text{eff}}$ can be mapped on to the relaxation time of the quiescent system as a function of $T$, using a scale factor that varies only weakly with the ratio $T/T_{\text{eff}}$. This suggests that shear unjams the system because it gives rise to a $T_{\text{eff}}$ that is higher than the glass transition temperature.

*This work was supported by DOE grant DE-FG02-03ER46087.

**SESSION G35: NANOPARTICLES, NANOTUBES AND NANOCRYSTALS: OPTICAL AND STRUCTURAL PROPERTIES**
**Tuesday Morning, 14 March 2006**
**338, Baltimore Convention Center at 8:00**
**Alexander Efros, Naval Research Laboratory, presiding**

**8:00**

**G35 1 Simulations of the Optical Properties of Silicon Nanoparticles Embedded in Silicon Nitride** SEBASTIEN HAMEL, *Lawrence Livermore National Laboratory* ANDREW WILLIAMSON, GIULIA GALLI, LUCA DAL NEGRO, *Massachusetts Institute of Technology* JAE HYUNG YI, VICTOR NGUYEN, YASHA YI, JURGEN MICHEL, LIONEL C. KIMERLING, There is currently a strong interest in the material science community in the optical properties of silicon nanoparticles embedded in silicon nitride. These nanostructures are CMOS-compatible materials which exhibit efficient and fast light emission. The optical properties of these embedded silicon nanoparticles are studied using first-principles Density Functional Theory simulations. We present simulations of the structural, electronic and optical properties of nitrogen-doped silicon nanoparticles both in the gas phase and embedded in a silicon nitride environment. These simulations point to the crucial role played by nitrogen atoms bonded to the surface of small ( $\sim$ 1nm) silicon nanoparticles in the light emission mechanism of $SiN_x$ films. We compare the calculated optical gaps and radiative lifetimes of the nanoparticles with recent experimental measurements of light-emitting silicon-rich silicon nitride films obtained by PE-CVD deposition followed by low tem-

perature (500-900 °C) thermal annealing. This work was performed under the auspices of the U.S. Dept. of Energy at the University of California/Lawrence Livermore National Laboratory under contract no. W-7405-Eng-48.

**8:12**

**G35 2 Multi-valued analog information storage using self-assembled nanoparticle films.** AL-AMIN DHIRANI, YOSHINORI SUGANUMA, *Department of Chemistry, University of Toronto* Digital computers use binary states, typically represented by 0 and 5 V, to store and process information at all stages of a calculation. If more states (ideally a continuum) were available in between, density of information could be dramatically increased. Here we show that self-assembled nanoparticle films can feature such continuous state or analog information storage. Nanoparticle films were prepared on gate oxides by alternate immersion in solutions of gold nanoparticle and dithiol linker molecules. These films afford microlithography-free fabrication bridging nanometer to micrometer length scales as well as a layer-by-layer assembly yielding three-dimensional functional structures. Information provided by an arbitrary gate voltage was 'written' by trapping charges in local, gate-modified potentials when films were cooled below 175 K. The information was 'read' using the film's built-in ability to sense charge via Coulomb blockade. Application of a time-dependent, multi-step writing gate voltage generates conductance maps corresponding to multi-valued analog information. As a proof of concept, we exploited this technique to store 'UT' in Morse code.

**8:24**

**G35 3 Using Accumulated Charge to Monitor Nanoparticle Deposition Rates Via Electrospray Ionization** JOEL THERRIEN, AMIR DINDAR, DAVID SMITH, *U. Massachusetts-Lowell, ECE Dept.* Electro-Spray Ionization (ESI) is a handy technique for depositing nanoparticles onto a substrate directly from a liquid suspension. ESI atomizes the suspension via high electric fields. The solvent in which the particles were suspended rapidly evaporates resulting in a stream of charged particles. This technique can be used to deposit a sub-monolayer dispersion of particles on any conducting substrate. AFM studies have been performed on ESI deposited samples to determine the correlation between the net charge deposited on the substrate via the deposition and the surface density of particles. This correlation may be used as a means of rate monitoring to assure higher reliability in achieving desired particle densities.

**8:36**

**G35 4 Enhanced optical luminescence in ZnO nanostructures following O 1s to $p_z$ excitation*** R.A. ROSENBERG, G.K. SHENOY, *Argonne National Laboratory* X.-T. ZHOU, T.K. SHAM, *University of Western Ontario* Room temperature ultraviolet ( $\sim$ 385 nm) lasing in ZnO nanostructures has recently been demonstrated.[1] This phenomenon is thought to arise from the natural cavity formed by the wurtzite nanostructure and its faceted ends. X-ray excited optical luminescence (XEOL) provides the capability to determine the nature of the sites responsible for producing low energy (1-6 eV) fluorescence. We will present XEOL excitation curves taken at the Zn L and O K edge obtained using both the defect ( $\sim$ 510 nm) and bandgap ( $\sim$ 370 nm) transitions as signals. Results obtained at the Zn L edge resemble the x-ray absorption curve of the nanostructure. However, striking differences are observed at the O K edge. Excitation to states of $p_z$ symmetry (along the c axis) leads to enhanced luminescence while excitation to $p_{x,y}$ states (lying in the basal plane) decreases the yield. We interpret this phenomenon as resulting from the lower probability of quenching by near surface defects for states excited along the c-axis as opposed to those excited perpendicular to it. 1. M.H. Huang, et al., Science **292**, 1897 (2001).

*Work supported by the U.S. Department of Energy, Office of Basic Energy Sciences, under Contract No. W-31-109-ENG-38.

**8:48**

**G35 5 Silicon nanoporous pillar array: template for fabricating silicon-based nanocomposites with enhanced physical properties*** XIN JIAN LI, *Zhengzhou University, China* XIAO NAN FU, *Zhengzhou University, China* HAI JUN XU, *Zhengzhou University, China* WEI FENG JIANG, *Zhengzhou University, China* A triple hierarchical structure, silicon nanoporous pillar array (Si-NPA), was formed on silicon wafers by a hydrothermal method. The structure of Si-NPA is characterized by the regular array of micron-sized silicon pillars, quasi-identical nanopores densely distributing over each pillar, and silicon nanocrystalllites composing the walls of the nanopores. Utilizing the excellent structural regularity and high chemical reactivity of Si-NPA, patterned nanocomposites of CdS, carbon nanotubes (CNTs), Au, and Fe3O4/Si-NPA were fabricated. Their element compositions, morphologies and microstructures were characterized. Ideal physical properties of I-V curve in CdS/Si-NPA heterojunction, field emission in Si-NPA, CNTs/Si- NPA, Au/Si-NPA, and humidity/gas sensitivity in Fe3O4/Si-NPA were observed and the corresponding mechanisms were analyzed. These results indicate that Si-NPA could be employed as an ideal template to assembly silicon-based functional nanosystems, and might find multiple applications in fabricating novel electronic devices.

*Supported by the National Natural Science Foundation of China.

**9:00**

**G35 6 Excitons in Negative Band Gap Nanocrystals** JAMES SIMS, GARNETT W. BRYANT, HOWARD HUNG, *National Institute of Standards and Technology* Exploiting quantum confinement in nanocrystals made from materials with negative bulk band-gap will be critical for nanosensor applications in the far infrared. However, understanding quantum confinement, excitonic states and optical response in negative band-gap nanocrystals provides challenges not posed for usual nanocrystals with positive bulk band-gaps. We show that intrinsic surface states occur in nanocrystals made from negative gap semiconductors such as HgS. We use atomistic tight-binding theory that accounts for band mixing critical in negative-gap semiconductors but unimportant in positive-gap systems. Such band mixing makes effective mass theory inadequate for negative-gap nanocrystals. In small HgS dots, the lowest conduction band states are cation-derived and the band-edge valence states are anion-derived, as for finite-gap dots. However, in bigger HgS dots, the lowest conduction band state has a high density at the surface that slowly decays into the dot. As the dot size increases, this conduction state crosses the valence band edge, reaching a limit inside the bulk negative gap for very large dots. In this limit, the state is localized to the surface. The excitonic states and optical response of HgS dots are discussed to identify signatures for intrinsic surface states and to assess nanosensor applications with these systems.

**9:12**

**G35 7 Freely-Suspended Monolayers of Gold Nanocrystals: Fabrication and Elastic Properties*** KLARA ELTETO, *University of Chicago* XIAO-MIN LIN, *Argonne National Laboratory* SANG-KEE EAH, *Rensselaer Polytechnic Institute* HEINRICH M. JAEGER, *University of Chicago* We present a method to produce freely-suspended monolayers of 5.5nm-diameter gold nanocrystals, ligated with dodecanethiol, over holes with widths up to 2microns (about 250 particles). The holes are etched through a 120nm thick silicon nitride membrane. A water droplet initially covers the substrate. When nanocrystals suspended in toluene are added, they spread over the water-air interface, forming an extended, compact monolayer. As the water dries, the monolayer settles over the substrate and drapes itself over the holes. The resulting freely-suspended monolayers are stable in air and vacuum, as observed with optical, atomic force and transmission electron microscopy. No additional polymer or crosslinking of the ligands is required. Possible mechanisms for the stability of the monolayer include ligand interdigitation and van der Waals interaction between the gold cores. We report on measurements of the elastic properties of such monolayers, obtained by applying point forces to the suspended areas with an atomic force microscope and measuring the vertical elastic deformation.

*This work was supported by the UC-ANL Consortium for Nanoscience Research, by NSF MRSEC under DMR-0213745, and by the DOE under #W-31-109-ENG-38.



**9:24**

**G35 8 Mapping Elastic Strain in Electrophoretically-Deposited CdSe Nanocrystal Films** IRVING HERMAN, SARBAJIT BANERJEE, SHENGGUO JIA, DAE-IN KIM, RICHARD ROBINSON, JEFFREY KYSAR, JOZE BEVK, *Materials Research Science and Engineering Center, Columbia University, New York, NY* The mechanical stability of nanocomponent films is critical for applications and yet is a largely unexplored area of research. Raman microprobe analysis has been used to probe elastic strain in the cores of thick, fractured electrophoretically-deposited CdSe nanocrystal films. Strain in these films arises from solvent evaporation and can be as much as 2.5% in the cores of CdSe nanocrystals for 3.2 $\mu$m thick films. The overall strain in these films, as determined by optical microscopy, is $\sim$ 11.7%. The in-plane stress developed in these films is $\sim$ 1.6 GPa. The biaxial modulus of the films is determined to be $\sim$ 13.8 GPa. Using micromechanics models, a value of $\sim$ 5.1 GPa is inferred for the biaxial modulus of the trioctylphosphine oxide ligand matrix. Since, solvent loss leads to strain in most ensembles of colloidal nanocrystals, this method has the potential for being broadly generalizable to other films made of nanocrystalline components. Support for this work was provided by the Materials Research Science and Engineering Center of the NSF under Grant No. DMR-0213574 and by NYSTAR.

**9:36**

**G35 9 White-Light Emission from Magic-Sized Cadmium Selenide Nanocrystals*** MICHAEL BOWERS, *Vanderbilt University* JAMES McBRIDE, *Vanderbilt University* SANDRA ROSENTHAL, *Vanderbilt University* Magic-sized cadmium selenide (CdSe) nanocrystals have been pyrolytically synthesized. These ultra-small nanocrystals exhibit broadband emission (420 -710 nm) that covers most of the visible spectrum while not suffering from self absorption. This behavior is a direct result of the extremely narrow size distribution and unusually large Stokes shift (40-50 nm). The intrinsic properties of these ultra-small nanocrystals make them an ideal material for applications in solid state lightingand also the perfect platform to study the molecule−to−nanocrystal transition.

*This work was supported by the U.S. Department of Energy and the National Institutes of Health

**9:48**

**G35 10 Antenna Effects in Arrays of Aligned Carbon Nanotubes** K. KEMPA, J. RYBCZYNSKI, Y. WANG, Z. REN, *Boston College* Z. P. HUANG, D. CAI, *NanoLab* J. B. KIMBALL, J. CARLSON, *US Army Natick Soldier Center* G. BENHAM, *MegaWave Corporation* We have demonstrated earlier [1], that carbon nanotubes respond to light as radio antennas. Specifically, we have demonstrated the polarization and length antenna effects. Here we show yet another, a more subtle antenna effect: the multi-lobe reflection pattern with the specular enhancement. We demonstrate this effect in a random array of aligned, widely spaced carbon nanotubes. We show via calculation and computer simulations that these effects are results of the conventional antenna theory. [1] Y. Wang, K. Kempa, B. Kimball, J. B. Carlson, G. Benham, W. Z. Li, T. Kempa, J. Rybczynski, A. Herczynski, and Z. F. Ren, Applied Physics Letters **85**, 2607 (2004).

**10:00**

**G35 11 Aligned carbon nanotubes as nanocoax cables for subwavelenght light transmission** JAKUB RYBCZYNSKI, KRZYSZTOF KEMPA, YANG WANG, *Boston College, MA* ZHONGPING HUANG, DONG CAI, DAVID CARNAHAN, *NanoLab Inc., USA* RENATA JARZEBINSKA, MICHAEL GIERSIG, *CAESAR Institute, Bonn, Germany* ZHIFENG REN, *Boston College, MA* We are presenting for the first time that vertically aligned carbon nanotubes can be used for fabrication of large-scale arrays of nanocoax cables. Multicoating with insulating and metallic layers results in a coaxial structure where light can be transmitted along the nanotube axis in the visible frequency range. We have shown that unlike simple optical waveguides, coaxial nanocables exhibit subwavelength transmission of light. Results obtained with near-field optical microscope confirm our predictions. Some aspects of nanocoax cables farbication and optical properties studies will be presented.

**10:12**

**G35 12 Theory of plasmon excitations in coaxial cylindrical geometries: finite magnetic field** MANVIR KUSHWAHA, *Institute of Physics, University of Puebla, Mexico* BAHRAM DJAFARI-ROUHANI, *Department of Physics, University of Science and Technology of Lille, France* We report on a theoretical investigation of the plasmon propagation in the coaxial cylindrical geometries using Green's function (or response function) theory in the presence of an applied axial magnetic field ($\vec{B}\|\hat{z}$). Green's function theory generalized to be applicable to such quasi-one dimensional (1D) systems enables us to derive explicit expressions for the corresponding response functions (associated with EM fields), which can in turn be used to compute numerous physical properties of the system under consideration. As an application, we present several illustrative examples on the dispersion characteristics of the confined and extended magnetoplasmons in the single- and double-interface structures. These dispersive modes are also substantiated through the computation of local as well as total density of states (DOS). It is found that, unlike the zero-field

case, the magnetoplasma propagation is nonreciprocal with respect to the sign of the index *m* of the Bessel functions involved. We also briefly clarify some delusive traces of the edge magnetoplasmpons for a plasma shell embedded between two identical or unidentical dielectrics. Our theoretical framework can also serve as a powerful technique for studying the intrasubband plasmons and magnetoplasmons in the emerging multiwall carbon nanotubes.

**SESSION G37: FOCUS SESSION: NANOSCALE MATERIALS PHYSICS OF PHASE TRANSITIONS I**
**Tuesday Morning, 14 March 2006**
**340, Baltimore Convention Center at 8:00**
**Richard Haglund, Vanderbilt University, presiding**

*Contributed Papers*

**8:00**
**G37 1 Adsorbate-Induced Ferroelectricity in Nanostructures***
JONATHAN SPANIER, *Drexel University* ALEXIE KOLPAK, ILYA GRINBERG, *University of Pennsylvania* JEFFREY URBAN, LIAN OUYANG, WANSOO YUN, *Harvard University* ANDREW RAPPE, *University of Pennsylvania* HONGKUN PARK, *Harvard University* DREXEL UNIVERSITY TEAM, UNIVERSITY OF PENNSYLVANIA TEAM, HARVARD UNIVERSITY TEAM, We discuss recent progress in understanding the size-dependent evolution of ferroelectricity in perovskite nanostructures and ultrathin films obtained via variable-temperature scanning probe microscopy investigations of individual nanorods and other ferroelectric nanostructures. We propose a mechanism in which the surface polarization charge is passivated by molecular adsorbates. A combination of density functional theory simulations, modified phenomenological Landau theory, and thermodynamic analysis demonstrates that the experimental behavior is well described by this mechanism.

*Work supported by NSF, ONR and ARO.

**8:12**
**G37 2 Nucleation process on the 180° domain wall of $PbTiO_3$ by the external electric field** YOUNG-HAN SHIN, ILYA GRINBERG, I-WEI CHEN, ANDREW RAPPE, *University of Pennsylvania* Ferroelectric oxides are extremely useful as nonvolatile memory storage materials, and the speed at which polar domains can be reversed is a critical characteristic for future development of these materials. However, the size of the critical nucleus during the polarization reversal is still unknown experimentally. If we assume that the magnitudes of local polarizations are the same and their directions are along the external field, it will be triangular and the height of the nucleus along the external field should be much larger than its width following the Miller and Weinreich's study in 1960s. We made an atomic potential for perovskite ferroelectrics based on the first-principles calculation, and performed molecular-dynamics simulations to understand the nucleation and growth process of ferroelectric domains. We find that its shape is close to a square not a triangle and its size much smaller than Miller and Weinreich's. It stems from the small polarizations and the voltex-like flow around the nucleus. To increase the system size we used the stochastic study using the nucleation and growth rates which were obtained from the molecular dynamics simulations. The overall speed of the domain wall motion can be estimated from this stochastic calculation.

**8:24**
**G37 3 Critical Behaviors in $Pb(Zr,Ti)O_3$ Ultrathin films** EMAD ALMAHMOUD, IGOR KORNEV, LAURENT BELLAICHE, *Physics Department, University of Arkansas, Fayetteville, Arkansas 72701, USA* The first-principles-derived approach of Ref. [1] is used to determine the thickness dependency of Curie temperature and of the spontaneous polarization in $Pb(Zr,Ti)O_3$ (PZT) thin films that are under stress-free and open-circuit boundary conditions. It is found that, above a thickness of 7 (B-) monolayers (ML), the Curie temperature follows the finite-size relation of Ref. [2] with a critical exponent $\lambda = 1.04$. On the other hand, the Curie temperature deviates from this ''usual'' relationship for thickness of 6 monolayers and below, characterizing a crossover from a three- to a two-dimensional behavior. This striking crossover is also reflected in the critical exponent it $\beta$, that is associated with the power law describing the behavior of the polarization with thickness. As a matter of fact, such exponent decreases drastically from 0.14 to 0.1 between 7 and 4 ML. This work is supported by ONR grants N 00014-01-1-0365, N00014-04-1-0413 and 00014-01-1-0600, by NSF grants DMR-0404335 and DMR-9983678, and by DOE grant DE-FG02-05ER46188. [1] E. Almahmoud, Y. Navtsenya, I. Kornev, H. X. Fu, and L. Bellaiche, Phys. Rev. B 70, 220102 registered (2004) [2] G. A. T. Allan, Phys. Rev. B1, 352 (1970).

*Invited Papers*

**8:36**
**G37 4 Phase transitions in ferroelectric superlattices.**
MATTHEW DAWBER, *DPMC, University of Geneva*

The construction of artificial ferroelectric superlattices with fine periodicity presents exciting possibilities for the development of new materials with extraordinary properties and furthermore a probe for understanding the fundamental physics of ferroelectric materials. Our superlattices of $PbTiO_3/SrTiO_3$ are prepared on conducting 0.5% Nb doped (001) $SrTiO_3$ substrates using off-axis RF magnetron sputtering. Cross-sectional TEM investigations were performed on several samples and reveal the coherent growth and artificial layering of the samples. Further structural characterization using standard $\theta$-$2\theta$ x-ray diffraction was performed on a series of 20 bilayer superlattices in which the $PbTiO_3$ thickness was varied from 54 to 1 unit cells while the $SrTiO_3$layer thickness was maintained at 3 unit cells. Intuitively one expects, as the thickness of the $PbTiO_3$ layers relative to the $SrTiO_3$ layers is reduced, a decrease of the ferroelectric polarization

which should result in a concomitant decrease of the average lattice parameter. This is indeed the behaviour we observe for superlattices $PbTiO_3/SrTiO_3$ n/3 where n is greater than 3. However, surprisingly, the 2/3 and 1/3 superlattices display larger average lattice parameters which indicate a recovery of ferroelectricity at very small $PbTiO_3$ layer thicknesses, a finding we confirmed using atomic force microscopy. The experimental finding thus stands in stark contrast to the intuitive expectation of a ferroelectric-paraelectric phase transition in this system as the ferroelectric component is reduced and we find further that the temperature of the ferroelectric-paraelectric phase transition is also greatly modified. Due to the excellent quality of the samples we are able to present the results of a number of detailed structural and electrical characterizations, along with the development of first principles based theoretical models, which cast further light on the fascinating phase transition behaviour of this system. Through this we can gain an insight into how we can understand and control the behaviour of ferroelectricity as the physical dimensions are reduced and the relevant boundary conditions are modified.

*Contributed Papers*

**9:12**

**G37 5 Generalized thermodynamics of solid surfaces applied to size effects on equilibrium** ROBERT CAMMARATA, *Johns Hopkins University* In his thermodynamics of liquid interfaces, Gibbs introduced the ''dividing surface'' and rigorously derived the general conditions for equilibrium, and showed how the size of phases can affect the equilibrium state. However, the case of systems with solid surfaces, he imposed certain restrictions, such as considering only single component solids, which limited the applicability of his approach. In the case of finite size and multicomponent solids, difficulties arise when defining the chemical potentials for the interface, which leads to difficulties in defining the surface energy. It will be shown how these difficulties can be overcome by using the concept of ''surface availability,'' analogous to the availability used in bulk thermodynamics. A generalized surface thermodynamics can be formulated consistent with Gibbs' analysis for liquid surfaces but that can be used for general multicomponent solid systems. Also, employing the surface availability allows one to dispense with the dividing surface construction and treat the interfacial region as a separate inhomogeneous phase. Applications to nanoscale materials will be discussed.

**9:24**

**G37 6 Theory of the Melting of Confined Nanocrystals** DARYL CHRZAN, Q. XU, I.D. SHARP, *Materials Science and Engineering, University of California, Berkeley and Materials Sciences Division, Lawrence Berkeley National Laboratory* D.O. YI, *Applied Science and Technology, University of California, Berkeley* C.W. YUAN, C.Y. LIAO, A.M. GLAESER, *Materials Science and Engineering, University of California, Berkeley and Materials Sciences Division, Lawrence Berkeley National Laboratory* J.W. AGER III, *Materials Sciences Division, Lawrence Berkeley National Laboratory* E.E. HALLER, *Materials Science and Engineering, University of California, Berkeley and Materials Sciences Division, Lawrence Berkeley National Laboratory* Recent measurements of the melting point of Ge nanocrystals embedded within a silica matrix reveal that the nanocrystals can be heated approximately 200 K above the bulk melting point before melting, and cooled approximately 200 K below the bulk melting point before solidification. This behavior is in marked contrast to that observed for free standing nanocrystals. We have developed a classical, continuum thermodynamic model which demonstrates that the phenomenon is caused by kinetic barriers to the nucleation of the liquid phase. The kinetic barriers are associated with the density increase upon melting of Ge and the fact that liquid Ge does not wet silica. The model provides a quantitative description of the experimental observations. This research is supported by the U. S. Department of Energy under contract No. DE-AC02-05CH11231.

**9:36**

**G37 7 Theory of the Jahn-Teller Soliton** DENNIS CLOUGHERTY, *University of Vermont* It is demonstrated that under common conditions a molecular solid subject to Jahn-Teller interactions supports stable Q- ball-like non-topological solitons. Such solitons represent a localized lump of excess electric charge in periodic motion accompanied by a time-dependent shape distortion of a set of adjacent molecules. The motion of the distortion can correspond to a true rotation or to a pseudo-rotation about the symmetric shape configuration. These solitons are stable for Jahn-Teller coupling strengths below a critical value; however, as the Jahn- Teller coupling approaches this critical value, the size of the soliton diverges signaling an incipient structural phase transition. The soliton phase mimics features commonly attributed to phase separation in complex solids.

**9:48**

**G37 8 Finite-size scaling of the critical temperatures of magnetic thin films with variable range of interactions.** TIMOTHY BRAMFELD, *The Pennsylvania State University* ROY F. WILLIS, *The Pennsylvania State University* Finite-size scaling in magnetic (spin) systems with an arbitrary range of spin interactions was first discussed by Domb and Dalton [1]. These authors explored the effect on the various critical exponents of the thermodynamic quantities of a generalized Ising model in which each spin interacts equally strongly with neighbors within some finite interaction distance beyond which the interaction goes to zero. Such a model was used by Zhang & Willis [2] to explain the thickness dependence of the Curie temperatures of ferromagnetic nickel films. Specifically, they showed that Tc followed a power law, reduced temperature $t \sim L^{-\lambda}$down to a critical thickness Lo = Ro, at which point the critical temperature reduced linearly with further decreasing thickness L. In this talk, we show that the demarcation point Lo = Ro scales with the range of spin interactions in alloy films. This parameter Ro is a function of the changing dimensions of the Fermi surface i.e. related to the period of RKKY oscillations in these itinerant ferromagnets. We examine the ramifications of an increasing range of spin interactions Ro on the finite-size critical behavior of a magnetic system. [1] C. Domb & N.W. Dalton, Proc. Phys. Soc. 89, 859 (1966). [2] R. Zhang & R.F. Willis, Phys. Rev. Lett. 86, 2665 (2001).

**10:00**

**G37 9 Phase Diagrams, Crossovers and Charge-Spin Separation in Small Clusters** ARMEN KOCHARIAN, *California State University* GAYANATH FERNANDO, KALUM PALANDAGE, *University of Connecticut* JAMES DAVENPORT, *Brookhaven National Laboratory* The charge-spin separation effect and response thermodynamics in the presence of a magnetic field are calculated using exact analytical diagonalization and grand canonical ensemble method for small clusters. Rigorous criteria for the Mott-Hubbard, Néel and zero-magnetic field (spin) weak singularities (*saddle points*) in the thermodynamic charge and spin densities of states *versus* chemical potential and magnetic field are found in the exactly solvable two and four site Hubbard ($U \mp 0$) clusters. Large quantum spin fluctuations are signaled by the presence of spin and charge density peaks, pseudogaps and corresponding temperature driven crossovers. The numerically evaluated, exact expressions for the charge, spin susceptibilities and specific heat demonstrate separation of charge and spin degrees and presence of pseudogaps that disappear at the distinct critical temperatures of crossovers. The phase diagram in the ground state, when monitored as a function of doping, displays the presence of clearly identifiable quantum phase transitions and critical points (QCP). In overall, the obtained spin pseudogap, magnetic correlations with antiferromagnetic (spin) pseudogap structure and crossovers in small clusters at $U > 0$ closely resemble the pseudogap phenomena and the normal-state phase diagram in high $T_c$ superconductors.

**10:12**

**G37 10 Electron-Spin Resonance of Chromium-Doped Vanadium Dioxide** PATRICK BUNTON, D. BLANE BAKER, KENNETH MAYNES, KENNETH HARTMAN, *William Jewell College* ANDREJ HALABICA, RENE LOPEZ, RICHARD HAGLUND, *Vanderbilt University* We have investigated the metal insulator transition (MIT) in vanadium dioxide using the electron-spin resonance (ESR) response of a chromium probe. Our goal is to elucidate information regarding potential trigger mechanisms for the MIT such as extrinsic defects or thermal excursion associated with soft modes. A chromium-doped vanadium dioxide film was prepared on fused-silica by pulsed laser deposition in oxygen followed by annealing in an oxygen atmosphere. The chromium dopant proved to be sensitive to the MIT, exhibiting a hysteretic dependence of chromium intensity. A 140 nm-thick film exhibits a factor of four decrease in chromium line intensity as the temperature increases across the MIT. ESR can yield information regarding thermal excursions of lattice ions as well as symmetry information – typically through either linewidth or axial spin Hamiltonian parameter. In addition, decreases in ESR signal intensities are discussed in relation to changes in electron spin-lattice relaxation times. Extensions to two-dimensional films of contiguous nanoparticles and to nanoparticle arrays will be discussed.

**10:24**

**G37 11 Percolation effects in networks of vanadium dioxide nanocrystals*** JOHN ROZEN, RENÉ LOPEZ, RICHARD HAGLUND, LEONARD FELDMAN, *Department of Physics and Astronomy & Institute of Nanoscale Science and Engineering, Vanderbilt University, Nashville, Tennessee 37235* Bulk vanadium dioxide undergoes a phase transition from a semiconductor to a metal near 68 $^{o}$C upon heating. A unique aspect of $VO_2$ nanocrystals is that their small size leads to meta-stable states and to the widening of the hysteresis loop traced out by the semiconductor-to-metal phase transition. We report simultaneous measurements of the transmittance and of the resistance made on thin $VO_2$ nanocrystalline films. An offset between the effective electrical and optical switching temperatures is observed. Indeed, there is an intermediate state where the films are optically metallic but electrically semiconducting (opening the possibility of designing tri-state devices). This is explained in terms of current percolation through a network of nanometer-scale grains of different sizes undergoing the transition at distinct temperatures. An effective-medium approximation can model this behavior and proves to be an indirect method to calculate the surface coverage of the films. Also, the understanding of the collective properties of the nanocrystals leads to the reconstruction of the electrical hysteresis of the phase transition.

*This work was supported by the National Science Foundation under grants DMR-0210785 & DMR-9871234.

**10:36**

**G37 12 Transmission modulation through sub-wavelength hole arrays in metal-$VO_2$ double-layer nanostructures** J. Y. SUH, E. U. DONEV, R. LOPEZ, L. C. FELDMAN, R. F. HAGLUND JR., *Vanderbilt University* Nanoscale optical systems require active devices able to control light in sub-wavelength structures. We report the use of a unique double layer structure which provides this function. Enhanced transmission of near-infrared light through a subwavelength hole arrays patterned in Ag-$VO_2$and Au-$VO_2$ double-layer films shows that it is possible to modulate transmitted intensity by means of a semiconductor-to-metal phase transition in $VO_2$. The transmitted intensity in the near-infrared for the metallic phase of $VO_2$ is a factor of $\sim$ 10 greater than the intensity for the semiconducting phase. We explain this modulation in terms of the switchable permittivity difference of the $VO_2$ phases.

**10:48**

**G37 13 Optical diffraction in ordered $VO_2$ nanoparticle arrays** RENE LOPEZ, LEONARD FELDMAN, RICHARD HAGLUND, *Deparment of Physics and Astronomy & Institute of Nanoscale Science and Engineering, Vanderbilt University, Nashville, TN, 37235* The potential of oxide electronic materials as multifunctional building blocks is one of the driving concepts of the field. In this presentation, we show how nanostructured particle arrays with long-range order can be used to modulate an optical response through exploiting the metal-insulator transition of vanadium dioxide. Arrays of $VO_2$ nanoparticles with long-range order were fabricated by pulsed laser deposition in an arbitrary pattern defined by focused ion-beam lithography. The interaction of light with the nanoparticles is controlled by the nanoparticle size, spacing and geometrical arrangement and by switching between the metallic and semiconducting phases of $VO_2$. In addition to the near-infrared surface plasmon response observed in previous $VO_2$ studies, the $VO_2$ nanoparticle arrays exhibit size-dependent optical resonances in the visible region that likewise show an enhanced optical contrast between the semiconducting and metallic phases. The collective optical response as a function of temperature gives rise to an enhanced scattering state during the evolving phase transition, while the incoherent coupling between the nanoparticles produces an order-disorder-order transition.

**SESSION G38: FOCUS SESSION: SUPERCONDUCTIVITY-CARBON ALLOYING OF MAGNESIUM DIBORIDE AND RELATED COMPOUNDS**
**Tuesday Morning, 14 March 2006; 341, Baltimore Convention Center at 8:00**
**Paul Canfield, Iowa State University, presiding**



*Invited Papers*

**8:00**
**G38 1 Tuning the Superconducting Properties of $MgB_2$.**
RUDEGER H.T. WILKE, *University of Wollongong*

The relatively high superconducting transition temperature of 39 K in $MgB_2$ has garnered much interest over the past several years in both fundamental and applied research. $MgB_2$ is a conventional phonon mediated BCS superconductor with the unconventional property of two superconducting gaps. These gaps ($\sigma$ and $\pi$) arise from the coupling of boron phonons with two different orthogonal sheets of the Fermi surface. In a conventional single gap superconductor the upper critical field can be tuned by the introduction of nonmagnetic impurities. For $MgB_2$ the situation becomes more complex because there are 3 important scattering channels (inter and intra-band). Theoretical calculations predict different developments of the upper critical field and anisotropy ratio if the scattering can be selectively tuned to a specific channel. In this talk I will present data on two different types of perturbations to $MgB_2$: carbon doping and neutron irradiation. Low level carbon doping enhances the upper critical field with only a minor decrease in $T_c$. Whereas $T_c$ suppression is the result of carbon electron doping the system, the enhancement of $H_{c2}(T=0)$ is the result of an increase in scattering, with evidence to suggest carbon doping enhances intra-$\pi$-band scattering. In contrast, $H_{c2}(T=0)$ values tend to scale with $T_c$ in heavily neutron irradiated samples and the superconducting properties can be understood in terms of a decrease in the density of states at the Fermi surface and an increase in interband scattering.

*Contributed Papers*

**8:36**
**G38 2 Upper critical field and anisotropy in carbon alloyed $MgB_2$ thin films*** QI LI, VALERIA FERRANDO, JUN CHEN, ALEXEJ POGREBNYAKOV, JOAN REDWING, XIAOXING XI, *Penn State University* ALEX GUREVICH, DAVID LARBALESTIER, *University of Wisconsin - Madison* J. B. BETTS, C. H. MIELKE, *Los Alamos National Lab* We have studied the upper critical field and its anisotropy $\gamma$ of C-alloyed $MgB_2$ thin films grown on (0001) SiC single crystal substrates by hybrid physical-chemical vapor deposition (HPCVD). Different concentrations of C were introduced during the deposition, which increased the residual resistivity systematically but did not affect $T_c$ seriously. The upper critical field was found to increase to above 60 T for $H$ parallel to the ab plane and up to $\sim$ 40T for $H$ parallel to the $c$ axis with even moderate amounts of C doping. Moreover, we show that $H_{c2}$ stays at these levels in a wide range of C doping. The $H_{c2}$ anisotropy was found to decrease as the C concentration increases. The $H_{c2}(T)$ curves for both $H\|ab$ and $H\|c$ directions were explained by a theoretical model of dirty limit two band superconductivity, which takes into account different scattering rates in $\pi$ and $\sigma$ bands, as well as interband scattering. The differences in the $H_{c2}(T)$ and $\gamma(T)$ for different samples can be explained by the differences of the relative scattering rates in each band which make it possible to adjust the $\pi$ and $\sigma$ scattering such that $H_{c2}$ perpendicular to $ab$ can attain almost 20T at 20K.

*This work is supported NSF and ONR.

**8:48**
**G38 3 Accentuated lattice parameters in carbon doped MgB2 thin films with enhanced upper critical fields** JONATHAN GIENCKE, *University of Wisconsin - Madison* ALEXEJ POGREBNYAKOV, *Penn State University* BEN SENKOWICZ, *University of Wisconsin - Madison* XIAOXING XI, *Penn State University* DAVID LARBALESTIER, CHANG BEOM EOM, *University of Wisconsin - Madison* We report a strong correlation between the accentuation of the a- and c-lattice parameters in carbon doped $MgB_2$ thin films grown via HPCVD and their enhanced upper critical fields. This phenomenon is in strong contrast to the behavior seen in carbon doped single crystals, where the a-lattice parameter is depressed while the c-lattice parameter remains unchanged. This has lead us to believe that the defects leading to the enhancement of the upper critical fields differ in single crystals and thin films, and is due to the non-thermodynamic equilibrium growth environment unique to thin film processes. In addition, the presence of secondary phases present only in thin films exhibiting the enhanced critical field will be discussed. Understanding the nature of these defects is essential to controlling the superconducting properties of $MgB_2$.

**9:00**
**G38 4 Carbon Inhomogeneity and Superconducting Properties of $Mg(B,C)_2$*** L. D. COOLEY, A. J. ZAMBANO,[†] A. R. MOODENBAUGH, *Condensed Matter Physics and Materials Science Department* R. F. KLIE, *Center for Functional Nanomaterials, BROOKHAVEN NATIONAL LABORATORY* Mg and $B_4C$ mixtures (molecular ratio of [1:2]) were reacted in a single step in stainless steel from 850[r]C to 1300[r]C to produce nominal $MgB_{1.8}C_{0.2}$ as estimated from unit cell volumes. Reactions from 850 to 1100°C produced an inhomogeneous superconducting phase despite the initial atomic $B_4C$ compound, suggesting that

carbon segregation is an important part of these reactions. For reactions above 1100°C, the critical temperature $T_c$ increased from 18 to 28 K as the strain (as estimated from x-ray diffraction peak broadening) decreased at nominally constant carbon content, suggesting that structural order is also important. These changes will be discussed with regard to the formation and coarsening of amorphous and crystalline impurity phases observed by electron microscopy, which affect electron scattering and connectivity. Since only scattering affects the upper critical field, whereas both scattering and connectivity affect the transport properties, optimization of these reactions is crucial to understanding the potential for $Mg(B,C)_2$ as a high-field superconductor.

*Work supported by the US Department of Energy under contract number DE-AC02-98CH10886.

†Present address: NSF MRSEC for Superconductivity Reserach, University of Maryland

**9:12**

**G38 5 Towards the development of a high quality doped boron precursor and the effect on the superconducting properties of $MgB_2$** JAMES MARZIK, *Specialty Materials, Inc.* ALBERT KUMNICK, *Specialty Materials, Inc.* Gas phase plasma synthesis techniques were used to produce nano-sized doped boron powder from vapor phase precursors. The powders were reacted with magnesium to make $MgB_2$. The measurement of the resultant superconducting properties suggests that boron made by this synthetic method may result in $MgB_2$ superconductors with enhanced critical currents and upper critical fields. The values of $J_c$ and $H_{c2}$ obtained using plasma synthesized boron precursors are compared with those values for $MgB_2$ obtained using crystalline and amorphous boron powder made by other techniques, as well as boron fiber made by chemical vapor deposition. The roles of processing temperature and time, particle and grain size, purity, dopant concentration, and chemical homogeneity are evaluated in terms of their relative effects on the critical current and upper critical field of $MgB_2$.

**9:24**

**G38 6 Boron powder purification and its effects on the microstructure and superconducting properties of $MgB_2$.** JIANYI JIANG, BEN SENKOWICZ, XUEYAN SONG, ERIC HELLSTROM, DAVID LARBALESTIER, *University of Wisconsin-Madison* APPLIED SUPERCONDUCTIVITY CENTER TEAM, $MgB_2$ wires can be easily fabricated by reacting Mg powder with amorphous boron powder. But commercial boron powder normally contains impurities such as $B_2O_3$. The presence of $B_2O_3$ could lead to the formation of oxides in $MgB_2$ wire, which may reduce the connectivity. In this work, $B_2O_3$ in amorphous boron powder was removed. $MgB_2$ samples were made both from purified and unpurified boron powders. X-ray diffraction showed that removing $B_2O_3$ in the boron powder resulted in a significant decrease in the content of MgO in the sample. The effects of boron powder purification on microstructure, critical temperature, critical field and connectivity will be presented.

**9:36**

**G38 7 Calorimetric transition widths, microstructure and magnetic relaxation of $MgB_2$ with and without additives** CARMINE SENATORE, *DPMC, University of Geneva, CH-1211, Switzerland* PAOLA LEZZA, *GAP, University of Geneva, CH-1211, Switzerland* GIUSEPPE CUSANELLI, *GAP, University of Geneva, CH-1211, Switzerland* SHI XUE DOU, *ISEM, University of Wollongong, NSW 2522, Australia* RENE FLUKIGER, *DPMC, University of Geneva, CH-1211, Switzerland* The addition of nanometric powders of SiC is known to improve the pinning properties of $MgB_2$. Nevertheless, the underlying physical mechanism remains yet unclear. In this frame we report on specific heat measurements of sintered polycrystalline samples of $MgB_2$ and itin situ $MgB_2$ wires, both pure and with SiC nano-additions. A comparison is made with results obtained from microstructural analysis (X-Ray diffraction, SEM, EDX). Specific heat has been measured as a function of temperature (2-45 K) at zero field and at 14 T. Our goal is to relate the broadening of the superconducting transition observed in the samples with additives to the variation in the lattice structure induced by the nano-additions. Furthermore, magnetic relaxation measurements have been performed in order to investigate the effect of the nano-additions on the pinning mechanism.

**9:48**

**G38 8 Critical Current Density and Connectivity Properties of High Jc Ex-situ $Mg(B_{1-X}C_X)_2$** B. J. SENKOWICZ, R. J. MUNGALL, J. R. MANTEI, E. E. HELLSTROM, D. C. LARBALESTIER, *University of Wisconsin - Madison, Applied Superconductivity Center* Using high-energy milling we have obtained $J_c$ (4.2K, 8T) $>$ $5*10^4$ A/cm$^2$ with H*(4.2K) $>$ 16T despite high normal state resistivity ($\rho$(40K) $>$ 100 $\mu\Omega$-cm). Analyzing resistivity curves by the Rowell method has led to the realization that as a result of overmilling and the presence of unincorporated carbon, our active cross section is only one tenth to one third of our total cross section. Therefore the potential exists to improve $J_c$ by a factor of several by increasing connectivity and decreasing grain boundary current obstruction. We examine the effect of composition and milling time on connectivity and superconducting properties. This research was performed under an appointment to the Fusion Energy Sciences Fellowship Program, administered by ORISE under contract between the U.S. DOE and the Oak Ridge Associated Universities. This work was supported by the NSF – FRG on $MgB_2$, and by DOE – Understanding and Development of High Field Superconductors for Fusion - DE-FG02-86ER52131.

**10:00**

**G38 9 Role of SiC Nanoparticles in the Electromagnetic Properties of SiC-doped $MgB_2$ Tapes*** PAUL VOYLES, YE ZHU, *University of Wisconsin* MATSUMOTO AKIYOSHI, *National Institute for Materials Science, Tsukuba* DAVID LARBALESTIER, *University of Wisconsin* $MgB_2$ tapes with $H_{c2}$(2.3K) = 42 T and $J_c$(4.2K) $\sim$ $4\times 10^5$ A/cm$^2$ have recently been demonstrated by Matsumoto et al. These tapes are synthesized by powder-in-tube-processing from $MgH_2$, B, and nanoparticle SiC precursors. TEM and scanning TEM analysis of samples as a function of SiC content and reaction temperature shows that the role of SiC is more complicated than simply providing a source of C to dope the

$MgB_2$. The sample with the highest $H_{c2}$ and $J_c$ contains unreacted SiC nanoparticles, which may act as pinning centers directly or may distort the adjoining $MgB_2$ lattice, increasing intraband scattering. Compared to pure $MgB_2$ samples, samples with SiC contain a significantly higher concentration of oxygen, leading to a higher density of second phases. SiC also tends to reduce the already small grain size of the pure $MgB_2$ from $\sim$ 50 nm to $\sim$ 20 nm, making grain boundaries another import source of pinning.

*This work is supported by the FRG on $MgB_2$ through the US National Science Foundation (DMR -0514592).

**10:12**

**G38 10 Enhancement of Critical Current Properties of $MgB_2$ Bulks by Controlling Microstructure and Crystallinity** JUNICHI SHIMOYAMA, *University of Tokyo* AKIYASU YAMAMOTO, YUKARI KATSURA, ISAO IWAYAMA, SHINYA UEDA, SHIGERU HORII, KOHJI KISHIO, Critical current properties of $MgB_2$ bulks with various grain size, crystallinity and bulk density were systematically studied. Samples with low crystallinity, which was achieved by the low temperature reaction and/or carbon substitution for boron, exhibited high $J_c$ in fields and high irreversibility fields, reflecting enhanced $H_{c2}$. In addition, a strong relationship was found between pinning force density and grain size controlled by changing starting particle size of boron, heating conditions and molar ratio between magnesium and boron. The highly dense $MgB_2$bulks prepared by a diffusion method showed excellent $J_c$ characteristics particularly in low fields. The carbon substitution for the dense bulk was effective for enhancement of $J_c$ under high fields. Essential pinning potential of the $MgB_2$was also evaluated using the dense bulks. Based on these results, a guiding principle to improve critical current properties of practical $MgB_2$ conductors will be discussed from various viewpoints.

**10:24**

**G38 11 Global and local flux jumps in $MgB_2$ films: Magneto-optical imaging and theory** D.V. SHANTSEV, D.V. DENISOV, Y.M. GALPERIN, T.H. JOHANSEN, *Department of Physics, University of Oslo, Norway* SUNG-IK LEE, *Pohang University of Science and Technology, Korea* A.L. RAKHMANOV, *Inst. for Theoretical and Applied Electrodynamics, Moscow* A.V. BOBYL, *Ioffe Physico-Technical Institute, St. Petersburg, Russia* $MgB_2$ is one of the most unstable superconducting materials, where flux jumps are commonly observed at low temperatures jeopardizing its potential for applications. We present a detailed MO imaging study of the jumps in $MgB_2$ films, where we observe large dendritic flux patterns as well as much smaller jumps down to 50 flux quanta. The large jumps destroy the critical state and dramatically suppress $\mathbf{J}_c$. The small jumps, instead, lead to a new type of the critical state where $\mathbf{J}_c$ is determined not only by the pinning, but also by the jump characteristics. A linear theory assuming a thermal origin of dendritic jumps gives the threshold fields for the instability to start and to form a dendritic pattern and reproduces its experimental temperature dependence. We also determine the size of flux jumps in the adiabatic approximation. Its field dependence as well as the flux density profiles after jumps, are in good agreement with the direct observations, see Denisov et al., cond-mat/0508679, and Shantsev et al. Phys. Rev. B 72, 024541 (2005).

**10:36**

**G38 12 Evolution of Anomalous Angular Dependence of $H_{c2}$ in $CaAl_{1-x}Ga_xSi$** TSUYOSHI TAMEGAI, KENTARO UOZATO, MASASHI TOKUNAGA, *Department of Applied Physics, The University of Tokyo* UNIV. OF TOKYO TEAM, In CaAlSi, the angular dependence of the upper critical field, $H_{c2}(\theta)$, shows an anomalous cusp when the field is applied parallel to the superconducting layer. $H_{c2}(\theta)$ can be reasonably well fitted by the Tinkham model for thin film superconductors. On the other hand, $H_{c2}(\theta)$ in CaGaSi does not show such an anomaly. Concomitant with these features, a lattice modulation along the *c*-axis exists only in CaAlSi. We have grown single crystals of the alloy $CaAl_{1-x}Ga_xSi$, and studied the evolution of the anomalous angular dependence of $H_{c2}$ and the superstructure. The superstructure.is sustained at least up to x = 0.2, although the period of the modulation changes from $\sim 6c$ to $\sim 3c$. On the other hand, the cusp-like feature in $H_{c2}(\theta)$ is strongly suppressed by the Ga substitution, and only evident at low temperatures. We have also investigated the homogeneity of the crystal by inspecting the vortex penetration using magneto-optical technique. We have found an inhomogeneous penetration of vortices along the superconducting plane in the itac plane, suggesting the presence of modulation of superconducting parameters. Based on these results, we will discuss the origin of the anomalous $H_{c2}(\theta)$.

**10:48**

**G38 13 Anisotropic s-wave superconductivity and peak effect in single crystals CaAlSi** R. PROZOROV, *Ames Laboratory and Department of Physics and Astronomy, Iowa State University, Ames, Iowa 50011* T. OLHEISER, R.W. GIANNETTA, *Department of Physics, University of Illinois at Urbana-Champaign, 1110 W. Green Street, Urbana, IL 61801* K. UOZATO, T. TAMEGAI, *Department of Applied Physics, The University of Tokyo, Hongo, Bunkyo-ku, Tokyo 113-8656, Japan* In- and out- of plane London penetration depths were measured in single crystals of CaAlSi by using radio-frequency resonant technique. The obtained temperature variation of the anisotropic superfluid density can be explained by an ellipsoidal s-wave gap with a weak-coupling BCS value in the ab-plane and larger gap amplitude in the c-direction. In a mixed state, similar measurements yield Campbell length, which was used to study the peak effect (PE) in the critical current. The position of the PE line on an H-T phase diagram, the influence of anisotropy and sample parameters are discussed.

**SESSION G39: FOCUS SESSION: SUPERCONDUCTIVITY: THEORY AND COMPUTATION I**
**Tuesday Morning, 14 March 2006; 342, Baltimore Convention Center at 8:00**
**Alexander Balatsky, Los Alamos National Laboratory, presiding**

*Invited Papers*

**8:00**
**G39 1 d-wave Pairing in the Two-Dimensional Hubbard Model.***
DOUGLAS SCALAPINO

In this talk we will review numerical evidence showing that the 2D Hubbard model can exhibit antiferromagnetism, stripes, d(xx-yy) pairing and pseudogap behavior. These numerical studies show that the different phases are delicately balanced with respect to small changes in parameters, reminding one of the cuprate materials. We will then discuss the structure of the pairing mechanism in this model.

*This research was supported by NSF Grant DMR-02-11166.

*Contributed Papers*

**8:36**
**G39 2 Andreev states in 2D finite size systems** LUCIAN COVACI, FRANK MARSIGLIO, *University of Alberta* Andreev reflection occurs at the interface between a normal metal and a superconductor. An electron with energy lower than the superconducting gap is reflected back as a hole while a pair enters the superconductor. In 1D systems, for energies smaller than the superconducting gap, the allowed states in the normal metal layer are quantized. For 2D systems these energies become continuous due to the extra degree of freedom in the direction parallel to the interface. With the use of a mean field extended Hubbard Hamiltonian to describe s-wave and d-wave superconductors, we employ a Lanczos recursion method to calculate the local density of states in these systems. Different shapes are considered, such as squares, triangles and circles. We observe the finite size properties of the Andreev bound states and present the different modes of the localized states. We also consider the effect of rough surfaces on the formation of the bound states.

**8:48**
**G39 3 *d*-wave Pairing Amplitude and Particle-hole Asymmetry of the $t - J$ type models: Implication from the Spectral Weight Analysis** CHUNG-PIN CHOU, *National Tsing-Hua University, Taiwan* TING-KUO LEE, *Academia Sinica, Taiwan* CHANG-MING HO, *Tam Kang University* By using the projected variational wave functions (VWF), we study the quasiparticle spectral weight (QPSW) of hole-doped cuprates in the $t - J$ type models. The QPSW $Z^+$ for adding an electron shows a pocket structure outside the Fermi surface that is related to the momentum distribution function $n_{\mathbf{k}}$. Based on our VWF, $Z^-$ for removing an electron can be proven to have a simple relation among the pairing amplitude and $Z^+$. In addition, we also find that strong correlations mainly causes the particle- hole asymmetry of the low-energy tunneling spectra.

**9:00**
**G39 4 The Structure of the Pairing Interaction in the 2D Hubbard Model** THOMAS MAIER, *Oak Ridge National Laboratory* MARK JARRELL, *University of Cincinnati* DOUGLAS SCALAPINO, *University of California* We present a detailed analysis of the effective pairing interaction in the doped two-dimensional Hubbard model. Using dynamical cluster Monte Carlo calculations we have studied the irreducible particle-particle vertex responsible for pairing in this model. The leading low temperature eigenvalue of the Bethe-Salpeter equation for the particle-particle channel is shown to have $d_{x^2-y^2}$-wave symmetry. The irreducible particle-particle vertex increases with increasing momentum transfer and decreases when the energy transfer exceeds a scale associated with the $Q = (\pi, \pi)$ spin susceptibility. Using an exact decomposition of this vertex into a fully irreducible two-fermion vertex and charge and magnetic exchange channels, the dominant contribution to the effective pairing interaction is found to come from the magnetic, spin $S = 1$ exchange channel.

**9:12**
**G39 5 Fluctuation exchange theory for superconductivity of *f*-electron systems with multipole degrees of freedom** KATSUNORI KUBO, TAKASHI HOTTA, *Advanced Science Research Center, Japan Atomic Energy Agency* Recently, an interesting possibility of superconductivity induced by multipole fluctuations has been discussed in some *f*-electron materials. In order to clarify such exotic superconductivity from a microscopic viewpoint, we apply fluctuation exchange (FLEX) approximation to an *f*-electron model with active orbital degree of freedom on the basis of a *j-j* coupling scheme. In this study, we consider a square lattice, for simplicity. First, we evaluate orbital dependent fluctuations and effective paring interactions within the FLEX approximation. Then, we determine the symmetry of the gap function among possible superconducting states by solving the Eliashberg equation. In particular, we pay our attention to the effect of crystalline electric field on the appearance of superconductivity. By further decomposing complex orbital dependent fluctuations into multipole components, we also discuss possible relevance of multipole fluctuations to exotic superconductivity.

**9:24 U. and MIT**
**G39 6 New Phases, Superfluid Weights, Free Carrier Densities: RG Theory of Hubbard, tJ Models** A. NIHAT BERKER, *Koç U. and MIT* MICHAEL HINCZEWSKI, *F. Gürsey Res. Cent. and MIT* We have studied the Hubbard and tJ models in d=3 with renormalization-group theory, obtaining phase diagrams and thermodynamic properties for all temperatures, densities, and coupling strengths. In the Hubbard model, at low temperatures and around half filling, the antiferromagnetic phase is obtained. (1) At strong coupling and 30-35% doping from half filling, (2) at weak and intermediate coupling and 10-18% doping, two novel phases ($\tau$

phases) were found. In these phases, the hopping expectation value is non-zero at all length scales. The weak-intermediate coupling $\tau$ phase exhibits, as in BCS superconductivity, an excitation spectrum gap and, in the specific heat, a low-temperature exponential decay and a cusp phase transition singularity. The strong coupling $\tau$ phase exhibits, as in BEC superconductivity, in the specific heat, an $\alpha \sim -1$ phase transition singularity and a pair-formation peak above the phase transition temperature. In the tJ model, we find that the superfluid weight increases with hole doping, passes through a maximum within the $\tau$ phase at 32-37% doping, and decreases, and that the free carrier density also increases to a maximum value at 32-37% doping but remains at this value under further doping. Calculations with spatially anisotropic d=3 systems yield a chemical potential shift as a function of hole doping in good agreement with experiments. Recent results with magnetic and non-magnetic impurities will also be presented.

**9:36**

**G39 7 Pseudogap and antiferromagnetic correlations in the Hubbard model** ALEXANDRU MACRIDIN, *University of Cincinnati* MARK JARRELL, *University of Cincinnati* THOMAS MAIER, *Oak Ridge National Laboratory* PAUL KENT, *University of Tennessee* CARSTEN HONERKAMP, *University of Wurzburg* Using the dynamical cluster approximation we calculate the single-particle spectra of the Hubbard model with next-nearest neighbor hopping t' at small doping. We find that the pseudogap along the zone diagonal in the electron doped systems is due to long range antiferromagnetic correlations. The physics in the proximity of $(0,\pi)$ is dramatically influenced by t'and determined only by the short range correlations. The effect of t' on the low energy ARPES spectra is weak except close to the zone edge. The short range correlations are sufficient to yield a pseudogap in the magnetic susceptibility and produce occupied states in the second antiferromagnetic Brillouin zone which develop a gap with decreasing temperature. We compare our self-energy with the one obtained form renormalization group (RG) calculations. In order to analyze the importance of scattering in different channels we analyze the self energy using a simple ansatz motivated by RG calculations.

**9:48**

**G39 8 Nonmonotonic gap in the coexisting antiferromagnetic and superconducting state for electron-doped cuprates** QINGSHAN YUAN, FENG YUAN, CHIN-SEN TING, *Texas Center for Superconductivity, University of Houston, Houston, TX 77204* Recent measurements on the superconducting (SC) electron-doped cuprates $Nd_{1.85}Ce_{0.15}CuO_4$ and $Pr_{0.89}LaCe_{0.11}CuO_4$ (both at optimal doping) have revealed that the excitation gap does not fit the simplest commonly assumed *d*-wave function $\cos k_x - \cos k_y$, but exhibits a nonmonotonic behavior with the gap maxima locating midway between the Brillouin zone boundaries and the zone diagonals. This observed gap was naturally regarded as the SC gap and the previous theoretical explanations were limited to extending the SC gap out of the simplest *d* wave. Here we propose a new idea that the observed gap at optimal doping is the lowest quasiparticle excitation energy in the *coexisting* antiferromagnetic (AF) and SC state, which is not purely the SC gap. The idea is implemented by simply studying the coexistence of AF and SC orders within the slave-boson mean-field approach based on the $t$-$t'$-$t''$-$J$ model. Although the pairing gap itself is assumed to be the simplest *d* wave which is monotonic, we have found that the quasiparticle excitation gap in the coexisting state is nonmonotonic, with the maxima around the hot spots where the Fermi surface is missing due to the AF gap. Within the same coexisting state the spectral function is also calculated at optimal doping. The obtained results are all consistent with experiments.

**10:00**

**G39 9 Hole correlation in the $t - J$ model with four holes on a 32-site lattice*** P. W. LEUNG, *Hong Kong University of Science and Technology* We study the $t - J$ model with four holes on a 32-site square lattice using exact diagonalization. This system corresponds to doping level $x=1/8$. At the ''realistic'' parameter $J/t=0.3$, holes in the ground state of this system are unbound. They have short range repulsion due to lowering of kinetic energy. There is no antiferromagnetic spin order and the electron momentum distribution function resembles hole pockets. Furthermore, we show evidence that in case antiferromagnetic order exists, holes form *d*-wave bound pairs and there is mutual repulsion among hole pairs. This presumably will occur at low doping level. This scenario is compatible with a checkerboard-type charge density state proposed to explain the ''1/8 anomaly'' in the LSCO family, except that it is the ground state only when the system possesses strong antiferromagnetic order.

*Supported by the Hong Kong Research Grants Council (Project number 602004)

**10:12**

**G39 10 LDOS and Angle-Resolved Photoemission Spectral Function of An inhomogeneous Superconductor** MING CHENG, W.P. SU, *Texas Center for Superconductivity, University of Houston* Nanoscale inhomogeneity seems to be a central feature of the d-wave superconductivity in the cuprates. Such a feature can strongly affect the local density of states (LDOS) and the spectral weight functions. Within the Bogoliubov-de Gennes formalism we examine various inhomogeneous configurations of the superconducting order parameter to see which ones better agree with the experimental data. Nanoscale large amplitude oscillations in the order parameter seem to fit the LDOS data for the underdoped cuprates. The one-particle spectral function for a general inhomogeneous configuration exhibits a coherent peak in the nodal direction. In contrast, the spectral function in the antinodal region is easily rendered incoherent by the inhomogeneity. This throws new light on the dichotomy between the nodal and antinodal quasiparticles in the underdoped cuprates.

**10:24**

**G39 11 Distinguishing Patterns of Charge Order in 2 dimensions; Stripes or Checkerboards** JOHN ROBERTSON, STEVEN KIVELSON, AHARON KAPITULNIK, *Stanford University* EDUARDO FRADKIN, *University of Illinois at Urbana-Champaign* Charge ordered states are common in strongly correlated materials, including especially the cuprate high temperature superconductors. Identifying where such phases occur in the phase diagram, and where they occur as significant fluctuating orders is a critical step in understanding what role they play in the physics. However, the both the presence of quenched disorder, and the smallness of the charge modulations make the detection of such order difficult in experiments. We discuss strategies for identifying the nature of the underlying ''clean'' order (such as ''stripes'' or ''checkerboards'') in experiments, particularly in STM. We use a model of an effective Hamiltonian in the presence of quenched disorder to simulate experimental data, and further apply our techniques to real experimental data.

**10:36**

**G39 12 Inhomogeneous states with checkerboard order in the t-J Model** CHUNHUA LI, *Boston College* SEN ZHOU, ZIQIANG WANG, We study inhomogeneous states in the *t-J* model using an unrestricted Gutzwiller approximation. We find that $pa \times pa$ checkerboard order, where $p$ is a doping dependent number, emerges from Fermi surface instabilities of both the staggered flux phase and the Fermi liquid state with realistic band parameters. In both cases, the checkerboard order develops at wave vectors $(\pm 2\pi/pa,0)$, $(0, \pm 2\pi/pa)$ that are tied to the peaks of the wave-vector dependent susceptibility, and is of the Lomer-Rice-Scott type. The properties of such periodic, inhomogeneous states are discussed in connection to the checkerboard patterns in the local tunneling density of states discovered in underdoped cuprates.

**10:48**

**G39 13 Hidden D-Wave Checkerboard Order in Cuprates** JIANGPING HU, *Purdue University* KANGJUN SEO, *Purdue University* We propose a new hidden order, D-wave checkerboard order, to explain the local charge checkerboard ordering observed in STM studies of the High Tc superconductors. We show that even a weak D-wave checkerboard order can have a strong effect on the STM spectrum in superconducting states and can nicely explain experimental observations. The D-wave checkerboard order also generates a Fermi arc with little dispersion around nodal points, which are consistent with results from angle resolved photoemission spectroscopy measurements. Therefore, the D-wave checkerboard order can naturally connect the pseudo-gap physics with the checkerboard structure featured in STM measurements.

**SESSION G40: FOCUS SESSION: MATERIALS FOR QUANTUM COMPUTING I**
**Tuesday Morning, 14 March 2006**
**343, Baltimore Convention Center at 8:00**
**Jason Petta, Harvard University, presiding**

**8:00**

**G40 1 Single-Atom Indexing of Quantum State Superpositions*** CHRISTOPHER R. MOON, *Stanford University* C. P. LUTZ, *IBM Almaden* D. M. EIGLER, *IBM Almaden* H. C. MANOHARAN, *Stanford University* The ultimate miniaturization of electronic devices will likely require the local control of single-electron wavefunctions. One system where this may be accomplished consists of two-dimensional metallic electron states confined within atomically engineered nanostructures. Here we describe experiments showing that an individual atom inside a 44-atom quantum corral can index arbitrary coherent superpositions of spatial quantum states. We demonstrate how the quantum mirage effect can be harnessed to image the resulting quantum superposition. We also present a straightforward method for determining the appropriate atom location for any desired superposition. The atom provides a real-space handle for an abstract Hilbert space, providing a simple, novel technique for coherently manipulating quantum states.

*This work was supported by the ONR and NSF, and by the DoD NDSEG program.

**8:12**

**G40 2 Valley Splitting in a Silicon Two-Dimensional Electron Gas*** SRIJIT GOSWAMI, MARK FRIESEN, *University of Wisconsin-Madison* J.L. TRUITT, *Lincoln Laboratory, MIT* CHARLES TAHAN, *Cavendish Laboratory, Cambridge, U.K.* J.O. CHU, *IBM T. J. Watson Research Center* D.W. VAN DER WEIDE, S.N. COPPERSMITH, ROBERT JOYNT, M.A. ERIKSSON, *University of Wisconsin-Madison* We have performed low-temperature microwave transport spectroscopy of low-lying valley states in a silicon two-dimensional electron gas. The magnitude of this splitting determines whether the ground state is degenerate for purposes of quantum computing with spins. The valley splitting varies linearly with magnetic field from 0.3 to 3 T, reaching 75 $\mu$eV, with no sign of saturation. We unambiguously identify the observed resonance as a valley excitation by comparing with Shubnikov-de Haas oscillations. The origin of the splitting is the coupling of the two $z$ conduction valleys in the silicon band structure, due to quantum well confinement. Previous theory suggests that the valley splitting can be of order 1 meV. However, we present a theory incorporating atomic steps, which are present in experimental systems. The theory leads to small valley splittings at zero magnetic field, and a linearly increasing splitting at nonzero fields, as observed in experiments.

*Research supported by NSA, ARDA, ARO and NSF.

**8:24**

**G40 3 Valley Splitting Theory for Silicon 2DEGs Grown on a Vicinal Surface*** MARK FRIESEN, S. CHUTIA, SRIJIT GOSWAMI, M. A. ERIKSSON, S. N. COPPERSMITH, *University of Wisconsin-Madison, Madison WI 53706* We develop a theory for the energy splitting of the two-fold degenerate conduction valleys of a silicon 2DEG. We assume that the quantum well is not perfectly aligned with the crystallographic axes, as consistent with typical experimental conditions. Under these general conditions, the valley splitting can be suppressed by many orders of magnitude from its theoretical upper bound. However, the confined electrons are able to recover some of their valley splitting, and thus lower their total energy, by a variety of means. We discuss two recovery methods, which apply to the cases of zero and nonzero magnetic fields, respectively. The results show a linear dependence of the valley splitting on the magnetic field, as consistent with the experimental data.

*Research supported by NSA, ARDA, ARO and NSF.

**8:36**

**G40 4 Quantum theory of decoherence in solid-state spin quantum computing architectures*** WAYNE WITZEL, SANKAR DAS SARMA, *University of Maryland* Decoherence is the adversary of any proposed quantum computer. In order to overcome it, we must understand it. Nuclear induced spectral diffusion, a type of electron spin decoherence caused by interaction with a nuclear spin bath, is a predominant source of information loss for solid-state spin quantum computing architectures. All previous theories for this 50-year-old problem have used phenomenological, semi-classical models. This talk presents our cluster expansion method which provides the first fully microscopic and quantum mechanical solution to this problem. With our method it becomes possible to ascertain the effectiveness of pulse sequences designed to enhance spin coherence.

*This work is supported by ARO-ARDA and LPS-NSA.

**8:48**

**G40 5 Effect of exchange interaction on spin dephasing in a double quantum dot*** EDWARD LAIRD, JASON PETTA, ALEX JOHNSON, *Harvard University* AMIR YACOBY, *Weizmann Institute of Science* CHARLES MARCUS, *Harvard University* MICAH HANSON, ART GOSSARD, *University of California, Santa Barbara* We use a pulsed-gate technique to study mixing of singlet and triplet spin states in a two-electron double quantum dot with a tunable exchange interaction. Spin dynamics in this system are governed by the interplay of exchange (which tends to preserve spin correlations) and hyperfine interaction with the lattice nuclei (which tends to destroy them.) When the two interaction strengths are comparable, we observe saturation of dephasing and damped temporal oscillations, persisting well beyond the hyperfine dephasing time, of the spin correlator. Both features of the data show good agreement with predictions from a quasistatic model of the hyperfine field.

*Supported by the ARO under W911NF-05-1-0476, DARPA under the QuIST program, and the Harvard NSEC

**9:00**

**G40 6 Exchange in singlet-triplet qubits: spin funnel and magnetic field structure*** MICHAEL STOPA, *Harvard University* CHARLES MARCUS, *Harvard University* We employ density functional (DF) calculated eigenstates as a basis for exact diagonalization studies of lateral semiconductor double quantum dots through the transition from the symmetric bias regime to the regime where both electrons occupy the same dot. The DF basis allows us to maintain the geometric fidelity of the device in the calculation while still capturing all of the many-body effects. Recent experiments by Petta et al. [Science **309**, 2184 (2005)] have shown the existence of a ''spin funnel'' in the behavior of the singlet-triplet splitting (the exchange coupling) as a function of bias detuning J($\varepsilon$) in the vicinity of the crossover from the (1,1) to the (0,2) honeycomb stability cells. Here we calculate the spin funnel and explain its origin and functional form. For an applied magnetic field B we predict the existence of local minima where dJ($\varepsilon$,B)/d$\varepsilon$ =0, and suppression of voltage noise can be expected.

*We acknowledge support from the National Nanotechnology Infrastructure Network Computation project

**9:12**

**G40 7 Competition between Coulomb localization and barrier modulation of the exchange energy in two-electron laterally coupled quantum dots** DMITRIY MELNIKOV, JEAN-PIERRE LEBURTON, *Beckman Institute for Advanced Science and Technology, University of Illinois at Urbana-Champaign, Urbana, IL 61801* We present calculations of the singlet-triplet energy separation (exchange energy) in the two-electron system confined in the double quantum dot system used in recent experiments on coherent manipulation of coupled electron qubits. The hybrid multiscale approach where the confined electrons are described by the direct diagonalization of the Schrödinger equation within the full quantum dot device environment was used to perform the calculations. We analyze the behavior of the exchange in the magnetic fields and find large changes from meV to sub-$\mu$eV value as the confinement gate biases (effective barrier) are varied, while the singlet-triplet transition magnetic field remains at about 1 T independently of the gate biases. The small values of the exchange in this structure are attributed to the large separation between the electrons leading to an almost classical description of the system due to the dominance of the Coulomb repulsion.

**9:24**

**G40 8 Entanglement of two strongly correlated electrons in a lateral quantum dot*** CONSTANTINE YANNOULEAS, UZI LANDMAN, *Georgia Institute of Technology* Exact-diagonalization calculations for two electrons in an elliptic lateral quantum dot show that the electrons can localize and form a molecular dimer even for screened interelectron repulsion. The calculated singlet-triplet splitting ($J$) as a function of the magnetic field ($B$) agrees with cotunneling measurements;[1] its behavior reflects the effective dissociation[2] of the electron dimer for large $B$. Knowledge of the dot shape and of $J(B)$ allows determination of two measures of entanglement (concurrence and von Neumann entropy for *indistinguishable* fermions), whose behavior correlates also with the dissociation of the dimer. The theoretical value for the concurrence at $B = 0$ agrees with the experimental estimates.

*Supported by the U.S. D.O.E. (FG05-86ER-45234) and the NSF (DMR-0205328)

[1]D.M. Zumbühl *et al.*, Phys. Rev. Lett. **93**, 256801 (2004).
[2]C. Yannouleas and U. Landman, Int. J. Quantum Chem. **90**, 699 (2002)

**9:36**

**G40 9 Detection and measurement of the Dzyaloshinskii-Moriya interaction in double quantum dot systems*** SUCISMITA CHUTIA, MARK FRIESEN, ROBERT JOYNT, *Department of Physics, UW-Madison* Spins in quantum dots can act as qubits for quantum computation. In this context we point out that spins on neighboring dots will experience the Dzyaloshinskii-Moriya interaction, which mixes the spin singlet and triplet states. This will have a strong influence on spin-dependent tunneling. We show that the effects of this interaction depend strongly on the direction of the external field, and demonstrate how to detect and measure the effect.

*Research supported by NSF,NSA,ARDA,ARO

**9:48**

**G40 10 Engineering Double Quantum Dots in Si/SiGe using Shottky Top Gates** NAKUL SHAJI, *Electrical and Computer Engineering, University of Wisconsin-Madison* LEVENTE KLIEN, *Department of Physics, University of Wisconsin-Madison* DON SAVAGE, *Material Science and Engineering, University of Wisconsin-Madison* MARK ERIKSSON, *Department of Physics, University of Wisconsin-Madison* ROBERT BLICK, *Electrical and Computer Engineering, University of Wisconsin-Madison* Quantum information processing in silicon based semiconductors have gained importance lately due to its inherent advantages like low spin orbit coupling and thus very large spin coherence times, as compared to competing III-V devices. Previous work done on silicon based low dimensional devices include successful fabrication of etch defined quantum dots in Si/SiGe quantum wells, whose potentials are modulated by lateral side gates. Another way of forming quantum dots is by using shottky top gates to deplete the underlying two dimensional electron gas (2DEG) in selected areas. Quantum dots formed by shottky top gates are preferred over etched ones to achieve better control over the tuning of tunnel barriers and to minimize etch induced depletion of the 2DEG. Unlike III-V materials, shottky gates formed in SiGe/Si quantum wells have been found to be very leaky. In this talk we discuss the issues of gate leakage, formation of tunnel junctions and engineering double quantum dots (Qubits) in SiGe/Si quantum wells with the help of an additional back-gate.

**10:00**

**G40 11 Stability Diagram of a Few Electron Triatom** ANDREW SACHRAJDA, *IMS, NRC, Ottawa, Canada K1A 0R6* LOUIS GAUDREAU, *IMS/NRC and Sherbooke University, Quebec* STUDENIKIN SERGEI, ALICIA KAM, JEAN LAPOINTE, PIOTR ZAWADZKI, MAREK KORKUSINSKI, PAWEL HAWRYLAK, *IMS, NRC, Ottawa, Canada K1A 0R6* A lateral few electron triple quantum dot system has been studied and the stability diagram mapped out using charged detection techniques. All three quantum dots are coupled together. The device could be tuned to observe quadruple points including the fundamental ones for quantum information applications, associated with the confinement of one, two and three electrons. The stability diagram includes a series of novel elements, including the cloning of charge transfer lines. The main results are successfully modeled by both capacitive and Hubbard models.

**10:12**

**G40 12 External field control of donor electrons at the Si-$SiO_2$ interface*** MARIA J. CALDERON, *Condensed Matter Theory Center, Department of Physics, University of Maryland* BELITA KOILLER, *Instituto de Fisica, Universidade Federal do Rio de Janeiro, Brazil, and Condensed Matter Theory Center, Department of Physics, University of Maryland* XUEDONG HU, *Department of Physics, University at Buffalo, SUNY* SANKAR DAS SARMA, *Condensed Matter Theory Center, Department of Physics, University of Maryland* Prospects for the quantum control of electrons in the silicon quantum computer architecture are considered theoretically. In particular, we investigate the feasibility of shuttling donor-bound electrons forth and back between the impurity in the bulk and the Si-$SiO_2$ interface by tuning an external electric field. We calculate the shuttling time to range from subpicoseconds to nanoseconds depending on the distance ( $\sim$ 10-50 nm) of the donor from the interface. For a certain range of parameters, the state at the interface is localized in all three dimensions, which allows to take the electron back to the donor. The size of the wave-function at the interface can be manipulated by applying a perpendicular magnetic field. Our results establish that quantum control in such nanostructure architectures should be achievable.

*This work is supported by LPS and NSA. BK also acknowledges support by CNPq and FAPERJ.

**10:24**

**G40 13 Experimental Stark tuning the donor electron spin resonance in silicon*** FORREST BRADBURY, ALEXEI TYRYSHKIN, GUILLAUME SABOURET, *Princeton University* THOMAS SCHENKEL, *Lawrence Berkeley Nat'l Lab* STEPHEN LYON, *Princeton University* We measure the hyperfine and spin-orbit shifts due to electric fields applied to bound electrons in silicon. The ability to electrically tune resonances allows for selective single qubit operations on electron spins without localized magnetic fields. We study $^{31}$P donors in natural silicon epilayers and $^{121}$Sb donors implanted into isotopically purified $^{28}$Si. The E-fields ( $\sim$ kV/cm) are applied by lithographically-patterned, interdigitated metal top-gates. Small shifts in resonant energies are measured by pulsed electron spin resonance using a modified two-pulse (Hahn) spin echo experiment with an electrical pulse applied to the gates between microwave pulses. At $B_0 \approx 0.35$T, we find the $2^{nd}$ order hyperfine and spin-orbit Stark shifts to be comparable in magnitude. Though the literature has heretofore focused on the hyperfine Stark shift, we predict that the spin-orbit Stark shift will be the dominant tuning parameter at higher magnetic fields where a future quantum computer is likely to operate.

*Supported in part by the ARO and ARDA

**10:36**

**G40 14 Nuclear Spin of Phosphorus Donors in Silicon: Spin Relaxation Times and Environmental Decoupling*** ALEXEI TYRYSHKIN, STEPHEN LYON, *Princeton University* JOHN MORTON, ARZHANG ARDAVAN, *Oxford University* All shallow donors in silicon (and their various isotopes) have non-zero nuclear spins and thus, both the electron and nuclear spins of neutral donors have been proposed for coding, manipulating and storing quantum information. We have recently demonstrated that the spin of electrons bound to donors have extremely long coherence times of at least $T_{2e} = 60$ms at liquid helium temperatures which permits $10^6$ single-qubit operations before the electron spin decoheres [1]. Here we extend this work and demonstrate that spin states of both the electron and nucleus of a $^{31}$P donor can be accurately controlled using resonant microwave and RF pulses in pulsed electron nuclear double resonance (ENDOR) experiments. We measure the spin relaxation times of the $^{31}$P nuclear spin and observe long longitudinal relaxation times $T_{1n} = 70$s at 6K, limited by hyperfine interaction with the electron spin residing on the donor. We implement a recently proposed bang-bang strategy which decouples the nuclear spin from a decohering environment, through repeated manipulation of the coupled electron spin [2]. This highlights the potential benefits of physical qubit systems beyond the simple 2-level structure. [1] A. M. Tyryshkin et al. PRB, 68, 193207 (2003); [2] J. J. L. Morton et al. Nature Physics in press (2005).

*Supported in part by the ARO and ARDA

**10:48**

**G40 15 Experimental realization of single electron confinement in an InAs quantum dot** G. M. JONES, *Department of Electrical and Computer Engineering, University of Maryland* B. H. HU, *Department of Electrical and Computer Engineering, University of Maryland* C. H. YANG, *Department of Electrical and Computer Engineering, University of Maryland* M. J. YANG, *Naval Research Laboratory* Y. B. LYANDA-GELLER, *Department of Physics, Purdue University* We demonstrate an enhancement-mode lateral single electron transistor (SET). In contrast to the depletion-mode SETs that reach one-electron regime by expelling electrons from multi-electron QDs, our SET structure uses a single top gate to create two symmetric tunnel barriers and make electrons tunnel into this empty quantum dot one at a time. The sample used in this work to demonstrate this novel SETs concept is an InAs/GaSb composite quantum well, whose bandgap is tunable by the thicknesses of the two QWs and is $\sim$ 100meV in our case. Using a gated Hall bar geometry, we show that the device can undergo a transition from hole accumulation to the inversion of electrons. As the widths of the conducting channel and the top gate are reduced to sub-micron, the conductance displays single electron tunneling. The data indicate a 15meV Coulomb charging energy and a 20meV orbital energy spacing, which imply a quantum dot of 20nm in diameter. Combining with the inherent advantage of a large electron g* factor in InAs, our demonstration is significant for solid state implementation of scalable quantum computing.

**SESSION G41: SUPERSOLID**
**Tuesday Morning, 14 March 2006**
**344, Baltimore Convention Center at 8:00**
**Norbert Mulders, University of Delaware, presiding**

*Contributed Papers*

**8:00**
**G41 1 Bose-Glass to Superfluid Transition in the 3d Boson Hubbard Model: z=d** PETER HITCHCOCK, ERIK SORENSEN, *McMaster University* Recent experiments on cold atomic gases in disordered optical lattices (Schulte et al. PRL 95, 170411 (2005)) have renewed interest in the bose-glass to superfluid phase transition in the boson Hubbard model. The dynamical critical exponent z is of central importance to understanding this transition, yet its value at $d > 2$ remains unclear. We present a Monte Carlo study of this transition in the three dimensions. Simulations are performed on the classical $(3 + 1)$ dimensional link-current representation using the geometrical worm algorithm. Finite-size scaling analysis (on lattices as large as 16x16x16x512 sites) of the superfluid stiffness and the compressibility is consistent with the value $z = 3$ for the dynamical critical exponent, in agreement with existing scaling and renormalization group arguments that $z = d$. We calculate a value of $\nu = 0.66(2)$ for the correlation length exponent, satisfying the relation $\nu \geq 2/d$ as an equality.

**8:12**
**G41 2 Superfluid Glass of He-4** BORIS SVISTUNOV, *University of Massachusetts* MASSIMO BONINSEGNI, *University of Alberta* NIKOLAY PROKOF'EV, *University of Massachusetts* With a recently developed worm algorithm, we simulate 800 atoms of He-4 at the density corresponding to the zero-$T$ melting point of the hcp crystal. We find that low-$T$ properties of the system— in our case, at $T = 0.2$K—crucially depend on the initial state and cooling protocol. An ideal hcp crystal is a clear-cut insulator. But if we start with a high-$T$ liquid state and quench-cool the sample down to $T = 0.2$K, we end up with a new state of matter, 'superglass',—a metastable amorphous solid that features off-diagonal long-range order and superfluidity.

**8:24**
**G41 3 Dynamic Structure Function of a Model Supersolid** CHI-DEUK YOO, ALAN DORSEY, *Department of Physics, University of Florida* Second sound, which is a fingerprint of superfluid behavior, can be observed in light scattering through the splitting of the central Rayleigh peak of the thermal diffusion mode into an additional Brillouin doublet of the second sound [1,2]. Since a supersolid undergoes a similar transition as a superfluid, we expect that the Rayleigh peak due to the defect diffusion mode in a normal solid will split into a Brillouin doublet of propagating modes in the supersolid phase. In this work, we have derived the hydrodynamic equations of motion including defects, and obtained both the second sound mode and the dynamic structure function for an isotropic and isothermal supersolid. We find the splitting occurs not only in the transition from a normal fluid to a superfluid but also from a normal solid to a supersolid, which might be observable in light scattering. [1] G. Winterling, F. S. Holmes, and T. J. Greytak, Phys. Rev. Lett. **30**, 427 (1973). [2] J. A. Tarvin, F. Vidal, and T. J. Greytak, Phys. Rev. B **15**, 4193 (1977).

**8:36**
**G41 4 Landau Theory for the Normal Solid-Supersolid Transition** ALAN DORSEY, *University of Florida* PAUL GOLDBART, *University of Illinois at Urbana-Champaign* JOHN TONER, *University of Oregon* Kim and Chan [1,2] have reported an anomalous decoupling transition of solid $^4$He in a torsional oscillator measurement, and interpret their results as evidence for non-classical rotational inertia and a possible supersolid phase of $^4$He. Motivated by these results, we [3] have developed a phenomenological Landau theory of the normal-solid to supersolid (NS-SS) transition in which superfluidity is coupled to the elasticity of the crystalline $^4$He lattice. We find that the elasticity does not affect the universal properties of the superfluid transition, so that in an unstressed crystal the well-known $\lambda$-anomaly in the heat capacity of the superfluid transition should also appear at the NS-SS transition. We also find that the onset of supersolidity leads to anomalies in the elastic constants near the transition, that should be observable in sound speed measurements; conversely, inhomogeneous strains in the lattice can induce local variations of the superfluid transition temperature, leading to a broadened transition. [1] E. Kim and M. H. W. Chan, Nature (London) **427**, 225 (2004). [2] E. Kim and M. H. W. Chan, Science **305**, 1941 (2004). [3] A. T. Dorsey, P. M. Goldbart, and J. Toner, cond-mat/0508271.

**8:48**
**G41 5 Effect of Quantum Correlations on the Vibrational Spectrum of Bosonic Quantum Solids** JORGE SOFO, *Department of Physics, The Pennsylvania State University* We study the effects of quantum correlations on the vibrational spectrum of solids. In particular, we are interested on the description of delocalized zero point vacancies and systems of light atoms interacting through weak dispersion forces, like Helium. We write the interaction Hamiltonian in a basis set of localized oscillators. A decoupling similar to the Random Phase Approximation of the equations of motion exhibits the dependence on particle correlations of the dispersion relation for phonons and consequently the sound speed. The approximation recovers the normal phonon modes in the case of a system described by an uncorrelated wave function. We show that the onset of correlations, as the temperature is lowered, changes the speed of sound, and the vibrational response of the solid. Implications for recent experimental observations of the supersolid state are discussed.

**9:00**
**G41 6 Exploration of Vacancies in Solid 4He** BRYAN CLARK, DAVID CEPERLEY, *UIUC Physics Dept.* Experiments by Kim and Chan [1] have renewed interest in the understanding of supersolids and whether mechanisms exist in solid $^4He$ to allow for supersolid-like effects. Ground state vacancies would lead to bose condensation and superfluidity. Using Path Integral Monte Carlo we examine vacancy formation energies, vacancy-vacancy interactions and the effect of vacancies on supersolid behavior in solid $^4He$. [1] E. Kim and M. H. Chan, Science **305**, 1941 (2004).

**9:12**
**G41 7 Observation of Nonclassical Rotational Inertia in Bulk Solid $^4$He Confined to a Cylindrical Cavity*** KEIYA SHIRAHAMA, MOTOSHI KONDO, SHUNICHI TAKADA, YOSHIYUKI SHIBAYAMA, *Department of Physics, Keio University, Yokohama 223-8522, Japan* Recent observation of nonclassical rotational inertia (NCRI) in solid $^4$He by Kim and Chan has attracted great interest in physics of supersolid, and motivated

a number of theoretical studies. However, there have been surprisingly few experiments to pursuit the nature of their observation. Thus, we have begun a torsional oscillator experiment for bulk solid $^4$He. In order to study the effects of sample geometry and crystal quality, we employ a cylindrical cell, 8 mm high and 8 mm in diameter, which is mounted on an aluminum alloy torsion rod. The resonant torsion frequency is about 1750 Hz, which is 2 $\sim$ 5 times the frequencies in the Kim and Chan's experiments. In a preliminary experiment we have observed an increase in the frequency below about 250 mK, indicating the existence of NCRI. The frequency shift shows a substantial driving amplitude dependence, which is also consistent with the previous observation.

*This work is supprted by Grant-in-Aid for Scientific Research on Priority Area, MEXT, Japan

**9:24**

**G41 8 Effect of $^3$He impurity on the supersolid transition of $^4$He*** EUNSEONG KIM, MOSES H. W. CHAN, *The Pennsylvania State University* The supersolid phase of $^4$He was revealed by a series of torsional oscillator experiments. [1] One of the most intriguing features of the supersolid transition is the broadening of the transition and the enhancement of $T_c$ by the addition of extremely small amount of $^3$He impurity. This effect is very different from that in superfluid film and that in 'bulk' superfluid helium. We have investigated the influence of$^3$He on the supersolid transition by systematically diluting isotopically−pure 4He (3He impurity less than 0.3ppb) with 3He. [1] E. Kim and M. H. W. Chan, Science **305**, 1941 (2004); Nature **425**, 227 (2004); J. Low Temp. Phys. **138**, 859 (2005).

*This research is supported by NSF Grant DMR 0207071.

**9:36**

**G41 9 Ballistic Phonon Propagation in Solid $^4$He at Low Temperature*** YUKI AOKI, HARRY KOJIMA, Phonon propagations in hcp solid $^4$He are being studied down to 30 mK including the recently discovered supersolid phase range. Phonons are generated with 2 $\mu$s long heat pulses by applying current into a metal film resistor (of area 5.2 mm$^2$) deposited onto a planar silicon substrate. The power applied to the heater is varied between 20 and 200 $\mu$W/mm$^2$. The phonons travel through 4.3 mm of solid $^4$He and are detected by superconducting edge sensor of 60 nm thick titanium film. In agreement with earlier studies, the main propagation peak detected by the sensor is the transverse sound propagation. Crossover from second sound in normal solid to ballistic propagation is observed between 100 mK and 300 mK at 25 bars. Measurements of ballistic phonon propagation are extended up to 50 bars for the first time. The velocity of transverse phonon propagation increases from 220 m/s at 25 bars to 250 m/s at 50 bars. It is expected that supersolid transition modifies the velocity of transverse sound propagation. It is found, within $\pm$ 1.5 % scatter of data, the ballistic phonon propagation velocity (measured at 200 $\mu$W/mm$^2$) remains constant below 100 mK at both 25 and 50 bars. At 30 mK, the velocity is independent of heater power within $\pm$ 1 %.

*Supported by NSF.

**9:48**

**G41 10 Specific heat of solid helium** XI LIN, *Penn State University* ANTHONY CLARK, EUNSEONG KIM, MOSES CHAN, Recently superflow in solid $^4$He was found below 200mK via a torsional oscillator technique[1]. While there were a number of measurements on the specific heat of solid helium carried out down to 100mK, there is no evidence of a heat capacity signature related to the onset of the supersolid phase[2]. A serious experimental challenge is discerning the small specific heat of solid helium from that of the metallic cells which are typically used to confine the solid. We have recently begun a new measurement of the heat capacity of solid helium contained in a silicon cell. The heat capacity of the silicon cell below 300mK is always less than that of the solid helium sample. Results of the measurement will be presented. This work is supported by NSF under grant number 0207071. [1] E. Kim and M. H. W. Chan, Nature **427**, 225 (2004); E. Kim and M. H. W. Chan, Science **305**, 1941 (2004); E. Kim and M. H. W. Chan, J. Low Temp. Phys. **138**, 859 (2005). [2] S. H. Castles and E. D. Adams, J. Low Temp. Phys. **19**, 397 (1975); B. Hébral et al., Phonons in Condensed Matter, edited by H. J. Maris (Plenum, New York, 1980), pg. 169; A. C. Clark and M. H. W. Chan, J. Low Temp. Phys. **138**, 853 (2005).



## SESSION G42: PHYSICS EDUCATION RESEARCH AND UNDERGRADUATE EDUCATION

**Tuesday Morning, 14 March 2006**
**345, Baltimore Convention Center at 8:00**
**Paula Heron, University of Washington, presiding**

**8:00**

**G42 1 Light Quanta and Photochemistry** M. BAUBLITZ, *Northeastern University & Boston University* M. HERSEK, *Northeastern University* N. A. GROSS, *Northeastern University* A. BANSIL, *Northeastern University* For many undergraduate students the photoelectric effect and quantum nature of light seem abstract because of their lack of first-hand experience with these phenomena. This is particularly true for non-science students taking general science courses. At Northeastern University through the Embedded Learning MOdules (ELMO) Project, developed with support from NSF and FIPSE, non-science students take part in experiments [1] related to the photoelectric effect that help them understand photochemical processes and the quantum nature of light. Photosensitive materials are produced by depositing thin layers of silver nitrate on paper, and various light sources and light filters are used that permit light from only a specific part of the spectrum to expose the photosensitive material. The dependence of the silver nitrate's photosensitivity on the color of the incident light provides students with an example that can be understood in terms of the quantum nature of light. [1] M. Hersek, N. A. Gross, E. J. Mason, and A. Bansil, J. College Sci. Teaching (in press); N. A. Gross, M. Hersek, and A. Bansil, Am. J. Phys. **73**, 986 (2005)

**8:12**

**G42 2 Generalizing the definition of buoyant force** CARL MUNGAN, *Physics Department, U.S. Naval Academy* I propose that buoyant force be defined as the negative of the weight of the displaced fluids, rather than as the net force exerted by fluid pressures on the surface of an object. In the case of a fully submerged

object, these two definitions are equivalent. However, if the object makes contact with a solid surface (such as the bottom of a beaker of liquid), only the first definition is well-defined, while the second depends on the ambiguous issue of how much fluid penetrates between the object and the solid surface.

**8:24**

**G42 3 Integrating computation and simulation into the undergraduate physics curriculum** GUS L. W. HART, *Northern Arizona University* At Northern Arizona University, we have been integrating computation and simulation into the curriculum at all levels. We hope to achieve a number of objectives: (i) increase student retention during the first three semesters of the program, (ii) train students in this ''third branch'' of science, (iii) provide students with scientific computing skills, (iv) expand the coverage of the upper-division course content. I will discuss two courses required during the freshman and sophomore years and how computation and simulation is integrated into the upper-division courses. The percieved successes and remaining shortcomings of the current curriculum will addressed.

**8:36**

**G42 4 Computational Physics in the Undergraduate Physics Curriculum** J.E. HASBUN, *University of West Georgia* Recent efforts to incorporate computational physics in the undergraduate physics curriculum have made use of Matlab, IDL, Maple, Mathematica, Fortran, and C[1] as well as Java.[2] The benefits of similar efforts in our undergraduate physics curriculum are that students learn ways to go beyond what they learn in the classroom and use computational techniques to explore realistic physics applications. In so doing students become better prepared to perform undergraduate research that will be useful throughout their scientific careers.[3] Our standard computational physics course uses some of the above tools.[1] More recently, we have developed a first draft of a textbook for the junior level mechanics physics course that incorporates computational techniques. The text being developed in addition to employing the invaluable traditional analytical approach to problem solving, it incorporates computational physics to build on those problems. In particular, the course makes use of students abilities to use programming to go beyond the analytical approach and complement their understanding. Selected examples of representative lecture problems will be presented. [1]''Computation and Problem Solving in Undergraduate Physics,'' David M. Cook, Lawrence University (2003), http://www.lawrence.edu/dept/physics/ccli. [2]''Simulations in Physics: Applications to Physical Systems,'' H. Gould, J. Tobochnik, and W Christian; see also, http://www.opensourcephysics.org. [3]R. Landau, APS Bull. Vol 50, No.1, 1069 (2005)

**8:48**

**G42 5 Using the Open Source Physics Java Library to do Computer Simulations*** HARVEY GOULD, *Clark University* JAN TOBOCHNIK, *Kalamazoo College* WOLFGANG CHRISTIAN, *Davidson College* Computation has become a common feature of many physics courses. However, the computation is usually an add-on and students do not learn how to write simulations in a way that is similar to how they are done in a research context. We describe how to teach students to learn physics by writing and modifying programs in Java using the objected oriented Open Source Physics library available at <www.opensourcephysics.org>.

*Supported in part by NSF DUE-0442481 and DUE-0127363.

**9:00**

**G42 6 Data Visualization in Physics I: Java applets for interactive demonstration of physics concepts** ELIZABETH M. CHERRY, *Cornell University* STEVEN J. EVANS, *Beth Israel Medical Center* HAROLD M. HASTINGS, *Hofstra University* FLAVIO F. FENTON, *Cornell University* As computing resources continue to develop toward increased flexibility and power, illustration of scientific concepts has become significantly easier. Java applets in particular form an especially appropriate medium through which simulations and animations can be shared easily across platforms. In this talk, we will show several Java applets that illustrate different concepts in physics, particularly in biophysics, complex systems, and excitable media. Various graphical interfaces will be shown for 0d to 2d systems. In addition, we will demonstrate how to incorporate Java applets into PowerPoint for easy presentation of results in classes and seminars.

**9:12**

**G42 7 Data Visualization in Physics II: VRML and Java for three-dimensional imaging and fully three-dimensional movies** FLAVIO H. FENTON, *Cornell University* STEVEN J. EVANS, *Beth Israel Medical Center* HAROLD M. HASTINGS, *Hofstra University* ELIZABETH M. CHERRY, *Cornell University* Presentation and analysis of large three-dimensional data sets is in general hard to do using only two-dimensional figures and plots. In this talk, we will demonstrate techniques for illustrating static and dynamic three-dimensional objects and data using Virtual Reality Modeling Language (VRML) as well as Java. The advantage of these two languages is that they are platform-independent, which allows for easy sharing of data and visualizations. In addition, manipulation of data is relatively easy as rotation, translation and zooming can be done in real- time for static objects as well as for data and objects that vary and deform in time. Examples of fully three-dimensional movies will be shown, including dendritic growth and propagation of electrical waves in cardiac tissue. In addition, we will show how to include VRML and Java viewers in PowerPoint for easy presentation of results in classes and seminars.

**9:24**

**G42 8 Advanced Lab Consortium ''Conspiracy''** JONATHAN F. REICHERT, *TeachSpin, Inc.* Advanced Laboratory instruction is a time-honored and essential element of an undergraduate physics education. But, from my vantage point, it has been neglected by the two major professional societies, APS and AAPT. At some schools, it has been replaced by ''research experiences,'' but I contend that very few of these experiences in the research lab, particularly in the junior year, deliver what they promise. It is time to focus the attention of APS, AAPT, and the NSF on the advanced lab. We need to create an Advanced Lab Consortium (ALC) of faculty and staff to share experiments, suppliers, materials, pedagogy, ideas, in short to build a professional network for those committed to advanced lab instruction. The AAPT is currently in serious discussions on this topic and my company stands ready with both financial and personnel resources to support the effort. This talk is a plea for co-conspirators.

**9:36**

**G42 9 Building and Sustaining a Successful Undergraduate Research Program** VIJENDRA AGARWAL, GUBBI SUDHAKARAN, *University of Wisconsin-La Crosse* The multidisciplinary Undergraduate Research (UR) program initiated about ten years ago continues to be one of the institutional priorities at the University of Wisconsin- La Crosse (UW-L). While, UR program has boosted overall student retention at UW-L, the physics program has very definitely experienced a phenomenal growth in the number of majors (from 5 to 130) and external grants (over a million dollars) in the last few years. In no uncertain terms, this kind of growth is attributed to the nurturing environment of the department and faculty mentored research with undergraduate students. This presentation will focus on various elements, shared responsibility, and resources that are critical to initiating and building a sustainable UR program in physics but even more importantly how to institutionalize it. We shall further discuss our overall experiences from the modest beginnings to our continuous growth.

**9:48**

**G42 10 Adaptations of the Physics By Inquiry Curriculum** LEON HSU, *University of Minnesota* KAREN CUMMINGS, *Southern Connecticut State University* JACK TAYLOR, *Baltimore City Community College* We report on the initial stages of a collaborative investigation into ways in which the Physics by Inquiry (PbI) curriculum (McDermott) can be implemented in larger enrollment courses using undergraduate peer instructors and cooperative grouping techniques. Typically, PbI is implemented in small classes with Physics graduate students as teaching assistants. However, many institutions, such as community colleges, do not have graduate students available. In other cases, there is a need for a larger enrollment class. We present three models we are investigating as responses to our local constraints. This work was partially supported by NSF DUE-0410804.

**10:00**

**G42 11 Science on the Table: Motivating Non-Science Majors to Learn Physical Science** MARTHA WELLER, JUDITH IRIARTE-GROSS, *Middle Tennessee State University* Most undergraduates in non-scientific fields view personal science knowledge as both irrelevant and unnecessary for their future well-being. Attempts by universities to address the problem of an increasingly scientifically illiterate citizenry through the incorporation of science requirements in the general education curriculum are viewed by students as one more obstacle in their quest for an undergraduate degree, not as an opportunity to develop the skills needed for personal and civic decision making related to scientific and technologic issues. We have modified the laboratory portion of our existing Physical Science course (previously a catch-all course intended to cover concepts in physics, chemistry, earth science, and astronomy in one semester) to incorporate activities that draw attention to the impact of science on society and individuals. These activities include classroom debates on current issues with scientific content as well as experiments that draw attention to the science of everyday materials and phenomena. We will discuss these activities and the skills students are expected to develop from them.

**10:12**

**G42 12 A Statistical Analysis of Activity-Based and Traditional Introductory Algebra Physics Using the Force and Motion Conceptual Evaluation*** CECELIA TRECIA MARKES, *University of Nebraska at Kearney* With a three-year FIPSE grant, it has been possible at the University of Nebraska at Kearney (UNK) to develop and implement activity- based introductory physics at the algebra level. It has generally been recognized that students enter physics classes with misconceptions about motion and force. Many of these misconceptions persist after instruction. Pretest and posttest responses on the ''Force and Motion Conceptual Evaluation'' (FMCE) are analyzed to determine the effectiveness of the activity- based method of instruction relative to the traditional (lecture/lab) method of instruction. Data were analyzed to determine the following: student understanding at the beginning of the course, student understanding at the end of the course, how student understanding is related to the type of class taken, student understanding based on gender and type of class. Some of the tests used are the t-test, the chi-squared test, and analysis of variance. The results of these tests will be presented, and their implications will be discussed.

*This work was supported by the US DOE's FIPSE Grant No. P116B51449.

**10:24**

**G42 13 To Hold A Class When You Can Not Be There** TARLOK AURORA, *Univ. of the Sciences in Philadelphia* Sometimes it is not possible for faculty to be physically present in class because of a need to participate in off-campus conferences or seminars. Due to scheduling conflicts, it may not be possible to find a substitute instructor. Under these conditions, one could cancel the class and make it up later on. Instead, it could also be productive for teaching and learning to make assignments that students could work on during the scheduled class time in the absence of the instructor. This would make learning student-centered and foster teamwork. To do this, students were instructed to meet in the classroom to work together on the specified day and an assignment was made visible on the Blackboard Learning Platform. The completed assignment was due no later than the next class period. The assignment involved reading selected pages from the physics textbook, answering questions and a quiz. It was found that on the specified day, thirteen (out of the fourteen) sophomore students got together and correctly completed the group assignment without supervision. This was not done for extra credit. Students liked working in a collaborative environment. This approach may be used in larger classes with multiple assignments made to small group of students. Details will be discussed.

**10:36**

**G42 14 Medical Physicists and AAPM** HOWARD AMOLS, *American Association of Physicists in Medicine* The American Association of Physicists in Medicine (AAPM), a member society of the AIP is the largest professional society of medical physicists in the world with nearly 5700 members. Members operate in medical centers, university and community hospitals, research laboratories, industry, and private practice. Medical physics specialties include radiation therapy physics, medical diagnostic and imaging physics, nuclear medicine physics, and medical radiation safety. The majority of AAPM members are based in hospital departments of radiation oncology or radiology and provide technical support for patient diagnosis and treatment in a clinical environment. Job functions include support of clinical care, calibration and quality assurance of medical devices such as linear accelerators for cancer therapy, CT, PET, MRI, and other diagnostic imaging devices, research, and teaching. Pathways into a career in medical physics require an advanced degree in medical

physics, physics, engineering, or closely related field, plus clinical training in one or more medical physics specialties (radiation therapy physics, imaging physics, or radiation safety). Most clinically based medical physicists also obtain certification from the American Board of Radiology, and some states require licensure as well.

**SESSION G44: CHARGE-DENSITY WAVES**
**Tuesday Morning, 14 March 2006**
**347, Baltimore Convention Center at 8:00**
**Robert Thorne, Cornell University, presiding**

**8:00**
**G44 1 Dynamics of the Electro-Optic Response of Blue Bronze** LUIS LADINO, MIRAJ UDDIN, MARIO FREAMAT, JOSEPH BRILL, *University of Kentucky* We have measured the frequency, voltage, and position dependence of the electro-transmittance and electro-reflectance of the charge-density-wave (CDW) conductor blue bronze at T $\sim$ 80 K when square-wave voltages are applied to the sample. The electro-optic response, assumed to be proportional to the local strain of the CDW, is characterized in terms of a relaxation time and a surprisingly long ( $>$ 0.1 ms) ''inertial'' delay for CDW repolarization. At a given position in the sample, the relaxation time increases with decreasing voltage, as expected. Both time constants increase away from the current contacts, indicating that the inertia is not due to barriers at the contacts. For one sample, the electro-optic response is also observed to decay for times $\sim$ 10 ms. This research was supported by NSF grants # DMR-0100572 and DMR-0400938.

**8:12**
**G44 2 Temperature Dependence of the Electro-Optic Relaxation Time of Blue Bronze** JOSEPH BRILL, LUIS LADINO, MARIO FREAMAT, MIRAJ UDDIN, *University of Kentucky* DAMIR DOMINKO, *University of Kentucky and Institute of Physics, Zagreb* We have measured the temperature dependence of the electro-transmittance of the quasi-one dimensional charge-density-wave (CDW) conductor blue bronze at temperatures between 55 K and 125 K when square-wave voltages are applied to the sample. For voltages well-above the threshold for nonlinear current, the characteristic electro-optic relaxation time, at a given position in the sample, depends primarily on the CDW current, whereas the magnitude of the relative change in transmittance decreases with decreasing temperature even for constant CDW current. At lower voltages, the frequency dependence of the response broadens, suggesting non-uniform and temperature dependent barriers to CDW repolarization. This research was supported by NSF grant # DMR-0400938.

**8:24**
**G44 3 Structure and Charge Density Waves of K0.3MoO3 (blue bronze) (20-1) Surfaces by Variable Temperature STM** MAXIM NIKIFOROV, *University of Pennsylvania* ABDEL ISAKOVIC, *Cornell University* ROBERT THORNE, *Cornell University* DAWN BONNELL, *University of Pennsylvania* Scanning Tunneling Microscopy has been used extensively in the study of charge density waves in hexagonal compounds such as NbSe2, $\alpha$-TaSe2, $\alpha$-TaS2, NbSe3 etc. A limited number of studies have been done of the surfaces of K0.3MoO3 (blue bronze), a monoclinic compound. To date, charge density waves on blue bronze have not been imaged by STM. In this work we demonstrate unit cell spatial resolution on the blue bronze (20-1) surface at room temperature and at 110K. The contrast in images obtained at room temperature is attributed to the surface atomic structure. The role of the tip atom in the contrast formation is demonstrated by comparison of three different images of the (20-1) surface of K0.3MoO3. At low temperatures charge density waves are superimposed on the unit cell resolution pattern. To the best of our knowledge this is the first observation of charge density waves on blue bronze by STM.

**8:36**
**G44 4 The Phase Diagram of Driven Density Waves*** ROBERT THORNE, *Cornell University* Despite nearly 30 years of study, the physics of the velocity-driving force relation of density wave (DW) conductors has remained controversial. Recent experiments indicate that at low temperatures collective DW motion begins at a threshold field $E_T$, but occurs via a new mechanism that we call coherent collective creep. A first-order transition from creep to high velocity sliding occurs when the DW reaches a critical velocity. As the temperature is increased, the transition vanishes at a critical point, and collective sliding begins immediately at $E_T$. This phase diagram is inconsistent with all existing models of driven elastic media in the presence of disorder, which assume a single length and energy scale associated with pinning. As emphasized by Larkin and Brazovskii, there are, in fact, two length and energy scales associated with local and collective pinning, respectively. This interpretation has broad consequences for our understanding of driven disordered systems.

*Supported by the NSF (DMR 04-05500)

**8:48**
**G44 5 Spatial and temporal correlations in CDW dynamics*** ZACHARY M. STUM, ABDEL F. ISAKOVIC, ROBERT E. THORNE, *Physics Department, LASSP, Cornell University, Ithaca, NY* Noise phenomena associated with the collective mode provide a powerful probe of charge-density-wave (CDW) dynamics. We have developed a setup to allow measurements of spatial and temporal correlations in the noise on length scales of hundreds of microns at frequencies of up to 1 GHz. Details of the electric field, temperature and sample quality dependence of these correlations will be discussed. Our goal is to observe long-sought evidence for critical dynamics as the depinning transition is approached from above.

*This work is supported through NSF DMR 04-05500

**9:00**
**G44 6 End current injection contacts for transport studies in CDW materials*** ABDEL F. ISAKOVIC, *Physics Dept., LASSP, Cornell University* KATARINA CICAK, *NIST, Boulder* ROBERT E. THORNE, *Physics Dept., LASSP, Cornell University* Current contacts to whisker- or rod-like crystals of quasi-one-dimensional conductors are generally applied to their sides. Effects associated with the resulting anisotropic current injection have long complicated interpretation of transport measurements. We have developed a method to microfabricate end current contacts. This method allows direct injection along the one-dimensional axis, greatly reduces spreading and contact resistances, and produces more uniform current densities. Using these contacts, we have been examining the physics of phase slip and

single-particle to collective current conversion in the CDW conductors $NbSe_3$ and $TaS_3$, and in particular how the excess voltage required for phase slip varies with current and temperature. End contacts also modify the magnitude and temperature dependence of the CDW's depinning threshold. Our analysis shows that the activation voltage for the nucleation of topological dislocations increases with decreasing temperature, and varies from typically 20 mV at 110 K to 80 mV at 80 K.

*Thsi work is supported through NSF DMR 04-05500

**9:12**

**G44 7 Electronic Structure of $LaTe_2$** DANIEL GARCIA, GEYHONG GWEON, *Department of Physics, University of California, Berkeley* SHUYUN ZHOU, *Department of Physics, University of California, Berkeley; Materials Sciences Division, Lawrence Berkeley National Laboratory, Berkeley* JEFF GRAF, *Materials Sciences Division, Lawrence Berkeley National Laboratory, Berkeley* CHRIS JOZWIAK, *Department of Physics, University of California, Berkeley* M.H. JUNG, *National Research Laboratory for Material Science, KBSI* Y.S. KWON, *Department of Physics, Sung Kyun Kwan University, Suwon* ALESSANDRA LANZARA, *Department of Physics, University of California, Berkeley; Materials Sciences Division, Lawrence Berkeley National Laboratory, Berkeley* Current work on the charge density wave system $LaTe_2$ indicates the existence of near Fermi energy gapping due to $\mathbf{q}_{CDW}=\mathbf{a}^*/2$ and $\mathbf{b}^*/2$. We find this band gapping to be weaker than originally thought, particularly for the near $\Gamma$ point contour. In addition, we find evidence of gap anisotropy which maintains the expected four fold symmetry of the crystal. Finally, we observe evidence of non-negligible kz dependence, originally considered minor. This appears to alter the CDW nesting as well as the gap anisotropy and has considerable importance to future studies of Rare-Earth Dichalcogenides.

**9:24**

**G44 8 Effect of Pressure on the Competition between Charge Density Wave and Superconductivity in $ZrTe_3$ Single Crystal** Y. UWATOKO, M. ABLIZ, M. HEDO, *ISSP, Univ. of Tokyo, Kashiwa, Chiba 277-8581, Japan* R. YOMO, K. YAMAMYA, *Dept. of Appl. Phys., Hokkaido Univ., Sapporo 060-8628, Japan* Competition and coexistence of CDW and superconductivity are studied from ancient times by $NbSe_2$, $NbSe_3$, etc. The rivalry of CDW and superconductivity was changed with pressure and the method of investigating the situation has been used. We report on an intricate competition between charge density wave (CDW) formation and superconductivity under pressure up to 11 GPa in the low-dimensional conductor $ZrTe_3$. The electrical resistivity measurements up to 11 GPa in the temperature 2.4K to 300K were performed using a standard 4-probe method. Hydrostatic pressure was produced by using a cubic anvil pressure cell in the Teflon cell filled with a fluid pressure transmitting medium of mixture of Fluorinert. As pressure increases, the CDW transition temperature $T_{CDW}$ initially increases, then begins to decrease at 2 GPa and abruptly disappears near 5 GPa. On the other hand, while the superconducting transition temperature $T_C$ falls to below 1.2 K at $\sim$ 0.5 GPa and is not observed at up to 5 GPa above 2.5 K, a superconducting transition emerges beginning at $\sim$ 5 GPa and $T_C$ increases steeply up to 11 GPa. This is an observation of pressure-induced reentrant superconductivity. The results are discussed in terms of the change in the reduced area of the Fermi surface due to CDW formation.

**9:36**

**G44 9 Incommensurate lattice modulation in CDW compound $TbTe_3$** N. RU, A. FANG, A. KAPITULNIK, I. R. FISHER, *Dept. of Applied Physics, Stanford University* M. F. TONEY, *Stanford Synchrotron Radiation Laboratory, Stanford Linear Accelerator Center* The layered materials $RTe_3$ ($R$ = rare earth) are simple charge-density wave (CDW) compounds, for which large regions of the original quasi-2D Fermi surface are nested by a single incommensurate wavevector. We use high resolution x-ray diffraction and scanning tunneling microscopy (STM) to study how the lattice responds to the incommensurate ordering. The superlattice of $TbTe_3$ reveals a unidirectional lattice modulation characterized by $q_{CDW} = 0.296$ c*. Higher harmonics are several orders of magnitude lower in intensity, implying an almost sinusoidal lattice modulation. The CDW is well correlated within and between planes, with correlation lengths in excess of 1000 Å. STM measurements reveal the CDW gap and real-space lattice modulation.

**9:48**

**G44 10 Stripes in quasi 2D rare-earth tellurides** HONG YAO, *Department of Physics, Stanford University, Stanford, CA 94305* JOHN ROBERTSON, *Department of Physics, Stanford University, Stanford, CA 94305* EUN-AH KIM, *Department of Physics, Stanford University, Stanford, CA 94305* STEVEN KIVELSON, *Department of Physics, Stanford University, Stanford, CA 94305* Even though the rare-earth tellurides are tetragonal materials with quasi-2D band structure, they have a hidden 1D character. The consequent, near-perfect Fermi surface nesting results in the formation of a charge density wave (CDW) state. Interestingly, the CDW is unidirectional (?striped?), spontaneously breaking not only translational symmetry, but the discrete rotational symmetry, as well. We show that there are two possible ordered phases consistent with the band structure: A bidirectional ?checkerboard? state would occur if the CDW transition temperature is sufficiently low, whereas the observed striped state is favored when the transition temperature is larger. We comment, as well, on the implications of this finding for the issue of stripes vs. checkerboards in more strongly correlated systems, such as the cuprates.

**10:00**

**G44 11 The dimensionality of charge density waves in the presence of quenched disorder** ADRIAN DEL MAESTRO, *Department of Physics, Harvard University* BERND ROSENOW,* *Institut für Theoretische Physik, Universität zu Köln* SUBIR SACHDEV, *Department of Physics, Harvard University* We present the effects of quenched disorder on a model of charge density wave (CDW) ordering on the square lattice. Our model may be applicable to the cuprate superconductors, where a random electrostatic potential exists in the CuO planes as a result of the presence of charged dopants. We argue that the presence of a random potential can affect the uni-directionality of the CDW order. Coupling to a uni-directional CDW, the random potential can lead to the formation of domains with 90 degree relative orientation, thus tending to restore the rotational symmetry of the underlying lattice. For a checkerboard CDW on the other hand, disorder generates spatial anisotropies on short length scales and thus some degree of uni-directionality. Using both numerical and analytical techniques, we quantify these disorder effects. Contact will be made with different experimental approaches on various materials that seem to observe both stripe and checkerboard charge ordering.

*Currently visiting Harvard University

**10:12**

**G44 12 Inhomogeneous and glassy electronic phases driven by competing orders** I. VEKHTER, *Louisiana State University* Z. NUSSINOV, *Washington University* A. V. BALATSKY, *Los Alamos National Laboratory* Emergence of inhomogeneous and glassy states in interacting systems has been a focus of much attention recently. It has been well established that such states may arise a) in the presence of disorder; b) in pure systems in the presence of interactions at competing length scales. Here we investigate the emergence of inhomogeneous states as a result of competing orders. We use a Ginzburg-Landau theory and find that, even if the theory is local, negative amplitude-gradient coupling leads to states of inhomogeneous coexistence of order parameters. Proliferation of low lying modes in such systems triggers slow dynamics and low critical temperatures.

**10:24**

**G44 13 Dynamic Compressibility and aging in Wigner crystals and quantum glasses*** THIERRY GIAMARCHI, *University of Geneva, DPMC, 24 Quai Ernest Ansermet, CH-1211 Geneva 4, Switzerland* LETICIA CUGLIANDOLO, *Laboratoire de Physique Theorique et Hautes Energies, 4 Place Jussieu, 75252 Paris Cedex 05, France* PIERRE LE DOUSSAL, *LPTENS CNRS UMR 8549 24, Rue Lhomond 75231 Paris Cedex 05, France* We study the non-equilibrium linear response of quantum elastic systems pinned by quenched disorder with Schwinger-Keldysh real-time techniques complemented by a mean-field variational approach. We find (i) a quasi-equilibrium regime in which the analytic continuation from the imaginary-time replica results holds provided the marginality condition is enforced; (ii) an aging regime. The conductivity and compressibility are computed. The latter is found to cross over from its dynamic to static value on a scale set by the waiting time after a quench, an effect which can be probed in experiments in e.g. Wigner glasses.

*Supported by Swiss Science Foundation, ACI-France grant and IUF

**10:36**

**G44 14 Wigner crystallization in $Na_3Cu_2O_4$ and $Na_8Cu_5O_{10}$ chain compounds.** P. HORSCH, *Max-Planck-Institute for Solid State Research, D-70569 Stuttgart, Germany* M. SOFIN, M. MAYR, M. JANSEN, We report the synthesis of novel doped edge-sharing chain compounds $Na_3Cu_2O_4$ and $Na_8Cu_5O_{10}$, which form insulating states with commensurate charge order [1]. We identify these systems as one-dimensional Wigner lattices, where the charge order is determined by the long-range Coulomb interaction and the number of holes in the d-shell of Cu. Our interpretation is supported by X-ray structure data as well as by an analysis of magnetic susceptibility and specific heat data. Remarkably, due to large second neighbor Cu-Cu hopping, these systems allow for an unambiguous distinction between the classical Wigner lattice and the $4k_F$ charge-density wave of quantum mechanical origin. Finally, we briefly discuss the domain-wall type charge excitations and the theoretical expectation for the optical conductivity of 1D Wigner lattices [2]. [1] P. Horsch, M. Sofin, M. Mayr, and M. Jansen, Phys. Rev. Lett. 94, 076403 (2005). [2] M. Mayr and P. Horsch, (unpublished).

**10:48**

**G44 15 Fermi surface nesting and the origin of the charge density wave in NbSe2** CHRISTOPHER HOWELLS, MICHELLE JOHANNES, IGOR MAZIN, *Naval Research Laboratory* The origin of a charge density wave (CDW) transition in $NbSe_2$ and related transition metal dichalcogenides has been studied and hypothesized about for the past four decades. The idea that CDW formation is the result of Fermi surface nesting was put forward as early as 1978 and continues to be suggested in current papers. Using highly accurate density functional calculations, we make a detailed study of the band structure and Fermi surfaces of equilibrium and pressurized $NbSe_2$. We calculate the real part of the non-interacting susceptibility, $\Re\chi_0(\mathbf{q})$, which is the relevant quantity for a CDW instability and the imaginary part,$\Im\chi_0(\mathbf{q})$, which directly shows Fermi surface (FS) nesting. We show that there are very weak peaks in $\Re\chi_0(\mathbf{q})$ near the CDW wave vector, but that no such peaks are visible in $\Im\chi_0(\mathbf{q})$, definitively eliminating FS nesting as a factor in CDW formation. We discuss the effects of pressure and provide calculated de Haas van Alphen frequencies and effective masses that can be compared to experiment.

**SESSION G45: PHASE TRANSITIONS IN RUTHENATES**
**Tuesday Morning, 14 March 2006**
**348, Baltimore Convention Center at 8:00**
**Sung Chang, Ames Lab, presiding**

**8:00**

**G45 1 Time-resolved Kerr effect in $SrRuO_3$: observation of oscillatory dynamics** M. LANGNER, C.L.S. KANTNER, C.P. WEBER, J. ORENSTEIN, L.W. MARTIN, R. RAMESH, *UC Berkeley and Lawrence Berkeley National Lab* We report measurements of magnetization dynamics in thin films of the perovskite transition metal oxide $SrRuO_3$, a metallic compound that is ferromagnetic below approximately 150 K. The dynamics of the magnetization vector, $\vec{M}$, were measured using the time-resolved magneto-optic Kerr effect. In this technique a pump laser pulse, at photon energy 1.5 eV, perturbs the magnet by reducing the magnitude of $\vec{M}$ and changing the direction of the anisotropy field. The subsequent dynamics of $\vec{M}$ are measured by detecting the rotation of the plane of polarization of a time-delayed probe beam that is reflected from the surface of the sample. Below $\sim$ 100 K, we observe a damped oscillation in the Kerr rotation with frequency 250 GHz. The damping decreases with decreasing temperature down to $\sim$ 50 K and remains constant below this temperature. We tentatively identify this oscillation as the q=0 magnon, or ferromagnetic resonance frequency (FMR), of SrRuO3. The rather large value of the FMR frequency is consistent with the known large magnetocrystalline anisotropy of this compound. We will report measurements of $\vec{M}$(t) as a function of film thickness, residual resistance, and orientation of crystalline axes.

**8:12**

**G45 2 Itinerant Ferromagnetism in Cr Doped Perovskite Ruthenates*** V. DURAIRAJ, E. ELHAMI, S. CHIKARA, X.N. LIN, A. DOUGLASS, G. CAO, *University of Kentucky* P. SCHLOTTMANN, E.S. CHOI, *National High Magnetic Field Lab* R.P. GUERTIN, *Tufts University* We report results of structural, magnetic and transport properties of single crystal $CaRu_{1-x}Cr_xO_3$ ($0 \leq x \leq 0.36$) and $SrRu_{1-x}Cr_xO_3$ ($0 \leq x \leq 0.20$). Cr substitution as low as $x=0.08$ drives $CaRu_{1-x}Cr_xO_3$ from paramagnetic state to an itinerant ferromagnetic state with an abrupt jump in isothermal magnetization leading to a sizeable saturation moment ( $\sim 0.4\mu_B$/f.u. within the ab plane). Ferromagnetism occurs abruptly and reaches as high as $T_C=123$ K for $x=0.22$. The Cr-driven ferromagnetism is highly anisotropic, suggesting an important role for spin-orbit coupling. Lattice constant and magnetic measurements strongly support the valence of the Cr to be tetravalent ($Cr^{4+}$, $3d^2$ configuration). The Cr substitution for Ru in $SrRuO_3$ ($T_C=165$ K) enhances the itinerant ferromagnetism, consistent with Cr-induced ferromagnetism in paramagnetic $CaRuO_3$, but without significant magnetic anisotropy. Preliminary pressure-dependent magnetization of $CaRu_{0.85}Cr_{0.15}O_3$ shows strong enhancement of the saturation magnetization (25% for P$\sim$ 0.7 GPa). All results indicate a coupling of Ru 4d and Cr 3d electrons that is unexpectedly favorable for itinerant ferromagnetism which often exists delicately in the ruthenates.

*This work was supported by NSF grant DMR-0240813

**8:24**

**G45 3 Borderline magnetism in $Sr_4Ru_3O_{10}$: Impact of dilute La and Ca doping on itinerant metamagntism and ferromagnetism*** SHALINEE CHIKARA, V. DURAIRAJ, W.H. SONG, Y.P. SUN, X.N. LIN, A. DOUGLASS, G. CAO, *University of Kentucky* The triple-layered $Sr_4Ru_3O_{10}$ features ferromagnetic behavior with Tc=105 K along the c-axis (interlayer) and a first-order metamagnetic transition below 50 K in the basal plane [1]. The coexistence of ferromagnetism and metamagnetism suggests $Sr_4Ru_3O_{10}$ be on the borderline that separates its closest neighbors: the itinerant ferromagnet $SrRuO_3$ and the enhanced paramagnet $Sr_3Ru_2O_7$. We report our results on $Sr_4Ru_3O_{10}$with Sr slightly substituted by La and Ca ions. The La doping drastically changes the magnetic and transport properties. In particular, it effectively suppresses Tc along the c-axis, but simultaneously induces ferromagnetic behavior in the basal plane with Tc=30 K, entirely different from that of the c-axis. Associated with these changes, the metamagnetism disappears in the basal plane but appears along the c-axis. In sharp contrast, the Ca doping significantly enhances the ferromagnetism along c-axis but drastically weakens the magnetic ordering in the basal plane where an unusual $T^{3/2}$-power law for the resisitivity is developed. The vastly different responses to the La and Ca doping, despite similar ionic radii of $La^{3+}$ and $Ca^{2+}$, highlight the role of the extra electron from the La ion added to the $t_{2g}$ orbitals. [1] G. Cao, et al., Phys. Rev. B **68** 174409 (2003)

*This work was supported by NSF grant DMR-0240813.

**8:36**

**G45 4 Infrared Hall effect in $SrRuO_3$ and $CaRuO_3$** M.-H. YANG, G. ACBAS, A. MARKELZ, J. CERNE,* *Physics Dept., Univ. at Buffalo, Buffalo, NY* I. OHKUBO, *Dept. of Applied Chemistry, Univ. of Tokyo, Tokyo, Japan* P. KHALIFAH, *Chemistry Dept., Univ. of Massachusetts, Amherst, MA* H. CHRISTEN, D. MANDRUS,† *Condensed Matter Sciences Div., Oak Ridge National Lab., Oak Ridge, TN* Z. FANG, *Inst. of Physics, Chinese Academy of Science, Beijing, China* The mid-infrared (MIR: 115-366 meV) Hall effect is studied in $SrRuO_3$ and $CaRuO_3$ films. In $SrRuO_3$, below 200 meV the MIR Hall response changes sign as a function of temperature near 120 K, similar to the dc Hall effect. Above 200 meV, no sign change occurs and the temperature dependence of the MIR Hall response is similar to the dc magnetization. On the other hand, in $CaRuO_3$, the MIR Hall effect is nearly independent of frequency above 100 meV, has a similar temperature dependence as the dc magnetic susceptibility, and does not change sign, unlike the dc Hall effect. In $SrRuO_3$, the complex Faraday and Kerr angles measured in the MIR at 10 K are in good qualitative and quantitative agreement with first-principles band calculations [Z. Fang et al., Science 2003].

*Supported by the Research Corporation Cottrell Scholar Award and NSF CAREER Award.
†Oak Ridge National Laboratory is managed by UT-Battelle, LLC, for the U.S. Department of Energy under contract DE-ACO5-00OR22725.

**8:48**

**G45 5 Oscillatory magnetoresistance periodic in 1/$B$ and $B$ and specific heat of $Ca_3Ru_2O_7$*** X.N. LIN, V. DURAIRAJ, S. CHIKARA, A. DOUGLASS, G. CAO, V. VARADARAJAN, V.A. BONDARENKO, J.W. BRILL, *Univ. of Kentucky* Z.X. ZHOU, *ORNL* P. SCHLOTTMANN, *NHMFL* We report magnetoresistance oscillations in high magnetic fields, B, up to 45 T and over a wide range of temperature in the Mott-like system $Ca_3Ru_2O_7$ [1]. For B rotating within the itac-plane, slow and strong Shubnikov-de Haas (SdH) oscillations periodic in 1/B are observed for T$\leq$ 1.5 K in the presence of metamagnetism. These oscillations are highly angular dependent and intimately correlated with the spin-polarization of the ferromagnetic state. For B$||$ [110], oscillations are also observed itbut periodic in B (rather than 1/B)it which persist up to 15 K. While the SdH oscillations are a manifestation of the presence of small Fermi surface (FS) pockets in the Mott-like system, the B-periodic oscillations, an exotic quantum phenomenon, may be a result of anomalous coupling of the magnetic field to the $t_{2g}$-orbitals that makes the extremal cross-section of the FS field-dependent. In addition, measurements of the specific heat show sharp anomalies at 48 K and 56 K, the former with a strong frequency dependence consistent with a sluggish first-order transition. Much less entropy is removed at the upper, second-order transition. All results will be presented and discussed along with comparisons drawn from impurity doped $Ca_3Ru_2O_7$. [1] XN Lin, et al., Phys. Rev. Lett. 95, 017203 (2005).

*This work was supported by NSF grant DMR-0240813

**9:00**

**G45 6 ARPES study on $Ca_{1.8}Sr_{0.2}RuO_4$** MADHAB NEUPANE, *Department of Physics,Boston College, MA* A.K.P. SHEKHRAN, Z.-H. PAN, J. -H. MA, H. DING, *Department of Physics,Boston College, MA* R. JIN, D. MANDRUS, *Condensed Matter Science Division, Oak Ridge National Laboratory, Tennessee* Owing to the discovery of triplet superconductivity in $Sr_2RuO_4$, much effort has been devoted in the past few years to the understanding of the $Ca_{2-x}Sr_xRuO_4$ family. These compounds exhibit a rich phase diagram which connects the p-wave superconductor $Sr_2RuO_4$ to the Mott insulator $Ca_2RuO_4$. Particularly, the x = 0.2 compound is at the boundary between a magnetic metal and a canted antiferomagnetic insulator. It has been suggested recently that this compound

has d−electron heavy−fermion behavior due to modulations in the magnetic correlations induced by the structural distortion. For such behavior, flat electronic b and s are expected. However,our angle resolved photo emission measurements observed only highly dispersive b and s.

**9:12**

**G45 7 Investigation of the Competition between Structural and Ferromagnetic Transitions in $GdRu_2$ using the Mossbauer Effect*** DERMOT COFFEY, MICHAEL DEMARCO, RYAN HEARY, *Dept. of Physics, Buffalo State College, NY 14222* PEI-CHUN HO, TODD SAYLES, M. BRIAN MAPLE, *Dept. of Physics, University of California, San Diego, CA 92093* STEVE TOORONGIAN, MICHAEL HAKA, *Nuclear Medicine Department, State University of New York at Buffalo, NY 14260* We use the $^{99}$Ru Mossbauer Effect(ME) to investigate magnetism in the Laves phase $Ce_{1-x}Gd_xRu_2$ series. This series of compounds is superconducting for small $x$ and has been thought to be ferromagnetic for large $x$ on the basis of extrapolations of Curie-Weiss fits to the $\chi$(T) data. We have studied the temperature dependence of the ME spectra for a number of these compounds and found no evidence of a hyperfine magnetic field due to ferromagnetic order. In $GdRu_2$, a Curie-Weiss fit to the $\chi$(T) data above 120K yields a Curie-Weiss temperature of 93K. However, at $\sim 120K$, $\chi^{-1}$ deviates from a straight line fit. The ME spectra show that there is a qualitative change in the environment of the Ru nucleus in this temperature re gion pointing to a structural phase transition. Below this transition the width of the ME spectrum grows with decreasing temperature by 50% between 100K and 4.2K. We analyze this temperature dependence in terms of a slowing down of the fluctuations of the local field due to Gd moments.

*This work is supported by the U.S. Dept. of Energy (Grants: DE-FG02-03ER46064 and DE-FG02-04ER46105).

**9:24**

**G45 8 Evidence for high temperature orbital fluctuations in $La_4Ru_2O_{10}$** PETER KHALIFAH, *University of Massachusetts - Amherst* BRIAN SALES, DAVID MANDRUS, *Oak Ridge National Laboratory* QINGZHEN HUANG, *National Institute of Standards and Technology* RAYMOND OSBORN, *Argonne National Laboratory* STEPHEN NAGLER, MARK LUMSDEN, *Oak Ridge National Laboratory* CHRISTOPHER KENDIZORA, *Naval Research Laboratory* EMIL BOZIN, SIMON BILLINGE, *Michigan State University* ROBERT CAVA, *Princeton University* Among ruthenates, the compound $La_4Ru_2O_{10}$ is unique in having a complete orbital ordering transition. Upon cooling below $T_{OO}$ = 160K, the magnetism of this compound is abruptly quenched. Initial crystallographic studies of this phase [1] showed that strong distortions in the Ru-O bond lengths appear only below $T_{OO}$. We have found distinctly different thermal conductivities of single-crystal $La_4Ru_2O_{10}$ above and below $T_{OO}$. At high temperatures, this material unexpectedly behaved as a thermal glass, providing strong evidence for dynamic orbital fluctuations in $La_4Ru_2O_{10}$. This is supported by a detailed analysis of the atomic displacement parameters (ADPs) of this material. We will discuss our current model for orbital ordering in $La_4Ru_2O_{10}$, the differences in the local and average structure of this material, and the reasons for the strong magnetoelastic coupling in this phase. [1] P. Khalifah, R. Osborn, Q. Huang, H. W. Zandbergen, R. Jin, Y. Liu, D. Mandrus, and R. J. Cava. ''Orbital ordering transition in $La_4Ru_2O_{10}$,'' Science, **297**, 2237-40 (2002).

**9:36**

**G45 9 Magnetic Field Induced Phases of $Ca_2RuO_4$ and $Ca_3Ru_2O_7$** J. F. KARPUS, R. GUPTA, H. BARATH, S. L. COOPER, *Department of Physics and Frederick Seitz Materials Research Laboratory, University of Illinois Urbana-Champaign* G. CAO, *Department of Physics and Astronomy, University of Kentucky* We present a Raman scattering study of the magnetic field induced phases in the layered ruthenates $Ca_2RuO_4$ and $Ca_3Ru_2O_7$. Single-layer $Ca_2RuO_4$ has an antiferromagnetic ground state, is a paramagnetic (PM) insulator above $T_N$ = 113 K and is a PM metal above $T_{MI}$ = 357 K, while double-layer $Ca_3Ru_2O_7$ has an antiferromagnetic insulating ground state, is metallic above $T_{MI}$ = 48 K, and is paramagnetic above $T_N$ = 56 K. Applied fields oriented in the a-b planes of both these materials produce dramatic changes to both the magnetic and vibrational spectra; these changes are associated with field-induced changes in the Ru orbital populations of these materials. In this talk, we compare the field induced orbital, magnetic, and conducting phases observed in $Ca_2RuO_4$ and $Ca_3Ru_2O_7$. *Work supported by NSF DMR02-44502, NSF DMR02-40813, and DOE DEFG02-91ER45439.

**9:48**

**G45 10 Crystal structure, electronic and magnetic properties of $SrRuO_3$ under epitaxial strain*** ALEXEY ZAYAK, KARIN RABE, *Rutgers University, 136 Frelinghuysen Rd., Piscataway 08854, New Jersey* XIANGYANG HUANG, *RJ Mears, LLC 1100 Winter Street, Suite 4700, Waltham, MA 02451* JEFFREY NEATON, *The Molecular Foundry, Material Science Devision, Lawrence Berkeley National Laboratory, Berkeley CA 94720* Using density functional theory, properties of $SrRuO_3$ have been investigated. We focused both on general properies of the orthorhombic distortion in $SrRuO_3$ and the effects of applying epitaxial constraints, whereby the influence of large in-plane strain resulting from coherent epitaxy have been isolated and investigated. The overall pattern of the structural relaxations revealed coherent distortions of the oxygen octahedra network which are sensitive to the magnetic order. The magnetic parameters exhibit substantial changes allowing us to discuss possibilities of magneto-structural tuning of the $SrRuO_3$-based thin film structures.

*This work was supported by NSF MRSEC DMR-00-80008.

**10:00**

**G45 11 Spectroscopic Investigation on the Electronic Structure of $Sr_2MO_4$ (M=Ru, Rh, and Ir)** S.J. MOON, M.W. KIM, K.W. KIM, T.W. NOH, *ReCOE & School of Physics, Seoul National University, Seoul 151-747, Korea* J.-Y. KIM, *PAL, Postech, Pohang, Korea* J.-H. PARK, *Department of Physics & Electron Spin Science Center, Postech, Pohang, Korea* I. NAGAI, S.I. IKEDA, *NeRI & AIST, Tsukuba, Japan* G. CAO, *Deparment of Physics and Astronomy, University of Kentucky, Lexington, Kentucky 40506, USA* We investigated the intriguing metal-insulator transition and the electronic structure change of the layered perovskite $Sr_2MO_4$ (M=Ru, Rh, and Ir) by optical and O 1s x-ray absorption (XAS) spectroscopy. $Sr_2RuO_4$ (four 4d electrons) is a superconductor. $Sr_2RhO_4$ (five 4d electrons) is a poor metal. $Sr_2IrO_4$ (five 5d electrons) is a small gap insulator. All the compounds have similar crystal structures, yet their unoccupied d-bands show intriguing change as the M is changed from Ru to Rh, and to Ir. In this presentation, we will discuss the possible origin of the electronic structure change in terms of the change in

local structural deformation, Coulomb energy, electron occupation, and the orbital degeneracy by comparing the optical conductivity with XAS spectra. We will also suggest a possible link between the electronic structure change and the metal (Sr2RuO4)-insulator (Sr2IrO4) transition.

**10:12**
**G45 12 Metamagnetism and domain formation in $Sr_3Ru_2O_7$** ANDREW MACKENZIE, RODOLFO BORZI, SANTIAGO GRIGERA, ROBIN PERRY, *University of St Andrews* YOSHITERU MAENO, *Kyoto University* The bilayer perovskite $Sr_3Ru_2O_7$ offers the possibility of creating a quantum critical point by tuning the end-point of a line of first-order metamagnetic transitions towards zero temperature[1,2]. In the purest samples, with residual resistivity less than 1 $\mu\Omega$cm, the quantum critical point is not reached, due to a bifurcation of the original first-order phase transition, possibly associated with the formation of a new phase [3,4]. Here we present the results of new measurements which give strong evidence for the existence of magnetic domains throughout the region of the phase diagram enclosed by the bifurcated transition lines. The effect of these domains on the electrical resistivity can be controlled by varying the relative directions of current and the in-plane component of the applied magnetic field. [1] S.A. Grigera et al., Science Science **294**, 329 (2001). [2] S.A. Grigera et al. Phys. Rev. B **67**, 214427 (2003). [3] S.A. Grigera et al. Science **306**, 1155 (2004). [4] A.G. Green et al. Phys. Rev. Lett. **95**, 086402 (2005).

**10:24**
**G45 13 Magnetic domain formation in the itinerant metamagnetic transition of $Sr_4Ru_3O_{10}$** ZHIQIANG MAO, MENG ZHOU, JOE HOOPER, *Tulane University* MINGHUI YU, CHARLES O'CONNOR, *University of New Orleans* We have performed systematic investigation on the electronic transport properties of the triple-layered ruthenate $Sr_4Ru_3O_{10}$. We observed surprising anomalous features near its itinerant metamagnetic transition, including ultrasharp magnetoresistivity steps and a non-metallic temperature dependence in resistivity for upward field sweeps. These features suggest that the metamagnetic transition of $Sr_4Ru_3O_{10}$ occurs via a phase separation process with magnetic domain formation. We have also identified the phase separated regime in the magnetic field-temperature phase diagram.

**10:36**
**G45 14 Modification of the Fermi Surface of a Ferromagnetic Metal at a Metamagnetic Transition: Shubnikov de Haas Effect in High Quality Single Crystals of $Sr_4Ru_3O_{10}$** YOUNJUNG JO, LUIS BALICAS, *National High Magnetic Field Lab* NAOKI KIKUGAWA, *School of Physics and Astronomy, University of St. Andrews, St. Andrews, Fife KY16 9SS, United Kingdom* KEVIN STORR, *Department of Physics, Prairie View A&M University, Prairie View, Texas 77446-0519, USA* ANDREW MACKENZIE, *School of Physics and Astronomy, University of St. Andrews, St. Andrews, Fife KY16 9SS, United Kingdom* ZHIQIANG MAO, *Department of Physics, Tulane University, New Orleans, Louisiana 70118, USA* We performed a detailed electrical transport study at low temperatures and high magnetic fields in high quality single crystals of the tri-layered ferromagnetic metal $Sr_4Ru_3O_{10}$. We observed Shubnikov de Haas oscillations for several frequencies. The most prominent orbits have two-dimensional character and display frequencies $F_\alpha = 9959$ T, $F_\beta = 3949$ T, $F_\gamma = 1877$ T corresponding respectively to 73.5, 29.2 and 13.9% of the area of the orthorhombic first Brillouin zone (FBZ). Several additional orbits, mostly with frequencies below 2 kT have also been identified, whose spectral weight and frequencies are shifted by a metamagnetic transition induced by an in-plane field component.

## SESSION G46: QHE, INCLUDING GRAPHENE
**Tuesday Morning, 14 March 2006**
**349, Baltimore Convention Center at 8:00**
**Allan MacDonald, University of Texas, presiding**

**8:00**
**G46 1 Edge States in Graphene*** NIKOLAI SINITSYN, *Department of Physics, The University of Texas, Austin* JASON HILL, HONGKI MIN, ALLAN H. MACDONALD, *Department of Physics, The University of Texas, Austin* We investigate edge states in graphene subject to both realistically described spin-orbit coupling and an external magnetic field. Localized edge states are responsible for the charge and spin transport when the electron chemical potential is in a gap of the bulk spectrum. We derive expressions for the edge state energy dispersions and wave functions both analytically and numerically and discuss specific features that distinguish them from conventional edge states due to magnetic field in electron gas. Finally we discuss the relationship between edge state characteristics and both spin and charge response functions.

*The work was supported by Welch Foundation, by DOE grant DE-FG03-02ER45958 and by NSF grant DMR-0115947

**8:12**
**G46 2 Quantum Hall effect and edge states in graphene.** LUIS BREY, *CSIC-Madrid* The experimentally observed quantum Hall effect (QHE) in graphene has renewed the interest in the study of multivalley semiconductors in high magnetic fields. In this work we study some properties of graphene in presence of a high magnetic field. 1) We discuss the form of the quantization of the Hall conductivity. We argue that the Hall conductance can be understood in the general framework of the theory of the QHE in two-dimensional systems. 2) We study the properties of undoped graphene in the QHE regime. We find that the Zeeman coupling combined with the electron-electron interaction favors a spin-polarized ground state against a valley-polarized state. This ground state support low energy collective excitations that are combinations of spin and valley density waves. We discuss the possibility that spin texture excitations, Skyrmions, become the low energy charged excitations in the spin-polarized ground state. 3) Finally we analyze the properties of the edge states in the QHE regime. Due to the valley degeneracy occurring in graphene, electron-like and hole-like Landau levels with different spin and valley orientation cross at the edge of the sample. In the undoped samples Coulomb interaction produces repulsion between the states and forces the states to anti-cross, creating a valley and spin coherent stripe at the edge of the sample. We analyze the excitations occurring in this stripe and discuss their possible relevance in tunnelling experiments.

**8:24**

**G46 3 Quantum Hall Effect in Graphene*** ANTONIO H. CASTRO NETO, *Department of Physics, Boston University* FRANCISCO GUINEA, *Instituto de Ciencia de Materiales de Madrid, Spain* NUNO M.R. PERES, *Universidade do Minho, Portugal* We study the integer and fractional quantum Hall effect on a honeycomb lattice at half-filling (graphene) in the presence of disorder and electron-electron interactions. We show that the interactions between the delocalized chiral edge states (generated by the magnetic field) and Anderson-localized surface states (created by the presence of zig-zag edges) lead to edge reconstruction. As a consequence, the point contact tunneling on a graphene edge has a non-universal tunneling exponent, and the Hall conductivity is not perfectly quantized in units of $e^2/h$. We argue that the magneto-transport properties of graphene depend strongly on the strength of electron-electron interactions, the amount of disorder, and the details of the edges.

*A. H. C. N. was supported by the NSF grant DMR-0343790.

**8:36**

**G46 4 Band Collapse as Route to Odd-Integer Quantum Hall Effect In Graphene** B. ANDREI BERNEVIG, TAYLOR HUGHES, HANDONG CHEN, CONGJUN WU, SHOUCHENG ZHANG, *Stanford University* STANFORD/SPINAPPS TEAM, The recent Quantum Hall experiments in graphene have confirmed the theoretically well-understood picture of the quantum Hall (QH) conductance in fermion systems with continuum Dirac spectrum. In this paper we take into account the lattice, and perform an exact diagonalization of the Landau problem on the hexagonal lattice. At very large magnetic fields the Dirac argument fails completely and the Hall conductance, given by the number of edgestates present in the gaps of our spectrum, is dominated by lattice effects. As the field is lowered, the experimentally observed situation is recovered through a phenomenon which we call band collapse. As a corollary, for low magnetic field, graphene will exhibit two qualitatively different QHE's: at low filling, the QHE will be dominated by the ''relativistic'' Dirac spectrum and the Hall conductance will be odd-integer; above a certain filling, the QHE will be dominated by a non-relativistic spectrum, and the Hall conductance will span all integers, even and odd.

**8:48**

**G46 5 Quantum Hall Ferromagnetism in Graphene** ALLAN H. MACDONALD, JASON HILL, HONGKI MIN, NIKOLAI SINITSYN, *Department of Physics, The University of Texas, Austin* In a magnetic field non-interacting electrons with the graphene band structure have four nearly degenerate Landau levels close to the intrinsic Fermi level. The four levels are associated with different spin states and with the two different sites in the honeycomb lattice unit cell. In a single-particle theory weak spin-orbit coupling and Zeeman fields split the four levels by an amount that is small compared to the electronic self-energy. We discuss the quantum Hall effect in graphene using at integer filling factors $\nu = -1$, $\nu = 0$, and $\nu = 1$ in a picture where the ground state is a broken symmetry SU(4) ferromagnet and these weak single-particle terms act as symmetry breaking external fields. We also discuss the consequences of the difference in interaction strength beteween electrons on the same and different sublattice and sample quality criteria necessary to realize quantum Hall ferromagnetism in graphene.

**9:00**

**G46 6 Local defects and ferromagnetic interactions in 2D graphite*** M.P. LÓPEZ-SANCHO, *Ins. Ciencia de Materiales de Madrid (CSIC) Cantoblanco 28049-Madrid* M.A.H. VOZMEDIANO, *Unidad ASociada CSIC-UC3M E28911 Leganés Madrid* F. GUINEA, *Inst de Ciencia de Materiales de Madrid (CSIC) Cantoblanco 28049 MADRID* Recent experiments have shown unexpected properties in carbon-based materials. Ferromagnetic behavior enhanced by proton bombardment has been reported in graphite and, more recently, quantum Hall effect has been experimentally observed in graphene sheets. These results suggest that electronic correlations play an important role in these materials. The anomalous electronic and transport properties reported by the experiments agree with theoretical predictions of 2D models considering only $\pi$-electrons. The vanishing of the density of states at the Fermi energy and the absence of a true Fermi surface have important consequences in the electronic behavior of 2D graphite. Although at present there is not a microscopic explanation of the graphite ferromagnetic properties, they seem to be related to topological defects, as pointed out by AFM measurements. In this work we show that lattice defects and vacancies in the graphene structure give rise to localized states at the Fermi energy. Repulsive electron-electron interactions lead to the formation of local moments by polarization of local states. Due to the lack of a Fermi surface the RKKY-like interaction does not have oscillations instead it decays as $r^{-3}$, where $r$ is the distance between defects. The interaction is then ferromagnetic.

*MCYT Grant No. MAT2002-0495-C02-01

**9:12**

**G46 7 Disorder and the integer quantum Hall plateau-to-plateau transition** WANLI LI, D.C. TSUI, *Princeton University* J.S. XIA, *University of Florida and NHMFL* L.N. PFEIFFER, K.W. WEST, *Bell Labs* We have studied the temperature scaling of integer quantum Hall plateau-to-plateau transition in various disordered systems down to 10mK. The samples are $Al_xGa_{1-x}As$-$Al_{0.33}Ga_{0.67}As$ heterostructures with different Al concentration $x$. Previous work has shown a perfect power law $(dR_{xy}/dB)|_{Bc} \propto T^{-\kappa}$ with $\kappa=0.42$ over two decades of temperatures in the sample with $x=0.85\%$. In the sample of $x=0$, $\kappa=0.58$ was observed at high temperatures, while we have now found $\kappa=0.42$ restored below a crossover temperature $T_c=120$mK. $T_c$ increases to 250mK for $x=0.21\%$, and is not observable in the experimental temperature range in the sample of $x=0.85\%$. We propose that the quantum phase coherence length exceeds the disorder correlation length below $T_c$, shifting the nature of the disorder in the system from long-ranged to short-ranged. On the other end of the sample series with $x=4.1\%$, where alloy clustering is believed to be significant, $\kappa=0.58$ is found to persist down to the lowest temperature of the measurement limit, suggesting a different universal class of the transition in long-range disordered systems.

**9:24**

**G46 8 Resistively-Detected NMR in a 2DES near $\nu = 1$: Clues to the Origin of the Dispersive Lineshape** J.P. EISENSTEIN, L.A. TRACY, *Caltech* L.N. PFEIFFER, K.W. WEST, *Bell Labs* Resistively-detected NMR (RDNMR) measurements on 2D electron systems near the $\nu = 1$ quantum Hall state are reported. In agreement with previous RDNMR studies, we observe a dispersive lineshape, where $R_{XX}$ vs. frequency shows both negative and positive excursions from the equilibrium $R_{XX}$ value. However, in

contrast to recent results of Gervais, et al. [Phys. Rev. Lett. 94, 196803 (2005)], this dispersive lineshape is found at all RF powers, and a conventional, Korringa temperature dependence ($T_1T = const$) of the nuclear spin- lattice relaxation rate is observed. The shape of the unexplained dispersive lineshape is found to invert when then temperature derivative of the longitudinal resistance changes sign. This suggests that both Zeeman and thermal effects are important to RDNMR in this regime.

**9:36**

**G46 9 Anisotropic Electronic Transport in a Two-dimensional Hole System under a Tilted Magnetic Field** ZHIGANG JIANG, *Dept. of Physics, Columbia Univ. and National High Magnetic Field Lab* M.J. MANFRA, *Bell Labs, Lucent Technologies* Y.-W. TAN, H.L. STORMER, *Dept. of Physics, Columbia Univ.* D.C. TSUI, *Dept. of Electrical Engineering, Princeton Univ.* L.N. PFEIFFER, K.W. WEST, *Bell Labs, Lucent Technologies* We study the electrical transport properties of a high mobility two-dimensional hole system (2DHS) confined in a GaAs/AlGaAs quantum well grown on the (100) surface of GaAs. We observed a remarkable magnetotransport anisotropy in the $N = 1$ Landau level, different from the two-dimensional electron gas (2DEG), in which the anisotropy shows exclusively in the higher Landau levels ($N \geq 2$). Under a tilted magnetic field, we find that the anisotropy can be either reduced or enhanced by the in- plane magnetic field, depending on the direction of the field with respect to the lattice orientation of the sample. This behavior is again different from the previous reported results in 2DEG, where we expect the anisotropy will collapse precipitously as applying a much smaller in-plane magnetic field than what we have applied on the 2DHS. Particularly, at high tilting angles, we observed a ''spike'' like feature developed in the magnetoresistance ($R_{xx}$) at the filling factor $2 < \nu \leq 5/2$. However, unlike the resistance spike features associated with the first order magnetic transition between quantum Hall ferromagnets, no correlated spike has been observed in the Hall resistance ($R_{xy}$) of our sample.

**9:48**

**G46 10 Evidence for reentrant striped phases in a two-dimensional hole system** MICHAEL MANFRA, *Bell Laboratories* Z. JIANG, *NHMFL* HORST STORMER, *Dept. of Physics, Columbia University* D. C. TSUI, *Princeton University* LOREN PFEIFFER, K. W. WEST, A. M. SERGENT, *Bell Laboratories, Lucent Technologies* Anisotropic transport is observed at low temperatures in the N=1 and N=2 Landau levels of a very clean two-dimensional (2D) hole system. At $\nu = 7/2$ and $\nu = 11/2$, the longitudinal magnetoresistance develops strong anisotropies which depend on the direction of current flow and temperature. Interestingly, the transport at $\nu=9/2$ is *isotropic* for all temperatures. Our results for a two-dimensional hole system contrast sharply with 2D electron transport where no anisotropy has been observed in the N=1 Landau level, the strongest anisotropy occurs at $\nu=9/2$, and no reentrant behavior is evident.

**10:00**

**G46 11 Spin Transition in a 2DES at $\nu = 1/2$** L.A. TRACY, J.P. EISENSTEIN, *Caltech* L.N. PFEIFFER, K.W. WEST, *Bell Labs* The transition from partial to complete electron spin polarization as a function of density in a 2DES at $\nu = 1/2$ has been probed using a resistively-detected NMR (RDNMR) technique. Both the nuclear spin lattice relaxation time $T_1$ of $^{71}$Ga and the response in resistance to a change in the nuclear spin polarization appear to reflect this transition. At low densities, where the electron spin polarization is partial, the $T_1$ time is relatively short, due to the presence of both electron spin states at the Fermi level. In this regime $T_1$ is density independent and has a Korringa-like temperature dependence. Above a critical density $T_1$ increases and the RDNMR signal eventually vanishes, consistent with a transition to complete electron spin polarization. In the transition region we observe a non- Korringa $T_1$ temperature dependence and an unexpected enhancement of the RDNMR signal.

**10:12**

**G46 12 Spin polarization at fractional filling factors** JAVIER GROSHAUS,*P. PLOCHOCKA, M. RAPPAPORT, I. BAR-JOSEPH, *Weizmann Inst.* B. DENNIS, L. PFEIFFER, K. WEST, *Bell Labs* A. PINCZUK, *Columbia U. & Bell Labs* We measure the spin polarization of a two-dimensional electron system (2DES) in the Quantum Hall regime by photocurrent interband absorption spectroscopy. The sample is a single GaAs quantum well that is placed in a dilution fridge with optical windows at low temperatures down to 70 mK. The 2DES density is tuned by a back-gate. We illuminate with circularly polarized light. This allows us to discriminate optical transitions into each electronic spin level. We show that the spectra consist of many-body electron-hole complexes. The lowest in energy is a singlet trion-like transition *T* (J.G. Groshaus *et.al.*, *Phys. Rev. Lett.* **93**, 96802, 2004). In the *T*-absorption process, the photocreated electron- hole pair binds to an electron from the 2DES with spin that is opposite to that of the photocreated one. We model this process taking into account correlations and phase space considerations. Using this model and measurements of the *T*-absorption, we obtain the spin polarization of the 2DES. We find that at $\nu = 1/3$ the 2DES is fully polarized. As $\nu$ is increased there is loss of spin polarization. Around $\nu = 2/3$ the 2DES is half polarized. At this $\nu$, the 2DES remains half polarized for the relatively wide range of magnetic fields of 2 Tesla. This points to the existence of spatial magnetic domains, as proposed by G. Murthy (*Phys. Rev. Lett.* **84**, 350, 2000).

*Also Bell Labs.

**10:24**

**G46 13 Small length-scale probes of 2D electron conduction and correlations.** ROBERT WILLETT, KEN WEST, LOREN PFEIFFER, *Bell Laboratories, Lucent Technologies* An important approach to revealing correlation effects in high mobility 2D electron systems is through conduction measurements, and this is particularly true when a conduction measurement can be applied over small length-scales. Relevant but attainable significant length-scales include composite fermion mean-free-paths for the various composite particle constructions throughout the magnetic field spectrum. These length-scales are dependent upon the sample quality such that higher mobilities will typically allow a larger conductance probe to examine the correlation effects. The specific correlations will present different length-scales: composite fermion mean-free-path at filling factor 1/2 is substantially larger than the mean-free-path of the 5/2 state precursor particle at high temperatures. We will present here various probes recently used to try to access these small length scale effects. The various techniques will be reviewed and the complicating factors for these probes will be discussed, in addition to prospects for improved examination of relative small correlation energy states.

**10:36**
**G46 14 High Frequency Magneto Oscillations in low Electron Density GaAs/AlGaAs Quantum Wells** Y.-W. TAN, *Phys. Dept., Columbia Univ.* H. L. STORMER, *Phys. Dept., Appl. Phys. and Math. Dept., Columbia Univ., and Bell Labs* L. N. PFEIFFER, K. W. WEST, *Bell Labs* We have observed exceptional magneto oscillations in modulation doped GaAs/AlGaAs quantum well structures with low (10%) Al barriers. These reproducible, rapid oscillations appear in our low density samples ($n \sim 6.5 \times 10^{10}/cm^2$) after standard illumination and are robust against thermal cycling. They are periodic in itinverse magnetic field (1/B) and the amplitude increases with temperature up to $\sim 600mK$. With increasing temperature, these oscillations shift from the $\nu \sim 1/2$ range towards the $\nu \sim 1/3$ range of the underlying, low density 2DES. Some aspects are reminiscent of recent work by G. A. Csáthy et al. (PRL, **92**, 256804(2004)) Under tilt, these oscillations follow the standard $\cos\theta$ behavior of a 2D system. The period, if naively translates into density, yields $1.4 \times 10^{13}/cm^2$, which significantly outnumbers all countable carriers in the device. A backside gate affects the QHE in the 2DES as well as the rapid oscillations, although the density shifts for the latter are highly incompatible with dimensions and screening considerations.

**10:48**
**G46 15 Linear magnetoresistance in a high quality two-dimensional electron system** W. PAN, *Sandia National Labs* H.L. STORMER, *Columbia University and Bell Labs, Lucent Technologies* D.C. TSUI, *Princeeton University* L.N. PFEIFFER, K.W. BALDWIN, K.W. WEST, *Bell Labs, Lucent Technologies* In a high quality two-dimensional electron system of density $n \sim 1 \times 10^{11}$ cm$^{-2}$ and mobility $\mu \sim 10 \times 10^6$ cm$^2$/Vs, at the temperature ($T$) of 1.2K, the diagonal magnetoresistance, $R_{xx}$, shows a strictly linear magnetic ($B$) field dependence, except for sharp spikes at $B$- fields where the integer quantum Hall effect develops. As $T$ is lowered to $\sim$ 35 mK, the main feature of $R_{xx}$ is now dominated by multiple minima and peaks, due to the formation of integer and fractional quantum Hall states. However, when plotting $R_{xx}$ at the even-denominator fillings ($\nu = 1/4$, 1/2, 3/4, and 3/2) as a function of $B$ field, the same linear $B$ field dependence is recovered. Interestingly, this linear magnetoresistance cannot be understood under the composite fermion model. Rather, it can be explained in terms of a slight, unintentional electron density gradient in our sample: Practically all $R_{xx}$ features can be reproduced quantitatively through $R_{xy}$. We will discuss the implications of this finding.



**SESSION H1: QUANTUM INFORMATION, CONCEPTS AND COMPUTATION**
**Tuesday Morning, 14 March 2006; Ballroom IV, Baltimore Convention Center at 11:15**
**Barry Sanders, University of Calgary, presiding**

**11:15**
**H1 1 Recent progress in trapped-ion quantum information processing.***
RAINER BLATT, *University of Innsbruck*

Trapped strings of cold ions provide an ideal system for quantum information processing. The quantum information can be stored in individual ions and these qubits can be individually prepared, the corresponding quantum states can be manipulated and measured with nearly 100% detection efficiency. With a small ion-trap quantum computer based on two and three trapped Ca+ ions as qubits we have generated in a pre-programmed way genuine quantum states. These states are of particular interest for the implementation of an ion quantum register: we have demonstrated selective read-out of single qubits and manipulation of single qubits of the register conditioned on the read-out results. Moreover, entangled states of up to eight particles were generated using an algorithmic procedure and the resulting states were analyzed using state tomography proving genuine multi-partite entanglement. With a new cavity QED setup we create an ion-qubit to photon-qubit interface for interconnecting ion-trap based quantum computers. With this device a source of deterministically generated single photons can be built and atom-photon entanglement can be investigated.

*This work is supported by the Austrian Science Fund (FWF), by the European Commission (QGATES, CONQUEST) and in parts by ARDA and ARO.

**11:51**
**H1 2 Quantum optics and quantum information processing with solid state systems.**
YOSHIHISA YAMAMOTO

A single semiconductor quantum dot embedded in a monolithic microcavity with a large spontaneous emission enhancement (Purcell) factor is capable of producing identical single photons on demand. Those single photons realize a multi-particle interference effect as quantum mechanically indistinguishable particles. Various quantum phenomena, such as violation of Bell's inequality and quantum teleportation, can be demonstrated with only such single photons and linear optics. An important challenge for quantum information system applications is to replace a man-made quantum dot by a natural substitutional donor impurity with suppressed inhomogeneous linewidth and electron/nuclear spin capability. In this talk we will discuss the recent experimental progress on this new quantum dot system.

**12:27**
**H1 3 Direct Observation of Atomic Number Squeezing in a Degenerate Bose Gas.**
MARK RAIZEN, *The University of Texas at Austin*

I will discuss recent work in my group on many-body quantum control towards the creation of atomic Fock states. In our rubidium experiment, a single Bose-Einstein condensate is optically trapped in crossed TEM01 modes, and we achieve confinement in two dimensions that is comparable to an optical lattice, but with single-atom addressability and detection. Using this system we have directly observed sub-Poissonian atom number statistics for a degenerate Bose gas with numbers as small as 20 atoms. The number squeezing was produced by starting with a Bose-Einstein condensate in an optical box trap and slowly lowering the walls in one dimension, a process we call quantum evaporation. The final atom number is determined by the energy of the N-body state in the box and can be precisely controlled. The observed squeezing is nearly a factor of two below the Poissonian (shot noise) limit. More importantly, known sources of noise can account for the residual fluctuations, so our results are consistent with the production of N-body Fock states. I will discuss the current limit to Fock state creation for even smaller numbers which we believe is due to many-body quantum tunneling. This effect can be controlled by the use of carefully tailored optical potentials and experiments are in progress. I will also discuss applications of our system to quantum computing and to the study of quantum critical phenomena.

**13:03**
**H1 4 General properties of Nonsignaling Theories.***
NICOLAS GISIN, *Geneva University*

We present a series of properties, usually associated to quantum physics, and show that they are common to all theories that do not allow for superluminal signalling and predict violation of Bell inequalities. These include intrinsic randomness, no cloning, monogamy of correlations, uncertainty relations, privacy of correlations, bounds on the shareability of some states. Finally, we emphasize that correlation data must violate some Bell inequality in order to contain distillable secrecy and introduce a new QKD protocol and prove its security against any individual attack by an adversary only limited by the no-signalling condition.

*Co-authors: Antonio Acin, Lluis Masanes and Valerio Scarani

**13:39**
**H1 5 Quantum control and robust quantum information.**
BIRGITTA WHALEY, *Department of Chemistry, University of California, Berkeley*

Controlling the time evolution of quantum states and quantum logic operations in an optimal manner gives rise to various desiderata depending on the physical constraints. In addition to fidelity optimization with respect to systematic and environmental errors, there may be requirements to optimize with respect to time or energy. We describe several approaches to control of logic operations on quantum bits that illustrate these different aspects, including both analytic and numerical tools. Applications are made to high fidelity quantum operations on solid state quantum bits.



## SESSION H2: SPIN LIQUIDS IN 2D FRUSTRATED QUANTUM MAGNETS
**Tuesday Morning, 14 March 2006; Ballroom III, Baltimore Convention Center at 11:15**
**Matthew Fisher, University of California, Santa Barbara, presiding**

**11:15**
**H2 1 Phase diagram of the 2D frustrated quantum magnet $Cs_2CuCl_4$ in applied field.**
RADU COLDEA, *University of Bristol, UK*

We use neutron scattering, magnetization and specific heat to probe how the ground state of the 2D spin-1/2 anisotropic triangular lattice antiferromagnet $Cs_2CuCl_4$ evolves as a function of applied magnetic field. We observe that the zero-field incommensurate spin spiral is suppressed by relatively small in-plane fields giving way to a commensurate 2D antiferromagnetic pattern stable over most of the intermediate field region, with incommensurate order appearing again for a narrow field range just below ferromagnetic saturation. The commensurate phase is not captured by a classical mean-field approach, suggesting that quantum fluctuations may be important in stabilizing this type of order.

**11:51**
**H2 2 Algebraic vortex liquid in spin-1/2 triangular antiferromagnets: Scenario for $Cs_2CuCl_4$.**
JASON ALICEA, *University of California, Santa Barbara*

Motivated by inelastic neutron scattering data on $Cs_2CuCl_4$, we explore spin-1/2 triangular lattice antiferromagnets with both spatial and easy-plane exchange anisotropies, the latter due to an observed Dzyaloshinskii-Moriya interaction. Exploiting a duality mapping followed by a fermionization of the dual vortex degrees of freedom, we find a novel ''critical'' spin-liquid phase described in terms of Dirac fermions with an emergent global SU(4) symmetry minimally coupled to a non-compact U(1) gauge field. This ''algebraic vortex liquid'' supports gapless spin excitations and universal power-law correlations in the dynamical spin structure factor which are consistent with those observed in $Cs_2CuCl_4$. We suggest future neutron scattering experiments that should help distinguish between the algebraic vortex liquid and other spin liquids and quantum critical points previously proposed in the context of $Cs_2CuCl_4$.

**12:27**
**H2 3 Spin liquid and Mott transition in organics with triangular lattice.**
KAZUSHI KANODA, *Department of Applied Physics, University of Tokyo*

The layered organics, k-(ET)2X, are model systems for the study of strongly correlated half-filled-band electrons. The Mott insulator k-(ET)2Cu2(CN)3 has a nearly isotropic triangular lattice and is a model system of frustrated quantum spins. The 1H and 13C NMR experiments show no indication of magnetic ordering down to 30 mK in spite of an exchange interaction of 250 K deduced from the susceptibility analysis. The spins are in the quantum liquid state. Under magnetic fields, an anomalous inhomogeneous spin state appears. Under pressure, it undergoes Mott transition to a Fermi liquid which shows superconductivity at low temperatures. The phase diagram and the nature of the superconductivity emerging from the spin liquid are also discussed.



**13:03**
**H2 4 Spinon Fermi sea state as a candidate spin liquid in $\kappa$-$(ET)_2Cu_2(CN)_3$.**
OLEXEI MOTRUNICH, *Kavli Institute for Theoretical Physics, University of California-Santa Barbara*

Experimental studies of the quasi-two-dimensional organic compound $\kappa$-$(ET)_2Cu_2(CN)_3$ strongly suggest a spin liquid state in the insulating phase at ambient pressure. This material is modelled as a half-filled triangular lattice Hubbard system close to the Mott transition. By applying trial wave function approach to an effective spin Hamiltonian with significant ring exchanges, it is proposed that a spin liquid state with spinon Fermi surface is realized in this system. Properties of this state are reviewed and compared with experiments. Further experiments find that an inhomogeneous spin state is induced by strong magnetic field. It is argued that the origin of this anomalous response is magneto-orbital effects, whereby spinons see significant orbital field and have strong back action on the internal gauge field. The spin liquid ground state itself is readjusting in the magnetic field, possibly in a discontinuous manner in an ideal system; this persists in a broad temperature range and may be responsible for the inhomogenuous state in the real system.

**13:39**
**H2 5 Spin excitations in frustrated Kagomé lattice systems.**
YOUNG LEE, *MIT, Department of Physics*

We present experimental results on the behavior of interacting spins on the two-dimensional frustrated Kagomé lattice. Basic concepts of geometrical frustration will be reviewed, and measurements on single crystal and powder samples of ideal Kagomé systems (both classical and quantum) will be described. For a system with S=5/2, our inelastic neutron scattering measurements of the spin wave excitations reveal a novel ''flat mode'' which is a direct consequence of the high degree of frustration. We observe interesting behavior related to spin chirality (both vector and scalar). Recently, we have performed measurements on a material with spin-1/2 ions in an ideal Kagomé lattice arrangement. We discuss our results in relation to the excitations proposed for novel quantum spin liquid states.

**SESSION H3: SOFT INTERFACES**
**Tuesday Morning, 14 March 2006; Ballroom I, Baltimore Convention Center at 11:15**
**Thomas Powers, Brown University, presiding**

**11:15**
**H3 1 A few Landau-Levich films.**
DAVID QUERE, *College de France*

We describe a few situations which produce a Landau-Levich films, such as the withdrawal of a solid plate out of a bath of wetting liquid or the air withdrawal by a jet plunging in a bath of liquid. We show why such antagonist situations can be described by similar arguments. We also discuss the shape and the stability of the film, and the way it bursts, in particular when it is surrounded by a viscous environment. Other contributors to this work: Etienne Reyssat, Jens Eggers and Elise Lorenceau

**11:51**
**H3 2 Humps, Spouts & Tendrils: Topological Transition Driven by Viscous Flow.**
WENDY ZHANG, *University of Chicago*

Viscous flows with large-scale spatial gradients can create small-scale structure on a steady-state interface separating two liquids. Here we focus on how an axisymmetric large-scale withdrawal flow in one liquid can break the interface between two liquids and thereby entrain a second liquid. Above the entrainment transition, thin spouts or tendrils of entrained liquid that persist over time form. Below the entrainment transition, the interface is deflected upwards by the flow and can form a hump with a strongly curved tip. To understand what mechanism allows a large-scale withdrawal flow to create small-scale feature on an initially flat interface, we analyze two simple scenarios. First, we consider the hump formed on an interface separating immiscible liquids. As the entrainment transition is approached from below, the minimum radius of curvature at the hump tip is determined by the maximum interface deflection height. Second, we consider the steady-state tendril formed on an interface between two miscible liquids. Again, the tendril radius is determined by the zero-entrainment deflection height of the interface.

**12:27**
**H3 3 Surfactant mass transfer effects on drop detachment.***
KATHLEEN STEBE, *Chemical and Biomolecular Engineering Department, Johns Hopkins University*

When a buoyant viscous drop is injected into a viscous fluid, it evolves to form a distended shape that detaches via the rapid formation and pinching of a neck. The effects of surfactants in altering this process are studied numerically. In the absence of surfactants, surface contraction is fastest in the vicinity of the neck. When surfactants are present, they accumulate there and alter the ensuing dynamics by reducing the surface tension that drives the contraction. When surfactant adsorption-desorption is very slow, interfaces dilute significantly during drop expansion, and drops form necks which are only slightly perturbed in their dynamics from the surfactant-free case. When adsorption-desorption dynamics are comparable to rate of expansion, a family of drop necks are predicted. Drops break at the primary neck at low surfactant coverage, at both the primary and secondary necks at moderate coverages, only at the secondary neck at higher coverages, or fail to neck at elevated coverages. When adsorption-desorption kinetics are rapid, the surface remains in equilibrium with the surrounding solution, and drops break like surfactant-free drops with a uniform surface tension. A map of neck/no-neck thresholds is constructed as a function of surfactant coverage and sorption dynamics, suggesting that drop detachment can be used as a means of characterizing surfactant dynamics. Co-authors: Mr. Fang Jin, Prof. Nivedita Gupta.

*This research was supported by NASA NCMR (Grant number NCC3-812).

**13:03**
**H3 4 Bubble microstreaming: Force focusing on lipid membranes.**
SASCHA HILGENFELDT, *ESAM and Mechanical Engineering, Northwestern University*

Ultrasound-driven oscillating microbubbles at container walls excite steady streaming flows of surprising speed that can be directed and controlled by patterning of the substrate. This new kind of microfluidics is simple to set up and does not need microchannels to guide flow transport. Hydrodynamic forces are locally focused around the oscillating bubbles and can be used to deform and rupture soft objects, such as the lipid membranes of vesicles and cells. We demonstrate these processes in experiment and quantify the stress exerted onto soft objects in the flow, investigating small and large deformations. We point out applications in bio-MEMS and biomedical studies of cellular response to hydrodynamic stimuli.

**13:39**
**H3 5 Topographies and Instabilities in Surfactant Monolayers.**
AJAY GOPAL

This abstract was not received electronically.

**SESSION H4: PHYSICS FOR EVERYONE AND DEPLETION FORCES IN VITRO AND OUT OF EQUILIBRIUM**
**Tuesday Morning, 14 March 2006; 308, Baltimore Convention Center at 11:15**
**Ivan Schuller, University of California, San Diego, and John Crocker, University of Pennsylvania, presiding**



**11:15**
**H4 1 The Physics Force- Physics for ages 6 to 106.**
E. DAN DAHLBERG, *University of Minnesota, School of Physics and Astronomy, Minneapolis, MN 55455*

The Physics Force is a very successful and entertaining outreach program of the Institute of Technology in the University of Minnesota developed to make science exciting and fun for students of all ages, from 6 to 106. Although all attendees, including high school and college students and guests from retirement homes, praise our performances, the primary focus is on K-6 students. The original Force consists of six k-12 teachers, Hank Ryan, Jon Barber, Jack Netland, Fred Orsted, Aaron Pinski, and Jay Dornfeld and Dan Dahlberg of the University of Minnesota Physics Department. The Force performed variations of The Physics Circus, our most popular show, at Disney's Epcot Center, parts of it were shown on Newton's Apple and several of us have performed demonstrations on the Knoff-Hoff Show, a very successful German T.V. science program. The goal of The Physics Force is to show students and the public **Science is Fun, Science is Interesting, and Science is Understandable**. By all measures we have available, we are extremely successful in reaching our goals. In the last three year cycle of our University support almost 100,000 residents of Minnesota (or about 2% of the total population) saw a Physics Force performance; it appears we will surpass those numbers in the present cycle.

**11:51**
**H4 2 The Science of Optics; The History of Art.***
CHARLES FALCO, *University of Arizona*

Recently, renowned artist David Hockney observed that certain drawings and paintings from as early as the Renaissance seemed almost ''photographic'' in detail. Following an extensive visual investigation of western art of the past 1000 years, he made the revolutionary claim that artists even of the prominence of van Eyck and Bellini must have used optical aids. However, many art historians insisted there was no supporting evidence for such a remarkable assertion. I will show a wealth of optical evidence for his claim that Hockney and I subsequently discovered during an unusual, and remarkably productive, collaboration between an artist and a scientist. I also will discuss some of the implications this work has for the history of science as well as the history of art. These discoveries convincingly demonstrate optical instruments were in use – by artists, not scientists – nearly 200 years earlier than commonly thought possible, and account for the remarkable transformation in the reality of portraits that occurred early in the 15th century. http://www.optics.arizona.edu/ssd/FAQ.html.

*This work done in collaboration with David Hockney.

**12:27**
**H4 3 Science as Performance: A Proactive Strategy to Communicate and Educate Through Theater, Music and Dance.***
BRIAN SCHWARTZ, *The Graduate Center of the City University of New York*

Theater, music, dance, the literary and the visual arts can convey the joys and controversies of science. We describe a program at the Graduate Center entitled Science as Performance which is designed to communicate to the public the excitement and wonder of science, technology, engineering and mathematics. Over the past few years there have been major successes in communicating science to the public through the arts. This is especially evident in theater and film with such recent plays as Copenhagen and the Oscar winning film A Beautiful Mind. The performance series Science and the Arts has been developed and tested at the Graduate Center of the City University of New York (CUNY) in mid-Manhattan for more than four years, see http://web.gc.cuny.edu/sciart/. We have developed working relationships with actors, playwrights, dancers, choreographers, musicians, composers, artists and scientists who work at the intersection of science and the arts. In this presentation we will illustrate many of our collaborations in theater, dance, music and art. The response to the series has shown that the arts can make the sciences accessible, relevant, and exciting to diverse

audiences in ways that provide both scientific content and significant artistic and entertainment values. The National Science Foundation has awarded a grant to the Graduate Center to help replicate similar Science and the Arts programs on other campuses by involving both their science departments and their performing arts departments. Some results of campus visits will be described. The author will also describe his involvement with producing two musical versions of a play, Einsteins Dreams based on the novel by Alan Lightman. One production opened at the Teatro da Trindade in Lisbon, Portugal at on October 21, 2005 for a four month run and a second and different production opens at the Prince Music Theater in Philadelphia in March 2006.

*Supported in part by the National Science Foundation, NSF PHY-0431660

**13:03**
**H4 4 Entropically Driven Helix Formation.**
YEHUDA SNIR, *University of Pennsylvania*

We model the folding of helices via the depletion interaction between a semi-flexible tube and hard spheres. We find that the lowest-entropy geometry of the tube depends on both the concentration and size of the spheres. In the limit of small spheres, the helix becomes optimally tight, that is, maximally thick for a fixed length. We discuss this effect when both the tube and spheres are confined in a cylinder, as a model of the ribosomal channel. The depletion interaction alone forces the tube to lie against the wall, as opposed to the tight helix. Hydrophobicity and electrostatics can stabilize the compact tube and we estimate the strength of these effects necessary to favor a tight helix.

**13:39**
**H4 5 Phase Behavior, Structure, and Assembly of Microsphere-Nanoparticle Mixtures.**
JENNIFER LEWIS, *University of Illinois*

The phase behavior, structure, and assembly of microsphere-nanoparticle mixtures have been investigated. A new mechanism for regulating the stability of colloidal particles, known as nanoparticle haloing, has been identified in binary mixtures that possess both high charge and size asymmetry. Negligibly charged colloidal microspheres, which flocculate when suspended alone in aqueous solution, undergo a remarkable stabilizing transition upon the addition of critical volume fraction of highly charged nanoparticle species. Using confocal microscopy, we have characterized the structural evolution of colloidal phases formed during sedimentation on patterned and non-patterned substrates as a function of varying composition. Through nanoparticle engineering, we have created robust colloidal crystals that can be harvested from solution without introducing drying related defects as well as colloidal gels whose structure and rheological properties vary dramatically.



## SESSION H5: FORUM: WHAT HAS ACTUALLY CHANGED IN PHYSICS DEPARTMENTS IN THE SITUATION FOR WOMEN, GRADUATE STUDENTS AND OTHER PEOPLE?

**Tuesday Morning, 14 March 2006; 309, Baltimore Convention Center at 11:15**
**Anthony Nero, Lawrence Berkeley National Laboratory, presiding**

**11:15–14:15**

The decade of the 90's was a period of intense scrutiny of climate issues in physics departments, e.g. the status of women, the job situation for new Ph.D.'s and postdocs, and the preparation of physicists for careers inside and outside of physics. There were many conference sessions on these topics, and both APS members and leadership instigated important efforts to focus on specific areas. These efforts included the program of visiting committees to departments to examine the situation for women by the Committee on the Status of Women in Physics, the AIP's various studies of a statistical nature, and the creation by the APS of a Committee on Careers and the Forum on Graduate Student Affairs, as well as the recent APS-AAPT task force on graduate education. This forum—patterned after similar sessions 10 years ago—will examine how physics departments have changed as a result of such efforts. It will begin with short (12-minute) talks by a panel of experts to describe what has happened in key areas. The greater part of the session will be a period of observations, questions, and discussion from the audience and the panel together. The purpose is to have an interchange

on these interrelated topics from which we can all learn.

Chair: Anthony Nero, Lawrence Berkeley National Laboratory.

**Patrick Mulvey**, AIP. Changes in graduate enrollment, composition, and subsequent jobs.

**Rachel Ivie**, AIP. Women in physics and astronomy departments 2005.

**David Campbell**, Boston University. Changes in graduate curricula and environment.

**Margaret Murnane**, University of Colorado-Boulder. The CSWP site visits to physics departments—what's been accomplished and learned.

**Kate Kirby**, Harvard-Smithsonian Center for Astrophysics. Survey of ethical issues in physics departments and the physics profession: results and reactions.

**Anne Catlla**, Duke University. Physics departments from the point of view of younger physicists.

**The bulk of the session will be a public forum, on these and related issues, among the audience and the panel.**

## SESSION H6: THE RESPONSE OF EXTENDED SYSTEMS TO ELECTRICAL AND MAGNETIC FIELDS: NOVEL, THEORETICAL, AND COMPUTATIONAL METHODS

**Tuesday Morning, 14 March 2006; 310, Baltimore Convention Center at 11:15**
**Nicola Marzari, Massachusetts Institute of Technology, presiding**



**11:15**
**H6 1 Orbital Magnetization in Periodic Insulators.***
TIMO THONHAUSER, *Rutgers University*

Recent years have seen a surge of interest in issues of charge and spin transport in magnetic materials and nanostructures, including anomalous Hall and spin Hall effects. In this context, it is quite surprising that the theory of orbital magnetization has remained in a condition similar to that of the polarization before the early 1990s, when the problem of computing finite polarization changes was solved by the introduction of the Berry-phase theory.[1] The essential difficulty, that the matrix elements of the position operator $\mathbf{r}$ are not well-defined in the Bloch representation, could be overcome by reformulating the problem in the Wannier representation. In order to derive an analogue theory for the orbital magnetization, we again work in the Wannier representation and assume a periodic insulator with broken time-reversal symmetry, vanishing (or commensurate) magnetic field, and zero Chern numbers. We show that by replacing the dipole operator $\mathbf{r}$ with the circulation operator $\mathbf{r} \times \mathbf{v}$, only one contribution to the magnetization is found, i.e., the magnetization associated with the internal circulation of bulk-like Wannier functions. The missing contribution arises from net currents carried by the Wannier functions at the boundary of the sample. We prove that both contributions can be expressed as bulk properties in terms of Bloch functions in a gauge-invariant way.[2] Our expression for the orbital magnetization is verified by comparing numerical tight-binding calculations for finite and periodic samples. Possible extensions to metals or insulators with non-zero Chern numbers will also be discussed.

*In collaboration with Davide Ceresoli, David Vanderbilt, and R. Resta.

[1]R. D. King-Smith and D. Vanderbilt, Phys. Rev. B **47**, 1651 (1993).
[2]T. Thonhauser, Davide Ceresoli, David Vanderbilt, and R. Resta, Phys. Rev. Lett. **95**, 137 205 (2005).

**11:51**
**H6 2 Spin Transport in Metals and Semiconductors.***
ALLAN H. MACDONALD, *University of Texas at Austin*

I will discuss a number of recent issues connected with spin-dependent transport in metals, semiconductors, and molecules with an emphasis on circumstances in which sophisticated electronic structure calculations can help achieve qualitative understanding. The specific topics that I will mention the anomalous Hall effect in ferromagnetic metals and semiconductors, the spin Hall effect, giant magnetoresistance and spin-torques in circuits containing antiferromagnetic metals, and current induced magnetization dynamics in transport through magnetic molecules.

*Supported by DOE grant DE-FG03-02ER45958

**12:27**
**H6 3 Ab Initio Calculations in a Uniform Magnetic Field Using Periodic Supercells.**
WEI CAI, *Stanford University*

This abstract was not received electronically.

**13:03**
**H6 4 Linear and Non-Linear Dielectric Response of Periodic Systems from Quantum Monte Carlo.**
PAOLO UMARI, *Department of Materials Science and Engineering, MIT, Cambridge, MA 02139, USA*

We present a novel approach that allows to calculate the dielectric response of periodic systems in the quantum Monte Carlo formalism. We employ a many-body generalization for the electric enthalpy functional, where the coupling with the field is expressed via the Berry-phase formulation for the macroscopic polarization. A self-consistent local Hamiltonian then determines the ground-state wavefunction, allowing for accurate diffusion quantum Monte Carlo calculations where the polarization's fixed point is estimated from the average on an iterative sequence. The polarization is sampled through forward-walking. This approach has been validated for the case of the polarizability of an isolated hydrogen atom, and then applied to a periodic system. We then calculate the linear susceptibility and second-order hyper-susceptibility of molecular-hydrogen chains whith different bond-length alternations, and assess the quality of nodal surfaces derived from density-functional theory or from Hartree-Fock. The results found are in excellent agreement with the best estimates obtained from the extrapolation of quantum-chemistry calculations. P. Umari, A.J. Williamson, G. Galli, and N. Marzari Phys. Rev. Lett. **95**, 207602 (2005).

**13:39**
**H6 5 Non-linear response of infinite periodic solids to homogenous electric fields and collective atomic displacements.**
PHILIPPE GHOSEZ, *Universite de Liege, Departement de Physique*

The non-linear response of infinite periodic solids to homogenous electric fields and cooperative atomic displacements will be discussed in the framework of density functional perturbation theory. The approach is based on the 2n + 1 theorem applied to an electric field dependent energy functional. We will focus on the non-linear optical susceptibilities, Raman scattering efficiencies and electrooptic coefficients. Different formulations of third-order energy derivatives will be examined and their convergence with respect to the k-point sampling will be discussed. The method will be applied to conventional semiconductors and to ferroelectric oxides. In the latter case, we will also describe how the first-principles results can be combined to an effective Hamiltonian approach in order to provide access to the temperature dependence of the optical properties. This work was done in collabration with M. Veithen and X. Gonze and was supported by the VolkwagenStiftung, FNRS-Belgium and the FAME-NoE.



## SESSION H7: NANOPORE BIOPHYSICS
**Tuesday Morning, 14 March 2006; 307, Baltimore Convention Center at 11:15**
**Xinsheng Sean Ling, Brown University, presiding**

**11:15**
**H7 1 Interaction of DNA and Proteins with Single Nanopores.***
J.J. KASIANOWICZ, *NIST, EEEL, Gaithersburg, MD 20899-8120*

The bacterial toxins Staphylococcus aureus alpha-hemolysin and itBacillus anthracis protective antigen kill cells in part by forming ion channels in target membranes. We are using electrophysiology, molecular biology/protein biochemistry and computer modeling to study how biopolymers (e.g., single-stranded DNA and proteins) bind to and transport through these nanometer-scale pores. The results provide insight into the mechanism by which these toxins work and are the basis for several potential nanobiotechnology applications including ultra-rapid DNA sequencing, the sensitive and selective detection of a wide range of analytes and high throughput screening of therapeutic agents against several anthrax toxins. In collaboration with V.M. Stanford, M. Misakian, B. Nablo, S.E. Henrickson, NIST, EEEL, Gaithersburg, MD; T. Nguyen, R. Gussio, NCI, Ft. Detrick, MD; and K.M. Halverson, S. Bavari, R.G. Panchal, USAMRIID, Ft. Detrick, MD.

*Supported in part by NIST, NIST ATP and NSF.

**11:51**
**H7 2 Force measurements on a DNA molecule inserted into a solid-state nanopore.**
CEES DEKKER, *Delft University of Technology*

Single nanometer-sized pores (nanopores) in an insulating membrane are an exciting new class of nanosensors for rapid electrical detection of and actuation on single biomolecules. I will report (i) our fabrication of solid-state nanopores and translocation measurements of single dsDNA molecules through these pores, and (ii) our recent demonstration of measurements of the force acting on a single DNA molecule that is inserted in the nanopore. Ad (i): Siliconoxide nanopores are fabricated with single nanometer precision and direct visual TEM feedback. Translocation of double-strand

DNA is monitored in the conductance of a voltage-biased pore. We find that DNA molecules can pass the pore both in a straight linear fashion and in a folded state. On molecules with a length from 3,000-100,000 base pairs, we observe a power-law scaling of the translocation time versus length, which we attribute to an effect of the hydrodynamic drag on the section of the polymer outside the pore. Measurements of DNA translocation at various salt concentrations reveal a crossover from a high-salt regime where current dips are seen, to a low-salt regime where current enhancements are observed. Ad (ii) For force measurements during the voltage-driven translocation of DNA and RNA, we have added an optical tweezer to our setup. With the tweezer, we hold a bead with a DNA molecule attached. Upon insertion of the DNA into the nanopore, the induced bead deflection yields a measure of the local force that acts on the DNA in the pore. The magnitude of the force involved is of fundamental importance in understanding and exploiting the translocation mechanism, yet so far has remained unknown. We obtain a value of 0.24 +/- 0.02 pN/mV for the force on a single DNA molecule, independent of salt concentration. Our data allow the first direct quantitative determination of the effective DNA charge of 0.53 +/- 0.05 electrons per base pair, corresponding to a 73% reduction of the bare DNA charge. Our novel single-molecule technique for local force sensing and actuation bears great promise for biophysical studies, e.g. for the study of DNA-protein binding or unfolding of RNA.

**12:27**
**H7 3 Protein unraveling through a single protein nanopore.**
LIVIU MOVILEANU, *Syracuse University*

The ability to respond to an external stimulus is a fundamental process in living systems. Based on this principle, we were able to design an unusual temperature-responsive pore-based nanostructure with a single movable elastin-like-peptide (ELP). The peptide is placed within the cavity of the alpha-Hemolysin protein pore. The temperature-dependent properties of single engineered pores were monitored by single-channel current recording in planar lipid bilayers. If a voltage bias was applied, the engineered pores exhibited transient current blockades, the nature of which depended on the length and sequence of the inserted ELP. These blockades are associated with the peptide excursions into the narrowest region of the pore. At low temperatures, the ELP is fully expanded and blocks reversibly and completely the pore. At high temperatures, the ELP is dehydrated and structurally collapsed, thus enabling a substantial ionic flow. Potential applications of this nanostructure in several arenas will be discussed.



**13:03**
**H7 4 Detecting Single DNA and Proteins Using a Solid-state Nanopore Device.**
JIALI LI, *Physics Department, University of Arkansas, Fayetteville, AR72701*

Charged single proteins and DNA molecules can be detected as they are driven through a solid-state nanopore by an applied electric field. The solid-state nanopores are fabricated in a free standing silicon nitride membrane using low energy noble gas ion beams. We demonstrate the silicon nitride nanopore based sensor can measure the properties of single molecules of proteins, double stranded DNA, and single stranded DNA molecules at different temperature, pH, and ionic strength. This technique allows us to discriminate between different types of molecules, different conformations of the same molecules, and also determine the configuration of individual molecules as well as their configuration distribution. We demonstrate the silicon nitride nanopore sensing system is robust and capable of detecting structural information of protein and DNA at extreme conditions.

**13:39**
**H7 5 Microscopic Kinetics of DNA Translocation through Synthetic and Biological Nanopores.**
ALEKSEI AKSIMENTIEV, *University of Illinois at Urbana-Champaign*

Using highly focused electron beams, artificial pores of nanometer diameters can be manufactured in ultra-thin silicon membranes with a sub-nanometer precision. A trans-membrane voltage bias can drive DNA strands through such pores; the resulting electrical signals can be recorded. As the diameter of the pore as well as the thickness of the silicon membrane can be made to match precisely the dimensions of a DNA nucleotide, the electrical signals produced by the interaction of DNA with the pore were proposed to contain information about the DNA sequence. In order to relate the DNA sequence to the measured electrical signals we characterized DNA conformations inside the pore through molecular dynamics simulations. A typical simulated system included a patch of a silicon membrane dividing electrolyte solution into two compartments connected by the nanopore. External electrical fields induced capturing of the DNA molecules by the pore from the solution and subsequent translocation. To calibrate our methodology, we carried out MD simulations of DNA translocation through an $\alpha$-hemolysin channel suspended in a lipid bilayer. Our results suggest that the rate-limiting step for DNA translocation through narrow synthetic pores is not the actual transit of DNA, but rather the search for such initial conformation that facilitates subsequent translocation. At the same time, hydrophobic adhesion of DNA

bases to the pore walls may considerably slow down or halt DNA translocation. We observed a threshold electric field for translocation of double stranded DNA through pores smaller in diameter than a DNA double helix occurring due to the overstretching transition at load forces of $\sim$ 60 pN. In narrow pores, DNA bases were observed to tilt collectively towards the 5'-end of the strand, which explains experimentally observed directionality of single stranded DNA in the transmembrane pore of $\alpha$-hemolysin.

**SESSION H8: FOCUS SESSION: JAMMING IN GLASSES, GRAINS, AND GELS I**
**Tuesday Morning, 14 March 2006**
**314, Baltimore Convention Center at 11:15**
**Andrea Liu, University of Pennsylvania, presiding**

*Contributed Papers*

**11:15**
**H8 1 Random-Packing Dynamics in Dense Granular Flow** MARTIN Z. BAZANT, CHRIS H. RYCROFT, KENNETH KAMRIN, *Department of Mathematics, MIT* The jamming transition of disordered hard spheres has attracted much recent attention, but how do slightly less dense random packings flow? Here, we propose a simple mechanism based on diffusing ''spots'' of free volume, which cause correlated displacements of neighboring particles. A multiscale algorithm, alternating between coarse-grained spot dynamics and microscopic particle relaxation, can produce realistic flowing packings, and yet is also convenient for mathematical analysis of mean flow and diffusion. We apply the model to granular drainage from a silo and fit three basic parameters (spot size, volume, and diffusivity) to brute-force simulations by the discrete-element method. For a wide silo, we find that the spot simulations can largely reproduce the dynamics of 100,000 frictional, visco- elastic spheres in the DEM simulations, while running over 100 times faster, although a general model for the spot dynamics in different geometries is still lacking. This may come from a stochastic reformulation of Mohr-Coulomb plasticity, where spots undergo random walks along slip planes.

**11:27**
**H8 2 Contact Numbers in 2D Granular Systems*** MATTHIAS SPERL, TRUSHANT MAJMUDAR, ROBERT BEHRINGER, *Duke University* There exists a critical density below which a granular system is no longer mechanically stable. Above this threshold, the particles form stable contacts with each other, while below there are no permanent contacts. We introduce a method to determine the number of contacts per particle with high accuracy: Using stress induced birefringence to identify contact points, the critical density can be identified with an uncertainty of 0.5%. For a binary mixture of frictional disks we find a discontinuous transition in the number of contacts per particle from zero to a value around 2.5; the transition point is located at an area fraction of 0.845. For higher densities, the increase in the contact number is compatible with a square-root law; however, different exponents close to 0.5 cannot be ruled out yet. At the same transition point, the average force in the system increases linearly with density.

*Support: NSF-DMR0137119, NSF-DMS0244492, and DFG-SP714/3-1

**11:39**
**H8 3 A hydrodynamic view on elasticity** ANAËL LEMAîTRE, *Institut Navier – France* LAURENTIU PASOL, *LadHyX – France* XAVIER CHATEAU, *Institut Navier – France* Considerable attention was drawn in the recent years on the non-affine displacement fields that accompany elastic deformation of non-crystalline materials. These non-affine displacements bring order unity corrections to the sound speed and Lamé constants that would be estimated using the traditional Born-Huang approximation. Bearing on standard homogenization tools and a compatibility theorem, we provide a simple analytical framework to write exact expressions for the elastic constants. We show that, in the thermodynamic limit, exact microscopic expressions reduce to integrals over the pair correlation function. We next show that the corrective terms may be further reduced to a simple integral involving the Green function of the disordered packing. This brings hope to be able to devise systematic procedures to estimate the real elastic constants of amorphous solids.

*Invited Papers*

**11:51**
**H8 4 Non-affine elasticity in jammed systems.**
CRAIG MALONEY, *Johns Hopkins University, Dept. of Physics and Astronomy; UC Santa Barbara, KITP*

Symmetry dictates that perfect crystals should deform homogeneously, or *affinely*, under external load, and computing the elastic moduli from the underlying interaction potential is then straightforward. For disordered materials no such simple procedure exists, and recent numerical works have demonstrated that non-affine corrections can dramatically reduce the naive expectation for the shear modulus in a broad class of disordered systems and may control rigidity loss in the zero pressure limit in purely repulsive systems, i.e. the unjamming transition (c.f. [O'Hern et al. PRE 68, 011306 (2003)]). We present numerical results and an analytical framework for the study of these non-affine corrections to the elastic response of disordered packings.

*Contributed Papers*

**12:27**

**H8 5 Effects of Nonaffinity on Jammed Materials*** DANIEL VERNON, ANDREA J. LIU, TOM LUBENSKY, *Department of Physics and Astronomy, University of Pennsylvania* If an amorphous solid such as a jammed particle system is subjected to an external stress, the induced displacements of internal particles are necessarily nonaffine. Using numerical minimization procedures, we investigate the response to stress of a disordered packing of purely repulsive spheres. We calculate the correlations of the nonaffine part of the displacements of individual particles just above the jamming threshold (point J)[1]. We find that these correlations are consistent with those predicted by a continuum theory and verified numerically in simple model random elastic systems[2].

*Work supported by the NSF through grant DMR 04-04670.

[1]C.S. O'Hern, L.E. Sibert, A.J. Liu, and S.R. Nagel, Phys. Rev. E **68**, 011306 (2003)
[2]B. DiDonna and T.C. Lubensky, Phys. Rev. E (to be published)

**12:39**

**H8 6 Compactivity measurements for a bidimensional granular** FREDERIC LECHENAULT, *CEA* FREDERIC DACRUZ, OLIVIER DAUCHOT, *CEA SPEC* ERIC BERTIN, *Department of Theoretical Physics, University of Geneva* We investigate experimentally the statistical properties of the free volumes inside a bidimensional granular packing. Having in mind the more general issue of the measure of intensive thermodynamical parameters in out-of-equilibrium systems, we propose an experimental procedure to access the compactivity of the packing from the free volume distributions over clusters of grains, varying the size of the cluster. Our main result is that the logarithm of the probability to find a given free volume in a cluster scales in a nonextensive way. The compactivity of the packing is then extracted from the corresponding scaling function for two different kinds of grains, and two levels of compaction.

**12:51**

**H8 7 How does friction affect the distribution of mechanically stable disk packings?*** ERIK BROWN, *Department of Physics, Yale University* GUO-JIE GAO, JERZY BLAWZDZIEWICZ, *Department of Mechanical Engineering, Yale University* COREY O'HERN, *Departments of Mechanical Engineering and Physics, Yale University* In recent work (*Physical Review E* **71** (2005) 061306), we generated nearly all of the mechanically stable packings in small systems composed of up to 20 bidisperse frictionless disks that interact via normal forces. Complete enumeration allowed us to decompose the probability distribution $P(\phi)$, for obtaining a mechanically stable state at packing fraction $\phi$ into algorithm-dependent and independent contributions, $\beta(\phi)$ and $\rho(\phi)$. $\rho(\phi)$ is the probability density to obtain a distinct mechanically stable packing at $\phi$, while $\beta(\phi)$ is the frequency with which each distinct state occurs. In the present study, we add frictional interactions between grains that vanish when the particles are rest. We will compare distributions of mechanically stable packings in systems with and without friction. In particular, we will comment on whether a well-defined random loose-packed state exists in 2D.

*We acknowledge support from NSF Grant DMR-044883.

**13:03**

**H8 8 Jamming as a critical phenomenon: A field theoretical approach** SILKE HENKES, BULBUL CHAKRABORTY, *Brandeis University* The proposed jamming diagram (Nature **396**, 21 (1998)) features a special point, termed point J, along the packing fraction axis where the jamming transition is sharp. Recent simulation work (PRE **68**, 011306 (2003)) has shown that point J has some features of a critical point. To model the jamming transition along the packing fraction axis, a field theory of frictionless, zero-temperature grain packings in two dimensions has been constructed (PRL **95**, 198002 (2005)). A mean-field theory involving two order parameters, $\langle\phi\rangle$, the average force per contact, and $\langle z\rangle$, the deviation of the average contact number from its isostatic value, predicts a transition from a jammed to an unjammed phase. The transition is of mixed order with a jump in $\langle\phi\rangle$ and divergent fluctuations. Current work focuses on application of this formalism to simulation data. This allows for the study of spatial fluctuations of $\phi$ and attempts are made to relate these to the concept of force chains. The $\phi$-field emerges as an excellent tool for data analysis and allows quantification of the structures seen in granular packings. Work supported by NSF-DMR 0403997.

**13:15**

**H8 9 Emergence of a critical scale in jamming of frictional grains** ELLAK SOMFAI, *University of Leiden and University of Oxford* MARTIN VAN HECKE, WOUTER ELLENBROEK, WIM VAN SAARLOOS, *University of Leiden* We probe the characteristic scale of two-dimensional frictional granular media close to the jamming transition by studying their vibrational properties as function of the applied pressure $P$ and friction coefficient $\mu$. The density of vibrational states exhibits a crossover from a plateau at frequencies $\omega > \omega^*(P,\mu)$ to a linear growth for $\omega < \omega^*(P,\mu)$. Both for large and for zero friction, this characteristic frequency $\omega^*$ vanishes when $P$ is lowered towards zero. For moderate friction, however, $\omega^*$ saturates at a finite value for $P \downarrow 0$. We show that $\omega^*$ is proportional with $\Delta z$, the excess number of contacts per grains relative to the minimally allowed, isostatic value, and that only for zero and infinitely large friction, systems at the jamming threshold have $\Delta z \to 0$ and hence are critical.

**13:27**

**H8 10 Granular dynamics in compaction and stress relaxation** PING WANG, *City College of New York* JASNA BRUJIC, *Schlumberger Doll Research* CHAOMING SONG, *City College of New York* DAVID JOHNSON, OLIVIER SINDT, *Schlumberger Doll Research* HERNAN MAKSE, *City College of New York* LEVICH INSTITUTE AND PHYSICS DEPARTMENT, CITY COLLEGE OF NEW YORK, NEW YORK, NY 10031 COLLABORATION, SCHLUMBERGER DOLL RESEARCH, OLD QUARRY ROAD, RIDGEFIELD, CT 06877 COLLABORATION, Elastic and dissipative properties of granular assemblies under uniaxial compression are studied both experimentally and by numerical simulations. Following a novel compaction procedure at varying oscillatory pressures, the stress response to a step-strain reveals an exponential relaxation followed by a slow logarithmic decay. Simulations indicate that the latter arises from the coupling between damping and collective grain motion predominantly through sliding. We characterize an analogous ''glass transition'' for packed grains, below which the system shows aging in time-dependent sliding correlation functions.

**13:39**
**H8 11 Jamming in Quasi-One Dimensional Systems** PRASANTA PAL, *Department of Applied Physics, Yale University* COREY O'HERN, *Department of Mechanical Engineering, Department of Physics, Yale University* We study the dynamics of hard rods undergoing Brownian motion in narrow channels. Our system is in the shape of a ''figure-8'' and composed of a horizontal and a vertical channel that intersect. In our preliminary studies, we allow the particles to switch at the ends of the channels, but not at the intersection. We calculate the mean-square displacement (msd), the residence time that a particle spends in the intersection, and other important dynamical quantities as a function of the density of rods and system size. In contrast to purely one-dimensional systems, we find that the figure-8 system jams (i.e. the msd possesses a plateau at long times) above a characteristic density that increases with system size. In addition, we have studied the effects of a biasing field on the dynamics and find that the jamming transition is pushed to much lower densities than at zero field. We also compare our results to those found in model glass-forming liquids in two and three dimensions.

**13:51**
**H8 12 Voronoi Volumes in Dense Granular Flow** CHRIS H. RYCROFT, MARTIN Z. BAZANT, *Department of Mathematics, MIT* The concept of free volume in amorphous materials has a long history, including void-based theories of viscous flow (Eyring 1936), the glass transition (Turnbull and Cohen 1957), and granular drainage (Mullins 1972), although it has become clear that particle displacements are highly correlated and not mediated by single-particle voids. Recently, we have shown that dense random packings can be made to flow cooperatively at nearly uniform density by diffusing ''spots'' of influence and find good agreement with discrete-element (DEM) simulations of frictional spheres in the case of granular drainage. Spots are presumed to carry a slight excess of interstitial volume, but verifying this would require tracking changes in local volume fraction of only a few percent. In flowing random packings, this is a significant computational challenge, which we address here by computing the evolving Voronoi tesselation with an efficient new algorithm. We study the distribution of local Voronoi volumes in simulations of granular drainage using the spot model and DEM and observe some intriguing differences. The Voronoi volume also provides a sensitive measure of whether a given region is ''liquid-like'' of ''solid-like'' in dense granular flow.

**14:03**
**H8 13 Correlated Dynamics in Dense Granular Flow** SHUBHA TEWARI, *Mount Holyoke College* ALLISON FERGUSON, BULBUL CHAKRABORTY, *Brandeis University* We report on studies of dense, gravity-driven granular flow via simulations of two-dimensional, inelastic, bidisperse hard disks in a vertical tube geometry. We analyze the flow in terms of coarse-grained velocity and stress fields. We find that as the flow rate decreases towards jamming, there is an increase in the timescale over which stress autocorrelations decay. While the spatial correlations of the stress do not increase significantly, there is a marked increase in the spatial correlation of the velocity, which is indicative of an increasing length scale that approaches the system size as the flow rate decreases. We further analyze the flow in terms of two different four-point correlation functions of the stress and the velocity analogous to those used to characterize dynamical heterogeneities in supercooled liquids. These allow us to extract a dynamical length scale as well as a relaxation time for this system.



## SESSION H10: FOCUS SESSION: FRONTIERS IN COMPUTATIONAL CHEMICAL PHYSICS I
**Tuesday Morning, 14 March 2006; 302, Baltimore Convention Center at 11:15**
**Eugene Mele, University of Pennsylvania, presiding**

***Invited Papers***

**11:15**
**H10 1 A Revisit to Soliton Theory.**
XI LIN, *MIT*

Our recent studies on the soliton theory of conjugated polymers, via Hubbard model and first-principles computations, reveal two subtle points concerning electron-electron correlation and electron-phonon coupling. Significant three-dimensional conformational changes and a sequence of self-localized electronic states are identified and attributed to the presence of soliton. The soliton-induced conformational deformations provide an intrinsic high strain-rate actuation mechanism in optical excitation processes, while the sensitivity of new self-localized states to the presence of local fields provides a high-resolution sensing mechanism for ions and radicals.

***Contributed Papers***

**11:51**
**H10 2 Auxiliary field quantum Monte Carlo with a localized basis−applications to atoms and molecules*** WISSAM A. ALSAIDI, SHIWEI ZHANG, HENRY KRAKAUER, *College of William and Mary* We extended the recently introduced phaseless auxiliary field quantum Monte Carlo approach [1] to any single-particle basis, and applied it to study atoms and molecules using localized Gaussian basis. This method maps the interacting many-body problem into a linear combination of non-interacting problems using a complex Hubbard-Stratonovich transformation, and controls the phase/sign problem using a trial wave function. It employs a random walk approach in Slater determinant space to project the many-body ground state of the system. The computational cost scales as a low power of system size. In all of the presented results the trial wave function was from a Hartree-Fock calculation. The obtained total energies of the atoms and molecules agree to within a few milli Hartrees with the exact value from full configuration interaction or density matrix renormaliza-

tion group. The results are comparable in accuracy to those of CCSD(T) for equilibrium geometries but are superior for bond breaking. [1] S. Zhang and H. Krakauer, Phys. Rev. Lett. **90**, 136401 (2003).

*Supported by ONR and DOE/CMSN.

**12:03**

**H10 3 Monte Carlo Studies of Soft Pentagonal Rotors and Polymer Self-Assembly** MICHAEL WINOKUR, *University of Wisconsin* MARCUS MUELLER, *Georg August Universitaet* Side chain substitution is widely used in $\pi$-conjugated polymers to promote processibility and reduce interchain aggregation. However this functionalization also creates diverse materials that self-organize at molecular length scales. Small modifications in the chemical architecture often produce large variations in the observed structures and phase behavior. An example of this is poly(9,9-bis(2-ethylhexyl)fluorene) (PF2/6) in which single chains form helices that subsequently undergo a supramolecular self-assembly to give a three chain unit cell or, equivalently, a $\sqrt{3} \times \sqrt{3}$ superlattice. Direct structure studies indicate that PF2/6 incorporates a heterogeneous sequence of conformational isomers approximating a 5-fold helix and this construction defines the overall shape of the chain. In terms of more conventional polymers we consider PF2/6 to be representative of a sparse brush with, on average, a columnar type structure. However PF2/6 structure studies already indicate that the potential is not uniformly cylindrical because of the 5-fold helix and the spontaneous formation of a 3 chain unit cell. Through construction of a representative ansatz Hamilton we have mimicked the interaction between soft pentagonal shaped rotors. Monte Carlo calculations employing this Hamiltonian identify a range of parameters that reproduce the experimentally observed $\sqrt{3} \times \sqrt{3}$ superlattice. Moreover we find that small changes in this orientational pair potential strongly alter the phase behavior.

**12:15**

**H10 4 Particle-Hole Corrections for Accurate DFT-based Charge Transfer Energetics** TUNNA BARUAH, *University of Texas at El Paso* M. PEDERSON, *Naval Research Laboratory* Density functional theory (DFT) is primarily a ground state theory because it lacks a rigorous prescription for the calculation of excited states. However, a formalism due to Theophilou showed that a Hohenberg-Kohn like theorem is extendable to an ensemble of ground and excited states provided the states are mutually orthogonality. This condition is also a necessary for a variational approach to individual excited states as shown by Levy. We present a way for obtaining accurate single-electron excitation energies from the ground-state Hamiltonian and orbitals. Our approach explicitly guarantees mutual orthogonality and removes spurious interactions between the electron and hole states. The method yields excellent results for inert gas atoms, closed-shell atoms and molecules, and to charge transfer systems such as the dissociated Na-Cl molecule and a 50 nm long organic molecule containing 200 atoms. Initial applications rely entirely upon standard GGA functionals but the approach is equally amenable to any mean-field method such as Hartree-Fock or DFT with SIC.

**12:27**

**H10 5 Low Energy Inelastic Helium Atom Scattering from Monolayers** L.W. BRUCH, *Department of Physics, University of Wisconsin-Madison* F.Y. HANSEN, *Department of Chemistry, Technical University of Denmark* A time-dependent wave packet calculation for inelastic low energy helium atom scattering (HAS) by a physisorbed monolayer[1] is extended to much longer propagation times by adding an absorbing potential at large distances. This enables a treatment of transiently trapped helium atoms for He/Xe/Pt(111) and shows that the lifetimes are in the range 10-30 ps. The scattering of the wave packet is essentially complete when the propagation is terminated. Systematic trends for an experiment on a Xe/Pt(111) monolayer[2] are discussed. The remarkable inelastic intensity for the shear horizontal (SH) monolayer branch is predicted to be strongly enhanced for incident energies in the range 4 to 6 meV, somewhat below the 8.2 meV energy used in most of that experiment.

[1]L. W. Bruch and F. Y. Hansen, J. Chem. Phys. **122**, 114714 (2005)
[2]L. W. Bruch, A. P. Graham, and J. P. Toennies, J. Chem. Phys. **112**,314 (2000)

*Invited Papers*

**12:39**

**H10 6 A time-dependent density functional theory approach for the excited state dynamics of nanostructures and biomolecules.***

RUBIO ANGEL, *Dpto. Fisica de Materiales, Facultad de Quimicas, U. Pais Vasco, San Sebastian and European Theoretical Sepctroscopy Facility (ETSF)*

We will review the recent implementations of TDDFT to study the optical absoprtion of biological chromophores, one-dimensional polymers and layered materials. In particular we will show the effect of electron-hole attraction in those systems. We will folow two routes: one based on solving the Bethe-Salpeter equation and the other on an orbital-dependent OEP method on top of the GW approximation for the self-energy. Virtues and deficiencies of both methods will be illustrated.

*Work done in collaboration with A. Castro, M. Marques, L. Wirtz, A. Marini, M. Gruning, L. Wirtz and D. Varsano and supported by the NANOQUANTA network of excellence and the Humboldt Foundation under the Bessel research award (2005).

*Contributed Papers*

**13:15**

**H10 7 Energetic, structural and vibrational properties of carbon monoxide on transition-metal surfaces: a linear-response approach to the energy puzzle** ISMAILA DABO, *MIT* ANDRZEJ WIECKOWSI, *UIUC* NICOLA MARZARI, *MIT* We have studied the energetic, structural and vibrational properties of carbon monoxide adsorbed on platinum and platinum-ruthenium surfaces using density-functional theory within the generalized-gradient approximation (GGA) and its molecular U variant (GGA + molecular U) introduced by Kresse *et al. [Phys. Rev. B 68, 73401 (2003)]*. Our study puts in evidence that the GGA frequency predictions for the C-O stretching mode are in excellent agreement with spectroscopic measurements. This agreement is made more remarkable by the generally-poor performance of standard exchange-correlation functionals which fail even in predicting the most stable adsorption site for CO on platinum. It is also shown that the molecular U correction to the electronic hybridizations and adsorption energies does not affect the excellent accuracy of the GGA vibrational-property predictions. Based on the linear-response approach proposed by Cococcioni and de Gironcoli *[Phys. Rev. B 71, 35105 (2005)]*, we provide a theoretical justification for this observation. The accurary of density-functional theory in predicting accurate vibrational spectra while paradoxically failing in determining correct adsorption energies is also discussed.

**13:27**

**H10 8 y-induced chaotic Whispering Gallery modes** ARACELI GONGORA-TREVINO, *UNAM, Mexico and Northeastern USA* STUART SCHAFFNER, *Northeastern University* JORGE JOSE, *SUNY at Buffalo* A free particle inside a circular billiard bouncing elastically from the boundary produces classically bounded caustic orbits and Whispering Gallery (WG) modes in the quantum case. If a sector is taken out from the circle, forming a Pacman-like billiard, the classical caustic orbits remain. However, in the quantum case the WG modes have fractional quantum angular momentum described by Bessel functions of fractional order. In this work we have considered the case when the straight walls of the Pacman are not fixed in time but oscillate periodically or non-periodically. The structure of the WG modes changes; there are cases where the WG mode intensity increases significantly in certain spatial locations when compared with the situation in the Pacman stationary case. This intensity increase is analyzed in detail, and it may be implemented and tested in the type of micro-cavity used in quantum dot lasers.

**13:39**

**H10 9 A generalization of the charge equilibration method** RAZVAN A. NISTOR, JELIAZKO G. POLIHRONOV, MARTIN H. MUSER, NICK J. MOSEY, *Department of Applied Mathematics, University of Western Ontario* Charge-equilibration (C-Eq) methods are an efficient means of calculating the effective partial charges of the atoms in molecules. The aim of obtaining the partial charges is to reconstruct the electrostatic field of a molecule, which then may be used as an accurate replacement to *ab initio* interatomic potentials. However, the inability of the C-Eq method to consistently predict the correct charges for a wide range of molecular geometries has limited its potential use in molecular simulations. A generalization to a split charge (split-Q) formalism, where the semi-empirical fit parameters are defined not in terms of atom-type, but in terms of bond-type, greatly improves the quality, and more importantly, the transferability of the fits. The flexible formalism of the split-Q approach allows for a number of generalizations over traditional C-Eq methods at the cost of additional fit parameters in the model. However, the split-Q approach can reproduce the charges on a variety of different molecules containing H, C, O, and Si, up to three times more accurately than previous methods when comparing to *ab initio* calculations.

**13:51**

**H10 10 Atomization energies using analytic density functional theory*** RAJENDRA ZOPE, *George Washington University, Washington DC* BRETT DUNLAP, *US Naval Research Laboratory, Washington DC* Our recent formulation of analytic and variational Slater-Roothaan (SR) method uses Gaussian basis sets to express the molecular orbitals, electron density and the one-body effective potential of density functional theory. It allows arbitrary scaling of the exchange potential around each atom in heteroatomic systems. We examine the performance of the SR method for atomization energies using values of Slaters scaling parameters determined from the Hartree-Fock and the exact total atomic energies. We also present another set of scaling parameters for atomization energies. The performance of the computationally efficient SR method for the atomization energies of a set of 148 molecules using this third set of parameters is comparable to that of the Perdew-Burke-Ernzerhof generalized gradient approximation.

*The Office of Naval Research, directly and through the Naval Research Laboratory, and the DoD's High Performance Computing Modernization Program, through the Common High Performance Computing Software Support Initiative, Project MBD-5, supported this work

**14:03**

**H10 11 Comparison of two simple models for high frequency friction: Exponential vs. Gaussian wings** STEVEN ADELMAN, *Purdue University* We describe new methods for ruling out unphysical forms for the high frequency friction $\lim_{\omega\to\infty}\beta(\omega)$ needed to compute vibrational energy relaxation times. These are based on the fluctuating force autocorrelation function($faf$) $C(t) = \langle\tilde{\mathfrak{J}}^2\rangle_0^{-1}\langle\tilde{\mathfrak{J}}(t)\tilde{\mathfrak{J}}\rangle_0$, which is proportional to the Fourier transform of $\beta(\omega)$. Here we compare two model faf's $C_{se}(t) = \mathrm{sech}\,(t/\tau)$ and $C_{ga}(t) = \exp[-\frac{1}{2}(t/\tau)^2]$. These give respective high frequency frictions which have incompatible exponential and Gaussian forms. We apply our procedures to eliminate $C_{se}(t)$. We do this by showing from $\beta_{se}(\omega) \equiv \langle\mathfrak{J}^2\rangle_0/k_BT\int_0^\infty\cos\omega t C_{se}(t)dt$ that $\lim_{\omega\to\infty}\beta_{se}(\omega)$ derives from the long time ''tail'' of $C_{se}(t)$. We then note that $C_{se}(t)$ is built only from short time quantities, rendering the form of this ''tail'' artifactual. Thus the exponential form of $\lim_{\omega\to\infty}\beta(\omega)$, is also artifactual.

**SESSION H11: FOCUS SESSION: CHEMICAL AND SPECTROSCOPIC APPLICATIONS OF NONLINEAR OPTICS I**
**Tuesday Morning, 14 March 2006; 303, Baltimore Convention Center at 11:15**
**Peer Fischer, Harvard University, presiding**

*Invited Papers*

**11:15**
**H11 1 Second Harmonic and Sum Frequency Studies of Aqueous Interfaces.***
KENNETH EISENTHAL, *Columbia University*

Among the topics to be discussed are ultrafast electron transfer at aqueous/organic interface, method for measurement of the absolute orientation of molecules at interfaces, second harmonic imaging studies of live nerve cells, time permitting second harmonic studies of gold nanorods at the air/aqueous interface.

*I thank the National Science Foundation and Office of Basic Energy Sciences DOE

*Contributed Papers*

**11:51**
**H11 2 Ultrafast Vibrational Dynamics of Water Interfaces Probed by Sum-frequency Vibrational Spectroscopy*** JOHN A. McGUIRE, Y.R. SHEN, *Department of Physics, University of California and Material Sciences Division, Lawrence Berkeley National Laboratory, Berkeley, CA 94720* Using sum-frequency generation (SFG) as a surface-specific probe, we measured the ultrafast population and dephasing dynamics of excitations of OH-stretch modes of water at fused-silica/water interfaces. A tunable femtosecond IR pulse was used to pump the vibrational mode. Another independently tunable femtosecond IR pulse, after a time delay, was used to probe the vibrational excitation and then up-converted by SFG for detection. Experiments on the hydrophilic fused-silica/water interface reveal population relaxation of the hydrogen-bonded OH modes on time scales of 200-500 fs, more rapid on the red side than the blue side. The width of transient spectral holes produced by the IR pump pulse correspond to homogeneous dephasing times of $\sim$ 50 fs. Measurements of the dangling OH bonds at the hydrophobic silica/*n*-octadecyltrichlorosilane/water interface reveal a population relaxation time of about 1.2 ps.

*The work was supported by DOE

**12:03**
**H11 3 Phase-sensitive sum-frequency vibrational spectroscopy on water/vapor interfaces*** VICTOR OSTROVERKHOV, NA JI, CHAO-YUAN CHEN, YUEN-RON SHEN, *Department of Physics, University of California, Berkeley* Water/vapor interfaces are ideal hydrophobic interfaces relevant to many important applications. They have been studied extensively by sum-frequency vibrational spectroscopy (SFVS) in recent years. Unfortunately, different interpretations of the spectra from different research groups have led to a great deal of confusion. The problem arises because in conventional SFVS, only the magnitude of the spectrum is recorded. We present here a phase-sensitive (PS) SFVS study of water/vapor interfaces that captures both the magnitude and the phase of an interfacial vibrational spectrum. The results allow us to decompose unequivocally the various OH stretch peaks in the spectrum and the net polar orientations of the water species contributing to the peaks.

*This work was supported by NSF/STC Water CAMPWS (CTS-0120978) and by DOE.

**12:15**
**H11 4 Measuring solvation dynamics using sum-frequency cross-correlation frequency resolved optical gating (SF XFROG)*** NANCY LEVINGER, *Colorado State University* BENJAMIN LANGDON, *Colorado State University* Solvation dynamics has been used to measure the dynamical response of a solvent to an electronic perturbation. The response is typically followed through sum-frequency conversion of sample emission with short light pulses to time-resolve spectral shifting of a fluorescent probe molecule. In contrast to traditional fluorescence up-conversion techniques where the time resolved fluorescence signal is approximated from 10-15 different sum-frequency gated decays distributed across the fluorescence spectrum, sum-frequency cross-correlation frequency resolved optical gating offers the opportunity to determine the electric field of the sample fluorescence as a function of time. Dynamic quantities associated with changes in the sample emission, such as solvent relaxation, can then be obtained directly from the electric field without assumption of a particular spectral lineshape. We show that the time evolving phase of the SF XFROG signal corresponds to the solvent response function, $C(t)$, and that the technique also reveals details about vibrational modes associated with the relaxation.

*This material is based upon work supported by the NSF under Grant No. 0415260

**12:27**
**H11 5 Time- and Frequency-Domain Surface Spectroscopy of Polymers and Langmuir-Blodgett films** ANDREY BORDENYUK, HIMALI JAYATHILAKE, ALEXANDER BENDERSKII, *Wayne State University* We combine frequency- and femtosecond time-domain IR+visible Sum Frequency Generation (SFG) measurements for spectroscopic characterization of material surfaces. Vibrational quantum beats observed in Langmuir-Blodgett monolayers are demonstrated to be sensitive to the molecular order/disorder in the film, depending on the two-dimensional phase. Nearly vertical alignment of all-trans alkyl chains is observed in films transferred at high surface pressure, while at lower surface pressure, changes in chain tilt angle and onset of gauche-defects are observed. The time- and frequency-domain data are analyzed simultaneously based on optical Bloch equations, allowing to utilize the information redundancy for more

accurate determination of the spectral parameters. Polymer surfaces used as alignment layers in liquid crystal displays were investigated to elucidate how the mechanical rubbing affects the molecular orientation and conformation. Rubbing was found to induce pronounced azimuthal anisotropy of the alkyl side chain orientation, observed in the CH-stretch SFG spectra of the $CH_3$ and $CH_2$ groups. Orientational analysis of the SFG vibrational spectra as a function of azimuthal and tilt angles (in- and out-of-surface plane) of the polymer side chains shows their preferential tilt along the rubbing direction.

*Invited Papers*

**12:39**
**H11 6 Small Molecules and Sum Frequency Generation Probes of Nanoparticulate $TiO_2$.**
MARY JANE SHULTZ, *Tufts University*

Anatase $TiO_2$ is known to photo catalytically mineralize a wide variety of pollutants and pathogens, both airborne and in aqueous solution. One of the major benefits of basing water treatment systems on $TiO_2$ is that it is environmentally benign and so non toxic that it is used as a colorant in creamy salad dressing. The primary impediment to wide spread implementation of a $TiO_2$ based system for water decontamination is that the quantum efficiency in contact with condense phase water is less than 5%. Since the quantum efficiency for destruction of airborne materials is greater than 80%, the potential for increased efficiency is very real. To convert the potential to practice, the oxidation mechanism needs to be more fully understood. We will report on the results of using a nonlinear optical spectroscopy, sum frequency generation (SFG) as an itin situ probe of interactions at the $TiO_2$ surface. Results suggest that the dominant oxidation mechanism converts from a direct to an indirect mechanism as the water content (vapor pressure) increases. This presentation will discuss the probe technique as well as the results.

*Contributed Papers*

**13:15**
**H11 7 Molecular Adsorption on Nano Colloidal Particles Probed by Second Harmonic Generation** SHIH-HUI JEN, HAI-LUNG DAI, *Department of Chemistry, University of Pennsylvania, Philadelphia, PA 19104-6323* It is shown that second-harmonic generation (SHG), detected at 90 degree angle from the fundamental beam propagation direction, can be used to probe molecular adsorption on spherical nano colloidal particles with diameter as small as 50 nm. Measurements done with the malachite green dye adsorbed on polystyrene particles with diameters ranging from 50 to 250 nm show that the SHG signal from these surface adsorbed molecules tilts toward larger scattering angles when the particle size becomes smaller. This phenomenon can be rigorously described by the nonlinear Rayleigh-Gans-Debye theory and used for measuring the density and adsorption free energy of molecules adsorbed on nanometer size colloidal particles.

**13:27**
**H11 8 Spectrally- and Time-Resolved Sum Frequency Generation (STiR-SFG): a new tool for ultrafast hydrogen bond dynamics at interfaces.** ALEXANDER BENDERSKII, ANDREY BORDENYUK, CHAMPIKA WEERAMAN, *Wayne State University* The recently developed spectrally- and time-resolved Sum Frequency Generation (STiR-SFG) is a surface-selective 3-wave mixing (IR+visible) spectroscopic technique capable of measuring ultrafast spectral evolution of vibrational coherences. A detailed description of this measurement will be presented, and a noniterative method or deconvolving the laser pulses will be introduced to obtain the molecular response function. STiR-SFG, combined with the frequency-domain SFG spectroscopy, was applied to study hydrogen bonding dynamics at aqueous interfaces ($D_2O/CaF_2$). Spectral dynamics of the OD-stretch on the 50-150 fs time scale provides real-time observation of ultrafast H-bond rearrangement. Tuning the IR wavelength to the blue or red side of the OD-stretch transition, we selectively monitor the dynamics of different sub-ensembles in the distribution of the H-bond structures. The blue-side excitation (weaker H-bonding) shows monotonic red-shift of the OD-frequency. In contrast, the red-side excitation (stronger H-bonding structures) produces a blue-shift and a recursion, which may indicate the presence of an underdamped intermolecular mode of interfacial water. Effect of electrolyte concentration on the H-bond dynamics will be discussed.

**13:39**
**H11 9 Non-linear vibrational spectroscopies for characterizing thin films of semi-conducting polymers** MARC GURAU, *National Institute of Standards and Technology* ZACHARY SCHULTZ, DEAN DELONGCHAMP, BRANDON VOGEL, JOSEPH KLINE, YOUNGSUK JUNG, ERIC LIN, LEE RICHTER, CHEMICAL SCIENCE AND TECHNOLOGY LAB, NATIONAL INSTITUTE OF STANDARDS AND TECHNOLOGY TEAM, MATERIALS SCIENCE AND ENGINEERING LAB, NATIONAL INSTITUTE OF STANDARDS AND TECHNOLOGY TEAM, The ongoing development of conjugated polymer electronic materials has shown that alterations of the structure of these materials and the means of processing can lead to large variations in the performance observed. Continued growth in this field requires the development of new metrologies suited to the examinations of thin polymeric films on a variety of substrates. Spectroscopic characterization of the vibrational structure of these systems provides a non-destructive means of monitoring such changes. The work presented in this talk demonstrates the use of nonlinear optical broadband coherent anti-stokes raman spectroscopy (CARS) and broadband sum frequency generation (SFG) to monitor both the bulk and interfaces of ultra-thin ( $<$ 50 nm) semiconducting polymer films. SFG provides insight into order at the critical buried polymer/dielectric interface of thin-film transistors while CARS provides insight into chemical degradation of the films.

**13:51**
**H11 10 Ferroelectric domains in dipolar liquids observed by hyper-Rayleigh scattering.** DAVID SHELTON, *U. Nevada Las Vegas* Hyper-Rayleigh scattering (HRS) is a sensitive probe of polar modes in isotropic media. For the dipolar liquids water, acetonitrile, nitromethane and nitrobenzene the depolarized HRS

spectrum is observed to contain a narrow spike at zero frequency shift due to a polar collective mode with a relaxation time greater than 30 ns. This spike in the HRS spectrum is attributed to ferroelectric domains in the liquid. The spike disappears when dilution of a dipolar liquid with a non-polar liquid reduces the dipole coupling strength of the solution below the predicted ferroelectric threshold. The size and dipole order parameter for the ferroelectric domains have been determined from HRS spectra for binary solutions of dipolar molecules.

**14:03**

**H11 11 Surfaces of alcohol-water mixtures studied by sum-frequency generation vibrational spectroscopy** JAEHO SUNG, KYUNGSU PARK, DOSEOK KIM, *Department of Physics and Interdisciplinary Program of Integrated Biotechnology, Sogang University, Seoul 121-742 Korea* Sum frequency generation vibrational spectroscopy in the $CH_x$ stretch vibration range used to investigate the surface of binary mixtures of water and short chain alcohols (methanol, ethanol, and propanol) at the air/liquid interface. It was found that the sum frequency signals from mixtures at low alcohol concentration are larger than that of pure alcohols. For example, the signal from a propanol mixture surface at 0.1 bulk mole fraction was $\sim$ 3 times larger than that from a pure propanol surface. On the other hand, the ratio between the sum-frequency signals taken at different polarization combinations was found to be constant within experimental errors as the bulk alcohol concentration was changed. This suggested that the orientation of surface alcohol molecules does not vary appreciably with the change of concentration, and that the origin of the signal enhancement is mainly due to the increase in the surface number density of alcohol molecules contributing to the sum-frequency signal for the alcohol/water mixture as compared to the pure alcohol surface.



**SESSION H12: THIN FILM GROWTH AND INTERFACES**
**Tuesday Morning, 14 March 2006**
**304, Baltimore Convention Center at 11:15**
**Michael Scarpulla, University of California, Berkeley, presiding**

**11:15**

**H12 1 Imaging of ALD Grown W Atoms on $\alpha$-TiO2(110) by X-ray Standing Wave Fourier Inversion** CHANG-YONG KIM, *Northwestern University* JEFFREY ELAM, MICHAEL PELLIN, *Argonne National Laboratory* DIPAK GOSWAMI, STEVEN CHRISTENSEN, MARK HERSAM, PETER STAIR, MICHAEL BEDZYK, *Northwestern University* Supported metal oxides are among the most important of catalytic materials systems. However, there is a lack of experimental atomic-scale structural information for describing the relevant interfaces. We combine atomic layer deposition (ALD) and x-ray standing wave (XSW) atomic-imaging to address this challenge. As a first case, we determine the precise registry of W atoms on a rutile TiO2(110) surface. The ALD W layer was formed by first exposing the $TiO_2$ surface to disilane ($Si_2H_6$) and then to tungsten hexafluoride ($WF_6$). The direct-space image reveals that W occupies the Ti-site that would be occupied by Ti if the bulk structure were extended above surface. The tungsten atoms are vertically shifted upward from the ideal Ti-site location by +0.23 Å. These XSW measurements of ALD heterolayer growth clearly show for the first time that ALD conformal layers can be highly coherent with the substrate lattice. The ALD method for supported catalyst material preparation provides a bridge over the ''materials preparation gap'' that typically separates practical, high-surface-area and single crystal model catalytic materials.

**11:27**

**H12 2 Beating Effects on X-ray Reflectivity for Pulsed Laser Deposition of TiN** YEN-RU LEE, *Dep. of Physics, University of Illinois at Urbana-Champaign* AARON GRAY, *Dep. of Physics, University of Illinois at Urbana-Champaign* PETER CZOSCHKE, JON TISCHLER, *Solid State Division, Oak Ridge National Laboratory* HAWOONG HONG, *Frederick-Seitz Material Research Laboratory, University of Illinois at Urbana-Champaign* TAI-CHANG CHIANG, *Dep. of Physics, University of Illinois at Urbana-Champaign* We grew TiN on sapphire (0001) substrates by pulsed laser deposition (PLD). The growth was monitored, in situ, in real time by x-ray diffraction at the $(0,0,\frac{1}{2})$ anti-Bragg position using a synchrotron beam. The experiment was carried out at the UNICAT undulator beamline at the Advanced Photon Source. The measured x-ray intensity shows atomic-layer-resolved oscillations superimposed on a beating pattern with changing wavelength. Numerical modeling shows that the results can be well described in terms of an evolving island height distribution. Implications in regard to film structure and morphology will be discussed.

**11:39**

**H12 3 Characterization of Graphene Films and Ribbons on Silicon Carbide** TIANBO LI, ASMEROM OGBAZGHI, XUEBIN LI, ZHIMIN SONG, CLAIRE BERGER, WALT DE HEER, PHILLIP FIRST, *Georgia Institute of Technology* Ultrathin graphite films, 1-6 graphene layers thick, were grown on both the Si-terminated (0001) and C-terminated $(000\bar{1})$ faces of 4H- and 6H-SiC via thermal desorption of silicon in UHV. Through investigations of the thinnest films (monolayer graphene) by LEED and STM, we show the existence of a complex $\sqrt{3} \times \sqrt{3}R30°$ reconstructed layer between the lowest graphene layer and the SiC substrate. The $6\sqrt{3} \times 6\sqrt{3}R30°$ LEED pattern obtained after annealing above $1250°C$ can be explained predominantly by kinematic scattering from the slightly $6 \times 6$ corrugated graphene, from the reconstruction, and from the SiC substrate. Low-order double-scattering is required to explain all of the diffraction features. LEED and STM on graphene ribbons patterned from these films (80-400 nm width) show that graphene layers remain intact after photolithography and plasma etching.

**11:51**

**H12 4 A new work function measurement technique allowing simultaneous material deposition, and reflectivity measurements.*** B. J. HINCH, A.V. ERMAKOV, E. Z. CIFTLIKLI, S. E. SYSOEV, I. G. SHUTTLEWORTH, *Dept. of Chemistry and Chemical Biology, Rutgers University, Piscataway, NJ 08854.* We report on the application of a novel technique for relative work function measurements, of single crystal surfaces, employing grazing incidence electron reflection. This technique cannot suffer from photo or e- beam induced surface damage effects, and yet does enable free access to the surfaces for simultaneous deposition/evaporation, and/or application of other surface characterization methods. We discuss the optimization of experi-

mental parameters in this method, and demonstrate its application in concurrent measurements of helium atom reflectivity and work function changes, taking place during oxygen exposure of a Cu(001) surface. Observed work function changes reproduce well the trends seen in earlier polycrystalline film measurements. In addition, the work function changes indicate structural changes that are not apparent in helium atom scattering at oxygen exposures in excess of ~ 50L.

*NSF support acknowledged

**12:03**

**H12 5 Si/Cu Interface Structure and Adhesion** XIAO-GANG WANG, JOHN SMITH, *Delphi Research Labs* An *ab initio* investigation of the Si(111)/Cu(111) interfacial atomic structure and adhesion is reported [1]. Misfit dislocations appear naturally, as do hcp interfacial silicide phases that vary with temperature. The silicides form in the interface even at relatively low temperatures. These results are consistent with available experimental data. [1] Xiao-Gang Wang, John Smith, Physical Review Letters 95, 156102 (2005).

**12:15**

**H12 6 Modeling the formation of nanoscale pores in metal oxides during anodization** CHRISTINE SAMPLE, ALEXANDER GOLOVIN, *Northwestern University* A theory of the formation of nanoporous metal oxides grown by anodization is developed. Linear stability analysis of an oxide layer is performed for the case of field-dependent conductivity, and parameter regions are determined corresponding to the onset of instability and the growth of pores. It is shown that competition between the destabilizing effect of field-assisted dissolution and the stabilizing effect of surface energy provides the selection mechanism of the pore diameter. The weakly nonlinear evolution of the oxide layer is shown to be governed by the Kuramoto-Sivashinsky equation whose solutions exhibit spatio-temporal chaos. A system of strongly nonlinear long-wave equations describing the evolution far from the instability threshold is described. It's numerical solution illustrates the formation of deep pores.

**12:27**

**H12 7 Local field distribution near corrugated interfaces: Green function formalism versus effective medium theory** CHUN WING CHOY, JUN JUN XIAO, KIN WAH YU, *The Chinese University of Hong Kong* The Green function formalism (GFF) has been established recently [1,2] to study the local field electric field distribution near a periodic interface separating two homogeneous media of different dielectric constants. In GFF, the integral equations can be solved conveniently because of the existence of an analytic expression for the kernel (Greenian). However, due to a severe singularity in the kernel, the formalism was formerly applied to compute the electric fields away from the interface region [1,2]. In this work, we have been succeeded in extending GFF to compute the electric field inside the interface region, by taking advantage of a sum rule. To our surprise, the strengths of the electric fields are quite similar in both media across the interface, despite of the large difference in the dielectric constants. Moreover, we propose a simple effective medium approximation (EMA) to compute the electric field inside the interface region. We show that EMA can indeed give an excellent description of the electric field except near a geometric resonance. [1] K. W. Yu and Jones T. K. Wan, Comput. Phys. Commun. 142, 368 (2001). [2] H. F. Tam and K. W. Yu, Annual APS March Meeting, abstract Q31.009 (2002).

**12:39**

**H12 8 Textbook adsorption at non-textbook adsorption sites: alkali atoms on alkali halide surfaces** BO LI, ANGELOS MICHAELIDES, MATTHIAS SCHEFFLER, *Fritz-Haber-Institut der Max-Planck-Gesellschaft* Density-functional theory (DFT) and second order Møller-Plesset perturbation theory (MP2) calculations for F, Cl and Br adatoms on the (100) surfaces of NaF, NaCl and NaBr indicate that on these surfaces the halide adatoms adsorb preferentially above halide substrate sites, rather than above Na substrate sites as might be anticipated. Analysis of the electronic structures in each system reveals that this hitherto unheard of adsorption mode is stabilized by the formation of perfectly conventional covalent bonds between the halide adatoms and the halide substrate atoms. This finding has implications to, for example, alkali-halide crystal growth, atomic manipulation on insulator surfaces, and the design of accurate empirical potentials to describe insulator-adatom interactions.

**12:51**

**H12 9 Adsorption and desorption of hydrogen on Cu(111) and Xe-covered Cu(111).*** YIYAN FEI, XIANGDONG ZHU, *University of California at Davis* Using an optical ellipsometry technique to monitor adsorbate coverage in-situ, we studied activated adsorption of filament-heated molecular hydrogen on Cu(111) and the isothermal desorption of hydrogen adatoms from Cu(111). The adsorption follows a zeroth order kinetics such that the net sticking probability, though small, is independent of the hydrogen adatom coverage until a saturation coverage is reached. The desorption follows a second-order kinetics with an activation energy of 0.63 eV and a pre-exponential factor of $1 \times 10^9$/s. A pre-adsorbed monolayer of Xe atoms on Cu(111) prohibits subsequent adsorption of filament-heated molecular hydrogen, making physisorbed Xe useful templates for spatial patterning of hydrogen adatom density on Cu(111).

*This work is supported by a grant from Petroleum Research Fund, administered by American Chemical Society

**13:03**

**H12 10 Pattern formation of hydrogen adatom density on Cu(111) using patterns of xenon adatoms as templates.*** XIANGDONG ZHU, YIYAN FEI, *University of California at Davis* We formed grating-like patterns of hydrogen adatom density on Cu(111) by using complementary patterns of xenon adatom density as the template. The template was pre-formed by laser-induced thermal desorption of a Xe monolayer on Cu(111) using the interference pattern of two coherent laser pulses. The ''patterned'' surface was subsequently exposed to hot hydrogen molecules which dissociate and adsorb preferentially on the uncovered part of the surface. We removed the Xe template by laser-induced thermal desorption which left behind a grating-like hydrogen density pattern intact on Cu(111). By following the evolution of hydrogen density gratings on Cu(111) from 153 to 183 K with linear

optical diffraction, we found that the diffusion of hydrogen atoms on Cu(111) in this temperature range was characterized by an activation energy barrier $E_{diff}$ = 6.4 kcal/mol (or 279 meV) and a pre-exponential factor $D_0 = 2.0 \times 10^{-3}$ cm$^2$/sec.

*This work is supported by a grant from Petroleum Research Fund, administered by American Chemical Society.

**13:15**

**H12 11 CRDS Detection of HS Radical in HFCVD Diamond Thin Film** MADALINA BUZAINAU, VLADIMIR MAKAROV, GERARDO MORELL, BRAD WEINER, *UPR* In the present study, the HS radical was detected using the Cavity Ring Down Spectroscopic (CRDS) method in hot filament diamond CVD for the $CH_4$(0.4%)/$H_2$ mixture doped by $H_2S$ (400 ppm). The HS radical was detected both by the 0 - 0(A —X) and 1 - 0(A — X) transitions. The absolute absorption density spectrum of the HS radical was obtained as well as the absolute HS concentration estimation. This study proofs that the HS radical is an intermediate produced during the diamond CVD synthesis.

**13:27**

**H12 12 The CRDS method application for study of the gas-phase processes in the hot CVD diamond thin film.** VLADIMIR BUZAIANUMAKAROV, ARTURO HIDALGO, GERARDO MORELL, BRAD WEINER, MADALINA BUZAIANU, *UPR* For detailed analysis of problem related to the hot CVD carbon-containing nano-material growing, we have to detect different intermediate species forming during the growing process as well as investigate dependences of concentrations of these species on different experimental parameters (concentrations of the $CJH_4$, $H_2S$ stable chemical compounds and distance from the filament system to the substrate surface). In the present study, the HS and CS radicals were detected using the Cavity Ring Down Spectroscopic (CRDS) method in the hot CVD diamond thin film for the $CH_4$(0.4 %) + $H_2$ mixture doped by $H_2S$ (400 ppm). The absolute absorption density spectra of the HS and CS radicals were obtained as a function of different experimental parameters. This study proofs that the HS and CS radicals are an intermediate, which forms during the hot filament CVD process. The kinetics approach was developed for detailed analysis of the experimental data obtained. The kinetics scheme includes homogenous and heterogenous processes as well as processes of the chemical species transport in the CVD chamber.

**13:39**

**H12 13 A Density Functional Study of the Americium (001) Surface*** DA GAO, ASOK KUMAR RAY, *University of Texas at Arlington* Electronic structure properties of the fcc americium (001) surface, modeled by periodically repeated fcc Am (001) surface slabs, have been studied with the full-potential linearized augmented plane wave (FP-LAPW) method. The alternative basis set APW+lo is used inside the atomic spheres for chemically important orbitals that are difficult to converge, whereas LAPW is used for others. The core states are treated fully relativistically and for valence states, two levels of treatments are implemented: (1) a scalar relativistic scheme including the mass-velocity correction and the Darwin s-shift and (2) a fully relativistic scheme with spin-orbit coupling included in a second variational treatment using the scalar-relativistic eigenfunctions as basis. Our results indicate that the ground state of Am (001) surface is antiferromagnetic. The quantum size effects in the surface energies and the work functions of the (001) fcc americium ultra thin films (UTF) have been examined up to seven layers. In addition, the Am (001) surface properties are compared with our earlier study of the Am (111) surface.

*This work is supported by the Chemical Sciences, Geosciences and Biosciences Division, Office of Basic Energy Sciences, Office of Science, U. S. Department of Energy (Grant No. DE-FG02-03ER15409) and the Welch Foundation, Houston, Texas (Grant No. Y-1525)

**13:51**

**H12 14 A Density Functional Study of Carbon Monoxide Adsorption on (100) Surface of $\gamma$-Uranium** ASOK RAY, PRATIK DHOLABHAI, *University of Texas at Arlington* Adsorption of the CO molecule on the $\gamma$-U (100) surface has been studied at both non-spin-polarized and spin-polarized levels using the generalized gradient approximation to density functional theory (GGA-DFT) with Perdew and Wang (PW) functionals. The bridge position with the vert2 approach is found to be most favorable site with a chemisorption energy of 2.93eV for the non-spin-polarized case, and 3.19eV for the spin-polarized case. The distances of the carbon atom from the uranium surface are found to be 1.59Å and 1.72Å for the non-spin-polarized and spin-polarized cases, respectively. The inter-atomic distances between the carbon and oxygen atoms for the most favorable position are found to be 1.13Å and 1.21Å for the non-spin-polarized and spin-polarized cases, respectively. The magnetic moment for the most favorable site is found to be 0.04$\mu_B$ per atom. A significant charge transfer from the first layer of the uranium surface to the carbon and oxygen atoms is found to occur, implying that the bonding is partly ionic. Significant hybridization between the U 5*f* and CO 2*p* orbitals are also observed. This work is supported by the Chemical Sciences, Geosciences and Biosciences Division, Office of Basic Energy Sciences, Office of Science, U. S. Department of Energy (Grant No. DE-FG02-03ER15409) and the Welch Foundation, Houston, Texas (Grant No. Y-1525).

**14:03**

**H12 15 A Density Functional Study of Atomic Oxygen and Carbon Adsorptions on the (100) Surface of $\gamma$-Uranium*** PRATIK DHOLABHAI, ASOK RAY, *University of Texas at Arlington* Atomic oxygen and carbon adsorptions on the $\gamma$-U (100) surface have been studied using the generalized gradient approximation to density functional theory (GGA-DFT) with Perdew and Wang (PW) functionals. Different chemisorption sites at both non-spin-polarized and spin-polarized levels of theory have been thoroughly investigated. For O adsorption, the bridge position is the most favorable site with chemisorption energies of 7.887eV and 7.965eV for the non-spin-polarized and spin-polarized cases, respectively. The distances of the O adatom from the U surface are found to be 1.19Å and 1.22Å, respectively. For C adsorption, the center position is the most favorable site with a chemisorption energy of 7.816eV for the non-spin-polarized case, and 7.895eV for the spin-polarized case. The distances of the C adatom from the U surface are 0.62Å for the non-spin-polarized and 0.52Å for the spin-polarized cases. A study of the density-of-states (DOS) for O and C adsorbed uranium surfaces shows that the hybridization between U 5*f* orbitals and the O and C 2*p* orbitals is weak and

the bonding is primarily ionic. Comparisons with published results will be presented.

*This work is supported by the Chemical Sciences, Geosciences and Biosciences Division, Office of Basic Energy Sciences, Office of Science, U.S. Department of Energy and the Welch Foundation, Houston, Texas.

**SESSION H13: COLLOID AND POLYMER INTERFACES**
**Tuesday Morning, 14 March 2006**
**305, Baltimore Convention Center at 11:15**
**Hai-Lung Dai, University of Pennsylvania, presiding**

**11:15**
**H13 1 Confinement-induced restructuring of colloidal particles** YINGXI ELAINE ZHU, CINDY LEI, YANGHAI YU, PRASAD SARANGAPANI, *Department of Chemical and Biomolecular Engineering, University of Notre Dame* Packing configuration of colloidal particles in the bulk suspension is determined by interparticle interaction and volume fraction. However, many modern technological applications of colloidal suspensions entail applications of surface confinement and significantly modify the packing structure of colloidal particles. The effect of surface confinement on particle packing is yet poorly understood. We have custom designed a compression apparatus that is well equipped with a confocal microscope, allowing us to vary the gap spacing between two flat solid substrates confining colloidal suspension and image the 3-D microstructure of colloidal particles simultaneously. We observe enhanced layering of confined colloidal particles and a well-ordered 2D crystal structure of each layer formed after quasi-static compression. Surprisingly, we have also observed disordered layers of colloidal particles and the jamming of multi-layers against one another after rapid quench. These observations suggest the intriguing confinement-induced restructuring of dense colloidal suspensions, and provide a unifying perspective from which to pack the particles more efficiently than in bulk. In preliminary experiments, we have also studied the effect of surface chemistry and topography on the packing configuration of confined colloidal particles.

**11:27**
**H13 2 Wetting Behavior of Nitrous Oxide Near its Critical Point** ROBERT WEILER, MORDECAI WAEGELL, RAFAEL GARCIA, *Worcester Polytechnic Institute* A liquid is said to ''not wet'' a surface if its beads on it and thus exhibits a nonzero contact angle. However, if the liquid spreads out uniformly on the surface, with a contact angle of zero, then it is said to ''wet'' the surface. Given any liquid whatsoever that initially does not wet a surface, the Cahn theory [1] predicts that the liquid will eventually wet the surface as we increase the temperature and follow along the liquid-vapor coexistence line. For liquids on solid surfaces, the wetting transition, from non-wetting to wetting, is predicted to be first order and occur sharply at a wetting temperature Tw [2]. Tw can be calculated from our knowledge of interatomic potentials that characterize the adatom-adatom attraction and the adatom-surface attraction. The Cahn theory has been verified for non-polar liquids on solid surfaces but so far there exist no experiments for polar liquids. Nitrous Oxide is polar and has a critical point slightly above room temperature. We will report on initial experiments to verify the Cahn theory for this system. [1] J. W. Cahn, J. Phys. Chem. 66, 3667 (1977). [2] M. Gatica, X. Zhao, J. K. Johnson and M. W. Cole, J. Phys. Chem. B 108, 11704 (2004) and References Therein.

**11:39**
**H13 3 Effects of contact line hysteresis and surface tension on contact line pinning of inclined droplets.** VIATCHESLAV BEREJNOV, ROBERT E. THORNE, *Physics Department, Cornell University, Ithaca, NY, 14853-2501* The stability and pinning of drops on inclined surfaces is of fundamental and technological interest. Contact line dynamics depends on the properties of the liquid, the solid surface and the manner in which line motion is driven. Achieving reproducible final contact line and drop shapes is important in biotechnology applications where drops are used as mini-reactors, such as in structural genomics where sessile drops are used for protein and virus crystallization. We will describe experiments investigating pinning and deformation of drops containing pure liquids, proteins and colloids, placed on substrates with a range of surface treatments. Proteins affect contact angle hysteresis at low concentrations, and surface tension at high concentration, leading to two different regimes of pinning. Theoretical approaches that can be useful in understanding our results will also be presented.

**11:51**
**H13 4 Contact Line Pinning by Microfabricated Patterns** YEVGENIY KALININ, VIATCHESLAV BEREJNOV, ROBERT THORNE, *Cornell University* Interactions of the liquid-solid contact line with micrometer-sized features on solid surfaces can provide a method for controlling contact line stability and shape. We have investigated how the size, shape and chemical properties of regular features affect the contact angle and its hysteresis. Microfabrication techniques are used to create 4-50 micrometer-size patterns on otherwise homogeneous flat surfaces, and the relative importance of geometric and chemical factors are determined. We discuss applications to protein crystallization, and in particular show that the volumes, shape stability and shape reproducibility of 10-100 microliter aqueous drops containing proteins and surfactants can be greatly increased. Surface patterning provides greater reproducibility in crystallization outcomes and greater flexibility in the design of crystallization experiments.

**12:03**
**H13 5 The kinetic coefficient of hard-sphere crystal-melt interfaces from molecular-dynamics simulations** MAJEED AMINI, *Department of Physics, University of Kansas, Lawrence, KS 66045 USA* BRIAN LAIRD, *Department of Chemistry, University of Kansas, Lawrence, Kansas 66045 USA* The kinetic coefficient for a crystal melt interface, $\mu$, is the ratio of the interface growth velocity to the undercooling $(T_M - T)$, where $T_M$ is the melting point. In this work we determine the kinetic coeffiecient for the hard-sphere system by analyzing capillary fluctuations in interface position using molecular dynamics (MD) simulation [Hoyt *et al*, Mat. Sci. Eng. **R41**, 121-163 (2003)]. We report the kinetic coefficient for the three interfaces: (100), (110), and (111). Our results for $\mu_{100}$, $\mu_{110}$, and $\mu_{111}$ are 1.15(4) $(k_B/(mT_M))^{1/2}$, 0.85(6) $(k_B/(mT_M))^{1/2}$, and 0.57(8) $(k_B/(mT_M))^{1/2}$, respectively, which gives the relation $\mu_{100} > \mu_{110} > \mu_{111}$. This ordering is consistent with the recent results of MD simulations for a variety

of metals. The anisotropy ratios $\mu_{100}/\mu_{110}$, and $\mu_{100}/\mu_{111}$ are 1.35(11), and 2.0(3), respectively. We compare our results to those of classical density functional theory (DFT) of [Mikheev and Chernov, J. Cryst. Growth **112**, 591-596 (1991)].

**12:15**

**H13 6 Quasielastic neutron scattering study of the dynamics of 1,3-diphenylpropane grafted to the pore surface of MCM-41** EDWARD KINTZEL, KENNETH HERWIG, MICHELLE KIDDER, A.C. BUCHANAN, PHILLIP BRITT, *Oak Ridge National Laboratory* ALAN CHAFFE, *Monash University* An initial study of the dynamics of 1,3-diphenylpropane (DPP, $\equiv$ Si-O-$C_6H_4(CH_2)_3C_6H_5$) attached to the surface of the mesoporous silica MCM-41 has been carried out using quasielastic neutron scattering. Measurements of the elastic intensity were carried out in the temperature range 50-380 K and indicate a trend in DPP dynamics with changing grafting density and pore size. Full quasielastic scans over an energy range of $\pm$ 17 $\mu$eV were carried out at temperatures of 240 K, 280 K, and 320 K. Initial analysis employed a stretched exponential to model the Fourier transformed data in the time domain. An average relaxation time, defined as $< \tau > = (\tau/\beta)\Gamma(1/\beta)$ where $\beta$ is the stretched exponent in the model, shows a dependence on temperature, pore size, and DPP grafting density. Molecular dynamics simulations using a model for DPP grafted onto the surface of MCM-41 was compared with the experimental results.

**12:27**

**H13 7 Experimental two-point microrheology of two-dimensional systems** VIKRAM PRASAD, ERIC WEEKS, *Emory University* Microrheology is often used to determine the bulk viscoelasticity of materials such as polymer solutions, by tracking the diffusion of tracer particles. For heterogeneous materials, where single particle microrheology breaks down, a modified technique known as two-point microrheology has been established where motions of particles with varying spatial separations are correlated. In 3-d systems, this correlated motion decays as 1/R, and can be used to identify the long wavelength modes in the system, and therefore the bulk viscoelasticity. For 2-d systems, theory has predicted a logarithmic decay, but to date, this prediction has gone untested. We look at the correlated motions of colloidal particles in two types of quasi 2-d systems (protein molecules at an air-water interface, and thin soap films), and observe a transition from 3-d to 2-d, by continuously varying the Boussinesq number, $B_0 = (\eta_s/\eta a)$ from 0 to $\infty$, where $\eta_s$ is the surface viscosity, $\eta$ is the bulk viscosity, and a is the size of the colloidal particle. The experimental results are compared to theory, and consequences for microrheology at interfaces are discussed.

**12:39**

**H13 8 Thermal response of polymer coated colloidal diffusion near surfaces** STEPHEN ANTHONY, HUILIN TU, LIANG HONG, PAUL BRAUN, STEVE GRANICK, *Departments of Chemistry and of Material Science, University of Illinois* Thermally responsive poly(/N/-isopropylacrylamide) (PNIPAAm) tethered silica particles represent a potential building block for new materials. For this research, Surface-initiated Atom Transfer Radical Polymerization (ATRP) was chosen for its ability to generate well defined, homogeneous polymer brushes on silica nanoparticles and surfaces. Phase contrast optical microscopy was used along with single particle tracking methods to characterize the motion of these particles in suspension as well as close to brush modified surfaces. Temperature dependence experiments reveal that increased temperature decreases the radius of the particles. Additionally, heating may trigger a transition from ''sticky'' surfaces to ''slippery'' surfaces. Below LCST, swelled PNIPAAm chains may interdigitate and slow down particle motion. Thermal hysteresis was also apparent; kinetic trapping of particles resulted in the retention of an immobilized population upon cooling. Furthermore, the analysis of the diffusion dynamics also implies interparticle interactions and particle-surface interactions. Understanding the kinetics of this complex fluid system facilitates the design and control of novel materials.

**12:51**

**H13 9 Surface patterns on co-assembled fibers from charged, amphiphilic molecules** KEVIN KOHLSTEDT, *Northwestern University* FRANCISCO SOLIS, *Arizona State University* MONICA OLVERA DE LA CRUZ, *Northwestern University* We analyze local segregation of species in charged multicomponent cylindrical micelles. In particular, we consider co-assemblies of cationic and anionic heterogeneous molecules such as lipids and peptide amphiphiles. Charge heterogeneities can develop at the surface of the fibers due to the competition between the short-range incompatibility of the co-assembled components and the electrostatic interactions. The system can be described by a line tension between domains $\gamma$, which favors growth of the domains of segregated components, and the electrostatic energy of the domains with charge density $\sigma$, which increases rapidly with the size of the segregated domain L. The competition results in the formation of domains with a characteristic size $L_o = (\gamma\varepsilon/\sigma^2)^{1/2}$. In stoichiometric mixtures the constraints of the geometry and the long range correlations lead to lamellar stripes of different pitch. We present results on the different orientations of the lamellar patterns as a function of the ratio between the lamellar size and the cylinder radius. We find the critical salt concentration, which is a function of radius and lamellar size, at which the patterns grow to macroscopic sizes due to the screening of the Coulomb interactions.

**13:03**

**H13 10 Ion and neutral particle emission from polytetrafluoroethyene under 157-nm irradiation** STEPHEN LANGFORD, SHARON JOHN, THOMAS DICKINSON, *Washington State University* Polytetrafluoroethylene (PFTE) is an important electronic material. Interactions with 157-nm laser radiation are of interest in the deposition and patterning of thin films of PTFE and similar materials. We have characterized the desorption of neutral and charged species from PTFE surfaces during 157-nm irradiation by time-resolved quadrupole mass spectroscopy. The principal neutral species are $(CF_2)_x$ units. The neutral time-of-flight signals have a fast component with kinetic energies on the order of an eV, consistent with direct photochemical emission. These energetic neutrals are presumably created by scission of the C-C backbone by UV excitation. Slower neutral emissions are consistent with thermal emission from the surface at temperatures of several hundred kelvin above ambient. Much of the slower emission is attributed to thermally activated unzipping of the polymer

backbone after photoelectronic scission. The principal positive and negative ions are $C^+$ and $F^-$. A large number of positive and negative charges are electrostatically coupled and travel together until separated by the electric fields of the mass filter.

**13:15**

**H13 11 Dual Syringe Electrospinning of FNfds-modified Hyaluronic Acid** YUAN JI, *Dept. of Materials Science, SUNY at Stony Brook* KAUSTABH GHOSH, *Dept. of Biomedical Engr., SUNY at Stony Brook* XIAOZHENG SHU, *Dept. of Medicinal Chemistry, the University of Utah* JONATHAN SOKOLOV, *Dept. of Materials Science, SUNY at Stony Brook* GLENN PRESTWICH, *Dept. of Medicinal Chemistry, the University of Utah* RICHARD CLARK, *Dept. of Biomedical Engr., SUNY at Stony Brook* MIRIAM RAFAILOVICH, *Dept. of Materials Science, SUNY at Stony Brook* We described the fabrication of a unique HA nanofibrous scaffold using dual syringe reactive electrospinning. 3′-dithiobis(propanoic dihydrazide)-modified HA (HA-DTPH) and Poly (ethylene glycol)-diacrylate (PEGDA) were selected as the cross-linking system. PEO was blended with HA-DTPH to facilitate the fiber formation. Fibronectin functional domains (FNfds) were incorporated with PEGDA and covalently linked to HA via conjugate addition to improve the cell attachment. The as-spun scaffold was soaked into DI water to remove PEO and yield an FNfds-modified HA-DTPH nanofibrous scaffold. Human dermal fibroblasts CF31 were seeded on FNfds-modified HA-DTPH scaffolds. The CF31 fibroblasts showed a unique extended dendritic morphology which is opposed to the typical flattened morphology of cells on regular 2D geometries. Supported by NSF-MRSEC.

**13:27**

**H13 12 Single Electron Tunneling to Individual Gold Nano-Particles** NING ZHENG, *Physics Dept* GANGLI WANG, *Chemistry Dept* EZRA BUSSMANN, *Physics Dept* LIN ZHAO, *Physics Dept* CLAYTON WILLIAMS, *Physics Dept, Univeristy of Utah* Single electron tunneling to naked gold clusters and monolayer protected gold clusters on a thermally grown silicon dioxide film has been performed by single-electron tunneling force microscopy (SETFM) at room temperature.[1,2] In this technique, single electron tunneling events are detected by electrostatic force measurement. We observe several abrupt steps in the smooth frequency shift curve as the tip approaches a cluster. These steps correspond to single or multiple electron tunneling events to the gold particle. Since the tunneling electron changes the charge on the particle, it is also detected as a change in surface potential. The electron can be manipulated to and from the gold particle by changing the voltage applied to the tip. These tunneling events can be used to determine the electronic structure and charging energy of the individual gold particle. The technique will be described and the single electron tunneling results will be discussed. A theoretical model of the tunneling measurements is in agreement with the measurements. [1] E. Bussmann, D. J. Kim, and C.C. Williamsit, Appl. Phys. Lett. **85**, 2538 (2004) [2] E. Bussmann, N. Zheng, and C.C. Williams, itAppl. Phys. Lett. **86**, 163109 (2005)

**SESSION H15: METALS: ELECTRONIC STRUCTURE, FERMIOLOGY, TRANSPORT**
**Tuesday Morning, 14 March 2006**
**311, Baltimore Convention Center at 11:15**
**Wei Ku, Brookhaven National Laboratory, presiding**

**11:15**

**H15 1 Angle Resolved Photoemission Spectroscopy of Single Crystal Uranium (001)*** C.P. OPEIL, R.K. SCHULZE, R.C. ALBERS, B. MIHAILA, K.B. BLAGOEV, M.E. MANLEY, J.C. LASHLEY, J.L. SMITH, *Los Alamos National Laboratory* P.B. LITTLEWOOD, *Cavendish Laboratory, University of Cambridge* Using Angle Resolved Photoemission Spectroscopy (ARPES) we measured the energy dispersion for binding energy (BE) $<$ 8 eV at 173 and 373 K on a high quality uranium single crystal (001) along the principle crystallographic directions $\Gamma$ to Y, $\Sigma$, and S. These measurements are compared with WIEN2K band structure calculations. We report significant correspondence between our band dispersion and theoretical calculations. Temperature and electron correlation effects will be discussed.

*Work performed under the auspices of the US Dept. of Energy.

**11:27**

**H15 2 Orbital-Resolved Soft X-ray Spectroscopy Measurnents of $Sr_2RuO_4$ Electronic Structure.** TIM SCHULER, *MPT Polymers* J. HOOPER, *Tulane University* ZHIQIANG MAO, *Tulane University* DAVID EDERER, *Tulane University* GUO-PING ZHANG, *Indiana State University* TOM CALLCOTT, *University of Tennessee* Strontium ruthenate ($Sr_2RuO_4$) is a spin-tripletsuperonductor[1] of the Ruddlesden-Popper (RP) series with n=1. We have studied the electronic structure of single crystals of this system by density functional theory (DFT) calculations and soft x-ray emission and absorption measurements at the oxygen K edge (530 eV) and find that DFT calculations provide an excellent model to characterize the molecular orbitals corresponding to the inequivalent O sites in this perovskite compound. The linearly polarized radiation excites primarily O [1] (planar) sites at almost normal incidence and O [2] (apical) sites at grazing incidence. Our results suggest a larger level of hybridization between the Ru d and the O p states in the $RuO^2$ planes than between the Ru and apical O atoms, which also implies more localized bonding along the apical direction than the planar direction. This work was supported by DOE grant No. DE−FG02−05ER−46183. 1)Y. Maeno, et al, Nature 372, 532 (1994).

**11:39**

**H15 3 Electronic Structure and Bulk Spin Valve Behavior in $Ca_3Ru_2O_7$** DAVID SINGH, *Oak Ridge National Laboratory* SUSHIL AULUCK, *IIT Roorkee, India* The perovskite based ruthenates show a remarkable range of electronic and magnetic properties, even though they are all based on $Ru^{4+}$ ions in octahedral environments with corner sharing bonding topologies. These behaviors include robust itinerant ferromagnetism, paramagnetic bad metal properties, unconventional superconductivity, Mott insulating properties and metamagnetic quantum critical behavior. The bilayer, so- called 327 compounds are of particular interest because of their borderline properties. We report density functional calculations of the magnetic properties and Fermiology of $Ca_3Ru_2O_7$. The ground state consists of ferromagnetic bilayers, stacked antiferromagnetically. The bilayers are almost but not exactly half-metallic. In the ferromagnetic state opposite spin polar-

izations are found for in-plane and out-of-plane transport. Relatively high out of plane conductivity is found for the majority spin, which is relatively weakly conductive in- plane. In the ground state in-plane quantities are essentially the same, but the out of plane transport is strongly reduced. This work was supported by the Department of Energy.

**11:51**

**H15 4 First Observation of MCD at O and Ru sites in $Sr_4Ru_3O_{10}$** YINWAN LI, ZHIQIANG MAO, MENG ZHOU, DAVID EDERER, *Tulane University* JOHN FREELAND, *Argonne National Laboratory* TOM CALLCOTT, *University of Tennessee* Perovskite strontium ruthenates of the Ruddlesden-Popper (RP) series $Sr_{n+1}Ru_nO_{3n+1}$show a variety of complex behavior including superconductivity and metamagnetism. $Sr_4Ru_3O_{10}$ is a trilayer member of the RP series with n=3 that is metamagnetic and shows an electronic phase separation[1]. We wanted to test if this material showed magnetic behavior at low fields and performed magnetic circular dichroism measurements (MCD) at the O K and Ru L edges. The measurements were carried out at the Sector 4 polarization beam line of the Advanced Photon Source at grazing (10°) and normal incidence angles at the characteristic temperature 50K below which metamagnetic behavior occurs[2] and above the ordering temperature (150K). We observed dichroic behavior at both temperatures although the dichroism was reduced by a factor of 10 at 150K relative to the measurements at 50K. It is significant to note that only the lowest unoccupied orbital (LUMO) associated with the planar O site showed dichroic behavior. This research was supported in part by DOE grant No. DE-FG02-05ER-46183, and the Advanced Photon Source is supported by DOE grant W-31-109-ENG-38.

Z.Q. Mao et al, submitted to Physical Review Letter. G. Cao et al, Phys. Rev. B **68**, 174409 (2003)

**12:03**

**H15 5 Zero bias anomaly in the low-temperature scanning tunneling spectra of Sr3Ru2O7*** R. MATZDORF, B. NANSSEU, J. HAGER, *Institute of Physics, University of Kassel, 34109 Kassel, Germany* H. YAGUCHI, Y. MAENO, *Kyoto University, Japan* J. ZHANG, *Department of Physics, Florida International University, Miami, Florida 33199, USA* R. MOORE, E.W. PLUMMER, *Condensed Matter Science Division, Oak Ridge national Laboratory, Oak Ridge, Tennessee 37831, USA* We have studied a zero bias anomaly in scanning tunneling spectra of Sr3Ru2O7 as function of temperature. The dip-like feature in the dI/dV spectra is observed in an energy range of −20meV to +20meV around Fermi energy. The depth of the dip decreases with increasing temperature in a temperature range of 5 to 30 Kelvin. The temperature dependence of the dip is not due to the thermal broadening connected to the tunneling process. The results on Sr3Ru2O7 are compared with temperature dependent scanning tunneling spectra of Sr2RuO4. Finally, we discuss different effects as possible explanations for the zero bias anomaly.

*Work supported jointly by NSF and DOE (DMS) NSF -DMR-0451163, NSF DMR-0346826 and by U.S. DOE under DE-FG02-04ER46125

**12:15**

**H15 6 Fermi-liquid-like quasiparticle excitations in $Sr_2RhO_4$** WILLIAM DUNKEL, FELIX BAUMBERGER, WORAWAT MEEVASANA, DONGHUI LU, *Stanford University* ROBIN PERRY, ANDY MACKENZIE, *St. Andrews University* ZHIXUN SHEN, *Stanford University* The layered 4d transition metal oxide $Sr_2RhO_4$ supports a highly anisotropic, well-defined Fermi-liquid-like electron fluid. Angle resolved photoemission spectroscopy shows a Fermi surface and quasiparticle effective masses in quantitative agreement with bulk de Haas-van Alphen data. Sr $_2RhO_4$ thus presents a prime opportunity to study the electronic self energy in a well-defined model system. To this end, we present a comprehensive spectral function analysis of high resolution angle resolved photoemission data from $Sr_2RhO_4$. Preliminary data at very low photon energies are presented and compared to state-of-the-art data taken at conventional UV photon energies.

**12:27**

**H15 7 Quantum oscillations in $RAgSb_2$ (R = La, Sm, Y) as seen via magnetostriction measurements** S.L. BUD'KO, S.A. LAW, P.C. CANFIELD, *Ames Laboratory and Dept. of Physics and Astronomy, Iowa State University* G.M. SCHMIEDESHOFF, *Dept. of Physics, Occidental College, Los Angeles* We present low temperature longitudinal magnetostriction measurements taken using a capacitance dilatometer in a PPMS-14 instrument for several $RAgSb_2$ (R = rare earth) compounds. The quantum oscillations in magnetostriction were observed up to temperatures as high as 25 K. These data are compared with the results of de Haas - van Alphen and Shubnikov - de Haas measurements. Using these data the uniaxial stress dependencies of the extremal Fermi surface orbits can be evaluated.

**12:39**

**H15 8 Local Flattening of the Fermi Surface and Quantum Oscillations in the Magnetoacoustic Response of a Metal** GREGORY ZIMBOVSKY, NATALYA ZIMBOVSKAYA, *University of Puerto Rico - Humacao* In the present work we theoretically analyze the effect of the Fermi surface local geometry on quantum oscillations in the velocity of an acoustic wave travelling in metal across a strong magnetic field. We show that local flattenings of the Fermi surface could cause significant amplification of quantum oscillations [1]. This occurs due to enhancement of commensurability oscillations modulating the quantum oscillations in the electron density of states on the Fermi surface. The amplification in the quantum oscillations could be revealed at fitting directions of the magnetic field. [1] N. A. Zimbovskaya, cond-mat/0505301.

**12:51**

**H15 9 Theory of the Cyclotron Resonance in Al,Pb,Zn and Cd** SHIGEJI FUJITA, ROHIT SINGH, ROBERT SIMION, *University of Buffalo* SEIICHI WATANABE, *Hokkaido University, Japan* SALVADOR GODOY, *UNAM, Mexico* A quantum theory of the cyclotron resonance is developed. For a face-centered-cubic (fcc) metal the obvious candidates for the Cyclotron Planes (CP) in which the conduction electron (''electron,'''hole'') circulates are the three families of planes {100}, {110} and {111}. Following Dresselhaus-Kip-Kittel (DKK,1955) we assume a quadratic energy-momentum ($\hbar k$) relation with the effective mass ($m_1, m_2, m_3$) and analyze the angle- dependent resonance peaks in terms of Shockley's formula (a generalization of the DKK formula).For aluminum Al (fcc) an ''electron'' ellipsoid with the major axes in [110] with ($m_1, m_2, m_3$) = (0.108,0.156,1.96)$m$ is obtained. For lead (Pb) (fcc) a hyperboloid in [110] with

$(m_1, m_2, m_3) = (1.18, 0.244, -8.71)m$ and an ''electron'' sphere with $m^* = 1.30m$ associated with the CP {100} are obtained. For a hexagonal- closed-pack (hcp) metal,the CP is the hexagonal base plane. The effective mass $m_b$ for the basal-plane motion and the mass $m_c$ along the c-axis for zinc (Zn) [cadmium (Cd)] (both hcp)are $(m_b, m_c) = (1.04, 0.212)$m [(1.14,0.217)m], which characterize the spheroids with the major axis along the c-axis.

**13:03**

**H15 10 Magnetic and Transport Properties of $RCoIn_5$(R=Pr,Nd) and $RCoGa_5$ (R=Tb-Tm)** JACOB HUDIS, *Department of Physics and Astronomy, Johns Hopkins University* RONGWEI HU, *Department of Physics, Brown University/ Brookhaven National Lab* COLLIN BROHOLM, *Department of Physics and Astronomy, Johns Hopkins University* V.F. MITROVIC, CEDOMIR PETROVIC, *Department of Physics, Brookhaven National Lab* We report on magnetic and transport properties of single crystals of the light rare earth containing series of compounds $RCoIn_5$ (R=Pr,Nd) and heavy rare earth con- taining series $RCoGa_5$ (R=Tb-Tm). All the compounds crystallize in the tetragonal $HoCoGa_5$ crystal structure and are very good metals with small defect scattering at low temperatures. $NdCoIn_5$ and members of the $RCoGa_5$ series with large de Gennes factors order antiferromagnetically.

**13:15**

**H15 11 Anomalous Nernst Effect in Ferromagnets** DI XIAO, QIAN NIU, *Department of Physics, The University of Texas, Austin, TX 78703* We study the intrinsic contribution to the anomalous Nernst effect in ferromagnets at low temperatures. It is shown that the anomalous Nernst conductivity is of topological nature and can be related to the Berry phase of occupied Bloch states. In ferromagnets, there may be nonzero magnetization current even in thermodynamic equilibrium. It can significantly change the thermoelectric transport coefficients. The Onsager relation is established for the charge and heat transport coefficients. Our theory well explains recent experimental result.

**13:27**

**H15 12 Giant Nernst effect in the Pr-filled skutterudite $PrFe_4P_{12}$** KAMRAN BEHNIA, ALEXANDRE POURRET, *ESPCI (Paris)* DAISUKE KIKUCHI, YUJI AOKI, HIDEYUKI SATO, *Tokyo Metropolitan University* The phase transition of $PrFe_4P_{12}$ at $T_O = 6.5$ K, probably associated with antiferroquadrupolar ordering, is explored by measuring thermal and thermoelectric transport coefficients. The transition leads to a drastic increase in lattice thermal conductivity pointing to a large drop in carrier concentration induced by the transition and a strong electron-phonon coupling. The low level of carrier density in the ordered state is confirmed by the anomalously large values of the Seebeck and Nernst coefficients. The latter attains a magnitude larger than what is reported for any metal. The results are reminiscent of the hidden-order state of $URu_2Si_2$. According to our analysis of the data, most carriers disappear at the transition, paving the way for an enhanced mean-free-path of both phonons and the residual quasi-particles. Thus, the ordered state of $PrFe_4P_{12}$ emerges as a heavy-fermion semi-metal.

**13:39**

**H15 13 Magnetoresistance and Hall Effect in cubic FeGe*** C. CAPAN, J.F. DITUSA, *Louisiana State University* H. LEE, L. PHAM, Z. FISK, *UC Davis* G. AEPPLI, *University College London* A. BANSKTON, E. THOMAS, J. CHAN, *Louisiana State University* An anomalous contribution to Hall Effect is observed in a variety of ferromagnetic systems ranging from simple metals and oxides to manganites, ruthenates and spinel compounds. Its nature (intrinsic or extrinsic) and microscopic mechanism is still an open issue and is being heavily investigated. It was originally attributed to skew or side jump scattering, which corresponds to an asymmetric scattering of conduction electrons by magnetic moments. More recent developments in the field seem to favor a scenario where an electron orbiting around the Fermi Surface at a finite field acquires a Berry phase when the direction of its moment is locked in presence of a strong spin-orbit interaction. FeGe is an itinerant helimagnet with a high Curie temperature of 280K. The lack of inversion symmetry of the crystal structure leads to helimagnetic order via Dzyaloshinskii-Moriya interaction, signature of a strong spin-orbit coupling in an otherwise cubic lattice. We will present new results of magnetoresistance, Hall Effect and magnetization in a single crystal of cubic FeGe and discuss the origin of the Anomalous Hall effect in this system.

*We acknowledge NSF-DMR grants 0406140 and 0433560

**13:51**

**H15 14 Electrical conductivity of warm expanded aluminum** GERALD FAUSSURIER, CHRISTOPHE BLANCARD, PATRICK RENAUDIN, *CEA* PIER-LUIGI SILVESTRELLI, *Università di Padova* CEA COLLABORATION, UNIVERSITÀ DI PADOVA COLLABORATION, The electronic and ionic structures of warm expanded aluminum are determined self-consistently using an average-atom formalism based on density-functional theory and Gibbs-Bogolyubov inequality. Ion configurations are generated using a least-square fit of the pair distribution function deduced from the average-atom model calculations. The electrical conductivity is computed from the Kubo-Greenwood formula for the optical conductivity implemented in a molecular dynamics scheme based on density-functional theory. This method goes beyond the Ziman approach used in the average-atom formalism. Moreover, it is faster than performing quantum molecular dynamics simulations to obtain ion configurations for the conductivity calculation. Numerical results and comparisons with experiments are presented and discussed.

**14:03**

**H15 15 The Kondo effect in the presence of magnetic impurities** HUBERT B. HEERSCHE, ZEGER DE GROOT, JOSHUA A. FOLK, LEO P. K. KOUWENHOVEN, HERRE S. J. VAN DER ZANT, *Kavli Inst. of Nanoscience, Delft University of Technology, The Netherlands* ANDREW A. HOUCK, JAROSLAW LABAZIEWICZ, ISAAC L. CHUANG, *MIT Media Lab, Cambridge MA* We measure transport through gold grain quantum dots fabricated using electromigration, with magnetic impurities in the leads. A Kondo interaction is observed between dot and leads, but the presence of magnetic impurities results in a gate-dependent zero-bias conductance peak that is split due to an RKKY interaction (I) between the spin of the dot and the static spins of the impurities. Both ferromagnetic and anti- ferromagnetic interactions have been observed in different samples. A magnetic field restores the single Kondo peak in the case of an anti-ferromagnetic

RKKY interaction, whereas the splitting is enhanced in the case of ferromagnetic interaction. A gate electrode can change the relative interaction strength $T_K/I$. This system provides a new platform to study Kondo and RKKY interactions in metals at the level of a single spin.

**SESSION H16: FOCUS SESSION: HYDROGEN STORAGE II**
**Tuesday Morning, 14 March 2006**
**312, Baltimore Convention Center at 11:15**
**Gregory P. Meisner, General Motors, presiding**

*Contributed Papers*

**11:15**
**H16 1 Infrared Spectroscopy of Hydrogen in Fullerite and MOF-5 Hosts** STEPHEN FITZGERALD, HUGH CHURCHILL, PHIL KORNGUT, CHRISTIE SIMMONS, YORGOS STRANGAS, *Oberlin College* We present a novel use of diffuse reflectance infrared spectroscopy to study the quantum dynamics of hydrogen molecules trapped within a host material. This technique is particularly useful for the study of hydrogen storage materials since it provides detailed information about the intermolecular potential at the binding site. Because $H_2$ has no intrinsic infrared activity any observed features arise solely through interaction with the host material and as such are very sensitive to the symmetry of the binding site. The drawback is that the induced spectra are quite weak. However, a technique based on diffuse reflectance has been shown to produce a sufficiently large signal [1]. We have now constructed a cryogenic system that allows spectra to be obtained in this manner at pressures as high as 100 atm. and at temperatures as low as 10 K. Data will be presented for $H_2$ in both $C_{60}$ and MOF-5 showing a series of absorption features arising from the quantized vibrational, rotational, and translational motion of the trapped $H_2$. At the lowest temperature these peaks become quite sharp, FWHM less than 1 $cm^{-1}$, with a detailed fine structure arising from the $H_2$ host interactions. 1. S. A. FitzGerald et al., Phys. Rev. B **65**, 140302. (2002)

**11:27**
**H16 2 Hydrogen Adsorption and Its Displacement of Carbon Dioxide in Microporous Transition Metal Cyanides** SITTICHAI NATESAKHAWAT, JEFFREY CULP, CHRISTOPHER MATRANGA, BRADLEY BOCKRATH, *U. S. Dept. of Energy, National Energy Technology Laboratory* The adsorption properties of $H_2$ and $CO_2$ have been investigated in $M_3$ $[Co(CN)_6]$ (M = Cu, Zn) Prussian blue analogues and $M[Fe(CN)_5NO]$ (M= Co, Ni) metal nitroprussides. Adsorption isotherms show that both materials adsorb between 1.4 to 1.7 wt % of $H_2$ at 77 K and 1 atm. The isosteric heat of adsorption was between 6.5 to 7.5 kJ/mol. Kinetic measurements are conducted in a specially designed vacuum system which is coupled to a Fourier-Transform Infrared Spectrometer. In a typical experiment, an infrared active gas (i.e $CO_2$) is physisorbed in the transition metal cyanide and the system is later back-filled with $H_2$. The infrared intensity of the physisorbed $CO_2$ is monitored to deduce the kinetics and energetics associated with its displacement from the transition metal cyanide by $H_2$. We have identified several kinetic steps, measured the rate constants, and examined the temperature dependence of this displacement process.

**11:39**
**H16 3 Adsorption study of Hydrogen in Carbon based Materials as measured by Nuclear Magnetic Resonance*** ALFRED KLEINHAMMES, SHENGHUA MAO, MARCELO BEHAR, YUE WU, *Department of Physics and Astronomy and Curriculum in Applied and Materials Sciences, University of North Carolina at Chapel Hill, NC 27599-3255* Nuclear magnetic resonance is shown to be a sensitive tool to probe hydrogen adsorption. The technique distinguishes between adsorbed $H_2$, hydrogen in the gas phase and can discriminate against protons brought in through contaminants. NMR provides a quantitative measurement of the number of molecules adsorbed. An estimate of the adsorption energy can be obtained from the measured isotherm. Adsorption measurements of $H_2$ in several materials – metal organic frameworks, conducting polymers, and doped single walled carbon nanotubes – are reported. Boron doped SWNTs when loaded with $H_2$ produce intriguing $^1$Hspectra indicative of adsorption and possibly several adsorption sites

*Funding provided by the US Department of Energys Office of Energy Efficiency and Renewable Energy within the Center of Excellence on Carbon-based Hydrogen Storage Materials as part of DOEs National Hydrogen Storage Grand Challenge

*Invited Papers*

**11:51**
**H16 4 Hydrogen cryo-adsorption; comparing low pressure and isosteric heats.***
CHANNING AHN, *California Institute of Technology*

The two criteria for effective physisorbents for hydrogen storage are high surface area and high adsorption heats. There are two heats that can be determined readily from the sorption isotherm. At very low pressures corresponding to low surface coverages, we can consider the differential enthalpy at zero coverage, determined from the temperature dependence of the Henry's Law constant which is in turn determined by the low pressure isotherm slope. The differential enthalpy can also be determined from isosteric heat measurements from the same data, provided that data is taken over a higher pressure range that includes the saturation limit. We have found that the two quantities are of similar magnitude, and while the direct measurement of the differential enthalpy is the easiest to perform, the requirements necessary in determining the isosteric heat yield the most useful data. Ideally, the sorption heats are constant as a function of ad-atom/molecule coverage density. This is typically not the case due to sorption site heterogeneities that are typical of real surfaces, and due to hydrogen-hydrogen interactions that occur at higher pressures. Consequently, this value drops

as a function of pressure. The consequence of this is that materials that show initially high sorption values at low pressure, do not typically yield high gravimetric saturation values. We will discuss this behavior in metal organic frameworks, activated carbons and carbon aerogels. All of these materials can have high surface area but the adsorption heats are typically 4–7 kJ/mole. We have measured the highest gravimetric hydrogen sorption in an activated carbon.

*This work was supported by the Dept. of Energy (DE-FC36-05GO15079)

*Contributed Papers*

**12:27**

**H16 5 Inelastic Neutron Scattering of $H_2$ Adsorbed on Boron Doped ( $\sim$ 1%) Single Walled Carbon Nanotubes** D. NAREHOOD, *Department of Physics, The Pennsylvania State University, University Park, PA 16802 USA* Y. LIU, C.M. BROWN, D.A. NEUMANN, *National Institute of Standards and Technology, NIST Center for Neutron Research, Gaithersburg, MD 208991, USA* PETER EKLUND, *Department of Physics, The Pennsylvania State University, University Park, PA 16802 USA* It is clear from this study that $H_2$ is preferentially adsorbed at boron sites in SWNTs and in these sites the $H_2$ experiences an orientational component in the potential. Thus, this study shows that the substitution of boron for carbon in the SWNT lattice produces higher energy binding sites for $H_2$ adsorption. We report here an inelastic neutron scattering investigation of $H_2$ adsorbed on $\sim$ 200 mg of purified boron doped ( $\leq$ 1%) SWNT bundles. At $H_2$ coverages $\leq$ 1 $H_2$/ B and at T = 3K, a clear splitting of $\sim$ 1.4 meV is observed for the sublevels of the J=1 state. As the $H_2$ coverage is increased, the rotational spectrum converges to that of the bulk like rotor observed for $H_2$adsorbed on undoped SWNTs with the appearance of a peak at 14.7 meV. As the temperature is increased from 3K, the bulk like peak decreases in intensity until only the split rotational peaks are present; the intensity of these peaks decreases with increasing temperature until about 75 K at which point no rotational peak is observable. Funding provided by the US DOE Office of Energy Efficiency and Renewable Energy within the Center of Excellence on Carbon-based Hydrogen Storage Materials.

**12:39**

**H16 6 Quantum Monte Carlo studies of the non-dissociative absorption of hydrogen to doped fullerenes** ANDREW WILLIAMSON, *Lawrence Livermore National Laboratory* YONGHYUN KIM, SHENGBAI ZHANG, *National Renewable Energy Laboratory* The reversible storage of hydrogen at room temperature requires an adsorption energy in the range of 0.2 to 0.6 eV per hydrogen molecule. However, there are currently no storage materials which have been shown to bind hydrogen with this energy. Typically, hydrogen either retains its molecular form, and binds only weakly via a van der Waals interaction, or it dissociates into atoms and forms strong covalent bonds. Here we present the results of first-principles density functional and Quantum Monte Carlo calculations of the non-dissociative absorption of hydrogen molecules to doped carbon fullerenes. These calculations reveal significantly enhanced binding of hydrogen to substitutional B and Be doped fullerenes. Our Quantum Monte Carlo and benchmark quantum chemistry calculations are used to evaluate the accuracy of different exchange correlation functionals for describing the hydrogen adsorption interaction. We find that the LDA functional significantly overestimates the binding energy of hydrogen, while GGA functionals underestimate the binding energy. This work was performed under the auspices of the US Department of Energy by the University of California, Lawrence Livermore National Laboratory under contract No. W-7405-Eng-48

**12:51**

**H16 7 Theoretical study of Hydrogen Storage in Nanotubes and Nanoscrolls.** GEORGE FROUDAKIS, *University of Crete* A combination of itab-initio and Molecular Dynamics methods is used for investigating the nature of atomic and molecular hydrogen interaction with C, SiC and BN Nanotubes and Nanoscrolls. The curvature of the tube wall together with the direction of the hydrogen approach is considered and evaluated. In addition the improvement of the storage capacity is tested under various conditions of doping, pressure and temperature.

**13:03**

**H16 8 The effect of metal clustering on hydrogen storage** PURU JENA, *Virginia Commonwealth University* QIAN WANG, *Virginia Commonwealth University* QIANG SUN, *Virginia Commonwealth University* YOSHIYUKI KAWAZOE, *IMS, Japan* Hydrogen has been recognized as an ideal energy carrier and has the potential to reduce our dependence on fossil fuels which are not only limited but also are harmful to the environment. The success of a new hydrogen economy, however, depends upon our ability to find materials that can store hydrogen reversibly with high gravimetric and volumetric density and operate under moderate temperatures and pressures. Although a great deal of effort has recently been devoted to searching of such materials, none are known to meet the above conditions. Nanostructures offer new possibilities for hydrogen storage due to the novel chemistry. It has been shown very recently that coating of carbon nanostructures with **isolated transition metal atoms** such as Sc and Ti can increase the binding energy of hydrogen and lead to high storage capacity up to 8 wt% hydrogen, However, this prediction depends on the assumption that the metal atoms coated on the fullerene surface will remain isolated. Using first principles calculations based on density functional theory, and we show that Ti atoms would prefer to cluster on the $C_{60}$ surface which can significantly alter the nature of hydrogen bonding, thus affecting not only the amount of stored hydrogen but also their thermodynamics and kinetics.

**13:15**

**H16 9 Storing hydrogen in graphene layers with tunable interlayer spacing*** YANG LEI, *Queen Mary, University of London* WENGUANG ZHU, *Harvard University* YAN SONG, *Queen Mary, University of London* ENGE WANG, *Institute of Physics, CAS* ZHENYU ZHANG, *University of Tennessee & ORNL* ZHENGXIAO GUO, *Queen Mary, University of London* Carbon nanostructures are being studied for hydrogen storage. However the nature of H-C interactions in such structures is unclear. We use first-principles simulation to model H adsorption between graphene layers. The adsorption of $H_2$ between layers is evaluated, particularly with respect to inter-layer variation thus simulating the effect of stressing the graphite for H storage. We note that $H_2$ dissociates when the inter-graphene distance is reduced (the graphite is compressed). When the ratio of H:C=1:1, the graphene changes from a planar to a diamond-like structure. The H-C interaction changes from weak physisorption to strong chemisorption. When the pressure is reduced, H atoms can recom-

bine to form $H_2$ by overcoming a small energy barrier. Based on this work, we propose a new scheme for H storage in C nanostructures: by way of altering the inter-graphene distance, the C structure can effectively ''inhale,'' store and release hydrogen in a controlled manner.

*Supported by USNSF, UCDOE, & EPSRC/UK-SHEC.

**SESSION H17: FOCUS SESSION: EMERGING RESEARCH DEVICES AND MATERIALS FOR MICROELECTRONICS INDUSTRY II**
**Tuesday Morning, 14 March 2006**
**313, Baltimore Convention Center at 11:15**
**Bruce White, Freescale Semiconductor, Inc., presiding**

*Contributed Papers*

**11:15**
**H17 1 Modeling spintronic devices** IGOR ZUTIC, *SUNY Buffalo and Naval Research Laboratory* JAROSLAV FABIAN, *University of Regensburg, Germany* STEVEN ERWIN, *Naval Research Laboratory* Conventional spintronic devices are based on metallic magnetic multilayers which utilize the magnetic moment associated with the spin to read magnetically stored information, leading to a nonvolatility and a substantial improvement in the performance of computer hard drives and magnetic random access memories. However, these applications employ two-terminal spin valves which are of limited use for advanced functionalities appropriate for signal processing and digital logic. While semiconductor-based three-terminal devices are natural candidates for spin logic, they remain inadequately investigated and even a simple understanding of their integration with CMOS is still missing [1]. We illustrate here several basic elements for modeling spin transport in spintronic devices and propose schemes for spin injection and detection in silicon [2], as well as for spin-controlled gain [1,3]. Supported by the US ONR, DARPA, and the National Research Council. [1] I. Zutic, J. Fabian, S. Das Sarma, Rev. Mod. Phys. **76**, 323 (2004). [2] I. Zutic, J. Fabian, and S. C. Erwin, eprint: cond-mat/0412580. [3] J. Fabian and I. Zutic, Appl. Phys. Lett. **86**, 133506 (2005); Phys. Rev. B **69** 115314 (2004).

**11:27**
**H17 2 Non-metal spintronics: study of spin-dependent transport in InSb- and InAs-based nanopatterned heterostructures** J.J. HEREMANS, HONG CHEN, *Department of Physics, Virginia Tech* J.A. PETERS, *Department of Physics and Astronomy, Ohio University* N. GOEL, S.J. CHUNG, M.B. SANTOS, *Department of Physics and Astronomy, University of Oklahoma* W. VAN ROY, G. BORGHS, *IMEC, Leuven, Belgium* Spin-orbit interaction in semiconductor heterostructures can lead to various spin-dependent electronic transport effects without the presence of magnetic materials. Mesoscopic samples were fabricated on InSb/InAlSb and InAs/AlGaSb two-dimensional electron systems, where spin-orbit interaction is strong. In mesoscopic devices, the effects of spin-orbit interaction are not averaged out over the geometry, and lead to observable electronic properties. We experimentally demonstrate spin-split ballistic transport and the creation of fully spin-polarized electron beams using spin-dependent reflection geometries and transverse magnetic focusing geometries. Spin-dependent transport properties in the semiconductor materials are also investigated using antidot lattices. Spin-orbit interaction effects in high-mobility semiconductor devices may be utilized toward the design of novel spintronics implementations. We acknowledge NSF DMR-0094055 (JJH), DMR-0080054, DMR-0209371 (MBS).

**11:39**
**H17 3 Novel nanopattern assisted Mn-implanted Ge for spintronic applications** JINGJING CHEN, *UCLA, Department of Electrical Engineer-Device Research Laboratory (DRL)* KOS GALATSIS, *UCLA-DRL* KANG WANG, *UCLA-DRL* UCLA-DRL TEAM, Mn-Ge is one of the most promising Diluted Magnetic Semiconductors (DMS) materials as reports indicate room temperature ferromagnetism. Our investigation focuses on fabricating Mn-Ge via novel diblock copolymer patterning methods to control Mn implantation within a Ge lattice. We foresee such methods could enable consistent tailoring of Mn-Ge magnetic properties by improving uniform solubility of Mn in Ge, along with decreasing defects. Sample fabrication is based on a 20nm-scale periodic nanodot patterning Ge substrate. Ion-implantation was performed with Mn at 40KeV and with a dose of $4.0 \times 10^{14}/cm^2$ then annealed at 400-700°C. Material characterization included XRD, SEM and TEM. XRD detected the presence of $Mn_5Ge_3$ and $Mn_{11}Ge_8$phase, which is theoretical known to have a Tc near room temperature. Ferromagnetic hysteresis loops were obtained at 5K using a SQUID magnetometer ranging from -5 to 5 kOe. Samples at various annealing temperatures showed the saturation magnetization reaches an optimum value at 450°C. The difference in the temperature-dependent remnant magnetization between the implanted n-type and p-type Ge is also observed.

*Invited Papers*

**11:51**
**H17 4 Beyond CMOS – The Semiconductor Industry's Nanoelectronics Research Initiative.**
HANS COUFAL, *NERC*

The tremendously powerful scaling of transistors, that has enabled Moore's Law for the past forty years, can not continue forever. Some of the reasons, such as the atomistic nature of matter, are obvious. Others are less obvious and will be briefly reviewed before some of the potential alternatives to charge based logic will be analyzed. Such an analysis had the semiconductor industry initiate a Nanoelectronics Research Initiative. The current status of this program will be reviewed.

*Contributed Papers*

**12:27**

**H17 5 Nanoscale Molecular-Electronic Device Fabrication enabling Complete Chemical and Physical Characterization** JASON J. BLACKSTOCK, *Quantum Science Research, HP Labs* DUNCAN T. STEWART, *Quantum Science Research, HP Labs* CARRIE L. DONLEY, *Quantum Science Research, HP Labs* R. STANLEY WILLIAMS, *Quantum Science Research, HP Labs* The limitation of most nanoscale molecular-electronic devices is the lack of physical/chemical characterization accompanying electrical data. Such characterization is typically impossible, because the critical layers and interfaces being inaccessibly buried in the final device structure. We present new fabrication techniques that enable a range of conventional characterization tools to be employed during and after nanoscale device fabrication. These techniques include: the fabrication of atomically-flat, patterned template-stripped bottom metal electrodes with well-defined atomic structure (elucidated by UHV-STM); and the formation of a new stencil-based nanopore device geometry enabling detailed characterization of the internal nanoscale physical/chemical properties of the final devices. The combination of these techniques allows for molecular-electronic devices with lateral sizes ranging from tens of nanometers to hundreds of microns. The fabrication, characterization and electrical properties of metal/molecular-monolayer/metal devices using these techniques (including UHV-STM, AFM, SEM, XPS and IR data) will be presented.

**12:39**

**H17 6 Carbon nanotube Y-junctions for Nanoscale Electronics** PRABHAKAR BANDARU, CHIARA DARAIO, SUNGHO JIN, *Univ. of California San Diego* APPARAO RAO, *Clemson University* Carbon Nanotube (CNT) based electronics offer significant potential, as a nanoscale alternative to silicon based devices, for novel molecular electronics technologies. To realize truly nanoelectronic architecture, it is desirable to have a fully integrated nanotube based technology, where both devices and interconnects are based on CNTs. With this aim in mind, we report on the electrical properties of CNT based Y-junctions. The carrier delocalization and the inevitable presence of catalyst particles, introduced during growth, at the junction region induce a net charge and scattering which can be exploited in constructing electronic devices. We have assembled and electrically characterized the DC resistance and the AC impedance of several Y-junction devices[2] with possibilities for switching and transistor related applications. These experiments alert us to the vast potentialities of Y-junction devices in the development of nanoelectronic components including inverters, logic gates, and frequency mixers. An electrical impedance model of a MWNT Y-junction will be presented which will help gain an understanding of the current transport mechanisms in these nanostructures. 1. P. Bandaru et al, ''Novel electrical switching behavior and logic in carbon nanotube Y-junctions,'' Nature Materials, vol. 4(9), 663-666, (2005) 2. N. Gothard, et al. ''Controlled growth of Y-junction nanotubes using Ti-doped vapor catalyst,'' Nanoletters **4**, 213-217 (2004).

**12:51**

**H17 7 Low Frequency Noise in Carbon Nanotube Field Effect Transistors*** FEI LIU, *UCLA* KANG L. WANG, DAIHUA ZHANG, *USC* CHONGWU ZHOU, UCLA TEAM, USC TEAM, It is critical to understand the noise performance of the carbon nanotube field effect transistors (CNT-FETs) due to their ultra-small diameters and large surface to volume ratios. In the abstract, we will describe the noise study of an ambipolar CNT-FET with a negative threshold of 5V and a positive threshold of 15V. The noise power spectra densities (PSDs) are obtained for frequencies from 0.0625Hz to 10.24kHz, showing $1/f^{\alpha}$ behavior. The exponential $\alpha$ of this $1/f^{\alpha}$ increases from about 0.6 to 1.2 for a gate bias from -6V to -15V at a small source-drain bias (-0.1V) and this exponential gate bias dependence comes from schottky contacts, where shot noise is the dominant noise component. We also observe a greater excess 1/f noise for electron conducting than that for hole conducting, suggesting higher defect density near the CNT conduction band. The characteristics of the CNT-FET noise are different from conventional MOSFET, and thus, additional studies are needed to understanding the noise in CNT-FETs.

*The work was in part supported by MARCO Focus Center on Functional Engineered Nano Architectonics FENA

**13:03**

**H17 8 Use of a Novel Fluidic Microplotter in Macroelectronics, Photonics, and Sensors** B. LARSON, D. LAGALLY, J. BAIER, *SonoPlot LLC, Madison, WI 53714* P. RUGHEIMER, B. TANTO, P. GOPALAN, M. G. LAGALLY, *University of Wisconsin-Madison, Madison WI 53706* Many future applications of microelectronics will focus not on computing but on broader uses in fast flexible electronics, imaging and displays, energy, and environmental and health monitoring. Such uses will require in many cases integration on the mesoscale, and the combination of the fast microelectronics with materials that provide other benefits. One need is the deposition of a wide range of materials from the fluid state. We describe a new fluidic microplotter that enables the deposition of a wide range of materials at the 1 $\mu$m and larger scale. The dispensing depends on a novel axial ultrasonic resonance of a fluid micropipette that allows a gentle noncontact deposition of spots, lines, curves, and 3D objects with high precision and very good CV values. We will demonstrate some of the capabilities of the plotter in 1) writing patterns on MEMS membranes, 2) writing a polymer LED, 3) writing parallel lines separated by 1 $\mu$m, 4) making bioarrays with very small spots, and 5) writing polymer waveguides, and writing on Si nanomembranes that serve as the basis for very fast flexible electronics. The physical basis for the unique dispensing action in this device, as well as broader features of the plotter will be described. Potential additional applications will be discussed.

**13:15**

**H17 9 Integration of top-down and bottom-up methods: generating templates for nanowire devices.** MATTHEW SHAW, *Intel / University College Cork* THOMAS FITZGERALD, *UCC* BARBARA KOSMALA, *UCC* MICK MORRIS, *UCC* Self-assembly can realize spatially controlled nanostructure arrays rivaling the lithography. However, self-assembled constructs to develop nano-circuitry on the macroscopic scale remains distant but combination of lithography and self-assembly might be used for sub-20 nm feature sizes. Spatially constrained block co-polymers can be used to generate these patterns and selective removal of one component can provide 'templates' to generate nanowire arrays. This work focuses on generating nm-size features across a real substrate. We use state of the art lithography to generate sub-$\mu$m features and within these generate nm sized co-polymer arrays. Spatial control is determined only by the block size of the co-polymers and not processing variables. Selective 'etching' and phase enhancement techniques were used to provide depth variations across the substrate and form the 'template' for nanowire

development. The results of sputtering and electrochemical deposition used to fill the templates are outlined. The results demonstrate an exciting nanofabrication technique for creating high density nanowire arrays for the nanoelectronic industry.

**13:27**

**H17 10 High Density Germanium Nanowire Assemblies: Contact Challenges, Electrical Characterization and Photoconductivity Dynamics** BRIAN DALY, *University College Cork* BORIS POLYAKOV, DONATS ERTS, *University of Latvia* MICHAEL MORRIS, JUSTIN HOLMES, *University College Cork* The conductivity and photoconductivity properties of vertically aligned germanium nanowires, within anodised aluminium oxide (AAO) templates have been characterized by C-AFM and macro-contact measurements. Contact resistance between the nanowires and metal macro-contacts was minimized by polishing and gradual etching of the AAO surface, to expose the nanowires, prior to deposition of the contacts. Conductivity data from C-AFM and macro-contact measurements were found to be comparable suggesting that both methods are inherently suitable for evaluating the electrical transport properties of encapsulated nanowires within a matrix. Photoconductivity measurements indicate a photocurrent/dark current ratio of up to 40% in the Ge nanowire matrix during illumination with an Ar laser between 457 – 514 nm. These results are significant as the ability to make good ohmic contacts to nanowires, within well defined arrays, is key for the future 'bottom-up' fabrication of multi-layered device architectures for future electronic and optoelectronic devices.

**13:39**

**H17 11 Excitonic states and carrier recombination in ZnO quantum dots** VLADIMIR A. FONOBEROV, ALEXANDER A. BALANDIN, *Nano-Device Laboratory (http://ndl.ee.ucr.edu), Dept. of Electrical Engineering, University of California, Riverside, CA 92521* ZnO quantum dots and related Mn-doped ZnO/ZnMgO nanostructures have recently attracted significant attention as a new nano-engineered functional material for spintronic and optoelectronic applications. We have studied the carrier recombination processes in ZnO-based quantum dots both theoretically and using the photoluminescence (PL) spectroscopy in the temperature range T=8.5 K - 300 K [1]. The obtained experimental data suggest that below T = 70 K, the ultraviolet PL in ZnO quantum dots originates from recombination of the donor-acceptor pairs, while above T = 70 K it is due to recombination of the acceptor-bound excitons. The latter is in agreement with our theoretical predictions [2]. No strong inhomogeneous broadening has been observed in ultraviolet PL from ZnO quantum dots. Our results shed new light on the carrier-recombination processes in ZnO quantum dots and can be used for the ZnO nanostructure optimization for the proposed applications. The authors acknowledge the support of MARCO and its Functional Engineered Nano Architectonics (FENA) Focus Center. [1] V.A. Fonoberov, K.A. Alim, A.A. Balandin et al., Phys. Rev. B, submitted (2005); [2] V.A. Fonoberov and A.A. Balandin, Phys. Rev. B 70, 195410 (2004); Appl. Phys. Lett. 85, 5971 (2004).

**13:51**

**H17 12 Mechanical Property Characterization for Nanowires** RUSTOM BHILADVALA, MINGWEI LI, THERESA MAYER, JAMES SIOSS, CHRISTINE KEATING, JOAN REDWING, *The Pennsylvania State University* Understanding and predicting the behavior of NEMS (nanoelectromechanical systems) resonators made by assembling template-grown nanowires requires characterization of the elastic modulus and intrinsic damping for such materials. In this work, we present results of resonance measurements using cantilevers made by electroplating clamps which fully enclose one end of nanowires (NWs) made from Si, Rh and Au. Data from 16 such Si NWs made by the VLS (Vapor-Liquid-Solid) technique reveal a typical Q-factor of 5000, a geometric scaling ( $\sim D/L^2$, diameter D, length L) of the frequency consistent with linear elastic beam theory, and a higher value of Young's modulus for single-crystal silicon than reported from experiments with thin-film Si resonators. The low scatter in the modulus data and the high value of Q are both indicative of low clamping losses. Similar-sized wires of polycrystalline Rh and Au made by electroplating, show net damping values (using Q-factor, mass and stiffness) for these materials to be close to each other and roughly 14 times that for silicon.

**14:03**

**H17 13 Selective epitaxy of III-V semiconductor on Si substrates patterned by diblock copolymer*** ZUOMING ZHAO, *Dept. of Electrical Engr., UCLA* TEA-SIK YOON, YA-HONG XIE, *Dept. of Materials Science and Engineering, UCLA* KANG L. WANG, *Dept. of Electrical Engr., UCLA* DUYEOL RYU, THOMAS P. RUSSELL, *Polymer Science and Engr. Dept., Univ. of Massachusetts, Amherst, MA, 01003* III-V semiconductors, GaAs and InAs, were grown on Si substrates using molecular beam epitaxy. Si substrates were patterned with $SiO_2$ using thin films of diblock copolymer, PS-*b*-PMMA. Using a thin film of a random P(S-r-MMA) copolymer to balance interfacial interactions, spin coated film of PS-b-PMMA, having cylindrical microdomains, were annealed 170$^o$C to orient the microdomais normal to the surface. [ P. Mansky et al, Science, 275, 1997 (1458)] After removal of the PMMA cylinders, RIE was used to transfer the copolymer template to the substrate yielding a hexagonal array of $\sim$ 20 nm pores in the substrate. GaAs and InAs were selectively filled in pores. Images from scanning electron microscopy show that GaAs and InAs quantum dots with density of $8\times 10^{10}$ cm$^{-2}$ and diameter of 30nm were achieved by selective epitaxy. This provides the possibility of patterning of nanostructures for integration of III-V materials on Si and offers new potentials for electronic and optoelectronic applications based on regular or homogeneous structures.

*Marco Focus Center on Functional Engineered Nano Architectonics

**SESSION H18: FOCUS SESSION: CARBON NANOTUBES: ELECTRONIC AND OPTICAL PROPERTIES II**
**Tuesday Morning, 14 March 2006; 315, Baltimore Convention Center at 11:15**
**Vasili Perebeinos, IBM, presiding**

*Invited Papers*

**11:15**
**H18 1 Two-photon photoluminescence and exciton binding energies in single-walled carbon nanotubes.**
CHRISTOPH LIENAU, *Max-Born-Institute, Berlin, Germany*

The optical properties of carbon nanotubes are thought to be dominated by excitonic effects. Exciton binding energies between 100 meV and 1 eV have been predicted, depending on diameter, chiral angle, and surrounding medium. Experimental proof for these large binding energies, however, has been missing so far. Here we present direct experimental evidence that the elementary optical excitations of carbon nanotubes are strongly Coulomb-correlated, quasi-one dimensionally confined electron-hole pairs, stable even at room temperature. By comparing one-photon and two-photon luminescence excitation spectra, we probe excitonic states with distinctly different wavefunction symmetry [1]. The energy splitting between one-photon active and two-photon active states is a distinct fingerprint of excitonic interactions in carbon nanotubes and binding energies between 300 and 500 meV are derived. Our results are strongly supported by itab initio calculations of two-photon absorption spectra [2]. We discover that for all the tubes studied, excitonic effects are very strong and are crucial for the one-photon as well as the two-photon spectra in both the peak shapes and positions. The implications of these results for the fluorescence yield and lifetime of single-walled carbon nanotubes [3] will be discussed. [1] J. Maultzsch et al., Phys. Rev. B 72, Rxxx (2005); cond-mat/0505150. [2] E. Chang, G. Bussi, A. Ruini, and E. Molinari, Phys. Rev. Lett. 92, 196401 (2004). [3] A. Hagen et al., Phys. Rev. Lett. 95, 197401 (2005).

**11:51**
**H18 2 Ab initio study of the optical properties of carbon nanotubes.**
ERIC CHANG, *CNR-INFM National Research Center S3 and Univ. of Modena and Reggio E., Italy*

We present an ab initio study of the optical properties of carbon nanotubes. We use state-of-the-art electronic structure methods based on many-body perturbation theory to compute the optical absorption and resonance Raman spectra of large tubes which have up to 200 atoms [1,2]. Our symmetry-based method makes the study of large tubes feasible within the many- body framework and also allows us to understand the symmetry properties of the excitons and selection rules. We include a study of the so-called dark excitons which are crucial for understanding luminescence efficiency in carbon nanotubes. The mechanism that explains the dark-bright splitting can be understood within our symmetry-based approach. Finally, we present an analysis of the two-photon spectra for several carbon nanotubes, a theoretical analysis which, in conjunction with combined one- and two-photon experiments, allows one to measure the binding energy of excitons. We find in all cases that the excitonic binding energy is large, ranging from 0.5 to 0.9 eV depending on the diameter of the tube, and that the excitonic wavefunction is Wannier-like and extended over many atoms. Our studies for the one- and two-photon absorption and resonance Raman spectra have been fruitful for understanding the corresponding experiments. In particular, our theoretical results are in good agreement with one- and two-photon absorption experiments [3-5]. The results for resonance Raman show that such a spectroscopic technique is a good alternative to optical absorption since it allows for the selection of tubes of a given diameter while probing the same excited states.

1. E.K. Chang, G. Bussi, A. Ruini, and E. Molinari, Phys. Rev. Lett. 92, 196401 (2004). 2. E.K. Chang, G. Bussi, A. Ruini, and E. Molinari, Phys. Rev. B 72, 195423 (2005). 3. M. Y. Sfeir et al., Science 306, 1540 (2004). 4. J. Maultzsch et al., to be published in Phys. Rev. B, see also cond-mat/0505150. 5. Z. M. Li et. al., Phys. Rev. Lett. 87, 127401 (2001).

*Contributed Papers*

**12:27**
**H18 3 Structural Dependence of Excitonic Optical Transitions and Band-Gap Energies in Carbon Nanotubes** GORDANA DUKOVIC, FENG WANG, DAOHUA SONG, MATTHEW SFEIR, TONY HEINZ, LOUIS BRUS, *Columbia University* The optical transitions in semiconducting carbon nanotubes have recently been ascribed to excitons. We have used two-photon excitation spectroscopy to measure the energies of exciton states of different symmetries by taking advantage of the different selection rules for two-photon absorption and one-photon fluorescence in this quasi-one-dimensional molecule. The measured exciton binding energies are on the order of hundreds of meV. Here we report the investigation of structural dependence of the exciton energies for different nanotube species, ranging in diameter from 0.76 to 1.2 nm. The exciton binding energies vary inversely with nanotube diameter, ranging from 420 to 270 meV in this sample. This result is in agreement with theoretical predictions. In addition, we have found that the measured band-gap energies are significantly blue-shifted from those predicted by tight-binding calculations, which may have implications for the transport properties of semiconducting carbon nanotubes.

**12:39**

**H18 4 Ultrafast decay of $E_{22}$ subband excitons in semiconducting SWNTs** TOBIAS HERTEL, JARED J. CROCHET, ZIPENG ZHU, *Vanderbilt University* We use CW and time-resolved spectroscopy for an investigation of intra- and interband relaxation of excited states in micelle suspended SWNTs. We observe that the dynamics of $E_{22}$ subband exciton decay in SWNTs is surprisingly similar to the dynamics of photoexcited carriers in bulk graphite. Moreover we find a clear correlation of the $E_{22}$ exciton decay rate with the excited state energy. We compare these results with earlier theoretical studies of quasi-particle decay in graphite and discuss the role of electron-electron and electron-phonon coupling for the dynamics of higher excited states.

**12:51**

**H18 5 Real-time *ab initio* simulations of excited carrier dynamics in carbon nanotubes.*** YOSHIYUKI MIYAMOTO, *Fundamental and Environmental Res. Labs. NEC* ANGEL RUBIO SECADES, *Universita Pais Vasco* DAVID TOMANEK, *Michigan State University* Combining time-dependent density functional calculations for electrons with molecular dynamics simulations for ions, we investigate the dynamics of excited carriers in a (3,3) carbon nanotube at different temperatures. Following an $h\nu = 6.8$ eV photo-excitation, the carrier decay is initially dominated by efficient energy transfer to the electronic degrees of freedom. About 200 fs after the photoexcitation in a nanotube initially at room temperature, the electron-hole gap is reduced to nearly half its initial value and the decay mechanism becomes dominated by coupling to phonons. We show that the onset point and damping rate within the phonon regime change with the initial ion velocities, which is a manifestation of a temperature dependent electron-phonon coupling.

*This work was supported by the Earth Simulator Center.

**13:03**

**H18 6 Pump-probe excitation spectroscopy of chirality enriched SWNT suspensions** ZIPENG ZHU, *Vanderbilt University* MICHAEL ARNOLD, *Northwestern University* JARED J. CROCHET, *Vanderbilt University* MARK HERSAM, *Northwestern University* CLAY McPHEETERS, *Rice University* DANIEL E. RESASCO, *University of Oklahoma* HENDRIK ULBRICHT, *University of Vienna* TOBIAS HERTEL, *Vanderbilt University* We study the transient optical response of chirality enriched SWNT samples by conventional pump-probe and pump-probe excitation spectroscopy using visible pump and white-light continuum probe pulses. Comocat starting material is suspended using either SDBS or DNA as surfactants. In addition, DNA suspended samples have been isopycnically fractionated. Transient spectra of these sample are significantly less congested than multi-disperse suspensions, which greatly simplifies the interpretation of photobleaching and photo-absorption transients. The newly developed technique of pump-probe excitation spectroscopy (PPES) also allows to study previously inaccessible aspects of the dynamics of the second subband $E_{22}$ exciton decay. Experiments indicate that $E_{22} \rightarrow E_{11}$ interband relaxation rates are higher than the decay of *G*-mode phonon sidebands seen not only in PPES but also in photoluminescence excitation spectra.

**13:15**

**H18 7 Intrinsic and extrinsic effects in the temperature dependent photoluminescence of semiconducting carbon nanotubes** DENIS KARAISKAJ, CHAIWAT ENGTRAKUL, TIMOTHY McDONALD, MICHAEL J. HEBEN, ANGELO MASCARENHAS, *Center for Basic Science, National Renewable Energy Laboratory, 1617 Cole Boulevard, Golden, Colorado 80401, USA* The temperature dependence of the band gap of semiconducting carbon nanotubes was measured for ten different nanotube species. The unprecedented effectiveness in avoiding the effect of external strain, or any other effects originating from the surrounding environment, lead to an accurate measurement of the band gap temperature dependence, giving fundamental insight into the nanotube electron-phonon interaction. Small but reproducible energy shifts of the emission lines with temperature were observed, showing a moderate chirality dependence, well in agreement with recent theoretical calculations [1]. In addition to the energy shift, a substantial narrowing of the emission lines was also observed. The removal of the temperature shift of the band gap, allows the precise measurement of the effect of external strain on carbon nanotubes in different environments. [1] Rodrigo B. Capaz, Catalin D. Spataru, Paul Tangney, Marvin L. Cohen, and Steven G. Louie, Phys. Rev. Lett. **94**, 036801 (2005).

**13:27**

**H18 8 Strong anisotropy in the THz absorption spectra of stretch-aligned single walled carbon nanotubes** Y. IWASA, N. AKIMA, H. MATSUI, N. TOYOTA, *Tohoku University* S. BROWN, A. M. BARBOUR, J. CAO, J. L. MUSFELDT, *University iof Tennessee* M. SHIRAISHI, *Osaka University* H. SHIMODA, O. ZHOU, *University of North Carolina* Polarized THz spectroscopy is crucial for understanding the low-energy electronic structure and carrier dynamics in single walled carbon nanotubes (SWNTs), as well as for exploring polarization-sensitive THz applications. We prepared stretch-aligned SWNT/polymer composites, and measured the polarized absorption spectra from the THz through the visible region. The low-frequency electronic excitations are predominantly polarized parallel to the tube direction. The peak centered near 100 $cm^{-1}$ is discussed in terms of a curvature-induced gap and a plasmon resonance due to a finite size/wavelength effects in the SWNTs. The broad middle infrared structure that is observed in unoriented films with spaghetti-like morphology disappears in stretch-aligned samples, suggesting that this middle infrared feature may be due to in-gap states in the semiconducting tubes caused by the highly disordered morphology of the unoriented films. Hole doping effects were also investigated, and conversion of semiconducting tubes to more conducting ones is demonstrated.

**13:39**

**H18 9 Ultrafast dynamics of the mid-infrared response of carbon nanotubes** CHRISTIAN FRISCHKORN, *Physics Department, Freie Universitat Berlin, Germany* TOBIAS KAMPFRATH, LUCA PERFETTI, MARTIN WOLF, We report on time-resolved measurements of low-energy excitations in carbon nanotubes and compare these with results obtained for graphite. The systems mid-infrared response has been obtained from time-resolved THz spectroscopy data in the 10 - 30 THz spectral range. We find essentially two processes governing an electronic current

dynamics in carbon nanotubes. First, strongly bound excitons are the main photoproduct in large-band gap tubes and thus prevent a typical free-carrier response, while in small-gap and metallic tubes carrier localization due to defects is observed as manifested in a substantial dichroism. In these measurements, the reduced polarizability perpendicular to the tube axis is exploited. In the case of graphite, our results show that strongly coupled optical phonons in the graphite layer dominate the ultrafast energy and transport relaxation dynamics after optical excitation [1]. These phonon modes heat up on a femtosecond time scale and cool down with a time constant of several picoseconds. Moreover, the observed pronounced increase in the Drude relaxation rate significantly originates from these few active lattice vibrations. - [1] PRL 95, 187403 (2005).

**13:51**
**H18 10 Photoluminescence excitation spectroscopy of individual single walled carbon nanotubes** JACQUES LEFEBVRE, *National Research Council* JEFFERY BOND, *University of Ottawa* YOSHIKAZU HOMMA, *NTT Basic Research Laboratories* PAUL FINNIE, *National Research Council* Photoluminescence excitation spectroscopy is an essential tool for understanding the optical properties of single walled carbon nanotubes. In many cases, such measurements are performed on large ensembles and, aside from the main spectral features, reliable assignment is most often difficult. In order to address the existence of additional emission and absorption levels/bands in PLE spectra, this work has focused on the study of individual and small ensembles of single walled carbon nanotubes. Such carbon nanotubes are grown by chemical vapor deposition on pre-patterned substrates allowing individual nanotubes to be suspended in free space. The measurements are performed in air, at room temperature, without post growth processing of the nanotubes.

**14:03**
**H18 11 Optical Spectroscopy of individual Single-Walled Carbon Nanotubes of Defined Chiral Structure** MATTHEW SFEIR, *Columbia University* TOBIAS BEETZ, *Brookhaven National Lab* FENG WANG, LIMIN HUANG, X.M. HENRY HUANG, JAMES HONE, STEPHEN O'BRIEN, *Columbia University* JAMES MISEWICH, *Brookhaven National Lab* TONY HEINZ, *Columbia University* YIMEI ZHU, *Brookhaven National Lab* LOUIS BRUS, *Columbia University* Single-walled carbon nanotubes (SWNTs) constitute of a family of nanostructures with over one hundred members. Each specific structure has distinct electronic and optical properties, varying from semiconducting to metallic. Here we study the correlation between electronic structure and physical structure in SWNTs by combing high-sensitivity Rayleigh spectroscopy and electron diffraction techniques. Simultaneous application of these experimental techniques on individual SWNTs allows for measurement of electronic transitions in tubes of fully and independently determined structure. In this manner, we directly verify the ''family behavior'' that has guided previous spectroscopic assignment of optical transitions in semiconducting SWNTs. We also demonstrate the previously unobserved, but theoretically predicted splitting of optical transitions in metallic SWNTs.



**SESSION H19: FOCUS SESSION: III-V MAGNETIC SEMICONDUCTORS II**
**Tuesday Morning, 14 March 2006; 316, Baltimore Convention Center at 11:15**
**Nitin Samarth, Pennsylvania State University, presiding**

***Invited Papers***

**11:15**
**H19 1 Optical Properties of Ferromagnetic Semiconductors.**
KENNETH BURCH, *University of California, San Diego*

Ferromagnetic semiconductors hold great promise for numerous magneto-optics applications. In this talk I detail recent optical spectroscopic studies of as grown and annealed thin films and digitally doped superlattices of $Ga_{1-x}Mn_xAs$, prepared in the group of D.D. Awschalom (UCSB) and annealed in the group of N.Samarth (PSU). Annealing induces a large strengthening of the optical conductivity ($\sigma_1(\omega)$), while the frequency dependence of $\sigma_1(\omega)$ remains unchanged. This indicates that the scattering rate and Fermi level have not been effected by annealing, despite the large increase in hole density. Our Infrared work on Digital Ferromagnetic Heterostructures reveals a unique ability to tune their optical properties as well as their intrinsic electronic structure without changing the doping/defect level. This work is in collaboration with D.B. Shrekenhamer, E.J. Singley, D.N. Basov (University of California, San Diego) J. Stephens, R.K. Kawakami, D.D. Awschalom (University of California, Santa Barbara), B.L. Sheu, and N. Samarth (Pennsylvania State University).

*Contributed Papers*

**11:51**

**H19 2 Faraday and Kerr effect studies in optimally annealed $Ga_{1-x}Mn_xAs$ random alloys.*** GHEOGHE ACBAS, A. MARKELZ, J. CERNE, *Physics Dept., Univ. at Buffalo, SUNY, Buffalo, NY* M. CUKR, V. NOVAK, *Institute of Physics, Acad. of Sciences of the Czech Republic, Prague, Czech Republic* J. SINOVA, *Physics Dept., Texas A&M Univ., College Station, TX* The mid-infrared (MIR: 115-366 meV) complex Faraday and Kerr effect are studied in $Ga_{1-x}Mn_xAs$ random alloy films (x = 0.05, and x = 0.07) as a function of frequency and temperature. The samples are optimally annealed with $T_C$ around 100K. The strong MIR magneto-optical response shows clear ferromagnetic behavior that is consistent with dc magnetization measurements. The real and imaginary parts of the measured Faraday and Kerr angles are in qualitative and quantitative agreement with the values predicted by an effective Hamiltonian model within a mean field treatment [E. M. Hankiewicz, J. Sinova et al., PRB 2004]. The Kerr and Faraday rotation peak at approximately 220 meV, which is consistent with theoretical predictions.

*This work was supported by DARPA/ONR N0001400-1-0951, Research Corporation Cottrell Scholar Award and NSF CAREER Award

**12:03**

**H19 3 Ferromagnetic resonance (FMR) study of ultra-thin $Ga_{1-x}Mn_xAs$ films as a function of layer thickness*** YINGYUAN ZHOU, Y.J. CHO, Z. GE, X. LIU, M. DOBROWOLSKA, J.K. FURDYNA, *Department of Physics, University of Notre Dame, Notre Dame, IN 46556* We report a detailed study of ferromagnetic resonance (FMR) in a series of $Ga_{1-x}Mn_xAs$ (x = 0.05) thin films grown on (100)GaAs substrates by low-temperature MBE. The thicknesses of the specimens ranged from 10nm to 200nm. We measured angular and temperature dependences of FMR and fitted the data to obtain the cubic and the uniaxial anisotropy parameters and g- factors for each specimen. The quality of the theoretical fitting results clearly indicates that FMR data can be reliably used to determine magnetic anisotropy parameters of $Ga_{1-x}Mn_xAs$. Our experiment indicates a strong thickness dependence of the in-plane uniaxial anisotropy field; on the other hand, the cubic anisotropy field, perpendicular uniaxial anisotropy field, and the g-factors depend on the hole concentration, but show little if any dependence on the film thickness, at least for as-grown specimens. The measurements and analysis of annealed specimens are presently underway.

*Supported by NSF Grant DMR02-10519

**12:15**

**H19 4 Ultrafast light-induced demagnetization in (III,Mn)V ferromagnetic semiconductors** L. CYWINSKI, L. J. SHAM, *University of California San Diego, Department of Physics* J. WANG, C. SUN, J. KONO, *Dept. of Elec. and Comp. Engineering, Rice University* A. OIWA, *University of Tokyo* H. MUNEKATA, *Tokyo Institute of Technology* An ultrafast (subpicosecond) demagnetization process induced by intense laser irradiation has been recently observed in InMnAs [1]. We propose a theoretical model of magnetization dynamics on such a timescale which is based on the sp-d exchange interaction between the delocalized carriers' spins and localized Mn spins. Light excitation heats up a population of holes, taking it out of equilibrium with the Mn spins. This triggers the process of energy and angular momentum exchange between the two spin systems. Fast spin relaxation of holes sustains the flow of spin polarization leading to the possibility of significant demagnetization of the Mn system. Ultrafast magnetization dynamics in GaMnAs will also be discussed. This work was supported by DARPA, NSF, ONR and MEXT. [1] J. Wang et al., Phys. Rev. Lett. 95, 167401 (2005).

**12:27**

**H19 5 Pressure Dependent Magnetotransport Properties of Dilute Magnetic Semiconductors** M. CSONTOS, G. MIHALY, *Department of Physics, Budapest University of Technology and Economics, 1111 Budapest, Hungary* T. WOJTOWICZ, *Institute of Physics, Polish Academy of Sciences, 02-668 Warsaw, Poland* B. JANKO, X. LIU, J. K. FURDYNA, *Department of Physics, University of Notre Dame, Notre Dame, Indiana 46556, USA* The $Mn^{2+}$ ions in (III,Mn)V ferromagnetic semiconductors provide magnetic moment and at the same time they act as a source of valence-band holes that mediate the $Mn^{2+}$-$Mn^{2+}$ interactions. This coupling results in the ferromagnetic phase. By using hydrostatic pressure to continuously tune the wavefunction overlap, one can control the strength of the ferromagnetic coupling resulting in a spectacular enhancement of the magnetization and the Curie-temperature [M. Csontos et al. Nature Materials **4**, 447 (2005)]. Magnetoresistance measurements on the magnetic semiconductor (In,Mn)Sb suggest that magnetic scattering in this material is dominated by isolated $Mn^{2+}$ ions located outside the ferromagnetically ordered regions [M. Csontos et al. Phys. Rev. Lett. **95**, 227203 (2005)]. The transport properties in presence of high magnetic field and hydrostatic pressure have also been investigated by Hall-effect and thermoelectric power measurements.

**12:39**

**H19 6 Magnetoresistance anomalies during hard axis magnetization reversal in (Ga,Mn)As epilayers.** MENG ZHU, GANG XIANG, BEN LI SHEU, XIA LI, PETER SCHIFFER, NITIN SAMARTH, *Physics Department, Penn State University, University Park PA 16802* The ferromagnetic semiconductor (Ga,Mn)As is known to display striking magnetoresistance (MR) during magnetization reversal. Here, we use temperature- and field-dependent MR measurements to probe hard axis magnetization switching processes in (Ga,Mn)As epilayers grown on (001) GaAs. MR is measured using Hall bars oriented along the three principal crystalline directions ([100], [$\bar{1}$10] and [110]) over a temperature range 0.35 mK $\leqslant T \leqslant$ 120 K, with the magnetic field normal to the sample plane. We find that the longitudinal MR exhibits distinct signatures corresponding to different types of magnetization reversal processes. While domain wall nucleation and propagation produce large MR anomalies ( $\sim 50\Omega - 100\Omega$), coherent domain rotation is accompanied by surprisingly weak MR. We discuss our experimental measurements using analytical simulations that incorporate SQUID magnetization data as additional input. Supported by DARPA/ONR and NSF.

**12:51**

**H19 7 Magnetotransport studies of $Ga_{1-x}Mn_xSb$ Random Alloys.** M. EGINLIGIL, G.B. KIM, S. WANG, H. LUO, B.D. MCCOMBE, *Department of Physics, University at Buffalo, SUNY* We report magnetotransport and magnetization measurements from two sets of well-characterized $Ga_{1-x}Mn_xSb$ samples grown by molecular beam epitaxy: set 1 - varying Sb/Ga flux ratios and constant nominal Mn concentration of 2.3%; set 2 - constant flux ratio (Sb/Ga=5.7) and varying nominal Mn content. Plots of $R_{sheet}$vs. temperature show both metallic and thermally activated

behavior. Two samples (one from each set) having the highest effective Mn content (as determined from measurements of saturation magnetization at low temperatures) but different flux ratios, exhibited thermally activated transport. Hole densities in the range $2.6x10^{19}cm^{-3}$ to $1.3x10^{20}cm^{-3}$ were extracted from plots of $R_{Hall}/ R^{\alpha}_{Sheet}$ vs. $B/ R^{\alpha}_{Sheet}$ at high fields and low temperatures; for the metallic samples $1 < \alpha < 2$ and for the samples showing thermally activated behavior $\alpha < 1$. The two samples that showed thermally activated transport, although they had the highest measured Mn content, have hole densities at the low end of the measured range. Both of these samples also exhibit extrema in the remnant hall resistance vs. temperature, with the sample from set 1 also showing very complex behavior of the anomalous Hall coefficient (a change of sign) vs temperature. This complex behavior is attributed to movement of the chemical potential through a region of non-monotonic behavior of the density of states vs. energy. Supported in part by DARPA ONR SpinS and NSF ECS0224206.

**13:03**

**H19 8 Transport Properties of $Ga_xCr_{1-x}N$ thin films synthesized by MBE** STEPHEN WU, HONGXUE LIU, RAKESH SINGH, NATHAN NEWMAN, *Arizona State University* The electrical transport properties of ferromagnetic single phase Cr-doped gallium nitride films grown by reactive molecular beam epitaxy were investigated by performing Hall and resistivity measurements as a function of temperature over a wide range of dopant concentrations. For Cr concentrations at 3%, the films are highly resistive and the thermally activated electron transport follows the exponential law, $R=R_o\exp[(T_o/T)]^{-1/4}$, characteristic of variable range hopping between localized states in an impurity band [1]. This relationship does not explicitly hold over a significant temperature range for other Cr concentrations. The physical mechanism responsible for the differences in the electrical properties of these films will be elucidated by comparing the transport processes involved with the fraction of Cr atoms situated on Ga substitutional sites as measured by RBS ion channeling and the ferromagnetic properties determined using a variable temperature vibrating sample magnetometer. [1] N.F. Mott, Philos. Mag., **19**, 835 (1969).

**13:15**

**H19 9 Controlling ferromagnetism in GaMnAs by arsenic defect engineering*** R. C. MYERS, A. W. JACKSON, A. C. GOSSARD, D. D. AWSCHALOM, *Center for Spintronics and Quantum Computation, University of California, Santa Barbara, CA 93106* B. L. SHEU, P. SCHIFFER, N. SAMARTH, *Department of Physics, The Pennsylvania State University, University Park, PA 16802* We manipulate the Curie temperature and hole density of $Ga_{1-x}Mn_xAs$ for $x = 0.75\%$ to 3% by systematically varying the arsenic compensation by As-flux control. The As:Ga flux ratio is varied using a new technique of non-rotated GaMnAs growth, where the geometry of the molecular beam epitaxy system provides a continuous variation in As-flux across a wafer. In this manner, As-stoichiometry can be calibrated in a single growth run for any Mn doping density. The hole density and Curie temperature are maximized at the same position on each wafer suggesting that minimizing As-defect compensation improves magnetic properties. Surprisingly, changes in the arsenic flux of as little as 10% can quench ferromagnetism in the low Mn-doped material causing an apparent shift in the paramagnetic to ferromagnetic cross over transition toward higher Mn concentrations. The results suggest that proper control of arsenic compensation is critical for optimizing Curie temperatures in the low Mn-doping regime.

*Work supported by DARPA, ONR, AFOSR, and NSF.

**13:27**

**H19 10 Evidence of MnAs precipitates in a diluted magnetic semiconductor (Ga,Mn)As** TAESOON HWANG, SOONCHIL LEE, *Dept of physics, Korea Advanced Institute of Science and Technology, Daejeon Korea* S. H. CHUN, *Dept of Physics, Sejong University, Seoul Korea* H.K. CHOI, Y.S. KIM, Y.D. PARK, *School of Physics, Seoul National University, Seoul Korea* Local magnetic field in (Ga,Mn)As epilayers with 500 nm thickness having 3.6% and 5.8% Mn was studied by zero field nuclear magnetic resonance (NMR) at liquid helium temperatures. The macroscopic magnetic and transport properties of the epilayers are quite similar to other previously reported low temperature molecular beam epitaxy prepared samples. We carefully searched for NMR signal from 20 MHz to 250 MHz, but only the spectrum of MnAs precipitations of hexagonal NiAs structure was observed. No evidence for the magnetism due to the substituted Mn ions was observed by NMR within the frequency range investigated. About 1/7 of Mn atoms incorporated into the sample participates in the formation of precipitates whose size is as small as to favor formation of single magnetic domains. Temperature dependence of magnetic moment of MnAs precipitations estimated by NMR frequency below 12 K indicates that its Tc should be much lower than that of bulk. The magnetization of MnAs precipitations decreases faster with increasing temperature for samples with a lower transition temperature. The origin of this correlation between the critical temperatures of MnAs precipitates and the single phase (Ga,Mn)As is not fully understood at this moment.

**13:39**

**H19 11 Magnetic Properties of Ferromagnetic (Ga,Mn)As Grown on (511) GaAs Substrates** CHONG XIE, Y. J. CHO, R. CHAKARVORTY, Y. Y. ZHOU, Z. GE, W. L. LIM, X. LIU, J. K. FURDYNA, M. DOBROWOLSKA, *Department of Physics, University of Notre Dame, Notre Dame, IN 46556* Ferromagnetic (Ga,Mn)As films were successfully grown on SI GaAs (511)A and (511)B substrates by LT-MBE. We have performed SQUID, magnetotransport, ferromagnetic resonance (FMR), and Magneto-Optic Kerr Effect (MOKE) measurements to characterize the magnetic properties of these samples. A conspicuous feature observed on these samples is an asymmetric shift of the Hall resistance caused by the superposition of the Planar Hall Effect (PHE) and the Anomalous Hall Effect (AHE), in agreement with our earlier studies of (Ga,Mn)As grown on vicinal GaAs (001) substrates. This asymmetric shift is a direct manifestation of the strength of the magnetocrystalline anisotropy, which confines the magnetization to the preferred crystalline plane, thus resulting in a non-zero component of the magnetization normal to the (Ga,Mn)As layer. The results are also compared with the magnetic properties measured in (Ga,Mn)As films grown on GaAs substrates with other orientations, e.g., (001) and (311). Supported by NSF Grant DMR02-10519.

**13:51**

**H19 12 Large spin polarization in $Ga_{1-x}Mn_xP$ synthesized by ion implantation and pulsed-laser melting** M.A. SCARPULLA, P.R. STONE, R. FARSHCHI, I.D. SHARP, E.E. HALLER, O.D. DUBON, *Dept. of Materials Science and Engineering, University of California and Lawrence Berkeley National Laboratory, Berkeley CA 94720* J.W. BEEMAN, *Lawrence Berkeley National Laboratory, Berkeley, CA 94720* E. ARENHOLZ, *Advanced Light Source, Lawrence Berkeley National Laboratory, Berkeley, CA 94720* We have recently demonstrated that the mediating holes in $Ga_{1-x}Mn_xP$ reside in an impurity band separated from the valence band by a gap [Scarpulla et al., Phys. Rev. Lett. **95** 207204 (2005)]. For samples with x≈ 0.06 and Curie temperature 60 K, this gap is approximately 25 meV. In this work, we demonstrate a very large spin polarization of states near the Fermi level across a range of Mn compositions using Mn $L_{3,2}$ X-ray magnetic circular dichroism (XMCD). We find that the X-ray absorption spectrum at the Mn $L_{3,2}$ edge is very similar to that observed in $Ga_{1-x}Mn_xAs$ [Edmonds et al., Appl. Phys. Lett. **84** 4065 (2004)], indicating that the Mn bonding environment is similar between $Ga_{1-x}Mn_xAs$ and $Ga_{1-x}Mn_xP$. The magnitude of the X-ray fluorescence XMCD signal reaches approximately 70% at the Mn $L_3$ edge across the range of compositions, indicating a large spin asymmetry in the density of states. This is consistent with (but not exclusive to) the existence of a spin-polarized impurity band near the Fermi level.

**14:03**

**H19 13 Evidence of room temperature itsp-d exchange in InMnAs epitaxial films** PHILIP CHIU, BRUCE WESSELS, *Northwestern University* InMnAs grown by metal organic vapor phase epitaxy (MOVPE) is a promising ferromagnetic semiconductor due to its high Curie temperature ($T_c$) of 330 K. However, the nature of itsp-d exchange in this material is not well understood. Since enhancement of magnetic circular dichroism (MCD) at band structure critical points is indicative of sp-d exchange, the reflection MCD of MOVPE InMnAs was measured. At room temperature and an applied field 0.5 T, the MCD spectrum is composed of two types of transitions: a negative peak centered between 2.60-2.68 eV and a broad featureless negative response from 1.6-3.0 eV. At both transitions, ferromagnetic hysteresis and saturation are observed in the MCD field dependence. The negative peak occurs between the *L*-point critical transitions of InMnAs, at 2.53 and 2.79 eV respectively. The single negative peak is also similar to that observed in MBE InMnAs in both the peak energy and width. The MCD enhancement at the *L*-point is consistent with room temperature itsp-d exchange splitting in MOVPE grown InMnAs. The itsp-d exchange is tentatively attributed to the presence of Mn dimers and trimers in the InMnAs that result in a $T_c$ of 326-327 K. The assignment of the broad spectral response is currently under way.



**SESSION H20: FRUSTRATION IN 3D**
**Tuesday Morning, 14 March 2006**
**317, Baltimore Convention Center at 11:15**
**Sarah Dunsiger, McMaster University, presiding**

**11:15**

**H20 1 Spin-nematic order in the frustrated pyrochlore-lattice quantum rotor model*** KAROL GREGOR, DAVID A. HUSE, S.L. SONDHI, *Princeton University* As an example of ordering due to quantum fluctuations, we examine the nearest-neighbor antiferromagnetic quantum $O(N)$ rotor model on the pyrochlore lattice. Classically, this system remains disordered even at zero temperature; we find that adding quantum fluctuations induces an ordered phase that survives to positive temperature, and we determine how its phase diagram scales with the coupling constant and the number of spin components. We demonstrate, using quantum Monte Carlo simulations, that this phase has long-range spin-nematic order, and that the phase transition into it appears to be first order.

*Supported by NSF MRSEC grant DMR-0213706

**11:27**

**H20 2 Engineering order−from−disorder** YUKITOSHI MOTOME, *RIKEN (The Institute of Physical and Chemical Research)* KARLO PENC, *Research Institute for Solid State Physics and Optics* NIC SHANNON, *H. H. Wills Physics Laboratory, University of Bristol* One of the most intriguing features of frustrated magnetism is the prevalence of *order–from–disorder* effects, where fluctuations conspire to select a unique state from a disordered manifold of degenerate classical ground states. Quite generally, order−from−disorder effects favour collinear spin configurations, and therefore lead to magnetization plateaux in many two−dimensional frustrated spin systems. Much less is known about order from disorder in three dimensions. Here we use classical Monte Carlo and low−T expansion techniques to show how thermal fluctuations stabilize a half−magnetization plateau in a Heisenberg model on the highly frustrated, three−dimensional Pyrochlore lattice if — and only if — they are given a ''helping hand'' by additional longer−ranged interactions. Our results provide the first example of fluctuation−driven magnetization plateau which can be tuned at will between different ordered states.

**11:39**

**H20 3 Inelastic Neutron Scattering Studies of $GeCo_2O_4$** M.K. CRAWFORD, R.L. HARLOW, *DuPont Company, Wilmington, DE* Y. CHEN, Q. HUANG, J.W. LYNN, Y. QUI, J.R.D. COPLEY, *NCNR, NIST, Gaithersburg, MD* S. HARA, Y. YOSHIDA, S.I. IKEDA, *AIST, Tsukuba, Japan* D.T. ADROJA, *ISIS, United Kingdom* R.W. STEVENS, B.F. WOODFIELD, J. BOERIO-GOATES, *Brigham Young University, Provo, UT* P.L. LEE, Y. ZHANG, *APS, ANL, Argonne, IL* R.A. FISHER, *LBNL, Berkeley, CA* $GeCo_2O_4$ is a normal spinel in which the magnetic spin- 3/2 $Co^{2+}$ ions are located on the crystallographic *B*-sites. $GeCo_2O_4$has a Néel transition ($T_N$ = 20.6 K) that coincides closely with a cubic-to-tetragonal structural phase transition, below which $c/a > 1$. Inelastic neutron scattering measurements show that there is an energy gap in the Néel state of magnitude 3 meV. We have measured the dispersion of the lowest energy spin wave branch along the (100), (110) and (111) directions for single crystals grown by the floating zone technique. In addition, inelastic neutron powder diffraction data have been obtained to study the higher energy crystal field levels of $Co^{2+}$. These data will be described and compared with results for other *B*-site spinels.

**11:51**

**H20 4 Suppressing magnetic order in $GeNi_2O_4$ and $GeCo_2O_4$** M. JAIME, A.V. SILHANEK, *LANL, Los Alamos, NM* P GODDARD, S.J. BLUNDELL, *Clarendon Lab, Oxford, UK* J.C. LASHLEY, *LANL, Los Alamos, NM* R.A. FISHER, *LBNL, Berkeley, CA* M.K. CRAWFORD, *DuPont, Willmington, DL* Spin S = 3/2 $GeCo_2O_4$ and spin S = 1 $GeNi_2O_4$ are both frustrated spinels, but they nevertheless order magnetically a low temperatures. $GeCo_2O_4$ achieves this by undergoing a structural phase

transition, but the mechanism adopted by $GeNi_2O_4$ is still an open question. We measured the magnetization, specific heat and magnetocaloric effect in polycrystalline samples of the title materials in high fields up to 45 T, and obtained detailed H,T phase diagrams. In the case of $GeNi_2O_4$ an almost degenerate double phase transition in zero field splits into two transitions separated by a wide magnetic field gap. The possibility of a spin-flop transition driven by single-ion anisotropy that also relieves the frustration in the Ni compound will be discussed.

**12:03**

**H20 5 Spin singlet state due to heptamer formation in $AlV_2O_4$** KEISUKE MATSUDA, NOBUO FURUKAWA, *Aoyama Gakuin University* YUKITOSHI MOTOME, *RIKEN* Spinel $AlV_2O_4$ is a mixed-valent system, where V ions construct a pyrochlore lattice with an average valence of 2.5+. This compound shows a phase transition at $T_c \sim$ 700K, and a doubling of the unit cell along the [111] direction is observed below $T_c$. A 3-1 type ''valence-skipping'' charge-ordering (CO) due to the strong correlation has been proposed to describe this transition. [1] Recently, a more careful analysis reported a trimer formation on [111] Kagomé layers. [2] It is also pointed out that the temperature dependence of the magnetic susceptibility can be decomposed into the Curie-Weiss contribution from $S = 1$ local moments on 1/8 of V sites and a spin-gap contribution from the rest V sites. [2] In the present study, instead of the CO scenario, we focus on the pairing of the Kagomé layers which leads to seven V-sites clusters (heptamers) by two trimers and a V site between the trimers. On the basis of the exact diagonalization study, we found that this model explains well the magnetic susceptibility in experiments. Hence, the heptamer formation appears to be the origin of the phase transition in this compound rather than the CO due to the electron correlation. [1] K. Matsuno *et al.*, J. Phys. Soc. Jpn. **70**, 1456 (2001) [2] Y. Horibe, *et al.*, unpublished

**12:15**

**H20 6 Entropy and susceptibility of ''stuffed'' spin ice – $Ho_2(Ho_xTi_{2-x})O_{7-x/2}$** B.G. UELAND, R.S. FREITAS, P. SCHIFFER, *Department of Physics and Materials Research Institute, Pennsylvania State University* G.C. LAU, B.D. MUEGGE, E.L. DUNCAN, R.J. CAVA, *Department of Chemistry, Princeton University* The spin ice material $Ho_2Ti_2O_7$ has been studied extensively due to its apparent residual ground state entropy, which is similar to that seen in water ice. This material has a pyrochlore structure in which the $Ho^{3+}$ and $Ti^{4+}$ cations form two interpenetrating sets of corner sharing tetrahedra. Here we present thermodynamic measurements on $Ho_2(Ho_xTi_{2-x})O_{7-x/2}$, with $0 \leqslant x \leqslant 0.67$, where we have replaced some Ti with Ho – effectively stuffing the lattice with more magnetic ions. We find that the zero field magnetic entropy remains essentially unchanged with stuffing. AC susceptibility measurements show the $T = 2$ K peak associated with the spin ice freezing decreases in magnitude with increasing $x$, indicating that spin freezing has been suppressed. While the residual entropy in $Ho_2Ti_2O_7$ is reduced with the application of a magnetic field, our measurements show that the entropy becomes less sensitive to applied field as $x$ is increased. This work is supported by the NSF.

**12:27**

**H20 7 Spin dynamics in the kagomé ice state** YOSHIKAZU TABATA, *Osaka University, Japan* HIROAKI KADOWAKI, *Tokyo Metropolitan University, Japan* KAZUYUKI MATSUHIRA, *Kyushu Institute of Technology, Japan* ZENJI HIROI, NAOFUMI ASO, *ISSP, University of Tokyo, Japan* BJÖRN FÅK, *CEA-Grenoble, France* Macroscopic degeneracy of the spin ice state in the geometrically frustrated pyrochlore oxide $Dy_2Ti_2O_7$ is partly or fully released under magnetic fields. For field along a [111] axis, it was proposed that another macroscopic degeneracy with a finite zero- temperature entropy occurs in the frustrated kagomé layers, which are built in the pyrochlore lattice. We have investigated this kagomé ice state using single-crystalline neutron scattering experiments. Spin correlations, i.e. scattering intensity maps, will be discussed based on Monte-Calro simulations of the spin-ice model with the dipolar interatction.

**12:39**

**H20 8 Spontaneous Strains in the Ground State of the Frustrated Pyrochlore $Tb_2Ti_2O_7$** JACOB RUFF, KIRRILY RULE, PATRICK CLANCY, JOHN PAUL CASTELLAN, JOSE RODRIGUEZ, BRUCE GAULIN, *McMaster University* The geometrically frustrated pyrochlore antiferromagnet $Tb_2Ti_2O_7$ has been the focus of much recent attention due to the spin liquid physics it displays at low temperatures. We have carried out high resolution x-ray scattering measurements of the principal Bragg peaks of $Tb_2Ti_2O_7$ which show substantial longitudinal broadening below approximately 20 K. Measurements on the non-magnetic pyrochlore $Y_2Ti_2O_7$ show no such broadening, suggesting this effect is driven by strong magnetoelastic coupling, as had been concluded from earlier anomolous low temperature Young's modulus measurements [Mamsurova et.al, JETP Letters, 1986]. We compare our x-ray scattering results to similar measurements in $TbVO_4$, which undergoes a cooperative Jahn-Teller phase transition near 34 K, and conclude that the longitundinal broadening is due to cubic-tetragonal fluctuations near a zero temperature phase transition, which acts to relieve the magnetic frustration.

**12:51**

**H20 9 Crystal Field Fluctuations in a Frustrated Pyrochlore Antiferromagnet $Tb_2Ti_2O_7$.** HAMID R. MOLAVIAN, MICHEL J. P. GINGRAS, *Department of physics, University of Waterloo* The antiferromagnetic pyrochlore $Tb_2Ti_2O_7$ presents a challenging puzzle to experimentalists and theorists studying frustrated magnets. Results from muon spin resonance and neutron scattering experiments for $Tb_2Ti_2O_7$ reveal a paramagnetic structure down to 50mK despite an antiferromagnetic Curie-Weiss temperature, $\theta_{CW} = -20$K. Crystal field calculations show that the $Tb^{3+}$ ion in $Tb_2Ti_2O_7$ is a ground state doublet with local $\langle 111 \rangle$ anisotropy and is separated from the first excited doublet state by a gap of 20K. We apply the Rayleigh-Schrodinger method to map the four states problem with exchange and dipole-dipole interactions onto an effective Hamiltonian with two states per ion. We give some properties of this effective Hamiltonian and discuss the possible classical and quantum phases of $Tb_2Ti_2O_7$.

**13:03**

**H20 10 Nematic order in square lattice frustrated ferromagnets** TSUTOMU MOMOI, *Condensed Matter Theory Laboratory, RIKEN* NIC SHANNON, *H. H. Wills Physics Laboratory, University of Bristol* PHILIPPE SINDZINGRE, *LPTMC, UMR 7600 of CNRS, Universite P. et M. Curie* We present a new scenario for the breakdown of ferromagnetic order in a two–dimensional quantum magnet with competing ferromagnetic and antiferromagnetic

interactions. In this, dynamical effects lead to the formation of two–magnon bound states, which undergo Bose–Einstein condensation, giving rise to bond–centered nematic order. This scenario is explored in some detail for an extended Heisenberg model on a square lattice. In particular, we present numerical evidence confirming the existence of a state with d– wave nematic correlations but no long range magnetic order, lying between the saturated ferromagnetic and collinear antiferromagnetic phases of the ferromagnetic $J_1$–$J_2$ model. We argue by continuity of spectra that this phase is also present in a model with 4–spin cyclic exchange. The case of the multiple spin exchange model on a triangular lattice, relevant to magnetism of solid $^3$He films, is also discussed.

**13:15**
**H20 11 A metamagnetic critical point in a three dimensional frustrated antiferromagnet** NIC SHANNON, *University of Bristol (UK)* KARLO PENC, *KFKI (Hungary)* YUKITOSHI MOTOME, *RIKEN (Japan)* The competition between different forms of order is central to the problem of strong correlation. This is particularly true of frustrated systems, which frequently exist at or near to a zero–temperature critical point. Here we show that a state with a half–magnetization plateau but no long range order can arise when a three dimensional frustrated antiferromagnet is tuned to a critical point bordering a metamagnetic state. We use classical Monte Carlo simulation and low–temperature expansion techniques to accurately characterize this ''spin pseudogap'' state, and show how its properties relate to those of the critical point. Our results provide an example of three dimensional spin model which can be used to study the relationship between gap and ''pseudogap'' — i.e. long range and preformed local order — near a metamagnetic critical point.

**13:27**
**H20 12 Transverse susceptibility of Ising spins** D. M. SILEVITCH, C. ANCONA-TORRES, T. F. ROSENBAUM, *James Frank Institute/University of Chicago* G. AEPPLI, *University College, London* The ac vector magnetic susceptibility of the Ising magnet $LiHo_xY_{1-x}F_4$ is studied as a function of frequency, excitation amplitude, transverse field and temperature. In the spin liquid ($x = 4.5\%$), application of a dc magnetic field projects the linear susceptibility transverse to the Ising axis. In addition, pumping the system along the Ising axis produces non-linear excitations in the transverse plane; these excitations can encode information and are potentially useful for quantum computation. In the ferromagnet ($x = 65\%$), measurements of the transverse susceptibility are used to probe the dynamics of domain wall tunneling and to estimate the mass of the domain walls.

**13:39**
**H20 13 $LiHo_xY_{1-x}F_4$ and the quantum Ising spin glass** MOSHE SCHECHTER, *Department of Physics and Astronomy, University of British Columbia* PHILIP STAMP, NICOLAS LAFLORENCIE, $LiHo_xY_{1-x}F_4$ in transverse field is considered to be the experimental realization of the transverse field Ising model, and a main tool in the study of quantum magnetism. For different values of $x$, ranging from 1 to $10^-3$, the system exhibits ferromagnetism, spin glass order, single large spin tunneling and various other interesting phenomena. Here we consider the spin glass regime, and in particular address two long standing puzzles posed by the experiments, i.e. the large disordering transverse field and the diminishing of the cusp in the nonlinear susceptibility as temperature is decreased. The solution of these puzzles emphasizes the significance of the hyperfine and offdiagonal dipolar interactions in this system. We then show that the latter destroys the spin glass order at any finite transverse field in this system, as well as in a general dipolar Ising spin glass. The nature of the disordering of the spin glass phase by quantum fluctuations will be discussed.

**13:51**
**H20 14 Random Field Effects in the Transverse Field Ising Spin-Glass $LiHo_xY_{1-x}F_4$ Magnetic Material.** S.M. ALI TABEI, MICHEL J.P. GINGRAS, *Department of Physics, University of Waterloo* Magnetic $LiHo_xY_{1-x}F_4$ in a transverse field has attracted a lot of attention recently because it is an ideal system to study quantum effects in disordered systems. When a magnetic field is applied transversely to the Ising magnetic moments in $LiHo_xY_{1-x}F_4$, the field-induced transition behaves quite differently from theoretical expectations. For $x = 0.167$ a paramagnet to spin glass transition has been studied experimentally in some detail. In particular,experiments find that the cusp in the nonlinear susceptibility signaling the glass state decreases in size as the temperature is lowered and the critical transverse field increases. We will show that the combination of applied transverse field and random off-diagonal dipolar interactions lead to random longitudinal field in $LiHo_xY_{1-x}F_4$. Using a simple model, we will show how this random field phenomenology accounts semi-quantitatively for the behavior of the nonlinear susceptibility in $LiHo_xY_{1-x}F_4$.



## SESSION H21: FOCUS SESSION: MICROFLUIDIC PHYSICS I
**Tuesday Morning, 14 March 2006; 318, Baltimore Convention Center at 11:15**
**Patrick Doyle, Massachusetts Institute of Technology, presiding**

***Invited Papers***

**11:15**
**H21 1 Experimental Studies of the Effects of Mixing on Reacting Systems.***
MATTHEW PAOLETTI, *University of Maryland at College Park*

Experimental studies of the effects of mixing on reacting systems are presented. The experiments can be divided into two classifications: (1) the effects of chaotic mixing on front propagation and (2) synchronization via superdiffusive mixing in an extended, fluid system. The front propagation studies are conducted in an oscillating vortex chain flow. The velocities of the propagating fronts are measured as a function of the frequency and amplitude of the external forcing. In the absence of mixing the Fisher-Kolmogorov result correctly predicts the front velocity; however these experiments show that this result is not extendable to chaotically mixed systems. Instead, the fronts are shown to mode-lock onto the

external forcing, propagating an integer number of vortices in an integer number of drive periods. The flow used in the synchronization studies is an oscillating/drifting vortex chain, which may be used to produce both enhanced diffusion and superdiffusion. We show that the key to synchronization in an extended, fluid system is superdiffusive transport produced by Lévy flights, where tracers undergo rapid jumps between distant regions of the flow.

*Supported by NSF and Bucknell University Research Experience for Undergraduates

*Contributed Papers*

**11:51**

**H21 2 Electrophoresis of Large DNA Molecules in Microcontractions** PATRICK DOYLE, GREG RANDALL, JU MIN KIM, *MIT* The ability to controllably position and stretch large DNA molecules in a microfluidic format is important for gene mapping technologies such as Direct Linear Analysis (DLA). Current technologies developed for DLA use controlled hydrodynamic flows created in a microfluidic device. The downside to this approach is that the imposition of the no-slip condition at the channel walls generates vorticity which can lead to DNA chain tumbling and incomplete stretching. We have recently shown that electric field gradients can be readily generated in a microfluidic device and the resulting field is purely elongational. We present here single molecule studies of DNA molecules driven by an electric field through a microfabricated contraction. Analogous to the hydrodynamic deformation of DNA, we can define an electrophoretic Deborah number (De) for our problem. We will discuss the effectiveness of the device to fully stretch DNA as a function of De and compare to stretching achieved in hydrodynamic flows. A detailed analysis of molecular stretching and the role of a non-homogeneous electric field will be discussed.

**12:03**

**H21 3 Measuring Streaming Current/Potential in Microchannel Arrays** ALI MANSOURI, AYDIN JAFARNEJAD, *U of Alberta* DANIEL KWOK, *U of Calgary* LARRY KOSTIUK, *U of Alberta* Streaming current/potential measurements have been commonly used to estimate interfacial properties. This paper explores challenges in conducting these measurements in an array of parallel microchannels, which is akin to flow through porous media. The issue that arise with these arrays is that increasing the number of channels subsequently increases the total conductance across an array. In situations with a large number of channels this array conductance can become comparable to the conductance in the bulk fluid in the reservoirs where electrodes are placed. In these cases, current drawn through an external electrical circuit connecting the two reservoirs (i.e. streaming current) become highly dependent on the location, material and surface area of the electrodes. However, with fewer channels the relative magnitude of conductances can be made such that this externally measured current is independent of these parameters and more representative of the streaming current. Streaming potential measurement, since they do not involve external current flow, also do not show these dependencies. In this study variations in the electrode materials (bright platinum, platinized platinum, silver and stain steel), size of electrodes, placement of the electrodes and electrolyte concentration ($10^{-3}$M KCL, $10^{-4}$M KCL and 0 M KCL) were used to affect the relative conductance in the system and to highlight these characteristics.

**12:15**

**H21 4 Electrophoretic extraction of ions from a pressure-driven flow*** HAO LUO, BOYD EDWARDS, SCOTT MILLER, BRENT RESCHKE, AARON TIMPERMAN, WVU TEAM, Coupling pressure-driven and electrokinetically driven flow streams in microfluidics is a critical issue for developing multi-dimensional separations systems. A promising method of coupling these flows is to electrokinetically extract the charged components from the pressure driven flow stream while minimizing the hydrodynamic flow in the electrokinetically driven channel. To model this extraction process we calculate the fraction f of ions in a pressure-driven microchannel that are diverted electrophoretically to a perpendicular side channel. The channel cross sections are rectangular, with aspect ratio $\gamma$. In the main channel, we use truncations of an exact series solution to describe the laminar velocity profile of the aqueous solution. The aqueous solution in the side channel is stationary; individual ions move through this channel in response to a uniform applied electric field at an electrophoretic velocity that is proportional to this field. We calculate f as a function of $\gamma$ and the ratio R between the flow rate in the main stream and that in the side stream. We find that f decreases with increasing R, as expected, and is nearly independent of $\gamma$.

*WVNano Initiative

**12:27**

**H21 5 The effect of fluid density on the transport of particles in nanochannels** ZHIGANG LI, GERMAN DRAZER, *Department of Chemical and Biomolecular Engineering, Johns Hopkins University* Understanding particle transport in nanochannels is crucial for the development of micro and nanofluidic devices. In this work, we investigate the effect of fluid number density on the transport of particles in nanochannels, by means of molecular dynamics simulations. Specifically, we examine the motion of a Lennard-Jones nanoparticle, under the action of a constant external force, in a Platinum nanochannel that contains a Lennard-Jones fluid. In the limiting case of a nanochannel free of fluid molecules the particle adsorbs to the surface of the nanochannel and moves at a very low velocity, due to dry friction with the wall. As the number density of the fluid increases the mobility of the nanoparticle is greatly enhanced, due to the formation of adsorbed fluid layers on the surface of both the nanochannel and the particle, which substantially reduce friction between the particle and the wall. Then, if the number density of the fluid is increased further the particle mobility drops, due to viscous drag. In fact, there is an optimal value at low fluid densities, at which the particle mobility can be significantly enhanced. We also examine the existence of a second peak at higher densities, when the fluid density is high enough to prevent the adsorption of the nanoparticles, and how these phenomena depend on the fluid-solid molecular interactions.

**12:39**

**H21 6 Molecular Dynamics simulations of polymers in Brownian ratchets.** MARTIN KENWARD, GARY W. SLATER, *University of Ottawa* Brownian ratchets rely on a combination of thermal *noise* and an asymmetry in a system to induce directed transport of particles (e.g., pumping in ion channels). This is

somewhat counter intuitive since thermal motion is often a detriment to transport mechanisms. In particular a Brownian ratchet can be used to manipulate polymers, for example in separation systems. We present a Molecular Dynamics study (with explicit hydrodynamic interactions) of short polymer chains in a fluid subjected to a periodic, asymmetric, saw-tooth potential (with zero net force) which is switched on and off for given time intervals, $\tau_{on}$ and $\tau_{off}$ repectively. We examine how variations of $\tau_{on}$ and $\tau_{off}$ affect the net migration of the polymer chains. We also examine how the width of the trapping potential and the degree of asymmetry affects the dynamics of the molecules.

**12:51**
**H21 7 Self-Assembly of Paramagnetic Beads in Rotating Magnetic Fields*** ERIC KEAVENY, *Division of Applied Mathematics, Brown University* MARTIN MAXEY, *Division of Applied Mathematics, Brown University* Paramagnetic beads, about 1 $\mu m$ in diameter, suspended in a liquid will aggregate to form chains when an initially random dispersion is subject to a uniform, static magnetic field. In a rotating field, the chains deform and, depending on the rotation rate, form S-shaped chains or aggregate clusters. A correct determination of the final shape requires an accurate calculation of the interparticle forces. We developed new methods to efficiently and accurately calculate the far-field and near-field magnetic interactions. Hydrodynamic interactions are resolved through the force-coupling method. We study the dynamics of single chains and suspensions of beads in rotating fields using these models and compare results from our simulations with recent experiments by Melle et al. (Phys. Rev. E **68**, 041503). At high rotations rates, the observed particle oscillations provide information on the particle properties affecting near-contact hydrodynamic forces.

*Supported by NSF award CTS-0326702

**13:03**
**H21 8 Semiflexible magnetic filaments** ANDREJS CEBERS, *Institute of Physics, Salaspils, LV-2169* Extension of the Kirchhoff model of an elastic rod by taking into account the long-range magnetic interactions allows one to describe the semiflexible filaments with body couples. Their behaviour in some aspects is similar to the flagellas of different microorganisms driven by internal torques due to molecular motors. Basing on the model different new phenomena are described - buckling instability due to the action of body torques, selfpropulsion of the filament in an ac field, a periodic regime of the magnetic filament motion under the action of the shear flow and the field and others. Taking into account the thermal noise the crossover from $t^{3/4}$ to $t^{1/2}$ for the time dependence of the mean square displacement of the filament at magnetic field increase is predicted. The characteristics of semiflexible magnetic filaments can be studied by measuring their magnetic susceptibility in small ac magnetic field for which in the high- frequency range the scaling law $\omega^{-3/4}$ is obtained. Application of these results for the study of the properties of magnetotactic bacteria is discussed.

**13:15**
**H21 9 Using nanowires to perform in-vivo measurements of elastic and viscous properties of an anisotropic fluid** CHRIS SMITH, *University of Western Ontario* COLIN DENNISTON, *University of Western Ontario* The immersion of a small wire within an anisotropic fluid is studied using a lattice Boltzmann algorithm. A magnetic field is used to manipulate and rotate the wire. The field and the anisotropic fluid each impose a torque on the wire. Our simulations agree well with experiments on the dynamics of high aspect ratio wires within a liquid crystal. In addition, our simulations are able to extend the range of predictive measurements to low aspect ratio wires, more suitable for use in biological environments. We are able to predict elastic and viscous properties of the anisotropic fluid environment based on the torque response of the rotating wire.

**13:27**
**H21 10 Experimental and theoretical study of mixing and transport due to the motion of a slender body sweeping out a cone.*** TERRY JO LEITERMAN, *University of North Carolina at Chapel Hill* RICHARD M. MCLAUGHLIN, ROBERTO CAMASSA, UNC RTG FLUIDS GROUP TEAM, We have used singularity theory to construct an exact solution for the fluid motion induced by a spheriod spinning about its center sweeping out a double cone in a low Reynolds number flow. We have additionally used slender body theory to construct an asymptotic solution for a slender cylinder attached to a no-slip plane spinning about its base sweeping out an upright cone. These time-varying, three-dimensional hydrodynamic solutions have been used to benchmark micro-fluidic experiments which have immediate consequences to understanding transport and mixing in ciliated tissues. A similar macro-scale experiment that is absent of thermal flucutations has been designed which validates the theory.

*RTG NSF DMS-0502266

**13:39**
**H21 11 Field Effect Modulation of Ion Transport in Single Nanotubes** RONG FAN, PEIDONG YANG, *Department of Chemistry, University of California at Berkeley* Field effect control in metal-oxide semiconductor field effect transistors (MOSFETs) has revolutionized how information is processed and stored, and created the modern digital age. Introducing field effect in fluidic systems would enable the manipulation of ionic and molecular species at a similar level and even logic operation. Due to strong Debye screening, field effect control in ionic solutions has to be occurring in nanoscale. Here we present the integration of chemically synthesized inorganic nanotubes into metal-oxide-solution field effect transistors (MOSolFETs), and demonstrated a rapid field effect modulation of ionic conductance. Surface modification, functioning as doping in semiconductors, alters the nanofluidic transistors from p-type field effect transistors, to ambipolar FETs, and n-type field effect transistors. Ambipolar behavior is of special interests in this gapless transport system. Possion-Boltzmann model has been employed to extract two key physical parameters – zeta potential and surface charge density. Furthermore, transient study was conducted, leading to the first kinetic model of field effect in ionic solutions. Nanofluidic FETs would be the key elements in sub-femtoliter analytical techniques and the integration of large-scale nanofluidic circuits.

**13:51**
**H21 12 Performance based applications of the Ultrasound Contrast Agents in the bio-medical field** PANKAJ JAIN, *University of Delaware* KAUSIK SARKAR, *University of Delaware* Ultrasound Contrast Agents are micron size bubbles encapsulated by nanometer-thick layer of surface active materials such as proteins and lipids. They are injected to patients to improve the quality of ultrasound images. They are also being used for drug delivery and arteriogenesis. We present results of itin-vitro ultrasound investigation on two such contrast agents, Definity and Optison.

We measure attenuation and scattering of ultrasound through emulsion of these agents. We investigate destruction of contrast agents and measure sub- and super-harmonic contents in their scattered response. Optison has a much lower threshold excitation level compared to Definity. Definity has a persistent sub-harmonic generation compared to Optison, for which the sub-harmonics go down above a certain pressure level. Both agents experiences transient bubble growth at lower excitation pressures due to increased permeability of the membrane to dissolved air outside. The results along with their implications on the applications such as drug delivery and imaging will be discussed.

**14:03**
**H21 13 Tuning the orbital angular momentum in optical vortices** CHRISTIAN SCHMITZ, KAI UHRIG, JOACHIM SPATZ, JENNIFER CURTIS, *Max-Planck-Institute for Metals Research, Dept. of New Materials and Biosystems, D-70569 Stuttgart, Germany* Optically-driven micromachines rely upon the precise definition of the intensity distribution and the angular momentum content of the controlling light fields. One such manipulation tool is the optical vortex (OV), which employs orbital angular momentum to spin particles around a ring of light. The orbital angular momentum of an OV is tuned by changing the helicity of its electric field's wavefronts or by tuning the input power. However, changing wavefront helicity has the undesirable effect of altering the vortex diameter. Thus, making complex patterns of OVs with fixed sizes but adjustable rotational frequencies is difficult. We introduce a new class of OVs with an additional independent tuning parameter to overcome these limitations. With these OVs, it is possible to smoothly increase particles' rotational frequency without changing the radius or power. We show that this tunability can be extended to groups of OVs with similar or different radii, allowing for complete flexibility to construct optical micromachines, or large arrays of OVs for parallel assays of biomolecules and cells.

**SESSION H22: FOCUS SESSION: NANOPARTICLES AND NANOCOMPOSITES**
**Tuesday Morning, 14 March 2006**
**319, Baltimore Convention Center at 11:15**
**Meigan Aronson, University of Michigan, presiding**

***Contributed Papers***

**11:15**
**H22 1 Magnetocaloric Effect in Nanoparticle Systems and Clathrates** D.J. REBAR, J. GASS, S. SRINATH, H. SRIKANTH, *Functional Materials Laboratory, Physics Department, University of South Florida, Tampa, FL 33620 USA* G.S. NOLAS, *Department of Physics, University of South Florida, Tampa, FL 33620* We report the magnetocaloric effect (MCE) in cobalt ferrite, manganese ferrite, and nickel ferrite nanoparticle systems and also the first observation of a large MCE in $Eu_8Ga_{16}Ge_{30}$ clathrate compounds. The ferrite nanoparticles were synthesized using organometallic precursors in a wet chemical technique and characterized by XPS and XRD. Change in entropy ($\Delta S^{mag}$) was calculated using the Maxwell relation from the family of M-H curves at different temperatures. The maximum entropy change in these nanoparticle systems is influenced by the particle size, overall distribution in anisotropy, and moments. Even though the entropy change for these nanoparticles is reasonably large in comparison to previous reports, it is much smaller in comparison to the bulk systems exhibiting giant MCE. We also investigated MCE in a bulk clathrate system and observed large entropy changes of 6 and 9.3 J/kg-K for the Type I and Type VIII clathrate phases, respectively. These results indicate that the clathrates known to possess excellent thermoelectric properties are also promising candidates as magnetic refrigerant materials. HS acknowledges support from NSF grant CTS-0408933.

**11:27**
**H22 2 Magnetotransport properties and microwave experiments on Co nanoparticles embedded in a Ag matrix*** NEUS DOMINGO, JOAN MANEL HERNÁNDEZ, ANTONIO FERNÁNDEZ, *Universitat de Barcelona* ALBERTO MARIA TESTA, *Istituto di Struttura della Materia - CNR* CHRIS BINNS, *University of Leicester* DINO FIORANI, *Istituto di Struttura della Materia - CNR* JAVIER TEJADA, *Universitat de Barcelona* The magnetic and magnetotransport properties of Co nanoparticles (1.6 nm diameter) embedded in Ag matrix with different volume fraction have been investigated. Magnetic measurements give evidence of blocking temperatures $T_B$ = 10 K (1.5% volume fraction) and $T_b$ = 15 K (9.8 % volume fraction). Such values, quite high for so small particle sizes, reveal an important surface contribution to the total anisotropy energy. From magnetoresistance measurements we have obtained typical values of GMR of the order of 10 %. The data were analyzed with respect to the relationship $\Delta R / R \sim [M(H)]^{\wedge 2}$. Then we have also studied the response of the samples with microwave radiation measuring the absorption properties of these nanoparticles as a function of the applied magnetic field at different temperatures. The relationship between magnetic and transport measurements is discussed.

*This work was supported by the EC NANOSPIN Project

**11:39**
**H22 3 Examination of Giant Magnetoresistance in Cu-Co Granular Films with Two-Particle Size Distribution** JIANQING WANG, *Binghamton University* NAM KIM, JORDAN PECK, Giant Magnetoresistance (GMR) effect and magnetization curves above the blocking temperature were studied for Cu80Co20 granular thin films. The attempt was to understand the relationship between the GMR effect, magnetization, and the degree of interface contribution to the spin-dependent scattering in a unified scheme. When the magnetization curve is fitted to the Langevin function using an averaged single particle size, the average size of the estimated Co particles is 2.8 nm.1 However, when the magnetization curve is used to fit the GMR curve, there is a lack of agreement between the experimental data and the fitting. The discrepancies were resolved by assuming that there are two size distributions in the Co nano-particle population. Under such assumptions, good fittings can be achieved with the experimental curves for both the GMR and the magnetization, using the same set of parameters. The obtained average particle sizes for the smaller and the larger particles, and their respective populations, are 1.1 nm and 2.7 nm, and 0.35 and 0.65, respectively. The smaller particles are responsible for the high field GMR effect while the large ones are for the low field. The study has revealed that a certain degree of magnetic bulk scattering is present in the spin-dependent scattering in this system. 1. L.M. Malkinski, J.-Q. Wang, et al, Appl. Phys. Lett. 75, 844 (1999).

**11:51**

**H22 4 Understanding the Role of Oxygen in $CoFeO_x$ Superparamagnetic Nanoparticles** PAMELA JEPPSON, TONY CARUSO, DOUG SCHULZ, ROB SAILER, SUPERPARAMAGNETISM TEAM, There is a present need for materials which provide both magnetic flux isolation and concentration. The primary application of such materials regards coatings for very sensitive (picotesla) magnetic field measurement or applied magnetic fields. The coatings help reduce 1/f noise and provide a means of controlling wanted or unwanted, internal and/or external magnetic fields. For the high permeability superparamagnetic materials that are presently in use, severe thin film limitations are keeping picotesla resolution from being realized. An example of such present limitations is the strain encountered in thin permalloy films. Beyond strain, there is also brittleness which impedes many inorganic, metallic films. The original goal of this research was to develop flexible and insulating superparamagnetic materials to help fulfill the present thin film limitations and to provide new applications, which utilize the insulating and/or flexible nature of the composite films. However, after optimizing the magnetic properties, we found an extreme saturation moment for some parameters of the transition metal oxide based films. The extreme saturation moments are attributed to the oxygen ratio and termination at the surface of the nanoparticle. This talk will focus on the surface magnetic structure and how it can enhance or suppress the soft properties of transition metal based oxide superparamagnetic nanoparticles.

**12:03**

**H22 5 Magnetic Properties of Fe-alloy Catalyst Nanoparticles for Carbon Nanofiber Synthesis*** K. D. SORGE, TH. LEVENTOURI, C. FINKEL, O. MALKINA, *Florida Atlantic University* P. D. RACK, *University of Tennessee* A. V. MELECHKO, J. D. FOWLKES, K. L. KLEIN, M. L. SIMPSON, *University of Tennessee and Oak Ridge National Lab* The magnetic properties of Fe-alloy nanoparticles, used as catalysts in vertically-aligned carbon nanofiber (VACNF) growth, has been investigated. First, Fe and Co or Ni were co-sputtered onto Si substrates in order to make a catalyst alloy film. These substrates were then placed in a plasma-enhanced CVD chamber with a substrate temperature of 700°C and a flowing mixture of acetylene ($C_2H_2$) and ammonia ($NH_3$) gas. During the PECVD, the catalyst film breaks into nanoparticles of 50–200 nm and VACNFs are grown. EDX shows that the catalyst nanoparticles nominally have the deposited alloy ratio. In addition, the nanoparticles are still magnetic and have a non-negligible remanence and hysteresis. Their magnetic properties are investigated by SQUID magnetometry in applied field of $|H| \leqslant 50$ kOe and temperatures of 5–400 K. In addition, AC susceptibility studies give energy loss characteristics of the co-synthesized VACNF system.

*Part of this research was conducted at the Center for Nanophase Materials Sciences, which is sponsored at Oak Ridge National Laboratory by the Division of Scientific User Facilities, U.S. Department of Energy.

**12:15**

**H22 6 Size Effects in Nanostructured MnBi*** LAURA H. LEWIS, KYONGHA KANG, ARNOLD MOODENBA, *Brookhaven National Laboratory* In addition to variations in temperature, pressure and magnetic field, nanostructuring can tailor the magnetostructural transition; in particular, transition temperatures and anisotropies may change as the material expresses large surface:volume ratios. Compositions near the Mn-Bi eutectic (Mn5Bi95, Mn10Bi90) were rapidly solidified to produce the ferromagnetic low-temperature phase (LTP) NiAs-type MnBi embedded in a Bi matrix. High-resolution TEM reveals that the two compositions have different microstructures: the Mn5Bi95 composition consists of isolated nanorods (10 nm $x$ 30 nm) self-assembled along the major hexagonal symmetry directions of the Bi matrix. In contrast, the Mn10Bi90 composition exhibits regions of equiaxed clustered MnBi precipitates (50 100 nm) in addition to regions of isolated nanorods. SQUID magnetometry shows that the Mn5Bi95 composition has an abrupt magnetization decrease for $T > 520$ K associated with a first- order hysteretic magnetostructural transformation from LTP MnBi to high-temperature phase (HTP) MnBi. This transition temperature is 100 degrees lower than that of the Mn5Bi95 composition, which exhibits the bulk MnBi transition temperature of 633 K with second-order character.

*Research performed under the auspices of the U.S. Dept. of Energy, Division of Materials Sciences, Office of Basic Energy Sciences under contract No. DE-AC02-98CH1-886.

***Invited Papers***

**12:27**

**H22 7 Phase and Heterostructure Controlled Fabrication of Freestanding Magnetic Nanocrystals.*** JIAN-PING WANG,

Magnetism at the nanoscale is still not fully understood. One of the major issues involved is the lack of precise experimental results. For nanoparticles, as their size shrinks the importance of surface atoms increases to such a level that they may dominate the overall magnetic performance. Clean and well defined surfaces on nanocrystals are therefore desirable to understand the surface effect with sufficient accuracy. Unfortunately, conventional fabrication techniques usually require specific surfactants or surface passivation agents, which may conceal the role of surface atoms. Here we report a unique technique that can prepare freestanding nanocrystals with controlled crystalline phase as well as desirous heterostructures. As an example, uniform $L1_0$ FePt nanoparticles with room temperature coercivity of 8.25 kOe were achieved. HRTEM analysis shows that these particles have perfect octahedron shape with only {111} surfaces exposed UHV compatible gas phase aggregation technique was used for the generation of nanoparticles. Atoms were generated from metal targets by using a magnetron sputtering gun, in which the plasma can be manipulated to provide certain circumstances for particle nucleation and growth. The materials were carried on by carrier gas from source to substrate

so the nucleation and growth stages were separated in space. Monodispersity is therefore achieved together with controlled phase and structure.

*INSIC NIST-ATP Program.

***Contributed Papers***

**13:03**

**H22 8 Synthesis and characterization of functional magnetic nanocomposites** J. GASS, J. SANDERS, S. SRINATH, H. SRIKANTH, *Functional Materials Laboratory, Physics Department, University of South Florida, Tampa, FL 33620, USA* Magnetic nanoparticles and carbon nanotubes have been excellent functional materials that could be dispersed in polymer matrices for various applications. However, uniform dispersion of particles in polymers without agglomeration is quite challenging. We have fabricated PMMA/polypyrrole bilayer structures embedded with $Fe_3O_4$ magnetite nanoparticles synthesized using wet chemical synthesis. Agglomeration-free dispersion of nanoparticles was achieved by coating the particles with surfactants and by dissolving both the particles and PMMA in chlorobenzene. Structural characterization was done using XRD and TEM. Magnetic properties of the bilayer structures indicated superparamagnetic behavior that is desirable for RF applications as the magnetic losses are reduced. Our polymer nanocomposite bilayer films with conducting polymer coatings are potential candidates for tunable RF applications with integrated EMI suppression. We will also report on our studies of pumped ferrofluids flowing past carbon nanotubes that are arranged in microchannel arrays. Magnetization under various flow conditions is investigated and correlated with the hydrodynamic properties. This scheme provides a novel method of energy conversion and storage using nanocomposite materials.

**13:15**

**H22 9 Iron nanoparticles embedded in $SrTiO_3$ via ion implantation1*** P.V. WADEKAR, Q.Y. CHEN, X.M. WANG, H.W. SEO, O. LOZANO, D.H. KIM, Z.H. ZHANG, J.R. LIU, Y.Y. XUE, WEI-KAN CHU, *Dept. of Physics & Texas Center for Superconductivity, University of Houston, Texas, USA*. Magnetic nanoparticles are interesting because of their possible applications ranging from biomedicine to data storage. Syntheses of iron nanoparticles embedded in YSZ and $Al_2O_3$ matrices by ion implantation have already been reported in literature. It is thus natural to ask if $SrTiO_3$ would be a good alternative matrix material because of its compatibility with silicon and the unique dielectric behaviors. In this work, 60 keV $Fe^+$ ions were implanted at room temperature into single-crystalline substrates of $SrTiO_3$ to a dosage of $5x10^{16}$ ions/cm$^2$. The specimens were then annealed at different temperatures in various ambient to bring about the nanoprecipitation. Spectrophotometry, SQUID magnetometry, X-ray diffraction, electron microscopy, and electrical measurements were conducted to understand the magnetic and electrical properties in relation to the structures of the nano-composites formed under various conditions of ion implantation and post-annealing.

*Supported by NSF grant DMR-0404542 and by DOE grant DE-FG02-05ER46208. Partial support by the Welch Foundation and the State of Texas through TcSUH are also acknowledged.

**13:27**

**H22 10 $^1$H NMR Spectra vs. the Bulk Magnetization of Magnetically Heterogeneous Systems with Nano- and Micro-scale Magnetic Inclusions** E.M. LEVIN, *Ames Laboratory and Department of Physics, Iowa State University (ISU), Ames, IA* A. RAWAL, *Ames Laboratory and Department of Chemistry, ISU, Ames, IA* S.L. BUD'KO, *Ames Laboratory and Department of Physics, ISU, Ames, IA* K. SCHMIDT-ROHR, *Ames Laboratory and Department of Chemistry, ISU, Ames, IA* The bulk magnetization of magnetically heterogeneous systems, where magnetic nano- and micro-particles are dispersed in a diamagnetic matrix, is correlated with their $^1$H static and magic angle spinning (MAS) NMR spectra. Mixtures containing magnetic $Fe_2O_3$ nano- and micro-particles varying from 0.5 to 8 mass % in a matrix of diamagnetic laponite layered silicate were studied as model systems. Laponite has two characteristic centerbands in $^1$H NMR, which allow us to exclude contributions that can arise from protons possibly associated with the iron oxide particles. An increase in the concentration of magnetic particles results in an increase of the width of static $^1$H NMR spectra. In contrast, all $^1$H MAS spectra show a very narrow centerband and a clear sideband pattern, which is due to magnetic dipole-dipole interactions and depends on the concentration of the $Fe_2O_3$ particles. Unexpectedly, $^1$H MAS NMR spectra are observed even if the materials have a very large magnetization of 4.8 emu/g. The width of the NMR signal increases linearly with the total bulk magnetization, which can be explained by a scaling model.

**13:39**

**H22 11 Defect Induced Magnetism in Carbon Nanostructures** S. TALAPATRA, T. KIM, R. VAJTAI, S. KAR, JI YU CHEN, M. SHIMA, P. AJAYAN, *Rensselaer Nanotechnology Center, Department of MS&E, RPI,Troy,NY 12180* M. HUANG, *Department of Physics, SUNY Albany, NY 12203, USA*. D. SRIVASTAVA, *NASA Ames Research Center, Moffett Field, CA 94035, USA* We report on the effect of nitrogen (N) and carbon (C) implantations on the magnetic properties of nanosized diamond particles, which show ferromagnetic hysteresis behavior at room temperature. The saturation magnetization in the N-implanted samples exceeds that of the C-implanted samples for dose sizes greater than $10^{14}$/cm$^2$. The observed enhanced ferromagnetic ordering in N doped samples is explained on the basis of the structural modification (defects) and C-N bonding states, as investigated by high resolution transmission electron microscopy, Raman Spectroscopy and X-Ray Photo Electron Spectroscopy (XPS).

**13:51**

**H22 12 Magnetic Properties of Hetrostructured Layered Thin Films Based on Prussian Blue Derivatives[1]** J.-H. PARK, M.W. MEISEL, *Department of Physics, University of Florida* F. FRYE, D. R. TALHAM, *Department of Chemistry, University of Florida* By utilizing a sequential deposition method and controlling the chemical composition of each layer, a series of hetrostructured layered thin films of different Prussian blue derivatives were fabricated. As a starting material, a thin film of 20 cycles of sequentially deposited $Rb_jNi_k\ [Cr(CN)_6]_l \cdot nH_2O$ film was generated, and the magnetization studies showed a ferromagnetic ordering at $T_C \sim$ 84 K and a frequency dependent susceptibility. A similar film of $Rb_jCo_k\ [Fe(CN)_6]_l \cdot nH_2O$ is known to show anisotropic photoinduced magnetism.[2] A hetrostructured film was also prepared with $Rb_jNi_k\ [Cr(CN)_6]_l \cdot nH_2O$ and $Rb_jCo_k\ [Fe(CN)_6]_l$

$\cdot\ n\mathrm{H_2O}$ alternately deposited for 10 cycles. The preliminary magnetooptical study of the hetrostructured film shows the presence of magnetic interactions between the layers of the two different Prussian blue derivatives. [1]This work was supported, in part, by the National Science Foundation DMR-0305371 (MWM) and NSF DMR-0543362 (DRT). [2]J.-H. Park, E. Čižmár, M. W. Meisel, Y. D. Huh, F. Frye, S. Lane, and D. R. Talham, Appl. Phys. Lett. 85, 3797 (2004).

**14:03**

**H22 13 Photoinduced Magnetism in Nanoparticles of Prussian Blue Derivatives*** N. E. ANDERSON, J.-H. PARK, M. W. MEISEL, *Department of Physics, University of Florida* F. FRYE, D. R. TALHAM, *Department of Chemistry, University of Florida* Nanoparticles of the Prussian blue family are of great interest due to the possibility for applications in magnetic memory, biosensing, and magnetic filtering. Nanoparticles also serve to better investigate fascinating phenomena, such as the anisotropic photomagnetic properties seen in thin films of Prussian blue derivatives.[1] Here, we present results on $\mathrm{Rb}_j\mathrm{Co}_k\ [\mathrm{Fe(CN)_6}]_l\ \cdot\ n\mathrm{H_2O}$ Prussian blue analog nanoparticles, which exhibit photoinduced magnetism. The nanoparticles are synthesized in a controlled manner, which allows for particle growth in the range of 5-50 nm. Early experiments show that upon irradiation with light at 5 K for a period of 2 hours, the final magnetization increases on the order of 10-100% compared to the initial dark state value. This increase is comparable in magnitude with the results reported for bulk materials. The change in magnetization is also accompanied by an increase in $T_c$. Furthermore, the effect of the dispersing agent on the photomagnetism, the size effect on characteristic magnetic properties, and ac susceptibility data will be presented.

*This work was supported, in part, by the National Science Foundation DMR-0305371 (MWM) and NSF DMR-0543362 (DRT).

[1]J.-H. Park, E. Cižmár, M. W. Meisel, Y. D. Huh, F. Frye, S. Lane, and D. R. Talham, Appl. Phys. Lett. **85**, 3797 (2004).



**SESSION H23: GMR AND AMR**
**Tuesday Morning, 14 March 2006**
**320, Baltimore Convention Center at 11:15**
**Pete Eames, NVE Corporation, presiding**

**11:15**

**H23 1 Magnetoresistance of atomic-scale electromigrated nickel nanocontacts** ZACHARY KEANE, LAM YU, DOUGLAS NATELSON, *Rice University* We report measurements of the electron transport through atomic-scale constrictions and tunnel junctions between ferromagnetic electrodes. Structures are fabricated using a combination of e-beam lithography and controlled electromigration. Sample geometries are chosen to allow independent control of electrode bulk magnetizations. As junction size is decreased to the single channel limit, conventional anisotropic magnetoresistance (AMR) increases in magnitude, approaching the size expected for tunneling magnetoresistance (TMR) upon tunnel junction formation. Significant mesoscopic variations are seen in the magnitude and sign of the magnetoresistance, and no evidence is found of large ballistic magnetoresistance effects.

**11:27**

**H23 2 Retention of Giant Magnetoresistance in Thin Films on Very Rough Substrates** S.M. WATSON, A.C. REILLY, D.M. VLASSAREV, K. SMITH,* *College of William and Mary* B.C. HOLLOWAY,† *College of William and Mary* W.F. EGELHOFF, JR, *National Institute of Standards of Technology* Interfacial roughness is known to affect GMR. Past studies have measured increases, decreases or negligible changes in GMR produced by increasing interfacial roughness. Most studies have explored small scale interfacial roughness induced by changes in growth parameters or annealing[1]. We present a study of the effects of large scale roughness ($\sigma_{rms} > 5$ nm) on the properties of GMR multilayers. GMR thin films were deposited on glass substrates chemically etched for different lengths of time producing a range of lateral and vertical roughness. We found that this long length scale does not have a significant detrimental effect suggesting that viable GMR multilayers can be deposited on a wide variety of surfaces, even with large roughness. M. C. Cyrille et al. Phys. Rev. B, 62, 3361 (2000), J. M. Colino et al., Phys. Rev. B, 54, 13030 (1996). [2]W. F. Egelhoff, Jr. et al., J. Appl. Phys., 82, 6142 (1997) [3]J. Alicea and S. Hershfield, J. Appl. Phys., 93, 7930 (2003)

*Department of Physics
†Department of Applied Science

**11:39**

**H23 3 Electrical Resistance of Sputtered Chromium Thin Films** Z. BOEKELHEIDE, D. COOKE, F. HELLMAN, *University of California - Berkeley* D. J. SMITH, *Arizona State University* M. J. CAREY, *Hitachi Global Storage Technologies* We have measured a large variation in the electrical resistivity of magnetron sputtered chromium thin films. The resistivity ranges from anomalously high (up to 20 times the bulk value) to comparable with the bulk value, and depends strongly on the deposition parameters, in particular the sputtering gas pressure. The range of sputtering gas pressure was 0.75 mTorr to 8 mTorr, with the resistivity increasing with pressure. We have also measured the structure and composition of the films, and the high resistivity does not appear to be caused by exotic structural phases, gross impurities, or grain size effects. The impact on the antiferromagnetism of sputtered chromium films and their role in magnetic multilayers will be discussed.

**11:51**

**H23 4 Non-saturating Magnetoresistance of Inhomogeneous Conductors** JINGSHI HU, *University of Chicago* T. F. ROSENBAUM, *University of Chicago* MEERA M. PARISH, *Cavendish Laboratory, Cambridge, UK* J. B. BETTS, *NHMFL Los Alamos* The inhomogeneous distribution of excess/deficient silver atoms, introducing spatial conductivity fluctuations with length scales independent of the cyclotron radius, lies behind the large, positive and linear transverse magnetoresistance displayed by $\mathrm{Ag}_{2\pm\delta}\mathrm{Se}$ and $\mathrm{Ag}_{2\pm\delta}\mathrm{Te}$. We report here a systematic measurement of the $\rho_{xx}(\mathrm{H})$, $\rho_{xy}(\mathrm{H})$ and $\rho_{xz}(\mathrm{H})$ components of the resistivity tensor with various sample geometries, showing clear evidence of distorted current paths as seen in theoretical simulations. Comparison of the (positive) transverse and (negative) longitudinal magnetoresistance for different sample thicknesses and electrical contact separations points to a characteristic length scale set by the spatial inhomogeneity that is as large as ten microns.

**12:03**

**H23 5 Electronic and Magnetic Structure of $CrO_2$ and $CrO_2$-$RuO_2$ Interfaces*** W. H. BUTLER, *MINT Center, University of Alabama* HUNTER SIMS, *Department of Physics, Tulane University* KRISHNA CHETRY, ZHIHONG LU, SANJOY SARKER, *MINT Center, University of Alabama* $CrO_2$ and $RuO_2$ share the same (rutile) crystal structure and have similar lattice constants. We have used Density Functional Theory within both the generalized gradient and LDA+U approximations to calculate the electronic and magnetic structure of $CrO_2$, $RuO_2$ and their interfaces. Consistent with previous calculations and experiment we find (for both GGA and LDA+U) that the $CrO_2$ Fermi energy lies in a band gap for the minority channel. $RuO_2$, in agreement with experiment, is predicted to be a metal by both types of calculations. We find relatively good matching between the majority energy bands of $CrO_2$ and either channel of $RuO_2$ in the (100), (110) and (001) directions. The nearest neighbor exchange interaction in $CrO_2$ is calculated and used to estimate a Curie temperature of 411K. For (100) interfaces of $CrO_2$ and $RuO_2$, we find that the $CrO_2$ moments remain collinear if the interfaces are abrupt, but our models of intermixed interfaces yielded non-collinear moment configurations with neighboring Cr moments making an angle of approximately 150° and a small induced Ru moment oriented opposite to that of the sum of the Cr moments. We speculate that non-collinear spins at interfaces may be a common problem in oxides that may be a challenge to overcome to achieve large GMR and TMR effects in some of these materials.

*Work supported by NSF MRSEC DMR0213985.

**12:15**

**H23 6 Spin-Orbital Coupling Effects on Magnetoresistance in Organic Materials** YUE WU, ZHIHUA XU, BIN HU, *University of Tennessee* We report the studies on magnetoresistance of organic materials based on the light-emitting diode of phosphorescent iridium complex $Ir(ppy)_3$ molecules dispersed in fluorescent poly(N-vinylcarbazole) (PVK). The magnetic field-dependent injection current indicates that the PVK of weak spin-orbital coupling exhibits a significant magnetoresistance while the resistance of $Ir(ppy)_3$ of super-strong spin-orbital coupling shows an independence of magnetic field up to 3000 Gauss. We find that the magnetoresistance from the $Ir(ppy)_3$/PVK composite displays a gradual decrease with increasing the concentration of $Ir(ppy)_3$. The magnetic field-dependent electroluminescence confirms that the dispersed $Ir(ppy)_3$ molecules account for the change of magnetorsistance in the $Ir(ppy)_3$/PVK composite. From the uniform dispersion of $Ir(ppy)_3$ molecules observed from transmission electron microscope, we suggest that the spin-orbital coupling is modified by the interface interaction and consequently varies the magnetoresistance in the $Ir(ppy)_3$/PVK composite.

**12:27**

**H23 7 Single domain ferromagnet/superconductor nanoscale heterostructures** ANDREI URSACHE, JAMES GOLDBACH, THOMAS RUSSELL, MARK TUOMINEN, *University of Massachusetts Amherst* Nanoscopic single-domain ferromagnetic elements promise simple model behavior for future generations of spintronic devices. In this work, ferromagnetic/superconductor (Co/Pb) multilayer nanowire devices with point contact interfaces are fabricated by electrodeposition in P(S-b-MMA) diblock copolymer derived nanoporous templates, which can produce lateral dimensions as small as 10 nm. Using a single two ion species electrolyte, selective electrodeposition of Co and Pb is achieved by electrode potential control, and the process is characterized in situ by an electrochemical quartz crystal microbalance technique. This fabrication scheme provides the possibility of probing the transport spin polarization of a a single domain ferromagnetic nanowire by means of point contact Andreev reflection (PCAR) spectroscopy. Preliminary electron transport measurements will be presented. This work is supported by NSF grants DMR-0306951, DMI-0103024 and MRSEC.

**12:39**

**H23 8 Inverse proximity effect in Ferromagnet/ Superconductor composite*** JIYEONG GU, *Department of Physics and Astronomy, California State University, Long Beach, 1250 Bellflower Blvd. Long Beach, CA 90840-3901* Recently, a theoretical study of spin-screening effect in ferromagnet ($F$)/superconductor ($S$) heterojunctions has been reported [1]. From the physics involved in $F/S$ junctions it is clear that the inverse proximity effect (the magnetization of the system changes due to the presence of the superconducting correlations) is related to the properties of the conducting electron. Either bi-layer or granular ($F$ particles embedded in $S$ matrix, for example, Co particles embedded in Nb matrix) types of $F/S$ thin films have been made using co-sputtering method. We measured the magnetization as a function of temperature, especially above and below the superconducting critical temperature, to determine the screening or antiscreening effect in $F/S$ hybrid system. This experiment is useful to examine the electronic properties at the Fermi level and the distribution of magnetic moments of ferromagnetic metals. Not only inverse proximity effect but also other properties such as regular proximity effect have been investigated. [1] F. S. Bergeret and N. Garcia, Phys. Rev. B 70, 052507 (2004)

*Characterization of the thin films at low temperature and high magnetic field was carried out in the Molecular Materials Research Center at the Beckman Institute of the California Institute of Technology.

**12:51**

**H23 9 Proximity effect in four-layered ferromagnet/ superconductor nanostructures: decoupled superconductivity and hierarchy of critical temperatures** NAIL G. FAZLEEV, *University of Texas at Arlington, Arlington, Texas, USA* YURII N. PROSHIN, *Kazan State University, Kazan, Russia* MANSUR G. KHUSAINOV, *Vostok branch, Kazan State Technical University, Chistopol, Russia* The four-layered nanostructure consisting of rather dirty superconducting (S) and ferromagnetic (F) metals is studied within the theory of the proximity effect taking detailed account of the boundary conditions. The F/S nanostructures with four and more F and S layers are shown to have considerably richer physics than the F/S/F trilayer and F/S superlattices. The dependence of the critical temperatures versus the F layers thicknesses is investigated. It is shown that the F/S/F′/S′ nanostructure can experience decoupled superconductivity. The latter manifests itself through a hierarchy of the critical temperature Tc, which can be different for different S and S′ layers. An optimal set of parameters is determined, for which the difference between the critical temperatures becomes significant, and the corresponding phase diagrams are constructed. A conceptual scheme of a new control device based on the F/S/F′/S′ nanostructure with superconducting and magnetic recording channels that can be controlled separately using a weak external magnetic field is proposed.

**13:03**

**H23 10 Giant Magneto-Refractive Effect in Pseudo-Valve Thin Films** JARED D. ROKITOWSKI, NAM H. KIM, JIAN-QING WANG, *Binghamton University* Magnetic-field-induced changes in infrared transmission of Co/Cu/Co pseudo spin-valve (PSV's) thin films are studied for the Magnetorefractive Effect (MRE). Samples are deposited on a Si (100) wafer under a high vacuum using magnetron sputtering, followed by annealing at various temperatures up to 6000C to enhance the GMR effect. A Thermo Electron Nexus 670 FT-IR spectrometer is used to measure a mid-IR spectrum with wavelengths ranging from 2.5$\mu$m to 30$\mu$m. The transmitted spectra through the thin films, placed in a magnetic field, were measured by a KBr detector at room temperature. The measured GMR value for a sample made up of several layers, Fe(5nm)/Co(5nm)/Cu(3nm)/Co(2nm), that has been annealed at 2500C is about 2% at room temperature. This sample exhibits a sharp low switching field at about 20G and a gradual high field switching at half peak height, approximately 400G. Variations of about 1.0% in the intensity of the transmitted IR spectrum are observed for a range of magnetic field strengths up to $\pm$ 1300G with special attention focused in the low field response (roughly -100 to 100 Gauss). The MRE is analyzed for a particular wavelength of 4m. The results of this graph produce a typical GMR curve. Earlier studies of Spin-vales have yielded comparable MRE results. Detailed experimental results (1) and possible explanations will be discussed. 1. S. Uran et al., Phys. Rev. B 57, 2705 (1998).

**13:15**

**H23 11 Tunneling Magnetoresistance in Magnetic Tunnel Junctions with a (Zn,Cr)Te electrode.*** WEIGANG WANG, *Physics and Astronomy, University of Delaware* CHAOYING NI, *Materials Science and Engineering, University of Delaware* TA-KAHIRO MORIYAMA, JUN WAN, ED NOWAK, JOHN XIAO, *Physics and Astronomy, University of Delaware* Tunnel magnetoresistance (TMR) of 21% is observed at low temperature in hybrid magnetic tunnel junctions composed of a magnetic semiconductor (Zn,Cr)Te and Co electrodes separated by a Al2O3 barrier. The MTJs were deposited in a magnetron sputter system with structure as Si / (Zn,Cr)Te(50)/ Al (0.75 – 2.75)+oxidation / Co (15) / Cu (70), where the numbers in parentheses are layer thickness in nanometers. The Cr atomic concentration in the (Zn-,Cr)Te layer is controlled to be at 20%. The TMR value decreases with increasing temperature but sustains up to 250K, which is a considerable improvement over the MTJs with semiconductor electrodes in previous studies. The temperature and bias dependence of TMR are understood in the context of spin polarized tunneling and spin independent hopping through impurity states. The observed zero bias anomaly in the dI/dV curve is correlated to the existing of a soft coulomb gap at the $E_F$ in the (Zn,Cr)Te electrode which leads to $T^{-1/2}$ dependence of logarithmic resistance, logR, at low temperature. The TMR characteristic can be significantly improved by optimizing the interface and barrier quality.

*This work is supported by NSF DMR Grant No. 0405-136

**13:27**

**H23 12 Giant electroresistance and giant magnetoresistance of Fe-doped amorphous carbon film on Si substrate** XIAOZHONG ZHANG, PENG TIAN, QINGZHONG XUE, *Dept of Materials Science and Engineering, Tsinghua University, PR China* Amorphous $Fe_x$-$C_{1-x}$ films are deposited on Si substrates at different temperatures using pulsed laser deposition (PLD). It is found that the resistance of $Fe_x$-$C_{1-x}$ films on Si (100) substrates are controlled by the measuring current within a given temperature range. Correspondingly, giant electroresistance (ER) and giant magnetoresistance (MR) were found in this material. For example, $Fe_{0.011}$-$C_{0.989}$ film has a positive MR of 138% at temperature of 300K and magnetic field of 5T. It is found that the switching of the conducting channel from the $Fe_x$-$C_{1-x}$ film to the Si substrate plays an important role in the current-dependent resistance of $Fe_x$-$C_{1-x}$ films. The multilayer of $Fe_x$-$C_{1-x}$ films on Si (100) substrate was also prepared by PLD. This multiplayer material has a positive MR of over 30% at low magnetic filed, and the MR sensitivity is comparable to the spin-vale structure of traditional GMR materials. However, this material has a novel MR mechanism. It is believed that this multiplayer material can find application in magnetic information storage such as magnetic sensors, magnetic recording head and magnetic random access memory.

**13:39**

**H23 13 Orbitronics: The Intrinsic Orbital Hall Effect in p-doped Silicon** TAYLOR HUGHES, *Stanford University* ANDREI BERNEVIG, SHOU-CHENG ZHANG, The spin Hall effect depends crucially on the intrinsic spin-orbit coupling of the energy bands in semiconductors. However materials with small spin-orbit coupling such as silicon will only exhibit a much reduced spin Hall effect. We show that the electric field in p-doped silicon will induce a dissipationless orbital current in a fashion reminiscent of the spin Hall effect. The effect is robust against disorder because the vertex correction due to impurity scattering vanishes due to symmetry. This orbital Hall effect can lead to the accumulation of local orbital angular momentum at the edge of the sample, and can be detected by the Kerr effect.

**SESSION H24: POLYMERS AT INTERFACES**
**Tuesday Morning, 14 March 2006**
**321, Baltimore Convention Center at 11:15**
**Chris Soles, National Institute of Standards and Technology, presiding**

**11:15**

**H24 1 Adsorption-induced fracture of branched macromolecules.*** SERGEI SHEIKO, FRANK SUN, DAVID SHIRVANYANTS, MICHAEL RUBINSTEIN,[†]HYUNG-IL LEE, KRZYSZTOF MATYJASZEWSKI, *Carnegie Mellon University* Recently, we have discovered the remarkable phenomenon that brush-like macromolecules with long side chains undergo scission of the backbone bonds as a result of adsorption onto a substrate. The macromolecule's self-destruction occurs because its side chains stretch the polymer backbone as the macromolecule struggles to reconfigure and maximize the number of contacts with the substrate. We show that the tension imposed by the surface attraction is unevenly distributed over the covalent bonds of the molecular skeleton. Along the brush axis, a major fraction of the tensile force is carried by the backbone, while in the perpendicular

direction the tension is distributed over many side chains. Using molecular visualization and computer simulation, we confirmed the first order kinetics and measured the corresponding rate constant, which revealed strong dependence on the attraction to the substrate.

*This research program was supported by the National Science Foundation (ECS 0103307 and DMR 0306787)
†University of North Carolina at Chapel Hill

**11:27**

**H24 2 The swelling and dissolution kinetics of polymer thin films** ARINDAM KUNDAGRAMI, M. MUTHUKUMAR, *Polymer Science & Engineering, University of Massachusetts, Amherst* We consider a theoretical analysis of the swelling and dissolution phenomena in polymer thin films. To determine the overall kinetics, we first consider the swelling process in a two-component system(solvent and polymer) and then apply this theory in conjunction with the theory of diffusive penetration of the solvent into the thin film. We also consider the dissolution of a pre-formed swelled gel of cross-linked polymers. Both analyses involve multiple moving boundaries. A comparison of our theoretical results with experimental data will be presented.

**11:39**

**H24 3 Sum-Frequency Vibrational Spectroscopy on Rubbed Poly(vinyl cinnamate) films for Liquid Crystal Alignment.** PASQUALE PAGLIUSI, *University of Calabria* ERIC C.Y. CHEN, *University of California at Berkeley* Y. R. SHEN, *University of California at Berkeley* Rubbing or uv-irradiation of poly-(vinyl cinnamate) (PVCi)-coated substrates can effectively align liquid crystal (LC) films deposited on them. We report here the use of surface-specific sum-frequency vibrational spectroscopy (SFVS) to investigate how rubbing affects the interfacial molecular structure of PVCi. The stretch modes of the pendant side-chain phenyl groups dominate the spectra, from which the average orientation of the phenyl groups is deduced. The results show that rubbing aligns the main chains of PVCi along the rubbing direction. While hard rubbing also aligns the phenyl rings toward the rubbing direction, soft rubbing preferentially aligns them perpendicular to the rubbing direction. The observations are correlated with the fact that hard-rubbed substrates induce LC alignment along the rubbing direction, and soft-rubbed substrates induce LC alignment perpendicular to the rubbing direction. This work was supported by NSF.

**11:51**

**H24 4 Structure of Confined Fluid between an Elastomer and a Flat Surface*** KUMAR NANJUNDIAH, *The University of Akron* ALI DHINOJWALA, The behavior of simple fluids under spatial restrictions is of considerable technological and fundamental interest. Experiments using force measurements have indicated that viscosity of confined fluids is different from that in the bulk. We have studied the confinement of linear alkanes between a poly (dimethyl siloxane) and a sapphire surface using surface sensitive infrared sum frequency generation spectroscopy (SFG). The results indicate ordering of the alkane molecules upon confinement above their bulk melting temperature. The SFG spectra of confined alkanes cooled below the bulk melting temperature shows a structure that is very different from the crystal structure of unconfined alkanes. A simple model will be presented that shows the alkane molecules crystallizing with the chains lying flat next to the sapphire surface.

*Financial Support from NSF (CTS-0355305 and DMR-0512156)

**12:03**

**H24 5 Resonant Soft X-ray Reflectivity of Polymer Thin Films** CHENG WANG, TOHRU ARAKI, HARALD ADE, *NC State University* Resonant Soft x-ray reflectivity [1], a new method for low Z materials that combines aspects of neutron reflectivity and x-ray reflectivity, is presented and its usefulness delineated. Resonant reflectivity provides enhanced and selective sensitivity to specific chemical moieties near the absorption edges of constituent elements and was demonstrated through the characterization of a bilayer polymer thin film. The relative reflectivity of a particular interface could be tuned by adjusting the incident photon energy. Using photons in the 270-320 eV energy range, measurements were performed on thin film bilayers of polystyrene on top of poly(methyl methacrylate). Large changes in reflectivity at an interface and the resulting interference in thin films and multilayers were observed as the complex index of refraction, $n = 1\text{-}\delta\text{-}i\beta$, changed rapidly as a function of photon energy. Through the use of specific energies, the sensitivity to the polymer-polymer or polymer-vacuum interface can be selectively enhanced. The resulting chemical specificity is analogous to using deuteration as a marker in neutron reflectivity, but without requiring special sample preparation. The interfacial width determined with resonant reflectivity is virtually identical to that measured previously by XR and NR confirming that RXR is an excellent, complementary tool for the study of low-Z material thin films. [1] C. Wang, T. Araki, and H. Ade, Appl. Phys. Lett. 87, 214109 (2005).

**12:15**

**H24 6 Possible explanation of polymer surface diffusion anomaly** DEBASHISH MUKHERJI, *Department of Physics and Astronomy, The University of Western Ontario, London, Ontario N6A 3K7, Canada* MARTIN H. MUSER, *Department of Applied Mathematics, The University of Western Ontario, London, Ontario N6A 5B7, Canada* Surface diffusion of polymer is studied with molecular dymanics simulation. Our simulation result shows the non-monotonic behavior of the polymer surface-diffusion coefficient D as a function of surface coverage. D first increased with increasing polymer surface concentration, then suddenly drops at a critical value. This finding shows striking similarities with the experimental result [1]. We found that the strong reduction of D above the threshold concentration is related to the spontaneous formation of double-layered structures, whose bottom layers manage to lock into the registry of the substrate much better than the single-layer pancakes that form at smaller concentration. This increases the barriers for lateral diffusion and is thus consistent with small values of D at larger concentration. [1] J. Zhao and S. Granick, J. Am. Chem. Soc. 126, 6242 (2004).

**12:27**

**H24 7 Unconventional Spinodal Surface Fluctuations on Polymer Films*** YONG JIAN WANG, OPHELIA K. C. TSUI, *Department of Physics and Institute of Nano Science and Technology, Hong Kong University of Science and Technology* We study the temporal growth pattern of surface fluctuations on a series of spinodally unstable polymer films where the instability is adjustable by the film thickness, $h_0$. For the most unstable film studied (whose $|h_0 - h_{sp}/h_{sp}| = 0.988$; $h_{sp}$ is the thickness where the second derivative of the interfacial potential of the film equals to zero), the growth rate function of the surface modes as a function

of the wavevector fits well to the mean-field theory. As the film thickness is increased such that $|h_0 - h_{sp}/h_{sp}| \leq 0.977$, the mean-field theory demonstrates marked disagreement with experiment, notwithstanding provision of the known corrections from high-order terms and thermal noises. We show that the deviations arise from large-amplitude fluctuations induced by homogeneous nucleation, which is not accounted for in the conventional treatments.

*We acknowledge financial support of the Research Grant Council of Hong Kong through the projects HKUST6070/02P and 603604.

**12:39**

**H24 8 Interfacial Characterization of Contact in Aqueous Environments with a Quartz Crystal Microbalance** DAVID A. BRASS, KENNETH R. SHULL, *Northwestern University* Adhesion of a material to a surface in an aqueous environment requires the removal of a water layer coating the surface. The evolution of this water layer between a micron thick polymer membrane and a quartz crystal microbalance has been investigated. This quartz crystal microbalance is highly surface sensitive, allowing determination of the water thickness during membrane contact. To improve this sensitivity, the thin, polymer membrane is backed by an ambient air environment. The surface of the quartz crystal is coated with a gold layer that acts as an electrode. This same surface allows for surface modification through the grafting of thiol terminated poly(ethylene oxide) brushes. These brushes can also by established with a coating of poly(ethylene oxide-b-styrene) diblock copolymer micelles.

**12:51**

**H24 9 Humidity influence on atomic force microscopy electrostatic nanolithography** SERGEI LYUKSYUTOV, *The University of Akron, OH* SHANE JUHL, RICHARD VAIA, *AF Research Laboratory, WPAFB OH* The formation and sustainability of water menisci and bridges between solid dielectric surface and nanoasperity under external electrostatic potential is a mystery, which must be adequately explained. The goal of our study is twofold: (i) To address the influence of an ambient humidity through the water meniscus formation on the nanostructure formation in soften polymeric surfaces; (ii) Estimate an electric charge generation and transport inside the water meniscus in vicinity of nanoscale asperity taking into consideration an induced water ionization in strong non-uniform electric field of magnitude up to $10^{10}$ $Vm^{-1}$. It is suspected that strong electric field inside a polymer matrix activates the hoping mechanism of conductivity. The electrons are supplied by tunneling of conductive tip, and also through water ionization. Electric current associated with these free carriers produces Jule heating of a small volume of polymer film heating it above the glass transition temperature. Nanostructures are created by mass transport of visco-elastic polymer melt enabling high structure densities on polymer film.

**13:03**

**H24 10 Comparison of thermal and chemical treatments of ultrathin chitosan films** CHRIS MURRAY, JOHN DUTCHER, *University of Guelph* Chitosan is a biodegradable polysaccharide derived from seashell waste products. The high water absorbency and biocompatibility of chitosan have enabled its use as a hydrogel in specialty biomedical applications. Chitosan can be dissolved in weakly acidic solutions enabling its use in applications such as films and gels, which can be converted into chitin by a chemical process known as acetylation. We present the results of several experiments in which changes in the thickness, index of refraction and molecular environment in response to changes in relative humidity for ultrathin films of chitosan are examined as a function of exposure to temperatures above 150 degrees Celsius. Measurements made by ellipsometry and FTIR spectroscopy indicate that changes in the thickness and index of refraction of the films are accompanied by a change in the infrared absorption spectra similar to that associated with acetylation, which is typically accomplished by exposure of chitosan to acetic anhydride. We believe that these changes are responsible for reduced equilibrium water content in the films at all relative humidity values studied, and may offer a simple method for converting chitosan into a chitin-like material.

**13:15**

**H24 11 Glucose/galactose binding protein changes its mechanical properties: Novel AFM method of detection in-situ.** VENKATESH SUBBA RAO, LINDA LUCK, IGOR SOKOLOV, *Clarkson University* Recently a periplasmic glucose/galactose binding protein, GGRQ26C, immobilized on gold surface has been used as an active part of a glucose biosensor based on quartz microbalance technique (QCM). However the nature of the glucose detection was not clear. Here we have found that the receptor protein film immobilized on the gold surface increases its rigidity when glucose is added, which explains the unexpected detection signal. To study the rigidity change, we developed a new fast and simple method based on using atomic force microscopy (AFM) in tapping mode. The method was verified by explicit measurements of the Young's modulus of the protein film by conventional AFM methods. Since there are a host of receptors that undergo structural change when activated by ligand, AFM can play a key role in the development and/or optimization of biosensors based on rigidity changes in biomolecules. From fundamental point of view, the developed method can be used for study of mechanics of proteins in different environments. This can be compared with molecular simulations to get additional information about the protein structure.

**13:27**

**H24 12 Modifying Surfaces with Light.** JEFF KOBERSTEIN, *Columbia University* GREG CARROL, FENG PAN, PENG WANG, NICHOLAS TURRO, The ability to locate particular functional groups at surfaces is an enabling aspect of many important technologies. Unfortunately, high energy functional groups are not thermodynamically stable at the surface of polymers and other low surface tension materials. We show that this difficulty can be overcome through the synthesis of surface active block copolymers and self-assembled monolayers that contain photoactive functional groups. Photoactive functional groups are protected during the synthesis step, but can be deprotected upon exposure to light. To accomplish this task we borrow from photoresist technology and employ photoacid generators to deprotect carboxylic acid groups delivered to a surface upon exposure to light. Since all modifications are accomplished with light, direct micropatterning of surface functional groups is possible simply by exposure through a mask. The technique is thus a simple, direct alternative to other patterning techniques such as stamping. We also demonstrate that polymers and carbohydrates can be photografted to a surface using photoactive groups that are capable of hydrogen abstraction. Applications that are demonstrated include prevention of thin film dewetting, general surface functionalization, micropat-

terning of functional groups, polymers and biopolymers, and the creation of the first covalently bound carbohydrate microarrays. This work is funded by grants from the Polymer Program of the National Science Foundation Division of Materials Research and the U.S. Army Research Office.

**13:39**

**H24 13 Dynamical simulations of rheology and phase behavior of ternary polymer blend systems.** BHARADWAJ NARAYANAN, VENKAT GANESAN, VICTOR PRYAMITSYN, *Department of Chemical Engineering, The University of Texas at Austin* We present the results of a multiscale simulation approach which combines Brownian dynamics simulations with polymer self-consistent field theory to study flow induced phase transitions in microemulsion phases of ternary polymer blends with homopolymers A and B with added copolymer AB. The results match qualitatively with the experimental observations and suggest flow transition of microemulsion phases into a three-phase coexistence followed by macrophase separation at stronger shears. We explore the effect of viscoelastic asymmetry (by varying polymer mobilities) and the copolymer (AB) to homopolymer length ratio ($\alpha$) on flow induced phase transitions. Though the series of phase transitions remain unchanged, quantitative differences arise as a function of viscoelastic asymmetry and $\alpha$. These transitions are also accompanied by a strong shear-thinning behavior in the rheological response. The results suggest significant differences between ternary polymeric systems and oil-water-surfactant systems. We rationalize the above results from a molecular viewpoint.

**13:51**

**H24 14 Orientation competition of lamellar phases in sheared block copolymers via hydrodynamic instability** ZHI-FENG HUANG, JORGE VINALS, *McGill University* We study the shear alignment of three dimensional lamellar diblock copolymers for achieving macroscopic order in defected, multidomain systems. We find that the competition between differently oriented microdomains, and thus the orientation selection between lamellar phases, is determined by the domain viscosity contrast which originates from different uniaxial domain symmetries relative to the imposed shear. This variation of domain viscosity causes hydrodynamic instability at high enough shear frequencies, breaking the degeneracy between parallel and perpendicular orientations in the system. The instability is found to obey a thin layer effect, inducing a size dependence of perpendicular domain expansion. Our calculations also suggest that the effective boundary of the experimentally observable regime with predominant perpendicular alignment follows a power law behavior between shear amplitude and frequency, with an exponent equal to 3/4.

**14:03**

**H24 15 Defects in a Noncentrosymmetric Lamellar Block Copolymer Blend** SHUJUN CHEN, SAMUEL P. GIDO, *Dept. of Polymer Sci. and Eng., Univ. of Massachusetts, Amherst, MA 01003* THODORIS TSOUKATOS, APOSTOLOS AVGEROPOULOS, NIKOS HADJICHRISTIDIS, *Dept. of Chemistry, Univ. of Athens, Panepistimiopolis, Zografou, 15771 Athens, Greece* KUNLUN HONG, JIMMY W. MAYS, *Dept. of Chemistry, Univ. of Tennessee, Knoxville, TN 37996, and Chem. Sci. Div., Oak Ridge National Lab, Oak Ridge, TN 37831* Here we report results from a defect study on the noncentrosymmetric (NCS) lamellar blend of an ABCD tetrablock copolymer and an AD diblock copolymer. The block copolymers used were polystyrene-block-polybutadiene-block-polyisoprene-block-polycyclohexadiene and polystyrene-block-polycyclohexadiene. Coexisting tetrablock-rich mixed centrosymmetric (CS) and NCS lamellar morphologies were seen in TEM, as predicted by the mean-field theory. NCS grain boundary defects similar to those in CS lamellar systems were observed as well as new defects unique to NCS layered systems, such as chain polarity reversals and kink bands with dilation or compression of the layers. In addition to morphology observations, geometrical and energetic calculations were performed on several new NCS defects, which are in good agreement with experimental results.

**SESSION H25: FOCUS SESSION: PARTICLE DYNAMICS AND ORGANIZATION**
**Tuesday Morning, 14 March 2006**
**322, Baltimore Convention Center at 11:15**
**Lynn Walker, Carnegie Mellon University, presiding**

**11:15**

**H25 1 Noncontinuum Effects in Dynamics of Nanoparticles in Polymer Matrices** GANESAN VENKATRAGHAVAN, VICTOR PRYAMITSYN, *The University of Texas at Austin* The dynamics and rheology of particulate suspensions have long been well-understood in a continuum fluid-mechanical framework dating back to Stokes and Einstein. These theories predict that the mobility of the particles decreases with an increase in the viscosity of the fluid and that the addition of particles increases the overall viscosity of the suspension. However, in many recent applications such as polymer-nanoparticle composites, the particle size is comparable to or smaller than the structural scale of the solvent and the dynamics exhibits many ''non-continuum'' effects, such as the mobility becoming independent of the molecular weight (and viscosity) of the polymer, a decrease in the suspension viscosity due to the addition of nanoparticles etc. Here we propose a new theoretical formulation for the dynamics of particulate suspensions, which within a single framework encompasses for the first time both the ''macroparticle'' limit of particles larger than the structural scale of solvent and the ''nanoparticle'' limit where the particles are smaller than such scales. We present theoretical predictions for the case of polymer-nanoparticle suspensions which quantitatively explain the preceding observations and also delineates the size scales at which the particles cross-over from behaving dynamically as a ''particle suspension in polymers'' to a ''solvent for the polymers.''

**11:27**

**H25 2 Mechanisms of Steady State Rheological Behavior of Polymer Nanoparticle Composites** VICTOR PRYAMITSYN, VENKAT GANESAN, *University of Texas at Austin* We use a mesoscale computer simulation framework to delineate the the mechanisms behind the linear and nonlinear dynamical properties of polymer-nanoparticle composites. Our studies specifically focus on the regimes where the particle sizes and the interparticle distances become comparable to the polymer sizes. Our results indicate that the zero shear viscosities of the composite can be described in a manner similar to colloidal suspensions in a simple fluid when both the particle-induced changes in the polymer relaxation spectra and the polymer slip effects are accounted. The

nonlinear shear rheology and the first normal stresses of the composite exhibits a subtle interplay between the shear thinning arising from the polymer and particle stresses. Overall, at dilute and semidilute nanoparticle concentrations, the composite shear rheology is dominated by the shear thinning of the polymer chains which in turn is modified by the presence of the particles. For higher particle loads, especially in regimes where particle jamming manifests, the polymeric contribution to the rheology becomes much less important and the shear thinning is dominated by the particles stresses. These competing efffects lead to intriguing polymer molecular weight, particle loading dependencies for the steady shear rheological behavior. Our results and mechanistic explanations are in excellent agreement with associated experimental observations.

**11:39**

**H25 3 Surface Modification of Plate-Like Nanoparticles and Their Assembly into Nematic Organogels** BANI CIPRIANO, SRINIVASA RAGHAVAN, *Department of Chemical and Biomolecular Engineering, University of Maryland, College Park, MD 20742* Plate-like clay nanoparticles (e.g., laponite) form gels in water at sufficiently high concentration. A remarkable feature of these gels is the appearance of birefringent textures characteristic of nematic liquid crystals. Here we report the counterpart of this phenomenon in organic solvents, i.e., the formation of nematic textures by adding organically modified clay nanoparticles into non-polar liquids such as toluene and chloroform. We present the phase diagram (isotropic/nematic phases) for these gels. The viscoleastic properties of the resulting gels are characterized by use of rheological methods. The quality of the dispersions and the birefringent textures are evaluated using optical microscopy and x-ray scattering techniques. The finding that organoclays self assemble into a nematic phase in non-polar mediums may well provide a route for in-situ formation of nematic polymer nanocomposites. We also describe preliminary efforts towards achieving nematic ordering of particles in polymers.

**11:51**

**H25 4 Gelation and structural characteristics of nanoparticles in solutions of adsorbing polymers** MEGHA SURVE, VICTOR PRYAMITSYN, VENKAT GANESAN, *University of Texas at Austin, TX* In the present talk, we examine the gelation, clustering behavior and structural characteristics of nanoparticles in presence of adsorbing polymers. We implement a polymer self consistent field theory to obtain the structural conformations of the polymer chains between two spherical particles. By solving the self-consistent field theory equations numerically in bispherical coordinates we account for size disparities between the particles and polymers. We present the effect of different molecular parameters such as adsorption strength, particle size, polymer concentration on the size, number and probability distribution of polymer bridges and anchors. The structure of polymer-nanoparticle mixtures is examined using Monte Carlo simulations. By incorporating the microscopic bridging statistics into the simulation framework, we predict the structure and clustering statistics of polymer-nanoparticle gels formed in mixtures of nanoparticles and adsorbing polymers. We further extend our formalism to predict the elastic and mechanical properties of the polymer-nanoparticle mixtures. Our analysis provides a molecular insight into the nanoscale phenomena such as prevalent gelation and significant lowering of percolation thresholds observed in nanoparticle regime and quantifies the role played by various nanoscale parameters such as particle curvature and strength of polymer-particle interactions in determining the macroscopic properties of polymer nanocomposites.

**12:03**

**H25 5 Shear induced alignment in thin bilayer films: a simulation study** JOERG ROTTLER, *Dept. of Physics and Astronomy, University of British Columbia, 6224 Agricultural Road, Vancouver, BC V6T 1Z1* DAVID J. SROLOVITZ, *Dept. of Mechanical and Aerospace Engineering, Princeton University, Princeton, NJ 08544* PAUL CHAIKIN, *Physics Dept., New York University, 4 Washingon Place, New York, NY 10003* Motivated by recent experimental progress, we study ordering mechanisms in confined bilayer systems under shear via Brownian dynamics simulations. In sphere-forming thin block copolymer films, spherical nanodomains arrange in grains of local hexagonal symmetry, but random orientation. If the film has precisely the bilayer thickness, the application of simple shear leads to global, macroscopic alignment in a triangular lattice (D. Angelescu et al., Adv. Mat. 17, 1878 (2005)). By representing each nanodomain a as purely repulsive sphere on a coarse-grained level (therefore making the model also applicable to colloidal assemblies), our simulations reveal that the long range order can develop through the shear induced motion of grain boundaries rather than global melting and recrystallization. The time dependence of this process may be described by Avrami growth laws. In order to gain further insight into the microscopic mechanism of shear induced ordering, we study the motion of single domain walls in simplified geometries and determine the dependence of the grain boundary migration velocity on geometry, shearing conditions and the resulting local stress gradients.

**12:15**

**H25 6 Field-theoretic nanocomposite simulations: preliminary results of hybrid particle/SCFT simulations** SCOTT SIDES, *Tech-X Corporation* GLENN FREDRICKSON, *University of California at Santa Barbara* Using block copolymers as mesoscale templates for organic/inorganic nanoparticles has the potential to create patterned particle aggregates that could be used as magnetic storage media and semiconductor materials. More generally, polymer nanocomposites such as these are being investigated for the potential to develop materials with specifically tailored optical, electrochemical, thermal and mechanical properties. The overall behavior of the nanocomposite system depends on the morphology of the polymer chains as well as the arrangement of the particles in the polymer matrix. Self-consistent field theory (SCFT) for dense polymer melts has been highly successful in describing complex morphologies in block copolymers. Field-theoretic simulations such as these are able to access large length and time scales that are difficult or impossible for particle-based simulations such as molecular dynamics, while still incorporating more realistic polymer models than many macroscopic, continuum simulations. In this talk I will outline the SCFT method, discuss some efficient methods of numerically solving the SCFT equations and present results for spherical nanoparticles embedded in an AB diblock copolymer melt. These results have been obtained using a hybrid particle/SCFT approach that treats the polymer in a field theory framework while explicitly retaining the individual nanoparticle coordinates as degrees of freedom.

**12:27**

**H25 7 Distributed Polymeric Stickers and their Role in Colloidal Interactions and Selective Adhesion Dynamics.** MARIA SANTORE, NATALIA KOZLOVA, *Department of Polymer Science and Engineering University of Massachusetts Amherst* BING MEI, *Department of Chemical Engineering University of Massachusetts Amherst* Polyelectrolytes are frequently added to colloidal dispersions as flocculants. When they are high in molecular weight and low in backbone charge, as they adsorb to particles they extend (at least temporarily) into solution from the surface of a first particle to trap a second. This is the basis for bridging flocculation, which is often reversible to the extent that backbone relaxation ultimately causes the chain to release the second particle and more completely coat and stabilize the first. By contrast, addition of small amounts of densely-charged low molecular weight chains produces irreversible flocculation via a patchwise mechanism: A localized region on a first particle is charge-overcompensated by an adsorbing chain, and adheres to a bare spot on an approaching particle. We show here, with a model system, how the dynamics of patchwise flocculation depend on fluctuations in the distribution of adsorbing chains, and gives rise to a curvature-based selectivity for particle destabilization.

**12:39**

**H25 8 Barrier Hopping, Viscous Flow and Kinetic Gelation in Nanoparticle-Polymer Suspensions** KENNETH SCHWEIZER, YENG-LONG CHEN, VLADIMIR KOBELEV, *University of Illinois at Urbana-Champaign* Ideal mode coupling theory is combined with the polymer reference interaction site model theory of structural correlations to predict depletion-induced physical gelation and elasticity of suspensions of nonadsorbing polymers and hard particles. The approach has been extended to treat the alpha relaxation process in the ultra-slow activated barrier hopping regime. The dynamic barrier is a rich function of polymer concentration, polymer-particle size asymmetry ratio and particle volume fraction. All these dependences can be collapsed on to a single master curve that is an effective power law function of a composite variable. Over a range of material parameters commonly studied experimentally the alpha relaxation time is an exponential function of colloid volume fraction and reduced polymer concentration. The theory has been applied to compute kinetic gel boundaries and the shear viscosity, and also to address the phenomenon of delayed sedimentation.

**12:51**

**H25 9 Soft X-ray Resonant Scattering of Structured Polymer Nanoparticles** HARALD ADE, T. ARAKI, *NCSU* G. MITCHELL, *Dow Chemical* J. STUBBS, D. SUNDBERG, *U. New Hampshire* J. KORTRIGHT, A.L.D. KILCOYNE, *LBNL* We present the development and application of resonant soft x-ray scattering (RXS) to chemically heterogeneous, i.e. structured, soft condensed matter materials. Polymer composite latex particles $\sim$ 200 nm in diameter were utilized to determine the potential utility of this technique. Two styrene-acrylic polymer latex systems were prepared on silicon nitride membranes. Scattering measurements were performed in transmission. Angular scans at photon energies corresponding to strong scattering contrast between specific chemical moieties made it possible to infer the relative effective radii corresponding to the two polymer phases in the structured latex particles. The results show that resonant soft x-ray scattering should be a powerful complementary tool to neutron- and hard x-ray scattering and NEXAFS spectromicroscopy for the characterization of structured soft condensed matter nanomaterials.

**13:03**

**H25 10 Studies of the formation of microporous polymer films in 'breath figure' condensation processes** MOHAN SRINIVASARAO, JUNG PARK, *School of Polymer, Fiber and Textile Engineering, Georgia Institute of Technology, Atlanta, GA* MATTHEW BARROW, RICHARD JONES, CHRIS WRIGHT, P. RHODRI WILLIAMS, *Center for Complex Fluids Processing, University of Wales, Swansea* We report studies of the formation of ordered microporous polymer films by the evaporation of polymer solutions following exposure to a humid atmosphere. High speed microphotographic (HSMP) studies of the formation process reveal that near the surface of the polymer solution, vapor condensation produces near monodisperse water droplets which form a close-packed monolayer (or 'breath figure'). Following the evaporation of the solvent, characterization of the solid by Atomic Force Microscopy confocal microscopy and white light interferometry reveals that the surface of the polymer film features extensive regions of hexagonally close-packed microscopic pores, whose spatial arrangement replicates that of the initial droplet monolayer. Defects recorded by HSMP in the packing of the colloidal monolayer of liquid droplets formed above the surface of the polymer solution are found to correspond to those transferred into the eventual solid film, providing the first direct evidence of the structure templating role of the droplet monolayer.

**13:15**

**H25 11 Filling Small Pores With Polymer Melts** PRIYANKA DOBRIYAL, MINGFU ZHANG, JIUN TAI CHEN, THOMAS RUSSELL, *Department of Polymer Science and Engineering, University of Massachusetts, Amherst* Wetting of nanoporous inorganic templates by polymer melts is a well known and convenient way to generate polymeric nanostructures. In this work, we carried out a systematic study of wetting of nanoporous aluminum oxide membranes by polystyrene melts and obtained very different polymeric nanostructures (rods or tubes) under different conditions. When the annealing of polystyrene was done at temperature slightly above its glass transition temperature ($T_g$), nanorods were generated. When the annealing temperature was well above $T_g$, the resultant nanostructure depended on polymer molecular weight: for low molecular weight polystyrenes, nanotubes were obtained; for polystyrenes with very high molecular weights, however, nanorods formed. Thus, the viscosity of polymer melt controlled the nanostructure formation. When the viscosity of polymer melt was high, the capillary force was the dominant driving force which gave rise to the formation of nanorods; but when the melt viscosity was low, nanotubes formed and the wetting of the nanopores was achieved through the formation of precursor film.

**13:27**

**H25 12 Shear Rate Dependent Structure of Polymer Stabilized $TiO_2$ Dispersions - 1. $TiO_2$ Structure** ALAN NAKATANI, *Rohm and Haas Company* ANTONY VANDYK, LIONEL PORCAR, *NIST* JOHN BARKER, We measured the shear rate dependent structure of $TiO_2$ dispersions (37% volume fraction) stabilized with commercial polymer dispersants in water. The $TiO_2$ is a commercial grade $TiO_2$ with a particle diameter of approximately 400 nm (when the dispersions were diluted and measured

by Nanotrac 150). The solvent compositions were adjusted to the contrast match point of each dispersant to isolate the behavior of the $TiO_2$. Two different molecular weight poly acid dispersants (Referred to as ''low MW acrylate polymer salt'' and ''high MW acrylate polymer salt'') and two different molecular weight alkali soluble acrylate copolymers (Referred to as ''low MW hydrophobic acrylate copolymer salt'' and ''high MW hydrophobic acrylate copolymer salt'') were used in this study. The experiments were conducted at the NIST Center for Neutron Research (NCNR) on the perfect crystal diffractometer (PCD) for ultra-high resolution small-angle neutron scattering (USANS) measurements. The results for the $TiO_2$ scattering show that shear induced agglomeration occurs for certain dispersants and shear induced breakup of $TiO_2$ aggregates is observed for other dispersants. The results suggest new ways to consider dispersion of particles.

**SESSION H27: COMPUTATIONAL METHODS: MULTISCALE MODELING**
**Tuesday Morning, 14 March 2006**
**324, Baltimore Convention Center at 11:15**
**Jean-Luc Fattebert, Lawrence Livermore National Laboratory, presiding**



**11:15**
**H27 1 Coarse Molecular Dynamics Applied to the Study of Structural Transitions in Condensed Matter** MIGUEL A. AMAT, *Department of Chemical Engineering, University of Massachusetts, Amherst, MA* IOANNIS G. KEVREKIDIS, *Department of Chemical Engineering, Princeton University, Princeton, NJ* DIMITRIOS MAROUDAS, *Department of Chemical Engineering, University of Massachusetts, Amherst, MA* We report results from application of two coarse molecular-dynamics (MD) methods to determining the onset of structural transitions in condensed matter focusing on the melting of crystalline silicon. The two techniques require properly defined coarse variables that are slow and attracting. The first method is coarse projective integration. It allows wrapping a coarse time stepper around an MD simulator to extract the corresponding itcoarse-level description resulting from short MD bursts, which is used to extrapolate forward over coarse time steps. The second method is used to construct the underlying effective free energy landscape. Proper multi-system initialization at representative points in coarse-variable space along with analysis of the coarse-variable trajectories yields the effective free energy landscape upon integration of the reconstructed Fokker-Planck equation. Subsequent application of a coexistence criterion yields the thermodynamic melting point.

**11:27**
**H27 2 Adaptive Resolution Molecular Dynamics Scheme** LUIGI DELLE SITE, MATEJ PRAPROTNIK, KURT PRAPROTNIK, *Max Planck Institute for Polym.Res.* A new adaptive resolution scheme for efficient particle-based multiscale molecular dynamics (MD) simulations is presented. The key feature of the method is that it allows for a dynamical change of the number of molecular degrees of freedom during the course of the MD simulation by an on-the-fly switching between the atomistic and coarse-grained levels of detail. The new approach is tested on a model system of a liquid of tetrahedral molecules. The simulation box is divided into two regions: one containing only atomistically resolved tetrahedral molecules, and the other containing only one particle coarse-grained spherical molecules. The molecules can freely move between the two regions while changing their level of resolution accordingly. The hybrid and the corresponding all-atom systems have the same statistical properties.

**11:39**
**H27 3 A Multiscale Field Theory for Atomistic Multi-element Systems*** YOUPING CHEN, JAMES LEE, Formulas for local densities of fundamental physical properties, including stress and heat flux fields, are derived for atomistic systems with many-body potentials. The obtained formulas are then generalized to multi-element systems and the field representation of the corresponding conservation equations is obtained. The resulting formulas are calculable within an atomistic simulation, in consistent with the conservation laws of the thermodynamics continuum, and can be applied to single- and multi-element systems involving general two- and three-body interaction forces. It is found that, for multi-element systems, fluxes are composed of homogeneous and inhomogeneous parts and the energy conservation equation takes a different form from single-element systems. At atomic level, stress is nonlinear and nonlocal in displacements and consists of higher order strain gradients, and heat flux is a function of both strain and temperature gradients. With the derived balance equations and constitutive relations, it is shown that the atomistic formulation is able to completely define a field theory that exactly represents the classical many-body dynamics and is able to work as an alternative to, but computationally more efficient than, atomic-level molecular dynamics simulations in studying statistical and finite temperature properties of finite size multi-element materials. Numerical examples will be presented. Potential applications of the obtained field theory will be discussed.

*This work is supported by National Science Foundation under Award Numbers CMS-0301539 and CMS-0428419.

**11:51**
**H27 4 Wavelet-based Multiresolution Particle Methods** MICHAEL BERGDORF, *ETH Zurich* PETROS KOUMOUTSAKOS, *ETH Zurich* Particle methods offer a robust numerical tool for solving transport problems across disciplines, such as fluid dynamics, quantitative biology or computer graphics. Their strength lies in their stability, as they do not discretize the convection operator, and appealing numerical properties, such as small dissipation and dispersion errors. Many problems of interest are inherently multiscale, and their efficient solution requires either multiscale modeling approaches or spatially adaptive numerical schemes. We present a hybrid particle method that employs a multiresolution analysis to identify and adapt to small scales in the solution. The method combines the versatility and efficiency of grid-based Wavelet collocation methods while retaining the numerical properties and stability of particle methods. The accuracy and efficiency of this method is then assessed for transport and interface capturing problems in two and three dimensions, illustrating the capabilities and limitations of our approach.

**12:03**
**H27 5 Multiscale model for the study of phase separation in alloys with elastic misfit*** DANNY PEREZ, LAURENT LEWIS, *Université de Montréal* We present a multiscale model developed for the study of phase separation and microstructure evolution in

binary alloys. The model is based on the classical time-dependent DFT formalism for lattice systems generalized so that elastic effects are taken into account. A multi-scale implementation of this formalism is then performed using the finite volume method to obtain the evolution of the diffusive degrees of freedom while the quasicontinuum method is used to relax the elastic degrees of freedom. The combination of these two methods allows for a seamless coupling between different length-scales using a single formalism, while reducing exactly to the original TDDFT model as the mesh size is reduced to atomic dimensions. As a first application of this model, we study the effect of elastic heterogeneity on the chemical potential of inclusions as a result of inclusion-matrix and inclusion-inclusion interactions, and infer the consequences on the coarsening behaviour of a collection of inclusions.

*Work supported by NSERC and FQRNT.

**12:15**

**H27 6 Multiscale Modeling of Polymer Rheology** SUBHRANIL DE, JACOB FISH, MARK SHEPHARD, PAWEL KEBLINSKI, SANAT KUMAR, We propose a novel simulation method which can be used to readily parallelizesimulations on systems with a large spatial extent. We simulate small parts of thesystem with independent molecular dynamics simulations, and only occasionally passinformation between these simulations through a constitutive model free continuumapproach. We illustrate the power of this method in the case of a polymeric fluidundergoing rapid one dimensional shear flow. Since we show that this flow problemcannot be modeled by using a steady-state constitutive model, this method offers the unique capability for accessing the non-linear viscoelasticity of complex fluids.

**12:27**

**H27 7 PUPIL: A New Concept of Software Integration in Multi-scale Simulations.** JUAN TORRAS-COSTA, ERIK DEUMENS, SAMUEL TRICKEY, *QTP, University of Florida* We present a relatively straightforward way to incorporate existing software packages systematically into a fully automated multi-scale simulation framework. The **PUPIL** (itProgram for User Package Interfacing and Linking) architectural concept is to provide a simulation manager, enabled by small, minimally intrusive wrapper routines installed within each software package. Thus prepared, the different packages (''Calculation Units'') are plugged into the **PUPIL** system which one then operates as a software driver. A protocol is defined to communicate between the different Calculation Units and the **PUPIL** system to exchange information. The system has been designed using the OO paradigm and implemented in Java as a fast prototyping language. A test has been carried out joining three different packages to do a MD calculation with pattern recognition to identify the QM region and an external QM force calculation. The results show the ease of operation and maintenance of this software system with little overhead. Work supported by NSF ITR award DMR-0325553.

**12:39**

**H27 8 Multi-scale Simulation of Ferroelectric Properties in Perovskite Solid** YAJIE LEI, *George Washington University* JAMES LEE, YOUPING CHEN, LIMING XIONG, The first principles calculations provide us with the fundamental information for the study of ferroelectric materials, including the atomic structures of morphotropic phases, ferroelectric double-well potentials, dynamical effective charges and phonon spectra. Building on such information obtained from the electronic-structure calculations by density functional theory, we developed a multi-scale approach with parameterization of the classical Buckingham potential. Applying the empirical potentials to the atomistic modeling method and a newly developed continuum theory, the ferroelectric behaviors of BiScO3 are investigated through dynamical simulations. This approach illustrates the capability to study ferroelectric materials with finite temperature and external electromechanical loadings, with no limitation to a small system with zero temperature as being imposed in the first principles calculations.

**12:51**

**H27 9 Anisotropy of Step Stiffness and Its Implications*** T. L. EINSTEIN, T. J. STASEVICH, F. SZALMA, *U. of Maryland, College Park* Based on a lattice gas viewpoint, we have derived[1] a simple expression for the [in-plane] orientation dependence of step stiffness which is accurate for, e.g., noble metals at room temperature except near orientations with close-packed steps. We have extended our result to deal with this narrow but important range of angles. In addition to previous applications to Cu (001) and (111), we consider, e.g., simulations of fluctuations of island edges on Pb (111) in conjunction with experimental data.[2] We find that the numerical data in an Arrhenius plot is dominated by the contributions from highly kinked regions of the step edge. We emphasize that our expression is far superior to the standard phenomenological forms and is continuous and differentiable, so well suited to continuum models and finite-element calculations.

*Work supported by NSF MRSEC DMR 0520471, with partial funding from DOE-CMSN DEFG0205ER46227.

[1]T. J. Stasevich et al., Phys. Rev. B 70, 245404 (2004); 71, 245414 (2005)
[2]F. Szalma et al., Phys. Rev. B 71, 035422 (2005) & to be published.

**13:03**

**H27 10 Grain Boundary Cohesive Laws as a Function of Geometry** VALERIE COFFMAN, *Cornell University* JAMES SETHNA, *Cornell University* Cohesive laws are stress-strain curves used in finite element calculations to describe the debonding of interfaces such as grain boundaries. It would be convenient to describe cohesive laws as a function of the parameters needed to describe the grain boundary geometry; two parameters in 2D and 5 parameters in 3D. However, we find that the cohesive law is not a smooth function of these parameters. In fact, it is discontinuous at all geometries for which the two grains have repeat distances that are rational with respect to one another. Using atomistic simulations, we extract cohesive laws of grain boundary fracture in 2D with a Lennard-Jones potential for all possible geometries which can be simulated within periodic boundary conditions with a maximum box size. We connect the atomistic result to analytic calculations of fracture toughness as a function of dislocation density.

**13:15**

**H27 11 Water-Silica Interactions from Quantum Calculations and Non-Markovian Meta-Dynamics*** YINGXIA WAN, HAIPING CHENG, *University of Florida* The interaction of silica clusters and water molecules has been investigated using first-principles Born-Oppenheimer molecular dynamics (BOMD)

method. A small silica nano-rod that contains 108 atoms is chosen to illustrate the effects of external stress. Our results show clearly that the hydration energy between the nano-rod and water increases as a function of strain, which suggests that the water is more reactive under stress. Further simulations have been performed in which the nano-rod is twisted or squashed. We have also implemented a meta-dynamics based on the ideas of the extended Lagrangian and coarse-grained Non-Markovian dynamics. Hopefully, the method can be used to explore free energy barriers of chemical reactions.

*Acknowledgement: NSF/ITR under grant number DMR-0325553

**13:27**

**H27 12 POP-ART: thermodynamically correct activated event sampling in complex materials*** M.V. CHUBYNSKY, *Université de Montréal, Montréal, QC, Canada* HENK VOCKS, *Universiteit Utrecht, Utrecht, The Netherlands* NORMAND MOUSSEAU, *Université de Montréal* G.T. BARKEMA, *Universiteit Utrecht* Dynamics of complex systems with a rugged energy landscape can be represented as a sequence of rare activated events during which the system jumps between different potential energy minima. The activation-relaxation technique (ART) [1] is an efficient method of sampling such events; however, because of an unknown bias in selecting these events it cannot easily provide thermodynamical information. We present a modification of ART, the properly obeying probability ART (POP-ART) [2]. POP-ART combines short molecular dynamics runs with ART-like activated moves, with an additional accept/reject step designed to satisfy detailed balance and thus reproduce correct thermodynamics. Both correctness and efficiency of the method have been tested using a variety of systems. We mention briefly some ways of extending the approach to obtain correct dynamics as well. [1] G.T. Barkema and N. Mousseau, Phys. Rev. Lett. 77, 4358 (1996) [2] H. Vocks, M.V. Chubynsky, G.T. Barkema and N. Mousseau, J. Chem. Phys., accepted

*Work supported by the MESL (Québec), FQRNT, NSERC, the Canada Research Chair program, the Dutch NWO

**13:39**

**H27 13 Microstructural Effects in a Fully-Resolved Simulation of 1,024 Sedimenting Spheres*** LORENZO BOTTO, ZHONGZHEN ZHANG, ANDREA PROSPERETTI,† *Johns Hopkins University* The results of a fully-resolved simulation of 1,024 particles settling under gravity in a periodic domain are described and analyzed. The particle volume fraction is about 13% and the single-particle terminal Reynolds number about 10. Single and two-particle diffusivities are explored in the vertical and horizontal directions and their values related to the anisotropy of the system. Examination of the microstructure reveals that that the formation of nearly-horizontal particle pairs is an important phenomenon affecting the mean settling velocity as well as the velocity fluctuations.

*Supported by NSF and NASA
†Department of Mechanical Engineering

**13:51**

**H27 14 Finite element modeling of heat and oxygen atom diffusion in nuclear fuel rods.** JUAN RAMIREZ, PETRICA CRISTEA, MARIUS STAN, *Los Alamos National Laboratory* We present finite-element simulations of coupled heat and oxygen atom diffusion for $UO_2$ fuel pellets. The thermal conductivity, specific heat and oxygen diffusivity for the fuel element are obtained from atomistic calculations, while all other properties are obtained from experimental measurements. We examine the temperature and non-stoichiometry distributions for a varying range of conditions. Simulations are performed for steady state and transient one-dimensional (purely radial) configurations as well as steady three-dimensional cases. We examine the influence of pores or voids on the temperature and non- stoichiometry distribution with three-dimensional simulations. All simulations are performed with the commercial code COMSOL Multiphysicstrademark.

**14:03**

**H27 15 Information-Based Examination of Variable Hierarchy in Radiation Detection** KIM FERRIS, BOBBIE-JO WEBB-ROBERTSON, *Pacific Northwest National Laboratory* DUMONT JONES, *Proximate Technologies, LLC* Of considerable importance in the development of a general program of information-based materials design is the manner in which materials data are stored, retrieved and analyzed. In the area of radiation detection materials, the variable spaces tend to be large and property measurements (and computations) of candidate materials are not abundant. Moreover, measurements and calculations of the same nominal quantity (e.g. bandgap) are typically based on differing and incompletely defined environments, and may not be directly comparable. The identification of parameter degeneracies, reduced spaces and transferability within the information hierarchy have become critical issues for the development of effective structure mappings for making inferences on these systems. As the initial framework for a materials-informatics approach to radiation detection materials, we have explored the use of both supervised (Support Vector Machines (SVM); Linear Discriminant (LDA)) and unsupervised (Principal Component (PCA)) learning methods for the development of structural signature models. Application of these methods yields complementary results, both of which are necessary to reduce parameter space and variable degeneracy. Using a crystal structure classification test, nonlinear SVM significantly increases predictive performance, suggesting trade-offs between smaller descriptor spaces and simpler linear models.

**SESSION H28: FOCUS SESSION: ENERGETICS AND TRANSPORT IN CONJUGATED ORGANICS**
**Tuesday Morning, 14 March 2006; 325, Baltimore Convention Center at 11:15**
**David Gundlach, National Institute of Standards and Technology, presiding**

*Invited Papers*

**11:15**
**H28 1 Exciton Trapping at Heterojunctions in Polymer Blends.***
CARLOS SILVA, *University of Montreal*

Optoelectronic devices made from semiconductor polymers often employ partially phase-separated binary polymer blends with 'distributed heterojunctions' in the polymer film and the migration of bulk excitons towards these heterojunctions crucially influences the device performance. Here, we investigate exciton migration in blend films of two polyfluorene derivatives. Localized exciplex states form in electron-hole capture at the heterojunction between the two polymers and these can be thermally excited to transfer to bulk excitons. Rapid radiative emission from these excitons can then allow efficient light-emitting diode operation. We show here that when these excitons migrate to another heterojunction site within their lifetime they are re-trapped at the interface and again form exciplex states or dissociate completely. We demonstrate that in polymer blend light-emitting diodes this can reduce the exciton population by more than 54% and strongly influences the emission spectrum. We then analyze exciton re-trapping in detail using time-resolved photoluminescence spectroscopy on blends with different morphologies and find that for nm-scale phases exciton emission is completely suppressed. We show that the data agrees well with a simple kinetic model which confirms the importance of the blend morphology for the exciton trapping efficiency.

*Co-authors: Arne C. Morteani and Prof. Sir Richard Friend, Cavendish Laboratory, University of Cambridge

*Contributed Papers*

**11:51**
**H28 2 Narrow Band Tails in Organic Semiconductor Crystals** C. KRELLNER, S. HAAS, D. J. GUNDLACH, B. BATLOGG, *ETH Zurich, Switzerland* In order to study the electronic states in the bulk of high quality organic semiconductor crystals, we have applied the technique of temperature-dependent SCLC measurements. The result is a quantitative density of states curve extending from typically 0.5 eV to (0.05–0.1) eV above the valence band mobility edge. We have studied dozens of crystals of pentacene, rubrene and related compounds, and find in the purest samples a very low DOS in the range of $10^{15}\mathrm{cm}^{-3}\mathrm{eV}^{-1}$ and a characteristic exponential distribution parameter of $\sim$ 180 meV. Close to the mobility edge, a rapidly rising DOS is found with a narrow typical energy of $\sim$ 10 meV. Extrapolated to the mobility edge, these curves meet the DOS derived from electronic structure calculations. The band tails are significantly narrower than in amorphous Si:H, or derived for pentacene in previous measurements, where surface or interface effects might play a significant role.

**12:03**
**H28 3 Hückle $\pi$-electron theory of self-assembled metalloporphyrin films** W. SCHWALM, J. MORENO, *University of North Dakota* A. BRANDT, *Moorhead State Univ.* Porphyrin-based thin films including transition metal ions can be formed by self-assembly (Y. Ni and Q. Huo, J. of Porphyrins and Phthalocyanines **9**, 275 (2005)). They have significant magnetic and optical properties. Assuming that the structures are planar and two-dimensionally periodic, the $\pi$-electron theory, though highly approximate, may give some rough insight into their electronic properties. We model the two-dimensional array of metalloporphyrin molecules using a double-exchange Hamiltonian, that couples the local moments on the metal ions with the metal-like extended $\pi$-orbitals. Within a parametrized Local Combination of Atomic Orbitals (LCAO) approximation the electronic wavefunction is treated in a minimal basis of states odd in reflection through the plane of the molecule. Local Density of States and other simple properties are computed by Green function methods. The support surface interaction breaks the reflection symmetry and contributes self energy. This effect is included through a simple model approximation.

**12:15**
**H28 4 Triplet exciton formation and decay in polyfluorene light emitting diode** H.H. LIAO, H.F. MENG, S.F. HORNG, J.T. SHY, K CHEN, C.S. HSU, We study the triplet excitons in poly (9,9-dioctylfluorene-2,7-diyl) (PFO) light emitting diode using infrared induced absorption. The infrared absorption is exclusively due to the triplet excitons and there is no spectral overlap with any other species. A strong suppression of the triplet exciton density relative to the singlet by voltage is observed. Through an unique independent measurement on the triplet exciton lifetime it is shown that the suppression solely comes from triplet exciton quenching by current injection. The triplet-to-singlet exciton formation ratio is independent of voltage as well as temperature, implying a spin-independent exciton formation.

**12:27**
**H28 5 Estimating the electronic conductivity of size-expanded DNA: a complex bandstructure study** MIGUEL FUENTES-CABRERA, JACK C. WELLS, *Oak Ridge National Laboratory* OSCAR HUERTAS, F. JAVIER LUQUE, *Facultat de Farmacia, Universitat de Barcelona* HAO WANG, JAMES P. LEWIS, *Department of Physics and Astronomy, Brigham Young University* MODESTO OROZCO, *Institut de Recerca Biomedica and Facultat de Quimica, Universitat de Barcelona* OTTO F. SANKEY, *Department of Physics and Astronomy, Arizona State University* xDNA is a new class of synthetic nucleic acid with one of the bases larger than the natural congeners. The larger bases, called x-bases, can be viewed as a synthesis of benzene and a natural base. We recently have found that the x-bases have HOMO-

LUMO gaps smaller than their natural congeners, and that size-expanded duplexes have stronger $\pi$-$\pi$ stacking interactions than B-DNA duplexes. These findings suggest that xDNA is likely to have a smaller band gap than B-DNA, which could make xDNA a candidate for molecular wire applications. Here we use the complex band-structure method to estimate the conductive properties of polyxG.polyC and polyxG.polyxC. These results are compared to those we obtained previously on polyG.polyC. In this manner, we systematically probe how changes in the $\pi$-$\pi$ stacking interactions affect the conductivity of DNA-like molecules.

**12:39**

**H28 6 Excitonic effects in molecular crystals built up by small organic molecules** PETER PUSCHNIG, CLAUDIA AMBROSCH-DRAXL, *University Leoben, Chair of Atomistic Modelling and Design of Materials* KERSTIN HUMMER, *University of Vienna, Institute of Materials Physics* STEPHAN SAGMEISTER, *University of Graz, Institute of Physics* The excitonic effects of biphenyl and 2,2'-bithiophene are investigated within an ab-initio framework. For this purpose the Bethe-Salpeter equation for the two-particle Greens function is solved. Therefrom the imaginary part of the dielectric function is derived, which includes the electron-hole interaction in the absorption process. It turns out that these organic molecular crystals, which are built by small molecules, give rise to sizeable exciton binding energies, which are between 0.7 and 0.8 eV. To study the influence of the intermolecular interaction, the exciton binding energy of crystalline biphenyl is calculated as a function of pressure. The decrease of both, the band gap and the exciton binding energy, results in a slight red-shift of the lowest optically active singlet exciton.

**12:51**

**H28 7 Doping Induced Energy Level Shift in Organic Semiconductors** HUANJUN DING, *University of Rochester* KATE GREEN, *University of Michigan (REU student)* YONGLI GAO, *University of Rochester* Using photoemission and inverse photoemission spectroscopy (UPS, XPS and IPES), we investigated the electronic structure of alkali metal (Cs and Na) doped copper phthalocyanine (CuPc) and tris(8-hydroxyquinoline) aluminum (Alq) films. We found that doping induces energy level shift, which can be seen as in two different stages. The first stage is predominantly due to the Fermi level moving in the energy gap as a result of the doping of electrons from the alkaline metal to the organic, and the second stage is characterized by the significant modification of organic energy levels such as the introduction of a new gap state and new core level components. In addition, we observed that the energy level shift in the first stage depended in a semi-logarithmic fashion on the doping concentration, whose slope could not be explained by the conventional model used in inorganic semiconductors. Furthermore, we also observed a reversal shift by depositing Au on alkali metal doped Alq film. The initial Au deposition quenches the Alq gap state, as well as the new component in N 1s core level, caused by the alkali metal doping. Further Au depositions shift gradually the energy levels opposite to that induced by doping. The results indicate that the gap state and energy level positions can be decoupled in the organic semiconductors, and that it's possible to fine tune the electronic structure by selective doping in the interface region.

**13:03**

**H28 8 Optical Studies of Excited States in Polyfluorene*** MINGHONG TONG, CHUANXIANG SHENG, Z. VALY VARDENY, *Physics Department, University of Utah* Polyfluorene is an attractive $\pi$-conjugated polymer for display applications owing to efficient blue emission and relatively large hole mobility with trap free transport. The understanding of its photophysics is important for improving its applications. We have applied a variety of ps transient and cw optical techniques to study the optical properties of poly(9,9-dioctyl) fluorene (PFO). These spectroscopies include absorption, photoluminescence, electroabsorption (EA), two-photon absorption (TPA), and ps transient photoinduced absorption. Using these techniques we probed odd- and even-parity excited states that are complementary to each other. We fitted the EA and TPA spectra by calculating the imaginary part of the third order optical susceptibility using a summation over states model, which include the effects of strongly coupled vibrations and distribution of conjugation lengths.

*Supported in part by the DOE.

**13:15**

**H28 9 On the Charge transport regime of crystalline organic semiconductors: diffusion limited by thermal off-diagonal electronic disorder** ALESSANDRO TROISI, *University of Warwick* In organic crystalline semiconductor molecular components are held together by very weak interactions and the transfer integrals between neighboring molecular orbitals are extremely sensitive to small nuclear displacements. We used a mixed quantum chemical and molecular dynamic methodology to assess the effect of thermal structural fluctuations on the modulation of the transfer integrals between close molecules. We have found that the fluctuations of the transfer integrals are of the same order of magnitude of their average value for pentacene and anthracene. This condition makes the band description inadequate because a dynamic localization takes place and the translational symmetry is completely broken for the electronic states. We also present a simple one-dimensional semiclassical model that incorporates the effects of dynamical localization and allows the numerical computation of the charge mobility for ordered organic semiconductors. These results explain several contrasting experimental observations pointing sometimes to a delocalized ''band-like'' transport and sometimes to the existence of strongly localized charge carriers.

**13:27**

**H28 10 Charge Transport Simulations for Amorphous Organic Thin Film Devices** CONOR MADIGAN, VLADIMIR BULOVIC, *EECS, MIT, Cambridge, MA* We employ Monte Carlo simulations to analyze charge transport through amorphous organic thin films using the well-established ''Miller-Abrahams'' hopping model within a disordered manifold of molecular energies. Whereas most existing studies calculate non-dispersive, equilibrium mobilities at low carrier concentrations, in this work we instead calculate current densities for film thicknesses (i.e. 10 to

100 nm) and applied voltages (i.e. 0.1 to 100 V) typical of common thin film devices (e.g. organic light emitting devices and photovoltaics). We find that at these thicknesses one can not assume the non-dispersive, equilibrium condition. Also, since conduction typically occurs at high carrier concentrations and is space charge limited, we must employ simulations which treat both conditions. We compare our results with those predicted by existing analytic theories, and find that the analytic theories are often highly inaccurate, mainly due to faulty use of Fermi statistics and improper calculation of backward hopping.

**SESSION H29: FOCUS SESSION: PHYSICAL ASPECTS OF MORPHOGENESIS: COMPUTATIONAL APPROACHES**
**Tuesday Morning, 14 March 2006; 326, Baltimore Convention Center at 11:15**
**Shane Hutson, Vanderbilt University, presiding**

***Invited Papers***

**11:15**
**H29 1 From Genes to Morphogenetic Movements: How Cell-level Modeling Makes such Connections Possible.**
G. WAYNE BRODLAND, *University of Waterloo*

New understanding provided by computational modeling makes it possible to identify, in detail, the sequence of events by which gene expression gives rise to specific morphogenetic movements. Convergent extension (CE), an important developmental process in which embryonic tissues undergo self-driven narrowing in one in-plane direction and expansion in the other, is one such example. CE is triggered by gene expression and, in amphibian gastrulae, involves cephalocaudal (CC) gradients of the morphogens Xbra and Chordin and signalling molecules that include planar cell polarity (PCP) and Wnt/Ca2+ (Nature 2004, 430: 305-306). When these pathways have established suitable biochemical conditions, cellular protrusions called lamellipodia, which previously arose with random orientations, form preferentially in the mediolateral (ML) direction. To investigate whether lamellipodium action has the mechanical capacity to drive cell intercalation and its attendant cell reshaping, the cell-level finite element model of Chen and Brodland (ASME J. Biomech. Eng., 2000, 122: 394-401) was modified so that lamellipodia could originate from randomly selected cells, connect to next-neighboring cells in the ML direction and then contract. The simulations show that lamellipodia with these characteristics can, indeed, drive CE and that adjacent tissue must resist ML narrowing in order for characteristically elongated cells to result, predictions that have been confirmed experimentally. When these meso-scale findings are integrated with tissue- and whole-embryo mechanics, multi-scale ''mechanical pathways'' become evident. These pathways, in turn, interface directly with known biochemical pathways to produce an unbroken causal sequence from gene expression to specific morphogentic movements.

**11:51**
**H29 2 Myxobacteria Fruiting Body Formation.***
YI JIANG, *Los Alamos National Laboratory*

Myxobacteria are social bacteria that swarm and glide on surfaces, and feed cooperatively. When starved, tens of thousands of cells change their movement pattern from outward spreading to inward concentration; they form aggregates that become fruiting bodies, inside which cells differentiate into nonmotile, environmentally resistant spores. Traditionally, cell aggregation has been considered to imply chemotaxis, a long-range cell interaction mediated by diffusing chemicals. However, myxobacteria aggregation is the consequence of direct cell-contact interactions. I will review our recent efforts in modeling the fruiting body formation of Myxobacteria, using lattice gas cellular automata models that are based on local cell-cell contact signaling. These models have reproduced the individual phases in Myxobacteria development such as the rippling, streaming, early aggregation and the final sporulation; the models can be unified to simulate the whole developmental process of Myxobacteria.

*Collaboration with M. Alber, D. Kaiser, O. Sozinova, and M. Kiskowski

***Contributed Papers***

**12:27**
**H29 3 Quantifying the Intercellular Forces during Drosophila Morphogenesis** XIAOYAN MA, M. SHANE HUTSON, *Dept of Physics and Astronomy, Vanderbilt University; and VIIBRE - Vanderbilt Institute for Integrative Biosystem Research and Education* In many models of morphogenesis, cellular movements are driven by differences in interfacial tension along cell-cell boundaries. We have developed a microsurgical method to determine these tensions in living fruit fly (Drosophila) embryos. Cell edges in these embryos are labeled with green fluorescent protein chimeras; and line scan images that intersect several cell edges are recorded with a laser-scanning confocal microscope at a time resolution of 2 ms. While recording these scans, a Q-switched Nd:YAG laser is used to cut a single cell edge. The recoil of adjacent cell edges is evident in the line scans and the time-dependent cell edge positions are extracted using custom ImageJ plugins based on the Lucas-Kanade algorithm. The post-incision recoil velocities of cell edges are determined by fitting the cell edge positions to a double exponential function. In addition, a power spectrum analysis of cell-edge position fluctuations is used to determine the viscous damping constant. In the regime of low

Reynolds number, the tension along a cell-cell boundary is well-approximated by the product of the viscous damping constant and the initial recoil velocity of adjacent cell edges. We will present initial results from two stages of Drosophila development – germ band retraction and early dorsal closure.

**12:39**

**H29 4 Mechanisms of Biological Neural Network Development** H.G.E. HENTSCHEL, *Emory University* Functionality of the nervous system depends to a large extent on the precise patterns of connections between neurons. Neuronal connections form during development when neurons send out axons which migrate to their targets. We will describe briefly how such networks form including guidance by diffusible cues and the influence of nerve fiber bundling on network growth and form.

**12:51**

**H29 5 Upregulation of Tissue Dynamics in Response to UV Laser Perturbations** XOMALIN G. PERALTA, Y. TOYAMA, *Department of Physics* S. VENAKIDES, *Department of Mathematics* D. P. KIEHART, *Department of Biology* G. S. EDWARDS, *Department of Physics, Duke University* We investigate tissue dynamics *in vivo* using a steerable UV-laser microbeam coupled to a scanning laser confocal microscope. We follow a stage in the morphogenesis of the fruit fly known as dorsal closure, which largely occurs in 2D. Dorsal closure is a consequence of four biological processes that are coordinated in space and are synchronized in time. During dorsal closure, two advancing flanks of epidermal tissue demarcate an eye-shaped opening on the dorsal side of the embryo, exposing the underlying amnioserosa tissue. As closure progresses, the two flanks of epidermal tissue approach each other and, via an adhesion mediated process, ''zip'' to form seams at the two canthi, i.e. the corners of the opening. In our studies, we target the microbeam to selectively remove specific tissues and track the resulting dynamics. We account for the results with a quantitative model. When we inhibit zipping by repeatedly targeting the microbeam to one canthus, we find evidence for an increase in the zipping rate of the seam at the other, unperturbed canthus. The upregulation occurs in a region remote from the tissue targeted by the microbeam and involves many cells. This upregulation of zipping is an example of a compensatory mechanism that ensures successful closure and highlights the resiliency of dorsal closure to perturbations. Supported by the NIH (GM33830 and GM61240).

**13:03**

**H29 6 Pattern Scaling Achieved by Oppositely Directed Morphogen Gradients** PETER McHALE, *UCSD* WOUTER-JAN RAPPEL, *UCSD* HERBERT LEVINE, *UCSD* Morphogens are proteins, often produced in a localised region, whose concentrations spatially demarcate regions of differing gene expression in developing embryos. The boundaries of expression must be set accurately and in proportion to the size $L$ of the developing field; this cannot be accomplished by a single one-dimensional gradient. Here, we show how a pair of morphogens produced at opposite ends of a developing field can solve the pattern-scaling problem. In the most promising scenario, two morphogens interact according to $A + B \rightarrow \varnothing$ and the switch occurs according to the absolute concentration of the first gradient. In this case scaling occurs in a window of developing-field sizes centred at a few times the morphogen decay length.

**13:15**

**H29 7 Shape and Size of the Fission Yeast Nucleus are governed by Equilibrium Mechanics** GERALD LIM, *Baylor College of Medicine (BCM)* GREG HUBER, *University of Connecticut Health Center* JONATHAN MILLER, *BCM* SHELLEY SAZER, *BCM* Nuclear morphogenesis in the asexual reproduction of itSchizosaccharomyces pombe (fission yeast) consists of two stages: (i) volume-doubling growth, in which a round nucleus inflates uniformly, and (ii) division, in which the nucleus undergoes shape changes from round to oblong to peanut to dumbbell before it resolves into two smaller, round daughter nuclei, driven by the formation and elongation of a microtubule-based spindle within the nucleus. The combined volume of the daughter nuclei immediately after division is the same as the volume of the single nucleus at the onset of division. Consequently, the nuclear envelope (NE) area must increase by 26% during division. We are developing a model in order to determine the mechanics governing these shape and size changes. It is based on current knowledge of the nuclear structure, insight from normal and abnormal nuclei, and concepts from the mechanics governing lipid-bilayer membranes. We predict that (a) the NE prefers to be flat, (b) the NE is under tension, (c) the nucleus has an internal pressure, (d) nuclear growth is governed by the Law of Laplace, and (e) some abnormal nuclei behave like vesicles with encapsulated microtubules.

**13:27**

**H29 8 A surprising answer in the search for a comprehensive health protection exposure metric for radiofrequency (RF) fields** MARJORIE LUNDQUIST,* *The Bioelectromagnetic Hygiene Institute* Matter can interact with light in 3 different ways (known by 1910): by absorption of energy [*thermal* hazard] or by absorption of linear momentum (radiation pressure) or of angular momentum (torque) or of both [*nonthermal* hazards].[1,2] The same is true for RF fields; indeed, microwave wattmeters may operate on a momentum absorption principle.[3,4] But most RF health protection standards today are based solely on *thermal* effects, ignoring nonthermal effects. Formal expressions for scientifically valid exposure metrics will be presented. It will be shown that nonthermal effects depend on field frequency, polarization and spatial configuration as well as on field strength, so a *general* metric valid for *all* fields may not exist. But with some approximations, the *magnetic induction current* may constitute an adequate *practical* exposure metric for RF fields. [1]M. Lundquist, BAPS **50** (1):620(2005). [2]M. Lundquist, BAPS **50** (1):1178(2005). [3]A. L. Cullen, Proc. IEE **99** Pt4(2):100-110(Apr 1952). [4]A. L. Cullen & I. M. Stephenson, Proc. IEE **99** Pt4(4):294-301 (Dec 1952).

*P.O. Box 11831, Milwaukee WI 53211-0831 USA

**13:39**

**H29 9 Nonlinear Analysis of Electromyography Time Series of Low Back Muscles** ULRICH ZURCHER, KAUFMAN MIRON, PAUL SUNG, *Cleveland State University* We have calculated the mean-square displacement $\Delta(t)$ from the EMG time series and have found that increases diffusively, $\Delta(t) \sim t$, for short times $t < 10$ms, and shows a plateau-like behavior, $\Delta(t) \sim t^0$, for interintermediate times $10\,\text{ms} < t < 0.5,\text{s}$. The plateau-like behavior implies the presence of correlations in the signal. We characterize these correlations and relate them to properties of the power spectrum of the signal.

**SESSION H30: PADDEN AWARD SYMPOSIUM**
**Tuesday Morning, 14 March 2006**
**327, Baltimore Convention Center at 11:15**
**Anne Mayes, Massachusetts Institute of Technology, presiding**

**11:15**
**H30 1 Electrochemically Controlled Self-Assembly of an Organometallic Block Copolymer** HANY EITOUNI, NITASH BALSARA, *U.C. Berkeley, LBNL* We have established a technique for exerting localized reversible control over the formation of block copolymer microphases. The application of electrical fields as low as 2 V/cm across a 17 weight % solution of a disordered, partially oxidized poly(isoprene-itblock-ferrocenyldimethylsilane) copolymer in dichlorobenzene results in the formation of ordered domains near the positive electrode. Spatially- and temporally-resolved small-angle neutron scattering (SANS) and birefringence measurements on the sample in the presence of the electric field were used to follow the order formation process. After reversal of the electrical bias on the system, the ordered regions underwent order-to-disorder transitions and new ordered regions were formed at the opposite electrode. Optical birefringence measurements indicated that the ordered regions possessed significant long-range orientational order.

**11:27**
**H30 2 Anomalous Segregation of Deuterium Labeled PS at hPS:dPS/hPMMA Interfaces as Characterized by SIMS and Mean-Field Theory*** SHANE HARTON, FRED STEVIE, HARALD ADE, *North Carolina State University* Secondary ion mass spectrometry (SIMS) was used to measure real- space depth profiles of deuterium labeled polystyrene (dPS) in hPS:dPS/poly(methyl methacrylate) (hPMMA) bilayers, with the hPS:dPS blend being well within the single-phase region of the phase diagram. Profound changes in the thermodynamic behavior of this system at the polymer/polymer interface are observed in the form of significant segregation of dPS to the hPS:dPS/hPMMA interface. Furthermore, a depletion hole was observed during the early stages of formation of an equilibrium excess of dPS, implying that the energetic gain at the interface per dPS chain has to be $>$ kT. The observed interfacial excess is quantified by generating theoretical profiles, using self-consistent mean- field theory (SCMF), and fitting an effective interaction energy parameter $\Delta\chi$ as a function of temperature. The temperature dependency of $\Delta\chi$ was found to be a factor of $3 - 4$ greater than any of those reported for $\chi$ of PS/PMMA. It was also found that SCMF accurately describes the concentration dependency of dPS segregation at a constant dPS molecular weight using a concentration independent $\Delta\chi$, however $\Delta\chi$ was found to be dependent on dPS molecular weight. A novel method of using carbon-13 labeling is demonstrated as an alternative to deuterium labeling, providing a true tracer for investigations of such phenomena as polymer chain mobility near surfaces and interfaces and reactive coupling at polymer/polymer heterogeneous interfaces.

*In collaboration with Fred Stevie and Harald Ade, North Carolina State University.

**11:39**
**H30 3 Toward Single-Chain Crystallisation Kinetics** MICHAEL V. MASSA, KARI DALNOKI-VERESS, *Physics and Astronomy, McMaster University* By dewetting a thin film of a crystallisable polymer on an unfavourable substrate, one can create an ensemble of isolated and impurity-free droplets, in which homogeneous crystal nucleation can occur. Previously we have demonstrated (PRL, 92, 255509, 2004) that for bulk-like droplets (containing on the order of 10 [9] chains) the homogenous nucleation rate scales with the itvolume of the droplet. However, as the domain size is reduced far below these length scales, the confinement of polymer chains to dimensions less than the radius of gyration, the increase in the ratio of surface area to volume, and the decrease in the number of neighbouring chains can all potentially lead to changes in the crystallisation kinetics. With the same sample geometry, we extend our study of homogeneous nucleation to smaller droplet length scales. Crystallisation is monitored using ellipsometry, which offers a very sensitive probe to changes in the sample density, even for extremely small quantities of material. With complimentary results from atomic force microscopy, we follow the homogeneous crystallisation of a supercooled melt, from bulk length scales down to single-chain dimensions.

**11:51**
**H30 4 Fabrication of Three-Dimensional Nanostructures from Self-Assembling Block Copolymers on Two-Dimensional Chemically Patterned Templates with Mismatched Symmetry** MARK STOYKOVICH, *University of Wisconsin* KOSTAS DAOULAS, *University of Goettingen* HARUN SOLAK, *Paul Scherrer Institute* SANG-MIN PARK, YIORYOS PAPAKONSTANTOPOULOS, JUAN DE PABLO, *University of Wisconsin* MARCUS MUELLER, *University of Goettingen* PAUL NEALEY, *University of Wisconsin* A combined experimental and theoretical approach is used to examine the direct fabrication of complex three-dimensional (3D) nanostructures by the self-assembly of block copolymer materials on two-dimensional templated surfaces. Here a lamella-forming ternary block copolymer – homopolymer blend is considered on periodically patterned substrates consisting of square arrays of spots. The blend follows the substrate pattern and forms a quadratically perforated lamella (QPL). At intermediate film thicknesses necks connect this QPL to the film surface, resulting in a bicontinuous morphology. For thicker films bicontinuous morphologies are observed that consist of a sequence of parallel lamellae with disordered perforations. The principal concept of this work extends beyond this initial demonstration and can be generalized to the fabrication of complex 3D structures that have potential applications in nanoelectronics, separation membranes, and catalysis.

**12:03**
**H30 5 Slaved Diffusion in Phospholipid Bilayers** LIANGFANG ZHANG, *Department of Chemical & Biomolecular Engineering, UIUC* STEVE GRANICK, *Department of Materials Science & Engineering, of Chemistry, of Physics, and of Chemical & Biomolecular Engineering, UIUC* Dual-color fluorescence correlation spectroscopy (FCS) was employed to simultaneously investigate the translational diffusion of phospholipids in supported fluid bilayers and polymers which adsorb on these bilayers at incomplete surface coverage. It was found that the translational diffusion of phospholipids split into two populations due to polymer adsorption. A slow mode, whose magnitude was the same as that of adsorbed polymers, coexisted with a fast mode characteristic of naked lipid diffusion. Using 2-color fluorescence, cross-

correlation between the diffusion of phospholipids and polymers suggested the plausible interpretation that polymer adsorption created nanodomains of lipid whose mobility was determined by the occluded area of the adsorbed polymer. That is, those lipids inside the nanodomains were enslaved by the adsorbed polymers and diffused collectively. Variations of the polymer molar mass showed that the slow mode of phospholipid diffusion varied inversely with molar mass of the adsorbate, as predicted by our notion of slaved diffusion. This work offers a new mechanism to explain how naonsized domains with reduced mobility arise in lipid membranes.

**SESSION H31: FOCUS SESSION: SIMULATION OF COMPLEX MATERIALS II**
**Tuesday Morning, 14 March 2006**
**328, Baltimore Convention Center at 11:15**
**Giulia Galli, University of California, Davis, presiding**

*Contributed Papers*



**11:15**
**H31 1 Persistent Current and Drude Weight in Mesoscopic Rings** F. CARVALHO DIAS, I.R. PIMENTEL, *University of Lisbon, Portugal* M. HENKEL, *Universite Henri Poincare, Nancy I, France* We study the persistent current and the Drude weight of a system of spinless fermions, with repulsive interactions and a hopping impurity, on a mesoscopic ring pierced by a magnetic flux, using a DMRG algorithm for complex fields. We find that the persistent current changes from an algebraic to an exponential decay with the system size, as the system crosses from the Luttinger Liquid (LL) to the Charge Density Wave (CDW) phase with increasing interaction $U$. We also find that in the interacting system the persistent current is invariant under the impurity transformation $\rho \rightarrow 1/\rho$, for large system sizes, where $\rho$ is the defect strength. In the LL phase the Drude weight decreases algebraically with the number of lattice sites $N$, due to the interplay of the electron interaction with the impurity, while in the CDW phase it decreases exponentially, defining a localization length which decreases with increasing interaction and impurity strength. Our results show that the impurity and the interactions always decrease the persistent current, and imply that the Drude weight vanishes in the limit $N \rightarrow \infty$, in both phases.

**11:27**
**H31 2 Applying Time-dependent DMRG to Calculate the Conductance of Nanostructures** KHALED AL-HASSANIEH, *Oak Ridge National Laboratory, Oak Ridge TN, and University of Tennessee, Knoxville TN 37831* A. E. FEIGUIN, *Kavli Institute for Theoretical Physics, University of California, Santa Barbara, CA 93106* J. A. RIERA, *Universidad Nacional de Rosario, Avenida Pellegrini 250,2000-Rosario, Argentina* C. A. BÜSSER, *Ohio University, Athens, OH 45701* E. DAGOTTO, *Oak Ridge National Laboratory, Oak Ridge TN, and University of Tennessee, Knoxville TN 37831* DMRG provides a powerful tool to study quantum 1D systems. We present a detailed procedure for applying the recently developed time-dependent DMRG to calculate the conductance of nanostructures, such as quantum dots (QD's). The leads are modelled using tight-binding Hamiltonians. The ground state at time zero is calculated at zero bias. Then a small bias is applied between the two leads, the wave-function is evolved in time and the current is measured as a function of time. Typically, the current saturates at a steady state after a short period of time. The conductance is obtained from the steady-state current. To test this approach We study several cases of interacting and non-interacting systems. Our results show excellent agreement with the exact results in the non-interacting case. We also reproduce quantitatively the well-established results in the case of one interacting QD and two coupled interacting QD's. [1] K. A. Al-Hassanieh *et al*, in preparation. [2] Steven R. White and Adrian E. Feiguin, Phys. Rev. Lett. **93**, 076041 (2004).

**11:39**
**H31 3 Structural and electronic properties of solvated benzene and hexafluorobenzene from itab initio simulations** MARKUS ALLESCH, *Department of Theoretical and Computational Physics, Graz University of Technology, Austria, and Lawrence Livermore National Laboratory, Livermore, CA* ERIC SCHWEGLER, *Lawrence Livermore National Laboratory, Livermore, CA 94550* GIULIA GALLI, *Lawrence Livermore National Laboratory, Livermore, CA 94550 and University of California at Davis, Davis, CA 95616* We have studied the aqueous solvation of benzene and hexafluorobenzene using extensive first principles molecular dynamics simulations. By employing a rigid water approximation [1], we have been able to efficiently address long time-scale simulations ( $\sim$ 100 ps) within a first-principles context. Our analysis of radial, spatial and tilt angle distribution functions of first shell water molecules reveals structural details in the axial and equatorial regions of the solute. In particular, we have identified strong orientational ordering near the faces of the rings and cage-like spacial structures in the equatorial regions. The structural properties of the first solvation shell lead to subtle changes in the electronic structure of water, e.g. changes in dipole moments. [1] M. Allesch, et al. J. Chem. Phys. 120, 5192 (2004) This work was performed under the auspices of the U.S. Dept. of Energy at the University of California/Lawrence Livermore National Laboratory under contract no. W-7405-Eng-48.

*Invited Papers*

**11:51**
**H31 4 Boron: do we know the ground state structure?***
TADASHI OGITSU, *Lawrence Livermore National Laboratory*

Boron is only the fifth element in the periodic table, having a simple electronic configuration, yet, it is known to form one of the most complicated crystal structures, $\beta$-rhombohedral structure. Up to date, the best estimate on the number of atoms in its hexagonal unit cell is 320.1, not even an integer number. The key concept to understand its complexity is

covalency and electron deficiency: It does not have enough valence electrons to form a simple covalent crystal, like carbon or silicon. Instead it forms a complicated packing of icosahedrons. The structural model of $\beta$-boron was developed in the 1960s based on X-ray experiment. Although this model structure captures the most of the structural characteristics of $\beta$-boron, it has a crucial pitfall; the number of atoms per cell estimated by X-ray experiment does not agree with the number of atoms estimated by the pycnometric density. In 1988, Slack et al. discovered four more POS, by which the discrepancy in the number of atoms is reconciled [J. of Solid State Chem. 76, 52 (1988)]. There still remains an unanswered question; how are these POS atoms configured? Is it completely random? Or there is some kind of order as it has been suggested in Slacks paper? A major challenge here is the astronomical number of possible configurations, roughly 150 million even for the irreducible cell. We tackle this problem using *ab-initio* simulated annealing coupled with a Lattice Model Monte Carlo simulated annealing. Our results reveal that the stable structure, indeed, has a certain type of correlation in its POS configuration. More detail on the structural property and its impact on electronic property of $\beta$-boron will be discussed at the presentation. This work was performed under the auspices of the U.S. Dept. of Energy at the University of California/ LLNL under contract no. W-7405-Eng-48.

*This work was done in collaboration with Giulia Galli, Francois Gygi, and John Reed.

***Contributed Papers***

**12:27**

**H31 5 First principles thermodynamics studies on the surface structures of Pt-alloy catalyst as a function of the surface segregation, co-adsorption and particle size** BYUNGCHAN HAN, GERBRAND CEDER, *Massachusetts Institute of Technology* Segregation in alloy catalysts can be significantly affected by the chemical environments. Using density functional theory coupled to the cluster expansion technique we study how adsorption of chemical species and bulk alloying change the surface structures and hence reactivity of Pt. We find that chemical adsorbates (O, OH, CO and water etc,) can change surface segregation energy of alloy elements dramatically in both bulk and nano-sized Pt. It implies that the interactions between adsorbates and surface atoms are important to understand the surface morphology and catalyst activities. We also find that Pt oxide (Pt-O or Pt-OH) has a higher reactivity to CO oxidation than pure Pt. On the other hands, Ru alloying on the Pt surface without adsorbates enhances the CO adsorption on Pt. We also investigate the effect of nanoparticle size of the on surface segregation and CO oxidation.

**12:39**

**H31 6 Structural and Vibrational Properties of Boron Nitride Analogues of Diamondoids** STEVEN L. RICHARDSON, *Howard University* KYUNGWHA PARK, *Virginia Polytechnic Institute and State University* TUNNA BARUAH, MARK R. PEDERSON, *Naval Research Laboratory* Diamondoids are stable cage-like hydrocabon molecules that possess a structure that is superimposable upon the diamond crystal. These highly symmetric structures have a generic structural formula $C_{4n+6}H_{4n+12}$, and they have been isolated from petroleum oil. Because of their various shapes and sizes, there has been speculation in the literature that diamondoids might be suitable building blocks for possible applications in nanotechnology. One could ask whether boron nitride (BN) analogues of diamondoids might exist. It is known experimentally that cyclotriborazane ($B_3N_3H_{12}$), the BN-analogue of the smallest diamondoid molecule adamantane exists, but there is no experimental evidence for the existence of higher-order BN-diamondoids at the present time. In this work we perform accurate all-electron density-functional theory (DFT) calculations to study the structural and vibrational properties of a small set of lower order BN-diamondoids (e.g. BN-adamantane ($B_6N_4H_{16}$), BN-diamantane ($B_7N_7H_{20}$), BN-triamantane ($B_{10}N_8H_{24}$), and BN-itanti-tetramantane ($B_{11}N_{11}H_{24}$)). We discuss the relative stability of each of these representative BN-diamondoid molecules and provide theoretical infrared and Raman spectra for future identification of this novel class of molecules. *This work was supported by the National Science Foundation and the Office of Naval Research.

**12:51**

**H31 7 High quality molecular dynamics simulation of carbon nanotubes in** DEYU LU, YAN LI, UMBERTO RAVAIOLI, *Beckman Institute, University of Illinois at Urbana-Champaign* GIANCARLO CICERO, *Istituto Superiore Mario Boella, Italy* GIULIA GALLI, *Chemistry department, University of California, Davis* KLAUS SCHULTEN, *Beckman Institute, University of Illinois at Urbana-Champaign* Biological applications of carbon nanotubes (CNTs) rely on mechanical, electrical, and chemical interactions between CNTs and biomolecules in water. Efficient computational methods for such nanoscale disordered systems have been developed that take into account the electronic degree of freedom of the CNTs interacting with biological media with thousands of atoms. For this purpose we combined in a molecular dynamics program an empirical CNT model employing a tight-binding CNT Hamiltonian with a classical description of the biological medium (water, ions, protein, DNA). The first application of this new method [1,2] described a potassium ion-CNT complex [3] and revealed a terahertz frequency oscillation of the ion inside a 16 angstrom long CNT segment. At a greatly reduced computational expense, our result showed good agreement with a Car-Parrinello molecular dynamics simulation. [1] D. Lu, Y. Li, U. Ravaioli, and K. Schulten. J. Phys. Chem. B, 109 (2005)11461. [2] D. Lu, Y. Li, S. V. Rotkin, U. Ravaioli, and K. Schulten. Nano Lett., 4 (2004) 2383. [3] D. Lu, Y. Li, U. Ravaioli, and K. Schulten. Phys. Rev. Lett., (2005) in press.

**13:03**

**H31 8 Realistic, quantitative descriptions of electron-transfer reactions: diabatic free-energy surfaces from first-principles molecular dynamics** P. H.-L. SIT, *Department of Physics, Massachusetts Institute of Technology* M. COCOCCIONI, *Department of Materials Science and Engineering, Massachusetts Institute of Technology* NICOLA MARZARI, *Department of Materials Science and Engineering, Massachusetts Institute of Technology* A general approach to calculate the diabatic surfaces for electron-transfer reactions is presented, based on first-principles molecular dynamics of the active centers and their surrounding medium. The excitation energy corresponding to the transfer of an electron at any given ionic configuration (the Marcus energy gap) is accurately assessed within ground-state density-functional theory via a

novel penalty functional for oxidation-reduction reactions that appropriately acts on the electronic degrees of freedom alone. The self-interaction error intrinsic to most exchange-correlation functionals is also corrected using the same penalty functional. The free-energy diabatic surfaces are then constructed with umbrella sampling on large ensembles of configurations. As a paradigmatic case study, the self-exchange reaction between ferrous and ferric ions in water is studied in detail.

**13:15**

**H31 9 Role of Interfaces and Effect of Impurities in Nitride-based Superhard Nanocomposites** HAO SHIQIANG, *The University of Sydney* BERNARD DELLEY, *Paul-Scherrer-Institut* CATHERINE STAMPFL, *The University of Sydney* Recently, a hardness similar to that of diamond has been reported for the ternary nitride-based nanocomposite, *nc*-TiN/ *a*-$Si_3N_4$/*a*- and *nc*-$TiSi_2$ [1]. The reproducibility, however, has proved difficult, as has the superhardness of the related, prototypical, binary nanocomposite *nc*-TiN/*a*-$Si_3N_4$. Extensive density- functional theory calculations indicate that the hardness enhancement in the latter system is due to the preferential formation of TiN(111) polar interfaces with a thin Si-layer which is N-coordinated and tetrahedrally bonded [2]. The tensile strength of TiN in the [111] direction is very similar to the weakest bonding direction in diamond. Oxygen impurities cause a significant reduction of the interface strength which could partly explain the conflicting results, and signals the importance of avoiding such contaminants for achieving super- and ultra-hard nanocomposites. [1] S. Veprek et al. Surf. Coat. Technol. 133-134, 152 (2000). [2] S. Hao, B. Delley, and C. Stampfl, to be published.

**13:27**

**H31 10 Spectral functions of fullerene molecules and solids** FEI LIN, ERIK SORENSEN, CATHERINE KALLIN, JOHN BERLINSKY, *McMaster University* There have been lots of interests in producing and engineering the fullerene materials, either because of their highly symmetric molecular geometry, the discovery of superconductivity in doped C60 materials, or their potential applications in nano devices. In this talk I will report some Quantum Monte Carlo/exact diagonalization calculations of the single-particle spectral properties on the Hubbard C20 molecule and its possible lattices. Similar calculations on the C36 and C60 materials may also be presented.

**13:39**

**H31 11 Static Polarizabilities of Nanoclusters** HYE-YOUNG KIM, JORGE SOFO, *Physics Department, The Pennsylvania State University, University Park, PA* DARRELL VELEGOL, *Chemical Engineering Department, The Pennsylvania State University, University Park, PA* MILTON COLE, *Physics Department, The Pennsylvania State University, University Park, PA* GAUTAM MUKHOPADHYAY, *Physics Department, Indian Institute of Technology-Bombay, India* In the present work, we evaluate the static polarizability of a cluster using a microscopic method that is exact within the linear and dipolar approximations. Numerical examples are presented for various shapes and sizes of clusters composed of identical atoms, where the term ''atom'' actually refers to a generic constituent, which could be any polarizable entity. The results for the clusters' polarizabilities are compared with those obtained by assuming simple additivity of the constituents' atomic polarizabilities; in many cases, the difference is large, demonstrating the inadequacy of the additivity approximation. Comparison is made (for symmetrical geometries) with results obtained from continuum models of the polarizability. Also, the surface effects due to the nonuniform local field near a surface or edge are shown to be significant.

## SESSION H32: FOCUS SESSION: COMPUTATIONAL NANOSCIENCE III

**Tuesday Morning, 14 March 2006**
**329, Baltimore Convention Center at 11:15**
**Byounghak Lee, Lawrence Berkeley National Laboratory, presiding**

***Contributed Papers***

**11:15**

**H32 1 First-Principles Study of Atomistically Engineered 2D-Boron Sheets** KAH CHUN LAU, RAVINDRA PANDEY, *Department of Physics, Michigan Technological University, Houghton, MI* Based on density functional theory with a planewave basis set, the stability, morphology and electronic properties of 2D boron sheets are studied. We suggest that a 2D boron sheet can be stable, and can posses metallic, half-metallic and semiconducting properties, depends on their distinct configurations. In contrast to previous studies, we predict the stability of a new novel 2D reconstructed {1221} boron sheet over the idealized {1212} triangular plane, together with their corresponding buckled configurations. Despite the high stability in cohesive energy, the unique features in geometry and electronic properties found in both configurations, suggest strong variations in electronic and mechanical properties, which might occur when the plane is rolled into different chiral structures of single-wall boron nanotubes.

**11:27**

**H32 2 Density Functional Investigation of Surface Stress-Induced Phase Transformations in FCC Metallic Nanowires** MICHAEL HAFTEL, *Naval Research Laboratory* KEN GALL, *Georgia Institute of Technology* We use density functional theory (DFT) to study the relaxation of narrow Cu, Ni, Au, Pt and Ag nanowires originally oriented in the $< 001 >$ direction with a FCC structure. For a small enough diameter ($D < 2$ nm) each nanowire, under the compressive influence of its own surface stress, spontaneously relaxes to either a $< 110 >$ orientation (Cu, Ni, Ag) or to a BCT $< 001 >$ (Au, Pt) orientation, both of which are characterized by a compression of the wire axis of at least 30%. To analyze the stability of BCT structures, we calculate the elastic constants for the BCT phases of these metals under bulk, slab, and nanowire conditions. We find that the surface contribution to the elastic constant for shear, $C_{66}$, helps stabilize the BCT phase in Au which would otherwise be unstable under bulk conditions. A large stabilization contribution from the surface also occurs in Ni and Cu, but not enough to overcome the shear instability in the bulk, and these nanowires do not transform to BCT. We discuss the implications of these results on the superelastic shape-memory effect for FCC metals.

**11:39**
**H32 3 First principles investigation of polymer-ceramic interfaces and composites** V. RANJAN, L. YU, M. BUONGIORNO NARDELLI, J. BERNHOLC, *North Carolina State University* Composite structures with high-k dielectrics are important future technologies for high-performance capacitors. We perform generalized-gradient approximation calculations to study interfacial properties of ceramic-polymer composites, focusing in particular on the strength of polymer adhesion to ceramic surfaces. Our results show that several polymers of interest do not bind directly to the ceramic. However, it is possible to functionalize the surface so that polymer attachment occurs. We present various possibilities for attachment to ceramic surfaces, which should lead to the formation of stable composites.

***Invited Papers***

**11:51**
**H32 4 Inverse Design of Surface-Based Magnetic Nanostructures.***
ZHENYU ZHANG, *Oak Ridge National Lab*

Multiscale modeling is gaining an increasingly important role in guiding the fabrication of artificially structured nanomaterials with atomic-scale precision and desirable physical properties. In this talk, two recent examples will be presented to illustrate its predictive power in modern materials research. The modeling approaches range from electronic-scale calculations based on first principles to mesoscopic-scale continuum elasticity theory. Specific examples include: (a) fabrication of ordered magnetic atom wires on non-magnetic metal substrates; (b) optimal dopant control in dilute magnetic semiconductors via ''Subsurfactant Epitaxy.'' Emphasis will be made on the substantially improved structure-property relationships achieved through such synergetic efforts between theory and experiment, including in the second example the striking observation of magnetic ordering temperatures well above 300 K.

*Supported by USDOE, USNSF, & NSF of China, in collaboration with W.G. Zhu, Y.N. Mo, C.G. Zeng, J.D. Guo, K. Varga, E.G. Wang, H.H. Weitering, and E. Kaxiras.

***Contributed Papers***

**12:27**
**H32 5 Design of Nano-Ears for Surface Enhanced Raman Scattering*** FERNANDO A. REBOREDO,† CHAD E. TALLEY, STEPHEN M. LANE, *Lawrence Livermore National Laboratory* Metallic structures optimized for surface enhanced Raman scattering (SERS) must combine i) large dipole moments, for stronger coupling with the external field E, and ii) highly localized plasmon modes, which increase Raman Scattering cross sections (proportional to E4) and improve spatial resolution. Since typical molecules are much smaller than the visible wave lengths, the design of nanostructured surfaces for SERS involves an electrodynamical problem analogous to the one solved with ear shapes in acoustics. In this limit, retardation effects can be ignored, which reduces the problem to the response at the metal surface. We have developed a finite element computational tool that allows the calculation of surface plasmons on arbitrary metallic shapes. We have found that an accurate description of the surface curvature is crucial. Our numerical results agree with exact analytical solutions for the quasi-static model known for spheres and spherical shells. Using this method, we have compared several shapes, where analytical results are not available, and uncover ear-shaped structures that are 12 orders of magnitude more efficient than spheres.

*This work was performed under the auspices of the U.S. Dept. of Energy at the University of California/Lawrence Livermore National Laboratory under contract no. W-7405-Eng-48.
†Present address ORNL

**12:39**
**H32 6 Tip-based simulations of nanotribology of self-assembled monolayers** MICHAEL CHANDROSS, CHRISTIAN D. LORENZ, MARK J. STEVENS, GARY S. GREST, *Sandia National Laboratories* While nanotribological simulations are generally performed for two opposing parallel surfaces, the Atomic Force Microscopy (AFM) experiments to which they are often compared measure the interactions between a curved probe tip and a sample. The parallel plate geometry cannot capture many effects seen in experiments, including load-dependent contact areas and molecular transfer of material from the substrate to the tip. We present the results of true dynamical nanotribological simulations of alkylsilane self-assembled monolayers (SAMs) with realistic tip/substrate geometries. Tips matching experimental dimensions (up to $\sim$ 30 nm radius of curvature) were cut out of an amorphous silica substrate (a-$SiO_2$) and either coated with SAMs or annealed for uncoated tips. The adhesion and friction of the tip in contact with a SAM-coated amorphous a-$SiO_2$ substrate were studied with massively parallel molecular dynamics simulations. The effects of load-dependent contact areas are compared to previous simulations with flat plate geometries, and to AFM measurments. Conditions leading to tip fouling, and the effects on nanotribological measurements will also be discussed. Sandia is a multiprogram laboratory operated by Sandia Corp., a Lockheed Martin Company, for the United States Departme nt of Energy's National Nuclear Security Administration under Contract DE-AC04-94AL85000.

**12:51**
**H32 7 Defects Assisted Growth Carbon-Based Nanomaterials*** M.N. YOON, ZHENYU ZHANG, DOUG LOWDNES, *Oak Ridge National Laboratory* A multiscale approach has been applied to study the growth mechanism of carbon-based nanomaterials such as graphite flakes, fullerenes, nanotubes, and nanohorns. Especially, the role of defects during the growth of different morphologies will be discussed. At high temperatures, interesting structural transitions among given morphologies are observed when defects are introduced. The transitions are driven by entropy which plays a crucial role in determining the structural stability at these temperatures. The stability of large structures is also studied

using molecular dynamics simulations and analytical calculations based on ab initio density functional techniques. We will further discuss the role of catalytic particles in determining the structural stabilities of experimentally observed nanomaterials.

*Supported by DOE

**13:03**

**H32 8 Ab-Initio Simulations of the Growth of Short Carbon Nanobells** G.L. ZHAO, *Southern University and A&M College; Visiting Fellow, Princeton University* D. BAGAYOKO, *Southern University and A&M College* We performed ab-initio density functional simulations to study the structural and growth properties of short carbon nanobells. We used a real space approach and the linear combination of atomic orbitals (LCAO) formalism. In the nitrogen-doped carbon nanobells, the nitrogen atoms that are attracted to the open-edge sites of the carbon nanobells play an important role in the growth of the short carbon nanostructures. We also present the calculated electronic structure of the short nanobells. The calculated local density of states of the nanobells revealed field emission characteristics that agree with experimental observations. Acknowledgments: this work was funded in part by NASA (Award No. NCC 2-1344), NSF (Award No. 0508245), and ONR (Grant No: N00014-05-1-0009).

**13:15**

**H32 9 Modeling the catalytic action of supersaturated Ni droplets for the initial stage of growth of single-walled nanotubes*** I. CHAUDHURI, M. YU, C.S. JAYANTHI, S. Y. WU, *University of Louisville* Transition metal nanoparticles are the catalysis of choice for the growth of single-walled carbon nanotubes because of the high miscibility of carbon atoms with their supersaturated liquid droplets. This suggests that, at least for modeling the initial stage of growth, the droplets may be represented by the jellium medium and catalytic action of the droplets may be modeled by the electron redistribution for carbon atoms mediated by the medium. We have tested this scenario by comparing stable configurations of cage-structured C clusters in vacuum with those in jellium, with an average charge transfer from the jellium to C atoms $n_{av} \approx$ 0.2e to model the effect of nickel atoms. The structural optimization was carried out using the semi-empirical self-consistent and environment- dependent Hamiltonian in the framework of linear combination of atomic orbitals developed by our group [1]. Our results showed that the pentagons are more stable with substantial charge transfer occurrence in the defects in the vicinity of pentagons, consistent with previous results [2]. We also found that for a cage-structured cluster of a given size, increasing $n_{av}$ tends to elongate the hexagonal rings. Thus it appears that the catalytic action provided by Ni-droplet may be modeled by the charge fluctuations on C atoms mediated by the jellium. [1] S. Y. Wu et.al. Handbook of Material Modeling Vol. I, p.2935 (2005). [2] X. Fan et. al. Phys. Rev. Lett. **90**, 145501 (2003).

*This work was supported by the DOE (DE-FG02-00ER4582)

**13:27**

**H32 10 Molecular Functionalization Mechanism of Hydrogenated Si Surfaces** YOSUKE KANAI, *Princeton University* ANNABELLA SELLONI, *Princeton University* NOBORU TAKEUCHI, *Universidad Nacional Autonoma de Mexico* ROBERTO CAR, *Princeton University* Within the current effort to understand and develop the organic functionalization of silicon surfaces, recent experiments have identified the radical chain reaction of unsaturated organic molecules with H-terminated silicon surfaces as a particularly promising route for controlled formation of such functionalized surfaces. Using periodic Density Functional Theory calculations, we theoretically study and characterize the basic steps of the radical chain reaction mechanism for different (conjugated and unconjugated) aldehyde molecules reacting with the H-Si(111) surface, under the assumption that a Si dangling bond is initially present on the surface. Molecular conjugation is found to play a crucial role in the viability of the reaction, by controlling the delocalization of the spin density at the reaction intermediate. Interesting differences are observed and discussed between our present results for aldehydes and our previous study for the reactions of alkene/alkyne molecules with H-Si(111) [Takeuchi, et al *J. Am. Chem. Soc.* **2004**, *126*, 15890.]

**13:39**

**H32 11 Density Functional Calculation of Hydrogen Storage in a $C_{60}$ Molecule*** CHIH-KAI YANG, *Chang Gung University* Storage of hydrogen molecules is a research topic that has deep scientific interests and enormous applications in providing a clean type of energy for the future. Recent experimental breakthrough in encapsulating hydrogen molecules in fullerene $C_{60}$ promises a wider role for the versatile carbon cage in this regard. Probing further, we use density functional theory to study how the enclosed hydrogen molecules interact with the carbon cage. The calculations show that quite a few molecules can be exothermically inserted into the cage and as many as 35 hydrogen molecules can be stored inside without rupturing the cage structure.

*Supported by the National Science Council of the Republic of China



## SESSION H33: FOCUS SESSION: FRICTION, FRACTURE AND DEFORMATION II

**Tuesday Morning, 14 March 2006**
**336, Baltimore Convention Center at 11:15**
**Udo D. Schwarz, Yale University, presiding**

***Contributed Papers***

**11:15**

**H33 1 Effect of Counterface Roughness on Sliding Friction of Alkane Monolayers** KEVIN VAN WORKUM, *United States Naval Academy* GINGER CHATEAUNEUF, GUANGTU GAO, DAVID SCHALL, JUDITH HARRISON, Classical molecular dynamics simulations of carbon-based counterfaces sliding against a monolayer of alkane chains are presented. The tribological behavior three carbon-based counterfaces of varying roughness are compared. The distribution of contact forces between individual monolayer chain groups and the counterface shows a strong dependence on the surface roughness of the counterface. Distinctions between contact forces which oppose and those which assist the counterface motion are made and are related to the net friction. A perfectly smooth counterface shows a realitively narrow distribution

of contact forces. The width of the distribution of contact forces increases with increasing counterface roughness. The local motion of the alkane chain end-groups is also discussed in terms of the roughness of the sliding counterface.

**11:27**
**H33 2 Molecular dynamic simulations of the contact between elastic solids and fractal substrates** CARLOS E. CAMPANA, MARTIN H. MÜSER, *University of Western Ontario* The contact mechanics and friction between unlubricated, elastic solids with fractal surfaces is studied using molecular dynamics. Large interfaces could be studied, owing to the use of elastic Green's functions for semi-infinite, elastic lattices. Our simulations confirm the emerging picture that friction and pressure distribution depend mainly on the mean slope of the walls in contacts (unlubricated and chemically passivated solids). Besides, the level of discreteness of the description plays an essential role. This supports another emerging picture, namely that the detailed structure of the very last layer is crucial for friction between two solids.

**11:39**
**H33 3 Friction and plasticity between self-affine surfaces*** BINQUAN LUAN, MARK ROBBINS, *Johns Hopkins University* JUDITH HARRISON, *U.S. Naval Academy* Simulations are used to study the contact area and adhesion between two amorphous solids with self-affine fractal surfaces, and the results are compared to continuum calculations. The friction between non-adhesive surfaces is proportional to load, but the coefficient of friction increases with roughness. The friction is much higher than expected for elasticallly deforming surfaces,* and substantial plastic deformation is observed. Indeed, friction forces for different surface roughness collapse when plotted against the number of plastic rearrangements per unit sliding distance. Including adhesion leads to an increase in both friction and plasticity.* M. H. Müser, L. Wenning, and M. O. Robbins, Phys. Rev. Lett. **86**, 1295 (2001).

*This research was supported in part by the National Science Foundation under Grants DMR-0454947 and PHY99-07949

***Invited Papers***

**11:51**
**H33 4 Superlubricity and atomic-scale energy dissipation in ultrahigh vacuum.***
ENRICO GNECCO, *University of Basel*

''Superlubricity'' has been recently achieved on ionic crystals in ultra-high vacuum in two different ways. First, the normal load exerted by a sharp AFM tip on the crystal surface has been reduced below a critical threshold under extremely low noise conditions, and kept constant while scanning in the usual way. The transition from the stick-slip motion commonly observed on the atomic scale to the superlubricated regime occurs in a continuous way, and can be theoretically described introducing a parameter $\eta$, which is, respectively, larger or smaller than 1 in the two regimes. A comparison with the Tomlinson model allowed us to carefully estimate the contact stiffness and the interaction between tip and surface down to the superlubricated regime [1]. The ''static'' superlubricity obtained in such way cannot be easily extended to systems of practical interest, like micro- and nano-electromechanical devices. The main problem is the smallness of the applied loads (below 1 nN), which must be maintained for a long time. This obstacle is removed if superlubricity is achieved in a different ''dynamic'' way. When an $ac$ voltage is applied between the tip and a counterelectrode on the other side of the crystal sample, and the actuation frequency corresponds to a normal resonance of the system, a sistematic decrease of friction to negligible values is also observed. In such case the magnitude of the applied load is not subject to upper limitations. This effect is probably due to a delicate interplay between thermal activation and the fast variation of the tip-surface interaction, as suggested by recent computer simulations. [1] A. Socoliuc, R. Bennewitz, E. Gnecco, and E. Meyer, Phys. Rev. Lett. 92 (2004) 134301.

*The Swiss NCCR-Nanoscale Science is gratefully acknowledged.

***Contributed Papers***

**12:27**
**H33 5 Study of nano-scale kinetic friction using vortices in superconductors and charge-density waves** A. MAEDA, Y. INOUE, H. KITANO, *Department of Basic Sciences, University of Tokyo* S. SAVELEV, F. NORI,* *Frontier Reserach System, RIKEN* I. TSKADA, *Central Research Institute of Electric Power Insdustry* S. OKAYASU, *Japan Atomic Research Institute* In analogy with the standard macroscopic friction in massive blocks, we present a comparative study of the friction force felt by moving quantized vortices in high-$T_c$ superconductors and charge-density waves (CDWs). Using $I - V$ characteristic measurement and a model for this data, our observations: (1) provide a link between friction at the micro- and macroscopic scales; (2) explain the roundness of the static-kinetic friction transition in terms of system sizes (critical-phenomena view) and thermal fluctuations; and (3) explain the crossing of the kinetic friction $F_k$ versus velocity $v$ for our pristine (high density of very weak defects) and our columnar-defect-irradiated samples (with lower density of deeper pinning defects). We will also investigate any possibilities of the observation of the scaling relation between the velocity dependence of the kinetic friction and the waiting time dependence of the static friction in these systems.

*also Department of Physics and MCTP, University of Michigan

**12:39**
**H33 6 Friction Measurements With Dewetted Polymer Droplets: Bridging the Gap in Contact Area Between Lateral Force Microscopy and the Surface Forces Apparatus** ANDREW B. CROLL, KARI DALNOKI-VERESS, *Physics and Astronomy, McMaster University* Lateral Force Microscopy (LFM) is an important tool that essentially created the field of nano-tribology some 20 years ago. The interest in this technique stems from its ability to measure true single asperity surface contact. Although

tremendously successful, LFM lacks the ability to vary contact area without complicated tip modifications, most of which require modeling to determine contact area. At the other end of the contact area length scale is the Surface Forces Apparatus (SFA). This technique allows for extremely high precision friction measurements, but only on macroscopic lateral length scales. Here we present a simple technique that uses dewetted polystyrene droplets (spherical caps) to overcome these obstacles. Droplets are reversibly attached to conventional atomic force microscope tips, and scanning takes place much as in LFM. The dewetted droplets have the advantage of very flat, well-defined, rigid contact with the substrate, over several orders of magnitude in area ( $\sim 10\ \mu m^2$ – $10000\ \mu m^2$). Measurements on an extremely thin poly(dimethyl siloxane) layer yield insight into the complex interplay between viscosity and elasticity in thin polymer lubricants.

**12:51**

**H33 7 Formation of nanoscale water bridges*** ELISA RIEDO, *Team 1* ROBERT SZOSZKIEWICZ, *Team 1* TAI-DE LI, *Team 1* JIANPING GAO, *Team 2* UZI LANDMAN, *Team 2* SCHOOL OF PHYSICS, GEORGIA INSTITUTE OF TECHNOLOGY TEAM, The water bridges provide stability to sand castles, act as transport channels for dip-pen nanolitography and increase adhesion and friction in micro- and nano- devices such as MEMS. The kinetics of capillary condensation and growth at the nanoscale is studied here using friction force microscopy and molecular dynamics calculations. At 40% relative humidity we find that the meniscus nucleation times increase from 0.7 ms up to 4.2 ms when the temperature decreases from 332 K to 299 K. The nucleation times grow exponentially with the inverse temperature 1/T obeying an Arrhenius law. We obtain a nucleation energy barrier of 7.8*10{-20}$\sim$ J and an attempt frequency ranging between 4-250 $\sim$ GHz, in excellent agreement with theoretical predictions. These results provide direct experimental evidence that capillary condensation is a thermally activated phenomenon.

*R. Szoszkiewicz and E. Riedo, Nucleation time of nanoscale water bridges Phys. Rev. Lett. 85 135502 (2005).

**13:03**

**H33 8 The effect of packing density on self-assembled monolayer friction: Investigation of frictional contrast between OTS phase-separated regions** ERIN FLATER, ROBERT CARPICK, *Univ. of Wisconsin-Madison* Motivated by the lack of fundamental understanding of friction, and that friction and wear are major limiting factors for surface micromachined devices, we use atomic force microscopy (AFM) to determine the nanoscale frictional properties of alkylsilane monolayers commonly used in these microscale devices to reduce adhesion and friction. Quantitative nanoscale single asperity measurements of friction and contact stiffness are performed using monolayer-terminated AFM tips on monolayer-terminated silicon. By comparing the two structural phases present in octadecyltrichrolosilane (OTS) monolayers, we observe that friction depends on the local molecular packing density. The liquid condensed phase shows measurably lower friction at low loads than the liquid expanded phase, demonstrating that lower friction is associated with higher molecular packing density. However, the phases exhibit the same frictional response at higher loads, suggesting that compressed forms of both phases are structurally and tribologically equivalent. We discuss these results in terms of stress-induced molecular conformational changes in the confined interface. We acknowledge our collaborators: W. Robert Ashurst at Auburn University, who provided the OTS samples, and Maarten P. de Boer and Alex D. Corwin at Sandia National Laboratories.

**13:15**

**H33 9 Coverage dependence of 1-propanol adsorption on the Si(001) surface and fragmentation dynamics** JIAN-GE ZHOU, FRANK HAGELBERG, *Jackson State University* The chemisorption of organic molecules on silicon surfaces is a highly topical subject of current research, both experimental and computational. This interest may be ascribed to both the fundamental nature of this problem, involving the interaction between finite units and periodic substrates, but also to its relevance to various areas of recent technology, such as insulator films, nanolithography, chemical and biological sensors, and molecular electronics. The organic layers are formed by depositing organic compounds on the semiconductor surface. In order to optimize this process, the understanding of the interaction between the surface and the organic species is crucial. The geometric, electronic, energetic, and dynamic properties of 1-propanol absorbed on the Si(001)-(2x1) surface are studied from first principles by use of a slab approach. The 1-propanol molecule initially interacts with the Si surface through formation of a dative bond, subsequently the physisorbed 1-propanol molecule reacts with the surface by cleavage of the O-H bond, and the Si(001)-(2x1) surface undergoes further reconstruction as a result of the adsorption of the organic species. The band structure and density of states (DOS) are first analyzed for this system. The band gap of the Si-1-propanol film increases as the coverage level is enhanced. Good agreement is found with available experimental data.

**13:27**

**H33 10 Buckling Instability In Bilayer Membranes** A. CONCHA, J. McIVER, P. MELLADO, R.L. LEHENY, *Johns Hopkins University* We have analyzed the patterns generated when a stress field is introduced to the inner layer of a cylindrically symmetric bilayer membrane through a combination of analytic calculations, numerical simulations, and experiments. A wrinkled structure forms that we explain in terms of a competition between bending and stretching energies under a suitable geometrical constraint. The wavelength, $\lambda$, at the onset of the instability is found theoretically and experimentally to be $\lambda = \pi\sqrt{8B/T_c}$, where $T_c$ is the critical tension of the inner layer marking the onset of the instability, and $B$ is the bending modulus of the membrane. We have also investigated the formation of pseudo-fractal structures that emerge beyond the onset of the instability. We further explain the existence of defects in the regular pattern as a consequence of multiple metastable states in the effective potential that describes this system.

**SESSION H35: ELECTRONIC PROPERTIES OF QUANTUM WELLS AND SUPERLATTICES**
**Tuesday Morning, 14 March 2006**
**338, Baltimore Convention Center at 11:15**
**Joe Tischler, Naval Research Laboratory, presiding**

***Contributed Papers***

**11:15**
**H35 1 Improving optical performance of W-structured type-II superlattices by adjusting $As_2$ and In flux** J.C. KIM, J.G. TISCHLER, I. VURGAFTMAN, J.R. MEYER, E.H. AIFER, L.J. WHITMAN, *Naval Research Laboratory* C.L. CANEDY, E.M. JACKSON, *SFA Inc.* We are investigating ''W-structured'' type-II superlattices (W-SLs) for use in IR photodiodes. A typical W-SL period consists of a hole quantum well (QW) sandwiched by two electron QWs, which are in turn bounded by barrier layers (*e.g.*, InAs/InGaSb/InAs/AlGaInSb), such that the bulk band-edges form a ''W'' pattern. The mini-band straddles the GaSb valence and InAs conduction bands, with a direct gap that can be varied from mid- to very long-wave IR. Photoluminescence (PL) has proven to be a sensitive indicator of photodiode performance, and here we present results correlating the PL intensity of W-SL's grown under varying conditions with their structure. X-ray diffraction is used to measure overall strain and periodicity, and cross-sectional STM (XSTM) is used to directly image the atomic-scale structure. We have discovered that roughness at InAs-on-InGaSb interfaces can be controlled by adjusting the $As_2$:In flux ratio and thereby reducing Sb cross-incorporation in the InAs. The smoother interfaces and reduced strain correlate with stronger PL. By independently adjusting the $As_2$ and In flux, W-SLs with low strain can be fabricated across a range of wavelengths with PL up to 20% greater than we have previously achieved. We discuss our analysis using XSTM to correlate the PL spectra with the structure of the W-SLs as a function of $As_2$ and In flux.

**11:27**
**H35 2 Equilibration of Two-dimensional Excitons in an In-Plane Harmonic Potential** ZOLTAN VOROS, DAVID SNOKE, *University of Pittsburgh* LOREN PFEIFFER, KEN WEST, *Bell Labs, Lucent Technologies* We report on the equilibration dynamics of a 2D gas of long-lifetime (10 $\mu$s), high-mobility excitons trapped in an in-plane harmonic potential produced by inhomogeneous external stress. Spatially indirect excitons are created in a GaAs/AlGaAs double quantum well structure by a quasi-continuous laser pulse. After excitation, the excitons approach equilibrium with a well-defined volume and constant temperature. When the system is far from quantum degeneracy, the effective temperature can be deduced from the spatial profile of the exciton cloud. We show that at the lowest temperatures, the disorder prevents the excitons from reaching the lattice temperature and that the external confining potential is greatly reduced by exciton-exciton repulsion. We discuss the implications of these two phenomena on the possibility of Bose-Einstein condensation of quantum well excitons.

**11:39**
**H35 3 Quantum well structure for a test of intersubband plasma instability** P. BAKSHI, C. DU, K. KEMPA, *Boston College* T. ROCHELEAU, M. SHERWIN, A. GOSSARD, *UCSB* We have shown theoretically that a resonant interaction of an intersubband plasmon emission mode with an absorption mode creates a plasma instability [1]. This can be tested experimentally in an asymmetric double quantum well where the lowest three levels, with appropriate occupancy, provide near resonant emission and absorption modes. The third level is to be partially populated by THz laser pumping from the first level. An applied bias tunes the second level in relation to the other two. The two modes attract each other to form a pair of complex conjugate modes, thus creating a plasma instability. Such a structure has been designed, grown and characterized through absorption measurements without pumping. The results are in good agreement with theory calculations. Narrow Lorentzian lineshapes are observed, indicating a low level of collisions. A realistic pumping fraction can produce sufficiently strong instability to overcome the collisional damping. Characteristic instability criteria, including a modified lineshape are predicted, to be tested with pumping in the next phase of the program. [1] P. Bakshi and K. Kempa, Cond. Matter Theories, 12, 399 (1997); 20, 45 (2005); Physica E7, 63 (2000).Work supported by ARO and NSF.

**11:51**
**H35 4 Mapping the Copper energy band using the quantum well states** J. WU, J. CHOI, T. OWENS, Z. Q. QIU, *Dept. of Phys., UC-Berkeley, Berkeley* E. ROTENBERG, N. V. SMITH, *Advanced Light Source, LBNL, Berkeley, CA 94720* Quantum well states (QWS) of copper electrons in Cu/Co/Cu(100) system are investigated using Angle Resolved Photoemission Electron Spectroscopy (ARPES). The samples were grown epitaxially at room temperature and measured in situ at beamlime 7 of the Advanced Light Source (ALS). Photoemission intensity oscillates with both the electron energy and the Cu film thickness. By counting the thickness oscillation periodicity at a given energy, we can determine the out-of-plane electron momentum without the need of the phase value in the phase accumulation model. This allows the experimental determination of the E-k relation (energy band) for the Cu film. We here report the Cu energy band determined in this way at different in-plane momentum. In addition, by fitting the oscillation as a function of the Cu thickness, we also determined the phase value of the quantization condition as a function of the energy and in-plane momentum.

**12:03**
**H35 5 Coulomb drag in coupled quantum wells: effects of bandstructure and q-dependent scattering*** RICHARD W. DENEEN III, *University of Akron* BEN YU-KUANG HU, *University of Akron* We study the effects of non-parabolicity of the bandstructure and wavevector-dependent scattering rates on the Coulomb drag in coupled quantum wells, using a theoretical formulation that takes these effects into account [K. Flensberg and B. Y.-K. Hu, Phys. Rev. B **52**, 14796 (1995)]. We examine the conditions in which this formulation reduces to the result given by von Oppen *et al.* [F. von Oppen, S. Simon and A. Stern, Phys. Rev. Lett. **87**, 106803 (2001)], in which the effects of band-structure are included through the terms $d\hat{\sigma}_i/dn_i$, where $\hat{\sigma}$ is the (single-layer) conductivity tensor and $n$ is the (single-layer) density and $i$ is the

layer index. The effect of scattering that is strongly wavevector-dependent will also be discussed.

*Supported by the Department of Energy

**12:15**

**H35 6 Dependence of current switching dynamics on contact conductivity in semiconductor superlattices** STEPHEN W. TEITSWORTH, HUIDONG XU, *Duke University* Numerical simulation results are presented for a discrete drift-diffusion electronic transport model appropriate to weakly-coupled semiconductor superlattices [1]. Sequential resonant tunneling between adjacent quantum wells is the primary conduction mechanism for this model which also incorporates an effective contact conductivity $\sigma_c$. We study the dependence on $\sigma_c$ of time-averaged current-voltage characteristics and transient current response to abrupt steps in applied voltage. For intermediate values of $\sigma_c$, three qualitatively distinct transient responses – each associated with a different mechanism for the itrelocation of a static charge accumulation layer [1] - are observed for different values of voltage step $V_{step}$; these involve, respectively, 1) the motion of a single charge accumulation layer, 2) the simultaneous motion of one depletion and two accumulation layers [2], and 3) the simultaneous motion of two accumulation layers. The range of $V_{step}$ values for each mechanism and the relocation times associated with each are studied as a function of $\sigma_c$; a critical value of $\sigma_c$ is identified above which the second relocation mechanism is not observed for any value of $V_{step}$. Relocation times are found to depend sensitively on specific values of $\sigma_c$ and $V_{step}$. [1] L. L. Bonilla and H. T. Grahn, Rep. Prog. Phys. **68**, pp. 577-683 (2005), and Refs. therein. [2] A. Amann, A. Wacker, L. L. Bonilla, and E. Schoell, Phys. Rev. E **63**, 066207 (2001).

**12:27**

**H35 7 Scanning probe study of dopant charging in a semiconductor heterostructure*** IRMA KULJANISHVILI, CEMIL KAYIS, JAMES HARRISON, CARLO PIERMAROCCHI, THOMAS KAPLAN, STUART TESSMER, *Michigan State University* LOREN PFEIFFER, KEN WEST, *Bell Laboratories, Lucent Technologies* The smallest possible semiconductor nano device is a single dopant atom. The properties of such a structure are most prominent at low temperature, where multiple electrons or holes can be localized at the parent donor or acceptor. Using a scanning probe method, we study dopant atom charging in an AlGaAs/GaAs heterostructure with a delta-doped Si layer. The method is based on the Scanning Charge Accumulation (SCA) imaging technique that allows for studying a subsurface electronic system. Here we report on our results resolving the single-electron addition spectra of small numbers of dopant atoms. These highly localized capacitance measurements are contrasted to gated capacitance measurements. The SCA data are compared to a simple model based on a donor-molecule picture.

*Research supported by the MSU Institute for Quantum Sciences and the National Science Foundation grant No DMR03-05461.

**12:39**

**H35 8 Theoretical Carrier Mobilities in $\delta$-doped AlInSb/InSb Hereterostructures*** Y. SHAO, S. A. SOLIN, *Washington University in St. Louis* L. R. RAM-MOHAN, *Worcester Polytechnic Institute* Ultrathin films with thicknesses ( $<$ 100 nm) and very high ( $>$ 1 $m^2$/Vs) room temperature carrier mobility are of immense practical importance in a number of magnetic sensor applications.[1] The electron transport mobilities in $\delta$-doped AlInSb/InSb heterostructures had been studied. The sub-band electron occupation and the energy levels were numerically obtained by solving the Schrödinger and Poisson equations self-consistently as a function of spacer layer thickness, well width and temperature. The quantum energy levels were found within the quasi-classical approximation. The electron mobilities were calculated by combining ionized impurity, background impurity, deformation potential acoustic phonon and polar optic phonon scattering. The dependencies of the electron mobility on temperature, spacer layer thickness and quantum well thickness were simultaneously obtained. At 0K and room temperature, mobilities as high as $1.3x10^3$ and 10 $m^2$/V s, respectively, were obtained at larger spacer layer (400nm) and well widths (400nm). In contrast to privious work, for the application of device design, the product of electron density and mobility was studied to maximize the transconductance. The model we used can be adaped to study other heterostructure.

*Supported by NSF ECS-0329347 and WU Center for Materials Innovation

[1]S.A. Solin, and D.R. Hines, J. Magn. Magn. Mater., **226,** 1976 (2000).

**12:51**

**H35 9 Three novel effects in nanostructures** GAGIK SHMAVONYAN, *State Engineering University of Armenia* To achieve the broadband characteristics, a sequence of non-identical multiple quantum well (MQWs) were designed. When designing a broadband semiconductor optical amplifier (SOA) using a non-identical MQW structure, factors such as QW transition energy, number and sequence of different QWs, the thickness of the separate confinement heterostructure (SCH) layer, the selection of the dominant carrier, the ability of the QW to trap the 2D carrier, the uniformity of the 2D carrier within the QWs, etc. must be taken into account. For SOAs fabricated on the substrate with five 6 nm InGaAsP quantum wells and two 150 nm InGaAsP quantum wells, a very broad emission spectrum is obtained. The spectral width is 400 nm, covering range from 1250 to 1650 nm. The broadest bandwidth for SOA ( $\sim$ 400 nm) allows us to observe three novel effects: Bi-directional guided effect of lasing mode in a bending waveguide of SOA. An optical switching effect in one SOA The SCH layer thickness effect.

**13:03**

**H35 10 Mesoscopic Anisotropic Magnetoconductance Fluctuations in Ferromagnets** SHAFFIQUE ADAM, MARKUS KINDERMANN, SAAR RAHAV, PIET W. BROUWER, *Laboratory of Atomic and Solid State Physics, Cornell University, Ithaca, NY 14853-2501* The conductance of a ferromagnetic particle depends on the relative orientation of the magnetization with respect to the direction of current flow. This phenomenon is known as ''anisotropic magnetoresistance.'' Quantum interference leads to an additional, random dependence of the conductance on the magnetization direction. These ''anisotropic magnetorestance fluctuations'' are caused by spin-orbit scattering, which couples the electron motion to the exchange field in the ferromagnet. We report a calculation of the dependence of the conductance autocorrelation function on the rotation angle of the magnetization direction.

**13:15**

**H35 11 Minigap plasmons in a periodically modulated two-dimensional electron gas: single-particle necktie spectra** HIROYUKI SAKAKI, *Institute of Industrial Science, University of Tokyo, Japan* MANVIR KUSHWAHA, *Institute of Physics, University of Puebla, Mexico* We investigate the plasmon excitations in a two-dimensional electron gas (2DEG) subjected to a one-dimensional (1D) weak periodic potential. We derive and discuss the dispersion relations for both intrasubband and intersubband excitations within the framework of Bohm-Pines' random-phase approximation (RPA). For such an anisotropic system with spatially modulated charge density, we observe a splitting of the 2D plasmon dispersion. The splitting is caused by the superlattice effect of the charge-density modulation on the collective excitation spectrum. In addition, We observe how the energy-tunneling allows the intersubband single-particle excitations (SPE) to attain a finite width at the zone center and to contain the gaps inside. The resulting gaps inside the intersubband SPE give rise to an intriguing structures of *neckties* appearing at the zone boundaries in the excitation spectra illustrating plasmon energy versus Bloch vector. We discuss how the tunneling and the potential amplitude affect such a *necktie* spectrum.

**13:27**

**H35 12 Work function oscillations of atomic-layer-resolved Pb films** JINFENG JIA, *Institute of Physics, The Chinese Academy of Sciences, Beijing 100080, China* YUN QI, XUCUN MA, SHUAIHUA JI, YINGSHUANG FU, QIKUN XUE, By scanning tunneling microscopy, the local work function (LWF) dependance on thickness was studied on Pb quantum wedges with flattop grown on stepped Si(111) substrate. The oscillatory behavior of LWF was observed due to the quantum well state formation induced by the electrons confined in the [111] direction of Pb wedges. The electronic density of state, which is believed to play an important role in such physical property as LWF, was also obtained by scanning tunneling spectroscopy. It is found that the highest occupied quantum well state near Fermi level presented by dI/dV curve has great relationship with the LWF oscillating. Our results show good agreement with the theoretical predictions. This work directly proves that the local work function and the related physical properties are also modulated by quantum well state.

**13:39**

**H35 13 The classical limit of coherent transport properties** SAAR RAHAV, PIET BROUWER, *Laboratory of Atomic and Solid State Physics, Cornell University* We investigate the behavior of weak localization, conductance fluctuations, and shot noise of a chaotic scatterer in the semiclassical limit. Time resolved numerical results, obtained by truncating the time-evolution of a kicked quantum map after a certain number of iterations, are compared to semiclassical theory. Considering how the appearance of quantum effects is delayed as a function of the Ehrenfest time gives a new method to compare theory and numerical simulations. We find that both weak localization and shot noise agree with semiclassical theory, which predicts exponential suppression with increasing Ehrenfest time. However, conductance fluctuations exhibit different behavior, with only a slight dependence on the Ehrenfest time.

**13:51**

**H35 14 Composite-fermion antiparticle description of the hole excitation in the maximum-density droplet** ALEV DEVRIM GUCLU, *Cornell University* GUN SANG JEON, *Pennsylvania State University* CYRUS J. UMRIGAR, *Cornell University* JAINENDRA K. JAIN, *Pennsylvania State University* The maximum-density droplet of quantum dots is a finite-size realization of the state at filling factor one. For a sufficiently small number of electrons, it becomes unstable to the creation of a central hole as the magnetic field is increased or the strength of the confinement potential reduced. The simplest model for the hole is a vortex at the center, which, however, is renormalized by edge excitations. We show that a remarkably accurate description of the actual hole state is achieved in terms of a ''composite-fermion antiparticle,'' which is surprising in view of the fact that composite fermions are thought to be relevant only in the fractional Hall regime. The composite-fermion antiparticle description also allows us to study the effect of Landau level mixing through variational and diffusion Monte Carlo calculations in a very efficient manner. Generalizations to systems containing several holes, as well as to the quasiholes of fractional quantum Hall states are presented.

**14:03**

**H35 15 Giant piezoresistance in AlAs 2D electron systems with antidot lattice** O. GUNAWAN, Y.P. SHKOLNIKOV, K. VAKILI, E.P.D. POORTERE, M. SHAYEGAN, *Princeton University* We report a novel giant piezoresistance effect in AlAs wide quantum well 2D electron system, patterned with an antidot lattice of about 1.0 $\mu$m period. At a low density of $\sim$ $3.5\times 10^{11}/\mathrm{cm}^2$ and at T=0.3 K, the piezoresistance exhibits a strain gauge factor as large as 20,000, the largest value reported so far without magnetic field. Compared to the region without the antidot pattern, this antidot region represents $\sim$ $3.5\times$ larger gauge factor and $\sim$ $5\times$ wider dynamic range in piezoresistance. Such device may find important applications for super sensitive strain detection in mechanical microstructures.



**SESSION H36: FOCUS SESSION: SINGLE MOLECULE CONDUCTANCE**
**Tuesday Morning, 14 March 2006; 339, Baltimore Convention Center at 11:15**
**Doug Natelson, Rice University, presiding**

***Invited Papers***

**11:15**

**H36 1 Probing molecular electronics with mechanical break junctions.**
HEIKO WEBER, *University of Erlangen*

We will report on experiments with single molecule junctions, performed with the mechanically controlled break-junction technique. A review is given on the capabilities of the technique and the results obtained so far. The importance of the

molecular structure, the local environment, the contacts, and of the electronic polarizability will be elucidated. As a particular example, we will present an experiment with a molecule that was designed to form a single-molecule diode when contacted from two sides. The concept is closely related to Aviram-Ratner's Gedankenexperiment. Indeed, the IVs show a pronounced asymmetry, whereas a blind experiment with symmetric molecules resulted in symmetric IVs. A closer analysis of the data, involving theoretical models, suggests that the bias-dependent charge reconfiguration of the electronic structure is responsible for the diode-like characteristics.

*Contributed Papers*

**11:51**

**H36 2 Pulling gold nanowires with a hydrogen clamp** SZABOLCS CSONKA, *Budapest University of Technology and Economics* ANDRAS HALBRITTER, GEORGE MIHALY, ELECTRON TRANSPORT RESEARCH GROUP OF THE HUNGARIAN ACADEMY OF SCIENCES AND DEPARTMENT OF PHYSICS TEAM, Gold nanojunctions were found to be perfect candidates for studying the quantum nature of the conductance. It was shown that monoatomic gold contacts have a single conductance channel with perfect transmission. During the elongation of a single-atom gold contact stable atomic chain can be formed [2]. We have performed an experimentally study of the interaction of gold nanowires with hydrogen molecules by the Mechanically Controllable Break Junction technique [1]. Our results show, that in hydrogen environment the conductance of the chain is strongly reduced compared to the perfect transmission of pure Au chains. The comparison of the experiments with recent theoretical prediction for the hydrogen welding of Au nanowires [3] implies that a hydrogen molecule can even be incorporated in the gold nanocontact, and this hydrogen clamp is strong enough to pull a chain of gold atoms. [1] Csonka et al., to be published in Phys. Rev. B, cond-mat/0502421 (2005). [2] Agrait et al., Phys. Rep. **377**, 81 (2003). [3] Barnett, Nano Letters **4**, 1845 (2004).

**12:03**

**H36 3 Gold point-contact measurements of molecular junctions** LATHA VENKATARAMAN, JENNIFER KLARE, IRIS TAM, COLIN NUCKOLLS, MARK HYBERTSEN, MICHAEL STEIGERWALD, *Columbia University* The conductance of molecular junctions, formed by breaking gold point-contacts dressed with various thiol-functionalized organic molecules, is measured at 293 K and at 30 K. In the presence of molecules, individual conductance traces measured as a function of increasing gold electrode displacement show clear steps below the quantum conductance steps of the gold contact. These steps are distributed over a wide range of molecule-dependent conductance values. Histograms constructed from all conductance traces therefore do not show clear peaks either at room and low temperatures. Filtering of the data sets by an objective automated procedure does only marginally improve the visibility of such features. We conclude that the geometrical junction to junction variations dominate the conductance measurements.

**12:15**

**H36 4 Theoretical Exploration of the Impact of Link Chemistry on Single Molecule Junction Conductance*** MARK S. HYBERTSEN, *Applied Physics and Applied Math. Dept, Columbia University* MICHAEL STEIGEWALD, *Chemistry Dept., Columbia University* LATHA VENKATARAMAN, *Physics Dept., Columbia University* JENNIFER E. KLARE, IRIS W. TAM, COLIN NUCKOLLS, *Chemistry Dept., Columbia University* Measurement of molecular conductance by repeatedly breaking an Au point contact in an environment of molecules allows for the study of a large number of fresh junctions and presents a statistical picture of the junction conductance. However, there is no direct control or knowledge of the atomic scale structure in each individual junction. It is important to distinguish effects on the conductance related to the structure of the metal-molecule link from those that are intrinsic to the backbone of the molecule in the junction. To that end, we examine the energetics and frontier electronic states of various link groups such as thiolate and isonitrile coupled to candidate Au structures using DFT based calculations. We discuss systematic trends in comparison with experiments.

*This work is supported by the NSF under award number CHE-0117752 and by NYSTAR.

**12:27**

**H36 5 Charge Storage Based Hysteretic Negative-Differential-Resistance in Metal-Molecule-Metal Junctions** RICHARD KIEHL, *University of Minnesota* JOHN LE, *University ofo Minnesota* PANGLIJEN CANDRA, *University ofo Minnesota* REBECCA HOYE, *University ofo Minnesota* THOMAS HOYE, *University ofo Minnesota* Experimental results on the electrical characteristics of Hg-alkanethiol//arenethiol-Au molecular junctions are used to develop a physical model for the hysteretic negative differential resistance observed for these, and possibly other, metal-molecule-metal junctions. The dependence of the current-voltage characteristic on sweep direction and rate are examined together with the voltage dependence of the junction's ac conductance. Based on several specific electronic properties, it is concluded that the observed behavior is caused by a slow charge storage process. The implications of this model on potential electronic applications are discussed.

**12:39**

**H36 6 Kondo resonances and anomalous gate dependence of electronic conduction in single-molecule transistors** D. NATELSON, L.H. YU, Z.K. KEANE, *Rice University, Dept. of Physics and Astronomy* J.W. CISZEK, L. CHENG, J.M. TOUR, *Rice University, Dept. of Chemistry* T. BARUAH, M.R. PEDERSON, *Naval Research Laboratory* We report Kondo resonances in the conduction of single-molecule transistors based on transition metal coordination complexes. We find Kondo temperatures in excess of 50 K, comparable to those in purely metallic systems. The observed gate dependence of the Kondo temperature is inconsistent with observations in semiconductor quantum dots and a simple single-dot-level model. We discuss possible explanations of this effect, in light of electronic structure calculations.

**12:51**

**H36 7 Self-aligned lithography and in-situ assembly of chemically responsive single-molecule transistors*** JINYAO TANG, JENNIFER KLARE, YILIANG WANG, ETIENNE DE POORTERE, COLIN NUCKOLLS, SHALOM WIND, *Columbia University* We report the fabrication and assembly of single-molecule transistors comprising ultrathin metal electrodes separated by a nanoscale gap, which is bridged by a single molecule or a small number of molecules. The electrodes sit upon a conductive sub-

strate, which serves as a gate, separated by a thin gate dielectric, and the gap is defined by a completely self-aligned process involving the lateral oxidation of a sacrificial thin film of Al. Devices with gaps ranging from $\sim$ 2 - 10 nm are fabricated with yields approaching 80%. Highly conjugated bis-oxazole molecules are assembled within the gaps in a sequential fashion, relying upon individually designed end-group chemistry to control the attachment of molecular units to the metal electrodes and the modular assembly of the bis-oxazole units, respectively. In addition, metal ion complexes are used to reversibly attach and detach terpyridyl molecular units from one another. Fully assembled devices display distinctive electrical response, which is strongly modulated by the molecular assembly and attachment.

*This work was supported primarily by the Nanoscale Science and Engineering Initiative of the National Science Foundation under NSF Award Number CHE-0117752 and by the New York State Office of Science, Technology, and Academic Research (NYSTAR).

**13:03**

**H36 8 Prevalence of Coulomb blockade in conjugated and non-conjugated molecules on gold versus palladium electromigrated junctions*** ARTUR ERBE, LARUE DUNKLEBERGER, KIRK BALDWIN, ROBERT WILLETT, *Bell Laboratories, Lucent Technologies* ANAT DE PICCIOTTO, JENNIFER KLARE, KENJI SUGO, COLIN NUCKOLLS, *Department of Chemistry and The Nanoscience Center, Columbia University* The conduction properties of electro-migration gap junctions made with Au or Pd and with various organic molecules incorporated in the gaps are studied to expose the full range of possible transport processes, and their prevalence. Primarily comparisons are made between molecules with an electron delocalized vs. electron-localized backbone, between molecules with one vs. two thiol end groups, and between molecules with and without large side chains on the Au junctions. Within these junctions Coulomb blockade can be observed in all molecular species tested, including bare junctions and those coated by molecules with no electron-accepting properties, but at significantly lower prevalence than molecules with delocalized electron backbones. Importantly, Coulomb blockade with high charging energy values is seen almost exclusively on junctions with molecules possessing the delocalized electrons. An overall lower prevalence of Coulomb blockade is observed in the Pd junctions, but with the same relative molecular dependence. These results indicate the scope of variation in transport possible for molecules on electro-migrated junctions of various metals.

*Under NSF Award Number CHE-0117752.

**13:15**

**H36 9 Control of topography, stress and diffusion at molecule-metal interface** NIKOLAI ZHITENEV, DONALD TENNANT, RAYMOND CIRELLI, *Bell Labs.* WEIRONG JIANG, ERIC GARFUNKEL, *Rutgers* ARTUR ERBE, *U. Konstanz* ZHENAN BAO, *Stanford* The electronic properties of molecular devices that are just a few atomic layers thick are determined not solely by the properties of the molecules but are equally dependent on dopants, defects and electronic states at the interfaces. We study the phenomena affecting the conductance of molecular devices by systematically varying the growth conditions at the metal-molecule interface. Transport properties of metal-molecule-metal junctions containing monolayer of conjugated and saturated molecules with characteristic dimensions in the range of 30-300 nm are correlated with microscopic topography, stress and chemical bonding at metal-molecule interfaces. Small shadow masks defined within a stack of $Si/SiO_2/SiN_x/SiO_2$ layers are used to obtain features below the usual lithographic limits. We demonstrate that the defects/interfaces can be rationally controlled and that their properties are often more important than the electronic properties of molecules in determining the device conductance. The density of defects caused by metal penetration into monolayers is significantly reduced yielding $>$ 95% of non-shorted devices. Our statistically significant dataset allows us to conclude that the conductivity of organic molecules $\sim$ 1.5 nm long is at least 4 orders of magnitude lower than is commonly believed.

**13:27**

**H36 10 Electronic Transport through Organic Monolayer Devices** DUNCAN STEWART, JASON BLACKSTOCK, CARRIE DONLEY, ZHIYONG LI, DOUGLAS OHLBERG, R. STANLEY WILLIAMS, *Hewlett-Packard Laboratories, Palo Alto, CA USA* SEHUN KIM, *KAIST, Daejeon, Korea* REGINA RAGAN, *UC Irvine, Irvine, CA, USA* We report experimental studies of electronic transport through molecular monolayers. Particular emphasis is placed on combining detailed chemical, physical and electronic characterization in a single test structure, and to whatever degree possible, fabricating well-defined interfaces that enable quantitative chemical and physical analysis. To this end, we describe physical characterization of ultra-flat template-stripped Au and Pt metal electrodes including UHV-STM imaging and incorporation into a new stencil-based nanopore structure. In-situ XPS and IR spectroscopy are used to characterize the organic monolayers and the buried inorganic/organic interfaces. Using this well-characterized device structure, we present detailed I-V characterization including temperature dependence and IETS spectroscopy of several alkane self-assembled and Langmuir-Blodgett monolayers, correlating both electrical switching behavior and IETS spectral responses to the measured chemical and physical structure of the device.

**13:39**

**H36 11 Structural Characterization of a Molecular Junction by X-ray Reflectivity** JULIAN BAUMERT, *Brookhaven National Laboratory* MICHAEL LEFENFELD, *Columbia University* ELI SLOUTSKIN, *Bar-Ilan University* PETER PERSHAN, *Harvard University* MOSHE DEUTSCH, *Bar-Ilan University* COLLIN NUCKOLLS, *Columbia University* BEN OCKO, *Brookhaven National Laboratory* In the field of molecular electronics, the nature and pathways of charge transfer through molecules is among the most intensely studied open questions. Experimental studies, employing both single molecules and self-assembled monolayers attached to the electrodes, have demonstrated that the electronic characteristic of these junctions is difficult to reproduce. We report x-ray reflectivity studies of the structure of organic mono- and bi-layers self-assembled between two conducting electrodes: silicon and mercury. At high molecular coverage, the Angstrom resolution high-energy synchrotron x-ray measurements reveal densely-packed layers of roughly interface-normal molecules. The interface normal structure is stable and relatively insensitive to electric fields when a voltage is applied across the junction. Furthermore, our x-ray studies reveal that variation of the molecular coverage of the electrodes influences the structure and quality of the molecular junctions.

**13:51**

**H36 12 Charge addition effects in phenylene ethynylene oligomers: the effect of -$NO_2$ substitution** S. W. ROBEY, C. D. ZANGMEISTER, R. D. VAN ZEE, *NIST-Gaithersburg* Interest in aromatic systems based on phenylene ethynylene oligomers (OPE) has been spurred by reports of interesting negative differential resistance/hysteretic behavior in metal-molecule-metal junctions. Theoretical work has invoked the importance of charge addition effects on conformation and electronic structure and polaronic effects to provide potential explanations for this behavior. We have investigated the influence of charge addition, via ''doping'' with K, in pristine versus nitro-substituted OPE using photoelectron spectroscopies. Sequential addition of K in unsubstituted OPE produces a gradual shift to higher binding energy, reminiscent of ''rigid band'' behavior, with relative shifts of $\pi$ levels suggesting some distortion/conformation change. For a nitro-substituted oligomer, a markedly different behavior is observed with K addition. After an initial shift, the electronic levels are pinned for subsequent K addition before a final shift brings the spectrum to near coincidence with that for the pristine oligomer. Potential explanations for this behavior are provided based on model calculations of the effects of charge addition on the molecular electronic structure. We have also investigated differences in the reorganization energy that accompanies charge addition/removal in these systems by a combination of photoelectron and optical spectroscopies and theoretical calculation.



**SESSION H37: FOCUS SESSION: NANOSCALE MATERIALS PHYSICS OF PHASE TRANSITIONS II**
**Tuesday Morning, 14 March 2006**
**340, Baltimore Convention Center at 11:15**
**Eric Mazur, Harvard University, presiding**

***Contributed Papers***

**11:15**

**H37 1 Electronic Transport in Molecularly-Linked Gold Nanoparticle Films Near the Metal-Insulator Transition.** AL-AMIN DHIRANI, JEFFREY DUNFORD, YOSHINORI SUGANUMA, *Department of Chemistry, University of Toronto* We have investigated the temperature ($T$) dependence of the conductance ($g$) of 1,4-butane dithiol linked Au nanoparticle films. Over a wide range of temperatures (20 K to 300 K), the conductance behaves as $g = g_0 \exp(-(T_0/T)^{1/2}))$. Such a temperature dependence is predicted by an Efros-Shklovskii variable-range hopping model based on a competition between Coulombic and intercluster tunneling processes. However, we find that hopping distances are too large (62 nm to 720 nm at 100 K) to be consistent with tunneling between clusters, and tend to scale with cluster size. We propose a modified ''quasi-localized hopping'' model based on competition between single-electron cluster charging and intra-cluster electron backscattering to explain this temperature dependence.

**11:27**

**H37 2 Plasticity and energy absorption at the nanoscale: kinetics and chemical control** MATTEO COCOCCIONI, GERBRAND CEDER, NICOLA MARZARI, *Department of Materials Science and Engineering and Institute for Soldier Nanotechnologies, MIT* Shock-induced phase transitions of group-IV nanoparticles are investigated using first-principles molecular dynamics in the electronic-enthalpy formalism [1]. In some of these systems a shock compression can induce plastic deformations, leading to the absorption of the mechanical energy coming from the impact. Kinetic factors greatly affect phase transformations, and so only some of the thermodynamically stable structures are explored. Still, transitions are always nucleated in the core of the nanoparticles, and are accompanied by the formation of small close-packed clusters of characteristic shape. Also, as the particle's size grows, amorphization remains confined in the core region. Finally, we highlight how chemical doping can be used to affect nucleation, and to tune pressure thresholds; this could be relevant e.g. for target applications such as the design of novel impact-absorbing nanostructured materials. [1] M. Cococcioni, F. Mauri, G. Ceder and N. Marzari, PRL (2005).

**11:39**

**H37 3 Magnetic response and enhanced Tc in the 1D to 2D crossover regime of mesoscopic superconducting aluminum rings.** NICHOLAS C. KOSHNICK, HENDRIK BLUHM, *Stanford University* MARTIN E. HUBER, *University of Colorado, Denver* KATHRYN A. MOLER, *Stanford University* We have studied more than 40 mesoscopic Aluminum rings by positioning a scannable SQUID susceptometer over each ring individually, and have found a striking non-monotonic dependence of Tc on linewidth. By measuring the magnetic response, or current in the ring, as a function of applied flux and temperature, it is possible to extract $\lambda(T)$ and $\xi(T)$. The rings vary in width (40-350nm) and diameter (1-4um) with a nominal thickness of 35nm. For rings with linewidths above 150nm ( $\approx 2\xi(T = 0)$), the extracted superfluid density shows a high-temperature tail up to temperatures as high as 15% above the 1D and bulk thin film critical temperatures. In this regime, we also find evidence for the saturation of $\xi(T)$ on the order of the ring's linewidth. We speculate that these results indicate the particular importance of Tc disorder in the crossover from quasi-1D to 2D superconductivity.

**11:51**

**H37 4 Fluctuation diamagnetism in mesoscopic Aluminum rings** HENDRIK BLUHM, NICHOLAS C. KOSHNICK, *Stanford University* MARTIN E. HUBER, *University of Colorado, Denver* KATHRYN A. MOLER, *Stanford University* We have measured the magnetic response of mesoscopic, superconducting Al rings using a high sensitivity scanning SQUID microscope. We find that for sufficiently small, quasi one- dimensional rings, the rounding of the superconducting transition due to thermal fluctuations is in good agreement with theoretical preditctions. The main effects are a fluctuation tail in the amplitude of the response near $T_c$ and a suppression of the apparent $T_c$ as determined from the temperature dependence of the superfluid density below the fluctuation tail compared to the extracted mean field $T_c$ by several mK. In larger rings, the tail is less pronounced due to the lack of phase coherence.

**12:03**
**H37 5 Magnon characterization in magnetic quantum dots**
MOHAMMAD-REZA MOZAFFARI, KEIVAN ESFARJANI, *Dept. of Physics, Sharif University of Technology, Tehran, Iran*
The spin structure in a magnetic dot is studied as a function of exchange coupling strength or dot size, within the semiclassical approximation on a discrete lattice. In addition to the exchange term, the dipole interaction has also been included in our calculations. As the exchange coupling is decreased or the size is increased, the ground state undergoes a phase change from a single domain ferromagnet to a spin vortex. The line separating these two phases has been calculated numerically for small system sizes. Magnon frequencies in such a dot have also been calculated in both phases by the linearized equation of motion method. These calculations have also been checked by comparing them to the spin autocorrelation function spectrum. Furthermore, the modes have been characterized for both the ferromagnetic and the vortex phase. The modes responsible for the instability of the vortex and the ferromagntic phases have been identified, and can provide the mechanism for spin reorientation in these phases.

***Invited Papers***

**12:15**
**H37 6 Magnetic multilayers on nanospheres.**
MANFRED ALBRECHT, *University of Konstanz*

In modern magnetic recording materials the 'superparamagnetic effect' [1] has become increasingly important as new magnetic hard disk drive products are designed for higher storage densities. In this regard, nanoparticle media [2], where two-dimensional arrays of monodisperse nanoparticles with high magnetic anisotropy are used, is assumed to be the ideal future magnetic recording material. In this presentation a novel magnetic gradient nanomaterial, which has been created by depositing Co/Pd multilayers onto two-dimensional arrays of self-assembled nanoparticles [3] will be introduced. The magnetic nanostructures formed on top of the particles are in a magnetically exchange-isolated quasi-single-domain state. This nanoscale system is quite distinct from the classical geometries: Neither extrinsic properties nor the intrinsic properties are uniform in space. The film is extended over a wide region of the sphere and thus shows substantial curvature. The film thickness varies and so do the intrinsic magnetic properties most notable the magneto-crystalline anisotropy, which is a key factor affecting the fundamental nature of the reversal process. The specific magnetic characteristics of such a gradient nanomaterial and in particular its impact on the reversal mechanism will be discussed. Angle-dependent reversal studies were performed for different particle sizes and the experimental results were interpreted using micromagnetic simulations. The simulations account for the angular dependence of the hysteresis loops and provide a detailed picture of how the local magnetization evolves during reversal, offering new opportunities in the functionalization of magnetic nanostructures for storage applications. [1] A. Moser et al., J. Phys. D: Appl. Phys. 35, (2002) R157. [2] S. Sun et al., Science 87, (2000) 1989. [3] M. Albrecht et al., Nature Mater. 4, (2005) 203.

***Contributed Papers***

**12:51**
**H37 7 Coulomb effects and hopping transport in granular metals** ANDREI LOPATIN, IGOR BELOBORODOV, VALERII VINOKUR, *Argonne National Laboratory* We investigate effects of Coulomb interaction and hopping transport in the insulator phase of granular metals and quantum dot arrays considering both spatially periodic as well as irregular grain/dot arraignments. We study the Mott transition between the insulating and metallic phases in a strictly periodic system and find the dependence of the Mott gap on the intergranular coupling. In this case the conductivity of the insulating state has the activation form with the Mott gap entering the exponent. In the irregular arrays the electrostatic disorder induces the finite density of states near the Fermi level giving rise to the variable range hopping conductivity. We derive the transport properties of the irregular array in the dielectric, low coupling limit and show that the conductivity follows the Efros-Shklovskii law. We develop a theory of tunneling through a chain of grains and discuss in detail both elastic and inelastic cotunneling mechanisms; the former dominates at very low temperatures and very low applied electric fields, while the inelastic mechanism controls tunneling at high temperature/fields.

**13:03**
**H37 8 Distinguishing Magnetic Behavior on the Slater-Pauling Curve applied to nanoscale thin films.** K.R. PODOLAK, M.G. BIRKE, *Penn State Univ.* N. JANKE-GILMAN, *Latrobe Univ. (present affiliation)* R.F. WILLIS, *Penn State Univ.* The Slater-Pauling curve is a plot of the stoichiometric mean saturation magnetization per atom as a function of the electron filling of the d-bands in the transition metals and their alloys. When the elemental magnetic moments are aligned, the volcano-shape curve plots the variation of the mean magnetic moment. It has been predicted that a narrowing of the d-bands in nanostructured magnetic materials will influence both the magnitude of the magnetic moments as well as the overall magnetic alignment through increased spin-orbit coupling [1]. In this paper, we report dichroism in the core-level x-ray photoemission spectra of the elements which reveals and distinguishes the changing magnitudes of the magnetic moments and the changing alignment of these moments with changing composition. The 3p core-level spectral densities of multiplet spin-ordered states show a width W proportional to the local Zeeman splitting of levels, and a magnetic dichroism amplitude A sensitive to the non-local magnetic order (anisotropy). In nanoscale epitaxial layers, small deviations from the bulk Slater-Pauling curve are observed due to enhanced moments due to d-band narrowing [2]. It is predicted that a plot of the spectral parameters W, A will show a different dependence of temperature approaching Tc, the critical ordering temperature. [1] S. Handschuh & S. Blügel, Solid State Communications. 105, 633 (1998). [2] R.F. Willis & N. Janke-Gilman, Europhysics Letters. 69, 411 (2005).

**13:15**

**H37 9 Localization of coupled plasmon modes in graded plasmonic chains*** JUN JUN XIAO, *Chinese Univ. of Hong Kong* K. YAKUBO, *Hokkaido Univ., Japan* K. W. YU, *Chinese Univ. of Hong Kong* Electromagnetic energy propagation and localization in plasmonics offer the potential for integrated nanophotonics. Plasmonic waves occur naturally inside the subwavelength scale with lateral confinement below the diffraction limit. However, controlling their localization/delocalization behavior in the propagating (longitudinal) direction is also desirable. We present results of longitudinal localization-delocalization tuning of coupled plasmon modes in graded chains of metallic nanodots. Two graded models will be studied: incremental spacing between the nanoparticles and graded index of refraction in the host medium. The coupled plasmons in these systems exhibit strong localization when detuned from the Mie plasmon frequency, showing a tunable passband in finite size system. To understand the localization mechanism, we map the problem onto an equivalent system of one-dimensional chain of coupled harmonic oscillators, whose coupling strength is gradually varied from one end to the other, with additional on-site potentials. The results can be applied to analogous graded systems. Confining and transmitting electromagnetic energy in these structures may pave new way for many fruitful applications in plasmonics.

*Work supported by the RGC Earmarked Grant of the Hong Kong SAR Government (K.W.Y), and in part by a Grant-in-Aid for Scientific Research from Japan Society for the Promotion of Science (No.16360044).

**13:27**

**H37 10 A study of Co thin films grown on Si(111) with Al buffer layer** ZI Q. QIU, J. WU, J. CHOI, J. LI, *Dept. of Phys., UC-Berkeley, Berkeley, CA 94720* A. SCHOLL, A. DORAN, *Advanced Light Source, LBNL, Berkeley, CA 94720* Growth and magnetic properties of Co/Si(111) and Co/Al/Si(111) were investigated using Scanning Tunneling Microscopy (STM), Surface Magneto-Optic Kerr Effect (SMOKE), and Photoemission Electron Spectroscopy (PEEM). For Co film grown directly on Si(111), silicide is formed at the interface which leads to a loss of magnetization for ultrathin Co film. By growing an Al buffer layer at the Co/Si interface, we found that the Al buffer layer effectively reduces the silicide formation and SMOKE signal was detected at a much thinner Co thickness as compared with Co film directly deposited on Si(111). Magnetic domain imaging using PEEM confirms the SMOKE measurement. STM measurements were also performed to study morphology change after inserting the Al buffer layer.

**13:39**

**H37 11 Experimental Evidence for a Dynamic Phase Transition in Ultra-thin Magnetic Films*** D.T. ROBB, *Florida State University* Y.H. XU, *University of Minnesota* O. HELLWIG, *Hitachi Global Storage Technologies* A. BERGER, *Hitachi Global Storage Technologies* M.A. NOVOTNY, *Mississippi State University* P.A. RIKVOLD, *Florida State University* We present the first convincing evidence for an experimental observation of a Dynamic Phase Transition (DPT) in a magnetic system: an ultrathin $[Co(0.4nm)/Pt(0.7nm)]_3$ multilayer, which is well modeled by a two-dimensional kinetic Ising system. This DPT, as a function of the period $P$ of an applied alternating magnetic field, has been observed previously in simulations of magnetic systems [1]. For several values of $P$ and bias field $H_b$, the magnetization was measured for 50 cycles of the field [2]. The order parameter, which was identified in simulations as the magnetization averaged over the $i$th cycle, $Q_i$, was obtained from the experimental data as a time series. Kinetic Monte Carlo simulations produced close agreement with the experimental data for the order parameter averaged over the final 30 cycles, $< Q_i >$, as a function of $P$ and $H_b$. The experimental fluctuations in the order parameter are also consistent with a DPT. [1] S.W. Sides, P.A. Rikvold, and M.A. Novotny, Phys. Rev. Lett. **59**, 2710 (1999). [2] D.T. Robb, Y.H. Xu, O. Hellwig, A. Berger, M.A. Novotny, and P.A. Rikvold, submitted to PRL.

*Computational work supported by NSF Grants No. DMR-0120310 and DMR-0444051

**13:51**

**H37 12 Structural and Magnetic Phase Diagrams of Co and Mn Doped Ge (100) Epitaxial Films** BRIAN COLLINS, LIANG HE, FRANK TSUI, *University of North Carolina* YUNCHENG ZHONG, STEFAN VOGT, YONG CHU, *Advanced Photon Source* We present studies of structural and magnetic properties of epitaxial films of $Co_xMn_yGe_{1-x-y}$ magnetic semiconductors, grown by combinatorial MBE on Ge (100) substrates. Structural effects were examined in-situ by reflection high energy electron diffraction and ex-situ by microbeam x-ray diffraction. A ternary epitaxial phase diagram has been determined for doping concentrations (x and y for Co and Mn respectively) up to 30 at %, where regions of coherent epitaxy and associated strain states, and regions of rough disordered growth and the nature of the disorders have been examined and identified. Specifically, within a narrow range of compositions around the atomic ratio between Co and Mn (x/y) of 3, the observed epitaxial strain is low ( $< 0.1\%$) and coherent epitaxial growth is most stable, where the thin film lattice constants obey Vegard's law and they match those of the Ge at x/y $=3$. Within this region of compositions, high quality epitaxial films of p-type magnetic semiconductors can be stabilized for total doping concentration of transition metal dopants as high as 13 at % and with $T_C$ as high as 300 K. A ternary magnetic phase diagram has been measured using magnetooptic Kerr effect. The interplays between structural effects and magnetism have been investigated.

## SESSION H38: SUPERCONDUCTIVITY-DISORDERED THIN FILMS AND QUANTUM PHENOMENA

**Tuesday Morning, 14 March 2006**
**341, Baltimore Convention Center at 11:15**
**A. M. Goldman, University of Minnesota, presiding**

**11:15**

**H38 1 Quantum Superconductor-Insulator transition and Nernst effect in NbxSi1-x** HERVE AUBIN, ALEXANDRE POURRET, KAMRAN BEHNIA, JEROME LESUEUR, *CNRS-ESPCI; 10 rue Vauquelin, Paris, France* CLAIRE MARRACHE-KIKUCHI, LAURENT BERGÉ, LOUIS DUMOULIN, *CSNSM-IN2P3, Orsay, France* We show that the nature of magnetic-field tuned superconductor- insulator transitions in amorphous $Nb_{0.15}Si_{0.85}$ thin films depends on the orientation of the magnetic with respect to the film. In perperndicular magnetic field, the transition is driven by quantum fluctuations, characterized by an isobestic point (Bc,Rc) in the resistance measurements, and a kink

in the temperature profile of the critical magnetic field – that indicates a temperature scale below which quantum fluctuations control the dynamics of the system. The isobestic point and the kink are not found when the magnetic field is applied parallel to the films, where the transition is classical, driven by the breaking of Cooper pairs at the temperature dependent critical field $H_{c2}$. In addition, we will present the first study of Nernst coefficient in such a disordered superconductor. As previous studies on the cuprates have suggested, we show that the Nernst signal is particularly sensitive to superconducting fluctuations, where a sizable signal is observed in a large temperature (T>Tc) and magnetic field range.

**11:27**

**H38 2 The interplay between localization and superconductivity in ultrathin amorphous beryllium films*** WENHAO WU, *Texas A&M University* E. BIELEJEC, *Sandia National Laboratories* Near the superconductor-insulator transition (SIT), quench-condensed ultrathin Be films show a highly anisotropic magnetoconductance (MC). The conductance can drop orders of magnitude in a weak perpendicular field ( $<$ 1 T). In the high field regime, 2 $\sim$ 10 T, the MC in a perpendicular field is positive and can vary orders of magnitude with increasing field. These features disappears when a small amount of Mn impurities are introduced. Our results indicate that superconductivity is the origin of the observed MC. We have carried out simultaneous electron transport and tunneling measurements across the SIT, which allow us to determine, itindependently and up to a constant on the order of unity, the localization length, $\xi_L$, and the dielectric constant, $\kappa$, for the films. We have found that, as the normal-state sheet resistance of the films at 20 K is reduced with increasing film thickness, $\xi_L$ increases exponentially. The SIT occurs when $\xi_L$ crosses the Ginzburg-Landau coherence length, $\xi_S$.

*Supported by NSF Grant No. DMR-0551813.

**11:39**

**H38 3 Field-Induced Superconductor to Metal and Superconductor to Insulator Transitions in Thin Indium Oxide Films** K. H. SARWA B. TAN, KEVIN A. PARENDO, ALLEN M. GOLDMAN, *School of Physics and Astronomy, University of Minnesota* Z. OVADYAHU, *The Racah Institute of Physics, The Hebrew University* The application of magnetic fields to ultra-thin superconducting films is believed to bring about superconductor-insulator transitions which are quantum phase transitions. We will present measurements in perpendicular and parallel magnetic fields of R(T) of amorphous indium oxide films. In contrast with what has been reported for films with similar $T_c$'s, scaling, although successful for the superconducting curves, fails for the insulating ones. For a 150 Angstrom thick film with a zero-field $T_c$ = 2.8K, the high-field behavior is governed by a $T^{1/3}$ law suggestive of a 3D dirty metal. For a 100 Angstrom film with $T_c$ =1.8K the high-field regime is governed by Efros-Shklovskii hopping. This suggests that the former is superconductor-metal transition, whereas the latter is a superconductor-insulator transition. Further studies related to quantum corrections and film morphology are still in progress. This work was supported in part by the National Science Foundation under grant NSF/DMR-0455121.

**11:51**

**H38 4 Vortices and quasiparticles near the ''superconductor-insulator'' transition in thin films.** VICTOR GALITSKI, *University of Virginia* GIL REFAEL, *Caltech* MATTHEW P. A. FISHER, *KITP, UCSB* T. SENTHIL, *IISc* We consider the low temperature behavior of an amorphous superconducting film driven normal by a perpendicular magnetic field. We introduce a new two-fluid formulation consisting of fermionized field-induced vortices and electrically neutralized Bogoliubov quasiparticles interacting via a long-ranged statistical interaction. This approach allows us to access a novel non-Fermi liquid phase which naturally interpolates between the low field superconductor and the high field normal metal. We also discuss the transport, thermodynamics, and tunneling properties of the resulting ''vortex metal'' phase.

**12:03**

**H38 5 Anomalous Insulating State Induced by Application of Parallel Magnetic Fields to 2D Superconducting Films** KEVIN A. PARENDO, K. H. SARWA B. TAN, ALLEN M. GOLDMAN, *School of Physics and Astronomy, University of Minnesota* Superconductor-insulator transitions in ultrathin films of amorphous Bi have been investigated by electrostatic electron doping, incrementing film thickness, and applying parallel magnetic fields. When superconductivity was induced in an insulating film by electrostatic tuning, a quantum phase transition was observed down to 60 mK. When superconductivity was quenched by parallel magnetic fields, above $\sim$ 150 mK, R(T) was best described by 2D Mott variable range hopping at the highest fields and scaling was successful. However, an anomalous insulating state was induced by the field below $\sim$ 150 mK in which the resistance becomes larger than expected from extrapolation of R(T) from higher temperatures, causing scaling to break down. This anomalous state has not been observed in zero field thickness- or electrostatic-tuned transitions in bismuth. It has also been observed in amorphous $In_2O_3$films in parallel fields, but not in perpendicular fields. This work is supported in part by the National Science Foundation under grant NSF/DMR-0455121.

**12:15**

**H38 6 Insulating State of Granular Superconductors in a Strong Coupling Regime** IGOR BELOBORODOV, *Argonne National Laboratory* YASHA FOMINOV, *Landau Institute for Theoretical Physics* ANDREI LOPATIN, VALERII VINOKUR, *Argonne National Laboratory* We analyze the possibly of the formation of a magnetic field induced insulating state in a two-dimensional granular superconductor with relatively strong intergranular coupling and show that such a state appears in a model with spatial variations of the single grain critical magnetic field. This model well describes realistic granular samples with the dispersion in grain sizes and explains qualitatively the recent experimental observation of a giant peak in the magnetoresistance of dirty superconducting films.

**12:27**

**H38 7 The effect of 3*d* paramagnetic impurities on superconductivity in quench-condensed amorphous Pb films** ASHWANI KUMAR, DAN E. READ, JEFFREY S. PARKER, H JEFFREY GARDNER, PENG XIONG, *Department of Physics and MARTECH, Florida State University* A modified dilution refrigerator equipped with Sb, Pb and NiCr sources is used to carry out an itin situ study of the effect of magnetic impurities (MI) on the same quench-condensed Pb films. Si substrate with pre-deposited

Au contacts is mounted in dilution unit and cool down to 5K. To ensure the electrical and possibly structural homogeneity down to monolayer thickness, we deposit a thin layer of Sb prior to the Pb evaporation. At a thickness above 8 ? the film exhibits superconductivity with well-defined resistive transition and $T_c$ controlled by the film thickness. When a film of desired $T_c$ is obtained we incrementally evaporate itMI onto the film by heating a NiCr wire at constant current and perform itin situ measurements. We observe that $T_c$ is continuously suppressed with increasing itMI density while the resistive transitions remain sharp, although the itMI induces significant filling of states inside the gap. The $T_c$ as a function of itMI density is well described by the Abrikosov-Gorkov theory regardless of the starting $T_c$ and the pair-breaking strength of the itMI appears to be independent of the degree of disorder.

**12:39**

**H38 8 Confirmation of the discrepancy between experiment and theory in the superconducting proximity effect** MANJIANG ZHANG, *Dept. of Physics and Astronomy, Univ of Southern California* GO TATEISHI, GERD BERGMANN, The transition temperature $T_c$ of a superconducting film S is reduced when it is covered with a normal metal N. Recently we investigated the superconducting proximity effect in double layers of Pb and alkali metals and found the initial slope $dT_c/dd_n$ of $T_c$ as a function of the thickness of the normal metal $d_n$ was smaller than the theoretical value by a factor of 2. The theory shows that the \QTR normalized initial slope $S_{sn} = (d_s/T_s)|dT_c/dd_n| = \Gamma^*_{sn}(N_n/N_s)$ depends only on the density of states ratio of the two metals, $N_n/N_s$, but not on the mean free paths or the interface. A literature search showed that this initial slope is rarely measured. The few experiments in the literature where the initial slope can be derived yield the same disagreement with the theory. In the present work we investigated systematically the initial slope of S/N sandwiches (S for Pb and N for the normal conductor) and also extended the investigation to $S_1/S_2$ sandwiches ($S_1$=Pb, $S_2$= Cd, Zn, Al, In, Sn). The normalized initial slope $S_{sn}$ is confirmed to be independent of the Pb thickness. Again for S/N sandwiches the value of $\Gamma_{sn}$ is more than a factor 2 smaller than the theoretical value. For the $S_1/S_2$ sandwiches this discrepancy decreases with increasing $T_c$ of $S_2$.

**12:51**

**H38 9 Vortex Glass is a Metal*** JIANSHENG WU, *University of Illinois* PHILIP PHILLIPS, *University of Illinois* We consider the disordered quantum rotor model in the presence of a magnetic field. We analyze the transport properties in the vicinity of the multicritical point between the superconductor, phase glass and paramagnetic phases. We find that the magnetic field leaves metallic transport of bosons in the glassy phase in tact. In the vicinity of the superconductivity to the intervening metallic state transition, the resistivity turns on as $(H - H_c)^2$ with $H_c$. This functional form is in excellent agreement with the experimentally observed turn-on of the resistivity in the metallic state in MoGe, namely $R \approx R_c(H - H_c)^\mu$, $1 < \mu < 3$. The metallic state is also shown to presist in three spatial dimensions. As the phase glass in $d = 3$ is identical to the vortex glass, we conclude that the vortex glass is, in actuality, a metal rather than a superconductor at $T = 0$.

*DMR-0305864

**13:03**

**H38 10 Quantum phase transition and possible phase separation in ultrathin doubly-connected superconducting cylinders of Al** HAOHUA WANG, NEAL STALEY, BENJAMIN CLOUSER, YING LIU, *Department of Physics, Penn State University* Fluxoid quantization demands that the superfluid velocity, $v_s$, of a doubly-connected superconducting cylinder increase as its diameter, $d$, decreases, leading to a destructive regime and a quantum phase transition (QPT) in one dimension (1D) - Superconductivity is suppressed around half-integer flux quanta even at zero temperature for cylinders with a $d$ less than the zero-temperature superconducting coherence length, $\xi(0)$. We have fabricated ultrathin doubly-connected superconducting cylinders of Al over a wide range of $d/\xi(0)$ ratios, with the smallest cylinder down to 100 nm in diameter. Electrical transport measurements revealed the presence of robust step-like features in resistance $vs.$ temperature curves as the destructive regime is approached. These field-induced step-like features, present only in the smallest cylinders with $d/\xi(0)$ close to or less than 1, are unrelated to sample inhomogeneity or phase slip centers, and are most likely resulted from a phase separation close to the QPT. We have also found that the normal state in the destructive regime becomes less stable as the $d/\xi(0)$ ratio increases, with the resistances at the half-flux quantum suppressed continuously from its full normal-state value. Resistance $vs.$ magnetic field measurements show that the field tuned QPT is very sharp (less than 1G) with little evidence for hysteretic behavior.

**13:15**

**H38 11 Hysteresis and Noise from Electronic Nematicity** ERICA CARLSON, *Purdue University* KARIN DAHMEN, EDUARDO FRADKIN, *University of Illinois at Urbana-Champaign* STEVEN KIVELSON, *Stanford University* An electron nematic is a translationally invariant state which spontaneously breaks the discrete rotational symmetry of a host crystal. In a clean square lattice, the electron nematic has two preferred orientations, while dopant disorder favors one or the other orientations locally. In this way, the electron nematic in a host crystal maps to the random field Ising model (RFIM). Since the electron nematic has anisotropic conductivity, we associate each Ising configuration with a resistor network, and use what is known about the RFIM to predict new ways to test for electron nematicity using noise and hysteresis. In particular, we have uncovered a remarkably robust linear relation between the orientational order and the resistance anisotropy which holds over a wide range of circumstances. We discuss the consequences of this for noise and hysteresis in transport anisotropy, as well as possible extensions to other experimental probes such as neutron scattering and STM.

**13:27**

**H38 12 Enhancement of superconductivity by local inhomogeneities** IVAR MARTIN, *Los Alamos National Laboratory* DANIEL PODOLSKY, *University of California, Berkeley* STEVEN KIVELSON, *Stanford University* We study the effect of inhomogeneity of the pairing interaction or the background potential on the superconducting transition temperature, $T_c$. In the weak coupling BCS regime, we find that inhomogeneity, which is incommensurate with the Fermi surface nesting vectors, enhances $T_c$ relative to its value for the uniform system. For a fixed modulation strength we find that the highest $T_c$ is reached when the characteristic modulation length scale is of the order of the superconducting coherence length.

**13:39**
**H38 13 Nanosecond, Transient Resistive State in Two-Dimensional Superconducting Stripes** JENNIFER KITAYGORSKY, I. KOMISSAROV, A. JUKNA, ROMAN SOBOLEWSKI, *University of Rochester* O. MINAEVA, N. KAUROVA, A. KORNEEV, B. VORONOV, I. MILOSTNAYA, GREGORY GOL'TSMAN, *Moscow State Pedagogical University* We have observed, nanosecond-in-duration, transient voltage pulses, generated across two-dimensional (2-D) NbN stripes (width: 100–500 nm; thickness: 3.5–10 nm) of various lengths (1–500 $\mu$m), when the wires were completely isolated from the outside world, biased at currents close to the critical current, and kept at temperatures below the mean-field critical temperature $T_{co}$. In 2-D superconducting films, at temperatures below the Kosterlitz-Thouless transition, all vortices are bound and the resistance is zero. However, these vortices can get unbound when a large enough transport current is applied. The latter results in a transient resistive state, which manifests itself as spontaneous, 2.5–8-ns-long voltage pulses with the amplitude corresponding to the unbinding potential of a vortex pair. In our 100-nm-wide stripes, we have also observed the formation of phase slip centers (PSCs) at temperatures close to $T_{co}$, and a mixture of PSCs and unbound vortex-antivortex pairs at low temperatures.

**SESSION H39: FOCUS SESSION: SUPERCONDUCTIVITY-JOSEPHSON JUNCTIONS AND PAIRING STATE SYMMETRY**
**Tuesday Morning, 14 March 2006**
**342, Baltimore Convention Center at 11:15**
**Mac Beasley, Stanford University, presiding**

*Contributed Papers*

**11:15**
**H39 1 Tunneling spectroscopy studies of the interplay between *s*- and *p*-wave pairings in a Ru microdomain embedded in bulk single-crystal $Sr_2RuO_4$** ZHENYI LONG, CHRYSAFIS ANDREOUS, ZHIQIANG MAO, YOSHITERU MAENO, YING LIU, *Department of Physics, Penn State University* We have performed detailed tunneling spectroscopy measurements on In-Ru/$Sr_2RuO_4$ junctions prepared by pressing freshly cut pure In wire onto $Sr_2RuO_4$ single crystals containing Ru microdomains (the 3-K phase). We have observed a superconducting transition with a $T_c = 0.5$ K and an energy gap of 0.08 meV, both of which correspond to those of the bulk Ru. We have also observed a Josephson coupling between In and Ru, suggesting that conventional *s*-wave pairing is present in the Ru microdomains. On the other hand, a zero bias conductance peak (ZBCP) in the tunneling spectrum and an enhanced critical magnetic field over the bulk value for Ru were observed as well, indicating that *p*-wave pairing exists simultaneously in the Ru microdomain. The temperature and the magnetic field dependences of the tunneling spectrum suggest a non-trivial interplay of the *s*- and *p*-wave pairings and a novel phase modulation of the order parameter at the boundary of the Ru microdomain. We observed an oscillation of the Ru energy gap as the magnetic field is applied along the c axis of the $Sr_2RuO_4$ crystal. Such oscillation was not observed with the field applied along the ab plane. We will discuss the implication of the above observations in this unique superconducting system.

**11:27**
**H39 2 Probing the configuration and dynamics of order parameter domains in $Sr_2RuO_4$ by Josephson interferometry** FRANCOISE KIDWINGIRA, JOEL STRAND, DALE VAN HARLINGEN, *University of Illinois at Urbana-Champaign* YOSHITERU MAENO, *Kyoto University, Kyoto, Japan* We observe anomalous features in the magnetic field dependence of the critical current of Josephson junctions formed between conventional superconductors and the ruthenate superconductor $Sr_2RuO_4$, including magnetic hysteresis, switching noise, and a wide variation of qualitatively different diffraction pattern shapes. All of this behavior can be explained by assuming a complex p-wave order parameter of the form $p_x+ip_y$ that supports a dynamical structure of domains of different chirality and orientation. To test this hypothesis, we are studying the effects of magnetic field cooling on the junction critical current. We find a substantial enhancement of the critical current in field cooled samples, consistent with chiral domains that couple to an applied magnetic field.

**11:39**
**H39 3 Phase-sensitive tests of the pairing state symmetry in $Sr_2RuO_4$** IGOR ZUTIC, *State University of New York at Buffalo* IGOR MAZIN, *Naval Research Laboratory* Exotic superconducting properties of $Sr_2RuO_4$ have provided strong support for an unconventional pairing symmetry. However, the extensive efforts over the past decade have not yet unambiguously resolved the controversy about the pairing symmetry in this material. While recent phase-sensitive experiments using flux modulation in Josephson junctions consisting of $Sr_2RuO_4$ and a conventional superconductor have been interpreted as conclusive evidence for a chiral spin- triplet pairing [1], we propose here an alternative interpretation [2]. We show that an overlooked chiral spin- singlet pairing is also compatible with the observed phase shifts in Josephson junctions and propose further experiments which would distinguish it from its spin-triplet counterpart. Supported by the US ONR and the National Research Council. [1] K. D. Nelson, Z. Q. Mao, Y. Maeno, and Y. Liu, Science **306**, 1151 (2004); T. M. Rice, Science **306**, 1142 (2004). [2] I. Zutic and I. Mazin, Phys. Rev. Lett. **95**, 217004 (2005).

*Invited Papers*

**11:51**
**H39 4 The Phase-sensitive *c*-Axis Twist Experiments on $Bi_2Sr_2CaCu_2O_{8+\delta}$ and Their Implications.** RICHARD KLEMM, *Kansas State University*

There are presently three sets of *c*-axis twist experiments on $Bi_2Sr_2CaCu_2O_{8+\delta}$ (Bi2212)[1]: the bicrystal experiments of Li *et al.*[2], the artificial cross-whisker experiments of Takano *et al.*[3], and the natural cross-whisker experiments of Latyshev *et al.*[4] We summarize these experiments and the extensive theoretical analyses of their possible implications, so

that reliable conclusions can be inferred. The theoretical discussion includes the allowable order parameter symmetries, the twist theorem for the *c*-axis critical current of *d*-wave superconductors across a 45° twist junction, treatments of weak, first-order *c*-axis tunneling with coherent and incoherent components, and effects of the Fermi surface, strong coherent tunneling, orthorhombicity, nanoscale disorder, and OP twisting near the physical twist junction. As a minimum, all three experiments can only be understood in terms of a substantial *s*-wave superconducting order parameter component in Bi2212 for $T \leqslant T_c$. An anisotropic *s*-wave order parameter can fit all three experiments quantitatively. The bicrystal and natural cross-whisker experiments are also consistent with the preponderance of other data that the *c*- axis tunneling in Bi2212 is strongly incoherent, so that all of the *c*-axis critical current arises from the *s*-wave order parameter component. These three sets of experiments appear to rule out a purely repulsive pairing interaction.

[1]R. A. Klemm, Phil. Mag. **85**, 801-853 (2005).
[2]Q. Li, Y. N. Tsay, M. Suenaga, R. A. Klemm, G. D. Gu, and N. Koshizuka, Phys. Rev. Lett. **83**, 4160 (1999).
[3]Y. Takano *et al.*, Phys. Rev. B **65**, 140513 (2002); Physica C **408-410**, 296 (2004), etc.
[4]Yu. Latyshev, A. P. Orlov, A. M. Nikitina, P. Monceau, and R. A. Klemm, Phys. Rev. B **70**, 094517 (2004).

***Contributed Papers***



**12:27**

**H39 5 Josephson effect with d+ip superconductors** BRIGITTE LERIDON, *CNRS/ESPCI, 10 rue Vauquelin, 75005 Paris* TAI-KAI NG, *Physics Department, HKUST, Hong-Kong* C. M. VARMA, *Department of Physics, University of Riverside, CA 92521* Two different experiments, namely ARPES with circularly polarized photons and neutron diffraction have observed a time-reversal and inversion symmetry breaking in the pseudogap state of the cuprates. This phase had actually been predicted in the framework of a general model for the normal and superconducting state of high-Tc superconductors. This symmetry breaking should also affect the superconductive symmetry and lead to the admixture of a p-wave component to the dominant d-wave order parameter. We show here that this allows to make specific predictions for the Josephson effect between a ''d+ip'' superconductor and an ordinary s-wave superconductor, or between two ''d+ip'' superconductors, according to the orientation of the surface. We propose a set of experiments where, for some particular orientations, an anomalous Josephson effect should be observed whenever a pseudogap is present.

**12:39**

**H39 6 Direct test of pairing fluctuations in the pseudogap phase of an underdoped cuprate** NICOLAS BERGEAL, JEROME LESUEUR, MARCO APRILI, BRIGITTE LERIDON, *LPQ ESPCI/UPR5-CNRS, 10 rue Vauquelin 75005 Paris (France)* GIANCARLO FAINI, *LPN-CNRS, Route de Nozay, 91460 Marcoussis (France)* JEAN-PIERRE CONTOUR, *UMR 137 CNRS/ THALES, Route departementale 128, 91767 Palaiseau Cedex (France)* In underdoped cuprates, many experiments have provided evidence for the presence of a gap-like structure in the electronic excitations spectrum, in a region above the critical temperature and below a characteristic temperature T*. The origin of this so-called pseudogap is still hardly debated and the answer to this question turns out to be essential for the understanding of high-$T_c$ superconductivity. One doesn't know if the pseudogap is related to superconductivity or to an order in competition. In the former case, it has been suggested that superconducting pairing fluctuations may be responsible for the partial suppression of electronic excitations. This remains to be tested experimentally, but most of the probes used to investigate the pseudogap are not sensitive to pairs and therefore cannot provide such a test. Here, we report for the first time on a direct test of pairing fluctuations in the pseudogap regime using a Josephson-like experiment. Our results shows that fluctuations survive only in a restricted range of temperature close to $T_c$ ($T-T_c < 15K$), well below T*, and therefore cannot be responsible for the opening of the pseudogap at high temperature.

**12:51**

**H39 7 Josephson (001) tilt grain boundary junctions of high temperature superconductors** GERALD ARNOLD, *University of Notre Dame* RICHARD KLEMM, *Kansas State University* We calculate the Josephson critical current $I_c$ across in- plane (001) tilt grain boundary junctions of high temperature superconductors. We solve for the electronic states corresponding to the electron-doped cuprates, two slightly different hole-doped cuprates, and an extremely underdoped hole- doped cuprate in each half-space, and weakly connect the two half-spaces by either specular or random Josephson tunnelling. We treat symmetric, straight, and fully asymmetric junctions with *s*-, extended-*s*, or $d_{x^2-y^2}$-wave order parameters. For symmetric junctions with random grain boundary tunnelling, our results are generally in agreement with the Sigrist-Rice form for ideal junctions that has been used to interpret ''phase-sensitive'' experiments consisting of such in- plane grain boundary junctions. For specular grain boundary tunnelling across symmetric junctions, our results depend upon the Fermi surface topology, but are usually rather consistent with the random facet model of Tsuei *et al.* [Phys. Rev. Lett. **73** 593(1994)]. Our results for asymmetric junctions of electron-doped cuprates are in agreement with the Sigrist- Rice form. However, our results for asymmetric junctions of hole- doped cuprates show that the details of the Fermi surface topology and of the tunnelling processes are both very important, so that the ''phase-sensitive'' experiments based upon in-plane Josephson junctions are less definitive than has generally been thought.

**13:03**

**H39 8 Josephson junctions and arrays fabricated via nanolithography and ion damage** SHANE CYBART, JOHN CLARKE, ROBERT DYNES, *University of California Berkeley* KE CHEN, YI CUI, QI LI, XIAOXING XI, *Penn State University* In the years to come, the size and cost of cryo-coolers will get smaller and the demand for a VLSI Josephson junction technology will increase. One possible candidate to fill this need is the ''ion-damage'' Josephson junction. These junctions are fabricated by using ion bombardment to create localized narrow regions of defects in the plane of a thin film of superconductor. These regions have a superconducting transition temperature lower than that of the bulk film and act as hysteretic Josephson junctions. The advantage of these junctions over other technologies is that they have

no interfaces between different materials, and can be placed over 10 times closer to each other in comparison to competing techniques. Individual junctions and series arrays were fabricated from YBCO and magnesium diboride. Junction current-voltage characteristics near the critical temperature follow the resistively shunted junction model however at lower temperatures the barrier becomes strongly coupled and flux flow behavior is evident. Series arrays of up to 20 junctions have been fabricated with sufficient parameter uniformity to achieve giant Shapiro steps under microwave radiation.

**13:15**

**H39 9 Quantum dynamics of a d-wave YBCO Josephson junction** FLORIANA LOMBARDI, *Chalmers University of Technology* THILO BAUCH, TOBIAS LINDSTRÖM, FRANCESCO TAFURI, GIACOMO ROTOLI, TORD CLAESON, We present direct observation of macroscopic quantum properties in an all high critical temperature superconductor d-wave Josephson junction. Although dissipation caused by low energy excitations is expected to strongly suppress macroscopic quantum effects we demonstrate macroscopic quantum tunneling [1] and energy level quantization [2] in our d-wave Josephson junction. We have investigated specific YBCO grain boundary Josephson junction's geometry, where tunneling in the node of the order parameter sensibly contributes to the transport properties. In such a case the Josephson current-phase relation is significantly modified and we have found that the fundamental state of the junction is doubly degenerate. The results indicate that the role of dissipation mechanisms in high temperature superconductors has to be revised, and may also have consequences for the class of solid state ''quiet'' quantum bit with superior coherence time. [1] T. Bauch et al., Phys. Rev. Lett. **94**, 087003 (2005). [2] accepted for publication in Science.

**13:27**

**H39 10 Biot-Savart correlations in anisotropic superconductors** KUMAR RAMAN, *University of Illinois at Urbana-Champaign* VADIM OGANESYAN, *Yale University* SHIVAJI SONDHI, *Princeton University* We study the normal-superconducting phase transition of layered type II superconductors in the limit of very weak Josephson coupling. By extending previous renormalization grouptreatments we investigate the importance of interlayer Biot-Savart interactionsfor three dimensional correlations near the transition and the recent weak-field magnetization experiments in BSSCO.

**13:39**

**H39 11 Electromagnetic wave generation by mesoscopic intrinsic Josephson junctions of single crystal $Bi_2Sr_2CaCu_2O_{8+\delta}$** KAZUO KADOWAKI, TAKUYA YAMAZAKI, ITSUHIRO KAKEYA, TAKASHI YAMAMOTO, UNIV. OF TSUKUBA TEAM, It is known that the junction resistance $R_c$ of mesoscopic intrinsic Josephson junctions of single crystal $Bi_2Sr_2CaCu_2O_{8+\delta}$ in a sweeping magnetic field parallel to the $ab$-plane exhibits a strong quantum oscillating behavior with periods of a unit of magnetic quantum flux $\phi_0$ or $\phi_0/2$, which penetrate through each insulating layer between superconducting $CuO_2$ layers of $Bi_2Sr_2CaCu_2O_{8+\delta}$ above or below a certain magnetic field $H^*$, respectively. This happens only at low level of currents, whereas at high currents this oscilating behavior fades away and $R_c$ becomes rather smooth saturation behavior. In such a condition it is expected that the collective motion of Josephson vortices would generate Josephson plasma in a junction, which may continuously emit the coherent THz electromagnetic waves. In reaching a current levels at $\sim$ 0.3-0.7$J_c$ in rather low fields, we were indeed able to detect electromagnetic radiation emitted from the junctions by a bolometer detecter located near the junction. The power observed is very large, reaching a few 100 W/cm$^2$, and is extremely efficient, showing 3-7% of the total input current energies. This is compared with the other methds such as cascade lasers using quantum dots and parametric oscillators using laser mixing in a non-linear optical materials.

**13:51**

**H39 12 Magnetic oscillations of critical current in Josephson-junction stacks** ALEXEI KOSHELEV, *Argonne National Laboratory* We consider magnetic oscillations of critical current in stacks of Josephson junctions, which are realized in mesas fabricated from layered high-temperature superconductors. Depending on the stack lateral size and magnetic field, oscillations may have either period of half flux quantum per junction (large-size regime) or one flux quantum per junction (small-size regime). We study in detail the crossover between these two regimes. In the small-size regime the lattice structure experiences periodic series of phase transitions between aligned rectangular configuration and triangular configuration. Triangular configurations in this regime realize only in narrow regions near magnetic-field values corresponding to integer number of flux quanta per junction. This work was supported by the U. S. DOE, Office of Science, under contract # W-31-109-ENG-38.

**14:03**

**H39 13 Effects of topological excitations in Josephson junction arrays.** SAID SAKHI, *American University of Sharjah* We study the zero-temperature physics of planar Josephson junction arrays in the self-dual approximation in the presence of external offset charges and magnetic fluxes. We introduce a new Landau-Ginzburg formulation to describe both types of topological excitations (electric and magnetic) that determine the quantum phase structure of the model. Through the condensation of the boson fields, this approach captures with ease various phases of Josephson junction arrays including the superconducting phase, the insulating phase, in addition to a novel quantum Hall phase that results from the condensation of composites formed by electric and magnetic topological excitations.

**SESSION H40: FOCUS SESSION: MATERIALS FOR QUANTUM COMPUTING II**
**Tuesday Morning, 14 March 2006**
**343, Baltimore Convention Center at 11:15**
**Britton Plourde, Syracuse University, presiding**

***Contributed Papers***

**11:15**

**H40 1 Microwave absorption by electrons on helium in a tilted magnetic field** SOLOMON DUKI, H. MATHUR, *Case Western Reserve University* Microwaves can be used to drive transitions between the ground and low-lying excited states of electrons bound to the surface of liquid helium. Such microwave absorption

has been observed since the 1970s and is the basis of quantum computing schemes that use electrons on helium. We study theoretically the effect of a tilted magnetic field on the microwave absorption. It is found that the absorption lineshape will change from a symmetric Lorentzian to an asymmetric Fano lineshape as the tilted field is increased. Thus application of the tilted field permits control of the lineshape.

**11:27**
**H40 2 Measurement of the charge transfer efficiency of electrons on liquid helium in a CCD-like architecture*** GUILLAUME SABOURET, E. A. SHANER, S. A. LYON, *Princeton University* Electrons floating on the surface of liquid helium are possible qubits in quantum computing; the necessary two quantum levels can either be the charge states or the spin states of the electrons. Varying electric potentials do not modify spin states, which allows the transport of qubits on the surface of liquid helium using a CCD-like array of underlying gates. A quantum computer will require the controlled movement of single electrons and the reliability of this scheme depends on how readily an electron can be transferred from one gate to another and on the absence of electron traps along the way. We will present a measurement of the charge transfer efficiency (CTE) of electrons clocked back and forth above a short CCD-like structure submerged under liquid helium. This was achieved by using a special clocking sequence that ejects any electrons left above a chosen gate at the end of each clock cycle. The CTE obtained at low clocking frequencies is very high with an electron density of about 0.3 electrons/cm$^2$, comparable to the CTE of silicon CCD's with much higher electron densities. We find no evidence for deep electron trapping in our system.

*Supported in part by ARO and ARDA.

**11:39**
**H40 3 A photoelectron source for electrons on liquid helium*** SHYAM SHANKAR, GUILLAUME SABOURET, WEI ZHAO, FABRICE AMY, ANTOINE KAHN, S. A. LYON, *Princeton University* Manipulation of the spins of electrons on the surface of liquid helium is a promising method to implement a quantum computer. One of the challenges in this method is to generate electrons on the helium surface in a reliable and controlled manner. The traditional approach is to use thermionic emission from a tungsten filament. This approach generates many electrons in an uncontrolled manner and heats the low temperature system. An electron source relying on photoemission from a zinc film has been previously described [1] using a high power light source coupled to a fiber. This work has been reproduced in a more compact manner by using a small modular lamp and proximity focussing. However, zinc films tend to oxidize rather quickly. We are studying the use of alternative low work function materials such as samarium that promise better stability. [1] L. A. Wilen and R. W. Gianetta, Rev. Sci. Instrum. 56(11), November 1985.

*Supported in part by the ARO and ARDA



***Invited Papers***

**11:51**
**H40 4 Oxygen Instabilities and the Electronic Properties of Oxide Tunnel Barrier Layers.**
ROBERT BUHRMAN, *Cornell University*

Very thin $AlO_x$ layers, usually formed by the controlled dose, RT oxidation of the surface of Al thin films, have long been the most successful and most reproducible approach for the fabrication of high-quality superconducting Josephson junctions, as well as for the formation of the gate-insulator for myriad non-conventional electronics studies. $AlO_x$ has also been widely employed as the barrier in magnetic tunnel junctions (MTJs). In recent years, however, it has become clear that for demanding applications, most notably Josephson junction qubit devices, the performance of the $AlO_x$ barrier layer is far below what is needed, particularly with respect to 1/f noise behavior; a determination that has given new urgency to the task of better understanding and significantly improving the properties of this barrier layer material, or of developing a better alternative. I will describe the results of a series of scanning tunneling spectroscopy, XPS and electronic transport studies on ultra-thin AlOx layers, in both half-formed and fully-formed junction configurations. These results demonstrate the inherently unstable nature of a significant portion of the oxygen component of the oxide. As the result of this instability, the process that forms a completed AlOx tunnel junction is much more complex than the reproducibility of the process might otherwise suggest. I will compare this character of amorphous AlOx barrier layers with the oxygen stability in crystalline MgO layers such as are currently being employed in MTJs, and on the basis of these findings discuss some approaches that might lead to more stable, lower noise Josephson junctions. Finally I will discuss some preliminary results that suggest that a low T tunnel-junction 1/f noise level that is much more than 10x less than the best that has been reported to date may indeed be achievable.

*Contributed Papers*

**12:27**

**H40 5 Eliminating Junction Fluctuators using Epitaxial Barrier in Josephson Qubit** SEONGSHIK OH, K. CICAK, M. S. ALLMAN, JEFFREY S. KLINE, K. D. OSBORN, G. PROKOPENKO, M. A. SILLANPAA, A. J. SIROIS, J. A. STRONG, J. D. WHITTAKER, R. W. SIMMONDS, D. P. PAPPAS, *NIST, Boulder* R. MCDERMOTT, JOHN M. MARTINIS, *UC, Santa Barbara* Before a multi-qubit solid-state quantum computer is realized, many obstacles need to be overcome. The most significant problem with any solid- state qubit implementation is strong coupling to sources of decoherence in the environment. Accordingly, identifying and removing these sources is an important prerequisite for construction of a solid-state quantum computer. Among other things, all the present-day superconducting qubits use amorphous $AlO_x$ as a tunnel barrier. However, there is growing evidence that the amorphous $AlO_x$ tunnel barriers have undesirable two-level fluctuators that adversely affect the qubit. Along this line, we have fabricated the first epitaxial Josephson phase qubit with single-crystal $Al_2O_3$ barrier and observed substantially reduced density of two-level fluctuators in this new type of qubit. This is the first clear evidence showing the relationship between crystallinity of the tunnel barrier and the two-level fluctuators. With this new epitaxial Josephson qubit technology, we are one-step closer to realization of a practical multi-qubit solid-state quantum computer. This talk will be focused more on the fabrication side of the epitaxial qubit and the following talk will discuss the details of its measurement.

**12:39**

**H40 6 Improved Phase Qubits with Re-$Al_2O_3$-Al Junctions with Epitaxial Barriers.*** K. CICAK, M.S. ALLMAN, JEFFREY S. KLINE, SEONGSHIK OH, K.D. OSBORN, G. PROKOPENKO, M.A. SILLANPAA, A.J. SIROIS, J.A. STRONG, J.D. WHITTAKER, *National Inst. of Standards and Tech. - Boulder* JOHN M. MARTINIS, *UC Santa Barbara, Dept. of Physics* D.P. PAPPAS, R.W. SIMMONDS, *National Inst. of Standards and Tech. - Boulder* In our efforts to identify and eliminate sources of decoherence in our qubits we have established that dielectric loss, both from substrate and from insulating layers in the device, can compromise qubit coherence. This has lead to significant improvements of our phase qubits. Now we show that the structural quality of the Josephson junction barrier itself can significantly improve qubit performance in a specific way. As compared to qubits with amorphous barriers, our latest measurements using qubits fabricated with epitaxial Josephson tunnel barriers show a significant decrease in density and coupling strength of individual spurious resonator defects.

*This work was supported by ARDA through Grant No. MOD717304

**12:51**

**H40 7 Epitaxial growth of Mo/$Al_2O_3$/Mo trilayers for Josephson junction qubits** JEFFREY S. KLINE, KRISTINE M. LANG, SEONGSHIK OH, KEVIN D. OSBORN, RAYMOND W. SIMMONDS, *National Institute of Standards and Technology* ROBERT MCDERMOTT, JOHN M. MARTINIS, *University of California-Santa Barbara* DAVID P. PAPPAS, *National Institute of Standards and Technology* The growth of ultrathin epitaxial $Al_2O_3$ tunnel barriers on Re has been proven to reduce the number of spurious resonators in Josephson phase qubits when compared to qubits fabricated with amorphous tunnel barriers. Other refractory metals might also be used as base layers for epitaxial $Al_2O_3$ growth. In this work, Mo films were deposited onto $Al_2O_3(11\bar{2}0)$ substrates by UHV magnetron sputtering. To achieve epitaxy, the substrate was held at elevated temperature during the deposition. Post-deposition high temperature anneals increase the terrace size and occurrence of step-bunching as observed by STM. Ultrathin films of $Al_2O_3$ were then deposited at room temperature onto the Mo base layer by reactive evaporation of Al in a controlled oxygen background. A high temperature anneal in an oxygen background crystallizes the amorphous $Al_2O_3$ layer. Finally, the structure is capped with polycrystalline Mo by sputter deposition at room temperature. Dielectric loss measurements on LC oscillators fabricated from these structures will be reported.

**13:03**

**H40 8 Josephson Tunnel-Junctions Fabricated From Epitaxial Niobium-Based Multi-Layers** PAUL B. WELANDER, TIM J. MCARDLE, JAMES N. ECKSTEIN, *Department of Physics, Frederick Seitz Materials Research Laboratory, University of Illinois at Urbana-Champaign, Urbana, Illinois 61801* We report on the investigation of Josephson tunnel-junctions fabricated from epitaxial multi-layers. The foundation of these devices is the growth of a single-crystal niobium base electrode on sapphire. Niobium films grown near 800 °C typically have critical temperatures around 9.4 K and residual resistance ratios above 100. Diffraction measurements show excellent crystallinity, and microscopy reveals surfaces with mono-layer step-edges and rms roughness less than 0.2 nm. Tunnel barriers are formed using a range of methods. On one hand, epitaxial alumina is grown on niobium above 700 °C by evaporating aluminum metal in an oxygen gas background of about 1 microtorr. On the other hand, an aluminum single- crystal film about 20 nm thick is deposited on niobium at room temperature and then oxidized in 10-100 torr oxygen gas for about one hour. The counter-electrode in both cases is amorphous niobium deposited at ambient temperature. The latter method of barrier formation produces tunnel-junctions with critical current densities around 100 A/cm$^2$.

**13:15**

**H40 9 Enhanced Macroscopic Quantum Tunneling in $Bi_2Sr_2CaCu_2O_{8+\delta}$ Intrinsic Josephson Junction Stacks** X.Y. JIN, J. LISENFELD, Y. KOVAL, A. LUKASHENKO, A.V. USTINOV, P. MÜLLER, *Physikalisches Institut III, Universität Erlangen-Nürnberg* We have investigated macroscopic quantum tunneling in $Bi_2Sr_2CaCu_2O_{8+\delta}$ intrinsic Josephson junctions and performed microwave absorption experiments. Classical-to- quantum crossover temperatures of up to 700mK were found. Plasma frequencies of up to 1.13 THz have been observed. In uniformly switching intrinsic Josephson stacks, the escape rate from zero-voltage state is enhanced by several orders of magnitude in comparison to single intrinsic junctions having comparable junction parameters. This enhancement is due to the unique stacking structure of intrinsic Josephson junctions.

**13:27**

**H40 10 Coupled Quantum Dots in the Kondo regime: interference and filtering effects.** LUIS DIAS DA SILVA, NANCY SANDLER, *Department of Physics and Astronomy, Ohio University* KEVIN INGERSENT, *Department of Physics, University of Florida* SERGIO ULLOA, *Department of Physics and Astronomy, Ohio University* Double quantum-dot systems (DQDs) provide a vast array of possibilities for both theoretical and experimental investigations of the Kondo regime. In this work, we propose

DQDs as a possible experimental realization of a Kondo impurity coupled to an effective structured (non-constant) density of states (DoS). We consider a DQD in parallel configuration coupled to metallic leads. By changing the lead-dot and dot-dot couplings, the effective hybridization function for an individual dot displays sharp resonances and/or pseudogaps, allowing for an experimental probe into the transition between both regimes. Using numerical renormalization group methods, we calculate the dot's spectral function in different regimes. For a dot weakly coupled to the leads and strongly coupled to the second dot, the effective DoS has a sharp resonance with width $\Delta$ and the spectral density shows a splitting in the Kondo resonance for $T_K > \Delta$, although the Kondo singlet is itpreserved. Furthermore, for small inter-dot coupling, second order dot-dot interactions through the conduction electrons lead to the formation of a pseudo-gap. The spectral density goes to zero as a power-law $|\epsilon - \epsilon_F|^2$ and the Kondo screening is suppressed. Supported by NFS-NIRT.

**13:39**

**H40 11 Spin polarized current in a double quantum dot with time-dependent interdot tunneling*** ERNESTO COTA, FRANCISCO MIRELES, FERNANDO ROJAS, *CCMC-UNAM* SERGIO E. ULLOA, *Ohio University* A bipolar spin filter has been proposed using a few-electron double quantum dot (DQD) in a 'hanging-dot' configuration [1], and tunable by controlling the molecular hybridization (interdot tunneling) between dots. The bipolar nature of the electron spin current arises from a singlet-triplet transition in the ground state of the two-electron DQD. The transition occurs due to the competition among Zeeman energy, exchange interaction and interdot coupling, favoring a lower (higher) energy for the triplet (singlet) configuration in the weak (large) interdot tunneling regime. In this work we use a density matrix equation to study the dynamical behavior of the DQD, by considering the adiabatic variation of the interdot tunneling in time. We report on the spin-polarized current through the DQD as a function of the relevant physical parameters. A bipolar spin filtering effect in the time domain is observed to arise on time scales smaller than the relevant coherent and spin relaxation times in typical QDs. Spin-orbit coupling is included in our approach but found to not significantly affect our results. [1] F. Mireles, E. Cota, F. Rojas and S.E. Ulloa, submitted.

*Work supported by DGAPA-UNAM project IN114403 and CONACYT project 43673, and the 21st Century Indiana Fund

**13:51**

**H40 12 Charge sensing in Si/SiGe quantum dots using single electron transistors** FENG PAN, TIM GILHEART, ALEXANDER RIMBERG, *Dartmouth College* KEITH SLINKER, LISA MCGUIRE, MARK ERIKSSON, *University of Wisconsin-Madison* J. O. CHU, *IBM Research Division, T. J. Watson Research Center* Qubit schemes based on silicon technology have obvious economic appeal as well as compelling physical motivations, such as a long spin-spin dephasing time. Proposed silicon solid-state qubit schemes include quantum dots coupled to fast readout devices, such as a quantum point contact or single electron transistor (SET). Recently, Si/SiGe quantum dots defined by Schottky gates deposited on a Si/SiGe heterostructure containing a high mobility two-dimensional electron gas have been fabricated. [1] Here we report the integration of a SET with such a Si/SiGe quantum dot. Several such devices have been produced, and recent measurements, including transport and sensing of the dot charge with the SET, will be discussed. [1] K A Slinker et al 2005 New J. Phys. **7** 246.

**14:03**

**H40 13 Few Electron Si/SiGe Quantum Dots** LEVENTE KLEIN, *University of Wisconsin* SRIJIT GOSWAMI, DON SAVAGE, KEITH SLINKER, LISA MCGUIRE, MAX LAGALLY, MARK ERIKSSON, Fully top-gated silicon/silicon-germanium quantum dots have been fabricated and characterized at low temperatures. For the quantum dots with few electron occupation, by varying the gate voltages two regimes may be accessed: at large negative voltages sharp Coulomb diamonds and classical Coulomb blockade is observed with a charging energy of 3.8 meV. At more positive gate voltage, co-tunneling features appear and a zero-bias conductance anomaly is observed with a behavior closely resembling the quantum dot Kondo effect. The increased zero-bias conductance vanishes with increasing temperature, and this peak splits into two peaks at finite drain-source voltage with increasing perpendicular magnetic field. The peak splitting increases linearly with increasing magnetic field. We discuss the various conductance regimes and the application of these types of quantum dots for quantum information processing.

**SESSION H41: DIELECTRIC, FERROELECTRIC, AND PIEZOELECTRIC OXIDES I**
**Tuesday Morning, 14 March 2006**
**344, Baltimore Convention Center at 11:15**
**Eugene Tsiper, Naval Research Laboratory, presiding**

**11:15**

**H41 1 Constrained polarization study of ferroelectric $KNO_3$*** OSWALDO DIÉGUEZ, DAVID VANDERBILT, *Rutgers University* Potassium nitrate has an interesting phase diagram that includes a reentrant ferroelectric phase (phase III, *R3m*), and it has been proposed as a promising material to be used in random-access memory devices.[1] Recently, we have developed a method to compute the ground-state of an insulator under a fixed value of its polarization[2] that can be used to gain insight into the properties of polar materials. In this talk we show the results of applying this method to study the structural behavior of potassium nitrate under polarization reversal, describing an unusual mechanism in which the reversal is accompanied by a rotation of the $NO_3$ unit by 60°. We also use our calculations as a basis for constructing first-principles based models that can be used to gain a deeper understanding of the switching behavior of this material.

*This work was supported by ONR.

[1]J. F. Scott, M. S. Zhang, R. B. Godfrey, C. Araujo, and L. McMillan, Phys. Rev. B **35**, 4044 (1987).
[2]See: cond-mat/0511711 (www.arXiv.org).

**11:27**

**H41 2 Surface passivation of III-V compound semiconductors using atomic-layer-deposition grown Al2O3** M.L. HUANG, M. HONG, Y.C. CHANG, C.H. CHANG, Y.J. LEE, P. CHANG, T.B. WU, J. KWO, DEP. OF MAT. SCI. & ENG., TSING HUA U., HSINCHU, TAIWAN TEAM, DEP. OF PHYS., TSING HUA U., HSINCHU, TAIWAN TEAM, Al2O3 was deposited on In0.15Ga0.85As/GaAs using atomic layer deposition (ALD). Without any surface preparation or post thermal treatment, excellent electrical properties of Al2O3/InGaAs/GaAs heterostructures

were obtained, in terms of low electrical leakage current density (10-8 to 10-9 A/cm2) and low interfacial density of states (Dit) in the range of 1012 cm-2eV-1. The interfacial reaction and structural properties studied by HRXPS and HRTEM. The depth profile of HRXPS, using synchrotron radiation beam and low energy Ar+ sputtering, exhibited no residual arsenic oxides and elemental arsenic at interface. The removal of the arsenic oxides from Al2O3/InGaAs heterostructures during ALD process ensures the Fermi level unpinning, which was observed in the C-V measurements. The HRTEM shows sharp transition from amorphous oxide to single crystalline semiconductor. The bandgap of ALD grown Al2O3 was measured by O 1s core level loss spectra as 6.55 eV, and valence band offset was 3.78 eV between Al2O3 and In0.15Ga0.85As layers.

**11:39**

**H41 3 Electronic and vibrational properties of tungsten-bronze niobates** MARCO FORNARI, *Dept. of Physics, Central Michigan University* We investigated the electronic and vibrational properties of complex niobates with tetragonal tungsten-bronze structure. Our first principles results show that, in $PbNb_2O_6$, the largest contribution to the polarization is from the four 15-coordinates Pb sites ($A^{XV}$). The interaction between these sites favors the orthorhombic ground-state. The substitution of Ba on the $A^{XV}$ site drives the system to a tetragonal phase forming a morphotropic phase boundary. Replacing Ba with Pb breaks the cooperative behavior a the origin of the orthorhombic phase. Octahedral rotations do not seem to play a significant role even if they influence the energetic of the position of Pb in the $A^{XV}$ cage. Chemical substitutions are tried to explore novel ferroelectric materials.

**11:51**

**H41 4 Cubic HfO2 Doped with Y2O3 for Advanced Gate Dielectrics by MBE.** ZHIKAI YANG, W.C. LEE, PEN CHANG, MOLIN HUANG, YI LIN HUANG, MINGHWEI HONG, *Dept. of MSE NTHU Taiwan* C.M. HUANG, C.H. HSU, *NSRRC Taiwan* RAYNIEN KWO, *Dept. of Phys. NTHU Taiwan* NATL SYNCHROTRON RAD. RES. CTR.TAIWAN COLLABORATION, High $\kappa$ $HfO_2$ ($\kappa$ =20) is currently employed as an alternative gate dielectric replacing $SiO_2$ in CMOS scaling. There are three known crystal structures of $HfO_2$, monoclinic, cubic, and tetragonal with varying dielectric constants [1]. Recently we showed $HfO_2$ films epitaxially grown on GaAs(100) formed the stable monoclinic phase ($\alpha = \gamma = 90$ and $\beta \sim 99$) with the *a* and *b* axes aligned with the in-plane GaAs{100} axes resulting in four equivalent domains. This work demonstrates the successful alteration of the crystal structure of $HfO_2$from the lower $\kappa$ monoclinic phase to the higher $\kappa$ ($\kappa$ =30) cubic phase stabilized through epitaxy on GaAs(100) and Si(100) with the aid of $Y_2O_3$ doping ( $\sim$ 20% based on XPS). X-ray diffraction scans on these films clearly indicated the cubic symmetry. Doping $Y_2O_3$ is also to enhance the thermal stability of amorphous $HfO_2$. $Y_2O_3$doping was shown to help raise the re-crystallization temperature of $HfO_2$to be compatible with high temperature processing.[1] X. Zhaoetal, PRB **65**, 233106 (2002).

**12:03**

**H41 5 Hydrogen bistability in non-magnetic oxides** JACOB GAVARTIN, ALEXANDER SHLUGER, MARSHALL STONEHAM, *University College London, U.K.* STEVE COX, *ISIS Facility, Rutherford Appleton Lab, U.K.* Recent extensive muonium spectroscopy measurements ($\mu$SR) [1] suggest a general correlation between stable muonium (Mu) forms in non magnetic oxides and their band gap, $E_g$ : in the materials with Eg$<$ 4 eV, Mu is, as a rule, fully ionized; in the oxides with Eg$>$ 7 eV, most of the Mu exists in the atomic form, while both ionized and atomic forms of Mu coexist in the oxides with the band gap in the interval 4$<$ Eg $<$ 7 eV. Based on the analogy between muonium and hydrogen, we propose a general model which may explain such a correlation and makes important predictions about hydrogen behavior in non-magnetic oxides. As an example, we use ab initio calculations to extract the parameters for this model to explain difference in hydrogen behavior in $HfO_2$, $ZrO_2$ films and in their silicates at low hydrogen concentrations [2]. We further discuss the role of hydrogen in mechanisms of tetragonal to a monoclinic phase transformations in $ZrO_2$ and $HfO_2$. 1. S.F.J. Cox, J.L. Gavartin, J.S. Lord et al. J. Phys. : Condens. Matter, 2006 (in press). 2. R.P. Pezzi, L. Miotti, K.P. Bastos et al. Appl. Phys. Lett. **85** 3540 (2004).

**12:15**

**H41 6 Growth of highly oriented monoclinic $HfO_2$ thin films after Co and Fe doping by pulsed laser deposition** S. DHAR, M.S.R. RAO, S.B. OGALE, D.C. KUNDALIYA, S.R. SHINDE, T. VENKATESAN, *Center for Superconductivity Research, Department of Physics, University of Maryland, College Park, MD 20742, USA* S.J. WELZ, R. ERNI, N.D. BROWNING, *Lawrence Berkeley National Laboratory, NCEM, One Cyclotron Road, Berkeley, CA 94720, USA* Above room-temperature ferromagnetism in undoped and Co doped high-k dielectric $HfO_2$thin films opens up the possibility for using spin functionality in various new electronic devices. In the present work, we report on the growth of high quality epitaxial $HfO_2$ thin films stabilized in monoclinic phase after 5% Co or Fe doping at 700-800$^o$C in an oxygen partial pressure of $10^{-4}$ torr on (001) yttria stabilized zirconia and (001) Si substrates by pulsed laser deposition. On the one hand, pure $HfO_2$ film did not grow epitaxally under various deposition conditions. On the other hand, the formation of single crystalline phase after Co or Fe doping was confirmed by X-ray analysis. Ion channeling analysis in Co and Fe doped films showed 8-24% minimum yield indicating highly oriented film growth, whereas, a very poor minimum yield was observed in the undoped case. Angular scans showed the $HfO_2$ to grow in a monoclinic phase with a 9.1 degree tilt with respect to the substrate. High resolution transmission electron microscopy showed very sharp interface while Electron energy loss spectroscopy revealed that Co is in 2+ state indicating the substitution of Co in ionic form into the $HfO_2$lattice.

**12:27**

**H41 7 Anomalous behavior of the dielectric constant of hafnium silicates** CARLO ANTONIO PIGNEDOLI, ALESSANDRO CURIONI, WANDA ANDREONI, *IBM Research, Zurich Research Laboratory, 8803 Rueschlikon (Switzerland)* Hafnium silicates (HfSiO) are among the materials most frequently investigated in the search for a replacement of silicon dioxide as gate dielectric in CMOS devices. Measurements of the dielectric constant as a function of the relative concentration of the two binary oxides exhibit an anomalous behavior. Large-scale DFT-based calculations reveal that this is due to the change of the relative stability of different structures with composition and their strong

influence on the permittivity. These results also help to rationalize the wide scatter in the experimental data for the dielectric constant for some concentrations and suggest ways to optimize the integration of these materials in the device.

**12:39**

**H41 8 Nucleation and Growth of ALD Hafnium Oxide High-k Dielectric Films by GISAXS.** ANDREW ALLEN, *NIST* MARTIN GREEN, *NIST* Atomic layer deposition (ALD) is an important film growth technique that enables accurate growth of ultrathin layers for high-k gate dielectrics. Results will be presented of grazing incidence small angle x-ray scattering (GISAXS) studies of the nucleation and growth of ALD hafnium oxide films. The scattering is related to surface roughness and internal interfaces within the films, resulting from film coalescence of the nuclei. Films grown on H-terminated Si are rough and nonplanar, exhibit greater scattering, and have greater internal surface area than films grown on chemically oxidized Si. These films have 5 times the internal surface area of films grown on chemically oxidized Si, and may be significantly porous. The characteristic scattering features are the film nuclei, which coalesce and become inherited features of the films. The nuclei size is about 2 nm, consistent with TEM observations. Films grown on chemically oxidized Si reach coalescence at about 25 cycles, or 1.3 nm thickness, consistent with electrical data. Implications arising from the different film morphologies discussed.

**12:51**

**H41 9 Self-interaction corrected extrinsic levels of oxygen vacancies in hafnia** GIORGIA M. LOPEZ, VINCENZO FIORENTINI, ALESSIO FILIPPETTI, *SLACS-CNR and University of Cagliari, Italy* To identify fixed-charge (generally negative) centers in thin hafnia layers on silicon, the position and nature of the electronic levels of candidate defects should be known accurately. Due to the DFT gap problem, this is still a controversial issue in ab initio calculations, especially for high-gap insulators and near-conduction states. Here we apply a self-interaction corrected DFT method, which dealt successfully with a variety of systems dominated by localized and correlated states, to study the electronic structure of oxygen vacancies in monoclinic hafnium oxide in various charge states. We set the position of the extrinsic levels within the gap, and relative to the Si gap position as determined by interface band offsets. In the positive states, the partially filled levels are well below the Si gap, hence the Fermi level, and play a minor role. For the neutral vacancy, a filled extrinsic state sits within the Si gap and may tend to pin the Fermi level. A negative center may be realized upon occupation of a near-conduction shallow state, which would occur under typical device operation bias. While a conclusive identification of fixed-charge centers remains an open issue, the nature of this level is compatible with the experimentally observed kinetics of trapping and detrapping.

**13:03**

**H41 10 A Novel Template Approach by MBE for ALD Growth of High k Dielectrics** K.Y. LEE, *Dept. of Mat. Sci. and Eng., National Tsing Hua Univ., Taiwan,* W.C. LEE, M.L. HUNG, Y.C. LEE, C.H. CHANG, Y.K. CHIOU, M. HONG, J. KWO, *Dept. of Phys., National Tsing Hua Univ., Taiwan.* Although growth of high k dielectrics by ALD on H-Si is feasible, it undergoes an incubation period during which the formation of SiO2 layer seems inevitable. Recently we showed the MBE growth of HfO2 on Si produced atomically abrupt interfaces, and achieved excellent electrical performance. Here we employed the MBE-grown high k dielectrics thin film as a template to suppress the interfacial layer formation during the ALD growth, and to improve the electrical properties of ALD films. The first demonstration is a bi-layer composite made of a lower HfO2 (MBE) layer 2.5nm thick, and an upper Al2O3 (ALD) film 4.0nm thick. The electrical properties are consistent with the two capacitors in series from two individual dielectric layers. The second demonstration is an MBE and ALD composite Al2O3 6.6nm thick. Studies are underway for the third structure of Al2O3 (MBE) and HfO2 (ALD) composite, which offers dual advantages of interfacial layer suppression and leakage current reduction during HfO2 recrystalization.

**13:15**

**H41 11 Dielectric Relaxation of $CaCu_3Ti_4O_{12}$ synthesized from a pyrolysis method*** JIANJUN LIU, W. N. MEI, *Department of Physics, University of Nebraska at Omaha, Omaha, Nebraska 68182-0266* R. W. SMITH, *Department of Chemistry, University of Nebraska at Omaha, Omaha, Nebraska 68182-0109* J. R. HARDY, *Department of Physics and Center for Electro-Optics, University of Nebraska, Lincoln, Nebraska 68588-0111* Giant dielectric constant material $CaCu_3Ti_4O_{12}$ has been synthesized by using a pyrolysis method. A stable solution was made by dissolving calcium nitrate, copper nitrate, and titanium isopropoxide in 2-methoxyethanol; the solution was then heated at 500 and 700 $^oC$ for 2 hours to obtain a pure phase of $CaCu_3Ti_4O_{12}$. The frequency and temperature dependences of dielectric permittivity were examined in the ranges of $10^{-1} \sim 10^6$ Hz and -150 $\sim$ 200 $^oC$. We found that the dielectric properties of the sample were the same as those made from solid state reaction. Specifically, there is a Debye-like relaxation at low temperature and its giant dielectric constant about 11000 is independent of the temperature and frequency over a wide range.

*This work was supported by the Nebraska Research Initiative and the U.S. Army Research Office under grant No. DAAD 19-02-1-0099.

**13:27**

**H41 12 Cathodoluminescence Studies of Rare Earth Ions in $LiNbO_3$ and GaN*** S. TAFON PENN, ZACK FLEISCHMANN, *Dept. of Physics, Lehigh University* G.S. CARGILL, *Dept. of Material Sciences, Lehigh University* V. DIEROLF, *Dept. of Physics, Lehigh University* In most host materials, rare earth ions have intra-atomic transitions that exhibit a sensitivity to the local environment through the crystal field splitting of their Stark sub-levels and the modification of the free ion parameters (e.g.: Slater parameters). Moreover, in crystals that lack inversions symmetry the transitions exhibit linear Stark shifts that makes them good probes for local electric fields that are created for instance by local charging and a ferroelectric domain inversion. We present cathodoluminescence emission spectra of $Eu^{3+}$ ions and $Er^{3+}$ in two host materials ($LiNbO_3$ and GaN) for a temperature range between 12 and 300K using the electron beam in JEOL JSM-6400 SEM with a voltage of 10keV, various beam currents and beam scanning modes. We observe a pronounced saturation effect in the emission of the rare earth ions that depends on details of the scan mode, the electron beam deflection frequency, and magnification. The saturation effect is absent in the intrinsic emission of GaN that is recorded simultaneously. We will present an interpretation of the effect that takes into account charging effects and the excitation and relaxation dynamics of the free carriers and the rare earth ions.

*Supported by ARO-grant W9111NF-04-1-0323

**13:39**

**H41 13 Electronic Structure Calculations of BiFeO3*** DAVID SULOCK, LUCAS K. WAGNER, LUBOS MITAS, *North Carolina State University* Bismuth Ferrite (BiFeO3) is a potentially useful material because it exhibits both ferroelectricity and antiferromagnetism, providing a link between magnetic and ferroelectric action in the same material. Experimentally BiFeO3 has been reported to have a spontaneous polarization ranging from.06 C/m2 to 1.50 C/m2, possibly indicating a large dependence on experimental setup. Theoretical efforts thus far within Density Functional Theory in the LDA approximation have settled on a value of around 0.95 C/m2; however, it is not clear that LDA provides a sufficient description of the material as it predicts a lattice constant in error by .2 angstroms and zero band gap for some parts of the ferroelectric distortion. To check the results provided by LDA we use Quantum Monte Carlo (QMC), which allows us to treat the system in a fully correlated way. We use the Reptation Monte Carlo algorithm of Moroni and Baroni to calculate the polarization and other properties, allowing us to then evaluate the accuracy of QMC versus LDA.

*Supported by NSF and ONR

**13:51**

**H41 14 Calculated polarizations and piezoelectric constants of wurtzite ZnO, CdO and MgO** PRIYA GOPAL, *UCSB* The macroscopic polarization in wurtzite crystal structures such as GaN and ZnO has a strong influence on the electrical and optical properties. This property has been exploited in GaN/AlGaN heterostructures, where the difference in the polarizations between layers induces an electric field at the interface forming a high mobility two-dimensional electron gas (2DEG)[1]. Here we calculate the polarization and the piezoelectric properties of the corresponding wurtzite-structure binary oxides ZnO, MgO and CdO. The knowledge of these properties is essential to explore the possibility of creating similar high mobility polarization induced 2DEGs in the ZnO-based material system. However, since wurtzite-structure MgO and CdO are not experimentally accessible, the values can be obtained computationally. We use the recently developed self-interaction corrected pseudopotential (pseudo-SIC) implementation[2] of the density functional theory and the widely used Berry phase method[3] for obtaining the polarization and piezoelectric constants. We find that the polarization gradients between the end-point compounds in the MgO-ZnO-CdO are larger[4] than in the GaN analogues.

[1]U. K. Mishra,Y. Wu, B.P. Keller, S. Keller and S.P. Denbaars IEEE Transactions on Microwave theory and Techniques, **46**, 6 (1998)
[2]A. Filippetti and N.A. Spaldin Phys. Rev. B **67**, 125109 (2003).
[3]R. D. Kingsmith and D. Vanderbilt Phys. Rev. B **49**, 5828 (1994).
[4]P. Gopal and N.A. Spaldin submitted

**14:03**

**H41 15 A More Accurate Generalized Gradient Approximation for Solids*** ZHIGANG WU, RONALD E. COHEN, *Carnegie Institution of Washington* We present a new nonempirical density functional generalized gradient approximation (GGA) based on a diffuse radial cutoff for the exchange-hole in real space and the analytic gradient expansion of the exchange energy for small gradients. There are no adjustable parameters, the constraining conditions of PBE are maintained, and the functional is easily implemented in existing codes. For the 18 testing solids including simple and transition metals, and ionic and covelent crystals, the new functional improves equilibrium lattice constants and bulk moduli significantly over the most popular Perdew-Burke-Ernzerhof (PBE) GGA and the local density approximation (LDA), and its accuracy for cohesive energies is similar to PBE. It also predicts highly accurate ground states of ferroelectrics, better metal surface energies and sublimation energy of ice than PBE and LDA, and correct ground states of magnetic iron and alpha quartz.

*This work was supported by the Center for Piezoelectrics by Design (CPD) and the Office of Naval Research (ONR) under ONR Grants No. N00014-02-1-0506.



## SESSION H42: FOCUS SESSION: DYNAMIC COMPRESSION
**Tuesday Morning, 14 March 2006; 345, Baltimore Convention Center at 11:15**
**Hector Lorenzana, Lawrence Livermore National Laboratory, presiding**

***Invited Papers***

**11:15**

**H42 1 Analyzing Isentropic Compression Wave Experiments.**
DENNIS HAYES, *Sandia National Laboratories*

Some common assumptions that are used to analyze shock wave experiments are inadequate for analyzing ramp wave compression experiments. Analysis of a Doppler shift through a window usually assumes a steady wave in the window, a condition that is violated when a ramp compression wave steepens as it propagates, requiring separate consideration during the analysis (LiF to 20GPa). Introduction of a free or windowed interface produces large perturbations to the flow in the sample that must be reconciled to achieve required timing accuracy: when the specimen has a unique stress-strain compression relation, the equations of motion are hyperbolic so that stress-strain relation can be directly deduced from measurements on two samples. If the sample is hysteretic like an elastic plastic material, there is not a unique solution to the flow and a separate drive measurement is needed. Time-dependent plasticity (spall in aluminum or twinning in U6Nb) has parabolic equations and backward solutions are unstable. Analyses that compare experiment and simulation have very broad minima in the parameters used to model stress-strain; unconstrained polynomial stress-strain expansions can wander and converge to unreasonable results. Better convergence is achieved with constrained models like certain forms of the Mie-Gruneisen EOS (copper to 18GPa) but those poorly represent materials with large changes in com-

pressibility with strain (HMX to 50GPa). Maintaining small sample thickness to eliminate shock-up while maximizing thickness for accurate wave velocity measurement produces problems for designing high stress experiments and leads to hybrid experimental designs. Sandia is a multi-program laboratory operated by Sandia Corporation, a Lockheed Martin Company, for the United States Department of Energy's National Nuclear Security Administration under contract DE-AC04-94AL85000.

**11:51**
**H42 2 From solitons to shocks: entropy generation and quasi-isentropic compression.**
ROGER MINICH, *LLNL*

Recently a number of experimental platforms have demonstrated the ability to produce stress waves that have thermodynamic paths intermediate between an ideal isentrope and the Hugoniot. It is of interest to quantify the entropy generated for a given path in order to accurately determine the equation of state. Stationary propagating structures known as solitons have recently been observed in particle velocity time histories and provide insight as to how entropy is generated in quasi-isentropic flows. The origin of the structures is discussed in terms of dispersion and dissipation and a metric for quantifying the entropy generated is derived. A generalization of Lagrangian analysis is presented that allows an experimental determination of the relative contributions of nonlinear steepening, dispersion and dissipation. Finally, wavelet analysis is introduced as a powerful tool for the quantification of nonlinear wave dispersion and energy dissipation.

***Contributed Papers***

**12:27**
**H42 3 Application of Ellipsometry to Shock-Compressed Materials*** J. REED PATTERSON, JEFFREY H. NGUYEN, NEIL C. HOLMES, *Lawrence Livermore National Laboratory* Measurements of optical properties, such as the dielectric tensor, along the shock Hugoniot can be achieved in real time and *in-situ* via ellipsometry. Since standard Hugoniot-EOS and sound speed experiments do not provide crystal structure information, our knowledge of the phase diagrams of high-pressure high-temperature materials is limited. Complementary to x-ray diffraction techniques, ellipsometry of dynamically compressed materials provides data that can be coupled with calculations, yielding information on phase transitions and crystal structures. Single-wavelength ellipsometry experiments demonstrate our ability to observe solid-solid ($\alpha - Fe \rightarrow \epsilon - Fe$) and solid-liquid (e.g. Sn) phase transitions. In addition, changes in the complex index of refraction are related to changes in the strain state of a material, as observed in preliminary experiments on LiF, which demonstrated stress-incduced birefringence. Time-resolved ellipsometric measurements have the potential to provide insight into dynamic phenomena such as elastic/plastic deformation/relaxation and phase transition kinetics. We will also discuss our efforts to extend the applicability of ellipsometry of dynamically compressed materials by incorporating multiple wavelengths.

*This work was performed under the auspices of the U.S. Department of Energy by the University of California, Lawrence Livermore National Laboratory under Contract W-7405-Eng-48.

**12:39**
**H42 4 Experimental Measurement of Compression Isentropes to Multimegabar Pressures*** JEAN-PAUL DAVIS, *Sandia National Laboratories* Isentropic ramp-wave loading of condensed matter has been hailed as a potential means to obtain accurate equation-of-state (EOS) data in the solid phase at relatively low temperatures and multimegabar pressures. In this range of pressure, isothermal diamond-anvil techniques have limited accuracy due to reliance on theoretical EOS of calibration standards; accurate isentropic compression data would help immensely in constraining EOS models. An isentropic compression technique developed using the Z Machine at Sandia as a magnetic drive has been extended to the multimegabar regime. Diagnostics typically consist of time-resolved velocity interferometry to monitor the back surfaces of samples having different thickness but subjected to the same magnetic loading. A number of design and analysis issues arise when attempting to extract a stress-density curve from such data. Following a brief discussion of these issues, recent results will be presented for quasi-isentropic compression of several materials to greater than 200 GPa.

*Sandia is a multiprogram laboratory operated by Sandia Corporation, a Lockheed Martin Company, for the United States Department of Energy's National Nuclear Security Administration under contract DE-AC04-94AL85000.

**12:51**
**H42 5 Recent Advances in Tailored Dynamic Compression*** JEFFREY H. NGUYEN, JEREMY R. PATTERSON, DANIEL ORLIKOWSKI, LOUIS P. MARTIN, P. ASOKA-KUMAR, KLAUS WIDMANN, NEIL C. HOLMES, *Lawrence Livermore National Laboratory* In the past few years, the functionally graded density impactor has been used in dynamic compression experiments that are tailored to reach previously inaccessible dynamic thermodynamic states beyond the principal Hugoniot and isentrope. These experiments demonstrated complex loading paths that included a combination of shocks, quasi-isentropic compressions, and controlled releases. The quasi-isentropic compression experiments last microseconds, and are capable of bridging the timescales of static experiments and current dynamic compression experiments. Some of the interesting experiments that were carried out included phase transition and equation of state studies. Our recent efforts have been concentrated on improving reproducibility and planarity of the impactors. Here, we will report the efforts and progresses on impactor manufacturing as well as experiments characterizing these impactors. We employed both line-VISAR and multi-PDV probes to characterize the planarity of the impactor as the target undergoes tailored dynamic compression.

*Work performed under the auspices of the U.S. DOE at the University of California/Lawrence Livermore National Laboratory under contract W-7405-ENG-48.

**13:03**

**H42 6 Dynamic Response of Shock-Loaded Multi-Component Glasses*** C.S. ALEXANDER, W.D. REINHART, T.J. VOGLER, D.E. GRADY, L.C. CHHABILDAS, *Sandia National Laboratories* Glass, in various formulations, may be useful as a transparent armor material. Fused quartz ($SiO_2$), modified with either $B_2O_3$ (13 % wt.) or $Na_2O$ (15 % wt.), was studied to determine the effect on the dynamic response of the material. Utilizing powder and two-stage light gas guns, plate impact experiments were conducted to determine the effect on strength properties, including the elastic limits and plastic deformation response. Further, the effect of glass modification on known transitions to higher density phases in fused quartz was evaluated. Results of these experiments will be presented and discussed.

*Sandia is a multiprogram laboratory operated by Sandia Corporation, a Lockheed Martin Company, for the United States Department of Energy's National Nuclear Security Administration under Contract DE AC04-94AL85000.

**13:15**

**H42 7 Coherent optical photons from shock waves in polarizable crystals** EVAN REED, *Lawrence Livermore National Laboratory* MARIN SOLJACIC, *Massachusetts Institute of Technology* RICHARD GEE, *Lawrence Livermore National Laboratory* JOHN JOANNOPOULOS, *Massachusetts Institute of Technology* We predict that coherent electromagnetic radiation can be generated in polarizable crystalline materials when subject to a shock wave or soliton-like propagating excitation. To our knowledge, this phenomenon represents a new source of coherent optical radiation source in the 1-100 THz frequency range that is distinct from lasers and free-electron lasers. The radiation is generated by the synchronized motion of large numbers of atoms when a shock wave propagates through a crystal. Analytical theory, finite-difference time-domain simulations of Maxwell's equations, and molecular dynamics simulations demonstrate coherence lengths on the order of mm (at 16 THz) and potentially greater.

**13:27**

**H42 8 kinetics of solid to solid phase transitions in bismuth** RICKY CHAU, FREDERICK STREITZ, *Lawrence Livermore National Laboratory* The role of kinetics in determining the time scale for transition from one phase to another is not known, but has been cited as contributing to the often observed discrepancy between phase boundaries determined in dynamic versus static pressure experiments. In this study, we demonstrate the use of real-time electrical conductivity as a phase diagnostic by presenting preliminary measurements of the conductivity of Bi under dynamic loading conditions. By exploiting the drastic variation in electrical conductivies among the low pressure phases, we are able to correlate changes in measured conductivity with phase changes in the sample. We will discuss the observed timescale for the phase transitions as well as possible effects due to the competition of phases. In addition, we will present results from experiments where both the electrical conductivity and particle velocity profiles are measured simultaneously, allowing observation of both the bulk and the local response of the system. This work was performed under the auspices of the U.S. Department of Energy by University of California, Lawrence Livermore National Laboratory under Contract W-7405-Eng-48.

**13:39**

**H42 9 Pressure Induced Metallization of Light Group IV Hydrides** AITOR BERGARA, MIGUEL MARTINEZ-CANALES, *University of the Basque Country (UPV/EHU) and Donostia International Physics Center (DIPC)* JI FENG, *Department of Chemistry and Chemical Biology, Cornell University.* WOJCIECH GROCHALA, *Department of Chemistry, University of Warsaw.* ROALD HOFFMANN, *Department of Chemistry and Chemical Biology, Cornell University.* N.W. ASHCROFT, *Laboratory of Atomic and Solid State Physics and Department of Physics, Cornell University.* Recently reported superconductivity in lithium under pressure has renewed the interest on hydrogen and hydrogen-rich systems in the long standing conquest of room temperature superconductivity. Although the required metallization of pure hydrogen cannot be achieved within current experimental capabilities, chemical precompression exerted by heavier atoms in compounds with a large hydrogen content is expected to imply that lower pressures might be required to attain the metallic transition in these alloys. In this work we present an itab initio analysis of pressure induced metallization of methane, silane and germane, as light group IVa hydrides. According to our calculations, although metallization in methane cannot be reached at pressures lower than 400 GPa, silane and germane are predicted to become metallic at experimentally accessible pressures of around 90 GPa and 70 GPa, respectively. Possible superconducting transitions of these compounds will be also analyzed.

**13:51**

**H42 10 Core/Shell Nanocrystalline Clusters in a Glass Matrix: A High Pressure Synchrotron X-Ray Diffraction Study*** PATRICIA E. KALITA, *High Pressure Science and Engineering Center, Dept. of Physics, UNLV* GINO MARIOTTO, *Dipartimento di Fisica, Università di Trento, Italy* YOSHIMICHI OHKI, *Dept. of Electrical Eng. and Bioscience, Waseda University, Tokyo, Japan* KRISTINA E. LIPINSKA-KALITA, *Center for Nanoscale Device Research, Dept. of Electrical and Computer Eng. University of Nevada Las Vegas* Synchrotron x-ray diffraction studies up to 50 GPa were performed on an optically transparent composite with nanometer-sized $ZrTiO_4/LiAlSi_2O_6$ core/shell clusters embedded in a host glass. In the low-pressure range the shift and broadening of the x-ray diffraction lines was consistent with the densification of the $LiAlSi_2O_6$ shell phase. At higher pressures, the considerable diffraction line broadening pointed to a partial amorphization of the nanocrystalline phase. With pressure increase the x-ray patterns progressively revealed the presence of the $ZrTiO_4$ core phase. Upon decompression from 50 GPa to ambient conditions the pressure-induced changes were not fully reversible, however the diffraction pattern of the pressure-quenched material suggested that the decompressed structure carries the signature of the initial ambient $LiAlSi_2O_6$ phase.

*Use of the HPCAT facility was supported by DOE-BES, DOE-NNSA (CDAC), NSF, DODTACOM, and the W.M. Keck Foundation

**SESSION H43: FOCUS SESSION: STRONGLY INTERACTING FERMI GASES AND THE BCS-BEC CROSSOVER II**
**Tuesday Morning, 14 March 2006**
**346, Baltimore Convention Center at 11:15**
**Murray Holland, University of Colorado, presiding**

*Contributed Papers*

**11:15**
**H43 1 Understanding the Superfluid phase diagram in trapped Fermi gases*** KATHY LEVIN, QIJIN CHEN, *University of Chicago* We address previous experimental observations of the condensation of fermionic atom pairs involving trapped Fermi gases which can be tuned from the BCS to BEC regime, with the application of magnetic fields. In the intermediate regime, condensation is demonstrated experimentally by a sweep technique that pairwise projects fermionic atoms onto molecules. While the condensate fraction is measured after a fast sweep to BEC, the temperature is measured by a slow adiabatic sweep to the Fermi gas regime. In this paper we compare the normal-superfluid phase boundary in this temperature-magnetic field plane as obtained in this way for $^{40}$K and computed theoretically. We demonstrate good agreement between the two. References: arXiv:cond-mat/0411090; Phys. Rev. Lett., in production.

*NSF-MRSEC Grant No. DMR-0213745

**11:27**
**H43 2 Critical Temperature and Thermodynamic Properties of Attractive Fermions** EVGENI BUROVSKI, NIKOLAY PROKOF'EV, BORIS SVISTUNOV, *University of Massachusetts, Amherst* MATTHIAS TROYER, *ETH, Zurich* The unitarity regime of the BCS-BEC crossover can be realized by diluting a system of two-component lattice fermions with an on-site attractive interaction. We perform a systematic-error- free finite-temperature simulations of this system by diagrammatic determinant Monte Carlo. We report the data obtained on the Cray X1E ''Phoenix'' of the Oak Ridge National Laboratory. The critical temperature in units of Fermi energy is found to be $T_c/E_F = 0.152(7)$. We also report the behaviour of the thermodynamic functions, and discuss the issues of thermomentry of ultracold Fermi gases.

**11:39**
**H43 3 Dynamical Mean-Field Equations for Strongly Interacting Fermi Gas in a Trap** WEI YI, LUMING DUAN, *University of Michigan* FOCUS TEAM, We derive the time evolution equations at zero temperature for the wavefunctions of the molecular bosons and the fermion pairs in a trapped Fermi gas near a wide Feshbach resonance. The derivation of the equations is based on the variational principle and the BCS-like ansatz state: $|\Phi\rangle = \mathcal{N} e^{\int \phi_b(\mathbf{r}) \Psi_b^\dagger(\mathbf{r}) d^3\mathbf{r}} e^{\int \rho(\mathbf{r},\mathbf{r}') \Psi_\uparrow^\dagger(\mathbf{r}) \Psi_\downarrow^\dagger(\mathbf{r}') d^3\mathbf{r} d^3\mathbf{r}'} |0\rangle$. In deriving the equations, we have assumed that the external trapping potential and the wavefunction of the molecular bosons are spatially slow-varying on the length scale of the size of the fermionic atom pairs, which should be valid over a wide range on the BEC side of resonance, including the resonance point. In the bosonic region ($\mu \leqslant 0$, where $\mu$ is the chemical potential), the equations will reduce to one that resembles a Gross- Pitaevskii (GP) equation. We solve the the stationary ground state of the system at different detunings near the crossover region and self-consistently checked our assumptions. The time evolution equations provide macroscopic description for the wavefunctions of the molecular bosons and of the fermion pairs near the interesting BCS-BEC crossover region. In future studies, these equations can be used to analyze the interesting physics of vortices or the excitation spectrum in the Fermi condensate.

*Invited Papers*

**11:51**
**H43 4 Studying the BCS-BEC crossover regime with a Fermi gas of $^{40}$K atoms.**
CINDY REGAL, *JILA: NIST and the University of Colorado and Department of Physics, University of Colorado*

Recent years have seen the emergence of an intriguing Fermi system achieved with ultracold atomic gases. With these systems it is possible to widely tune the s-wave interatomic interaction strength using a Feshbach resonance. Of particular interest is the strongly interacting regime ($-1 < 1/k_F a < 1$) where a crossover between BCS theory of superconductivity and Bose-Einstein condensation (BEC) of molecules occurs. Recently experiments with $^6$Li and $^{40}$K have succeeded in studying many aspects of this superfluid Fermi system. In my talk I will discuss recent experiments performed at JILA on this Fermi system using $^{40}$K.

*Contributed Papers*

**12:27**
**H43 5 Counting Statistics of Density Fluctuations in a Quantum Gas** WOLFGANG BELZIG, *University of Konstanz, Theoretical Solid State Physics, Department of Physics, D-78457 Konstanz, Germany* CHRISTIAN SCHROLL, CHRISTOPH BRUDER, *Dept. of Physics and Astronomy, University of Basel, Klingelbergstr. 82, CH-4056 Basel, Switzerland* We investigate the statistics of density fluctuations in a coherent ensemble of interacting fermionic atoms around the BEC-BCS crossover. Adapting the concept of full counting statistics, well-known from quantum optics and mesoscopic electron transport, we study second-order as well as higher-order correlators of density fluctuations. This method is applied to the crossover from a molecular BEC state to a fermionic BCS state and yields a transition from Poissonian statistics to binomial statistics. The large Poissonian fluctuations confirm the picture of independent molecules on the BEC side of the transition. Strongly suppressed fluctuations on the BCS side reflect the correlation among Cooper pairs and the in-

ertness of a Fermi sea. In the transition region the third cumulant is a measure of the particle hole symmetry of the distribution function. The statistics can thus be used as an experimental tool to gain information on the many-body ground states.

**12:39**

**H43 6 A mean-field model for condensates in the BEC-BCS crossover regime** CHENG CHIN, *The University of Chicago* We present a new mean-field model to describe Fermionic condensates in the BEC-BCS crossover regime. By introducing an effective mean-field potential, this approach allows us to analytically evaluate the chemical potential, the equation of states, and the pair wave function. The results agree surprisingly well with recent quantum Monte Carlo calculations. Density profiles and the collective mode frequencies of a trapped gas can thus be analytically determined. In particular, the pair wave function can be expressed in terms of Airy function. We show that this wave function naturally approaches molecular wave function in the BEC limit. In the presence of strong interaction, the wave function is compressed to a smaller size, which implies an upshift of the pairing energy. This effect can be understood based on the repulsive interaction between two pairs (Petrov et al.) and has been observed in rf spectroscopy experiment. Although the mean-field approach does not explicitly include anti-symmetric fermionic correlations, it does provide a complementary picture to view the crossover physics. The validity of this approach is based on the fact that a degenerate Fermi gas constitutes the same quantum phase as that of a condensate of pairs. Both descriptions should therefore be similarly effective in the crossover. One advantage of the bosonic approach is that the molecular mean-field term can conveniently capsulate four-fermion interactions. It is, however, more difficult to do so in the BCS-type calculation.

**12:51**

**H43 7 FFLO State in a Rotating Cold Fermionic Atom System** YUN-PIL SHIM, REMBERT DUINE, ALLAN H. MACDONALD, *University of Texas at Austin* Superconductors with a large Zeeman splitting are expected to have an inhomogeneous order parameter. This Fulde-Ferrell-Larkin-Ovchinnikov (FFLO) state was proposed in the early 1960's, and recent experiments in various solid state systems have shown some progress in realizing this state. We study the FFLO state for rotating fermionic atom systems consisting of two hyperfine species with different populations. The fermi surface mismatch due to the population imbalance effectively plays the role of Zeeman splitting. In recent experiments [1,2], vortex structures were observed in rotating cold fermion systems over the whole range of the BEC-BCS crossover, but the exotic vortex structures expected for the FFLO state have yet to be observed. We use a fully quantum mechanical approach to include the Landau level quantization effect due to the rotation and present a phase diagram for superconducting phase transition with center of mass (COM) motion of the paring atoms in different Landau levels. The FFLO state is expected over small range of parameters and as the population imbalance increases, the paring condensation occurs at higher COM Landau level. [1] M. W. Zwierlein et al, Nature 435, 1047 (2005) [2] M. W. Zwierlein et al, cond-mat/0511197.

**13:03**

**H43 8 Spin-polarized fermionic superfluidity in a trap** DANIEL E. SHEEHY, LEO RADZIHOVSKY, *University of Colorado* Recent research on Feshbach resonantly paired superfluids has focused on the fate of such superfluidity upon changing the relative population of the two hyperfine states undergoing pairing. I will discuss recent work [1] showing that such imposed spin polarization frustrates pairing and leads to a rich phase diagram consisting of a polarized superfluid, phase separation, and Fulde-Ferrell-Larkin-Ovchinnikov phases. In the spatially inhomogeneous environment of a trap, the local spin polarization (magnetization) is also inhomogeneous, providing a direct signature of these phases. I will discuss this and other signatures of such phases in degenerate atom experiments. This work was supported by NSF DMR-0321848 and the Packard Foundation. [1] D.E. Sheehy and L. Radzihovsky, cond-mat/0508430.

**13:15**

**H43 9 Density profile and collective modes of the unpolarized and partially polarized trapped Fermi gas in the BCS-BEC crossover region.** THEJA DE SILVA, ERICH MUELLER, *LASSP, Cornell University* We study the zero temperature BCS-BEC crossover physics of both the unpolarized and partially polarized 2-component trapped Fermi gas near a Feshbach resonance. We investigate the spatial distribution of the partially polarized atomic system; studying superfluid and normal fluid phase separation and coexistence within a local density approximation. We calculate collective mode frequencies as a function of the interaction strength, finding quantitative agreements with experiments.

**13:27**

**H43 10 Pairing in Feshbach-resonant trapped fermionic atom gases with unequal species populations** MASUDUL HAQUE, HENK STOOF, *Utrecht University, the Netherlands* Interest in BCS-like pairing with unequal Fermi surfaces has recently been revived due to the possibility of its realization in ultracold atomic gases, and the first experimental measurements have appeared in the past few months. We briefly review zero-momentum pairing with unequal chemical potentials for the two species. We then describe effects of an external trapping potential on the pairing process, and the resulting shell structure of different phases in the trap.

**13:39**

**H43 11 Strong coupling theory for the superfluidity of Bose-Fermi mixtures** DAW-WEI WANG, *Physics Department, National Tsing-Hua University, Hsinchu, Taiwan, ROC* We develop the strong coupling theory for the superfluidity of fermion *s*-wave pairing state in a Bose-Fermi mixture. Dynamical screening, self-energy renormalization, and pairing gap function are included self-consistently in the regime where the phonon velocity is smaller than the Fermi velocity. Analytical form for the transition temperature ($T_c$) is derived within reasonable approximations. In typical $^{40}$K-$^{87}$Rb mixtures, the obtained $T_c$ is several times larger than that in the weak coupling theory and can be as high as several percents of Fermi temperature.

**SESSION H44: QUANTUM PHASE TRANSITIONS**
**Tuesday Morning, 14 March 2006**
**347, Baltimore Convention Center at 11:15**
**T. Vojta, University of Missouri, Rola, presiding**



**11:15**
**H44 1 Quantum Phase Transition in Hard-Core Bosons Due to Background Potentials** ANAND PRIYADARSHEE, JI-WOO LEE, SHAILESH CHANDRASEKHARAN, HAROLD BARANGER, *Duke University* We study the zero temperature phase diagram of hard-core bosons hopping on a two dimensional lattice under the influence of three types of background potentials: (1) staggered, (2) uniform, and (3) random (on-site disorder). Using the directed-loop quantum Monte Carlo algorithm on large square lattices, we examine the susceptibility, superfluid density, compressibility, and particle-particle correlation length. For all three types of potentials, the system undergoes a quantum phase transition from a superfluid phase at small potential to a normal phase when the applied potential is large. For a staggered or uniform potential, the transition is to an insulating phase; as expected, the staggered case shows XY universality, while the uniform case belongs to the mean field universality class with dynamic exponent z=2. In contrast, the disorder driven transition is clearly different from either of these. We find a transtion to a phase with non-zero compressibility with critical exponents $\nu \sim 1$, $\beta \sim 0.6$ and $z \sim 1.4$

**11:27**
**H44 2 Thermal Transport at the Superfluid–Insulator Transition** MIRACULOUS BHASEEN, *Oxford University* ANDREW GREEN, *University of St Andrews* SHIVAJI SONDHI, *Princeton University* We investigate the finite temperature thermoelectric response in the vicinity of the Superfluid–Insulator quantum phase transition. We present results for the Nernst coefficient in the disorder free Bose–Hubbard model.

**11:39**
**H44 3 The quasi-particle gap in a disordered boson Hubbard model in two dimensions** JI-WOO LEE, *School of Physics, Korea Institute for Advanced Study, Dongdaemun-gu, Seoul 130-722, Korea* MIN-CHUL CHA, *Department of Applied Physics, Hanyang University, Ansan, Kyunggi-do 426-791, Korea* We investigate the behavior of the quasi-particle energy gap near quantum phase transitions in a two-dimensional disordered boson Hubbard model at a commensurate filling. Via Monte Carlo simulations of ensembles with fixed numbers of particles, we observe the behavior of the gap as a function of the tuning parameter for various strength of diagonal disorder. For weak disorder, we find that gapped Mott insulating phase is sustained up to the transition point and disappears only in a superfluid, strongly supporting a direct Mott-insulator-to-superfluid transition. Bose glass behavior, insulating with vanishing gap, appears only when the strength of disorder is bigger than a critical value.

**11:51**
**H44 4 Current noise near to the 2D superconductor-insulator quantum critical point** ANDREW G. GREEN, *University of St Andrews* JOEL E. MOORE, ASHVIN VISHWANATH, *UC Berkeley* SHIVAJI L. SONDHI, *Princeton University* We consider current fluctuations near to the two-dimensional superconductor-insulator transition described by a quantum XY model. This model displays metallic conductivity at criticality. We consider the system both in thermal equilibrium and when a large electric field drives it far from thermodynamic equilibrium. As the strength of the electric field is increased, we find a crossover from thermal, Johnson-Nyquist noise (whose form is demanded by the fluctuation dissipation relation) to a high-field non-linear ''shot noise'' or Schwinger regime, where the current noise is proportional to $\sqrt{E}$. Comparison with noise in diffusive electronic systems and the possible relevance of using noise measurements in experiments on S-I systems will be discussed.

**12:03**
**H44 5 Quantum Monte Carlo studies of charged monolayer Bose fluids** EFSTRATIOS MANOUSAKIS, *MARTECH, Physics Department, Florida State University and University of Athens, Greece* KEOLA WIERSCHEM, *MARTECH, Physics Department, Florida State University* Computational studies of phase separation due to competing forces are implemented on monolayers of charged bosons above a smooth substrate (effectively a two dimensional Bose fluid). Hard-core bosons with van der Waals attraction are modeled with a Lennard-Jones potential, and to this is added a Coulomb repulsion of variable strength. The long range interparticle repulsion induces the Bose fluid to phase separate into ordered clumps of equilibrium liquid and low density gas, instead of a single domain of equilibrium liquid surrounded by its vapors. The ''clumps'' form bubbles or stripes (or a combination of these states), depending on the particle density as well as the repulsion strength. A Bose fluid with weak van der Waals attraction and large quantum fluctuations will become superfluid at low temperatures (as is the case with helium). The possibility of superfluidity in the microscopically phase separated state is also investigated. Path integral Monte Carlo is employed to include the effects of quantum fluctuations and particle permutations.

**12:15**
**H44 6 Phases, RK Points and Possible Deconfined Transitions in a Model of Bosons on the Honeycomb Lattice** ASHVIN VISHWANATH, CENKE XU, JOEL MOORE, *UC Berkeley* We consider a model of hard-core bosons (or S=1/2 spins) on the sites of the honeycomb lattice with an interaction that favors exactly three bosons per hexagon. A rich phase diagram of insulating states is obtained, which includes a solvable point of the Rokhsar-Kivelson type where the ground-state wavefunction is related to a constrained version of the three-color model. On introducing charge fluctuations a superfluid phase obtains. We study transitions between the different insulating phases and between the superfluid and insulating states utilizing a duality due to Motrunich. The unusual aspect of these transitions is that when continuous, they lead to 1/3 charged fractional excitations and an emergent U(1)xU(1) gauge structure in the vicinity of the critical point. The phase diagram of this model makes it a promising candidate for numerically studying 'deconfined' quantum criticality using Quantum Monte Carlo techiniques.

**12:27**
**H44 7 Comparison of the Superconductor to Insulator Transition in Nano-Perforated and Conventional Homogeneous Films*** M.D. STEWART, JR., JAMES M. VALLES, JR., *Dept. of Physics, Brown University* AIJUN YIN, J.M. XU, *Division of Engineering, Brown University* Near a critical resistance of 6.5 kOhms a quantum Superconductor to Insulator Transition (SIT) occurs in homogeneous ultra-thin films. We have measured this transition at dilution refrigerator temperatures in conventional

Bi/Sb films as well as Bi/Sb films that are perforated by a regular array of holes. The perforations are separated by an amount ( $\sim$ 100nm) that is much less than the penetration depth but on the same scale as the coherence length. We will compare these transitions to determine whether the macroscopic normal state sheet resistance (measured over many perforations) or the microscopic (characteristic of the links between holes) normal state sheet resistance determines whether a film is on the insulating or superconducting side of the transition. We will discuss how the results provide insight into the relative influences of vortex and quasiparticle fermionic degrees of freedom on the SIT.

*This work has been supported by the NSF through DMR-0203608, AFRL, and ONR.

**12:39**

**H44 8 Continuous Phase Transition of the Fully Frustrated 3D XY Model with a Magnetic Field in the [111] Direction*** KWANGMOO KIM, DAVID STROUD, *The Ohio State University* We study the fully frustrated three-dimensional XY model on a simple cubic lattice. This model describes a 3D array of superconducting grains in an applied magnetic field $\mathbf{H} = (\Phi_0/a^2) \times(1/2,1/2,1/2)$. Using standard Metropolis Monte Carlo simulations with periodic boundary conditions, we obtain the internal energy $U$, the specific heat $C_V$, and the helicity modulus $\gamma$ of our system. Our results support the conclusion that our system has a continuous phase transition between two liquid-like phases. Disorder in the low-temperature phase is suggested by the behavior of the vortex density-density correlation function at a very low temperature, $T = 0.01J/k_B$. By contrast, previous results for $\mathbf{H} = (\Phi_0/a^2)(1/3,1/3,1/3)$ indicate a first-order phase transition. Mean-field theory suggests a possible explanation for the liquid-like low-temperature phase: there are four degenerate unstable modes at the mean-field transition temperature $T_c^{\mathrm{MF}}$. We also use finite-size scaling and two renormalization group methods to determine the critical exponents $\alpha$, $\upsilon$, and $\nu$ for $C_V$, $\gamma$, and the correlation length $\xi$. We compare our values of these critical exponents with those for other phase transitions.

*This work was supported by NSF Grant DMR04-13395. All calculations were carried out on the P4 Cluster at the Ohio Supercomputer Center.

**12:51**

**H44 9 Noise and Phase Transitions** ZHI CHEN, CLARE C. YU, *University of California, Irvine* Noise is present in many physical systems and is often viewed as a nuisance. Yet it can also be a probe of microscopic fluctuations. There have been indications recently that the noise in the resistivity increases in the vicinity of the metal-insulator transition. But what are the characteristics of the noise associated with well-understood first and second order phase transitions? It is well known that critical fluctuations are associated with second order phase transitions, but do these fluctuations lead to enhanced noise? We have addressed these questions using Monte Carlo simulations to study the noise in the 2D Ising model which undergoes a second order phase transition, and in the 5-state Potts model which undergoes a first order phase transition. We monitor these systems as the temperature drops below the critical temperature. At each temperature, after equilibration is established, we obtain the time series of quantities characterizing the properties of the system, i.e., the energy and magnetization per site. We apply different methods, such as the noise power spectrum, the Detrended Fluctuation Analysis (DFA) and the second spectrum of the noise, to analyze the fluctuations in these quantities.

**13:03**

**H44 10 Percolation quantum phase transitions in diluted magnets** THOMAS VOJTA, *Department of Physics, University of Missouri-Rolla* JOERG SCHMALIAN, *Department of Physics and Astronomy and Ames Laboratory, Iowa State University* We show that the interplay of geometric criticality and quantum fluctuations leads to a novel universality class for the percolation quantum phase transition in diluted magnets. All critical exponents involving dynamical correlations are different from the classical percolation values, but in two dimensions they can nonetheless be determined exactly. We develop a complete scaling theory of this transition, and we relate it to recent experiments in $La_2Cu_{1-p}(Zn,Mg)_pO_4$. Our results are also relevant for disordered interacting boson systems.

**13:15**

**H44 11 Competing order in a 3D antiferromaget** KEVIN BEACH, *Boston University* It has long been believed that systems of interacting spins can support, in addition to the usual collinear Néel state, a variety of paramagnetic ground states with resonating or static valence bond order. Confirmation of their existence in candidate models has been complicated by the fact that the frustrating interactions that might support these exotic phases are generally sign problematic and not amenable to exact numerical simulation. Recent advances in projector valence bond Monte Carlo [A. W. Sandvik, Phys. Rev. Lett. **95**, 207203 (2005)], however, have expanded the limited class of models that can be simulated. This algorithm is compatible with a class of SU(2) invariant interactions that suppress antiferromagnetism. In particular, a continuous transition (a candidate for a deconfined quantum-critical point) between an antiferromagnetic and columnar bond phase in 2D can be engineered by tuning the strength of a four-spin interaction. We consider a generalization of this interaction in a 3D antiferromagnet, where it is suspected that the Néel and bond-ordered phases are separated not by a single quantum critical point but by an extended spin liquid phase. New developments for the valence bond basis allow us to calculate higher-order spin correlations, Binder cumulants, and the spin stiffness.

**13:27**

**H44 12 Néel and disordered phases of coupled Heisenberg chains*** SAMUEL MOUKOURI, *University of Michigan* We use the recently proposed two-step density-matrix renormalization group method to study the effects of frustration in Heisenberg models with $S=\frac{1}{2}$ to $S=4$ in a two- dimensional spatially anisotropic lattice. We find that the system is made of nearly disconnected chains at the maximally frustrated point, $J_d/J_\perp = 0.5$, i.e., the transverse spin-spin correlations decay exponentially. This leads to the following consequences: (i) all half-integer spins systems are gapless, behaving like a sliding Luttinger liquid; (ii) for integer spins, there is an intermediate disordered phase with a spin gap, with the width of the disordered state is roughly proportional to the 1D Haldane gap.

*This work was supported by the NSF grant No DMR-0426775

**13:39**

**H44 13 Relevance of Disorder to Critical Behavior of Antiferromagnets** OMID NOHADANI, *University of Southern California* STEFAN WESSEL, *University Stuttgart, Germany* STEPHAN HAAS, *University of Southern California* We study the magnetic-field-induced antiferromagnetic order in cubic dimer systems with bond disorder. The critical exponents, in absence of randomness, were reported to be mean-field-like in 3D. Using stochastic series expansion quantum Monte Carlo simulations at ultra-low temperatures, we investigate the relevance of disorder to the critical behavior in the vicinity of a quantum critical point. Furthermore, we demonstrate that in the presence of bond disorder, a new Bose-glass phase separates the dimer spin liquid regime from the antiferromagnetically ordered phase. Since most of the experimentally probed compounds reveal traces of disorder, our results are significant for quantum phase transition studies.

**13:51**

**H44 14 Quantum disordered phase in bond-diluted two-dimensional Heisenberg antiferromagnets** RONG YU, TOMMASO ROSCILDE,*STEPHAN HAAS, *Department of Physics and Astronomy, University of Southern California* We investigate quantum phase transitions in the spin-1/2 Heisenberg antiferromagnet on square lattices with *inhomogeneous* bond dilution. It is shown that quantum fluctuations can be continuously tuned by inhomogeneous bond dilution, eventually leading to the destruction of long-range magnetic order on the percolating cluster. We find two multicritical points at which the magnetic transition separates from the percolation transition, taking a quantum nature. Beyond these multicritical points a quantum-disordered phase appears, characterized by an infinite percolating cluster with short ranged antiferromagnetic order. In this phase, the low-temperature uniform susceptibility diverges algebraically with non-universal exponents. This is a signature that the novel quantum-disordered phase is a *quantum Griffiths phase*, as also directly confirmed by the statistical distribution of local gaps. This study thus presents evidence of a genuine quantum Griffiths phenomenon in a two-dimensional Heisenberg antiferromagnet.

*Current address: Max-Planck-Institut fuer Quantenoptik, Hans-Kopfermann-Str. 1, D-85748 Garching, Germany

**14:03**

**H44 15 Universal adiabatic dynamics in the vicinity of a quantum critical point** ANATOLI POLKOVNIKOV, *Boston University* I will discuss temporal behavior of a quantum system under a slow external perturbation, which drives the system across a second order quantum phase transition. Despite the conventional adiabaticity conditions are always violated near the critical point, the number of created excitations still goes to zero in the limit of infinitesimally slow variation of the tuning parameter. It scales with the adiabaticity parameter as a power related to the critical exponents $z$ and $\nu$ characterizing the phase transition. I will support general arguments by direct calculations for the Boson Hubbard and the transverse field Ising models.

## SESSION H45: THEORETICAL METHODS IN STRONGLY CORRELATED ELECTRON SYSTEMS

**Tuesday Morning, 14 March 2006**
**348, Baltimore Convention Center at 11:15**
**A.J. Millis, Columbia University, presiding**

**11:15**

**H45 1 Analytic derivation of the equivalence between the Gutzwiller-projected BCS Hamiltonian and the t-J model at half filling** KWON PARK, *Korea Institute for Advanced Study* A connection between quantum antiferromagnetism and high $T_C$ superconductivity is theoretically investigated by analyzing the *t-J* model and its relationships to the Gutzwiller- projected BCS Hamiltonian. In particular, it is analytically shown that the ground state of the *t-J* model at half filling (i.e., the 2D antiferromagnetic Heisenberg model) is entirely equivalent to the ground state of the Gutzwiller- projected BCS Hamiltonian with strong pairing. The relationship between the ground state of the projected BCS Hamiltonian and Anderson's resonating valence bond state (i.e., the projected BCS ground state) is discussed.

**11:27**

**H45 2 Implications of the Low-Temperature Instability of Dynamical Mean Theory for Double Exchange Systems** CHUNGWEI LIN, ANDREW MILLIS, *Department of Physics, Columbia University* The single-site dynamical mean field theory approximation to the double exchange model is found to exhibit a previously unnoticed instability, in which a well-defined ground state which is stable against small perturbations is found to be unstable to large-amplitude but purely local fluctuations. The instability is shown to arise either from phase separation or, in a narrow parameter regime, from the presence of a competing phase. The instability is therefore suggested as a computationally inexpensive means of locating regimes of parameter space in which phase separation occurs.

**11:39**

**H45 3 A continuous-time impurity solver for dynamical mean field theory*** PHILIPP WERNER, ANDREW J. MILLIS, *Department of Physics, Columbia University* MATTHIAS TROYER, *Theoretical Physics, ETH Zurich* We present a new continuous-time impurity solver for dynamical mean field theory. The method is based on a diagramatic expansion in the quadratic part of the effective action, in contrast to a previous approach [A. N. Rubtsov et al., cond-mat/0411344], which uses an expansion in the interaction part. Interactions and chemical potentials are taken into account during the Monte Carlo sampling of certain collections of diagrams. Comparison to Hirsch-Fye QMC simulations shows that the new approach allows an efficient calculation of the Greens function even at very low temperatures.

*PW and AJM acknowledge support from NSF DMR 0431350

**11:51**

**H45 4 Correlated hybridization in transition metal complexes*** ARND HUBSCH, *Max-Planck-Institut für Physik komplexer Systeme, Nöthnitzer Str. 38, 01187 Dresden, Germany* JONG-CHIN LIN, JIANPING PAN, DANIEL L. COX, *Department of Physics, University of California, Davis, CA 95616* We apply local orbital basis density functional theory (using SIESTA) coupled with a mapping to the Anderson impurity model to estimate the Coulomb assisted or correlated hybridization between transition metal

d-orbitals and ligand sp-orbitals for a number of molecular complexes. We find remarkably high values which can have several physical implications including: (i) renormalization of effective single band or multiband Hubbard model parameters for the cuprates and, potentially, elemental iron, and (ii) spin polarizing molecular transistors.

*Research supported by NSF grant PHY 0120999 (the Center for Biophotonics Science and Technology), by the US Department of Energy, Division of Materials Research, Office of Basic Energy Science, and by DFG grant HU 993/1-1.

**12:03**

**H45 5 Exactly solvable Hamiltonian for the chiral spin liquid** DARRELL SCHROETER, *Occidental College* ELIOT KAPIT, *Reed College* An exact spin Hamiltonian for the chiral spin liquid will be presented. The model starts with the quantum Hall wave function on a lattice of N sites in a toroidal geometry, a state that describes a spin liquid that violates the symmetries of parity and time reversal. A parent Hamiltonian for which the state is the exact ground state is constructed out of vector operators that annihilate the ground state. This model avoids the subtle error that has been identified [D. F. Schroeter, Ann. Phys. **310**, 155 (2004)] in Laughlin's original solution to the problem [R. B. Laughlin, Ann. Phys. **191**, 163 (1989)]. The construction of the model and its numerical verification will be presented.

**12:15**

**H45 6 Spin Glass Solution to the Double-Exchange Model in Infinite Dimensions** RANDY FISHMAN, *Oak Ridge National Lab* JUANA MORENO, *University of North Dakota* THOMAS MAIER, GONZALO ALVAREZ, *Oak Ridge National Lab* FLORENTIN POPESCU, *Florida State University* Using dynamical mean-field theory, we have evaluated the magnetic instabilities and T=0 phase diagram of the double-exchange model on a Bethe lattice in infinite dimensions. In addition to ferromagnetic (FM) and antiferromagnetic (AF) phases, we also study a broad class of spin-glass (SG) solutions with extensive entropy and short-range magnetic order. In the weak-coupling limit, a SG has a higher transition temperature than the AF phase for all fillings p below 1 and can even have a higher transition temperature than the FM phase. At T=0 and for small Hund's coupling, a SG has lower energy than either the FM or AF phases for $0.26 < p < 1$. Phase separation is absent as the Hund's coupling vanishes but appears for any non-zero value. Our T=0 phase diagram agrees remarkably well with Monte-Carlo results in two and three dimensions. The stability of a SG at T=0 can be understood by examining the interacting density-of-states, which is gapped for any nonzero Hund's coupling in an AF but only when the Hund's coupling exceeds a critical value in a SG.

**12:27**

**H45 7 Bound states, symmetry breaking, and memory effects in doped $t - J$ $Y$-junctions** JURIJ SMAKOV, SASHA CHERNYSHEV, STEVE WHITE, *UC Irvine* The effect of strong electronic correlations on the properties of the weakly doped $Y$-junctions is studied within the $t - J$ and $t - J_z$ models using an analytical Green's function approach and DMRG. It is shown that the bound state at the junction depends counter-intuitively on the strength of the correlation: the bound state exists for the range of $0 < J/t < J/t|_c$, where at $J = 0$ ($U \to \infty$) the problem maps on the free-electron one, while the bound state disappears above the critical value of $J/t|_c \approx 0.47$ as the correlations weaken. Such a bound state also shows a dynamic symmetry breaking between the legs of the junction: the charge density is distributed unevenly among the legs. It is also demonstrated that the $Y$-junction with the Ising anisotropy can exhibit peculiar type of memory effects for charge transport.

**12:39**

**H45 8 Quasiparticle self-consistent GW method applied to f systems** MARK VAN SCHILFGAARDE, ATHANASIOS CHANTIS, TAKAO KOTANI, *Arizona State University* ANDRE PETUKHOV, *South Dakota Tech* We have applied the recently-developed quasi-particle self-consistent $GW$ method (QPsc$GW$) to several f systems, Gd, GdN, GdAs, ErAs, and CeO2. The QPsc $GW$ is desigened to determine the best independent particle picture; it can cover rather wide-range of materials, semiconductor to transion metal oxides with acceptable accuracy [1] [2] without any parameters. We found that QPsc$GW$ gives reasonable description of the f level positions and exchange splitting, though it predicts unoccupied f levels a little too high. In addition, the Fermi surface analysis shows that SdH frequencies and carrier concentration are in good agreement with available experimental data. [1] Mark van Schilfgaarde, Takao Kotani, and Sergey V. Faleev, cond-mat/0510408 [2] A. N. Chantis, Mark van Schilfgaarde, Takao Kotani, cond-mat/0508274.

**12:51**

**H45 9 Fermi arcs and hidden zeros of the Green function in the pseudogap state** TUDOR STANESCU, *University of Illinois at Urbana Champaign* GABRIEL KOTLIAR, *Rutgers University* We investigate the evolution of the low energy properties of a correlated metal in the proximity of a Mott insulator within the planar Hubbard model. We use a generalized version of the Cellular Dynamical Mean Field Theory having cumulants as the basic irreducible objects for re-constructing the lattice quantities from their cluster counterparts. We find that the zero temperature one particle Green function is characterized by the appearance of lines of zeros, in addition to a Fermi surface which changes topology as a function of doping. We show that these features are directly related to the opening of a pseudogap in the one particle spectrum and provide a simple picture for the appearance of Fermi arcs.

**13:03**

**H45 10 Incompressible Quantum Liquids and New Conservation Laws** ALEXANDER SEIDEL, HENRY FU, DUNG-HAI LEE, JOEL MOORE, *Materials Sciences Division, Lawrence Berkeley National Laboratory, Berkeley, CA 94720* JON MAGNE LEINAAS, *Department of Physics, University of Oslo, P.O. Box 1048 Blindern, 0316 Oslo, Norway* We discuss a class of Hamiltonians which, in addition to the usual center-of-mass (CM) momentum conservation, also have center-of-mass position conservation. We find that regardless of the particle statistics, the energy spectrum is at least $q$-fold degenerate when the filling factor is $p/q$, where $p$ and $q$ are coprime integers. Interestingly, the simplest form of Hamiltonian respecting this type of symmetry encapsulates two prominent examples of novel states of matter, namely the fractional quantum Hall liquid and the quantum dimer liquid. We explore the connection to the Hall liquid in some detail, and also discuss the possible relevance of this class of Hamiltonian to the search for featureless Mott insulators.

**13:15**

**H45 11 High-Temperature Criticality in Strongly Constrained Quantum Systems*** CLAUDIO CASTELNOVO, CLAUDIO CHAMON, *Boston University Physics Department* CHRISTOPHER MUDRY, *Paul Scherrer Institut* PIERRE PUJOL, *Ecole Normale Superieure de Lyon* The exotic nature of many strongly correlated materials at reasonably high temperatures, for instance cuprate superconductors in their normal state, has lead to the suggestion that such behavior occurs within a quantum critical region where the physics is controlled by the influence of a phase transition down at zero temperature. Such a scenario can be thought of as a bottom-up approach, with the zero temperature mechanisms finding a way to manifest critical behavior at high temperatures. Here we propose an alternative, top-down, mechanism by which strong kinematic constraints that can only be broken at extremely high temperatures are responsible for critical behavior at intermediate but still high temperatures. This critical behavior may extend all the way down to zero temperature, but this outcome is not one of necessity, and the system may actually order at low temperatures. We provide explicit examples of such high-temperature criticality when extra strong interactions are added to quantum Heisenberg, transverse field Ising, and some lattice bosonic models.

*This work is supported in part by the NSF Grants DMR-0305482 and DMR-0403997

**13:27**

**H45 12 Search for ferromagnetism in a generalized Hubbard model with disorder** ERIK NIELSEN, R.N. BHATT, *Dept. of Electrical Engineering, Princeton University* While the Hubbard model on a hypercubic lattice in two and three dimensions is believed to have a ferromagnetic phase away from half filling, its extent and precise location has remained controversial. With the introduction of positional disorder, a random singlet/valence-bond glass state is stabilized at half filling over the conventional antiferromagnetic phase, which could lead to a considerable reduction in the regime of ferromagnetism. In this study, we have used a variety of numerical techniques, including exact diagonalization of small systems and numerical mean field methods to search for the possibility of ferromagnetism in a generalized Hubbard model with and without positional disorder, aimed at the system of hydrogenic centers in semiconductors. We will present our results showing the effects of positional disorder, of electron-hole asymmetry, and other properties applicable to real experimental systems of doped semiconductors. The possibility of setting up a renormalization scheme as for the half-filled case will be discussed.

**13:39**

**H45 13 Quantum Phase Transitions of Hard-Core Bosons on the Kagome Lattice** S. V. ISAKOV, *University of Toronto* R. G. MELKO, *Oak Ridge National Laboratory* K. SENGUPTA, *Saha Institute of Nuclear Physics* S. WESSEL, *University of Stuttgart* YONG BAEK KIM, *University of Toronto* We study hard-core bosons with nearest-neighbor repulsion on the kagome lattice at different filling factors using quantum Monte Carlo simulations and a dual vortex theory. At half-filling, the ground state of the system is always a uniform superfluid in contrast to the case of the triangular lattice. There exists a quantum phase transition from a superfluid to a valence bond solid phase away from half-filling. The possibility of unusual quantum criticality is investigated.



## SESSION H46: FOCUS SESSION: WIDE BAND GAP SEMICONDUCTORS IV

**Tuesday Morning, 14 March 2006; 349, Baltimore Convention Center at 11:15**
**Michael Stavola, Lehigh University, presiding**

***Invited Papers***

**11:15**

**H46 1 Gallium Nitride-Based Nanowire Radial Heterostructures for Nanophotonics.**
FANG QIAN, *Harvard University*

Semiconductor nanowires are attractive building blocks for the assembly of active photonics devices, providing a unique and flexible pathway for creating multicolor integrated nanophotonic systems beyond the limit of conventional planar structures. Realizing this potential will require novel electrically driven and interconnected nanowire building blocks with emission wavelengths that can be rationally tuned. To achieve this goal, we have exploited the controlled growth of well-defined GaN-based nanowire radial heterostructures, and their application as efficient and synthetically tunable multicolor light sources. Prepared by metal-organic chemical vapor deposition, these nanowire heterostructures consist of an n-GaN core and diverse multishells, including n-GaN/InGaN/p-GaN double heterostructures, n-GaN/InGaN/GaN/p-AlGaN/p-GaN single quantum well, and n-GaN/(InGaN/GaN)m/p-AlGaN/p-GaN multi-quantum well structures, where variation of indium mole fraction is used to tune emission wavelength. Transmission electron microscopy analysis shows that these nanowires are dislocation-free single crystals with triangular cross-sections and chemically distinct shells, while composition and thickness of individual shells are well controlled during synthesis. Under optical excitation, they exhibit strong photoluminescence consistent with bandgap emission of InGaN inner shell, and behave as freestanding Febry-Pérot optical cavities. Moreover, by contacting simultaneously n-GaN core and p-GaN shell, electroluminescence results demonstrate that in forward bias they function as high-brightness light-emitting diodes with tunable emission from 365 to 600 nm and high quantum efficiencies. The ability to synthesize rationally GaN-based nanowire radial heterostructures as electrically-driven, efficient and color-tunable light sources should open up significant potential for integrated photonics.

*Contributed Papers*

**11:51**

**H46 2 GaN nanorods grown on Si(111) substrates by plasma-assisted molecular beam epitaxy** CHING-LIEN HSIAO, LI-WEI TU, TONG-WEI CHI, MIN CHEN, *Department of Physics and Center for Nanoscience and Nanotechnology, National Sun Yat-Sen University, Kaohsuing 80424, Taiwan, Republic of China* Various GaN nanorod structures grown on Si(111) substrate are realized by plasma-assisted molecular-beam epitaxy. Evolution of the nanorod structure from isolated regular nanorods, to isolated non-regular nanorods, and to dense nanorods is well controlled by the GaN buffer structure. Adding the parameter of beam-equivalent pressure of N/Ga ratio to the nanorod growth, the density of the regular nanorod becomes also a controllable item. There are several combinations of rod density and diameter in the nanorod growth. High density-small diameter and low density-large diameter can be grown directly on the surface without buffer layer. Low density-small diameter, low density-large diameter, and high density-large diameter can be achieved by inserting a GaN buffer. Nanorod of single crystal wurtzite structure without dislocation was characterized by high-resolution transmission electron microscopy. Only Ga and N signals were detected by energy-dispersion x-ray spectroscopy analysis. Single freestanding nanorod was prepared to perform micro-Raman spectroscopy. Wurtzite-type Raman modes at different scattering configurations have small line width and indicate the high crystalline quality of the nanorod. Frölich interaction and the surface vibrational modes are observed at high laser power densities which will be discussed in detail.

**12:03**

**H46 3 GaN Overgrowth on GaN Nanocolumns by Molecular Beam Epitaxy*** K. L. AVERETT, J. E. VAN NOSTRAND, J. BOECKL, *Materials and Manufacturing Directorate* R. CORTEZ, J. D. ALBRECHT, *Sensors Directorate, Air Force Research Laboratory, Wright-Patterson Air Force Base, OH* GaN nanocolumns grown by plasma-assisted molecular beam epitaxy are explored as host structures for overgrowth of bulk-like GaN films. We investigate the layers of vertical GaN nanocolumns 90 $\pm$ 10nm in width which were grown on sapphire and alternate substrates. We present photoluminescence, x-ray diffraction, and microscopy data that indicates that the columns are unstrained, low-defect wurtzite GaN nanostructures. The nanocolumns form discontinuous layers with areal densities controlled by grown conditions. The nanocolumn layers are subsequently overgrown with thick GaN films and compared with commercial GaN template materials used for device fabrication. The overgrowth of GaN is studied as a function Ga flux and growth temperature. We present photoluminescence and Hall effect characterization of the overgrown layers. The microstructure and morphology are probed by atomic force, scanning and transmission electron microscopy, as well as x-ray diffraction.

*Supported by the Air Force Office of Scientific Research.

**12:15**

**H46 4 Growth of ZnO Nanotube without catalyst and templates** YOKE KHIN YAP, *Michigan Tech University* SAMUEL MENSAH, *Michigan Tech University* VIJAYA KAYSTHA, *Michigan Tech University* Nanotubular structures of oxides materials have recently gained attention for their hydrophilic properties. These oxide nanotubes are attracting interest for biological applications including nanofuidic devices for single DNA molecule sensing, rapid disease diagnosis and DNA sequencing. Here we show that tubular cavities of ZnO can be directly grown on substrates without the use of catalyst and templates. This is obtained by the evaporation and the condensation of a mixture of ZnO and graphite powders in a double-tube vapor-phase transport system. Field-emission scanning electron microscopy (FESEM), high-resolution transmission electron microscopy (HRTEM), X-ray powder diffraction, Raman spectroscopy and photoluminescence (PL) were employed to study and characterize the tubular structures. Results show that these tubular structures were single crystals of pure hexagonal Wurtzite structure. Our results show that rapid cooling rate and deficiency of oxygen during cooling contributed to the tubular ZnO nanostructures. A growth model and possible reasons for the growth of ZnO nanotubes will be discussed at the meeting.

**12:27**

**H46 5 Growth of ZnO Nanowires without the mixture of other ZnO nanostructures** SAMUEL MENSAH, *Michigan Tech University* VIJAYA KAYSTHA, *Michigan Tech University* YOKE KHIN YAP, *Michigan Tech University* We describe a new procedure to grow pure ZnO nanowires without the mixture of other ZnO nanostructures like nanobelts and nanocombs. A variety of ZnO nanostructures have been grown on oxidized Si substrates by a vapor phase transport process at temperatures ranging from 900 –500 deg. C. A mixture of ZnO and graphite powders are used as raw materials and result in the growth of nanobelts, nanocombs, and nanorods at various temperature zones when Au catalysts are used. We found that pure ZnO nanowires can be grown on catalyst free substrates. This is obtained at the temperature zone 500 to 600 deg. C, a region beyond those for growing nanobelts and nanorods. The crucial step is the need of an Au-coated substrate adjacent to the plain substrates. Long nanowires with uniform diameter less than 50 nm were obtained. Field-emission scanning electron microscopy (FESEM) analysis shows that the gold vapor from the adjacent substrates creates the nucleation sites on the catalyst free substrates to initiate the nanowire growth. Characterization of these ZnO nanostructures was conducted by X-ray powder diffraction (XRD), high-resolution transmission electron microscopy (HRTEM), Raman spectroscopy and photoluminescence (PL). Details of these will be discussed in the meeting.

**12:39**

**H46 6 Exceptionally Bright Visible-wavelength Luminescence from Sulfur-doped ZnO Nanowires** JOHN V. FOREMAN, *U.S. Army Aviation and Missile RDEC, Redstone Arsenal, Alabama 35898 and Department of Physics, Duke University, Durham, North Carolina 27708* HONGYING PENG, *Department of Physics, Duke University* JIANYE LI, *Department of Chemistry, Duke University* SOOJEONG CHOI, *Department of Physics, Duke University* HENRY O. EVERITT, *U.S. Army Aviation and Missile RDEC and Department of Physics, Duke University* JIE LIU, *Department of Chemistry, Duke University* Sulfur-doped ZnO nanowires have been grown by the vapor-liquid-solid technique using ZnS and carbon as starting materials. The broadband, visible-wavelength emission of unprecedented brightness from these nanowires is characterized by steady-state and time-resolved spectroscopy. Energy transfer is explored by simultaneously studying the fast ( $<$ 50 ps) decay of band edge emission and the slow ( $>$ 5 ns) decay of the visible-wavelength emission as a function of temperature and excitation intensity. The contributions of sulfur doping and nanostructuring to the generation of this intense visible-wavelength emission are clarified by characterizing

ZnO nanowires and micropowders of different morphologies and dopant concentrations. The results can be understood in terms of a physically motivated rate equation model, for which several of the key parameters are experimentally constrained.

**12:51**

**H46 7 Optical properties of AlGaN/AlGaN microcavities containing GaN quantum wells** OLEG MITROFANOV, STEFAN SCHMULT, MICHAEL MANFRA, MICHAEL SERGENT, *Bell Labs, Lucent Technologies* RICHARD MOLNAR, *Lincoln Lab, MIT* The large oscillator strength and binding energy of excitons in GaN make GaN based microcavities attractive for studies of light-matter coupling. Lattice mismatch within the family of Nitride alloys, however, results in formation of many extended defects, which degrade optical quality of heterostructures and substantially increase inhomogeneous broadening of excitons. We will discuss optical properties of AlGaN/AlGaN microcavities for the spectral region around 350 nm grown by molecular beam epitaxy on thick GaN templates. The structural quality of the microcavities is maintained by compensating the compressive and tensile strains in the layers of the distributed Bragg reflectors (DBR). This approach results in the lowest elastic strain energy and allows the growth of thick coherently strained DBRs with reflectivity higher than 99%. We will present photoluminescence studies on GaN quantum wells incorporated inside microcavities and discuss exciton-photon coupling.

**13:03**

**H46 8 Studies of Enhanced Internal Quantum Efficiency of Photoluminescence from $Al_xGa_{1-x}N$ Alloys Displaying Nanoscale Compositional Inhomogeneities** GREGORY A. GARRETT, A. V. SAMPATH, C. J. COLLINS, W. L. SARNEY, H. SHEN, M. WRABACK, *US Army Research Lab, Sensors and Electron Devices Directorate, Adelphi, MD* AlGaN epilayers, grown by plasma-assisted molecular beam epitaxy, show internal quantum efficiency (IQE) for photoluminescence (PL) much higher than expected for growth on sapphire where high defect densities ( $> 10^{10}$ $cm^{-2}$) are generated. Results are similar to earlier successes seen in blue- green light emitting diodes (LEDs) incorporating InGaN active regions where carrier localization is seen due to indium segregation. With no predicted immiscibility gap for aluminum in GaN and no observed aluminum segregation, the IQE increase in our AlGaN layers is attributed to localization of carriers to regions of nanoscale compositional inhomogeneities (NCI) that inhibit movement of carriers to nonradiative sites. Subpicosecond time-resolved PL, using gated downconversion in a nonlinear optical crystal, is used to measure carrier capture dynamics from the bulk epilayers into these NCI regions. Rate equation modeling is used to estimate the density of NCI regions and to help understand the observed changes in IQE for NCI AlGaN epilayers grown under different conditions.

**13:15**

**H46 9 Wide bandgap semiconductor nanoclusters: Magnetism and UV photoluminescence** JIJI ANTONY, *University of Idaho* DAVID E. McCREADY, MARK ENGELHARD, CHONGMIN WANG, *Pacific Northwest National Laboratory* AMIT SHARMA, JOSEPH NUTTING, DANIEL MEYER, YOU QIANG, *University of Idaho* PACIFIC NORTHWEST NATIONAL LABORATORY COLLABORATION, Transition metal-doped ZnO is of great interest to current research due to its wide variety of applications in spintronic materials. We prepared 5% Ti, V, Co or Ni-doped ZnO nanoclusters using a third generation nanocluster source. TEM images show that the nanoclusters are monodispersive with a nanocrystalline size $<$ 10 nm. XRD patterns are identical to the bulk ZnO wurtzite structure. XPS detected the dopant elements in clusters and showed Ti in +4 oxidation state, V in +4 and +5, Co in +2, and Ni in +2 and +3. These analyses indicate that dopant elements do not exist as independent aggregates but are incorporated into the ZnO structure. All the doped ZnO nanoclusters are ferromagnetic above room temperature. Magnetic moments of Ni or V-doped ZnO are much larger than Ti or Co doped ZnO clusters at 300K. Double exchange interactions due to the mixed valance states can be the reason that Ni or V-doped ZnO clusters a better magnetic moment than the Ti or Co-doped clusters. UV-photoluminescence is observed at pure and low dopant concentration ZnO nanoclusters.

**13:27**

**H46 10 Microbeam High Resolution X-ray Diffraction and Reciprocal Space Mapping Characterization of Selective Area Grown InGaN/GaN Waveguides** A.A. SIRENKO, *New Jersey Institute of Technology* A. KAZIMIROV, S. CORNABY, D. H. BILDERBACK, *Cornell High Energy Synchrotron Source, CU* A. OUGAZZADEN, *Georgia Institute of Technology, GTL/Metz, France* B. NEUBERT, F. SCHOLZ, *Universitaet Ulm, Germany* We present microbeam high-resolution x-ray diffraction (HRXRD) and Reciprocal Space Mapping (RSM) analysis of InGaN/GaN-based MQW ridge-waveguide arrays for monolithically integrated optoelectronic devices. InGaN/GaN waveguides were produced by the MOVPE technique in the Selective Area Growth (SAG) regime with the width of 6 microns and the oxide mask widths varied between 2 and 14 microns. Synchrotron Radiation-based triple- axis HRXRD measurements with the angular resolution of 13 arcsec were carried out at CHESS with the x-ray beamsize of 10 microns. Strain, thickness, and Indium composition variation in the active region of the ridge waveguides have been measured for different configurations of the SAG mask. Gas-phase diffusion coefficients have been determined for In and Ga precursors. Strain-induced relaxation effects in the active regions have been studied using RSM analysis.

**13:39**

**H46 11 Magnetotransport investigation of spin-orbit interactions in high-mobility GaN/AlGaN heterostructures.** STEFAN SCHMULT, MICHAEL MANFRA, ALEX PUNNOOSE, MICHAEL SERGENT, *Bell Laboratories, Lucent Technologies* RICHARD MOLNAR, *MIT, Lincoln Laboratory* Spin-splitting in the conduction band of a two-dimensional electron gas (2DEG) in GaN/AlGaN single interface heterostructures with mobilities of $\sim$ 80.000$cm^2$/Vs is investigated utilizing low field magnetoconductivity measurements. The observation of a distinct antilocalization feature near zero magnetic field signals the presence of significant spin-orbit coupling. A spin-orbit coupling value in the Rashba formalism of $6x10^{-13}$eVÅ is extracted. For a typical 2DEG density of $\sim 10^{12}cm^{-2}$ this value of the coupling strength corresponds to a spin-splitting energy of 0.3meV at the Fermi edge. The observed value is unexpectedly high for a wide-bandgap semiconductor. This talk summarizes our studies of the carrier density, mobility, and temperature dependence of the magnetoresistance data.

**13:51**

**H46 12 Low-temperature peculiarities of AlGaN/GaN heterostructure transport.*** ANDRIY KURAKIN, SVETLANA VITUSEVICH, SERHIY DANYLYUK, NORBERT KLEIN, *Forschungszentrum Juelich, ISG 2, Germany* ALEXANDER BELYAEV, *Institute of semiconductor physics, Kiev, Ukraine* At present, AlGaN/GaN heterostructures are attracting a lot of scientific interest in semiconductor research and are extensively studied. Despite this there are a number of open questions concerning the low temperature properties of such systems with two-dimensional electron gas (2DEG). We report here our recent results on transmission-line model (TLM) patterns and high electron mobility transistor (HEMT) measurements in the temperature range of 0.3-10.0 K. A set of samples with different Al fractions of the barrier layer, wide bandgap spacer and different substrates were tested. It is important that accurate information on 2DEG systems becomes available with the systematic analysis of current-voltage characteristics of TLM patterns. The latter enables channel resistance to be extracted from total device resistance. It was found that channel conductance in low electric field shows metal-like temperature dependence. The peculiarities observed in low-temperature characteristics of AlGaN/GaN heterostructures are analyzed.

*The research is supported by Deutsche Forschungsgemeinschaft (Project KL 1342)

**14:03**

**H46 13 Electron Mobility in InGaN and InAlN Alloys** LEON HSU, *University of Minnesota* WLADEK WALUKIEWICZ, *Lawrence Berkeley National Laboratory* III-Nitride alloys containing In offer the possibility of engineering materials with bandgaps as small as 0.7 eV. We have calculated electron mobilities in InGaN and InAlN alloys taking into account the standard scattering mechanisms of acoustic and optical phonons, Coulomb scattering from charged impurities, and alloy disorder scattering. Effects of the non-parabolicity of the conduction band have also been included. We compare our calculations with experimental results on composition and concentration dependencies of the electron mobility in as-grown and in high-energy particle irradiated materials. This work was partially supported by the US DOE under Contract No. DE-AC03-76SF00098.

**SESSION J1: POSTER SESSION II**
**Tuesday Afternoon, 14 March 2006**
**Exhibit Hall, 2:00pm–5:00pm Baltimore Convention Center at 14:00**

**J1 1 METALS POSTER SESSION**

**J1 2 Mechanical Spectral Hole Burning – A Technique to Characterize Dynamic Heterogeneity*** XIANGFU SHI, QIAN QIN, GREGORY MCKENNA, *Texas Tech University* The Mechanical Spectral Hole Burning (MSHB) technique was developed and initially used to qualitatively characterize dynamic heterogeneity of polymer melts and solutions. Here we attempt to develop a quantitative relationship between the heterogeneity and the length scale, by developing a ''calibration'' for the dynamic heterogeneity, i.e. the frequency and magnitude of the burned hole and the size or length scale. Here we consider the local heterogeneity and well characterized structures of macroscopically homogeneous systems, such as miscible polymer blends and block copolymers in the disordered state, but approaching the phase boundary. We interrogate these materials using the MSHB method at different temperatures going through the phase boundary. Presently and for a styrene-isoprene-styrene triblock copolymer, we find that the hole amplitudes increase as the phase boundary is approached from the one-phase region, i.e., as the order-disorder transition is approached. Further work is ongoing to use miscible blends and other block copolymer systems to determine if the MSHB response can be related quantitatively to the known heterogeneities of the systems.

*Thanks to the ACS-PRF grant # 40615-AC7 for support of this project.

**J1 3 Ferromagnetic single-electron transistors fabricated by atomic force microscopy*** RUISHENG LIU, HAKAN PETTERSSON, *Center for Applied Matematics and Physics, Halmstad University, Sweden* LUKASZ MICHALAK, CARLO CANALI, *Div. of Physics Dept of Chemistry and Bimedical Sciences, Kalmar University, Sweden* LARS SAMUELSON, *Solid State Physics/Nanometer Consortium, Lund University, Sweden* We report on the fabrication and magneto-transport measurements of Ni/Au/Ni ferromagnetic single-electron transistors (F-SETs), fabricated by atomic force microscopy. By positioning a single Au disc (30 nm in diameter) into the gap between the Ni drain and source electrodes (of width 220 nm and 80 nm, respectively) step-by-step with Angstrom precision, and using plasma-processed $NiO_x$ as tunneling barriers, we can successfully fabricate F-SETs of high quality and substantial stability. The characteristic time interval of the device between two successive tunneling events is $\sim$ 10ps. The absence of any clear features in the transport related to the applied external magnetic field indicates that no spin-accumulation is maintained in the central Au disc. This interesting result indicates that the spin-relaxation time inside the central island should be shorter than 10ps. Based on these findings, we will discuss possible mechanisms of spin-relaxation in metal nanostructures triggered by spin-orbit interaction.

*This work is supported by the SSF as well as by VR in Sweden.

**J1 4 Molecular dynamics simulations of equilibrium and undercooled liquid Ni*** ALVARO POSADA-AMARILLAS, EFRAÍN URRUTIA-BAÑUELOS, ROBERTO NÚÑEZ-GONZALEZ, *Universidad de Sonora* I.L. GARZÓN, *Universidad Autonoma de México* Molecular dynamics computer simulations were performed for equilibrium and undercooled liquid Ni. The Gupta potential was used to mimic the interatomic metallic interaction for different thermodynamic states. The inherent structures formalism is used to explore the potential energy landscape, showing a competition between periodic crystalline order (fcc, rhcp and bcc) and regular and distorted icosahedral order. For undercooled liquid Ni, a correlation between the entropy and the change in the crystalline (fcc) and icosahedral order is shown. This is the first simulation study which shows an interplay between the

microstructural ordering in undercooled liquid metals and the entropy of the system.

*Acknowledge to POMEP for support and Dirección de Investigación y Posgrado, UNISON for computational resources on ACARUS

**J1 5 Elastic properties and phase stability of AgCl under external pressure*** ALEJANDRO BAUTISTA-HERNÁNDEZ, PEDRO H. HERNÁNDEZ, GREGORIO HERNÁNDEZ-COCOLETZI, J. FRANCISCO RIVAS-SILVA, *Universidad Autónoma de Puebla* Ab initio total energy calculations have been performed to study AgCl phase stabilities. Our calculations are done using the density functional theory within the local density approximation, for the exchange and correlation energies. The ion-electron interactions are treated with the Troullier-Martins pseudopotentials. We determine the equation of state and free energy in the B1 (NaCl) and B2 (CsCl) phases. To obtain the elastic constants, we take the second derivative of the total energy respect to the applied deformations in both B1 and B2 phases. Our calculated structural parameters of the phases B1 and B2 of AgCl are compared with those available experimental data and theoretical calculations based on the local density approximation. The stability analysis based on elastic coefficients yields a critical pressure of 6 GPa at which the ideal lattice of B1 structure becomes unstable against homogeneous tetragonal shear deformation. The B2 structure is unstable in the interval of pressures 0-25 GPa. Therefore, a pressure induced phase transition between the structures B1 and B2 is not allowed elastically. We also explore the atomic structure of AgCl in the KOH phase.

*PROADU (SEP-CONACyT), Grant 2003-01-21-001-051 and VIEP28/G/EXC/05.

**J1 6 Single-Wall Gold Nanotubes** R. TUGRUL SENGER, *Bilkent University, Turkey* SEFA DAG, *Oak Ridge National Laboratory, USA* SALIM CIRACI, *Bilkent University, Turkey* In recent ultra-high-vacuum transmission-electron-microscopy experiments evidence is found for the formation of suspended single-wall nanotubes (SWNTs) of gold. Similar to carbon nanotubes, the (n,m) notation defines the structure of the gold SWNTs. Experimentally, only the (5,3) tube has been observed to form among several other possible alternatives. Using first-principles calculations we demonstrate that gold atoms can form both freestanding and tip-suspended, chiral, single-wall nanotubes. Although freestanding, infinite (5,5) tube is found to be energetically the most favorable, the experimentally observed suspended (5,3) tube corresponds to a local minimum in the variation of wire-tension with the radius of the structure, which explains the experimental finding. Similarly, we predict the (4,3) tube as a favorable structure yet to be observed experimentally. Analysis of band structure, charge density, and quantum ballistic conductance suggests that the current on these nanotubes is less chiral than expected, and there is no direct correlation between the numbers of conduction channels and helical strands. [1] R.T. Senger, S. Dag, and S. Ciraci, Phys. Rev. Lett. **93**, 196807 (2004).

**J1 7 Role of relativity in electron impact ionization** BIDHAN C. SAHA, *Florida A&M University, Florida-32307* ARUN K. BASAK, *University of Rajshahi, Rajshahi, Bangladesh* M. ALFAZ UDDIN, *University of Rajshahi, Rajshahi, Bangladesh* The recently modified MBELL parameters [1] are generalized in terms of nl quantum numbers and applied to few selective systems. We intend to describe the procedure and to report the excellent predictive role of this simple procedure [2]. [1] A. K. F. Haque, M. A. Uddin, A.K. Basak, K. R. Karim and B. C. Saha, Phys. Rev. A 76 (in press) [2] A. K. F. Haque, M. A. Uddin, A.K. Basak, K. R. Karim, B. C. Saha, and F. B. Malik, Phys. Rev. Lett (under consideration).

**J1 8 Density-Functional Calculation for the Junction between Metal and Semimetal** CHIN-SHENG WU, *Center for General Education, Yuan-Ze University, Nei-Li, Taiwan* . We apply the density-functional theory to calculate the junction characteristics between the metal and semimetal. We obtain the self-consistent solution of the charge distribution both when Fermi levels of the metal and semimetal are set equal and when they are set unequal. The differential junction capacitance is obtained by differentiating the areal charge density with respect to the shift of Fermi levels. The electronic structure, potential, differential junction capacitance for the interface are reported. Our calculations for the metal with the conduction electron densities r=2, 6, and 12 a.u., and the semimetal with r=24 a.u.

**J1 9 Asymmetric confinement of an electron in a double-well potential and its relation with molecular lasers** IVAN MARIN-ENRIQUEZ, JOSE LUIS MARIN-FLORES, GERMAN CAMPOY-GUERENA, RAUL RIERA-AROCHE, *Departamento de Investigacion en Fisica, Universidad de Sonora* The confinement of an electron in an asymmetric double-well is proposed as an alternative system in which transitions and tunneling between bound states can have a similar behavior as in double-square well structures, regarding lasing properties. We show that this system would be more reliable than actual devices, since the relevant factor related to its efficiency is sharper and can be shifted in wavelength in a wide range as compared with, namely, its closest partner, the square double-well potential. Since nowadays technology allows the deposition of atom by atom (or molecule by molecule) layers of active materials, we think that such a device is feasible of construction, and represents a very attractive subject for research at both experimental and theoretical physics.

**J1 10 Wannier-Like Functions of Cesium Under High Pressure** EVA ZUREK, *Max Planck Institute for Solid State Research* OVE JEPSEN, *Max Planck Institute for Solid State Research* OLE KROGH ANDERSEN, *Max Planck Institute for Solid State Research* At ambient pressures cesium metal is found in the body centered cubic structure. At higher pressures, it undergoes a series of phase transitions which are accompanied by an electronic transition of the valence *s* electron to *d*-like states. We first of all propose a procedure which may be used to obtain Wannier-like functions for metallic systems using the newly developed NMTO (Muffin Tin Orbitals of order *N*) method. Wannier-like orbitals for a subset of the experimentally determined crystal structures of cesium are calculated. The electron density obtained from these orbitals is compared with that obtained from standard LMTO calculations. These orbitals give clear evidence of the electronic transition: they are primarily *s*-like at ambient volumes and display an increasing amount of *d*-character for structures found at higher pressures.

**J1 11 The effect of M (M=Ti, Cr, V, Nb) on transport and elastic properties of nanolayered ternary carbides $M_2AlC$** JEFF HETTINGER, PETER FINKEL, SAM LOFLAND, *Rowan University* MICHEL BARSOUM, ADRISH GUPTA, *Drexel University* We report on a systematic investigation of the electronic, magneto-transport, thermal and elastic properties of the family of materials $M_2AlC$ where M is Ti, V, Cr or Nb in the temperature

range 4 to 300K. The elastic constants were measured for all compounds ultrasonic technique. The bulk moduli and anisotropic Young's moduli found to be varied in these compounds for various transition metal M. The Debye temperatures were high in the 640-710 K range and quite insensitive to composition. The Seebeck coefficient was a non-monotonic function of a temperature: at the lowest temperatures is small but increases with increasing temperature and saturates at 60-80 K and goes through zero again manifesting change in the dominating charge carrier type. The electrical conductivity, Hall coefficient and magnetoresistances are analyzed within a two-band framework assuming a temperature-independent charge carrier concentration. We concluded that there is little correlation between the Seebeck voltage and Hall number. As with other MAX-phase materials, all these materials are nearly compensated. Comparisons of these results will be presented. Results will be discussed in relation to theoretical work and recent measurements on related systems.

**J1 12 Vacancy Scanning Tunneling Spectroscopy of Ag (111)** DANDA P. ACHARYA, *Ohio University* KAI-F. BRAUN, *Ohiu University* SAW-WAI HLA, *Ohio university* We investigate the vacancy electronic structures on a Ag(111) surface at 4.6 K by using scanning-tunneling-microscopy (STM) manipulation and spectroscopy in an ultra-high-vacuum environment. The vacancies with single atom to over a hundred-atom sizes are created on atomically cleaned Ag(111) surface by controlled tip-sample contact and single atom manipulation. Conductance tunneling spectroscopy data are then acquired by using a lock-in amplifier attached to the STM. The shift of the on-set of Ag(111) surface state is observed in few-atom vacancies. For the larger vacancies, we are able to probe the bulk silver unoccupied s-p band using tunneling spectroscopy. This experiment demonstrates a unique capability of a combined STM manipulation and spectroscopy to probe bulk and surface properties of materials through engineered atom and nanoscale cavities. This work is financially supported by a US-DOE grant, DE-FG02-02ER46012, and a NSF-NIRT grant, DMR-0304314.

**J1 13 Analytic treatment of metallic multilayer strength at all length scales** LAWRENCE FRIEDMAN, LEI FANG, *Pennsylvania State University, Dept. of Engineering Science and Mechanics* Metallic multilayers can be used as ultra-high strength coatings. They exhibit a very pronounced size-effect where the mechanical strength depends on the layer thickness. Traditionally, the Hall-Petch Relation is used to describe the size effect. The Hall-Petch Relation is based on dislocation pileup theory, which states that the macroscopically observable strength is determined by dislocation obstacles and stress multiplication from pileups. However, more rigorous application of dislocation pileup theory as applied to multilayers predicts significant deviation from the Hall-Petch Relation due to elastic inhomogeneity, discreteness of dislocations and dislocation source operation. The necessary modifications to the Hall-Petch Relation are presented. An analytic formula accounting for these effects can only be obtained in a piecewise fashion. The variation of strength with layer thickness must be broken down into four length-scale regimes, and a simple analytic formula is obtained for each regime. This formulation allows one to bridge the length scales and predict multilayer strength from microscopic parameters (interface strength and dislocation source characteristics) and fundamental material parameters (elastic moduli, layer thickness and crystal structure). Finally, the theory is applied to Cu/Ni multilayers and theory prediction is compared with experimental data.

**J1 14 Low-temperature Superplasticity of Dual-phase $Ti_3Al$ Based Alloy** KAI-LIN YANG, CHIH-CHING HUANG, To date, the $Ti_3Al$ based alloys have been widely reported their admirable superplasticity within the temperature ranges of 900-1000$^o$C. However, the superplastic behavior of temperature lower than 900$^o$C was seldom reported. The current paper will be aimed on the superplastic behavior at lower temperatures (700-900$^o$C). The phase transformation of $\beta \rightarrow \alpha_2$ in the two-phase ($\alpha_2 + \beta$) region during static annealing and superplastic straining at 700-1000$^o$C was occurred in this ($\alpha_2 + \beta$) dual-phase alloy. In addition, the misorientation angle distributions and texture characteristics of the $\beta$ and $\alpha_2$ phases were examined by the electron backscattered diffraction (EBSD) to complete the deformation behavior. Under the optimum LTSP condition at 850$^o$C and the strain rate of $5x10^{-4}$ $s^{-1}$, texture evolution is also investigated. From the texture characteristics associated with microstructure, the transformation behavior related to the deformation behavior could be demonstrated more clearly. In this current study, the texture characteristics, phase transformation phenomena, and the deformation mechanism at lower temperatures (below 900$^o$C) will be related and discussed.

**J1 15 Abstract Withdrawn**

**J1 16 Designing Laser Pulses to Control Molecular Motion** QINGHUA REN, GABRIEL BALINT-KURTI, FREDERICK MANBY, *School of Chemistry, University of Bristol, Bristol, BS8 1TS, UK* MAXIM ARTAMONOV, TAK-SAN HO, HERSCHEL RABITZ, *Department of Chemistry, Princeton University, Princeton, New Jersey 08544* A new method for incorporating polarization effects of the strong electric field into optimal control calculations is presented. An Electric-Nuclear Born-Oppenheimer approximation is introduced in which both the nuclear motion and the fluctuations of the external electric field are assumed to be slow compared with the speed at which the electronic wavefunction responds to these changes, which permits the generation of a potential energy surface that depends not only on the geometry of the nuclei, but also on the electric field strength and on the orientation of the molecule with respect to the electric field. As an illustration, it is firstly applied to the optimal control of the vibrational excitation of a hydrogen molecule aligned along with the field direction.[1] And then it is extended to full three dimensions by allowing the $H_2$ molecules to rotate as well as vibrate.[2] All calculation results show that it is possible to design shaped laser pulses that can excite $H_2$ either vibrationally, rotationally or both with a probability higher than 90%. [1] G. G. Balint-kurti, F. R. Manby, Q. Ren, M. Artamonov, T. Ho, and H. Rabitz, J. Chem. Phys. 122, 084110 (2005). [2] Q. Ren, G. G. Balint-kurti, F. R. Manby, M. Artamonov, T. Ho, and H. Rabitz, J. Chem. Phys. (in press).

**J1 17 Auger Parameter of Aluminum in aluminum compounds*** A. CHOURASIA, R. MILLER, G. NIXON, *Texas A&M University-Commerce* X-ray photoelectron spectroscopy has been employed to study 1s core level of aluminum in elemental aluminum, and in various aluminum compounds. The XPS spectra in the various regions have been recorded in the high resolution mode. The zirconium anode (energy = 2042 eV) has been used to access the 1s core level of aluminum. The energy difference between the 1s core level and the x-ray excited Auger line of aluminum in the XPS spectrum has been used to calculate the Auger

parameter. Wagner plot has been constructed from these data. In this plot the insulating materials appear lower on the grid as compared to those showing metallic nature. The points do not lie on the same line with slope +1, distinctly indicating that aluminum exists in different chemical states in these materials. The estimation of bonding characteristics from this plot will be discussed.

*Faculty Enhancement Grant, TAMU-Commerce

**J1 18 Electronic Structure of $Sr_2RhO_4$ investigated by ARPES** SEUNGHYEOK LEE, BUM-JOON KIM, JAEJUN YU, SE-JUNG OH, *School of Physics and Center for Strongly Correlated Materials Research, Seoul National University, Seoul, Korea* CHANGYUNG KIM, *Institute of Physics and Applied Physics, Yonsei University, Seoul, Korea* I. NAGAI, S.I. IKEDA, *National Institute of Advanced Industrial Science and Technology, Tsukuba, Ibaraki 305-8568, Japan* We investigated the electronic structure of 4d-transition metal oxides $Sr_2RhO_4$by high-resolution ARPES(angle-resolved photoemission spectroscopy) and compared the results with density-functional electronic structure calculation. $Sr_2RhO_4$has the same crystal structure with $Sr_2RuO_4$and just one more electron than $Sr_2RuO_4$ in 4d orbitals. But ARPES data reveal very different Fermi surface from that expected in the simple rigid-band picture, and especially the electronic structure related to the $d_{xy}$ band-the full occupation and missing at Fermi surface of the $d_{xy}$ band- is qualitatively different from $Sr_2RuO_4$. This turns out to be due to the fact that $RhO_6$ octahedra are rotated about the c-axis. We will discuss how the rotation of octahedra change the electronic structure by comparing the ARPES experimental results with density-functional electronic structure calculation in real crystal structure of $Sr_2RhO_4$.

**J1 19 A Generalized Model for Dielectric Relaxation and Resonance** JAMES BAKER-JARVIS, MICHAEL JANEZIC, PAVEL KABOS, *NIST* In this paper we develop a very general model from our previously developed statistical mechanical theory that describes relaxation, resonance, with temperature dependence. We also analyze the model in terms of entropy and a generalized Lyddane-Sachs-Teller relationship. The model is based on a correlation function approach and complex relaxation time from our previously developed theory. The commonly used Cole-Cole, Cole-Davidson and other models are related to this model as a special case. Using a fluctuation-dissipation theorem, we develop an algorithm for extraction of the loss properties of nanowires.

## J1 20 SEMICONDUCTORS POSTER SESSION

**J1 21 HgSe Semiconductor Nanoclusters in Zeolite*** A.M.M. ABEYKOON, *University of Houston* E.A. ANOKHINA, MIGUEL CASTRO-COLIN, W. DONNER, A.J. JACOBSON, SIMON C. MOSS, Our primary challenge has been to produce HgSe semiconductor nanoclusters with a precise, controllable and narrow size distribution. Since a zeolite framework constrains the size and shape of species encapsulated within a pore, we use zeolite pores to contain our nanoclusters. Two different zeolite frameworks, Linde type L (tubular pore) and Faujesite (nearly spherical pore) are used in our study. Elemental Hg and Se are embedded into dehydrated zeolite cavities via vapor phase deposition. The AXS (Anomalous X-ray Scattering) technique is used in combination with the PDF (atomic Pair Distribution Function) technique to solve for the structure of the nanocluster. Optical absorption measurements are used to determine the band gap of the cluster. We intend to perform Raman Spectroscopy to complement our determination of local structure and to probe the electronic properties of the semiconductor nanoclusters. AXS and PDF data sets were collected at X7A beam line at the NSLS. Optical measurements were carried out in the UH Chemistry Department. Currently we are analysing our x-ray data sets to yield a successful model for the nanoclusters.

*DOE

**J1 22 Crystallographic analysis on growth process of GaAs nanocrystals deposited onto Si(100) surface** HIROYUKI USUI, *Venture Business Laboratory, Kobe University, Nada, Kobe 657-8501, Japan* KENSUKE YAMADA, *Department of Mechanical Engineering, Kobe University, Nada, Kobe 657-8501, Japan* HIDEHIRO YASUDA, *Department of Mechanical Engineering, Kobe University, Nada, Kobe 657-8501, Japan* HIROTARO MORI, *Research Center for Ultra-High Voltage Electron Microscopy, Osaka University, Yamadaoka, Suita, 565-0871, Japan* Crystallographic analysis on growth process was carried out for GaAs nanocrystals deposited onto Si(100) by molecular beam epitaxy. Equilibrium crystal shapes of the GaAs nanocrystals at each growth stage were observed by cross-sectional transmission electron microscopy. At the initial growth stage, Stranski-Krastanov wetting layer and facetted nanocrystals with lower aspect ratio were formed. The GaAs nanocrystals at the middle growth stage formed regular pyramids consisting of {111} planes. At the later stage, the shape of GaAs nanocrystals was changed to dome structure consisting of {111} and {311} planes which has lower aspect ratio. This indicates that the GaAs nanocrystals introduced {311} facets to minimize the total surface free energy at the later stage because the surface free energy of {311} facets is smaller than that of {111} facets.

**J1 23 Study of Interfacial Water Layer during Pentacene Monolayer Deposition** SONGTAO WO, BINRAN WANG, YIPING WANG, RANDALL HEADRICK, *University of Vermont* ALEXANDER KAZIMIROV, *Cornell High Energy Synchrotron Source, Cornell University* This study includes the formation of pentacene monolayer on SiO2 substrate. itIn situ synchrotron x-ray scattering was used to probe the early stages of pentacene growth in real time and under conditions relevant to the fabrication of Organic Thin Film Transistors (OTFTs). Reflectivity measurements reveal that there is interfacial water layer between the pentacene monolayer and SiO2, which initially present on the substrate, and is trapped at the interface when the pentacene film is deposited. Anti-Bragg oscillations, observed for the first time during organic film growth, reveal that the first monolayer of pentacene completes fully before the second one nucleates.

**J1 24 3D Simulation of Phonon Modes in Semiconductor Nanocrystals*** NICHOLAS JURASEK, SHANG-FEN REN, WEI CHENG, *Illinois State University* The goal of this current research is the visualization of different phonon modes of NCs with 3D simulation to help in the understanding of their behavior. In order to realize this goal, the numeric data output from the previous atomistic model calculations is used that provides a list of

positions of atoms in NCs, the vibration frequencies and the displacement vectors of atoms in each phonon mode. These phonon modes are organized in different symmetries. Methods of visualizing the movement of these atoms are searched, and VMD from the University of Illinois is chosen as the best method to carry out it. VMD can create a 3-D image based on the positions and displacements of atoms, and it allows the user to rotate the structure around and to also ''fly'' through the structure. To use VMD, a program to convert the output of the simulation program into something that VMD can read is created. In this presentation, how VMD is used to carry out the 3D simulation of phonons in NCs will be discussed, and some interesting simulation results will be presented. These simulations can be used to understand more about the phonons and their related properties of NCs.

*This research is supported by an award from the Research Corporation (CC6274).

**J1 25 Determination of electron penetration depth and stopping power of amorphous AlN using luminescence of Tm and Ho ions** MUHAMMAD MAQBOOL, *Mount Olive College* MARTIN KORDESCH, *Ohio University* Electron penetration depth and stopping power of amorphous AlN is determined using luminescence of $Tm^{+3}$ and $Ho^{+3}$ ions. Thin film bilayers of AlN:Ho and AlN:Tm are deposited on flat Silicon substrates by RF Magnetron sputtering at liquid nitrogen temperatures. In making a bilayer, 15.3 nm thick AlN:Ho film is first deposited on a flat Si(111) substrate of $2\times$ 2 $cm^2$ surface area. On the top of this AlN:Ho film 37.8 nm thick AlN:Tm film is deposited to make it a bilayer. Electron beam of different energies, obtained from electron gun of the CL apparatus, is allowed to penetrate in the AlN:Tm/AlN:Ho bilayer film. Blue emission from $Tm^{+3}$ as a result from $^1D_2 \rightarrow {}^3F_4$ transition and green emission from $Ho^{+3}$ as a result from $^5S_2 \rightarrow {}^5I_8$ transition were used to track the electron beam penetrating in the bilayer. Energy of the beam just crossing 37.8 nm AlN:Tm film is recorded to obtain the stopping power experimentally. Experimental results are compared to the theoretical value using the established mathematical equations for stopping power. A percent deviation of 6.6% is found in the experimental and theoretical results.

**J1 26 Diffusion doping and Infrared Optical Properties of Transition Metal Ions in ZnSe windows and $Cd_{0.55}Mn_{0.45}Te$ crystals** EI NYEIN, UWE HOMMERICH, IVY JONES, MONIQUE CALHOUN, ERICA HAYNES, *Hampton University* SUDHIR TRIVEDI, *Brimrose Corporation of America* Transition metal (TM) doped II-VI semiconductors are of current interest for tunable solid state lasers in the mid-infrared (IR) spectral region as well as passive optical Q-switches. Laser action has been demonstrated at $\sim$ 2.3 $\mu$m from Cr: ZnSe, Cr: ZnS, Cr: CdSe, Cr: CdTe, Cr: Cr: CdMnTe, and at $\sim$ 4 $\mu$m from Fe: ZnSe. In this work, we report on the material preparation and IR optical properties of diffusion-doped TM ions ($Cr^{2+}$, $Fe^{2+}$, $Co^{2+}$) in polycrystalline ZnSe windows and $Cd_{0.55}Mn_{0.45}Te$ crystals. Different dopant sources were employed in thermal diffusion experiments including TM chloride compounds, TM selenides, and elemental TM powders. The characteristic IR absorption bands from $Cr^{2+}$, $Co^{2+}$, and $Fe^{2+}$ doped II-VI hosts were observed in all samples, independent of the dopant source. Details of the absorption and luminescence properties of these TM: ZnSe and TM: CdMnTe samples will be presented at the conference.

**J1 27 On the transfer matrix method and WKB approximation for systems with spatial-dependent effective mass** CHUN-FENG HUANG, *National Measurement Laboratory, Center for Measurement Standards, Industrial Technology Research Institute, Hsinchu 200, Taiwan, R. O. C.* S.D. CHAO, *Institute of Applied Mechanics, National Taiwan University, Taipei, Taiwan, R. O. C.* D.R. HANG, *Department of Materials Science and Optoelectronic Engineering, National Sun Yat-sen University, Kaohsiung 804, Taiwan, R. O. C.* Y.C. LEE, *Institute of Materials Science and Engineering, National Sun Yat-sen University, Kaohsiung 804, Taiwan, R. O. C.* A set of coupled differential equations is derived by considering the continuous limit of the transfer matrix method, which is a numerical approach for the one-dimensional structures such as the semiconductor heterostructures. By decoupling such a set of equations, an extension to the Wentzel-Kramers-Brillouin (WKB) method is obtained to incorporate effects due to the spatial-dependent effective mass. For a traveling wave, the decoupling is to ignore the reflection resulting from the variations of both the potential and effective mass. By considering a solvable fully-quantized system, it is shown that the extended WKB method provides good approximation for the states with the high eigenenergies.

**J1 28 Unusual excitation spectra of magnesium-related donor impurities in silicon** L.T. HO, *Institute of Physics, Academia Sinica, Taipei, Taiwan* It is well known that the group-II magnesium, when diffused into silicon, enters the silicon lattice interstitially and behaves as a helium-like double donor. Magnesium has also been found to be able to pair with dispersed oxygen in silicon to form magnesium-oxygen complex impurity, which is an interstitial double donor as well. Previous studies on the excitation spectra of these helium-like impurities indicate that the excited states of neutral magnesium donor or neutral magnesium-oxygen complex donor are all similar to those of hydrogen-like group-V donor impurities in silicon. Recently, however, from further study of the excited spectra of these magnesium-related donor impurities, we have observed some very unusual result totally unexpected and clearly different from a typical donor spectrum in silicon.

**J1 29 LDA density functional study of lithium intercalated compounds in grephite** JUAN SALVADOR ARELLANO, *Area de Fisica Atomica Molecular Aplicada, UAM Azcapotzalco, 02200, Mexico D.F.* PABLO DE LA MORA, *Depto. de Fisica, Fac. de Ciencias, UNAM, Mexico* M. J. LOPEZ, L. M. MOLINA, J. A. ALONSO, *Departamento de Fisica Teorica, Universidad de Valladolid, 47011, Valladolid, Spain* Local Density Functional (LDA) calculations have been done for different lithium intercalated graphite compounds. We have explored the most common ones namely $LiC_6$, and $LiC_2$. Also the $LiC_3$ has been studied. To explain some details about the structural and electronic properties of the last one, we have used two computer codes, FHI98MD and WIEN2k. This was motivated by a recent work for the $LiC_3$compound, where it is said that lithium atoms positions are not in the middle plane between the graphene layers formed by the carbon atoms. Discussion of the three mentioned lithium intercalated compounds and somewhat about the superconductivity will be given during the presentation.

**J1 30 Electronic structure of V-doped TiO2** YUSHAN WANG, *University of Delaware* First-principles calculations using the full-potential linearized augmented plane-wave method have been performed to investigate the electronic structure of V-doped TiO2 in the anatase modification. In calculations with local density approximation (LDA) plus U ( Hubbard coefficient) approach, V 3d states were found to be completely spin- polarized with net magnetic moment generated.

**J1 31 Structural deformation and instability of strong covalent solids*** CHANGFENG CHEN, *University of Nevada, Las Vegas* HONG SUN, *Shanghai Jiaotong University* We employ first principles total-energy calculations to study the structural deformation modes at large strains and the lattice instabilities beyond the elastic limit for several strong covalent solids. We examine the atomistic bonding changes to elucidate the microscopic mechanism for the stress response and the orientational dependence of the peak stresses along different crystallographic directions and the bond breaking modes. Implications for the mechanical properties will be discussed.

*This work was supported in part by the Department of Energy

**J1 32 The 4x4 spin 1/2 representation in electron polarization in a magnetic field** KESHAV SHRIVASTAVA, *University of Hyderabad* We introduce a 4x4 spin representation for spin 1/2. There are two spin orientations for a given value of $g_+$ and two for $g_-$ which arise for two signs of spin. This theory produces factors which affect the product m*g* so that if these factors are not taken into account, much larger values of the electron mass than those of the electron mass in a band arise. This predicted phenomenon is in accord with the experimental data. Similarly we find that factors arise in cyclotron frequency which affect the magnetoresistance and hence the g values. Accordingly, large g values are measured in the experimental data. When our factors are taken into account, the g values compare well with band values. The $g^* = g_\pm - \delta$ describes the shift due to many-body interactions.

**J1 33 An alternative model of the integer quantum Hall effect** TOBIAS KRAMER, *Physics Department Harvard University* Contrary to common belief, the current emitted by a contact embedded in a two-dimensional electron gas (2DEG) is quantized in the presence of electric and magnetic fields. This observation suggests a simple, clearly defined model for the quantum current through a Hall device that does not invoke disorder or interactions as the cause of the integer quantum Hall effect (QHE), but is based on a proper quantization of the classical electron drift motion. The theory yields a quantitative description of the breakdown of the QHE at high current densities that is in agreement with experimental data. Furthermore, several of its key points are in line with recent findings of experiments that address the dependency of the QHE on the 2DEG bias voltage, results that are not easily explained within the framework of conventional QHE models. For additional information, see also http://arxiv.org/abs/cond-mat/0509451 (accepted by IJMPB) and the article references on http://people.deas.harvard.edu/~tkramer.

**J1 34 Determination of the structure of ZnS:$ErF_3$ TFEL phosphors using XAFS** STANISLAV STOUPIN, *Illinois Institute of Technology* CARLO SEGRE, *Illinois Institute of Technology* MARK DAVIDSON, *University of Florida* PAUL HOLLOWAY, *University of Florida* Many phosphor systems that provide useful levels of IR emission have a poor match between dopant atom and the host structure. An example of such a system is ZnS doped with rare-earth elements incorporated into the host as trivalent ions. For example, the size of Er is quite large compared to Zn and it does not easily substitute into the same crystallographic site. We have prepared a number of $ErF_3$ 1 mol% doped ZnS thin film electroluminescent (TFEL) phosphors using RF magnetron sputtering followed by annealing at various temperatures. The intensity of the IR emission is found to be very sensitive to the post-deposition annealing. As the local chemical and structural environment of the dopant atom is very important to the performance of the phosphor we have used x-ray absorption fine structure spectroscopy (XAFS) to provide detailed information on the local environment surrounding the Er atom. The XAFS spectra are consistent with Er-F complex substitution into the Zn site accompanied by creation of S vacancies. The ZnS host lattice reveals significant disorder effects in the first Zn-S coordination shell. These structural features change with annealing temperature and are likely responsible for the observed changes in intensity of the various Er emission lines.

**J1 35 Surface modification of InP wafers by pulsed UV laser radiation below ablation threshold** OMAR MUSAEV, *UMKC* O.-S. KWON, *UMKC* D.-M. ZHU, *UMKC* D. WIELICZKA, *UMKC* J. WROBEL, *UMKC* SURFACXE SCIENCE TEAM, Under multi-pulse laser irradiation below the threshold of ablation modification of surface layer of semiconductor can happen. The creation of point defects may lead to their subsequent aggregation and cause macroscopic damage of the irradiated surface if the number of pulses is large enough despite that the fluency is lower than ablation threshold. Low energy pulsed laser irradiation may also cause different structural changes in the surface layer of a compound semiconductor which manifests itself in changes of physical and chemical parameters of the surface. The surface of InP wafer irradiated by different numbers of pulses with different fluences below ablation threshold was analyzed with AFM and XPS. Mechanisms of defect creation and aggregation in InP surface under low intensity laser irradiation are discussed.

**J1 36 Capacitance Dispersion in GaN Grown by Molecular Beam Epitaxy** MO AHOUJJA, REX BERNEY, SAID ELHAMRI, *University of Dayton, Dayton OH* YUNG KEE YEO, *ENP/AFIT, W-PAFB OH* UNIVERSITY OF DAYTON, DAYTON OH TEAM, GaN semiconductors are of great interest for applications in high-temperature and high-frequency electronic devices as well as blue to UV light emitting and detecting devices. However, an understanding of the role of dopants and defects in these semiconductors is essential for the realization of high performance devices. Si doped GaN samples grown by radio-frequency plasma activated molecular beam epitaxy on sapphire substrates were characterized by capacitance-voltage (C-V) measurements. The C-V measurements were performed with an LCR meter in series mode with an AC modulation level of 50 mV in the frequency range of 500 Hz to 1MHz. The junction capacitance of the Schottky diodes varied with both temperature and frequency. The variation of capacitance with frequency is known as capacitance dispersion. This dispersion is generally attributed to the slow response of deep levels to the high frequency AC signals. Consequently, it is suggested that native defects in GaN play a role in the observed capacitance dispersion.

**J1 37 Intervalley Transitions in GaN Single Crystals** S. WU, D. WANG, R. SOBOLEWSKI, *University of Rochester, Rochester, NY 14627* P. GEISER, J. JUN, J. KARPINSKI, *ETH, CH-8093 Zurich, Switzerland* We present the direct observation of the intervalley transition of electrons between the conduction band $\Gamma$ valley and the L valley in GaN single crystals, using the two-color

(ultraviolet-near infrared), femtosecond, pump-probe spectroscopy technique. We have found that scattering of electrons from the Γ to L valley is faster than the optical phonon emission time, while the return process of electrons from L to Γ is measurably slower. The developed model based on three-state rate equations fitted very well our experimental results. The fitting parameters showed that the Γ– L scattering time is ~ 250 fs, while the L–Γ return time is ~ 1 ps. The optical phonon emission time was found to be equal to ~ 500 fs. The characteristic scattering times obtained in our experiments demonstrate that the dynamics of the intervalley transition process in GaN is substantially slower than the similar transitions earlier observed for GaAs.

**J1 38 Positron annihilation induced Auger electron emission from silicon carbide surfaces** S. MUKHERJEE, M. NADESALINGAM, *University of Texas at Arlington* G. BRAUER, *Institut für Ionenstrahlphysik und Materialforschung, Forschungszentrum Rossendorf* T. NOZAWA, A. KOHYAMA, *Institute of Advanced Energy, Kyoto University* A.H. WEISS, *University of Texas at Arlington* Silicon carbide (SiC) in monocrystalline, hexagonal polytype form is a very interesting material for a wide class of novel applications in electronics. SiC fiber-reinforced SiC matrix composite materials (SiC/SiC) are considered to be the attractive candidates as materials for advanced energy systems, such as high performance combustion systems, fuel-flexible gasification systems, fuel cell / turbine hybrid systems, nuclear fusion reactors, and high temperature gas-cooled fission reactors. Positron Annihilation induced Auger Electron Spectroscopy (PAES) is an established tool to characterize the top most atomic surface layer of solids. Here, PAES has been used to study the surface of 6H-SiC after annealing under different thermal and ambient conditions. In addition, results of investigating the surface of a composite consisting of sintered SiC Nanopowder and fibres of pyrolytic carbon are presented and discussed. This research supported by the Welch Foundation under Y-1100.

**J1 39 Anisotropy in the Amplitude of Shubnikov-de Haas Oscillations in AlGaN/GaN Heterostructures** S. ELHAMRI, R. BERNEY, M. AHOUJJA, G. LANDIS, *University of Dayton* W. MITCHEL, W. MITCHELL, *Wright Patterson Air Force Base* Variable temperature resistivity and Hall effect measurements were performed on several AlGaN/GaN heterostructures. The temperature dependence of the mobility and carrier density extracted from these measurements indicated the presence of a good quality two dimensional electron gas. At liquid helium temperatures, the carrier density and mobility in these samples ranged from about 2 x $10^{12}$ to roughly 1 x $10^{13}$ $cm^{-2}$ and from about 4000 to more than 50000 $cm^2$/Vs respectively. Variable field magnetoresistance studied were also conducted on several of these van der Pauw shaped samples at 1.2 K in fields up to 8 T. These measurements revealed the presence of Shubnikov-de Haas oscillations in the longitudinal magnetoresistance. However, the amplitude of the Shubnikov-de Haas oscillations originating from perpendicular van der Pauw positions were not isotropic. This anisotropy varied with the carrier density which was changed by illumination. The results of this study suggest that the anisotropy is either a manifestation of spatial carrier density inhomogeneities and/or an indication of a nonuniform scattering mechanism arising from an anisotropic interface roughness.

**J1 40 Spin-Orbit Interaction for Cylindrical Nanotubes** GODFREY GUMBS, *Hunter College of CUNY* YONATAN ABRANYOS, *Hunter College of CUNY* When a gate voltage is applied perpendicular to the axis of nanotubes, this can lead to spin-orbit interaction (SOI) effects. This is of the same nature as the Rashba-Bychkov SOI at the interface of an asymmetric semiconductor heterojunction. We use a continuum model to obtain analytical expressions for the spin-split energy eigenstates for electrons on the surface of nanotubes in the presence of SOI. Each energy level could then be used to accommodate the two types of spin. For qubit functionality, one can use either one nanotube or a pair of coupled nanotubes. We investigate this scheme by calculating the exchange interaction energy and subsequently the entanglement of electron spins as they occupy allowed subbands. We also calculate the effect which SOI has on the plasma excitations since the exchange interaction can be mediated by long-range collective excitations.

**J1 41 Conductivity for a Spin-Split 2D Electron System** GODFREY GUMBS, *Hunter College of CUNY* Recent research on spintronic systems has examined a wide variety of their transport and optical properties from both a theoretical and experimental perspective. By including spin-orbit interaction (SOI) in a model Hamiltonian, we calculate the low-frequency local conductivity, starting with Kubo's formula. For long mean-free paths, we obtain a closed-form analytical result which is a generalization of the Drude conductivity. By adding vertex corrections using maximally crossed Feynman diagrams to our result, we also obtain, to lowest order in the scattering parameter, the non-local conductivity is given in terms of function which shows that there is an ''interference'' effect due to the SOI. This means that the electrons do not diffuse through the sample when the SOI is neglected, as it demonstrated several years ago.

**J1 42 Effect of SOI on the Acoustoelectric Current** YONATAN ABRANYOS, GODFREY GUMBS, *Hunter College of CUNY* With a need to increase the accuracy of the measured acoustoelectric current for metrological applications, we investigate the role played by the Rashba spin-orbit (SO) coupling. With a model Hamiltonian which takes into account the confinement of electrons within a narrow channel between split metal gates, we demonstrate that the SO interaction increases the confinement of a captured electron in a moving quantum dot and may consequently improve the quenching of the quantized acoustoelectric current.

**J1 43 A kinetic equation approach to the spin Hall effect in *p*-type bulk semiconductors** S. Y. LIU, *Stevens Institute of Technology and Shanghai Jiaotong University, China* NORMAN J. M. HORING, *Stevens Institute of Technology* X. L. LEI, *Shanghai Jiaotong University, China* V. FESSATIDIS, *Fordham University* A two-band kinetic equation method is employed here to investigate the spin-Hall effect (SHE) in a *p*-type Luttinger semiconductor. We find that the previously predicted solely intrinsic SHE arises from a dc-field induced polarization directly, or in other words, a stationary Rabi process, associated with all hole states below the Fermi surface. The total SHE, encompassing a mix of both extrinsic and intrinsic features, results essentially from a related polarization process involving electric field excitations between heavy- and light-hole bands, both directly and indirectly through scattering. In particular, we examine effects of long-range disorder on spin-Hall current (SHC) within the self-consistent

Born approximation. In contrast to the vanishing SHC contribution due to short-range disorder, we show that long-range impurity scattering produces a nonvanishing SHC, independent of impurity density, having its sign opposite to that of the intrinsic SHC contribution and leading to a significant reduction of the total SHC. This disorder-generated SHE arises from a disorder-mediated interband polarization, related only to hole states near the Fermi surface. We analyze the hole density dependencies of SHC and spin mobility numerically: with increasing hole density, the SHC first increases and then decreases, while the spin mobility decreases monotonically.

**J1 44 Kane model for the spin-splitting of holes in semiconductor heterostructures*** ARTURO WONG, FRANCISCO MIRELES, *Centro de Ciencias de la Materia Condensada, UNAM* We present a theoretical study of the Rashba-like spin-orbit coupling in two dimensional hole systems formed in zincblende semiconductor heterostructures. Using an 8X8 band Kane model within the envelope function approximation we derive exact analytical expressions for the Rashba-like Hamiltonians of the heavy, light and split-off holes [1]. The linear and cubic dependence in the wave vector of such Hamiltonians will be discussed. Simple analytical expressions for the spin-orbit coupling parameters can be also extracted from our model. A variational approach has been used in order to estimate the hole spin-splitting energies in typical III-V semiconductor quantum wells. Our preliminary results indicate that the magnitude of the spin-splitting energies for heavy holes is generically larger than their counterparts for electrons. This results could be of relevance for the design and implementation of novel (hole) transport spintronic devices. [1] A. Wong and F. Mireles (in preparation).

*This work has been supported in part by CONACYT/México, projects No. J40521F and 43673.

**J1 45 Structural, Magnetic and Transport Properties of Cobalt doped ZnO Epitaxial Thin Films** HYOJIN LEE, SUNGHO LEE, FIKRET YILDIZ, YOON HEE JEONG, *Dept. of Physics, POSTECH* Semiconductors with ferromagnetism at room temperature has been actively searched for in recent years; a prospect of spintronic devices using both charge and spin continuously gives impetus to the activities. Co substituted ZnO thin films, for example, were reported to show ferromagnetic properties at room temperature. However, various subsequent studies including ours do not seem to converge on a definite picture and controversy continues. What is needed is well synthesized and thoroughly characterized samples. A series of $Zn_{1-x}Co_xO$ ($0 = x = 0.2$) thin films on sapphire (0001) substrates were epitaxially grown by using Laser MBE deposition technique, controlling laser fluence, substrate temperatures and oxygen partial pressures. In-situ RHEED pattern showed that the films grew in the layer by layer growth mode. We performed high resolution X-ray diffraction (XRD), SEM, TEM, and AFM measurements to confirm the structure and morphology of the films. XRD figures showed that the films were of single phase with the pure ZnO wurtzite structure. AFM measurements showed that the RMS values of roughness of the films were about 2Å. Magnetization, resistivity, and Hall coefficient measurements were also carried out systematically as a function of $x$. These measurements revealed that Co doping brings about self-curing of oxygen vacancies. These results will be presented in detail.

**J1 46 Magnetic and transport properties of cobalt doped ZnO Epitaxial thin films.** HYO-JIN LEE, *Department of Physics & Electron Spin Science Center, Pohang University of Science and Technology, Pohang 790-784, S. Korea* FIKRET YILDIZ, S.-H LEE, YOON-HEE JEONG, *Department of Physics & Electron Spin Science Center, Pohang University of Science and Technology, Pohang 790-784, S. Korea* Transition metal doped ZnO has become an important topic of scientific interest in view of diluted magnetic semiconductor (DMS) at room temperature. A series of $Zn_{1-x}Co_xO$ ($0 \leq x \leq 0.2$) thin films on sapphire (0001) substrates were epitaxially grown by using Laser MBE deposition technique, controlling laser fluence, substrate temperatures and oxygen partial pressures. RHEED, X-ray diffraction (XRD), Atomic force microscope (AFM) scanning, magnetization and transport measurements were performed to investigate their structural, morphological, transport and magnetic properties. During the film growth, layer by layer growth mode were seen on RHEED pattern. XRD measurements showed that the films have the single phase of the pure ZnO wurtzite structure, there was not any secondary phase. The RMS values of roughness of the films were determined about 2Å range from AFM images. The electric and magnetic properties will be presented.

**J1 47 Investigations of the magnetocrystalline anisotropy by the Planar Hall Effect in (Ga,Mn)As epilayers grown on vicinal GaAs substrates*** W. L. LIM, X. LIU, K. DZIATKOWSKI,† Z. GE, S. SHEN, J. K. FURDYNA, M. DOBROWOLSKA, *Department of Physics, University of Notre Dame, IN 46556 USA* An asymmetric shift of the Planar Hall resistance is observed in the ferromagnetic (Ga,Mn)As epilayers grown on vicinal GaAs substrates, due to the superposition of both the in-plane Planar Hall Effect (PHE) and the out-of-plane Anormalous Hall Effect (AHE). The asymmetric shift reveals the direct manifestation of the strong magnetocrystalline anisotropy that confined the magnetization to the crystalline plane, providing a non-zero normal component of the magnetization with respect to the sample plane at low fields. This shift allows one to measure both components of AHE and PHE simultaneously in these (Ga,Mn)As thin films. We found that the ratio of the AHE resistance to the average PHE resistance change is independent of the vicinal angles. The asymmetry shift is found to be reduced with the increase of the temperature. At the temperature around 30K, the anisotropic magnetoresistance obtained by the PHE measurements shows a significant different profile near the switching fields during the magnetization reversal processes, indicating a complex competition between the cubic magnetocrystalline anisotropiy and the uniaxial anisotropy in these samples grown on vicinal GaAs substrates.

*Supported by the NSF grants DMR02-10519 and DMR02-45227
†Also at Institute of Experimental Physic, Warsaw University, Poland

**J1 48 Hydrostatic pressure enhancement of the Curie temperature and anomalous Hall effect in $Sb_{2-x}Cr_xTe_3$*** JEFFREY S. DYCK, ANDREW J. LUCIANA, *Department of Physics, John Carroll University* CESTMIR DRASAR, PETR LOSTAK, *Faculty of Chemical Technology, University of Pardubice, Czech Republic* The narrow band gap tetradymite-type semiconductors with the form $A_2^VB_3^{VI}$ (A = Sb, Bi and B = Se, Te) are normally associated with thermoelectric cooling devices. However, $Sb_2Te_3$ doped with V or Cr and $Bi_2Te_3$ doped with Fe display a ferromagnetic transition at low temperatures. We have investigated electrical transport properties of bulk single crystals of

the ferromagnetic diluted magnetic semiconductor $Sb_{2-x}Cr_xTe_3$ under varying pressure (0 GPa to 1.5 GPa), temperature (2 K to 300 K), and magnetic fields (0 T to 6 T). High pressure measurements afford a reversible way to tune both the electronic structure and magnetic interactions of these materials. The behavior of the Curie temperature $T_C$ can be monitored via the position of the peak in the resistance data associated with the ferromagnetic transition. We observe that $T_C$ increases with increasing pressure in this compound. The anomalous Hall effect with clear hysteresis is also observed below $T_C$, and trends with pressure will be discussed.

*C.D. and P.L. thank the Ministry of Education of the Czech Republic for the support under the project No. MSM 0021627501 and J.D. and A.L. gratefully acknowledge support from the Research Corporation.

## J1 49 INSULATORS AND DIELECTRICS POSTER SESSION SION

**J1 50 Polarizing and phase-shifting properties of multilayered X-ray mirrors with fluctuating parameters** ARKADY SATANIN, *Institute for Physics of Microstructures RAS* MARIA BARYSHEVA, NIKOLAY CHKHALO, It is well known that the multilayered periodical structures (MS) may be used for different X-ray optics applications: dispersion elements, mirrors, polarimeters etc. At the present the polarizing and phase-shifting properties of the MS attract much attention. It was found an intriguing behavior of the MS when the structures having almost the same reflection coefficients demonstrate the strong variations of the polarizing and phase-shifting characteristics. To understand this phenomenon we have investigated the distribution functions of polarization and phase-shift fluctuations for an array of identical MS depending on layer thickness fluctuations. It was shown both analytically and numerically that the relative small fluctuations of layer thickness and the deterministic (systematic) local period deviations may change dramatically the polarization and phase-shift of the MS. In our work we have shown that the polarization and phase-shift of the MS may be found from the reflection measurements.

**J1 51 Crystal Structure, Magnetism, and Infrared Reflectivity of Double Perovskites$Sr_2B\ UO^6$ and Sr2B $UO_{6-d}$, B =Mn,Fe,Co,Ni,Zn** R. M. PINACCA, M. DELC. VIOLA, J. C. PEDREGOSA, *FQBF, UNSL, SanLuis, Argentina* R. E. CARBONIO, *INFIQC, UNC, Córdoba, Argentina* M. J. MARTINEZ−LOPE, J. A. ALONSO, *ICMM, CSIC, Cantoblanco, Madrid, Spain* F. P. DELACRUZ, N. E. MASSA, *LANAISEFO−CEQUINOR, U.N.L.P., C.C. 962, (1900) LaPlata, Argentina* Double perovskites$Sr^2B\ UO_6$ where B'=Mn, Fe, Co, Ni, Zn have been prepared as a polycrystalline powder by solid-state reaction. and studied by X-ray diffraction and magnetic measurements. At 300K, they present the same monoclinic distorted crystal structure, space group $P2_1$ /n. The perovskite lattice consists of a completely ordered array of B $O^6$ and $UO^6$ octahedra exhibiting a slight tilting of the type a − b + a − . Magnetic measurements show antiferromagnetism for the phases with B =Co, Ni and Mn at low temperature. The effective magnetic moment at T ⩾ $T_{Neel}$ (5.22l B/f.u. for Co phase and 3.26 B/f.u. for Ni phase) suggests an unquenched orbital contribution. The value for the Mn phase (5.74 B/f.u.) is consistent with that expected for high-spin $Mn^{2+}$ (5.91 B/f.u.). The topotactic reduction of the stoichiometric sample leads to oxygen deficient disordered perovskites, SrB0.5U0.5O3 − d having an orthorhombic distorted structure, space group Pbnm, at 300K. We will also comment on the temperature dependent infrared reflectivity of Sr2CoUO6 and isomorphous compounds.

**J1 52 Epitaxial Thin Films of the Oxynitride $BaTaO_2N$ Grown by Pulsed-laser Deposition** WEIDONG SI, SANGMOON PARK, ELI SUTTER, THOMAS VOGT, *Brookhaven National Laboratory* YOUNG-IL KIM, PATRICK WOODWARD, *Department of Chemistry, The Ohio State University* Pulsed-laser deposition has been used to grow epitaxial thin films of the oxynitride $BaTaO_2N$ on MgO substrates and $SrTiO_3$ substrates with and without $SrRuO_3$ buffer layers. The thin films have a relatively high dielectric constant in the order of 200 - 250 from room temperature down to 4.2K with no significant frequency dependence. This special property, which has not been found before in other materials, potentially makes it a good candidate for many dielectric applications. We argue that a new mechanism is required to understand the dielectric properties of $BaTaO_2N$.

**J1 53 Time-dependent space-charge-limited conduction** HOKEI CHAN, *School of Physics and Astronomy, University of Manchester, Manchester (U. K.)* YAN ZHOU, CHI-HANG LAM, F.G. SHIN, *Department of Applied Physics, Hong Kong Polytechnic University, Hong Kong* The concept of time-dependent space-charge-limited conduction (TDSCLC) was introduced in 2004 to account for the well-known observation of polarization offsets in compositionally graded ferroelectric films [1]. It is a generalization of Mott's steady-state SCLC model ($J \sim V^2$) [2] to include two carrier types ($p$ and $n$) and time dependence. Subsequently it was found to have a wider applicability in explaining the imprint phenomenon commonly observed in homogeneous ferroelectric films [3]. Here we would like to review the derivation of the TDSCLC formula and its relation to the steady-state SCLC model, and discuss its applicability to other electrical insulators. [1] H. K. Chan, C. H. Lam, and F. G. Shin, J. Appl. Phys. 95, 2665 (2004) [2] R. Coelho, Physics of Dielectrics for the Engineer (Elsevier Scientific, New York, 1979), pp. 123-125 [3] Y. Zhou, H. K. Chan, C. H. Lam, and F. G. Shin, J. Appl. Phys. 98, 024111 (2005).

**J1 54 Mossbauer studies of mixed Fe-Mo oxides** H.H. HAMDEH, H. AL-GHANEM, J.C. HO, *Wichita State University* R.J. WILLEY, E. MARCHESE, W. JABLONSKI, *Northeastern University* Mossbauer spectroscopy was carried out in conjunction with a catalytic study on mixed Fe-Mo oxides, among which $Fe_2(MoO_4)_3$ has been widely used in selective oxidation of certain hydrocarbons. With the specific activity being sensitive to the catalyst particle size and morphology, an aerogel process was employed to prepare the samples covering Fe/Mo ratios from 1/2 to 2/1. Each set of Mossbauer data were well fitted to reflect one Fe3+ and two or three non-equivalent Fe2+ sites. Their isomer shift, quadruple splitting and molar fraction are analyzed in terms of temperature and Fe/Mo-ratio dependence. The Fe-rich samples exhibit magnetic ordering at low temperatures.

**J1 55 Mid-infrared spectroscopy of Praseodymium doped $KPb_2Br_5$ and $KPb_2Cl_5$** PETER AMEDZAKE, EI NYEIN, UWE HOMMERICH, *Hampton University* SUDHIR TRIVEDI, *Brimrose Corporation of America* JOHN ZAVADA, *US Army Research Office* Rare-earth doped low phonon energy hosts are promising materials for mid-infrared (MIR) solid-state laser applications. Room temperature laser activity has been demonstrated at 7.2 $\mu$m, 5.2 $\mu$m and 1.6 $\mu$m from Pr: $LaCl_3$. In this work, we report on the material preparation and optical properties of Pr doped $KPb_2Br_5$ (KPB) and $KPb_2Cl_5$ (KPC). KPB and KPC are both non-hygroscopic and have low maximum phonon energies of 140cm$^{-1}$ and 200cm$^{-1}$, respectively. The small phonon energies lead to reduced non-radiative decay rates due to multiphonon relaxation. The preparation of Pr: KPB and Pr: KPC was based on a careful purification of the host materials followed by self-seeded Bridgman crystal growth. The characteristic absorption bands were obtained in the visible and IR spectral region. Under 1907 nm and 1550 nm excitations, both crystals exhibited broad MIR emission spectra centered $\sim$ 4.7 $\mu$m with a room-temperature lifetime of 4.5 ms. Results of temperature dependent and time-resolved emission spectroscopy of Pr: KPB and Pr: KPC will be presented at the conference.

**J1 56 Planar faults in metastably retained hexagonal $BaTiO_3$.** YU-CHUAN WU, HONG-YANG LU, Hot-pressed $BaTiO_3$ ceramic samples contain predominantly h-$BaTiO_3$ as determined by XRD, and with a trace amount of t-$BaTiO_3$ as revealed by TEM. Extended planar stacking faults (EPSF's) found ubiquitously in hot-pressed samples having the eligible fault vectors $\mathbf{R}_{F(I)} = (1/2)\mathbf{c} + \mathbf{p}_{(I)}$ and $\mathbf{R}_{F(II)} = (n/6)\mathbf{c} + \mathbf{p}'_{(II)}$, containing both $\mathbf{p}_{(I)} = 1/3\langle 2110\rangle$, $\mathbf{p}'_{(II)} = 1/3\langle 1010\rangle$, n = 1, 2, 4, and 5, and $\mathbf{c} = [0001]$, have been determined by contrast analysis using the $2\pi\mathbf{g}\cdot\mathbf{R}_F = 0$ or $2n\pi$ criteria crystallographically, and the number of layers along **c** confirmed by high-resolution imaging uniquely. Two general types of EPSF's are found; one group with only three vectors of the six degeneracies of the **p**-component $\langle 1010\rangle$ eligible and the other with all six degeneracies of the **p**-component $\langle 2110\rangle$ eligible for the fault vector. The latter is analogously a $\pi$-rotation fault (as in $DO_{19}$ intermetallics) that a rotation about [0001] by 180$^o$ (or 60$^o$) arrives at another eligible fault vector. The metastable retention of the high-temperature h-$BaTiO_3$ phase is discussed in favour of oxygen deficiency.

**J1 57 PIMC simulation of Ps in a dielectric solid** ZACHARY WOLFSON, *Swarthmore College* AMY BUG, *Swarthmore College* Positronium (Ps) is commonly used to probe the pore space in insulating materials like polymers and low-k dielectrics. Such studies require an accurate model relating the lifetime to the size of the pore. The standard Tao-Eldrup approach models Ps as one quantum particle in the ground state of a spherical box. We go beyond Tao-Eldrup by modeling Ps exactly as two quantum particles at arbitrary temperature, using Path Integral Monte Carlo (PIMC) to simulate the electron and positron each as a classical polymer. As a further correction, we also include the dielectric response of the surrounding material. The total annihilation rate, which is the inverse of the lifetime, may be calculated from the pickoff and self annihilation rates via $\Gamma = \Gamma_{p.o.} + \kappa\Gamma_{self}$ We find that the material's polarization causes the Ps to be more attracted to the wall, decreasing its pickoff lifetime. The internal contact density, $\kappa$, decreases with increasing dielectric constant. The combination of using the two particle model as well as polarizable walls yields a lifetime close to the Tao-Eldrup result.

**J1 58 Scaling laws In PZT/Si(001) Thin Films** JUAN RAMÍREZ, ALEXANDER CORTES, WILSON LOPERA, MARIA ELENA GÓMEZ, PEDRO PRIETO, *Universidad del Valle, Physics Department* THIN FLIM GROUP TEAM, Self-affine scaling behavior of ferroelectric $Pb(Zr_{1-x}Ti_x)O_3$ (PZT) thin films grown on Si(001) substrates has been investigated by AFM Atomic Force Microscope. PZT thin films were grown via Rf-sputtering technique at high oxygen pressures and at substrate temperatures 600 $^o$C varying the deposition time and keeping all parameters. growth constant. The $\alpha$-global rough-exponent was founded close to 0.7 indicating a correlated growth. Anomalous scaling behavior was founded in all PZT/Si surfaces. A value of 0.5 for the $\alpha$-local value was founded. The local value of the roughness exponent is associated to the diffusional process on the first stage growth. Saturation roughness showed oscillation dependence with the PZT-thickness. This dependence can be explained by the mismatch between Si substrate and PZT thin film. These results are corroborated calculating the grain size for all samples. This work was supported by COLCIENCIAS under the Excellence Center for Novel Materials Contract no 0043-2005.

**J1 59 Crystal Structure and Relaxor-Type Transition In Praseodymium Doped SBT** JORGE MATA*, ALEJANDRO DURAN*, RAUL ESCAMILLA, *IIM-UNAM Mexico* EDUARDO MARTINEZ*, JESUS HEIRAS*, JESUS SIQUEIROS*, **Centro de Ciencias de la Materia Condensada-UNAM, MEXICO* The effects of Pr substitution and ferroelectric response for the $Sr_{1-x}Pr_xBi_2Ta_2O_9$ ceramic system were studied. Rietveld refined X-ray diffraction indicates that Pr ion progressively replaces Sr in the $A2_1$itam space group structure. The solubility of Pr in the solid solution is around 15 %. The replacement induces change in the crystal structure and as consequence dielectric properties are affected. The displacement of $TiO_6$ octahedra with respect to $Bi_2O_2$ along the polarization axis decreases as Pr is increased. A notable decrease in the transition temperature (Tm) is observed. With Pr substitution the Tm shifts gradually from $\sim$ 305 $^o$C to $\sim$ 120 $^o$C. Apparently, the rotation at the ab-plane ($\beta$) as well the octahedral distortion observed are strongly related to the coupling between Tm and x. However, the tilt angle ($\alpha$) associated to the c-axis don't play an important role as it remains essentially constant. Relaxor type transition is observed as Pr increases due to polar microregions above the nominal ferroelectric transition. Local disorder induced by Pr ion is confirmed by the continuous increase in the diffuseness coefficient according to Isupov's model. Thanks to DGAPA-UNAM and CONACYT for funds through Proj. No. 40604-F, 47714-F, IN116703, IN100903 and to P. Casillas, J. Peralta, M. Sainz.

**J1 60 Thermal stability and interfacial properties of $ZrAl_xSi_yO_z$ films prepared by pulse-laser deposition in high vacuum** XIAOYAN QIU, *Nanjing National Laboratory of Microstructures, Nanjing University & Institute of Physics, Southwest University* HONGWEI LIU, JUNMING LIU,* *Nanjing National Laboratory of Microstructures, Nanjing University* The thermal stability and interfacial properties of $ZrAl_xSi_yO_z$ film prepared by pulse-laser deposition (PLD) in high vacuum have been investigated. X-ray diffraction (XRD) and differential scanning calorimeter (DSC) investigation show that the crystallization temperature of $ZrAl_xSi_yO_z$ film is above 900°C. A dielectric constant of 12.9 (at 1MHz) is obtained by measuring a Pt/$ZrAl_xSi_yO_z$/Pt structure. High-resolution transmission electron microscopy (HRTEM) and X-ray photon spectroscopy (XPS) analyses reveal that an amor-

phous Zr-silicide interfacial layer is formed at 700°C, but $Pt/ZrAl_xSi_yO_z$/Zr-silicide/Si capacitors still have good electrical properties, such as small equivalent oxide thickness of 0.5nm, flat band voltage of 0.43V and low leakage current density of 2.76mA/cm2 at 1V gate voltage.

*Corresponding author

**J1 61 Fatigue endurance property of PZT thin films enhanced by Sr and Ba doping.** YANG WANG, ZHENYU LI, QIYUE SHAO, *Nanjing National Laboratory of Microstructures, Nanjing University* JUNMING LIU,* *Nanjing National Laboratory of Microstructures, Nanjing University & International Center for Materials physics, Chinese Academy of Sciences* PZT thin films with Sr and Ba doping at A site, deposited by sol-gel and PLD method respectively, were investigated in our work. The enhancement of fatigue resistance property with increasing doping content were both observed in two kinds of samples. The experiments of dc conductivity vs temperature reveal that this behavior can be attributed to the reduction of oxygen vacancies, due to the stronger chemical bonding of Sr-O and Ba-O bonds compared to that of Pb-O bond suppressing the volatility of Pb ions and intensifying the stability of the metal-oxygen octahedron, since the defect chemistry is believed to play a key role in the fatigue of perovskite ferroelectrics.

*Corresponding author

**J1 62 Trends in behavior for tunable ferroelectric material** DANIEL POTREPKA, *US Army Research Laboratory* Measurements in an environmental chamber pose problems in effectively coupling to rf- and microwave-tunable, ferroelectric devices. Capacitance can be measured but true device loss is shrouded by losses due to calibration error, impedance matching error from cables and packaging, and vibration interference. In this study, the true device losses of pulsed-laser deposited Barium Strontium Titanate films, at rf frequencies under DC bias are sought using a probe station, calibrated for matching. Breakdown of the device at the higher end of applied voltage and thin film material structure are characterized. Resulting losses and tunability versus temperature are commented upon.

**J1 63 Thermal analysis and evidence of structural transition induced by praseodymium in $SrTiO_3$** *ALEJANDRO DURAN, **FRANCISCO MORALES, *IIM-UNAM* ***LUIS FUENTES, +JAVIER CASTRO, *JESUS SIQUEIROS, **Centro de Ciencias de la Materia Condensada-UNAM, **IIM-UNAM, ***CIMAV-Chihuahua, Chih. MEXICO, +UACJ-Ciudad Juarez, Chih. MEXICO* To explore the nature of ferroelectric behavior induced by Pr ion in the $SrTiO_3$ ceramic, we brought together a combination of Synchrotron x-ray powder diffraction and thermal analysis. Rietveld analysis shows a clear peak splitting strongly suggesting a cubic-tetragonal structural transition when 15 % Pr substitutes the Sr site. To determine the temperature of the structural instability differential thermal analysis at high temperatures (30-900 °C) and specific heat at low temperatures (2-300 K) were performed. The difference in the heat capacity for Pr doped and undoped samples is very small. A plateau in Cp/T-T at 110 K is a clear evidence of the competing effect of two kinds of order parameters, one represented by the polarization and the other by the rotation of the oxygen octahedral in the perovskite structure. Upon heating, DTA analysis shows an unexpected single endothermal broad anomaly at about 118 °C. The occurrence of this thermal anomaly could be related to displacive structural contributions providing unambiguous evidence of diffuse phase transition and of the ferroelectric behavior observed at room temperature. Thanks are due to CONACYT P. 47714-F, DGAPA P. IN100903 and to P. Casillas for technical help.

**J1 64 Structural and Dielectric Characterization of $SrBi_2Ta_2O_9$ Doped with Gadolinium** JORGE MATA, ALEJANDRO DURAN, RAUL ESCAMILLA*, EDUARDO MARTINEZ, JESUS SIQUEIROS, *Centro de Ciencias de la Materia Condensada, UNAM. Apdo. Postal 2681, Ensenada, B.C., Mexico.*IIM-UNAM, Apartado Postal 70-360, Mexico, D. F. 04510.* The results of the study of polycrystalline samples of $SrBi_2Ta_2O_9$ (SBT) doped with Gd, Sr-vacancies and a Bi-excess are presented. XRD structural characterization using Rietveld refinement revealed that the Gd-doped SBT with Sr-vacancies and Bi-excess ($Sr_{0.70}?_{0.15}Gd_{0.15}Bi_2Ta_2O_9$) is single phase. Furthermore, cationic disorder on the $Bi^{3+}$ and $Sr^{2+}$ crystallographic sites is promoted by the addition of the $Gd^{3+}$ ions. Replacement of Gd ions for Sr and vacancies in the SBT structure produces a shift toward lower values of the Curie Temperature (Tc) from 400 to 200 $^o$C in contrast with previous reports in the literature where a notable increase in Tc and the dielectric permittivity are found when the Sr- site is replaced with vacancies. Bi and Gd substitution and the cation vacancies at the Sr site in the $Sr_{0.70}?_{0.15}Gd_{0.15}Bi_2Ta_2O_9$ compound, enhance the structural distortion in the $TaO_6$ octahedra and leads to a larger ferroelectric spontaneous polarization. Acknowledgments: This work was partially supported by DGAPA-UNAM Project N$^o$ IN100903 and CONACYT No. 47714-F and 40604-F. The authors thank Pedro Casillas, M. Sainz, J. Peralta for their technical assistance.

**J1 65 Thermo-Electromechanical Coupling Effects on Ferroelectric Perovskites** XIAOWEI ZENG, *George Washington University* JAMES LEE, *George Washington University* YOUPING CHEN, *George Washington University* We are investigating the thermo-electromechanical coupling effects on ferroelectric perovskite materials. This work is based on a shell model potential with parameters obtained from first-principles calculation. Molecular dynamics simulations are performed to investigate the dynamic response of the ferroelectric perovskites under thermal, mechanical and electric loadings. The phenomena of finite temperature phase transitions and polarization reorientation are observed. The temperature-pressure phase diagram is also obtained.

## J1 66 SUPERCONDUCTIVITY POSTER SESSION

**J1 67 Effects of triplet pairing amplitudes in hybrid junctions of superconductor, ferromagnet, and normal metal.** NA YOUNG LEE, HAN-YONG CHOI, HYEONJIN DOH, We calculate the critical temperature Tc and pairing amplitude of the hybrid junctions of superconductor (S), ferromagnet (F), and normal metal (N) by solving the Usadel equation in the dirty limit. S is a conventional singlet s-wave supercondcutor like Nb. The interface between S and N is modeled in terms of the interface

resistance without the spin flips, while the interface between F and S or F and N is modeled by both the interface resistance and spin flip scatterings, parameterized by, respectively, $\gamma_b$ and $\gamma_m$. The spin flip scatterings induce the triplet pairing components from the singlet component. The Tc of the junction is determined by the critical order parameter, ie., the singlet pairing component. The $\gamma_b$ or $\gamma_m$ changes the Tc of the junctions indirectly by altering the singlet component by modifying the boundary conditions at the interfaces. We calculate the Tc and pairing amplitudes of S/N/F and F/S/F trilayers including $\gamma_b$ and $\gamma_m$ and investigate the effects of the triplet pairing components on the Tc and pairing amplitudes of the trilayers.

**J1 68 Domain patterns in type-I superconducting films.** ANDREJS CEBERS, *Institute of Physics, Salaspils, LV-2169, Latvia* CATHERINE GOURDON, VINCENT JEUDY, TAKANORI OKADA, *Institut des Nanosciences de Paris, CNRS UMR 7588, Universities Paris 6 and 7, France* INSTITUTE OF PHYSICS, UNIVERSITY OF LATVIA TEAM, INSTITUT DES NANOSCIENCES DE PARIS,CNRS UMR 7588, UNIVERSITIES PARIS 6 AND 7 TEAM, Like many other systems (magnetic fluids, Langmuir polarized layers . . . ) type-I superconducting (SC) films exhibit a phase modulation known as the intermediate state (IS). It consists of coexisting domains of the normal state (NS) and SC phases. The striking similarity of the domain patterns for various systems has stimulated the development of general models [1] based on the competition between the interface energy and the long-range interaction between domains. However, for superconductors, the long-range magnetic interaction between domains has to be modified to take properly into account screening currents [2]. This leads to substantial improvement of the description of the IS as it will be illustrated through 3 examples: (i) the impeded growth of NS circular domains, (ii) the stability limit of the circular shape, (iii) the nucleation and collapse of SC domains in the NS phase. [1] A.T. Dorsey and R.E. Goldstein, Phys. Rev. B 57, 3058 (1998) [2] A. Cebers et al, Phys. Rev. B 72, 014513 (2005).

**J1 69 Specific heat of bosons among periodical layers*** MIGUEL A. SOLÍS, *Instituto de Física, UNAM, Apartado Postal 20-364, 01000 México, D.F., MEXICO* MARCELA GRETHER, *Facultad de Ciencias, UNAM, Apartado Postal 70-542, 04510 México, D.F., MEXICO* It is well known that the specific heat of a 3D ideal boson gas shows continuity as a function of the temperature. However, interactionless bosons among periodic plane layers with variable penetrability, show a specific heat jump at the critical temperature, which increases as a function of the layer impenetrability. The jump resembles that of a conventional superconductor instead of that of a laminar cuprate. We expect that inclusion of inter-boson interaction leads to a more realistic specific heat.

*We thank PAPIIT IN111405 and CONACyT 43234-F

**J1 70 Thermodynamic properties of $Ca_{1.82}Na_{0.18}CuO_2Cl_2$ single crystals** KYUNG-HEE KIM, HEON-JUNG KIM, JUNG-DEA KIM, H.-G LEE, SUNG-IK LEE, *POSTECH* NATIONAL CREATIVE RESEARCH INITIATIVE CENTER FOR SUPERCONDUCTIVITY AND DEPARTMENT OF PHYSICS, POHANG TEAM, We report the experimental results on the reversible magnetization of high quality $Ca_{1.82}Na_{0.18}CuO_2Cl_2$ single crystals in the high-pressure condition of about 5.2 GPa. The superconducting transition temperature $T_c$ ( $\sim$ 27 K) of this single crystal is the highest reported in this family. The magnetizations are analyzed using the Hao-Clem model and the high-field scaling law. From these analysis, we have obtained various thermodynamic parameters such as the penetration depth and the critical fields, and clarified the dimensional nature of the superconductors. Even though the doping content between $Ca_{1.82}Na_{0.18}CuO_2Cl_2$ and $La_{1.82}Sr_{0.18}CuO_4$ is same, the physical properties of these materials are quite different. For example, $\lambda_{ab}(0)$ is estimated to be 440 nm, which is larger than that of $La_{1.82}Sr_{0.18}CuO_4$. These changes are totally unexpected in this iso-structural superconductor.

**J1 71 Linear Temperature Dependence of the Resistivity in the Pseudogap State** A.A. ABRIKOSOV, *Materials Science Division, Argonne National Laboratory, USA* A concept is proposed, explaining the characteristic features of the in-plane resistivity of high-$T_c$ layered cuprates above$T_c$: quasi-linear temperature dependence and absence of the residual resistance in the extrapolation of the curve $\rho(T)$ from $T > T_c$ to $T = 0$. This concept is based on the idea of the pseudogap state structure described in previous works by the present author. This work was supported by the Department of Energy under the contracts # W-31-109- ENG-38.

**J1 72 Changes in the superconducting temperature by pressure in $Nb_3Sn$ and its influence in the martensitic transition.** RICHART FALCONI, *UJAT* FRANCISCO MORALES, ROBERTO ESCUDERO, *IIMUNAM* R. WEBB, *UCSD* High pressure experiments performed in a $Nb_3Sn$ single crystal shows changes on the superconducting temperature and in the martensitic transition. Specific heat measurements performed in this crystal shows an anomaly at about 50 K associated to the martensitic transition. At ambient pressure, the electrical resistivity as a function of temperature shows a $T_C$ of 18.7 K with a transition width $\Delta T_C$ (10 to 90 %) of 0.7 K. At low temperatures the R vs T curve show a $T^2$ behavior, specifically in the temperature range from 52 down to 23 K. The superconducting transition temperature decreases in linear form with a rate dTc/dP = - 0.79 K/GPa. The results are discussed in terms of the pressure effects on the martensitic transition via changes in the density of electronic states.

**J1 73 Generating spin current by AC magnetic field** MINHUI SHANGGUAN, *Center of theoretical and computational physics and Department of Physics, The University of Hong Kong, Pokfulam Road, Hong Kong, China* QINGFENG SUN, *Institute of Physics, Chinese Academy of Sciences, Beijing, P.R. China* JIAN WANG, *Center of theoretical and computational physics and Department of Physics, The University of Hong Kong, Pokfulam Road, Hong Kong, China* HONG GUO, *Department of Physics, McGill University, Montreal, Quebec, Canada* We report a theoretical investigation on the possibility of generating pure spin current without an accompanying charge current, by applying a train of magnetic field pulses on the leads of a tunnel junction. When the duration of on-state of the pulse is shorter than the spin relaxation time while the off-state is longer than it, a spin current is driven through the two-probe device coherently. The time averaged spin current is found to be almost a periodic function of the pulse strength. A negative spin current can also be produced for a positive spin chemical potential, due to quantum interference among the Fourier modes of the photon assisted tunneling.

**J1 74 Effect of Electron-Electron Scattering on the Conductance of a Single Quantum Wire*** DANHONG HUANG, *USAF Research Lab* KEN LYO, *Sandia National Labs* Electron-electron scattering conserves momentum and does not dissipate momentum in a low-density system where the Umklapp process becomes forbidden. However, it can still affect the conductance through the energy relaxation of carriers. We show that this effect can be studied with an arbitrary accuracy in a multi-level single quantum wire system with impurity and phonon scattering using a formally exact solution of the Boltzman transport equation. We study the effect of electron-electron scattering on the temperature and density dependence of the conductance at low temperatures. Some unique features in the calculated conductance as functions of the temperature and the density are predicted and physically explained.

*Sandia is a multiprogram laboratory operated by Sandia Corporation, a Lockheed Martin Company, for the U.S. DOE under Contract No.DE-AC04-94AL85000.

**J1 75 Density-matrix renormalization group study of pairing in Holstein-Hubbard model: effect of electronic band structure*** MASAKI TEZUKA, *University of Tokyo* RYOTARO ARITA, *Max-Planck Institute Stuttgart and University of Tokyo* HIDEO AOKI, *University of Tokyo* The density-matrix renormalization group, with a modification [1], is used to directly obtain correlation functions [2] when both electron-electron and electron-phonon interactions are strong with the Holstein-Hubbard model in a region intermediate between the adiabatic (Migdal's) and antiadiabatic limits. We found that the pairing correlation for a one-dimensional system at half-filling does not dominate over the charge density- wave (CDW) correlation, even when the phonon-induced attraction is comparable with the electron-electron repulsion. However, the pairing is shown to become dominant in a trestle lattice where the electron-hole symmetry is absent, which indicates that superconductivity can appear in a manner dependent on the lattice (hence the electronic band) structure even for the Holstein-Hubbard model with on-site interactions. Band- filling dependence is also discussed. [1] M. Tezuka, R. Arita, and H. Aoki, Physica 359B-361B, 708 (2005). [2] M. Tezuka, R. Arita, and H. Aoki, Phys. Rev. Lett. 95, 226401 (2005).

*This work is in part supported by a Grant-in-Aid for Science Research on Priority Area from the Japanese Ministry of Education.

**J1 76 Dynamics of magnetic flux jumps in highly dense $MgB_2$ samples** C. ROMERO, O.A. HERNANDEZ, *IF-UAP* F. MORALES, *IIM-UNAM* A. DURAN, D.H. GALVAN, *CCMC-UNAM* R. ESCUDERO, *IIM-UNAM* Flux jumps in magnetization curves were investigated experimental and theoretically in a polycrystalline $MgB_2$ dense sample. We performed magnetization cycles of M-H at different temperatures. Theoretical calculation were performed using an adiabatic critical-state model, that considers the heating effects due to the motion of flux lines, the instability process that originates flux jumps, and the flux redistribution towards a new metastable critical state. The flux jump and temperature dependence in the final state were successfully reproduced from experimental M-H curves. The number of the flux jumps and the jump size increase as the temperature is decreased corroborating the typical flux jump in hard type-II superconductor.

**J1 77 Flux jumps in irradiated $MgB_2$ dense samples** E. VERDIN, *DF-UNISON* C. ROMERO, *IF-UAP* F. MORALES, *IIM-UNAM* E. ADEM, J. RICKARDS, *IF-UNAM* A. DURAN, D.H. GALVAN, M.B. MAPLE, *UCSD* R. ESCUDERO, *IIM-UNAM* This work shows magnetic flux jumps and changes in specific heat measurements studied in $MgB_2$ dense bulk samples irradiated: with $^{60}Co$ (500 mrad), electrons (500 mrad), and protons ($1x10^6$ $cm^2$). Magnetic susceptibility measurements $\chi(T)$ show that the Tc ( $\sim$ 38.5 K) is independent of irradiation doses. M vs H data display flux jumps strongly dependent of the temperature. Specific heat measurements show an increase in the magnitude of Cp/T vs T curves just in the transition temperature for the irradiated protons, suggesting enhanced local disorder. The behavior of specific heat data at low temperature is analyzed using a two band model in order to clarify the effect of local disorder with the gap superconducting structure.

**J1 78 Vortex nucleation in a Layered Superconductor*** PATRICIA SALAS, *Posgrado en Ciencia e Ingenieria de Materiales, UNAM, MEXICO* MIGUEL A. SOLIS, *Instituto de Fisica, UNAM, Apartado Postal 20-364, 01000 Mexico, D.F., MEXICO* We propose that the paired fermions (electrons) in a layered superconductor, such as cuprates, be treated as interacting bosons in the Bose-Einstein regime. We solve the time dependent Gross-Pitaevskii equation for these bosons inside a rotating layered superconductor which is simulated by an external periodical potential of the Kronig-Penney type perpendicular to the planes while bosons are allowed to be free in the other two directions [1]. Among the several numerical methods that exist to solve the Gross-Pitaevskii Equation, we use a time iteration procedure, based on the discretization of time and space [2]. We annalize the vortex nucleation and its influence in the thermodynamic properties of the superconductor. [1] See M.A. Solis and M. Grether, ''Specific heat of bosons among periodical layers,'' in this proceedings. [2] S. K. Adhikari and P. Muruganandam, J. Phys. B **35**, 2831 (2002).

*We thank PAPIIT- IN111405 and CONACyT 43234-F

**J1 79 Gap Distributions in Cuprate Superconductors*** ASHOT MELIKYAN, *University of Florida* BRIAN M. ANDERSEN, *University of Florida* TAMARA S. NUNNER, *Institute of Theoretical Physics, Berlin* P. J. HIRSCHFELD, *University of Florida* Recent Scanning Tunneling Microscopy (STM) data on $Bi_2Sr_2CaCu_2O_{8+x}$ impose stringent restrictions on the spatial distribution of the superconducting order parameter and scalar potential due to impurities. In Ref. [1] it was shown that these distributions are inconsistent with a conventional mean-field approach where the inhomogeneities in the LDOS are driven by a scalar impurity potential. It was further demonstrated that the salient experimental features of the LDOS spatial modulations can be obtained if the pairing coefficient itself is assumed to be enhanced by the dopant atoms. Here, we report additional features of the LDOS that support the conclusions of Ref. [1]. [1] T. S. Nunner, B. M. Andersen, A. Melikyan, and P. J. Hirschfeld, Phys. Rev. Lett. 95, 177003 (2005).

*This work was supported by A. V. Humboldt Foundation (T.S.N.), Institute of Fundamental Theory (A.M.), and ONR Grant No. N00014-04-0060 (P.J.H. and B.M.A.)

**J1 80 Holonomic quantum computation using rf superconducting quantum interference devices coupled through a mi-**

**crowave cavity** JIADA SUN, PENG ZHANG, ZIDAN WANG, CHANGPU SUN, We propose a different scheme to realize holonomic quantum computation with rf superconducting quantum interference device (SQUID) qubits in a microwave cavity. In this scheme associated with the non-Abelian holonomies, the single-qubit gates and a two-qubit controlled-PHASE gate as well as a controlled-NOT gate can be easily constructed by tuning adiabatically the Rabi frequencies of classical microwave pulses coupled to the SQUIDs. The fidelity of these gates is estimated to be possibly higher than 90% with the current technology.

**J1 81 An improved system for SQUID-detected MRI at microtesla fields** S. BARRIGA, P. KOO, A. HUNT, S. BUSCH, D. KINION, M. HATRIDGE, W. MYERS, M. MÖßLE, A. PINES, JOHN CLARKE, *UC Berkeley and LBNL* M. MÜCK, *U. of Giessen* We perform magnetic resonance imaging (MRI) by detecting protons precessing at 5.6 kHz in a 132-$\mu$T field with a superconducting gradiometer coupled to a superconducting quantum interference device (SQUID). We have designed, built, and tested an improved system with an increased signal to noise ratio, intended to reduce data acquisition time and/or increase spatial resolution. By using a SQUID with a lower noise and an input coil inductance optimally matched to that of the gradiometer we have reduced the intrinsic magnetic field noise referred to one pickup loop by a factor of four to 0.4 fT $Hz^{-1/2}$. To take advantage of this reduced noise we have enclosed the entire system in a 6-mm thick aluminum shield that attenuates 5.6-kHz magnetic noise by a factor of about 60. Our new coils provide more homogeneous imaging fields and field gradients and are more compact than those employed in our prototype. Finally, we align the precession field perpendicular to the fields generated by the building elevator to minimize shifts in the precession frequency. We present images obtained in our new system. This work was supported by the USDOE.

**J1 82 Pulsed Tera-hertz Radition from Femto-second Laser Excited Superconductive $YBa_2Cu_3O_{7-\delta}$ Antenna** SHYH-SHII PAI, CHENG-CHUNG CHI, *Department of Physics, National Tsing Hua University, Hsinchu, Taiwan, R. O. C.* We have observed the ultrashort electromagnetic pulse radiation from a current-biased bow-tie structure of $YBa_2Cu_3O_{7-\delta}$ thin film dipole antenna on MgO using 100 fs, 750 nm laser pulses. With the electro-optic detection, we obtained the THz pulses with 1.0 ps full width at half maximum, containing frequency components up to 1.0 THz. The THz peak amplitude dependence shows the saturation and a nonlinear behavior with a higher excitation pumping power and with the applied bias currents. The saturation on the dependence with the excitation powers exhibits the bolometric heating in nature. However, the nonlinear characterization of the THz radiation from the superconductive thin film antenna revealed that the inadequacy of pure supercarrier approximation on a two-fluid model. The ultrashort transient response and the deviation from the classical theory are discussed in relation to the quasiparticle dynamics of the nonequilibrium mechanism.

**J1 83 Vortex avalanche in gold-coated and finite-sized $MgB_2$ thin films.** EUN-MI CHOI, HYUN-SOOK LEE, SUNG-IK LEE, *POSTECH* Å. A. F. OLSEN, D.V. SHANTSEV, T.H. JOHANSEN, *University of Oslo* The vortex avalanches in carbon-free $MgB_2$ thin films were studied using magneto-optical imaging. The main focus of this study was the effect of a gold coating and the sample size on the occurrence of the dendritic flux avalanches. For this purpose, we prepared two different sets of $MgB_2$ films. In the first, the films had gold coatings of various thicknesses, and in the second set bare $MgB_2$ films were patterned into long strips of different widths. The dendritic flux avalanches essentially disappeared for gold coatings thicker than 2.5 $\mu$m. Also for strip widths less than 0.33 $mm^2$ the formation of flux dendrites are suppressed. The results are consistent with a thermomagnetic origin of the dendritic instability.

**J1 84 Effect of disorder in neutron irradiated $MgB_2$ thin films investigated by transport measurements in high magnetic field** VALERIA FERRANDO, *CNR-INFM-LAMIA, University of Genova* ILARIA PALLECCHI, *CNR-INFM-LAMIA* CHIARA TARANTINI, MARINA PUTTI, *CNR-INFM-LAMIA, University of Genova* XIAOXING XI, *The Pennsylvania State University* CARLO FERDEGHINI, *CNR-INFM-LAMIA* We analyse a series of $MgB_2$ thin films grown by Hybrid Physical Chemical Vapor Deposition (HPCVD), where disorder is introduced by neutron irradiation. Increasing progressively the neutron fluence, $T_c$ monotonously decreases down to 2K and $\rho_0$ increases by one order of magnitude. A complete characterization of this series of samples is presented. In particular, we propose high field magnetoresistivity and critical field as a method to study the effect of disorder in the two bands. Differently from polycrystalline samples, $H_{c2}$, after a first increase at the lowest neutrons fluences, only weakly depends on the irradiation level. This suggests that in thin films $H_{c2}$ and resistivity are affected by different mechanisms induced by irradiation. From a quantitative analysis of the magnetoresistivity curves as a function of the angle between the field and the crystalline axes, we extract the scattering times in $\pi$- and $\sigma$-bands. We find that the unirradiated films have less mobile $\pi$ − bands than $\sigma$ − ones; upon irradiation, the scattering rates of both bands progressively increase, allowing to estimate resistivity values consistent with the measured ones.

**J1 85 Tuning inter-band scattering mechanism in $MgB_2$ through ion irradiation*** S. PATNAIK, S.D. KAUSHIK, *School of Physical Sciences, Jawaharlal Nehru University, New Delhi 110067, India* The effect of light and heavy ion irradiation on Magnesium Diboride thin films is studied. $MgB_2$ is a two-band superconductor and its electromagnetic response is determined by the relative strength of scattering between the isotropic $\pi$ band vis á vis the planar $\sigma$ band. Our results indicate that by suitably choosing the type of ion, fluence, and energy we can control the inter and intra band scattering and thereby alter the physical properties of this intermetallic superconductor. For example, we find that while the anisotropy in upper critical field can be increased with point defects created by $Si^{+8}$ ions, it can only be decreased by extended defects formed by heavy ion $Au^{+15}$ at same fluence. Similarly while the upper critical field in the direction parallel to c-axis of the film shows enhancement post irradiation with heavy ions, it exhibits some decrease with light ion irradiation. The curvature in H-T phase diagram is also dependent on the defect type. We understand these phenomena within the framework of disorder in multiband superconductivity.

*This work was funded by DST & CSIR, India

**J1 86 Study of $MgB_2$ Films on Niobium Substrate*** CHENGGANG ZHUANG, DAN YAO, FEN LI, KAICHENG ZHANG, QINGRONG FENG, ZIZHAO GAN, *School of Physics and State Key laboratory for Artificial Microstructure and Mesoscopic*

*Physics, Peking University, Beijing 100871, P. R. China* We have successfully fabricated polycrystalline $MgB_2$ films on metal niobium by using the hybrid physical-chemical vapor deposition technique. $T_C$ (onset) of these samples ranged from 38.5 K to 39.4 K, with $\Delta T$, 0.1 K $\sim$ 0.3 K. The observed $T_C$ was the highest among all the $MgB_2$ films over metal substrates reported to date. Thicknesses of the films were about 1.0 $\mu$m. XRD indicated that lattice constants approached the values of the bulk. The film surface was visible with hexagonal plate-shaped $MgB_2$ crystallites but not dense enough, shown by SEM observation. A line scanning spectra of EDX on the cutting cross section exhibited that there was an oxygen-rich region at the interface. Also, the diffusion of the Mg atoms deeply into the film has resulted in the tenacity and adherence of the film to the substrate. TEM investigation proved the existence of this buffer layer, $\sim$ 100 nm. Estimated using magnetic hysteresis loops and Bean model, $J_C$ was above $2.30 \times 10^4$ A/cm$^2$ at 10 K in zero field. The synthesis of $MgB_2$/Nb films with thickness above one micron, showing certain tenacity, is an important and significant step towards the application of the $2^{nd}$ generation $MgB_2$ superconductor wires or tapes.

*This work is supported by NSFC under contract No. 50572001

**J1 87 Nonequilibrium Photoresponse of Current-Biased, Epitaxial $MgB_2$ Microbridges** M. KHAFIZOV, D. WANG, X. LI, R. SOBOLEWSKI, *University of Rochester, Rochester, NY 14627* Y. CUI, X. X. XI, *Pennsylvania State University, University Park, PA 16802* We report nonequilibrium, subnanosecond-wide voltage transients generated by current-biased $MgB_2$ microbridges excited by 100-fs optical pulses. Our epitaxial $MgB_2$ films were grown by the HPCVD technique and the microbridge structures, embedded into coplanar waveguides, were patterned by a conventional photolithography and ion milling. The electrical photoresponse transients, measured in the superconducting state, could be decomposed into two elements: the fast, $\sim$ 100-ps-wide, dominating pulse attributed to the kinetic inductive response, and the slow, several-ns-long signal representing the thermal resistive response. The characteristics of the fast response follow the Rothwarf-Taylor model, although in order to explain the peculiar features of this nonequilibrium signal one needs to incorporate into the model the two distinct superconducting gaps. The nonequilibrium photoresponse of $MgB_2$ microbridges makes them attractive as fast photodetectors.

**J1 88 The loss of the anisotropy in the electrical conductivity in $MgB_2$ under pressure** ULISES ESTEVEZ, PABLO DE LA MORA, *Depto. de Fisica, Fac. de Ciencias, UNAM, Mexico* $MgB_2$ is a multiple band superconductor, with two $\sigma$-bands and two $\pi$-bands. The $\sigma$-bands that are highly anisotropic are the responsible of the superconductivity in this compound. It has been shown that with Sc, C and Al doping the $\sigma$-bands reduce their anisotropy, but for the case of Al and C doping the bands fill up and as consequence the number of $\sigma$-carriers reduce and disappear which leads to $T_c$ reduction. In this work it is shown that pressure reducing the $MgB_2$-cell parameters which leads to an increase of the interplane $\sigma$-orbitals overlap. This leads to an increase of the $\sigma$-bands electrical conductivity in the c-direction, in other words, a reduction of the anisotropy of the $\sigma$-bands, on the other hand there is no band filling therefore no reduction of $\sigma$-carriers. This reduction as function of pressure follows a similar trend as $T_c$, thus showing that the anisotropy in the $\sigma$-bands could be an important factor of the high $T_c$ in $MgB_2$.

## J1 89 MAGNETISM POSTER SESSION

**J1 90 Research on Dynamic Model Building of Active Magnetic Bearing** JIAN SHI, GUO-ZHENG YAN, KUN-DONG WANG, *820 Institute, School of Electron, Information and Electrical Engineering, Shanghai Jiao Tong University, Shanghai, 200240, China* As for AMB(active magnetic bearing), many researchers and engineers use theoretical method presented by G. Schweitzer to get the dynamic model. But the model built in this way can not suspend the magnetic system effectively sometimes. Furthermore if any original physical parameter is changed or lost, the theoretical method will be out of work at all. This paper presents a simple and convenient experimental method to build the primary dynamic model of AMB. There is a special advantage that this process has no relation to any original parameter except the mass of rotor which can be obtained easily however. Base on the dynamic model, feedback control system is designed which can make AMB system suspended stably. Through online identifying with frequency method we get the so-called precise model. Finally three models from experiment, theoretical method and online identification respectively, are compared. Result shows that the model from experiment is much closer than that from theoretical method to the precise model.

**J1 91 Spin liquids of a frustrated SU(3) quantum magnets on a triangular lattice** PENG LI, SHUN-QING SHEN, *Dept. of Phys., The Univ. of Hong Kong, Pokfulam Road, Hong Kong, China* The spin disorder state of the bilinear-biquadratic model near the edge of antiferromagnetic region on a triangular lattice is studied in a point of view of frustrated SU(3) quantum magnets. A mean field theory in the quasi-particle representation is established. From the quasi-particle spectra, we show that the density-of-states rise linearly from zero in the region where the SU(3) symmetry is broken. As a consequence, the specific heat at low-temperature in this region exhibits the power law, $C \propto T^2$, which may give an explanation for a recent experiment on NiGa2S4. A finite susceptibility is also obtained in the zero temperature limit, which is also in agreement with the experiment.

**J1 92 Linear and nonlinear magneto-optical properties of Fe/Au multilayered films and Fe-Au alloy films** Y. H. HYUN, Y. P. LEE, *q-Psi and Dept. of Physics, Hanyang Univ., Seoul, Korea* K. W. KIM, *Dept. of Physics, Sunmoon Univ., Asan, Korea* R. YANG, Q. Y. JIN, *Dept. of Optical Science & Engineering, Fudan Univ., Shanghai, China* In this study, the magnetic and the magneto-optical properties of Fe/Au multilayered films (MLF) and Fe-Au alloy films were comparatively studied to elucidate the peculiar magneto-optical properties of Fe/Au MLF. (3.0 nm Fe / $t_{Au}$)$_{20}$ MLF (where $t_{Au}$ = 1.0, 2.0, 2.5 and 3.0 nm) and $Au_{1-x}Fe_x$ ($0 < x < 1$) alloy films of about 100 - 150 nm in thickness were prepared by rf-sputtering onto glass substrates at room temperature. The structures of these films were studied by

x-ray diffraction. The magnetic properties were investigated by using a vibrating sample magnetometer. The magneto-optical properties of Fe-Au alloys and Fe/Au MLF were measured by using magneto-optical Kerr effect (MOKE) and magnetization-induced second-harmonic generation (MSHG). The MOKE was obtained in the equatorial mode, and the MSHG measurements were performed in the longitudinal mode. The MSHG results were analyzed in connection with the MOKE and the VSM results.

**J1 93 Magnetic Properties and Electronic Structure in Transition Metal Doped $La_{0.5}Ca_{0.5}MnO_3$** K.K. YU, S.J. JUN, J.S. PARK, J.Y. KIM, Y.P. LEE, *q-Psi and Dept. of Physics, Hanyang University, Seoul, Korea* K.H. HAN, *Proton Engineering Frontier Project, Korea Atomic Energy Research Institute, Dejeon, Korea* Y.S. LEE, *Division of information Communication and Computer Engineering, Hanbat National University, Daejeon, Korea* J.-H. KANG, *Department Nano and Electronic Physics, Kookmin University, Korea* The magnetic properties of $La_{0.5}Ca_{0.5}Mn_{0.98}TM_{0.02}O_3$ (TM = Cr, Ti) perovskites were studied by using the temperature dependences of magnetization and coercive field. The transition-metal doping like $La_{0.5}Ca_{0.5}Mn_{1-y}TM_yO_3$ (TM = transition metal) can alter the $Mn^{3+}/Mn^{4+}$ ratio, and lead to significant modifications in the magnetic properties. The observed reductions of Curie temperature and magnetization are interpreted with the calculated ratio of $Mn^{3+}/Mn^{4+}$ according to the Curie- Wiess law. The value is determined to be 0.48 for the TM-doped samples. The Mn L- and O K-edge were also measured by x-ray absorption fine-structure spectroscopy. The domain- wall pinning was investigated, as well, with the temperature dependence on coercivity at a constant field.

**J1 94 Magnetic behaviour of $Sr_{2-x}La_xIrO_4$** CARLOS COSIO, GUSTAVO TAVIZON, *Depto. de Fis. y Quimica Teorica, Fac. de Quimica, UNAM, Mexico* PABLO DE LA MORA, *Depto. de Fis., Fac. de Ciencias, UNAM, Mexico* ROBERTO ESCUDERO, *Inst. de Inv. en Materiales, UNAM, Mexico* Magnetic properties of $Sr_2IrO_4$ are an interesting topic because the anisotropic behaviour showed in the single crystal case, as well to the variable valence states of iridium. By solid state reaction we have obtained polycrystalline samples of the solid solution $Sr_{2-x}La_xIrO_4$ and performed structural refinements based on the X-ray powder pattern. We have observed that, as a consequence of distortions in the [IrO6] octahedra, the symmetry of the compounds in the solid solution $Sr_{2-x}La_xIrO_4$ goes from the $K_2NiF_4$ (SG 139) type to $I4_1/acd$ (SG 142). This explanation also is supported by internal parameters optimization with electronic structure calculations using the Wien2K code. On the other hand, magnetic and electrical behaviour characterization of samples in the range of 2-300 K shows that this system can be thought as a weak ferromagnet in all the solubility range. For the high temperature regime the observed effective magnetic moment of iridium ion diverges from the free ion case.

**J1 95 Field dependence of RF susceptibility in the vicinity of a ferromagnetic transition in single crystals $CeAgSb_2$** R. PROZOROV, M.D. VANNETTE, S.A. LAW, S.L. BUD'KO, P.C. CANFIELD, *Ames Laboratory and Department of Physics and Astronomy, Iowa State University, Ames, Iowa 50011* A 10 MHz resonant technique was used to study ferromagnetic transition in single crystals $CeAgSb_2$. Detailed measurements of field and temperature dependencies of the dynamic susceptibility in the vicinity of the ordering temperature were performed. It was found that a sharp peak in zero-field response rapidly smears out in a weak ( $\sim$ 100 Oe) magnetic field. Obtained results are compared to DC magnetic susceptibility and resistivity, - both showing no similar effect. The possible relation our measurements to study dynamics of a ferromagnetic transition is discussed.

**J1 96 Determination of complex magnetism in a homologous series of compounds.*** R.W. MCCALLUM, Y. JANSSEN, TA. LOGRASSO, K.A. GSCHNEIDNER, JR., V.K. PECHARSKY, B.N. HARMON, *Ames Laboratory, Iowa State University, Ames IA 50011* $Pr_{(n+1)(n+2)}Ni_{n(n-1)+2}Si_{n(n+1)}$, where n = 2, 3, and 4, forms a homologous series of hexagonal compounds whose basic structural unit is a trigonal prism of Pr atoms with its axis parallel to the c-axis. Between 100 and 400 K, their dc susceptibility, $\chi$s measured with H$||$c and H$\perp$ c on a single crystal follows a Curie-Weiss law. In all compounds, the component of M$||$c orders ferromagnetically with T*c* increases with n. For H$\perp$ c, a peak is observed in the low−field M vs T plots below Tc suggesting antiferromagnetic order. For H$\perp$ c at 5 K, all three compounds exhibit a metamagnetic transition between 2 T and 3 T. Based on the systematics of the properties of the members of the series, a model for site specific interactions has been developed for comparison with first principles calculations.

*Ames Laboratory is operated for the US Department of Energy by Iowa State University under contract number W−7405−ENG−82.

**J1 97 The spin structure of maghemite investigated by $^{57}Fe$ NMR** SEONG-JOO LEE, SOONCHIL LEE, *Korea Advanced Institute of Science and Technology* Maghemite( $\gamma$-$Fe_2O_3$) is a ferrimagnetic material known for a long time but its detailed spin structure is not fully understood yet. Interpretation of the hyperfine field measured by the Mössbauer study, which has been the main tool to study local spin structure of this material, has been controversial. Maghemite has an inverse spinel structure where magnetic Fe ions can occupy either the octahedral or the tetrahedral sites. The NMR spectrum shows two separate peaks in zero external field. We split these peaks clearly by applying external magnetic field and compared the peak intensities. The result shows that the hyperfine field at the nuclear spins in the octahedral site is larger than that in the tetrahedral site. The field dependence of the resonance frequency shows that the spins at the octahedral site are antiparallel with external field while those at the tetrahedral site are canted and parallel to external field.

**J1 98 Spin structure of NiFe/FeMn/NiFe trilayers** A.M. ALSMADI, *Physics Department, Hashemite University, 13115 Zarqa, Jordan and Intense Pulse Neutron Source, Argonne National Laboratoy, Argonne IL 60439* S.G.E. TE VELTHUIS, G.P. FELCHER, *Material Science Division, Argonne National Laboratory, Argonne, IL 60439* H.G. YOON, C.G. KIM, *Department of Material Science and Engineering, Chungnam National University, Daejon 305-764, South Korea* Using polarized neutron reflectometry we studied the layer-by-layer spin structure of NiFe(t)/FeMn(15nm)/NiFe(5nm) trilayers with, t = 3.8, and 12 nm in. For both samples the hysteresis curves show two clearly separated loops, each corresponding to the magnetization reversal of one of the two NiFe layers. For the first sample of t = 3.8 nm the neutrons were reflected without undergoing a spin inversion, indicating that at all fields the magnetization of both NiFe layers are

either parallel or antiparallel to the field. However for the second sample of t = 12 nm, at the field where the magnetization of the top NiFe layer starts being hysteretical, the presence of non-zero neutron spin-flip reflectivities signals that some component of the magnetization is perpendicular to the applied field at some depth in the film. The data are consistent with a magnetic configuration where the NiFe layer magnetizations are canted with respect to each other. The polarized neutron results are discussed in terms of the detail FM/AF/FM interactions.

**J1 99 Superlattice effects on spin precession in lateral ferromagnetic heterostructures*** NIKOLAY POLUSHKIN, STEVEN MICHALSKI, ROGER KIRBY, *Department of Physics and Astronomy, University of Nebraska-Lincoln, 68588-0111, Lincoln, NE* FAST MAGNETIZATION DYNAMICS LABORATORY TEAM, Wang and Tilley have developed a model to describe spin wave behavior in systems of magnetic stripes separated by non-magnetic spacers.[1] A key parameter defining spin-wave excitation features in periodic systems is the QD product, where Q is the wavenumber of excited magnons and D the superlattice period. In the long-wavelength limit when QD$<<$1, spin-wave frequencies can be calculated analytically. We have extended the Wang and Tilley model to describe spin-wave behavior in striped media with stripes of two different magnetizations. The analysis reveals the existence of a basic difference in the spectra for different geometries of the applied magnetic field. For instance, two dominating modes occurring under parallel field orientation reduce to a single mode if the field is oriented in the transverse direction. This crossover reflects the different arrangement of the effective medium permeability tensor, which depends on the geometry of the field. This analysis is applied to our pump-probe studies of patterned heterostructures of submicron-width Fe-V stripes. [1]X.Z. Wang and D.R. Tilley, Phys. Rev. B 50, 13472 (1994).

*Work supported by NSF-MRSEC and the W. M. Keck Foundation

**J1 100 Spin-state Transition Associated with the Magnetization Jump on $Y_{1-x}Sr_xCoO_{3-\delta}$ Compounds (x=0.67, 0.75)** M. IZUMI, Y.F. ZHANG, S. SASAKI, *Tokyo University of Marine Science and Technology* O. YANAGISAWA, *Yuge National College of Maritime Technology* Perovskite-type compounds $Y_{1-x}Sr_xCoO_3$ (x=0.67, 0.75) were prepared by the conventional solid state method and sintered under air and $O_2$ flow. There is a DC magnetization jump during the field cooling at 0.01 T and then it comes normally back to high temperature in the specimens, which is called as magnetic memory effect. The $Co^{3+}$ ions spin state transition from low to intermediate state results in the magnetization jump. The jump temperature ($T_J$) and magnetization increase with the x increases. With increasing the magnetic field, the magnetization jump disappears. Air-processed samples exhibit higher $T_J$ and larger magnetization than $O_2$-processed samples. The main reason is the different content of $Co^{3+}$ ions due to the oxygen deficiency under the different prepared conditions. Samples with x=0.75 show the higher Curie temperature ($T_C$) and at almost the same temperature the cusp appears in the zero-field curve. At the same time, there is another small cusp in the zero-field curve in x = 0.75 samples.

**J1 101 Scaling of hysteresis in phenomenological models of thin ferromagnetic films** ESHEL FARAGGI, *Physics Department, Florida International University, Miami, Florida 33199* Explicit solutions are derived for several phenomenological models of magnetization reversal in thin ferromagnetic films driven by a saw-tooth magnetic field. For a domain wall velocity that is linear in the magnetic field it is found that the dynamic coercive field, and hence the scaling of hysteresis, follows a square-root power-law in the slope of the magnetic field, shifted by the depinning field. For a more general domain wall velocity different power-law exponents are found, yet the overall form for the scaling of the area of the hysteresis loop remains a power-law shifted by the depinning field. This shifted power-law could be interpreted to be a crossover between adiabatic and dynamic regimes.

**J1 102 Magnetic Properties and Magnetization Dynamics in Amorphous Ferromagnetic Microwires*** JOÃO PAULO SINNECKER, RAFAEL NOVAK, *Instituto de Física - Universidade Federal do Rio de Janeiro - CP 68528 - 21941-972 - Rio de Janeiro - BRAZIL* The dynamics of the domain walls during magnetization reversal processes in amorphous ferromagnetic microwires is studied. The studies have been based in measurements made in bmagnetic bistable $Fe_{77.5}Si_{7.5}B_{15}$ microwires. In bistable microwires the magnetization reversal process generally happens through the propagation of a single domain wall along the axial direction, i.e., a large Barkhausen jump. This reversal process is initiated at the wire ends, where a complex domain structure, characterized by the presence of closure domains, is found. Samples with diameters between 20 and 40 $\mu$m, and lengths between 7 and 12 centimeters have been studied. The dynamics has been investigated through the analysis of the signal induced in search coils by the domain walls movement. The influence of externally applied magnetic fields in the dynamics of domain wall propagation has been investigated. Through these studies it was possible to distinguish the different magnetization processes taking place at the extremities and the central part of the microwires.

*Authors would like to thank FAPERJ and CNPq.

**J1 103 Dissipative dynamics of vortices in a spiral state and transport in the spin-glass phase of $La_{2-x}Sr_xCuO_4$** V. JURICIC, *Institute for Theoretical Physics, Univ. of Utrecht* L. BENFATTO, *Dept. of Physics, Univ. of Rome ''La Sapienza,'' Italy* A.O. CALDEIRA, *Inst. of Physics, Univ. of Campinas, Brazil* C. MORAIS SMITH, *Institute for Theoretical Physics, Univ. of Utrecht* Doping of an antiferromagnet with holes may lead to a spiral rearrangement of the spins, as it has been argued by Shraiman and Siggia. The formation of a spiral is consistent with the incommensurate magnetic order observed by the neutron scattering experiments in the spin-glass phase of $La_{2-x}Sr_xCuO_4$. The spiral state has a chiral degeneracy that leads to the formation of topologically nontrivial vortex-like defects. We propose that the dissipative dynamics of these defects is responsible for the transport properties in the spin-glass phase of cuprates [1]. Using the collective-coordinate method, we show that the defects are coupled to a bath of magnons. The resulting effective action, after the magnons have been integrated out, indicates that the motion of the defects is damped due to the scattering by the magnons. Assuming that the holes are attached to the vortices, we have calculated the corresponding in-plane resistivity, which exhibits an anisotropy and linear temperature dependence in agreement with experimental data. References: [1] V. Juricic, L. Benfatto, A. O. Caldeira, and C. Morais Smith, Phys. Rev. B **71**, 064421 (2005).

**J1 104 Spin fluctuations and quantum criticality in a CePt ferromagnetic Kondo lattice** JULIO LARREA J., M.B. FONTES, E. BAGGIO-SAITOVITCH, *Centro Brasileiro de Pesquisas Físicas, Brazil* A. EICHER, *Technical University of Braunschwaig, Germany* M. CONTINENTINO, *Instituto de Física, Universidade Federal Fluminense, Brazil* We report on an study of the quantum critical behavior of a ferromagnetic (FM) CePt Kondo lattice using ac susceptibility ($\chi_{ac}$) and electrical resistance ($R(T)$) measurements under high pressures ($P \leqslant 15$ GPa). Our results shows that the FM ordering disappears at the critical pressure $P_C \sim 12.1$ GPa, which is seen as a vanishing of the Curie temperature ($T_C$) and the anisotropic FM magnons ($\Delta$). This $P_C$ is taken as a quantum critical point (QCP) and separates the FM ordering from paramagnetic (PM) state at zero temperature. In the vicinity of $P_C$, a non Fermi liquid behavior (NFL) is observed in the $R(T)$ data as a temperature dependence $T^{1.3}$, which is ascribed to the FM-QCP transition. Beyond the QCP, the system recovers the truly Fermi liquid (FL) behavior. For our knowledge, CePt is the only Ce Kondo lattice that shows a direct FM-QCP transition [1]. Our analysis of the $R(T)$ data, using scaling relations and a spin wave scenario, suggest that the two dimensional FM spin fluctuations is the mechanism to accounts for this ferromagnetic instability. [1] J. Larrea J. et al, Phys. Rev. B 72, 035129 (2005).

**J1 105 Magnetism and hybridization effects in UCuSn** SAMI EL-KHATIB, ANNA LLOBET, *LANSCE-LC, Los Alamos National Laboratory, Los Alamos* AGUS PURWANTO, *Neutron Scattering Laboratory, BATAN, Serpong, Tangerang 15314, Indonesia* A. ALSMADI, *Physics Department, Hashemite University, 13115 Zarqa, Jordan* HEINZ NAKOTTE, *Physics Department, New Mexico State University, Las Cruces NM 88003* UCuSn crystallizes in an orthombically-distorted structure that is closely related to the hexagonal GaGeLi structure. Bulk studies reveal that UCuSn undergoes two magnetic transitions at about 60 and 25 K. Here, we present more detailed neutron-diffraction studies that performed on the High-Intensity Powder Diffractometer (HIPD) at the Manuel Lujan, Jr. Neutron Scattering Center at Los Alamos. Neutron-diffraction studies provide clear evidence for a non-collinear configuration of the magnetic moments in both magnetic phases. We propose a simultaneous existence of two magnetic allowed-symmetry structures as one possible explanation to fit the observed magnetic intensities below 25 K. We will discuss the relationship between magnetic and structural properties in UCuSn. We observe regular thermal contraction with decreasing temperature down to 60 K, below which we observe discontinuities for the interatomic spacings, $d_{U-U}$, $d_{U-Cu}$ and the cell parameters, which provides a measure of the hybridization effects in UCuSn. We were able to correlate the structural changes with the magnetism in UCuSn.

**J1 106 Hartree-Fock calculations of the frustrated 2D Hubbard model*** MATTHEW ENJALRAN, *Southern CT State University* Motivated by recent work on the materials $Na_xCoO_2 \cdot yH^2O$ and a class of organic conductors ($\kappa-(BEDT-TTF)^2X$), where strongly correlated electrons are confined to a geometrically frustrated triangular lattice, we investigate the frustrated Hubbard model via mean−field theory. Were port preliminary results from Hartree−Fock calculations of the charge and magnetic properties of our model on the triangular and square lattices. We also discuss the potential application of the constrained path quantum Monte Carlo (CPQMC) method to the study of frustrated 2D Fermi systems.

*We acknowledge the support of the CSU Research Grant program.

**J1 107 Colossal resistivity change besides magnetoresistance: an extended theoretical framework for electronic transport of manganites** SHUAI DONG, KEFENG WANG, *Nanjing National Laboratory of Microstructures, Nanjing University* HAN ZHU, *Department of Physics, Princeton University, Princeton* XIAOYAN YAO, *Nanjing National Laboratory of Microstructures, Nanjing University* JUNMING LIU,* *Nanjing National Laboratory of Microstructures, Nanjing University & International Center for Materials physics, Chinese Academy of Sciences* Current theoretical approaches to manganites mainly stem from magnetic framework, in which the electronic transport is thought to be spin-dependent. However, quite a number of experimental observations can yet not be reasonably explained. An extended framework for electronic transport of manganites has been proposed, in which the total resistivity has been partitioned into two parts: $\rho_s$ and $\rho_c$ in terms of two different mechanisms: spin-dependent and charge-dependent. Correspondingly, the colossal magnetoresistance (CMR) classification inherited from Aliaga et al has been extended as: CMR2 and XR, where CMR2 is the classical spin-dependent process while XR is spin-independent. We emphasize the important role of XR which helps to understand the true mechanism of CMR.

*Corresponding author

**J1 108 The enhanced magnetoresistant effects and cluster-glass state induced by A-site cational size disorder** KEFENG WANG, LIFENG WANG, *Nanjing National Laboratory of Microstructures, Nanjing University* JUNMING LIU,* *Nanjing National Laboratory of Microstructures, Nanjing University & International Center for Materials Physics, Chinese Academy of Sciences* In pervoskite-structure oxides, not only the A-site cational mean radii, but also the variance of the A-site cational radii, controls the physical properties of the sample. The disorder effects induced by A-site cational size mismatch in large band-width manganite $La_{0.55}Sr_{0.45}MnO_3$ have been carefully studied by preparing a series of samples which have the same $< r_A > = 1.25$Å with different variance of the A-site ionic radii. The ground state of the system changed from a ferromagnetic metal to a cluster-glass insulator with increasing of the variance of the A-site ionic radii. Moreover, the magnetoresistant effects is enhanced significantly in the sample with intermediate disorder. We argued that the A-site disorder enhanced the fluctuation between the competing ordered states and then induced the cluster-glass state and the enhanced magentoresistant effects.

*Corresponding author

**J1 109 Resistor-network study of tunneling magnetoresistance in ordered arrays of magnetic nanoparticles** DIMITRIS KECHRAKOS, KALLIOPI TROHIDOU, *Institute of Materials Science, NCSR Demokritos, 15310 Athens, GR* The tunneling magnetoresistance (TMR) of a hexagonal array of dipolar interacting magnetic nanoparticles is studied using a resistor network model and micromagnetic configurations obtained from Monte Carlo simulations. Analysis of the field-dependent TMR and the corresponding magnetization curve shows that dipolar interparticle

interactions suppress the maximum TMR effect, increase or decrease the field-sensitivity depending on the direction of applied field and produce strong dependence of TMR on the direction of applied magnetic field. The peak in TMR for a unipolar sweep of the magnetic field is associated with the critical field for irreversible rotation of the magnetization, rather than the coercive field as commonly interpreted. This behavior is evident in strongly interacting arrays with the magnetic field at a nearly right angle to the array. Under these conditions the difference between the coercive and critical field is maximized. The relation of our simulations to recent TMR measurements in self-assembled Co nanoparticle arrays is discussed.

**J1 110 Epitaxial half metallic/oxide semiconductor schottky contacts** J. JHAVERI, *Department of Physics, University of Florida, Gainesville, FL* A. VENIMADHAV, QI LI, *Department of Physics, Pennsylvania State University, PA16801* Half metallic/semiconductor junctions are useful for spintronic devices. With such an interface, one can potentially inject a large percentage of spin polarized electrons into the semiconductor in a active spintronic device. We fabricated half-metallic $Sr_2FeMoO_6$ (SFMO) and 0.1% Nb doped $SrTiO_3$(Nb: STO) schottky contacts using Pulsed Laser Deposition (PLD). $Sr_2FeMoO_6$films were grown epitaxially on Nb-$SrTiO_3$ with Ar and small amounts of $O_2$ (0.02%) while the substrate was kept at $800^o$ C. The current versus voltage characteristics of the junction were measured on 1 $mm^2$ contact area. The I-V curves were measured at several temperatures and in each case, the junction exhibited a clear rectifying behavior. A strong rectifying behavior was observed at room temperature with a small activation voltage of 0.2 V. Temperature dependence of I-V characteristics shows a clear schottky nature of the contacts. The barrier height and ideality factor of the junction were calculated using the thermionic model given by $I = I_s(e^{V/nkT} - 1)$. Here, $I_s = AA^* T^2 e^{q\phi/kT}$, where $A$ is the active area, $A^*$ is the effective Richardson constant, $\phi$ is the Schottky barrier height, and $n$is the ideality factor. We found that the ideality factor was approximately constant as the temperature was varied with small deviations, and the barrier height decreased with temperature and more abruptly below 100K.

**J1 111 Spin-polarized sources for Si-based spin injection-detection devices** SEBASTIAAN VAN DIJKEN, *Trinity College Dublin* C. BOOTHMAN, *Trinity College Dublin* M. THIEBAULT, *Trinity College Dublin* C. MURRAY, *Trinity College Dublin* G. FENG, *Trinity College Dublin* J.M.D. COEY, *Trinity College Dublin* We have explored magnetite/Si and Fe/MgO/Si contacts as possible sources of highly spin-polarized currents. Reactive sputtering of magnetite from a pure Fe target results in the growth of single crystal films with a (111) texture on both Si(001) and Si(111) substrates. The evolution of the film magnetization with temperature exhibits a sudden decrease around 120 K, which is characteristic for the Verwey transition in magnetite and indicates high quality film growth. Electrical transport across the magnetite/Si interface is dominated by tunneling through (at low temperatures) and thermionic emission across (at elevated temperatures) a Schottky barrier. The Schottky barrier height is 0.52 eV and 0.65 eV for magnetite films on Si(111) and Si(001), respectively. Direct rf magnetron deposition of MgO on Si(001) results in tunnel barriers with a weak (001) film texture. The injector current (at fixed bias voltages) varies non-monotonically with tunnel barrier thickness. This dependence is qualitatively explained by a competition between a reduction in current due to a thicker tunnel barrier and an increase in current due to a reduction of the Schottky barrier height and Si depletion width.

**J1 112 High coercive cobalt ferrite $Co_xFe(3\text{-}x)O4$ nano−composite thin films prepared by spin−on process' *** P. TALAGALA, R. NAIK, *Wayne State University* G.M. TSOI, L.E. WENGER, *University of Alabama at Birmingham* R. SURYANARAYANAN, *Universite of Paris−Sud* V.M. NAIK, *University of Michigan−Dearborn* Spin coating technique have been employed to synthesize $CO_xFe_{3-x}O_4$ ($0.5 \leqslant x \leqslant 1.9$) nano−composite thin films of $\sim$ 10nm crystalline size on sapphire, glass, and aluminum substrates. The films were annealed invarious environments such as air, H2/Ar, and vacuum. The structural properties were characterized by XRD and Raman Spectroscopy. The magnetic hysteresis measurements of the films exhibit a large coercivity HsC (15−17kOe) at 5K. Low temperature processed films demonstrate super magnetic characteristics with HC=$\sim$ 150 Oe and reduced remanence $M_{rs}/M_s = \sim 0.05 at 300$ K.These films show a spin−glass behavior with the blocking temperature $T_B \propto H^2$ for low fields and $T_B \propto H^{2/3}$ for high fields. High temperature processed films with various annealing conditions demonstrate $H_C$ as high as 1.8kOe at 300K. Estimated magnetic anisotropy value of the films is in the range of $0.8-2.4x10^6$ erg/$cm^3$. Optical absorption spectra exhibit band gaps in the visible range of 1.4−1.7eV and in the I Rrange (1.0eV and 0.7eV). Annealing in hydrogen shows are duction of resistivity. Further details of the structural, electrical and magnetic properties of the films will be presented.

*This Work is supported by NSF−REU grant No. EEE0097736

**J1 113 Structural and Magnetic Ordering of the Interface of Fe/Gd Multilayers** ATAUR CHOWDHURY, *University of Alaska Fairbanks* ANDREA FREITAG, *Brookhaven National Laboratories* Multilayers of Fe/Gd were fabricated with magnetron sputtering to study the magnetic and structural ordering of the interfaces of these multilayers. Two groups of samples, one with fixed Gd layer thickness and one with fixed Fe layer thickness, were prepared to study the effect of layer thickness on the structural properties of these multilayers. The samples were investigated using x-ray diffraction and Mossbauer spectroscopy. Two major structures were identified with x-ray diffraction, and two more minor structures were identified from Mossbauer measuremnt. The composition and the thickness of the interface was found to change with both Fe and Gd layer thicknesses. Results of Mossbauer measurement also show that an amorphous Gd-Fe component at the interface with an average composition close to that of the intermetallic compound $GdFe_2$ is likely to be the origin of perpendicular magnetic anisotropy (PMA) of Fe/Gd multilayers. Experimental results clearly suggest that PMA in Fe/Gd multilayers and amorphous Gd-Fe films may have the same origin.

**J1 114 Properties of magnetoelectric susceptibility*** JUNYI ZHAI, JIEFANG LI, DWIGHT VIEHLAND, *Virginia Tech* M.I. BICHURIN, *Novgorod State University, Russia* VIRGINIA TECH TEAM, NOVGOROD STATE UNIVERSITY TEAM, The magnetoelectric (ME) susceptibility is the principle property of ME materials, determining the connection between polarization (or electric induction) and an external magnetic field. Since measurement of the ME susceptibility over a wide frequency range [1]

and the design of new ME devices require more information about the ME susceptibility, the present work has focused on this property in detail. First, we consider the ME susceptibility as a complex parameter with both real and the imaginary parts, advancing a methodology for measurement of these values. Second, we have analyzed the ME susceptibility, for example a trilayer laminate composite of Terfenol-D/PZT, Terfenol-D, and found a maximum value of $\sim$ 3.5x10-7s/m in the electromechanical resonance range. In addition, we have studied the internal structure of the ME susceptibility: i.e., its dependencies on phase volume fractions, layer thickness, and choice of materials couple. Our results for the ME susceptibility will allow it to be more correctly used both as a fundamental materials property and also in potential ME device applications. [1] M.I. Bichurin, V.M. Petrov, Yu.V. Kiliba, and G. Srinivasan. Phys. Rev. B 66, 134404 (2002).

*The work was supported by grants from the Office of Naval Research.

**J1 115 Domain wall phase diagram and wall widths** M. KLAUI, M. LAUFENBERG, D. BACKES, U. RUDIGER, *Fachbereich Physik, University of Konstanz* C. A. F. VAZ, J. A. C. BLAND, *Cavendish Laboratory, University of Cambridge* L. J. HEYDERMAN, F. NOLTING, *PSI, Villigen* SPELEEM GROUP, ELETTRA TRIESTE COLLABORATION, The details of the spin structure of domain walls have recently become the focus of intense research due to the fundamental physical questions associated with domain walls (wall width, magnetoresistance, current-induced domain wall propagation). Using photoemission electron microscopy (XMCDPEEM) we have obtained high-resolution images of the spin structure of the domain walls, which allows us to determine the wall type and the wall width for different Co [1] and NiFe wire and ring geometries. We determine the phase transition between the different domain wall types as a function of the geometrical parameters (width, thickness) [1]. Comparison with theoretical calculations [2] and micromagnetic simulations reveals the importance of local energy minima and the geometry-dependent height of the energy barriers separating the two wall types can be derived. The energy barrier height is then directly measured by high-temperature (up to 600 K) imaging of thermally activated transitions from transverse to vortex walls. By varying the spacing between domain walls, we determine the coupling strength that leads to a shift in the phase boundary. [1] M. Klaui et al., APL **85**, 5637 (2004); [2] R.D. McMichael and M.J. Donahue, IEEE Trans. Magn. **33**, 4167 (1997).

**J1 116 Electric Dipole Transitions at Magnetoacoustic Resonance** M.I. BICHURIN, V.M. PETROV, O.V. RYABKOV, A.V. FILIPPOV, A.A. IVANOV, *Novgorod State University, Russia* G. SRINIVASAN, *Oakland University* Ferromagnetic-ferroelectric composites show giant magnetoelectric (ME) effects that are facilitated by the sample response to electric, magnetic, and elastic forces. Composites consisting of magnetostrictive ferrites and piezoelectric lead zirconate titanate (PZT) or lead magnesium niobate-lead titanate (PMN-PT) are found to show strong ME coupling. Such materials also provide us with unique opportunities for theoretical and experimental studies on ME coupling when the magnetic and/or electric subsystems show resonance behavior. Two types of resonances are of importance: electromechanical resonance (EMR) for the piezoelectric component and ferromagnetic resonance (FMR) for the magnetic component. At the coincidence of EMR and FMR, i.e., at the magneto-acoustic resonance (MAR) ME interaction becomes stronger [1]. This work focuses on electric dipole transitions in multilayer ferromagnetic-ferroelectric composites, such as yttrium iron garnet (YIG) and PZT, at MAR. Expressions have been obtained for ME susceptibility and the ME coefficient. The results indicate the potential for novel microwave devices based on ME interactions at MAR. Supported by grants from the ARO, ONR and NSF. [1] M.I. Bichurin, V.M. Petrov, O.V. Ryabkov, S.V. Averkin and G. Srinivasan, Phys. Rev. B. **72**, 060408(R) (2005).

**J1 117 Enhancement in Magnetoelectric Effects at Thickness Modes of Layered Ferromagnets and Ferroelectrics** D.A. FILIPPOV, M.I. BICHURIN, V.M. PETROV, *Novgorod State University, Russia* V.M. LALETSIN, *Inst. Tech. Acoustics, Belarus* G. SRINIVASAN, *Oakland University* C.W. NAN, *Tsinghua University, China* Magnetoelectric (ME) effects in magnetic - piezoelectric heterostructures are caused by mechanical coupling between magnetic and piezoelectric layers. We reported earlier on the theory and observation of a resonant enhancement in the ME effects when the electrical subsystem is driven to resonance, i.e., electromechanical resonance (EMR) associated with radial acoustic modes [1]. Here we discuss the theory and data for ME effects associated with thickness EMR modes. Profiles of ME voltage coefficients versus frequency were estimated for trilayers based lead zirconate titanate and the following ferromagnetic phases: cobalt ferrite, nickel ferrite and lithium ferrite and Fe, Co and Ni. The results are compared with data on samples 10 mm in diameter and 2 mm in thickness. An enhancement in the ME voltage due to radial modes is observed at 350 kHz. A similar behavior due to the thickness mode is observed at 1.5-2 MHz, in agreement with the theory. Calculated ME voltage coefficients versus frequency profiles are in excellent agreement with data. - supported by an NSF grant. [1] D. A. Filippov, M. I. Bichurin, V. M. Petrov, V. M. Laletin, G. Srinivasan, Phys. Solid State **46**, 1674, (2004).

**J1 118 Nonextensivity in Magnetic Nanocluster Ensembles*** CHRISTIAN BINEK, *Dept. of Physics and Astronomy* SRINIVAS POLISETTY, XI HE, TATHAGATA MUKHERJEE, RAJESH RAJASEKERAN, *Dept. of Chemistry* JODY REDEPENNING, *University of Nebraska-Lincoln* We study the scaling behavior of dipolar interacting nanoparticles in 3D samples of various sizes but constant particle density. Ferromagnetic $\gamma$-$Fe_2O_3$ clusters embedded in a polystyrene matrix are fabricated by thermal decomposition of metal carbonyls. Transmission electron microscopy reveals a narrow size distribution of 12 nm clusters. They are randomly dispersed in the matrix with an average separation of 80 nm. Magnetization isotherms of these single domain particle ensembles are measured by SQUID magnetometry above the blocking temperature $T_B$ =115K where non-equilibrium effects are avoided. After demagnetization corrections which convert the applied magnetic fields into internal fields, H, a data collapse is achieved when scaling the magnetic moment, m, and H by appropriate factors. The latter are theoretically predicted functions of the number of particles and determined here numerically. Scaling of H takes into account the nonextensive (NE) behavior of dipolar interacting particles. In the case of long range interactions a scaling schema has been proposed by Tsallis and confirmed by simulations. The controversial field of NE thermodynamics requires however experimental evidence provided here.

*Work supported through NSF-MRSEC

**J1 119 Magnetic and magneto-optical properties of $Co_2MnSi$ magnetic grating** J.B. KIM, G.J. LEE, Y.P. LEE, *q-Psi and Dept. of Physics, Hanyang Univ., Seoul, Korea* C.S. YOON, *Dept. of Materials Science and Engineering, Hanyang Univ., Seoul, Korea*

J.Y. RHEE, *Dept. of Physics, Sungkyunkwan Univ., Suwon, Korea* K.W. KIM, *Dept. of Physics, Sunmoon Univ., Asan, Korea* The magnetic and the magneto-optical properties of periodic magnetic structure, produced by the femtosecond-laser induced crystallization of amorphous $Co_2MnSi$ films, were elucidated. The amorphous $Co_2MnSi$ films have been prepared by rf-magnetron sputtering on a glass substrate at room temperature. In order to form a grating structure, two-beam interference of femtosecond laser pulses was employed. The atomic-force-microscopy and the transmission-electron-microscopy results show regularly-spaced alternating lines with a periodicity of 2 $\mu$m. The magnetic-force-microscopy results reveal the periodic patterns of magnetic domains. The Kerr hysteresis loops of sample were measured by using a magneto-optical microscope. The enhanced magneto-optical properties were observed in the first-order diffracted beam. It was also found that the films with a spatially periodic magnetic structure can be relatively easily fabricated by selectively crystallization of a paramagnetic $Co_2MnSi$ amorphous film, which crystallizes into a ferromagnetic phase upon illumination with sufficiently intense laser light.

**J1 120 Non-lithographic Fabrication of Magnetic Nanodot Arrays*** BI-CHING SHIH, *University at Buffalo, the State University of New York* MIN NI, *University at Albany, State University of New York* HAO ZENG, *Department of Physics, University at Buffalo, the State University of New York, Buffalo, NY14260* Highly-ordered magnetic nanodot arrays with tunable size and interdot spacing have been fabricated by electron-beam evaporation through ultra thin porous anodic alumina (PAA) templates. The PAA templates were fabricated by a 2-step anodization process in a 0.3 M oxalic acid electrolyte at room temperature, with an anodization voltage ranging from 20 to 60 V. The aspect ratio were controlled by the second anodization time. In order to get porous arrays with through holes, the aluminum layer and the barrier layer were removed by wet chemical etching. The template was then placed on a solid substrate as a shadow mask for subsequent deposition of magnetic nanodots. The magnetic properties of Ni nanodot arrays with 50 nm diameter and 80 nm spacing were studied in detail. The dots are superparamagnetic at room temperature. They become ferromagnetic at approximately 170 K. The coercivity at low temperatures is found to be much higher than that of continuous Ni films, due to a transition of magnetization reversal mechanisms from domain wall motion to spin rotation. A significant reduction in the Curie temperature is observed, which is attributed to the finite size effect.

*Work supported by IRCAF at Ubiversity at Buffalo.

**J1 121 Magnetic Thermal Hysteresis in (Co, Fe)/Tb Multilayers** MARIA HOSSU, *Department of Physics, University of Texas at Arlington, Arlington, TX, 76019* ALI KOYMEN, *Department of Physics, University of Texas at Arlington, Arlington, TX, 76019* In plane and out of plane magnetic thermal hysteresis have been measured to investigate the ferrimagnetic behavior of (Co, Fe)/Tb multilayers. Due to antiferromagnetic coupling between the (Co, Fe) and Tb, the multilayers behave like artificial ferrimagnets. For $[Co\ (30Å)/Tb\ (45\ Å)]_8$ the measurement of magnetic moment (M) as a function of temperature shows that magnetic phase transition occurs at different temperatures during the heating (superheating) and cooling (supercooling) cycles resulting in a characteristic **bow-tie** shaped thermal hysteresis curve for **M (T)**.The width of the thermal hysteresis was measured to be to be around 90 K in an external magnetic field of 2000 Oe. Increasing the field to 4000 Oe reduces the thermal hysteresis width to about 40 K and above 6000 Oe the thermal hysteresis disappears. Co/Tb multilayers with thicker layers show the same trend, however, the width of the thermal hysteresis is generally smaller at a given magnetic field.

**J1 122 Magnetic properties of double-layer vanadium oxides and vanadium oxide nanotubes.** NATASHA A. CHERNOVA, SAMUEL T. LUTTA, CHRIS JACOBS, M. STANLEY WHITTINGHAM, *Institute for Materials Research, SUNY at Binghamton, Binghamton NY 13902-6000* PETER Y. ZAVALIJ, *Department of Chemistry and Biochemistry, University of Maryland, College Park, MD 20742-4454* Double-layer $V_8O_{20}$ compounds[1] intercalated with various cations and the vanadium oxide nanotubes (VONTs) $VO_{2.4}\ [C_{12}H_{28}N]_{0.31} \cdot 0.56H_2O$ were prepared using hydrothermal method and characterized by x-ray diffraction, TGA, TEM, FTIR. Magnetic properties were studied using SQUID magnetometer. Depending on the intercalated cation type, the magnetic susceptibility of $V_8O_{20}$ compounds reveal presence of small clusters or infinite linear chains with antiferromagnetic (AF) exchange. VONTs show a spin gap, which is well described by the simple model of magnetic dimers with AF exchange. Various ion exchange and red-ox reactions are performed on VONTs. Structure and magnetic properties of the resulting compounds are discussed. No ferromagnetic response from the VONTs reacted with BuLi is found[2]. The work is supported by the National Science Foundation through grant DMR 0313963.

[1]P. Y. Zavalij and M. S. Whittingham, Acta Cryst. B55, 627 (1999).
[2]L. Krusin-Elbaum, D. M. Newns, H. Zeng, V. Derycke, J. Z. Sun and R. Sandstrom, Nature 431, 627 (2004).

**J1 123 Thermal and Quantum Peierls Transitions in Organic Charge-Transfer Salts** SHARON BEWICK, ZOLTAN SOOS, *Princeton University* The choice of donors (D) and acceptors (A) governs the charge-transfer $\rho$ in organic CT salts with mixed one-dimensional DADA stacks. Strong D and A yield $\rho \sim 0.9$ stacks of radical ions with thermally accessible spin and charge degrees of freedom whose Peierls transition can be described by a Hubbard model with site energies. The same microscopic model describes CT salts with smaller and variable $\rho \sim 0.5$ in which neutral-ionic and/or Peierls transitions occur in the ground electronic state. Quantum transitions are driven by volume changes, with negligible thermal population of excite states. CT salts with thermal or quantum Peierls transitions are identified. Conflicting magnetic, vibrational and structural data in several CT salts are resolved in terms of mobile spin solitons, a dimerized ground state and a Peierls transition beyond the crystal's thermal stability.

**J1 124 Avalanches in Mn12-Acetate: ''Magnetic Burning''** SEAN McHUGH, Y. SUZUKI, D. GRAYBILL, M.P. SARACHIK, *Department of Physics, City College of New York/CUNY, New York, New York* N. AVRAHAM, Y. MYASOEDOV, H. SHTRIKMAN, E. ZELDOV, *Department of Condensed Matter, Weizmann Institute of Science, Rehovot, Israel* R. BAGAI, N.E. CHAKOV, G. CHRISTOU, *Department of Chemistry, University of Florida, Gainesville, FL* From local time-resolved measurements of fast reversal of the magnetization in single crystals of the molecular magnet $Mn_{12}$-acetate, we have shown [1] that the magnetization avalanche spreads as a narrow interface that propagates through the crystal at a constant velocity roughly two orders of magnitude smaller than the speed of sound. This phenomenon is

closely analogous to the propagation of a flame front (deflagration) through a flammable chemical substance. The propagation speed of the avalanche depends on the energy stored in each molecule, which can be controlled and tuned using an external magnetic field. We report studies of propagation speed with different external fields in $Mn_{12}$-acetate. [1] Yoko Suzuki, M.P. Sarachik, E.M. Chudnovsky, S. McHugh, R. Gonzalez-Rubio, N. Avraham, Y. Myasoedov, H. Shtrikman, E. Zeldov, N.E. Chakov and G. Christou, Phys. Rev. Lett. 95, 147201 (2005).

**J1 125 Time Evolution of the Magnetization of Mn-12 Acetate above 1.8 K.** REEM JAAFAR, Y. SUZUKI, D. GRAYBILL, M.P. SARACHIK, *City College of New York* R. BAGAI, G. CHRISTOU, *University of Florida, Gainesville* It is well known that the decay of the magnetization of the molecular magnet Mn12-acetate is not a simple exponential. From measurements using a commercial Quantum Design MPMS magnetometer between 3 K and 1.8 K, we present the results of a detailed study of the time evolution of the magnetization as it increases from zero (following zero-field cooling) in response to longitudinal magnetic fields up to 400 Oe. Fits to the data will be shown for distributions of characteristic times (Gaussian, Lorentzian and others) of different widths in response to magnetic fields near and away from a tunneling resonance. The effect of temperature and transverse field will be discussed.

**J1 126 Edge excitations in quantum spin chains*** CHANGFENG CHEN, *University of Nevada, Las Vegas* We explore the nature of the topological edge excitations in quantum spin chains using both analytical valence-bond-solid analysis and numerical simulations. The results reveal new excitation modes that are associated with a topological order in the spin chains. Experimental implications will be discussed.

*This work was supported in part by the Department of Energy.

**J1 127 Record Two-Halide Exchange in Cu(2,5-dmpz)$Br_2$: Theory and Experiment** R. BUTCHER, C.P. LANDEE, M.M. TURNBULL, *Clark University, Worcester, MA 01610* J. NOVOA, J. RIBAS, *Departament de Quimica Fisica, Universitat de Barcelona, Barcelona, Spain.* Cu(2,5-dmpz)$Br_2$ (2,5-dmpz = 2,5-dimethylpyrazine) is an antiferromagnetic rectangular lattice, with the S=1/2 copper ions bridged along one axis through the pyrazine molecules and through Cu-Br.. Br-Cu contacts in a transverse direction. Large orbital overlap is obtained by the very short Br-Br distances plus the linear arrangement of the copper and bromine atoms. The magnetic susceptibility corresponds to an exchange strength of $J/k_B \approx$ 160 K, a record for exchange for two bromide contacts. Numerical techniques have been developed for calculating two-halide contact magnetic exchange interactions from first principles [1,2]. They predict the same exchange strength for Cu(2,5-dmpz)$Br_2$ based only on the structural parameters of the compound. We present the magneto-structural correlations in Cu(2,5-dimethylpyrazine)$Br_2$ and compare this to two other known pyrazine complexes; Cu(pyrazine)$CuBr_2$ and Cu(2,3-dimethylpyrazine)$Br_2$. 1. M. Deumal et al, Polyhedron **22** 2235-2239 (2003). 2. M. Deumal et al, Euro. J. Inorg. Chem. **2005**, 4697-4706.

**J1 128 Magnetic properties of Co-Rh and Ni-Rh nanostructures** JAVIER GUEVARA, *Escuela de Ciencia y Tecnología, Universidad de San Martín, Argentina and Dept Física, CAC-CNEA, Argentina* TRISTANA SONDON, *Dept Fisica, CAC-CNEA, Argentina and Instituto Sabato, UNSAM, Argentina* ANDRES SAUL, *CRMCN-CNRS, Campus de Luminy Case 913, 13288 Marseille Cedex 9 France* We study the evolution of the magnetic properties of Co-Rh and Ni-Rh nanostructures (free-standing monolayers and wires) on Rh content ($x$). It is known that dimensionality affects the magnetic properties of the materials. Rh is non magnetic in bulk, but shows magnetic order as free-standing monolayer or nano- wire, being $1.03\mu_B$ and $0.26\mu_B$ the corresponding magnetic moments, calculated by using the *abinitio* Wien-2k code. In the case of $Co_{1-x}Rh_x$ and $Ni_{1-x}Rh_x$ wires, the evolution of the Rh magnetic moment is similar for both cases, being enhanced with respect to pure Rh wire value and reaching the largest values at x=.5 ($1.36\mu_B$ and $1.31\mu_B$ respectively). For $x > 0.5$ all the magnetic moments fall. For $x < .5$ the Co and Ni magnetic moments reach values larger than the corresponding pure wire and than their saturation magnetic moments. In the case of mixed monolayers the Rh and Ni magnetic moments are not enhanced as Co or Ni content increases, however Co $\mu$ is enhanced without crossing its saturation value. By alloying with Co or Ni, Rh wires enhanced their magnetic moments, while mixed monolayers' Rh magnetic moments are not enhanced.

**J1 129 $^{51}$V-NMR investigation of the spin-frustrated magnet $Ni_3V_2O_8$.*** W.G. CLARK, P. RANIN, GUOQING WU, G. GAIDOS, *UCLA Physics and Astronomy* G. LAWES, *Wayne State U. Physics* A.P. RAMIREZ, *Lucent Bell Labs* R.J. CAVA, *Princeton U. Chem.* M. HORVATIC, C. BERTHIER, *Grenoble High Magnetic Field Lab.* The $Ni^{2+}$ ions in the Kagomé-staircase lattice compound $Ni_3V_2O_8$ form an electron spin $S = 1$ system with a geometrically frustrated magnetization and a rich variety of phases below 10 K. Here, we report a study of the local magnetic field and its fluctuations using $^{51}$V NMR measurements of the spectrum, the spin-phase memory time ($T_2$), and the spin-lattice relaxation rate ($1/T_1$) over a broad range of magnetic field and temperature. Above 10 K, the local field from the $Ni^{2+}$ ions follows a Curie-Weiss law. In the ordered phases below 10 K, the NMR spectrum has a very broad structure that changes according to the particular phase. Also, below 10 K, $1/T_1 \propto T^2$. These features suggest that $1/T_1$ is dominated by $Ni^{2+}$ electron moment fluctuations whose dynamics are driven by two-dimensional antiferromagnetic coupling.

*The work done at UCLA was supported by NSF Grant DMR-0334869.

**J1 130 Variation of critical temperature with dilution in a 3D-XY insulating ferromagnet*** G.C. DEFOTIS, R.A. HUDDLESTON, B.C. ROTHERMEL, J.H. BOYLE, E.S. VOS, Y. MATSUYAMA, A.T. HOPKINSON, *College of William and Mary* A very rare 3D-XY insulating ferromagnet is the molecular material Fe(III) bis(diselenocarbamate) chloride, ordering near 3.4 K. The XY anisotropy arises because of a large zero-field splitting of the quartet crystal field ground term, with a positive axial splitting parameter making the (+1/2,-1/2) Kramers doublet low-lying. Intermolecular exchange interactions operate via Fe-Se...Se-Fe contacts. We have succeeded in diluting this material to significant degrees with a diamagnetic near structural isomorph, Zn(II) bis (dithiocarbamate). Analysis of dc susceptibility and magnetization data leads to estimates of the ferrromagnetic ordering temperature in undiluted, 0.137, and 0.202 Zn-mole fraction diluted material. Compositions are determined by atomic absorption spectropho-

tometry. The ordering temperature decreases moderately with increasing dilution, at a rate typical of three-dimensional systems and much slower than in two-dimensional materials. It is more difficult to distinguish among spin interaction models based on the data.

*Supported by NSF-SSC Grant No. DMR-0085662 and by an ACS-PRF grant.

**J1 131 A Yttrium Iron Garnet-Lead Zirconate Titanate Phase Shifter** G. SRINIVASAN, A.S. TATARENKO, *Oakland University* M.I. BICHURIN, *Novgorod State University, Russia* Tunable microwave phase shifters are of interest for miniature oscillators and phased array antenna systems. Traditional ferrite phase shifters use magnetic tuning systems that are slow, demand high power, and are not miniature in size. Here we discuss the design, fabrication and characterization of a novel electric field tunable phase shifter based on a yttrium iron garnet (YIG) – lead zirconate titanate (PZT) bilayer. The electrical control of the phase shift is realized through magnetoelectric (ME) interaction. The phase shifter consisted of a microstrip transmission line with stubs of $\lambda/8$ and $3\lambda/8$ lengths for generating circularly polarized microwave magnetic field in the YIG-PZT resonator. The ME resonator was made from 124 micron thick (100) YIG film on GGG and 0.5 mm thickness PZT with electrodes. The operating frequency of the phase shifter was set by applying appropriate bias magnetic field. The phase shift vs. electric field E characteristics was linear or quadratic in E, depending on the operating frequency. The maximum phase shift was 180 deg. and showed an insertion loss of 1.5-2.0 dB at 5 GHz and 3-4 dB at the frequency 10 GHz. The ME phase shifter is capable of rapid tuning, miniature in size and dissipates practically zero power. – The work was supported by grants from ONR, ARO and NSF.

**J1 132 A Magnetic Field Tunable Lens of Left-Handed Material** A.S. PETROV, R.V. PETROV, M.I. BICHURIN, *Novgorod State University, Russia* G. SRINIVASAN, *Oakland University* D. VIEHLAND, *Virginia Tech.* The design, fabrication and characterization of lenses of left handed materials (LHM) based on ferrite spheres are presented. A unit-cell constructed from cross-wire resonators with 2-mm diameter polycrystalline yttrium iron garnet spheres at the center was used. The ferrite sphere facilitated LHM elements with magnetic-field dependent permeability. The focal length of the LHM lens, therefore, could be tuned with a magnetic field. The studies show that the YIG-cross-wire resonators are ideal tunable LHM lenses. The lens characteristics were measured in the frequency range from 1 to 18 GHz. For example, the focal point of the lens could be tuned over a length of 2 cm by varying the magnetic field from 4100 to 4125Oe at 11.5 GHz. - supported by a grant from the NSF.

**J1 133 A Negative-Index Metamaterial Unit Cell** R.V. PETROV, M.I. BICHURIN, *Novgorod State University, Russia* D. VIEHLAND, *Virginia Tech.* G. SRINIVASAN, *Oakland University* Metamaterials with a negative index of refraction can be realized in an array of straight wires and split-ring resonators (SRRs). Such structures will have a negative permittivity and permeability at a specific frequency. Here we provide the details on the design and characterization of a modified negative-index material (NIM) that uses cross-wire resonators (CWR). The resonators were made of copper wires having a diameter of 0.2 mm. Comparison of properties at 11.5 GHz for NIMs constructed with SRR and CWR is presented. For the NIM lens with CWR, precise control of the focal point is possible; the edges in the profile for intensity vs. distance are well defined, and the maximum achievable focal length is higher than for the split-ring NIMs. - supported by a grant from the NSF.

**J1 134 Study of Complete Elliptic Integrals with a goal of Improving Computation of Axisymmetric Fields** JOSEPH W. RUDMIN, *Physics Dept. James Madison Univ* In recent years I have been investigating the Complete Elliptic Integral of the First Kind, K, with a goal of finding a rapidly convergent power series R such that K can be written in terms R with the non-analyticities subtracted off or divided out. The singularities in K are logarithmic in nature, so that power series expressions of K converge slowly. Progress in this study will be presented.

**J1 135 Magnetization dynamics of two interacting spins in an external magnetic field** WILLIAM COFFEY, *Dept. Electronic & Electrical Engineering, Trinity College, Dublin 2, Ireland* HAMID KACHKACHI, *Lab. Magnétisme et d'Optique, Université de Versailles St. Quentin* YURI KALMYKOV, *Université de Perpignan, 52 Avenue Paul Alduy, 66860 Perpignan Cedex, France* SERGEY TITOV, *Institute of Radio Engineering and Electronics of the Russian Academy of Sciences, Fryazino, 141190, Russia* The longitudinal relaxation time of the magnetization of a system of two exchange coupled spins subjected to a strong magnetic field is calculated exactly by averaging the stochastic Gilbert-Landau-Lifshitz equation for the magnetization, i.e., the Langevin equation of the process, over its realizations so reducing the problem to a system of linear differential-recurrence relations for the statistical moments (averaged spherical harmonics). The system is solved in the frequency domain by matrix continued fractions yielding the complete solution of the two spin problem in external fields for all values of the damping and barrier height parameters. The magnetization relaxation time extracted from the exact solution is compared with the inverse relaxation rate from Langer's theory of the decay of metastable states [J. S. Langer, Ann. Phys. (N.Y.) **54**, 258 (1969)], which yields in the high barrier and intermediate-to-high damping limits the asymptotic behavior of the greatest relaxation time.

**J1 136 A Comparison of Various Update Schemes Used in Monte Carlo Simulations of Stoner-Wohlfarth Particles*** CHRISTOPHER RUSSELL, KARL UNRUH, *University of Delaware* The hysteresis loops for non-interacting Stoner-Wohlfarth particles have been simulated by the Monte Carlo (MC) method as a function of the temperature, the magnitude of the angular aperture used to update the magnetization direction, and the total number of MC steps. Comparing the coercivity obtained from these hysteresis loops with those obtained from Néel's relaxation model has allowed two different sets of consistent MC parameters to be determined (in the sense that the simulated hysteresis loops will reproduce the temperature dependence of the Néel coercivity). The first set allows the use of a physical temperature but requires the magnitude of the update aperture to be temperature dependent (at a fixed number of MC steps). The second set allows the use of a constant update aperture but requires the introduction of an effective temperature (again at a fixed number of MC steps).

*This work has been supported by ARO DEPSCOR grant no. W911NF-04-1-0264

**J1 137 Toy model of an electron interacting with two classical spins** WILLIAM SCHWALM, JUANA MORENO, *Physics Univ. N. Dakota* We consider a single electron governed by a tight-binding Hamiltonian, $H = H^{(o)} + V$, where $H^{(o)}$ stands for the band structure of the crystal and $V$ is a double-exchange type interaction between the electron and two localized classical spins, $\vec{S}_1 \cdot \vec{J} + \vec{S}_2 \cdot \vec{J}$, where $\vec{S}_1$ and $\vec{S}_2$ are classical spins and $\vec{J}$ is electron angular momentum. We study the dynamics of the system as a function of the distance and the angles between the two spins. By summing over electron states we learn about the effective interaction between the two spins. We discuss the connection of this model with ferromagnetism in dilute magnetic semiconductors.

**J1 138 Relaxation of the magnetization in biaxial superparamagnetic particles in the presence of a strong uniform magnetic field** Y. KALMYKOV, *MEPS, Université de Perpignan, 52 Avenue Paul Alduy, 66860 Perpignan, France* W. COFFEY, *Dept. Electronic & Electrical Engr., Trinity College, Dublin, Ireland* B. OUARI, *MEPS, Université de Perpignan, 52 Av. Paul Alduy, 66860 Perpignan, France* S. TITOV, *Inst. of Radio Eng. & Electronics, Russian Acad. Sci., Fryazino, 141190, Russia* The longitudinal relaxation time of the magnetization and the spectrum of the complex magnetic susceptibility are evaluated for biaxial single domain ferromagnetic particles in the presence of a strong uniform magnetic field. The relaxation time is estimated for all dissipation regimes, i.e., very low damping, intermediate-to-high damping, and turnover, using the method of Coffey et al. [Adv. Chem. Phys. **117**, 483 (2001)]. It is shown that the simple asymptotic formulae for the greatest relaxation time so obtained are in complete agreement with the relaxation time calculated from the infinite hierarchy of linear differential-recurrence equations for the statistical moments. This hierarchy, which governs the relaxation of the magnetization of an individual particle, is derived by averaging the governing stochastic Gilbert equation over its realizations. The exact solution of the system of moment equations is obtained by matrix continued fractions. Simple analytic equations, which allow one to accurately predict the spectrum of the longitudinal complex susceptibility for wide ranges of the barrier height and dissipation parameters, are also proposed.

**J1 139 A Novel Class of Helical Nanostructures: Paradigms for their Design and Synthesis Using Imprint Lithography and Carbon Nanotubes** DAVID SMALLING, *Undergraduate* This research focuses on the use of solenoid-like configurations which are both microscopic and macroscopic, to make energy conversions between electrical energy and other forms. Numerous conceptual models are to be evaluated for the construction of an environment in which a charged particle could be allowed travel along a helical path of extremely small pitch and comparatively large large radius. The two main types of solenoid designs discussed, are lithographically synthesized solenoids and coiled carbon nano tube solenoids. For future identification the family of structures described will be referred to as Zeta ($\zeta$) Structures. In the case of a $\zeta$ solenoid, the objective would be to create a solenoid whose general structure is macroscopic but comprises a conductive trace which is on the nano-scale, In the case of such a solenoid the current flowing $I$ and the magnetic flux $B$ would be related approximately by $B \approx 1.256 \times 10^3 I$. Such a situation gives rise to a very fascinating relationship between B and I. This means that if a current of say 1 ampere was made to flow through the solenoid, a magnetic flux of 1250 Tesla would be generated. The defining characteristic of $\zeta$ structures is their overall macroscopic dimensions which comprise high level nano-scale repetition. This research discusses theoretical propositions for the development of a class sub micron structures defined by a unique helical foundation, to be used for the generation of magnetic fields.

**J1 140 Comparative Study of the Magnetic Properties of Ba-Ferrite Thin Films Deposited on Different Substrates*** W. J. YEH, JOEL KREHBIEL, A. R. ABUZIR, *Department of Physics, University of Idaho* The Barium ferrite ($BaFe_{12}O_{19}$) film is an attractive candidate for the self-biased microwave circulator application. The requirement for this application is that the Barium ferrite films have excellent c-axis orientation with moderate $H_c$ value and good squareness, so that Barium ferrite films can be self-biased to eliminate the requirement of the external DC magnetic field. We have used the magnetron sputtering to deposit Ba-ferrite films onto silicon, MgO and sapphire substrates. All of the films were deposited in the same $Ar + O_2$ atmosphere at elevated substrate temperatures to optimize the magnetic properties in terms of c-axis orientation. The films were studied by VSM, XRD, SEM and MOKE. It was found that Barium ferrite thin films on silicon substrates had coercivity value of 3000 Oe with squareness of 0.6 with moderate c-axis orientation. Films deposited on MgO showed better c-axis orientation. However, the values of $H_c$ and squareness were low. Films deposited on sapphire showed the best c-axis orientation. The coercivity value of 3000 Oe and the squareness of 0.93 in perpendicular direction were achieved. Based on our results sapphire is the promising substrate choice for growing Barium ferrite films for the self- biased circulator application.

*Work was supported by ONR grant N000140210925

**J1 141 Control of magnetic and ferroelectric phase in multiferroic (Tb, Bi)$MnO_3$ system** TAE-HWAN JANG, MURALIDHARAN RAJARAM, CHAN-HO YANG, TAE YEONG KOO, YOON HEE JEONG, *Dept. of Physics and Electron Spin Science Center and Pohang Accelerator Laboratory, Pohang University of Science and Technology* Various magnetic ferroelectrics have been discovered and extensively studied because of the possibility of coupling between electric and magnetic degrees of freedom and their potential technological applications. However, the two transitions from electric and magnetic origins have a big difference in their temperature range of occurrence and there is a rare possibility to get two critical points in the same temperature region. We report highly polarizable cation modification effects of multiferroic $TbMnO_3$ polycrystalline system on magnetic and ferroelectric phase transition. Random replacement of $Tb^{3+}$ with $Bi^{3+}$ induces low frequency relaxation in magnetic susceptibility reminiscent of relaxor behavior. The special role of $Bi^{3+}$ ions is emphasized because the anomalous behavior has not been observed in other non-magnetic cation substituted $TbMnO_3$ systems. Various accompanying phenomena such as magnetic and ferroelectric relaxational behavior, structural anisotropy, and tuning of electromagnetic coupling are also discussed. Controllability of both magnetic and ferroelectric phase by the combination of Bi-substitution and driving frequency suggests a new possibility for getting two transitions having different origin at the same temperature point.

**J1 142 Role of oxygen vacancy in ferromagnetic Mn-doped ZnO films** S.Y. PARK, Y.J. YOO, P.J. KIM, Y.P. LEE, *Hanyang University* T.H. KIM, *Ewha Woman University* J.-H. KANG, *Kookmin University* We report that $Zn_{1-X}Mn_XO$ (x = 0.4) films grown by reactive magnetron co-sputtering have ferromagnetism at temperatures above 300 K. The ferromagnetic behavior is sensitive to not only the carrier concentration but also the film growth parameters, such as the substrate, substrate temperature, deposition rate and oxygen partial pressure ($P_{O2}$) during deposition. In this study, we focused on the role of oxygen vacancy for the ferromagnetism in $Zn_{1-x}Mn_xO$ films with $x \leqslant 0.05$. In order to fabricate high-quality samples, the preparation was performed in an ultrahigh vacuum, and the accurate $P_{O2}$ was monitored using a residual gas analyzer during deposition. The magnetic and the structural properties of films were characterized by SQUID and XRD, respectively. The normal-mode and oxygen-resonance-mode RBS were carried out to confirm the mount of Mn, Zn and O contents. The film, prepared at an oxygen partial pressure of $2.2x10^{-7}$ Torr, exhibits a strong ferromagnetism with *T*c above 300 K, while the films at an partial pressure of higher than $1.2x10^{-6}$ Torr show the nonmagnetic behaviors. Our results can be elucidated with a theoretical model by Coey [1] that the oxygen vacancy could results in the magnetic ordering of Mn-doped ZnO film by the enhancement of overlap between *s*-band and imputity *d*-band. [1] J. M. D. Coey et al., Nat. Mater. **4**, 173 (2005).

**J1 143 Magnetoelectric effect in $HoMnO_3$** N. HUR, A. SAXENA, M.F. HUNDLEY, *Los Alamos National Laboratory, Los Alamos, NM 87545* S.B. KIM, S.-W. CHEONG, *Dept. of Physics & Astronomy, Rutgers University, Piscataway, NJ 08854* Multiferroic rare earth manganites have attracted a renewed interest because of recent observations of the giant coupling between ferroelectricity and magnetism in these materials. In particular, hexagonal $HoMnO_3$ has been one of the most actively studied systems among them. For incidence, novel dielectric phase transitions and electric field induced ferromagnetism have been observed recently. However, any direct observation of magnetoelectric effect has not been made. In this presentation, I will discuss the effect of magnetic structure change on the electric polarization in $HoMnO_3$ studied by measuring the polarization change as a function of the temperature and magnetic fields.

**J1 144 Negligible Magnetism in transition metal (Cr, Mn, Fe, Co) doped Nb:SrTiO3*** SHIXIONG ZHANG, SATISH OGALE, WEGDAN RAMADAN, SANKAR DHAR, DARSHAN KUNDALIYA, THIRUMALAI VENKATESAN, *Center for Superconductivity Research, Department of Physics, University of Maryland, College Park, MD 20742-4111* LIANFENG FU, NIGEL BROWNING, *Lawrence Berkeley National Laboratory, NCEM, 1 Cyclotron Road, MS 72-150, Berkeley, CA 94720* In order to realize the possibility of carrier induced ferromagnetism in transition metal (TM) doped $SrTiO_3$, we have performed magnetic, electronic transport, and micro-structural measurements on 2% TM doped $SrTi_{0.98-x}Nb_xO_{3-\delta}$ (x=0.000, 0.005,0.010) thin films. Unfortunately, no unambiguous signature of ferromagnetism is observed in this system, even though its conductivity is seen to be greatly improved by the enhancement of carrier density due to Niobium doping. High-resolution Z-contrast Scanning Transmission Electron Microscopy shows no evidence of clustering, while Electron Energy Loss Spectroscopy indicates that the TM is enriched on the surface of the film whereas Niobium is mostly distributed in the bulk. It is believed that the absence of strong ferromagnetism in this system may be attributed to a spatial separation of the spins contributed by the TM and the carriers from Nb in the $SrTiO_3$ matrix.

*Work Supported under DARPA SpinS program; Supported under Fulbright Program

**J1 145 Dependence of Ferromagnetic Properties on Carrier Transfer in $(Ga_{1-x}Mn_x)N$** H. C. JEON, S. J. LEE, T. W. KANG, T. W. KIM, JOONGOO KANG, K. J. CHANG, QSRC, DONGGUK UNIVERSITY SEOUL TEAM, ELECTRICAL AND COMPUTER ENGINEERING, HANYANG UNIVERSITY SEOUL COLLABORATION, DEPARTMENT OF PHYSICS, KAIST DAEJEON COLLABORATION, Among many types of DMS materials, $(Ga_{1-x}Mn_x)As$ DMS have been mostly studied. However, since the highest $T_c$ obtained from the $(Ga_{1-x}Mn_x)As$ has been 172 K, which is too low for practical applications. As alternative DMS materials with the high $T_c$, $(Ga_{1-x}Mn_x)N$ DMSs are of current interest because their $T_c$ values can be as high as room temperature. Theory predicts that the ferromagnetic properties observed in GaMnN material system depends on the occupancy of the Mn energy band in GaMnN and the position of the Fermi level relative to this band. Carriers (holes) in the Mn energy band are needed to mediate ferromagnetic interaction: the depletion and enhancement of carrier concentration in the band will change the ferromagnetic properties of GaMnN. Even though many studies concerning the growth and characterization of $(Ga_{1-x}Mn_x)N$ have been carried out, systematic studies are required to understand the carrier-mediated ferromagnetism which is assumed to play an important role in enhancing the Tc by increasing hole carrier concentrations. This work will demonstrate this concept by studying the carriers to mediate ferromagnetism in various GaMnN structures, hence affecting the ferromagnetic properties of the GaMnN.

**J1 146 Magnetism of Discrete, $L1_0$ Ordered FePt Nanoparticles** HAO ZENG, *Department of Physics, the State University of New York, Buffalo, NY 14260* MICHAEL DEMARCO, *Department of Physcs, Buffalo State College* DAREN LI, PING LIU, *Department of Physics, University of Texas at Arlington* Discrete, $L1_0$ ordered FePt nanoparticles have been made by annealing the as-synthesized nanoparticles in the presence of NaCl powder.[1] These particles exhibit high degree of chemical ordering and very large coercivity at room temperature. The temperature dependent magnetic properties of these non-aggregated nanoparticles have been studied systematically as a function of particle size. The magnetization reversal behavior of 4 nm particles can be well explained by Stoner-Wohlfarth coherent rotation model, while that of 8 nm and 15 nm particles is more complicated. Mossbauer spectroscopy measurements indicate the existence of a paramagnetic phase in these highly ordered nanoparticles. The amount of the second phase decreases with temperature but persists even in liquid He temperature. This is attributed to canted spins at the particle surfaces. [1]K. Elkins, D. Li, N. Poudyal, V. Nandwana, Z. Jin, K. Chen and J.P. Liu, J. Phys. D: Appl. Phys. 38, 2306 (2005).

**J1 147 Silicon and III-V compound nanotubes: Structural and electronic properties** ENGIN DURGUN, SEFAATTIN TONGAY, SALIM CIRACI, *Bilkent University* Unusual physical properties of single-wall carbon nanotubes have started a search for similar tubular structures of other elements. We present a theoret-

ical analysis of single-wall nanotubes of silicon and group-III-V compounds. Starting from precursor graphenelike structures we investigated the stability, energetics, and electronic structure of zigzag and armchair tubes using the first-principles pseudopotential plane wave method and finite temperature ab initio molecular dynamics calculations. We showed that (n,0) zigzag and (n,n) armchair nanotubes of silicon having $n \geq 6$ are stable but those with $n < 6$ can be stabilized by internal or external adsorption of transition metal elements. Some of these tubes have a magnetic ground state leading to spintronic properties. We also examined the stability of nanotubes under radial and axial deformation. Owing to the weakness of radial restoring force, stable Si nanotubes are radially soft. Undeformed zigzag nanotubes are found to be metallic for $6 \leq n \leq 11$ due to the curvature effect; but a gap starts to open for $n \geq 12$. Furthermore, we identified stable tubular structures formed by the stacking of Si polygons. We found AlP, GaAs, and GaN (8,0) single-wall nanotubes stable and semiconducting. Our results are compared with those of single-wall carbon nanotubes. [1] E. Durgun, S. Tongay, and S. Ciraci Phys. Rev. B 72, 075420 (2005).

## J1 148 COMPLEX STRUCTURED MATERIALS POSTER SESSION



**J1 149 Self-Assembly of Nanoporous Silica: Synthesis, Morphogenesis, Functionalization, and Applications** YAROSLAV KIEVSKY, IGOR SOKOLOV, *Clarkson University* We study the process of self-assembly and growth of nano(meso)porous silica particles and film via surfactant templating. Process of formation of the mesoporous silica includes growth of the liquid crystalline template and solidification of this template via polymerization of silica precursor. Material obtained as a result of such synthesis (e.g., MCM-41) features highly uniform porosity, a large variety of shapes and their sizes. To control the assembly of the desired shapes, we study their morphogenesis. New conditions of self-assembly are found to form monoshaped nanoporous fibers. Recently suggested Origami-type mechanism for synthesizing a rich family of nanoporous silica shapes (cones, hollow tubes, and helixes) is examined. Shape details and their evolution are analyzed by means of XRD, SEM, TEM, AFM, and optical microscopy techniques. The shapes can possibly serve as templates for various electronic and optical applications. Nanoporous shapes are the prospective hosts for lasing dyes (sealing laser dye molecules inside the silica pores saves them from oxidation and prevents their dimerization). Color coded silica beads are interesting for tagging in security applications and labeling in biology. Diffusion from the nanoporous shapes can be used for a control drug release. Another application of mesoporous silica is the coating of optical fibers by uniform low refractive index film with a good adhesion – a possible host for laser dyes or quantum dots.

**J1 150 Synthesis of Hollow Carbon Nanofibers and Filled Carbon Nanotubes using Chemical Vapor Deposition Technique.** KEVIN SHAY, EVGENIYA MOISEEVA, GAMINI SUMANASEKERA,* *Department of Physics, Universityof Louisville* Hollow carbon nanofibers (CNFs) and filled carbon nanotubes were created using chemical vapor deposition (CVD). Hollow carbon nanofibers were synthesized in porous anodic aluminum oxide templates (AAO) by CVD of methane ($CH_4$) with ferrocene ($C_{10}H_{10}Fe$), indium tin oxide (ITO) and iron nitride ($Fe(NO_3)_3$) as catalyst at 910°C. Carbon nanotubes were filled with iron using CVD of methane. The source of iron in this process was ferrocene. Both the nanostructures were viewed under SEM and TEM. The CNFs grown within the pores of the aluminum oxide membranes are uniform with lengths of about 50 mm and outer diameters of about 200 nm. A diameter of 20-30 nm was measured for the iron filled sample. The magnetic transport properties of the samples will be presented.

*Primary Reference

**J1 151 Raman studies of crystallization and photo-darkening in HARP a-Se targets*** R.E. TALLMAN, B.A. WEINSTEIN, *Physics Department, SUNY at Buffalo, NY* A. REZNIK, J.A. ROWLANDS, *Sunnybrook Women's College Health Science Center, Toronto* M. KUBOTA, K. MIYAKAWA, Y. OHKAWA, K. TANIOKA, *NHK Science and Technical Labs., Tokyo* T. KAWAI, *Hamamatsu Photonics, Tokyo* The build-up of light-induced defects in the a-Se targets of High-gain Avalanche Rushing Photoconductor (HARP) cameras is important for the robustness of these detectors. Recent experiments show that the photo-induced dark spots in HARP targets exhibit irreversible and reversible components, i.e., spot transparency is only partly restored by heating to 35C, $\sim$ 1C below the a-Se glass transition. [1] We report Raman studies of laser(2mW HeNe)-induced crystallization in a-Se camera targets. The rate of increase in the trigonal c-Se Raman intensity (233 $cm^{-1}$ peak) is measured itvs. exposure time for local temperatures in the range 25 – 65 C, as found from Stokes-to-anti-Stokes ratios. Lateral- and depth- profiling by optical microscopy easily correlate the Raman-detected crystallization regions with visual damage. Further studies itvs. temperature and HARP-target usage are in progress to unravel the damage mechanisms. [1] A. Reznik et. al., submitted to J. Non-Cryst. Solids.

*Work supported in part by a grant from Sunnybrook and Women's College HSC, Toronto, Canada

**J1 152 Equilibrium Atomic Configurations Studies and Electron Paramagnetic Resonance of Binuclear Niobium Molecules in Li-Nb Phosphate Glass Dielectrics.** SABRINA ARRINGTON-PEET, RAKHIM RAKHIMOV, VLADIMIR GAVRILENKO, *Center of Materials Research, Norfolk State University, Norfolk VA 23504* Equilibrium atomic configurations of binuclear niobium complexes Nb-O-Nb both free-standing and that embedded in lithium niobium phosphate glass (LNPG) are studied by total energy minimization method using itab initio pseudopotentials within density functional theory. Measurements of electron paramagnetic resonance revealed nonequivalent distribution of the charge and electron spin density between two Nb atoms. Measurements and theoretical analysis indicate that niobium atoms could exist in either of the two forms, $Nb^{4+}$-$Nb^{4+}$ or $Nb^{3+}$-$Nb^{5+}$. The Nb atoms in freestanding molecule are equivalent with oxygen atom having only one local equilibrium position in the center of the molecule, indicating centro-symmetric structure. When the Nb complex is embedded into the glass the effect of external potential in LNPG resulted in an appearance of two non-equivalent configurations for the central oxygen atom in the molecule. Predicted nonequivalent geometries of the Nb-O-Nb complex embedded into LNPG is confirmed experimentally. Mechanism of the distortion is discussed.

**J1 153 X-ray absorption spectroscopic studies of the coordination environment of rare earth ions in novel rare earth phosphate glasses** HASITHA GANEGODA, KANISHKA MARASINGHE, *University of North Dakota* NATHANIEL WYCKOFF, RICHARD BROW, CARLO SEGRE, *Illinois Institute of Technology* MALI BALASUBRAMANIAN, *Argonne National Laboratory* Rare earth (RE) phosphate glasses ($RE_2O_3$-$P_2O_5$) have exciting magnetic and optical properties with numerous potential applications. These properties depend heavily on the atomic structure, especially the rare earth coordination environment. A series of rare earth (namely neodymium, praseodymium, gadolinium, and erbium) phosphate glasses having low rare earth ion concentrations have been studied with rare earth $L_{III}$ edge X-ray absorption spectroscopy (XAS). Rare earth coordination environment appears to undergo an abrupt change when the $RE_2O_3$ concentration exceeds approximately 15 mol%. Implications of this structural change will be discussed and results from XAS technique will be compared with those obtained with X-ray and neutron diffraction techniques.

**J1 154 Electron density, geometric structure and vibration spectra of endohedral $M_{1-3}@C_{60}$ (M = Mn, Co, Fe, Gd) metallofullerenes** G. P. LI, R. SABIRIANOV, W. N. MEI, *Department of Physics, University of Nebraska at Omaha, Omaha, Nebraska 68182* P. A. DOWBEN, *Department of Physics, University of Nebraska, Lincoln, Lincoln NE 68588-0416* X. C. ZENG, *Department of Chemistry, University of Nebraska, Lincoln, Lincoln NE 68588-0416* Endohedrally doped buckminster fullerene C60 with metallic clusters of $M_{1-3}$, (M = Mn, Co, Fe and Gd) are studied by using density functional theory (DFT), projector augmented wave (PAW) and pseudo-potential (PP) methods. Optimized molecular geometries are obtained from varying the positions of these two/three metal atoms together with the $C_{60}$ cage and finding the energy minimum while considering different multiplicities and magnetic configurations. Subsequently the vibrational frequencies of the cluster, electric and magnetic dipole moments are calculated and compared with experiments. Upon the molecular properties are thoroughly studied, we construct different crystal models utilizing these metallofullerenes and employ the local density approximation (LDA)+U techniques to account for many-body effects.

**J1 155 Energy Radiation from Plasmons on Nanotubes** ANTONIOS BALASSIS, GODFREY GUMBS, *Hunter College of CUNY* A formalism has been developed for calculating the rate of transfer of energy from a current of charged particles to multiwalled and a linear array of nanotubes. Numerical calculations are presented for tubules of various radii and impact parameters of the moving charged particles. The dispersion relation of the coupled tubules interacting through the Coulomb interaction has several branches corresponding to excitation of electrons within a subband as well as between energy subbands. The electric field of the current excites these modes but one of them is unstable and radiates energy. This is demonstrated in the spectrum of energy transfer with a ''dip'' unlike the other plasmon modes which have a ''peak'' for arbitrary impact parameter. The single-particle excitation spectrum does not have an instability for any charged particle velocity or impact parameter.

**J1 156 Hysteresis in single-walled carbon nanotube field–effect transistors: Experiments, a model, and implications** S. KAR, *Department of Materials Science and Engineering, Rensselaer Polytechnic Institute, Troy New York* S. TALAPATRA, *Rensselaer Nanotechnology Center, Rensselaer Polytechnic Institute, Troy New York* A. VIJAYARAGHAVAN, *Department of Materials Science and Engineering, Rensselaer Polytechnic Institute, Troy New York* C. SOLDANO, *Department of Physics, Applied Physics and Astronomy, Rensselaer Polytechnic Institute, Troy New York* R. VAJTAI, *Rensselaer Nanotechnology Center, Rensselaer Polytechnic Institute, Troy New York* S.K. NAYAK, *Department of Physics, Applied Physics and Astronomy, Rensselaer Polytechnic Institute, Troy New York* O. NALAMASU, P.M. AJAYAN, *Department of Materials Science and Engineering, Rensselaer Polytechnic Institute, Troy New York* Hysteresis in carbon nanotube FETs is understood to be due to charge injection from the nanotube to its surrounding dielectric. We present a simple yet effective model to understand and analyze this phenomenon, wherein the charge injection and its subsequent redistribution has been modeled as a series RC circuit. A set of experiments validates this model, and also fits previously published data by other groups. Our work provides an in-depth picture of the parameters, which play a crucial role in modifying the transfer characteristics in nanotube FETs under different experimental conditions.

**J1 157 Networking Carbon Nanotubes for Integrated Electronics.** J.M. ROMO-HERRERA, M. TERRONES, H. TERRONES, *Advanced Materials Dept IPICyT, Camino Presa Sn Jose 2055 Lomas 4a Sec, SLP 78216 Mexico* V. MEUNIER, *Computer Science & Mathematics Div and CNMS, ORNL POBox 2008, TN 37831-6367 USA* The unique electronic and mechanical properties of individual Carbon Nanotubes (CNTs) have attracted much interest as candidates for molecular electronic devices and reinforced materials. However, their integration in organized architectures remains a major challenge. Recent breakthroughs reported on the Self-Assembly of 1D Nanostructures [1], and on the coalescence mechanism for interconnecting CNTs [2], point to the possibility of designing and obtaining Ordered Networks based on CNTs (ON- CNTs). We propose a set with different complex architectures of ON- CNTs based on –but not limited to– armchair and zigzag nanotubes. In addition to the study of the energetics of the structures, we have systematically investigated their electronic transport properties in the framework of the Landauer-Buttiker formalism and equilibrium Green functions. To take curvature into account, we employed a semi-empirical Hamiltonian based on 4 orbitals (s,px,py,pz) per carbon atom. Further insight is obtained analyzing the electron pathways from a scattering point of view, which allows a real-space analysis of the wave function from the transmitted electrons across the structure. [1] Whang D., etal. Nanoletters, **3** (2003). Tao A., etal. Nanoletters, **3** (2003). [2] Terrones M., etal. PRL, 89 (2002). Endo M., etal. Nanoletters, 5 (2005).

**J1 158 Band structure and absorption spectrum of double-walled zigzag carbon nanotubes in an electric field*** YEN-HUNG HO, G. W. HO, M. F. LIN, *Department of Physics, National Cheng Kung University* C. P. CHANG, *Center for General Education, Tainan Woman's College of Arts and Technology* The electronic structure of the (9,0)-(18,0) double-walled zigzag carbon nanotubes in the presence of a uniform transverse electric field is studied by the tight-binding model. The electric field could induce the semiconductor-metal transition, change the direct gap into the indirect gap, alter the subband curvatures, destroy the double degeneracy, produce the new band- edge states, make more

subbands group around the Fermi level, and widen the $\pi$-band width. Such effects are directly reflected in density of states and optical excitation spectra. The absorption spectra exhibit a lot of prominent peaks, mainly owing to the rich one-dimensional energy subbands. The intensity, the number, and the frequency of absorption peaks are strongly modulated by the electric field. The modulation of electronic and optical properties is amplified by the parallel magnetic field. The predicted electronic and optical properties can be, respectively, verified by the conductance measurements and the optical spectroscopy.

*NSC 93-2112-M-006-002, NSC 93-2112-M-145-001; NSC 93-2112-M-165-001

**J1 159 Electronic and optical properties of finite carbon nanotubes in an electric field** R.B. CHEN, *Center of General Studies, National Kaohsiung Marine Univ.* C.H. LEE, M.F. LIN, *Dept. of Physics, Natl. Cheng Kung Univ.* C. P. CHANG, *Center for General Education, Tainan Woman's College of Arts Tech.* The effects, caused by the geometric structure and a transverse electric field (**E**), on the electronic and optical properties of quasi-zero-dimensional finite carbon nanotubes are explored by employing the tight-binding model coupled with a curvature effects. It is found that the electronic properties (discrete state energies, symmetry of electronic states, energy spacing, and state degeneracy) are significantly affected by **E** and the geometric structure (radius, length, and chirality). The electric field, by lowering the symmetry of finite carbon nanotubes, modifies the electronic properties. Thus, the optical excitation spectra, excited by electric polarization parallel to the nanotube axis, exhibit rich delta- function-like peaks, which reveal the characteristics of the electronic properties. Therefore it follows that geometric structure and **E** influence the low-energy absorption spectra, i.e., the change of frequency of the first peak, the alternation of the peak height, and the production of the new peaks. Moreover, the very complicated optical absorption spectra are characteristic for individual the chiral carbon nanotube due to its specific geometric structure. Above all, the predicted absorption spectra and the associated electronic properties could be verified by optical measurements. Supported by NSC 94-2112-M-022-001; NSC 94-2112-M-165-001; NSC 94-2112-M-006-002.

**J1 160 Electronic excitations and deexcitations in narrow-gap carbon nanotubes*** C. W. CHIU, Y. H. HO, M. F. LIN, *Department of Physics, National Cheng Kung University* F. L. SHYU, *Department of Physics, Chinese Military Academy* Temperature could induce some free carriers in narrow-gap carbon nanotubes. Such carriers exhibit rich intraband single- particle excitations and collective excitations. Only the low- frequency e-h excitations are the effective deexcitation channels in the carrier decay. The Coulomb decay rates are dominated by the screened loss function and the carrier distribution function. They are very sensitive to the changes in nanotube radius and temperature, but not wave vector. Narrow- gap carbon nanotubes quite differ from moderate-gap and metallic carbon nanotubes in electronic excitations and carrier relaxation.

*NSC 93-2112-M-006-002; NSC 93-2112-M-145-001

**J1 161 Efficacy of the Thermalized Quantum Potential Approach for Modeling Nanoscale Semiconductor Devices.** SHAIKH AHMED, *Dept. of Electrical and Computer Engr., Purdue University* DRAGICA VASILESKA, *Dept. of Electrical Engr., Arizona State University* GERHARD KLIMECK, *Dept. of Electrical and Computer Engr., Purdue University* CHRISTIAN RINGHOFER, *Dept. of Mathematics, Arizona State University* We propose a novel parameter-free effective potential scheme for use in conjunction with particle-based simulations of alternative semiconductor device technologies. The method is based on perturbation theory around thermodynamic equilibrium and leads to a quantum potential which depends on the energy and wavevector of each individual electron. The computation of the quantum potential involves only the evaluation of pseudo-differential operators and can be effectively facilitated using Fast Fourier Transform (FFT) algorithms. Our investigations suggest that for low doping densities, as it is usually the case in alternative device structures, such as dual-gate, FinFET and nanowire devices, the Hartree correction term (computationally expensive) can be neglected and the quantum correction for the Barrier potential/field term (one-dimensional and time-independent adding no additional computational cost) needs be included in the model only. Excellent agreement has been obtained with our Effective Potential Monte Carlo device simulations data and the results that utilize the NEGF formalism.

**J1 162 Optical Trapping and Torquing of C60 Nanorods*** DOUGLAS BONESSI, KEITH BONIN, *Wake Forest University* THAD WALKER, *University of Wisconsin* We have optically trapped and studied C60 polymer nanorods with diameters of 300-500 nm and lengths of 1-3 microns. The primary goal is to measure opto-electronic properties of the C60 polymer rods. This is accomplished by observing the rotational motion of the rods in a water sample when a light torque is applied. We also hope to report on opto-electronic properties of even smaller rod-shaped objects (of diameters less than 100 nm).

*This research was supported by an award from the Research Corporation.

**J1 163 Heavy Ion Interactions with Nanotubes and Nanowires** B.W. JACOBS, V.M. AYRES, R.M. RONNINGEN, A.F. ZELLER, E.H. CAREY, M.A. CRIMP, *Michigan State University, East Lansing, MI 48824* M.P. PETKOV, *NASA JetPropoulsionLaboratory, Pasdena, CA 91109* S.L. RUTLEDGE, J.B. BENAVIDES, H.C. SHAW, *NASA Goddard Space Flight Center, Greenbelt, MD 20771* D. LIU, *Muniz Engineering, Inc., Greenbelt, MD 20771* J.B. HALPERN, M.Q. HE, G.L. HARRIS, *Howard University, Washington, DC 20059* We will present investigations of the response of single and multi wall carbon nanotubes, electrospun carbon nanofibers and gallium nitride nanowires to high-Z heavy ion radiation that simulates space radiation environments. The heavy ion radiation experiments were performed at the National Superconducting Cyclotron Laboratory at Michigan State University, whose available beams and beam energies well match the energy spectra of abundant charged particles in galactic cosmic rays. In these experiments, the nanotubes and nanowires were irradiated in two separate series of experiments using Krypton primary beams with mass numbers 86 and 78 respectively. Explorations of the fundamental mechanisms of radiation interactions and damage propagation in reduced dimensionality systems, and in nanoscale systems with high surface to bulk ratios and small overall volumes, will be presented.

**J1 164 A Novel Vibrational Mode in Carbon Systems** MORINOBU ENDO, *Shinshu University, Japan* MAURICIO TERRONES, *IPICYT, Mexico* Y.A. KIM, TAKUYA HAYASHI, HIROYUKI MURAMATSU, *Shinshu University, Japan* RIICHIRO SAITO, *Tohoku University, Japan* FEDERICO VILLALPANDO-PAEZ, SHIN GRACE CHOU, MILDRED S. DRESSELHAUS, *MIT, USA* We report on the identification of a novel resonant Raman mode located at itca. 1850 $cm^{-1}$, which is related to vibrations of linear carbon chains. This mode, termed ?the coalescence inducing mode? (CIM), was observed during the merging of highly purified double-walled carbon nanotubes (DWNTs) induced by thermal annealing and boron doping. In our case, the CIM mode arises from the generation of short 1D carbon chains established covalently between adjacent tubes. These chains trigger nanotube coalescence via a zipper model, and as the tubes merge the CIM vibration disappears. Theoretical calculations demonstrate that this vibrational frequency corresponds to linear chains with a few carbon atoms. The CIM mode could now be used to identify sp hybridized carbon in various systems such as irradiated graphite, polymerized $C_{60}$ molecules, functionalized fullerenes and nanotubes, carbynes, polymers, nanographites, etc.

**J1 165 Growth and characterization of aligned ZnO nanorods** T. WILLIAMS, K. ZHANG, D. HUNTER, K. LORD, A.K. PRADHAN, *Center for Materials Research, Norfolk State University* We report the growth of aligned ZnO nanostructures on pulsed-laser deposited ZnO epitaxial film-substrates synthesized by vapor transport of the evaporation of pure Zn metal powders followed by subsequent condensation. Remarkable arrangements of uniform ZnO nanorods were found on ZnO film by varying the synthesis conditions. The nanorods grow preferentially from a hexagonal ZnO base. High-density aligned nanorods of 60-100 nm diameter and 10-20 $\mu$m in length grew at the center of the substrate over a large area. Structural and spectroscopic properties clearly indicate that the nanorods are of superior and defect-free in quality. The ZnO nanorods have also been grown on Si and sapphire substrates. Details of the results will be presented.

**J1 166 Intensity dependent Raman spectra of pristine and functionalized carbon nanotubes.*** CHARLES BLACKLEDGE, *Oklahoma State University* DEOKJIN YU, *Oklahoma State University* MAXIM TCHOUL, *Oklahoma State University* XIAOMING JIANG, *Oklahoma State University* WARREN FORD, *Oklahoma State University* JAMES WICKSTED, *Oklahoma State University* Raman spectra of polymer functionalized and pristine single wall carbon nanotubes (SWNTs) are presented. The intensity ratio of the disorder (D band) to the tangential (G band) increases after polymer functionalization. Generally Raman spectra of ensembles of SWNTs indicate sample inhomogeneity such as the presence of many different nanotube symmetries and diameters. Laser induced changes in SWNT Raman spectra were also investigated. We observe temporally the laser induced loss of the intensities of the RBMs from small SWNTs and the metallic G band. This is attributed to selective oxidation of smaller carbon nanotubes that primarily consist of metallic SWNTs in our samples. Under identical conditions, the spectral changes of pristine samples are greater than those of polymer functionalized SWNTs. These results confirm that pristine small diameter SWNTs are more reactive than large ones.

*Funding from NSF EPSCoR is gratefully acknowledged.

**J1 167 Percolation Model of Magnetoelectric Effects in Ferrite/Piezoelectric Bulk Composite** V.M. PETROV, M.I. BICHURIN, D.S. TUSKOV, *Novgorod State University, Russia* G. SRINIVASAN, *Oakland University* A bulk composite consisting of ferrite-ferroelectric phases shows magnetoelectric (ME) effects that are product properties of the magnetostrictive deformation and piezoelectric charge generation.Bulk composites with strong ME effects are desirable over layered samples due to superior mechanical strength. Here we discuss a percolation approach for modeling the ME effect in bulk composite [1]. We calculated percolation threshold corresponding to structural phase transition of bulk composites from the state with ME interactions to a state with no ME interactions.Expressions for longitudinal and transverse low-frequency ME voltage coefficients have been obtained. Volume fractions corresponding to peak ME voltage coefficients are given. We obtained a piezoelectric volume fraction of 0.45 for maximum ME effect in bulk samples of lead zirconate titanate and nickel-cobalt ferrite. These estimates are in excellent agreement with data. supported by a grant from the NSF. [1] V. M. Petrov, M. I. Bichurin, V. M. Laletin, N. Paddubnaya, and G. Srinivasan, itMagnetoelectric Interaction Phenomena in Crystals-NATO Science Series II. Vol. 164, Eds. M. Fiebig, V. V. Eremenko, and I. E. Chupis (Kluwer Academic Publishers, London, 2004), p.65-70.

**J1 168 Analysis of the Behaviour of Nanocomposites by Multiscale Simulation*** WOONG LEE,† *Yonsei University* WOO-SUNG JUNG, *Korea Advanced Institute of Science and Technology* JAE-MIN MYOUNG, *Yonsei University* Hierarchical multiscale simulation scheme was introduced for the analysis of the mechanical behaviour of nanocomposites. Aluminium matrix composites reinforced with uniformly dispersed carbon nanotube (CNT) was chosen as a model system. Ab initio simulation was first carried out to estimate inter-atomic potential between a CNT and an Al atom and to determine type of bonding between CNT and Al. This fundamental information was then passed onto the molecular dynamic (MD) simulation in which the interface properties between the matrix and the reinforcement was characterised in terms of load-displacement behaviour by simulating a CNT pullout test. Continuum analysis wad carried out with this interface properties to finally extract representative properties of CNT-reinforce Al matrix nanocomposites using representative volume element approach. Fracture behaviour was also estimated by analysing possible crack paths within the nanocomposites.

*This work was supported in part (WL and JMM) by the Korea Research Foundation Grant funded by Korean Government (MOEHRD) R08-2004-000-10193-0.
†Corresponding author

**J1 169 Microscopic Mechanism of Reinforcement and Conductivity in Polystyrene/Carbon Nanotube Composites** T.-E. CHANG, S. RHODES, A. KISLIUK, W. J. BRITTAIN, A. P. SOKOLOV, *University of Akron* Carbon nanotube (CNT) is one of the most studied materials for the polymer reinforcement due to their extraordinary mechanical properties, superior thermal and electronic properties, and high aspect ratio. However, to unlock the potential of CNTs for applications, CNTs must be well dispersed in polymer matrix and the microscopic mechanism of polymer reinforcement by CNTs must be understood. The main goal of the presented research is to analyze structure and conductivity and enhance mechanical properties of polystyrene/carbon nanotube composites. Polystyrene matrix composites reinforced with single-wall carbon nanotubes (SWNTs) were prepared with different

nanotubes concentrations. Microscopic structure and conductivity of composites is analyzed using Raman scattering and dielectric measurement. Studies on the tangential mode in the Raman spectra indicated well-dispersed SWNTs in polymer matrix. We show that conductivity appears in composites already at very low concentrations, hinting at the formation of a 'percolative' network even below 0.5% of the SWNT.

**J1 170 Adsorption of Supercritical Carbon Dioxide in Aerogels as Studied by SANS and Neutron Transmission Techniques*** GEORGE WIGNALL, YURI MELNICHENKO, DAVID COLE, *Oak Ridge National Laboratory* HENRICH FRIELINGHAUS, *Forschungszentrum, Julich* Small-angle neutron scattering (SANS) has been used to study the adsorption behavior of supercritical carbon dioxide (CO2) in porous Vycor glass and silica aerogels. Measurements were performed at T = 35C and 80C as a function of pressure up to P = 25 MPa. The neutron transmission data were used to monitor the ''excess'' adsorption of CO2 at different pressures. The adsorption of CO2 is significantly higher in aerogels than in activated carbons and silica gels. SANS data have revealed the existence of highly compressed adsorbed phase with the density close to the density corresponding to van der Waals volume of carbon dioxide. The results demonstrate the utility of SANS combined with transmission measurements to study the adsorption of supercritical fluids in porous materials.

*This work was supported by the Division of Materials Sciences, under Contract No. DE-AC05-00OR22725 with the Oak Ridge National Laboratory, managed by UT-Battelle, LLC.

**J1 171 First-principles phonon calculation for Al-(Re,Mn)-Si 1/1-1/1-1/1 approximants** N. NAGASAKO, *Toyota Central R&D Labs., Inc.* R. ASAHI, *Toyota Central R&D Labs., Inc.* T. TAKEUCHI, *Nagoya University* A very low thermal conductivity ( $\sim$ 1 W/Km) and a relatively large Seebeck coefficient in Al-based Mackay-type icosahedral quasicrystal have attracted much interest aiming for thermoelectric applications. We performed first-principles phonon calculations for the Al-(Re,Mn)-Si 1/1-1/1-1/1 approximants [1] to elucidate mechanism of their low thermal conductivity. The total energy and atomic force were calculated for a modeled $Al_{17}(Re,Mn)_4Si_2$ unit cell containing 138 atoms using the projector augmented wave method implemented in VASP code [2], and were then utilized for obtaining a phonon dispersion by the direct method [3]. The calculated lattice specific heat showed very good agreement with experiment, confirming validity of the present calculations. We found localized optical modes with a relatively low frequency ( $\sim$ 2 THz) in the phonon dispersion. We discuss the low thermal conductivity in comparison between the Al-Re-Si and Al-Mn-Si systems via averaged group velocity and umklapp phonon scattering related to these optical modes. [1] Takeuchi et al., Phys. Rev. B70, 144202 (2004). [2] G. Kresse, J. Furthmuller, Phys. Rev. B54, 11169 (1996). [3] MedeA-Phonon, Materials Design, Inc. (2003) based on K. Parlinski, Phonon 3.11 (2002).

**J1 172 Interaction of Surface Modified Carbon Nanotubes with Supercritical Carbon Dioxide*** NIHAT BAYSAL, BANU UNSAL, *Department of Chemical Engineering, Yeditepe University, Istanbul 34755, Turkey* RAHMI OZISIK, *Materials Science and Engineering, Rensselaer Polytechnic Institute, Troy, NY 12180, USA* The properties of carbon nanotube (CNT)-polymer nanocomposites are far below than those calculated, mainly due to poor dispersion or interface quality. This is particularly difficult for single walled carbon nanotubes (SWNTs) as they tend to form bundles or ropes that are difficult to exfoliate. Supercritical fluid (SCF) assisted processing is one of the methods that can be used to exfoliate/disperse CNTs along with modifiying the interface of the CNTs. Molecular dynamics simulations were performed to understand how the surface modifiers behave near SWNT surface with and without the presence of SCF molecules. It is also important to understand the diffusivity of SCF molecules between SWNT bundles and the effect of surface modifiers on diffusion. Octane and itn-perflourooctane molecules were used as surface modifiers with varying tethering density and carbon dioxide ($CO_2$) was chosen as the SCF. Results showed that the system with highest number of itn-perfluorooctanes presented the highest degree of success in separating the SWNTs in the presence of $CO_2$.

*This material is based upon work supported by the National Science Foundation under Grant 0500324.

**J1 173 The influence of electric field on optical properties of the few-layer graphene with AB-stacking*** CHILANG LU, Y.C. HUANG, M.F. LIN, *Department of Physics, National Cheng Kung University* C.P. CHANG, *Center for General Education, Tainan Woman's College of Arts & Technology* R.B. CHEN, *Center for General Education, National Kaohsiung Marine University* The effect of perpendicular electric field **E** on optical properties of the AB-stacked few-layer graphene, made up of two, three, or four graphite sheets, is explored through the gradient approximation. In contrast to the featureless optical spectra of graphene, the low-energy absorption spectra of few-layer graphene with AB-stacking exhibit many jumping structures, which result from the band edge states caused by the stacking effect, in the absence of electric field. Remarkably, **E** causes the subband (anti)crossing, changes the subband spacing, produces the scillating bands, and increases the edge states. It, therefore, follows that the field-modulating-spectra with sharp peaks are generated. Moreover, the frequency of peak, which is strongly dependent on the layer number and the field strength, is predicated. Above all, the predicted absorption spectra and the associated electronic properties could be verified by the optical measurements.

*Supported by NSC 94-2112-M-165-001; NSC 94-2112-M-006-0002.

**J1 174 Cluster Formation and Corralling Effect in Two Dimensional Binary Mixtures*** DONGSHENG ZHANG, MARCELO CARIGNANO, IGAL SZLEIFER, *Department of Chemistry, 560 Oval Dr., Purdue University, West Lafayette, IN 47907-1393* We study the formation of ordered clusters of nanoparticles in binary mixtures in two dimensions using Monte Carlo simulations. The necessary conditions for the formation of highly ordered clusters are: the size mismatch between the two components and a long-range soft repulsions between the large particles. The degree of order of the clusters depends on the concentration of large particles. We show the conditions upon which compression of the layer induces squeezing out of the large particles from the interface. Our findings explain recent experimental observations on

poloxamer-lipid mixtures and provide guidelines for how to form ordered clusters of nanoparticles in two dimensions.

*This work is supported by the National Science Foundation, under grant CTS-0338377

**J1 175 A molecular-dynamics study of defects and failure mechanisms in strained heteroepitaxial interfaces*** JARROD E. SCHIFFBAUER, *West Virginia University, Physics Department* MARTINA E. BACHLECHNER, *West Virginia University, Physics Department* The formation and growth of pits and pit-like structures through a delamination-driven mechanism have been observed in the analysis of comprehensive molecular dynamics simulations of a laterally strained $Si(111)/Si_3N_4(0001)$ interfacial system. These phenomena contribute to the ultimate mechanical failure of the simulated samples. Several factors play a key role the nucleation and growth of the pits including temperature and strain rate. Here we present an overview of the dependence of pit nucleation and morphology on both global and local conditions for a representative range of temperatures and applied strain rates.

*Supported in parts by NASA.

**J1 176 The hierarchy of 1D-, 2D- and 3D-dimensional LPS in Cu-Pd and Ag-Pd: A first-principles study*** S. BÄRTHLEIN, E. WINNING, S. MÜLLER, *Universität Erlangen-Nürnberg, Germany* G.L.W. HART, *Northern Arizona University, Flagstaff, Arizona 86011-6010* A. ZUNGER, *National Renewable Energy Lab, Golden, Colorado 80401* Throughout many decades the marvelous variety of so-called long-periodic superlattices (LPS) - being constructed from stacks of $L1_2$ with a certain period $M$ after which an anti-phase boundary is introduced - has been a matter of interest for binary compounds consisting of Pd and noble metals such like Cu, Ag and Au. Whereas $Au_{0.75}Pd_{0.75}$ puts forth the $D0_{23}$ (i.e. $M = 2$) structure as ground state [1], $Cu_{0.75}Pd_{0.75}$ and $Ag_{0.75}Pd_{0.75}$ exhibit LPS3 (i.e. $M = 3$) as $T = 0$K ground state. Moreover, the formation enthalpies for a whole class of superlattices are almost degenerated. In order to control the energetical hierarchies of *all* LPS in question the usual 1D-LPS configuration space must be overcome. We therefore demonstrate how for each system a set of suitable interactions can be constructed by first principles means. Questions concerning a complete description and exhaustive predictive power will be asked and answered by a mixed-space cluster expansion that allows us to handle 1D-LPS with average $M$, 2D- and 3D-LPS with arbitrary integer $M$ and to predict their energies in order to investigate their abilities to serve as ground state candidates. [1] S. Barabash et al., submitted to Phys. Rev. B.

*Supported by DFG and NSF

**J1 177 Statistical studies of the propagation of a signal through a disordered system** JOSHUA DACHMAN-SOLED, *Department of Physics, Yeshiva University* GABRIEL CWILICH, *Department of Physics, Yeshiva University* We have considered the propagation of a signal through a certain layered nanostructure by modeling it as a collection of random one- dimensional interfaces, through which a coherent wave can be transmitted or reflected while being scattered at each interface. We have previously used a simple model where a persistent random walk ( the ''t-r'' model in 1- D) is used as a representation of the propagation of the signal in such a medium [(1)] We will present here some extensions of those results to analyze the total transmission through a chain when a random distribution of the transmittance of the scatterers is included. Some of the statistical properties of the system will be discussed, and some results of possible extensions to more than one dimension in the context of this model will be presented. (1) Nanotechnology, v13, 274, (2002).

**J1 178 Density Functional Study of a Typical Thiol on Perfect Au(111) Surfaces** GUAN WANG, *National Research Council Research Associate* WILLIAM SANDBERG, *Laboratory for Computational Physics and Fluid Dynamics, Naval Research Laboratory, Washington, DC* STEVEN KENNY, *Univ. of Loughborough, U. K.* We investigated systematically the static, dynamical and mechanical properties of a typical thiol-Au surface system at the density functional level. The computational approach uses optimized atomic-like orbits for efficiency and parallel computation. Ab initio results show the equilibrium configuration of the thiol on gold surfaces is in agreement with other computational methods. We found, from ab initio molecular dynamics simulations, that this tethering system keeps stable at 300, 350, and 370 degrees K. We studied the energy profiles that reflect the behaviors of the tethered thiol under normal and parallel stretches. The obtained rupture force is comparable with AFM measurements. We found the rupture force of thiols on gold surfaces is directional. We also show the process by which multiple successive ruptures of the tether occur with the surface. These results should be useful in understanding failure dynamics of tailored biosurfaces in microfluidic devices where fluidic sheer and normal forces are of concern.

**J1 179 Magnetic, magneto-optical and dielectric properties of ferromagnetic semiconductors $CdCr_2S(Se)_4$ from first-principles calculations** GUANG-YU GUO,*HAI-QING LIN, *Department of Physics, Chinese University of Hong Kong, Shatin, Hong Kong* Recently, $CdCr_2S_4$ has been found to exhibit fascinating relaxor ferroelectricity and colossal magnetocapacitive effect.To understand this and other interesting properties, we have calculated the electronic structure, exchange coupling, optical dielectric constant and magneto-optical Kerr rotation of $CdCr_2S_4$ and $CdCr_2Se_4$. The calculations are based on density functional theory with generalized gradient approximation plus on-site Coulomb correlation (GGA+U). The all-electron full potential linearized augmented plane wave (FLAPW), frozen core full potential projector augmented wave (PAW), and also all-electron tight-binding linear muffin-tin orbital methods (TB-LMTO) are used. In this contribution, we will present the obtained exchange coupling parameters, magneto-optical Kerr rotation spectra and dielectric constants. In particular, we will discuss the possible origins of the obtained ferroelectricity in these materials.

*On sabbatical leave from Department of Physics, National Taiwan University, Taipei, Taiwan

**J1 180 Ferromagnetic properties of epitaxial manganite films on $SrTiO_3$/Si heterostructures** D. HUNTER, B. LASLEY, K. LORD, T.M. WILLIAMS, R.R. RAKHIMOV, A.K. PRADHAN, *Center for Materials Research, Norfolk State University* We report on the growth and magnetic properties of epitaxial LSMO films on Si (100) and Si (111) substrates using $SrTiO_3$ template layer, which demonstrate magnetic and electrical properties at and above room temperature. The growth conditions were optimized by varying substrate temperature and oxygen partial pressure. The grain of 20 nm in size coalesced with increasing substrate temperature,

revealing very smooth film surface. The magnetization data show magnetic transition and magnetic hysteresis at and above room room-temperature. The ferromagnetic resonance studies show anisotropic effects related to ferromagnetic properties of films. The details of the structural and magnetic properties will be presented.

**J1 181 Polarizability of carbon nanotube peapods from first-principles*** KISEOK CHANG, YOUNG-GUI YOON, *Chung-Ang University* We calculate polarizability of carbon nanotube peapod from first-principles. The calculated result gives information about electronic screening effects of carbon nanotubes. Recently, the structure has been suggested as bucky shuttle memory devices and three-terminal switching devices. The polarizability and the screening effects may play an important role for the control of that type of devices. We discuss our results in the context of nanoelectronics application.

*The authors would like to acknowledge the computational support from KISTI under 'the 7th Strategic Supercomputing Applications Support Program' with Dr. S. M. Lee as the technical supporter.

**J1 182 Structural and electronic properties of a bucky-ferrocene molecule from first-principles*** JINWOO JEONG, YOUNG-GUI YOON, *Chung-Ang University* Bucky-ferrocene molecules have been synthesized from fullerene and ferrocene molecules. The molecules have features of both components. We performed first-principles electronic structure calculations of a bucky-ferrocene based on $C_{60}$ fullerene and ferrocene molecules in a supercell geometry. We got local minimum structures with geometry optimization from different initial configurations. Orientation of methyl groups and pentacene leads to states in small energy range. Possible device applications of the molecule are discussed.

*This work was supported by the Korea Research Foundation Grant funded by the Korean Government(MOEHRD) (KRF-2005-070-C00041) in which main calculations were performed by using the supercomputing resource of KISTI.

**J1 183 Supramolecular Lysophospholipid-Carbon Nanotube Complexes Enable Cellular Studies** APPARAO RAO, YONNIE WU, JESSICA MOORE, PU-CHUN KE, *Clemson University* LABORATORY OF SINGLE-MOLECULE BIOPHSYICS AND POLYMER PHYSICS TEAM, NANOMATERIALS LABORATORY TEAM, PROTEOMICS LABORATORY TEAM, Single walled carbon nanotubes (SWNTs) have found tremendous applications in electronics, nanophotonics, chemical and biosensing, and very recently, in nanomedicine. The bottleneck for many of these applications is the inherent insolubility of SWNTs due to their mutual interactions. Here we report that lysophospholipids, or single-chained phospholipids offer unprecedented solubility for SWNTs. The biocompatibility of lysophospholipids is unsurpassed since they occur naturally in the cell membrane. Using transmission electron microscopy we show lysophospholipids wrap SWNTs as striations whose size and regularity are affected by the polarity of the lysophospholipids. These findings shed light on the debate over the binding mechanism of amphiphilic polymers and cylindrical nanostructures and has implications on the design of novel supramolecular complexes and nanodevices. Since the head groups of lysophospholipids can be functionalized with tags such as quantum dots, antioxidants, and monoclonal antibodies, our method opens the door for utilizing nanomaterials for itin vivo imaging, gene and drug therapy, and novel nanomedicine.

**J1 184 Time-resolved photoluminescence of single wall carbon nanotubes** CHRISTOPHE VOISIN, SÉBASTIEN BERGER, GUILLAUME CASSABOIS, CLAUDE DELALANDE, PHILIPPE ROUSSIGNOL, *LPA-ENS, 24 rue Lhomond, 75005 Paris, France* XAVIER MARIE, *LNMO-INSA, Toulouse, France* Time-resolved photoluminescence measurements are performed on ensembles of isolated (6,5) single wall carbon nanotubes after a selective picosecond excitation of the second transition of the semiconducting nanotubes. These measurements give insight into the carrier dynamics in the bright nanotubes. The carrier dynamics in bright nanotubes is non exponential reflecting the inhomogeneous distribution of life times. However two contributions to the relaxation are distinguishable within the experimental resolution: a fast component of the order of 10 ps and a smaller long living component of about 100 ps. When cooling the sample down to 10 K, the relative weight of the slow component increases with a characteristic temperature of 150 K. Only a small increase of about 30% of the quantum yield is observed at low temperature. No clear relation between emission energy and life time is observed. In light of recent publications these results suggest that the monoexponential relaxation process in one single nanotube might be either fast or slow and that the proportion of both kind of processes is modified by the temperature with a typical energy of 15 meV.

**J1 185 Effects of the Modification of Single- and Double-Wall Carbon Nanotubes: A Theoretical Study of Field Emission Properties** BRAHIM AKDIM, *Air Force Research Lab* TAPAS KAR, *Utah State University* XIAOFENG DUAN, *ASC/MSRC* RUTH PACHTER, *Air Force Research Lab* In this work, we report first principles calculations of modified single-wall carbon nanotubes (SWCNTs) by $O_3$ and –COOH functionalization, as well as of double-wall carbon nanotubes (DWCNTs) by Cs surface adsorption. Properties related to field emission, including the effects of an applied electric field to mimic the emission environment, as well as structural parameters, are discussed. The results, which suggest a suppression of the emission upon ozone adsorption and carboxy-functionalization in SWCNTs, but an enhancement with Cs surface adsorption, are explained in detail. Finally, the effects of treating DWCNTs with Cs adsorption, as compared to our previous results for SWCNTs, are summarized.

**J1 186 Dissociation of Water on Ti-Decorated C nanostructures*** YANG LEI, *Queen Mary, University of London* WENGUANG ZHU, *Harvard University* SHENG MENG, *University of Texas & ORNL* ZHENYU ZHANG, *University of Tennessee & ORNL* ZHENGXIAO GUO, *Queen Mary, University of London* Direct thermal splitting of water produces pure hydrogen but requires exceptionally high temperatures, making practical implementation challenging. Here we use first-principles simulations to show that water can dissociate on Ti decorated carbon nanostructures, such as graphenes and nanotubes. The behavior of water molecules approaching a Ti adatom is investigated. A single water molecule dissociates freely on a Ti-decorated graphene layer. A small energy barrier has to be overcome to dissociate a second water molecule, with the released H atoms readily combining to form $H_2$. As the number of water molecules further increases, the Ti adatom will dissociate from the graphene layer. We find similar results for when a Ti atom is adsorbed on a carbon nanotube. When more Ti atoms are adsorbed on the outside of the carbon nanotube, the energy barrier against dissociating water

molecules is greatly decreased. We also explore the effects of replacing Ti by other potential catalytic elements.

*Supported by UCDOE, USNSF, & EPSRC/UK-SHEC.

**J1 187 Field Emission of Electrons From Transparent Carbon Nanotube Sheets.** ALEXANDER KUZNETSOV, *NanoTech Inst., The Univ. of Texas at Dallas* ALEXANDER ZAKHIDOV, *Dept. of Phys., Moscow State Univ., Moscow, Russia* MEI ZHANG, SERGEY LEE, RAY BAUGHMAN, ANVAR ZAKHIDOV, *NanoTech Inst., The Univ. of Texas at Dallas* The well-ordered aligned arrays of multiwalled carbon nanotubes were used to make strong and transparent carbon nanotube sheets, prepared by dry spinning from oriented MWCNT forests [1]. Study of electron field emission (FE) shows phenomenally low threshold fields $<$ 0.5 V/mm with very high current densities and steep I-V curves. Also some unusual features observed in IV curves including step-like current increase and hysteresis behavior. Some possible explanations are proposed. Such CNT transparent sheets can be used as high current, high stability field emission sources which are at the same time transparent and can be used as an optical polarizer. The prototype of high luminosity fluorescent lamp with CNT sheets as a cathode was created. [1] M. Zhang, S. Fang, A. Zakhidov, S.B. Lee, A. Aliev et.al., Science, 309,(2005) 1215.

**J1 188 Microwave plasma enhanced chemical vapor deposition growth of small-diameter CNTs using the polymer based catalysts** PENG WANG, *U. of North Carolina at Chapel Hill* JENNIFER LU, *Agilent Inc.* OTTO ZHOU, *Dept. of Physics and Astronomy U. of North Carolina at Chapel Hill* DEPT. OF PHYSICS AND ASTRONOMY COLLABORATION, AGILENT INC. COLLABORATION, Microwave plasma enhanced chemical vapor deposition (MPECVD) has emerged to be a promising candidate method to realize the growth of carbon nanotubes (CNTs) at a temperature of several hundred degrees Celsius. Among various catalysts, metal-containing polymers have the advantage of easy particle size and density controlling. Here we report to produce carbon nanotubes by using metal-containing polymers at 604 $^{o}$C. There are two to six wall layers. The diameter is consistently in the range of 4 to 7 nm. The control of the density and the length of the as grown nanotubes are discussed. The field emission property is characterized.

**J1 189 Hückel theory of large-scale planar organic structures** WILLIAM SCHWALM, *University of North Dakota* MIZUHO SCHWALM, *University of Minnesota-Crookston* Hückel theory applies, if at all, to the $\pi$ orbitals of planar organic molecules, treating only one $p_z$-like basis function for each atomic site. The only advantage of this is that one has closed formulas for properties of rather large, complex structures. We develop $\pi$-orbital Green function calculations for $\vec{k}_{\|}$ resolved density of states of ordered layers of organic adsorbates, such as might pertain to angle-resolved photoemission. Simple-minded though it may be, the theory leads to closed formulas for a wide variety of molecular architectures.

**J1 190 Quantum transport through a carbon nanotube under a time-dependent electric field.** MONICA PACHECO, *Universidad Santa Maria, Valparaiso, Chile* PEDRO ORELLANA, *Universidad Catolica del Norte, Antofagasta, Chile* We investigate quantum transport through single-wall carbon nanotubes (CNT) connected to leads in the presence of an externally imposed time-dependent transverse electric field. A time-oscillating potential uniform in space induces the apparition of side-bands in the spectrum and therefore the tunneling current is drastically modified. To obtain the conductance and the density of states of the CNT, we adopt the equation of motion approach and we calculate the retarded and advanced Green's function defined in terms of the creation and annihilation operator of the electron in the CNT. We analyze the conductance spectra as a function of the frequency and amplitude of the external time-varying potential. We found that above a critical value of the electric field intensity, an enhancement of the conductance, or suppressed resistance, as a function of the electric field strength occurs. This effect can be explained in terms of photon-assisted transport. The conductance increases displaying oscillations which amplitude shows a strong dependence on the frequency of the electric field. For low frequencies, in the microwave range, the oscillations evolve to a structure of well defined steps. The steps in the normalized resistance as a function of the field strength appear for energies corresponding to the Van Hove singularities of the LDOS of the CNT.

**J1 191 Carbon Nanotubes as Counter Electrodes for Gratzel Solar Cells** HASAN SHODIVE, ALI ALIEV, MEI ZHANG, SERGEY LEE, RAY BAUGHMAN, ANVAR ZAKHIDOV, *The University of Texas at Dallas, NanoTech Institute, BE 26, P.O. Box 830688, Richardson, TX 75083* The role of interfaces is very critical for solar cell devices which use nanostructured materials. Dye Sensitized Solar Cells (DSSC) are devices which parts are interfacial in character and physico –chemical processes occur at the interface of two distinct media. DSSC are of great interest due to combination of their high efficiency and relatively low cost. An effective counterelectrode with high electrochemical activity is an important component of DSSC to enhance its practical utility. Presently used Pt coated ITO counterelectrode can not be applied in flexible DSSC architectures, while there is a growing need for flexible anodes which are transparent and have desired interface characteristics. In this work in order to search for such materials for counter electrode in dye sensitized solar cells, newly developed strong and transparent and modified carbon nanotube sheets [1] are used in interfacial counter electrode. To increase the electrochemical activity of the anode the CNT sheets are coated with highly conductive SWCNT and compared with pure multiwall CNT sheets. We show that the transparent sheets of SWCNT/MWCNT perform as a flexible anode and as electrochemical catalyst and also can be used in tandems of dye sensitized solar cells as transparent charge recombination or interconnect layers. [1] M. Zhang, S. Fang, A. Zakhidov, S.B. Lee, A. Aliev et.al., Science, 309, (2005) 1215.

**J1 192 Is a DNA-Wrapped Metallic Nanotube Still Metallic?** S.E. SNYDER, S.V. ROTKIN, *Department of Physics, Lehigh University, Bethlehem, PA, email: ses7@lehigh.edu* Modeling suggests that essential changes in electronic band structure can result from the helical wrapping of single-stranded DNA around a single-walled carbon nanotube (SWNT). The metal-to-semiconductor transition of a metallic nanotube is one of many possible changes. As SWNT/DNA hybrids become more popular, it is of great practical importance to determine how the charged backbone of single-stranded DNA may affect SWNT properties. As a first approximation, the change in band structure is modeled by considering the Coulomb interaction with a charged helical wrap. A range of models is developed to address a variety of wrappings of both metallic and semiconducting tubes. Parameters

of the model include width, charge profile, and axial and angular displacement of the helix, periodicity along the helix, and, indirectly, chiral angle of the wrap. Band gap changes are shown to be fairly robust for axial and angular shifts of the helix. Trends of the band gap and strength of the potential perturbation with tube diameter and wrapping angle are explored. DNA is just one of several polymers which are presumed to helically wrap SWNTs and thereby disperse SWNTs in solution. Therefore, our study is relevant for electronics applications which require individual nanotubes dispersed via polymer wrapping.

**J1 193 Parameter identification procedure for the Density-Gradient model*** PETRU ANDREI, *Florida State University* The existing methods for the computation of parameters of the Density-Gradient model [M. G. Ancona et al, Phys. Rev. B **39**, 9536 (1989)] are based on the comparison of the model with one-dimensional Poisson-Schrödinger computations. While this approach gives good results for devices in which the carriers are confined in only one direction, it is not appropriate for devices in which the carriers are confined in more than one direction. Such devices include short-channel MOSFET and SOI devices, FinFETs, etc. In this presentation we propose a new identification technique based on the effective-mass Schrödinger equation. Our identification technique can be easily applied to 2- and 3-dimensional semiconductor systems. The model parameters are found by using the electron and hole concentrations computed in the framework of the effective-mass Schrödinger equation. Special attention is paid to the computation of the electron effective mass entering in the Density-Gradient equations since these equations are widely used in n-channel nanoscale transistor simulations.

*This work is supported by the Army High Performance Computing Research Center under agreement number DAAD19-01-2-0014.

**J1 194 The Lowest Energy Structures of Si-24 Cluster*** J. RUFINUS, *Widener University* We present the results of computational calculations of the lowest energy structures of Silicon 24 cluster. The calculations were done in the framework of DFT with PBE exchange functional. The initial structures were calculated using a Genetic Algorithm. Approximately 1000 structures were recalculated using Gaussian 03 (with the basis set 6-31G) to determine the lowest energy structures.

*The computations were performed in part on the NSF Terascale Computing System at the Pittsburgh Supercomputing Center.

**J1 195 Density Functional Study of Strain Effects on the Energy Gap in Silicon Nanoclusters** XIHONG PENG, AZAR ALIZADEH, NITIN BHATE, SURYA GANTI, *GE Global Research, Niskayuna, NY 12309* PRADEEP SHARMA, *Department of Mechanical Engineering, University of Houston, Houston, TX 77204* SAROJ NAYAK, SANAT KUMAR, *Departments of Physics and Chemical Engineering, Rensselaer Polytechnic Institute, Troy, NY 12180* It is well known that nanoscale Si clusters are photo luminescent. In parallel, industry routinely exploits the dramatic strain dependence of the band gap of bulk Si for electronics applications. We have discovered, using density functional calculations that the combined role of finite size and strain leads to previously unanticipated effects on the energy gap in Si clusters. Both hydrostatic and non-hydrostatic strains were applied to the clusters with sizes up to 2nm. For the hydrostatic strain, which maintains the tetrahedral bonding network in Si, the effects of strain on the energy gap exhibits size dependence. The behavior can be classified in three distinct regimes that will be discussed in detail. For non-hydrostatic strains, which result in distortion of the tetrahedral bonds, the coupling between the energy gap and strain is largely independent of the cluster size. The mechanisms responsible for the coupling between the gap and strain are proposed. The relative shifts of the energy gap for hydrostatic and non-hydrostatic strains are compared.

## J1 196 FLUIDS AND SOFT MATTER POSTER SESSION

**J1 197 Anomaly in the heat capacity of triethylamine and water** RUTH SHEWMON, RYAN HARTSCHUH, D.T. JACOBS, *Physics Department, The College of Wooster, Wooster OH 44691* The heat capacity $C_p$ of the liquid-liquid mixture triethylamine-water has been precisely measured using our own computer-based data acquisition and control, adiabatic calorimeter. A step process of adding heat and then waiting several minutes for a stable temperature assures equilibrium values for the heat capacity from the known heat added and the resulting change in temperature. For a sample with a much larger concentration of triethylamine than the critical concentration, we observe strikingly different behavior in the heat capacity than that observed near-critical. The unusual behavior is reproducible and may be due to a structure forming in the sample. We acknowledge support from NSF-REU grant DMR 0243811.

**J1 198 Extrinsic homogeneity of non-cubic periodic minimal surface families** GERD E. SCHROEDER, *Applied Maths, RSPhysSE, Australian National University, 0200 ACT, Australia* ANDREW FOGDEN, *Institute for Surface Chemistry, P.O. Box 5607, SE-11486 Stockholm, Sweden* STEPHEN T. HYDE, *Applied Maths, RSPhysSE, Australian National University, 0200 ACT, Australia* Infinite periodic minimal surfaces (IPMS) form the structural basis of cubic phases in copolymer, lipid or surfactant self-assemblies. Although few non-cubic equilibrium phases have been reported to date, there are compelling reasons to study non-cubic IPMS: first, they offer possible transition structures between bicontinuous cubic phases. Second, the reason why soft systems (that favour homogeneity but not explicitly symmetry) exhibit phases of cubic symmetry is still uncertain. We use the concept of *medial surfaces* to quantify *packing homogeneity*, i.e. variations of the channel radius within the structure. This analysis is carried out on IPMS families that are degradations of the cubic P, D and G surfaces (the rPD, rG, tG, tD tP, and H). We show that the cubic G and D are locally maximally homogeneous, whereas the cubic P has at least one relative that is more homogeneous. We discuss the implications for molecular self-assembly (chain stretching), and compare this result to analyses of curvature fluctuations. G.E. Schöder, S.J. Ramsden, A. Fogden, S.T. Hyde, Physica A **339**, 137–144 (2004) and G.E. Schröder, S.J. Ramsden, A.G. Christy, S.T. Hyde, Eur. Phys. J. B **35**, 551–564 (2003)

**J1 199 Synchrotron studies of nanocrystal thin film self-assembly*** DIEGO PONTONI, KYLE ALVINE, *DEAS, Harvard University, Cambridge,MA, 02138* ANTONIO CHECCO, OLEG GANG, BEN OCKO, *BNL, Upton, NY, 11973* PETER PERSHAN, *DEAS, Harvard University, Cambridge, MA, 02138* FRANCESCO STELLACCI, *MIT, Cambridge, MA, 02129* This work is aimed at exploring the mechanisms of formation and dissolution of nanocrystal 2D and 3D assemblies in the presence of nano-thin wetting films. In particular monolayers of bimodal/polydisperse thiol-stabilized gold nanocrystals are studied. In-situ synchrotron X-ray grazing incidence diffraction reveals that upon adsorption of a good solvent for the nanocrystals, the monolayer first expands and then undergoes a transition to a bilayered/disordered state. A detailed physical model for the corresponding X-ray reflectivity data suggests that the transition starts when the substrate is completely covered by the monolayer as a result of its expansion into 2D voids. Further liquid adsorption forces the expulsion of nanocrystals from the monolayer by vertical displacement. The first nanocrystals to be expelled are the large ones. The whole process is reversible upon slow decrease of the adsorbed liquid.

*Work supported by the NSF (NSF03-03916). Synchrotron measurements performed at X22B, National Synchrotron Light Source, Brookhaven National Lab and supported by DOE grants DE-FG02-88ER45379 and DE-AC02-98CH10886.

**J1 200 Self-Assembly of Porphyrin J-Aggregates** VALENTINAS SNITKA, *Research Center for Microsystems and Nanotechnology, Kaunas University of Technology, Lithuania* MINDAUGAS RACKAITIS, *Bridgestone CRT, Akron OH, USA* GINTARE NAVICKAITE, *Research Center for Microsystems and Nanotechnology, Kaunas University of Technology, Lithuania* The porphyrin nanotubes were built by ionic self-assembly of two oppositely charged porphyrins in aqueous solution. The porphyrins in the acid aqueous solution self-assemble into J-aggregates, wheels or other structures. The electrostatic forces between these porphyrin blocks contribute to the formation of porphyrin aggregates in the form of nanotubes, enhance the structural stability of these nanostructures. The nanotubes were composed mixing aqueous solutions of the two porphyrins - anionic Meso-tetra(4- sulfonatophrnyl)porhine dihydrochloride ($TPPS_4$) and cationic Meso-tetra(4-pyridyl)porphine ($T_4MPyP$). The porphyrin nanotubes obtained are hollow structures with the length of 300 nm and diameter 50 nm. Photocatalytic porphyrins are used to reduce metal complexes from aqueous solution and to control the deposition of Au from $AuHCl_4$ and Au nanoparticles colloid solutions onto porphyrin nanotubes. Porphyrin nanotubes are shown to reduce metal complexes and deposit the metal selectively onto the inner or outer surface of the tubes, leading to nanotube-metal composite structures.

**J1 201 Longitudinal complex dielectric polarizability and relaxation times of polar molecules in a biaxial liquid crystal phase** YURI KALMYKOV, *MEPS, Université de Perpignan, 52 Avenue Paul Alduy, 66860 Perpignan Cedex, France* WILLIAM COFFEY, *Department of Electronic and Electrical Engineering, Trinity College, Dublin 2, Ireland* BACHIR OUARI, *MEPS, Université de Perpignan, 52 Avenue Paul Alduy, 66860 Perpignan Cedex, France* SERGEY TITOV, *Institute of Radio Engineering and Electronics of the Russian Academy of Sciences, Fryazino, Moscow Region, 141190, Russia* The longitudinal relaxation time and the complex dielectric polarizability of rod-like molecules with dipole moment parallel to the long axis in a biaxial nematic liquid crystal are calculated using as model the rotational Brownian motion in a mean field potential so reducing the problem to a set of linear differential-recurrence relations for the appropriate equilibrium orientational correlation functions. The solution of this set is obtained by matrix continued fractions. Simple analytic equations (based on the exponential separation of the time scales of the intrawell and overbarrier (interwell) relaxation processes), allowing one to understand the qualitative behavior of the system and accurately predicting the longitudinal complex polarizability for a wide range of the barrier height and anisotropy parameters, are proposed.

**J1 202 Critical behavior at the isotropic to nematic phase transition in a bent-core liquid crystal** DAVID WIANT, STRAHINJA STOJADINOVIC, KRISHNA NEUPANE, SUNIL SHARMA, *Physics Dept. Kent State U.* KATALIN FODOR-CSORBA, *Hungarian Research Institute for Solid State Physics and Optics* ANTAL JAKLI, *Liquid Crystal Institute Kent State U.* JAMES GLEESON, SAMUEL SPRUNT, *Physics Dept. Kent State U.* Magnetic birefringence and dynamic light scattering measurements of orientational order parameter fluctuations at the isotropic- nematic phase transition of a bent-core liquid crystal reveal a pretransitional temperature dependence consistent with the standard Landau-deGennes mean field theory. However, the transition in the bent-core compound is more weakly first-order ($T_{NI} - T^* \approx 0.4°C$), the leading Landau coefficient is $\sim$ 10 times lower, and the viscosity associated with nematic order fluctuations is $\sim$ 50 times higher, than typically observed in calamitic (rod- shaped) liquid crystals. These anomalies can be explained by an unconventional optically isotropic phase composed of complexes of bent-core molecules. Also, we will present preliminary magnetic birefringence and density measurements at temperatures above the nematic-isotropic transistion which support the existence of an optically isotropic state.

**J1 203 Dielectric Properties of Binary Mixtures of MBBA and 7CB** JOHN GAMBLE, SHILA GARG, *Physics Department, The College of Wooster, Wooster OH 44691* The dielectric properties of mixtures of 4-methoxyybenzylidene-4-butylaniline (MBBA) and 4-n-heptyl-4'-cyanobiphenyl (7CB) were investigated at different molar concentrations. The isotropic-nematic phase boundary was determined for various mixtures in order to calculate the nematic range. For some concentrations, there was a second transition to a higher order smectic phase, most likely a Smectic G. Our previous work on MBBA and 5CB indicated that there was strong interaction between the two mesogens at certain concentrations. We find similar strong interactions for mixtures around the 1:1 molar concentration. Planar and homeotropic cells were constructed in order to measure the two different dielectric permittivities, $\varepsilon_{||}$ and $\varepsilon_{\perp}$. The cells were maintained at a fixed reduced temperature $\tau$ during the measurements, since the nematic range and transition temperatures were different for each mixture. From the $\varepsilon_{||}$ and $\varepsilon_{\perp}$ data, we calculated the dielectric anisotropy $\Delta\varepsilon = \varepsilon_{\parallel} - \varepsilon_{\perp}$ as a function of molar concentrations of the mixtures.

**J1 204 Thermal Conductivity of Silica Aerogels from Computer Simulations** BRIAN GOOD, *NASA Glenn Research Center* Aerogels are of current interest to the aerospace community; their light weight and low thermal conductivity make them suitable for use in lightweight thermal insulation. The gels typically exhibit a

complex structure; the smallest observed feature is a 2-5nm ''primary'' particle of amorphous silica. The primary particles aggregate to form ''secondary'' particles an order of magnitude larger, and these, in turn, form pearl-necklace structures whose details depend on the density. The gels appear to exhibit fractal dimensionality, at least over a small range of length scales. In this work, we investigate the relationship between the structure of the gels, their dimensionality and density, and their thermal conductivity. We model the secondary-particle aggregate structure using a modified diffusion limited cluster aggregation (DLCA) scheme, which produces qualitatively different structures at low and high densities that are consistent with experimental observation. At lower densities, we find evidence for a transition from fractal behavior at small length scales to compact mass scaling at larger lengths. We model the thermal conductivity by assigning a size-dependent thermal conductance to each secondary particle, and an effective thermal conductivity to the gas assumed to be present in the pores between the particles. The conductivity of the gel-gas network is obtained using standard numerical techniques. The scaling of the thermal conductivity with density, fractal dimension, and the ratio of silica to gas conductivities is discussed.

**J1 205 Dynamics of multiple glass states** NORA GRANETO, ANDRZEJ LATKA, PIOTR HABDAS, *Dept. of Physics, Saint Joseph's University* We study concentrated colloidal suspensions, a model system which exhibits a glass transition. Using microscopy techniques we directly observe the microscopic behavior of the colloidal particles as the glass transition is approached. Moreover, by adding polymer to the colloidal suspension we induce ''sticking'' between the colloidal particles. When such attractive force is introduced to a hard-sphere colloidal glass, the system enters a liquid phase. Increasing the polymer concentration even further causes the system to enter another glass state – an attractive glass. We investigate the particle dynamics as system enters multiple glass states. Particularly, we focus on single particle jumps and effect of caging on the particles' dynamics.

**J1 206 Statistical Mechanics of Hydrodynamically Coupled Colloidal Spheres in Optical Vortices** YAEL ROICHMAN, *New York University* DOV LEVINE, *Technion, Israel Institute of Technology* DAVID G. GRIER, *New York University* Optical vortices are ring-like optical traps created by strongly focusing a helical mode of laser light. Colloidal particles trapped in an optical vortex are driven around its circumference by the vortex's orbital angular momentum flux. A set of such circulating spheres may be viewed as a system of perpetually sedimenting particles. Like sedimenting spheres, colloid in a vortex experience a uniform body force. They also interact with each other hydrodynamically. Unlike sedimenting spheres, those in an optical vortex remain in the field of view indefinitely and can be studied in great detail. In addition, the circulating colloid can be subjected to a nonuniform static potential energy landscape created by varying the intensity of light around an optical vortex's circumference. This elegant model system allows us to study the effect of hydrodynamic coupling on the mutual sedimentation of several particle with varying sizes. We find that sedimentation of a bidispered mixture of colloids forms stable couples of particles as opposed to the less stable structure of monodipersed particles sedimenting. We also demonstrate that fluctuations in the particles' trajectories can be used to gauge their system's departure from equilibrium.

**J1 207 Measuring the transverse magnetization of rotating ferrofluids** MANFRED LÜCKE, J. EMBS, S. MAY, C. WAGNER, A. KITYK, A. LESCHHORN, *University Saarbrücken* We report on measurements of the transverse magnetization of a ferrofluid rotating as a rigid body in a constant magnetic field, $\mathbf{H}_0$, applied perpendicular to the axis of rotation. The rotation of the fluid leads to a non-equilibrium situation, where the ferrofluid magnetization, $\mathbf{M}$, and the magnetic field within the sample, $\mathbf{H}$, are no longer parallel to each other. The off-axis magnetization perpendicular to $\mathbf{H}_0$ is measured as a function of both the applied magnetic field, $H_0$, and the angular frequency $\Omega$. The latter ranges from a few Hz to frequencies well above a characteristic inverse Brownian relaxation time. Our experimental results strongly indicate that the transverse magnetization is caused only by a small fraction of the collodial ferromagnetic particles. The effect of the polydispersity of the ferrofluid is discussed. Experimental results are compared to predictions based on several theoretical models. A single-time relaxation approach for the so-called effective field and a field dependent Debye relaxation of $\mathbf{M}$ yield reasonably good shapes of the curves of transverse magnetization versus $\Omega$. However, like the other models they overestimate their magnitudes.

**J1 208 Effect of Associative Polymers on the Foaming Properties of Surfactant Solutions*** ALFREDO CERVANTES, EMMANUEL ROBLES, *Departamento de Investigación en Polímeros y Materiales, Universidad de Sonora* HERIBERTO ACUÑA, ROGELIO GAMEZ, AMIR MALDONADO, *Departamento de Física, Universidad de Sonora* Aqueous foams are materials which have many industrial applications. Their stability is affected by three mechanisms: bubble coalescence (film rupture), coarsening (gas diffusion) and drainage (gravity-driven liquid flow). The aim of this work is to obtain some insight into the effect of associative polymers on the foamability, foam stability and drainage of surfactant solutions. The foams were produced by air bubbling and by the turbulent mixing method. The surfactant is SDS and the associative polymers studied are HEUR and POE-Stearate. We studied the effect of polymer concentration for each macromolecule. The results show that two opposite effects are present when the polymer concentration is increased: for low polymer concentrations, foamability and foam stability is higher than for high concentrations. Results are discussed in terms of the properties of the solution: surface tension, electrical conductivity, bulk viscosity, etc.

*We acknowledge financial support from Universidad de Sonora.

**J1 209 Elasticity of the FCC Hard Sphere Crystal from two point microrheology** MATTHEW SULLIVAN, *Princeton University / Schlumberger-Doll Research* KUN ZHAO, ANDREW HOLLINGSWORTH, P.M. CHAIKIN, *Princeton University / New York University* WILLIAM B. RUSSEL, *Princeton University* We present a measurement of the full elastic tensor of a hard sphere colloidal crystal. Our system consists of concentrated suspensions of monodisperse PMMA-PHSA particles suspended in a density-matching solvent mixture of decalin and tetrachloroethylene. Single crystals are heterogeneously nucleated from a surface template to produce large face centered cubic (FCC) single crystals. The two-point displacement correlations are measured using confocal microscopy and video analysis. These show a $1/r$ decay with distance and an angular dependence that can be used to determine the three elastic constants of the FCC crystal.

**J1 210 Computer simulations of SDS/dodecanol (hexadecanol) monolayers at water/air interface*** HECTOR DOMINGUEZ, *Instituto de Investigaciones en Materiales, Universidad Nacional Autonoma de Mexico (UNAM). Mexico 04510* MARGARITA RIVERA, *Instituto de Fisica, Universidad Nacional Autonoma de Mexico. Mexico 01000* Simulations of monolayer mixtures of amphiphlic molecules were investigated to study the effects of the polar head groups in the structure of the monolayer at the water/air interface. The binary mixture was composed of sodium dodecyl sulfate (SDS) and dodecanol (hexadecanol) molecules For the low dodecanol concentration molecules two monolayer mixtures were prepared. In the first monolayer all the dodecanol molecules were placed together in the center of the simulation box whereas in the second monolayer those molecules were uniformly distributed in the surface area in such a way that they were a part from each other. Simulations of both systems indicate that the dodecanol tails in the first monolayer are more straight and more ordered than those in the second monolayer. When simulations of SDS/hexadecanol are performed it is observed that the tilt angle and the order of the tails are different respect to the SDS/dodecanol mixtures.

*We acknowledge CONACYT- Mexico grant 42842-F

**J1 211 Role of membrane composition in the formation and stability of buds** KURT A. SMITH, ANNA C. BALAZS, *University of Pittsburgh* Using dissipative particle dynamics we study the behavior of buds in amphiphilic bilayer membranes. These buds occur during phase separation when line tension between the two phases comes to dominate the bending rigidity of the membrane. We show that the inclusion of twin-tail amphiphiles, which segragate to the interface between the two phases, is a means to controlling the onset of budding. In addition they stabilize the neck when budding does occur, by acting essentially as stitches, thereby increasing the energy needed to detach the bud from the membrane.

**J1 212 Competing interactions in two dimensional Coulomb systems: Surface charge heterogeneities in co-assembled cationic-anionic incompatible mixtures** SHARON LOVERDE, YURI VELICHKO, MONICA OLVERA DE LA CRUZ, *Department of Materials Science and Engineering, Northwestern University* A binary mixture of oppositely charged components confined to a plane such as cationic and anionic lipid bilayers may exhibit local segregation. The relative strength of the net short range interactions, which favors macroscopic segregation, and the long range electrostatic interactions, which favors mixing, determines the length scale of the finite size or microphase segregation. The free energy of the system can be examined analytically in two separate regimes, when considering small density fluctuations at high temperatures, and when considering the periodic ordering of the system at low temperatures (F. J. Solis, S. I. Stupp and M. Olvera de la Cruz J. Chem. Phys. 122 (5), 054905 (2005)). A simple Molecular Dynamics simulation of oppositely charged monomers, interacting with a short range Lennard Jones potential and confined to a two dimensional plane, is examined at different strengths of short and long range interactions. The system exhibits well-defined domains that can be characterized by their periodic length-scale as well as the orientational ordering of their interfaces. By adding salt, the ordering of the domains disappears and the mixture macroscopically phase segregates in agreement with analytical predictions.

**J1 213 Circular Couette cell for two-dimensional turbulence experiments in sheared flow: initial results.*** JOHN V. ULMEN, PAUL W. FONTANA, MARTIN KEARNEY-FISCHER, *Seattle University* An experiment to study turbulence in quasi-two-dimensional flows with a controlled mean flow shear has been built. Experiments are underway to investigate the suppression of turbulent transport by sheared flow as seen in geostrophic flows and laboratory fusion plasmas. The apparatus, a circular Couette cell, uses a liquid film of dilute soap solution suspended freely in an annular channel with a rotating outer boundary. The channel is $7cm$ wide with an average radius of $46.5cm$, and can be rotated at angular speeds exceeding $10rad/s$. Mean flow profiles will be presented showing the effect of air resistance on the flow; damping lengths on the order of $1mm$ are observed. Turbulence is driven independently via electromagnetic forcing. The rate of turbulence injection can be varied continuously, and its spatial scale corresponds to the spatial frequency of an array of NdFeB magnets. Diagnostics include particle imaging velocimetry, two-point laser Doppler velocimetry, and thickness measurements via reflection interferometry. Initial results and plans for upcoming measurements will be presented.

*Supported by the M. J. Murdock Charitable Trust, Research Corporation, and the NSF-MRI program.

**J1 214 Droplet pinch off of diluted polymer solutions** CHRISTIAN WAGNER, RAINER SATTLER, *Universitaet des Saarlandes* JENS EGGERS, *University of Bristol* Tiny amounts of polymers can alter the flow behaviour of simple liquids dramatically. An aesthetic and instructive example is the detachment process of a droplet of a polymer solution, e.g. a diluted DNA solution. It is characterized by the suppression of the pinch off finite time singularity and the formation of a cylindrical filament between the droplet and the nozzle. On later stages of the experiments beads on a string a formed. Their generation can be well explained with scaling arguments of the intrinsic time scales of the experiment. The dramatic increase of resistance against the flow is macroscopically described by the elongational viscosity. It is a crucial parameter in many different industrial processes where contraction flows are generic. A pure elongational flow stretches the macromolecules at maximum and we use different experimental techniques simultaneously to relate macroscopic flow profiles with microscopic polymer configurations.

**J1 215 Motility in multicomponent fluids*** ROBERT MAGERLE, STEPHAN WEISS, NICOLAUS REHSE, *Technische Universitaet Chemnitz* During annealing in air thin films of polystyrene-block-polypropylene and similar block copolymers decompose and form a phase separating multi-component polymeric fluid where domains coarsen similar as in a binary mixture. At a certain threshold of domain size, two domains form a droplet which starts to move spontaneously across the surface. We show that a chemical reaction with oxygen is required for this motion for which we have determined the effective activation energy. We discus a model for droplet motion and speculate about the relevance of the underlying physics for the motility of biological cells and their ultra-cellular compartments.

*Supported by Deutsche Forschungsgemeinschaft (SFB 481)

**J1 216 Characterization of diffusion in supersaturated solutions using T-sensors*** KRISTEN BLOSCHOCK, *Georgetown University Department of Physics* RUSSEL ROSS, *Georgetown University Department of Physics* EDWARD VAN KEUREN, *Georgetown University Department of Physics* Measurement of the molecular diffusivity has provided much of the evidence for cluster formation in supersaturated solutions. The recent development of the T-sensor, a microfluidics laminar flow device, enables rapid determination of molecular diffusion coefficients. In this device, fluids in two channels meet and undergo laminar flow, with diffusion occurring perpendicular to the direction of flow in the channel. We have used fluorescence imaging of molecules in a T-sensor to study diffusion in supersaturated solutions of several dyes. When they self-assemble, these molecules exhibit characteristic changes in fluorescence emission. Therefore, using imaging we can determine both the state of aggregation and the diffusion coefficient. We will present results of experiments with one channel containing a molecular solution and the second a miscible non-solvent; the diffusional mixing induces nucleation and growth of nanocrystals.

*This work was supported by the National Science Foundation, Grant DMR 0348955.

**J1 217 Self-organizing flow in a multi-component driven system - interacting lattice gas simulation** RAS PANDEY, *Naval Research Laboratory and University of Southern Mississippi* JOE GETTRUST, *Naval Research Laboratory* We consider a mixture of mobile particles $(A,B)$ described by their molecular weight, interaction, and miscibility gap on a discrete lattice of size $L_x \times L_y \times L_z$. The source of particles is at the bottom $(z = 1)$ of the lattice with open top $(z = L_z)$. The Metropolis algorithm is used for stochastic moves of particles with a hydrostatic pressure bias (H). Periodic boundary conditions are used along the transverse directions with open longitudinal ends. Particles continue to enter the lattice from the source and are driven by bias, concentration gradient, and thermal energy against gravity. Net flow of particles occurs and a steady-state is reached with a self-organized morphology. Self-organizing structures and flow flux rates are examined as a function of bias for a range of molecular weight ratios for non-equilibrium steady-state system with non-conservative mass/volume. Response of the flux density shows linear and nonlinear behavior depending on the range of the bias with an eruptive response at extreme values of the bias.

**J1 218 Distributions and seeps of driven mixture around a slit in porous media - interacting lattice gas simulation** JOE GETTRUST, *Naval Research Laboratory* RAS PANDEY, *Naval Research Laboratory and University of Southern Mississippi* We consider a porous medium with a slit on a discrete lattice of size $L_x \times L_y \times L_z$. The porous matrix is generated by a random distribution of immobile barriers on a fraction of the lattice sites. A longitudinal slit of width $L_s$ spans from bottom to top through the center of the lattice. The source of particles specified by their molecular weight, interaction, and miscibility gap is connected to the bottom $(z = 1)$ of the lattice with an open top $(z = L_z)$. The Metropolis algorithm is used for stochastic moves of particles with a hydrostatic pressure bias $(H)$. Periodic boundary conditions are used along the transverse directions with open longitudinal ends. Particles continue to enter the lattice from the source. Particles flow from bottom to top reaching a steady-state where we examine their seeps and distributions. We find that the steady-state distributions of constituents and their local mobility in the slit and the surrounding regions depend on bias and porosity with strong correlations at high bias.

**J1 219 Self-Organized Criticality in a Bead Pile** MEGAN MILLER, TUAN NGUYEN, ELIZABETH BAKER, D.T. JACOBS, *Physics Department, The College of Wooster, Wooster OH 44691* This experiment examined a conical bead pile and the distribution of avalanche sizes when using uniform 3mm stainless steel spheres (''beads''). A bead pile is built by pouring beads onto a circular base where the bottom layer of beads has been glued randomly. Beads are then individually dropped from a fixed height after which the pile is massed. This process is repeated for thousands of bead drops. By measuring the number of avalanches of a given size that occurred during the experiment, the resulting distribution could be compared to a power law description as predicted by self-organized criticality. We had found in an earlier experiment that glass beads dropped from a small height were consistent with a simple power-law, but if dropped from larger heights then a power-law times an exponential was needed. The stainless steel beads always had a distribution that deviated from a simple power-law with larger deviations as the beads were dropped from larger heights. In addition, we observed a different power-law exponent than that found for glass beads yet a similar dependence on drop height. We acknowledge support from NSF-REU grant DMR 0243811.

**J1 220 Effect of Relative Material Stiffness of Binary Mixture Components to Compression*** CRAIG BENTHAM, *Pfizer Ltd., Sandwich, Kent, UK* MEENAKSHI DUTT, *University of Cambridge* BRUNO HANCOCK, *Pfizer Inc., Groton, Connecticut, USA* JAMES ELLIOTT, *University of Cambridge* Typical powder blends will have constituent particles which will differ in material properties, such as stiffness, resulting in variation of coordination number and contact slipping state, at a local particle scale. At a macroscopic scale, the relative properties of the various components will influence the force and stress response of the blend to an external load or strain. Of particular curiosity is the distribution of load as a function of contact stiffness. We present numerical results from our studies on binary mixtures with components whose relative stiffness (Young's modulus) has been varied systematically. These mixtures settle under gravity followed by compression at a constant strain rate. In addition, we discuss the correlations between the contact slipping state, stiffness, and the load sustained.

*Special Acknowledgements to Pfizer for funding

**J1 221 Granular templating: effects of boundary structure on particle packings under simultaneous shear and compression*** BRUNO HANCOCK, *Pfizer Inc., Groton, Connecticut, USA* MEENAKSHI DUTT, *University of Cambridge* CRAIG BENTHAM, *Pfizer Ltd., Sandwich, Kent, UK* JAMES ELLIOTT, *University of Cambridge* We present our findings on the effect of various confining substrates, both crystalline and amorphous, on spherical granular particles, packed under gravity followed by the simultaneous application of shear and compressive strains. We show that a substrate templated with the BCC (100) plane, whose void and particle packing structures are identical, is most suitable for inducing crystallization mimicking the substrate structure. Our results for both templated substrates show the compressive strain dominating the shear strain.

*Special Ackowledgements to Pfizer for funding

**J1 222 A Particle-Substrate Model and Its Applications to Cooling and Driven Granular Systems*** ROBERT BEHRINGER, *Duke University* MEENAKSHI DUTT, *University of Cambridge* A complete understanding of the microscopic dynamics of a monolayer of identical spheres moving on a substrate must encompass the effects of collisions and the substrate on the particles. We begin from first principles by considering collections of spherical frictional particles that roll and slip on a flat static substrate. We present a numerical model which accounts for collisional and surface frictional dissipation and their influence on particle dynamics for a quasi 2-dimensional cooling granular material. We apply this model to a simulation of the granular collider experiment (Painter et al., Physica D (2003)), in which collections of particles collided as they moved radially inward on a substrate. We find an agreement between the experimental and numerical results. We extend this model further to study a horizontally vibrated particle-substrate system. We show that the ratio of the substrate acceleration to the particle-substrate static frictional force per unit mass (Kondic, Phys Rev. E (1999)) dominates the individual particle dynamics and the collision dynamics. We will present results from our numerical experiments which further higlight the critical role of static friction, relative to the driving acceleration.

*Special acknowledgements to NSF support: NSF-DMR-0137119

**J1 223 Flux from a vibrated granular medium** KE CHEN, MATTHEW STONE,*RACHEL BARRY, MATTHEW LOHR, WILLIAM McCONVILLE, *Dept. of Physics and Materials Research Inst., Penn State University* KIT KLEIN, *Dept. of Computer Engr., Penn State University* BEN-LI SHEU, *Dept. of Physics and Materials Research Inst., Penn State University* ANDREW MORSS,† *Dept. of Physics and Materials Research Institute, Penn State University* THOMAS SCHEIDEMANTEL, PETER SCHIFFER, *Dept. of Physics and Materials Research Inst., Penn State University* We have studied vertically vibrated granular media by measuring the flux through a hole in the container's bottom surface. We find that when fully fluidized, the flux is controlled by the peak velocity of the vibration, $v_{max}$, i.e., the flux is nearly independent of the frequency and acceleration amplitude for a given value of $v_{max}$. The flux decreases with increasing peak velocity and then becomes constant for the largest values of $v_{max}$. We demonstrate that the data at low peak velocity can be quantitatively described by a hydrodynamic model. By contrast, the nearly constant flux at larger peak velocity signals a crossover to a state in which the granular density near the bottom is insensitive to the energy input to the system. This research was supported by the NASA through grant NAG3-2384 and the NSF REU program through grant DMR 0305238.

*Currently at Condensed Matter Sciences Division, Oak Ridge Natl. Lab

†Currently at Dept. of Physics, Ohio State University

**J1 224 Quicksand** DANIEL BONN, *ENS/LPS and WZI, UvA* Quicksand is the generic name for unstable soils reputed to trap anyone who treads on it. Popular wisdom has it that one should not move when trapped in quicksand, as motion makes one sink in even deeper and that once trapped, it is difficult to escape. We provide an explanation for these observations by studying the most commonly encountered form of natural quicksand. We show that a spectacular liquefaction of the material occurs when a stress is applied to the material: the liquefaction is the reason why one sinks away, and it is more pronounced for larger stresses. By constructing laboratory quicksand, we demonstrate that the liquefaction is due to the structure: quicksand is a loose granular packing of sand particles stabilized by a clay matrix that forms a particulate gel. The stress liquefies the clay matrix, and the granular assembly collapses, expulsing water. This results in a densely packed system that practically impossible to dilate: it is for this reason that once trapped it is difficult to get out of quicksand. A sinking test demonstrates that, due to buoyancy, it impossible to drown in the quicksand.

**J1 225 Properties of uniformly heated and sheared granular gases. A DSMC simulation.** FRANCISCO VEGA REYES, *Departamento de Fisica, Universidad de Extremadura, E-06071 Badajoz, Spain* We study a monodisperse hard sphere granular gas by means of the Direct Monte Carlo Simulation (DSMC) of the associated Enskog-Boltzmann equation. Due to the kinetic energy loss in the interparticle collisions, the granular temperature decays to the zero unless there is some kind of energy input. We consider two types of energy input. One, heating, process through which kinetic energy is added directly to the particles; and two, shearing of the granular gas. We focus particularly in the uniform steady states. Contrary to elastic hard sphere gases, in granular gases the steady uniform shear state is possible (i.e., a constant linear velocity profile with steady uniform density and temperature). This state is a reference point in the study of granular gases. We analyse the relevant magnitudes (like stress tensor) in the different energy input cases, as a function of the inelasticity.

**J1 226 Networks of Liquid Bridges and Clusters in Wet Granular Systems** MARIO SCHEEL, STEPHAN HERMINGHAUS, RALF SEEMANN, *MPI for Dynamics and Self-Organization, Bunsenstr. 10, D-37073 Göttingen, Germany* The macroscopic mechanical properties of a dry granulate change dramatically when small amounts of liquid are added. This is due to capillary bridges forming between mutually adjacent grains in the pile, which exert an attractive force by virtue of the surface tension of the liquid. If much more liquid is added, the liquid clusters, and the stability of the pile is reduced. Although the tensile strength of wet granulates can be roughly estimated from the capillary forces, a quantitative theory of the mechanical properties of granulate requires a detailed understanding of the topology of the complex network of capillary bridges and clusters. We have determined the macroscopic properties in model granulates with a vertical fluidization experiment, as well as the microscopic geometry of the distribution of liquid within the pile via x-ray microtomography. The transition from capillary bridges to clusters or the percolation can be clearly observed in both the fluidization experiments and the tomographic imaging.

**J1 227 Flow of Polymer Solutions in Nansocale Slit Pores** JAIME A. MILLAN, MOHAMED LARADJI, *Physics Dept., University of Memphis* YONGMEI WANG, *Chemistry Dept., University of Memphis* We present results from extensive and systematic molecular dynamics simulations of semi-dilute and cocentrated polymer solutions in nanoscale slit pores. We will particulary report on the effects of the polymer concentration, molecular weight and flow rate on the profiles of the velocity field, polymer concentration, and radii of gyration of the polymer chains across the slit.

**J1 228 Kinematics of a sphere moving through a non-Newtonian liquid** HANS WHEELERSBURG, NORA GRANETO, PIOTR HABDAS, *Dept. of Physics, Saint Joseph's University* When a sphere moves through a non-Newtonian liquid, it creates an envelope of sheared liquid around the sphere. By using different tube sizes and pulling the sphere at different velocities we examine the dimensions of the envelope and study the effect of the walls of the tube on the sphere in motion. Also we study how the drag force acting on the sphere varies with the tube size, sphere velocity, sphere size, and the properties of the non-Newtonian liquids (i.e. yield stress). In a Newtonian liquid, the drag force acting on the sphere is proportional to the velocity of the sphere and follows the Stokes Law. The drag force acting on a sphere moving through a non-Newtonian liquid does not follow this dependence and we are currently investigating the relationship of the drag force on velocity in non-Newtonian liquids.

**J1 229 Spreading of Advected Tracers in a Creeping Flow in a Rectangular Channel** MIRON KAUFMAN, We have developed an analytical solution [M. Kaufman, 2003 AIChE Annual Meeting Conference Proceedings] of the Navier-Stokes equation for the two-dimensional incompressible flow in a rectangular cavity in the limit of zero Reynolds number. An analytical solution for the fluid velocity along the axis of a parallelepiped, again in the Stokes limit, is also known. In this work we combine the two solutions to get analytically the three-dimensional creeping flow inside a channel in the shape of a parallelepiped. We integrate numerically the velocity vector to get trajectories of tracers advected by the fluid. We analyze the spreading in space of the tracers by calculating the time evolution of the entropy.

**J1 230 Spinning Rods: Experiment & Theory*** JONATHAN TOLEDO, *University of North Carolina at Chapel Hill* RICHARD M. McLAUGHLIN, ROBERTO CAMASSA, TERRY JO LEITERMAN, RICHARD SUPERFINE, JING HAO, LEANDRA VICCI, ADAM BROOKS, *University of North Carolina, UNC RTG FLUIDS GROUP* UNC RTG FLUIDS GROUP TEAM, Mixing and transport properties of the fluid motion induced by a slender rod attached to a plane sweeping out a cone are examined in a table- top experiment. This experiment is used to validate an exact solution for the motion of a spheroid sweeping out a double cone in free space and an asymptotic solution for a slender body attached to a plane. Validation of the theory is used to examine mixing and transport of the same experiment on the microscale.

*RTG NSF DMS-0502266

**J1 231 Influence of Pressure on Fast Dynamics in Polymers** B. BEGEN, A. KISLIUK, A.P. SOKOLOV, *University of Akron* V.N. NOVIKOV, *IA&E, Russian Academy of Sciences* K. NISS, A. CHAUTY-CAILLIAUX, C. ALBA-SIMIONESCO, *Université de Paris-Sud* B. FRICK, *Institut Laue-Langevin* Recent experiments reveal a strong correlation between the fast dynamics and the fragility of glass forming liquids. It is known that both density and thermal energy influence significantly the structural relaxation and the glass transition in most of the glass forming systems. However, not much is known about the influence of volume and temperature on the fast dynamics. In this contribution, we present light and neutron scattering study of the influence of pressure on fast dynamics and elastic properties in polymers. Our results show that the boson peak frequency increases with pressure stronger than the sound velocity. We observed that the boson peak intensity decreases under pressure stronger in Raman scattering than in neutron scattering suggesting a decrease in the light-to-vibrations coupling coefficient $C(v)$. We argue that variations in $C(v)$ might be related to amplitude of structural fluctuations. We speculate that change in disorder and/or overall density under pressure is the main cause for the observed variations.

**J1 232 Fragility, spatially heterogeneous dynamics, and enhanced translational self-diffusion in low molecular weight glassformers*** MARIE K. MAPES, STEPHEN F. SWALLEN, M.D. EDIGER, *University of Wisconsin, Madison* Recent measurements of self-diffusion coefficients in prototypical small molecule glassformers reveal behaviors believed to be universal for low molecular weight fragile glasses. These behaviors include enhanced translational motion and a self-diffusion controlled crystallization regime. Similar enhancements in self-diffusion relative to the Stokes-Einstein relation have been found for two glassformers of similar fragility: *o*-terphenyl with around 100 times faster self-diffusion than expected at $T_g$ +3 K, and ittris-naphthylbenzene, with around 400 times faster diffusion at $T_g$. The temperature range of enhanced motion also overlaps a range of self-diffusion controlled crystal growth. The origin of enhanced diffusion is often attributed to spatially heterogeneous dynamics thought to exist in fragile glassformers. Relaxation time distributions in the literature for *o*-terphenyl and ittris-naphthylbenzene, and their relationships with enhancement of self-diffusion, fragility, and heterogeneous dynamics are discussed.

*The authors acknowledge support for this work from NSF Chemistry (NSF-CHE 0245674).

**J1 233 Dynamics of magnetic colloids** ARTUR ERBE, MICHAEL KOEPPL, LARYSA BARABAN, FLORIAN MERKT, PAUL LEIDERER, *FB Physik, Universitaet Konstanz, Germany* Colloidal suspensions are fascinating examples of soft matter, but also model systems for studying the behavior of atoms and molecules. Here we present the dynamic behavior of superparamagnetic particles and the fabrication and characterization of magnetically anisotropic particles. Transport of the superparamagnetic particles (diameter of 4.7 $\mu$m) is characterized through narrow constrictions on the scale of 60 $-$ 100 $\mu$m in an externally applied magnetic field. In this system we observe the formation of lanes depending on the interparticle interactions and the particle densities. In order to create a larger range of interparticle interactions we also produce anisotropic particles by evaporation of metallic caps on top of the colloidal particles (for these experiments we use nonmagnetic silica colloids). These particles can have a well-defined magnetic moment, given by the material of the cap. We determine this moment using the magnetooptic technique.

**J1 234 Informational Self Organization in Isotopically Random Soft Structures** ALEXANDER A. BEREZIN, *McMaster University* Stable isotopicity can potentially account for self organization and informational proliferation in soft matrices, gels and even fluids. This can be a key to explain seeming ''impossibility'' of such claims as memory effects in water. Within isotopicity paradigm (A.A. Berezin, Isotopic diversity in natural and engineering design, In: Design and Nature, WIT Press, 2004, 411-419) pattern enhancement upon successive dilutions can be attributed to ''avalanche'' cascade formation of informationally rich and numerically redundant ''Arnold tongues'' akin to strange attractors. Furthermore, even biological and medical ''phenomenol-

ogy'' which we currently put under umbrella term ''immune systems'' can be operationally interpreted through quantum computer informational processing in isotopic neural networks using diversity of nuclear spins of different isotopes. Under action of informational attractor (analogy with Aristotelian causa finalis) ''decay'' process of patterns can be slower than build up of informational redundancy (morphic resonance). The latter can be envisioned as a kind of informational ''Huygens principle'' in which formation of global (wave) front (here: informational front) results from superposition of virtual sources at previous stage of cascade process. Nonlocal aspects of isotopic quantum computing can potentially provide connector to infinititude (perhaps even Cantor uncountable) library of patterns and serve as yet another bridge between physics and biology.

**J1 235 Quantifying spatiotemporal chaos in Rayleigh-Benard convection** MAGNUS EINARSSON, *Virginia Tech* M.R. PAUL, *Virginia Tech* P.F. FISCHER, *Argonne National Laboratory* One of the biggest challenges of modern science is to gain further understanding of large spatially extended systems driven far-from-equilibrium. Such systems often exhibit spatiotemporal chaos yielding aperiodic behavior in both space and time that is difficult to characterize. Diagnostics based upon the Lyapunov exponents and eigenvectors are explored as a way to quantify spatiotemporal chaos in Rayleigh-Benard convection in an experimentally realistic cylindrical domain. This is done through large-scale parallel numerical simulations and the results are used to gain new physical insight into the behavior of spatiotemporal chaotic systems.

**J1 236 Modeling microcapsules moving through microchannels of differing geometries** ALEXANDER ALEXEEV, ROLF VERBERG, ANNA BALAZS, *Chemical Engineering Department, University of Pittsburgh, Pittsburgh, PA* We study the dynamic behavior of deformable microcapsules in microchannels, which are roughly comparable in size to the diameter of the capsules. The capsules model synthetic polymeric microcapsules or biological cells, such as leukocytes. The microcapsules are driven to move through the channels by an imposed pressure gradient or flow field. Each microcapsule consists of an elastic shell that is filled with a viscous fluid. To model this multi-component system, we combine the lattice Boltzmann model for fluid dynamics and the lattice spring model for the micromechanics of elastic solids. We determine the effects of the mechanical properties of the elastic capsule and the characteristics of the imposed flow on the dynamics of the capsules as they move inside microchannels with sinusoidal and undulating geometries. We also isolate conditions that lead to a trapping of the capsule inside the channel. The findings provide insight into the behavior of cells within biological vessels and provide guidelines for regulating the motion of polymeric microcapsules with microfluidic devices.

**J1 237 Deviation of a Jet at a T junction at low Reynolds number** PASCAL PANIZZA, WILFRIED ENGL, *LOF/CNRS* KOUSKE OHATA, *LOF* ANNIE COLIN, *LOF/CNRS* We study the hydrodynamic behaviour of a laminar jet flowing through a channel when it reaches a junction. We observe the existence of two possible flow regimes, namely the splitting and deviation of a jet in the most simple microfluidic configuration, namely a T junction. The transition between the two regimes is not monitored by the shape of the T junction nor by capillary effects, but can be easily anticipated in terms of the hydrodynamic properties of the flow. We present a simple hydrodynamic model which is in very good agreement with observed experimental jet behaviour. The transition between both regime acts as a flow or viscosity comparator. We show how this effect can be used for the design of digital and integrated microfluidic devices

**J1 238 Fluids Moving Past Smooth Hydrophilic Surfaces – Slip?** JANET WONG, SUNG-CHUL BAE, LIANG HONG, STEVE GRANICK, *Department of Materials Science and Engineering, University of Illinois at Urbana-Champaign* Recent experiments challenge the traditional view that fluids satisfy the ''no-slip'' boundary condition. While the amount of slip observed differs between research groups, it is now generally accepted that the no-slip boundary condition need not hold strictly – if the surface is smooth and hydropobic. What happens if the surface is wetted by the moving fluid? This work describes hydrodynamic studies of fluid between two crossed cylinders in a surface forces apparatus, using a new method of mica cleaving that appears to produce different findings from those obtained from classical methods. Aqueous salt solutions with various ion concentrations were used with mica as the confining surface. The role of salt concentration was explored. Independently, the fluorescence lifetime of fluorescent dyes was used to measure the near-surface ionic conditions independent of a force measurement.

**J1 239 Enhanced Fluid Mixing in Nanochannels: A Molecular Dynamics Study** ERIC C.J. OLIVER, GARY W. SLATER, *University of Ottawa* The efficient mixing of fluids is of paramount importance in several applications such as lab-on-a-chip and microfluidic devices. The main limitation to efficiency is that on small scales where the Reynolds number of the flow is low, mixing is dominated by diffusion. Purely diffusive motion is very slow and is an inefficient mixing mechanism unless the channel width is extremely small. Starting with the basic result for diffusive mixing of a binary fluid in a Poiseuille flow we explore methods to enhance the level of mixing between the two fluid species. We simulate the system using Molecular Dynamics and model the fluids as assemblies of Lennard-Jones beads. In order to increase the rate of mixing we have forced lateral motion in the fluid using configurations of mid-stream posts. Specifically, posts set in a prism-like structure have proven to be extremely well suited to reducing the channel length required to achieve complete mixing. In order to measure efficiency we have proposed a mathematical function that quantifies the level mixing associated with a fluid element. Furthermore, we have developed a basic theory for the position of the mixing front in a flow with spatially dependent velocity and diffusion coefficient.

**J1 240 Effects of Membrane Material Properties on the Deformation of Elastic Capsules in a Shear Flow*** KIT YAN CHAN, CHARLES EGGLETON, *UMBC* The deformation process of elastic capsules in a simple shear flow is studied numerically using the immersed boundary method to probe the influence of membrane material properties. Membrane models that are representative of linear elastic membrane (Hookean law), strain hardening membrane (Skalak), and strain softening membrane (Mooney-Rivlin, neo-Hookean) and the Evans-Skalak model developed from thermodynamic principles to represent the behavior of a lipid bilayer and a cytoskeletal network, are used to study the effects of membrane material properties on the response of the capsule at various shear rates. Simulation results indicate that both

the time to reach steady state and the final steady shape of the capsule are sensitive to the choice of the membrane model and parameter values used. These experimentally measurable quantities may be compared with computations for determining suitable model of a particular capsule of interest, and the associated material properties. Local strain and energy distributions computed also provide additional information that is not easily accessible experimentally.

*Supported by NIH/NIAID RO1O63366

**J1 241 Molecular dynamics modeling of nanoparticle dielectrophoresis** EMPPU SALONEN, EMMA TERAMA, *Lab of Physics and HIP, Helsinki Univ of Tech, Finland* ILPO VATTULAINEN, *Lab of Physics and HIP, Helsinki Univ of Tech, Finland; Memphys-Center of Biomembrane Physics, SDU; Inst of Physics, Tampere Univ of Tech, Finland* MIKKO KARTTUNEN, *Lab of Computat Engineering, Helsinki Univ of Tech, Finland; Dept of Applied Math, Univ of Western Ontario, Canada* We have used molecular dynamics simulations to study nanoparticle dielectrophoresis (DEP), i.e., motion induced by a coupling of the particle polarization to a non-uniform electric field. In the first simulations we have considered the case of a single spherical colloid in a non-conductive solvent [1]. This approach has given qualitative information on the limitations of DEP transport due to the thermal motion of the manipulated particles at different DEP coupling strengths. In addition, we have studied changes in the DEP transport efficiency due to particle aggregation. The results of the modeling are compared to analytical studies [2,3] as well as experiments. [1] E. Salonen et al., Eur. Phys. J. E. 18 (2005) 133. [2] J. P. Huang et al., Phys. Rev. E 67 (2003) 021403. [3] J. P. Huang et al., Phys. Rev. E 69 (2004) 051402.

**J1 242 An internal splash: Levitation and Long Transients of Falling Spheres in Stratified Fluids*** RICHARD PARKER, BYRON HUFF, RICHARD McLAUGHLIN, ROBERTO CAMASSA, *University of North Carolina* UNC RTG FLUID GROUP TEAM, We present measurements regarding new phenomena arising with falling bodies in sharply stratified (two layer) fluids.[1] Specifically, the newly observed phenomena in which a heavy falling sphere stops and reverses its motion before ultimate descent to the bottom is further explored through careful adjustment of the bottom layer fluid density. An experimental study is presented which documents the bounce amplitude and long layer residence times as function of the bottom layer density for several spheres of different densities. Finally, we present the behavior associated with beads of adjustable density and varying size.

*RTG NSF DMS-0502266

[1]N. Abaid, D. Adalsteinsson, Akua Agyapong, and R. M. McLaughlin, ''An Internal Splash: Falling Spheres in Stratified Fluids,'' Physics of Fluids, 16, no. 5, 1567-1580, 2004.

**J1 243 Flow through a laboratory sediment sample: hydraulic conductivity by computer simulation modeling** EDWARD BRAITHWAITE, *Naval Research Laboratory* ALLEN REED, *Naval Research Laboratory* RAY SEYFARTH, *University of Southern Mississippi* RAS PANDEY, *Naval Research Laboratory and University of Southern Mississippi* JOE GETTRUST, *Naval Research Laboratory* Digitized catscan image of a three dimensional laboratory sediment sample provides a host matrix of size $100^3$. The porosity of the sample is 0.282, i.e., below the site percolation threshold of a cubic lattice. Despite a high fraction of sediment barriers, visualizations reveal that the ramified channels of connected pores span across the sample. A coarse grained description is used to model fluid by interacting particles in spirit of classical lattice gas. As in experiments, the source of the fluid is connected at one end of the sample in our computer simulations. The fluid constituents execute their stochastic motion via Metropolis algorithm and flow through the sample with periodic boundary condition across transverse boundaries. From the net flow of fluid, we estimate the flux density and the hydraulic conductivity in steady-state. We also consider pressure bias (H) to investigate the response. Results of transport, flux rate, and distribution of fluid will be presented.

**J1 244 Acoustic modulation of pharmaceutical sprays** SORIN MITRAN, *UNC* HUGH SMYTH, *UNM* ANTHONY HICKEY, *UNC* We consider the effect of acoustical radiation upon the particle size distribution in pharmaceutical sprays. A mixed particle hydrodynamic-Eulerian technique is used to model the propagation of acoustic waves through the spray and the effect of the acoustic radiation upon spray droplets. A model for droplet breakdown based upon normal mode oscillations is employed to capture acoustically induced modifications of the particle size distribution. Measurements are presented for metered dose inhalers and compared to theoretical predictions.

**J1 245 Arranging Droplets for Microfluidics** CRAIG PRIEST, ENKHTUUL SURENJAV, MAGDALENA ULMEANU, STEPHAN HERMINGHAUS, RALF SEEMANN, *Max-Planck-Institute for Dynamics and Self-Organization* The online generation, organization and manipulation of monodisperse droplets in confinement present new possibilities for microfluidics. Droplets make excellent compartments for handling minute quantities of chemical, biological and particulate materials. When confined, a high dispersed phase volume fraction emulsion, i.e. gel emulsion, will self-organize into well-defined arrangements. The possible arrangements are dependent on the droplet size and the length-scale of the confining geometry. In this work, we have studied the organization of monodisperse gel emulsions in microchannels for application in microfluidic processing. The high degree of spatial order exhibited by gel emulsions facilitates the precise manipulation of a droplet, or group of droplets, using geometry alone.

**J1 247 Critical Behavior Of Uniformly Uniaxial Magnets** DEMETRIS NICOLAIDES, *Bloomfield College* Real magnetic systems never obey rotational invariance because the lattice itself is not completely rotation-invariant. The simple case of phase transitions in a magnetic system with broken rotational symmetry, described by a single, m-component vector order parameter, with uniform uniaxial perturbation in only the first component, is a prototype example. Renormalization group theory found that this kind of magnets experience phase transition of the second order, into either the easy axis of magnetization, or that they have critical behavior analogous to an (m-1)-component spin system. The present work extends this study to cover the more complex case of two coupled, continuous, anisotropic, m-component vector order parameters, having frozen-in, uniform, uniaxial anisotropies. These anisotropies are due to nonmagnetic impurities, and affect

the trial (mean-field) critical temperature of only the first component of each order parameter. The study is done with the help of a phenomenological model which considers fluctuations partially. It is shown that when both coupled vector order parameters are anisotropic, the order-disorder phase transition is always of the second order, into either the uniaxial or the (m-1)- isotropic phase. This is despite the fact that for the isotropic case of two coupled order parameters, the phase transition is a fluctuation-induced first order.

**J1 248 Dynamical mean-field theory of the Hubbard-Holstein model at half-filling: electron-phonon interaction effects on the finite temperature Mott transition** JAE HYUN YUN, HANYONG CHOI, GUN-SANG JEON, HYUN C. LEE, TAE-HO PARK, We study the Hubbard-Holstein (HH) model which indludes both the electron-electron and electron-phonon interactins characterized by $U$ and $g$, respectively, by empolying the dynamical mean-field theory in combination with Wilson's numerical renormalization group technique. We fix $g = 0.1W$ ($W$=bandwidth of the conduction electrons) and calculate the finite temperature phase diagram of metal-insulator transition in the $U - T$ plane. We will discuss in particular how the critical $U$ values, $U_{c1}$ and $U_{c2}$, and the critical temperature $T_c$ of the Mott transition are changed by the electron-phonon interaction.

**J1 249 Magnetic and transport properties of V-doped $La_{0.7}Ca_{0.3}MnO_3$** J.S. PARK, K.K. YU, Y.P. LEE, *q-Psi and Dept. of Physics, Hanyang Univ., Seoul, Korea* Y.S. LEE, *Division of Information Communication and Computer Engineering, Hanbat National University, Daejeon, Korea* J.-H. KANG, *Department of Nano and Electronic Physics, Kookmin University, Seoul, Korea* The effects of substitution of V for Mn on the electronic and the magnetic properties of $La_{0.7}Ca_{0.3}MnO_3$ have been investigated. The samples show a reentrant magnetic behavior as the V doping is increased. The V doping into the Mn sites leads to a mixed-phase ground state consisting of the ferromagnetic insulating and the ferromagnetic metallic phases at low temperatures. The magnetic relaxation was observed in both the ferromagnetic and the reentrant spin-glass phases, which means the existence of frustration and magnetic disorder in the samples. It was found that the V-doped manganites with aging effect bear the characteristics of a reentrant ferromagnet.

**J1 250 Heat bath approach to Landau damping and Pomeranchuk quantum critical points** JOHAN NILSSON, ANTONIO CASTRO NETO, *Boston University* We study the problem of the damping of collective modes close to a Pomeranchuk quantum critical point in a Fermi liquid. In analogy with problems in dissipative open quantum systems, we derive the Landau damping of a Fermi liquid by integrating out a macroscopic number of degrees of freedom from a generating functional. Being a reformulation of the linearized Boltzmann equation this approach reproduces well-known results from the theory of Fermi liquids. We also study the Bethe-Salpeter equations within the Landau theory and discuss the implications of these results on quantum phase transitions of the Pomeranchuk type and its dynamical exponent, z. We apply our results to the electronic nematic instability and find z=3 in the collisionless limit.

**J1 251 Magnetic Phases of λ-$(BETS)_2FeCl_4$ investigated by proton NMR spectroscopy.** GUOQING WU, W.G. CLARK, P. RANIN, S.E. BROWN, *UCLA Physics and Astronomy* L. BALICAS, *NHMFL Tallahassee* L.K. MONTGOMERY, *Indiana U. Chem.* The organic conductor λ-$(BETS)_2FeCl_4$, is of interest because of its unusual phases, which include a paramagnetic metal (PM), an antiferromagnetic insulator (AFI), and a field-induced superconducting phase. Important drivers for these phases are the 3d $Fe^{3+}$ moments (spin $S_d = 5/2$) from the $FeCl_4^-$ anions and the $\pi$ conduction electrons (spin $S_\pi = 1/2$) in the BETS donor molecules, which generate a correlated $\pi$-d electron system. Here, we report a proton NMR spectroscopy study of these phases in a small ($\sim 3\ \mu$g) single crystal of λ-$(BETS)_2FeCl_4$ using an applied field of 9 T over the temperature ($T$) range 2-180 K. The results show a complex spectrum that broadens and is shifted as $T$ is lowered in the PM phase, and additional changes associated with the PM-AFI transition. The main spectral features at all $T$ are attributed to the large dipolar field from the 3d $Fe^{3+}$ ions at the proton sites. A phenomenological model provides a reasonable fit to them. On lowering $T$ through the PM-AFI transition at 3.5 K, the spectrum smears and its second and first moments change discontinuously. These features indicate that the transition is first order and that the $\pi$-d interaction is important for its properties. The work at UCLA is supported by NSF Grants DMR-0334869 (WGC) and 0203806 (SEB).

**J1 252 Improved thermoelectric characteristics of misfit-layered cobaltites $Ca_3Co_{4-x}Fe_xO_{9+\delta}$.*** CHIA-JYI LIU, LI-CHEN HUANG, WEN-CHING HUNG, *Department of Physics, National Changhua University of Education* JENG-LUNG CHEN, CHING-LIN CHANG, *Department of Physics, Tamkang University* We have measured the electrical resistivity, Seebeck coefficients and thermal conductivity as a function temperature for a new series of oxides $Ca_3Co_{4-x}Fe_xO_9$ (x=0, 0.05, 0.1, 0.15, 0.2) prepared by the conventional solid state reaction. Structural parameters were refined with a superspace group of X2/m(0b0)s0 using powder X-ray diffraction data. With the substitution of $Fe^{+2}$ for $Co^{+3}$, the resistivity ($\rho$) decreases, while the thermoelectric power (S) also increases simultaneously. In the low temperature regime from 15 K to 60 K, the electrical conductivity follows the Mott's law of the form $\exp[T_0/T^{-1/4}]$, suggesting the variable-range-hopping transport. The thermoelectric power also shows the same transport mechanism in the same temperature regime. The x = 0.05 sample exhibits a higher power factor value (3.3 $\mu W/K^2$-cm) than that of undoped $Ca_3Co_4O_9$ (1.2 $\mu W/K^2$-cm) at 300K, indicating the improvement of the thermoelectric characteristics upon Fe substitution for Co.

*This work was supported by National Science Council of R. O. C. under the Grant No. NSC 94-2112-M018-001.

**J1 253 Computational Toolkit for First-Principles Multicomponent Alloy Thermodynamics*** TECK TAN, NIKOLAI ZARKEVICH, D.D. JOHNSON, *Materials Science and Engineering, University of Ilinois Urbana-Champaign* A ''toolkit'' for the simulation of alloy thermodynamics has been developed by integrating first-principles, electronic-structure calculations and the cluster expansion (CE) with Monte Carlo (MC) methods. This Thermal Toolkit (TTK) is aimed at producing reliable thermodynamics of alloys with limited input from the user. Given an alloy, TTK first generates a comprehensive set of structures, automatically submits an electronic-structure calculation to determine the

structural energies, stores the structure and its energy in a database,[1] then constructs the CE via the structural inversion method that conforms to a set of mathematical conditions to produce an optimal truncated cluster expansion.[2] Using this optimal CE, a MC code (included in TTK) can be used to calculate thermodynamic properties, such as structural phase diagram (T vs c). We present here example application and functionality of TTK on binary and ternary alloy.

*We acknowledge funding from NSF ITR grant DMR-03-25939 and DOE grant DE-FG02-03ER46026.

[1]The ''Structural Database'' http://data.mse.uiuc.edu

[2]Nikolai Zarkevich and D.D. Johnson, Phys. Rev. Letts 92, 255702 (2004)

**J1 254 Resonant X-ray Scattering Study of Quadrupolar Ordering in $DyB_4$** SUNGDAE JI, C. SONG, J. KOO, K.-B. LEE, *eSSC and Dept. of Physics, Pohang University of Science and Technology, Pohang, 790-784, South Korea* Y.J. PARK, *Pohang Accelerator Laboratory, Pohang University of Science and Technology, Pohang, 790-784, South Korea* J.S. RHYEE, B.K. CHO, *Center for Frontier Materials and Dept. of Materials Science and Engineering, GIST, Gwangju, 500-712, South Korea* Resonant x-ray scattering was performed on $DyB_4$ to observe a quadrupolar ordering. It is demonstrated that anisotropic tensor susceptibility (ATS) resonances due to ordering in Dy 4*f* states can be seperated from those due to atomic displacements, such as Jahn-Teller distortion, by tuning the incident x-ray energies. An ATS resonance at 7.792 keV, corresponding to antiferro-type quadrupolar (AFQ) ordering, was observed to have different azimuthal angular dependence and polarizations from those of magnetic resonance. The AFQ order parameter is developed concomitantly with monoclinic phase transition below 12.3 K, and its magnitude is proportional to quadratic of the monoclinic angle.

**J1 255 Smoothing and Bootstrapping in Numerical Studies of Lattice Statistical Models** VOLTAIRE TEODORESCU, *Northern Illinois University* We investigate the applicability and estimate efficiency for Monte Carlo type simulations in lattice models of magnetic materials. In particular, an improved algorithm based on smoothed bootstrapping of Markov chains is applied to the two-dimensional Ising model. We report the results based on several smoothing functions.

**J1 256 Magnetic and transport properties of $La_{0.7}Ca_{0.3}MnO_3/BaTiO_3$ and $La_{0.7}Sr_{0.3}MnO_3/BaTiO_3$ bilayered films** V.G. PROKHOROV, *Institute of Metal Physics, Academy of Science of Ukraine, Kiev, 03142 Ukraine* Y.P. LEE, K.K. YU, S.Y. PARK, *q-Psi and Department of Physics, Hanyang University, Seoul, 133-791* V.L. SVETCHNIKOV, *National Center for HREM, TU Delft, 2628AL, The Netherlands* The magnetic and the transport properties of $La_{0.7}Ca_{0.3}MnO_3/BaTiO_3$ (LCMO/BTO) and $La_{0.7}Sr_{0.3}MnO_3/BaTiO_3$ (LSMO/BTO) bilayered films, prepared by the rf-magnetron sputtering, have been investigated. For comparison, the same data for the LCMO and the LSMO films, deposited on the bare $LaAlO_3$ (LAO) substrates, are obtained as well. The microstructural analysis reveals that LCMO/BTO and LSMO/BTO have the biaxial tensile in-plane and compressive out-of-plane strains, while LCMO/LAO and LSMO/LAO are reversely in the compressive in-plane and tensile out-of-plane strains. The films with biaxial tensile in-plane lattice strains undergo the magnetic transition at a higher temperature than those with biaxial compressive ones. This suggests that the Mn-O-Mn bond angle, controlled by the lattice strain, plays more important role in the formation of spin ordering in the manganite film than the modification of Mn-O bond length. The observed enhancement of magnetoresistance at room temperature in LSMO/BTO provides an advance for the development of new hybrid ferromagnetic/ferroelectric devices.

**J1 257 Kondo Transport at Low Temperature and Electron-electron Interaction in Dilute Mn-doping $Na_{0.7}CoO_2$ Systems** JINCANG ZHANG, ZAIQING ZHANG, YAN XU, CHAO JING, SHIXUN CAO, *Shanghai University* DEPARTMENT OF PHYSICS, SHANGHAI UNIVERSITY TEAM, The layer transition-metal oxide $Na_\gamma CoO_2$ engendered much interest to physicists due to its promising thermoelectric properties. Its anomalous large thermoelectric power and low electrical resistivity in combination with low thermal conductivity is difficult to be understood in the framework of conventional band picture. In this paper, we present the results of low-temperature transport behaviour and its dependence on applied magnetic field for dilute Mn doping $Na_{0.7}Co_{1-x}Mn_xO_2$ systems with x=0, 0.03, 0.07, 0.1. The results show that the transport properties are very sensitive to Mn doping and a novel resistivity minimum was found with a characteristic of metallic-semiconductor transition at low temperature for all the doping samples. And the best fitting was made in the framework of Kondo scattering and the electron-electron (e-e) interaction in a wide temperature range of 2-100 K. The weak dependent on the external field prove that the present $Na_{0.7}Co_{1-x}Mn_x$ is a strong disorder system and there exists an enhancing e-e interaction, which reflects a typical characteristic of strong correlation systems. The results prove that the layer $Na_\gamma CoO_2$ is a kind of typical Kondo-like oxide as like the dilute convention alloys.

**J1 258 Study of the one-band model for colossal magnetoresistive manganites using the Truncated Polynomial Expansion Monte Carlo Method** CENGIZ SEN, *National High Magnetic Field Laboratory and Department of Physics, Florida State University, Tallahassee, FL* ELBIO DAGOTTO, *Oak Ridge National Laboratory, Oak Ridge, TN and Department of Physics, University of Tennessee, Knoville, TN* The recently proposed Truncated Polynomial Expansion Method (TPEM) for spin-fermion systems is tested using the one-band double exchange model with finite Hund coupling $J_H$ in the clean limit. Two dimensional lattices as large as $48\times 48$ are studied, far larger than those that can be handled with standard exact diagonalization (DIAG) techniques for the fermionic sector. Phase diagrams are obtained, showing first-order transitions separating ferromagnetic metallic from insulating states. A huge magnetoresistance is found at low temperatures by including small magnetic fields, in excellent agreement with experiments. By comparing results between the two methods, TPEM and DIAG, on small lattices, and by analyzing the systematic behavior with increasing cluster sizes, it is concluded that the TPEM is accurate to handle realistic manganite models on large systems. Our results pave the way to a frontal computational attack of the colossal magnetoresistance phenomenon using double-exchange like models, on large clusters, and including quenched disorder.

**J1 259 The effect of substrate induced strain on the electronic soft matter in thin films of the manganite**

**$(La_{1-y}Pr_y)_{0.67}Ca_{0.33}MnO_3$ ($y$ = 0.5, 0.6)** JACOB TOSADO, TARA DHAKAL, SUNGHEE YUN, AMLAN BISWAS, *Department of Physics, University of Florida, Gainesville, FL* For most hole-doped manganites, the low temperature phase is either a ferromagnetic metal (FMM) or charge-ordered insulator (COI). At certain compositions the competition between the FMM and COI phases leads to a mixed phase state in which both these phases coexist. In this mixed phase state, changing the temperature, magnetic field or strain modifies the spatial arrangement and relative proportions of these two phases. This property of manganites is reminiscent of electronic soft matter. We have studied the effect of substrate-induced strain on this electronic soft matter by measuring the magneto-transport properties of $(La_{1-y}Pr_y)_{0.67}Ca_{0.33}MnO_3$ (LPCMO,$y$ = 0.5, 0.6) thin films of different thicknesses. The temperature –magnetic field ($T - H$) phase diagram of LPCMO shows four distinct phases itviz., the COI phase, the FMM phase, a static phase separated (SPS) state and a fluid phase separated (FPS) state. Our experimental results show that as the thickness of the thin film increases (i.e. the substrate induced strain decreases), the SPS state expands and covers more area in the phase diagram at the expense of the FPS state.

## J1 260 SURFACES, INTERFACES, AND THIN FILMS POSTER

**J1 261 Structure of Photonic Multilayer Films Created by Plasma Enhanced Chemical Vapor Deposition (PECVD)** SOMESHWARA PERI, BRIAN HABERSBERGER, BULENT AKGUN, MARK FOSTER, *Institute of Polymer Science* HAO JIANG, TIMOTHY BUNNING, *Air Force Research laboratory* CHARLES MAJKRZAK, *NIST Center for Neutron Research* The structures of copolymer films created by PECVD were studied for the first time using neutron reflectivity (NR) and x-ray reflectivity (XR). Both homopolymer films of benzene (PP-B) and octafluorocyclobutane (PP-OFCB) and copolymer films of HMDS and OFCB made using different feed ratios were considered. In HMDS-OFCB copolymer films, we observed a transient structure next to the substrate as seen previously for homopolymer OFCB films. PP-B films swelled approximately 200 % in deuterated-THF vapor and PP-OFCB swelled approximately for 30 % in deuterated-toluene vapor, indicating that for these processing conditions PP-B films are much less highly crosslinked than are PP-OFCB films. We have measured for the first time the variation in crosslink density with depth for homopolymer films created by PECVD.

**J1 262 TOF MS studies of the BN and carbon laser ablated plasma (YAG-laser, $\lambda_{exc}$ = 1064 nm).** VLADIMIR MAKAROV, DACHUN HUANG, *University of Puerto Rico, Dept of Chem* ARTUTO HIDALGO, GERARDO MORELL, *University of Puerto Rico, Dept of Phys* BRAD WEINER, *University of Puerto Rico, Dept of Chem* In the present study, TOF MS spectra of the ablated ions from the BN-ceramic, amorfus carbon, graphite and fullerene-60 surfaces were recorded for different distances between the target surface and work (analytical) area of the TOF MS and for different radiation density of the laser radiation. The averaged energy and temperature of the ablated ions were estimated. The mechanism of the plasma formation in all cases studied was analyzed and discussed.

**J1 263 Pair distribution functions of silicon/silicon nitride interfaces*** DENG CAO, MARTINA E. BACHLECHNER, *West Virginia University, Physics Department* Using molecular dynamics simulations, we investigate different mechanical and structural properties of the silicon/silicon nitride interface. One way to characterize the structure as tensile strain is applied parallel to the interface is to calculate pair distribution functions for specific atom types. The pair distribution function gives the probability of finding a pair of atoms a distance $r$ apart, relative to the probability expected for a completely random distribution at the same density. The pair distribution functions for bulk silicon nitride reflect the fracture of the silicon nitride film at about 8 % and the fact that the centerpiece of the silicon nitride film returns to its original structure after fracture. The pair distribution functions for interface silicon atoms reveal the formation of bonds for originally unbound atom pairs, which is indicative of the interstitial-vacancy defect that causes failure in silicon.

*Supported in parts by NASA.

**J1 264 Interaction of H atom with Si(111)4x1-In surface** SANG-YONG YU, *Korea Research Inst. of Standards and Science* GEUNSEOP LEE, *Inha Univ., Inchon, Korea* HANCHUL KIM, *Korea Research Inst. of Standards and Science* D. LEE, *Chungnam Univ., Daejeon, Korea* JA-YONG KOO, *Korea Research Inst. of Standards and Science* Using scanning tunneling microscopy (STM) measurements and itab initio calculations, the interaction of an H atom with the Si(111)4x1-In surface at room temperature is investigated. It is found that the H atom preferentially adsorbs at the bridge site between the In chain and the Si Seiwatz chain and break an In-Si bond to form a Si-H bond. Experimentally, the adsorption of H is influenced by the registry of the Si substrate and preferentially occupies one of the two zigzag In chains to the other, while the little difference is found in the calculated adsorption energy. The adsorbed H atom induces not only a localized lattice distortion but also a distant electronic perturbation near the Fermi level, which appears as out-of-phase period-doubled (x2) charge ordering in the filled- and the empty-state STM images. These perturbations induced by the two nearby H atoms in the same row interfere to make the inbetween x2 modulation enhanced or suppressed depending on the H-H distance. The x2 perturbed region remains metallic, distinguishing it from the insulating low-temperature 4x2 (8x2) phase. The observed x2 perturbation away from the H-adsorbate is found to be the theoretical ground state of the In/Si(111) surface predicted by density-functional theory, which is stabilized by the presence of the surface defect.

**J1 265 Tetracene thin film morphology on hydrogen-passivated Si(100)*** JUN SHI, ANDREW TERSIGNI, XIAORONG QIN, *Department of Physics, University of Guelph* Initial stage of vacuum evaporated tetracene films on hydrogen-passivated Si(100) substrates has been investigated by scanning probe microscopy. Three-dimensional crystalline islands and dendrites have been obtained at low deposition rates, exhibiting contributions of lateral and vertical edge-diffusions in growth and

local surface effects. The absence of the 3D structures has been achieved at a proper range of deposition rates and a layer-by-layer thin film growth mode has been obtained. Results suggest that the obtained thin film phase defines a kinetic path for the formation of uniform films.

*Supported by Natural Sciences and Engineering Research Council (NSERC) of Canada

**J1 266 Oxidation of Hafnium studied by X-ray photoelectron spectroscopy.*** A CHOURASIA, W. JOHNSTON, *Texas A&M University-Commerce* The oxidation of hafnium has been studied by X-ray photoelectron spectroscopy. Two types of experiments were conducted. In both types, thick films of hafnium were deposited on a metal substrate using the electron beam deposition technique. In one set of experiments, the substrate temperature was in the range between 100C and 500C. The deposition chamber was filled with oxygen at a very low pressure while the film was getting deposited. In the second set of experiments, substrate was kept at room temperature during the hafnium film deposition. The film was then subjected to post-deposition annealing in an oxygen atmosphere. The hafnium XX core level and oxygen 1s core level were recorded in the high resolution mode. The thickness of the oxide films have been determined from the XPS spectra using the Quantitative Analysis by SES software. The study provides a comparison of the oxide formation as a function of substrate temperature in the two cases.

*Research Corporation Award; Faculty Research Enhancement TAMU-Commerce

**J1 267 Self Alignment of Wafer Stacks via Pattern Modification of Self Assembled Monolayer Surface Energies*** ERNEST WALKER, *North Carolina State University* HANS HALLEN, *North Carolina State University* Self assembled monolayers (SAMs) are deposited on oxide layer, and characterized by ellipsometry and contact angle. Vinyl-terminated SAMs are oxidized to carboxyl-termination, which changes the wetting characteristics. Measurements of sliding friction between combinations of these layers is measured and discussed. The relative surface energies can also be obtained. From these data, the relative importance of friction and forces resulting from surface energy gradients can be determined, and wafer self-alignment masks evaluated.

*Air Force grant

**J1 268 Reciprocal Space Mapping of Thin $La_x$ Mn $O_3$ Films of Varying Thickness** M.A. DELEON, T. TYSON, *New Jersey Institute of Technology, Applied Physics* C. DUBOURDIEU, *Laboratoire des Máteriaux et du Génie Physique UMR CNRS 5628, INPG, 38402 St.Martin d'Héres, France* J. BAI, *ORNL* In order to understand the growth of ultrathin manganite films on substrates, we made reciprocal space maps in the 004, 404, and 044 pseudocubic directions of $La_xMnO_3$ films deposited on $LaAlO_3$ (LAO) via metal-organic chemical vapor deposition. The x-ray maps exhibit the strain effects of the lattice-substrate mismatch and the effects of a twinned interface on the growth of films. Reciprocal space mapping provides more accurate lattice parameters and strain effects from lattice-substrate interface mismatch. A characteristic feature of the LAO substrates is twinning, which results in multiple structural components of the films, similar lattice parameters but differing orientation. These characteristics reveal crucial aspects of deposition processes to be inspected in assuring high-quality films. This research is supported by NSF DMR-0209243 and DMR-0512196.

**J1 269 H Adsorption on RH (110) Surface** SHAO-PING CHEN, *Los Alamos National Laboratory* We have used the density functional theory to study the H adsorption phenomena on Rh (110) surface with H coverage from 0.33 to 2.00 mono-layers. We found H atom favors the three- fold coordinated site as observed experimentally. We confirmed the existence of 1x3-H, 1x2-H, 1x3-2H, 1x1-2H ordered structures. We also found that the proposed 1x2-2H structure for coverage of 1.0 is not the lowest energy configuration. We have proposed a new 1x2-2H structure which needs to be tested by future experiments.

**J1 270 Influence of diffusion on submonolayer island growth during hyperthermal deposition onto Cu(100) and Cu(111)** MIKA JAHMA, MARKO RUSANEN, *Laboratory of Physics, Helsinki University of Technology* ISMO KOPONEN, *Department of Physical Sciences, University of Helsinki* TAPIO ALA-NISSILA, *Laboratory of Physics, Helsinki University of Technology* We consider the influence of realistic island diffusion rates to homoepitaxial growth on metallic surfaces using a recently developed rate equation model [1] which describes growth in the submonolayer regime with hyperthermal deposition. To this end, we incorporate realistic size and temperature-dependent island diffusion coefficients for the case of homoepitaxial growth on Cu(100) and Cu(111) surfaces [2]. We demonstrate that the generic features of growth remain unaffected by the details of island diffusion, thus validating the generic scenario of high density of small islands found experimentally and theoretically for large detachment rates. However, the details of the morphological transition and scaling of the mean island size are strongly influenced by the size dependence of island diffusion. This is reflected in the scaling exponent of the mean island size, which depends on both temperature and the surface geometry. [1] I.T. Koponen et. al, Phys. Rev. Lett. **92**, 086103 (2004) [2] M.O. Jahma et. al, Surface Science, in press.

**J1 271 Self-assembly of nanoparticle/copolymer mixtures** JINBO HE, RAVISUBHASH TANGIRALA, KEVIN SILL, TODD EMRICK, THOMAS RUSSELL, *Department of Polymer Science & Engineering, University of Massachusetts, Amherst, MA 01003* XUEFA LI, JIN WANG, YAO LIN, *Argonne National Laboratory, Argonne, IL 60439* ALEXANDER BOKER, *Lehrstuhl fur Physikalische Chemie II, Universitat Bayreuth, 95440 Bayreuth, Germany* ANNA BALAZS, *Department of Chemical and Petroleum Engineering, University of Pittsburgh, Pittsburgh, Pennsylvania 15261* Mixtures of polystyrene-itblock-poly (2-vinylpyridine) with tri-*n*-octylphosphine oxide-(TOPO)-covered CdSe nanoparticles were chosen to test the theoretical prediction of synergistic effects between two self-organization systems. Preliminary results confirmed that hierarchical structures were provided, with poly (2-vinylpyridine) cylindrical microdomains oriented normal to the surface and CdSe-TOPO nanoparticles self-assembly at the surface, that balanced the surface tensions of the P2VP with that of PS. Detailed structure evolution was revealed by in-situ grazing incidence small angle x-ray scattering (GISAXS) during thermal annealing. Results from these studies indicated that the orientation of the mcrodomains began at the free surface and propagated in the film towards the substrate. This

one-step self-orienting, self-assembly process, without the use of external fields, opens a simple route for fabrication of nanostructured materials having hierarchical order, with applications including chemical sensing, separation, catalysis, high-density data storage and photonic materials.

**J1 272 Equilibrium shape and dislocation nucleation in strained epitaxial nanoislands** J. JALKANEN, *Helsinki University of Technology, Finland* O. TRUSHIN, *Institute of Microelectronics and Informatics, Russia* K. ELDER, *Oakland University* E. GRANATO, *Instituto Nacional de Pesquisas Espaciais, SP Brasil* T. ALA-NISSILÄ, *Helsinki University of Technology, Finland* S.-C. YING, *Brown University* We study numerically the equilibrium shapes, shape transitions and dislocation nucleation of small strained epitaxial islands with a two-dimensional atomistic model, using simple pair potentials [1]. We first map out the phase diagram for equilibrium island shapes as a function of island size and lattice misfit with the substrate. When the interactomic potential minimum depth $\epsilon$ is the same for substrate and adsorbate, the latter either wets the surface or has one of three generic equilibrium island shapes. As $\epsilon$ favours substrate-adsorbate interface, Stranski-Krastanow growth mode emerges between complete wetting and island formation zones while in the opposite case the islanding zone is extended. A simulation based extrapolation scheme predicts an optimal island shape for attractive $\epsilon$. The energy barriers and transition paths between different island shapes and dislocation nucleation in initially coherent islands are investigated with Nudged Elastic Band method. We also discuss the elastic behaviour of these systems in terms of the Phase Field Crystal model [2]. [1] J. Jalkanen, O. Trushin, E. Granato, S. C. Ying, and T. Ala-Nissila, Phys. Rev. B 72, 081403 (2005) [2] K. Elder and M. Grant, Phys. Rev. E **70**, 051605 (2004).

**J1 273 The Structure of Adsorbed Methane on the MgO(100) Surface from Inelastic Neutron Scattering and First-Principles Calculations** M.L. DRUMMOND, B.G. SUMPTER, W.A. SHELTON, JR., *Oak Ridge National Laboratory* J.Z. LARESE, *University of Tennessee* The adsorption of molecules onto a solid surface is a phenomenon with important ramifications in areas such as catalysis, corrosion, and electronics. We have used plane-wave, psuedopotential-based density functional calculations, in conjunction with inelastic neutron scattering (INS), to evaluate the structure of methane on the MgO(100) surface. The combination of high-resolution INS and high-quality calculations has proven extremely versatile in determining the structural arrangement, despite the existence of multiple energetically favorable arrangements. The structures for adsorbed methane mono-, bi-, and higher order adlayers are discussed.

**J1 274 c(4x2) Reconstruction of Manganese Tetramers on Mn3N2 (001) Studied by Scanning Tunneling Microscopy** RONG YANG, *Ohio University* HAIQIANG YANG, *Ohio University* ARTHUR SMITH, *Ohio University* We have investigated the growth of antiferromagnetic Mn3N2 on MgO(001) by molecular beam epitaxy. Two orientations [(010) and (001)] of this structure are grown controllably on MgO(001), depending on the growth conditions. The bulk structure is face- centered tetragonal with 2 layers of MnN followed by 1 layer of Mn. Here we present results for the (001) surface. STM images show smooth terraces and atomic steps. On some of the terraces a unique and new reconstruction is seen, resolved as square Mn tetramers in a c(4$\times$ 2) structural arrangement. Two domains of the tetramer reconstruction, rotated by 90 $^\circ$ to each other, occur. A model is presented for this square Mn tetramer reconstruction, in which the Mn atoms of the tetramer layer belong to the Mn layer at the surface in the MnN- MnN-Mn stacking sequence. The work is supported by NSF9983816 and 0304314.

**J1 275 Intrinsic Surface Reconstructions of Zinc-Blende GaN(001) Studied by Scanning Tunneling Microscopy*** ARTHUR R. SMITH, MUHAMMAD HAIDER, RONG YANG, COSTEL CONSTANTIN, HAMAD AL-BRITHEN,[†] ERDONG LU, NANCY SANDLER, *Nanoscale & Quantum Phenomena Institute, Ohio University* PABLO ORDEJON, *Instituto do Ciencia de Materiales de Barcelona, Bellaterra, Barcelona, Spain* The intrinsic structures of semiconductor surfaces are important for epitaxial growth and future applications. Here we present a scanning tunneling microscopy study of the clean zinc-blende GaN(001) surface, free from the presence of arsenic. We find a sequence of reconstructions for the clean surface, beginning with 4x3 and including c(4x12), 4x7, c(4x16), 4x9, and c(4x20). Generally, all of these reconstructions are row-like. The 4x3 is a semiconducting surface structure with a bandgap, measured using tunneling spectroscopy, of 1.14 eV; the 4x3 is obtained under Ga-poor surface conditions and is compared with a model calculated using ab-initio techniques. The other reconstructions are metallic, obtained under Ga-rich surface conditions. They can be modeled using simple adatom schemes on top of a bulk-like Ga atom termination.

*Work supported by National Science Foundation Grant #s 9983816 & 0304314

[†]Currently: King Saud University

**J1 276 First-principles study of adsorption and migration on the (001) surfaces of cubic BN*** HIROAKI KOGA, TSUYOSHI MIYAZAKI, *National Institute for Materials Science* SATOSHI WATANABE, *The University of Tokyo* TAKAHISA OHNO, *National Institute for Materials Science* This first-principles study examines the behavior of boron and nitrogen adatoms on the dimer-reconstructed (001) surfaces of cubic boron nitride (cBN), to find low-barrier migration pathways that control the vapor-growth of cBN. Adatom dynamics on the surfaces of wide band gap semiconductors such as cBN (with $\sim$ 6 eV gap) and diamond is an uncharted field of surface science: Because these materials have very strong, directional bonds, the adatoms may choose unlikely adsorption sites and migration pathways, to minimize the induced strains. For example, we have found that a N adatom on a N dimer row of cBN(001) migrates using a site-exchange reaction, rather than migrating on the dimer row. The calculated energy barrier for the site-exchange pathway is mere 0.9 eV, in contrast with the large barrier (over 4 eV) of the dimer row pathway. At the meeting, we report such low-barrier pathways on cBN(001), and also discuss a new approach to cBN epitaxy that exploits them.

*H. K. is supported by the JSPS Research Fellowships for Young Scientists. This work was in part supported by a Grant-in-Aid from the Ministry of Education, Culture, Sports, Science and Technology.

**J1 277 Anchoring to the Nanoworld: Spectroscopic Investigation of Atomic Metal Strings Adsorbed on GaN** CHE-CHEN CHANG, CHIEN-HUA LUNG, *National Taiwan University* It is now possible to produce structures that are only a few tens to a few nanometers in size using techniques which involve the self assembly or the chemical functionality-guided arrangement of atoms, molecules and nanospecies. Their devices, however, are useless unless they are able to communicate with the outside world and with one another. This study explored the possibility of fabricating metal contacts from the bottom up on semiconductors using a linear metal atom string complex, which was chelated by dipyridylamino ligands and terminated at both ends by one Cl atom each, for CVD. More than 75% of the string complex exposed at 105 K to the GaN(0001) surface was chemisorbed dissociatively, with one of its terminal Cr-Cl bonds disrupted and the other pointing freely outwards. The chelate structure of the adsorbed complex was stable until reaching $\sim$ 340 K, at which temperature detachment of some of its ligands occurred. The ligand desorption followed the first-order kinetics, with a desorption energy of 21.5 kcal/mol. The detachment of the ligand from the complex caused the metal chain axis to lie down on the surface. Consequently, the Cr-Cl bond on the free end of the chain interacted with the surface, causing other ligands to desorb from the surface at the higher substrate temperature of $\sim$ 540 K.

**J1 278 Negative differential resistance of TEMPO on Si(111)** ANN-SOFIE HALLBACK, HAROLD J W ZANDVLIET, BENE POELSEMA, *University of Twente* Negative differential resistance (NDR) has been observed for individual 2,2,6,6-tetramethyl-1-piperidinyloxy (TEMPO) molecules, adsorbed on Si(111) at room temperature. Measurements were performed in ultra high vacuum (UHV) using scanning tunneling microscopy (STM) and -spectroscopy (STS). NDR effects were observed exclusively at negative bias voltage on the used n-type Si(111) sample. TEMPO was observed to adsorb preferentially at corner adatom sites of the Si(111)-7x7 structure. Although the Si(111)-7x7 reconstruction was conserved, local defects were observed in the vicinity of the TEMPO adsorbates.

**J1 279 Reflectance anisotropy spectra of CdTe(001) surfaces*** RAUL VAZQUEZ, BERNARDO MENDOZA, NORBERTO NARZATE, *Centro de Investigaciones en Optica A. C.* We calculate reflectance anisotropy (RA) spectra of a clean Cd-terminated CdTe(001) surface which exhibits $c(2 \times 2)$ reconstruction, and clean Te-terminated CdTe surfaces with $(2 \times 1)$, $(1 \times 2)$ and $c(2 \times 2)$ surface reconstructions. Theoretical spectra are obtained from two aproaches: an *ab initio* pseudopotential calculation in the framework of the density functional theory and within the local density approximation (DFT-LDA), and a microscopic formulation based on a semi- empirical tight binding approach which includes spin-orbit (SO) interactions[1]. We show how RA spectrum changes when SO coupling is taken into account and compare our theoretical results with experimental results[2]. We find a good agreement between experimental and theoretical spectra. [1] R. A. Vázquez-Nava, B. S. Mendoza and N. Arzate, Phys. Stat. Sol. b **242** 3022 (2005); R. A. Vázquez-Nava, B. S. Mendoza and C. Castillo Phys. Rev. B **70**, 165306 (2004) [2] R. E. Balderas-Navarro, K. Hingerl, W. Hilber, D. Stifter, A. Bonanni and H. Sitter, J. Vac. Sci. Technol. B **18** 2224 (2000).

*We acknowledge partial support from CONACYT-México grant SEP-2004-C01-48142 and CONCYTEG-México grant 05-04-k117-026 anexo 1.

**J1 280 Local Valence Structure of Fe in Fe3Si/GaAs(001)** KUAN-LI YU, HSUEH-HSING HUNG, LING-YUN JANG, *National Synchrotron Radiation Research Center* MING-WEI HONG, *Department of Materials Science and Engineering, National Tsing Hua University* RAY NIEN KWO, *Department of Physics, National Tsing Hua University* A high quality, eptiaxial magnetic films of $Fe_3Si$ on GaAs(001) substrates were studied in our experiment. $Fe_3Si$ is ferromagnet and can be regarded as a Heusler-like alloy with a composition of $Fe_2FeSi$. There is possibility that $Fe_3Si$ is a half metal which is an ideal candidate for spin injection, although the calculated density of states for bulk $Fe_3Si$ does not predict half-metallic behavior. By using diffraction anomalous fine structure measurement, there is chance to look at the anomalous effect on the different atom sites. Two diffraction of $Fe_3Si$ were measured as (002) and (004) to understand the local electron density structure in different Fe sites and the spectra show significant different features. By carefully handling these DAFS results, there is chance to understand the structure of the local density of state of the Fe atoms in different crystal sites.

**J1 281 Angle-resolved Ultra-violet Photoelectron Spectroscopy Study of Epitaxial $CrO_2$ films grown on $TiO_2$ Substrates** DANIEL BORST, *University of New Orleans* CARL VENTRICE, *Unversity of New Orleans* G. MIAO, *University of Alabama* ARUN GUPTA, *University of Alabama* Chromium dioxide is predicted to be a half-metallic oxide. Although there is experimental evidence that $CrO_2$ is half-metallic at low temperature, attempts to make devices based on $CrO_2$ have yielded very low efficiencies. To study the electronic properties of the surface region of $CrO_2$, we have performed ARUPS measurements on epitaxial $CrO_2$ films. The $CrO_2$ thin films have been deposited on (100) and (110)-oriented TiO2 substrates by chemical vapor deposition, using $CrO_3$ as a precursor. The effects of sputtering of the $CrO_2$ films to remove the outer layer of $Cr_2O_3$ and of annealing the films in oxygen to heal surface defects has been studied. Sputtering results in shifts in the onset of valence emission away from the Fermi edge by as much as 0.5 eV, which is opposite of what would be expected for a half-metallic system. Annealing of the films above 450 $^o$C results in spectra similar to $Cr_2O_3$.

**J1 282 Ga-doping effect on superconductivity for Ba8Si46 clathrates*** RUIHONG ZHANG, YANG LIU, XINGQIAO MA, NING CHEN, GUOHUI CAO, YANG LI, *Department of Physics, University of Science and Technology Beijing* We present a joint experimental and theoretical study of the superconductivity and electronic structures in type-I Ga-doped silicon clathrates. The superconducting critical temperature in Ba8Si46-xGax is shown to decrease strongly with gallium content increasing. These results are corroborated by first-principles simulations calculated from the density-functional theory with plane waves and pseudopotentials. The simulations show that Ga doping results in a large decrease of electronic density of states in Fermi level, which can explain the superconducting critical temperature decrease with Ga-doping in the BCS theoretical frame.

*National Natural Science Foundation of China (Grant No.50372005)

**J1 283 The Ferromagnetic Hafnium Dioxide Thin Films Prepared by Pulsed Laser Deposition** YUNG M. HUH, R. VASELAAR, *Physics Department, South Dakota State University, Brookings, SD 57007* J. ZHANG, D.J. SELLMYER, *Department of Physics and Astronomy, University of Nebraska, Lincoln, NE*

*68588* The ferromagnetic hafnium dioxide (HfO2) thin films were prepared using pulsed laser deposition (PLD) system. Ferromagnetic moment was completely suppressed and revived as HfO2 film was annealed in vacuum and air. The variation of ferromagnetic moment was investigated to study the origin of the ferromagnetism in HfO2 system. X-ray diffraction showed that the c-plane is perpendicular to the growth direction. Strong anisotropic moment was observed for applied magnetic fields along the parallel and perpendicular to the c-plane.

**J1 284 Inelastic electron tunneling spectroscopy of decanethiol on Au(111) at elevated temperatures** ANN-SOFIE HALLBACK, HAROLD J W ZANDVLIET, BENE POELSEMA, *University of Twente* We have studied decanethiol self-assembled monolayers (SAMs) on Au(111) in UHV by inelastic electron tunneling spectroscopy (IETS) performed with a scanning tunneling microscope (STM). This study reveals inelastic peaks, which can successfully be assigned to molecular vibration modes (Au-S or S-C stretch modes, and C-C stretch mode or $CH_2$ modes). It is remarkable that these modes can be detected already at 77 K, i.e. at a much higher temperature than commonly used in IETS measurements.

**J1 285 Quantum size effect on the diffusion barriers and growth morphology of Pb/Si(111)** TZU-LIANG CHAN, CAI-ZHUANG WANG, MYRON HUPALO, MICHAEL TRINGIDES, KAI-MING HO, *Ames Laboratory-U.S. DOE. and Department of Physics and Astronomy, Iowa State University* Using first-principles total energy calculations, we have studied the diffusion barriers of Pb adatoms on a free-standing Pb(111) film as a function of film thickness. We found that diffusion of an adatom on the Pb film has very low barriers (less than 60 meV). A bi-layer oscillation in the diffusion barriers due to quantum size effect (QSE) is observed, with lower barrier on the odd-layered,relatively unstable Pb films. The diffusion barrier difference between the odd-and even-layered film is found to be as large as 40 meV. This big difference in the diffusion barriers due to QSE is the origin of the intriguing growth morphology of Pb islands on Si(111) surface observed in the STM experiments: the growth of a Pb layer on Pb islands with unstable heights starts from the periphery and moves towards the center, while the nucleation of the next layer on stable Pb islands starts away from the periphery.

**J1 286 Substrate Dependence on the Allotropic Transformation and the Morphology of Ultrathin Bi Films on Si(111)*** S. YAGINUMA, T. NAGAO, K. NAGAOKA, *NIMS, Tsukuba, Japan* M. MAEKAWA, *Kanazawa Univ.* J.T. SADOWSKI, *IMR. Tohoku Univ.* M. SAITO, *Kanazawa Univ.* Y. FUJIKAWA, T. SAKURAI, *IMR. Tohoku Univ.* T. KAKAYAMA, *NIMS. Tsukuba, Japan* Bismuth film grows via an intriguing thickness-driven allotropic transformation from a {012}-oriented phase to a bulk-like (001) phase. We compare the growth of Bi films on the Si(111)-7x7 surface with that on the Si(111)-$\beta - \sqrt{3}$x$\sqrt{3}$-Bi surface by use of electron diffraction and scanning tunneling microscopy. Small amount of Bi(001) nanocrystals can nucleate on the 7x7 substrate from the very beginning of the growth $\sim$ 1 monolayer (ML). They stabilize with 3 bilayer height in a perfect commensurate manner on the 7x7 substrate because of lattice contraction as predicted from our itab initio calculations, and thus lead to the growth of the highly-crystalline (001) films. On the $\beta - \sqrt{3}$x$\sqrt{3}$-Bi surface, on the contrary, the (001) nuclei is not observed in the initial stage of the growth and the Bi{012} films survive, and thus the nucleation of the (001) phase is inhibited up to $\sim$ 15 ML.

*This work has been supported by ICORP JST and Grants-in-Aid from JSPS

**J1 287 Comparative studies of Pb films on different substrates by first-principles calculations*** YU JIA, *Zhengzhou University, China & ORNL* BIAO BU, *Inst. of Phys. CAS, China* H.H. WEITERING, *The University of Tennessee & ORNL* ZHENYU ZHANG, *ORNL & The University of Tennessee* Quantum growth of ultrathin Pb on Ge(111) and Cu(111) substrates up to more than 25 monolayers are studied using total energy calculations within density functional theory. Our studies show that the surface energy, work function, and lattice relaxation of these films all oscillate strongly with the film thickness. The oscillation pattern is always even-odd with interruptions by crossovers, in good agreement with experimental observations. However, the positions of the crossovers and the separation between the crossovers depend on which substrate is used. These results are rationalized based on the interplay between Friedel oscillations, quantum size effects, and charge transfer effects.

*Supported by US DOE, US NSF, & NSF of China.

**J1 288 Characterization of Noble Gas Ion Beam Fabricated Single Molecule Nanopore Detectors** RYAN ROLLINGS, *University of Arkansas* BRADLEY LEDDEN, *University of Arkansas* JOHN SHULTZ, *University of Arkansas* DANIEL FOLOGEA, *University of Arkansas* JIALI LI, *University of Arkansas* JOHN CHERVINSKY, *Harvard University* JENE GOLOVCHENKO, *Harvard University* Nanopores fabricated with low energy noble gas ion beams in a silicon nitride membrane can be employed as the fundamental element of single biomolecule detection and characterization devices [1,2]. With the help of X-ray Photoelectron Spectroscopy (XPS) and Rutherford Backscattering (RBS), we demonstrate that the electrical noise properties, and hence ultimate sensitivity of nanopore single molecule detectors depends on ion beam species and nanopore annealing conditions. 1. Li, J., D. Stein, C. McMullan, D. Branton, M.J. Aziz, and J.A. Golovchenko, Ion-beam sculpting at nanometre length scales. Nature, 2001. **412** (12 July): p. 166-169. 2. Li, J., M. Gershow, D. Stein, E. Brandin, and J.A. Golovchenko, DNA Molecules and Configurations in a Solid-state Nanopore Microscope. Nature Materials, 2003. **2**: p. 611-615.

**J1 289 Simulation of self-organized evolution of patterned GaAs(001) surfaces during homo-expitaxial growth*** ERIN FLANAGAN, *Department of Materials Science and Engineering, University of Maryland, College Park* HUNG-CHIH KAN, *Department of Physics, University of Maryland, College Park and the Laboratory for Physical Sciences* TABASSOM TADAYYON-ESLAMI, *Department of Materials Science and Engineering, University of Maryland, College Park and the Laboratory for Physical Sciences* SUBRAMANIAM KANAKARAJU, *The Laboratory for Physical Sciences* CHRIS RICHARDSON, *The Laboratory for Physical Sciences* RAYMOND PHANEUF, *Department of Materials Science and Engineering, University of Maryland, College Park and the Laboratory for Physical Sciences* We report on both physically based and phenomenological simulations for morphological evolution of patterned GaAs(001) surface during homo-

epitaxial growth. We compare these simulations with the experimental observations of homo-epitaxial growth on substrates patterned with arrays of cylindrical pillars. Our atomic force microscope (AFM) characterization indicates that the pillars evolve in a self-organized manner, i.e. the shape evolution of the pillars seems to be insensitive to its initial diameter in the [-110] direction.

*This work is supported by the Laboratory for Physical Sciences and an NSF-MRSEC Grant No. DMR-0080008

**J1 290 Study of Nanopore Sculpting with Noble Gas Ion Beams at Various Energies** BRADLEY LEDDEN, ERIC KRUEGER, JIALI LI, *University of Arkansas* We report on experiments using noble gas beams: Helium, Neon, Argon, Krypton, and Xenon, at energies of 1keV, 3keV, and 5keV to controllably fabricate nanopores in freestanding silicon nitride membranes. Utilizing computer simulations (SRIM and TRIM), and a surface adatom diffusion model to describe the phenomenon of nanopore formation, we evaluate the conditions, specifically the ion energy, responsible for highly controllable fabrication of solid state nanopores. Additionally, we present methods to determine the thickness of the grown film as well as the thickness profile of the nanopore.

**J1 291 Surface-enhanced Raman spectroscopy of the nitrided $SiO_2$/SiC interface*** S.H. CHOI, *Vanderbilt University* M. PARK, D. WANG, J.R. WILLIAMS, *Auburn University* W. LU, *Fisk University* S. DHAR, L.C. FELDMAN, *Vanderbilt University* AUBURN UNIVERSITY COLLABORATION, FISK UNIVERSITY COLLABORATION, Performance of silicon carbide (SiC) field effect devices is limited by poor channel mobility due to the high density of oxide/dielectric interface states, ($D_{it}$). In general $D_{it}$ is crystal-face dependent. Carbon clusters generated by the high temperature oxidation process, are assumed to be the major contributor to this high defect density. Nitric oxide (NO) annealing reduces the interface states and results in an enhanced mobility, although the physical/chemical mechanisms are not yet established. We report a surface enhanced Raman spectroscopy (SERS) analysis of the 4H-SiC/$SiO_2$ interface, clearly showing carbon cluster bands, on the C (carbon-terminated) face. The concentration of the carbon clusters on the C-terminated interface is much higher than that of the Si-face, consistent with the higher $D_{it}$ on the C-face. Furthermore, NO annealing results in a reduction of the cluster concentration. This result provides direct experimental evidence that carbon clusters exist at the as-grown interface and the effect of NO anneal at atmospheric pressure suggest removal of these interfacial carbon defects.

*Supported by the Ministry of Information and Telecommunication (MIC, Republic of Korea) and DARPA/ONR

**J1 292 Surface Demixing in a AuSn Liquid Alloy*** VENKAT BALAGURUSAMY, REINHARD STREITEL, OLEG SHPYRKO*, PETER PERSHAN, *DEAS and Physics Dept, Harvard University, Cambridge, MA 02138* BEN OCKO, *Brookhaven National Laboratory, Upton, NY 11973* MOSHE DEUTSCH, *Bar-Ilan University, Ramat-Gan 52900, Israel* We present results of X-ray reflectivity studies of the eutectic AuSn alloy liquid-vapor interface. The analysis shows that in common with the BiSn eutectic, there is surface demixing that extends to more than one monolayer. This is in contrast to a common presumption that the Gibbs adsorption predicts complete demixing only in the surface monolayer. The composition profiles can be explained by surface segregation theory for attractive interaction between Sn and Au atoms, similar to BiIn [1] and BiSn [2]. [1] E. DiMasi, H. Tostmann, O. G. Shpyrko, P. Huber, B. M. Ocko, P. S. Pershan, M. Deutsch, and L. E. Berman, Phys. Rev. Lett. **86**, 1538 (2001) [2] O. G. Shpyrko, A. Y. Grigoriev, R. Streitel, D. Pontoni, P. S. Pershan, M. Deutsch, and B. M. Ocko, Phys. Rev. Lett. **95**, 106103 (2005) *Present address: Center for Nanoscale Materials, ANL.

*Synchrotron measurements performed at ChemMatCARS, Advanced Photon Source, ANL and supported by DOE grants DE-FG02-88-ER45379 and DE-AC02-98-CH10886



## SESSION K1: OPTICAL FREQUENCY CLOCKS AND EXPERIMENTAL QUANTUM OPTICS
**Tuesday Afternoon, 14 March 2006; Ballroom IV, Baltimore Convention Center at 14:30**
**David Weiss, Penn State University, presiding**

**14:30**
**K1 1 Trapped Ion Optical Clocks.**
PATRICK GILL

For the last fifty years, the international standard of time has been the caesium atomic clock, which is based on the 9.2 GHz microwave absorption in caesium-133 atoms. The recent Nobel Physics award to T W Haensch and J L Hall for their development of widespan femtosecond comb metrology has recognised the major role that femtosecond combs have made to the progress of optical frequency standards, and their use, going forward, as optical clocks. Such single trapped ion and cold atom optical clocks are now capable of challenging the best caesium fountain microwave clocks available. High accuracy frequency measurement of the single trapped ion optical frequency standards such as $^{199}Hg^+$ [1], $^{88}Sr^+$ [2], and $^{171}Yb^+$ [3] by means of femtosecond combs referenced to the primary caesium fountain standard has now resulted in uncertainties at the $10^{-15}$ level. These measurements are close to being limited by the caesium standard itself. Looking forward, it now becomes attractive to reverse the ''directionality'' of accuracy provision by referencing the comb to the optical frequency standard itself, and this concept has already been demonstrated [4]. The optical clock so formed can then deliver full accuracy of the optical standard to about a million comb modes across the visible and near infra-red, and,

through the comb repetition rate frequency, to the microwave and rf regions. This presentation will review recent results and expected future capabilities of these optical clocks, particularly in respect of the single cold $^{88}Sr^{+}$ ion quadrupole and $^{171}Yb^{+}$ ion octupole clock transitions. [1] J C Bergquist et al 2005, submitted to Nature [2] H S Margolis et al. Science **306** 1355 (2004) [3] T Schneider et al Phys. Rev. Lett. **94** 230801 (2005) [4] S A Diddams et al. Science **293** 825 (2001).

**15:06**
**K1 2 Precision Spectroscopy of Hydrogen and Femtosecond Laser Frequency Combs.**
THOMAS UDEM, *MPI fuer Quantenoptik*

A femtosecond frequency comb is a simple and compact tool that allows the phase coherent connection of the radio frequency domain (below 100 GHz) with the optical domain (above 200 THz). It greatly simplified high precision optical frequency measurements and provides the long awaited clockwork mechanism for an all-optical atomic clock. We have used such a frequency comb to measure the absolute frequency of the 1S-2S two-photon transition in atomic hydrogen, i.e. comparing it with the Cs ground state hyperfine splitting. By comparing data taken in 2003 with earlier measurements in 1999 we can set an upper limit on the variation of the 1S-2S transition frequency of ( $-$ 29 $\pm$ 57) Hz within 44 months. To derive limits on the drift rates of fundamental constant such as the fine structure constant, we combine these measurements with other optical frequency measurements in $Hg^{+}$ and in $Yb^{+}$ performed at NIST, Boulder/USA and at PTB, Braunschweig/Germany respectively. This combined method gives precise and separate restrictions for the fractional time variation of the fine structure constant and the Cs nuclear magnetic moment measured in Bohr magnetons. The latter is a measure of the drift rate of the strong interaction. We also report on efforts to convert the frequency comb technology to much shorter wavelength. Based on intra cavity high harmonic generation an XUV (up to 60 nm) frequency comb is generated with a repetition rate of more than 100 MHz useful for high resolution laser spectroscopy in this region.

**15:42**
**K1 3 Precision measurement meets ultrafast science.***
JUN YE, *JILA, NIST and Univ. of Colorado*

Phase control of a single-frequency continuous-wave laser and the electric field of a mode-locked femtosecond laser has now reached the same level of precision, resulting in sub-optical-cycle phase coherence being preserved over macroscopic observation times exceeding seconds. The subsequent merge of CW laser-based precision optical-frequency metrology and ultra-wide-bandwidth optical frequency combs has produced remarkable and unexpected progress in precision measurement and ultrafast science. A phase-stabilized optical frequency comb spanning an entire optical octave ( $>$ 300 THz) establishes millions of marks on an optical frequency ''ruler'' that are stable and accurate at the Hz level. Accurate phase connections among different parts of electromagnetic spectrum, including optical to radio frequency, are implemented. These capabilities have profoundly changed the optical frequency metrology, resulting in recent demonstrations of absolute optical frequency measurement, optical atomic clocks, and optical frequency synthesis. Combined with the use of ultracold atoms, optical spectroscopy and frequency metrology at the highest level of precision and resolution are being accomplished at this time. The parallel developments in the time domain applications have been equally revolutionary, with precise control of the pulse repetition rate and the carrier-envelope phase offset both reaching the sub-femtosecond regime. These developments have led to recent demonstrations of coherent synthesis of optical pulses from independent lasers, coherent control in nonlinear spectroscopy, coherent pulse addition without any optical gain, and coherent generation of frequency combs in the VUV and XUV spectral regions. Indeed, we now have the ability to perform completely arbitrary, optical, waveform synthesis, complement and rival the similar technologies developed in the radio frequency domain. With this unified approach on time and frequency domain controls, it is now possible to pursue simultaneously coherent control of quantum dynamics in the time domain and high precision measurements of global atomic and molecular structure in the frequency domain. These coherent light-based precision measurement capabilities may be extended to the XUV spectral region, where new possibilities and challenges lie for precise tests of fundamental physical principles.

*The work is supported by ONR, NASA, AFOSR, NIST, and NSF

**16:18**
**K1 4 The Hg/Al single-atom, optical clocks: on the path to inaccuracies below $10^{-17}$.***
JAMES BERGQUIST, *NIST*

For the past fifty years, atomic standards based on the frequency of the cesium ground-state hyperfine transition have been the most accurate timepieces in the world. Recently, we reported a comparison between the cesium fountain standard NIST-F1, which has been evaluated with an inaccuracy of about $4 \times 10^{-16}$, and an optical frequency standard based on an ultraviolet transition in a single, laser-cooled mercury ion for which the fractional systematic frequency uncertainty was below $7.2 \times 10^{-17}$ [1]. We have also compared the frequency of the mercury ion optical clock to that of an optical standard based on the $^{1}S_0 \leftrightarrow {}^{3}P_0$ transition of $^{27}Al^{+}$ at 267 nm, which offers several attractive features as a single-ion optical clock. Its sharp natural linewidth, small electric quadrupole moment, and low quadratic Zeeman coefficient (0.7 $Hz/B^2$) allow for high stability and accuracy, but until recently, precision spectroscopy of $Al^{+}$ had not been possible, because it lacked an accessible, laser-cooling transition. However, with the development of quantum logic based spec-

troscopy [2, 3] a single aluminum ion can be efficiently probed. In our realization of this scheme, a single $^{9}Be^{+}$ ion is trapped together with the single Al ion in a linear Paul trap and is used to sympathetically cool the Al ion and to detect its internal state after the clock radiation is applied. We will report the latest results of the frequency comparison of the two optical standards and the implication these comparisons might have toward improved tests of the stability of Fundamental Constants. [1] W. H. Oskay et al., submitted for publication. [2] D. J. Wineland et al., Proc. 6th Symp. on Freq. Standards and Metrology, 361 (2002). [3] P. O. Schmidt et al., Science 309, 749 (2005).

*This work was partially supported by ONR and ARDA/NSA

**16:54 ge de France and ENS Paris**
**K1 5 Exploring the states of light: from photon counting to quantum information.**
SERGE HAROCHE, *Collège de France and ENS Paris*

Forty years ago, the seminal papers of Roy Glauber have given a complete analysis of photon counting and light coherence, combining in a single theoretical framework a description of the granular and wave-like features of radiation. Glauber's theory has since then explained countless landmark experiments in quantum optics and has become an essential tool to understand the role played by photons in the physics of quantum information. We will describe a few experiments which illustrate the importance of Glauber's work in modern quantum optics. In addition, we will stress that complementary wave and particle behaviors are not restricted to light. They are also exhibited by atomic matter in Bose Einstein condensates. As we will see, Glauber's formalism of coherent states and particle counting has also found a remarkable testing ground in this new domain of research at the boundary between atomic and condensed matter physics.



**SESSION K2: EXOTIC ORDERING IN SPINELS**
**Tuesday Afternoon, 14 March 2006; Ballroom III, Baltimore Convention Center at 14:30**
**Sang-Wook Cheong, Rutgers University, presiding**

**14:30**
**K2 1 Metal-insulator transition in $CuIr_2S_4$: XAS results, structure revisited, electronic structure proposed.**
MARK CROFT, *Rutgers University*

Interestingly, the magnetism in the spinel compound $Fe_3O_4$ (loadstone), constitutes the correlated electron material/problem of the greatest antiquity known to man. The Verwy transition problem in $Fe_3O_4$ is, by comparison, young at only 67 years of age. Recently experimental and theoretical insights into such exotic magnetic, charge, and orbital orderings in transition metal (T) spinel compounds have been rapidly emerging. The leitmotifs in these works involve: frustrated tripartite crossing 1D chains of edge-sharing T-ligand octahedra; T-d($t_{2g}$) orbital ordering onto subsets of these chains which involve d-d overlap; dimmer formation on these chains; and/or charge ordering on the chains dependent on band filling. Understanding the low temperature structural and metal (M) to insulator (I) transition in the spinel compound $CuIr_2S_4$ provides a key link in the generalization to other such systems. S *K*-edge X-ray absorption spectroscopy (XAS) measurements across this M-I transition reflect a dramatic Ir *d*-electronic state redistribution[1]. These results stimulated a detailed re-evaluation of the of *I*-phase crystal structure in terms of: decoupled chains of $IrS_6$ octahedra along the (110)-type directions; and an $Ir^{3+}$ ($Ir^{4+}$-$Ir^{4+}$) $Ir^{3+}$ repeat pattern ordering, where the ($Ir^{4+}$-$Ir^{4+}$) pair forms a dimmer. Further, the electronic state changes, evidenced by the XAS, motivated a model in which the I-phase involves: an orbital ordering of the highest lying $t_{2g}$ electron into 1D chains; the 3/4 filling of this 1D band dictating the periodicity of the orbital/charge ordering; and the direct $t_{2g}$-$t_{2g}$ dimmer bonding production of an antibonding state prominent in the S-K edge spectrum. The generalization of these concepts to other transition metal spinels will be addressed. [1]M. Croft, W. Caliebe, H. Woo, T. A. Tyson, D. Sills, Y. S. Hor, S-W. Cheong, V. Kiryukhin, and S-J. Oh, Phys. Rev. B 67 (Rapid Comm.), 201102 (2003).

**15:06**
**K2 2 Charge carriers in spinel $AlV_2O_4$ order below 700K.**
YOICHI HORIBE, *Department of Physics, Osaka Prefecture University*

$AlV_2O_4$ with the spinel structure shows some magnetic and electric anomalies around 700K, which originate from the formation of the charge ordered (CO) structure. [1,2] In this talk, we will report a structural model of the CO structure in $AlV_2O_4$, which was obtained by electron diffraction, synchrotron x-ray diffraction and magnetic measurements. The CO structure is characterized by the formation of V clusters ''heptamers,'' each of which is consisting of 7 vanadium

atoms and is in a spin- singlet state as a total. Note that the number of electrons per site is still fractional in this CO structure. In addition, theoretical consideration suggests that this unique molecular-like V heptamer is stabilized by a strong bonding of vanadium $t_{2g}$ orbitals. This work has been done in collaboration with Drs. S. Mori, T. Katsufuji, Y. Motome, N. Furukawa, H. Ishibashi, N. Ikeda and K. Kato. [1] K. Matsuno, et al., J. Phys. Soc. Jpn. **70**, 1456 (2001). [2] K. Matsuno et al., Phys. Rev. Lett. **90**, 096404 (2003).

**15:42**
**K2 3 Orbital Superstructures in Spinels.**
DANIEL KHOMSKII, *II.Physikalisches Institut, Universitaet zu Koeln*

Orbital degrees of freedom often lead to specific types of orbital and spin ordering. Complicated and interesting superstructures are observed in B-sublattice of spinels. This is connected with the geometric frustration of this lattice and with the interconnection of edge-sharing $MO_6$ octahedra, which is especially important for transition metals with partially-filled $t_{2g}$ levels. In some such systems ($MgTi_2O4$, $CuIr_2S_4$, $AlV_2O_4$) there appears strange superstructures with the formation of spin gap states. In other cases ($ZnV_2O_4$) structural transitions, apparently connected with orbital ordering, are followed by long-range magnetic ordering. Last but not least, the famous Verwey transition in magnetite $Fe_3O_4$ leads to a very complicated structural pattern, accompanied by the appearance of ferroelectricity. In this talk I will discuss all these examples, paying main attention to an interplay of charge, spin and orbital degrees of freedom. In particular, for $MgTi_2O4$, and $CuIr_2S_4$ we proposed the picture of orbitally-driven Peierls state [1]. Similar phenomenon can also explain situation in $ZnV_2O_4$ [2], although the corresponding superstructure has not yet been observed experimentally. Finally, I propose the model of charge and orbital ordering in magnetite [3], which uses the idea of an interplay of site- and bond-centered ordering [4] and which seems to explain both the structural data and the presence of ferroelectricity in Fe $_3O_4$ below Verwey transition. [1] D.I. Khomskii and T. Mizokawa, Phys. Rev. Lett. **94**, 156402 (2005); [2] Hua Wu, T. Mizokawa and D.I. Khomskii, unpublished; [3] D.I. Khomskii, unpublished; [4] D.V. Efremov, J. van den Brink and D.I. Khomskii, Nature Mater. **3**, 853 (2004).

**16:18**
**K2 4 Probing spin correlations with phonons in the strongly frustrated magnet: ZnCr2O4.***
ANDREI SUSHKOV, *Materials Research Science and Engineering Center, University of Maryland*

Geometrically frustrated magnets can resist magnetic ordering and remain in a strongly correlated paramagnetic state well below the Curie-Weiss temperature. The spin-lattice coupling can play an important role in relieving the frustration in these systems. In ZnCr2O4, an excellent realization of the Heisenberg antiferromagnet on the pyrochlore network, a lattice distortion relieves the geometrical frustration through a spin- Peierls-like phase transition at Tc=12.5 K with a lowering of the symmetry from cubic to tetragonal. Conversely, spin correlations strongly influence the elastic properties of a frustrated magnet. By using infrared spectroscopy and published data on magnetic specific heat, we demonstrate that the frequency of the Cr optical phonon triplet in ZnCr2O4 tracks the nearest-neighbor spin correlations above Tc.* Below Tc, the triplet splits into a singlet and a doublet, separated by 11 cm- 1. This splitting gives a direct measurement of the spin- Peierls order parameter. From analysis of the ion displacements in the phonon modes we can conclude that direct Cr-Cr exchange dominates in ZnCr2O4. These experiments result in a clear understanding of spin-phonon coupling in ZnCr2O4 in contrast to other oxide magnets. Recent ab initio calculations** confirm the magnetic origin of both the phonon splitting in ZnCr2O4 and the frequency shifts in the ferromagnetic insulating spinel CdCr2S4. *A.B. Sushkov et al., Phys. Rev. Letters 94 (2005) 137202. ** C.J. Fennie and K.M. Rabe, cond-mat/0508136 and Mar06 APS Meeting.

*This work was done in collaboration with O. Tchernyshyov, W. Ratcliff II, S.W. Cheong, and H. D. Drew. This work supported in part by NSF-MRSEC Grant DMR-0520471.

**16:54**
**K2 5 Orbital ordering in transition-metal spinels.**
PAOLO G. RADAELLI, *ISIS facility, Rutherford Appleton Laboratory, Chilton, Didcot, OXON OX11 0QX, UK*

Transition-metal spinels (general formula $AB_2X_4$) have been for many years the subject of intense experimental and theoretical activity. Structurally, the most interesting feature of these systems is the fact that the *B* cation occupies the nodes of a pyrochlore lattice, which is known to be geometrically frustrated. Therefore, one can explore how their natural tendency to order in the charge, magnetic and orbital sectors is affected by geometrical frustration. Orbital Ordering (OO) occurs when the orbital degeneracy of an extended concentrated system is lifted, typically through a distortion of the lattice. This may result in either single orbital occupation or alternation/modulation of the orbital occupancy, with or without an associated charge ordering. The degree of charge localization is another important issue: in highly localized systems, one can speak of a cooperative Jahn-Teller (JT) effect, but this paradigm is no longer sufficient in the present of significant electronic hopping. Both $e_g$ and $t_{2g}$ orbitals are relevant for transition-metal spinels; $e_g$ systems, such as $ZnMn_2O_4$, tend to display the strongest JT effects, with direct coupling to the lattice. More recently, significant attention has been devoted to the possibility of orbital ordering in ions with partial $t_{2g}$ occupation, such as $Ti^{3+}$ and $V^{4+}$ ($3d^1$) and $V^{3+}$ ($3d^2$) and their electron/hole-symmetric counterparts. With respect to $e_g$ systems, $t_{2g}$ systems have a greater

degeneracy and weaker coupling to the lattice, and can give rise to significant hopping, due to the direct overlap of the $t_{2g}$ orbitals along the $<110>$ crystallographic directions of the spinel structure. Recent results on Ti, V, Fe and Ir spinels will be discussed, with particular reference to the relation between the complex crystallographic superstructures and the changes in transport (metal-insulator transitions) and magnetic (paramagnetic-diamagnetic transitions) properties at the ordering temperatures.

**SESSION K3: ELECTRON DOPED HIGH TC SUPERCONDUCTORS**
**Tuesday Afternoon, 14 March 2006; Ballroom I, Baltimore Convention Center at 14:30**
**Martin Greven, Stanford University, presiding**



**14:30**
**K3 1 Evidence for Quantum Criticality in Electron-doped Cuprates.***
YORAM DAGAN, *School of Physics and Astronomy Tel Aviv University*

The electron-doped cuprates have attracted a lot of scientific interest recently. The antiferromagnetic (AFM) phase in these cuprates may persist well into the superconducting dome and vanish in a quantum critical point. We describe experimental evidence for a quantum phase transition near optimum doping in the electron-doped material $Pr_{2-x}Ce_xCuO_{4-\delta}$: The normal state Hall coefficient, at 350mK, exhibits a remarkable change at this doping. This singular behavior is accompanied by significant changes in the temperature dependence of the resistivity below 20K [1]. In addition, at low temperatures, a spin scattering magnetoresistance appears in the underdoped region, increases in magnitude at optimum doping and suddenly vanishes at the critical doping where also the upturn in resistivity ($d\rho/dT < 0$) disappears. [2] Supporting evidence for the quantum critical scenario from neutron scattering and infrared measurements and the nature of the ordered phase will be discussed. Our tunneling experiments show that the normal state tunneling gap is not directly related to the AFM order. T*, the temperature at which the normal state tunneling gap disappears, is greater than $T_c$ for the underdoped region and it follows $T_c$ on the overdoped side. [3] This behavior suggests finite pairing amplitude above $T_c$ on the underdoped side. [1] Y. Dagan et al., PRL., **92**, 167001 (2004). [2] Y. Dagan et al., PRL., **94**, 057005 (2005). [3] Y. Dagan et al., PRL., **94**, 187003 (2005).

*NSF Grant No. DMR-0352735 supported this work.

**15:06**
**K3 2 Evolution of superconductivity in electron-doped cuprates.***
GIRSH BLUMBERG, *Bell Labs, Lucent Technologies*

The superconducting (SC) phase diagram of the electron-doped cuprates has been explored by Raman spectroscopy as a function of polarization, temperature and magnetic field. The SC gap magnitudes in optimally- and over-doped samples are in agreement with the single particle spectroscopy measurements. An in-gap collective mode has been observed in the $B_{2g}$ channel for the under-doped samples. The SC coupling strength decreases with increasing Ce concentrations from the strong- coupling regime for the under-doped sample to a weak-coupling at optimal doping and beyond. The persistence of SC coherence peaks in the $B_{2g}$ channel for all dopings implies that superconductivity is mainly governed by interactions in the vicinity of $(\pm \pi/2a, \pm \pi/2a)$ regions of the Brillouin zone (BZ). Well- defined SC coherence peaks in the $B_{1g}$ channel occur for optimally-doped samples and this implies that the electron-like carriers near the $(\pm \pi/a, \pm \pi/4a)$ and $(\pm \pi/4a, \pm \pi/a)$ regions of the BZ are also gapped at this doping. Low energy scattering below the SC coherence peak energies for all dopings and Raman symmetries is due to nodal QPs. However, the order parameter is more complicated than a simple monotonic $d_{x^2-y^2}$. We have studied the field and temperature dependence of the SC gap magnitude and the integrated intensity of the $2\Delta$ coherence peaks and extract an effective upper critical field line $H^*_{c2}(T,x)$ at which the superfluid stiffness vanishes. The field dependence of the measured SC gap reveals an estimate of $H^{2\Delta}_{c2}(T,x)$, an upper critical field at which the SC amplitude is suppressed by field. For optimally-doped samples, the field effectively suppresses the superfluid stiffness while the SC amplitude survives higher fields suggesting a phase fluctuation regime for these samples.

*Work done in collaboration with M. M. Qazilbash, A. Koitzsch, B. S. Dennis, C. A. Kendziora, and R. L. Greene

**15:42**
**K3 3 Recent Photoemission Results for the Electron-Doped Superconductors.**
TAKASHI TAKAHASHI, *Tohoku University*

Recent improvement in the energy and angular resolution of angle-resolved photoemission spectroscopy (ARPES) enabled us to investigate the detailed electronic structure in electron-doped high-temperature superconductors (HTSC), which have a relatively smaller energy-scale of superconductivity compared to hole-doped systems. In this talk, we report our recent ARPES results[1,2] focusing on the many-body interaction and the superconducting-gap symmetry in electron-doped HTSC. We have performed high-resolution ARPES measurements on $Nd_{2-x}Ce_xCuO_4$ and observed that the quasiparticle (QP) effective mass around o$\pi$sg_p is strongly enhanced due to opening of an antiferromagnetic (AF) pseudogap. Both the QP effective mass and the AF pseudogap are strongly anisotropic with the largest magnitude near the hot spot, which is defined as an intersection point of the Fermi surface and the AF zone boundary. Temperature-dependent measurements have revealed that the AF pseudogap survives at temperatures much higher than $T_N$ (Néel temperature), possibly due to the short-range AF correlation remaining even above $T_N$. The AF pseudogap gradually decreases with doping and is abruptly filled up near the boundary between the AF and superconducting phases. To study the anisotropy of superconducting gap in electron-doped HTSC, we have performed high-resolution ARPES on $Pr_{0.89}LaCe_{0.11}CuO_4$. We observed that the momentum dependence of superconducting gap is basically consistent with the $d_x2_{-y}2$–wave symmetry, but it obviously deviates from the simple $d_x2_{-y}2$ gap function. The maximum superconducting gap is not observed at the zone boundary as expected from the simple $d_x2_{-y}2$ gap symmetry, but it is located around the hot spot where electrons are thought to be strongly coupled to the AF spin fluctuation. All these ARPES results suggest that the electronic stricture and the superconducting behavior are strongly dominated by the AF interaction in electron-doped HTSC. 1) H. Matsui, K. Terashima, T. Sato, T. Takahashi, S.-C. Wang, H.-B. Yang, H. Ding, T. Uefuji, and K. Yamada, Phys. Rev. Lett. **94** (2005) 047005. 2) H. Matsui, K. Terashima, T. Sato, T. Takahashi, M. Fujita and K. Yamada, Phys. Rev. Lett. **95** (2005) 017003.



**16:18**
**K3 4 Recent Magnetic Neutron Scattering Experiments on the Electron-Doped Superconductor $Nd_{2-x}Cu_xCuO_4$.**
EUGENE MOTOYAMA, *Stanford University*

The study of the fascinating properties of the high-$T_c$ superconductors has arguably been one of the most important themes in physics during the past two decades. One of the fundamental issues in this quest is the investigation of the different roles of hole vs. electron doping of the Mott insulator parent compounds in order to attain superconductivity. While the vast majority of experimental studies has focused on the properties of the hole-doped materials, there has been renewed interest in the electron-doped side of the of the high-$T_c$ phase diagram. We present recent magnetic neutron scattering experiments on the prototypical compound $Nd_{2-x}Ce_xCuO_4$. Our work takes advantage of the fact that the upper critical field is relatively small for the electron-doped materials, and it provides new insight into the connection between antiferromagnetism and superconductivity. Among our new findings are a linear magnetic field effect on the superconducting magnetic gap and the evolution of the instantaneous spin correlations from the antiferromagnetic to the superconducting phase.

**16:54**
**K3 5 New Class of T'-structure Cuprate Superconductors.***
MICHIO NAITO, *Tokyo University of Agriculture and Technology (TUAT)*

High-temperature superconductivity has been discovered in $La_{2-x}Ba_xCuO_4$ that derives from the undoped mother compound $La_2CuO_4$ crystallizing in the $K_2NiF_4$ (so-called $T$) structure with oxygen octahedra surrounding the copper ions. It has been common sense that high-temperature superconductivity develops upon doping such an antiferromagnetic Mott-insulator with charge carriers. $La_2CuO_4$ is also the basis of the electron-doped cuprate superconductors of the form $La_{2-x}Ce_xCuO_{4+y}$, which however crystallize in the $Nd_2CuO_4$ ($T'$) structure without apical oxygen above or below the copper ions of the $CuO_2$-plane. Due to the vicinity to the structural phase transition into the $T$-structure the study of the undoped or low doped mother compound with $T'$-structure is difficult. However, using the itisovalent substituents Y, Sm, Eu, Gd, Tb, or Lu for La, nominally undoped $La_2CuO_4$ can be synthesized by molecular beam epitaxy in the $T'$-structure. The surprising result is that all these nominally itundoped $T'$-compounds are itsuperconductors with fairly high critical temperatures over 20 K. This suggests a phase diagram for this new class of electron doped cuprates, in which the Mott-insulating, antiferromagnetic ground state is not obtained.

*This work has been performed in collaboration with Akio Tsukada (TUAT), Yoshi Krockenberger (MPI), Masumi Noda (NTT), Hideki Yamamoto (NTT), Dirk Manske (MPI) and Lambert Alff (Darmstadt University of Technology).

**SESSION K4: DMP/CSWP PRIZE SYMPOSIUM**
**Tuesday Afternoon, 14 March 2006; 308, Baltimore Convention Center at 14:30**
**Lynn Boatner, Oak Ridge National Laboratory, presiding**

**14:30**
**K4 1 Nanocrystals, Nanowires and the Role of Quantum Confinement.***
JAMES CHELIKOWSKY, *University of Texas at Austin*

One of the most challenging issues in materials physics is to predict the properties of matter at the nanoscale. In this size regime, new structural and electronic properties exist that resemble neither the atomic, nor solid state. By changing the size of the system, inherently intensive properties become extensive properties, which can be strongly altered from the macroscopic limit. Such properties can have profound technological implications, e.g., at small length scales a poor optical material like silicon can be converted to an optically active one. Unfortunately, the development of theoretical methods to predict the properties of these systems is formidable challenge. Nanoscale systems may contain thousands of electrons and atoms, and often possess little symmetry. I will illustrate some recent advances in this area based on methods that are designed to exploit high performance computational platforms. I will present real space pseudopotential techniques for solving the electronic structure problem within density functional theory (see http://www.ices.utexas.edu/parsec). I will apply these techniques to systems ranging from clusters of a few dozen atoms to systems containing over a thousand atoms. I will present predictions for the structural and electronic properties of semiconductor nanowires and nanocrystals, intrinsic and doped, and will resolve some outstanding issues in the literature.

*Supported by the NSF (DMR-0551195) and DOE (DE-FG02-03ER25585 and -03ER15491)



**15:06**
**K4 2 Near-field intensity correlations in metal-dielectric nano-composites.**
HUI CAO, *Northwestern University*

Spatial correlations of field and intensity are indicative of the nature of wave transport in random media and have been widely investigated in the context of electromagnetic wave propagation in disordered dielectric systems However, less is known of near-field intensity correlations in metallic random systems, which can exhibit rich phenomena due the involvement of intrinsic resonance effects-surface plasmons. Neither is clear the difference between correlation functions in metallic and dielectric systems. This paper presents the first experimental study of near-field intensity correlations in metal-dielectric systems in regimes where localization and delocalization are expected. Significant differences are observed between the spatial intensity correlations functions in metal-dielectric systems and those of purely dielectric random media. In disordered metallic nanostructures, surface plasmon modes are governed by the structural properties of the system and may be strongly localized. Recent theoretical studies of metallic nanoparticle aggregates suggest that the eigenmodes of such systems may have properties of both localized and delocalized states. However, it is not clear how such eigenmodes impact the propagation or localization of surface plasmon polaritons excited by impinging light, an issue addressed in this study. In the current experiment, the concentration of metal particles on a dielectric surface $p$ was varied over a wide range to control the amount of scattering. Spatial intensity correlations obtained from near-field optical microscopy (NSOM) images show a transition from propagation to localization and back to propagation of optical excitations in planar random metal-dielectric systems with increase in metal filling fraction.

**15:42**
**K4 3 Carbon Nanotubes: Recent Results and Directions.**
HONGJIE DAI, *Stanford University*

This talk will present our latest research on single walled carbon nanotubes. We have been using carbon nanotube as a model system to study interesting nanoscale problems concerning materials synthesis, solid-state physics and devices, surface science and nanobiotechnology. This presentation will cover our latest results in, (1) Controlled synthesis of nanotube structures on surfaces. (2) Coherent quantum electron transport and diffusive electron-phonon scattering phenomena in suspended nanotubes. (3) Pushing the performance limit of nanotube transistors, and (4) interfacing carbon nanotubes with biological systems including living cells.

**16:18**
**K4 4 Exploiting the unique electronic and mechanical properties of carbon and boron nitride nanotubes.**
ALEX ZETTL, *University of California at Berkeley*

Carbon and boron nitride nanotubes have unusual geometrical features that affect their electronic, thermal, and mechanical properties. I will discuss relevant experimental studies of the underlying physics, as well as possible applications including sensors, nanoscale electric motors, high frequency tunable resonators, and phonon waveguides.

**SESSION K5: MICROELECTRONICS FOR MID-INFRARED THROUGH TERAHERTZ**
**Tuesday Afternoon, 14 March 2006; 309, Baltimore Convention Center at 14:30**
**Mark Lee, Sandia National Laboratories, presiding**

**14:30**
**K5 1 Multi-Wavelength and Nonlinear Quantum Cascade Lasers.**
CLAIRE GMACHL, *Princeton University*

Quantum Cascade (QC) lasers are a rapidly evolving mid-infrared technology well suited for chemical sensing applications. For sensing of trace gas mixtures, large molecules, or liquids, probing at a single wavelength is often not sufficient, but the analyte must be sampled at various wavelengths. Here, we will discuss various means of providing multi-wavelength emission from QC lasers. Four different routes are currently being investigated. First, the active waveguide core of a QC laser can be subdivided into substacks of different active regions, hence allowing for multi-wavelength emission. We will discuss the design optimization procedures employed to develop a multi-wavelength laser module with several wavelengths covering the 7 – 13 $\mu$m wavelength range. Second, QC lasers can be designed to emit different wavelength light when operated at different (positive or negative) bias settings. We have recently developed such a QC laser capable of emitting at $\sim$ 8 and $\sim$ 11 $\mu$m. Third, nonlinear QC lasers that in addition to QC laser active regions also include nonlinear mixing regions emit light not only at the fundamental frequency, but also at nonlinear frequencies. Second harmonic generation with up to 2 mW of nonlinear light has recently been demonstrated. Finally, QC lasers with very broad gain spectra can in principle be used to tune over significant wavelength ranges using an external cavity. A key component for such tunability is a low reflectance laser facet to suppress laser action based on feedback from the laser facets. We will show approaches to facet reflection reduction through sub-wavelength facet patterning. This work is supported through collaboration with Pacific Northwest National Labs / Battelle by DARPA L-PAS, the DOE, and the NSF ECS-0400615. This work is being conducted in collaboration with A. Dirisu, S.S. Howard, Z. Liu, O. Malis, G. Shu, D.L. Sivco, and F. Toor.

**15:06**
**K5 2 Ultrasensitive Quantum-Limited Far-Infrared Detectors.***
DANIEL PROBER, *Yale University*

Superconducting tunnel junction (STJ) direct detectors have been developed for submillimeter astronomy. Photons with energy greater than the superconducting gap of the aluminum absorber break Cooper pairs and generate excess quasiparticles, inducing an extra tunneling current through the STJ. To monitor the response of the STJ with large readout bandwidth and maximal sensitivity, we use a novel readout which uses radio frequency (RF) reflectometry, like the readout invented for the RF-SET. (1) For calibration of the detector, we have developed a in-situ, on-chip, hot-cold submillimeter photon source, a gold microbridge. When it is voltage biased, emitted noise from the microbridge couples via a microstripline to the detector. This provides a calibrated photon source with near unity coupling, very fast ( $<$ ns) chopping, and calculable power output. Cooling is by outdiffusion of hot electrons (2). We present recent detection results in the range 100 140 GHz. These demonstrate the expected good responsivity, high sensitivity, and fast response times. The readout approach is easily used with a frequency multiplexed readout, allowing economy of cold electronics. Ultimate sensitivity may require the use of an RF-SET as the readout, for NEP below NEP below $10^{-20}$ W/(Hz)$^{1/2}$. -Research with J.D. Teufel, M. Shen, L. Frunzio, C. M. Wilson, T.J. Stevenson and R.J. Schoelkopf. -(1). R.J. Schoelkopf et al., Science v. 280 p.1238 (1998). -(2). D.E. Prober, Appl. Phys. Lett. v. 62 p.2119 (1993). -(3). D.E. Prober, LTD11 Conf. (2005), invited, to appear.

*Supported by NASA, Goddard SFC, and NSF-AST

**15:42**
**K5 3 Electronically Tunable Terahertz Detection Using Plasmons.**
ERIC SHANER, *Sandia National Labs*

Spectroscopy in the millimeter-wave to THz frequencies has received a great deal of recent interest for security applications and chemical identification. This talk will address detectors that utilize plasmons in high-mobility GaAs/AlGaAs quantum well structures to provide a frequency tunable detector response. While there are various competing detection schemes based on plasmons, here we will cover the grating-gate detector along with a variant having enhanced performance called the split-grating gate detector. The basic device consists of source and drain electrical contacts along with a single grating-gate that spatially modulates both the incident radiation and the carrier density in a quantum well channel. The plasmon frequency underneath the gate lines is tuned by changing the carrier density with an applied gate bias. When this plasmon frequency is in resonance with the incident radiation field, a resonant peak is found in the photoresponse. The split-gate devices work in a similar fashion, except with additional gates in the device used to build larger nonlinearities into the system. By doing so, we have observed a several order of magnitude increase in responsivity. Currently, the grating-gate style of detector covers a frequency range from 150GHz to 800GHz at temperatures ranging

from 4K to 80K, however, the ultimate frequency and temperature limits of these detectors are not currently known. The ability to tune the detector response by simply changing a gate voltage leads to an attractive spectrometer-on-a-chip where no moving parts would be needed for THz spectral analysis. Sandia is a multiprogram laboratory operated by Sandia Corporation, a Lockheed Martin Company, for the United States Department of Energy's National Nuclear Security Administration under contract DE-AC04-94AL85000.

**16:18**
**K5 4 Designing the emission of THz Quantum Cascade Lasers with surface plasmon photonic structures.**
ALESSANDRO TREDICUCCI, *NEST CNR-INFM and Scuola Normale Superiore*

The development of quantum cascade lasers operating at terahertz frequencies is proceeding at a very rapid pace. For their successful practical implementation, specific requirements have now to be addressed, particularly concerning the properties of the emitted radiation. Single-mode THz lasers with distributed feedback resonators have been achieved and a new technique involving surface plasmon gratings has been demonstrated to improve performances. The latter also offers the possibility of constructing distributed Bragg gratings as a replacement for high-reflection coatings or to implement vertical emitting devices. Solutions allowing broad tuneability are examined, either relying on external cavity set-ups or more unconventional external electrical control.

**16:54**
**K5 5 Mid-Infrared Through Terahertz Cameras Based on Superconducting Technology.***
DAN SCHMIDT, *NIST, Boulder*

A new generation of cameras is set to make a tremendous impact on the field of mid-infrared to Terahertz astronomy. Take for example, the SCUBA-II instrument to be deployed on the James Clerk Maxwell Telescope at Mauna Kea, Hawaii. The existing SCUBA instrument has two arrays of 37 and 91 pixels, observing at 850 $\mu$m and 450 $\mu$m. The SCUBA-II arrays have 5120 pixels each and the noise contribution from the detectors is less than the sky load noise. As a result, large regions of the sky can be mapped about 1000 times faster. Superconducting thin film devices play multiple critical roles in these large format arrays. We will discuss the superconducting detector, multiplexing, and amplifier technology developed at NIST Boulder by the Quantum Sensors Project and the integration all of these technologies into a science grade imaging array. We will also survey the role that superconducting detectors, multiplexers, and thin film refrigerators will play in future instruments at both longer and shorter wavelengths.

*Quantum Sensors Project: Jim Beall, Randy Doriese, Will Duncan, Lisa Ferreira, Gene Hilton, Rob Horansky, Kent Irwin, Ben Mates, Nathan Miller, Galen O'Neil, Carl Reintsema, Joel Ullom, Leila Vale, Barry Zink, and Yizi Xu.



**SESSION K6: MINORITIES IN THE NANOSCIENCES**
**Tuesday Afternoon, 14 March 2006; 310, Baltimore Convention Center at 14:30**
**James Dickerson, Vanderbilt University, presiding**

***Invited Papers***

**14:30**
**K6 1 Controlling Carbon Nanotube Quantum Devices.**
NADYA MASON, *University of Illinois at Urbana-Champaign*

The unique properties of nanotubes make them attractive candidates for a variety of quantum devices. We present transport data on nanotube-based quantum devices that demonstrate both one-dimensional physics and quantum-dot behavior. We show how voltages applied to narrow metallic gates can be used to produce localized depletion regions in the underlying tubes. A single depletion region in a nanotube with ohmic contact electrodes creates a quantum point contact, while a pair of depletion regions defines the quantum dot. Local gate voltages tune the conduction through point contacts, the transparencies of tunnel barriers, and electrostatic energies within single and multiple dots. We will show how this full gate control allows us to measure and control quantum phenomena such as quantized conductance steps and ''Honeycomb'' charge stability patterns in nanotube devices.

**15:06**

**K6 2 Dielectrophoretic gating and phase separation of particles for micro- and nano-fluidic biodetection applications.***

CONRAD JAMES, *Sandia National Laboratories*

Performance metrics for biological detection systems are significantly impacted by their ability to separate target analytes from background materials, a process that aids in the elimination of false positives. We report here several implementations of an electro-hydrodynamic technique for separating analytes in nanoliter sample volumes. This technique, AC dielectrophoresis (DEP) accompanied by field-induced phase transitions, includes electric field- and shear-induced phenomena to modify local concentrations of suspended particles. This non-optical separation technique relies upon intrinsic electric polarizability, and thus requires no time-consuming and costly labeling steps. We have demonstrated biological and non-biological particle separation, and both batch-mode and continuous flow configurations have been developed. The dielectrophoretic gating technique has been optimized to produce large electric field gradients ($\nabla E^2 \sim 10^{20} V^2/m^3$) and we are currently applying this technique for particle chaperone preconcentration and nucleic acid purification. For the first application, we have achieved 100x preconcentration factors and high efficiency particle valving with no degradation in flowrate. This technique will prove useful for bead-based assay systems utilizing packed beds or high throughput flow cytometry. In the second application, we have preconcentrated dsDNA target molecules, and shown that preconcentration of false-positive inducing ssDNA reporter oligonucleotides is negligible. This method can be integrated on-chip, providing a significant advantage over conventional off-chip purification technologies such as centrifugation and precipitation. We will also present our results in traveling wave DEP, a technique which utilizes phase-quadrature signals to preconcentrate and transport particles without the use of hydrodynamic forces.

*Sandia is a multiprogram laboratory operated by Sandia Corporation, a Lockheed Martin Company, for the United States Department of Energy under contract DE-AC04-94AL85000.

***Contributed Papers***

**15:42**

**K6 3 Enhanced Physical Properties of Quantum-Confined Europium Sulfide Nanocrystals** MARCELA REDIGOLO, DMITRY S. KOKTYSH, SANDRA J. ROSENTHAL, JAMES H. DICKERSON, *Vanderbilt University* Synthesis and characterization of sub-2.0 nm europium sulfide nanocrystals is presented. Of particular interest is the behavior of the optical, magnetic, and magneto-optical properties as the nanocrystal diameter decreases, approaching the quantum confinement regime. The physical properties of these materials are dominated by 4f ionic transitions, which are affected directly by the nanocrystal size, due to nearest and next-nearest neighbor couplings. We believe that nanocrystal size, surface strain, and surface passivation will enhance the observable physical characteristics of the nanomaterials. To our knowledge, this would be the first evidence of quantum confinement effects in europium chalcogenide nanocrystals. Calculations of the Bohr radii of the 4f transition establish the upper limit on the nanocrystal size that exhibits blue shifts in the fluorescence and, perhaps, enhancements on the magnetic moment ($\mu_{eff}$). Structural properties are characterized by transmission electron microscopy, selected area electron diffraction, and x-ray diffraction. Absorption and photoluminescence spectroscopy measurements also are presented to describe the optical properties of the nanocrystals.

**15:54**

**K6 4 Network Structures in ABC Block Copolymers** THOMAS EPPS, MICHAEL FASOLKA, *NIST, Polymers Division* FRANK BATES, *University of Minnesota* At mesoscopic length scales interfacial curvature and packing geometry often reflect the self-assembly of molecules with prescribed architectures and directed interactions. It is well known that block copolymers microphase separate into periodic structures controlled by interaction parameters, volume fractions, and degree of polymerization. Some of the most promising morphologies in block copolymers are the periodic network phases, which generally have superior mechanical properties when compared to their one- and two-dimensional counterparts. We investigated the phase behavior of linear poly(isoprene-*b*-styrene-*b*-ethylene oxide) (ISO) triblock melts and discovered three triply-periodic networks. Two cubic network phases were found, along with an orthorhombic network in our bulk studies. It is also important to expand knowledge of free and substrate surface energy effects on triblock films, as the greater surface to volume ratio, relative to bulk materials, increases the influence of these parameters on thin film morphologies. To this end, we studied the effects of surface energy on the structure of the same ISO triblocks mentioned above. These films were examined on gradient substrates using AFM and XPS. Surface energy and PI content were found to influence the polymer nanostructures. The results we obtained demonstrate the importance of exploring both the thin film and bulk behavior of polymeric materials.

**16:06**

**K6 5 Local Structure and Photoluminescence Decay Dynamics in Undoped and $Mn^{2+}$ Doped ZnSe Nanoparticles** THADDEUS NORMAN, *Lawrence Livermore National Lab* CHRISTIAN GRANT, *Rutgers University* EDWARD OLANO, *University of California, Santa Cruz* EDWARD CASTNER, *Rutgers University* FRANK BRIDGES, JIN ZHANG, *University of California, Santa Cruz* Undoped and $Mn^{2+}$-doped ZnSe nanoparticles were synthesized from molecular cluster precursors. The nanoparticles were characterized using UV-VIS, PL, ESR, and XAFS. These studies confirmed the presence if $Mn^{2+}$ dopant in the host ZnSe lattice, and suggested the existence of two distinct $Mn^{2+}$ sites in the ZnSe lattice. Energy transfer dynamics in $Mn^{2+}$-doped ZnSe nanoparticles were also studied using time-integrated and time-resolved spectroscopic techniques. Time-resolved picosecond PL and femtosecond transient absorption studies show that the $Mn^{2+}$ doping substantially shortens the lifetimes of both the band-edge excitonic states and the shallow trap states. Energy transfer from ZnSe to $Mn^{2+}$ likely follows two mechanisms: one that involves mediation through trap states and another without.

*Invited Papers*

**16:18**
**K6 6 New Approach Towards Aqueous Functional Nanostructures via Amphiphilic Coordination Networks.**
JUAN NOVERON, *University of Texas at El Paso*

The unprecedented use of designed amphiphiles with coordination- capable head groups that allow for the traditional coordination- directed networks to further self-assemble into nanostructures with novel complexity and function will be presented. With this approach the versatile chemistry of transition metals and the properties that amphiphiles exhibit in aqueous media are combined to generate extraordinary materials with interesting functions such as gene-encapsulation and delivery, drug- delivery vehicles, and hydrogen storage materials.

**16:54**
**K6 7 Effects of interfacial bonds and strain on the formation of InAs/GaSb Self Organized Nanostructures.***
DONNA STOKES, *University of Houston*

Interfacial effects play an important role on the formation of self-organized nanostructures based on the morphological instability of strained semiconductor multilayers. For many III-V systems with a misfit of less than 1%, instability occurs at some critical layer thickness, which is typically large ( $>$ 150 Å). However, for the non-common anion strained system, InAs/GaSb, the instability is observed at a thickness of a few monolayers. In this presentation, the results of a structural analysis by x-ray diffraction of an InAs/GaSb planar and nanowire superlattice grown by molecular beam epitaxy (MBE) with different interfacial bonds will be presented. Cross sectional scanning tunneling microscopy (XSTM) and atomic force microscopy (AFM) were also used to probe the physical structure of the superlattices. The effects of the strain and interfacial bond on the formation of the nanostructures will be discussed as well as how they may be manipulated to control the formation of these nanostructures in this system and other III-V systems. Also presented will be the results from a preliminary analysis of the effects of the nanostructure on the optical properties of the system.

*Co-authors are J.H. Li, O.Caha, S.L. Ammu, J. Bai, K.E. Bassler, J. Wickett and S.C. Moss. We are grateful to the National Science Foundation for support of this work.



**SESSION K7: NEW METHODS AND ALGORITHMS FOR BIOMOLECULAR MODELING**
**Tuesday Afternoon, 14 March 2006; 307, Baltimore Convention Center at 14:30**
**Christopher Roland, North Carolina State University, presiding**

**14:30**
**K7 1 Adaptive Biasing Force Method for Vector Free Energy Calculations.**
ERIC DARVE, *Stanford*

The adaptive biasing force method is an efficient technique to compute the potential of mean force along a reaction coordinate and for alchemical transformations. We present recent developments of the method for vector free energy calculations (i.e. for several reaction coordinates or for multiple alchemical transformations). General formulas are derived and their relative merit is discussed. In particular, many techniques require the ability to calculate second order derivatives and are therefore cumbersome to implement for complex reaction coordinates. We present new formulations requiring first derivatives only. Our approach will be compared with other popular techniques such as metadynamics. Application examples will be provided for simple examples, such as alanine dipeptide, and a more advanced one: the insertion of an amphipathic helix inside a cell membrane. For the latter, we will examine the stability of the inserted peptide relative to the interfacial configuration and its role in the association of individual peptides into larger multimeric structures, such as cellular channels. Our candidate for studies is the synthetic peptide $(LSLLLSL)_3$. It was shown experimentally that, in the presence of an electric field, the orientation changes from parallel to the membrane to perpendicular and the location of the center-of-mass (COM) changes from the membrane surface to the center of the lipid bilayer. Experimental results, however, provide no information about stability of individual helices in the transmembrane orientation. We will present results on the free energy surface of insertion of $(LSLLLSL)_3$ as a function of two coordinates: the distance of the COM of the peptide to the center of the membrane and the orientation of the helix relative to the membrane surface. Our results show that there is a global minimum corresponding to the parallel orientation at the water-membrane interface. The transmembrane arrangement of a single peptide is only metastable, i.e. it corresponds to a local minimum.

**15:06**
**K7 2 New Distributed Multipole Methods for Accurate Electrostatics for Large-Scale Biomolecular Simultations.**
CELESTE SAGUI, *North Carolina State University*

An accurate and numerically efficient treatment of electrostatics is essential for biomolecular simulations, as this stabilizes much of the delicate 3-d structure associated with biomolecules. Currently, force fields such as AMBER and CHARMM assign ''partial charges'' to every atom in a simulation in order to model the interatomic electrostatic forces, so that the calculation of the electrostatics rapidly becomes the computational bottleneck in large-scale simulations. There are two main issues associated with the current treatment of classical electrostatics: (i) how does one eliminate the artifacts associated with the point-charges (e.g., the underdetermined nature of the current RESP fitting procedure for large, flexible molecules) used in the force fields in a physically meaningful way? (ii) how does one efficiently simulate the very costly long-range electrostatic interactions? Recently, we have dealt with both of these challenges as follows. In order to improve the description of the molecular electrostatic potentials (MEPs), a new distributed multipole analysis based on localized functions – Wannier, Boys, and Edminston-Ruedenberg – was introduced, which allows for a first principles calculation of the partial charges and multipoles. Through a suitable generalization of the particle mesh Ewald (PME) and multigrid method, one can treat electrostatic multipoles all the way to hexadecapoles all without prohibitive extra costs. The importance of these methods for large-scale simulations will be discussed, and examplified by simulations from polarizable DNA models.

**15:42**
**K7 3 Flexibility in Biomolecules: Beyond Molecular Dynamics.***
MICHAEL THORPE, *Center for Biological Physics, Arizona State University*

Molecular dynamics is unable to explore the conformations large protein complexes, viral capsids etc. Using Lagrange constraints for covalent bonds, hydrogen bonds, hydrophobic tethers, and van der Waals excluded volumes, Monte Carlo dynamics uses ghost templates to efficiently guide rigid clusters via the flexible joints between them. The generation a new protein conformation typically requires about 100 milliseconds CPU time. Specifically, input from a single X-ray crystallographic structure can generate an ensemble of structures remarkably similar to those observed in NMR. Further applications are pathways for ligand docking, misfolding proteins and viral-capsid swelling. The software used for this work is available either interactively or for downloading via flexweb.asu.edu.

*Work done in collaboration with Stephen Wells, Dan Farrell, Scott Menor and Brandon Hespenheide - see Constrained Geometric Simulation of Diffusive Motion in Proteins, Physical Biology (October 2005).

**16:18**
**K7 4 Enhanced conformational sampling via novel variable transformations and very large time-step molecular dynamics.***
MARK TUCKERMAN, *New York University*

One of the computational grand challenge problems is to develop methodology capable of sampling conformational equilibria in systems with rough energy landscapes. If met, many important problems, most notably protein folding, could be significantly impacted. In this talk, two new approaches for addressing this problem will be presented. First, it will be shown how molecular dynamics can be combined with a novel variable transformation designed to warp configuration space in such a way that barriers are reduced and attractive basins stretched. This method rigorously preserves equilibrium properties while leading to very large enhancements in sampling efficiency. Extensions of this approach to the calculation/exploration of free energy surfaces will be discussed. Next, a new very large time-step molecular dynamics method will be introduced that overcomes the resonances which plague many molecular dynamics algorithms. The performance of the methods is demonstrated on a variety of systems including liquid water, long polymer chains simple protein models, and oligopeptides.

*This work was supported by NSF-EIA-0081307, NSF CHE-0121375, NSF CHE-0310107, the Camille and Henry Dreyfus Foundation (TC-02-012) and an NYU Whitehead Fellowship in Biological and Biomedical Sciences

**16:54**
**K7 5 Reaction Path Reaction path potential for complex biomolecular systems derived from mixed QM/MM methods.***
WEITAO YANG, *Department of Chemistry Duke University*

The reaction path potential (RPP) follows the ideas from the reaction path Hamiltonian of Miller, Handy and Adams for gas phase reactions but is designed specifically for large systems described with QM/MM methods. RPP is an analytical energy expression of the combined QM/MM potential energy along the minimum energy path (J. Chem. Phys. 121, 89, 2004). An expansion around the minimum energy path is made in both the nuclear and the electronic degrees of freedom for the QM subsystem, while the interaction between the QM and MM subsystems is described as the interaction of the

MM charges with polarizable QM charges. The input data for constructing the reaction path potential are energies, frequencies and electron density response properties of the QM subsystem. RPP provides a potential energy surface for rigorous statistical mechanics and mixed quantum/classical reaction dynamics calculations of complex systems, as will be shown for several enzymes. Recent further development in determining QM/MM free energy reaction paths will also be presented.

*In collaboration with Zhenyu Lu, Hao Hu and Steven Burger.

**SESSION K8: FOCUS SESSION: JAMMING IN GLASSES, GRAINS AND GELS II**
**Tuesday Afternoon, 14 March 2006**
**314, Baltimore Convention Center at 14:30**
**Corey O'Hern, Yale University, presiding**

*Contributed Papers*

**14:30**
**K8 1 Mechanisms of Reversible Shear Thickening in Concentrated Colloidal Dispersions** NORMAN WAGNER, *Center for Mol. & Eng. Thermodynamics, Dept. of Chemical Engineering, Univ. Delaware, Newark, DE 19711* Experimental studies on model systems of colloidal and nanoparticles dispersions of spherical, elliptical and plate-like particles, where both rheology and mictrostructure are measured, are summarized and compared to illustrate the salient features of reversible shear thickening in well-defined model systems. Reversible shear thickening is shown to be stress-controlled and a connection between the transition from ''continuous'' to ''discontinuous'' shear thickening and underlying thermodynamic phase transitions (liquid-crystal, and liquid- nematic) is demonstrated. Theoretical models based on particle micromechanics which include lubrication hydrodynamics are shown to successfully predict the onset of reversible shear thickening. Small angle neutron scattering and light scattering measurements indicate the formation of ''hydroclusters'' as the source of the increased viscous dissipation and validate the micromechanical modeling. A comparison is made between reversible shear thickening and jamming in concentrated colloidal and nanoparticles dispersions under shear and extensional flows.

**14:42**
**K8 2 Nature of Strain-Induced Nonlinearity in Filled Rubbers** XIAORONG WANG, *Bridgestone Americas, Center for Research & Technology, Akron, OH 44317* CHRISTOPHER G. ROBERTSON, We present evidence suggesting the existence of an analogy between dynamic strain-induced nonlinearity in modulus of filled rubbers and physics of the glass transition of glass-forming materials and the jamming transition of vibrated granular materials. This analogy stems from the fact that shear strain in dynamic measurements introduce fluctuations in fillers that can be described by an ''effective temperature.'' The nonlinearity in modulus of filled rubbers simply reflects a de-jamming transition of fillers in rubber matrices. Filled rubbers with respect to strain therefore display many unusual phenomena, including the asymmetric kinetics, crossover effects, and the glass-like transitions. In addition, the jamming transition in filled rubbers also behaves as an isoenergetic thermodynamic transition. This evidence suggests that although jamming is kinetic, it may also be thermodynamic in nature. The coexistence of kinetic and thermodynamic descriptors of the jamming transition is analogous to observations of thermoreversible gels. Based on those results, we propose a unified phase diagram for jamming transitions. The significance of the new jamming phase diagram is that it has incorporated variables that are all derivable from Hamiltonians and may facilitate crucial comparisons between theories and experiments. [1]. C. G. Robertson and Xr. Wang, Phys. Rev. Lett. 95, 075703, 2005. [2]. Xr. Wang and C. G. Robertson, Phys. Rev. E 72, 031406, 2005.

**14:54**
**K8 3 Transition rates in the Lennard-Jones binary mixture*** YASHENG YANG, BULBUL CHAKRABORTY, JANÉ KONDEV, *Martin Fisher School of Physics, Brandeis University* The slow relaxation in glass forming liquids approaching the glass transition is often described by the Vogel-Fulcher-Tammann (VFT) equation which predicts a diverging viscosity at a non-zero temperature. The origin of this anomalously slow relaxation is an outstanding problem. Recent work (PRE 70, 060501(R) (2004)) shows that a system will obey the VFT equation near a critical point if the transition rates between different macrostates have an asymmetric form: energy lowering rates depend only on the entropy change and energy raising rates depend only on the energy change. Here we investigate this mechanism for glassy dynamics in the the Lennard-Jones binary mixture (LJBM); a well-known glass former. The transition rates between different inherent structures (local minima of the potential energy) are calculated using the interval-bisection method. We find that the energy lowering transition rates are not temperature-sensitive, while the energy raising ones depend on the temperature. The dynamics in the IS energy space is however, non Markovian. We discuss these findings in light of the proposed mechanism for glassy relaxation characterized by a VFT form.

*This work has been supported by NSF-DMR-0207106. JK is a Cotrell Scholar of Research Corporation.

*Invited Papers*

**15:06**
**K8 4 Pushing on colloids: How a gel can stress a glass.**
DANIEL BLAIR, *Harvard University*

We employ a novel technique to for the application of external mechanical and osmotic stress on dense suspensions of colloidal particles. Thermally expandable NIPA hydrogels are used to confine a sediment of colloidal particles. By allowing the gel to expand up to ten times it's initial volume, we dramatically compress the sediment. Using laser

scanning confocal microscopy, we directly measure the effects of increased stress on the properties of a colloidal hard sphere suspensions. We observe the appearance of heterogeneities as the particles are pushed together. We will present results on the analysis of the local volume and dynamical properties of these heterogeneities and postulate their equivalence to characteristic features of analogous systems near their jamming transition.

*Contributed Papers*

**15:42**

**K8 5 Microscopic dynamics of recovery in sheared concentrated depletion gels** R. L. LEHENY, B. CHUNG, R. BANDYOPADHYAY, D. LIANG, *Johns Hopkins U.* S. RAMAKRISHNAN, C. F. ZUKOSKI, *UIUC* J. L. HARDEN, *U. of Ottawa* We describe x-ray photon correlation spectroscopy and diffusing wave spectroscopy investigations of concentrated depletion gels formed from nanoscale silica colloids in solutions of nonabsorbing polymer. The experiments track the changing microscopic dynamics as these jammed, nonergodic systems recover following the cessation of large shear. The two techniques provide a quantitatively coherent picture of the dynamics as ballistic or convective motion of colloidal clusters whose internal motion is arrested. While the evolution of the dynamics possesses features characteristic of nonergodic soft solids, including a characteristic relaxation time that grows linearly with the time since cessation of shear, comparison with the behavior of quenched supercooled liquids indicates the dynamics are not directly related to traditional aging and rejuvenation phenomena in glasses.

**15:54**

**K8 6 Local Disturbances of Binary Colloidal Glass Systems** BENJAMIN BLUTH, *Emory University* PIOTR HABDAS, *St. Joseph's University* ERIC R. WEEKS, *Emory University* We look at local disturbances in colloidal systems as they approach the glass transition. A colloidal system is a fluid filled with microscopic particles which can serve as a model for the atoms of a glass. When the concentration of these particles becomes sufficiently large the particles can no longer move. This is the point which we refer to as the glass transition. We study systems at concentrations just below the glass transition by ''pulling'' a magnetic bead through the sample using an external magnetic field. In our samples there are particles of two distinct sizes that have been dyed such that they fluoresce at different wavelengths. This allows the microscope to differentiate between the two sizes and gives us the ability to isolate and analyze their respective motions independently. From this we examine the motion of the surrounding colloids as the magnetic bead is pulled through the sample, and characterize the behavior as the glass transition is approached.

**16:06**

**K8 7 Polymer Statics and Dynamics in Confined Geometries** JOSHUA KALB, BULBUL CHAKRABORTY, *Brandeis University* Current work on biological systems and glass forming polymers (JCP 106, 6176 (1997)) has led to an interest in the study of single polymer systems. The main questions concern relaxation phenomena and the shape adopted by single polymers under hard and soft boundaries. Little is known about the possibility of inducing a glass transition through pure dimensional confinement. We are concerned with whether or not there is a critical value of the confining length scale. Both structure and relaxation can be described using scaling arguments and tested with Monte Carlo simulations using the bond-fluctuation algorithm (Macromolecules 21,2819 (1988)), which uses a lattice representation of the polymer chain with excluded volume effects. We look at the effects of confinement on a itsingle polymer chain by measuring quantities such as the magnitude end-to-end vector, the radius of gyration, and single monomer motion (JACS 124, 20 (2004)). A primary question is whether the self-avoidance constraint manifests itself in a manner similar to kinetically constrained models of the glass transition. Understanding how these quantities change with various confining geometries will lead to a deeper understanding of biological structures and glass formation. Work supported by NSF-DMR 0403997.

**16:18**

**K8 8 Nonlinear behavior of a driven probe in a colloidal suspension near the Glass Transition.** JASON HAY, *Emory University* PIOTR HABDAS, *St. Joseph's University* ERIC R. WEEKS, *Emory University* By applying a force to isolated microscopic magnetic particles embedded in a PMMA colloidal suspension a nonlinear relationship between the applied force and the measured velocity was measured with the assistance of a confocal microscope. Over short time scales it is possible to observe a threshold force, below which no apparent motion is detected. The value of this threshold force is highly dependent upon the concentration of the sample. At stronger forces, the velocity of a driven magnetic particle displays a power law dependence upon the applied force. In particular, the behavior becomes increasingly nonlinear as the concentration is raised toward the colloidal glass transition point. This behavior was consistent across numerous samples with different concentrations and a varying size ratio of PMMA to magnetic particle.

**16:30 Bordeaux 1**

**K8 9 Yielding in concentrated emulsions** ANNIE COLIN, *LOF Université Bordeaux 1* SÉBASTIEN MANNEVILLE, *CRPP* LYDIANE BECU, *CRPP* We studied the non linear rheological response of two kinds of soft glassy materials: direct concentrated emulsions with and without a short range interparticle attraction induced by adding surfactant. Using high frequency ultrasonic velocimetry, the velocity profiles in a Couette cell are recorded simultaneously to the global rheological data during start up experiments. Under applied shear rate in the vicinity of the yielding transition, the gel ie the adhesive emulsion separates into a liquid state sheared rapidly at a rate higher than a substantial critical shear rate and a static solid region. The static region disappears at high shear rate. On the contrary, the glass ie the non adhesive emulsions flows homogeneously. Below the yield stress the emulsions remains solid like whereas above it becomes liquid like. Under applied shear rate no coexisting states between a liquid like phase and a solid like phase are evidenced. Our data point out that ''glass'' and ''gel'' flow differently in the vicinity of the yielding transition suggesting that the involved mechanisms are not universal.

**16:42**

**K8 10 Numerical studies of two-dimensional *k*-core percolation** ANDREA LIU, *University of Pennsylvania* LINCOLN CHAYES, *UCLA* JEN SCHWARZ, *Syracuse University* The disconnected-connected phase transition in *uncorrelated* percolation has long been known to exhibit a continuous phase transition.

Is this property retained when *correlations* between occupied sites are incorporated into percolation? An example of such a model is *k*-core percolation. In *k*-core percolation a constraint is introduced where a site can remain occupied only if it has at least *k* occupied neighbors; otherwise it is removed from the lattice. The mean field *k*-core transition is random first-order (or hybrid). What then is the nature of the *k*-core transition in finite-dimensions? We show numerical evidence for a hybrid transition in two-dimensions for a variant of *k*-core where there is an additional constraint of pseudo-force-balance. Using finite-size scaling analysis we demonstrate that there is a jump in the usual order parameter at the transition along with, not one, but two, diverging correlation length exponents, neither of which scale as 1/2 (or 1). This model may have some implications for the jamming transition.

**16:54**
**K8 11 Generic rugged landscapes under strain and the possibility of rejuvenation in glasses** DANIEL LACKS, BRITTANY ISNER, *Case Western Reserve Universty* A strain-dependent random landscape model shows that many aspects of the mechanical response of disordered materials are universal, and arise from the rugged nature of the energy landscape. Simulations with this model demonstrate that states produced by mechanical deformation will generally be distinct from the states traversed during thermal aging. This behavior is a generic consequence of a rugged energy landscape, and is independent of any specific microstructure of the material. Thus, mechanical deformation does not literally ''rejuvenate'' a material, although the states produced by mechanical deformation may in some ways resemble less aged systems.

**17:06**
**K8 12 The frequency distribution of mechanically stable packings** GUO-JIE GAO, JERZY BLAWZDZIEWICZ, COREY O'HERN, *Yale University* We generate mechanically stable packings of soft particles in 2D using an algorithm in which we successively grow or shrink purely repulsive grains and minimize the total energy at each step until particles are just at contact and at rest. We focus on small systems of up to 20 particles, and thus we are able to enumerate nearly all of the possible mechanically stable packings. Complete enumeration allows us to factorize the probability distribution, $P(\phi)$, for obtaining a mechanically stable state at packing fraction $\phi$ into algorithm-dependent and independent contributions, $\beta(\phi)$ and $\rho(\phi)$. $\rho(\phi)$ is the probability density to obtain a distinct mechanically stable packing at $\phi$, while $\beta(\phi)$ is the frequency with which each distinct state occurs. We found several remarkable features of the frequency distribution. For example, the frequency averaged over bins of width $d\phi$ grows exponentially with increasing packing fraction. In addition, distinct mechanically stable packings within $d\phi$ can occur with frequencies that differ by orders of magnitude. We also add thermal fluctuations to these stable configurations to understand the relationship between the frequency and shape of the potential landscape near the stable configurations.

**17:18**
**K8 13 Collision Times and Stress Distributions in Mono and Polydisperse Granular Flows** JOHN DROZD, *University of Western Ontario* COLIN DENNISTON, *University of Western Ontario* We investigate, using simulations, collision times and stress distributions in two and three-dimensional steady-state granular matter in jammed versus diffuse flows. We find that the level of order or disorder in the grains dictates values of collision time power-laws. This observation is consistent in both two and three dimensions. We compare our simulations to experimental results.



## SESSION K10: FOCUS SESSION: FRONTIERS IN COMPUTATIONAL CHEMICAL PHYSICS II

**Tuesday Afternoon, 14 March 2006; 302, Baltimore Convention Center at 14:30**
**Rigoberto Hernandez, Georgia Tech, presiding**

***Invited Papers***

**14:30**
**K10 1 First-principles statistical mechanics for heterogeneous catalysis.**
KARSTEN REUTER, *Fritz-Haber-Institut, Faradayweg 4-6, D-14195 Berlin*

We present a first-principles approach to heterogeneous catalysis that quantitatively describes the activity over a wide range of realistic environmental situations of varying temperatures and pressures. Within a first-principles statistical mechanics setup [1], density-functional theory is first used together with transition state theory to accurately obtain the energetics of all relevant processes. Subsequently the statistical mechanics problem is solved by kinetic Monte Carlo simulations. This two-step approach enables us to gain microscopic insight into the system, following its full dynamics from picoseconds up to seconds and explicitly considering the detailed statistical interplay of all elementary processes, i.e., by fully accounting for the correlations, fluctuations and spatial distributions of the chemicals at the catalyst surface. In the application to CO oxidation at a $RuO_2(110)$ model catalyst, we compute the composition and structure of the catalyst surface in reactive environments ranging from ultra- high vacuum to technologically relevant conditions with pressures of the order of atmospheres and elevated temperatures [2]. For all these conditions the obtained conversion rates are in unprecedented quantitative agreement with existing experimental data. The catalytic activity is narrowly peaked in environments, where the surface kinetics builds a disordered and dynamic adsorbate composition at the surface. In the full concert of the large number of processes occurring in this active state, the chemical reaction with the most favorable energy barrier contributes only little to the overall $CO_2$ production. [1] K. Reuter, D. Frenkel, and M. Scheffler, Phys. Rev. Lett. 93, 116105 (2004). [2] K. Reuter and M. Scheffler, Phys. Rev. B, submitted.

*Contributed Papers*

**15:06**

**K10 2 Kinetics and equilibrium properties of supercooled salt solutions in contact with ice and water vapor** MARCELO CARIGNANO, PAUL SHEPSON, IGAL SZLEIFER, *Purdue University* The kinetics of ice growth from salt solutions and the final equilibium systems are studied by Molecular Dynamics simulations. Two systems are investigated. In one a liquid layer of supercooled salt solution is sourronded by ice walls. In the other, the liquid layer is in contact with an ice block on one side and water vapor on the other side. We found that the kinetics of ice growth in both cases is slower than the corresponding system with no ions. A faster ice growth is obserbed on the prismatic plane than on the basal plane of the ice. In the cases where complete freezing is achieved, the final systems have all the ions participating in cluster formations. In the system with water/vapor interface, complete freezing is not reached, leaving the ions solvated in a quasi liquid layer. The density profiles of the ions show their preference to be closer to the water/ice interface than to the water/vapor interface. The simulations enable the understanding of the mechanisms for ice formation under different solution conditions, and the final equilibrium properties of the studied systems.

**15:18**

**K10 3 Thermodynamic and Kinetic differences between solid superheating and liquid supercooling** XIAN-MING BAI, MO LI, *School of Materials Science and Engineering, Georgia Institute of Technology* When surface melting is properly suppressed, a solid can be heated above its melting temperature, which is called superheating. Although many explanations were proposed for solid superheating in the past century, its nature and extent still remain veiled. It is commonly assumed that solid superheating is a reverse process of liquid supercooling. The classical nucleation theory was directly applied to estimate the liquid nucleation rate and the upper limit of superheating despite the lack of decisive test of this analogy. Here we present our investigation of the thermodynamic and kinetic differences between superheating and supercooling via molecular-dynamics simulations. It is shown that the large elastic energy associated with internal melting and solid-liquid interface disorder play important roles in superheating. The growth rate is anisotropic for supercooling, but isotropic for superheating. Supercooling can be well described by the classical nucleation theory, whereas superheating shows many exceptions. The underlying mechanisms for these differences are discussed.

**15:30**

**K10 4 Why does 5-mthyl-2-pyrimidinone fluoresce? An ab initio study of the photophysics of a fluorescent DNA pyrimidine analog.** KURT KISTLER, SPIRIDOULA MATSIKA, *member* The photophysical properties of gas phase 5-methyl-2-pyrimidinone, a fluorescent DNA/RNA pyrimidine analog, have been calculated using multi-reference configuration-interaction with three levels of dynamical electron correlation included. The bright state at vertical excitation is $S_2$ ($\pi\pi^*$) at 4.42 eV. An $S_1$-$S_2$ seam originates close to vertical, and a gradient pathway from this seam leads to a global minimum on the $S_1$ surface. A conical intersection between $S_1$ and $S_0$ (itci01) was found, but all levels of theory show that this conical intersection is significantly higher than the minimum, supporting fluorescence from $S_1$. The details for this energetic inaccessibility, and the emission energy calculated (2.36 - 2.75 eV), depend on the level of theory used. Pathways along the $S_1$ surface when no dynamical or intermediate dynamical correlation is included show a small barrier along with a second minimum in the $S_1$ path from vertical to ci01. When higher level of correlation is included ( $\sim$ 130,000,000 configurations) the barrier vanishes, the secondary minimum becomes global, the energy of ci01 increases, and the fluorescence energy becomes closer to experimental. Thus the importance of dynamical correlation when studying the photophysics of the DNA/RNA bases theoretically is underscored.

**15:42**

**K10 5 Interactions between nanoparticles in supercritical fluids** SERGEI EGOROV, *University of Virginia* This talk presents a theoretical study of interactions between sterically stabilized spherical nanoparticles in a supercritical solvent. The theory is used to analyze the effect of particle size, solvent density, and solvent-ligand interaction strength on the potential of mean force between the particles. Experimentally observed size- selective precipitation of nanoparticles is rationalized in terms of the behavior of the density profiles of stabilizing ligands as a function of particle size and solvent thermodynamic conditions. The theory yields the same general trends as observed in experiments, namely, an increased stability of nanoparticle dispersions at higher solvent densities and for smaller particle sizes.

**15:54**

**K10 6 Effects of co-adsorbed C and K on energetics of CO oxidation on Pd(111)*** FAISAL MEHMOOD, SERGEY STOLBOV, TALAT S. RAHMAN, *Department of Physics, Kansas State University, Manhattan, KS 66506* In the course of catalytic oxidation of CO, carbon may atomically adsorb on catalyst surface and change (presumably poison) its reactivity. On the other hand, the reactivity of many catalysts is enhanced upon alkali co-adsorption. To gain insight into the nature of these effects, we carried out ab initio electronic structure calculations based on density functional theory with the generalized gradient approximation. The energetics and reaction pathways for CO oxidation on the clean Pd(111) and on Pd(111) co-adsorbed with C or K are calculated. We find that even at coverages as small as 1/12 ML, co-adsorbed C increases the activation energy barrier for the reaction by 20%, while K reduces it by 10%. This clearly shows the role of K as a promoter and C as a poison for this catalytic reaction. To understand the microscopic mechanism of these phenomena, we analyze the effects of the co-adsorbate coverage and the CO — co-adsorbate distance on the activation energy barriers and the local densities of electronic states and valence charge densities calculated for the initial and transition states of the reaction.

*We acknowledge financial support from DOE under grant No. DE-FGO3-03ER15445, NSF under grant No. CHE-0205064 and computational resources provided by NSF Cyberinfrastructure and TeraGrid grant No. DMR050039N.

**16:06**

**K10 7 Parallel Temperature-Accelerated Dynamics Simulations of Epitaxial Growth*** Y. SHIM, J. G. AMAR, *University of Toledo* B. P. UBERUAGA, A. F. VOTER, *Los Alamos National Laboratory* The temperature-accelerated dynamics (TAD) method is a powerful tool for carrying out non-equilibrium simulations of systems with infrequent events over extended timescales. However, since the computational time for a typical TAD simulation

increases rapidly with the number of atoms $N$, TAD simulations have so far been limited to relatively small system sizes. By applying a recently proposed synchronous sublattice algorithm to parallel TAD simulations, we have been able to simulate the evolution of systems over much larger length- as well as time-scales. As a first test of our method, we have carried out simulations of the surface diffusion of Cu atoms on the Cu(100) surface. In contrast to serial TAD simulations for which the computational time scales as $N^{2.5} - N^3$, in our parallel TAD simulations the computational time scales as $log(N)$ and may even be independent of $N$ for larger system sizes. In particular we find that for intermediate size systems our parallel TAD simulations are several orders of magnitude faster than the corresponding serial TAD simulations. Preliminary results for low-temperature multilayer Cu/Cu(100) growth obtained using parallel TAD simulations are also presented.

*Supported by NSF DMR-0219328 and CCF-0428826

**16:18**

**K10 8 Hydration and Dewetting near Fluorinated Superhydrophobic Plates** RUHONG ZHOU, XIN LI, JINGYUAN LI, MARIA ELEFTHERIOU, The water dynamics near a nanoscale fluorinated ($CF_3(CF_2)_7(CH_2)_2SiH_3$) surface as well as the possible dewetting (water drying) transition within two such superhydrophobic surfaces (plates) have been studied with molecular dynamics simulations. A partial water dewetting with an expansion of approximately 7-8Å and a water density $\sim$ 20% lower than the bulk is found near the single superhydrophobic surface. More remarkably, a strong dewetting transition is found in the inter-plate region for the double plates with a critical distance $D_c$ up to 10Å (3-4 water diameters). This transition, although occurring on a microscopic length scale, is reminiscent of a first order phase transition from liquid to vapor. Furthermore, simulation results show that the fluorinated carbons are more hydrophobic than their hydrogenated counterparts (with $D_c = 8.0$Å) in terms of the dewetting transition critical distance, despite their much larger partial charges and dipoles. The unusual superhydrophobicity of fluorocarbons is found to be related to their larger surface areas, while the intrinsic hydrophobicity is roughly the same for both fluorocarbons and hydrocarbons based on a detailed water-plate interaction energy profiling. Somewhat surprisingly, we find that even though the electrostatic energies do contribute slightly more in the fluorocarbon plates than the hydrocarbon plates, the van der Waals energies dominate the water-plate interactions (with more than 90% contributions for close shells) and they contribute almost the same in both plates.

**16:30**

**K10 9 Metastable States and Population Dynamics in the Linkage Isomer Compound Sodium-nitro-prusside** BERNARD DELLEY, JÜRG SCHEFER, *Paul Scherrer Institut Switzerland* DOMINIK SCHANIEL, THEO WOIKE, *U. Cologne* Two long-lived metastable states S1 and S2 can be produced in $Na_2$ $[Fe(CN)_5NO]2H_2O$ by illumination with light in the spectral range 380-580 nm. Local minima in the ground state energy hypersurface as given by density functional theory are in agreement with the linkage isomerism model. We identify S2 with a side on bonded NO configuration and S1 with an inverted one. We have shown that that thermal properties, vibrational spectrum, optical properties and the Mossbauer spectrum are predicted in agreement with experiment. We find that the crystal model gives a significantly improved account of spectral differences between the ground and S1 state as compared to the free anion model. On the basis of the energy surfaces we estimate thermal depopulation rates and explore the dynamics of direct population of S1 induced by blue light.

**16:42**

**K10 10 Effect of the substrate-adsorbate coupling on the dispersion of phonons of CO on Cu(001).*** TALAT S. RAHMAN, *Kansas State University* KLAUS PETER BOHNEN, *Forschungzentrum Karlsruhe* MARISOL ALCANTARA ORTIGOZA, *Kansas State University* In order to understand the effect of the substrate on the dynamics of the adsorbate we have carried out first principle calculations of the dispersion of phonons of the c(2x2) CO overlayer on Cu(001) based on the Density Functional Theory, using ultrasoft pseudopotentials and the PBE-GGA approximation for the exchange-correlation energy. Comparing with frozen-substrate calculation, at the gamma point, we found that the frequencies of the C-O stretch mode, $\nu 1$, and the adsorbate-substrate stretch mode, $\nu 2$, are almost independent of the substrate. However, while $\nu 2$ is dispersionless, $\nu 1$ presents a 10 meV dispersion at the M-point. The frustrated translation and frustrated rotation modes present a dispersion of less than 5 meV, nevertheless having the frustrated translation mode such a low energy a $\sim$ 1 meV dispersion is rather considerable. Moreover, Helium atom scattering studies of this mode found that it splits into two branches everywhere other than the $\Gamma$ point; they attributed one branch to the frustrated translation mode of a perfect c(2x2) CO overlayer, and the other one to defects in the same. Here we show that the splitting is an intrinsic feature of the perfect c(2x2) CO overlayer.

*DOE under grant No. DE-FG03-ER15445 and NSF under grant No. CHE-0205064

**16:54**

**K10 11 Theory of Electronic Structure and Nuclear Quadrupole Interactions in the BF3-NH3 Complex** R.H. PINK, DIP N. MAHATO, M.B. HUANG, T.P. DAS,* *SUNY Albany* ARCHANA DUBEY, LEE CHOW, *UCF Orlando* MAHENDRA K. MAHANTI, *NEHU Shillong, India* R.H. SCHEICHER, *MTU Houghton* Boron Trifluoride is widely used as a catalyst in chemical research and industry forming complexes in the process with other molecules like $NH_3$, $H_2O$, and $CH_3OH$. We have studied the $BF_3$-$NH_3$ molecular complex using Hartree-Fock procedure combined with many-body perturbation theory. The B-N bond is found to involve about 75% covalent and 25% van der Waals characters. The calculated geometry of the complex compares well with experimental results. The nuclear quadrupole interaction parameters for the $^{19}F$* nucleus [1] show good agreement with experiment for both solid $BF_3$ and the complex including the nuclear quadrupole coupling constants and the sizable asymmetry parameters. The $^{11}B$ quadrupole coupling constant is however found to be about 1.5 times the available experimental value [2] for solid $BF_3$, possibly

due to the influence of intermolecular bonding. [1] K. Bertholdt et al. J. Mol. Struct. 192, 199 (1989) [2] P.A. Casabella and T. Oja J. Chem. Phys. 50, 4814 (1969).

*Also UCF Orlando

**17:06**
**K10 12 Theory of Nuclear Quadrupole Interaction in Trifluoro-Aminoboranes [$BF_3$-$NH_{3-X}(CH_3)_X$]** MAHENDRA K. MAHANTI, *NEHU Shillong, India* ARCHANA DUBEY, H.P. SAHA, LEE CHOW, *UCF Orlando* R.H. SCHEICHER, *MTU Houghton* R.H. PINK, DIP N. MAHATO, M.B. HUANG, T.P. DAS,* *SUNY Albany* The understanding of the catalytic properties of $BF_3$ of great current interest require information about the electronic structures of the associated complexes of $BF_3$ with the molecules involved in the process. In this work we have studied the corresponding complexes for methylamines using the Hartree-Fock procedure combined with many-body perturbation theory. Results will be presented for the natures of the three complexes and the $^{19}F$* quadrupole coupling constants and asymmetry parameters for which experimental data [1] are available. Comparisons will be made with the corresponding properties for $BF_3$-$NH_3$, allowing valuable insights into the trends in the electron distributions in this family of complexes. [1] K. Bertholdt et al., J. Mol. Struct. 192, 199 (1989).

*Also UCF Orlando

**17:18**
**K10 13 Electron Distribution in Solid $BF_3$ and $BF_3 - NH_3$ – Associated Nuclear Quadrupole Interactions** DIP N. MAHATO, R.H. PINK, M.B. HUANG, T.P. DAS,* *SUNY Albany* ARCHANA DUBEY, LEE CHOW, *UCF Orlando* MAHENDRA K. MAHANTI, *NEHU Shillong, India* R.H. SCHEICHER, *MTU Houghton* The electronic structures of $BF_3$ and the complex $BF_3 - NH_3$in the solid state[1] have been studied by the Hartree-Fock Cluster Procedure and including many-body effects by perturbation theory. The motivation is to understand the nature of the bonding between the individual molecules in the solid and changes in the bonding within the molecules. We also have attempted to understand the differences in the nuclear quadrupole interactions of $^{11}B$ and $^{19}F$* nuclei in the free molecules and the solid state systems and have compared the results of theory with available experimental results [2] in solid state. Nuclear quadrupole interaction results for $^{14}N$ and deuteron will also be presented in the complex. [1] D. Mootz and M. Steffen, Angew. Chem. Int. Ed. Engl. 19, 483(1980). [2] P.A. Casabella and T. Oja, J. Chem. Phys. 50, 4814(1969); K. Berthholdt et al, J. Mol. Struct. 192, 199(1989).

*Also UCF Orlando



**SESSION K11: FOCUS SESSION: CHEMICAL AND SPECTROSCOPIC APPLICATIONS OF NONLINEAR OPTICS II**
**Tuesday Afternoon, 14 March 2006; 303, Baltimore Convention Center at 14:30**
**Alexander V. Benderskii, Wayne State University, presiding**

***Invited Papers***

**14:30**
**K11 1 Sum-Frequency Spectroscopy as a Novel Probe for Molecular Chirality.***
Y. RON SHEN, *University of California at Berkeley*

Conventional techniques to probe molecular chirality, such as circular dichroism (CD), suffer from poor sensitivity because they are electric-dipole forbidden. Sum-frequency generation (SFG) is electric-dipole allowed even in chiral liquids, and therefore could be a more sensitive spectroscopic technique for probing molecular chirality in both electronic and vibrational transitions. We describe here a series of experiments that explore such a possibility. Despite the finding that chiral SFG is intrinsically weak for various reasons, we have succeeded in observing chiral SFG at both electronic and vibrational transitions with monolayer sensitivity. This work was supported by the U.S. Department of Energy.

*In collaboration with Na Ji and Mikhail Belkin, University of California at Berkeley.

**15:06**
**K11 2 Chiral Phenomena in Nonlinear Optic.**
GARTH SIMPSON, *Purdue University*

Frequency doubling (second harmonic generation, SHG) and frequency mixing (sum frequency generation, SFG) are remarkably sensitive probes of interfacial structure. The application of these techniques in studies of biological systems and interfaces is particularly exciting, given their high sensitivity to chirality. Whereas absorbance measurements yield circular dichroic (CD) ratios of a few fractions of a percent, these same molecular systems can easily produce CD ratios approaching 100% in thin films. In order for these emerging techniques to successfully undergo the transformation from academic curiosities to practical instrumental tools for biological characterization, experimental and theoretical advances are required. Novel ellipsometric approaches for polarization analysis have been developed to yield greater information content with simpler instrumentation. As a complement to these experimental studies, new and relatively simple theories

have been proposed for interpreting the relationships between the detected signals and the molecular/macromolecular structures at the interfaces. Applications of these combined experimental and theoretical techniques include the demonstration of label-free methods for real-time biosensing, chiral-specific detection and analysis with ultra-high sensitivity, and the quantification of changes in protein secondary structure from polarization analysis.

*Contributed Papers*

**15:42**

**K11 3 Multiple-Sequence Two-Dimensional Infrared Spectroscopy of *N*-Acetyl-L-Prolinamide*** SOOHWAN SUL, DENIS KARAISKAJ, YING JIANG, NIEN-HUI GE, *Department of Chemistry, University of California at Irvine* Femtosecond nonlinear 2D IR spectroscopy has been applied to study the conformational distribution of a model dipeptide, *N*-acetyl-L-prolinamide, in chloroform. Using rephasing, non-rephasing, and reverse photon echo pulse sequences at several polarization conditions, we resolved new spectral features associated with multiple conformers that were difficult to discern by linear IR spectroscopy. Ab initio calculations in vacuo suggested the existence of a major ittrans-$C_7$ and a minor itcis structure. Calculated 2D spectra based on these structures agree reasonably well with experimental spectral features obtained at parallel polarizations, but better agreement between the calculated and experimental cross-peak patterns can be reached if the major conformer takes a structure deviated from the $C_7$ form. We will discuss our results in relationship with earlier findings from NMR studies and MD simulations.

*Supported by ACS PRF and NSF

**15:54**

**K11 4 Investigation of Surface Mounted Molecular Rotors Through Optical Second Harmonic Generation** JAMES D. WALKER, CHARLES T. ROGERS, *Dept. of Physics, Univ. of Colorado, Boulder, CO 80309* GREGG S. KOTTAS, JOSEF MICHL, *Dept. of Chemistry, Univ. of Colorado, Boulder, CO 80309* Exploiting the lack of inversion symmetry near a surface, optical surface second harmonic generation (SHG) can be a powerful tool for probing molecular monolayers (or multilayers) adhered to such a surface. In particular, spectroscopy by resonant SHG (Ti:Sapph laser pulses plus Optical Parametric Oscillators and frequency doubling) can provide insight into the orientation of the different sections of the molecular rotor (rotator and axle). The molecular population's orientation can then be studied in the presence of externally applied electric fields, given that the rotator has an intrinsic electric dipole moment, as well in variable temperature UHV environments (down to approx. 30 Kelvin). Concentrating on an anthracene based rotor molecule, synthesized in-house and utilizing silane attachment chemistry on fused silica substrates, we will describe progress made in probing the population's orientation through SHG as well as sample preparation and characterization (linear UV-VIS spectroscopy, FTIR, and XPS).

**16:06**

**K11 5 VSFS studies of soluble monolayers formed by linear and branched alcohols at the air/water interface** SÜLEYMAN CAN, DEESHA MAGO, ROBERT WALKER, *Department of Chemistry and Biochemistry, University of Maryland* Vibrational Sum Frequency Spectroscopy (VSFS) was used to examine the molecular structure and organization of linear and branched octanol and nonanol monolayers adsorbed to the air/water interface. Vibrational bands in the CH stretching region – specifically the symmetric and antisymmetric normal modes of the methyl and methylene groups as well as bands resulting from Fermi Resonance interactions – were used to characterize molecular orientation. Complementing these studies were a full series of surface tension measurements designed to measure surface excess concentrations at full monolayer coverage. VSFS data show that branched alcohols attached to an odd carbon (such as 3-nonanol) create monolayers having very similar surface structures and surface coverages, regardless of where the alcohol functional group is attached. Functional substitution at an even-carbon (2-octanol), however, leads to a monolayer having expanded surface coverage (44 sq. Angstroms/molecule) but a surprisingly high degree of conformational order. These results are examined in terms of a competition between hydrogen bonding of the alcohol with the water sub-phase and the tendency of alkyl chains to pack together in close registry.

*Invited Papers*

**16:18**

**K11 6 Recent Progress in Molecular Dynamics Simulation of Vibrational Sum Frequency Generation Spectroscopy.**

AKIHIRO MORITA, *Institute for Molecular Science*

While the visible-IR Sum Frequency Generation (SFG) spectroscopy is a powerful probe of interfaces using a second-order optical process, understanding of the experiments involves many factors to be addressed, including surface density and thickness, molecular orientation, local environment, and higher-order bulk terms. Assignment of the spectra is also complicated by overlap or interference of vibrational components. Therefore, practical methods of analysis with the help of reliable theoretical calculations will greatly benefit the SFG experiments. We have developed computational methods of vibrational SFG spectroscopy in combination of ab initio molecular modeling and molecular dynamics simulation. These methods allow direct calculation of SFG spectra from a molecular model without resorting to empirical spectral fitting. An essential ingredient of the theoretical methods is calculation of frequency-dependent nonlinear susceptibility that may be dominated by vibrational effects. We have proposed two ways of modeling of the nonlinear susceptibility, based on the energy representation and the time-dependent representation. This talk summarizes the progress of these theoretical methods and application to aqueous interfaces.

*Contributed Papers*

**16:54**

**K11 7 Vibrational Spectroscopy and Symmetry Specific Vibrational Energy Relaxation of Ethanol Molecule: A Study with Sum Frequency Generation and Photoacoustic Stimulated Raman Spectroscopy** HONG-FEI WANG,* *Institute of Chemistry, Chinese Academy of Sciences* SHI-LIN LIU,† *Department of Chemical Physics, University of Science and Technology of China* Orientational analysis of Sum Frequency Generation Vibrational Spectroscopy (SFG-VS) of un-deuterated ethanol indicated that the assignment of its C-H stretching vibrations in the literature was troublesome. The assignments were clarified using deuterated ethanols with their SFG-VS spectra at the vapor/liquid interface, and photoacoustic stimulated Raman spectra in the vapor phase. Comparison of SFG-VS spectra at vapor/liquid interface, infrared and Raman spectra in liquid phase, and photoacoustic stimulated Raman spectra in vapor phase of both un-deuterated and deuterated ethanol at room temperature indicated that the vibrational energy relaxation dynamics of ethanol molecule is significantly different for its symmetric and asymmetric C-H vibrational modes. These results showed that surface nonlinear spectroscopic methods can be used as effective tools for interrogating spectroscopy of molecules in bulk and vapor phases.

*Department of Chemical Physics, University of Science and Technology of China

†Also: Heifei National Laboratory for Physical Sciences at the Microscale (HFNL)

**17:06**

**K11 8 New forms of chiral spectroscopy: optical activity revisited** PEER FISCHER, AMBARISH GHOSH, *Rowland Institute at Harvard, Harvard University* Fresnel showed that an isotropic medium gives rise to optical rotation if its refractive indices for left- and right-circularly polarized light are unequal. Such is the case in optically active liquids, i.e. non-racemic solutions of chiral molecules. Nonlinear optical techniques have recently been developed that do not require the use of circularly polarized light to detect chirality. Here we present a new form of chiral spectroscopy which arises in linear optics and which yields information identical to that of conventional optical rotatory dispersion, yet without the need for a polarization analysis. The technique is independent of the optical path-length through the sample and permits optical activity to be imaged.

**17:18**

**K11 9 Structural properties and organization of hexadecanol isomers at the air/water interface** ROBERT WALKER, *Department of Chemistry and Biochemistry, University of Maryland* SÜLEYMAN CAN, *Department of Chemistry and Biochemistry, University of Maryland* DEESHA MAGO, *Department of Chemistry and Biochemistry, University of Maryland* A wealth of experimental data and theoretical modeling has led to well-honed intuition about the surface properties and structure of symmetric amphiphiles adsorbed to liquid surfaces. Less clear is how asymmetric amphiphiles organize in two dimensions at different surface coverages. We have studied the structure and two dimensional phase behavior of hexadecanol isomers adsorbed to the air/water interface. These isomers include the linear, n-hexadecanol as well structures with the alcohol functional group in the 2-, 3-, and 4-positions. Surface pressure methods are employed to study thermodynamic behavior of these insoluble monolayers, and vibrational sum frequency generation – a vibrational spectroscopy with surface specificity – is used to probe the molecular conformation and orientation of molecules within films. At their equilibrium spreading pressures, both 1- and 2- hexadecanol form very compact films having a high degree of conformational order and molecular areas of 19 and 28 sq. Angstroms/molecule in the tightly packed limit. In contrast, monolayers formed by 3-hexadecanol and 4-hexadecanol are much more disordered - but very similar to each other - and occupy much larger areas/molecule (75 sq. Angstroms/molec) in the tightly packed limit.



## SESSION K12: FOCUS SESSION: MAGNETIC THIN FILMS AND NARROW GAP SEMICONDUCTORS

**Tuesday Afternoon, 14 March 2006; 304, Baltimore Convention Center at 14:30**
**Juliet Correa, University of Muenster, presiding**

*Invited Papers*

**14:30**

**K12 1 Subsurfactant Epitaxy for Ferromagnetic Semiconductors.**
HANNO H. WEITERING, *The University of Tennessee and Oak Ridge National Laboratory*

In this talk, I will discuss a discovery that is expected to have due impacts in two forefront areas of materials research. First, I will introduce ''subsurfactant epitaxy'' as a novel kinetic pathway toward the synthesis of non-equilibrium structures and materials [1,2]. The discovery of subsurfactant growth is of broad fundamental- and paramount practical interest, particularly within the context of doping functional materials. Secondly, we have successfully applied this conceptual advance to alleviate a major bottleneck problem in spintronics, namely how to fabricate dilute magnetic semiconductors with ferromagnetic ordering temperatures that exceed room temperature by a comfortable margin while minimizing the structural disorder and inhomogeneities that are intrinsic to high doping levels. Here, we demonstrate that controlled Mn doping of Ge via subsurfactant epitaxy produces ferromagnetic ordering temperatures well above room temperature at doping levels that are at least 20 times lower than those typically invoked in other fabrication techniques. Detailed comparison between samples grown by conventional MBE [3-5], and samples grown via the subsurfactant procedure [2] indicates the vastly superior structure-property relationship of the latter. Subsurfactant epitaxy thus stands as a new and powerful avenue toward superior dopant control in dilute magnetic semiconductors and potentially other semiconductor applications that require doping levels far above the thermodynamic solubility limit. Work done in

collaboration with M. Chisholm, L.C. Feldman, A.P. Li, J.R. Thompson, C. Zeng, and Z.Y. Zhang. Funded by NSF-DMR-0306239. ORNL is managed by UT-Battelle, LLC, for the U.S. DOE under constract No. DE-AC-5-00OR22725
[1] W. Zhu et al., Phys. Rev. Lett. 93, 126102 (2004). [2] C. Zeng et al., submitted [3] A.P. Li et al, Appl. Phys. Lett. 86, 152507 (2005) [4] A.P. Li et al., Phys. Rev. B 72, 195205 (2005) [5] Y.D. Park et al., Science 295, 651 (2002).

*Contributed Papers*

**15:06**

**K12 2 Manganese silicide thin films on Si(001).** MICHAEL KRAUSE, ANDREW STOLLENWERK, VINCENT LABELLA, *College of Nanoscale Science and Engineering, University at Albany-SUNY, Albany, New York 12203* Theoretical considerations suggest that epitaxial MnSi thin films should order ferromagnetically on Si(001). This substantiates the hope that the Mn-Si system might be utilized as spin injectors through a Schottky barrier in future spintronics applications. Both thin and ultrathin films of manganese silicide on Si(001) have been investigated with different STM based techniques. In the ultrathin film regime three-dimensional manganese silicide islands form upon annealing. No closed and flat films have been found. With increasing annealing time the density of islands per surface area decreases while the average size of the remaining islands increases. The time dependence of the coarsening shows the typical characteristics of surface diffusion limited Ostwald Ripening. The activation energy for the clustering of Mn on Si(001) has been found to be 2.6 eV. Thicker (6 nm) continuous MnSi films were investigated using ballistic electron emission microscopy (BEEM) at 80 K to study the electrical properties. The BEEM spectra indicate a complex band structure at the MnSi/Si(001) interface. The MnSi overlayers show a high elastic scattering rate compared to Au/Si(001).

**15:18**

**K12 3 Kinetic stabilization of Fe ultra-thin film on GaAs(100) grown at low temperature** JAE-MIN LEE, SE-JUNG OH, *School of Physics & CSCMR, Seoul National University, Seoul 151-747, Korea* J.-Y. KIM, K.-J. KIM, *Pohang Accelerator Laboratory, Pohang University of Science and Technology, pohang 790-784, Korea* S.-U. YANG, J.-S. KIM, *Department of Physics, Sookmyung womens University, Seoul, Korea* We grew ultra-thin Fe films on GaAs(100) at low temperature (around 130K) to suppress chemical reactions between Fe and substrate atoms (interface alloying and As- surface segregation). For various Fe film thickness ranging from 1 to 30Å, we preformed photoemission experiment using synchrotron radiation to characterize the growth kinetics, and compared them with Fe films of similar thickness grown at room temperature. We confirmed that the interface alloying is obviously decreased at low temperature, and the surface segregation of As is blocked when Fe film is grown around 130K. As a result, more abrupt interface can be obtained in the low temperature growth. Furthermore, these Fe films grown at low temperature are found to be stable against As segregation even when the sample is annealed up to room temperature.

**15:30**

**K12 4 In-Situ Atomic-Scale Scanning Tunneling Microscopy Investigations of Cr on GaN Surfaces*** ARTHUR R. SMITH, MUHAMMAD HAIDER, ERDONG LU, WENZHI LIN, RONG YANG, COSTEL CONSTANTIN, HAMAD AL-BRITHEN,† *Ohio University* SMITH GROUP TEAM, Currently there is much interest in the magnetic properties of magnetically-doped nitride semiconductors. For purposes of doping GaN with Mn or Cr, it is important to investigate the action of these dopants on the clean surface under epitaxial growth conditions. In this study, we investigate the surface of GaN which has been doped with Cr during molecular beam epitaxial growth using in-situ scanning tunneling microscopy. In addition, we also investigate the surface of GaN which has been exposed to a fraction of monolayer of Cr deposited directly on the clean surface. For low concentrations, we find that the Cr can incorporate into the Ga lattice positions, participating in the known 3x3 and 6x6 reconstructions of GaN(000-1). For higher percentages of Cr, a novel Cr nanowire structure forms at the surface. Efforts are underway to study the magnetic properties of these surfaces.

*Work supported by National Science Foundation Grant #s 9983816 & 0304314
†Current address: King Saud University

**15:42**

**K12 5 Epitaxial Growth of Binary Ferromagnetic $Mn_{3-\delta}Ga$ Thin Films on Wurtzite GaN(0001) and Investigation by Atomic Scale Scanning Tunneling Microscopy** E.D. LU, R. YANG, M.B. HAIDER, C. CONSTANTIN, A.R. SMITH, *Condensed Matter and Surface Science Program, Department of Physics and Astronomy, Ohio University, Athens, OH 45701* J.W. KNEPPER, F.Y. YANG, *Physics Department, Ohio State University, 191 Woodruff Avenue, Columbus, OH 43210* Due to increasing interest in developing new magneto-optical and magneto-electronic devices, and spin injection sources in spintronics applications, ferromagnetic (FM)\MnxGay is an attractive candidate system to explore. Here we report that binary FM $Mn_{3-\delta}Ga(1.14< \delta < 2.0)$ single crystalline thin films has been epitaxially grown on (*w*)-GaN(0001)surfaces using molecular beam epitaxy. The face-centered tetragonal structure of $Mn_{3-\delta}Ga$ thin films with CuAu-$L1_0$ type ordering has been determined *insitu* by both reflection high energy electron diffraction and atomic-scale scanning tunneling microscopy. The epitaxial relationship of the $Mn_{3-\delta}Ga$ with GaN(0001) is $(111)[1\bar{1}0]_{MnGa} \parallel (0001)[1\bar{1}00]_{GaN}$ and $(111)[11\bar{2}]_{MnGa} \parallel (0001)[11\bar{2}0]_{GaN}$. The hysteresis loops of the thin films show magnetic anisotropy along itin-plane and itout-of-plane directions. It is found that Curie temperature and magnetic moments of the $Mn_{3-\delta}Ga$ thin films are closely related to the Mn content, and the reconstruction changes from $1\times$ 1 to $2\times$ 2 by increasing the ratio of Mn to Ga during the growth. Thus, we have achieved reconstruction-control of magnetic properties.

**15:54**

**K12 6 Indium nitride growth on Si(100) by femtosecond pulsed laser deposition** MOHAMED HAFEZ, HANI ELSAYED-ALI, *Old Dominion University* Deposition of indium nitride (InN) on Si(100) is performed under ultrahigh vacuum with an amplified Ti:sapphire laser (130 fs) operating at a wavelength of 800 nm. The objective is to grow single crystal InN films on Si(100). An intermediate layer of indium on Si(100)-($2\times$ 1) is prepared to avoid surface nitridation and decrease the lattice mismatch between the InN and Si(100). Reflection high-energy electron diffraction (RHEED) is used in situ during the deposition to study the growth dynamics and the surface structure of the grown

films. Growth of indium on Si(100)-(2× 1) by femtosecond pulsed laser deposition showed high-quality 2D films. The initial 2D indium layers on Si(100)-(2× 1) formed in the In-(2× 1) structure at room temperature and the In-(4× 3) structure at a substrate temperature of 653-693 K. Growth of InN on the In-(2× 1) and In-(4 × 3) buffer layer is discussed. The morphology of the InN films is examined by ex situ atomic force microscopy (AFM) and scanning electron microscopy (SEM).

**16:06**

**K12 7 Influence of temperature on mobility and carrier density of InN films** JAGDISH THAKUR, *Wayne State University* V.M. NAIK, *University of Michigan-Dearborn* R. NAIK, D. HADDAD, G.W. AUNER, *Wayne State University* H. LU, W.J. SCHAFF, *Cornell University* We have investigated temperature dependence of Hall mobility and carrier density for thin InN films with low and high carrier density grown by Molecular Beam Epitaxy (MBE) and Plasma Source Molecular Beam Epitaxy (PSMBE), respectively. At very low temperatures, a large concentration of carriers which are temperature independent is observed in both the low and high density films. However, the behavior of mobility for the low density film is different from that of the high density film particular for temperatures less than 300K. For the low density film, mobility increases with temperature and passes through a maximum around 250 K in contrast to temperature independent mobility observed for the high density film for T $<$ 300K. Theoretically, we investigated the temperature dependence behavior of the mobility using Born-scattering and found the presence of charged dislocation in the low density film. At higher temperatures the mobility is determined by the electrons scattering from the longitudinal-optical (LO) phonons.

**16:18**

**K12 8 Electrolyte-based capacitance voltage analysis of InN** J.W. AGER III, K.M. YU, *Lawrence Berkeley National Laboratory, Berkeley, CA* R.E. JONES, D.M. YAMAGUCHI, S.X. LI, *Lawrence Berkeley National Laboratory and UC Berkeley, Berkeley, CA* W. WALUKIEWICZ, *Lawrence Berkeley National Laboratory, Berkeley, CA* E.E. HALLER, *Lawrence Berkeley National Laboratory and UC Berkeley, Berkeley, CA* H. LU, W.J. SCHAFF, *Cornell University, Ithaca, NY* The electron affinity of InN, 5.8 eV, is larger than for any other known semiconductor. As a result, InN has a surface accumulation layer of electrons reflecting pinning of the Fermi level ca. 0.9 eV above the conduction band edge. In addition, all metals form an ohmic contract to InN, so that it is not possible to measure the space charge distribution using standard capacitance voltage (CV) measurements. We show that electrolyte solutions can be used to make blocking contacts to InN and that under reverse bias conditions, the surface accumulation layer and up to ca. 10 nm of the underlying InN can be depleted. Analysis of CV data obtained under these conditions using the Poisson equation allows net charge as a function of depth to be modeled. In n-type InN, good agreement with bulk Hall effect data is obtained when the depletion region is extended to $>$ 5 nm below the surface. In Mg-doped InN, modeling of the CV data produces evidence for ionized acceptors below a surface inversion layer.

**16:30**

**K12 9 Observation of Quantized Electron Accumulation States in InN(0001−)** LEYLA COLAKEROL, HAE-KYUNG JEONG, LUKASZ PLUCINSKI, SHANCAI WANG, ALEX DEMASI, KEVIN SMITH, *Department of Physics, Boston University* PAPO CHEN, THEODORE MOUSTAKAS, *Department of Electrical and Computer Engineering, Boston University* We report a study of the surface and bulk electronic structure of InN(0001–) thin films using high resolution synchrotron radiation excited angle-resolved photoemission. The InN thin films were grown by plasma-assisted molecular beam epitaxy on *c*-plane sapphire. Samples were cleaned both by annealing in ultra-high vacuum (UHV) and by cycles of nitrogen ion bombardment followed by UHV annealing. We have observed a series of quantized states above the Fermi level ($E_F$), for a narrow range of excitation energies and band momenta. These states have a parabolic dispersion around the surface Brillouin zone center and are due to an electron accumulation layer in the conduction band. The number of states observed is a function of annealing temperature. We observe an increase in the number of states following sputtering, which is likely due to segregation of In metal to the surface. Up to four individual free electron states are observed. Supported in part by the NSF, the U.S. ARO, and by the U.S. AFOSR. Experiments were performed at the NSLS.

**16:42**

**K12 10 Electron Mobility of InN*** REBECCA JONES, SONNY LI, EUGENE HALLER, *Materials Sciences Div., Lawrence Berkeley National Laboratory, and Dept. of Materials Science and Engineering, University of California, Berkeley, CA* KIN MAN YU, WLADEK WALUKIEWICZ, HENRICUS VAN GENUCHTEN, JOEL AGER, *Materials Sciences Division, Lawrence Berkeley National Laboratory, Berkeley, CA* LEON HSU, *General College, University of Minnesota, Minneapolis, MN* HAI LU, WILLIAM SCHAFF, *Dept. of Electrical and Computer Engineering, Cornell University, Ithaca, NY* We use irradiation with 2 MeV $H^+$ and $He^+$ ions to create donor-like point defects in InN films and thereby predictably control the free electron concentration and mobility over a large conductivity range. Calculations of theoretical electron mobilities coupled with experimental annealing studies (at temperatures up to 500$^o$C) suggest at least two types of donor-like defects are formed by the irradiation: singly-charged nitrogen vacancies and triply-charged, relaxed indium vacancies. Under annealing at these temperatures, the nitrogen vacancies appear stable, while the indium vacancies are removed. The annealing creates InN films with electron mobilities well above those of as-grown films at similar concentrations. We use these results to analyze the factors limiting the mobility in as-grown InN films.

*Funded by DOE, ONR and DOD

**16:54**

**K12 11 Role and Effect of Native Defect Complexes in InN** XIANGMEI DUAN, CATHY STAMPFL, *School of Physics, The University of Sdyney* CONDENSED MATTER THEORY TEAM, We have carried out the first-principles density-functional theory calculations to investigate the structural and electronic properties and the formation energies of native point defect complexes in InN. We report an extensive and systematic study of possible configurations and different concentrations, focusing on the nitrogen- and indium-vacancies. Nitrogen vacancies prefer to be situated close to one another resulting in local metallic indium-rich regions or ''clustering''; while indium vacancies prefer to be separated, or to cluster together, where neighbouring under-

coordinated N atoms spontaneously form N2 molecules. These defect structures induce marked changes in the states in the egion of the band gap, which may explain the wide variation in experimentally determined band-gaps (see e.g. [1]). [1] T. V. Shubina, et al. Phys. Stat. Sol. (a) 202, 377 (2005).

**17:06**

**K12 12 Photoinduced magnetic and electronic phenomena in organic magnetic semiconductor $V(TCNE)_{x\sim2}$** JUNG-WOO YOO, R. SHIMA EDELSTEIN, A. J. EPSTEIN, *The Ohio State University, Columbus, OH 43210* K. I. POKHODNYA, JOEL S. MILLER, *Univeristy of Utah, Salt Lake City, UT 84112* $V(TCNE)_{x\sim2}$ is a fully spin-polarized half- semiconductor, whose magnetic order exceeds room temperature ($T_c > 350$ K), and electronic transport follows hopping mechanism in the Coulomb energy split in $\pi^*$ band. Substantial decrease of magnetization by illuminating with light ($\lambda = 457.9$nm) has been found at low temperature ($T < 100$K). The photo-excited metastable state has a lifetime $> 10^6$s at low temperatures and completely relaxes to the state before illumination after annealing upto 250K. Photoinduced ESR analysis indicates strong increase of magnetic anisotropy by light irradiation. We also report substantial increase of conductivity induced by illumination with light ($\lambda = 457.9$nm). The temperature dependence of resistivity clearly indicates substantial decrease in activation energy for electronic hopping. The photoinduced effect is proposed to originate from structural changes triggered by $\pi \rightarrow \pi^*$ excitation in (TCNE) molecules, which leads modification of the orbital wavefunction resulting in changes of magnetic exchange energy $J$ and the activation energy $\Delta E$. *Supported in part by AFOSR Grant No. F49620-03-1-0175 and DOE Grant No. DE-FG02-01ER45931 and DE-FG02-86ER45271.



**SESSION K13: ATOMIC AND MOLECULAR PROCESSES AT SOLID SURFACES**
**Tuesday Afternoon, 14 March 2006**
**305, Baltimore Convention Center at 14:30**
**Eric Borguet, Temple University, presiding**

**14:30**

**K13 1 Thermal Chemistry of $N_2$, $CO_2$, and $CH_4$ on Cesiated Pt(111)** KRISTY DEWITT, LETICIA VALADEZ, IAN HARRISON, *Department of Chemistry, University of Virginia, Charlottesville, VA 22904* MERRICK DEWITT, *SPARTA, Inc., 1911 N. Fort Myer Drive, Suite 1100, Arlington, VA, USA 22209* Promoting transition metal surfaces with alkali metals is known to drastically reduce the surface work function. We have investigated the effect of Cs promotion on the thermal chemistry of $CH_4$, $N_2$ and $CO_2$ using temperature programmed desorption (TPD). At low Cs coverage the $CH_4$TPD peak broadens and shifts to higher temperature. As the Cs coverage increases further three $CH_4$ peaks develop: one at higher temperature than on a bare Pt surface, and two at lower temperatures. With Cs coverage of one saturation monolayer (it$\theta_{sat} = 0.41$ ML) or more only the lowest temperature peak remains. $CH_4$ sticking also varies as a function of Cs coverage. $N_2$ displays similar behavior to $CH_4$ in response to coadsorption of Cs, but does not stick to Cs multilayers. $CO_2$ exhibits very unusual behavior as a function of Cs coverage. At low Cs coverage the physisorbed $CO_2$ peak broadens, then splits into a doublet, with one peak at higher temperature than the ''normal'' $CO_2$ peak, and the other at lower temperature. With increasing Cs coverage $CO_2$ begins to dissociate, evidenced by high temperature recombinative desorption and the presence of chemisorbed CO. As the Cs coverage approaches $\theta_{sat}$ the physisorbed peak disappears entirely, and only dissociative chemisorption is seen.

**14:42**

**K13 2 Observation and Manipulation of Subsurface Hydride in Pd(111)** CHARLES SYKES, *Tufts University* LUIS FERNANDEZ-TORRES, *University of Puerto Rico at Cayey* SANJINI NANAYAKKARA, *Penn State University* BRENT MANTOOTH, *Geo-Centers* RYAN NEVIN, *University of Wisconsin-Madison* PAUL WEISS, *Penn State University* We have observed and manipulated hydrogen atoms beneath the surface of a Pd(111) crystal using low-temperature scanning tunneling microscopy (STM). The subsurface region of Pd can be populated with hydrogen atoms from the bulk by applying voltage pulses from a STM tip. Topographic and local electronic data characterizing subsurface hydrogen in these stable sites is presented. We discuss our ability to selectively populate subsurface sites with hydrogen and present a full STM characterization of this state. This phenomenon is explained with an inelastic excitation mechanism, whereby hydrogen atoms in the bulk are excited by tunneling electrons and are promoted to more stable sites in the subsurface region.

**14:54**

**K13 3 Oxygen-Induced Faceting of Ir(210)** TIMO JACOB, PAYAM KAGHAZCHI, MATTHIAS SCHEFFLER, *Fritz-Haber Institute, Faradayweg 4-6, D-14195 Berlin, Germany* Although rough clean metal surfaces usually have higher surface free energies than their closed-packed analogs, adsorbates are able to modify this behavior and cause changes in surface morphology through reconstructions or facet formations. Using different surface sensitive techniques (e. g. STM or LEED) Madey *et al.* [1] found that Ir(210) shows interesting surface faceting at high oxygen coverages ($\theta > 0.5$ ML). The facets were identified as three-sided nanoscale pyramids with two (311) and one (110) planes. In oder to understand this effect we used density functional theory in combination with the *ab initio* atomistic thermodynamics and studied the influence of an oxygen atmosphere on the structure of Ir(210). Assuming an oxygen partial pressure of 1 atm, it turned out that below $T < 1000$ K the oxygen-covered facets are thermodynamically more stable than non-faceted O/Ir(210). Further heating reverts the substrate structure to planar O/Ir(210). While most nanoscale pyramids consist of smooth and unreconstructed planes, some (110) facets show a complex reconstructed superstructure. Thus, present studies aim on the stability and an atomistic understanding of those structures. [1] I. Ermanoski *et al.*, *Surf. Sci.* **549**, 1 (2004).

**15:06**

**K13 4 The Nature of Metal-Oxygen Bonding at Corundum (0001) Surfaces in the Presence of Oxygen** EMILY JARVIS,* ORKID COSKUNER, ANNE CHAKA, *National Institute of Standards and Technology, Physical and Chemical Properties Division, Computational Chemistry Group* Metal oxides are of critical importance in a variety of applications ranging from gas sensing to catalysis to environmental containment of heavy metals. In all of these cases, it is the surface chemistry that is essential to the necessary function. The detailed surface structure is heavily de-

pendent on the physical and chemical features of the surroundings, and its reactivity is largely dictated by the nature of the local bonding character. We use all electron density functional calculations combined with itab initio thermodynamic predictions to explore surfaces of several corundum-structured metal oxides as a function of oxygen partial pressure, which is a crucial first step in understanding corrosion, passivation, and catalysis. Additionally, we apply quantum mechanical wavefunction-based methods with the goal of elucidating the local bonding character of these surfaces. Our calculations provide detailed insight into the nature of the chemical bonding at chromia and hematite (0001) surfaces with M=O termination, i.e., the chromyl- and ferryl-terminated surfaces, and explain the dissimilar thermodynamic predictions for the alumina (0001) surface relative to these transition metal oxide surfaces.

*Membership Pending

**15:18**

**K13 5 Theoretical treatment of excited electronic states of adsorbates on metals: electron attachment to $CO_2$ adsorbed on Pt(111)*** JERRY WHITTEN, LAURA SREMANIAK, *North Carolina State University* Photochemistry involving adsorbates on metals often proceeds by photoexcitation of the metal followed by transient attachment of photoemitted electrons to the adsorbate. First principles theoretical methods suitable for describing electronic states embedded in a near continuum of metal to metal excitations are described and an application to electron attachment to $CO_2$ adsorbed on Pt(111) is reported. Wavefunctions are constructed by itab initio configuration interaction methods which allow a rigorous resolution of states and differentiation between competing pathways of molecular desorption and dissociation. An embedding theory is used to achieve high accuracy in the adsorbate-surface region. The overall process can be understood as formation of an electron attached state at an energy lower than the work function of the metal, localization of the metal hole and attraction of the charged adsorbate to the metal. Optimum geometries are calculated and pathways between these geometries determine whether molecules will desorb, dissociate by bond rupture directly in the excited electronic state, or dissociate after return to the ground state potential energy surface via vibrational processes. The influence of a coadsorbed potassium electron donor atom on the energy required to form the electron attachment state is also reported.

*Supported by the U.S. Department of Energy

**15:30**

**K13 6 Quantum Nature of Hydrogen on Metals: Ground-State Geometry of Vacancies** SUNGHO KIM, SEONG-GON KIM, *Mississippi State University* STEVEN C. ERWIN, *Naval Research Laboratory* When hydrogen is adsorbed on a Pd(111) surface, very simple vacancy defects – which form quite commonly – exhibit fundamentally quantum wavelike behavior. Conventional wisdom has it that the quantum nature of hydrogen and other light atoms is only rarely manifested, typically in specially designed experimental protocols. A great many studies have proceeded under the assumption that, for most purposes, as long as the electronic motion is handled quantum mechanically, the nuclear motion of hydrogen can be treated classically. We show that this approximation fails badly in a very simple system. Moreover, by treating the problem fully quantum mechanically, several recent experimental finding [Mitsui et al, Nature 422, 705 (2003)] can be plausibly interpreted as having a fundamentally quantum origin. In particular, we present new ground-state geometry of hydrogen vacancies on Pd(111) surface that are obtained from a full quantum treatment of the hydrogen nuclear motion. This new structures enable us to predict that all vacancy defects to have an unexpected triangular appearance in scanning tunneling microscopy; recent experiments have found precisely this behavior.

**15:42**

**K13 7 Positron annihilation induced Auger electron spectroscopic study of the changes in the top layers of electrodeposited $Cu_2O$ surfaces resulting from vacuum annealing** M. NADESALINGAM, *University of Texas at Arlington* J. ZHU, N. FAZLEEV, S. MUKHERJEE, N. R. DE TACCONI, S. SOMASUNDARAM, C.R. CHENTHAMARAKSHAN, K. RAJESHWAR, A. H. WEISS, Positron Annihilation induced Auger electron Spectroscopy (PAES) and electron stimulated Auger Spectroscopy (EAES) were used to measure changes in the surface of electrodeposited $Cu_2O$ resulting from vacuum annealing. The PAES measurements show a very large increase in the intensity of the Cu MVV Auger peak after annealing at 535 K. Similar but significantly smaller changes were observed in the EAES spectra consistent with the fact that PAES is primarily sensitive to the top-most atomic layer due to the fact that the positrons are trapped just outside the surface prior to annihilation while EAES samples several atomic layers. The PAES and EAES data indicate that vacuum annealing of $Cu_2O$ results in a surface with a high concentration of Cu in the top-most atomic layer. Research supported by the Welch Foundation Y-1100 and NSF DMR 98-12628.

**15:54**

**K13 8 Atomic-scale study of the Rh/$\gamma$-alumina catalytic system** SHUPING ZHUO, *School of Chem. Eng., Shandong Univ. of Tech.* YIPING PENG, *Condensed Matter Sci. Div., ORNL* STEPHEN PENNYCOOK, *Condensed Matter Sci. Div., ORNL* KARL SOHLBERG, *Chem. Dept., Drexel Univ.* Prerequisite to the non-empirical design and refinement of improved heterogeneous catalysts is the identification of the atomic-scale structure and properties of the catalytically active sites. We report an investigation of the Rh/$\gamma$-alumina system, which is representative of many common heterogeneous catalysts that consist of transition metals dispersed on a high surface area support. Previous atomic-resolution Z-contrast STEM observations have shown Rh-containing ''rafts'' on the (100) exposure. This finding is surprising given that the preferred exposure of $\gamma$-alumina is (110). First-principles density functional studies and image simulations suggest that these Rh-containing structures consist of the high-pressure rhodium sesquioxide (II) phase growing on the surface. The high pressure phase of rhodium sesquioxide and $\gamma$-alumina (100) exposure yield improved interface match over the regular rhodium sesquioxide phase and $\gamma$-alumina (110) exposure.

**16:06**

**K13 9 Nature of Versatile Chemisorption on TiC(111) and TiN(111)*** BENGT I LUNDQVIST, CARLO RUBERTO, ALEKSANDRA VOJVODIC, *Department of Applied Physics, Chalmers University of Technology, SE-412 96, Göteborg, Sweden* Extensive density-functional calculations on the polar TiX(111) (X = C, N) surfaces show (i) for the clean surfaces strong Ti3d-derived surface resonances (SR's) at the Fermi level, unlike on the stable TiX(001) surfaces, and X2$p$-derived SR's in the upper valence band, and (ii) for chemisorption of atoms in the first three periods pyramid-shaped trends in atomic adsorption energies Eads, with an extremely strong O-atom bond. The adsorption is

successfully described by a by us proposed concerted-coupling model (CCM), where adsorbate states couple to both kinds of SR's in a concerted way, and which is consistent with trends in the adsorbate-induced DOS and explains the characteristic variations in Eads and in bond lengths, as well as radical differences between TiX(111) and TiX(001), and similarities and small differences between TiC and TiN. The versatility of chemisorption on TiX(111) and the general nature of CCM indicate both ramifications and predictive abilities in, e.g., growth and catalysis.

*Support from the Swedish Research Council and the Swedish Foundation for Strategic Research via the ATOMICS consortium is gratefully acknowledged, as well as allocation of computer time at UNICC (Chalmers) and SNIC (Swed. Nat. Infrastr. for Computing).

**16:18**

**K13 10 Depth Profiling and Interface Analysis by Time-of-Flight Secondary Ion Mass Spectrometry (TOF-SIMS): Potential, Performance and Limitations.** COREY FOSTER, *ION-TOF USA* SVEN KAYSER, THOMAS GREHL, RUDOLF MOELLERS, EWALD NIEHUIS, *ION-TOF GmbH* TOF-SIMS has always been a very sensitive tool for surface spectroscopy and imaging. In recent years TOF-SIMS has improved significantly for traditional dynamic SIMS applications. Operated in the so-called dual-beam mode, where the sample is sputtered with a low energy sputter beam, while the analysis is performed in the center of the sputter crater using a high energy beam, TOF-SIMS provides high-sensitivity depth profiling capabilities comparable to quadrupole or magnetic sector mass spectrometers. Providing parallel mass detection, high mass resolution, advanced charge compensation and 3D imaging capabilities, TOF-SIMS has developed considerable advantages for the characterization of technologically advanced materials. In this study we investigated the depth resolution, detection limits, quantification and reproducibility now available with TOF-SIMS. During this talk we will show examples and applications of TOF-SIMS depth profiling in the field of inorganic materials and compare the depth profiling capabilities of TOF-SIMS instruments with other dynamic SIMS machines.

**16:30**

**K13 11 Insight into the mechanisms of metal ion binding in hexagonal tungsten bronze** SHANE KENNEDY, SUZANNE SMITH, MAXIM AVDEEV, ALEX FUCHS, *Bragg Institute and Institute of Materials Engineering Science, Australian Nuclear Science and Technology Organisation, Lucas Heights, NSW, Australia* Tungsten trioxides and their alkali-metal-intercalated products $M_zWO_{3+}$ show potential for application in electrodes, as ion exchangers, catalysts and the treatment of radioactive waste. Hexagonal tungsten bronze (HTB) was selected for the present work because its structure features hexagonal channels, of diameter $\sim$ 0.54 nm, that may be useful for selective and reversible binding of metal ions. X-ray and neutron powder diffraction were used to provide an insight into the mechanisms of metal ion binding of the Mo doped HTB's. Combined Rietveld refinement of the X-ray and neutron diffraction shows that doping with Mo degrades the crystallinity of HTB, in particular by creating a high degree of disorder in the a-b planes. Structural information combined with solution chemistry indicates several potential mechanisms of binding and metal ion exchange sites. This type of investigation provides invaluable information for new strategies in the design of inorganic sorbents and their optimization for metal ion separation.

**16:42**

**K13 12 Adsorption of NO on Rh(111) studied by STM.** J.H.A. HAGELAAR, *Eindhoven University of Technology* C.F.J. FLIPSE, The ability of Rhodium to efficiently dissociate NO makes it the most suitable metal for the removal of nitrogen oxides from automotive exhaust gasses in catalytic converters. Using a STM, the adsorption of NO on Rh(111) was studied in ultra high vacuum. First, the NO is adsorbed at T=200 K, giving rise to two structures with coverages of 0.5 ML and 0.75 ML. These structures differ from the 0.5 ML (4x2)-2NO and 0.75 ML (2x2)-3NO structures found in literature. Once a structure was obtained, the sample was cooled down to 4.8K to perform inelastic electron tunneling spectroscopy (IETS) on the individual molecules within the structure. The molecules in the 0.5 ML structure showed a significant shift in the NO-stretch frequency compared to the expected frequency of 1600 $cm^{-1}$. These results will be presented and discussed in detail.

**16:54**

**K13 13 Picosecond real time observation of low energy electron scattering from large molecules on surfaces** CLAUDIO CIRELLI, *Physik Institut, Universitaet Zuerich, CH-8057, Switzerland and Physikalisch-Chemisches Institut, JL-Universitaet, D-35392 Giessen, Germany* MATTHIAS HENGSBERGER, ANDREI DOLOCAN, JUERG OSTERWALDER, THOMAS GREBER, *Physik Institut, Universitaet of Zuerich, CH-8057, Switzerland* HERBERT OVER, *Physikalisch-Chemisches Institut, J.L. Universitaet, D-35392 Giessen, Germany* In order to observe in real time structural changes of molecules, it is necessary to develop a technique providing both nanometer and picosecond resolution. This task is tackled with a time resolved Low Energy Electron Diffraction (LEED) experiment in a pump-probe scheme. The pump pulses are 800 nm 100 fs laser light pulses and the probe 60eV energy electron pulses. Using a novel electron gun with a measured energy resolution of 0.7eV at 100eV, we observe transient changes in the differential scattering cross section and an energy shift of the diffracted LEED spot up to about 250meV. As this energy shift is pump fluence dependent, we can assign it to the onset of a space charge effect created by the pump beam on the sample surface. Conclusions about surface space charge and molecular dynamics can be drawn by tracking this effect on the picosecond timescale. Results on the response of the bare Cu(111) surface and of $C_{60}$/Cu(111) will be presented. [1] A. Dolocan et al., Jap. J. Appl. Phys. 45 (2006)

## SESSION K16: FOCUS SESSION: MOLECULAR-SCALE ELECTRONICS II

**Tuesday Afternoon, 14 March 2006**
**312, Baltimore Convention Center at 14:30**
**Ravindra Pandey, Michigan Technological University, presiding**

***Contributed Papers***

**14:30**

**K16 1 Inelastic scattering effects on single molecule spectroscopy: Consequences for Negative Differential Resistance** JASON PITTERS, *National Institute for Nanotechnology - NRC* ROBERT WOLKOW, *University of Alberta* The adsorption of styrene and cyclopentene on Si(100) has been studied with scanning tunneling microscopy and spectroscopy. Blinking of mol-

ecules in images and irregularities in current-voltage spectra and in current-time traces are analyzed. It is also shown that NDR-like features in IV spectra of both styrene and cyclopentene molecules are not consistently present. Such erratic behavior cannot be accounted for by voltage controlled resonant alignment of adsorbate and substrate energy levels but is consistent with random configuration change driven by inelastically scattered electrons. These random processes, which include molecular rearrangement, desorption and/or decomposition occur with increasing frequency at larger voltage and current settings. It is concluded that the molecules studied do not exhibit negative differential resistance due to a resonant tunneling mechanism. Conditions where resonant NDR may be observed are discussed.

**14:42**
**K16 2 Calculations of the structural, electronic and transport properties of self-assembled monolayers of porphyrins on the Si(001) surface** FILIPE J. RIBEIRO, W. LU, J. BERNHOLC, *North Carolina State University* Self-assembled monolayers (SAMs) of organic molecules on surfaces have very promising technological applications. The oxidation states of porphyrins are currently being explored to store charge in a controllable way, aiming at the development of multi-state molecular memories. We present the results of theoretical calculations on the structural, electronic and transport properties of chemisorbed porphyrins on a hydrogen-passivated Si(001) surface. Density-functional calculations were performed to optimize the structural parameters of the adsorbed porphyrins using a real-space multi-grid approach. Electron transport properties for a porphyrin molecule attached to two Si(001) leads were calculated using a non-equilibrium Green's function method in a basis of optimally localized orbitals. Our results show that the current, negligible at low voltages, exhibits a very strong non-linear behavior for bias voltages above 1.5 V, including multiple regions of negative differential resistance (NDR). The multiple NDRs may lead to multi-state molecular devices.

**14:54**
**K16 3 Theory of molecular hysteresis switch** MORTKO KOZHUSHNER, *Institute of Chemical Physics, RAS* IVAN OLEYNIK, *University of South Florida* Molecular hysteresis switching has been recently observed in a series of experiments that measured the I-V spectrum of bipyridyl-dinitro oligophenylene-ethylene dithiol (BPDN) based molecular devices [1]. The experimental observations clearly show the presence of Coulomb blockade in single organic molecules that is responsible for the voltage-induced switching. We present the theory of the hysteresis switch which explains the non-linear hysteresis I-V characteristics based on the mechanisms of Coulomb blockade and the existence of two different molecular conformations of neutral and charged states of the molecule. [1] A.S. Blum, J.G. Kushmerick, D.P. Long, C.H. Patterson, J.C. Yang, J.C. Henderson, Y.X. Yao, J.M. Tour, R. Shashidhar, and B.R. Ratna, it''Molecularly inherent voltage-controlled conductance switching'', Nature Materials **4,** 167 (2005).



***Invited Papers***

**15:06**
**K16 4 Theory of Molecular Electron Transport.**
SHASHI KARNA, *US Army Research Laboratory*

Thanks to the curiosity and devoted research of physicists and chemists over the past century and a half, electron transport in extended system has been a well understood phenomenon and has lead to today's all pervasive, monolithic, microelectronics technology. However, despite intense interest and ensuing research since the 1950s, an understanding of electron transport in confined systems, such as molecules and nano-scale atomic particles, remains limited. In this talk, I shall present an overview of our current understanding of the physics and chemistry of electron transport in molecules and at the molecule-solid interface. The effect of electronic structure, chemical bonding, physical dimension, stereochemistry, and external perturbation on molecular electron transport will be discussed.

***Contributed Papers***

**15:42**
**K16 5 Electrical and structural switching in [2] rotaxane molecular electronic devices** YONG-HOON KIM, *Korea Institute for Advanced Study* WILLIAM A. GODDARD III, *California Institute of Technology* In the effort to identify good candidates of molecular electronics, two-families of redox-controllable mechanically interlocked supramolecular complexes – bistable catenanes and bistable rotaxanes – have attracted much attention. Carrying out large-scale first-principles matrix Green function calculations combined with classical force-field molecular dynamics simulations, we study the charge transport properties of a monolayer of full (including stoppers) bistable rotaxane molecules in their realistic folded conformations. We will discuss (i) the universal nature of the identified switching mechanism in comparison with the [2] catenane device, (ii) the robustness of the switching signal with respect to thermal fluctuations, and (iii) the nature of molecule-electrode barriers that play an important role in inducing a structural switching between the bistable conformations of the molecule, a precondition of observing the electrical switching.

**15:54**
**K16 6 Low temperature transport study of the nitro molecules** NABANITA MAJUMDAR, Z. MARTIN, N. SWAMI, L. HARRIOTT, *University of Virginia* Y. YAO, J. TOUR, *Rice University* D. LONG, R. SHASHIDHAR, *Geo Center R&D Center* Various research groups, including ours, have observed switching with memory behavior at room temperature from a monolayer of oligo(phenylene ethynylene) (OPE) molecules with a nitro sidegroup.[1,2] This switching behavior has the potential to be used in molecular electronic devices. However, the transport mechanisms of this ''nitro'' molecule are not well understood. Understanding the transport mechanisms of the nitro molecules may help identify the underlying cause of the switching behavior. We performed a systematic study of the transport characteristics of OPE molecules

with and without a nitro side group in our nanowell test device[3] at various temperatures between 60K and 300K. We observed non-switching exponential current-voltage characteristics from OPEs without the nitro side group. The mechanism of transport was determined to be hopping with a transport barrier of 0.03± .01 V between 100K to 300K. Switching with memory behavior as well as non-switching exponential I-V characteristics were observed from the nitro molecules at various temperatures. The transport mechanism in switching devices was determined to be hopping with an activation barrier of 0.26± .08 V between 200K and 300K. However, a significantly lower activation barrier similar to that of OPEs without a nitro group was estimated for the nitro molecule devices that did not show any switching behavior.

**16:06**

**K16 7 Theoretical Study of Spin-Polarized Electron Tunneling via $C_{60}$ Molecules** HAIYING HE, RAVINDRA PANDEY, *Department of Physics, Michigan Technological University, Houghton, MI 49931* SHASHI KARNA, *US Army Research Laboratory, Weapons and Materials Directorate, Aberdeen Proving Ground, MD 21005-5069* The controlled injection and transport of spin-polarized electrons through organic molecules has drawn increasing attention in recent years due to its potential applications in molecular and molecular-nano hybrid electronics and sensors. In this talk, we will present the results of a theoretical study of spin-polarized electron tunneling via $C_{60}$ molecules in contact with ferromagnetic nickel electrodes. In this system, the resistance varies as the magnetic moments in the two electrodes are tuned from parallel to anti-parallel alignment. Particular attention is given to the chemical bonding features in the molecule-electrode interface, which leads to the observed difference in magnetoresistance.

**16:18**

**K16 8 Is Electron Transport In Boron Nanotube Ballistic?** KAH CHUN LAU, RANJIT PATI, RAVINDRA PANDEY, *Department of Physics, Michigan Technological University, Houghton, MI* SHASHI P. KARNA, *US Army Research Laboratory, Weapons and Materials Research Directorate, ATTN: AMSRD-ARL-WM, Aberdeen Proving Ground, MD 21005-5069* The electron transport in single-walled boron nanotube is studied using the Landauer-Buttiker multi-channel approach in conjunction with the tight-binding method. The calculated results predict a ballistic transport in boron nanotubes, with a relatively lower resistances as compared to that of a single-walled carbon nanotube. The electron-deficient character in bonding of elemental boron may be attributed to its higher conductivity.

**16:30**

**K16 9 Active Transport Orbitals in Electron Propagator Calculations on Molecular Wires.** YURI DAHNOVSKY, *Department of Physcs & Astronomy, University of Wyoming* V.G. ZAKRZEWSKI, *Department of Chemistry, Kansas State University* ALEXEY KLETSOV, *Department of Electrical Engineering, University of Wyoming* J.V. ORTIZ, *Department of Chemistry, Kansas State University* YURI DAHNOVSKY AND ALEXEY KLETSOV COLLABORATION, V. J. ORTIZ AND V. G. ZAKRZEWSKI COLLABORATION, Ab initio electron propagator methodology may be applied to the calculation of electrical current through a molecular wire. A new theoretical approach is developed for the calculation of the retarded and advanced Green functions in terms of the electron propagator matrix for the bridge molecule. The calculation of the current requires integration in a complex half-plane for a trace that involves terminal and Green function matrices. Because the Green function matrices have complex poles represented by matrices, a special scheme is developed to express these ''matrix poles'' in terms of ordinary poles. An expression for the current is derived for a terminal matrix of arbitrary rank. For multi-terminal terminals, the analytical expression for the current is given in terms of pole strengths, poles and terminal matrix elements of the electron propagator. It is shown that Dyson orbitals with high pole strengths and overlaps with terminal orbitals are most responsible for conduction of electrical current.

**16:42**

**K16 10 Electron Propagator Calculations on Molecular Wires.** J.V. ORTIZ, V.G. ZAKRZEWSKI, *Department of Chemistry, Kansas State University, 111 Willard Hall, Manhattan, KS 66506-3701* ALEXEY KLETSOV, *Department of Electrical Engineering, University of Wyoming, 1000 E. University Avenue, Laramie, WY 82071* YURI DAHNOVSKY, *Department of Physics & Astronomy/3905, University of Wyoming, 1000 E. University Avenue, Laramie, WY 82071* J. V. ORTIZ AND V. G. ZAKRZEWSKI COLLABORATION, YURI DAHNOVSKY AND ALEXEY KLETSOV COLLABORATION, Several molecular wires are studied by an itelectron propagator method using a non-self-consistent formalism for the calculation of Keldysh functions. This approach is based on diagrammatic approximations for describing electron correlation in a bridge molecule that have been successful in the itab initio determination of electron binding energies. In this work, we compute nonequilibrium Keldysh functions in order to find the dependence of current on applied voltage for particular molecular wires. Quantum chemical calculations are performed for several molecular bridges and require additional computational method development of established electron propagator techniques. The extended molecule approach is adopted. Results are compared with experimental data and other quantum chemical approaches, especially those based on density functional theory.

**16:54**

**K16 11 Molecular conductance at finite voltage: bias driven evolution of Kohn-Sham-orbitals** MAX KOENTOPP, *Rutgers University, Department of Chemistry* FERDINAND EVERS, *Institute of Nanotechnology, Research Center Karlsruhe, Germany* KIERON BURKE, *Rutgers University, Department of Chemistry* Ground state density functional theory calculations yield the exact electron density if the exact exchange-correlation functional is employed. The evolution of the equilibrium density with parametric changes in the Hamiltonian, e.g. realized by a change in the electrostatic potential, can provide crucial information about transport properties, like the Coulomb blockade. To test our ideas, we perform model calculations using the quantum chemistry package TURBOMOLE for a diode molecule, which exhibits the structure of a double quantum dot and has been investigated experimentally [1]. In particular, we explain the origin of the characteristic peak structure in the differential conductance. Our results are consistent with the interpretation that the stepwise increase of the conductance occurs when the number of occupied levels of one of the dots, that have an energy above the lowest unoccupied level of the other dot, increases by one. [1] M. Elbing, R. Ochs, M. Koentopp, M. Fischer, C. von Hänisch, F. Weigend, F. Evers, H. Weber, M. Mayor, Proc. Nat. Acad. Sci. USA **102**, 8815 (2005).

**SESSION K17: FOCUS SESSION: SI, GE AND SIGE NANOSTRUCTURES**
**Tuesday Afternoon, 14 March 2006; 313, Baltimore Convention Center at 14:30**
**Leonid Tsybeskov, New Jersey Institute of Technology, presiding**

*Invited Papers*

**14:30**
**K17 1 Dynamic studies of the growth of Si and Ge nanostructures.**
FRANCES ROSS, *IBM TJ Watson Research Center*

By making observations in real time during the growth of nanostructures, it is possible to obtain kinetic data which help us to determine the physical phenomena controlling growth. In this presentation we will describe the growth of Si and Ge nanowires by the vapour-liquid-solid process. Observations were made in a transmission electron microscope during ultra high vacuum chemical vapour deposition of Si and Ge onto substrates covered by Au catalyst. We will show that wire length and diameter are controlled by the diffusion of the catalyst along the wire surfaces, and that this diffusion is driven by a coarsening process. We will compare nanowire growth with the formation of Ge quantum dots by self-assembly during strained layer epitaxy, in which surface diffusion of Ge driven by coarsening also plays an essential role in controlling the structures formed. We will describe spontaneous roughening of Si and Ge nanowire surfaces, a phenomenon which may have analogues in the formation of surface roughness in SiGe alloy thin films. We will finally discuss the control of wire structure for the fabrication of novel devices.

*Contributed Papers*

**15:06**
**K17 2 Silicon nanostructures grown by solid phase epitaxy** PETER HADLEY, *Kavli Institute, TU Delft* YANN CIVALE, *DIMES, TU Delft* LIS NANVER, *DIMES, TU Delft* Silicon nanocrystals can be grown by depositing amorphous silicon (a-Si) on a thin metal layer and then annealing this bilayer. The silicon diffuses through the metal and forms crystals at the metal substrate interface in a process called solid phase epitaxy (SPE). This process has been investigated for many metals (Au, Al, Pd, Ni, Cr, Fe, Co, Ti, V, Rh) and it is observed that the temperature where the significant diffusion takes place is roughly half the eutectic temperature for metals that form a eutectic composition with silicon and it is roughly half the melting temperature for the metals that form a silicide. Using this process, it is possible to deposit crystalline silicon at low temperature. In the past, uniform metal/a-Si bilayers were used. Here we describe experiments where contact windows were opened through silicon oxide before the bilayer was deposited and the metal was patterned before the annealing step. This results in the selective deposition of the silicon crystals. Devices made by this process will be described.

**15:18**
**K17 3 Patterning of Ge nanoparticles by focused electron beam*** NAN JIANG, *Department of Physics, Arizona State University* We demonstrate that Ge nano-particles can be precipitated in $GeO_2$ and $GeO_2$-$SiO_2$ efficiently by the high-energy focused electron beam. The dynamic process of nanoparticle precipitations in these oxides were observed from the TEM images in real time, and analyzed using time-resolved electron energy loss spectroscopy (TREELS). The composition and structure of the precipitated nanoparticles were determined using both high-spatial resolution EELS and diffraction techniques. It was found that the particles are pure Ge and the average size increases slightly with the irradiation time. The dependences of size of nanoparticles on dose and dose rate of electron beam were also statistically analyzed, which is important to optimize experimental conditions to control the size of patterned nanoparticles. The mechanism involving the nucleation and growth process on surfaces is responsible for the precipitation of Ge in $GeO_2$. This was obtained through the thickness dependence of precipitation process. The patterned nanoparticles were then fabricated using the scanning (STEM) mode in a single step process. We noted that the production of Ge nanoparticles using this method is impressively efficient; less than a second is needed to create a large assembly of nanoparticles simultaneously under parallel illumination mode in TEM. Using the focused electron probe, a single particles can be formed within several tens milliseconds.

*This work is supported by NSF Grant DMR0245702.

**15:30**
**K17 4 Near-infrared photoluminescence of germanium nanocrystal synthesized in inverse micelle** ZHIFENG REN, *Boston College* WENZHONG WANG, *Boston College* KEDA WANG, *Boston College* DAXING WANG, *Boston College* In this work we study photoluminescence (PL) properties of Ge nanocrystals prepared via a low-temperature inverse micelle solvothermal route. The as-prepared nanocrystals have an average diameter of $\sim$ 24 nm. Visible- and near-IR PL is observed from the pure nc-Ge samples at room temperature. We present the PL results in the near-IR range. The PL was excited using either 488-nm or 632-nm laser lines. The luminescence signal was dispersed by a grating monochromator and then collected by a liquid-nitrogen cooled Ge detector. The lock-in technique was used with a light chopper at a frequency of 17 Hz. We found two peaks located at $\sim$ 1.37 eV (905 nm) and $\sim$ 1.45 eV (855 nm). Those are within the wavelength range for optical communications. Upon oxidation the relative intensity of the 1.45 eV peak was enhanced. And then the intensity decreased after hydrogen annealing. Meanwhile, the changes of 1.37 eV peak is negligible upon either oxidation or

hydrogen annealing. The origination of the near-IR luminescence peaks is discussed. The 1.45 eV peak is more likely related with the surface states of the nc-Ge particles; while, the 1.37 eV peak is more likely originated from the bulk of the nc-Ge.

**15:42**
**K17 5 Strain driven organization of SiGe islands on ultra-thin Si cantilevers*** CLARK S. RITZ, *University of Wisconsin, Madison* FRANK S. FLACK, MICHELLE M. ROBERTS, DONALD E. SAVAGE, MAX G. LAGALLY, Silicon/germanium 3-D islands have long been studied, both to improve understanding of growth mechanisms in strained epitaxial films and for potential applications as quantum dots (QDs). Self assembly of these QDs into ordered arrays is technologically important, and has been partially achieved through various forms of substrate strain patterning. We experimentally study the effects of substrate local compliancy on the organization of epitaxially grown Ge and Si(1-x)Ge(x) QDs. We form the QDs through the Stranski-Krastanov growth mode on single-crystal ultra-thin Si cantilevers with thicknesses on the order of 20nm. Films are deposited using molecular beam epitaxy and ultra-high vacuum chemical-vapor deposition (CVD) to grow islands on one or both sides of the cantilevers, respectively. Both types of samples show QD ordering along cantilever edges; however, CVD-grown films exhibit additional ordering. Angled SEM imaging shows a strong anti-correlation between the positions of islands grown on the top and bottom faces of the cantilevers. The crystallographic orientation of the cantilevers also plays a role, as islands order better when edges are aligned along [100] (the soft elastic direction). Results will be interpreted in the context of continuum elasticity theory.

*Supported by DOE

**15:54**
**K17 6 Controlled Movement of SiGe/Si Microtubes in Suspension** MINRUI YU, ROBERT BLICK, *Department of Electrical and Computer Engineering, University of Wisconsin-Madison* Microtubes are potential vehicles for chemical or drug delivery. By applying electric potentials on specially arranged electrodes, SiGe/Si microtubes suspended in liquids are moved in a controllable fashion to designated positions. Such manipulation mechanism is also applicable to smaller entities such as nanotubes.

**16:06**
**K17 7 Field Emission from a Nanomechanical Pillar*** HYUN KIM, HUA QIN, ROBERT BLICK, *Laboratory for Molecular Scale Engineering, Electrical and Computer Engineering, University of Wisconsin-Madison* MICHAEL WESTPHALL, LLOYD SMITH, *Department of Chemistry, University of Wisconsin-Madison* We have measured the field emission in a nano-electromechanical structure in which a nanometre silicon pillar oscillates in between the source and drain electrodes. The device consists out of a mechanically flexible pillar with a length of some 200 nm and a diameter of some 50 nm and allows for mechanical resonant excitations at radio frequencies (10 $\sim$ 1000 MHz) and mechanical clocking of the field emitted electrons. Operation of the device at room temperature in the frequency range of 300 $\sim$ 400 MHz is presented. For AC and DC drive, the current shows a rich frequency dependent response. A modified Fowler-Nordheim field emission curve is observed and attributed to the effect of oscillating pillar excited by an alternating electric field.

*This work was supported by AFOSR (F49620-03-1-0420)



***Invited Papers***

**16:18**
**K17 8 Silicon Nanowire Devices.**
THEODORE KAMINS, *Quantum Science Research, Hewlett-Packard Laboratories, Palo Alto CA 94304*

Metal-catalyzed, self-assembled, one-dimensional semiconductor nanowires are being considered as possible device elements to augment and supplant conventional electronics and to extend the use of CMOS beyond the physical and economic limits of conventional technology. Such nanowires can create nanostructures without the complexity and cost of extremely fine scale lithography. The well-known and controllable properties of silicon make silicon nanowires especially attractive. Easy integration with conventional electronics will aid their acceptance and incorporation. For example, connections can be formed to both ends of a nanowire by growing it laterally from a vertical surface formed by etching the top silicon layer of a silicon-on-insulator structure into isolated electrodes. Field-effect structures are one class of devices that can be readily built in silicon nanowires. Because the ratio of surface to volume in a thin nanowire is high, conduction through the nanowire is very sensitive to surface conditions, making it effective as the channel of a field-effect transistor or as the transducing element of a gas or chemical sensor. As the nanowire diameter decreases, a greater fraction of the mobile charge can be modulated by a given external charge, increasing the sensitivity. Having the gate of a nanowire transistor completely surround the nanowire also enhances the sensitivity. For a field-effect sensor to be effective, the charge must be physically close to the nanowire so that the majority of the compensating charge is induced in the nanowire and so that ions in solution do not screen the charge. Because only induced charge is being sensed, a coating that selectively binds the target species should be added to the nanowire surface to distinguish between different species in the analyte. The nanowire work at Hewlett-Packard Laboratories was supported in part by the Defense Advanced Research Projects Agency.

*Contributed Papers*

**16:54**

**K17 9 Carrier transport in Ge nanowires / Si substrate heterojunction** E.-K. LEE, B. KAMENEV, L. TSYBESKOV, *New Jersey Institute of Technology* S. SHARMA, T.I. KAMINS, *Hewlett-Packard Laboratories* Semiconductor nanowires (NWs) attached to lattice-mismatched single-crystal substrates form quasi-one-dimensional (QOD) heterojunctions (HJs) where efficient structural relaxation might occur due to high surface-to-volume ratio. Current-voltage characteristics in Ge NW/(p+)Si samples with nearly micron-long Ge NWs exhibit metal-type conductivity with ohmic behavior and little conductivity temperature dependence. In contrast, Ge NW/(n+)Si samples display significant change in conductivity as a function of temperature with an activation energy up to 200 meV. In a narrow temperature interval near 150 K we observed current instabilities and oscillations for Ge NW/(n+)Si. At higher temperatures we find negative differential photoconductivity at low forward biases. Our experimental results are explained using a model of nearly ideal Si substrate/Ge NW hetero-interfaces.

**17:06 sica, Universidade de São Paulo**

**K17 10 A theoretical study of Si and Ge nanowires.** A. FAZZIO, J. T. ARANTES, CEDRIC ROCHA LEÃO, ANTÔNIO J. R. DA SILVA, *Instituto de Física, Universidade de São Paulo* We have performed a systematical itab initio study of the electronic and structural properties of pure Ge and Si nanowires (NWs), as well as Ge nanowires doped with Mn atoms. All our results are obtained via total energy Density Functional Theory (DFT) calculations within the generalized gradient approximation and pseudopotentials. The growth directions for all wires were considered to be along the (110) direction, and they present a hexagonal cross section formed by the intersection of <111> and <001> planes, with all the dangling bonds saturated with H atoms. We have considered three different diameters of SiNW's of similar shapes: 2.01 nm, 2.67 nm e 3.61 nm. In particular, we analyze how their properties, such as dispersion relations, band gaps and structural properties, like nearest neighbor distances, vary with the diameter. Similar calculations were also performed for the Ge NWs. In this latter case we have also investigated Mn doping. We focused on tetrahedral interstitial and substitutional sites, and conclude that the most stable position for Mn is substitutional at the surface of the nanowire.

**17:18**

**K17 11 Single-hole tunneling and Coulomb blockade in the strain-relaxation-induced quantum ring** GUOHUA WANG, D. TAMBE, A. ZASLAVSKY, V. SHENOY, *Department of Physics and Division of Engineering, Brown University* D. SYPHERS, *Physics Department, Bowdoin College* We fabricated an ultrasmall Si/SiGe strained vertical quantum dot in the Coulomb blockade regime, where strain relaxation in the SiGe quantum well creates a ring-like confinement potential. [1] The resonant tunneling characteristics contains features near the threshold due to single-hole tunneling and Coulomb blockade. The features are steps in one bias polarity and peaks in the other, which we attribute to the differences in the dynamic occupation of the dot due to double Si barrier asymmetry. The spacing of the features gives the charging energy of the quantum ring. When magnetic fields are applied parallel to the tunneling direction, the evolution of the single-hole tunneling features with magnetic fields reveals cusps arising from the angular-momentum transition of the single-particle ground state of the quantum ring in the magnetic field, and the periodicity of the cusps in magnetic field is consistent with the calculated one from h/e, the magnetic flux quantum. Unlike single-carrier tunneling into quantum dots, our data on the tunneling into a quantum ring show no evidence of a singlet-triplet transition. [1] J. Liu et al, Phys. Rev. Lett. 89, 096804 (2002).



**SESSION K18: FOCUS SESSION: DILLON MEDAL SYMPOSIUM**
**Tuesday Afternoon, 14 March 2006; 315, Baltimore Convention Center at 14:30**
**Hiroshi Watanabe, Kyoto University, presiding**

*Invited Papers*

**14:30**

**K18 1 Stimuli Responses of Topology-Controlled Polymer Networks and Liquid Crystalline Gels.**
KENJI URAYAMA, *Kyoto University*

In this talk I will present and discuss the stimulus-response relationships of topology-controlled polymer networks and liquid crystalline gels. I will assess several modern entanglement theories of rubber elasticity on the basis of the multi-axial stress-strain data of end-linked polydimethylsiloxane (PDMS) networks with well-characterized structures. The dynamics of guest linear PDMS in host PDMS networks will also been discussed as a function of mesh size and molecular mass of guest chains. I will also demonstrate the highly extensible or damping elastomers of PDMS by simply controlling the topological characteristics such as the conformation of network chains, the amount of trapped entanglement and pendant chain. Furthermore, I will present the volume transition accompanying the shape variation induced by nematic-isotropic transition in liquid crystalline gels. I will also reveal the electrically-driven deformation coupled to director rotation in nematic gels.

*Contributed Papers*

**15:06**

**K18 2 Self-Assembly of Magnetic Particles into Polymer Chains and Networks** JACK DOUGLAS, *Polymers Division, NIST* WOLFGANG LOSERT, JUSTIN STAMBAUGH, *Department of Physics, University of Maryland* KEVIN VAN WORKUM, *Polymers Division, NIST* The increasing demand to manufacture structures at the nanoscale has made it necessary to pursue new fabrication strategies based on self-assembly. Although it is generally appreciated that this type of ordering process relies on the interplay of directional and isotropic interactions to guide the organization process, the theoretical principles governing this process remain uncertain. There is clearly a need for the development of itreal model systems exhibiting self-assembly and for their intensive investigation by experimental and simulation studies, in conjunction with analytic modeling. Since particle size is not an intrinsic limitation in this type of study, we investigate the self-assembly of vertically vibrated magnetic 'beads' (spheres with embedded magnets) into dynamic polymer chains where the effective temperature of the fluid is determined by the shaking velocity. Self-assembly is assumed to be described by equilibrium polymerization and we perform Monte Carlo simulations for this model fluid at thermodynamic equilibrium. The experiments, simulations and analytic calculations lead to a self-consistent description of the self-assembly process in this fluid. We regulate polymer branching by adding beads having relatively short embedded magnets that are characterized by appreciable itmultipoleinteractions in addition to the dipole interaction.

**15:18**

**K18 3 Electrical Properties of Poly(ethylene oxide)-based Ionomers as Single Ion Conductors** RALPH H. COLBY, SHICHEN DOU, SHIHAI ZHANG, ROBERT J. KLEIN, JAMES P. RUNT, KARL T. MUELLER, *Materials Research Institute, Pennsylvania State University* Polyethers, such as poly(ethylene oxide) (PEO) are of interest for development of advanced lithium batteries because $Li^+$ ions have facile transport in this media. We make ionomers based on PEO by reacting poly(ethylene glycol) (PEG) oligomers with the sodium salt of dimethyl 5-sulfoisophthalate. Since the sulfonate group is covalently bonded to the chain, it is essentially immobile and hence these materials are single-ion conductors. The charge spacing on the chain can be directly controlled by the molar mass of the PEG oligomers (we use M = 400, 600 and 900) used in the synthesis. Conductivity depends strongly on temperature, with nearly identical conductivities in all of our samples at the same $T - T_g$, suggesting that $Li^+$ ion transport is controlled by segmental motion of the PEO. Using the onset of electrode polarization (usually considered a nuisance in dielectric spectroscopy) we quantitatively estimate the free ion concentration and mobility, based on work of MacDonald (1952 & 1974) and Coelho (1983 & 1991). The temperature dependence of the free ion concentration is described by a simple pairing energy, which decreases in going from $Li^+$ to $Na^+$ to $Cs^+$, consistent with larger ions being less strongly bound to the sulfonate groups. The ion mobility shows a Vogel-Fulcher temperature dependence, as anticipated by the polymer's segmental motion controlling ion mobility.

**15:30**

**K18 4 Rheological Properties of Nanotube – Polymer Nanocomposites** RAMANAN KRISHNAMOORTI, TIRTHA CHATTERJEE, *University of Houston* Single walled carbon nanotubes represent the next generation of nanoparticles for the development of polymer nanocomposite materials with potential in multifunctional applications. We have successfully dispersed such SWNTs in various polymer nanocomposites and have recently examined the linear and non-linear viscoelastic measurements. The nanocomposites in the melt state of the polymer demonstrate solid – like behavior beyond a percolation threshold, which in many of these nanocomposites is below 0.1 wt % SWNT. The plateau modulus (corresponding to the stress supported by the percolated nanoparticle network structure) scales as the volume fraction of the SWNTs to the third power and inconsistent with current fractal models. The onset of the non-linear behavior occurs at progressively lower strain values with increasing SWNT concentration and is similar to other filled polymers. Interestingly the recovery of the polymer network following large strain is extremely slow and is similar to materials that are classified as soft- glassy materials.

**15:42**

**K18 5 Non-Newtonian Behavior of Diblock and Triblock Copolymer Solutions** HIROSHI WATANABE, *ICR, Kyoto University* Non-Newtonian flow behavior was examined for butadiene-styrene (BS) diblock and BSB triblock copolymers dissolved in a S-selective solvent, dibutyl phthalate (DBP). Spherical domains of the non-solvated B blocks were arranged on a bcc lattice in both solutions at equilibrium, as revealed from SANS. The solutions exhibited significant thinning under steady flow, which was well correlated with the disruption of the bcc lattice detected with SANS. The lattice disruption was most prominent at a shear rate comparable to the frequency of B/S concentration fluctuation. For the BS/DBP solution, the recovery of the lattice structure after cessation of flow was the slowest for the most heavily disrupted lattice, as naturally expected. In contrast, for the BSB/DBP solution, the recovery rate was insensitive to the magnitude of lattice disruption. This peculiar behavior of the BSB solution suggests that the rate-determining step of the recovery in this solution is the transient B/S mixing required for reformation of the S bridges connecting the B domains.

**15:54**

**K18 6 Arm Retraction of Star and Dangling Polymers in the Absence of Dynamic Dilution** DANIEL A. VEGA, *Department of Physics. Universidad Nacional del Sur. CONICET. Argentina* The dynamic response of model polymer networks containing low contents of star shaped and linear dangling polymers was studied through stress relaxation experiments. As compared with their melts, the behavior of star and dangling polymers leads to a dynamic response with unprecedented large relaxation times. By comparing data of star melts with those corresponding to stars and dangling chains residing in polymer networks, the effects of dynamic dilution were clearly identified. Since in polymer networks the dynamic dilution effect is suppressed, we were able to experimentally test the validity of the potential for arm retraction proposed by Pearson and Helfand.

**16:06**

**K18 7 Consequences of Switchable Solvent Quality on the Self-Assembly of Block Copolymers in a Nematic Liquid Crystal**

**Solvent** JULIA KORNFIELD, The microstructure of a diblock copolymer having a coil and liquid crystalline blocks dissolved in liquid crystal (LC) solvent is exceptionally sensitive to changes in the LC order; the quality of the solvent changes discontinuously across the LC phase transitions. This ''switchable solvent quality'' manifests itself in the nanostructure and rheology of solutions of AB diblocks with a polystyrene (PS) block (''coil'' type) and a side-group liquid crystalline polymer block (SGLCP) dissolved in the LC solvent 5CB. The nematic order of the solvent presents a large entropic penalty to solvation of the PS block, but in the isotropic phase it is a good solvent for PS. The SGLCP is soluble in both the nematic and isotropic phases. In these block copolymers, the LC solvent switches from being strongly selective toward the SGLCP block to being a good solvent for both blocks at the isotropization point. Pairwise thermodynamic interactions between the LC solvent, PS, and the SGLCP are inferred from the ternary phase diagram of homopolymer solutions in 5CB. In the nematic phase, unfavorable 5CB-PS interactions dominate at all concentrations. In the isotropic phase, segregation occurs even though 5CB is a good solvent for both blocks driven by either the slight preference of isotropic 5CB for SGLCP at $c < c^*$ or SGLCP-PS interactions at $c > c^*$.

**16:18**

**K18 8 Swelling and Elasticity of Entangled Polymer Networks** MICHAEL RUBINSTEIN, *University of North Carolina* JONATHAN CAMPBELL, *Massachusetts Institute of Technology* SERGEY PANYUKOV, *Russian Academy of Sciences* We develop and solve a molecular model for nonlinear elasticity of entangled polymer networks, called non-affine slip-tube model. Each chain passes through a sequence of slip-links. The topological constraints imposed by neighboring network chains on a given one are represented by the confining potential acting on the slip-links. This topological potential restricts fluctuations of the network chains to the non-affinely deformed confining tube and changes upon network deformation. The non-affine tube model puts softer restriction on swelling gels, leading to larger equilibrium swelling ratio. It also predicts that weakly-entangled networks initially swell following the dependencies of entangled gels, but as soon as affine length reaches the size of network strand, further swelling is described by unentangled gel relations. The non-affine tube model predicts stronger concentration dependence of elastic modulus, $G$, than affine model, as well as weaker dependence of $G$ on preparation concentration. The non-affine tube model also predicts a cross-over at the preparation condition to a much stronger concentration dependence of elastic modulus, $G$, upon de-swelling and weaker dependence of $G$ on preparation concentration.

**16:30**

**K18 9 Electric Field Response of Electroclinic Liquid Crystal Elastomers** BANAHALLI RATNA, *Naval Research Laboratory* CHRISTOPHER SPILLMANN, JAWAD NACIRI, Supramolecular ordered assemblies such as liquid crystal elastomers provide an excellent framework for incorporating anisotropy as well as functionalities in materials that respond to external stimuli. Electroclinic Liquid Crystal Elastomers (ELCEs) are of particular interest due to their ability to exhibit linear actuation under an applied voltage. The crosslinked elastomer network consists of chiral liquid crystal mesogens attached to a polymer backbone and exhibiting a chiral smectic A phase with large field induced tilt angle. The response of these materials to electric field and their mechanical properties will be discussed.

**16:42**

**K18 10 Brownian dynamic simulations of electrophoresis and electro-stretching of DNA molecules in polymer gels.** RONALD LARSON, *University of Michigan* RICHARD GRAHAM, *University of Leeds* We derive a model for the motion of long DNA chains entangled in a concentrated gel matrix in the presence of a strong electric field. The model is adapted from a tube-based slip-link approach, which was originally intended to model the rheology of entangled polymer fluids, and is suitable for solution by Brownian dynamic simulation. We account for the constraining effect of the surrounding matrix, motion due to the electric field and finite extensibility of the DNA chain. We are able investigate the effect of molecular weight and field strength on the DNA drift velocity in a constant electric field, along with molecular stretching in an oscillating field. Both examples have applications in DNA separation and sequencing. Our approach includes a detailed treatment of the chain end motion through the matrix, which our simulations demonstrate has a significant role in the DNA dynamics, particularly in oscillating fields. The model provides a convenient formalism for further refinements. For example, large fields may tend to cause hernia-like chain loops to protrude from the main tube. Furthermore, to model matrices comprised of linear polymers we can include the effect of constraint release, in which the confinement experienced by the DNA is diminished by the motion of the matrix chains.

**16:54**

**K18 11 Diffusion and Equilibration in Surfactant-Bearing Interfaces** NITASH BALSARA, BENEDICT REYNOLDS, MEGAN RUEGG, CLAYTON RADKE, *University of California, Berkeley* The efficacy of surfactants for stabilizing interfaces between immiscible fluids depends on both thermodynamic and dynamic effects. Dynamic effects are especially important when the fluids are immiscible high molecular weight polymers. Block copolymers are used to stabilize interfaces between immiscible polymers. The chain-like character of polymers leads to molecular entanglement, which leads to extremely slow dynamics. We have prepared two surfactant-bearing polymeric interfaces that are initially out of equilibrium. The distance between the interfaces was varied from 50-600 nm, and the transport of the surfactant molecules was measured by dynamic secondary-ion mass spectroscopy. This transport depends on diffusion coefficients and the depth of the thermodynamic potential wells that trap the surfactant molecules at the interfaces. The diffusion coefficients were measured in independent experiments. The depth of the thermodynamic potential well was calculated using self-consistent field theory (SCFT), which required Flory-Huggins interaction parameters and statistical segment lengths measured by small angle neutron scattering. This enables a comparison of our experimental interfacial transport measurement and theoretical predictions with no adjustable parameters.

**17:06**

**K18 12 Thermodynamically Self-Consistent Theory of Crystalline Polymer Blends*** THEIN KYU, *University of Akron* Thermodynamically self-consistent theory has been developed to determine phase diagrams of binary crystalline polymer blends. The original Flory diluent theory, although captures the liquidus line, is unable to account for the solidus line due to the inherent assumption of complete immiscibility of solvent in the solid crystal. This over-simplification has led to the $\chi$ parameter obtained from the melting point depression curve to be at variance with the $\chi$ parameter by small-angle neutron scattering. The present theory

takes into account all possible interactions such as amorphous-amorphous, crystal-amorphous, amorphous-crystal, and crystal-crystal interactions to predict various phase diagrams involving liquid-liquid, liquid-solid, and solid-solid coexistence regions bound by liquidus and solidus lines. It was found that the crystal-amorphous interaction is the major contributor to the melting point depression rather than the conventional Flory-Huggins $\chi$ parameter. However, in the limit of the complete insolubility of the solvent in the crystal phase, the original Flory diluent theory is recovered. In collaboration with Rushikesh Matkar, University of Akron.

*Supported by NSF DMR 05-14942

**17:18**
**K18 13 Polymer nano-adhesion promoted by surface mobility**
KEIJI TANAKA, TOSHIHIKO NAGAMURA, *Kyushu University* KYUSHU UNIVERSITY TEAM, We here propose a novel nano-adhesion technique on the basis of enhanced surface mobility in polymer films. As materials, monodisperse polystyrene and deuterated polystyrene (PS and dPS) with number average molecular weight of 29k were used. The surface and bulk glass transition temperatures were 294 and 373 K, respectively. PS bilayers were prepared, and were annealed at a temperature between the surface and bulk Tgs for a given time. Then, interfacial adhesion strength (G) was measured. In addition, adhesion measurement by a scanning force microscope using a probe tip covered with the PS layer was made. In this case, the adhesion area was also on nanometer level. Hence, this experiment is denoted as nano-adhesion hereafter. For both experiments, G value first increased with increasing time and then reached a constant. This implies that segments moved across the interface even at a temperature below the bulk Tg and thus adhesion took place at the interface. To confirm this, the interfacial evolution for the (PS/dPS) bilayers was examined by dynamic secondary ion mass spectroscopy. Since G value was linearly proportional to interfacial thickness, it was claimed that the adhesion at the bilayer interface was mainly governed by the interfacial thickening. Interestingly, G value by nano-adhesion measurement was much larger than that for a bilayer at a given time. The difference can be explained in terms of the completeness of the interfacial formation.

## SESSION K19: FOCUS SESSION: III-V MAGNETIC SEMICONDUCTORS III
**Tuesday Afternoon, 14 March 2006; 316, Baltimore Convention Center at 14:30**
**Brian Kirby, Los Alamos National Laboratory, presiding**



***Invited Papers***

**14:30**
**K19 1 Exchange interactions of DMS alloys in the GW approximation.***
MARK VAN SCHILFGAARDE, *Arizona State University*

Dilute Magnetic semiconductors are a new but little understood class of materials, and in particular the origin of ferromagnetism in these materials. As we will show, the LSDA combined with the rigid-spin approximation fails to predict the observed magnetism in many of these materials, and a key question is whether the failing is due to the approximations made, or is something else going on? The best understood of DMS is zincblende $Mn_xGa_{1-x}As$, with $x \lesssim 0.1$. Optimally grown thin films have been recently shown to exhibit conventional temperature-dependent magnetization behavior with $T_c \sim 170$K. Using a standard LDA linear-response technique the LSDA total energy is mapped analytically onto a Heisenberg hamiltonian, which is analyzed for random and partially ordered structures. Temperature-dependent properties were investigated using a form of the Cluster Variation method for the Heisenberg model. The calculated $T_c$ is predicted to increase with $x$ to $x=15\%$, reaching $T_c \sim 250$K. For still larger $x$, $T_c$ is predicted to fall and turn antiferromagnetic when $x > 50\%$. Clustering and spin-orbit coupling are both found to reduce $T_c$. Thus in this case the theory falls in good agreement with observed values for low concentration. An analysis shows the Mn $e_g$ levels are responsible for the antiferromagnetic contribution. We show that suitable short-period superlattices can minimize this contribution, thus signficantly enhancing $T_c$. Many other less well studied DMS alloys–particularly nitride and oxide compounds–have now been reported with $T_c$ exceeding 300K. Several of these cases were investigated, and the LSDA linear-response predicts low $T_c$, typically $T_c < 100$K. Moreover, the LDA results for $Mn_xGa_{1-x}As$ at large $x$ are at variance, with observed ferromagnetism in a quantum dot of MnAs in the zincblende phase[1]. To address validity of the LSDA+rigid approximation, a we present results from a recent implementation of self-consistent *GW* calculation of the spin susceptibility. As will be described *GW* alters the exchange parameters in even in elemental transition metals, and the changes in transition metal compounds can be dramatic. [1]K. Ono et al, J. Appl. Phys. **91**, 8088 (2002).

*In collaboration with Takao Kotani. Supported by the Office of Naval Research

*Contributed Papers*

**15:06**

**K19 2 Combinatorial design of high-temperature ferromagnetic semiconductors from first principles** ALBERTO FRANCESCHETTI, SERGEY DUDIY, SERGEY BARABASH, ALEX ZUNGER, *National Renewable Energy Laboratory, Golden, CO 80401* J. XU, M. VAN SCHILFGAARDE, *Arizona State University, Tempe, AZ 85287* The Curie temperature $T_C$ of Mn-doped GaAs depends strongly on the arrangement of the substitutional Mn dopants. For example, the highest $T_C$ reported so far was attained in thin GaMnAs layers embedded in GaAs. However, an exhaustive search of all possible configurations to find those that maximize $T_C$ is difficult, due to the astronomically large number of possibilities. Here we address this problem by parametrizing the Curie temperature of a set of $\sim$ 50 input configurations, calculated from first principles using linear-response theory and Monte Carlo simulations, in terms of configuration variables (cluster expansion). Once established, this expansion allows us to search almost effortlessly the Curie temperature of arbitrary configurations of Mn dopants in GaAs. We find that the highest $T_C$ ($>$ 350K) is achieved for $(GaAs)_m/(MnAs)_n$ superlattices in the (201) crystallographic orientation, with (m,n)=(4,1). Our general approach of cluster expanding *electronic or magnetic properties* of complex systems opens the way to first-principles combinatorial design of materials with prescribed transition temperatures. This work was supported by DARPA, under NREL contract No. DEAC36-98-GO10337.

**15:18**

**K19 3 First-principles study of the effects on ferromagnetic coupling in Mn/GaAs digital ferromagnetic heterostructure by free holes Injection and Be co-dopant** MEICHUN QIAN, WARREN PICKETT, C.Y. FONG, *Department of Physics, Univ. of California Davis* We use density functional theory to study the effect of free holes injection and Be co-dopant on the ferromagnetic coupling in Mn/GaAs digital ferromagnetic heterostructure (DFH). The injection of free holes is simulated by assigning a range of concentrations of missing electrons in unit cell. The $\delta$-layer doping of Mn atoms in GaAs introduces three spin-polarized hole bands which are the consequence of hybridization between the *d*-states of the Mn atoms and the *p*-states of the nearest neighboring As atoms. The distribution of hole charge density shows that these spin-polarized holes are confined to the vicinity of the Mn $\delta$-layer. After the injection of free holes, the Fermi energy $E_F$ is lowered, then the number of spin-polarized holes in the layer of MnAs is increased monotonously. We characterize the ferromagnetic coupling by the total energy difference between the ferromagnetic and the antiferromagnetic phases, $E_{FA}$, per one pair of Mn atoms. The results of $E_{FA}$, $E_F$, and the projected spin-polarized holes at Mn and the nearest neighboring As atoms are shown as a function of concentration of the injected free holes. We demonstrate the enhancement of the ferromagnetic coupling, which is in agreement with the experimental results of Nazmul et al.[1]. In contract, after the Be co-dopant in Mn/GaAs-DFH, the ferromagnetic coupling is deteriorated. We will give the explanation. [1] A. M. Nazmul et at. Phys. Rev. B67, 241308(R) (2003).

**15:30**

**K19 4 Mn doped InP nanowires: An ab initio study** TOME SCHMIDT, *Universidade Federal de Uberlandia* PEDRO VENEZUELA, *Universidade Federal Fluminense* JEVERSON ARANTES, ADALBERTO FAZZIO, *Universidade de Sao Paulo* We investigated the electronic and magnetic properties of Mn doped InP nanowires. Our study was based on total energy density functional calculations. The Mn dopants were placed substitutionally in In atom sites. We have found that the most energetically favorable position for the Mn atom is near the surface. However, a small amount of Mn atoms will be located at ''bulk-like'' positions in the wire. When the Mn atoms are in ''bulk-like'' positions, the Mn-3d majority-spin-orbitals appear in two different regions of the valence band (VB): about 2.0 eV below the top of the VB and resonant with the top of the VB. In these cases there is also an empty orbital in the gap whit p-character. The total valence spin-densities ($\rho_\uparrow - \rho_\downarrow$), for a single Mn atom in any of the configurations studied here, show a strong localized magnetic moment around the Mn atom site. In order to study the magnetic coupling we also did calculations with two Mn atoms in each cell. For several configurations studied, we concluded that if both Mn atoms are in ''bulk-like'' positions the system presents ferromagnetic ordering. On the other hand, if at least one of the Mn atoms is located near the surface, there is no magnetic ordering or the system is antiferromagnetic.

**15:42**

**K19 5 Ab-initio Prediction of Conduction Band Spin Splitting in Zincblende Semiconductors** ATHANASIOS CHANTIS, MARK VAN SCHILFGAARDE, TAKAO KOTANI, *Arizona State University* We use a recently developed self-consistent *GW* approximation to present systematic *ab initio* calculations of the conduction band spin splitting in III-V and II-V zincblende semiconductors. The spin orbit interaction is taken into account as a perturbation to the scalar relativistic Kohn-Sham hamiltonian. These are the first calculations of conduction band spin splittings based on a quasiparticle approach. We show that the self-consistent *GW* scheme accurately reproduces the relevant band parameters, and is therefore expected to be a reliable predictor of spin splittings. The results are compared to the few available experimental data and a previous calculation based on a model one-particle potential. We show that the commonly used $\mathbf{k} \cdot \mathbf{p}$ hamiltonian is missing contributions, and cannot reliably reproduce the splittings.

**15:54**

**K19 6 Microscopic Hamiltonian for dilute magnetic semiconductors** YUCEL YILDIRIM, *ORNL, UT, FSU* ADRIANA MOREO, *ORNL, UT* GONZALO ALVAREZ, *ORNL* ELBIO DAGOTTO, *ORNL, UT* We formulated a real space Hamiltonian to study the effect of dilute magnetic doping of III-V semiconductors. A p-type valence band is considered and nearest neighbor hopping of holes in a diamond lattice is allowed. The relevant hopping parameters between orbitals are obtained using the Slater technique. Considering the effects of the spin-orbit interactions the number of degrees of freedom per site is reduced from 6 (3 orbitals and two spin orientations for the p bands) to 4 (the four projections corresponding to j=3/2 which is the quantum number of the heavy and light hole bands). The ferromagnetic interaction between the doped magnetic impurities and the spin of the mobile holes is written in the appropriated base. The numerical values of the hopping parameters and Hund interaction are obtained from the literature for the different compounds and, thus, there are no free

parameters. The properties of the materials are calculated using numerical techniques. The newly developed TPEM method allows us to consider lattices as big as 6x6x6 cubes containing 8 ions each. Finite size effects are very small when systems larger than 3x3x3 cubes are considered. For Mn doped GaAs we reproduce the experimentally observed Curie temperatures for all the studied values of effective hole dopings. For Mn doped GaN our results predict above room temperature Tc's.

**16:06**

**K19 7 Electron-mediated ferromagnetism and negative $s-d$ exchange splitting in semiconductors*** SU-HUAI WEI, GUSTAVO M. DALPIAN, *National Renewable Energy Laboratory* Magnetic semiconductors have many unique physical properties that can be used for magneto-optical and spintronic applications. Currently, most of the studies on magnetic semiconductors are focused on hole-mediated FM systems. In this work we discuss several approaches that can enhance the spin-splitting at the conduction band edge and consequently induce electron-mediated stabilization of ferromagnetic semiconductors. We show that kinetic $s-d$ coupling can be introduced through chemical ordering and/or strain. We find that quantum confinement has a large effect on the spin- splitting at the conduction band edge. It can effectively reverse the sign of the conduction band splitting, thus, sheding light on the recent puzzling experimental observation that $s-d$ exchange splitting is negative in semiconductor superlattices. Finally, we show that, using rare-earth elements as magnetic dopants, the symmetry-allowed $s-f$ coupling can lead to a large splitting at the conduction band edge.

*This work is supported by DOE/BES

**16:18**

**K19 8 Theory of magnetic circular dichroism in GaMnAs*** JIAN-MING TANG, MICHAEL E. FLATTÉ, *University of Iowa* We present a newly developed theoretical approach to calculate the magnetic circular dichroism in diluted magnetic semiconductors. Our approach uses the tight-binding method to incorporate the spin-orbit coupling and to obtain the electronic structure over a sufficiently wide energy range. The optical transitions from the valence band to the impurity band that can not be treated in the effective mass theories are included in our calculations. We consider GaMnAs, in which the Mn dopants interact with the GaAs host through the p-d exchange interaction. Our calculations show spin-polarized acceptor states, and resonances within the valence bands. The local density of states near the valence band edge is significantly enhanced by these resonances and qualitatively different from what is obtained from models based on rigid-band shift. We find that the optical transition from deep in the valence band to the impurity band can be stronger than the transition from the valence band edge to the conduction band edge, and can account for the broad positive peak in the magnetic circular dichroism data.

*This work is supported by ARO MURI DAAD19-01-1-0541.

**16:30**

**K19 9 Electrical conductivity in disordered spin-dependent media: application to diluted magnetic semiconductors*** FEDIR KYRYCHENKO, CARSTEN ULLRICH, *Department of Physics and Astronomy, University of Missouri-Columbia* Most theoretical calculations of the electrical conductivity and optical response in diluted magnetic semiconductors (DMSs) treat disorder in relaxation time approximation, using phenomenological relaxation times. However, the role of disorder in III-V DMS materials, particularly the non-trivial effects of spin-dependent scattering from magnetic impurities, requires more careful consideration. In this work we go beyond the relaxation time approximation and derive the electrical conductivity in spin-dependent disordered systems based on the equation of motion for the paramagnetic current-current response function. The general expression relates the full current response function to the set of full system spin-density response functions and is valid for any strength of disorder. We present numerical results for conductivities and dielectric functions in the weak disorder limit, treating carriers with a simple parabolic band model and electron interactions within RPA. For various system parameters we study the relative importance of Coulomb and spin-dependent scattering processes. Special attention is paid to the effects of spatially correlated versus random scattering centers.

*This work is supported by DOE Grant DE-FG02-05ER46213

**16:42**

**K19 10 Ferromagnetism of $Ga_{1-x}Mn_xAs$ and Weiss theory of Curie temperature in the coherent potential approximation*** SZE-SHIANG FENG, MOGUS MOCHENA, *Florida A&M University* Using spin-$\frac{1}{2}$ description of valence holes and Kondo coupling between local spins and carriers, the zinc-blende GaAs-based III-V diluted magnetic semiconductors (DMS) are studied in the coherent potential approximation (CPA). We use the exact Hilbert transformation of the face-centered cubic (fcc) density of states (DOS). Our calculated relation of ground-state energy and impurity magnetization shows that ferromagnetism is always favorable at low temperatures. For very weak Kondo coupling, the density of states (DOS) of the host semiconductor is modified slightly. Impurity band can be generated at the host band bottom only when Kondo coupling is strong enough. Using Weiss molecular theory, we predict a nonlinear relation of Curie temperature with respect to Kondo coupling. Our calculated $T_C$ agrees with measured values very well.

*This work is supported in part by the Army High Performance Computing Research Center (AHPCRC) under the auspices of the Department of Army, Army Research Laboratory (ARL) under Cooperative Agreement Number DAAD 19-01-2-0014.

**16:54**

**K19 11 The ($T = 0$) Phase Diagram of the RKKY model*** DONALD PRIOUR, JR., SANKAR DAS SARMA, *University of Maryland* We consider magnetic moments (e.g. Mn ions in $Ga_{1-x}Mn_xAs$) coupled via the indirect exchange RKKY interaction. We obtain via Monte Carlo the $T = 0$ phase diagram as a function of Mn density $n_i$ and the relative carrier (hole) concentration $n_c/n_i$. As evidenced by a diverging correlation length and the magnetic susceptibility, the boundary between the ferromagnetic (FM) and paramagnetic (PM) phases constitutes a line of zero temperature critical points with behavior very similar to that of a percolation transition. In particular, ferromagnetic clusters increase in size and ultimately coalesce to span the system as the phase boundary is approached from the PM side. In the dilute limit, we find that bulk ferromagnetism vanishes for $n_c/n_i > 0.1$. We also incorporate the local antiferromagnetic superexchange coupling between nearest neighbor magnetic impurities, eliminating ferromagnetism above a Mn density threshold $n_i^{\mathrm{crit}}$. We discuss the impact of a finite carrier mean free path $l$, which we include as a damping factor in the RKKY range function.

Among our findings for an $l$ on the order of the lattice constant $a$ is an expansion of the ferromagnetic region in the phase diagram, though with a suppression of the Curie Temperature $T_c$. We determine the values of $n_i, n_c$, and $l$ which maximize $T_c$.

*Work supported by US-ONR and LPS

**17:06**
**K19 12 Photo-induced ferromagnetism in dilute magnetic semiconductors through Bogoliubov-Valatin transformation**
SUBODHA MISHRA, SASHI SATPATHY, *Department of Physics and Astronomy, University of Missouri-Columbia, Columbia, MO 65211* GOURI S. TRIPATHI, *Department of Physics, Berhampur University, Orissa, India* The dilute magnetic semiconductor is an emerging area of interest because of their possible applications in spintronics. One can control ferromagnetism in these materials by shining light on the sample. The incident light creates extra carriers (electrons and holes) across the band gap, thereby enhancing the carrier-mediated ferromagnetism between the localized Mn moments. The effect is studied by a model Hamiltonian that includes the kinetic energy and Columb interaction terms and the coupling of carriers to light. The Hamiltonian is solved by B-V transformation and then minimizing the ground-state energy by a variational method. We study how the critical temperature varies with light frequency and coupling of light to the carrieres.

**17:18**
**K19 13 Intrinsic Resistance of Magnetic Topological Defects**
ANH KIET NGUYEN, ROMAN SHCHELUSKIN, ARNE BRATAAS, *Norwegian University of Science and Technology* We show that magnetic topological defects in zincblende magnetic semiconductors have an intrinsic resistance against ballistic transport of holes with spin-orbit coupling. The intrinsic resistance is independent of the real space size and detailed shape of the defects, provided that their spatial variations are sufficiently smooth. Rather, it depends on the shape of the defects in the magnetic orderparameter space. For typical parameters, the intrinsic resistance of a domain wall defect is as large as the geometrical resistance and should therefore be experimentally measurable.

## SESSION K20: FOCUS SESSION: MULTIFERROICS II—HEXAGONAL SYSTEMS
**Tuesday Afternoon, 14 March 2006; 317, Baltimore Convention Center at 14:30**
**Alois Loidl, Augsburg University, presiding**



***Invited Papers***

**14:30**
**K20 1 Spin-lattice coupling from first principles.**
CRAIG FENNIE, *Rutgers University*

The hexagonal manganites are a class of multiferroic materials that are simultaneously ferroelectric and antiferromagnetic, in which many physically interesting and potentially technologically relevant manifestations of spin-lattice coupling have been observed. Chromium spinels such as $ZnCr_2O_4$ and $CdCr_2S_4$ are antiferromagnetic and ferromagnetic insulators respectively, each displaying a differrent manifestation of a spin-lattice effect. In $ZnCr_2O_4$ a large magnetically induced phonon anisotropy has been observed while mode-dependant phonon anomalies have been measured in $CdCr_2S_4$. With the continuing advances in theoretical algorithms such as the LSDA+U method and in computational power it is now possible to study structurally and magnetically complex solids such as these using density-functional first-principles methods. Here, I describe a first-principles approach to study the influence of magnetic order on the phonons and dielectric properties of $YMnO_3$, $ZnCr_2O_4$, and $CdCr_2S_4$, our ongoing investigation of the coupling between the magnetic order and polarization in hexagonal manganites, and the search for ferroelectric behaviour in the simple ferromagnet $CdCr_2S_4$.

***Contributed Papers***

**15:06**
**K20 2 Magnetic Phase Diagrams of Hexagonal $ErMnO_3$, $TmMnO_3$ and $HoMnO_3$***
F. YEN, C. R. DELA CRUZ, B. LORENZ, Y. Y. SUN, *Department of Physics and TcSUH, University of Houston* C. W. CHU, *also in LBNL, Berkeley and HKUST, Hong Kong* M. M. GOSPODINOV, *Institute of Solid State Physics, Bulgarian Academy of Sciences, Bulgaria* Multiferroic rare earth manganites have attracted special attention because of the coexistence of ferroelectric and magnetic orders resulting in higher-order magnetoelectric effects and complex phase diagrams at low temperature. We investigate the magnetic phase diagrams of $RMnO_3$ (R = Er, Tm, Ho) and show that all phase boundaries are well determined by sharp changes in their dielectric properties proving the existence of strong spin-lattice coupling. The stability range of the AFM order below the Neel temperature of $RMnO_3$ (R=Er, Tm) extends to far higher magnetic fields than previously assumed. For the case when R = Ho, the magnetic phase diagram was found to be extremely complex including new phases with yet unknown magnetic structures. Hence, we extend the phase diagram to higher external magnetic fields up to 14 Tesla for all of the three aforementioned compounds. The detection of these phase boundary lines is through anomalies of the dielectric constant, DC and AC magnetization.

*Supported by the NSF, DoE and the State of Texas through TCSUH.

**15:18**
**K20 3 Molecular beam epitaxy of $YMnO_3$ on GaN (0001)***
YEWHEE CHYE, TAO LIU, DEBIN LI, KYOUNGNAE LEE, THOMAS MYERS, DAVID LEDERMAN, *Multifunctional Materials Laboratory, Dept of Physics, West Virginia University*

Ferroelectric oxide thin films on semiconductors have attracted considerable attention from the physics and engineering communities for their potential applications in nonvolatile memory, piezoelectric, microwave devices, etc. In this work, we describe the molecular beam epitaxial (MBE) growth of the ferroelectric oxide $YMnO_3$ on GaN. $YMnO_3$ is an obvious candidate of oxide films on GaN because they both have hexagonal lattice structure and the lattice constant of $YMnO_3$ is approximately 2 times that of GaN. $YMnO_3$ films are grown on GaN (0001)-on-sapphire templates using MBE. Y and Mn are evaporated using effusion cells. Reactive oxygen was generated by a RF plasma source. The structure of the films as characterized by in-situ RHEED, x-ray diffraction, and atomic force microscopy will be discussed.

*Supported by the ONR (grant N00014-02-1-0974), the AFOSR (MURI Grant F49620-03-1-0330), and the NSF (grant CIAM 0502825).

**15:30**

**K20 4 Dependence of the Properties of MBE-grown Multiferroic $YMnO_3$/GaN Heterostructures on the Growth Temperature and Post-growth Annealing Processes*** TAO LIU, YEWHEE CHYE, CAMERON KEENAN, THOMAS MYERS, DAVID LEDERMAN, *Multifunctional Materials Laboratory, Dept of Physics, West Virginia University* We report on the molecular beam epitaxy (MBE) of multiferroic $YMnO_3$ on c-plane GaN. Study and understanding of these $YMnO_3$/GaN heterostructures are important for potential applications in multifunctional materials and structures. Atomic force microscopy revealed that the $YMnO_3$ films grown at different temperatures have significantly different morphologies. X-ray diffraction showed that there is a $30^o$ rotation between the unit cells of $YMnO_3$ and GaN. Samples grown at the optimal growth temperature are ferroelectric at room temperature, with a large remnant polarization, and magnetic at low temperatures. The difference between magnetic field-cooled and zero-field-cooled behavior at low temperatures indicates the presence of antiferromagnetic frustration or ferromagnetic behavior. The effects of different growth temperatures and post-growth annealing will be discussed.

*Supported by the ONR (grant N00014-02-1-0974), the AFOSR (MURI Grant F49620-03-1-0330), and the NSF (grant CIAM 0502825).

**15:42**

**K20 5 Structural, ferroelectric, and magnetic properties of epitaxial $YMnO_3$ thin films grown on wurtzite-structure materials** AGHAM POSADAS, JENG-BANG YAU, JUNG HAN, CHARLES AHN, *Yale University* KAREN JOHNSTON, KARIN RABE, *Rutgers University* JEFFREY NEATON, *Lawrence Berkeley National Laboratory* STEFANO GARIGLIO, *University of Geneva* Thin films of the multiferroic oxide $YMnO_3$ have been grown on single crystal substrates with the wurtzite crystal structure, including GaN and ZnO with different polarities. Films have also been grown on the wurtzite derivative 6H-SiC. X-ray diffraction reveals epitaxial, c-axis oriented growth on all of these crystals. The measured ferroelectric polarization is similar to that of single crystal $YMnO_3$, and magnetization measurements reveal frustrated antiferromagnetic ordering in the plane of the film. X-ray diffraction also reveals an epitaxial relationship that is associated with a very large ( $\sim$ 10%) in-plane strain for growth on GaN. This unusual observation is explained by first principles calculations of the strain and bonding energies.

**15:54**

**K20 6 Doping effect on ferroelectric microstructure in $YMnO_3$.** S. MORI, J. TOKUNAGA, Y. HORIBE, *Department of Physics, Osaka Prefecture University* T. ASADA, Y. KOYAMA, *Department of Materials Sceince, Waseda University* T. KATSUFUJI, *Department of Physics, Waseda University* $YMnO_3$ is one of the typical multiferroic materials showing the coexistence of the antiferromagnetic and ferroelcrric orders at low temperature. In this work, we have investigated doping effect on ferroelectric microstructure in $YMnO_3$ by both electron diffraction and real-space imaging techniques. We found that the large ferroelectric domains with several micron meters change into the ferroelectric microdomains with the size of 20-30nm by substituting $Y^{3+}$ ions for $Ca^{2+}$ and $Zr^{4+}$ ions. In addition, diffuse scatterings elongated along both the [110] and [001] directions were found, which were similar to those found in $YMn_{0.825}Ti_{0.175}O_3$ exhibiting the enhanced magnetocapacitance effect. [1] The lattice instability in the Mn triangle lattice induced by the partial substitution at $Y^{3+}$ site should have some influence on the coupling between magnetic and ferroelectric orders. [1] S.Mori et al., Phys.Rev.B (in press).

**16:06**

**K20 7 Multiferroicity of $RMn_{1-x}Ga_xO_3$ (R = Ho, Y) and $Ho_{1-x}Y_xMnO_3$** H.D. ZHOU, J.C. DENYSZYN, JOHN. B. GOODENOUGH, *The University of Texas at Austin* $RMn_{1-x}Ga_xO_3$ (R = Ho or Y) and $Ho_{1-x}Y_xMnO_3$ single-crystals have been prepared. The experimental results revealed that the $c$ axis decreases with increasing temperature with a larger $|dc/dT|$ above $T_C$ than below it. This shows that the cooperative $MnO_5$ site rotations responsible for the ferrielectricity expend energy to induce the ferroic $R^{3+}$-ion displacements along the $c$ axis. Ga doping raises the ferrielectric Curie temperature $T_C$ and the Mn-spin reorientation temperature $T_{SR}$ while lowering $T_N$ of the Mn spins and the Ho magnetic ordering temperature $T_2$. The data show (i) an important coupling between the $Mn^{3+}$-ion and $Ho^{3+}$-ion spins; (ii) a $T_{SR}$ that is driven by the cooperative $MnO_5$ site rotation and $R^{3+}$-ion displacements that control the $c$ lattice parameter. Y doping favors the formation of $P6_3'$cm' magnetic phase below $T_N$, and enhances the temperature region of $P6_3'$cm' phase. Therefore, $T_{SR}$ for the transition from $P6_3'$c'm to P6'$_3$cm' phase increases with increasing $x$, but $T_{SR}$ disappears for $x > 0.8$ samples because the $P6_3'$cm' phase already occupies the whole temperature region below $T_N$. The thermal conductivity data also support an enhanced spin-lattice interaction above $T_N$ in the geometrically frustrated (GF) Mn-spin system.

**16:18**

**K20 8 Multiferroicity in the Mixture of Orthorhombic and Hexagonal $RMnO_3$ (R=rare earths)** CHENGLIN ZHANG, GUHA SABYASACHI, SANG-WONK CHEONG, *Rutgers University* Orthorhombic perovskite $RMnO_3$ (R = Tb, Dr) shows an incommensurate magnetic/lattice modulation below $\sim$ 40 K and a lock-in transition below $\sim$ 25 k. The system becomes ferroelectric at the lock-in transition. On the other hand, hexagonal $RMnO_3$ (R = Ho-Lu, Y) exhibits ferroelectricity with a much higher transition temperature ( $\approx$ 1000 K) and a magnetic ordering transition at $\sim$ 100 k. We will report the results of our comprehensive study of

what happens when these two types of ferroelectric 113 compounds are mixed.

**16:30**
**K20 9 Magneto-thermal conductivity in multiferroic $HoMnO_3$** YOUNG JAI CHOI, PETER A. SHARMA, SANG-WOOK CHEONG, It is well known that multiferroic $HoMnO_3$ exhibits a rich phase H-T diagram. We have discovered that thermal conductivity of hexagonal $HoMnO_3$ shows an unconventional diversity of anomalies at low temperatures under external magnetic fields. In order to understand the origin of these anomalies, we have performed comprehensive characterization experiments on the multiferroic compound, including measurements of dielectric constant, DC and AC magnetic susceptibility, and polarization as functions of temperature and applied magnetic field.

**16:42**
**K20 10 Magnetoelectric and magnetoelastic effects in a triangular lattice antiferromagnet $CuFeO_2$** T. KIMURA, A.P. RAMIREZ, *Bell Laboratories, Lucent Technologies* J.C. LASHLEY, *Los Alamos National Laboratory* Magnetoelectric and magnetoelastic effects related to a phase transition into noncollinear magnetic phase have been investigated for single crystals of $CuFeO_2$ with a frustrated triangular lattice. $CuFeO_2$ exhibits several long-wavelength magnetic structures related to the spin frustration, and it is found that finite electric polarization, namely inversion symmetry breaking, occurs with noncollinear but not at collinear magnetic phases. This result demonstrates that the noncollinear spin structure is a key role to induce electric polarization, and suggests that frustrated magnets which often favor noncollinear configurations can be plausible candidates for magnetoelectrics with strong magnetoelectric interaction.

**16:54**
**K20 11 Landau Theory of the Magnetic Phases of Hexagonal Rare Earth Manganites*** IRAM MUNAWAR, STEPHANIE CURNOE, *Department of Physics and Physical Oceanography/ Memorial University of Newfoundland* A group theoretical analysis is presented on the magnetic structure of rare earth atoms in the multiferroic hexagonal manganites $RMnO_3$ (R=Ho, Er, Tm, Yb, Sc, Y) which exhibit the coexistence of ferroelectricity ($T_c \sim 900$ K) and antiferromagnetism ($T_N \sim 100$ K). Using Landau theory, a phenomenological model of the free energy based on four one-dimensional magnetic order parameters has been developed. Coupling of the various order parameters leads to complex magnetic field – temperature phase diagrams in qualitative agreement with experimental data. References: [1] S. H. Curnoe and I. Munawar, Magnetic Phases of Rare Earth Hexagonal Manganites, Proceedings of The International Conference on Strongly Correlated Electron Systems SCES '05, July $26^{th}$ - $30^{th}$, 2005, Vienna, Austria, (accepted on July 29, 2005 to be published in Physica B) [2] Manfred Fiebig. (2005) Revival of the magnetoelectric effect, Journal of Physics D: Applied Physics, 38, R123-R152.

*This work was supported by NSERC of Canada

**SESSION K21: COLLOIDS V**
**Tuesday Afternoon, 14 March 2006**
**318, Baltimore Convention Center at 14:30**
**D. Grier, New York University, presiding**

**14:30**
**K21 1 Giant Enhancement of Colloidal diffusion in a Corrugated Optical Vortex** SANG-HYUK LEE, DAVID G. GRIER, *Department of Physics and Center for Soft Matter Research New York University* We experimentally study thermally driven velocity fluctuations of a Brownian particle in a tilted washboard potential. Our system consists of a single fluid-borne colloidal sphere driven by a holographically projected superposition of optical vortices. A single optical vortex is a ring-like optical trap created by focusing a helical mode of laser light. Torque exerted by an optical vortex's orbital angular momentum flux drives a trapped colloidal particle around its circumference. Superposing two optical vortices with opposite helicities and different amplitudes creates a corrugated optical vortex with sinusoidal intensity variations around its circumference. The resulting tilted washboard potential admits both static trapped states and dynamic running states. Digital video microscopy measurements of the resulting particle trajectories reveal a hundred-fold enhancement of the effective self-diffusion coefficient near the static-to-running transition.

**14:42**
**K21 2 Diffusion Limited Branched Polymers*** CARLOS MENDOZA, *Instituto de Investigacion en Materiales, UNAM (MEXICO)* GUILLERMO RAMIREZ-SANTIAGO, *Instituto de Fisica, UNAM (MEXICO)* We introduce an algorithm to construct polymers with defined branching structure and whose morphology is determined by diffusion. We apply this procedure for the case of star-branched polymers and calculate their fractal dimension. We also carried out a finite size scaling analysis and determine the scaling properties of the radius of gyration. This procedure may be useful to construct large branched polymers near their relaxed configurations which in turn may help to determine equilibrium configurations of dilute solutions made of these polymers.

*Supported by DGAPA-UNAM IN110103 & CONACYT 43596-F

**14:54**
**K21 3 A Constant Force Dielectrophoretic Cell** MARIA KILFOIL, VINCENT PELLETIER, ANDREW SCOTT, ALLAN HALDANE, *McGill University* We fabricated an especially designed cell to study colloidal suspension under an isomotive dielectrophoresis force. Under such conditions, the effects of a uniaxial force on gel structure and crystallization can be studied with an absolute control on its magnitude. Since the force is horizontal by design, we can take advantage of the higher resolution on the horizontal axis to obtain more precise particle locations. Preliminary results are shown.

**15:06**
**K21 4 Electric Double Layer Structures near Rough Surfaces: Molecular Dynamics Simulation** DAEJOONG KIM, ERIC DARVE, *Stanford University* S. S. Dukhin in Surface and Colloid Science (1974) mentioned both the possibility of increase in zeta potential due to surface roughness and the possibility of decrease, depending on Debye length relative to surface roughness. In this work we report our results of molecular dynamic (MD) simula-

tions on electric double layer structures near solid surfaces having roughness with the order of magnitude of Debye length. For computational simplicity only counter-ions are present. We computed static and dynamics properties including density profiles of water and ions, electrostatic potential distributions due to ions, polarization density profiles and self-diffusivities of water and ions. We also performed nonequilibrium MD to simulate electroosmotic flows. From electrostatic potential distributions and slip plane locations, we computed zeta potential and found that it decreases with surface roughness. It also showed a dependency on the spatial frequency of surface roughness. For comparison we used the Helmholtz-Smoluchowski relation and found the same trend. Currently we are studying pressure-driven flows, a computational counterpart to streaming current experiments. One of the purposes is to find more exact locations of slip planes by fitting to Poiseuille flow solutions. We are also simulating model systems with co-ions to investigate the possibility of charge inversion and other effects.

**15:18**

**K21 5 Heterogeneities in Two-Dimensional Pinned Liquids** JING-XIAN LIN, *T-12 and T-CNLS, Los Alamos National Laboratory; University of California, Riverside* CHARLES REICHHARDT, *T-13 and T-CNLS, Los Alamos National Laboratory* ZOHAR NUSSINOV, *T-11, Los Alamos National Laboratory* LEONID P. PRYADKO, *University of California, Riverside* CYNTHIA J. OLSON REICHHARDT, *T-12 and T-CNLS, Los Alamos National Laboratory* We introduce a model system in which the amount of heterogeneous motion in a liquid phase just above melting can be controlled directly. Using numerical simulations, we place a two-dimensional assembly of repulsively interacting colloids on a commensurate triangular substrate of pinning sites, and then randomly deactivate a fraction $n_p$ of the pinning sites. Heterogeneous motion is induced when the unpinned colloids melt at lower temperatures than the pinned colloids, and this heterogeneity can be controlled by changing the fraction of active pinning sites. The melting transition occurs in a single step for $n_p = 0$ or 1, and is considerably broadened for partially pinned samples. We measure the noise fluctuations of the dislocation density as a function of time and find a maximum noise power when $n_p = 0.5$. Signatures of a two step melting process appear for up to 3/4 of the pinning sites removed. We also correlate the regions of high mobility with regions of high dislocation density, and analyze the heterogeneity using the Van Hove correlation function.

**15:30**

**K21 6 Computation of Super-Hydrophobic States and Stability*** YONGKANG CHEN, *Portland State University* DANNY BOLLEDDULA, RYAN JENSON, MARK WEISLOGEL, Super-hydrophobic fluid phenomena have been the focus of an increasing number of research investigations over the past decade. Perhaps the greatest achievements recently have come by way of the highly controlled surfaces that can be produced using any one of a number of rapidly expanding surface microfabrication techniques. In this work we present a numerical approach to systematically probe both the states and stability of certain (super- or ultra-) hydrophobic surfaces as they depend on surface porosity, specific surface feature size and geometry, and fluid properties such as 'equilibrium' contact angle and surface tension. Drop stability in terms of critical roll-off angles, advancing and receding contact angles (hysteresis), Bond number, and effective contact angle is computed and used as a measure of 'superhydrophobicity.' Both Wenzel and Cassie hydrophobic states are analyzed by the numerical method.

*Support for this research provide by the National Science Foundation (CTS-0521890)

**15:42**

**K21 7 Design of Porous Wick Structures: Steady Flows*** MARK WEISLOGEL, RYAN JENSON, YONGKANG CHEN, LAWRENCE MELVIN III, Methods of analysis developed for capillary flows in large complex containers for spacecraft are applied to microscale networks of interconnected repeat units to develop design methodologies to compute optimal geometries for high performance microporous materials and structures on Earth. The fundamental transport mechanism in the media is the interior corner geometry. The specific objectives of the research focus on the optimization of high performance wick structures employed in advanced two-phase passive cooling systems for microelectronic thermal control. The analysis employs the governing transport equations in a cell-by-cell approach to compute optimal pore structures in the low saturation limit where the media may be effectively modeled as a nodal network of interconnected interior corners and solved by matrix methods. The 'all analytic' method under development does not employ empirically determined constants or highly varying numerical coefficients as other pore-scale investigations. Example pore geometries solved to date for steady flows clearly identify the origins of the manifold improvements possible in select porous structures. Applications for such methods are also helpful to improving transport processes in porous media such as fabrics and membranes.

*Support for this work provide by the National Science Foundation (CTS-0521890)

**15:54**

**K21 8 Capillary waves at the water liquid-vapor interface** AHMED E. ISMAIL, GARY S. GREST, MARK J. STEVENS, *Sandia National Laboratories* Evidence for capillary waves at the liquid-vapor interface of water is presented from molecular dynamics simulations. The total interfacial width includes a correction term which depends logarithmically on the length $L_\parallel$ of the simulation cell parallel to the interface, and which is inversely proportional to the surface tension $\gamma_{cw}$. Comparison of $\gamma_{cw}$ for system sizes up to $10^5$ molecules to $\gamma_p$, obtained from the difference between the pressure parallel and the pressure perpendicular to the interface, yields adequate agreement only if one fits the interfacial profile to an error function and not to a hyperbolic tangent, as often assumed. Results for $\gamma$ for a number of atomistic three-site (SPC/E, TIP3P, TIP3P-CHARMM, and TIP3P-Ew) and four-site (TIP4P and TIP4P-Ew) non-polarizable water models are compared to experiment for temperatures from 300 K to 500 K, and for a variety of interaction cutoffs and reciprocal-space mesh refinements. Our results show that the SPC/E model is more accurate than the other available three-site models, while the original TIP3P model is closer to experimental data than its more recent parameterizations.

**16:06**

**K21 9 Self-assembly of Colloid-Polymer Mixtures Confined by Soft Walls** YU-QIANG MA, *National Laboratory of Solid State Microstructures, Nanjing University, Nanjing 210093, China* We discuss how to control self-assembled ordering structures in colloid-polymer systems confined by soft walls, and find that with varying the colloidal concentration, the colloidal self- assembly undergoes a series of symmetry-changing transitions, due to the competition between the elastic entropy effect of soft walls and steric packing effect of colloids.

**16:18**

**K21 10 Rheological response of emulsions of drops immersed in electric fields.** ARTURO FERNANDEZ, *The Catholic University of America* Direct numerical simulation is used to examine the temporal response of an emulsion of drops immersed in an electric field. When a drop is immersed in a suspending fluid of different electrical properties, and an electric field is applied, surface electric charges accumulate on the boundary between drop and suspending fluid. These charges, coupled with an electric field, lead to the appearance of electric stresses at the interface between the fluids. When an emulsion is immersed between two plates moving at different velocities, the microstructure and rheological properties depend on the competition between electric and hydrodynamical forces. We present a study of these phenomena for DC and AC electric fields. The effect on microstructure is quantified by the PDF, and on rheological properties by effective viscosity and normal stress difference. The numerical simulations show that fluid shear, electrical properties of both fluids, frequency for an AC electric field, and intensity are the main parameters governing the response of the system.

**16:30**

**K21 11 Applications of Quartz Tuning Forks to Liquid Property Measurements** JAMES BENNETT, LEONID MATSIEV, OLEG KOLOSOV, *Symyx Technologies* Sensor technology for fluid samples often measures a single physical parameter per sensor and for many applications this is sufficient. In some cases however, characterization of the state or condition of a fluid can be improved through the simultaneous measurement of multiple physical parameters. We will discuss our work in the application of flexural mechanical resonators such as quartz tuning forks to the characterization of fluids. We have previously shown that if a tuning fork resonator is immersed in a fluid, the changes in resonator response can be used to determine physical properties of the fluid. We will describe the development of a measurement system based on a tuning fork resonator, the associated electronics and analysis software. This system can provide simultaneous measurement of liquid properties such as viscosity, density, dielectric constant and ac conductivity. We have applied the tuning fork sensor to the characterization of fluids over a range of temperatures and conditions. Simultaneous measurement of viscosity, density and dielectric constant can provide information about the state or condition of the fluid. For example, for motor oils, clear differences in the measured parameters are observed between fresh and used oils and may be correlated to the oil condition.

**16:42**

**K21 12 Phase Segregation and Patterning in Two Dimensional Systems: Competition Between Van der Waals and Electrostatic interactions** SHARON LOVERDE, *Department of Materials Science and Engineering, Northwestern University* FRANCISCO SOLIS, *Department of Biophysics, Arizona State University* MONICA OLVERA DE LA CRUZ, *Department of Materials Science and Engineering, Northwestern University* The formation of heterogeneities on surfaces, such as microdomains found in synthetic and natural lipid membranes, has not yet been yet fully explored from a theoretical point of view. It has been proposed, for example, that lipid rafts arise in membranes due to lipid-lipid and/or lipid-protein interactions. We consider a coarse-grained model of a mixture of charged lipids interacting within a monolayer. We analyze this model both analytically and with molecular dynamics simulations, and find a rich phase diagram. The complex phase behavior is generated by the competition between the short range van der Waals interactions and long range electrostatic interactions. In particular, we observe phase coexistence between an ''ionic gas'' phase with a dense patterned solid phase. We have examined the phase diagram of the system as a function of net charge density and charge asymmetry.

**16:54**

**K21 13 Binary Lennard-Jones Fluids: A Look Through Time Series Analysis*** THEODOROS KARAKASIDIS, ATHANASIOS FRAGKOU, ANTONIOS LIAKOPOULOS, *Hydromechanics Laboratory, School of Engineering, University of Thessaly, 38334 Volos, Greece* In this paper we discuss the dynamical behavior of a binary Lennard-Jones fluid simulated at the atomic scale using Molecular Dynamics. The system was simulated at several fluid states as a function of system density and temperature and its instantaneous temperature was recorded. We report preliminary results on time-series analyses of the instantaneous system temperature as well as of the temperature of its two constituents. In this course we employ both linear (autocorrelation function and power spectrum) and non-linear tools (average mutual information and correlation dimension). It turns out that the time series present a complex $1/f^{\alpha}$ behavior. The dependence of the regimes on the physical state of the system is discussed.

*Acknowledgements: This research has been partially supported by the program ''PYTHAGORAS-EPEA K II'' jointly funded by the European Community and the Greek Ministry of Education.

**17:06**

**K21 14 2D Lennard-Jones as complex liquid** ALEXANDER PATASHINSKI, *Northwestern University* RAFAL ORLIK, ANTONI MITUS, *Polytechnic University, Wroclaw, Poland* MARK RATNER, *Northwestern University* The high viscosity, large relaxation times, and other signature features of complex liquids are associated with substantial local order and long-living significant liquid structures in these liquids. In 3D Lennard-Jones liquids, representing simple liquids, no detectible structural local order in 13-atom clusters was found at the melting line. In contrast to that, the 2D Lennard-Jones liquid appears locally ordered: about half of the atoms are, at any time, in recognizable hexagonal cages. We present results of a study of the statistics and dynamics of local order in 7-atom clusters in 2D Lennard-Jones-based system. The study includes states along a supercritical isotherm in the range of densities where the system changes from disordered liquid to ordered solid state.

**SESSION K22: FOCUS SESSION: MAGNETIZATION DYNAMICS**
**Tuesday Afternoon, 14 March 2006**
**319, Baltimore Convention Center at 14:30**
**Paul Crowell, University of Minnesota, presiding**

*Contributed Papers*

**14:30**
**K22 1 Time-domain diffracted magnetooptic Kerr probing of magnetization dynamics of patterned magnet arrays*** XIAOBIN ZHU, *University of Alberta* FABIAN GIESEN, ZHIGANG LIU, MARK FREEMAN, *University of Alberta* HIROYUKI AKINAGA, *AIST, Japan* We probe the ultrafast magnetooptic Kerr effect in the diffracted spots of a patterned array of magnets, which serve as diffraction grating. This technique, diffracted MOKE, provides valuable information, as the off-specular spots contain the finite spatial frequencies of the magnetic moment configuration [1-3]. In this talk, we will present the D-MOKE study in the time domain of a 2 $\mu$m sized Permalloy square array and a 1 $\mu$m sized Permalloy disk array. The time-domain measurements are performed using a time resolved scanning Kerr microscopy in its spectroscopic mode [4]. Due to spatial averaging, we find that time-domain curve shows faster damping compared with individual magnets. We also find that the sensitivity of the Kerr signal is enhanced at the first order. Through Fourier transformation of the time-domain data, and through comparison with micromagnetic simulation, information about magnetic normal modes in individual magnets is extracted. [1] M. Grimsditch, et al., J. Phys.: Condens. Matter **16** R275 (2004); [2] R. Antosit, et al., Appl. Phys. Lett., **86**, 231101 (2005); [3] N. Kida, et al., Phys. Rev. Lett. **94**, 077205 (2005). [4] W. K. Hiebert, et al., Phys. Rev. Lett., 79, 1134 (1997).

*Supported by NSERC,NRC,CRC,iCORE and AIST

**14:42**
**K22 2 Ultrafast Laser Spin Wave Measurement of Temperature Dependent Magnetic Anisotropy of Half-Metallic Chromium Dioxide** ANNE REILLY, *College of William and Mary* HAILONG HUANG, *College of William and Mary* KEOKI SEU, *College of William and Mary* Recent work has shown that the all-optical ultrafast laser production and detection of spin waves can provide useful measurements of anisotropy in magnetic thin films [1,2]. A pump laser pulse momentarily affects the magnetic anisotropy, perturbing the magnetization, which relaxes towards a new equilibrium by means of coherent oscillation. The coherent oscillation is detected by the magnetoopitcal Kerr effect. We present a study of the temperature dependence of the magnetocrystalline anisotropy of half-metallic CrO2 thin films from temperatures 10 K to 363 K. At higher temperatures, the oscillations are approximately single frequency. The anisotropy constants obtained by analyzing the oscillation frequencies as a function of applied fields using the Landau Lifshitz Gilbert equation agrees with measurements made by other techniques, particularly ferromagnetic resonance. Interesting features of the temperature dependence, as compared to ferromagnetic metals such as Co, Ni and Fe, will be highlighted. 1. M. Van Kampen et al., Phys. Rev. Lett. 88, 227201 (2002) 2. D. Talbayev et al., Appl. Phys. Lett., 86, 182501 (2005)

**14:54**
**K22 3 Interface magnetization switching and precession in Fe/AlGaAs (001)** GUNTER LUEPKE, HAIBIN ZHAO, DIYAR TALBAYEV, *College of William and Mary* AUBREY HANBICKI, CONNIE LI, BEREND JONKER, *Naval Research Laboratory* Understanding of interface magnetic properties is a key for efficient spin-polarized injection in semiconductor spintronic devices. Here, we have measured the reversal process of the Fe interface layer magnetization in Fe/AlGaAs (001) using magnetization-induced second harmonic generation (MSHG), and compared it with the bulk magnetization obtained from magneto-optic Kerr effect (MOKE). The switching characteristics are distinctly different – single step switching occurs at the interface layer, while two-jump switching occurs in the bulk Fe for the magnetic field orientations employed. The different switching processes lead to a deviation angle of 40-85$^o$ between interface and bulk magnetization, which may result from reduced exchange interaction and different magnetic anisotropies at the interface. We also use time-resolved MSHG to investigate the coherent magnetization precession at the interface, and compare with the bulk spin precession obtained from time-resolved MOKE. The different switching behaviors are further revealed in the precession dynamics. The field dependence of precession frequency provides a quantitative analysis of magnetic anisotropies of the interface layer.

**15:06**
**K22 4 Excitation of single-frequency spin waves in exchange-biased IrMn/Co by ultrafast laser repinning** KEOKI SEU, HAILONG HUANG, ANNE REILLY, *Department of Phyiscs, College of William and Mary* We have excited and detected coherent spin waves in exchange-biased IrMn/Co using the all-optical ultrafast laser pump probe technique. The laser pump produces changes in the exchange biasing which launches spin waves which are detected by the magnetooptical Kerr effect. The oscillations are single frequency and can be described according to ferromagnetic resonance equations. Unlike previous work in these systems [1-3], oscillations have been detected when the applied magnetic field is along any direction relative to the pinning axis, including directly along the easy axis, and in fields larger than the magnetic saturation. This is contrary to energetic arguments and predictions from the Landau Lifshitz Gilbert equation [1]. Our suggested mechanism for these oscillations is a destruction and re-pinning of the exchange-bias interaction, introducing a 'kick' required for the magnetization to precess. Evidence of this ultrafast laser repinning will be presented. 1 Ganping Ju, et al., Phys. Rev. B. 62 1171 (2000). 2 M. C. Weber, et al., Eur. Phys. J. B. 45 243 (2005). 3 Ganping Ju, et al., Phys. Rev. Lett. 82 3705 (1999).

**15:18**
**K22 5 Optically induced magnetization dynamics in manganite films studied by time-resolved magneto-optical Kerr effect 1.** DIYAR TALBAYEV, HAIBIN ZHAO, GUNTER LUEPKE, *The College of William and Mary* ADYAM VENIMADHAV, JUN CHEN, QI LI, *Pennsylvania State University* Magnetization precession is the fastest way to switch magnetic memory elements. We studied optically-induced magnetization dynamics in epitaxial $La_{2/3}Sr_{1/3}MnO_3$ (LSMO) and $La_{2/3}Ca_{1/3}MnO_3$ (LCMO) films on different substrates. Both uniform precession of magnetization and spinwaves were observed. The precession frequency is governed by magnetic anisotropy that depends on the strain state of the films. In LSMO, compressive and tensile strain induces uniaxial normal-to-plane anisotropy. Similar behavior was observed in

tensile-strained LCMO. However, a large in-plane anisotropy was discovered in LCMO on $NdGaO_3$. The field-dependent relaxation times of the decaying precession are in 100 – 1400 ps range. The corresponding Gilbert damping parameter is field-dependent and decreases sharply with increasing field in LSMO films. The research was supported in part by the National Science Foundation and the Department of Energy.

**15:30**

**K22 6 Laser induced ultrafast magnetization dynamics in CoPt multilayer** A. BARMAN, S. WANG, H. SCHMIDT, *School of Engineering, University of California Santa Cruz, 1156 High Street, Santa Cruz, CA 95064* A. BERGER, *Hitachi Global Storage Technologies, San Jose Research Center, 650 Harry Rd., San Jose, CA 95120* We study femtosecond laser induced magnetization dynamics in CoPt multilayer structures in the presence of an externally applied magnetic field. The dynamics revealed three different time regimes. The first few hundred femtoseconds show an instantaneous demagnetization, followed by a quick recovery within next few picoseconds. Subsequently, an oscillatory motion comes into play whose frequency is field dependent and attributed to the precessional motion of magnetization. The sudden heating with laser pulses causes a rapid change in the anisotropy of the sample that results in a change in the equilibrium orientation of magnetization and triggers a precession. The precessional dynamics completely decays within 100ps leaving it to a slower recovery of magnetization. Analysis of the time-resolved magnetization shows a single precessional mode at higher fields, while several modes become apparent at lower fields. The dependence of different frequency modes and their damping on the applied field are studied to understand the dynamics in more detail. The effects of the anisotropy field distribution and different multilayer compositions on the dynamic response will also be discussed.

***Invited Papers***

**15:42**

**K22 7 Ultrafast coherent control of Spin- and magnetization dynamics.**
THEO RASING,* *Insitute for Molecules and Materials*

The manipulating of the electron spin is not only relevant for magnetic storage but may also lead to the development of novel electronic devices with new characteristics (so-called spintronics). Therefore, the investigations of the physical mechanisms underlying the manipulation of electron spin in ferromagnets, semiconductors and hybrid ferromagnet/semiconductor structures constitute at present an exciting area of research. Due to the fact that in antiferromagnets no angular momentum is associated with the order parameter, spin dynamics in these materials is intrinsically much faster than in ferromagnets, expanding the area of spin-dynamics even more [1]. Femto-second laser excitation opens the way to excite magnetic systems on a time scale much shorter than fundamental time scales such as spin-lattice relaxation or precession times. This has already lead to surprising and exciting results like changes in magnetization on a sub-picoscond time scale [2]. Fs laser pulses can also be used to generate short magnetic field pulses, that allow coherent control of the magnetization dynamics [3]. Recent progress in this area will be discussed, demonstrating in particular the use of time resolved magneto-optical methods to investigate the static and dynamic properties of magnetically ordered structures and the possibility of direct spin manipulation with optical fields[4,5]. [1] A. V. Kimel, A. Kirilyuk, A. Tsvetkov, R. V. Pisarev, and Th. Rasing, Nature 429 850 (2004). [2] Spin Dynamics in Confined Magnetic Structures I-II, edited by B. Hillebrands and K. Ounadjela (Springer-Verlag, Berlin, 2002-2003). [3] Th. Gerrits, H. A. M. van den Berg, J. Hohlfeld, L. Bär, and Th. Rasing, Nature 418, 509 (2002). [4] A. Kimel, A. Kirilyuk, P.A. Usachev, R.V. Pisarev, A.M. Balbashov and Th. Rasing, Nature 435, 655 (2005) [5] F. Hansteen, A.V. Kimel, A. Kirilyuk and Th. Rasing, PRL 95, 047402-1 (2005). **Acknowledgements** This work was partially supported by the European IST network SPINOSA, the RTN network DYNAMICS, the Russian Foundation for Basic Research (RFBR), Nederlandse Organisatie voor Wetenschappelijk Onderzoek (NWO) as well as Stichting voor Fundamenteel Onderzoek der Materie (FOM).

*Radboud University Nijmegen.

***Contributed Papers***

**16:18**

**K22 8 Ferromagnetic Resonance of a Single Nanoscale Magnet Driven by an RF Spin-Transfer Torque.** JACK SANKEY, *Cornell University* P.M. BRAGANCA, I.N. KRIVOROTOV, A.G.F GARCIA, D.C. RALPH, R.A. BUHRMAN, By applying a spin-polarized RF current through Py/Cu/$Py_{0.65}Cu_{0.35}$ spin-valve nanopillar devices approximately 100 nm in cross section, we have excited ferromagnetic resonance modes in the Cu-doped Py ''free'' layer. We detect the resonance via a DC voltage generated through mixing of the RF current and the oscillating magnetoresistance from the precessing magnetization. We find two different regimes of behavior. For small applied DC currents, we observe simple ferromagnetic resonance. The frequency-widths of the resonant peaks are related to the intrinsic magnetic damping, with the damping decreasing approximately linearly with DC current. In this regime we can also characterize the nonlinearities of the resonances from peak-shape analysis at larger RF currents. For DC currents large enough to excite spontaneous magnetic precession, we find a second regime in which the applied RF current produces phase locking, with a distinctive line shape. In both regimes, we observe dynamical modes not seen previously in DC-driven dynamical measurements.

**16:30**

**K22 9 FMR spectroscopy of individual nanopillars** GREGOIRE DE LOUBENS, VLADIMIR V. NALETOV,*OLIVIER KLEIN, *CEA Saclay, Service de Physique de l'Etat Condense* We have performed FMR spectroscopy on perpendicularly magnetized hybrid nanopillars (lateral sizes range between 500 nm and 2 $\mu$m) using a Magnetic Resonance Force Microscope. The sensitivity of this technique allows us to measure an individual sample. Firstly, 100 nm thick Permalloy (Py) disks sandwiched by Cu have been

studied. It is found that the lowest energy mode is an edge mode localized at surfaces instead of being the uniform precession. The study of the dynamics in the non linear regime shows that the damping of this edge mode decreases with increasing power, which favors its excitation at high power level compare to the other modes. Secondly, Py100/Cu10/Py10 (nm) devices showing GMR effect have been measured and we have studied the spectral changes induced by high DC current densities J flowing through them. FMR spectra at J=0 are compared to those of single magnetic layer disks and qualitatively interpreted. The influence of the Oersted field and of the temperature increase when J$\neq$ 0 is quantified and a small effect of spin transfer is extracted.

*Also at Physics Department, Kazan State University

**16:42**

**K22 10 Ferromagnet dynamics in a driven spin valve** JOERN N. KUPFERSCHMIDT, SHAFFIQUE ADAM, PIET W. BROUWER, *Laboratory of Atomic and Solid State Physics, Cornell University, Ithaca, NY, 14853* The magnetoresistance of a ferromagnet/normal-metal/ferromagnet trilayer depends on the relative orientation of the two magnetic moments. We analyze out-of-plane precession of the magnetization for a soft ferromagnetic layer in such a geometry, where the system is driven by an alternating charge current. We consider the effect of both spin-torque and spin-pumping on the magnetization dynamics and find that these have signatures in the magnetoresistance.

**16:54**

**K22 11 Strong interactions between a nanomagnet and a microcavity mode*** ÖNEY O. SOYKAL, M.E. FLATTÉ, *Department of Physics and Astronomy, University of Iowa, Iowa City, IA* We consider the interaction of a nanomagnet with a single mode of a microcavity in a fully quantum treatment. We derive the interaction Hamiltonian from Maxwell's equations by introducing the fully quantized forms of the spherical electromagnetic solutions. For a nanomagnet acting as a macrospin, within a cavity roughly 1 $mm^3$ in volume, the magnet-microwave mode coupling is $\sim 10^{-7}$eV. Strong coupling can therefore be seen if the quality factor of the cavity exceeds 1000.

*Work supported by an ARO MURI.

**17:06**

**K22 12 Magnetic permeability and dielectric permittivity of ferrite materials in millimeter waves.** KONSTANTIN KOROLEV, *Institute of Radioengineering and Electronics of RAS, Moscow, Russia; Tufts University, Medford, MA 02155, USA* LAKSHMI SUBRAMANIAN, MOHAMMED AFSAR, *Tufts University, Medford, MA 02155, USA* Magneto-optical approach for the measurements of complex magnetic permeability and dielectric permittivity of solid and powdered strontium ferrite materials have been performed in the frequency range of 34-120 GHz. Free-space quasi-optical millimeter wave spectrometer equipped with a backward wave oscillator as a tunable source of coherent radiation provides the transmittance spectra in transverse magnetic field up to 7.5 kOe. Frequency dependences of dielectric and magnetic parameters of strontium ferrites have been calculated by matching theoretical curves to the experimental transmittance spectra. Shift of the ferromagnetic resonance to higher frequencies and the broadening of the zone of strong absorption in transverse magnetic field have been observed for solid ferrite materials. A relation between the specific gravity and the saturation of magnetization for these materials has been found. The shift of ferromagnetic resonance frequency vs. specific gravity has been observed. The correlations between complex dielectric permittivity and magnetic permeability and density of the samples have been observed.

**17:18**

**K22 13 Multiphoton antiresonance in large-spin systems** CHRISTIAN HICKE, MARK DYKMAN, *Michigan State University* We show that multiphoton resonance in a $S > 1$ spin system is accompanied by anticrossing of the responses in resonating states. This anticrossing accompanies the standard anticrossing of quasienergy levels. It leads to antiresonance: the ratio of the vibration amplitude to the modulation amplitude in one of the states becomes much less and in the other state much larger than in the weak-modulation limit. The response anticrossing can be observed by adiabatically sweeping the modulation frequency through multiphoton resonance. The shape and overall width of the dip/peak of the response as function of frequency strongly depend on the modulation amplitude. The effect has no analog in two-level systems and is sensitive to the parameters of the spin. It is most pronounced when the spin Hamiltonian in the absence of driving is $H_0 = \omega_0 S_z + \gamma S_z^2$. In this case several states experience multiphoton resonance at a time. The higher-order terms in $S_z^2$ lead to smearing of the antiresonance. We also study the response of the spin when the modulation is sharply turned on. The antiresonance leads to oscillations of the response with the multiphoton Rabi frequency. Their amplitude strongly depends on the modulation amplitude. The effect is compared with multiphoton antiresonance in a nonlinear oscillator [1]. [1] M. I. Dykman and M. V. Fistul, Phys. Rev. B **71**, 140508(R) (2005).

## SESSION K23: QUANTUM MAGNETS: BEC AND 2D

**Tuesday Afternoon, 14 March 2006**
**320, Baltimore Convention Center at 14:30**
**Collin Broholm, Johns Hopkins University, presiding**

**14:30**

**K23 1 Thermodynamic and Magnetostriction Measuremetns of the Bose-Einstein Condensate $NiCl_2$-4SC$(NH_2)_2$** V.S. ZAPF, *National High Magnetic Field Lab at Los Alamos National Lab* V. CORREA, *NHMFL, Tallahassee, FL* D. ZOCCO, M. JAIME, N. HARRISON, A. LACERDA, *NHMFL, LANL* C.D. BATISTA, *T-11, LANL* T. MURPHY, E. PALM, S. TOZER, *NHMFL, Tallahassee, FL* A. PADUAN-FILHO, *Universidade de Sao Paulo, Brazil* We investigate Bose-Einstein condensation (BEC) of magnons in the organic magnet $NiCl_2$-4SC$(NH_2)_2$ (DTN). For magnetic fields applied along the tetragonal c-axis, the antiferromagnetically (AFM) ordered Ni spins can be recharacterized as a system of effective bosons with a hard-core repulsive interaction where the AFM transition corresponds to BEC. New, detailed data of the field-temperature phase diagram of DTN have been taken by means of thermodynamic measurements to dilution fridge temperatures. The magnetic field-temperature quantum phase transition line $H_c$-$H_{c1} \sim T^{\alpha}$ approaches a power law at low temperatures, with an exponent $\alpha$ at the quantum critical point that is consistent with the BEC theory prediction of $\alpha = 3/2$. In addition, new magnetostriction data at dilution refrigerator temperatures

will be presented. In the AFM ordering regime, field-induced $2^{nd}$ order changes in the lattice parameters create field-dependent AFM and spin-orbit coupling parameters, which can in turn distort the phase diagram at high fields.

**14:42**

**K23 2 High Magnetic Field Susceptibility Measurements for $BaCuSi_2O_6$** K. M. PURCELL, C. MARTIN, T. P. MURPHY, E. C. PALM, S. W. TOZER, *NHMFL-FSU* S. E. SEBASTIAN, I. R. FISHER, *Stanford University* We have measured the change in magnetic susceptibility of the spin gap system $BaCuSi_2O_6$ at high magnetic fields (33T) utilizing the change in the resonant frequency of a tunnel diode oscillator (TDO). At temperatures below T$\sim$ 3K, measurements reveal the presence of a critical field $H_{c1}$, characterized by a jump in magnetic susceptibility. The evolution of $H_{c1}$ with temperature is in good agreement with the previous magnetization and specific heat measurements and with the theoretical predictions for the realization of Bose-Einstein condensate by the spin system of $Cu^{2+}$ dimers. This technique provides the opportunity for future investigation of this material at high pressures.

**14:54**

**K23 3 Dimensional reduction at the BEC quantum critical point in $BaCuSi_2O_6$.** SUCHITRA SEBASTIAN, IAN FISHER, *Stanford University* NEIL HARRISON, MARCELO JAIME, PETER SHARMA, *NHMFL, Los Alamos National Laboratory* CRISTIAN BATISTA, *Theoretical Division, Los Alamos National Laboratory* LUIS BALICAS, *NHMFL, Tallahassee* NAOKI KAWASHIMA, *Institute for Solid State Physics, University of Tokyo* We present results on the magnetic spin dimer system $BaCuSi_2O_6$, which can be tuned across a Bose-Einstein condensation (BEC) quantum critical point (QCP) to an ordered BEC of spins by applying an external magnetic field. Experimental results reveal a continuous crossover in critical scaling behaviour near the QCP from 3d to 2d BEC universality, indicating that dimensionality itself is an emergent property at the QCP of this particle density-tuneable BEC. Geometrical frustration leading to inter-layer decoupling is identified as the mechanism responsible for this unique manifestation of a lower dimensional QCP in the 3d $BaCuSi_2O_6$ spin system. While the theoretical concept of dimensional reduction has been extensively discussed in many different contexts as a route to low dimensionality in bulk materials, this is the first experimental realisation of dimensionally reduced criticality.

**15:06**

**K23 4 Field-Induced Quantum Criticality in a Two-Dimensional Antiferromagnet*** TAO HONG, MICHEL KENZELMANN, MATTHEW BOULOUBASIS, DANIEL REICH, COLLIN BROHOLM, *Johns Hopkins University* MATTHEW STONE, *Oak Ridge National Laboratory* EMILY DUNKEL, SUBIR SACHDEV, *Harvard University* We describe neutron scattering measurements on the two-dimensional spin gap antiferromagnet piperanzium hexachlorodicuprate (PHCC) in the vicinity of quantum critical point at which the spin gap is closed by an applied magnetic field. We measure the energy and damping of the propagating $S_z = 1$ mode above the spin gap; both quantities become strongly temperature dependent at the critical field. The temperature dependence of the mode energy is successfully described by a self-consistent Hartree-Fock theory of interacting spin excitations.

*Work at the Johns Hopkins University was supported by the NSF under Grants No. DMR-0306940. Work at Harvard University was supported by NSF under Grants No. DMR-0537077. Work at NCNR was supported by NSF under Grants No. DMR-0086210

**15:18**

**K23 5 Magnon decay in gapped quantum spin systems** ALEXEI KOLEZHUK,*SUBIR SACHDEV, *Harvard University, Department of Physics* In the O(3) $\sigma$-model description of gapped spin systems, $S = 1$ magnons can only decay into *three* lower energy magnons. We argue that the symmetry of the quantum spin Hamiltonian often allows decay into *two* magnons, and compute this decay rate in model systems. For a realistic model describing two-dimensional spin dimer material $(C_4H_{12}N_2)Cu_2Cl_6$ (known as PHCC), we compare our results for the momentum-dependent magnon linewidth with recent measurements by Stone *et al.* (e-print cond-mat/0511266) and extract new information on the exchange coupling pattern in this material. For $S = 1$ Haldane chains, we show that two-magnon decay is allowed in the full lattice description, even though it cannot be induced by any allowed term written in powers and gradients of the $\sigma$-model field. We present estimates for the behavior of the magnon linewidth in Haldane gap chains and discuss relation to the recent experimental work.

*Supported by the Heisenberg Fellowship of DFG; on leave from Institute of Magnetism, National Academy of Sciences of Ukraine.

**15:30**

**K23 6 Impurity induced Knight shifts in 2D antiferromagnets** SEBASTIAN EGGERT, *University Kaiserslautern, Germany* FABRIZIO ANFUSO, *Chalmers University, Gothenburg, Sweden* The local response to a uniform field around vacancies in the two-dimensional (2D) spin-1/2 Heisenberg antiferromagnet is determined by numerical quantum Monte Carlo simulations as a function of temperature. It is possible to separate the Knight shifts into uniform and staggered contributions on the lattice which are analyzed and understood in detail. The contributions show interesting long and short range behavior that may be of relevance in NMR and susceptibility measurements. For more than one impurity remarkable non-linear enhancement and cancellation effects take place. We predict that the Curie impurity susceptibility will be observable for a random impurity concentration even in the thermodynamic limit.

**15:42**

**K23 7 Variational ground states of 2D antiferromagnets in the valence-bond basis*** JIE LOU, ANDERS SANDVIK, *Boston University* We use a variational method to study two-dimensional $S = \frac{1}{2}$ Heisenberg antiferromagnets in the valence bond basis. The wave function is of the form $|\psi\rangle = \Pi h(x_{ij}, y_{ij})(i,j)$, where $(i,j)$ represents a singlet formed by the spins at sites $i$ and $j$; $(i,j) = 1/\sqrt{2}\,(\uparrow_i\downarrow_j - \downarrow_i\uparrow_j)$, and $h(x_{ij}, y_{ij})$ is the amplitude corresponding to a bond coneenting two spins with seperation $(x_{ij}, y_{ij})$. The form $h \sim 1/r^p$, where $r$ is the distance, was studied prevously. The best variational energy was obtained for $p = 4$. Now we optimize all $h(x,y)$by combining a standard Newton method and a conjugate gradient method. For systems with up to 16 $\times$ 16 spins, the energy of the optimized wave function deviates by

less than 0.1% from the exact ground state energy. The spin-spin correlations are also very well reproduced. The exponent $p = 3$ in agreement with recent Monte Carlo simulations. We also investigates this class of wave functions for a quantum-critical bilayer model.

*Supported by NSF grant No. DMR-0513930

**15:54**

**K23 8 Dynamics of $S = 1/2$ Antiferromagnetic clusters*** LING WANG, ANDERS SANDVIK, *Boston University* A site diluted 2-d Quantum Heisenberg Antiferromagnet undergoes a Neel to disordered phase transition at the classical percolation density $p^*$, since the sublattice magnetization $m$ has a nonvalishing value on the percolating cluster. Although this implies that some of the exponents of the transition are equal to those of classical percolation, exponents involving dynamics are non-classical. We investigate the quantum dynamics of diluted systems at the percolation point by Lanczos diagonalization, generating histograms of the singlet to triplet excitation gap $\Delta$ for clusters of different size $N$. We investigate the finite-size scaling of the average and typical $\Delta$, to determine the dynamic exponent $z$. In a clean d-dimensional system with Neel order, $\Delta$ scales as $1/L^z$ with $z = d$, which arises from the quantum rotor states when the rotational symmetry has not been broken. As a direct generalization, it has been proposed that $z = D_f$ holds for the percolating clusters, where $D_f$ is the fractal dimensionality; $D_f = 91/48$. This has not been confirmed numerically, however, and there remains the possibility that there could be other excitations of the clusters leading to $z > D_f$. In addition to the Lanczos calculations, we also investigate the the distribution of the stagged susceptibility $\chi(\pi,\pi)$ and the stagged structure factor $S(\pi,\pi)$, which give information on the quantum dynamics through sum rules.

*Supported by NSF grant No. DMR-0513930

**16:06**

**K23 9 Variational Study of the Two-dimensional Hubbard Model at half-filling** YUNG-CHUNG CHEN, *Department of Physics, Tunghai University, Taiwan* H.C. CHIEN, *Physics, National Tsing Hua University, Taiwan* CHIH-TIN SHIH, *Physics, Tunghai University, Taiwan* The ground-state properties of the half-filled two-dimensional Hubbard model is systematically investigated by the variational wave function with d-wave supercondcting and anti-ferromagnetic correlations. The enhanced pairing correlation observed in the previous Gutzwiller approximation is found to be strongly suppressed by the doublon-holon and antiferromagnetic correlations. In order to check this result, power-Lanczos method is employed to improve the variational wave function. It is found that that pairing is not stable against antiferromagnetic long-range order. Possible models for the theory Gossamer superconductivity will be discussed in this paper.

**16:18**

**K23 10 Investigations of the 2D Isinglike magnet, $ZnMn_2O_4$** WILLIAM RATCLIFF, YING CHEN, YIMING QIU, QING HUANG, JEFFREY LYNN, *National Institute of Standards and Technology, NCNR* SUNMOG YEO, SANG CHEONG, *Rutgers University, Department of Physics* PAULA PICCOLI, ARTHUR SCHULTZ, *Argonne National Lab, IPNS* $ZnMn_2O_4$ crystallizes at high temperatures in the spinel structure. At lower temperatures, it undergoes a Jahn Teller distortion which lowers its symmetry to tetragonal. At lower temperatures ($T_N \sim 60$K), the system orders magnetically. Fits to the order parameter, line shape of powder diffraction peaks, and the direct observation of rods of scattering in single crystal diffraction experiments show the system to be two dimensional. This is likely due to an interplay of orbital ordering and frustration. In this talk, I present the results of recent neutron diffraction experiments performed on this compound and discuss the nature of the magnetism.

**16:30**

**K23 11 Novel magnetic structure of one monolayer Fe on Ir(111)** STEFAN HEINZE, KIRSTEN VON BERGMANN, ELENA VEDMEDENKO, MATTHIAS BODE, ROLAND WIESENDANGER, *Institute of Applied Physics, University of Hamburg, Jungiusstrasse 11, 20355 Hamburg, Germany* GUSTAV BIHLMAYER, STEFAN BLÜGEL, *Institut für Festkörperforschung, Forschungszentrum Jülich, 52425 Jülich, Germany* Due to the interplay between symmetry, nearest-neighbor spacing, and hybridization with the substrate surprising magnetic ground-states can occur for monolayer films such as the two-dimensional antiferromagnetism of Fe on W(001) [1]. Much more complex magnetic structures have been predicted for monolayer thick films of an antiferromagnet on a triangular lattice given e.g. by an (111) fcc surface. To our knowledge, however, there is no experimental proof. Here, we report a novel, nanometer scale magnetic structure for one monolayer Fe on Ir(111). Based on the observed contrast in spin-polarized scanning tunneling microscopy (SP-STM) measurements a giant magnetic unit cell consisting of 15 Fe atoms is suggested. Our first-principles calculations show that the proposed magnetic state is indeed more favorable than all possible magnetic solutions describable by the classical Heisenberg model including interactions between neighbors of arbitrary distance. We find that the $3d - 5d$ hybridization between the Fe ML and the Ir substrate plays a key role for the unusual magnetic behavior. [1] A. Kubetzka *et al.*, Phys. Rev. Lett. **94**, 087204 (2005).

**16:42**

**K23 12 Magnetic order and lattice anomalies in the $J_1$-$J_2$ model system $VOMoO_4$** ALESSANDRO BOMBARDI, *Diamond Light Source* LAURENT CHAPON, *ISIS-Rutherford Laboratory* IRENE MARGIOLAKI, *ESRF* CLAUDIO MAZZOLI, *ESRF* SABINE GHONTIER, *CNRS* FABIENNE DUC, *CNRS-Toulouse* PAOLO RADAELLI, *ISIS-Rutherford Laboratory* High resolution x-ray and neutron powder diffraction measurements were performed on polycrystalline $VOMoO_4$. Below $\simeq 40$ K the system orders in a simple Néel antiferromagnetic state (propagation vector $\vec{k} = 0$), indicating a dominant role of the nearest-neighbor interactions. The order is three dimensional but the reduced saturated magnetic moment $m$ of 0.41 (1) $\mu_B/V^{4+}$ at 2 K indicates strongly 2D character and enhanced quantum fluctuations. On cooling, there is no evidence of a reduction of the crystal symmetry. However, neutron diffraction indicates an anomalous evolution of the lattice parameters, which can be related to the onset of magnetic correlations.

**16:54**

**K23 13 Field-induced thermal transport in low-dimensional antiferromagnets*** ALEXANDER CHERNYSHEV, *UC Irvine* Recent thermal transport experiments in a number of low-dimensional antiferromagnets such as $K_2V_3O_8$, $Nd_2CuO_4$, $Pr_2CuO_4$, $TlCuCl_3$ and others have shown that the low-temperature thermal conductivity can be strongly increased by a modest magnetic field. It was suggested that this effect could be due to the field-induced heat transport by spin excitations. We show that in most of the reported cases the observed enhancement

of the thermal conductivity is not of spin, but of phononic nature. That is, the increase in the thermal conductivity occurs because of the decrease of the scattering of phonons on spin excitations. This decrease is due to the field-induced gaps in the spin-excitation spectra. Our calculations reproduce quantitatively all characteristic field-dependencies observed in experiments such as increase of the thermal conductivity and its saturation in higher fields. A number of suggestions for future experiments is made.

*This work is supported by DOE under grant DE-FG02-04ER46174

**17:06**

**K23 14 Magnetic Properties of a Novel Fe(II) itmeso-tetra(4-pyridyl)porphyrin Network** DUSAN DANILOVIC, CHYAN LONG LIN, TAN YUEN, *Department of Physics, Temple University* LONG PAN, JING LI, *Department of Chemistry & Chemical Biology, Rutgers University, Piscataway, NJ 08854* Magnetic properties of Fe(II) itmeso-tetra(4-pyridyl)porphyrin [Fe(TpyP)], a newly discovered metalloporphyrin network, were investigated using magnetic susceptibility $M(T)/H$, isothermal magnetization $M(H)$, and heat capacity $C(T)$ measurements. The crystal structure of Fe(TpyP) at room temperature is orthorhombic with a space group Cmca (No. 64). And this network gives rise to an unprecedented two-dimensional paddle-wheel-like pattern (a $4^4$ topology). The results of $M(T)/H$ on powder samples of Fe(TpyP) show that the effective moment $\mu_{eff}$ of $Fe^{2+}$ is 5.52 $\mu_B$ at 340 K, close to the expected value for a high spin $Fe^{2+}$ ($S = 2$) ion. $\mu_{eff}$ increases to 5.90 $\mu_B$ as $T$ decreases to the range of 170 K $< T <$ 220 K, and then decreases monotonically as $T$ decreases further. The behavior of $\mu_{eff}$ in the high temperature region may be attributed to a positive $Fe^{2+}$-$Fe^{2+}$ coupling. The low field ($H \leq$ 4 kG) $M(T)/H$ data reveal an anomalous behavior of this compound in the low temperature region which seems spin-glass-like. A small hysteresis was observed in $M(H)$ measured at 2 K. No anomaly was seen in the $C(T)$ data from 1.6 to 25 K.

**17:18**

**K23 15 Signatures of one-dimensional localization of magnetically quantized carriers in graphite: power-law hopping mechanism.** ARTHUR HEBARD, *University of Florida* XU DU, *Rutgers University* DMITRI MASLOV, RONOJOY SAHA, *University of Florida* We present results of a transport study on highly oriented pyrolytic graphite (HOPG) in ultra-quantum limit magnetic fields (B$>$ 8T) applied along the c-axis (z direction). For temperatures in the range 2K$<$ $T <$ 20K, the measured in-plane resistivity $\rho_{xx}$ follows a metallic-like $T^{1/3}$ dependence while the c-axis **resistivity** $\rho_{zz}$ exhibits an insulating-like linear temperature dependence. We show that the c-axis transport behavior can be explained within the context of a power-law hopping mechanism, in which phonons cause localized electrons to hop over distances on the order of the localization length with a frequency of $1/\tau_\phi \propto T$. The corresponding resistivity behaves as $\rho_{zz.} \propto \tau_\phi \propto T^{-1}$. The temperature range for this picture to hold is justified by the semimetal-like properties of HOPG. Both the in-plane and c-axis behavior agree well with the model of electrons almost localized by strong magnetic fields in the presence of long-range disorder, which predicts that $\rho_{xx} \propto \rho_{zz}^{1/3} \propto T^{1/3}$ [1] [1] S. S. Murzin, JETP Lett. **45**, 283 (1987).

**SESSION K24: POLYMER NANOMATERIALS II**
**Tuesday Afternoon, 14 March 2006**
**321, Baltimore Convention Center at 14:30**
**Azar Alizadeh, General Electric, presiding**

**14:30**

**K24 1 Coffee Break**

**15:06**

**K24 2 Cracks and Topological Defects in Nematic Nanotube Gels** A.G. YODH, M.F. ISLAM,*A.M. ALSAYED, Z. DOGIC, M. NOBILI, J. ZHANG, FANGFU YE, T.C. LUBENSKY, *Department of Physics & Astronomy, University of Pennsylvania* We have created [1] and studied [2] lyotropic nematic gels composed of aligned single wall carbon nanotubes (SWNTs) in a crosslinked N-isopropyl acrylamide (NIPA) polymer matrix. These composites are created by dispersing surfactant stabilized SWNTs at low concentration in a solution of NIPA monomer that is then polymerized and crosslinked to form a gel, and then inducing a temperature-dependent volume-compression transition of the NIPA gel. Quantitative measurements of SWNT order parameter reveal a concentration-dependent crossover from isotropic to nematic phases. Due to the coupling of nematic order and elasticity of the polymer matrix, we also observe: (i) undulations and then cusping of the gel sidewalls, (ii) a nematic director that evolves as the gel sidewalls deform, (iii) networks of surface cracks that are orthogonal to the nematic director, and (iv) fissures at the sidewall cusps and associated topological defects that would not form in liquid nematics. This work is supported by grants from NSF (MRSEC DMR 05-20020 and DMR-0505048) and NASA NAG8-2172. References: 1. Islam, Alsayed, Dogic, Zhang, Lubensky, Yodh, PRL **92**, 088303 (2004). 2. Islam, Nobili, Ye, Lubensky, Yodh, PRL **95**, 148301 (2005).

*Current Address: ChemE & MSE, Carnegie Mellon University

**15:18**

**K24 3 Composite Polymer Nanofibers with Carbon Nanotubes and Titanium Dioxide Particles with Photocatalytic Activity** SHAHAR KEDEM, YARON PAZ, YACHIN COHEN, *Technion, Israel* Composite nanofibers containing Multi Walled Carbon Nanotubes (MWCNT) and nanometric $TiO_2$ particles dispersed in poly(acrylonitrile) (PAN) were prepared by the electrospinning (ES) technique. The fabricated nanofibers, the diameters of which were in the 20-200 nm range, contained well-oriented nanotubes and spherical $TiO_2$ nanoparticles in close proximity. The carbon nanotubes stabilize the polymer nanofibers against photodegradation by UV radiation, as compared with nanofibers composed only of PAN and $TiO_2$. Preliminary results on the photocatalytic activity of these nanofibers in decomposition of organic molecules will be reported.

**15:30**

**K24 4 The Impact of Sample Preparation on Polymer Carbon Nanotube Nanocomposites.** CHANG-UK LEE, *University of Tennessee, Knoxville* MARK DADMUN, *University of Tennessee, Knoxville* The dispersion of multi-walled carbon nanotubes (MWNTs) in a polymer matrix is a critical parameter that impacts the ability of that MWNT to improve the properties of the polymer matrix. In this study, the impact of the sample preparation process on the dispersion and properties of the resultant nanocomposite is discussed. Additionally, the impact of intermolecular interactions

between the MWNT and polymer matrix on the mechanical properties of the polymer nanocomposites was investigated. Polymer nanocomposites composed of 1 wt% MWNT and poly(styrene-co-4-vinyl phenol) (PS-co-VPh) random copolymers were prepared by three different methods, including melt-mixing and solution casting. The MWNT are either oxidized to incorporate oxygenated defects or utilized as received. DMA results suggest that solution casting allows the formation of more intermolecular hydrogen bonding between MWNT and polymers than melt mixing. DMA data also suggests that more intermolecular hydrogen bonding results in improved mechanical properties of the resultant polymer nanocomposites.

**15:42**

**K24 5 NMR Characterization of the Interface in Polyurethane/Carbon Nanotube Composites** PETER MIRAU, *Air Foirce Research Laboratory* DANIEL POWERS, *Air Foirce Research Laboratory* JENNIFER GARBER, *Wright State University* HILMAR KOERNER, *Air Force Research Laboratory* RICHARD VAIA, *Air Force Research Laboratory* Solid-state proton NMR has been used to investigate the structure and dynamics of shape recovery polymers and composites with carbon nanotubes (CNTs). The thermoplastic polyurethane (Morthane) has both soft and hard segments. The soft segments are mobile at ambient temperature and give rise to a 2 kHz-wide proton signal. The protons signals shift and broaden with the introduction of CNTs. The proton spin- lattice and spin-spin relaxation times are relatively insensitive to the presence of CNT, demonstrating that the broadening is a consequence of proximity of the CNTs rather than a change in the molecular dynamics. The structures of the films in the stretched and relaxed states are probed using proton spin diffusion experiments. The results show the hard segments form 12 nm-sized domains and that the spin diffusion curves are very sensitive to the onset of soft-segment crystallinity as the samples are stretched. The effect of CNTs on the domain sizes and spacings are also measured in stretched and relaxed films.

**15:54**

**K24 6 Single-wall carbon nanotube aerogels** M. B. BRYNING, *University of Pennsylvania* M. F. ISLAM, *Carnegie Mellon University* L. A. HOUGH, *Rhodia* A. G. YODH, *University of Pennsylvania* Aerogels of single-wall carbon nanotubes (SWNTs) were created by freeze drying and critical point drying of aqueous SWNT gels. The resulting aerogels maintain the strongly-connected three-dimensional SWNT network of the original gel and have density less than 0.1 g/cm3. While these pure SWNT aerogels are self-supporting, reinforcement with small amounts of added polyvinylalcohol (PVA) produces much stronger structures that are easy to handle. Electrical conductivity of order 1 S/cm is observed in the self-supporting aerogels, and similar conductivity can be achieved in PVA-reinforced aerogels through additional processing. The aerogels can be backfilled with polymers such as epoxy to create composite materials that retain the high conductivity of the network. Other potential applications for these structures, such as sensors, actuators, and thermoelectric devices, are currently being explored. This work is supported by grants from NSF (MRSEC DMR05-20020 and DMR-0505048) and NASA NAG8-2172.

**16:06**

**K24 7 Polymer crystallization-driven, periodical patterning on carbon nanotubes** LINGYU LI, CHRISTOPHER LI, *Drexel University* We report herein a unique means to periodically pattern polymers on carbon nanotubes (CNTs) using controlled polymer crystallization method. CNTs were periodically decorated with polymer lamellar crystals, resulting in nano hybrid shish-kebab (NHSK) structures. The periodicity of adjacent kebabs varies from 20 - 150 nm. The kebabs are approximately 5 nm thick (along CNT direction) with a lateral size of $\sim$ 20 nm to micrometers, which can be readily controlled by varying crystallization conditions. Both polyethylene and Nylon 66 were successfully decorated on single-walled carbon nanotubes (SWNT), multi-walled carbon nanotubes (MWNT), as well as vapor grown carbon nanofibers (CNF). The formation mechanism was attributed to ''size dependent soft epitaxy.'' NHSK structure was discussed with an emphasis on the periodicity of adjacent kebabs. The influence of experimental parameters on the periodicity was investigated in details Since NHSK formation conditions depend upon CNT structures, it further provides a unique opportunity for CNT separation. The reported method opens a gateway to periodically patterning polymers and different functional groups on individual CNTs in an ordered and controlled manner, an attractive research field that is yet to be explored.

**16:18**

**K24 8 Alignment and Alignment Modulation of Single Wall Carbon Nanotubes Using Lyotropic Chromonic Liquid Crystals** M. F. ISLAM, *Department of Chemical Engineering and Department of Materials Science & Engineering, Carnegie Mellon University, Pittsburgh, PA 15213* I. I. SMALYUKH, O. D. LAVRENTOVICH, *Chemical Physics Interdisciplinary Program and Liquid Crystal Institute, Kent State University, Kent, Ohio 44242* A. G. YODH, *Department of Physics & Astronomy, University of Pennsylvania, Philadelphia, PA 19104-6396* We report alignment and local alignment modulation of single wall carbon nanotubes (SWNTs) dispersed in a nematic solvent of lyotropic chromonic liquid crystals (LCLCs). Polarized optical absorption suggests that when SWNTs are coated with surfactant molecules, e.g., sodium dodecyl benzene sulfonate (NaDDBS), the SWNTs align along the nematic director of the LCLCs, possibly due to elastic interaction between the anisotropic SWNTs and the nematic field of the LCLCs. In contrast, if the SWNTs are not coated with surfactant, then SWNTs align normal to the LCLC nematic director, possibly due to $\pi - \pi$ interactions between the aromatic groups of the LCLCs and the graphitic surface of SWNTs. We describe these observations and show that SWNTs can easily be realigned via realignment of nematic LCLCs using a magnetic field of only a few KGauss. This work is supported by grants from NSF (MRSEC DMR 05-20020 and DMR-0505048) and NASA NAG8-2172.

**16:30**

**K24 9 Theoretical investigation of the atomic and electronic structure of amino acids on Si(100) surfaces** XUAN LUO, GEFEI QIAN, CELESTE SAGUI, CHRISTOPHER ROLAND, *Department of Physics, NCSU* There are currently considerable efforts underway to combine silicon-based device technology with myriad of organic molecules, thereby fabricating new structures that take advantage of the tunable electronic and optical properties of organic molecules. A key aspect of this integration process is binding of the organics to the silicon surfaces. As part of this effort, we have been investigating the binding of several amino

acids – the building blocks for proteins – on the Si (100) surface with state-of-the art density functional theory methods. Specifically, the binding between the buckled Si(100) and the NH2, CH2, COOH, C=0 and NC entities at various surface sites have been investigated. We report and discuss on the resulting structures and their electronic properties.

**16:42**
**K24 10 Dynamics of poly(ethylene oxide)/$Li^+$ complexes confined in 1nm slits** GEORGIOS POLIZOS, *Penn State University* VIKRAM KUPPA, *Massachusetts Institute of Technology* ANDREAS SCHÖNHALS, *Federal Institute of Materials Research and Testing, Berlin, Germany* EVANGELOS MANIAS, *Materials Science and Engineering, Penn State University, University Park, PA* Poly(ethylene oxide) (PEO)/$Li^+$ complexes were nanoscopically confined in 1nm slit pores between inorganic solids of controlled $Li^+$ charge surface density (*cf.* varied cation exchange capacity $Li^+$ montmorillonites). The experimental systems were prepared by direct melt intercalation and investigated by dielectric relaxation spectroscopy over broad frequency and temperature ranges. Ionic conductivity/diffusion effects and the interfacial polarization relaxation process (due to the motion of the $Li^+$ ions in the slits) are systematically explored and analyzed. We present their dependences on frequency, temperature, $Li^+$ surface density, and PEO/$Li^+$ interactions. The above results are discussed in the context of previous Molecular Dynamics computer simulations, and mechanisms associated with the existence of water in the slit are thus identified.

**16:54**
**K24 11 Development of New Elastomers and Elastic Nanocomposites from Plant Oils** LIN ZHU, *Dept Chemical Engineering* RICHARD WOOL, *University of Delaware* Economic and environmental concerns lead to the development of new polymers from renewable resources. In this research, new elastomers were synthesized from plant oil based resins. Acrylated oleic methyl ester (AOME), synthesized from high oleic triglycerides, can readily undergo free radical polymerization and form a linear polymer. To achieve the elastic properties, different strategies have been developed to generate an elastic network and control the crosslink density. The elastomers are reinforced by nanoclays. The intercalated state has a network structure similar to thermoplastic elastomers in which the hard segments aggregate to give ordered crystalline domains. The selected organically modified clay and AOME matrix have similar solubility parameters, therefore intercalation of the monomer/polymer into the clay layers occurs and the nano-scale multilayered structure is stable. itIn situ intercalation and solution intercalation were used to prepare the elastic nanocomposites. Dramatic improvement in mechanical properties was observed. Changes of tensile strength, strain, Young's modulus and fracture energy were related to the clay concentration. The fracture surface was studied to further understand clay effects on the mechanical properties. Self-Healing of the intercalated nanobeams, thermal stability, biocompatibility and biodegradability of this new elastomer were also explored.

**17:06**
**K24 12 Simulations of Polymer Nanocomposites** THOMAS CLANCY, *National Institute of Aerospace* Simulations of polymer nanocomposites were undertaken in order to determine the effect of molecular structure on macroscopic properties. Due to the large amount of interfacial area present in nanostructured materials, the effect of structural details at this interface is influential in the resulting material properties. These simulations focus on variation in molecular structural details at this interface and the effect on the resulting macroscopic properties of the nanocomposite.

**17:18**
**K24 13 Characterizing the structural properties of organic-inorganic hybrid semiconductors by first-principles calculations** CHANG-YOUN MOON, GUSTAVO DALPIAN, YONG ZHANG, SU-HUAI WEI, *National Renewable Energy Laboratory* XIAOYING HUANG, JING LI, *Department of Chemistry and Chemical Biology, Rutgers University* Recently, a new type of hybrid materials $A_{II}B_{VI}(en)_{0.5}$, consisting inorganic II-VI semiconductor slabs connected by organic molecule spacers have been synthesized. [1] These materials have the advantage of possessing both inorganic and organic constituents: good electric and optical properties of the inorganic part, and the easiness of assembly of the organic part. [1,2] In this work, using first principles method, we study the stability and structural properties of $A_{II}B_{VI}(en)_{0.5}$ (A=Zn or Cd, B=S, Se, or Te, and en=ethylenediamine) in the known $\alpha$ and $\beta$ phases. We found that the relative stability of the $\alpha$ and $\beta$ phases of the hybrids is closely related to the intrinsic stability of the two phases of the inorganic semiconductor constituent: wurtzite (WZ) and zincblende (ZB). An inorganic compound with WZ ground state will prefer to exist in the $\alpha$ phase, whereas a ZB compound will prefer to exist in the $\beta$ phase.The relative stability is also affected by the size of the inorganic constituents and the spacing and bond angle of the en molecules. The results are analyzed by considering the contribution from the organic and inorganic part separately. [1] X. Huang et al., J. Am. Chem. Soc. 122, 8789 (2000); 125, 7049 (2003). [2] B. Fluegel et al., Phys. Rev. B 70, 205308 (2004)



**SESSION K25: POLYMER ELECTROLYTES AND CONDUCTION**
**Tuesday Afternoon, 14 March 2006**
**322, Baltimore Convention Center at 14:30**
**Bulent Ozbas; Princeton University, presiding**

**14:30**
**K25 1 Coffee Break**

**15:06**
**K25 2 Conformational transition of polybenzimidazole in N,N-Dimethylacetamide/lithium chloride.** CHRISTOPHER SHOGBON, *Rensselaer Polytechnic Institute* HAIFENG ZHANG, BRIAN BENICEWICZ, YVONNE AKPALU, *Rensselaer Polytechnic Institute, Troy,NY.* JEAN-LUC BROUSSEAU, *Brookhaven Instruments Corporation, Holtsville, NY.* Static light scattering and circular dichroism techniques have been used for the first time to study the chain conformation of a previously synthesized *m*-PBI sample in DMAc/LiCl. The chain conformation was studied as a function of a) polymer concentration (0.1 to 20 mg/mL) at a fixed salt concentration of 4 % LiCl and b) salt concentration (0.05 to 7 %) at a fixed polymer concentration of 0.3 mg/mL. As polymer or salt concentration was increased, the chains collapsed initially, and then underwent fluctuations in size without a significant decrease in their average size. The collapse

was associated with a conformational transition from random coil to an ''extended wormlike'' chain. At polymer concentrations greater than 9 mg/mL, the average size of the polymer chain is relatively constant at 31.2 ± 1.7 nm. Circular dichroism measurements confirmed the conformational transitions that had been observed by indicating optical activity at polymer concentrations above 2 mg/mL. These results contribute to our overall understanding of chain stiffness and conformational transitions in PBI polymers, which may play an important role in the preparation of polymer electrolyte membranes via sol-gel processing.

**15:18**

**K25 3 Nanostructured Polymer Electrolytes** OMOLOLA ODUSANYA, *University of California, Berkeley* MOHIT SINGH, *Lawrence Berkeley National Laboratory* NITASH BALSARA, *University of California, Berkeley* We present results on work on polystyrene-b-polyethyleneoxide copolymer electrolyte membranes. The volume fraction of the ethylene oxide block is 0.38 and molecular weight of each block is 36 kg/mol and 25 kg/mol respectively for the polystyrene and ethyleneoxide blocks. These electrolytes were made by doping with lithium bis(trifluoromethylsulfonyl)imide salt with the ratio of Li ion / ethylene oxide units ranging from 0.02 to 0.1. The salt/polymer samples were pressed into 1.0mm thick and 4.0 mm ID pellets in an air-free environment and measurements were made from 80$^o$C to 120$^o$C. Transmission Electron Microscopy and Small Angle X-ray Scattering experiment results indicate that our samples have a perforated hexagonal morphology. Conductivity results using AC impedance spectroscopy show that we are able to achieve values of $\sim$ 0.0001 S/cm, well within the theoretical upper limit expected for these samples while maintaining a high mechanical integrity of about 0.1GPa as determined from rheology. Achieving the combination of high conductivity with mechanical strength, which we observe in our results, has been a major problem in the battery research community.

**15:30**

**K25 4 Proton Conducting Membranes from Fluorinated Poly(Isoprene)-itblock-Sulphonated Poly(Styrene): A Structure Vs Property Study.*** AKINBODE ISAACS-SODEYE, SAMUEL GIDO, *University of Massachussetts Amherst* TIANZI HUANG, JIMMY MAYS, *University of Tennessee Knoxville* Proton Conducting Membranes used in Fuel Cells typically comprise of ionomers, having hydrophobic backbones and hydrophilic acid bearing side chains. Cell Efficiencies are limited by membrane morphology amongst other things. This study is a step towards tuning the morphology and ultimately properties of our relatively cheaper fluorinated Poly(Isoprene)-block-sulphonated Poly(Styrene) block copolymer ionomer membranes, made from post polymerization modified PS-PI. Work on random and graft copolymer ionomers especially Nafion $^{TM}$ have shown that morphologies of membranes from such materials vary with temperature, water content, counterion and No. of acid groups per chain etc. Analysis of our membranes using USAXS and SANS aims to explore the above mentioned variables; furthermore methanol permeability and proton conductivity will be studied using a diffusion Cell and impedance spectroscopy respectively.

*Acknowledgement: U.S Army

**15:42**

**K25 5 Proton transport through polymeric membranes** XINYU WANG, *Dept. of Physics, Univ. of Mass.* RICH WOUDENBERG, *Dept. of Polymer Science and Engr., Univ. of Mass.* OZGUR YAVUZCETIN, *Dept. of Physics, Univ. of Mass.* SERGIO GRANADOS, *Dept. of Polymer Science and Engineering, Univ. of Mass.* BRYAN COUGHLIN, *Dept. of Polymer Science and Engr., Univ. of Mass* MARK TUOMINEN, *Dept. of Physics, Univ. of Mass.* M.T. TUOMINEN TEAM, E.B. COUGHLIN COLLABORATION, Hydrogen fuel cells have drawn increasing attention from researchers because of the steadily declining supply of fossil fuels. A key component of a fuel cell is a membrane that is an efficient conductor of protons, but not electrons or molecules. Nafion currently is the dominant material chosen for this purpose, with proton conductivity facilitated by an imbibed network of water. Unfortunately, this material loses its conductivity as it becomes dehydrated at elevated temperatures. In this work we make a detailed examination of the physics of proton conductivity in anhydrous polymeric membranes though temperature-dependent DC current-voltage characterization, AC impedance spectroscopy and Hall effect measurements. We assess the relevance of fundamental proton conductivity models involving thermo-mechanical and electro-mechanical transport mechanisms. This work is supported by DOE grant 10759-001-05, NSF grant DMR-0306951 and MRSEC.

**15:54**

**K25 6 Performance of Nanostructured Polymer Electrolytes in Li Batteries** MOHIT SINGH, *LBNL* LOLA ODUSANYA, *UC berkeley* NITASH BALSARA, *UCB/LBNL* Batteries that employ Li anodes for high energy density applications suffer from failures due to side reactions and dendrite growth on the Li electrodes. A recent theory by Newman and Monroe (2005) shows that dendrite formation can be prevented if the shear modulus of the electrolyte can be increased by several orders of magnitude without a concomitant decrease in conductivity. The nanostructured polymer electrolyte (PE) in our study has a modulus of a glassy polymer. AC impedance measurements on Li/PE/Li systems show that the PE has high ionic conductivity. We present experimental data on the performance of a novel nanostructured dry PE in a Li/PE/Li battery. We report the DC cycling measurements, interfacial resistance measurements, and dendrite growth characteristics in Li/PE/Li cells. The performance of the nanostructured PE is compared with that of PE based on the homopolymer poly(ethylene oxide), which is a benchmark for dry polymer electrolytes.

**16:06**

**K25 7 PEO mobility in nanoparticle-filled polymer electrolytes as measured by neutron scattering** SUSAN FULLERTON, JANNA MARANAS, *Penn State* VICTORIA GARCIA SAKAI, *NIST Center for Neutron Research* The mobility of poly(ethylene oxide) [PEO] is measured for solid polymer electrolyte systems of PEO/LiClO4 and PEO/LiClO4/Al2O3, where LiClO4 is the lithium salt and Al2O3 is the nanoparticle filler. While the addition of nanoparticles has been shown to improve conductivity in solid polymer electrolytes, the molecular mechanism is unclear. Some suggest the addition of nanoparticles increases PEO mobility, while others suggest nanoparticles act like crosslinkers, pinning PEO at the ether oxygen atoms - decreasing PEO mobility. The glass transition temperatures of polymer electrolytes filled and unfilled with nanoparticles differs by only a few degrees, making it difficult to interpret the influence of nanoparticle fillers on PEO mobility. However, mobility can be directly measured by quasi-

elastic neutron scattering, and has previously been used to measure a system of PEO/LiClO4. We measure PEO mobility using the High-Flux Backscattering Spectrometer [HFBS] and the Disk Chopper Time-of-Flight Spectrometer [DCS] at the NIST Center for Neutron Research in Gaithersburg, Maryland. The two techniques measure motion on a timescales ranging from 240 ps to 2 ns, and 0.1 ps to 40 ps respectively. PEO mobility is measured for filled and unfilled solid polymer electrolytes at 323K. The addition of LiClO4 imparts a second, slower process, and the addition of nanoparticle fillers increases PEO mobility.

**16:18**

**K25 8 Effects of Temperature and Dissolved $LiClO_4$ on the Viscoelastic and Dynamic Properties of Poly(ethylene oxide), (PEO) Melts** R.B. BOGOSLOVOV, J.C. SELSER, S. PENG, *Department of Physics, University of Nevada, Las Vegas* Poly(ethylene oxide)/lithium perchlorate ($PEO/LiClO_4$) complexes are widely studied as a prototype solid polymer electrolyte in rechargeable lithium-polymer batteries. Characterizing the structure and dynamics of the system in its molten state is important for understanding the role of the polymer environment in lithium ion transport and conductivity. A fiber-optic coupled Fabry-Perot interferometer is employed in the investigation of the electrolyte viscoelastic and dynamic properties, which are both related to the intrachain local mobility and therefore to ion diffusion. The properties of the system are studied as a function of composition, temperature, and frequency. Structural relaxation processes are observed both in the neat polymer melt and in the salt containing electrolytes. A unique *q*-dependent measurement is performed, allowing the investigation of the Brillouin frequency and linewidth as a function of frequency. It revealed a double-step relaxation in the gigahertz frequency range. The two relaxations are identified as secondary relaxations with Maxwell-Debye character.

**16:30**

**K25 9 Local Ion Motion and Interactions in Single-Ion Polymer Electrolytes via Dielectric Spectroscopy** ROBERT KLEIN, SHIHAI ZHANG, SHICHEN DOU, RALPH COLBY, JAMES RUNT, *Materials Science and Engineering, Pennsylvania State University* A novel method is presented whereby the parameters quantifying the conductivity of polymer electrolytes can be extracted from the phenomenon of electrode polarization in dielectric spectroscopy. The validity of the model was confirmed by examining the effects of sample thickness and temperature, as well as by comparison of predicted and measured conductivities. Ion mobilities and mobile ion concentrations of neat and 'gel' forms are compared for poly(ethylene oxide)-based sulfonated ionomers. The mobile ion concentration of the neat ionomers was found to be a surprisingly low fraction of the total ion concentration, but increases substantially in the gel ionomers. Furthermore, the temperature dependence of mobility changes from VFT-like for the neat ionomers, to more Arrhenius-like for the gel ionomers. In addition, adding plasticizers to the ionomer significantly influences the local beta process, and the effects are quantified as a function of the dielectric constant and donor number of the plasticizer, and related to the conductivity.

**16:42**

**K25 10 Confined Water in Ionic Membranes: Studied by NMR** LILIN HE, *Department of Chemistry, Clemson University, South Carolina, 29634-0973* CY FUJIMOTO, *Chem.and Bio. Technologies, Sandia National Laboratories, Albuquerque, New Mexico 87185-0888* CHRISTOPHER CORNELIUS, *Chem.and Bio. Technologies, Sandia National Laboratories, Albuquerque, New Mexico 87185-0888* DVORA PERAHIA, *Department of Chemistry, Clemson University, South Carolina, 29634-0973* Proton NMR studies have been carried out to identify the location and dynamics of water confined within highly rigid sulfonated ionomer membranes. Understanding the dynamics and location of water molecules within polymeric ionic membrane, is critical to their many potential uses from fuel cell application to water purifying membranes. The magnetic relaxation times are sensitive to the degree of confinement of the molecules and the chemical environment affects the resonance frequency (chemical shift) of the water. Three different environments have been identified, highly mobile, almost free water molecules, partially confined in hydrophilic environment and water molecule that penetrated into the hydrophobic regime. Where surprisingly no fast exchange between these sites was detected even at room temperature. The distribution between these sites strongly depend on the degree of ionization of the polymers.

**16:54**

**K25 11 E-Field Dependent Conduction Mechanisms in Low Density Polyethylene*** JERILYN BRUNSON, J.R. DENNISON, *Utah State University* Successful conduction mechanisms have been developed for amorphous solids and semi-conductors for electric field dependent charge carrier mobility. Where electrons are the primary charge carriers, their mobility is dependent on their probability of hopping between potential well trapping sites. Extending these conduction mechanisms to polymers, resistivity can be directly related to carrier mobility within the bulk. A series of low electric field resistivity measurements at constant temperature have been made to test the Poole-Frenkel theory of field-enhanced hopping conduction in low density polyethylene.

*Supported by the Rocky Mountain Space Grant Consortium and NASA SEE Program

**17:06**

**K25 12 Ab initio study of a class of metalorganic systems** HARALD O. JESCHKE, L. ANDREA SALGUERO, ROSER VALENTI, *Institut für theoretische Physik, Johann Wolfgang Goethe-Universität, Max-von-Laue-Str. 1, 60438 Frankfurt/Main, Germany* BADIUR RAHAMAN, TANUSRI SAHA-DASGUPTA, *S.N.Bose National Centre for Basic Sciences, J.D Block, Sector 3, Salt Lake City, Kolkata 700098, India* CHRISTIAN BUCHSBAUM, MARTIN U. SCHMIDT, MATTHIAS WAGNER, *Institut für Anorganische und Analytische Chemie, Johann Wolfgang Goethe-Universität, Marie Curie-Str. 11, 60439 Frankfurt/Main, Germany* We use first principles methods to study the electronic properties of a Cu(II) coordination polymer. We have introduced two substitutions on the polymer in order to investigate the influence of the change of constituents in the hydroquinone molecule on the interactions between the metal centers. Furthermore, we have introduced two different ligand molecules in order to simulate the effect of satellite molecules in a real sample in the laboratory. In the preparation and analysis of the structures, we optimize computational efficiency and precision by employing four different methods: We initially prepare structures with classical force field methods, then we relax the rough structure by ab initio molecular dynamics. The analysis is done with a

full-potential linearized augmented plane-wave (LAPW) method and by downfolding with the N-th order muffin tin orbitals (NMTO) method. We find subtle changes of the interaction between the metal centers and of the band structure with each substituent or ligand molecule.

**17:18**

**K25 13 Computer simulation of supramolecular assembly by metal-ligand complexation*** SHIHU WANG, CHUN-CHUNG CHEN, ELENA E. DORMIDONTOVA, *Macromolecular Science and Engineering, Case Western Reserve University, Cleveland, OHIO 44106* Monte Carlo simulations were employed to study the supramolecular assembly of oligomers end-functionalized by ligands capable of complexation with metal ions. The properties of these metallo-supramolecular polymers strongly depend on the oligomer concentration, strength of complexation, and metal-to-ligand ratio. At high oligomer concentration the average molecular weight exhibits a maximum near the stoichiometric composition and decreases for higher or lower metal content. On the other hand, at low oligomer concentration the molecular weight shows a local minimum around the stoichiometric composition. This unusual behavior is attributed to the larger population of small rings around the stoichiometric composition, which make up a significant fraction of the overall molecular weight at low oligomer concentration. This effect is especially pronounced at low temperature, where the fraction of rings is higher. The fraction of chains and rings for different concentrations, temperatures and oligomer lengths were calculated and compared with experimental data.

*This work was supported by the NSF Career Award CHE-0348302



**SESSION K26: FOCUS SESSION: SINGLE MOLECULE BIOPHYSICS I**
**Tuesday Afternoon, 14 March 2006**
**323, Baltimore Convention Center at 14:30**
**David Nelson, Harvard University, presiding**

***Contributed Papers***

**14:30**

**K26 1 Conformational Dynamics of Adenylate Kinase: The Effects of Temperature and Mutation on Friction, Memory, and Reactivity** LUCAS WATKINS, KARL DUDERSTADT, SUCHARITA BHATTACHARYYA, HAW YANG, *Department of Chemistry, University of California Berkeley* Enzymes reside on a convoluted free energy surface. This free energy surface generates the conformational dynamics that control activity. We use single molecule Förster Resonance Energy Transfer measurements to study these conformational dynamics and the physics that underly them in a model enzyme, Adenylate Kinase (AK), which catalyzes the disproportionation of ADP into AMP and ATP. Our microscope records time-dependent single-molecule trajectories as a list of single photon arrival times. We treat the distance trajectory that generates this data as a manifestation of a many-dimensional Langevin equation, projected onto the coordinate defined by our two labeling sites. Using a likelihood-based approach, we can then directly extract the potential of mean force and the friction coefficient from the raw photon-by-photon trajectories. Temperature-dependent studies allow calculation of entropy and enthalpy profiles from the measured potentials of mean force, while mutants in functionally-important regions allow us to understand the role of individual residues in dynamics and catalysis. Ultimately, this newly-developed method allows us to begin to draw direct connections between structure, dynamics, and reactivity.

**14:42**

**K26 2 Single Human Plasma Fibrinogen Molecule Imaging by PEEM and AFM** XIANHUA KONG, JACOB GARGUILO, CRISSY RHODES, ROBERT NEMANICH, Human Plasma Fibrinogen (HPF), which is a protein involved in thrombosis, was studied by photoelectron emission microscopy (PEEM) and Atomic Force Microscopy (AFM). PEEM, using the spontaneous emission output of the Duke OK-4 free electron laser (FEL), clearly reveals the trinodular structure of the single fibrinogen molecule absorbed on oxidized silicon substrates. Moreover, PEEM images excited using various wavelengths between 249 and 310 nm reveal ionization thresholds of 4.6 eV for HPF. In addition, hydrogen-terminated silicon (H-Si) substrates and oxidized silicon substrates serving as model hydrophobic and hydrophilic surfaces were used to investigate the absorption coverage difference of fibrinogen molecules using ambient AFM. The images show that the fibrinogn absorption on H-Si substrates is significantly greater than that on the oxidized substrates.

**14:54**

**K26 3 Probing the low-resolution dynamics of biopolymers under force** RUXANDRA DIMA, *University of Massachusetts* CHANGBONG HYEON, D. THIRUMALAI, *IPST, University of Maryland* Single molecule force experiments are a major source of information for probing the structure and the dynamics of biopolymers. While the response of a biopolymer to the application of force, which is readily obtained from the force versus the extension curve, provides a glimpse of the underlying energy landscape, the much more interesting molecular-level behavior is not as easy to extract. In this context, we introduce a minimal model suitable for simulating the dynamics under force of biomolecules for long time-scales and with modest computational expenses. We will show that forced unfolding pathways predicted using this minimal model on systems that are challenging to simulate with conventional methods correlate very well with the results of recent force-unfolding experiments. Our findings underline the importance of understanding the interplay between tension propagation and the molecular relaxation time in pulling experiments.

**15:06**

**K26 4 Motion of single MreB bacterial actin proteins in Caulobacter show treadmilling in vivo*** W.E. MOERNER, SOYEON KIM, *Stanford University* ZEMER GITAI, *Princeton University* ANIKA KINKHABWALA, HARLEY MCADAMS, LUCY SHAPIRO, *Stanford University* Ensemble imaging of a bacterial actin homologue, the MreB protein, suggests that the MreB proteins form a dynamic filamentous spiral along the long axis of the cell in Caulobacter crescentus. MreB contracts and expands along the cell axis and plays an important role in cell shape and polarity maintenance, as well as chromosome segregation and translocation of the origin of replication during cell division. In this study we investigated the real-time polymerization of

MreB in Caulobacter crescentus using single-molecule fluorescence imaging. With time-lapse imaging, polymerized MreB could be distinguished from cytoplasmic MreB monomers, because single monomeric MreB showed fast motion characteristic of Brownian diffusion, while single polymerized MreB displayed slow, directed motion. This directional movement of labeled MreB in the growing polymer implies that treadmilling is the predominant mechanism in MreB filament formation. These single-molecule imaging experiments provide the first available information on the velocity of bacterial actin polymerization in a living cell.

*Supported in part by DOE Grant No. DE-FG02-04 ER63777 and NIH Grant No. 1 P20 HG003638-01.

**15:18**

**K26 5 Co-operative unfolding of protein domains** BUDDHAPRIYA CHAKRABARTI, *Lyman Laboratory of Physics, Harvard University, Cambridge MA 02138* TANNIEMOLA B. LIVERPOOL, *Department of Applied Mathematics, University of Leeds, LS2 9JT, UK.* ALEX J. LEVINE, *Department of Chemistry, University of California at Los Angeles, Los Angeles, CA 90095* How well does the worm-like chain force extension curve fit single-molecule protein unfolding data? Careful analysis of dynamic force spectroscopy data for different proteins [1] suggests that the compliance of a protein is generically larger than that predicted by the worm-like chain model. We propose that the observed excess compliance is due to pre-transitional conformational rearrangements within the protein domain that occur before the more dramatic failure of the domain as a whole. Using a generalization of the formalism introduced by Evans and Ritchie [2], we study protein–unfolding kinetics in our model where these internal conformational rearrangements are represented by a number of interacting Ising-type variables, which cooperatively escape over a barrier to the unfolded state. From this model, we predict a relation between the statistics of the fluctuations of the peak domain–unfolding force and the deviations of the force extension curves from the worm-like chain prediction. We suggest that, by using this approach, one can extract further details on the domain–unfolding pathway from extant force spectroscopy data. [1] D. J. Brockwell (private communication). [2] E. Evans, and K. Ritchie, Biophys. J., **72** 1541 (1997).

**15:30**

**K26 6 Quantitative analysis of tethered particle motion** PHILIP NELSON, *Dept. of Physics, Univ. Pennsylvania* CHIARA ZURLA, *Dept. of Biology, Univ. Milan* DARREN SEGALL, *Div. of Engr. and Applied Science, Caltech* DORIANO BROGIOLI, *Dept. of Biology, Univ. Milan* ROB PHILLIPS, *Div. of Engr. and Applied Science, Caltech* DAVID DUNLAP, *Dept. of Cell Biology, Emory Univ.* LAURA FINZI, *Dept. of Physics, Emory Univ.* Tethered particle motion (TPM) is a single-molecule technique that consists in tethering a bead to a slide through a DNA molecule. The Brownian amplitude of motion of the bead provides information about the conformational changes of the DNA molecule. We describe an improved experimental protocol, and a data analysis algorithm to extract quantitative conclusions from the data. We then apply a theoretical model for the statistics of the bead motion, which are quite different from those of a free polymer. Our experimental data for chain extension versus tether length are in good agreement with the model, showing that TPM is a useful tool for monitoring large conformational changes such as DNA looping. Moreover, we present the first experimental determination of the full probability distribution function of bead displacements, and find excellent agreement with theory over a range of tether lengths. Knowing this distribution a priori enhances our ability to extract events such as loop formation from observed time series.



***Invited Papers***

**15:42**

**K26 7 The Role of Fluctuations in Enzymatic Activity.** STEVEN CHU, *Lawrence Berkeley National Laboratory*

In ''What is Life,'' a set of lectures delivered in 1944, Erwin Schrodinger states '' . . . from all we have learnt about the structure of living matter, we must be prepared to find it working in a manner that **cannot** be reduced to the ordinary laws of physics [not because] there is any 'new force', . . . but because the construction is different from anything we have yet tested in the physical laboratory.'' I will briefly discuss how this prediction fared 60 years after these lectures were given. With the advent of molecular, structural and single molecule biology, we are developing an increasingly mechanistic understanding of bio-molecular systems. The molecular machinery of life is imbedded in a viscous fluid where friction and thermal fluctuations are huge. In particular, studies of RNA enzymes such as the ribosome and other ribozymes show that their construction and operation itis different than human designed machines that work in an environment where fluctuations and dissipation or minimized.

***Contributed Papers***

**16:18**

**K26 8 Protein Unfolding Energy Determined by Jarzynski's Equality** CHING-HWA KIANG, *Physics & Astronomy, Rice University* NOLAN HARRIS, LEIMING LI, YANG SONG, WEI LIAO, *Physics & Astronomy, Rice University* The dynamic response of single protein molecules to mechanical forces and the relation of dynamics to equilibrium properties of biomolecules has been a subject of intense recent study. Characterization of the fluctuations in these small systems plays an important role in successful application of Jarzynski's equality to determine equilibrium free energies from nonequilibrium measurements. Here we used the atomic force microscope to manipulate single titin I27 molecules to unfold the protein, and we have applied Jarzynski's equality to calculate the free energy landscape for stretching this heart muscle protein.

**16:30**

**K26 9 Protein folding in a force-clamp** MAREK CIEPLAK, *Polish Academy of Sciences* PIOTR SZYMCZAK, *Warsaw University* Kinetics of folding of a protein held in a force-clamp are compared to an unconstrained folding. The comparison is made within a simple topology-based dynamical model of ubiquitin. We demonstrate that the experimentally observed rapid changes in the end-to-end distance mirror microscopic events during folding. However, the folding scenarios in and out of the force-clamp are distinct.

**16:42**

**K26 10 Using a Microcantilever Array for Detecting DNA Melting** SIBANI BISWAL, *UC Berkeley* DIGVIJAY RAORANE, *UC Berkeley* ALISON CHAIKEN, *HP Labs* ARUN MAJUMDAR, *UC Berkeley* Microcantilever based sensors translate changes in Gibbs free energy due to macromolecular interactions into mechanical responses. We utilize the microcantilevers to observe surface stress changes in response to thermal dehybridization of surface grafted double stranded DNA oligonicleotides. We begin by immobilizing and hybridizing 20, 25, and 30 base pair DNA strands. Once the cantilever is heated, the DNA undergoes a transition as the complementary strand melts which results a cantilever deflection change. This deflection is due to changes to the electrostatic, ionic, and hydration interaction forces between the remaining immobilized DNA strands. For example, using a 20mer DNA strand in a 50 mM PBS buffer, the cantilever deflection shows an abrupt discontinuity at T $\sim$ 39$^o$C. When the salt concentration is lowered to 25 mM, we see a shift in the discontinuity to a lower temperature, T $\sim$ 30$^o$C. We also observe that DNA strands grafted onto the cantilever melt at lower temperatures compared to bulk solution due to the interactions between neighboring strands and the surface. We are also probing how base mismatches affect the cantilever deflection. This new technique has allowed us to probe DNA melting dynamics and leads to a better understanding of the stability of DNA complexes on surfaces.

**16:54**

**K26 11 Exploring the Electrical Conductivity of Cytochrome P450 by Nano-Electrode and Conductive Atomic Force Microscopy*** DEBIN LI, JIANHUA GU, YEWHEE CHYE, DAVID LEDERMAN, *Dept of Physics, West Virginia University* JAROD KABULSKI, PETER GANNETT, *Basic Pharmaceutical Sciences, West Virginia University* TIMOTHY TRACY, *Dept of Experimental and Clinical Pharmacology, University of Minnesota* There is a growing interest in measuring the conductivity of electron-transfer proteins. The cytochrome P450 (CP450) enzymes represent an important class of heme-containing enzymes. Immobilizing CP450 enzymes on a surface can be used for studying a single enzyme with respect to electron transfer. The spin state of the heme iron can change upon binding of a substrate. In our experiment, CP450 (diameter $\sim$ 5 nm) has been bonded to a metal surface. Nano-electrodes (gap $<$ 10 nm) were fabricated by defining a bridge via e-beam lithography and then breaking the junction by electromigration at low temperatures. We have examined the electronic properties of CP450 by itself and after binding CP450 with flurbiprofen. The room temperature I-V conductivity is reminiscent to cyclic voltammetry measurements, indicating the presence of strong ionic transfer. At lower temperatures (100 K) the I-V characteristics indicate electronic transport dominated by tunneling processes. The conductive AFM is an additional method used to examine the enzyme's electronic properties. The results from two methods will be discussed.

*Supported by the West Virginia University WVNano Initiative.

**17:06**

**K26 12 Traveling wave tracking of individual molecular motors** IRENE DUJOVNE, M. VAN DEN HEUVEL, *Kavli Inst. of NanoScience, Delft University of Technology* C. SYMONDS, G. CAPPELLO, *Institut Curie, Paris, France* CEES DEKKER, *Kavli Inst. of NanoScience, Delft University of Technology* Insight into the mechanisms of motility can be obtained by the study of the movement of motor proteins along biological filaments. Optical tweezer techniques are now able to track the motion of motor proteins with nanometer spatial resolution and 1-10 Hz bandwidth. Recently, G. Cappello developed an optical technique to track the movement of beads with sub-nanometer and microsecond resolution [1]. A unique aspect of this technique, based on total-internal-reflection traveling wave, is that no force is applied on the object under study. In this work we present modifications of this optical technique with the goal of larger scattering intensities that allow shorter acquisition times. Here we present this system to the study of microtubules traveling on kinesin-coated structures. The impact of fabricated nanostructures on the scattering intensities is discussed together with the feasibility of the application of this experimental scheme to the study of DNA-processing enzymes. 1 L. Busoni, A. Dornier, Jean-Louis Viovy, J.Prost, and G. Cappello, J. Appl. Phys. 98, 064302 (2005).

**17:18**

**K26 13 Steering and Trapping Multiple Particles by Feedback Flow Control: Theory and Experiments** MIKE ARMANI, SATEJ CHAUDHARY, ROLAND PROBST, BENJAMIN SHAPIRO, On the macro scale, feedback control is routinely applied to improve performance and enable new tasks in complex and uncertain systems operating in noisy environments. Our lab has focused on applying feedback control ideas to systems on the micro scale. We show how to combine micro-fluidics and feedback control to independently steer multiple particles with micrometer accuracy in two spatial dimensions. The particles are steered by creating a spatially and temporally varying fluid flow that carries all the particles from where they are to where they should be at each time step. Our control loop comprises sensing, computation, and actuation to steer particles along user-input trajectories, to hold particles in place, or both. Particle locations are identified in real-time by an optical system and sent to a control algorithm that then determines the electrode voltages necessary to create a flow field to carry all the particles to their next desired locations. The process repeats at the next time instant. We have demonstrated flow steering of multiple particles at once both in simulations and in experiments. The steering algorithm is robust to uncertainty and works even when conditions of the particles (size, surface charge), conditions of the buffer (pH, temperature, electro-chemistry, impurities), and attributes of the devices (errors in fabrication geometry, parasitic pressure flows driven by surface tension) vary and/or are unknown.

**SESSION K27: DENSITY FUNCTIONAL THEORY**
**Tuesday Afternoon, 14 March 2006**
**324, Baltimore Convention Center at 14:30**
**Kieron Burke, Rutgers University, presiding**

**14:30**
**K27 1 Long-range excitations in time-dependent density functional theory** DAVID G. TEMPEL, NEEPA T. MAITRA, *Hunter College of CUNY* Within TDDFT linear response, an adiabatic approximation such as ALDA to the exchange correlation kernel is most often used. It is local in time, or when considered in the frequency domain, frequency independent. We show that this neglected frequency dependence leads to drastic consequences for all excitations of a heteroatomic molecule composed of two open shell fragments at large separation. Strong frequency dependence of the kernel is needed for excitations of both local and charge transfer character. The needed frequency dependence arises from static correlation due to the step in the Kohn Sham potential between the fragments. An approximate kernel is derived to undo the static correlation and restore excited molecular dissociation curves at large separation. Leading order polarization and local dynamic correlation effects are also included. Future challenges for TDDFT will be discussed including molecular Feshabch resonances in stretched systems.

**14:42**
**K27 2 A physical interpretation of the Kohn-Sham energy in time-dependent current-density functional theory** ROBERTO D'AGOSTA, *Department of Physics, University of California - San Diego* GIOVANNI VIGNALE, *Department of Physics and Astronomy, University of Missouri - Columbia* It is well known that in static density functional theory the Kohn-Sham energy plays a fundamental role because it gives, by construction, the ground state energy of the system under study. In time-dependent density functional theory, it is not possible to attach to the Kohn-Sham energy the same physical interpretation. For example we know that for an isolated system the Kohn-Sham energy can be ''dissipated'' while the total energy of the real system is conserved.[1] However, the Kohn-Sham energy can be given a new physical interpretation as the maximum work that can be extracted from the system and it is related to the production of entropy during the time evolution of the system.[1] Project supported by NFS Grant No. DMR-0313681 [1]R. D'Agosta and G. Vignale, accepted by Phys. Rev. Lett., cond-mat/0508175.

**14:54**
**K27 3 Memory and exact exchange in time-dependent density-functional theory*** HARSHANI O. WIJEWARDANE, CARSTEN A. ULLRICH, *Department of Physics and Astronomy, University of Missouri-Columbia* Most applications in time-dependent density-functional theory (TDDFT) are being carried out using adiabatic approximations, such as the ALDA, for the exchange-correlation potential $V_{\rm xc}(r,t)$ at time $t$. In these approximations, the previous history of the system at times $t' < t$ is ignored in constructing $V_{xc}(r,t)$. In this talk, we consider the exact exchange potential in TDDFT and show that it has a memory. The exact exchange potential is obtained from the time-dependent optimized effective potential (TDOEP) method. We solve the associated TDOEP integral equation in space and time for a quantum well with two occupied subbands. We compare exact results with the KLI, Slater and ALDA approximations, discussing the memory effects and their relation to the elasticity of the electron liquid.

*Work supported by NSF Grant No. DMR-0553485 and Research Corporation.

**15:06**
**K27 4 The Generating-Coordinate Method in Static and Time-Dependent Density Functional Theory*** EDNILSOM ORESTES, *Instituto de Quimica de Sao Carlos, Universidade de Sao Paulo and Department of Physics and Astronomy, University of Missouri-Columbia* A. B. F. DA SILVA, *Instituto de Quimica de Sao Carlos, Universidade de Sao Paulo* KLAUS CAPELLE, *Instituto de Fisica de Sao Carlos, Universidade de Sao Paulo* CARSTEN A. ULLRICH, *Department of Physics and Astronomy, University of Missouri-Columbia* The generating-coordinate method represents a many-body wave function as a superposition of non-orthogonal Kohn-Sham Slater determinants arising from different Hamiltonians. This method provides additional variational degrees of freedom in the calculation of static and dynamical properties of electronic systems. We present results for atomic ground- and excited- state energies for various choices of generating coordinates. We then apply our variational approach to discuss a particularly challenging problem in TDDFT, the calculation of correlated double-ionization processes. We present results for single- and double-ionization probabilities of a strongly driven two-electron Hookes atom.

*Work supported by NSF Grant No. DMR-0553485 and Research Corporation.

**15:18**
**K27 5 The quantum defect: the true measure of TDDFT results for atoms** META VAN FAASSEN, KIERON BURKE, *Department of Chemistry and Chemical Biology, Rutgers University* We apply quantum defect theory to (time-dependent) density-functional calculations of Rydberg series for some closed shell atoms. We will compare several potentials by considering the quantum defect instead of the excitation energies. The quantum defect has the property of amplifying errors, allowing us to show that results that seem accurate from tables of excitation energies are not always so, especially for larger values of the principle quantum number $n$. In this way the quantum defect provides the appropriate tool for comparing time-dependent density-functional results for atoms.

**15:30**
**K27 6 Atom-Atom Scattering with TDDFT - Beyond the Born-Oppenheimer Approximation.*** RYAN M. HATCHER, ALAN R. TACKETT, MATTHEW J. BECK, SOKRATES T. PANTELIDES, *Vanderbilt University* We report results of calculations of atom-atom scattering going beyond the Born-Oppenheimer (B-O) approximation. We use time-dependent density functional theory with an adiabatic approximation to the scalar exchange-correlation potential in the local-density approximation. We use pseudopotentials, keeping the nearest approach larger than the core radius. The ions are treated as classical particles while the electrons have full freedom to evolve off their instantaneous ground state. If radiative energy loss is not included, energy is conserved; part of the initial ion kinetic energy is transferred to

electrons and stays there after separation, a clear sign of effects beyond the B-O approximation. Results of treating radiative losses at two levels of approximation will be discussed. Further results of ongoing calculations of scattering of a Si atom by a solid Si matrix will be described.

*The work was supported in part by DOE grant DE-FG02-02ER45972 and AFOSR grant FA9550-05-1-0306

**15:42**

**K27 7 Effects of core-valence interaction in the screened-exchange density functional method*** BYOUNGHAK LEE, LIN-WANG WANG, *Lawrence Berkeley National Lab* We present a new development for the screened-exchange (sX) density functional method using a planewave basis. In the screened-exchange density functional method, an explicit screened exchange interaction term is included in the total energy expression. When implemented with a planewave basis, the LDA derived norm-conserving pseudopotentials have usually been used without any change for the sX calculation. While this works well for valence *s* and *p* orbitals with the same quantum numbers, we found that there is a problem when *d* orbitals with a different quantum number are included. This is due to an error in the exchange integral between *d* and *s*, *p* orbitals stemming from the use of pseudowavefunctions. As a result, the calculated bulk electronic structures have much smaller band gaps compared to all electron sX calculations and experiments. We propose a scheme to correct the *d-s/p* exchange integrals using atomic orbital projection operators. We test our scheme on ZnTe, CdSe, and GaAs, and discuss the effects of shallow core states in comparison with other implementations such as the full potential linearized augmented planewave method. We will also compare our scheme with other Hartree-Fock pseudopotentials.

*This work was supported by U.S. Department of Energy under Contract No. DE-AC02-05CH11231 and used the resources of the National Energy Research Scientific Computing Center.

**15:54**

**K27 8 Non-Uniqueness of Local Effective Potential Energy in Density Functional Theory** VIRAHT SAHNI, XIAO-YIN PAN, *The Graduate School, CUNY* MARLINA SLAMET, *Sacred Heart University* As a consequence of the first Hohenberg-Kohn (HK) theorem, in the mapping from a *ground* state of an interacting system to an S system of noninteracting fermions with equivalent density, the effective potential energy of the latter is *unique*. But it is so *only* if these fermions are in their *ground* state. It can be shown via Quantal Density Functional Theory,[1] that the *ground* state density of an interacting system can also be reproduced by S systems that are in an *excited* state. Hence, in principle, there are an infinite number of functions that can reproduce a *ground* state density. Similarly, in the mapping from an *excited* state of the interacting system to an S system with equivalent density, the state of the latter is *arbitrary*. Hence, there are an infinite number of functions that can reproduce the excited state density. The latter proves the lack of a first HK theorem for *excited* states. The difference between the potential energy functions in either case is due solely to Correlation-Kinetic effects.

[1]*Quantal Density Functional Theory*, V. Sahni (Springer-Verlag, 2004)

**16:06**

**K27 9 Dynamical exchange-correlation potentials beyond the local density approximation*** JIANMIN TAO, GIOVANNI VIGNALE, *University of Missouri* Approximations for the static exchange-correlation (xc) potential of density functional theory (DFT) have reached a high level of sophistication. By contrast, time-dependent xc potentials are still being treated in a local (although velocity-dependent) approximation [G. Vignale, C. A. Ullrich and S. Conti, PRL **79**, 4879 (1997)]. Unfortunately, one of the assumptions upon which the dynamical local approximation is based appears to break down in the important case of d.c. transport. Here we propose a new approximation scheme, which should allow a more accurate treatment of molecular transport problems. As a first step, we separate the exact adiabatic xc potential, which has the same form as in the static theory and can be treated by a generalized gradient approximation (GGA) or a meta-GGA. In the second step, we express the high-frequency limit of the xc stress tensor (whose divergence gives the xc force density) in terms of the exact static xc energy functional. Finally, we develop a perturbative scheme for the calculation of the frequency dependence of the xc stress tensor in terms of the ground-state Kohn-Sham orbitals and eigenvalues.

*Work supported by DOE Grant No. DE-FG02-05-ER46203

**16:18**

**K27 10 Beyond the LDA in density functional theory: empirical Laplacian-based models for the exchange-correlation energy.** ANTONIO C. CANCIO, *Ball State University* M.Y. CHOU, *Georgia Tech* We report recent work in developing a simple GGA-level density functional theory using primarily the Laplacian of the density $\nabla^2 n$ as an input beyond the LDA, obtained by a fit to the exchange-correlation energy density of the Si crystal and atom[1]. Preliminary tests of this model with LDA pseudopotentials for several solids and molecules show a modestly improved treatment of structural properties over that of conventional GGA's, particularly for covalently bonded systems. We discuss an all-electron generalization of our model constructed by fitting to all-electron data for the energy density and potential of closed-shell first row atoms (He, Be, Ne)[2]. The use of $\nabla^2 n$ trivially avoids the singularity in the Kohn-Sham potential that gradient-based models suffer due to the cusp in electron density at the nucleus. Using an expansion in $1/\nabla^2 n$ we are able to fit exchange energy densities in the cusp region with a great degree of accuracy, while obtaining reasonable potentials.

[1]A. C. Cancio and M. Y. Chou, cond-mat/ 0506462.
[2]C. J. Umrigar and X. Gonze, Phys. Rev. A **50**, 3827 (1994).

**16:30**

**K27 11 Local self-interaction correction in LSMS.** MARKUS EISENBACH, G. M. STOCKS, *ORNL* While local density approximation (LDA) calculations have proven to be exceptionally successful for performing first principles calculations materials generally thought of as being strongly correlated (e.g. transition metal oxides) are poorly described. However, for many of these systems, it is now clear that an important factor in this failure is the self-interaction error that results in an unphysical Coulomb interaction of an electron with itself. This error can be readily accounted for by use of self-interaction corrected (SIC) LDA [1,2]. Here we report on our implementation of the recently developed local SIC (L-SIC) formulation developed by Lüders et al. [3] and which is particularly well suited to multiple scattering theory based electronic structure methods. Here we will describe

the implementation of L-SIC in our order-N locally self-consistent multiple scattering (LSMS) code as well results for example applications f-electron and TMO systems. 1. J. P. Perdew & A. Zunger, PRB 23, 5048 (1981). 2. Z. Szotek et al., J. Phys.:CM 16, S5587-S5600 (2004). 3. M. Lüders et al., PRB 71 205109 (2005). This research is sponsored by DOE-OS, BES-DMEP under contract number DE-AC05-00OR22725 with UT-Battelle LLC.

**16:42**
**K27 12 One-to-one Correspondence of the Normalization and Coulomb Hole Sum Rules for Approximate Wave Functions.[1]**
XIAO-YIN PAN, VIRAHT SAHNI, LOU MASSA, *The Graduate School, CUNY* For approximate wave functions, we prove the theorem that there is a one-to-one correspondence between the constraints of normalization, and of the Fermi-Coulomb and Coulomb hole sum rules. This correspondence is surprising because normalization depends on the probability of finding an electron at some position, whereas the Fermi-Coulomb/Coulomb hole sum rules depend on the probability of two electrons staying apart due to Pauli-Coulomb/Coulomb correlations. We demonstrate the theorem by example using wave function functionals[2]. The significance of the theorem for DFT lies in the fact that the extensively employed LYP correlation energy functional[3] is based on a wave function (that of Colle-Salvetti[4]) which satisfies the Coulomb hole sum rule only approximately, and that wave function is therefore not normalized. 1 Supported by RF CUNY 2 X.-Y. Pan*et al*, Phys. Rev. Lett. **93**, 130401 (2004) 3 C. Lee *et al*, Phys. Rev. B **37**, 785 (1988) 4 R. Colle and O.Salvetti, Theor. Chim. Acta **37**, 329 (1975).

**16:54**
**K27 13 Wave Function Arbitrariness of Noninteracting Fermion Model in Quantal Density Functional Theory[1](QDFT)**
MARLINA SLAMET, *Sacred Heart University* VIRAHT SAHNI, *The Graduate School, CUNY* In the QDFT mapping from a *ground* or *excited* state of the interacting system to one of noninteracting fermions in a particular *excited* state with equivalent density, there is an arbitrariness in the wave function of the model system. For example, in the case of a two-electron atom, the mapping to the excited singlet $2^1S$ state of the model system, there are three wave functions that lead to the *same* density: two single Slater determinants of the orbitals that are eigen functions of only $S_z$, and a linear combination of Slater determinants of these orbitals that is an eigen function of both $S_z$ and $S^2$. Neither of the wave functions is more appropriate than the other, since all three wave functions deliver the same density. However, based on the choice of wave function, the structure of the corresponding Fermi and Coulomb holes, and therefore the values of the resulting Pauli and Coulomb correlation energies, will differ. Their sum, the Fermi-Coulomb holes, and the Pauli-Coulomb energy, remains unchanged. The wave function arbitrariness will be demonstrated via the Hooke's atom. 1 *Quantal Density Functional Theory*, V. Sahni (Springer-Verlag, 2004).

**17:06**
**K27 14 Rydberg transitions from the local density approximation*** KIERON BURKE, *Rutgers University* ADAM WASSERMAN, *Harvard University* Using quantum defect theory, we show how to extract accurate Rydberg transitions (both frequencies [1] and oscillator strengths [2]) from density functional calculations using the local density approximation, despite the short-ranged potential. For the case of He and Ne, the asymptotic quantum defects predicted by the calculations are in less than 5% error, yielding transition frequency errors of less than 0.1 eV. [1] Rydberg transition frequencies from the Local Density Approximation A. Wasserman and K. Burke, Phys. Rev. Lett. 95, 163006 (2005). [2] Accurate Rydberg Excitations from Local Density Approximation A. Wasserman, N.T. Maitra, and K. Burke, Phys. Rev. Lett. 91, 263001 (2003).

*Work supported by NSF CHE-0355405

**17:18**
**K27 15 Ions on the verge of ionization*** VAZGEN SHEKOYAN, *Rutgers University, Department of Physics and Astronomy* KIERON BURKE, *Rutgers University, Department of Chemistry and Chemical Biology* The behavior of negative ions on the verge of ionization is studied. Electron-electron correlation plays a significant role for negative ions, especially for the outermost electron. Answering questions such as what negative ions exist, what the behavior of its electronic density is at the ionization threshold or why negative ions are particularly hard to treat in Density Functional Theory(DFT) are important. A general formalism (a differential equation for the square root of the electronic density) has been developed to treat such systems. It has been applied on a 1-d model of 2-electron negative ion, and its behavior on the verge of ionization has been studied in detail.

*This work is supported by NSF/CHE-0355405.



**SESSION K28: FOCUS SESSION: MICROPHYSICAL PROPERTIES OF BLOCK COPOLYMER AGGREGATES II**
**Tuesday Afternoon, 14 March 2006; 325, Baltimore Convention Center at 14:30**
**Dennis Discher, University of Pennsylvania, presiding**

***Invited Papers***

**14:30**
**K28 1 Coffee Break.**

**15:06**
**K28 2 Polymer Vesicles in Biomimetic Applications.**
MARIA SANTORE, *UMass Amherst Polymer Science and Engineering*

The performance of phospholipid vesicles in targeted pharmaceutical delivery is greatly improved by the addition of water-soluble polymeric tethers. The resulting solvated brush resists protein adsorption and access of biological entities

to the hydrophobic membrane core, evading immune response. Polymeric vesicles have, due to their increased stability and greater variability in chemical and mechanical properties, huge potential relative to lipsomes. They may ultimately form the basis for artificial cells and scavengers, or in non-biomedical applications, distributed microreactors. To this end, we explore the incorporation of biomimetic features in polymer lamellae: membrane phase separation and ''rafts,'' bending fluctuations and budding, triggered release, and dynamic engulfment. Vesicle phase separation, bending, lamellar disruption, and lamellar wetting all are rooted in block copolymer and polymer brush physics. For instance, vesicles blended from two block copolymers, polystyrene-co-poly(ethylene oxide) (PS-PEO) and poly(butadiene)-PEO (PBD-PEO) exhibit no macroscopic phase separation, though blends of PS and PBD at the same molecular weight do. This represents either an upward shifting of the UCST or a suppression of large-scale morphology. Also interesting is the ability of PS-PEO to form robust, vesicle-sized, capsules carrying aqueous phase cargo. While we doubt the true vesicular nature of these structures, they are often robust to passing of a liquid-air contact line. Their morphology is highly dependent on copolymer composition. The capsules are subject to buckling instabilities and in some instances, glassy fracture with sudden content release. Lamellar physics also plays an important role in the scavenging and adhesion capabilities of polymer vesicles: While the density of adhesive groups on the chain ends of incorporated tethers acts in ways easy to anticipate, engulfment dynamics depends dramatically on dynamic membrane bending.

*Contributed Papers*

**15:42**

**K28 3 Transition from Unilamellar to Bilamellar Vesicles Induced by an Amphiphilic Biopolymer** SRINIVASA RAGHAVAN, JAE-HO LEE, *Department of Chemical and Biomolecular Engineering, College Park, MD 20742* GREGORY PAYNE, *Center for Biosystems Research, University of Maryland Biotechnology Institute, College Park, MD 20742* VIVEK AGARWAL, ARIJIT BOSE, *Department of Chemical Engineering, University of Rhode Island, Kingston, RI 02881* We report some unusual structural transitions upon the addition of an amphiphilic biopolymer to unilamellar surfactant vesicles. The polymer is a hydrophobically modified chitosan and it embeds its hydrophobes in vesicle bilayers. We study vesicle-polymer mixtures using small-angle neutron scattering (SANS) and cryo-transmission electron microscopy (cryo-TEM). When low amounts of the polymer are added to unilamellar vesicles of itca. 120 nm diameter, the vesicle size decreases by about 50%. Upon further addition of polymer, lamellar peaks are observed in the SANS spectra at high scattering vectors. Using a model developed by Nallet et al., we show that the SANS data corresponds to a co-existence of unilamellar vesicles and bilamellar vesicles (i.e., vesicles with two bilayers). The transition to bilamellar vesicles as well as the changes in unilamellar vesicle size are further confirmed by cryo-TEM. A mechanism for the polymer-induced transition from uni- to bilamellar vesicles is proposed.

**15:54**

**K28 4 Temperature and pH Response of PB-P(Lys) Block Copolymer Assemblies** DANIEL A. SAVIN, KAY E. GEBHARDT, GOPAL R. VENKATACHALAM, *University of Vermont* Amphiphilic block copolymers consisting of poly(butadiene) and poly(L-lysine) (PB-P(Lys)) were synthesized and their solution properties studied using dynamic light scattering and transmission electron microscopy. We exploit secondary structure changes that occur in the P(Lys) chain to observe changes in solution morphology as a function of solution conditions. At high pH, the P(Lys) chain assumes either an $\alpha$-helical or a $\beta$-sheet conformation depending on temperature, while at lower pH the side chains become protonated, resulting in an expanded coil configuration. In these studies, four molecular weights and compositions of PB-P (Lys) were studied. For short P(Lys) blocks, these block polymers assemble into vesicles that swell with decreasing pH. For longer P(Lys) blocks, cylindrical micelles are formed that undergo a morphological shift to spherical micelles with decreasing pH.

**16:06**

**K28 5 Understanding the Self-Assembly of Amphiphilic Diblock Copolypeptides for Controlled Biomaterial Design** LISA PAKSTIS, *Univ. of Delaware* ANDREW NOWAK, ERIC HOLOWKA, TIMOTHY DEMING, *UCLA* DARRIN POCHAN, *Univ. of Delaware* Copolypeptides with a hydrophilic lysine (K) block and a hydrophobic leucine (L) block were designed to self-assemble due to their amphiphilic nature and the defined secondary structure of the hydrophobic block. In aqueous solution, these copolypeptides assemble into stiff, porous hydrogels at low volume fractions of polymer (vol. fraction polypeptide (0.5 wt%). Assembly is dictated by the secondary structure of the hydrophobic block and the polyelectrolytic character of the hydrophilic block, as revealed through microscopy and neutron scattering experiments. Understanding the self-assembly mechanism of amphiphilic diblock copolypeptides has led to the formation of a disparate range of materials. Vesicles can be produced by inducing curvature at the interface between the hydrophilic to hydrophobic blocks by altering either the charge density or the molecular weight of the polypeptide. Manipulation of the assembly kinetics, by dissolution of the polypeptide into an organic solvent with subsequent addition of water followed by evaporation of the organic component, produces twisted fibrils and hexagonal platelets. Characterization of these materials demonstrates that assembly is intrinsically controlled on the nanoscale by molecular design, most importantly by the presence of the alphahelical hydrophobic block, and can also be influenced by assembly kinetics and manipulation of electrostatic interactions of the charged blocks.

**16:18**

**K28 6 Laminated, Nontwisting Beta-Sheet Fibrils Constructed via Peptide Self-Assembly** MATTHEW S. LAMM, *University of Delaware - Department of Materials Science and Engineering* KARTHIKAN RAJAGOPAL, *University of Delaware - Department of Chemistry and Biochemistry* JOEL P. SCHNEIDER, *University of Delaware - Department of Chemistry and Biochemistry* DARRIN J. POCHAN, *University of Delaware - Department of Materials Science and Engineering* A de novo designed peptide has been characterized that self-assembles into beta-sheet fibrils exhibiting a nontwisted, laminated morphology. The laminated morphology is constituted by 2.5nm wide filaments that laterally associate to form flat fibril laminates exceeding 100nm in width and microns in length. The height of each fibril is determined by the length of exactly one peptide momomer in an extended beta-strand conformation, approximately 7nm. Once formed, these fibrils are highly stable over a range of temperatures and pH and exhibit characteristics similar to those of amyloid fibrils. Kinetic

parameters of pH and temperature can be used to affect the rate of beta-sheet formation and, consequently, the degree of lamination. Finally, the importance of peptide sequence on the resultant fibril morphology is demonstrated via rational peptide design and discussed in the context of current theories of fibril twisting.

**16:30**
**K28 7 Physical Properties of Anionic Peptide Amphiphile Fibers Grown in the Presence of Cationic Proteins** MEGAN GREENFIELD, MONICA OLVERA DE LA CRUZ, SAMUEL STUPP, *Northwestern University* We analyze the structure and mechanical properties of fibers formed by anionic peptide amphiphiles (PA) in the presence of cationic proteins with varying charge. The PA molecules, which are composed of a hydrophobic alkyl tail, a beta-sheet forming region, and a hydrophilic epitope region, self-assemble into cylindrical micelles in water at 1% weight concentration in the presence of multivalent salts. The fibers grow in one dimension by forming an internal beta sheet along the middle segment; the hydrophobic tail hides inside the micelle and the epitope region is exposed to the water. Rheology and electron microscopy are used to investigate the physical properties of the resulting PA gels. The correlation between the charge of the cationic proteins used for gelation and the resulting PA gel's structure and mechanical properties are discussed.

**16:42**
**K28 8 Dewetting instability during formation of polymerosomes from block-copolymer-stabilized double emulsions** RYAN HAYWARD, *University of Massachusetts, Amherst* ANDREW UTADA, DAVID WEITZ, *Harvard University* We study the formation of polymer vesicles, or polymerosomes, from double emulsion droplets of controlled architecture produced via a microfluidic device. A volatile organic solvent containing an amphiphilic diblock copolymer is employed as the middle phase of a water-in-oil-in-water emulsion. The block copolymer assembles at the oil-water interfaces, stabilizing the interior water droplet against coalescence with the exterior aqueous phase. Upon evaporation of the organic solvent, a thin vesicle of the block copolymer is formed. We find that the presence of excess diblock copolymer in the oil phase gives rise to a dewetting phenomenon, in which the shrinking oil droplet partially wets a thin film of solvated block copolymer. This yields acorn-like morphologies similar to those commonly encountered in systems of three immiscible fluids, ultimately resulting in an inhomogeneous polymerosome structure. We propose that the dewetting may be driven by a depletion effect due to the excess diblock copolymer.

**16:54**
**K28 9 Condensed States of a Semiflexible Copolymer in a Poor Solvent: Figures of Eight and Discrete Toroids** DAVID WILLIAMS, ERNESTO HERNANDEZ-ZAPATA, IRA COOKE, *Australian National University* We examine the problem of a semiflexible (stiff) copolymer chain in a selective solvent. In the homopolymer case toroids often result. In the copolymer case the phase diagram is much richer. One can obtain striped toroids, figure eights, cages and many other stuctures. We will present simple analytical results for some of these along with computer simulations showing a variety of morphologies. One major result, is that for copolymers the structures must be discrete so the size of the toroids is effectively quantised.

**SESSION K29: PROTEINS STRUCTURE AND FUNCTION**
**Tuesday Afternoon, 14 March 2006**
**326, Baltimore Convention Center at 14:30**
**F. A. Ferrone, Drexel University, presiding**

**14:30**
**K29 1 Biochemical Reversal of Aging** JOHN T.A. ELY, *Radiation Studies, University of Washington* We cite our progress on biochemical reversal of aging. However, it may be circa 2 years before we have necessary substances at low cost. Meanwhile, without them, a number of measures can be adopted providing marked improvement for the problems of aging in modern societies. For example, enzymes are needed to excrete toxins that accelerate aging; Hg is the ultimate toxin that disables all enzymes (including those needed to excrete Hg itself). Low Hg level in the urine, due to loss of excretory ability, causes the diagnosis of Hg toxicity to almost always be missed. Hg sources must be removed from the body! Another example is excess sugar; hyperglycemia decreases intracellular ascorbic acid (AA) by competitively inhibiting the insulin- mediated active transport of AA into cells. Thus, immunity is impaired by low leucocyte AA. AA is needed for new proteins in aging tissues. Humans must supplement AA; their need same as in AA-synthesizing mammals.

**14:42**
**K29 2 A Unified Approach to Sickle Hemoglobin Gelation and Phase Separation** F.A. FERRONE, *Drexel University* M.U. PALMA, M.B. PALMA-VITTORELLI, *University of Palermo* Protein aggregation has been identified as a major component in a number of diseases of which the earliest known and most thoroughly studied is sickle cell disease. Because of its direct bearing on pathophysiology, HbS polymer formation has been extensively described. The principal challenge now lies in the need of reconciling well documented but apparently contrasting properties of HbS solutions. These are the purely hard-sphere behavior of HbS under non-gelling conditions (extending to the 7th order in virial coefficients), and the equally well documented existence of a region of liquid-liquid demixing of the solution, from which notable deviations from hard-sphere behavior would be expected. We present a strategy to circumvent this impasse by including explicit and well known activity coefficients in a Flory-Huggins like term in the monomer chemical potential. This preserves the successful thermodynamic treatment of polymer formation while introducing a term leading to a spinodal. The formulation is consistent with known data, and implications for kinetics will be described.

**14:54**
**K29 3 Fluorescence photocycle of GFP studied by trapping phototransformation intermediates** GEORGI GEORGIEV, *Assumption College* TIMOTHY SAGE, *Northeastern University* JASPER VAN THOR, *Oxford University* OXFORD/NORTHEASTERN COLLABORATION, NORTHEASTERN/ASSUMPTION TEAM, The fluorescence photocycle consists involves excited state proton transfer (ESPT) from chromophore to Glu222, ionizing chromophore and neutralizing Glu222. A competing low quantum yield phototransformation process ionizes chromophore, and decarboxylates Glu222. We report spectroscopic measurements on cryotrapped reaction intermediates of the phototransformed GFP that electrostatically mimic intermediates in the fluorescence photocycle. Illumination at 100K leads to ap-

pearance of both a visible absorption band at 497nm, indicating an ionized chromophore in a non-equilibrium environment, and of multiple IR bands due to photogenerated carbon dioxide, confirming the decarboxylation of Glu222. Additional changes in the IR spectrum reflect numerous rearrangements of surrounding side chains and internal water molecules even at 100K. Polarized IR measurements on single crystals, measurements on mutant GFP, and solvent exchange measurements allow us to identify IR difference signals due to Gln69, Cys70, and weakly hydrogen-bonded internal water molecules. These spectroscopic changes highlight the role of the chromophore environment in preventing nonradiative decay of the excited state, and thereby enhancing the quantum efficiency.

**15:06**

**K29 4 Mechanisms of triggering H1 helix in prion proteins unfolding revealed by molecular dynamic simulation*** CHIH-YUAN TSENG, *Dept. of Physics, National Central University* H.C. LEE, *Dept. of Physics and Dept. of Life Science, National Central University* In template-assistance model, normal Prion protein ($PrP^{normalC}$), the pathogen to cause several prion diseases such as Creutzfeldt-Jakob (CJD) in human, Bovine Spongiform Encephalopathy (BSE) in cow, and scrapie in sheep, converts to infectious prion ($PrP^{normalSc}$) through a transient interaction with $PrP^{normalSc}$. Furthermore, conventional studies showed S1-H1-S2 region in $PrP^{normalC}$ to be the template of S1-S2 $\beta$-sheet in $PrP^{normalSc}$, and Prion protein's conformational conversion may involve an unfolding of H1 and refolding into $\beta$-sheet. Here we prepare several mouse prion peptides that contain S1-H1-S2 region with specific different structures, which are corresponding to specific interactions, to investigate possible mechanisms to trigger H1 $\alpha$-helix unfolding process via molecular dynamic simulation. Three properties, conformational transition, salt-bridge in H1, and hydrophobic solvent accessible surface (SAS) are analyzed. From these studies, we found the interaction that triggers H1 unfolding to be the one that causes dihedral angle at residue $Asn^{normal143}$ changes. Whereas interactions that cause S1 segment's conformational changes play a minor in this process. These studies offers an additional evidence for template-assistance model.

*This work is partially supported by grant NSC 93-2811-B-008-001

**15:18**

**K29 5 Analyzing knots in protein structures** PETER VIRNAU, MEHRAN KARDAR, *Department of Physics, MIT* LEONID MIRNY, *Harvard-MIT Division of Health Sciences & Technology* Although globular homopolymers display an abundance of knots (Virnau et al, J. Am. Chem. Soc. 127, 15102 (2005)), only about one in a thousand protein structures are knotted. Can this absence of entanglement be explained in terms of statistical mechanics or is there an evolutionary bias? Do knots in proteins serve a purpose and how do they actually fold? To elaborate on this, we will present an overview of knotted proteins from the current version of the Protein Data Bank. We will also discuss some particularly intriguing examples of this set.

**15:30**

**K29 6 Designing novel kinases using evolutionary sequence analysis** AREEZ MODY, JOAN WEINER, LAKSHMAN IYER, SHARAD RAMANATHAN, *Bauer Center for Genomics at Harvard University* Cellular pathways with new functions are thought to arise from the duplication and divergence of proteins in existing pathways. The MAP kinase pathways in eukaryotes provide one example of this. These pathways consist of the MAP kinase proteins which are responsible for evoking the correct response to external stimuli. In the yeast *Saccharomyces cerevisiae* these pathways detect pheromones, osmolar stresses and nutrient levels, leading the cell into dramatic changes of morphology. Despite being homologous to each other, the MAP kinase proteins show specificity of function. We investigate the nature of the amino acid sequences conferring this specificity. To this end, we i) search the sequences of similar proteins in other Eukaryote species, ii) make a study of simple theoretical models exploring the constraints felt by these protein segments and iii) experimentally construct, a large suite of hybrid proteins made of segments taken from the homologous proteins. These are then expressed in Yeast cells to see what function they are able to perform. Particularly we also ask whether it is possible to design a new kinase protein possessing new function and specificity.

**15:42**

**K29 7 Phase Diagram for Urate Oxidase** NATHANIEL WENTZEL, JAMES D. GUNTON, *Lehigh University* Urate Oxidase from itAsperigillus flavus has been shown to be a model protein in terms of understanding the effects of PEG on the crystallization of large proteins. Extensive experimental studies based on SAXS (Vivares et al, J. Phys. Chem. B 108, 6498 (2004)) have determined the effects of salt, pH, temperature, and most importantly polyethylene glycol (PEG), on the crystallization of this protein. Recently, some aspects of the phase diagram have also been determined. In this paper we use Monte Carlo techniques to predict phase diagrams for urate oxidase in solution with PEG. The model used includes an electrostatic interaction, van der Waals attraction, and a polymer-induced depletion interaction (Vivares et al, Eur. Phys. J. E 9, 15 (2002)). Results of the simulation are compared with experimental results.

**15:54**

**K29 8 Inter-Domain Dynamics in a Two-Domain Protein Studied by NMR** YAROSLAV RYABOV, *University of Maryland at College Park* DAVID FUSHMAN, Domain orientation and dynamics often play an important role in regulation of multi-domain proteins function. Here we consider a two-domain system, Lys48-linked di-ubiquitin ($Ub_2$), which is the simplest model of the polyubiquitin chain involved in the ubiquitin-proteasome pathway. Under physiological conditions $Ub_2$ adopts a compact conformation, in which the functionally important hydrophobic residues are sequestered at the interface between the two $Ub_2$ domains. Here we present a dynamic model that combines the anisotropic overall rotational diffusion with intra- and interdomain dynamics. This model describes the interdomain motion as a transition between two distinct conformational states. The model is applied to experimental $^{15}N$ relaxation data for Lys48-linked $Ub_2$ acquired at neutral (pH 6.8) and acidic (pH 4.5) conditions. The model provides complete picture of $Ub_2$ domain mobility including domain orientations, time scales of domain motions, and occupation probabilities for both states of $Ub_2$. The obtained results are consistent with independent data on chemical shift perturbation mapping and spin labeling.

**16:06**

**K29 9 Discovering the recognition code bacteria use to sense their environment by tracking co-evolutionary patternsBacteria typically posses tens of distinct signaling pathways that allow the organism to translate diverse environmental conditions into action** ROBERT WHITE, *The Scripps Research Institute (TSRI)* TERRY HWA, *The Center for Theoretical Biological Physics (UCSD)* JIM HOCH, *TSRI* Bacteria typically posses tens of distinct signaling pathways that allow the organism to translate diverse environmental conditions into action. A common signaling mechanism is a bucket brigade of phosphate triggered by the autophosphorylation of ''sensor kinase'' (SK) then passed to a protein called a ''response regulator'' (RR). The phosphorylation state of the RR regulates its function, thereby completing the signaling pathway. In one organism—but in pathways responsible for sensing diverse signals—the domains at which the transfer of the phosphate group occurs show surprising homology to each other. What keeps the organism from getting its signals crossed? We present a detailed bioinformatic study of over 1500 cognate SK/RR pairs that reveals patterns that can be used to predict the presence of evolved crosstalk and shed light on the paralogous divergence of these essential messengers.

**16:18**

**K29 10 Simple Model of Sickle Hemoglobin** ANDREY SHIRYAYEV, XIAOFEI LI, JAMES GUNTON, A microscopic model is proposed for the interactions between sickle hemoglobin molecules based on information from the protein data bank. A Monte Carlo simulation of a simplified two patch model is carried out, with the goal of understanding fiber formation. A gradual transition from monomers to one dimensional chains is observed as one varies the density of molecules at fixed temperature, somewhat similar to the transition from monomers to polymer fibers in sickle hemoglobin molecules in solution. An observed competition between chain formation and crystallization for the model is also discussed. The results of the simulation of the equation of state are shown to be in excellent agreement with a theory for a model of globular proteins, for the case of two interacting sites.

**16:30**

**K29 11 Antifreeze Protein Binds Irreversibly to Ice*** I. BRASLAVSKY, N. PERTAYA, C.L. DI PRINZIO, L. WILEN, *Ohio University, Athens, OH* E. THOMSON, J.S. WETTLAUFER, *Yale University, CT* C.B. MARSHALL, P.L. DAVIES, *Queen's University, ON, Canada* Many organisms are protected from freezing by antifreeze proteins (AFPs), which bind to ice and prevent its growth by a mechanism not completely understood. Although it has been postulated that AFPs would have to bind irreversibly to arrest the growth of an ice crystal bathed in excess liquid water, the binding forces seem insufficient to support such a tight interaction. By putting a fluorescent tag on a fish AFP, we were able to visualize AFP binding to ice and demonstrate, by lack of recovery after photo-bleaching, that it is indeed irreversible. Because even the most avid protein/ligand interactions exhibit reversibility, this finding is key to understanding the mechanism of antifreeze proteins, which are becoming increasingly valuable in cryopreservation and improving the frost tolerance of crops.

*Supported by CIHR, the Bosack and Kruger Foundation, Yale and Ohio Universities.

**16:42**

**K29 12 Fluorescence microscopy studies of the hyperactive antifreeze protein from an insect*** N. PERTAYA, C.L. DI PRINZIO, L. WILEN, *Ohio University, Athens, OH* E. THOMSON, J.S. WETTLAUFER, *Yale University, CT* C.B. MARSHALL, P.L. DAVIES, *Queen's University, ON, Canada* I. BRASLAVSKY, *Ohio University, Athens, OH* Antifreeze proteins (AFPs) protect animals from freezing by binding to extracellular ice and inhibiting its growth. Since the initial discovery of AFPs in fish, non-homologous types have been found in insects, plants, bacteria, fungi, and vertebrates. Different AFP types have diverse structures and varied activities. For example, AFPs produced by insects are much more active in inhibiting ice crystal growth compared to most AFPs found in fish or plants. By putting a fluorescent tag on an insect AFP we were able to visualize AFP binding to ice, to determine the ice crystal surfaces to which the AFP adheres, and to follow the kinetics of AFP binding to ice. We expect this approach will contribute to a better understanding of the mechanism of AFP activity and in particular the hyperactivity of insect AFPs.

*Supported by CIHR, the Bosack and Kruger Foundation, Yale and Ohio Universities.

**16:54**

**K29 13 Self-assembly of type 1 collagen : Interaction between normal and mutant collagen** SEJIN HAN, WOLFGANG LOSERT, *University of Maryland* We investigate the self-assembly of type 1 collagen, termed fibrillogenesis. Fibrillogenesis of type I homozygous mutations revealed a substantial difference in the kinetics, in particular, rapid growth of fibers and the absence of lag time. We developed a technique for differential fluorescent labeling of collagen combined with laser scanning confocal microscopy for time dependent observation of fibrillogenesis kinetics and structural properties in 3D. We observed that co-assembly of heterotrimers (normal) and homotrimers (mutant) in mixtures within the same fibrils during fibrillogenesis, despite their very different fibrillogenesis kinetics. Turbidity measurements of fibrillogenesis of mixture of hetero- and homotrimers showed the normal S-shaped curve with a lag time typical of heterotrimers. We characterized the structural topology of the collagen 3D network through Betti numbers that are primarily describing the connections between different components. We found that homotrimers has fewer intersections per disjoint fiber than normal heterotrimers, demonstrating finer and straighter network structure in images.

**17:06**

**K29 14 MutY: optimized to find DNA damage site electronically?*** JONG-CHIN LIN, DANIEL COX, RAJIV SINGH, Iron sulfur clusters are present in the DNA repair protein MutY in a region highly homologous in species as diverse as *E. Coli* and Homo Sapiens, yet their function remains unknown. In MutY, this mixed valence cluster exists in two oxidation states, $[Fe_4S_4]^{2+/3+}$, with the stability depending upon the presence of DNA. We have studied the electronic structure and stability of these clusters using the local orbital based SIESTA implementation of density functional theory. We find that the iron-sulfur cluster in MutY can undergo 2+ to 3+ oxidation when coupling to DNA through hole transfer, especially when MutY is near an oxoguanine modified base(oxoG). Employing the Marcus theory for electron transfer, we find (i) near optimal Frank-Condon(FC) factor for 2+ transfer to oxoG; (ii) reduced FC factor for transfer to G due to a high oxidation potential; (iii) reduced FC factor with

the mutation L154F; (iv) reduced tunning matrix element with the mutation R149W. Both L154F and R149W mutations dramatically reduce or eliminate repair efficiency. Hence, redox modulation of MutY search and binding appears plausible and may have broader implications for DNA-protein interactions.

*Work initiated with the support of NSF grant PHY 0120999 (the Center for Biophotonics Science and Technology).

**SESSION K30: CARBON NANOTUBES: APPLICATIONS AND NOVEL PHENOMENA**
**Tuesday Afternoon, 14 March 2006**
**327, Baltimore Convention Center at 14:30**
**Jun Kono, Rice University, presiding**



**14:30**
**K30 1 Weighing Molecules with Carbon Nanotubes** ABHIJAT GOYAL, TADIGADAPA SRINIVAS, *Department of Electrical Engineering, The Pennsylvania State University, University Park, PA 16802* PETER EKLUND, *Department of Physics, The Pennsylvania State University, University Park, PA 16802* We have constructed a sensitive mass balance by coating a thin quartz transducer with debundled carbon nanotubes. The transducer operates in theshear mode at 29 MHz. Application of the nanotube film to the transducer downshifts the frequency as expected (mass loading), but we observe an unexpected increase in the Q-factor, i.e., the nanotube loading reduces the mechanical losses in the resonator. This nanomechanical resonator is also sensitive to mass loading of the internal pores of the nanotubes. By exposing the nanotube-coated resonator to various gases (e.g., inert gases, N2, SF6, etc.), we are able to easily observe the adsorption/desorption of the gases. At constant temperature and pressure, we observe an interesting M0.45 shift in the resonance frequency, where M is the molecular mass. The mass exponent we observe in these mass-balance experiments results is in good agreement with that published recently [1] on the collision-induced changes in the resistance and thermolectric power of thin nanotube films. The theory behind exponential mass dependence will be discussed and relates to the deformation of the nanotube wall and the residence time of the molecule on the tube wall.

**14:42**
**K30 2 Probing Mechanical Properties of Carbon Nanotubes by Light Scattering** YANG WU, FENG WANG, MINGYUAN HUANG, LIMIN HUANG, MATTHEW Y. SFEIR, LOUIS E. BRUS, STEPHEN O'BRIEN, JAMES HONE, TONY F. HEINZ, *Columbia University, New York, NY 10027* An important capability for studying and exploiting the remarkable mechanical properties of carbon nanotubes is the detection of their physical motion. Here we present a scheme based on light scattering by a nanotube placed slightly off-center of a tightly focused laser beam. The approach permits measurement of the movement of individual single-walled carbon nanotubes with nanometer sensitivity and high detection bandwidth. The method can be readily combined with optical characterization by Rayleigh scattering spectroscopy for studies of well-defined nanotube structures [1]. The technique is demonstrated for suspended pristine nanotubes, as well as for nanotubes modified by mass loading. By passing a current through the nanotube in the presence of a magnetic field, we can apply static and oscillating Lorentz forces. In this fashion, we have produced both static deflection and vibration excitation of nanotubes. Sharply defined nanotube vibrational modes are observed by sweeping the frequency of the driving force. We discuss the nature of these resonances and how to extract fundamental nanotube properties from the measurements. [1] M. Y. Sfeir, Science **306**, 1540 (2004).

**14:54**
**K30 3 Continuum Theory for Nanotube Piezoelectricity** PAUL J. MICHALSKI, NA SAI, E. J. MELE, *University of Pennsylvania* We develop and solve a continuum theory of the piezoelectric response in 1-D nanotubes and nanowires. We find that the piezoelectric response depends on the aspect ratio, the chiral angle, and two dimensionless parameters giving the relative strengths of the two elastic constants to the piezoelectric constant. Solutions for several limiting cases in the parameter space are discussed. The low dimensionality of the model system gives rise to several interesting effects not seen in conventional 3-D systems. We find that a uniform axial stress will induce a spatially non-uniform polarization and a non- linear variation of the electrostatic potential along the tube. The model predicts a strong coupling between longitudinal strain and torsional strain in chiral nanotubes and nanowires. The theory is applied to estimate the piezoelectric response of boron-nitride nanotubes.

**15:06**
**K30 4 Analysis of band-gap formation in squashed armchair CNTs** H. MEHREZ, A. SVIZHENKO, M. P. ANANTRAM, *Mail Stop: 229-1, Center for NanoTechnology and NASA Advanced Supercomputing Division, NASA Ames Research Center, Moffett Field, California 94035-1000* M. ELSTNER, T. FRAUENHEIM, *heoretische Physik, Universitat Paderborn, D-33098 Paderborn, Germany* The electronic properties of squashed arm-chair CNTs are modeled using constraint free density functional tight binding molecular dynamics simulations. Independent from CNT diameter, squashing path can be divided into *three* regimes. In the first regime, the CNT deforms with negligible force. In the second one, there is significantly more resistance to squashing with the force being $\sim 40 - 100$ nN/per CNT unit cell. In the last regime, the CNT looses its hexagonal structure resulting in force drop-off followed by substantial force enhancement upon squashing. We compute the change in band-gap ($E_g$) as a function of squashing and our main results are: (i) $E_g$ initially opens due to interaction between atoms at the top and bottom sides of CNT. The $\pi -$ orbital approximation is successful in modeling the $E_g$ opening at this stage. (ii) In the second regime of squashing, large $\pi - \sigma$ interaction at the edges becomes important, which can lead to $E_g$ oscillation. (iii) Contrary to a common perception, nanotubes with broken mirror symmetry can have *zero* $E_g$. (iv) All armchair nanotubes become metallic in the third regime of squashing. [Phys. Rev. B 71, 155421 (2005)].

**15:18**
**K30 5 Conductivity, Rheology and Processing of Carbon Nanotube Composites** KALMAN MIGLER, *NIST* SAM KHARCHENKO, JAN OBRZUT, JACK DOUGLAS, PAUL START, The primary application for CNT composites is the enhancement of their electrical properties relative to pure polymers. The conductivity is controlled by the alignment and the dispersion of the nanotubes in the polymer matrix during processing. Understanding the interplay between conductivity, processing, alignment and rheology is key their efficient use. We present simultaneous

measurements of the Rheology and conductivity of molten polymer nanotube composites over a range of concentrations near the percolation threshold. We find that simple shear fields can change the conductivity by orders of magnitude. Surprisingly, upon cessation of shear, the conductivity returns to its quiescent value.

**15:30**

**K30 6 Focused electron beam from open-tip single-wall carbon nanotubes** SANGBONG LEE, SEUNGCHUL KIM, JISOON IHM, *School of Physics, Seoul National University, Seoul, Korea* Open-tip single-wall carbon nanotubes can produce focused electron spot in the field emission. We calculate direct evolution of the nanotube wavefunction under applied electric field by solving the time dependent Shrödinger equation in the first principles scheme. (5,5), (10,10), and (12,12) carbon nanotubes are investigated and We obtain the focused spot size of a few angstroms. The spot size of electron beam from the (10,10) tube is smaller than that of the (5,5) or (12,12) tube. We also find that s-like state near the Fermi level contributes most to the field emission current.

**15:42**

**K30 7 Controlling the diameter of carbon nanotubes** T.D. YUZVINSKY, W. MICKELSON, S. ALONI, G.E. BEGTRUP, A. ZETTL, *University of California at Berkeley* We report a method to control the diameter of an individual carbon nanotube. Electronic transport measurements performed in situ reveal a striking dependence of conductance on nanotube geometry. As the diameter of the nanotube is reduced to near zero, we observe negative differential resistance.

**SESSION K31: FOCUS SESSION: SIMULATION OF COMPLEX MATERIALS III**
**Tuesday Afternoon, 14 March 2006**
**328, Baltimore Convention Center at 14:30**
**Alberto Franceschetti, National Renewable Energy Laboratory, presiding**

*Contributed Papers*

**14:30**

**K31 1 Integrated Density of States Lloyd's Formula for Disordered Alloys with Short-Range Order via a KKR-based Dynamical Cluster Approximation*** D. A. BIAVA, SUBHRADIP GHOSH, W. A. SHELTON, D. D. JOHNSON, *Physics and Materials Science and Engineering, University of Illinois Urbana Champaign* Within Korringa, Kohn and Rostoker (KKR) multiple scattering theory, we have formulated[1] a static version of the Dynamic Cluster Approximation (DCA)[2], which is a cluster (or nonlocal) generalization of the coherent potential approximation (NLCPA)[3] that includes environmental effects, including short-range order. Within our KKR-DCA/NL-CPA we present an analytic expression for configurationally-averaged integrated density of states $< N(E) >$ , or generalized Lloyd's formula. We show also that this Lloyd's formula is stationary with respect to changes in the DCA/NLCPA effective medium, providing a rigorous electronic density functional theory and total-energy formalism for (partially) disordered alloys with(out) short-range order that is exact for infinite sized clusters and reduces to the single-site CPA for a cluster size of one. We show applications to various alloys with-(out) short-range order.

*Support from NSF under grant DMR-0312448 and DOE under grant DE-FG02-03ER46026

[1]D.A. Biava et al, Phys. Rev. B 72 113105 (2005)
[2]M. Jarrell and H R Krishnamurthy, Phys. Rev. B 63 125102 (2001)
[3]D.A. Rowlands et al, Phys. Rev. B 67 115109 (2003)

**14:42**

**K31 2 New modeling approach for the deformation of fractal hierarchical structures.** CATALIN PICU, MONICA SOARE, *Rensselaer Polytechnic Institute* A new formulation is proposed to address the deformation of multiscale hierarchical structures with a self-similar geometry across scales for which the classical formalism of continuum mechanics either does not apply or it is too expensive from computational point of view. Examples of such structures are porous materials (rocks, aerogels, glasses) in which pores with a wide range of dimensions are found, many biological materials and some of the newly developed nanostructured hierarchical composites. To this end, the equations of solid mechanics are reformulated to include information about the geometry. The procedure to solve boundary value problems with the new formulation will be presented. Examples will be discussed in which the variation of the solution with the number of scales in the hierarchy is studied.

**14:54**

**K31 3 Medium-Range Structural Properties of Vitreous Germania Obtained through First-Principles Analysis of Vibrational Spectra** LUIGI GIACOMAZZI, PAOLO UMARI, ALFREDO PASQUARELLO, *Ecole Polytechnique Fédérale de Lausanne (EPFL), Institute of Theoretical Physics, CH-1015 Lausanne* We analyse the principal vibrational spectra of vitreous $GeO_2$ and derive therefrom structural properties referring to length scales beyond the basic tetrahedral unit. We generate a model structure which yields a neutron structure factor in accord with experiment. The inelastic-neutron, the infrared, and the Raman spectra, calculated within a density-functional approach, also agree with respective experimental spectra. The accord for the Raman spectrum supports a Ge-O-Ge angle distribution centered at 135°. The Raman feature $X_2$ is found to result from vibrations in three-membered rings, and therefore constitutes a distinctive characteristic of the medium-range structure.

*Invited Papers*

**15:06**

**K31 4 Predicting complex ground state structures from first principles: genetic algorithm for finding accurate coarse-grained Hamiltonians.**

VOLKER BLUM, *Fritz-Haber-Institut, Faradayweg 4-6, 14195 Berlin, Germany*

First-principles quantum-mechanical (QM) calculations allow to evaluate many interesting properties of a *given* nanoscale configuration of atoms with high accuracy. However, *predicting* stable structures or finite-$T$ thermodynamic configurational averages with QM accuracy remains a challenge: even for a binary solid with $N$ atoms per unit cell, $2^N$ distinct configurations must be evaluated. Such large numbers of calculations can be made affordable by mapping the QM Hamiltonian onto a computationally simpler ''coarse-grained'' Hamiltonian. The ability to predict ground state structures then depends on the shape of the coarse-grained Hamiltonian, but this shape is not a priori clear. For instance, a few simple assumed generic interactions will allow only a few simple ground states, but any more complex structures will be missed. For the generalized Ising model for binary alloys (cluster expansion), I show how a genetic algorithm[1,2] can identify the leading interactions which characterize a given system. I illustrate the method for the bcc binary alloys of Nb, Ta, Mo, W. A rich spectrum of ground state structures is found, including both well-known and unsuspected complex structures, far beyond what is envisioned from ''usual-suspect'' structure listings or from simple generic interactions. At the same time, order-disorder temperatures are significantly lower than those from simple intuition-based interactions, in agreement with experimental observations for these systems. This work was done at the National Renewable Energy Laboratory, supported by DOE-SC-BES, in collaboration with A. Zunger and G. Hart. [1]G. Hart, V. Blum, M. Walorski and A. Zunger, Nature Materials **4**, 391 (2005); [2]V. Blum, G. Hart, M. Walorski and A. Zunger, Phys. Rev. B **72**, 165113 (2005).

*Contributed Papers*



**15:42**

**K31 5 Accurate prediction of x-ray absorption spectra using density functional theory*** GIULIA GALLI,[†]DAVID PRENDERGAST,[‡] *Lawrence Livermore National Laboratory* The increasing availability of x-ray absorption spectroscopy measurements for materials in the condensed phase is providing new opportunities to explore the local structure of disordered materials. However, the spectra produced by such experiments rely heavily on theoretical interpretation to infer the underlying atomic structure. We make use of density functional theory calculations to accurately approximate the initial and final state electronic structure associated with the absorption of an x-ray photon in the condensed phase. We outline some efficient computational approaches applied to ordered and disordered systems, concentrating on the K-edge absorption of oxygen. We report simulated x-ray absorption spectra for ice I, liquid water and magnesium oxide. Our results indicate excellent agreement with experiment for ice I and magnesium oxide, and our results for water, modelled using the classical TIP4P potential, indicate a reasonable qualitative agreement with experiment.

*This work was performed under the auspices of the U.S. Department of Energy at the University of California/Lawrence Livermore National Laboratory under Contract No. W-7405-Eng-48.

[†]University of California, Davis
[‡]University of California, Berkeley

**15:54**

**K31 6 A First-principles Investigation of Superprotonic Activity in $CsHSO_4$** BRANDON WOOD, *MIT* NICOLA MARZARI, With the recent push to realize the hydrogen economy, there has been a surge of interest in viable solid-state materials for use as fuel cell electrolytes. Among the candidates are various derivatives of the anhydrous superprotonic conductor $CsHSO_4$, which exhibits reasonably high ionic conductivity at relevant operating temperatures while remaining electronically insulating. However, despite being widely characterized experimentally, a truly atomistic picture of the diffusion pathways and mechanisms in the material is missing. To this end, we have characterized this material with extensive first-principles static and dynamical calculations on 112-atom supercells of $CsHSO_4$. We isolate the dominant atomistic mechanisms involved in the superprotonic behavior and discuss the effect of correlated diffusive events in enhancing proton transport. We also offer a detailed description of the dynamics of the hydrogen bond network topology as the diffusing protons propagate through the lattice structure. The role of our findings in understanding superionic behavior are discussed.

**16:06**

**K31 7 First-principles study of the Hume-Rothery electron concentration rule in Al-Cu-(Fe,Ru)-Si 1/1-cubic approximants*** RYOJI ASAHI, *Toyota Central R&D Labs., Inc.* O.Y. KONTSEVOI, *Northwestern University* U. MIZUTANI, *Toyota Phys.&Chem. Res. Inst.* T. TAKEUCHI, *Nagoya University* A.J. FREEMAN, *Northwestern University* To elucidate the Hume-Rothery electron concentration rule, we determined the self-consistent electronic structures of the $Al_{108}Ru_{24}Cu_6Si_6$ and $Al_{108}Fe_{24}Cu_6Si_6$ 1/1-1/1-1/1 approximants containing 144 atoms in each it Pm-3 cubic unit cell using the full-potential linearized augmented plane wave (FLAPW) method [1], now running on massively parallel computer platforms. A significant pseudogap was found around the Fermi level for both alloys in the calculated densities of states, which should contribute to stabilization of the system. The FLAPW wave functions provide a direct observation of the Brillouin zone resonance in the Fermi surface [2]: a Fourier analysis of the wave functions confirms the Hume-Rothery matching rule $2k_F = K$ where the reciprocal lattice vectors $K$ consist of {543}, {550}, and {710} planes highly degenerate at the $N$ point. Consequently, an effective electron concentration per atom $(e/a)$ was evaluated to be 0.8 for both Ru and Fe in these structures

making a sharp contrast with the previously assumed empirical value of -2.7 proposed by Raynor [3]. [1] Wimmer et al., Phys. Rev. B **24**, 864 (1981). [2] Asahi et al., Phys. Rev. B **72**, 125102 (2005). [3] Raynor, Prog. Metal Phys. **1**, 1 (1949).

*Work at NU supported by the AFOSR (Grant FA9550-04-1-0013)

**16:18**

**K31 8 High-precision mixed-space cluster expansion for Cu-rich Cu-Pd alloys: Explaining the "$L1_{2''}$" phase*** S. BÄRTHLEIN, S. MÜLLER, *Universität Erlangen−Nürnberg, Germany* G.L.W. HART, *Northern Arizona Univieersity, Flagstaff, Arizona 86011−6010* A. ZUNGER, *National Renewable Energy Lab, Golden, Colorado 80401* A remarkable feature of Cu−Pd alloys is the existence of long−periodic superlattices (LPS) on the Cu−rich side of the phase diagram. Whereas earlier studies did not include necessary information about the diversity of important, but until then inaccessible formation enthalpies, we are able by combining DFT calculations with a mixed−space cluster expansion, genetic algorithms [1] and Monte Carlo to predict the phase stability from millions of possible candidates. Effective interactions were constructed, enabling us to predict the ground state line in order to determine the stable configurations a T=0 K. As a matter of special interest, we investigate the so −called ″L12″ phase, whiche merges as a domain −mixture between the LPS3 and a newly discovered low −temperature phase at xPd=0.125. Examination of the system's short−range order reveals a continuous transition from the domain−mixture to the disordered solid solution. Hence a natural explanation for the existence of this off−stoichiometry phase can be given. [1] G.L.W. Hartetal., Nat. Mater. **4**, 391 (2005)

*Supported by DFG and NSF.

**16:30**

**K31 9 Nanoscale Patterning of $L1_2$ Chemical Order in $Ni_3Al$ Alloy Processed by Energetic Ions** JIA YE, YOUHONG LI, ROBERT AVERBACK, PASCAL BELLON, JIANMIN ZUO, We recently predicted that alloys forming chemical ordered phases at equilibrium can be forced into stable nanoscale patterns of chemical order by irradiation with energetic particles. We have tested this prediction on the $Ni_3Al$ compound by combining MD and KMC simulations. For 1MeV Kr and 70KeV He ions, MD simulation is used to simulate the disordered zones, which are then incorporated into KMC simulations to reach long irradiation times. We introduce a new method based on scaling behavior of structure factor to identify reliably the transition boundary between patterning and disordered states. These simulations indicate that 1MeV Kr ion irradiation can lead to patterning, whereas 70KeV He ion cannot. These results are compared to experimental results, obtained by performing ion irradiations on $Ni_3Al$ thin films grown by sputtering.

**16:42**

**K31 10 Maximally fast coarsening algorithms** MOWEI CHENG, *Center for Theoretical and Computational Materials Science, National Institute of Standards and Technology* ANDREW RUTENBERG, *Department of Physics and Atmospheric Science, Dalhousie University* We present maximally-fast numerical algorithms for conserved coarsening systems that are stable and accurate with a growing natural time-step $\Delta t = At_s^{2/3}$. We compare the scaling structure obtained from our maximally-fast conserved systems directly against the standard fixed-timestep Euler algorithm, and find that the error scales as $\sqrt{A}$ — so arbitrary accuracy can be achieved. For non-conserved systems, only effectively finite timesteps are accessible for similar unconditionally stable algorithms.

**16:54**

**K31 11 Mesoscopic modeling of the response of human dental enamel to mid-infrared radiation** ANA VILA VERDE, *Department of Chemical Engineering, Penn State University* MARTA RAMOS, *Department of Physics, University of Minho, Portugal* A.M. STONEHAM, *Centre for Materials Research, Department of Physics and Astronomy, University College London, UK* Ablation of human dental enamel, a composite biomaterial with water pores, is of significant importance in minimally invasive laser dentistry but progress in the area is hampered by the lack of optimal laser parameters. We use mesoscopic finite element models of this material to study its response to mid-infrared radiation. Our results indicate that the cost-effective, off-the-shelf $CO_2$ laser at $\lambda = 10.6\ \mu$m may in fact ablate enamel precisely, reproducibly and with limited unwanted side effects such as cracking or heating, provided that a pulse duration of $\approx 10\ \mu$s is used. Furthermore, our results also indicate that the Er:YAG laser ($\lambda = 2.94\ \mu$m), currently popular for laser dentistry, may in fact cause unwanted deep cracking in the enamel when regions with unusually high water content are irradiated, and also provide an explanation for the large range of ablation threshold values observed for this material. The model may be easily adapted to study the response of any composite material to infrared radiation and thus may be useful for the scientific community.

**17:06**

**K31 12 The isotope effect in the ferroelectric phase transition of KDP using *ab-initio* path intergal simulations** VARADHARAJAN SRINIVASAN,* ROBERTO CAR, *Princeton University, Princeton, NJ 08544, US* DANIEL SEBASTIANI, *Max Planck Institute for Polymer Research, Ackermannweg 10 / 55128 Mainz, Germany* We perform *ab-initio* path integral simulations on protonated and deuterated KDP at different temperatures and lattice constants in order to probe the origin of the isotope effect of the ferroelectric phase transition in this material. By taking into account the quantum nature of the proton/deuteron our simulations are capable of distinguishing the direct effects of a pure mass change versus the indirect structural effect in the hydrogen bonding geometry upon deuteration. In reality, the direct and indirect effects amplify each other in a self-consistent manner, leading to the huge isotope effect on the transition temperature. With our calculation we can selectively investigate the manisfestation of the two phenomena. We characterize the ferro and paraelectric phases with the help of a recent modification of the path integral implementation in the CPMD package which enables us to compute momentum distributions of the proton/deuteron both above and below the transition temperature in order to characterize the extent of proton/deuteron delocalization in both phases.

*Max Planck Institute for Polymer Research, Ackermannweg 10 / 55128 Mainz, Germany

**SESSION K32: FOCUSED SESSION: COMPUTATIONAL NANOSCIENCE IV**
**Tuesday Afternoon, 14 March 2006**
**329, Baltimore Convention Center at 14:30**
**Milen Kostev, North Carolina State University, presiding**



**14:30**

**K32 1 Trends in the structure of neutral, cationic, and anionic Ag and Au clusters from DFT calculations*** IGNACIO L. GARZON, *Instituto de Fisica, UNAM* LUIS A. PEREZ, KARO MICHAELIAN, The physical and chemical properties of small coinage metal clusters, with atomic structures $nd^{10}(n+1)s^1$ ($n=$ 3,4,5 for Cu, Ag and Au, respectively), are of great interest since, for example, can be viewed as a bridge between those existing in the ''simple'' *s*-only alkali metal and the more complicated transition metal clusters. Several theoretical calculations and indirect experimental evidence have shown that $Au_N$ clusters prefer planar structures up to sizes around $N=13$, cage-like structures for the $T_d$ $Au_{20}$ and $I_h$ $Au_{32}$ and low- symmetry (amorphous) configurations for $Au_{55}$. In this work, we present a theoretical study of the structural and electronic properties of Ag and Au neutral, cationic and anionic clusters with up to $N=55$ atoms, using density functional theory in the generalized gradient approximation. A different behavior is found in the physical properties of Ag and Au clusters, mainly due to the stronger relativistic effects present in the Au clusters. Another trend indicates that not only the size (number of atoms) and shape (isomer geometry) of a given cluster determine its properties, but also the charge present in the system may affect the cluster behavior even in the larger sizes with N=55. A discussion of the structural motifs existing in neutral, cationic and anionic Ag and Au clusters with up to N=55 atoms and their connection with recent experimental data will be presented.

*We acknowledge support from Conacyt-Mexico under grant 43414-F

**14:42**

**K32 2 Enantiospecific adsorption study at chiral gold nanoclusters from DFT calculations*** XOCHITL LOPEZ-LOZANO, *Instituto de Fisica, UNAM, Mexico.* LUIS A. PEREZ, IGNACIO L. GARZON, Chiral structures have been found as the lowest energy isomers of bare and passivated gold nanclusters from density functional theory (DFT) studies. Recently, experimental evidence on the existence of chiral gold nanoclusters has been published. In this work, DFT calculations are performed to study the adsorption of chiral molecules (like cysteine) on chiral and achiral (icosahedral) $Au_{55}$ clusters. Different locations on the metal cluster surfaces are used to identify the most favorable adsorption sites of the chiral molecule. Enantioselectivity is investigated through the comparison of the binding energies of the (S) and (R)-cysteine molecule adsorbed on the different $Au_{55}$ cluster enantiomers.

*We acknowledge the support from Conacyt Mexico grant No. 43414F

**14:54**

**K32 3 Structural and electronic properties of sodium nanoclusters*** LUIS A. PEREZ, *Instituto de Fisica, UNAM* JUAN A. REYES-NAVA, *IPICYT* IGNACIO L. GARZON, *Instituto de Fisica, UNAM* Recent advances on mass selection of sodium nanoclusters and their characterization by photoemission electron spectroscopy [1] have given useful data for a variety of clusters sizes. These data may lead to assignments of the relevant structures by comparing the measured photoelectron spectra (PES) with the electronic density of states (DOS) obtained from DFT calculations. In this work, the lowest energy structures modeled by the many-body Gupta potential, are obtained by using molecular dynamics simulations for $Na_n$ (n= 178, 204, 271, 298-300, 309). DFT calculations were then performed for neutral, positively- and negatively-charged $Na_n$ clusters. A comparison between the DOS of clusters of the same size but different charge will be presented, as well as between the available experimental PES and the theoretical obtained DOS. [1] H. Haberland, T. Hippler, J. Donges, O. Kostko, M. Schmidt, B. von Issendorff, Phys. Rev. Lett. 94, 035701 (2005).

*This work was supported by CONACyT No. 43414-F.

**15:06**

**K32 4 Electron-Stimulated Emission of Na Atoms from NaCl Nanocubes** DAVIDE CERESOLI, TANYA ZYKOVA-TIMAN, *SISSA, Trieste* ERIO TOSATTI, *SISSA and ICTP, Trieste* Emission of neutral cations/anions from solid akali halides can in principle be provoked by donating/subtracting electrons to the surface of alkali halide crystals, but generally constitutes a very endoenergetic process. The amount of energy required is expected to decrease for atoms located in less favorable positions, such as at surface steps and kinks, where the local coordination is smaller. The most favorable case of all should be represented by corner atoms of alkali halides cubes, where ionic binding is the weakest. We carried out first principles density functional calculations and simulations of magic-size neutral and charged NaCl nanocubes, to ascertain the stability and extractibility of neutralized corner ions. We find that detachment of neutral Na atoms upon donation of an excess electron is possible for a very modest energetic cost of the order of 0.6 eV, in line with early experimental observations. The atomic and electronic structure of the resulting $Na^+$ vacancy is analyzed in detail.

**15:18**

**K32 5 Comparison of TDLDA and GW-Bethe-Salpeter Methods for Optical Excitations in Noble Metal Clusters** SHING F. YIP, JUAN C. IDROBO, SERDAR OGUT,* *University of Illinois at Chicago* MURILO TIAGO, JAMES R. CHELIKOWSKY,† *University of Texas at Austin* JINLAN WANG, JULIUS JELLINEK,‡ *Argonne National Laboratory* We perform a comparative analysis of first principles results for optical spectra of $Ag_n$ and $Au_n$ ($n \leqslant 8$) clusters calculated within the time-dependent local density approximation (TDLDA) and the GW-Bethe-Salpeter (GW-BSE) technique. Both the TDLDA and GW-BSE calculations are performed entirely in real space based on the higher-order finite difference *ab initio* pseudopotential method. In the GW-BSE method, the screened Coulomb potential is calculated from the TDLDA polarizability. The convergence of the

results with respect to various computational parameters is carefully examined. In general, the TDLDA and GW-BSE methods are in reasonable agreement with respect to peak positions at low energies, while high-energy excitations and oscillator strengths can be different. The GW-BSE results are found to be in a somewhat better agreement with the available experimental data.

*Supported by DOE Grant No. DE-FG02-03ER15488
†Supported by DOE Grant No. DE-FG02-03ER15491
‡Supported by the Office of Basic Sciences, Division of Chemical Sciences, Geosciences, and Biosciences, U. S. Department of Energy under Contract No. W-31-109-Eng-38

**15:30**

**K32 6 *Ab initio* calculations for the photoelectron spectra of iron clusters*** SHEN LI, *Department of Physics and Astronomy, Rutgers the State University of New Jersey, Piscataway, NJ 08854,USA* MANUEL ALEMANY, *Departamento de Física de la Materia Condensada,Facultad de Física, Universidad de Santiago de Compostela, E-15872, Spain* JAMES CHELIKOWSKY, *Department of Physics and Chemical Engineering, Institute of Computational Engineering and Sciences, University of Texas, Austin, Texas 78712, USA* We studied negatively charged iron clusters $Fe_n^-$ $(n = 3 - 6)$. We use a real-space pseudopotential approach based on the density-functional theory within local spin density approximation. The real space approach assumes no explicit basis. Wave functions are evaluated on a uniform grid; only one parameter, the grid spacing, is used to control the convergence of the electronic properties. Charged states are easily handled in real space, in contrast to method based on supercells where electrostatic divergences require special handling. For each cluster, we determined the ground state structure. To compare with the experimental photoelectron spectra, we calculated the electron binding energies, which include the final state relaxation effects. Our results for the photoelectron spectra, are able to reproduce the main features of the experiments. Our results for the magnetic moment of each cluster agree well with the other theories.

*This work was supported by National Science Foundation, Minnesota Supercomputing Institute, the Department of Energy and the National Energy Research Scientific Computing Center

**15:42**

**K32 7 Size Dependence of the Static Polarizabilities and Absorption Spectra of Gold Clusters** SERDAR OGUT, JUAN CARLOS IDROBO,* *University of Illinois at Chicago* JINLAN WANG, JULIUS JELLINEK,† *Chemistry Division, Argonne National Laboratory* We present results for static polarizabilities and absorption spectra for ground state structures of $Au_n$, $n = 2 - 14,20$, clusters calculated within static and time-dependent density functional theory. The static polarizabilities of the clusters with less than 14 atoms exhibit even-odd oscillations. The polarizabilities of $Au_{14}$ and $Au_{20}$ are noticeably lower. This change in the behavior of static polarizability is correlated with the transition from two-dimensional to three- dimensional structures at $n = 14$. The *d* electrons have a large effect on the optical spectra as they quench the oscillator strengths significantly and are heavily involved in low-energy excitations. The calculated spectra are compared with available experimental data and spectra obtained for $Ag_n$ clusters.[1]

*Supported by DOE Grant No. DE-FG02-03ER15488
†Supported by the Office of Basic Sciences, Division of Chemical Sciences, Geosciences, and Biosciences, U. S. Department of Energy under Contract No. W-31-109-Eng-38

[1]J. C. Idrobo, S. Ogut, and J. Jellinek, Phys. Rev. B **72**, 085445 (2005)

**15:54**

**K32 8 Interactions of water and oxygen molecules with gold clusters** SEUNG BUM SUH, BOKWON YOON, MINDE SUN, UZI LANDMAN, *School of Physics. Georgia Institute of Technology, Atlanta, GA 30332-0430* The interaction of water and oxygen molecules with neutral gold clusters, $Au_n$ for n=2-8, is investigated using the first- principles calculations based on the density functional theory with generalized gradient correction. The $O_2$ binding energy, the intramolecular bond-length of $O_2$, and the excess charge on the adsorbed $O_2$ show even-odd alternations as a function of the number of gold atoms, correlating with the vertical electron detachment energy of $Au_n$ . The influence of pre-adsorbed $H_2O$ on the $O_2$ adsorption is pronounced when the $O_2$ is adsorbed with an Au-O bond with the gold cluster and an O-H bond with pre- adsorbed $H_2O$, while the influence is relatively small for $O_2$ adsorbed with double Au-O bonds. Compared to the $O_2$ adsorption in the absence of $H_2O$, the binding energy of $O_2$ are increased by 0.4 eV, and the intramolecular bond- length are stretched by up to 0.03 Å.

**16:06**

**K32 9 Density-Functional Study of $Au_n^-$ $(n = 16 - 24)$: Atomic and Electronic Structures and Interaction with $O_2$** BOKWON YOON, UZI LANDMAN, *Georgia Institute of Technology* PEKKA KOSKINEN, MICHAEL MOSELER, *Fraunhofer Institute for Mechanics of Materials* HANNU HAKKINEN, *University of Jyvaskyla* Anionic gold clusters with 16 to 24 atoms are studied using the Born-Oppenheimer local-spin-density molecular dynamics method. The structures of the ground-state clusters and energetically lowest-lying isomers are 3-dimensional, while the ground-state structures of smaller $Au_n^-$ with up to 14 atoms were reported to be planar (Häkkinen, et al., J. Chem. Phys. 117, 6982 (2002)). The calculated vertical electron detachment energies ($vDE$) are in good agreement with the experimental results (Taylor, et al., J. Chem. Phys. 98, 3319 (1992)); $vDE$'s are smaller for even $n$'s and larger for odd $n$'s, with the exception of $n = 16$. Compared to the other even-numbered clusters, $Au_{16}^-$ exhibits relatively large $vDE$, $vDE(Au_{16}^-)$=4.03 eV. The smallest $vDE$ is measured for $n = 20$, $vDE(Au_{20}^-)$=2.71 eV, The adsorption of $O_2$ to $Au_n^-$ is also sensitive to the cluster size; the $O_2$ adsorption is relatively strong for the even-numbered clusters with the exeption of $Au_{16}^-$. The $O_2$ binding energy, the intramolecular bond-length of $O_2$, and the excess charge on $O_2$ correlate strongly with the vertical electron detachment energy of $Au_n^-$ .

**16:18**

**K32 10 Properties of $Pt_{37}$ and $Pt_6Ru_{31}$ Clusters on Carbon: comparison of theory and experiment*** LIN-LIN WANG, DUANE D. JOHNSON, *Department of Materials Science and Engineering, UIUC* Using DFT calculations, we analyze the structures of self-organizing nanoparticles formed by Pt and Ru-Pt on a carbon support and clarify complex behaviors noted in earlier experimental studies. With clusters deposited via metallo-organic Pt or

PtRu5 complexes and annealed at 670 K in hydrogen atmosphere, the Pt and Pt-Ru based clusters were observed to form fcc(111)-stacked cuboctahedral geometry and essentially bulk-like metal-metal bond lengths, even for the 10-40 atom nanoparticles for which the average coordination number is much smaller than that in the bulk, and that Pt in bimetallic clusters segregates to the ambient surface. We explain these observations and characterize the cluster structures with graphite as a model for the support. Our study reveals the origin of the observed bulk-like metal-metal bond lengths and bond-length disorder, and demonstrates the profound consequences that result from the cluster/support interactions and hydrogen passivation on their structural and electronic properties.

*DOE Grants DE-FG02-91ER45439 and DE-FG02-03ER15476

**16:30**
**K32 11 Structure and functionality of a prospective (Pt, Ru)/MgO nanocatalyst** RYSZARD BUCZKO, *Oak Ridge National Laboratory* ALBINA BORISEVICH, *Oak Ridge National Laboratory* RICHARD ADAMS, *University of South Carolina* MICHAEL AMIRIDIS, *University of South Carolina* STEPHEN PENNYCOOK, *Oak Ridge National Laboratory* SOKRATES PANTELIDES, *Vanderbilt University* The atomic structure of metal nanoparticles in the prospective catalyst (Pt, Ru)/MgO was imaged by Z-contrast scanning transmission electron microscopy. On the MgO (110) surface we find regular monolayer-like particles; all atoms show uniform intensity in the image and are likely to be Pt because of the large atomic number. Density functional theory calculations have been used to determine the structure of possible particles. We find that regular monolayer-like structures can be formed, with Pt bonded to surface oxygen. The Pt particles are loosely connected to the substrate in agreement with microscopic observations. The influence of surface defects on cluster structure and mobility will be analyzed, and the implications for the catalytic activity of the (Pt, Ru)/MgO system will be discussed.

**16:42**
**K32 12 Vibrational Dynamics and Thermodynamics of AgCu nanoparticles*** ABDELKADER KARA, HANDAN YILDIRIM, TALAT S. RAHMAN, *Physics Department, Kansas State University* RICARDO FERRANDO, *INFM and IMEM-CNR, Dipartimento di Fisica dellUniversita' di Genova, via Dodecaneso 33, 16146 Genova, Italy* We present results of a systematic study of the structure, vibrational dynamics and thermodynamics of $Ag_nCu_{34-n}$ nanoparticles including. The starting structure were generated using a structural optimization using a genetic algorithm [1]. Using the embedded atom method potentials, we have calculated the vibrational densities of states for all stoichiometries and the corresponding vibrational free energies, in the harmonic approximations. At 300K, the vibrational free energy is found to behave linearly with the increasing number of Ag atoms in the nanoparticles. The vibrational contributions to the free energy increase from 5.5% for $Ag_0Cu_{34}$ to 8.3% $Ag_{34}Cu_0$. Selected force constants for several nanoparticles were calculated using density functional theory (DFT) and were found to be very close to those determined using EAM potentials. [1] G. Rossi, A. Rapallo, C. Mottet, A. Fortunelli, F. Baletto and R. Ferrando Phys. Rev. Lett, **93**, 105503 (2004)

*Work supported in part by DOE under grant No: BES DE-FGO3-97ER45650.

**16:54**
**K32 13 Selective modification of the surface structure of oxide nano-particles using sub-bandgap photons** A. SHLUGER, P. TREVISANUTTO, P. SUSHKO, A. STONEHAM, *Department of Physics and Astronomy, University College London, Gower St., London, WC1E 6BT, UK* M. HENYK, K. BECK, A. JOLY, W. HESS, *Pacific Northwest National Laboratory, P.O.Box 999, Richland, WA 99352 USA* Controlled manipulation of the physical and chemical properties of nano-structured materials requires correlating their spectroscopic properties and reactivity with specific surface sites. We have demonstrated experimentally that laser excitation of MgO nano-crystalline films and nanocube samples with 4.66 eV photons desorbs neutral O and Mg atoms with hyperthermal kinetic energies in the range of 0.1–0.4 eV. Using an ab initio embedded cluster approach we developed the mechanisms for the hyper-thermal emission of atomic species. We demonstrate that the desorption of O atoms from 3-coordinated (3C) surface sites occurs via the following steps: i). an exciton is excited at the 3C site; ii) the exciton is ionized, while the remaining electronic hole is trapped at the 3C O site converting it to an $O^-$ radical; iii) absorption of another 4.66 eV photon in the vicinity of the 3C site forms an excited state, which relaxes with desorption of a neutral O atom. Similar process was identified for Mg-terminated 3C site. The proposed general mechanism can be used to control atomic scale modification of insulating surfaces. [1] P.E. Trevisanutto et al., itSurf. Sci., **593**, 210 (2005); W.P. Hess et al, itJ. Phys. Chem. B, **109**, 19563 (2005).



## SESSION K33: NOVEL MOVING BOUNDARY PROBLEMS
**Tuesday Afternoon, 14 March 2006; 336, Baltimore Convention Center at 14:30**
**Wim Saarloos, Leiden University, presiding**

**14:30**
**K33 1 Nonlinear shape evolution of electromigration-driven single-layer islands.*** JOACHIM KRUG, *University of Cologne*

Electromigration is the transport of matter induced by an electric current in the bulk or at the surface of a conducting material. Electromigration along interfaces and grain boundaries is a central factor limiting the reliability of integrated circuits. This has motivated numerous theoretical studies of the shape evolution of voids in metallic thin films caused by electromigration along the void boundary [1]. In this case the coupling of the void shape to the current distribution in the film leads to a nonlocal moving boundary problem driven by a mass current tangential to the boundary. Here we are concerned with the itlocal version of the problem, which applies to the electromigration of single-layer islands on metallic

surfaces [2]. We show that the introduction of crystal anisotropy in the mobility of atoms along the island boundary induces a rich variety of dynamical behaviors, ranging from spontaneous symmetry breaking to periodic and chaotic modes of island migration [3]. Under suitable physical conditions these phenomena can be reproduced in kinetic Monte Carlo simulations of a realistic microscopic model of the Cu(100) surface. Finally, we discuss recent results on the electromigration of vacancy islands in the kinetic regime dominated by exchange with the adatom diffusion field itinside the island. The talk is based on joint work with P. Kuhn, F. Hausser, A. Voigt and M. Rusanen. [1] M. Schimschak, J. Krug, J. Appl. Phys. **87**, 685 (2000). [2] O. Pierre-Louis, T.L. Einstein, Phys. Rev. B **62**, 13697 (2000). [3] P. Kuhn, J. Krug, F. Hausser, A. Voigt, Phys. Rev. Lett. **94**, 166105 (2005).

*Supported by DFG within SFB 616 and project KR 1123/1-2.

**15:06**
**K33 2 Fluctuation-regularized front propagation dynamics in reaction-diffusion systems.***
DAVID KESSLER, *Bar-Ilan University*

We introduce and study a new class of fronts in finite particle number reaction-diffusion systems, corresponding to propagating up a reaction rate gradient. We show that these systems have no traditional mean-field limit, as the nature of the long-time front solution in the stochastic process differs essentially from that obtained by solving the mean-field deterministic reaction-diffusion equations. Instead, one can incorporate some aspects of the fluctuations via introducing a density cutoff. Using this method, we derive analytic expressions for the front velocity dependence on bulk particle density and show self-consistently why this cutoff approach can get the correct leading-order physics.

*Work supported in part by the Israel Science Foundation

**15:42**
**K33 3 Spark formation as a moving boundary process.**
UTE EBERT, *CWI Amsterdam and TU Eindhoven*

The growth process of spark channels recently becomes accessible through complementary methods. First, I will review experiments with nanosecond photographic resolution and with fast and well defined power supplies that appropriately resolve the dynamics of electric breakdown [1]. Second, I will discuss the elementary physical processes as well as present computations of spark growth and branching with adaptive grid refinement [2]. These computations resolve three well separated scales of the process that emerge dynamically. Third, this scale separation motivates a hierarchy of models on different length scales. In particular, I will discuss a moving boundary approximation for the ionization fronts that generate the conducting channel. The resulting moving boundary problem shows strong similarities with classical viscous fingering. For viscous fingering, it is known that the simplest model forms unphysical cusps within finite time that are suppressed by a regularizing condition on the moving boundary. For ionization fronts, we derive a new condition on the moving boundary of mixed Dirichlet-Neumann type ($\phi = \epsilon\partial_n\phi$) that indeed regularizes all structures investigated so far. In particular, we present compact analytical solutions with regularization, both for uniformly translating shapes and for their linear perturbations [3]. These solutions are so simple that they may acquire a paradigmatic role in the future. Within linear perturbation theory, they explicitly show the convective stabilization of a curved front while planar fronts are linearly unstable against perturbations of arbitrary wave length. [1] T.M.P. Briels, E.M. van Veldhuizen, U. Ebert, TU Eindhoven. [2] C. Montijn, J. Wackers, W. Hundsdorfer, U. Ebert, CWI Amsterdam. [3] B. Meulenbroek, U. Ebert, L. Schäfer, Phys. Rev. Lett. **95**, 195004 (2005).

**16:18**
**K33 4 Stalactite Growth as a Free-Boundary Problem.***
RAYMOND GOLDSTEIN, *University of Arizona*

As far back in recorded history as the writings of the Elder Pliny in the first century A.D. are found references to the fascinating structures found in limestone caves, particularly stalactites. Although the subject of continuing inquiry since that time, the chemical mechanisms responsible for their growth have only been well-established since the 19th century, and there has been no quantitative understanding of the morphological evolution of these strange and beautiful forms. In this talk I will describe a synthesis of calcium carbonate chemistry, diffusion, thin-film fluid dynamics, and nonlinear dynamics which shows that stalactites evolve according to a novel geometric growth law which exhibits extreme amplification at the tip. Studies of this model show that a broad class of initial conditions is attracted to an ideal parameter-free shape, not previously known in science, which is strikingly close to a statistical average of natural stalactites. Similar hydrodynamic and geometric considerations lead to a quantitative theory for the shapes of icicles, and an understanding of why stalactites and icicles look so similar, despite the vastly different physics underlying their growth.

*Supported by NSF ITR Grant PHY0219411

**16:54**
**K33 5 Unsteady Crack motion and branching.**
ALAIN KARMA, *Northeastern University*

This abstract was not received electronically.

**SESSION K34: PANEL DISCUSSION**
**Tuesday Afternoon, 14 March 2006**
**337, Baltimore Convention Center at 14:30**

**SESSION K35: ELECTRONIC PROPERTIES AND THE KONDO EFFECT IN QUANTUM DOTS**
**Tuesday Afternoon, 14 March 2006**
**338, Baltimore Convention Center at 14:30**
**Michael Scheibner, Naval Research Laboratory, presiding**



**14:30**
**K35 1 Exotic few-particle ground states in charged self-assembled InAs/GaAs quantum dots*** LIXIN HE, GABRIEL BESTER, ALEX ZUNGER, *National Renewable Energy Laboratory, Golden, Colorado 80401* Three-dimensionally confined quantum dots can be loaded with a few carriers. However, unlike real atoms, in self-assembled InAs/GaAs quantum dots, the Coulomb repulsion between holes $J_{hh} \sim$ 15 -25 meV is comparable to the single-particle energy spacing between levels $\Delta\epsilon \sim$ 10 - 20 meV. This opens the possibility of observing stable, exotic spin configurations that defy the rules of atomic physics (Hund's rule and the Aufbau principle). We have applied a combination of atomistic pseudopotential description for the single-particle level structure, with a many-body configuration interaction (CI) description of many-particle effects to predict both electron and hole charged states in InGaAs/GaAs self-assembled quantum-dots. We find that while electron charging follow both the Aufbau principle and Hund's rule, hole charging gives rise to stable but unusual spin configurations. Our theory [1] offer a self-consistent interpretation to recent experimental observations [2], where the simple 2D effective mass parabolic models fail. [1] L. He, G. Bester and A. Zunger, Phys. Rev. Lett. (in press), cond-mat/0505330. [2] Reuter *et al*, Phys. Rev. Lett. **94**, 026808 (2005).

*Supported by DOE-SC-BES-DMS, under NREL Contract No. DEAC36-99-GO10337.

**14:42**
**K35 2 A variational wave function for two-dimensional quantum-dot helium*** M. GOLAM FARUK, *Department of Electrical Engineering and Department of Physics, Prairie View A&M University, Prairie View, Texas 77446* ORION CIFTJA, KEVIN STORR, *Department of Physics, Prairie View A&M University, Prairie View, Texas 77446* We introduce a variational wave function for two-dimensional quantum dot helium (a system of two interacting electrons in a two-dimensional parabolic confinement potential) in an arbitrary perpendicular magnetic field. This variational wave function contains a Jastrow pair correlation factor of displaced Gaussian form in addition to the commonly used Laughlin correlation factor. The Gaussian correlation factor assures the overall quality of the variational wave function at all values of the magnetic field including weak (or zero) and strong magnetic fields. The accuracy of the variational wave function is gauged through exact numerical diagonalization results. We find out that this trial wave function is a very accurate representation of the true ground state for the whole range of magnetic fields.

*This research was supported by the U.S. D.O.E. (Grant No. DE-FG52-05NA27036)

**14:54**
**K35 3 Spin-Orbit effects in Quantum Dots: Interplay of disorder and interactions** HAKAN E. TÜRECI, Y. ALHASSID, A. DOUGLAS STONE, *Center for Theoretical Physics, Sloane Physics Laboratory, Yale University, New Haven, CT 06520* Disordered or chaotic quantum dots with a large Thouless conductance g provide a tractable experimental and theoretical system for studying electron-electron interactions within the framework of the universal Hamiltonian. In particular, good agreement between theory and experiment is observed for the mesoscopic fluctuations of the conductance in dots with negligible spin-orbit scattering [1]. Here we focus on the effects of a tunable spin-orbit scattering within the universal Hamiltonian model. The presence of spin-orbit scattering was shown to introduce new symmetry limits of the single-particle Hamiltonian [2]. We present results for ground state and finite temperature properties in the crossover regime between symmetries. Furthermore, we study the signatures of a quantum critical regime dominated by collective critical fluctuations [3].
Y. Alhassid and T. Rupp, Phys. Rev. Lett. 91, 056801 (2003). I.L. Aleiner and V.I. Fal'ko, Phys. Rev. Lett. **87**, 256801 (2001). G. Murthy, Phys. Rev. B **70**, 153304 (2004).

**15:06**
**K35 4 A many-polaron system in a background-charge potential*** F. BROSENS, S. N. KLIMIN, J.T. DEVREESE, *–TFVS, Departement Natuurkunde, Universiteit Antwerpen* The ground state energy of an *N*-polaron system confined to a quantum dot with a neutralizing background charge is investigated within an all-coupling many-body path-integral variational principle taking into account both Fermi statistics of polarons and the electron-electron interaction. The treatment of the ground-state energy is performed for both closed-shell and open-shell systems. The electron-phonon contribution to the ground-state energy as a function of the number of fermions demonstrates a trend to a constant value when increasing *N*. For a finite number of polarons, the dependencies of the ground-state energy and of the polaron contribution on the parameter $r_s^*$, which determines the average fermion density in a quantum dot, are very similar to those for a polaron gas in bulk. Herefrom, we can conclude that the ground-state properties of a polaron gas in bulk can be qualitatively described using a model of a finite number of polarons in a confinement potential provided by a background charge.

*Work supported by the GOA BOF UA 2000, IUAP, FWO-V project G.0435.03 and the WOG WO.035.04N (Belgium).

**15:18**

**K35 5 Spectroscopy of the Kondo Problem in a Box** DENIS ULLMO, RIBHU KAUL, GERGELY ZARAND, SHAILESH CHANDRASEKHARAN, HAROLD BARANGER, *Duke U, Karlsruhe U, Budapest U, and LPTMS Orsay* We study the spin quantum numbers and energy eigenvalues of the ground state and low lying excitations of a quantum dot with a single spin-S impurity. We prove an exact theorem that allows us to infer the ground state spin for an arbitrary spin-S of the impurity and for even/odd electrons on the quantum dot. Additionally, strong and weak coupling perturbation theory backed up with quantum Monte-Carlo simulations enable us to map out the spin structure of the excited states and the energy splittings between them as the ratio $\Delta/T_K$ is tuned. We propose a simple transport experiment involving the tunneling spectroscopy of a double quantum dot, where these results can be observed. Finally, we make explicit contact with experiment by calculating the transport properties of the proposed double dot device that exhibit signatures of tunneling into the Kondo-correlated state.

**15:30 teborg University**

**K35 6 Charge Fluctuations in a Nanoscale Structure: Interplay of Kondo and Luttinger Liquid Physics** PAATA KAKASHVILI, *Chalmers University of Technology* HENRIK JOHANNESSON, *Göteborg University* We propose a setup which allows to study the interplay of Kondo and Luttinger liquid physics. It consists of a quantum box, biased by a gate voltage, and side-coupled to a quantum wire by a point contact. Close to the degeneracy points of the Coulomb blockaded box the setup can be described as a Luttinger liquid interacting with an effective Kondo impurity. By applying a magnetic field one drives the system from an effective two-channel to a one-channel situation, allowing for the study of the crossover between the two. Using bosonization and boundary conformal field theory we predict that for the case of spin-polarized electrons the differential capacitance of the box will exhibit distinctive Luttinger liquid scaling with temperature and gate voltage. In the limit of zero field the Luttinger liquid behavior gets masked by two-channel Kondo screening, leading to a logarithmic scaling of the differential capacitance with temperature and gate voltage. These effects should be possible to study experimentally using the recently developed SET electrometer technique.

**15:42**

**K35 7 Universality and non-universality for a time-dependent quantum dot in the Kondo regime** ALI GOKER, PETER NORDLANDER, *Rice University* We employ time-dependent noncrossing approximation for single electron transistor and calculate the transient response of the conductance for a variety of temperatures in infinitesimal bias when the dot-lead tunneling constant is suddenly changed such that the Kondo effect is present in the final state. In non-universal timescale, we see rapid oscillations. The frequency of these oscillations depends on the dot level and their amplitude is modulated by initial and final tunneling constants. We explain this observation qualitatively by exact solution of the resonant level model. In universal timescale, we compute the conductance for two systems which have different Kondo temperatures and test universality. Our results indicate that universality is well preserved as a function of $T/T_K$ in spite of tiny deviations at low temperatures.

**15:54**

**K35 8 Universal Scaling Behavior of the Kondo Effect in a Quantum Dot.** DAVID GOLDHABER-GORDON, ILEANA RAU, *Stanford University* RONALD POTOK, *Harvard University* MICHAEL GROBIS, *Stanford University* At zero temperature, a many-body Kondo singlet forms between a spin-1/2 quantum dot and electrons in nearby, tunnel-coupled reservoirs. This Kondo singlet can be broken by sufficiently large temperature T or bias V across the dot. Differential conductance G(V,T) is predicted to show universal scaling in eV/kT. However, such behavior has not been examined thoroughly in experiments. To address this issue, we have performed detailed transport measurements through a Kondo quantum dot at finite bias and temperature. We will present our results and discuss the scaling behavior seen in this system.

**16:06**

**K35 9 The Two-channel Kondo Effect in a Semiconductor Nanostructure** ILEANA RAU, *Stanford University* RON POTOK, *Harvard University* DAVID GOLDHABER-GORDON, *Stanford University* Quantum dots have proven to be excellent systems for studying the single-channel Kondo effect, the many-body ground state resulting from the interaction between a spin 1/2 quantum dot and a reservoir of conduction electrons. The two-channel Kondo effect is achieved by coupling the dot with equal strength to two independent reservoirs. In this case the reservoirs compete to independently form a Kondo state with the dot, resulting in overscreening of the excess spin. In a new semiconductor double quantum dot geometry, proposed by Y. Oreg and D. Goldhaber-Gordon (1), we observe spin two-channel Kondo physics. Low temperature transport measurements through the smaller of the two dots reveals that the double dot – leads system undergoes a quantum phase transition from one competing single-channel Kondo state to another. By tuning between these two Fermi liquid regimes, we observe the non-Fermi liquid signature of the two-channel Kondo state. I will explore recent experimental progress and open questions. (1) Y. Oreg, D. Goldhaber-Gordon, PRL **90** 136602 (2003).

**16:18**

**K35 10 Jahn-Teller / Kondo Interplay in a Three-Terminal Quantum Dot** R.C. TOONEN, *University of Wisconsin (UW)* H. QIN, *UW* A.K. HUETTEL, *Ludwig-Maximilians-Universitaet* S. GOSWAMI, *UW* D.W. VAN DER WEIDE, *UW* K. EBERL, *Max-Planck-Institut fuer Festkoerperforschung* R.H. BLICK, *UW* The Jahn-Teller effect is the spontaneous geometric distortion of a nonlinear molecular entity. The Kondo effect, an expression of asymptotic freedom, arises from the hybridization between localized states of a magnetic impurity and the itinerant states of its environment. The interplay of these two phenomena has attracted the attention of theorists studying the growth and interactions of heavy-fermion systems. Because of the technical difficulties associated with probing isolated impurities in bulk materials, this composite effect has remained experimentally unexplored. We have investigated co-tunneling transport phenomena in a three-terminal quantum dot with triangular symmetry. Our measurements of anomalous spectral signatures reveal interplay between the Jahn-Teller and Kondo effects. This discovery suggests a means of controlling the correlation of spatially separated pairs of entangled electrons (EPR pairs)—a necessary condition for the physical realization of a quantum computer (DiVincenzo's 7th requirement).

**16:30**

**K35 11 Quantum Dot Coupled to a Mesoscopic Fabry-Perot Resonator.** MICHAEL GROBIS, *Stanford University* ILEANA RAU, *Stanford University* RONALD POTOK, *Harvard University* DAVID GOLDHABER-GORDON, *Stanford University* We will present our study of a quantum dot coupled to a Fabry-Perot resonator. The Fabry-Perot resonator is created by tunnel coupling a lithographically defined two-lead quantum dot to an additional finite reservoir of tunable length. Fabry-Perot oscillations are observed in transport through the quantum dot caused by interference between the direct tunneling path through the dot and the multi-step path that includes tunneling in and out of the finite reservoir. These oscillations are dependent on the phase shifts acquired during the transmission events and the nature of the electron path through the Fabry-Perot cavity. Tuning the quantum dot through a Kondo resonance allows us to extract information about the Kondo transmission phase shift and the nature of Kondo screening cloud in this system.

**16:42 guezsica, Universidad Nacional Autónoma de México**

**K35 12 Electron Dynamics in AC-Driven Quantum Lenses** AREZKY HERNÁNDEZ-RODRíGUEZ, *Instituto de Física, Universidad Nacional Autónoma de México* LILIA MEZA-MONTES, *Instituto de Física, Universidad Autónoma de Puebla* CARLOS TRALLERO-GINER, *Dept. de Física Teórica, Univ. de La Habana* SERGIO ULLOA, *Dept. of Physics and Astronomy, Ohio Univ.* We have applied the Floquet formalism to study the effects of an ac electric field applied to quantum dots with lens shape. The electric field is applied along and perpendicular to the direction of the axial symmetry and the time-dependent Hamiltonian in the effective mass approximation is solved. A complete set of orthonormal functions is found to characterize the physical problem while keeping the full lens symmetry. When the electric field is along the axial symmetry axis, we show that the Hilbert space of solutions is separated into orthogonal subspaces with different $z$-component of the angular momentum. In case of a perpendicular field, the appearance of new dynamical symmetry is studied. We give an explicit analytical representation for the quasi-energy spectrum and electronic states, and show numerical results for different lens parameters and intensity and direction of the electric field. The interplay between the lens shape geometry and the ac driven field (intensity and frequency) are analyzed. Our approach applies to the full range of intensities.

**16:54**

**K35 13 Toward Strong Interactions in Circular Quantum Dots: Correlation Induced Inhomogeneity** AMIT GHOSAL, *University of California Los Angeles* ALEV GUCLU, CYRUS UMRIGAR, *Cornell University* DENIS ULLMO, *LPTMS Orsay* HAROLD BARANGER, *Duke University* Physical properties of the electron gas, which describes conduction electrons interacting via Coulomb forces, change dramatically depending on the balance between the strength of the kinetic energy and the Coulomb repulsion. For weak interactions (high density), the system behaves as a Fermi liquid, with delocalized electrons. In contrast, in the strongly interacting limit (low density), the electrons localize and order in a Wigner crystal phase. The physics at intermediate densities is phenomenally rich and not adequately understood. Here we present a study of the intermediate density electron gas (up to $r_s = 18$) confined to a circular quantum dot containing up to 20 electrons. Using an accurate quantum Monte Carlo technique, we show that the correlation induced by increasing interaction strength smoothly causes, first, ring structure and, then, angular modulation in the pair-density without any signature of a cross-over. The excitation energy for certain high-spin states decreases significantly with $r_s$. Dots with smaller number of electrons are typically more affected by correlation effects.

**17:06**

**K35 14 Kondo Physics in Exactly Solvable SU(4) Double Dots** ROBERT KONIK, *Brookhaven National Laboratory* I study a dot-lead system composed of two quantum dots arranged in series. I consider dots that are both capacitive and tunnel coupled and where the applied gate voltage to the individual dots is unequal. This system admits an exact solution via the Bethe ansatz even in the presence of finite (as opposed to infinite) Coulomb repulsion. From this solution, the transport properties of the dot system can be ascertained analytically. In particular transport can be determined everywhere from the empty orbital to the mixed valence to an SU(4) Kondo regime. While double dots are the focus, natural generalizations to systems with $N > 2$ dots are similarly integrable.

**17:18**

**K35 15 Kondo Shadows in Hybrid Magnetic Molecular Solids** MIKHAIL KISELEV, *Institute for Theoretical Physics, Universität Würzburg, Würzburg D-97074, Germany* KONSTANTIN KIKOIN, *Ben-Gurion University of the Negev, Beer Sheva 84105, Israel* We discuss the properties of layered Anderson/Kondo lattices with metallic electrons confined in 2D xy planes and local spins in insulating layers forming chains in z direction. Each spin in this model possesses its own 2D Kondo cloud, so that the Nozieres' exhaustion problem does not occur. The high-temperature perturbational description is matched to exact low-T Bethe-ansatz solution. The excitation spectrum of the model is gapless both in charge and spin sectors. The disordered phases and possible experimental realizations of the model are briefly discussed.

**SESSION K36: MAGNETIC DOMAINS AND APPLIED MAGNETIC MATERIALS**
**Tuesday Afternoon, 14 March 2006**
**339, Baltimore Convention Center at 14:30**
**John Unguris, National Institute of Standards and Technology, presiding**

**14:30**

**K36 1 Real Space Observation of Helical Spin Order by Lorentz Microscopy** MASAYA UCHIDA, *ERATO, Japan Science and Technology Agency (JST), Tsukuba, Japan* YOSHINORI ONOSE, *ERATO-JST, Tsukuba, Japan* YOSHIO MATSUI, *AML, National Institute for Materials Science (NIMS), Tsukuba, Japan* YOSHINORI TOKURA, *Univ. Tokyo, Tokyo, Japan* Helical spin order is widely observed and its average structure has been investigated so far in reciprocal space mainly by neutron diffraction. Here the helical spin order and dynamics are visualized in real space by means of Lorentz electron microscopy. Our system of choice is $Fe_{1-x}Co_xSi$, which exhibits a helical spin order with a long period ($> 30$ nm) in a concentration range $0.05 \leqslant x \leqslant 0.8$. The Néel temperature $T_N$ and the helix period for $x = 0.5$ take about 38 K and 90 nm along the [100] direction, respectively. The

helical spin order is due to the Dzyalosinsky-Moriya (DM) interaction because of the lack of centrosymmetry of the lattice. The observations were made by means of a Lorentz transmission electron microscope operated at 300 kV. The magnetization distribution was obtained by the transport of intensity equation (TIE) analysis. The real world of the helical spin order proves to be much richer than expected from the averaged structure, as manifested by variegated magnetic defects like atomic boundary and dislocation in the crystal lattice. By applying magnetic fields we can directly observe the deformation processes of the helical spin order, accompanied by nucleation, movement, and annihilation of the magnetic defects.

**14:42**

**K36 2 Imaging chiral domains and magnetic phase coexistence in holmium metal*** A. CADY, J. C. LANG, D. HASKEL, G. SRAJER, *Argonne National Laboratory* D. B. MCWHAN, *Brookhaven National Laboratory (retired)* In the rare-earth metal holmium, the magnetic moments in the atomic planes form a magnetic spiral structure below $T_N = 133$ K with an incommensurate repeat unit along the crystal c-axis. This spiral structure forms with different chirality in different regions of the samples, giving rise to chiral domains. The pitch of the spiral evolves with temperature decreasing toward six atomic layers as the crystal is cooled to $T = 19$ K where the magnetic moments cant toward the c-axis, and a commensurate conical magnetic structure results. This magnetic phase transition leads to the formation of a second type of domains where the spiral phase coexists with the conical phase over a temperature range of approximately 1 K. We have combined micro-diffraction with phase-retarding x-ray optics to image both types of magnetic domains simultaneously as a function of temperature. Using circularly polarized x-rays, the satellite peaks associated with the magnetic ordering become sensitive to the chirality of the spirals, and the micro-focused beam provides spatial resolution of a couple microns. We will present images of both chiral domains and spiral/conical domains, which have been shown to occur over length scales of many microns.

*Work supported by the U.S. Department of Energy, Office of Basic Energy Sciences, under Contract No. W-31-109-ENG-38.

**14:54**

**K36 3 Inverse Transition of Magnetic Domain Patterns in Ultrathin Fe Films on Cu(001): A Quantitative Analysis** OLIVER PORTMANN, ALESSANDRO VINDIGNI, TUOMAS KNOWLES, ANDREAS VATERLAUS, DANILO PESCIA, *Laboratory for Solid State Physics, ETH Zurich* The magnetization of ultrathin Fe films on Cu(001) is perpendicular to the film plane. Due to the competition between exchange and dipolar interactions such films break up into domains of opposite magnetization. As the temperature is increased, the magnetic domain pattern undergoes an inverse transition[1]: a more ordered stripe phase is found at higher temperatures than a less ordered labyrinthine phase. The domain structure has been imaged by means of a SEMPA (Scanning Electron Microscope with Polarization Analysis). We characterize this pattern sequence quantitatively in terms of domain width, correlations, single-configuration energy and density of defects, directly extracted from SEMPA images. [1] O. Portmann, A. Vaterlaus, and D. Pescia, Nature **422**, 701 (2003).

**15:06**

**K36 4 Magnetic bubble domains in the spin reorientation transition region of Fe/Ni/Cu(001)** J. CHOI, J. WU, T. OWENS, Z. Q. QIU, *Dept. of Phys., UC-Berkeley, Berkeley, CA 94720* C. WON, *MSD, Argonne Nat. Lab., Argonne, IL 60439* Y. Z. WU, *Dept. of Phys. Fudan Univ., Shanghai, P. R. China* A. SCHOLL, A. DORAN, *Advanced Light Source, LBNL, Berkeley, CA 94720* Spin reorientation transition (SRT) in Fe/Ni/Cu(001) system was investigated using photoemission electron microscopy (PEEM). In addition to the previously found stripe domains, we also observed bubble domains within a narrow thickness region of the SRT after applying an in-plane magnetic field. Because of the up-down asymmetry of the bubble domains, a small off-normal component of the in-plane magnetic field is necessary to generate the bubble domains. By applying the magnetic field along different directions related to the sample surface, we found that the bubble domains disappear if the field direction is more than $\sim$ 10 degrees off the sample surface. A temperature dependent study shows that the bubble domains are unstable against annealing and will be converted back to the stripe phase, indicating that the bubble domain phase is a meta-stable phase.

**15:18**

**K36 5 Regular magnetic domain pattern in $TbNi_2B_2C$ due to strong magneto-elastic coupling** A. KREYSSIG, J.-W. KIM, L. TAN, A. I. GOLDMAN, *Ames Laboratory USDOE, Department of Physics and Astronomy, Iowa State University, Ames, IA 50011* C. DETLEFS, *ESRF Grenoble, 38043 Grenoble, France* B. GRENIER, *ILL Grenoble, 38042 Grenoble, France* M. LOEWENHAUPT, *Technische Universitaet Dresden, IFP, D-01062, Germany* $RNi_2B_2C$ compounds are of strong interest due to the competition between superconductivity and magnetism. The crystal electric field effects yield strong magnetoelastic effects. The strongest tetragonal-to-orthorhombic distortion is observed for $TbNi_2B_2C$ with a relative distortion of 0.6 % in the antiferromagnetic state at 1.5 K. The lowering of the symmetry forces the development of domains of two forms, in which the magnetic moment direction are align along the a or b axis, respectively. For both kind of domains, the lattice distortion is opposite in the ab plane. We investigated the resulting domain using scattering techniques. Temperature-dependent topographic x-ray images show that the domains are very large in (110) directions where as they are very narrow in the direction perpendicular in the ab plane. In X-ray and neutron diffraction sattelite reflections are found, which are produced by the regular pattern of domains with dimensions of 10 nm. A model describing this pattern and consequences for magnetic and superconducting properties will be discussed.

**15:30**

**K36 6 Disorder Induced Magnetic Memory** MICHAEL S. PIERCE, *University of Washington* To test theories of random microscopic disorder, we first developed and then applied coherent x-raymetrology to a series of thin multilayer films with perpendicular magnetic anisotropy anddegrees of disorder. We used coherent x-rays to generate speckled scattering patterns. The ''random'' arrangement of the speckles is due to the exact configuration of the magneticin the sample. Changes in the domain structure change the speckles, and comparison of thespeckle patterns provides a quantitative determination of how much the domain structure has. We asked (and answered) two important questions. How is the magnetic domain configuration at one point on the major hysteresis loop related to the configurations at the same point on the loop during subsequent cycles: microscopic

return point memory (RPM)? We found the RPM is partial and imperfect in the disordered samples. How are the magnetic domains at one point on the major loop related to the domains at the inversion symmetric point on the loop, during the same and during subsequent cycles: microscopic complementary point memory (CPM)? We found the CPM is also partial and imperfect in the disordered samples. In addition, we found that RPM is always larger than CPM. No existing theory was capable of reproducing our results. We developed newthat do fit our observations. Our experimental and theoretical results set new benchmarks for work.

**15:42**

**K36 7 Kerr Imaging of Co/Pt multilayers with perpendicular anisotropy** M. ROBINSON, Y. AU, J. KNEPPER, F. YANG, R. SOORYAKUMAR, *The Ohio State University* Co/Pt multilayer films are promising materials for applications such as in high density magnetic recording media. For very thin Co layers these structures exhibit perpendicular magnetization. The exchange coupling between adjacent Co layers is ferromagnetic and the coupling strength oscillates as the nonmagnetic Pt layer thickness ($t_{Pt}$) ranges from 3 to 75°A. In order to understand the magnetization reversal process in these structures, we report on magneto-optical images of a series of $[\text{Co}(4\ \text{Å})/\text{Pt}(t_{Pt})]_N$ multilayers obtained with Kerr microscopy as a function of $t_{Pt}$ and layer repetition N. The images reveal the evolution of the magnetic reversal process that strongly depends on $t_{Pt}$ and therefore on the interlayer coupling. For Co/Pt multilayers with small $t_{Pt}$, e.g., 11 Å, when Co layers are strongly coupled, the whole multilayer switches as a single ferromagnet. As Co layers are farther separated and decoupled, e.g., at $t_{Pt}$ =41 Å, Co layers switch independently and layer by layer switching was observed by Kerr imaging. The response of these distinct magnetic phases to external magnetic fields and their relationship to details of the hysteresis loops will be discussed.

**15:54**

**K36 8 Sagnac type fiber interferometer for magneto-optic Kerr effect measurement at cryogenic temperatures*** JING XIA, *Stanford University* PETER BEYERSDORF, *San Jose State University* MARTIN FEJER, AHARON KAPITULNIK, *Stanford University* We describe a Sagnac type magneto-optical interferometer operating at 1550 nm wavelength in which the fast and slow axis of a single 10-meter long Polarization-Maintaining fiber were used as the Sagnac loop. The last 2 meters of this PM fiber were fed into a cryogenic probe to measure Kerr rotation. This zero-area-Sagnac-loop design is virtually immune to temperature fluctuations and mechanical bending of the fiber, and can work at much lower temperature ( $<$ 1 K) compared to apparatus with optical windows. Most important, no perturbing AC magnetic field is needed. Up to now, we have achieved a Kerr rotation sensitivity of $2.5 \times 10^{-7} rad/\sqrt{Hz}$ down to liquid Helium temperature, with $4\mu W$of optical power at the detector. Drifts of this apparatus were observed to be less than$0.5 \times 10^{-7} rad/Hour$. We studied ferromagnetic transition and magnetic domains of thin (3 to 30 nm) $SrRuO_3$ films by cooling them through Tc in zero fields ( $<$ 5 mG) and measuring polar Kerr rotations.

*supported by CPN, NSF grant PHY-0425897

**16:06**

**K36 9 Fluctuation in the depinning of edge magnetic domains due to edge defects in ultrathin films** ADEBANJO ORIADE, SIU-TAT CHUI, *Bartol Research Institute* Magnetic memory devices utilize an optimal reversal field to change the magnetic state of a magnetic memory element. Edge pinned domains (EPD) can lead to the restoration of the original magnetic state. Failure in reversal can occur when the external field is withdrawn before EPD's are completely depinned [1],[2]. We study, via Monte-Carlo simulations, the reversal of edge pinned domains in NiFe ultrathin films with dimensions $0.33\mu m \times 0.50\mu m \times 50$ Å and $0.20\mu m \times 1.00\mu m \times 50$ Å (aspect ratio 2:3 and 1:5 respectively) at different temperatures. Fluctuations in reversal field were computed relative to that of samples without edge defects, our control. Defects in the edges parallel to the easy axis increase the switching field by an average of 29% in 1:5 samples and 6.7% in 2:3 samples. Defects in the edges perpendicular to the easy axis reduce the switching field by an average of 3.6% in 1:5 samples and 4.2% in 2:3 samples. The averages are quoted for word ($H_{ext,x}$) and digit ($H_{ext,y}$) line fields that result in a net external field at an angle of 5° to 55° to the easy axis (digit line). We show the mechanism for edge pinned domain reversal is by the removal of 180° domain walls. This removal is by the nucleation of solitons propagating from one end of the sample to the other. Most of the time, the upper and lower walls are removed simultaneously from opposite ends. [1] J. Shi et al, Appl. Phys. Lett. 77, 1692 (2000). [2] A. A. Oriade et al, Jour. App. Phys. 97, 023905 (2005).

**16:18**

**K36 10 A study of magnetic domain formation and motion in perpendicularly magnetized ultrathin film using the magnetic ac-susceptibility** NIDAL ABU-LIBDEH, DAVID VENUS, *McMaster University* The Complex, low-frequency ac magnetic susceptibility $\chi$ has been used to study magnetic domain formation and motion in perpendicularly magnetized ultrathin Fe films on a 2ML Ni/W(110) substrate. Analysis of the real and imaginary part of $\chi$ reveals that below a characteristic temperature $T_{sat}$, the stripe-domain density cannot change quickly enough to maintain equilibrium. This is due to the fact that domain wall creation and/or annihilation is itself an activated process, with nucleation energy $E_n$, distinct from the pinning of existing domain walls by defects in film structure, with activation energy $E_a$. $T_{sat}$, is set by the time scale of the measurements, which is determined by the rate of change of temperature (R). The Magnetic susceptibility was recorded as a function of temperature at different heating rates between 0.03 (K/s) to 1 (K/s). Our results show that below heating rate $R_c$(= 0.2 K/s for 1.5ML Fe film) the susceptibility peak temperature ($T_{peak}$) decreases as dT/dR = -200.0 (s). Above $R_c$, the susceptibility peak temperature increases as dT/dR = 16.6 (s). Preliminary model calculation show the movement of $T_{peak}$ is due to the change in $T_{sat}$ as the heating rate changes. $R_c$ is set by the relative values of $E_n$and $E_a$.

**16:30**

**K36 11 Imaging Antiferromagnetic Domain Walls with the Hall Effect*** RAFAEL JARAMILLO, T.F. ROSENBAUM, *University of Chicago* E.D. ISAACS, O.G. SHPYRKO, *Argonne Nat'l. Lab* P.G. EVANS, *University of Wisconsin* G. AEPPLI, *University College, London* Z. CAI, *Advanced Photon Source, Argonne Nat'l. Lab* We find that the Hall effect in the

spin-density-wave state of elemental chromium is sensitive to the underlying magnetic domain structure. A modest hysteresis in the linear Hall coefficient emerges as a function of temperature in the antiferromagnetic phase. By measuring all three components of the resistivity tensor in the plane of the sample we are able to separately consider the effects of domain rearrangement on carrier mobility and density. We also present direct images of hysteretic domain rearrangement, acquired via spatially resolved X-ray charge and magnetic scattering, and we show that these images can be correlated to the transport measurements.

*This material is based upon work supported under a National Science Foundation Graduate Research Fellowship

**16:42**

**K36 12 Anhysteretic magnetization and magnetostriction of thin NiFe films under stress and plastic deformation** PETER FINKEL, ED GARRITY, *Thomson* SAM LOFLAND, *Rowan University* The magnetic properties of thin samples of a thin film NiFe sample under tensile stress are investigated. The magnetostriction contribution to dc magnetization under elastic stress and the effect of the plastic strain on the hysteresis loops are discussed. Also, a role of the plastic deformation interrelated with the elastic stress in the magnetization process is established. An experimental system based on a conventional vibrating sample magnetometer equipped with the specially designed loading fixture and optical resonant spectroscopy tension monitoring technique is used to measure anhysteretic permeability and magnetization curve as a function of stress and temperature. This method used to measure anhysteretic permeability and magnetization curve of Ni-Fe as a function of stress and temperature. Anhysteretic permeability was extracted from the anhysteretic $B - H$ curves constructed by degaussing the sample at given longitudinal (parallel to the stresses) dc field. The large positive magnetostriction constant of FeNi samples leads to higher susceptibility and lower coercivity with tensile stress while the large volume magnetostriction results in reduced saturation magnetization. Large stresses imposed on the sample result in plastic strain of the sample which induces increase in dislocation density and domain wall pinning. This causes the gain in hysteresis loss and coercivity to increase at the highest stresses. We also discuss the effect of the Ni composition on results of the measurements.

**16:54**

**K36 13 Soft magnetic layers for low-field detection in spin-valve and magnetic-tunnel-junction sensors** WILLIAM EGELHOFF, ROBERT McMICHAEL, CINDI DENNIS, MARK STILES, ALEXANDER SHAPRIO, BRIAN MARANVILLE, CEDRIC POWELL, *NIST* We have investigated a wide variety of soft magnetic layers as sense layers for magnetic-field sensors. We find that in thin-film form, some of these soft materials can have susceptibilities approaching those of the corresponding bulk material. In general, the highest susceptibilities occur in tri-layer structures with a non-magnetic film separating two soft magnetic films. The alloy $Ni_{77}Fe_{14}Cu_5Mo_4$ of the mu-metal family is the softest thin-film material we have found, and we can achieve hard-axis susceptibilities of $\sim 10^5$ in tri-layer structures. The hard axis is preferred for magnetic sensors due to its near-linear response. The major impediment we have found to using these very soft layers in low-field sensors is that the susceptibility decreases by almost two orders of magnitude when the soft structure is incorporated in a standard spin valve or magnetic tunnel junction. In this talk, we will illustrate the problem, show how the structural modifications can minimize the problem, discuss the outlook for the complete elimination of the problem, and assess the prospects for significant improvements in thin-film, low-field magnetic sensors.

**17:06**

**K36 14 Minimizing 1/f Noise in Magnetic Sensors Using MEMS Flux Concentrators** ALAN EDELSTEIN, GREG FISCHER, *U.S. Army Research Laboratory* MICHAEL PEDERSEN, WILLIAM BERNARD, *MEMS Exchange* SHU-FAN CHENG, *Naval Research Laboratory* EDMUND NOWAK, *University of Delaware* The 1/f noise of new types of magnetoresistance sensors based on GMR and MTJ limits their sensitivities at low frequencies. Our approach for dealing with this problem is to shift the operating frequency to higher frequencies where the 1/f noise is much lower. The shift is accomplished by placing flux concentrators on MEMS flaps. Springs connecting the flaps are used to establish the proper normal mode. The motion of the MEMS structure, driven to oscillate at 15 kHz by electrostatic comb drives, modulates the field at the position of the sensor. The device was fabricated using SOI wafers, deep reactive ion etching (DRIE), and flip chip bonding. The motion of the permalloy on the MEMS flaps modulates the field by a factor of 2. Driving the motion only requires microwatts of power. Noise measurements indicate that the device is likely to increase the sensitivity of many magnetic sensors at low frequencies by orders of magnitude.

**17:18**

**K36 15 Enhanced coercivity in melt-spun Sm-Co-Fe-Cu ribbons after low temperature aging*** D. SULTANA, M. MARINESCU, Y. ZHANG, G.C. HADJIPANAYIS, *Department of Physics & Astronomy, University of Delaware, 223 Sharp Lab., Newark, DE 19716* MAGNETICS LAB. TEAM, We have studied systematically the influence of the microstructure refinement on the change of coercivity in melt-spun Sm $(Co_{0.45}Cu_{0.4}Fe_{0.15})_5$ alloys after thermal aging. The specimens have been prepared in the form of ribbons with a thickness in the range of 35 - 80 $\mu$m for values of the quenching wheel speed between 5-25 m/s. X-ray diffraction spectra of the as-spun ribbons showed a single phase 1:5 structure. The as-spun ribbons had a coercivity $H_c = 8$ kOe. The as-spun ribbons have been subjected to low temperature aging between 350-400 °C for different periods of time, in Ar atmosphere. Our results showed that the highest coercivity of 44 kOe was obtained in a sample aged at 400 $^o$C for 133 h. Microstructural investigations by transmission electron microscopy reveal that the average grain size of the specimens with the enhanced coercivity is about 500 nm. In order to have an insight into the mechanism of the coercivity enhancement, we are investigating the microchemistry at the grain boundaries by energy dispersive X-ray analysis and measuring the change in the Curie temperature through thermomagnetic measurements.

*Work supported by DOE under the grant PHYS 372115.

**SESSION K37: SUPERCONDUCTIVITY—TIME RESOLVED OPTICAL AND INELASTIC X-RAY SCATTERING IN CUPRATES**
**Tuesday Afternoon, 14 March 2006**
**340, Baltimore Convention Center at 14:30**
**David Tanner, University of Florida, presiding**



**14:30**
**K37 1 Ultrafast, Time-Resolved Quasiparticle Dynamics in Hg-Based High Temperature Superconductors** X. LI, M. KHAFIZOV, R. SOBOLEWSKI, *University of Rochester, Rochester, NY 14627* S. CHROMIK, V. STRBIK, *Slovak Academy of Sciences, SK-84104 Bratislava, Slovakia* D. DE BARROS, P. ODIER, *CNRS, F-38042 Grenoble, France* We present our all optical and optoelectronic time-domain studies of the quasiparticle and Cooper pair dynamics in Hg-based superconductors. The samples were mixed phase (Hg-1212 and Hg-1223), *c*-axis-oriented thin films, fabricated by magnetron sputtering, followed by itex-situ mercuration. The films exhibited the onset of the superconducting transition at $T_c = 123$ K and the zero-resistance at 110 K. Far below $T_c$, our femtosecond pump-probe spectroscopy studies clearly demonstrated the bi-molecular-type relaxation of photoexcited quasiparticles, governed by the direct Cooper pair formation process. At temperatures close to $T_c$, we observed a severe phonon bottleneck, and the quasiparticle relaxation time was limited by the phonon anharmonic decay/escape process. The photoresponse studies performed on current-biased microbridges, illuminated by femtosecond optical pulses demonstrated the picosecond nonequilibrium response on top of the much slower bolometric signal.

**14:42**
**K37 2 Time-resolved infrared spectroscopy of superconducting NbTiN films*** H. ZHANG, D.H. REITZE, C.J. STANTON, D.B. TANNER, *Department of Physics, University of Florida* R.P.S.M. LOBO, *ESPCI-CNRS* G.L. CARR, *Brookhaven National Laboratory* Time-resolved, pump-probe measurements of superconducting thin NbTiN films were performed at the National Synchrotron Light Source, Brookhaven National Laboratory. Near-infrared Ti:sapphire laser pulses break Cooper pairs, producing an excess of non-thermal quasiparticles. The recombinations of these excess quasiparticles are probed by time-synchronized, far-infrared, synchrotron pulses, with a time resolution of order 200 picoseconds. The main process probed is the bottleneck between gap-edge quasiparticles and excess $2\Delta$ phonons. (The phonons, generated by recombination of quasiparticles into Cooper pairs, are pairbreaking, producing gap-edge quasiparticles.) We will report the temperature, magnetic field, and laser fluence dependence of the spectrum-averaged far-infrared photoinduced transmission and reflection. We will also report the changes in the photoinduced far-infrared transmission spectrum.

*Supported by the DOE through grant DE-FG02-02ER45984 and contract DE-AC02-98CH10886 at BNL.

**14:54**
**K37 3 Finite bandwidth effects in time-domain measurements of fast electronic processes** OFER NAAMAN, JOSÉ AUMENTADO, *NIST, 325 Broadway, Boulder CO., 80305* Using rf reflectometry, we have observed individual quasiparticle tunneling events in a superconducting single- charge transistor. These events follow a Poisson process on microsecond time scales. We show that when the measurement is done with a finite bandwidth receiver, the experimentally observed process is no longer Poissonian, and the measured transition rates always underestimate those in the underlying system. We will present a model that accounts for bandwidth effects in these time-domain measurements, and show how to obtain the underlying rates from their measured values. We compare the results of our model to simulated and experimental data. We argue that these effects, which are significant even if the receiver is 10 times faster than the process, are a general feature in time domain experiments.

**15:06**
**K37 4 Determination of electron−phonon interaction parameters from time−domain terahertz spectroscopy** J. STEVEN DODGE, M. A. GILMORE, SAEID KAMAL, D. M. BROUN, *Simon Fraser University* We present an analytical framework for determining metallic electron−phonon interaction parameters from time−domain terahertz spectroscopy measurements in the normal state. We apply this analysis to the case of lead, where we obtain values that are consistent with existing estimates. We discuss the statistical and systematic errors that limit the uncertainty in the parameter estimates.

**15:18**
**K37 5 Hole doping in $YBa_2Cu_3O_{6+\delta}$ from polarization dependent x-ray absorption spectroscopy** DAVID HAWTHORN, DARREN PEETS, KYLE SHEN, SUMAN HOSSAIN, GEORGE SAWATZKY, *University of British Columbia* THOMAS KROLL, *IFW-Dresden* JONATHAN DENLINGER, *Lawrence Berkeley National Lab* RUIXING LIANG, DOUG BONN, WALTER HARDY, *University of British Columbia* We present detailed polarization dependent x-ray absorption spectroscopy (XAS) measurements of the cuprate $YBa_2Cu_3O_{6+\delta}$ as a function of oxygen concentration for ($0 \leqslant \delta \leqslant 1$). By adding O into the chain layer of YBCO, holes are doped into both the $CuO_2$ planes and $CuO_3$ chains. The presence of O induced states is directly observed by measurements of the O K edge and Cu L edge XAS, which probes unoccupied states in the O $2p$ and Cu $3d$ orbitals respectively. Owing to the different symmetry of the Cu d orbitals in the planes ($d_{x^2-y^2}$) and chains ($d_{y^2-z^2}$), the contribution to the total XAS from the chains and planes is clearly separated by measuring the polarization dependence of the x-ray absorption. Comparison to LDA calculations of the unoccupied density of states are used to obtain a quantitative measure of the hole doping in the planes and chains as a function of O concentration. In addition, the doping of holes into the $CuO_2$ planes as a function of degree of oxygen order in the chains is observed by measuring $YBa_2Cu_3O_{6.5}$ in both the chain ordered (ortho II) and chain disordered phases. This provides direct evidence for the role of chain ordering on hole doping in YBCO.

**15:30**
**K37 6 Doping Dependence of Resonant Inelastic X-ray Scattering (RIXS) in Electron and Hole-doped Cuprates*** ARUN BANSIL, ROBERT MARKIEWICZ, *Northeastern University* YINWAN LI, DONG QIAN, ZAHID HASAN, *Princeton University* Resonant inelastic X-ray scattering (RIXS) can in principle access all intra- and inter-band transitions over a wide range of energies and momenta. For these reasons, RIXS is emerging as an important probe of Mott gap physics in strongly correlated materials. Here we discuss evolution of RIXS spectra in electron and hole doped cuprates within the framework of a three-band model Hamiltonian [1]. The theoretical predictions are compared and

contrasted with the corresponding experimental results in NCCO and LSCO [2]. Interband (magnetic) transitions are found to shift to lower energy with increasing doping, while intraband features appear away from half-filling and spread over a wider energy range as the bandwidth grows with doping. Higher energy features arising from transitions deeper within the cuprate valence band complex will also be discussed. 1: R.S. Markiewicz and A. Bansil, cond-mat/0506474. 2: M.Z. Hasan, *et al.*, cond-mat/0406654.

*Work supported by the USDOE.

**15:42**

**K37 7 Resonant Inelastic X-ray Scattering (RIXS) Studies in the Cuprates*** ROBERT MARKIEWICZ, ARUN BANSIL, *Northeastern University* Resonant inelastic X-ray scattering (RIXS) is emerging as a probe of Mott gap physics in strongly correlated materials. Here we discuss some details of our recent three-band model [1] calculations for the cuprates. We discuss Mott vs Slater physics in the three-band model, aspects of magnetic gap collapse in the cuprates, and calculational details including polarization and initial energy dependence and relation of the band model to cluster calculations. 1: R.S. Markiewicz and A. Bansil, cond-mat/0506474.

*Work supported by U.S.D.O.E.

**15:54**

**K37 8 Electronic Excitations in the Resonant X-Ray Scattering Spectra of $La_2CuO_4$*** DAVID ELLIS, *Department of Physics, University of Toronto* JOHN HILL, *Department of Physics, Brookhaven National Laboratory* SHUICHI WAKIMOTO,† *Department of Physics, University of Toronto* DIEGO CASA, *CMC-CAT, Advanced Photon Source, Argonne National Laboratory* THOMAS GOG, *CMC-CAT, Advanced Photon Source, Argonne National Laboratory* YOUNG-JUNE KIM, *University of Toronto* Resonant inelastic X-Ray scattering (RIXS) experiments were done on the insulating cuprate $La_2CuO_4$ (LCO), tuning the incident energy to the copper k-edge at 8.99 keV to probe excitations on the order of an eV. With an energy resolution of 130 meV, a number of new features in the electronic excitations could be resolved. The momentum dependence of these features was studied in detail. In LCO, distinct peaks were seen above 2 eV, the first of which is associated with the charge-transfer excitation between the copper and the neighboring oxygen atoms. The amplitude of this peak decreased with increasing momentum transfer q, and energy increased with an observed dispersion of at least 0.2 eV. These results were interpreted using a 1-band model calculation. Also seen was a non-dispersive feature at 1.8 eV thought to be an orbital d-d excitation.

*Work supported by NSERC Canada and U.S DOE
†currently at Japan Atomic Energy Research Institute

**16:06**

**K37 9 Quantum melting of the hole crystal in the spin ladder of $Sr_{14-x}Ca_xCu_{24}O_{41}$** ANDRIVO RUSYDI, *University of Hamburg* P. ABBAMONTE, *UIUC* H. EISAKI, *AIST* Y. FUJIMAKI, S. UCHIDA, *University of Tokyo* G. BLUMBERG, *Bell Laboratories* M. RUEBHAUSEN, *University of Hamburg* G.A. SAWATZKY, *UBC* The ''spin ladder'' is a reduced-dimensional analogue of the high temperature superconductors that was predicted to exhibit both superconductivity and an electronic charge density wave or ''hole crystal'' (HC). Both phenomena have been observed in the doped spin ladder system $Sr_{14-x}Ca_xCu_{24}O_{41}$ (SCCO), which at x = 0 exhibits a HC which is commensurate at all temperatures. To investigate the effects of discommensuration we used resonant soft x-ray scattering (RSXS) to study SCCO as a function of doped hole density, $\delta$. The HC forms only with the commensurate wave vectors $L_L = 1/5$ and $L_L = 1/3$ (Not at 1/4!) and exhibits a simple temperature scaling $\tau_{1/3}/\ \tau_{1/5} = 5/3$. For incommensurate values the HC ''melts.'' During this study, the distribution of holes in ladder ($n_L$) and chain ($n_c$) of SCCO are redetermined as a function of $x$ using polarization-dependence x-ray absorption spectroscopy (XAS). An interpretation of polarization dependent XAS is proposed. Based on our interpretation, for $x = 0$, the estimation of $n_L$ and $n_c$ is 2.8 and 3.2, respectively. The number of holes in the ladder is linearly increasing with $x$. For $x = 11$, the estimation of $n_L$ and $n_c$ is 4.4 and 1.6, respectively. This number of holes is matching well with the model of paired of holes needed to explain the RSXS result.

**16:18**

**K37 10 Shedding New Light on Spin Excitations: Magnon-Magnon Scattering in a High-$T_c$ Parent Compound Using Soft X-rays** B. FREELON, *LBNL- UC Berkeley* P.G. MEDAGLIA, A. TEBANO, G. BALESTRINO, *INFM COHERENTIA Tor Vergata* P.A. GLANS, T.E. LEARMONTH, K. SMITH, *Boston University* K. OKADA, *Okayama University* A. KOTANI, *RIKEN-Spring8* D.E. KILCOYNE, B. RUDE, I. FURTADO, J.-H. GUO, *LBNL* The struggle to understand high-temperature superconductivity (HTSC) has taken place in the field of condensed matter physics for a relatively long time. The difficulty in discovering a HTSC mechanism seems to originate from the confluence of two very complicated problems; electron correlation and quantum magnetism. Novel techniques that specifically probe the electronic or magnetic behavior of these materials are highly sought. We report the direct observation of spin-flip (SF) excitations using resonant inelastic soft x-ray scattering (RIXS). The antiferromganetic (AFM) charge transfer insulator, $CaCuO_2$, was irradiated by soft x-rays tuned to the Cu M-edge ( $\sim$ 75 eV). Magnon-magnon (2 spin-flips) excitations were revealed as low-energy loss (0.39 eV) features in photon-in/photon-out experiments. The process is analogous to 2-magnon laser Raman scattering. Collected RIXS spectra provide a measurement of the 2 spin-flip excitation energy and the extraction of the AFM exchange of $CaCuO_2$. These results mark the first report of two-spin-flip magneto-optical excitations revealed through Raman scattering using x-rays. This work reveals the utility of RIXS as a new probe of the spin structure in strongly correlated electron materials.

**16:30**

**K37 11 Theoretical Study of Orthorhombic Distortions in High-Temperature Superconductors** ANDREAS SCHNYDER, *Paul Scherrer Institute, CH-5232 Villigen PSI, Switzerland* DIRK MANSKE, *Max Planck Institut für Festkörperforschung, Heisenbergstrasse 1, D-70569 Stuttgart, Germany* CHRISTOPHER MUDRY, *Paul Scherrer Institute, CH-5232 Villigen PSI, Switzerland* MANFRED SIGRIST, *Institut für Theoretische Physik, ETH Zürich, Hönggerberg, CH-8093 Zürich, Switzerland* Using a Fermi-liquid-based theory we calculate the response function for various spectroscopic probes in hole-doped high-$T_C$ superconductors, and determine the effects of orthorhombic distortions in the crystal lattice and asymmetry in the superconducting gap function. Employing the two-dimensional one-band Hubbard model and a generalized RPA-type theory we consider anisotropic hopping parameters ($t_x \neq t_y$) and a mixing of *d*- and *s*-wave symmetry of the superconducting order parameter. Within this model, both the

electronic Raman spectra and the dynamical magnetic susceptibility [1] are studied in detail. The relevance of these calculations to electronic Raman scattering measurements and inelastic neutron scattering experiments [2] on untwinned $YBa_2Cu_3O_{6+x}$ are discussed. [1] A. P. Schnyder, D. Manske, C. Mudry, and M. Sigrist, cond-mat/0510790. [2] V. Hinkov, S. Pailhes, P. Bourges, Y. Sidis, A. Ivanov, A. Kulakov, C. T. Lin, D. P. Chen, C. Bernhard, and B. Keimer, Nature **430**, 650 (2004).

**16:42**

**K37 12 Doping dependence of the coupling of electrons to bosonic modes in the single-layer high-temperature superconductor, $Bi_2Sr_2CuO_6$*** W. MEEVASANA, D.H. LU, F. BAUMBERGER, W.S. LEE, T. CUK, J. ZAANEN, Z.-X. SHEN, *Stanford University* N.J.C. INGLE, K.M. SHEN, *U. of British Columbia, Canada* J.R. SHI, *U. of Texas, Austin* H. EISAKI, *Nanoelectronic Research Institute, AIST, Japan* T.P. DEVEREAUX, *U. of Waterloo, Canada* N. NAGAOSA, *CREST, U. of Tokyo, Japan* S. SAHRAKORPI, M. LINDROOS, R. S. MARKIEWICZ, A. BANSIL, *Northeastern University* A recent highlight in the study of high-$T_c$ superconductors is the observation of band renormalization/self-energy effects on the quasiparticles in the form of kinks in their dispersions as measured by photoemission, interpreted as signatures of collective bosonic modes coupling to the electrons. Here we compare for the first time the self-energies in an optimally doped and strongly overdoped, non-superconducting single-layer Bi-cuprate, $Bi_2Sr_2CuO_6$. Besides a strong overall weakening we also find that weight of the self-energy in the overdoped system shifts to higher energies. We present evidence that this might well be related to the coupling to c-axis phonons which are unscreened at optimal doping, being particularly sensitive to the rapid change of the c-axis screening in this doping range. We also discuss doping dependencies of the FS maps and dispersions in terms of the corresponding band structure and one-step photointensity computations.

*DOE No. DE-AC03-765F00515, NSF DMR-0304981 and ONR N00014-98-1-0195

**16:54**

**K37 13 Unusual photoemission resonances of oxygen-dopant induced states in $Bi_2Sr_2CaCu_2O_{8+x}$** P. RICHARD, Z.-H. PAN, M. NEUPANE, Z. WANG, H. DING, *Department of Physics, Boston College, Chestnut Hill, MA 02467* A. V. FEDOROV, *Advanced Light Source, Lawrence Berkeley National Laboratory, Berkeley, CA 94720* T. VALLA, P. D. JONHSON, G. D. GU, *Physics Department, Brookhaven National Laboratory, Upton, NY 11973* A rising interest for the doping impurities in cuprates have been stimulated by a recent STM report on $Bi_2Sr_2Ca_1Cu_2O_{8+x}$ [McElroy *et al.*, Science **309**, 1048 (2005)], which identified oxygen dopants and investigated their local influence on the $CuO_2$ plane electronic properties. The nature of the perturbation induced by the dopants, which is of crucial importance, is thus questioned by these results. In order to investigate further this issue, we have performed an angular-resolved photoemission study of underdoped, optimally doped and overdoped $Bi_2Sr_2Ca_1Cu_2O_{8+x}$ samples using a wide photon energy range (14 - 100 eV). We report the presence of a non-dispersive peak, which we assign to a local impurity state similar to the one observed by STM and attributed to oxygen dopants. Unusual resonances in the peak intensity are observed around 50 and 75 eV for both the nodal and anti-nodal orientations, which suggest a hybridization of the local state with in-plane Cu.



**SESSION K38: SUPERCONDUCTIVITY—MESOSCOPICS AND THEORY**
**Tuesday Afternoon, 14 March 2006**
**341, Baltimore Convention Center at 14:30**
**Timir Datta, University of South Carolina, presiding**

**14:30**

**K38 1 Charge dynamics in a single electron trap** JULIE WYATT, *Yale University* ROBERT SCHOELKOPF, *Yale University* We report on measurements made using a radio frequency single electron transistor (RF-SET) capacitively coupled to a small metallic island to study the dynamics of single tunneling events. A circuit consisting of two small metallic islands and two tunnel junctions provides an architecture with which to tune the tunneling rates of single electrons up to the micro-second time scale. Thermal and cotunneling (quantum tunneling) events as well as the cross-over between the two regimes can be studied with this system. Characterization of devices will be shown including stability diagrams and the dependence of tunneling rates on bias conditions.

**14:42**

**K38 2 Measuring the Quantum Capacitance of a Differential Single Cooper-Pair Box*** MATTHEW SHAW, JUSTIN SCHNEIDERMAN, *University of Southern California* PER DELSING, *Chalmers University of Technology, Microtechnology and Nanoscience, MC2* HANS BOZLER, *University of Southern California* PIERRE ECHTERNACH, *Jet Propulsion Laboratory, California Institute of Technology* We present a simple method for measuring the quantum capacitance (QC) of a charge qubit based on a Differential Single Cooper-Pair Box using a Differential Radio-Frequency Single Electron Transistor. Measurement of the QC, which is proportional to the second derivative of the energy bands, can in principle be used for state readout at the degeneracy point, where decoherence due to charge fluctuations is at a minimum. The QC is measured by examining the response of the qubit to a small-amplitude AC excitation. Using this technique, we make an independent measurement of the qubit energy relaxation time. Although we have performed this experiment with a differential SCB and differential charge readout, the technique can easily be applied to a conventional SCB.

*This work was made possible by a grant from the National Security Agency.

**14:54**

**K38 3 A solid-state refrigerator for cooling cm-scale payloads below 300 mK*** N.A. MILLER, D.R. SCHMIDT, J.A. BEALL, W.D. DUNCAN, G.C. HILTON, G.C. O'NEIL, L.R. VALE, K.D. IRWIN, J.N. ULLOM, *National Institute of Standards and Technology (NIST) - Boulder* State-of-the-art x-ray and infrared sensors require bath temperatures near 100 mK. Currently, the two main options for cooling devices below 300 mK are the dilution refrigerator and adiabatic demagnetization refrigerator. We have developed a compact, lightweight alternative. Solid-state refrigerators based on Normal metal/Insulator/Superconductor (NIS) tunnel junctions can cool from temperatures near 300 mK to below 100 mK. The physical cooling mechanism is the preferential tunneling of the highest energy (hottest) electrons through a biased NIS junction. Recently, we have cooled both thin-film and bulk thermistors from 320 to 240 mK. Here, we present progress towards NIS refrigerators capable of cooling user-supplied payloads. In particular, we demonstrate a NIS-based refrigerator capable of

cooling 6 x 6 $mm^2$ silicon chips. This refrigerator, in combination with a $^3$He cryostat (base temperature $\sim$ 300 mK), forms a simple, compact cooling platform for ultralow temperature x-ray and infrared sensors. NIS refrigerators are fabricated lithographically on wafers, making the technology inherently scaleable to wafer-sized detector arrays.

*Contribution of an agency of the U.S. Government; not subject to copyright.

**15:06**

**K38 4 Quantum Calorimetry for Nonproliferation*** B. L. ZINK, *NIST* J. N. ULLOM, J. A. BEALL, K. D. IRWIN, W. B. DORIESE, R HORANSKY, W. DUNCAN, G. C. HILTON, C. D. REINTSEMA, D. R. SCHMIDT, L. R. VALE, *NIST Quantum Sensors Project, Boulder CO* High resolution $\gamma$-ray spectroscopy is an important tool for non-destructive analysis of nuclear materials and is often used by safeguards inspectors to help verify the inventories of nuclear materials held around the world. The energy spectrum of photons emitted from isotopes of uranium or plutonium in the 40 $-$ 1000 keV energy range give unique signatures that, if accurately measured, give inspectors important information about the age and enrichment of the material and therefore its intended purpose. In this talk I will describe our recent demonstration of a $\gamma$-ray spectrometer based on a superconducting transition-edge sensor microcalorimeter detector. This device has more than an order of magnitude better energy resolution than standard high resolution $\gamma$-ray detectors. We present high-resolution $\gamma$-ray spectra of Pu isotopic mixtures, describe the physics of the microcalorimeter and overview our plans for a realistic spectrometer for meeting real-world challenges such as measuring the mass of plutonium in spent nuclear fuel.

*NIST-EEEL, DOE, NNSA

**15:18**

**K38 5 Tunable magnetic coupler for a superconducting adiabatic quantum computer** ANDREW BERKLEY, PAUL BUNYK, SERGEI GOVORKOV, MARK W. JOHNSON, MURRAY THOM, BROCK WILSON, *D-Wave Systems Inc. Burnaby, BC Canada* We report on measurements of a superconducting sign-tunable magnetic coupling element. This device could be used as part of a programmable adiabatic quantum computer utilizing flux qubits. The sign-tunability is achieved by mediating the coupling between two flux qubits through a third rf SQUID device [1]. We are able to tune the resulting coupling from antiferromagnetic through zero to ferromagnetic. [1] A. Maassen van den Brink, A. J. Berkley, M. Yalowsky, New J. Phys. 7 230 (2005).

**15:30**

**K38 6 Giant oscillations of energy levels in mesoscopic superconductors*** VALERII VINOKUR, *Argonne National Laboratory* NIKOLAY KOPNIN, *Low Temperature Laboratory, Helsinki* ALEXANDER MELNIKOV, VALENTINA POZDNYAKOVA, DENIS RYZHOV, IGOR SHERESHEVSKII, *Institute for Physics of Microstructures, Nizhny Novgorod, GSP-105, Russia* The interplay of geometrical and Andreev quantization in mesoscopic superconductors leads to giant mesoscopic oscillations of energy levels as functions of the Fermi momentum and/or sample size. Quantization rules are formulated for closed quasiparticle trajectories in the presence of normal scattering at the sample boundaries. Two generic examples of mesoscopic systems are studied: (i) one dimensional Andreev states in a quantum box, (ii) a single vortex in a mesoscopic cylinder.

*supported, in part, by the US DOE Office of Science, contract No. W-31-109-ENG-38, by RFBR grant03-02-17402-a, by Program ''Quantum Macrophysics'' of RAS, byRussian Presidential Program grant MD-141.2003.02

**15:42**

**K38 7 Dynamics of a Nanomechanical Resonator Coupled to a Superconducting Single Electron Transistor*** MILES BLENCOWE, *Dartmouth College* JARA IMBERS, *University of Nottingham* ANDREW ARMOUR, *University of Nottingham* We present an analysis of the dynamics of a nanomechanical resonator coupled to a superconducting single electron transistor (SSET) in the vicinity of the Josephson quasiparticle (JQP) and double Josephson quasiparticle (DJQP) resonances. For weak coupling and wide separation of dynamical timescales, we find that for either superconducting resonances the dynamics of the resonator are given by a Fokker-Planck equation, i.e., the SSET behaves effectively as an equilibrium heat bath, characterised by an effective temperature, which also damps the resonator and renormalizes its frequency. Depending on the gate and drain-source voltage bias points with respect to the superconducting resonance, the SSET can also give rise to an instability in the mechanical resonator marked by negative damping and temperature within the appropriate Fokker-Planck equation. Furthermore, sufficiently close to a resonance, we find that the Fokker-Planck description breaks down. We also point out that there is a close analogy between coupling a nanomechanical resonator to a SSET in the vicinity of the JQP resonance and Doppler cooling of atoms by means of lasers.

*Supported by the NSF under NIRT grant CMS-0404031

**15:54**

**K38 8 Dipolon Theory of Superconducting Regular and Pseudo- Energy Gap Parameters at Finite Temperature and Transition Temperatures $T_C$ and $T^*$ in High-Temperature Superconductors** RAM SHARMA, *University of Illinois at Chicago, Chicago, IL* First temperature dependent regular and pseudo- energy gap parameters and regular ($T_C$)and pseudo-($T^*$) transition temperatures have been obtained arising from the same physical origin by developing many-body field-theoretic techniques making use of dipolon propagator and electron Green's function with dressed dipolons as mediators of superconductivity, screened Coulomb repulsion, nonrigid electron energy bands, retardation and damping effects and electron-hole asymmetry, as an extention of our previous zero temperature formalism [1]. The theory contains all essential and important electron correlations. The Migdal vertex correction is found to be small ( $\sim$ 1%). Our calculated results of temperature dependent regular and pseudo-energy gap parameters and regular ($T_C$) and pseudo- ($T^*$) transition temperatures for Bi-cuprates agree well with available experimental data. In comparison it is concluded that the models (such as the Hubbard and t-j models) should contain additionally electron correlations due to dipolons to visualize superconductivity. 1. R.R. Sharma, Phys. Rev. **B 63**, 054506, (2001).

**16:06**
**K38 9 Bad Screening and Applicability of Migdal's Theorem to Layered Cuprates** ALEXEI ABRIKOSOV, *Materials Science Division, Argonne National Laboratory, USA* A proof is presented, that in the model of high-$T_c$ layered cuprates with long-range phonon-mediated attraction, due to bad screening of Coulomb forces, the ''Migdal's theorem,'' permitting to neglect vertex corrections, still holds, despite the absence of the small ''adiabatic parameter.'' The calculation of the superconducting critical temperature for this model permits to explain the high values of $T_c$ observed in experiment. This work was supported by the Department of Energy under the contracts # W-31-109-ENG-38.

**SESSION K39: FOCUS SESSION: SUPERCONDUCTIVITY—THEORY AND COMPUTATION II**
**Tuesday Afternoon, 14 March 2006; 342, Baltimore Convention Center at 14:30**
**Richard Klemm, Kansas State University, presiding**



***Invited Papers***

**14:30**
**K39 1 Kondo Physics and Strongly Correlated Superconductivity in Model Fullerene Conductors.*** MICHELE FABRIZIO, *International School for Advanced Studies (SISSA) and The Abdus Salam Center for Theoretical Physics (ICTP)*

The effects of electronic correlations on superconductivity are investigated by means of Dynamical Mean Field Theory (DMFT) in a model for alkali doped fullerenes. It is shown that the proximity to a Mott transition actually amplifies the *s*-wave phonon-mediated pairing mechanism built into the model. It leads to a superconduting pocket adjacent the Mott insulator with a superconducting gap which is huge in comparison with the corresponding BCS value.The physical properties of this strongly correlated superconductor are compatible with the experimental data available on fullerenes. Yet, contradicting the common belief for fullerenes, superconductivity in this model is not of the BCS-type nor is the normal state a conventional Fermi-liquid. We find on the contrary several aspects which rather resemble those of cuprate superconductors, such as an increase of Drude weight accompaning the onset of superconductivity. We identify the origin of these anomalies to the unconventional properties displayed by the Anderson impurity model for a $C_{60}^{n-}$ molecule onto which the lattice model maps within DMFT. We also argue that this behavior should be common to other models that contain pairing mechanisms able to survive inside the Mott insulator, which translate within DMFT into impurity models where Kondo screening competes against an internal mechanism that tends to freeze the impurity in a low-spin state.

*(In collaboration with M. Capone, L. De Leo, E. Tosatti and C. Castellani).

***Contributed Papers***

**15:06**
**K39 2 Renormalization Group approach to anisotropic-pairing superconductivity** RAFAEL ROLDAN, *Instituto de Ciencia de Materiales de Madrid, CSIC, Spain* SHAN-WEN TSAI, *Physics Dept., Univ. of California, Riverside* The Renormalization Group (RG) approach to interacting fermions [R. Shankar, *Rev. Mod. Phys.* **66** 129 (1994)] has been extended to the case where both electron-electron and electron-phonon interactions are present [S.-W. Tsai *et al*, *Phys. Rev. B* **72** 054531 (2005)]; [S.-W. Tsai *et al*, cond- mat/0505426]. There Eliashberg's equations are derived for the case of a two dimensional Hubbard model with a circular Fermi surface (FS) in the presence of isotropic Einstein phonons. However, there are materials where the isotropic electron-phonon coupling is not a good approximation. In this work we study the problem of superconductivity mediated by anisotropic electron-phonon couplings, and derive a generalization of the Eliashberg's equations for this case. We solve, for the case of a circular FS, the flow equations for the interaction vertices in the particle-particle channel up to one loop, taking into account the retardation effects due to the presence of phonons. Retardation effects lead to important corrections to the imaginary part of the self-energy. For a generic anisotropic electron- phonon coupling these corrections are momentum dependent and the RG flow equations for superconducting couplings with different symmetries become coupled. We find an instability of the Fermi liquid state towards superconductivity for various momentum-dependent el-ph couplings, with competition between superconducting channels with different symmetries of the order parameter.

**15:18**
**K39 3 Correlations in Dynamic Hubbard Model: A DMRG Study** FATIH DOGAN, FRANK MARSIGLIO, *University of Alberta, Edmonton, Canada* The Dynamic Hubbard model has been introduced to study how holes behave in the Hubbard Model with dynamic degrees of freedom modelled by pseudo-spins. It has previously been analyzed using exact diagonalization on small clusters. However the lattice sizes used are not sufficiently large to understand the behaviour of the system in the thermodynamic limit. We present our analysis using the density-matrix-renormalization- group (DMRG) to understand the behaviour of two holes for different system sizes. We observed a decrease in kinetic energy, and an increase in the effective nearest neighbor attraction, even for moderate on-site repulsion, which indicates pairing of the holes through effective nearest neighbor attraction.

**15:30**

**K39 4 Dynamical Mean-Field calculation of kinetic energy for the one-band doped Hubbard Model*** ARMIN B. COMANAC, *Columbia University Department of Physics, NY 10027 USA* LUCA DE' MEDICI, *École Polytechnique - CPHT, F91128 PALAISEAU CEDEX FRANCE* ANDREW J. MILLIS, *Columbia University Department of Physics, NY 10027 USA* We present a Dynamical Mean-Field calculation of the interaction, doping and temperature dependence of the kinetic energy for the one-band doped Hubbard model. We combine Quantum Monte-Carlo and an improved finite temperature Exact Diagonalization method to obtain results over a wide range of temperatures. The overlapping temperature region for the two methods enables an improved error estimation. The results are compared to recent experimental data.

*This work is supported by Columbia University and École Polytechnique through the 'Alliance' Program and the NSF-DMR grant No. 0431350

**15:42**

**K39 5 Fermi surface splittings in multilayered high-$T_c$ cuprates with charge imbalance** M. MORI, T. TOHYAMA, S. MAEKAWA, *IMR, Tohoku Univ; CREST, JST* Cuprate superconductors have layered structure of $CuO_2$ planes, which makes conducting blocks separated by an charge- reservoir block. Multilayered high-$T_c$ cuprates, e.g., $Ba_2Ca_3Cu_4O_8(O_{1-y}F_y)_2$ and $HgBa_2Ca_4Cu_5O_y$, have two kinds of $CuO_2$ planes in a unit cell; the outer-pyramidal-coordinated-planes (OP's) and the inner-square-coordinated-planes (IP's). The carrier density in the OP is generally different from that in the IP. We call such an inhomogeneous charge-distribution [**lq**]charge imbalance'. We study doping dependence of interlayer hoppings, $t_\perp$, in such a charge-imbalance system in the Gutzwiller approximation. When the double occupancy is forbidden in the $CuO_2$ plane, an effective amplitude of $t_\perp$ is shown to be proportional to the square root of the product of doping rates in adjacent two planes. Therefore, the charge imbalance in more than three-layered cuprates results in two different values of $t_\perp^{\rm eff}$, i.e., $t_{\perp 1}^{\rm eff} \propto t_\perp\sqrt{\delta_{\rm IP}\delta_{\rm IP}}$ between IP's, and $t_{\perp 2}^{\rm eff} \propto t_\perp\sqrt{\delta_{\rm IP}\delta_{\rm OP}}$ between IP and OP, where $\delta_{\rm IP}$ ($\delta_{\rm OP}$) is the doping rates in IP (OP). Fermi surfaces are calculated in the four-layered $t$-$t'$- $t''$-$J$ model by the mean-field theory. The order parameters, the renormalization factor of $t_\perp$, and the site- potential making the charge imbalance between IP and OP are self-consistently determined for several doping rates. We show the interlayer splitting of the Fermi surfaces, which may be observed in the angle resolved photoemission spectroscopy measurement. *cond-mat/0511249.

**15:54**

**K39 6 Effective theory of underdoped cuprates and the puzzle of superfluid density** IGOR HERBUT, *Simon Fraser University* I will discuss the recently proposed low-energy description of fluctuating d-wave superconductors (I. F. Herbut, PRL 94, 237001 (2005)), and its implications for the evolution of the superfluid density with doping and temperature. Recent experiments find that while the T=0 superfluid density becomes reduced by more than two orders of magnitude by going from optimal to extremely underdoped regime in single crystals of YBCO, the slope of the temperature dependence stays roughly the same. This apparent violation of the Ioffe-Larkin rule, argued otherwise rather generally to hold in the underdoped regime, is explained as being due to the particular form of the bosonic (fluctuation) term, which resembles the condensate of the weakly interacting layered Bose gas. This suggests that, its linear appearance notwithstanding, the reduction of the superfluid density with temperature in extremely underdoped cuprates may be due to phase fluctuations over most of the temperature range. Further experimental tests of this idea will be proposed.

**16:06**

**K39 7 Magnetic Origin of the Tetragonal-Orthorhombic Phase Transition in the Cuprates** JIANGPING HU, *Purdue University* CHEN FANG, STEVEN KIVELSON, *Stanford University* STUART BROWN, *UCLA* It is shown that a quasi two dimensional (layered) Heisenberg antiferromagnet with fully frustrated interplane couplings generically exhibits two thermal phase transitions with lowering temperature – an upper transition (''order from disorder without order'') in which the lattice point-group symmetry is spontaneously broken, and a lower Neel transition at which spin-rotational symmetry is broken. We therefore suggest that it may primarily be the magnetic interactions between planes, rather than strains associated with a mismatch of ionic radii, that are responsible for the tetragonal to orthorhombic (T-O) structural phase transition seen in many of the cuprates.

**16:18**

**K39 8 A 4D-XY model of the superfluid density of strongly underdoped cuprate superconductors** ANDREW IYENGAR, *Indiana University* MARCEL FRANZ, *University of British Columbia* A new phenomenology is proposed for the superfluid density of strongly underdoped cuprate superconductors based on data for ultra-clean single crystals of YBCO. The data feature a puzzling departure from Uemura scaling and a decline of the slope as the $T_c = 0$ quantum critical point is approached. We argue that the proximity of a Mott insulator drives quantum fluctuations of the superconducting phase which are described by a (3+1)-dimensional XY model. The subsequent renormalization of the superfluid density is computed using variational methods and then studied systematically as a function of c-axis anisotropy, interaction strength, and doping. We find that non-critical phase fluctuations explain key features of the new cuprate phenomenology, which is expected to fail in the true critical regime.

**16:30**

**K39 9 Microscopic Spectral Model of High Temperature Superconductors** J.C. PHILLIPS, *Dept. of Physics and Astronomy, Rutgers University* The self-organized dopant percolative filamentary model [1], entirely orbital in character (no spins), explains the evolution with doping of Fermi arcs observed by ARPES, including the abrupt transitions in quasiparticle strength observed near optimal doping in cuprate high temperature superconductors [2]. Similarly abrupt transitions are also observed [3] in time-resolved picosecond relaxation spectroscopy at 1.5 eV, and these are explained as well, using no new assumptions and no adjustable parameters. The anomalous ''precursive'' temperature-dependent strains observed by EXAFS [4] are associated with relaxation of filamentary ends. [1] J. C. Phillips, Phys. Rev. Lett. 88, 216401 (2002). [2] T. Yoshida, X. J. Zhou, T. Sasagawa et al., Phys. Rev.

Lett. 91, 027001 (2003). [3] N. Gedik, M. Langer, J. Orenstein et al., Phys. Rev. Lett. 95, 117005 (2005). [4] N. L. Saini and H. Oyanagi, Phys. C 412, 152 (2004).

**16:42**

**K39 10 Pairing in Marignal Fremi Liquid and Luttinger Liquid in Terms of the Bethe-Salpeter Equation** YURIY MALOZOVSKY, *Department of Chemistry and Physics, Southeastern Louisiana University* The pairing between two fermions in the fermionic systems with the smeared Fermi distribution is considered in terms of the Bethe-Slapeter equation. The examples of the systems with the smeared Fermi distribution are the marginal Fermi liquid and the Luttinger liquid where the quasiparticle pole is absent in the Green's function. Although the pairing between two fermions in the systems with the smeared Fermi distribution is, in general, absent, the pairing similar to the Cooper's pairing can occur and the conditions for such pairing to exist are discussed.

**16:54**

**K39 11 High-$T_c$ superconductivity does not originate in cuprate-planes.*** JOHN D. DOW, *Arizona State U.* $CuO_2$ planes are not needed for high-$T_c$ superconductivity, as demonstrated by $Sr_2YRuO_6$ and $Ba_2YRuO_6$, weakly doped on Ru sites with Cu, with onset $T_c$'s of 49K and 93K, but no cuprate-planes. $Gd_{2-z}Ce_zSr_2Cu_2RuO_{10}$ and $GdSr_2Cu_2RuO_8$ do not superconduct in their cuprate- planes, which are magnetic, but in their SrO layers (with onset $T_c \approx 45$K). High-temperature superconductivity resides in SrO, BaO, or interstitial oxygen regions, not in cuprate-planes. In $YBa_2Cu_3O_7$, Harshman *et al.* [1], using muon spectroscopy, found *s*-wave character, not *d*-wave character (to better than one percent) which measures the *superconducting* layers. This contradicts scanning tunneling microscopy and photoemission, which claim *d*-wave behavior after measuring *near-surface* layers (which often do not superconduct). High-temperature superconductivity originates in the BaO, SrO, or interstitial oxygen regions, not in the cuprate planes. [1] D. R. Harshman, *et al.*, Phys. Rev. **B 69,** 174505 (2004).

*Supported by ARO.

**17:06**

**K39 12 Feasibility of Superconductivity in Semiconductor Superlattices** KENNETH P. WALSH, *U. S. ArmyEnergetics, Pyrotechnic Research and Technology* ANTHONY T. FIORY, N. M. RAVINDRA, *New Jersy Institute of Technology* DALE R. HARSHMAN, *Physikon Research Corporation* JOHN D. DOW, *Arizona State University* The possibility of designing a semiconducting superlattice of alternating electron and hole layers that exhibits high temperature superconductivity is studied by numerical simulation of modulation-doped $GaAs/Al_xGa_{1-x}As$ superlattices. The feasibility of superconductivity is based on observations of high-temperature superconductors by Harshman and Mills[1], who concluded that the mechanism for Cooper pairing is a Coulomb interaction that is optimum when the mean distance between charge carriers within the layers equals the distance between the layers. Superlattice design considers optimum layer spacings, doping concentrations, and alloy concentration, x. The program employed in the superlattice simulations is a one-dimensional Schrödinger-Poisson solver developed by Snider[2]. 1. D. R. Harshman and A. P. Mills, Concerning the nature of high-Tc superconductivity, Phys. Rev. B 45, 707 (1992). 2. G. Snider, 1D Poisson/Schrödinger User's Manual: A Band Diagram Calculator, (http://www.nd.edu/~ gsnider, Univ. Notre Dame, Notre Dame, Indiana).

**17:18**

**K39 13 Unconventional Pairing in 2D lattice with an ''Inherent Gap''** RENYUAN LIAO, KHANDKER QUADER, *Department of Physics, Kent State University* We investigate superconducting pairing in 2D lattice with an ''inherent gap.'' In this calculation, we take this gap to be a constant, and thus similar to that in semiconductors. We consider different pairing symmetries, namely, s-wave, extended-s-wave, p-wave and d-wave. We calculate superconducting gap parameters, critical temperatures, chemical potential, etc in terms of interaction strength and filling factor. There is a sharp transition fom the ''inherent gapped state'' to a superconducting state for half filling f=1/2, corresponding to the undoped case. For finite doping, the transition becomes a smooth crossover. We also explore other features, such as the effect of phase fluctuations and the resulting Kosterlitz-Thouless transition; tunneling density of states, etc.



**SESSION K40: FOCUS SESSION: MATERIALS FOR QUANTUM COMPUTING III**
**Tuesday Afternoon, 14 March 2006; 343, Baltimore Convention Center at 14:30**
**Seongshik Oh, National Institute of Standards and Technology-Boulder, presiding**

***Invited Papers***

**14:30**

**K40 1 Decoherence in Josephson Qubits.**
ROBERT McDERMOTT, *UC Santa Barbara*

The Josephson junction can be thought of as an artificial atom, with energy levels determined by the circuit design parameters and bias. This system shows great promise for quantum computing, since it should be straightforward to scale to many-qubit circuits using standard integrated circuit technology. To date, however, device performance has been severely limited by coupling of the qubit to spurious materials defects. Here I discuss a recent breakthrough which has enabled striking improvements in phase qubit coherence and visibility, and which has deep implications for other Josephson qubits. I present a model of qubit decoherence induced by two-level defect states, and describe an intimate connection between intrinsic (low-temperature and low-power) dielectric loss and qubit performance: coupling to individual defects in the tunnel barrier of the Josephson junction results in a loss of visibility of coherent qubit oscillations, while coupling to a continuum of defects in the wiring dielectric leads to energy relaxation from the qubit $|1>$ to the $|0>$ state. Optimization of the phase qubit proceeds along two lines. The first approach involves a novel circuit architecture

which promotes statistical avoidance of resonant defects, and leads to dramatic enhancements in qubit visibility and measurement fidelity. The second approach is to explore novel high-Q dielectrics for qubit circuits. Recent improvements in materials have led to a factor of 30 increase in qubit coherence time. I describe progress in the development of novel epitaxial dielectrics grown on epitaxial refractory metal underlayers for qubit applications. These results open the door to the realization of many-qubit algorithms in superconducting circuits.

*Contributed Papers*

**15:06**

**K40 2 Developing Phase Qubits Without Dielectric Materials*** R.W. SIMMONDS, M.S. ALLMAN, K. CICAK, JEFFREY S. KLINE, SEONGSHIK OH, K.D. OSBORN, G. PROKOPENKO, M.A. SILLANPAA, A.J. SIROIS, J.A. STRONG, J.D. WHITTAKER, D.P. PAPPAS, *National Inst. of Standards and Tech. - Boulder* Recently amorphous insulating materials have been found to be detrimental to the energy retention of Josephson phase qubits. Most of this amorphous material has presently been used as an insulating layer between two wiring layers used in fabricating trilayer based Josephson phase qubits. In an effort to improve phase qubit performance we have developed two new fabrication techniques in order to produce phase qubits that do not require insulating layers. Here we will describe the fabrication processes and recent measurements on these systems.

*This work was supported by ARDA through Grant No. MOD717304.

**15:18**

**K40 3 Using Phase Qubits to Evaluate Dielectrics Materials*** J.A. STRONG, M.S. ALLMAN, K. CICAK, JEFFREY S. KLINE, SEONGSHIK OH, K.D. OSBORN, G. PROKOPENKO, M.A. SILLANPAA, A.J. SIROIS, J.D. WHITTAKER, *National Inst. of Standards and Tech. - Boulder* JOHN M. MARTINIS, *UC Santa Barbara* D.P. PAPPAS, R.W. SIMMONDS, *National Inst. of Standards and Tech. - Boulder* It has been known since the late 1970's that Amorphous insulating materials contain defects that can be modeled as a bath of interacting two-level fluctuators. Measurements of LC oscillator microwave circuits have identified these two-level systems as an inherent energy loss mechanism in Josephson phase qubits. By developing methods to reduce the volume of dielectric material in the fabrication of Josephson phase qubits, we have been able to conclusively show that the energy relaxation time can be improved in these systems. Furthermore, by using a different dielectric material with less intrinsic low temperature loss, it is possible to further improve this situation. In addition, we have fabricated new phase qubits which have strong coupling to substrate materials in an effort to evaluate loss from different substrates. We show that substrate materials with high crystalinity result in qubits with improved relaxation times.

*This work was supported by ARDA through Grant No. MOD717304.

**15:30**

**K40 4 Further Microwave Resonator Studies of Loss Mechanisms to Improve Qubits*** K.D. OSBORN, M.S. ALLMAN, K. CICAK, JEFFREY S. KLINE, SEONGSHIK OH, G. PROKOPENKO, M.A. SILLANPAA, A.J. SIROIS, J.A. STRONG, J.D. WHITTAKER, *National Inst. of Standards and Tech. - Boulder* JOHN M. MARTINIS, *UC Santa Barbara, Dept. of Physics* D.P. PAPPAS, R.W. SIMMONDS, *National Inst. of Standards and Tech. - Boulder* Microwave resonators have been previously used to identify materials that limit the coherence time of Josephson phase qubits. For example, amorphous silicon dioxide was found to exhibit an unsaturated loss tangent of 0.005 in resonators at low temperatures. Minimized use of this dielectric has shown improved phase qubit performance as well as using lower loss materials like silicon-nitride. Furthermore, superconducting aluminum, the major superconductor used in many present types of qubits, forms a native surface oxide which may also contribute to dielectric loss. To prevent any native oxides on superconducting circuits, we have fabricated resonators with superconducting wiring that has been covered with a thin layer of gold. We will measure the power dependence of resonant peaks in these circuits in order to determine losses in these systems as well as investigate various substrate materials and compare these results to losses from silicon-oxide and silicon-nitride.

*This work was supported by ARDA through Grant No. MOD717304

**15:42**

**K40 5 Ohmic and step noise from a single trapping center hybridized with a Fermi sea†*** ROGERIO DE SOUSA, K. BIRGITTA WHALEY, *Department of Chemistry and Pitzer Center for Theoretical Chemistry, University of California, Berkeley, CA 94720-1460, USA* FRANK K. WILHELM, JAN VON DELFT, *Department Physik, CeNS, and ASC, Ludwig-Maximilians-Universität, Theresienstrasse 37, D-80333 München, Germany* We show that single electron tunneling devices such as the Cooper-pair box or double quantum dot can be sensitive to the zero-point fluctuation of a single trapping center hybridized with a Fermi sea. If the trap energy level is close to the Fermi sea and has line-width $\gamma > k_B T$, its noise spectrum has an Ohmic Johnson-Nyquist form, whereas for $\gamma < k_B T$ the noise has a Lorentzian form expected from the semiclassical limit. Trap levels above the Fermi level are shown to lead to steps in the noise spectrum that can be used to probe their energetics, allowing the identification of individual trapping centers coupled to the device. [ ]†R. de Sousa, K.B. Whaley, F.K. Wilhelm, and J. von Delft, Phys. Rev. Lett. in press; cond-mat/0504149.

*We acknowledge support from NSF, DARPA SPINS, DFG, and ARDA.

**15:54**

**K40 6 Quasiparticle Poisoning in a Cooper-Pair Box** B. S. PALMER, C. A. SANCHEZ, A. NAIK, M. A. MANHEIMER, *Laboratory for Physical Sciences* J. F. SCHNEIDERMAN, *Department of Physics, University of Southern California* P. M. ECHTERNACH, *Jet Propulsion Laboratory* F. C. WELLSTOOD, *Center for Superconductivity Research, Department of Physics, University of Maryland* We have used a single-electron transistor (SET) to measure the Coulomb staircase of a single Cooper-pair box (CPB) from a temperature of 30 mK to 300 mK. At the lowest temperature, the data shows that the CPB, which is fabricated from $Al/AlO_x/Al$ tunnel junctions, is poisoned by nonequilibrium quasiparticles. As the temperature is increased from 30 to 150 mK, the width of the odd step in the staircase, which corresponds to a quasiparticle on the island of the box, decreases linearly with temperature. Above 180 mK, the width of the odd step increases,

eventually producing a staircase with 1ite steps. The low-temperature poisoning is consistent with the assumptions of Aumentado et al. that quasiparticles are spontaneously generated in the leads.[1] For particular gate voltages it is energetically favorable to have a nonequilbrium quasiparticle occupy a state on the island; hence poisoning the pure 2e staircase. The data above 180 mK is consistent with the quasiparticle states of the island being thermally populated.

[1]J. Aumentado, M. Keller, J. Martinis, & M. Devoret, Phys. Rev. Lett. **92**, 066802 (2004).

**16:06**

**K40 7 Kinetics of the superconducting charge qubit in the presence of a quasiparticle** R. LUTCHYN, L. GLAZMAN, A. LARKIN, *U of Minnesota* We investigate the energy and phase relaxation of a superconducting qubit caused by a quasiparticle. In our model, the qubit is an isolated system consisting of a small island (Cooper-pair box) and a larger superconductor (reservoir) connected by a Josephson junction. If such system contains an odd number of electrons, then even at lowest temperatures a single quasiparticle is present in the qubit. The quasiparticle resides in the reservoir with an overwhelming probability, but its quick round-trips to the box lead to the relaxation of the qubit. We derive master equations governing the evolution of the qubit coherences and populations. We find that the kinetics of the qubit can be characterized by two time scales - quasiparticle escape time from reservoir to the box $\Gamma_{in}^{-1}$ and quasiparticle relaxation time $\tau$. The former is determined by the normal-state conductance $g_T$ of the Josephson junction and one-electron level spacing $\delta_r$ in the reservoir ($\Gamma_{in} \sim g_T \delta_r$), and the latter is due to electron-phonon interaction. The phase coherence is damped on the time scale of $\Gamma_{in}^{-1}$. The qubit energy relaxation depends on the ratio of the two characteristic times, $\tau$ and $\Gamma_{in}^{-1}$, and also on the ratio of temperature $T$ to the Josephson energy $E_J$. In the limit $\Gamma_{in}\tau \gg 1$ and $T \ll E_J$, the relaxation of the qubit populations occurs in two stages. In the first stage, $t \sim 1/g_T\delta_r$, the initial population of the excited state changes only by a small amount $\sim (T/E_J)1/2$. This quasi-stationary state relaxes to full equilibrium over a longer time scale $t \sim \tau(E_J/T)^{1/2}$.

**16:18**

**K40 8 Charge motion near metallic single electron transistors on oxidized Si substrates** K. R. BROWN, L. SUN, B. E. KANE, *University of Maryland* Many proposals for spin qubits in semiconductors rely on spin-charge conversion combined with charge measurement for determination of the final state. In pursuit of such a measurement for donor spins in Si we have performed systematic experiments using Al-$AlO_x$-Al single electron transistors (SETs) on doped, oxidized Si substrates. One of the first priorities has been to identify other sources of charge motion that could disguise or overwhelm the signals from donors. We have identified reproducible peaks in the ac susceptibility of our samples as a function of electric field, similar to the response that would be expected from donor electrons moving between two different states. Nevertheless, preliminary results indicate that these peaks are associated with defects above the interface and not with charge motion in the Si itself. We will discuss planned device refinements to eliminate these and other defects and to isolate donor electron signals.

**16:30**

**K40 9 Design of a metallic SET gated by lateral Schottky gates for measurements of electric-field-dependent ionization of donors** LUYAN SUN, K. R. BROWN, B. E. KANE, *Laboratory for Physical Sciences, University of Maryland* Spins associated with donors in silicon are ideally suited as qubits for a solid state quantum computer due to their long coherence times and potential scalability. One method for spin measurement incorporates electric-field-dependent ionization of two-electron systems to distinguish singlet and triplet spin states. Therefore the electric field at donor sites needs to be known accurately. The electric field can be applied via a heavily doped back gate, but sharp density profiles are difficult to obtain both with ion implantation (due to straggle) and with molecular beam epitaxy. To resolve this issue, we have fabricated lateral PtSi Schottky gate devices. Schottky gates should make the transition from conducting layer to intrinsic Si far more abrupt. They can also tune the Fermi level in the substrate, so that we can populate donors in the substrate by applying an appropriate bias and shining an LED. By studying the Coulomb blockade peak spacing of an Al/$AlO_x$/Al SET while sweeping a nearby Schottky gate, we can identify the flat band condition. We will present preliminary data for the filling and emptying of $Si/SiO_2$ interface states and for the determination of electric field below the SET island from such devices.

**16:42**

**K40 10 Experimental demonstration of an oscillator stabilized Josephson flux qubit** R. H. KOCH, G. A. KEEFE, F. P. MILLIKEN, J. R. ROZEN, C. C. TSUEI, J. R. KIRTLEY, D. P. DIVINCENZO, *IBM Research, Yorktown Heights, NY 10598* We experimentally demonstrate the use of a superconducting transmission line, shorted at both ends, to stabilize the operation of a tunable flux qubit. Our qubit consists of three Josephson junctions and three loops coupled to a fixed-length superconducting transmission line. The bare qubit has two control parameters, the flux and the control flux. This allows the qubit to have a tunable difference frequency between the ground and first excited states and at the same time to be biased at a degenerate point with respect to the flux parameter. This condition can be met for a wide range of junction critical currents. This flexibility of our structure is a very desirable property for a scalable qubit. To stabilize the operation of our qubit and increase its coherence time, we couple the bare qubit to the lowest mode of a superconducting transmission line, which we model as a harmonic oscillator. Using harmonic oscillator stabilization and pulsed dc operation, we have observed Larmor oscillations with a single shot visibility of 90 percent and a coherence time of 100 ns. In another qubit the visibility was 60 percent and there was no measurable visibility reduction after 35 ns.

**16:54**

**K40 11 Design and Implementation of Devices for Flux Qubit Entanglement Experiments*** PAUL REICHARDT, TRAVIS HIME, *University of California, Berkeley* BRITTON PLOURDE, *Syracuse University* TIMOTHY ROBERTSON, CHENG-EN WU, *University of California, Berkeley* ALEXEY USTINOV, *University of Erlangen-Nuremberg* JOHN CLARKE, *University of California, Berkeley* We report measurements on two superconducting flux qubits coupled to a readout Superconducting QUantum Interference Device (SQUID). The chosen device parameters allow for the implementation of a fast, controllable qubit coupling scheme based on variations in the current bias of the readout SQUID in the zero-voltage state. The devices have Al-AlOx-Al

tunnel junctions and were fabricated with e-beam lithography on a single substrate. Two on-chip flux bias lines allowed independent flux control of any two of the three elements. By applying microwave radiation, we observed resonant excitation of each qubit and thereby individually mapped out energy dispersions for both qubits. These dispersions displayed the expected hyperbolic dependence with tunnel splittings of 9.0 ± 0.2 GHz, which agreed well with the calculated and measured device parameters. Single qubit coherence properties including relaxation times, Rabi oscillations, Ramsey fringes, and echoes were also measured.

*Supported by AFOSR, ARO, ARDA, NSF, BaCaTeC

**17:06**

**K40 12 Variable Coupling of Two Flux Qubits*** T. HIME, *University of California, Berkeley* P.A. REICHARDT, B.L.T. PLOURDE, *Syracuse University* T.L. ROBERTSON, *University of California, Berkeley* C.-E. WU, A.V. USTINOV, *University of Erlangen-Nuremberg* JOHN CLARKE, *University of California, Berkeley* We report observations of variable coupling of two flux qubits. The qubits are coupled inductively to each other and to a readout Superconducting Quantum Interference Device (SQUID). By applying microwave radiation to the device, we observed resonant absorption in each of the qubits when the level splitting in the qubit matched the energy of the microwave photons. Using the two on-chip flux bias lines we adjusted the bias of each qubit so that the energy levels of the two qubits were equal; we then observed a splitting of the resulting absorption peak characteristic of coupling between the qubits. We varied the coupling between the qubits by changing the current bias in the SQUID in the zero voltage state, thereby changing its dynamic inductance and thus modifying the effective mutual inductance between the qubits. We compare the resulting changes in splitting with our predictions. This controllable coupling should be extendable to many qubits.

*Supported by AFOSR, ARO, ARDA, NSF, BaCaTeC

**17:18**

**K40 13 Actively Tuned and Spatially Trapped Polaritons** RYAN BALILI, DAVID SNOKE, *Department of Physics and Astronomy, University of Pittsburgh* LOREN PFEIFFER, KENNETH WEST, *Bell Labs, Lucent Technologies* The resulting eigenstate of the strong coupling of light and excitons in a two-dimensional semiconductor microcavity produces the quasiparticles called polaritons. Owing to their light mass and bosonic character, these particles are predicted to Bose condense at much higher temperatures and lower densities than their atomic counterparts. However, standard methods of producing strongly coupled semiconductor microcavities are very inefficient. Only tiny regions of the microcavity wafer end up in the strong coupling regime due to the wedge of the layer thicknesses formed during the growth process. Here we present a method to actively control the exciton coupling with cavity photon modes and at the same time create an in-plane spatial trap for polaritons, which is necessary for two-dimensional BEC. The exciton energy of quantum well excitons in a semiconductor microcavity is actively tuned using applied stress. Starting with the quantum well exciton energy higher than the cavity photon mode, stress is used to reduce the exciton energy and bring it into resonance with the photon mode. At the point of zero detuning, line narrowing and strong increase of the photoluminescence are seen. By the same means, an in-plane harmonic potential for the polaritons is created, which allows trapping, potentially making possible BEC of polaritons analogous to trapped atoms. Drift of the polaritons into this trap is also demonstrated.

## SESSION K41: FOCUS SESSION:DIELECTRIC, FERROELECTRIC, AND PIEZOELECTRIC OXIDES II

**Tuesday Afternoon, 14 March 2006**
**344, Baltimore Convention Center at 14:30**
**Darrell Schlom, Penn State University, presiding**

***Contributed Papers***

**14:30**

**K41 1 Ferroelectricity of Perovskites under Pressure*** IGOR KORNEV, L. BELLAICHE, *Physics Department, University of Arkansas* P. BOUVIER, *LEPMI, CNRS, France* P.-E. JANOLIN, B. DKHIL, *SPMS, CNRS-UMR8580, France* J. KREISEL, *LMGP, ENSPG, INPG, France* Ab-initio simulations and experimental techniques are combined to reveal that, unlike commonly accepted for more than 30 years, perovskites and related materials *enhance* their ferroelectricity as hydrostatic pressure increases above a critical value [1]. This unexpected high-pressure ferroelectricity is different in nature from conventional ferroelectricity because it is driven by an original electronic effect rather by long-range interactions. [1]. Igor A. Kornev, L. Bellaiche, P. Bouvier, P.-E. Janolin, B. Dkhil, and J. Kreisel, Phys. Rev. Lett. 95, 196804 (2005).

*This work is supported by ONR grants N00014-04-1-0413, N00014-01-1-0365 and N00014-01-1-0600, NSF grants DMR-0404335 and DMR-9983678, DOE grant DE-FG02-05ER46188.

**14:42**

**K41 2 NMR quadruopole spectra of PZT from first-principles*** DANDAN MAO, *College of William and Mary* ERIC J. WALTER, *College of William and Mary* HENRY KRAKAUER, *College of William and Mary* High performance piezoelectric materials are disordered alloys, so it can be difficult to determine the local atomic geometry. Recently, high field NMR measurements have shown great promise as a microscopic probe of ABO3 perovskite-based alloys[1] by their ability to resolve line-splittings due to nuclear quadrupolar coupling with the electric field gradient (EFG) at the nucleus. We report first-principles LDA calculations of the EFG's in monoclinic and tetragonal $Pb(Zr_{0.5}Ti_{0.5})O_3$ systems using the linear augmented planewave (LAPW) method, and we compute NMR static powder spectra for $^{91}Zr$, $^{47}Ti$, and $^{17}O$ atoms as a function of applied strain. With decreasing $c/a$ ratio PZT converts from tetragonal to monoclinic symmetry. We observe that the calculated NMR spectra show dramatic deviations with decreasing $c/a$ from that in tetragonal $P4mm$ well before the electric polarization begins to rotate away from the [001] direction. This indicates that NMR measurements

can be a very accurate probe of local structural changes in perovskite piezoelectrics.

*Supported by ONR and the Center for Piezoelectrics by Design

[1]G. L. Hoatson, D. H. Zhou, F. Fayon, D. Massiot, and R. L. Vold, Phys. Rev. B, **66**, 224103 (2002).

**14:54**
**K41 3 A First Principles Approach to Modelling $Ba_{(1-x)}Ca_{(x)}ZrO_3$** JOSEPH BENNETT, ILYA GRINBERG, ANDREW RAPPE, *University of Pennsylvania* Dielectric properties are often optimized by varying material composition, so there is a need to understand the impact of doping on the local structure and properties of a material. One study showed that the dielectric constant of $BaZrO_3$ (BZ) can be increased by up to 50% by doping with small amount of Ca [1]. This is interesting because $CaZrO_3$ (CZ) actually has a lower epsilon than BZ. We use first principles methods to characterize the local structure of $Ba_{(1-x)}Ca_{(x)}ZrO_3$ (BCZ) at various compositions and compute the contribution to the dielectric response of each normalized mode at 0 K. There arise low frequency phonon modes related to Ca-O motions and a transformation of Raman modes to IR modes caused by the introduction of Ca. [1] Levin, I. et al. J Sol. State Chem. 175 (2003) 170-181.

*Invited Papers*

**15:06**
**K41 4 Pressure-Induced Ferroelectric-to-Relaxor Crossover in PSN and Isomorphs.***
EUGENE VENTURINI, *Sandia National Laboratories*

We discuss the influences of pressure (P) and bias field on the dielectric properties and phase behavior of a single crystal of the chemically-disordered ABB'$O_3$ perovskite $Pb(Sc_{0.5}Nb_{0.5})O_3$ or PSN. On cooling from high temperatures (T), PSN first enters a relaxor (R) state and then spontaneously transforms to a ferroelectric (FE) phase at a temperature $T_c$ substantially below the maximum in the dielectric susceptibility. The R state indicates the presence of polar nanoregions, arising from the B-site chemical disorder, that increase in size with decreasing T. At ambient P, these regions grow to macroscopic size, leading to a first-order FE transition at $T_c$. Hydrostatic P offers a unique method to systematically decrease the dielectric polarizability of PSN by reducing the unit cell volume and, hence, increasing the frequency of the soft transverse optic phonon modes. As P increases, the size of the polar regions decreases, enhancing the R state at the expense of the FE phase. It appears that the FE phase vanishes somewhat above the highest P reached in the experiments, making the R state the ground state of the crystal at reduced volume. This suggests a T-P phase diagram with a $T_c$(P) phase line that terminates between 10 and 15 kbar in a manner akin to a critical point; however, in the case of PSN this feature represents a FE-to-R crossover. In contrast, a biasing electric field favors the FE phase over the R state, and the data indicate that the R state vanishes above 5 kV/cm. Additional insight is provided by comparison to dielectric results on isomorphous $Pb(Sc_{0.5}Ta_{0.5})O_3$ in both its compositionally ordered and disordered forms.

*With G.A. Samara and R.K. Grubbs, Sandia Labs, Y. Bing and Z.-G. Ye, Simon Fraser Univ. Work at Sandia supported by Division of Materials Sciences and Engineering, Office of Basic Energy Sciences, U.S. Dept. of Energy, under contract DE-AC04-94AL85000.



*Contributed Papers*

**15:42**
**K41 5 Dielectric Behavior of Compositionally Graded Ferroelectrics** MOHAMED EL-NAGGAR, KAUSHIK DAYAL, DAVID GOODWIN, KAUSHIK BHATTACHARYA, *California Institute of Technology* Graded ferroelectric thin films offer the possibility of engineering the dielectric response by spatial variations in composition. While a homogenous ferroelectric material achieves very high dielectric constants near the phase transition, heterogeneous compositions can result in high dielectric responses over a wide range of temperatures. This can be understood as an ''aggregate'' response of the graded film, and has been experimentally observed. It is a promising candidate for tunable microwave applications that benefit from temperature-insensitivity. We examine this issue through a continuum model that accounts for the spatial variation in properties and the long-range electrostatic interaction. This model is applied to graded Barium Strontium Titanate and Lead Barium Titanate films in a single-domain system where the polarization gradient is normal to the film surface. We examine the effect of grading and the geometry of electrode/ferroelectric layers on the dielectric behavior with temperature and provide results that are useful as design tools for functionally graded devices.

**15:54**
**K41 6 Origin of Curie temperature non-linearity in ferroelectric $BiBO_3$-$PbTiO_3$ solid solutions** ILYA GRINBERG, *Department of Chemistry, University of Pennsylvania* ANDREW M. RAPPE, *Department of Chemistry, University of Pennsylvania* We use first-principles density functional theory calculations to investigate compositional trends in ferroelectric $BiBO_3$-$PbTiO_3$ solid solutions. We find that cation displacements which give rise to ferroelectricity in these materials follow a linear relationship with the average displacive characteristics of the B-site. The transition temperatures in these materials are well correlated with polarization magnitudes computed from our calculations. The coupling between composition of the B-site and A- and B-site displacements explains the highly nonlinear and sometimes non-monotonic dependence of the Curie temperature ($T_c$) on composition observed in these materials.

**16:06**
**K41 7 Atomistic simulation of strained $BaTiO_3$/$SrTiO_3$ superlattices** SILVIA TINTE, *NIST, MD* MARCELO SEPLIARSKY, *IFIR, Argentina* BENJAMIN P. BURTON, *NIST, MD* The $BaTiO_3$(BT)/$SrTiO_3$(ST) superlattice is one of the most intensively studied because of the possibility of polarization enhancement by manipulating strain and layer thicknesses. In this work, we apply an

atomistic-level description to explore the structural, polar and dielectric properties of epitaxial 001-oriented BT/ST superlattices. The shell-model potentials used here have previously described well the phase diagram and properties of BT perfect crystals and ST in the high-temperature limit, and in combination, these potentials reproduced the FE properties of $Ba_xSr_{1-x}TiO_3$ random solid solutions. Here, we focus on asymmetric BT/ST superlattices with in-plane lattice parameter matched to a ST substrate, and periods ranging from 6 to 18 unit cells. These structures have strain induced tetragonal symmetry at low temperature with polarization along the modulation direction and transform to a paraelectric phase at high temperature. Ferroelectric transition temperatures and static dielectric constant are reported as functions of the BT/ST ratio. Also, we show values for local strain and local spontaneous polarization.

**16:18**

**K41 8 Effects of Pressure and Electric Field on the Relaxational Dielectric Properties of $K_{0.97}Li_{0.03}O_3$ (KLT-3)*** GEORGE SAMARA, ROBERT GRUBBS, EUGENE VENTURINI, *Sandia Labs* LYNN BOATNER, *Oak Ridge* The temperature dependence of the dielectric response of KLT-3 shows no evidence of a thermodynamic phase transition, but reveals two prominent relaxational features associated with the off-center $Li^+$ ion, one attributed to the hopping of the $Li^+$ dipole and the other with the reorientation of $Li^+$ - $Li^+$ ion pair. Both relaxations are Debye-like and follow Arrhenius kinetics, the energy barriers decreasing with pressure. While pressure favors the relaxational behavior, a biasing itdc electric field favors long-range order of the dipolar system. The interplay between pressure and field provides additional insight. Pressure suppresses the magnitude of the $\varepsilon'(T)$ response over the whole temperature range The results allow evaluation of the contributions of the soft mode and of the $Li^+$ dipoles to the measured $\varepsilon'(T)$ response.

*The work is supported by Division of Materials Sciences and Engineering, Office of Basic Energy Sciences, U.S. Dept. of Energy at Sandia under contract No.DE-AC04-94AL85000 and at Oak Ridge under contract DE-AC05-00OR22725.

**16:30**

**K41 9 Ferroelectricity in $PbTiO_3$ and $BaTiO_3$ under Pressure** R.E. COHEN, Z. WU, *Carnegie Institution of Washington* First-principles total energy and linear response calculations reveal a complicated pressure-induced phase transition sequence for $PbTiO_3$ (PT) under pressure. The previously proposed $P4mm$-to-$Cm$-to-$R3m$-to-$Pm\bar{3}m$ transition sequence [1] is not complete because only zone-center ($\Gamma$) instabilities and pressures $P$ less than 30 GPa were considered. Recently Kornev *et al.* reported an unexpected enhancement of ferroelectric instability at high pressures [2]. Our computations confirm this result, and in addition, the zone-boundary R-point rotational instability is enhanced with pressure. Preliminary results show $R3m$-to-$R3c$-to-$R\bar{3}c$-to-$R3c$ phase transitions in PT for 18 GPa $< P <$ 120 GPa due to the competition and interaction of zone-center and zone-boundary instabilities. On the other hand, there is no instability in cubic $BaTiO_3$ for $P >$ 10 GPa up to 120 GPa, resulting in a single $R3m$-to-$Pm\bar{3}m$ transition at 0 K. We are investigating whether the covalency of Pb is responsible for the unusual enhancement of ferroelectricity under high pressure. The electromechanical coupling constants become enormous in the transition regions from the tetragonal to high pressure phases for PT, suggesting that the large coupling in PT solid solutions such as PZT, PMN-PT, and PZN-PT, simply tune this transition to zero pressure [1]. Supported by ONR. [1] Z. Wu and R. E. Cohen, Phys. Rev. Lett. **95**, 037601 (2005). [2] Kornev *et al.*, Phys. Rev. Lett. **95**, 196804 (2005).

**16:42**

**K41 10 A-site driven ferroelectricity in $K_{0.5}Li_{0.5}NbO_3$** DANIEL I. BILC, D.J. SINGH, *Condensed Matter Sciences Division, Oak Ridge National Laboratory, Oak Ridge, Tennessee 37831, USA* Mixed A-site ferroelectric materials have gained recent attention. Here we report density functional calculations of $K_xLi_{1-x}NbO_3$ perovskite supercells in order to understand the interplay between various lattice instabilities with size mismatch on the A-site and the role of the A and B site ions in this case. The calculations were done using the general potential LAPW method. For x=0.5, we find a ferroelectric ground state, even though the average tolerance factor is significantly smaller than unity and there is no stereochemically active A site ion. This is due to frustration due to the very different ionic radii of K and Li. We find very large off-centering of the Li ions, which distinguishes this compound. Relative to this the Nb off-centering is quite small. This is in contrast to most perovskite ferroelectrics where there is significant off-centering of all ions, and resulting cooperativity. Also because of the large Li off-centering it contributes strongly to the anisotropy between tetragonal and rhombohedral ground states, yielding a tetragonal ground state. Normally the anisotropy is determined by the interplay of B site off-centering and strain coupling. This work was supported by the Office of Naval Research and the Department of Energy.

**16:54**

**K41 11 Effective Hamiltonian study of $PbSc_{1/2}Nb_{1/2}O_3$ under pressure** ERIC COCKAYNE, SILVIA TINTE, BENJAMIN P. BURTON, *NIST* UMESH V. WAGHMARE, *JNCASR* In general, increasing pressure depresses the transition temperature $T_{FE}$ of ferroelectric transitions, and sufficient pressure yields a FE $\rightarrow$ paraelectric (PE) transition. A more complicated behavior is observed for disordered $PbSc_{1/2}Nb_{1/2}O_3$ (PSN). At atmospheric pressure, PSN exhibits relaxor ferroelectric (RFE) properties within a small temperature range before transforming to a FE phase at low temperatures. Pressure of approximately 1.5 to 2.5 GPa induces a low-temperature RFE state without a RFE/FE phase boundary.[E. L. Venturini et al.] To investigate the effects of pressure on phase transitions in PSN, we used a first-principles based effective Hamiltonian. Our effective Hamiltonian includes a local field term arising from the charge difference between the $Sc^{3+}$ and $Nb^{5+}$ ions. Under pressure, the local field term changes little, while the FE well depths decrease, increasing the relative importance of the local fields. Molecular dynamics simulations show that $T_{FE}$ decreases with temperature and that the phase transition broadens.

**17:06**

**K41 12 Pressure-induced phase transitions in $PbTiO_3$*** MUHTAR AHART, P. DERA, R. E. COHEN, RUSSELL J. HEMLEY, *Carnegie Institution of Washington* We have investigated $PbTiO_3$ under pressure in a diamond anvil cell for temperatures of 20K to 300K using micro-Raman spectroscopy and x-ray diffraction. The Raman spectra show large changes: three peaks, centered at 200, 240 and 250 $cm^{-1}$ disappeared above 20, 19 and 17 GPa at 20, 47 and 77 K, respectively. Furthermore, a new peak centered at 300 $cm^{-1}$ appears above transition points. The disappearance of peaks and the appearance of new peaks are consistent with theo-

retical calculations of Z. Wu et al., Phys. Rev. Lett. 95, 37601, 2005, and suggest a zone boundary instability at high pressures. The experimental results also indicate that pressure induced phase transitions at low temperature are reversible. At room temperature the first order Raman spectrum disappears above 12 GPa consistent with a transition to the cubic phase, but x-ray diffraction data suggests a rhombohedral or monoclinic phase between the tetragonal and cubic phases, consistent with the predictions of Z. Wu et al. The experimental results provide a new phase diagram for $PbTiO_3$.

*This work is supported by the ONR under the contract number N000140210506 and the Carnegie/Department of Energy Alliance Center (DE-FC03N00144)

**17:18**

**K41 13 Electronic structure and lattice distortion in $PbMg_{1/3}Nb_{2/3}O_3$** MALLIGA SUEWATTANA, DAVID SINGH, *Oak Ridge National Laboratory* We investigated the local structural distortions of PMN($PbMg_{1/3}Nb_{2/3}O_3$) within the density functional theory using the linearized augmented plane-wave method. Structural relaxations were performed on 30 atom unit cells with B-cations arranged in 1:1 chemical ordering along [111]. The direction and magnitude of Mg and Nb off-centering within $O_6$ octahedral cages and Pb within its cage as well as electronic structures were examined. The results are discussed in terms of the Nb 4d - O 2p and Pb 6p - O 2p hybridizations and their interplay. A significant role is found for the on-site Ewald potential of different Nb sublattices, which is correlated with the off-centering. †This work was supported by ONR and DOE.



**SESSION K42: FOCUS SESSION: PLANETARY MATERIALS II**
**Tuesday Afternoon, 14 March 2006**
**345, Baltimore Convention Center at 14:30**
**Eric Schwegler, Lawrence Livermore National Laboratory, presiding**

**14:30**

**K42 1 Shock Hugoniot Calculations of Dense Liquid Helium*** BURKHARD MILITZER, *Carnegie Institution of Washington* By combining two first-principles computer simulation techniques, path integral Monte Carlo and density functional molecular dynamics, the properties of dense liquid helium are studied. From the equation of state we derive the shock Hugoniot curves. Results at low pressures agree well with gas gun experiments. For higher pressures, we predict that helium is compressible to more than five times its initial density. This behavior is in contrast to hydrogen, for which we predicted a maximum compression ratio of only 4.25. In the case of helium, the conditions for 5-fold compression are attainable with existing shock facilities. Studying this material will enable us to verify new experimental and theoretical techniques, and may help us to understand the existing controversy in the experimental shock results for deuterium. The characterization of dense liquid hydrogen and helium allows us to build models describing the interior of Giant Planets and answer fundamental questions of their evolution.

*Supported by NASA's PGG program (NNH04ZSS001N).

**14:42**

**K42 2 Simulations of dense hydrogen and hydrogen-helium mixtures at conditions relevant to gas planet interiors*** ISAAC TAMBLYN, *Dalhousie University* JAN VORBERGER, *Carnegie Institution of Washington Geophysical Laboratory* BURKHARD MILITZER, *Carnegie Institution of Washington Geophysical Laboratory* STANIMIR A. BONEV, *Dalhousie University* The principle components of all gas giants are hydrogen and helium. In order to improve models describing the formation and evolution of planets such as Jupiter and Saturn, we investigate the properties of these materials under extreme conditions. itAb initio molecular dynamics simulations are performed on both pure hydrogen and hydrogen-helium mixtures. The equation of state and structural properties of these liquids are determined at characteristic temperatures, pressures, and mixing ratios relevant for the interior of Jupiter-like planets. Results are compared with previous investigations, both experimental and theoretical, with improvements highlighted. In particular, effects originating from the dissociation of molecular hydrogen are discussed.

*Work supported by Carnegie Canada and the NSERC of Canada.

**14:54**

**K42 3 Hydrogen-Helium Mixtures under Giant Gas Planet Conditions** JAN VORBERGER, *Geophysical Laboratory, Carnegie Institution of Washington, Washington D.C.* ISAAC TAMBLYN, STANIMIR A. BONEV, *Dalhousie University, Halifax, Canada* BURKHARD MILITZER, *Geophysical Laboratory, Carnegie Institution of Washington, Washington D.C.* We use density functional molecular dynamic simulations to investigate equilibrium properties of mixtures of hydrogen and helium. We consider a range of temperature, density and mixing ratio which enables us to study the equation of state for these mixtures under extreme conditions relevant, e.g., for giant gas planets. We focus on the atomic and molecular phase of hydrogen helium mixtures. We consider the structure of the liquid and how the presence of helium influences the bond length and suppresses the dissociation of the hydrogen molecules. We present binary distribution functions illustrating that helium leads to lower dissociation in the system. We will demonstrate constraints concerning the validity of the linear mixing rule. We will show comparisons to different methods and present results for Jupiters isentrope.

**15:06**

**K42 4 Equation of state and electronic structure of liquid Helium at high pressure** LARS STIXRUDE, *University of Michigan* RAYMOND JEANLOZ, *University of California at Berkeley* As the second most abundant element, the properties of fluid Helium form an important part of our understanding of stellar and giant planetary structure. Yet the physics of Helium at pressure-temperature conditions characteristic of these bodies is uncertain. We perform first principles molecular dynamics simulations of fluid Helium over a wide range of pressure ( $<$ 1 Gbar) and temperature ( $<$ 5 eV). The simulations are based on finite-temperature density functional theory in the generalized gradient approximation, and are performed in the canonical ensemble with a Nose thermostat. We find that both temperature and compression have a strong influence on the electronic structure as revealed by the band gap. At a density of 1 g $cm^{-3}$ the band gap varies from 20 eV for the static crystal to 0 for the fluid at 4 eV. The gap is closed at all temperatures for density greater than 20 g $cm^{-3}$. We find that the equation of state varies smoothly through the band gap closure transition with no indication of a high-order phase transformation. The decrease in band gap with increasing tempera-

ture at constant density results from enhanced mixing of 1s- and 2s-like states with increasing disorder (i.e., enhanced vibrational amplitudes and melting) that has profound implications for understanding the deep interiors of planets.

**15:18**

**K42 5 Raman spectroscopy of hot compressed hydrogen and nitrogen - implications for the intramolecular potential** ALEXANDER F. GONCHAROV, *Geophysical Laboratory, Carnegie Institution of Washington* JONATHAN C. CROWHURST, *Lawrence Livermore National Laboratory* Raman measurements of molecular hydrogen, deuterium, and nitrogen have been made under simultaneous conditions of high temperature and high static pressure. Measurements have been made on hydrogen and deuterium to 50 GPa and 1600 K, and on nitrogen to 50 GPa and 2000 K. In all three materials the familiar molecular stretching mode (vibron) is accompanied in the high temperature Raman spectra by one or more lower frequency peaks due to transitions from excited vibrational states. We find the frequency differences between these bands decreases with pressure, implying that the anharmonicity of the corresponding part of the intramolecular potential also decreases. This is accompanied by an increase in the measured line widths of the bands that is consistent with a decrease of the depth of the potential and an approaching molecular dissociation.

**15:30**

**K42 6 First-principles study of the effect of helium on the onset of dissociation in liquid hydrogen** KYLE CASPERSEN, SEBASTIEN HAMEL, TADASHI OGITSU, FRANÇOIS GYGI, *University of California Davis* ERIC SCHWEGLER, *Lawrence Livermore National Laboratory* The onset of molecular dissociation in liquid hydrogen under high-pressures is known to occur abruptly, possibly involving a first-order liquid-liquid phase transition [1,2]. We have examined this transition in detail by performing a series of large-scale first-principles molecular dynamics simulations of liquid hydrogen and mixtures of hydrogen with small concentrations of helium. In addition, we have examined the electronic properties of hydrogen-helium mixtures by using hybrid density functional theory to analyze snapshots from our molecular dynamics simulations. This work was performed under the auspices of the U.S. Department of Energy by the University of California, Lawrence Livermore National Laboratory under contract No. W-7405-Eng-48. [1] S. Scandolo, PNAS 100, 3051 (2003). [2] S.A. Bonev, et al. Phys. Rev. B 69, 014101 (2004).

**15:42**

**K42 7 Reentrant Phase Diagram in Ortho-Para Mixtures of Solid $H_2$ at High Pressure** BALAZS HETENYI,* *SISSA, Trieste (Italy)* SANDRO SCANDOLO, *The Abdus Salam ICTP and INFM-CNR Democritos, Trieste (Italy)* ERIO TOSATTI, *SISSA, ICTP, and Democritos, Trieste (Italy)* Quantum effects dominate the low temperature phase diagram of solid molecular hydrogen in a wide range of pressures from ambient up to about 100 GPa. Important differences exist in the behavior of pure even-$J$(para-$H_2$ and ortho-$D_2$), and odd-$J$ (ortho-$H_2$ and para-$D_2$) species, but little is known about the phase diagram of ortho-para mixtures. We develop a multiorder parameter mean-field formalism for systems of coupled quantum rotors and apply it to solid $H_2$ and $D_2$. For a thermal distribution of ortho-para molecules we find an anomalous reentrant orientational phase transition in the pressure - temperature phase diagram of both systems [Hetenyi et al., PRL 94, 125503 (2005)]. The correlation functions of the order parameter indicate short-range order at low temperatures. As the temperature is increased the correlation increases along the phase boundary. We also find that even extremely small itodd-$J$concentrations (1%) can trigger short-range orientational ordering.

*Present address: TU Graz, Austria

**15:54**

**K42 8 Observability of a projected new state of matter: a metallic superfluid hydrogen*** EGOR BABAEV, *Cornell University* ASLE SUDBO, *NTNU Trondheim* N.W. ASHCROFT, *Cornell University* Dissipationless quantum states, such as superconductivity and superfluidity, have attracted interest for almost a century. A variety of systems exhibit these macroscopic quantum phenomena, ranging from superconducting electrons in metals to superfluid liquids, atomic vapours, and even large nuclei. It was recently suggested that liquid metallic hydrogen could form two new unusual dissipationless quantum states, namely the metallic superfluid and the superconducting superfluid. Liquid metallic hydrogen is projected to occur only at an extremely high pressure of about 400 GPa, while pressures on hydrogen of 320 GPa having already been reported. The issue to be adressed is if this state could be experimentally observable in principle. We propose experimental probes for detecting it and discuss recent developments in superconducting/superfluid properties of the projected metallic state of hydrogen or its isotopes.

*Supported by STINT and Swedish Research Council, National Science Foundation and Norwegian Research Council

**16:06**

**K42 9 Observation of a metallic superfluid in a numerical experiment*** ASLE SUDBO, JO SMISETH, EIVIND SMORGRAV, EGOR BABAEV, *Norwegian University of Science and Technology* We report the observation, in Monte Carlo simulations, of a novel type of quantum ordered state: *the metallic superfluid*. The metallic superfluid features ohmic resistance to counter-flows of protons and electrons, while featuring dissipationless co-flows of electrons and protons. One of the candidates for a physical realization of this remarkable state of matter is hydrogen or its isotopes under high compression. This adds another potential candidate to the presently known quantum dissipationless states, namely superconductors, superfluid liquids and vapours, and supersolids.

*Work supported by US National Science Foiundation and the NANOMAT Program, Research Council of Norway

**16:18**

**K42 10 The melting of water under pressure*** ERIC SCHWEGLER, *Lawrence Livermore National Lab* FRANCOIS GYGI, GIULIA GALLI, *University of California, Davis* We have investigated the melting of water under high-pressure conditions with a series of first-principles molecular dynamics simulations. In particular, the two-phase approach [1] has been used to determine the melting temperature of water under pressures ranging from 10 to 50 GPa. The effect of molecular dissociation on the structural, dynamical and melting properties of water will be discussed in detail. [1] T. Ogitsu, E. Schwegler, F. Gygi and G. Galli, Phys. Rev. Lett. 91, 175502 (2003).

*This work was performed under the auspices of the US Department of Energy by the University of California at the LLNL under contract no W-7405-Eng-48.

**16:30**

**K42 11 Scaling fields and equation of state near the liquid-liquid critical point in supercooled water** DAPHNE FUENTEVILLA, MIKHAIL ANISIMOV, *University of Maryland, College Park* We have developed a scaled parametric equation of state to describe and predict thermodynamic properties of water in supercooled conditions. The equation of state is built on the assumption that in the supercooled water an additional critical point, the critical point of liquid-liquid separation, does exist. Although this second critical point of water is not accessible experimentally, the pre-critical anomalies affect thermodynamic and transport properties of water in the metastable and even in stable regions and can be observed experimentally. Our approach is based on the principle of critical-point universality. The equation of state is universal in terms of theoretical scaling fields and belongs to the three-dimensional Ising-model class of universality. The theoretical scaling fields are postulated to be analytical combinations of physical fields (pressure and temperature). The proposed equation of state enables us to accurately locate the ''Widom line'' (the locus of stability minima) and the position of the critical point, as well as to predict the thermodynamic properties in the regions that are not accessible to experiments.

**16:42**

**K42 12 The metastable limit of isentropically compressed water** D.H. DOLAN, *Sandia National Laboratories* M.D. KNUDSON, *Sandia National Laboratories* J.P. DAVIS, *Sandia National Laboratories* C. DEENEY, *Sandia National Laboratories* C. HALL, *Sandia National Laboratories* Although freezing is normally a slow process, it can be observed on very short time scales using isentropic compression techniques. For isentropic compression beyond 2 GPa, liquid water becomes metastable with respect to the ice VII phase and can freeze on nanosecond time scales if heterogeneous nucleation sites are present [D.H. Dolan et al., J. Chem. Phys. **123**, 64702 (2005)]. Such nucleation sites are typically found on the surfaces of crystalline and amorphous silica windows used to compress a water sample; in the absence of such windows, water remains in a metastable liquid state for some time. Recent gas gun and Z machine experiments at Sandia National Laboratories suggest a sharp metastable limit for isentropically compressed water, beyond which the liquid phase rapidly transforms to a solid without the aid of a nucleating window. This rapid transition is expected because the liquid phase is increasingly unfavorable at high pressure, but has not been previously observed. Comparison of the new freezing observations with prior results reveals stark qualitative differences, suggesting that this newly observed freezing is very different from a heterogeneously nucleated transition.

**16:54**

**K42 13 Infrared study of high-pressure HD: observation of the A-phase*** AKOBUIJE CHIJIOKE, ISAAC SILVERA, *Lyman Laboratory of Physics, Harvard University, Cambridge MA 02138* Infrared absorption was used to investigate the phase diagram of solid HD up to pressures of 156 GPa at temperatures ranging from 4 to 200K. A re-entrant phase line between the low-pressure and broken-symmetry phases (BSP) was observed, in agreement with Raman scattering results, with a 0 K transition pressure of $\sim$ 65-70 GPa. A phase transition was observed with an onset at $\sim$ 154 GPa (at 5K), consistent with the transition to the A-phase, previously observed in $H_2$ and $D_2$. The infrared spectra in the compressed low-pressure and BSP phases complement existing Raman spectra in these phases.

*Research supported by the US Army Missile Command

**17:06**

**K42 14 Water in $MgSiO_3$ melt at high pressure** MAINAK MOOKHERJEE, LARS STIXRUDE, *University of Michigan* The presence of water is thought to play important role in modifying the equilibrium and transport properties of earth materials including silicate liquids. In our study we want to address the following questions: How does the presence of water modifies density of melts? What is the partial molar volume of water in melts? What structural species of $H_2O$ are present at high pressure? In order to address these issues we explore the high-pressure behaviour of hydrous $MgSiO_3$ melt with 11 wt% $H_2O$, using first principles molecular dynamics simulation, based on local density approximation (LDA) and the plane-wave-pseudopotential method. The simulations are performed in the canonical ensembles with periodic boundary conditions and a Nose' thermostat. Melting was confirmed by the radial distribution function displaying no long-range order. By comparing our results with that of the anhydrous counterpart (Stixrude and Karki, 2005), we find that the partial molar volume of water decreases along the 3000 K isotherm from 20 cc/mol at 2 GPa to 6.6 cc/mol at 80 GPa. The water component is substantially more compressible than the silicate component. The partial molar volume of water is much less than the volume of pure water at the same conditions (Pitzer and Sterner, 1994), indicating a difference in structure. Analysis of our simulations shows a range of $H_2O$ species including hydroxyls, water molecules and H-O-H-O groups.

**17:18**

**K42 15 Optical studies of compressed silane up to 40 GPa** VIKTOR V. STRUZHKIN, XIAOJIA CHEN, OLGA DEGTYAREVA, MUHTAR AHART, YANG SONG, HANNS-PETER LIERMANN, JIAN XU, HO-KWANG MAO, RUSSELL J. HEMLEY, *Geophysical Laboratory, Carnegie Institution of Washington, Washington, DC 20015* Under sufficiently strong compression, hydrogen is believed to be a metal and eventual superconductor with high transition temperatures. Despite an unrelenting experimental assault at ultra-high pressures, dense solid hydrogen has so far defined all attempts at metallization. Recently, Ashcroft suggested that the dense group IVa hydrides would undergo a transition to eventual metallic and superconducting states at pressures considerably lower than may be necessary for hydrogen. We have performed the vibrational study of silane at high pressures up to 31.6 GPa by Raman spectroscopy. By using the fully symmetrical stretching mode as a probe for exploring the phase transition, we find one fluid-solid transition at around 4.0 GPa and two solid-sold transitions near 6.5 GPa and 26.5 GPa at 300 K. After 26.5 GPa, the solid silane becomes opaque. Our x-ray diffraction data also confirmed the high-pressure phase transitions. Moreover, the observed high-pressure structure is irreversible. Although there is no evidence for possible metallization in this pressure regime from our IR measurements, the observation of black hydrogen in solid silane is significant since the pressure used is ten times smaller than that in solid hydrogen.

**SESSION K43: TRAPPED FERMI GASES**
**Tuesday Afternoon, 14 March 2006**
**346, Baltimore Convention Center at 14:30**
**C. Sa de Melo, Georgia Institute of Technology, presiding**

**14:30**
**K43 1 Population of closed-channel molecules in trapped Fermi gases with broad Feshbach resonances*** QIJIN CHEN, K. LEVIN, *University of Chicago* We compute the fraction of closed-channel molecules in trapped atomic Fermi gases, over the entire range of accessible fields and temperatures. We use a two-channel model of BCS–Bose-Einstein condensation (BEC) crossover theory at general temperature $T$, and show that this fraction provides a measure of the $T$ dependent pairing gap. Our calculations, containing no free parameters, are in good quantitative agreement with recent low $T$ measurements in $^6$Li. We present readily testable predictions for the dependencies of the closed-channel fraction on temperature and Fermi momentum. Reference: arXiv:cond-mat/0505689; Phys. Rev Lett. 95, Dec 31, 2005.

*NSF-MRSEC Grant No. DMR-0213745

**14:42**
**K43 2 Quantum Monte Carlo Simulations of Dilute Fermion Gases at Finite Temperature** VAMSI AKKINENI, DAVID CEPERLEY, *University of Illinois at Urbana-Champaign* NANDINI TRIVEDI, *The Ohio State University* In a system of fermions with attractive interactions at low temperature, the crossover from the BCS regime to a molecular BEC, with increasing interaction strengh, is a problem of particular interest in many-body physics. The development of successful experimental techniques to trap and cool dilute gases of fermionic alkali atoms, and to tune the effective inter-atomic interaction over a wide range, have opened exciting possibilities for studying the physics of interacting fermions in this crossover region. The composition of the ground state, nature of fermion pairs, nature of excitations, pairing energy scale, and the pairing and condensation transitions are all important considerations in this crossover regime. Ab initio quantum simulations are invaluable tools for obtaining accurate values of various physical quantities of interest. We utilize the Restricted Path Integral Monte Carlo (RPIMC) technique to calculate to the energy, pairing energy, and the superfluid density at the unitarity point. We present these results along with an estimate of the critical temperature for the superfluid transition.

**14:54**
**K43 3 Evolution from BCS to BEC superfluidity in p-wave Fermi gases** MENDERES ISKIN, CARLOS SA DE MELO, *Georgia Institute of Technology* We consider the evolution of superfluid properties of a three dimensional $p$-wave Fermi gas from weak (BCS) to strong (BEC) coupling as a function of scattering volume. We analyse the order parameter, quasi-particle excitation spectrum, chemical potential, average Cooper pair size and the momentum distribution in the ground state ($T = 0$). We also discuss the critical temperature $T_c$, chemical potential and number of unbound, scattering and bound fermions in the normal state ($T = T_c$). Lastly, we derive the time-dependent Ginzburg-Landau equation for $T \approx T_c$ and extract the Ginzburg-Landau coherence length.

**15:06**
**K43 4 Many body exchange effects close to the s-wave Feshbach resonance in two component Fermi systems: is a triplet superfluid possible?** SERGIO GAUDIO, *Los Alamos National Laboratory and Department of Physics, Boston College* JASON JACKIEWICZ,*KEVIN BEDELL, *Boston College* We suggest that the fluctuations close to a Feshbach resonance in a two component Fermi gas can result in an effective p-wave attractive interaction. On the BCS side of the resonance, the magnitude of this effective interaction is comparable to the s-wave interaction, therefore leading to the possibility of a spin-triplet superfluid in the range of temperatures of actual experiments. We compare the results for our effective scattering length to the mean field result and to the observed binding energy. Finally, we show that by including particle-hole exchange in the fluctuations, the divergence of the effective scattering length disappears.

*now at Max Planck Institute, Katlenburg-Lindau, Germany

**15:18**
**K43 5 Spin noise spectroscopy to probe quantum states of ultracold fermionic atom gases** BOGDAN MIHAILA, SCOTT CROOKER, KRASTAN BLAGOEV, DWIGHT RICKEL, *Los Alamos National Laboratory* PETER LITTLEWOOD, *Cavendish Laboratory, Cambridge University, UK* DARRYL SMITH, Physical systems are often studied by measuring their response to an external perturbation. Measuring the intrinsic noise of a physical system can provide the same information as measuring its response to a perturbation, but noise spectroscopy measurements often disturb the physical system less strongly and scale more favorably with system size reduction. For quantum systems at very low temperature, noise from quantum fluctuations in the ground state of an observable that does not commute with the Hamiltonian can be used as a probe of the system properties. We describe the use of electron spin noise spectroscopy to probe the quantum states of ultracold fermionic atomic gases. The electron spin is not a good quantum number of the atomic gases and fluctuations of electron spin can be measured using optical Faraday rotation. We show that electron spin noise spectroscopy gives unique signatures for different models describing the interatomic interactions in the ultracold fermionic gases, can be used to probe the BCS/BEC crossover in these systems, and weakly disturbs the atomic gases. Measurements of spin noise in classical Boltzmann gases of alkali atoms are used to estimate the expected signal strength for spin noise measurements in ultracold atom systems and to show that these measurements are tractable.

**15:30**
**K43 6 Atomic Fermi gases with unequal spin populations** MEERA PARISH, *University of Cambridge* We investigate the properties of a gas of fermionic atoms where the two spin populations are unequal. By considering how the ground state evolves as a function of inter-atomic interaction and population imbalance, we will determine what the measurable differences are between the various theoretical models of the BCS-BEC crossover in atomic gases.

**15:42**
**K43 7 Spontaneous Vortices in Imbalance Populated Fermion Gas, Finite Size System** JUNG-JUNG SU, YUN-PIL SHIM, REMBERT DUINE, ALLAN H. MACDONALD, *Department of Physics, University of Texas at Austin* Atomic Fermion gases with mismatched densities have attracted much interest recently both experimentally and theoretically. These gases are related to super-

conductors in a magnetic field, to color superconductivity in high density QCD and to other systems. The main focus of recent research is on the possibility of unusual pairing states, the Larkin-Ovchinnikov-Fulde-Ferrel(LOFF) [1] phase, the Deformed Fermi surface(DFS) [2] and other states have been suggested in the past few years. We work specifically on two-dimensional systems with circular hard walls which contain atoms with two different hyperfine states and different populations. In addition to phase separation, a phenomenon that has already been observed [3], we consider the possibility of the spontaneous formation of vortices and giant vortices in some regions of parameter space. [1] Qinghong Cui, C.-R. Hu, J.Y.T. Wei, and Kun Yang, cond-mat/0510717 [2] A. Sedrakian et al., cond-mat/0404577 [3] R. Hulet, preprint.

**15:54**

**K43 8 Superfluid properties across the BEC/BCS transition*** JACQUES TEMPERE, JOZEF DEVREESE, *Universiteit Antwerpen* The superfluid properties of a Bose-Einstein condensate (BEC) and of the Bardeen-Cooper-Schrieffer (BCS) state are reasonably well understood. Recent experimental breakthroughs allow investigating the transition region between the BEC and BCS limits. In this contribution, we apply the path-integral formalism to study how the vortex core size, the superfluid critical velocity and the pair-pair scattering length vary in the crossover region. These quantities depend on the interaction strength of the atoms and change quantitatively from BEC to BCS side. In particular we discuss how the pair-pair scattering length obtained here relates to the mean-field results and to the four-body scattering result.

*Financial support from FWO, BOF NOI UA, IUAP is acknowledged.

**16:06**

**K43 9 Relaxation and persistent oscillations of the order parameter in the non-stationary BCS theory** EMIL YUZBASHYAN, *Center for Materials Theory, Rutgers University, Piscataway, New Jersey 08854, USA* OLEKSANDR TSYPLYATYEV, *Physics Department, Lancaster University, Lancaster LA1 4YB, UK* BORIS ALTSHULER, *Physics Department, Columbia University, New York, New York 10027, USA* We determine the limiting dynamics of a fermionic condensate following a sudden perturbation for various initial conditions. We demonstrate that possible initial states of the condensate fall into two classes. In the first case, the order parameter asymptotes to a *constant* value. The approach to a constant is oscillatory with an inverse square root decay. This happens, e.g., when the strength of pairing is abruptly changed while the system is in the paired ground state and more generally for any *nonequilibrium* state that is in the same class as the ground state. In the second case, the order parameter exhibits persistent oscillations with several frequencies. This is realized for nonequilibrium states that belong to the same class as excited stationary states. Our *classification* of initial states extends the concept of excitation spectrum to nonequilibrium regime and allows one to predict the evolution without solving equations of motion.

**16:18**

**K43 10 Dynamical properties of the pairing gap in ultra-cold Fermi gases** MAXIM DZERO, *DOE Ames Laboratory* EMIL YUZBASHYAN, *Rutgers University* We study the dynamics of a condensate of an atomic ultra-cold Fermi gas following an abrupt change in the pairing strength. At long times the order parameter asymptotes to a constant value, which we determine exactly. Under certain conditions, the system reaches a novel steady state with peculiar properties.

**16:30**

**K43 11 Exploring the Possibility of Collapse in a Degenerate Fermi Gas*** J. VON STECHER, S. T. RITTENHOUSE, C. H. GREENE, *Department of Physics and JILA, University of Colorado, Boulder, Colorado 80309-0440* M. J. CAVAGNERO, *Department of Physics and Astronomy, University of Kentucky, Lexington, Kentucky 40506-0055* Trapped ultracold atomic gases with tunable attractive interactions can, in principle, collapse to a deep many-body bound state. Mean-field theories have predicted collapse of Bose-Einstein condensates with negative scattering length $a$ [1], which has been confirmed experimentally [2]. Mean field treatments of degenerate Fermi gases have also predicted collapse [3]. In a recent study, we proposed [4] a hyperspherical coordinate treatment of a two-component degenerate Fermi gas in an isotropic oscillator trap, for which the atoms interact through a zero-range pseudopotential. Ref. [4] predicts a ($T = 0$) collapse at $k_f a = -1.21$. Using Monte Carlo methods, we study variationally the collapse for different two body finite range interactions. We introduce Jastrow-type correlations in the many-body wave function, which allows us to test the validity of the mean-field approach and the zero-range interaction. [1] E. V. Shuryak, Phys. Rev. A 54, 3151 (1996). [2] E. A. Donley et al, Nature 412, 295-299 (2001). [3] M. Houbiers et al, Phys. Rev. A 56, 4864 (1997). [4] S. T. Rittenhouse et al, arXiv:cond-mat/0510454.

*This work was supported in part by NSF.

**16:42**

**K43 12 Viscous relaxation and transport in a 2d Fermi liquid*** DMITRY NOVIKOV, *Princeton University* Long-wavelength transport and relaxation properties of interacting systems are naturally described in terms of hydrodynamic modes. Here we focus on the viscosity of the two-dimensional (2d) interacting fermions. It is well-known that the viscosity of a clean Fermi liquid in three dimensions is proportional to the quasiparticle lifetime, scaling as $E_F/T^2$. We find that for the 2d fermions, the viscosity is logarithmically enhanced by the factor of $\ln(E_F/T)$, that arises from the phase-space restrictions for quasiparticle scattering in two dimensions. In particular, these restrictions enforce the dominant contributions of the collisions between quasiparticles from opposite sides of the Fermi surface, the effect specific to the 2d geometry. We discuss the effects of viscous modes that can manifest themselves in the electron transport in the metallic phase, and in the momentum relaxation of cold fermion gases.

*This work was supported by NSF MRSEC grant DMR 02-13706.

**SESSION K44: TRANSPORT IN DISORDERED ELECTRONIC SYSTEMS**
**Tuesday Afternoon, 14 March 2006**
**347, Baltimore Convention Center at 14:30**
**A. Punnose, University of Wisconsin, presiding**

**14:30**
**K44 1 Metals and insulators at infinite temperature** DAVID HUSE, *Princeton University* VADIM OGANESYAN, *Yale University* Numerical exact diagonalization results for spectral correlations and finite temperature transport of strongly disordered and interacting lattice fermions are presented. We study the finite temperature metal-insulator transition recently proposed by Basko and collaborators (condmat/0506617) focussing in particular on establishing the existence of the insulating phase.

**14:42**
**K44 2 Magnetism near the percolation transition in two-dimensional electron systems** KEIVAN ESFARJANI, MAHDI FAZELI, *Department of Physics, Sharif University of Technology, Tehran, IRAN* BILAL TANATAR, *Department of Physics, Bilkent University, Ankara, Turkey* Recent thermodynamic measurements on two-dimensional (2D) electron systems have found divergence in the magnetic susceptibility and appearance of ferromagnetism as the electron density is lowered. The critical density for these phenomena coincides with the metal-insulator transition (MIT) recorded in transport measurements. Based on density functional calculations within the local spin-density approximation, we have investigated the compressibility and magnetic susceptibility of a 2D electron gas in the presence of remote impurities. A correlation between the minimum in the inverse capacitance, which is identified with the percolation transition, and the maximum of magnetization and magnetic susceptibility was found. This is also coincident with the MIT point based on values we obtain for the inverse participation ratio.

**14:54**
**K44 3 Melting of the electron Wigner Crystal: Theory of the metal-insulator transition in two dimensions (2DMIT)** JOHN JANIK, SERGEY PANKOV, VLADIMIR DOBROSAVLJEVIC, *NHFML/FSU National High Magnetic Field Laboratory and Department of Physics, Florida State University, Tallahassee, FL 32310* Past theoretical work in explaining the 2D metal-to-insulator transition at $T = 0$ has focused on perturbative approaches around the Fermi Liquid state, and has met with limited success [1]. Starting from the opposite limit we propose a charge transfer model with vacancy-interstitial pair formation as the mechanism for the phase transition. A new picture of the phase diagram has emerged [2], which our theory explains. At low carrier density we find an insulating phase with short-range order, at high density a metallic phase with no order, and a persistent intermediate density metallic phase with short range order. Our theory also explains the experimentally observed strong effective mass enhancements, as the metal-insulator transition is approached from the metallic side. 1. Abrahams, E., Kravchenko, S. V., and Sarachik, M. P., Rev. Mod. Phys. 73, 251-266 (2001). 2. Falakshahi, H. & Waintal, X., Phys. Rev. Lett. 94, 046801 (2005).

**15:06**
**K44 4 Transport of GaAs two-dimensional holes in strong Coulomb interaction regime** JIAN HUANG, D.C. TSUI, *Princeton University* L.N. PFEIFFER, K.W. WEST, *Bell Labs, Lucent Technologies* We report experimental findings on the 2D holes in a GaAs/AlGaAs heterojunction insulated-gate field-effect transistor in the strong interaction regime ($E_{ee} > > E_F, kT$) with the carrier densities (p) varying from $7 \times 10^9\ cm^{-2}$ to $7 \times 10^8\ cm^{-2}$. Though the temperature dependence of the resistivity ($\rho$) resembles that observed in typical 2D Metal-to-Insulator Transition (MIT), there are two things strikingly different. First, for each density, a kink/dip appears in the $T$-dependence of the conductivity ($\sigma$) around a characteristic temperature which we call $T_c$. In the $T_c$-$p$ relation, there is a sudden change at a characteristic density which is the same as the critical density $p_c$ where the apparent MIT is observed. The linear $T_c$-$p$ at high densities suggests that $T_c$s for $p > p_c$ correspond to the Fermi temperature $T_F$s. However, $T_c$ shows little $p$- dependence at $p < p_c$ ($p_c = 4 \times 10^9\ cm^{-2}$). Second, $T_c$ divides the $\sigma$-$T$ into a linear part for $T > T_c$ and a power-law part for $T < T_c$. The $\sigma$ is finite at the base temperature of 35mK even for the lowest density $7 \times 10^8\ cm^{-2}$. These results rule out the possibility of hopping transport, or the insulator of a pinned Wigner crystal.

**15:18**
**K44 5 Metal-insulator transition in 2D: comparison between experiment and Punnoose-Finkelstein's theory*** S. ANISSIMOVA, A. A. SHASHKIN, S. V. KRAVCHENKO, *Northeastern University* T. M. KLAPWIJK, *TU Delft* New theory of the 2D metal-insulator transition (Punnoose and Finkelstein, Science 310, 289 (2005)) explains all most striking features of this phenomenon — temperature- independent separatrix between metallic and insulating phases, destruction of the metallic state by magnetic field, critical behavior of the spin susceptibility and dramatic enhancement of the effective mass in the vicinity of the transition. We will report detailed comparison between our experiments and this theory.

*Supported by NSF and PRF

**15:30**
**K44 6 Hall coefficient and magnetoresistance of 2D spin-polarized eletron system*** EUYHEON HWANG, *University of Maryland* SANKAR DAS SARMA, *University of Maryland* Recent measurements of the Hall resistance show that the Hall coefficient is independent on the applied in-plane magnetic field which gives rise to the spin-polarization of the system. We calculate the weak-field Hall coefficient and the magnetoresistance of a spin polarized system based on the screening theory. We solve the coupled kinetic equations of the two carrier system including electron-electron interaction. We find that the in-plane magnetic field dependence of the Hall coefficient can be suppressed by the weakening of the screening and the electron-electron interaction. However, the in-plane magnetoresistance is barely affected by the electron-electron interaction.

*Supported by US-ONR, LPS-NSA, and NSF.

**15:42**

**K44 7 Unified scaling picture for electronic transport in two-dimensions at low temperatures*** DAVID NEILSON, *University of Camerino* D.J. WALLACE GELDART, *Dalhousie University* We focus on generic features of the phase diagram for the 2D metal-insulator transition phenomenon. The diagram has a line of critical points corresponding to a conducting region (but not necessarily Fermi-liquid-like). The line terminates at a critical end point which controls an extended quantum critical region encompassing not only the conventional quantum critical sector but also a wide range of low temperature data extending deep into the insulator region. This permits us to unify analysis of transport data from the insulating region and the quantum critical sector, and allows us to determine the $z$ and $\nu$ critical exponents from a single experiment. We present strong evidence for the connection between data in the quantum critical sector and insulating critical region, pointing to the presence of a quantum critical point.

*Supported by grants from PRIN Italy, Australian ARC, and NSERC Canada

**15:54**

**K44 8 Temperature-Dependent Weak Field Hall Resistance in 2D Carrier Systems** THEODORE CASTNER,* *University of Rochester* Das Sarma and Huang [1] have attempted to explain the T- dependent Hall coefficient $R_H(T)$ of Gao et al. [2] for the 2D GaAs hole system solely with the T-dependent Hall factor $r_H(T) = <\tau^2>/<\tau>^2$. They employed $R_H = r_H(T)/en$ with n the total hole density which is independent of T. However $r_H = 1$ at T=0 and $r_H > 1$ at finite T. Thus $r_H(T)$ cannot explain the observed decrease of $R_H(T)$ with increasing T. Employing the known relation $R_H(T) = r_H/ep_i(T)$, where $p_i(T)$ is the itinerant hole density, one can explain the decrease in $R_H$ with increasing T with $p_i(T)$ increasing faster than $r_H(T)$. Using the mobility data $[\mu(T) \alpha <\tau>]$ one can determine $r_H(T)$, which differs from the calculated curves in [1] in that it is asymmetrical about $r_{H,max}$. Using the Hall data and $r_H(T)$ inferred from the data one can obtain the increase in $p_i(T)$ with T and compare it with calculations of $p_i(T)$ done with Fermi Liquid theory taking account of the soft Coulomb gap in the density-of-states. This approach gives good agreement, but doesn't take account of inhomogeneity. Other features of the Gao et al. data will be discussed. 1. S. Das Sarma and E.H. Huang, Phys. Rev. Lett. 95, 0164011 (2005) 2. X.P.A. Gao et al., Phys. Rev. Lett. 93, 256402 (2004).

*Note address and e-mail change

**16:06**

**K44 9 The transmission of a quantum particle through 2D disordered clusters.** MD ISLAM, HISAO NAKANISHI, *Purdue University* We study quantum percolation model in two dimensions by directly calculating the conductance of finite disordered clusters. In extrapolating to the limit of very large clusters we find evidence that states are localized for any amount of disorder except at the limit of zero disorder where resonance transmission may occur. The nature of localization, however, depends on the amount of disorder present in the clusters. When disorder exceeds certain critical value, transmission decreases exponentially with the size of the clusters whereas below that value it is consistent with power laws. We also investigate how the energy affects the transmission in 2D disordered systems.

**16:18**

**K44 10 Mean-field description of Anderson localization transition** JINDRICH KOLORENC, *Center for High Performance Simulation and Department of Physics, North Carolina State University, Raleigh, NC 27695-8202* VACLAV JANIS, *Institute of Physics, Academy of Sciences of the Czech Republic, Na Slovance 2, CZ-18221 Praha 8, Czech Republic* The Anderson model of noninteracting disordered electrons is studied in high spatial dimensions. In this limit the coupled Bethe-Salpeter equations determining two-particle vertices (parquet equations) reduce to a single algebraic equation for a local vertex. We find a disorder-driven bifurcation point in this equation signaling vanishing of electron diffusion and onset of Anderson localization. There is no bifurcation in $d = 1,2$ where all states are localized. In dimensions $d \geqslant 3$ the mobility edge separating metallic and insulating phase is found for various types of disorder and compared with results of other treatments.

**16:30**

**K44 11 Anomalously Localized States at the Anderson Transition** HIDEAKI OBUSE, *Condensed Matter Theory Laboratory, RIKEN, Wako, Saitama 351-0198, Japan* KOUSUKE YAKUBO, *Department of Applied Physics, Graduate School of Engineering, Hokkaido University, Sapporo 060-8628, Japan* Anomalously localized states (ALS) at the critical point of the disorder induced metal-insulator transition, namely, the Anderson transition, are investigated. ALS are states in which most of amplitudes of a wave function concentrate on a narrow spatial region even in a metallic phase. While the existence of ALS in the metallic phase was analytically predicted and confirmed by numerical and experimental works, ALS at the critical point are far from understood due to lack of proper analytical methods describing critical phenomena of this phase transition. In this work, it is numerically shown that ALS exist at the critical point of the Anderson transition in both the three-dimensional orthogonal class and the two-dimensional symplectic class by quantifying non-multifractality of critical wave functions due to a characteristic length originating in their concentration nature of ALS. These results may suggest that the existence of non-multifractal states at criticality is generic in many disordered systems.

**16:42**

**K44 12 New Glassy Phases of Electrons in Disordered Potentials** ROGER HAYDOCK,* *University of Oregon* NIGEL GOLDENFELD, *University of Illinois at Urbana-Champaign* Critical disorders are found analytically for the Anderson model of independent electrons in two and three-dimensional random potentials. At large disorders the states are exponentially localized, then with decreasing disorder the model goes through a sequence of less strongly localized phases ending with power-law localization just above the transition to extended states. These results follow from an analytic transformation of the Anderson model into augmented space where disorder is removed from matrix-elements by constructing a basis of extended states correlated with the potential. For different disorders, the states are dominated asymptotically by different sectors of augmented space, and these sectors are identified by path-counting.

*Work supported by the Richmond F. Snyder Fund

**16:54**
**K44 13 Noise in an Electron Glass, Amorphous Indium Oxide** STEPHEN ARNASON, *University of Massachusetts Boston* Amorphous Indium Oxide is a material that manifests a rich spectrum of physical phenomena. It undergoes both the disorder driven and the magnetic field driven superconductor to insulator transitions. In addition, in highly disordered samples, it shows electron glass behavior, where correlations amongst the electrons leads to memory and aging effects. It is hypothesized that this glassy behavior is the consequence of a hierarchy of multielectron relaxation processes. To study this hierarchical relaxation we are measuring conductance fluctuations in samples in the glassy regime, where the spectrum of fluctuations is related to the relaxation processes, leading to a 1/f type of spectral dependence.

**17:06**
**K44 14 Proposal for a pre-exponential dependent Efros-Shklovskii regime** MIGUEL RODRIGUEZ, ISMARDO BONALDE, ERNESTO MEDINA, *Centro de Fisica, IVIC, Caracas, Venezuela* We address the variable range hopping regime in the range for which the measured temperatures are of the order of the characteristic Mott or Efros-Shklovskii temperatures $T_M$ and $T_{ES}$ respectively. In such a range present theories imply $R_{hop}/\xi < 1$ where $R_{hop}$ is the hopping length and $\xi$ is the localization length. Using the Mott optimization procedure, including prefactor corrections in the wavefunction overlap, we obtain expressions for the dependence on temperature for the typical hopping length and the resistivity in an Anderson insulator with coulombic interactions. Such expressions lead to a regular Efros-Shklovskii law when $T << T_{ES}$ while for $T \sim T_{ES}$ they can lead to a meaningful pre-exponential dominated regime such that $R_{hop}/\xi > 1$. We propose that the optimization procedure can consistently explain contradictory results in the critical regime and recent experimental results showing a maximum in resistivity due to a interplay between prefactor and exponential terms.

**17:18**
**K44 15 Universal and Non-universal Behavior at the Metal Insulator Transition.*** ERIK HELGREN, LI ZENG, DAMIEN QUERLIOZ, FRANCES HELLMAN, DEPT. OF PHYSICS, UC BERKELEY TEAM, A metal-insulator transition in amorphous metal semiconductor alloys is known to exist at dopant concentrations much higher ( $\sim$ 12 at. %) than their crystalline counterparts [1]. We have studied the MIT in alloys grown using MBE for a series of semiconductor matrices, Si, Ge and both C and H-C (hydrogenated carbon) for various dopants (magnetic Gd and non-magnetic Y and Nb), as a function of concentration and magnetic field tuning. We compare the temperature dependence of the DC conductivity in the magnetically doped systems to the non-magnetic systems and to crystalline doped semiconductors (i.e. Si:P). Results are discussed in terms of a theoretical model that incorporates both disorder and electronic correlations [2]. This model correctly describes many universally observed aspects including the remarkably similar temperature dependence of the metallic and insulating DC conductivity of crystalline and amorphous systems, despite the vastly different disorder and electron concentration. There are however very significant variations in the prefactors that control the magnitude of the conductivity, which we correlate with the microscopic physics of each system. [1] F. Hellman et al. PRL 77, 4652 [2] Lee and Ramakrishnan RMP 57, 287.

*We thank the NSF for funding this research.

**SESSION K45: HEAVY FERMIONS: EXPERIMENT**
**Tuesday Afternoon, 14 March 2006**
**348, Baltimore Convention Center at 14:30**
**M. Aronson, University of Michigan, presiding**

***Contributed Papers***

**14:30**
**K45 1 Thermal and Magnetic Properties of Ferromagnetic $YbPt_2$*** MOO SUNG KIM, *University of Michigan* MARCUS BENNETT, *University of Michigan* MEIGAN ARONSON, *University of Michigan* JASMINE MILLICAN, *Louisiana State University* JULIA CHAN, *Louisiana State University* We present the results of magnetization and heat capacity measurements carried out on needle-like single crystals of $YbPt_2$. Above 250 K, the magnetic susceptibility is well described by a Curie-Weiss expression with a moment of 3.35 $\mu_B$ per Yb and a Weiss temperature of 73 K, indicating ferromagnetic interactions among almost localized moments. At the lowest temperatures, the magnetization is increasingly nonlinear in field, approaching a saturation value of 3.5 $\mu_B$/Yb at 1.8 K. However, an Arrott plot analysis indicates that ferromagnetic order occurs at a much lower temperature, approximately 0.85 K. Above $\sim$ 10 K,we find that the heat capacity $C = \gamma T + \beta T^3$, with $\gamma = 0.358$ J/mol-K$^2$, while between 10 K and 3 K, C/T drops by a factor of four, perhaps due to the opening of a gap at the Fermi surface. A large anomaly is found in the heat capacity at 0.83 K, suggesting that the transition to the ferromagnetic state is weakly first order. Our results imply that $YbPt_2$ is a rare example of a heavy fermion ferromagnet.

*Work at the University of Michigan supported by the National Science Foundation.

**14:42**
**K45 2 Magnetic Field Suppression of Ferromagnetism in $Yb_2Pt_3$** MARCUS BENNETT, *University of Michigan* DMITRY SOKOLOV, *University of Michigan* WILLIAM GANNON, *University of Michigan* MEIGAN ARONSON, *University of Michigan* CARL HENDERSON, *University of Michigan* JASMINE MILLICAN, *Louisiana State University* JULIA CHAN, *Louisiana State University* We have measured the heat capacity, resistivity and magnetization of single crystals of $Yb_2Pt_3$ grown from Pb flux. The magnetization is anisotropic and strongly non linear with field, with an Arrott plot analysis indicating ferromagnetic order. The zero field AC susceptibility is peaked at 2.4 K, where the zero field heat capacity shows a first order paramagnetic to ferromagnetic transition. This transition is suppressed by magnetic field, disappearing at a critical point, 1.75 T and 1.3 K. The zero field resistivity shows a metallic temperature dependence, and for all fields we find $\rho(T,H) = \rho_0(H) + A(H)T^2$ at sufficiently low temperature. The coefficient, A(H), has a strong maximum for H=1.75 T. It is remarkable that the application of a magnetic field decreases $T_C$ in $Yb_2Pt_3$, contradicting conventional expectations.

**14:54**
**K45 3 Complete Elastic Constants of the Heavy Fermion YbAgGe*** I. MIHUT, J. BETTS, S. HARRINGTON, A. MIGLIORI, *National High Magnetic Field Laboratory, LANL, Los Alamos, NM, 87545* S. L. BUD'KO, P. C. CANFIELD, *Ames Laboratory, Iowa State University, Iowa 50011, USA* We measured the elastic constants of the heavy fermion YbAgGe using resonant ultrasound spectroscopy at temperatures from 300K to

0.5K and magnetic fields to 7T. As a function of magnetic field and below 7K, the elastic constants show strong non-monotonic behavior, suggesting a field-induced quantum critical point. Only at the lowest magnetic fields is there a strong temperature dependence.

*The work at NHMFL was carried under the auspices of the National Science Foundation, the state of Florida, and the U.S. Department of Energy.

**15:06**

**K45 4 Studies of the Non-Fermi Liquid Kondo System $Lu_{1-x}Yb_xRh_2Si_2$.*** SAMUEL MAQUILON, LONG PHAM, HAN-OH LEE, PETER KLAVINS, ZACH FISK, *UC Davis* Single Crystalline Platelets of the $YbRh_2Si_2$ system show strong magnetic anisotropy. Specific Heat, Magnetic Susceptibility and Electrical Resistivity data are presented for the alloy system $Lu_{1-x}Yb_xRh_2Si_2$across the entire composition range. The data suggests that the effective Kondo scale for $YbRh_2Si_2$is smaller than that for the dilute alloys of $Yb$ in $LuRh_2Si_2$. This work was supported by NSF DMR-0433560.

*NSF DMR-0433560

**15:18**

**K45 5 Quantum critical behaviour of heavy Fermion CeNi2Ge2*** BILAL ZOGHBI, *Kent State University* ALMUT SCHROEDER, *Kent State University* COLLIN BROHOLMS, *Johns Hopkins University* Neutron scattering data of CeNi2Ge2 collected at SPINS at NIST will be presented to characterize the magnetic correlations and dynamics close to an antiferromagnetic quantum critical point (AF QCP). The dynamical susceptibility $\chi''$(q,E) has been measured in a temperature range 0.1K$<$ T $<$ 30K. While the q-independent fluctuations remain unchanged for T$<$ 30K, the enhanced susceptibility $\Delta\chi''$ close to the wavevector q=(0.5,0.5,0), shows a relaxation rate following the absolute temperature kBT down to 5K but then remains finite towards the lowest T = 0.1 K. The Lorentzian linewidth is reduced to about 0.4 meV, a factor of ten smaller than the rate observed in the q- independent spectrum. The energy, q, and T dependence of $\Delta\chi''$ shows characteristics of the fluctuations expected close to an AF QCP in 3 dimensions, stating that CeNi2Ge2 lies beside the AF QCP.

*Work in collaboration with Y. Qiu, D.F. McMorrow, N. Christensen, J. Mydosh, O. Tegus, G. Aeppli, M. Adams. Work supported by NSF DMR 0306766

**15:30**

**K45 6 Time-resolved optical spectroscopy of the itinerant antiferromagnets $UMGa_5$ (M=Ni, Pt)** EE MIN ELBERT CHIA, HAE JA LEE, *MST-CINT, Los Alamos National Laboratory* ERIC BAUER, NAMJUNG HUR, *MST-10, Los Alamos National Laboratory* RICHARD AVERITT, ANTOINETTE TAYLOR, *MST-CINT, Los Alamos National Laboratory* JOHN SARRAO, *MST-10, Los Alamos National Laboratory* We present time-resolved optical conductivity measurements of the itinerant antiferromagnets $UNiGa_5$ ($T_N$=85K) and $UPtGa_5$ ($T_N$=25K), as well as the parent material $UGa_3$, using a pump-probe technique. The relaxation time $\tau$ diverges near $T_N$, which we attribute to the opening of a spin gap. $\tau$ also diverges at the lowest temperatures, which is similar to that shown by the heavy fermion $YbAgCu_4$, but with no blocking of electron-phonon scattering within the DOS peak. The transient amplitude exhibits a sign change at $T_N$, whose temperature dependence is also consistent with the appearance of a spin gap. We will also attempt to analyze our data using the Rothwarf-Taylor model.

**15:42**

**K45 7 Ferromagnetism and Crystalline Electric Field Effects in Cubic $UX_2Zn_{20}$ (X=Co, Rh, Ir)** E.D. BAUER, *LANL* F. RONNING, A. SILHANEK, N. HARRISON, J.D. THOMPSON, J.L. SARRAO, R. MOVSHOVICH, M.F. HUNDLEY, M. JAIME, *LANL* E. DANIEL, *Cidade Universitaria* C.H. BOOTH, *LBNL* The properties of a new class of cubic $UX_2Zn_{20}$ (X=Co, Rh, Ir) heavy fermion compounds have been investigated by means of magnetic susceptibility, specific heat, electrical resistivity, and x-ray absorption spectroscopy. Both $UCo_2Zn_{20}$ and $URh_2Zn_{20}$ show peaks in $C(T)$ and $\chi(T)$ at $\sim$ 5-10 K suggesting the presence of crystalline electric field (CEF) effects in these materials, i.e., a localized $5f^2$ configuration of uranium. In addition, measurements in high magnetic fields up to 40 T are consistent with a CEF model of a nonmagnetic ground state and a magnetic first excited state separated by $\sim$ 20 K. In contrast, $UIr_2Zn_{20}$ exhibits a first-order ferromagnetic transition at $T_c$=2.75 K with a saturation moment $\mu_{sat}$=0.5 $\mu_B$ in the ferromagnetic state. All compounds in this series are heavy fermion materials with enhanced electronic specific heat coefficients $\gamma \sim$ 150-300 mJ/molK$^2$. The physical properties of $UX_2Zn_{20}$ (X=Co, Rh, Ir) will be discussed.

**15:54**

**K45 8 NMR Probes Two Kinds of HO Effects in $URu_2Si_2$ Single Crystals*** O.O. BERNAL, J. SEUNGHUN, *California State University, Los Angeles* A.P. REYES, P.L. KUHNS, *National High Magnetic Field Lab, Tallahassee* D.E. MacLAUGHLIN, *University of California, Riverside* J.A. MYDOSH, *Institute of Physics II, University of Cologne, Germany* T.J. GORTENMULDER, *Kamerlingh Onnes Lab, Leiden University, The Netherlands* We performed $^{29}$Si NMR experiments in two single crystals of $URu_2Si_2$ for $4 < T <$ 50 K and $9 < H <$ 15 T. Crystal # 1 (50 mg) had an irregular trapezoidal shape with base dimensions of $\sim$ 6 (major) and $\sim$ 4 (minor) mm, height $\sim$ 4 mm, and 1 mm thickness. Crystal # 2 (10 mg) was rectangular: 2 mm by 3 mm, with a 0.5 mm thickness. We will describe NMR spectra from $T$ sweeps at orientation angles of 90° (Crystal # 1) and 70° (Crystal # 2) between the corresponding crystal's $c$-axis and $H$. Our results for Crystal #1 indicate a homogeneous, field- independent internal field, increasing from zero just below $T_0$ = 17.5 K@ and reaching a value of order 5 G at the lowest temperatures. Crystal #2 displayed a different kind of hidden order effect. In this case, the NMR intensity dropped continuously with decreasing $T$, becoming a minimum at $T_0$. We will describe the NMR conditions used to acquire the signal in the two cases, and discuss possible ways to understand the results.

*Supported by NSF/DMR-0203524 (CSULA) and 0084173 (NHMFL); the State of Florida, and DOE (NHMFL)

**16:06**

**K45 9 Ordered states of $URu_2Si_2$ under hydrostatic pressure** J. R. JEFFRIES, N. P. BUTCH, J. PAGLIONE, M. B. MAPLE, *Department of Physics and Institute for Pure and Applied Physical Sciences, University of California, San Diego* Oriented single crystalline samples of $URu_2Si_2$ have been synthesized and investigated under nearly hydrostatic pressure via electrical resistivity and ac susceptibility measurements. The heavy fermion compound $URu_2Si_2$ exhibits three distinct ordered states as a function of temperature and pressure: ''hidden order'' (HO), in which the order parameter has yet to be determined; antiferromagnetism (AFM), which seemingly develops out of the HO state at $P \leqslant 15$ kbar; and superconductivity (SC), which exists at ambient pressure. Careful measurements of the HO transition, occurring at $T_{HO} \sim 16.5$ K at ambient pressure, have been performed at several different pressures, yielding a *P-T* phase diagram for the HO state as a function of pressure. In addition, measurements of the superconducting critical temperature, $T_c \sim 1.4$ K at ambient pressure, and the upper critical field $H_{c2}$ have been performed at low temperatures using a $^3$He-$^4$He dilution refrigerator, revealing the superconducting *H-T-P* phase diagram. Possible correlations between the HO, AFM, and SC states will be discussed. This research was supported by the National Nuclear Security Administration under the Stewardship Science Academic Alliances program through DOE Research Grant No. DE-FG52-03NA00068.

**16:18**

**K45 10 Hall Effect Evolution Across a Field-Induced Quantum Critical Point in $U(Ru_{0.96}Rh_{0.04})_2Si_2$** YOON SEOK OH, KEE HOON KIM, *School of Physics and CSCMR, Seoul National University* N. HARRISON, P. A. SHARMA, *NHMFL-LANL* H. AMITSUKA, *Hokkaido University* J. A. MYDOSH, *Leiden University* The heavy fermion compound $U(Ru_{0.96}Rh_{0.04})_2Si_2$ has been recently identified as a unique system in which a magnetic field-induced quantum critical point (QCP) is avoided by the creation of a single magnetic phase [1]. To further understand the nature of phase formation across the putative QCP, we have measured the Hall effect of $U(Ru_{0.96}Rh_{0.04})_2Si_2$ between 0.6 and 30K using a 50T mid-pulse magnet. We find that the Hall coefficient $R_H$ abruptly increases inside the new phase formed between 28 and 38T, around $B_{QCP} \sim$ 34T, evidencing formation of a gap in the Fermi surface. Furthermore, low temperature $R_H$ at $B >$ 38T is much smaller than that at $B <$ 28T, indicating the different Fermi surface area in each Fermi liquid states. While the field-induced phase disappeared above 9.5K, $R_H$ still exhibits a broad maximum near $B_{QCP}$, signaling a finite temperature crossover of the Fermi surface change. All of above findings are consistent with an electronic structure evolution from a heavy fermion to spin-polarized Fermi liquids across $B_{QCP}$. [1] K. H. Kim *etal.*, Phys. Rev. Lett. **93**, 206402 (2004).

**16:30**

**K45 11 Irreversible dynamics of the phase boundary in $U(Ru_{1-x}Rh_x)_2Si_2$** VICTOR FANELLI, *Dep. of Phys. and Astron., University of California, Irvine, CA and MST-NHMFL, LANL, Los Alamos, NM* A.V. SILHANEK, M. JAIME, N. HARRISON, *MST-NHMFL, LANL, Los Alamos, NM* C.D. BATISTA, *T11, LANL, Los Alamos, NM* H. AMITSUKA, *Grad. School of Science, Hokkaido University, Japan* L. BALICAS, *NHMFL-FSU, Tallahassee, FL* J.L. SARRAO, *MST, LANL, Los Alamos, NM* J.A. MYDOSH, *II Physikalisches Institut, Universitat zu Koln, Germany* Specific heat and magneto-caloric effect measuments on the systems: $U(Ru_{1-x}Rh_x)_2Si_2$ and $Yb_{1-x}Y_xIn\ Cu_4$ were carried out at high magnetic fields. Thermodynamic similarities are found at the phase boundary into the magnetic field-induced phase (phase II) of the former and at the valence transition of the latter. We show that the irreversible properties of the transition into the phase II of $U(Ru_{1-x}Rh_x)_2Si_2$ are very similar to that associated with the valence transition of $Yb_{1-x}Y_xIn\ Cu_4$. To explain these results, we propose a bootstrap mechanism by which lattice degrees of freedom within phase II become coupled to the 5f-electron hybridization, giving raise to a valence change at the transition.

**16:42**

**K45 12 Neutron scattering studies of itinerancy and ''hidden order'' in $URu_2Si_2$** C.R. WIEBE, J.A. JANIK, *Florida State University/NHMFL* G.J. MACDOUGALL, G.M. LUKE, J.D. GARRETT, *McMaster University* Y. QIU, J.R.D. COPLEY, *CHRNS, NIST* C. BROHOLM, *Johns Hopkins University* W.J.L. BUYERS, *CNBC,Chalk River* The heavy fermion superconductor $URu_2Si_2$ has been of interest for the last two decades but the nature of the ''hidden order'' in the phase below $T_0 = 17.5$ K has not been identified. The large specific heat jump at this temperature cannot be accounted for by the weak ordered moment which is only a fraction of a Bohr magneton on the uranium site (0.03 $\mu_B$). In recent neutron scattering experiments we set new limits for the maximum size of an ordered moment which could be observed in the ''hidden order'' phase, and we investigated the possibility of orbital currents. Furthermore, our experiments have unveiled a new feature in the inelastic spectrum – the precursor phase above 17.5 K exhibits incommensurate fluctuations that are highly correlated in Q and extend to high energies. This suggests that (1) the spins are itinerant, rather than localized and (2) these excitations must play a role in the heat capacity anomaly at the phase transition, as they become gapped at incommensurate wavevectors below $T_0$ and cover a large region of phase space. Implications of these new measurements will be discussed.

**16:54**

**K45 13 Region of Quantum Critical Behavior in $Ce(Ru_{1-x}Rh_x)_2Si_2$*** G.R. STEWART, J.S. KIM, D.J. MIXSON, D. BURNETTE, *Dept. of Physics, Univ. of Florida* The magnetic phase diagram of $Ce(Ru_{1-x}Rh_x)_2Si_2$ is quite rich, with a spin density ordering temperature approaching T=0 around $x_{QCP} = 0.4$ and with - from the Rh rich side where $T_N$ of $CeRh_2Si_2$ is 36 K - a long range, local moment ordering temperature approaching T=0 at approximately $x_{QCP} = 0.6$. Specific heat data down to 0.04 K for a number of compositions indicate a itregion of non-Fermi liquid behavior between x=0.4 and 0.6 associated with the two quantum critical points. The nature of the nFl temperature dependence in the specific heat changes from Moriya-like weak spin fluctuation behavior at the Ru rich side to strong fluctuation, $C/T \propto \log T$ behavior at the Rh rich end. How this smooth progres-

sion of behavior with increasing x provides insights into our understanding of non-Fermi liquid behavior in general will be discussed. The disagreement in the literature over whether C/T is Moriya-like or follows logT at x=0.5 is resolved in favor of the former temperature dependence.

*Work at Florida supported by the US DOE, contract no. DE-FG05-86ER45268.

**17:06**

**K45 14 Magnetic ordering and valence instability in Kondo system $CeMn_{2-x}Cu_xSi_2$** GAN LIANG, SHELLEY KEITH, JESSE VERNON, *Sam Houston State University* F. YEN, *University of Houston* The transition from a 3d-antiferromagnetically ordered mixed valence system to a Kondo lattice system has been studied for the $CeMn_{2-x}Cu_xSi_2(0 \leqslant x \leqslant 1)$ series. The Ce $L_3$-edge x-ray absorption result shows that the series evolves from a Ce mixed valence system at $x = 0$ to a nearly trivalent system at $x = 2$. The resistivity results show that in the low Ce valence region ($x$ greater than 1.0), the system exhibits a crystalline-field modified Kondo lattice behavior. In the high valence region, however, the system displays a behavior of the prototype mixed valence compound $CePd_3$. Magnetization (M) data were taken in both zero-field-cooled (ZFC) and field cooled (FC) processes. It is found that for $0 \leqslant x < 0.4$, Neel temperature decreases rapidly with the increase of the Cu concentration $x$. In the range of $x$ from $0.4 \leqslant x < 0.8$, ferromagnetic phase is observed below 150 K, and both the ordering temperature $T_c$ and Qurie-Weiss temperature $\theta$ decrease with the increase of $x$. For $x \geqslant 0.8$, the $M$ (T) curves are reversible and display paramagnetic behavior. Thus, the system is non-magnetic as it approaches heavy-fermion compound $CeCu_2Si_2$. Finally, a magnetic phase diagram is proposed for this compound series.

**17:18**

**K45 15 Deviations from Drude response in $CaRuO_3$** SAEID KAMAL, STEVE DODGE, *Department of Physics, Simon Fraser University, B.C., V5A-1S6, Canada* DONG-MIN KIM, CHANG-BEOM EOM, *Department of Materials Science and Engineering, University of Wisconsin-Madison, Madison, Wisconsin 53706* We report on the low frequency optical conductivity measurements of epitaxial thin films of $CaRuO_3$, obtained with time-domain terahertz spectroscopy. We find that the conductivity does not follow a simple Drude form, even at low temperatures and frequencies; alternative power-law forms also fail to describe it adequately. To achieve a good fit to the experimental data, we find it necessary to use a multi-component model consisting of multiple *Drude* terms and a finite frequency Lorentzian. This parameterization allows us to set an upper bound on the free-carrier spectral weight, from which we can set a lower bound on the renormalized mass of $m^*/m \cong 10$. If the scattering is assumed to be isotropic, our results imply a frequency dependence in the mass enhancement and scattering rate that extends well below terahertz frequencies. However, our results are also consistent with frequency-independent carrier dynamics that vary strongly over the Fermi surface.



## SESSION K46: SPECTROSCOPY OF SEMICONDUCTORS

**Tuesday Afternoon, 14 March 2006**
**349, Baltimore Convention Center at 14:30**
**Giti Khodaparast, Virginia Polytechnic Institute and State University, presiding**

**14:30**

**K46 1 Microwave cyclotron resonance of two-dimensional holes in GaAs/AlGaAs quantum wells on (100) substrates** HAN ZHU, K. LAI, D. C. TSUI, N. P. ONG, *Princeton University* M. MANFRA, L. PFEIFFER, K. WEST, *Bell Labs* Cyclotron resonance at microwave frequencies is used to measure the band mass ($m_b$) of two-dimensional holes (2DHs) in the $GaAs/Al_xGa_{1-x}As$ quantum wells grown on (100) GaAs substrates [1]. The measured $m_b$ shows strong dependences on both the 2DH density ($p$) and the well width ($W$). For a fixed $W$, in the density range ($0.4\times 10^{11}$ to $1.1\times 10^{11}cm^{-2}$) studied here, $m_b$ increases with $p$, consistent with previous studies of the 2DHs on the (311)A surface [2]. However, the density dependence is significantly weaker on the (100) surface than that on the (311)A surface for the same well width of 30nm. For a fixed $p = 1.1\times 10^{11}cm^{-2}$, $m_b$ increases from $0.22m_e$ at $W = 10$nm to $0.54\ m_e$ at $W = 20$nm, and stays around $0.51m_e$ for $W$ up to 1000nm. With the transport measurement at 0.3K in the dark, the DC scattering time $\tau_{DC}$ deduced for $p = 1.1\times 10^{11}cm^{-2}$ shows a maximum of 0.6ns at $W = 20$nm. [1] M. J. Manfra *et al.*, Appl. Phys. Lett. 86, 16 (2005). [2] W. Pan *et al.*, Appl. Phys. Lett. 83, 3519 (2003).

**14:42**

**K46 2 Magnetoplasmons and cyclotron resonance in a two-dimensional electron gas** GERARD MARTINEZ, *Grenoble High Magnetic Field Laboratory* C. FAUGERAS, *Thales Group, Paris, France* YU. A. BYCHKOV, *L. D. Landau Institute, Moscow, Russia* A. RIEDEL, R. HEY, K.J. FRIEDLAND, *Paul Drude Institute, Berlin, Germany* Cyclotron resonancen (CR) transitions in quasi two-dimensional electron gas (2DEG) are known to involve magnetoplasmons (MP) dispersion. It has been recently [1] possible to derive in the frame of the MP picture, assuming the Hartree-Fock approximation, the magneto conductivity response of such systems for any value of the filling factor $\nu$ and including non-parabolicity effects. As compared to the one-electron picture, the MP theory predicts specific behavior of the response concerning both the oscillator strength as well as the energy variation of the CR transitions as a function of $\nu$. These predictions are confronted to absolute magneto-transmission results obtained on high mobility 2DEG embedded in GaAs quantum wells. It is shown that the MP theory reproduces quite well the experimental findings for $2n+1 < \nu < 2n+2$ whereas clear discrepancies appear for $2n < \nu < 2n+1$. The possible origin of these discrepancies are discussed. [1] Yu. A. Bychkov and G. Martinez, Phys. Rev. B**72**, 195328 (2005).

**14:54**

**K46 3 Infrared Magneto-Optical Probe of Landau Levels of Graphite in the Extreme Quantum Limit** DIMITRI BASOV, ZHIQIANG LI, WILLIE PADILLA, *UCSD* SASA DORDEVIC, *University of Akron* KENNETH BURCH, *UCSD* YONG-JIE WANG, *National High Magnetic Field Laboratory* UCSD COLLABORATION, UNIVERSITY OF AKRON COLLABORATION, NATIONAL HIGH MAGNETIC FIELD LABORATORY COLLABORATION, We present a systematic investigation of the ab plane magneto- reflectance R($\omega$,H) of highly oriented pyrolytic graphite (HOPG) in magnetic fields up to 18T, with magnetic field parallel to the c axis of the sample. A linear magnetic field dependence of the Landau level energies is observed in contrast to the square root field dependence predicted by Dirac fermion description of the quasiparticles in HOPG. We show that the conventional graphite band model can quantitatively account for the totality of the magneto-optical data. We also find that the resonance linewidth of the lowest inter-Landau-level transition shows an unconventional linear field dependence. These results provide new insights into the magneto- transport of HOPG.

**15:06**

**K46 4 Ultrahigh spatial and spectral resolution photoluminescence experiments on excitons bound to the isoelectronic nitrogen impurities in GaAs.** DENIS KARAISKAJ, ANGELO MASCARENHAS, *Center for Basic Science, National Renewable Energy Laboratory, 1617 Cole Boulevard, Golden, Colorado 80401, USA* Optical spectroscopy with diffraction limited resolution allows the measurement of luminescence from single impurity centers. Selectively studying individual centers makes it possible to unveil their otherwise concealed polarization anisotropy, identify their particular configuration, map their spatial distribution, and demonstrate the presence of diversity of local environments [1]. Experiments on several single nitrogen impurity pairs in GaAs allowed us to gain valuable insight into their orientation, distribution, and local environment. The nanoscale photoluminescence experiments have been combined with ultrahigh spectral resolution studies in order to better understand the optical transitions of excitons bound to nitrogen pairs in GaAs. The high spectral resolution studies have revealed a new excitonic transition originating most likely from excitons bound to two or more nitrogen impurity atoms, unprecedented since the discovery of isoelectronic impurity bound excitons in the sixties [2]. The temperature dependence demonstrates that all involved transitions originate from the same center, while the polarization dependent studies give insight into the orientation of the different nitrogen atoms in the cluster. [1] S. Francoeur, J. F. Klem, and A. Mascarenhas, Phys. Rev. Lett. **93**, 067403 (2004). [2] D. G. Thomas and J. J. Hopfield, Phys. Rev. **150**, 680 (1966).

**15:18**

**K46 5 Nuclear spin-lattice relaxation in n-GaAs close to the metal-insulator transition** W.G. MOULTON, JUN LU, M.J.R. HOCH, P.L. KUHNS, *National High Magnetic Field Laboratory* Dynamic nuclear polarization is of considerable interest in semiconductors particularly in GaAs. Nuclear spin-lattice relaxation interactions are important in the polarization process. The coupling of electron and nuclear spins in n-GaAs close to the metal-insulator (MI) transition changes significantly as the dopant concentration n increases through the MI critical concentration $n_C = 1.2\text{x}10^{16}$ cm$^{-3}$. The changes correspond to the evolution of localized donor states into itinerant states close to the bottom of the conduction band. Measurements of the $^{71}$Ga relaxation rates $^{71}W$ made as a function of magnetic field (1 – 13 T) and temperature (1.5 – 300 K) for n-GaAs samples with n = $5.9\text{x}10^{15}$, $7\text{x}10^{16}$ and $2\text{x}10^{18}$ cm$^{-3}$ show marked changes in the relaxation behavior with n. Korringa-like relaxation is found in the metallic samples for $T < 30$ K and power law dependence at lower n. For $T > 30$ K phonon-induced nuclear quadrupolar relaxation is dominant. Knight shift measurements made on the $2\text{x}10^{18}$cm$^{-3}$ sample using magic-angle spinning, confirm a small value for the hyperfine coupling constant and permit comparison of the Korringa product with predictions. At lower n, local moments play an important role in relaxation producing striking changes in the $H$ dependence of $^{71}W$. A model will be presented.

**15:30**

**K46 6 Low-temperature scanning tunneling spectroscopy of Si(111) 7x7 near the Fermi energy** SHENGYONG QIN, DAEJIN EOM, CHIH-KANG SHIH, *Department of Physics, the University of Texas at Austin, Austin TX 78712* Si(111) 7x7 is probably the most widely studied surface in surface sciences. Scanning tunneling microscopy/spectroscopy (STM/S) have been applied extensively to and have provided very detailed understanding of the atomic and electronic structures of this surface, revealing adatom, dangling bond and backbond states. Most spectroscopic studies however, have focused on the electronic structures far away from the Fermi energy. The metallic nature of this surface, however, makes it interesting to explore the electronic states near Fremi energy. Moreover, theoretical studies of this surface suggested important correlation effects. By using a low temperature STM (about 5K), we reported studies of electronic structures near the Fermi energy. In addition to the real-space distribution of density of states directly revealed by STS, Fourier analysis is used to obtain k-space electronic structures. We confirm that the surface is metallic with appreciable DOS, however with a small gap (about 0.15 eV) below the Fermi energy. Moreover, Fourier space analysis reveals what appears to be a Fermi surface in the extended zone scheme, although further investigation is needed to confirm this observation.

**15:42**

**K46 7 Electrostatic potential screened by a two-dimensional electron system: A real-space observation by scanning tunneling spectroscopy** MASANORI ONO, YOSHIHIRO NISIGATA, TAKAHIRO NISHIO, TOYOAKI EGUCHI, *The Institute for Solid State Physics, The University of Tokyo* YUKIO HASEGAWA, *The Institute for Solid State Physics, The University of Tokyo; PRESTO, Japan Science and Technology Agency* Scanning tunneling spectroscopy at 5K was used to investigate the electrostatic potential profile on the Si(111)-$\sqrt{3}\times\sqrt{3}$ Ag surface at subnanometer spatial resolution. The potential was measured from an energy-level shift of electronic states on the surface. The potential images obtained reveal that the potential drops around the steps and Ag adsorbates, upon which positive charges are presumably accumulated. The profiles of the reduced potentials are explained with the screening of potential due to the charges by two-dimensional electron gas (2DEG) existing on the surface. The Friedel oscillation, which results from the screening and has a period of the half Fermi wavelength of the 2DEG, was also observed in the potential images as well.

**15:54**

**K46 8 Phonon Confinement and Laser Heating Effects on Germanium Nanowires.** ROMANEH JALILIAN, *University of Louisville, Department of Physics* HARI CHANDRASEKHAR, MAHENDRA SUNKARA, *University of Louisville, Department of Chemical Engineering* GAMINI SUMANASEKERA, *University of Louisville, Department of Physics* We explore the combined effects of phonon confinement, local heating and stress on the Raman spectra of Germanium nanowires with varying diameters. Germanium nanowires were synthesized using spontaneous nucleation and basal growth from gallium droplets. The asymmetric broadening and downshifting of the first order Raman band is studied as a function of average diameter, local temperature of the nanowires. This basic phenomenological model with a modified confinement function incorporated with thermal effects and stress are in agreement with our experimental results. Fano-resonance effect was excluded from this study.

**16:06**

**K46 9 Optical and Electronic Properties of Ge-Sb-Te films*** HENG LI, *University of Utah* P. C. TAYLOR, *Colorado School of Mines* Amorphous and crystalline films in the system Ge-Sb-Te are of interest because of their use in reversible phase change optical storage media or electrical switches. These applications utilize differences in optical or electrical properties between the crystalline and amorphous phases of the same material. The most commonly employed composition is $Ge_2Sb_2Te_5$, which lies along the pseudobinary tie line GeTe-$Sb_2Te_3$. We present data on amorphous films of GeTe, $Sb_2Te_3$, $Ge_2Sb_2Te_5$, and $Ge_2Sb_2Te_7$ grown by rf sputtering and examine the effects of growth rate and oxygen impurities on the optical and electronic properties. For Ge2Sb2Te5, the optical gap decreases with increasing growth rate, and the inverse slopes of the exponential band tails (Urbach tails) extending into the gap also decrease with increasing growth rate (i.e., the band tails become sharper at slower growth rate). The increase of the optical gap for oxygen concentrations greater than about $10^{21}$ $cm^{-3}$ is almost certainly due to the presence of oxygen at levels approaching alloy compositions. On the other hand, the sharpening of the band tail absorption is probably due to increased diffusion on the surface during growth with decreasing growth rate.

*Research supported by the Air Force Research Laboratory under grant no. F29601-03-01-0229 and by the National Science Foundation under grant no. DMR 0307594

**16:18**

**K46 10 Structural, Vibrational, and Electronic Properties of Ternary SiGeSn Alloys*** VIJAY R. D'COSTA, JOSÉ MENÉNDEZ, ANDREW V.G. CHIZMESHYA, JOHN TOLLE, JOHN KOUVETAKIS, *Arizona State University* The recent demonstration of ternary SiGeSn alloys represents a significant breakthrough that adds new levels of flexibility to the design of microelectronic and optoelectronic devices based on group-IV materials. We present a systematic experimental and theoretical study of the structural, vibrational, and electronic properties of this material. X-ray reciprocal lattice maps are used to determine the equilibrium lattice constant of the alloys, whose composition is measured independently by Rutherford Backscattering. It is found that the system follows Vegard's law quite closely, in contrast to GeSn alloys, which show evidence for bowing in the compositional dependence of the lattice constant. The Raman spectrum shows the three standard Si-Si, Ge-Si, and Ge-Ge peaks found in GeSi alloys. No evidence for Sn-Ge or Sn-Si modes is seen, but the three observed peaks shift in frequency as a function of the Sn concentration. The energy of the direct optical transitions display significant bowing as a function of the alloy composition. The dominant source of bowing appears to be the simultaneous presence of Si and Sn atoms in the ternary alloy.

*Supported by NSF-DMR-0221993, the U.S. Air Force AFRL/SNHC (F19628-03-C-0056), and Intel Corporation.

**16:30**

**K46 11 Two-photon Photoemission Electron Microscopy Imaging of $TiO_2$** GANG XIONG, ALAN JOLY, WAYNE HESS, S. CHAMBERS, T. KASPAR, KENNETH BECK, *Pacific Northwest National Laboratory, P O Box 999, Richland, WA 99352, USA* Photoemission electron microscopy (PEEM) utilizing two-photon excitation was used to image a novel $TiO_2$ thin film sample grown by molecular beam epitaxy. The $TiO_2$ thin film consists of small (50-100 nm) $TiO_2$ rutile nanocrystallites embedded in an epitaxial anatase $TiO_2$ film. Individual rutile crystallites can be identified from the anatase background, in part due to the work function difference and morphology contrast. For both phases the photoelectron signals result from electrons at the surface defect levels in the gap rather than valence band electrons. We compare the two-photon PEEM images excited by p- and s-polarized light. The greater image intensity excited by p-polarized light can be attributed to a stronger refracted wave and is further enhanced by the two-photon effect. How the differences in optical refraction, absorption and photoelectron yield affect the contrast between rutile nanocrystallites and anatase background is discussed. We summarize the contrast mechanisms for PEEM imaging and discuss the role of the complex dielectric constant in PEEM contrast mechanisms. Enhanced photoemissions from localized regions are also discussed.

**16:42**

**K46 12 Electron Paramagnetic Resonance Study of Amorphous $V_2O_5$** D.B. BAKER, K. HARTMAN, K.C. MAYNES, P.H. BUNTON, *William Jewell College* S. FELLER, *Coe College* Vitreous $V_2O_5$ is generally non-stoichiometric when cooled from above the melt, leading to the formation of paramagnetic $V^{4+}$ ions. At low temperature ( $\sim$ 120 K), previous workers have observed well-resolved EPR spectra associated with these centers. By contrast, recent results from our laboratory show EPR spectra that remain broad ( $\sim$ 20 mT, peak-to-peak) from ambient down to 120 K, with no apparent hyperfine interactions. EPR spin counting analyses also indicate high concentrations ( $\sim$ $10^{20}$ spins/$cm^3$) of paramagnetic centers, suggesting that linewidths are limited by spin-spin relaxation of the electron spin system. In addition, current results reveal that EPR signal intensities increase more rapidly than $(\text{Temperature})^{-1}$, as indicated by monitoring signal intensities over the temperature range from 120-300 K. In particular, when temperature is decreased by a factor of two (from 240 to 120 K), signal intensity increases by a factor of approximately 10. Such observations indicate the possibility of superparamagnetic or spin glass behavior within the amorphous $V_2O_5$ system. In order to further investigate the magnetic behavior of amorphous $V_2O_5$, several experimental EPR parameters are evaluated over the temperature range from 120-370 K.

**16:54**
**K46 13 Analysis of Reflectivity Measurements*** WILLIAM KARSTENS, *Saint Michael's College* D. Y. SMITH, *University of Vermont and Argonne National Laboratory* Reflectivity measurements over a limited wavelength range do not uniquely determine a material's optical constants. To achieve the latter, reflectivity must be known over a sufficient range to apply phase dispersion analysis, or reflectivity at several angles of incidence must be measured in order to solve Fresnel's equations. An approximate alternative is to fit reflectivity data with a model for the optical constants that is consistent with the material's known, or at least plausible, electronic and/or phonon structure. We have explored this procedure for analysis of IR and visible reflectivity of crystalline, amorphous, and porous silicon using both theoretical and empirical models. Limitations of this procedure, especially at the extremes of the measured range will be discussed.

*Supported by US Department of Energy, Office of Science, Materials Science Division under Contract No. DE-FG02-02ER45964, and Office of Nuclear Physics under contract W-31-109-Eng-38.

**SESSION L10: DCP BUSINESS MEETING**
**Tuesday Evening, 14 March 2006**
**302, Baltimore Convention Center at 17:30**

**SESSION L16: FIAP BUSINESS MEETING**
**Tuesday Evening, 14 March 2006**
**312, Baltimore Convention Center at 17:30**

**SESSION L18: DPOLY BUSINESS MEETING**
**Tuesday Evening, 14 March 2006**
**315, Baltimore Convention Center at 17:30**

**SESSION L23: GMAG BUSINESS MEETING**
**Tuesday Evening, 14 March 2006**
**320, Baltimore Convention Center at 17:30**

**SESSION L29: DBP BUSINESS MEETING**
**Tuesday Evening, 14 March 2006**
**326, Baltimore Convention Center at 17:30**

**SESSION L33: GSNP BUSINESS MEETING**
**Tuesday Evening, 14 March 2006**
**336, Baltimore Convention Center at 17:30**
**Daniel Lathsop, University of Maryland, presiding**

**SESSION L40: TGQI BUSINESS MEETING**
**Tuesday Evening, 14 March 2006**
**343, Baltimore Convention Center at 17:30**

**SESSION L48: FIP BUSINESS MEETING**
**Tuesday Evening, 14 March 2006**
**Galena, Marriott Waterfront Hotel at 17:30**

**SESSION L49: DCMP BUSINESS MEETING**
**Tuesday Evening, 14 March 2006**
**Dover A, Marriott Waterfront Hotel at 19:00**

**SESSION L50: DMP BUSINESS MEETING**
**Tuesday Evening, 14 March 2006**
**Dover B, Marriot Waterfront Hotel at 19:00**

**SESSION L7: FLEXIBLE MOLECULAR RECOGNITION: THE NEW PARADIGM**
**Tuesday Evening, 14 March 2006; 307, Baltimore Convention Center at 17:45**
**Jin Wang, Stony Brook University, presiding**



**17:45**
**L7 1 Mis-folding and self-association: opportunities for alternative modes of self-recognition during the folding of TIM barrel proteins.***
C. ROBERT MATTHEWS, *University of Massachusetts Medical School*

The $(\beta\alpha)8$ or TIM barrel motif is one of the most common in biology, represented in all three super-kingdoms of life. Detailed thermodynamic and kinetic analysis of the folding reactions of three members of the TIM barrel family of proteins reveal a common propensity to mis-fold to an off-pathway intermediate in less than a few milliseconds. The unfolding of this stopped-flow burst-phase intermediate controls access to an on-pathway intermediate that is highly-populated at moderate denaturant concentrations. Curiously, the equilibrium intermediate for two of the three nominally monomeric proteins spontaneously adopts a dimeric form; the native state of the third also dimerizes at micromolar concentrations. The early mis-folding reactions may reflect the rapid access to non-native folds enabled by the simple, repetitive $\beta\alpha$ topology of this motif. The propensity of stable forms, either intermediate or native, to form dimers may reflect a segment-swapping mechanism enabled by the modular folding of these single structural domain proteins. Off-pathway intermediates and non-native dimers serve as examples of important, alternative intra- or inter-molecular self-recognition events.

*This work was supported by NIH grant GM23303.

**18:21**
**L7 2 Dynamics of enzymes. Magnetic resonance methods.**
DOROTHEE KERN, *Brandeis University*

This abstract was not received electronically.

**18:57**
**L7 3 Protein kinases/signal transduction: structure/function.**
SUSAN S. TAYLOR, *University of California at San Diego*

This abstract was not received electronically.

**19:33**
**L7 4 Flexible protein-protein interactions.**
PATRICIA A. JENNINGS, *University of California at San Diego*

This abstract was not received electronically.

**20:09**
**L7 5 Single Molecule Dynamics Reveals the Role of Flexibility in Bio-molecular Recognition.**
JIN WANG, *SUNY at Stony Brook*

With combined single molecule study of flexible protein binding with an energy landscape inspired microscopic model, we found strong evidences of a new paradigm that bio-molecular recognition is determined by flexibilities in addition to structures. The single-molecule study show conformational fluctuations of the protein complex that involves bound and loosely bound states, which can be quantitatively explained in our model as a result of cooperative binding. Theoretical predictions on the key residues are consistent with mutational experiments. The combined study provides a test ground for fundamental mechanisms and insights for future explorations on recognition with large conformational changes.

**SESSION M50: INTELLIGENT DESIGN: ITS IMPACT AND RESPONSES TO IT**
**Tuesday Evening, 14 March 2006; Grand Salon V, Marriot Waterfront Hotel at 19:30**
**Robert Eisenstein, Santa Fe Institute, presiding**



**19:30**
**M50 1 Legal Perspectives on Religion in Public School Science Classes.**
JEREMY GUNN, *American Civil Liberties Union*

In the 1920s, state legislatures in the United States became involved in enacting laws prohibiting the teaching of evolution in public schools. The famous itTennessee v. John Scopes trial of 1925 was the most famous test case to determine the constitutionality the first phase of the laws. Scopes was convicted of violating one such law and many of these anti-evolution laws continued to be in effect for the next forty years. During the 1950s, for a number of reasons, the teaching of evolution became more common as the anti-evolution laws were either repealed or ignored. In 1968, the Supreme Court in *Epperson v. Arkansas* ruled that the prohibition of the teaching of evolution was unconstitutional. Since the itEpperson decision, there have been several other federal court decisions that have considered the constitutionality of allowing religious theories to be taught in the science curriculum. For all practical purposes, federal courts since 1968 have prohibited the teaching of creationism. The new current battleground is on the issue of intelligent design. The first court decision on intelligent design, from Dover, Pennsylvania, is expected by January 2006. The significance of this decision, and the fallout from it, will be discussed. In many ways, the current controversy over the teaching of intelligent design may be only the tip of a far larger public controversy involving the roles of science, law, politics, and religion. Suggestions will be made as to how the scientific community can contribute to the legal and cultural issues that underlie this debate.

**20:06**
**M50 2 Science and Society Under Attack: The Need for Political As Well As Scientific Responses.**
MARSHALL BERMAN, *Sandia National Laboratory, retired, and past Vice-President of the New Mexico State Board of Education*

Today science and scientists are under attack. This is not new in human history. Copernicus delayed publishing for fear of possible persecution. Bruno was burned at the stake. Galileo was forced to recant. Darwin worked for 20 years without publishing his ideas, perhaps out of fear of possible consequences. In the US today, fundamentalist evangelicals have launched an attack on science, from intelligent design creationism, to stem cell research, global warming, vaccines to prevent cervical cancer, even museums that show exhibits on evolution. In the $21^{st}$ century, this medieval mentality must be strenuously resisted. Rational thought can co-exist with religious faith, unless extremism becomes the norm. Scientists have often ignored politics in their pursuit of new knowledge. But they must understand that public opinion is strongly influenced by non-scientific elements of society, from the pulpit, from politicians and bureaucrats, from a scientifically illiterate public, and from a media that frequently treats all points of view as equal, when they are most certainly not. Will science eventually be required to pass muster for religious fundamentalists in the near future?

**20:42**
**M50 3 APS Activities with Other Professional Societies.**
FRANCIS SLAKEY, *American Physical Society*

In 1981, the APS Council issued a statement that opposed ''equal time'' presentation in public school science classes of creationism and evolution. The statement clarified that ''Scientific inquiry and religious beliefs are two distinct elements of the human experience. Attempts to present them in the same context can only lead to misunderstandings of both.'' The APS Council revisited the issue in 1999 when a school board in Kansas attempted to eliminate the Big Bang, among other issues, from the science curriculum. Since that time, the APS has been more directly involved in confronting efforts that would dilute the teaching of science in public school science classes. This talk will review the APS activities and describe a developing multi-science society activity.

**21:18**
**M50 4 Media Coverage of Evolution and Intelligent Design.**
CORNELIA DEAN, *New York Times*

This abstract was not received electronically.

## C

## E

## F

## G

## H

## M

## O

## P

## Q

## R

## S

## U

**V**

## W

## X

## Y

## Z

# NOTES

# NOTES

# NOTES

# NOTES

# NOTES

# NOTES

# NOTES

# NOTES

# NOTES

# NOTES

# The Baltimore Convention Center Overview

## Level 400

- 36,672 square foot ballroom.
- Divides into 4 sections.
- Ceiling height 28 feet.
- Prefunction space.

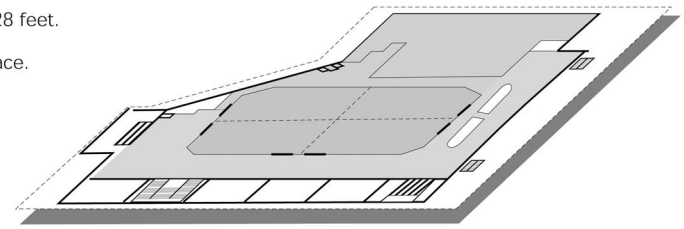

## Level 300

- 50 meeting rooms accommodate 85 to 1,600 people.
- Information kiosk.
- Prefunction space.

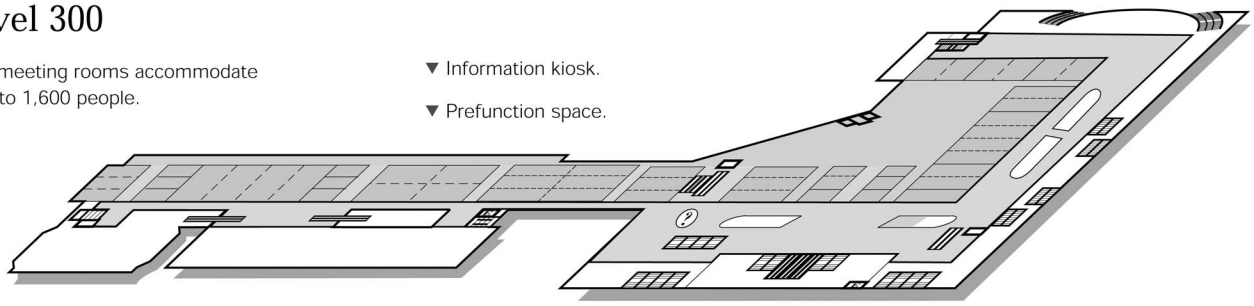

## Level 200

- Access to all areas of Convention Center.
- Convention Center Offices.
- Access to Skywalk, Inner Harbor and hotels.
- Information kiosk.

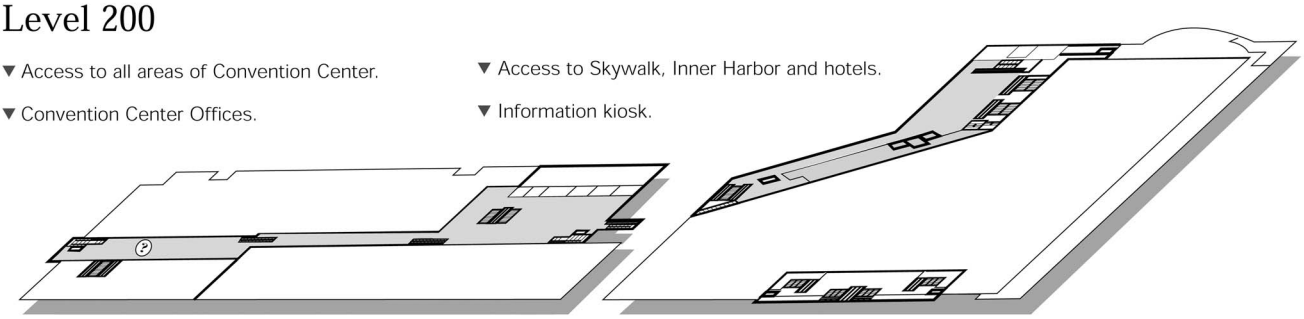

## Level 100

- 300,000 square feet of exhibit space.
- Divides into 7 separate halls.
- Ceiling height 30 feet at center.
- 32 covered loading docks.

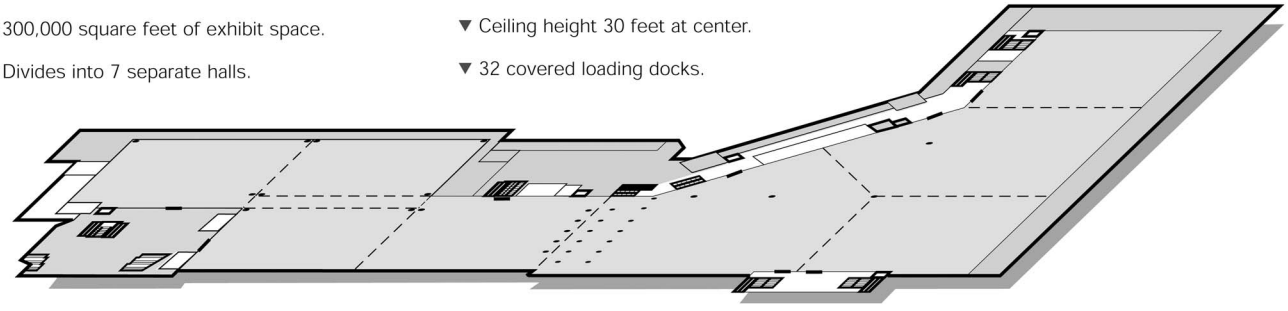

# The Baltimore Convention Center

## Level 100

- 300,000 square foot exhibit space divides into 7 sections.
- Ceiling height 30 feet at center.
- 120/208V and 277/480V electrical services at approximately 30-foot spacing on the floor.
- Cold water, sanitary drain, compressed air available.
- Direct drive-in access for vehicles through 15'x18' overhead doors.
- 32 covered loading docks.
- All halls have available public address system and telephone outlets.
- Complimentary show offices come with exhibition halls.
- VIP Suite available in Charles Lobby.
- The entire exhibition space is relatively column-free.

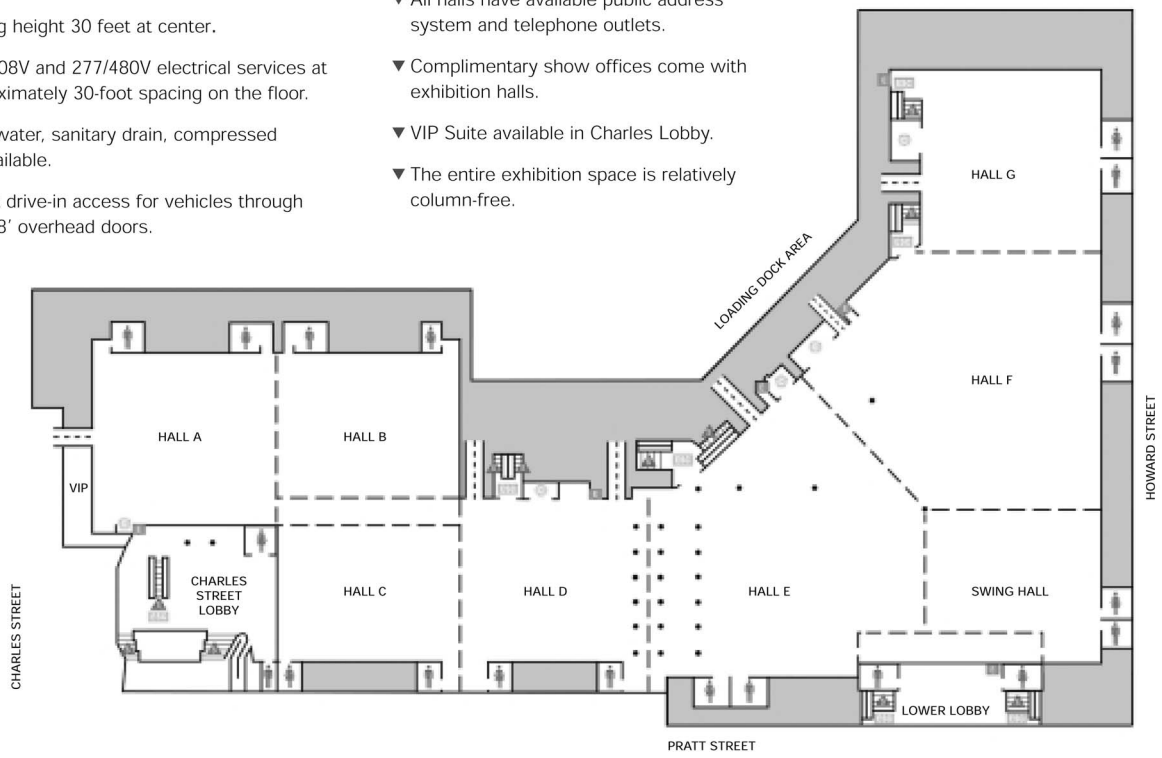


| key | concessions | elevator | escalator | stairs |
|---|---|---|---|---|

# The Baltimore Convention Center

## Level 200

- Includes Otterbein and Sharp Street Lobbies, Pratt Street Entrance and Convention Center Offices.
- Access to Skywalk, Inner Harbor, and hotels. Access to Baltimore's Light Rail System providing a direct route to BWI Airport. Walking distance to the MARC train system with service to Washington, D.C.
- Prefunction space.
- Visitor information kiosk.

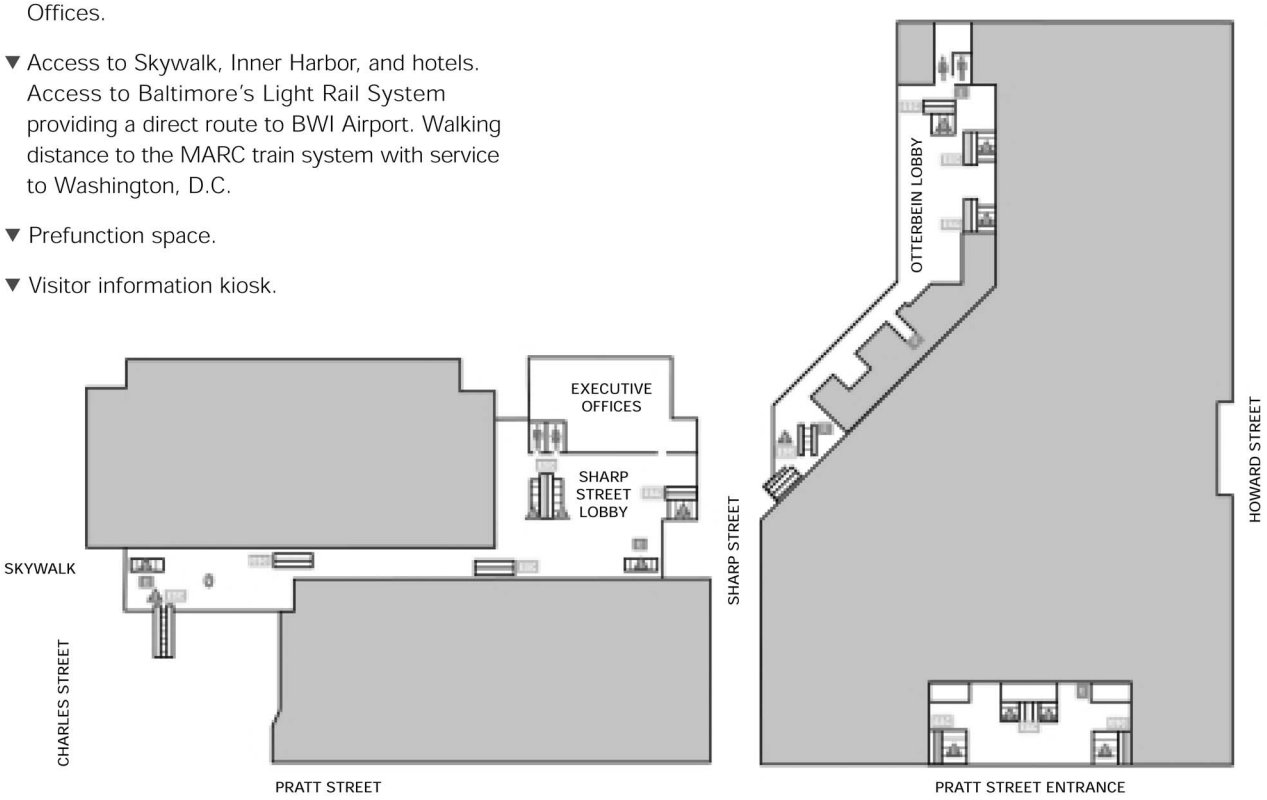


| key | restrooms – public restrooms are handicap accessible | handicap accessible restroom and assistant | drive in access | visitor kiosk |
|---|---|---|---|---|

# The Baltimore Convention Center

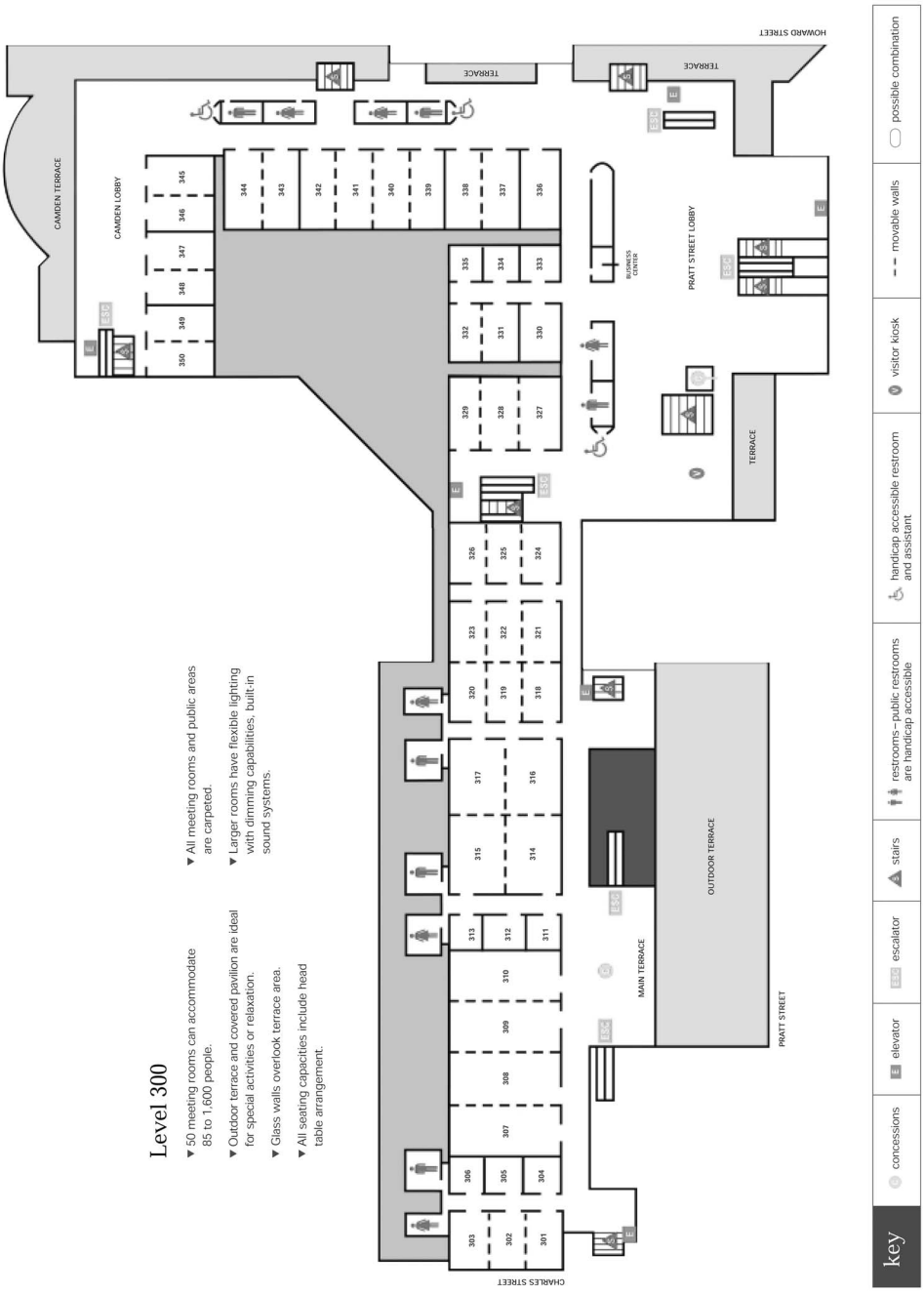

# The Baltimore Convention Center

## Level 400

- 36,672 square foot ballroom.
- Divisible into 4 sections.
- Ceiling height 28 feet.
- Complete kitchen/catering facilities.
- Built-in sound system.
- Fluorescent and incandescent lighting with dimmers.
- VIP Suites available.
- Ballroom foyer provides spacious prefunction space.

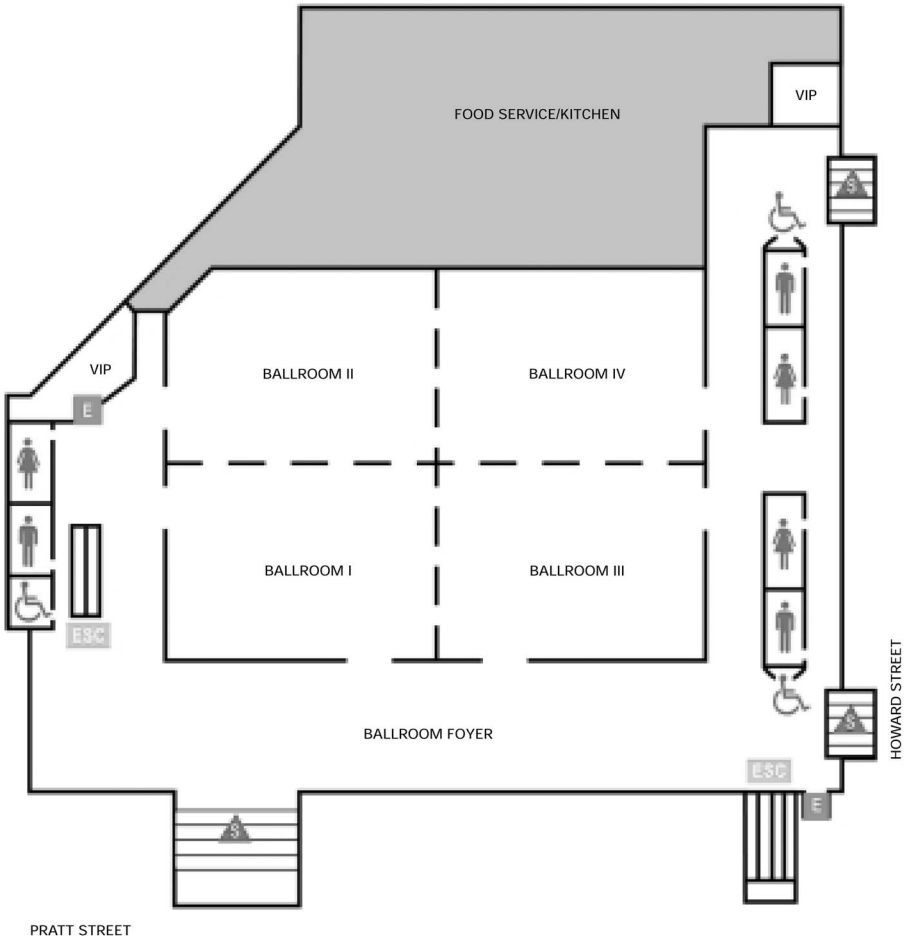


| key | | | | |
|---|---|---|---|---|
| | C concessions | E elevator | ESC escalator | stairs |
| | restrooms<br>public restrooms are handicap accessible | handicap accessible restroom & assistant | V visitor kiosk | |

BULLETIN
OF THE AMERICAN PHYSICAL SOCIETY

Vol. 51, No. 1, Part 2, March 2006

# March Meeting 2006

## TABLE OF CONTENTS

# APS MARCH MEETING 2006

March 13–17, 2006
Baltimore Convention Center
Baltimore, MD

## General Information

Welcome to the Annual March Meeting of the American Physical Society. All scientific sessions and some APS-sponsored sessions will be held at the Baltimore Convention Center (BCC). APS affiliated meetings and satellite meetings will be held at the Marriott Waterfront Hotel, headquarters hotel for the meeting. Consult the schedule of APS affiliated and satellite meetings, in this Bulletin for exact locations.

An outstanding scientific program has been planned by the March Meeting Program Committee. The five-day program consists of approximately 6,900 papers to be presented in invited, contributed, focus and poster sessions. A larger, enhanced exhibit show will complement the scientific program. Attendees are encouraged to visit with exhibitors who will be displaying the latest products, instruments and equipment, computer software, as well as science publications related to the research and application of physics.

## Participating APS Units

**Divisions:** Condensed Matter Physics (DCMP); Materials Physics (DMP); Polymer Physics (DPOLY); Chemical Physics (DCP); Biological Physics (DBP); Fluid Dynamics (DFD); Computational Physics (DCOMP); Atomic, Molecular and Optical Physics (DAMOP); Laser Science (DLS).

**Topical** Groups: Instrument and Measurement Science (GIMS); Magnetism and Its Applications (GMAG); Quantum Information, Concepts, and Computation (GQI); Shock Compression of Condensed Matter (SCCM); Statistical and Nonlinear Physics (GSNP).

**Forums:** Industrial and Applied Physics (FIAP); Physics and Society (FPS); History of Physics (FHP); International Physics (FIP); Education (FEd); Graduate Student Affairs (FGSA).

## Registration Location/Hour

Pratt Street Lobby
Baltimore Convention Center (BCC)

The APS Registration Desk will open and close at the following times.

| | |
|---|---|
| Sunday, March 12 | • 1:00pm –7:00pm |
| Monday, March 13 | • 7:00am – 5:00pm |
| Tuesday, March 14 | • 7:00am – 5:00pm |
| Wednesday, March 15 | • 7:00am – 4:00pm |
| Thursday, March 16 | • 7:30am – 3:00pm |
| Friday, March 17 | • 7:30am – 10:00am |

## Badge Monitoring

All attendees must register for the meeting. Attendees must wear their badges at all times. Security personnel will be checking for badges before allowing admission to the sessions. Attendees without badges will not be admitted to sessions or exhibits. If you have lost your badge, please go to the APS registration desk for a new one. We will give you one replacement badge free. After that replacement badges will be charged $10.00.

## Wireless Connection at the Convention Center

The Baltimore Convention Center has wireless internet connection available free of charge, sponsored by the American Physical Society.

## APS Job Fair

Whether you are looking for a job or recruiting, the American Physical Society Annual March Meeting Job Fair is the place to be! The Job Fair will provide job seekers and hiring managers with unsurpassed recruitment and networking opportunities. Last year, we assisted hundreds of job seekers and more than 50 employers.

*March 12 –16*
*Job Fair Schedule*

| | | |
|---|---|---|
| *March 12* | • | Employer/Job Seeker on-site pre-registration and check-in<br>1:00pm – 4:00pm |
| March 13 | • | Job Fair hours of operation<br>10:00am – 5:00pm |
| March 14 | • | Job Fair hours of operation<br>10:00am – 5:00pm |
| March 15 | • | Job Fair hours of operation<br>10:00am – 4:00pm |
| March 16 | • | Last day to view/search jobs and résumés online |

Join in with hundreds of individuals specializing in the following areas:

*Computational Physics*
*Insulators and Detectors*
*Polymeric and Organic Materials*
*Metals History and Physics*
*Statistical and Nonlinear Physics*
*Phase Transitions and Strongly Correlated Systems*
*Artificially Structured Materials*
*Surface, Interfaces and Thin Films*
*Physics and Society Magnetism*

*International Physics Instrumentation and Measurement*
*Quantum Information, Concepts and Computation*
*Education Chemical Physics*
*Biological Physics*
*Superconductivity*
*Fluids*
*Complex Structured Materials*
*Industrial and Applied Physics*

## Job Seekers utilize the Job Fair services to:

- Network with technical staff and human resource recruiters
- Post your résumé and search open positions
- Interview for positions

## Employers utilize the Job Fair services to:

- Showcase your company with a Recruitment Booth
- Advertise open positions
- Interview qualified job seekers
- Search résumés specific to this meeting

*For more information contact abrice@aip.org*

## APS Store

| | |
|---|---|
| Monday – Wednesday | • 9:30am – 5:00pm |
| Thursday | • 9:30am – 1:00pm |

Come browse our t-shirts, bumper stickers, and more.

## APS Exhibit Show/APS Lounge

*Exhibit Hall E*

| | |
|---|---|
| Monday, March 13 | • 10:00am – 5:00pm |
| Tuesday, March 14 | • 10:00am – 5:00pm |
| Wednesday, March 15 | • 10:00am – 4:00pm |

The annual exhibit show days are Monday through Wednesday. The exhibits are an important adjunct to the meeting, offering information on a wide variety of physics-related products and services. In addition, book and periodical publishers will be participating as exhibitors. The poster sessions, and food concessions will be located in the exhibit hall, as will the E-mail Pavilion. A wine and cheese reception will be held in the exhibit hall on Monday and Tuesday from 4:00pm – 5:00pm. Plan to stop by to visit the exhibits, view the posters and enjoy the refreshments. **NOTE:** *You must wear your badge to be admitted to the exhibit hall.*

## APS Membership Booth

The APS Membership Booth is located near APS Registration in the Pratt Street Lobby. Membership Department staff will be on hand to answer questions about APS Membership and journal subscriptions.

## E-mail Service

E-mail service will be available on Monday, Tuesday and Wednesday in the Exhibit Hall during exhibit hours only. E-mail will be available on Thursday and Friday in the Pratt Street Lobby. Email stations will be available for your use during the following hours:

| | |
|---|---|
| Monday, March 13 | • 10:00am – 5:00pm (exhibit hall) |
| Tuesday, March 14 | • 10:00am – 5:00pm (exhibit hall) |
| Wednesday, March 15 | • 10:00am – 4:00pm (exhibit hall) |
| Thursday, March 16 | • 7:00am – 6:00pm (Pratt Street Lobby) |
| Friday, March 17 | • 7:00am – 12:00noon (Pratt Street Lobby) |

Please be advised that e-mail access is provided as a service to attendees, and that we cannot provide unlimited access to e-mail stations, both in terms of the number of stations provided and the length of time that they are available.

## Speaker-Ready Room

*BCC/Room 330*

The speaker-ready room will be open as follows:

| | |
|---|---|
| Sunday, March 12 | • 1:00pm – 7:00pm |
| Monday, March 13 | • 7:00am – 5:00pm |
| Tuesday, March 14 | • 7:00am – 5:00pm |
| Wednesday, March 15 | • 7:00am – 5:00pm |
| Thursday, March 16 | • 7:00am – 5:00pm |
| Friday, March 17 | • 7:00am – 12:00noon |

## Press Room

*Press Room: BCC/Room 334*
*News Conference Room: BCC/Room 333*

| | |
|---|---|
| Monday through Thursday | • 8:00am – 5:00pm |
| Friday | • 8:00am – 12:00noon |

Phone: 410–649–6498
Fax: 410–649–6494

## Press Conference Room

*BCC/Room 333*

A schedule of news conferences can be obtained from the Press Room (Room 334).

## City Information Desk

The Baltimore Convention and Visitors Bureau will host an information desk in the BCC/Pratt Street Lobby:

| | |
|---|---|
| Sunday, March 12 | • 2:00pm – 6:00pm |
| Monday, March 13 | • 11:00am – 5:00pm |
| Tuesday, March 14 | • 11:00am – 5:00pm |

Stop by to inquire about restaurants in the city and sightseeing.

## Business Center

The Baltimore Convention Center business center is located off the Pratt Street Lobby across from Room 333. The business center offers a full range of services and is open Monday through Friday 8:30am – 4:30pm.

## Hotel List - March Meeting

- Marriott Waterfront Hotel (HQ)
  700 Aliceanna Street
  *Bussing provided to and from Convention Center*
- Sheraton Inner Harbor
  300 South Charles Street
  *Within walking distance*
- Days Inn
  100 Hopkins Place
  *Within walking distance*
- Renaissance Harborplace Hotel
  202 East Pratt Street
  *Within walking distance*
- Hyatt Regency Baltimore
  300 Light Street
  *Connected to Center*
- Holiday Inn
  301 West Lombard Street
  *Within walking distance*
- Wyndham Inner Harbor
  101 West Fayette Street
  *Within walking distance*

# PRE-MEETING PROGRAMS

**DPOLY Short Course – Baltimore Convention Center (BCC)**
Polymers in Existing and Emerging Patterning Technologies (no on-site registration – you must be pre-registered to attend this course)
**Room 304**
Saturday March 11 • 8:30am – 5:00pm
Sunday March 12 • 8:30am – 3:00pm

**Tutorials – Baltimore Convention Center (BCC)**
*(No on-site registration – you must be pre-registered to attend a tutorial)*
**Sunday, March 12**
**Baltimore Convention Center**
**Morning Tutorials #1–4**
*8:30am –12:30pm*
T1 Spintronics: What's New – Room 307
T2 Molecular Magnetics – Room 301
T3 Current Interpretations of Quantum Mechanics – Room 302
T4 Thermoelectric Energy Conversion – Room 303

**Afternoon Tutorials #5–8**
*1:30pm – 5:30pm*
T5 Solid State Implementations of Cavity QED – Room 301
T6 Spallation Neutron Sources – Room 302
T7 Forefront Methods and Limits of Lithography – Room 303
T8 Polymeric Templating – Room 305

**Professional Skills Development for Women Physicists**
**Sunday, March 12**
*8:00am – 5:00pm*
*Reception 5:00pm – 6:30pm*
Marriott Waterfront Hotel/Dover A (workshop)
Marriott Waterfront Hotel/Grand Salon I (reception)
This one-day workshop will offer training on persuasive negotiation and communication skills for tenure track and newly-tenured women physicists. Workshop will be led by professional facilitators using an interactive format that encourages highly personal learning. Lunch will be provided and a reception for participants will follow the workshop. Limited to 30 participants. Pre-registration required.

**Workshop on Opportunities in Biology for Physicists**
**Organized by APS Division of Biological Physics**
**Sunday, March 12**
*8:00am – 5:00pm*
Lunch break on your own.
BCC/Room 310
Biology is a rapidly changing field that has been making tremendous strides forward in recent years. Biology is changing from a descriptive to a quantitative and conceptually profound field. This workshop will showcase a sample of the rich opportunities in biology for physicists. It is aimed at physicists, especially graduate students and postdocs, who are curious about how a background in physics can provide a unique perspective of biological systems. We believe that physicists will make a substantial contribution to this revolution by working together with biologists.

**Invited speakers include:**
- William Bialek (Princeton)
- Steven Block (Stanford) (tentative)
- Robijn Bruinsma (UCLA)
- Hans Frauenfelder (Los Alamos)
- Klaus Lehnertz (Bonn)
- Yale Goldman (Penn)
- Boris Shraiman (Santa Barbara) (tentative)
- Charles Stevens (Salk Institute)
- Zuzanna Siwy (Irvine)
- Sunney Xie (Harvard)

Co-chairs of Organizing Committee:
Dean Astumian, DBP Vice Chair, astumian@maine.edu
Clare Yu, cyu@uci.edu

On-site registration is available but payable in cash only – no credit cards or checks.
Students: $50
Post Docs: $75
Regular Members: $100

**Special Workshop: Quantum Mechanics with Interactive Computer-based Tutorials**
Sponsored by the APS Forum on Education
**Sunday, March 12**
1:30pm – 5:30pm
BCC/Room 306
• No cost to attend the workshop - all are welcome.
Although quantum mechanics is one of the most widely taught topics on the college/university level in the physical sciences, the teaching of quantum mechanics has not changed significantly since the 1940s. This workshop will present recently developed computer-based curricular material that has shown to improve understanding of traditional quantum topics and that makes many heretofore inaccessible topics in quantum mechanics accessible to undergraduate and graduate students. Participants will receive a CD containing curricular material from the Quantum Interactive Learning Tutorials (QUILT) project as well as a collection of ready to run Java programs from the Open Source Physics (OSP) project. All programs are freely distributable under the GNU GPL license.
This workshop will benefit anyone teaching or planning to teach quantum mechanics as well as computational physicists wishing to adopt the OSP Java libraries for their own teaching and research. We will discuss the general pedagogical and technical issues in the design of interactive computer-based tutorials as well as how OSP programs can be adapted to your local situation. Additional information can be obtained at www.opensourcephysics.org

**Speakers:**
- Chandralekha Singh, University of Pittsburgh
- Wolfgang Christian, Davidson College
- Mario Belloni, Davidson College

**Career Workshop**
**Sunday, March 12**
*3:00pm – 7:00pm*
BCC/Room 308

Attendance is free. All are welcome.

# PRE-MEETING PROGRAMS

**NRC/NAS Town Meeting**
**Sunday, March 12**
*7:30pm – 9:30pm*
Marriott Waterfront Hotel, Grand Ballroom Salon V

**Condensed Matter and Materials Physics In the Next Decade**

M. A. Kastner, Chair, Solid State Sciences Committee of the National Research Council and Department of Physics, MIT

• The National Research Council (NRC) will soon appoint a committee to carry out a decadal study of condensed-matter and materials physics called CMMP2010. The study, which will result in an NRC report, is supported by the NSF and DOE. The committee will assess the current and future opportunities of our field. It will identify the most important fundamental scientific problems, as well as problems whose solutions are likely to help meet national or societal needs. It will also examine the current status and future needs for resources that will be necessary to solve these problems, such as small and large facilities, individual and multi-investigator research support, as well as university, national and industrial laboratories. After a brief introduction to the work done so far, under the auspices of the Solid State Sciences Committee, attendees will be invited to offer their views about issues to which the panel should pay special attention.

# APS MEETINGS / EVENTS
***(In chronological order)***

**Contact Congress**
**Mon-Thurs 9:00am–6:00pm**
Sponsored by DCMP and DMP
BCC/Pratt Street Lobby

Worried about the slashing of NSF, DOE and NASA funding? Concerned about the dearth of science literacy in our high-schoolers? Anxious about where the country's security is heading? YOU can have an impact on national science policy! Come write your representatives in Congress to let them know how you feel about science issues of interest to you. The most important letters that a Member of Congress receives are the ones from his or her constituents – you elect them, and you matter. The American Physical Society feels that it is incumbent on all of us to interact with the government, to offer technical assistance where we can, and to remind our Members of Congress that scientists have much to offer the country, in areas of basic science R&D funding, education, and energy policy. We have set up computers in the entrance area where you can send a letter to your Senators and Representatives - you can use our template or write your own letter on issues that matter to you. If the state of affairs in Washington, DC, interests you, we have another way for you to get involved: the APS "Physics and Government Network," a group of APS members who volunteer to contact their representatives in Congress a few times a year at critical junctures. PGNet signup fliers will be available at the registration desk and at the "Contact Congress" computers. Come help make science more visible in Congress!

**Awards Program**
**Monday, March 13**
*5:45pm – 6:30pm*
BCC/Room 309
Prizes and awards will be bestowed on individuals for outstanding contributions to physics. Please plan on attending the Awards Program and join us in honoring these individuals. See page 829 for a list of award and prize winners. The Awards Program will be followed by the Welcome Reception at 6:45pm.

**Welcome Reception**
**Monday, March 13**
*6:45pm – 8:00pm*
BCC/Ballroom II

All Attendees welcome.

## *Special Symposium:*

**Emerging Emergent Phenomena (Session F50)**
**Monday, March 13**
Sponsored by DCMP
*8:00pm – 10:00pm*
Marriott Waterfront Hotel, Grand Ballroom Salons V-VI

Session Chair: Leo Kadanoff, University of Chicago
*Speakers:*
- Edward Witten: Emergent Phenomena In Particle Physics
- Susan J. Lolle: Revisiting Mendel and the Paradox of Gene Restoration
- Albert Laszlo Barabas: Complex Networks: From the Internet to Biology
- Bernard Sadoulet: Condensed Matter Physics and the Nature of Dark Matter in the Universe

**Wine and Cheese Reception**
**Monday and Tuesday • 4:00pm – 5:00pm**
BCC/Exhibit Hall E

**APS Journal Editors Panel Discussion**
**Tuesday, March 14**
*2:30pm – 3:30pm*
BCC/Room 337
All are invited to a panel discussion with the Editors of the American Physical Society journals. The panel will include Editors from Physical Review Letters, Physical Review B, and Physical Review E. They will briefly discuss some current issues facing the journals such as how to express appreciation for good refereeing, possible inclusion of popular abstracts in PRL to make Letters accessible to physicists in all fields, the challenge posed by open access, etc. The Editors look forward to hearing opinions on these and other issues. They will also respond to questions and comments. The Panel Discussion will be followed by the Meet the Editors Reception.

**Meet the Journal Editors of AIP and APS**
**Tuesday, March 14**
*3:30pm – 5:30pm*
BCC/Camden Lobby

The Editors of the AIP and APS journals cordially invite you to join them for conversation and refreshments. Your questions, criticisms, compliments, and suggestions about the journals are welcome. We hope you will be able to join us.

**Journals of the American Institute of Physics:**
- Applied Physics Letters
- Chaos
- Journal of Applied Physics
- The Journal of Chemical Physics
- Journal of Mathematical Physics
- Physics of Fluids
- Physics of Plasmas
- Review of Scientific Instruments

**Journals of the American Physical Society:**
- Physical Review A
- Physical Review B
- Physical Review E
- Physical Review Focus
- Physical Review Letters
- Reviews of Modern Physics

# APS MEETINGS / EVENTS
*(In chronological order)*

### *Special Symposium:*

**Intelligent Design: Its Impact and Responses to It**
**Tuesday, March 14**
*7:30pm – 9:30pm*
Marriott Waterfront Hotel/Grand Ballroom Salon V

Session Chair: Robert Eisenstein
Speakers:

- Jeremy Gunn, ACLU - Dover, PA Case
- Marshall Berman - Action at the Local Level
- Cory Dean, New York Times - Media Coverage
- Francis Slakey, APS Office of Public Affairs - APS Activities

**Congressional Visits during March Meeting 2006**
**Congressional Visits Office –**
**BCC/East Pratt Show Office, Lower Level**

The APS Office of Public Affairs (OPA) is organizing Congressional visits during the 2006 APS March Meeting in Baltimore. The advantageous location of this year's Meeting provides an exciting opportunity to have attendees from as many districts and states as possible travel down to Washington, DC to educate Congress on the importance of science research funding. The visit days are scheduled for Wednesday, March 15th and Thursday March 16th.

Carrying the message to individual offices remains one of the best means of influencing a Member of Congress. The timing of these visits is excellent since Congress will have just started its considerations of the appropriations for the next fiscal year. In addition to influencing Congress, we hope that participants see first-hand the importance of informing their elected officials about what physicists do. While our members are getting more active in this regard and more APS meeting attendees write letters at the Contact Congress computers, there is much more to do.

OPA will assist the participants in all aspects of the congressional visits from scheduling to follow up. Leading up to the meeting, OPA will contact participants to inform them of the organizational logistics of the visits and provide a means of coordination of their meetings on the Hill with other participants in their state or district. During the March Meeting, briefings will be held in Baltimore in the evenings preceding the visits to outline a common message, offer advice on how to conduct an effective meeting, and cover the logistics of a congressional visit. We will also provide materials to be left with each office that will present useful talking points and have state specific information. Shuttle bus transportation to and from the Meeting and Washington, DC will be provided for participants.

We would like you and all APS members to view Congressional visits as part of developing a relationship with an office rather than a one-time event. We would hope that you would follow up with the Congressional office at opportune times, make visits to the home offices and perhaps invite staff or Members of Congress to visit their labs. You may also become resources for a Member's office.
For more information visit the Congressional Visits office as noted above.

**Session on Refereeing**
**Wednesday, March 15**
*9:30am – 11:00am*
BCC/Room 337

Editors from Physical Review Letters and the Physical Review will provide useful information and tips for referees. Following short presentations from the editors, there will be a moderated discussion where questions relevant to refereeing will be addressed. Refreshments will be served.

**Estate Planning Seminar**
**Wednesday, March 15**
*1:00pm – 2:00pm*
BCC/Room 301

### *Special Symposium:*

**Perspectives on our Energy Future**
**Wednesday, March 15**
*7:30pm – 9:00pm*
Marriott Waterfront Hotel/Grand Ballroom Salon V

Session Chair: George Crabtree, Argonne National Laboratory
Speakers:

- Steven E. Koonin, Chief Scientist, BP
- Patricia Dehmer, Office of Basic Energy Sciences, DOE

**Physics Sing-a-Long/Listen-a-Long**
**Wednesday, March 15**
9:00pm – 10:00pm
Grand Salon II, Marriott Waterfront Hotel

**Changing Dynamics of Industrial Research as a Consequence of Global Trends (Session V19)**
Sponsored by APS and AIP
**Thursday, March 16**
BCC/Room 316

Session Chair: Mark Bernius, The Dow Chemical Company
Speakers:

- **Alan Taub**: General Motors' R&D: Managing Innovation Globally
- **Hans Stork**: Not Only Texas is Flat …
- **Mark Durcan**: Micron R&D: Global Scope and Nano-Scale in N-Dimensions
- **Abel Weinrib**: Leap Ahead: Global R&D at Intel
- **Thomas Feist**: Sustaining Breakthrough Research in a Changing Global Environment

# APS EVENTS FOR SPECIAL GROUPS

***(In chronological order)***

**Companions Breakfast**
**Monday, March 13**
*8:00am – 9:30am*
Marriott Waterfront Hotel/Dover A

Companions of the attendees of the March Meeting are invited to a complimentary breakfast to meet other companions and learn about the city of Baltimore. Presentations will be made by a representative of the Baltimore Convention and Visitors Bureau. At the breakfast you will receive information about the sites and attractions in the city.

**SPS Undergraduates and Mentors Gathering**
**Monday, March 13**
*1:50pm – 2:20pm*
BCC/Room 345

Undergraduates and their mentors, as well as graduate school representatives, are especially invited to hear the student presentations and mingle with the presenters during this gathering. The event is sandwiched between two exciting undergraduate research sessions - B42 and D42 in room 345. Light refreshments will be available for those attending the talks.

**CSWP/FIAP Networking Breakfast for Women in Physics**
**Tuesday, March 14**
*7:30am – 9:30am*
Marriott Waterfront Hotel, Grand Ballroom Salon VII
$20 (pre-registration only)

The Committee on the Status of Women in Physics (CSWP) and the Forum on Industrial and Applied Physics (FIAP) will host a networking breakfast for women in physics. All are welcome, both men and women. Thanks to the generosity of FIAP, the breakfast is free for physics students who pre-register. Only a limited number of walk-ins can be accepted.

**High School Physics Teachers Day**
**Tuesday, March 14**
*8:00am – 2:30pm*
Marriott Waterfront Hotel, Grand Ballroom Salons II–III

In conjunction with the 2006 March Meeting, the APS Department of Education & Outreach is sponsoring a High School Physics Teachers' Day for teachers in the Baltimore region. For more information contact Ed Lee: lee@aps.org

*The day's program includes:*

- Hands-on workshops presenting innovative, class room-ready activities
- Research talks on cutting-edge physics
- A welcoming breakfast, and a chance to network with fellow teachers
- Lunch with a physicist

**Congressional Visits Meeting**
**Tuesday, March 14**
*5:00pm – 6:30pm*
BCC/Room 337

**DCMP/DMP/DCOMP Fellows & Awards Reception**
**Tuesday, March 14**
*5:30pm – 7:00pm*
Marriott Waterfront Hotel/Grand Salon VI

**FIP Reception**
**Tuesday, March 14**
*6:30pm – 8:00pm*
Marriott Waterfront Hotel/Dover C

**Students Lunch with the Experts**
**Wednesday, March 15**
*1:00pm – 2:30pm*
BCC/Ballroom II

Students can sign up on-site to enjoy a complimentary box-lunch while participating in an informal discussion with an expert on a topic of interest to them. Sign-up will take place beginning on Monday, March 13 at 1:00pm at the APS registration desk, and will be on a first-come, first-served basis. Attendance is limited to eight students per topic.
See page 828 for list of topics and experts.

**Congressional Visits Meeting**
**Wednesday, March 15**
*5:00pm – 6:30pm*
BCC/Room 311

**Status of Funding Opportunities in NSF's Division of Materials Research**
**Wednesday, March 15**
*5:00pm – 7:00pm*
BCC/Room 338

**Student Reception**
**Wednesday, March 15**
*5:30pm – 6:30pm*
BCC/Ballroom II
Sponsored by the Forum on Graduate Student Affairs (FGSA)

All students are welcome. Plan to attend and socialize with your fellows and enjoy the refreshments. The Forum on Graduate Student Affairs (FGSA) will present a short program.

# APS EVENTS FOR SPECIAL GROUPS

***(In chronological order)***

## APS Unit Business Meetings

### SUNDAY, MARCH 12

**GSCCM Business Meeting**
*3:00pm – 4:00pm*
Falkland Room, Marriott Waterfront Hotel

### TUESDAY, MARCH 14
### 5:30pm – 6:30pm

**DPOLY Business Meeting**
BCC/Room 315

**FIAP Business Meeting**
BCC/Room 312

**FIP Business Meeting**
Marriott Waterfront Hotel, Galena

**DCP Business Meeting**
BCC/302

**GSNP Business Meeting**
BCC/Room 336

**GMAG Business Meeting**
BCC/Room 320

**GQI Business Meeting**
BCC/Room 343

**GIMS Business Meeting**
BCC/Room 301

### TUESDAY, MARCH 14
### 7:00pm–8:00pm

**DCMP Business Meeting**
Marriott Waterfront Hotel/Dover A

**DMP Business Meeting**
Marriott Waterfront Hotel/Dover B

### WEDNESDAY, MARCH 15

**FED Business Meeting and Reception**
*5:30pm – 7:00pm*
Marriott Waterfront Hotel/Grand Ballroom Salon III

**DCOMP Business Meeting**
*6:30pm – 730pm*
Marriott Waterfront Hotel, Dover C

# SATELLITE MEETINGS

***(ancillary events sponsored by non-APS groups)***

**Sunday, March 12**
**High Magnetic Field Laboratory Users Group**
*5:00pm – 9:00pm*
Marriott Waterfront Hotel/Grand Ballroom Salon X

**Sunday, March 12**
**Socialize with Science - Oxford Instruments**
*7:00pm – 9:00pm*
Marriott Waterfront Hotel/Grand Salons VIII–IX

**Monday, March 13**
**Discussions and Updates on the Nanoscale Ordered Materials Diffractometer at the Spallation Neutron Source (NOMAD)**
11:00am – 2:00pm
Marriott Waterfront Hotel/Dover C

**Tuesday, March 14**
**Research Corporation Reception**
*5:00pm – 7:00pm*
Marriott Waterfront Hotel/Grand Ballroom Salon I

**Tuesday, March 14**
**Alumni Reunions**
*6:00pm – 8:00pm*
Marriott Waterfront Hotel
- Cornell University, Grand Ballroom Salons IX–X
- University of Illinois, Grand Ballroom Salons II–III
- Michigan State University, Bristol
- IBM, Grand Salon VIII
- Brown University, Falkland
- State of Florida Universities, Harborside Ballrooms AB
- Sigma Pi Sigma, Essex B
- Brandeis Alumni Reunion, Essex C

**Tuesday, March 14**
**Chinese Academy of Sciences Reception**
*6:00pm–8:00pm*
Marriott Waterfront Hotel/Essex A

**Tuesday, March 14**
**American Chapter of the Indian Physics Association**
*7:30pm – 9:30pm*
Marriott Waterfront Hotel/Grand Ballroom Salon IV

**Wednesday, March 15**
**RSI Editorial Board Meeting**
*12:00noon – 2:00pm*
Marriott Waterfront Hotel/Grand Salon IX

**Wednesday, March 15**
**Status of Funding Opportunities in NSF's Division of Materials Research**
*5:00pm – 7:00pm*
BCC/Room 338

**Wednesday, March 15**
**MRFM Workshop**
**(Magnetic Resonance Force Microscopy)**
*6:30pm – 10:30pm*
Marriott Waterfront Hotel/Atlantic Room

# STUDENTS LUNCH WITH THE EXPERTS

**Wednesday, March 15**
*1:00pm – 2:30pm*
Ballroom II

Students can sign up on-site to enjoy a complimentary box-lunch while participating in an informal discussion with an expert on a topic of interest to them. Topics are listed below. Sign-up will take place beginning on Monday, March 13 at 1:00pm at the APS registration desk, and will be on a first-come, first-served basis. Attendance is limited to eight students per topic/expert. You must show your ticket and badge at the door, and sit at the table for which you have a ticket.

Lunch topics
sponsored by:

| | | |
|---|---|---|
| **1. DMP** | **Jaqueline Krim** | **Nanotribology: Applications and Implications of Friction at the Atomic Scale** |
| 2 DMP | Lynn Boatner | Smart Nanocomposite Materials and How to Make Them |
| **3. DFD** | **Ray Goldstein** | **Biological Physics** |
| 4. DFD | Wolfgang Losert | Complex Fluids from Sand to Cells |
| **5. DFD** | **Dave Weitz** | **Squishy Physics** |
| 6. FPS | Francis Slakey | The Issue of Intelligent Design |
| **7. GMAG** | **Jeff Childress** | **Research in Magnetic Recording - Industrial and Academic Perspectives** |
| 8. GMAG | Jim Rhyne | Neutron Scattering Insights into Condensed Matter Systems |
| **9. DCMP** | **Allen Goldman** | **Superconductivity** |
| 10. DCMP | Art Ramirez | Frustrated Magnetism |
| **11. DCMP** | **Gwyn P. Williams** | **Careers in the National Labs: Development of the Jefferson Lab FEL** |
| 12. DCMP | David Awschalom | Spin Dynamics and Spin Coherence in Condensed Matter Systems (Spintronics) |
| **13. DCMP** | **Julia Phillips** | **Sandia & Los Alamos Center for Integrated Nanotechnologies** |
| 14. DCMP | Alan Dorsey | Supersolids |
| **15. DCMP** | **Garnett Bryant** | **Quantum Nano-optics and Quantum Dots** |
| 16. DCMP | Arthur F. Hebard | Magnetism in Reduced Dimensions: Ultra Thin Films and Thin-Film Interfaces |
| **17. DCMP** | **Christopher Homes** | **Optical Spectroscopy of Superconductors** |
| 18. DCMP | Richard Newrock | One Dimensional Conductance: Coulomb Drag and Luttinger Liquids |
| **19. DCMP** | **Eric Shirley** | **Optical Properties of Materials: From Basic Theory to Industrial Impact** |
| 20. DCMP | Lia Krusin-Elbaum | Can Disorder be Useful? |
| **21. DCMP** | **David Reitze** | **Ultrafast Spectroscopy in High Magnetic Fields: Experiments at the NHMFL** |

# 2006 PRIZES AND AWARDS

**Award Session (Session E5)**
**Monday, March 13**
*5:45pm – 6:45pm*
*BCC/309*

## Biological Physics Prize

**Alfred G. Redfield**
*Brandeis University*

"For his seminal contributions to the theory and technical development of nuclear magnetic resonance spectroscopy, and for pioneering applications of this technique to the study of biological molecules."

## Lars Onsager Prize

**Rodney Baxter**
*Australian National University*

"For his original and groundbreaking contributions to the field of exactly solved models in statistical mechanics, which continue to inspire profound developments in statistical physics and related fields."


## Oliver E. Buckley Prize

**Noel A. Clark**
*University of Colorado*

**Robert Meyer**
*Brandeis University*

"For groundbreaking experimental and theoretical contributions to the fundamental science and applications of liquid crystals, particularly their ferroelectric and chiral properties."

## George E. Pake Prize

**Charles B. Duke**
*Xerox Innovation Group*

"For groundbreaking theoretical contributions to the understanding of tunneling in solids, and inelastic scattering of low-energy electrons in solids, and for his outstanding contributions to Xerox Corporate Research both as an intellectual leader and research manager."

## Frank Isakson Prize

**Roberto Merlin**
*University of Michigan*

"For original contributions to spontaneous Raman and ultrafast spectroscopy of fundamental excitations in solids."

## Earle K. Plyler Prize

**Mark Johnson**
*Yale University*

"For the applications of spectroscopic methods towards the understanding of solvation on the microscopic scale, especially the solvation of protons and hydroxide anions by water."


## James C. McGroddy Prize

**Hongjie Dai**
*Stanford University*

**Alex Zettl**
*University of California, Berkeley*

"For developing novel synthesis pathways for preparing carbon and boron nitride nanotubes and for pioneering applications of these for sensing, electronics and nanomechanics."

## Polymer Prize

**Ludwik Leibler**
*Ecole Superieure de Physique et Chimie Industrielles, Paris*

"For outstanding theoretical contributions to the fundamental understanding of self-assembly of diblock copolymers and gels, and wetting."

# 2006 PRIZES AND AWARDS

## Aneesur Rahman Prize

**David Vanderbilt**
*Rutgers University*

"For his conceptual breakthroughs in his development of the ultrasoft pseudopotential and the modern theory of polarization, and their impact on first-principles investigations of the properties of materials."


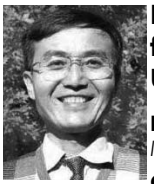

## Prize to a Faculty Member for Research in an Undergraduate Institution

**Rainer Grobe**
*Illinois State University*

**Q. Charles Su**
*Illinois State University*

"For their outstanding effort at creating a successful and renowned optical theory research program at Illinois State University, and for their exemplary involvement of undergraduates in this research."

## David Adler Lectureship Award

**James Chelikowsky**
*University of Texas*

"For his creative and outstanding research in computational materials physics and for his effectiveness in communicating research results through lectures and publications."


## LeRoy Apker Award

**Nathaniel Craig**
*Harvard University*

**Matthew Paoletti**
*Bucknell University*

"Tunable Nonlocal Spin Control in a Coupled Quantum Dot System."
"Experimental Studies of the Effects of Chaotic Mixing on an Advection-Reaction-Diffusion System."

## Edward A. Bouchet Award

**Angel Garcia**
*Rensselaer Polytechnic Institute*

"For his contributions to the understanding of the role of water in the dynamics and folding of proteins through computer simulations."

Photo not available

## John H. Dillon Medal

**Kenji Urayama**
*Kyoto University*

"For insightful experiments that probe the nature of polymer networks."

## Keithley Award

**Frances Hellman**
*University of California, Berkeley*

"In recognition of using emerging micromachining techniques to significantly extend the range of calorimetry into the realm of nano-scale science, by construction of Si based microcalorimeters capable of operating in extreme environments with unprecedented sensitivity and accuracy."

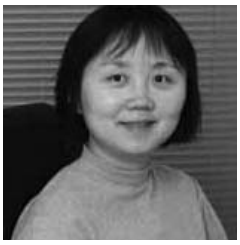

## Maria Goeppert-Mayer Award

**Hui Cao**
*Northwestern University*

"For her groundbreaking contributions to the experimental studies of coherent light generation and transport in disordered media, including her invention of microlasers based on disordered media."

Photo not available

## Nicholas Metropolis Award

**Joseph A. Barranco**
*University of California, Berkeley*

"For the development of computational techniques to handle 3D compact vortices in rotating shear flows, and for the application of these techniques to solve longstanding problems in the theory of planet and star formation."

**Additional Awards:**

**Marshak Lectureship Award: Zohra ben Lakhdar (Session D3)**

**Beller Lectureship Award: Pierre-Gilles de Gennes (Session Y29)**

Each year, the APS Committee on International Scientific Affairs (CISA) will award the APS Beller and Marshak Lectureships to bring distinguished foreign scientists to speak at the March and April meetings.

The Beller Lectureship was endowed by Esther Hoffman Beller for the purpose of bringing distinguished physicists from abroad as invited speakers at APS meetings. The Marshak Lectureship, endowed by Ruth Marshak, in honor of her late husband and former APS president, Robert Marshak, provides travel support for physicists from a developing country or Eastern Europe invited to speak at APS meetings.

# FOCUS SESSIONS

**DAMOP**
A43 - Focus Session: Strongly Interacting Fermi Gases and the BCS - BEC Crossover I
D43 - Focus Session: Vortices and Vortex Lattices in Fermi and Bose Superfluid Gases
H43 - Focus Session: Strongly Interacting Fermi Gases and the BCS - BEC Crossover II
U43 - Focus Session: Novel Phases in Low Dimensional Quantum Gases

**DAMOP/GQI**
W43 - Focus Session: Cold Atoms in Optical Lattices

**DBP**
G26 - Focus Session: Trapping of Nanoscale Biological Objects
G29 - Focus Session: Physical and Engineering Constraints on the Function of Biological Systems
H29 - Focus Session: Physical Aspects of Morphogenesis: Computational Approaches
N29 - Focus Session: Physical Models of Ion Channel Function
R26 - Focus Session: Counterion Dynamics in Charged Biopolymer Systems
R28 - Focus Session: Biological Networks: Structure, Dynamics and Function
W26 - Focus Session: Biological Photophysics
Y26 - Focus Session: Physics of Physiological Systems

**DBP/DCMP**
K26 - Focus Session: Single Molecule Biophysics I

**DBP/DCP**
P26 - Focus Session: Protein Dynamics in Folding and Function

**DBP/DFD**
N26 - Focus Session: DNA and Protein Analysis with Micro and Nano Fluidics

**DBP/DPOLY**
B26 - Focus Session: Single Molecule Biophysics: DNA & RNA
D26 - Focus Session: Dynamics of Nuclei Acid-Protein Interaction: Single Molecule
U29 - Focus Session: Nonequilibrium Fluctuation in Biomolecules and Artificial Nanodevices
Y29 - Focus Session: Noise and Fluctuation in Biological Systems

**DBP/GSNP**
B29 - Focus Session: Micro-Organism Motility
A39 - Focus Session: Magnesium Diboride and Related Compounds: Multi Gap Superconductivity
D15 - Atomic Tunneling, Films, Nanostructures
H39 - Focus Session: Josephson Junctions and Pairing State Symmetry

**DCMP/DCOMP**
*G39* - Focus Session: Superconductivity: Theory and Computation I

**DCMP/GSCCM**
R42 - Focus Session: Plasticity and Phase Transitions

**DCOMP**
D27 - Focus Session: Novel Computational Algorithms I
G27 - Focus Session: Novel Computational Algorithms II

**DCOMP/DFD**
V8 - Focus Session: Simulations Using Particles

**DCOMP/DCMP**
K39 - Focus Session: Superconductivity: Theory and Computation II
P39 - Focus Session: Superconductivity: Theory and Computation (Mainly First Principles)
V39 - Focus Session: Superconductivity: Theory and Computation III
Z39 - Focus Session: Superconductivity: Theory and Computations (Mostly Phonons)

**DCOMP/DMP**
B32 - Focus Session: Computational Nanoscience I
D32 - Focus Session: Computational Nanoscience II
G31 - Focus Session: Simulation of Complex Materials I
H31 - Focus Session: Simulation of Complex Materials II
H32 - Focus Session: Computational Nanoscience III
K31 - Focus Session: Simulation of Complex Materials III
K32 - Focus Session: Computational Nanoscience IV
R32 - Focus Session: Computational Nanoscience V

**DCOMP/GSCCM/DMP**
N42 - Focus Session: Simulations of Matter at Extreme Conditions I
U42 - Focus Session: Simulations of Matter at Extreme Conditions II
W42 - Focus Session: Simulations of Matter at Extreme Conditions III

**DCOMP/GQI**
P40 - Focus Session: Pathways to Practical Quantum Computing I
R40 - Focus Session: Pathways to Practical Quantum Computing II

**DCOMP/GQI/DAMOP**
U40 - Focus Session: Pathways to Practical Quantum Computing III

**DCP**
A10 - Focus Session: Physical Chemistry of Nanoscale Systems I
A11 - Focus Session: Promises and Challenges in Chemical Dynamics I
B10 - Focus Sessions: Physical Chemistry of Nanoscale System II
B11 - Focus Session: Promises and Challenges in Chemical Dynamics II
D10 - Focus Session: Physical Chemistry of Nanoscale System III
D11 - Focus Session: Promises and Challenges in Chemical Dynamics III
G10 - Focus Sessions: Physical Chemistry of Nanoscale System IV
G11 - Focus Session: Promises and Challenges in Chemical Dynamics IV
H10 - Focus Session: Frontiers in Computational Chemical Physics I
H11 - Focus Session: Chemical and Spectroscopic Applications of Nonlinear Optics I
K10 - Focus Session: Frontiers in Computational Chemical Physics II
K11 - Focus Session: Chemical and Spectroscopic Applications of Nonlinear Optics II

# FOCUS SESSIONS

N10 - Focus Session: Frontiers in Computational Chemical Physics III
N11 - Focus Session: Aerosols, Clusters, Droplets: Physics and Chemistry of Nanoobjects I
N13 - Focus Session: Ultrafast and Ultrahigh Field Chemistry I: Strong Field Phenomena
P10 - Focus Session: Frontiers in Computational Chemical Physics IV
P11 - Focus Session: Aerosols, Clusters, Droplets: Physics and Chemistry of Nanoobjects II
P13 - Focus Session: Ultrafast and Ultrahigh Field Chemistry II: Quantum Control
R10 - Focus Session: Surfaces and Interfaces in Electronic Materials I
R11 - Focus Session: Aerosols, Clusters, Droplets: Physics and Chemistry of Nanoobjects III
R13 - Focus Session: Ultrafast and Ultrahigh Field Chemistry III: Ultrafast Processes
U10 - Focus Session: Surfaces and Interfaces in Electronic Materials II
U11 - Focus Session: Aerosols, Clusters, Droplets: Physics and Chemistry of Nanoobjects IV
V10 - Focus Session: Surfaces and Interfaces in Electronic Materials III
V11 - Focus Session: Aerosols, Clusters, Droplets: Physics and Chemistry of Nanoobjects V
W10 - Focus Session: Surfaces and Interfaces in Electronic Materials IV
W11 - Focus Session: Aerosols, Clusters, Droplets: Physics and Chemistry of Nanoobjects VI

**DCP/DBP**

A13 - Focus Session: Spectroscopy of Biomolecules from Isolated Molecules to Cell Environoment I
B13 - Focus Session: Spectroscopy of Biomolecules from Isolated Molecules to Cell Environoment II
D13 - Focus Session: Spectroscopy of Biomolecules from Isolated Molecules to Cell Environoment III
G13 - Focus Session: Spectroscopy of Biomolecules from Isolated Molecules to Cell Environoment IV

**DFD**

H21 - Focus Session: Microfluidic Physics I

**DFD/DBP**

R21 - Focus Session: Biological Hydrodynamics I
U28 - Focus Session: Biological Hydrodynamics II

**DFD/GSNP**

P8 - Focus Session: Jets, Shocks & Splashes

**DMP**

A18 - Focus Session: Carbon Nanotubes: Synthesis and Growth I
A35 - Focus Session: Nanoscale Thermal, Thermoelectricity and Mass Transport: Measurement and Characterization
A46 - Focus Session: Wide Bandgap Semiconductors I
B18 - Focus Session: Carbon Nanotubes: Synthesis, Processing and Characterization
B35 - Focus Session: Nanoscale Thermal, Thermoelectricity and Mass Transport: Theory and Simulation
B46 - Focus Session: Wide Band Gap Semiconductors II
D18 - Focus Session: Carbon Nanotubes: Synthesis and Growth II
D35 - Focus Session: Thermal Transport and Thermoelectricity in Nanotubes and Graphene
D38 - Focus Session: Magnesium Diboride and Related Compounds: Properties of Doped and Irradiated MgB2
D46 - Focus Session: Wide Band Gap Semiconductors III
G18 - Focus Session: Carbon Nanotubes: Electronic and Optical Properties I
G37 - Focus Session: Nanoscale Materials Physics of Phase Transitions I
G38 - Focus Session: Magnesium Diboride and Related Compounds: Carbon Alloying of MgB2
G40 - Focus Session: Materials for Quamtum Computing I
H18 - Focus Session: Carbon Nanotubes: Electronic and Optical Properties II
H36 - Focus Session: Single Molecule Conductance
H37 - Focus Session: Nanoscale Materials Physics of Phase Transitions II
H40 - Focus Session: Materials for Quantum Computing II
H46 - Focus Session: Wide Band Gap Semiconductors IV
K40 - Focus Session: Materials for Quantum Computing III
K41 - Focus Session:Dielectric, Ferroelectric, and Piezoelectric Oxides II
N18 - Focus Session: Carbon Nanotubes: Transport I
N36 - Focus Session: Optical Properties of Nanostructures with S, Se, Te, and Ge
N37 - Focus Session: Nanoscale Fabrication, Assembly and Semiconductor Nanowires
N39 - Focus Session: Magnesium Diboride and Related Compounds: MgB2 Thin Films and Junctions
P18 - Focus Session: Carbon Nanotubes: Opto-Electronics
P36 - Focus Session: Plasmon Resonances in Nanostructures
P41 - Focus Session: Dielectric, Ferroelectric, and Piezoelectric Oxides III
R18 - Focus Session: Carbon Nanotubes: Transport II
R36 - Focus Session: Optical and X-ray Properties of Nanostructures
R37 - Focus Session: Nanoscale Conductance Theory I
R41 - Focus Session: Dielectric, Ferroelectric, and Piezoelectric Oxides IV
U18 - Focus Session: Carbon Nanotubes: Transport III
U36 - Focus Session: Optical Properties of Nano-Dots, Holes, and Wires
U37 - Focus Session: Nanowire and Nanodot Quantum Devices
V18 - Focus Session: Carbon Nanotubes: Transport IV
V36 - Focus Session: Optical Properties of Carbon Nanotubes and C60
V41 - Focus Session: Dielectric, Ferroelectric, and Piezoelectric Oxides V
W18 - Focus Session: Carbon Nanotubes: Electronic and Optical Properties IV
W36 - Focus Session: Optical Properties of Nanostructures of Si & GaAs
Y18 - Focus Session: Carbon Nanotubes: Adsorption and Gas Surface Interactions with Carbon Nanotubes
Y37 - Focus Session: Probing Novel Nanostructures
Z18 - Focus Session: Carbon Nanotubes: Double Wall Nanotubes, Sheets and Chains
Z37 - Focus Session: Nanoscale Conductance Theory III

**DMP/DCMP**

A12 - Focus Session: Steps, Growth, and Smoothing
D15 - Focus Session: Atomic Tunneling, Films, Nanostructures
K12 - Focus Session: Magnetic Thin Films and Narrow Gap

# FOCUS SESSIONS

Semiconductors
N12 - Focus Session: Alloy and Interface Composition
U12 - Focus Session: Electrochemical and Related Growth
V12 - Focus Session: Wetting and Hard-Soft Interfaces

**DMP/DCOMP**
A42 - Focus Session: Planetary Materials I
K42 - Focus Session: Planetary Materials II
P42 - Focus Session: Planetary Materials III

**DMP/DPOLY**
N32 - Focus Session: Carbon Nanotubes: Composites and Applications

**DMP/GMAG**
A20 - Focus Session: Complex Oxide Thin Films Surfaces and Interfaces I: Superlattice Fabrication and Properties
D20 - Focus Session: Multiferroics I: Improper Ferroelectrics
G20 - Focus Session: Complex Oxide Thin Films Surfaces and Interfaces II: Surfaces and Theory
G32 - Focus Session: Orbital/Charge Order in Complex Oxides
K20 - Focus Session: Multiferroics II - Hexagonal Systems
N20 - Focus Session: Complex Oxide Thin Films Surfaces and Interfacess III: New Materials, New Techniques, and Effects of Strain
P20 - Focus Session: Cobaltites, Nickelates and Vanadates
R20 - Focus Session: Multiferroics III: Perovskites
U20 - Focus Session: Metal-Insulator Transition and Electron Phonon Coupling in Perovskites
W20 - Focus Session: Multiferroics IV

**DMP/GSNP**
D33 - Focus Session: Friction, Fracture and Deformation I
H33 - Focus Session: Friction, Fracture and Deformation II
P33 - Focus Session: Friction, Fracture and Deformation III
R33 - Focus Session: Friction, Fracture and Deformation IV

**DPOLY**
A30 - Focus Session: Block Copolymer Dynamics
D25 - Focus Session: Particle Dynamics and Organization; Polymer Tethers and Interfacial Segregation
G28 - Focus Session: Microphysical Properties of Block Copolymer Aggregates I
H25 - Focus Session: Particle Dynamics and Organization
K18 - Focus Session: Dillon Medal Symposium
K28 - Focus Session: Microphysical Properties of Block Copolymer Aggregates II
U30 - Focus Session: Mechanical Properties: Deformation, Rupture and Failure
V30 - Focus Session: Mechanical Properties: Microscale Deformation and Failure
W24 - Focus Session: Lithography

**DPOLY/DBP**
W30 - Focus Session: Biopolymers at Interfaces
Y30 - Focus Session: Biopolymers I: Phase Transitions

**DPOLY/DMP**
A24 - Focus Session: Organic Interfaces
A25 - Focus Session: Organic Field Effect Transistors
G30 - Focus Session: Electronic Transport in Organic Films
H28 - Focus Session: Energetics and Transport in Conjugated Organics
N25 - Focus Session: Organic Photovoltaics

**FIAP**
A16 - Focus Session: Hydrogen Storage I
A17 - Focus Session: Structure and Properties of Nanoscale Oxide Films
B16 - Focus Session: Molecular-Scale Electronics I
B17 - Focus Session: Phase Transitions and Domains in Ferroelectric Nanostructures I
D16 - Focus Session: Negative Refractive Index I
D17 - Focus Session: Phase Transitions and Domains in Ferroelectric Nanostructures II
G17 - Focus Session: Emerging Research Devices and Materials for Microelectronics Industry I
H16 - Focus Session: Hydrogen Storage II
H17 - Focus Session: Emerging Research Devices and Materials for Microelectronics Industry II
K16 - Focus Session: Molecular-Scale Electronics II
K17 - Focus Session: Si, Ge and SiGe Nanostructures
N16 - Focus Session: Hydrogen Storage III
N17 - Focus Session: Semiconductors for THz and IR I
P16 - Focus Session: Molecular-Scale Electronics III
R17 - Focus Session: Semiconductors for THz and IR II

**GMAG/DMP**
A19 - Focus Session: Optical and Electrical Spin Generation in Semiconductors
B19 - Focus Session: Transition Metal Oxide Ferromagnetic Semiconductors
B20 - Focus Session: Phase Competition and Separation in Pervoskite Oxides
D19 - Focus Session: Semiconductor Spin Injection and Detection
D22 - Focus Session: Magnetic Nanopatterns
G19 - Focus Session: III-V Magnetic Semiconductors I
G22 - Focus Session: Magnetic Nanoparticles I
H19 - Focus Session: III-V Magnetic Semiconductors II
H22 - Focus Session: Nanoparticles and Nanocomposites
K19 - Focus Session: III-V Magnetic Semiconductors III
N22 - Focus Session: Magnetic Vortices and Exchange Biased Thin Films
P19 - Focus Session: Spin Interference and Spin Hall Effect
R19 - Focus Session: Spin Hall Effect and Spin Transport
R22 - Focus Session: Biomagnetism and Exchange Biased Thin Films
U19 - Focus Session: Semiconductor Spin Nanostructures for Quantum Computing
V20 - Focus Session: Semiconductor Spin Dynamics: Optics
W19 - Focus Session: Semiconductor Spin Transport: Noise/Theory
W22 - Focus Session: Magnetic Nanoparticles II
Y19 - Focus Session: Novel Ferromagnetic Semiconductors I
Y20 - Focus Session: Ruddlesden-popper Phase Manganites
Z19 - Focus Session: Spin Dynamics in Quantum Dots
Z20 - Focus Session: Novel Ferromagnetic Semiconductors II

**GMAG/DMP/DCOMP**
D23 - Focus Session: MAG.THY I / Spin Structures and Dynamics
G23 - Focus Session: MAG.THY II / Transport & General
N23 - Focus Session: MAG.THY III: Oxides and Phase Transitions
W23 - Focus Session: MAG.THY IV / ab initio Studies

# FOCUS SESSIONS

*Focus Sessions (cont'd)*

**GMAG/FIAP**
R23 - Focus Session: Theory and Simulation for Information Storage Applications
Y22 - Focus Session: Coupled Thin-Film Structures for Magnetic Recording
Z22 - Focus Session: FePt Nanoparticles for Information Storage

**GMAG/FIAP/DMP**
A22 - Focus Session: Current Driven Magnetization Dynamics I
B22 - Focus Session: Current Driven Magnetization Dynamics II
K22 - Focus Session: Magnetization Dynamics
P22 - Focus Session: Spin Transport in Metals
U22 - Focus Session: Magnetic Tunneling I
V22 - Focus Session: Magnetic Tunneling II

**GSCCM/DCMP**
H42 - Focus Session: Dynamic Compression

**GSNP**
A33 - Focus Session: Econophysics
H8 - Focus Session: Jamming in Glasses, Grains, and Gels I
K8 - Focus Session: Jamming in Glasses, Grains and Gels II
N33 - Focus Session: Instabilities & Turbulence in Complex Fluids
N35 - Focus Session: Organization of Complex Networks
V33 - Focus Session: Social Networks

**GSNP/DBP**
P7 - Focus Session: Physics of Transcriptional Regulatory Networks
U26 - Focus Session: Cytoskeletal Dynamics

**GSNP/DFD**
B8 - Focus Session: Granular Materials Near Jamming
W8 - Focus Session: Nonlinear Electrokinetics

**GQI/DCMP**
D40 - Focus Session: Foundations of Quantum Theory
V40 - Focus Session: Linear Optics Quantum Computation

# POSTER SESSIONS

**Poster Sessions**
*Exhibit Hall*
Poster sessions will be held Monday, Tuesday and Wednesday. Posters will be on display from 10:00am to 5:00pm on Monday and Tuesday and from 10:00am to 4:00pm on Wednesday. Authors should be in attendance at the times listed below. APS is not responsible for poster materials that are left in the exhbiti hall after the session is over. No A/V is allowed in poster sessions.

**C1: Poster Session 1**
**Monday, March 13**
Authors in attendance from 2:00pm – 5:00pm
(DPOLY Session from 11:15am – 2:15pm)

Posters 1-99: DPOLY Posters I
Posters 100-152: Biological Physics
Posters 153-184: Chemical Physics
Posters 185-215: Statistical and Nonlinear Physics
Posters 216-256: Artificially Structured Materials
Posters 257-270: Instrumentation and Measurements

**J1: Poster Session II**
**Tuesday, March 14**
Authors in attendance from 2:00pm – 5:00pm

- Posters 1-19: Metals
- Posters 20-48: Semiconductors
- Posters 49-65: Insulators and Dielectrics
- Posters 66-88: Superconductivity
- Posters 89-147: Magnetism Poster
- Posters 148-195: Complex Structured Materials
- Posters 196-245: Fluids and Soft Matter Poster
- Posters 246-259: Phase Transitions and Strongly Correlated Systems
- Posters 260-292: Surfaces, Interfaces and Thin Films

**Q1: Poster Session III**
**Wednesday, March 15**
Authors in attendance from 1:00pm – 4:00pm
(DPOLY Session from 11:15am – 2:15pm)

- Posters 1-97: DPOLY Posters II
- Posters 98-122: Applications
- Posters 123-144: General Theory
- Posters 145-154: General Physics
- Posters 155-157: Quantum Fluids and Solids
- Posters 158-173: Atomic, Molecular & Optical (AMO) Physics
- Posters 174-186: Physics Education
- Posters 187-199: Quantum Information, Concepts, and Computation
- Posters 200-333: Post-Deadline Posters

# PROGRAM FORMAT

**Program Time-Blocks**

Normally contributed and invited sessions at APS general meetings are three hours in length - three sessions per day at 8:00am, 11:15am, and 2:30pm. The time blocks are designated in alpha order beginning with time-block "A" on Monday at 8:00am, and ending with "Z" designating the 11:15 time-block on Friday.

**Session Codes**

The number following the alpha that designates the time-block represents the sequential numbering of the sessions within the time-block. Session A1 is one of several sessions taking place in parallel in the first time-block on Monday. The number following the decimal in the session code represents the sequence of the papers to be presented in that session. For *example:* B3.004 = Time-block B (Monday at 11:15am); Session 3 (of several) within that time-block; and the 4th paper to be presented in that session.

**Poster Codes**

The poster sessions will take place on Monday, Tuesday, and Wednesday in the Exhibit Hall. A breakdown of the topics presented in each category is listed on page 835.

- Monday poster sessions = Sessions C1
- Tuesday poster session = Sessions J1
- Wednesday poster sessions = Sessions Q1

Each poster presentation (board) within each poster session is numbered sequentially.

## GUIDELINES FOR SPEAKERS

**Oral Presentations**

Please arrive at least 15 minutes prior to the scheduled time of your talk. Contributed papers are allocated 12 minutes each - 10 minutes for presentation and 2 minutes for questions from the audience, unless otherwise specified. Invited papers are allocated 36 minutes - 30 minutes for presentation and 6 minutes for questions from the audience.

Note: Occasionally (and unfortunately) the chair for a session may not appear, in which case we ask that the first presenter serve as chair of the session.

**Poster Presentations**

If you are presenting a poster, please be sure to have your poster up prior to 10:00am on the day of your poster presentation to which you have been assigned, and taken down immediately at the end of the day. You must be on hand at the beginning of the poster session (see epitome for times). APS will not be responsible for posters left up after the end of each poster session. No A-V is allowed in the poster sessions. Posters will be on display between the hours of 10:00am to 5:00pm Monday, Tuesday; 10:00am to 4:00pm, Wednesday. Consult the Poster Session Schedule for exact times and a breakdown of poster topics.

## GUIDELINES FOR SESSION CHAIRS

- Prior to the session, check the Corrigenda distributed with the Bulletin, as well as the Program-Changes Board in the registration area to see if any papers in the session you are chairing have been withdrawn.
- Arrive at the meeting room about 15 minutes prior to the start of the session and familiarize yourself with the controls for lights, microphones, A-V equipment and the timer. Technicians will be on hand to assist. If you encounter problems, you should immediately alert the Meetings Manager and/or the A-V specialist.
- Start the session on time. Briefly introduce yourself, announce the first paper and author, and start the timer.
- Please adhere to the time schedule listed in the Bulletin, so that simultaneous sessions are as closely synchronized as possible. Many attendees move from session to session in order to hear specific papers.

Note: any time used by the speaker and/or technicians to set up laptops for LCD (Powerpoint) presentations is deducted from the time allocated for the talk.

- The allotted time for contributed papers is 12 minutes; for invited papers - 36 minutes. If you are chairing a session that includes both contributed and invited papers please be aware of the different times allocated for each and set the timer as follows:

*Contributed papers* - set timer for 8 minutes to give initial warning, then set the final bell to go off 2 minutes later. When this time is up, allow 2 additional minutes for questions relating to the paper, thank the speaker and promptly introduce the next paper and speaker.

Invited papers - set timer for 25 minutes for initial warning, and the final bell to ring 5 minutes later. Then set the timer for 6 additional minutes for questions from the audience.

Explain the timing system to the audience prior to the start of the session, and as often during the session as you think necessary.

- The By-Laws of the Society request that speakers be asked to stop when their allotted time is up in a courteous but firm manner. Keep in mind that the session must end on time, and that the last speaker has just as much right to an audience as does the first speaker.
- Should a speaker fail to appear, you must wait 12 minutes before going on to the next speaker. At the end of the session, call again for the regularly scheduled paper, if time allows.
- When two or more papers are submitted by an author, only one of these will be assigned a scheduled presentation time within that session. It is assumed that the first author listed in the abstract is the person who will present the paper at the meeting. A second abstract submitted by the same author is automatically assigned to a poster.
- If any problems arise that you are unable to handle relative to successfully chairing the session, please inform the A-V tech in the room, or go immediately to the APS registration desk to alert the APS staff.

**General A-V Policy**

In keeping with our legally binding contract with our A-V vendor, speakers are not permitted to bring their own projection equipment for use at the meeting.

**Standard A-V in all Sessions**

The standard A-V package consists of an LCD projector, overhead projector, screen, laser pointer and 2 lapel microphones – one for the chair and one for the speakers. Any additional A-V equipment must be rented by the speaker directly through APS's designated A-V provider located in Rooms 331-332. The speaker is responsible for the cost of renting any additional equipment.

# PROGRAM FORMAT

**Policy and Guidelines on Use of LCD Projectors**

The responsibility for a smooth, technically trouble-free presentation ultimately rests with the presenter. Speakers who plan to use LCDs must do the following:

• Bring your own laptop computer, power cord, and any proprietary cords required for your computer. Do not bring your own projector to the meeting. NOTE: APS is not responsible for the security of personal laptop computers.

• Visit the Speaker-Ready room located in Room 330 to run through the presentation to ensure a smooth and technically trouble-free talk. Testing your presentation in the Speaker-Ready room prior to your presentation is strongly recommended to minimize equipment compatibility difficulties. Remember that time used to set up equipment reduces the time you have to make your presentation.

• Bring a back-up vu-graph presentation in case there are set-up difficulties with the LCD equipment.

# PROGRAM FORMAT & UNIT ACRONYMS

**Divisions**

DAMOP ..... Division of Atomic, Molecular and Optical Physics
DAP ..... Division of Astrophysics
DBP ..... Division of Biological Physics
DCP ..... Division of Chemical Physics
DCMP ..... Division of Condensed Matter Physics
DCOMP ..... Division of Computational Physics
DFD ..... Division of Fluid Dynamics
DLS ..... Division of Laser Science
DMP ..... Division of Materials Physics
DNP ..... Division of Nuclear Physics
DPB ..... Division of the Physics of Beams
DPF ..... Division of Particles and Fields
DPP ..... Division of Plasma Physics
DPOLY ..... Division of Polymer Physics

**Topical Groups**

GFBS ..... Few Body Systems Topical Group
GFC ..... Precision Measurement and Fundamental Constants Topical Group
GGR ..... Gravitation
GHP ..... Topical Group on Hadronic Physics
GIMS ..... Instrumentation and Measurement
GMAG ..... Magnetism and Its Applications Topical Group
GPAP ..... Topical Group on Plasma Astrophysics
GQI ..... Quantum Information, Concepts and Computation
GR ..... Gravitation Topical Group
GSNP ..... Statistical and Non-linear
GSCCM ..... Shock Compression of Condensed Matter

**Forums**

FEd ..... Forum on Education in Physics
FGSA ..... Forum on Graduate Student Affairs
FHP ..... Forum on History of Physics
FIAP ..... Forum on Industrial and Applied Physics
FIP ..... Forum on International Physics
FPS ..... Forum on Physics and Society

**Committees**

COM ..... Committee on Minorities
CSWP ..... Committee on the Status of Women in Physics

# MARCH EXHIBIT SHOW GUIDE 2006

The following is a list of exhibitors participating in the March Meeting 2006. For complete information on exhibiting companies and their booth numbers, consult the Pocket Epitome/Exhibitor Guide distributed at registration. Please take time during the meeting to visit the exhibits. You must wear your badge to be admitted to the exhibits.

**APS Exhibit Hours:**
Monday, March 13 • 10:00am–5:00pm
Tuesday, March 14 • 10:00am–5:00pm
Wednesday, March 15 • 10:00am–4:00pm

A&N Corporation
ADE Phase Shift
Advanced Research Systems, Inc.
AIP Education & Society of Physics Students
AJA International, Inc.
Ambios Technology
American Institute of Physics
American Magnetics Inc.
American Physical Society
Amuneal Manufacturing Corporation
Andeen-Hagerling, Inc.
Applied Surface Technologies
AR Worldwide
Asylum Research
ATOMISTIX
Attocube Systems AG
Blake Industries, Inc.
Bruker BioSpin Corporation, EPR Division
Cambridge Magnetic Refrigeration
Cambridge University Press
COMSOL, Inc.
Cryo Industries of America, Inc.
Cryogenic Control Systems, Inc.
Cryogenic Ltd.
Cryomagnetics, Inc.
Cryomech Inc.
DCA Instruments
Easylab Technologies
Elsevier
Gatan
GMW Associates
Hamamatsu Corporation
Hinds Instruments, Inc.
Horiba Jobin Yvon
ICEoxford®
IEE/Inspec
IOP Publishing
J.A. Woollam Co., Inc.
Janis Research Company, Inc.
Keithley Instruments
Kimball Physics, Inc.
KLA Tencor Corporation
Kurt J. Lesker Co.
Lake Shore Cryotronics, Inc.
Lay Tec GmbH
MacKichan Software
Mad City Labs, Inc.
Mantis Deposition
Material Research Society
MDC Vacuum Products/Insulator Seal
Molecular Imaging
NanoAndMore USA Corp.
Nanomagnetics Instruments
Nanonics Imaging Ltd.
National High Magnetic Field Laboratory
National Nanotechnology
Infrastructure Network
National Research Council of the National Academies
Nature Publishing Group
Neocera, Inc.
Nor-Cal Products, Inc.
NOVOControl
NRC Research Press
Ocean Optics, Inc.
Omicron Nanotechnology USA
Origin Lab Corporation
Oxford Applied Research
Oxford Instruments Superconductivity
Oxford University Press
Photonics Specta
Physics Today
PI (Physik Instrumente) LP
Princeton University Press
Quantum Design
Raith USA, Inc.
RHK Technology, Inc.
Rigaku Molecular Metrology
Royal Society of Chemistry
Scientific Cryomagnetics Ltd.
Scientific Instruments, Inc.
Signal Recovery
Smithsonian/NASA ADS
SPECS GmbH
SPECS Scientific Instruments, Inc.
Springer
Staib Instruments, Inc.
Stanford Research Systems
STAR Cyroelectronics
Stone Ridge Technology
Taylor & Francis Group LLC - CRC Press
Teachspin, Inc.
Tristan Technologies, Inc.
Varian Inc.
VAT, Inc.
Veeco Instruments
Vericold Technologies GmbH
VG Scienta
WebAssign
Wiley
Witec Instruments Corp.
Wolfram Research
World Scientific Publishing Company

# *Epitome of the March Meeting 2006*

**15:00 SUNDAY AFTERNOON 12 MARCH 2006**

1B GSCCM: **GSCCM Business Meeting**
Falkland, Marriott Waterfront Hotel

**19:30 SUNDAY EVENING 12 MARCH 2006**

1A **NAS Town Meeting**
Grand Ballroom Salon V, Marriott Waterfront Hotel

**8:00 MONDAY MORNING 13 MARCH 2006**

A1 DCMP: **Quantum Properties of Superconducting Nanowires**
*Sachdev, Tian, Rogachev, Khlebnikov, Arutyunov*
Ballroom IV, Baltimore Convention Center

A2 DCMP: **Magnetic-Ferroelectric Coupling in Multiferroics**
*Cheong, Vajk, Harris, Chu, Mostovoy*
Ballroom III, Baltimore Convention Center

A3 DCMP: **Bilayer 2D Systems: Interlayer Drag and Spontaneous Coherence**
*Pillarisetty, Das Sarma, Kivelson, Simon, Pellegrini*
Ballroom I, Baltimore Convention Center

A4 DPOLY: **Particle Self Assembly**
*Crocker, Starr, Hammond, Douglas, Walker*
308, Baltimore Convention Center

A5 DMP/ FIAP: **Advanced Materials for Energy Applications**
*Dresselhaus, Kanatzidis, Christensen, Mavrikakis, Schubert*
309, Baltimore Convention Center

A6 DCOMP: **Frontiers of Computational Materials**
*Asta, Johnson, Marzari, Hart, Kolmogorov*
310, Baltimore Convention Center

A7 DBP: **Bacterial Flagellar Dynamics, Polymorphism, and Conformational Spread**
*Powers, Stark, Darnton, Shaevitz*
307, Baltimore Convention Center

A8 DFD/ GSNP: **Pattern Formation and Nonlinear Dynamics**
314, Baltimore Convention Center

A9 DCMP: **Electronic Structure on Surfaces and in Reduced Dimensions**
301, Baltimore Convention Center

A10 DCP: **Focus Session: Physical Chemistry of Nanoscale Systems I**
*Nesbitt, Van Duyne*
302, Baltimore Convention Center

A11 DCP: **Focus Session: Promises and Challenges in Chemical Dynamics I**
*Shapiro, Lin*
303, Baltimore Convention Center

A12 DMP/ DCMP: **Focus Session: Steps, Growth, and Smoothing**
*Margetis*
304, Baltimore Convention Center

A13 DCP/ DBP: **Focus Session: Spectroscopy of Biomolecules from Isolated Molecules to Cell Environment I**
*Anfinrud, Spence*
305, Baltimore Convention Center

A15 DCMP: **Metals: 1D, 2D, 3D**
311, Baltimore Convention Center

A16 FIAP: **Focus Session: Hydrogen Storage I**
*Frederick Pinkerton*
312, Baltimore Convention Center

A17 FIAP: **Focus Session: Structure and Properties of Nanoscale Oxide Films**
*Pennycook, Freund*
313, Baltimore Convention Center

A18 DMP: **Focus Session: Carbon Nanotubes: Synthesis and Growth I**
*Hata*
315, Baltimore Convention Center

A19 GMAG/DMP: **Focus Session: Optical and Electrical Spin Generation in Semiconductors**
*Sipe*
316, Baltimore Convention Center

A20 DMP/GMAG: **Focus Session: Complex Oxide Thin Films Surfaces and Interfaces I: Superlattice Fabrication and Properties**
*Varela*
317, Baltimore Convention Center

A21 DFD: **Colloids I: Emulsions, Foams, and Suspensions**
318, Baltimore Convention Center

A22 GMAG/FIAP/DMP: **Focus Session: Current Driven Magnetization Dynamics I**
*Pufall*
319, Baltimore Convention Center

A23 GMAG: **Strongly Correlated Electrons I**
320, Baltimore Convention Center

A24 DPOLY: **Semi-Crystalline and Structured Polymers**
321, Baltimore Convention Center

A25 DPOLY/DMP: **Focus Session: Organic Field Effect Transistors**
*Marks*
322, Baltimore Convention Center

A26 DBP: **Biomolecular Computation**
323, Baltimore Convention Center

A28 DPOLY: **Polymer Blends**
325, Baltimore Convention Center

A29 DBP: **Experimental Techniques in Biophysics**
326, Baltimore Convention Center

A30 DPOLY: **Focus Session: Block Copolymer Dynamics**
*Morse*
327, Baltimore Convention Center

A31 DCMP: **Metallic Nanostructures**
328, Baltimore Convention Center

A32 DCMP: **Fullerenes**
329, Baltimore Convention Center

A33 GSNP: **Focus Session: Econophysics**
*Yakovenko*
336, Baltimore Convention Center

A35 DMP: **Focus Session: Nanoscale Thermal, Thermoelectric and Mass Transport: Measurement and Characterization**
*Fon*
338, Baltimore Convention Center

A36 DCMP: **Structural, Optical, and Electronic Properties of Nanostructures**
339, Baltimore Convention Center

A38 DCMP: **Superconductivity—Vortex Matter**
341, Baltimore Convention Center

A39 DMP: **Focus Session: Magnesium Diboride and Related Compounds: Multi Gap Superconductivity**
342, Baltimore Convention Center

A40 TGQI/DCMP: **Quantum Entanglement**
343, Baltimore Convention Center

A41 DCMP: **Quantum Fluids and Solids**
344, Baltimore Convention Center

A42 DMP/DCOMP: **Focus Session: Planetary Materials I**
*Gironcoli, Lin*
345, Baltimore Convention Center

A43 DAMOP: **Focus Session: Strongly Interacting Fermi Gases and the BCS-BEC Crossover I**
*Denschlag*
346, Baltimore Convention Center

A45 GMAG: **Cuprates and Nickelates**
348, Baltimore Convention Center

A46 DMP: **Focus Session: Wide Bandgap Semiconductors I**
*Wetzel*
349, Baltimore Convention Center

**11:15 MONDAY MORNING**
**13 MARCH 2006**

B1 DCMP: **DCMP/DCOMP Prize Session**
*Clark, Meyer, Merlin, Vanderbilt*
Ballroom IV, Baltimore Convention Center

B2 DCMP: **Solid Helium**
*Clark, Beamish, Dai, Reatto, Ceperley*
Ballroom III, Baltimore Convention Center

B3 GSNP: **Uncovering the Structure of Complex Networks**
*Newman, Guimera, Vicsek, Muñoz, Almaas*
Ballroom I, Baltimore Convention Center

B4 DMP/ FIAP: **Advances in ZnO Materials Physics and Applications**
*Van de Walle, Tsukazaki, Brillson, Hsu, Norton*
308, Baltimore Convention Center

B5 FPS: **Nuclear Proliferation & Nuclear Terrorism**
*Cirincione, Fetter, Park, Carter*
309, Baltimore Convention Center

B6 DCMP: **Spin-Based Quantum Computing**
*Hanson, Ghosh, Flatté, Finley, Burkard*
310, Baltimore Convention Center

B7 DBP/ DCMP: **Bionanotechnology: Application and Fundamental Aspects of Processes at Nano-scale**
*Eisenberg, Kosztin, Stein, Yu, Kohli*
307, Baltimore Convention Center

B8 GSNP/ DFD: **Focus Session: Granular Materials Near Jamming**
*Campbell, Daniels*
314, Baltimore Convention Center

B9 DCMP: **Phase Transitions, Dynamics, and Excitations**
301, Baltimore Convention Center

B10 DCP: **Focus Sessions: Physical Chemistry of Nanoscale System II**
*El-Sayed, Dexheimer*
302, Baltimore Convention Center

B11 DCP: **Focus Session: Promises and Challenges in Chemical Dynamics II**
*Jortner, Brus*
303, Baltimore Convention Center

B12 DCMP/ DMP: **Quantum Metal Films and Overlayer Structures**
304, Baltimore Convention Center

B13 DCP/ DBP: **Focus Session: Spectroscopy of Biomolecules from Isolated Molecules to Cell Environment II**
*de Vries, Jarrold, Jockusch*
305, Baltimore Convention Center

B15 DCMP: **Metals: Lattice, Low D, Phonons**
*Burin*
311, Baltimore Convention Center

B16 FIAP: **Focus Session: Molecular-Scale Electronics I**
*Champagne*
312, Baltimore Convention Center

B17 FIAP: **Focus Session: Phase Transitions and Domains in Ferroelectric Nanostructures I**
*Levanyuk*
313, Baltimore Convention Center

B18 DMP: **Focus Session: Carbon Nanotubes: Synthesis, Processing and Characterization**
*Arnold*
315, Baltimore Convention Center

B19 GMAG/ DMP: **Focus Session: Transition Metal Oxide Ferromagnetic Semiconductors**
*Ogale*
316, Baltimore Convention Center

B20 GMAG/ DMP: **Focus Session: Phase Competition and Separation in Pervoskite Oxides**
*Wu*
317, Baltimore Convention Center

B21 DFD: **Colloids II: Colloidal Crystals, Gels, and Glasses**
318, Baltimore Convention Center

B22 GMAG/ FIAP/ DMP: **Focus Session: Current Driven Magnetization Dynamics II**
*Beach*
319, Baltimore Convention Center

B23 GMAG: **Quantum Spin Chains I**
320, Baltimore Convention Center

B26 DBP/ DPOLY: **Focus Session: Single Molecule Biophysics: DNA & RNA**
*Nelson*
323, Baltimore Convention Center

B28 DBP: **Experimental Techniques in Biomaterials Science**
325, Baltimore Convention Center

B29 DBP/ GSNP: **Focus Session: Micro-Organism Motility**
*Bodenschatz*
326, Baltimore Convention Center

B31 DCMP: **Insulating Nanostructures**
328, Baltimore Convention Center

B32 DCOMP/ DMP: **Focus Session: Computational Nanoscience I**
*Roundy*
329, Baltimore Convention Center

B33 GSNP: **Financial Markets and Other Applications of Statistical Physics**
336, Baltimore Convention Center

B35 DMP: **Focus Session: Nanoscale Thermal, Thermoelectric and Mass Transport: Theory and Simulation**
*Heinze*
338, Baltimore Convention Center

B36 DCMP: **Electronic Properties of Nanowires**
339, Baltimore Convention Center

B37 DCMP: **High-Tc: STM and Pseudogap**
340, Baltimore Convention Center

B38 DCMP: **Superconducting Devices and Applications**
341, Baltimore Convention Center

B39 DCMP: **Superconductivity—Magnetic Properties**
342, Baltimore Convention Center

B40 TGQI/ DCMP: **Topics in Quantum Foundations**
343, Baltimore Convention Center

B42 **SPS Undergraduate Research I**
345, Baltimore Convention Center

B43 DAMOP: **BEC in Trapped Atomic Gases**
346, Baltimore Convention Center

B46 DMP: **Focus Session: Wide Band Gap Semiconductors II**
*Wright*
349, Baltimore Convention Center

**13:30 MONDAY AFTERNOON 13 MARCH 2006**

B34 **Session on Authoring**
337, Baltimore Convention Center

**14:00 MONDAY AFTERNOON 13 MARCH 2006**

C1 **Poster Session I**
Exhibit Hall 2:00pm–5:00pm (DPOLY session: 11:15am–2:15pm), Baltimore Convention Center

**14:30 MONDAY AFTERNOON 13 MARCH 2006**

D1 DCMP: **Fluctuation and Relaxation Near Jamming**
*Langer, Makse, Abate, Silbert, Losert*
Ballroom IV, Baltimore Convention Center

D2 DCMP: **Quantum Hall Effect in Graphene**
*Kim, Geim, Sharapov, De Heer*
Ballroom III, Baltimore Convention Center

D3 FIP: **Scientists from Developing Countries: Is There an Effective Way to Support Meaningful Research?**
*Kofane, Ben lakdar, de Brito Cruz, M'Passi-Mabiala*
Ballroom I, Baltimore Convention Center

D4 DPOLY/ DMP: **Organic Electronics**
*Friend, Martin, Loo, Chabinyc, Lin*
308, Baltimore Convention Center

D5 FIAP: **Catalysis and Complexity: Ken Hass Memorial**
*Schneider, Wolverton, Carlsson, Davis*
309, Baltimore Convention Center

D6 DCOMP: **Simulating Hydrogen Storage: From Current Challenges to Future Promises**
*Johnson, Tse, Zhao, Jena, Goddard*
310, Baltimore Convention Center

D7 GMAG: **New Results in Geometrically Frustrated Magnets**
*Mendels, Moessner, Gardner, Schiffer, Lunkenheimer*
307, Baltimore Convention Center

D8 DFD/GSNP: **Patterns and Instabilities I**
314, Baltimore Convention Center

D9 DBP: **Methods in Nanobiotechnology**
*Roukes, Austin, Michl, Wiseman, Hla*
301, Baltimore Convention Center

D10 DCP: **Focus Session: Physical Chemistry of Nanoscale System III**
*Leone, Xie*
302, Baltimore Convention Center

D11 DCP: **Focus Session: Promises and Challenges in Chemical Dynamics III**
*Kawasaki*
303, Baltimore Convention Center

D12 DCMP/DMP: **Morphological Evolution and Instabilities**
304, Baltimore Convention Center

D13 DCP/DBP: **Focus Session: Spectroscopy of Biomolecules from Isolated Molecules to Cell Environment III**
*Baumgart, Ha*
305, Baltimore Convention Center

D15 DCMP: **Focus Session: Atomic Tunneling, Films, Nanostructures**
*Enss*
311, Baltimore Convention Center

D16 FIAP: **Focus Session: Negative Refractive Index I**
*Brueck*
312, Baltimore Convention Center

D17 FIAP: **Focus Session: Phase Transitions and Domains in Ferroelectric Nanostructures II**
*Gregg*
313, Baltimore Convention Center

D18 DMP: **Focus Session: Carbon Nanotubes: Synthesis and Growth II**
315, Baltimore Convention Center

D19 GMAG/DMP: **Focus Session: Semiconductor Spin Injection and Detection**
*Crowell*
316, Baltimore Convention Center

D20 DMP/GMAG: **Focus Session: Multiferroics I**
317, Baltimore Convention Center

D21 DFD: **Colloids III: Particles at Interfaces and in Confined Geometries**
318, Baltimore Convention Center

D22 GMAG/DMP: **Focus Session: Magnetic Nanopatterns**
*Chien*
319, Baltimore Convention Center

D23 GMAG/DMP/DCOMP: **Focus Session: MAGTHY I/Spin Structures and Dynamics**
*Dobrovitski*
320, Baltimore Convention Center

D25 DPOLY: **Focus Session: Particle Dynamics and Organization; Polymer Tethers and Interfacial Segregation**
*Smith*
322, Baltimore Convention Center

D26 DBP/DPOLY: **Focus Session: Dynamics of Nuclei Acid-Protein Interaction: Single Molecule**
*Wang, Wuite*
323, Baltimore Convention Center

D27 DCOMP: **Focus Session: Novel Computational Algorithms I**
*Hu, Aspuru-Guzik*
324, Baltimore Convention Center

D28 DPOLY: **Block Copolymer Thin Films**
325, Baltimore Convention Center

D29 DBP/GSNP: **Molecular Machines and Motors**
*Flood, Goldman*
326, Baltimore Convention Center

D30 DPOLY: **Multiphase Polymer Materials**
327, Baltimore Convention Center

D31 DCMP: **Properties of Semiconducting Nanostructures**
328, Baltimore Convention Center

D32 DCOMP/DMP: **Focus Session: Computational Nanoscience II**
329, Baltimore Convention Center

D33 DMP/GSNP: **Focus Session: Friction, Fracture and Deformation I**
*Dickinson*
336, Baltimore Convention Center

D35 DMP: **Focus Session: Thermal Transport and Thermoelectricity in Nanotubes and Graphene**
*Shi*
338, Baltimore Convention Center

D38 DMP: **Focus Session: Superconductivity—Properties of Doped and Irradiated Magnesium Diboride and Related Compounds**
*Putti*
341, Baltimore Convention Center

D39 DCMP: **Spin Properties of Superconductors**
342, Baltimore Convention Center

D40 TGQI/DCMP: **Focus Session: Foundations of Quantum Theory**
*Hardy*
343, Baltimore Convention Center

D42 SPS: **SPS Undergraduate Research II**
345, Baltimore Convention Center

D43 DAMOP: **Focus Session: Vortices and Vortex Lattices in Fermi and Bose Superfluid Gases**
*Zwierlein*
346, Baltimore Convention Center

D45 GMAG: **Strongly Correlated Electrons on Triangular Lattices**
348, Baltimore Convention Center

D46 DMP: **Focus Session: Wide Band Gap Semiconductors III**
*Huang*
349, Baltimore Convention Center

## 17:45 MONDAY EVENING 13 MARCH 2006

E5 **APS Prizes and Awards Ceremony**
309, Baltimore Convention Center

## 18:45 MONDAY EVENING 13 MARCH 2006

E6 **Welcome Reception**
Ballroom II, Baltimore Convention Center

## 20:00 MONDAY EVENING 13 MARCH 2006

F50 DCMP: **Emerging Emergent Phenomena**
*Witten, Lolle, Barabási, Sadoulet*
Grand Salons V-VI, Marriott Waterfront Hotel

## 8:00 TUESDAY MORNING 14 MARCH 2006

G1 **Nobel Prize Symposium and Special Prize Session**
*Hänsch, Hall, Glauber, Su, Grobe*
Ballroom IV, Baltimore Convention Center

G2 DCMP: **Quantum Criticality in Cuprates**
*Chamon, Tallon, Shibauchi, Lake, Broun*
Ballroom III, Baltimore Convention Center

G3 DCMP: **Coupled Superconducting Qubits**
*Shnirman, Martinis, Schuster, Plantenberg, Morpurgo*
Ballroom I, Baltimore Convention Center

G4 DPOLY: **Polymer Physics Prize**
*Leibler, Möller, Fredrickson, Candau, Colby*
308, Baltimore Convention Center

G5 DMP/FIAP: **Advanced Materials for Solar Energy Utilization**
*Lewis, Kurtz, Yong, Moore, Carlson*
309, Baltimore Convention Center

G7 GSNP: **Shear-Induced Patterns in Complex Fluids and Granular Matter**
*van Saarloos, Reichmann, Register, Davidovitch, Jaeger*
307, Baltimore Convention Center

G8 DFD/GSNP: **Patterns and Instabilities II**
314, Baltimore Convention Center

G10 DCP: **Focus Sessions: Physical Chemistry of Nanoscale System IV**
*Yang, Xia*
302, Baltimore Convention Center

G11 DCP: **Focus Session: Promises and Challenges in Chemical Dynamics IV**
*Shafer-Ray*
303, Baltimore Convention Center

G12 DCMP/DMP: **Self-Assembled Nanostructures: Growth and Patterning**
304, Baltimore Convention Center

G13 DCP/DBP: **Focus Session: Spectroscopy of Biomolecules from Isolated Molecules to Cell Environment IV**
*Zwier, Hochstrasser, Mons*
305, Baltimore Convention Center

G15 DCMP: **Mechanical Properties of Metals**
311, Baltimore Convention Center

G16 FIAP: **Focus Session: Negative Refractive Index II**
*Narimanov*
312, Baltimore Convention Center

G17 FIAP: **Focus Session: Emerging Research Devices and Materials for Microelectronics Industry I**
*Vogel*
313, Baltimore Convention Center

G18 DMP: **Focus Session: Carbon Nanotubes: Electronic and Optical Properties I**
*Spataru*
315, Baltimore Convention Center

G19 GMAG/DMP: **Focus Session: III-V Magnetic Semiconductors I**
*Poggio*
316, Baltimore Convention Center

G20 DMP/GMAG: **Focus Session: Complex Oxide Thin Films Surfaces and Interfaces II: Surfaces and Theory**
317, Baltimore Convention Center

G21 DFD: **Colloids IV: Polymeric and Colloid-Polymer Systems**
318, Baltimore Convention Center

G22 GMAG/DMP: **Focus Session: Magnetic Nanoparticles I**
*Leslie-Pelecky*
319, Baltimore Convention Center

G23 GMAG/DMP/DCOMP: **Focus Session: MAGTHY II/ Transport & General**
*Yao*
320, Baltimore Convention Center

G24 DPOLY: **Polymer Nanomaterials I**
321, Baltimore Convention Center

G25 DPOLY: **Structure and Dynamics of Functional Macromolecules**
322, Baltimore Convention Center

G26 DBP: **Focus Session: Trapping of Nanoscale Biological Objects**
*Cohen, Gratton*
323, Baltimore Convention Center

G27 DCOMP: **Focus Session: Novel Computational Algorithms II**
*Bai, Baroni*
324, Baltimore Convention Center

G28 DPOLY: **Focus Session: Microphysical Properties of Block Copolymer Aggregates I**
*Discher*
325, Baltimore Convention Center

G29 DBP: **Focus Session: Physical and Engineering Constraints on the Function of Biological Systems**
*Lezon, Doyle*
326, Baltimore Convention Center

G30 DPOLY/DMP: **Focus Session: Electronic Transport in Organic Films**
*De Feyter, Charra*
327, Baltimore Convention Center

G31 DCOMP/DMP: **Focus Session: Simulation of Complex Materials I**
*Wagner*
328, Baltimore Convention Center

G32 DMP/GMAG: **Focus Session: Orbital/Charge Order in Complex Oxides**
*Ye*
329, Baltimore Convention Center

G33 GSNP: **GSNP Student Award Session and Glasses**
336, Baltimore Convention Center

G34 DFD: **Glassy Dynamics and Jamming**
337, Baltimore Convention Center

G35 DCMP: **Nanoparticles, Nanotubes and Nanocrystals: Optical and Structural Properties**
338, Baltimore Convention Center

G37 DMP: **Focus Session: Nanoscale Materials Physics of Phase Transitions I**
*Dawber*
340, Baltimore Convention Center

G38 DMP: **Focus Session: Superconductivity—Carbon Alloying of Magnesium Diboride and Related Compounds**
*Wilke*
341, Baltimore Convention Center

G39 DCMP/ DCOMP: **Focus Session: Superconductivity: Theory and Computation I**
*Scalapino*
342, Baltimore Convention Center

G40 DMP: **Focus Session: Materials for Quantum Computing I**
343, Baltimore Convention Center

G41 DCMP: **Supersolid**
344, Baltimore Convention Center

G42 FEd: **Physics Education Research and Undergraduate Education**
345, Baltimore Convention Center

G44 DCMP: **Charge-Density Waves**
347, Baltimore Convention Center

G45 GMAG: **Phase Transitions in Ruthenates**
348, Baltimore Convention Center

G46 FIAP: **QHE, Including Graphene**
349, Baltimore Convention Center

## 11:15 TUESDAY MORNING 14 MARCH 2006

H1 GQI: **Quantum Information, Concepts and Computation**
*Blatt, Yamamoto, Raizen, Gisin, Whaley*
Ballroom IV, Baltimore Convention Center

H2 DCMP: **Spin Liquids in 2D Frustrated Quantum Magnets**
*Coldea, Alicea, Kanoda, Motrunich, Lee*
Ballroom III, Baltimore Convention Center

H3 DCMP: **Soft Interfaces**
*Quere, Zhang, Stebe, Hilgenfeldt, Gopal*
Ballroom I, Baltimore Convention Center

H4 DCMP: **Physics for Everyone and Depletion Forces In Vitro and Out of Equilibrium**
*Dahlberg, Falco, Schwartz, Snir, Lewis*
308, Baltimore Convention Center

H5 FEd/ FGSA/ FPS/ CSWP: **Forum: What Has Actually Changed in Physics Departments in the Situation for Women, Graduate Students and Other People?**
309, Baltimore Convention Center

H6 DCOMP: **The Response of Extended Systems to Electrical and Magnetic Fields: Novel, Theoretical, and Computational Methods**
*Thonhauser, MacDonald, Cai, Umari, Ghosez*
310, Baltimore Convention Center

H7 DBP: **Nanopore Biophysics**
*Kasianowicz, Dekker, Movileanu, Li, Aksimentiev*
307, Baltimore Convention Center

H8 GSNP: **Focus Session: Jamming in Glasses, Grains, and Gels I**
*Maloney*
314, Baltimore Convention Center

H10 DCP: **Focus Session: Frontiers in Computational Chemical Physics I**
*Lin, Angel*
302, Baltimore Convention Center

H11 DCP: **Focus Session: Chemical and Spectroscopic Applications of Nonlinear Optics I**
*Eisenthal, Shultz*
303, Baltimore Convention Center

H12 DCMP/ DMP: **Thin Film Growth and Interfaces**
304, Baltimore Convention Center

H13 DCP: **Colloid and Polymer Interfaces**
305, Baltimore Convention Center

H15 DCMP: **Metals: Electronic Structure, Fermiology, Transport**
311, Baltimore Convention Center

H16 FIAP: **Focus Session: Hydrogen Storage II**
*Ahn*
312, Baltimore Convention Center

H17 FIAP: **Focus Session: Emerging Research Devices and Materials for Microelectronics Industry II**
*Coufal*
313, Baltimore Convention Center

H18 DMP: **Focus Session: Carbon Nanotubes: Electronic and Optical Properties II**
*Lienau, Chang*
315, Baltimore Convention Center

H19 GMAG/ DMP: **Focus Session: III-V Magnetic Semiconductors II**
*Burch*
316, Baltimore Convention Center

H20 GMAG: **Frustration in 3D**
317, Baltimore Convention Center

H21 DFD: **Focus Session: Microfluidic Physics I**
*Paoletti*
318, Baltimore Convention Center

H22 GMAG/ DMP: **Focus Session: Nanoparticles and Nanocomposites**
*Wang*
319, Baltimore Convention Center

H23 GMAG/ DMP/ FIAP: **GMR and AMR**
320, Baltimore Convention Center

H24 DPOLY: **Polymers at Interfaces**
321, Baltimore Convention Center

H25 DPOLY: **Focus Session: Particle Dynamics and Organization**
322, Baltimore Convention Center

H27 DCOMP: **Computational Methods: Multiscale Modeling**
324, Baltimore Convention Center

H28 DPOLY/ DMP: **Focus Session: Energetics and Transport in Conjugated Organics**
*Silva*
325, Baltimore Convention Center

H29 DBP: **Focus Session: Physical Aspects of Morphogenesis: Computational Approaches**
*Brodland, Jiang*
326, Baltimore Convention Center

H30 DPOLY: **Padden Award Symposium**
327, Baltimore Convention Center

H31 DCOMP/ DMP: **Focus Session: Simulation of Complex Materials II**
*Ogitsu*
328, Baltimore Convention Center

H32 DCOMP/ DMP: **Focus Session: Computational Nanoscience III**
*Zhang*
329, Baltimore Convention Center

H33 DMP/ GSNP: **Focus Session: Friction, Fracture and Deformation II**
*Gnecco*
336, Baltimore Convention Center

H35 DCMP: **Electronic Properties of Quantum Wells and Superlattices**
338, Baltimore Convention Center

H36 DMP: **Focus Session: Single Molecule Conductance**
*Weber*
339, Baltimore Convention Center

H37 DMP: **Focus Session: Nanoscale Materials Physics of Phase Transitions II**
*Albrecht*
340, Baltimore Convention Center

H38 DCMP: **Superconductivity—Disordered Thin Films and Quantum Phenomena**
341, Baltimore Convention Center

H39 DCMP: **Focus Session: Superconductivity—Josephson Junctions and Pairing State Symmetry**
*Klemm*
342, Baltimore Convention Center

H40 DMP: **Focus Session: Materials for Quantum Computing II**
*Buhrman*
343, Baltimore Convention Center

H41 DMP: **Dielectric, Ferroelectric, and Piezoelectric Oxides I**
344, Baltimore Convention Center

H42 GSCCM/ DCMP: **Focus Session: Dynamic Compression**
*Hayes, Minich*
345, Baltimore Convention Center

H43 DAMOP: **Focus Session: Strongly Interacting Fermi Gases and the BCS-BEC Crossover II**
*Regal*
346, Baltimore Convention Center

H44 DCMP: **Quantum Phase Transitions**
347, Baltimore Convention Center

H45 DCMP: **Theoretical Methods in Strongly Correlated Electron Systems**
348, Baltimore Convention Center

H46 DMP: **Focus Session: Wide Band Gap Semiconductors IV**
*Qian*
349, Baltimore Convention Center

## 14:00 TUESDAY AFTERNOON 14 MARCH 2006

J1 **Poster Session II**
Exhibit Hall, 2:00pm–5:00pm, Baltimore Convention Center

## 14:30 TUESDAY AFTERNOON 14 MARCH 2006

K1 DAMOP: **Optical Frequency Clocks and Experimental Quantum Optics**
*Gill, Udem, Ye, Bergquist, Haroche*
Ballroom IV, Baltimore Convention Center

K2 DCMP: **Exotic Ordering in Spinels**
*Croft, Horibe, Khomskii, Sushkov, Radaelli*
Ballroom III, Baltimore Convention Center

K3 DCMP: **Electron Doped High Tc Superconductors**
*Dagan, Blumberg, Takahashi, Motoyama, Naito*
Ballroom I, Baltimore Convention Center

K4 DMP/ CSWP: **DMP/CSWP Prize Symposium**
*Chelikowsky, Cao, Dai, Zettl*
308, Baltimore Convention Center

K5 FIAP: **Microelectronics for Mid-Infrared through Terahertz**
*Gmachl, Prober, Shaner, Tredicucci, Schmidt*
309, Baltimore Convention Center

K6 COM: **Minorities in the Nanosciences**
*Mason, James, Noveron, Stokes*
310, Baltimore Convention Center

K7 DBP: **New Methods and Algorithms for Biomolecular Modeling**
*Darve, Sagui, Thorpe, Tuckerman, Yang*
307, Baltimore Convention Center

K8 GSNP: **Focus Session: Jamming in Glasses, Grains and Gels II**
*Blair*
314, Baltimore Convention Center

K10 DCP: **Focus Session: Frontiers in Computational Chemical Physics II**
*Reuter*
302, Baltimore Convention Center

K11 DCP: **Focus Session: Chemical and Spectroscopic Applications of Nonlinear Optics II**
*Shen, Simpson, Morita*
303, Baltimore Convention Center

K12 DMP/DCMP: **Focus Session: Magnetic Thin Films and Narrow Gap Semiconductors**
*Weitering*
304, Baltimore Convention Center

K13 DCP: **Atomic And Molecular Processes at Solid Surfaces**
305, Baltimore Convention Center

K16 FIAP: **Focus Session: Molecular-Scale Electronics II**
*Karna*
312, Baltimore Convention Center

K17 FIAP: **Focus Session: Si, Ge and SiGe Nanostructures**
*Ross, Kamins*
313, Baltimore Convention Center

K18 DPOLY: **Focus Session: Dillon Medal Symposium**
*Urayama*
315, Baltimore Convention Center

K19 GMAG/DMP: **Focus Session: III-V Magnetic Semiconductors III**
*van Schilfgaarde*
316, Baltimore Convention Center

K20 DMP/GMAG: **Focus Session: Multiferroics II—Hexagonal Systems**
*Fennie*
317, Baltimore Convention Center

K21 DFD: **Colloids V**
318, Baltimore Convention Center

K22 GMAG/FIAP/DMP: **Focus Session: Magnetization Dynamics**
*Rasing*
319, Baltimore Convention Center

K23 GMAG: **Quantum Magnets: BEC and 2D**
320, Baltimore Convention Center

K24 DPOLY: **Polymer Nanomaterials II**
321, Baltimore Convention Center

K25 DPOLY: **Polymer Electrolytes and Conduction**
322, Baltimore Convention Center

K26 DBP/DCMP: **Focus Session: Single Molecule Biophysics I**
*Chu*
323, Baltimore Convention Center

K27 DCOMP: **Density Functional Theory**
324, Baltimore Convention Center

K28 DPOLY: **Focus Session: Microphysical Properties of Block Copolymer Aggregates II**
*Santore*
325, Baltimore Convention Center

K29 DBP: **Proteins Structure and Function**
326, Baltimore Convention Center

K30 DMP: **Carbon Nanotubes: Applications and Novel Phenomena**
327, Baltimore Convention Center

K31 DCOMP/DMP: **Focus Session: Simulation of Complex Materials III**
*Blum*
328, Baltimore Convention Center

K32 DCOMP/DMP: **Focus Session: Computational Nanoscience IV**
329, Baltimore Convention Center

K33 GSNP: **Novel Moving Boundary Problems**
*Krug, Kessler, Ebert, Goldstein, Karma*
336, Baltimore Convention Center

K34 **Panel Discussion**
337, Baltimore Convention Center

K35 DCMP: **Electronic Properties and the Kondo Effect in Quantum Dots**
338, Baltimore Convention Center

K36 GMAG: **Magnetic Domains and Applied Magnetic Materials**
339, Baltimore Convention Center

K37 DCMP: **Superconductivity—Time Resolved Optical and Inelastic X-ray Scattering in Cuprates**
340, Baltimore Convention Center

K38 DCMP: **Superconductivity—Mesoscopics and Theory**
341, Baltimore Convention Center

K39 DCOMP/DCMP: **Focus Session: Superconductivity—Theory and Computation II**
*Fabrizio*
342, Baltimore Convention Center

K40 DMP: **Focus Session: Materials for Quantum Computing III**
*McDermott*
343, Baltimore Convention Center

K41 DMP: **Focus Session: Dielectric, Ferroelectric, and Piezoelectric Oxides II**
*Venturini*
344, Baltimore Convention Center

K42 DMP/DCOMP: **Focus Session: Planetary Materials II**
345, Baltimore Convention Center

K43 DAMOP: **Trapped Fermi Gases**
346, Baltimore Convention Center

K44 DCMP: **Transport in Disordered Electronic Systems**
347, Baltimore Convention Center

K45 DCMP: **Heavy Fermions: Experiment**
348, Baltimore Convention Center

K46 FIAP: **Spectroscopy of Semiconductors**
349, Baltimore Convention Center

**17:30 TUESDAY EVENING**
**14 MARCH 2006**

L9 GIMS: **GIMS Business Meeting**
301, Baltimore Convention Center

L10 DCP: **DCP Business Meeting**
302, Baltimore Convention Center

L16 FIAP: **FIAP Business Meeting**
312, Baltimore Convention Center

L18 DPOLY: **DPOLY Business Meeting**
315, Baltimore Convention Center

L23 GMAG: **GMAG Business Meeting**
320, Baltimore Convention Center

L29 DBP: **DBP Business Meeting**
326, Baltimore Convention Center

L33 GSNP: **GSNP Business Meeting**
336, Baltimore Convention Center

L40 TGQI: **TGQI Business Meeting**
343, Baltimore Convention Center

L48 FIP: **FIP Business Meeting**
Galena, Marriott Waterfront Hotel

**17:45 TUESDAY EVENING**
**14 MARCH 2006**

L7 DBP: **Flexible Molecular Recognition: The New Paradigm**
*Matthews, Kern, Taylor, Jennings, Wang*
307, Baltimore Convention Center

**19:00 TUESDAY EVENING**
**14 MARCH 2006**

L49 DCMP: **DCMP Business Meeting**
Dover A, Marriott Waterfront Hotel

L50 DMP: **DMP Business Meeting**
Dover B, Marriott Waterfront Hotel

**19:30 TUESDAY EVENING**
**14 MARCH 2006**

M50 FPS: **Intelligent Design: Its Impact and Responses to It**
*Gunn, Berman, Slakey, Dean*
Grand Salon V, Marriott Waterfront Hotel

**8:00 WEDNESDAY MORNING**
**15 MARCH 2006**

N1 DCMP: **Topological Phases and Quantum Computing**
*Kitaev, Hermele, Freedman, Stern, Fendley*
Ballroom IV, Baltimore Convention Center

N2 DCMP: **Nanoscale Crystals**
*Craig, Alivisatos, Drndic, Krauss*
Ballroom III, Baltimore Convention Center

N3 DCMP: **Insulating Cobaltates: Mottness on a Triangular Lattice**
*Gasparovic, Hasan, Zandbergen, Balicas, Imai*
Ballroom I, Baltimore Convention Center

N4 DPOLY/DMP: **Polymer Crystallization**
*Cheng, Hsiao, Ungar, Muthukumar, Granasy*
308, Baltimore Convention Center

N5 FIAP: **Pake and AIP Industrial Physics Prizes**
*Duke, Semerjian, Palffy-Muhoray, Lubell, Edelstein*
309, Baltimore Convention Center

N6 DAMOP: **Fermi Superfluid Gases: Non-equal Spin Polarization (FFLO State) and p-Wave pairing**
*Son, Yip, Hulet, Diener, de Melo*
310, Baltimore Convention Center

N7 DCOMP: **Recent Advances in the Computation of Optical and Transport Properties of Nanostructures**
*Weissker, Bester, Gebauer, Sanvito, Pecchia*
307, Baltimore Convention Center

N8 DFD: **Granular Flows**
314, Baltimore Convention Center

N10 DCP: **Focus Session: Frontiers in Computational Chemical Physics III**
*Cui*
302, Baltimore Convention Center

N11 DCP: **Focus Session: Aerosols, Clusters, Droplets: Physics and Chemistry of Nanoobjects I: Helium Nanodroplets I**
*Drabbels, Tiggesbäumker*
303, Baltimore Convention Center

N12 DMP/ DCMP: **Focus Session: Alloy and Interface Composition**
*Hannon*
304, Baltimore Convention Center

N13 DCP: **Focus Session: Ultrafast and Ultrahigh Field Chemistry I: Strong Field Phenomena**
*Jones, Yamanouchi*
305, Baltimore Convention Center

N16 FIAP: **Focus Session: Hydrogen Storage III**
*Yildirim*
312, Baltimore Convention Center

N17 FIAP: **Focus Session: Semiconductors for THz and IR I**
*Perera*
313, Baltimore Convention Center

N18 DMP: **Focus Session: Carbon Nanotubes: Transport I**
*Strunk*
315, Baltimore Convention Center

N19 GMAG/ DMP: **Semiconductor Spin Transport**
316, Baltimore Convention Center

N20 DMP/ GMAG: **Focus Session: Complex Oxide Thin Films Surfaces and Interfacess III: New Materials, New Techniques, and Effects of Strain**
317, Baltimore Convention Center

N21 DFD: **Microfluidic Physics II**
318, Baltimore Convention Center

N22 GMAG/ DMP: **Focus Session: Magnetic Vortices and Exchange Biased Thin Films**
*Roshchin*
319, Baltimore Convention Center

N23 GMAG/ DMP/ DCOMP: **Focus Session: MAGTHY III: Oxides and Phase Transitions**
*Schulthess*
320, Baltimore Convention Center

N24 DPOLY: **Structure and Dynamics in Polymer Thin Films**
321, Baltimore Convention Center

N25 DPOLY/ DMP: **Focus Session: Organic Photovoltaics**
*Inganäs*
322, Baltimore Convention Center

N26 DBP/ DFD: **Focus Session: DNA and Protein Analysis with Micro and Nano Fluidics**
*Riehn, Hansen*
323, Baltimore Convention Center

N27 DCOMP: **Electronic Structure I**
324, Baltimore Convention Center

N28 DPOLY: **Polymer Adsorption and Surface Modification**
325, Baltimore Convention Center

N29 DBP: **Focus Session: Physical Models of Ion Channel Function**
*Gillespie, Coalson*
326, Baltimore Convention Center

N30 DPOLY: **Block Copolymer Phase Behavior**
*327, Baltimore Convention Center*

N31 DCMP: **Carbon Nanotubes: Theory**
*328, Baltimore Convention Center*

N32 DMP/ DPOLY: **Focus Session: Carbon Nanotubes: Composites and Applications**
*Baughman*
329, Baltimore Convention Center

N33 GSNP: **Focus Session: Instabilities & Turbulence in Complex Fluids**
*Sureshkumar*
336, Baltimore Convention Center

N35 GSNP: **Focus Session: Organization of Complex Networks**
*Mendes*
338, Baltimore Convention Center

N36 DMP: **Focus Session: Optical Properties of Nanostructures with S, Se, Te, and Ge**
339, Baltimore Convention Center

N37 DMP: **Focus Session: Nanoscale Fabrication, Assembly and Semiconductor Nanowires**
*Misra*
340, Baltimore Convention Center

N38 DCMP: **Transport Properties of High-Tc Superconductors**
341, Baltimore Convention Center

N39 DMP: **Focus Session: Superconductivity—Thin Films and Junctions Magnesium Diboride and Related Compounds**
*Xi*
342, Baltimore Convention Center

N41 DCMP: **Insulating and Dielectric Oxides**
344, Baltimore Convention Center

N42 DCOMP/ GSCCM/ DMP: **Focus Session: Simulations of Matter at Extreme Conditions I**
*Johansson*
345, Baltimore Convention Center

N43 DAMOP: **Quantum Optics and Strong Field Physics**
346, Baltimore Convention Center

N44 DCMP: **Quantum Criticality and Nematic Ordering**
347, Baltimore Convention Center

N45 DCMP: **Exotic Phases in Strongly Correlated Systems**
348, Baltimore Convention Center

N46 FIAP: **Semiconductor Devices/ Semiconductors General**
349, Baltimore Convention Center

## 9:30 WEDNESDAY MORNING 15 MARCH 2006

N34 **Session on Referreeing**
337, Baltimore Convention Center

## 11:15 WEDNESDAY MORNING 15 MARCH 2006

P1 DCMP: **Electron Transport in Single Molecules**
*Tao, Yao, Flensberg, Wolkow, Bar-Joseph*
Ballroom IV, Baltimore Convention Center

P2 DCMP: **The Electronic Properties of Overdoped Cuprates: The Clean Gateway to High-Tc Superconductivity**
*Hussey, Damascelli, Slezak, Taillefer, van der Marel*
Ballroom III, Baltimore Convention Center

P3 FEd: **Physics Teacher Preparation at a Crisis: Innovative Programs Addressing a National Need**
*Heron, Marder, Stewart, Finkelstein, Hein*
Ballroom I, Baltimore Convention Center

P4 GIMS: **Keithley Award Session**
*Hellman, Jach, Fortune, Migliori*
308, Baltimore Convention Center

P5 DFD: **Shedding Light on the Enigma of the Transition to Turbulence in Pipes and other Shear Flows**
*Mullin, Henningson, Waleffe, Kerswell, Tumin, Eckhardt*
309, Baltimore Convention Center

P6 GMAG: **Quantum Spin Dynamics in Molecular Nanomagnets**
*Waldmann, Chudnovsky, Sessoli, Harmon, Park*
310, Baltimore Convention Center

P7 GSNP/DBP: **Focus Session: Physics of Transcriptional Regulatory Networks**
*You, Buchler, Li, Huang, Vazquez*
307, Baltimore Convention Center

P8 DFD/GSNP: **Focus Session: Jets, Shocks & Splashes**
*Xu, Lohse*
314, Baltimore Convention Center

P10 DCP: **Focus Session: Frontiers in Computational Chemical Physics IV**
*Martinez*
302, Baltimore Convention Center

P11 DCP: **Focus Session: Aerosols, Clusters, Droplets: Physics and Chemistry of Nanoobjects II: Helium Nanodroplets II, Aerosols, and Miscellaneous**
*Signorell*
303, Baltimore Convention Center

P12 DCMP/DMP: **Metal Islands and Clusters**
304, Baltimore Convention Center

P13 DCP: **Focus Session: Ultrafast and Ultrahigh Field Chemistry II: Quantum Control**
*Silberberg, Girard*
305, Baltimore Convention Center

P16 FIAP: **Focus Session: Molecular-Scale Electronics III**
*Janes*
312, Baltimore Convention Center

P18 DMP: **Focus Session: Carbon Nanotubes: Opto-Electronics**
*Chen*
315, Baltimore Convention Center

P19 GMAG/DMP: **Focus Session: Spin Interference and Spin Hall Effect**
*Sih*
316, Baltimore Convention Center

P20 DMP/GMAG: **Focus Session: Cobaltites, Nickelates and Vanadates**
317, Baltimore Convention Center

P21 DFD: **Microfluidic Physics III**
318, Baltimore Convention Center

P22 GMAG/FIAP/DMP: **Focus Session: Spin Transport in Metals**
*Garzon*
319, Baltimore Convention Center

P23 GMAG: **Quantum Spin Chains II**
320, Baltimore Convention Center

P26 DBP/DCP: **Focus Session: Protein Dynamics in Folding and Function**
*Mildvan, de Alba, Miller, Summers, Campbell, Hall, Pastor, Redfield*
323, Baltimore Convention Center

P27 DCOMP: **Electronic Structure II**
324, Baltimore Convention Center

P29 DBP: **Biomolecular Structure and Functions**
326, Baltimore Convention Center

P30 DPOLY/DMP: **Focus Session: Organic Interfaces**
*Rosei*
327, Baltimore Convention Center

P31 DCMP: **Nanotubes: Theory and Experiment**
328, Baltimore Convention Center

P32 GMAG: **Spin Glasses**
329, Baltimore Convention Center

P33 DMP/GSNP: **Focus Session: Friction, Fracture and Deformation III**
*Falk*
336, Baltimore Convention Center

P35 DCMP: **Nanostructure Fabrication, Quantum Point Contacts, and Single Electron Transistors**
338, Baltimore Convention Center

P36 DMP: **Focus Session: Plasmon Resonances in Nanostructures**
339, Baltimore Convention Center

P38 DCMP: **Superconductivity—Optical Spectroscopy of Cuprates**
341, Baltimore Convention Center

P39 DCOMP/DCMP: **Focus Session: Superconductivity—Theory and Computation (Mainly First Principles)**
*Mazin*
342, Baltimore Convention Center

P40 DCOMP/TGQI: **Focus Session: Pathways to Practical Quantum Computing I**
*DiVincenzo*
343, Baltimore Convention Center

P41 DMP: **Focus Session: Dielectric, Ferroelectric, and Piezoelectric Oxides III**
*Dierolf*
344, Baltimore Convention Center

P42 DMP/ DCOMP: **Focus Session: Planetary Materials III**
345, Baltimore Convention Center

P43 DAMOP: **Novel Phases in Quantum Gases**
346, Baltimore Convention Center

P44 DCMP: **Organic Conductors**
347, Baltimore Convention Center

P45 DCMP: **Structural and Ferroelectric Phase Transitions**
348, Baltimore Convention Center

P46 FIAP: **FQHE**
349, Baltimore Convention Center

## 13:00 WEDNESDAY AFTERNOON 15 MARCH 2006

Q1 **Poster Session III**
Exhibit Hall, 1:00pm–4:00pm (DPOLY session: 11:15am–2:15pm), Baltimore Convention Center

## 14:30 WEDNESDAY AFTERNOON 15 MARCH 2006

R1 DCMP DBP: **Cytoskeletal Dynamics and Mechanics**
*Svitkina, Julicher, Gopinathan, Gardel, Storm*
Ballroom IV, Baltimore Convention Center

R2 DCMP: **Fractional Quantum Hall Systems**
*Csathy, Gallais, Peterson, Kim, Schulze-Wischeler*
Ballroom III, Baltimore Convention Center

R3 DCMP: **Lateral Spin Transport**
*Ji, Bauer, Valenzuela, Otani*
Ballroom I, Baltimore Convention Center

R4 DPOLY: **Ionic, Dipolar and H-bonding Polymers**
*Breedveld, Dormidontova, Pochan, Cremer, Prabhu*
308, Baltimore Convention Center

R5 FGSA/ FIAP: **Paths from Academics to Employment**
*Czujko, Silbernagel, Seiler, Stanton, Garg*
309, Baltimore Convention Center

R6 CSWP: **U.S. Women in Physics: An International Perspective**
*Michelman-Ribeiro, Whitten, Horton, Ong, Hodari*
310, Baltimore Convention Center

R7 DBP/ FEd/ FPS: **The Experimental and Theoretical Foundations of Evolution**
*Keymer, Deem, Fisher, Lenski, Shapiro*
307, Baltimore Convention Center

R8 DFD: **Monolayers, Membranes & Microemulsions**
314, Baltimore Convention Center

R9 GIMS: **Imaging, Signal Detection and Processing**
301, Baltimore Convention Center

R10 DCP: **Focus Session: Surfaces and Interfaces in Electronic Materials I**
*Wieckowski, Switzer*
302, Baltimore Convention Center

R11 DCP: **Focus Session: Aerosols, Clusters, Droplets: Physics and Chemistry of Nanoobjects III: Molecular Clusters**
*Johnson*
303, Baltimore Convention Center

R12 DCMP/ DMP: **Dynamics at Silicon Surfaces**
304, Baltimore Convention Center

R13 DCP: **Focus Session: Ultrafast and Ultrahigh Field Chemistry III: Ultrafast Processes**
*Schafer, Villeneuve, Matsumoto*
305, Baltimore Convention Center

R16 FIAP: **Thermoelectrics**
312, Baltimore Convention Center

R17 FIAP: **Focus Session: Semiconductors for THz and IR II**
*Zhang*
313, Baltimore Convention Center

R18 DMP: **Focus Session: Carbon Nanotubes: Transport II**
*Roche*
315, Baltimore Convention Center

R19 GMAG/DMP: **Focus Session: Spin Hall Effect and Spin Transport**
*Engel*
316, Baltimore Convention Center

R20 DMP/GMAG: **Focus Session: Multiferroics III: Perovskites**
317, Baltimore Convention Center

R21 DFD/DBP: **Focus Session: Biological Hydrodynamics**
*Aranson*
318, Baltimore Convention Center

R22 GMAG/DMP: **Focus Session: Biomagnetism and Exchange Biased Thin Films**
*Hoffmann*
319, Baltimore Convention Center

R23 GMAG/FIAP: **Focus Session: Theory and Simulation for Information Storage Applications**
*Schrefl*
320, Baltimore Convention Center

R24 DPOLY: **Block Copolymer Applications**
321, Baltimore Convention Center

R25 DPOLY: **Adhesion and Viscoelasticity in Polymer Thin Films**
322, Baltimore Convention Center

R26 DBP/DPOLY: **Focus Session: Counterion Dynamics in Charged Biopolymer Systems**
*Wong, Netz*
323, Baltimore Convention Center

R27 DCOMP: **Many-Body/Strongly Correlated**
324, Baltimore Convention Center

R28 DBP: **Focus Session: Biological Networks: Structure, Dynamics and Function**
*El-Samad, Suel*
325, Baltimore Convention Center

R29 DBP: **Biomolecular Structure and Function**
326, Baltimore Convention Center

R30 DPOLY: **Polymer Nanocomposites**
327, Baltimore Convention Center

R31 DCMP: **Properties of Carbon Nanotubes**
328, Baltimore Convention Center

R32 DCOMP/DMP: **Focus Session: Computational Nanoscience V**
*Tangney*
329, Baltimore Convention Center

R33 DMP/GSNP: **Focus Session: Friction, Fracture and Deformation IV**
*Houston*
336, Baltimore Convention Center

R34 DFD: **Turbulence**
337, Baltimore Convention Center

R36 DMP: **Focus Session: Optical and X-ray Properties of Nanostructures**
*Vasiliev*
339, Baltimore Convention Center

R37 DMP: **Focus Session: Nanoscale Conductance Theory I**
*Baranger*
340, Baltimore Convention Center

R38 DCMP: **Superconductivity—Optical Spectroscopy of Cuprates: IR Hall Effect**
341, Baltimore Convention Center

R39 DCMP: **Superconductivity—Sodium Cobaltate**
342, Baltimore Convention Center

R40 DCOMP/TGQI: **Focus Session: Pathways to Practical Quantum Computing II**
*Laflamme*
343, Baltimore Convention Center

R41 DMP: **Focus Session: Dielectric, Ferroelectric, and Piezoelectric Oxides IV**
*Streiffer*
344, Baltimore Convention Center

R42 DCMP/GSCCM: **Focus Session: Plasticity and Phase Transitions**
*Robinson, Lorenz*
345, Baltimore Convention Center

R43 DAMOP: **One Dimensional Bose Gases**
346, Baltimore Convention Center

R44 DCMP: **Experimental Studies of 115 Materials**
347, Baltimore Convention Center

R45 DCMP: **Strong Correlation in Metals: Mott Transition**
348, Baltimore Convention Center

R46 FIAP: **Electronic and Optical Properties of Semiconductors: First Principals**
349, Baltimore Convention Center

**17:30 WEDNESDAY EVENING 15 MARCH 2006**

S48 FED: **FED Business Meeting & Reception**
Grand Ballroom Salon III, Marriott Waterfront Hotel

**17:45 WEDNESDAY EVENING 15 MARCH 2006**

T7 DBP: **Physics, Chemistry and Biology of the Hydrophobic Effect**
*Li, Widom, Chandler, Truskett*
307, Baltimore Convention Center

**18:30 WEDNESDAY EVENING 15 MARCH 2006**

S49 DCOMP: **DCOMP Business Meeting**
Dover C, Marriott Waterfront Hotel

**19:30 WEDNESDAY EVENING 15 MARCH 2006**

T50 **Perspectives on our Energy Future**
*Koonin, Dehmer*
Grand Salon V, Marriott Waterfront Hotel

**8:00 THURSDAY MORNING 16 MARCH 2006**

U1 DCMP: **Spin Liquids and Superconductivity near the Mott Transition**
*Lee, Schmalian, Tremblay, Mook, Bourges*
Ballroom IV, Baltimore Convention Center

U2 DCMP: **Quantum Magnets in High Magnetic Fields**
*Broholm, Grenier, Zheludev, Hagiwara, Essler*
Ballroom III, Baltimore Convention Center

U3 DCMP: **Nanomechanical Architecture of Strained Thin Films**
*Prinz, Liu, Schmidt, Blick*
Ballroom I, Baltimore Convention Center

U4 DPOLY: **Lithography**
*Willson, Dammel, Nealey, Jones, Hinsberg*
308, Baltimore Convention Center

U5 FHP: **Low Temperature Physics, A Historical Perspective**
*Wheeler, Donnelly, Meyer, Lee*
309, Baltimore Convention Center

U6 DCOMP: **Strong Electronic Correlation in Solids: Applications of the LDA+U method**
*Louie, Janotti, Lichtenstein, Kunes, Cococcioni*
310, Baltimore Convention Center

U7 FIAP: **Nanoscale Pattern Generation and Lithography**
*Hector, Smith, Baglin, Kim, Russell*
307, Baltimore Convention Center

U8 DFD: **Granular Materials**
314, Baltimore Convention Center

U9 GIMS: **Scanning Probe Microscopy**
301, Baltimore Convention Center

U10 DCP: **Focus Session: Surfaces and Interfaces in Electronic Materials II**
*Buriak, Wang*
302, Baltimore Convention Center

U11 DCP: **Focus Session: Aerosols, Clusters, Droplets: Physics and Chemistry of Nanoobjects IV: Metal Clusters I**
*Duncan, Woeste*
303, Baltimore Convention Center

U12 DMP/ DCMP: **Focus Session: Electrochemical and Related Growth**
*Wang*
304, Baltimore Convention Center

U16 FIAP: **Nanotechnology: Applications and Measurements**
312, Baltimore Convention Center

U17 DBP: **Physics and Imaging in Medicine**
*Amols, Soares, Baird, Gueye*
313, Baltimore Convention Center

U18 DMP: **Focus Session: Carbon Nanotubes: Transport III**
*Ferrari*
315, Baltimore Convention Center

U19 GMAG/ DMP: **Focus Session: Semiconductor Spin Nanostructures for Quantum Computing**
*Mizel*
316, Baltimore Convention Center

U20 DMP/ GMAG: **Focus Session: Metal-Insulator Transition and Electron Phonon Coupling in Perovskites**
*Alvarez*
317, Baltimore Convention Center

U21 DFD: **Liquid Crystals I**
318, Baltimore Convention Center

U22 GMAG/ FIAP/ DMP: **Focus Session: Magnetic Tunneling I**
*Yang*
319, Baltimore Convention Center

U23 GMAG: **Frustration in 2D**
320, Baltimore Convention Center

U24 DPOLY: **Liquid-Crystalline Polymers**
321, Baltimore Convention Center

U25 DPOLY/ DMP: **Focus Session: Oligoacene Semiconductors**
322, Baltimore Convention Center

U26 GSNP/ DBP/ DPOLY: **Focus Session: Cytoskeletal Dynamics**
*Danuser*
323, Baltimore Convention Center

U27 DCMP: **Computational Methods: Monte Carlo/Molecular Dynamics I**
324, Baltimore Convention Center

U28 DBP/ DFp: **Focus Session: Biological Hydrodynamics II**
*Groisman, Brenner*
325, Baltimore Convention Center

U29 DBP/ DPOLY: **Focus Session: Nonequilibrium Fluctuation in Biomolecules and Artificial Nanodevices**
*Astumian, Janko*
326, Baltimore Convention Center

U30 DPOLY: **Focus Session: Mechanical Properties: Deformation, Rupture and Failure**
*Marder*
327, Baltimore Convention Center

U31 DCMP: **Nanotubes, Experiment**
328, Baltimore Convention Center

U33 GSNP: **Dynamics and Systems Far From Equilibrium**
336, Baltimore Convention Center

U35 DCMP: **Nanowires**
338, Baltimore Convention Center

U36 DMP: **Focus Session: Optical Properties of Nano-Dots, Holes, and Wires**
339, Baltimore Convention Center

U37 DMP: **Focus Session: Nanowire and Nanodot Quantum Devices**
*Doh*
340, Baltimore Convention Center

U38 DCMP: **1-D Superconductors and Organics**
341, Baltimore Convention Center

U39 DCMP: **Superconducting Proximity Effect—S/N and S/F**
*Eschrig*
342, Baltimore Convention Center

U40 DCOMP/ TGQI/ DAMOP: **Focus Session: Pathways to Practical Quantum Computing III**
*Cirac*
343, Baltimore Convention Center

U41 DCMP: **Dielectrics: Response Properties**
344, Baltimore Convention Center

U42 DCOMP/ GSCCM/ DMP: **Focus Session: Simulations of Matter at Extreme Conditions II**
*Ashcroft*
345, Baltimore Convention Center

U43 DAMOP: **Focus Session: Novel Phases in Low Dimensional Quantum Gases**
*Porto, Ho*
346, Baltimore Convention Center

U44 DCMP: **Models of Strongly Correlated Electrons**
347, Baltimore Convention Center

U45 DCMP: **Structural, Surface and Other Phase Transitions**
348, Baltimore Convention Center

U46 FIAP: **Optical Properties of Semiconductors: Excitons and Phonons**
349, Baltimore Convention Center

**11:15 THURSDAY MORNING 16 MARCH 2006**

V1 DCMP: **Quantum Hall Edges**
*Grayson, Yang, Rezayi, Roddaro, Papa*
Ballroom IV, Baltimore Convention Center

V2 DCMP: **Excitons in Single-Walled Carbon Nanotubes**
*Lanzani, Sheng, Zhao, Mirlin, Reich*
Ballroom III, Baltimore Convention Center

V3 DCMP: **Nonequilibrium Nano-oscillators**
*Cleland, Chan, Dykman, Vijayaraghavan, Clerk*
Ballroom I, Baltimore Convention Center

V4 DAMOP: **Dynamics and Non-equilibrium Phenomena in Optical Lattices**
*Batrouni, Polkovnikov, Weiss, Rigol, Minguzzi*
308, Baltimore Convention Center

V5 DMP: **Surfaces and Interfaces of Correlated Oxides**
*Kawasaki, Ahn, Santamaria, Bozovic, Mannhart*
309, Baltimore Convention Center

V7 GSNP/DBP: **Noise in Biological Systems**
*Cluzel, Tu, Levine, Setayeshgar, Sourjik*
307, Baltimore Convention Center

V8 DCOMP/DFD: **Focus Session: Simulations Using Particles**
*Koplik, Cottet*
314, Baltimore Convention Center

V9 GIMS: **Magnetic Force Microscopies**
301, Baltimore Convention Center

V10 DCP: **Focus Session: Surfaces and Interfaces in Electronic Materials III**
*Uosaki, Wei*
302, Baltimore Convention Center

V11 DCP: **Focus Session: Aerosols, Clusters, Droplets: Physics and Chemistry of Nanoobjects V: Metal Clusters II**
*Schooss, Cheshnovsky*
303, Baltimore Convention Center

V12 DMP/DCMP: **Focus Session: Wetting and Hard-Soft Interfaces**
*Cicero*
304, Baltimore Convention Center

V16 FIAP: **Nanotechnology: Biological and Polymer**
312, Baltimore Convention Center

V17 DBP: **Medical Physics Panel Discussion**
313, Baltimore Convention Center

V18 DMP: **Focus Session: Carbon Nanotubes: Transport IV**
*Gruner*
315, Baltimore Convention Center

V19 APS/AIP: **The Changing Dynamics of Industrial Research as a Consequence of Global Trends**
*Taub, Stork, Durcan, Weinrib, Feist*
316, Baltimore Convention Center

V20 GMAG/DMP: **Focus Session: Semiconductor Spin Dynamics: Optics**
*Hall*
317, Baltimore Convention Center

V21 DFD: **Liquid Crystals II: Nano & Bio**
318, Baltimore Convention Center

V22 GMAG/FIAP/DMP: **Focus Session: Magnetic Tunneling II**
319, Baltimore Convention Center

V23 GMAG: **Spin Waves**
320, Baltimore Convention Center

V24 DPOLY: **Charged and Ion-Containing Polymers: Properties**
321, Baltimore Convention Center

V25 DPOLY: **Polymer Composites—Nanotubes and Nanoclays**
*Dhinojwala*
322, Baltimore Convention Center

V26 DBP: **Cellular Biomechanics**
323, Baltimore Convention Center

V27 DCOMP: **Computational Methods: Monte Carlo/Molecular Dynamics II**
324, Baltimore Convention Center

V28 DPOLY: **Rheology of Biopolymer Solutions**
325, Baltimore Convention Center

V29 DBP/ DCMP: **Nonlinear Phenomena & Pattern Formation in Biology**
326, Baltimore Convention Center

V30 DPOLY: **Focus Session: Mechanical Properties: Microscale Deformation and Failure**
*Sue*
327, Baltimore Convention Center

V31 DCMP: **Nanotubes: Transport**
328, Baltimore Convention Center

V33 GSNP: **Focus Session: Social Networks**
*Redner*
336, Baltimore Convention Center

V35 DCMP: **Photonic Crystals**
338, Baltimore Convention Center

V36 DMP: **Focus Session: Optical Properties of Carbon Nanotubes and C60**
*Ma*
339, Baltimore Convention Center

V38 DCMP: **Superconductivity—Thermodynamics and Structure**
341, Baltimore Convention Center

V39 DCOMP/ DCMP: **Focus Session: Superconductivity—Theory and Computation III**
342, Baltimore Convention Center

V40 TGQI/ DCMP: **Focus Session: Linear Optics Quantum Computation**
*Rudolph*
343, Baltimore Convention Center

V41 DMP: **Focus Session: Dielectric, Ferroelectric, and Piezoelectric Oxides V**
*Warusawithana*
344, Baltimore Convention Center

V42 FHP/ FEd: **History and Physics Outreach**
345, Baltimore Convention Center

V43 DAMOP: **Atomic/Molecular Structure and AMO Processes on Surfaces and in Condensed Matter**
346, Baltimore Convention Center

V44 DCMP: **Kondo Physics and Luttinger Liquids**
347, Baltimore Convention Center

V45 GMAG: **Spin Structure and Phase Transitions: Theory**
348, Baltimore Convention Center

V46 FIAP: **Defects and Impurities in Si/Ge**
349, Baltimore Convention Center

V47 FIAP: **Spectroscopy and Transport in 2D Semiconductors**
350, Baltimore Convention Center

## 14:30 THURSDAY AFTERNOON 16 MARCH 2006

W1 DCMP: **ARPES in High Tc Superconductors**
*Dessau, Valla, Chubukov, Cuk, Ino*
Ballroom IV, Baltimore Convention Center

W2 DCMP: **Imaging Charge and Spin and Semiconductors**
*Steele, Komiyama, LeRoy, Aidala, Hasegawa*
Ballroom III, Baltimore Convention Center

W3 DCMP: **Topological Aspects of Electron Transport in Solids**
*Nagaosa, Haldane, Kane, Bernevig*
Ballroom I, Baltimore Convention Center

W4 DPOLY: **Carbon Nanotube Dispersions**
*Hobbie, Pasquali, Poulin, Windle, Winey*
308, Baltimore Convention Center

W5 FHP: **A Century of Critical Phenomena**
*Sengers, Voronel, Ahlers, Fisher, Kadanoff*
309, Baltimore Convention Center

W6 FIAP: **New Applications of Silicon in Photonics and Biomedicine**
*Manalis, Jalali, Lipson, Murphy, Vlasov*
310, Baltimore Convention Center

W7 DBP/ DPOLY: **Physics of Cell Elasticity, Interactions and Tissue Formation**
*Riveline, Bruinsma, Janmey, Safran, Suresh*
307, Baltimore Convention Center

W8 GSNP/ DFD: **Focus Session: Nonlinear Electrokinetics**
*Rubinstein*
314, Baltimore Convention Center

W9 GIMS: **X-ray, Light, and Particle Scattering and Diffraction**
301, Baltimore Convention Center

W10 DCP: **Focus Session: Surfaces and Interfaces in Electronic Materials IV**
*Penner, Goesele*
302, Baltimore Convention Center

W11 DCP: **Focus Session: Aerosols, Clusters, Droplets: Physics and Chemistry of Nanoobjects V: Nanocatalysis, Supported Clusters I**
*Heiz, Moseler*
303, Baltimore Convention Center

W12 DCMP/ DMP: **Molecules on Surfaces**
304, Baltimore Convention Center

W16 FIAP: **Semiconductor Applications**
312, Baltimore Convention Center

W18 DMP: **Focus Session: Carbon Nanotubes: Electronic and Optical Properties III**
*Maruyama*
315, Baltimore Convention Center

W19 GMAG/ DMP: **Focus Session: Semiconductor Spin Transport: Noise/Theory**
316, Baltimore Convention Center

W20 DMP/ GMAG: **Focus Session: Multiferroics IV**
*Loidl*
317, Baltimore Convention Center

W21 DFD: **Liquid Crystals III**
318, Baltimore Convention Center

W22 GMAG/ DMP: **Focus Session: Magnetic Nanoparticles II**
*Dvorak*
319, Baltimore Convention Center

W23 GMAG/ DMP/ DCOMP: **Focus Session: MAGTHY IV/ab initio Studies**
*Stepanyuk*
320, Baltimore Convention Center

W24 DPOLY: **Focus Session: Lithography**
*Soles, Jonas*
321, Baltimore Convention Center

W25 DPOLY: **Gels and Networks**
322, Baltimore Convention Center

W26 DBP: **Focus Session: Biological Photophysics**
*Zhong, Venugopalan*
323, Baltimore Convention Center

W28 DPOLY/ DMP: **Focus Session: Ordered Optoelectronic Organics**
325, Baltimore Convention Center

W29 DBP: **Biological Networks and System Biology**
326, Baltimore Convention Center

W30 DPOLY/ DBP: **Focus Session: Biopolymers at Interfaces**
*Ober*
327, Baltimore Convention Center

W31 DCMP: **Nanotubes: Devices**
328, Baltimore Convention Center

W32 DCMP: **Glassy and Amorphous Systems**
329, Baltimore Convention Center

W33 DFD: **Nonequilibrium and Templated Assembly**
336, Baltimore Convention Center

W34 DFD: **Fluid Structure & Properties**
337, Baltimore Convention Center

W36 DMP: **Focus Session: Optical Properties of Nanostructures of Si & GaAs**
*Chou, Dal Negro*
339, Baltimore Convention Center

W37 DMP: **Nanoscale Conductance Theory II**
340, Baltimore Convention Center

W38 DCMP: **Flux Pinning and Critical Currents**
341, Baltimore Convention Center

W39 DCMP: **Superconductivity—Josephson Junctions and Qubits**
342, Baltimore Convention Center

W40 TGQI/ DAMOP: **Quantum Communication, Cryptography and Computation**
343, Baltimore Convention Center

W41 DCMP: **Cold Fusion**
344, Baltimore Convention Center

W42 DCOMP/ GSCCM/ DMP: **Focus Session: Simulations of Matter at Extreme Conditions III**
*Streitz*
345, Baltimore Convention Center

W43 DAMOP/ GQI: **Focus Session: Cold Atoms in Optical Lattices**
*Demler*
346, Baltimore Convention Center

W45 GMAG: **Spin Structure in Magnetic Materials**
*348, Baltimore Convention Center*

W46 FIAP: **Compound Semiconductor Defects and Dopants**
349, Baltimore Convention Center

W47 FIAP: **Quantum Transport in Semiconductors: Theory and Experiment**
350, Baltimore Convention Center

**8:00 FRIDAY MORNING 17 MARCH 2006**

Y1 DCMP/ DBP: **Engineering Biomolecules and Circuits by Rational Design and Genetic Selection**
*Hwa, Guet, Goulian, Liao, Noireaux*
Ballroom IV, Baltimore Convention Center

Y2 DCMP: **Electrostatic Levitation and High Energy X-rays**
*Rogers, Hyers, Goldman, Fadley, Lee*
Ballroom III, Baltimore Convention Center

Y4 GMAG: **High TMR MgO Tunneling and Spin Momentum Transfer Materials, Physics, and Devices**
*Parkin, Yuasa, Fuchs, Huai, Sun*
308, Baltimore Convention Center

Y5 FIAP: **New Functionalities in Glasses and Nanomaterials**
*Chakravorty, Gopalan, Jain, Kieffer, Mazur*
309, Baltimore Convention Center

Y6 DCOMP: **Is the Hubbard/t-J Model a High Temperature Superconductor?**
*Pryadko, Putikka, Troyer, Ogata*
310, Baltimore Convention Center

Y7 DCMP: **Challenges and Issues in Nanowire Nanodevices**
*Friedman, Hashizume, Cobden, Aono*
307, Baltimore Convention Center

Y8 DFD: **General Fluid Dynamics**
*Barranco*
314, Baltimore Convention Center

Y12 DCMP/ DMP: **Oxide Surface and Interfaces**
304, Baltimore Convention Center

Y16 FIAP: **Optics and Optoelectronics**
312, Baltimore Convention Center

Y18 DMP: **Focus Session: Carbon Nanotubes: Adsorption and Gas Surface Interactions with Carbon Nanotubes**
315, Baltimore Convention Center

Y19 GMAG/ DMP: **Focus Session: Novel Ferromagnetic Semiconductors I**
*Saito*
316, Baltimore Convention Center

Y20 GMAG/ DMP: **Focus Session: Ruddlesden-popper Phase Manganites**
*Hayward*
317, Baltimore Convention Center

Y22 GMAG/ FIAP: **Focus Session: Coupled Thin-Film Structures for Magnetic Recording**
*Thiele*
319, Baltimore Convention Center

Y23 GMAG: **Single Molecule Magnets**
320, Baltimore Convention Center

Y24 DPOLY: **Polymer Melts & Solutions: Structure & Solubility**
321, Baltimore Convention Center

Y25 DPOLY: **Charged and Ion-Containing Polymers: Computation**
322, Baltimore Convention Center

Y26 DBP: **Focus Session: Physics of Physiological Systems**
*Ben-Jacob*
323, Baltimore Convention Center

Y28 DPOLY/DMP: **Focus Session: Magnetic and Doping Effects in Cojugated Organics**
325, Baltimore Convention Center

Y29 DBP/DPOLY: **Focus Session: Noise and Fluctuation in Biological Systems**
*van Oudenaarden, de Gennes*
326, Baltimore Convention Center

Y30 DPOLY/DBP: **Focus Session: Biopolymers I: Phase Transitions**
*Garcia, Onuchic*
327, Baltimore Convention Center

Y31 DCMP: **Quasicrystals, Adsorption on Quasicrystals, Porous and Random Materials**
329, Baltimore Convention Center

Y33 GSNP: **Statistical Physics: Dynamics and Transitions**
336, Baltimore Convention Center

Y37 DMP: **Focus Session: Probing Novel Nanostructures**
*Fölsch*
340, Baltimore Convention Center

Y38 DCMP: **Superconductivity—Vortex Lattices and Pinning Center Arrays**
341, Baltimore Convention Center

Y39 DCMP: **Superconductivity—Materials and Processing**
342, Baltimore Convention Center

Y40 TGQI/DCMP: **Solid State Quantum Computing I**
343, Baltimore Convention Center

Y45 GMAG: **Magnetic Phase Transitions**
348, Baltimore Convention Center

Y46 FIAP: **Bilayers, Wigner Crystals**
349, Baltimore Convention Center

## 11:15 FRIDAY MORNING 17 MARCH 2006

Z1 DCMP: **Strong Interaction Effects in Small Conductors**
*Petta, Matveev, Steinberg, Fiete, LeHur*
Ballroom IV, Baltimore Convention Center

Z2 DCMP: **Resonant Inelastic X-ray Scattering in Complex Oxides**
*Kim, Hancock, Ishii, Ghiringhelli, Li*
Ballroom III, Baltimore Convention Center

Z4 DPOLY/DBP: **Biopolymers**
*Vogel, Sheetz, Perkins, Greer, Horkay*
308, Baltimore Convention Center

Z7 DBP: **Synchrony and Complexity in Brain Activity and Function**
*Towle, Nadkarni, Schiff, Lehnertz, Zochowski*
307, Baltimore Convention Center

Z18 DMP: **Focus Session: Carbon Nanotubes: Double Wall Nanotubes, Sheets and Chains**
*Kuzmany*
315, Baltimore Convention Center

Z19 GMAG/DMP: **Focus Session: Spin Dynamics in Quantum Dots**
*Abstreiter*
316, Baltimore Convention Center

Z20 GMAG/DMP: **Focus Session: Novel Ferromagnetic Semiconductors II**
317, Baltimore Convention Center

Z22 GMAG/FIAP: **Focus Session: FePt Nanoparticles for Information Storage**
*Weller*
319, Baltimore Convention Center

Z23 GMAG: **Strongly Correlated Electrons II**
320, Baltimore Convention Center

Z24 DPOLY: **Polymer Melts & Solutions: Rheology & Dynamics**
321, Baltimore Convention Center

Z25 DPOLY: **Molecular Dynamics: Theory and Simulation**
322, Baltimore Convention Center

Z26 DBP: **Radiation Therapy and Medical Imaging Techniques**
323, Baltimore Convention Center

Z28 DBP/GSNP: **Methods of Statistical Physics, Population Dynamics and Epidemiology**
*Brockmann*
325, Baltimore Convention Center

Z31 DCMP: **Complexed Structured Materials, Glasses and Clathrates**
329, Baltimore Convention Center

Z33 GSNP: **Statistical and Nonlinear Physics**
336, Baltimore Convention Center

Z37 DMP: **Focus Session: Nanoscale Conductance Theory III**
340, Baltimore Convention Center

Z38 DCMP: **High Tc Cuprates: ARPES**
341, Baltimore Convention Center

Z39 DCOMP/DCMP: **Focus Session: Superconductivity—Theory and Computations (Mostly Phonons)**
342, Baltimore Convention Center

Z40 TGQI/DCMP: **Solid State Quantum Computing II**
343, Baltimore Convention Center

Z45 GMAG: **Mostly Spinels**
348, Baltimore Convention Center

Z46 FIAP: **2D Multi-Valley Systems: QHE Experiment**
349, Baltimore Convention Center

# MAIN TEXT

**SESSION N1: TOPOLOGICAL PHASES AND QUANTUM COMPUTING**
**Wednesday Morning, 15 March 2006; Ballroom IV, Baltimore Convention Center at 8:00**
**Eduardo Fradkin, University of Illinois, presiding**

**8:00**
**N1 1 Protected qubits and quantum computation using Josephson junctions.**
ALEXEI KITAEV, *Caltech & Microsoft*

Several schemes of topological protection have been proposed, in which qubits are realized as degenerate ground states of quantum many-body systems so that all likely perturbations are exponentially suppressed. In the realm of Josephson junction physics, this approach was pioneered by Doucot, Vidal, Ioffe, and Feigelman in 2002. I will report a variation of their scheme that offers greater robustness and flexibility. Its key element is a ''quantum transformer,'' a superconducting current mirror operated in the quantum regime. This is a four-terminal device whose energy depends only on $\phi_1 - \phi_2 + \phi_3 - \phi_4$, with exponentially small ''error terms'' like $\cos(\phi_1 - \phi_4)$. The qubit is implemented by connecting terminal 1 with 3 and 2 with 4. I will describe a realization of the basic element, qubit measurements and unitary gates, and also discuss some parameter tradeoffs.

**8:36**
**N1 2 Quantum critical phases in two dimensions: U(1) spin liquids.**
MICHAEL HERMELE, *Physics Department, Massachusetts Institute of Technology*

Usually, we expect that stable phases of matter can be described in terms of quasiparticle excitations that interact only weakly at low energies. However, it is now clear that certain quantum spin liquids dramatically violate this expectation, but can nonetheless exist as stable zero-temperature phases in two-dimensional systems. These are the critical or algebraic spin liquids, which have no broken- symmetry ordering, but support gapless spin-carrying excitations. These states are promising candidates for the longstanding goal of the unambiguous experimental detection of a quantum spin liquid state; they have been suggested to play a role in certain strongly correlated materials, and they possess a variety of striking, and measurable, properties. I will discuss recent work on the simplest algebraic spin liquids. These are a type of two-dimensional U(1) spin liquid, and can be described at low energies by gapless Dirac fermions (spinons) coupled to a compact U(1) gauge field (photon). I will outline an argument that establishes the stability of these states in a large-N limit, and thus resolved a longstanding controversy. Next, I will discuss some of the remarkable properties of these states, and conclude with a discussion of open issues.

**9:12**
**N1 3 Non-Abelian topological phases.**
MICHAEL FREEDMAN, *Microsoft*

I will discuss the role of topology in the storage and processing quantum information. Chern-Simons theories in their chiral and doubled versions will be discussed. The Fractional quantum hall effect is the leading example of topological phases and may be home to striking nonabelian examples such as the $\nu = 5/2$ state. These examples will be considered within a larger mathematical framework.

**9:48**
**N1 4 Proposed experiments to probe the non-abelian $\nu = 5/2$ quantum Hall state.***
ADY STERN, *Weizmann Institute of Science*

We propose several experiments to test the non-abelian nature of quasi-particles in the fractional quantum Hall state of $\nu = 5/2$. One set of experiments studies interference contribution to back-scattering of current, and is a simplified version of an experiment suggested recently by Das Sarma et al. A second set looks at thermodynamic properties of a closed system. A third set looks at electronic transport in an array of immobile quesi-particles. The first two sets are only weakly sensitive to disorder-induced distribution of localized quasi-particles.

*Work done with B.I. Halperin (Harvard) and E. Grosfeld (Weizmann).

**10:24**
**N1 5 Realizing non-Abelian statistics in time-reversal invariant systems.**
PAUL FENDLEY, *University of Virginia*

Motivated by the search for a quantum computer robust against errors, much theoretical effort has been devoted to finding systems with quasiparticles obeying non-abelian statistics. I discuss a general method of constucting quantum loop gases with such behavior, focusing in particular on the simplest time-reversal-invariant model (P. Fendley and E. Fradkin, Phys. Rev. B 72 (2005) 024412 [cond-mat/0502071]). The quasiparticles of this model are called ''Fibonacci anyons,'' and their braiding is related to SO(3) Chern-Simons theory. I also discuss the quantum critical point governing the transition from a topological phase to a conventionally-ordered phase.

**SESSION N2: NANOSCALE CRYSTALS**
**Wednesday Morning, 15 March 2006; Ballroom III, Baltimore Convention Center at 8:00**
**Dmitri Talapin, Lawrence Berkeley Laboratory, presiding**

**8:00**
**N2 1 LeRoy Apker Award (2005): Tunable Nonlocal Spin Control in a Coupled Quantum Dot System.**
NATHANIEL CRAIG, *Stanford University*

The effective interaction between magnetic impurities in metals that can lead to various magnetic ground states often competes with a tendency for electrons near impurities to screen the local moment (known as the Kondo effect). The simplest system exhibiting the richness of this competition, the two-impurity Kondo system, was realized experimentally in the form of two quantum dots coupled through an open conducting region. We demonstrate nonlocal spin control by suppressing and splitting Kondo resonances in one quantum dot by changing the electron number and coupling of the other dot. The results suggest an approach to nonlocal spin control that may be relevant to quantum information processing.

**8:36**
**N2 2 Electrical Transport Through a Single Semiconductor Nanocrystal Tetrapod.**
A. PAUL ALIVISATOS, *University of California, Berkeley, and Lawrence Berkeley National Laboratory*

Semiconductor nanocrystal tetrapods represent a unique complex nanostructure of interest for multiterminal electrical and electromechanical studies. We demonstrate by single electron transport measurements the electronic coupling between the nanotetrapod core quantum dot and the four arm quantum rods. Either ionic or covalent bonding-type of coupling can exist when the interaction between quantum dot at the junction and arm rods is weak or strong. In addition, we demonstrate a new integrated single electron transistor scheme enabled by the unique coupled nanotetrapod systems: one arm can be used as a sensitive arm-gate to control the electrical transport through the whole system. The work here reveals that nanotetrapods and other branched colloidal nanocrystals represent a new class of chemically controlled ''artificial molecules'' of coupled quantum dots.

**9:12**
**N2 3 Controlled assembly and electronics in semiconductor nanocrystal-based devices.**
MARIJA DRNDIC, *University of Pennsylvania*

I will discuss the assembly of semiconductor nanocrystals (CdSe and PbSe) into electronic devices and the basic mechanisms of charge transport in nanocrystal arrays [1-4]. Spherical CdSe nanocrystals show robust memory effects that can be exploited for memory applications [1]. Nanocrystal memory can be erased electrically or optically and is rewritable. In PbSe nanocrystal arrays, as the interdot coupling is increased, the system evolves from an insulating regime dominated by Coulomb blockade to a semiconducting regime, where hopping conduction is the dominant transport mechanism [2]. Two-dimensional CdSe nanorod arrays show striking and anomalous transport properties, including strong and reproducible non-linearities and current oscillations with dc-voltage [4]. I will also discuss imaging of the charge transport in nanocrystal-based electronic devices. Nanocrystal arrays were investigated using electrostatic force microscopy (EFM) and transmission electron microscopy (TEM) [3]. Changes in lattice and transport properties upon annealing in vacuum were revealed. Local charge transport was directly imaged by EFM and correlated to nanopatterns observed with TEM. This work shows how charge transport in complex nanocrystal networks can be identified with nm resolution [3]. This work was supported by the ONR grant N000140410489, the NSF grants DMR-0449553 and MRSEC DMR00-79909, and the ACS PRF grant 41256-G10. References: 1) Fischbein M. D. and Drndic M., ''CdSe nanocrystal quantum-dot memory,'' Applied Physics Letters, 86 (19), 193106, 2005. 2) H. E. Romero and Drndic M., ''Coulomb

blockade and hopping conduction in PbSe quantum dots,'' Physical Review Letters 95, 156801, 2005. 3) Hu Z., Fischbein M. D. and Drndic M., ''Local charge transport in two-dimensional PbSe nanocrystal arrays studied by electrostatic force microscopy,'' Nano Letters 5 (7), 1463, 2005. 4) Romero H.E., Calusine G. and Drndic M., ''Current oscillations, switching and hysteresis in CdSe nanorod superlattices,'' Physical Review B 72 (23), 2005.

**9:48**
**N2 4 Localized charge of single CdSe quantum rods and the role of lattice imperfections.**
TODD KRAUSS, *University of Rochester*

The local electronic structure of colloidal semiconductor nanoparticles is of significant fundamental and technical interest. Electrostatic force microscopy was used to determine that single CdSe quantum rods (QRs) have a permanent polarization surface-charge density, an unexpected observation for supposedly well-shaped, neutral dielectric particles. To investigate the source of the surface charge, we performed electron nanodiffraction studies with a scanning transmission electron microscope (STEM). Electron nanodiffraction patterns suggest that rotations exist between various ''sections'' of individual QRs, and that the rotation axes may form substantial angles with the c-axis. Thus, the surface charge results from the slight angle between the QR sides and the direction of internal electric polarization. Despite the large dipole moment expected for CdSe QRs, none was observed. The unavoidable presence of permanently charged surfaces on CdSe QRs has the potential to impede the development of novel devices incorporating these materials.

## SESSION N3: INSULATING COBALTATES: MOTTNESS ON A TRIANGULAR LATTICE
**Wednesday Morning, 15 March 2006; Ballroom I, Baltimore Convention Center at 8:00**
**Patrick Lee, Massachusetts Institute of Technology, presiding**

**8:00**
**N3 1 Neutron scattering study of novel magnetic order in $Na_{0.5}CoO_2$.***
GORAN GASPAROVIC, *MIT*

The layered sodium cobaltates, $Na_xCoO_2$, have attracted much recent attention, due to their unusual thermodynamic properties, as well as the recent discovery of superconductivity in the hydrated composition. These strongly correlated systems exhibit a rich electronic phase diagram as a function of sodium doping, $x$. A particularly intriguing insulating phase is realized at $x = 1/2$, featuring a long range sodium order, a metal-insulator phase transition at 51 K, and a magnetic ordering transition at 88 K. We present polarized and unpolarized neutron scattering measurements of the magnetic order in single crystals of $Na_{0.5}CoO_2$. Our data indicate that below $T_N = 88$ K the spins form a novel antiferromagnetic pattern within the CoO2 planes, consisting of alternating rows of ordered and non-ordered Co ions. The domains of magnetic order are closely coupled to the domains of Na ion order, consistent with such a two-fold symmetric spin arrangement. Magnetoresistance and anisotropic susceptibility measurements further support this model for the electronic ground state.

*Work done in collaboration with R. A. Ott, J.-H. Cho, F. C. Chou, Y. Chu, J. W. Lynn, and Y. S. Lee. Supported by DOE DE-FG02-04ER46134, and NSF MRSEC DMR02-13282.

**8:36**
**N3 2 Quasiparticles, Fermi surface topology and Phase transitions in $Na_xCoO_2$.***
M. ZAHID HASAN, *Dept. of Physics, Princeton University, Princeton, NJ*

Recently discovered triangular cobaltate class is a novel realization of doped Mott insulators on a triangular spin- lattice. This system exhibits superconductivity, spin-density- waves, charge-order, metal-insulator phase transitions and colossal thermopower as well as Mott and Band insulation. We employ state-of-the-art ARPES to uncover the nature of electron motion in the cobaltates over the phase diagram. Quasiparticle dynamics (Fermi velocity, bandwidth, FS topology, correlation parameters, quasiparticle coherence) we extract from the data provides valueable insights into the novel phases of matter realized on this first realization of a triangular lattice Mott system. Low-T metal-insulator (order-disorder) phase transition will be discussed in this presentation.

*Work in collaboration with D. Qian, R.J. Cava, Z. Hussain and A. Fedorov. This work is supported by U.S. DOE, NSF and Princeton Center for Complex Materials and partially carried out at the Advanced Light Source.

**9:12**

**N3 3 Sodium Ion Ordering in double-layered and triple-layered $Na_xCoO_2$.**

HENNY ZANDBERGEN, *Dept. of Chemistry and Princeton Materials Inst., Princeton University; National Centre for HREM, Dept. of Nanoscience, Delft University of Technology*

The layered sodium cobalt oxide $Na_xCoO_2$ is studied by electron diffraction for a wide range of sodium contents, $0.15 < x < 0.75$. This range in compositions is obtained by removal of Na by various methods for the starting materials $Na_{0.7}CoO_2$, and $Na_{1.0}CoO_2$ The structure of $Na_xCoO_2$ is based the stacking of triangular O-Co-O layers with Na planes. The Co atoms are in edge-sharing $CoO_6$ octahedra. For the starting compound $Na_{0.7}CoO_2$, the $Na^+$ ions are in a trigonal prismatic coordination whereas for $Na_{1.0}CoO_2$ the $Na^+$ coordination is octahedral. Prismatic coordination occurs when the close packed oxygen planes directly adjacent to the Na plane have the same projection into the basal plane (A-Na-A), whereas octahedral coordination of Na occurs when the directly adjacent oxygen planes have different projections (A-Na-B) into the basal plane. Due to this difference in stacking the a axis is about 1.08 nm and 1.65 nm for $Na_{0.7}CoO_2$ and $Na_{1.0}CoO_2$respectively. For $Na_{0.7}CoO_2$ as well as $Na_{1.0}CoO_2$a series of superstructures are observed, which can be explained with ordered Na ion-Na vacancy superlattices. The structural principle for some of the observed ordering schemes, particularly near $x=0.5$, is, surprisingly, the presence of lines of Na ions and vacancies rather than simply maximized Na-Na separations. With $Na_{0.7}CoO_2$ as starting material, the most strongly developed superlattice is found for the composition $Na_{0.5}CoO_2$. With $Na_{1.0}CoO_2$ as starting material, the most strongly developed superlattice is found for the compositions $Na_{0.75}CoO_2$and $Na_{0.5}CoO_2$. In particular the superstructure $Na_{0.75}CoO_2$of is very complicated. In collaboration with M.L. Foo, Department of Chemistry and Princeton Materials Institute, Princeton University, Princeton, NJ 08544 USA; Q. Xu and V. Kumar, National Centre for HREM, Department of Nanoscience, Delft University of Technology, Rotterdamseweg 137, 2628 AL Delft, The Netherlands ; L. Viciu, Department of Chemistry and Princeton Materials Institute, Princeton University; Q. Huang, NIST Center for Neutron Research, NIST, Gaithersburg, MD 20899; and R.J. Cava, Department of Chemistry and Princeton Materials Institute, Princeton University.

**9:48**

**N3 4 Magnetic-Field-Induced Suppression of the Charge Ordered State in $Na_{0.5}CoO_2$ and the observation of Shubnikov−de Haas Oscillations in $Na_xCoO_2$.**

LUIS BALICAS, *National High Magnetic Field Lab*

We performed electrical transport measurements at low temperatures and high magnetic fields in $Na_xCoO_2$ single crystals for both $x = 0.5$ and $x = 0.3$. For $x = 0.5$ Shubnikov de Haas oscillations corresponding to only 1% of the area of the orthorhombic Brillouin zone (BZ) were clearly observed, indicating that most of the original Fermi surface vanishes at the charge ordering (CO) transition. While in-plane magnetic fields were found to strongly suppress the charge ordered state observed for $x = 0.5$ via a field-induced strongly hysteretic transition. When the external fields are rotated within the conducting planes, we observe angular magnetoresistance oscillations whose periodicity changes from two-to six-fold at the transition suggesting the reconstruction of the Fermi surface of this material. These facts indicate that the charge order is a delicate one, more akin to a charge-density-wave, and consistent with the small gap observed in the optical conductivity. While for $x = 0.3$ we clearly observe quantum oscillatory phenomena for two frequencies $f_1 \cong 480$ and $f_2 \cong 800$ T corresponding respectively to only 0.8 and 1.36% of the first Brillouin zone (FBZ), with very weak indications of possible additional frequencies. These values contrast markedly with what is predicted by band structure calculations for $x = 0.3$, i.e., 2.26% and 22.3% of the FBZ for the pockets resulting from the $e_g'$ and the $a_{1g}$ bands, respectively. We speculate that the Na superstructures seen for both concentrationsm re-define the Brillouin zone and thus the geometry of the Fermi surface explaining perhaps such discrepancies.



**10:24**

**N3 5 $^{17}O$ and $^{59}Co$ NMR Studies of Strongly Correlated Electrons in $Na_xCoO_2$.**

TAKASHI IMAI, *McMaster University*

The anomalous electronic properties of triangular-lattice system $Na_xCoO_2$ has been attracting strong interest over the last several years since the discovery of superconductivity in hydrated $Na_{1/3}CoO_2 \cdot {}_{4/3}[H_2O]$. The electronic phase diagram of these materials is quite rich, as the physical properties depend very strongly on Na concentration. Here we report our $^{17}O$ and $^{59}Co$ NMR studies of the local electronic properties and low-frequency spin dynamics in these materials for a variety of Na concentrations [1,2]. [1] F.L. Ning, T. Imai, B.W. Statt, and F.C. Chou, PRL 93 (2004) 237201. [2] F.L. Ning and T. Imai, PRL 94 (2005) 227004.

**SESSION N4: POLYMER CRYSTALLIZATION**
**Wednesday Morning, 15 March 2006; 308, Baltimore Convention Center at 8:00**
**Freddy Khoury, National Institute of Standards and Technology, presiding**

**8:00**
**N4 1 A new approach to study of the onsets of tethered chain overcrowding and highly stretched brush regime utilizing crystalline-amorphous diblock copolymers.**
STEPHEN CHENG, *Maurice Morton Institute and Department of Polymer Science, University of Akron, Akron, Ohio 44325-3909 USA*

Two series of diblock copolymers, PEO-*b*-PS and PLLA-*b*-PS, were used as templates to generate tethered PS blocks on the single crystal surfaces. Controlled and tunable reduced tethering density, $\tilde{\sigma}$, defined by it$\sigma\pi R_g^2$ (where it$\sigma$ is the tethered chain density), could be achieved in a broad range (up to 24) by changing the molecular weights (MW's) of the crystalline and amorphous blocks and by varying the crystallization temperature ($T_x$) of different PEO-*b*-PS and PLLA-*b*-PS solutions. The $\tilde{\sigma}$ of the tethered PS chains on the crystal surface increased with increasing $T_x$ because at a fixed MW of the PEO or PLLA block, an increase in the lamellar thickness ($d_{CRYST}$) was evidence of a decrease in the number of folds. When we plotted the relationships between $1/d_{CRYST}$ and $T_x$ for these two series of diblock copolymers, sudden and discontinuous changes of the slopes in some of these were observed at $\tilde{\sigma} = 3.7$ ($\tilde{\sigma}$*). This was as a result of the drastic interaction change of the neighboring PS tethered chains. An average reduced surface free energy of the tethered PS chains ($\Gamma^{PS}$) was used as a parameter to characterize the PS tethered chain interactions. The relationship between $\Gamma^{PS}$ and $\tilde{\sigma}$ showed a discontinuous transition at $\tilde{\sigma}$*. This could be identified as the onset of the tethered PS chain overcrowding in solution. This transition indicates that the extra entropic surface free energy created by the repulsion of tethered PS chains started to affect the nucleation barrier of the PEO or PLLA block crystallization. Based on the scaling laws, the onset of highly stretched brush regime could be identified at $\tilde{\sigma} = 14.3$ ($\tilde{\sigma}$**). In the $\Gamma^{PS}$ versus $\tilde{\sigma}$ plot, the transition appears to be continuous. Thus, a crossover regime in the tethered PS chains exists between $\tilde{\sigma}^* = 3.7$ and $\tilde{\sigma}^{**} = 14.3$. It is defined as the regime where the interaction of the tethered PS chains undergo changes from being non-interacting towards penetration to, finally, chain stretching normal to the surface.

**8:36**
**N4 2 Flow-Induced Crystallization Precursor Structure in Entangled Polymer Melt.***
BENJAMIN HSIAO, *Stony Brook University*

Flow-induced crystallization has long been an important subject in polymer processing. Varying processing conditions can produce different morphologies, which lead to different properties. Recent studies indicated that the final morphology is in fact dictated by the initial formation of crystallization precursor structures (i.e., shish kebabs) under flow. In this talk, factors that affect the shish-kebab formation in entangled polymer melts are systematically reviewed, including the concept of coil-stretch transition, chain dynamics, critical orientation molecular weight, phase transition during shish and kebab formations. In particular, recent experimental results from in-situ rheo-X-ray studies and ex-situ microscopic examinations have been presented to illustrate several new findings of flow-induced shish-kebab structures in polymer melts. (1) The shish entity consists of stretched chains (or chain segments) that can be in the amorphous, mesomorphic or crystalline state. (2) The kebab entity mainly arises from the crystallization of coiled chains (or chain segments), which seems to follow a diffusion-control growth process. (3) A shish-kebab structure with multiple shish was seen in the ultra-high molecular weight polyethylene (UHMWPE) precursor. Based on the above results and recent simulation work from other laboratories, a modified molecular mechanism for the shish-kebab formation in entangled melt is presented.

*This work was supported by the National Science Foundation (DMR-0405432).

**9:12**
**N4 3 Curved faces in polymer crystals with asymmetrically spreading growth patches.**
GORAN UNGAR, *U. Sheffield*

Polymer crystals often have curved faces. Understanding such morphology is of major interest since it allows distinction between fundamentally different theories of polymer crystallization. E.g., Sadler's ''roughness-pinning'' theory assumes that the curvature is a result of roughening transition on lateral faces. It has since been shown by Mansfield that the curvature can be explained quantitatively, essentially within the Lauritzen-Hoffman nucleation theory. However, the step propagation rates $v$ implied in their treatment are substantially lower than predicted by the LH theory. The retardation appears to be due to the ''self-poisoning'' or ''pinning'' effect of incorrect chain attachment, effectively demonstrated by the extreme cases of growth rate minima in long-chain monodisperse n-alkanes. Recently crystals of poly(vinylidene fluoride) and alkanes $C_{162}H_{326}$ and $C_{198}H_{398}$ have been found with habits that can be best described as bounded by curved {110} faces. The interesting feature is the asymmetry of the curvature: while the faces are curved at one end, they are straight at the other. We carried out mathematical analysis of the curvature, generalizing the Mansfield model. We

suggest that such asymmetric curvature arises from the propagation rates to the left, $v_l$, and to the right, $v_r$, being different because of the lack of mirror bisecting planes such as (110). By solving appropriate equations with moving boundaries, we obtained the shape of the growth front $y(x,t)$. Calculated crystal habits gave excellent fits to the observed growth shapes of $a$-axis lenticular crystals of long alkanes and PVDF, as well as of single crystals of PEO. This explains some hitherto poorly understood morphologies and, in principle, allows independent measurements of step initiation and propagation rates in all polymers.

**9:48**
**N4 4 New Paradigms for Polymer Crystallization.**
MURUGAPPAN MUTHUKUMAR, *University of Massachusetts*

The ordering process of topologically connected chains into a crystalline state is distinctly different from that of low molar mass substances. One of the key differences arises fundamentally from entropic barriers due to substantial reduction in configurational entropy of the system during the ordering process. We have derived a new theoretical model with the following essential features: (1) For a single lamella, the free energy landscape exhibits many metastable states (separated by free energy barriers), and a globally stable state. Among the metastable states, even the first viable state with its free energy just below that of the melt is long-lived, due to the barrier for thickening. The thickness of this long-lived metastable state increases with temperature. However, if enough time is granted for this metastable state to evolve, then the equilibrium thickness would be reached for each temperature. The equilibrium thickness decreases with temperature, until the approach of the equilibrium melting temperature. The equilibrium melting temperature does not correspond to that of extended chain dimensions. (2) The lateral growth faces a free energy barrier, due to temporal crowding of entangled chains at the growth front. A general formula is derived for the growth kinetics of the growth front, providing a crossover description for crystallization of low and very high molar mass polymer chains. The predictions are compared with available experimental data.

**10:24**
**N4 5 Growth and form of spherulites: A phase field study.**
LASZLO GRANASY, *Research Institute for Solid State Physics and Optics*

Polycrystalline patterns termed spherulites are present in a broad variety of systems including metal alloys, polymers, minerals, and have biological relevance as well (see e.g. semi-crystalline amyloid spherulites and spherultic kidney stones). The fact that similar polycrystalline patterns are observed in systems of very different nature suggests that a minimal model based on coarse-grained fields, which neglects the details of molecular interactions, might be appropriate. Although such a field-theoretic approach disregards most of the molecular scale details of formation, some features such as crystal symmetries can be incorporated via the anisotropies of the model parameters. The rationale for developing such coarse-grained models is the current inability of fully molecular models to address the formation of large scale morphologies. A phase field theory of polycrystalline growth, we developed recently, is applied for describing spherulitic solidification in two and three dimensions. Our model consists of several mechanisms for nucleating new grains at the perimeter of the crystallites, including homogeneous (trapping of orientational disorder and branching in certain crystallographic directions) and heterogeneous (particle-induced nucleation) processes. It will be shown that the diversity of spherulitic growth morphologies arises from a competition between the ordering effect of discrete local crystallographic symmetries and the randomization of the local crystallographic orientation that accompanies crystal grain nucleation at the growth front. This randomization in the crystal orientation accounts for the isotropy of spherulitic growth at large length-scales and long times. We find the entire range of observed spherulite morphologies can be reproduced by this generalized phase field model of polycrystalline growth.



## SESSION N5: PAKE AND AIP INDUSTRIAL PHYSICS PRIZES
**Wednesday Morning, 15 March 2006; 309, Baltimore Convention Center at 8:00**
**Thomas Theis, IBM, presiding**

**8:00**
**N5 1 The Future of Research in Industry.**
CHARLES DUKE,* *Xerox Wilson Center for R&T*

Since 1990 the environment for and execution of industrial research has changed profoundly. See, e.g., R. Buderi, Engines of Tomorrow (Simon and Shuster, New York, 2000); H. W. Chesbrough, Open Innovation (Harvard Business School Press, Boston, 2003); C. B. Duke, Creating Economic Value from Research Knowledge (The Industrial Physicist, Aug-Sept. 2004, pp. 29-31). According to Thomas L. Friedman (''The World is Flat,'' Farrar, Straus and Giroux, New York, 2005) a new global communications-collaboration platform has ''flattened'' the world. National alarms have been

raised about the US capability to compete in this changed environment. See, e.g., ''America's Tech Might Slipping?,'' Business Week, March 14, 2004; ''Globalization and Engineering,'' The Bridge, National Academy of Engineering, Fall 2005; ''Rising Above the Gathering Storm,'' National Academy of Sciences, 2005. In this presentation I indicate why firms perform research and how they generate economic value from it. Then I discuss the profound changes in the environment for these activities since 1990. This leads to a consideration of how firms are modifying their Research and Development activities to deal with this situation. I close by noting implications of these developments on the role of physics and the careers of physical scientists in the 21st century.

*Vice President and Senior Fellow.

**8:36**
**N5 2 NIST Role in Advancing Innovation.**
HRATCH SEMERJIAN, *NIST*

According to the National Innovation Initiative, a report of the Council on Competitiveness, innovation will be the single most important factor in determining America's success through the $21^{st}$ century. NIST mission is to promote U.S. innovation and industrial competitiveness by advancing measurement science, standards, and technology – in ways that enhance economic security and improve the quality of life for all Americans. NIST innovations in measurement science and technology often become the basis for new industrial capabilities. Several examples of such developments will be discussed, including the development of techniques for manipulation and measurement of biomolecules which may become the building blocks for molecular electronics; expansion of the frontiers of quantum theory to develop the field of quantum computing and communication; development of atomic scale measurement capabilities for future nano- and molecular scale electronic devices; development of a lab-on-a-chip that can detect within seconds trace amounts of toxic chemicals in water, or can be used for rapid DNA analysis; and standards to facilitate supply chain interoperability.

**9:12**
**N5 3 Liquid Crystals: From Discovery to Products.**
PETER PALFFY-MUHORAY, *Kent State University*

Liquid crystals, constituting a new phase of matter, were discovered in 1888. They remained a scientific curiousity until the late 1960s, when liquid crystal displays were invented by Heilmeier at RCA and Fergason at Kent State University. Today, LCDs dominate the flat panel display industry, with production primarily in the Far East. In this talk, I will briefly review the history of liquid crystals and LC devices, discuss emerging LC technologies and speculate on their commercial potential. I will outline new directions in liquid crystal research and describe some of the remarkable new products that may result. I will conclude by considering the connection between support for basic and applied research and successful product commercialization.

**9:48**
**N5 4 Benchmarking Competitiveness: Is America's Technological Hegemony Waning?**
MICHAEL S. LUBELL, *CCNY Department of Physics*

For more than half a century, by almost every standard, the United States has been the world's leader in scientific discovery, innovation and technological competitiveness. To a large degree, that dominant position stemmed from the circumstances our nation inherited at the conclusion of the World War Two: we were, in effect, the only major nation left standing that did not have to repair serious war damage. And we found ourselves with an extraordinary science and technology base that we had developed for military purposes. We had the laboratories – industrial, academic and government – as well as the scientific and engineering personnel – many of them immigrants who had escaped from war-time Europe. What remained was to convert the wartime machinery into peacetime uses. We adopted private and public policies that accomplished the transition remarkably well, and we have prospered ever since. Our higher education system, our protection of intellectual property rights, our venture capital system, our entrepreneurial culture and our willingness to commit government funds for the support of science and engineering have been key components to our success. But recent competitiveness benchmarks suggest that our dominance is waning rapidly, in part because other nations have begun to emulate our successful model, in part because globalization has ''flattened'' the world and in part because we have been reluctant to pursue the public policies that are necessary to ensure our leadership. We will examine these benchmarks and explore the policy changes that are needed to keep our nation's science and technology enterprise vibrant and our economic growth on an upward trajectory.

**10:24**
**N5 5 MRI from 400 gauss to 1.5 tesla and beyond.**
WILLIAM EDELSTEIN, *GE Global Research Center (Retired)*

Magnetic Resonance Imaging (MRI) is arguably the most novel and important medical imaging modality since the advent of the X-ray. MRI grew out of the long development of atomic spectroscopy, atomic and molecular beam resonance and, finally, nuclear magnetic resonance (NMR) in condensed matter. The operation and economics of MRI systems depend

on the performance of magnets, pulsed magnetic field gradient windings and rf (radiofrequency) coils. Physics and physicists have made critical contributions to these technologies. Superconducting magnets have come to be the magnet of choice. Magnetic gradient windings present theoretical electromagnetic and practical challenges. The need for rf antennas that resonate at high frequencies while surrounding sizable spatial regions inspired large coils producing uniform rf magnetic fields while minimizing electric field interactions with the imaging subject. This development enabled MRI at high magnetic fields. Additionally it is possible to use arrays of small rf coils to obtain MRI images with the high signal-to-noise ratio of a small surface coil and the field of view of a large coil. We recently investigated the intense acoustic noise (110 dB or more) produced in MRI scanners. Surprisingly, eddy currents induced in the magnet cryostat inner bore make a major contribution to this noise. Calculations indicate that a thin layer of Cu on the outside of the gradient assembly could substantially decrease eddy currents and help reduce noise. GE R&D work was focused on the science underlying MRI, MRI technology and the MRI product. Corporate management sometimes discourages technical publication related to evolving products because it might help rivals. Our practice of extensive publication and participation in open scientific exchange—after filing appropriate patent applications—served as quality control for company science and technology. GE conference presentations and journal publications helped establish technical leadership and determine which ideas were most important. GE scientists built reputations leading to leadership prominent within the MRI technical community. Openness underpinned a highly effective development process that enabled GE to pull ahead of competitors.

## SESSION N6: FERMI SUPERFLUID GASES: NON-EQUAL SPIN POLARIZATION (FFLO STATE) AND P-WAVE PAIRING

**Wednesday Morning, 15 March 2006; 310, Baltimore Convention Center at 8:00**
**Erich Mueller, Cornell University, presiding**

**8:00**
**N6 1 Phase Diagram of Cold Polarized Fermi Gas.**
DAM THANH SON, *University of Washington*

We propose the phase diagram of cold polarized atomic Fermi gas with zero-range interaction. We identify four main phases in the plane of density and polarization: the superfluid phase, the normal phase, the gapless superfluid phase, and the modulated phase. We argue that there exist a Lifshitz point at the junction of the normal, the gapless superfluid and the modulated phases, and a splitting point where the superfluid, the gapless superfluid and the modulated phases meet. We show that the physics near the splitting point is universal and derive an effective field theory describing it. We also show that subregions with one and two Fermi surfaces exist within the normal and the gapless superfluid phases.

**8:36**
**N6 2 Superfluid stability in polarized Fermi atomic gases.**
SUNGKIT YIP, *Inst. Physics, Academia Sinica*

For a two-species atomic Fermi gas with equal populations, it is now widely accepted that a smooth BCS-BEC cross-over occurs when the Feshbach resonance is crossed. However, the situation is very different if the populations of the two species are different. In particular, the uniform state is stable only either (a) for sufficiently negative detuning, where the system is a gapless mixture of Bose condensed pairs and unpaired normal Fermions, or (b) for sufficiently positive detuning, where Fermions are unpaired and the system is in the normal state. No uniform state is stable in between. Phase transition(s) must therefore occur when the resonance is crossed. We discuss the theoretical phase diagram of this system in this talk.

**9:12**
**N6 3 Pairing and Phase Separation in a Polarized Fermi Gas.***
RANDALL HULET,† *Rice University*

BCS pairing can only occur when the Fermi energies of the individual particles are equal. There has been great interest, however, in the consequences of mismatched Fermi energies that may arise in several important situations, including magnetized superconductors or cold dense quark matter at the core of neutron stars. Pairing is qualitatively altered by the Fermi energy mismatch, and there has been considerable speculation regarding the nature and relative stability of various proposed exotic phases. We have created a two-component gas of $^6$Li atoms in which the relative Fermi energies are altered by changing the relative numbers of each component[1]. The BEC/BCS crossover with tunable interactions is realized via a Feshbach resonance. Above a critical number polarization, which depends on the interaction energy, the gas

separates into a superfluid paired core surrounded by a shell of normal unpaired atoms. Below the critical polarization the gas exists in a paired state with asymmetric Fermi surfaces. The critical polarization is largest in the BEC regime, and becomes small in the BCS regime. We also measure the universal interaction parameter $\beta$ for a strongly interacting Fermi gas to be -0.54 (5), in good agreement with recent Monte-Carlo calculations.

*Supported by NSF, ONR, NASA, and the Welch Foundation.
†Co-authors: G.B. Partridge, Wenhui Li, R.I. Kamar, Yean-an Liao.

[1]G.B. Partridge et al., cond-mat/0511752.

**9:48**
**N6 4 Fermi superfluids with p-wave pairing near a Feshbach resonance.**
ROBERTO DIENER, *Department of Physics, The Ohio State University*

Fermi superfluids with s-wave pairing near an s-wave Feshbach resonance are being extensively studied both theoretically and experimentally. Recently, Feshbach resonances in the p-wave channel have been observed in both $^{40}$K and $^{6}$Li, raising the possibility that fermionic superfluids with p-wave pairing could be attained at low temperatures. Since the pairing wavefunction in this case breaks rotational symmetry, the superfluid properties of this system in the BEC-BCS crossover will be much different from the s-wave case. In particular, I will discuss the symmetry of the ground state as well as the experimental signatures of these novel superfluids as a function of the parameters defining the resonance. Other new results on resonance physics will also be reported.

**10:24**
**N6 5 Evolution from BCS to BEC Superfluidity in Dilute Fermi Gases.***
CARLOS A. R. SA DE MELO, *Georgia Institute of Technology*

I will review briefly some old results [1,2] of the evolution from BCS to BEC superfluidity in dilute Fermi gases, including critical temperature, order parameter amplitude, chemical potential and time dependent Ginzburg-Landau theory for the s-wave channel in three dimensions. Following this discussion, I will present new results for the BCS to BEC evolution of Fermi gases in the p-wave channel [3]. I will make comparisons between s-wave and p-wave superfluidity and point out the main differences between the two cases. Lastly, I will discuss supefluidity of s-wave and p-wave Fermi gases in a restricted two-dimensional geometry (one dimensional optical lattice), where a Berezinkii-Kosterlitz-Thouless-type transition is proposed as the system evolves from the weak to the strong attraction limit. In this case, I will show that spontaneous vortex-antivortex pairs form and that they can condense into a vortex-antivortex lattice at lower temperatures [4]. [1] C. A. R. Sa de Melo, M. Randeria, and J. R. Engelbrecht, PRL 71, 3202 (1993). [2] J. R. Engelbrecht, M. Randeria, and C. A. R. Sa de Melo, PRB 55, 15153 (1997). [3] M. Iskin, and C. A. R. Sa de Melo, cond-mat/0510300 (2005). [4] S. S. Botelho, and C. A. R. Sa de Melo, cond-mat/0509387 (2005).

*I would like to thank NSF (DMR-0304380) for financial support.



## SESSION N7: RECENT ADVANCES IN THE COMPUTATION OF OPTICAL AND TRANSPORT PROPERTIES OF NANOSTRUCTURES

**Wednesday Morning, 15 March 2006; 307, Baltimore Convention Center at 8:00**
**Marco Buongiorno Nardelli, North Carolina State University, presiding**

**8:00**
**N7 1 Optical Properties of Nano-Crystallites.***
HANS-CHRISTIAN WEISSKER, *European Theoretical Spectroscopy Facility (ETSF) France and Laboratoire des Solides Irradies, Ecole Polytechnique, France*

The optical properties of nanostructured materials are interesting due to the tunability of the electronic structure, of the lifetimes, and of the excitation spectra. This calls for precise knowledge of the physical effects which create the desired properties. Thereby it is of utmost importance to settle the question as to how many-body effects have to be incorporated in the description of the excitation aspects inherent in any optical process. Static DFT-LDA itab initio calculations have now become possible for systems of about 1000 atoms for the ground state. Time-dependent DFT (TDDFT) can in principle describe excitations as exhibited in optical spectra. However, approximations for the exchange and correlation contributions that are valid in a wide range of situations and efficient enough to be applied to large nanostructures are still to be found. GW calculations deal only with charged (electron addition and removal) excitations. The solution of the Bethe-Salpeter equation (BSE) gives good answers for neutral excitations like absorption but is numerically heavy and so far tractable for rather small systems only. In my talk I will briefly review the state of the calculation of optical

properties. Using bulk semiconductors and Ge, Si, and alloy nanocrystals as illustrations, I will then discuss the following points: Manifestation of confinement effects in various spectra; Importance of surface effects; Interplay between many-body effects and confinement and surface effects; Importance of short- and long-range contributions. How are they adequately described? (Important, e.g., for embedded nanostructures.) These questions will be discussed in view of the optical properties, but also for loss spectra and photo-emission. Methods used are DFT-LDA, TDDFT in various approximations, GW, and BSE.

*Supported by the European Union through the Network of Excellence NANOQUANTA (Contract NMP4-CT-2004-500195).

**8:36**
**N7 2 Atomistic Pseudopotential Calculations of the Electronic and Optical Properties of Self-Assembled Quantum Dots.***
GABRIEL BESTER, *National Renewable Energy Laboratory*

The optical spectrum and the charging energies of semiconductor quantum dots have been recently measured with high accuracy. Both of these experimental techniques probe many-body states that are not directly described by independent particle theories such as the density functional theory. On the other hand, quasi- particle theories that can in principle address the problem, such as GW, are computationally too demanding for the study of nanostructures (as opposed to clusters) where many thousands of atoms are involved. One way to approach this problem is to use the effective mass approximation or the k.p method and choose a confinement potential that reproduces a few known experimental facts (e.g. the splitting between confined levels). These methods can provide a good initial guess but were shown to be too crude to enable a quantitative comparision with recent experiments. We therefore adopt a bottom-up atomistic approach where instead of starting from a simplified approach, such as effective mass, and progressively increase the complexity by adding parameters, we start from the accurate atomistic description (LDA or GW) and work ourselves up using a few well controlled approximations. I will first present the method, namely (i) the scheme that is used to derive the empirical pseudopotentials including the piezoelectric effect, (ii) the choices that have to be made for the basis used to expand the wave functions, (iii) the inclusion of corelations through Bethe-Salpeter-like treatment. I will then present recent applications of the theory to calculate the fine-structure [1] of excitons and charged excitons, the charging spectra of holes [2] and the degree or entanglement stored in a quantum dot molecule [3]. [1] G. Bester, S.V. Nair, A. Zunger, PRB **67**, 161306 (2003). [2] L. He, G. Bester, A. Zunger, PRL (in press). [3] G. Bester, J. Shumway, A. Zunger, PRL **93**, 047401 (2004).

*In collaboration with A. Zunger, L. He, S.V. Nair and J. Shumway. Supported by DOE-SC-BES-DMS under the LAB 03-17 Program under NREL contract AC3699GO10377.



**9:12**
**N7 3 Density Functional Theory of the electrical conductivity of molecular devices.**
RALPH GEBAUER, *The Abdus Salam International Centre for Theoretical Physics (ICTP)*

The theoretical modeling of electrical transport through nanoscale devices is a very challenging task: On one hand, the conduction properties of a molecular junction depend crucially on details of the chemical bonding, particularly at the interface. Such properties are routinely studied using methods based on density-functional theory (DFT). On the other hand, ground-state theories like DFT cannot be directly applied to systems with a finite current, because such devices are out of equilibrium. One possibility to overcome this problem is to study electron transport in the time domain. In the spirit of what is done in semiclassical Boltzmann approaches, one considers the system subject to both an external electrical field and to dissipation due to inelastic scattering. The combined influence of the external driving force and dissipation leads to a steady state with finite current. In this presentation I will first show how time-dependent DFT can be formally extended to dissipative systems, described by a Liouville master equation for the reduced density matrix. In a second step this formalism is then applied to calculate the current-voltage characteristics of molecular junctions, like e.g. carbon nanotubes suspended between metallic contacts.

**9:48**
**N7 4 Self-interaction errors in density functional calculations of electronic transport.**
STEFANO SANVITO, *Trinity College Dublin*

All density functional (DFT) calculations of single-molecule transport to date have used continuous exchange-correlation approximations, such as the local density approximation (LDA) or the generalized gradient approximation (GGA). These usually provide a good description of metallic systems, but fail in predicting the correct I-V curve for molecules weakly coupled to the current/voltage probes. Most of the problem can be attributed to the lack of the derivative discontinuity of the DFT potential in local approximations. These in fact continuously connect the orbital levels for different integer occupations, leading to qualitative errors such as the erroneous prediction of the dissociation of heteronuclear molecules into fractionally charged ions In this talk I will first describe the typical errors arising from neglecting the derivative discontinuity in transport calculations [1], namely the erroneous prediction of metallic transport for insulating molecules. Then I will present a simple and computationally undemanding atomic self-interaction correction scheme for transport. This preserves the computational and conceptual simplicity of standard LDA, and nevertheless re-introduces part of the derivative discontinuity. The method is implemented in our quantum transport code Smeagol [2] (www. smeagol.tcd.ie) and several examples will be given. [1] C. Toher, A. Filippetti, S. Sanvito, and K. Burke, Phys. Rev. Lett. 95, 146402, (2005). [2] A.R. Rocha, V.M. Garcia Suarez, S.W. Bailey, C.J. Lambert, J. Ferrer, and S. Sanvito, cond-mat/0510083.

**10:24**
**N7 5 Electron-vibration interaction in molecular electronics and GW approximation for the e-e interaction in transport theory.**
ALESSANDRO PECCHIA, *Roma 'Tor Vergata'*

The field of molecular electronics has seen a tremendous expansion in recent years, thanks to the realization of ingenious experimental setups and the fundamental achievement of reproducible results and behaviours. Significant progresses have also been made from a theoretical point of view, although the agreement with experiments is still not satisfactory. The challenges for a complete understanding of transport in such systems are still considerable. Inelastic electron tunnelling spectroscopy is becoming very popular in the field thanks to its powerful capability of probing molecular vibrational properties and could provide in the future a valuable characterization tool if correctly related to theoretical calculations. We simulate IETS spectra of various molecules between metal contacts and show the importance of such simulation for the interpretation of the experiments. Particular attention is devoted to the evaluation of Joule heating and thermal dissipation. The problem is tackled within the formalism of NEGF by the calculation of appropriate electron-phonon self-energies. The electron-phonon coupling is derived from the DFTB Hamiltonian. The Power dissipated is calculated from the virtual contact current originated from phonon emission and absorption processes. Preliminary results of thermal dissipations of molecules coupled to Au and Si substrates will be shown. As well known, all DFT methods tend to underestimate the electronic band-gap of semiconducting and insulating materials. In particular the band-gap of conjugated organic molecules is usually underestimated by few electronvolts. However, band-gap corrections are crucial for quantitatively correct calculations of the tunneling current through organic molecules. We show a novel implementation of the itGW correction applied to our DFTB method and show its applications to molecular systems sandwitched in-between electrodes to obtain a first-principle correction of the $e - e$ interaction energy. The resulting self-energy is used to improve the system itGF and to obtain a correction of the tunneling current. We also apply the itGW correction in the context of the computation of the complex band-structures of polymers such as poly-acetylene or poly-phenylene and show how the energy gap and decay lengths of the evanescent states should be corrected by quasi-particle effects.

**SESSION N8: GRANULAR FLOWS**
**Wednesday Morning, 15 March 2006**
**314, Baltimore Convention Center at 8:00**
**Erin Rericha, University of Maryland, presiding**

**8:00**
**N8 1 Assessing a Continuum Description of Wide Shear Zones in Slow Granular Flow by Discrete Element Simulations** JEREMY B. LECHMAN, GARY S. GREST, *Sandia National Laboratories** MARTIN DEPKEN, *Instituut-Lorentz for Theoretical Physics* MARTIN VAN HECKE, *Kamerlingh Onnes Lab* While the rheology of rapid granular flows is becoming well established, slow, dense flows are not well characterized in part because the strain localization (i.e., shear bands) they often exhibit is not easily amenable to continuum descriptions. Recently, a novel experimental system (split-bottom Couette Cell) was developed with promising potential to give new insight into these flows due to its wide, smooth shear zones (Fenistein et al. PRL **92**, 94301). Subsequent experimental and numerical studies have lead to a good understanding of the nature of the flow in this device, which has lead Depken et al. (cond-mat/0510524) to propose a set of testable constitutive relations between the internal stresses and flow field. In particular, they suggest that the bulk, effective friction coefficient between sliding layers of particles is not constant, but has a subtle dependence on the orientation of the layers with respect to the bulk force. Here we present large-scale Discrete Element Simulations to analyze the bulk flow in both circular, above and below the critical height, and linear, where no critical height for slip at the base is found, split-bottom geometries. We check the proposed form of the stress tensor and assess the validity of the claim that the effective friction coefficient depends on the shape of the shear zone with respect to gravity.

**8:12**

**N8 2 Dynamical heterogeneities in dense granular flow: timescales and large-scale particle rearrangements** ALLISON FERGUSON, BULBUL CHAKRABORTY, *Brandeis University* Recent interest in understanding the dynamical arrest leading to a fluid $\rightarrow$ solid transition in both thermal and athermal systems has led to questions about the nature of these jamming transitions (PRL **86**, 111 (2001), Nature **411**, 772 (2001)). It is believed that these jamming transitions are dependent on the influence of extended structures on the dynamics of the system (Science **287**, 627 (2000)). Simulations of steady-state gravity-driven flows of inelastically colliding hard disks show the formation of large-scale linear chains of particles with a high collision frequency even at flow velocities well above the jamming transition (EPL **66**, 277 (2004)). These chains can be shown to carry much of the collisional stress in the system due to a dynamical correlation that develops between the momentum transfer and time between collisions in these ''frequently-colliding'' particles. While measurements of slowly decaying stress correlations yield an average lifetime for these structures which scales inversely with the flow velocity (cond-mat/0505496), distributions of time scales associated with the stress chains may provide more information about their effect on the dynamics of the flowing granular medium. These distributions may be obtained by considering time scales related to large-scale rearrangements of neighbouring particles in analogy with measurements done on supercooled fluids.

**8:24**

**N8 3 Dense granular flows down an inclined plane** ROBERT ECKE, TAMAS BORZSONYI,* *Los Alamos National Laboratory* Granular flow on a rough inclined plane is an important model system in which to study the basic rules of the dynamics of granular materials. Despite intensive study, many features of such flows are still incompletely understood. For uniformly flowing layers at relatively shallow inclination, we consider experimentally the the basic flow rheology of the granular media and propose new scalings to collapse our data for glass beads and rough sand as a function of inclination angle and particle diameter. At steep inclinations above some angle $\theta_s$ ($\tan\theta_s/\tan\theta_r \approx 1.3 - 1.5$, where $\theta_r$ stands for the angle of repose) for flowing grains, numerics and theory predict that the surface roughness is inadequate to dissipate energy gained in the gravitational field, and the flow should continue to accelerate. We report on our experimental results on the properties of granular flows on a steeply inclined plane and define the domains of steady flows. We also discuss the instabilities of such flows leading to spatial patterns.

*Currently at Hungarian Academy of Sciences, Budapest, Hungary.

**8:36**

**N8 4 Transverse Instability of Avalanches in Granular Flows down Incline*** IGOR ARANSON, *Argonne National Laboratory* FLORENT MALLOGGI, ERIC CLEMENT, *ESPCI, France* Avalanche experiments on an erodible substrate are treated in the framework of ''partial fluidization'' model of dense granular flows. The model identifies a family of propagating soliton-like avalanches with shape and velocity controlled by the inclination angle and the depth of substrate. At high inclination angles the solitons display a transverse instability, followed by coarsening and fingering similar to recent experimental observation. A primary cause for the transverse instability is directly related to the dependence of soliton velocity on the granular mass trapped in the avalanche.

*This research was supported by US DOE, contract #W-31-109-ENG-38.

**8:48**

**N8 5 Swirling in a Vibrated Monolayer of Rods** VIJAY NARAYAN, SRIRAM RAMASWAMY, *Indian Institute of Science, Bangalore* NARAYANAN MENON, *U. of Massachusetts, Amherst* We report observations of the spatiotemporal behaviour of a vertically vibrated horizontal monolayer of copper rods (aspect ratio $\approx$ 5) etched to a rolling-pin-like shape. The spatial organization of the rods resembles a highly-defected nematic state with large, coherently moving swirls. We measure spatiotemporal correlations of the single-particle and collective velocities, and study the structure and dynamics of the system as a function of density and vibration amplitude. We analyze the observed patterns in the light of theories[1] of orientational ordering, dynamics, and topological defects in systems of driven particles. We make comparisons to related but different experiments[2], as well as to our earlier measurements[3] on similar particles with higher aspect ratio.

[1]J. Toner, Y. Tu and S. Ramaswamy, Ann. Phys. 318 (2005) 170.
[2]D.L. Blair, T. Neicu, and A. Kudrolli, Phys. Rev. E 67, 031303 (2003).
[3]V. Narayan, N. Menon and S. Ramaswamy, J. Stat. Mech. (2005) in press; cond-mat/0510082.

**9:00**

**N8 6 Simple Power Law for Transport Ratio with Bimodal Distribution of Coarse Sediment** CHRISTOPHER THAXTON, *Appalachian State University* JOSEPH CALANTONI, *Naval Research Laboratory* Using a discrete particle model, we have simulated sheet flow transport of coarse bimodal sediment distributions in the bottom boundary layer over a range of oscillatory waves and steady currents. The ratio of large grain to small grain diameter was varied as 5:4, 3:2, and 2:1. For each bimodal distribution, the mass ratio $M_L/M_S$ ($M_L$ and $M_S$ are the masses of large and small grains respectively – the total mass was fixed for all runs) was varied from 1/9 up to 9/1. We find that, independent of wave and current forcing for the range of conditions considered, the ratio of large to small grain time-average transport rate obeys the power law $Q_L/Q_S = C(M_L/M_S)^k$, where $Q_L$ and $Q_S$ are the time-average transport rates of the large grains and small grains respectively and $C$ and $k$ are regression constants. A linear regression in log space (including 81 different simulations per diameter ratio) suggests that itk$\approx D_L/D_S$ with $R^2 > 0.9$. The robust nature of the results suggests that the new power law may have a broad range of applications for shear flows of bimodal granular mixtures.

**9:12**

**N8 7 Large scale surface flow generation in driven suspensions of magnetic microparticles.** MAXIM BELKIN, ALEXEY SNEZHKO, IGOR ARANSON, *Materials Science Division, Argonne National Laboratory, 9700 South Cass Avenue, Argonne IL 60439* Nontrivially ordered dynamic self-assembled snake-like structures are formed in an ensemble of magnetic microparticles suspended over a fluid surface and energized by an external alternating magnetic field. These self-assembled multi-segment structures emerge as a result of the collective interaction between the particles oscillations induced by an external magnetic field and the standing waves on the surface of fluid. Surprising large-scale vortex flows

are generated by these snake-like structures. The flows can be as fast as 2 cm/sec and strongly depend on the driving magnetic field parameters. We report on systematical experimental study of the vortex flow properties and generation mechanisms.

**9:24**

**N8 8 Green-Kubo expressions for transport coefficients of a granular fluid.** APARNA BASKARAN, JAMES DUFTY, *Department of Physics, University of Florida* A formal derivation of linear hydrodynamics for a granular fluid is given. The linear response to small spatial perturbations of the homogeneous state is studied in detail using methods of nonequilibrium statistical mechanics. A transport matrix for macroscopic excitations in the fluid is defined in terms of the response functions. An expansion in the wavevector to second order allows identification of all phenomenological susceptibilities and transport coefficients through Navier - Stokes order [1]. The transport coefficients in this representation are the generalization of Helfand and Green-Kubo relations to granular fluids. The analysis applies to a wide range of collision rules. Several differences from the corresponding expressions in the elastic limit are noted. Then, the particular case of inelastic hard spheres is considered and some approximate analytical evaluations illustrated. [1] A preliminary report of these results can be found in J. W. Dufty, A. Baskaran and J. J. Brey cond-matt/0507609.

**9:36**

**N8 9 Dynamics angle and surface flow properties of wet and cohesive granular matter** QING XU, ARSHAD KUDROLLI, *Physics Dept., Clark University* We will discuss an experimental study of the flow of grains mixed with a small amount of liquid using a horizontally rotated drum apparatus, extending on our previous work on the maximum angle of stability of wet granular materials [1]. We focus on the continuous avalanching regime observed at high rotation rates, and examine the shape of the granular surface and depth of flow with imaging techniques as a function of amount, viscosity and surface tension of the liquid. Glass beads with 1mm diameter, and a drum with a diameter 295 mm and a width of 145mm is used to minimize the effect of the boundary. We find that the shape of the surface may be approximated by two linear segments in the upper and lower halves. The slope of the upper segment corresponding to the dynamical angle of repose $\theta_d$ is observed to initially increase with rotation rate and volume fraction of liquid as expected, while the lower segment has an approximately constant slope. Interestingly, $\theta_d$ is observed to peak before decreasing to an approximately constant value as the volume fraction is increased. The rate of increase of $\theta_d$ is observed to decrease with rotation rate and viscosity. The role of the time scale over which wet grains shear past each other and the time over which grains actually come into contact due to lubrication forces on the observed change in scaling will be discussed. [1]: S. Nowak, A. Samadani, and A. Kudrolli, Nature Physics **1**, 50 (2005).

**9:48**

**N8 10 Characterizing the banded state of granular material in a rotating drum.*** MICHAEL NEWEY, *University of Maryland* KENNETH DESMOND, *Rochester Institute of Technology* WOLFGANG LOSERT, *University of Maryland* Why do particles of different size segregate axially in a horizontal rotating tumbler? We aim to understand the microscopic mechanisms for axial segregation through direct measurements of the motion of individual particles. Imaging the surface of the flowing layer, we extract flow angles, velocities, drift and diffusion for different particle types and mixtures of particles. Surprisingly, the direction of surface drift and steepest flow angle do not coincide and that surface drift cannot explain the axial segregation in our mixtures. On the other hand, particles in small particle bands flow significantly faster then particles in large particle bands, and this can be observed before visible band formation. We discuss the possible role of velocity differences in the axial segregation process. We characterize the fluidity of the flowing layer from its response to gentle sideways forcing.

*Supported by NASA Grant NAG-32736.

**10:00**

**N8 11 Mechanisms in size segregation of binary granular mixtures** STEPHAN ULRICH, *University of Göttingen* JENNIFER KREFT, MATTHIAS SCHRÖTER, JACK SWIFT, HARRY SWINNEY, *Center for Nonlinear Dynamics, University of Texas at Austin* Shaking of a mixture of large and small particles can lead to segregation. One distinguishes between the Brazil-nut effect (large particles go to the top) and its opposite, the reverse Brazil-nut effect. In this talk, experiments of vertically shaken binary mixtures are presented. Using image analysis, the number of large particles visible at the top and bottom of the granulate are counted to determine the state of segregation. By complementing these results with molecular dynamics simulations, we are able to identify different segregation mechanisms discussed in recent theoretical approaches: a geometrical mechanism called void filling, transport of particles in sidewall-driven convection rolls, and thermal diffusion, a mechanism predicted by kinetic theory.

**10:12**

**N8 12 Upward penetration through a granular medium** D. COSTANTINO, T.J. SHEIDEMANTEL, M.B. STONE, J. COLE, C. CONGER, K. KLEIN, M. LOHR, W. McCONVILLE, Z. MODIG, P. SCHIFFER, *Penn State University* We measure the force needed to push a flat plunger upwards through a granular medium. The plunger begins flush with the base of the grains' container, and we focus upon the force necessary to initiate motion. The data show that this break-out force increases monotonically with plunger diameter and pile height as expected. In contrast to previous measurements of the force needed for vertical penetration from above and of the horizontal drag force, this break-out force has a strong dependence on bead diameter. Research supported by NASA grant NAG3-2384 and the NSF REU program.

**10:24**

**N8 13 Correlation in granular shear flows** GREGG LOIS, *University of California, Santa Barbara* JEAN CARLSON, *University of California, Santa Barbara* We investigate the effects of long-range correlation in simulations of sheared granular materials and develop theories to model force propagation in the dense regime. Measurements of spatial force correlations determine the size of force networks that emerge as the density is increased. The magnitude of the correlation length separates the dilute regime, where kinetic theory holds, from a dense regime where its assumptions break down. In the dense regime we introduce theories that successfully predict constitutive relations for the stress tensor, using geometrical properties of the force networks. Additionally, we observe that the behavior of the contact force distribution at small forces is highly dependent on the size of the force networks.

**10:36**
**N8 14 Shear reversal in granular flows** MASAHIRO TOIYA, *University of Maryland* WOLFGANG LOSERT, *University of Maryland* The reversal of the shear direction in flow of monodisperse and bidisperse granular matter in a shear cell of Taylor-Couette type is characterized experimentally. By changing the boundary conditions we tune the location and width of the shear band in steady state flow. When the shear direction is reversed, the system compacts over a characteristic length of half a particle diameter, and shear forces reach a steady state over a chacteristic length of 1-3 particle diameter. A linear strain is found at the onset of shear reversal before a steady state shear band develops. We associate this extra strain during shear reversal with the displacement needed to jam particles in regions away from the shearband. We find that the strain decreases with increasing particle size for a fixed system size. We also find radial components in average particle velocities at the top surface, suggesting a convection current in the bulk.

## SESSION N10: FOCUS SESSION: FRONTIERS IN COMPUTATIONAL CHEMICAL PHYSICS III
**Wednesday Morning, 15 March 2006; 302, Baltimore Convention Center at 8:00**
**Jeffrey Saven, University of Pennsylvania, presiding**

***Invited Papers***

**8:00**
**N10 1 Development of effective models for vectorial biological processes.***
QIANG CUI, *UW-Madison*

Progress towards understanding vectorial processes in biological systems using theoretical and computational approaches will be discussed. The specific problems of interest include mechanochemical coupling in the molecular motor myosin and vectorial proton pumping in cytochrome c oxidase. Several related methodological developments will be discussed, which include boundary potential for QM/MM simulations, effective QM methods for treating long-range proton transfers and phosphate chemistry, and coarse-grained models for describing large-scale motions in biomolecules. Quantitative benchmark calculations of these methods have been carried out using both model and realistic biological systems. The application of these methods to myosin and cytochrome c oxidase will be briefly presented.

*Projects were supported via grants from the National Science Foundation and the National Institutes of Health.

***Contributed Papers***

**8:36**
**N10 2 Hierarchical Coarse-Grained Models for Polymer Simulations*** SHENG D. CHAO, *Institute of Applied Mechanics, National Taiwan University* Structural and thermodynamic properties of industrial and bioengineering materials can be better investigated using atomistic simulations. However, current large-scale atomistic simulations remain computationally demanding. It is thus desirable to seek alternatives to perform efficient and informative mesoscopic simulations. We have developed a coarse-grained intermolecular force (CGIF) model for polymer nanostructures and nanocomposites. This model can effectively capture the stereochemical response to anisotropic long-range interactions. The coarse-graining procedure forms the basis to perform a hierarchy of simulations starting with the quantum-chemistry calculations to coarse-grained molecular dynamics toward continuum modeling. We have applied this procedure to several cases from alkane to benzene to fullerene. For liquid methane, molecular dynamics simulations using the CGIF model reproduce the structural properties calculated using the atomistic force field. The coarse-grained energetics of benzene clusters has well reproduced the results using electronic structure calculations. The subtle anisotropy in the interaction potential of fullerene dimer is also well represented by the CGIF model and is consistent with that calculated using the Brenner force field.

*This work was supported by the National Science Council of Taiwan, ROC.

**8:48**
**N10 3 Dynamic Phase Transitions in Coupled Motor Proteins** ANATOLY KOLOMEISKY, EUGENE STUKALIN, *Rice University* The effect of interactions on dynamics of coupled motor proteins is investigated theoretically. A simple stochastic discrete model, that allows to calculate explicitly the dynamic properties of the system, is developed. It is shown that there are two dynamic regimes, depending on the interaction between the particles. For strong interactions the motor proteins move as one tight cluster, while for weak interactions there is no correlation in the motion of the proteins, and the particle separation increases steadily with time. The boundary between two dynamic phases is specified by a critical interaction that has a non-zero value only for the coupling of the asymmetric motor proteins, and it depends on the temperature and the transitions rates. At the critical interaction there is a change in a slope for the mean velocities and a discontinuity in the dispersions of the motor proteins as a function of the interaction energy.

**9:00**
**N10 4 Reduced-Dimensional Models for Chemical Dynamics in Complex Environments** RIGOBERTO HERNANDEZ, ALEX V. POPOV, ELI HERSHKOVITS, *School of Chemistry and Biochemistry, Georgia Institute of Technology, Atlanta, GA 30332-0400* Nonstationary Langevin models have been developed that are capable of capturing feedback between complex environments and the underlying molecular constructs which in turn collectively comprise the environment. Although initial justifications for this formalism were heuristic and phenomenological, in recent work we have shown that in some cases it arises as the projection of a

simple model of a chemical system bilinearly coupled to a harmonic bath with a time-dependent coupling. Moreover, the stochastic model can be used to surmise the diffusion of a tagged particle in a colloidal suspension which swells or shrinks with time. Alternatively, a liquid crystal, modelled as a colloidal suspension of orientable bodies, can also exhibit driven (time-dependent) behavior by way of the rotation of a magnetic field. Once again, the diffusion of a tagged particle under such time-dependence, can be surmised by the stochastic model. Thus these models allow for a substantial reduction of the dimensionality of a complex environment while retaining its multiple-time-scale features.

**9:12**

**N10 5 Structure of Alzheimer's 10-35 $\beta$ peptide from replica-exchange molecular dynamics simulations in explicit water** ANDRIY BAUMKETNER, JOAN-EMMA SHEA, *University of California Santa Barbara* We report a replica-exchange molecular dynamics study of the 10-35 fragment of Alzheimer's disease amyloid $\beta$ peptide, A$\beta$10-35, in aqueous solution. This fragment was previously seen [J. Str. Biol. 130 (2000) 130] to possess all the most important amyloidogenic properties characteristic of full-length A$\beta$ peptides. Our simulations attempted to fold A$\beta$10-35 from first principles. The peptide was modeled using all-atom OPLS/AA force field in conjunction with the TIP3P explicit solvent model. A total of 72 replicas were considered and simulated over 40 ns of total time, including 5 ns of initial equilibration. We find that A$\beta$10-35 does not possess any unique folded state, a 3D structure of predominant population, under normal temperature and pressure. Rather, this peptide exists as a mixture of collapsed globular states that remain in rapid dynamic equilibrium with each other. This conformational ensemble is seen to be dominated by random coil and bend structures with insignificant presence of $\alpha$-helical or $\beta$-sheet structure. We find that, overall, the 3D structure of A$\beta$10-35 is shaped by salt bridges formed between oppositely charged residues.Of all possible salt bridges, K28-D23 was seen to have the highest formation probability, totaling more than 60% of the time.

**9:24**

**N10 6 Orbital Energetics and Molecular Recognition** AARON GEORGE, *Targacept, Inc.* REBECCA HARRIS, VISHALI MOGALLAPU, YONAS ABRAHAM, ROBERTO CAR, *Princeton University* JEFFREY SCHMITT, We present data demonstrating that orbital eigenenergy fluctuation recorded in the course of ab initio molecular dynamics calculations contains information relevant in determining molecular behavior and recognition. A simple scheme is presented that maps these data to molecular descriptors. Using computational drug design as the context, these descriptors are compared with previous electronic eigenvalue descriptor methods with encouraging results. Finally we discuss further methods of mapping electronic structure based molecular dynamics trajectories to Quantitative Structure Activity Relationships (QSAR).

**9:36**

**N10 7 Unrestricted Hartree-Fock Investigation of the Electron Distribution on the Heme System in Azidohemoglobin-$^{57m}$Fe and $^{14}$N Hyperfine Interactions.** ARCHANA DUBEY, H.P. SAHA, LEE CHOW, *UCF, Orlando* R.H. SCHEICHER, *MTU, Houghton* N. SAHOO, R.H. PINK, DIP N. MAHATO, M.B. HUANG, T.P. DAS*, *SUNY Albany* We have a program of investigations in progress on the electronic structure of azidohemoglobin by the first-principles Unrestricted Hartree-Fock procedure to understand the substantial amount of magnetic (g-tensor), magnetic hyperfine, and nuclear quadrupole interaction, data available [1] from electron paramagnetic resonance, Mosbauer and electron-nuclear double resonance measurements. Earlier semi-empirical Self-Consistent Charge Extended Huckel investigations have provided semiquantitative results [2] with different degrees of agreement for the available properties and suggested the need for more accurate and quantitative investigations. Results of our investigations will be presented for the $^{57m}$Fe and $^{14}$N nuclear quadrupole and magnetic hyperfine interaction properties and compared with experimental data. *Also UCF Orlando [1] See Refs. 2-4 listed in Ref.[2]. [2] Santosh K. Mishra, J.N. Roy, K.C. Mishra and T.P. Das, Theo. Chim. Acta 75, 195 (1989).

**9:48**

**N10 8 Polymer dynamics and the folding rates of fast folding proteins** JOHN PORTMAN, *Kent State University* In recent years, minimal models of fast folding proteins has enabled considerable agreement between computation, theory, and experiment. The assumptions associated with most simple models of fast folding proteins (Go-models) give rather robust results in terms of coarse grained description of the transition state ensemble. One aspect of the folding mechanism that has received less attention is describing the conformational dynamics responsible for the folding rate prefactor, $k_0$. Here, we consider the distribution of prefactors of fast folding proteins: does local dynamics influence $k_0$, or can one reasonably expect that $k_0$ is essentially the same regardless of contact order or mean structure of the transition state ensemble. We address this question by considering the folding routes of a wide variety of fast folding proteins using a polymer based model in which structural ensembles are parameterized by the degree of localization about the native structure.

**10:00**

**N10 9 A United Atom Model for Simulation of DNA from Angstroms to Microns in Length** THOMAS KNOTTS IV, NITIN RATHORE, JUAN DE PABLO, *Department of Chemical and Biological Engineering - University of Wisconsin-Madison* For several years, single molecule pulling experiments have given insights into the stability of DNA. Many descriptions of DNA, from atomistic to continuum, have proven successful at reproducing observed behavior. We have found, however, that there is no suitable model for several problems of interest, including viral packaging of DNA and microarray interactions, where the size of the molecules prohibits atomistic representations, but continuum and linear bead-spring models do not contain the required molecular level of detail. Emerging technologies require that mesoscopic models of DNA be developed, capable of describing length scales in the 5 to 500 nm range. One of the main challenges is to preserve a coupling between the phenomena seen at longer length scales (e. g. a persistence length of 50 nm) while incorporating the features needed for smaller scales (e. g. charge effects, geometry, and base specificity). We have developed a coarse grain description of DNA which reduces the complexity of a nucleotide to three interaction sites. The model is capable of describing sequence information,

bubble formation, and salt effects in simulations of DNA up to a few microns in length. The predictions are in remarkable, quantitative agreement with experiment, and shed light into the coupling of multiple length scales and interactions to yield unique behaviors and functions.

**10:12**
**N10 10 Diffusion Monte Carlo applied to weak interactions - hydrogen bonding and aromatic stacking in (bio-)molecular model systems** M. FUCHS, J. IRETA, M. SCHEFFLER, *Fritz-Haber-Institut der MPG, Berlin* C. FILIPPI, *Instituut Lorentz, Univ. Leiden* Dispersion (Van der Waals) forces are important in many molecular phenomena such as self-assembly of molecular crystals or peptide folding. Calculating this nonlocal correlation effect requires accurate electronic structure methods. Usual density-functional theory with generalized gradient functionals (GGA-DFT) fails unless empirical corrections are added that still need extensive validation. Quantum chemical methods like MP2 and coupled cluster are more accurate, yet limited to rather small systems by their unfavorable computational scaling. Diffusion Monte Carlo (DMC) can provide accurate molecular total energies and remains feasible also for larger systems. Here we apply the fixed-node DMC method to (bio-)molecular model systems where dispersion forces are significant: (dimethyl-) formamide and benzene dimers, and adenine-thymine DNA base pairs. Our DMC binding energies agree well with data from coupled cluster (CCSD(T)), in particular for stacked geometries where GGA-DFT fails qualitatively and MP2 predicts too strong binding.

**10:24**
**N10 11 Computational Methods for Enhanced Conformational Kinetics** IOAN ANDRICIOAEI, *University of Michigan* We present and analyze two general method to calculate time-correlation functions from molecular dynamics on scaled potentials or from molecular dynamics with artificial momenta distributions. They are useful for complex systems whose simulations are affected by broken ergodicity. Depending on the value of the scaling factor or of the details of the momentum distributions, correlation functions can be accurately calculated for times that can be orders of magnitude longer than those accessible to current molecular dynamics simulations. We show that the exact value of the correlation functions of the original system can be obtained, in principle, using an action-reweighting scheme based on a stochastic path-integral formalism. Tests on model systems and peptides are exemplified. We also show that free energy profiles using Jarzynski's identity can be more effectively calculated within this scheme.

## SESSION N11: FOCUS SESSION: AEROSOLS, CLUSTERS, DROPLETS: PHYSICS AND CHEMISTRY OF NANOOBJECTS I: HELIUM NANODROPLETS I

**Wednesday Morning, 15 March 2006; 303, Baltimore Convention Center at 8:00**
**Giacinto Scoles, Princeton University, presiding**

*Invited Papers*

**8:00**
**N11 1 Imaging the Photodynamics of Doped Helium Droplets.**
MARCEL DRABBELS, *Institute of Chemical Sciences and Engineering, Swiss Federal Institute of Technology Lausanne, Switzerland*

During the last decade helium nanodroplets have been established as an ideal spectroscopic matrix. Helium droplets are also thought to be ideal low temperature nanoreactors because of their ability to stabilize weakly bound species. As the focus is nowadays shifting to the study of chemical reactions in liquid helium droplets, question related to the energy relaxation and solvation dynamics become more and more prominent. To address these questions experiments have been performed in with species with a well defined kinetic energy distribution have been created via the photodissociation molecules residing inside helium droplets. The velocity distributions of the photofragments that have escaped from the droplets have been determined using ion imaging techniques. The analysis of speed distributions as function of droplet size and precursor has enabled to obtain a consistent picture of the mechanisms underlying the translational motion of these non-thermal species through this quantum liquid. Additional information on the solvation dynamics could be obtained by using non-resonant ionization techniques in these experiments. More recently the translational dynamics of quasi-free electrons in helium droplets has been investigated by means of photoelectron spectroscopy. The results on these experiments indicate that the relaxation of the electrons is governed by the same mechanism responsible for the kinetic energy relaxation of non-thermal neutral molecules.

*Contributed Papers*

**8:36**

**N11 2 Photoionization and photoelectron spectroscopy of doped helium nanodroplets** DANIEL NEUMARK, *University of California, Berkeley* Photoionization and photoelectron spectra for helium nanodroplets doped with rare gas atoms and $SF_6$ will be reported. The experiments were conducted using tunable synchrotron radiation at the Advanced Light Source in the photon energy range of 14-26 eV. Time-of-flight mass spectra will be presented, along with photoion and photoelectron images. The results will be compared to previous electron impact ionization data.

**8:48**

**N11 3 Photoinitiated processes in and on liquid helium** ELENA POLYAKOVA, DANIIL STOLYAROV, CURT WITTIG, *Columbia University* Photoinitiated processes that involve molecules in $He_n$ droplets are examined. Excitation to states that contain Rydberg character results in repulsion between the electronically excited embedded molecules and the surrounding helium. Even after the helium has, moved further from the molecular core, the situation is unstable in the sense that the electronically excited species prefer the surface. The timescale for transport to the surface is $<$ 10 itns duration of the laser pulse. The resulting surface-bound species can be ionized, yielding small clusters of the form $He_mNO^+$, where $\langle g \rangle$ is of order 10,000. The possibility of observing high Rydberg states in which the electron is outside the helium droplet will be discussed. A vastly different case of photoexcitation occurs when the excited potential is coupled to a lower one via conical intersection.

**9:00**

**N11 4 Wave packet propagation of alkali dimers attached to helium nanodroplets** FRANK STIENKEMEIER, *Universitaet Freiburg, Germany* PATRICK CLAAS, *Universitaet Bielefeld, Germany* CLAUS-PETER SCHULZ, *Max-Born-Institut Berlin, Germany* Real-time spectroscopy of alkali dimers attached to helium nanodroplets has been studied by femtosecond pump-probe spectroscopy. Wave packet propagation in different electronic states of $Na_2$ and $K_2$ molecules was investigated. The perturbation of the helium environment allows in particular to observe electronic ground state vibrational motion. Furthermore, for the first time wave packets in alkali dimer triplet states are observed. Finally, the slight change of the vibrational structure when desorbing from the helium droplet can be utilized to determine desorption times upon laser excitation.

**9:12**

**N11 5 Metal clusters in helium droplets: Fulfilling the promise** PAUL L. STILES, ROGER E. MILLER,* *University of North Carolina* In 2001 we demonstrated that superfluid helium droplets, coupled to high-resolution infrared spectroscopy, could be used to investigate the intermolecular interactions and structures of metal cluster-adsorbate systems. The HCN-$Mg_n$ (n = 1-6) clusters investigated provided several interesting surprises and taught us many valuable lessons but nevertheless remained a somewhat uninteresting system from the point of view of catalysis and reactivity. Recently, we have overcome some significant experimental challenges and are finally beginning to fulfill the promise of using superfluid helium droplet spectroscopy for the investigation of more ''chemically interesting'' systems. In this talk we will present the infrared spectra of a single HCN molecule bound to copper and silver clusters. From these spectra we were able to obtain information about the adsorbate-metal cluster interactions, as well as obtaining direct structural information through high-resolution spectra.

*Deceased.

**9:24**

**N11 6 Adaptive Clustering of Adatoms Around Ionic Dopants in He Droplets: Quantum Calculations** FRANCESCO A. GIANTURCO, *Dept. of Chemistry, University of Rome ''La Sapienza''* The structuring and collocation of individual He atoms as quantum objects around simple atomic and molecular impurities has been the subject of a great number of studies, both experimentally and from the theoretical viewpoint [1,2] since the advent of droplets experiments, where such nanoscopic containers have been exploited to provide a sort of nanocryostat for the analysis of the dopant's spectroscopic behavior [3]. We have carried out computations of potential fields within small clusters which contain a variety of ionic dopants using post-Hartree-Fock, ab initio methods and have further endeavoured to extract from them the corresponding classical and quantum structuring of such impurities within clusters of variable size. For the latter enquiry we have employed both classical optimization methods and Quantum Diffusion Monte Carlo analysis. Results for both atomic ($Li^+$) and molecular ($LiH^+$, $OH^+$, $OH^-$) ionic dopants will be presented at the meeting. [1] J.P. Toennies and A.F. Vilesov, Angewandte Chemie **43**, 2622 (2004). [2] e.g. see: F. Paesani, A. Viel, F.A. Gianturco and K. Whaley, Phys. Rev. Lett. **90**, 073401 (2003). [3] J.P. Toennies and A.F. Vilesov, Ann. Rev. Phys. Chem. **49**, 1 (1998).

**9:36**

**N11 7 Electron-impact ionization mass-spectrometry of molecules and clusters in a pulsed helium droplet source** SHENGFU YANG, SCOTT BRERETON, ANDREW M. ELLIS, *University of Leicester, UK* A pulsed helium droplet source has been developed and characterized. The nozzle geometry was found to be critical in allowing controlled tuning of helium nanodroplet size by variation of the stagnation pressure and temperature. The average droplet size scales according to a simple $\{p, T\}$ scaling law, placing pulsed helium nanodroplet sources on a par with cw sources for the first time. Using this pulsed source, the ability of helium nanodroplets to impede ion fragmentation in electron impact mass spectrometry has been explored. A number of haloalkanes and $C_1$–$C_6$ alcohols were selected as the target species. The presence of helium alters the fragmentation patterns when compared with the gas phase, with some ion product channels being more strongly affected than others. Parent ion intensities are also enhanced by the helium for alcohols, but only for the two cyclic alcohols studied, cyclopentanol and cyclohexanol, is this effect large enough to transform the parent ion from a minor product (in the gas phase) into the most abundant ion in the helium droplet experiments. The results obtained are difficult to explain solely by rapid cooling of the excited parent ions by the surrounding superfluid helium, although this undoubtedly takes place. A second factor also seems to be involved, a cage effect which favors hydrogen atom loss over other fragmentation channels.

*Invited Papers*

**9:48**
**N11 8 Electron and Ion Emission from Clusters exposed to Strong Laser Fields.**
JOSEF TIGGESBÄUMKER, *Institut of Physics, University of Rostock, Germany*

When clusters interact with intense optical laser pulses energetic and highly charged atomic fragment ions e.g. are generated[1]. In contrast to atoms the efficiency of the process could be enhanced by choosing a pair of optical delayed pulses instead of a single but more intense femtosecond pulse[2]. In metals the stronger charging of the clusters can qualitatively be explained by a plasmon enhanced ionization process. We extended our studies and have made a compared analysis of the emission of highly charged ions and energetic electrons the interaction dynamics of intense femtosecond laser fields with nanometer-sized silver clusters. Using a pair of laser pulses with variable optical delay the time-dependent cluster response is resolved. A dramatic increase both in the atomic charge state of the ions and the maximum electron kinetic energy is observed for a certain delay of the pulses. Corresponding Vlasov calculations on a metal cluster model system indicate that enhanced cluster ionization as well as the generation of fast electrons coincide with resonant plasmon excitation.[3]

[1]L. Köller, M. Schumacher, J. Köhn, S. Teuber, J. Tiggesbäumker, and K.-H. Meiwes-Broer, Phys. Rev. Lett. **82**, 3783 (1999).

[2]T. Döppner, Th. Fennel, Th. Diederich, J. Tiggesb äumker, and K.-H. Meiwes-Broer, Phys. Rev. Lett. **94**, 013401 (2005).

[3]Th. Fennel, G.F. Bertsch, and K.-H. Meiwes-Broer, Eur. Phys. J. D **29**, 367 (2004).

*Contributed Papers*

**10:24**
**N11 9 Energy and angular momentum densities of states of ripplons on the surfaces of helium nanodroplets and bubbles***
VITALY KRESIN, MICHAEL JOHNSON, *University of Southern California* KLAVS HANSEN, *Gothenburg University* We present an analytical evaluation of the statistical densities of states of surface excitations (ripplons) of (1) isolated liquid-drop helium nanoclusters and (2) large multielectron bubbles in bulk liquid helium [1]. For the former case, the calculation of the energy density of states, $\rho(E)$, can be accurately performed in a micro-canonical ensemble formalism [2] and yields an expression which is extremely close both to the exact numerical calculation and to its fitted form [3]. For case (2) the canonical ensemble formulation is appropriate. For both systems, the calculation is then extended to yield the energy- and angular-momentum- resolved density of states $\rho(E,L)$ (c.f. [3]); in other words, the ripplon moment of inertia is described. [1] J. Tempere, I.F. Silvera, J.T. Devreese, Phys. Rev. Lett. **87**, 275301 (2001). [2] J.U. Andersen, E. Bonderup, K. Hansen, J. Chem. Phys. **114**, 6518 (2001). [3] K.K. Lehmann, J. Chem. Phys. **119**, 3336 (2003).

*Supported by NSF and VR.

**10:36**
**N11 10 Excited states of $He_NH^-$Clusters*** PAULO ACIOLI,† *Physics Department, Northeastern Illinois University* FREDERICO V. PRUDENTE, *Instituto de Fisica, Universidade Federal da Bahia* We use correlation function quantum Monte Carlo (CFQMC) method to compute the excited states of the weakly bonded Helium clusters with the $H^-$ impurity ($He_N$ $H^-$, N=1, . . . ,5). The methodology was tested through comparison with previously published results for the ground state of the system with N=1-11. Our test basis set consists of a standard pair-product ground state multiplied by a polynomial. Our tests for $HeH^-$ and $He_2H^-$ demonstrated very good agreement with previously published discrete variable representation (DVR) results. We believe the lowest excited states of the larger clusters to be of similar quality and they can reveal important properties of these weakly bound systems, mainly on the effect of the impurity on the cluster and vice versa.

*This work was supported by CNPq (Brazil).
†On leave from Departamento de Fisica, Universidade de Brasilia, Brazil.

**10:48**
**N11 11 Microwave Spectroscopy in Helium Nanodroplets.**
RUDOLF LEHNIG, *University of Alberta* WOLFGANG JAEGER, *University of Alberta* We have implemented a microwave resonator, i.e. a Fabry-Perot cavity, into a helium nanodroplet instrument. The cavity consists of two spherical aluminum mirrors with radius of curvature of 13 cm and diameter of 10 cm. The cavity is mounted in a coaxial fashion into the instrument to maximize the interaction length between radiation and doped helium droplets. The helium droplet beam enters and exits the cavity through a hole in each of the mirrors. One of the mirrors can be adjusted to tune the cavity into resonance. The output of a cw microwave synthesizer can be amplified by a traveling wave tube amplifier to powers of about 25 Watt and is coupled into the cavity through a simple wire hook antenna. Detection is accomplished using the depletion technique. We have measured the spectrum of the J=2-1 transition of carbonylsulfide demonstrating the sensitivity of this method. Power saturation was observed and will be analyzed as will be the observed line width of the transition.

**SESSION N12: FOCUS SESSION: ALLOY AND INTERFACE COMPOSITION**
**Wednesday Morning, 15 March 2006**
**304, Baltimore Convention Center at 8:00**
**Karsten Pohl, University of New Hampshire, presiding**

*Contributed Papers*

**8:00**
**N12 1 Boron nitride nanostructures: complete layers and nanomeshes** MARTINA CORSO, MARTIN MOERSCHER, SIMON BERNER, THOMAS GREBER, JUERG OSTERWALDER, *Physik-Institut, Universitaet Zuerich, Winterthurerstr. 190, CH-8057, Zuerich, Switzerland* ANDRII GORIACHKO, *Physikalisch-Chemisches Institut, J. L. Unversitaet, D-35392 Giessen, Germany* A highly ordered self-assembled nanomesh grows on a hot (1000 K) Rh(111) surface during 40 L (1 Langmuir=$10^{-6}$ $torr \times s$) of borazine $(HBNH)_3$ exposure [1]. Hexagonal boron nitride (ith–BN) units aggregate to form this double-layer network of 3 nm periodicity and 2 nm hole size. The two layers are offset so that nearly the entire underlying metal surface is covered. This system can be used as a template for supramolecular structures, as demonstrated with $C_{60}$ molecules, or for any purpose where a nanopatterned surface that is stable at high temperatures (1000 K) is needed. One of the driving forces for its formation is the large lattice mismatch of 6.9 % between the ith–BN film and the Rh substrate. The growth of similar nanomeshes on different substrates is investigated, with the purpose to control hole size and shape. It is found that not only the lattice mismatch and the symmetry of the underlying metal play an important role but also the bonding between the nitrogen atoms and the substrate. In fact nanomeshes can be grown on Ru(0001) and on Ir(111) thin films but it does not form on Pd(111) nor on Pd(110). [1] M. Corso et al. Science, 303 (2004) 217.

**8:12**
**N12 2 Measurements of Molecular Dynamics in Atomically Engineered Molecular Nanostructures*** JOSEPH A. STROSCIO, ROBERT J. CELOTTA, *Electron Physics Group, National Institute of Standards and Technology, Gaithersburg, MD 20899-8412* The quantum yield for exciting the motion of a single atom within a molecular nanostructure was measured with atomic spatial resolution. The molecular nanostructures consisted of a series of $CoCu_n$ and $CoCu_nCo$ linear molecules fabricated on a Cu(111) surface. The Co atoms at the end of the molecules were induced to switch between two lattice positions using electron excitation in a scanning tunneling microscope (STM). The electron excitation and quantum yield were found to be spatially localized on an atomic scale. Above an electron energy threshold, the Co atom motion resulted from a predominantly single electron process. By systematically varying the molecular structure, atom motion within the molecule was shown to be dependent on molecular length and composition.

*This work is supported in part by the Office of Naval Research.

**8:24**
**N12 3 Formation and Vibrational Entropy-Driven Disordering of Mo(100) and W(100) Surface Alloys** M.S. ALTMAN, K.L. MAN, Y.J. FENG, C.T. CHAN, *Hong Kong University of Science and Technology* Atoms that are deposited on a surface of a dissimilar material may either remain on the surface or they may become incorporated in a surface or bulk alloy. Although the energetic differences between alloy and overlayer structures at T = 0 can now be understood from first principles in many systems, the entropic contribution to the system free energy, which governs the equilibrium structure, is less well understood. The formation and stability of Cu, Ag and Au-induced c(2x2) alloys at the Mo(100) and W(100) surfaces have been investigated with low energy electron microscopy and diffraction. The dependence of the c(2x2) diffraction intensity upon metal deposition flux reveals that alloy formation is governed by atomistic processes that are analogous to those that dictate overlayer island nucleation. An order-disorder transition is also observed that converts the surface from ordered alloy to disordered overlayer structure. Combined with knowledge of energetics that is obtained from first principles calculations, a comparison of disordering temperatures for alloys of the different metal species and substrates provides information on the decisive contribution of vibrational entropy to the system free energy. Effective Debye temperatures for metal adatoms are determined that are substantially lower than bulk values, but exhibit the expected mass and bond strength dependence.Vibrational entropy may also play a role in the stability of alloys at other surfaces.

*Invited Papers*

**8:36**
**N12 4 Measuring 3D Alloy Composition Profiles at Surfaces.**
JAMES HANNON, *IBM Research Division*

A key challenge in thin-film growth is controlling structure and composition. Of particular importance is understanding how and why atomic-scale heterogeneity develops during growth. We have used low-energy electron microscopy (LEEM) to measure how the three-dimensional composition of an alloy film evolves with time at the nanometer length scale. By quantitatively analyzing the reflected electron intensity in LEEM, we determine the alloy composition and structure, layer by layer near a surface, with 9 nm lateral spatial resolution. As an example, we show that heterogeneity during the growth of Pd on Cu(001) arises naturally from a generic step-overgrowth mechanism that is likely to be relevant in many growth systems. This work was performed in collaboration with Jiebing Sun (UNH), Karsten Pohl (UNH), and Gary Kellogg (Sandia Labs).

*Contributed Papers*

**9:12**

**N12 5 Threading Dislocation Pair Annihilation as a Mechanism for the Growth of Ordered 2D Nanocluster Arrays*** BOGDAN DIACONESCU, KARSTEN POHL, *Physics Department and Material Science Program, University of New Hampshire* The bottom-up approach of growing nanostructured ordered arrays of clusters on the misfit dislocation networks of strained metallic thin films requires a detailed understanding of the nucleation and film-adsorbate interaction processes. In the case of S adsorption on submonolayer Ag / Ru(0001), the Ag's short herring bone rectangular misfit dislocation unit cell of 54Åx40Å (19x16 Ag atoms) reconstructs into a well ordered triangular array of S filled vacancy islands 50Å apart. Atomically resolved VT-STM measurements show that the S cluster growth mechanism involves a local restructuring of the misfit dislocation network of Ag with the final structure free of threading dislocations. The new symmetry and morphology of the composed S/Ag films is obtained via a threading dislocation annihilation mechanism where adjacent and opposite pairs of threading dislocations are replaced by the S filled Ag vacancy islands. The local character of the annihilation process is shown by the conservation of the unit cell size area of 21.5nm$^2$.

*Supported by NSF-CAREER-DMR-0134933 and ACS-PRF-37999-G5.

**9:24**

**N12 6 Highly-spatial resolved surface structure and composition by LEEM image intensity analysis** J. SUN, *Univ. of New Hampshire* J. B. HANNON, *IBM Research Division* G.L. KELLOGG, *Sandia Natl. Labs* K. POHL, *University of New Hampshire, Department of Physics, Durham, NH 03824* Controlling the local structure and composition of a surface alloy is of great importance in thin film technologies. However, measuring the alloy's heterogeneity is very difficult, because existing experimental techniques either assume lateral homogeneity or have limited subsurface or chemical sensitivity. In this work we have analyzed the electron diffraction intensity vs. incident energy curves of the (00) beam acquired from low-energy electron microscopy (LEEM) images. In contrast to conventional LEED-IV we are able to extract structural and local composition in the surface region with a lateral resolution of 8 nm. Two challenges in applying multiple electron scattering calculations to the analysis of LEEM data are the low and limited electron energy range (10 to 100 eV), which we address by a careful choice of the energy-dependent real and imaginary part of the optical potential. Our analysis of the LEEM IV curves for the clean Cu(001) and Pd/Cu(001) surfaces gives excellent agreement between experimental and best-fit data and good agreement with previous structural investigations. Our new analysis technique is capable of determining surface structure and composition with high accuracy.

**9:36**

**N12 7 Structure of an ultra-thin Ag film on the Al(100) surface*** M. KOPCZYK, *Montana State University* A. KAYANI, *Montana State University* R.J. SMITH, *Montana State University* D.S. CHOI, *Kangwon National University, Chunchon, Korea* The surface structure for one monolayer of Ag deposited on the Al(100) surface at room temperature has been studied using low energy electron diffraction (LEED), ion scattering spectroscopy (ISS) and Rutherford back-scattering spectroscopy (RBS). The Ag coverage was determined with RBS. We conclude that the Ag atoms form two domains of a buckled, quasi-hexagonal structure that is incommensurate with the Al(100) surface unit cell, having a repeat distance of 5 Al(100) interatomic spacings in the [110] direction. The LEED pattern shows a double-domain (5x1) structure with additional intensity in those spots corresponding to a (111) close-packed hexagonal layer. The analysis of the ISS results suggests that the heights of the adsorbed Ag atoms above the Al surface are not all the same, leading to the proposed buckling model. In addition, some Al atoms apparently move from the substrate up into the Ag adlayer.

*Work Supported by NSF Grant DMR-0516603.

**9:48**

**N12 8 MEAM Potentials for Al-Mg Alloy: Application to Defects** BOHUMIR JELINEK, *Mississippi State University* JEFFERY HOUZE, *Mississippi State University* SEONG-GON KIM, *Mississippi State University* MARK F. HORSTEMEYER, *Mississippi State University* M. I. BASKES, *Los Alamos National Laboratory* The ab-initio calculations based on density functional theory (DFT) are performed for the Al and Mg crystals and their alloy in reference structures, such as NaCl structure. The lattice constant (volume), bulk modulus and shear moduli for each element and the alloy are determined from the total energy calculations. These material parameters are then used to determine the Modified Embedded Atom Method (MEAM) potentials for these elements and their alloys. The transferability of these parameters are tested by obtaining relevant physical quantities on structures different than the reference structures and compare them with the results from ab-initio calculations. MEAM potentials determined for these materials are used to study the structure and morphology of various form of defects of these materials.

**10:00**

**N12 9 Disorder and Roughening at Surfaces of Silver/Gold Alloys*** GREGORY DERRY, *Loyola College In Maryland* RUNDONG WAN, *University of Maryland Baltimore County* Attempts to obtain a clean and well-ordered surface in ultrahigh vacuum for several low index faces of a 50 at% silver/gold alloy gave rise to an unexpected phenomenon. After several cycles of sputtering and annealing, the surfaces appeared clean using Auger spectroscopy but yielded low energy electron diffraction spots of poor quality (in the case of AgAu(110), no diffraction was observed at all). Many further time/temperature annealing protocols were attempted with no improvement. In addition to the diffraction results, which indicate a lack of long-range microscopic order at the surface, continued processing resulted in macroscopic roughening of the surfaces. Electron microscopy revealed the presence of features with sizes on the order of microns at the roughened surfaces. Analysis of the lineshapes of the diffuse LEED beams for the AgAu(111) surface indicates that the sizes of the ordered patches on the surface are less than a nanometer. These results will be presented in more detail and possible explanations for this extraordinary behavior will be discussed.

*Funded by the National Science Foundation, grant DMR-9903108.

**10:12**

**N12 10 Surface Freezing in Liquid Gold-Silicon Eutectic Alloy investigated with Surface X-ray Diffraction** REINHARD STREITEL, OLEG SHPYRKO,*ALEXEI GRIGORIEV,†VENKAT BALAGURUSAMY, PETER PERSHAN, *Harvard University* BEN OCKO COLLABORATION,‡MOSHE DEUTSCH COLLABORATION,§ The formation of a 2D AuSi crystalline lattice on top of liquid AuSi eutectic alloy was found in surface X-ray diffraction experiments. Up to 12 degree above bulk melting temperature ($T_{melt} = 361°C$) we observe a powder like, 2D crystalline lattice. Increasing the temperature we find a first order phase transition. GID diffraction data was used to determine the 2D lattice parameters and the domain size was estimated to be larger than 0.9 $\mu m$. Normalized X-ray reflectivity shows an increase of a factor of 20 in comparison to classical systems, indicating that atomic layering normal to the surface is significantly enhanced for AuSi. Synchrotron measurements were performed at ChemMatCARS, Advanced Photon Source, Argonne National Lab and supported by DOE grants DE-FG02-88-ER45379 and DE-AC02-98CH10886.

*Center for Nanoscale Materials, Argonne, IL.
†University of Wisconsin, Madison, WI.
‡Brookhaven National Laboratory, Upton, NY 11973.
§Bar-Ilan University, Ramat-Gan 52900, Israel.

**10:24**

**N12 11 Determination of interface compositions by X-ray three-beam resonance diffraction** H.-H. WU, Y.-R. LEE, C.-M. HSUEH, H.-H. CHEN, S.-L. CHANG, *National Tsing Hua University* X-ray three-beam diffraction$(200/\bar{3}\,\bar{1}\,1)$under resonant conditions is used to measure the concentrations of the constituent elements of the interface between a (100) CdTe thin film and a (100) InSb substrate. The three-beam diffraction profiles versus the azimuth angle of rotation around [200] reveal a wide variety of change in phase shift due to resonance for photon energies in the vicinity of the Cd $L_{III}$ absorption edge. At different momentum transfers $q_r$ along [200], sensitive to the interfacial structure, the phase shift in the resonant state also provides sufficient information about the distributions of Cd and Te concentrations. With theoretical analysis for the crystallographic phase of the structure-factor triplets and the resonance phase shifts involved in the three-beam diffraction, it allows us to determine the composition of Cd and Te as a function of depth normal to the interface. Via the propagation of the secondary$(\bar{3}\,\bar{1}\,1)$reflected beam along the surface, possible interface structures parallel to the surface could also be deduced.

**10:36**

**N12 12 LEED and Ab-Initio Study of the SmSi(111)-3x2 Reconstruction** CHRISTOPHER EAMES, STEVE TEAR, MATTHEW PROBERT, *Dept of Physics, University of York, UK* The Si(111)3x2-Sm reconstruction that has been observed by STM produces a 3x1 pattern when viewed using LEED [1]. It has been suggested that similar behaviour for Si(111)3x2-Ba is due to the interference of the emergent electron amplitudes between adjacent registry shifted unit cells [2]. We have gathered LEED I(V) curves from this surface and here we present a quantitative comparison of these with a structural model that has been suggested in the literature [3] and with the results of our own ab-initio calculations done using the CASTEP [4] code. [1] C. Wigren et al, Phys. Rev. B., **48** 11014-11021 (1993). [2] J. Schafer et al, Phys. Rev. B., **67** 85411-85415 (2003). [3] E. Ehret et al, Surf. Sci., **569** 23-32 (2004). [4] M. D. Segall et al, J. Phys.: Cond. Matt., **14** 2717-2743 (2002).

**10:48**

**N12 13 Investigation of the interface structure in sputtered $WSi_2$/Si multilayers by in-situ synchrotron X-ray scattering.** YIPING WANG, HUA ZHOU, LAN ZHOU, RANDALL L. HEADRICK, *University of Vermont, Department of Physics, Burlington, VT 05405* ALBERT. T. MACRANDER, *Advanced Photon Source, Argonne National Laboratory, Argonne, Illinois 6043* KARL F. LUDWIG, *Boston University, Department of Physics, Boston, MA 02215* Multilayer X-ray optics have many applications such as X-ray microscopy, X-ray lithography, and X-ray microanalysis. The interface imperfections are critical to the optical performance of the multilayer structures. We report on the growth of $WSi_2$ and Si amorphous thin films by dc magnetron sputtering in a vacuum chamber with $10^{-9}$ Torr base pressure. In-situ synchrotron X-ray scattering with high temporal resolution has been employed to probe the surface and interface roughness evolution during film deposition. X-ray reflectivity simulations were performed using the IMD software package. It is found that the structure of $WSi_2$/Si multilayers is with an alternately smooth and rough interface. While Si layer roughens, $WSi_2$ layer is observed to smooth out an initially rough surface. The ion energy and flux assisting the growth may play a role in inducing this asymmetry in the interface roughness.



## SESSION N13: FOCUS SESSION: ULTRAFAST AND ULTRAHIGH FIELD CHEMISTRY I: STRONG FIELD PHENOMENA

**Wednesday Morning, 15 March 2006; 305, Baltimore Convention Center at 8:00**
**Robert Levis, Temple University, presiding**

***Invited Papers***

**8:00**

**N13 1 Strong-Field Physics with Coherently Prepared Molecular Targets.***
ROBERT JONES, *University of Virginia*

Intense, short laser pulses can create rotational wavepackets in molecules, resulting in transient preferential molecular alignment in a field free environment. The availability of aligned rather than randomly oriented molecular samples is

enabling new strong-field molecular physics experiments which offer additional insight into a variety of complex phenomena. For example, high harmonic generation (HHG) is mediated by electrons that are first tunnel-ionized and then driven back into their parent ions by an intense laser field. Both the initial ionization and recollision events can be strongly dependent on the orientation of the molecular axis with respect to the laser field. Once this dependence is well understood, information regarding the structure of the parent molecule at the instant of the electron/ion recollision might be extracted from the resulting electron and/or photon emission. I will describe methods for manipulating and probing molecular alignment, as well as our recent measurements of the dependence of intense laser ionization rates, HHG yields, and the polarization of high-order harmonics on the alignment of the molecular axis relative to the polarization direction of the intense laser field.

*Supported by DOE BES.

*Contributed Papers*

**8:36**

**N13 2 Non-adiabatic Electronic Excitation of Linear Polyenes in the Strong Field Regime** STANLEY SMITH, *Wayne State University, Detroit, MI* XIAOSONG LI, *University of Washington, Seattle, WA* ALEXEI MARKOVICH, DMITRI ROMANOV, ROBERT J. LEVIS, *Temple University. Philadelphia, PA* H. BERNHARD SCHLEGEL, *Wayne State University, Detroit, MI* Using a newly developed unitary transform time-dependent Hartree-Fock (UT-TDHF) algorithm, the electronic response to an ultrashort strong-field laser pulse was studied on a series of molecules – ethylene, butadiene, and hexatriene – in which molecular size and conjugation increase systematically. The evolution of electronic subsystem of molecules exposed to 760 nm $8.75\times 10^{13}$ W/cm$^2$ of 7 fs duration was calculated using the 6-31G(d,p) basis set. Two scenarios are envisioned: in the first, the molecule interacts with the pulse immediately after ionization; in the second, sufficient time elapses for the molecular geometry to relax. The non-adiabatic behavior of the instantaneous dipole moment and the charge distribution in a molecule is more pronounced for the monocations than for the dications or neutrals. For a given charge state and geometry, the non-adiabatic effects increase with the length of the molecule. As Fourier analysis reveals, the residual (after-pulse) oscillations of the dipole moment are mainly due to non-resonant excitations of the lowest excited states with significant oscillator strength. For each molecule, the non-adiabatic coupling is greater for geometry with the lower excitation energies.

**8:48**

**N13 3 A new type of wavelength dependence in strong-field ionization** DMITRI ROMANOV, *Dept. of Physics, Center for Advanced Photonics Research, Temple University* KATHARINE MOORE, RYAN COMPTON, ROBERT J. LEVIS, *Dept. of Chemistry, Center for Advanced Photonics Research, Temple University* It is commonly assumed that in mid-IR region the strong-field ionization approaches quasistatic limit (tunneling, or ADK regime) and ceases to depend on the laser wavelength. Contrary to this notion, ionization yields for the noble gas Xe at intensities from $10^{13}$-$10^{15}$ W cm$^{-2}$ for wavelengths spanning from 800 to 1500nm reveal strong and counterintuitive wavelength dependence. There is an increasing ionization probability in the strong field regime as the excitation wavelength increases from 800nm to 1500 nm at fixed field intensity. The measured thresholds for the ionization event scale approximately as $\lambda^{-2}$. We developed a simple quantitative model that extends through-the-barrier tunneling with single photon ionization from a Rydberg intermediate state and captures the observed wavelength dependence. This wavelength dependence will be reduced to some degree if the ionization occurs in a strong DC electric field that is capable to independently ionize the Rydberg states. The wavelength dependence of ionization rate in the quasitstatic regime is of considerable importance for ascertaining the correct physics for various strong field processes.

**9:00**

**N13 4 Orientation effects in Coulomb explosion of $H_2S$ in intense laser fields studied by coincidence momentum imaging** AKIYOSHI HISHIKAWA, EIJI TAKAHASHI, *Institute for Molecular Science, National Institute for Natural Sciences and The Graduate University for Advanced Studies (SOKENDAI)* The Coulomb explosion of $H_2S$ in an ultrashort intense laser field (12 fs, 0.33 PW/cm$^2$), $H_2S^{3+} \rightarrow H^+ + S^+ + H^+$, has been studied by the coincidence momentum imaging method to study how the nuclear dynamics depends on the molecular orientation with respect to the laser polarization vector. When the molecular plane, defined as the plane spanned by the fragment momentum vectors, is perpendicular to the laser polarization vector ($\varepsilon$), the distribution of the total kinetic energy release E shows a peak at E = 21(1) eV. On the other hand, the distribution peak is observed at a substantially smaller value, E = 15(1) eV, when the molecular plane is perpendicular to $\varepsilon$, showing that the Coulomb explosion dynamics of $H_2S$ depends sensitively on the orientation of the molecular frame to the laser polarization vector. The difference in the peak kinetic energies indicates that the geometrical structure for the perpendicular orientation is less elongated prior to the Coulomb explosion than that for the perpendicular orientation.



*Invited Papers*

**9:12**

**N13 5 Ultrafast hydrogen atom dynamics of small hydrocarbon molecules in intense laser fields - Ejection of H3+ and hydrogen migration.**

KAORU YAMANOUCHI, *The University of Tokyo*

In ultrashort intense laser fields, molecules are decomposed into fragments via a variety of dissociation pathways. Among them, ultrafast migration of hydrogen atoms within molecules as well as efficient ejection of H3+ molecular ions are noteworthy [1]. By referring to our recent studies on small hydrocarbon molecules in intense laser fields [2] by the

coincidence momentum imaging method [3], I will show how ultrafast dynamics of hydrogen atoms are induced within duration of ultrashort intense laser pulses. [1] Y. Furukawa, K. Hoshina, K. Yamanouchi, H. Nakano, Chem. Phys. Lett. 414, 117 (2005). [2] T. Okino, Y. Furukawa, P. Liu, T. Ichikawa, R. Itakura, K. Hoshina, K. Yamanouchi, and H. Nakano, Chem. Phys. Lett. 419, 223 (2005). [3] H. Hasegawa, A. Hishikawa, K. Yamanouchi, Chem. Phys. Lett. 349, 57 (2001).

***Contributed Papers***

**9:48**

**N13 6 Femtosecond Laser Ionization of Organic Amines with Very Low Ionization Potential.** TOMOYUKI YATSUHASHI, TAKASHI OBAYASHI, MICHINORI TANAKA, MASANAO MURAKAMI, NOBUAKI NAKASHIMA, *Graduate School of Science, Osaka City University* The interaction between high intensity femtosecond laser and molecules is one of the most attractive areas in laser chemistry and ionization is the most fundamental subject. Theoretical consideration successfully reproduced the ionization behavior of rare gases. However, the understanding of ionization mechanisms of large molecules is difficult more than those of rare gases due to their complexity. Generally speaking, molecules are harder to ionize than rare gases even if they have the same ionization potential. The suppressed ionization phenomena are one of the important features of molecular ionization. Hankin et al. examined 23 organic molecules with ionization potentials between 8.25 and 11.52 eV. We have examined ionization and/ or fragmentation of many organic molecules, including aromatic compounds, halogenated compounds, methane derivatives etc. at various wavelengths below $10^{16}$ $Wcm^{-2}$. In order to investigate the nature of molecular ionization, it is interesting to examine a variety of molecule in a wide range of ionization potential. In this study, we examined several organic amines because we can explore the uninvestigated ionization potential range down to 5.95 eV. In addition to the significant suppression of the ionization rates, stepwise ionization behavior, which was not observed in rare gases, was observed.

**10:00**

**N13 7 All-solid-state, ultraviolet, high power laser system using Ce:LiCAF as a gain medium** NOBUHIKO SARUKURA, *Osaka University* SHINGO ONO, HIDETOSHI MURAKAMI, ALEX QUEMA, ELMER ESTACIO, *Institute for Molecular Science* TSUGUO FUKUDA, *Tohoku University* High peak-power, femtosecond, ultraviolet (UV) lasers have attracted new interest. Chirped pulse amplification (CPA) in the UV region has been demonstrated using Ce:LiCaAlF6 (Ce:LiCAF) crystal as the gain medium. The peak power of the amplified and compressed pulse (115 fs) reached 30 GW at 290 nm. To increase the peak power to the terawatt (TW) level, further pulse compression is desired. Since Ce:LiCAF has a tunability of 281nm to 315nm, it holds promise for 3-fs pulse generation which are required for seeding TW-class Ce:LiCAF lasers. The pulse-width of the frequency-tripled Ti:sapphire regenerative amplifier was measured to be 210 fs. The seed pulses were then focused into a hollow fiber filled with argon to spectrally broaden the pulses due to self-phase-modulation. The pulses were then compressed to 25 fs by dispersion-compensation. The fourth harmonics of a Nd:YAG laser (266 nm) is an ideal pump source as it falls within the absorption band Ce:LiCAF. We have generated 430 mJ fourth harmonics with a total conversion efficiency of 30.5% using Li2B4O7

$$(LB4)crystals.ACe{:}LiCAF$$

double-pass power-amplifier was then designed with a peak energy of 98 mJ for a 13 mJ seed pulse and an extraction efficiency of 25%.

**10:12**

**N13 8 Influence of linear chirp on non-vertical transitions in a dye solution** ELIZABETH CARROLL, ANDREI FLOREAN, PHILIP BUCKSBAUM, ROSEANNE SENSION, *FOCUS Center, University of Michigan, Ann Arbor, MI* KEN SPEARS, *Department of Chemistry, Northwestern University, Evanston, IL* Chirped laser pulses can manipulate vibrational coherences in dye solutions. We show that the effect of linear chirp also depends strongly on the power spectrum of the ultrafast pulse. We use a programmable phase mask to control the spectral phase of 25-fs visible pulses generated in a noncollinear optical parametric amplifier (NOPA). Following chirped pulse excitation of the oxazine laser dye LD690, coherent oscillations are observed in the time-resolved transient absorption. When a vertical transition is excited, negative chirp leads to strong ground state vibrational coherences as resonant stimulated Raman processes are enhanced by the frequency sweep of the laser pulse. When the chirped pulse excitation is higher frequency than the Franck-Condon transition, the optical response of the dye is significantly affected by excited state absorption. In this case, coherences are established in excited states but no chirp-enhancement of the ground state wavepacket is observed.

**10:24**

**N13 9 Terahertz absorption spectrum of water vapor at different humidity at room temperature** XUYING XIN, HAKAN ALTAN, DAVID MATTEN, ANGELAMARIA SAINT, ROBERT ALFANO, *Institute for Ultrafast Spectroscopy and Lasers, Physics Department, the City College of New York* We measured the absorption spectrum of water vapor in 0.2-2.4THz range at different humidity from 17% to 98% at room temperature using Er: doped fiber laser (IMRA America Inc.) based terahertz time-domain spectroscopy. The experiments were performed in a nitrogen-purged cage at atmosphere environment to obtain the reference and water absorption information. The seventeen absorption lines were observed due to water molecular rotations in the ground vibration state. The first three absorption lines at low frequencies increase with humidity, following the Beer-Lambert Law, while some of high frequency lines were found to decrease with humidity. These effects will be discussed. The observed line broadening is due to collisions occurring among water and nitrogen molecules.

**SESSION N16: FOCUS SESSION: HYDROGEN STORAGE III**
**Wednesday Morning, 15 March 2006**
**312, Baltimore Convention Center at 8:00**
**Jan F. Herbst, General Motors, presiding**

*Contributed Papers*

**8:00**
**N16 1 Ambient and High Pressure Structural Studies on $TiH_2$*** PATRICIA KALITA, RAVHI KUMAR, ANDREW CORNELIUS, *University of Nevada, Las Vegas* Currently metal hydrides attract intense research interest because of their potential application as hydrogen storage materials. We performed in situ high-pressure synchrotron x-ray diffraction as well as high-pressure Raman spectroscopy studies on $TiH_2$ at pressures up to 20 GPa. Low temperature ambient pressure x-ray diffraction studies were also carried out. A phase transition from a high symmetry cubic structure to a lower symmetry tetragonal structure was observed as temperature is lowered below room temperature. The unit cell parameters as well as the equation of state were calculated. To the best of our knowledge this is the first report of high pressure synchrotron x-ray diffraction as well as high-pressure Raman spectroscopy studies on $TiH_2$.

*We acknowledge support from DoE Award No. DE-FG36-05GO08502.

**8:12**
**N16 2 Optical Spectroscopy of PdO and Pd thin Films under hydrogen exposure*** J.I. AVILA, M. FAVRE, U.G. VOLKMANN, A.L. CABRERA, *Departamento de Fisica, Universidad Catolica de Chile* D. LEDERMAN, *Physics Department, West Virginia University* Palladium oxide (PdO) is a p-type semiconductor with a bandgap appropriate to absorb light in the visible range an thus generating an electrical current. This bandgap, being of the order of 2.5 eV, remains yet not accurately determined. We are currently setting up a new experiment in which we are able to monitor the evolution of reflectivity or transmission, for several wavelengths in the visible spectrum, and the resistivity as a function of the exposure time to hydrogen. We should be able to calculate the evolution of bandgap of the semiconductor as a function of reduction from the reflectivity data. Pd films also change reflectivity properties during hydrogen absorption. The experimental set up consist of a tungsten light, Spectrapro 275 monochromator with a diffraction grid of 1200 lines/mm, and a silicon diode detector. Preleminary results will be shown. Based on these data we expect to depict a model for the changes measured.

*FONDECYT 1030642, CIAM 009-1-2004,DIPUC 2005/03P.

**8:24**
**N16 3 First-principles prediction of a new metallic carbon hydride: bcc-$CH_2$*** CESAR CAB, ROMEO DE COSS, GERKO OSKAM, *Department of Applied Physics, CINVESTAV-Merida, Mexico* GABRIEL MURRIETA, *Facultad de Matematicas, UADY, Yucatan, Mexico* GABRIEL CANTO, *CCMC-UNAM, Ensenada, Mexico.* The observation of a new carbon phase in nanoparticles having the body-centered-cubic structure (bcc) has been reported very recently. However, has been suggested that hydrogen is present in the samples forming solid $CH_2$ with the anti-cuprite structure. The structural and electronic properties of bcc-C and bcc-$CH_2$ are unknown. In the present work we have studied the elastic stability and the electronic structure of these systems by means of first-principles total-energy calculations. The results were obtained with the pseudopotentials LCAO method (SIESTA code) and the Generalized Gradient Approximation (GGA) for the exchange-correlation potential. We have evaluated the structural stability via the elastic properties, we find that bcc-$CH_2$ is stable with a lattice parameter very close to the experimental value. In addition, we find that the electronic structure of bcc-$CH_2$ exhibits metallic behavior with a relatively high density of states at the Fermi level. The relevance of this new hydride to the problem of hydrogen storage is discussed.

*This research was supported by CONACYT under Grants No. 43830-F, No. 44831-F, and No. 43828-Y.



*Invited Papers*

**8:36**
**N16 4 Combined neutron scattering and first principles study of novel hydrogen.**
TANER YILDIRIM, *National Institute of Standards and Technology*

This abstract was not received electronically.

*Contributed Papers*

**9:12**
**N16 5 Ab Initio Thermochemistry and Elastic Properties of Alkaline Earth Hydrides** LOUIS HECTOR, JR., JAN HERBST, *GM R&D Center* WALTER WOLF, PAUL SAXE, *Materials Design* In addition to comprising a scientifically interesting class of materials, the binary alkaline earth hydrides are important components of hydrogen sorption/desorption reactions. Of critical importance for predicting the thermodynamic stability of hydrides is the enthalpy of hydride formation, $\Delta H$, which links the temperature and pressure of hydrogen sorption via the van't Hoff relation. We compare LDA and GGA predictions of the heats of formation and elastic properties of alkaline earth metals and their binary hydrides $BeH_2$, $MgH_2$, $CaH_2$, $SrH_2$, and $BaH_2$ using a plane wave density functional method. Phonon calculations using the direct method enabled prediction of the zero point energies of each material and the 0K and 298K heats of formation. We also computed the 0K and 298K cohesive energies for the alkaline earth metals. Born effective charge tensors were computed via the Berry phase method and enabled prediction of the phonon dispersion curves with LO/TO zone center splittings. It was found that the LO/TO splittings have no effect on the computed zero point energies and heats of formation. The elastic constants were computed with a least squares fitting method using a set of sequentially-applied strains to improve the accuracy of each calculation. Comparison of results from the least squares methodology with prior results using the Hartree-Fock method suggest that the former is substantially more accurate for predicting hydride elastic properties.

**9:24**

**N16 6 Hydrogen uptake and the 18-eletron rule** KIRAN BOGGAVARAPU, ANIL KANDALAM, PURU JENA, *Virginia Commonwealth University* Hydrogen is considered to be an ideal energy carrier in the foreseeable future; however, the key problem is its storage. Solid state materials capable of storing hydrogen with high gravimetric (9 wt %) and volumetric density (70 g/L) operating under ambient thermodynamic conditions and exhibiting fast hydrogen sorption kinetics are of practical importance. It is clear that the storage material should consist of light elements such as Li, B, and C etc. Hydrides of these elements are too strongly bound to be easily desorbed. Attempts were made to deposit light weight transition metals on carbon surfaces such as fullerenes, nanotubes etc., however, they tend to cluster together reducing hydrogen uptake dramatically. One way to achieve high storage is to functionalize simple organic molecules such as $C_4H_4$, $C_5H_5$ etc. with light weight metals such as Sc and Ti. In this presentation, we will discuss based on DFT computations, the dependence of hydrogen uptake on the nature of substrate, the desportion energies, and the nature of bonding.

**9:36**

**N16 7 Ab initio simulation of hydrogen storage in BN systems** * STEPHEN SHEVLIN, *Queen Mary, University of London* ZHENGXIAO GUO, *Queen Mary, University of London* We model via first principles simulation hydrogen storage in boron nitride systems, such as h-BN sheets, the paradigm BN molecule borazine ($B_3N_3H_6$) and ammonia-borane ($BNH_6$). We found $H_2$ preferentially adsorbs on the perfect h-BN surface but strongly bound atomic hydrogen prefers to adsorb on vacancies, with consequences for hydrogen storage. The addition of TM (transition metal) atoms to boron nitride, to act as adsorbents for hydrogen, was investigated using borazine as a prototype system for h-BN. The binding of TM atoms (Sc, Ti, V etc.) to borazine was determined, with the variation in bonding intimately related to the electronic structure. The dopants were found to promote the binding of both hydrogen atoms and molecules to borazine, increasing binding energy by $\sim$ 300% and 1500%, respectively. Initially TM dihydrides form but as hydrogen concentration increases molecular hydrogen becomes preferred. Bound hydrogen is stable at room temperature and the maximum hydrogen capacity and kinematics of this prototype system will be presented. In addition, the dissociation of $BNH_6$ itin vacuo, on the surface of $MgH_2$, and in the presence of TM catalysts is modeled.

*Funding support from EPSRC UK-SHEC.

**9:48**

**N16 8 Atomic and Molecular Hydrogen Interaction with Ti-Doped Al (100): Hydrogen Dissociation and Surface Alane Formation** ERIK MULLER, PETER SUTTER, PERCY ZAHL, *Center for Functional Nanomaterials, Brookhaven National Laboratory* SANTANU CHAUDHURI, JAMES MUCKERMAN, *Department of Chemistry, Brookhaven National Laboratory* A comprehensive research effort on the atomistic mechanisms underlying hydrogen storage in Ti-doped $NaAlH_4$ is aimed at deriving a knowledge base for the rational optimization of this and other related complex hydride materials. Our investigation focuses on the role of the Ti dopants in promoting reversible hydrogenation, a key requirement for any practical hydrogen storage material. The re-hydrogenation reaction proceeds from the crucial initial step of dissociative adsorption of molecular hydrogen on Al or NaH. A specific Al:Ti complex was recently predicted as an active site for $H_2$ dissociation on extended Al(100) surfaces [1]. Combining high-resolution surface imaging experiments (scanning tunneling microscopy, low-energy electron microscopy) with density functional theory, we are investigating the dissociative adsorption of $H_2$ on Ti-doped Al(100) prepared in ultrahigh vacuum. We will discuss our progress toward identifying catalytically active sites for H2 dissociation on this surface, as well as pathways toward the formation of mobile Al-species. [1] S. Chaudhuri and J.T. Muckerman, J. Phys. Chem. B 109, 6952 (2005).

**10:00**

**N16 9 Theoretical Study of Hydrogen Dissociation on the $TiAl_3$ Surface*** YAN WANG, M. Y. CHOU, *School of Physics, Georgia Institute of Technology* In order to better understand the catalytic role played by Ti in enhancing the reaction kinetics of sodium alanate, we present a first-principles investigation of hydrogen dissociation and adsorption on the pure Al surface as well as on the Ti doped surface with a local alloy composition of $TiAl_3$. The most energetically favorable location for Ti near the surface is identified. It is found that the presence of Ti promotes H adsorption on the surface with the H atom sitting on top of an Al atom. The binding between Ti and Al modifies the surface charge distribution near the adsorption site and facilitates the adsorption process. The potential energy surface for $H_2$ dissociation over both pure Al and the alloy surfaces are also discussed.

*Supported by the Department of Energy.

**10:12**

**N16 10 Phase Stability of Mixed-Alkali Alanates** ZHU MA, *School of Physics, Georgia Institute of TeZhuchnology, Atlanta, GA 30332* MEI-YIN CHOU, *School of Physics, Georgia Institute of Technology, Atlanta, GA 30332* To date sodium alanate $NaAlH_4$ is the only reversible complex hydride that satisfies the international density targets for hydrogen storage materials of 5 wt.% and 70 kg/m$^3$. The reversible hydrogenation process takes place at reasonable conditions. Therefore, it is desirable to increase the H wt.partially replacing Na with a lighter alkali metal such as Li. To study the stability of these mixed-alkali alantes, we perform first-principles calculations for the alloy systems $Na_{1-x}Li_xAl\ H_4$ and $Na_{3(1-x)}Li_{3x}AlH_6$ within the framework of density functional theory and pseudopotentials. For the compositions we have considered for the tetrahydrides, the mixing energies are all positive, indicating that the sodium and lithium alanates prefer being phase separated. For the hexahydrides, one stable intermediate compound is found. The binding characteristics of these mixed-alkali alanates will be discussed.

**SESSION N17: FOCUS SESSION: SEMICONDUCTORS FOR THZ AND IR I**
**Wednesday Morning, 15 March 2006; 313, Baltimore Convention Center at 8:00**
**K. K. Choi, Army Research Laboratory, presiding**

*Invited Papers*

**8:00**
**N17 1 Terahertz Semiconductor Detectors: Designs to Applications.**
UNIL PERERA, *Georgia State University*

The work describes terahertz photon detectors based on semiconductor micro- and nano-structures using homojunctions, and heterojunctions. A Homojunction or HEterojunction Interfacial Workfunction Internal Photoemission (HIWIP or HEIWIP) infrared detector, formed by a doped emitter layer, and an intrinsic layer acting as the barrier followed by another highly doped contact layer, can detect Terahertz photons due to intraband transitions. The threshold can be tailored by adjusting the band offset between the emitter and the barrier. This principle can be used with any semiconductor material combination. HIWIPs have the same material (doped and undoped) in the emitters and barriers, while HEIWIPs have different band gap material in the two layers. The detection mechanism involves free carrier absorption in the emitter, followed by the internal photoemission of photoexcited carriers across the junction barrier, and then the collection of carriers by the applied electric field at the contacts. Utilization of nanoplasmonic resonances to enhance the terahertz absorption using engineered and self-assembled metal nanostructures on HEIWIP detectors will also be discussed. The metal nanostructures will act as enhanced frequency couplers, which will allow more efficient absorption of terahertz radiation as it is converted into surface plasmons. The near field of SPs will affect the electron gas in the photodetectors the same way as the far-field does. Thus the local field enhancement known for other phenomena and devices could be achieved. Work supported in part by US NSF and US Airforce.

*Contributed Papers*

**8:36**
**N17 2 III-V Semiconductor Diodes and the Terahertz Technology Gap** THOMAS CROWE, *Virginia Diodes, Inc.* The terahertz frequency band, spanning from roughly 100 GHz through 10 THz, is often sited as the most scientifically rich, yet unexplored region of the electromagnetic spectrum. Scientific applications include radio astronomy, chemical spectroscopy, plasma diagnostics, compact range radar, atmospheric remote sensing and electron paramagnetic resonance studies of organic molecules. Recently, many groups have developed rudimentary imaging systems for this frequency band, either for basic scientific investigations or defense and security scanners. However, the inherent difficulty of creating sources of terahertz power that are sufficiently powerful, tunable, reliable and robust is a primary difficulty. Researchers in the field generally speak of the terahertz technology gap, which spans the transition from classical electronics to quantum photonics. This talk will consider the nature of the terahertz technology gap and the technological transition from electronics to photonics. Efforts to develop useful sources and receivers of terahertz energy based on III-V semiconductor diodes will be discussed. Also, important recent results, including the development of all-solid-state sources and receivers for the 0.1 – 3 THz frequency range will be presented. Finally, the fundamental limitations of this technology will be considered.

**8:48**
**N17 3 Spontaneous emission from accelerated Bloch electrons – Bloch oscillation radiation*** VALERIY SOKOLOV, GERALD IAFRATE, *Dept. of Electrical and Computer Engineering, NCSU, Raleigh, NC 27695-8617* JOSEPH KRIEGER, *Dept. of Physics, Brooklyn College, CUNY, Brooklyn, NY 11210* A theory of spontaneous emission of radiation for a Bloch electron traversing a single band in an external electric field is presented. The radiation field is described by a free space quantized electromagnetic field in the Coulomb gauge. It is shown that the spontaneous emission occurs with frequencies equal to integral multiples of the Bloch frequency without any itad hoc assumptions concerning the existence of Wannier-Stark levels. An explicit expression for the transition probability is derived in first-order perturbation theory relative to the radiation field. Although the output frequency of the radiation can be operationally tuned from the gigahertz to terahertz spectral range by varying the constant electric field, it is estimated that a spontaneous emission power output of only about 0.1 of a microwatt is available using GaAs-based superlattices. In this regard, it is noted that the atomic spontaneous emission probability and related transition rates can be enhanced by properly tailoring the surrounding electromagnetic environment. Therefore, considering Bloch oscillations in a resonant microcavity to enhance the spontaneous emission is a noteworthy alternative for exploring tunable gigahertz to terahertz radiation sources.

*This work is presently supported by the US Army Research Office.

**9:00**
**N17 4 Developing a voltage tunable two-color corrugated QWIP focal plane array** KWONG-KIT CHOI, CARLOS MONROY, *U. S. Army Research Laboratory* THEODOR TAMIR, MING LEUNG, *Polytechnic University* JINJIN LI, DANIEL TSUI, *Princeton University* Single color quantum well infrared photodetector focal plane array (QWIP FPA) has been fully developed. The trend is toward FPAs with spectral analysis and target discrimination capabilities. The challenges of achieving a two-color QWIP FPA are the identification of an effective coupling scheme for both wavelengths and a voltage tunable QWIP material. The former is needed to ensure high sensitivity in both wavelengths and the latter is needed in high resolution FPAs

where only one external connection per pixel may be permissible. In this talk, we will discuss the detector parameters needed for high performance infrared imaging, the corrugated light coupling scheme, and the voltage tunable two-color QWIP materials based on superlattices (SLs). In the coupling design, one approach is to use Fabry-Perot oscillations in the triangular cavities to enhance both incident intensities. In the material design, the focus is on the electron energy relaxation rate in the energy relaxation layers (ERL) lying between the active SL periods. By computing the hot-electron distribution after traversing through the ERL layer, one can determine the doping required to eliminate cross-talk between the two colors.

**9:12**

**N17 5 Study of a broadband high-gain InGaAs/InGaAsP quantum-well infrared photodetector** J. LI, *Princeton University* K.K. CHOI, *US Army Research Laboratory* J.F. KLEM, J.L. RENO, *Sandia National Laboratories* D.C. TSUI, *Princeton University* PRINCETON UNIVERSITY TEAM, US ARMY RESEARCH LABORATORY COLLABORATION, SANDIA NATIONAL LABORATORIES COLLABORATION, Lattice-matched InGaAs/InP quantum well infrared photodetectors (QWIPs) exhibit high photoconductive gain but nonadjustable detection wavelength because of their fixed barrier height. The use of $In_xGa_{1-x}As_yP_{1-y}$ (InGaAsP) as the barrier material is superior to that of InP with regard to flexibility of the operating wavelength. In this work we investigate the use of InGaAsP barriers in QWIPs for long-wavelength infrared detection applications. We studied a broadband quantum well InGaAs/InGaAsP detector covering 8-14 $\mu$m and found excellent agreement between observed and calculated responsivity spectra. This result shows the validity of our design model. To determine the usefulness of InGaAsP in long-wavelength detection, we also designed a GaAs/AlGaAs quantum well detector with a similar spectrum and compared its performance with that of the InGaAs/InGaAsP detector. Dark current noise measurement indicates that the gain of InGaAsP is 4.6 times larger than that of AlGaAs, showing that InGaAsP is a good candidate for long-wavelength high-speed infrared detection.

**9:24**

**N17 6 Interfaces as tools in the design of short period type-II InAs/GaSb superlattices for mid-IR detection** FRANK SZMULOWICZ,*HEATHER HAUGAN,†GAIL BROWN, K. MAHALINGAM,‡ *Air Force Research Laboratory* B. ULRICH, *Bowling Green State University* S. MUNSHI, *Air Force Research Laboratory* The effect of interface anisotropy on the electronic structure of InAs/GaSb type-II superlattices is exploited in the design of thin-layer superlattices for mid-IR detection threshold. The design is based on a theoretical envelope function model that incorporates the change of anion and cation species across InAs/GaSb interfaces, in particular, across the preferred InSb interface. The model predicts that a given threshold can be reached for a range of superlattice periods with InAs and GaSb layers as thin as a few monolayers. A number of superlattices with periods ranging from 50.6 to 21.2 angstroms for the 4 micron detection threshold were grown by molecular beam epitaxy based on the model design. Low temperature photoluminescence and photoresponse spectra confirmed that the superlattice band gaps remained constant at 330 meV although the period changed by the factor of 2.5.

*Also University of Dayton Research Institute.
†Also Universal Technology Corporation.
‡Also Universal Technology Corporation.

**9:36**

**N17 7 Quantum Hall Devices as efficient and fast THz photodetectors** NIKOLAI G. KALUGIN, *Dept. of Physics, Texas A&M University* CHRISTIAN STELLMACH, *Inst. of Applied Physics, TU Braunschweig, Germany* YURI B. VASILYEV, *Ioffe Physicotechnical Inst., St. Petersburg, Russia* RENE BONK, ALEXANDER HIRSCH, *Inst. of Applied Physics, TU Braunschweig, Germany* GÜNTER HEIN, *Physikalisch-Technische Bundesanstalt, Germany* GEORG NACHTWEI, *Inst. of Applied Physics, TU Braunschweig, Germany* Efficient THz photodetectors on the basis of quantum Hall (QH) system have been developed during the recent years. Engineering of the device shape and selection of the parameters of operation allow to implement QH detectors with response times ranging from 10 ns to milliseconds. The spectral resolution of QH detectors, ranging between 1-2 meV at energies of 8-12 meV of the incoming radiation, is a function of the electron mobility and of the bias voltage. QH photodetectors are tunable by the magnetic field and a gate voltage. The combination of these properties together with the high sensitivity of QH THz detectors serves as a basis for an implementation of reliable spectrometer-on-chip devices for THz spectroscopy and imaging.

**9:48**

**N17 8 Type-II Strained Layer InAs-GaSb Superlattice Photodiodes For Long Wave IR Detection** MARK FIELD, GERARD SULLIVAN, AMAL IKHLASSI, BERINDAR BRAR, *Rockwell Scientific* MICHAEL FLATTE, *University of Iowa* CHRISTOPHER GREIN, *University of Illinois* MICHAEL WEIMAR, *Texas A&M University* We have fabricated and tested p-i-n photodiodes in InAs-GaSb superlattice material with measured cutoff wavelengths from 8.5 – 10 $\mu$m, and compared their performance with mercury cadmium telluride (MCT) detectors of the same cutoff wavelengths. Impedance area (R0A) products approaching the MCT devices have been demonstrated with quantum efficiencies of over 14 % per micron depth of the intrinsic layer. Progress towards designs with longer cutoff wavelengths, up to 16 $\mu$m, will be discussed along with issues and latest results on fabrication of a focal plane array using this material.

**10:00**

**N17 9 Electro-optically tunable compact terahertz source** DONG WU, *Naval Research Laboratory* The promise of terahertz technology for surveillance and reconnaissance applications is huge. Despite the technical advantages, the major challenge today in terahertz technology is the development of a portable high-power terahertz source. Of the several available terahertz source technologies those based on the difference frequency technique are very promising, as they can produce a relatively high power terahertz beam over the frequency from 100 GHz to 3.5 THz, which is tunable. However, earlier this technique suffered from a high loss of terahertz signal, and produced a weak terahertz beam, in part due to a large impedance mismatching. Also its frequency tuning was cumbersome and its tuning range was limited since it was typically performed by rotating a nonlinear optical crystal against the pumping beam. In our recent experiments we modified the technique to improve the impedance matching and to replace the mechanical tuning with an electro-optical tuning. With this

new technique we demonstrated a terahertz beam output power exceeding 10 mW (occasionally ~ 100 mW) at frequencies around 1 THz. Our new technique the frequency tuning is very convenient and not limited by the geometry of the experimental set up. Detailed experiments and experimental results will be discussed

**10:12**
**N17 10 Terahertz time domain spectroscopy of hollow polycarbonated metal waveguides** APARAJITA BANDYOPADHYAY, AMARTYA SENGUPTA, JOHN FEDERICI, *New Jersey Institute of Technology* VALENCIA JOHNSON, JAMES HARRINGTON, *Rutgers-The State University of New Jersey* Recently, the terahertz region of the electromagnetic spectrum has gained critical significance in various technical applications and fundamental research problems, involving nondestructive evaluation of material parameters, bio-medical imaging, remote sensing and security screening. However, for applications in which THz radiation needs to be transmitted over a long distance without atmospheric absorption, a flexible waveguide could have potential applications simplifying the propagation of THz radiation in remote locations. Different structures like rigid hollow metallic waveguides, solid wires, or short lengths of solid-core transparent dielectrics such as sapphire and plastic have already been explored for THz guiding purposes. Recently, it has been reported that Cu coated flexible, hollow polycarbonate waveguide has a low loss of less than 4 dB/m in single mode operation, at 1.89 THz. In the present study, using a broadband THz source of photoconductive antennae, we characterize the loss and dispersion profile of Cu coated flexible, hollow polycarbonate waveguide having an inner diameter of 2mm. Insertion loss and the attenuation coefficient were calculated using waveguides of lengths between 40mm and 70mm.

**10:24**
**N17 11 Single Crystal Si Passive Optical Components for itmm-Astronomy** ARI BROWN, *Goddard Space Flight Center* JAMES CHERVENAK, DAVID CHUSS, EDWARD WOLLACK, ROSS HENRY, S. HARVEY MOSELEY, Construction of ultrasensitive, cryogenic-focal-planes for itmm-radiation detection requires simultaneous maximization of detector quantum efficiency and minimization of stray light effects, e.g., optical ''ghosting.'' To achieve this task in the focal plane detector arrays of the Atacama Cosmology Telescope, integration of two technologies are envisioned; (1) an antireflective (AR) coating for reducing ghosting from the reflected component and increasing absorption at the focal plane, and (2) a backside absorber for suppressing reflections of the transmitted component. We propose a novel approach, involving single crystal Si components, to fabricate AR coatings and backside absorbers. AR coatings are made from Si dielectric honeycombs, in which their dielectric constant may be tuned via honeycomb dimension and wall thickness. Backside absorbers consist of AR Si honeycomb coated-resistors, and the resistors consist of P-implanted Si wafers. This approach enables us to circumvent the mechanical complexities arising from thermal expansion effects, because the detector array, back-short, and AR coating are fabricated out of the same material. We also extend the functionality of single crystal Si in the field of itmm-radiation detection by fabricating curved, low-loss, broadband waveguides. These waveguides may enable compact structures for applications requiring variable pathlength, e.g., interferometric spectroscopy.

## SESSION N18: FOCUS SESSION: CARBON NANOTUBES: TRANSPORT I
**Wednesday Morning, 15 March 2006; 315, Baltimore Convention Center at 8:00**
**Jun Kono, Rice University, presiding**



***Invited Papers***

**8:00**
**N18 1 Quantum Interference in Multiwall Carbon Nanotubes.**
CHRISTOPH STRUNK, *University of Regensburg, Germany*

Recent low temperature conductance measurements on multiwall carbon nanotubes in perpendicular and parallel magnetic field are reported. An efficient gating technique allows for a considerable tuning of the nanotube doping level. This enables us to study extensively the signature of nanotube bandstructure in electron quantum interference effects like weak localization, universal conductance fluctuations and the Aharonov-Bohm effect. We show that the weak localization is strongly suppressed at peaks at certain gate voltages which can be linked with the bottoms of one-dimensional electronic subbands. This assignment allows a detailed comparison of theoretical calculations with the experimental data. In agreement with the theory, we find clear indications for a pronounced energy dependence of the elastic mean free with a strong enhancement close to the charge neutrality point. In large parallel magnetic field, we observe a superposition of h/2e-periodic Altshuler-Aronov-Spivak oscillations and an additional h/e-periodic contribution. The latter contribution shows a diamond-like pattern in the B/$V_{gate}$-plane, which reflects the magnetic field dependence of the density of states of the outermost shell of the nanotube.

***Contributed Papers***

**8:36**
**N18 2 Three-dimensional images of contact geometry between carbon nanotubes and metal contacts using electron tomography** JUDY CHA, MATTHEW WEYLAND, *School of Applied and Engineering Physics, Cornell University* JAMES SETHNA, *Physics Department, Cornell University* DAVID MULLER, *School of Applied and Engineering Physics, Cornell University* A significant barrier to the widespread application of carbon nanotube transistors is the variability in contact resistance between

metallic leads and nanotubes. Varying by orders of magnitude, the contact resistance has recently been reported to depend on the size of the nanotube. To understand why, we study the three-dimensional contact geometry between metal contacts and nanotubes using electron tomography. Spatially resolved core-level electron energy-loss spectroscopy reveals a change in the local electronic structure of the nanotube in contact with gold-palladium We report successful three-dimensional reconstructions of the metal-nanotube interface for gold, gold-palladium and titanium contacts that explain the change in the electronic structure of the nanotube.

**8:48**

**N18 3 Electrically Tunable Magnetic Properties of Defective Metallic Carbon Nanotubes*** YOUNG-WOO SON, MARVIN L. COHEN, STEVEN G. LOUIE, *Department of Physics, University of California at Berkeley and Materials Sciences Divisions, LBNL* We present a first-principles study of the magnetic properties of metallic carbon nanotubes with various defects under a homogeneous transverse electric field. Single carbon adatoms, hydrogen passivated single carbon adatoms, and the various vacancies in (10,10) nanotubes are shown to play the role of magnetic impurities. The relative energy levels of quazi-localized states of such magnetic impurities with respect to the Fermi level are changeable with the application of a transverse electric field so that the corresponding magnetic ground states are shown to be tunable. Our results suggest that a pure organic nanomagnet could be realizable and their magnetic properties are controllable by electric fields.

*This work was supported by NSF Grant No. DMR04-39768 and DOE Contract No. DE-AC03-76SF00098. Computational resources have been provided by NSF at the NPACI and DOE at the NERSC.

**9:00**

**N18 4 Band structure modulation in carbon nanotube-metal junction** VADIM PULLER, SLAVA V. ROTKIN, *Lehigh University, Physics Dept, 16 Memorial E Dr, Bethlehem, PA 18015* In transport experiments carbon nanotubes (NTs) are embedded in metallic contacts. Distortion of NT shape within the NT-metal junction region may result in the change of NT electronic structure: the deformation can open a band gap in otherwise metallic nanotube, and reduce or completely close the gap in a semiconducting one. Local band structure modulation has non-negligible effect on the electron transmission through NT-metal interface, e.g. the Shottky barrier transparency is changing exponentially with the gap width. To analyze the deformation-induced change of the NT band structure in the contact region, we develop a comprehensive theory of the inhomogeneous deformations in NT, which combines the tight-binding approach with continuous description of the deformation field, and is applicable for NT of any chirality. We calculate the band gap variation in the contact region, and discuss the effect of the deformation on the NT-metal contact resistance.

**9:12**

**N18 5 Ab initio Calculation of Contact Effects on Transport Properties of Carbon Nanotubes Connected to Metallic Electrodes** NOBUHIKO KOBAYASHI, *Nanotech Res Inst, AIST, JAPAN* TAISUKE OZAKI, *Res Inst Comp Sci, AIST, JAPAN* KENJI HIROSE, *Fund Env Res Lab, NEC, JAPAN* Recently, a number of studies have been performed to make carbon nanotube devices. One of the important issues in the developments of the carbon nanotube devices is the control of contact effects of the electrodes. To detect electric signals through nanotubes, electrodes must be connected to the nanotubes. Contact with the electrodes sensitively influences the transport properties. Therefore, it is important to discuss the transport properties on the basis of the detailed electronic state calculation that includes the effect of contact with the electrodes. We have developed a first-principles method of analyzing quantum transport in nanometer-scale systems between electrodes. The electronic states are calculated using a numerical atomic orbital basis set in the framework of the density functional theory, and the conductance is calculated using the Green's function method. We apply the method to calculating transmission spectra of carbon nanotubes connected to metallic electrodes, and discuss the contact effect of the electrodes on the transport properties in the finite size of metallic and semiconducting nanotubes.

**9:24**

**N18 6 Electronic Structure of Metal-covered Semiconducting Carbon Nanotubes** WENGUANG ZHU, *Harvard University* EFTHIMIOS KAXIRAS, *Harvard University* Carbon nanotube field-effect transistor (CNFET) are regarded as potential building blocks for future nanoelectronics. The interaction between a carbon nanotube and metal contacts and the resulting electronic structure effects are crucial for device properties. In this talk, we present recent results on the properties of semiconducting single wall carbon nanotubes in contact with Pd, in a fully covered geometry that resembles experimental setups. We use first-principles calculations to determine the electronic structure, charge transfer effects, electrostatic potential and Fermi level alignment at the interfaces between the metal contact and various semiconducting single-wall carbon nanotubes.

**9:36**

**N18 7 Atomic-Scale Theory and Modeling of Electronic and Molecular Transport through Carbon Nanotubes** YONG-QIANG XUE, *SUNY-Albany* In this talk, we investigate the application of carbon nanotubes as novel transport channels for electrons and molecules using atomistic simulation. (1) Electronic transport: In this talk, we present a Green's function based self-consistent tight-binding study of electron transport through SWNT junction devices, which takes fully into account the 3D atomistic nature of the electronic processes. We discuss insights obtained from such atomistic study on the contact/diameter dependence of junction conductance and self-consistent study of current transport through metal-SWNT-metal junctions. (2) Molecular transport: Carbon nanotube could also be used to build assemblies for controlled transport of biomolecules for nanofluidic devices. Water confinement inside such nanoscale cylindrical core plays a significant role in determining the insertion and flow of biomolecules through the nanotube channel, which can be strongly affected by surface functionalization. Molecular dynamics simulations have been carried out to study the structure and thermodynamics of water in carbon nanotube and its effect on the spontaneous insertion of DNA molecules inside the nanotube channel. The simulations can provide valuable insights into the transport of molecules through nanoscale pore or channel structures.

**9:48**

**N18 8 Signatures of Chemical Defects in Carbon Nanotube Electronic Devices** BRETT R. GOLDSMITH, A. KANE, PHILIP G. COLLINS, *Department of Physics and Astronomy, University of California Irvine, Irvine, CA 92697-4576* The study of chemical defects in carbon nanotubes has important implications for their operation as electronic devices, and many synthesis and fabrication techniques for such devices result in non-zero defect densities. Scanned probe microscopy techniques are particularly useful for identifying these sites and then examining their electronic properties. We have examined a number of electronic devices in which single defects play important roles in determining the two- and three-terminal device behavior. Using conducting-tip atomic force microscopy to measure local electronic properties, we distinguish one type of defect from another and correlate this with the device characteristics. Furthermore, we can chemically modify and reinvestigate the same defect site. Ultimately, the goal is to use the device characteristics as a kind of signature to reliably infer the presence of particular chemical defects. This work is partly supported by NSF grant DMR-0239842.

**10:00**

**N18 9 Gated Spin Transport through an Individual Single Wall Carbon Nanotube*** BHASKAR NAGABHIRAVA, TANESH BANSAL, *Department of Electrical and Computer Engineering, University of Louisville, Louisville* GAMINI SUMANASEKERA, *Department of Physics, University of Louisville, Louisville* LEI LIU, *Department of Physics, McGill University, Montreal* BRUCE ALPHENAAR,† *Department of Electrical and Computer Engineering, University of Louisville* We report on the fabrication and characterization of ferromagnetically contacted ''short channel'' SWNT devices that show clear hysteretic switching in the magnetoresistance, and provide strong evidence for SWNT spin transport. The main difference between our work and previous studies is that we have greatly reduced the transport length separating the ferromagnetic contacts to distances on the order of 10 nm. Preliminary measurements demonstrate this reduction to be extremely beneficial. We have observed clear hysteretic switching in the magnetoresistance in 75% of our devices, and are able to modify the magnetoresistance between +15% and -10% as a function of gate voltage. The gate mediated change in magnitude itand sign of the magnetoresistance switching allows us to discount other non-spin related sources for the observed signal and provides the basis for the first SWNT spin transistor. We note that the short channel contacting scheme is generally applicable to non-ferromagnetic contacts as well, and provides a straightforward technique for fabricating SWNT quantum dot devices.

*ONR/NSF, NASA.
†Primary Reference.

**10:12**

**N18 10 Spin transport studies in mesoscopic graphite** BARBAROS OEZYILMAZ, PHILIP KIM, *Department of Physics, Columbia University, New York, NY 10027* We present experimental studies on spin transport in mesoscopic graphite. Two dimensional graphite sheets have been fabricated by means of micromechanical exfoliation. Spin injection has been achieved by employing ferromagnetic Co electrodes. We use the shape anisotropy of the electrodes to uniquely define the magnetic state of the device. Typical two terminal resistances are in the order of 1 $k\Omega$. We will discuss the switching behavior of the device magnetoresistance as a function of temperature, the gate bias voltage and of the source drain bias.

**10:24**

**N18 11 Ballistic conductance in narrow graphene strips*** D. ARESHKIN, *GWU* J.W. MINTMIRE, *OSU* C.T. WHITE, *NRL* With structures making them suitable for in-plane device processing, high aspect ratio graphene strips with widths down to tens of nanometers or smaller could ultimately provide important components in carbon-based quantum electronics. However, in comparison to corresponding single-wall carbon nanotubes, such strips will likely have a higher degree of imperfection due to variations in their widths and interactions with the substrate which will degrade their conductance. Also, unlike nanotubes, they can exhibit highly localized edge states which are degenerate with their more extended states at or near the Fermi level. On the other hand, their more extended states near the Fermi level have properties similar to those exhibited by related states in nanotubes, which should suppress the effects of back scattering both due to short and long-range disorder. Stimulated by these observations and recent experiments on graphene sheets, simulations were performed to assess the effects of various types of disorder on the conductance of narrow graphene strips. The results indicate that these strips can exhibit ballistic conductance over large distances in the presence of reasonable disorder making them excellent synthetic targets for carbon-based device applications.

*Supported by ONR.

**10:36**

**N18 12 Probing Biological Processes on Supported Lipid Bilayers with Single-Walled Carbon Nanotube Field-Effect Transistors** XINJIAN ZHOU, *LASSP, Cornell University* JOSE MANUEL MORAN-MIRABAL, *School of Applied and Engineering Physics, Cornell University* HAROLD CRAIGHEAD, *School of Applied and Engineering Physics, Cornell University* PAUL MCEUEN, *LASSP, Cornell University* We have formed supported lipid bilayers (SLBs) by small unilamellar vesicle fusion on substrates containing single-walled carbon nanotube field-effect transistors (SWNT-FETs). We are able to detect the self-assembly of SLBs electrically with SWNT-FETs since their threshold voltages are shifted by this event. The SLB fully covers the NT surface and lipid molecules can diffuse freely in the bilayer surface across the NT. To study the interactions of important biological entities with receptors imbedded within the membrane, we have also integrated a membrane protein, GT1b ganglioside, in the bilayer. While bare gangliosides can diffuse freely across the NT, interestingly the NT acts as a diffusion barrier for the gangliosides when they are bound with tetanus toxin. This experiment opens the possibility of using SWNT-FETs as biosensors for label-free detection.

**10:48**

**N18 13 First Principles Properties of Polymeric Photovoltaic Materials** T. JAYASEKERA, J. W. MINTMIRE, *Department of Physics, Oklahoma State University* Recent reports suggest that the acceptor-donor junction for bulk heterojunction photovoltaic devices can be achieved using single wall carbon nanotubes (SWNT) and polymers such as poly-3-octothiophenes (P3OT). Optical excitation is believed to occur in the organic polymer which acts as a good hole conductor, with electron transfer to the SWNT which acts as a good electron conductor. An appropriate theoretical understanding of the photovoltaic effect requires knowledge of the electronic states near the Fermi level in these materials. We calculate the electronic structure of infinitely long quasi one-dimensional nanostructures such as carbon nanotubes or electroactive chain polymers, such as polythiophenes using a first

principles, all electron, self consistent local density functional (LDF) approach. We present and compare electronic structure calculations for SWNTs and poly-3-alkyl-thiophenes. Further we discuss the variation of effective mass of charge carriers in polymers and SWNTs in the vicinity of Fermi level. This work was supported by the US Office of Naval Research and the DoD HPCMO CHSSI program through the Naval Research Laboratory.

**SESSION N19: SEMICONDUCTOR SPIN TRANSPORT**
**Wednesday Morning, 15 March 2006**
**316, Baltimore Convention Center at 8:00**
**Jim Chelikowsky, University of Texas, presiding**

**8:00**
**N19 1 High field magnetoresistance in *p*-(In,Mn)As/*n*-InAs heterojunctions** BRUCE WESSELS, STEVEN MAY, *Materials Science and Engineering, Northwestern University* The high field magnetoresistive properties of a *p*-$In_{0.96}Mn_{0.04}As$/*n*-InAs junction have been measured. The heterojunctions were formed by epitaxially depositing an InMnAs thin film on an InAs substrate using metal-organic vapor phase epitaxy. Under forward bias, a large, nonsaturating magnetoresistance is observed at temperatures from 25 to 295 K in fields up to 9 T. At room temperature, the magnetoresistance increases linearly with magnetic field from 1.5 to 9 T and is greater than 700 % at 9 T. The magnetoresistance can be simulated using a modified diode equation, including a field-dependent series magnetoresistance.

**8:12**
**N19 2 Room Temperature Tunnel Magnetoresistance and Spin Polarized Tunneling Studies with Organic Semiconductor Barrier** T. S. SANTOS, P. MIGDAL, I. C. LEKSHMI, J. S. MOODERA, *Francis Bitter Magnet Lab, MIT, Cambridge, MA* J. S. LEE, *Nano-device Research Center, KIST, Seoul, Korea* Organic semiconductors, $\pi$-conjugated, with a weak spin-orbit interaction, show promise for spin-conserved transport applications.[1,2] An organic spin-valve utilizing the molecular organic semiconductor tris (8-hydroxyquinolinato)aluminum ($Alq_3$), demonstrated giant magnetoresistance at LHe temperatures.[1] The $Alq_3$ films in this spin-valve were $>$ 130nm, and the spin diffusion length was 45nm. Our current study demonstrates spin polarized tunneling through an ultra-thin layer of $Alq_3$ in a magnetic tunnel junction. Significant tunnel magnetoresistance was measured in a MTJ structure at room temperature, which increased when cooled to low temperatures. Tunneling characteristics, such as the I-V behavior and temperature and bias dependence of the TMR, show good quality of the organic tunnel barrier. Spin polarization of the tunnel current from Co, Fe and NiFe electrodes through the $Alq_3$ layer was directly measured using a superconducting Al electrode as the spin detector. This demonstration of spin-conserved transport through an organic semiconductor at room temperature shows the potential of this material for further study. Supported by KIST-MIT Program and NSF. 1) Z. H. Xiong, et al, Nature **427**, 821 (2004). 2) V. Dediu, et al, Solid State Commun. **122**, 181 (2002).

**8:24**
**N19 3 Diluted Magnetic Double Barrier Resonant Tunneling Structures for Novel Magnetically-Defined Quantum Dot and Nano Structures*** ZAILI FANG, A.M. CHANG, *Department of Physics, Duke University, Durham, NC 27708* X.Y. LIU, J.K. FURDYNA, *Department of Physics, University of Notre Dame, Notre Dame, IN 46556* The further development of Spintronics requires the direct control of the spin degree of freedom. A milestone on the path towards this accomplishment has been recently achieved by the demonstration of the successful operation of a magnetic resonant tunneling diode[1]. We will report our results on manganese doped double barrier tunneling structures (II-IV group) with varying doping, confining potential and well width. These structures, in which both the barrier and well are doped with manganese, show a Zeeman splitting tendency in the vertical transport through the barrier in magnetic field. This tendency can be exploited as spin filter for spintronic applications. Based on this spin voltage transport property of diluted magnetic semiconductor heterostructures and the interaction of superconductors and semiconductors, we propose a novel spin aligned vertical quantum dot device. Progress on the fabrication of this device will also be reported.

*Research supported in part by NSF DMR-02105191.

[1]A. Slobodskyy et al., Phys. Rev. Lett. **90**, 246601 (2003).

**8:36**
**N19 4 Spin dependent tunnelling in indirect double-barrier structures** TITUS SANDU, *Departement de Chimie, Universite de Montreal, Canada* Spin-dependent tunelling and polarization in GaAs/AlAs/GaAs based resonant tunelling diode are studied by a tight-binding model. We compare the GaAs/AlAs/GaAs case with similar structures where the barriers are direct and show the advantages of a GaAs/AlAs/GaAs configuration.

**8:48**
**N19 5 Magnetic Resonances in the circular polarization of light emitted by Fe/InAs QD spin LEDs** M. YASAR, S. DELIKANLI, R. MALLORY, A. PETROU, *SUNY Buffalo* G. KIOSEOGLOU, A.T. HANBICKI, C.H. LI, B.T. JONKER, *Naval Research Laboratory* The circular polarization $P_{circ}$ of the light emitted from InAs QD LEDs was studied as function of applied magnetic field $B$ in the 5-75 K temperature range. The quantum dots are incorporated at the center of a GaAs quantum well of width $L_W$. At$T$ = 5 K we observed two distinct resonances in the $P_{circ}$ versus $B$ plot. For $L_W$ = 430 Å the resonances occur at $B$ = 4.6 T (strong) and $B$ = 2.3 T (weak). The strength of the resonances depends critically on bias voltage $V$ (very pronounced at low $V$values) The resonances become weaker with increasing temperature and disappear completely by $T$ = 60 K. No resonances were observed in LEDs in which the QDs were not incorporated in a quantum well. We propose a model that takes into account the confinement conduction subbands of the GaAs quantum well and the dependence of their energies on magnetic field. Acknowledgements: This work is supported by the DARPA SpinS Project, ONR, and NSF.

**9:00**
**N19 6 Tailoring magnetic anisotropy in ferromagnetic metal / semiconductor contacts for spin injection*** C. H. LI, G. KIOSEOGLOU, A. T. HANBICKI, T. J. ZEGA, R. M. STROUD, B. T. JONKER, *Naval Research Lab, Washington, DC* Robust spin injection across an Fe/AlGaAs interface has recently been demonstrated, producing an electron spin polarization $>$ 32% in a GaAs QW. In an effort to incorporate a spin injecting metal contact with perpendicular remanence and to explore interface effects on spin

injection, we have grown MnGa thin films epitaxially on GaAs(001) LED structures by MBE. Streaky RHEED patterns indicate single crystalline films. Although lattice matched to GaAs, TEM shows that while MnGa crystallizes nicely away from the interface, defects exist at the interface. The insertion of a thin ( $\sim$ 5ML) Fe seed layer between MnGa and AlGaAs promotes the initial nucleation of MnGa and provides a means to control the structure of the spin-injecting interface, while the magnetic behavior is determined by the MnGa. Samples are processed to form surface emitting LEDs, and the EL is dominated by QW excitonic emission. A 0.5% remanent circular polarization is observed, which tracks the MnGa magnetization obtained by independent SQUID measurements. Comparison between MnGa spin-LEDs with and without the Fe seed layer (including interface properties), and magneto absorption effects in these heterostructures, will be discussed.

*Supported by DARPA and ONR.

**9:12**

**N19 7 Quasi-one-dimensional spin polarized states in T-shaped nanostructures** PAWEL REDLINSKI, BOLDIZSAR JANKO, *University of Notre Dame* We present results of theoretical and numerical investigations of T-shaped semiconductor nano-wire structures. Such structures have been synthesized in Molecular Beam Epitaxy laboratories by using traditional (GaAs) and magnetic (GaMnAs) semiconductors. The wire is formed in a three-stage MBE process and in its final form, the structure looks as if one quantum well (QW) called Stem well grew perpendicularly into the second QW, the so-called Arm well. The quasi 1D states are formed at the intersection of the two QWs. Typically in the T-shaped structures the thickness of the wire is of order of few nm. For such thickness there is only one conduction channel and the energy states of quasi-particles are indexed by a single quantum number, the 1D linear momentum $k$, and by its spin. There are two distinctive features present in this type of systems: strong spin-orbit coupling, and the lack of square symmetry of the wire cross section. These features have profound implications and make this system very important from theoretical point of view. Results, obtained within the **kbullet p** formalism, show that at $k \neq 0$ the valence band states are non-degenerate with respect to the spin degree of freedom. Both dispersions of spin up and spin down states are well modeled as parabolic bands but with different effective masses. It opens possible to manipulate the spin degrees of freedom in a T-shaped quantum structure.

**9:24**

**N19 8 Atomistic spin-orbit effects on the electronic structure of T-shaped quantum wires** JAVIER AIZPURUA, *Donostia Intl Physics Center, Donostia, Spain* GARNETT W. BRYANT, *NIST, Gaithersburg, MD* The electronic structure and optical properties of GaAs/AlGaAs T-shaped quantum wires are studied by use of an empirical tight-binding method (ETB). This model allows us to study atomistic effects on the electronic structure of wires that have a complicated geometrical cross section. We find that the electronic structure for electrons is similar to that described by effective mass models whereas the electronic structure for holes shows important modifications when spin-orbit coupling is included in the atomistic model. The binding energies of the holes in a T-wire agree with previous effective mass model calculations. However, we find that asymmetries in the spatial distribution of these hole states are induced by atomistic spin-orbit effects. Moreover, the atomistic tight-binding model predicts complex band crossings for hole states that are not predicted by simpler effective mass theories. Consequences for the optical response of T-wires and for excitonic and electron-hole plasma phases in T-wires are discussed.

**9:36**

**N19 9 Quasi-one-dimensional spin field-effect transistors** JAESEUNG JEONG, HYUN-WOO LEE, *Pohang University of Science and Technology* We study a spin field effect-transistor(SFET) with multiple transport modes. Energy dispersion relations and spin profiles of eigen-transport modes are examined numerically and analytically for weak and strong Rashba spin-orbit coupling parameters. Electron transport properties of the multiple-mode SFET are investigated including the Fabry-Perot-type interference due to multiple reflections and the peak splitting by external magnetic fields. Impurity scattering effects are also addressed.

**9:48**

**N19 10 Lateral diffusive spin transport in layered structures*** HANAN DERY, LUKASZ CYWINSKI, LU J. SHAM, *Department of Physics, University of California San Diego* A one dimensional theory of lateral spin-polarized transport is derived from the two dimensional flow in the vertical cross section of a stack of ferromagnetic and paramagnetic layers. This takes into account the influence of the lead on the lateral current underneath, in contrast to the conventional 1D modeling by the collinear configuration of lead/channel/lead. Our theory is convenient and appropriate for the current in plane configuration of an all-metallic spintronics structure as well as for the planar structure of a semiconductor with ferromagnetic contacts. For both systems we predict the optimal contact width for maximal magnetoresistance and propose an electrical measurement of the spin diffusion length for a wide range of materials. This work was supported by NSF DMR-0325599.

*Preprint cond-mat/0510770.

**10:00**

**N19 11 Microscopic calculation of the Gilbert damping in a spin-polarized two-dimensional electron liquid with Rashba spin-orbit interaction*** GIOVANNI VIGNALE, EWELINA HANKIEWICZ, *University of Missouri* We present a microscopic calculation, based on mode-coupling theory, of (i) the Gilbert damping constants for in-plane and out-of-plane relaxation and (ii) the magnetic anisotropy tensor of the spin-polarized two-dimensional electron liquid in the presence of a spin-orbit interaction of the Rashba form.

*Work supported by NSF Grant No. DMR-0313681.

**10:12**

**N19 12 Controlling spin in an electronic interferometer with spin-active interfaces** CHRISTOPH BRUDER, *Dept. of Physics and Astronomy, University of Basel, CH-4056 Basel, Switzerland* AUDREY COTTET, *Laboratoire de Physique des Solides, Université Paris Sud, F-91405 Orsay Cedex, France* TAKIS KONTOS, *Laboratoire Pierre Aigrain, Département de Physique, ENS, 24, rue Lhomond, F-75231 Paris Cedex 05, France* WOLFGANG BELZIG, *University of Konstanz, Theoretical Solid State Physics, Department of Physics, M703, D-78457 Konstanz, Germany* CHRISTIAN SCHÖNENBERGER, *Dept. of Physics and Astronomy, University of Basel, Klingelbergstr. 82, CH-4056*

*Basel, Switzerland* We consider electronic current transport through a ballistic one-dimensional quantum wire connected to two ferromagnetic leads. We study the effects of the spin-dependence of interfacial phase shifts (SDIPS) acquired by electrons upon scattering at the boundaries of the wire. The SDIPS produces a spin splitting of the wire resonant energies which is tunable with the gate voltage and the angle between the ferromagnetic polarizations. This property could be used for manipulating spins. In particular, it leads to a giant magnetoresistance effect with a sign tunable with the gate voltage and the magnetic field applied to the wire.

**10:24**

**N19 13 Interferometric detection of spin-polarized transport** G. SALIS, S. F. ALVARADO, *IBM Research, Zurich Research Laboratory, 8803 Rüschlikon, Switzerland* It is shown that in addition to its sensitivity to spin polarization, the magneto-optic Kerr effect strongly depends on the spatial distribution of spin-polarized charge carriers. Using time-resolved Kerr rotation, the dynamics of spin- polarized electrons can thus be monitored on the nanometer length scale. This is demonstrated experimentally for optically- excited electron spins in the depletion layer of *n*-doped GaAs close to a metallic electrode. The Kerr rotation exhibits fast oscillations that originate from an interference of the light reflected at the electrode with that reflected at the front of the electron distribution moving into the semiconductor. From these oscillations, the dynamics of the electron front is obtained, which is strongly screened by the space-charge field of the excited electron-hole pairs and can be controlled by an electric bias across the Schottky barrier. In addition, the dynamics provides information on the Schottky-barrier height, the depletion-layer thickness and the doping concentration.

**10:36**

**N19 14 Spin Resolved Current Focusing in InSb Heterostructures*** ARUNA DEDIGAMA, DAVID DEEN, SHEENA MURPHY, NITI GOEL, JOEL KEAY, MICHAEL SANTOS, *University of Oklahoma* KYOICHI SUZUKI, SEN MIYASHITA, YOSHIRO HIRAYAMA, *NTT Basic Research Laboratories* Spin-resolved current focusing has been observed in InSb/AlInSb structures. While InSb has the most significant Rashba and Dresselhaus effects of any of the III-V semiconductors, Dresselhaus effects are expected to dominate in the symmetrically doped structures used here. The double quantum point contact devices were designed with typical dimensions of 0.5 micron which preserve ballistic transport up to 185K as measured in previous experiments. Focusing peaks were observed near the expected values of perpendicular magnetic field; however the first focusing peak was a doublet. With application of a parallel magnetic field the doublet evolved into a singlet as expected for spin resolved focusing.

*This work is supported by the National Science Foundation under grants DMR-0510056 and DMR-0520550.

**10:48**

**N19 15 Spintronic Ratchet** SAYEEF SALAHUDDIN, SUPRIYO DATTA, *School of Electrical and Computer Engineering, Purdue University, West Lafayette, IN-47907* Carefully designed ratchets are of great interest, practically and conceptually, as means to convert fluctuations into useful work. We argue that a recently proposed ''Spin-Capacitor'' [Appl. Phys. Lett. **87**, 013115 (2005)] exhibits characteristics that have close resemblance to ratchets. It shows unidirectional current-voltage (I-V) characteristics that depend on the spin excitation spectrum of a neighboring array [http://arxiv.org/abs/cond-mat/0511566]. More interestingly, if the spins in the array are out of equilibrium, useful work can be extracted at the expense of energy/entropy. This is manifested as a **non-zero current at zero bias** and we argue that a recent experiment in an integer quantum hall system [http://link.aps.org/abstract/PRL/v95/e056802] shows evidence for this general principle.

## SESSION N20: FOCUS SESSION: COMLEX OXIDE THIN FILMS SURFACES AND INTERFACESS III: NEW MATERIALS, NEW TECHNIQUES, AND EFFECTS OF STRAIN

**Wednesday Morning, 15 March 2006**
**317, Baltimore Convention Center at 8:00**
**Anand Bhattacharya, Argonne National Laboratory, presiding**

**8:00**

**N20 1 Growth and Properties of a New Correlated Electron Perovskite Thin Film – $PbVO_3$.** LANE W. MARTIN, QIAN ZHAN, WENKAN JIANG, *Materials Science and Engineering, University of California, Berkeley* MIAOFANG CHI, NIGEL BROWNING, *Chemical Engineering and Materials Science, University of California, Davis and National Center for Electron Microscopy, Lawrence Berkeley Nat. Lab.* YURI SUZUKI, R. RAMESH, *Materials Science and Engineering, University of California, Berkeley* We report the growth of single phase, fully epitaxial thin films of a relatively new perovskite material, lead vanadate ($PbVO_3$), using pulsed laser deposition. This growth realizes the first production of $PbVO_3$ outside of high-temperature and high-pressure techniques through growth of epitaxial thin films on various substrates. Structural analysis of the $PbVO_3$ thin films using transmission electron microscopy, x-ray diffraction, and Rutherford backscattering spectroscopy reveals films that are single phase, highly crystalline, and have a tetragonally distorted perovskite structure, with $a = 3.79$Å and $c = 5.02$Å (c/a = 1.32). Electron energy loss spectroscopy and x-ray absorption spectroscopy were used to show the stabilization of vanadium in the $V^{4+}$ state, thereby proving the creation of a new $d^1$ system for intensive physical study. Films exhibit semiconducting behavior in plane of the film with thermally activated behavior and distinctly different properties from other $d^1$ $AVO_3$ thin films. Studies of the magnetic and ferroelastic/ferroelectric nature of $PbVO_3$ are also underway.

**8:12**

**N20 2 Phase Transitions of $SrFeO_3$ Studied Using a Single-Crystalline Film** NAOAKI HAYASHI, SHIGETOSHI MURANAKA, *Graduate School of Human and Environmental Studies, Kyoto University* TAKAHITO TERASHIMA, *Research Center for Low temperature and Materials Sciences, Kyoto University* MIKIO TAKANO, *Institute for Chemical Research, Kyoto University* To study the electronic nature of $SrFeO_3$ (SFO), which is a cubic perovskite containing $Fe^{4+}$ equipped with deep *d* levels and is, therefore, dominated by *p*-hole character, a single crystalline film was grown and the resistivity (it$\rho$), Hall effect, magnetoresistance (itMR) and susceptibility were measured. It is known

that this oxide in bulk form becomes antiferromagnetically ordered in a screw spin structure. The $T_N$ of the film has been found to be at 120~ 125 K from the susceptibility measurement, while the transport properties showed well-defined anomalies at 105 K, rather than at the $T_N$. The metallic film (it$\rho$ = 9× $10^{-4}\Omega$cm at 300 K) exhibited a hysteretic, inflectional drop in the it$\rho$ -*T*curve at 105 K after showing a very small anomaly at 125 K; the Hall coefficient was positive and temperature-independent above 110 K but increased quickly below ~ 100 K; the itMR changed its sign from negative to positive quite steeply at 105 K. Considering these results together with what is known about bulk samples, we conclude that SFO undergoes its antiferromagnetic transition in two stages, passing an incompletely coherent stage before entering the final coherent state.

**8:24**

**N20 3 Magnetic Properties of PLD Grown Expitaxial Double Perovskite Thin Films*** D.E. BROWN, S. TOTAPALLY, Y. YOO, S. KOLESNIK, J. MAIS, O. CHMAISSEM, J. CHURILLA, B. DABROWSKI, C. KIMBALL, *Physics Dept., Northern Illinois University* M. HAJI-SHEIK, *Electrical Engineering Dept.,Northern Illinois University* Transition metal oxides with a double perovskite structure $A_2FeMoO_6$ and (A = Ca, Ba, Sr) has attracted a great deal of attention owing to their high magnetic transition temperatures and spin dependent transport properties. Electronic structure calculations and experimental results show that these materials are half-metallic ferrimagnets with localized up-spin electrons on the Fe ions and itinerant down-spin electrons shared between Fe and Mo. The Fe and Mo atoms are ordered on alternating, corner-shared octahedral sites, however, the ordered array can have imperfections that are dependent upon synthesis conditions. We have grown, using a pulsed laser deposition device, epitaxial double perovskite thin films. These films have been characterized by SQUID, resistivity, and x-ray crystallography measurements. The measurements show that double perovskite thin films can be grown with a high degree of order between the Fe and Mo atoms. Thus these materials can be attractive candidates for spin electronic devices.

*Work at NIU is supported by the Department of Education.

**8:36**

**N20 4 Exotic Single Crystal Thin Films Made From Cobalt Ferrite.** H. CORCORAN, *Morgan State University* A. COLEMAN, *Morgan State University* A. LISFI, *Morgan State University* C. M. WILLIAMS, *Morgan State University* W. MORGAN, *Morgan State University* A. KUMAR, *Morgan State University* The search for new magnetic materials is driven by technological demands such as increasing the magnetic recording density. Materials possessing a large magnetic anisotropy are suitable media to meet such requirements since a stable magnetization can be promoted in nano-structures. Hard ferrites such as the hexagonal ($BaFe_{12}O_{19}$) and the cubic ($CoFe_2O_4$) are attractive for such kind of applications due to their large magnetocrystalline anisotropy and high chemical stability. In this talk we report on exotic properties of films made from $CoFe_2O_4$. Epitaxial $CoFe_2O_4$ thin films have been grown by pulsed laser deposition (PLD) on (100) MgO substrate. Two types of spin-reorientation have been observed in such films upon annealing or increasing the film-thickness. In the as-deposited layers and at low thickness the easy axis of the magnetization is confined to the normal to the film plane whereas at large thickness the film plane becomes the preferential direction of the magnetization. On the other hand annealing induces a reorientation of magnetic anisotropy, which switches from the normal to the film plane in the as-deposited film to be in-plane aligned in the annealed state. The origin of both reorientations is explained in term of competition between stress and magnetocrystalline anisotropies.

**8:48**

**N20 5 Magnetic Anisotropy of Cr-Substituted Magnetostrictive Cobalt Ferrite** YEVGEN MELIKHOV, JOHN SNYDER, CHESTER LO, PAUL MATLAGE, SANG-HOON SONG, KEVIN DENNIS, *Iowa State University, Ames, IA 50011, USA* DAVID JILES, *Cardiff University, Cardiff CF243AA, UK* In order to tailor the magnetomechanical response of substituted cobalt ferrite for strain sensing and actuating applications, more needs to be known about the variation of the basic magnetoelastic and magnetic properties with temperature and composition. In this study, the variation of magnetic anisotropy with temperature and composition for a series of Cr-substituted cobalt ferrites, $CoCr_xFe_{2-x}O_4$, ($0 \leq x \leq 0.8$) was investigated. In order to determine the cubic anisotropy constant $K_1$,the ''high field'' regime (from 1 T to 5 T) of the major magnetic hysteresis loops, which were measured at temperatures over the range 10-400 K using a SQUID magnetometer, was fitted using the law of approach approximation $M(T) = M_S(1\text{-}8/105K_1^2/(\mu_0 H M_S)^2)$ plus a forced magnetization term linear in applied field *H*. It was found that anisotropy increases with decreasing temperature, with the steepest increase coming at progressively lower temperatures for increasing Cr content. For fixed temperatures, anisotropy decreases with increasing Cr content. For the pure cobalt ferrite and x=0.2 Cr samples it appears that for temperatures less than 150 K, 5 Tesla is not enough to saturate the samples, so anisotropy cannot be computed correctly by this method. This research was supported by NSF, Grant No.DMR-0402716, and by NASA, Award No.NAG-1-02098.

**9:00**

**N20 6 Influence of substrate strain on $(La_{1-x}Pr_x)_{1-y}Ca_yMnO_3$ phase transition*** DANE GILLASPIE, J.X. MA, *Univ. of Tenn Physics Dept. and ORNL* H-Y. ZHAI, *ORNL* Z. WARD, E.W. PLUMMER, *Univ. of Tenn Physics Dept. and ORNL* H. CHRISTEN, *ORNL* J. SHEN, *Univ. of Tenn Physics Dept. and ORNL* The large-scale phase separation between ferromagnetic metallic (FMM) and charge-ordered insulating (COI) domains observed in $(La_{1-x}Pr_x)_{1-y}Ca_yMnO_3$ (LPCMO) crystals has attracted a lot of attention. This coexistence of phases is very sensitive to structural and magnetic changes, and is responsible for the enhanced magnetoresistance in LPCMO compared to its parent compounds. The energy balance of the FMM and COI phases is still not well understood. We can change the energy balance by changing the substrate, and therefore the strain on the thin film, and thereby improve our understanding of the phase transition. We have grown and characterized several different thicknesses of LPCMO on $LaAlO_3$, $SrLaGaO_4$, $NdGaO_3$ and $SrTiO_3$ substrates. We have observed that the compressive strain from the $LaAlO_3$ substrate suppresses the long-range charge ordering in the sample, and enhances magnetoresistance and magnetic hysteresis. The charge ordering is also suppressed in the films on $SrLaGaO_4$, even though the strain is negligible. Conversely, the tensile strain from the $NdGaO_3$ and $SrTiO_3$ substrates enhances the long-range charge ordering and reduces the magnetoresistance and magnetic hysteresis.

*Oak Ridge National Laboratory, managed by UT Battelle for the U.S. Dept. of Energy under contract DE-AC05-00OR22725.

**9:12**

**N20 7 The role of strain in the magnetic properties of $La_{0.7}Sr_{0.3}MnO_3$ films studied by magnetic force microscopy** RAVI KUMMAMURU, YEONG-AH SOH, *Dept. of Physics and Astronomy, Dartmouth College, Hanover, NH 03755.* NEIL MATHUR, LUIS HUESO, *Department of Materials Science, University of Cambridge, Cambridge CB2 3QZ, UK* CONDENSED MATTER, DEPARTMENT OF PHYSICS AND ASTRONOMY, DARTMOUTH COLLEGE TEAM, DEVICE MATERIALS GROUP, DEPARTMENT OF MATERIALS SCIENCE, UNIVERSITY OF CAMBRIDGE COLLABORATION, In order to elucidate the role of strain in the magnetic properties of manganite films, we studied the behavior of the magnetic domains in $La_{0.7}Sr_{0.3}MnO_3$ (LSMO) films grown on $SrTiO_3$ (STO) and $NdGaO_3$ (NGO) substrates, which are differently strained. Our previous studies on the magnetic properties of $La_{0.7}Sr_{0.3}MnO_3$ films grown on STO substrates using magnetic force microscopy showed a distinct magnetic texture within magnetic domains, and spin reorientation and enhancement of $T_C$ near grain boundaries. These results were attributed to the strain in the film caused by the lattice mismatch with the substrate and the strain relaxation at the grain boundaries. Our new studies on $La_{0.7}Sr_{0.3}MnO_3$ films grown on NGO substrates, which have very low strain due to a close lattice match between the film and substrate, show no presence of magnetic texture and a very sharp transition from the paramagnetic to ferromagnetic phase.

**9:24**

**N20 8 Strain Induced Crystal Superstructure in Manganite Films** YEONG-AH SOH, *Dartmouth College* ZAHIRUL ISLAM, JONATHAN LANG, GEORGE SRAJER, *Argonne National Laboratory* NEIL MATHUR, MARK BLAMIRE, *University of Cambridge* Using xray diffraction we studied in detail the crystal structure of a 100 nm thick $La_{0.7}$ $Sr_{0.3}MnO_3$ film grown on a $SrTiO_3$ substrate. Satellite peaks are observed at $(H \pm \delta h, K, L)$ for nonzero $K$ and $(H, K \pm \delta k, L)$ for nonzero $H$. No satellite peaks are observed around $(0\ 0\ L)$ reflections. Our measurements show that the modulation wave vectors and polarization vectors representing the atomic displacements are perpendicular to each other and point in the direction parallel to the plane of the film. $L$ scans around the main Bragg peaks and around the satellite peaks exhibit strong Laue oscillations indicating that the superstructure is coherent throughout the whole thickness of the film. We will discuss the results of the xray measurements in connection with the scanning probe microscopy measurements done on the same film.

**9:36**

**N20 9 Electronic properties of structural twin and antiphase boundaries in materials with strong electron-lattice couplings*** K. H. AHN, *Advanced Photon Source, Argonne National Laboratory, Argonne, IL 60439* T. LOOKMAN, A. SAXENA, A. R. BISHOP, *Theoretical Division, Los Alamos National Laboratory, Los Alamos, NM 87545* Using a symmetry-based atomic scale theory of lattice distortions, we show that in functional materials with strong electron lattice coupling, the electronic properties are distinctly modified near elastic textures such as twin boundaries (TBs) and antiphase boundaries (APBs), which can be directly measured by STM. The results also show that the heterogeneities of electron local DOS are not confined within TBs and APBs, but can propagate into domains in the form of Friedel oscillations for TBs and with the wave vector related to short wave length lattice distortions for APBs. The results are discussed in relation with perovskite manganites and other functional electronic materials. Reference: Ahn, Lookman, Saxena, and Bishop, Phys. Rev. B 71, 212102 (2005).

*This work is supported by US DOE.

**9:48**

**N20 10 Ultra-thin Perovskite Manganite films on $SrTiO_3$ and $SrTiO_3$/Si heterostructures** A. PRADHAN, *Norfolk State University* D. HUNTER, K. ZHANG, B. LASLEY, K. LORD, T.M. WILLIAMS, R.R. RAKHIMOV, *Center for Materials Research, Norfolk State University* We report on the growth and characterization of high-quality ultra-thin $La_{0.7}Ba_{0.3}MnO_3$ and $La_{0.7}Sr_{0.3}MnO_3$ epitaxial films on $SrTiO_3$ and $SrTiO_3$-buffered Si (100) and Si (111) substrates by pulsed-laser deposition. The films demonstrate remarkable magnetic and electrical properties associated with the colossal magnetoresistance behavior at and above room temperature. The enhanced transition temperature of manganite films on buffered Si substrates is discussed in terms of the strain relaxation at the interface between the manganite film and the $SrTiO_3$ buffer layer which is caused by the smaller grain size. We also report the doping of Ru (x=0.3 to 0.4) into Mn sites in LSMO films grown both on STO and STO buffered Si. The films display remarkable hardening of $H_c$ due to the charge-transfer-enhanced exchange coupling. We have optimized doping for the compensation of hole doping by the valence effect of Ru, This effect has been explained in terms of the charge transfer between the $Mn^{4+}$ and $Ru^{4+}$ species and ferromagnetic interaction between the resultant $Mn^{3+}$ and $Ru^{5+/4+}$. The electrons in $Ru^{4+}$ partially occupy the degenerated $t_{2g}$ orbitals due to the fact that Ru is a heavy metal, we expect a single-ion anisotropy of Ru spins through a spin-orbit channel. This structure is highly applicable for fabrication of the magnetic tunnel junctions.

**10:00**

**N20 11 Variation of magnetic domain structure correlated to low-field magnetoresistance hysteresis in $La_{0.66}Ca_{0.34}MnO_3$ film as observed by magnetic force microscopy.*** CHANGBAE HYUN, CASEY ISRAEL, WEIDA WU, ALEX DE LOZANNE, *Department of Physics, University of Texas at Austin* ALAKA P. VALANJU, RODGER M. WALSER, *Electrical and Computer Engineering, University of Texas at Austin, Austin, TX 78712* M.E. GOMEZ, J. G. RAMIREZ, *Thin Films Group. Universidad del Valle, A.A. 25360 Cali, Colombia* G.A. MENDOZA, *Magnetic Materials and Nanostructures Group. Universidad del Quindío, Armenia, Colombia* The ferromagnetic domain structure of a 150-nm-thick $La_{0.66}Ca_{0.34}MnO_3$ film was imaged by magnetic force microscopy (MFM) as a function of in-plane applied field at 240K, just below $T_C$. The film was grown by sputtering on a (001) $SrTiO_3$ substrate. The variation of the domain structure is correlated with the hysteresis in both magnetization and magnetoresistance. The resistance peak in the magnetoresistance coincides with the coercivity of the film and sweeping changes in the MFM images. We show the effect of applying the in-plane magnetic field along both in-plane crystalline axes.

*This work is supported by NSF DMR-0308575.

**10:12**

**N20 12 Anisotropic magnetoresistance in colossal magnetoresistive $La_{1-x}Sr_xMnO_3$ thin films** JENG-BANG YAU, *Yale University* X. HONG, *Yale University* C. H. AHN, Y. BASON, *Bar Ilan University* L. KLEIN, *Bar Ilan University* We report on magnetic field and temperature dependent measurements of the anisotropic magnetoresistance (AMR) in epitaxial $La_{1-x}Sr_xMnO_3$ (LSMO) thin films. While in 3*d* ferromagnetic alloys increasing the magnetization, either by reducing the temperature or increasing the magnetic field, increases the AMR, in LSMO films the AMR dependence on magnetization displays non-monotonic behavior which becomes particularly pronounced in lightly doped compounds. This could imply that these samples may be electronically inhomogeneous, in which increased magnetization yields enhanced uniformity which suppresses spin-dependent scattering and hence reduces the AMR.

**10:24**

**N20 13 Size effect in percolative phase separation of colossal magnetoresistive (La,Pr,Ca)$MnO_3$ films.** HONG-YING ZHAI, *Oak Ridge National Laboratory* JIANXING MA, DANE GILLASPIE, THOMAS WARD, *Oak Ridge National Laboratory and University of Tennessee* ANTHONY HMELO, *Vanderbilt University* LEONARD FELDMAN, *Vanderbilt University* JIAN SHEN, *Oak Ridge National Laboratory and University of Tennessee* $La_{1-x-y}Pr_yCa_xMnO_3$(LPCMO) (where x=3/8) is electronically phase-separated into a sub-micrometre-scale mixture of ferromagnetic metallic (FMM) and charge-ordered insulating (COI) domains. Transport through the ferromagnetic network depends sensitively on the domain structure, which can be controlled by magnetic field, light, and strain, etc. Enhanced CMR effect can be achieved in the vicinity of the percolative threshold. Using optical lithography, e-beam lithography, and focused ion beam techniques, we can fabricate series micron and sub-micron structures on LPCMO films grown on $LaAlO_3$ and $SrTiO_3$ using pulsed laser deposition. Size dependant transport properties will be addressed in detail. Research sponsored by the U.S. Department of Energy under contract DE-AC05-00OR22725 with Oak Ridge National Laboratory.

**10:36**

**N20 14 Combinatorial Hall Effect System for Oxide Films*** JEFFREY CLAYHOLD, *Physics Department, Miami University, Oxford, OH 45056* BRYAN KERNS, DAVID RENCH, MICHAEL SCHROER, IVAN BOZOVIC, *Brookhaven National Laboratory* Combinatorial film growth techniques have made it possible to produce large numbers of high-quality oxide films at one time. Characterizing the samples by traditional methods would be far too slow. Certain measurements, such as the the Hall effect, require careful temperature control and lock-in amplifiers to resolve the small signal. We have built special-purpose, multichannel resistance bridges to measure the Hall effect simultaneously in 32 samples. The voltage resolution is less than 2 nV for signals on the order of 1 $\mu$V, for a signal-to-noise ratio of 500. We will discuss Hall effect data from samples of $La_{2-x}Sr_xCuO_4$.

*Supported by Brookhaven National Laboratory and the Department of Energy.

**10:48**

**N20 15 B-site substitution in $LaTiO_3$ thin films: influence on the titanium oxidation state.** A. GUILLER, C. MARCHIORI, M. SOUSA, R. GERMANN, J. P. LOCQUET, J. FOMPEYRINE, *IBM Research GmbH* J. W. SEO, *IPMC, Ecole Polytechnique Federale de Lausanne* $LaTiO_3$ (LTO) is a Mott insulator, antiferromagnetic at RT, and exhibits a Metal Insulator Transition (MIT) at the Neel temperature. Despite its complex chemistry, it is an interesting candidate to fabricate field-effect devices. A full device requires the deposition of a dielectric in contact with the LTO thin film such as $HfO_2$. This choice will be discussed, and we will present issues related to a possible interdiffusion. Adding Hf in the LTO layer leads to a clear change of the resistivity measured as a function of temperature, and strongly influences the MIT temperature. Starting from a semiconducting LTO, 20% Hf substitution on the perovskite B-site makes the layer become metallic from RT down to 4.2K. The average valence of Ti is increasing from $Ti^{3+}$ towards $Ti^{4+}$ with the substitution of Hf, as shown by XPS. Several explanations can be proposed beyond a real incorporation of Hf into the LTO matrix. Besides a pure electronic effect, structural and catalytic effects have been then investigated in details by means of XRD, XPS and HRTEM. Multilayers as well as single-phase thin films have been fabricated to disentangle these different effects. Our results will be discussed taking also into account a possible material loss in the structure. We will in particular explore the behavior of La-deficient structure to qualitatively explain our data.

## SESSION N21: MICROFLUIDIC PHYSICS II
**Wednesday Morning, 15 March 2006**
**318, Baltimore Convention Center at 8:00**
**Patrick Tabeling, Ecole Sup, presiding**

**8:00**

**N21 1 Microfluidics with Gel Emulsions** CRAIG PRIEST, ENKHTUUL SURENJAV, STEPHAN HERMINGHAUS, RALF SEEMANN, *Max-Planck-Institute for Dynamics and Self-Organization* Microfluidic processing is usually achieved using single phase liquids. Instead, we use monodisperse emulsions to compartment liquids within microchannel geometries. At low continuous phase volume fractions, droplets self-organize to form well-defined arrangements, analogous to foam. While it is well-known that confined geometries can induce rearrangement of foam compartments at the millimeter-scale, similar dynamics are also expected for gel emulsions. We have studied online generation, organization and manipulation of gel emulsions using a variety of microchannel geometries. ''Passive'' reorganization, based on fixed channel geometries, can be supplemented by ''active'' manipulation by incorporating a ferrofluid phase. A ferromagnetic phase facilitates reorganization of liquid compartments on demand using an electromagnetic trigger. Moreover, coalescence between adjacent compartments within a gel emulsion can be induced using electrical potential. Microfluidics using gel emulsions will be well-suited for combinatorial chemistry, DNA sequencing, drug screening and protein crystallizations.

**8:12**

**N21 2 In-situ Generation of Focal Conic Defects in Flow of Smectic-A Liquid Crystals in Microchannels*** SHAHAB SHOJAEI-ZADEH, SHELLEY ANNA,† *Carnegie Mellon University* The response of ordered phases of layered liquids such as smectic-A liquid crystals to flow is often dominated not by the direct coupling of flow to molecular degrees of freedom, but by the driven motion of defects in these systems. This is because flow generates instabilities in these systems that lead to the formation of defects. Most attention to date focuses on the global viscoelastic behavior and shear alignment of layered liquids, while little work has been done to understand defect motion and defect/flow interaction in these systems. Here we introduce a new approach, which enables simultaneous generation and observation of focal conic defects in pressure-driven flow of smectic-A liquid crystals. We observe that introducing a sudden change in the cross-sectional area of a microchannel via a small obstacle leads to the formation of a steady stream of defects. Generated defects move along the microchannel and interact with each other and with the flow itself. We measure the pressure drop and defect velocity and relate these to observed defect size and microchannel geometry. These results provide a novel way of probing nonlinear behavior of layered fluids under flow.

*This research is supported by NSF Grant CTS-0527909.
†Department of Mechanical Engineering.

**8:24**

**N21 3 Folding and swirling of viscous threads in microfluidics** THOMAS CUBAUD, THOMAS G. MASON, *UCLA, Chemistry and Biochemistry Dept.* We study miscible multiphase flows with large viscosity contrast in microchannels. We investigate the folding instability of a viscous thread surrounded by a less viscous liquid that flow into a diverging microchannel. In this situation, extensional viscous stresses cause the thread to bend and fold rather than dilating in order to minimize dissipation. We show that diffusive mixing at the boundary of the thread can significantly modify the folding flow morphologies. We relate the folding frequency to the characteristic shear rate. We also examine the hydrodynamic coupling between multiple threads and the threads' rupturing into arrays of viscous swirls, reminiscent of the Kelvin-Helmholtz instability.

**8:36**

**N21 4 Observations of Tipstreaming and Thread Formation in a Microfluidic Flow Focusing Device** SHELLEY ANNA, *Carnegie Mellon University* HANS MAYER, *Department of Mechanical Engineering, Carnegie Mellon University* We present a novel method of generating sub-micron scale droplets in a microfluidic device. In particular we utilize the interaction of fluid motion and surfactant transport during the tipstreaming mode of droplet formation, which is achieved using a flow focusing microfluidic design. Tipstreaming is a mode of drop breakup in which daughter droplets, usually orders of magnitude smaller than the parent drops, are ejected from the pointed tips of parent droplets or bubbles. An attractive characteristic of tipstreaming is that droplets produced are not limited by the device feature size. In this work we observe that tipstreaming occurs within a specific range of capillary number (Ca $\sim$ 0.1 to 1, consistent with literature values for tipstreaming), flow rate ratio, and surfactant concentration, and that tipstreaming is preceded by the formation of thin threads that follow the pinchoff of larger droplets. We measure the thread diameter and length as a function of dimensionless parameters and discuss our results with respect to surfactant diffusion and kinetic timescales relative to flow timescales.

**8:48**

**N21 5 Drops and Jets in two Phase Coaxial Flows** ANDREW UTADA, ALBERTO FERNANDEZ-NIEVES, DAVID WEITZ, *Harvard University* We discuss the transition from dripping to jetting from a nozzle in a coaxially flowing fluid. The fact that the outer fluid is viscous and moving affects the transition from dripping to jetting as well jet shape and drop formation mechanism. We relate the physics of drop formation to a recently reported microcapillary device (1,2) that generates monodisperse double emulsions. (1) A. S. Utada, E. Lorenceau, D. R. Link, P. Kaplan, H. A. Stone, D. A. Weitz, Science 308, 537 (2005) (2) E. Lorenceau, A. S. Utada, D. R. Link, G. Cristobal, M. Joanicot, D. A. Weitz, Langmuir in press, (2005).

**9:00**

**N21 6 Geometrically controlled jet-like instabilities in microfluidic two-phase flows** KATHERINE HUMPHRY, *Department of Physics, Harvard University, Cambridge MA 02138, USA* ARMAND AJDARI, *Laboratoire de Physico-Chimie Theorique, ESPCI, Paris, F-75005, France* HOWARD STONE, ALBERTO FERNANDEZ-NIEVES, *Division of Engineering and Applied Sciences, Harvard University, Cambridge MA 02138, USA* DAVID WEITZ, *Department of Physics and Division of Engineering and Applied Sciences, Harvard University, Cambridge MA 02138, USA* We demonstrate effects of confinement in microfluidic devices with a two phase co-flowing system. When the flow rate of the inner fluid is small compared to the flow rate of the outer fluid, and the resulting width of the inner fluid is smaller than the height of the channel, the inner fluid breaks into droplets, as expected for a three-dimensional system. On the other hand, when the width of the second phase becomes comparable to the height of the microfluidic device, Rayleigh capillary instabilities are suppressed, and the inner fluid forms a jet that does not break, as might be expected for a purely two-dimensional system. We show that by changing the dimensions of the microfluidic channel we can transition from a stable co-flow to drop break-up. The experimental results are compared with of model of this two-phase flow.

**9:12**

**N21 7 Playing with Microfluidic Droplets and Actuators** PATRICK TABELING, *ESPCI-CNRS* VALESSA BARBIER, *Univ Paris XIII* HERVÉ WILLAIME, *ESPCI-CNRS* MMN TEAM, In the lab-on a chips of the future, flows will be handled at the microscale through mazes of microchannels using actuators. Here we concentrate on PDMS based microfluidic systems and we use actuators to introduce localized perturbations on a chip, close to where droplets are formed, i.e. near the intersection of a main and a side channel along which oil and water flows are driven. We observe Arnold tongues and devil staircases leading to the formation of regular or quasiperiodic-like droplets. These behaviors are well accounted for by modelling the system as a non linear oscillator driven by an external forcing. The characteristics of the regimes that are observed depend on the flow-rate conditions. In some range of flow-rates, we show that the droplet sizes can be varied by one order of magnitude by changing the actuation frequency, without modifying the flow-rates.These findings are used to understand the complex behavior of droplet emittors placed in parallel.

**9:24**

**N21 8 Droplet Traffic Control at a simple T junction** PASCAL PANIZZA, WILFRIED ENGL, ANNIE COLIN, *LOF/CNRS* ARMAND AJDARI, *ESPCI* A basic yet essential element of every traffic flow control is the effect of a junction where the flow is separated into several streams. How do pedestrians, vehicles or blood cells divide when they reach a junction? How does the outcome depend on their density? Similar fundamental questions hold for much simpler systems: in this paper, we have studied the behaviour of periodic trains of water droplets flowing in oil through a channel as they reach a simple, locally symmetric, T junction. Depending on their dilution, we observe that the droplets are either alternately partitioned between both outlets or sorted exclusively into the shortest one. We show that this surprising behaviour results from the hydrodynamic feed-back of drops in the two outlets on the selection process occurring at the junction. Our results offer a first guide for the design and modelling of droplet traffic in complex branched networks, a necessary step towards parallelized droplet-based ''lab-on-chip'' devices.

**9:36**

**N21 9 Manipulation and stretching of bacteria and liposomes by Microfluidics** EYAL ZUSSMAN, WAEL SALALHA, *Faculty of Mechanical Eng., Technion, Israel* Microfluidic technology can be useful in lab-on-a-chip applications of biological assays, environmental monitoring, detection of toxic materials, as well as for assembly of nano- and micro-scale objects into more complex systems. In this work we focused on the orientation of rod-shaped bacteria (Bacillus) by employing shear flow and a high rate elongation flow, and stretching of giant liposomes with diameter size of tens of microns, which can be used as a simplified model for cell behavior. This was achieved by flows of dilute rod-like bacteria and liposome suspensions within a micro-channel by means of a capillary-driven motion. Fluidic alignment situations were tested, firstly by Venturi-like flow which produces a sufficiently converging and diverging flow, and secondly by sink-like flow in a converging microchannel. In the first method we found that the converging part of the flow aligns rod-like bacteria, whereas the diverging part disaligns them, while in the second method the rod-like bacteria can perfectly align along the streamlines. In addition we used the same technology to test liposome deformation while they are flowing through a Venturi-like microchannel. The microfluidics devices were fabricated from poly(dimethylsiloxane) (PDMS) by soft lithographic techniques.

**9:48**

**N21 10 Continuous separation of serum from human whole blood within a microfluidic device** JOHN DAVIS, *Princeton University* DAVID INGLIS, *Princeton University* JAMES STURM, *Princeton University* ROBERT AUSTIN, *Princeton University* We were able to demonstrate separation of red and white blood cells from their native blood plasma, using a technique known as deterministic lateral displacement. The device takes advantage of asymmetric bifurcation of laminar flow around obstacles. This asymmetry creates a size dependent deterministic path through the device. All components of a given size follow equivalent migration paths, leading to high resolution. A subsequent version of the device will focus on the removal of platelets from whole blood. Samples will be extracted from the microfluidic device and analyzed by conventional flow cytometry.

**10:00**

**N21 11 Reversible Dialysis in a Microfluidic Formulator.** SEILA SELIMOVIC, JUNG-UK SHIM, SETH FRADEN, *Brandeis University* In order to facilitate the screening of conditions for protein crystallization, we have been using the Microfluidic Formulator chip (Stephen Quake, PNAS Vol. 101, 40). This PDMS device allows us to mix up to 40 different reagents and protein solutions. We use this combinatorial approach along with a ''drop-on-demand'' method whereby we employ on-chip positive displacement pumps to form aqueous droplets containing protein and separate them by plugs of oil. Subsequently, the aqueous drops containing protein are guided by surface tension forces into storage chambers. To control the chemical potential of these sub-nanoliter protein samples, we fabricate reservoirs underneath the storage compartments. A thin PDMS membrane that is permeable to water, but not to protein or salt, separates the reservoirs from the storage chambers. Water can permeate into or out of the stored samples until the chemical potentials of the reservoir and the protein solution are equal leading to protein crystallization in some chambers.

**10:12**

**N21 12 A noble microfluidic device for protein crystallizations.** JUNG-UK SHIM, SETH FRADEN, *Brandeis University* A high throughput, low volume microfluidic device has been constructed out of poly(dimethylsiloxane) elastomer. We have demonstrated that sub-nanoliter water-in-oil drops of protein solutions of different composition can be rapidly stored in individual wells, which allows screening of 1000 conditions while consuming a total of only 1 microgram protein on a 20 $cm^2$ chip. This reduction in protein needed for crystal screens allows high-throughput crystallization of mammalian proteins expressed in tissue culture. A significant advance over current microfluidic devices is that each pot is in contact with a reservoir through a dialysis membrane which only water and other low molecular weight organic solvents can pass, but not salt, polymer or amphiphile. This enables the concentration of all solutes in a solution to be reversibly, rapidly, and precisely varied in contrast to current microfluidic methods, which are irreversible. This microfluidic dialysis technology solves a major problem in protein crystallization, the decoupling of nucleation from growth. The device will also be useful for general studies of the phase behavior of protein solutions.

**10:24**

**N21 13 Shear induced particle migration in binary colloidal suspensions*** DENIS SEMWOGERERE, ERIC R. WEEKS, *Emory University* JEFFREY F. MORRIS, *City College of New York* We present experimental investigations of the spatial and temporal evolution of particle migration in pressure driven flows of Brownian particle suspensions. Binary suspensions of 1 $\mu$m- and 3 $\mu$m-diameter colloidal particles at a variety of concentration ratios and volume fractions are pumped through a 50 $\mu$m x 500 $\mu$m rectangular-cross-section capillary tube. Shear rate gradients caused by the resulting parabolic velocity profile drive particles away from the walls towards the center of the channel where the shear rate is lowest. Size segregation is observed. We measure the development of the size segregation by tracking the evolution of the particle concentration down the center of the tube of the small and large sized particles. The flows are directly imaged using high-speed confocal microscopy (up to 300 images/second).

*Supported by NSF (DMR-0239109).

**10:36**
**N21 14 Using permeable microcapsules to deliver nanoparticles on substrates** ROLF VERBERG, ALEXANDER ALEXEEV, ANNA BALAZS, *University of Pittsburgh* We present a novel algorithm to simulate nanoparticles in the presence of a substrate, microcapsules and an externally driven flow. Here, the microcapsules consist of an elastic shell that encloses a fluid with either a dissolved chemical component or a suspension of nanoparticles that are small enough to be treated as so-called tracer particles (mutually non-interacting particles without excluded volume). The model couples a lattice-Boltzmann model for the fluid flow, a lattice-spring model for the elastic shell, and a Brownian dynamics model to simulate tracer trajectories. We then apply the model to simulate the release of nanoparticles from a microcapsule as it rolls along a substrate, as well as the subsequent particle adsorption on the wall. We study the effect of flow conditions, reaction kinetics, capsule elasticity, and capsules-substrate interaction on the rate of deposition and the size of the area of deposition at the substrate. The results provide guidelines for designing effective micro-scale delivery systems.

**SESSION N22: FOCUS SESSION: MAGNETIC VORTICES AND EXCHANGE BIASED THIN FILMS**
**Wednesday Morning, 15 March 2006**
**319, Baltimore Convention Center at 8:00**
**Jian Shen, Oak Ridge National Laboratory, presiding**

***Contributed Papers***

**8:00**
**N22 1 Field Dependence of Magnetic Vortex Dynamics** R.L. COMPTON, J.P. PARK, P.A. CROWELL, *University of Minnesota* We have used time-resolved Kerr microscopy (TRKM) to investigate the dynamical behavior of micron diameter disks patterned from sputtered Permalloy (Py) films. Different growth conditions yielded grain diameters of $\sim$ 35 nm and $\sim$ 80 nm while average roughness (Ra) remained less than 1 nm for 50 nm thick films. The magnetization of the disks relaxes into a vortex ground state, in which broadband spin dynamics include a low frequency vortex translational mode (vortex mode) that is expected to be nearly independent of field, based on simulations and analytical theory. We measured the field dependence of the vortex dynamics of individual disks using 5 Oe field steps from 0 Oe through the vortex annihilation field ($H_a$). For a 1 $\mu$m diameter disk the vortex mode has a mean frequency of $\sim$ 300 MHz, but the frequency fluctuates throughout the entire field range ($H_a \sim$ 350 Oe) with a magnitude $\Delta f \sim$ 200 MHz and a characteristic period $\sim$ 30 Oe. The fluctuations are not symmetric about zero field and look different in detail for different disks, but are highly repeatable for the same disk. We have also observed non-linear effects including the presence of up to 3 higher harmonics of the vortex mode, with a higher harmonic occasionally dominating the spectrum. A consistent interpretation is that the vortex core samples a distribution of pinning potentials, some of which are anharmonic, as it traverses the disk under the influence of the static applied field. Supported by NSF DMR 04-06029.

**8:12**
**N22 2 Fractional vortices and composite domain walls in flat nanomagnets*** OLEG TCHERNYSHYOV, GIA-WEI CHERN, *Johns Hopkins University* We provide a simple explanation of complex magnetic patterns observed in ferromagnetic nanostructures. To this end we identify elementary topological defects in the field of magnetization: ordinary vortices in the bulk and vortices with *fractional* winding numbers ( $\pm$ 1/2) confined to the edge [1]. Domain walls found in experiments and numerical simulations in strips and rings are composite objects containing two or more of the elementary defects. Allowed compositions of a domain wall in a strip or ring are constrained by simple selection rules of topological origin: (i) An edge contains an odd number of edge defects. (ii) The net winding number of all edge and bulk defects is zero. The walls observed most frequently in experiments and simulations contain a halfvortex and an antihalfvortex (transverse walls in thin and narrow strips) or two antihalfvortices and a vortex (vortex walls in thicker and wider strips). [1] O. Tchernyshyov and G.-W. Chern, Phys. Rev. Lett. **95,** 197204 (2005).

*Supported by the NSF Grant No. DMR05-20491.

**8:24**
**N22 3 Magnetic domains in ferromagnetic particles with perpendicular anisotropy** STAVROS KOMINEAS, CHRISTOFOROS MOUTAFIS, TONY BLAND, *University of Cambridge* We derive a Derrick-like virial theorem for static states in a disc-shaped ferromagnetic particle with an axially symmetric magnetic configuration. This is applied to elementary magnetic states such as a single domain and a vortex. We calculate the vortex state in a disc-shaped particle with no anisotropy and study the very thin and very thick limits. In the very thin limit the virial relation effectively gives the vortex core radius. We also consider a particle with significant perpendicular anisotropy and show that a vortex is a static state for sufficiently thin particles. For thicker particles the vortex core expands to become comparable to the particle lateral size while the magnetization at the periphery of the particle tilts out of plane opposite to the vortex core region. In sufficiently thick particles, the magnetic state takes the form of a magnetic ''bubble'' (well-known in films) viewed here as a bidomain state. The signature of a bubble is its magnetostatic field which consists of two concentric regions of opposite sign above the particle top surface. Higher order states of multiple concentric domains of opposite magnetization are found in larger particles. We finally study the effect of an external field on magnetic bubble states.

**8:36**
**N22 4 Composite domain walls in flat nanomagnets: the dipolar limit*** GIA-WEI CHERN, HYUN YOUK, KATHLEEN MERIT, OLEG TCHERNYSHYOV, *Johns Hopkins University* Topological defects play an important role in nanoscale ferromagnets. We have previously demonstrated that domain walls in thin strips and rings are composite objects made of bulk vortices (winding numbers $n = \pm 1$) and edge defects (fractional winding numbers $n = \pm 1/2$) and given analytical solutions in the exchange limit [1]. Experimentally accessible systems are in the opposite regime where the dipolar interaction dominate. In this limit the vortex solution remains unchanged, the antivortex and antihalfvortex are deformed but survive, whereas the halfvortex acquires a high magnetostatic energy and becomes unstable. Accordingly, domain walls in this limit consist of two antihalfvortices and a vortex between them. We present a model of the domain wall in the magnetostatic limit in which the location of the vortex

core is a variational parameter. As the width and thickness of a strip change, the global and local minima of the total magnetic energy yield the familiar transverse and vortex walls, as well as more exotic configurations such as the ''diagonal wall'' with a vortex hanging close to an edge. [1] O. Tchernyshyov and G.-W. Chern, Phys. Rev. Lett. **95**, 197204 (2005).

*Work supported by the NSF Grant No. DMR05-20491.

**8:48**

**N22 5 Single vortex dynamics in patterned ferromagnetic ellipses*** KRISTEN BUCHANAN, *Argonne National Laboratory* PIERRE ROY, *Angstrom Laboratory, Sweden* MARCOS GRIMSDITCH, FRANK FRADIN, KONSTANTIN GUSLIENKO, SAM BADER, VAL NOVOSAD, *Argonne National Laboratory, USA* ARGONNE NATIONAL LABORATORY, USA TEAM, ANGSTROM LABORATORY, SWEDEN TEAM, Measurements of low frequency dynamics of single magnetic vortices confined in elliptic ferromagnetic dots made of Permalloy with dimensions 2x1 $\mu m^2$ and 3x1.5 $\mu m^2$, 40-nm thick, have been performed using a microwave reflection method. Resonances were recorded in the sub-GHz range that can be attributed to the vortex translational mode where the vortex core follows an elliptic trajectory around its equilibrium position. The existence of single vortex states in the samples was confirmed by magnetic force microscopy. The frequency of this translational mode varies little under the influence of an in-plane static field H along the easy axis, however, it increases by more than a factor of two when H is applied along the hard axis. Micromagnetic simulations are used to explore the origin of the observed field dependence.

*This work was supported by the U.S. Department of Energy, Basic Energy Sciences, Material Sciences under Contract No. W-31-109-ENG-38, NSERC Canada (K. B.), and the Swedish Research Council and Swedish Foundation for Strategic Research (P. R.).

**9:00**

**N22 6 The relationship between the sign of exchange bias and the magnetization depth profile of Co/$FeF_2$** MICHAEL FITZSIMMONS, BRIAN KIRBY, *Los Alamos National Laboratory, Los Alamos NM 87545* SUJOY ROY, ZHI-PAN LI, IGOV V. ROSHCHIN, R. MORALES, S.K. SINHA, IVAN K. SCHULLER, *Department of Physics, University of California at San Diego, La Jolla CA 92093* We have used the unique spatial sensitivity of polarized neutron beams in reflection geometry to measure the depth dependence of magnetization across the interface between a ferromagnet (Co) and an antiferromagnet ($FeF_2$). Our Co/$FeF_2$ bilayer sample is one that exhibits either positive or negative exchange bias depending upon the magnitude of the cooling field. For positive exchange bias, pinned magnetization at the Co/$FeF_2$ interface is directed opposite to the cooling field, while in the $FeF_2$ bulk, the net pinned magnetization is parallel to the cooling field. For negative exchange bias, the net pinned magnetization near the Co/$FeF_2$ interface is parallel to the direction of the cooling field. We propose a model that explains the cooling field dependence of the sign of exchange bias. Work at LANL and UCSD was funded by the U.S. Department of Energy, BES-DMS, and by a University of California Campus-Laboratory Collaboration grant.

***Invited Papers***

**9:12**

**N22 7 Vortex State in Sub-100 nm Magnetic Nanodots.**

IGOR V. ROSHCHIN, *Physics Department, UCSD, La Jolla, CA*

Magnetism of nanostructured magnets, which size is comparable to or smaller than ferromagnetic domain size, offers a great potential for new physics. Detailed knowledge of magnetization reversal and possible magnetic configurations in magnetic nanostructures is essential for high-density magnetic memory. Many theoretical and experimental studies are focused on a magnetic vortex which in addition to a circular in-plane configuration of spins has a core, - the region with out-of-plane magnetization. We present a quantitative study of the magnetic vortex state and the vortex core in sub-100 nm magnetic dots. Arrays of single-layer and bilayer nanodots covering over 1 $cm^2$ are fabricated using self-assembled nanopores in anodized alumina. This method allows good control over the dot size and periodicity. Magnetization measurements performed using SQUID, VSM, and MOKE indicate a transition from a vortex to a single domain state for the Fe dots. This transition is studied as a function of the magnetic field and dots size. Micromagnetic and Monte Carlo simulations confirm the experimental observations. Thermal activation and exchange bias strongly affect the vortex nucleation field and have a much weaker effect on the vortex annihilation field. Direct imaging of magnetic moments in sub-100 nm dots is extremely difficult and has not been reported yet. Polarized grazing incidence small angle neutron scattering measurements allow dot imaging in reciprocal space. Quantitative analysis of such measurements performed on 65 nm Fe dots yields the vortex core size of $\sim$ 15 nm, in good agreement with the 14 nm obtained from the simulations. This work is done in collaboration with Chang-Peng Li, Zhi-Pan Li, S. Roy, S. K. Sinha, (UCSD), Xavier Batlle (U. Barcelona), R. K. Dumas, Kai Liu, (UC Davis), S. Park, R. Pynn, M. R. Fitzsimmons (LANL), J. Mejia Lopez (Pontificia U. Catolica de Chile), D. Altbir, (U. de Santiago de Chile), A. H. Romero (Cinvestav-Unidad Queretaro), and Ivan K. Schuller (UCSD) and supported by AFOSR, US DOE, NSF, UC-CLE, Spanish MECD, Catalan DURSI, FONDECYT, Millennium Initiative, and Conacyt Mexico.

*Contributed Papers*

**9:48**

**N22 8 Using multiple antiferromagnet/ferromagnet interfaces as a probe of grain size dependent exchange bias in polycrystalline Co/$Fe_{50}Mn_{50}$*** B. BOLON, M.A. HAUGEN, A. ABINFUENTES, J. DENEEN, C.B. CARTER, C. LEIGHTON, *Dept. of Chemical Engineering and Materials Science, University of Minnesota, Minneapolis, MN 55455* We have used ferromagnet/antiferromagnet/ferromagnet trilayers and ferromagnet/antiferromagnet multilayers to probe the grain size dependence of exchange bias in polycrystalline Co/FeMn. X-ray diffraction and transmission electron microscopy characterization show that the FeMn grain size increases with increasing FeMn thickness in the Co (30 Å) / FeMn system. Hence, in Co (30 Å) / FeMn / Co (30 Å) trilayers the two Co layers ''sample'' different FeMn grain sizes at the two antiferromagnet/ferromagnet interfaces. For FeMn thicknesses above $\sim$ 100 Å, where simple bilayers have a thickness independent exchange bias, we are therefore able to deduce the influence of grain size on the exchange bias and coercivity (and their temperature dependence) by measuring trilayer and multilayer samples with varying FeMn thickness. Increasing the average grain size results in a large decrease in exchange bias energy. We interpret the results as being due to a decrease in uncompensated spin density with increasing grain size, further evidence for the importance of defect generated uncompensated spins.

*Work supported by NSF MRSEC.

**10:00**

**N22 9 Interplay between reversal asymmetry, training, and anisotropy, in epitaxial NiMn/Ni exchange biased bilayers** M.S. LUND, C. LEIGHTON, *University of Minnesota* We have employed electron and x-ray diffraction, x-ray reflectivity, conventional magnetometry, and polarized neutron reflectivity to probe epitaxial NiMn/Ni bilayers. Binary alloys such as NiMn often require an annealing procedure to induce AF ordering which leads to interdiffusion at the AF/ F interface and a subsequent, and poorly understood, reduction in exchange bias. Our previous work with neutron reflectivity revealed a 35 Å interdiffused region that contains competing AF and F interactions resulting in a very unusual temperature dependant magnetic interface location (M.S. Lund, M.R. Fitzsimmons, S. Park, and C. Leighton, APL 2004). In this work we find that at low temperatures there is a rapid divergence of the exchange bias field, coincident with the onset of strong training, an obvious reversal asymmetry, and the appearance of higher order induced anisotropies. We show in a simple way that the rapid increase in bias field, strong training, and reversal asymmetry are all consequences of the induced anisotropies. In addition, we are able to demonstrate in a single sample that uniaxial anisotropy favors low training, while biaxial anisotropy results in large training, confirming a recent theoretical prediction (A. Hoffmann, PRL 2004). Research was supported by NSF MRSEC.

**10:12**

**N22 10 Effect of Hard Layer Demagnetization on the Magnetization Reversal of Epitaxial Fe/SmCo Spring Magnets*** KAI LIU, J.E. DAVIES, *UC - Davis* E.E. FULLERTON, *Hitachi Global Storage Tech* J.S. JIANG, S.D. BADER, *Argonne National Lab* In epitaxial Fe/SmCo, a classical spring magnet, irreversible magnetization reversal is observed once the SmCo hard layer starts switching [1,2]. To distinguish the soft and hard layer reversibility separately, we studied the effect of partial SmCo layer demagnetization on the reversal behavior of the entire bilayer using the first and second order reversal curve methods (FORC and SORC, respectively). The FORC distribution [2,3] shows two distinct features during the hard layer reversal: a negative/positive pair of features and a single positive peak. The negative/positive pair is from the soft Fe layer reversal and is a manifestation of the interlayer exchange coupling. The single positive peak occurs at larger applied fields and corresponds to the reversal of the hard SmCo layer. A SORC measurements were done at several reversal fields to determine the reversibility along different FORCs. We observe that the Fe layer remains mostly reversible. The partially demagnetized SmCo layer is the main source of irreversibility, particularly when the applied field approaches the hard layer nucleation/saturation field. [1] Fullerton, PRB 58, 12193 (1998). [2] Davies, et al, APL 86, 262503 (2005). [3] Davies, et al, PRB 70, 224434 (2004); PRB 72, 134419 (2005).

*Work is supported by ACS-PRF, Alfred P. Sloan Foundation and DOE (BES-MS contract #W-31-109-ENG-38).

**10:24**

**N22 11 Electrically controlled exchange bias for spintronic applications*** XI HE, SRINIVAS POLISETTY, CHRISTIAN BINEK, *University of Nebraska-Lincoln* Electrically controlled exchange bias (EB) is proposed for novel spintronic applications [1]. Basic effects of electrically controlled EB and its magnetoelectric (ME) switching are studied in a $Cr_2O_3(111)/(Co/Pt)_3$ heterostructure. Exchange coupling between the ME antiferromagnet $Cr_2O_3$ and a ferromagnetic CoPt multilayer exhibits perpendicular EB. The latter is controlled by applied axial electric fields inducing excess magnetization at the interface. The enhancement of this hitherto weak tuning effect is explored when replacing ME bulk pinning systems by epitaxal thin films. Recently, the sign of the EB field has been tuned via field cooling the system in either parallel or antiparallel axial magnetic and electric fields [2]. Here, the crossover from bulk to thin film ME pinning systems is studied and spintronic applications are suggested based on the electrically controlled EB. Pure voltage control of magnetic configurations of tunneling magneto resistance spin valves is proposed as an alternative to current−induced magnetization switching. In addition we suggest an XOR operation realized in a ME ally pinned giant magneto resistance structure. [1] Ch. Binek, B. Doudin, J. Phys. Condens. Matter **17**, L39 (2005). [2] P. Borisovetal, Phys. Rev. Lett. **94**, 117203 (2005).

*Work supported through NSF−MRSEC.

**10:36**

**N22 12 Exchange bias training effect in coupled all ferromagnetic bilayer structures*** SRINIVAS POLISETTY, XI HE, CHRISTIAN BINEK, *University of Nebraska-Lincoln* ANDREAS BERGER, *Hitachi Global Storage Technologies* We study exchange coupled bilayers of soft and hard ferromagnetic (FM) thin films by means of Alternating Gradient Force Magnetometry. A CoCr thin film realizes the magnetically soft layer (SL) which is exchange coupled via a Ru-interlayer with a hard CoPt-CrB pinning layer (HL). This new class of all FM bilayers shows remarkable analogies to conventional antiferromagnetic (AF)/FM exchange bias (EB) heterostructures. Not only do these all FM bilayers exhibit a tunable EB effect, they also show a distinct training behavior upon cycling the SL through consecutive hysteresis loops. Training resembles the cycle dependent evolution of the bias field and is to a large extend analogous to the gradual

degradation of the EB field observed upon cycling the FM top layer of a AF/FM EB heterostructure through consecutive hysteresis loops. However, in contrast to these conventional EB systems, our all FM bilayer structures allow the observation of training induced changes in the bias-setting HL by means of simple magnetometry. Our experiments show unambiguously that the training effect is driven by deviations from equilibrium in the pinning layer. A comparison of the experimental data with predictions from a theory based upon triggered relaxation phenomena shows excellent agreement.

*Work supported through NSF-MRSEC.

**10:48**

**N22 13 Alignment-Sensitive Reversal Mechanisms of Epitaxial-$FeF_2$/Polycrystalline-Ni Exchange Biased Thin Films*** JUSTIN OLAMIT, KAI LIU, *UC Davis Physics Department* ZHI-PAN LI, IVAN K. SCHULLER, *UC San Diego Physics Department* Magnetization reversal mechanisms of epitaxial-$FeF_2$/polycrystalline-Ni exchange biased thin films were investigated with vector magnetometry and a First Order Reversal Curve (FORC) technique [1]. The FORCs were measured **without** remounting the sample after the vector magnetometry measurements, ensuring consistency between the two methods. Samples were exchange biased by field cooling along the $FeF_2$ spin axis. When the applied field is aligned with the spin axis, the transverse hysteresis loop is flat and FORC analysis shows that the magnetization switching is highly irreversible ( $\sim$ 80%), indicating that domain nucleation and motion is the reversal mechanism. With a misalignment of 5[r], the transverse hysteresis loop shows that the reversal is predominantly by rotation [2] and FORC analysis shows that the majority of the magnetic switching is by a reversible mechanism (only $\sim$ 40% irreversible). These results demonstrate that the magnetization reversal mechanisms are **itextremely sensitive** to the alignment of the applied field with the antiferromagnet spin axis and the exchange bias direction [3]. 1. J. E. Davies, et al., Phys. Rev. B **70**, 224434 (2004); Phys. Rev. B **72**, 134419 (2005). 2. J. Olamit, et al., Phys. Rev. B **72**, 012408 (2005). 3. A. Tillmans et al, cond-mat/0509419.

*Work supported by ACS-PRF, Alfred P. Sloan Foundation, and DOE.



**SESSION N23: FOCUS SESSION: MAG.THY III: OXIDES AND PHASE TRANSITIONS**
**Wednesday Morning, 15 March 2006**
**320, Baltimore Convention Center at 8:00**
**Bruce Harmon, Ames Laboratory, presiding**

***Contributed Papers***

**8:00**

**N23 1 Antiferromagnetic Heisenberg Spin Layers coupled with Dipolar Interaction – a Monte Carlo study of $Rb_2MnF_4$*** CHENGGANG ZHOU, THOMAS C. SCHULTHESS, *Computer Science and Mathematics Division, Oak Ridge National Laboratory, P.O. Box 2008, Oak Ridge, TN 37831-6164* DAVID P. LANDAU, *Center for Simulational Physics, University of Georgia, Athens GA, 30602* $Rb_2MnF_4$ is a quasi-2D antiferromagnetic (AF) system, in which $Mn^{2+}$ ions carrying spin-5/2 occupy square lattices perpendicular to the c-axis of the tetragonal unit cell. These spins interact via mostly nearest neighbor isotropic AF exchanges, while the dipolar interaction contributes to the effective anisotropy that stabilizes the AF phase at low temperatures. In a magnetic field parallel to the c-axis, the AF phase is terminated along a spin-flop line, and a transverse (XY) phase appears. We perform large scale extensive Monte Carlo simulations to map out the phase diagram and investigate the critical behavior along the phase boundaries. A novel reweighting technique is used to efficiently handle the dipolar interaction. Our results suggest that both the AF phase and the XY phase experience continuous transitions across the spin-flop line, which is consistent with a bicritical point at zero temperature. We also found that the effect of the weak inter-planar coupling is not completely negligible for the spin-flop transition and the properties of the XY phase.

*This research is supported by the Department of Energy through the Computational Materials Science Network of the Division for Materials Science and Engineering as well as by NSF DMR-034187.

**8:12**

**N23 2 RVB liquid phase of a quantum dimer model with competing kinetic terms** FRANCOIS VERNAY, *University of Waterloo, Ontario, Canada* ARNAUD RALKO, *ITP - Ecole polytechnique Federale de Lausanne, Switzerland* FEDERICO BECCA, *SISSA, Trieste, Italy* FREDERIC MILA, *ITP - Ecole polytechnique Federale de Lausanne, Switzerland* Starting from a spin-orbital model adapted to the case of $LiNiO_2$, we derived an effective quantum dimer model including 6-dimer loops. We argue that the relevant terms of this model are of kinetic type. Using numerical techniques like exact diagonalizations and Green's function Monte-Carlo we show that a competition between two kinetic terms can lead to a resonating valence bond state for a finite range of the parameters.

**8:24**

**N23 3 Dynamical correlations of the Quantum Dimer Model on the triangular lattice** ARNAUD RALKO, *ITP, Ecole Polytechnique Fédérale de Lausanne, Switzerland* MICHEL FERRERO, FEDERICO BECCA, *INFM-Democritos, SISSA, Trieste, Italy* DMITRI IVANOV, FRÉDÉRIC MILA, *ITP, Ecole Polytechnique Fédérale de Lausanne, Switzerland* Using Green's function Monte Carlo simulations, we have studied the zero-temperature properties of the quantum dimer model (QDM) on the triangular lattice [1] on clusters with up to 588 sites. A detailed comparison of the static properties in different topological sectors as a function of the cluster size and for different cluster shapes has allowed us to identify different phases, and to to show explicitly the presence of topological degeneracy in a phase close to the Rokhsar-Kivelson point, in agreement with an earlier suggestion [2]. We have also extended the Green's function Monte Carlo algorithm to calculate dynamical correlation functions. Preliminary results on the dimer-dimer correlations confirm the extension of the RVB phase and bring new insight on the nature of the transition to the $\sqrt{12} \times \sqrt{12}$ phase and on the type of long-range order realized in that phase. [1] A. Ralko, M. Ferrero, F. Becca, D. Ivanov and F. Mila, Phys. Rev. B, **71**, 224109 (2005). [2] R. Moessner and S.L. Sondhi, Phys. Rev. Lett, **86**, 1881 (2001).

*Invited Papers*

**8:36**
**N23 4 Towards material-specific simulations of high-temperature superconducting cuprates.***
THOMAS SCHULTHESS, *Oak Ridge National Laboratory*

Simulations of high-temperature superconducting (HTSC) cuprates have typically fallen into two categories: (1) studies of generic models such as the two-dimensional (2D) Hubbard model, that are believed to capture the essential physics necessary to describe the superconducting state, and, (2) first principles electronic structure calculations that are based on the local density approximation (LDA) to density functional theory (DFT) and lead to materials specific models. With advent of massibely parallel vector supercomputers, such as the Cray X1E at ORNL, and cluster algorithms such as the Dynamical Cluster Approximation (DCA), it is now possible to systematically solve the 2D Hubbard model with Quantum Monte Carol (QMC) simulations and to establish that the model indeed describes *d*-wave superconductivity [1]. Furthermore, studies of a multi-band model with input parameters generated from LDA calculations demonstrate that the existence of a superconducting transition is very sensitive to the underlying band structure [2]. Application of the LDA to transition metal oxides is, however, hampered by spurious self-interactions that particularly affects localized orbitals. Here we apply the self-interaction corrected local spin-density method (SIC-LSD) to describe the electronic structure of the cuprates. It was recently applied with success to generate input parameters for simple models of Mn doped III-V semiconductors [3] and is known to properly describe the antiferromagnetic insulating ground state of the parent compounds of the HTSC cuprates. We will discus the models for HTSC cuprates derived from the SIC-LSD study and how the differences to the well-known LDA results impact the QMC-DCA simulations of the magnetic and superconducting properties. [1] T. A. Maier, M. Jarrell, T. C. Schulthess, P. R. C. Kent, and J. B. White, Phys. Rev. Lett. 95, 237001 (2005). [2] P. Kent, A. Macridin, M. Jarrell, T. Schulthess, O. Andersen, T. Dasgupta, and O. Jepsen, Bulletin of the American Physical Sosciety 50, 1057 (2005). [3] T. C. Schulthess, W. Temmerman, Z. Szotek, W. H. Butler, and G. M. Stocks, Nature Materials 4, 838 (2005).

*Work enabled by computational resources of the Center of Computational Sciences at Oak Ridge National Laboratory and supported by the Division of Materials Science and Engineering, U. S. Department of Energy.

*Contributed Papers*

**9:12**
**N23 5 Mechanism of Noncollinearity and Magnetoelectric Coupling in Incommensurate Multiferroics** IVAN SERGIENKO, ELBIO DAGOTTO, *Oak Ridge National Laboratory* Using extensive Monte-Carlo simulations of a modified orbitally degenerate double-exchange model applied to the multiferroic perovskites $R\mathrm{MnO}_3$ ($R$ = Gd, Tb, Dy), we show that the spiral magnetic phase results from the interplay between the double exchange coupling, superexchange, Jahn-Teller and Dzyaloshinskii-Moriya (DM) interactions. The DM interaction also induces a small ferroelectric moment and provides the mechanism of the strong coupling between the unusual magnetism and ferroelectricity. We also discuss the magnetoelectric effects in the applied magnetic fields.

**9:24**
**N23 6 Numerical Study of Magnetism in the Periodic Anderson Model*** YONG-QIANG WANG, HAI-QING LIN, *Institute of Theoretical Physics and Department of Physics, The Chinese University of Hong Kong, Hong Kong SAR, China* JAMES GUBERNATIS, *Los Alamos National Laboratory, USA* The periodic Anderson model is believed as a candidate of the minimal lattice models for itinerant ferromagnetism. Several numerical methods, including exactly diagonalization, constrained-path Monte Carlo method and mean field method, are employed to investigate the magnetic properties of the model in one dimension and two dimensions. By changing the band-filling, chemical potential of the impurity band and the hybridyzation between conduction band and impurity band, we found that in some parameter regions, different magnetic ordering exist. Some of results confirm the previous works and some are new.

*This work is partially supported by the Earmarked Grant for Research, HKSAR.

**9:36**
**N23 7 Bond-diluted Heisenberg spin systems on coupled ladders** DAOXIN YAO, ANDERS W. SANDVIK, A.H. CASTRO NETO, DAVID K. CAMPBELL, *Department of Physics, Boston University, MA 02215* We study spin-1/2 Heisenberg spin systems with bond dilution on coupled ladders or striped phases. The diluted bond configurations can be static or dynamic. The dynamic case with motion of the bonds is described by pseudo-spins and modeled by anisotropic Heisenberg spin chains in an external field. The systems are studied using the stochastic series expansion quantum Monte Carlo method. We find the quantum critical point for real spins from the ordered phase to the disordered phase is sensitive to the bond configuration. A study of the ground state energy shows strong differences for different bond configurations, which may be related to phase separation. Under certain conditions, real spin systems with bond-dilution can be described by a coupling-weakened fully coupled spin systems. For the pseudo-spins, an effective field induced by the real spins is observed.

**9:48**
**N23 8 Thin Ising films with both competing surface fields and a magnetic field gradient: A Monte Carlo study*** LIJUN PANG, D.P. LANDAU, *Center for Simulational Physics, University of Georgia, Athens, GA30602* K. BINDER, *Institute of Physics, University of Mainz, Germany* Extensive Monte Carlo simulations are used to study the interesting effects resulting from a linearly varying magnetic field on a thin Ising film (equivalent to applying gravity to the corresponding lattice-gas model). Besides

competing surface fields acting on two LxL free surfaces a distance D apart from each other, we also apply a magnetic field g that varies linearly between the surfaces and which competes with the surface fields. To determine the phase diagram, we look for bulk two-phase conexistence at different values of g and temperature T. In situations with only competing surface fields applied, the interface unbinding transition[1] happens at temperature $T_c(D)$. The addition of the g field produces a phase diagram in which, as g increases, the temperature bounding bulk two-phase coexistence first goes up from $T_c(D)$, and then decreases. For small g, we find a second order transition, whereas for large g, the transition appears to be first order. We will compare our simulation results with theoretical predictions[2].

*Research supported by NSF.

[1]K. Binder, D.P. Landau, A.M. Ferrenberg, Phys. Rev. E **51**, 2824 (1995).
[2]J. Rogiers, J.O. Indekeu, Europhys. Lett. **24**, 21 (1993).

**10:00**
**N23 9 Electronic structure and excitation spectra of transition metal monoxides investigated via orbital-dependent functionals*** J. ASHLEY ALFORD, OSCAR D. RESTREPO, ADOLFO G. EGUILUZ, *Oak Ridge National Laboratory/Univ. of Tennessee* THOMAS C. SCHULTHESS, *Oak Ridge National Laboratory* We are investigating the electronic structure of strongly correlated 3d transition metal monoxides with two orbital dependent functionals, the self-interaction corrected local spin-density method (SIC-LSD) as well as the LDA+U method. Both functionals are known to reproduce the antiferromagnetic insulating ground state of, for example, CoO and NiO. We perform a detailed comparison of magnetic moments, exchange, and electronic structure calculated with the two methods. In addition, we study the interplay between the electronic structure and the electron-hole excitations in both the insulating and the metallic phases. Our results are compared with available experimental data.

*Work supported by the Division of Materials Science and Engineering and the Computational Materials Science Network of the US Dept. of Energy.

**10:12**
**N23 10 Ab initio calculations on the frustrated magnet $ZnCr_2O_4$** KEVIN T. CHAN, JAY D. SAU, MARVIN L. COHEN, *UC Berkeley and Lawrence Berkeley National Laboratory* PEIHONG ZHANG, *University at Buffalo* The complex oxide $ZnCr_2O_4$ is a good realization of the Heisenberg antiferromagnet on a pyrochlore lattice and is a strongly frustrated magnetic system. Recent experiments have shown that $ZnCr_2O_4$ undergoes a lattice distortion and a transition from paramagnetic to antiferromagnetic order at $T_c = 12.5K$. Infrared spectroscopy has shown a large splitting of a phonon mode involving magnetic ions. We perform ab initio total energy calculations of the exchange coupling constant and phonon modes using the plane-wave pseudopotential formalism with the LSDA+U method, and we compare the results to experiment. This work was supported by National Science Foundation Grant No. DMR04-39768 and by the Director, Office of Science, Office of Basic Energy Sciences, Division of Materials Sciences and Engineering, U.S. Department of Energy under Contract No. DE-AC03-76SF00098. Computational resources have been provided by NPACI and NERSC.

**10:24**
**N23 11 Anisotropic magnetic phases** JULIO F. FERNANDEZ, *ICMA, CSIC, Zaragoza, Spain* JUAN J. ALONSO, *Universidad de Malaga, Spain* We study how magnetic phases vary with uniaxial and fourfold anisotropy constants, C and D. We do this for classical magnetic dipoles on cubic lattices with dipolar and nearest neighbor exchange interactions. By mean field and by Monte Carlo calculations, results are obtained for bulk and n-layer film systems under no applied external field. We pay special attention to the spin reorientation (SR) transition. We find (1) a reentrant SR transition for a narrow range of C/D values, and (2) that the ratio of the ordering temperature to the SR temperature varies with C/D but depends rather weakly on the exchange constant.

**10:36**
**N23 12 Alternative methods to characterize phase transitions in Ising systems*** EUGENIO E. VOGEL, BERNARDO FIERRO, FERNANDO BACHMANN, *Universidad de La Frontera, Temuco, Chile* The Binder cumulant (BC) is defined in terms of average values of second and fourth momenta of an order parameter q. Simulations for Ising systems show that the curves for BCs they all cross at the same temperature regardless of the size of the system. We present here two alternative and different methods to obtain the critical temperature after finding the time evolution of any order parameter q(t), after equilibration. First, we consider the time autocorrelation functions for the absolute value of a site order parameter, $|q|$, for different system sizes, showing that they also cross at the same temperature where BCs cross. Second, we show that the ''weight'' in bites of the compressed file containing vector q(t) maximizes at a temperature close to the critical temperature; a scaling analysis takes us back to the temperature of previous crossing. The main advantage of the new methods is its easy physical interpretation.

*Partly funded by Fondecyt and Millennium Scientific Iniciative (Chile).

**SESSION N24: STRUCTURE AND DYNAMICS IN POLYMER THIN FILMS**
**Wednesday Morning, 15 March 2006**
**321, Baltimore Convention Center at 8:00**
**Steve Granick, University of Illinois at Urbana Champaign, presiding**

**8:00**
**N24 1 Unique refractive index and thickness values for polymer films via ellipsometry** ALAN R. ESKER, UFUK KARABIYIK, MIN MAO, *Virginia Tech, Department of Chemistry (0212), Blacksburg, VA 24061* SUSHIL K. SATIJA, *Center for Neutron Research, National Institute of Standards and Technology, Gaithersburg, MD 20899* In this study, elliposometry using multiple ambient media at Brewster's angle is used to determine unique values of refractive index and film thickness for polymer thin films. Measurements were made for polymer thin films on HF etched silicon wafers against air and water. Results obtained for poly(t-butyl acrylate), polystyrene, and trimethylsilyl cellulose

confirm that the refractive indices agree well with the literature values and that the film thicknesses agree with values obtained from X-ray reflectivity. This technique provides a rapid unambiguous method for determining a film's thickness and refractive index for polymers.

**8:12**

**N24 2 Watching How Molecules Orient in a Surface Forces Apparatus, Using Confocal Raman Spectroscopy** SHAN JIANG, *UIUC, Materials Science and Engineering Department* MINSU KIM, *UIUC, Physics Department* SUNG CHUL BAE, STEVE GRANICK, *UIUC, Materials Science and Engineering Department* Much is known about surface forces, less about where they come from. This laboratory is engaged in direct vibrational spectroscopic measurements of how molecules orient in confined geometries. Regarding force measurements, PDMS (polydimethylsiloxane) was a model system for many years. In this study, we describe direct experiments using a novel version of confocal Raman spectroscopy. This experiment allows direct measurement of how the PDMS molecules orient under confinment as well as under subsequent shear. When the thickness of the fluid film is less than the unperturbed radius of gyration of the polymer, we obtain two novel findings: (a) linewidth analysis of peaks reveals that vibrational relaxation times are perturbed in this confined geometry; (b) orientation of the chain backbone is not everywhere the same within the molecularly-thin film; domains of various orientation are observed instead.

**8:24**

**N24 3 Polymer dynamics at local scales: origin of ripples formation** ROBERT SZOSZKIEWICZ, *School of Physics, Georgia Institute of Technology, Atlanta, GA 30332* TAKASHI OKADA, *School of Chemistry and Biochemistry, Georgia Institute of Technology, Atlanta, GA 30332* ENRICO GNECCO, *Institute of Physics, University of Basel, Switzerland* WILLIAM KING, *School of Mechanical Engineering, Georgia Institute of Technology, Atlanta, GA 30332* SETH MARDER, *School of Chemistry and Biochemistry, Georgia Institute of Technology, Atlanta, GA 30332* ELISA RIEDO, *School of Physics, Georgia Institute of Technology, Atlanta, GA 30332* A plethora of nanowear patterns in polymers has been obtained by heating the polymers and scanning their surfaces with an atomic force microscope (AFM) tip (1, 2). These morphologies represent the nanoscale realization of aeolian ripples in sandy deserts and are similar to patterns obtained during evolution of surfaces during ion sputtering (3). By means of locally heated AFM probes we studied ripples on various polymer films. While the theory of aeolian ripples formation is very complicated (3), we show that the key morphological features in our results can be explained in terms of the elastic and diffusive properties of the polymer. From measurements of the ripple spacing we study the local dynamics of polymers in the vicinity to the glass transition. (1) B. Gotsmann and U. Durig, Langmuir 20, 1495 (2004) (2) R. H. Schmidt, G. Haugstad and W. L. Gladfelter, Langmuir 15, 317 (1999) (3) T. Aste and U. Valbusa, New Journal of Physics 7, 122 (2005).

**8:36**

**N24 4 Probing surface relaxation of polystyrene films using gold nano-particles** ZAHRA FAKHRAAI, *Physics Department, University of Waterloo, Waterloo, ON, N2L 3G1 Canada* JAMES A FORREST, *Physics Department, University of Waterloo, Waterloo, ON, N2L 3G1 Canada* Polymer thin films are usually used to probe the confinement effects on the dynamics of glass former materials. Many studies show that the glass transition temperature of thin polymer films is decreased below bulk Tg for very thin films. There is evidence that this Tg reduction is due to the existence of a more mobile region near the surface of the film. However, it is very hard to directly measure the existence of this layer, let alone more quantitative aspects such as thickness or viscoelastic properties. In this work we probe the near surface behaviour of thin polystyrene films using a nanorheological technique. To do this, we uniformly distribute gold nanoparticles on the surface. A particle's motion on the surface is then driven by surface capillary waves. The motion of nanoparticles is detected by dynamic light scattering. Since the particles only interact with the surface region (determined independently using AFM), these experiments tell us about the viscoelastic properties of the near surface region.

**8:48**

**N24 5 Grazing-incidence x-ray scattering studies on surface melting in ultrathin polymer films*** TADANORI KOGA, Y. WANG, M. RAFAILOVICH, J. SOKOLOV, *Stony Brook University* A. TIKHONOV, D. SCHULTZ, M. LEE, *University of Chicago* M. TOLAN, *Dortmund University* The aim of this study is to investigate surface crystal structures formed in ultrathin (thickness below 100 nm) polymer films by using surface-sensitive x-ray scattering techniques. This study was motivated by our current experimental finding that showed a drastic suppression (the decrease of $\sim$ 50[r]C) in the surface melting temperature ($T_m$) of ultrathin polymer films, which was determined as the onset of surface softening by using the shear modulation force microscopy (SMFM) method[1]. In order to clarify the relationship between the melting behavior and surface crystal structures, we integrated a variety of grazing-angle x-ray scattering techniques including reflectivity, diffuse scattering, grazing-incidence diffraction, and grazing-incidence small-angle scattering. As a result, we found that diffuse scattering, which is sensitive to surface roughness, drastically changed at $T_m$ determined from SMFM, while the surface crystallinity decreased with increasing temperature, but remained up to the bulk melting temperature. A model to explain the mechanism of the surface melting will be discussed. [1] Wang, Y. et al. Macromolecules, **37**, 3319 (2004).

*This work was supported by the SRC-NY CAIST funding and by NSF (the Garcia MRSEC).

**9:00**

**N24 6 The Tg-Nanoconfinement Effect and the Relaxation of Residual Stresses in Spin-Coated Films of Polystyrene and Styrene-Containing Copolymers: Characterization by Intrinsic Fluorescence.** MANISH K. MUNDRA, CHRISTOPHER J. ELLISON, ROSS BEHLING, JOHN M. TORKELSON, *Northwestern University, Evanston, IL 60208* The glass transition temperatures (Tgs) of films of polystyrene (PS) and styrene (S)-methyl methacrylate (MMA) copolymers have been determined using intrinsic fluorescence from styrene units. The Tgs are measured by a break in the temperature dependence of fluorescence intensity measured upon cooling from the equilibrium liquid state. As the film thickness decreases below 50 nm, there is a substantial deviation in Tg from bulk Tg, with PS and high S-content copolymers exhibiting a reduction in Tg and high MMA-content copolymers exhibiting an increase in Tg. This is explained by a competition of free surface effects and the effects of attractive polymer-substrate interactions. As the intrinsic fluorescence is a combination of monomer and excimer fluorescence, it reflects the local conformational population. This is used to determine the conditions at which residual stresses induced by spin coating are relaxed away, leading to a steady-state conformational population

and fluorescence signal independent of annealing time. Films must be heated to temperatures well above Tg (Tg + 30 K) for several minutes to achieve constant fluorescence independent of further annealing. Annealing for short times close to Tg is insufficient to achieve an equilibrium conformational population.

**9:12**

**N24 7 Dynamics of very thin polymer films on supported surface** CHUNHUA LI, *State University of New York at Stony Brook* HYUNJUNG KIM, *Sogang University, Korea* JUN JIANG, CLIVE LI, TADANORI KOGA, *State University of New York at Stony Brook* LAURENCE LURIO, *Northern Illinois University* SUNIL SINHA, *University of California San Diego* JONATHAN SOKOLOV, MIRIAM RAFAILOVICH, *State University of New York at Stony Brook* STATE UNIVERSITY OF NEW YORK AT STONY BROOK TEAM, SOGANG UNIVERSITY, KOREA COLLABORATION, NORTHERN ILLINOIS UNIVERSITY COLLABORATION, UNIVERSITY OF CALIFORNIA SAN DIEGO COLLABORATION, In this work, we study the effect of solid substrate surface on the viscosity of polymer thin films. We found that the viscosity of polymer thin film increased about two orders of magnitude near the solid substrate. Measurements performed on split layer substrates indicated that this layer was responsible for trapping the subsequent layers, and propagating the effect of the surface interactions to the chains without direct contacts to the surface. If this layer was applied prior to the rest of the film, it in fact screened the surface interactions and even caused auto-dewetting of the other layers in the film. These results will be discussed in terms of the ''two fluid'' hypothesis. This surface interaction was also found to induce the ''melt fracture'' of the polymer thin film during the dewetting process where we see the cracks in the less viscous bottom layer.

**9:24**

**N24 8 The Distribution of Tgs in Thin and Ultrathin Methacrylate-Based Polymer Films: Percolation of Free Surface and Interface Effects over Tens and Hundreds of Nanometers.** RODNEY D. PRIESTLEY, MANISH K. MUNDRA, PERLA RITTIGSTEIN, LINDA J. BROADBELT, JOHN M. TORKELSON, *Northwestern University, Evanston, IL 60208* A multilayer/fluorescence method is used to measure the distribution of Tgs in poly(methyl methacrylate) (PMMA) films. The average Tg increases with decreasing total film thickness (h) below 90 nm. In bulk, bilayer films, the free surface layer exhibits a reduced Tg at a thickness of 30 nm or less. The Tg reduction at the free surface is a fraction of that in polystyrene (PS) films; a 14-nm-thick free surface layer exhibits a Tg reduction of $\sim$ 6 K in PMMA and $\sim$ 32 K in PS. The Tg increase observed in the substrate layer of a PMMA bilayer, bulk film exceeds the Tg reduction observed at the free surface and occurs over longer length scales. An amazing effect of confinement of the total multilayer film on the free surface layer Tg of PMMA has been observed. When h $<$ 250 nm, a 12-nm-thick free surface layer exhibits an increase in Tg with decreasing h, and the free surface layer Tg exceeds that of bulk Tg when h $<$ 90 nm. This is the first demonstration that a free surface layer can exhibit Tg $>$ bulk Tg and means that the perturbation of Tg dynamics at the substrate can percolate over hundreds of nanometers in PMMA films. These results will be contrasted with those of poly(isobutyl methacrylate) films which exhibit no average Tg-confinement effect.

**9:36**

**N24 9 Dynamics of Polymer Thin Film Mixtures** BRIAN M. BESANCON, *Department of Chemical Engineering, University of Texas at Austin* PETER F. GREEN, *Department of Materials Science and Engineering, University of Michigan* CHRISTOPHER L. SOLES, *NIST Polymers Division* We examined the influence of film thickness and composition on the glass transition temperature ($T_g$) and mean square atomic displacements (MSD) of thin film mixtures of deuterated polystyrene (dPS) and tetramethyl bisphenol-A polycarbonate (TMPC) on Si/$SiO_x$ substrates using incoherent elastic neutron scattering (ICNS). The onset of dissipative motions, such as those associated with the glass transition and sub-Tg relaxations, are manifested as ''kinks'' in the curve of elastic intensity (or MSD) versus temperature. From the relevant kinks, the $T_g$ was determined as a function of composition and of film thickness. The dependence of the $T_g$ on film thickness exhibited qualitatively similar trends, at a given composition, as determined by the ICNS and ellipsometry measurements. However, with increasing PS content, the values of $T_g$ measured by INS were consistently larger then those measured by ellipsometry. These results are examined in light of existing models on the thin film glass transition and component blend dynamics.

**9:48**

**N24 10 Dynamics of Block copolymer films*** HYUNJUNG KIM, *Dept. of Physics and Interdiscplinary Program of Integrated Biotechnology, Sogang University, Korea* HEEJU LEE, YOUNG JOO LEE, *Dept. of Physics, Sogang University, Korea* ZHANG JIANG, SUNIL SINHA, *Dept. of Physics, UC San Diego and LANSCE* XUESONG JIAO, *Northern Illinois University* ADRIAN RUEHM, *Max Planck Institute for Metal Research, Germany* S. G. J. MOCHRIE, *Yale Univ.* We have investigated the dynamics of thin block copolymer films of ploy(styrene)-b-poly(dimethylsiloxane) using X-ray Photon Correlation Spectroscopy (XPCS). The films were supported on Si substrates and measured at melt. The results are compared with the theory of overdamped thermal capillary waves on thin films. The lateral length scales examined were between 600 and 6000 nm. We selectively measured the dynamics from the surface and from the micelles by changing incident angles and found the different behaviors between them.

*This research was supported by International Cooperation Research Program of Ministry of Science & Technology of Korea, Interdisciplinary Program of Integrated Biotechnology of Sogang University and NSF (DMR -0209542),U.S.A.

**10:00**

**N24 11 Conformational Anisotropy and the Glass Transition in Polymer Thin Films** FOLUSHO OYEROKUN, *UCSB* ANNA CAVALLO, *Uni-Mainz* MARCUS MUELLER, *Uni-Gottingen* KENNETH SCHWEIZER, *UIUC* A segmental level theory of the ideal kinetic glass transition, or dynamic crossover, temperature ($T_c$) in confined polymer films has been developed. The theory is based on an anisotropic generalization of a coarse grained polymer mode coupling theory which utilizes conformational and thermodynamic information from anisotropic PRISM theory and computer simulations. Confinement is found to enhance the bulk compressibility and induce anisotropic segmental dynamics. For noncapped films (free standing or supported films on neutral substrates) the theory predicts suppression of $T_c$, with confinement. The underlying mechanism is reduction of the degree of coil interpenetration and intermolecular repulsive contacts due to segmental scale alignment and deformation. The predicted suppres-

sion of $T_c$ is nonuniversal and follows an inverse power law dependence on film thickness in reasonable agreement with experiments. For capped films simulations find a weak variation of the dimensionless compressibility with confinement suggesting little or no shift of $T_g$.

**10:12**
**N24 12 Radial Thickness Profiles of Spincoated Thickness Gradient Films** MONIKA MICHALEK, BERNIE NICKEL, JOHN DUTCHER, *University of Guelph* By dropping a polymer solution onto a spinning substrate at a position displaced from the axis of rotation, one can produce a film in which the thickness increases with increasing radial distance (thickness gradient film). Since each film contains a continuous range of thickness values, one can track subtle changes in the physical properties with film thickness by using a local probe of the film properties. We have used two such local probes, focused ellipsometry and atomic force microscopy, to measure the radial thickness profiles. We have also developed a simple, fluid flow model that describes the dependence of the polymer film thickness on radial distance from the axis of rotation. A detailed comparison between the measured and calculated radial thickness profiles will be discussed.

**10:24**
**N24 13 Internal Phase Separation Induces Dewetting in Multicomponent Polymer Films** HYUN-JOONG CHUNG, RUSSELL J. COMPOSTO, *MSE and LRSM, U. of Pennsylvania* KOHJI OHNO, TAKESHI FUKUDA, *ICR, Kyoto U.* Thin liquid films that dewet from their substrate are ubiquitous as demonstrated by the beading of paint on oily surface. Although most coatings contain more than one component, the dewetting mechanisms in multicomponent films are not understood. Using dPMMA:SAN (50:50) films (550 nm) with or without nanoparticles (NP), we demonstrate, for the first time, that the Laplace pressure induced by internal phase-separated structure is the driving force for roughening and rupture in polymer blend films. Three NP were investigated, namely $NP_A$, $NP_B$, and $NP_C$ which either partition into dPMMA or weakly and strongly segregate to the dPMMA/SAN interface, respectively. $NP_B$ are more effective than $NP_A$ at stabilizing the film, whereas $NP_C$ are able to prevent film rupture. Upon annealing, roughened films display a periodic, lacey structure, resembling patterns from spinodal dewetting. The fluctuation periodicity scales with roughness evolution as $it\lambda_s \propto R_q^{1/4}$ for neat blends and blends with $NP_A$, whereas the scaling breaks down for blends containing $NP_B$ and $NP_C$. These studies show that phase separation is responsible for film roughening.

**10:36**
**N24 14 Dewetting Morphology and Dynamics of Ordered Symmetric Block Copolymer Films: Stability of Nanoscopic Liquid Bilayers** MATTHEW J. FARRAR, ANDREW B. CROLL, KARI DALNOKI-VERESS, *Physics and Astronomy, McMaster University* Symmetric diblock copolymers, which form lamella upon micro-phase separation, can have unique dewetting properties. In this experimental study we explore the effects of the microphase separation on the dewetting of three different systems. We begin with the dewetting of disordered thin poly(styrene)-b-poly(methyl methacrylate) films on poly(dymethyl siloxane) coated Silicon. In this case, the film is not allowed to relax to its lamellar state before dewetting begins. The complex interplay between dewetting and microphase separation leads to hole growth that appears dendritic and deviates dramatically from the conventional circular hole growth. In a second experiment, the thin films are arrange into their lamellar equilibrium before being transferred onto an unfavourable substrate, which initiates dewetting. On an unfavourable substrate, these films show remarkable stability. Holes that do form are cylindrical but grow at a much-reduced rate when compared to a homopolymer system. Finally, hole growth in free-standing ordered lamellar films is explored. Here we again see significant stability and extremely slow dynamics – an ordered free-standing film is stable, or nearly stable, even though the liquid film is well above the glass transition temperature and only of order 1 lamella ( $\sim$ 30nm) thick!

**10:48**
**N24 15 Interfacial segregation and micellization of hydrogen bonding copolymers** MICHELLE LEFEBVRE, MURAT GUVENDIREN, MONICA OLVERA DE LA CRUZ, KENNETH SHULL, *Department of Materials Science and Engineering, Northwestern University* An AB diblock copolymer in which A and B have unfavorable interactions will segregate to an interface between A and B homopolymers. The driving force for segregation is increased if the B homopolymer is replaced by a C homopolymer and B and C have favorable interactions. When copolymer accumulates at the interface, the preferred interfacial curvature changes as a function of the copolymer composition. This change in curvature leads to a variety of possible morphologies, including micelles, swollen micelles, or inverted micelles. To examine this effect we use a model system where A is polystyrene (PS), B is poly(4-hydroxystyrene) (PHS), and C is poly(2-vinylpyridine) (PVP), and the PHS and PVP can undergo hydrogen bonding. We measure the interfacial segregation of PS- PHS copolymers at an interface between PS and PVP using dynamic secondary ion mass spectrometry.



**SESSION N25: FOCUS SESSION: ORGANIC PHOTOVOLTAICS**
**Wednesday Morning, 15 March 2006; 322, Baltimore Convention Center at 8:00**
**Max Shtein, University of Michigan, presiding**

***Invited Papers***

**8:00 sping University**
**N25 1 Organic photovoltaics - towards high performance low bandgap polyfluorene/fullerene bulk heterojunction devices.**
OLLE INGANÄS, *Linköping University*

We use alternating copolymers of polyfluorene (APFOs) in polymer/fullerene blends as used in plastic solar cells. APFO-3/PCBM devices typically give power conversion efficiencies up to 3.4 % (AM1.5, 100 mW/cm$^2$). The APFO's are stable, have high mobility and may be fashioned for liquid crystalline phases, as well as for broad optical absorption.

By chemical design it is possible to move the optical absorption edge out to 1000 nm, and also to extract this absorption in photocurrent generation out to 1000 nm. As polymer bandgap is reduced, LUMO and HOMO orbitals shift. This requires the use of modified fullerene acceptors, with shifted orbitals, necessary to give the conditions for photoinduced charge transfer with the low bandgap polymers. The APFO polymers therefore give the necessary variability to catch a larger fraction of the solar spectrum. We have developed full optical and electrical model, predicting device performance for multilayer cells and for tandem cells, and using as input empirical determination of optical and electronic transport properties. We find the hole mobility to be a limiting parameter for device function.

*Contributed Papers*

**8:36**

**N25 2 High Performance Organic Light-Emitting Diodes Based on Intramolecular Charge Transfer Emission from Donor-Acceptor Molecules** ABHISHEK KULKARNI, XIANGXING KONG, SAMSON JENEKHE, *Departments of Chemical Engineering and of Chemistry, University of Washington, Seattle WA, 98195* A clear understanding of the key factors governing the electroluminescence (EL) efficiency of emissive donor-acceptor (D-A) molecules in OLEDs is currently lacking, but is essential to a rational molecular design of future emissive materials. In this study, OLEDs based on intramolecular charge transfer emission from 3,7-[bis(4-phenyl-2-quinolyl)]-10-methylphenothiazine (BPQ-MPT) and 3,6-[bis(4-phenyl-2-quinolyl)]-9-methylcarbazole (BPQ-MCZ) had device performances that differ by orders of magnitude. High performance (44360 cd/m$^2$, 21.9 cd/A, 5.78% external quantum efficiency (EQE) at 1140 cd/m$^2$) green OLEDs were achieved from BPQ-MPT which has a HOMO level at 5.09 eV and a non-planar geometry. In contrast, diodes with far lower performance (2290 cd/m$^2$, 1.4 cd/A, 1.7% EQE) were obtained from BPQ-MCZ which has a HOMO level of 5.75 eV and a planar geometry. These results highlight the pronounced influence of the electron donor strength and molecular geometry on the EL efficiency of D-A molecules.

**8:48**

**N25 3 Reversible Persistence and Effects of Oxygen on the Photoconductivity of Porphyrin Nanorods** E. A. MULLER, V. H. JOINES, W. F. SMITH, *Haverford College* A. D. SCHWAB, *Appalachian State U.* J. C. DE PAULA, *Lewis and Clark College* D. E. JOHNSTON, A. T. JOHNSON, *U. of Pennsylvania* Tetrakis(4-sulfonatophenyl) porphine ($TPPS_4$) self assembles[1] into well-defined nanorods with intriguing photoelectronic properties.[2] New experiments show that illumination under Ar for several hours induces a change to persistent behavior, i.e. conductivity decays slowly when light is removed, rather than dropping to zero. After resting 24 hours, the sample recovers non-persistent behavior. The dark conductivity of $TPPS_4$ aggregates formed by a different technique is sensitive to $O_2$ .[3] We find that the conductivity under illumination of nanorod aggregates decreases when 0.2% $O_2$ is added, but this change is reversible. By contrast, if the sample is exposed to 21% $O_2$ shortly after light is removed, the photoconductivity is permanently lowered. These effects may be due to a combination of $O_2$-mediated quenching of excited state porphyrin and oxidation.

[1]A.D. Schwab et al., J. Phys. Chem. B **107**, 11339 (2003).

[2]A.D. Schwab et al., Nano Letters **4**, 1261 (2004).

[3]Y. Otsuka et al., Nanotechnology **15**, 1639 (2004).

**9:00**

**N25 4 Photoinduced Charge Transport Spectra for Porphyrin and Naphthalene Derivative-based Dendrimers** J.H. PARK, Y. WU, J.R. PARQUETTE, A.J. EPSTEIN, *The Ohio State University, Columbus OH 43210* Dendrimers are important chemical structures for harvesting charge. We prepared model dendrimers using two porphyrin derivatives and a naphthalene derivative. Films of these porphyrin derivatives have a strong Soret band ( $\sim$ 430nm) and four significant Q-bands; the naphthalene derivative has strong absorption at 365 and 383nm. Two kinds of photovoltaic cell structures [ITO/BaytronP/(thick or thin) dendrimer/Al] are constructed to investigate the optical response spectra of dendrimers under electric potential($V$) on the cell (range from -1V to 2V). To obtain pure optical responses, incident light is modulated with an optical chopper and a lock-in amplifier is used to measure current ($I_{AC}$) and phase ($\theta$). For the excitation of the Soret band, $I_{AC}$ and $\theta$ do not change substantially with change of sign and amplitude of $V$. For Q-bands and naphthalene absorption bands, $\theta$ nearly follows the polarity of V on the cells and $I_{AC}$ is linear with $V$. Hence, $I_{AC}$ is nearly ohmic for Q- band although there are shifts due to built-in-potential. $I_{AC}$ for Soret band is almost same for thick and thin active layer cells. In contrast, $I_{AC}$ increases with thickness increase for Q bands. Mechanisms of photogeneration and charge transport will be discussed.

**9:12**

**N25 5 Carbon nanotube sheets as transparent charge injectors in organic light-emitting diodes** CHRISTOPHER WILLIAMS, MEI ZHANG, RAQUEL OVALLE, KRUTARTH TRIVEDI, ALEXANDER KUZNETSOV, SERGEY LEE, RAY BAUGHMAN, ANVAR ZAKHIDOV, *The University of Texas at Dallas* Carbon nanotubes (CNTs) have been recognized for their potential in many applications ranging from high strength materials and fibers to true nanoscale electronics. Recently a method for making strong and transparent CNT sheets has been developed, producing free-standing multiwall nanotube sheets which are easy to process [1]. Their mechanical and electrical properties allow them to meet the needs of a wide range of applications, particularly in optoelectronics. We show here the potential for using these thin, flexible CNT sheets in the development of flexible organic light-emitting diode (OLED) displays. The high transparency of the sheets, the high degree of orientation of tubes and the high work function of the material make them suitable hole injectors for typical hole transport materials used in OLEDs and polymeric LEDs (PLEDs). We show that CNT sheets can be used as anodes for both PLEDs and molecular OLEDs. We also introduce a method for producing inverted OLEDs on existing drive electronics for active matrix displays and a design for a transparent display using CNT sheets as both the electron and hole injector. [1] M. Zhang, S. Fang, A. Zakhidov, S. Lee, A. Aliev, C. Williams, K. Atkinson, R. Baughman, Science **309**, 1215 (2005).

**9:24**

**N25 6 Dissociation Processes of Singlet and Triplet Excitons in Organic Photovoltaic Cells** ZHIHUA XU, YUE WU, BIN HU, *University of Tennessee* The dissociation processes of singlet and triplet excitons were studied based on single-layer photovoltaic cells using: fluorescent Aluminum (III) 8-hydroxyquinoline ($Alq_3$) and phosphorescent itfactris (2-phenylpyridine) iridium ($Ir(ppy)_3$) molecules. We found that triplet exciton dissociation leads to a more efficient photovoltaic response as compared to singlet excitons. The short-circuit photocurrent action spectra suggest that the triplet excitons dissociate mainly at the metallic electrode interface while the singlet excitons exhibit bulk dissociation. This interface dissociation of triplet excitons forms a mechanism for phosphorescent organic materials to show efficient photovoltaic responses. Therefore, control of singlet-to-triplet exciton ratio presents a new pathway to enhance photovoltaic response from organic materials.

**9:36**

**N25 7 Multilayer polymer devices: light emitting diode and vertical hot carrier transistor** HSIN-FEI MENG, *National Chiao Tung University* SHENG-FU HORNG, CHAIN-SHU HSU, SHIN-RON TZENG, YU-CHIANG CHAO, SYUAN-LIN YANG, Two new devices based on polymer multilayers are presented:charged-balanced LED and hot carrier transistor. 1. An intermediate liquid buffer layer is introduced to overcome the dissolution problem of solution-processed multilayer polymer light-emitting diodes. This method can be applied to arbitrary combinations of polymers with no restriction on solvents. As an example, a hole-blocking layer is successfully spin-coated on the emissive polymer layer. Three typical p-type polymers, The electron-hole balance is improved by the addition of hole-blockinglayer. The electroluminescence efficiency can be increased up to 5 times, while the luminance up to 7 times. Electron-blocking layer is applied to blue polyfluorene copolymer and the brightness is as high as 30,000 $cd/m^2$ while the yield is 4 cd/A. 2. Metal-base hot-carrier transistor with conjugated polymer emitter and collector is demonstrated. The device is fabricated by multiple spin-coating with the metal base sandwiched between two polymers. A thin insulating layer of LiF is inserted between emitter and base to enhance the hot carrier kinetic energy and reduce the mutual dissolution. Using poly(9-vinylcarbazole) as the emitter, Al as base, and poly(3-hexylthiophene) as the collector, common-emitter current gain of 26 is obtained with operation voltage as low as 5V.

**9:48**

**N25 8 Single-crystal films of a combination of materials (co-crystal) involving DAST and IR-125 for electro-optic applications** A. NARAYANAN, J. TITUS, H. RAJAGOPALAN, P. VIPPA, M. THAKUR, *Photonic Materials Research Laboratory, Auburn University, AL* Single-crystal film of DAST (4'-dimethylamino-N-methyl-4-stilbazolium tosylate) has been shown [1] to have exceptionally large electro-optic coefficients ($r_{11} \sim$ 770 pm/V at 633 nm). In this report, single crystal film of a combination of materials (co-crystal) involving DAST and a dye molecule IR-125 will be discussed. Modified shear method was used to prepare the co-crystal films. The film has been characterized using polarized optical microscopy, optical absorption spectroscopy and x-ray diffraction. The optical absorption spectrum has two major bands: one at about 350–600 nm corresponding to DAST and the other at about 600-900 nm corresponding to IR-125. The x-ray diffraction results show peaks involving the presence of DAST and IR-125 within the co-crystal film. Since the co-crystal has strong absorption at longer wavelengths it is expected to show higher electro-optic coefficients at longer wavelengths. Preliminary measurements at 1.55 $\mu$m indicate a high electro-optic coefficient of the co-crystal film. [1] Swamy, Kutty, Titus, Khatavkar, Thakur, Appl. Phys. Lett. **85**, 4025 (2004); Kutty, Thakur, Appl. Phys. Lett. **87**, 191111 (2005).

**10:00**

**N25 9 Highly efficient third-order optical nonlinearities and their frequency dependence in donor-substituted cyanoethynylethene molecules.** JOSHUA C. MAY, IVAN BIAGGIO, *Department of Physics and Center for Optical Technologies, Lehigh University* TSUYOSHI MICHINOBU, FRANÇOIS DIEDERICH, *Laboratorium für Organische Chemie, ETH-Hönggerberg* We report on a new class of organic molecules with record efficiency for application in third-order nonlinear optics (NLO). The third-order polarizability, $\gamma$, of several donor-substituted cyanoethynylethene molecules was determined at the off-resonant wavelength of 1.5 microns using four-wave mixing. The nonlinearities were found to be extraordinarily large relative to the small molecular masses and were found to be within 50 times Kuzyk's fundamental limit,[1] with $53 \times 10^{-48}$ $m^5V^{-2}$ as the highest $\gamma$ value. Select molecules were further investigated at wavelengths on and surrounding their two-photon (TP) absorption peaks, revealing large TP cross sections and the resonant influence on the real and imaginary parts of $\gamma$. Several members of this molecular family can be vapor-deposited and are likely candidates for third-order NLO devices. When considering their small mass, the *specific* $\gamma$ ($\gamma$ per molecular mass) for this family (off resonance, at 1.5$\mu$m) is up to $6.5 \times 10^{-23}$ $m^5V^{-2}Kg^{-1}$, approximately one order of magnitude larger than previously known large $\gamma$ molecules.[2]

[1]M. G. Kuzyk, Opt. Lett. 25, 1218 (2000).
[2]J. C. May et al, Opt. Lett. 30, 3057 (2005).

**10:12**

**N25 10 A Time-Dependent Density Functional Theory Study of One-and Two-Photon Absorption: Donor-Acceptor Chromophores.** RUTH PACHTER, PAUL N. DAY, KIET A. NGUYEN, *Air Force Research Laboratory, Materials & Manufacturing Directorate, Wright-Patterson Air Force Base, Ohio 45433-7702* We report time-dependent density functional theory (TDDFT) calculations of one-photon, and two-photon absorption spectra, for a series of compounds, in which electron donating and accepting groups are attached to a core having a delocalized pi-electron structure, such as stilbene or fluorene. We find that the calculated excitation energies are in better agreement with experimental data upon the application of (x-c) functionals that take into account long-range interactions, and also by the inclusion of solvent effects. Furthermore, two-photon absorption cross-section predictions are improved with the application of quadratic response TDDFT, in comparison to experiment.

**10:24**

**N25 11 Two Photon Absorption in a Novel Nano-optical Material Based on the Nonconjugated Conductive Polymer, Poly(beta-pinene)** JITTO TITUS, MRINAL THAKUR, *Photonic Materials Research Laboratory, Auburn University, AL* As recently reported, the electrical conductivity of the nonconjugated polymer, poly(beta-pinene) increases by more than ten orders of magnitude upon doping with iodine [1]. The FTIR, optical absorption and EPR measurements have shown that radical cations are formed upon doping and charge-transfer involving the isolated

double-bond in poly(beta-pinene). In this report, exceptionally large two-photon absorption in iodine-doped poly(beta-pinene) will be discussed. The linear absorption spectrum of medium-doped poly(beta-pinene) have peaks at about 4 eV and 3.1 eV. The first peak is due to the radical cation and the second due to the charge-transfer between the double bond and the dopant. The two-photon absorption of the medium-doped polymer has been measured at 730-860 nm using open-aperture z-scan with 150 femtosecond pulses from a Ti:Sapphire laser. A two-photon peak at about 1.5 eV with a magnitude of more than 1 cm/MW has been observed. The large magnitude of the two-photon absorption coefficient which is proportional to the imaginary part of the third order susceptibility has been attributed to the special structure of the radical cation and the confinement within a sub-nanometer dimension. [1] Vippa, Rajagopalan and Thakur, J. Poly. Sci. Part B: Poly. Phys., 43, 3695 (2005).

**10:36**
**N25 12 Temperature dependent electrical and optical characterization of polyfluorene based organic light-emitting-diodes*** MOHAMMAD ARIF, S. GUHA, *Department of Physics, Univ. of Missouri-Columbia* M.S. YUN, S. GANGOPADHYAY, *Department of Electrical Engineering,Univ. of Missouri-Columbia* Polyfluorene (PF) conjugated polymers have received widespread attention due to their strong blue emission, high charge mobility and excellent chemical and thermal stability which creates great prospect for optoelectronic device applications. Efficient and well balanced injection of charge carriers and transport capabilities are of paramount importance for high luminescence efficiency of organic light emitting diodes (OLEDs). The maximum current flowing through metal/semiconductor is limited by available space and trapped charges, barrier heights, applied electric field and mobility of the carriers. In this work we present detailed current- voltage (I-V) measurements as a function of temperature from 2- ethylhexyl substituted PF (PF2/6) based OLEDs. PF2/6 is characterized by Tg of 80 $^{o}$C and a nematic liquid crystalline phase above 150 $^{o}$C. Barrier heights for current injection were calculated as a function of thermal cycling. The characteristic I-V measurements were fitted with ideal space charge limited conduction (SCLC) with traps to calculate carrier mobilities and trap concentration. Preliminary studies of Raman scattering from these working devices will be discussed.

*This work was supported by NSF-ECS # 0523656.

**10:48**
**N25 13 Pi-Conjugated Dendrimers for Organic Photovoltaics** SEAN SHAHEEN, WILLIAM MITCHELL, NIKOS KOPIDAKIS, JOSEPH BOZELL, GARRY RUMBLES, *National Renewable Energy Lab* Polymer-based organic photovoltaic (OPV) devices are promising candidates for low-cost solar cell fabrication. The operation of such devices is known to be strongly dependent upon the morphology and carrier mobility of the polymer. Here we discuss the use of pi-conjugated dendrimers in OPV devices. Dendrimers have a precisely defined molecular weight, in contrast to pi-conjugated polymers, which leads to a well-defined morphology. This morphology can be highly ordered owing to strong pi-electron interactions between dendrimers. We have synthesized a family of phenyl-cored thiophene dendrimers with a variable number of arms and and variable number of thiophenes in each arm. The optical band gaps of these materials in thin film form range from 2.3 to 2.6 eV. Time-resolved microwave conductivity measurements of the dendrimers showed a power-law dependence of lifetimes extending into the millisecond regime, indicative of a very pure material. Preliminary OPV devices fabricated by blending the dendrimers with a soluble fullerene yielded maximum open-circuit-voltages of 900 mV and external quantum efficiencies of 22%. A reduced band gap dendrimer was also synthesized by adding strong electron withdrawing groups onto the phenyl core, resulting in an optical band gap of 1.82 eV. This material show good molecular ordering as evidenced by x-ray diffraction.

## SESSION N26: FOCUS SESSION: DNA AND PROTEIN ANALYSIS WITH MICRO AND NANO FLUIDICS
**Wednesday Morning, 15 March 2006**
**323, Baltimore Convention Center at 8:00**
**Steven Quake, Stanford University, presiding**

***Contributed Papers***

**8:00**
**N26 1 Formation of bi-nanopores in silicon chips*** SANG RYUL PARK, HONGBO PENG, X. S. LING, *Brown University* Solid-state nanopores are holes with diameter and length on the order of 20 nm or smaller embedded in an insulating solid membrane. These nanopores have been shown to allow linear translocation of DNA molecules in buffer conditions and can be used as an electronic device for detecting and characterizing nucleic acids and proteins. Here we report a novel method of fabricating bi-nanopores in silicon chips using feedback electrochemical etching. The simplicity and low-cost of our approach, taking advantage of the well-known anisotropic etching behavior of silicon in alkaline solutions, bring solid-state nanopores closer to industrial-scale applications.

*This work was supported by the NSF-NIRT program.

**8:12**
**N26 2 Fabrication of nanopores in wax using laser-induced shrinking*** SHANSHAN WU, SANG RYUL PARK, X. S. LING, *Brown University* We developed a simple laser heating induced shrinking technique for making plastic nanopore bio-sensing devices. Our technique is capable of shrinking thermoplastic pores of diameters up to several hundred micrometers to a few nanometers. We have made nanopore devices by applying this technique to Apiezon W wax (thermoplastics) micropores. Our DNA translocation experiments with 48 kilo base pairs (kbp) double-stranded λ DNA (λ dsDNA) have yielded convincing results of the functionality of these devices as biomolecular nanosensors.

*This work is supported by an NSF-NIRT (Nanoscale Interdisciplinary Research Team) grant.

**8:24**
**N26 3 Ion Valence and Solution Temperature Effects on DNA Translocations in Solid-State Nanopores** JAMES UPLINGER, *Physics Department, University of Arkansas* DANIEL FOLOGEA, *Physics Department, University of Arkansas* JIALI LI, *Physics Department, University of Arkansas* Solid-state nanopore device provides a sensitive and robust environment for single DNA analysis. When a nanopore is the only partition between two reservoirs filled with an ionic solution and electrical conduction is established any DNA molecule translocation through the nanopore will partially block the open pore current. The current blockage and dwell time depends on both the external parameters, such as applied voltage, ionic strength and on characteristics of the DNA molecule itself, such as the charge and geometry. The properties of the molecule can be modulated by interactions with the ionic solution, and these will produce modifications of the current blockage and translocation time. Here we report on how the DNA translocation signature is modified when: (1) salts of varied valences are used and concentration of the surrounding solution changes; (2) the temperature of ionic solution changes. The mobility and diffusion coefficient of DNA molecule at above conditions are estimated.

***Invited Papers***

**8:36**
**N26 4 DNA in nanofluidic devices.**
ROBERT RIEHN, *Princeton University*

Nanochannels with a channel cross-section of around 100 nm x 100 nm or less are emerging as a powerful new technique for single-molecule DNA analysis. In these nanochannels, DNA is linearized to a constant fraction of its contour length, and thus spatial locations measured by fluorescence microscopy can be directly related to genomic locations. Because the stretching in nanochannels is caused by lateral confinement, molecules are free to undergo longitudinal fluctuations. Hence, time-averaging over a single molecule is meaningful, and a high resolution can be achieved even using few molecules. We will present how DNA imaging in nanochannels can be applied to common tasks in molecular biology that go beyond simple sizing. In particular, we will discuss the genomic identification of human DNA fragments using fluorescent markers, and how to perform enzymatic reactions, such as restriction mapping using endonucleases, in nanochannels. We will also present our recent progress in the development of ''nanoplumbing,'' that is devices that contain junctions of nanochannels. We will show how device dimensions influence the transport of DNA at those nanochannel junctions, and how those properties can be utilized in the design of devices and exotic materials.

***Contributed Papers***

**9:12**
**N26 5 Nanoscale electrical detection of DNA** CHIH-KUAN TUNG, *Department of Physics, Princeton University* ROBERT REIHN, *Department of Physics, Princeton University* LUKAS URBAN, *Department of Physics, Unversity of Illinois, Urbana-Champaign* ALI YAZDANI, *Department of Physics, Princeton University* ROBERT AUSTIN, *Department of Physics, Princeton University* We try to detect DNA electrically by different nano-devices, including single-walled carbon nanotubes and platinum nano- wires. We will demonstrate the responses of carbon nanotubes conductance to the exposure to DNA, and ac lock-in measurements across metal nano-wires based on the biochemical properties of the DNA bases. The effects of different bases are also studied, which may provide us a real opportunity to sequence DNA electrically.

**9:24**
**N26 6 DNA Translocation Dependence on Ionic Solution Concentration in a Solid-State Nanopore Device** BRIAN THOMAS, *Physics Department University of Arkansas Fayetteville Arkansas 72701* DANIEL FOLOGEA, *Physics Department University of Arkansas Fayetteville Arkansas 72701* JIALI LI, *Physics Department University of Arkansas Fayetteville, Arkansas 72701* Our work describes dsDNA translocations through a silicon nitride nanopore subjected to an applied electric field in solutions of different ionic strengths. We demonstrate how the ion concentration affects DNA shielding and, consequently, its effective negative charge. These modifications alter key parameters of the translocation process, such as the dwell time and current drop of the event. In this way, the DNA/salt interaction process can be explored by translocation experiments.

**9:36**
**N26 7 DNA size and conformations analysis using a synthetic nanopore** DANIEL FOLOGEA, *University of Arkansas, Physics Department, Fayetteville, AR72701* JAMES UPLINGER, *University of Arkansas, Physics Department, Fayetteville, AR72701* BRIAN THOMAS, *University of Arkansas, Physics Department, Fayetteville, AR72701* BRADLEY LEDDEN, *University of Arkansas, Physics Department, Fayetteville, AR72701* ERIC BRANDIN, *Harvard University, Department of Molecular and Cellular Biology, Cambridge, MA02138* DANIEL BRANTON, *Harvard University, Department of Molecular and Cellular Biology, Cambridge, MA02138* JIALI LI, *University of Arkansas, Physics Department, Fayetteville, AR72701* Our work reveals the ability of a synthetic nanopore made in a silicon nitride membrane to discriminate between different conformations and lengths of DNA molecules and presents a comparative analysis with the electrophoretic behavior of the same DNA. Double stranded linear, supercoiled and relaxed form of the same DNA, linear restriction fragments, as well as single stranded DNA, are passed through a synthetic nanopore filled with a buffered ionic solution, and a subsequent analysis in terms of current blockage, translocation time and integrated events area shows the analytical ability of such a device. Also, we prove that an intercalating agent increases the temporal resolution by increasing the translocation time up to a factor of two.

*Invited Papers*

**9:48**
**N26 8 Microfluidic Protein Crystallography.**
CARL HANSEN, *University of British Columbia*

Due to their impressive economies of scale and unique mass transport properties microfluidic devices have become viable technologies for nano-volume protein crystallization screening and growth. In particular, soft microfluidic devices based on multilayer soft lithography (MSL) have been successfully applied to systematic protein solubility studies and efficient nanoliter volume screening by free interface diffusion. While these systems have proven highly effective in identifying crystallization conditions for a large number challenging crystallization targets, realizing the full potential of microscale crystallization requires complementary technologies for crystal optimization and harvesting. In this talk I will briefly review previous studies of protein phase space mapping and crystallization screening, and will present recent work on a microfluidic device which provides a link between chip-based nanoliter volume crystallization screening and structure analysis through ''kinetic optimization'' of crystallization reactions and direct in situ structure determination. Using this device we demonstrate control over crystal quality, reliable scale-up from nanoliter volume reactions, facile harvesting and cryo-protectant screening, and protein structure determination at atomic resolution from data collected in-chip.

*Contributed Papers*

**10:24**
**N26 9 Statics and Dynamics of Single DNA Molecules Confined in Nanoslits** PO-KENG LIN, *Department of Physics, National Taiwan University, Taipei, Taiwan* CHI-CHENG FU, *Institute of Atomic and Molecular Science, Academia Sinica, Taipei, Taiwan* Y.R. CHEN, *Graduate Institute of Electronics Engineering and Department of Electrical Engineering, National Taiwan University, Taipei, Taiwan* WUNSHAIN FANN, *Institute of Atomic and Molecular Science, Academia Sinica,Taipei, Taiwan* C.H. KUAN, *Graduate Institute of Electronics Engineering and Department of Electrical Engineering, National Taiwan University, Taipei, Taiwan* de Gennes provided the scaling predictions for the linear polymer chain trapped in slit with dimension close to the Kuhn length decades ago; however, it has yet to be compared with experiments. We have fabricated nano-slits with vertical dimension similar to the Kuhn length of ds-DNA, $\sim$ 100nm, using standard photolithography. Single DNA molecules with length range from 2 to75 micrometers were successfully inject into the slits and the Brownian motions were imaged by fluorescence microscopy. The distributions of the radius of gyration and the two-dimensional asphericity were measured and it is found that the DNA exhibit highly anisotropic shape distribution. The scaling exponents for the chain extension and the center-of-mass diffusion coefficient will also be discussed.

**10:36**
**N26 10 Slowing down DNA translocation using magnetic and optical tweezers*** HONGBO PENG, SHANSHAN WU, SANG RYUL PARK, ANDREW POTTER, X. S. LING, *Brown University* Electric-field driven DNA translocation through nanopores can be exploited for DNA sequencing and other applications. However, the DNA translocation under normal patch-clamp-type measurement is too fast to allow detailed measurements of individual or few nucleotides. We propose a concept to slow down the DNA translocation through the nanopore by using magnetic (or optical) tweezers. The 3' end of a single-strand DNA can be attached to a streptavidin-coated magnetic bead through a single biotin molecule. During DNA translocation, the 5' end of DNA will be electrophoretically drawn through the nanopore to the itrans side while the 3' end of DNA stays in the itcis side with the magnetic bead. A set of permanent magnets or electric coils can be used to generate a magnetic field gradient large enough to pull the bead, hence the DNA out of the nanopore. The net force on the magnetic bead will determine this back-translocation speed. By carefully tuning the magnetic field gradient and the voltage bias on the nanopore, one can make the back-translocation much slower than the conventional forward-translocation in which case the DNA is driven only by the electric force. We will report our experimental design as well as the preliminary results.

*This work was supported by NSF-NIRT.

**10:48**
**N26 11 Patterned Periodic Nanofilter Array for Continuous-Flow Bimolecular Separation** JIANPING FU, *Department of Mechanical Engineering, MIT* JONGYOON HAN, *Department of Electrical Engineering and Computer Science, Division of Biological Engineering, MIT* We present an experimental study on sieving process of small biomolecules (i.e., proteins and small DNAs) in one- and two-dimensional periodic arrays of nanofilter. The nanofilters served as artificial sieves with precise pore size characterization and showed exceptional size selectivity and separation efficiency from the periodicity of the environment. A kinetic model is developed to explain the electrophoretic drift of charged molecules across periodically modulated free energy landscapes. Further experimental evidence shows the crossover from Ogston-like sieving to entropic trapping mechanism depending on nanofilter thickness and on electric field strength. We also demonstrate continuous-flow biomolecule separation with a device containing of two-dimensional periodic nanofilter arrays. The interaction between migrating molecules and the two-dimensional physical landscapes cause molecules of different sizes to follow radically different paths leading to separation. Continuous-flow fractionations of small DNA molecules (50bp-766bp) as well as SDS-protein complexes (11kDa-200kDa) were achieved in about 5 minutes with a resolution of 10%. By virtue of its gel-free and continuous-flow operation, this device suggests himself a key component to an integrated biomolecule sample preparation and analysis microsystem.

**SESSION N27: ELECTRONIC STRUCTURE I**
**Wednesday Morning, 15 March 2006**
**324, Baltimore Convention Center at 8:00**
**Michael Mehl, Naval Research Laboratory, presiding**

**8:00**
**N27 1 Tight binding calculations of vibrational and thermal properties of amorphous silicon** MICHAEL MEHL, *Naval Research Laboratory* JOSEPH FELDMAN, DIMITRIS PAPACONSTANTOPOULOS, *Naval Research Laboratory and George Mason University* NOAM BERNSTEIN, *Naval Research Laboratory* By displacing atoms by different amounts and computing atomic forces within the NRL tight binding method we obtain all second order (harmonic) and some third order (anharmonic) coupling constants of a 1000 atom TB-relaxed Wooten CRN model of amorphous silicon. The harmonic force constant results allow us to study various properties including vibrational density of states, dynamic structure factors, specific heat and thermal conductivity within Kubo theory. We shall present results of these applications and compare to experiment and previous work based on the Stillinger Weber potential.

**8:12**
**N27 2 Manifestation of Negative Compressibility in Low-Density Electron Liquids: Anomaly in the Ion-Pair Distribution Function in Supercritical Fluid Rb** YASUTAMI TAKADA, *ISSP, Univ. of Tokyo* It is a well-known fact that the electronic compressibility $\kappa$ diverges in the 3D electron gas as the density parameter $r_s$ approaches 5.25. A recent investigation clarifies that this divergence is due to the excitonic effect in the electron-hole pair excitation, in particular, to its zero-energy excitation [1]. For $r_s > 5.25$, $\kappa$ becomes negative, leading to the negative static dielectric function $\varepsilon(q,0)$ for at least small $q$ owing to the compressibility sum rule. Then we can expect that two positive test charges do not repel but attract to each other in such a system. Keeping this situation in mind, we have calculated the ion-pair distribution function g(R) in the expanded Rb liquid metal by using the Monte Carlo method and found interesting features in g(R) characteristic to the negative $\varepsilon(q,0)$ [2]. Such features have been observed by the recent measurement of g(R) in the supercritical fluid Rb metal with continuously increasing $r_s$ from 5.25 [3]. This confirms the situation of $\kappa < 0$ in the low-density 3D electron gas for the first time. [1] YT, J. Superconductivity **18**, No.3 (2005). [2] H. Maebashi and YT, to be submitted. [3] K. Matsuda and K. Tamura, private communication.

**8:24**
**N27 3 Finite temperature quasiparticle self-consistent GW approximation** SERGEY FALEEV, *Sandia National Laboratories* MARK VAN SCHILFGAARDE, TAKAO KOTANI, *Arizona State University* FRANCOIS LEONARD, MICHAEL DESJARLAIS, *Sandia National Laboratories* We present a new ab initio method for electronic structure calculations of materials at finite temperature (FT) based on the all-electron quasiparticle self-consistent GW (QPscGW) approximation and Keldysh time-loop Green's function approach. We apply the method to Si, Ge, GaAs, InSb, and diamond and show that the band gaps of these materials universally decrease with temperature in contrast with the local density approximation (LDA) of density functional theory (DFT) where the band gaps universally increase. At temperatures of a few eV the difference between quasiparticle energies obtained in FT-QPscGW and FT-LDA approaches significantly reduces. This result suggests that existing simulations of very high temperature materials based on the FT-LDA are more justified then it might appear from well-known LDA band gap errors at zero-temperature.

**8:36**
**N27 4 Iterative minimization by Kohn–Sham inversion and potential mixing** ROOPE ASTALA, MALCOLM STOTT, *Department of Physics, Queen's University, Kingston, Ontario, Canada* Applications of Hohenberg–Kohn–Sham density functional theory to problems in materials physics are critically dependent on algorithms for iterating the Kohn–Sham equations to self-consistency. We present an approach for obtaining the self-consistent solution, which explores a connection between iterative minimization and Kohn–Sham inversion, iti.e. finding a self-consistent potential for a given density. The central idea is to perform the Kohn–Sham inversion using a position-dependent Lagrange multiplier and to construct a new trial potential from the result. The method is variational, in contrast to commonly-used density mixing approaches, and has excellent convergence. We demonstrate the method using a real-space pseudopotential implementation with applications to small molecules.

**8:48**
**N27 5 Atomic Forces and Geometry Optimisation with the ONETEP Linear-Scaling DFT Method** ARASH MOSTOFI, *Massachusetts Institute of Technology, USA* PETER HAYNES, *Cavendish Laboratory, University of Cambridge, UK* CHRISKRITON SKYLARIS, *Physical and Theoretical Chemistry Laboratory, University of Oxford, UK* MIKE PAYNE, *Cavendish Laboratory, University of Cambridge, UK* ONETEP[1] (Order-*N* Electronic Total Energy Package), is a density functional method, based on plane-waves, whose computational cost scales only linearly with the number of atoms. ONETEP uses a localised yet orthogonal basis of periodic cardinal sine (psinc) functions[2], also known as Dirichlet or Fourier Lagrange-mesh functions, which are formed from a discrete sum of plane-waves. The localised non-orthogonal generalised Wannier functions (NGWFs) which span the occupied subspace are represented in terms of these psinc functions and are optimised during the calculation. This choice of basis and optimisation of the NGWFs results in smooth potential energy surfaces and enables the use of the Hellmann-Feynman theorem for the calculation of atomic forces. These have been implemented within a quasi-Newton geometry optimisation scheme and preliminary results are presented. [1] J. Chem. Phys. **122**, 084119 (2005). [2] J. Chem. Phys. **119**, 8842 (2003).

**9:00**
**N27 6 Optimized norm-conserving Hartree-Fock pseudopotentials*** ERIC J. WALTER, *College of William and Mary* WISSAM A. AL-SAIDI, *College of William and Mary* We report soft Hartree-Fock based pseudopotentials obtained using the optimized pseudopotential method[1]. The spurious long range tail due to the non locality of the exchange potential is removed using a self-consistent damping mechanism as employed in exact exchange[2] and recent Hartree-Fock pseudopotentials[3]. The

binding energies of several dimers computed using these pseudopotentials within a planewave Hartree-Fock code show good agreement with all-electron results.

*Supported by the Center for Piezoelectrics by Design / ONR.

[1]A. M. Rappe, K. M. Rabe, E. Kaxiras, and J. D. Joannopoulos, Phys. Rev. B **41**, 1227 (1990).
[2]E. Engel, A. Höck, R. N. Schmid, R. M. Dreizler, and N. Chetty, Phys. Rev. B **64**, 125111 (2001).
[3]J. R. Trail and R. J. Needs, J. Chem. Phys. **122**, 014112 (2005).

**9:12**

**N27 7 Effect of Ti and metal vacancies on the dehydrogenation of $Na_3AlH_6$*** SA LI, PURU JENA, *Virginia Commonwealth University* RAJEEV AHUJA, *Uppsala University* VIRGINIA COMMONWEALTH UNIVERSITY TEAM, UPPSALA UNIVERSITY COLLABORATION, Electronic and structural properties of sodium-aluminum hexahydride ($Na_3AlH_6$) formed during the decomposition reaction of sodium alanate ($NaAlH_4$) are calculated using density functional theory and generalized gradient approximation for exchange and correlation potential. The roles of Ti substitution at the Na and Al sites as well as that of Na and Al vacancies on the desorption of hydrogen have also been investigated. We show that the improvement in dehydrogenation of $Na_3AlH_6$is due to the addition of Ti much the same way as that in $NaAlH_4$, namely through the weakening of the metal-hydrogen bond. However, as in the case of $NaAlH_4$, vacancies are found to be more effective in desorbing hydrogen at lower temperatures than Ti substitution at the Na or Al sites.

*This work was supported in part by grants from the Department of Energy (DOE), Swedish Research Council (VR) and by the Swedish Foundation for International Cooperation in Research and Higher Education (STINT).

**9:24**

**N27 8 Excitation Energies from Time-Dependent Density Functional Theory within Modified Linear Response: Inclusion of the Electron-Hole Hartree-Fock Interaction** CHUNPING HU, OSAMU SUGINO, *Institute for Solid State Physics, University of Tokyo, and also CREST, Japan Science and Technology Agency* YOSHIYUKI MIYAMOTO, *Fundamental and Environmental Res. Labs, NEC, Japan* Time-dependent density functional theory (TD-DFT) within linear response (LR) has gained enormous popularity in the calculation of electronic excitations, whereas it is known to give considerably underestimated excitation energies for Rydberg and charge-transfer excitations. Although the incorrect long-range behavior of exchange-correlation (XC) potentials has been blamed for this problem, a different point of view on the LR scheme without any correction of XC potentials is presented here. Analyzing approximate excitation energies from LR within adiabatic local density approximation (ALDA) and the exact exchange (EXX) scheme, we propose a modified LR theory to strictly include the electron-hole Hartree-Fock interaction kernel, and to make excitation energy expression in ALDA explicitly similar to the EXX one. TD-LDA calculations within modified LR on typical diatomic molecules show that excitation energies of both Rydberg and charge-transfer excitations can be greatly improved to the EXX-level accuracy.

**9:36**

**N27 9 Quasiparticle Corrections to the Electronic Properties of Point Defects*** ARNO SCHINDLMAYR, *Forschungszentrum Jülich and Fritz-Haber-Institut der Max-Planck-Gesellschaft, Berlin, Germany* MAGNUS HEDSTRÖM, PHILIPP EGGERT, MATTHIAS SCHEFFLER, *Fritz-Haber-Institut der Max-Planck-Gesellschaft, Berlin, Germany* We present a quantitative ab initio method for calculating defect states and charge-transition levels of point defects in semiconductors. It relies on a separation into lattice and electronic energy contributions, which are treated within density-functional theory and many-body perturbation theory, respectively. We use the $GW$ approximation for the self-energy to determine the quasiparticle corrections to defect states in the band gap. As an example, we consider anion vacancies on the (110) surfaces of III-V semiconductors. The calculated charge-transition levels, in particular, show a clear improvement over the local-density approximation and are in close agreement with the available experimental data. As the surface is simulated by a slab within the supercell approximation, we place special emphasis on a convergence analysis of the quasiparticle properties in this approach. The dynamic polarization between the periodic images can be understood within a simple model, which also allows an a posteriori correction.

*This work was funded in part by the EU through the Nanoquanta Network of Excellence (Contract No. NMP-4-CT-2004-500198).

**9:48**

**N27 10 Probing the Ab-initio Fermi Surface Efficiently using Wannier Interpolation** JONATHAN YATES, IVO SOUZA, *LBNL and University of California, Berkeley* XINJIE WANG, DAVID VANDERBILT, *Rutgers University* Modern *ab-initio* techniques are able to provide an accurate description of the electronic structure for a wide range of materials. However, evaluation of the transport properties of metals requires an extremely detailed, and hence computationally expensive, sampling of the Fermi surface. We show that the electron group velocity and effective mass can be obtained directly from the Wannier representation of a system. This leads to an efficient and precise method for the calculation of transport properties using Wannier interpolation. We will present calculations of the ordinary Hall coefficient and thermoelectric power for a variety of materials.

**10:00**

**N27 11 Nonlinear Optical Response of Polar Semiconductors in the Terahertz Range** ERIC ROMAN, JONATHAN YATES, *University of California, Berkeley* MAREK VEITHEN, *Université de Liège* DAVID VANDERBILT, *Rutgers University* IVO SOUZA, *University of California, Berkeley* Using the Berry-phase finite-field method, we compute from first-principles the recently measured[1] infrared (IR) dispersion of the nonlinear susceptibility $\chi^{(2)}$ in III-V zincblende semiconductors. At far-IR (terahertz) frequencies, in addition to the purely electronic response $\chi_\infty^{(2)}$, the total $\chi^{(2)}$ depends on three other parameters, $C_1$, $C_2$, and $C_3$, describing the contributions from ionic motion. They relate to the TO Raman polarizability and the second-order displacement-induced dielectric polarization and forces, respectively. Contrary to a widely-accepted model,[2] but in agreement with the recent experiments on GaAs,[1] we find that the contribution from mechanical anharmonicity dominates over electrical anharmonicity. By using Richardson extrapolation to evaluate the Berry's phase in $k$-space by finite differences, we are able to improve the

convergence of the nonlinear susceptibility from the usual[3] $\mathcal{O}[(\Delta k)^2]$ to $\mathcal{O}[(\Delta k)^4]$, dramatically reducing the computational cost.

[1]T. Dekorsy, V. A. Yakovlev, W. Seidel, M. Helm, and F. Keilmann, Phys. Rev. Lett. **series 90**, 055508 (2003).
[2]C. Flytzanis, Phys. Rev. B **6**, 1264 (1972).
[3]P. Umari and A. Pasquarello, Phys. Rev. B **68**, 085114 (2003).

**10:12**
**N27 12 Breathing oscillations accompanying Bloch oscillations of wavepackets in periodic potentials*** MIGUEL PRUNEDA, *UC Berkeley* IVO SOUZA, *UC Berkeley* Using a 1D tight-binding model, we study the evolution of a well-localized wavepacket of Bloch states under an applied electric field. We apply a novel algorithm[1] for solving numerically the equations of motion which does not rely on the single-band approximation and can thus be used to explore interband Zener tunneling effects. In addition to the well-known Bloch oscillations of the center of the packet, we show that as the waveform moves in k-space, its real-space width varies in response to the change in the local quantum metric,[2] $g(k)$, of the underlying Bloch states. A generalized uncertainty relation is obtained between the spread in position and in *crystal* momentum of a wavepacket. It differs from the usual position/momentum uncertainty relation because of the interband matrix elements of the position operator in the crystal-momentum representation, which introduce a correction in terms of $g(k)$.

*Marie Curie OIF programme.

[1]Along the lines of I. Souza *et. al.*, Phys. Rev. B **69**, 085106 (2004).
[2]N. Marzari and D. Vanderbilt, Phys. Rev. B **56**, 12 847 (1997).

**10:24**
**N27 13 Nonadiabatic Transition in the Quantum Hall Effect** MANABU MACHIDA, NAOMICHI HATANO, *IIS, University of Tokyo* JUN GORYO, *Aoyama Gakuin University* We analyze the nonadiabatic transition in a 2D electron system with a periodic potential in the quantum Hall regime. We obtain corrections to the Chern-number term of the Hall conductance and a non-vanishing diagonal conductance. We treat the electric field as a time-dependent vector potential in the Hamiltonian. We calculate the time evolution of the density operator taking account of the first order of the electric field, and thereby study the electric conduction when the system evolves nonadiabatically. We thus obtain analytical expressions of the diagonal and off-diagonal conductances and calculate them numerically.

**SESSION N28: POLYMER ADSORPTION AND SURFACE MODIFICATION**
**Wednesday Morning, 15 March 2006**
**325, Baltimore Convention Center at 8:00**
**Eric Lin, National Institute of Standards and Technology, presiding**

**8:00**
**N28 1 PEG Surface Modification by Thermoreversible Ligand Cleavage in Nanoparticle Composites.** RICK BEYER, PHILIP COSTANZO, *Army Research Laboratory* The control of surface chemistry is an increasingly important area of research in the polymer science community; a simple example of a need for controlled surface properties can be found in the need for surfaces that are resistant to bacterial growth for medical applications. In this study, we have successfully modified the surface properties of solvent cast poly(ethylene glycol) (PEG) films, triggered by exposure to an elevated environmental temperature. PEG matrices of varying molecular weights have modified with gold nanoparticles functionalized with thiol terminated, poly(styrene)-PEG block copolymer (P(S-*b*-PEG)) ligands. Gold nanoparticles approximately 15 nm in diameter were first synthesized via reduction of $HAuCl_4$ with oleyl amine. Diels-Alder chemistry was then used to create P(S-*b*-EG) ligands that, with increasing temperature, dissociate into simple thiol-terminated PS ligands and PEG oligomers. The ligand-modified gold particles were characterized via small-angle X-ray scattering and TEM. After dissociation occurs, around 90 [r]C, the gold particles are suddenly functionalized with only a PS ligand and thus immiscible in the surrounding PEG matrix. The gold nanoparticles are then driven to the surface of the films, measurably denoted by a change in contact angle. After cooling below 60 [r]C, the Diels-Alders linkages reform, stabilizing the film surfaces with the new morphology trapped both chemically and kinetically.

**8:12**
**N28 2 Smart Polymeric Surfaces: Responsiveness and Reconstruction** JULIE CROWE, JAN GENZER, *N.C. State University* The ultimate responsive surface is one that instantaneously responds to its environment with a measurable property change. In our research we utilize model poly(vinylmethyl)siloxane elastomer (SE) networks modified with thiol alkanes to provide hydrophobic or hydrophilic surface properties. The cooperative effects of polymer mobility, arising from the high flexibility of the siloxane backbone, and the enthalpic interactions between the outside medium and the SE functionalized surface control the degree of responsiveness as measured by dynamic and static contact angle. The initial parameters screened were alkane chain length, medium temperature, and end-group functionality. Real-time wetting force measurements have been obtained with dynamic contact angle, where the surface reconstruction is measured continuously providing a means to determine the kinetics of reconstruction and reversibility. Our examples show that not only are SE networks excellent stimuli-responsive substrates, but that the magnitude of change and repeated reversibility are unparallel to most polymeric surfaces.

**8:24**
**N28 3 Conformations of Amphiphilic Comb Copolymer Chains Confined to Two Dimensions Through Self-Organization at the Polymer/Water Interface** WILLIAM KUHLMAN, ELSA A. OLIVETTI, LINDA G. GRIFFITH, ANNE M. MAYES, *Massachusetts Institute of Technology* Amphiphilic comb copolymers composed of a hydrophobic poly(methyl methacrylate) (PMMA) backbone and short, hydrophilic PEO side chains (PMMA $-$ *g* $-$ PEO) are known to self-organize at the polymer/water interface, resulting in the effective confinement of the backbone to two dimensions for chains at the surface of a PMMA-*g*-PEO film. Conformations of polymers thus confined were studied through selective nanoparticle labeling of PEO side chains of polymer molecules at the film surface. Transmission electron microscopy was used trace the backbone trajectory of nanoparticle labeled chains. The distribution of observed chain lengths is found in good agreement with the distribution determined by gel permeation chromatography. The 2D radius of gyration ($R_g$) calculated from the observed conformations was found

to scale with number of backbone segments ($N$) as $R_g \sim N^{0.69\pm0.02}$. This value agrees with Monte Carlo simulations for a system of similar polydispersity, which yield a scaling exponent between that for 2D isolated chains and monodisperse polymer melts ($R_g \sim N^{0.64\pm0.03}$).

**8:36**

**N28 4 Temperature-responsive polymers and brushes with tunable onset of response** THERESA FOLEY, *Penn State University* KIRIL EFIMENKO, *North Carolina State University* JAN GENZER, *North Carolina State University* EVANGELOS MANIAS, *Materials Science and Engineering, Penn State University* Temperature-responsive polymers are of high interest in the scientific field of stimuli responsive materials, in particular water soluble polymers with a response at $\sim 36.5^{o}$C. However, difficulties in tailoring this T-response, as illustrated for example from studies of PNIPAM in numerous functionalized and copolymer forms, has hampered their proliferation. Here we present a systematic series of temperature-responsive polymers, which were designed, synthesized, and studied, and we show that we can tailor with high sensitivity their onset of T-response via the design of their monomer. Specifically, we demonstrate lower critical solution temperature (LCST) in water finely tuned between 5 and $70^{o}$C, by controlling the hydrophilic/hydrophobic balance in the monomer (closely following predictions of phase behavior theories). In addition, we will also show that these polymers maintain their T-responsive characteristics when end-tethered to solid surfaces, over a wide range of grafting densities in combinatorial brushes. This approach allows for controlling contact angle, adhesion and tackiness as a function of temperature.

**8:48**

**N28 5 Single Molecule Experiments with Adsorbed Polyelectrolytes*** SERGIY MINKO, YURI ROITER, We report on the AFM study of single polyelectrolyte (positively charged) molecules (PE) adsorbed on mica surfaces at different conditions (we vary pH and salt concentration). The study was carried out under aqueous solutions in a liquid cell. We observed behavior of PE in real time. The AFM experiments were experiments when possible effects of the AFM tip on PE conformations were minimized. A series of experiments were carried out when PE was adsorbed between two electrodes at applied electrical potential. The AFM images were processed to extract contour length, end-to-end distance, and radii of center of mass. The experiments revealed several interesting facts about adsorption of PE. The chain statistics was found to be consistent with the 2D random walk model. A decrease of charge density resulted in the coil-to-globule transition. The globules appear as a strongly deformed swollen polymer globule. In saline solutions the globules resemble necklace-like globules. PE chains were mobile if an electrical field was applied. The motion of PE chains can be describes as a caterpillar-like motion.

*Support from NATO NSF Grant DGE-0411649.

**9:00**

**N28 6 Quantifying How Polymer Interfacial Diffusion Differs from Bulk** LIANG HONG, *Materials Science and Engineering Department, University of Illinois at Urbana-Champaign* STEVE GRANICK, *Department of Materials Science and Engineering, Chemistry, Physics, Chemical Engineering, University of Illinois at Urbana-Champaign* Whereas polymer adsorption-desorption kinetics are reasonably well explored, in-plane diffusion is not. This talk will describe the molecular weight (M) and surface coverage dependence of two polymers, polystyrene (PS) and polydimethylsiloxane (PDMS) adsorbed to quartz from organic solvent. The M scaling of surface diffusion is quantified, and a surprising dependence on surface coverage is described. Time permitting, additional studies will be described in which, for the first time, polymer self-diffusion has been studied within a surface forces apparatus designed for fluorescence spectroscopy. Using FRAP (fluorescence recovery after photobleaching) to study slow diffusion and FCS (fluorescence correlation spectroscopy) to study rapid diffusion, we quantify how the self-diffusion coefficient of PDMS oligomer melts slows with diminishing surface separation, when PDMS is confined between mica surfaces.

**9:12**

**N28 7 Balancing size exclusion and adsorption of polymers in nanopores** WON KIM, CHANG Y. RYU, *Rensselaer Polytechnic Institute, Department of Chemistry and Chemical Biology* The liquid chromatography at critical condition (LCCC) presents the condition, at which the size exclusion and adsorption of polymer chains are balanced upon interactions with nanoporous substrates. In this study, we investigate how the polymer interactions with nanopores are affected by the solvent quality and nanopore size. Specifically, we measure the retention times of monodisperse polystyrenes in C18-bonded nanoporous silica column as a function of molecular weight, when a mixed solvent of methylene chloride and acetonitrile are used as elutent. C18-bonded silica particles with 70, 100, and 250 A pore size are used as a stationary phase to study how the transition from SEC-like to IC-like retention behavior depends on the condition of temperature and solvent composition. To locate the LCCC at various nanopore sizes, the temperature and solvent composition have been varied from 0 to 60 C and from 51 to 62 v/v% of methylene chloride, respectively.

**9:24**

**N28 8 Polymer brushes dynamics by evanescent wave dynamic light scattering** BENOIT LOPPINET, VASSILIKI MICHAILIDOU, GEORGE FYTAS, *IESL-FORTH* JUERGEN RUEHE, *IMTEK Freiburg Germany* Dynamics of swollen brush is experimentally measured by dynamic light scattering in the total internal reflection geometry. Dense thick polymer polystyrene brushes with varying grafting densities are obtained through grafting from synthesis. When highly swollen in good solvent, concentration fluctuations are found to decay through a fast diffusive mechanism, attributed to the expected cooperative diffusion, akin to semi-dilute polymer solutions. Its hydrodynamic size is found to be comparable to the estimated distance between grafting chains. De-swelling of the brush by lowering solvent quality (using cyclohexane at different temperatures) leads to qualitative different dynamics. An extra slower relaxation with a broad distribution of relaxation times is observed, which strongly depends on solvent quality, with an extensive slow down of it characteristic time and an increase of scattered intensity upon cooling. This complex dynamics is discussed in relation to the dynamics in entangled semi-dilute solution in theta solvent. Finally, the brownian dynamics of colloidal particles (radius from 17nm to 100nm) in contact with the brushes are reported. The particles are found to marginally penetrate the brush, but to nonetheless exhibit dynamics reflecting their interactions with the outer part of the brush.

**9:36**

**N28 9 Electromechanical Recognition of Molecules Adsorbed on Microcantilevers** SANGMIN JEON, DONGKYU LEE, *POSTECH* THOMAS THUNDAT, *ORNL* An alternating current was applied to gold-coated silicon microcantilevers in sodium chloride solution. The cantilever is coated on one side with a thin layer of gold. Since the applied electric field through the cantilever attracts oppositely charged ions onto the gold layer, the variation of surface charges induces the oscillation of the cantilever. The larger the applied voltage is, the more the cantilever oscillates. When the experiment was repeated with self-assembled monolayer coated cantilever, the amplitude of the oscillation is decreased because the monolayer hinders the ions from approaching to the cantilever. In-situ measurements of the adsorption of mercaptohexanol molecules under the electric field clearly showed that the decrease of the oscillation resulted from the formation of the layer. When a square electric field was applied to 1-mercaptoethanol, 1-mercaptopropanol, and 1-mercaptohexanol coated cantilever, the bending profile of the cantilever depended on the kinds of the monolayer. This method can be used to study the diffusion of small ions through thin films as well as the structure of self-assembled monolayer.

**9:48**

**N28 10 Dependence of surface diffusivity on the molecular conformation of single hydrophobic polyelectrolytes molecules*** JIANG ZHAO, SHENGQIN WANG, *Institute of Chemistry, Chinese Academy of Sciences, Beijing 100080, China* Hydrophobic polyelectrolytes are found to have their conformation change from an extended chain to globule via neck- lace structures. In this work, surface diffusion of single poly (2-vinylpryridine) (P2VP) molecule was studied under different chemical environment (pH value and ionic strength). Via hydrophobic interaction, P2VP molecules adsorbed to a hydrophobic surface. By fluorescence correlation spectroscopy, fluorescence labeled P2VP molecules were found to raise their surface diffusivity moderately but monotonously when the pH value was tuned from 2.0 to 6.5. The physical mechanism of the diffusivity dependence on molecular conformation is discussed.

*Supported by Natural Science Foundation of China (NSFC) and Chinese Academy of Sciences (CAS).

**10:00**

**N28 11 Adsorption of polymers onto selective mixed brushes.** A.I CHERVANYOV, G. HEINRICH, *Leibniz-Institut fur Polymerforschung Dresden, Hohe Str. 6, 01069 Dresden, Germany* Reversible adsorption of polymers onto selective mixed brushes is studied theoretically. Mixed brushes are recently developed self-adoptive materials that reversibly change their morphology in response to altering external factors (e.g. quality of the solvent). The above changes in the morphology result in the formation of different patterns on the outer surface of the brush. It is shown that thus achieved patterning of the adsorbing surface of the mixed brush drastically enhances the adsorption of polymers, as compared to the adsorption onto the homogeneous brush surface. The density profiles and absorbances of the selected homo- and copolymers are calculated for the three different morphologies ('ripple', 'dimple' and random) of the binary brush. The interplay between conformational entropy and binding energy of the adsorbed polymer leads to the reach adsorption-desorption behavior that is described by the developed theory. The calculated isotherms are compared with the experimental data and Monte-Carlo simulation results. In addition, the developed theory is applied to the study of the polymer adsorption onto the non-uniform binary brush in the presence of the gradient of chemical composition.

**10:12**

**N28 12 Nano-meter structured three-phase contact line and its surface-guided alignment effect*** GANG LIU, JIANG ZHAO, *Institute of Chemistry, Chinese Academy of Sciences, Beijing 100080, China* We report our studies on the air-liquid-solid three-phase contact line on the periodically patterned surface made of polystyrene-b-polymethylmethacrylate (PS-b-PMMA). The difference of the contact angle of the liquid (water and polymer solution) on PS and PMMA generates the contact line with periodic structures of 40 nm length scale. Such a structured contact line was found to produce surface guided alignment effect for single DNA molecules by the molecular combing process and to generate surface-guided morphology of the polymer films through a combination of de-pinning and de- wetting process.

*Supported by Natural Science Foundation of China (NSFC) and Chinese Academy of Sciences (CAS).

**10:24**

**N28 13 Surface diffusion of adsorbed polymers studied by molecular dynamics simulation** WONKI ROH, ERIK LUIJTEN, *University of Illinois at Urbana-Champaign* We study the diffusion of adsorbed polymers near a flat surface by means of molecular dynamics simulations, as a function of chain length $N$, adsorption energy, and surface coverage $\phi$. We find that the two-dimensional diffusion coefficient scales as $D \sim N^{-1.017\pm0.011}$, in agreement with other experimental and simulation results. The relation between lateral diffusion coefficient and surface coverage shows an exponential decay. We also investigate the conformation of the adsorbed chains. The number of ''trains,'' ''loops,'' and ''tails'' per chain, as well as the number of monomers in tails and loops increase as surface density increases and adsorption energy decreases, whereas the number of monomers in trains decreases. The parallel radius of gyration increases as a power law of the chain length, $\langle R_{g\|}^2 \rangle \sim N^{2\nu}$, with a power that is in good agreement with the Flory exponent $\nu = 3/4$ for two-dimensional chains. $\langle R_{g\|}^2 \rangle$ decreases with increasing surface density and decreasing adsorption energy, whereas $\langle R_{g\perp}^2 \rangle$ remains almost constant with increasing surface density and increases with decreasing surface energy.

**10:36**

**N28 14 Solvent and salt effects on the adsorption of polymers to charged surfaces** GOVARDHAN REDDY, ARUN YETHIRAJ, *Univeristy of Wisconsin - Madison* The effect of solvent quality and salt concentration on the adsorption of charged polymers to a planar uniformly charged surface is studied using molecular dynamics simulation. The polyion chains are modeled as chains of charged spheres, the counter ions to the polyions and the surface are modeled as charged spheres, and the solvent molecules are modeled as uncharged spheres. The polyion adsorption is studied as a function of monomer and salt concentration, solvent quality and surface charge density of the surface. The amount of polyion adsorbed on the surface increases with the decrease in solvent quality as the system approaches a bulk phase transition. There are some surprising and counter-intuitive results in this re-

gime. For example, incoprporating a short-ranged attraction between the polymers and the surfaces decreases the number of adsorbed polymers, and the amount of polyion adsorbed decreases as the salt concentration increases.

**10:48**

**N28 15 Mean-field theory of planar absorption of RNA molecules*** TOAN NGUYEN, *Dept. of Physics and Astronomy, University of California, Los Angeles* ROBIJN BRUINSMA, *Dept. of Physics and Astronomy, University of California, Los Angeles* WILLIAM GELBART, *Dept. of Chemistry and Biochemistry, University of California, Los Angeles* Interaction between the viral RNA and the protective protein capsid plays a very important role in the cell infection and self-assembly process of a virus. To better understand this interaction, we study a similar problem of absorption of RNA on an attractive wall. It is known that the secondary structure of a folded RNA molecules without pseudo-knots has the same topology as that of a branched polymer. We use a mean-field theory for branched polymers to analytically calculate the RNA concentration profile. The results are compared to known exact scaling calculations and computer simulations.

*Supported by NSF under DMR Grant 0404507 and CHE 0400363.

## SESSION N29: FOCUS SESSION: PHYSICAL MODELS OF ION CHANNEL FUNCTION

**Wednesday Morning, 15 March 2006**
**326, Baltimore Convention Center at 8:00**
**Bob Eisenberg, Rush University, presiding**

***Contributed Papers***

**8:00**

**N29 1 The metabolic energy cost of action potential velocity** PATRICK CROTTY, *University of Virginia Health System* THOMAS SANGREY, *Emory University* WILLIAM LEVY, *University of Virginia Health System* Voltage changes in neurons and other active cells are caused by the passage of ions across the cell membrane. These ionic currents depend on the transmembrane ion concentration gradients, which in unmyelinated axons are maintained during rest and restored after electrical activity by an ATPase sodium-potassium exchanger in the membrane. The amount of ATP consumed by this exchanger can be taken as the metabolic energy cost of any electrical activity in the axon. We use this measure, along with biophysical models of voltage-gated sodium and potassium ion channels, to quantify the energy cost of action potentials propagating in squid giant axons. We find that the energy of an action potential can be naturally divided into three separate components associated with different aspects of the action potential. We calculate these energy components as functions of the ion channel densities and axon diameters and find that the component associated with the rising phase and velocity of the action potential achieves a minimum near the biological values of these parameters. This result, which is robust with respect to other parameters such as temperature, suggests that evolution has optimized the axon for the energy of the action potential wavefront.

**8:12**

**N29 2 The Dependence of Ionic Conduction on the Dielectric Properties of Ion Channels** MARCO SARANITI, DAVID MARREIRO, *Illinois Institute of Technology* SHELA ABOUD, *Worcester Polytechnic Institute* The ion channel OmpF porin is a water filled trimer found in the outer membrane of itEscherichia coli. Each monomer is a hollow barrel structure with a physical constriction near the center that reduces the width of the pore to approximately 6 Å. Highly charged residues line the inside of the pore constriction, generating an intense electric field that facilitates the dynamics of ions through the channel. The cost of simulating these systems for long times is an oversimplification of key physical features of the ion channel system, most notably, the polarization effects related to the solvent (water) and the protein are poorly represented by a stepwise constant dielectric constant. While the use of this model for the aqueous solution inside the permeation pore is arguably suitable because the ionic hydration shell remains intact (at least away from the central constriction), its validity is questionable when used to describe the polarization response of the protein. In this work, a previously validated $P^3M$ force-field scheme, self-consistently coupled to a Brownian Dynamics kernel, is used to investigate the influence of the protein dielectric constant on permeation in OmpF porin. The computed channel conductivity is in agreement with experimental measurements. Increased cation selectivity at low ionic concentrations is also observed in the simulations and appears to be dependent on the rings of aspartic acid residues around the mouths of the porin.

**8:24**

**N29 3 Rocking and Flashing Ratchet Mechanisms of Ion Current Rectification in Asymmetric Nanopores in the Presence of Calcium** ZUZANNA SIWY, MATTHEW POWELL, ERIC KALMAN, *Univ. of California, Irvine* BOB EISENBERG, *Rush University Medical Center, Chicago* We have investigated an engineered system of a single nanopore in a plastic membrane that shows rectification depending on the chemical composition of the surrounding solutions. No lipid bilayer is involved so the system is simple and robust with $>$ 10 gigohm leak resistance. The single nanopores are tapered cones with openings of diameter $\sim$ 600 nm and $\sim$ 5 nm. The single nanopores were prepared by the track-etching technique. The walls of the pores have carboxylate groups with surface density $\approx$ 1.5 ($\mathbf{e}/[\mathrm{nm}]^2$). Transport properties of these nanopores were studied by recording current-voltage curves in a variety of solutions. In KCl solutions these single asymmetric nanopores are cation selective and rectify with a ratio of limiting conductances $\approx$ 4-10. The K ions flow with lower resistance from the smaller to larger opening. Adding millimolar Ca to both sides reverses the direction of rectification and produces a negative incremental resistance; i.e., larger magnitudes of voltage produce smaller magnitudes of ion current. The rectifying properties of these asymmetric nanopores are described by rocking and flashing ratchet models of directional motion. It will be interesting to compare permeation, selectivity, and gating properties of the polymer nanopores and biological voltage-gated calcium channels.

*Invited Papers*

**8:36**
**N29 4 Ion selectivity in the ryanodine receptor and other calcium channels.**
DIRK GILLESPIE, *Rush University Medical Center*

Biological ion channels passively conduct ions across cell membranes, some with great specificity. Calcium channels are selective channels that range in their $Ca^{2+}$ affinity depending on the channel's physiological role. For example, the L-type calcium channel has micromolar affinity while the ryanodine receptor (RyR) has millimolar affinity. On the other hand, both of these channels have the chemically-similar EEEE and DDDD amino acid motifs in their selectivity filters. An electrodiffusion model of RyR that reproduces and predicts $>$ 50 data curves will be presented. In this model, ions are charged, hard spheres and the chemical potential is computed using density functional theory of fluids. Ion selectivity arises from a competition between the need for cations to screen the negative charges of the channel and the crowding of ions in the tiny space of the channel. Charge/space competition implies that selectivity increases as the channel volume decreases (thereby increasing the protein charge density), something that has recently been experimentally confirmed in mutant channels. Dielectric properties can also increase selectivity. In Monte Carlo simulations, $Ca^{2+}$ affinity is much higher when the channel protein has a low dielectric constant. This counterintuitive result occurs because calcium channel selectivity filters are lined with negatively-charged (acidic) amino acids (EEEE or DDDD). These permanent negative charges induce negative polarization charge at the protein/lumen interface. The total negative charge of the protein (polarization plus permanent) is increased, resulting in increased ion densities, increased charge/space competition, and there in increased $Ca^{2+}$ affinity. If no negative protein charges were present, cations would induce enough positive polarization charge to prevent flux.

*Contributed Papers*

**9:12**
**N29 5 Modeling Activity: Ions to Hydrophobics in Crowded Biological Solutions** MONTGOMERY PETTITT, *University of Houston* Nonideal solutions play a role in many aspects of chemistry. As concentrations increase, concentration itself becomes a less useful quantity to understand equilibria. Industrial and medicinal chemistry often fail due to the difference between concentration and activity. An understanding of the impact of the crowded conditions in the cytoplasm on its biomolecules is of clear importance to biochemical, medical and pharmaceutical science. Work on the use of small biochemical compounds to crowd protein solutions indicates that a quantitative description of their non-ideal behavior is possible and straightforward. Here, we will show what the structural origin of this non-ideal solution behavior is from expression derived from a semi grand ensemble approach. We discuss the consequences of these findings regarding protein folding stability and solvation in crowded solutions through a structural analysis of the m-value or the change in free energy difference of a macromolecule in solution with respect to the concentration of a third component.

**9:24**
**N29 6 Entropy driven insulator-metal crossover in ion channels and water filled nanopores** JINGSHAN ZHANG, ALEX KAMENEV, BORIS SHKLOVSKII, ANATONY LARKIN,* *University of Minnesota* We consider ion transport of an ion channel in a lipid membrane or a water filled nanopore in silicon films [1]. It is known that due to the large ratio of dielectric constants of water (80) and lipid (2), the electric lines of an ion in the channel are squeezed. This should lead to a large electrostatic self-energy barrier for Ohmic resistance [2]. Nevertheless biological channels are well transparent at least for some selected ions. To address this paradox, we study reduction of the electrostatic barrier by a finite concentration of salt in water and/or by immobile charges on the internal channel walls. We show that both types of charges reduce the barrier, leading to insulator-metal crossover resembling metal-insulator transition in excited gas or in doped semiconductors. But here entropy plays the role of quantum mechanics. Evolution of ion channels took into account biological concentration of monovalent salt, and more importantly, made some channels charged from inside to reduce electrostatic barrier for a given sign of ions (cation/anion selectivity). We also show that in the channel with negative wall charges fractionalization of divalent Ca ions into monovalent excitations leads to good Ca-Vs.-Na selectivity of Ca channels. [1] A. Kamenev, J. Zhang, A. I. Larkin, B. I. Shklovskii, Physica A 359, 129 (2006); J. Zhang, A. Kamenev, B. I. Shklovskii, Phys. Rev. Lett. 95, 148101 (2005); cond-mat/0510327. [2] A. Parsegian, Nature 221, 844 (1969).

*Deceased.

**9:36**
**N29 7 Measurement of gating forces of mechanosensitive channels of large conductance in Escherichia coli** ELVIS PANDZIC, PAUL WISEMAN, MARIA KILFOIL, *Physics McGill* J. L. NADEAU TEAM,*J. A. MAURER COLLABORATION,† In order to sense and respond to external mechanical stimuli, cells have evolved schemes to incorporate mechanosensors within their plasma membranes. Mechanosensitive channels of large conductance (MscL) are used by bacterial cells to respond quickly and effectively to hypo-osmotic shock: the opening of this channel permits cells to quickly release large amounts of osmolytes in order to quickly equalize unbalanced osmotic pressure across a membrane. In this study, we are investigating the physical mechanism of the MscL gating within the native environment of the itEscherichia coli cells. We are using the green fluorescent protein (GFP) and derivative proteins (CFP, BFP) to label the C-termini of MscL subunits in order to observe the channels in live bacteria by fluorescence microscopy. Moreover, we label the opposite termini with a different chromophore system that constitutes an excellent fluorescence resonance energy transfer (FRET) pair with CFP. Channels are activated within the bacterial membrane by osmotic stress and interactions between differently labeled subunits are measured by fluorescence microscopy.

*Biomedical Engineering at McGill University.
†Chemistry Dept. at Washington University in St-Louis.

*Invited Papers*

**9:48**
**N29 8 Calculating Ion Permeation through Biological Channel Proteins.***
ROB COALSON, *University of Pittsburgh*

We have developed methodology to simulate the current of ions (Na+, Cl-, etc.) through a general three-dimensional ion channel structure embedded in a lipid bilayer when an electric potential is applied across the membrane. These calculations are done at the level of Brownian dynamics, i.e., ions are treated as particles and their motion is computed using a stochastic algorithm which simulates Brownian motion. Water solvent is treated as a dielectric continuum, which both supplies the thermal agitation underlying the motion of the ions and influences the electrostatic forces on these ions by virtue of its dielectric constant (which differs substantially from that of the protein-membrane complex). Application is made to the Glycine Receptor channel, emphasizing physico-chemical influences on ion current, e.g., charges of critical pore-lining amino acids, channel geometry, etc.

*This work is supported by NSF and DOD-MURI.

*Contributed Papers*

**10:24**
**N29 9 Morphometric approach to selectivity and gating of ion channels** ROLAND ROTH, *MPI fuer Metallforschung, Heisenbergstrasse 3, 70569 Stuttgart, Germany* A physical understanding of selectivity and gating of ion channels requires the free energy of the fluid confined in the channel pore. The free energy depends not only on fluid properties like its density, but also on the interaction between fluid particles and the confining protein, which gives rise to a potentially complicated dependence of the free energy on the conformation of the protein. Here we propose a simple thermodynamic approach that employs the idea that the free energy can be separated into geometrical measures and corresponding thermodynamic coefficients. Our approach enables us to calculate the change in the free energy caused by a change of the pore conformation such as that underlying the gating of an ion channel. We study the connection between the geometrical change of a hydrophobic pore and capillary evaporation, i.e. the effect that water is expelled from the permeation pathway and ion flow is thereby stopped although the pore remains wider than the water or ion diameters. We estimate the energy it takes to remove the water from the pore. Within the same thermodynamic framework, we can also study effects of pore conformation on the equilibrium absorption of ions and thus on ionic selectivity of the channel.

**10:36**
**N29 10 Voltage Sensor in Voltage-gated ion channels** FRANCISCO BEZANILLA, *Institute for Molecular Pediatric Science. University of Chicago* Voltage-gated ion channels are intrinsic membrane proteins that play a fundamental role in the generation and propagation of the nerve impulse. Their salient characteristic is that the probability of the ion channel of being open depends steeply on the voltage across the membrane where those channels are inserted. Thus, in a membrane containing many channels, the ionic conductance is controlled by the membrane potential. The voltage exerts its control on the channel by reorienting intrinsic charges in the protein, generally arginine or lysine residues located in the 4th transmembrane segment of the channel protein, a region that has been called the voltage sensor. Upon changing the membrane potential, the charged groups reorient in the field generating a transient current (gating current). The properties of the gating current may be studied with a small number of channels to infer the operation of the sensor at the single molecule level by noise analysis or with a large number of channels to infer the details of the energy landscape the sensor traverses in opening the pore. This information is global in nature and cannot pinpoint the exact origin of the charge movement that generates the gating current. The movement of physical charges in the protein has been inferred with site-directed mutagenesis of the charged residues to histidine that allows the study of proton accessibility. The actual movement has been studied with fluorescence spectroscopy, fluorescence resonance energy transfer. The combined information of site-directed mutagenesis, gating currents, fluorescence studies and emerging crystal structures have started to delineate a physical representation of the conformational changes responsible for voltage sensing that lead to the opening of the conduction pore in voltage-gated ion channels.



## SESSION N30: BLOCK COPOLYMER PHASE BEHAVIOR
**Wednesday Morning, 15 March 2006**
**327, Baltimore Convention Center at 8:00**
**Thomas Epps, National Institute of Standards and Technology, presiding**

**8:00**
**N30 1 Equilibrium Phase Diagram of a Model Rod-Coil Block Copolymer** B.D. OLSEN, R.A. SEGALMAN, *University of California Berkeley and Lawrence Berkeley National Lab* Rod-coil block copolymers can be used to form important self-assembled structures containing functional blocks such as helical polypeptides or conducting polymers. The thermodynamics of these materials is distinct from classical block copolymers due to the conformational asymmetry of the polymer chain and the effect of liquid crystallinity on the microphase structure. We have recently developed a weakly segregated model system, poly(alkoxyphenylene vinylene-b-isoprene) (PPV-b-PI), in which rod-rod and rod-coil interactions are modulated by the presence of short side chains on the rod. We present the phase diagram for rod-coil block copolymers in the weak segregation limit, demonstrating equilibrium lamellar, nematic, and isotropic phases. As molecular weight is increased, subtle order-order transitions in the lamellar phase become obvious. In particular, we will discuss the relative stabilities of smectic phases based on scattering data. Finally, we will discuss the non-lamellar hexagonal phases that are observed as the relative rod-fraction of the block copolymer is decreased.

**8:12**

**N30 2 Phase behavior of linear ABC triblock copolymer** JOON CHATTERJEE, FRANK S. BATES, *Department of Chemical Engineering and Material Science, University of Minnesota* We report the study of melt phase behavior of poly(isoprene-*b*-styrene-*b*-ethylene oxide) as our model ABC triblock copolymer. Previous investigations on this system have discovered a network phase with $O^{70}$ space group symmetry in an orthorhombic lattice adjacent to network phases with cubic lattice symmetries, namely, alternating gyroid and core-shell gyroid. The present study investigates and expands the phase diagram with varying monomer compositions and temperature. Nearly monodisperse triblock copolymers with controlled molecular weights and block compositions are synthesized by anionic polymerization techniques. Blending of homopolymers with the triblock copolymer is used to refine the phase boundaries. Dynamic mechanical spectroscopy, small angle x-ray scattering, TEM and optical experiments are used to characterize the equilibrium morphologies. Other new phases such as hexagonal cylinders and bcc spheres have been observed. We observe that the phase diagram is not symmetric across the $f_A = f_C$ isopleth.

**8:24**

**N30 3 Electron tomography of a novel non-cubic network phase in ABC copolymers** GERD E. SCHROEDER, STEPHEN T. HYDE, *Applied Maths, RSPhysSE, Australian National University, 0200 ACT, Australia* HERMIS IATROU, NIKOS HADJICHRISTIDIS, *Chemistry Dept, Univ of Athens, Panepistimiopolis, Zografou 15771, Athens, Greece* SATOSHI AKASAKA, HIROKAZU HASEGAWA, *Dept of Polymer Chemistry, Grad School of Engineering, Kyoto Univ, Katsura, Nishikyo-ku, Kyoto 615-8510, Japan* We report the discovery of a novel bicontinuous tetragonal phase in the linear ABC triblock terpolymer system polystyrene (PS), polyisoprene (PI) and polydimethylsilocane (PDMS). The data is consistent with spacegroup Fddd and is distinctly non-cubic. The channel topology is distinct from the better-known cubic bicontinuous mesophases (diamond and gyroid types, with channels). It consists in 2 identical intertwined labyrinths with 3- and 4-connected nodes. Our mesophase differs from an earlier report of a copolymer phase (also in a linear terpolymer system) with the same spacegroup by Epps *et al* (Macromolecules **37**, 8325-41, 2004), who deduced a single channel morphology, based on TEM and SAXS data. Our proposal is based on 3D $e^-$-tomography data. The channel geometry is identified via a medial surface (MS) algorithm. For a labyrinth, the MS is a generalised channel graph consisting in surface patches. In contrast to line graphs, the MS is a complete descriptor of both topology and geometry. It provides robust shape characteristics, and is a useful tool for visualisation of complicated hyperbolic mazes.

**8:36**

**N30 4 Phase behavior of poly(pentafluorostyrene-b-methyl methacrylate) block copolymers** TRACY BUCHOLZ, YUEHLIN LOO, *University of Texas at Austin* Fluorine-containing polymers have garnered interest for properties such as chemical inertness, high thermal stability, and low dielectric constants. Previously, the controlled synthesis of fluoropolymers has been difficult due to the electron-withdrawing nature of fluorinated monomers. This issue, however, has been addressed with the development of atom transfer radical polymerization. Using this technique, we have been able to synthesize diblock copolymers containing polypentafluorostyrene (PPfS) and poly(methyl methacrylate), PMMA. The resulting diblock copolymers exhibit narrow molecular weight distributions ( $\leqslant$ 1.1) and undergo microphase separation to form highly-ordered nanostructures at moderate molecular weights. Comparisons of order-disorder transition temperatures with anionically synthesized poly(styrene-b-isoprene), PS/PI, diblocks of comparable molecular weights and compositions suggest that the segregation strength of PPfS/PMMA is within a factor of two of that of PS/PI. This observation is surprising given the chemical uniqueness of PPfS and PMMA but is in fact in agreement with the theoretical segregation strength relative to PS/PI predicted by differences in their solubility parameters.

**8:48**

**N30 5 Perforated layer structures in liquid crystalline block copolymers** KISHORE TENNETI, *Drexel University* XIAOFANG CHEN, *Peking University* CHRISTOPHER LI, *Drexel University* YINGFENG TU, XINHUA WAN, QI-FENG ZHOU, *Peking University* IGORS SICS, BENJAMIN HSIAO, *University of Stony Brook* DREXEL UNIVERSITY TEAM, PEKING UNIVERSITY COLLABORATION, UNIVERSITY OF STONY BROOK COLLABORATION, Phase structures of a series of poly(styrene-block-(2,5-bis-(4- methoxyphenyl)oxycarbonyl)styrene) (PS-b-PMPCS) liquid crystalline rod-coil block copolymers (LCBCPs) were investigated using thermal analysis, X-ray analysis and transmission electron microscopy. In the low molecular weight asymmetric BCP system, perforated layer structures were observed where the excessive PS molecules punctured the PMPCS domains and these perforations uniquely possess tetragonal in-plane symmetry. In the high molecular weight system, these perforated layer structures were observed in symmetric samples. Randomly initiated perforations became more regular and uniform upon blending with PS homopolymer in symmetric BCPs. These regular perforations also possess tetragonal in-plane symmetry.

**9:00**

**N30 6 Self-assembly of polydisperse acrylic block copolymers** ANNE-VALERIE RUZETTE, LUDWIK LEIBLER, *Laboratoire Matiére Molle et Chimie, UMR 7167 ESPCI-CNRS, Paris, France* FLORENCE CHAUVIN,*DENIS BERTIN, *Chimie, Biologie et Radicaux Libres, UMR 6517, Marseille, France* PIERRE GERARD, *ARKEMA, Lacq, France* Self-assembled block copolymers present great interest since they combine at the nanometer scale intrinsic properties of different homopolymers. Over the past decade, remarkable progress in synthetic chemistry has unveiled new opportunities to prepare tailored block copolymers of judiciously chosen monomer type and architecture at reasonable cost. In particular, controlled radical polymerizations (CRP) are suitable to all kinds of vinyl monomers in common mass, suspension or even emulsion processes. Most synthetic efforts in this field have focused on developing a ''living'' character of free radical chain-ends and control polydispersity in length and composition. Here, we discuss a different, though quite common, situation where only one of the copolymer blocks is controlled. Overall composition and molecular weight polydispersities are thus large. Self-assembly and mesoscopic order in these ''asymmetrically polydisperse'' block copolymers and their blends is discussed.

*Present address: ARKEMA, King of Prussia, PA, USA.

**9:12**

**N30 7 Electrospun poly(styrene-b-isoprene) fibers that exhibit internal structure** SERGIO MENDEZ, VIBHA KARLA, PRASHANT KAKAD, MARLEEN KAMPERMAN, YONG JOO, *Cornell University* We have used the elelctrospinning process to fabricate fibers from THF / poly(styrene-b-isoprene) (PS-PI) diblock copolymer solutions. We spun fibers with copolymers that had various volume fractions of PI. These fibers had diameters ranging from 200 nm to 5 microns depending on the processing conditions such as solution concentration, needle size, electric field, etc. The goal of this investigation was to observe the formation of self-assembled microstructures within the fibers. SAXS data indicates that the copolymer microphase separates and that there is some degree of globally ordered domains; however, TEM images indicate that this order is more local which might be due to the short residence time in the electrospinning process. By comparison, SAXS and TEM data of PS-PI films exhibits unambiguous global ordering. In an attempt to improve the long range order within the fibers, we performed various annealing treatments, and found that heating at temperatures below the glass transition temperature only had a small effect.

**9:24**

**N30 8 Confinement induced novel morphologies of block copolymers** AN-CHANG SHI, *McMaster University* BIN YU, BAOHUI LI, *Nankai University* Self-assembly of block copolymers confined in cylindrical nanopores is studied systematically using a simulated annealing method. For diblock copolymers which form two-dimensional hexagonally-packed cylinders with period $L_0$ in the bulk, novel structures such as helices and stacked toroids spontaneously form inside the cylindrical pores. These confinement induced morphologies have no counterpart in the bulk system and they depend on the pore diameter ($D$) and the surface-polymer interactions, reflecting the importance of structural frustration and interfacial interactions. On tightening the degree of confinement, transitions from helices to toroids to spheres are observed. Mechanisms of the morphological transitions can be understood based on the degree of structural frustration parametrized by the ratio $D/L_0$.

**9:36**

**N30 9 Self-assembly of three-dimensional morphologies in a diblock copolymer melt confined in a cylindrical nanopore*** WEIHUA LI, ROBERT A. WICKHAM, *Department of Physics, STFX, Antigonish, NS* The microdomain morphologies of an AB diblock copolymer melt confined in a cylindrical nanopore are investigated using three- dimensional real-space self-consistent mean-field theory. We find that many structures self-assemble in the pore, including cylinders, helices, toroids, disks, and spheres. We compute the relative stability of these structures and locate transitions between phases as the diameter of the pore is varied. We focus on narrow pores for simplicity since it appears that the number and complexity of the structures formed increases as the pore size increases. For each of our morphologies, we measure the inter-domain distance, the degree of chain stretching, the area of A/B interface, and the A/B interfacial curvature. We identify which of these factors are driving the structural transitions. Our results will be compared with recent experiments and simulations.

*NSERC, CFI.

**9:48**

**N30 10 Effects of confinement on the order-disorder transitionin diblock copolymer melts and crystallization** DADONG YAN, BING MIAO, CHARLES C. HAN, *PPCL, Joint Laboratory of Polymer Science and Materials, Institute of Chemistry, Chinese Academy of Sciences, Beijing 100080, China* AN-CHANG SHI, *Department of Physics and Astronomy, McMaster University, Hamilton, Ontario L8S 4M1, Canada* The effects of confinement, in terms of size and geometry, on the order-disorder transition (ODT) in diblock copolymer melts are studied theoretically. Confinements are applied by restricting diblock copolymers in given geometries of slab, cylinder and sphere, respectively. Within the frame of self- consistent field theory, the second-order fluctuation of free energy functional is studied, and its minimum determines the spinodal point of the homogeneous phase. For the slabs and cylindrical cases the spinodal point $(\chi N)_s$ of the homogeneous phase is independent of the confinement, while in spherical case $(\chi N)_s$ is increased except some suitable radius of the sphere. In addition, using the idea that before nucleation there are fluctuations of the orientation of polymer chains, the puzzling direction of lamellae in the crystallization under confinement can be explained.

**10:00**

**N30 11 Effect of Cross-linking on the Structure and Thermodynamics of Lamellar Block Copolymers** ENRIQUE GOMEZ, NITASH BALSARA, *University of California, Berkeley* JAYAJIT DAS, ARUP CHAKRABORTY, *Massachusetts Institute of Technology* The effect of cross-linking on the structure and thermodynamics of a lamellar poly(styrene-itblock-isoprene) copolymer was studied using small angle X-ray scattering (SAXS), depolarized light scattering (DPLS) and transmission electron microscopy (TEM). The selective cross-linking of the polyisoprene block took place either in the disordered state, in an isotropic ordered state, or in a shear-aligned ordered state. Using DPLS and TEM, the grain structure as a function of cross-linking density was studied. The order-disorder transition temperature for various block copolymer networks was determined as function of cross-linking density, and comparisons are made to a mean-field theory.

**10:12**

**N30 12 Influence of Conformational Asymmetry on the Phase Behavior of Ternary Homopolymer/Block Copolymer Blends around the Bicontinuous Microemulsion Channel** NING ZHOU, TIMOTHY LODGE, FRANK BATES, *University of Minnesota* We have developed a new ternary polymeric system, poly(ethylene-alt-propylene) (PEP) / poly(butylene oxide) (PBO) / PEP-PBO, to study the complex phase behavior near the bicontinuous microemulsion phase channel. The molecular weights of the PEP and PBO homopolymers are 2600 and 3050 g/mol, respectively, and copolymer is 23.4 kg/mol with volume fraction composition fPBO = 0.49. A combination of small-angle neutron scattering, small-angle X-ray scattering, rheology, optical microscopy and visual oil bath measurements was employed to map out the phase diagrams at five fixed homopolymer PBO/PEP ratios, ranging from 40/60 to 60/40 by volume, with copolymer concentrations ranging from 0 to 100%. It was found that the bicontinuous microemulsion channel is consistently cut off at low temperature by a hexagonal phase. We attribute this phenomenon to the effect of the conformational asymmetry between the PEP and PBO

species, whereby the more flexible PBO component induces a spontaneous curvature toward the PBO domains. These findings complement previous descriptions of the isopleth phase diagrams for the A/B/A-B systems, and identify a new design variable for preparing bicontinuous phases.

**10:24**
**N30 13 Swelling and Shrinkage of Lamellar Domain of Conformationally Restricted Block Copolymers by Metal Chloride*** DONG HYUN LEE, JIN KON KIM, *Department of Chemical Engineering, Pohang University of Science and Technology* JUNE HUH, *School of Materials Science and Engineering, Seoul National University* DU YEOL RYU, *Department of Chemical Engineering, Yonsei University* The lamellar domain spacing (D) of symmetric polystyrene-block- poly(2-vinyl pyridine) copolymer (PS-P2VP) and PS-block-poly(4- vinyl pyridine) copolymer (PS-P4VP) with cadmium chloride (CdCl2) were studied by using rheometry, small angle X-ray scattering and transmission electron microscopy. With increasing amount of CdCl2, D of PS-P2VP increased greatly, but it decreased for PS-P4VP. This is due to different types of the coordination between CdCl2 and nitrogen atoms in the 2-position of pyridine ring (intra-chain coordination), compared with nitrogen atoms in the 4-position (inter-chain coordination).

*This work was supported by the Creative Research Initiative Program (KOSEF).

**10:36**
**N30 14 Azimuthal Orientational Correlations due to Excluded Volume Epitaxy in Growing Anisotropic Grains** ASHOUTOSH PANDAY, SAMUEL GIDO, *University of Massachusetts, Amherst, MA 01003* The understanding of the microstructure of anisotropically shaped grains can have a strong influence on a range of material properties, including transport, mechanical and electro-optical properties. A grain-structure related phenomenon, called Excluded Volume Epitaxy (EVE) is reported in this study. EVE is a local, inter-grain orientational correlations effect, which results from a combination of sporadic nucleation of anisotropic grains and impingement of growing grains. Due to EVE, the anisotropically shaped grains have a tendency to be similarly aligned in a local neighborhood, despite the fact that there is no global orientation in the sample. This effect has been verified by transmission electron microscope (TEM) images of lamellar block copolymers and optical micrographs of small molecule crystals. Additionally, to quantify the effect of EVE, a modeling and simulation study involving random nucleation and subsequent growth of anisotropic grains was performed. The simulation study revealed a tendency for azimuthal, inter-grain orientational correlation and re-confirmed the experimental observation of EVE.

**SESSION N31: CARBON NANOTUBES: THEORY**
**Wednesday Morning, 15 March 2006**
**328, Baltimore Convention Center at 8:00**
**Dimitrios Papaconstantopoulos, Naval Research Laboratory, presiding**

**8:00**
**N31 1 Cyanide Nanotubes** YINA MO, EFTHIMIOS KAXIRAS, *Harvard University* The discovery of carbon nanotubes (CNTs) has given birth to an entire field devoted to the study of these one-dimensional (1D) nano-scale structures with extraordinary properties and tremendous promise for applications. To mention but a few, single wall carbon nanotubes are reported to exhibit Luttinger liquid behavior and proximity-induced superconductivity, and can be efficient hydrogen storage systems. The electronic properties of a carbon nanotube are fully determined by its helicity and range from metallic to semiconducting. However, when growing nanotubes, it is not possible to control the helicity; thus, carbon nanotube properties are not a result of design but luck. To overcome this limitation, Cohen and coworkers predicted the existence of insulating boron-nitride nanotubes (BNTs) and Zettl produced such tubes experimentally; these tubes are semiconducting and their properties vary less with helicity. Here we propose another type of structurally simple and energetically stable nanotubes consisting of transition metals and cyanide units. which are semiconductors with large band gaps ( $\sim 2 - 3$ eV). Using first-principles calculations, we study the properties of these nanotubes and find that their helicity does not significantly affect the electronic band gap. The nature of bonding in these systems singles out a particular helicity as energetically more stable, suggesting that only one type of tube will be predominantly formed with well defined electronic properties.

**8:12**
**N31 2 Electronic Structure of Core-Shell Semiconductor Nanowires** LI YANG, MEI-YIN CHOU, *Georgia Institute of Technology* We investigate the electronic structure of silicon/germanium core-shell nanowires with first-principles calculations using the local density approximation (LDA) with pseudopotentials and plane waves. The atomic configurations of the core-shell nanowires are fully relaxed. By examining the wave functions in real space, the electronic states at the band edge are found to be localized in either the core or the shell part of the nanowire. The band offsets are calculated for different core-shell structures. Given the cylindrical band offsets and the associated confined electronic states, a novel doping mechanism in nanowires is proposed for the manufacturing of high-speed nano-devices.

**8:24**
**N31 3 Dielectric properties of carbon nanotubes from first principles*** BORIS KOZINSKY, NICOLA MARZARI, *Massachusetts Institute of Technology* We characterize the response of single- (SWNT) and multi-wall (MWNT) carbon nanotubes to static electric fields using first-principles calculations and density-functional theory. The longitudinal polarizability of SWNTs scales as the inverse square of the band gap, while in MWNTs it is given by the sum of the polarizabilities of the constituent tubes. The transverse polarizability of SWNTs is insensitive to band gaps and chiralities and is proportional to the square of the effective radius; in MWNTs the outer few layers dominate the response. The transverse response is intermediate between metallic and insulating, and a simple electrostatic model based on a scale-invariance relation captures accurately the first-principles results. Dielectric response in both directions remains linear up to very high values of the applied field.

*Supported by NSF/NIRT.

**8:36**
**N31 4 Atomic-scale and electronic structure of double-walled carbon nanotubes.** KYLE RITTER, NOUREDDINE TAYEBI, JOSEPH LYDING, *Beckman Institute for Advanced Technology, University of Illinois, Urbana-Champaign* Ultra-high vacuum scanning tunneling microscopy (STM) and spectroscopy have been used to elucidate the electronic and atomic-scale structure of double-walled carbon nanotubes[1] (DWNTs) on the Si(100) 2x1:H

surface. Atomically clean DWNT-surface interfaces were facilitated by an itin situ deposition method[2] which enables simultaneous resolution of the DWNT chirality and surface atomic structure. A key result includes the observation of periodic 2.7 nm spatial modulation superimposed on the nanotube chirality at both positive and negative scanning biases for a 2 nm diameter semiconducting DWNT. The periodic modulation of the DWNT topography suggests the lattices of the inner and outer nanotubes produce an interference pattern depending on the relative alignment of the constituent carbon atoms. Experimental data (diameter, chiral angle, and local density of state measurements) will be supplemented with simulated STM images which illustrate subtle changes in the outer nanotube topography depending on the inner nanotube chirality. 1. DWNTs synthesized by Nanocyl (www.nanocyl.com) 2. P.M. Albrecht and J.W. Lyding. Appl. Phys. Lett. 83, 5029 (2003).

**8:48**

**N31 5 All-electron electronic properties of carbon nanotubes through multiresolution analysis** IVAN P. DAYKOV, TOMÁS A. ARIAS, *Department of Physics, Cornell University, Ithaca, NY, 14853* Utilizing our latest developments of density functional calculations using multiresolution wavelet-like basis we compute the electronic properties of carbon nanotubes by including all electrons.

**9:00**

**N31 6 Molecular Dynamics Simulations of DNA-Functionalized Carbon Nanotube Chemical Sensors** ROBERT JOHNSON, MICHAEL KLEIN, ALAN JOHNSON, *University of Pennsylvania* We have conducted all-atom classical molecular dynamics simulations onDNA-functionalized carbon nanotube chemical sensors, including the presence of water. Our simulations verify that single stranded DNA (ssDNA) binds to a single-wall carbon nanotube (swCN) via a pi-pi stacking interaction. Preliminary simulations of a partially hydrated system also suggest that the ssDNA conformation about a swCN exhibits nanoscale pockets that can result in additional binding sites for analytes. Molecular dynamics simulations have also been performed to determine binding orientations of analytes adsorbed to the swCN-ssDNA system. To determine possible chemical gating effects of analytes on the swCN, we numerically calculate changes in the electric potential at the surface of the swCN due to the introduction of ssDNA and analytes. Results of further simulations of a fully hydrated system will also be presented.

**9:12**

**N31 7 Fluxional handles for direct control of conductance in functionalized carbon nanotubes** YOUNG-SU LEE, NICOLA MARZARI, *Department of Materials Science and Engineering, Massachusetts Institute of Technology* A class of covalent functionalizations for single-wall carbon nanotubes is identified — from extensive first-principles calculations — that preserves the conduction channels of metallic nanotubes. Cycloaddition of carbenes or nitrenes can induce bond cleaving between two adjacent sidewall carbons, restoring their original $sp^2$ hybridization and recovering in the process a transparent $\pi$ manifold, radically at variance with the strong scattering permanently induced by other common covalent functionalizations. The chirality and curvature of the nanotube and the chemistry of the addends can force or inhibit this bond cleavage, that in turn controls very distinctly the transport properties of the functionalized conductor. A well-defined range of diameters can be found for which certain addends —such as dicyanocarbene—exhibit a bistable switchable state, where the opening or closing of the sidewall bonds, and the accompanying on/off switch in the conductance, can be directed with chemical, electrochemical or optical means.

**9:24**

**N31 8 Silicon-carbon nano-structures to nano-tubes.*** M.N. HUDA, LEONARD KLEINMAN, *University of Texas at Austin, Austin, Texas 78712* A.K. RAY, *University of Texas at Arlington, Arlington, Texas-76019* There have been continuing efforts to stabilize silicon cage-type nano-structures or nano-tubes which can be used in similar ways as the carbon-based fullerene structures. This is due to the fact that the current semiconductor industries are based on silicon. Silicon carbide is the focus of scientific research due to its potential use even in extreme conditions, such as extreme high-temperature, high-power capabilities and high radiation conditions. In the present study, a set of novel silicon carbon nanosructures ($Si_{2n}C_n$) in tubular form have been studied which can be extended to form silicon carbide nano-tubes. Generalized gradient approximation to density functional theory has been used with an all electron basis set to study the stability of these structures. A frequency analysis has been performed to ensure that all the frequencies are real. A slight structural shift has been predicted between the hydrogen saturated and –unsaturated nano-tubes.

*Work supported by the Welch Foundation, Houston, Texas (Grant Nos. F-0934 and Y-1525).

**9:36**

**N31 9 *Ab initio* study of semiconducting carbon nanotubes adsorbed on the Si(100) surface: diameter- and registration-dependent atomic configurations and electronic properties*** SALVADOR BARRAZA-LOPEZ, PETER M. ALBRECHT, NICHOLS A. ROMERO,[†] KARL HESS, *University of Illinois* We present a theoretical study within density functional theory in the local density approximation of semiconducting carbon nanotubes adsorbed on the unpassivated Si(100) surface. We find that the interaction between the nanotube and silicon surface results in significant atomic re-arrangment of the surface atoms. Since the spatial configuration of the surface dimers determines to a great extent the electronic properties of the surface, our first-principles calculations indicate a tendency towards metallicity for the semiconducting tube-Si(100) surface system. We confirm this for nanotubes of different diameters and chiral angles, and find the effect to be independent of the orientation of the nanotubes on the surface. Reference: cond-mat/0510477 and references therein.

*Work supported by the National Computational Science Alliance under grant number DMR050032N, Office of Naval Research (N00014-98-1-0604), NSF (DMR-0325939) and DoE (DEFG02-91ER45439).

[†]Current Address: U.S. Army Research Laboratory, Aberdeen Proving Ground, MD 21005-5069.

**9:48**

**N31 10 A plasmon absorption model for a super-lattice of single-walled carbon nanotubes** M. E. MARKES, *University of Nebraska-Kearney* P. F. WILLIAMS, *University of Nebraska-Lincoln* Several years ago one of us (P. F. Williams*) developed a self-consistent dielectric response model for one-dimensional metals at high frequency using a tight-binding approximation. At the time this model was found useful in a study of the single-particle excitations and plasmon dispersion curves of tetrathiofulvalene-tetracyano-quinodimethane (TTF-TCNQ). This paper is a report of

work in progress to extend this model to arrays of single-walled carbon nanotubes. First the quasi one-dimensional model is extended to represent free electrons confined to the surfaces of cylindrical shells arranged in a 2-D square array. The collective electronic excitations of this system are characterized by a frequency and wavelength dependent complex dielectric constant obtained using the method of self-consistent fields in the random phase approximation. Progress in extending the model to arrays of shells with surface structure will also be discussed.

*P. F. Williams and A. N. Bloch, Phys. Rev. B, **10,** 1097 (1974).

**10:00**
**N31 11 Numerical Results for SU(4) and SU(2) Kondo Effect in Carbon Nanotubes** GEORGE MARTINS, *Department of Physics, Oakland University, Rochester, MI 48309* CARLOS BUSSER, *Condensed Matter Sciences Division, Oak Ridge National Laboratory, Oak Ridge, Tenessee, 37831* New numerical results are presented for the Kondo effect in Carbon Nanotube (CNT) quantum dots (QDs). As recently reported by P. Jarillo-Herrero *et al.* (Nature **434**, 484 (2005)), the Kondo effect in CNTs presents an SU(4) symmetry, which arises from the entanglement of orbital and spin degrees of freedom. As the number of cotunneling processes increases, thanks to the extra (orbital) degree of freedom, the Kondo temperature reaches a high value of $T_K = 7.7K$. Interesting considerations can be drawn regarding the change from SU(4) to SU(2) symmetries depending on the hopping matrix elements between the leads and the CNT QD. Our results will analyze the transition between the SU(4) and the so-called two-level SU(2) (2LSU(2)) Kondo regimes induced by the variation of the coupling of the QD to the leads. The effect of an external magnetic field along the tube direction will also be analyzed. Our results will be compared with available Numerical Renormalization Group (NRG) results by M-S Choi *et al.* (Phys. Rev. Lett. **95**, 067204 (2005)). A comparison with the experimental results will be made to gauge the adequacy of the model and approximations made.

**10:12**
**N31 12 Deep levels in the band gap of the carbon nanotube with vacancy-related defects*** GUNN KIM, *N.C. State University, USA* BYOUNG WOOK JEONG, JISOON IHM, *Seoul National University, Korea* We study the modification in the electronic structure of the carbon nanotube induced by vacancy-related defects using the first-principles calculation. Three defect configurations which are likely to occur in semiconducting carbon nanotubes are considered. A vacancy-adatom complex is found to bring about a pair of localized states deep inside the energy gap. A pentagon- octagon-pentagon topological defect produced by the divacancy is structurally stable and gives rise to an unoccupied localized state in the gap. We also discuss the character of partially- occupied localized state produced by a substitutional impurity plus a monovacancy.

*This work is supported by the SRC program (Center for Nanotubes and Nanostructured Composites) of MOST/KOSEF, the BK21 project of KRF and the MOST through the NSTP (grant No. M1-0213-04-001).

**10:24**
**N31 13 Transport Properties in Carbon Nanotubes films for Hydrogen Sensor Applications*** JIANWEI ZHANG, YAO HE, CHAO CAO, LEX KEMPER, HAI-PING CHENG, *Department of Physics and Quantum Theory Project, University of Florida* Thin single-walled carbon nanotue (CNT) films doped with palladium (Pd) on surface are shown to be promising in hydrogen(H2) sensor applications. We study electronic transport properties of CNT/Pd/H2 system by combining first-principles band structure calculations with Boltzmann transport theory. The coupling between Pd atoms and carbon nanotues is described by the Kondo model. An effective scattering potential, which creates the major resistance in nanotubes, is calculated by fitting potential parameters to the calculated band structures. In addition, intersection resistance between the nanotubes is also included in our simulations. We will present the band structure of the CNT/Pd system with and without the hydrogen atoms or hydrogen molecules. The conductance change of the whole nanotube films in the presence of hydrogen gas will be shown.

*Acknowlegment: DOE/BES under grant FG02-02ER45995.

**10:36**
**N31 14 Theoretical Study of Iron Filled Carbon Nanotubes** MARIANA WEISSMANN, *C.N.E.A., Buenos Aires, Argentina* GRISELDA GARCIA, MIGUEL KIWI, RICARDO RAMIREZ, *Facultad de Fisica, PUC, Chile* CHU-CHUN FU, *CEA, Saclay, France* We have investigated, using ab-initio methods, the geometry and magnetic structure of free standing and encapsulated iron nanowires, both in perfect and defective single wall carbon nanotubes. The geometries adopted consist of two layers of iron atoms per unit cell, arranged in hcp(0001) and bcc(011) structures, repeated periodically along the wire axis, When the ratio of the nanowire to nanotube diameter is small there is an attractive interaction among them and the density of states at the Fermi energy corresponds to a single spin orientation, as for the free standing nanowires. These systems are therefore potentially interesting for spintronics. When the same ratio is close to one the systems are less stable and a tendency towards antiferromagnetic ordering is observed due to the confinement.



**SESSION N32: FOCUS SESSION: CARBON NANOTUBES: COMPOSITES AND APPLICATIONS**
**Wednesday Morning, 15 March 2006; 329, Baltimore Convention Center at 8:00**
**Andrew Rinzler, University of Florida, presiding**

***Invited Papers***

**8:00**
**N32 1 The Solid-State Fabrication, Structure, and Multifunctional Applications of Strong Carbon Nanotube Yarns and Transparent Sheets .***
R.H. BAUGHMAN, *University of Texas at Dallas*

We describe novel methods for producing polymer-free carbon nanotube yarns and transparent sheets (self-assembled textiles), and describe their application as multifunctional materials. These fabrication methods are conducted at room

temperature in the solid state for multi-walled carbon nanotubes, which are much cheaper to produce that our previously used single-walled carbon nanotube fibers. The yarns have a maximum failure strength of above 460 MPa (850 MPa after polymer infiltration), they are highly resistant to creep and to knot or abrasion-induced failure, and they provide a giant Poisson's ratio for stretch in the fiber direction. The nanotube textiles have higher gravimetric strength than the strongest steel sheet or the polymers used for ultralight air vehicles and proposed for solar sails. Applications evaluations are described for artificial muscles, thermal and light harvesting, energy storage, field-emission electron sources, electrically conducting appliques, three types of lamps and displays, and sensors.

*Co-authors: M. Zhang, S. Fang, A. A. Zakhidov, M. Kozlov, S. B. Lee, A. E. Aliev, C. D. Williams (University of Texas at Dallas), and K. R. Atkinson (CSIRO Textile & Fibre Technology, Belmont, Victoria, Australia).

***Contributed Papers***

**8:36**

**N32 2 Mechanical Reinforcement of Functionalized Carbon Nanotube-Polyethylene Polymer Composites** MERLYN PULIKKATHARA, VALERY KHABASHESKU, *Rice Quantum Institute, Rice University* Carbon nanotube-polymer composites are promising materials for a variety of applications including space exploration and the aerospace industry. In this work, we functionalized and fabricated a series of single walled carbon nanotube (SWNT) composite samples using medium density polyethylene (MDPE). The composites were made by shear mixing melt processing of MDPE with up to 1 wt.% added pristine and functionalized SWNTs including fluoro (F), undecyl and urea SWNT-derivatives. The former two were prepared as described earlier, while the synthesis of the latter is a novel method that has been developed utilizing a solvent free reaction of fluoro-SWNT with molten urea. FTIR, Raman, and AFM data confirm that urea bonds covalently to the SWNT surface and displaces most of the fluorine. Initial tensile strength (TS) of the MDPE composites loaded with urea-F-SWNT reinforced 48% and undecyl-functionalized SWNTs show unprecedented reinforcement up to 185% compared to neat MDPE. These preliminary results show that these functionalized SWNT increased the mechanical strength in of MDPE composites. The FTIR, Raman, AFM, SEM, TEM, XPS, TGA, and TS data of studied materials will be presented.

**8:48**

**N32 3 Adhesion and Reinforcement in Carbon Nanotube Polymer Composite** CHENYU WEI, *NASA Ames Research Center* The temperature dependent adhesion behavior and reinforcement in carbon nanotube(CNT)-polymer (polyethylene) composite is studied through molecular dynamics (MD) simulations. The interfacial shear stress through van der Waals interactions is found to increase linearly with applied tensile strains along the nanotube axis direction, until the non-covalent bonds between CNTs and molecules break successively. A lower bound value about 46 MPa is found for the shear strength at low temperatures. Direct stress-strain calculations show significant reinforcements in the composite in a wide temperature range, with $\sim$ 200% increase in the Young's modulus when adding 6.5% volume ratio of short CNTs, and comparisons with the Halpin-Tsai formula are discussed.

**9:00**

**N32 4 Multi-scale Real-Space Characterization of Carbon Nanofiber Composites** BENJI MARUYAMA, *Air Force Research Laboratory, Materials & Manufacturing Directorate* SIRINA PUTTHANARAT, *University of Dayton Research Institute* LAWRENCE DRUMMY, RICHARD VAIA, JONATHAN SPOWART, *AFRL, Materials & Manufacturing Directorate* CARLA LEER, FERRIE VAN HATTUM, *University of Minho, Portugal* Good dispersion of the reinforcement phase in nanocomposites is recognized as critical to achieving material property goals. Hierarchical nanocomposite morphologies can be quantified by a combination of 1) Reciprocal space methods such as scattering, 2) Real space imaging such as AFM and TEM, and/or 3) Inference from established structure-property models. However, none of these techniques alone has proven satisfactory to quantitatively characterize nanocomposite morphologies across multiple length scales and link them to properties. Nor have they been adequate to define quality control metrics for dispersion. The current effort is devoted to characterizing dispersion in carbon nanofiber composites from the nano- to meso-scales (i.e., 10 nm - 10 mm) using the Multi-Scale Analysis of Area Fractions (MSAAF) technique of Spowart et al. This technique uses a fractal analysis of real space images to generate a homogeneous length scale (scale at which the statistical variability in concentration is at some threshold), and a fractal dimension characteristic of the dispersion over a wide range of length scales. This work is part of a larger effort to determine structure/property relations of complex materials systems.

**9:12**

**N32 5 Radial Elasticity of Nanotubes** ISMAEL PALACI, STEPHAN FEDRIGO, HARALD BRUNE, *Swiss Federal Institute of Technology (EPFL), Institute of the Physics of Nanostructures, Lausanne, Switzerland* CHRISTIAN KLINKE, *IBM Watson Research Center, Nanoscale Science Department, New York, USA* ELISA RIEDO, *Georgia Institute of Technology, School of Physics, Atlanta, USA* The last decade has lead to the discovery of many nanostructures like nanotubes, nanowires or nanobelts. Industrial applications of these nanostructures need practical tools to characterize their optical, electrical or mechanical properties. Here we propose to use state of the art atomic force microscopy to characterize the radial elasticity of nanotubes of different diameters. The nanostructures were elastically strained in the radial direction by applying small indentation amplitudes. In the case of multiwalled carbon nanotubes, this method enables to extract the radial Young modulus from compliance measurements. We find 600 GPa for our smallest tubes with a radius $R = 2.2$ nm. The values strongly decrease with increasing radii until they reach an asymptotic value of $30 \pm 10$ GPa at $R \geqslant 4$ nm. The normal force vs. indentation curves are in qualitative agreement with molecular dynamics simulations.

**9:24**

**N32 6 Dissipation in suspended carbon nanotube oscillators*** P. ALEX GREANEY, JEFFREY C. GROSSMAN, *University of California, Berkeley* The vibrational properties of doubly clamped suspended single walled carbon nanotubes are studied numerically using continuum, and atomistic methods. Of interest is the dissipation of energy in athermally excited modes. Simple continuum arguments may be used to bound the limits of energy dissipation that arise due to the scale of the nanotubes; however, more detailed atomistic descriptions are required to capture the dissipation due to coupling between phonon modes. This work has implication for the use of carbon nanotubes as high frequency resonators in nanomechanical systems.

*This material is based upon work supported by the National Science Foundation under Grant No.EEC- 0425914.

**9:36**

**N32 7 Structure and Mechanical Properties of Model Nanotube Composites** ANDREW B. SCHOCH, KENNETH R. SHULL, L. CATHERINE BRINSON, WESLEY R. BURGHARDT, THOMAS O. MASON, NEIL J. KIDNER, SUPAPORN WANSOM, LETA Y. WOO, *Northwestern University* Thermoreversible gels based on solutions of acrylic triblock copolymers have been infused with multi-walled carbon nanotubes at various loadings. The fast transition between liquid and solid states allows for the nanotubes to be frozen into their positions. These composite materials exhibit distinct mechanical and electrical properties from the bulk gel. The storage modulus of the filled gels persists at temperatures well above the gel transition and signifies elasticity that comes solely from the nanotube inclusions. The magnitude of this additional elasticity at high temperatures increases dramatically with increasing nanotube volume fraction above a ''percolation'' threshold that is extremely low. Sensitivity to nanotube interactions is enhanced by the low background levels of gel elasticity above the gel transition temperature. Complementary alternating current impedance spectroscopy measurements were performed to asses the onset of electrical percolation in these systems.

**9:48**

**N32 8 In vivo MRI of single-wall carbon nanohorns through magnetite nanoparticle attachment** JIN MIYAWAKI, *JST/SORST* MASAKO YUDASAKA, *JST/SORST and NEC* HIDETO IMAI, *NEC* HIDEKI YORIMITSU, HIROYUKI ISOBE, EIICHI NAKAMURA, *The University of Tokyo* SUMIO IIJIMA, *JST/SORST and NEC* Superparamagnetic magnetite (SPM) is used as a contrast agent in magnetic resonance imaging (MRI). Thus, the SPM-attachment to carbon nanotubes (CNTs) will enable to visualize motional behaviors of CNTs in the living body through MRI. We found that the strong attachment of the SPM nanoparticles (ca. 6 nm size) to one type of CNTs, single-wall carbon nanohorns (SWNHs), could be achieved through a deposition of iron acetate clusters on SWNHs in ethanol at room temperature, followed by heat-treatment in Ar. In vivo MRI visualized that the SWNHs attached with the SPM nanoparticles accumulated in several organs of mice when injected into mice via tail veins. This simple method for the SPM-attaching on CNTs would facilitate the toxicity assessment of CNTs and the applications of CNTs in bioscience and biotechnology.

**10:00**

**N32 9 Sensor applications and spin-transport measurements in carbon nanotube nanocomposites** J. SANDERS, J. GASS, H. SRIKANTH, *Functional Materials Lab, Dept. of Physics, University of South Florida-Tampa, 33620, USA* F.K. PERKINS, E.S. SNOW, *Nanotechnology Section, U.S. Naval Research Lab, Washington, D. C* Vertical and horizontal carbon nanotubes have been grown at USF using CVD and PECVD techniques with Ni and Fe nanoparticle catalysts. At NRL we have used CVD to produce carbon nanotube networks on $SiO_2/Si^{++}$ substrates to build sensors for chemical and bio agents by measuring capacitance and conductance. Various chemical vapors are able to be sensed with a fast response and recovery as well as a high degree of selectivity. A microfluidic flow system has been developed to extend the sensing applications to biological analytes. It is also known that carbon nanotubes are excellent transmission channels for charge and spin transport. In addition to the biosensors, we will also report on our experiments probing charge and spin transport through nanotube networks using point contact Andreev reflection (PCAR) based on superconducting and ferromagnetic junctions. Work at USF supported by DARPA/ARO through grant # W911NF-05-1-0354.

**10:12**

**N32 10 Characterisation of a Hydroxyapatite and Carbon Nanotube Bioceramic Composite** C. KEALLEY, B. BENNISSAN, *University of Technology, Sydney, Australia* A. VAN RIESSEN, *Curtin University of Technology, Australia* M. ELCOMBE, *Australian Nuclear Science and Technology Organisation, Australia* A biocompatible composite for bone replacement applications was investigated. The effects that the microstructure may have on the mechanical properties of the bioceramic have been assessed. Hydroxyapatite was prepared as reported previously[1] with 2, 5 and 10 wt% of carbon nanotubes (CNTs) being incorporated during the production before hot isostatic pressing. Microstructural analysis of the composite has been undertaken by SEM/EDS, TEM/EDS, XRD and ND. The effects of concentration of the CNTs on the mechanical properties of the composite material have been determined. At 2 wt% excellent densification has been achieved, and there is a significant improvement in Vickers Hardness and Young's Modulus. However, as expected fracture toughness is reduced. [1] Lewis, K., Kealley, C., Elcombe, M., van Riessen, A., and Ben-Nissan, B. (2005), J. Aust. Ceram. Soc., 41(2), p52-55.

**10:24**

**N32 11 The physical properties and possible applications of metal coated carbon nanotubes** ENGIN DURGUN, *Bilkent University* SEFA DAG, *ORNL* SALIM CIRACI, *Bilkent University* We show that Ti atoms can form a continuous coating of carbon nanotubes at various amounts of coverage. The circular cross section of the tubes changes to a square-like form, and the semiconducting tube becomes a ferromagnetic metal with high quantum ballistic conductance. Metallicity is induced not only by the metal-metal coupling, but also by the band gap closing of SWNT at the corners of the square. The magnetic properties of Ti coated tubes depend strongly on the geometry, amount of Ti coverage and also on the elastic deformation of the tube. While the magnetic moment can be pronounced significantly by the positive axial strain, it can decrease dramatically upon the adsorption of additional Ti atoms to the monolayer coting of the nanotube. Besides, electronic structure and spin- polarization near the Fermi level can also be modified by radial strain. On the other hand, it is found that Ti and V

decorated carbon nanotubes of various radii and chirality can adsorb large amounts of hydrogen molecules and can be possible candidates for hydrogen storage applications. The other transtions metals like Fe, Co, Cr, and Mn cannot cover nanotube surface uniformly but can only be adsorbed in clustered forms. Depending on the geometry and amount of adsorption these systems can posses high polarization near Fermi level with variable magnetic moments which can be useful in spintronic devices.

**10:36**
**N32 12 Field Emission from Carbon Nanotubes: From Isolated Nanotubes to Matrix Cathodes.** DAVID CAREY, RICHARD SMITH, RAVI SILVA, *University of Surrey* The high aspect ratio and current carrying ability of carbon nanotubes (CNTs) make them an attractive material for electron sources. Field screening effects are known to occur at high nanotube densities and most large area field emission characteristics (FECs) reflect ensemble averages of the sites with the lowest effective potential barriers. We have studied the FECs and enhancement factor from isolated nanotubes mounted on high resolution manipulators within a scanning electron microscope. We have further developed an in-situ three terminal characterisation facility allowing estimates of the screening factor of the gate electrode and gate transparency. Measurements of the FEC of carbon nanotube – polymer spin cast composites cathodes have also been made. A range of samples with arc discharge nanotube mass fractions up to 7 % was prepared. Electron emission at low applied electric fields is observed. The transport and emission mechanism of the electrons is discussed in terms of a polymer coating that surrounds the nanotube and acts as a tunnel barrier. This gives rise to fluctuation induced tunnelling between the nanotubes which affects the field emission. The effects of the disordered percolation control network on the field emission along with prospects for applications are discussed.

**10:48**
**N32 13 Thermal Field Emission from a Single Carbon Nanotube** GONGPU ZHAO, JIAN ZHANG, QI ZHANG, HAN ZHANG, *Department of Physics and Astronomy, University of North Carolina at Chapel Hill, Chapel Hill, NC 27599-3255* TIE TANG, *National Institute for Materials Science, Tsukuba 305-0047, Japan* OTTO ZHOU, LU-CHANG QIN, *Department of Physics and Astronomy, University of North Carolina at Chapel Hill, Chapel Hill, NC 27599-3255* Carbon nanotubes (CNTs) exhibit excellent characteristics in field-induced electron emission with high brightness, stable emission current, long service time and narrow energy distribution. But it is still not clear how carbon nanotubes behave under high electric field and high temperature. We have characterized the thermal field emission properties of an individual multiwalled carbon nanotube fabricated by a two step process. The characterization was conducted in the transition zone between thermionic emission and field emission. An approximation has been made to the Murphy-Good equation so that the temperature at the CNT apex can be extracted. The boundary of transition zone was determined experimentally by activating thermal field emission at various temperatures. We also show that higher temperature will improve the emission stability and remove disruptions in the emission current.

## SESSION N33: FOCUS SESSION: INSTABILITIES & TURBULENCE IN COMPLEX FLUIDS
**Wednesday Morning, 15 March 2006; 336, Baltimore Convention Center at 8:00**
**Daniel Lathrop, University of Maryland, presiding**



***Invited Papers***

**8:00**
**N33 1 Nonlinear dynamics and flow transitions in viscoelastic shear flows.***
R. SURESHKUMAR, *Washington University, St. Louis, MO 63130*

Dynamical explorations of viscoelastic flows are of fundamental and practical interest. Elastic forces cause flow instability even in the absence of inertia (creeping flow) and greatly modify the onset and ensuing sequence of flow transitions in flows with finite inertia. While past research has yielded much progress, literature on several intriguing nonlinear phenomena has been only slowly emerging. These include: (i) nonlinear transitions in itlinearly itstable, parallel shear flows, (ii) influence of elastic instability on itpressure-flow rate relationship under creeping flow conditions, (iii) effect of elasticity on itpattern formation in itcurved shear flows and (iv) novel instabilities caused by thermal effects induced by itviscous heating. The recent advances and challenges in the abovementioned areas will be discussed.

*NSF CTS 9874813, 0132730, 0335348; ACS/PRF; DARPA.

***Contributed Papers***

**8:36**
**N33 2 Low-dimensional models for coherent states in viscoelastic turbulent shear flows** ANSHUMAN ROY, *University of Michigan, Ann Arbor* ALEXANDER MOROZOV, WIM VAN SAARLOOS, *Leiden University* RONALD LARSON, *University of Michigan, Ann Arbor* We present low-dimensional models for the sustenance of turbulence in shear flows of viscoelastic liquids. We develop these models by systematically investigating the effect of incremental amounts of elasticity on the self-sustaining process maintaining turbulence in shear flows. The recently proposed (Waleffe, 1997) self-sustaining process for shear flows consists of streamwise rolls leading to redistribution of the mean shear into spanwise streaks. A Kelvin-Helmholtz instability of the spanwise streaky flow then results in the regeneration of the streamwise rolls via nonlinear interactions. With the help of our low-dimensional model, we are able to identify which part of the cycle is interrupted or enhanced by the presence of elasticity. Additionally, we explore the effect of fluid rheology on the flow kinematics, particularly the role played by the first and second normal

stress differences. For Newtonian liquids, such low-dimensional models have demonstrated their utility by helping to understand the features of full numerical solutions of turbulent flows. We believe that our low dimensional model for viscoelastic turbulent flow will help interpret experiments and direct numerical simulations of turbulent drag reduction by polymers.

**8:48**

**N33 3 Instabilities in the oscillatory flow of a complex fluid** JORDI ORTIN, MIREIA TORRALBA, *Dept. ECM, Universitat de Barcelona, Spain* ALFONSO A. CASTREJON-PITA, GABRIELA HERNANDEZ, GUADALUPE HUELSZ, JOSE ANTONIO DEL RIO, *Centro de Investigacion en Energia, UNAM, Mexico* The dynamics of both a Newtonian and a viscoelastic shear- thinning fluid, subjected to an oscillatory pressure gradient in a vertical tube, is studied experimentally. PIV is used to determine the 2d velocity fields in the vertical plane of the tube axis, for driving amplitudes from 0.8 to 2.5 mm and driving frequencies from 2.0 to 11.5 Hz. The Newtonian fluid exhibits always a laminar flow regime, independent of the axial position. For the complex fluid, instead, the parallel shear flow regime exhibited at low amplitudes [Torralba et al., Phys. Rev. E **72**, 016308 (2005)] becomes unstable at higher drivings against the formation of symmetric vortices, equally spaced along the tube. At even higher drivings the vortex structure itself becomes unstable, and complex nonsymmetric structures develop. The system studied represents an interesting example of the development of shear-induced instabilities in nonlinear complex fluids in purely parallel shear flow.

**9:00**

**N33 4 Instability of a Sheared Fluid-Gel Interface** SATISH KUMAR, *University of Minnesota* SHENG LIN-GIBSON, ERIK K. HOBBIE, *NIST* The planar interface between a viscous fluid and an elastic gel is known to be unstable to simple steady shear flow [V. Kumaran and R. Muralikrishnan, Phys. Rev. Lett. **84**, 3310 (2000)]. By embedding a small number of micron-sized Latex particles at the planar interface between a Newtonian fluid and a soft viscoelastic gel, we use stroboscopic particle tracking to study the onset of this instability in the limit of large gel-to-fluid thickness ratios. The mean-square displacement of the interface and the power spectrum of displacement fluctuations are measured as a function of applied shear rate and gel modulus. Long-wavelength fluctuations with a periodic component are observed in the plane of flow and vorticity, with limited motion normal to the plane of the interface. By relating the power spectrum of fluctuations to the viscoelasticity of the gel, we discuss potential applications in the area of non-Brownian microrheology, where one exploits this instability to optically infer the rheological properties of an otherwise inaccessible soft phase.

**9:12**

**N33 5 DNS of Viscoelastic Turbulent Channel Flow at High Drag Reduction** ANTONY BERIS, *University of Delaware* KOSTAS HOUSIADAS, *Aegian University, Greece* LUO WANG, *University of Delaware* A new method has been developed to enable Direct Numerical Simulations (DNS) of viscoelastic turbulent channel flow with high accuracy spectral methods at high values of drag reduction (HDR), when the polymer molecules undergo high extensional deformation. To faithfully represent that we have expressed the conformation tensor, c, as the exponential of another tensor a, c=exp(a) and we solve for a instead of c. Thus, by construction, the positive definite property of c is always preserved. In addition, a stabilizing artificial diffusion has been added to the viscoelastic constitutive model and efficiently implemented numerically using a multigrid method. The Finite-Elasticity Non-Linear Elastic Dumbbell model with the Peterlin approximation (FENE-P) is then used to represent the effect of polymer molecules in solution. To achieve HDR we used high values of the key model parameters: (a) the maximum extensional viscosity, which for the FENE-P constitutive model is proportional to the quantity (1-$\beta$)*L[2], where $\beta$ is the solvent viscosity ratio and L is the maximum extensibility parameter and (b) the friction Weissenberg number, We$\tau$.

**9:24**

**N33 6 Time Dependent Drag Reduction by Long Chain Polymers in Taylor-Couette Flow** DANIEL D. LANTERMAN, *IREAP, Dept. of Physics, University of Maryland, College Park 20740* MATHEW FERGUSON, *IREAP, Dept. of Physics, University of Maryland, College Park 20740, National Institute of Health, Bethesda Maryland 20892* DANIEL P. LATHROP, *IREAP, Dept. of Physics, University of Maryland, College Park 20740* The addition of small amounts of long chain polymers has been shown to dramatically reduce the drag in some aqueous turbulent flows. We examined this effect in flow between concentric rotating cylinders (Taylor-Couette flow). The apparatus is instrumented to measure torque on the inner cylinder and can achieve Reynolds numbers up to $Re = 1.4 \cdot 10^6$. Reductions in drag of up to 47% are seen immediately after the addition of the polymer (typical concentrations 10-20 ppm), but this value decays over a time scale of tens of minutes. While the scission of individual polymer molecules may also be important, light scattering measurements, performed on liquid samples, suggest the formation of entangled aggregates of polymer molecules. The polymers used are polyacrylamide with mean molecular weights of 5.5 and 18 MDaltons. Tested concentrations range from 0.5 to 100 parts per million by mass. We examine the dependence on concentration and shear rate (Reynolds number).

**9:36**

**N33 7 Nonlinear traveling waves as a framework for understanding turbulent drag reduction** WEI LI, LI XI, MICHAEL GRAHAM, *Univ. of Wisconsin-Madison* Nonlinear traveling waves that are precursors to laminar-turbulent transition and capture the main structures of the turbulent buffer layer have recently been found in all the canonical parallel flow geometries. We study the effect of polymer additives on these ''exact coherent states'' (ECS), in the plane Poiseuille geometry. Many key aspects of the turbulent drag reduction phenomenon are found, including: delay in transition to turbulence; drag reduction onset threshold; diameter and concentration effects. The examination of the ECS existence region leads to a distinct prediction, consistent with experiments, regarding the nature of the maximum drag reduction regime. Specifically, viscoelasticity is found to completely suppress the normal (i.e. streamwise-vortex-dominated) dynamics of the near wall region, indicating that the maximum drag reduction regime is dominated by a distinct, and perhaps intrinsically elastic, flow structure.

**9:48**

**N33 8 Complex dynamics in simple models of shear banding** SUZANNE FIELDING, *School of Mathematics, University of Manchester* HELEN WILSON, *Department of Mathematics, University College London* PETER OLMSTED, *School of Physics and Astronomy, University of Leeds* Complex fluids commonly undergo flow instabilities and flow-induced transitions that result in spatially heterogeneous ''shear banded'' states. Often, these

banded states display oscillatory or chaotic dynamics, measured in the bulk rheological signals and in the motion of the interface between the bands. Until recently, however, theory predicted a steady state comprising stationary bands separated by a flat interface. We discuss recent theoretical progress in capturing complex dynamics of the banded state: first in a model in which the interface (or interfaces) remains flat but moves in a chaotic way; second in a model that explicitly allows for undulations along the interface.

**10:00**
**N33 9 Elastic Instabilities of Polymer Solutions in Extensional Flows*** PAULO ARRATIA, *University of Pennsylvania* JERRY GOLLUB, *Haverford College & University of Pennsylvania* When flexible polymer molecules (in dilute solution) pass near the hyperbolic point of a microchannel cross flow, they are strongly stretched. As the strain rate is varied at low Reynolds number $< 0.01$, tracer and particle-tracking experiments show that molecular stretching produces two flow instabilities, one in which the velocity field becomes strongly asymmetric, and a second in which it fluctuates non- periodically in time. The flow is strongly perturbed even far from the region of instability, and this phenomenon can be used to produce mixing. Bulk flow instabilities are not observed in dilute solutions of rigid polymers or Newtonian fluids under similar conditions.

*Work supported primarily by NSF DMR-0405187, with additional support by NSF DMR05-20020.

**10:12**
**N33 10 Delay of Disorder by Diluted Polymers** CHRISTIAN WAGNER, *Universitaet des Saarlandes* ANDRIY KITYK, *Technical University of Czestochowa* We study the effect of diluted flexible polymers on a disordered capillary wave state. The waves are generated at an interface of a dyed water sugar solution and a low viscous silicon oil. This allows for a quantitative measurement of the spatio-temporal Fourier spectrum. The primary pattern after the first bifurcation from the flat interface consists of squares. With increasing driving strength we observe a melting of the square pattern. It is replaced by a weak turbulent cascade. The addition of a small amount of polymers to the water layer does not affect the critical acceleration but shifts the disorder transition to higher driving strengths and the short wave length - high frequency fluctuations are suppressed.

**10:24**
**N33 11 Shear thickening, shear localization and elastic turbulence.** DANIEL BONN, *LPS/ENS and WZI Amsterdam* The vast majority of complex fluids is shear thinning. The mechanisms of shear thinning are relatively well understood, and the phenomenon is widely used to tailor the rheology of complex fluids. Shear thickening is the exception to this rule, is incompletely understood and hardly ever used to tailor fluid properties. We study shear thickening in granular pastes (cornstarch), and show that shear localization (banding) is an essential ingredient for shear thickening. For high flow rates, the shear banding is followed by elastic turbulence. Our measurements provide us with the mechanism of both shear thickening and the flow instabilities that result from it.

**10:36**
**N33 12 A Transitional Pathway to Turbulence in Elastic Fluids** BRUCE SCHIAMBERG, LAURA SHEREDA, HUA HU, RONALD LARSON, *University of Michigan* Multiple scenarios have been discovered by which laminar flow transitions to turbulence, where transitions are caused by inertia or temperature, in Newtonian fluids. Here we show in non-Newtonian fluids a transition sequence that is due to elasticity from polymers, with negligible inertia. Multiple states are found linking the stable base flow to ''elastic turbulence'' in the flow between a rotating and stationary disk, including circular and spiral rolls, and stationary and time-dependent modes. Also, a surprising progression from apparently ''chaotic'' flow to periodic flow and then to ''elastic turbulence'' is found. In these experiments, either shear stress or shear rate is incrementally increased and then held at fixed values. The modes we discover have distinct rheological signatures, and we also image the accompanying secondary-flow field kinematic structures. Finally, we have explored how polymer concentration and gap-to-radius ratio affect (and possibly limit) the transitional pathway. The most concentrated solution tested appears to stabilize an additional, time-periodic mode. In conclusion, we have studied an unexplored route, which we hope, in time, will make it possible to compare experimentally and theoretically the routes to purely elastic turbulence with those for inertial turbulence, leading to a richer understanding of both.

**SESSION N34: SESSION ON REFERREEING**
**Wednesday Morning, 15 March 2006; 337, Baltimore Convention Center at 9:30**

**SESSION N35: FOCUS SESSION: ORGANIZATION OF COMPLEX NETWORKS**
**Wednesday Morning, 15 March 2006; 338, Baltimore Convention Center at 8:00**
**Sidney Redner, Boston University, presiding**

*Invited Papers*

**8:00**
**N35 1 Structural properties of Complex networks.**
JOSÉ MENDES, *University of Aveiro*

The k-core decomposition was recently applied to a number of real-world networks (the Internet, the WWW, cellular networks, etc and was turned out to be an important tool for visualization of complex networks and interpretation of cooperative processes in them. Rich k-core architectures of real networks were revealed. The k-core is the largest subgraph where vertices have at least k interconnections. We find the structure of k-cores, their sizes, and their birth points — the bootstrap percolation thresholds. I will show a derivation of exact equations describing the k-core organization of a randomly damaged uncorrelated network with an arbitrary degree distribution. This allows us to obtain the sizes and other structural characteristics of k-cores in a variety of damaged and undamaged random networks and find the nature of the k-core percolation in complex networks. These general results will be applied to the classical random graphs and to scale-free networks, in particular, to empirical router-level Internet maps. We find that not only the giant connected components in infinite networks with slowly decreasing degree distributions are resilient against random damage, as was known, but their entire k-core architectures are robust.

*Contributed Papers*

**8:36**
**N35 2 Skeleton and fractal scaling in complex networks** KWANG-IL GOH,*GIOVANNI SALVI, BYUNGNAM KAHNG, DOOCHUL KIM, *Seoul National University* We find that the fractal scaling in a class of scale-free networks originates from the underlying tree structure called skeleton, a special type of spanning tree based on the edge betweenness centrality. The fractal skeleton has the property of the critical branching tree. The original fractal networks are viewed as a fractal skeleton dressed with local shortcuts. An in- silico model with both the fractal scaling and the scale- invariance properties is also constructed. The framework of fractal networks is useful in understanding the utility and the redundancy in networked systems.

*Present address: University of Notre Dame; Dana-Farber Cancer Institute, Harvard Medical School.

**8:48**
**N35 3 Analysis of structure of small-world networks** TAO JIA, RAHUL KULKARNI, EIVIND ALMAAS, *Lawrence Livermore National Labs* We study the distribution function for minimal paths in small-world networks. We express this distribution in a convex combination form, and use numerical studies to obtain a functional fit for the convex coefficient in the limit of large system sizes and small disorder. Finally, we find analytic expressions for minimal paths distribution based on the functional fit for the convex coefficient. Our analysis can also be considered from the perspective of 1D random walks, our work thus provides a mapping between the structure of small-world networks and the exit problem for a class of 1D random walks.

**9:00**
**N35 4 Inverted Berezinskii-Kosterlitz-Thouless Behavior on Scale-Free Hierarchical-Lattice Small-World Net** MICHAEL HINCZEWSKI, *F. Gürsey Res. Cent. and MIT* A. NIHAT BERKER, *Koç U. and MIT* We have obtained exact results for a hierarchical lattice incorporating three key features of real-world networks: a scale-free degree distribution, a high clustering coefficient, and the small-world effect. By varying the probability $p$ of long-distance bonds, the entire spectrum from an unclustered non-small-world network to a highly-clustered small-world system is studied. Expressions for the degree distribution $P(k)$ and clustering coefficient $C$ are obtained for all $p$, as well as for the average path length $\ell$ for $p = 0,1$. The Ising model on this network is studied by exact renormalization-group transformation of the quenched bond probability distribution, using up to 562,500 renormalized probability bins for the distribution. For $p < 0.494$, we find power-law critical behavior of the magnetization and susceptibility, with exponents continuously varying with $p$, and exponential decay of correlations away from $T_c$. For $p \geq 0.494$, where the network exhibits a small-world character, the critical behavior radically changes: We find an inverted Berezinskii-Kosterlitz-Thouless singularity, between a low-temperature phase with nonzero magnetization and finite correlation length and a high-temperature phase with zero magnetization and infinite correlation length, with power-law decay of correlations. Approaching $T_c$ from below, the magnetization and the susceptibility respectively exhibit $\exp(-C/\sqrt{T_c - T})$ and $\exp(D/\sqrt{T_c - T})$ singularities.

**9:12**
**N35 5 Origin of Fractality in the Growth of Complex Networks** CHAOMING SONG, *Levich Institute and Physics Department, City College of New York* SHLOMO HAVLIN, *Minerva Center and Department of Physics, Bar-Ilan University* HERNAN MAKSE, *Levich Institute and Physics Department, City College of New York* The emergence of self-similarity and modularity in complex networks raises the fun- damental question of the growth process according to which these structures evolve. The possibility of a unique growth mechanism for biological networks, WWW and the Internet is of interest to the specialist and the laymen alike,

as it promises to uncover the universal origins of collective behavior. Here, we present the concept of renormalization from critical phenomena as a mechanism for the growth of fractal and non-fractal modular networks. We show that the key principle that gives rise to the fractal architecture of networks is a strong effective ''repulsion'' between the most connected nodes (hubs) on all length scales, rendering them very dispersed.

**9:24**

**N35 6 A rescaling procedure for complex networks** FRANCESCO RAO, *Centro Studi e Ricerche Enrico Fermi, Rome Italy* GUIDO CALDARELLI, *CNR-INFM Istituto dei Sistemi Complessi, Rome Italy* PAOLO DE LOS RIOS, *Ecole Polytechnique Federale de Lausanne, Switzerland* CENTRO FERMI ROME ITALY TEAM, ISTITUTO DEI SISTEMI COMPLESSI ROME, ITALY TEAM, ECOLE POLYTECHNIQUE FEDERALE DE LAUSANNE TEAM, We present here a renormalization scheme for graphs. We introduce a decimation procedure by weighting the different nodes through their centrality. In such a way we obtain rescaled graphs with the same statistical properties of the one at the finest scale. We present the results of such method for some numerical simulations of various models. We also apply this procedure to the real graph composed by Internet Autonomous System. We believe that this procedure can help in detecting the scale free-properties of such structures and can be fruitfully applied whenever the size of a system is that large that it is impossible to be visualized as well as described as a whole.

**9:36**

**N35 7 Statistical Properties of Sampled Networks** SANG HOON LEE, PAN-JUN KIM, HAWOONG JEONG, *Department of Physics, KAIST* We study the statistical properties of the sampled scale-free networks, deeply related to the proper identification of various real-world networks. We exploit three methods of sampling, and investigate the topological properties such as degree and betweenness centrality distribution, average path length, assortativity, and clustering coefficient of sampled networks compared with those of original networks. It is found that the quantities related to those properties in sampled networks appear to be estimated quite differently for each sampling method. We explain why such a biased estimation of quantities would emerge from the sampling procedure, and give appropriate criteria for each sampling method to prevent the quantities from being overestimated or underestimated.

**9:48**

**N35 8 Routing and Congestion in Power Law Graphs** SAMEET SREENIVASAN, *Boston University* EDUARDO LOPEZ, ZOLTAN TOROCZKAI, *Center for Non Linear Studies, Los Alamos National Laboratory* We investigate a simple model of packet routing on a power law (scale free) graph where packets arrive at each node at a given rate and are routed to a randomly chosen destination along the shortest path between the source and destination. This mimics the Shortest Path Routing protocol used in the internet. It was previously found that there is a critical rate of packet arrival beyond which there is an onset of congestion and packets start accumulating on the network. This critical rate depends on the maximum betweenness incurred on the network when shortest path routing is used. We analytically find a bound on the maximal betweenness incurred in shortest path routing and compare it to the optimal (least possible) maximal betweenness that can be acheived using an arbitrary routing protocol. This provides an effective quantitative measure of the optimality of Shortest Path Routing.

**10:00**

**N35 9 Connectivity and Cost Trade-offs in Multihop Wireless Networks*** MAY LIM, *New England Complex Systems Institute and Brandeis University* DAN BRAHA, *New England Complex Systems Institute and University of Massachusetts Dartmouth* SANITH WIJESINGHE, *New England Complex Systems Institute* STEPHENSON TUCKER, *Sandia National Laboratory* YANEER BAR-YAM, *New England Complex Systems Institute* Ad-hoc wireless networks are of increasing importance in communication and are frequently constrained by energy use. Here we propose a distributed, non-hierarchical adaptive method using preferential detachment for adjusting node transmission power to reduce overall power consumption without violating network load limitations. We derive a cost and path length trade-off diagram that establishes the bounds of effectiveness of the adaptive strategy and compare it with uniform node transmission strategy for several node topologies. We achieve cost savings as high as 90% for specific topologies.

*This work was supported in part by Sandia National Laboratories under US DoE Contract DE-AC04-94AL85000.

**10:12**

**N35 10 Locating overlapping dense subgraphs in gene (protein) association networks and predicting novel protein functional groups among these subgraphs** GERGELY PALLA, *(a) Biological Physics Research Group of HAS and (b) Department of Biological Physics, Eotvos University* IMRE DERENYI, *(b)* ILLES J. FARKAS, *(a,b)* TAMAS VICSEK, *(a,b)* Most tasks in a cell are performed not by individual proteins, but by functional groups of proteins (either physically interacting with each other or associated in other ways). In gene (protein) association networks these groups show up as sets of densely connected nodes. In the yeast, Saccharomyces cerevisiae, known physically interacting groups of proteins (called protein complexes) strongly overlap: the total number of proteins contained by these complexes by far underestimates the sum of their sizes (2750 vs. 8932). Thus, most functional groups of proteins, both physically interacting and other, are likely to share many of their members with other groups. However, current algorithms searching for dense groups of nodes in networks usually exclude overlaps. With the aim to discover both novel functions of individual proteins and novel protein functional groups we combine in protein association networks (i) a search for overlapping dense subgraphs based on the Clique Percolation Method (CPM) (Palla, G., et.al. Nature 435, 814-818 (2005), http://angel.elte.hu/clustering), which explicitly allows for overlaps among the groups, and (ii) a verification and characterization of the identified groups of nodes (proteins) with the help of standard annotation databases listing known functions.

**10:24**

**N35 11 Scaling Properties of Topological Neural Nets*** ALFRED HUBLER, *Department of Physics, University of Illinois at Urbana-Champaign* JOSEPH JUN, *Department of Physics, Penn State University* We study the agglomeration of metallic particles in an electric field. Earlier it has been shown that this system is a hardware implementation of a neural net [1]. In this paper we study the growth and topological properties of the emerging net-

works. In contrast to other networks the conductivity of the connections has a fixed value, but the completeness and number of connections depends on the training patterns. We find that the patterns grow in three stages: growth of shooters, ramification, and expansion [2]. The emerging patterns are hierarchical. For the limiting patterns certain properties are highly reproducible, such as the number of end points and the number of branching points, while other properties are not well reproducible, such as the number of tree structures. Further there are power law relations between the mass and the number of branching points and the number of end points. [1] M. Sperl, A. Chang, N. Weber, and A. Hubler, Hebbian Learning in the Agglomeration of Conducting Particles, Phys. Rev. E. **59**, 3165-3168 (1999). [2] J. K. Jun and A. Hubler, Formation and structure of ramified charge transportation networks in an electromechanical system, PNAS 102, 536–540 (2005).

*Supported by the National Science Foundation Grant No. NSF PHY 01-40179, NSF DMS 03-25939 ITR, and NSF DGE 03-38215.

**SESSION N36: FOCUS SESSION: OPTICAL PROPERTIES OF NANOSTRUCTURES WITH S, SE, TE, AND GE**
**Wednesday Morning, 15 March 2006**
**339, Baltimore Convention Center at 8:00**
**Janica Whitaker, Naval Research Laboratory, presiding**

**8:00**
**N36 1 Symmetry considerations for semiconductor nanocrystals** GUSTAVO M. DALPIAN, *University of Texas* MURILO L. TIAGO, MARIE LOPEZ DEL PUERTO, *University of Minnesota* JAMES R. CHELIKOWSKY, *University of Texas* Semiconductor nanocrystals or quantum dots show a wide range of physical properties with respect to their size or shape. In this paper we show that symmetry is also an important characteristic that can lead to different electronic and optical properties, mainly for small nanocrystals. This means that two spherical nanocrystals with similar sizes but different symmetries have different optical and electronic signatures, which should be accessible experimentally. We use pseudopotential density- functional theory, on a real space approach, to address the differences between spherical nanocrystals with similar sizes but different symmetries. We will report differences in the energy gap, the crystal field splitting and the absorption spectra for CdSe nanocrystals. The symmetry of the nanocrystal is also important when studying doping of nanocrystals.

**8:12**
**N36 2 Optical transitions and the nature of Stokes shift in spherical CdS quantum dots*** DENIS DEMCHENKO, LIN-WANG WANG, *Lawrence Berkeley National Laboratory, Berkeley, California 94720* Resonant Stokes shift observed in CdS quantum dots (QDs) has been previously studied theoretically using $\mathbf{k} \cdot \mathbf{p}$ approach. The large values of measured Stokes shift along with the structure of the excitonic levels obtained by the $\mathbf{k} \cdot \mathbf{p}$ calculations have suggested an optically forbidden *P* envelope valence state, thus forming a spatial symmetry induced ''dark exciton'' in CdS QDs, in contrast with the spin-forbidden exchange interaction induced ''dark exciton'' found in CdSe QDs. Since the $\mathbf{k} \cdot \mathbf{p}$ method has been known to incorrectly predict the energy levels in other QDs, here we apply *ab initio* accuracy methods to study this problem. Using the LDA-based charge patching method to generate the Hamiltonian, combined with the folded spectrum method to solve the single particle states of thousand-atom nanostructures, we find that the top of the valence band state is *S*-like, thus optically bright, in contrast with all the previous $\mathbf{k} \cdot \mathbf{p}$ calculations. Our results also indicate the range of applicability of the $\mathbf{k} \cdot \mathbf{p}$ method. The calculated electron-hole exchange splitting suggests that the spin-forbidden valence state may explain the nature of the ''dark exciton'' in CdS quantum dots.

*This work was supported by U.S. Department of Energy under Contract No. DE-AC02-05CH11231 and used the resources of the National Energy Research Scientific Computing Center.

**8:24**
**N36 3 Bright Exciton Fine Structure Observed in Single CdSe Nanocrystal Quantum Dots** S.A. CROOKER, M. FURIS, *National High Magnetic Field Laboratory, Los Alamos, NM* H. HTOON, M.A. PETRUSKA, V.I. KLIMOV, *Chemistry Division, Los Alamos National Laboratory, Los Alamos, NM* The fine structure splitting of bright excitons in epitaxial quantum dots provides a basis for many quantum computation and entanglement schemes. We demonstrate the existence of a similar splitting in single colloidal CdSe nanocrystals through high- resolution, polarization-resolved, low-temperature photoluminescence (PL) experiments. At 4K, single-dot spectra reveal emission from two distinct, linearly- (and orthogonally- ) polarized bright exciton states. This splitting of the nominally degenerate spin $\pm$ 1 bright excitons ranges from 1 to 2 meV, depending on nanocrystal size. These values agree well with the splitting recently inferred from spin-polarized resonant PL of nanocrystal ensembles measured in high magnetic fields to 33 Tesla [1]. Similarly to epitaxially-grown quantum dots, the observed fine structure likely results from shape anisotropy of the nanocrystal (i.e. a reduction of axial symmetry), leading to a long-range, anisotropic electron-hole exchange. [1] M. Furis et al., cond-mat/0511567.

**8:36**
**N36 4 The Peculiar electronic structure of PbSe quantum dots*** JOONHEE AN, ALBERTO FRANCESCHETTI, S. DUDIY, ALEX ZUNGER, *National Renewable Energy Laboratory, Golden, Colorado 80401* PbSe quantum dots have recently emerged as promising systems that may realize direct carrier multiplication (DCM) for solar cell applications. We have calculated the underlying electronic/optical structure of PbSe nanocrystals with an atomistic pseudopotential method, finding that the electronic structure is more subtle than k · p or tight-binding calculations have previously suggested. The following two effects emerge from our calculations: (i) The bulk-degenerate L states forming the VBM and CBM are split due to (1) valley-valley coupling, (2) valence-conduction interband coupling, and (3) the strong anisotropy of the bulk L valleys. Optical absorption is dictated by transitions among anisotropic dot states characteristic of transverse and longitudinal effective masses. Our calculated optical absorption spectrum is in good agreement with experiment. In particular, our calculation reproduces the measured second obsorption peak that had previously been attributed to forbidden transitions $1S_h \rightarrow 1P_e$ or $1P_h \rightarrow 1S_e$ on the basis of k · p and tight-binding

calculations. (ii) Using our calculated single-particle states, we evaluate DCM mechanism, showing that the rate of X-to-XX (exciton to biexciton) transitions far exceeds the reverse, XX-to-X rate, thus opening the way to efficient DCM.

*Supported by DOE-SC-BES-DMS under NREL contract No. DE-AC36-99GO10337.

**8:48**

**N36 5 Study of colloidal quantum dot surfaces using an innovative thin-film positron 2D-ACAR method** B. BARBIELLINI, A. BANSIL, *Northeastern U.* S. W. H. EIJT, H. SCHUT, *Delft University of Technology* P. E. MIJNARENDS, *Northeastern U. and Delft University of Technology* A. B. DENISON, *Lawrence Livermore National Laboratory* Despite a wealth of information, many fundamental questions regarding the nature of the surface of nanosized inorganic particles and its relationship with the electronic structure remain unsolved. We have investigated the electron momentum density (EMD) of colloidal CdSe quantum-dots via depth-resolved positron 2D angular correlation of annihilation (2D-ACAR) spectroscopy at the Delft intense variable-energy positron beam. This method, in combination with first-principles calculations of the EMD, shows that implanted positrons are trapped at the surface of CdSe nanocrystals. They annihilate mostly with the Se electrons and monitor changes in composition and structure of the surface while hardly sensing the ligand molecules. We thus unambiguously confirm [1] the strong surface relaxation predicted by first-principles calculations [2]. Work supported by the USDOE. [1] S.W.H. Eijt et al., Nature Materials (in press). [2] A. Puzder, , Phys. Rev. Lett. 92, 217401 (2004).

**9:00**

**N36 6 Fluorescence blinking statistics from single CdSe nanorods*** SIYING WANG, *University of Pennsylvania* NATHAN LANDY, *Swarthmore College* TARA FINLEY, *Swarthmore College* HUGO ROMERO, *University of Pennsylvania* MARIJA DRNDIC, *University of Pennsylvania* CATHERINE CROUCH, *Swarthmore College* We report that room temperature fluorescence from single colloidally synthesized CdSe nanorods exhibits intermittency (blinking) with truncated power-law off-time and on-time statistics. The nanorods have cross-sectional diameter 5 nm and length 20 nm and are deposited on mica substrates. The aggregated off-time statistics from 67 single nanorods follow a power law: $P(t_{off}) \sim t_{off}^{-\alpha}$, with $\alpha \approx 1.1$. Power-law behavior extends to off-times of roughly 10 s; longer-time probabilities fall below the best-fit power law. Individual nanorods also show power-law off-time statistics with $1 \leqslant \alpha \leqslant 1.3$. On-time probabilities drop below a power law after only $\sim$ 0.6 s; no on-times longer than $\sim$ 3 s are observed. These results differ somewhat from those observed with spherical CdSe or CdSe/ZnS core-shell nanocrystals, for which power-law statistics persist to much longer on- and off-times.

*M.D. acknowledges support from NSF DMR-0449553 and ONR DURIP N00014-05-1-0393.

**9:12**

**N36 7 Time-resolved photoluminescence of individual CdS nanowires** L.V. TITOVA, THANG B. HOANG, H.E. JACKSON, L.M. SMITH, *Dept. of Phys., Univ. of Cincinnati, Cincinnati, OH 45221* J.M. YARRISON-RICE, *Dept. of Phys., Miami Univ., Oxford, OH 45056* J.L. LENSCH, L.J. LAUHON, *Dept. of Mat. Sci. and Eng., Northwestern Univ., Evanston, IL 60208* We study photoluminescence (PL) dynamics of single VLS-prepared CdS nanowires. AFM imaging reveals that while some nanowires are straight and uniform, the others show significant morphological irregularities. Low temperature PL of uniform nanowires displays a single near band edge (NBE) peak. Spectra of the irregular nanowires exhibit a broad PL band with a high energy shoulder in the same energy range as the NBE peak of the uniform nanowires, as well as an array of narrow peaks at the lower energy. Spatially-resolved PL images indicate that the narrow lines originate at specific locations along the nanowire. Time-resolved PL (TRPL) measurements show that NBE emission in all nanowires is short-lived (lifetime $<$ 50 ps), indicating the presence of non-radiative recombination channels. On the other hand, TRPL of the localized states exhibit are significantly longer (400 ps to 1 ns) and vary from line to line. At room temperature, the PL spectra of all nanowires, regardless of the morphology, consist of the single short-lived NBE emission peak. We acknowledge the support of ACS through the PRF, and NSF through grants 0071797, 0216374, and a graduate fellowship (JLL).

**9:24**

**N36 8 Morphology and temperature dependence of single CdS nanowire photoluminescence** THANG B. HOANG, L.V. TITOVA, H.E. JACKSON, L.M. SMITH, *Univ. of Cincinnati, Cincinnati, OH* J.M. YARRISON-RICE, *Miami Univ., Oxford, OH* J.L. LENSCH, L.J. LAUHON, *Northwestern Univ., Evanston, IL* We study the optical properties of single CdS nanowires (grown by VLS method using 50 nm catalysts) using the technique of micro-PL. We studied ten wires, several that were straight and uniform, and others with morphological irregularities. At room temperature, the PL spectra of all wires are alike and consist of a single line around 2.41 eV. At low temperature (5 K), the PL properties of these two groups of wires differ significantly: the spectra of the uniform wires display a single peak near the band edge, and the spectra of the irregularly shaped wires exhibit a series of sharp lines at lower energies. Detailed PL imaging reveals that the sharp lines are emitted only from particular positions along the wires. Moreover, most of the photons emitted at low temperatures occur at energies below the band edge PL of bulk CdS. This suggests that the sharp lines result from defects or surface states which rapidly trap carriers from the bulk of the wires. As the temperature increases, the sharp lines begin to weaken at about 30 K and completely disappear at 85 K, while a peak which emerges from the high energy shoulder of the low-T emission band becomes dominant and survives up to room temperature. We acknowledge the support of ACS through PRF, and NSF through grants 0071797, 0216374, and a graduate fellowship (JLL).

**9:36**

**N36 9 Probing the Electronic and Vibronic Structure of Single and Ensemble CdS Nanowires using Resonant Raman Scattering.** A. ABDI, L.V. TITOVA, L.M. SMITH, H.E. JACKSON, *Dept. of Physics, Univ. of Cincinnati, Cincinnati, OH 45221* J.M. YARRISON-RICE, *Dept. of Physics, Miami Univ., Oxford, OH 45056* J.L. LENSCH, L.J. LAUHON, *Dept. of Materials Science and Engineering, Northwestern Univ., Evanston, IL 60208* Semiconductor nanostructure electronic and vibrational states can be sensitively probed using resonant Raman scattering (RRS) even when such states are not accessible through photoluminescence or transport techniques. We present an investigation of the electronic and vibrational states in both a single CdS nanowire and in an ensemble of CdS nanowires using RRS at room temperature. The CdS nanowire samples were grown using a chemical vapor deposition and gold-catalyzed vapor liquid solid growth technique. We

observe strong 1-LO and 2-LO Raman resonances within the broader photoluminescence emission. The energy separation between the peaks of the 1-LO and 2-LO resonance of an ensemble of CdS nanowires was found to be 34 meV. Raman scattering from a single nanowire exhibits similar behavior but with a narrower resonance. These results demonstrate that RRS is a powerful tool for probing the electronic and vibrational properties of semiconductor nanostructures. We acknowledge the support of ACS through PRF, and NSF through grants 0071797, 0216374, and a graduate fellowship (JLL).

**9:48**

**N36 10 Investigation of the optical gap in Ge nanowires.*** JIAXIN HAN, *The University of Texas at Austin* S. P. BECKMAN, *The University of Texas at Austin* JAMES CHELIKOWSKY, *The University of Texas at Austin* We investigate the role of quantum confinement for the optical and electronic properties of Ge nanowires. Real space pseudopotentials constructed within density functional theory were used to solve the electronic structure problem. We predict the quasi-particle and optical gaps as a function of the diameter up to approximately 3 nm for wires oriented along the (110) and (111) directions. We compare our results to previous work on Si wires.

*Financial support by DOE under grants DE-FG02-03ER25585/15491, NSF grant DMR-0551195. Computational resources provided by the Texas Advanced Computing Center (TACC).

**10:00**

**N36 11 Exciton-polariton emission and absorption in inorganic-organic hybrid crystals $ZnTe(en)_{0.5}$*** YONG ZHANG, G. M. DALPIAN, B. FLUEGEL, SU-HUAI WEI, A. MASCARENHAS, *National Renewable Energy Laboratory* XIAOYING HUANG, JING LI, *Rutgers University* LINWANG WANG, *Lawrence Berkeley National Laboratory* The ultimate accuracy and quality test of nanotechnologies based on either MBE or MOCVD growth is perhaps to make an ultra-short-period superlattice with one monolayer thick alternating components. However, neither artificially nor spontaneously ordered monolayer superlattices (e.g., GaAs/AlAs or GaP/InP) that have been grown by either MBE or MOCVD have been shown to have the desired perfection [1,2]. Recently, we have successfully synthesized a group of II-VI based inorganic-organic crystalline hybrid superlattices with single atomic-layer thick inorganic slabs and single molecular-length organic spacers [3]. We will report experimental and/or theoretical studies on the exciton-polariton emission and absorption, exciton binding energies, and dielectric properties for a prototype hybrid superlattice $ZnTe(en)_{0.5}$ [4,5]. [1] J. Li et al., PRL 91, 106103 (2003). [2] Spontaneous Ordering in Semiconductor Alloys, edited by A. Mascarenhas. [3] X. Huang et al., JACS 122, 8789 (2000); 125, 7049 (2003). [4] B. Fluegel et al., PRB 70, 205308 (2004). [5] Y. Zhang et al., PRL (in press).

*Supported by DOE, NREL, and NSF.

## SESSION N37: FOCUS SESSION: NANOSCALE FABRICATION, ASSEMBLY AND SEMICONDUCTOR NANOWIRES

**Wednesday Morning, 15 March 2006**
**340, Baltimore Convention Center at 8:00**
**Latha Venkataraman, Columbia University, presiding**

***Contributed Papers***

**8:00**

**N37 1 Single electron transistors without tunnel junctions tailored by local oxidation of metallic ultra thin films** VINCENT BOUCHIAT, *CNRS* MARC FAUCHER, CÉCILE DELACOUR, THIERRY FOURNIER, BERNARD PANNETEIR, *CNRS/CRTBT* We present the fabrication and low temperature electric properties of nanoscale metallic constrictions made by local oxidation with an Atomic Force Microscope of weakly localized niobium ultra-thin (3nm) strip lines. These constrictions implements nanoscale resistors with resistance of the order of the resistance quantum. Both laterally constrained and variable thickness junctions are made with a lateral gate coupled to the interjunction electrode. Circuits following both geometries exhibits reproducible low contrast gate oscillations at 4K which phase inverts with drain source voltage. The gate modulation of the current is in strong disagreement with the orthodox theory that involves tunnelling. Transport is interpreted as single or multiple islands in series for which Coulomb blockade is induced by the highly resistive sheet resistance.

**8:12**

**N37 2 Single-Walled Carbon Nanotubes as Shadow Masks for Nanogap Junction Fabrication*** ETIENNE DE POORTERE, LIMIN HUANG, MINGYUAN HUANG, SHALOM WIND, JAMES HONE, STEPHEN O'BRIEN, HORST STORMER, COLUMBIA NANOSCALE SCIENCE AND ENGINEERING CENTER COLLABORATION, We report a technique for fabricating nanometer-scale gaps in Pt wires on insulating substrates, using individualit single-walled carbon nanotubes as shadow masks during metal deposition. 83% of the devices display current-voltage dependencies characteristic of direct electron tunneling. Fits to the current-voltage data yield gap widths in the 0.8 - 2.3 nm range for these devices, dimensions that are well suited for single-molecule transport measurements.

*Supported by the Nanoscale Science and Engineering Initiative of the National Science Foundation (NSF Award Number CHE-0117752), by NYSTAR, by the NSF grant PHY-0103552, and by the W. M. Keck Foundation.

**8:24**

**N37 3 Self-Assembly for Large Scale Fabrication of Integrated Electronic Devices Based on 1-D Nanostructures.*** JUNTAE KOH, MINBAEK LEE, JIWOON IM, SUNG MYUNG, SEUNGHUN HONG, *School of Physics, Seoul National University, Seoul, Korea* Recently, electronic devices based on 1-dimensional (1-D) nanostructures (e.g. carbon nanotubes (CNTs) and nanowires) have been drawing much attention as next-generation device architecture. However, the shortage of reliable nanomanufacturing methods for such circuits has hindered their practical applications. One promising nanomanufacturing method can be 'surface-programmed assembly' process, where functional molecular monolayer on the substrate guides the 'selective assembly' and

'alignment' of nanowires and nanotubes on the substrate without relying on any external forces. Using this method, we successfully assembled and aligned carbon nanotubes and vanadium oxide nanowires on various substrates including Au, silicon oxide, Si, Al, and polymer. Furthermore, by additional microfabrication process, we demonstrated large-scale fabrication of various device structures such as junctions and top-gate transistors based on CNTs and vanadium oxide nanowires. Significantly, since this process does not require any high-temperature processing steps, it can be applied to virtually general substrates and may remove current difficulty in manufacturing of electronic devices based on 1-D nanostructures.

*This work was supported by NSI-NCRC and SAIT.

***Invited Papers***

**8:36**
**N37 4 Integrating molecular electronics with silicon.** VEENA MISRA, *NC State U.*

This abstract was not received electronically.

***Contributed Papers***

**9:12**
**N37 5 Nanoscale devices on thin films by ultra-high-resolution lithography*** MICHAEL FISCHBEIN, *University of Pennsylvania* MARIJA DRNDIC, *University of Pennsylvania* It is possible to achieve exceptionally high resolution with lithographic techniques that use scanning and transmission electron beams by using a thin film as a substrate. With this approach, numerous structures such as nanowires, nanorings, nanogaps and quantum dots can be made with dimensions under ten nanometers and in some cases even less than one nanometer. The flexibility of this fabrication approach also allows these extremely small structures to be easily contacted by large electrodes and therefore integrated into full electronic devices that exhibit effects due to carrier confinement. Furthermore, because these devices are on thin films, they are compatible with imaging by transmission electron microscopy (TEM). Basic devices made with this approach will be introduced. Extensions to devices with more complicated geometries and those which also include non-lithographically prepared nanostructures will be discussed as well.

*This work was supported by ONR (N000140410489), NSF (DMR-0449553), NSF MRSEC (DMR00-79909) and NSF-IGERT (DGE 022166).

**9:24**
**N37 6 Correlated electrostatic force microscopy and transmission electron microscopy study of nanostructures on silicon nitride membranes** ZONGHAI HU, MICHAEL FISCHBEIN, MARIJA DRNDIC, *University Of Pennsylvania* Silicon nitride membrane windows allow correlated electrostatic force microscopy and transmission electron microscopy (EFM/TEM) study of electrical and structural properties of the same nanoscale electronic devices fabricated on top of them. Under EFM, nanoscale charge transport patterns are distinguished and correlated with structural details as imaged by high resolution TEM. Examples of nanostructures studied include lithographically fabricated devices and self-organized nanocrystal arrays. Implications of the results on the transport mechanisms of these nanostructures will also be discussed. This work is supported by ONR Young Investigator Award N000140410489, ACS PRF Grant 41256-G10, NSF Career Grant DMR-0449553, and NSF NSEC Grant DMR-0425780.

**9:36**
**N37 7 Local Photocurrent Mapping of Nanowire Photodetectors with Ohmic and Schottky Contacts** YI GU, JOHN P. ROMANKIEWICZ, JESSICA L. LENSCH, TERI W. ODOM, LINCOLN J. LAUHON, *Northwestern University* Near-field scanning photocurrent microscopy (NSPM) was used to determine the mechanisms of carrier transport and collection in CdS nanowire photodetectors. NSPM employs an apertured NSOM probe as a local ( $<$ 100 nm) illumination source to map the local photocurrent as a function of the tip position along the device, i.e., from one metal contact to the other. Striking differences between Schottky and ohmically contacted devices have been observed in maps of the local photocurrent. In the Schottky devices, the photoinduced current is localized to the reverse biased diode, whereas in ohmic devices, the peak photoresponse position shifts continuously with applied bias. Modeling of the photocurrent profiles in ohmically contact devices gives the mobility-lifetime product for electrons and for holes. When independent carrier lifetime measurements are considered, one can extract electron and hole mobilities. As expected for CdS, the electron mobility exceeds the hole mobility, producing the observed shift of the photocurrent peak towards the hole collector. The effects of surface passivation and trap filling on carrier transport have also been explored.

**9:48**
**N37 8 Negative Differential Resistance in CdSe Nanorod Devices.*** HUGO ROMERO, DONG TRAN, GREGORY CALUSINE, MARIJA DRNDIC, *Department of Physics and Astronomy, University of Pennsylvania, Philadelphia, Pennsylvania 19104* Semiconductor quantum rods are expected to exhibit interesting novel behaviors because of their well-defined shape with the long axis preferably grown along the unique c axis. They would also allow for efficient quasi-1D electrical transport. Thus, when organized into arrays of aligned quantum rods separated by insulating barriers, improved and unconventional electronic transport could be achieved compared to that of ''spherical'' nanocrystal arrays. Here, we report on the observation of interesting charging properties in electronic devices consisting of CdSe quantum rod thick films as the active components. The low bias regime of the current-voltage characteristics of such devices displays mul-

tiple negative differential resistance behavior and step-like structures at room temperature. This effect may be related to the alignment of localized trap levels in the insulating barriers with the carrier levels in the quantum rods.

*This work was supported by ONR grant N000140410489 and NSF grant DMR-0449553.

**10:00**

**N37 9 Electron transport of nanoscale P-donor wires in silicon*** T.-C. SHEN, *Utah State University* S. J. ROBINSON, J. R. TUCKER, *University of Illinois at Urbana-Champaign* Three dimensional carrier transport in doped semiconductors has been extensively investigated. However, transport in low-dimensions is much less clear because of the difficulty to confine dopant distribution in a crystal. In the past few years we have created 2D embedded dopant sheets by exposing Si(100) surfaces to phosphine molecules in ultrahigh vacuum followed by growing epitaxial silicon over-layers at room temperature. Electron density in these delta layers can be as high as $\sim 1.5 \times 10^{14}$ cm$^{-2}$. We find that surface roughness dictates the carrier mobility and activation, even though all surfaces are atomically clean and locally ordered. Furthermore, applying STM e-beam lithography on a single-layer H-resist enables us to define P-donor wires at widths from 200 nm to 5 nm in 2-terminal device templates. The As-implanted electrodes in the device templates provide ohmic contact with P-donor wires. In this presentation we will discuss our electrical and magneto-resistance measurement of various P-donor nanostructures at cryogenic temperatures. The goal of this research is to apply 2D P-donor patterns as building blocks for nanoscale integrated circuits.

*This work is supported by NSF under Grant No. 0404208.

**10:12**

**N37 10 Confined Doping for Control of Transport Properties in Nanowires and Nanofilms*** JIANXIN ZHONG, G. MALCOLM STOCKS, *Oak Ridge National Laboratory* Doping, an essential element for manipulation of electronic transport in traditional semiconductor industry, is widely expected to play important role as well in control of transport properties in nanostructures. However, traditional theory of electronic disorder predicts that doping in one-dimensional and two-dimensional systems leads to carrier localization, limiting practical applications due to poor carrier mobility. Here, a novel concept is proposed that offers the possibility to significantly increase carrier mobility by confining the distribution of dopants within a particular region [1]. Thus, the doped nanostructure becomes a coupled system comprising a doped subsystem and a perfect crystalline subsystem. We showed that carrier mobility in such a dopped nanowire or a nanofilm exhibits counterintuitive behavior in the regime of heavy doping. In particular, the larger the dopant concentration the higher the carrier mobility; we trace this transition to the existence of quasi-mobility-edges in the nanowires and mobility edges in nanofilms. J.X. Zhong and G.M. Stocks, Nano Lett., in press, (2005).

*Supported by the Material Sciences and Engineering Division Program of the DOE Office of Science under contract DE-AC05-00OR22725 with UT-Battelle, LLC.

**10:24**

**N37 11 Field emission characteristics of GaN nanorods on self-implanted (111) Si*** H.W. SEO, X.M. WANG, Q.Y. CHEN, *Dept. of Physics & Texas Center for Superconductivity, University of Houston, Texas, USA.* L.W. TU, Y.J. TU, C.L. HSIAO, M. CHEN, *Dept.of Physics & Center for Nanoscience and Nanotechnology, National Sun Yat-Sen University, Taiwan, Republic of China.* O. LOZANO, D.H. KIM, P.V. WADEKAR, WEI-KAN CHU, *Dept. of Physics & Texas Center for Superconductivity, University of Houston, Texas, USA.* Periodic arrays of GaN nanostructures have been fabricated by MBE growth on self-implanted (111) Si substrates. Nano-capillary condensation was found to be an effective catalytic process fostering the formation of epitaxially aligned GaN nanorods supported by a thin film matrix. Changes of Si substrate surface morphology as a result of ion bombardments prior to the thin-film deposition are responsible for the enhanced nanorod growth. The density of nanorods in relation to implanted ion dosages was studied. Field emission measurement was performed to understand the physical characteristics of functional devices based on such nanostructures. Experimental details and their implications for the future development of nanostructure and nano-device fabrications will be presented.

*Supported by NSF grant DMR-0404542 and by DOE grant DE-FG02-05ER46208. Partial support by the Welch Foundation and the State of Texas through TcSUH are also acknowledged.

**10:36**

**N37 12 Conductance measurement of GaN nanorods*** O. LOZANO, H.W. SEO, Q.Y. CHEN, *Dept. of Physics & Texas Center for Superconductivity, University of Houston, Texas, USA.* L.W. TU, Y.J. TU, C.L. HSIAO, M. CHEN, *Dept.of Physics & Center for Nanoscience and Nanotechnology, National Sun Yat-Sen University, Taiwan, Republic of China.* D.H. KIM, P.V. WADEKAR, WEI-KAN CHU, *Dept. of Physics & Texas Center for Superconductivity, University of Houston, Texas, USA.* GaN nanorods have been grown by molecular beam epitaxy over a thin-film GaN matrix on Si substrate. We have studied the conductance behaviors of a single nanorod and clusters nanorods. Transport measurement of internal emission of electrons from nanorod-clusters was carried out with metallic contacts over the nanostructure. Vacuum tunneling of externally emitted electrons from individual nanorod was measured using a scanning tunneling microscope-first in constant voltage mode to locate the more conductive nanorods, which was then followed by measurements at various applied voltage. Observations are made to distinguish thin film matrix from the nanorods by their efficiencies of electron emission. The characteristics of I-V curves will be reported and the applications of these nanorods to electron-emission devices will be discussed.

*Supported by NSF grant DMR-0404542, DOE grant DE-FG02-05ER46208, the Welch Foundation and the State of Texas.

**10:48**

**N37 13 Structural and Electronic Properties of GaN and InN Nanowires grown using Hot-Wall CVD** ELENA CIMPOIASU, ERIC STERN, GUOSHENG CHENG, RYAN MUNDEN, ARIC SANDERS, MARK A. REED, *Departments of Electrical Engineering, Applied Physics, and Physics, Yale University, New Haven, CT* We study the electron-mobility dependence on the free carrier concentration itn exhibited by hot-wall chemical-vapor deposition-grown gallium nitride (GaN) and indium nitride (InN) nanowires. The growth involves flow of ammonia over solid sources of gallium or indium and the substrate, which is covered

with metal catalyst (in case of GaN) or is catalyst-free (in case of InN). The nanowires are subsequently deposited on oxidized silicon wafers and fabricated in field-effect transistors using optical lithography. In this way, more than 1000 devices were characterized at room temperature. Both types of nanowires show high carrier concentration ($10^{19} - 10^{20}$ $cm^{-3}$ for GaN and $10^{20} - 10^{21}$ $cm^{-3}$ for InN), with mobility decreasing with increasing free carrier concentration, consistent with ionized impurity scattering. Mobility levels range between below 1 to 100 $cm^2/Vs$. Estimations of the ionized impurity mobility indicate that GaN wires grow heavily compensated, and subsequent anneals in ammonia result in even higher compensation levels. We were also successful in doping GaN nanowires with magnesium, for p-type doping. Similar chemical, structural, and electronic analysis will be presented. This work was partially supported by DARPA through AFOSR, ARO, AFOSR, NASA, by the Department of Homeland Security, and by NSF.

**SESSION N38: TRANSPORT PROPERTIES OF HIGH-TC SUPERCONDUCTORS**
**Wednesday Morning, 15 March 2006**
**341, Baltimore Convention Center at 8:00**
**Patrick Fournier, University of Sherbrooke, presiding**

*Contributed Papers*

**8:00**
**N38 1 Anomalous dimensional crossover in critical microwave-conductivity fluctuations of superconducting $La_{2-x}Sr_xCuO_4$ thin films** HARUHISA KITANO, TAKEYOSHI OHASHI, ATSUTAKA MAEDA, *Department of Basic Science, University of Tokyo* ICHIRO TSUKADA, *Central Research Institute of Electrical Power Industry* We demonstrate that there are two dimensional crossover lines separating the phase diagram of $La_{2-x}Sr_xCuO_4$ (LSCO) into three regions with different universality classes, by using a dynamic scaling analysis of the microwave complex conductivity. For underdoped LSCO from x=0.07 to x=0.14, we show clear evidence for the 2D-itXY universality class (the BKT transition in the nearly decoupled $CuO_2$ planes), while the 3D-itXY universality class is observed for nearly optimally doped region (x=0.15, 0.16). Surprisingly, for overdoped LSCO with x> 0.17, we found that the critical behavior strongly suggested the 2D universality class, in contrast to the reduction of anisotropic properties with hole-doping. We discuss the implication of these results in terms of the effect of the quantum critical fluctuations.

**8:12**
**N38 2 Finite Size Effects in YBCO Films in Zero and Non-Zero Field*** SU LI, *Center for Superconductivity Research, Department of Physics, University of Maryland, College Park* HUA XU, *Center for Superconductivity Research, Department of Physics, University of Maryland, College Park* M. C. SULLIVAN, *Department of Physics, Ithaca College* STEVEN M. ANLAGE, *Center for Superconductivity Research, Department of Physics, University of Maryland, College Park* C. J. LOBB, *Center for Superconductivity Research, Department of Physics, University of Maryland, College Park* The phase transition in high Tc superconductors in a magnetic field has been intensely studied. However, only a few papers have discussed finite-size effects (Phys. Rev. B **69**, 214524 (2004)). Neglecting finite size effects can cause misinterpretation of the experimental data leading to incorrect critical exponents. We will report results of DC transport measurements on YBa2Cu3O6.95 films in zero field (less than 50 nT) as well as in fields up to 6 T. The results will be analyzed in terms of field-induced finite size effects and thickness-induced finite size effects.

*This work was supported by NSF grant number DMR-0302596.

**8:24**
**N38 3 Fluctuations at the superconductor/normal phase transition of YBCO thin films** HUA XU, SU LI, CHRISTOPHER LOBB, STEVEN ANLAGE, *Center for Superconductivity, Department of Physics, University of Maryland, College Park, MD 20742* The zero-field phase transition of high $T_c$ superconductors has been studied by a number of techniques, such as penetration depth, magnetic susceptibility, specific heat and thermal expansion, which reveal information about the static, properties of fluctuations. Transport properties (such as the conductivity) which probe the dynamics near $T_c$ are less explored, and a wide range of critical exponents were reported experimentally. We investigated fluctuation effects of $YBa_2Cu_3O_{7-d}$ (YBCO) around $T_c$ by doing frequency-dependent microwave conductivity measurements and dc current-voltage characteristics on the same film. For each experiment the scaling behavior of the data was investigated. The critical exponents $\nu$ and z from the two different experiments will be extracted and compared. We also investigated YBCO frequency-dependent conductivity fluctuation effects for different powers or currents and for different film thickness. The finite size effects in both the microwave and DC voltage current experiments will also be discussed. (This work was supported by NSF grant number DMR-0302596).

**8:36**
**N38 4 Transport and Noise Properties of High Temperature Superconductor Nanostructures** D.S. CAPLAN, X. ZHAI, J.N. ECKSTEIN, D.J. VAN HARLINGEN, *University of Illinois at Urbana-Champaign* The study of transport and noise properties of high-$T_c$ superconductor nanostructures provides a sensitive probe of their local electronic structure and may give insight into the proposed mechanisms for the superconductivity and the nature of the anomalous normal phases. We discuss a novel technique for fabricating nanostructures based on the growth of cuprate films on substrates pre-patterned by Focused Ion Beam etching. We report measurements in underdoped YBCO and BSCCO nanostructures fabricated by this technique that are designed to understand anomalous switching noise observed in the pseudogap phase above $T_c$. Our goal is to test if these signal show the existence of dynamical domains characterized by inhomogeneous conductivity or by anisotropic charge stripes.

**8:48**
**N38 5 Thermoelectric power as evidence for a Quantum Phase Transition in electron-doped cuprates $Pr_{2-x}Ce_xCuO_{4-y}$.*** PENGCHENG LI, R.L. GREENE, *Center for Superconductivity Research and Department of Physics, University of Maryland, College Park, MD, 20742* K. BEHNIA, *Laboratoire de Physique Quantique (CNRS), ESPCI, 10 Rue Vauquelin, 75005 Paris,*

*France* We report magnetic field driven normal state thermoelectric power (S) measurement in electron-doped cuprate system $Pr_{2-x}Ce_xCuO_{4-y}$ as a function of doping (x from 0.11 to 0.19) down to 2K. Consistent with the normal state Hall effect[a], S in the underdoped region (0.11-0.15) is negative. S changes sign at certain temperatures in overdoped samples (0.16-0.18), which supports the picture of a spin density wave rearrangement of the Fermi surface[b]. More significantly, both S and S/T at 2K (at 9T) increase dramatically from x=0.11 to 0.16, and then saturate in the overdoped region. This kink around x=0.16 is similar to the previous Hall effect result[a] in $Pr_{2-x}Ce_xCuO_{4-y}$. Our results are further evidence for antiferromagnetism to paramagnetism quantum phase transition in electron-doped cuprates. a. Y. Dagan et al, Physical Review Letters, 92 (16) 167001, 2004 b. A. Zimmers et al, Europhysics Letters 70 (2) 225, 2005.

*This work is supported by NSF Grant DMR-0352735.

**9:00**

**N38 6 Anomalous Nernst Effect in High-$T_c$ Superconductors by Layer Decoupling** JOSE P. RODRIGUEZ, *California State University at Los Angeles* The extended vortex-liquid phase found in high-$T_c$ superconductors at temperatures and magnetic fields that lie above the vortex-lattice melting line can be attributed to weak inter-layer coupling. We compute the diamagnetic contribution to the equilibrium magnetization there, $M$, using the corresponding uniformly frustrated $XY$ model, given in terms of the phase of the superconducting order parameter[1]. A high-temperature expansion that is valid in the vicinity of the mean-field phase transition yields (i) that $-M$ increases monotonically with the external magnetic field, and (ii) that it vanishes as the mean-field phase transition is approached from below. Further, we show (iii) that the assumption of a direct dependence between $M$ and the Peltier transport coefficient results in an anomalous Nernst signal inside of the vortex-liquid phase. These results are compared to recent experimental determinations of the equilibrium magnetization and of the Nernst effect in the vortex-liquid phase of high-$T_c$ superconductors[2]. [1] J.P. Rodriguez, PRB **66**, 214506 (2002); **69**, 069901(E) (2004). [2] Y. Wang, et al., PRL, in press (arXiv: cond-mat/0503190).

**9:12**

**N38 7 Thermoelectric transport near the pair breaking quantum phase transition out of a *d*-wave superconductor** DANIEL PODOLSKY, ASHVIN VISHWANATH, JOEL MOORE, *University of California at Berkeley* SUBIR SACHDEV, *Harvard University* We study electric, thermal, and thermoelectric conductivities in the vicinity of a $z = 2$ superconductor-diffusive metal transition in two dimensions, both in the high and low frequency limits. We find violation of the Wiedemann-Franz law, with a Lorentz ratio *below* the Sommerfeld value (more charge than heat transport). In addition, the dc thermoelectric conductivity $\alpha$ does not vanish at low temperatures, in contrast to Fermi liquids. We introduce a Langevin equation formalism to study critical dynamics over a broad region surrounding the quantum critical point.

**9:24**

**N38 8 Competing orders in LSCO probed by heat transport** SHIYAN LI, *University of Sherbrooke, Canada* D. G. HAWTHORN, *University of Toronto, Canada* LOUIS TAILLEFER, *University of Sherbrooke, Canada and Canadian Institute for Advanced Research* K. YAMADA, *Tohoku University, Japan* We elucidate the nature of the thermal metal-to-insulator transition in $La_{2-x}Sr_xCuO_4$ (LSCO) [1] through measurements of the thermal conductivity $\kappa$ performed very close to the transition, down to temperatures as low as 50 mK and in magnetic fields $H$ up to 17 T. For a single crystal with x = 0.15, a monotonic increase in the residual linear term $\kappa_0/T$ is observed up to 17 T, as expected for a d-wave superconductor. For a crystal with x = 0.144, however, we observe an initial increase in $\kappa_0/T$ at low field, followed by a decrease when $H$ exceeds a critical field $H^*$. This result is consistent with recent neutron scattering measurements on a similar sample [2], which show that static spin-density-wave (SDW) order is not present in zero field, but sets in at a critical magnetic field $H^*$, and then co-exists/competes with superconductivity (SC) for $H > H^*$. Taken together, these two measurements reveal that the SC phase gives way to a phase which is both magnetic and insulating, whether by increasing magnetic field or by decreasing doping. Using low-energy quasiparticle transport, we map out the $T = 0$ field-doping ($H - x$) phase diagram of LSCO. [1] D.G. Hawthorn et al., Phys. Rev. Lett. 90, 197004 (2003); X.F. Sun et al., Phys. Rev. Lett. 90, 117004 (2003). [2] B. Khaykovich et al., Phys. Rev. B 71, 220508(R) (2005).

**9:36**

**N38 9 Existence of a boson mode in underdoped YBCO** NICOLAS DOIRON-LEYRAUD, S.Y. LI, *Université de Sherbrooke* M. SUTHERLAND,* *University of Toronto* L. TAILLEFER, *Université de Sherbrooke and CIAR* R. LIANG, D.A. BONN, W.N. HARDY, *University of British Columbia and CIAR* We have examined the underdoped region of the cuprate phase diagram via a study of heat transport at temperatures down to 50 mK in samples of YBCO with a hole concentration in the vicinity of 5%. The measured thermal conductivity was found to be well described by a sum of three terms, $\kappa(T) = aT + bT^{\alpha} + cT^3$, which we associate with, respectively, fermionic quasiparticles, phonons, and a new bosonic mode. By comparing data taken at different doping levels on the same sample it was possible to track the evolution of the $T^3$ term. Its coefficient was found to increase with decreased doping, i.e., with proximity to magnetism. We speculate that this term may be associated with the transport of heat by magnons, as observed recently by Li et al. [1] in the undoped cuprate material $Nd_2CuO_4$. This would suggest that long range magnetic order in YBCO appears at a doping level very close to that at which superconductivity ends. [1] S.Y. Li et al., Phys. Rev. Lett. **95**, 156603 (2005).

*Now at University of Cambridge UK.

**9:48**

**N38 10 Low-Temperature Normal State Hall Effect in High-$T_c$ $La_{2-x}Sr_xCuO_4$*** FEDOR BALAKIREV, *Los Alamos National Laboratory, Los Alamos, NM 87545, USA* JONATHAN BETTS, *Los Alamos National Laboratory, Los Alamos, NM 87545, USA* ALBERT MIGLIORI, *Los Alamos National Laboratory, Los Alamos, NM 87545, USA* ICHIRO TSUKADA, *Central Research Institute of Electric Power Industry, Komae, Tokyo 201-8511, Japan* YOICHI ANDO, *Central Research Institute of Electric Power Industry, Komae, Tokyo 201-8511, Japan* GREGORY BOEBINGER, *National High Magnetic Field Laboratory, Tallahassee, FL 32310, USA* We report Hall effect measurements in the normal state of the high-$T_c$ superconductor $La_{2-x}Sr_xCuO_4$. The Hall resistivity was measured by suppressing superconductivity in 60T magnetic field, thus revealing the normal-state behavior in the low

temperature limit. The carrier concentration is varied from overdoped to underdoped regimes by partially substituting La with Sr in a set of thin film samples. We find a discontinuity in the doping dependence of the Hall coefficient suggestive of a phase transition near optimal doping.

*The work at the National High Magnetic Field Laboratory was supported by the National Science Foundation and DOE Office of Science.

**10:00**

**N38 11 Effect of Disorder Outside the $CuO_2$ Planes on $T_c$ of Copper Oxide Superconductors.** KAZUHIRO FUJITA, *Department of Advanced Materials Science, University of Tokyo, L.A.S.S.P. Department of Physics, Cornell University* KENJI KOJIMA, *Department of Physics, University of Tokyo* HIROSHI EISAKI, *Nanoelectronics Research Institute, National Institute for Advanced Industrial Science and Technology (AIST)* SHIN-ICHI UCHIDA, *Department of Physics, University of Tokyo, Department of Advanced Materials Science, University of Tokyo* The effect of disorder on the superconducting transition temperature $T_c$ of cuprate superconductors is examined. Disorder is introduced into the cation sites in the plane adjacent to the $CuO_2$ planes of single-layer systems, $Bi_2Sr_{1.6}Ln_{0.4}CuO_{6+y}$. Disorder is controlled by changing rare earth (Ln) ions with a different ionic radius with the doped carrier density kept constant. We show that this type of disorder works as weak scatterers in contrast to the in-plane disorder produced by Zn, but remarkably reduces $T_c$, suggesting novel effects of disorder on high-$T_c$ superconductivity.

**10:12**

**N38 12 Mixed State $c-$ axis Resistivity of $Y_{0.54}Pr_{0.46}Ba_2Cu_3O_{7-\delta}$ Single Crystals*** T. KATUWAL, V. SANDU, C.C. ALMASAN, *Kent State University* B.J. TAYLOR, M.B. MAPLE, *University of California at San Diego* We report temperature $T$, magnetic field $H$, and angle $\theta$ dependent out-of-plane resistivity $\rho_c$ measurements on $Y_{0.54}Pr_{0.46}Ba_2Cu_3O_{7-\delta}$ single crystals. We performed these measurements in order to investigate the origin of the large $\rho_c$ of layered superconductors like cuprates and of its T, H, and $\theta$ dependence. The $\rho_c(T,H,\theta)$ data are very well fitted by the Ambegaokar $-$ Halperin expression [V. Ambegaokar and B. I. Halperin, Phys. Rev. Lett. 22, 1364 (1969)] for temperatures up to the critical temperature $T_c$ and applied magnetic field up to 14 T. This implies that in the underdoped cuprates the layered structure can be depicted as stacks of Josephson junctions. We calculated the value of the critical current density $J_c$ at different temperatures by using the above model and the values of the fitting parameters. Both the magnitude and $T$ dependence of $J_c$ are consistent with previous reports. This result supports the applicability of the model and indicates that the mixed state $c-$ axis dissipation is mainly due to the Josephson effect.

*This work was supported by the National Science Foundation Grant No. DMR-0406471 at KSU and by the U. S. Department of Energy Grant No. DE-FG03-86ER-45230 at UCSD.

**10:24**

**N38 13 C-axis Resistivity and Magnetoresistance of the Electron-doped Cuprate $Pr_{1.85}Ce_{0.15}CuO_4$** WEIQIANG YU, B. LIANG, R. L. GREENE, *Center for Superconductivity Research, Department of Physics, University of Maryland, College Park, MD 20742* C-axis resistivity and magnetoresistance have been studied extensively in the hole-doped high temperature superconductors. Observations, such as a resistivity upturn and associated negative magnetoresistance (n-MR), were attributed to the pseudogap. Recently similar phenomena were reported in the electron-doped superconductor $Sm_{1.85}Ce_{0.15}CuO_4$ (SCCO), and a universal Zeeman splitting of a spin gap (pseudogap) state was proposed [1]. Here we report transport properties of $Pr_{1.85}Ce_{0.15}CuO_4$ (PCCO) ($T_C \approx 25K$) single crystals for comparison. Our c-axis n- MR can be explained by superconducting fluctuations due to the Aslamazov-Larkin (AL) process and the fluctuating electronic density of states (FDOS) above $H_{C2}$. We find that PCCO does not follow the Zeeman scaling behavior as reported for SCCO. This work is supported by NSF (Grant DMR 0352735).

[1]T. Kawakami et al., Phys. Rev. Lett. 95, 017001 (2005).

**10:36**

**N38 14 Resistivity and Hall effect measurements in $Pr_{2-x}Ce_xCuO_{4-y}$ up to 60 T*** R.L. GREENE, PENGCHENG LI, *Center for Superconductivity Research and Department of Physics, University of Maryland, College Park, MD, 20742* F. BALAKIREV, *National High Magnetic Field Lab in Los Alamos National Lab, Los Alamos, NM, 87545* We report resistivity and Hall effect measurements in the electron$-$doped cuprate system $Pr_{2-x}Ce_xCuO_{4-y}$ in magnetic field up to 60 T. We found negative magneto resistance (MR) in the under doped region for all magnetic field values, similar to the low field data reported previously a. The MR becomes positive at high field in the optimal doped (x=0.15) sample at low temperature. Most surprisingly, we observed a substantial magnetic field dependence of the Hall coefficient at high field (above $\sim$ 40 T) in optimal dopedand over doped samples (from x=0.15 to 0.19) in a certain temperature range. As pin density wave induced Fermi surface reconstruction model can be used to explain this phenomenon. We also report for the first time the parallel upper critical field (H//abplane) for $Pr_{2-x}Ce_xCuO_{4-y}$. (A.Y. Daganetal, Physical Review Letters **94**(5), 11 2005).

*This work is supported by NSF Grant DMR$-$0352735.

**10:48**

**N38 15 Role of Disorder and Oxygen Reduction on Transport Properties in $Pr_{1.83}Ce_{0.17}CuO_{4\pm\delta}$*** J. S. HIGGINS, Y. DAGAN,† M. C. BARR, R. L. GREENE, *Center for Superconductivity Research, Physics Department, University of Maryland, College Park, Maryland, USA 20742* B. D. WEAVER, *Naval Research Laboratory, Code 6818, Washington, DC, USA 20375* We present a study on the effects of changing the oxygen content in the electron-doped superconducting cuprate $Pr_{2-x}Ce_xCuO_{4\pm\delta}$ (PCCO). Epitaxial, c-axis oriented, overdoped (x = 0.17) thin films were grown using a pulsed laser deposition technique, and the oxygen content was adjusted during a post-growth annealing

process. In addition to the transition temperature ($T_c$), measurements of the Hall effect and resistivity were performed at low temperatures ($T < T_c$, $H > H_{C2}$) in several films of different oxygen content. We compare the disorder observed in these oxygenated samples with disorder induced by proton irradiation in an optimally annealed ($x = 0.17$) film. An analysis of the data demonstrates that a change in the oxygen content of PCCO has two separable effects: 1) a disorder effect, and 2) a doping effect similar to that of cerium.

*This work was supported by NSF Grant DMR-0352735 and, in part, by ONR.

†Current address: School of Physics and Astronomy, Raymond and Beverly Sackler Faculty of Exact Sciences, Tel Aviv University, Tel Aviv 69978, Israel.

## SESSION N39: FOCUS SESSION: SUPERCONDUCTIVITY-THIN FILMS AND JUNCTIONS MAGNESIUM DIBORIDE AND RELATED COMPOUNDS

**Wednesday Morning, 15 March 2006; 342, Baltimore Convention Center at 8:00**
**John Rowell, Arizona State University, presiding**

### *Invited Papers*

**8:00**
**N39 1 Clean and Dirty $MgB_2$ Thin Films by Hybrid Physical-Chemical Vapor Deposition.***
XIAOXING XI, *Penn State University*

The interband and intraband scattering in $MgB_2$ have significant influences on various properties of this two-band superconductor. In order to explore new physical phenomena and realize the potential for applications in $MgB_2$, it is desirable to control the interband and intraband scattering arbitrarily and independently. Hybrid physical-chemical vapor deposition (HPCVD) is a promising technique towards this goal. It has produced very clean $MgB_2$ films with a residual resistivity ratio of 60. The tensile strain in the films due to crystallite coalescence results in a softening of the $E_{2g}$ phonon and higher-than-bulk $T_c$ values. The long mean free path of the films, which are the cleanest $MgB_2$ materials reported, allow magnetoresistance measurements that reveal rich features of the two-band Fermi surfaces. The HPCVD technique also allows doping of the clean films in a controlled manner, which modifies the interband and intraband scattering and results in record-high upper critical field $H_{c2}$ of over 60 T. The demonstrations of HPCVD for high quality polycrystalline coatings on coated conductor fibers, high deposition speed and thick films, and on various polycrystalline substrates make it a promising technology for high field applications of $MgB_2$.

*This work is supported by ONR and NSF.

### *Contributed Papers*

**8:36**
**N39 2 Hybrid Physical-Chemical Vapor Deposition of $MgB_2$ Film on Flexible Dielectric and Metallic Substrates** ERIC MAERTZ, A. V. POGREBNYAKOV, J. M. REDWING, X. X. XI, *The Pennsylvania State University* The need for flexible dielectric and metallic substrates arises when considering making wires or tapes for high field applications. To accomplish this, Cu wire and foil with a buffer layer, flexible yttrium stabilized zirconium (YSZ), as well as Nb, Ta, and stainless steel foil were used as substrates for polycrystalline $MgB_2$ film growth. The foil substrates used range from 1 to 3 mil thickness. The buffer layers deposited on Cu were Ni plating (on 28 BSG wire) as well as $TiB_2$ and Nb deposited by sputtering. These served as a barrier to prevent the chemical reaction between Cu and Mg that occurs during deposition of $MbB_2$. The resistance vs. temperature (R-T) dependences were recorded for the films successfully grown on these substrates. For the films on YSZ, R-T was recorded initially and then after bending of the film on the substrate over a diameter of 20mm. The $T_C$ of $MgB_2$ on stainless steel was 38K; on YSZ and Nb it was 38.5K. This is lower than epitaxial films on SiC substrate with $T_c$ up to 41.5K. The R-T curve for $MgB_2$ on YSZ remained almost completely unchanged after bending. These films hold promise for electromagnetic field generation applications. This work is supported by NSF and ONR.

**8:48**
**N39 3 Planar $MgB_2$ superconductor-normal metal-superconductor Josephson junctions** KE CHEN, Y. CUI, QI LI, *Department of Physics, The Pennsylvania State University, University Park* X. X. XI, *Department of Physics and Department of Materials Sciene and Engineering, The Pennsylvania State University, University Park* SHANE A. CYBART, *Department of Physics, University of California, San Diego* R. C. DYNES, *Department of Physics, University of California, Berkeley* X. WEN, J. M. REDWING, *Department of Materials Sciene and Engineering, The Pennsylvania State University, University Park* We have fabricated planar superconductor-normal metal-superconductor (SNS) $MgB_2$ Josephson junctions using $MgB_2$ films grown by hybrid physical chemical vapor deposition (HPCVD). The junctions exhibit resistively-shunted-junction-like (RSJ-like) current-voltage characteristics up to 31 K. Ac Josephson effect was observed and the behavior of the Shapiro steps are in good agreement with theoretical predictions. The magnetic field modulation of the critical current also agrees with the thin film planar junction be-

havior. The junction's behavior can be described by Likharev's proximity effect model with rigid boundary at dirty limit. A dc SQUID with modulation depth of 45 $\mu$V at 29 K has been demonstrated. This work is supported by ONR, NSF, and AFOSR.

**9:00**

**N39 4 Fabrication and characterization of $MgB_2$/ thermal oxide barrier /Pb Josephson tunnel junctions** YI CUI, KE CHEN, QI LI, XIAOXING XI, *Department of Physics, The Pennsylvania State University* JOHN M. ROWELL, *Arizona State University* Cross-bridge Josephson tunnel junctions were fabricated, using $MgB_2$ films grown by hybrid physical-chemical vapor deposition (HPCVD) and barriers made by thermal oxidation at different temperatures. The junctions showed clear Josephson tunneling characteristics with high supercurrents, high $I_cR_N$ products ($I_cR_N$ products $\sim$ 1.8 mV at 4.2 K), and small subgap current leakage. The external DC magnetic field dependence was also measured and showed clear Fraunhofer pattern. The properties of the thermal oxide barrier depend sensitively on the oxidation temperature. The potential height and barrier thickness of 0.7 eV and 1.8 nm, respectively, were inferred from conductance measurements at high bias voltage. Two superconducting gaps of 2.0 meV and 7.5 meV for $MgB_2$ were observed from these sandwich-type tunnel junctions. These results suggest the potential of using $MgB_2$ thermal oxide layers as a barrier for practical Josephson tunnel junction fabrication. This work is supported by ONR and NSF.

**9:12**

**N39 5 MgB2 Tunnel Junctions with Native or Thermal Oxide Barriers** RAKESH SINGH, *Arizona State University* RAGHURAM GANDIKOTA, JIHHON KIM, NATHAN NEWMAN, JOHN ROWELL, $MgB_2$ tunnel junctions ($MgB_2$/barrier/$MgB_2$) were fabricated using an oxide (or a mixture of oxides) grown on the first $MgB_2$ film as the tunnel barrier, by exposure to air at 20$^o$C (native oxide) or 160$^o$C (thermal oxide). Such barriers therefore survived the deposition of the second electrode at 300$^o$C, even over junction areas of $\sim$ 1mm$^2$. The sum of the superconducting gaps of the top and bottom electrodes, from conductance-voltage data, was as high as 4.3 mV and this sum gap remained non-zero for temperatures above 30 K. Conductance vs. voltage dependencies of all-$MgB_2$ junctions and those of the type $MgB_2$/Native or Thermal Oxide/Metal (Pb, Au, or Ag) were used to characterize the height and width of the barriers formed. Such barriers have surprisingly low barrier heights, with typical values for barrier height and width being 0.2 V and 4.5 nm respectively. These values are very different from those reported in the literature. These results show that tunnel barriers grown on $MgB_2$ can have different properties (barrier height and width), depending on the film growth, surface composition and oxidation conditions.

**9:24**

**N39 6 All $MgB_2$ tunnel junction with $Al_2O_3$ tunnel barrier*** HEEJAE SHIM, JAGADEESH S. MOODERA, *Francis Bitter Magnet Laboratory, MIT, Cambridge, MA* $MgB_2$ tunnel junctions are attractive not only from superconducting electronics application part of view but also from the fundamental physics to understand multi-gap superconductors. All $MgB_2$ planar junctions with $Al_2O_3$ tunnel barrier were fabricated in situ in an MBE system by coevaporation of Mg and B for $MgB_2$ and plasma oxidized Al for tunnel barrier on Si (111) substrate. The junctions exhibit the current-voltage characteristic for quasiparticle and Josephson tunneling including microwave induced Shapiro steps. From conductance spectrum at 1 K, we clearly observe features that correspond to different $\pi$ and $\sigma$ superconducting energy gaps for the two $MgB_2$ electrodes. The observed multi-gap structure will be discussed with the difference of crystallographic orientation of $MgB_2$ at the interface between tunnel barrier and both superconducting layers.

*This work was supported by ONR Grant and H. Shim was supported by the Post-doctoral Fellowship Program of KOSEF.

**9:36**

**N39 7 Scanning tunneling spectroscopy and high-frequency response of MgB2 films** M.S. RZCHOWSKI, D.M. KIM, J. GIENCKE, C.B. EOM, *University of Wisconsin-Madison* T.W. HEITMANN, *Syracuse University* The critical issues governing thin-film MgB2 applications can be traced to factors both microscopic, arising from the two-gap structure and scattering mechanisms, as well as mesoscopic, determined by connectivity and grain boundary characteristics. These are intertwined to the extent that substitutional doping to control gap characteristics and band scattering can strongly affect connectivity through grain boundary segregation and growth of second phases. These issues can be addressed with a combined approach of gap characterization by low-temperature scanning tunneling spectroscopy, and temperature-dependent microwave conductivity measurements. We discuss preliminary results characterizing gap properties with low-temperature superconducting-tip scanning tunneling microscopy, and 10 GHz cavity-based microwave conductivity measurements.

**9:48**

**N39 8 Thickness dependence of the properties of $MgB_2$ films grown by hybrid physical-chemical vapor deposition** ALEXEJ POGREBNYAKOV, *Department of Physics and Department of Materials Science and Engineering, The Pennsylvania State University* ARSEN SOUKIASSIAN, JOAN REDWING, *Department of Materials Science and Engineering, The Pennsylvania State University* XIAOXING XI, *Department of Physics and Department of Materials Science and Engineering, The Pennsylvania State University* Properties of pure $MgB_2$ films of different thicknesses (up to $\sim$ 1 $\mu$m) grown by hybrid-physical-chemical vapor deposition on sapphire substrates were studied. In accordance with the previous results for the films with thicknesses up to about 400 nm, $T_c$ of the films on $Al_2O_3$ levels off at a value of 40.0 - 40.5 K at thicknesses larger than 200 nm. The residual resistivity, $\rho_0$, monotonically decreases with thickness, which is caused by a reduction of the surface and interface scattering (size effect on resistivity). For films with thickness over $\sim$ 800 nm, $\rho_0$ is below 0.15 $\mu\Omega$.cm and $RRR >$ 60. X-ray studies of the films did not reveal any other phases besides $MgB_2$. In this talk, $MgB_2$ films of even larger thickness and the thickness dependence of critical current density will also be reported.

**10:00**

**N39 9 Far-infrared Studies of the Two-Gap Behavior in Epitaxial $MgB_2$ Films*** JIUFENG TU, *The City College of New York* G.L. CARR, *BNL* R.P.S.M. LOBO, *ESPCI* P. ORGIANI, X.X. XI, *Penn State* Far-infrared transmission and reflectivity measurements have been carried out for a series of pure and carbon-doped epitaxial $MgB_2$ films. While the carbon-doped film exhibits the typical characteristics for a dirty BCS superconductor in the $T_S$ /$T_N$ and $R_S$ /$R_N$ ratios, the pure $MgB_2$ films can only be understood knowing the multi-gap nature of the superconducting

state in $MgB_2$. As a function of increasing $T_c$, the fraction of the Cooper pairs having the larger gap increases. Both gaps appear to follow the BCS temperature dependence. However, the two gaps exhibit different behavior when a magnetic field is applied along c-axis. While the smaller gap can be suppressed by a relatively small field, the larger gap can persist up to 10 T. These infrared measurements indicate that the two superfluids coexist quite independently in the superconducting state of $MgB_2$.

*Supported by CUNY-RF-80212-13-04, DOE-AC02-98CH10886, ONR-N00014-00-1-0294 and NSF-DMR-0306746.

**10:12**

**N39 10 Penetration Depth Anisotropy in $MgB_2$ measured by Small-Angle Neutron Scattering** D. PAL, L. DEBEER-SCHMITT, T. BERA, M.R. ESKILDSEN, *Department of Physics, University of Notre Dame, Notre Dame, IN 46556* C.D. DEWHURST, R. CUBITT, *Institut Laue-Langevin, 6 Rue Jules Horowitz, F-38042 Grenoble, France* J. JUN, N.D. ZHIGALDO, J. KARPINSKI, *Laboratory for Solid State Physics, ETH, CH-8093 Zurich, Switzerland* V.G. KOGAN, *Ames Laboratory and Department of Physics and Astronomy, Iowa State University, Ames, Iowa 50011* Traditionally the anisotropy of a type-II superconductor is described either by $\gamma_\lambda = \lambda_c/\lambda_{ab}$ or $\gamma_H = H_{ab}/H_c = \xi_{ab}/\xi_c$. with the two considered to be identical. However, in materials with anisotropic gaps this is generally not the case. $MgB_2$ represents an extreme case in which $\gamma_\lambda \neq \gamma_H$. While there is consensus on the value of $\gamma_H(T)$, measurements of $\gamma_\lambda$ are still contradictory. Here we demonstrate a novel use of small-angle neutron scattering to determine $\gamma_\lambda$ in $MgB_2$, by measuring the misalignment between the applied field and the direction of the flux-line lattice as the field is rotated between the *c* axis and the basal plane. Using a two-band/two-gap model we can fit the angular dependence of the misalignment, yielding $\gamma_\lambda = 1.1 \pm 0.2$ at 4.9 K and 0.4 T.

**SESSION N41: INSULATING AND DIELECTRIC OXIDES**
**Wednesday Morning, 15 March 2006**
**344, Baltimore Convention Center at 8:00**
**Seong Gon Kim, Mississippi State University, presiding**

**8:00**

**N41 1 Oxygen-deficient defects and hydrogen in irradiated Si/SiO2 systems** RENEE VAN GINHOVEN, *Sandia National Labs* HAROLD HJALMARSON, *Sandia National Labs* Performance of Si/SiO2 devices is degraded by ionizing radiation through the production of interface traps and buildup of trapped charge in the oxide. This process is connected to the presence of hydrogen in the oxide. Exposure to ionizing radiation stimulates release of mobile hydrogen, which can migrate through the oxide to the Si/SiO2 interface and depassivate H-terminated Si-dangling bonds. The resulting interface trap states act as charge recombination centers. Our calculations focus on the interaction of hydrogen with oxygen deficient centers in the oxide. In the bulk oxide, these defects can release hydrogen from Si-H groups, or crack H2 molecules. These active sites may also act as border trap recombination centers when near the interface. Our presentation will describe molecular scale mechanisms for radiation-induced generation of free hydrogen using density functional theory applied to fully periodic models. The oxide is represented by both crystalline and amorphous configurations. Sandia is a multiprogram laboratory operated by the Sandia Corporation, a Lockheed Martin Company, for the United States Department of Energy under contract DE-AC04-94AL85000.

**8:12**

**N41 2 Photo-catalytic studies of transition metal doped titanium dioxide thin films processed by metalorganic decomposition (MOD) method** P. TALAGALA, X. MARKO, K.R. PADMANABHAN, R. NAIK, *Wayne State University, Detroit MI* D. RODAK, Y.T. CHENG, *General Motors R&D Center, Warren MI* We have synthesized pure and transition element (Fe, Co and V) doped Titanium oxide thin films of thickness $\sim$ 350 nm on sapphire, Si, and stainless steel substrates by Metalorganic Decomposition (MOD) method. The films were subsequently annealed at appropriate temperatures ( 500-750C) to obtain either anatase or the rutile phase of $TiO_2$. Analysis of the composition of the films were performed by energy dispersive X-ray(EDAX) and Rutherford backscattering spectrometry(RBS). Ion channeling was used to identify possible epitaxial growth of the films on sapphire. Both XRD and Raman spectra of the films exhibit that the films annealed at 550C are of anatase phase, while those annealed at 700C seem to prefer a rutile structure. The water contact angle measurements of the films before and after photoactivation, demonstrate a significant reduction in the contact angle for the anatase phase. However, the variation in contact angle was observed for films exposed to UV ( $< 10^o$-$30^o$) and dark ($25^o$-$50^o$). Films doped with Fe show a trend towards lower contact angle than those doped with Co. Results with films doped with V will also be included.

**8:24**

**N41 3 Proton Conduction and Microstructure of Lanthanum Phosphates*** GABRIEL HARLEY, LINDSEY KARPOWICH, LUTGARD DE JONGHE,† *University of California, Berkeley, 94720* Lanthanum phosphate (LaPO4) has been recently studied as a potential proton conducting ceramic electrolyte for fuel cells. The complexity of the La2O3 - P2O5 system, particularly in the 1000 - 1600K range, leads to the difficulty in forming phase pure LaPO4 by traditional synthesis methods. Complex microstructures involving amorphous and crystalline phases at grain boundaries have been detected by high resolution transmission electron microscopy, and have been shown to affect proton conductivity by several orders of magnitude. A simple model is used to predict conductivity of the material based on grain size and grain-boundary phases, and experimental results match up well with the model. Conductivities as high as 3.6E-5 S/cm at 773 K were found for undoped LaPO4.

*Supported by the Director, Office of Science, Office of Basic Energy Sciences, Materials Sciences and Engineering Division, of the U.S. Department of Energy under Contract No. DE-AC02-05CH11231

†All authors also at the Materials Science Division, Lawrence Berkeley National Labs, 1 Cyclotron Rd. Berkeley, CA, 94720

**8:36**

**N41 4 Comparison of the electronic structures of four crystalline phases of $FePO_4$*** PING TANG, N. A. W. HOLZWARTH, *Wake Forest University* $LiFePO_4$ in the olivine structure is a promising cathode material for Li-ion batteries. During normal battery operation, an olivine form of $FePO_4$ is formed. Experimen-

tal evidence suggests that the olivine phase is meta-stable relative to a quartz-like trigonal phase. In addition, several other meta-stable phases have been reported[1] including a monoclinic and a high pressure $CrVO_4$ structure. We have carried first-principles electronic structure calculations on all of these phases in order to investigate their relative stability and other properties using both LAPW and PWPAW methods.[2] We find that the LSDA approximation systematically underestimates the lattice constants and the calculated stability ordering of the phases is inconsistent with experiment. In contrast the GGA approximation models the phase stability in closer agreement with experiment, although the lattice constants are systematically over-estimated.

*Supported by NSF Grant No. DMR-0405456.

[1]M. S. Whittingham, Chem. Rev. **104**, 4271 (2004); Y. Song and co-workers, Inorg. Chem. **41**, 5778 (2002); H. N. Ng and C. Calvo, Can. J. Chem. **53**, 2064 (1975); J. P. Attfield and co-workers, J. Solid State Chem. **57**, 357 (1985); A. S. Andersson and co-workers, Solid State Ionics **130**, 41 (2000)http://www.wien2k.at/; http://pwpaw.wfu.edu/

[2]5); A. S. Andersson and co-workers, Solid State Ionics **130**, 41 (2000) http://www.wien2k.at/; http://pwpaw.wfu.edu/

**8:48**

**N41 5 First-principles study of phase stability and phase transition in $Ga_2O_3$*** JIANJUN DONG, BIN XU, *Department of Physics, Auburn University* Gallium oxide ($Ga_2O_3$) is a promising opto- and/or electronic wide-band-gap semiconductor. For example, it has been considered as a gate dielectric oxide for MOS device based on GaN or GaAs. In addition to the ground-state monoclinic $\beta$-phase, a rhombohedral $\alpha$-phase metastably exists at ambient conditions. The conditions of stability of either phase are not well understood. In this talk, we will present our recent itab initio calculation results of thermodynamic properties of the $\alpha$ and $\beta$ phase. We have computed Gibbs free energies of the two phases based on the total energy density functional theory (DFT) and the statistical quasi-harmonic approximation (QHA), calculated the thermal equations of states, and estimated the equilibrium phase boundary. We have further calculated the pressure dependence of Raman and IR frequencies in the two phases. Our results will be compared with some recent experimental data.

*This work is partially funded by DOE (DE-FG02-03ER46060).

**9:00**

**N41 6 Phase transition of Ta-modified $Pb(Sc_{0.5}Nb_{0.5})O_3$ nanoceramics** MARGARITA CORREA, RAM CHOUDHARY, RAM KATIYAR, *Department of Physics, University of Puerto Rico, San Juan PR00931-3343* Ferroelectric relaxors are promising candidates for multilayer ceramic capacitors. We have synthesized nanocrystalline $Pb(Sc_{0.5}Nb_{(1-x)/2}Ta_{x/2})O_3$, $(0.1< x < 0.9)$ by a high-energy ball milling technique. Analysis of as prepared powders using an X-ray technique shows the formation of materials in the tetragonal phase. TEM micrographs reveal that the particle size decreases to $\sim$ 20nm from $\sim$ 200nm on increasing the milling time These particles are nanocrystalline as evident by the diffraction rings of the selected area diffraction patterns of the activated powders. Studies of dielectric properties as a function of temperature (200-600K) and frequency (1 kHz – 1 MHz) of the sintered samples at different temperatures have shown that the materials have relaxor ferroelectric behavior and diffuse phase transition for $x \leqslant 0.5$. However, for $x \geqslant 0.6$ a diffuse phase transition without the frequency dispersion has been observed. The dielectric/relaxor properties of the compounds are dependent upon the sintering temperature, time, and composition. Detailed results will be presented.

**9:12**

**N41 7 Substrate-induced strain effects on the transport properties of pulsed laser deposited Nb doped $SrTiO_3$ films.*** WEGDAN RAMADAN, SATISH OGALE, SANKAR DHAR, SHIXIONG ZHANG, DARSHAN KUNDALIYA, ISSEI SATOH, THIRUMALAI VENKATESAN, *Center for Superconductivity Research, Department of Physics, University of Maryland, College Park, MD 20742-4111* Thin films of Nb doped $SrTiO_3$(NSTO) are grown via pulsed laser deposition (PLD) on $LaAlO_3$ (LAO, 001), $MgAl_2O_4$ (MAO, 001), $SrTiO_3$ (STO, 001), and Y-stabilized $ZrO_2$(YSZ, 001) substrates. The film growth is examined under various growth conditions. The dependence of film properties on the film-substrate lattice mismatch, film thickness, and substrate temperature is investigated. The electrical transport in NSTO films is shown to exhibit a strong sensitivity to strain, which is suggested to arise from the dependence of carrier mobility on bond distortions/stretching and related changes in phonon modes.

*Wedgan Ramadan acknowledges support under Fulbright program

**9:24**

**N41 8 Blue-light emission at room temperature from $Ar^+$-irradiated $SrTiO_3$** DAISUKE KAN, *Institute for Chemical Research, Kyoto University* TAKAHITO TERASHIMA, *Research Center for Low Temperature and Materials Sciences, Kyoto University* RYOKO KANDA, ATSUNOBU MASUNO, *Institute for Chemical Research, Kyoto University* ATSUSHI ISHIZUMI, *Graduate School of Material Science, Nara Institute of Science and Technology* YOSHIHIKO KANEMITSU, YUICHI SHIMAKAWA, MIKIO TAKANO, *Institute for Chemical Research, Kyoto University* $SrTiO_3$ is a key material for fabricating oxide-based electronic devices. We found that $Ar^+$-irradiated, metallic $SrTiO_3$ crystals emit 430-nm blue-light at room temperature. Oxygen-deficient metallic $SrTiO_3$ thin films also show the blue-light emission. Reciprocal mapping using synchrotron x-ray radiation at SPring-8 reveals a slight elongation of the lattice parameter along the out-of-plane direction both for these samples. We, therefore, suggest that the $Ar^+$-irradiation introduces oxygen deficiency in the crystal surface, and that the deficiencies generate conduction carriers which wait ready for the recombination with photo-exited holes, and play an important role in the emission. It is emphasized that the emitting region could be patterned into any size and shape by combining conventional photolithography and $Ar^+$-milling. These new features of $SrTiO_3$ will open up new possibilities for the oxide-based electronic devices.

**9:36**

**N41 9 Measurement of the Electric Field Gradient at $^{181}$Ta in $ZrSiO_4$and $HfSiO_4$ using Perturbed Angular Correlation Spectroscopy** HERBERT JAEGER, *Miami University* SEAN McBRIDE, *University of Nebraska-Lincoln* Perturbed angular correlation spectroscopy (PAC) is a nuclear technique often used to probe the hyperfine interaction of a nuclear moment with extra-nuclear fields. For example the electric field gradient (EFG) at a $^{181}$Ta probe nucleus in zircon ($ZrSiO_4$) depends on the arrange-

ment of the Zr, Si, and O-atoms and is very sensitive to structural rearrangements. Our PAC experiments with zircon show that a very subtle rearrangement of Si-atoms within the unit cell leads to a change in the temperature dependence of the EFG. We are currently performing a series of PAC experiments on the isostructural hafnon ($HfSiO_4$). Preliminary results show no evidence of a similar structural rearrangement. In addition to the EFG, we also measure the anisotropy of the $\gamma\gamma$-cascade emitted during the decay of a $^{181}$Ta nucleus. The measured anisotropy depends somewhat on the geometry of the sample and detector arrangement. However, with a given nucleus and a fixed geometry one would not expect a substantial change in the anisotropy during a series of measurements, say as a function of temperature. Yet our PAC spectra of zircon show a consistent decrease of the anisotropy in the temperature range between 650 and 800°C. Preliminary PAC spectra of hafnon show no change of the anisotropy. Reasons for this apparent loss in anisotropy will be discussed.

**9:48**

**N41 10 Structure, Energetics, and Clustering Interactions for Cu on $TiO_2$ (110) at Various Coverages** SCOTT J. THOMPSON, STEVEN P. LEWIS, *University of Georgia* $TiO_2$ (110) is one of the prototypical metal-oxide surface systems, studied extensively and under a variety of different conditions by experimentalists and theorists alike. Recent experiments have enhanced our understanding of the structure of the stochiometric surface, and our Density Functional Theory calculations show excellent quantitative agreement with these latest results. In addition, strong interactions between metal catalysts and their supporting oxide substrates give rise to enhanced catalytic properties, and we are exploring this phenomenon for the prototypical system of Cu on the (110) surface of rutile $TiO_2$. In this talk, we will present our theoretical results for the surface structure and elaborate on the agreement with the latest experimental findings as well as the differences from previous theoretical work on this important system. We will also discuss predictions of the structure and energetics for Cu on $TiO_2$ (110) at various coverages and on both stoichiometric and reduced surfaces, where specific focus will be upon clustering interactions and the formation of Cu islands, which has been observed experimentally.

**10:00**

**N41 11 *Ab initio* molecular dynamics of a proton in amorphous $SiO_2$ illustrating the hopping mechanism** JULIEN GODET, ALFREDO PASQUARELLO, *Ecole Polytechnique Fédérale de Lausanne, Institute of Theoretical Physics, CH-1015 Lausanne* The scaling of metal-oxide-semiconductor devices to smaller dimensions is a major issue in current silicon technology. In order to understand the role of hydrogen at silicon-oxide interfaces, we here investigate charged states of hydrogen in amorphous $SiO_2$ ($a$-$SiO_2$) using first-principles calculations (DFT-GGA). We first show that the formation energies of $H^0$, $H^+$ and $H^-$ in $a$-$SiO_2$ are essentially equivalent to those in $\alpha$-quartz. In particular, the $H^+$ and $H^-$ species are always more stable than their neutral counterpart. Then, we focus on the basic diffusion mechanism of the proton in $a$-$SiO_2$. Our molecular dynamics simulations show that the proton hops between O atoms. The hopping does not occur between first O neighbors connected through the network, but takes place across rings when the O–O distance is about 2.3 Å. The hopping process is favored by the thermal vibrations of the O atoms.

**10:12**

**N41 12 Unusual compressibility in the negative-thermal-expansion material $ZrW_2O_8$*** ALBERT MIGLIORI, C. PANTEA, H. LEDBETTER, Y. ZHAO, T. KIMURA, *LANL* PETER B. LITTLEWOOD, *Cavendish Lab., Univ. of Cambridge* J. VAN DUIJN, *Dept. of Physics and Astronomy, Johns Hopkins Univ.* G.R. KOWACH, *Dept. of Chemistry, The City College of NY* The negative thermal expansion (NTE) compound $ZrW_2O_8$ has been well-studied because it remains cubic with a nearly constant, isotropic NTE coefficient over a broad temperature range. However, its elastic constants seem just as strange as its volume because NTE makes temperature acts as itpositive pressure, decreasing volume on warming and, unlike most materials, the thermally-compressed solid it softens. Does $ZrW_2O_8$ also soften when pressure alone is applied? Using pulse−echo ultrasound in a hydrostatic SiC anvil cell, we determine the elastic tensor of monocrystalline ZrW2O8 near 300 K as a function of pressure. We indeed find an unusual decrease in bulk modulus with pressure. Our results are inconsistent with conventional lattice dynamics, but do show that the thermodynamically−complete constrained−lattice model can relate NTE to elastic softening as increases in either temperature or pressure reduce volume, establishing the predictive power of the model, and making it an important concept in condensed−matter physics.

*Work performed under the auspices of the National Nuclear Security Administration, Florida State University, and the National High Magnetic Field Laboratory

**10:24**

**N41 13 Oxide films imaged on a nanometer-scale by single-electron tunneling force microscopy*** CLAYTON C. WILLIAMS, EZRA BUSSMANN, NING ZHENG, *University of Utah* Recently, we reported a scanning probe technique to manipulate a single electron to and from states in a nonconducting surface by electron tunneling. Each electron is detected by electrostatic force as it tunnels between a scanning probe and the surface. Electrons are manipulated by tuning the probe Fermi level with respect to the states by a dc voltage. This manipulation serves as the mechanism for imaging and for performing electronic spectroscopy of states in dielectric films. The energy distribution of the states is measured by counting the electrons tunneling to the surface at incrementally varied voltages. The spatial distribution of states is imaged on a nanometer-scale by counting each electron tunneling on a 2-D grid. We present spectroscopic and imaging results from silicon dioxide and hafnium oxide. The density and spatial distribution of states is compared for various growth parameters. The measurements reveal evidence for energy relaxation and charge movement in the states. This new nanometer-scale approach provides the means to locate and identify electronic states in nonconducting surfaces, opening for exploration a whole class of materials not accessible to the STM. [1] E. Bussmann, N. Zheng & C. C. Williams, Appl. Phys. Lett. **86**, 163109 (2005).

*This work supported by the Semiconductor Research Corporation.

**10:36**

**N41 14 A novel approach to the growth of polycrystalline hydroxyapatite thin films*** ZHENDONG HONG, LAN LUAN, SEBUM PAIK, BIN DENG, DONALD ELLIS, JOHN KETTERSON, *Department of Physics and Astronomy, Northwestern University* ALEXANDRE MELLO, ALEXANDRE ROSSI, JOICE TERRA, *Centro Brasileiro de Pesquisas Fisicas, Brasil* NORTHWESTERN UNIVERSITY COLLABORATION, CBPF COLLABORATION, Hydroxyapatite (HA) thin films on metals have been extensively studied in connection with bioimplants. Conventional sputtering techniques have shown some advantages

over the commercially utilized plasma spray method; however, the as-sputtered films are usually amorphous which can cause serious adhesion problems when post-deposition heat treatment is necessitated. We present a novel opposing RF magnetron sputtering approach for the room temperature preparation of HA thin films on various substrates at low power levels. The as-sputtered films are found to be polycrystalline and the preferred orientations of the films vary with the substrate material and orientation. The effects of different sputtering parameters on the physical, chemical and structural properties was also studied. Finally, patterned films fabricated both before and after deposition have been prepared for further in vitro cell culture experiments.

*Work supported by the National Science Foundation under grant DMR-0303491 and in Brazil through the CNPq.

**10:48**

**N41 15 Finite temperature properties of $(Ba,Sr)TiO_3$ disordered alloys and $BaTiO_3/SrTiO_3$ superlattices from first-principles*** SERGEY LISENKOV, LAURA WALIZER, LAURENT BELLAICHE, *University of Arkansas* We develop and use a first-principles-based scheme to predict properties of $(Ba,Sr)TiO_3$-based systems at finite temperature. This scheme yields a composition-versus-temperature phase diagram of disordered $(Ba_{1-x}Sr_x r)TiO_3$ solid solutions that is in rather good agreement with experimental data. We further use this scheme to reveal and understand the strain-versus-temperature phase diagram of several $BaTiO_3/SrTiO_3$ superlattices. A wide variety of dipole patterns, including homogeneous ferroelectric phase and periodic stripe patterns, are predicted to occur depending on the interplay between temperature, strain and superlattice periods.

*This work is supported by ONR grants N00014-01-1-0365, N00014-04-1-0413 and N00014-01-1-0600, by NSF grants DMR-0404335 and DMR-9983678, and by DOE grant DE-FG02-05ER46188.



**SESSION N42: FOCUS SESSION: SIMULATIONS OF MATTER AT EXTREME CONDITIONS I**
**Wednesday Morning, 15 March 2006**
**345, Baltimore Convention Center at 8:00**
**Larry Fried, Lawrence Livermore National Laboratory, presiding**

***Contributed Papers***

**8:00**

**N42 1 Shock-Induced Chemical Reactions of Polycyclic Aromatic Hydrocarbons** MARK ELERT, *U. S. Naval Academy* SERGEY ZYBIN, *California Institute of Technology* SHANNON REVELL, *U. S. Naval Academy* CARTER WHITE, *Naval Research Laboratory* Polycyclic aromatic hydrocarbons (PAHs) have been found in the atmospheres of Jupiter and Titan, and also in meteorites, interplanetary dust, and circumstellar graphite grains. The ubiquity of these complex organic structures and their stability under extreme conditions make them a significant factor in discussions of brebiotic chemistry in the solar system. To study the shock-induced chemistry of PAHs under conditions appropriate for astrophysical impacts, molecular dynamics simulations have been carried out for solid naphthalene and anthracene using a reactive empirical potential. The major reaction channels for these two closely related compounds were found to be substantially different. Product distributions were also found to depend strongly on the orientation of the PAH crystal relative to the shock propagation direction.

**8:12**

**N42 2 Interatomic bond-order potentials for atomistic simulations of materials at extreme conditions** YONGXUE YU, IVAN OLEYNIK, *Univ. of South Florida* Molecular dynamics simulations provide an excellent opportunity to address fundamental physics and chemistry of materials at extreme conditions. However, the results of MD modeling can only be as reliable as the ability of the interatomic potentials to properly describe a variety of chemical effects including bond-breaking and bond-making. Our recent MD simulations of shock compression of covalently bonded materials such as diamond and silicon using REBO interatomic potential for diamond and EDIP potential for Si showed that the properties of C and Si systems at large pressures and temperatures are not well described in spite of the fact that the near equilibrium properties of both diamond and silicon are well reproduced. We present new results on development of analytic bond-order potentials (BOPs) for covalently bonded materials at extreme conditions. These BOPs are derived using the powerful concepts of moments of density of states, Green's function and Lanczos recursion, applied within the two-center, orthogonal tight-binding bond representation of electronic structure. Importantly, they include explicit analytic expressions for both the $\sigma$ and $\pi$ bonds. We will describe details of BOP construction including devising a first-principle database of fundamental materials properties, its fitting by the tight-binding (TB) model, and devising the analytic BOPs using the direct link between TB and analytic BOPs via the bond orders. Validation of analytic BOPs by comparison with first-principles high-pressure data will also be discussed.

**8:24**

**N42 3 First-principles modeling of energetic materials** MIKE CONROY, *University of South Florida* IVAN OLEYNIK, *University of South Florida* CARTER WHITE, *Naval Research Laboratory* The prediction of properties of energetic materials using atomic-scale simulation techniques is one of the promising areas of energetic materials (EM) research. One of the challenges is to understand the initial response of EM to shock loading based on fundamental atomic-scale properties of EM crystals. We report the results of first-principles density-functional calculations of static and thermodynamic properties of PETN, HMX and RDX molecular crystals including properties of different crystalline phases and their equations of states (EOS). The EOS are extended beyond simple isotropic constitutive relationships to include materials response upon uniaxial compressions and high pressures up to 100 GPa. The predictions of the theory are compared with recent experimental results.

**8:36**

**N42 4 Direct Simulation of Detonations: Applications to the $H_2$-$Cl_2$ System*** PATRICK D. O'CONNOR, *Pennsylvania State University* LYLE N. LONG, *Pennsylvania State University* JAMES B. ANDERSON, *Pennsylvania State University* Earlier simulations in our laboratory showed that ultrafast detonations having steady-state velocities greater than predicted by the Chapman-Jouguet (CJ) and the Zeldovich-von Neumann-Döring (ZND) theories could be produced by very fast model reactions. In

this paper we will report matching studies incorporating a realistic treatment of the reaction $H_2 + Cl_2 \rightarrow 2\ HCl$ reacting by the Nernst chain reaction mechanism with ignition, propagation and termination steps along with the inclusion of rotational and vibrational degrees of freedom for diatomic species and the realistic treatment of energy exchanges among all species. The $H_2$-$Cl_2$ system is the prototypical system for studying detonations both experimentally and theoretically, and is an ideal candidate for investigation. Our simulations are made using Bird's direct simulation Monte Carlo method which produces the full details of the coupled gas-dynamic and reaction effects as well as temperature, velocity, density, pressure, and species profiles for the detonation waves. By comparing predictions with available experimental measurements for the system, we will be able to predict the likelihood that ultrafast detonations can be observed for the $H_2$-$Cl_2$ reaction.

*NSF IGERT Grant No. NSF-DGE-9987589

**8:48**

**N42 5 Molecular Dynamics Simulations of Thermal Induced Chemistry in TATB*** JASON QUENNEVILLE, TIMOTHY GERMANN, *Los Alamos National Laboratory* Equilibrium molecular dynamics (MD) simulation of high explosives can provide important information on their thermal decomposition by helping to characterize processes with timescales that are much longer than those attainable with non-equilibrium MD shock studies. A reactive force field is used with MD to probe the chemisty induced by intense heating ('cook-off') of 1,3,5-triamino-2,4,6-trinitrobenzene (TATB). The force field (ReaxFF) was developed by van Duin, Goddard and coworkers† at CalTech and has already shown promise in predicting the chemistry in small samples of RDX under either shock compression or intense heat. Large-system simulations are desired for TATB because of the high degree of carbon clustering expected in this material. We will show results of 100,000-particle simulations at several temperatures, carried out with the massively parallel GRASP MD software developed at Sandia National Lab. Finally, we will compare the reactions and reaction timescales with those of RDX and HMX. † A. C. T. Van Duin, itet al, itJ. Phys. Chem. A, **1005**, 9396 (2001).

*This work was performed under the auspices of the United States Department of Energy (Contract No. W-7405-ENG-36)

**9:00**

**N42 6 Decomposition of Energetic Materials at Extreme Conditions** RIAD MANAA, LAURENCE FRIED, *Lawrence Livermore National Laboratory* Detailed description of chemical reaction mechanisms of solid energetic materials at high-density and temperatures is essential for understanding events that occur at the reactive front of these materials, and for the subsequent development of predictive models of materials properties. In this talk, we will report the results of our ongoing ab initio based molecular dynamic simulation of the chemistry of TATB, at density of 2.9 g/cm$^3$ and temperature of 1500K, and at density of 2.87 g/cm$^3$ and temperature of 2500 K. These conditions are similar to those experienced at the CJ and von Neumann spike Following the dynamics for a time scale of up to forty picoseconds allows the construction of approximate rate laws for typical products such as $H_2O$, $N_2$, CO, and $CO_2$. The approximate reaction rates obtained for these products at the CJ state will be compared to those obtained recently for HMX at similar conditions. This work was performed under the auspices of the U.S. Department of Energy by the Lawrence Livermore National Laboratory under contract number W-7405-Eng-48.

**9:12**

**N42 7 Transitions between strong shock and elastic-plastic shock regimes in tin and Lennard-Jonesium.** J.M.D. LANE, MICHAEL MARDER, *Center for Nonlinear Dynamics/Dept. of Physics* SHOCK TEAM, We have recently developed the Continuous Hugoniot Method as an efficient numerical approach to study the front dynamics of steady shocks. This method produces a continuous set of shock states as a function of the shock strength driving parameter. We use our method to investigate the shock states at and near the transition between the strong shock and elastic-plastic shock regimes in both single-crystal tin and Lennard-Jonesium along the $\langle 100 \rangle$ directions.

**9:24**

**N42 8 Multi-scale molecular dynamics simulations of steady shock waves in Lennard-Jones and nitromethane** EVAN REED, *Lawrence Livermore National Laboratory* LAURENCE FRIED, M. MANAA, WILLIAM HENSHAW, CRAIG TARVER, *Lawrence Livermore National Laboratory* We compare spatial profiles of steady shock waves using our multi-scale simulation technique (Phys. Rev. Lett. 90, 235503 (2003)) and direct simulation techniques and find good agreement. Multi-scale simulations of shocked amorphous Lennard-Jones are in good agreement with NEMD simulations and multi-scale simulations of shock waves in analytical equations of state of explosives are in good agreement with hydrodynamic simulations. In both cases, agreement improves with distance behind the shock front. We have applied the multi-scale technique to the study of chemically reactive shock waves in condensed nitromethane (CH3NO2) using the density-functional tight-binding (DFTB) method. We study shock waves with speeds ranging from 5.5 km/s to 8 km/s for durations up to 0.5 ns behind the shock front. We believe these are the longest duration tight-binding simulations of shocked matter ever performed.

**9:36**

**N42 9 First-principles approach to reactivity in the presence of shockwave** CHRISTOPHER MUNDY, *LLNL* I.-F. WILL KUO, *LLNL* ALESSANDRO CURIONI, *IBM* EVAN REED, *LLNL* LARRY FRIED, *LLNL* Gaining insight into the mechanisms leading to detonation in energetic materials within a planar shock geometry had been thought to be computationally prohibitive. The use of the Multiscale Shock Method (MSSM) of Reed et. al has opened the possibilities to study the chemistry of complex molecular systems undergoing uniaxial shock compression using Kohn-Sham density functional theory (KS-DFT). Here, we present results of nitromethane under various levels of shock loading and reveal the chemical mechanisms underlying the detonation process. We will also discuss an alternative non-Hamiltonian formulation of the MSSM. The aforementioned formulation is present in both CPMD and CP2K software packages. We also will compare and contrast different formulations of KS-DFT (both plane- wave and hybrid schemes) and discuss future of scaling the MSSM method to tera- scale platforms such as Blue Gene/L.

**9:48**

**N42 10 Finding the structure of phosphorus in phase IV by the first-principles calculation** TAKAHIRO ISHIKAWA, HITOSE NAGARA, KOICHI KUSAKABE, NAOSHI SUZUKI, *Osaka University* Phosphorus in phase IV (P-IV) had been unclear since first experimental report. Using the metadynamics combined with the first-principles calculation, we obtained a new structure. The structure is a monoclinic of sc: a=c=4.22Å, b=4.15Å, $\beta$=97.76° and a modulation is observed along the b-axis. We noted this modulated pattern and, for modulated structures having other wave-lengths, compared the x-ray diffraction patterns of these structures with experimental one. As a result, limited to the case of commensurate patterns because of the periodic boundary condition for the calculations, the structure whose period is 4 times as long as that of the non-modulated structure is the most compatible for the experimental result. For this pattern, calculating the enthalpy for pressure, it is lower than both sc and sh in the range from 118 GPa to 128 GPa. Recently Akahama et al. have determined the structure of P-IV, which is rather close to our structure. Our calculation shows the transition from sc to P-IV was the first order phase transition.

**10:00**

**N42 11 First Principles Phonon and Elasticity Computations for Iron under extreme conditions*** XIANWEI SHA, R.E. COHEN, *Carnegie Institutiion of Washington* We performed linear-response Linear-Muffin-Tin-Orbital (LMTO) and particle-in-cell (PIC) model calculations to understand and predict the lattice dynamical, thermal equation of state and elastic properties of bcc, fcc, and hcp iron as functions of pressure and temperature. The phonon dispersion and phonon density of states have been calculated at different volumes and show good agreement with experiment. We derived the Helmholtz free energy based on both the linear response LMTO and PIC calculations, and found that the calculated geometric mean phonon frequencies and free energies from these two different methods agree well under pressure, in contradiction to an earlier calculation. We performed detailed investigations on the behavior of elastic constants and various thermal equation of state parameters, including the bulk modulus, the thermal expansion coefficient, the Grüneisen ratio, and the heat capacity as functions of temperature and pressure. We made detailed comparison with experiment and earlier theoretical calculations. We do not find the large change in c/a axial change with T. Sound velocities at extreme conditions have also been examined. These first-principles data provide important information to understand shock dynamics and other interesting phenomena under extreme conditions.

*This work was supported by US Department of Energy ASCI/ASAP subcontract to Caltech, Grant DOE W-7405-ENG-48 (to REC).

**10:12**

**N42 12 Ab initio studies of magnetism at extreme volume and shape deformation** MOJMIR SOB, *Masaryk University, Brno* MARTIN FRIAK, *Institute of Physics of Materials, Academy of Sciences of the Czech Republic, Brno* DOMINIK LEGUT, *Institute of Physics of Materials, Academy of Sciences of the Czech Republic, Brno* MIROSLAV CAK, *Faculty of Mechanical Engineering, Brno University of Technology* MARTIN ZELENY, *Faculty of Chemistry, Brno University of Technology* Magnetic solids constitute a basis of many technologically important materials, however, very little is known how their magnetic behavior changes when a high-strain deformation is applied (as it is, for example, in heavily deformed regions of extended defects, such as grain boundaries, dislocation cores, crack tips etc.). In the present talk, we report on magnetic behavior of iron, nickel, FeCo, $Ni_3Al$ and $Fe_3Al$ at the extreme volume as well as tetragonal and trigonal deformation. The total energies are calculated by spin-polarized full-potential LAPW method and are displayed in contour plots as functions of tetragonal or trigonal distortion $c/a$ and volume; borderlines between various magnetic phases are shown. Stability of tetragonal magnetic phases of $\gamma$-Fe is discussed. In case of Fe, Ni and FeCo, the calculated phase boundaries are used to predict the lattice parameters and magnetic states of overlayers from these materials on various (001) substrates. Whereas magnetism does not play an important role in stabilization of the $L1_2$ structure in $Ni_3Al$, the magnetic effects in Fe and $Fe_3Al$ are vital.



***Invited Papers***

**10:24**

**N42 13 Electronic Structure of Actinides under Pressure.**
BORJE JOHANSSON, *Department of Physics, Uppsala University*

The series of heavy radioactive elements known as the actinides all have similar elemental properties. However, when the volume per atom in the condensed phase is illustrated as a function of atomic number, perhaps the most dramatic anomaly in the periodic table becomes apparent. The atomic volume of americium is almost 50% larger than it is for the preceding element plutonium. For the element after americium, curium, the atomic volume is very close to that of americium. The same holds also for the next elements berkelium and californium. Accordingly from americium and onwards the actinides behave very similar to the corresponding rare-earth elements - a second lanthanide series of metallic elements can be identified. This view is strongly supported by the fact that all these elements adopt the dhcp structure, a structure typical for the lanthanides. The reason for this behavior is found in the behavior of the 5f electrons. For the earlier actinides, up to and including plutonium, the 5f electrons form metallic states and contribute most significantly to the bonding. In Np and Pu they even dominate the bonding, while all of a sudden they become localized in Am, very much like the 4f electrons in the lanthanide series, and contribute no longer to the cohesion. This withdrawal of 5f bonding gives rise to the large volume expansion between plutonium and americium. This difference between the light and heavy actinide suggests that it would be most worthwhile to strongly compress the transplutonium elements, thereby forcing the individual 5f electron wave functions into strong contact with each other (overlap). Recently high pressure experiments have been performed for americium and curium and dramatic crystal structure changes have been observed. These results and other high pressure data will be discussed in relation to the basic electronic structure of these elements.

**SESSION N43: QUANTUM OPTICS AND STRONG FIELD PHYSICS**
**Wednesday Morning, 15 March 2006**
**346, Baltimore Convention Center at 8:00**
**V. Jacobs, Naval Research Laboratory, presiding**

**8:00**
**N43 1 Large Double-EIT and Mutual Phase Shifts in Rubidium*** BARRY SANDERS,† ZENG-BIN WANG, KARL-PETER MARZLIN, *Institute for Quantum Information Science, University of Calgary* We propose a scheme to achieve large double-EIT and mutual phase shifts for two slow, co-propagating pulses of light through a Rubidium gas, with the additional advantages of enabling equal group velocities for the two pulses and avoiding cancellations of nonlinearities at resonance.

*This project is supported by iCORE and NSERC.
†Also: Centre for Quantum Computer Technology, Macquarie University, Sydney

**8:12**
**N43 2 Electromagnetically induced transparency and precision measurement of atomic transitions in a laser-cooled sample of cesium atoms*** CHIN-CHUN TSAI, MING-DA TSAI, MEI-JU LU, RAY-YUAN CHANG, *Center for Quantum Information Science and Department of Physics, National Cheng-Kung University* Electromagnetically induced transparency (EIT) has observed in a cascade system of laser-cooled Cs atoms and the atomic energy levels have been measured to an accuracy of 0.0003 $cm^{-1}$. In our experiment, Cs atoms are loaded into the magneto-optical trap (MOT) from a background vapor that has a pressure of $10^{-9}$ torr. The number of Cs atoms is estimated using a CCD camera to be $10^7$ occupying a roughly spherical volume having a radius of 2 mm and the temperature of the atom cloud is measured using a time of flight technique to be about 100 $\mu$K. A diode laser excites the Cs atoms from $|6\,^2S_{1/2}, F = 4\rangle$ state to $|6\,^2P_{3/2}, F = 5\rangle$ state, then a dye laser couples the 6 $P_{3/2}$ state to the higher excited, $|9\,^2D_{3/2}\rangle$, $|9\,^2D_{5/2}\rangle$, $|10\,^2D_{3/2}\rangle$, $|10\,^2D_{5/2}\rangle$, and $|11\,^2S_{1/2}\rangle$ atates. The signal is monitored by detecting the trap loss while changing the pump or coupling laser frequency. The effect on the EIT signals by changing the pump laser detuning and the coupling laser power is also discussed. The line positions are measured by comparing the saturation absorption spectrum of molecular iodine (accuracy $<$ 3 MHz).

*We greatly acknowledge the support of the National Science Council, Taiwan.

**8:24**
**N43 3 Femtosecond Coherent Raman Spectroscopy in Biomolecules** ZOE-ELIZABETH SARIYANNI, YURI ROSTOVTSEV, *Dept. of Physics and Inst. for Quantum Studies, Texas A&M University, College Station, TX 77843* TORSTEN SIEBERT, WOLFGANG KIEFER, *Institut für Physikalische Chemie, Universität Würzburg, 97074 Würzburg, Germany* GUY BEADIE, JOHN REINTJES, *US Naval Research Lab, Code 5614, 4555 Overlook Ave., Washington, DC 20375* MARLAN SCULLY, *Dept. of Physics, Electrical and Chemical Engineering and Inst. for Quantum Studies, Texas A&M University, College Station, TX 77843* We present a scheme for identification of biomolecules in real time by using Coherent Anti-Stokes Raman Spectroscopy (CARS) with femtosecond pulses. The nonlinear interaction of the pulses with the molecules is calculated analytically as well as numerically and comparison is made with the experimental results. We show that the commonly used rotating wave approximation needs to be waved for our fast dephasing molecules. Propagation effects are simulated, in addition to the nonlinear interaction, and it is shown how one needs to balance the electronic resonance enhancement and the losses due to absorption, in order to maximize the signal at the output of the optically dense medium. In the transient regime, we present and analyze the generation of polarization beats. These beats are generated due to the very broad bandwidth of the femtosecond pulses, which allows for the coupling of more that one vibrational modes at a time.

**8:36**
**N43 4 Dephasing of excitons in single ZnSe quantum wells using 30 fs pulses** PRADEEP BAJRACHARYA, HANS-PETER WAGNER, SUVRANTA K. TRIPATHY, HANS-PETER TRANITZ, *Department of Physics, University of Cincinnati, Cincinnati, Oh, 45221* The dephasing of excitons in homogenously broadened 10nm wide ZnMgSe/ZnSe single quantum wells is investigated using ultra short ( $<$ 30fs) light pulses in two beam and three beam four wave mixing (FWM) configuration. The observed FWM traces show marked quantum beats due to excitation of higher exciton transitions within the 80 meV spectrally broad pulses. For pulse delay times shorter than 500 fs, non-Markovian signal decay is observed. For longer delay times the exciton dephasing becomes single exponential indicating the transition from quantum kinetics to classical Boltzmann kinetics. Intensity and polarization dependent FWM measurements give further information on the physical nature and scattering processes that take place in both time regimes. This work is supported by the National Science Foundation (DMR-0305076).

**8:48**
**N43 5 Dynamics of high amplitude coherent phonons in photoexcited bismuth*** DAVID REIS, *FOCUS Center and Department of Physics, University of Michigan* DAVID FRITZ, *FOCUS Center and Department of Physics, University of Michigan* EAMMON MURRAY, *Department of Physics and Tyndall National Institute, University College, Cork, Ireland* STEPHEN FAHY, *Department of Physics and Tyndall National Institute, University College, Cork, Ireland* JARED WAHLSTRAND, *JILA/University of Colorado* We report on studies of high amplitude coherent phonons in photoexcited bismuth. All optical experiments, in which two pump pulses are used to coherently control the amplitude $A_{1g}$ phonon at a fixed carrier density, allow us to separate the effects of carrier dynamics from anharmonicity. The results show that the the time dependent frequency of the phonon is dominated by electronic softening of the interatomic potential. Seperate first-principals theoretical calculations confirm these results for photoexcited carrier densities up to approximately 2% of the valence electrons. We comment on the possibility of x-ray diffraction and diffuse scattering as a means of measuring the detailed dynamics.

*Supported in part by the National Science Foundation FOCUS Physics Frontier Center, the Department of Energy, Basic Energy Sciences, Science Foundation Irealand and the Irish Research Council for Science, Engineering, and Technology

**9:00**
**N43 6 Optimization and Rate-Equation Model for Second-Harmonic Generation in Mid-Infrared Quantum Cascade La-**

**sers** JING BAI, DAVID CITRIN, *Georgia Institute of Technology* We present the rate-equation simulation of a mid-infrared quantum cascade laser with optimized second-harmonic generation. The simulation is performed by optimization of the structure design followed by self-consistently solving the rate equations for the carriers in the various levels. The optimized structure was obtained by supersymmetric quantum mechanics with both position-depended mass and band nonparabolicity included. In the rate-equation model, the second harmonic generation process is described by sequentially two single photon absorption and one second-harmonic photon generation. Nonunity pumping efficiency is accounted by all relevant electron-electron and electron-LO phonon scatterings between injector/collector and active region are included. The modal gain, linear power and second-harmonic power can then be calculated based on the steady-state populations in the active region. Results show that the optimized structure has higher modal gain and linear to nonlinear conversion efficiency.

**9:12**

**N43 7 Observation of a coherent exciton-LO phonon resonance in a ZnSe single quantum well** SUVRANTA K. TRIPATHY, HANS-PETER WAGNER, PRADEEP BAJRACHARYA, *Department of Physics, University of Cincinnati, Cincinnati, Oh, 45221* A. UETA, D. HOMMEL, *Institut für Festkörperphysik, Universität Bremen, D-28334 Bremen,Germany* A new coherent signal has been observed while performing two- beam degenerate four-wave mixing (FWM) experiments on a 3nm ZnMgSSe/ZnSe single quantum well (SQW) using 30fs laser pulses. In this SQW structure the exciton binding energy exceeds the LO-phonon energy (31.6 meV). The observed spectral feature is blue shifted with respect to the heavy-hole bound exciton transition by $\sim$ 32 meV and indicates the formation of a coherent exciton-LO phonon resonance with a dephasing time of $\sim$ 500 fs. This tentative assignment is further supported by photoluminescence excitation (PLE) and by reflection measurements. This work is supported by the National Science Foundation (DMR-0305076).

**9:24**

**N43 8 Vibrational Lifetimes and Frequency-Gap Law of Hydrogen Bending Modes in Semiconductors** BAOZHOU SUN, GUNTER LUEPKE, *Department of Applied Science, the College of William and Mary* GANG SHI, MICHAEL STAVOLA, *Department of Physics, Lehigh University* NAGESWARA SUNKARANAM, SRIRAM DIXIT, NORMAN TOLK, FELDMAN LEONARD, *Department of Physics and Astronomy, Vanderbilt University* Vibrational lifetimes of hydrogen and deuterium related bending modes in semiconductors are measured by transient bleaching spectroscopy and high-resolution infrared absorption spectroscopy. We find that the vibrational lifetimes follow a universal frequency-gap law, i.e., the decay time increases exponentially with increasing decay order, with values ranging from 1 ps for a one-phonon process to 265 ps for a four-phonon process. The temperature dependence of the lifetime shows that the bending mode decays by lowest-order multi-phonon process. Our results provide new insights into vibrational decay and the giant isotope effect of hydrogen in semiconductor systems.

**9:36**

**N43 9 High field gradient for electron acceleration and ultrashort electron pulse formation** ALEXANDER POKROVSKY, ALEXANDER KAPLAN, *Johns Hopkins University* We explore a possibility of strongly inelastic scattering and large energy exchange between the tightly focused laser and electron beams in the ''transverse'' geometry, whereby the beams propagate normally to each other. In the most basic configuration of the laser standing wave we demonstrate that multi-MeV electron acceleration per pass is attainable, if the field has large spatial gradient along the direction of electron motion. The electron motion in this case is relativistic, and the energy gain or loss can be retained by an electron with very high efficiency. The proposed scheme may provide enormous $\sim$ 0.1 TeV/cm acceleration gradient. We also show that the transverse electron and laser beam configuration can cause strong temporal electron focusing resulting in formation of ultra-short electron bunches. Such a system has a potential to operate as a full-switch laser gate for electrons, a new base element of a free-electron laser and laser electron accelerators.

**9:48**

**N43 10 Relativistic effect of ponderomotive force direction reversal in a standing laser wave** ALEXANDER KAPLAN, ALEXANDER POKROVSKY, *ECE Department, Johns Hopkins University* In our research, we theoretically discovered a relativistic effect of the direction reversal of the field-gradient (ponderomotive) force (PF) in a standing laser wave. This reversal makes the high-field areas attractive for electrons, in contrast to the regular PF, and it represents the only effect known so far that pins down a distinct borderline between relativistic and nonrelativistic motion. We demonstrated that the collinear configuration, in which the laser wave is linearly polarized with electric field, $\vec{E}$ parallel to the initial electron momentum, $\vec{p}_0$, is the optimal configuration for the relativistic reversal. In that case, the transverse PF reverses its direction when the incident momentum is $p_0 = mc$. The reversal effect vanishes in the cases of circular and linear with $\vec{E} \perp \vec{p}_0$ polarizations. We have discovered, however, that the counter-rotating circularly polarized standing waves develop attraction and repulsion areas along the axis of laser, in the laser field whose intensity is homogeneous in that axis, i.e. has no field gradient.

**10:00**

**N43 11 Spatial and pulse shape dependence of K$\alpha$ source from high contrast fs laser plasmas in regime of Relativistic Engineering** LIMING CHEN, *Advanced Photon Resaerch Center, Japan Atomic Energy Agency* Interaction of intense Ti: Sapphire laser with Cu foil targets has been studied by measuring hard X-ray generation. Hard x-ray spectroscopy and K$\alpha$ X-ray conversion efficiency ($\eta_K$) from Cu plasma have been studied as a function of laser intensity via pulse duration scan (60 fs $\sim$ 600 fs), laser pulse energy scan (60 mJ $\sim$ 600 mJ) and target displacement scan from best focus. For intensity I $>$ 1x10$^{17}$ W/cm$^2$, the Cu $\eta_K$ keep on increasing to reach a maximum value of $1x10^{-4}$ at an intensity $I = 1x10^{18}$ W/cm$^2$. The focusing was varied widely to give a range of intensities from $10^{15}$W/cm$^2$ $\sim$ $10^{18}$ W/cm$^2$. Two individual emission peaks are obtained, one is at best focal spot and the other is at larger target offset corresponding to $\sim$ $10^{15}$ W/cm$^2$. Each peak is corresponding to different energy absorption mechanism. In addition, when we introduce slightly detuning of compressor gratings at the best focal condition, it shows $\eta_K$ generated by negatively skewed 100 fs pulse width laser irradiation reach $5x10^{-4}$ and almost 7 times greater than the case of positively skewed pulse. Vacuum Heating is greatly stimulated in this case and preciously control of preplasma is the key factor in tuning control of X-ray emission in relativistic itfs regime.

**10:12**
**N43 12 Guiding of 100 TW Relativistic Laser Pulses by 10 mm Plasma Channels** LIMING CHEN, *Advanced Photon Resaerch Center, Japan Atomic Energy Agency* First experiments for laser-gas plasma interaction about electron acceleration have been performed with 30 fs, 100 TW relativistic Ti:Sapphier laser pulse interaction with long slit (1.2 x 10 $mm^2$) gas plasmas. The world record it10 mm length plasma channel formed that was longer than 20 times the Rayleigh length. Plasma density was the key factor for this long channel stimulation under 100 TW laser pulse irradiation that was much higher than critical power for relativistic self-focusing. For the first time, channel characteristics such as laser bending, hosing and cavity formation were demonstrated experimentally. In case of long channel guiding, accelerated electron bunch was tightly collimated with low emmitance it$<$ 0.8 $\pi$ mm mrad and quasi-monoenergetic electron bunch (it$\sim$ 70 MeV) was obtained as well. Accelerated electron charge current with electron energy $>$ 1 MeV was $\sim$ 10 nC/shot which was highest value in laser accelerator, to our knowledge, and ascribed to the contribution of long plasma channel.

**SESSION N44: QUANTUM CRITICALITY AND NEMATIC ORDERING**
**Wednesday Morning, 15 March 2006**
**347, Baltimore Convention Center at 8:00**
**Q. Si, Rice University, presiding**

**8:00**
**N44 1 The Effect of the Berry Phase on the Quantum Critical Properties of the Bose-Fermi Kondo model** STEFAN KIRCHNER, *Rice University* QIMIAO SI, *Rice University* The theory of the quantum critical point of a $T = 0$ transition is traditionally formulated in terms of a quantum-to-classical mapping, leading to a theory of its classical counterpart in elevated dimensions. Recently, it has been shown that this mapping breaks down in an SU(N)$\times$ SU(N/2) Bose-Fermi Kondo model (BFKM) [1], a BFKM with Ising anisotropy [2] and the spin-boson model [3]. Here we report the Quantum Monte Carlo results for the scaling properties of the quantum critical point of the BFKM with Ising anisotropy. In addition, using the Lagrangian formulation of the BFKM, we study the critical properties in the presence and absence of the spin Berry phase term. The results of the two cases are compared with the numerical results. [1] L. Zhu, S. Kirchner, Q. Si, and A. Georges, Phys. Rev. Lett. 93,267201 (2004). [2] M. Glossop and K. Ingersent, Phys. Rev. Lett. 95, 067202 (2005). [3] M. Vojta, N-H Tong, and R. Bulla, Phys. Rev. Lett. 94, 070604 (2005).

**8:12**
**N44 2 Quantum Critical Behaviour Near the Kondo Breakdown Fixed Point*** INDRANIL PAUL, *SPhT, CEA Saclay, L'Orme des Merisiers, 91191 Gif-sur-Yvette, France and Materials Science Division, Argonne National Lab, Argonne, IL-60439* CATHERINE PÉPIN, *SPhT, CEA Saclay* MIKE R. NORMAN, *Materials Science Division, Argonne National Lab* We study the Kondo-Heisenberg model using a fermionic representation for the localized spins. In this model, the mean field Kondo hybridization at $T = 0$ can be continuously tuned to zero as a function of the exchange interactions. We calculate the fluctuations of the hybridization and its associated gauge potential at the one loop level, and their contribution to the specific heat and spin susceptibility, near the quantum critical point.

*Work supported by the U. S. Dept of Energy, Office of Science, under contract No. W-31-109-ENG-38.

**8:24**
**N44 3 Kondo Screening and Fermi Surface in the Antiferromagnetic Metal Phase** SEIJI YAMAMOTO, *Rice University* QIMIAO SI, *Rice University* We address the Kondo effect deep inside the antiferromagnetic metal phase of a Kondo lattice Hamiltonian with SU(2) invariance. The local- moment component is described in terms of a non-linear sigma model. The Fermi surface of the conduction electron component is taken to be sufficiently small, so that it is not spanned by the antiferromagnetic wavevector. The effective low energy form of the Kondo coupling simplifies drastically, corresponding to the uniform component of the magnetization that forward-scatters the conduction electrons on their own Fermi surface. We use a combined bosonic and fermionic (Shankar) renormalization group procedure to analyze this effective theory and study the Kondo screening and Fermi surface in the antiferromagnetic phase. The implications for the global magnetic phase diagram, as well as quantum critical points, of heavy fermion metals are discussed.

**8:36**
**N44 4 Sign change of the Grüneisen parameter and magnetocaloric effect near quantum critical points** MARKUS GARST, *Theoretical Physics Institute, University of Minnesota, USA* ACHIM ROSCH, *Institute for Theoretical Physics, University of Cologne, Germany* Strong fluctuations near a quantum critical point lead to a singular entropy distribution in the phase diagram. This results in strong signatures of the Grüneisen parameter and the magnetocaloric effect. In particular, a sign change of the Grüneisen parameter coincides with the accumulation point of entropy in the phase diagram. If the quantum critical point is the endpoint of a line of finite temperature phase transitions the sign change generically occurs in the Ginzburg regime of the classical transition as observed in several heavy fermion compounds. In addition, we predict a sharp peak in the Grüneisen parameter at the critical temperature due to the contribution of classical critical fluctuations. For magnetic field tuning these signatures are also reflected in the magnetocaloric effect. Moreover, we discuss the case of metamagnetic quantum criticality where the sign change is located at the critical magnetic field.

**8:48**
**N44 5 Towards a unification of local moment magnetism and the Kondo lattice** JEROME RECH, *Rutgers University, CEA Saclay* PIERS COLEMAN, *Rutgers University* GERGELY ZARAND, *Budapest University of Technology and Economics* OLIVIER PARCOLLET, *SPhT CEA Saclay* We apply the Schwinger boson scheme to the fully screened Kondo model and generalize the method to include antiferromagnetic interactions between ions. Our approach unifies the Kondo impurity approach of Parcollet and Georges with the Schwinger boson description of antiferromagnetism of Arovas and Auerbach, enabling the formalism to describe magnetically correlated and magnetically ordered heavy electron phases. For the single impurity, our approach captures the Kondo crossover from local moment behavior to a Fermi liquid with a non-trivial Wilson ratio. When applied to the two

impurity model, the mean-field theory describes the ''Varma Jones'' quantum phase transition between a valence bond state and a heavy Fermi liquid. We will extend the method to the Kondo lattice, and explore the nature of the phase diagram connecting the heavy electron phase, the magnetic phase and the spin-liquid phase.

**9:00**

**N44 6 Quasi-particle linewidth close to a quantum critical point: Crossover from non-Fermi liquid to Fermi liquid behavior*** PEDRO SCHLOTTMANN, *Florida State University* Heavy fermion systems frequently display non-Fermi liquid behavior due to a nearby quantum critical point. A nested Fermi surface together with the remaining interaction between the carriers after the heavy particles are formed may give rise to itinerant antiferromagnetism. The order can gradually be suppressed by mismatching the nesting and a quantum critical point is obtained as $T_N \rightarrow 0$. The quasi-particle linewidth is calculated in the paramagnetic phase following an approach outlined by Virosztek and Ruvalds (Phys. Rev. B **42**, 4064 (1990)). The linewidth shows a crossover from non-Fermi liquid ( $\sim T$) to Fermi liquid ( $\sim T^2$) behavior with increasing nesting mismatch and decreasing temperature. The quasi-particle linewidth is a quantity relevant to the electrical resistivity and the width of the inelastic neutron scattering quasi-elastic peak.

*Support from DOE is acknowledged

**9:12**

**N44 7 Curie law, entropy excess, and superconductivity in heavy fermion metals and other strongly interacting Fermi liquids** V.A. KHODEL, M.V. ZVEREV, *Russian Research Centre Kurchatov Institute* VICTOR YAKOVENKO, *Department of Physics, University of Maryland* Low-temperature thermodynamic properties of strongly interacting, itinerant Fermi liquids with fermion condensate are investigated. We demonstrate that the spin susceptibility of these systems exhibits the Curie-Weiss law, and the entropy contains a temperature-independent term. The excessive entropy is released at the superconducting transition, enhancing the specific heat jump $\Delta C$ and rendering it proportional to the effective Curie constant. The theoretical results are favorably compared with the experimental data on the heavy fermion metal $CeCoIn_5$, as well as $^3$He films. Reference: cond-mat/0508275, Phys. Rev. Lett. (December 2005).

**9:24**

**N44 8 Super-frustration for strongly-correlated fermions in two dimensions** PAUL FENDLEY, *University of Virginia* KARELJAN SCHOUTENS, *University of Amsterdam* We prove that there exists an exotic ''super-frustrated'' state of strongly-correlated spinless fermions hopping on a two-dimensional lattice. This state is characterized by an extensive ground-state entropy, and very possibly is at a non-Fermi-liquid quantum critical point. We give explicit Hamiltonians which exhibit this behavior. Exploring various lattices and limits, we show how the ground states can be frustrated, quantum critical, or combine frustration with a Wigner crystal.

**9:36**

**N44 9 Domain formation in electronic nematic phase coupled to lattice deformation** HYEONJIN DOH, YONG BAEK KIM, *Dept. of Physics, Univ. of Toronto, Canada* KEUN HYUK AHN, *Advanced Photon Source, Argonne National Laboratory* Motivated by the experiments on $Sr_3Ru_2O_7$, we have investigated the possibility of domain formation in electronic nematic phase coupled to lattice deformations. It has been suggested that the formation of the nematic order may explain the two consecutive metamagnetic transitions observed in $Sr_3Ru_2O_7$. Our study may serve as the explanation of the high residual resistivity observed in a range of magnetic fields.

**9:48**

**N44 10 Non-Fermi Liquid Behavior of Nematic Fermi Fluids** MICHAEL LAWLER, EDUARDO FRADKIN, *University of Illinois at Urbana-Champaign* Following the initial study of Ref. 1, we explore the behavior of physically relevant quantities in the vicinity of the quantum critical point between a nematic Fermi fluid and a Fermi liquid. As shown in Ref. 1, this strong coupling fixed point is completely accessible within the method of high dimensional bosonization and we continue the analysis presented therein focusing on quasiparticle properties, such as the fermion residue and the fermion spectral function. We show in particular, that the fermion residue vanishes according to the essential singularity $\exp(-1/\sqrt{\delta})$ where $\delta$ is the dimensionless coupling constant measuring the distance to the critical point. Also, at low temperatures, we verify explicitly that the heat capacity obey's the non-Fermi liquid powerlaw of $T^{2/3}$. We conclude with a discussion of the signatures of the nematic phase that would appear in light scattering and angle resolved photo emission spectroscopy experiments. [1] Lawler, Barci, Fernandez, Fradkin and Oxman, unpublished; cond-mat/0508747.

**10:00**

**N44 11 Phase and amplitude fluctuations for the $l = 2$ Pomeranchuk instability in two dimensions.** JORGE QUINTANILLA, *ISIS facility, Rutherford Lab. (U. K.)* MASUDUL HAQUE, *Utrecht University, the Netherlands* For a two-dimensional fermionic system, we analyze models that produce shape-distortion instabilities of the Fermi surface in the $l = 2$ channel, leading to a non-Fermi liquid with nematic order. The finite-temperature phase diagram contains a transition of the Kosterlitz-Thouless type and a crossover at higher temperatures, corresponding respectively to the disordering of phase and amplitude degrees of freedom.

**10:12**

**N44 12 Interplay between parallel and diagonal electronic nematic phases in interacting systems** HAE-YOUNG KEE, HYEONJIN DOH, NIR FRIEDMAN, *Dept. of Physics, Univ. of Toronto, Canada* An electronic nematic phase is a spontaneous broken state of a discrete rotational symmetry of a given crystal. There exist two distinct electronic nematic phases in a square lattice. One is the parallel nematic order which breaks the symmetry in $x$- and $y$-direction, and the other is the diagonal nematic order which breaks the diagonal $(x + y)$ and the anti-diagonal $(x - y)$ symmetry. We investigate the different features and the mutual interaction between these two nematic orders. We also discuss the possible implication of our results in the context of neutron scattering and Raman spectroscopy measurements in high $T_C$ superconductors.

**10:24**

**N44 13 Interacting fermions in two dimensions: singularities in the perturbation theory and the role of collective modes.** SUHAS GANGADHARAIAH, *University of Utah* DMITRII GUTMAN, *University of Florida* DMITRII MASLOV, *University of Florida* We consider a system of interacting fermions in two dimensions. It is shown that even for an infinitesimally weak interaction a straight-forward perturbation theory is ill defined near the mass shell. Starting from the second order, the perturbative expansion for the self-energy is singular at the mass shell. We show that this singularity is a manifestation of a non- perturbative effect: the interaction of fermions with the collective mode. The singularities in the perturbation series for the self-energy is treated by resumming the most divergent diagrams. A threshold for emission of zero-sound waves leads to a non-monotonic variation of the self-energy. Consequently, the spectral function acquires a non-Lorentzian kink-like feature. This feature is reminiscent to spin-charge separation in 1D, as the kink is absent in a spin-polarized system. We examine the possibility of detecting the kink in momentum-conserving tunneling between two parallel layers of a 2D electron gas.

**10:36**

**N44 14 Ferromagnetic quantum phase transition in an itinerant three-dimensional system** RONOJOY SAHA, DMITRII MASLOV, *Dept. of Physics, University of Florida, Gainesville, FL 32611-8440, USA* ANDREY CHUBUKOV, *Dept. of Physics, University of Wisconsin-Madison, 1150 University Avenue, Madison, WI 53706-1390, USA* The non-analytic behavior of the spin susceptibility both away and near the quantum critical point signals the breakdown of the Hertz-Millis scenario for a ferromagnetic quantum phase transition in itinerant systems. It is believed that in both 2D and 3D $\chi_s$ increases as a function of the magnetic field ($H$) or momentum ($q$), which indicates a tendency to either first order transition or ordering at finite $q$. We show that the 3D case is different from the 2D one. Away from the 3D critical point, the non-analytic part of $\chi_s$ can be of either sign, depending on microscopic parameters. The non-analyticity in 3D arises from two physically distinct processes: excitations of a single and three particle-hole pairs. Both processes contribute a max $\{H^2,q^2\}\ln\max\{H^2,q^2\}$ term to $\chi_s$, but the signs of these contributions are opposite. The single-pair process leads to an increase of $\chi_s$ with $H,q$ whereas the three pair one corresponds to a decrease. In the paramagnon model, the three pair contribution always wins sufficiently close to the Stoner instability. We also discuss the behavior of $\chi_s$ in the immediate vicinity of the quantum critical point within the spin-fermion model.

**10:48**

**N44 15 Metallic phase in a two-dimensional disordered Fermi system with singular interactions** VICTOR GALITSKI, *Physics Department, University of Virginia* We consider a two-dimensional disordered system of gapless fermions interacting with a singular transverse gauge-field. We study quantum corrections to fermion conductivity and show that they are very different from those in a usual Fermi liquid. In particular, the weak-localization effect is suppressed by magnetic field fluctuations. We argue that these fluctuations can be considered static at time scales of fermionic diffusion. By inducing fluxes through diffusive loops that contribute to weak localization, they dephase via the Aharonov-Bohm effect. It is shown that while the flux-flux correlator due to thermal fluctuations of magnetic field is proportional to the area enclosed by the loop, the correlator due to quantum fluctuations is proportional to the perimeter of the loop. The possibility of dephasing due to these quasistatic configurations is discussed. We also study interaction induced effects and show that perturbation theory contains infrared divergent terms originating from unscreened magnetic interactions. We show that due to singular small-angle scattering, the corresponding contributions to the density of states and conductivity are very large and positive indicating that the fermion-gauge system remains metallic at low temperatures.

## SESSION N45: EXOTIC PHASES IN STRONGLY CORRELATED SYSTEMS

**Wednesday Morning, 15 March 2006**
**348, Baltimore Convention Center at 8:00**
**A. Sandvik, Boston University, presiding**

**8:00**

**N45 1 Fractionalization in a strongly correlated exciton system*** SUNG-SIK LEE, PATRICK LEE, *Massachusetts Institute of Technology* We show that fractionalized phases arise out of a strongly coupled exciton bose condensate in a multi-band insulator. Based on a world line picture of exciton, we demonstrate that the deconfinement phases can occur in a gauge theory of the exciton model despite an infinite bare gauge coupling. A world sheet of electric flux line in the emergent gauge theory is identified as a web of exciton world lines. It is shown that a deconfined U(1) gauge theory with ''photon'' and either fractionalized boson or fermion can emerge out of a single model depending on the coupling constants. The statistics and spin of the fractionalized particles are shown to be determined uniquely by the dynamics of the model. The exciton model can be numerically simulated without sign problem and some of our results will be shown.

*This work was supported by the NSF grant DMR-0517222.

**8:12**

**N45 2 Criticality in correlated quantum matter*** ANGELA KOPP, SUDIP CHAKRAVARTY, *UCLA* At quantum critical points (QCPs) quantum fluctuations occur on all length scales, from microscopic to macroscopic, which, remarkably, can be observed at finite temperatures, the regime to which all experiments are necessarily confined. But how high in temperature can the effects of quantum criticality persist? That is, can physical observables be described in terms of universal scaling functions originating from the QCPs? We answer these questions by examining exact solutions of models of systems with strong electronic correlations and find that QCPs can influence physical properties at surprisingly high temperatures. As a powerful illustration of quantum criticality, we predict that the zero temperature superfluid density, $\rho_s(0)$, and the transition temperature, $T_c$, of the copper-oxide superconductors are related by $T_c \propto \rho_s(0)^y$, where the exponent $y$ is different at the two edges of the superconducting dome, signifying the presence of the respective QCPs. This relationship can be tested in high quality crystals.

*supported by the NSF under grant DMR-0411931

**8:24**

**N45 3 Deconfined quantum-criticality in a 2D $S = 1/2$ Heisenberg model*** ANDERS SANDVIK, *Boston University* The two-dimensional $S = 1/2$ Heisenberg model including a four-spin interaction is studied using a ground state projector quantum Monte Carlo (QMC) method in the valence bond basis. The model is sign-problematic in standard QMC methods formulated in the $S^z$ basis, but not in the valence bond basis. The ground state is studied on lattices with up to $40 \times 40$ spins. The four-spin interaction is shown to suppress the antiferromagnetic order, leading to a phase transition into a valence-bond-solid (VBS) state. The finite-size scaling of the singlet-triplet gap (which can be calculated with the valence bond projector using an improved estimator) scales as $1/L$ at the transition point, indicating a quantum phase transition with dynamic exponent $z = 1$. This, and a large spin-spin correlation exponent, $\eta \approx 0.4$, suggests that the transition is a *deconfined quantum-critical point*. This would then be the first example of a model Hamiltonian for which this exotic Néel–VBS quantum-criticality has been observed.

*Supported by NSF grant No. DMR-0513930

**8:36**

**N45 4 Bilayer antiferromagnet with four-spin interaction*** THOMAS C. LANG, *Boston University, TU Graz, Austria* ANDERS W. SANDVIK, *Boston University* We investigate a spin-1/2 Heisenberg antiferromagnet with four-spin interaction on bilayer square and honeycomb lattices. In addition to the standard Neel and quantum disordered phases, these models can be expected to have a valence-bond-solid (VBS) phase [1]. Our aim is to locate the VBS phase and to investigate, in particular, a transition from quantum disorder to VBS. This is potentially a deconfined quantum critical point [1]. We use a recently introduced ground state projection Monte Carlo method which allows us to study these models without negative-sign problems [2]. [1] A. Vishwanath et al, Phys. Rev. B **69**, 224416 (2004). [2] A. W. Sandvik, Phys. Rev. Lett. **95**, 207203 (2005).

*Supported by NSF grant No. DMR-0513930

**8:48**

**N45 5 Simulations of Quantum Spin Models on 2D Frustrated Lattices** ROGER MELKO, *Oak Ridge National Laboratory* Algorithmic advances in quantum Monte Carlo techniques have opened up the possibility of studying models in the general class of the S=1/2 XXZ model (equivalent to hard-core bosons) on frustrated lattices. With an antiferromagnetic diagonal interaction (Jz), these models can be solved exactly with QMC, albeit with some effort required to retain ergodicity in the near-degenerate manifold of states that exists for large Jz. The application of the quantum (ferromagnetic off-diagonal) interaction to this classically degenerate manifold produces a variety of intriguing physics, including an order-by-disorder supersolid phase, novel insulating states, and possible exotic quantum critical phenomena. We discuss numerical results for the triangular and kagome lattices with nearest and next-nearest neighbor exchange interactions, and focus on the relevance of the simulations to related areas of physics, such as experiments of cold trapped atomic gasses and the recent theory of deconfined quantum criticality.

**9:00**

**N45 6 Quantum phase transition from a valence bond crystal to an antiferromagnet*** KENNETH GRAHAM, *University of Michigan, Dept. of Physics* SAMUEL MOUKOURI, *University of Michigan, Dept. of Physics and Michigan Center for Theoretical Physics* We use the recently proposed two-step density-matrix renormalization group to study a ground state phase transition from a dimerized phase to a Néel phase in a frustrated spatially anisotropic Heisenberg and $t - J$ models. We compute critical exponents for the gap and correlation functions.

*We thank the NSF for support via grant no. DMR-0426775.

**9:12**

**N45 7 Calculations of Domain Wall and $Z_4$ Vortex Energies in the Dimerized Phase of J1-J2 Heisenberg Model** TYLER BRYANT, RAJIV R.P. SINGH, *UC Davis* We develop a series expansion method to calculate the Domain Wall Energy per unit length and the $Z_4$ vortex energies in the dimerized phase of the J1-J2 Heisenberg Model. The energy difference between the state with and without domain walls is calculated by series expansions around two different dimer configurations. The calculations are used to study the transition away from the dimerized phase. These calculations are compared with other studies of the phase boundaries in this system.

**9:24**

**N45 8 The nature of quantum phase transition in quantum compass model** HAN-DONG CHEN, *Department of Applied Physics, Stanford University and Department of Physics, UIUC* CHEN FANG, *Department of Physics, Purdue University* JIANGPING HU, *Department of Physics, Purdue University* HONG YAO, *Departmenf of Physics, Stanford University* In this work, we show that the quantum compass model in two dimension can be mapped to a fermionic model with local density interaction and the quantum phase transition point at the symmetric point Jx=Jz marks a first order phase transition.

**9:36**

**N45 9 Quantum Nematic Phase in the Emery Model** KAI SUN, EDUARDO FRADKIN, *UIUC* STEVEN KIVELSON, *Stanford University* We investigate one strong coupling regime of the Emery model of a CuO plane in the strong coupling limit first discussed in Ref. [1]. In this regime the on-site repulsion energies are much larger than the inter site Coulomb repulsions and the hopping terms. By integrating out the copper sites, we mapped this model into an interacting fermionic model on an effective two-dimensional crossed-chains lattice. We will discuss the simpler case of spinless fermions on this effective lattice in the regime in which the residual interactions are weak. Using a mean-field approach, we discuss the isotropic-nematic phase transition in this system. We show that the nematic phase may exist even for infinitesimally weak interactions. We investigate this phase transition for a range of dopings, temperatures and interactions. For certain choice of parameters, the effective electronic states behave like those of a 2D square lattice model, but for some other choices, its properties are reminiscent of a quasi-one-dimensional system. [1] Steven A. Kivelson, Eduardo Fradkin, and Ted Geballe, PRB 69, 144505 (2004)

**9:48**

**N45 10 No sliding in time** KIRILL SHTENGEL, *UC Riverside* CHETAN NAYAK, *Microsoft* WAHEB BISHARA, *Caltech* CLAUDIO CHAMON, *Boston University* We analyse the following apparent paradox: As has been recently proved by Hastings, under a general set of conditions, if a *local* Hamiltonian has a spectral gap above its (unique) ground state, all connected equal-time correlation functions of local operators decay exponentially with distance. On the other hand, statistical mechanics provides us with examples of 3D models displaying so-called sliding phases which are characterised by the algebraic decay of correlations within 2D layers and exponential decay in the third direction. Interpreting this third direction as time would imply a gap in the corresponding (2+1)D quantum Hamiltonian which would seemingly contradict Hastings' theorem. The resolution of this paradox lies in the non-locality of such a quantum Hamiltonian.

**10:00**

**N45 11 Quantum dimer model on a two dimensional pyramid lattice.** HONG YAO, *Department of Physics, Stanford University, CA 94305* HANDONG CHEN, *Department of Physics, Uiversity of Illinois, Urbana-Champaign, IL 61801* CONGJUN WU, *Kavli Institute for Theoretical Physics, University of California, Santa Barbara, CA 93106* We study the Rokhsar-Kivelson (RK) quantum dimer model on a two dimensional corner-sharing pyramid lattice. Contrast to other lattices such as square and triangular lattice, on the RK line (V=t, V' arbitrary), the dimer-dimer correlation is exact zero as long as dimers are a few lattice constants away from each other. More interestingly, a deconfined dimer liquid phase (or RVB phase) is found to the left of the RK line in the phase diagram. There are two kinds of confined valence bond crystal (VBC) states to the very left of the RVB phase. And there is a VBC state to the right of the RK line. Surprisingly, the spinor excitations are deconfined within the model even though the underlining state breaks the translational symmetry and rotational symmetry.

**10:12**

**N45 12 A doped interacting quantum dimer model on the square lattice** STEFANOS PAPANIKOLAOU, ERIK LUIJTEN, EDUARDO FRADKIN, *University of Illinois at Urbana-Champaign* We introduce a generalized quantum dimer model [1] for interacting dimers on the square lattice [2] which can be mapped to generic 2D classical partition functions. More specifically, we show that the amplitudes of the exact ground state wavefunction are given by the Gibbs weights of a 2D classical doped interacting dimer model. We use this mapping to determine the phase diagram in the interaction - hole density plane. Analytically, we exploit a direct microscopic mapping of the classical dimer model on the square lattice to a special 8-vertex model and generalized Coulomb gases. Numerically, we use a novel rejection-free geometrical cluster algorithm [3] for classical interacting dimers on the square lattice, in the canonical ensemble. We also use simulations to study the system in the grand canonical ensemble. We discuss the structure of the phase diagram and its critical behavior. 1. D.S. Rokhsar and S.A. Kivelson, PRL 61, 2376 (1988), 2. F. Alet et al. PRL 94, 235702 (2005), 3. J. Liu and E. Luijten, PRL 92, 035504 (2004).

**10:24**

**N45 13 Possible New Physics at Quantum Critical Points: Skyrmions as Elementary Excitations of 2 + 1 D Antiferromagnets** ZAIRA NAZARIO, DAVID I. SANTIAGO, *Stanford University* It has recently been proposed that there are degrees of freedom intrinsic to quantum critical points that can contribute to quantum critical physics. We point out that intrinsic critical degrees of freedom exist quite generally below the upper critical dimension. We show that in 2 + 1 D antiferromagnets skyrmion excitations are stable at criticality and identify them as the critical excitations.

**10:36**

**N45 14 Possible New Physics at Quantum Critical Points: Skyrmions as critical Spin 1/2 Excitations of 2+1 D Antiferromagnets** DAVID SANTIAGO, *Stanford University* ZAIRA NAZARIO, *Stanford University* We show that despite the absence of a Hopf term and zero Berry phase terms, the Nèel ordered phase of 2 + 1 D quantum antiferromagnets have spin 1/2 excitations, i.e. *spinons*. The spinons are skyrmion excitations of a topological nature. Since skyrmion gap is proportional to the spin stiffness, quantum criticality corresponds to skyrmion gap collapse. We speculate that skyrmions are relevant at criticality and are, perhaps, related to recent suggestions of critical fractionalization.

**10:48**

**N45 15 Quartet condensation of fermions** ASEEM TALUKDAR, *University of Cincinnati* We investigate quartet condensation in fermion systems with four internal states. Physical examples include spin-3/2 fermionic atoms, transition metal oxides with orbital degeneracy, bi-layered systems with electrons and holes and quadra-layer spin-polarized electron hole systems. We consider a simple SU(4) symmetric model in which the fermions interact among themselves with point attractive interactions. The effective free energy functional of the Cooper Pairs (CP) is found to contain attractive interactions among certain types of CP's. This will allow the CP's to form bound states or quartets. Using a variational calculation based on the Bogoliubov inequality, we find that the system may undergo quartet condensation which will suppress the CP instability. By tuning the interaction away from the SU(4) limit, a phase transition from quartet to CP condensation can occur.



## SESSION N46: SEMICONDUCTOR DEVICES/ SEMICONDUCTORS GENERAL

**Wednesday Morning, 15 March 2006**
**349, Baltimore Convention Center at 8:00**
**Andrei Sergeev, University at Buffalo, presiding**

**8:00**

**N46 1 Dielectric and Photovoltaic Physics in Thin-Film Crystalline Sulfides*** RODNEY McKEE, *Oak Ridge National Laboratory* FRED WALKER, *Oak Ridge National Laboratory* Solar energy utilization has been the hope and sought-for solution to local energy needs at least since the late 1800's. In today's terms, solar energy is one of the few renewable energy sources with the potential to have a major impact on domestic energy independence. There is a rich, but incomplete scientific literature on the underpinning photovoltaic physics of solar cell development. This literature does however, clearly identify a pervasive, unsolved physics problem – itdeep level electronic states in wide band gap

semiconductors quench the electro-optic behavior of solar cells: either p-type or n-type doping is inhibited both of which are required for the basic function of a semiconducting p-n junction solar cell. We will report on our approach towards solving this problem via layer-sequenced stabilization of thin-film photovoltaics that enable symmetric p or n-type doping. We will bring interface phase physics to the synthesis process for sulfur-based chalcogenides to show that the valence and conduction band energy levels as well as defect formation energies in these systems can be systematically modified in wide bandgap photovolatics.

*Research sponsored by the Division of Materials Sciences and Engineering, Office of Basic Energy Sciences, U.S. Department of Energy at Oak Ridge National Laboratory under contract DE-AC05-00OR22725 with UT-Battelle, LLC.

**8:12**

**N46 2 Metal-semiconductor-metal junctions with silver sulphide barrier layers*** I. CHAITANYA LEKSHMI, YASMIN AFSAR, JAGADEESH S. MOODERA, *Francis Bitter Magnet Lab, MIT, Cambridge, MA* Atomic level electrical switching requires innovative methods of charge transport, wherein the device can be switched between ''on'' and ''off'' states at ambient temperatures by applying reasonably small voltages. Recently, the mixed conducting property of silver sulphide was utilized in making a quantized conductance atomic switch[1] which satisfies these requirements. We present the fabrication of metal-semiconductor-metal junctions where a $Ag_2S$ layer is sandwiched between two metal electrodes. Current-voltage measurement shows diode characteristics for these junctions at large thickness (100 Å) of $Ag_2S$. At lower thicknesses, the nature of transport changes over to a nonlinear tunnel junction like behaviour up to an applied external voltage of 1.5 V. The growth, morphology and transport properties of $Ag_2S$ layers depend critically on the deposition conditions. Using the tunnel junction, we investigate the effects of parameters such as growth and thickness of semiconducting layers, choice of metal electrodes and the metal-semiconductor interface on the charge transport across the junction. [1] K. Terabe et. al, Nature **433**, 47 (2005)

*Supported by NSF

**8:24**

**N46 3 Characterization of hydrogenation processes for c-Si photovoltaics** S. KLEEKAJAI, M. STAVOLA, F. JIANG, *Lehigh University* A commonly used method to introduce H into Si solar cells to passivate bulk defects is by the post-deposition annealing of an H-rich $SiN_x$ surface layer that also acts as an antireflection coating.[1] It previously had been impossible to characterize the small concentration of H that is introduced by this method. Our work on the properties of the transition-metal-H complexes in Si has led us to develop a novel method to characterize the introduction of H into Si.[2] We have used IR spectroscopy coupled with transition-metal impurities introduced into Si-test samples to act as traps for H. The transition-metal-H complexes can then be detected with high sensitivity to determine the concentration and penetration depth of H in the samples. This model system has been used to obtain insight into what solar-cell processing strategies lead to the best passivation of defects in the Si bulk. We thank V. Yelundur and A. Rohatgi for an enjoyable and fruitful collaboration. This work is supported by NSF Grant DMR 0403641 and NREL grant AAT-1-31605-04. 1. A. G. Aberle, Sol. Energy Mater. Sol. Cells **65**, 239 (2001). 2. F. Jiang et al., Appl. Phys. Lett. **83**, 931 (2003).

**8:36**

**N46 4 Optical switching and structural properties of Ge2Sb2Te5 and Ge2Sb2Te7 films*** T. W. HERRING, *University of Utah* P. C. TAYLOR, *Colorado School of Mines* C. E. INGLEFIELD, M. J. NELSON, *Weber State University* D. A. BAKER, M. A. PAESLER, *North Carolina State University* Ge2Sb2Te5 and Ge2Sb2Te7 are materials important in phase change memory applications, but the structures of both the amorphous and crystalline phases are not well known. Large areas of optically switched material are needed in order to probe the structure. Films of amorphous Ge2Sb2Te5 varying in thickness between 20 nm and 100 nm were crystallized by exposure to a focused beam of 532 nm laser light with a power density of approximately 50 $kW/cm^2$. Rastering of the crystallized spots produces areas of several square millimeters suitable for experiments to probe the structure of the films. The switching causes little change in surface topography as measured by atomic force microscopy. Ablation of the films occurs if the power density is too high. The structure of optically crystallized films studied by EXAFS will be discussed. Films of Ge2Sb2Te7 will also be discussed.

*Research supported by the Air Force Research Laboratory under grant no. F29601-03-01-0229 and by the National Science Foundation under grant no. DMR 0307594

**8:48**

**N46 5 Interface Dielectric Function in ZnO/Ag Structures for Applications as Back-Reflectors in Thin Film Solar Cells** DEEPAK SAINJU, NIKOLAS PODRAZA, JIAN LI, ROBERT COLLINS, *University of Toledo, Ohio* MAARIJ SYED, *Rose-Hulman Institute of Technology* Sequential deposition of optically-opaque Ag followed by the transparent conductor ZnO, both by magnetron sputtering on substrates such as stainless steel, is a key process for efficient optical back-reflectors (BRs) of thin film solar cells. The roughness scale investigated in our work is an order of magnitude smaller than that studied previously. We have first analyzed Ag deposition by real time spectroscopic ellipsometry (RTSE) over the energy range from 1.0 eV to 6.5 eV in order to establish the final roughness thickness on the Ag just prior to itin situ deposition of ZnO. Values from 10 to 50 Å are obtained, for a relatively narrow range of substrate temperature (20-90°C). We employ the same RTSE probe to analyze the interface and bulk optical properties of ZnO and thus deduce a complete optical model of the BR. Our model for the dielectric function of the interface layer helps explain the losses in the BR structure. It includes contributions from free electrons associated with the Ag component, and bound electrons associated with a metal particle plasmon resonance near 2.7 eV and with interband transitions from Ag and ZnO. The effect of the interface layer on reflectance of BR structures is evaluated.

**9:00**

**N46 6 High-performance ZnO/ZnMgO FET using a hetero-MIS stricture** SHIGEHIKO SASA, *Osaka Institute of Technology* MASASHI OZAKI, KAZUTO KOIKE, MITSUAKI YANO, MASATAKA INOUE, We propose a new structure of ZnO/ZnMgO field-effect transistors (FETs) for simplifying the fabrication process as well as for the improvement of the FET characteristics. Recently, we developed a ZnO/ZnMgO heterostructure FET (HFET) by utilizing a two-dimensional electron gas channel layer

formed in the selectively-doped single quantum well structure.[1)] In the HFET fabrication process, the ohmic contact formation is crucial because of the difficulty in removing the top ZnMgO barrier layer with the underlying ZnO channel remained. The use of a very thin (1-2 nm) ZnMgO top barrier layer enables the formations of both good ohmic contacts without the ZnMgO etching and the gate electrodeD We used metal-insulator semiconductor (MIS) gate structure with the use of a 50-nm-thick $Al_2O_3$ gate insulator. The thin ZnMgO barrier acts as a setback layer for the channel electrons from the ZnMgO/$Al_2O_3$ interface. The 1-$\mu$m-gate device showed a complete FET operation with a transconductance of as high as 28 mS/mm and the effective mobility of 62 $cm^2$/Vs. 1) K. Koike et al., Appl. Phys. Lett. **87**, 112106 (2005).

**9:12**

**N46 7 First-principles calculations of mobilities in novel MOSFETs** MATTHEW EVANS, *Vanderbilt University* SOKRATES PANTELIDES, *Vanderbilt University* Nanoscale metal-oxide-semiconductor field-effect transistors (MOSFETs) incorporating novel materials demonstrate unusual electron transport behavior. Straining the silicon lattice results in significant increases in electron and hole mobility. However, mobility calculations using standard approximations have difficulty explaining this increase. MOSFETs using novel gate dielectrics (e.g. hafnium oxide) have mobilities that are much lower than MOSFETs using silicon dioxide as the dielectric. ''Interface quality'' has been invoked as a likely cause of this difference, but few attempts have been made to tie the mobility decrease to scattering mechanisms associated with the novel dielectric structure. In this talk, we report results of mobility calculations in MOSFETs with a strained-Si channel and with alternate gate dielectrics. The calculations employed a recently developed first-principles method based on atomic-scale interface models.[1] Changes in the local environment of atomic-scale interface roughness defects are shown to potentially account for the increase in mobility under strain. Interstitial Hf defects near the silicon-oxide interface can act as traps and are shown to impact the mobility in MOSFETs with hafnium oxide gate dielectrics. [1] M. H. Evans, X.-G. Zhang, J. D. Joannopoulos, and S. T. Pantelides, Phys. Rev. Lett., v. 95, p. 106802 (2005).

**9:24**

**N46 8 Negative Bias Temperature Instability (NBTI) recovers fully with bake at 325 C or above and the device is equivalent to new.** ANASTASIOS KATSETOS, *IBM* Negative Bias Temperature Instability (NBTI) is one of the major degradation mechanisms of PMOSFET devices. When the p-channel Field Effect Transistor (PFET) gate is biased negatively with respect to the channel, as in CMOS inverter, at elevated temperature the threshold voltage (Vt) decreases (absolute value increases for application temperatures) and the drive current (Ion) decreases. This degrades the device performance and may lead to circuit failure. NBTI is process dependent and has strong dependence on temperature, gate voltage, time, and gate oxide thickness. It also depends on device area and or geometry. NBTI models used in industry are empirical. I have observed, on different technologies, in the last several years that NBTI recovers with bake. The recovery amount depends on the bake temperature, which can be the stress temperature, and happens very fast at any temperature. Full recovery is achieved at temperatures above 325 degrees C. After full bake recovery the device behaves like new with NBTI equal to the NBTI of the original stress.

**9:36**

**N46 9 Calculation of the Phonon Lifetime of Photoexcited Bismuth*** EAMONN MURRAY, *Department of Physics and Tyndall National Institute, University College, Cork, Ireland* DAVID PRENDERGAST,† TADASHI OGITSU, *Lawrence Livermore National Laboratory* STEPHEN FAHY, *Department of Physics and Tyndall National Institute, University College, Cork, Ireland* Phonon lifetimes of the zone-center longitudinal optical phonon in bismuth are calculated with respect to the fraction of valence band electrons excited into the conduction bands. Second order density-functional perturbation theory (DFPT), combined with the frozen phonon technique, is used to calculate the third-order anharmonic couplings between phonons. Calculations on the photoexcited system are performed by constraining the occupations of the valence and conduction bands, giving a certain excited electron-hole plasma density. It is found that the calculated decrease in the phonon lifetime with excitation is due both to the reduction of the phonon frequency and an increase in the coupling to other phonons.

*Supported by the Irish Research Council for Science, Engineering and Technology and SFI; and performed under the auspices of the U.S. Department of Energy by University of California Lawrence Livermore National Laboratory under contract No. W-7405-Eng-48.Present address: Department of Physics, University of California, Berkeley

†g-48.Present address: Department of Physics, University of California, Berkeley

**9:48**

**N46 10 Defect levels in semiconductors - is the band gap problem truly a problem?*** PETER A. SCHULTZ, *Sandia National Laboratories, Albuquerque, NM* Quantitative predictions of defect properties in semiconductors using density functional theory (DFT) have been crippled by standard supercell methods, which have incorrect boundary conditions for an isolated defect, and the band gap problem, where DFT drastically underestimates the band gap. I present a generalized supercell method with boundary conditions appropriate to point defects, to fix the electrostatic boundary conditions, remove ambiguity in charge reservoir, include bulk polarization effects, and specifically account for defect level dispersion. I compute formation energies for an extensive set of defects in silicon. The resulting defect level spectrum in silicon exhibits no band gap problem. The results agree remarkably well with experiment for those values that are experimentally known, and predict heretofore unobserved electronic transitions important for the electrical response of irradiated semiconductor devices.

*Sandia is a multiprogram laboratory operated by Sandia Corporation, a Lockheed Martin Company, for the United States Department of Energy's National Nuclear Security Administration under Contract DE-AC04-94AL85000.

**10:00**

**N46 11 Structural, optical, and electrochromic properties of $V_2O_5$ thin films by Metalorganic Decomposition** M.B. SAHANA, G. LAWES, K. R. PADMANABHAN, R. NAIK, *Wayne State University, Detroit,* V.M NAIK, *University of Michigan, Dearborn* $V_2O_5$ a n-type semiconductor has been widely used in variety of technological applications such as solid state battery cathodes, solar cell windows, and electrochromic devices as it

allows easy intercalation/deintercalation of different ions due its open layered structure. Recently the attention has been focused on the development of thin films of $V_2O_5$ as a cathode material in microbatteries owing to the miniaturization of electronic devices. We report the preparation of $V_2O_5$ thin films by cost effective easy method of metalorganic decomposition technique using vanadium naphthenate oxide precursor. The solution is spin coated on glass and ITO coated glass substrates. The resulting films on annealing at 450°C are comprised of $V_2O_5$ nanoparticles as evidenced from X-ray diffraction and Raman spectra. UV-VIS studies indicate band gap of $\approx$ 2.4 eV. The dependence of electrochromic properties of these films, heat treated at various temperatures, on microstructure and crystallinity will be presented.

**10:12**

**N46 12 Structure of III-Sb(001) Surfaces Under Extreme Sb-rich Conditions** JEFFERY HOUZE, SUNGHO KIM, SEONG-GON KIM, *Mississippi State University* STEVEN C. ERWIN, *Naval Research Laboratory* We use density functional theory to study the structure of III-Sb(001) (III = Al or Ga) growth surfaces. Various reconstruction models are considered to construct the surface stability diagram under different III-Sb growth conditions. We found that AlSb surface stability diagram identifies experimentally observed surface reconstructions quite well. For GaSb, however, all $(n \times 5)$-like reconstructions proposed to date have too high surface formation energies compared to the ones with wrong periodicities and thus cannot adequately model the structures observed experimentally under extreme Sb-rich growth conditions. Our results indicate that the existing reconstruction models for GaSb(001) surface require revisiting and demonstrate the need for a better reconstruction model.

**10:24**

**N46 13 A density functional study of the effect of pressure on GeTe** LEONARD KLEINMAN, B.R. SAHU, ADRIAN CIUCIVARA, *University of Texas at Austin* We compare local density approximation (LDA) and generalized gradient approximation (GGA) calculations of GeTe as a function of applied pressure. The LDA yields a poor result for the zero pressure trigonal angle but good to excellent results for the zero pressure lattice constants, energy gap, and relative positions of the two sublattices. More importantly, it yields results within the wide range of experimental values for the critical pressure at which the ferroelectric trigonal to rock-salt transition takes place. We also calculate the zero pressure polarization.

**10:36**

**N46 14 Pressure-Raman study of optical phonon anharmonicity and metastable phase in $^{68}Zn^{76}Se$*** R.E. TALLMAN, B.A. WEINSTEIN, *Physics Department, SUNY at Buffalo, NY* R. LAUCK, M. CARDONA, *Max Plank Institut fur Festkorperforschung, Germany* The effects of hydrostatic pressure on the one- and two-phonon Raman spectra of isotopic purity $^{68}Zn^{76}Se$ are studied to 15GPa at 300K. With increasing pressure the TO-TA(X,K) difference-mode shifts rapidly to higher energy, moving above the 2TA overtone band at 5.8GPa with no significant 4-phonon mixing. Above 10GPa, the one-phonon TO($\Gamma$) peak broadens rapidly, reaching $\sim$ 60cm$^{-1}$ FWHM and overlapping both TO-TA(X,K) and LO($\Gamma$). After the sample undergoes the forward and reverse high-pressure transitions, the sphalerite-structure Raman features return (including the strongly broadened TO($\Gamma$) peak) and a new sharp line attributed to a metastable ZnSe phase appears. The TO($\Gamma$) broadening in ZnSe is much stronger than that due to pressure-tuning of the anharmonic decay TO($\Gamma$) $=>$ TA+LA(X,W,K) in GaP and ZnS.[1] Our results suggest that the resonant anharmonic interactions in ZnSe may be strongly enhanced by spatial confinement and disorder in the domains of nucleating phases. [1] J. Serrano et. al., Phys. Rev. B69, 014301(2004).

*Work partially supported by University of Buffalo CSEQuIN Center.

**10:48**

**N46 15 Raman scattering in $Zn_{1-x}Fe_xTe$, a van Vleck diluted magnetic semiconductor*** X. LU, S. TSOI, I. MIOTKOWSKI, S. RODRIGUEZ, A.K. RAMDAS, *Purdue University* H. ALAWADHI, *Sharjah University, UAE* T.M. PEKAREK, *University of North Florida* $Zn_{1-x}Fe_xTe$, a zinc blende II-VI diluted magnetic semiconductor(DMSs), exhibits van Vleck paramagnetism, thanks to the electronic level structure of $Fe^{2+}$ with $T_d$ site symmetry, Subjected to crystal field and spin-orbit coupling, the lowest level of its ground state multiplet has a $\Gamma_1$ non-magnetic level, with a $\Gamma_4$ magnetic level just above it. This level ordering leads to its van Vleck paramagnetism. The Raman spectra of this DMS display the $\Gamma_1 \rightarrow \Gamma_4$electronic transition($\Gamma^*$) whose Zeeman splittings are interpreted in terms of symmetry considerations and numerical calculations. The magnetic field and the temperature dependence of the spin-flip Raman line of the donor-bound electron in $Zn_{1-x}Fe_xTe$ exhibit characteristics typical of van Vleck paramagnetism and, in combination with magnetization measurements, yield the s-d exchange constant $\alpha N_0 = 236.9 \pm 9$ meV. The Raman spectra also show $\Gamma^*$ in combination with LO phonons which exhibit an intermediate mode behavior.

*This work was supported by NSF Grant No. DMR 0405082 at Purdue University, and by the Donors of the American Chemical Society Petroleum Research Fund PRF#40209-B5M and by the NSF Grant No. DMR-03-05653 at the University of North Florida.

**SESSION P1: ELECTRON TRANSPORT IN SINGLE MOLECULES**
**Wednesday Morning, 15 March 2006; Ballroom IV, Baltimore Convention Center at 11:15**
**Allan MacDonald, University of Texas at Austin, presiding**

**11:15**
**P1 1 Electrochemical gate-controlled conductance of single molecules.**
N.J. TAO, *Arizona State University*

The ability to measure and control current through a single molecule is a basic requirement towards the ultimate goal of building an electronic device using single molecules. This ability also provides one with a rather unique opportunity to study charge transport, a phenomenon that plays vital roles in many chemical, electrochemical and biological processes, on a single molecule basis. To reliably measure the current, one must: 1) provide a reproducible contact between the molecule and two probing electrodes; 2) find a signature to identify that the measured conductance is due to not only the sample molecules but also a itsingle sample molecule; 3) provide a third gate electrode to control the current. The method that we have used to create individual molecular junctions is to bring two electrodes into and out of contact with each other in the presence of sample molecules terminated proper linkers that can bind covalently to the electrodes. The individually created molecular junctions vary in the atomic scale details of the contact configurations, and statistical analysis is used to extract the conductance of the molecular junction with the most probable configuration. When several configurations occur with comparable probabilities, the method may result in multiple conductance values. In order to control the current through a molecule, we use an electrochemical gate in which the molecular junction is immersed in an electrolyte and biased with respect to a reference. We have studied three types of molecules: electrochemically inactive molecules, electroactive molecules that undergo irreversible redox reactions, and electroactive molecules that undergo reversible redox reactions. These molecular systems exhibit rather different electrochemical gating behaviors.

**11:51**
**P1 2 Electron Transport in Molecular Transistors.**
ZHEN YAO, *Department of Physics, The University of Texas at Austin, Austin, TX 78712*

We have fabricated molecular transistors by depositing molecules between nanometer-spaced electrodes created via electromigration. Electron transport in these devices is dominated by the single-electron tunneling effect. Several examples will be discussed including (1) excitations of intramolecule vibrations in single trimetal-molecule transistors, (2) room-temperature single-electron tunneling transistors using alkanedithiols here the transport occurs through ultrasmall Au nanoparticles spontaneously formed during thiol assembly, and (3) Kondo resonance and co-tunneling behavior in metal-porphyrin and expanded-porphyrin molecule transistors.

**12:27**
**P1 3 Electron-vibron coupling in single molecule transistors.**
KARSTEN FLENSBERG, *Niels Bohr Institute*

I discuss coupling between electron transport and vibrational degrees of freedom in single-molecule and nanotube systems. The coupling gives rise several effects such as sidebands in the differential conductance, rectification due to polaron formation,and interesting interplay with the Kondo resonance.

**13:03**
**P1 4 Field Regulation of Single Molecule Conductivity by a Charged Atom.**
ROBERT WOLKOW, *National Institute for Nanotechnology*

A new concept for a single molecule transistor is demonstrated [1]. A single chargeable atom adjacent to a molecule shifts molecular energy levels into alignment with electrode levels, thereby gating current through the molecule. Seemingly paradoxically, the silicon substrate to which the molecule is covalently attached provides 2, not 1, effective contacts to the molecule. This is achieved because the single charged silicon atom is at a substantially different potential than the remainder of the substrate. Charge localization at one dangling bond is ensured by covalently capping all other surface atoms. Dopant level control and local Fermi level control can change the charge state of that atom. The same configuration is shown to be an effective transducer to an electrical signal of a single molecule detection event. Because the charged atom induced shifting results in conductivity changes of substantial magnitude, these effects are easily observed at room temperature. [1] Paul G. Piva1,Gino A. DiLabio, Jason L. Pitters, Janik Zikovsky, Moh'd Rezeq, Stanislav Dogel, Werner A. Hofer & Robert A. Wolkow, Field regulation of single-molecule conductivity by a charged surface atom, NATURE **435**, 658-661 (2005).

**13:39**
**P1 5 Measurement of the conductance of single conjugated molecules.**
ISRAEL BAR-JOSEPH, *Weizmann Institute of Science*

This abstract was not received electronically.

**SESSION P2: THE ELECTRONIC PROPERTIES OF OVERDOPED CUPRATES: THE CLEAN GATEWAY TO HIGH-TC SUPERCONDUCTIVITY**
**Wednesday Morning, 15 March 2006; Ballroom III, Baltimore Convention Center at 11:15**
**Andy Mackenzie, University of St. Andrews, presiding**

**11:15**
**P2 1 The origin of anomalous transport in a high temperature superconductor.**
NIGEL HUSSEY, *University of Bristol*

The metallic state of high-temperature superconductors is anomalous in that the Hall coefficient is strongly temperature dependent while the resistivity varies linearly in temperature over a wide temperature range. Although this *T*-linear resistivity gradually weakens with doping, crucially it survives until superconductivity is destroyed. Both the superconducting pairing interaction and the origin of this anomalous transport have yet to be determined, though most theoretical approaches consider them to be intrinsically linked. Through novel analysis of polar angular magnetoresistance oscillations, we have succeeded to determine the full temperature and momentum dependence of the mean free path of the charge carriers in highly doped $Tl_2Ba_2CuO_{6+\delta}$ ($T_c$ = 15K) up to 60K. From this, we have been able to identify the origin of the *T*-linear resistivity itand the temperature dependence of the Hall coefficient for this particular compound. Given the correlation between the appearance of the *T*-linear resistivity and the onset of superconductivity, this additional scattering is also a prime candidate for the pairing mechanism for high temperature superconductivity itself**.**

**11:51**
**P2 2 Nodal-antinodal quasiparticle anisotropy reversal in the overdoped high-$T_c$ cuprates.***
ANDREA DAMASCELLI, *University of British Columbia*

The cuprate superconductors can be tuned through a remarkable progression of states of matter by doping charge carriers into $CuO_2$ planes. The most generic feature of this tuning is a sequence from a Mott antiferromagnetic insulator, to the d-wave superconductor at intermediate doping, and eventually to an overdoped metal which is widely believed to be described by Fermi liquid theory. Of these three, the testing of Fermi liquid theory in the overdoped regime has been particularly hampered by a lack of compounds suitable for a wide range of experimental techniques. Important breakthroughs could come from the study of $Tl_2Ba_2CuO_{6+\delta}$ (Tl2201), a clean and structurally simple system with a very high $T_c$, whose natural doping range extends from optimal to extreme overdoping as one varies the oxygen content. Recent success in high-purity single crystal growth [1] gave us the opportunity of performing the first extensive ARPES study of the low-energy electronic structure of heavily overdoped Tl2201, which reveals a novel phenomenology: contrary to the case of under and optimally-doped cuprates, quasiparticles are sharp near ($\pi$,0), i.e. the antinodal region where the gap is maximum, and broad at ($\pi$/2, $\pi$/2), i.e. the nodal region where the gap vanishes [1,2]. This reversal of the nodal-antinodal quasiparticle anisotropy across optimal doping and its relevance to scattering, many-body, and quantum-critical phenomena in the high-Tc cuprate superconductors, is discussed. [1] D.C. Peets et al., cond-mat/0211028 (2002); [2] M. Platé et al., PRL **95**, 077001 (2005).

*This work was done in collaboration with D.C. Peets, M. Platé, J.D.F. Mottershead, I.S. Elfimov, N.J.C. Ingle, M. Raudsepp, Ruixing Liang, D.A. Bonn, W.N. Hardy, S. Chiuzbaian, M. Falub, M. Shi, and L. Patthey.

**12:27**
**P2 3 Scanning tunneling spectroscopy studies of $Bi_2Sr_2CaCu_2O_{8+x}$ from the strongly underdoped to strongly overdoped regime.**
JAMES SLEZAK, *Department of Physics, Cornell University*

Using atomically resolved scanning tunneling microscopy (STS), we investigate the electronic structure $Bi_2Sr_2CaCu_2O_{8+x}$ across a range of doping levels from x $\sim$ 0.1 up to as high as $\sim$ 0.23, with significant changes in electronic structure observed above p$\sim$ 0.21. New sample preparation processes [1] were used to produce heavily overdoped crystals suitable for the imaging of various forms of electronic heterogeneity. The evolution of the gap map $\Delta$(r), coherence peak height map A(r), the inelastic tunneling signatures $\omega$(r), and the quasiparticle interference LDOS modulations, as well as their interrelations across this range of doping levels, will be presented. Additional authors: J.

Lee, M. Wang, Laboratory of Atomic and Solid State Physics, Department of Physics, Cornell University, Ithaca, NY 14853, U.S.A; K. Fujita, Department of Advanced Materials Science, University of Tokyo, Tokyo 113-0033, Japan; H. Eisaki, National Institute of Advanced Industrial Science and Technology (AIST), 1-1-1 Central 2, Umezono, Tsukuba, Ibaraki 305-8568; S. Uchida, Department of Physics, University of Tokyo, Tokyo 113-0033; and J. C. Davis, Laboratory of Atomic and Solid State Physics, Department of Physics, Cornell University. [1] J. Slezak, K. Fujita, J. C. Davis, in preparation (2005).

**13:03**
**P2 4 Evolution of superconducting gap and metallic ground state in cuprates from transport.**
LOUIS TAILLEFER, *University of Sherbrooke & Canadian Institute for Advanced Research*

We report on fundamental characteristics of the ground state of cuprates in the limit of T=0, for both normal and superconducting states, obtained from transport measurements on high-quality single crystals of YBCO and Tl-2201, as a function of hole concentration. The superconducting gap is extracted from thermal conductivity; it is found to scale with the superconducting transition temperature throughout the overdoped regime, with a gap-to-Tc ratio of 5 [1]. The normal state is accessed by suppressing superconductivity with magnetic fields up to 60 T and is characterized by the limiting behavior of its electrical resistivity; while carrier localization is observed in YBCO at low temperature for carrier concentrations p below 0.1 hole/planar Cu, at p=0.1 and above the material remains highly metallic down to T=0 [2]. This shows that the non-superconducting state of underdoped cuprates, deep in the pseudogap phase, is remarkably similar to that of strongly overdoped cuprates, e.g. at p=0.3. We compare these results with similar measurements on other cuprates and discuss their implication for our understanding of the cuprate phase diagram. [1] In collaboration with: D.G. Hawthorn, S.Y. Li, M. Sutherland, E. Boaknin, R.W. Hill, C. Proust, F. Ronning, M. Tanatar, J. Paglione, D. Peets, R. Liang, D.A. Bonn, W.N. Hardy, and N.N. Kolesnikov. [2] In collaboration with: C. Proust, M. Sutherland, N. Doiron-Leyraud, S.Y. Li, R. Liang, D.A. Bonn, W.N. Hardy, N.E. Hussey, S. Adachi, S. Tajima, J. Levallois, and M. Narbone.

**13:39**
**P2 5 Optical properties of Cuprates in the Normal and superconducting state.***
DIRK VAN DER MAREL, *University of Geneva*

For superconducting materials it is interesting and important to determine the kinetic energy of the conduction electrons, $< <H> >_T$, because its behavior as a function of temperature dependence, in particular at the superconducting phase transition, provides a direct and profound insight in the mechanisms by which the superconducting phase is stabilized. The intra-band optical spectral weight, W(T), is, apart from a minus sign, closely related to the kinetic energy[1]. With modern optical techniques it is possible to measure W(T) very accurately as a function of temperature. Over the past few years several teams have reported that by the superconducting phase transition affects the optical conductivity over an energy range of several electron Volts[2-8]. Some of these results were accurate enough to determine the effect of superconductivity on W(T). Here we present new optical data for a large number of underdoped and optimally doped samples of various compositions. In order to clearly distinguish the effect of the superconducting phase transition from other temperature dependencies, we use a dense sampling of temperatures (1 spectrum every Kelvin) over a broad range of temperatures and frequencies. All our data support that the change at Tc of W(T) parallel to the CuO2-planes is opposite to the trend expected from the BCS prediction. For strongly overdoped samples the observed behavior of W(T) in the normal state and in the superconducting state is qualitatively different compared to underdoped and optimally doped superconductors. [1] P- F. Maldague, Phys. Rev. 16, 2437 (1977). [2] M. J. Holcomb, et al., Phys. Rev. Lett. 73, 2360 (1994). [3] D. N. Basov et al., Science 283, 49 (1999). [4] H. J. A. Molegraaf et al., Science 295 (2002) 2239 [5] A. F. Santander-Syro et al., Europhys. Lett 62 (2003) 568 [6] V. Boris et al., Science 304, 708 (2004). [7] B. Kuzmenko et al., Phys. Rev. B 72 (2005) 144503 [8] M. Ortolani et al., Phys. Rev. Lett. 94 (2005) 067002.

*This work was supported by the Swiss National Science Foundation through the NCCR 'Materials with Novel Electronic Properties.



## SESSION P3: PHYSICS TEACHER PREPARATION AT A CRISIS: INNOVATIVE PROGRAMS ADDRESSING A NATIONAL NEED

**Wednesday Morning, 15 March 2006; Ballroom I, Baltimore Convention Center at 11:15**
**Ramon Lopez, Florida Institute of Technology, presiding**

**11:15**
**P3 1 Improving the preparation of K-12 teachers: Contributions from physics education research.***
PAULA HERON, *University of Washington*

Physics education research can contribute to efforts by college and university faculty to improve the preparation of K-12 teachers to teach physics and physical science. Examples are used to demonstrate the need to help teachers deepen their

understanding of basic topics and to illustrate how a research-based curriculum can assist in this process. Evidence is presented of the impact on student learning in K-12 classrooms.

*Supported in part by the National Science Foundation.

**11:51**
**P3 2 UTeach: Secondary Teacher Preparation in Science and Mathematics at the University of Texas at Austin.**
MICHAEL MARDER, *The University of Texas at Austin*

The UTeach Program is a joint effort of the College of Natural Sciences, the College of Education and the Austin Independent School District to recruit, prepare and support math and science teachers for the State of Texas. UTeach uses early and on-going field experiences to capture the imagination of preservice teachers and provide a foundation for more advanced pedagogical courses. With over 400 students enrolled and over 80 graduates per year, UTeach is one of the largest programs producing secondary science, mathematics, and computer science teachers in the nation. Most UTeach students are undergraduates, but around 10% are people of many ages with strong backgrounds in mathematics or science who have decided to enter teaching. Hallmarks include: Four-year degree plans that enable undergraduates to obtain certification at no cost in time or money. Active recruitment and support including tuition reimbursement, paid internships, personal advising, and guidance by master teachers. Emphasis on preparing teachers who will be knowledgeable of their discipline, experienced with involving students in scientific inquiry, and practiced in employing new technologies to enhance student learning. A revised, streamlined professional education sequence drawing on research on learning, standards-based curricula, multiple forms of assessment, and proven strategies for achieving equity and integrating technology into math and science education. Program flexibility with multiple entry points (from freshman to post baccalaureate), integrated degree plans, and proficiency-based assessment, including the development of individual teaching portfolios. For more information on UTeach, see tthttp://uteach.utexas.edu.

**12:27**
**P3 3 Better prepared future teachers = better physics department!***
GAY STEWART, *University of Arkansas*

A more scientifically literate society benefits physics as a profession. It is best realized by better serving all undergraduate physics students. Arguably, the most important are future K-12 teachers. In better-serving all students, the department also benefits. University of Arkansas, Fayetteville has seen a drastic change in number of majors, the number of students active in research and the number of graduates pursuing graduate work while also increasing the number of majors who decide to teach. What works to build these numbers and strengthen these resources at Arkansas will be discussed, with additional examples from other members of the growing Coalition of institutions that are seeking to improve and promote physics and physical science teacher education within physics departments. This group, the Physics Teacher Education Coalition (www.PTEC.org), is bringing together innovative ideas and practices throughout the country to help meet the critical shortage of well prepared and actively supported teachers. The program will be described and information provided for those interested in taking advantage of these efforts.

*PhysTEC is supported in part by the National Science Foundation.

**13:03**
**P3 4 Sustainable and Scalable Reforms in Physics Education: Research studies from Colorado PhysTEC.**
NOAH FINKELSTEIN, *University of Colorado at Boulder**

While many practices developed within the physics education research community have been demonstrated as successful, they respond to calls and employ practices that echo efforts from the early part of the 20th Century. Are we bound to the same limited success as these precursors? We examine what it means to replicate proven reforms and to develop models for sustainable implementation of these reforms. As part of the Colorado Physics Teacher Education Coalition, we have implemented the Tutorials in Introductory Physics, which were developed by researchers at the University of Washington. We present research on the successful implementation of these reforms at the University of Colorado and begin to answer the questions: What does it mean to replicate an educational program? and How might these educational transformations be sustained? We present empirical data on the success of reforms and the fidelity of implementation as well as theoretical frames for analyzing these data. We also present a model (the Learning Assistant program) designed for sustaining these reforms and for increasing student interest and retention in teaching.

*In collaboration with Steven Pollock, University of Colorado at Boulder.

**13:39**
**P3 5 The AAPT/PTRA Program: Professional Development for Pre-College Physics Teachers Hosted by College and University Physics Departments.**
WARREN HEIN, *American Association of Physics Teachers*

The American Association of Physics Teacher's Physics Teaching Resource Agents (AAPT/PTRA) program has a twenty year history of providing professional development for in-service pre-college physics and physical science teachers. More than 500 teachers have been prepared through NSF-funded summer institutes to provide professional development for their peers in a wide variety of venues ranging from urban, inner-city classrooms to classrooms in low population rural areas. A wide variety of inquiry-based, active engagement workshops have been developed that can assist in-service teachers at all experience and preparation levels, from new and crossover teachers to those who have taught for many years. AAPT/PTRA presenters are typically active physics teachers who share lessons learned in their classrooms on how to adopt research-based practices. College and university physics and astronomy departments interested in providing in-service professional development for pre-college teachers in their geographic areas can enter into agreement with the AAPT/PTRA program to utilize the services of these trained professional development providers. United States Department of Education Math and Science Partnership funds that are allocated to each state are an excellent source of funds that physics and astronomy departments can use to support this type of professional development for physics and physical science teachers. An example of a funded program currently in place in Texas will be presented. AAPT/PTRA program is currently funded by NSF grant # ESI-0138617.

## SESSION P4: KEITHLEY AWARD SESSION
**Wednesday Morning, 15 March 2006; 308, Baltimore Convention Center at 11:15**

**11:15**
**P4 1 Nanocalorimetry: Using Si-micromachined Devices for Thermodynamic Measurements of Thin Films and Tiny Crystals.***
FRANCES HELLMAN, *Physics Dept., University of California, Berkeley, and Materials Sciences Division, Lawrence Berkeley Lab*

We have used Si micromachining to fabricate membrane-based calorimeters for measuring thermodynamic properties of microgram-quantity samples over a temperature range from 1.7 to 550K in magnetic fields to 8T. Prototype scaled down devices have been made which allow precise measurements of nanogram quantities. Different types of thermometers are used for different purposes and in different temperature ranges. Current development efforts are extending the temperature range to 0.3 - 800K, and we are collaborating with the national high magnetic field lab to extend the field range to 65T in pulsed magnets. These devices are particularly useful for specific heat measurements of thin film samples (100-400 nm thick) deposited directly onto the membrane through a Si micromachined evaporation mask. They have also been used for small bulk samples attached by conducting paint or In, and for powder samples dissolved in a solvent and dropped onto devices. The measurement technique used (relaxation method) is particularly suited to high fields because thermal conductance is measured in zero field and is field independent, while the relaxation time constant does not depend on thermometer calibration. The devices have been used with little modification for thermal conductivity and thermopower measurements, and are well suited to measurements of calorimetric signals such as those occurring at phase transitions or under irreversible thermal behavior. I will discuss device fabrication and thermal analysis which allow us to precisely identify heat flow in the devices and consequent limits on the absolute accuracy, as well as possible future directions for device development. I will also briefly discuss examples of measurements on several materials of current interest: 1) amorphous Si and its alloys, 2) high precision critical temperature studies of $La_{1-x}Sr_xMnO_3$ and $La_{1-x}Ca_xMnO_3$, 3) antiferromagnetic CoO nanoparticles and thin layers, 4) Fe/Cr giant magnetoresistance multilayers.

*I would like to thank the DOE and NSF for support.

**11:51**
**P4 2 High-Resolution Microcalorimeter Detectors for X-ray Spectroscopy.**
TERRENCE JACH, *National Institute of Standards and Technology, Gaithersburg, MD*

For many decades, standard wavelength- and energy-dispersive x-ray detectors have dominated experimental physics. Recently, microcalorimeter detectors of various types that count individual photons have started to make an appearance on the experimental scene. I shall describe the development of Transition Edge Sensor (TES) detectors at NIST, with particular emphasis on their use in high-resolution x-ray spectrometry. These detectors combine the broad energy range of a SiLi or Ge detector with energy resolution approaching that of diffraction-related methods. The technologies for producing ultra-cold temperatures and for fabricating superconducting electronics have made these detectors practical to

use on a daily basis. By means of careful matching of absorber and energy, detectors can be built to cover energy ranges from 1 keV to 100 keV. By extrapolating from single-pixel detectors to arrays, the possibility of large detection areas, high count rates, and even imaging is starting to look realistic. While embodying some challenging technical constraints, microcalorimeter x-ray detectors will provide attractive advantages and opportunities for physicists in a number of fields.

**12:27**
**P4 3 Angle-Resolved High Field Low Temperature Calorimetric Measurements of Low Dimensional Materials.**
NATHANAEL FORTUNE, *Smith College*

Quasi-two-dimensional materials exhibit a rich variety of magnetic-field-induced superconducting and magnetic states. These states are highly anisotropic with respect to magnetic field orientation; in some cases, the very existence of the state is field angle dependent. To establish the phase boundaries of these high-field, low temperature, angle-dependent states, we have fabricated miniature rotatable calorimeters for measurements of specific heat and the magnetocaloric effect at temperatures ranging from 0.1K to 20K in magnetic fields up to 20, 35 or 45 tesla. The sample orientation relative to the applied field can be continuously varied at low temperature along a single axis (with a resolution of 0.02 degrees) and at room temperature along a second axis (with a resolution of 2 degrees). The sample temperature can be programatically set and regulated to better than 0.1 percent over the entire field and temperature range, allowing field sweeps at constant temperature in addition to temperature sweeps at fixed fields. In this talk, I will discuss the design, performance, and evolution of our calorimeter and recently obtained results, including the calorimetric observation of an angle-dependent magnetically enhanced FFLO superconducting state in a heavy fermion superconductor and an angle-dependent quantum fluctuation induced ''plateau state'' at 1/3 of the saturation magnetization in a quasi 2D S = 1/2 Heisenberg antiferromagnet.

**13:03**
**P4 4 Some non-traditional approaches to thermal and thermodynamic measurements.***
ALBERT MIGLIORI, *Los Alamos National Laboratory*

Three non-traditional measurement methods for measurement of thermal and thermodynamic quantities are explored. Each method is not commonly used, has some astonishing advantages, and produces outstanding accuracy with little chance for error for several reasons. One reason in common is that for each method, only one quantity is measured. The methods include noise spectroscopy for the measurement of the elastic tensor of solids (and maybe other states of matter), third-harmonic measurements of thermal conductivity and specific heat, and impulse methods for obtaining the difficult-to-acquire ''ZT'' for thermoelectrics.

*This work was supported by the National Nuclear Security Administration, The State Of Florida, and the National Science Foundation.



**SESSION P5: SHEDDING LIGHT ON THE ENIGMA OF THE TRANSITION TO TURBULENCE IN PIPES AND OTHER SHEAR FLOWS**
**Wednesday Morning, 15 March 2006; 309, Baltimore Convention Center at 11:15**
**Tom Mullin, DFD; R.R. Kerswell, Bristol University, presiding**

**11:15**
**P5 1 The Transition to and from Turbulence in a pipe.***
TOM MULLIN, *DFD*

A discussion of experimental investigations of the stability of flow along a pipe will be given. The transition to turbulence is catastrophic when a well–defined amplitude of injected perturbations is exceeded. The stability threshold scales inversely proportional to the Reynolds number, $Re$, with a sharp cut off at low $Re$ values. On the other hand, the decay from the turbulent state exhibits systematic exponential behavior with diverging timescales which are indicative of critical behavior. The long transients contain spatio-temporal coherence which suggest connections with recent theoretical developments.

*Support from EPSRC 'Senior Fellowship'. Joint work with J. Peixhino.

**11:45**
**P5 2 Transient growth and subcritical transition in shear flows.**
DAN HENNINGSON, *KTH Mechanics*

The possibility for disturbance growth in shear flows which are linearly stable is discussed, and it is shown that a necessary condition is that the underlying linear operator is non-normal, i.e. that it is associated with non-orthogonal eigenfunctions. Since the non-linear terms are conservative it is only by utilizing linear growth mechanisms associated with the non-normal linearized operator that energy growth is possible also for subcritical finite amplitude disturbances. The non-normal effects are manifested in the possibility for large transient growth of the disturbance energy, large response to forcing and large sensitivity of the eigenvalues. The optimal transient growth and response to forcing are calculated as the norm of the matrix exponential and resolvent, respectively. The optimal disturbances are streamwise vortices and the optimal responses are streaks of high and low velocity in the streamwise direction. These flow structures are prevalent in all subcritical transitional shear flows, including pipes and channels. It is shown by direct numerical simulations that transition scenarios initiated by the optimal disturbances have low transition thresholds. The dependence of the thresholds on the Reynolds number is also presented. Finally, extensions of the transient growth concept to more complex flows are discussed and examples of its use given.

**12:15**
**P5 3 Self-Sustaining Process and Exact Coherent Structures in Shear Flows.**
FABIAN WALEFFE, *Depts. of Mathematics and Engineering Physics, University of Wisconsin-Madison*

The Self-Sustaining Process (SSP) is a weakly nonlinear theory of a fundamental three-dimensional nonlinear process in shear flows. It is the basic mechanism that enables enhanced momentum transport and the redistribution of the mean shear energy into smaller scales and, ultimately, turbulent motions. I will briefly review the 40 years of observations of streaks and coherent structures in the near wall region of turbulent shear flows that led to the formulation of the SSP theory. A primary impact of the SSP, besides providing some level of mechanistic understanding, has been to provide a method to calculate unstable traveling wave solutions of the Navier-Stokes equations. This approach has now been successfully carried out in all canonical wall-bounded shear flows with stress as well as velocity boundary conditions. The traveling waves thus obtained show striking similarity with the observed near-wall coherent structures, earning them the name of 'exact coherent structures'. Furthermore, those unstable waves have been shown to capture basic statistics of turbulent flows remarkably well, thereby providing hope for a quantitative theory of turbulence over smooth walls. The traveling waves come in many kinds: small scales, large scales and multi-scales. The asymptotics of the large scale traveling waves as the Reynolds number goes to infinity is remarkably simple and confirms the asymptotic validity of the SSP. These large scale coherent states may yield a new promising target for the control of turbulence in shear flows.

**12:45**
**P5 4 Travelling waves in pipe flow and their relevance for transition to turbulence.**
RICH KERSWELL, *Bristol University*

The problem of understanding the nature of pressure-driven fluid flow through a circular straight pipe remains one of the oldest problems in fluid mechanics. The steady, unidirectional parabolic (laminar) flow solution named after Hagen (1839) and Poiseuille (1840) is linearly stable yet temporally and spatially disordered 3-dimensional (turbulent) solutions can easily be triggered at sufficiently large flow rates (Reynolds 1883). In contrast with Rayleigh-Benard convection where transition to turbulence proceeds along an orderly sequence of bifurcations at well-defined values of the thermal driving, the transition in a pipe is abrupt, dependent on the level of ambient disturbances in the system and, at least close to the threshold flow rate, transient. The recent discovery of travelling wave solutions (which represent saddle points in phase space) in this system has at last provided a theoretical stepping stone towards rationalizing the transition process. We will discuss the structure of these waves as well as evidence of their relevance during the transition process.

**13:15**
**P5 5 Two scenarios for dynamics of perturbations in pipe Poiseuille flow.**
ANATOLI TUMIN,* *The University of Arizona*

Two experiments on perturbations in circular pipe flows and their possible theoretical interpretations are discussed to illustrate complexity of the problem. The experimental data by A. Kaskel (1961) are discussed within the framework of spatial transient growth theory, and we argue that the phenomenon of transient growth was observed in the pipe-flow experiments. Another experiment (Eliahou et al, 1998) illustrates how weak streamwise vortices provide instability of the secondary disturbances which, in turn, amplify the steady vertical structures. The latter is consistent with the self-sustaining process scenario. These examples, and more recent DNS and experimental studies represent typical controversies that arise in the study of complex systems.

*In collaboration with Prof. Eli Reshotko, CWRU.

**13:45**
**P5 6 Edge of chaos in the transition to turbulence.**
BRUNO ECKHARDT, *Philipps Universität Marburg*

We study the boundary of the laminar region near the onset of turbulence. Approaching the boundary from the laminar side, the lifetime of perturbations increases, diverges when the boundary is reached, and varies chaotically for larger amplitudes. In the chaotic region, lifetimes vary sensitively with amplitude, consistent with the strange saddle picture of the turbulence proposed earlier. The trajectory on the edge between the laminar and chaotic regions is asymptotic to a single well defined state, essentially independent of the type of perturbation. The edge then becomes the stable manifold of this structure. In the case of a model shear flow, the edge states are simple or period doubled or chaotic trajectories. The case of pipe flow shows less variability and the edge state seems to remain close to a state with simple vortical structure. This is joint work with T.M. Schneider (U Marburg), J.D. Skufca (Clarkson U) and J. Yorke (U Maryland).

## SESSION P6: QUANTUM SPIN DYNAMICS IN MOLECULAR NANOMAGNETS
**Wednesday Morning, 15 March 2006; 310, Baltimore Convention Center at 11:15**
**Andrew Kent, New York University, presiding**

**11:15**
**P6 1 Quantum Dynamics of the Neel Vector of Antiferromagnetic Nanomagnets.**
OLIVER WALDMANN, *University of Bern*

This abstract was not received electronically.

**11:51**
**P6 2 Universal Mechanism of Spin Relaxation in Solids.**
EUGENE CHUDNOVSKY, *Lehman College, CUNY*

Conventional elastic theory ignores internal local twists and torques. Meantime, spin-lattice relaxation is inherently coupled with local elastic twists through conservation of the total angular momentum (spin + lattice). This coupling gives universal lower bound (free of fitting parameters) on the relaxation of the atomic or molecular spin in a solid [1] and on the relaxation of the electron spin in a quantum dot [2]. [1] E. M. Chudnovsky, D. A. Garanin, and R. Schilling, Phys. Rev. B **72**, 094426 (2005). [2] C. Calero, E. M. Chudnovsky, and D. A. Garanin, Phys. Rev. Lett. **95**, 166603 (2005).

**12:27**
**P6 3 Organization of Single Molecule Magnets on Surfaces.***
ROBERTA SESSOLI, *Department of Chemistry, University of Florence, Italy*

The field of magnetic molecular clusters showing slow relaxation of the magnetization has attracted a great interest for the spectacular quantum effects in the dynamics of the magnetization that range from resonant quantum tunneling to topological interferences. Recently these systems, known as Single Molecule Magnets (SMMs), have also been proposed as model systems for the investigation of flame propagation in flammable substances. A renewed interest in SMMs also comes from the possibility to exploit their rich and complex magnetic behavior in nano-spintronics. However, at the crystalline state these molecular materials are substantially insulating. They can however exhibit significant transport properties if the conduction occurs through one molecule connected to two metal electrodes, or through a tunneling mechanism when the SMM is grafted on a conducting surface, as occurs in scanning tunnel microscopy experiments. Molecular compounds can be organized on surfaces thanks to the self assembly technique that exploits the strong affinity of some groups for the surface, e.g. thiols for gold surfaces. However the deposition of large molecules mainly comprising relatively weak coordinative bonds is far from trivial. Several different approaches have started to be investigated. We will briefly review here the strategies developed in a collaboration between the Universities of Florence and Modena. Well isolated molecules on Au(111) surfaces have been obtained with sub-monolayer coverage and different spacers. Organization on a large scale of micrometric structures has been obtained thanks to micro-contact printing. The magnetic properties of the grafted molecules have been investigated through magneto-optical techniques and the results show a significant change in the magnetization dynamics whose origin is still object of investigations.

*Matteo Mannini of the University of Florence and Andrea Cornia of the University of Modena & Reggio Emilia (Italy) are gratefully acknowledged.

**13:03**
**P6 4 First Principles Calculations and Spin Models.***
BRUCE HARMON, *Ames Laboratory*

Single magnetic molecules are fascinating entities. The individual transition metal ions have well defined spin states associated with localized d-orbitals bonded to ligands, which mediate the effective exchange or magnetic coupling among spins. At low temperatures and magnetic fields the internal complexity of the molecule can often (but not always) be ignored, with only the total collective spin determining the ground state and first few excited states. Using $Mn_{12}$ and $V_{15}$ as prototypes, this talk will describe a more reductionist approach and describe first principles electronic structure calculations used to gain insight into the electronic and magnetic structure of the individual transition metal ions and their interactions. Various spin coupling schemes and phenomenological Hamiltonians will be presented and compared to a variety of experimental results. Many colleagues and students from a number of institutions have contributed to this work and will be acknowledged during the talk.

*Supported by DOE Office of Science/BES under Contract No. W-7405-Eng-82.

**13:39**
**P6 5 Density-Functional Theory of Molecular Magnets.***
KYUNGWHA PARK, *Virginia Tech*

Molecular magnets are large (a few nanometers in diameter), well-defined, discrete molecules consisting of several transition metal ions interacting through organic and/or inorganic ligands. Among thousands of synthesized molecular magnets, there is a class of molecular magnets known as single-molecule magnets (SMMs) which have large effective magnetic moments and behave as single-domain magnetic nanoparticles in an external magnetic field. They are particularly interesting because of observed quantum tunneling of magnetization and their possible applications in magnetic recording and molecular electronics. In this talk, I will demonstrate how quantum mechanics can be used to study the properties of SMMs from a first-principles vantage point. In particular, I will present density-functional calculations of the electronic, vibrational, and magnetic properties of selected SMMs, such as the total magnetic moment, electronic energy gaps, Raman scattering spectra, exchange constants, spin excitation energetics, and magnetic anisotropy barriers. I will also discuss what types of molecular environmental changes can significantly influence the exchange interaction, magnetic anisotropy, and observed quantum tunneling in the SMMs.

*Supported by the ONR, the DoD HPC CHSSI program, and the W.M. Keck Foundation.

## SESSION P7: FOCUS SESSION: PHYSICS OF TRANSCRIPTIONAL REGULATORY NETWORKS
**Wednesday Morning, 15 March 2006; 307, Baltimore Convention Center at 11:15**
**Joshua Socolar, Duke University, presiding**



**11:15**
**P7 1 Programming bacterial dynamics by synthetic killer circuits.**
LINCHONG YOU, *Duke University*

This abstract was not received electronically.

**11:51**
**P7 2 Molecules, nonlinearity, and function in regulatory networks.**
NICOLAS BUCHLER, *Rockefeller University*

Biological regulatory networks are capable of sophisticated functions, such as integrating chemical signals, storing memories of previous molecular events, and keeping time. These networks often contain feedback loops, which can promote bistability and oscillation. However, feedback alone is not enough. Strong nonlinearities in the network dynamic are also needed. It is known that many regulatory proteins form higher-order complexes and multimers. I will discuss two important sources of nonlinearity in multimerization. First, ample experimental evidence suggests that protein subunits itin vivo can degrade less rapidly when associated in complexes. For homodimers, this effect leads to a concentration dependence in the protein degradation rate. Theoretical analysis of two model gene circuits in bacteria, i.e. switch and oscillator, demonstrates that this effect can substantially enhance the function of these circuits. Second, active proteins can often be sequestered into inactive complexes. This molecular titration can lead to sharp nonlinearities, and suggests a scenario for the rapid evolution of bistable or oscillatory circuits in nature.

**12:27**
**P7 3 Combinatorial Regulation in Yeast Transcription Networks.**
HAO LI, *University of California, San Francisco*

Yeast has evolved a complex network to regulate its transcriptional program in response to changes in environment. It is quite common that in response to an external stimulus, several transcription factors will be activated and they work in combinations to control different subsets of genes in the genome. We are interested in how the promoters of genes are designed to integrate signals from multiple transcription factors and what are the functional and evolutionary constraints. To answer how, we have developed a number of computational algorithms to systematically map the binding sites and target genes of transcription factors using sequence and gene expression data. To analyze the functional constraints, we have employed mechanistic models to study the dynamic behavior of genes regulated by multiple factors. We have also developed methods to trace the evolution of transcriptional networks via comparative analysis of multiple species.

**13:03**
**P7 4 Gene expression dynamics during cell differentiation: Cell fates as attractors and cell fate decisions as bifurcations.***
SUI HUANG, *Harvard Medical School*

During development of multicellular organisms, multipotent stem and progenitor cells undergo a series of hierarchically organized ''somatic speciation'' processes consisting of binary branching events to achieve the diversity of discretely distinct differentiated cell types in the body. Current paradigms of genetic regulation of development do not explain this discreteness, nor the time-irreversibility of differentiation. Each cell contains the same genome with the same $N(\sim 25{,}000)$ genes and each cell type $k$ is characterized by a distinct stable gene activation pattern, expressed as the cell state vector $S_k(t) = \{x_{k1}(t),.\, x_{ki}(t),.\, x_{kN}(t)\}$, where $x_{ki}$ is the activation state of gene $i$ in cell type $k$. Because genes are engaged in a network of mutual regulatory interactions, the movement of $S_k(t)$ in the $N$-dimensional state space is highly constrained and the organism can only realize a tiny fraction of all possible configurations $S_k$. Then, the trajectories of $S_k$ reflect the diversifying developmental paths and the mature cell types are high-dimensional attractor states. Experimental results based on gene expression profile measurements during blood cell differentiation using DNA microarrays are presented that support the old idea that cell types are attractors. This basic notion is extended to treat binary fate decisions as bifurcations in the dynamics of networks circuits. Specifically, during cell fate decision, the metastable progenitor attractor is destabilized, poising the cell on a 'watershed state' so that it can stochastically or in response to deterministic perturbations enter either one of two alternative fates. Overall, the model and supporting experimental data provide an overarching conceptual framework that helps explain how the specifics of gene network architecture produces discreteness and robustness of cell types, allows for both stochastic and deterministic cell fate decision and ensures directionality of organismal development.

*This work has been supported by the USAF/AFOSR.

**13:39**
**P7 5 Network theory and prediction of regulatory switches.**
ALEXEI VAZQUEZ, *University of Notre Dame*

While the influence of the high intracellular concentration of macromolecules on cell physiology is increasingly appreciated, its impact on the function of intracellular molecular interaction networks remains poorly understood. To test the effect of molecular crowding on the function of metabolic networks, we introduce a modified form of flux balance analysis that takes into account the constraint imposed by the limit on the attainable concentration of enzymes in the crowded cytoplasm. We demonstrate and experimentally confirm that the method can successfully predict the existence of regulatory points that allow switching from high to low biomass yield pathways when changing cellular growth rate. These results demonstrate that molecular crowding represents a bound on the achievable functional states of metabolic networks, and provide a systematic approach to uncover potential regulatory points in cellular metabolism.

**SESSION P8: FOCUS SESSION: JETS, SHOCKS & SPLASHES**
**Wednesday Morning, 15 March 2006; 314, Baltimore Convention Center at 11:15**
**Wendy Zhang, University of Chicago, presiding**

*Invited Papers*

**11:15**
**P8 1 The secret of splashing: interplay of air and roughness.**
LEI XU, *University of Chicago*

We studied splashing on both smooth and rough dry surfaces using high speed photography. For smooth substrates, a striking phenomenon is observed: splashing can be completely suppressed by decreasing the pressure of the surrounding gas. The threshold pressure where a splash first occurs is measured as a function of the impact velocity and found to depend on the molecular weight of the gas and the viscosity of the liquid. Both experimental scaling relations support a model in which the compressibility of the gas is responsible for creating the splash[1]. For the case of rough substrates, we systematically varied both the surface roughness and the pressure of the surrounding gas and found two distinct contributions to a splash. One is caused by air and has the same characteristics as the ''coronal'' splash observed on smooth substrates. A second, ''prompt'' splash, contribution is caused by surface roughness. We have also measured the size distribution of the droplets emitted from a splash. For a smooth surface, a broad distribution of droplet sizes is found at high gas pressures. As the gas pressure is lowered towards the splash/no-splash transition the distribution gets more and more peaked at a characteristic size. For a rough surface, the distribution is strongly correlated with the surface roughness.
[1] L Xu, W W Zhang and S R Nagel, Phys. Rev. Lett. 94, 184505 (2005)

*Contributed Papers*

**11:51**
**P8 2 Statistical Mechanics of a Geophysical Jet*** EMILY CONOVER, J.B. MARSTON, *Brown University* We investigate the equal-time statistics of an equatorial jet in a two-dimensional quasi-geostrophic model of a planetary atmosphere on a rotating sphere[1]. Potential vorticity is advected by the barotropic flow and at the same time relaxes towards the zonal shear flow of an underlying equatorial jet. A transition to turbulence occurs at sufficiently slow relaxation rates. Statistics accumulated by direct numerical simulation[2] are compared to those obtained by a simple cumulant expansion. We study rigorous upper bounds on the instability size[3] and discuss the limitations of the cumulant expansion.

*Supported in part by NSF DMR-0213818.

[1]R. S. Lindzen, A. J. Rosenthal, and R. Farrell, J. Atmos. Sci. **40**, 1029 (1983).
[2]Akio Arakawa, J. Comp. Phys. **1**, 119 (1966).
[3]T. G. Shepherd, J. Fluid. Mech. **196**, 291 (1988).

**12:03**
**P8 3 High-Speed X-ray Investigation of Granular Jets*** JOHN ROYER, ERIC CORWIN, ANDREW FLIOR, BRYAN CONYERS, MARIA-LUISA CORDERO, MARK RIVERS, PETER ENG, HEINRICH JAEGER, *James Franck Institute, The University of Chicago* When a heavy sphere is dropped onto a bed of loose, fine sand, a large, focused jet of sand shoots upward.[12] Experiments at reduced air pressure reveal that the jet in fact consists of two components: a wispy, thin jet that varies little with pressure followed by a thick air-pressure-driven jet[3]. To observe the initial stages of jet formation inside the granular bed, we employed x-ray radiography using the high-intensity beams available at the Advanced Photon Source. This technique allowed us to image the motion of the sphere and the evolution of the void left behind it at frame rates up to 6600 frames per second. The x-ray movies reveal that gravity-driven collapse produces the initial, thin jet, while the compression of an air pocket trapped below the surface drives up the thick jet. We also find that the interstitial air alters the compressibility of the sand bed. In vacuum a visible compaction front precedes the ball, while at atmospheric pressure the sand flows out of the way of the ball, behaving more like an incompressible fluid.

*This work was supported by NSF and DOE.

[1]Thoroddsen, S. T. and Shen, A. Q. Phys. Fluids **13**, 4-6 (2001).
[2]Lohse, D. et al. Phys. Rev. Lett. **93** (2004).
[3]Royer, J. et al. Nature Physics, December 2005.

**12:15**
**P8 4 Measurement of Stopping Force in Low Velocity Impact Cratering** JOSEPH AMATO, MICHAEL NITZBERG, *Colgate University* The time dependent stopping force on a ball dropped into a granular medium has been measured using an accelerometer embedded within the ball. The velocity dependence of the force shows two distinct behaviors: (1) for impacts with large (200 $\mu$m) irregularly shaped sand particles, $F(v) \propto v^{1/2}$; for impacts with 100 $\mu$m spherical glass beads, $F(v) \propto (v - v_0)$. The accelerator apparatus yields reproducible, low noise data that reveals peculiar features such as a downward acceleration pulse just before the ball comes to rest.

*Invited Papers*

**12:27**
**P8 5 Giant bubble-pinchoff.***
DETLEF LOHSE, *University of Twente*

Self-similarity has been the paradigmatic picture for the pinch-off of a drop. Here we will show through high-speed imaging and boundary integral simulations that the inverse problem, the pinch-off of an air bubble in water, does not obey self-similarity (of the first kind): A disk is quickly pulled through a water surface, leading to a giant, cylindrical void, which at collapse creates an upward and a downward jet. The neck radius h(tau) of the void does NOT scale with the inertial power law exponent 1/2 (i.e., does not obey ''Rayleigh-scaling''). This is due to a second length-scale, the inverse curvature of the void,which follows a power-law scaling with a different exponent. Only for infinite Froude numbers the scaling exponent 1/2 is recovered. In all cases we find the void-profile to be symmetric around the minimal void radius up to the time the airflow in the neck deforms the interface.

*In collaboration with Raymond Bergmann, Devaraj van der Meer, Mark Stijnman, and Andrea Prosperetti, University of Twente.

*Contributed Papers*

**13:03**
**P8 6 Nano-liquid bridges in ambient conditions** WEI KANG, UZI LANDMAN, *School of Physics, Georgia Institute of Technology, Atlanta, GA 30332* The dynamics of nano-liquid bridges in an ambient gaseous environment is studied using molecular dynamics simulations. Under these conditions new behavior close to break-up is found, compared to the behavior in vacuum. The probability for appearance of a long-thread structure close to pinch-off, versus the appearance of a double-cone profile in vacuum, depends on the density of the ambient gas. The stochastic lubrication equation that has been introduced by Moseler and Landman [1] for the case of break-up in vacuum is modified to include an additional term representing the effect of the ambient gas. Numerical integration of the modified stochastic lubrication equation shows good agreement with the molecular dynamics simulations. [1] M. Moseler and U. Landman, Science 289, 1165(2000).

**13:15**
**P8 7 Splashing on dry, smooth inclined surfaces** JAMES BIRD, *Harvard University* DAVID WEITZ, *Harvard University* HOWARD STONE, *Harvard University* MICHAEL BRENNER, *Harvard University* We investigate splashing of drops on dry, smooth inclined surfaces. The asymmetry of the impact leads to an azimuthal variation of the ejected rim. We show that under certain conditions only part of the rim splashes. A model for the azimuthal splash threshold is compared both with the data and with existing splash criteria.

**13:27**
**P8 8 Levitation of Falling Spheres in Stratified Fluids*** RICHARD McLAUGHLIN, ROBERTO CAMASSA, BYRON HUFF, RICHARD PARKER, *University of North Carolina* UNC RTG FLUIDS GROUP COLLABORATION, The motion of sphere's falling under the influence of gravity is a classical problem dating back to Galileo and earlier. How a falling body additionally interacts with its environment is an equally challenging problem and involves strong coupling between the body and fluid via hydrodynamic drag. We present new phenomena[2] concerning the motion of a sphere falling through a sharply stratified (two layer) fluid in which the falling heavy body stops and reverses its direction (bounces) before ultimately returning to descent. Shadowgraph imaging shows the physics responsible for this surprising motion is a coupling between the body and the ambient boundary layer fluid, which is endowed with a negative potential energy as it is drawn into the lower layer, forming a rising turbulent plume. The hydrodynamic coupling between the sphere and this plume temporarily arrests the motion, even causing the bead to rise back through the transition layer. We present measurements of this trapping phenomena, and report the long residence times in which the sphere is trapped within the transition layer as a function of the bottom layer fluid density field for an array of different sized spheres. [2] N. Abaid, D. Adalsteinsson, Akua Agyapong, and R. M. McLaughlin, ''An Internal Splash: Falling Spheres in Stratified Fluids,'' Physics of Fluids, 16, no. 5, 1567-1580, 2004.

*RTG NSF DMS-0502266

**13:39**
**P8 9 Sodium luminescence from laser-induced bubbles in salt water*** SONNY VO, TIM HSIEH, HAN-CHING CHU, GARY WILLIAMS, *UCLA* Luminescence from collapsing laser-induced bubbles in salt water (up to 1M NaCl) has been studied. We find a new emission pulse from the 589 nm sodium line that arrives about 50 ns prior to the main blackbody luminescence pulse. This may be related to the dynamics of the compressional heating process in the bubble. We have also noticed in the salt water that the time duration of the blackbody pulse is reduced by up to 30% from the duration in pure water, and this has been observed in several other alkali salt solutions.

*Work supported in part by the NSF, DMR 01-31111

**13:51**
**P8 10 The dynamics of a flexible loop in a high-speed flow** SUNGHWAN JUNG, *AML, Courant Inst., New York Univ.* KATHLEEN MARECK, *AML, Courant Inst., New York Univ.* MICHAEL SHELLEY, *AML, Courant Inst., New York Univ.* JUN ZHANG, *AML, Courant Inst., New York Univ.* We study the behavior of an elastic loop in a fast-flowing soap film. The loop is wetted into the film and is held fixed at a single point against the oncoming flow. We interpret this system as a 2D closed flexible body moving in a quasi-2D flow. The loop is deformed by the flow, and this coupled fluid-structure system shows bi-stability: stationary and oscillatory. In its stationary state, the loop essentially remains motionless and its wake is a von Kármán vortex street. In its oscillatory state, the loop sheds two vortex dipoles within each oscillation period. The frequency of oscillation of the loop is linearly proportional to the flow velocity.

**14:03**
**P8 11 Superfluid-like shock waves in nonlinear optics** WENJIE WAN, JASON W. FLEISCHER, *Princeton University* It is well-known, but often underappreciated, that condensate dynamics has analogies with nonlinear light propagation in optics. In both cases, a single, macroscopic wavefunction describes the coherent wave behavior of interest. Here, we take advantage of this correspondence and examine superfluid-like spatial shock waves by propagating coherent light through a nonlinear crystal. We report the observation of both 1D and 2D shock waves, their nonlinear behavior as a function of intensity, and double-shock wave collisions. Analytical calculations and numerical simulations show excellent agreement with the experimental results. The fine structures and features observed here match similar observations in previous shock studies using superfluids and BEC, obtained in this case in a table-top apparatus, without the need for vacuum isolation, ultracold temperatures, etc. Moreover, the inherent optical advantages of easy control of the wavefunction input and direct imaging of the output make us optimistic that the nonlinear photonic systems described here will lay the foundation for a whole series of condensate-inspired experiments, many of which would be difficult (if not impossible) to perform in the corresponding condensed matter environments.

## SESSION P10: FOCUS SESSION: FRONTIERS IN COMPUTATIONAL CHEMICAL PHYSICS IV
**Wednesday Morning, 15 March 2006; 302, Baltimore Convention Center at 11:15**
**Andrew Rappe, University of Pennsylvania, presiding**

*Invited Papers*

**11:15**
**P10 1 First Principles Dynamics Beyond the Born-Oppenheimer Approximation.***
TODD MARTINEZ, *UIUC*

The dynamics of molecules in excited electronic states almost invariably involves breakdown of the Born-Oppenheimer approximation, necessitating treatment of quantum mechanical effects for both electrons and nuclei. The ab initio multiple spawning (AIMS) method has been developed in order to model molecular dynamics in excited states from first principles, solving both the electronic and nuclear Schrödinger equations ''on the fly.'' We discuss some recent developments in the AIMS methodology and applications to photodamage in DNA bases. Theoretical results are compared directly to femtosecond spectroscopy experiments. Recent attempts to couple the AIMS approach with optimization algorithms to redesign fluorescent proteins will also be discussed, if time allows.

*In collaboration with Hanneli Hudock, Benjamin G. Levine, and Kristina Lamothe.

*Contributed Papers*

**11:51**
**P10 2 First principles studies of CO adsorption and oxidation on the $Cu_2O$(100) surface*** SERGEY STOLBOV, DUY LE, TALAT S. RAHMAN, *Physics Department, Kansas State University* This work is motivated by the experimental results [1] indicating that the rate of CO oxidation on $Cu_2O$ surface is much higher than that on Cu and CuO surfaces. To gain insight into the nature of this effect we study from first principles the energetics of adsorption and oxidation of CO on $Cu_2O$(100). Applying the itab initio thermodynamics approach [2] to the surface in contact with gaseous $O_2$, we find that the O-termination of $Cu_2O$(100) is preferred for all reasonable range of temperature and the $O_2$ pressure. We find that CO adsorbed on surface O associates with it to form $CO_2$ without any activation barrier. On the other hand, CO adsorbing on a surface Cu atom, it is found to slide first towards the neighboring O atom to form $CO_2$ as in the previous case. We analyze the local densities of electronic states and valence charge densities of the systems to rationalize the obtained results.
T.-J. Huang and D.-H. Tsai, Catal. Lett. 87, 173 (2003). K. Reuter and M. Scheffler, Phys. Rev. B **65**, 035406 (2002).

*Work supported in part by DOE under grant No. DE-FGO3-03ER15445. Computational resources provided by NSF Cyberinfrastructure and TeraGrid, grant No: DMR050039N

**12:03**
**P10 3 Electronic structure and bonding properties of K and $K^+$ on graphite under external electric field*** ALEJANDRO TAPIA, ROMEO DE COSS, *Department of Applied Physics, CINVESTAV-Merida, Mexico.* GABRIEL CANTO, *CCMC-UNAM, Ensenada, Mexico.* The effect of an external electric field on the adsorption of K and $K^+$ on the graphite (0001) surface, are studied by means of first- principles total-energy calculations. The results were obtained with the pseudopotentials LCAO method (SIESTA code) and the Generalized Gradient Approximation (GGA) for the exchange-correlation potential. The structural parameters, bonding properties, and electronic structure of the K and $K^+$-graphite system are studied in the triangular (2x2) overlayer phase as a function of the external electric field magnitude. We find an important change in the K and $K^+$-graphite bonding as a consequence of the charge transfer from the adatom towards the substrate induced by the electric field. However, we find that none of the investigated systems show diffusion of K or $K^+$ into graphite even with a strong electric field. The results are discussed in the light of the experimental observed diffusion of K into graphite, presumably induced by external electric fields.

*This work was supported by Consejo Nacional de Ciencia y Tecnologia (CONACYT, Mexico) under Grants No. 43830-F and No. 44831-F.

**12:15**

**P10 4 Carbon-based nanostructured materials for enhanced $H_2$ production** M.K. KOSTOV, E.E. SANTISO, A.M. GEORGE, K.E. GUBBINS, M.B. NARDELLI, *North Carolina State University* A key fundamental limit of the thermal splitting of bulk water is the fact that the ground state of oxygen is paramagnetic, whereas the ground state of water is diamagnetic. Here, we propose to explore a new paradigm in $H_2$ production: a process in which the system remains on the spin singlet potential surface throughout the reaction, by exploiting the catalytic role of defective carbon substrates. Using first principles modeling techniques, we found evidence that mono-vacancy defects in graphite and carbon nanotubes give rise to a rich chemistry, yielding many possible water dissociation pathways, some of which have activation barriers lower than half the value for the dissociation of bulk water. This reduction is caused by spin selection rules that allow the system to remain on the same spin surface throughout the reaction. These novel reactions enhance the hydrogen yield and the reaction rate. In the presence of water only, this reaction is self-limiting: when all of the defects are oxidized, the reaction is complete, and no further $H_2$ is produced. There are several possibilities to achieve regeneration of the active surface sites, such as photo-excitation, vibrational excitations or further reaction with other molecules. We will discuss this exploration in the context of a complete cycle of energy storage and release through the production of $H_2$.

**12:27**

**P10 5 Quantum dynamics with wavepackets and density matrices: A novel computational tool with applications to biological enzymes.*** SRINIVASAN IYENGAR, *Indiana University* A recently developed computational approach for simultaneous dynamics of electrons and nuclei is discussed. The approach is based on a synergy between quantum wavepacket dynamics and ab initio molecular dynamics. The quantum dynamics is performed using an efficient banded, sparse and Toeplitz representation for the discretized free propagator that is formally exact. Ab initio molecular dynamics is achieved by using (a) an extended Lagrangian formalism, known as atom-centered density matrix propagation, that effects an adjustment of time-scales of the electronic motion, (b) Born-Oppenheimer dynamics. The quantum dynamics and ab initio dynamics schemes are coupled through a time-dependent self consistent field-like procedure. Higher order coupling between the subsystems is inherent when the Born-Oppenheimer procedure is used as opposed to atom-centered density-matrix propagation. A fundamental computational bottleneck associated with the computation of the interaction potential between the ab initio and quantum dynamical subsystem are overcome through a novel importance sampling approach and this aspect is also discussed. Further generalization for periodic quantum dynamical treatment in extended systems is outlined.

*This work is supported by the Camille and Henry Dreyfus Foundation.

**12:39**

**P10 6 First-Principles pH Theory*** YONG-HYUN KIM, S. B. ZHANG, *National Renewable Energy Laboratory* Despite being one of the most important macroscopic measures and a long history even before the quantum mechanics, the concept of pH has rarely been mentioned in microscopic theories, nor being incorporated computationally into first-principles theory of aqueous solutions. Here, we formulate a theory for the pH dependence of solution formation energy by introducing the proton chemical potential as the microscopic counterpart of pH in atomistic solution models. Within the theory, the general acid-base chemistry can be cast in a simple pictorial representation. We adopt density-functional molecular dynamics to demonstrate the usefulness of the method by studying a number of solution systems including water, small solute molecules such as $NH_3$ and HCOOH, and more complex amino acids with several functional groups. For pure water, we calculated the auto- ionization constant to be 13.2 with a 95 % accuracy. For other solutes, the calculated dissociation constants, i.e., the so- called $pK_a$, are also in reasonable agreement with experiments. Our first-principles pH theory can be readily applied to broad solution chemistry problems such as redox reactions.

*Work supported by the U. S. DOE/BES and EERE under contract No. DE-AC36-99GO10337.

**12:51**

**P10 7 Efficiency and accuracy in transition-metal chemistry: a self-consistent GGA+U approach** HEATHER KULIK, MATTEO COCOCCIONI, NICOLA MARZARI, *DMSE, Massachusetts Institute of Technology* Transition-metal centers are the active sites for a broad variety of biological and inorganic chemical reactions. Notwithstanding this central importance, density-functional theory calculations based on local-density or generalized gradient approximations often fail qualitatively and quantitatively in describing energetics, multiplet structures, reaction barriers, and geometries around the active sites. We suggest here an alternative approach, mutuated from the Hubbard U correction to solid-state problems, that provides an excellent agreement with accurate, correlated-electron quantum chemistry calculations in paradigmatic test cases that range from the ground state of the $Fe_2$ dimer to the potential energy surfaces for the addition-elimination of molecular hydrogen on $FeO^+$. The Hubbard U is determined with a novel self-consistent procedure based on a linear-response approach.

**13:03**

**P10 8 First principles calculation of the x-ray absorption spectra of ice and liquid water*** DAVID PRENDERGAST,[†] GIULIA GALLI,[‡] *Lawrence Livermore National Laboratory* Recent interpretations of x-ray absorption spectra (XAS) of ice and liquid water propose that the standard, tetrahedral model of the liquid should be replaced with a model where each water molecule possesses two stronger and two weaker hydrogen bonds to nearest neighbor molecules. We have investigated this issue and find no conclusive evidence to discount the standard model. Using density functional theory (DFT) calculations we find an excellent agreement with experiment for the XAS of ice I. We perform TIP4P classical molecular dynamics simulations of the liquid at 300K. Using 10 statistically uncorrelated snapshots of 32 molecules in our DFT calculations, we compute the XAS of this standard liquid model and also find a reasonable agreement with experiment. The

spectral differences between liquid and solid arise from both structural disorder and the presence of dangling hydrogen bonds.

*This work was performed under the auspices of the U.S. Department of Energy at the University of California/Lawrence Livermore National Laboratory under Contract No. W-7405-Eng-48
†Present address: University of California, Berkeley
‡Present address: University of California, Davis

**13:15**

**P10 9 Exploiting unitary invariance in ab initio molecular dynamics: Applications to spectral decomposition and surface reactions*** MARK TUCKERMAN, *New York University* The methodology of ab initio molecular dynamics, wherein finite-temperature dynamical trajectories are generated using forces computed ''on the fly'' from electronic structure calculations, has benefited significantly from its combination with maximally localized electronic orbitals. The latter exploit the unitary invariance of the total energy to generate orbitals with maximum spatial locality. These orbitals resemble the classic textbook picture of molecular orbitals and, hence, are useful tools for analyzing electronic structure. In addition, maximally localized orbitals, expanded in localized basis sets, are a key component in linear scaling methods. In this talk, it will be shown how techniques from quantum field theory can be used to reformulate ab initio molecular dynamics in such a way that maximally localized orbitals are generated automatically and dynamically as the calculation proceeds. As an application of the technique, it will be shown how IR spectra can be decomposed to reveal particular structures in aqueous solutions. A second application will focus on the addition of organic molecules to the Si(100)-2x1 surface.

*This work was supported by NSF CHE-0121375 and NSF CHE-0310107

**13:27**

**P10 10 Engineering protein structure and function with computational protein design** JEFFERY SAVEN, *University of Pennsylvania* Understanding molecular folding has important applications to understanding biology and to developing new therapeutics and new materials. Protein design also opens new ways to probe the determinants of folding and to facilitate the study of proteins. Such design is complicated, however, by the conformational complexity of proteins and by the large numbers of possible sequences. Recent computational methods for identifying the properties of amino acid sequences likely to fold to a given three-dimensional structure will be presented. Several examples of structures so designed, which have been experimentally synthesized and characterized, will be presented.

**13:39**

**P10 11 First-Principles Calculations of van't Hoff Plots for Novel Hydrogen-Storage Materials*** NIKOLAI ZARKEVICH, D.D. JOHNSON, *Department of Materials Science and Engineering, and Materials Computation Center, University of Illinois at Urbana-Champaign* A van't Hoff plot, log(P) vs. 1/T, provides information on the free-energy change in a reaction and is widely used to characterize hydrogen-storage materials. Recently, a new reaction of $LiBH_4$ destabilized by $MgH_2$ (yielding over 11 wt.% of $H_2$) was proposed.[1] Here we investigate this reaction and its products by first-principles calculations and construct the van't Hoff plot for a direct comparison to experiment. Although it is often assumed that there is a constant slope in the van't Hoff plot for ease of interpretation, we find an important non-linearity arising from temperature-dependent vibrational entropy difference, etc. This non-linearity can be critical for an accurate comparison to experimental data, and between various reactions to determine optimal hydrogen-storage systems. Including these effects, we find agreement with recent measurements.

*This work was supported by the U.S. Department of Energy though grant DE-FC36-05GO15064, as part of the Metal-Hydride Center of Excellence.

[1]J.J. Vajo et al., J. of Phys. Chem. B 109, p.3719 (2005)

**13:51**

**P10 12 Application of Generalized Sturmians to the Bound States of Two-Electron Atoms and Molecules** EDDIE RED, ALBERT WYNN III, CHARLES WEATHERFORD, *Florida A&M University* A variation on the method of Generalized Sturmians [J. Avery, Hyperspherical Harmonics and Generalized Sturmians, Kluwer, 2000], is applied to the calculation of the ground and excited states of two-electron atoms and molecules (etc. He, $H_2$). In the present implementation of this method, each determinant formed from a set of primitive one-electron Sturmians, is required to separately solve the Schödinger equation. In the process, the screening constant of each one- electron Sturmian orbital is non-iteratively uniquely determined. The resultant generalized eigenvalue problem however has a non-positive- definite overlap matrix. The method of ''corresponding orbitals'' [H.F. King et. al. J. Chem. Phys. 47, 1936 (1967)] is used to produce a positive-definite overlap matrix. A CI calculation is then performed whereby the Hartree-Fock calculation is avoided. Results will be presented and compared with Hartree-Fock based CI calculations.

**14:03**

**P10 13 Characterizing the potential energy landscape by its geodesic paths** CHENGJU WANG, RICHARD M. STRATT, *Department of Chemistry, Brown University, Providence, RI 02912* We suggest that the time evolution of a condensed-matter system is related to a unique exploration path in its multidimensional potential energy surface. We show that sampling from what we call the potential energy landscape filling ensemble, we can study the potential energy landscape of a monatomic Lennard-Jones system without the complications of barrier hopping processes. The ensemble defined to include all the configurations with potential energy less than a specified value, allows us to sample the geodesic path between two randomly selected configurations. The geodesics were tentatively related to the dynamics of the system under the assumption that the geodesic path corresponds to the most efficient exploration route on its potential energy surface. The derived dynamic parameters were compared with those obtained from a molecular dynamics simulation. The agreement we found offers us a new method for relating the dynamics of a system to the topology of its static potential energy surface.

**SESSION P11: FOCUS SESSION: AEROSOLS, CLUSTERS, DROPLETS: PHYSICS AND CHEMISTRY OF NANOOBJECTS II: HELIUM NANODROPLETS II, AEROSOLS, AND MISCELLANEOUS**
**Wednesday Morning, 15 March 2006**
**303, Baltimore Convention Center at 11:15**
**Geoffrey Smith, University of Georgia, presiding**

***Contributed Papers***

**11:15**
**P11 1 High resolution infrared and microwave spectra of OCS solvated in helium clusters.** WOLFGANG JAEGER, *University of Alberta* ROBERT MCKELLAR, *National Research Council of Canada* YUNJIE XU, *University of Alberta* In recent years, exciting progress has been made in determining the onset and following the evolution of a bulk phase property, namely superfluidity, in the microscopic size regime. Our previous microwave and infrared studies of small $He_N$-OCS and $He_N$-$N_2O$ clusters extended up to N=8 and N=19, respectively, and the infrared spectra with CO or $CO_2$ as probe reached almost up to N=20. We have now been able to extend the studies on $He_N$-OCS to much larger N-values in both the infrared and microwave regions. The B rotational constants that were extracted from the spectra show unexpected, non-classical behavior as a function of N, the number of helium atoms. We will present the experimental techniques used and an interpretation of the observed trends in spectroscopic observables.

**11:27**
**P11 2 Recurrences in rotational dynamics and superfluid response in doped He-HCCCN and He-$N_2O$ clusters** NIKOLAY BLINOV, *Department of Chemistry, University of Alberta* PIERRE-NICHOLAS ROY, *Department of Chemistry, University of Alberta* WOLFGANG JÄGER, *Department of Chemistry, University of Alberta* Recent experiments on He-$N_2O$ complexes revealed the oscillatory behavior of the rotational constant in the range of cluster sizes corresponding to the completion of the first solvation shell. We use the path-integral Monte Carlo approach to show that this phenomenon can be associated with a non-monotonic size evolution of the non-classical rotational inertia and superfluidity, the origin of which can be traced back to combined solvent layering and bosonic exchange effects. Using the dopant molecule as an experimental microscopic probe of superfluidity, we show that in small doped helium clusters superfluidity builds up in stages correlated with the filling and completion of solvation shells.

**11:39**
**P11 3 Infrared spectra and intensities of $H_2O$-$N_2$, $H_2O$-$O_2$ and $H_2O$-Ar complexes in superfluid He droplets.** SUSUMU KUMA, *Kyoto University* MIKHAIL N. SLIPCHENKO, *University of Southern California* KIRILL KUYANOV, *University of Southern California* TAKAMASA MOMOSE, *University of British Columbia* ANDREY F. VILESOV, *University of Southern California* The infrared spectra of $H_2O$-$N_2$, $H_2O$-$O_2$ and $H_2O$-Ar complexes in superfluid He droplets were measured in the range of the stretching vibrational bands of water molecules. The infrared intensities of anti-symmetric stretching band of these complexes showed no significant increase with respect to that of a single $H_2O$ molecule as opposed to the predicted intensities in previous theoretical calculations. From the analysis of the observed spectra, it was found that $H_2O$ in $H_2O$-$O_2$ and $H_2O$-Ar rotates nearly freely inside the complexes, while that in $H_2O$-$N_2$ does not. The conformation of these complexes were estimated from the rotational constants obtained from the analysis.

***Invited Papers***

**11:51**
**P11 4 Spectroscopic Properties of Aerosols and their Microscopic Origin.**
RUTH SIGNORELL, *University of British Columbia*

Large molecular aggregates with sizes ranging from less than nanometers up to microns play an important role in atmospheric processes, as components of the interstellar medium, and as drug delivery systems in medicine. The vibrational dynamics of these particles can be strongly influenced by intrinsic particle properties such as size, shape, or surface area. These phenomena are discussed here for several pure and composite ice particles which consist of $CO_2$, $N_2O$, $NH_3$, $SO_2$, their isotopomers, and different carbohydrates. The aerosol are generated in collisional cooling cells, by supersonic expansions, and by rapid expansion of supercritical solutions [1]. The vibrational dynamics is studied in situ with a rapid scan Fourier transform infrared spectrometer. We demonstrate that only the combination of experiments with microscopic models leads to a comprehensive understanding of the various features observed in the infrared spectra. The corresponding molecular model (exciton model [1,2]) allows us not only to calculate spectra for large molecular aggregates, but also to derive propensity rules for the occurrence of characteristic effects in infrared spectra of particles. [1] R. Signorell, Mol. Phys. **101**, 3385, (2003). [2] R. Disselkamp and G. E. Ewing, J. Chem. Soc. Faraday Trans. **86**, 2369, (1990).

*Contributed Papers*

**12:27**

**P11 5 Kinetics and Products of Radical-Initiated Oxidation of Organic Particles Using Aerosol CIMS** GEOFFREY SMITH, JOHN HEARN, *University of Georgia* Ambient aerosol can contain a significant fraction of organic material which may react with trace gases in the atmosphere. Recently, it has been proposed that reactions with radical species, such as OH and Cl, may constitute a substantial loss mechanism for organic particles. In particular, the radical-initiated oxidation could lead to the creation of smaller, more volatile species which remove mass from the particles. An accurate assessment of the importance of these radical reactions requires measurements of their rates of reaction as well as identification of the subsequent products. We are exploring OH- and Cl-initiated reactions using Aerosol CIMS (chemical ionization mass spectrometry) to monitor changes in the compositions of the aerosol as well as the gas phase. This technique is well-suited to the study of organic species since the mass spectra contain very little fragmentation. These experiments provide insight into the oxidative processing which may potentially alter many critical properties of organic aerosol, including hygroscopicity and their ability to act as cloud condensation nuclei.

**12:39**

**P11 6 Gas-phase infrared spectroscopy of ionic uranyl coordination complexes*** DAVID MOORE, *UC Berkeley* ANITA GIANOTTO, *Idaho National Lab* NICK POLFER, *FOM Institute for Plasma Physics* JOS OOMENS, *FOM Institute for Plasma Physics* MIKE VAN STIPDONK, *Wichita State University* GARY GROENEWOLD, *Idaho National Lab* The uranyl dication ($UO_2^{2+}$) is the primary carrier of uranium in environmental and biological systems, yet relatively little is known about its chemical properties. Mass spectrometric studies have confirmed that the properties, and in particular the reactivity of the uranyl center is rather dependent on its coordination environment. The current study uses IRMPD spectroscopy of ionic uranyl complexes, recorded using a free-electron laser coupled to an FTICR mass spectrometer, to investigate the effects of cluster size and composition on the infrared spectra. The central observation from the current study is that the asymmetric uranyl stretch is quite sensitive to the coordination environment, showing clear, reproducible, incremental redshifts as the number and electron donating ability of the ligands is increased. These spectral trends are accurately reproduced by computed frequencies from DFT calculations. Results from complexes containing anionic ligands are also presented, and are consistent with the presence of a significant barrier to electron transfer within the complexes.

*Financial support was received from the NWO (DTM, JO, NP), the INL (GSG, AKG) and the NSF (MvS).

**12:51**

**P11 7 Stable highly symmetric dopant encapsulated binary clusters*** PETER LIEVENS, SVEN NEUKERMANS, EWALD JANSSENS, *Laboratory of Solid State Physics and Magnetism, K.U.Leuven, Celestijnenlaan 200D, B-3001 Leuven, Belgium* While clusters composed of rare gas atoms exhibit enhanced stabilities for high symmetry geometries, magic numbers in simple metal clusters are determined by the number of delocalized valence electrons. Altering the composition of binary clusters allows to tailor independently the cluster geometry (number of atoms) and electronic properties (number of delocalized electrons). We produce beams of binary clusters with a dual-target dual-laser vaporization source. Size and composition dependent stability fluctuations are investigated with photofragmentation and mass spectrometry, and ionization energies with threshold laser ionization spectroscopy. We recently studied clusters of noble metals doped with transition metal atoms, and of group IVa elements doped with di- and trivalent metal atoms. Evidence is presented for the existence of combined closures of shells of atoms and shells of electrons for specific binary species. Phenomenological interpretations of new electronic shell closures are compared with DFT calculations of their geometry and electronic structure.

*This work was supported by the Fund for Scientific Research Flanders (FWO), the Flemish Concerted Action (GOA) program, and the Belgian Interuniversity Poles of Attraction (IAP) program.

**13:03**

**P11 8 Factors Controlling Polymorph Formation in Nonphotochemical Laser-Induced Nucleation (NPLIN) of Aqueous Glycine Solutions** XIAOYING SUN, BRUCE A. GARETZ, *Polytechnic University, Brooklyn, NY 11201* The supersaturation and polarization dependence of nonphotochemical laser-induced nucleation (NPLIN) was studied in aqueous glycine solutions at wavelengths of 532 and 1064 nm, using linearly, circularly and elliptically polarized light. We observed a narrow supersaturation window (SS=1.45-1.54) for ''polarization switching,'' i.e. different polarizations producing different polymorphs. We also observed that, within this window, a small range of ellipticities near unity could induce the nucleation of the alpha polymorph, and that this range depended on supersaturation. Similar ''polarization switching'' behavior was observed at wavelengths of 1064 and 532 nm, although the supersaturation window became narrower at lower laser intensities at both wavelengths. Order-parameter ellipsoids and triangles based on optical Kerr alignment are presented to aid the interpretation of the experimental results.

**13:15**

**P11 9 Density Functional Studies of Magic Metal-$(C_{60})_2$ Clusters** EVA ZUREK, *Max Planck Institute for Solid State Research* JOCHEN AUTSCHBACH, *Department of Chemistry, University at Buffalo* Previous experimental studies of $C_{60}$-metal clusters revealed that clusters with composition $C_{60}Ba_{32}$ and $(C_{60}K_6)_nK^+$ appeared as magic peaks in the Time-of-Flight mass spectra due to geometric and electronic stability, respectively. Recent experiments using a new heating technique have revealed a different set of magic peaks, which cannot be explained by either one of the aforementioned mechanisms. We present theoretical studies addressing the stability and bonding of these newly observed magic clusters. Molecular density functional calculations have been performed to determine the most energetically stable geometrical configurations for $M_n(C_{60})_2$ clusters, with $M$ = K, Ba and $1 \leq n \leq 6$. The bonding mechanisms have been analyzed in some detail. The results indicate that for barium containing clusters, ionic bonding (transfer of the valence $6s$ electrons to the $C_{60} - \pi^*$ orbitals) and covalent bonding (between the barium $5d$ and $C_{60} - \pi^*$ orbitals) are the dominant mechanisms. Moreover, a metal cluster is formed between the two fullerenes (Ba-Ba bonding). For the potassium containing clusters, only ionic bonding was found. Calculations of the Gibbs free energies indicate that $Ba_3(C_{60})_2$ and $K_4(C_{60})_2$ are the most stable structures, in agreement with experimental results. The role of the entropy is found to be very important in determining which clusters are magic.

**13:27**
**P11 10 Photoelectron spectroscopy as a structural probe of intermediate size clusters** LEEOR KRONIK, OLGA GULIAMOV, *Weizmann Institute of Science* KOBLAR A. JACKSON, *Central Michigan University* We examine the utility of photoelectron spectroscopy (PES) as a structural probe of $Si_n^-$ in the n = 20 – 26 size range by determining isomers and associated photoelectron spectra from first principles calculations. Across the entire size range, we consistently obtain good agreement between theory and experiment [Hoffmann et al., itEur. Phys. J. D **16**, 9 (2001)]. We find that PES can almost invariably distinguish between structurally distinct isomers at a given cluster size, but that structurally similar isomers usually cannot be reliably distinguished by PES. For many, but not all, sizes the isomer giving the best match to experiment is the lowest-energy one found theoretically. Thus, combining theory with PES experiments emerges as a useful source of structural information even for intermediate size clusters.

**13:39**
**P11 11 Nearly Free Electron Gas in a Silicon Cage** J. ULISES REVELES, SHIV KHANNA, *Department of Physics, Virginia Commonwealth University, Richmond Va. 23284* Theoretical investigations of the ground state geometries, electronic structure, spin magnetic moment and the stability of the metal encapsulated $MSi_{12}$ ( M= Sc, Ti, V, Cr, Mn, Fe, Co, Ni) clusters have been carried out within a gradient corrected density functional formalism. The ground state of most $MSi_{12}$ clusters are shown to have the lowest spin multiplicity as opposed to the high spin multiplicity of free transition metal atoms. Consequently, a proper inclusion of the spin conservation rules is needed to understand the variation of the binding energy of M to $Si_{12}$ clusters. Using such rules, $CrSi_{12}$ and $FeSi_{12}$ are found to exhibit the highest binding energy across the neutral while $VSi_{12}^-$ has the highest binding energy across the anionic $MSi_{12}^-$series. It is shown that the variations in binding energy, electron affinity and ionization potential can be rationalized within an 18-electron sum rule commonly used to understand the stability of chemical complexes and shell filling in a confined free electron gas.

**13:51**
**P11 12 Single and Multiple Rings, and Cages in $SiO_x$ Clusters** PENEE CLAYBORNE, ARTHUR REBER, J. ULISES REVELES, SHIV KHANNA, *Department of Physics, Virginia Commonwealth University, Richmond Va, 23284* A. WELFORD CASTLEMAN, *Department of Chemistry and Physics, The Penn State University, University Park, Pa 16802* ASHRAF ALI, *Laboratory for Extraterrestrial Physics, Code 691 NASA Goddard Space Flight Center, Greenbelt Md, 20771* Theoretical studies on the geometry, electronic structure and stability of $Si_nO_m$ clusters have been carried out within a gradient corrected density functional formalism. It is shown that the ground states of small $Si_nO_n$ clusters containing upto 4 units are single rings. The first Si-Si bond appears at $Si_5O_5$, and starting at this size, the elementary rings begin to assemble into multiple rings that eventually lead to cages. The ground state structures at larger sizes have a central core of pure Si atoms decorated by outer shell of SiO units. An analysis of the fragmentation patterns shows that $Si_7O_7$ and $Si_{10}O_{10}$ are particularly stable species. The results of our investigations on the $Si_nO_{n-1}$ and $Si_nO_{n+1}$ species will also be presented. In particular, we will examine possible reaction mechanisms that could lead to the formation of $SiO_2$ from SiO molecules in interstellar space.



**SESSION P12: METAL ISLANDS AND CLUSTERS**
**Wednesday Morning, 15 March 2006**
**304, Baltimore Convention Center at 11:15**
**Jim Hannon, IBM T.J. Watson Research Center, presiding**

**11:15**
**P12 1 The crossover from collective motion to periphery diffusion for small adatom-islands on Cu(111) and Ag(111)*** ALTAF KARIM, *Kansas State University* ABDELKADER KARA, *Kansas State University* AHLAM AL-RAWI, *Kansas State University* OLEG TRUSHIN, *Academy of Science, Russia* TALAT RAHMAN, *Kansas State University* The diffusion of two dimensional adatom islands (containing 2-100 atoms) on Cu(111) and Ag(111) has been studied, using the newly developed self-learning Kinetic Monte Carlo (SLKMC) method [Phys. Rev. B 72, 115401, 2005]. A variety of multiple and single atom processes are revealed in the simulations and the size dependence of the diffusion coefficients and effective diffusion barriers are calculated. From the tabulated frequencies of events found in the simulation, we show a crossover from diffusion due to the collective motion of the island to a regime in which the island diffuses through the periphery dominated mass transport. This crossover occurs for island sizes of 8 to 11 atoms. For islands containing 19 to 100 atoms the scaling exponent is 1.5, which is in good agreement with previous work. The diffusion of islands containing 2 to 10 atoms can be explained primarily on the basis of a linear increase of the barrier for the collective motion with the size of the island.

*This work was supported by NSF-CRDF RU-P1-2600-YA-04, and NSF-ITR 0428826. T.A-N.

**11:27**
**P12 2 Excitation of frustrated translation and nonadiabatic adatom hopping induced by inelastic tunneling*** KAI LIU, *Institute of Physics, Chinese Academy of Science* SHIWU GAO, *Institute of Physics, Chinese Academy of Sciences, and Department of Physics, Goteborg University* The dynamics of lateral manipulation for cobalt/Cu(111) has been investigated combining the model of vibrational heating and first-principles density functional calculations [1]. The frustrated translational mode responsible for lateral excitation is identified as a vibrational resonance involving a concerted motion between the adatom and surface phonons. The calculated frequency shows good agreement with the onset energy for adatom hopping induced by inelastic tunneling. Simulation of the power law, compared with experiment, suggests that the atom hopping overcomes a nonadiabatic barrier due to the nonequilibrium local heating of the translational mode. [1] Kai Liu and Shiwu Gao, Phys. Rev. Lett. 95, 226102 (2005)

*Work supported by the 100-Talent Program, Chinese Academy of Sciences and Materials Consortium ATOMICS, SSF, Swden

**11:39**
**P12 3 Metal Island Coalescence Stress for Varying Surface Traction** STEVEN SEEL, EDMUND WEBB III, JONATHAN ZIMMERMAN, *Sandia National Laboratories* During Volmer-Weber thin film growth, discrete metal islands grow on a substrate. When the separation between their adjacent free surfaces becomes small enough, islands coalesce and trade surface energy for elastic strain energy. While it is understood that traction between island and substrate directly influences coalescence stress, questions re-

main. For instance, wafer curvature measurements during growth of low traction systems indicate zero stress in the growing film. This results from a lack of mechanical coupling between film and substrate so island stress cannot be accurately determined from experimental data. We examine, via atomistic simulations, coalescence between two metal islands as a function of island size and island-substrate traction. We reveal the stress state in the coalesced structure for low traction where entire islands are able to slide along the substrate. This is compared to higher traction where islands can only slide near the point of coalescence resulting in local tensile strain. We conclude by examining the dependence upon island size of the traction above which only local sliding is observed. Sandia is a multiprogram laboratory operated by Sandia Corporation, a Lockheed Martin Company, for the United States Department of Energy's National Nuclear Security Administration under Contract DE-AC04-94AL85000.

**11:51**

**P12 4 Effects of Strain on Island Morphology and Size Distribution in Submonolayer Island Growth*** G. NANDIPATI, J.G. AMAR, *University of Toledo* We have carried out kinetic Monte Carlo simulations of submonolayer heteroepitaxial growth using a model in which the strain energy is approximated by a long-range $1/r^3$ interaction. For the case of irreversible growth with rapid island relaxation due to edge-diffusion we find that the island-shape changes from square to rectangular in the presence of sufficient strain. However, in this case fluctuations play an important role and the scaled island-size distribution is only weakly affected by strain. General scaling forms for the island-width and island-length distributions are also derived. Simulation results for a reversible model of Cu/Ni(001) growth, for which an interesting shape transition has been experimentally observed, are also presented and compared with experiments.

*Supported by NSF DMR-0219328 and CCF-0428826

**12:03**

**P12 5 Incidence-angle dependence of optical reflectivity difference from an ultrathin film on a solid surface*** J. P. LANDRY, J. GRAY, M. K. O'TOOLE, X. D. ZHU, *Dept. of Physics, Univ. of California at Davis* The oblique-incidence reflectivity difference (OI-RD) technique is a special form of polarization-modulated nulling ellipsometry that has been judiciously used in studies of ultrathin films and other surface-bound changes on a solid or even liquid substrate. We have recently studied the incidence angle dependence of the optical reflectivity difference signals in response to ultrathin films on transparent and opaque substrates. We find that the classical three-layer model reproduces the experimentally obtained angular dependence for a monolayer of xenon on Nb(110) and for a monolayer of protein molecules on functionalized glass. We report the findings of this recent experimental investigation and explore the enhancement of the optical response near the Brewster angle (or its equivalent for opaque substrates) in thin film detection.

*This work was supported by a UC Biotechnology Research and Education Program GREAT Fellowship and the NSF Center for Biophotonics Science and Technology.

**12:15**

**P12 6 Time Resolved Study of Ordering Between Quantum Well Islands by Wide-Area k-Space Mapping** HAWOONG HONG, L. BASILE, P. CZOSCHKE, A. GRAY, T.-C. CHIANG, *Fredrick Seitz Materials Research Laboratory, University of Illinois at Urbana-Champaign* The growth of Pb quantum well islands on Si(111) was investigated in time resolved manners. The wide-area momentum space mapped in our x-ray diffraction techniques allows simultaneous observation of the lateral ordering and height distributions of Stranski-Krastanov (S-K) islands during deposition, annealing, and cycling between deposition and annealing. These islands are formed not by strain relaxation but through quantum phase separation. The ordering of these islands exhibits unusual behaviors not well described by existing strained island theories. The population of islands always decreases monotonically during all three processes. However, the island ordering was stable without coarsening with time, at least within the experimental condition. This study suggests that quantum well effect may provide a new mechanism for uniform self-assembled nanostructures.

**12:27**

**P12 7 Sublimation of Atomic Layers from a Chromium Surface** WACEK SWIECH, SHU-JUNG TANG, SUNEEL KODAMBAKA, IVAN PETROV, PETER FLYNN, TAI-CHANG CHIANG, *University of Illinois at Urbana-Champaign* We employ low-energy electron microscopy to study the kinetics of thermal etching, or sublimation, of Cr(001) at $\sim$ 1100 K. Atomic layers are removed from the surface by spontaneous nucleation and growth of two-dimensional vacancy islands, by rotation of spiral steps, and by island decay. The growth rates of vacancy islands and the rotation frequencies of double spirals are measured as a function of temperature, and the results are correlated with activation barriers of surface processes. Mass transport between the surface and bulk is shown to be unimportant.

**12:39**

**P12 8 Iso-coverage diffusion zones observed with LEEM during annealing of Ag on Si(001)*** KELLY ROOS, *Department of Physics, Bradley University* KIMBERLY ROOS, *Department of Materials Science and Engineering, University of Illinois at Urbana-Champaign* FRANK MEYER ZU HERINGDORF, MICHAEL HORN-VON HOEGEN, *Institute for Experimetnal Physics, University of Duisburg-Essen* JOACHIM KRUG, *Institute for Theoretical Physics, University of Cologne* During high temperature annealing of 3D Ag islands grown on Si(001) PEEM images reveal the emergence of a bright zone surrounding the decaying islands. Microdiffraction patterns from these bright areas display a (2x3) Ag reconstruction. The decaying Ag islands act as sources of Ag adatoms which then diffuse on the surface. The (2x3) reconstruction spreads away from the island to a distance determined by the interplay of diffusion and desorption, and by the local coverage of Ag: the outer boundary of the imaged diffusion zones constitutes an ''iso-coverage boundary.'' We describe the time and temperature behavior of these iso-coverage zones, and present a simple continuum model that describes the iso-zone size as a function of the diffusion and desorption rates.

*Financial support from the National Science Foundation through grants DMR-0203097 and DMR-0320908, and from Deutsche Forschungsgemeinschaft through SFB616 ''Energy Dissipation at Surfaces'' is gratefully acknowledged.

**12:51**

**P12 9 Imprinting Chirality into inorganic CuO Thin Films** ROLAND WIDMER, ROMAN FASEL, OLIVER GROENING, FRANZ-JOSEF HAUG, PIERANGELO GROENING, EMPA MATERIALS SCIENCE AND TECHNOLOGY, FEUERWERKERSTRASSE 39, CH-3602 THUN TEAM, Switzer et al. [1] have shown, that thick ( $>$ 300nm) films of CuO grown electrochemically in the presence of chiral tartaric acid (TA) acquires a chiral orientation with respect to the growth surface. We have investigated this growth on Au(100) in the presence of chiral TA for low film thicknesses by X-ray Photoelectrons Spectroscopy and X-ray Photoelectron Diffraction (XPD). The resulting XPD patterns were analyzed by single scattering cluster calculations. XPD revealed that using chiral L(+)- or D(-)-TA in the deposition process results in a chiral CuO surface which exhibits mirror-symmetric, non-superimposable patterns with the corresponding chirality imprinted already for film thicknesses below 3nm. Whereas the XPD patterns of the CuO films deposited with the racemic DL-TA and the ''achiral'' meso-TA are completely symmetric. The selectivity of enantiomeric CuO films was demonstrated by subsequent deposition of CuO from a solution containing DL-TA onto a CuO film grown with only one of the enantiomeric forms. Additionally, films with alternating chirality were produced. [1] J. A. Switzer, H. M. Kothari, P. Poizot, S. Nakanishi, E. W. Bohannan, Nature, 2003, 425, 490

**13:03**

**P12 10 Geometry and Electronic Structure of Alumina Supported Ag Clusters** ELIZABETH A. SOKOL, SARA E. MASON, *University of Pennsylvania* VALENTINO R. COOPER, *Rutgers, The State Univ. of N.J.* ANDREW M. RAPPE, *University of Pennsylvania* We use DFT/GGA to model silver clusters supported on Al-terminated alpha-alumina. A variety of cluster sizes and geometry are considered. We find that the adsorption of the Ag clusters causes dramatic surface relaxations and polarization of the Ag clusters as some Ag atoms of the clusters bond with O, while others bond with Al. For comparison, we also model adsorption of a single Ag atom, which bonds at a hollow site (relative to surface oxygen). We use the electronic structure of the adsorbed clusters to interpret the bonding interaction between the Ag atoms and surface O and Al atoms. The differences in Ag-surface bonds within the cluster give rise to different electronic environments at each Ag atoms. This effect has implications of this result to reactivity.

**13:15**

**P12 11 Adsorptive and chemical properties of supported silver clusters** SARA E. MASON, ELIZABETH A. SOKOL, *University of Pennsylvania* VALENTINO R. COOPER, *Rutgers, The State Univ. of N.J.* ANDREW M. RAPPE, *University of Pennsylvania* Unlike bulk metal slabs, clusters of transition metals on nonmetallic supports have a finite electron reservoir. Additionally, the interaction of clusters with the support can lead to polarization in the cluster. These effects give rise to adsorption properties quite different from those of bulk metal. We characterize the adsorption of different atomic and molecular species on silver clusters supported by Al-terminated alpha-alumina using DFT/GGA calculations. A range of cluster sizes and cluster geometries is onsidered and the adsorption energetics and geometries are compared with those of bulk silver metal.

**13:27**

**P12 12 Alkali ion scattering from sputter-induced Au nanoclusters** P. KARMAKAR, G.F. LIU, *Department of Physics, University of California, Riverside, California 92521* Z. SROUBEK, *Institute of Radio Engineering and Electronics, Czech Academy of Science, Chaberska 57, 182 51, Prague 8, Czech Republic* J.A. YARMOFF, *Department of Physics, University of California, Riverside, California 92521* The neutralization of scattered 3 keV $^{23}Na^{+}$ ions is used to probe the confined states of sputter induced Au nanoclusters on a $TiO_2(110)$ substrate. The neutral fraction of Na scattered from Au nanoclusters deposited on $TiO_2(110)$ is high compared to bulk Au, as described earlier (G.F. Liu, Z. Sroubek, J.A. Yarmoff, Phys. Rev. Lett. **92**, 216801 (2004)). Here, normal incidence 0.5 keV $Ar^{+}$ ion bombardment of a thin Au film is employed as an alternative method for the self-organized formation of Au nanoclusters. The interplay between curvature dependent sputtering and surface diffusion during $Ar^{+}$ bombardment works to develop the Au nanoclusters. The neutral fraction of the scattered Na gradually increases from 5% to 50% as the cluster dimensions decrease due to the $Ar^{+}$ sputtering. XPS is used to quantify the reduction of Au coverage with sputtering time. STM revels a decrease of both the rms roughness and the correlation length of Au nanoclusters with $Ar^{+}$ fluence.

**13:39**

**P12 13 CO oxidation reaction on Au clusters supported on the $TiO_2(110)$ surface** DAVIDE RICCI, ANGELO BONGIORNO, UZI LANDMAN, *Georgia Institute of Technology, School of Physics* ANKE WOERZ, MATTHIAS ARENZ, UELI HEIZ, *Technical University of Munich, Lehrstuhl fuer Phyzsikalische Chemie* We have studied by means of density functional theory (DFT) plane waves calculations, the CO oxidation reaction on $Au_8$ clusters adsorbed on both the stoichiometric and reduced rutile $TiO_2(110)$ surfaces. $O_2$ molecules bind at the interface between the $TiO_2(110)$ surface and the gold particle, where they become partially charged through the population of the anti-bonding molecular orbital, resulting in the extension of the O-O bond length to values of peroxo-like states. When CO is co-adsorbed on the gold-particles, the Langmuir-Hinshelwood and the Elay-Rideal mechanisms are possible for the oxidation reaction. Both the catalytic cycles have been considered and the theoretical results have been compared with experimental findings obtained on size-selected $Au_8$ clusters deposited on thin, oxidized and reduced $TiO_2$ films.

**13:51**

**P12 14 High photocatalytic activity of immobilized non-crystalline nanometric titanium oxide: key role of interface*** ANDREI KANAEV, *LIMHP, UPR1311 CNRS* MOHAMED BENMAMI, *LIMHP, University Paris-Nord* KHAY CHHOR, *LIMHP, University Paris-Nord* INORGANIC NANOMATERIALS TEAM, Thinnest coatings prepared by itchemical deposition ofit non-crystalline nanomertic titanium oxide particles (2R=5.0 nm) show important photocatalytic activity, which can be higher than that of the reference sample, crystalline itDegussa P-25 $TiO_2$. We describe an original method of the sol particles preparation and immobilization on complex supports in the sol-gel reactor. The effect of the coating thickness on its photocatalytic activity is studied. We show that the very first layer of the deposited nanoparticles possesses both high mechanically stability and the highest efficiency. We describe main features on the nanocoatings behavior in photocatalysis (gas-phase trichloroethylene deg-

radation) and show that their internal efficiency increases with the decrease of the deposited mass. These results suggest a new approach to the active component design, while earlier non-crystalline $TiO_2$ has been considered inactive.

*This work is supported by the COST D19 Action of European Commission

**14:03**
**P12 15 Ab-Initio Studies of Properties of 2D Rare-Earth Silicide Surfaces** CHRISTOPHER EAMES, STEVE TEAR, MATTHEW PROBERT, *Dept of Physics, University of York, UK* Rare Earth overlayers on the Si(111) surface have attracted interest due to their novel properties [1,2] and the unusual reconstruction that is formed with a flat rare earth layer buried inside the Silicon [3,4,5,6]. Here we present the results of ab-initio calculations done using the CASTEP [7] code to determine the structural and electronic properties of these reconstructions. We compare these to those derived experimentally. [1]F. P. Netzer, *J. Phys.: Cond. Matt.*, **7** (1995) 991-1022 [2]K. N. Tu *et al*, *App. Phys. Lett.*, **38** (1981) 626-628 [3]M. Lohmeier *et al*, *Phys. Rev. B.*, **54** (1996) 2004-2009 [4]D. J. Spence *et al*, *Phys. Rev. B.*, **61** (2000) 5707-5713 [5]D. J. Spence *et al*, *Surf. Sci.*, **512** (2002) 61-66 [6]C. Rogero *et al*, *Phys. Rev. B.*, **66** (2002) 235421-235427 [7]M. D. Segall *et al*, *J. Phys.: Cond. Matt.*, **14** (2002) 2717-2743

## SESSION P13: FOCUS SESSION: ULTRAFAST AND ULTRAHIGH FIELD CHEMISTRY II: QUANTUM CONTROL
**Wednesday Morning, 15 March 2006; 305, Baltimore Convention Center at 11:15**
**Kenji Ohmori, Institute of Molecular Science Japan, presiding**

***Invited Papers***

**11:15**
**P13 1 Quantum Control with Nonclassical Light.**
YARON SILBERBERG, *Weizmann Institute*

Most of the experimental advances in coherent quantum control in recent years have involved ultrashort pulses and pulse shaping techniques. These pulses have been an excellent source of coherent light with precise phase relationship between the various frequency components. In several recent works we have investigated the possibility of using broadband nonclassical light, generated by down-conversion of narrow-band lasers, for coherent control. Such light, for most purposes, exhibit the properties of a broadband thermal noise, but also unique quantum correlations between spectral mode pairs at the signal and idler frequencies that are required for quantum control. We have investigated both the single-photon limit, when the light was composed of individual entangled photon-pairs, and the large signal limit, when the light is not weak but does exhibit nonclassical phase correlations. In the high-intensity limit, we have shown that coherent control of two-photon absorption can be performed with incoherent non-classical light. We showed that the signal-idler phase correlations cause the spectral quantum interference to be completely constructive for two-photon interactions that have a final state energy equal to the pump laser frequency. Consequently, even though the broadband down converted light is neither coherent nor pulsed, it induces two-photon absorption just like a coherent ultrashort pulse, and may likewise be coherently controlled by pulse-shaping techniques. We also demonstrated that pulse shaping techniques can be used in the single-photon limit, where we shape the two-photon correlation function. We demonstrate control of the quantum interference of photons at a beam-splitter, and the generation of Bell-states using polarization pulse-shaping techniques. We believe that the combination of quantum control techniques with quantum optics could add an important ingredient to the toolbox of quantum information and computing.

***Contributed Papers***

**11:51**
**P13 2 Bell state generation in the presence of complicated entangling interactions*** KENJI MISHIMA, *JST-CREST* KOICHI YAMASHITA, *The University of Tokyo, JST-CREST* We present theoretical investigations on the entanglement generation of bipartite two- and three-level systems interacting with complicated entangling interactions and external electromagnetic fields. The theoretical method employed is based on rotating wave approximation (RWA). By using the partitioning of the complicated entangling interaction matrix, we propose a method of creating the Bell state from the initial separable state in bipartite two-level systems. In addition, by using the bipartite three-level model systems, we show how to create decoherence-free subspace when the Bell state is to be generated. The present work will be useful for realization of entanglement manipulation in the presence of complicated entangling interactions in molecular systems.

*The authors wish to thank CREST, JST for funding.

**12:03**
**P13 3 High-Precision Coherent Control of Molecular Wave Packets** HIROYUKI KATSUKI, *Institute for Molecular Science, National Institutes of Natural Sciences, Japan* KOUICHI HOSAKA, HISASHI CHIBA, KENJI OHMORI, INSTITUTE FOR MOLECULAR SCIENCE, NATIONAL INSTITUTES OF NATURAL SCIENCES, JAPAN TEAM, CREST, JAPAN SCIENCE AND TECHNOLOGY AGENCY, JAPAN COLLABORATION, THE GRADUATE UNIVERSITY FOR ADVANCED STUDIES (SOKENDAI), JAPAN COLLABORATION, The quantum interference of two vibrational wave packets has been

precisely controlled in the electronically excited state of a diatomic molecule by using a pair of fs laser pulses whose relative phase $\phi$ is locked within the attosecond time scale, and the real time evolution of that interference has been observed by another fs probe pulse. The real-time evolution shows a clear dependence on $\phi$. We have also measured a population code, which is a population ratio among the vibrational eigenstates within a WP. The population code also shows a clear dependence on $\phi$. The ordinary frequency domain interpretation based on the spectral interference of locked pulses may be useful to elucidate $\phi$ dependence of population codes, but is no longer suitable for the present real-time observation. The combination of a population code and real-time evolution is useful to obtain both phase and amplitude information stored in a WP.

**12:15**

**P13 4 Nanolocalized Nonlinear Electron Photoemission under Coherent Control*** MARK STOCKMAN, *Department of Physics and Astronomy, Georgia State University* We theoretically show that two-photon coherent control yields electron photoemission from metal nanostructures that is localized in nano-size hot spots whose positions are controllable on a nanometer scale, in agreement with recent experiments. We propose to use silver V-shapes as taylored nanoantennas for which the position of the coherently controllable photoelectron-emission hot spot can be deterministically predicted. We predict that the low-frequency, high-intensity (quasistationary) excitation of the photoemission leads to an exponentially high contrast of the coherent control. REFERENCES M. I. Stockman and P. Hewageegana, ''Nanolocalized Nonlinear Electron Photoemission under Coherent Control,'' Nano Lett. 5(11), 2325-2329 (2005)

*This work was supported by grants from the Chemical Sciences, Biosciences and Geosciences Division of the Office of Basic Energy Sciences, U.S. Department of Energy and a grant from National Science foundation.

**12:27**

**P13 5 Monitoring Molecular Dynamics using Coherent Electrons from High-Harmonic Generation** NICK WAGNER, ANDREA WÜEST, IVAN CHRISTOV, TENIO POPMINTCHEV, XIBIN ZHOU, MARGARET MURNANE, HENRY KAPTEYN, *University of Colorado and National Institute of Standards and Technology* In this talk, we will discuss the first observation of intramolecular vibrational dynamics using electrons rescattered during the process of high-order harmonic generation. We excite coherent vibrations in $SF_6$ using impulsive Raman scattering with a short laser pulse. A second, more-intense laser pulse generates high-order harmonics of the fundamental laser, at wavelengths of $\sim$ 20-50 nm. The high-order harmonic yield is observed to oscillate, at frequencies corresponding to all the Raman-active modes of $SF_6$, with an asymmetric mode most visible. This is in contrast to conventional impulsive stimulated Raman spectroscopy where only the symmetric breathing mode of the molecule is easily observed. The data also show evidence of relaxation dynamics following impulsive excitation of the molecule. Our results indicate that high harmonic generation is a sensitive probe of vibrational dynamics and may yield more information simultaneously than conventional ultrafast spectroscopic techniques. Since the de Broglie wavelength of the recolliding electron is on the order of interatomic distances, i.e. $\sim$ 1.5 Å, small changes in the shape of the molecule lead to large changes in the high harmonic yield. This work therefore demonstrates a new spectroscopic technique for probing ultrafast internal dynamics in molecules that uniquely combines ultrafast time resolution with atomic-scale structural information.

*Invited Papers*



**12:39**

**P13 6 Observation and control of ultrafast quantum interferences in atoms and molecules.**
BERTRAND GIRARD, *Lab. Collisions, Agrégats, Réactivité, IRSAMC, Univ. P. Sabatier - Toulouse 3*

I will present several examples of ultrafast interferences in atoms and molecules, at the femtosecond and picosecond time scale. In a two level atom, real-time quantum state holography is performed through interferences between quantum states created by a reference pulse and a chirped pulse resulting in coherent transients. A sequence of several measurements allows one to measure the real and imaginary parts of the excited state wave function. These measurements are performed during the interaction with the ultrashort laser pulse. The extreme sensitivity of this method to the pulse shape provides a tool for electric field measurement. In a molecule, the transient interferences between two oscillating wave-packets have been observed and controlled. In a first experiment, a vibrational wave packet is created in the iodine B state. Due to anharmonicity, the wave-packet spreads and recombines in one single wave packet (revival time) or two wave-packets (half revival time). When these two wave packets cross, they transiently create a stationary wave which is observed. In a second experiment, the same situation is created by launching two wave packets in the same potential well with an ultrastable relative phase. The delay, set to 1.5 vibrational periods, is stabilized with sub 100 attosecond precision. The same transient interference pattern is observed. Moreover, the relative phase between the counterpropagating wave packets can now be controlled by scanning the interpulse delay on an optical period.

*Contributed Papers*

**13:15**

**P13 7 Final resolution of the step-wise versus concerted mechanism controversy for excited-state double proton transfer in the 7-azaindole dimer in the gas phase** HIROSHI SEKIYA, KENJI SAKOTA, *Department of Chemistry, Faculty of Science, Kyushu University* CHIE OKABE, NOBUYUKI NISHI, *Institute for Molecular Science* The excited-state double-proton transfer (ESDPT) reaction in the 7-azaindole dimer has been extensively studied by spectroscopic methods in the gas phase and in solution. Two ESDPT mechanisms, stepwise and concerted mechanisms, have been proposed so far. However, a definite conclusion has not been provided due to a lack of clear evidence. We provide final resolution of the stepwise versus concerted mechanism controversy for the ESDPT reaction in the 7-azaindole dimer by electronic spectroscopy and picosecond-time resolved spectroscopy in the gas phase (K. Sakota, C. Okabe, N. Nishi, H. Sekiya, J. Phys. Chem. A, 109, 5245 (2005)). The ESDPT reaction in the 7-azaindole dimer proceeds via the concerted mechanism. We propose a dynamic cooperative effect, where the motions of the two transferring protons couple with each other through the electronic reorganization (K. Sakota ,H. Sekiya, J. Phys. Chem. A, 109, 2718 (2005); 109,2722 (2005)).

**13:27**

**P13 8 On the Control of Product Yields in the Photofragmentation of Deuteriumchlorid Ions ($DCl^+$) – Cl + $D^+$ < - - $DCl^+$ - - > $Cl^+$ + D.*** KARL-MICHAEL WEITZEL, GEORG BREUNIG, ALEXANDRA LAUER, *Philipps Universitaet Marburg, FB Chemie, Germany* MIKHAIL KOROLKOV, *Academy of Science, Minsk, Belarus* We have investigated the prospect of controlling the photofragmentation of deuterium chloride ions ($DCl^+$) via ultra short IR laser pulses both by experiments and by numerical solution of coupled Schrödinger equations. The calculations provide evidence that the ratio of product ion yields $Cl^+$ versus $D^+$ can be manipulated by appropriate choice of laser pulse parameters, in particular central laser wavelength, pulse duration, intensity and chirp [1]. The analysis of time dependent populations reveals phase sensitive competition between intra- and inter-electronic state excitation. Complementary, we have performed one- and two-color fs experiments looking at the dissociation of $DCl^+$ ions at 800 nm [2] and in the range from 3.5$\mu$m to 7.5$\mu$m (2857$cm^{-1}$ to 1333$cm^{-1}$) [3]. In particular we show, that the ratio of product yields $D^+/Cl^+$ can be controlled via the chirp of the laser pulse at 4.5$\mu$m. References [1] M.V. Korolkov, K.-M. Weitzel, J. Chem. Phys. 123, 164308, (2005) [2] H.G. Breunig, A. Lauer, K.-M. Weitzel, Proceedings of the Femtochemistry VII (2005) [3] H.G. Breunig, K.-M. Weitzel, in preparation.

*Supported by INTAS and the DFG.

**13:39**

**P13 9 Femtosecond pulse shaping in the mid infrared region using a Dazzler** TAKAMASA MOMOSE, *The University of British Columbia, Tokyo Institute of Technology, CREST, JST* MASAAKI TSUBOUCHI, *The University of British Columbia, CREST, JST* YUKI MIYAMOTO, *Kyoto University* We present a method to produce programmable phase- and amplitude-modulated femtosecond laser pulses in the mid infrared region (MIR: 3 – 10 $\mu$m) by difference-frequency generation (DFG). The signal output (NIR: 1.1 – 1.5 $\mu$m) of an optical parametric amplifier was shaped with an acousto-optic programmable dispersive filter (Dazzler), and mixed in a $AgGaS_2$ crystal with the idler pulse temporary stretched by passing a dispersion block to generate MIR pulses. A Dazzler provides convenient and precise way of shaping femtosecond pulses in NIR region. It is, however, not well understood how the phase and amplitude modulations are transferred from a NIR pulse to a MIR pulse via DFG process. We will discuss the analysis of the shaped NIR and MIR pulses using a frequency-resolved optical gating (FROG) and an FT-IR

**13:51**

**P13 10 Fast Transient Electron Magnetic Resonance at 240 GHz*** JOHAN VAN TOL, *National High Magnetic Field Lab* The zero-field splitting of the excited triplet states of organic molecules often is of the order of 1 GHz or less, and transient EPR at X-band is generally sufficient for the determination of the zero-field splitting and kinetic parameters in these type of molecules. However, information on the g-factor and g-anisotropy cannot be obtained at conventional EPR frequencies, and interpretations of the data in terms of electronic structure are mostly limited to symmetry considerations. On the other hand information of the g-anisotropy provides additional clues with respect to electronic structure, while a direct comparison with radical-ion forms of the molecules becomes possible. Experimental data of transient EPR at 240 GHz will be presented for a variety of system (fullerene-based and porphyrin-based). EPR at these very high frequencies can accurately determine the g-anisotropy and in some cases the orientation of the g-tensor with respect to the ZFS tensor. Also at these high frequencies sub nanosecond processes can be measured. Examples will be given.

*This research was funded by the NSF grant

**14:03**

**P13 11 Response of Dipicolinic Acid ($C_5H_5N(COOH)_2$) to Ultrafast Laser Pulses*** PETRA SAUER, ROLAND ALLEN, *Texas A&M University* Dipicolinic acid (DPA) and its salts are common constituents of bacterial spores, including those of anthrax. It has been proposed that such spores can be detected via spectroscopic techniques which employ ultrashort laser pulses. The development of these techniques should be enhanced by a detailed understanding of the microscopic processes that transpire when a molecule is subjected to femtosecond-scale pulses of various intensities, durations, and polarizations. We have recently developed a model that can be used to perform realistic simulations of the electronic and nuclear dynamics of biological molecules (containing carbon, hydrogen, oxygen and nitrogen) when they are subjected to such pulses. The bond lengths and vibrational frequencies for a variety of test molecules are in reasonable agreement with those obtained in experiment and itab initio calculations. Here we report results of simulations for DPA responding to femtosecond-scale laser pulses, with an analysis of the vibrational modes and electronic states which are most relevant for various choices of the laser pulse parameters.

*Work supported by Robert A. Welch Foundation (Grant A-0929).

**SESSION P16: FOCUS SESSION: MOLECULAR-SCALE ELECTRONICS III**
**Wednesday Morning, 15 March 2006**
**312, Baltimore Convention Center at 11:15**
**Shashi Karna, Army Research Laboratories, presiding**

***Contributed Papers***

**11:15**

**P16 1 Molecular sensing using point contact conductivity modulation** ADAM DICKIE, ROBERT WOLKOW, *University of Alberta* The electrical properties of semiconductors are sensitive to external influences, such as the adsorption of gaseous molecules. For single crystal Si surfaces, the change in conductivity induced by molecular adsorption is a very small fraction of the bulk conductivity, precluding their use as efficient sensors. Here we show that point contacts on Si surfaces in UHV environments can overcome this fundamental limitation, through the use of minority-carrier-induced conductivity modulation. Point contacts made to clean, low-doped $n-$ Si(100) produce significant surface inversion layers. The inversion layer minority-carrier population is exponentially dependent upon surface charge. Slight increases in the surface charge density, from gas molecule adsorption, are detected as large increases in sample conductivity, as electrons flow in to balance the positive hole space charge. The sensitivity of this simple device structure is so high that physisorption of inert gas molecules such as He, $N_2$, and Ar can be detected as conductivity increases of 2 – 100%; the specific response is proportional to the molecular ionization potential. Decreasing the point contact size, from micro- to nano- to atomic-scale, increases device sensitivity because of increased minority-carrier injection ratios.

**11:27**

**P16 2 Humidity dependence of molecular tunnel junctions with an AlOx/COOH- interface** XIAOHANG ZHANG, STEPHEN MCGILL, PENG XIONG, *Physics Department & MARTECH, Florida State University, Tallahassee, FL* We have studied the electron transport in planar tunneling junctions with aluminum oxide and an organic self-assembled monolayer (SAM) as the tunnel barrier. The structure of the junctions is Al/AlOx/SAM/(Au, Pb) with a junction area of $\sim$ 0.4mm$^2$. The organic molecules investigated include mercaptohexadecanoic acid (MHA), hexadecanoic acid (HDA), and octadecyltrichlorosilane (OTS); all of which form ordered SAMs on top of aluminum oxide. The use of a superconducting electrode (Al) enables us to determine unambiguously that these are high-quality tunnel junctions. For junctions incorporating MHA, the transport behavior is found to be strongly humidity dependent. The resistance of these junctions drops more than 50% when placed in dry nitrogen and recovers when returned into the ambient. The same drop also occurs when the sample is placed into a vacuum, and backfilling the vacuum with either dry N2 or O2 has negligible effect on the resistance. For comparison, junctions with HDA show the same humidity dependence, while OTS samples do not. Since both MHA and HDA have carboxylic groups and OTS does not, the results suggest that water molecules at the AlOx/COOH- interface play the central role in the observed behavior. Inelastic tunneling spectroscopy (IETS) has also been performed to understand the role of water. This work was supported by a FSU Research Foundation PEG grant.

**11:39**

**P16 3 Signatures of magnetism in an individual Mn12O12 molecule probed by single-electron tunneling.** MOON-HO JO, *Dept of Materials Science and Engineering, POSTECH* JACOB E. GROSE, DANIEL C. RALPH, *Dept of Physics, Cornell Univ* KANHAYALAL BAHETI, JEFFREY R. LONG, *Dept of Chemistry. UC Berkeley* WENJIE LIANG, MANDAR M. DESHMUKH, HONGKUN PARK, *Department of Chemistry & Chemical Biology and Department of Physics* We report low-temperature electron transport through individual molecular clusters, Mn12O12(O2C-R)16(H2O)4, [Mn12O12], where R is -CH3 and -CHCl2. Energy level spectroscopy with single-electron tunneling probes the ground state spin of the individual Mn12O12 molecules, and exhibits signatures of their magnetism. In particular the absence of the spin degeneracy is manifested as an energy splitting between low-lying energy manifolds of the ground state spin at zero-magnetic field, and it signifies the magnetic anisotropy of an individual Mn12O12 molecule. We also discuss the influence of this anisotropy to the electron tunneling spectrum in the presence of a magnetic field.

**11:51**

**P16 4 ESR-STM Spectrometer for Paramagnetic Molecular Adsorbates on Surfaces*** PAOLO MESSINA,[†] *MSD Argonne Nat. Lab., US* MATTEO MANNINI, *Dept. Chemistry University of Florence, Italy* ANDREA CANESCHI, DANTE GATTESCHI, LORENZO SORACE, PAOLO SIGALOTTI, *ApeResearch Trieste, Italy* CRISTIAN SANDRIN, PAOLO PITTANA, *Elettra Sincrotrone S.P.A. Trieste, Italy* YISHAY MANASSEN, *Bengurion University of the Negev, Israel* ESR-STM is a technique able to detect noise at the Larmor frequency in the tunnelling current associated with the spin dynamics of a single paramagnetic center on the surface. Several questions concerning details of this phenomenon in different magnetic fields and tunnelling currents, and for different paramagnetic centers are still debated. In this paper we describe the construction and the testing of an instrument able to detect the ESR-STM signal from organic paramagnetic molecules (DPPH and BDPA) deposed on Au(111) at different magnetic fields. First results on these molecules are presented.

*Financial support from the Italian MIUR, FIRB and FISR projects, EC HPRI-CT-2000-40022 SENTINEL and MRTN CT-2003 504880 ''QuEMolNa'' and NoE ''Magmanet'' are also acknowledged. Partial support from the US-Israel binational foundation is also acknowledged.I have just subscribed to be an APS member

[†]I have just subscribed to be an APS member

**12:03**

**P16 5 Exploring electron transport through organic monolayers using conductive tip AFM techniques** DENIS SCAINI, *Synchrotron Trieste, Trieste, Italy; Department of Physics, University of Trieste, Trieste, Italy* MATTEO CASTRONOVO, *Department of Physics, University of Trieste, Trieste, Italy* MARTINA

DELL'ANGELA, *Synchrotron Trieste, Trieste, Italy;* ROBERT HUDEJ, *Synchrotron Trieste, Trieste, Italy; International School for Advanced Studies (ISAS), Trieste, Italy* LOREDANA CASALIS, *Synchrotron Trieste, Trieste, Italy* GIACINTO SCOLES, *Synchrotron Trieste, Trieste, Italy; International School for Advanced Studies (ISAS), Trieste, Italy; Princeton University, Princeton, NJ* We follow an alternative approach to the study of Metal-molecule-Metal junctions that uses a combination of two atomic force microscopy (AFM) techniques. We use Nanografting to build a nanopatch of the molecules of interest and a second made of a reference molecule into a hosting self assembled monolayer (SAM) typically made of alkanethiols. After the tip is changed to a conductive one CT-AFM is used to characterized the whole system recording, at the same time, the system topography. Some of the advantages of this approach are the possibility to build and study a wide range of different M-m-M junctions and the in-situ control of the quality of the monolayers and patches. Results will be presented on saturated and unsaturated thiols self-assembled and nanografted on Au(111) surfaces. The results will be compared with those obtained by Liang and Scoles at Princeton using similar techniques.

**12:15**

**P16 6 A Novel Automated System for Assembling Films of Nanoparticles** EDNA CARDENAS, *Sandia National Laboratories* STEPHEN HOWELL, SHAWN DIRK, DAVE WHEELER, *Sandia National Laboratories* MICRO-TOTAL-ANALYTICAL SYSTEMS TEAM, Due to their interesting properties, nanoparticle films have emerged as useful platforms for miniaturized chemical sensing. For nanoparticle sensors to become practical in real world applications, a reproducible method of assembly has to be implemented. This project focuses on robotic assembly techniques that deposit nanoparticle films on various substrates. We have developed a process to iteratively assemble and electronically characterize nanoparticle films using a custom robotic preparation system. The robot's design uses commercially available pneumatic and electronic actuators, valves and regulators to manage precision movements. Control of the robot is obtained by a custom Labview program which uses a TTL and GPIB interface to control relays, power supplies, and measurement circuitry. Sandia is a multiprogram laboratory operated by Sandia Corporation, a Lockheed Martin Company, for the United States Department of Energy under contract DE-AC04-94AL85000.

***Invited Papers***

**12:27**

**P16 7 Electronic Conduction in Metal/Molecule/Semiconductor Devices.**
DAVID JANES, *School of Electrical and Computer Engineering, Purdue University*

In the field of molecular electronics, the contacts to the molecular elements are critical interfaces. The use of semiconductor contacts allows direct covalent bonding, provides an additional degree of freedom due to the semiconductor states, and, in certain circumstances, can minimize the effects of electrical shorting due to direct metal/substrate contacts. This talk will describe the development and electrical characterization of metal/molecule/semiconductor device structures on GaAs and Si active layers. In order to observe the conductance of the molecular species, rather than that of the semiconductor barrier, the semiconductor layers used in this study are generally highly doped. In these structures, the electronic conduction between the metal and semiconductor can be modulated by choice of molecular species. Several alkyl thiol and aromatic thiol molecules have been employed in order to determine the effects of molecular length, conjugation and intrinsic dipole moment. In certain molecules, conductance peaks or memory/switching effects have been observed. The current-voltage characteristics and conductance versus temperature both indicate that the molecular layers change the transport mechanism, generally involving a lower effective barrier height than that of a metal/semiconductor Schottky barrier. Studies on both n- and p- type substrates, including those with nanometer scale cap layers, allow the effects of the molecular and semiconductor barriers to be isolated. A basic conduction model has been developed, based on the electrostatics of the structure and thermionic-field-emission analysis of the semiconductor portion of the barrier.

***Contributed Papers***

**13:03**

**P16 8 Towards a 160 kBit molecular electronic memory at $10^{11}$ Bits/cm$^2$*** JONATHAN GREEN, J.W. CHOI, E. JOHNSTON-HALPERIN, E. DEIONNO, Y. LUO, A. BOUKAI, Y. BUNIMOVICH, B.A. SHERIFF, J.R. HEATH, *Division of Chemistry and Chemical Engineering, The California Institute of Technology, Pasadena, CA* Since its inception by Avirim and Ratner in 1974, molecular-based electronics has emerged as a promising alternative to scaled CMOS technology and its eventual integration limit. Here we present progress towards an electronically configurable, molecule-based 160,000 Bit random access memory at a Bit density approaching $10^{11}$ Bits/cm$^2$. This device is based on a cross-bar architecture in which the active switching elements are bi-stable [2]-rotaxane supramolecules sandwiched between perpendicular arrays of SNAP-fabricated [1] metallic and n-Si nanowires at 34 nm pitch. Challenges in memory fabrication and testing will be discussed. [1] Science **300**, 112 (2003); J. App. Phys. **96**, 5921 (2004).

*Funding provided by DARPA

**SESSION P18: FOCUS SESSION: CARBON NANOTUBES: OPTO-ELECTRONICS**
**Wednesday Morning, 15 March 2006; 315, Baltimore Convention Center at 11:15**
**Vasili Perebeinos, IBM T.J. Watson Research Center, presiding**

*Invited Papers*

**11:15**
**P18 1 Electrically-Induced Infrared Emission from Carbon Nanotube Devices.**
JIA CHEN,* *IBM T. J. Watson*

The optical properties of carbon nanotubes (CNTs) are currently the focus of intense study. CNTs are direct band gap materials and their optical spectra have long been attributed to transitions between free particle bands. We show that studies of electrically-excited infrared (IR) emission from single nanotube molecules provide new insights into the electron-hole interactions in quasi-1D systems. We demonstrate strongly-enhanced electroluminescence from a partially suspended CNTFET operated under unipolar transport conditions [1]. In our devices, carriers are generated locally, when a single type of carrier is accelerated under high local electric fields at intra-molecular junctions to energies sufficient to create strongly correlated e-h pairs (excitons). This excitation mechanism contrasts with emission from radiative recombination of carriers (electrons and holes) injected from the opposite ends (source and drain) of a CNTFET operated under ambipolar transport conditions. The new excitation mechanism is about 1000 times more efficient than recombination of independently injected electrons and holes, and it results from weak electron-phonon scattering and strong electron-hole binding caused by one-dimensional confinement. We show that the light emission intensity increases exponentially with the drive current in partially suspended CNTFETs, while in 3D materials light emission is usually proportional to the product of the electron and the hole currents. The strong Coulomb interaction between electrons and holes in a 1D CNT creates bound excitons whose binding energies are more than an order of magnitude larger that those in 3D materials, preventing them from dissociating under electrical fields thus contributing little to drive current compared with that in 3D. Finally, the much higher exciton density achieved in our devices than that in typical photoluminescence experiments allows us to detect emission from higher excitation states in CNTs. [1] J. Chen, V. Perebeinos, M. Freitag, J. Tsang, Q. Fu, J. Liu, Ph. Avouris, Science 310, 1171 (2005).

*This work is done in collaboration with V. Perebeinos, M. Freitag, J. Tsang, Q. Fu, J. Liu and Ph. Avouris.

*Contributed Papers*

**11:51**
**P18 2 Exciton Formation and Electroluminescence Quenching during 1D Impact Excitation of Carbon Nanotubes Field-Effect Transistors** LAËTITIA MARTY, *Regroupement Québécois sur les Matériaux de Pointe (RQMP) and Chemistry Department, University of Montreal* ELYSE ADAM, DAVID MÉNARD, *RQMP and Physical Engineering Department, Ecole Polytechnique of Montreal* RICHARD MARTEL, *RQMP and Chemistry Department, University of Montreal* There are few studies addressing the influence of excitonic effects on the electro-optical response of carbon nanotube (CNT) devices. We present here near infra-red electroluminescence (EL) from unipolar single-wall carbon nanotube field effect transistors (CNFETs) at high drain-source voltages. The conditions for emission at high field reveal that a single carrier type induces EL in CNFETs through a mechanism involving 1D impact excitation. Well-resolved spectra show that the emission is assigned to the radiative recombination of the $E_{1,1}$ exciton. An emission quenching is also observed at high field and attributed to an exciton-exciton annihilation process and free carrier generation. Excitons binding energy in the order of 270 meV for 1.4 nm CNTs is inferred from the spectral features.

**12:03**
**P18 3 Uni- and Ambipolar Light Emission From Inhomogeneous Carbon Nanotube FET's** JAMES TSANG, MARCUS FREITAG, JIA CHEN, PHAEDON AVOURIS, *IBM T. J. Watson Research Center* Heterogeneities in the environment of CNTFETs can produce stationary, unipolar, electroluminescence, in addition to the normal ambipolar emission. We compare the unipolar emission with the ambipolar emission in the same device to characterize the unipolar emission process and show how the heterogeneities modify the electronic properties of the CNT. If a CNTFET is partially covered by a PMMA overlayer, changes in the IV characteristics are observed which correlate with discontinuities in the motion of the ambipolar emission at the PMMA boundary, and the generation of unipolar emission at the boundary. These PMMA induced changes show there is a step in the potential along the CNT at the boundary. Similarly, localized effects in both the ambi- and unipolar emission are observed in CNTFETs containing closed loops. The unipolar emission requires the junction between the portions of the single carbon nanotube that form the base of a loop must support the voltage drop needed to generate the light. Direct comparison of the ambipolar and unipolar emission in the same device demonstrates the efficiency of the unipolar processes.

**12:15**
**P18 4 Carbon Nanotube p-n Junction Diodes** JI UNG LEE, *GE Global Research* We describe the formation of p-n junctions along individual single-walled carbon nanotubes (SWNTs) using electrostatic doping techniques. The electrostatic doping preserves the pristine nature of CVD grown SWNTs, and when suspended, these diodes can be described by the ideal diode equation. The low background leakage currents coupled with a built-in electric field region to transport the quasi particles also makes these diodes ideal for studying the optical responses of SWNTs. We will describe several characteristics of SWNT diodes such as the quantum efficiency, origin of the quasi-particles (electrons and holes) currents, and effects due to excitons.

**12:27**

**P18 5 Electronic Transport in Individual Carbon Nanotube P-N Junction Diodes** NATHANIEL GABOR, *Laboratory of Solid State Physics, Cornell University* KEN BOSNICK, *National Institute for Nanotechnology, National Research Council of Canada* PAUL MCEUEN, *Laboratory of Solid State Physics, Cornell University* We have investigated electronic transport in single-walled carbon nanotube p-n junction diodes formed using gates to electrostatically dope the tube. Previous measurements [1] have shown that such diodes demonstrate nearly ideal turn-on behavior at room temperature and low biases, consistent with thermal activation over the junction barrier. We have performed measurements over a broad temperature range and have verified that the transport is by thermal activation. From the temperature dependence of the current-voltage characteristics, we can extract the nanotube band gap and the transmission coefficient through the p-n junction region. [1] J.U. Lee et al, App. Phys. Lett. **85**, 145 (2004)

**12:39**

**P18 6 Negative differential conductance in suspended semiconducting carbon nanotubes** HAIBING PENG, ALEX ZETTL, *Center of Integrated Nanomechanical Systems and Department of Physics, University of California at Berkeley, Berkeley, CA 94720* Suspended single-wall carbon nanotubes (SWCNTs) have been grown directly on metal electrodes with electrical contact by chemical vapor deposition. Extraordinary negative differential conductance was observed for the first time in suspended semiconducting SWCNTs. The current-voltage characteristics show an abrupt drop of conductance as the source-drain voltage is increased, followed by a constant differential conductance at higher voltage. The effect is qualitatively different from the recently reported negative differential conductance in metallic SWCNTs (it-Phys. Rev. Lett. **95** 155505, 2005). We suggest that the observed negative differential conductance in semiconducting SWCNTs may be attributable to Schottky barriers between the as-grown suspended SWCNTs and the electrodes, instead of optical phonon scattering invoked in explaining the negative differential conductance in metallic SWCNTs. Our observations not only have potential applications for novel electronic devices, but also shed light on better understanding and manipulating SWCNTs transistors.

**12:51**

**P18 7 Nanotube Film Electrodes in Electro-Optic Devices*** ZHUANGCHUN WU, *[1]* JEREMIAH K. MWAURA, *[2]* MARIA NIKOLOU, *[1]* TIMOTHY STECKLER, *[2]* DAVID B. TANNER, *[1]* JOHN R. REYNOLDS, *[2]* ANDREW G. RINZLER, *[1] 1. Dept. of Physics, 2. Dept. of Chemistry, University of Florida, Gainesville, FL* The interface between conjugated polymers and conducting electrodes is crucial for the operation of organic electronic devices such as light emitting diodes (LEDs), electrochromics and photovoltaics. Transparent electrodes in these devices have been based mostly on indium tin oxide (ITO). There have been efforts to develop conducting polymer electrodes, and some success has been realized with films based on poly(3,4-ethylene-dioxythiophene)-poly(styrene sulfonate) (PEDOT-PSS).[1] In most cases however, the polymer conductivity is too low for such applications. Pure nanotube thin films, demonstrated to have much higher conductivities while exhibiting good transparency in the visible and near to mid IR, provide attractive alternatives.[2] Here we describe fabrication and performance of two devices: (1) an MEH-PPV polymer LED using a carbon nanotube film as the hole injecting electrode and (2) an infrared transmissive/absorptive electrochromic cell that makes use of the superior IR transmittance of the nanotube films. 1. A. A. Argun, A.Cirpan, J. R. Reynolds, Adv. Mater. 15, 1338 (2003). 2. Z. Wu, et al., Science 305, 1273 (2004).

*MN and DBT acknowledge support of the NSF, DMR-0305043

**13:03**

**P18 8 Measurements of exciton binding energies in single wall nanotubes using field dependent photocurrent spectroscopy** A.D. MOHITE, J.-T. LIN, G.U. SUMANASEKERA, B.W. ALPHENAAR, *Dept of Electrical & Comp. Engr., Univ. of Louisville* We have used electric field dependent photocurrent measurements to distinguish between band-to-band and excitonic transitions in the excitation spectrum of a single wall nanotube capacitor. The zero field photocurrent spectrum is limited to carriers excited into continuum states that can freely diffuse from the nanotubes and into the metal contact. Application of an applied field allows for the separation of the bound exciton states via field ionization. Near the $E_{11}$ resonance, both excitonic and band-to-band transitions are resolvable with a binding energy of 109 meV. This is in reasonable agreement with recent theory for 1.3 nm diameter nanotubes[1]. Near the $E_{22}$resonance, we observe only a single field independent peak in the photocurrent spectrum indicating a fast decay of the exciton into the lower energy continuum states. Surprisingly, we are also able to resolve an exciton resonance associated with metallic nanotubes. Theory shows that in metallic nanotubes, optical transitions between the overlapping states at the Fermi energy are disallowed, giving rise to a symmetry gap[2]. We measure the binding energy of the metallic exciton to be 49 meV for 1.3 nm diameter tubes. **References** (1) Perebeinos, V.; Tersoff, J.; Avouris, Ph., Phys. Rev. Lett. **2004**, 92, 257402. (2) Spataru, C.D.; Ismail-Beigi, S.; Benedict, L.X,; Louie, S.G. Phys. Rev. Lett. **2004**, 92, 077402.

**13:15**

**P18 9 Optical Properties of Aligned Carbon Nanotube Mats for Photonic Applications** G.L. ZHAO, *Southern University and A&M College; Visiting Fellow, Princeton University* D. BAGAYOKO, *Southern University and A&M College* L. YANG, *NASA Ames Research Center* We studied the optical properties of the aligned carbon nanotube (16, 0), (10, 0) and (8, 4) mats for photonic device applications. We employed the ab-initio density functional calculations in the linear combination of atomic orbital formalism. We calculated the electronic structure of the carbon nanotube mats and the real and imaginary parts of the dielectric functions as functions of photon energy. The calculated dielectric functions of the aligned carbon nanotube mats show a strong anisotropy when the electric field of light is parallel or perpendicular to the tube axes. Especially, there are strong peaks in the imaginary part of the dielectric function near the absorption edges, when the electric field of light is parallel to the carbon nanotube axes. The unusual optical properties of the semiconducting carbon nanotube mats present a new opportunity for applications in new electro-optical devices in the infrared energy region. Acknowledgments: this work was funded in part by NSF (Award No. 0508245), NASA (Award No. NCC 2-1344), and ONR (Grant No: N00014-05-1-0009).

**13:27**

**P18 10 Theory of Auger Recombination of Excitons in One-Dimensional Nanostructures*** FENG WANG, YANG WU, MARK S. HYBERTSEN, TONY F. HEINZ, *Columbia University* The effective Coulomb interaction is greatly enhanced in one-dimensional (1D) systems. As has been recently demonstrated for single-walled carbon nanotubes [1], this strong Coulomb interaction causes the formation of tightly bound exciton states upon optical excitation of semiconducting materials. The strength of the Coulomb interaction in 1D systems leads to a second consequence: Auger recombination of excitons, also known as exciton-exciton annihilation, can be very efficient. Here we investigate the 1D Auger process using a point-contact model for the Coulomb interaction. We show that the Auger process is essentially temperature independent, in contrast to the behavior of weakly bound excitons and free carriers in bulk semiconductors. We apply the explicit expression that we have derived to single-walled carbon nanotubes. We obtain an Auger rate of $\sim 0.6\,\mathrm{ps}^{-1}\,\mu\mathrm{m}$, comparable to the reported experimental value [2]. [1] F. Wang et al., Science **308**, 838 (2005); [2] F. Wang et al., Phys. Rev. B **70**, 241403 (2004).

*Supported by Columbia Nanoscale Science and Engineering Center

**13:39**

**P18 11 Measurement of Optical Stark Effect in Semiconducting Single-Walled Carbon Nanotubes** DAOHUA SONG, FENG WANG, GORDANA DUKOVIC, LOUIS E. BRUS, TONY F. HEINZ, *Columbia University, New York, NY 10027* M. ZHENG, G.B. ONOA, E.D. SEMKE, *DuPont Central Research and Development, Wilmington, DE 19880* The optical Stark effect in quantum-confined systems, such as quantum wells, has been the subject of active interest for many years. In this paper we present the first measurement of the optical Stark effect in carbon nanotubes. In our experiment we used two-color femtosecond spectroscopy to probe the $E_{11}$ transition in the nanotubes while applying a strong optical pump beam at significantly lower photon energy (the large detuning limit). The sample was an aqueous suspension of (6,5)-enriched single-walled carbon nanotubes. An instantaneous shift in the absorption line by up to 1 meV was observed; the magnitude of the shift scaled linearly with the pump intensity. The nature of the optical Stark effect in the carbon nanotube system, with its strong excitonic transitions, will be discussed.

**13:51**

**P18 12 Bandgap Modulation by Transverse Electric Fields in Single Wall Carbon Nanotubes** J. M. KINDER, *University of Pennsylvania* E. J. MELE, *University of Pennsylvania* We study the variation of the electronic bandgap of semiconducting carbon nanotubes in a static electric field perpendicular to the nanotube axis. We consider three models for the transverse field profile and find that the spectrum is sensitive to the spatial variation of the transverse field. For a uniform transverse field, we show the bandgap is fixed until the field strength exceeds a critical value, in agreement with previous theoretical work. In contrast, we find no critical behavior when the applied field is localized to a region of the nanotube much smaller than its length. An arbitrarily weak field produces bound states inside the unperturbed bandgap whose binding energy vanishes as the fourth power of the applied field strength. The field strengths required to reduce the gap by a few percent are the same order of magnitude as those commonly used in scanning tunneling microscopy.



## SESSION P19: FOCUS SESSION: SPIN INTERFERENCE AND SPIN HALL EFFECT

**Wednesday Morning, 15 March 2006**
**316, Baltimore Convention Center at 11:15**
**Jairo Sinova, Texas A&M University, presiding**

***Contributed Papers***

**11:15**

**P19 1 Direct observation of the Aharonov-Casher phase*** M. KÖNIG, *Physikalisches Institut(EP3) der Universitaet Wuerzburg, Am Hubland, D-97074 Wuerzburg, Germany* E. M. HANKIEWICZ, *Texas A&M University, College Station, TX 77843-4242 and University of Missouri-Columbia, Columbia, MO 65211* JAIRO SINOVA, *Texas A&M University, College Station, TX 77843-4242* A. TSCHETSCHETKIN, V. HOCK, V. DAUMER, M. SCHÄFER, C. R. BECKER, H. BUHMANN, L. W. MOLENKAMP, *Physikalisches Institut(EP3) der Universitaet Wuerzburg, Am Hubland, D-97074 Wuerzburg, Germany* We report the direct observation of Aharonov-Casher effect, which can occur when electrons propagate in a ring structure in the presence of spin-orbit interactions and external magnetic field perpendicular to the ring plane. The transport measurements have been conducted on the series of ring structures fabricated from HgTe/HgCdTe quantum wells. We study Aharonov-Bohm type conductance oscillations as a function of Rashba spin-orbit splitting strength. We observe non-monotonic phase changes indicating that an additional phase factor modifies the electron wave function. We associate these observations with the Aharonov-Casher effect and confirm it by numerical calculations of the magnetoconductance for a multichannel ring within the Landauer-Büttiker formalism.

*Work supported by Deutsche Forschungsgemeinschaft (SFB 410) and ONR (04PR03936-00).

**11:27**

**P19 2 Spin Interference Effect in a Square Loop Array including the Rashba and Dresselhaus Terms*** T. KOGA[2], H. OKUTANI, *GSIST, Hokkaido University and* [2]*CREST, JST* Y. SEKINE, [3]*NTT Basic Research Laboratories, NTT Corporation* J. NITTA[2,3], *GSEng., Tohoku University* The effect of electron wave interference to the electric conductivity ($\sigma$), including the effect of spin degree of freedom, is investigated through nanolithographically defined square (and other) loop array structures fabricated on $In_{0.52}Al_{0.48}As/In_{0.53}Ga_{0.47}As/In_{0.52}Al_{0.48}As$ quantum wells (QW). In this experiment, we measure $\sigma$'s of QWs as a function of magnetic field $B$ ($\mathbf{B}\perp$ QW plane). These samples had a gate electrode covering the entire loop array structures, where a gate voltage $V_g$ was applied between the metal gate electrode and the QW. We note that $V_g$ controls both the carrier density and the Rashba and Dresselhaus spin-orbit terms within the QWs. It turned out that the magnetoconductance $\sigma(B)$ oscillates as a function of $B$ with a period corresponding to $h/2e$, which is denoted as the

AAS oscillation. We found that the amplitude of the AAS oscillation in this system also oscillated as a function of $V_g$, which is called as a ''spin interference'' effect. We investigated this effect, which is also in close relation to the ''Aharonov-Casher'' effect (electric control of the phase of the electronic wave function), in detail including both the Rashba and Dresselhaus spin-orbit terms quantitatively.

*T.K. acknowledges the Inamori Foundation and the Murata Science Foundation for financial support.

**11:39**

**P19 3 Numrical simulation of a spin interferometer based on a single square loop with Rashba interaction** ZHENYUE ZHU, QING-FENG SUN, BIN CHEN, XIN-CHENG XIE, *Oklahoma State University* We numerically calculate the transverse conductance as a function of magnetic field in two models. One is an exact 1D model and the other is a quasi 1D square loop system which is similar to the experimental setup by Koga et. al. From the conductance curves, we employ FFT (Fast Fourier transform) and IFFT (inverse Fast Fourier transform) to extract separately the oscillatory part of conductance whose period correspond to the magnetic flux quanta (AB oscillation) and half quanta (AAS oscillation). We show that the spin precession angle $\theta$ is modulated by the Rashba interaction strength. From the curves about the amplitude of AB or AAS oscillations at B=0 versus $\theta$, we find that the node positions of $\theta$ in the exact 1D model fits well with previous theoretical calculations, but there are some deviations for the quasi 1D model.

**11:51**

**P19 4 Ahronov-Bohm oscillations in a GaAs 2D hole system** BABUR HABIB, EMANUEL TUTUC, MANSOUR SHAYEGAN, *Princeton University* We have grown shallow 2D hole samples in GaAs for implementing mesoscopic structures via local anodic oxidation using an AFM. In this talk we present our results of a ring device which shows clear Ahronov-Bohm oscillations. The amplitude of the resistance oscillations are about 10% of the ring resistance, the strongest seen in a 2D hole system to date.

**12:03**

**P19 5 Zero-field spin-splitting in $Al_xGa_{1-x}N$/GaN heterostructures** IKAI LO, M.H. GAU, W.T. WANG, J.K. TSAI, S.F. TSAY, J.C. CHIANG, *Department of Physics, Center for Nanoscience and Nanotechnology, National Sun Yat-Sen University, Kaohsiung, Taiwan, Republic of China.* DEPARTMENT OF PHYSICS, CENTER FOR NANOSCIENCE AND NANOTECHNOLOGY, NATIONAL SUN YAT-SEN UNIVERSITY, COLLABORATION, We have observed the beating Shubnikov-de Haas oscillations with respect to the zero-field spin splitting of 2DEG in $Al_xGa_{1-x}N$/GaN heterostructures. The spin-splitting energy was obtained about 9 meV from the beating SdH frequency derived by the non-linear curve fitting. A new mechanism ($\Delta_{C1} - \Delta_{C3}$ coupling) was proposed to describe the large spin splitting in wurtzite GaN, which is originated from the band folding effect and intrinsic wurtzite structure inversion asymmetry. The band-folding effect generates two conduction bands ($\Delta_{C1}$ and $\Delta_{C3}$), in which $p$-wave probability has tremendous change when $k_z$ approaches anti-crossing zone. The $\Delta_{C1} - \Delta_{C3}$ coupling can produce a spin-splitting energy much larger than traditional Rashba or Dresselhaus effects. This project is supported in parts by National Science Council, Core Facilities Laboratory in Kaohsiung-Pintung area, Taiwan (ROC).

**12:15**

**P19 6 Exact Landau Levels in Two-Dimensional Electron Systems with Rashba and Dresselhaus Spin-Orbit Interactions in a Perpendicular Magnetic Field** DEGANG ZHANG, C.S. TING, *Texas Center for Superconductivity, University of Houston, Houston, TX 77204* C.-R. HU, *Department of Physics, Texas A&M University, College Station, TX 77843* We study a two-dimensional electron system in the presence of both Rashba and Dresselhaus spin-orbit interactions in a perpendicular magnetic field. Defining a suitable boson operator and using the unitary transformations we are able to obtain the exact Landau levels in the range of all the parameters. When the strengths of the Rashba and Dresselhaus spin-orbit interactions are equal, the Zeeman and spin-orbit splittings are independent of the Landau level index $n$. Due to the Zeeman energy, new crossing between the eigenstates $|n,k,s = 1,\sigma>$ and $|n+1,k,s' = -1,\sigma'>$ is produced at certain magnetic field for larger Rashba spin-orbit coupling. This degeneracy leads to a resonant spin Hall conductance if it happens at the Fermi level.

***Invited Papers***

**12:27**

**P19 7 Spatial imaging of the spin Hall effect and current-induced polarization in two-dimensional electron gases.*** VANESSA SIH,† *Center for Spintronics and Quantum Computation, University of California, Santa Barbara, CA 93106*

Spin-orbit coupling in semiconductors relates the spin of an electron to its momentum, and provides a pathway for electrically initializing and manipulating electron spins in zero magnetic field for applications in spintronics and spin-based quantum information processing. This coupling can be regulated with strain in bulk semiconductors and quantum confinement in semiconductor heterostructures. Using Faraday and Kerr rotation spectroscopies with temporal and spatial resolution, current-induced spin polarization[1] and the spin Hall effect[2] have been observed in bulk semiconductors. More recently, we have investigated the spin Hall effect and current-induced spin polarization in a two-dimensional electron gas confined in (110) AlGaAs quantum wells using Kerr rotation microscopy[3]. In contrast to previous measurements, the

spin Hall profile shows complex structure and the current-induced spin polarization is out-of-plane. The experiments map the strong dependence of the current-induced spin polarization to the crystal axis along which the electric field is applied, reflecting the anisotropy of the spin-orbit interaction. These results reveal opportunities for tuning a spin source using quantum confinement, strain and device engineering in non-magnetic materials.

*This work was supported by ARO, DARPA, NSF and ONR.
†In collaboration with R. C. Myers, Y. K. Kato, W. H. Lau, A. C. Gossard and D. D. Awschalom.

[1]Y. K. Kato, R. C. Myers, A. C. Gossard, D. D. Awschalom, Phys. Rev. Lett. **93**, 176601 (2004).
[2]Y. K. Kato, R. C. Myers, A. C. Gossard, D. D. Awschalom, Science **306**, 1910 (2004).
[3]V. Sih, R. C. Myers, Y. K. Kato, W. H. Lau, A. C. Gossard and D. D. Awschalom, Nature Physics **1**, 31 (2005).

*Contributed Papers*

**13:03**
**P19 8 Spin Hall effect, spin-accumulation, and spin-currents in mesoscopic structures** MARIO BORUNDA, *Texas A&M University* KENTARO NOMURA, *University of Texas* JAIRO SINOVA, *Texas A&M University* Spin dependent transport effects in strongly spin-orbit coupled paramagnetic systems, such as the spin Hall Effect, have been studied extensively over the last few years. We explore how spin accumulation in a mesoscopic device could be used to observe the effect through electrical and optical means. We report calculations of spin flow in finite size samples with strong spin-orbit coupling using the non-equilibrium Green's function formalism in both the linear and the non-linear regimes. We explore different geometries and spin-orbit coupling mechanism to understand how spin relaxes near the interfaces. We will also report on the progress made in understanding the spin Hall Effect in the bulk regime and how it connects to the closely related effect of the anomalous Hall effect in ferromagnetic materials.

**13:15**
**P19 9 The finite spin Hall effect in semicondutors** NAOYUKI SUGIMOTO, *Department of Applied Physics, University of Tokyo* SHIGEKI ONODA, *Spin Superstructure Project, ERATO, Japan Science and Technology Agency* SHUICHI MURAKAMI, NAOTO NAGAOSA, *Department of Applied Physics, University of Tokyo* We formulate the theory of the spin Hall effect taking into account the impurity scattering effect as general as possible with the focus on the definition of the spin current. The conserved spin current (Zhang *et, al*. [cond- mat/0503505]) satisfying the continuity equation of spin in the bulk is considered in addition to the conventional one defined by the anti-symmetric product of the spin and velocity operators. The condition for the non-zero spin Hall current is clarified from a generic viewpoint and the following new results for explicit models are obtained: (i) spin Hall current in Rashba model is non-zero on the non-delta impurity scattering potential, and (ii) spin Hall current vanishes in cubic Rashba model on the delta impurity scattering potential.

**13:27**
**P19 10 What is intrinsic and what is extrinsic in the spin Hall effect?*** EWELINA HANKIEWICZ, GIOVANNI VIGNALE, *Univ. of Missouri-Columbia* MICHAEL FLATTÉ, *University of Iowa* Two different forms of the spin Hall effect, intrinsic and extrinsic, have been recently proposed and observed in experiments. The intrinsic effect is caused by spin-orbit coupling in the band structure of the semiconductor and survives in the limit of zero disorder, whereas the extrinsic effect is caused by spin-orbit coupling between Bloch electrons and impurities. We treat both effects on equal footing within the framework of the exact Kubo linear response formalism. We show that the ''side-jump'' term, which is usually considered part of the extrinsic spin Hall effect, is really intrinsic, because it is independent of disorder. Furthermore, it is the only non-zero *intrinsic* contribution to the spin-Hall effect for the linear Rashba (or Dresselhaus) spin-orbit coupling model. On the other hand, the skew scattering term is the only *extrinsic* contribution to the spin-Hall effect within this model. The proof based on gauge invariance holds at all orders in disorder and electron-electron interactions and to first order in spin-orbit coupling, but does not apply to more complex spin-orbit coupled bands (e.g the Luttinger model). We also study many-body effects and predict that the spin Coulomb drag will reduce the spin Hall conductivity.

*Work supported by NSF Grant No. DMR-0313681 and DARPA/ ARO DAAD19-01-1-0490.

**13:39**
**P19 11 Spin Hall Effect in Doped Semiconductor Structures*** WANG-KONG TSE, SANKAR DAS SARMA, *University of Maryland* We present a microscopic theory of the extrinsic spin Hall effect based on the diagrammatic perturbation theory. Side-jump (SJ) and skew-scattering (SS) contributions are explicitly taken into account to calculate the spin Hall conductivity, and we show their effects scale as $\sigma_{xy}^{SJ}/\sigma_{xy}^{SS} \sim (\hbar/\tau)/\varepsilon_F$, where $\tau$ being the transport relaxation time. Motivated by recent experimental work we apply our theory to n-doped and p-doped 3D and 2D GaAs structures, obtaining analytical formulas for the SJ and SS contributions. Moreover, the ratio of the spin Hall conductivity to longitudinal conductivity is found as $\sigma_s/\sigma_c \sim 10^{-3} - 10^{-4}$, in reasonable agreement with the recent experimental results of Kato et al. [Science 306, 1910 (2004)] in n-doped 3D GaAs system.

*This work is supported by NSF, ONR, and LPS-NSA.

**13:51**
**P19 12 Intrinsic spin Hall conductivity*** PAVEL KROTKOV, *University of Maryland* SANKAR DAS SARMA, *University of Maryland* In an isotropic 2D gas with general dispersion and linear-in-k spin-orbital interaction of the Rashba or Dresselhaus type in the presence of impurities we find that an intrinsic spin-Hall conductivity is finite and is of the order of the spin-orbit term squared. It vanishes only in the well-studied particular case of a quadratic dispersion.

*Supported by NSF, US-ONR, and LPS-NSA.

**14:03**

**P19 13 Imaging Stationary Flow of Spin Hall Effect-Induced Spin Densities in Mesoscopic Nanostructures** LIVIU ZÂRBO, *University of Delaware* SATOFUMI SOUMA, *Tokyo University of Science* BRANISLAV NIKOLIĆ, *University of Delaware* The spin Hall effect has recently attracted a lot of attention in semiconductor spintronics since it offers a novel way of all-electrical generation and manipulation of pure spin currents by employing spin-orbit (SO) couplings. To describe spin Hall transport on a scale of a few nanometers we introduce the concept of bond spin current and corresponding local flowing spin densities between the sites of the lattice model of a multiterminal SO coupled semiconductor nanostructure, and express them in terms of the nonequilibrium (Keldysh) Green functions. Our predictions for the out-of-plane polarized steady state spin densities flowing into the transverse interaction-free electrodes due to the longitudinal charge current injected into high-mobility two-dimensional electron gas (2DEG) with Rashba SO coupling crucially depend on the size of 2DEG in the units of spin precession length. In the presence of disorder, the flowing spin Hall densities remain non-zero in the bulk of the 2DEG. Moreover, we also find in-plane polarized spin densities flowing into the longitudinal leads due to the magneto-electric effect. These theoretically predicted images of mesoscopic spin Hall flow could be tested via recently advanced Kerr rotation microscopy.

**SESSION P20: FOCUS SESSION: COBALTITES, NICKELATES AND VANADATES**
**Wednesday Morning, 15 March 2006**
**317, Baltimore Convention Center at 11:15**
**Owen Vajk, National Institute of Standards and Technology, presiding**

**11:15**

**P20 1 Intrinsic nanoscale electronic phase separation and simple percolation in $La_{1-x}Sr_xCoO_3$*** J. WU, *Materials Science, Univ. of Minnesota* J. PARKER, *Physics, Univ. of Minnesota* C. PERREY, B. CARTER, *Materials Science, Univ. of Minnesota* J. LYNN, *Nist Center for Neutron Research, NIST* H. ZHENG, J. MITCHELL, *Materials Science Division, Argonne National Lab* C. LEIGHTON, *Materials Science, Univ. of Minnesota* The doped pervoskite cobaltite $La_{1-x}Sr_xCoO_3$ has been advanced as a model system for studying magnetoelectronic phase separation. We present here a combination of chemically sensitive high-resolution TEM, SANS, and transport data that reveal interesting new features of this phase separation. The TEM data show that the material is chemically homogenous down to nm length scales, proving that the phase separation is truly intrinsic electronic phase separation. The SANS data, which were performed at several compositions below $x = 0.18$ (where long-range ferromagnetism (FM) sets in), reveal that the FM clusters have a maximum size of about 2-3 nm, itindependent itof doping. This demonstrates that the percolation transition that occurs at $x = 0.18$ is due to an increasing density of clusters with increasing x, itnot an expansion of cluster size. These observations naturally explain the simple percolation observed in single crystal transport, i.e. conductivity exponents close to predicted values and a critical composition ($x = 0.18$) close to the expected value for the 3-D percolation limit.

*Work supported by NSF and ACS PRF.

**11:27**

**P20 2 Short-range magentic correlations and dynamic orbital ordering in the thermally activated spin state of $LaCoO_3$** S. ROSENKRANZ, *Argonne National Laboratory* D. PHELAN, D. LOUCA, S.H. LEE, *University of Virginia* P.J. CHUPAS, R. OSBORN, H. ZHENG, J.F. MITCHELL, *Argonne National Laboratory* The cobalt perovskites $La_{1-x}Sr_xCoO_3$ show intriguing spin, lattice, and orbital properties similar to the ones observed in colossal magnetoresistive manganites. The $x=0$ parent compound is a non-magnetic insulator at low temperatures, but shows evidence of a spin-state transition of the cobalt ions above 50K from a low-spin to an intermediate or high-spin configuration. Using high resolution, inelastic neutron scattering, we observe a distinct low energy excitation at 0.6meV coincident with the thermally induced spin state transition observed in susceptibility measurements. The thermal activation of this excited spin state also leads to short-range, dynamic ferro- and antiferromagnetic correlations. These observations are consistent with the activation of a zero-field split intermediate spin state as well as the presence of dynamic orbital ordering of these excited states. Work supported by US DOE BES-DMS W-31-109-ENG-38 and NSF DMR-0454672

**11:39**

**P20 3 Emergence of Magnetism in $La_{1-x}Sr_xCoO_3$** D. PHELAN, DESPINA LOUCA, S.-H. LEE, *University of Virginia, Dept. of Physics* S. ROSENKRANZ, J.F. MITCHELL, *Materials Science Division, Argonne National Laboratory* Orbital, spin, and charge degrees of freedom play a central role in the physics of CMR-type transition metal perovskite oxides. $La_{1-x}Sr_xCoO_3$ is a system in which a ferromagnetic, metallic state emerges when holes are doped into the parent compound, a non-magnetic, Mott insulator in the ground state. We have studied this system using elastic and inelastic neutron scattering techniques on single crystals with $0 \leqslant x \leqslant 0.2$. With hole doping the ferromagnetic correlations between Co spins become static and isotropically distributed due to the formation of ferromagnetic droplets. The correlation length and condensation temperature of these droplets increase rapidly with metallicity due to the double exchange mechanism. Diffuse spin dynamics appear as the correlation length increases. The dynamics are broad in energy indicative of a spin wave continuum.

**11:51**

**P20 4 Local Matrix-Cluster Interactions In $La_{1-x}$ $Sr_xCoO_3$.** SEAN GIBLIN, *CCLRC-Rutherford Appelton Lab, UK* IAN TERRY, *Durham University, UK* ANDREW BOOTHROYD, DHARMALINGIAM PRABHAKARAN, *University of Oxford, UK* JING WU, CHRIS LEIGHTON, *CEMS, University of Minnesota, USA* Magneto-electronic phase separation plays an integral part in many recent advances in the understanding of correlated electron systems. We have studied the magnetically phase separated material $La_{1-x}$ $Sr_xCoO_3$ and the parent compound $LaCoO_3$, using muon spectroscopy and magnetic susceptibility measurements. The muon as a local magnetic probe is sensitive to the magnetic field distribution in $LaCoO_3$ in the LS state, which is a direct consequence of magnetic excitons. We believe that these excitons are interacting with the Co ions undergoing the known thermally induced spin transition. By directly comparing the results of the parent compound with $La_{1-x}$ $Sr_xCoO_3$we can observe

the hole-rich ferromagnetic clusters interacting with the neighboring hole poor matrix for low x. This mechanism, detected here for the first time, may play an important role in the rich electrical and magnetic properties of $La_{1-x}$ $Sr_xCoO_3$.

**12:03**

**P20 5 Anisotropy-driven magnetic anomalies in $Pr_{1-x}Sr_xCoO_3$*** CHRIS LEIGHTON, DOUG STAUFFER, JING WU, *University of Minnesota* QING HUANG, JEFF LYNN, BRIAN TOBY, *NIST* JOHN MITCHELL, *Argonne National Lab* Interest in the perovskite cobaltites has been growing steadily due to the intriguing phenomena they exhibit. It is well known that the availability of various Co ion spin states in the cobaltites provides an additional degree of freedom in comparison to the manganites. In this work we demonstrate that the cobaltites also possess another factor of considerable importance not present in the manganites – large magnetocrystalline anisotropy. As previously reported [Mahendiran et al PRB 68 024427 (2003)] at $x > 0.30$ $Pr_{1-x}Sr_xCoO_3$ displays an additional anomaly below the Curie temperature, where the magnetization can dramatically increase or decrease depending on applied field. We demonstrate here, using magnetometry, transport, heat capacity, and neutron diffraction, that this results from a structural phase transition from a low symmetry to higher symmetry (tetragonal) phase on reducing T. Although the Co moment is unaffected, a sharp change in the magnetocrystalline anisotropy takes place and is reflected in the hysteresis loop shape, coercivity, and remnance. The complex and puzzling behavior of the field dependence of the magnetization vs. T curves is then simply explained by the T dependent variations in hysteresis loop shape.

*Work at UMN supported by NSF and ACS PRF

**12:15**

**P20 6 Magnetic properties and phase separation in $Pr_{1-x}Sr_xCoO_3$, using $^{59}$Co NMR** R. SMITH, P.L. KUHNS, M.J.R. HOCH, W.G. MOULTON, *National High Magnetic Field Laboratory* D. STAUFFER, J. WU, C. LEIGHTON, *University of Minnesota* Doped transition metal oxides including manganites and cobaltites have revealed a rich variety of properties that may be technologically important. The mixed valence cobaltite $Pr_{1-x}Sr_xCoO_3$(PSCO) has a phase diagram reminiscent of $La_{1-x}Sr_xCoO_3$(LSCO) but with a number of significant differences. For x=0.5 the system is ferromagnetic (FM) below $T_C$= 240 K but anomalous magnetization behavior is found close to 120 K with an associated crystal structure change from low symmetry to tetragonal with decreasing *T*. For $x < 0.3$ no change in magnetic properties or crystal structure is found below $T_C$. Zero-field $^{59}$Co NMR spectra show that differences in FM character between x=0.5 and x=0.3 samples are negligibly small at temperatures in the range 3-30 K No FM line was observed for x=0.2; a narrow paramagnetic- like signal only slightly shifted from the diamagnetic $^{59}$Co spectrum is observed in high- field NMR for all three x values, providing evidence of some form of phase separation where a paramagnetic phase coexists with the FM phase. The results will be compared with the very different phase separation data previously obtained for LSCO.

**12:27**

**P20 7 Structural and Magnetic Properties of the Kagomé Antiferromagnet $YbBaCo_4O_7$** JOHN MITCHELL, *Materials Science Division, Argonne National Laboratory* ASHFIA HUQ, *IPNS, Argonne National Laboratory* LAURENT CHAPON, PAOLO RADAELLI, KEVIN KNIGHT, *ISIS, Rutherford Laboratory* PETER STEPHENS, *SUNY Stonybrook* HONG ZHENG, *Materials Science Division, Argonne National Laboratory* The mixed-valent compound $YbBaCo_4O_7$ is built up of Kagomé sheets of $CoO_4$ tetrahedra, linked in the third dimension by a triangular layer of $CoO_4$ tetrahedra in an analogous fashion to that found in the known geometrically frustrated magnets such as pyrochlores and $SrCr_{9x}Ga_{12-9x}O_{19}$ (SCGO). We have undertaken a study of the structural and magnetic properties of this compound using combined high resolution powder neutron and synchrotron X-ray diffraction. $YbBaCo_4O_7$ undergoes a first order trigonal to orthorhombic phase transition at 175 K that breaks the trigonal symmetry of the structure. We show that this transition occurs as a response to a markedly underbonded $Ba^{2+}$ site in the high-temperature phase and does not appear to involve charge-ordering of $Co^{2+}/Co^{3+}$ ions in the tetrahedra. The symmetry-lowering relieves the geometric frustration of the structure, and a long-range ordered 3-D antiferromagnetic state develops below 80 K.

**12:39**

**P20 8 Crystal Structure and Magnetic Properties of an oxygen deficient n = 2 Ruddlesden-Popper phase $Sr_3Co_2O_{5.67}$** JULIENNE M. HILL, JOHN F. MITCHELL, *Materials Science Division, Argonne National Laboratory, Argonne, IL 60439* BOGDAN DABROWSKI, *Department of Physics, Northern Illinois University, DeKalb, IL 60115* Interest in charge, orbital, and spin state phenomena in perovskite and related cobalt oxides is a growing area of transition metal oxide physics. Recently, J. Matsuno et al.[1] have found that epitaxial films of the n = 1 Ruddlesden-Popper (R-P) phase $Sr_2CoO_4$ are metallic ferromagnets with relatively high $T_C \sim$ 250 K. This is particularly interesting in light of the formal oxidation state of Co, $Co^{4+}$, offering no clear source of carriers. To extend the materials chemistry and physics of the R-P series of cobaltites, we have synthesized the n = 2 R-P phase $Sr_3Co_2O_{7-\delta}$ in bulk form. The crystal structure [from neutron powder diffraction (NPD) data] of our most oxygen-deficient sample, $Sr_3Co_2O_{5.67}$ is orthorhombic itImmm with a = 3.94025(9) Å, b = 3.67479(9) Å and c = 20.6642(5) Å. The magnetization versus temperature data show two antiferromagnetic transitions at approximately 170 K and 220 K. To further elucidate the magnetic properties of this material, we have conducted a temperature-dependent NPD study. The low temperature magnetic structure is surprisingly complex and suggestive of an incommensurate ordering wave vector. Full details and results of the NPD study will be given.

[1]J. Matsuno et al., PRL **93**, 167202 (2004).

**12:51**

**P20 9 Complex magnetic structure of YBaCo4O7** LAURENT C. CHAPON, *ISIS Facility, Rutherford Appleton Laboratory, UK* JOHN F. MITCHELL, *Materials Science Division, Argonne National LAboratory, USA* PAOLO G. RADAELLI, *ISIS Facility, Rutherford Appleton Laboratory, UK* The new series of mixed-valent oxides RBaCo4O7 (R=Yb,Tb,Y) show complex structural and magnetic behavior. We have recently revealed, for the Yb analog, that a stuctural phase transition occurs in response to an extremely underbounded Ba2+ site. The symmetry lowering from orthorhombic to tetragonal, releases the frustration and allows the

system to order magnetically below 80K. Here we present our neutron diffraction study of the analog compound YBaCo4O7, that shows the same structural phase transition at high temperature and a magnetic transition at around 110K, where the system orders antiferromagnetically with propagation vector k=0. The magnetic structure, solved by global optimization algorithms, shows a non colinear Co-spins arrangement that results from the unique topology of the Co interactions. The magnetic structure is found to be strongly temperature dependent between 1.6K and 110K, which provide crucial information about the relative strengths of competing interactions.

**13:03**

**P20 10 The effect of transition metal ions distribution on magnetic properties of $Li_x(Ni_yMn_yCo_{1-2y})O_2$.** NATASHA A. CHERNOVA, MIAOMIAO MA, JIE XIAO, M. STANLEY WHITTINGHAM, *Institute for Materials Research, SUNY at Binghamton, Binghamton NY 13902-6000* PETER Y. ZAVALIJ, *Department of Chemistry and Biochemistry, University of Maryland, College Park, MD 20742-4454* $Li_x(Ni_yMn_yCo_{1-2y})O_2$ compounds have layered O(3) structure with an occupancy disorder as Ni ions migrate to the lithium layer. Ni ions provide strong antiferromagnetic (AF) exchange between the transition metal (TM) layers; therefore the degree of disorder has a pronounced effect on the magnetic properties. Ni migration is reduced when the amount of Co or Li is increased. In this work we study temperature and magnetic field dependences of magnetization and the ac susceptibility of $Li_x(Ni_yMn_yCo_{1-2y})O_2$ with various Li and Co contents. We have shown that in $LiNi_{0.5}Mn_{0.5}O_2$ compound large amount of Ni on Li sites facilitates AF order within the TM layer, while interlayer Ni ions contribute to the net magnetic moment. This is consistent with the ''flower'' order of the TMs proposed from the Monte-Carlo simulations. With increasing Co content, the ''flower'' structure is destroyed and a spin glass state is observed in Co-containing compounds. This work is financially supported by the US Department of Energy, Office of FreedomCAR and Vehicle Technologies, through the BATT program at LBNL.

**13:15**

**P20 11 Observation of Magnetic Memory Effect and Photo-induced Magnetism in $Y_{0.33}Sr_{0.67}CoO_{3-\delta}$** M. IZUMI, Y.F. ZHANG, S. SASAKI, *Tokyo University of Marine Science and Technology* O. YANAGISAWA, *Yuge National College of Maritime Technology* We prepared the $Y_{0.33}Sr_{0.67}CoO_{3-\delta}$by the conventional solid state method which sintered under the $O_2$ flow. The sample was finally annealed under the oxygen and nitrogen atmosphere. A DC magnetization jump was found about 200 K with a large thermal hysteresis at 0.01 T indicating a kind of magnetic memory effect. The magnetization jump comes from the inter-spin state transition on $Co^{3+}$ ion from low to intermediate spin state. The magnetic memory effect gradually disappears with the magnetic field increase and the jump temperature ($T_J$) shifts to low temperature. Annealed samples indicate high $T_J$, $T_C$ and the magnetization coming from the oxygen content difference. Under the irradiation of a pulsed near-infrared laser ($\lambda$ = 1050 nm), the $T_J$ shifts to low temperature and the magnetization below $T_J$ decreases. Photo-induced effect is weakened with the magnetic field. Laser irradiation may suppress spin-state transition of the part $Co^{3+}$ ions.

**13:27**

**P20 12 Local Electronic and Spin Structure of GdBaCo2O5.5 from X-ray Absorption Spectroscopy** KYLE SHEN, DAVID HAWTHORN, DARREN PEETS, ILYA ELFIMOV, GEORGE SAWATZKY, *University of British Columbia* ALEXEY TASKIN, YOICHI ANDO, *CRIEPI, Japan* The family of $RBaCo_2O_{5+\delta}$ cobaltates is known to exhibit a rich variety of magnetic behavior as a function of oxygen content and temperature. We present x-ray absorption measurements on detwinned single crystals of $GdBaCo_2O_{5.5}$, where the structure is comprised of alternating rows of $CoO_6$ octahedra and $CoO_5$ pyramids. $GdBaCo_2O_{5.5}$ exhibits successive paramagnetic, ferromagnetic, and antiferromagnetic phases, and also exhibits a ''spin blockade'' effect upon doping. These unusual behaviors are believed to stem from the nearly degenerate spin states of the $Co^{3+}$ ions which can potentially vary from low (S=0), intermediate (S=1), to high (S=2) spin states. Our recent x-ray absorption measurements provide the first measurements of the local electronic and spin states. Measurements of the temperature and polarization dependence of the x-ray absorption at the oxygen K edge clearly indicate an abrupt change in the orbital populations at the metal-insulator transition at T $\sim$ 360 K. We combine our spectroscopic measurements with atomic multiplet and LSDA+U calculations to provide a first insight into the true nature of the spin state transitions which govern the unusually rich magnetic properties of the $RBaCo_2O_{5+\delta}$ cobaltates.

**13:39**

**P20 13 High Pressure and High Resolution Magnetization of $GdBaCo_2O_{5.5}$** R. P. GUERTIN, *Tufts Univ., Medford, MA 02155* E. S. CHOI, P. SCHLOTTMANN, *NHMFL/Florida State Univ., Tallahassee, FL 32310* Z. X. ZHOU, *ORNL, Oak Ridge, TN 37830* We present the results of two rather diverse experiments designed to reveal new features of the complex magnetic properties of $GdBaCo_2O_{5.5}$ and, in particular, lanthanide/transition metal coupling in oxide materials. First, high resolution magnetization, M (H,T), measurements on an untwinned single crystal show a small but non-zero coupling between the 3d-shell Co-based magnetic order and the 4f shell Gd paramagnetism. Second, high pressure magnetization measurements on a polycrystalline sample suggest a weakening of the ferromagnetic interplane coupling at the expense of a strengthening of the antiferromagnetic interplane coupling. In the measured pressure range, however, no unambiguous pressure-induced spin transition was observed. Finally, low temperature isothermal magnetization measurements under pressure indicate a slight weakening of the effective Co-generated molecular field, affecting the Gd paramagnetism. The totality of data contained in this work suggests that there is a small but definitive molecular field effect at the Gd sites, which is a function of the strength of transition metal magnetism ordering at higher temperatures.

**13:51**

**P20 14 Electron-phonon coupling and low-temperature structure of $NaV_2O_5$** JUERGEN SPITALER, *Institute for Atomistic Modelling and Design of Materials,University Leoben* E. YA. SHERMAN, *Department of Physics, University of Toronto* H.G. EVERTZ, *Institute for Theoretical Physics, Graz Technical University* CLAUDIA AMBROSCH-DRAXL, *Institute for Atomistic Modelling and Design of Materials,University Leoben* INSTITUTE FOR ATOMISTIC MODELLING AND DESIGN OF MATERIALS,UNIVERSITY LEOBEN TEAM, INSTITUTE FOR THEORETICAL PHYSICS, GRAZ TECHNICAL UNIVERSITY

COLLABORATION, $NaV_2O_5$ is an extraordinary example of a structure where charge, spin and lattice degrees of freedom strongly interact. This low-dimensional compound is characterized by V atoms arranged in the form of ladders. At ambient conditions it is found to be quarter-filled with one electron distributed over one rung of the ladder. Going below $T_c = 34K$, $NaV_2O_5$ undergoes a phase transition involving a reordering of the V charges, a lattice deformation and a spin pairing. In order to investigate the mechanisms driving the phase transition, parameters of electron-phonon and spin-phonon for the $\Gamma$ point phonons are determined from ab initio calculations within density functional theory. They are compared to the corresponding parameters of the isostructural $CaV_2O_5$, where no phase transition occurs. Moreover, ab initio results of several candidates for the low-temperature supercell of $NaV_2O_5$ are presented and analyzed in terms of total energies and electric field gradients.

**14:03**

**P20 15 Quasi-one-dimensional electronic structure of $\beta'$-$Cu_xV_2O_5$ ($x$=0.33$\sim$ 0.65) studied by photoemission*** S.-K. MO, F. WANG, J. W. ALLEN, *Univ. of Michigan* J. HE, *Univ. of Tennessee* R. JIN, D. MANDRUS, *Oak Ridge National Lab* H. HÖCHST, *Synchrotron Radiation Center* $\beta'$-$Cu_xV_2O_5$ is a quasi-one-dimensional (quasi-1D) oxide that undergoes a metal to insulator transition (MIT) when $x$ decreases from 0.65 to below 0.60. It becomes a superconductor below 6K under pressure around 3GPa. In the metallic phase, the electrical resistivity along the chain direction is 30 times larger than that across the chain direction, making this material suitable for studies of quasi-1D electronic structures. We present the first photoemission spectra of $\beta'$-$Cu_xV_2O_5$ in both metallic (x=0.60, 0.65) and insulating (x =0.33, 0.55) phases. Angle-integrated spectra show a clear indication of the MIT. Nonetheless the intensity near the Fermi energy ($E_F$) is heavily suppressed in the metallic phase, just as in the spectra of $Li_{0.9}Mo_6O_{17}$ and certain other low dimensional oxides [1]. We observe a single band crossing $E_F$ along the chain direction, around the $\Gamma$-point of the Brillouin zone, only in the metallic phase angle-resolved spectrum. Fermi surface intensity maps have clear 1D character and the Fermi wavevector changes according to the concentration of the dopant. [1] G.-H. Gweon, J.W. Allen, and J.D. Denlinger, Phys. Rev. B **68**, 195117 (2003).

*Supported by U.S. NSF at UM (DMR-03-02825), at ORNL by the U.S. DoE, at UT by the NSF, at SRC by the NSF.



**SESSION P21: MICROFLUIDIC PHYSICS III**
**Wednesday Morning, 15 March 2006**
**318, Baltimore Convention Center at 11:15**
**Mark Robbins, John Hopkins University, presiding**

**11:15**

**P21 1 Multi-Point Holographic Micro-Velocimetry** ROBERTO DI LEONARDO, *INFM-CNR Dipartimento di Fisica, Universita' di Roma ''La Sapienza,'' Roma, Italy* JONATHAN LEACH, *Department of Physics and Astronomy, University of Glasgow, Glasgow, Scotland* HASAN MUSHFIQUE, *Department of Electrical Engineering, University of Glasgow, Glasgow, Scotland* JOHN COOPER, *Department of Electrical Engineering, University of Glasgow, Glasgow, Scotland* GIANCARLO RUOCCO, *INFM-CNR Dipartimento di Fisica, Universita' di Roma ''La Sapienza,'' Roma, Italy* MILES PADGETT, *Department of Physics and Astronomy, University of Glasgow, Glasgow, Scotland* We show how holographic optical trapping can be used for the multi-point measurement of fluid flow in microscopic geometries. An array of microprobes can be simultaneously trapped and used to map out the fluid flow in a microfluidic device. The optical traps are alternately turned on and off such that the probe particles are displaced by the flow of the surrounding fluid and then re-trapped. The particles' displacements are monitored by digital video microscopy and directly converted into velocity field values. The validity of the technique is demonstrated for the case of the flow around a spinning sphere and the flow at the outlet of a micro-channel.

**11:27**

**P21 2 A Hybrid Microwave Source and Irradiator for Biological Lab On a Chip Applications.** DAVID ISSADORE, *Harvard University, Department of Engineering and Applied Sciences* TOM HUNT, KRISTI ADAMSON, *Harvard University, Physics* ROBERT WESTERVELT, *Harvard University, Department of Engineering and Applied Sciences* RICK ROGERS, *Harvard Medical School* Using a standard lithographic process, we have built a hybrid microwave irradiator for use in microwave enhanced chemistry and localized, rapid heating. The device combines a 100mW microwave source with a near field antenna to produce an entirely on-chip system for delivering microwave energy into a thin( $< 100\mu$m) layer above a substrate. The antenna utilizes a serpentine wire pattern to produce a thin layer of intense microwave electromagnetic field intensity that falls off exponentially in distance away from the substrate. The device, including RF electronics, was built on a standard 1'' by 3'' glass slide, and several antenna pixel sizes are tested for Biological Lab On a Chip Applications. This work is made possible by the NSEC NSF grant PHY-0117795.

**11:39**

**P21 3 Simulations of Contact Line Motion in Partially Miscible Fluids** SHENGFENG CHENG, *Dept of Physics and Astronomy, The Johns Hopkins University, Baltimore, MD 21218, USA* COLIN DENNISTON, *Dept of Applied Mathematics, The University of Western Ontario, London, Ontario, Canada N6A 5B8* MARK ROBBINS, *Dept of Physics and Astronomy, The Johns Hopkins University, Baltimore, MD 21218, USA* We report on extensive molecular-dynamics simulations of contact line motion in partially miscible fluids confined between two solid walls and sheared in a Couette geometry. Our results show that diffusion alone cannot remove the stress singularities at the contact line or lead to no-slip boundary conditions on the fluid velocity. Computed velocity fields show that there is a substantial drop of the fluid velocity near the contact line, which is associated with the gradient of the fluid-solid interfacial tension in the same region. However, the fluid velocity does not fall to zero at the contact line, in contrast to the case where fluids are immiscible. The nonzero velocity leads to a net advective flux across the fluid-fluid interface, which is balanced by the diffusive flux induced by the concentration gradient. The advective and diffusive fluxes across the interface are only significant in the very first layer of fluid atoms.

**11:51**

**P21 4 Macromolecular Liquids Slip Over Solid Surfaces: Experimental Studies of the Slip Length*** KARIN JACOBS, RENATE FETZER, *Saarland University, Dept. of Experimental Physics, 66041 Saarbruecken, Germany* We present a novel method to asses the slip length and viscosity of thin films of highly viscous Newtonian liquids. We quantitatively analyze dewetting fronts of low molecular weight polystyrene melts on Octadecyl- (OTS) and Dodecyltrichlorosilane (DTS) polymer brushes [1]. Using a thin film (lubrication) model derived in the limit of large slip lengths, we can extract slip length and viscosity of films with thicknesses between 50 nm and 230 nm and temperatures above the glass transition. We find slip lengths from 100 nm up to 1 micron on OTS and between 300 nm and 10 microns on DTS covered silicon wafers. The slip length decreases with temperature. The obtained values for the viscosity are consistent with independent measurements [2]. [1] R. Fetzer, K. Jacobs, A. Muench, B. Wagner, T.P. Witelski, Phys. Rev. Lett. 95, 127801 (2005) [2] R. Fetzer, K. Jacobs, M. Rauscher (to be published)

*Priority Program SPP 1146 ''Nano- and Microfluidics'' of the German Science Foundation

**12:03**

**P21 5 Source of Shear Dependent Slip at Liquid/Solid Interfaces** NIKOLAI PRIEZJEV,* *Michigan State University* SANDRA TROIAN,† *Princeton University* Slippage at liquid/solid interfaces can strongly influence transport behavior in micro- and nanoscale systems. Previous molecular dynamics (MD) studies of simple and polymeric fluids subject to planar shear at small Reynolds number have shown that the slip length increases as a power law in the shear rate for moderate to high values. The corresponding boundary condition provides a new generalization of the Navier slip law. In this talk, we examine what physical mechanism is responsible for the shear rate exponent by focusing on the collision events between the fluid particles in the first layer and the adjacent wall particles comprising a crystalline surface. By examining the interfacial frictional force as a function of the fluid sliding velocity, we recover similar behavior as inherent in the generalized slip condition and determine that the dominant frictional response stems from the repulsive part of the Lennard-Jones interaction potential. A reduced kinetic model describing the scattering of a single molecule with a given slip velocity along a crystalline surface helps explain the saturation in the frictional force at large sliding velocities. These results elucidate how different is the slip behavior at liquid/solid interfaces from that observed in rarefied gases.

*Dept. Mechanical Engineering
†Dept. Chemical Engineering

**12:15**

**P21 6 Apparent Slip at Hydrophilic Surface: Flow Profile within 1 nm from the Surface** SUNG CHUL BAE, STEPHEN ANTHONY, STEVE GRANICK, *Departments of Materials Science and Engineering, of Chemistry, of Physcis, University of Illinois* Fluid dynamics within small channels draws great interest due to the development of microfluidic devices, yet details about flow immediately at a solid surface remain too vague. Here, by using fluorescence energy transfer (FRET and fluorescence quenching) approaches, we measured the flow rate of fluorescence quencher molecules within 1 nm from the quartz surface within a specially-designed microfluidic device. In parallel, we have simulated the flow dynamics at the surface, in order to separate cleanly the actual near-surface velocity from the confounding effects of near-surface diffusion.

**12:27**

**P21 7 Slip versus Friction : Modifying the Navier condition** EVANGELOS KOTSALIS, *ETHZ* JENS WALTHER, *ETHZ & TU Denmark* PETROS KOUMOUTSAKOS, *ETHZ* The modeling of fluid-solid interfaces remains one of the key challenges in fluid mechanics. The prevailing model, attributed to Navier, defines the fluid ''slip'' velocity as proportional to the wall shear and a parameter defined as the slip length. Several works have in turn proposed models for this slip length but no universal model for the slip velocity has been accepted. We present results from large scale molecular dynamics simulations of canonical flow problems, indicating, that the inadequacy of this classic model, stems from not properly accounting for the pressure field. We propose and validate a new model, based on the fundamental observation that the finite ''slip'' velocity is a result of an imbalance between fluid and solid intermolecular forces. An excess force on the fluid elements will lead to their acceleration which in turn may result in a slip velocity at the interface. We formulate the slip velocity in terms of fluid-solid friction $F_f$ and propose a generalized boundary condition: $F_f = F_s + F_p = \lambda_u u_s + \lambda_p p$ where p denotes the pressure, and $\lambda_u$and $\lambda_p$ the viscous and static friction coefficients, for which universal constants are presented. We demonstrate that the present model can overcome difficulties encountered by the classical slip model in canonical flow configurations.

**12:39**

**P21 8 Slip and Air-Entrainment at Water-Solid Interfaces** YINGXI ELAINE ZHU, PRASAD SARANGAPANI, *Department of Chemical and Biomolecular Engineering, Univerisity of Notre Dame* ASHIS MUKHOPADHYAY, *Wayne State University* A number of recent studies performed with water flow past hydrophobic microchannels have reported the existence of 'slip' at wall and suggested the existence of the interfacial gas layer as the underlying mechanism for the slip motion, yet the details are much disputed. We combine microscopy and advanced laser spectroscopy to directly and non-invasively detect the interfacial gas layer in flowing water past micro/nano-channels whose surface chemistry and gap spacing are varied. We observe that the dimension of the gas layer strongly depends on surface hydrophobicity and flow rates. Surprisingly, we have also observed the slip motion of water over hydrophilic surfaces with a strong dependence on liquid-loading conditions. We propose a mechanistic theory about air-entrainment that can account for our observations to elucidate the origin of the gas formation at water-solid interface and its consequence on slip motion.

**12:51**

**P21 9 Rheology of sub-nanometer thick water films** TAI-DE LI, ROBERT SZOSZKIEWICZ, ELISA RIEDO, SCHOOL OF PHYSICS, GEORGIA INSTITUTE OF TECHNOLOGY TEAM, Knowing the behavior of water in small volumes is essential for the understanding of many processes in biology, tribology, and geophysics. Water under nano-confinement plays a crucial role in biological and technological systems. Here, we report an experiment in which an atomic force microscope tip approaches a flat solid surface in purified water, while small lateral oscillations are applied to the tip. The normal and lateral forces acting on the tip

are measured directly and simultaneously as a function of water thickness. We find that, for hydrophilic surfaces, oscillatory solvation forces are present in the last four adjacent water layers where the dynamic viscosity is measured to grow up orders of magnitude in respect to bulk water. The same effects are present for atomically smooth surfaces and slightly rough surfaces. Oscillatory solvation forces have been detected also when the confining flat surface was hydrophobic.

**13:03**

**P21 10 Wetting morphologies on surfaces nanopatterned with chemical stripes*** ANTONIO CHECCO, OLEG GANG, BENJAMIN M. OCKO, *Condensed Matter Physics and Materials Science Dept. Brookhaven Natl. Laboratory* SOFT MATTER GROUP TEAM, Here we investigate the wetting of simple, volatile liquids on model chemical nanopatterns created using Local Oxidation Nanolithography. This technique makes use of a biased, metallic AFM tip to locally oxidize the methyl-terminations of a self-assembled monolayer (octadecylthrichlorosilane) into carboxylic acid termination[1]. With this method we have realized parallel, 50 to 500 nm wide, wettable stripes (carboxylic) embedded into a non-wettable (methyl) surface. Several organic (polar, non-polar), volatile liquids have been condensed onto the nanopatterned surface and the resulting wetting morphologies have been studied in-situ by using an environmental AFM. Initially the liquid only condenses on the wettable stripes to form a thin liquid film. Close to saturation the liquid morphology becomes drop-like. Eventually, when more and more liquid is condensed on the stripes, the liquid drops may ''spill over'' into the non-wettable spacer so that neighboring lines merge and undergo a ''morphological wetting transition.'' For all of these regimes we show that long-range forces are relevant to nanoliquid ''shape.'' Results will be compared with those of Density Functional Theory.[1] R. Maoz, S. Cohen, and J. Sagiv, Adv. Mater. **11**, 55 (1999)

*This work is supported by the U.S. DOE under contract No. DE-AC02-98CH10886

**13:15**

**P21 11 Self-propelled film-boiling liquids** HEINER LINKE, MICHAEL TAORMINA, BENJAMIN ALEMAN, LAURA MELLING, COREY DOW-HYGELUND, RICHARD TAYLOR, *University of Oregon* MATTHEW FRANCIS, *University of Sydney* We report that liquids perform self-propelled motion when they are placed in contact with hot surfaces with asymmetric (ratchet-like) topology. Millimeter-sized droplets or slugs accelerate at rates up to 0.1 g and reach terminal velocities of several cm/s, sustained over distances up to a meter. The pumping effect is observed when the liquid is in the film-boiling regime, for many liquids and over a wide temperature range. We propose that liquid motion is driven by a viscous force exerted by vapor flow between the solid and the liquid. This heat-driven pumping mechanism may be of interest in cooling applications, eliminating the need for an additional power source.

**13:27**

**P21 12 Ratcheting motion of capsules on tailored substrates** ANNA C. BALAZS, KURT A. SMITH, ALEXANDER ALEXEEV, ROLF VERBERG, *University of Pittsburgh* We study the motion of microcapsules on attractive surfaces. The capsules, modeled as fluid-filled elastic shells, represent polymeric microcapsules or biological cells. Certain periodic surface patterns give rise to directed capsule motion for a symmetric energy input, such as an oscillatory shear flow. We use a numerical model which integrates a lattice spring representation of the capsule shell and the substrate with a lattice Boltzmann representation for the fluid regions. We consider, as a surface pattern, a series of asymmetric ramps. The minimum shear necessary to drive a capsule ''forward'' over one ramp is less than that needed to drive the capsule ''backward'' over a ramp. We show under what conditions it is possible to move the capsule forward, in a ratcheting motion, via an imposed oscillatory flow. These patterned surfaces could be used to control capsule motion precisely, based on flow and surface properties. They coud also be used to efficiently sort capsules based on their size or material properties.

**13:39**

**P21 13 Electrowetting for Digital Microfluidics** TOM HUNT, KRISTI ADAMSON, *Harvard Physics* DAVID ISSADORE, ROBERT WESTERVELT, *Harvard Division of Engineering and Applied Science* Droplet based chemistry promises to greatly impact biomedical research, providing new avenues for high throughput, low volume assays such as drug screening. Electrowetting on Dielectric (EWOD) is an excellent technique for manipulating microscopic drops of liquid. EWOD uses buried electrodes to locally change the surface energy between a droplet and a substrate. We present microfabricated devices for moving droplets with EWOD. One example of such a device consists of a series of 16 interdigitated electrodes, decreasing in size from 1mm to 20 microns. Each electrode is addressable by an independent, computer controlled, high voltage supply. This work made possible by a gift from Phillip Morris and the NSEC NSF grant PHY-0117795.

**13:51**

**P21 14 Surface mediated liquid transport on nanotube** MIN-FENG YU, *Univ. of Illinois at Urbana-Champaign* KYUNGSUK YUM, The surface mediated liquid transport on nanotubes was studied using a nanotube-based liquid transport system. Micros-cale liquid droplets were formed and transferred to nanotubes using the liquid transport system integrated with a nano-manipulator. If the spreading parameter $S$ is larger than a threshold value $S_c$, the liquid spontaneously flows out of the liquid droplet through a thin precursor film formed along the nanotube surface. The liquid transport on nanotube surfaces was studied itin situ by measuring the volume flow rate which was obtained from a direct observation of the droplet. The flow rate dependence on the size of nanotubes and surface energy were also investigated. The surface mediated liquid transport phenomenon can be exploited for the development of nanoscale liquid transport system for nanofabrication and nanoscale devices for biological and chemical applications. Reference: Kyungsuk Yum and Min-Feng Yu, Surface-mediated liquid transport through molecularly thin liquid films on nanotubes, Phys. Rev. Lett. 95, 186101 (2005)

**SESSION P22: FOCUS SESSION: SPIN TRANSPORT IN METALS**
**Wednesday Morning, 15 March 2006**
**319, Baltimore Convention Center at 11:15**
**Branislav Nikolic, University of Delaware, presiding**

*Contributed Papers*

**11:15**
**P22 1 Disorder, itinerant ferromagnetism and the anomalous Hall effect in two dimensions** PARTHA MITRA, ARTHUR HEBARD, *Department of Physics University of Florida* This talk will describe research motivated by the lack of consensus on what happens in a band ferromagnet such as iron when the itinerancy of the electrons, which carry spin information, is compromised by disorder. We address this challenging problem by performing itin situ studies of magnetotransport in a series of films having sheet resistances varying from 50 to 1,000,000 Ohms. In the weakly disordered regime of this two-dimensional system, where the quantum corrections to the conductivity have logarithmic temperature dependence, we find a surprising scaling of the longitudinal and anomalous Hall (transverse) resistances. For higher disorder the scaling breaks down and the anomalous Hall resistance $R_{xy}$ saturates at a constant value near 100 Ohms. These results imply the presence of an itanomalous Hall insulating state where the longitudinal $L_{xx}$ and transverse $L_{xy}$ conductivities approach zero with a ratio $R_{xy} = L_{xy}/L_{xx}^2$ that remains constant.

**11:27**
**P22 2 Theory of Anomalous Hall Effect in Ferromagnets** SHIGEKI ONODA, *Spin Superstructure Project, ERATO, Japan Science and Technology Agency* NAOYUKI SUGIMOTO, NAOTO NAGAOSA, *Department of Applied Physics, University of Tokyo* Mechanism of the anomalous Hall effect (AHE) in ferromagnetic metals has been controversial over many decades. Karplus-Luttinger initiated the discussion by focusing on the intrinsic thermodynamic Hall current produced by the band structure with a spin-orbit interaction. Later, it was argued that instead, scattering by impurity or disorder together with the spin-orbit interaction distorts the electron motion as the skew scattering or the side jump and these extrinsic contributions dominate over the Hall current. Here, we reexamine this issue by fully taking account of both the impurity scattering and the anomalous velocity in terms of the quantum transport theory. We demonstrate that apart from the conventional nonequilibrium transport current, an equilibrium Hall current flows even in the presence of dissipation in metals. This equilibrium Hall current contains the intrinsic one which has a topological non-perturbative nature associated with degeneracy of the band dispersions in the momentum space. We also show that there appears a crossover from the extrinsic regime to the intrinsic as the electron damping rate becomes comparable to or larger than the energy scale of the spin-orbit coupling. This resolves the long standing puzzle on the mechanism and reveals a new small energy scale governing the quantum transport in multiband systems.

**11:39**
**P22 3 Quantum correction to the anomalous Hall conductivity of ferromagnetic metallic films** KHANDKER MUTTALIB, *University of Florida* PETER WOELFLE, *University of Karlsruhe, Germany* Motivated by new anomalous Hall effect (AHE) data on polycrystalline Fe films we calculate the interaction correction to the AHE for both the skew scattering and the side jump mechanisms. The correction to the longitudinal conductivity is also considered. We use a model of randomly located short range impurity potentials of arbitrary scattering strength, inducing spin-orbit scattering, and an isotropic band ferromagnet. The quantum correction is found to depend sensitively on the strengths of the scattering potential and the spin-orbit interaction. In the limit of weak scattering, known results are recovered.

**11:51**
**P22 4 Spin Hall effects in diffusive normal metals.** ROMAN SHCHELUSHKIN, ARNE BRATAAS, We study transport in normal metals in an external magnetic field. We employ the Keldysh formalism to find transport equations in the presence of the spin-orbit interaction, interaction with magnetic impurities, and nonmagnetic impurity scattering. This system exhibits an interplay between a transverse spin imbalance (spin Hall effect) caused by the spin-orbit interaction, a Hall effect via the Lorentz force, and spin precession due to the Zeeman effect. The spin and charge accumulations are computed numerically in experimentally relevant thin film geometries. The out-of-plane spin Hall potential is suppressed when the Larmor frequency is larger than the spin-flip scattering rate. The in-plane spin Hall potential vanishes at a zero magnetic field and attains its maximum at a finite magnetic field before spin precession starts to dominate. Spin injection via ferromagnetic contacts creates a transverse charge Hall effect that decays in a finite magnetic field due to spin precession.

**12:03**
**P22 5 Resistance and Scattering Anisotropy of Al Interfaces with Co, Fe, and Co(91)Fe(9).*** NIKOLETA THEODOROPOULOU, THIBAULT HAILLARD, AMIT SHARMA, REZA LOLOEE, WILLIAM PRATT JR., JACK BASS, *Dept. of Physics and Astronomy, Michigan State University* The properties of normal/ferromagnetic metal interfaces, described by the interface specific resistance, AR* (A = area, R = resistance) and spin scattering anisotropy, $\gamma$, are of both fundamental interest and practical interest for optimizing current-perpendicular-to-plane (CPP) magnetoresistance (MR) and current-induced magnetization-switching (CIMS) in nanopillars. From measurements of the CPP resistances and MRs of sputtered [Al/F]x$N$ (F= Fe, Co, Co(91)Fe(9)) multilayers with $N$-bilayers, and Al/F-based exchange-biased spin-valves, we are able to estimate 2AR* and $\gamma$ for each metal pair at 4.2K. In each case, 2AR* is large and $\gamma$ is small, comparable to values of 2AR* $\sim$ 9 f$\Omega$m$^2$ and $\gamma \sim 0.03$ for Permalloy (Py)/Al interfaces [1], and each differing by an order of magnitude from the parameters for well-studied Co/Cu and Py/Cu interfaces (2AR* $\sim$ 1 f$\Omega$m$^2$, $\gamma \sim 0.8$). The values of AR* with Al are too large to be explained by the resistivities of alloyed Al/F interfaces. The similarity of results for Py, Fe, Co, and Co(91)Fe(9) strongly suggests that spin dependent scattering at Al/F interfaces is determined mainly by the properties of Al. [1] N. Theodoropoulou et al., J. Appl. Phys. (In Press, 2006).

*Supported by NSF grant 05-01013 and Seagate Technology

**12:15**

**P22 6 Current-Perpendicular-to-Plane (CPP) Resistance of Cu/Al Interfaces*** AMIT SHARMA, NIKOLETA THEODOROPOULOU, REZA LOLOEE, WILLIAM PRATT JR., JACK BASS, *Department of Physics, Michigan State University, East Lansing, MI 48824* . The recent discovery [1] that the current-perpendicular-to-plane (CPP) interface specific resistance (area A times resistance R) of Py/Al (Py = Permalloy = Ni(84)Fe(16)) is almost 10 times larger than that of Py/Cu, led us to examine also the resistances and magnetoresistances of Py/Cu/Al/Cu/Py exchange-biased spin-valves (EBSV) and [Cu/Al]x*N* multilayers with *N* repeats. Using two different techniques, we estimate the interface specific resistance of sputtered Al/Cu interfaces as $2AR(Al/Cu) \sim 2$ f-ohm-$m^2$ at 4.2K. However, some of the data from these two techniques, as well as from the Cu/Al/Cu EBSV studies, show unusual behaviors that suggest that the Cu and Al atoms might not always stay where they are deposited. We will describe our CPP-resistance results, and plan to supplement them with x-ray and cross-sectional TEM studies. [1] N. Theodoropoulou et al., J. Appl. Phys. (In Press, 2006).

*Supported by NSF grant 05-01013 and Seagate Technology

***Invited Papers***

**12:27**

**P22 7 Spin transport and spin-flip scattering in magnetic multilayer structures.***
SAMIR GARZON, *University of South Carolina Nanocenter*

The existence of spin-flip scattering at the interface between ferromagnetic (F) and nonmagnetic (N) layers of magnetoresistive F/N/F structures can significantly reduce the size of the magnetoresistance, limiting the sensitivity and increasing the power consumption of F/N/F devices such as GMR magnetic field sensors, magnetic read heads, and MRAM's [1]. Detecting and measuring the degree of spin flip scattering in F/N/F structures can allow further optimization in such devices as well as increase the understanding of interfacial spin transport. Our nonlocal spin injection and detection experiments on mesoscopic Co-$Al_2O_3$-Cu-$Al_2O_3$-Co spin valves provide evidence for the existence of interfacial spin-flip scattering in magnetoresistive devices [2]. By extending the conventional picture of spin-dependent interfacial resistances ($R_\uparrow$, $R_\downarrow$) to include two additional spin-flip scattering channels ($R_{\uparrow\downarrow}$,$R_{\downarrow\uparrow}$) [3] we have shown that the nonlocal resistance contains information about both the degree of spin polarization and the degree of spin-flip scattering at the F/N interface. The magnitudes of $R_{\uparrow\downarrow}$ and $R_{\downarrow\uparrow}$ depend on the relative orientation of the detector magnetization and the nonequilibrium magnetization in the normal metal. We have observed that the difference in spin-flip scattering between up and down channels vanishes at low temperatures, but for T$>$ 100K it increases nonlinearly with temperature. Further evidence for the presence of interfacial spin-flip scattering can be obtained from noise measurements, which are extremely sensitive to the microscopic transport details. [1] Spin Dependent Transport in Magnetic Nanostructures, edited by S. Maekawa and T. Shinjo (Taylor & Francis, New York, 2002). [2] S. Garzon, I. Žutić, and R. A. Webb, Phys. Rev. Lett. **94**, 176601 (2005). [3] E. I. Rashba, Eur. Phys. J. B **29**, 513 (2002).

*This work was done with I. Žutić and R. A. Webb and was supported by NSF, NSA Laboratory for Physical Science, and NRC.

***Contributed Papers***

**13:03**

**P22 8 Measurement of spin-diffusion length in sputtered Ni films*** CHARLES MOREAU, *Albion College* WILLIAM PRATT, *Michigan State University* NORMAN BIRGE, *Michigan State University* The spin-diffusion length of the electron represents a fundamental transport parameter and plays a central role in the development of spintronic devices. While several measurements of the spin-diffusion length in normal metals and in ferromagnetic alloys exist, measurements in elemental ferromagnets (Ni, Fe, Co) have been scarce. We present a novel sample geometry using giant magnetoresistance (GMR) for the measurement of the spin-diffusion length in elemental ferromagnets with weak scattering asymmetry. We report the first measurement of the spin-diffusion length of Ni using an exchanged-biased Permalloy-based spin-valve, Py/Ni/Cu/Py, where the Ni layer acts as a GMR spoiler layer when its thickness becomes greater than the spin-diffusion length in Ni.

*Work supported by NSF DMR-0405238

**13:15**

**P22 9 Magneto-transport in $Fe_3O_4$/Nb:$SrTiO_3$ schottky junction diode** DARSHAN KUNDALIYA, S.B. OGALE, J. HIGGINS, T. VENKATESAN, *Center for Superconductivity Research, University of Maryland, College Park, MD-20742* L.F. FU, N.D. BROWNING, *LBNL, NCEM, One Cyclotron Road, Berkeley, CA-94720* Among the half metallic ferromagnets, $Fe_3O_4$ is of particular interest because of its half metallicity, high curie temperature and a charge ordering transition at 120K (popularly known as Verwey transition ($T_V$)). These materials are also expected to show 100% spin polarization. In view of these fascinating properties, we studied temperature dependent transport, magnetic, structural and interface characteristics of epitaxial schottky junctions between $Fe_3O_4$ and Nb:$SrTiO_3$ (with different Nb concentrations). Epitaxial thin films of $Fe_3O_4$ were grown on Nb:$SrTiO_3$ substrates by PLD technique. The films show epitaxial growth along (100)-axis direction. We also performed HR-TEM and EELS study to ensure a better quality interface. In the temperature range above $T_V$, 300K-130K, the I-V characteristic shifts towards higher forward bias voltage upon lowering temperature. On further decreasing temperature (below $T_V$), the trend is reversed. Junction parameters such as the Schottky barrier height (it $\phi_B$) and ideality factor (it $\eta$) are extracted using thermionic emis-

sion theory at all temperatures. These parameters show interesting and systematic trends above and below $T_V$. From the magnetic field dependence of non linear I-V characteristics data, a spin polarization of $\sim$ 80% is estimated for the magnetite electrode at $T_V$.

**13:27**

**P22 10 Spin filtering of hot electrons in ferromagnetic layers** DRISS LAMINE, *Laboratoire de Physique de la matière condensée, UMR 7643-CNRS, Ecole Polytechnique. 91128 Palaiseau Cedex, France* NICOLAS ROUGEMAILLE, *Lawrence Berkeley National Laboratory, 1 Cyclotron Road MS/72, Berkeley, CA 94720, USA* GEORGES LAMPEL, YVES LASSAILLY, JACQUES PERETTI, *Laboratoire de Physique de la matière condensée, UMR 7643-CNRS, Ecole Polytechnique. 91128 Palaiseau Cedex, France* We present a spin dependent transport experiment where spin polarized electrons, injected from vacuum, are spin-filtered when entering into a thin ferromagnetic layer. The role of the interface between this spin-filter layer and the ''current collector'' is analysed. In a first geometry, the ''current collector'' is a semiconductor and the transmitted current is measured through a Fe/Oxide/GaAs diode. In that case, the measured electrons are selected at the interface, at an energy higher than the Schottky barrier. In a second geometry, the spin filter is a self standing thin layer Au/Co/Au and the ''current collector'' is a faraday cup. In that case, only electrons that overcome the vacuum energy level of the gold are measured. In both cases, the spin dependent part of the collected current is measured when the ferromagnetic layer is reversed. We have found an energy domain where both the collected current and its spin dependence increase over orders of magnitude. The role of the interface in the spin-dependent transport is discussed and a spin dependent transport model is presented.

**13:39**

**P22 11 Mesoscopic Conductance Fluctuations in Cobalt Nanoparticles** YAGUANG WEI, XIYA LIU, LIYUAN ZHANG, DRAGOMIR DAVIDOVIC, *Georgia Institute of technology* SCHOOL OF PHYSICS, GEORGIA INSTITUTE OF TECHNOLOGY TEAM, We present measurements of mesoscopic conductance fluctuations in Cobalt particles of diameter 200nm. Samples are made by e-beam lithography and shadow metal deposition. Co particles are not single domain; domain walls are nucleated at the contacts between Co and Cu-reservoirs. We obtain the dependence of peaks in differential resistance with the applied voltage and the magnetic field during the magnetization reversal process at 0.03K temperature. The conductance fluctuations with the magnetic field are caused by a mechanism different from the usual Aharonov-ohm effect. In particular, domain walls are found to generate significant mesoscopic fluctuations. We obtain that electron transfer across the domain wall is associated with a phase change of about $5\pi$. We explain how this phase-shift arises from a not perfectly parallel spin-transport across domain walls. The dephasing time is very short, $\tau_\phi \sim ps$. Fast dephasing is correlated with the strong magnetocrystalline anisotropy in Co. This work was performed in part at the Georgia-Tech electron microscopy facility. We thank P. Brouwer for valuable discussions. This research is supported by the David and Lucile Packard Foundation grant 2000-13874 and Nanoscience/Nanoengineering Research Program at Georgia-Tech.

**13:51**

**P22 12 Spin transport through atomic scale chromium Coulomb islands*** MARC VAN VEENHUIZEN, JAGADEESH MOODERA, *Massachusetts Institute of Technology* Electrical current through metallic islands coupled via tunnel barriers to external leads is governed by the Coulomb repulsion and can be brought down to single electron transport. The spin-degeneracy of the electrons can be lifted by choosing both the leads and the islands to be magnetic. The combination of spin-splitting and Coulomb blockade creates a device geometry capable of resonant tunneling of a single spin-direction only. Maximum effect can be obtained by minimization of the size of the Coulomb islands in order to suppress spin-relaxation. We report on our efforts to make a spin-resonant tunneling device using atomic size clusters of chromium atoms, submerged in an alumina-barrier in a conventional magnetic tunnel junction set-up. The $300x300\ \mu m^2$ size magnetic tunnel junction consists of a cobalt bottom electrode, an aluminum-oxide tunnel barrier, a delta-doping layer of chromium in the range of $1 - 6$ Å, an alumina tunnel barrier, and a permalloy top-electrode. Transport measurements reveal Coulomb blockade behavior.

*Supported by NSF and KIST-MIT grants

**14:03**

**P22 13 Orbital nature of spin magnetic moment** CHIH-PIAO CHUU, *University of Texas* MING-CHE CHANG, *University of Texas* QIAN NIU, *University of Texas* In view of the application of spintronics, it is important to understand the physical observable of the spin, i.e. its magnetic moment. We show by constructing a wave-packet in the upper bands of the Dirac equation that the spin magnetic moment (Bohr magneton) is a direct result of the self-rotation in the wave-packet. In this sense, an non-relativistic electron is really a rotating charged object, confirming the original speculation on the physical nature of the electron spin. In a Bloch band of a crystal, a wave-packet can acquire additional self-rotating orbital angular momentum, giving rise to a change of the spin magnetic moment and causing a modification of the g-factor from 2.



**SESSION P23: QUANTUM SPIN CHAINS II**
**Wednesday Morning, 15 March 2006**
**320, Baltimore Convention Center at 11:15**
**Matthew Stone, Oak Ridge National Laboratory, presiding**

**11:15**

**P23 1 Thermal transport of dimerized and frustrated spin-1/2 chains*** FABIAN HEIDRICH-MEISNER, *Department of Physics and Astronomy, The University of Tennessee, Knoxville, and Condensed Matter Sciences Division, Oak Ridge National Laboratory* ANDREAS HONECKER, WOLFRAM BRENIG, *Institut für Theoretische Physik, Technische Universität Carolo-Wilhelmina zu Braunschweig, Germany* We present a numerical study of thermal transport in dimerized and frustrated spin-1/2 chains at finite temperatures. Since these models are nonintegrable, the thermal Drude weight scales to zero in the thermodynamic limit. The conductivity at finite frequencies, however, is non-zero and we discuss the scaling with system size as well as the extrapolation to the zero-frequency limit. Results for three cases are presented. First,

the dimerized chain is studied in the limit of weakly coupled dimers. In this case, interactions of the elementary triplet excitations are weak, which should allow for an analytical description based on a bond-boson operator representation. Second, we compare the thermal conductivity of the frustrated chain in the massless and the massive regime of this model. Finally, we extract the zero-frequency thermal conductivity of the isotropic two-leg spin ladder and discuss implications for the interpretation of recent experiments for $La_5Ca_9Cu_{24}O_{41}$.

*This work was supported by the Deutsche Forschungsgemeinschaft, DFG.

**11:27**

**P23 2 A systematic method for constructing a spin-singlet basis for quantum antiferromagnets*** VLADIMIR GRITSEV, *Department of Physics, Harvard University* JULIEN SUDAN, DIONYS BAERISWYL, *Department of Physics, University of Fribourg, Switzerland* We present a new method for constructing a complete orthonormal basis for the singlet states of quantum spin-1/2 lattice systems. Our approach can be used for any dimension and an arbitrary lattice symmetry. In this talk the main group- and graph-theoretical steps are explained. The general theory is then applied to the one-dimensional quantum antiferromagnet. Exploiting the symmetries of closed rings, we can drastically reduce the number of basis states for the different eigenstates of the Hamiltonian (in the singlet sector). The method allows to calculate in an efficient way expectation values of any operator.

*Supported by Swiss National Science Foundation

**11:39**

**P23 3 Crossed Spin-1/2 Heisenberg Chains as a Quantum Impurity Problem*** SEBASTIAN REYES, *Brookhaven National Laboratory and Stony Brook University* ALEXEI TSVELIK, *Brookhaven National Laboratory* Using equivalencies between different models we reduce the model of two spin-1/2 Heisenberg chains crossed at one point to the model of free fermions. The spin-spin correlation function is calculated by summing the perturbation series in the interchain interaction. The result reveals a power law decay with a nonuniversal exponent.

*This research was supported by US DOE under contract No. DE-AC02-98 CH 10886.

**11:51**

**P23 4 Comparison of Magnetic Field-Modified Electronic Excitations in Ni(II) Compounds** VIRGINIA LONG, E.C. SCHUNDLER, P.O. MAKUMBE, *Colby College, Waterville ME* X. WEI, *NHMFL, Tallahassee, FL* B.R. LANDRY, K.R. MAXCY, M.M. TURNBULL, C.P. LANDEE, *Clark University, Worcester MA* NTDN ($Ni[tn]_2[NO_2]_2$) can be considered a paramagnetic analog material to the Haldane compounds NENP and NENB ($Ni[en]_2NO_2ClO_4$ and $Ni[en]_2NO_2BF_4$; where en = $C_2N_2H_8$ and tn = $C_2N_3H_10$). Except for the different bonding of one $NO_2$ group and the absence or presence of spin chains, NTDN and the Haldane compounds have nearly identical electronic coordination around the $Ni^{2+}$ ions. Here, we report and compare the magnetic field ($H$)-dependent polarized optical transmittance of the three materials in the range 9,000 to 22,000 $cm^{-1}$. The $H$ dependence is manifest in the varying intensities of certain electronic absorptions with applied field. Although all three materials possess similar $H$- sensitive excitations, the details of the $H$ dependence differ with the magnetic ground states. In NTDN, the intensity changes commence at $H = 0$ and saturate at $\approx$ 10 T, whereas in the Haldane compounds, the onset of changes is at the gap- closing critical field, $H_C$, above which the intensity is linearly modified with field. The mechanism of the $H$- dependence is yet to be clarified and probably depends on the nature of the electronic excitation. Intensity variations with applied field are observed in both $Ni^{2+}$-to-$NO_2^-$ charge transfer transitions and $Ni^{2+}$ $d - d$ spin forbidden excitations.

**12:03**

**P23 5 Magnetic Chains Assembled with Atomic Precision** CYRUS F. HIRJIBEHEDIN, CHRISTOPHER P. LUTZ, ANDREAS J. HEINRICH, *IBM Research Division, Almaden Research Center* We report the first study of small magnetic chains constructed and studied itin-situ with atomic precision. By positioning Mn atoms one at a time with an STM, we are able to follow the low energy excitation spectrum of the chain as it changes dramatically with length. The low energy spectra of chains built from an odd number of atoms display a spin-flip excitation similar to that of a single Mn atom. In even-length chains the spin flip excitation is absent and is replaced by an excitation at higher energies that splits into three distinct modes in a magnetic field. We interpret these results as direct evidence of the antiferromagnetic coupling of the individual atomic spins. Quantitative comparison of our results with the Heisenberg model allows us to directly obtain the coupling strength J$\sim$ 6meV between atomic spins and suggests that the total spin of the individual Mn atoms on the surface is 5/2.

**12:15**

**P23 6 Resonant Quantum Tunneling of spin chains in 3D-magnetically ordered CoTAC** CARLEY PAULSEN, *CRTBT-CNRS Grenoble, France* ELSA LHOTEL, *CRTBT-CNRS Grenoble, France* EUGENE KHAYSKO, *National Academy of Sciences of Ukraine* CoTAC is a well know molecular spin chain system which orders in an antiferromagnetic canted state at $4.15K$. We show that, below $300mK$, the dynamics of the magnetization in the $c$-direction are governed by resonant quantum tunneling of the magnetization. This conclusion is based on a number of experimental observations: the temperature independence of the relaxation of the magnetization, speeding up of the relaxation at a well defined magnetic field value ($1025Oe$) and the increase of the magnetization each time this field is crossed during a succession of minor loops. The key to understanding this behavior could be the absence of resonance in zero field. We propose a mechanism to describe this behavior using a simple model of domain wall nucleation which explains many of the unusual experimental observations.

**12:27**

**P23 7 Extended Valence-Bond Solid Picture for Quasi-One-Dimensional Quantum Magnets** MUNEHISA MATSUMOTO, Ground-state gapped phases of quasi-one-dimensional quantum magnets are given an comprehensive interpretation based on an extended valence-bond solid (VBS) picture. We introduce composite spins with the enlarged spin magnitude in the ground state and regard the system as an effective single spin chain that consists of composite spins. The relevance of the composite spins in the ground state is revealed by the effects of dimerization in the spin-spin couplings. In order to characterize the gapped phases, we inspect the configuration of valence bonds by calculating the appropriate order parameters by the quantum Monte Carlo method

with the continuous-time loop algorithm. The so-called short-range resonating-valence bond solid state is identified to be an extended VBS state. Dimensional crossover to the two-dimensional systems is also discussed.

**12:39**

**P23 8 Luttinger sum rules in the 2-channel spin 1 Kondo chain** IAN McCULLOCH, *Institut fur Theoretische Physik C, RWTH-Aachen* We present numerical results, using the DMRG method, for the zero-temperature phase diagram of the one-dimensional 2-channel Kondo lattice model, coupled to $S = 1$ localized spins. Unlike the previously studied 1-channel $S = 1/2$ case, the $S = 1$ localized spins in the 2-channel model permit a gapped Haldane state, which stabilizes the weak-coupling (''small'' Fermi surface) paramagnetic phase. We focus on the paramagnetic region approaching half-filling, where the interesting possibility has been recently raised of a non-trivial crossover region where the Fermi wavenumber varies continuously.

**12:51**

**P23 9 Coupling of Spin and Charge Degrees of Freedom in a Hydrodynamic Two-Fluid Approach** FABIO FRANCHINI, *Stony Brook University* ALEXANDER ABANOV, *Stony Brook University* We use a hydrodynamic approach to study correlated quantum one- dimensional systems. One can derive an effective hydrodynamics in the limit of smooth densities and slow velocities. In the limit when gradients of density and velocity can be neglected, one obtains an integrable system. We discuss the origin of this integrability and, as an application, we calculate some non trivial correlation functions. The Hydrodynamic description is a useful tool to study the dynamics of a system. We introduce a two-fluid hydrodynamic description of one-dimensional spin 1/2 fermions with contact interactions. It is known that linearized hydrodynamics (bosonization) exhibits spin-charge separation. In the full *non-linear* theory, the spin and charge degrees of freedom are coupled to each other, therefore spin waves carry charge as well. We discuss the dynamics of such system.

**13:03**

**P23 10 Coupled one-dimensional magnetic systems: the truncated conformal spectrum approach*** YURY ADAMOV, ROBERT KONIK, ALEXEI TSVELIK, *Brookhaven National Laboratory* We develop a combined analytical/numerical technique in order to understand coupled, possibly strongly, one dimensional magnetic systems. The approach trades on exact knowledge of the underlying one dimensional subsystem and the concomitant ability to compute exactly matrix elements of operators coupling the subsystems together. With these matrix elements in hand, the fully coupled system is first truncated and then diagonalized numerically. In this way we obtain both the spectrum and correlation functions of the system. The truncation can be improved upon through a renormalization group procedure. As a test case we consider coupled quantum Ising chains.

*Supported by US DOE

**13:15**

**P23 11 Random antiferromagnetic spin chains with enlarged symmetry** JOSÉ A. HOYOS, EDUARDO MIRANDA, *IFGW, Unicamp, Campinas, SP, Brazil* We present the asympotically exact solution of some random antiferromagnetic spin chains with enlarged symmetry groups. Using a generalization of the strong disorder real space renormalization group method, we considered both the isotropic SU(N) and the anisotropic SU(4) chains with totally antisymmetric irreducible representations. In the first case, the system is governed by a universal infinite-randomness fixed point (IRFP), with activated dynamical scaling between energy ($\Omega$) and length ($L$) scales $\Omega \sim \exp(-L^{\psi})$ (with the tunneling exponent $\psi = 1/N$), and average correlation function decaying as a power law with exponent $\eta = 4/N$. All thermodynamic quantities are universal with exponents depending only on $N$. In the second case, relevant for systems with $SU(2)_{spin} \otimes SU(2)_{orbital}$ symmetry, we determined the full phase diagram as a function of the mean anistropy and its variance. All stable fixed points are of the IRFP variety with activated dynamical scaling. The tunneling exponents span a wide range of values and can even be larger than the SU(2) value, $\psi = 1/2$.

**13:27**

**P23 12 Thermodynamics and magnetization process of the frustrated ferromagnetic spin-1/2 chain** FABIAN HEIDRICH-MEISNER, *Department of Physics and Astronomy, The University of Tennessee and Condensed Matter Sciences Division, Oak Ridge National Laboratory* DANIEL C. CABRA, TEMO VEKUA, *Laboratoire de Physique Théorique, Université Louis Pasteur Strasbourg, France* ANDREAS HONECKER, *Institut für Theoretische Physik, Technische Universität Carolo-Wilhelmina zu Braunschweig, Germany* We report a study of the thermodynamics and magnetization curve of a $J_1$–$J_2$ spin-1/2 chain with a ferromagnetic nearest neighbor coupling $J_1$ and an antiferromagnetic next-nearest neighbor interaction $J_2$. This model has recently been suggested to describe the properties of different compounds such as $LiCuVO_4$ and $Rb_2Cu_2Mo_3O_{12}$. We present results for both the specific heat and the magnetic susceptibility for the whole parameter range of $J_2/4 <| J_1| < 0$ obtained by exact diagonalization of up to $N = 24$ sites. The specific heat exhibits a two-peak structure for $J_1 < 0$, originating from, first, the proximity to a ferromagnetic ground state and, second, antiferromagnetic fluctuations at higher energies. Furthermore, the magnetization process at zero temperature is analyzed by means of the density matrix renormalization group technique. Particular emphasis is given to the presence (or rather absence) of magnetization plateaus and a comparison with other theoretical results for the ground-state phase diagram.

**13:39**

**P23 13 The Magnetic phase diagram of the spin-chain system $Ca_{2+x}Y_{2-x}Cu_5O_{10-\delta}$: Oxygen hole-doping** KEESEONG PARK, *Department of Physics, The University of Texas at Austin* JOHN MARKERT, *Department of Physics, The University of Texas at Austin* Recently, K. Kudo et al.[1] studied the magnetic ground state in the edge-sharing $CuO_2$ chains in the spin- chain system $Ca_{2+x}Y_{2-x}Cu_5O_{10-\delta}$. In that study, the antiferromagnetic transition temperature decreases with increasing $x$ and disappears around $x=1.4$ followed by the appearance of a spin-glass phase at $x=1.5$. We propose that the oxygen content should be included in the hole doping effect by $p = 1/5(x - 2\delta)$ in the spin-chain system. We present x-ray diffraction, magnetic susceptibility, specific heat and iodometric titration measurements[2] which indicate that an oxygen deficiency shifts the magnetic features toward higher $x$. For example, for $x = 1$ samples, the single crystals of Ref.1 are equivalent to our oxygen deficient polycrystalline sample with $\delta \approx 0.5$. Such a composition has an only slightly suppressed Néel temperature, while for nearly fully oxygenated

$x = 1$ samples, the antiferromagnetic transition is completely suppressed.[3]

[1]K. Kudo, S. Kurogi, and Y.Koike, Physical Review B **71**, 104413 (2005)
[2]This work is supported by the Robert A. Welch Foundation grant No.F-1191 and the National Science Foundation grant No. DMR-0210383
[3]M. D. Chabot, and J. T. Markert, Physical Review Letters **86**, 163 (2001)

**13:51**
**P23 14 Low temperature magnetization and the excitation spectrum of antiferromagnetic quantum Heisenberg rings** LARRY ENGELHARDT, MARSHALL LUBAN, *Ames Laboratory and Department of Physics and Astronomy, Iowa State University, Ames, Iowa 50011* We have performed quantum Monte Carlo calculations to obtain the low temperature magnetization and differential susceptibility for finite, antiferromagnetic Heisenberg rings of intrinsic spins $s = 1/2,1,3/2,2,5/2,3,7/2$. From these data we have determined the level-crossing fields as well as the dependence of the minimal excitation energies on the total spin quantum number $S$. For large intrinsic spins ($s \geq 3/2$) we find that the data exhibit scaling behavior, approaching the classical limit proportional to $s^{-1.05}$. Since this limit is approached so slowly, even $s = 7/2$ spins are distinctly non-classical. We have also found for large $s$ that as the number of spins $N$ increases, the energy gap between the ground state and the first excited state approaches zero proportional to $1/N^{\alpha}$, where $\alpha \approx 0.76$ for $s = 3/2$ and $\alpha \approx 0.84$ for $s = 5/2$. Finally, we demonstrate the usefulness of our results by examining the $Fe_{12}$ molecular ring, leading to a new, more accurate estimate of the exchange constant for this system than has been obtained heretofore.

**14:03**
**P23 15 Magnetic Properties of a Coordination Polymer [$Mn_3$ [$(OH)_2Na_2(3\text{-}cnba)_6$]n** TAN YUEN, CHYAN LONG LIN, *Physics Dept., Temple University* PRINCY VARUGHESE, JING LI, *Dept. of Chemistry & Chemical Biology, Rutgers University* JING-TANG LI, JUN TAO, RONG-BIN HUANG, LAN-SUN ZHENG, *Dept. of Chemistry and State Key Laboratory for Physical Chemistry of Solid Surface, Xiamen University, Xiamen 361005, China* Magnetic properties of [Mn3($OH$)2$Na$2(3 − $cnba$)6]n(3−Hcnba=3−cyanobenzoic acid), a newly discovered three-dimensional coordination polymer, were investigated using magnetic susceptibility M(T)/H and isothermal magnetization M(H). The crystal structure of [Mn3($OH$)2$Na$2(3 − $cnba$)6]n is triclinic with a space group P−1. The lattice parameters area= 6.663Å,b= 12.971Å,c= 14.161Å,$\alpha$ = 70.13[$r$], $\beta$=88.43[r], and $\gamma$=76.47[r]. The results ofM(T) /Hon powder samples show that the effective moment $\mu$ effof Mn2+ is 5.88$\mu$Bat temperatures above 100K, close to the expected value for a free Mn2+ ion. Below 3K, [Mn3($OH$)2$Na$2 (3 − $cnba$)6]n orders antiferromagneticly. A sudden slope change in M(H)measured at is observed at a very small critical field of Hc≈20G, suggesting a metamagnetic transition. Above 20kG, M(H) starts to saturate, reaching a value equivalent to 1.7 $\mu$B per Mn2+ ion. The magnetic behavior of the complex is interpreted in terms of an effective ferrimagnetic Mn(II) chains in which spin moments are linked by interactions in an AF−F−AF(F= ferromagnetic and AF= antiferromagnetic) sequence in the triangular magnetic repeating unit.

## SESSION P26: FOCUS SESSION: PROTEIN DYNAMICS IN FOLDING AND FUNCTION
**Wednesday Morning, 15 March 2006; 323, Baltimore Convention Center at 11:15**
**Robert Callendar, Albert Einstein College, presiding**



***Invited Papers***

**11:15**
**P26 1 NMR Studies of Enzyme Structure and Mechanism.**
ALBERT MILDVAN, *Johns Hopkins U. School of Medicine*

At least three NMR methodologies pioneered by Al Redfield, have greatly benefited enzymology: (1) the suppression of strong water signals without pre-saturation; (2) sequence specific NH/ND exchange; and (3) dynamic studies of mobile loops of proteins. Water suppression has enabled us to identify unusually short, strong H-bonds at the active sites of five enzymes (three isomerases and two esterases), and to measure their lengths from both the chemical shifts and D/H fractionation factors of the deshielded protons involved (J. Mol. Struct. 615, 163 (2002)). Backbone NH exchange studies were used to detect regions of an NTP pyrophosphohydrolase in which NH groups became selectively protected against exchange on Mg(2+) binding, and further protected on product (NMP) binding, thus locating binding sites as well as conformationally linked remote sites (Biochemistry 42, 10140 (2003)). Dynamic studies were used to elucidate the frequency of motion of a flexible loop of GDP-mannose hydrolase (66,000/sec) containing the catalytic base His-124, from exchange broadening of the side chain NH signals of His-124 in the free enzyme. The binding of Mg(2+) and GDP-mannose lock His-124 in position to deprotonate the entering water and complete the reaction.

**11:27**
**P26 2 Interference between relaxation and parameters for protein structure determination.***
EVA DE ALBA, *National Institutes of Health*

The effect of cross-correlated relaxation on scalar and dipolar coupling measurements is analyzed. We compare one-bond proton-carbon scalar and dipolar couplings of protein methine and methylene sites obtained by monitoring proton and

carbon magnetization. Apparent J-coupling constants of the same pair of nuclei vary depending on the type of magnetization involved. The discrepancies are of different magnitude for methine and methylene moieties. Dynamic frequency shifts are partially responsible for the observed differences. More importantly, the largest observed variations can be explained by processes of magnetization transfer originated by cross-correlated relaxation. These later effects are not cancelled when obtaining residual dipolar couplings.

*In collaboration with Nico Tjandra, National Institutes of Health.

*Contributed Papers*

**11:39**
**P26 3 Multiple Quantum Relaxation Probes of Protein Dynamics on Multiple Timescales** RANAJEET GHOSE, *City College of New York* Several effects may lead to significant differences between the relaxation rates of zero-quantum coherences (ZQC) and double-quantum coherences (DQC) (collectively known as multiple-quantum coherences) generated between a pair of spin 1/2 nuclei in solution. These include the interference between the anisotropic chemical shifts of the two nuclei participating in formation of the ZQC or DQC, the individual dipolar interactions of each of the two nuclei with the same proton, and the slow modulation of the isotropic chemical shifts of the two nuclei due to conformational exchange. Motional events that occur on a timescale much faster than the rotational correlation time (picosecond-nanosecond) influence the first two effects, while the third results from processes that occur on a far slower timescale (microsecond-millisecond). An analysis of the differential relaxation of ZQC and DQC is thus informative about dynamics on the fast as well as the slow timescales. We present here a set of NMR experiments that measure the differential relaxation of ZQC and DQC involving several backbone and sidechain nuclei in proteins. These measurements provide significant insight into the complex dynamic modes that exist in the protein backbone and sidechains. A detailed understanding of these dynamic modes may provide clues into the role of dynamics in modulating protein function.

*Invited Papers*

**11:51**
**P26 4 A Plastic Explosive-Degrading Enzyme.***
ANNE-FRANCES MILLER, *University of Kentucky*

The enzyme nitroreductase catalyzes reduction of high explosives such as TNT and RDX. Although a well-resolved $^{1}H^{15}N$-HSQC is obtained at 37 °C, the HSQC at 4 °C is concentrated between 7.5 and 8.5 ppm and is comprised of sharp overlapped peaks. Thus, it appears that the protein denatures upon cooling. However, the non-covalently-bound FMN cofactor is not released at the lower temperature. Similarly, ultra-violet CD spectroscopy shows that the protein retains essentially full secondary structural content at 4 °C. Thus, it appears that nitroreductase exists as an ensemble of rapidly interconverting loose structures at lower temperature, only adopting a single long-lived structure above 20 °C. Both saturation transfer from water and solvent proton exchange measurements, demonstrate that resonances of the poorly-dispersed spectrum represent protons closer to water, and in faster exchange with it. Thus we propose that the single well-defined structure is favored entropically, by release of water molecules that solvate the protein at 4 °C. We propose that the loosely structured state plays a role in accommodating binding of diverse substrates.

*In collaboration with Peng Zhang, University of Kentucky.

*Contributed Papers*

**12:27**
**P26 5 Protein-Protein Interactions during Bacterial Chemotaxis using Methyl TROSY Nuclear Magnetic Resonance.** DAMON HAMEL, FREDERICK DAHLQUIST, *University of California Santa Barbara* During bacterial chemotaxis, the histidine autokinase CheA interacts with the chemotaxis receptors with the help of the coupling protein CheW. The CheA-CheW interaction is typical of many macromolecular complexes where protein-protein interactions play an important role. In this case a relatively small protein, CheW (18 kDalton), becomes part of a much larger complex. Here we describe a new method to map the residues at a protein-protein interface for macromolecular complexes of molecular weight greater than 100 kDalton. The method exploits the C13 methyl TROSY methodology developed in Lewis Kay's laboratory. The essence of the Kay approach is that a portion of the intensity of HMQC spectra of individual -(13)CH3 resonances in an otherwise deuterated macromolecule have much reduced dipole-dipole relaxation and remain sharp and relatively easy to detect, even in macromolecules of molecular mass 100 kD or greater. The reduction in dipolar interactions is lost if a given methyl group comes in close contact with other protons such as those supplied by the interface of a protonated interaction partner. Comparing the -(13)CH3 resonances of a protein of interest in the presence of a protonated versus deuterated interaction partner allows the methyls at the interface can be identified. The application of the approach for establishing points of contact between CheA and CheW will be discussed.

*Invited Papers*

**12:39**
**P26 6 Structural Basis for Specific Membrane Targeting by the HIV-1 Gag Protein.***
MICHAEL F. SUMMERS, *University of Maryland Baltimore County*

In HIV-1 infected cells, newly synthesized retroviral Gag polyproteins are directed to specific cellular membranes where they assemble and bud to form immature virions. Membrane binding is mediated by Gag's matrix (MA) domain, a 132-residue polypeptide containing an N-terminal myristyl group that can adopt sequestered and exposed conformations. Membane specificity was recently shown to be regulated by phosphatidylinositol-(4,5)-bisphosphate (PI(4,5)P2), a cellular factor abundant in the inner leaflet of the plasma membrane (PM). We now show that phosphoinositides, including soluble analogs of PI(4,5)P2 with truncated lipids, bind HIV-1 MA and trigger myristate exposure. The phosphoinositol moiety and one of the fatty acid tails binds to a cleft on the surface of the protein. The other fatty acid chain of PI(4,5)P2 and the exposed myristyl group of MA bracket a conserved basic surface patch implicated in membrane binding. Our findings indicate that PI(4,5)P2 acts as both a trigger of the myristyl switch and as a membrane anchor, and suggest a structure-based mechanism for the specific targeting HIV-1 Gag to PI(4,5)P2-enriched membranes.

*In collaboration with Jamil S. Saad, Jaime Miller, Janet Tai, Andrew Kim, and Ruba H. Ghanam, University of Maryland Baltimore County.

**12:51**
**P26 7 Vinculin Tail Dimerization and Paxillin Binding.**
SHARON CAMPBELL, *University of North Carolina*

Vinculin is a highly conserved cytoskeletal protein that is essential for regulation of cell morphology and migration, and is a critical component of both cell-cell and cell-matrix complexes. The tail domain of vinculin (Vt) was crystallized as a homodimer and is believed to bind F-actin as a dimer. We have characterized Vt dimerization by Nuclear Magnetic Resonance (NMR) Spectroscopy and identified the dimer interface in solution by chemical shift perturbation. The Vt dimer interface in solution is similar to the crystallographic dimer interface. Interestingly, the Vt dimer interface determined by NMR partially overlaps the paxillin binding region previously defined coarsely by deletion mutagenesis and gel-blot assays. To further characterize the paxillin binding site in Vt and probe relationship between paxillin binding and dimerization, we conducted chemical shift perturbations experiments using a paxillin derived peptide, LD2. Our NMR experiments have confirmed that the paxillin binding site and the Vt dimerization site partially overlap, and we have further characterized both of these two binding interfaces. Information derived from these studies was used to identify mutations in Vt that selectively perturb paxillin binding and Vt self-association. These mutants are currently being characterized for their utility in structural and biological analyses to elucidate the role of paxillin binding and Vt dimerization in vinculin function.

*Contributed Papers*

**13:03**
**P26 8 Protein dynamics and allostery** BABIS KALODIMOS, *Rutgers University, Chemistry Department, Newark NJ 07102* Cooperativity and allostery are phenomena of universal importance in biological systems. According to the classical ''mechanical'' view allosteric interactions are mediated by a series of discrete changes in bonding interactions that alter the protein conformation. Nevertheless, proteins may have adopted additional mechanisms for energetically linking distant sites, thereby allowing a signal to be propagated over long distances. We have identified a cooperative biological system wherein allosteric interactions appear to be mediated exclusively by transmitted changes in protein motions. Changes in the structure, fast and slow protein motions and the redistribution of the native-state ensemble along the cooperative reaction coordinate have been characterized.

*Invited Papers*

**13:15**
**P26 9 Protein Dynamics in an RNA Binding Protein.***
KATHLEEN HALL, *Washington University School of Medicine*

Using $^{15}N$ NMR relaxation measurements, analyzed with the Lipari-Szabo formalism, we have found that the human U1A RNA binding protein has ps-ns motions in those loops that make contact with RNA. Specific mutations can alter the extent and pattern of motions, and those proteins inevitably lose RNA binding affinity. Proteins with enhanced mobility of loops and termini presumably lose affinity due to increased conformational sampling by those parts of the protein that interact directly with RNA. There is an entropic penalty associated with locking down those elements upon RNA binding, in addition to a loss of binding efficiency caused by the increased number of conformations adopted by the protein. However, in addition to local conformational heterogeneity, analysis of molecular dynamics trajectories by

Reorientational Eigenmode Dynamics reveals that loops of the wild type protein undergo correlated motions that link distal sites across the binding surface. Mutations that disrupt correlated motions result in weaker RNA binding, implying that there is a network of interactions across the surface of the protein. (KBH was a Postdoctoral Fellow with Al Redfield from 1985-1990). This work was supported by the NIH (to KBH) and NSF (SAS).

*In collaboration with James Kranz, Johnson & Johnson; and Scott Showalter, Florida State University.

**13:27**
**P26 10 Axial Rotation of Lipids in Membranes.**
RICHARD PASTOR, *Food and Drug Administration*

This study was motivated by Mary Roberts and Al Redfield, who proposed that the observed 10 ns decay time in their phosphorous NMR measurements of DPPC in bilayers originated from axial rotation of the lipid. Analyses of correlation functions and average first passage times from 50 ns molecular dynamics of DPPC bilayers strongly support their interpretation. The rotational anisotropy of a lipid in a bilayer is close to 1.0, in contrast to the 2.5 expected for a hydrodynamic cylinder with lipid dimensions. This implies that axial rotation is dominated by headgroup, not tail, interactions.

**13:39**
**P26 11 High Resolution Field Cycling NMR in Biopolymers in Solution: Current and Potential Applications.**
ALFRED REDFIELD, *Brandeis University*

I have been exploring the feasibility and utility of performing high resolution relaxation and cross-relaxation (NOE) in an unmodified shared commercial NMR instrument (PNAS 101:17066-17071) in collaboration with Mary Roberts of Boston College and Elan Eisenmesser of Brandeis. We can move a sample from 11.7 T to low (fringe) field 40- 80 cm above the commercial probe, and back, in 0.3 to 0.5 sec. I am making the system move the sample more gently, to avoid protein denaturation, using a stepping-motor timing-belt linear-motor. I willreview our initial papers on a DNA octamer, and phospholipidvesicles using phosphorus NMR. We emphasize phosphorus,in part, because relaxation studies over a wide range can make behavior of this biologically important species more readily interpretable than at high field alone. Then I will discuss a range of biochemical experiments, not yet done, using the full capability of our commercial instrument for multidimensional preparation and detection before and after field-cycling, and utilizing other nuclear species (H, C, and N). These involve especially use of electron-paramagnetic species and/or studies of small molecules in fast binding exchange with larger ones, and/or increased hetero-NOE effects at low field, to get new information on dynamics and structural preferences. Predictably we have found that, once we start to work on a specific biopolymer problem, we think of more things to do than we expected at first.

**SESSION P27: ELECTRONIC STRUCTURE II**
**Wednesday Morning, 15 March 2006**
**324, Baltimore Convention Center at 11:15**
**Anne Chaka, National Institute of Standards and Technology, presiding**

**11:15**
**P27 1 Analytic structure of Bloch functions for linear molecular chains*** EMIL PRODAN, *PRISM, Princeton University* In this talk I will discuss Hamiltonians of the form $H = -\nabla^2 + v(x,y,z)$, with $v(x,y,z)$ periodic along the $z$ direction, $v(x,y,z+b) = v(x,y,z)$. The wavefunctions of $H$ are the well known Bloch functions $\psi_{n,\lambda}(x,y,z)$, with the fundamental property $\psi_{n,\lambda}(x,y,z+b) = \lambda\psi_{n,\lambda}(x,y,z)$ and $\partial_z\psi_{n,\lambda}(x,y,z+b) = \lambda\partial_z\psi_{n,\lambda}(x,y,z)$. I will give the generic analytic structure (i.e. the Riemann surface) of $\psi_{n,\lambda}(x,y,z)$ and their corresponding energy, $E_n(\lambda)$, as functions of $\lambda$. I will also discuss several applications, like a compact expression of the Green's function or the asymptotic behavior of the density matrix and other correlation functions for insulating molecular chains.

*Work supported by Grant. No. NSF-DMR03-13980

**11:27**
**P27 2 First-principles calculation of Hubbard parameter: Constrained local density functional approach with Maximally localized Wannier function** KAZUMA NAKAMURA, *Department of Physics, University of Tokyo, Japan* RYOTARO ARITA, *Department of Physics, University of Tokyo, Japan* YOSHIHIDE YOSHIMOTO, *Institute for Solid State Physics, University of Tokyo, Japan* SHINJI TSUNEYUKI, *Department of Physics, University of Tokyo, Japan* We present a new ab initio method for calculating effective onsite Coulomb interactions of itinerant and strongly correlated electron systems. The method is based on constrained local density functional theory formulated in terms of maximally localized Wannier functions. This scheme can be implemented with any basis, and thus allows us to perform the constrained calculation with plane-wave-based electronic-structure codes. We apply the developed method to the evaluation of the onsite interaction of 3d transition-metal series. The results are discussed using a heuristic formula for screened Coulomb interactions. This work was supported by NAREGI Nanoscience Project, Ministry of Education, Culture, Sports, Science and Technology, Japan.

**11:39**
**P27 3 Electronic structure of $Cu_{2-x}S$ and related compounds** PAVEL LUKASHEV, WALTER R. L. LAMBRECHT, *Case Western Reserve Univ.* TAKAO KOTANI, MARK VAN SCHILFGAARDE, *Arizona State Univ.* Chalcosite $Cu_2S$ and digenite $Cu_{1.8}S$ are possibly interesting semiconductors for photovoltaic applications. Their electronic structure is poorly understood because their crystal structure is complex. If consists of a close-

packed lattice of S with mobile Cu occupying various types of interstitial sites with a statistical distribution depending on temperature. As a starting point for understanding these materials, we investigated the simpler antifluorite structure. Both local density approximation (LDA) and self-consistent quasiparticle GW calculations with the full-potential linearized muffin-tin orbital method give a semimetallic band structure with the Fermi level pinned at a degenerate Cu-d band state at $\Gamma$. A random distortion of the Cu atoms from the perfect antifluorite positions inside each S cage is found to break the degeneracy of the *d* state at $\Gamma$ and thus opens up a small gap of about 0.1 eV in LDA. The experimental evidence for a semiconducting gap of about 1 eV is critically examined. To gain further insight into the Cu d and s-band shifts beyond LDA, we considered other Cu compounds such as $Cu_2O$ and CuBr. We compare their LDA and GW band structures and determined the effective masses and Kohn-Luttinger Hamiltonian parameters for CuBr.

**11:51**

**P27 4 The Applicability of Different Quantum Mechanical Methods to Transition Metal Oxides** ORKID COSKUNER, EMILY JARVIS, THOMAS ALLISON, CARLOS GONZALEZ, ANNE CHAKA, *National Institute of Standards and Technology, Physical and Chemical Properties, Gaithersburg, MD 20889* NIST, COMPUTATIONAL CHEMISTRY GROUP TEAM, Numerous quantum mechanical methods and basis sets have been applied extensively to organic molecules. However, the performance of these is not well understood for transition metal oxides. We employed different methods along with several basis sets for optimizing the geometries in the gas phase and calculating the IR spectra as well as thermodynamic properties including Gibbs free energy and enthalpy of linear, trigonal and tetrahedral metal oxides. The MCSCF and DFT methods generally give the most accurate results for organic and inorganic molecules. Surprisingly, our studies showed that the results obtained for iron(III) oxides at the GVB and MP2 levels gave more accurate results than the MCSCF and hybrid methods. Similarly, for aluminum and chromium oxides, the calculations with MP2 and PBE yielded thermodynamic properties, which are closer to experimental values.

**12:03**

**P27 5 Zeroth-moment dielectric sum rule applied to electron damping*** ERIC L. SHIRLEY, *NIST* J.A. SOININEN, *U. Helsinki* J.J. REHR, *U. Washington, Seattle* The first and inverse-first frequency moments of the dielectric function, epsilon(q,omega), are given by the f-sum rule and Kramers-Kronig transformation of the static dielectric function. Model expressions for these quantities are plentiful. The square of the zeroth moment must be less than the product of the above two, by Cauchy-Schwartz. (It equals that product in single-plasmon-pole models). In this work, we present simple ways to estimate the zeroth moment as a function of q. This facilitates an improved model for epsilon(q,omega) that requires minimal computation and exhibits realistic behavior without use of a pole model. We apply this to calculating the electron self-energy, particularly lifetime damping effects in insulators near the band gap.

*Supported in part by DOE Grant DE-FG02-97ER45623 and facilitated by the Computational Materials Science Network (CMSN).

**12:15**

**P27 6 Relativistic real-space multiple scattering calculations of EELS*** K. JORISSEN, *U. Antwerp* J.J. REHR, A. SORINI, *U. of Washington* Z.H. LEVINE, *NIST* We present an extension of the real space multiple scattering code FEFF8 for *ab initio*, relativistic calculations of electron energy loss spectra (EELS), which is applicable both to periodic and non-periodic systems. The approach explains the observed relativistic shifts in the magic angle.[1] In addition, the method can account for experimental parameters such as collection and convergence angles of the microscope and sample orientation. We also discuss relativistic effects on inelastic electron scattering including the density correction to the stopping power. Our results are compared with other approaches and with experiment.

*Supported by DOE Grant DE-FG02-97ER45623 (JJR and MP), NIST Grant 70 NAMB 2H003 (AS), NIH NCRR BTP grant RR-01209 (AS), and facilitated by the DOE Computational Materials Science Network (CMSN).

[1]B. Jouffrey, P. Schattschneider and C. Hebert, Ultramicroscopy **102**, 61 (2004).

**12:27**

**P27 7 Prediction of Born-Oppenheimer Interatomic Forces Using Orbital-Free Density Functional Theory with Approximate Kinetic Energy Functionals*** S.B. TRICKEY, V.V. KARASIEV, FRANK E. HARRIS,† *Quantum Theory Project and Department of Physics, U. of Florida* Rapid calculation of Born-Oppenheimer forces is essential for driving the so called quantum region of a multi-scale molecular dynamics (MD) simulation. The orbital-free (OF) DFT approach is appealing but has proven difficult to implement because of the challenge of constructing reliable orbital-free approximations to the kinetic energy functional. To be maximally useful for multi-scale simulations, an OF-KE functional must be local (i.e. one-point). In the face of these difficulties, we demonstrate that there is a way forward. By requiring only that the approximate functional deliver high-quality forces, by exploiting the ''conjointness'' hypothesis of Lee, Lee, and Parr, by enforcing a basic positivity constraint, and by parameterizing to a carefully selected, small set of molecules we are able to generate a OF-KE functional that does a good job of describing various $H_qSi_mO_n$ clusters as well as CO and $H_2O$ (providing encouraging evidence of transferability).

*Supported in part by U.S. NSF ITR Grant DMR-0218957
†also Dept. of Physics, U. of Utah

**12:39**

**P27 8 Fitting of Molecular Densities by Compact, Atom-Centered Expansion*** V.V. KARASIEV, S.B. TRICKEY, FRANK E. HARRIS,† *Quantum Theory Project and Dept. of Physics, U. of Florida* Use of an orbital-free (OF) version of DFT requires both a suitable approximate Kohn-Sham kinetic energy functional and a systematic but simple model of the system density. We report useful approximations to the KS density via a very compact expansion in atom-centered functions. Spherically averaged, isolated-atom densities are used as basis functions to expand spherically symmetric atom-centered contributions. A simplified expansion in real spherical harmonics is then added to the spherically symmetric contributions. Although drastically simplified, such representations of the density nevertheless result in impressively small mean square deviations relative to the target KS density. The fitted density can then be combined with an approximate

OF-KE functional we have developed[1] to generate energy surfaces. These energy surfaces have shapes similar to those arising from true KS densities, and are therefore suitable for calculation of forces to drive molecular dynamics simulations.

*Supported in part by U.S. NSF ITR Grant DMR-0218957
†also Dept. of Physics, U. of Utah

[1]V.V. Karasiev, S.B. Trickey, and F.E. Harris, J. Comp. Aided Mat. Des. (2005) (accepted).

**12:51**
**P27 9 Magnetic Field Effects upon Exchange-Correlation in the Hooke's Atom*** WUMING ZHU, SAMUEL TRICKEY, *Quantum Theory Project and Department of Physics, University of Florida, Gainesville, FL 32611* Extending Density Functional Theory (DFT) to coulombic systems in a non-vanishing magnetic field in a computationally feasible way is highly desirable. Even though the current DFT (CDFT) formalism is long-established, there still are no generally applicable, reliable $E_{xc}, \mathbf{A}_{xc}$ functionals analogous with the LDA. Progress can be made by comparison study on a solvable correlated system. Hooke's atom is well-known in ordinary DFT because its Schrödinger equation can be solved exactly for some coupling strengths and numerically with high accuracy for the rest. Hence exact Kohn-Sham quantities are readily available. Using our extensions (exact and numerical) to non-zero B-field, we examined the effects on exchange- correlation holes and energies and considered possible ways to include the essential ones in $E_{xc}, \mathbf{A}_{xc}$. In our tests, the CDFT vorticity variable, $\nu$, turns out to be a computationally difficult quantity which may not be appropriate in practice to describe external B field effects on $E_{xc}, \mathbf{A}_{xc}$.

*Work supported by US NSF ITR DMR-0218957.

**13:03**
**P27 10 The problems in the density functional theory with the total spin and space symmetry and the invariant properties of the electron density.** I.G. KAPLAN, *Instituto de Investigaciones en Materiales, UNAM, Apdo. Postal 70-360, 04510 México D.F. México* The problems in the density functional theory (DFT) arising when it is applied to the spin and space multiplets are discussed. It is rigorously proved that the electron density of an arbitrary *N*-electron system does not depend upon the value of the total spin *S* of the state and preserves the same analytical form for all states with the definite *S*. It is also proved that the diagonal element of the full density matrix is invariant respecting all operation of the group symmetry of the state, i.e, it is a group invariant. From these results follows that the problems in DFT with the total spin and degenerated states cannot be solved within the framework of density matrix formalism.

**13:15**
**P27 11 Dehydrogenation in catalyst activated $MgH_2$*** SA LI, PURU JENA, RAJEEV AHUJA, *Virginia Commonwealth University* VIRGINIA COMMONWEALTH UNIVERSITY TEAM, UPPSALA UNIVERSITY COLLABORATION, Dehydrogenation in catalyst activated magnesium hydride ($MgH_2$) has been investigated using itab initio Molecular Dynamics (MD) simulation and Nudged Elastic Band (NEB) method. Our calculation explains why small amount of $Nb_2O_5$ catalyst can substantially improve the thermodynamics and kinetics of $MgH_2$. We show that $Nb_2O_5$ promotes the creation of Mg vacancies and that the hydrogen desorption from the vicinity of Mg vacancies occurs in molecular form and is exothermic. The activation energy barrier for $H_2$ desorption in vacancy containing magnesium hydride (1.02 eV) is much lower than that in the pure magnesium hydride (3.30 eV). Therefore, the effective catalyst for dehydrogenation in $MgH_2$ will be one that can easily facilitate MgO formation.

*This work was supported in part by grants from the Department of Energy, Swedish Research Council (VR) and by the Swedish Foundation for International Cooperation in Research and Higher Education (STINT).

**13:27**
**P27 12 A method for biased surface electronic structure: a planewave non-repeated slab approach** MINORU OTANI, OSAMU SUGINO, *Institute for Solid State Physics, Tokyo University* We have developed a new formalism for calculating electronic structures in a symmetric/asymmetric slab model [1]. The method can treat not only surfaces exposed to vacuum but also biased surfaces. To solve the Kohn-Sham equation, we adopt a conventional Kohn-Sham solver in a repeated slab model. On the other hand, for the Poisson equation, we solve it in a whole space along surface normal direction. Owing to this treatment we can easily obtain work functions of the surface and we can calculate polarized surfaces without dipole correction. By introducing an effective screening medium and imposing appropriate boundary conditions to the Poisson equation, we can calculate a surface that is placed in front of electrode. In this model it is possible to apply a bias voltage to the surface by changing the Fermi energy of the surface. Thus we can calculate electronic and geometric structures of the biased surface. This model corresponds to the experimental setup for the scanning tunneling microscopy or back-gate field effect transistor. The important advantage of the method is that we can easily implement it in a conventional first-principles calculation method. References: [1] M. Otani and O. Sugino, submitted to PRB.

**13:39**
**P27 13 Many-Body Electronic Structure of Curium metal** ANTONINA TOROPOVA, *Center for Materials Theory, Department of Physics and Astronomy, Rutgers University* KRISTJAN HAULE, *Center for Materials Theory, Department of Physics and Astronomy, Rutgers University* GABRIEL KOTLIAR, *Center for Materials Theory, Department of Physics and Astronomy, Rutgers University* We report computer-based simulations for the many-body electronic structure of Curium metal. Cm belongs to the actinide series and has a half-filled shell with seven $5f$ electrons. As a function of pressure, curium exhibits five different crystallographic phases. At low temperatures all phases demonstrate either antiferromagnetic or ferrimagnetic ordering. In this study we perform LDA+DMFT calculations for the antiferromagnetic state of high-pressure fcc modification of Curium metal.



**SESSION P29: BIOMOLECULAR STRUCTURE AND FUNCTIONS**
**Wednesday Morning, 15 March 2006**
**326, Baltimore Convention Center at 11:15**
**Suzanna Zsiwy, University of California at Irvine, presiding**

**11:15**
**P29 1 Interactions between model bacterial membranes and synthetic antimicrobials.** LIHUA YANG, *Department of Materials Science and Engineering, University of Illinois at Urbana-*

*Champaign* ABHIJIT MISHRA, *Dept of Materials Science and Engineering, University of Illinois at Urbana-Champaign* ABHIGYAN SOM, GREGORY N. TEW, *Department of Polymer Science and Engineering, University of Massachusetts* GERARD C.L. WONG, *Department of Materials Science and Engineering, Department of Physics, Department of Bioengineering, University of Illinois at Urbana-Champaign* Antimicrobial peptides comprise a key component of innate immunity for a wide range of multicellular organisms. It has been shown that natural antimicrobial peptides and their analogs can permeate bacterial membranes selectively. There are a number of proposed models for this action, but the detailed molecular mechanism of the induced membrane permeation remains unclear. We investigate interactions between model bacterial membranes and a prototypical family of phenylene ethynylene-based antimicrobials with controllable hydrophilic and hydrophobic volume fractions, controllable charge placement. Preliminary results from synchrotron small angle x-ray scattering (SAXS) results will be presented.

**11:27**

**P29 2 Observation of membrane fusion between individual virus particles and supported lipid bilayers** LAURA WESSELS, KEITH WENINGER, *North Carolina State University* A portion of the host cell membrane is incorporated into newly produced, enveloped virus particles during an active infection. Fusion of that viral membrane with the membrane of targeted host cells is generally accepted to be a key step for the infection of normal cells as a virus spreads among a normal cell population. For the best studied enveloped viruses, viral proteins catalyze the membrane fusion reaction during a low pH step along the cellular endocytotic pathway. To gain a better understanding of the molecular mechanisms underlying viral membrane fusion, we have constructed an itin vitro fluorescence assay to allow high resolution, real time measurements of Sindbis viral fusion to supported lipid bilayers. Single particle tracking is used to observe individual virus particles. The mixing of a fluorescent dye incorporated into the viral membrane with the supported bilayer reports fusion. We present results regarding the effects of different lipid blends as well as different buffer conditions on membrane fusion for Sindbis virus. We compare the fusion of virus produced in mammalian cells to that from insect cells.

**11:39**

**P29 3 Simulating Domain Formation and Fusion in Lipid Bilayers** MARK STEVENS, *Sandia National Laboratories* The lipid dynamics is the source of the variety of membrane structures and dynamics found in celss. Many of the interesting phenomena of biomembranes involve time scales of at least microseconds, which have been beyond simulations until recently. Coarse-grained models of lipid molecules have been developed to reach these long time scales and maintain the essential physical character of the molecules. Using these models in molecular dynamics simulations, time scales in the $\mu$s to ms range are treatable. As examples, simulations of domain formation and membrane fusion will be presented. In mixed lipid systems, the formation of domains is now understood to be an active component in biological processes. Our simulations reveal the dynamics of the lipid molecules that form domains in binary systems. In particular, the correlation between the two monolayers of the bilayer is dependent on the molecular structure of the lipid molecules. Membrane fusion is a fundamental process of cellular transport and infection processes. Understanding the basic principles governing membrane fusion has many important consequences. The coarse-grained molecular dynamics simulations show how lipid molecular structure influences the fusion process.

**11:51**

**P29 4 Lipid Coupling in Asymmetric Supported Lipid Bilayers Revealed by Fluorescence Correlation Spectroscopy** YAN YU, *Dept. of Materials Science & Engineering, UIUC* LIANGFANG ZHANG, *Dept. of Chemical & Biomolecular Engineering, UIUC* STEVE GRANICK, *Dept. of Materials Science & Engineering, of Physics, of Chemistry, and of Chemical & Biomolecular Engineering, UIUC* In biological systems, phospholipids asymmetry in two leaflets is a key feature of cell membranes for membrane biogenesis, intracellular fusion and signal transduction. Detailed information of the interactions and dynamics of the asymmetric membranes is paramount for design of applications. Here we use fluorescence correlation spectroscopy (FCS) to measure the coupling between 1, 2-dilauroyl-itsn-glycero-3-phosphocholine (DLPC) and 1, 2-dipalmitoyl-itsn-glycero-3-phosphocholine (DPPC) in asymmetric planar-supported bilayers (PSLBs), at temperatures where DLPC is in the fluid phase but DPPC is in the gel phase. Asymmetric PSLBs were prepared by placing dilute fluorescent-labeled 1, 2-dimeristoyl-itsn-glycero-3-phosphoethanolamine (DMPE) in DLPC leaflet as the probe for measuring lateral diffusion within the host leaflet environment. By constructing asymmetric bilayers where DLPC is alternatively in the top and in the bottom leaflet, we compare lipid coupling between the two leaflets with frictional interaction between the leaflets and the nanometer-thick water layer that separates the bottom leaflet from the solid support.

**12:03**

**P29 5 Dissipative Particle Dynamics Simulation of Structure Properties of Lipid Micelles** JINSUO ZHANG, YI JIANG, *MSK-575, Los Alamos National Lab* We chose dissipative particle dynamics (DPD) simulation to study the micelle structure properties. The self-assembly lipid is modeled by a flexible chain with head and tail particles. By changing interaction parameters between the solution particles and the lipid particles, three types of solution are considered: water, oil and water-oil mixture. It is found that the tail/head chains forming the micelle core have a very disorder distribution. The relation between the core radius with the aggregation number as well as the number of oil particles inside is obtained based on the simulation results and the molecular packing parameter. The mean density of particles in the core is higher than that in the simulation box. For micelles without oils inside, the density depends on the number of head particles in a lipid molecule, and the dependence becomes weaker as more oil particles are captured. At the core surface, head particles form clusters with water particles incorporated between the clusters. Comparisons with results from other simulation method such as MD show that DPD achieves high performance in simulating micelle formation and structure properties.

**12:15**

**P29 6 Anomalously Slow Domain Growth in Membranes with Asymmetric Transbilayer Lipid Distribution** MOHAMED LARADJI, *Physics Department, University of Memphis, Memphis, TN 38152* P.B. SUNIL KUMAR,* *Center for Biomembrane Physics, University of Southern Denmark, Campusvej 55, DK-5230,*

*Odense-M, Denmark* The effect of asymmetry in transbilayer lipid distribution on the phase separation of self-assembled multicomponent fluid vesicles is investigated numerically via dissipative particle dynamics. We show that this asymmetry induces a spontaneous curvature wich alters significantly the morphology and dynamics of the lipid mixture. In particular, at intermediate tension, domain growth is found to be anomalously slow dynamics. In contrast, in the limiting cases of low and high tensions, the dynamics proceed toward full phase separation.

*Permanent address: Physics Dept., Indian Institute of Technology-Madras, Chennai-600036, India

**12:27**

**P29 7 Molecular simulation studies of tail-length effects in mixed-lipid bilayers** JAMES KINDT, JASON DE JOANNIS, FUCHANG YIN, FRANK YONG JIANG, HAO WANG, *Department of Chemistry and Emerson Center for Scientific Computation, Emory University* Because lipid lateral diffusion is slow on the time-scale accessible to atomistic molecular dynamics (MD) simulations, equilibrium clustering and segregation in mixed-lipid bilayers are impractical to study through conventional computational approaches. A hybrid MD-Monte Carlo method employing lipid mutation moves within the semi-grand canonical ensemble method has been implemented for mixtures of lipids of differing tail lengths. For DLPC:DPPC mixtures, equilibration is demonstrated during simulation runs nearly two orders of magnitude shorter than estimates for standard MD. Statistical measures of lateral association in bilayer slabs and of partitioning among membrane micro-environments (flat bilayers, inner and outer leaflets of curved bilayers, and bilayer edge) will be presented.

**12:39**

**P29 8 Stabilization of Model Membrane Systems by Disaccharides. Quasielastic Neutron Scattering Experiments and Atomistic Simulations** EMMANOUIL DOXASTAKIS, *Dept. of Chem. & Biol. Engr., Univ. of Wisconsin* VICTORIA GARCIA SAKAI, *NIST Center for Neutron Research and Univ. of Maryland* SATOSHI OHTAKE, *Dept. of Chem. & Biol. Engr., Univ. of Wisconsin* JANNA K. MARANAS, *Dept. of Chem. Engr., Penn. State University* JUAN J. DE PABLO, *Dept. of Chem. & Biol. Engr., Univ. of Wisconsin* Trehalose, a disaccharide of glucose, is often used for the stabilization of cell membranes in the absence of water. This work studies the effects of trehalose on model membrane systems as they undergo a melting transition using a combination of experimental methods and atomistic molecular simulations. Quasielastic neutron scattering experiments on selectively deuterated samples provide the incoherent dynamic structure over a wide time range. Elastic scans probing the lipid tail dynamics display clear evidence of a main melting transition that is significantly lowered in the presence of trehalose. Lipid headgroup mobility is considerably restricted at high temperatures and directly associated with the dynamics of the sugar in the mixture. Molecular simulations provide a detailed overview of the dynamics and their spatial and time dependence. The combined simulation and experimental methodology offers a unique, molecular view of the physics of systems commonly employed in cryopreservation and lyophilization processes.

**12:51**

**P29 9 Protein crystals on phase-separating model membranes** SULIANA MANLEY, MARGARET HORTON, SZYMON LESZCZYNSKI, ALICE GAST, *Massachusetts Institute of Technology* We study the interplay between the crystallization of proteins tethered to membranes and separation within the membranes of giant unilamellar vesicles (GUVs) composed of DOPC, sphingomyelin (SM), and cholesterol. These model membranes phase separate into coexisting liquid domains below a miscibility transition temperature. This phase separation captures some aspects of the formation of lipid rafts in cell membranes and demonstrates the influence of membrane composition on raft formation. Real cell membranes have a much more complicated structure. There are additional physical constraints present in cell membranes, such as their attachment to the cytoskeleton and the presence of membrane bound proteins. The self-association of membrane proteins can influence the membrane phase behavior. We begin to investigate these effects on model tethered protein- loaded membranes by incorporating a small amount of biotin-X- DPPE into our GUVs. The biotinylated lipid partitions into a cholesterol-poor phase; thus, streptavidin binds preferentially to one of the membrane phases. As streptavidin assembles to form crystalline domains, it restricts the membrane mobility. We examine the effect of this protein association on lipid phase separation, as well as the effect of the lipid phase separation on the crystallization of the tethered proteins.

**13:03**

**P29 10 Model systems to investigate the effect of cholesterol on the transfection efficiency of lipoplexes** ALEXANDRA ZIDOVSKA, HEATHER M. EVANS, KAI EWERT, CYRUS R. SAFINYA, *Materials, Physics, and Molecular, Cellular and Developmental Biology Departments, Santa Barbara, CA 93106* Motivated by its important role in lipid-mediated gene delivery, we have studied the effect of cholesterol on membrane fusion. While recent work in our group has identified the membrane charge density as a critical parameter for transfection efficiency (TE) of lamellar, DOPC containing cationic lipid-DNA (CL-DNA) complexes [1-3], this model cannot fully explain the effect of cholesterol, suggesting that a different mechanism is responsible for the observed enhancement of TE. A model system using negatively charged giant vesicles has been developed to mimic the interaction of the cell membrane with CL-DNA complexes containing cholesterol. Differences in fusogenic properties have been observed as a function of the amount of cholesterol present in the CL-DNA complexes, and a fluorescence resonance energy transfer based assay was employed to quantify this effect. X-ray diffraction confirms that the lamellar structure seen with CL- DNA complexes is retained with the addition of cholesterol. Funding provided by NIH GM-59288 and NSF DMR-0503347. [1] A.J. Lin et al, Biophys. J., 2003, V84:3307-3316. [2] K. Ewert et al, J. Med. Chem., 2002, V45:5023-5029. [3] A. Ahmad et al., J. Gene Med., 2005, V7:739-748.

**13:15**

**P29 11 Had a drink last night? How alcohol interacts with biological membranes** MIKKO KARTTUNEN, *Helsinki University of Technology, Finland* MICHAEL PATRA, *Lund University, Sweden* EMPPU SALONEN, EMMA TERAMA, ILPO VATTULAINEN, *Helsinki University of Technology, Finland* ROLAND FALLER, BRYAN LEE, *University of California, Davis* JUHA HOLOPAINEN, *University of Helsinki* We have performed extensive 100 ns molecular dynamics simulations to study the effect of methanol and ethanol on two different lipid bilayer sys-

tems (POPC and DPPC) in the fluid phase at 323 K [1,2]. We studied both structural changes induced by the alcohols and the dynamics of the system. It turned out that ethanol was able to penetrate the membranes whereas methanol was not able to do so. In particular, ethanol prefers to be accommodated in the vicinity of the lipid headgroup region. We also determined the dependence of lipid chain ordering on ethanol concentration and quite surprisingly found that to be non-monotonous. We explain that in terms of modified surface tension [2]. Finally, we determined lifetime of hydrogen bonds to be about 1 ns and found that be in excellent agreement with NMR results. [1] B.W. Lee, et al, Fluid Phase Equilibria 225, 63-68 (2004) [2] M. Patra et al, Biophys. J., in press 2005

**13:27**
**P29 12 Solid domain rafts in lipid vesicles and scars*** SLAVA CHUSHAK, *Iowa State University* ALEX TRAVESSET, *Iowa State University and Ames lab* The free energy of a crystalline domain coexisting with a liquid phase on a spherical vesicle may be approximated by an elastic or stretching energy and a line tension term. The stretching energy generally grows as the area of the domain, while the line tension term grows with its perimeter. We show that if the crystalline domain contains defect arrays consisting of finite length grain boundaries of dislocations (scars) the stretching energy grows linearly with a characteristic length of the crystalline domain. We show that this result is critical to understand the existence of solid domains in lipid-bilayers in the strongly segregated two phase region even for small relative area coverages. The domains evolve from caps to stripes that become thinner as the line tension is decreased. We also discuss the implications of the results for other experimental.

*funded by NSF-DMR-0426597

**13:39**
**P29 13 Efficient calculation of mechanical properties of multicomponent phospholipid bilayers with Monte Carlo simulations** MANAN CHOPRA, EMMANOUIL DOXASTAKIS, NICHOLAS L. ABBOTT, JUAN J. DE PABLO, *UW Madison* We present a systematic study of the mechanical properties of multicomponent phospholipid bilayers. Two sets of systems are considered. The first consists of a mixture of DioleoylPhosphatidylethanolamine (DOPE) and DioleoylPhosphatidylcholine (DOPC) phospholipids. These two molecules have different head groups but the same chain length. The second system consists of a mixture of DilauroylPhosphatidylcholine (DLPC) and DistearoylPhosphatidylcholine (DSPC); these molecules have different chain lengths but the same head group. We use atomistic and coarse grain models, coupled to advanced Monte Carlo simulation techniques, to examine the structure and mechanical properties of the bilayers. Our results for pure systems are in quantitative agreement with experiment. Experimental data for mixed bilayers are not available, but our results indicate that their mechanical behavior is highly non-linear, a finding that we can interpret in terms of the composition and the resulting structure of the mixtures.

**13:51**
**P29 14 Roughness effect on vesicle adhesion characterised by a novel micropipette-based technique** MARIE-JOSEE COLBERT, ADAM N. RAEGEN, KARI DALNOKI-VERESS, CECILE FRADIN, *Physics and Astronomy, McMaster University* Numerous biological processes have to go through a cell adhesion process, which make the fundamental study of the adhesion of cells on solid substrate a key research topic in cellular biophysics. We will present our work on the adhesion of a single vesicle on a substrate. A vesicle is held at the end of a micropipette mounted on a micromanipulator and put into contact with a surface. We developed a novel technique to directly measure adhesion using the spring-constant of an L-shaped micropipette when pulling the vesicle from the substrate. The substrate is made of a micropatterned polymer film coated with a thin layer of gold to promote adhesion with the vesicle. The effect of the surface roughness can therefore be carefully characterized.

**14:03**
**P29 15 Structure of Cholesterol Helical Ribbons, Self-Assembling Biological Springs.*** B. KHAYKOVICH, C. HOSSAIN, A. LOMAKIN, J. McMANUS, D. E. MONCTON, G. B. BENEDEK, *Department of Physics and Materials Processing Center, Massachusetts Institute of Technology, Cambridge, MA* Helical ribbons with characteristic pitch angles form spontaneously in a variety of quaternary surfactant-lipid-sterol-water solutions. These helical ribbons form in a variety of axial lengths, widths and radii. Surprisingly, however, they all have pitch angles of either 11 or 54[r]. Our X-ray diffraction studies of individual ribbons confirm that the remarkable stability of each of the two pitch angles is related to a crystalline nature of the ribbons. The small size (of 100 x 10 x 0.1 $\mu m^3$) and the significant curvature of the ribbons produce weak and broad Bragg peaks. Therefore, novel methods are used to analyze these data. The structure of these ribbons is similar to that of cholesterol monohydrate. Interestingly, there is an evidence for a superlattice structure, resembling that found in thick films of cholesterol grown at the air-water interface.

*This work is supported by the Department of Energy, Division of Materials Sciences and Engineering, Office of Basic Energy Sciences under Award No. DE-FG02-04ER46149.



**SESSION P30: FOCUS SESSION: ORGANIC INTERFACES**
**Wednesday Morning, 15 March 2006; 327, Baltimore Convention Center at 11:15**
**Lynn Loo, University of Texas, Austin, presiding**

***Invited Papers***

**11:15**
**P30 1 Properties of Organic Molecules at Metal Surfaces.**
FEDERICO ROSEI, *Universite du Quebec*

The adsorption and selfassembly of organic molecules at surfaces has recently been investigated extensively, both because of the fundamental interest and for prospective applications in nanoelectronics and nanophotonics [1, 2].

Moleculemolecule and moleculesubstrate interactions can be tuned by the appropriate choice of substrate material and symmetry. Upon molecular adsorption, surfaces typically do not behave as static templates, but often rearrange dramatically to accommodate different molecular species [3, 4]. This presentation reviews recent experimental work using Scanning Tunneling Microscopy, which is providing new insight into fundamental properties such as molecular diffusion [5, 6] and selfassembly via surface templating [7] and hydrogen bonding driven by co-adsorption [8]. [1] F. Rosei et al., Prog. Surf. Science **71**, 95 (2003). [2] F. Rosei, J. Phys. Condens. Matter **16**, S1373 (2004). [3] F. Rosei et al., Science **296**, 328 (2002). [4] R. Otero, F. Rosei, et al., Nanoletters **4**, 75 (2004). [5] M. Schunack, T.R. Linderoth, F. Rosei, et al., Phys. Rev. Lett. **88**, 156102 (2002). [6] J.A. Miwa, S. Weigelt, H. Gersen, F. Besenbacher, F. Rosei, T.R. Linderoth, submitted. [7] R. Otero, Y. Naitoh, F. Rosei et al., Angew. Chem. **43**, 4092 (2004). [8] K.G. Nath, O. Ivasenko, J.A. Miwa, H. Dang, J.D. Wuest, A. Nanci, D.F. Perepichka, F. Rosei, submitted.

***Contributed Papers***

**11:51**

**P30 2 Direct measurements of contact resistances in asymmetric pentacene thin-film transistors with polyaniline and gold electrodes** KWANG SEOK LEE, TIMOTHY SMITH, JOUNG EUN YOO, KEITH STEVENSON, YUEH-LIN (LYNN) LOO, *Department of Chemical Engineering, Department of Chemistry and Biochemistry, University of Texas at Austin* We have fabricated asymmetric pentacene thin-film transistors with one gold electrode and one polyaniline (PANI) electrode connected to the same pentacene channel. Surface potential measurements reveal large potential drops at the gold/pentacene contact, but not at the PANI/pentacene contact during operation. We observe, however, some potential drop along the PANI electrode outside the scan window due to the bulk resistance of PANI. To minimize the potential drop across the PANI electrode, we have fabricated asymmetric devices with one exposed gold electrode, and one PANI-coated gold electrode. The surface potential profiles of these asymmetric devices with the PANI-coated gold electrode as the source electrode and the exposed gold electrode as the drain electrode, and vice versa, reveal no additional potential drop across the PANI-coated gold electrode. Quantification of the contact resistance indicates that the PANI/pentacene contact is significantly less resistive than the gold/pentacene contact whether the PANI-coated gold electrode is used as the source, or the drain electrode. Additionally, charge injection from the exposed gold electrode and the PANI-coated electrode appears to be more difficult than charge extraction from these electrodes.

**12:03**

**P30 3 Nm-resolution studies of Au/molecular-film/GaAs junctions using ballistic electron emission microscopy (BEEM)** C. MARGINEAN, C. TIVARUS, J.P. PELZ, *The Ohio State University* HOSSAM HAICK, DAVID CAHEN, *The Weizmann Institute* BEEM was used to image and quantify lateral homogeneity and energy band alignments at molecule/electrode interfaces in Au/dC-X/GaAs structures, where dC-X are dicarboxylic ligands with X= H, $OCH_3$, $CF_3$, CN, or $CH_3$ [1]. Transport through such junctions was proposed to be dominated by ''pinholes'' in the dC-X film, with the Au/GaAs Schottky barrier height (SBH) at pinholes modified by the surrounding molecular film dipole [1]. BEEM images of dC-$CH_3$ with $V_{tip} < \sim 1.38$ eV indeed revealed isolated 20-40 nm sized ''pinholes'' with measured local SBHs ranging from 0.90 – 1.0 eV, consistent with the model [1]. However, between the pinholes we also observed a new conduction channel for $V_{tip} > \sim 1.38$ eV, possibly due to transport through the LUMO of the dC-$CH_3$ film itself. BEEM measurements for the other –X groups also showed non-uniform, film-dependent SBH, but for those films the pinholes were too dense or the films too transparent to resolve isolated pinholes. All dC-X films were stable under the BEEM hot-electron flux. [1] H. Haick et al., Adv. Mater. **16**, 2145 (2004).

**12:15**

**P30 4 A Possible Mechanism For Photoinduced Effects In Molecule-Based Magnets** SERKAN ERDIN, MICHEL VAN VEENENDAAL, *Dept. of Physics, Northern Illinois University, DeKalb, IL, 60615 & Argonne National Laboratory,Advanced Photon Source, Argonne, IL 60439* A mechanism based on charge transfer processes between ligand and metal, for photoinduced effects on magnetic order that are observed in manganese-tetracyanoethylene molecule-based magnet is proposed. In order to support the mechanism, Monte Carlo calculations for a double exchange model with antiferromagnetic interaction between nearest neighbor manganese core spins, $J_{AF}$ on two dimensional metal-ligand lattice are performed. Depending on strength of $J_{AF}$ and the number of electrons in the system, total average magnetization and average angles of core spins are calculated.

**12:27**

**P30 5 The electronic structure and polymerization of a self-assembled monolayer** DANQIN FENG, DAVID WISBEY, *University of Nebraska-Lincoln* YIAN TAI, *Universität Heidelberg* YAROSLAV LOSOVYJ, *Center for Advanced Microstructures and Devices* MICHAEL ZHARNIKOV, *Universität Heidelberg* PETER DOWBEN, *University of Nebraska-Lincoln* Irradiation-induced modifications of electronic structure in the monomolecular insulator [1,1';4',1''-terphenyl]-4,4''-dimethanethiol (TPDMT) films have been investigated by photoemission and inverse photoemission. A dominant effect is cross-linking of the TPDMT film, which result in a quasipolymeric material with a smaller gap between the highest occupied molecular orbital (HOMO) and lowest unoccupied molecular orbital (LUMO) but improved the dielectric properties. The cross-linking processes are also accompanied by changes in molecular orientation. The photoemission intensities of organic molecular layers generally obey the Debye-Waller temperature dependence but not always. With the example of a monomolecular film formed from [1,1';4',1''-terphenyl]-4,4''-dimethanethiol, we show that pronounced deviations from Debye-Waller temperature behavior are possible and are likely caused by temperature dependent changes in molecular orientation.

**12:39**

**P30 6 A first-principles study of $\pi$-stacking in charged oligothiophenes in the presence of counterions** NICHOLAS MILLER, *DMSE, Massachusetts Institute of Technology* DAMIAN SCHERLIS, *Universidad de Buenos Aires* NICOLA MARZARI, *DMSE, Massachusetts Institute of Technology* We investigate the structural and electronic properties of charged oligothiophenes and of their $\pi$-stacking interactions with extensive density-functional theory (PBE, B3LYP) and post-Hartree-Fock (MP2) calculations. We pay particular attention to the role of counterions and of the solvation medium in tuning the balance between electrostatic repulsion and chemical bonding, including explicitly hexafluorophosphate counterions, and exploring the role of polarizability and surface tension for different solvents. Our calculations show that Coulomb's repulsion of the charged oligothiophenes is rapidly screened by solvation, counterions, or both, leading to stable $\pi$-dimerized systems (or higher stackings) where binding is driven by $\pi$-bond hybridization. Furthermore, we studied the charge-transfer properties of the counterion-oligomer system, as well as site preferences for counterions, highlighting the relevance of a proper treatment of correlations and self-interaction in describing the electronic-structure of these systems.

**12:51**

**P30 7 Orientation of Fluorophenols on Si(111)** FAN ZHENG, *University of Wisconsin-Madison* J.L. McCHESNEY, *Lawrence Berkeley National Lab* XIAOSONG LIU, F.J. HIMPSEL, *University of Wisconsin-Madison* Oriented adsorption of switchable organic molecules at surfaces is an important prerequisite for single molecular electronics [1, 2]. As model systems we select polar fluorophenols with tailored dipole moments and investigate their adsorption on the Si(111)7$\times$ 7 surface by near edge x-ray absorption fine structure spectroscopy (NEXAFS). A strong polarization dependence of the $\pi^*$ transitions is observed in fluorinated phenols, while phenol itself is isotropic. A quantitative model is developed to convert polarization-dependent NEXAFS data into orientational information. The model includes three angular degrees of freedom, two of them fixed and the other with a Gaussian distribution. Such a situation is encountered in a variety of self-assembled monolayers (SAMs) with tailored end groups [3]. [1] T. A. Jung, R. R. Schlittler, J. K. Gimzewski, Nature **386**, 696, (1997) [2] A. J. Mayne, M. Lastapis, G. Baffou, L. Soukiassian, G. Comtet, L. Hellener and G. Dujardin, Phys. Rev. B **69**, 045409 (2004) [3] Y.Y. Luk, N. L. Abbott, J. N. Crain and F. J. Himpsel, J. Chem. Phys. **120,** 10792 (2004)



**SESSION P31: NANOTUBES: THEORY AND EXPERIMENT**
**Wednesday Morning, 15 March 2006**
**328, Baltimore Convention Center at 11:15**
**Nicholas Kioussis, California State, Northridge, presiding**

**11:15**

**P31 1 Building and Deploying Community Nanotechnology Software Tools on nanoHUB.org – Non-Equilibrium Green's Function Simulations of the Impact of Atomic Defects on the Performance of Carbon Nanotube Transistors.** NEOPHYTOS NEOPHYTOU, SHAIKH AHMED, DIEGO KIENLE, MARK LUNDSTROM, GERHARD KLIMECK, *Network for Computational Nanotechnology, Purdue University, W. Lafayette, IN 47907* The Network for Computational Nanotechnology (NCN) is a multi-university, NSF-funded initiative with a mission to lead in research, education, and outreach deploying a unique web-based infrastructure (http://nanoHUB.org) to serve the nation's National Nanotechnology Initiative. Around 30 research codes/community tools are available and all the NCN services are free of charge. One such community tool is the CNTFET simulator based on NEGF techniques and the Finite-Element-Method (FEM) to treat three-dimensional (3D) electrostatics. We are able to simulate electronic transport in experimentally demonstrated 3D CNT devices with atomistic potential and charge resolution. Currently, we are investigating the effects of atomistic defects in the CNT devices such as vacancies and charged impurities.

**11:27**

**P31 2 Separation of single-walled carbon nanotubes into metallic and semiconducting groups: a simple and large-scale method** JING LU, *Mesoscopic Physics Laboratory, Department of Physics, Peking University, Beijing 100871, Peoples Republic of China.* Y. MAEDA, *Department of Chemistry, Tokyo Gakugei University, Tokyo 184-8501, Japan* Separation of a large number of single-walled carbon nanotubes (SWNTs) into groups each with specifically metallic and semiconducting properties is an extremely important task for technology application. Even though effective methods (1, 2) have been devised, they suffer from drawbacks such as either the yield is low (3) or expense is high (4). In this work, we study the problem from a theoretical approach, we notice that based on the first principles calculations the binding strengths of methylamine to the semiconducting [13, 0] SWNT are only 36$\sim$ 61% of that to the metallic [7, 7] SWNT, which suggests that the amines is much more attractive toward the pure metallic than the semiconducting SWNTs. Therefore starting from as-prepared SWNTs and with the assistance of amines, we achieved SWNTs with enriched metallic properties over semiconducting in a convenient and large-scale manner. (1) D. Chattopadhyay, L. Galeska, F. Papadimitrakopoulos, Journal of the American Chemical Society 125, 3370 (MAR 19, 2003). (2) H. P. Li et al., Journal of the American Chemical Society 126, 1014 (FEB 4, 2004). (3) R. Krupke, F. Hennrich, H. von Lohneysen, M. Kappes, SCIENCE 301, 344 (JUL 18, 2003). (4) M. Zheng et al., Science 302, 1545 (NOV 28, 2003).

**11:39**

**P31 3 Polaron superconductivity model for Li-doped nanotube-zeolite composite** XIANXIANG HUANG, PING SHENG, *Department of Physics and Institute of Nano Science and Technology, The Hong Kong University of Science and Technology* We propose a polaron superconductivity model for Li-doped nanotube-zeolite composite, in which the 4 Angstrom carbon nanotubes are embedded in the zeolite matrix, with a nanotube-nanotube wall separation of less than 10 Angstroms. The small separation implies inevitable nanotube-nanotube coupling, leading to a 3D anisotropic superconductor. Here we calculate the mean-field superconducting transition temperature based on the fact that each adsorbed Li atom, situated in the middle of the nanotube, donates an electron to the nanotube so as to form an ion-electron system. In addition, the Li ion is trapped in a shallow well formed by the (5,0) nanotube, with a periodicity of 4.3 Angstroms. So the

Li vibration resembles that of an optical phonon. We have evaluated both the electron-electron interaction and the electron-phonon interactions in the presence of the screening effect, and solved the Eliashberg-Gorkov equation to obtain the superconducting transition temperature.

**11:51**

**P31 4 Theoretical Model for a Carbon Nanotube-Based Magnetometer at Non-Zero Temperatures** VLADIMIR DOBROKHOTOV, CHRIS BERVEN, *University of Idaho* We present a complete description of electronic current in metallic single-walled carbon nanotubes under the influence of axially oriented magnetic fields at nonzero temperatures. We include in our model [1] the diameter of the carbon nanotube, the temperature and length of the nanotube. We find that the current in a zigzag carbon nanotube that is metallic at zero magnetic field is strongly modulated by varying the magnitude of an axially oriented magnetic field. We use this property, to propose a design of a carbon nanotube based directional magnetometer that could be designed to sense magnetic fields from 1 T to 8 T and at temperatures from 0 K up to 100 K. [1] Vladimir Dobrokhotov and Christopher Berven, ''Electronic Transport Properties of Metallic CNTs in an Axial Magnetic Field at nonzero Temperatures: A Model of an Ultra-small Digital Magnetometer,'' accepted for publication 11-2005 Physica E

**12:03**

**P31 5 Effect of Short-Range Electron Correlation in Nanotubes** ANDREW KINCHEN, RUSSELL SELVA, YURIY MALOZOVSKY, *Southeastern Louisiana University* We study the effect of short-range electron correlation in the zigzag and armchair carbon nanotubes (CNT). We derived the dynamic pair interaction potential between two electrons in the tubule incorporating Hubbard type local field factor. The dispersion of plasma modes at different values of angular momentum, and chirality angle and single-particle excitations are derived as well. We also evaluate the self-energy part due to the interaction of an electron with acoustic mode.

**12:15**

**P31 6 Electron Standing Waves in Semiconducting Carbon Nanotubes: Spatially-Resolved Scanning Tunneling Spectroscopy** SE-JONG KAHNG, *Department of Physics, Korea University* HAJIN KIM, SUNGJUN LEE, YOUNG KUK, *School of Physics and Center for Science in Nanometer Scale, Seoul National University* Electronic modulation patterns were observed, from the gap states of semiconducting single-wall carbon nanotubes, using spatially-resolved scanning tunneling spectroscopy. Some modulations show single peaks, with the period twice of the lattice constants, while others show double peaks. Both modulations are localized within a few nano-meters, enclosed by exponential decay functions. The modulation patterns are well understood in terms of the squared wavefunctions, derived from the simple quantum mechanical potential well models. Our model can be applied to the bound states of metallic carbon nanotubes as well.

**12:27**

**P31 7 Electronic structure of carbon nanotubes adsorbed on Si(001) vicinal surfaces.** S. BERBER, A. OSHIYAMA, *University of Tsukuba* We have investigated adsorption of carbon nanotubes on Si(001) vicinal surfaces using Density Functional Theory total energy and electronic structure calculations. Energetically favorable adsorption orientations and positions of carbon nanotubes were searched by total energy calculations, and detailed atomic structure of carbon nanotubes adsorbed at most probable adsorption sites have been obtained by full structure relaxation. Adsorption energy shows both direction and site dependence since the carbon nanotube form covalent bonds with the clean vicinal surface. Charge transfer between the nanotube and the surface happens mainly at the interface, which results in a quasi one-dimensional electron channel. Electronic states of carbon nanotube and silicon surface are highly rehybridized and mixed. A metallic carbon nanotube could behave as small gap semiconductor depending on adsorption site. Insertion of $sp^3$ bonded carbon atoms in $sp^2$ bond network introduces energy gap in electronic structure of the nanotube near Fermi level. This energy gap could be eliminated if there are surface states available for charge transfer. But such surface states are not available for particular nanotube directions, and non-metallic electronic structure appears. Dangling bond states of silicon surface, which appears as energy bands near the Fermi level, attracts electrons from the nanotube provided that these states are localized near the nanotube. Termination of surface dangling bonds in the vicinity of adsorbed nanotube could help tune the electronic properties of adsorbed nanotube.

**12:39**

**P31 8 The II-VI nanostructure zoo** PHILIP LINDAN,* *School of Physical Sciences, University of Kent* SAMANTHA LISTER, *School of Physical Sciences, University of Kent* We present predictions of a completely new family of nanotubes, related nanostructures and fullerene-like cages formed from the II-VI semiconductor mercury telluride. Our predictions are supported by first-principles calculations on the structures. The structures are remarkable in several ways: They are all more stable than the planar form of HgTe from which they are formed; they are radically altered from the tetrahedral bulk forms, and a strong interaction with the electronic structure results in a semimetal-semiconductor transformation; and for the larger armchair tubes isomerisation leads to striking structures formed from heavy modification of the tube, accompanied by large changes in the bandgap. For the nanotubes two simple rules for preferred coordination of Hg and the Hg-Te-Hg bond angles explain the structural stability of the nanotubes, and the formation of their exotic isomers. The cage structures are based upon the Archimedean and Platonic solids, where key requirements in terms of numbers of vertices, number of triangular faces and their connectivity determine the viable subset of structures.

*Reciprocal society member - UK Institute of Physics

**12:51**

**P31 9 Nonlinear ac conductivity of disordered Luttinger liquids*** BERND ROSENOW, *Physics Department, Harvard University, USA* THOMAS NATTERMANN, *Insitut fuer Theoretische Physik, Universitaet zu Koeln, Germany* We consider low energy charge transport in one-dimensional electron systems with short range interactions under the influence of a random potential. At zero temperature, the linear ac conductivity vanishes like $\sim \omega^2(\ln(1/\omega))^2$. Much less is known about the *non-linear conductivity*. At zero temperature and frequency, charge transport is only possible by tunneling of charge carriers, which can be described by instanton formation. The nonlinear dc conductivity is characterized by $I \sim \exp(-\sqrt{E_0/E})$ provided the system is coupled to a dissipative bath [1]. Combining RG and instanton methods, we calculate the nonlinear ac conductivity and discuss the crossover between the nonanalytic field dependence of the

electric current at zero frequency and the linear ac conductivity at small electric fields and finite frequency [2].[0.5cm] [1] S. Malinin, T. Nattermann, and B. Rosenow, Phys. Rev. B **70**, 235120 (2004). [2] B. Rosenow and T. Nattermann, accepted for publication in Phys. Rev. B; preprint cond-mat/0408042.

*Research is supported by DFG grant Ro 2247/4-1

**13:03**

**P31 10 Renormalization of a single impurity potential of arbitrary strength in a Tomonaga-Luttinger liquid*** KENJI KAMIDE, YUJI TSUKADA, SUSUMU KURIHARA, *Department of Physics, Waseda University, 3-4-1, Okubo, Shinjuku, Tokyo 169-8555* We study the renormalization flow of a single impurity potential of arbitrary strength in a Tomonaga-Luttinger liquid (TL). It is known that an impurity potential in TL is effectively renormalized by electron-electron interaction, with different manners in weak and strong potential limits for spin dependent models $K_s \neq 1$. This fact strongly suggests that the fixed points of an impurity potential should shift as varying potential strength. In order to determine the scaling fixed points at arbitrary potential strength, we extend boundary bosonization scheme to the problem of arbitrary potential strength, and calculate the local density of states (LDOS) as a function of temperature and distance from the impurity. The impurity scaling flow is determined from the ratio between LDOS at the boundary and in the bulk. For $K_s = 1$, the phase boundary is given by $K_\rho = 1$ irrespective of the potential. For $K_s \neq 1$, we find that the fixed points shift from $K_\rho \sim 2 - K_s$ to $K_\rho = 1/K_s$ as increasing the potential strength from 0 to $\infty$. We also discuss how the scaling behavior appears in transport experiments.

*K. K. is supported by the Japan Society for promotion of Science.

**13:15**

**P31 11 Adsorbed monolayers on suspended single-walled carbon nanotubes** ZENGHUI WANG, JIANG WEI, ROBERT DORMAIER, OSCAR VILCHES, DAVID COBDEN, *University of Washington* A monolayer of adsorbates on a single-walled carbon nanotube presents the possibility of extending earlier studies of two-dimensional monolayer systems on graphite to the quasi-one-dimensional regime, by effectively imposing cylindrical boundary conditions. The monolayer can be detected either via its effect on the nanotube's conductance or by using the nanotube itself as a vibrating microbalance. Many adsorbates are known to affect the conductance, through a variety of mechanisms. Amongst these are $O_2$ and the noble gases Xe and Kr, whose phases and ordering on 2D graphite are well known. Our experiments so far have indicated that the presence of an $O_2$ layer on a nanotube close to liquid nitrogen temperatures can be detected using a threshold shift. We are now fabricating individual suspended nanotube devices with the initial aim of studying cylindrical commensurability effects on the phases of noble gases using the microbalance technique.

**13:27**

**P31 12 Superplastic single-walled carbon nanotubes** J.Y. HUANG, S. CHEN, Z. WANG, K. KEMPA, S.H. JO, *Department of Physics, Boston College, Chestnut Hill, MA 02467* Y.M. WANG, *Lawrence Livermore National Laboratory, Livermore, CA 94550* G. CHEN, *Department of Mechanical Engineering, MIT, Cambridge, MA 02139* M.S. DRESSELHAUS, *Department of Physics, Electrical Engineering and Computer Science, MIT, Cambridge, MA 02139* Z.F. REN, *Department of Physics, Boston College, Chestnut Hill, MA 02467* Theoretical prediction on the maximum achievable tensile strain of a single-wall carbon nanotube (SWCNT) is less than 20%, but experiments indicate a much lower attainable strain of less than $\sim$ 6%. Here we report that, at temperatures of above 2000[r]C, SWCNTs deform superplastically, with a tensile elongation to failure nearly 280%, and a diameter reduction of fifteen times. With this remarkable dimension change, the electronic property changes correspondingly from a metal with a pseudogap to a semiconducting state with a tunable gap up to 2 eV. Such superplastic deformation originates from plastic deformation mechanism dominated by the nucleation and motion of the kinks as well as atom diffusion in SWCNTs at high temperatures. Variable range hopping conduction is observed in the localized state due to scattering by point defects and kinks in the quasi-one-dimensional system.

**13:39**

**P31 13 Unoccupied electronic states of Multiwall Carbon Nanotubes Arrays** PATRICIO HÄBERLE, SAMUEL HEVIA, RODRIGO SEGURA, WLADIMIR IBÁÑEZ, *Universidad Técnica Federico Santa María, Valparaíso, Chile* We have grown multiwall carbon nanotube (MWCNT) arrays by CVD both from pyrolysis of Fe-Phthalocyanine and decomposition of Acetylene on Fe covered $SiO_2$/Si(111) substrates. The characteristic diameter of the tubes is 50 nm for both type of samples. Even though the films show good alignment in the bulk, they do present some disorder of the tubes at the top of the films. Inverse photoemission spectra from these samples are similar to those obtained from HOPG. The main differences are in: the non existence of what has been recognized as an image charge state on graphite and some additional intensity very close to the Fermi level ($\varepsilon_F$). A similar intensity has been measured previously by photoemission in a symmetrical position with respect to $\varepsilon_F$. This increased metallic character could, at this point, be interpreted as defects from the closure of the tubes or as a manifestation of van Hove oscillations in the unoccupied density of states.

**13:51**

**P31 14 Electrostatics of Straight and Wiggly Nanotubes in External Electric Field*** MIKHAIL RAIKH, EUGENE MISHCHENKO, *University of Utah* Distribution of charge induced in a straight nanotube (NT) by external electric field parallel to the NT axis is found as a function of the NT length and radius. As the voltage drop along the NT exceeds the gap, positive and negative charge regions emerge at the NT ends. These regions are separated by a neutral strip at the NT center. External field is unscreened within the neutral strip, while it is strongly suppressed outside the strip. For a NT of a wiggly shape, the induced charge distribution represents alternating positively and negatively charged regions separated by neutral strips.

*Supported by the Petroleum Research Fund

**SESSION P32: SPIN GLASSES**
**Wednesday Morning, 15 March 2006**
**329, Baltimore Convention Center at 11:15**
**G. Luke, McMaster University, presiding**

**11:15**

**P32 1 Effects of high magnetic fields on the spin-glass states in disordered manganites** NOBORU MIURA, PETER KERSCHL, NADJA V. KOZLOVA, KONSTANTIN NENKOV, KATHRIN DOERR, *IFW, Dresden, Germany* ALEXANDER KIRSTE, MICHAEL VON ORTENBERG, *Humboldt University, Berlin, Germany* DAISUKE AKABOSHI, YASUHIDE TOMIOKA, YOSHINORI TOKURA, *CERC, AIST, Tsukuba, Japan* IFW, DRESDEN TEAM, HUMBOLDT UNIVERSITY, BERLIN TEAM, CERC, AIST, TSUKUBA TEAM, Magnetization and magnetoresistance were measured in single crystals of random alloys $RE_{1-x}AE_xMnO_3$ (RE and AE denote the rare-earth and alkaline-earth ions at the perovskite A-site) in pulsed high magnetic fields up to 50 T with a long time duration ( $\sim$ 10 ms) and up to 140 T with a short time duration ( $\sim \mu$s). The crystals exhibit the spin glass behaviors at low temperatures in zero field. In high magnetic fields, $Sm_{1-x}(Ba_{1-y}Sr_y)_xMnO_3$ showed prominent metamagnetic transitions, whereas $RE_{1-x}Ba_xMnO_3$ (RE=Sm, Eu, Gd) showed a smooth magnetization saturation with just kinks in the derivative of the magnetization. Moreover, in the metamagnetic phase transitions, peculiar time dependence and the prehistory dependence were found in the hysteresis of the magnetization. It was also found that the magnetization is accompanied with a colossal magnetoresistance. These behaviors were interpreted in terms of the developments of the clusters and the orbital orders by magnetic fields, which are dependent on the average A-site ionic radius and the randomness.

**11:27**

**P32 2 What is new for spin-glass in a quasi-2D system*** WEI BAO, *Los Alamos National Lab* YING CHEN, *NIST* YIMING QIU, *NIST* J.E. LORENZO, *CNRS Grenoble* J.L. SARRAO, *Los Alamos National Lab* DEREK HO, *NIST* MIN Y. LIN, *NIST* In conventional spin glasses, magnetic interaction is not strongly anisotropic and the entire spin system is believed to be frozen below the spin-glass transition temperature. Along *any* direction, spin correlations are highly disordered. In $La_2Cu_{0.94}Li_{0.06}O_4$, for which the in-plane exchange interaction dominates the interplane one, only a fraction of spins with antiferromagnetic correlations extending to neighboring planes become spin-glass. The remaining spins with only in-plane antiferromagnetic correlations remain spin-liquid at low temperature. Spin correlations are highly disordered only along the interlayer direction, but highly ordered in-plane. Such a novel partial spin freezing out of a two-dimensional spin-liquid observed in this cold neutron scattering study is likely due to a delicate balance between disorder and quantum fluctuations in the quasi-two dimensional $S=1/2$ Heisenberg system.

*Ref.: PRB **72**, 184401 (2005). Supported by US DOE

**11:39**

**P32 3 Spin Glasses at the Bond Percolation Threshold*** EMILIANO MARCHETTI, STEFAN BOETTCHER, *Physics Department, Emory University, Atlanta GA* Low energy excitations for the Edwards-Anderson model on hyper- cubic lattices at the bond percolation threshold $p_c$ are investigated. At $T = 0$, $p_c$ separates paramagnetic and spin glass phases. At the ''edge'' of the ordered state, these excitations are characterized by a distinct scaling exponent. This exponent allows to determine the shape of the phase boundary, $T_c(p) \sim (p - p_c)^{\phi}$, for $p \to p_c^+$, which is experimentally measurable in $d = 3$. At $p_c$, very large spin glass systems can be studied with an *exact* reduction algorithm[1] to produce accurate scaling behavior. For more information, see http://www.physics.emory.edu/faculty/boettcher/

*This work has been supported by grant 0312510 from the Division of Materials Research at the National Science Foundation.

[1]Europhys. Lett. **67**, 453 (2004)

**11:51**

**P32 4 Spin-glass correlations in classical dipoles** VADIM OGANESYAN, *Yale University* We present analytic mean-field and high-temperature expansion results on thermodynamics of classical Ising dipoles in the strongly diluted regime. These display a broad distrubution of couplings resulting in strong enhancement of the spin-glass transition temperature from the naive estimate. We comment on reliability of these results and their relationship to other approaches.

**12:03**

**P32 5 Computing Barriers in Spin Glasses** A. ALAN MIDDLETON, *Syracuse University* The energy barriers $E_B$ between low-lying states in spin glasses are expected to scale as a power of the system size: $E_B \sim N^{\psi/d}$ for $N$ spins in a $d$-dimensional spin glass. Whether the barrier exponent $\psi$ is equal to the stiffness exponent $\theta$ (where the cost of minimal large scale excitations scales as $N^{\theta/d}$) is an unsolved question in general. In an attempt to solve this question with some rigor in large theoretical spin glass samples, numerical simulations for barriers in spin glasses on a hierarchical lattice have been carried out, using an exact algorithm for computing the barrier to the monotone growth of connected domains. The resulting $\psi$ is sensitive to the distribution of weights on the bonds between spins. These distributions give different weights to bonds that appear at different stages of the hierarchical generation of the lattice. Results for $\psi$ and $\theta$ will be presented for various lattices, including variations of Cayley trees and lattices that satisfy Migdal-Kadanoff approximations, and distributions that plausibly emulate finite-dimensional spin glasses.

**12:15**

**P32 6 The End of Aging in a Spin Glass** GREGORY KENNING, *Department of Physics, Indiana University of Pennsylvania* GILBERTO RODRIGUEZ, *Department of Physics, University of California Riverside* RAYMOND ORBACH, *Department of Energy, Office of Science* Aging phenomena in complex systems has been used as an important tool to investigate the physics of complexity. In particular aging effects in spin glasses, measured using the Thermoremenant Magnetization (TRM) decays, have been instrumental as a probe of complex equilibrium and non-equilibrium dynamics. Current theoretical and experimental analysis suggest that the TRM decay of spin glasses is mainly composed of two terms; The ''stationary'' term which does not depend on the sample history and dominates the short time decay ( $<$ 1s) and a long time aging term which depends on the samples history. We report finding that aging found in spin glass materials, has a finite lifetime and that after aging has ended there is a third component of the magnetization decay. This decay is independent of the waiting time, logarithmic in nature and part of the same mechanism that produces aging. Finally we find that the logarithmic decay

implies a maximum aging time (MAT) that is very strongly dependent on temperature and ranges from short times near the spin glass transition temperature to many times the current best estimates of the age of the universe for low temperature.

**12:27**

**P32 7 Memory and aging effect in hierarchical spin orderings of stage-2 $CoCl_2$ graphite intercalation compound** MASATSUGU SUZUKI, ITSUKO SUZUKI, *SUNY-Binghamton* MOTOHIRO MATSUURA, *Fukui University of Technology* Stage-2 $CoCl_2$ graphite intercalation compound undergoes two magnetic phase transitions at $T_{cl}$ (= 7.0 K) and $T_{cu}$ (= 8.9 K). The aging dynamics of this compound is studied near $T_{cl}$ and $T_{cu}$. The intermediate state between $T_{cl}$ and $T_{cu}$ is characterized by a spin glass phase extending over ferromagnetic islands. A genuine thermoremnant magnetization (TRM) measurement indicates that the memory of the specific spin configurations imprinted at temperatures between $T_{cl}$ and $T_{cu}$ during the field-cooled (FC) aging protocol can be recalled when the system is re-heated at a constant heating rate. The zero-field cooled (ZFC) and TRM magnetization is examined in a series of heating and reheating process. The magnetization shows both characteristic memory and rejuvenation effects. The time ($t$) dependence of the relaxation rate $S_{ZFC}(t) = (1/H)\mathrm{d}M_{ZFC}(t)/\mathrm{dln}t$ after the ZFC aging protocol with a wait time $t_w$, exhibits two peaks at characteristic times $t_{cr1}$ and $t_{cr2}$ between $T_{cl}$ and $T_{cu}$. An aging process is revealed as the strong $t_w$ dependence of $t_{cr2}$. The observed aging and memory effect is discussed in terms of the droplet model.

**12:39**

**P32 8 Bose glass vs. Mott glass in site-diluted S=1 Heisenberg antiferromagnets** TOMMASO ROSCILDE, *Max-Planck-Institut fuer Quantenoptik - Germany* STEPHAN HAAS, *Department of Physics and Astronomy - USC* Making use of large-scale quantum Monte Carlo simulations, we investigate the ground-state phase diagram of the square-lattice S=1 Heisenberg antiferromagnet with strong single-ion anisotropy and in presence of site-dilution of the magnetic lattice. Mapping the spins onto Holstein-Primakoff bosons, the single-ion anisotropy is seen to play the role of a repulsive on-site potential for the bosons. The clean limit of the model shows an anisotropy-driven quantum phase transition from an XY ordered (superfluid) phase to a quantum disordered (Mott insulating) phase. A similar transition is also driven by the application of a uniform field on the disordered state. Adding site dilution to the model, the non-trivial interplay between quantum fluctuations and lattice randomness gives rise to a novel quantum-disordered Mott-glass phase in zero field, with a gapless spectrum and yet a vanishing uniform susceptibility. Upon applying a field, such phase is turned into a Bose glass, with gapless spectrum and finite susceptibility. The above picture is directly relevant for experiments on doped quasi-low-dimensional Ni compounds, such as the recently investigated $NiCl_2$-4SC$(NH_2)_2$ (V.S. Zapf et al., condmat/0505562).

**12:51**

**P32 9 Impurity effects on frustrated ferro- and ferrimagnets in one dimension** MASANORI KOHNO, XIAO HU, *Computational Materials Science Center, National Institute for Materials Science, Tsukuba 305-0047, Japan* We have investigated impurity effects on magnetization for frustrated one-dimensional ferro- and ferrimagnets. Using the density-matrix renormalization group method and the exact diagonalization method, we confirmed that the magnetization decreases significantly by doping non-magnetic impurities. In a special case, the magnetization can vanish due to a single impurity in finite chains. Introducing the picture of magnetic domain inversion, we numerically investigated the impurity-density dependence of magnetization. In particular, we show that the magnetization substantially decreases down to less than 60% from that of the corresponding pure system by doping an infinitesimal density of impurities. We also formulate conditions for the materials which may show this anomalous impurity effect.

**13:03**

**P32 10 Frustrating interactions in oxides induced by non-magnetic impurities** SHIU LIU, *University of California, Irvine* SASHA CHERNYSHEV, *University of California, Irvine* An antiferromagnetic host material doped with non-magnetic impurities, such as Zn-doped $La_2CuO_4$, is generally believed to represent an excellent model case of the site-dilution of a magnetic substance. We demonstrate that there exist a significant qualitative correction to such a picture: an impurity can induce substantial frustrating interactions between spins that are nearest neighbors of the impurity site. Not only this effect explains discrepancies between experimental data and the site-dilution theory, but it could also lead to some important modification of the behavior of doped antiferromagnets close to the percolation. We study the 2D, $S = 1/2$ copper-oxide plane with Zn impurities starting from the microscopic three-band Hubbard model. We show that, for a wide range of the model parameters, the substantial superexchange interactions between the next- and next-next-nearest neighbor Cu spins around the impurity site can be generated via the virtual transitions through the oxygen orbitals. Surprisingly, the interaction across the impurity $J''_{Zn}$ is greater than the next-nearest neighbor interaction $J'_{Zn}$ due to a partial cancellation of the super- and the cyclic exchanges for the latter. This study is completed by the $T$-matrix calculation of the staggered magnetization $M(x)$ as a function of Zn doping $x$. The predicted range of $J'_{Zn}$ and $J''_{Zn}$ agrees with the values needed to explain experimental deviation of $M(x)$ from the results of the site-dilution theories.

**13:15**

**P32 11 Spin Polarization Measurments of $Co_{1-x}-Pt_x$ alloys by Point Contact Andreev Reflection Spectroscopy** MUHAMMAD FAIZ, RAGHAVA PANGULURI, B. NADGORNY, *Department of Physics, Wayne State University, Detroit, MI 48201* CHRISTIAN KAISER, *IBM Almaden Research Center, San Jose, California 95120 and Physikalisches Institut, RWTH-Aachen, Aachen, Germany* STUART S. P. PARKIN, *IBM Almaden Research Center, San Jose, California 95120* Recently Kaiser et al., [1] compared the spin polarization measured by spin resolved tunneling spectroscopy (Tedrow-Meservey) and the magnetic moment of $Co_{1-x}-Pt_x$ alloys. We have measured the transport spin polarization, $P_c$ and magnetic properties of the same series of samples using Point Contact Andreev Reflection Spectroscopy (PCAR). All films with x varying from 0 to 100% and a thickness of $\sim$ 1000 Å were grown on Si substrates covered with $\sim$ 250 Å of $SiO_2$ by magnetron sputtering. We will present a correlation between spin polarization and magnetization for this series of magnetic alloys and compare our results with the ones obtained in Ref. [1]. 1. C. Kaiser et al., PRL **94** 247203 (2005).

**13:27**
**P32 12 Charge degrees of freedom in frustrated lattices** JOSEPH BETOURAS, *Lorentz Institute, University of Leiden* FRANK POLLMAN, *Max Planck Institute for Physics of Complex Systems, Dresden, Germany* KIRILL SHTENGEL, *Department of Physics, University of California Riverside* PETER FULDE, *Max Planck Institute for Physics of Complex Systems, Dresden, Germany* We explore systematically the charge degrees of freedom in frustrated lattices. A model of spinless fermions on a checkerboard lattice with nearest-neighbor hopping t and Coulomb repulsion V is used at half and quarter fillings. Quantum fluctuations reduce the classical macroscopic degeneracy. For the strongly correlated limit V >> t, an added electron decays into two quasiparticles with fractional charge. We study the classical correlations and, by means of quantum field theory as well as axact diagonalisation, we also investigate the possibility of a confined or deconfined phase as well as the statistics of these quasiparticles.

**13:39**
**P32 13 Probing the Almeida-Thouless line away from the mean-field model** HELMUT G. KATZGRABER, *Theoretische Physik, ETH Zurich* A. PETER YOUNG, *University of California Santa Cruz* In order to test the existence of a spin-glass phase in a field at finite temperatures, results of Monte Carlo simulations of the one-dimensional long-range Ising spin glass with power-law interactions in the presence of a (random) field are presented. By tuning the exponent of the power-law interactions, we are able to scan the full range of possible behaviors from the infinite-range (Sherrington-Kirkpatrick) model to the short-range model. A finite-size scaling analysis of the correlation length indicates that there is no transition in a field with non-mean field critical behavior at zero field. This suggests that there is no Almeida-Thouless line for short-range Ising spin glasses away from the mean-field regime.

**SESSION P33: FOCUS SESSION: FRICTION, FRACTURE AND DEFORMATION III**
**Wednesday Morning, 15 March 2006**
**336, Baltimore Convention Center at 11:15**
**Yue Qi, General Motors Research and Development, presiding**

***Contributed Papers***

**11:15**
**P33 1 Atomistic Simulation of Size Effects in Bending a Single Crystal*** N. SCOTT WEINGARTEN, *The Catholic University of America* ROBIN SELINGER, *Kent State University* We perform atomistic Monte Carlo simulations of bending a Lennard-Jones single crystal in two dimensions. In examining initial yield, we find an apparent ''reverse'' size effect. However, when strain rate effects are taken into account, we demonstrate that the size effect disappears. Once geometrically necessary dislocations coalesce to form grain boundaries, we observe a size effect of the usual kind, e.g. smaller samples support a higher scaled bending moment than larger samples. We compare simulation results with recent experiments on bending of highly annealed nanowires [B. Wu et al, Nature Matls 4, 525, 2005.] Finally, we observe a topological instability in the evolution of a grain boundary intersecting a free surface under compressive stress. The grain boundary buckles and nucleates a protruding grain, suggesting a novel mechanism for the formation of a hillock on a compressed metal surface.

*NSF-DMR-0116090

**11:27**
**P33 2 Analytical calculation of energy barrier for dislocation nucleation from a crack tip** SERGIO PICOZZI, *George Washington University* ROBIN SELINGER, *Kent State University* In a ductile material a crack subjected to a subcritical applied load may respond by emitting dislocations via thermal activation. Computer simulations show the activation energy to be strongly dependent on the applied stress. To understand this result we use conformal mapping techniques to analyze the interaction of a straight screw dislocation with a parallel crack in a strip geometry. The energy barrier for dislocation escape from the crack tip is calculated explicitly and it is found to be a sensitive function of the applied stress, in qualitative agreement with simulation results. Scaling properties of the activation energy are also determined. This analytical result permits us to formulate hypotheses regarding the factors controlling the observed strain rate. To test such hypotheses we finally calculate the strain rate as a function of temperature and applied stress and compare our results with observations.

**11:39**
**P33 3 XRay Scattering in a Deformed Crystal by a Phase Field Method** ROBB THOMSON, *retired* MARISOL KOSLOWSKI, *Purdue Univ.* RICHARD LESAR, *LANL* We demonstrate the use of a phase field method for dislocated crystals, developed by one of us, for computing the scattering of Xrays. The model addresses deformation on a single slip plane by dislocations of a single burgers vector interacting with a set of point obstacles. The obstacles are introduced in two modes; one randomly on the slip plane, and the second in straight ''walls.'' The obstacles simulate blocking interactions by dislocations on different slip planes, and the ''walls'' represent the intersection of a secondary slip plane with the primary plane being simulated. In the small angle case, the scattering source is the local dilatation induced by the dislocations on the slip plane, and in the Bragg case, the scattering source is the change in local lattice constant. The small angle results show scattering with oscillations attributable to the width of the ''walls.'' In the Bragg case, the Laue spots are broadened by the dislocations, and the results directly confirm the picture of dipolar wall scattering introduced many years ago by H. Mughrabi.

**11:51**
**P33 4 Atomistic Dislocation Dynamics in Phase Field Crystals: Long Time Scale Properties** JOEL BERRY, *McGill University* K.R. ELDER, *Oakland University* MARTIN GRANT, *McGill University* The fundamental dislocation processes of glide, climb, and annihilation are studied on diffusive time scales within the framework of a continuum field theory, the Phase Field Crystals (PFC) model. Glide and climb are examined for single edge dislocations subjected to shear and compressive strain, respectively, in a two dimensional hexagonal lattice. It is shown that the natural features of these processes are reproduced without any explicit consideration of elasticity theory or ad hoc construction of microscopic Peierls potentials. Particular attention is paid to the Peierls barrier for dislocation glide/climb and the ensuing dynamic behavior as functions of strain rate, temperature, and dislocation density.

It is shown that the dynamics are accurately described by simple viscous motion equations for an overdamped point mass, where the dislocation mobility is the only adjustable parameter. The critical distance for the annihilation of two edge dislocations as a function of separation angle is also presented.

**12:03**
**P33 5 Studies of the Dislocation Glass** GERGELY ZIMANYI, *UC Davis* BOTOND BAKO, ISTVAN GROMA, GEZA GYORGYI, *Eotvos Lorand University, Budapest, Hungary* We report the large scale simulations of 2D dislocation systems with overdamped dynamics. 40,000-1,000,000 dislocations were studied with a combination of coarse graining, Fast Fourier Transform and stochastic methods. Both glide and climb processes were considered, as well as the local rotation of crystal axes. Simulations were performed at zero and finite temperatures, with and without dislocation annihilation. When climb processes were included, the system exhibited the formation of dislocation cells/patterns even in equilibrium, without the application of shear. This is in close correspondence with recent experiments on GaAs by P. Rudolph et al. (2005). The distribution function of cell sizes can exhibit a fractal dimension. At long times the system shows glassy dynamics. In particular, aging was observed through the waiting time dependence of the correlations and the effective diffusion. In certain parameter ranges the formation of cells leads to an initial exponential decay of correlations. This is followed by the growth of cells, generating a power law temporal decay in the long time domain. Data for both time domains and for all waiting times can be collapsed onto a single master curve when a t/tw scaling is applied.

**12:15**
**P33 6 Nonlinear acoustic effects from dislocation-based hysteretic kinking solids under stresses** PETER FINKEL, *Thomson/Rowan University* MATHIEU FRASCZKIEWICZ, *Drexel University* MICHEL BARSOUM, *Drexel University* We argue that proposed recently mechanism explaining inelastic hysteresis in non-linear elastic systems indeed can be explained by means of formation of dislocation-based incipient kink bands (IKB). Using acoustic waves we investigated possible dislocation related mechanisms responsible for nonlinear dynamic response of IKB solids. In this work, for the first time we observed IKB formation and reversibility directly using acoustic coupling technique (ACT) measuring ultrasonic waves attenuation as a function of stress and acoustic emission signatures during compression test of nanolaminated layered ternary carbide (MAX phases) samples. We confirm here that the dynamic behavior of these non-linear elastic systems is due to the interaction of dislocations with the stress waves.

***Invited Papers***

**12:27**
**P33 7 Simulations of Nano-indentation and Shear Banding in Amorphous Solids.**
MICHAEL FALK, *University of Michigan, Department of Materials Science and Engineering*

Molecular dynamics simulations of a number of amorphous systems reveal the structural changes that accompany plastic localization. We have simulated both two-dimensional and three-dimensional systems in nanoindentation[1], uniaxial tension[2] and compression in plane strain[3]. The degree of strain localization depends sensitively on the quench rate during sample preparation, with localization only arising in more gradually quenched samples. Careful analysis of the strain rate dependence of the localization allows us to extrapolate to the low strain rate limit. This analysis reveals a transition from localized flow to homogeneous flow at a critical value of the potential energy per atom prior to testing. This transition occurs in both two- and three- dimensional systems. The transition appears to be associated with the k-core percolation of short range order (SRO) in the two-dimensional system[2]. We have used a generalization of the Frank-Kasper criterion to identify SRO in the three-dimensional systems. Only in certain systems does this method predict a percolation transition corresponding to the transition in mechanical behavior. We discuss the non-uniqueness of this measure of SRO, and consider whether a more rigorous definition could be derived which applies to systems far from the hard-sphere limit.

[1]Y. Shi and M.L. Falk, ''Structural transformation and localization during simulated nanoindentation of a non-crystalline metal film,'' Applied Physics Letters, Vol. 86, pp. 011914 (2005).
[2]Y. Shi and M.L. Falk, ''Strain localization and percolation of stable structure in amorphous solids,'' Physical Review Letters, Vol. 95, pp. 095502 (2005).
[3]Y. Shi and M.L. Falk, ''Does metallic glass have a backbone? The role of percolating short range order in strength and failure,'' Scripta Materialia, Vol. 54, pp. 381 (2005).



***Contributed Papers***

**13:03 Mixte CNRS/Saint-Gobain**
**P33 8 A statistical model of plastic deformation in disordered media** MEHDI TALAMALI, DAMIEN VANDEMBROUCQ, STÉPHANE ROUX, *Unité Mixte CNRS/Saint-Gobain* Plastic deformation at the macroscopic scale is assumed to stem from series of successive localized plastic events. A random elastic limit is associated to each site of a discrete mesh. Using a quasi-static driving, one site at a time undergoes plastic shear. The local plastic threshold is then renewed. The localized slip induces long range elastic interactions of quadrupolar symmetry. These additional internal stresses are then used to determine the next weakest site. The model gives rise to a macroscopic plastic flow, corresponding to a genuine depinning transition. We obtain an asymptotic macroscopic yield stress. The transient regime can be associated to a hardening phenomenon of pure statistical origin. Beyond the average plastic behavior we observe stress fluctuations following a universal distribution (only dependent on the system size $L$). Shear deformation presents at all scales spatial and temporal fluctuations of universal character. We observe shear band-like structures which persist only during a finite time $\tau \propto L^{z}$ and which present a clear anisotropic character with a system size dependent width $w \propto L^{\zeta}$.

**13:15**

**P33 9 Scaling laws in fracture of metallic glasses** X.K. XI, *Department of Physics and Astronomy, University of North Carolina, Chapel Hill, North Carolina 27599-3255, USA* D.Q. ZHAO, M.X. PAN, W.H. WANG, *Inst Phys, Chinese Academy of Sciences, Beijing 100080, China* Y. WU, *Department of Physics and Astronomy, University of North Carolina, Chapel Hill, North Carolina 27599-3255, USA* J.J. LEWANDOWSKI, *Dept. of Mater Sci & Eng, Case Western Reserve University, 10900 Euclid Avenue, 44106 Cleveland, Ohio, USA* Brittle metallic glasses themselves can be seen as a model system to study the mechanical properties of metallic based glassy materials. We report a brittle Mg-based bulk metallic glass which approaches the ideal brittle behavior. However, a dimple-like structure is observed at the fracture surface by high resolution scanning electron microscopy, indicating some type of 'ductile' fracture mechanism in this very brittle glass. We also show a clear scaling correlation between the fracture toughness and plastic process zone size for various glasses. The results indicate that the fracture in brittle metallic glassy materials might also proceed through the local softening mechanism but at different length scales. The full text of this work has been published under the title itFracture of Brittle Metallic Glasses: Brittleness or Plasticity by the authors in Physical Review Letters 94, 125510 (2005).

**13:27**

**P33 10 Mapping Elasticity at the Nanoscale** GHEORGHE STAN, WILLIAM PRICE, *National Institute of Standards and Technology, MSEL/Ceramics Division, 100 Bureau Drive 217/ B107, Gaithersburg, MD 20899* In the last few years Atomic Force Acoustic Microscopy has been developed to investigate the elastic response of materials at the nanoscale [1],[2]. We have extended this technique to the real-time mapping of nanomechanical properties of material surfaces. This mapping allows us to investigate the local variation of elastic properties with nanometer resolution and to reduce the uncertainties that arise from single measurements. Quantitative measurements are acquired by first performing an accurate calibration of the elastic properties of the Atomic Force Microscopes probes with respect to single crystal reference materials. A wide variety of surfaces with different mechanical properties have been investigated to illustrate the applicability of this technique. [1] U. Rabe *et al.*, Surf. Interface Anal. **33**, 65 (2002) [2] D.C. Hurley *et al.*, J. Appl. Phys. **94**, 2347 (2003)

**SESSION P35: NANOSTRUCTURE FABRICATION, QUANTUM POINT CONTACTS, AND SINGLE ELECTRON TRANSISTORS**
**Wednesday Morning, 15 March 2006**
**338, Baltimore Convention Center at 11:15**
**Ilya Ponomarev, Naval Research Laboratory, presiding**

**11:15**

**P35 1 Atomic-Scale Modeling of Shape Stability-Regimes and Stacking in InAs/GaAs Quantum Dot Nanostructures** THOMAS HAMMERSCHMIDT, PETER KRATZER, MATTHIAS SCHEFFLER, *Fritz Haber Institute of the Max Planck Society, Faradayweg 4-6, 14195 Berlin, Germany* From a thermodynamic point of view, quantum dot (QD) growth is governed by the balance between energy gain due to strain relief and energy cost due to formation of QD side facets and edges. Both contributions are accounted for by an interatomic potential of the Abell-Tersoff type that we developed recently. We relax realistic InAs/GaAs QD nanostructures using this interatomic potential and compare the resulting total energies. To investigate the experimentally observed shape sequence of 'hut'-like QD's dominated by {317} facets and 'dome'-like QD's dominated by {101} facets, we compare the energy of a homogenous InAs film and differently sized InAs QD's with either shapes. We identify three regimes: For coverages below about 1.9 monolayers InAs the film is most stable, followed by small 'hut'-like QD's and larger 'dome'-like QD's. This is in line with the experimentally deduced critical coverage for the 2D to 3D growth transition, and the shapes of small and larger QD's. We can also explain the growth correlation in QD stacks: Our calculated potential-energy surfaces of free-standing QD's in different lateral positions above overgrown QD's show an energy gain of about 20 meV per In atom for the experimentally observed vertical QD alignment.

**11:27**

**P35 2 Raman Spectroscopy of InAs/GaAs Quantum Dots Patterned by Nano-indentation** MARTIN MUNOZ, *Physics Department, Virginia Commonwealth University* LINDSAY HUSSEY, *Physics Department, Virginia Commonwealth University* DURIG LEWIS, *Physics Department, Virginia Commonwealth University* CURTIS TAYLOR, *Mechanical Engineering Department, Virginia Commonwealth University* EUCLYDES MAREGA, *Department of Physics, University of Arkansas* AJAY MALSHE, *Mechanical Engineering Department, University of Arkansas* Patterns of InAs/GaAs quantum dots (QDs) grown by the combination of nanoindentation technique and molecular beam epitaxy were studied. The resulting QDs tend to preferentially nucleate on indented areas rather than other regions. We studied the strain on the indentations, regions surrounding the indents, and non-indented areas. The QD LO mode for the patterned areas shifted by 8 cm-1 when compared to the non-patterned area. The biaxial strain in the indented areas producing this shift is four times larger than that in non-indented areas, explaining the QD preference within these areas. This larger strain suggests that QDs on the indentations can be formed by depositing a smaller InAs amount than that required to form QDs on non-indented areas, thus obtaining QDs only on the pattern.

**11:39**

**P35 3 Self-Assembled Unstrained InGaAs Quantum Dashes** ALEXANDER UKHANOV, *US Naval Research Laboratory* ALLAN BRACKER, GEORO BOISHIN, JOE TISCHLER, JIM CULBERTSON, We describe a technique for MBE-based fabrication of unstrained quantum dashes with $Al_xIn_yGa_{1-x-y}As$ alloys lattice-matched to InP substrates. Templates for lattice-matched quantum dash growth are obtained by combining molecular beam epitaxy with itin situ etching by arsenic bromide. A seed layer of self-assembled InAs quantum dashes is converted into nanotrench templates through overgrowth followed by strain-enhanced etching. We have explored limitations on the accessible range of alloy compositions imposed by the etch process and found that strain-induced etching is limited to compounds with low Al content. Nanotrench templates can be filled with lattice-matched alloys of varied compositions to define barriers and quantum wires that could lead to optoelectronic devices in a spectral range around 1.5 $\mu$m. Here we also present Atomic Force Microscopy and Photoluminescence data obtained from self assembled unstrained $In_{0.53}Ga_{0.47}As$ Quantum Dashes.

**11:51**

**P35 4 Microanalysis of quantum dots with type II band alignments** WENDY SARNEY, JOHN LITTLE, STEFAN SVENSSON, *US Army Research Laboratory* We will discuss the structural characterization of a system consisting of undoped self-assembled InSb quantum dots having a type II band alignment with the surrounding $In_{0.53}Ga_{0.47}As$ matrix. This differs from systems using conventional type-I quantum dots that must be doped and that rely on intersubband transitions for infrared photoresponse. Type II dots grown in a superlattice structure combine the advantages of quantum dots (3-dimensional confinement) with the tunability and photovoltaic operation of the type II superlattice. We grew a high surface density of InSb quantum dots with a narrow distribution of sizes and shapes and free of dislocations within the body of the dots. The dots are relaxed due to an array of misfit dislocations confined at the basal dot/matrix interface. This makes burying the dots with InGaAs not feasible without generating dislocations due to the large dot/matrix lattice mismatch. We are experimenting with strain-compensating or graded strain overlayers to lower the lattice mismatch.

**12:03**

**P35 5 Feasibility Study of Directed Self-Assembly of Semiconductor Quantum Dots** LAWRENCE FRIEDMAN, JIAN XU, *Pennsylvania State University* Strain mismatched semiconductors are used to form Self-Assembled Quantum Dots (SAQDs). An important step in developing SAQD technology is to control randomness and disorder in SAQD arrays. There is usually both spatial and size disorder. Here, it is proposed to use spatially varying heating as a method of to direct self-assembly and create more ordered SAQD arrays or to control placement of single dots or dot clusters. The feasibility of this approach is demonstrated using a 2D computational model of Ge dots grown in Si based on finite element analysis of surface diffusion and linear elasticity.

**12:15**

**P35 6 Controlling the self-assembly of Ge quantum dots grown by pulsed laser deposition** MOHAMMED HEGAZY, HANI ELSAYED-ALI, *Old Dominion University* Growth dynamics and morphology of self-assembled Ge quantum dots (QD) on Si(100)-(2x1) by nanosecond pulsed laser deposition are studied by in situ reflection high-energy electron diffraction (RHEED) and post deposition atomic force microscopy (AFM). The effects of the laser fluence and substrate temperature on the QD formation are investigated. The QD density increased dramatically (from $3\times 10^7$ $cm^{-2}$ to $6.3\times 10^8$ $cm^{-2}$), while the average lateral size decreased (from 362 nm to 107 nm) when the laser fluence was increased from 23 J/$cm^2$to 70 J/$cm^2$. Their shape also changed from large huts, observed at 23 J/$cm^2$, to domes observed at the highest fluence. At 150° C, misaligned QDs formed resulting in diffused RHEED pattern. At 400° C and 500° C, transmission RHEED patterns were observed indicating the growth of oriented hut and dome QDs. Around 600° C, the QDs were formed on top of textured surfaces.

**12:27**

**P35 7 Defect engineering in periodic gradient-index optical thin films** MATTHEW HAWKEYE, ANDY VAN POPTA, JEREMY SIT, MICHAEL BRETT, *University of Alberta* For thin film deposition with obliquely incident vapour flux, ballistic shadowing limits growth to nucleation sites, forming a porous columnar microstructure. Combined with advanced substrate rotation in a technique known as glancing angle deposition (GLAD), precisely controlled nanoscale architectures are formed. In situ variation of the angle of incidence provides dynamic control of the resulting film porosity, allowing the design of continuously varying periodic refractive index profiles to produce thin film interference filters. Intentional nanostructural defects can be introduced, such as uniaxial and biaxial constant index layers or index profile discontinuities, creating defect modes in the filter optical stopbands. Structural and optical characterizations of these periodic structures were performed, with the goal of understanding the relationship between the spectral properties of the film and the engineered nanostructure, demonstrating the high degree of control obtainable over the resulting filter properties using the GLAD process.

**12:39**

**P35 8 Strontium titanate transformation to highly conductive nanolayers** VLADIMIR BUTKO, *Brookhaven National Laboratory* DAVID REAGOR, *Los Alamos National Laboratory* Developing fabrication methods for electronically active nanostructures is an important challenge of modern science and technology. Fabrication efforts for crystalline materials have been focused on state-of-the-art epitaxial growth techniques. These techniques are based on deposition of precisely controlled combinations of various materials on a heated substrate. We report a method that does not require deposition and transforms a nanoscale layer of a complex crystalline compound into a new material using low energy Ion Beam Preferential Etching (IBPE). We demonstrate this method by transforming a widely used insulator model system, SrTiO3, into a transparent conductor. Most significantly, the resistivity decreases with decreasing temperature as 2.5 power of T and eventually falls below that of room temperature copper. These transport measurements imply a crystal quality in the conduction channel comparable to that obtained with the highest quality growth techniques. The universality of low energy IBPE implies wide potential applicability to fabrication of other nanolayers. David W. Reagor, Vladimir.Y. Butko, Nature Materials, v.4, 593, August 2005.

**12:51**

**P35 9 Dependency of quantum pumping on transmission mode and dot size** KAI-MING LIU, SHIH-YING HSU, *Department of Electrophysics, National Chiao Tung University, Hsinchu, Taiwan* We have used e-beam lithography to fabricate sub-micron metal gates on a two dimensional electron gas with mean free path on the order of several micrometers. Negative biases were applied to the metal gates to confine electrons in a small area ( $\sim \mu m^2$) forming a so-called quantum dot. Two quantum point contacts (QPCs) served the entrance and exit of electrons in the dot are located in line. Quantum charge pumping phenomena of the open dot in the absence of an external bias was observed using two independent ac voltages with the same frequency, $1\sim$ 80MHz, but a phase difference between them. Similar pumping results were reported by Marcus et al. earlier. However, due to the differences in the geometrical arrangements, the behaviors are somehow different including that our pumping current is one order more magnitude bigger and does not increase linearly with frequency for the entire measuring range. Moreover, we found that the pumping current seems increase with decreasing transmission mode numbers of the two QPCs. When the mode number goes to zero and the open dot transforms to closed dot, the pumping current vanishes. The results and measurements of the dependences of quantum charge pumping on transmission mode and dot size will be presented and discussed.

**13:03**

**P35 10 Local Density of States of a Quantum Point Contact Near Pinchoff** LINDSAY MOORE, DAVID GOLDHABER-GORDON, *Stanford University* Over the last decade, there has been great interest in how electrons flow through a quantum point contact (QPC) as it is just opened up, before a fully transmitting 1D conduction channel is available. Remarkably, there does not seem to be a smooth transition from tunneling to ballistic transport. Instead, a shoulder appears in the conductance versus channel width, at a conductance of roughly 0.7 times that of an open spin-degenerate channel. Experiments have built a consensus that this so-called ''0.7 structure'' is related to electron spin and electron-electron interaction, but the detailed description remains controversial. To study this system, we have made devices where one of the two QPC gates is actually a tunnel barrier to a third lead, fabricated on a GaAs/AlGaAs heterostructure. With this third lead, it is possible to probe the density of states in the QPC channel from the side as the QPC opens from pinchoff through the first channel. We acknowledge support from the ONR Young Investigator Program, Award No. N00014-01-1-0569 and a Research Corporation Research Innovation Award, No. RI1260.

**13:15**

**P35 11 Single electron transistors in GaN/AlGaN heterostructures.*** H.T. CHOU, D. GOLDHABER-GORDON, *Stanford Univeristy* M.J. MANFRA, *Bell labs* R.J. MOLNAR, *MIT* We study transport properties of two single-electron transistors (SETs) in a GaN/AlGaN heterostructure. The first SET accidentally formed in a quantum point contact near pinchoff. Its small size produces large energy scales: a charging energy of 7.5 meV, and well-resolved excited states. The second, intentionally-fabricated SET is much larger. Hundreds of consecutive, uniformly-spaced Coulomb oscillations yield a charging energy of 0.85 meV. Excited states are not resolvable in Coulomb diamonds, and Coulomb blockade peak height remains constant with increasing temperature, indicating that transport is through multiple quantum levels even at the 450 mK base electron temperature of our measurements.

*The work at Stanford was sponsored by the Office of Naval Research Young Investigator Program under award no. N00014-01-1-0569 and Packard Fellowship.

**13:27**

**P35 12 Current Biased Real Time Charge Detection in a Single Electron Transistor** KENNETH MACLEAN, SAMI AMASHA, DOMINIK ZUMBUHL, IULIANA RADU, MARC KASTNER, *Massachusetts Institute of Technology* MICAH HANSON, ARTHUR GOSSARD, *University of California, Santa Barbara* Measurements of charge fluctuations in an AlGaAs/GaAs single electron transistor (SET) are presented. The SET consists of a lateral quantum dot created by confining a two-dimensional electron gas using nanometer-size surface electrodes. The charge on the quantum dot is detected by changes in conductance of a nearby quantum point contact. We discuss noise and bandwidth characteristics of our charge detection method, which uses commercially available voltage amplifiers. Our real time charge detection capabilities are used to investigate charge dynamics on the SET in a magnetic field parallel to the two-dimensional electron gas. This work is supported by the U.S. Army Research Office under Contract No. W911NF-05-1-0062, by the National Science Foundation under Grant No. DMR-0353209, and in part by the NSEC Program of the National Science Foundation under Award No. PHY-0117795.

**13:39**

**P35 13 Real Time Electron Hopping Phenomena in a Single-Electron Transistor** SAMI AMASHA, KENNETH MACLEAN, DOMINIK ZUMBUHL, IULIANA RADU, MARC KASTNER, *Massachusetts Institute of Technology* MICAH HANSON, ARTHUR GOSSARD, *University of California, Santa Barbara* Utilizing a current-biased quantum-point-contact charge sensor, we observe electrons hopping on and off a AlGaAs/GaAs single-electron transistor (SET) in real time. An electron tunnels between the extended states in the leads and the lowest-energy state localized in the lateral quantum dot created by nanometer-size surface electrodes. We observe changes in the tunneling rates, caused by the spin splitting in a magnetic field B applied parallel to the 2DEG. We have also observed single-electron photo-ionization of the SET by application of microwave radiation. This work is supported by the ARO (W911NF-05-1-0062), the NSF (DMR-0353209) and in part by the NSEC Program of the NSF (PHY-0117795).

**13:51**

**P35 14 Shot noise and strong feedback effects in nanoelectromechanical systems** STEVEN BENNETT, *McGill University* AASHISH CLERK, *McGill University* Quantum nanoelectromechanical systems have attracted much attention recently, offering potential for applications as well as insight into fundamental physics. Using a quantum noise approach, we study theoretically a nanomechanical oscillator coupled to a superconducting single-electron transistor (SSET). Incoherent Cooper pair tunneling processes in the SSET can lead to a negative damping instability, where the oscillator's amplitude increases as it absorbs energy from the SSET[1]. Here, we focus on the current noise of the SSET in the negative damping regime, in which the growing amplitude of the oscillator becomes large enough that the motion of the oscillator and the dynamics of the SSET depend strongly on each other. We describe the inherent non-linearity of this regime using effective, energy-dependent damping and temperature, and discuss characteristic timescales for dynamics in the system. The current noise is of particular interest because it can be directly observed, and current experiments are probing this regime[2].

[1]Clerk, Bennett, NJP **7**, 238 (2005).
[2]K. Schwab *et al.* (in preparation).

**14:03**

**P35 15 Finite size effects in the decay of metastable states in one-dimensional resonant tunneling structures*** OLEG TRETIAKOV, *Johns Hopkins University* KONSTANTIN MATVEEV, *Argonne National Lab* We study the current switching in a double-barrier resonant tunneling structure in the regime where the current-voltage characteristic exhibits intrinsic bistability, so that in a certain range of bias two different steady states of current are possible. Near the upper boundary $V_{th}$ of the bistable region the upper current state is metastable, and because of the shot noise it eventually decays to the stable lower current state. We find the time of this switching process in strip-shaped devices, with the width small compared to the length. The mean switching time $\tau$ increases exponentially as the bias $V$ is tuned inside the bistable region from its boundary value $V_{th}$. The one-dimensional geometry of the problem enables us to obtain analytically exact expressions for the exponential factor and to calculate the prefactor of $\tau$ for an arbitrary length of the strip. Furthermore, we evaluate the

mean time of switching in ring-shaped devices, with the widths small compared to their diameters.

*Work supported by U.S. DOE, Office of Science, Contract No. W-31-109-ENG-38.

**SESSION P36: FOCUS SESSION: PLASMON RESONANCES IN NANOSTRUCTURES**
**Wednesday Morning, 15 March 2006**
**339, Baltimore Convention Center at 11:15**
**Zachary Levine, National Institute of Standards and Technology, presiding**

**11:15**
**P36 1 Photoluminescence from a gold nanotip as an example of tabletop Unruh-Hawking radiation.** IGOR SMOLYANINOV, *University of Maryland* Conversion of zero-point quantum fluctuations into real thermal photons which may occur in a curved space-time is the main mechanism behind the Hawking radiation and the Unruh effect [1]. Up to date no experimental verification of these effects and the related dynamical Casimir effect has been reported. Here we argue that the recently observed infrared photoluminescence from a gold nanotip, which is mediated by surface plasmons (SP) propagating over a curved metal tip surface [2], constitutes an example of such zero-point to real photon conversion. Since SP wavelength may be very short, a surface plasmon wave packet propagating along a curved metal surface with radius of curvature $R \sim 1$ micrometer may be considered as a classical particle (this would correspond to the ray optics approximation). The centripetal acceleration of such particle may be as large as $a \sim c^2/R \sim 10^{22}g$. According to Ref. [1], such particle perceives vacuum as a bath of thermal radiation with temperature $T = \hbar a/2\pi kc \sim 1000K$. Nonlinear optical mixing of SPs with the thermal quanta from this bath looks like infrared photoluminescence in the laboratory reference frame. This work was supported in part by NSF grants ECS-0304046, CCF- 0508213 and ECS-0508275. [1] W.G. Unruh, Phys.Rev.D 14, 870 (1976). [2] M.R. Beversluis, A. Bouhelier, and L. Novotny, Phys.Rev.B 68, 115433 (2003).

**11:27**
**P36 2 Surface plasmon dielectric waveguides** CHRISTOPHER DAVIS, IGOR SMOLYANINOV, YU-JU HUNG, *University of Maryland* We demonstrate that surface plasmon polaritons can be guided by nanometer scale dielectric waveguides on top of a gold film. In a test experiment plasmons were coupled to a curved 3 micrometer radius dielectric stripe, which was 200 nm wide and 138 nm thick using a parabolic surface coupler. This experiment demonstrates that using surface plasmon polaritons the scale of optoelectronic devices based on dielectric waveguides can be shrunk by at least an order of magnitude.

**11:39**
**P36 3 Synthesis and Optical Properties of Star-shaped Gold Nanoparticles*** COLLEEN NEHL, *Physics and Astronomy Department, Rice University* HONGWEI LIAO, *Chemistry Department, Rice University* JASON HAFNER, *Physics and Astronomy, Chemistry Departments, Rice University* Here we describe the synthesis, structure, and optical properties of ca. 100 nm star-shaped gold nanoparticles. Seed mediated, surfactant directed synthesis yields nanoparticle solutions sufficiently monodisperse that extinction spectra reveal plasmon bands representative of their structure. Single particle spectroscopy measurements demonstrate that these nanoparticles exhibit multispectral, multidirectional polarized scattering. Through correlated structural characterization by electron microscopy, each scattering component can be assigned to the different points on the star-shaped structure. The plasmon resonances were also found to be extremely sensitive to the local dielectric encironment, yielding sensitivities as high as 1.41 eV photon energy shift per refractive index unit. These properties suggest that the star-shaped gold nanoparticles may be highly valuable for certain biosensing and microscopic imaging paradigms.

*This work supported by the Department of Defense and the Welch Foundation.

**11:51**
**P36 4 Nanorice: a new hybrid nanostructure** P. NORDLANDER, D. BRANDL, F. LE, H. WANG, N.J. HALAS, *Rice University* The plasmon hybridization method [1] is applied to nanorice, a new metallic nanostructure which combines the properties of two popular tunable plasmonic nanoparticle geometries: nanorods and nanoshells. The particle consists of a prolate spheroidal dielectric core and a thin metallic shell, bearing a remarkable resemblance to a rice grain. The nanorice particle shows far greater geometric tunability of the optical resonance, larger local field intensity enhancements and far greater sensitivity as a surface plasmon resonance (SPR) nanosensor than any previously reported dielectric-metal nanostructure. The tunability of the nanorice particle arises from the interaction of primitive plasmons associated with the inner and outer surfaces of the shell. The results from plasmon hybridization are compared to FDTD simulations. [1] E. Prodan and P. Nordlander, J. Chem. Phys. 120(2004)5444-5454

**12:03**
**P36 5 Photonic Crystal Effects in Surface Enhanced Raman Scattering from Nanocluster/Nanoshell Arrays*** KE ZHAO, *University of Tennessee* HONGXING XU, *Institute of Physics, Chinese Academy of Science & Lund University, Sweden* BAOHUA GU, *Oak Ridge National Laboratory* ZHENYU ZHANG, *Oak Ridge National Laboratory & University of Tennessee* We study the local optical properties of one-dimensional solid nanosphere dimer arrays with large array spacings, using the generalized Mie theory. We have obtained a large Raman cross section enhancement with magnitude of $10^{11}$ purely by electromagnetic effects, which is higher if compared with that of an isolated nanosphere dimer and in the literature. A coupled dipole approximation is used to understand this enhancement and the plasmon resonance shift relative to the isolated dimer. We have also studied the nanoshell dimer array and found even higher enhancement with magnitude of $10^{13}$. Our studies show that the nanoshell arrays with

proper spacings have clear advantages in single molecule surface enhanced Raman spectroscopy (SMSERS).

*Supported by DOE.

**12:15**

**P36 6 Strongly anisotropic optical composites** JUSTIN ELSER, *Oregon State University* EVGENII NARIMANOV, *Princeton University* VIKTOR PODOLSKIY, *Oregon State University* We study the macroscopic electromagnetic properties of nanostructured meta-materials formed by plasmonic nanowires embedded in a dielectric host. We show that nanowires have a significant effect on the effective dielectric constant of the system even in the case when their concentration is below 15%. The effect of dielectric properties of nanowires as well as the effect of inclusion concentration, shape and local configuration disorder on effective dielectric constant is explored via numerical simulations. Further, we develop an analytical description of the effective dielectric properties of nanowire composites and study the limit of its validity. We demonstrate that it is possible to use plasmonic nanowire composites to construct strongly anisotropic low-loss optical materials. Proposed applications include polarizers, reflectors, high-energy-density nano-waveguides, and the recently discovered non-magnetic low-loss left-handed media.

**12:27**

**P36 7 Metal Nanoparticle Enhanced Fluorescence – Role of Particle Plasmon Resonance*** SHY-HAUH GUO, *University of Maryland* TIM CORRIGAN, *University of Maryland* HENRYK SZMACINSKI, *Microcosm, Inc* RAY PHANEUF, *University of Maryland* We report on a systematic investigation of the enhancement of fluorescence by proximity to Ag nanoparticles whose size, shape and spacing are varied systematically using electron beam lithography. Our measurements indicate that enhancement of both absorption and radiative decay takes place. We compare our observations with expectactions based upon coupling to particle plasmons.

*Work supported by the Laboratory for Physical Sciences.

**12:39**

**P36 8 Role of Cylindrical Surface Plasmons in Enhanced Optical Transmission** MICHAEL HAFTEL, *Naval Research Laboratory* CARL SCHLOCKERMANN, GIRSH BLUMBERG, *Bell Laboratories, Lucent Technologies* We investigate the role of cylindrical surface plasmons in enhancing the optical transmission from nanoarrays of dielectric coaxial cylinders embedded in a metal film. Finite difference time domain (FDTD) simulations identify transmission peaks at long wavelengths as being associated with the fields produced by the individual coaxial cylinders, and these peaks move out to increasingly long wavelengths as the dielectric ring becomes narrower. An analysis of cylindrical surface plasmon dispersion relations show that these peaks are due to resonances from surface plasmons propagating on the cylindrical metal-dielectric interfaces whose wave functions increasingly overlap as the ring narrows. The counterintuitive behavior of the wavelength of the peak is a direct consequence of the negative dielectric constant of the metal film and would not occur for a perfectly conducting or dielectric film. This resonant surface plasmon mechanism closely accounts for the dependence of the position of the simulated transmission peaks on ring geometry and the length of the coaxial cylinders.

**12:51**

**P36 9 Plasmonic properties of non-concentric nanoshells** Y. WU, H. WANG, N.J. HALAS, P. NORDLANDER, *Rice University* The plasmon hybridization method [1]is applied to nanoeggs, i.e., nanoshells with a non-concentric (offset) core. In contrast to concentric nanoshells, the particle exhibits a multitude of dipole active plasmon resonances. These resonances are formed by hybridization of the multipolar plasmon resonances associated with the inner and outer surfaces of the metallic shell. The reduced symmetry introduced by the offset of the core causes a significant admixture of dipolar components in all plasmon modes. The hybridization is shown to depend strongly on the asymmetry of the particle. The results compare very well with results from FDTD simulations. The non-concentric nanoshell particles are shown to provide large electric field enhancements on open-ended surfaces. [1] E. Prodan and P. Nordlander, J. Chem. Phys. 120(2004)5444-5454

**13:03**

**P36 10 Plasmonic properties of the metallic nanosphere/thin wire system.** FENG HAO, P. NORDLANDER, *Rice University* The plasmon hybridization method [1] is applied to a metallic nanosphere positioned near an infinitely long metallic wire. The plasmon resonances of the sphere are found to be shifted and to depend on the polarization of the incident light. In the limit of a thin wire, a virtual state consisting of propagating low energy wire plasmons is induced. The state is similar in nature to the virtual thin film state recently predicted and observed for a nanosphere near a thin metallic film [2]. [1] E. Prodan and P. Nordlander, J. Chem. Phys. 120(2004)5444-5454. [2] F. Le, N. Z. Lwin, J.M. Steele, M. Kall, N.J. Halas, and P. Nordlander, Nano Lett. 5(2005)2009-2013.

**13:15**

**P36 11 Optical Response of Metal Nanoparticle Chains** KIN HUNG FUNG, CHE TING CHAN, *The Hong Kong University of Science and Technology* The excitation of surface plasmon on metal nanoparticles is interesting to many researchers because of its variety of applications. By arranging nanoparticles in different ways, many interesting properties can be observed. For metal nanoparticle chains, there is a red (blue) shift on the plasmon resonant frequency for longitudinal (transverse) excitation. We present the results on this splitting of plasmon resonant frequency for Ag nanoparticle chains with diameters around 10nm, calculated by the multiple scattering theory (MST) and the ways to understand the results using simple models. MST calculations are performed on the extinction of finite silver nanosphere chains embedded in glass matrix. The transmission and reflection of an infinite 2D arrays of silver nanospheres are also calculated to understand the interaction between nanoparticle chains. The results are in agreement with recent experiments. The splitting of plasmon-resonance modes associated with different polarizations of the incident light is further understood by employing simple models. Results on the effect of order and disorder in nanoparticle chains are also presented.

**13:27**

**P36 12 Emergence of collective plasmon excitation in a confined one-dimensional electron gas** ZHE YUAN, *Department of Engineering Physics, Chalmers University of Technology* SHIWU GAO, We present a theoretical study of the electronic excitation in a confined one-dimensional electron gas [1], which is utilized to model atomic chains created in recent experiments. The length

dependence of the excitation spectra is obtained from the linear response theory within the random phase approximation and time-dependent density functional theory. As the length of the chains increases, the dipole excitation spectra shows a transition from electron-hole pair excitations to collective plasmon excitation. The trend of the length-dependent plasmon resonance is predicted, and the nature of the plasmon resonance is also elaborated. [1] Shiwu Gao and Zhe Yuan, Phys. Rev. B 72, 121406(R) (2005).

**13:39**

**P36 13 Electron energy-loss spectroscopy study of surface plasmons in Au nano-particles.** CHENG-HSUAN CHEN, MING-WEN CHU, *Center for Condensed Matter Sciences, National Taiwan University, Taipei, Taiwan* JIN-PEI DENG, CHUNG-YUAN MOU, *Department of Chemistry, National Taiwan University, Taipei, Taiwan* We have studied the surface plasmon excitations of $\sim$ 10 nm Au nano-particles with various shapes (such as sphere, rod, and triangle) by electron energy-loss spectroscopy (EELS) using a 0.2 nm electron probe in a scanning transmission electron microscope (STEM). EELS spectra were investigated as a function of distance from the probe to the nano-particle surface, i.e., the impact parameter, and four surface plasmon peaks at 10, 15, 24, and 33 eV could be identified in the loss spectra in the 10 to 40 eV range where the dielectric constant of Au is positive (and still less than one). These high energy surface excitations are anomalous and in sharp contrast to the well-known surface plasmon of Au at 2.4 eV in the visible spectral range where the dielectric constant is negative. Spectral imaging studies also conclusively show that these high energy surface excitations are indeed localized at the surface of the nano-particles.

**13:51**

**P36 14 Plasmons in the metallic nanoparticle-film system as a tunable impurity problem** F. LE, N.Z. LWIN, N.J. HALAS, P. NORDLANDER, *Rice University* We show that the plasmon resonances of a metallic nanoparticle interacting with a metallic film is an electromagnetic analog of the spinless Anderson-Fano model [1]. The three characteristic regimes of this model are realized here, where the energy of the nanoparticle plasmon resonance lies above, within, or below the energy band of surface plasmon states. The latter regime is experimentally observed and identified. Our approach [1] is generalized to describe a nanoshell on a metallic film and to account for the screening effects caused dielectric backgrounds. These three interaction regimes are controlled by film thickness and the aspect ratio of the nanoshell. The results are compared with Finite-Difference Time-Domain (FDTD) simulations using realistic dielectric functions. [1] F. Le, N. Z. Lwin, J.M. Steele, M. Kall, N.J. Halas, and P. Nordlander, Nano Lett. 5(2005)2009-2013.

**14:03**

**P36 15 Surface plasmon interference spectroscopy of metal films*** VITALII VLASKO-VLASOV, *Argonne National Laboratory* ULRICH WELP, *Argonne National Laboratory* ANDREAS RYDH, *ANL and Dept. of Physics, Stockholm University* JOHN PEARSON, *Argonne National Laboratory* Circular nanoslits manufactured by focused ion beam in silver films were used to excite surface plasmon polaritons and to generate plasmon interference patterns. Changes of the plasmon interference periods at changing the excitation wavelength were imaged by a near-field scanning optical microscope and scaled by the known nanostructure dimensions allowing precise plasmon wavelength measurements. The plasmon dispersion curves for our film thickness were calculated in different approximations and a proper fitting function for the experimental data was chosen. This allowed to retrieve the frequency dependence of the dielectric function of our silver film, which is different from usually cited Johnson-Christy and Palik data but falls in the range of values reported in literature. The results of fitting indicate to the important role of losses, which can not be neglected in definition of the real part of the dielectric constant even in the Drude region. Our technique is a useful tool for the local characterization of the dielectric function sensitive to the structure of metal films potential for photonics applications.

*The work was supported by the U.S. Department of Energy, Basic Energy



**SESSION P38: SUPERCONDUCTIVITY—OPTICAL SPECTROSCOPY OF CUPRATES**
**Wednesday Morning, 15 March 2006**
**341, Baltimore Convention Center at 11:15**
**Tomas Timusk, McMaster University, presiding**

**11:15**

**P38 1 Optical Study of Optimally Doped and Overdoped YBCO*** MINGHAN CHEN, D.B. TANNER, *Department of Physics, University of Florida, Gainesville FL 32611-8440, USA* G. HAMMERL, J. MANNHART, *Center for Electronic Correlation and Magnetism, Institute of Physics, Augsburg University, Augsburg 86135, Germany* Thin films of the optimally-doped and overdoped high temperature superconductor ($YBa_2Cu_3O_{7-\delta}$ and $Y_{0.7}Ca_{0.3}Ba_2Cu_3O_{7-\delta}$ with $T_c$ = 90 K and 79 K, respectively) have been investigated by optical spectroscopy in the ab-plane. In the normal state, with increasing the carrier concentration in the $CuO_2$ planes, spectral weight is lost in the high-frequency charge-transfer band and transferred to lower frequencies. With increased doping, the free-carrier (Drude-like component) plasma frequency increases, consistent with a charge density increase. However, the superfluid density decreases in this regime (overdoped region) and a substantial normal-fluid component still exists in the low frequency part of the optical conductivity well below $T_c$.

*MC and DBT acknowledge support of the NSF, DMR-0305043.

**11:27**

**P38 2 The optical conductivity of Ortho II $YBa_2Cu_3O_{6.5}$.** THOMAS TIMUSK, JUNG-SEEK HWANG, JING YANG, SERGEI SHARAPOV, JULES CARBOTTE, *McMaster University* DOUG BONN, RUIXING LIANG, WALTER HARDY, *University of British Columbia* The a-axis optical properties of the ortho II phase of YBCO (every other chain filled, $T_c$ = 59 K) were derived from reflectance data over a wide frequency and temperature range. Above 200 K the spectra are dominated by a broad background of scattering that extends to 1 eV. Below 200 K, in the normal state, a shoulder in the reflectance signals the onset of scattering at 400 $cm^{-1}$. Below the superconducting transition temperature the superconducting condensate appears. Its spectral weight is consistent, to within experimental error, with the FGT sum rule and with independent measurements of Gd ESR. We also compare our data with magnetic neutron scattering on samples from the same source that show a strong resonance at 31 meV. Extrapolating the optical conductivity to zero frequency yields the

dc resistivity of Ortho II which is in good agreement with four-probe measurements. We find that the scattering rates can be modeled as the combined effect of the neutron resonance, a bosonic background and a density of states with a pseudogap.

**11:39**

**P38 3 Optical conductivity of $Bi_2Sr_2CuO_6$ in the optimally and overdoped regimes** R.P.S.M. LOBO, D. LYZWA, N. BONTEMPS, *ESPCI-CNRS, Paris, France* Z.Z. LI, H. RAFFY, *LPS, Université de Paris Sud, Orsay, France* $Bi_2Sr_2CuO_6$ has a much lower critical temperature ($T_c^{Max} \sim 20$ K) than other single layer cuprate superconductors, making this compound very useful to investigate normal state properties of cuprates. In addition, it is possible to oxygenate this material to a relatively high degree of overdoping ($T_c < 5$ K). We measured, from room temperature to 5 K, the optical conductivity of the same $Bi_2Sr_2CuO_6$ film thermally treated to be in the optimally and overdoped regimes. The in-plane resistivity in the optimally doped regime depends lineraly on the temperature. It develops a positive curvature in the overdoped regime as expected from its more Fermi liquid like behavior. Surprisingly, despite its linear resistivity, the frequency dependent scattering rate in the optimally doped sample has a quadratic behavior. We will discuss our results in terms of the possible scenarios for the normal state conductivity and infer its effects on the superconducting state.

**11:51**

**P38 4 Doping and temperature dependent optical properties of $Bi_2Sr_2CaCu_2O_{8+\delta}$** JUNGSEEK HWANG, THOMAS TIMUSK, *McMaster University* GENDA GU, *Brookhaven National Laboratory* MARTIN GREVEN, HIROSHI EISAKI, *Stanford University* We report on the ab-plane reflectance of underdoped (UD), optimally doped (OPT), and overdoped (OD) $Bi_2Sr_2CaCu_2O_{8+\delta}$ (Bi-2212) samples [$T_c$ = 69 K(UD), 96 K (OPT), 82 K (OD), 80 K (OD: annealed from the OPT sample), 65 K (OD) and 60 K (OD)]. We analyzed the measured reflectance data and previous data of two underdoped Bi-2212 samples ($T_c$ = 67 K (UD) and 82 K (UD)) to extract the doping dependent optical constants. Bi-2212 is one of the most important cuprate systems widely studied by ARPES and tunnelling. We also calculate the doping dependent dc resistivity from extrapolation of the optical conductivity and the doping dependent superfluid density and the optical self- energy by using the extended Drude model. With these quantities in hand, we will discuss some current issues: the kinetic energy change at $T_c$, the role of the magnetic resonance mode, and a possible quantum critical point.

**12:03**

**P38 5 Polarization dependence of charge-transfer excitations in $La_2CuO_4$** LI LU, GUILLAUME CHABOT-COUTURE, *Department of Applied Physics, Stanford University, Stanford, California 94305* JASON HANCOCK, *Stanford Synchrotron Radiation Laboratory, Stanford University, Stanford, California 94309* OWEN VAJK, GUICHUAN YU, *Department of Physics, Stanford University, Stanford, California 94305* KENJI ISHII, JUN'ICHIRO MIZUKI, *Synchrotron Radiation Research Center, Japan Atomic Energy Research Institute, Hyogo 679-5148, Japan* DIEGO CASA, THOMAS GOG, *CMC-CAT, Advanced Photon Source, Argonne National Laboratory, Argonne, Illinois 60439* MARTIN GREVEN, *Department of Applied Physics, Stanford University, Stanford, California 94305* We have carried out an extensive resonant inelastic x-ray scattering (RIXS) study of $La_2CuO_4$ at the Cu K-edge. Multiple charge-transfer excitations have been identified using the incident photon energy dependence of the cross section and studied carefully with polarizations E//c and E //ab. An analysis of the incident photon energy dependence, the polarization dependence, as well as the K-edge absorption spectra, indicates that the RIXS spectra reveal rich physics about the K-edge absorption process and momentum-dependent charge-transfer excitations in cuprates.

**12:15**

**P38 6 Evidence of an anisotropic charge-excitation gap in stripe-ordered $La_{2-x}Ba_xCuO_4$ with $x = 1/8$ *** C. C. HOMES, S. V. DORDEVIC, G. D. GU, Q. LI, T. VALLA, J. M. TRANQUADA, *Condensed Matter Physics & Materials Science Dept., Brookhaven National Laboratory* The *ab*-plane optical properties of a cleaved single crystal of $La_{2-x}Ba_xCuO_4$ for $x = 1/8$ ($T_c \simeq 2.4$ K) have been measured over a wide frequency and temperature range. The low-frequency conductivity is Drude-like and shows a metallic response with decreasing temperature. However, below $\simeq 60$ K, corresponding to the onset of charge-stripe order, there is a rapid loss of spectral weight below about 40 meV, resulting in a major reduction in the number of free carriers. This suggests a partial gapping of the Fermi surface. Surprisingly, the sample is still metallic and becomes a superconductor at low temperature. This material is a striking example of how charge and spin stripe order, metallic behavior and superconductivity can coexist.

*This work was supported by the DOE under contract number DE-AC02-98CH10886.

**12:27**

**P38 7 Anisotropic Drude response in $Mg(B_{1-x}C_x)_2$** TERUHISA KAKESHITA, SERGEY LEE, *SRL-ISTEC* SETSUKO TAJIMA, *Osaka University* SRL-ISTEC TEAM, OSAKA UNIVERSITY COLLABORATION, There exists an unsolved issue on $MgB_2$ that a plasma edge estimated from optical spectra so far is conspicuously inconsistent with a band calculation. It is mysterious since experimental band dispersions by ARPES are marvelously coincident with the band calculation. We report on a- and c-axis optical responses in $Mg(B_{1-x}C_x)_2$ using small single crystals and a FTIR spectrometer combined with an optical microscope. It was verified that the Drude responses show the anisotropy between a- and c-axis. The observed plasma frequencies $\omega_{p'}$ are considerably small compared to a theoretical value ( $\sim$ 7eV), whereas the bare ones $\omega_p$, estimated from a sum rule of optical conductivity $\int d\omega\sigma(\omega) = (\pi/2)\omega_p^2 = (\pi/2)\varepsilon_\infty\omega'^2_p$, are fairly coincident with it. We also discuss an effect of carbon-substitution on carrier concentration and scattering rate in a multiband system. This work was supported by the New Energy and Industrial TechnologyDevelopment Organization(NEDO) through ISTEC as the Collaborative Research and Development of Fundamental Technologies for Superconductivity Applications.

**12:39**

**P38 8 Mode coupling effect in infrared spectra of $Tl_2Ba_2Ca_{n-1}Cu_nO_x$ (n=1, 2, 3)** N.L. WANG, Y.C. MA, *Institute of Physics, Chinese Academy of Sciences, Beijing 100080* We performed in-plane optical reflectance measurements on $Tl_2Ba_2Ca_{n-1}Cu_nO_x$ with n=1, 2, 3. The single crystals were successfully grown by flux method with maximum $T_c$=90 K, 109 K, and 119 K for n=1, 2, 3, respectively. For all three phases near optimal doping, the reflectance roughly has a linear-frequency dependence in the normal state, but displays a pronounced knee

structure followed by a dip-like feature at higher frequency below $T_c$. Such characteristic features were commonly ascribed to the coupling of electrons with a bosonic mode. Very remarkably, we found that the energy levels of those features scale with $T_c$ for the three phases. The results suggest against a phonon origin for the bosonic mode. We also investigated the spectral evolution with doping for Tl-2201 crystals in the overdoped side. We found that the mode coupling effect weakens with doping and disappears in the heavily overdoped sample. Meanwhile, the optical scattering rate evolves from a linear- $\omega$ dependence to a shape with upward curvature in the normal state. Both the temperature and frequency dependence of the scattering rate can be described by a power law relation. Compared with ARPES results, we suggest that the overall decrease of the scattering rate may mainly originate from the increase of the quasiparticle life time near the $(\pi,0)$ region in the Fermi surface.

**12:51**
**P38 9 A Complete Charge Model For The High $T_c$ Superconductivity** YOUNG HOON KIM, PEI HERNG HOR, *University of Houston* Focusing on the recent transport, far-infrared (far-IR), and neutron scattering data, we establish a model for the high temperature superconductivity (HTS) built on the two-dimensional (2D) square electronic lattices in the $CuO_2$ planes and their three-dimensional ordering. We demonstrate that our model captures all the essential physics that bring about a coherent picture of the HTS and offers the key to the mechanism for the HTS.

**13:03**
**P38 10 Temperature Dependent of the Optical Spectral Weight in Correlated Metal $Nd_{1-x}TiO_3$(x=0.095)** JING YANG, JUNGSEEK HWANG, THOMAS TIMUSK, *Department of Physics and Astronomy, McMaster University* ATHENA SAFA-SEFAT, JOHN E. GREEDAN, *Department of Chemistry, McMaster University* We investigated the infrared reflectance of $Nd_{1-x}TiO_3$, which is a hole-doped transition-metal-oxide system. In the metallic sample with $x=0.095$ (hole concentration=3 $x=0.285$), the partial optical spectral weight, $\omega(\Omega,T) = \int_0^\Omega \sigma_1(\omega,T)d\omega$, turns out to be a linear function of $T^2$at different cutoff frequencies. Recent optical studies of LSCO [1] and BSCCO [2] also found that the optical spectral weight varies quadratically with temperature, i.e. $\omega(\Omega,T) \simeq \omega_0 - B(\Omega)T^2$, in both superconductors and nonsuperconducting metals. The coefficient $B(\Omega)$ was considered as a ''thermal response'' of the carriers. In our study, for $Nd_{1-x}TiO_3(x=0.095)$, $B(\Omega)$ exhibits distinct features which we compare to both cuprates and conventional metals. [1] M. Ortolani et al., Phys. Rev. Lett. **94**, 067002 (2005). [2] H. J. A. Molegraaf et al., Science **295**, 2239 (2002).

**13:15**
**P38 11 Phonon Shifts at the Superconducting Transition in it $\kappa$-(BEDT-TTF)$_2$-Cu(NCS)$_2$*** C. N. KODITUWAKKU, C. A. BURNS, X. WANG, *Dept. of Physics, Western Michigan University* H. SINN, A. SAID, A. ALATAS, *Advanced Photon Source, Argonne National Laboratory* We have measured the phonon spectra above and below the superconducting transition in it $\kappa$-(BEDT-TTF)$_2$-Cu(NCS)$_2$. This organic superconductor has a transition temperature near 10K. These measurements were carried out using inelastic x-ray scattering at sector 3ID at the Advanced Photon Source. The incident x-ray energy was 21.657 keV and the resolution of the spectrometer was about 2.0 meV. We have observed significant phonon shifts at several energies in these spectra at several points in the Brillouin zone. Here we discuss the behavior of the phonons and possible reasons for the shifts.

*Work Supported by DOE DE-FG02-99ER45772

**SESSION P39: FOCUS SESSION: SUPERCONDUCTIVITY—THEORY AND COMPUTATION (MAINLY FIRST PRINCIPLES)**
**Wednesday Morning, 15 March 2006; 342, Baltimore Convention Center at 11:15**
**Ole Andersen, Max Planck Institute, presiding**



*Invited Papers*

**11:15**
**P39 1 Effect of Spin Fluctuations on Electron-Phonon Superconductivity.***
IGOR MAZIN, *Naval Research Laboratory*

Most of our intuition regarding conventional superconductivity is derived from the McMillan formula. What are often believed to be generic properties of the Eliashberg equations, in reality hold only in the regime where the McMillan formula is applicable. I will show how common beliefs, such as a monotonic relation between the reduced gap and the coupling constant, or an exponential behavior of the NMR relaxation with the gap as the activation parameter, fail for more complicated spectral functions. Most interestingly, I will demonstrate that our conventional wisdom totally fails us in the rapidly developing field of superconductors near a magnetic instability. In particular, I will derive (and test against numerical solutions of the Eliashberg equations) an analogue of the McMillan formula, fully accounting for the pair-breaking effect of spin fluctuations, and will show that these *increase* the phonon isotope effect, sometimes by as much as a factor of two. This is counterintuitive and opposite to the effect of the high-energy Coulomb interactions (the so-called Coulomb pseudopotential). I will also discuss the possibility of observing this effect in specific materials, such as $MgCNi_3$. This work has been done in collaboration with Oleg Dolgov (MPI Stuttgart) and Alexander Golubov (U. Twente).

*I acknowledge the hospitality of the Max Planck Institute in Stuttgart where much of this work has been done.

*Contributed Papers*

**11:51**

**P39 2 Properties from spin-phonon coupling in high-$T_C$ superconductors: $HgBa_2CuO_4$ and $La_{(2-x)}Sr_xCuO_4$** THOMAS JARLBORG, *DPMC, University of Geneva, Switzerland* The mechanism of spin-phonon coupling (SPC) in high-$T_C$ copper oxides is explored from band calculations on LSCO and HBCO systems. The LMTO band calculations, based on the local density approximation, are made for cells containing frozen phonon displacements and/or spin waves within the CuO plane. The virtual crystal approximation is used for studies of hole doped systems. The main result is that phonons are favorable for spin waves and vice-versa, and that pseudogaps appear naturally in the band structures of striped materials with strong SPC. The wave length of the spin-phonon modulation is related to doping, and the mutual enhancement of SPC is strongest when the non-doped system is close to an anti-ferro magnetic ground state. The calculated band results are used for modelling of different properties, such as isotope effects, phonon softening, shear dependences and T-variations. The results are discussed and compared with experiment. It is speculated that perpendicular SPC, with different behavior along x- and y-directions, can produce double gap structures. A moderate correction to LDA, which stabilizes the AFM state for the undoped material, will enhance the coupling constant for spin fluctuations $\lambda_{sf}$ for doped cases. These results suggest that properties of high-$T_C$ superconductors should depend both on phonons and magnetic fluctuations.

**12:03**

**P39 3 Superconductivity of Li, Al and K under pressure** GIANNI PROFETA, *Univ. di L'Aquila (Italy)* C Franchini[β], N. N. Lathiotakis[†], A. Floris[†β], A. Sanna[β], M. A. L. Marques[†], M. Lüders[‡], S. Massidda[β], E. K. U. Gross[†], A. Continenza*. * *CASTI - INFM and Dip. Fis., Univ. di L'Aquila, I-67010 Coppito (L'Aquila) Italy;* [β] *SLACS INFM and Dip. Fis., Univ. di Cagliari, I-09042 Monserrato (Ca), Italy;* [†] *Institut für Theoretische Physik, Freie Universität Berlin, Arnimallee 14, D-14195 Berlin, Germany;* [‡] *Daresbury Lab., Warrington WA4 4AD, United Kingdom* Extreme pressure strongly affects the superconducting properties of ''simple'' metals, like Li, K and Al. Using the new ab-initio method of density functional theory of the superconducting state, we report investigations on the superconducting properties of dense Li, K and Al. Our results show an unprecedented agreement with experiments, assess the predictive power of the method over a wide range of densities and electron-phonon couplings, and provide predictions for K, where no experiments exist so far. For fcc K we predict a superconducting phase transition at 18 GPa, with a maximum critical temperature of about 2 K at 23 GPa, the pressure where the crossover between the fcc and the K *III* structure experimentally occurs. We studied the effect of pressure on the electronic and vibrational properties of alkali, showing a progressive phonon softening near the K point of the Brillouin zone and a concomitant enhancement of the electron-phonon coupling constant $\lambda$.

**12:15**

**P39 4 Superconductivity of Alkali Metals under High Pressure** LEI SHI, DIMITRIOS PAPACONSTANTOPOULOS, *School of Computational Sciences, George Mason University* We calculated the superconductivity properties of alkali metals under high pressure using the results of band theory and the rigid-muffin theory of Gaspari and Gyorffy. Our results suggest that at high pressures Lithium, Potassium, Rubidium and Cesium would be superconductors with transition temperatures approaching 10-20 K. Our calculations also show that Sodium would not be a superconductor under high pressure even if compressed to less than half of its equilibrium volume. We found that the compression of the lattice strengthens the electron-phonon coupling through a delicately balanced increase of both the electronic and phononic components of this coupling. This increase of the electron-phonon coupling in Li is due to an enhancement of the s-p channel of the interaction, while in the heavier elements the p-d channel is the dominant component.

**12:27**

**P39 5 Superconductivity and Lattice Instability in Compressed Lithium from Fermi Surface Hot Spots** DEEPA KASINATHAN, JAN KUNES, RICHARD SCALLETAR, WARREN PICKETT, *University of California, Davis* AMY LAZICKI, CHOONG-SHIK YOO, *Lawrence Livermore National Labratory, Livermore, CA* HELGE ROSNER, *Max-Planck Institute for Chemical Physics of Solids, Dresden, Germany* Lithium, a simple metal not superconducting above 5mK at ambient pressure, becomes a 20 K superconductor at 50 GPa. This high $T_c$ is shown to arise from critical (formally divergent) electron-phonon coupling to the transverse phonon branch along intersections of Kohn anomaly surfaces with the Fermi surface. First principles linear response calculations of the phonon spectrum and spectral function $\alpha^2F(\omega)$ reveal (harmonic) instability already at 25 GPa. Our results imply that the fcc phase is anharmonically stabilized in the 25-38 GPa range.

**12:39**

**P39 6 DFT Study of the Single-Band Layered TMO $LiNbO_2$** ERIK YLVISAKER, *UC Davis* WARREN PICKETT, *UC Davis* We establish using first principles methods that $LiNbO_2$ is a realization of a triangular lattice ''single band'' system. The bandwidth (less than 2 eV) suggests the interesting possibility of correlation effects that should be kept in mind. We present a tight-binding model for the valence band of $LiNbO_2$, composed primarily of Nb $d_{z^2}$ states, finding that intralayer second neighbor hopping $t_2$100 meV is dominant over the significantly smaller first neighbor interactions $t_1$70 meV. The nearest neighbor coupling is strongly modified by oxygen displacements, and the electron-phonon coupling may provide the coupling mechanism for superconductivity in Li-deficient samples ($T_c \approx 5$K). We will present the Nb-centered Wannier function, which provides insight into this unusual electronic structure. Calculations of the Born effective charges for the metal ions are also found to have anisotropy that reflects the layered nature of the electronic bonding. Their deviation from formal charge values indicates important covalent character, which is also evident in the Wannier function.

**12:51**

**P39 7 Electron-phonon Interaction in Graphite-Intercalation Compounds** LILIA BOERI, *Max-Planck-Institut für Festkörper-Forschung, Stuttgart, Germany* MATTEO GIANTOMASSI, *Unité de Physico-Chimie et de Physique des Matériaux, Université Catholique de Louvain, B-1348 Louvain-la-Neuve, Belgium* GIOVANNI B. BACHELET, *INFM Center for Statistical Mechanics and Complexity and Dipartimento di Fisica, Università ''la Sapienza,'' Roma, Italy* OLE KROGH ANDERSEN, *Max-Planck-Institut für FestkörperForschung, Stuttgart, Germany* After the discovery of superconductivity with a Tc of 11.5 K in Ca-intercalated graphite (CaC6)[1], the interest in graphite-

intercalation compounds has been revived. Different pairing mechanisms, based on excitons or electron-phonon interactions, have been put forward [2]. In this contribution we first analyze, using the NMTO[3] method, the electronic structure of CaC6. We then propose a simple model, based on pure graphite, to explain superconductivity in this class of compounds. Implications on the design of new materials with similar superconducting properties are also discussed. [1] T.E. Weller *et al.*, Nature Physics **1**, 39 (2005). [2] G. Csany *et al.*, Nature Physics **1**, 42 (2005); I. I. Mazin, cond-mat/0504127; M. Calandra and F. Mauri, [3] O.K. Andersen and T. Saha-Dasgupta, Phys. Rev. B 62, R16219 and O.K. Andersen, T. Saha-Dasgupta and S. Ezhov, Bull. Mat. Sci. 26, 19 (2003).

**13:03**

**P39 8 Gap anisotropy in density functional theory of the superconducting state** A. FLORIS, *Freie Universität Berlin Germany* A. CONTINENZA, C. FRANCHINI, E.K.U. GROSS, N.N. LATHIOTAKIS, M. LÜDERS, M. MARQUES, S. MASSIDDA, G. PROFETA, A. SANNA, The discovery of superconductivity in $MgB_2$ ($T_c$ = 39.5K), with the clear presence of two gaps, has renewed the interest not only in electron-phonon mediated superconductivity, but also on the problem of anisotropic superconductivity. Here we use the recently introduced density functional theory of the superconducting state, that allows calculations of material-specific properties without the use of any adjustable parameters. The method, extended to $\mathbf{k},\mathbf{k}'$ resolved matrix elements of phonon-mediated and coulomb interactions, allows for a fully $\mathbf{k}$-resolved gap structure. Within this approach, we obtain the critical temperature and the two gaps of $MgB_2$ in good agreement with experiment. We will report on the existence of two different gaps also in Pb, and show that this is related to the different strength of the electron-phonon coupling associated with the two bands crossing the Fermi level. The calculated anisotropy is in good agreement with experiment. The same aproach is used for Nb3Sn, where recent experiments (Guritanu et al., Phys. Rev. B 70, 184526 (2004)) point to a possible two-gap behaviour. Our calculations show how our formalism is able to capture, in absence of any ad-hoc model, the features of multi-gap superconductors.

**13:15**

**P39 9 Band structure trend in cuprates and correlation with T *cmax*** OVE JEPSEN, EVA PAVARINI, WENHUI XIE, OLE KROGH ANDERSEN, *Max-Planck-Institute FKF, Germany* INDRA DASGUPTA, *IIT Bombay, India* TANUSRI SAHA-DASGUPTA, *S. N. BoseCenter, Calcutta, India* Parameters in model Hamiltonians are derived from LDA band structures for cuprate high $T_c$ superconductors. The materials and structural dependences of these are discussed. The most essential material dependent parameter is the range of the intralayer hopping. Furthermore, the range of this hopping correlates with $T_c$, i.e. materials with larger hopping ranges have higher maximum $T_c$'s.

**13:27**

**P39 10 First-Principles Construction of the Zhang-Rice singlet: Role of the apical oxygen in the mobility of the doped hole.*** WEI KU, WEI-GUO YIN, *Condensed Matter Physics & Materials Science Department, Brookhaven National Laboratory, Upton, NY 11973* The Zhang-Rice singlet (ZRS) has been well accepted as the most relevant low-energy states in high $T_c$ cuprates. Based on a novel Wannier state analysis [1] of the LDA+$U$ electronic structure, a realistic ZRS is constructed from properly orthogonalized local Cu $d_{x^2-y^2}$ and symmetric combination of O-p states ($p^{(s)}$), leading to a realistic derivation of low-energy effective t-t'- t''-J Hamiltonian. Interestingly, symmetrized apical oxygen $p_z$ orbital with the Cu $d_{z^2}$ symmetry is found to be close to the ZRS in energy ( 0.7 eV) and thus significantly facilitates the hopping to the second and third nearest neighbors. [1] W.-G. Yin, D. Volja, and W. Ku, cond-mat/0509075.

*Work supported by DOE-CMSN

**13:39**

**P39 11 Band structure and Fermi surface of $Ba_2Ca_3Cu_4O_8F_2$** WENHUI XIE, OVE JEPSEN, OLE K. ANDERSEN, *Max-Planck-Institut FKF Stuttgart Germany* ZHI-XUN SHEN, *Stanford University* Recently Y. Chen itet ital. have measured the Fermi Surface (FS) of the fluorinated four $CuO_2$ layer superconductor, $Ba_2Ca_3Cu_4O_8F_2$, using angular resolved photoemission spectroscopy (ARPES). Surprisingly, they found only two large ($\pi$, $\pi$) centered hole FS sheets, while four would have been expected. In order to investigate the reason for this we have performed first-principles electronic band structure calculations for this compound. As expected four antibonding copper-oxygen bands cross the Fermi level of which the two have dominantly orbital character on the two inner-layers and the other two have most orbital character on the outer-layers. The splitting between these bands is, however,much smaller than the splitting between the two measured FS sheets. The fluorine were claimed to replace all apical oxygens, however, by partly substituting apical oxygen as well as oxygen in the four $CuO_2$ layers by fluorine, good agreement with the experimental FS could be obtained.

**13:51**

**P39 12 The role of the Fermi surface sampling in first-principles calculations of electron-phonon coupling*** FELICIANO GIUSTINO, MARVIN L. COHEN, STEVEN G. LOUIE, *University of California at Berkeley* A quantitative understanding of the electron-phonon interaction is crucial to the understanding of conventional and possibly high-$T_c$ superconductivity, as well as to the study of transport and spectroscopic (such as optical and photoemission) properties of bulk and nanoscale systems. Despite the enormous interest in calculating electron-phonon interaction from first principles, present methods carry severe practical limitations. We present here a comparative study of several existing methods for computing this quantity. We show that, independent of the approximation adopted, a common computational bottleneck is that the Fermi surface must be sampled with extremely high accuracy, leading to prohibitively expensive calculations for complex systems. We also reformulate the problem of evaluating phonon linewidths in terms of self-consistent linear response theory, and demonstrate our approach through application to magnesium diboride.

*This work is supported in part by the NSF and the U.S. Department of Energy

**SESSION P40: FOCUS SESSION: PATHWAYS TO PRACTICAL QUANTUM COMPUTING I**
**Wednesday Morning, 15 March 2006; 343, Baltimore Convention Center at 11:15**
**Gerardo Ortiz, Los Alamos National Laboratory, presiding**

***Invited Papers***

**11:15**
**P40 1 Solid state technologies for quantum computers.**
DAVID DIVINCENZO, *IBM Research Division*

Impressive progress is now being made in realizing the rudiments of quantum computers in solid state devices. I will discuss two of them. First, single electron quantum dots now offer a higly coherent spin state for use as a qubit. Decoherence effects, arising from hyperfine interactions and the spin-orbit interaction, are well on their way to being understood and controlled. Second, Josephson junction devices, in many forms, are showing promise as qubits. The dynamics of these electric circuits can be designed to exhibit a wide variety of quantum effects; good two-level systems can be produced by careful design, and careful schemes for decoupling from the environment. Coupling to harmonic modes offer a wide variety of ''quantum optic'' realizations in the microwave regime.

***Contributed Papers***

**11:51**
**P40 2 CNOT logic for Josephson phase qubits** MICHAEL GELLER, EMILY PRITCHETT, ANDREW SORNBORGER, *University of Georgia* MATTHIAS STEFFEN, JOHN MARTINIS, *University of California, Santa Barbara* Josephson junctions have demonstrated enormous potential as qubits for scalable quantum computing architectures. Here we study the speed and fidelity of four controlled-NOT gate implementations designed for capacitively coupled phase qubits. One gate applies to qubits fixed permanently in resonance, two require varying the dc current bias, and the fourth applies to permanently detuned qubits. Realistic simulations suggest that these implementations can be demonstrated with good fidelity using existing superconducting circuits.

**12:03**
**P40 3 Violation of Bell's Inequality using Josephson Phase Qubits** MARKUS ANSMANN, R. BIALCZAK, N. KATZ, E. LUCERO, R. MCDERMOTT, M. NEELEY, M. STEFFEN, E.M. WEIG, A.N. CLELAND, J.M. MARTINIS, *UC Santa Barbara* Recent improvements of the measurement visibility and coherence times in Josephson Phase Qubits have enabled first tests of two-qubit quantum gates and examination of quantum phenomena using these devices. Here, we present an experiment in which we attempt to violate Bells Inequality, which would be further proof that the system at hand behaves in a truly quantum mechanical way. The violation of Bells Inequality is the primary argument against the possible existence of a hidden- variable-theory as an alternative to quantum mechanics. This experiment illustrates the use of coherent control over capacitatively coupled qubits with always-on coupling, including the establishment of the system in eigenstates of the coupling, e.g. the singlet state. Single qubit rotations combined with a simultaneous, fast, high-visibility read-out allow for state- tomography on the system.

**12:15**
**P40 4 Experimental State Tomography using Superconducting Quantum Bits** M. STEFFEN, M. ANSMANN, R. BIALCZAK, N. KATZ, E. LUCERO, R. MCDERMOTT, M. NEELEY, E.M. WEIG, A.N. CLELAND, J.M. MARTINIS, *UC Santa Barbara* The superconducting approach to building a scalable quantum computer has enjoyed tremendous successes in the past several years with coherence times now sufficiently long to implement quantum gates on a system with coupled qubits. In order to quantify the performance or fidelity of the gates, quantum state tomography is required. Successful state tomography relies on high measurement fidelities and the ability to perform arbitrary rotations in the transverse plane of the Bloch sphere. Here, we have made significant progress towards overcoming these challenges and present, for the first time, experimental data on single and two-qubit state tomography.

**12:27**
**P40 5 Towards single shot read-out in circuit quantum electrodynamics (QED)** ANDREAS WALLRAFF, DAVID SCHUSTER, ALEXANDRE BLAIS, JAY GAMBETTA, LUIGI FRUNZIO, JOE SCHREIER, BLAKE JOHNSON, ANDREW HOUCK, WILL BRAFF, HANNES MAJER, MICHEL DEVORET, STEVE GIRVIN, ROB SCHOELKOPF, *Depts. of Applied Physics and Physics, Yale University* In recent experiments we have demonstrated the resonant coherent coupling of individual photons to a single qubit implemented as a Cooper pair box in a high quality superconducting cavity [1]. In the non-resonant case, the dispersive coupling between the qubit and the cavity field is used to perform quantum non-demolition (QND) measurements of the qubit state [2]. Using this read-out technique we have performed high visibility measurements of Rabi oscillations and Ramsey fringes [3]. Here we present a detailed experimental and theoretical analysis of the cavity response for continuous and pulsed measurements in a wide range of cavity drive amplitudes. We also discuss an optimal read-out strategy for qubits in a continuous QND measurement and aim at demonstrating single shot read-out in the circuit QED architecture [4]. [1] A. Wallraff et al. Nature (London) 431, 162 (2004) [2] D. I. Schuster et al. Phys. Rev. Lett. 94, 123602 (2005) [3] A. Wallraff et al. Phys. Rev. Lett. 95, 060501 (2005) [4] A. Blais et al. Phys. Rev. A 69, 062320 (2004)

**12:39**

**P40 6 Coherent control in circuit QED** ALEXANDRE BLAIS, JAY GAMBETTA, ANDREAS WALLRAFF, DAVID SCHUSTER, LUIGI FRUNZIO, JOHANNES MAJER, STEVEN M. GIRVIN, ROBERT J. SCHOELKOPF, *Yale University* Superconducting charge qubits fabricated inside a transmission line resonator have been used to successfully demonstrate strong interaction of an artificial atom with a single photon [1]. This architecture has also been used to show high-visibility and long coherence time ($T_1 \sim 7\ \mu$s, $T_2 \sim$ 500 ns) Rabi oscillations [2] and in the detailed study of measurement-induced dephasing [3]. Here we will discuss protocols to realize one and two-qubit logical gates in circuit QED. These are based on resonant and off-resonant irradiation of the transmission line resonator. First experimental results towards the realization of these gates will be presented. Supported by NSA and ARDA under ARO Contract No. W911NF-05-1-0365 and the NSF under Grants No. ITR-0325580 and No. DMR-0342157. [1] A. Wallraff et al., Nature 431, 162 (2004). [2] A. Wallraff et al., Phys. Rev. Lett., 95, 060501 (2005). [3] D. Schuster et al., Phys. Rev. Lett., 94, 123602 (2005).

**12:51**

**P40 7 Superconducting SET backaction on the Cooper-pair box** JOHANNES MAJER, BENJAMIN TUREK, *Yale University* AASISH CLERK, *McGill University* STEVEN GIRVIN, ROBERT SCHOELKOPF, *Yale University* KEVIN BLADH, DAVID GUNNARSSON, PER DELSING, *Chalmers Institue of Technology* We report on measurements of the backaction of a superconducting single electron transistor (SSET) measuring a Cooper-pair box qubit. During the weak, continuous measurement made by the SSET, the charge noise acts on the Cooper-pair box. The quantum nature of that noise is able to dephase, relax and even excite the qubit. This noise depends strongly on the operating point of the SSET. We operate the SSET near the double Josephson quasiparticle (DJQP) feature, where the backaction of the SSET is well understood (A. Clerk, et al., Phys. Rev. Lett. 89, 176804 (2002)), and where there are no quasiparticle poisoning effects. Measurements of the relaxation time of the Cooper- pair box reveal the symmetric component of the quantum noise and measurements of the steady-state polarization reveal the anti-symmetric component. Both measurements vary as expected with SSET operating point and confirm this model of SSET backaction.

**13:03**

**P40 8 Information Flow in the Readout of a Superconducting Quantum Bit** I. SIDDIQI, R. VIJAY, M. METCALFE, E. BOAKNIN, C. RIGETTI, L. FRUNZIO, R. SHOELKOPF, M.H. DEVORET, *Yale University* Quantum computation requires efficient and well controlled coupling between qubits. Superconducting qubits can be strongly coupled using passive electrical circuit elements, but one of the major remaining challenges is to eliminate uncontrolled coupling to parasitic degrees of freedom. I will present experimental results on charge qubits integrated with a novel readout device – the Josephson bifurcation amplifier (JBA). New experiments using the improved readout fidelity and speed of the JBA quantify parasitic losses and shed light on their mechanism.

**13:15**

**P40 9 Mach-Zehnder-type Interferometry in a Strongly Driven Persistent-Current Qubit*** WILLIAM OLIVER, *MIT Lincoln Laboratory* YANG YU,† *MIT EECS Department* JANICE LEE, *MIT EECS Department* KARL BERGGREN, *MIT EECS Department* LEONID LEVITOV, *MIT Physics Department* TERRY ORLANDO, *MIT EECS Department* We have demonstrated Mach-Zehnder-type interferometry with a niobium superconducting persistent-current qubit. The qubits ground and first-excited states exhibit an anti-crossing. Driving the qubit with a large-amplitude harmonic excitation sweeps it through this anti-crossing two times per period. The induced Landau-Zener (LZ) transitions act as coherent beamsplitters, and the accumulated phase between LZ transitions varies with the driving amplitude. We have observed quantum interference fringes as a function of the driving amplitude for 1 to 20 photon excitations. We present and discuss these results.

*This work at was supported by the AFOSR (F49620-01-1-0457) under the DURINT program and the DoD under Air Force contract FA8721-05-C-0002.

†present address: Nanjing University

**13:27**

**P40 10 Double Quantum Dot Molecule Coupled with Single-Electron Transistors for Quantum Computation Applications*** LIMIN CAO, PHILLIP WU, FABIO ALTOMARE, A. M. CHANG, *Department of Physics, Duke University, Durham, NC 27708* M. R. MELLOCH, *School of Electrical Engineering, Purdue University, West Lafayette, IN 47907* We describe the fabrication of a series-coupled double quantum dot (DQD) with side-coupled single-electron transistors (SETs). The DQD are intended to work as qubits, and the SETs perform the quantum spin measurements. The device was fabricated on a GaAs/AlGaAs heterostructure using a one-step, two-angle, evaporation of aluminum. Our design is compatible with modern semiconductor techniques, and if proven successful, can readily be scaled into larger integrated qubit systems with spin manipulation and measurement circuitry. Our preliminary experimental results indicate that both the QDs and SETs have single-electron tunneling behaviors with good reproducibility. We will report on progress towards the in-situ detection of the spin and charge of a single electron trapped in the semiconductor quantum dots.

*Research supported in part by NSF DMR-0401648

**13:39**

**P40 11 Charge fluctuation induced dephasing of exchange coupled spin qubits*** XUEDONG HU, *University at Buffalo, SUNY* S. DAS SARMA, *University of Maryland* Exchange coupled *spin* qubits in semiconductor nanostructures are shown to be vulnerable to dephasing caused by *charge noise* invariably present in the semiconductor environment. This decoherence of exchange gate by environmental charge fluctuations arises from the fundamental Coulombic nature of the Heisenberg coupling, and presents a serious challenge to the scalability of the widely studied exchange gate solid state spin quantum computer architectures. We explore the properties of the resulting exchange gate errors, and estimate dephasing times for coupled spin qubits in a

wide range (from 1 nanosecond up to more than 1 microsecond) depending on the exchange coupling strength and its sensitivity to charge fluctuations in a particular nanostructure.

*We acknowledge support by NSA, LPS, and ARO.

**13:51**
**P40 12 Solid-state quantum teleportation between nanomechanical modes** L. TIAN, S. M. CARR, *National Institute of Standards and Technology, 100 Bureau Drive, Stop 8423, Gaithersburg, MD 20899* We study a quantum teleportation scheme between two nanomechanical modes without local interaction. The nanomechanical modes are connected by and linearly coupled to the continuous variable modes of a superconducting circuit made of transmission line and Josephson junctions. The phase sensitive measurement during the teleportation can be conducted by a superconducting single electron transistor operated as an rf mixer. Using a Wigner function approach, we calculate the fidelity of transferring coherent state under finite temperature and non-unit detector efficiency. We show that a fidelity above the classical limit of 1/2 can be achieved for a large range of parameters.

**14:03**
**P40 13 Spin transport and quasi 2D architectures for donor-based quantum computing** AUSTIN FOWLER, *Institute for Quantum Computing, University of Waterloo, Canada* LLOYD HOLLENBERG, ANDREW GREENTREE, CAMERON WELLARD, *ARC Centre of Excellence for Quantum Computer Technology, University of Melbourne, Australia* The original Kane quantum computer architecture is based on a single line of $^{31}P$ atoms spaced a few tens of nm apart in an isotopically pure $^{28}Si$ lattice with electrodes above and between donor atoms. This architecture suffers from major technical issues including strong spatial oscillations in the nearest neighbour donor electron exchange coupling strengths at the scale of a single lattice site and an inability to limit the effect of a given electrode to its nearest donor or donor pair. Through the introduction of a new donor electron spin transport mechanism, a 2D donor electron spin quantum computer architecture is proposed. This new architecture addresses the exchange coupling and cross-talk issues, as well as a host of other physical barriers to implementation.

## SESSION P41: FOCUS SESSION: DIELECTRIC, FERROELECTRIC, AND PIEZOELECTRIC OXIDES III
**Wednesday Morning, 15 March 2006; 344, Baltimore Convention Center at 11:15**
**Nicola Spaldin, University of California, Santa Barbara, presiding**

***Invited Papers***

**11:15**
**P41 1 Luminescence and Raman based real time imaging of ferroelectric domain walls.***
VOLKMAR DIEROLF, *Physics Department, Lehigh University*

Novel methods for real-time imaging of ferroelectric domain walls open up new possibilities for advancing physical understanding of domain wall structure, properties, and defect interactions. Instead of destructive chemical etching and subsequent optical or electron microscopy, domain walls are imaged nondestructively in real-time by photoluminescence microscopy using dilute doping by rare earth ions as designer defects whose luminescence is affected by the domain walls. Uisng a combination of high spatial and spectral site-selectvity in laser confocal and near field opptical microscopy, domain structure changes on a 100 nm length scale can be observed with a temporal resolution of 5ms, as demonstrated in $LiNbO_3$ and $LiTaO_3$. Imaging using Raman spectroscopy (that does not require rare earth doping) will also be described. These new imaging methods reveal that domain wall widths and structures are velocity-dependent, and they provide active, real time feedback needed for precise laser-writing of ferroelectric domain patterns.

*Supported by NSF grant DMR -0349632 and ARO-grant W9111NF-04-1-0323.

***Contributed Papers***

**11:51**
**P41 2 Study of Ferroelectric Domains in a Phase Separated Multiferroic Mixture by Variable Temperature Electrostatic Force Microscopy*** ALEX DE LOZANNE, TIEN-MING CHUANG, WEIDA WU, CASEY ISRAEL, *Department of Physics, University of Texas at Austin* CHENGLIN ZHANG, SANG-WOOK CHEONG, *Department of Physics and Astronomy, Rutgers University* We present a variable temperature Electrostatic Force Microscopy (VTEFM) study on a mixed multiferroic crystal. The sample was synthesized by the floating zone method. It was cut and polished with the surface normal to the growth direction. The chemical phase separation is clearly seen by polarized optical microscopy. The transition temperature is about 25K and 900K for the two different phases. The VTEFM images taken at 77 K reveal the ferroelectric domains, with typical sizes in the order of micrometers.

*This work is supported by NSF DMR-0308575

**12:03**
**P41 3 A new fundamental limit of ferroelectric devices and its domain dynamics in ultrathin ferroelectric $BaTiO_3$ films** J.Y. JO, D.J. KIM, Y.S. KIM, T.W. NOH, *ReCOE & School of*

*Physics,Seoul National University, Seoul 151-747, Korea* T.K. SONG, *Department of Ceramic Science and Engineering, Changwon National University, Changwon, Kyungnam 641-773, Korea* J.-G. YOON, *Department of Physics, University of Suwon, Gyunggi-do 445-743, Korea* Phenomena in ultrathin ferroelectric (FE) films, such as the critical thickness and the domain structures, have attracted much interest for a few years. We fabricated fully-strained $SrRuO_3/BaTiO_3/SrRuO_3$ capacitors, whose $BaTiO_3$ layer thicknesses were between 5 and 30 nm, using the laser molecular beam epitaxy. We found that rapid decay of net polarization occurs due to large depolarization field [1]. Using the Monte-Carlo simulations, this decay can be explained by the domain formation dynamics, governed by the domain nucleation process. We found a universal relation between the decay exponent and nucleation energy barrier, regardless of film thickness and temperature. This universal relation will provide a fundamental thickness limit for practical FE devices, set by net polarization decay. [1] D. J. Kim et al. Phys. Rev. Lett, in press.

**12:15**

**P41 4 Raman Studies of Ferrolectric Domain Walls in Lithium Tantalate and Niobate*** PAVEL CAPEK, GREG STONE, VOLKMAR DIEROLF, *Physics, Lehigh University* CHAD ALTHOUSE, VENKAT GOPALAN, *MS&E, Pennsylvania State University* The local structure of ferroelectric domain walls and its dependence on intrinsic defects and dopants is of great interest both from a basic science and a application point of view. For instance, in the ferroelectrics $LiNbO_3$ and $LiTaO_3$ that are widely used in nonlinear and electro-optical devices, the stability, shape, switching fields and smallest achievable domain size are determined by the defect concentration. Using confocal Raman spectroscopy we investigated the perturbation of the phonon modes across a domain wall as a function of sample stoichiometry (i.e.: the number of intrinsic defects. For all samples, we find that in the spectral vicinity of the $E(TO_8)$ and $E(TO_9)$ the Raman intensity is enhanced in the domain wall region. In order to elucidate the origin of this enhancement, we investigate the directional dispersion of the observed change and perform measurements under variation of pump and probe light polarization and sample orientation. On the basis of these results, we will discuss structural models of the domain wall.

*supported by NSF-Grant DMR 0349632. ARO-Grant W911NF-04-1-0323 and the Center for Optical Technologies at Lehigh University

**12:27**

**P41 5 Time-Resolved Observations of Soft Phonon Modes in Strained $BaTiO_3$/Si Heterostructures*** CHENG CEN, JEREMY LEVY, *Department of Physics and Astronomy, University of Pittsburgh* VENUGOPALAN VAITHYANATHAN, JAMES LETTIERI, WEI TIAN, DARRELL SCHLOM, *Department of Material Science and Engineering, Pennsylvania State University* COSMQC TEAM, Ferroelectric thin films such as $BaTiO_3$, grown on Si(100) substrates, have enormous potential for applications ranging from non-volatile random access memories to electro-optic gates for quantum information processing architectures. Optical techniques provide powerful means for obtaining time-resolved information about the ferroelectric soft mode in these materials. Using a two-color pump-probe arrangement, we observe THz-frequency soft modes in strained $BaTiO_3$/Si heterostructures grown by oxide-molecular beam epitaxy.

*This work is supported by DARPA QuIST (DAAD-19-01-0650).

**12:39**

**P41 6 Distribution function of random electric fields in disordered ferroelectrics thin films** VLADIMIR STEPHANOVICH, ELENA KIRICHENKO, *Institute of Mathematics and Informatics, Opole University* We present the calculation of first moment $E_0$ and variance $\Delta E$ of distribution function of random fields in a ferroelectric of finite size. This defines completely the distribution function in gaussian limit. Specific calculations have been performed for the case of slab-shaped ferroelectric thin film. We have shown that $E_0$ and $\Delta E$ can be expressed through the integrals from first and second degree of Green's function of such confined geometry ferroelectric in $k$ - space. To obtain the Green's function, we solve the differential equation minimizing Landau free energy of a ferroelectric with respect to the boundary conditions on its surfaces. We show, that the distribution function of random fields in the finite-size ferroelectric differs from that of the unbounded bulk material. For example, both $E_0$ and $\Delta E$ depends on film thickness $L$. Knowledge of this distribution function permits to calculate the observable physical properties of ferroelectric thin films made from ferroelectric relaxors. Our method of calculation of $E_0(L)$ and $\Delta E(L)$ can be easily generalized for ferroelectric of arbitrary shape.

**12:51**

**P41 7 Interface Induced Ferroelectric Phase Transformation in SrTiO3.** DAWN BONNELL, *University of Pennsylvania* RUI SHAO, GERD DUSCHER, *North Carolina State University* MATTHEW CHISOLM, *Oak Ridge National Lab* The transport properties across bicrystal interfaces in SrTiO3 are quantified with 4-pt probe, Hall measurements, scanning impedance microscopy and scanning tunneling microscopy. The properties are related to the structure determined by transmission electron microscopy, energy loss spectroscopy and first principles calculations. An anomaly in the temperature dependence of the transport properties arises from the charge trapped at the interface, which induces dipole ordering adjacent to the boundary. This represents the first observation of interface induced ferroelectricity in SrTiO3.

**13:03**

**P41 8 Nanoscale structural dynamics of ferroelectric thin films** ALEXEY GRIGORYEV, DAL-HYUN DO, DONG-MIN KIM, CHANG-BEOM EOM, PAUL EVANS, *University of Wisconsin-Madison* ERIC DUFRESNE, BERNHARD ADAMS, *Advanced Photon Source, Argonne National Laboratory* The emerging capability to visualize dynamical phenomena at small scales in both distance and time simultaneously has important implications in understanding ferroelectric materials. We have used time-resolved synchrotron x-ray microdiffraction to probe polarization switching and piezoelectric response at the sub-nanosecond time scale and the sub-micrometer spatial scale in lead zirconium titanate thin films. Based on time resolved maps of the polarization and piezoelectric distortion, the polarization switching domain wall velocity can be measured directly. The magnitude of this velocity and its scaling with electric fields suggest that significant improvements in switching speed can be made in optimized thin film structures.

**13:15**

**P41 9 External and internal magnetic-field effects on ferroelectricity in orthorhombic rare-earth manganites** H. KUWAHARA, K. NODA, M. AKAKI, *Dept. of Phys., Sophia Univ.* We report the dielectric and magnetic properties of the perovskite $(Eu,Y)MnO_3$ crystal *without* the presence of the $4f$ magnetic moments of the rare earth ions. The subject compound, $(Eu,Y)MnO_3$,

was controlled the average ionic radius of the $A$ site so that it was the same as that of $TbMnO_3$ in which the intriguing magnetoelectric effect has been recently discovered. The (Eu,Y)$MnO_3$ crystal was found to have two distinct ferroelectric phases with polarization along the $a$ ($P_a$, $T \leqslant 23$K) and $c$ ($P_c$, $23\text{K} \leqslant T \leqslant 25$K) axes in the orthorhombic $Pbnm$ setting in a zero magnetic field. In addition, we have demonstrated a magnetic-field-induced switching between these ferroelectric phases: $P_a$ changed to $P_c$ by the application of magnetic fields parallel to the $a$ axis ($H_a$). In analogy to the case of $P_c$ in $TbMnO_3$, this result is possibly interpreted as follows. In the case of (Eu,Y)$MnO_3$, Mn $3d$ spins rotate in the $ab$ plane and $P_a$ would emerge in a zero field. In the $H_a$, the field will force the spins to rotate in the $bc$ plane, in which $P_c$ would be stabilized. Magnetization measurements supported this interpretation: We confirmed the change of the spin rotation axis of the helix from the $c$ axis to the $a$ axis induced by application of the $H_a$ because there is no $4f$ moments acting as an internal magnetic field and interacting with the $3d$ spins. Results obtained with other rare-earth manganites such as (Gd,Tb)$MnO_3$ and (Eu,Ho)$MnO_3$ will be presented.

**13:27**

**P41 10 Dielectric and vibrational properties of crystalline and amorphous high-k lanthanum aluminate** PIETRO DELUGAS, VINCENZO FIORENTINI, ALESSIO FILIPPETTI, *SLACS-CNR and University of Cagliari, Italy* High-k oxides are the focus of intense research for their applications in MOS and FLASH devices. A material currently in focus is $LaAlO_3$, with a dielectric constant of 23-24 in the crystal phase, and similar values of around 20-22 in the amorphous phase (although values as low as 15 have also been reported). We have studied $LaAlO_3$ in both phases [1] to identify possible reasons for this apparent conservation of the dielectric properties upon amorphization. Amorphous samples were generated by melt-and-quench using a combination of pair potentials and ab initio dynamics. The linear response density-functional perturbation-theory approach was used to study dynamical response and phonons. We indeed find a large dielectric constant ( 24) in the amorphous: the rationale is that the expected reduction of the anomalous effective charges is compensated by the appearance of new low-frequency (weakly) IR-active modes, whose character is a mixture of La translations (IR in the crystal) and Al-O octahedra rotations (Raman in the crystal). A similar behavior is expected in any rare earth aluminate exhibiting a similar perovskite-related structure (e.g. scandates). 1) P. Delugas, V. Fiorentini, and A. Filippetti, Phys. Rev. B 71, 134302 (2005), and to be published.

**13:39**

**P41 11 Composition dependence of the diffuse scattering in relaxor $(1\text{-}x)Pb(Mg_{1/3}Nb_{2/3})O_3\text{-}xPbTiO_3$ $(0 \leqslant x \leqslant 0.40)$** M. MATSUURA, K. HIROTA, *ISSP The University of Tokyo* P. M. GEHRING, *NIST Center for Neutron Research* ZUO-GUANG YE, W. CHEN, *Department of Chemistry Simon Fraser University* G. SHIRANE, *Deapartment of Physics Brookhaven National Laboratory* We have studied composition dependence of diffuse scattering in the relaxor system $(1\text{-}x)Pb(Mg_{1/3}Nb_{2/3})O_3\text{-}xPbTiO_3$ (PMN-$x$PT) with $x = 0$, 10, 20, 30, and 40% by neutron diffraction. The addition of ferroelectric $PbTiO_3$ (PT) modifies the ''butterfly'' and ''ellipsoidal'' diffuse scattering patterns observed in pure PMN ($x = 0$), which are associated with the presence of randomly oriented, polar nanoregions (PNR). The spatial correlation length $\xi$ derived from the width of the diffuse scattering increases from 12.6 Å for PMN ($x = 0$) to 350 Å for PMN-20%PT, corresponding to an enlargement of the PNR. The integrated diffuse scattering intensity, which is proportional to $\chi''$, grows and reaches a maximum at $x = 20\%$. Beyond $x = 30\%$ PT, a concentration very close to the morphotropic phase boundary (MPB), no diffuse scattering is observed below $T_C$, and well-defined critical behavior is observed. By contrast, the diffuse scattering for $x \leqslant 20\%$ persists to low temperatures, where the system retains an average cubic structure ($T_C = 0$). We can simulate the wave vector dependence of the diffuse scattering by assuming that it arises from the condensation of a soft transverse-optic (TO) phonon.

**13:51**

**P41 12 Multiresonance, multifrequency spectroscopy of rare-earth and transition ions in ferroelectrics.** GALINA MALOVICHKO, *Physics Department, Montana State University* VALENTIN GRACHEV, *Physics Department, Montana State University* The usual scheme of many methods for material investigation includes an emitter of electromagnetic waves and detectors for the wave registration. Typical output of one-frequency methods is an image with a space resolution of about the used wavelength. The methods are very successful for the study of lattice structures, their transformations at phase transitions, domains etc. Another approach uses sweeping of the frequency or another external parameter: electric or magnetic field, pressure etc. Typical result of a measurement is a spectrum or a dependence of measured characteristic on the sweeping parameter. The spectra do not contain direct evidence about the space structure of a lattice or defects. However, they contain very important information about the energetic characteristics of interactions of lattice ions, intrinsic and extrinsic defects. We present results of multifrequency research of defects in oxide crystals involving optical spectroscopy, microwave and radiofrequency spectroscopy: electron paramagnetic resonance, and electron nuclear double resonance.

**14:03**

**P41 13 Femtosecond Spectroscopy of $LuMnO_3$** SHITAO LOU, *Department of physics and Astronomy, Rutgers University* FRANK M. ZIMMERMANN, ROBERT A. BARTYNSKI, NAMJUN HUR, SANG-WOOK CHEONG, *Department of Physics and Astronomy, Rutgers University* Hexagonal $LuMnO_3$ manganite is a ferroelectric and strongly frustrated antiferromagnetic crystal. Strong coupling between lattice, electronic, and magnetic degrees of freedom makes it a promising electronic material. We have used femtosecond pump-probe spectroscopy to study the interaction of electron excitations with lattice vibrations in real time. Optical excitation of a Mn $d_{(x^2-y^2),(xy)} \rightarrow d_{(3z^2-r^2)}$transition served as the primary excitation step. With both pump and probe beam polarization perpendicular to the c axis, the probe reflectivity shows a sharp drop due to saturation of the transition, recovering on a timescale of 1 ps. We also observed displacive excitation of a coherent optical phonon vibration at 3.6 THz, which is assigned to an A1 symmetry mode involving Lu ion motion along the c axis. This mode was excited in longitudinal (LO) and transverse mode (TO) geometries. While the LO-TO frequency splitting is small ( $< 0.1$ THz), a remarkable phase reversal of the reflectivity curve was observed. This is attributed to a large linear electro-optic effect (Pockels effect), induced by the THz electric field associated with the LO mode.

**SESSION P42: FOCUS SESSION: PLANETARY MATERIALS III**
**Wednesday Morning, 15 March 2006**
**345, Baltimore Convention Center at 11:15**
**Lars Stixrude, University of Michigan, presiding**

**11:15**

**P42 1 Dissociation of $CaIrO_3$-type $MgSiO_3$ in the gas giants*** KOICHIRO UMEMOTO, RENATA WENTZCOVITCH, *Minnesota Supercomputing Institute and Department of Chemical Engineering and Materials Science, University of Minnesota* PHILIP ALLEN, *Department of Physics and Astronomy, Stony Brook University* $CaIrO_3$-type $MgSiO_3$ is the planet-forming silicate stable at pressures and temperatures (PTs) beyond those of Earth's core-mantle boundary. We have found using first principles quasiharmonic free energy computations that this mineral dissociates into MgO and $SiO_2$ at PTs expected to occur in the cores of the gas giants ( $> \sim$10 Mbar, 10,000 K). This transformation should be important also for modeling the internal structure of two recently discovered terrestrial exoplanets: a dense Saturn orbiting HD149026b and a super Earth orbiting GJ876d. We propose a low pressure route experiment to confirm this dissociation.

*Research supported by NSF/EAR 013533, 0230319, NSF/ITR 0428774 (VLab), and Minnesota Supercomputing Institute.

**11:27**

**P42 2 Thermal Electrons and Thermal Conductivity in Oxide Minerals at P and T Relevant to Terrestrial Exoplanets*** PHILIP B. ALLEN, *Stony Brook University* KOICHIRO UMEMOTO, *University of Minnesota* RENATA M. WENTZCOVITCH, *University of Minnesota* The recent discovery of an extrasolar planet, with 7.5 times the mass of the Earth, has prompted investigation of a new range of parameter space, 3 times higher in temperature T and 10 times higher in pressure P than the Earth's mantle. We estimate thermal conductivity k(T) of minerals under these extreme conditions. The radiative portion of k(T) is large above the mid-lower post-perovskite mantle, where T reaches 5000-6000K. At T higher than 5000 K, free electron carriers are thermally activated with the population n(T) increasing as exp(-E*/2kT), where E* is the band gap energy of around 5 eV. Free carriers damp electromagnetic waves at frequencies below the plasma frequency, estimated to be close to 1 eV, shutting down radiative heat transport. Although thermal holes have low mobility, we find that thermal electrons are quite mobile, with small effective masses and weak scattering. Therefore, they become dominant carriers of heat. We predict electrical resistivity as low as 1000 micro-ohm cm.

*Research supported by NSF/EAR 0230319, NSF/ITR 0428774, NSF/ITR 0426757, and VLab.

**11:39**

**P42 3 Elasticity of MgO Under Direct Pressure Measurement: Insights on Current Pressure Scales.*** BAOSHENG LI, *Stony Brook University* KELLY WOODY, *Division of Water Supply, The State of Tennessee* ROBERT LIEBERMANN, *Department of Geosciences, SUNY Stony Brook* Recent high pressure studies indicated that the inaccuracy and inconsistency of the pressure scales used for pressure determination in different studies might be an importance source that gives rise to the apparent discrepancy in the derived phase equilibrium and physical properties for mantle minerals. In this study, P and S wave velocities and unit cell parameters (density) of MgO are measured simultaneously up to 11 GPa 1073K using combined ultrasonic interferometry and in-situ X-ray diffraction techniques, from which the elastic bulk and shear moduli as well as their and temperature pressure derivatives are obtained independent of pressure. These properties are subsequently used to calculate the primary pressures at the observed strains for comparison with those derived from previous proposed MgO pressure scales. Additionally, a comparison of the primary pressure obtained from MgO with those inferred from the enclosed internal pressure calibrant (NaCl) gives an opportunity to evaluate the Decker NaCl scale as well. Our results suggest that current pressure scales may bear larger uncertainties than originally claimed.

*The research is supported by NSF grant EAR00135550.

**11:51**

**P42 4 A high PT scale based on density functional calculations of MgO*** Z. WU, R.M. WENTZCOVITCH, *Department of Chemical Engineering and Materials Science and Minnesota Supercomputing Institute, University of Minnesota, Minneapolis, MN 55455, USA* B. LI, *Mineral Physics Institute, Stony Brook University, Stony Brook, NY 11794, USA* K. UMEMOTO, *Department of Chemical Engineering and Materials Science and Minnesota Supercomputing Institute, University of Minnesota, Minneapolis, MN 55455, USA* In situ crystallography based on diamond anvil cells have recently been extended to the multi-Mbar regime. Temperatures in these experiments have crossed the 2,000 K mark. Yet, current high PT standards of calibration produce too large uncertainties to the point of inhibiting clear conclusions regarding the importance of certain phenomena for planetary processes at these high PTs, e.g., the post-perovskite transition in Earths mantle. We propose a calibration based on thermal equations of state (EoS) of MgO obtained from LDA quasiharmonic (QHA) calculations. These EoSs agree very well with several calibrations at relatively low PTs. This gives further support to our predictions made within the range of validity of the QHA.

*Research supported by NSF/EAR 0230319, 0135550, and NSF/ITR 0428774, VLab

**12:03**

**P42 5 Phase stability and elasticity of $CaSiO_3$ perovskite at high pressure and high temperature from Ab inito molecular dynamic calculations** DONALD WEIDNER, LI LI, *Stony Brook University* JOHN BRODHOLT, DARIO ALFE, DAVID PRICE, *University College London* STONY BROOK UNIVERSITY COLLABORATION, UNIVERSITY COLLEGE LONDON COLLABORATION, We report the dynamics of the structure and elastic properties of CaSiO3 perovskite from itab initio molecular dynamics (AIMD) calculations at high pressure (P up to 130 GPa) and high temperature (T up to 5000K). Our calculations indicate three separate stability fields: metrically orthorhombic, tetragonal and cubic, with the tetragonal phase dominating the pressure and temperature region between room temperature and 4000K. The cubic phase is not entirely stabilized even at temperatures of the Earth's lower mantle. Calculated X-ray diffraction patterns indicate small super- lattice reflections that could result from the octahedral rotations throughout the P-T region investigated. The calculated elastic constants and velocities are independent of temperature at constant volume. Referenced to room pressure and 2000K, we find: Grûneisen parameter is $\gamma(V) = \gamma0(V/V0)q$ with $\gamma0 = 1.53$ and $q = 1.02(5)$, and the Anderson Grûneisen param-

eter is given by ($\alpha$/ $\alpha$0) = (V/V0)$\delta$T in which $\alpha$0 = 2.89 x 10-5 K-1 and $\delta$T = 4.09(5). Using the third order Birch Murnaghan equation of state to fit our data, we have for ambient P and T, $K_0$ = 236.6(8) GPa, $K_0$' = 3.99(3), and $V_0$ = 729.0(6) Å3.

**12:15**

**P42 6 Computational study of the pressure behavior of post-perovskite phases** RAZVAN CARACAS, *Geophysical Laboratory, Carnegie Institution of Washington* RONALD COHEN, *Geophysical Laboratory, Carnegie Institution of Washington* The recent discovery of the post-perovskite phase transition ($CaIrO_3$ structure) in $MgSiO_3$ has lead to theoretical and experimental investigations of silicates, germanates and oxides that could take this structure. We have employed density functional-theory to explore a series of new compounds with the post-perovskite structure under pressure. We analyze the effects of the Si substitution by tetravalent cations on the perovskite-to-post-perovskite transition and on the crystal structure of post-perovskite. Cations $Ti^{4+}$ and $Zr^{4+}$ prefer the post-perovskite structure. We also explore the sesquioxides $Al_2O_3$ and $Rh_2O_3$ and compare their structural evolution with the one of $MgSiO_3$. For $Rh_2O_3$ we observe an enhancement of the ionic character of the type II structure with pressure.

**12:27**

**P42 7 Thermodynamics of $Mg_2SiO_4$ liquid from first principles molecular dynamics simulations** NICO DE KOKER, LARS STIXRUDE, *University of Michigan* As the main medium through which planetary differentiation occurs, silicate liquids have a central role in the study of the Earth. We determine the structural and thermodynamic properties of $Mg_2SiO_4$ liquid using first principles molecular dynamics in the framework of density functional theory and the local density approximation (LDA). Calculations, performed in the canonical ensemble with a Nose thermostat, span a range of pressures (0 - 150 GPa) and temperatures (3000 - 6000 K). Simulations are performed over 3000 time steps (femto seconds), yielding the total energy and average pressure from which the equation of state, heat capacity and Gruneisen parameter are determined. Preliminary results show that, in addition to the increase in Si coordination with pressure, about one third of the O atoms are not bound to Si at low pressure, a fraction which vanishes with increased Si coordination.

**12:39**

**P42 8 Dissociation of Ringwoodite investigated by first principles*** YONGGANG YU, RENATA WENTZCOVITCH, TAKU TSUCHIYA, KOICHIRO UMEMOTO, JUN TSUCHIYA, *Minnesota Supercomputing Institute and Department of Chemical Engineering and Materials Science, University of Minnesota* DONALD WEIDNER, *Center for High Pressure Research and Department of Geosciences, State University of New York, Stony Brook, NY 11794, USA* RENATA WENTZCOVITCH'S GROUP AT UNIVERSITY OF MINNESOTA TEAM, DONALD WEIDNER'S GROUP AT STATE UNIVERSITY OF NEW YORK AT STONY BROOK COLLABORATION, The dissociation of Ringwoodite, $Mg_2SiO_4$ gamma-spinel, into MgO and $MgSiO_3$ perovskite is believed to be associated with the 660-km discontinuity in Earth's mantle. Details of this transition are important to clarify its effect on mantle convection: it is believed to inhibit flow across the ''660'' discontinuity. We have investigated the phase boundary using quasiharmonic free energy computations within the LDA and GGA. Once more the GGA transition pressure, $P_{tr}$, is higher and in much better agreement with the limited experiments available. The higher GGA $P_{tr}$ can be rationalized by close inspection of the relationship between GGA and LDA functional forms. Our predictions of density, bulk modulus, and bulk velocity jumps across the transition are consistent with seismic observations.

*Research supported by NSF/EAR 013533, 0230319, NSF/ITR 0428774 (VLab), and Minnesota Supercomputing Institute

**12:51**

**P42 9 Structure and freezing of $MgSiO_3$ liquid in Earth's interior** BIJAYA KARKI, *Louisiana State University* LARS STIXRUDE, *University of Michigan* Silicate liquids are primary agents of mass and heat transport, yet little is known of their physical properties or structure over most of the mantle pressure regime. We have applied density functional theory within the local density approximation to the study of silicate liquids via Born-Oppenheimer first principles molecular dynamics. The simulations are performed in the NVT ensemble with a Nose thermostat. We find that over the pressure regime of Earth's mantle the mean Si-O coordination number increases nearly linearly with compression from four-fold to six-fold. The Grüneisen parameter of the liquid increases markedly on compression, in contrast to the behavior of mantle crystalline phases, and in accord with expectations based on the pressure-induced change in structure of the liquid. The density contrast between liquid and crystal decreases nearly five-fold over the mantle pressure regime and is 4 % at the core-mantle boundary. The melting curve, obtained via integration of the Claussius-Clapeyron equation yields a melting temperature of 5400 $\pm$ 600 K at the core mantle boundary. Our results support the notion of buoyantly stable silicate melts at the core-mantle boundary.

**13:03**

**P42 10 A laboratory method for modeling synthesis of coesite in the earth's surface by combining local mechanical collision with shear stress and high static pressure.** WEN-HUI SU, SHU-E LIU, *Center for the Condensed-Matter Science and Technology, Harbin Institute of Technology, Harbin 150001, P. R. China* DA-PENG XU, WEI-RAN WANG, *Center for Rare-Earth Solid State Physics, Jilin University, Changchun 130023, P. R. China* XIAO-MEI LIU, *Center for the Condensed-Matter Science and Technology, Harbin Institute of Technology, Harbin 150001, P. R. China* A laboratory method of combining the high-energy mechanical ball milling and high static pressure has been suggested for modeling synthesis of coesite in the earth's surface. A window of milling time, a mechanical collision-induced intermediate phase of $\alpha$-quartz and its condition of easily crystallizing into coesite induced by high static pressure 3.0 GPa, 923 K, $<$ 1.0 min have been discovered. The condition has a much shorter synthesizing time and lower synthesizing critical pressure than that obtained before. The Raman spectrum for the coesite synthesized by the present method has the biggest number of peaks, and have covered over the information of those natural and synthesized coesite reported before. Here We clarify the implications of the coesite synthesized by this method in geo-science, and suggest another possible formation mechanism of coesite in the earth's surface, which is different from the hypothesis of plate subduction-exhumation in the earth that was based on the coesite formation condition of high static pressure in laboratory.

**13:15**

**P42 11 Novel Perovskite Compounds Synthesized under Elevated High Pressure.*** C.Q. JIN, Q.Q. LIU, X.M. QIN, *Institute of Physics, Chinese Academy of Sciences* High pressure synthesis is very powerful to stabilize new compounds with perovskite-like structure, as it has been very well established in the studies of Earth mantle. This has been widely demonstrated in the research of transition metal oxides. Here we introduce some new transition metal compounds that have been recently synthesized under elevated high pressure.

*This work was supported by NSF and Ministry of Science and Technology of China through the research projects.

**13:27**

**P42 12 Structure of $MgO(MgSiO_3)_n$ in Earth's Lower Mantle: ab initio calculations** PATRIC OULEVEY, MOHAMMED SAHNOUN, *Department of Chemistry, University of Fribourg, CH-1700 Fribourg, Switzerland* SIMONPIETRO DI PIERRO, *Laboratoire de Sciences de la Terre, UMR CNRS 5570, École Normale Supérieure de Lyon, France* BERNARD GROBÉTY, *Department of Mineralogy, University of Fribourg, CH-1700 Fribourg, Switzerland* CLAUDE DAUL, *Department of Chemistry, University of Fribourg, CH-1700 Fribourg, Switzerland* Ruddlesden-Popper (RP) compounds are composed of alternating perovskite-type and rocksalt-type structural elements. $MgSiO_3$ and MgO are found as separate phases in Earth's lower mantle. Both structural elements occur also in the hypothetical RP-series $MgO(MgSiO_3)_n$. It is interesting to explore the high pressure-high temperature stability of such RP-structures. Using the augmented plane wave implementation of Density Functional Theory we investigate the structural stability at lower mantle conditions of the member with $n = 1$ e.g. $Mg_2SiO_4$. The goal of the present calculations is to test the stability of this Ruddlesden-Popper phase relative to $\gamma$-$(Mg,Fe)_2SiO_4$ and the assemblage $MgSiO_3$-perovskite + MgO magnesiowüstite. We will present our results of this study.

**13:39**

**P42 13 Heat capacity measurements of sub-milligram quantities of mantle minerals** DAVID W. COOKE, F. HELLMAN, *University of California at Berkeley* A. NAVROTSKY, M. DOROGOVA, C.E. LESHER, *University of California at Davis* Knowledge of heat capacities and standard entropies of mantle minerals is necessary for thermodynamic modeling of high P-T equilibria. However many of these materials can only be prepared in milligram quantities in a multianvil apparatus or in microgram quantities in a diamond anvil cell. This eliminates traditional adiabatic calorimetry techniques for Cp measurements. Our microcalorimeters have been used to successfully measure thin films, multilayers, and magnetic single crystals. Using these ''calorimeters on a chip,'' we are measuring the heat capacity of the $Fe_2SiO_4$ olivine and spinel polymorphs from 2 K to room temperature. This will provide a direct measurement of the entropy of the olivine-spinel transition and will uncover possible magnetic phase transitions at low temperature in the spinel phase. We would like to thank the DOE for funding this research.

**13:51**

**P42 14 Carbon under extreme conditions: phase boundaries from first-principles theory** ALFREDO A. CORREA, *Physics Department, University of California, Berkeley* STANIMIR A. BONEV, *Department of Physics, Dalhousie University, Halifax* GIULIA GALLI, *Department of Chemistry, University of California, Davis* We present predictions of diamond and BC8 melting lines and their phase boundary in the solid phase, as obtained from first principles calculations. Maxima are found in both melting lines, with a triple point located at $\sim$ 850GPa and $\sim$ 7400K. Our results show that hot, compressed diamond is a semiconductor which undergoes metalization upon melting. On the contrary, in the stability range of BC8, an insulator to metal transition is likely to occur in the solid phase. Close to the diamond/ and BC8/liquid boundaries, molten carbon is a low-coordinated metal retaining some covalent character in its bonding up to extreme pressures. Our data provide constraints to the carbon equation of state, which is of critical importance to devise models of, e.g., Neptune, Uranus and white dwarf stars, as well as of extra-solar carbon planets. This work was performed under the auspices of the U.S. Dept. of Energy at the University of California/Lawrence Livermore National Laboratory under contract no. W-7405-Eng-48.

**14:03**

**P42 15 Synthesis of New Cubic $C_3N_4$ Phase under High Pressure and High Temperature** LI CHUNG MING, PAVEL ZININ, *University of Hawaii* YUE MENG, *Argonne National Laboratory* XIU-RU LIU, SHI MING HONG, *Southwest Jiaotong University, China* YI XIE, *University of Science and Technology of China* Synchrotron-based X-ray diffraction studies were carried out on a graphite-like $C_3N_4$ ($g$-$C_3N_4$) phase subjected to high pressures up to 38 GPa and high temperatures of up to 3000 K using the laser-heated diamond-anvil cell. Laser-heating the sample to 1800 K at pressure between 20 and 38 GPa, a new set of diffraction pattern appeared, showing positively that a high-pressure phase was formed. Upon decompression of the post-lasered sample to 1 atmospheric pressure, the X-ray diffraction peaks of high-pressure phase were replaced completely by a new pattern, thus demonstrating a new metastable phase was formed retrogressively. X-ray diffraction data on the recovered phase show that it is a new cubic phase that does not match to any high-pressure phases in $C_3N_4$ predicted theoretically.

## SESSION P43: NOVEL PHASES IN QUANTUM GASES

**Wednesday Morning, 15 March 2006**
**346, Baltimore Convention Center at 11:15**
**B. Svistunov, University of Massachusetts, presiding**

**11:15**

**P43 1 Stability of Bosonic atomic and molecular condensates near a Feshbach Resonance** SOURISH BASU, ERICH MUELLER, *Laboratory of Atomic and Solid State Physics, Cornell University, Ithaca, New York 14853* Fermions near a Feshbach resonance exhibit a smooth crossover between a Bose-Einstein condensed state of molecules and a BCS superfluid of Cooper pairs. We study the analogous problem in Bosons, where there is a possibility of a phase transition between a molecular condensate (MC) and an atomic condensate (AC). We show that on the mo-

lecular side of the resonance at low densities, a MC-AC continuous transition is precluded by the AC state having a negative compressibility [cond-mat/0507460]. Instead, there is a mechanical collapse to a liquid-like state, analogous to a first order phase transition. We predict that sufficiently high densities (beyond those currently achieved in experiments) will push the system beyond its tricritical point and allow a continuous MC-AC phase transition.

**11:27**

**P43 2 Phase diagram of Bose-Fermi mixtures in one-dimensional optical lattices** LODE POLLET, MATTHIAS TROYER, *Institut Theoretische Physik, ETH Zurich, CH - 8093 Zurich, Switzerland* KRIS VAN HOUCKE, STEFAN ROMBOUTS, *Subatomaire en Stralingsfysica, Universiteit Gent, B - 9000 Gent, Belgium* The ground state phase diagram of the one-dimensional Bose-Fermi Hubbard model is studied in the canonical ensemble using a quantum Monte Carlo method. We focus on the case where both species have half filling in order to maximize the pairing correlations between the bosons and the fermions. In case of equal hopping we distinguish between phase separation, a Luttinger liquid phase and a phase characterized by strong singlet pairing between the species. True long-range charge density waves exist with unequal hopping strengths.

**11:39**

**P43 3 Luttinger's theorem and Phase Transitions in Bose-Fermi mixtures** STEPHEN POWELL, *Yale University* SUBIR SACHDEV, *Harvard University* HANS PETER BUCHLER, *University of Innsbruck* A mixture of bosonic and fermionic atoms with a Feshbach resonance between the two can exhibit a range of phases as the energy of a fermionic bound state is varied. In each uniform phase a generalized statement of Luttinger's theorem can be made regarding the two Fermi surfaces, one associated with the atomic fermion and one with the bound-state molecule. The various phases can then be characterized by their different Luttinger constraints, which also depend on the presence or absence of a bosonic condensate. Interesting parallels can be drawn between this system and two others: the transition to the fractionalized Fermi liquid in Kondo lattice models, and fermion-pair condensation in the presence of mismatched Fermi surfaces.

**11:51**

**P43 4 Spontaneous Symmetry Breaking and Defect Formation in a Quenched Ferromagnetic Spinor Bose-Einstein Condensate** LORRAINE SADLER, JAMES HIGBIE, MUKUND VENGALATORRE, SABRINA LESLIE, DAN STAMPER-KURN, *University of California, Berkeley* We observe spontaneous symmetry breaking in a spinor Bose condensate of $^{87}$Rb that is quenched across a quantum phase transition to a ferromagnetic state. Using high spatial resolution maps of the vector magnetization of the condensate, we directly observe the spontaneous formation of inhomogeneous ferromagnetic regions separated by unmagnetized defects. The growth of these ferromagnetic regions are due to a dynamical instability, which determines their typical size and the time for their formation in accord with our observations.

**12:03**

**P43 5 Thermodynamic properties of Bose-Hubbard model.** BARBARA CAPOGROSSO-SANSONE, NIKOLAY PROKOF'EV, BORIS SVISTUNOV, *Department of Physics, University of Massachusetts, Amherst, Massachusetts 01003* We perform Monte Carlo simulations of bosons in a three-dimensional optical lattice. We present accurate data for the ground state phase diagram and for the finite-temperature thermodynamic properties, including specific heat and entropy. Our data form a basis for an accurate thermometry of the system.

**12:15**

**P43 6 Existence of Roton Excitations in Bose Einstein Condensates: Signature of Proximity to a Mott Insulating Phase** ZAIRA NAZARIO, DAVID I. SANTIAGO, *Stanford University* Within the last decade, artificially engineered Bose Einstein Condensation has been achieved in atomic systems. Bose Einstein Condensates are superfluids just like bosonic Helium is and all interacting bosonic fluids are expected to be at low enough temperatures. One difference between the two systems is that superfluid Helium exhibits roton excitations while Bose Einstein Condensates have never been observed to have such excitations. The reason for the roton minimum in Helium is its proximity to a solid phase. The roton minimum is a consequence of enhanced density fluctuations at the reciprocal lattice vector of the stillborn solid. Bose Einstein Condensates in atomic traps are not near a solid phase and therefore do not exhibit roton minimum. We conclude that if Bose Einstein Condensates in an optical lattice are tuned near a transition to a Mott insulating phase, a roton minimum will develop at a reciprocal lattice vector of the lattice. Equivalently, a peak in the structure factor will appear at such a wavevector. The smallness of the roton gap or the largeness of the structure factor peak are experimental signatures of the proximity to the Mott transition.

**12:27**

**P43 7 Supersolid Bosons on Frustrated Optical Lattices** STEFAN WESSEL, *Institute for Theoretical Physics III, University of Stuttgart, Germany* MATTHIAS TROYER, *Institute for Theoretical Physics, ETH Zurich, Switzerland* We consider an ultra-cold Bose gas on a triangular optical lattice subject to nearest neighbor repulsion, and determine the phase diagram using quantum Monte Carlo simulations. Already in the hard-core limit the system is found to exhibit an extended supersolid phase emerging from an order-by-disorder effect as a novel way of a quantum system to avoid classical frustration. We analyze the nature of the supersolid phase and its stability in competition with phase-separation, which we find to occurs in other regions of parameter space. Possible experimental realizations of our scenario and extensions to other lattice geometries are discussed as well as the connection to the physics of frustated quantum antiferromagnets.

**12:39**

**P43 8 Frustrated two-dimensional XY models with cold atoms in optical lattices** ANTON BURKOV, EUGENE DEMLER, *Harvard University* We consider a system of cold bosonic atoms in a rotating optical lattice at finite temperature. We show that such system exhibits a non-trivial dependence of the condensation temperature and the superfluid order parameter on the vortex density due to commensuration effects of the vortex and optical lattices.

We identify several vortex filling/lattice geometry combinations for which the vortex ordering pattern exhibits subtle order-by-disorder effects due to an interplay between multiple degeneracy of frustrated vortex configurations and thermal fluctuations.

**12:51**

**P43 9 Winding Numbers in Rotating Bose Gases** ALEXIS G. MORRIS, *University of Calgary* DAVID L. FEDER, *University of Calgary* The exact ground states of zero-temperature rotating Bose gases confined in quasi-two-dimensional harmonic traps are investigated numerically, for small numbers of alkali atoms. As the rotation frequency increases, the interacting Bose gas undergoes a series of transitions from one quantum Hall state to another. By tracking the change in ground state energy with an applied phase twist, we are able to calculate the winding (Chern) number characterizing the topological nature of the various bosonic quantum Hall states.

**13:03**

**P43 10 Parafermionic states in rotating Bose-Einstein condensates** NICOLAS REGNAULT, *LPA, ENS-Paris, France* THIERRY JOLICOEUR, *LPTMS, Orsay, France* Rotating Bose-Einstein condensates in a trap are the place of a very rich physics. It has been predicted that, under appropriate conditions, they will behave like two dimensional electron systems in the fractional quantum Hall effect regime. In addition to the usual fractions, more exotic phases have also been predicted at filling factor $\nu = k/2$. These parafermionic states are described by the Read-Rezayi (RR) wave functions. We study how the system size and interaction act on the overlap between the true ground state and corresponding RR state. The quasihole excitations of the RR states are known to obey non-Abelian statistics. We numerically evaluate the degeneracy of these states and show it is in agreement with a formula given by E. Ardonne. We compute overlap between low-energy true eigenstates and quasihole ground states, and discuss in which cases such description is valid.

**13:15**

**P43 11 Quantum magnetism with multicomponent polar molecules in an optical lattice** RYAN BARNETT, DMITRY PETROV, MIKHAIL LUKIN, EUGENE DEMLER, *Harvard University* We consider dipolar molecules in an optical lattice prepared as a mixture of states with angular momentum $\ell = 0$ and $\ell = 1$. The $1/r^3$ interaction between molecules for this system is produced by exchanging a quantum of angular momentum between two molecules. We show that Mott states of such systems have a large variety of non-trivial spin orderings including SDW state at a wavevector that can be controlled by changing parameters of the system. As the Mott insulating phase is melted, we also show that an interesting winding in the phase of the order parameter can occur. Finally, we consider ways of detecting such phases experimentally.

**13:27**

**P43 12 Biaxial nematic phase of two dimensional disordered rotor models and spin-one bosons in optical lattices** JEAN-SEBASTIEN BERNIER, *University of Toronto* KRISHNENDU SENGUPTA, *Saha Institute of Nuclear Physics* YONG BAEK KIM,* *University of Toronto* We show that the ground state of disordered rotor models with quadrupolar interactions can exhibit biaxial nematic ordering in the disorder-averaged sense. We present a mean-field analysis of the model and demonstrate that the biaxial phase is stable against small quantum fluctuations. We point out the possibility of experimental realization of such rotor models using ultracold spin-one Bose atoms in a spin-dependent and disordered optical lattice in the limit of a large number of atoms per site and also suggest an imaging experiment to detect the biaxial nematicity in such systems.

*also affiliated with School of Physics Korea Institute of Advanced Study

**SESSION P44: ORGANIC CONDUCTORS**
**Wednesday Morning, 15 March 2006**
**347, Baltimore Convention Center at 11:15**
**Michael Naughton, Boston College, presiding**

**11:15**

**P44 1 Interlayer magnetoresistance as a probe of the quantum coherence of electronic excitations in layered metals** MALCOLM KENNETT, *Simon Fraser University* ROSS McKENZIE, *University of Queensland* Angle-dependent magnetoresistance oscillations (AMRO) have been used as a powerful tool to map out Fermi surfaces in layered metals, such as organic metals, strontium ruthenate, and an over-doped cuprate. We derive a general formula for AMRO in systems with anisotropic interlayer hopping, anistropic in-plane scattering and an anisotropic 2*d* Fermi surface. We discuss the ability of AMRO to discriminate between coherent transport when there is a 3*d* Fermi surface and weakly incoherent transport, where there is hopping between 2*d* Fermi surfaces that are only defined in each layer. We illustrate these ideas by comparison with experimental measurements of AMRO in thallium cuprate [1]. [1] N. E. Hussey *et al.*, Nature **425**, 814 (2003).

**11:27**

**P44 2 Interlayer Aharonov-Bohm interference in tilted magnetic fields in quasi-one-dimensional organic conductors** VICTOR YAKOVENKO, BENJAMIN COOPER, *Department of Physics, University of Maryland* Different types of angular magnetoresistance oscillations in quasi-one-dimensional organic conductors, such as $(TMTSF)_2X$, are explained in terms of Aharonov-Bohm interference in interlayer electron tunneling. A two-parameter pattern of oscillations for generic orientations of a magnetic field is visualized and related to the experimental data. Reference: cond-mat/0509039

**11:39**

**P44 3 Unified Theory of Magic Angles and Interference Commensurate Oscillations.** SI WU,*ANDREI LEBED,† *Dept. of Physics, University of Arizona* HEON-ICK HA, *Dept. of Physics, Harvard University* MICHAEL NAUGHTON, *Dept. of Physics, Boston College* We suggest the unification theory of angular magnetoresistance oscillations in low-dimensional metals with open sheets of Fermi surfaces. It is based on an idea that effective space dimensionality of electron spectrum and electron wave functions is changed at some special directions of a magnetic field. These 1D -> 2D dimensional crossovers are shown to be due to interference effects, which occur when electrons move in the extended Brillouin zone in a magnetic field. Our quantum mechanical approach allows to derive an equation which describes analytically

both Magic Angles and Interference Commensurate oscillations in resistivity component, perpendicular to conducting layers, and reveals their common physical origin. We compare our results with experimental data obtained on $(TMTSF)_2ClO_4$ and $(TMTSF)_2PF_6$.

*presenting author
†contact author

**11:51**

**P44 4 Lebed Magic Angles in $(TMTSF)_2X$ Probed by Torque, Transport and NMR*** J.I. OH, *Boston College* K. KOBAYASHI, *Princeton University* P.M. CHAIKIN, *NYU* J. SHINAGAWA, *UCLA* S.E. BROWN, *UCLA* M.J. NAUGHTON, *Boston College* We have investigated the Lebed effect [1] in the quasi −1D molecular organic conductor (TMTSF)2X for magnetic fields in the b′ −c* −plane, via angle−dependent torque, magnetoresistance, and NMR relaxation rate. In torque versus field angle measurements for X = ClO4 at 0.1 K, we observed distinct field induced spin density wave (FISDW) transitions but, to within our experimental accuracy of 3× 10−11 Nm, we found no evidential anomalies at the Lebed magic angles. We compare this result with earlier reports of torque measurements in X = ClO4 [2] and 77Se NMR relaxation rate measurements in X = PF6 [3]. In fixed angles T− (NMR) and B−sweeps (torque and magnetoresistance) in the vicinity of magic angles, no change in the FISDW position was observed. These measurements suggest that magic Lebed orientations have no effect on the metal−FISDW transition. [1] A. G. Lebed, JETP Lett. **43**, 174 (1986). [2] M. J. Naughton et al., Phys. Rev. Lett. **67**, 3712 (1991). [3] W. Wu et al., Phys. Rev. Lett. 94, 097004 (2005).

*This work was supported by the National Science Foundation Grants DMR−0308973 (MJN), DMR−0243001 (PMC), and DMR−0203806 (SEB).

**12:03**

**P44 5 Thermoelectric power and Nernst effect studies in the metallic and field-induced spin density wave states in $(TMTSF)_2ClO_4$** EUN SANG CHOI, JAMES S. BROOKS, *NHMFL/Florida State University* HAEYONG KANG, YOUNJUNG JO, WOUN KANG, *Ewha Womans University, Seoul, Korea* We have measured the angular dependence of thermoelectirc power (TEP) and Nernst effect of $(TMTSF)_2ClO_4$. At low temperatures and in the metallic state, Nernst effect shows giant resonant signals around the Lebed magic angles, while TEP is small without noticiable angular dependence. This behavior is very similar to what was observed in $(TMTSF)_2PF_6$ in the metallic state [Wu et al., Phys. Rev. Lett. **91** 56601(2003)]. By entering the field-induced spin density wave (FISDW) state, both TEP and Nernst signal show complicated behaviors reflecting the FISDW subphase transitions. Remarkably, the resonant Nernst effect still persists in the FISDW state and with even lager amplitude. By increasing the perpendicular field above ~ 6.5 T, both TEP and Nernst effect becomes small again at all angles. Our Nernst effect results are inconsistent with some proposed models for the metallic state of $(TMTSF)_2PF_6$, which may suggest this phenomenon is beyond the Fermi liquid description.

**12:15**

**P44 6 Coexistence of spin density wave and triplet superconductivity in quasi-one-dimensional Bechgaard salts** WEI ZHANG, CARLOS SA DE MELO, *Georgia Institute of Technology* The interplay between magnetic order and superconductivity is a very important problem in condensed matter physics. In the quasi-one-dimensional (quasi-1D) organic conductor $(TMTSF)_2PF_6$, an antiferromagnetic state charaterized by a spin density wave (SDW) order neighbors a triplet superconducting (TSC) state on the pressure-temperature phase diagram. Experiments [1,2] suggest a coexisting region of SDW and TSC orders in the vicinity of the phase boundary. We consider a tight-binding quasi-1D electron system, and construct the Ginzburg-Landau (GL) free energy with two order parameters. In the absence of a magnetic field, the rotational symmetry of this system is broken due to spin anisotropy and spin-orbit coupling. Thus, the GL free energy has a similar form as the ordinary $\phi_1$-$\phi_2$ model, except additional gradient terms. We calculate the GL coefficients microscopically and obtain a phase diagram in zero magnetic field. This phase diagram shows a coexistence region for SDW and TSC. Reference: [1] T. Vuletic *et al.*, Eur. Phys. J. B **25**, 319 (2002). [2] I. J. Lee *et al.*, Phys. Rev. Lett. **94**, 197001 (2005).

**12:27**

**P44 7 Anomalous temperature dependence of the single-particle spectrum in the organic conductor TTF-TCNQ** NEJAT BULUT, *IMR, Tohoku University and CREST, Japan Science and Technology Agency* HIROAKI MATSUEDA, *Department of Physics, Tohoku University* TAKAMI TOHYAMA, *IMR, Tohoku University* SADAMICHI MAEKAWA, *IMR, Tohoku University and CREST, Japan Science and Technology Agency* The angle-resolved photoemission spectrum of the quasi-one-dimensional organic-conductor TTF-TCNQ exhibits an unusual temperature dependence in the sense that a transfer of spectral weight over an energy range of $\approx$ 1iteV takes place as the temperature decreases below 260$K$. In order to investigate the origin of this behavior, we have performed Dynamical Density-Matrix-Renomalization-Group (DDMRG) calculations at zero temperature and Quantum Monte Carlo (QMC) calculations at finite temperatures for the single-particle spectral weight of the doped one-dimensional (1D) Hubbard model. We present DDMRG and QMC results for a range of the model parameters of the 1D Hubbard model and make comparisons with the photoemission data. In addition, we present zero-temperature DDMRG results on the doped 1D Hubbard-Holstein model in order to explore how the electron-phonon coupling influences the single-particle spectrum in 1D correlated conductors.

**12:39**

**P44 8 Multiple spin sites in an organic conductor without magnetic ions.*** TAKAHISA TOKUMOTO, *FSU/NHMFL* YUGO OSHIMA, *Tohoku University, Japan* DAVID GRAF, *NHMFL* JAMES BROOKS, *FSU/NHMFL* JOHAN VAN TOL, *NHMFL* LOIUS-CLAUDE BRUNEL, *NHMFL* GEORGE PAPAVASSILIOU, *National Hellenic Research Foundation, Greece* The anisotropic low dimensional organic conductors are attractive because of the variety of ground states with unusual and exotic electronic properties. One of them is tau-[P-($S$, $S$)-DMEDT-TTF]$_2$($AuBr_2$)$_{1+y}$ [where y~ 0.75 and P-($S$, $S$)-DMEDT-TTF stands for pyrazino-($S$, $S$)-dimethyl-ethylenedithio-tetrathiafulvane], which has tetragonal crystal structure with unit cell dimensions **a**=**b**=7.3546 Å and **c**=67.977 Å[1]. Even though there are no magnetic ions in the

compound, transport measurements show magnetic ordering at low temperature and in magnetic fields. To investigate the origin of the magnetic behavior, we are conducting an ESR study. We do observe multiple resonances which indicate the existence of the multiple spins although the system does not contain magnetic ions. Moreover, the in-plane angular dependent ESR measurements reveal 4 fold symmetry. Both in-plane and out of plane ESR signal show evidence of antiferromagnetic behavior below 12 K. It is possible that the ion stoichiometric charge transfer (1+y) is the origin of the magnetic effects. Further analysis will be presented.

*This work is supported by NSF-DMR 0203532 and NSF-DMR 0520481

**12:51**

**P44 9 Investigating the Charge Ordering Pattern in the Organic Spin Ladder $(DT\text{-}TTF)_2Cu(mnt)_2$*** S. BROWN, J. T. HARALDSEN, J. CAO, J. L. MUSFELDT, *University of Tennessee, Knoxville* M. MAS-TORRENT, C. ROVIRA, *Institut de Ci ència de Materials de Barcelona, Spain* J. C. DIAS, R. T. HENRIQUES, M. ALMEIDA, *Instituto Tecnológico e Nuclear, Portugal* Quantum spin ladders have attracted considerable interest as intermediaries between one-dimensional chains and two- dimensional square lattices. In order to elucidate the charge ordering pattern in a model organic spin ladder, we measured the temperature-dependent infrared spectra of the organic spin- ladder candidate $(DT\text{-}TTF)_2Cu(mnt)_2$. We interpret the results within the context of recent theoretical predictions of various charge ordering patterns in spin ladders [1]. Comparision with spectra of the isostructural Au analogue and neutral DT-TTF compound aid in this analysis. [1] R. T. Clay, S. Mazumdar, Phys. Rev. Lett. **94**, 207206 (2005)

*This work is supported by the NSF.

**13:03**

**P44 10 Magnetic field effects on the coexisting Bond-Charge-Density waves in the quasi-one-dimensional quarter-filled bands*** SUMIT MAZUMDAR, *University of Arizona* R. TORSTEN CLAY, *Mississippi State University* Magnetic field effects on spin-Peierls systems have been of interest for a long time. The theoretical phase diagram consists of three different regions containing the homogenous dimerized and undimerized phases, and a magnetic phase consisting of a soliton lattice or an incommensurate phase. We have investigated numerically spin excitations and magnetic field effects on the bond-charge-density wave (BCDW) that appears below the spin-Peierls transition in the quarter-filled band organic charge transfer solids (CTS), with the specific goal of determining whether the simplest phase diagram, obained within the spin model, applies also to the quarter-filled band where both charge and spin degrees of freedom exist. We also discuss recent experiments in quarter-filled band CTS within the context of our theory.

*Supported by NSF-DMR-0406604 and the PRF-ACS.

**13:15**

**P44 11 Temperature dependent competition between charge-ordering and spin-Peierls transition in $(TMTTF)_2X$: the role of quantum phonons*** R. T. CLAY, *Mississippi State University* R. P. HARDIKAR, *Mississippi State University* S. MAZUMDAR, *University of Arizona* The $(TMTTF)_2X$ salts are quasi-one-dimensional materials with complex phase diagrams that feature a large number of ordered states including superconductivity. The ground states of these materials are often spin-Peierls (SP) states. However, at intermediate temperatures (100 K) a transition to a charge ordered state is also present, which may compete with the ground state SP ordering. We investigate numerically models for these materials that include three components: electronic interactions, bond-coupled phonons, and Holstein-type phonons coupled to the local charge density. These three components have different energy scales are hence expected to dominate at different temperatures. We explicitely include finite phonon frequency in our calculations using quantum Monte Carlo methods. We present charge, spin, and bond susceptibilities as a function of temperature and discuss recent experiments on these materials.

*Supported by the Petroleum Research Fund and NSF-DMR-0406604

**13:27**

**P44 12 Discrete breather energy thresholds in Discrete Nonlinear Schrodinger (DNLS) systems Discrete breather energy thresholds in Discrete Nonlinear Schrodinger (DNLS) systems** JUN ZHOU, JEROME DORIGNAC, DAVID CAMPBELL, *Boston University* The DNLS equation has been used successfully to model physical systems as varied as the Holstein polaron, the Davydov soliton, local modes of small molecules and, more recently, optical wave guide arrays and Bose-Einstein condensates trapped in optical lattices. In addition, the DNLS also governs the slow modulations of plane waves in Klein-Gordon systems (network of oscillators). In one dimension and for a cubic nonlinearity, the DNLS is known to support discrete breather solutions - time-periodic, spatially localized excitations - with arbitrary low energy (or norm). In contrast, for higher nonlinearities or in higher dimensions, an energy (norm) threshold is known to exist, below which discrete breathers cannot be found. Using two different approaches to treat the DNLS equation–namely, an exponential ansatz and the so-called ''single nonlinear impurity'' approximation– we derive analytical expressions for these energy thresholds and compare them to the exact numerical solutions.

**13:39**

**P44 13 Bipolaron phase diagram of the 1D adiabatic Holstein-Hubbard model in the strong coupling limit** JEROME DORIGNAC, JUN ZHOU, DAVID CAMPBELL, *Boston University* We derive the phase diagram for bipolarons in the one-dimensional adiabatic Holstein-Hubbard model in the strong coupling (small hopping) limit. We show the existence of a threshold value for the Coulomb interaction beyond which the ground state of the system consists of two free polarons (infinitely far apart from each other). This result, obtained by means of an exact perturbative expansion, cannot be reproduced by the usual exponential ansatz for the wave function.

**13:51**

**P44 14 First-Principles Study of Electronic Structure in $\alpha$-$(BEDT\text{-}TTF)_2I_3$ at Ambient Pressure and under Uniaxial Strains.*** HIORI KINO, *National Institute for Materials Science* TSUYOSHI MIYAZAKI, We calculate the electronic structure of $\alpha$-$(BEDT\text{-}TTF)_2I_3$ at 8K and room temperature at ambient pressure and under the uniaxial strains along the a- and a-axes within the density functional theory. We discover itanisotropic Dirac cone dispersion near the chemical potential. We also extract the orthogonal tight binding parameters to analyze physical properties. An investigation of the electronic structure near the chemical potential clarify that effects of the uniaxial strain along the a-axis is

different from that along the b-axis. The Dirac cone dispersion yields the linear density of states to give $T^2$ dependence of the carrier density upto about 100K. It may explain the experimental findings not only qualitatively but also quantitatively.

*This work is partially supported by a Grant-in-Aid for Scientific Research on Priority Areas of Molecular Conductors (No. 16038227) of MEXT of the Japanese Government.

**14:03**

**P44 15 Power-law Current-Voltage Characteristics of Charge-Ordered Organic Crystals $\theta$-(BEDT-TTF)$_2$MZn(SCN)$_4$ (M =Cs, Rb)** YAMAGUCHI TAKAHIDE, TAKAKO KONOIKE, KENGO ENOMOTO, MITSUKA NISHIMURA, TAICHI TERASHIMA, SHINYA UJI, *National Institute for Materials Science, Japan* HIROSHI M. YAMAMOTO, *RIKEN(The Institute of Physical and Chemical Research), Japan* We have measured the current-voltage characteristics of charge- ordered organic crystals $\theta$-(BEDT-TTF)$_2$MZn(SCN)$_4$ (M=Cs, Rb) in a low current range down to $10^{-13}$ A. The current-voltage characteristics follow the power law $I \propto V^a$ with a large exponent (e.g., $a = 8.4$ at 0.3 K for M=Cs) over a wide range of currents. The power-law characteristics are attributed to electric field-induced unbinding of electron- hole pairs which are thermally excited in the background of the two-dimensional charge order. From analysis of crossover electric fields from ohmic to the power-law characteristics, we obtain strong evidence that the electron-electron Coulomb interaction is significantly long-ranged, i.e., the screening length is greater than 10 molecule sites. A novel magnetoresistance effect, possibly due to the Pauli exclusion principle, is also presented.

**SESSION P45: STRUCTURAL AND FERROELECTRIC PHASE TRANSITIONS**
**Wednesday Morning, 15 March 2006**
**348, Baltimore Convention Center at 11:15**
**Pavel Krotkov, University of Maryland, presiding**

**11:15**

**P45 1 Structural symmetry of $Cd_2Re_2O_7$ from nonlinear optics** JESSE C. PETERSEN, MICHAEL D. CASWELL, J. STEVEN DODGE, *Department of Physics, Simon Fraser University, Burnaby, British Columbia, Canada* JIAN HE,*DAVID MANDRUS, *Department of Physics and Astronomy, The University of Tennessee, Knoxville and Solid State Division, Oak Ridge National Laboratory* $Cd_2Re_2O_7$, a superconducting metallic pyrochlore, undergoes a second-order structural phase transition at 200 K from a cubic to tetragonal lattice. Landau theory predicts that any second-order cubic-to-tetragonal phase transition must also possess an order parameter associated with broken inversion symmetry. By observing optical second-harmonic generation, we provide a direct demonstration that the 200 K transition in $Cd_2Re_2O_7$ involves broken inversion symmetry. Moreover, we have used the polarization dependence of SHG to refine the crystal structure. We find that the low-temperature crystal symmetry is that of the $F\bar{4}2m$ space group.

*Now with Department of Physics and Astronomy, Clemson University, Clemson, SC

**11:27**

**P45 2 X-ray absorption spectroscopy on the phase transition of $Cd_2Re_2O_7$** SHIH-WEN HUANG, *Department of Electrophysics, National Chiao Tung University* J. M. CHEN, *National Synchrotron Radiation Research Center* H. T. JENG, *Institute of Physics, Academia Sinica* J-Y LIN, *Institute of Physics, National Chiao Tung University* J. M. LEE, *National Synchrotron Radiation Research Center* H. D. YANG, *Department of Physics, National Sun Yat Sen University* KENG LIANG, *National Synchrotron Radiation Research Center* H. BERGER, *Department of Physics, EPF Lausanne, CH-1015 Lausabbe* Pyrochlore $Cd_2Re_2O_7$ has received considerable attention and investigated extensively because of its manifold phase transitions accompanied by profound physical properties. In this study, the relations among the electronic structure, phase transition, and some physical properties of $Cd_2Re_2O_7$ single crystals have been investigated. We conducted the X-ray diffraction as well as Re $L_{2,3}$-edge extended X-ray absorption fine structure (EXAFS) at different temperatures to investigate the local structure of $Cd_2Re_2O_7$ and temperature-dependent O $K$-edge X-ray absorption near edge structure (XANES) to probe its electronic structure during the phase transition. We also performed the band structure calculations to understand the DOS near the Fermi level of $Cd_2Re_2O_7$ at different temperatures.

**11:39**

**P45 3 Pressure effects on a low carrier density metal's infrared response** N. PETER ARMITAGE, *University de Geneve* RICCARDO TEDIOSI, *University de Geneve* LASZLO FORRO, *Ecole Polytechnique Federale de Lausanne* DIRK VAN DER MAREL, *University de Geneve* We have performed pressure and temperature dependent infrared studies of semi-metal bismuth. Along with other semi-metals such as graphite and antimony, bismuth is a material of much current interest due to the interesting properties resulting from an extremely low carrier density, small effective mass, and long mean free path. A novel optical setup has been developed to measure low temperature infrared responses at pressures of up to 17kbar. We observe massive changes in bismuth's optical and infrared conductivity as a function of temperature and pressure. We discuss the origin of these changes both in terms of simple band structure effects, as well as in terms of the correlation effects that are expected in this very low-carrier density metal.

**11:51**

**P45 4 Ferroelectric phase transition in the incommensurate phase of the $K_2SeO_4$ crystal** TIGRAN ASLANYAN, *Institute for Physical Research, Armenian National Academy of Sciences* It is shown that in the incommensurate (IC) phase of the $K_2SeO_4$ crystal a phase transition takes place to the ferroelectric IC phase, prior to the lock-in transition to the triple-period commensurate phase. Such a behavior is due to the Lorentz microscopic electric field, which is induced by the IC domains on approaching the lock-in transition temperature. The proposed behavior of the $K_2SeO_4$ crystal explains the second-harmonic generation, observed in the IC phase, near the lock-in transition. It explains also the observed drop in the crystal's elastic constant c55 near the lock-in transition, which corresponds to a significant decrease of the z-polarized sound velocity in the x-direction. Continuous increasing of the polarization in the ferroelectric IC phase manifests itself as a continuous decreasing of the sound velocity. In the same

model one can explain also the observation of an overdamped Raman scattering in the z(xz)y geometry in the low temperature range of the IC phase existence. Dielectric properties of the ferroelectric crystals with artificially fabricated domains are discussed.

**12:03**

**P45 5 Normal and superconducting state properties of the $(Pr_{1-x}Nd_x)Os_4Sb_{12}$ system*** PEI-CHUN HO, WILLIAM YU-HASZ, TATSUYA YANAGISAWA, NEIL FREDERICK, NICHOLAS BUTCH, TODD SAYLES, JASON JEFFRIES, BRIAN MAPLE, *Physics & IPAPS/UCSD* YUICHI NEMOTO, TERUTAKA GOTO, *Grad. Sch. Sci. & Tech./Niigata U., Japan* Our previous experimental studies of the $(Pr_{1-x}Nd_x)Os_4Sb_{12}$ system revealed that: (1) superconductivity and ferromagnetism from both end compounds were suppressed almost monotonically toward $x = 0.55$, (2) retention of the antiferroquadrupolar order phase in $(Pr_{1-x}Nd_x)Os_4Sb_{12}$ to higher values of $x$ than in $Pr(Os_{1-x}Ru_x)_4Sb_{12}$, (3) two possible CEF energy level schemes in $NdOs_4Sb_{12}$, in which the ground state is either the $\Gamma_6$ doublet or $\Gamma_8^{(2)}$ quartet. Recent ultrasonic measurements in the $NdOs_4Sb_{12}$ sample ($x = 1$) revealed softening of the $C_{44}$ mode, which indicated that the CEF ground state in this compound is more likely to be the $\Gamma_8^{(2)}$ quartet. The lattice parameter in $(Pr_{1-x}Nd_x)Os_4Sb_{12}$ seems to increase slightly from $PrOs_4Sb_{12}$ ($x = 0$) toward $NdOs_4Sb_{12}$ ($x = 1$). The T-x and H-x phase diagrams related to superconductivity, ferromagnetism, antiferroquadrupolar order, and the CEF energy level scheme for the $(Pr_{1-x}Nd_x)Os_4Sb_{12}$ system for $0 \leqslant x \leqslant 1$ will be discussed.

*The research at UCSD is funded by U.S. DOE and NSF; the research at Niigata U. is supported by the Grant-in-Aid for Scientific Research Area ''Skutterudites'' of MEXT, Japan.

**12:15**

**P45 6 Elastic properties of ferromagnetic heavy fermion system $SmOs_4Sb_{12}$** YOSHIKI NAKANISHI, TOMOAKI TANIZAWA, TAKUYA FUJINO, ATSUSHI SUGIHARA, PEIJIE SUN, MASAHITO YOSHIZAWA, *Graduate School of Engineering, Iwate University* HITOSHI SUGAWARA, *Faculty of Integrated Arts and Sciences, The University of Tokushima* DAISUKE KIKUCHI, HIDEYUKI SATO, *Deoartment of Physics, Tokyo Metropolitan University* We report the elastic constants of the heavy fermion system $SmOs_4Sb_{12}$ by means of an ultrasonic measurement. A steep decrease associated with the ferromagnetic transition was observed at around 2 K in elastic constants C11, (C11-C12)/2 and C44. Furthermore a characteristic increase, possibly due to the ''rattling-motion'' was observed around 15 K in the elastic constants. The variation of the onset temperature and a degree of the increase as a function of the ultrasonic frequency is reasonably reproduced in terms of the Debye-type dispersion. The obtained parameters describing the rattling-motion such as a relaxation time, an activation energy and a mean square displacement will be discussed as compared with those of an isostructural compound $PrOs_4Sb_{12}$.

**12:27**

**P45 7 High-Energy X-Ray Study of Short Range Order and Phase Transformations in Ti-V** INGO RAMSTEINER,*ANDREAS SCHOEPS, HARALD REICHERT, HELMUT DOSCH, *Max-Planck-Institute for Metals Research Stuttgart, Germany* Phase transformations, especially precipitation processes, are a key factor in alloy design. Understanding these processes in the framework of statistical thermodynamics requires knowledge about the atomic interaction potentials between the alloy constituents. Experimentally, these parameters can be accessed via the diffuse x-ray scattering caused by the configurational short range order and lattice distortions. We employ a bulk sensitive high energy technique to study both phenomena simultaneously in situ, probing macroscopic single crystals in transmission geometry. The data recorded by a 2D detector reveal Bragg reflections from the precipitates superimposed on the diffuse scattering of the matrix. We present a detailed study of bcc Ti-V, a typical titanium $\beta$-alloy. The diffuse scattering is mainly due to lattice distortions induced by the atomic size mismatch. Depending on the annealing temperature, growth and dissolution of hcp $\alpha$-Ti precipitates and minute fractions of TiC are observed. HRTEM experiments have been conducted to complement our results.

*New Affiliation (2006): Harvard University, Cambridge MA, USA

**12:39**

**P45 8 Reversible Magnetostriction with Temperature in Single Crystal $Tb_5Si_{2.2}Ge_{1.8}$** A.P. RING, H.L. ZIEGLER, T. LOGRASSO, D. SCHLAGEL, J.E. SNYDER, *Materials and Engineering Physics Program, Ames Laboratory* D.C. JILES, *Wolfson Centre for Magnetics, Cardiff University, Cardiff, Wales, UK* The magnetostriction changes that accompany the phase transitions of single crystal $Tb_5(Si_{2.2}Ge_{1.8})$ have been investigated at temperatures between 20 K and 150 K, by measurements of the reversible component of the magnetostriction along the crystallographic ''a'' axis. Over this temperature range the shape and slope of the magnetostriction curves change, which are indicative of changes in the magnetic state, crystal structure and magnetic anisotropy. Results show a phase transition that occurs near 106 K (onset-completion range 100 - 116 K). The abrupt nature of the strain transition, its unusual hysteresis, and its temperature dependence appear to indicate a first order phase transition which can be activated by applied magnetic field or temperature. Magnetostriction measurements at temperatures below the transition region show a magnetostriction of small overall magnitude but with a high, temperature dependent anisotropy. Funded by USDoE-Office of Basic Energy Sciences

**12:51**

**P45 9 Magnetic phase transition and spin dynamics in Li(Ni1-xFex)PO4** JIYING LI, DAVID VAKNIN, JEREL ZARESTKY, *Ames Laboratory and Department of Physics and Astronomy, Iowa State University, Ames IA 50011* JAE-HO CHUNG, *NIST Center for Neutron Research, National Institute of Standards and Technology, Gaithersburg, MD 20899* Elastic and inelastic neutron scattering techniques were used to study the magnetic phase transition and spin dynamics in pure and Fe substituted LiNiPO4 single crystals. Pure LiNiPO4 undergoes a first-order magnetic phase transition from a long- range ordered incommensurate phase to an antiferromagnetic ground state at TN = 20.8 K. With the substitution of Fe for Ni, the magnetic phase transition changes from first-order to second-order, and moreover, the long-range ordered incommensurate phase of pure LiNiPO4 between 20.8 K to 21.5 K was suppressed in the LiNi0.75Fe0.15PO4 sample. Inelastic neutron scattering revealed a 2 meV energy gap and an anomalous soft mode in the spin wave dispersion curve along the [010] direction for pure LiNiPO4. For LiNi0.8Fe0.2PO4, however, the energy gap was reduced to 0.9 meV and the anomaly along the [010] direction reduced. The spin-wave dispersion curves were simulated using a Heisenberg Hamiltonian with Dzyaloshinski-Moriya interactions.

**13:03**

**P45 10 Phonon Anomalies in the Martensitic Phase of $Ni_2MnGa$*** S.M. SHAPIRO, *Brookhaven National Laboratory, Upton, NY* P. VORDERWISCH, *Hahn-Meitner Institute, Berlin, Germany* K. HRADIL, H. SCHNEIDER, *ICP, U. of Goettingen, Germany* $Ni_2MnGa$ is a cubic ferromagnetic shape memory alloy exhibiting phonon anomalies as precursors to the Martensitic phase transformation. By cooling in a small magnetic field (1.5T) through its transformation temperature it is possible to obtain a single domain of the tetragonal Martensite phase. One can, therefore, measure the phonon dispersion curves in the Martensite phase and compare them to the high temperature cubic phase. The TA branch propagating along the [qq0], with polarization along [q-q0], shows an anomaly near the wavevector of the charge density wave (CDW) peak at q=0.425, which differs from q=0.33 observed in the cubic phase. Most interesting is a new acoustic-like branch emerging from the CDW peak. This will be discussed in relationship to phasons and amplitude modes observed in other incommensurate systems.

*Work at Brookhaven supported by US-DOE under contract No. DE-AC02-98CH10886

**13:15**

**P45 11 Medium-range Structure of $La_{2-x}Sr_xCuO_4$ ($0.0 < x < 0.3$) by Pulsed Neutron PDF Analysis** JIN NAKAMURA, *University of Tennessee* THOMAS PROFFEN, *Los Alamos National Laboratory* TAKESHI EGAMI, *University of Tennessee and Oak Ridge National Laboratory* We studied the local and medium-range atomic structure in high- temperature superconductor (HTSC) $La_{2-x}Sr_xCuO_4$ ($0.0 < x < 0.3$) by the pulsed neutron pair-density function (PDF) analyses. The measurement was made with the NPDF of LANSCE, LANL. Because of the high $Q$-resolution of the NPDF the PDF was determined up to 20 $nm$. The measured PDF was compared with that calculated for the average structure determined by the Rietveld analysis of the same data. We found that the measured PDF deviates from the calculated PDF in two different ways. For $x = 0.16$ - 0.3 deviations were seen up to about 3 $nm$, strongly related to the oxygen in the $CuO_2$ plane displaced along the $c$-axis. These deviations reflect local fluctuations between the orthorhombic and tetragonal phases. A more interesting deviations were seen for $x = 0.04$ - 0.16 up to 2 $nm$ for all compositions. The lengthscale of this local fluctuation corresponds to the in-plane coherence length, suggesting that the structure that supports HTSC may be different from the average structure, and the size of the local domains is not limited by the dopant concentration. Further implications are discussed.

**13:27**

**P45 12 Inelastic neutron scattering study of $YBaFe_2O_5$** SUNG CHANG, *Ames Laboratory* P. KAREN, *Department of Chemistry, University of Oslo* M. P. HEHLEN, F. R. TROUW, *Los Alamos National Laboratory* R. J. MCQUEENEY, *Department of Physics and Astronomy and Ames Laboratory* $YBaFe_2O_5$ belongs to a new class of oxides with the chemical formula $RBaM_2O_5$ ($R$ = rare-earth, $M$ = transition metal), based on the perovskite structure with a doubled unit cell pyramids of five-coordinated $M$-sites. The $M$-site is mixed valent in the stoichiometric formula unit (with an average valence of +2.5). Therefore, charge and orbital ordering phenomena can exist on the $M$-site and be studied without introducing disorder. The charge ordered phase of $YBaFe_2O_5$ is unusual, since it does not satisfy the Anderson criterion (i.e. it is not the lowest energy electrostatic arrangement of charges), but rather orders into alternating chains of 2+/3+. This indicates that other interactions, such as electron-phonon coupling, are necessary to arrive at the chain structure. Here, we present the results of an inelastic neutron scattering study of polycrystalline $YBaFe_2O_5$. We find the spectrum of phonon and magnetic excitations are clearly modified at the charge- and magnetic ordering temperatures: $T_{CO} = 308$ K and $T_N = 430$ K, respectively.

**SESSION P46: FQHE**
**Wednesday Morning, 15 March 2006**
**349, Baltimore Convention Center at 11:15**
**Dmitri Feldman, Brown University, presiding**

**11:15**

**P46 1 Measuring Exchange Interactions by Tunneling Deep Into the Quantum Hall Liquid** O.E. DIAL, R.C. ASHOORI, *Massachusetts Institute of Technology, Cambridge, MA 02139* L.N. PFIEFFER, K.W. WEST, *Bell Laboratories, Lucent Technologies, Murray Hill, New Jersey 07974, USA* We present measurements of the tunneling density of states of a two dimensional electron gas (2DEG) in GaAs at energies up to 10 meV above and below the Fermi energy. Using time domain capacitance spectroscopy (TDCS), we determine the current-voltage (IV) characteristics for tunneling perpendicularly between a gated 2DEG and a 3D electron continuum separated by a thin tunneling barrier. In TDCS, sharp pulses are applied to the sample while measuring displacement currents from electrons entering or leaving the 2DEG, allowing tunneling IV measurements without direct electrical contact to the 2DEG. We observe changes in the Landau level structure far from the Fermi surface as we fill and empty individual Landau levels by varying the electron density and magnetic field. This provides a unique measurement of the exchange enhanced spin splitting of empty and filled Landau levels.

**11:27**

**P46 2 Thermal Dephasing in the Laughlin Quasiparticle Interferometer** F.E. CAMINO, WEI ZHOU, V.J. GOLDMAN, *Stony Brook University* We report experiments on thermal dephasing of the Aharonov-Bohm oscillations in the novel Laughlin quasiparticle (LQP) interferometer, [1] where quasiparticles of the 1/3 FQH fluid execute a closed path around an island of the 2/5 fluid. In the $10.2 \leqslant T \leqslant 141$ mK temperature range, qualitatively, the experimental results follow a thermal dephasing dependence expected for an electron interferometer, and show clear distinction from the activated behavior observed in resonant tunneling and Coulomb blockade devices, both in the chiral Luttinger liquid ($\chi$LL) and the Fermi liquid regimes. The data fit very well the $\chi$LL dependence predicted for a $g = 1/3$ two point-contact LQP interferometer. [2] The fit yields a value of the chiral edge excitation velocity, $u = 1.4 \times 10^4$ m/s obtained for the first time for a continuous FQH edge excitation spectrum. The small deviation from the zero-bias theory seen below 20 mK indicates yet unrecognized source of experimental decoherence, not included in theory. [1] F. E. Camino et al., Phys. Rev. B **72**, 075342 (2005). [2] C. de C. Chamon et al., Phys. Rev. B **55**, 2331 (1997).

**11:39**

**P46 3 Flux Period Scaling in the Laughlin Quasiparticle Interferometer** WEI ZHOU, F.E. CAMINO, V.J. GOLDMAN, *Stony Brook University* Aharonov-Bohm superperiod was rececently reported for electron interferometer devices in the quantum Hall regime, where electron paths circle a 2D electron island. The electron island main confinement is produced by etch trenches, into which front gate metal is deposited. We determine experimentally the A-B period $\Delta_B$ at several front gate voltages $V$ for electrons ($f = 1$) and Laughlin quasiparticles (2/5 embedded in 1/3). For moderate $|V| \leqslant 300$ mV, on each QH plateau, we find linear dependence of $\Delta_B$ on $V$. For $f = 1$, the electron A-B path area $S$ can be found from $\Delta_B$ using flux quantization condition $\Delta_\Phi = S\Delta_B = h/e$ for the flux period $\Delta_\Phi$. The A-B area enclosed by the $f = 1/3$ edge channel (the 2/5 island area) is not known independently if the FQH flux period is not known a priory. The front gate voltage dependence of $\Delta_B$ provides such independent determination of the 2/5 island area. The directly measured values of $\Delta_B$ and its slope $d\Delta_B/dV$ can be combined to derive the voltage $V(1e)$ attracting a unit charge to the area of the A-B path, assuming $S$ is known. For a many-electron ( $\sim$ 2000) 2D disc of radius $r$, the product $rV(1e)$ should be approximately constant, independent of the QH filling or the area. Thus the $f = 2/5$ island area can be determined directly with a $\sim$ 10% accuracy, which is quite sufficient to distinguish the physically reasonable possibilities of the flux periods $5h/e$, $5h/2e$, $1h/e$, and $h/2e$.

**11:51**

**P46 4 Extracting fractional statistics from superperiodic Aharonov-Bohm oscillations** EUN-AH KIM, STEVEN KIVELSON, *Stanford University* We consider a quantum Hall interferometer in which the quasiparticles of a fractional quantum Hall (FQH) liquid with filling factor $\nu_1 = 1/3$ propagate around a large ring of radius $r_1$, which is encircles an island with a smaller radius $r_2$ occupied by FQH liquid with filling factor $\nu_2 = 2/5$. We study the conductance oscillations that result from the incompressibility of the FQH liquid occupying the island and the constructive interference condition for the quasiparticles encircling the outer ring. Since the constructive interference condition depends on both the magnetic flux enclosed by the encircling path and the statistical phase gained by the encircling quasiparticle due to the presence of quasiparticles in the island, such conductance oscillations can be used to detect signatures of fractional statistics. We find that oscillatory period depends on both radii, $r_1$ and $r_2$. We discuss the relation between our results and the recent experiments by F.E. Camino, W. Zhou and V.J. Goldman in the context of our model.

**12:03**

**P46 5 Resonant tunneling in fractional Hall effect** CHUNTAI SHI, *Department of Physics,104 Davey lab,The Pennsyvania State University* JAINENDRA JAIN, *Department of Physics,104 Davey lab,The Pennsyvania State University* We study theoretically the possible transitions of a fractional quantum Hall island surrounded by another fractional quantum Hall state, induced by either the variation of the magnetic field or a backgate voltage, and find a rich set of possibilities in addition to the one considered previously[1],The elementary transitions correspond to the addition or removal of a composite fermion from the edge or the interior of the island; combinations of elementary transitions may occur simultaneously due to electrostatic constraints. Relevance to a recent experiment[2] is considered, which measures the resonant tunneling of composite fermions through their quasi-bound states around such a 2/5 island surrounded by the 1/3 sea. It is shown that the results are consistent with the notion of fractional braiding statistics, but can be explained on the basis of fractional charge alone. We also perform calculations based on microscopic composite fermion wavefunctions of finite systems to test the theoretical considerations. [1]J.K.Jain, S.A.Kivelson, and D.J.Thouless, Phys.Rev.Lett.**71**, 3003(1993). [2]F.E.Camino, W.Zhou, and V.J.Goldman, Phys.Rev.B **72**, 075342(2005).

**12:15**

**P46 6 Electronic Mach-Zehnder interferometer as a tool to probe fractional statistics** KAM TUEN LAW, DIMA FELDMAN, *Brown University* YUVAL GEFEN, *Weizmann Institute of Science* We study transport through an electronic Mach-Zehnder interferometer recently devised at the Weizmann Institute. We show that this device can be used to probe statistics of quasiparticles in the fractional quantum Hall regime. We calculate the tunneling current through the interferometer as the function of the Aharonov-Bohm flux and voltage bias, and demonstrate that its flux-dependent component is strongly sensitive to the statistics of tunneling quasiparticles.

**12:27**

**P46 7 Pauli-like principle for Abelian and non-Abelian FQHE quasiparticles*** F. D. M. HALDANE, *Princeton University* A general formulation of condensed matter physics describes the Hamiltonian as $H_0 + H_1$, where $H_0$ is a positive ''topological'' Hamiltonian with a highly-degenerate zero-energy ground state (extensive $T = 0$ entropy) and $H_1$ is the ''physical'' Hamiltonian that splits this huge multiplet. Usually, $H_0$ is a non-interacting Hamiltonian, with zero modes that form a simple Fock space spanned by Wannier orbitals of low-energy electron bands, or a Landau level, etc. Systems of Laughlin FQHE quasiholes are described by a more general $H_0$ that removes low-relative-angular momentum two-particle states from the zero-mode spectrum, and the non-Abelian Moore-Read and Read-Rezayi quasihole systems involve removal of $n > 2$ particle states. The latter are candidates systems for topological quantum computation. The zero-modes count has been previously obtained by counting the number of linearly-independent polynomials of various types. I give a simpler Pauli-principle-like formulation that transparently gives the counting rules, and allows the creation of subsets of lowest-Landau-level Slater determinant states from which the zero-mode states can be constructed. This aids numerical diagonalization of $P_0H_1P_0$, where $P_0$ is the projection into the zero-modes space of $H_0$, for exact-diagonalization simulations of the manipulations of non-Abelian quasiparticles proposed for topological quantum computations.

*Supported by NSF MRSEC DMR-0213706

**12:39**

**P46 8 Quantitative study of the non-Abelian statistics of quasiholes and quasiparticles in the nu=5/2 paired Hall state** CSABA TOKE, JAINENDRA JAIN, *Penn State University* We analyze quantitatively various properties of a collection of quasihole and quasiparticle excitations of the paired composite fermion state, described by a Pfaffian wave function proposed by Moore and Read (Nucl.Phys.B 360, 362, 1991), which are relevant to the validity of the notion of non-abelian braiding statistics. Working in the spherical geometry, we study the coupling of two quasiholes as a function of their distance by evaluating both the density profile and the interaction energy of a quasihole pair. Further, we perform a numerical study to check whether the $2^{n-1}$ independent

states of $2n$ quasiholes are almost degenerate, i.e. the coupling between these states is exponentially suppressed as a function of their separation, which will be crucial for any practical realization of non-Abelian statistics. We also compare the exact diagonalization spectra of the Coulomb interaction in the second Landau level and the model three-body contact interaction for which the Pfaffian state and its quasihole variants are known to be exact. Based on the connection between Halperin's 331 state and the Pfaffian state (Greiter, Wen, and Wilczek, PRL 66, 3205, 1991) we construct a class of quasiparticle wave functions, which we study with respect to both the three- body contact interaction and the Coulomb interaction to test their accuracy.

**12:51**

**P46 9 Probing Non-Abelian Statistics in the $\nu = 5/2$ Fractional Quantum Hall State** PARSA BONDERSON, *Caltech* ALEXEI KITAEV, *Caltech* KIRILL SHTENGEL,* *shtengel@physics.ucr.edu* We analyse an interferometric experiment to detect non-Abelian quasiparticle statistics – one of the hallmark characteristics of the Moore-Read state expected to describe the observed FQHE plateau at $\nu = 5/2$. The implications for using this state for constructing a topologically protected qubit as has been recently proposed by Das Sarma, Freedman and Nayak are also addressed.

*UC Riverside

**13:03**

**P46 10 Composite fermions and conformal field theory*** SUSANNE VIEFERS, *University of Oslo, Norway* HANS HANSSON, *Stockholm University, Sweden* JAINENDRA JAIN, CHIACHEN CHANG, *Penn State University* JON MAGNE LEINAAS, *University of Oslo, Norway* We show how Quantum Hall quasiparticle wave functions similar to those in the composite fermion theory are related to correlators of certain nonlocal operators in a conformal field theory. Charge and statistics are determined using both analytical and numerical methods.

*This work was supported in part by NordForsk and by the Instiute for Theoretical Sciences, a joint institute of Argonne National Laboratory and the University of Notre Dame through DOE contract W-31-109-ENG-38 and Notre Dame Office of Research.

**13:15**

**P46 11 An Exact Solution for the Half-filled Lowest Landau Level** EMIL BERGHOLTZ, ANDERS KARLHEDE, *Stockholm University* We present an exact solution for the interacting electron gas in the half-filled lowest Landau level on a thin torus. The low energy sector consists of non-interacting, one-dimensional, neutral fermions (dipoles). The ground state, which is homogeneous, is the Fermi sea obtained by filling the negative energy states and the excited states are the gapless neutral excitations out of this one-dimensional sea. We identify this ground state as a version of the Rezayi-Read state, and find that it develops continuously, as the circumference grows, into the Rezayi-Read state that is believed to describe the observed metallic phase in the two-dimensional system. This suggests a Luttinger liquid description of the half-filled Landau level.

**13:27**

**P46 12 One-Dimensional Theory of the Quantum Hall System** ANDERS KARLHEDE, EMIL J. BERGHOLTZ, *Stockholm University* We consider the lowest Landau level on a torus as a function of its circumference $L_1$. When $L_1 \to 0$, the ground state at general rational filling fraction is a crystal with a gap—a Tao-Thouless state. For filling fractions $\nu = p/(2pm + 1)$, these states are the limits of Laughlin's or Jain's wave functions describing the gapped quantum Hall states when $L_1 \to \infty$. For the half-filled Landau level, there is a transition to a Fermi sea of non-interacting neutral dipoles, or rather to a Luttinger liquid modification thereof, at $L_1 \sim 5$ magnetic lengths. This state is a version of the Rezayi-Read state, and develops continuously into the state that is believed to describe the observed metallic phase as $L_1 \to \infty$. Furthermore, the effective Landau level structure that emerges within the lowest Landau level follows from the magnetic symmetries.

**13:39**

**P46 13 Competing liquid and solid orders at $\nu = 1/5$** CHIACHEN CHANG, CSABA TOKE, *Department of Physics, The Pennsylvania State University* GUN SANG JEON, *School of Physics, Seoul National University, Seoul, Korea* JAINENDRA K. JAIN, *Department of Physics, The Pennsylvania State University* The lowest Landau level states at very low filling factors are accurately understood as topological quantum crystals of composite fermions. At higher fillings (but still in the lowest Landau level), on the other hand, the system forms an incompressible composite-fermion liquid. However at $\nu = 1/5$, both descriptions fail to give an accurate account to the true ground state. Our numerical calculations show that for small systems the crystal has lower energy than the liquid, and only for $N \geqslant 10$ does the liquid become the ground state. We find that a linear combination of the CF liquid and the CF crystal wave functions provides an excellent account of the actual state for small systems. These results indicate that the 1/5 fractional Hall state is highly susceptible to the formation of composite fermion crystallites in it. We will discuss the relevance of these results to experiment, and also the possibility of inducing a liquid-solid transition at 1/5 by tuning the interaction.

**13:51**

**P46 14 Electric field effects in the Hall conductivity*** ALEJANDRO KUNOLD, *Departamento de Ciencias Básicas, Universidad Autónoma Metropolitana-Azcapotzalco, Av. San Pablo 180, México D. F. 02200, México* MANUEL TORRES, *Instituto de Física, Universidad Nacional Autónoma de México, Apartado Postal 20-364, México Distrito Federal 01000, México* We study the Hall conductivity as a topological invariant under the influence of an intense electric field. We consider a model of a 2DEG in a two-dimensional lattice in the presence of an applied in-plain electric field and perpendicular magnetic field. The Hall conductivity is determined from quasiclassical calculations. In the presence of an electric field the longitudinal quasi-momentum is quantized leading to the appearance of a magnetic Stark ladder, in which the bands of the Hofstadter butterfly are replaced by a series of quasi discreet levels. We show that the transverse conductivity of this levels is an integer topological invariant independent of the intensity of the electric field thus leading to an integer Hall conductivity.

*We acknowledge the financial support endowed by CONACyT through grants 42026-F and J43110-F

**14:03**
**P46 15 Measurement of Spin Excitations in the Fractional Quantum Hall Regime of 1/2< $\nu$ < 1** JUN YAN, *Columbia University* YANN GALLAIS, *Columbia University* ARON PINCZUK, *Columbia University, Bell Labs* LOREN PFEIFFER, *Bell Labs* KEN WEST, *Bell Labs* We use inelastic light scattering methods to investigate quasiparticle excitations of the fractional quantum Hall liquid in the filling factor range 1/2< $\nu$ < 1. The long wavelength spin wave mode at the Zeeman energy shows intriguing behavior. The mode is observed at the filling factors nu=1, 2/3 and 3/5 of the quantized Hall states but its intensity collapses for filling factors away from these states. In the filling factor range 1/2< $\nu$ < 2/3 spin excitations are observed below the Zeeman energy. These modes are interpreted as spin flips where the composite fermion Landau level quantum number and spin orientation change. The spectral lineshapes of spin flip excitations suggest a spin polarization transition between $\nu$=3/5 and $\nu$=2/3 [1]. [1] Irene Dujovne et al, PRL 95, 056808 (2005)

**SESSION Q1: POSTER SESSION III**
**Wednesday Afternoon, 15 March 2006**
**Exhibit Hall, 1:00pm–4:00pm (DPOLY session: 11:15am–2:15pm) Baltimore Convention Center at 13:00**

**Q1 1 DPOLY POSTER SESSION II**

**Q1 2 Effect of Hydrogen Bonding End Groups on the Bulk Diffusion of Polymers** KATHLEEN SCHAEFER, CRAIG HAWKER, EDWARD KRAMER, *UCSB* Multiple hydrogen bonding (MHB) groups are being incorporated into an increasingly wide variety of polymer architectures, from short difunctional oligomers to high molecular weight multifunctional random copolymers. The addition of even weakly binding groups can have a drastic effect on rheological properties; generally this is due to dimerization of complementary groups, but these can also interact with the surrounding polymer matrix. To better understand this process we have synthesized linear polymers with a single hydrogen bonding end group and compared their bulk diffusion behavior to non-functional linear polymers. Deuterated poly(benzyl methacrylate) was synthesized via RAFT polymerization; the dithioester chain end was displaced by heating in the presence of an excess of radicals derived from AIBN or a functional azo compound. Thin films ( $\sim$ 100nm) of deuterated polymer were cast onto thick films ( $>$ 500nm) of protonated polymer and these bilayers annealed at various temperatures. The depth profiles of the bilayers were measured by dSIMS and fit to the solution of the diffusion equation to determine diffusion coefficients and the effect of a single hydrogen bonding end group on motion through the polymer matrix.

**Q1 3 Thermal Conductivity of Carbon Nanotube/Liquid Nanofluid** THOMAS ACCHIONE, FANGMING DU, JOHN FISCHER, KAREN WINEY, *Department of Material Science and Engineering, University of Pennsylvania* Nanofluids have been shown to be a potential heat-transferring medium due to nanofillers superior thermal conductivity and larger surface areas. Multiwall carbon nanotubes (MWNT) have quickly attracted much attention in this nanofluid field because of their unique thermal conductivity. Our studies on MWNT nanofluid show that there is a modest improvement in thermal conductivity at a high nanotube loading, $\sim$ 35% increase for a 1wt% MWNT nanofluid. We attribute this increase to the formation of a nanotube network with a higher thermal conductivity. However, at low nanotube loadings, $<$ 0.03wt%, we observe a decrease in thermal conductivity with the increase of the loading, $\sim$ 30% decrease for a 0.02wt% nanofluid. A thermal void mechanism is proposed to explain this unexpected decrease. Molecular size and polarity of the matrix liquids have been studied to gain more insights on the heat transportation inside nanofluids.

**Q1 4 Experimental and Theoretical Study of Raman Spectra of Polyisobutylene*** PRADEEP KUMAR, JAMIE MESSMAN, BRIAN ANNIS, *Chemical Sciences Division, Oak Ridge National Laboratory, Oak Ridge TN 37831* BOBBY SUMPTER, *Computer Science and Mathematics Division, Oak Ridge National Laboratory, Oak Ridge TN 37831* CHARLES FEIGERLE, *Department of Chemistry, University of Tennessee, Knoxville TN 37996* The effects of strain induced partial crystallization, partial deuteration, molecular weight and temperature on the Raman spectra of polyisobutylene (PIB) are determined. The Raman spectra of stretched PIB are correlated with the development of crystallinity as found by X-ray diffraction. One of the spectral regions altered by the stretching is in the vicinity of 200 $cm^{-1}$ which is often attributed to disordered longitudinal modes. The results are compared with spectra computed from $1^{st}$ principles electronic structure calculations using Density Functional Theory and Hartree-Fock approaches on model PIB systems.

*Research sponsored by the Division of Materials Sciences, Office of Basic Energy Sciences, U. S. Department of Energy under contract DE-AC0500OR22725 with Oak Ridge National Laboratory, managed and operated by UT-Battelle LLC.

**Q1 5 Examining the origin of spatial shear-rate variation in Couette flow of entangled polymer solutions** THOMAS Y. HU, *Unilever Research, CT* AMY PHILIPS, SHI-QING WANG, *Department of Polymer Science, University of Akron* The objective of this work is to determine the time-dependent velocity profile in Couette flow of entangled polymer solutions. In comparison to other flow apparatuses including cone-plate and sliding plate assemblies, the Couette flow can potentially avoid the complications arising from the boundary conditions. Both rheological and particle imaging velocimetric measurements have been carried out on model solutions to compare with results obtained for a cone-plate cell [1] and to shed light on the nature of non-homogeneous shear flow in the stress plateau region. [1] Tapadia, P.; Wang, S. Q. itPhys. Rev. Lett., in press (2005).

**Q1 6 Opening the black-box of entangled polymers in flow: A first time-resolved velocity profile determination upon step**

**shear** PRASHANT TAPADIA, SHAM S. RAVINDRANATH, SHI-QING WANG, *Department of Polymer Science,The University of Akron* We have recently revealed that entangled polymer solutions undergo a discontinuous bulk flow transition under controlled shear stress due to a chain entanglement-disentanglement transition (EDT) [1]. The implication of such results is far reaching, the least of which is that the assumed ithomogeneous shear would not occur in the stress plateau region, invalidating the previous efforts to explore the constitutive behavior of entangled polymers. The present work [2] applied a particle-tracking velocimetric method developed in our lab and confirmed the inevitable consequence of the EDT: presence of a spatial variation of the shear rate across the sample thickness in a cone-plate shear cell. The explicit velocity profile evolution sheds light onto such common features as shear overshoot during startup shear. [1] Tapadia, P.; Wang, S. Q. itPhys Rev. Lett, **91**, 198301 (2003); Tapadia, P.; Wang, S. Q. itMacromolecules **37**, 9083 (2004). [2] Tapadia, P.; Wang, S. Q. itPhys. Rev. Lett., in press (2005).

**Q1 7 Influence of Neutralization Methods on the Self-Assembly of Nanoscale Ionic Aggregates in Ionomers.** NICHOLAS BENETATOS, KAREN WINEY, *Department of Materials Science and Engineering, University of Pennsylvania, Philadelphia, Pa, 19104* Recent results show that scanning transmission electron microscopy (STEM) and small angle x-ray scattering (SAXS) have been used to obtain complementary morphological information for solvent cast poly(styrene-itran-methacrylic acid) (SMAA) ionomers neutralized with copper. In order to systematically explore the affect of neutralization methods on the nanoscale morphology, materials were isolated by three different methods: solvent casting, solution annealing, and precipitation. Each of these methods allows for a different rate of polymer structure formation. While solvent cast and solution annealed Cu-SMAA films exhibit isotropic ionomer scattering peaks and similar morphologies in STEM, the precipitated powder shows no scattered intensity in the region of the ionomer peak. These data suggest that isolating the polymer by precipitation induces a metastable morphology in which the ionic aggregates are only partially formed or are not uniformly distributed throughout the material. Upon thermal treatment, the scattering pattern of the precipitated powder begins to resemble that of the solvent cast films. SAXS and STEM experiments are underway to further investigate the nanoscale self-assembly mechanism.

**Q1 8 Cylindrical Polyelectrolyte Brushes*** RIKKERT NAP, IGAL SZLEIFER, *Department of Chemistry, Purdue University, 560 Oval Drive West-Lafayette, IN 47907* Polyelectrolytes tethered to a cylindrical surface are investigated. The surface can either be formed by e.g. another polymer, a carbon nanotube, or protein chain. The cylindrical polyelectrolyte brush is of interest to us because it forms a model system for the description of the properties of aggrecan, which is one of the main components of cartilage. We used a molecular theory to theoretically investigate the properties of aggrecan. We computed the potential of mean force between two aggrecan molecules. The influence of the cylindrical geometry, the salt concentration, and the pH of the solution upon the conformation of the aggrecans, was investigated. The findings for cylindrical electrolyte brushes were contrasted with the behavior of planar electrolyte brushes, which revealed a large influence of the geometry upon the properties of the brush layer.

*This research was supported by NSF-NIRT 0403903.

**Q1 9 Poly(Ethylene-Methacrylic Acid) Ionomers Neutralized by Solution and Melt Methods** CHRISTOPHER CHAN, *Department of Chemical and Biomolecular Engineering, University of Pennsylvania* KAREN WINEY, *Department of Material Science and Engineering, University of Pennsylvania* Poly(ethylene-methacrylic acid) has been traditionally neutralized in the melt although other methods, including solution, are also possible. Different neutralization methods may introduce morphological differences in the polyethylene crystallites and ionic aggregates. While the crystallization of the polyethylene chains can be controlled through thermal history, the ionic aggregates form during neutralization and there is no evidence to date of morphological changes after neutralization. In this study, we examine the effect of neutralizing 50% of the acid groups in P(E-itran-3.87%-MAA) with a weak zinc base in solution as compared with in the melt. We have found that solution neutralization with slow precipitation as compared with melt neutralization does not affect the size and distribution of the ionic aggregates. STEM indicates spherical aggregates in a liquid-like disorder with diameter of 2.84 nm $\pm$ 0.42 in the solution neutralized polymer as compared with 2.83 nm $\pm$ 0.56 in the melt neutralized polymer and X-ray scattering interpreted with the Yarusso-Cooper model has parameters of 0.88 nm in diameter versus 0.89 nm.

**Q1 10 Structure calculations for hydrated ionomer membranes*** PHILIP TAYLOR, MEHDI HAMANEH, *Case Western Reserve University* The structure of the perfluorinated ionomer Nafion is determined by a process of partial phase separation in which the ionic components form clusters within a matrix of hydrophobic material. The dipoles associated with the ionic groups tend to order in such a way as to form head-to-tail sequences. In this study we are investigating the effects of hydration on the structure and formation of the ionic clusters and their associated internal electric fields by a combination of atomistic molecular-dynamics simulations and analytical theory. We find that a useful concept is the vorticity of the electric dipole moments and its dependence on hydration. Various procedures have been used in order to develop realistic pictures of the nature of the ionic clusters and their interconnectedness, as the presence of continuous pathways through a Nafion membrane is a determining factor in the transport of protons in polymer-electrolyte membrane fuel cells.

*Work supported by the U. S. Department of Energy

**Q1 11 Direct observation of enhanced mobility near the surface of polymer nanocomposite thin films*** TADANORI KOGA, C. LIN, J. JIANG, J. KOO, M. RAFAILOVICH, J. SOKOLOV, *Stony Brook University* S. NARAYANAN, D. LEE, *Argonne National Lab.* L. LURIO, *Northern Illinois Univ.* S. SINHA, *UC San Diego* The x-ray photon correlation spectroscopy (XPCS) technique with grazing-incident geometry is currently being used to probe surface dynamics of a planer film on microscopic length scales. Sinha et al.[1] have shown that the viscosity of a polymer thin film could be derived from the relaxation rate of thermally induced surface roughness. As a further application of XPCS, we studied surface dynamics of polymer nanocomposite thin films. A combination of thiol-functionalized gold nanoparticles (4 nm in diameter, 4wt%) and polystyrene was chosen as a model system. The high x-ray contrast of Au nanoparticles enabled us to monitor their Brownian motion associated with polymer chain dynamics. In addition, making use of the advantage that the x-ray penetration depth can be tuned by varying the incidence

angle of the incoming beam, we could measured the Brownian motion at the topmost 10 nm of the film and in the bulk separately. As a result, it was found that the diffusion coefficient for the Brownian motion was 50% greater at the surface than in the bulk. That is, the viscosity of the polymer is much lower at the surface. [1] H. Kim, et al. itPhys. Rev. Lett., 90, 683020 (2003).

*This work was supported by the SRC-NY CAIST funding and by NSF (the Garcia MRSEC).

**Q1 12 Viscosity Measurements of Very Thin Polymer Films** CHUNHUA LI, TADANORI KOGA, CLIVE LI, JUN JIANG, *State University of New York at Stony Brook* LAURENCE LURIO, *Northern Illinois University* SUNIL SINHA, *University of California San Diego* SURESH NARAYANAN, *Argonne National Laboratory* MIRIAM RAFAILOVICH, JONATHAN SOKOLOV, *State University of New York at Stony Brook* STATE UNIVERSITY OF NEW YORK AT STONY BROOK TEAM, UNIVERSITY OF CALIFORNIA SAN DIEGO COLLABORATION, NORTHERN ILLINOIS UNIVERSITY COLLABORATION, ARGONNE NATIONAL LABORATORY COLLABORATION, We reported that the viscosity of ultra thin polymer films can be measured by three independent techniques: Bilayer dewetting measurements where the viscosity is derived from dewetting velocity; X-ray Photon Correlation Spectroscopy (XPCS) where the viscosity is determined from the relaxation rate of thermally induced surface roughness and Dynamic Secondary Ion Mass Spectroscopy (DSIMS) where the viscosity is derived from the measurements of the tracer diffusion coefficient. The results from three different techniques are in good agreement with each other. The scaling relationship, $\eta \sim$ Mw PS, yielded from dewetting and XPCS measurement was in excellent agreement with the bulk scaling of 3.4 and the prediction from reptation theory.

**Q1 13 Tethered Ligand-Receptor Binding in Confined Environments** G. LONGO, *Purdue University* I. SZLEIFER, *Purdue University* The binding of small proteins with ligands that are attached to polymers tethered to a surface is studied using a molecular theory. The effects of changing the intrinsic binding equilibrium constant, the polymer surface coverage, the polymer molecular weight, and protein size are studied. The results are compared with the case where the ligands are directly attached to the surface without a polymer acting as a spacer. Within biological range of binding constants the protein adsorption is enhanced by the presence of the polymer spacers. There is always an optimal surface coverage for which ligand-receptor binding is a maximum. This maximum increases as the binding energy or the polymer molecular weight increases. The presence of the maximum is due to the ability of the polymer bound proteins to form a thick layer by dispersing the ligand in space to optimize binding and minimize lateral repulsions. The binding of proteins is reduced as the size of the protein increases. The orientation of bound proteins can be manipulated by proper choice of the grafted layer conditions. A surface modified with a mixture of long ligand-conjugated polymers in low surface density and short polymers in high surface coverage will present optimal binding properties at the same time as nonspecific adsorption of proteins onto the surface is suppressed. The results of the theoretical calculations can be used in the design of experimental systems, providing the kind of polymer and the surface coverage required to optimize ligand-receptor binding.

**Q1 14 Growth of poly-DL-lysine hydrobromide single crystal on mica(001) surfaces.*** DIPAK GOSWAMI, XIAOGANG LIU, YI ZHANG, JOHN OKASINSKI, KHALID SALAITA, PENG SUN, MICHAEL BEDZYK, CHAD MIRKIN, *Northwestern University* CHAD A. MIRKIN COLLABORATION, MICHAEL J. BEDZYK COLLABORATION, We present a method for controlling the initiation and kinetics of polymer crystal growth using atomic force microscope tip coated with poly-DL-lysine hydrobromide (PLH). PLH form triangular prisms on freshly cleaved mica(001) surfaces. These prisms grow in a parallel or anti parallel fashion, which indicates epitaxial growth of the crystal with respect to underling mica lattice. Back reflection Laue on mica (001) surface along with optical microscopy measurements guided us to propose a model which showed that two preferred prism orientations exist along [100] direction of the mica lattice. Grazing incidence oscillation x-ray diffraction measurements revealed that the prisms grown on mica are single crystal with a lattice that has an in-plane orientational epitaxy with the underlying mica lattice. We have observed two growth exponents for the growth of the edge length of the PLH prisms. This reveals that in the early stage of the growth, the prisms grow faster and then the growth rate decreases.

*Supported by: NSEC, IBNAM, NIH, NSF, Baxter-Helthcare

**Q1 15 Electrostatic conformation and hydrodynamic properties of a polyelectrolyte studied using static light scattering and viscosity** CHARLES GORDON,* *Millsaps College* DEBBIE RIGNEY,† *Millsaps College* GINA SORCI, *Millsaps College* Using a combination of light scattering and viscometry we are able to observe the changes in the second and third virial coefficients as well as hydrodynamic properties for a continuous concentration gradient. The concentrations of various salts are observed in order to better describe how the molecule behaves when in the presence of different ionic species ranging from simple salts such as NaI to complex salts such as tetraethylammonium chloride. The ionic strength is varied up to 1M which is near physiological conditions. The goal of this work is to obtain a detailed explanation of how these molecules behave so that we will be able to use these models to describe the functions of these molecules within biological systems such as the kidney.

*undergraduate student
†undergraduate student

**Q1 16 Transport along freely suspended actin cortex models in a controlled microfluidic environment** SIMON SCHULZ, TAMAS HARASZTI, WOUTER ROOS, CHRISTIAN SCHMITZ, JENS ULMER, STEFAN GRAETER, JOACHIM P. SPATZ, *Max-Planck-Institute for Metals Research, New Materials and Biosystems; University of Heidelberg, Biophysical Chemistry, 70569 Stuttgart, Germany* Arrays of microfabricated pillars are constructed to serve as a template for mimicking the actin cortex of cells. The three-dimensional template surface prevents interaction of the actin filaments hanging between pillars. A special flow-cell design enables applying flow around a network of actin freely suspended between polydimethylsiloxane pillars. This opens new possibilities to study the mechanics of two-dimensional actin networks as a function of actin-crosslinkers, to observe the active diffusion of molecular motors operating on pending networks and to investigate the alternations in the transport of microscopic particles, coated by different proteins and molecular motors, along these actin cortex models under the drag of flow. The stiffness of the F-actin can be tuned by bundling through various

cross-linkers. Additionally, actin filaments act as tracks for guiding passive and active transport of cargo such as organelles or microspheres by molecular motors like myosin-V. These transport problems are biomimetic studies of tracks and external driving force on a statistical process of two-dimensional networks isolated from the complicated and undetermined cellular environment.

**Q1 17 Time-resolved electric force microscopy of charge traps in polycrystalline pentacene films** MICHAEL JAQUITH, *Department of Chemistry and Chemical Biology, Cornell University* ERIK MULLER, *Department of Physics, Cornell University* JOHN MAROHN, *Department of Chemistry and Chemical Biology, Cornell University* The microscopic mechanisms by which charges trap in organic electronic materials are poorly understood. Muller and Marohn recently showed that electric force microscopy (EFM) can be used to image trapped charge in working pentacene thin-film transistors [E. M. Muller *et al*, *Adv. Mater.* **17** 1410 (2005)]. We have extended their work by imaging trapped charge in pentacene films with much larger grains. In contrast to the previous study in which charge was found to trap inhomogeneously throughout the transistor gap, we find microscopic evidence for a new trapping mechanism in which charges trap predominantly at the pentacene/metal interface in large-grained devices. We have also made localized measurements of the trap growth over time by performing pulsed-gate EFM experiments. Integrated-rate kinetics data supports a charge trap mechanism which is second order in holes, e.g., holes trap in pairs, although the charge-trapping rate appears to depend on gate voltage.

**Q1 18 Shear flow induced unfolding of collapsed polymers.*** ALFREDO ALEXANDER-KATZ, ROLAND NETZ, *Technical University Munich* In the process of clotting in small vessels, platelets form a plug in an injured zone only in the presence of a protein known as the von Willebrand Factor (vWF). The absence or malfunction of the vWF leads to a bleeding disorder, the so-called von Willebrand disease. It is believed that the protein is collapsed (or globular) when released into the blood flow, and that it undergoes a transition at high shear rates that allows it to bind platelets. Using hydrodynamic simulations of a simple model of the vWF in shear flow, we show that a globular polymer undergoes a globule-stretch transition at a critical shear rate. Below this threshold shear rate the polymer remains collapsed and slightly deformed, while above it the chain displays strong elongations in the direction of the flow. Finally, we discuss the relevance of our results in the case of blood flow, and compare them to the physiological values present in the body.

*A. A. acknowledges support from the NSF through the International Postdoctoral Fellowship Program.

**Q1 19 Dynamics of polar guest molecules contained in cryptophane molecular crystals** ERICK WINSTON, ROBERT HORANSKY, MATTHEW MYERS, JOHN PRICE, *The University of Colorado, Boulder* JAROSLAV VACEK, *Academy of Sciences of the Czech Republic* Cryptophanes are a class of molecules with an interior cavity which can be occupied by smaller guest molecules non-covalently. In cases where the guest molecules are free to tumble within the cryptophane, and where the cryptophanes can be crystalized, it is possible to create ordered arrays of reorienting guest molecules. By using dipolar guests such as the methyl halides, the guest motions can be observed by dielectric spectroscopy and guests may order via strain or dipole-dipole interactions. We will present the results of dielectric spectroscopy experiments on single crystals of iodomethane in cryptophane-A. The observed rotational barriers are compared to computational molecular mechanics calculations based on the X-ray structure of the complex.

**Q1 20 Tethered Polymer Interactions with Attractive Surface Potentials** RYAN VAN HORN, JOSEPH X. ZHENG, HUIMING XIONG, WILLIAM Y. CHEN, KYUNGMIN LEE, RODERIC P. QUIRK, *University of Akron* BERNARD LOTZ, *Institut of Charles Sadron* EDWIN L. THOMAS, *MIT* AN-CHANG SHI, *McMaster University* STEPHEN Z.D. CHENG, *University of Akron* Due to their surface modification capabilities, tethered polymer chains have been a research focus for several years. Experimental and theoretical work has been done to understand the conformations and interactions of these systems at varying tethering densities. A new technique developed in our group makes it possible to use single crystals of crystalline-amorphous diblock copolymers to study tethered polymer chains. These systems have controlled density through defined fold numbers and controlled MW through living polymerization. Zheng and coworkers found that the reduced tethering density is 3.7 for the onset of interchain interaction and 14.3 for the highly-stretched brush. This work provides, for the first time, the values of these two onsets with high certainty; however, the systems studied do not provide general results. Both systems had repulsive interactions between the surface and the tethered chains. In order to broaden the scope of the physics behind tethered polymer chains, the study should include systems with attractive potentials. Preliminary studies of one such system, PMMA-b-PLLA, will be presented.

**Q1 21 Single crystal engineering of block copolymers*** HUIMING XIONG, JOSEPH X. ZHENG, RYAN M. VAN HORN, Y. GUO, RODERIC P. QUIRK, STEPHEN Z. D. CHENG, In the past two decades, tethered polymer systems have attracted attention due to, not only their theoretical interests, but also their applicable potentials. Usually, physical adsorption, ''grafting to'' and ''grafting from'' methods have been used to fabricate polymer brushes on solid substrates. Recently, we have proposed a novel method which can achieve narrow molecular weight distribution, and precisely control the tethering density by using amorphous-crystalline block copolymers. With a constant molecular weight of the crystalline block and crystallization temperature, the thickness of single crystals and thus, the number of folds are fixed. This leads to a constant tethering density. We can thus adjust the tethering density by controlling the thickness of the single crystals by changing undercooling and molecular weights of the crystalline blocks. Systems of triblock copolymers with one crystalline block at one end or in the middle will generate diblock copolymer brushes or mixed and/or unmixed polymer brushes. The morphologies of polymer brushes can be controlled by the crystallization condition of single crystal. Mutually, the tethered polymer brushes could also affect crystallization of the crystalline block.

*This work was supported by NSF (DMR-0516602).

**Q1 22 Overall Crystallization Kinetics of Polymorphic Poly (propylenes)** YSELA CHIARI, KIMBERLY THOMPSON, RUFINA ALAMO, *FAMU-FSU College of Engineering, Department of Chemical and Biomedical Engineering, Tallahassee, Fl* The isothermal crystallization of propylene ethylene random copolymers evolves with a simultaneous formation of two polymorphic forms, monoclinic crystals (alpha form) and orthorhombic crystals

(gamma form). The relative content of each modification changes during crystallization. The content of gamma crystals developed at high levels of transformation increases with the concentration of ethylene and with the crystallization temperature. The overall crystallization kinetics of copolymers with an ethylene content ranging from 0.8 to 7.5 mol % were followed by DSC and analyzed according to classical Avrami kinetics. For most copolymers, fits with single stage nucleation and growth models were poor. Following structural models for lamellar growth that account for epitaxial gamma branching from alpha surfaces, the experimental data were modeled with parallel two-stage crystallization kinetics with excellent fits up to 80 % transformations. The Avrami exponents obtained from the fits are consistent with a 3-D spherulitic growth with instantaneous nucleation for alpha and homogeneous nucleation (linear with time) for the gamma phase.

**Q1 23 Melting in Copolymer Blends** BUCKLEY CRIST, *Northwestern University* It is observed that the melting temperature $T_m$ of polyethylene is insensitive to blending with a melt-miscible random ethylene copolymer. On the other hand, the $T_m$ of an ethylene-rich copolymer is depressed strongly when blended with a less ethylene-rich copolymer. If A is a homopolymer that does not cocrystallize with B, the standard thermodynamic prediction for $T_m$ employs the small entropy of mixing of entire chains. The situation is quite different if A and B are random copolymers with different amounts of non-crystallizable comonomers. Copolymer melting is based on the mixing of crystallizable and non-crystallizable monomers during fusion, calculated for sequences, not for entire chains. In essence, $T_m$ for the copolymer blend depends on the total concentration of crystallizable monomers from both blend components, regardless of the chain to which a particular sequence belongs. This concept adequately accounts for the observations above.

**Q1 24 Ultra-Small Angle Neutron Scattering Study of Polyethylene Crystallization from Solution*** HOWARD WANG, NARAYAN DAS, KAIKUN YANG, *Department of Materials Science and Engineering, Michigan Technological University, Houghton, MI 49931* Crystallization of polyethylene in deuterated toluene solution has been investigated using time-resolved ultra small angle neutron scattering for the first time. Both slit-smeared and de-smeared scattering spectra were analyzed using Guiniers law to obtain time-dependent structural information. The average lateral dimension of crystallites grows linearly with time, while the degree of crystallinity increases as square of time. The results suggest that the number density of nuclei remains constant during the crystal growth.

*This work is supported by an NSF Career Award

**Q1 25 Holographic Patterning and Crystallization of a Semicrystalline polymer** MICHAEL BIRNKRANT, *Drexel University* CHRISTOPHER LI, *Drexel University* LALGUDI NATARAJAN, VINCENT TONDIGLIA, RICHARD SUTHERLAND, *Science Applications Intl Corp* TIMOTHY BUNNING, *Air Force Research Laboratory* Manufacturing dynamically controlled multifunctional photonic structures for application in optical elements and waveguides is crucial to control the flow of light. Holographic Patterning (HP) is a simple, fast and attractive means to fabricate complex photonic structures. During the HP process, a photopolymerizable syrup is exposed to two or more coherent laser beams. The resulting anisotropic photopolymerization leads to the spatial distribution of a crosslinked network polymer and homopolymer poly ethylene glycol (PEG). The HP of low molecular weight PEG and thiol-ene reactive monomers produced a long range uniform layered structure. The difference in refractive indexes of PEG and crosslinked polymer network results in unique transmission spectra and diffraction efficiencies. Furthermore, upon heating the holographically patterned PEG produces a red shift in the reflected wavelength of the material which reverses upon cooling. Closer analysis through X-ray scattering has found that PEG crystals contained within the confined layers preferentially crystallize.

**Q1 26 Comparative Determinations of Orientation in Injection-Molded Thermotropic Liquid Crystalline Copolyester (TLCP) Plaques** ROBERT BUBECK, *Michigan Molecular Institute* STANLEY RENDON, WESLEY BURGHARDT, *Northwestern University* DANIEL FISCHER, *NIST* Two-dimensional wide-angle X-ray scattering (2D-WAXS) in transmission and C K edge near edge X-ray adsorption fine structure (NEXAFS) spectroscopy were used to characterize anisotropy and catalog orientation states in injection-molded plaques fabricated under varying conditions using two commercial TLCP copolyesters. The observed 2D-WAXS patterns are usually bimodal in character due to contributions from the core and skin regions that result from extensional and shear flow, respectively, in the mold. Deconvolution of the 2D-WAXS patterns permits one to gain a measure of the Hermans orientation parameter of the core and skin for finite thicknesses of the plaques. The NEXAFS in partial electron yield mode is sensitive to the orientation of the molecular pi orbital of backbone phenyl groups of the top 3 nm of a surface. Updated analyses of the NEXAFS results indicate much greater localized molecular orientation at the very surface of the samples than for the more general orientations for the core and skin derived from the WAXS. The NEXAFS results are generally consistent with those obtained by using surface specific attenuated total reflectance Fourier transform infra-red spectroscopy.

**Q1 27 Coupling of Lithium-Polymer Complexes and Electric Field: Routes to Enhance the Alignment of Block Copolymer Thin Films** JIA-YU WANG, JULIE LEISTON-BELANGER, SURESH GUPTA, *University of Massachusetts, Amherst* TING XU, *Cold Neutrons for Biology and Technology (CNBT) at NIST* Recently, the unexpected experimental results indicated that lithium ionic impurities in block copolymer thin films might assist applied electric filed to overcome the interfacial interactions so that the alignment of microdomains was enhanced.1 But some questions are still open: whether lithium ions aid in overcoming interfacial interactions, what is the nature of the interactions of the lithium ions with the polymer chains, and what is the driving forces in this process? We designed a method to introduce lithium chloride into polystyrene-block-poly(methyl methacrylate) (PS-b-PMMA) copolymer thin films. The IR results show that lithium-PMMA complexes in copolymers were formed. These lithium-PMMA complexes markedly enhanced the dielectric constant of PMMA block. Thus the critical electric field strength for aligning the microdomains is significantly decreased so that the external electric field can overcome the interfacial interactions and increase the alignment of microdomains. The addition of ionic salts into one block of a diblock copolymer opens up a potential route to fabricate the long-range ordered nanostructures of block copolymer thin films. [1] Xu T.; Goldbach J. T.; Leiston-Belanger J.; Russell T. P. Colloid Polym. Sci., 2004, 282, 927.

**Q1 28 Structure of Rod-Coil Block Copolymer Thin Films** R.A. SEGALMAN, B.D. OLSEN, *University of California Berkeley and Lawrence Berkeley National Lab* The self-assembly of rod-coil block copolymers confined to thin films demonstrates new and unusual surface effects. Since the rod block does not experience chain stretching and instead undergoes liquid crystalline interactions, the surface induced order of the block copolymer system is drastically modified. Thin films of a model rod-coil block copolymer, poly(alkoxyphenylene vinylene-b-isoprene), form islands or holes with lamellae oriented primarily parallel to the substrate. These parallel lamellae form grains bounded by defect regions consisting of lamellae oriented out of the plane of the film. These defects appear to have long-range interactions with the surrounding grains resulting in regular, angular grain boundaries. As film thickness is increased toward 10 lamellar spacings, the surface induced order dies off and the lamellae at the vacuum interface are entirely oriented perpendicular to the substrate. We will discuss the kinetics of grain growth and the penetration depth of surface induced ordering as a function of thermal history.

**Q1 29 Renormalized One-Loop Theory of Fluctuations in Homopolymer Blends and Diblock Copolymer Melts** PIOTR GRZYWACZ, DAVID MORSE, *University of Minnesota* We construct a perturbation theory for the effects of composition fluctuations in polymer mixtures, which we apply to both binary homopolymer blends and diblock copolymer melts. The inverse structure function is divided into an inverse intramolecular correlation function and a direct correlation function, which are calculated separately to first order in a loop expansion. We show that corrections to mean-field theory that are sensitive to local fluid structure, as reflected by a dependence on the value of a microscopic cutoff length, can be absorbed into $q$-independent changes in the value of the direct correlation function (which is closely related to the Flory-Huggins $\chi$ parameter) and changes in statistical segment lengths. Predictions are presented for the changes in radii of gyration of chains in a binary solution near the critical point (which are extremely small) and for the behavior of the stucture factor in a block copolymer melt near the order-disorder transition.

**Q1 30 Investigation of the Phase Behavior of Amphiphilic Triblock Copolymers (PAA-itb-PMA-itb-PS in Mixed Solvents** KELLY HALES, HONGGANG CUI, ZHIBIN LI, DARRIN POCHAN, *Dept. of Materials Science and Eng, Univ. of Delaware* ZHIYUN CHEN, QAI KI, KAREN WOOLEY, *Dept. of Chemistry, Washington Univ. at St. Louis* Unique morphologies have been prepared from amphiphilic triblock copolymers of poly(acrylic acid)-b-poly(methyl acrylate)-b-polystyrene in water/tetrahydrofuran (THF) solvent mixtures. The length of the acrylic acid block and the methyl acrylate block were held constant for each copolymer while the polystyrene block length was varied. For self- assembly, the block copolymers were dissolved in THF in the presence of a divalent, organic counterion and water was added slowly. This resulted in a variety of unique structures including polymer nanoparticles with internal block phase separation, bulk phase separation, spherical micelles, cylindrical micelles, disks, as well as toroidal (ring-like) assemblies. The specific structure formed was dependent on the architecture of the triblock copolymer, the amount of counterion present, and the water to THF volume ratio. The focus of this work is the basic understanding and characterization of the phase separated structures present in low water content solutions. The understanding of this bulk phase behavior and its effects on the assemblies formed at higher water contents will be presented. Transmission electron microscopy (TEM), cryo-TEM and neutron scattering were used to examine the copolymer solutions.

**Q1 31 Overall static conformation of chain molecules in nanoscopic cylinders** KYUSOON SHIN, *School of Chemical and Biological Engineering, Seoul National Univeristy* JUIN-TAI CHEN, *Department of Polymer Science and Engineering, University of Massachusetts, Amherst* PRIYANKA DOBRIYAL, *Chemistry Department, University of Massachusetts, Amherst* PAPPANNAN THIYAGARAJAN, *Argonne National Laboratory* THOMAS RUSSELL, *Department of Polymer Science and Engineering, University of Massachusetts, Amherst* We explore the overall static conformation of chain molecules in nanopores. We used anodized aluminum oxide membrane with hexagonally packed, regular-sized nanopores with the pore diameter of 15 nm. Via strong capillary action, we have successfully filled different size polystyrene (molecular weight range 20,000 to 3,000,000) in these membranes. Polymers, whose size in the bulk is much larger than the diameter of the nanopores, should deform due to the confinement and the spatial configuration of the chain must deviate from that seen in the bulk. By examining the single chain scattering of the polymer confined within the nanopores via small angle neutron scattering, we examine whether the chain retains its random conformation or elongate along the nanopore.

**Q1 32 Effects of shear flow on reactive coupling of polymer chains at melt interfaces** JIANBIN ZHANG, *Department of Chemical Engineering and Materials Science, University of Minnesota* TIMOTHY LODGE, *Department of Chemical Engineering and Materials Science and Department of Chemistry, University of Minnesota* CHRISTOPHER MACOSKO, *Department of Chemical Engineering and Materials Science, University of Minnesota* The coupling reaction of functional polymers at static polymer-polymer interfaces is typically much slower than that at interfaces formed during mixing (see, for example, Reference 1). We have demonstrated that the imposed simple shear can accelerate coupling reactions at flat interfaces. For amine-terminal polystyrene ($PS\text{-}NH_2$)/anhydride terminal poly(methyl methacrylate) (PMMA-anh), the PMMA-anh conversion under dynamic oscillation even at strain amplitude as small as 1% is seven times that under static conditions. Reaction time and temperature and the total interfacial area were maintained the same. Similar behavior was found for both bilayer and multilayer samples. Under steady simple shear, the reaction conversion and the rate of interfacial area generation are comparable to that of batch mixing.
Macosko, C. W.; Jeon. H. K.; Hoye, T. R. Prog. Polym. Sci. **2005**, 30, 939.

**Q1 33 Cation Effects on Electroactive Responses of Conjugated Polymers*** XUEZHENG WANG, ELISABETH SMELA, *Dept. of Mech. Engr., UMCP* The ions present in the electrolyte in which a conjugated polymer actuator is cycled are known to affect performance such as response time and volume changes. Understanding how speed, force, strain, etc. are affected by ion size and other ion characteristics is critical to applications, but is not yet well understood. In this paper, we first present effects of monovalent and divalents cation mass on transport velocity and volume change in polypyrrole doped with dodecylbenzenesulfonate, PPy(DBS), which is a cation-transporting material. Volume change,

measured by mechanical profilometry, was greatest for $Li^+$ and decreased in order of atomic mass: $Na^+$, $K^+$, Rb, and $Cs^+$. This was expected because prior studies had shown that the ions are hydrated when they enter the PPy, and $Li^+$ has the largest hydration shell. Ion transport, measured by phase front propagation experiments, was also fastest for $Li^+$, however, contradicting the expectation that larger species would move more slowly. Possible explanations based on hydration shapes and ion-chain interactions will be discussed. In this paper, we also present effects of ion mixtures: $Li^+/K^+$ and $Li^+/Mg^{2+}$. The results show that small amount of slow moving ions increases the response time drastically. The experiments also show that the $Mg^{2+}$ ions are trapped in the polymer films and influence electroactivity of conjugated polymers.

*We would like to acknowledge funding through DuPont's Young Professor Grant and the Laboratory of Physical Sciences while completing this research.

**Q1 34 Modeling self-oscillation and waves in a reactive polymer gel** VICTOR YASHIN, ANNA BALAZS, *Department of Chemical Engineering, University of Pittsburgh, Pittsburgh, PA* We model the self-oscillation and wave propagation phenomena in a swollen polymer gel that participates in the Belousov-Zhabotinsky (BZ) reaction. The BZ reaction causes variations in the gel volume through reduction-oxidation changes of a metal catalyst, which is covalently bonded to the polymer chains. We employ the Oregonator model to describe the BZ reaction kinetics. The Flory and Flory-Huggins models are used to describe the gel elasticity, and the polymer-solvent interactions, respectively. We identify the model parameters that yield the oscillatory behavior, and demonstrate that the kinetics of the BZ reaction can be significantly affected by coupling the reaction to the polymer gel dynamics. To simulate the traveling waves of swelling-deswelling, we utilize the gel lattice spring model, which we have developed recently, and is equivalent to the two-fluid model. We demonstrate and discuss the effects of mechanical constraints on the generation and propagation of 1D and 2D swelling-deswelling waves in the reactive gel.

**Q1 35 Measuring the Local Modulus of Soft Polymer Networks** JESSICA ZIMBERLIN, ALFRED CROSBY, *University of Massachusetts* Biological tissues often rely upon local ''heterogeneities'' to define their structure –property relationship. An example is the integrated layered structure of the mitral valve. For most native tissues, these ''heterogeneities'' are attributed to the local arrangement and structure of the collagen fibril network. To guide the development of tissue scaffolds, we characterize and understand these structure-property relationships on local length scales. In our research we have developed a method to determine the local modulus at specific points within a material. The method involves inducing cavitation and monitoring the pressure of the cavity instability. This pressure is directly related to the local modulus of the material. Initial results focus on the network development of poly vinyl alcohol hydrogels. We monitor the process of gelation and the mechanical response of these hydrogels on length scales similar to their pore structure.

**Q1 36 Monte Carlo Simulation of Reversibly Associating Networks*** SHIHU WANG, CHUN-CHUNG CHEN, ELENA E. DORMIDONTOVA, *Macromolecular Science and Engineering, Case Western Reserve University, Cleveland, OHIO 44106* We applied Monte Carlo simulations to study the reversible network formation through oligomers end-functionalized by ligands capable of complexation in 3:1 ratio with metal ions acting as crosslinkers. By varying the oligomer concentration and metal-to-oligomer ratio, we studied the fractions of different associating species and the molecular weight distribution. The conditions for network formation (over the percolation threshold) were determined using three different criteria, which lead to similar results. The molecular weights of species in the corresponding sol and gel phases were obtained along with the fractions of small rings, dangling ends, and network mesh sizes. An analytical model based on the equilibrium among different associating species and classical gelation theory modified to account for unequal reactivity/cooperativity was developed. The predictions of the analytical model are in good agreement with the simulation results, which compare favorably with experimental observations.

*This work was supported by the NSF Career Award CHE-0348302

**Q1 37 Formation of nanoparticles during melt mixing a thermotropic liquid crystalline polyester and sulfonated polystyrene ionomers** HYUKSOO LEE, *Samsung Electro-mechanics Co.* LEI ZHU, *University of Connecticut* R. A. WEISS, *University of Connecticut* The formation of nanoparticles and the mechanism of their formation in a blend of a thermotropic liquid crystalline polyester (LCP) and the zinc salt of a lightly sulfonated polystyrene ionomer (Zn-SPS) were investigated using Fourier transform infrared, thermogravimetric analysis, and gas chromatograph-mass spectroscopy. Transmission electron microscopy and wide-angle X-ray scattering were used to study the morphology of the blends and structure of nanoparticles. The origin of nanoparticle formation appeared to be related to the development of phenyl acetate chain ends on the LCP that arose due to a chemical reaction between the LCP and residual catalytic amounts of zinc-acetate and/or acetic acid that were present from the neutralization step in the preparation of the ionomer. The origin of formation and kinetics of the nano-particle formation and the mechanical and rheological properties of these nanocomposites are briefly discussed.

**Q1 38 Characterization of Release Mechanism in Polymeric Drug Delivery Systems** ARTHUR JAMES LAPLANTE, ROBIN MARIE PLACHY, KAORU AOU, JAKE FERGUSON, SHAW LING HSU, *Polymer Science and Engineering Department, University of Massachusetts* Our polymeric drug delivery system is based on our understanding of phase behavior of polymers [e.g poly(lactic acid)], low molecular drugs and various solvents used in processing. Clearly the different morphologies achieved, based on different phase separation kinetics, can affect drug release rates. Release of drugs, in most cases, involves the exchange between the extraction media and drug. We have characterized the transport behavior using a number of unique techniques. Reflectance infrared spectroscopy has given us a detailed description of the release rate of drugs into the extraction media. Surface plasmon resonance has shown the overall mass loss. UV-visible spectroscopy has yielded the concentration of drug in the solution. These measurements are compared to the release mechanism based on Fickian diffusion. The two step release rates observed can only be explained by taking into account differences in the morphological features of the phase separated films.

**Q1 39 Transport behavior of small molecules out of various poly (vinylidene fluoride) copolymer morphologies** SURIYAKALA RAMALINGAM, GUOLIN WU, FENG YI, SHAW LING HSU, *Polymer Science and Engineering Department, University of Massachusetts* Due to its biocompatibility, durability and existence of various crystalline states, poly (vinylidene fluoride) (PVdF) have been used in medical applications. In this study, the hydrophobic poly (VdF-hexafluoropropylene) polymeric matrix was used to develop a durable matrix system and to control the transport of small molecules by diffusion. Films of this family of copolymers have been prepared from various solutions and with different thermal history. Various morphological features in terms of degree of crystallinity, crystalline phase and segmental orientation can be obtained. These morphological features at different length scales have been characterized by AFM, X-ray and confocal Raman microscopy. The changes in morphology and microstructures are especially interesting when the films of this family of copolymers are prepared using the electrospray technique. The dispersion of small molecular weight component in the various films has been evaluated. Their transport behavior has also been characterized.

**Q1 40 An Analysis of the Solidification Process in Immiscible and Crystallizable Polymer Blends.** YOUNG GYU JEONG, NATALIA POGODINA, SHAW LING HSU, *Polymer Science and Engineering Department, University of Massachusetts Amherst* Despite the tremendous number of studies in this area, the solidification process of binary and ternary blends is not clearly understood. Here we report the solidification process of immiscible and crystallizable blends, composed of crystallizable polyester and noncrystallizable polyether, in terms of crystallization kinetics, morphological features, and interaction between domains and matrix. All blends exhibited phase-separated morphology with polyester-rich dispersed domains and polyester-poor continuous matrix. The local composition, morphological features, crystallization and solidification process were characterized using $^1$H-NMR, optical microscopy, DSC, and small-amplitude oscillatory viscometry, respectively. The local composition and crystallinity in polyester-rich and –poor phases were varied, depending on blend composition and/or crystallization temperature. The solidification process of blends with low polyester content of 10-30 wt% was dominated by crystallization of the polyester-poor phase. The ultimate viscosity of the overall blend was also lower than that of the polyester-poor phase. The high ultimate viscosity in the polyester-poor phase was associated with the percolated morphology of 'curved leaf'-shape crystallites.

**Q1 41 The Role of Percolation in the Rheological Behavior of Binary and Ternary Blends.** NATALIA POGODINA, YOUNG GYU JEONG, SURIYAKALA RAMALINGAM, SHAW LING HSU, *Polymer Science and Engineering Department, University of Massachusetts Amherst* The rheological behavior of binary and ternary blends involving polyether [e.g. poly(propylene glycol) (PPG)], crystallizable aliphatic polyester [e.g. poly(hexamethylene adipate) (PHMA)] and acrylic copolymers has been studied. The phase behavior of these polymer mixtures at different temperatures is extremely fascinating depending on the nature of the polymers used. The morphological features formed during cooling from elevated temperatures involve phase separation and polyester crystallization. The existence of a percolating solid was established based on evidence from rheological (oscillatory shear) and morphological studies. Typically the blends form a phase-separated droplet-matrix morphology. The transition from the liquid to the solid state has been explicitly correlated to the crystallization behavior of the polyester poor phase. A step increase in the elastic (storage) modulus is observed at a precisely determined PHMA content. The high elasticity can be explicitly explained in terms of the percolation model. The contributions of the domains, interfacial layer and the matrix to the percolation ability of the blend are also discussed.

**Q1 42 Production of Exfoliated Polyethylene-Organoclay Nanocomposites and Its Effect on Mechanical Properties and Thermal Stability.** CYNTHIA PIERRE, JOHN M. TORKELSON, *Northwestern University, Evanston, IL 60208* Low density polyethylene (LDPE)-organoclay nanocomposites as well as linear low density polyethylene (LLDPE)-organoclay nanocomposites are prepared using solid-state shear pulverization (SSSP). The organoclay content in each nanocomposite is 5 wt%. X-ray diffraction indicates that the nanocomposites are exfoliated, because the basal beak at 3.6 degrees for organoclay is nearly eliminated in the nanocomposites made by SSSP. Transmission electron microscopy (TEM) provides further evidence that the nanocomposites are significantly exfoliated. Upon 2 hour annealing at temperatures 25 K above the melt transition of the polymer, x-ray diffraction patterns remain unchanged, indicating that the exfoliated structure of the nanocomposites is kinetically stable in the melt state of the polymer. Due to the stiffness of the clay sheets, the Young's modulus is increase $\sim$ 20% by nanocomposite formation. Thermogravimetric analysis reveals that the onset temperature of degradation is increased by $\sim$ 5 K in the nanocomposites and that the initial degradation of the nanocomposites is retarded relative to neat polymer up to 5% loss of sample weight.

**Q1 43 Oxygen Permeation as a Quantitative Means of Ranking Exfoliation in Polymer-Clay Nanocomposites.** KOSMAS G. KASIMATIS, CYNTHIA PIERRE, AMANDA M. WALKER, JOHN M. TORKELSON, *Northwestern University, Evanston, IL 60208* A series of polymer-clay nanocomposites have been made by solid-state shear pulverization (SSSP), which yields good exfoliation of clay based on x-ray diffraction and transmission electron microscopy results, and by melt mixing, which yields relatively little exfoliation of clay based on similar characterization. Here we demonstrate the utility of oxygen permeation as a quantitative tool for ranking exfoliation levels in polymer-clay nanocomposites; the basis for this approach is related to the fact that greater exfoliation of clay will lead to a more tortuous diffusion path for oxygen in the polymer matrix and thereby a reduction in permeability coefficient. A greater than factor of 3 reduction in permeability coefficient has been achieved in polymer clay nanocomposites processed by SSSP. A comparison of permeation results will be made to other characterization and properties that are known to reflect exfoliation.

**Q1 44 Origins of Linear Viscoelastic Behavior of Polymer-Nanoparticle Composites** VICTOR PRYAMITSYN, VENKAT GANESAN, *University of Texas at Austin* We use computer simulations to study the mechanisms governing the linear viscoelasticity behavior of composites of spherical nanofillers dispersed in polymer melt matrices. Our results suggest that particles can influence the viscoelastic properties of the system by a variety of different mechanisms. On the one hand, the particle-induced effects on the dynamics of polymer segments modify the relaxation

spectrum of the polymers. Secondly, particle jamming effects lead to slow relaxations and substantial enhancements in elasticity. Finally, our results suggest that the strain field distortion caused by the presence of rigid inclusions also affects the overall modulus of the composite. For our model system, we delineate the regimes and frequencies at which the different effects manifest and also suggest how the picture can be generalized for parametric conditions different from our simulations.

**Q1 45 Effect of Molecular Weight on Load Transfer in Nanotube / Polymer Composites** MINFANG MU, *Department of Materials Science and Engineering* FANGMING DU, *Department of Chemical and Biomolecular Engineering* RETO HAGGENMUELLER, KAREN WINEY, *Department of Materials Science and Engineering* The tensile moduli of nanocomposite fibers are being investigated with attention to the molecular weight of the polymer. Nanocomposites composed of single wall carbon nanotube (SWNT) and poly(methyl methacrylate) (PMMA) were prepared by our coagulation method and processed into composite fibers using melt fiber spinning. SWNT in the fibers are aligned and the nanotube - nanotube interactions are diminished, so that, the mechanical load on SWNT is mainly from polymer - SWNT interactions. The tensile moduli along the direction parallel to the SWNT were characterized at 1.0 mm / sec with the fiber length of 25.4 mm. At a weight-average molecular weight (Mw) 25 kDa, the tensile moduli of PMMA are the same with the composites. However, when the Mw is increased to 100kDa, the tensile moduli are improved greatly by adding SWNT. This indicates that the load in the composites is transferred to the SWNT more efficiently at 100 kDa molecular weight. A micromechanics model was used to relate the elastic shear stress on the polymer - SWNT interface to the polymer chain length. It showed that with increasing polymer chain length, the interfacial shear stress was enhanced. This study demonstrates the importance of the molecular weight of the polymer matrix to the load transfer in nanocomposites.

**Q1 46 Templated Nanocarbon Black Nanocomposite Electrodes for Rechargeable Lithium Batteries** OZGE AKBULUT, *MIT* ELSA A. OLIVETTI, *MIT* DONALD R. SADOWAY, *MIT* ANNE M. MAYES, *MIT* In this work, the fabrication of high energy density electrode materials for solid-state rechargeable batteries via block copolymer templating schemes was investigated. Atom transfer radical polymerization was used to synthesize the copolymer template poly((oligooxyethylene) methacrylate)-itblock-poly(butyl methacrylate), POEM-b-PBMA. Continuous, nanoscale phases of vanadium oxide were subsequently grown within the POEM domains of the microphase-separating block copolymer using sol-gel synthesis from a vanadium alkyoxide precursor. The in situ growth of cathodic components in ion-conducting POEM domains allows for control of morphology and increases the interface-to-volume ratio, thereby escalating the specific electrode area over which faradaic reactions can occur and decreasing ion diffusion distances within the electrode. Films incorporating up to 34 wt% $V_2O_5$ were flexible and semi-transparent. To achieve necessary electronic conductivity, the incorporation of nanocarbon black was investigated. Hydrophilic surface modification of carbon black nanoparticles provided a mechanism for their selective incorporation into POEM domains. Transmission electron microscopy (TEM) and small angle x-ray scattering (SAXS) were performed to probe the morphology of the nanocomposite electrodes.

**Q1 47 Creep and Recovery Behaviors of a Polythiophene-based Electrorheological Fluid** DATCHANEE CHOTPATTANANONT, *Chiangmai University* ANUVAT SIRIVAT, *PPC, Chulalongkorn University* We investigate the creep response of poly(3-thiopheneacetic acid) (PTAA) particles doped with perchloric acid. With increase of applied stress, these suspensions exhibit an evolution from a linear viscoelastic response, with three components of instantaneous elastic strain, retarded elastic strain and viscous strain, to a nonlinear viscoelastic response, where the retarded elastic and viscous strains monotonically decrease and a plastic contribution to the instantaneous strain grows, followed by a viscoplastic solid behavior, with fully plastic instantaneous strain, and finally a transition from plastic solid to a plastic liquid at the yield stress. With increase of electric field strength at fixed particle concentration and applied stress, the viscoplastic response diminishes, and more elastic behavior ensues. For highly-doped samples, at high electric field strengths, a fully elastic solid response is observed in the linear viscoelastic regime. The equilibrium compliance, $J_C$ and steady state recoverable compliance $J_R$, were investigated as a function of electric field strength, particle concentration and particle conductivity. The results are interpreted in terms of the field-induced formation of thick fibrillar aggregates spanning the gap between the electrodes, each consisting of bundles of particle strings.

**Q1 48 Electric Field Generated Stress Moduli in Polythiophene/Polyisoprene Elastomer Blends** TOEMPHONG PUVANATVATTANA, ANUVAT SIRIVAT, *PPC, Chulalongkorn University* The effects of crosslinking ratio and electric field strength on the rheological properties of polyisoprene and polythiophene/polyisoprene (Pth/PI) blendss were investigated as potential electroactive actuator. Electrorheological properties of polyisoprene and blends were measured under the oscillatory shear mode with the applied electric filed strength varying from 0 to 2 kV/mm. The dynamic moduli, G′ and G″, of the pure polyisoprene depend on the crosslinking ratio and the electric filed strength; the storage modulus (G′) increases but the loss modulus (G″) decreases with increasing crosslinking ratio. The storage modulus (G′) and the loss modulus (G″) of the pure polyisoprene fluid exhibit no change with increasing electric field strength. For PI with the crosslinking ratios of 2, 3, 5 and 7 (PI_02, 03, 05 and 07), the storage modulus sensitivity, $\Delta G'/G'_o$, increases with electric field strength and attains maximum values of 10%, 60%, 25%, and 30% at the electric field strength of 2 kV/mm, respectively. The loss modulus (G″) of the PI with the crosslinking ratios of 2 and 3 increases with the electric field, but for the blends of the crosslinking ratios of 5 and 7, it decreases. For the blends of polythiophene with PI at concentrations of 5%, 10% and 20% by vol, G′ and G″ are generally higher than those of pure polyisoprene.

**Q1 49 Electromechanical response of a silicone elastomer containing PPV** SUMONMAN NAIMLANG, ANUVAT SIRIVAT, *PPC, Chulalongkorn University* Electrorheological properties of PDMS gel and PPV/PDMS blend were investigated experimentally under an oscillatory shear mode at the temperature of 27°C to determine the effects of crosslink ratio, electric field strength and doping level. For the pure PDMS gels, the storage modulus, G′, increases with increasing crosslinking ratio and electric field at all frequencies between 0.1-100 rad/s. When an electric field is applied, the polymer molecules become polarized resulting in the interaction through the electrostatic force between the polarized

PDMS molecules. The PDMS gel system with the crosslinking ratio of 0.01 possesses the highest G sensitivity to electric field. For the PPV/PDMS blends (PPV/PDMS_10), the dynamic moduli, G′ and G″, are higher than those of pure PDMS in the absence of electric field because PPV particles act as a filler in PDMS matrix. The G′ sensitivity of PDMS increases up to 35% at the electric filed strength of 2 kV/mm. Moreover, the doped PPV/PDMS blend (doped PPV (1:10)/PDMS_10) shows the highest G′ sensitivity (170%) due to interacting electrostatic forces between electric field induced dipole moments of the conductive molecules.

**Q1 50 Creep and Recovery of Electroactive Polyaniline Suspension** PIYANOOT HIAMTUP, ANUVAT SIRIVAT, *PPC, Chulalongkorn University* Creep and recovery behaviors of the PANI/silicone oil suspensions were investigated under applied electric field to explore the effects of field strength and particle concentration. The data show that, at any applied shear stress, the creep curves of this ER fluid showed a large instantaneous elastic response, whereas the retarded elastic and the viscous responses were very small and they disappeared as applied stress was increased. After the removal of applied stress, the strain decreased but did not completely relax to its original value indicating that the fluid exhibited a partially elastic recovery. However, it was noted that the recovery after stress removals disappeared when the strain was higher than the critical values $\sim$ 0.4-0.5, independent of particle concentration and field strength. It was also found that creep resistance of EB/Silicone oil suspension were clearly dependent on both field strength and particle concentration.

**Q1 51 Anisotropy of Electroactive Strain in Textured Polypyrrole Actuators** RACHEL PYTEL, EDWIN THOMAS, IAN HUNTER, *Massachusetts Institute of Technology* Polypyrrole has been extensively studied as an electroactive material, but these studies have provided little insight to the influence that morphology has on actuation at the nanoscale. By discovering and exploiting the connection between nanoscale transport events and macroscale active strain, we can learn how to process polypyrrole and other conducting polymers for improved electroactive device performance. We show that by controlling polymer chain configuration and packing, a conducting polymer actuator can be engineered that shows a significantly larger macroscopic electroactive response for a given set of driving conditions. We utilize different modes of deformation to impart orientation textures that can be observed via synchrotron x-ray diffraction and electronic and ionic resistance measurements. Certain textures enhance pathways for ion transport between polymer chains, resulting in an anisotropic electroactive strain response that can be harnessed when making polypyrrole-driven devices. This response provides valuable insight to the mechanism of polypyrrole actuation on the nanoscale, supporting a mechanism where counterions migrate to locations between the oriented polymer chains.

**Q1 52 Detecting composition and monomer sequence distribution in random copolymers with interaction chromatography** JUNWON HAN, CHANG Y. RYU, *Rensselaer Polytechnic Institute* JAMES J. SEMLER, JAN GENZER, *North Carolina State University* We demonstrate that interaction chromatography (IC) is capable of discriminating among both the chemical composition and monomer sequence distribution in random copolymers. By fine-tuning the separation conditions in the IC (solvent type and stationary phase type), we were able to delineate the effect of both their chemical composition and the monomer sequence distribution of partially brominated polystyrenes on chromatographic retention. The degree of bromination and the 4-BrS sequencing was controlled by varying the bromine concentration in the reaction vessel, bromination reaction time, and solvent temperature. Our experiments suggest that 1) the blockiness of 4-BrS adsorption segments can further enhance the surface affinity of the copolymer chains at a fixed copolymer chemical composition, and 2) the adsorption-based molecular recognition of copolymer chains occurs by cooperative and synergistic adsorption of segments on surfaces along with neighboring adsorptive segments.

**Q1 53 Interplay between polymer and nanopore sizes for polymer adsorption in nanopores** CHANSU KIM, CHANG Y. RYU, *Rensselaer Polytechnic Institute* We investigated the adsorption and desorption of monodisperse polystyrene (Mw: 4K $\sim$ 3M) in cyclohexane into nanoporous silica (Rp, radius of pore: 4, 7, 14, and 24nm; particle diameter: 7 micron) to understand the interplay between polymer coil size and nanopore size for the polymer adsorption in nanopores. Regardless of the pore sizes, two regimes of polymer nanopore adsorption have been identified to universally describe the surface access (adsorbed mass per unit area) in terms of the relative size interplay, Rg/Rp. When polystyrene is much smaller than pore, the surface access increases with the radius gyration, Rg, essentially following the adsorption behavior on the flat surface. When polystyrene is similar or larger than pore, the surface access in nanopore surface is smaller than that on the flat surface. From SEM, we found morphological evidence to support that the steric crowding of polystyrene chains occurs at the nanopore entrance to offer the limited accessibility of polymers into the pore surfaces.

**Q1 54 Recent developments in multivariant surface-tethered polymer assemblies** RAJENDRA BHAT, MICHAEL TOMLINSON, JASON STONE, JAN GENZER, *N.C. State University* Surface-tethered polymer brushes prepared via surface-initiated controlled/''living'' radical polymerization represent an effective tool for tuning the physico-chemical properties of surfaces. We have recently developed methods leading to assemblies of surface-tethered polymers with continuously varying grafting density, molecular weight, and composition. In this presentation, we will demonstrate how these assembling concepts can be utilized to: 1) study the kinetics of surface-initiated controlled/''living'' radical polymerization, 2) systematically study the phase behavior of diblock and triblock copolymers upon exposure to selective solvents, 3) study the behavior of block copolymer polyampholyte brushes, and 4) explore the wettability transitions (superhydrophobic/superhydrophilic) using thermoresponsive polymer brushes on topologically corrugated substrates.

**Q1 55 Evaporation and interdiffusion of solvent in polymer films** MESFIN TSIGE, *Southern Illinois University Carbondale* GARY S. GREST, *Sandia National Laboratories* Solvent evaporation from homopolymer and heteropolymer films along with the interdiffusion of solvent into these films is studied using large scale molecular dynamics and grand canonical Monte Carlo simulations. As the solvent evaporates, a sharp increase in polymer density at the film/vapor interface is observed. The rate of solvent evaporation, for both homopolymer and heteropolymer films is found to decrease exponentially with time. For multiblock films

the resulting domain structure is found to be strongly affected by the relative stiffness of the two blocks. In the interdiffusion study, the shape of the solvent concentration profile and the weight gain by the film can be related to the diffusivity. For homopolymer films, although the diffusivity is found to be strongly concentration dependent especially as one approaches the glass transition temperature of the polymer, the weight gain scales as $t^{1/2}$ for all cases studied, which is expected for Fickian diffusion. For a multiblock copolymer film in which the stiffer block is below the glass transition temperature is also studied, even though the solvent swells only the softer block of the copolymer, the weight gain by the film remains Fickian.

**Q1 56 Adsorption of Biodegradable Diblock Copolymers PEO-PLA and PEO-PCL to Colloidal Polystyrene** KAREN A. MURPHY, JESSICA M. MENDES, DANIEL A. SAVIN, *University of Vermont* A series of amphiphilic block copolymers composed of poly (ethylene oxide) and either poly(lactide) or poly($\epsilon$-caprolactone) (PEO-PLA, PEO-PCL respectively) were synthesized and their solution properties studied using dynamic light scattering. The synthesis was performed using the same PEO macroinitiator while varying the fraction of the hydrophobic block. These materials were found to self-assemble in aqueous media with the hydrodynamic radius increasing with increasing hydrophobic fraction. In order to ascertain the potential for use of these materials as degradable coatings in delivery applications, block copolymers were adsorbed to colloidal polystyrene and the thickness of the adsorbed layer determined from changes in the hydrodynamic size. The adsorbed thickness ranged from 4 - 10 nm with varying block ratio, polymer concentration and colloid concentration. In general, the adsorption of PEO-PCL to colloidal polystyrene resulted in larger adsorbed thickness compared with PEO-PLA.

**Q1 57 Optical Properties of Molecules and Molecular Aggregates Adsorbed on Solid Surfaces. First Principle Study.** ALEXANDER GAVRILENKO, MIKHAIL NOGINOV, CARL BONNER, VLADIMIR GAVRILENKO, *Center of Materials Research, Norfolk State University, Norfolk VA 23504* Equilibrium atomic geometries of Ferrocene and Rhodamine 6G (R6G) dye molecules adsorbed on Si(111) and Ag(111) surfaces respectively are studied using density functional theory. Equilibrium atomic geometries are obtained through total energy minimization method. Electron energy structure and optical properties are calculated using generalized gradient approximation method with itab initio pseudopotentials. Modifications of electronic surface structures of Ag(111) and Si(111) caused by the adsorption of molecules as well as charge transfer between molecules and solids are studied. Red or blue shifts of optical absorption spectra of R6G dye molecules after aggregation in *J*- or *H*-dimmers respectively are predicted. Calculated optical absorption spectra are interpreted in terms of inter-molecular and molecular-solid interactions. Results of the calculations are discussed in comparison with experimental data.

**Q1 58 Wetting Morphologies in Triangular Grooves*** KRISHNACHARYA KAREH, MARTIN BRINKMANN, STEPHAN HERMINGHAUS, RALF SEEMANN, *MPI for Dynamics and Self-Organisation, D-37073 Goettingen* BRUCE LAW, *Kansas State University, Manhattan, KS 66506* We studied the wetting behavior of liquids in triangular grooves with chemically homogeneous walls. Droplets form elongated morphologies with negative mean curvature for contact angles, $\theta$, smaller than 90° minus half the opening angle of the groove. For larger $\theta$, the liquid either forms elongated filaments of finite length and positive mean curvature or drop-like morphologies. For in situ manipulation of small amounts of liquid on this substrate topography, we used electrowetting which allows varying $\theta$ as a function of the applied Voltage. The filling and drainage behavior of these grooves were studied as a function of time and $\theta$. In contrast to grooves with rectangular cross section, the liquid filaments in triangular grooves undergo a dynamic instability when being quenched from a filling to a non-filling situation. The liquid filament breaks up into isolated droplets with a preferred distance which compares favorably with a straightforward theoretical model.

*This work was partly funded by the German Science Foundation under grant number SE1118 within the priority program Nano- and Microfluidics SPP 1164.

**Q1 59 Freezing of Polymer Thin Films and Surfaces: The Small Molecular Weight Puzzle** STEPHAN HERMINGHAUS, RALF SEEMANN, *MPI for Dynamics and Self-Organization, D-37073 Goettingen* KARIN JACOBS, *Saarland University, D-66123 Saarbruecken* KATHARINA LANDFESTER, *University of Ulm, D-89069 Ulm* Experimental observations (ellipsometry, scanning force microscopy (AFM), and nuclear magnetic resonance (NMR)) of the freezing behavior of thin supported films as well as the free surface of atactic polystyrene are reported, taken at a particularly small molecular weight of 2 kg/mol. Remarkably, we find the same effect of reduction of the glass transition temperature, Tg, as observed earlier with much longer molecules. Furthermore, surface melting is observed by NMR, with the molten layer thickness similar to what has been observed with larger molecular weight. We conclude that molecular geometry effects cannot account for these observations, and that a consistent explanation must be presentable in a continuum picture. Based on the capillary wave spectrum of the free surface and of the supported films, we present such a model, and find that it accounts very consistently with all observations made so far with polystyrene.

**Q1 60 Film Formation with Reactive Hydrophobic and Polar Groups in Aqueous Solution: A Bond-Fluctuating Computer Simulation Model*** SHIHAI YANG, SAMUEL BATEMAN, RAS PANDEY, MAREK URBAN, *University of Southern Mississippi* We study film formation with reactive hydrophobic ($H$) and polar ($P$) components in evaporating aqueous ($A$) solution by Monte Carlo simulation to model the polyurethane film growth. Each component is represented by mobile particles with appropriate molecular weight, interaction, and reaction functionality on a simple three-dimensional lattice $L_x \times L_y \times L_z$ with an adsorbing substrate. $H$ and $P$ react by forming fluctuating covalent bonds proceeding from the substrate with probability $P_B$. Bonds may also be formed between $H$ and $A$ when $A$ is considered reactive. Growth of the film thickness ($h$) and surface roughness ($W$) are studied at a range of temperature ($T$). With non-reactive $A$, the saturated film thickness ($h_s$) and roughness ($W_s$) decay first before increasing linearly on raising the temperature. With reactive $A$, a fast increase of $h_s$ at low temperature is followed by a slow increase at high temperature. $W_s$ also shows non-monotonic dependence on temperature.

*We acknowledge support from NSF MRSEC program (DMR 023883)

**Q1 61 Enhancement of X-ray Reflectometry for the Depth-Profiling of Polymer Films using Polymeric Substrates*** MARIA I. LYGERAKI, HARIS RETSOS,† SPIROS H. ANASTASIADIS,‡ *Foundation for Research and Rechnology - Hellas, Heraklion Crete, Greece* CHRIS TOPRAKCIOGLU, ALEKOS A. VRADIS, *University of Patras, Rion Patras, Greece* YVES GALLOT, *Institut Charles Sadron, Strasbourg, France* The investigation of the internal structure of thin polymer films on conventional substrates by X-Ray reflectometry is restrained due to the high electron densities of these substrates compared to those of most polymers. A methodology is proposed and applied to circumvent this problem by utilizing polymeric substrates of appropriate thickness and roughness, which can be reproducibly deposited on the standard substrates in order to render them invisible to the X-rays. The resolution of the X-ray reflectometry is significantly enhanced as illustrated utilizing thin films of PS-b-PMMA diblock copolymers of various thicknesses. The proposed methodology will allow the study of internal polymer interfaces using in-house diffractometers/reflectometers.

*Sponsored by Greek General Secretariat of Research and Technology (?ENED) and by NATOs Scientific Affairs Division
†Present Address: Laboratoire de Physico-Chimie Structurale et Macromoleculaire, E.S.P.C.I., Paris, France
‡Also at Aristotle University of Thessaloniki, Thessaloniki, Greece

**Q1 62 Switchable Adhesion Properties From Low and High $T_g$ Polymeric Brushes** HARIS RETSOS, YVETTE TRAN, *E.S.P.C.I., PARIS* GANNA GORODYSKA, ANTON KIRIY, MANFRED STAMM, *I.F.P. Dresden, Germany* COSTANTINO CRETON, *E.S.P.C.I., PARIS* We investigated the adhesive properties of mono-component and bi-component polymeric brushes chemically grafted on silicon wafers from end-functionalized hydrophilic and/or hydrophobic chains by using the technically simple 'grafting to' method. The charge state and the molecular organization of high $T_g$ brushes could be varied reversibly by exposure to appropriate solvents or by varying the grafting density. Adhesive properties were tested against soft pressure-sensitive-adhesives (hydrophobic & hydrophilic) with a probe method. In the case of low $T_g$ brushes, an increase in contact time could selectively improve the adhesion with the soft hydrophobic or hydrophilic adhesive layer. This is due to reorganization of the interface at the molecular scale leading to the formation of entanglements or favorable interactions between the polymer brush and the polymers in the soft adhesive.

**Q1 63 Principles of resonant soft x-ray reflectivity – a novel tool in polymer research** CHENG WANG, TOHRU ARAKI, SHANE HARTON, *NC State University* TADANORI KOGA, *SUNY Stony Brook* HARALD ADE, *NC State University* Resonant soft x-ray reflectivity (RXR) has been reported to be a potentially excellent tool for the study of polymer thin films [1]. To further delineate the applicability of this method, detailed principles about RXR will be discussed. Near the carbon 1-s absorption edge, the complex index of refraction $n = 1-\delta-i\beta$ is changing rapidly as a function of photon energy in a manner that strongly depends on the chemical moieties of the polymer. This leads to enhanced contrast between two polymers at specific energies when compared to hard x-rays. This contrast enhancement mimics the contrast enhancement achieved through deuteration used in neutron reflectivity, yet does not require special chemical procedures. PS/PMMA, PBrS/PMMA, PS/SAN, PS/P2VP and PCHMA/PMMA bilayers were characterized by RXR at beamline 6.3.2 at the Advanced Light Source. For a subset of these samples, RXR results were directly compared to hard x-ray reflectivity characterization that uses a fourier analysis method [2], and the results showed good agreement. [1]C. Wang, T. Araki, and H. Ade, Appl. Phys. Lett. 87, 214109 (2005). [2]O. H. Seeck et al., Appl. Phys. Lett. 76, 2713 (2000).

**Q1 64 Calorimetric Tg and Heat Capacity of Polystyrene Thin Films*** YUNG KOH, GREGORY McKENNA, SINDEE SIMON, *Texas Tech University* The glass transition temperature and the absolute heat capacity of polystyrene thin films were measured using the step-scan method of differential scanning calorimetry. The glass transition temperature is found to be depressed 8 K for a sample of stacked 17 nm thick films and Tg is depressed 3 K for a sample of stacked 61 nm thick films. The results are consistent with data in the literature for the Tg depression in supported polystyrene films although our films are expected to be ''freely standing'' for the initial DSC scan. In addition, the absolute heat capacity in both the liquid and glassy states decreases with decreasing film thickness, the step change in heat capacity at the glass transition temperature decreases with decreasing film thickness, and the breadth of the transition region increases with decreasing film thickness. The effect of heating the thin film samples to 135 [r]C, approximately 40 [r]C above their Tgs, is a slight increase in the absolute heat capacity and a slight increase in Tg. No significant changes occur on subsequent scans. The ''thin film'' morphology is maintained in spite of scanning to above Tg where the stacked film sample is expected to lose its free surface.

*Funding from NSF DMR 0304640 is gratefully acknowledged.

**Q1 65 Dissipative particle dynamics simulations of dilute polymer solutions confined in a slit with interactive surfaces** WENHUA JIANG, *Department of Chemistry, The University of Memphis, Memphis, TN 38152* JIANHUA HUANG, *Department of Chemistry, The University of Memphis, Memphis, TN 38152; Department of Chemistry, Zhejiang Sci-Tech University, Hangzhou, 310018, China* MOHAMED LARADJI, *Department of Physics, The University of Memphis, Memphis, TN 38152* YONGMEI WANG, *Department of Chemistry, The University of Memphis, Memphis, TN 38152* Dynamics of polymer chains in confined geometries are significantly different from that in a bulk solution. Understanding the confinement effect on the chain dynamics is of great value to applications of microfluidic devices. We applied dissipative particle dynamics (DPD) to study polymer chain dynamics confined in slits with interactive surfaces. We first examined the dynamics and the static properties of polymers in dilute bulk solutions. After correcting for the effect of finite box size, our results unambiguously confirmed that the DPD has correctly accounted for hydrodynamic interaction within a polymer chain. We then extended the simulation to polymer solutions confined in a slit with interactive surfaces. For purely repulsive surfaces, the dynamics and the static properties of polymers show a broad crossover from a free solution to a confined solution. The attractive interactions of polymers with the walls were found to retard the dynamics of the chains significantly. The influence of surface interactions on polymer dynamics will be presented.

**Q1 66 Dissipative particle dynamic simulations of solvent flow through nanometer sized smart channel coated with stimuli**

**responsive polymer brush** JIANHUA HUANG, *Department of Chemistry, The University of Memphis, Memphis, TN 38152; Department of Chemistry, Zhejiang Sci-Tech University, Hangzhou, 310018, China* MOHAMED LARADJI, *Department of Physics, The University of Memphis, Memphis, TN 38152* YONGMEI WANG, *Department of Chemistry, The University of Memphis, Memphis, TN 38152* Various efforts have been focused on the development of smart materials which can respond to environmental stimuli such as pH or temperature. Nanometer sized channels coated with such stimuli responsive polymers can serve as smart gating or smart valve that are of interest for applications such as controlled drug release and tunable permeation and separations of toxic solutes. These systems involve the interplay of solvent flow with the structure of polymer brush in response to the external stimuli. We applied dissipative particle dynamic (DPD) method to investigate solvent flow through such smart channels. The external stimuli are modeled by the change in solvent quality that causes polymers undergoing a coil-to-globular transition. We investigate the ability of such smart channel to control the solvent flow under different stimuli. The interplay of the solvent flow and the properties of polymer brush are studied at the molecular level. The effects of the grafted density and the layer thickness of polymer brush on its controlling ability have also been investigated.

**Q1 67 Exfoliation of stacked sheets: effects of temperature and platelet size by a Monte Carlo simulation*** BARRY FARMER, *Air Force Research Laboratory* RAS PANDEY, *University of Southern Mississippi* Can a layer of stacked sheets (coarse grained description of clay platelets) exfoliate in a solvent? Computer simulations are performed to address this question with a stacked layer of four sheets. A sheet is modeled by nodes tethered together by fluctuating bonds on a cubic lattice; sheets of sizes $12^2 - 64^2$ are considered. The initial distance between sheets is small and kept constant for different sets of stacked sheets. There is an attractive interaction between sheets, i.e., their nodes and the empty lattice sites, the effective solvent medium. Nodes execute stochastic movement with the Metropolis algorithm subject to bond fluctuation and excluded volume constraints. Simulations are performed at different temperatures. Visual analysis shows that the exfoliation depends on the size of the sheet and temperature. We find that it is easier to exfoliate smaller sheets and that the exfoliation is enhanced by raising the temperature. The exfoliation becomes very slow for large sheets at low temperatures due to longer relaxation times.

*We acknowledge supports from the Materials and Manufacturing Directorate of the Air Force Research Laboratory.

**Q1 68 Correlations of System Mobility with Various Scalar Metrics** JULIEANNE HEFFERNAN, ROBERT BACA, JOHN McCOY, *New Mexico Institute of Mining and Technology* JOANNE BUDZIEN, DOUGLAS ADOLF, *Sandia National Laboratories* Molecular dynamic simulations of chain systems were performed in order to investigate the relationships between the system mobility and thermostatic quantities. Systems consisted of pearl-necklace chains along with single site penetrants. Both attractive and repulsive systems (based on the cut-off of the Lennard-Jones potential) were simulated. The diffusion coefficients, D, for the chains and penetrants were then found for a variety of temperatures (T) and density combinations. D/T was found to be a single-valued function of a thermostatic quantity that we denoted as a ''scalar metric.'' Four scalar metrics were found. Since, through the master curve, the mobilities for all temperature-density points can be extrapolated to a single zero, a unique ideal glass transition can be proposed to exist. Consequently, a scalar metric can be used as a ''distance'' measure to this ideal glass transition.

**Q1 69 A Monte Carlo Study of Frozen Lattices on Curved Surfaces** A. HEXEMER, E. J. KRAMER, G. H. FREDRIKSON, *UCSB* V. VITELLI, D. R. NELSON, *Harvard* We compare the defect structure and density of particles confined on 2d surfaces with different curvatures as well as different surface morphologies. All simulations are performed using a smart Monte Carlo algorithm while the particle system is cooled from a melted state to zero degree temperature. The surfaces show similar defect patterns. At low maximum Gaussian curvature a hexagonal lattice wraps defect-free onto the curved surface. We then observe a critical maximum curvature at which the creation of defects lowers the potential energy of the lattice with respect to the defect-free lattice. At this critical value we observe free dislocations located at the inflection points of the surface. Further increase in curvature results in the creation of more free dislocations which organize in grain boundaries aligned along the shortest connection between the positive and negative Gaussian curvature areas. A stronger curvature leads to the creation of free disclinations. The $-60^o$ disclinations are pinned to the area of positive curvature while the $+60^o$ disclinations occupy the negative areas. The transition from the defect free lattice to a defected lattice as the lowest energy state is compared to an analytic expression derived from continuum mechanics.

**Q1 70 A Molecular Dynamics Study of the Odd-Even Effect in Self-Assembled Monolayers*** LAWRENCE HERMAN, *United States Naval Academy, Midshipman First Class* PAUL MIKULSKI, *United States Naval Academy, Physics Department* JUDITH HARRISON, *United States Naval Academy, Chemistry Department* Classical Molecular Dynamics has been used to examine the friction in model systems consisting of an amorphous hydrocarbon tip sliding across self-assembled monolayers consisting of well-ordered densely-packed pure linear hydrocarbon chains. An odd monolayer composed of C13 chains is compared against an even monolayer composed of C14 chains at a number of loads. Periodic Boundary Conditions imposed in the horizontal plane are used to model infinite monolayers. The friction of the odd monolayer is seen to be roughly twice as large as that of the even monolayer at all loads. The difference is attributable to the differing orientation of terminal chain groups in odd versus even monolayers. Analysis of net forces exerted by the entire set of tip atoms on individual monolayer atoms lends insight into specific properties associated with the observed frictional difference.

*This work was supported by The Office of Naval Research (N00014-05-WX-20129) and The Air Force Office of Scientific Research (F1ATA04295G001 and F1ATA0429G002).

**Q1 71 Fabrication of Biopolymer Nanofibers of Hyaluronic Acid via Electrospinning** DENICE YOUNG,* *North Carolina State University* HAILEY QUEEN,† *North Carolina State University* WENDY KRAUSE,‡ *North Carolina State University* Electrospinning is a novel technology that uses an electric field to form fibrous materials from a polymer solution. Unlike traditional spinning techniques, electrospinning can produce fibers on the order of 100 nm that can be utilized in applications where nanoscale fibers

are necessary for successful implementation, including tissue engineering. Hyaluronic acid (HA) is a widely used biopolymer found in the extracellular matrix and currently marketed in medical applications for joint lubrications and tissue engineering. The high viscosity and surface tension of HA make it an unlikely candidate for electrospinning processes as viscosity is an important parameter in successful electrospinning. To promote HA fiber formation by electrospinning, the effects of salt (NaCl), which is used to reduce the viscosity of aqueous HA solutions; molecular weight of the HA; and an additional biocompatible polymer (e.g., PEO) are under investigation.

*Research Assistant
†Research Assistant
‡Professor

**Q1 72 Influence of D-Penicillamine on the Viscosity of Hyaluronic Acid Solutions** JING LIANG, *North Carolina State University* WENDY E. KRAUSE, *North Carolina State University* RALPH H. COLBY, *The Pennsylvania State University* Polyelectrolyte hyaluronic acid (HA, hyaluronan) is an important component in synovial fluid. Its presence results in highly viscoelastic solutions with excellent lubricating and shock-absorbing properties. In comparison to healthy synovial fluid, diseased fluid has a reduced viscosity. In osteoarthritis this reduction in viscosity results from a decline in both the molecular weight and concentration of hyaluronic acid HA. Initial results indicate that D-penicillamine affects the rheology of bovine synovial fluid, a model synovial fluid solution, and its components, including HA. In order to understand how D-penicillamine modifies the viscosity of these solutions, the rheological properties of sodium hyaluronate (NaHA) in phosphate-buffered saline (PBS) with D-penicillamine were studied as function of time, D-penicillamine concentration (0 – 0.01 M), and storage conditions. Penicillamine has a complex, time dependent effect on the viscosity of NaHA solutions—reducing the zero shear rate viscosity of a 3 mg/mL NaHA in PBS by itca. 40% after 44 days.

**Q1 73 Electrospinning of Biocompatible Nanofibers** ANDREW J. COUGHLIN,* *North Carolina State University* HAILEY A. QUEEN, *North Carolina State University* SETH D. McCULLEN, *North Carolina State University* WENDY E. KRAUSE, *North Carolina State University* Artificial scaffolds for growing cells can have a wide range of applications including wound coverings, supports in tissue cultures, drug delivery, and organ and tissue transplantation. Tissue engineering is a promising field which may resolve current problems with transplantation, such as rejection by the immune system and scarcity of donors. One approach to tissue engineering utilizes a biodegradable scaffold onto which cells are seeded and cultured, and ideally develop into functional tissue. The scaffold acts as an artificial extracellular matrix (ECM). Because a typical ECM contains collagen fibers with diameters of 50-500 nm, electrostatic spinning (electrospinning) was used to mimic the size and structure of these fibers. Electrospinning is a novel way of spinning a nonwoven web of fibers on the order of 100 nm, much like the web of collagen in an ECM. We are investigating the ability of several biocompatible polymers (*e.g.*, chitosan and polyvinyl alcohol) to form defect-free nanofiber webs and are studying the influence of the zero shear rate viscosity, molecular weight, entanglement concentration, relaxation time, and solvent on the resulting fiber size and morphology.

*Supported by NC State University's Undergraduate Research Awards Grants administered through the Office of Undergraduate Research.

**Q1 74 Structure and interactions of human respiratory mucin** KIRSTIN PURDY, *University of Illinois at Urbana Champaign* JOHN SHEEHAN, MICHAEL RUBINSTEIN, *University of North Carolina* GERARD WONG, *University of Illinois at Urbana Champaign* Human respiratory mucin plays a crucial role in the pathology of Cystic Fibrosis lung infections. Mucin is a flexible, linear polyelectrolyte, characterized by its many charged oligo-carbohydrate side chains that give it its bottle-brush structure. The macroscopic properties of a mucin suspension are known to change drastically with changes in ion concentration and solution pH, but little is known about the effect of these variables on individual mucin structure. We present preliminary results on the structural response of individual human respiratory mucin molecules to variations in concentration of ions of different valences via small angle x-ray diffraction.

**Q1 75 Theoretical simulation of compression of single bovine carbonic anhydrase II molecule by AFM tip** KATSUNORI TAGAMI, MASARU TSUKADA, *Waseda University, Japan* Based on all-atom force field model called CHARMM, we calculated the force distance curves of the single bovine carbonic anhydrase II molecule adsorbed on the graphite surface in the UHV condition. The AFM tip is modeled by the graphite sheet of monolayer thickness. The force distance curves show the nonlinear feature which can be classified into three regions, i.e., the attractive, weak repulsive, and strong repulsive force regions. We found that in the second region the surrounding alpha helices are compressed while in the third region the core beta sheets are also compressed. This finding indicates that the heterogeniousity in a single protein molecule can be measured by the AFM. We will also discuss the effect of the temperature on the force distance curves.

**Q1 76 Self Assembly of $\beta$-Hairpin Peptides into Hydrogel Networks: Tuning Supramolecular Properties Through Molecular Design** TUNA YUCEL, *Materials Science and Engineering, University of Delaware* CHRIS MICKLITSCH, JOEL SCHNEIDER, *Chemistry and Biochemistry, University of Delaware* DARRIN POCHAN, *Materials Science and Engineering, University of Delaware* Monomeric peptides were designed to undergo reversible, intramolecular folding with external stimuli (e.g. pH, temperature, salt) to form $\beta$-hairpins that consequently self assemble into a hydrogel network rich in $\beta$-sheet. The design was composed of a turn sequence ($V^DPPT$) flanked by extended strands containing alternating lysine and valine residues. The hydrophobicity of the peptides was altered through replacing valine residues in the arms with residues such as, norvaline, norleucine and isolecine. Circular dichroism spectroscopy illustrated that random-coil to $\beta$-sheet transition could be tuned from $35^oC$ to below $5^oC$ at pH 9, while the transition pH at $T_{room}$ could be shifted from pH 9 down to pH 7. TEM illustrated that all peptides self-assembled into fibrilar networks. Single fibril dimensions were 3 nm as measured using TEM and small-angle neutron scattering, consistent with the proposed self-assembly mechanismof

fibrils with a molecular bilayer cross-section. There was a direct correlation between fibril morphology and consequent changes in the nature of junction points and gel rigidity as observed by TEM, and oscillatory rheology, respectively.

**Q1 77 Flory $\chi$ of the homologous series of deuterated polystyrene-b-poly(n-alkyl methacrylates): small angle neutron scattering and theoretical studies** DU YEOL RYU, *Yonsei University* KRISTOPHER A. LAVERY, THOMAS P. RUSSELL, *University of Massachusetts at Amherst* JUNHAN CHO, *Dankook University* DONG HYUN LEE, JIN KON KIM, *Pohang University of Science and Technology* We have performed small angle neutron scattering and theoretical studies of the homologous series of deuterated polystyrene-b-poly(n-alkyl methacrylates) from methyl to n-hexyl groups that cover from UODT (upper order-disorder transition) to LODT (lower DOT), and barotropic to baroplastic behavior. It was shown that the effective Flory $\chi$ from the measurements reveal a monotonic dependence on 1/T for UODT (methyl, n-hexyl) systems and a complicated dependence for LDOT (ethyl to n-pentyl) systems. The recently developed compressible random-phase approximation (RPA) analysis has been applied to the copolymers to interpret in a unified way such diversified temperature and pressure dependence of $\chi$ and the transitions. Specific interactions (SI) and compressibility were incorporated through the RPA interaction fields in this theoretical approach. It was argued that the SI gives a major contribution to the LDOT behavior and the complicated dependence of $\chi$ on 1/T. The compelling changes in $\chi$ and the pressure responses of transitions according to the pendant group size were also interpreted successfully with the theory.

**Q1 78 A new field-theoretic simulation method for compressible systems containing block copolymers** JUNHAN CHO, *Dankook University* A new field-theoretic simulation method based on a compressible random-phase approximation (RPA) theory has been suggested to understand the self-assembly behavior and its pressure responses of compressible systems containing block copolymers. Finite compressibility is incorporated in the free energy functional for the dissipative dynamics through effective RPA interactions that account for the excluded volume and the attractive nonbonded interactions. It was shown for A-b-B copolymer melts in unconfined or confined geometry that basic equation-of-state parameters completely characterizing given block components readily yield stable and metastable morphologies without any presumed symmetry over a wide range of temperature-pressure-composition space. It was demonstrated that the simulation tool is capable of predicting in a unified way the self-assembly behavior not only exhibiting nanoscale ordering either upon cooling or reversely upon heating, but also revealing barotropicity and baroplasticity. The simulation of the self-assembly behavior of multiblock copolymers with diverse molecular architectures and also of block copolymers in a solvent covering from complex patterns to micellar structures was also discussed.

**Q1 79 Stability of the orthorhombic *Fddd* phase in diblocks using Landau theory of weak crystallization** AMIT RANJAN, DAVID MORSE, *Department of Chemical Engineering and Materials Science, University of Minnesota* Recent numerical SCFT caculations by Tyler and Morse [*Phys. Rev. Lett.*, **94**, 208302, 2005] predict a stable orthorhombic network phase with space group *Fddd* in weakly segregatd diblocks. In this work, we examine the stability of the *Fddd* phase using Landau theory. Our analysis and results suggest that *Fddd* structure with a special unit cell is expected to be a stable phase not only in weakly segregated diblocks but in any other weakly ordered material.

**Q1 80 Depletion interaction effects on diblock copolymer micelles in selective solvents** SAYEED ABBAS, TIMOTHY LODGE, *Department of Chemical Engineering and Materials Science, University of Minnesota* Block copolymers form micelles when dissolved in a selective solvent for one block. At higher concentrations the micelles pack into ordered microstructures. When non-adsorbing homopolymer is added to the solutions, we observe that the ordered morphologies can be disordered. Due to the addition of homopolymer the repulsive inter-micellar interactions are screened, which leads to the melting of the ordered microstructures. This phenomenon is analogous to depletion interactions in colloid/polymer mixtures. We have chosen the polystyrene-b-polyisoprene dissolved in dialkyl phthalates, as our model system. To these solutions polystyrene homopolymer is added. The molecular weight of the homopolymer has a significant effect on the phase behavior of the system. Our goal is to study the changes in phase behavior induced by addition of homopolymers and explore the underlying parameters which control the phase behavior.

**Q1 81 Order-Disorder Transition and Critical Micelle Temperature in Concentrated Block Copolymer Solutions** MOON JEONG PARK, KOOKHEON CHAR, *Seoul National University* JIN KON KIM, *Pohang University of Science and Technology* TIMOTHY P. LODGE, *University of Minnesota* The phase behavior of symmetric styrene-isoprene diblock copolymers in selective solvents in the vicinity of the order- disorder transition (ODT) was investigated by SANS and rheology. To understand morphological changes in more detail, one of the blocks is deuterated and the scattering length density of the solvents used were identical to the corona chains. We examined two different ODTs: body-centered cubic/disorder and hexagonal cylinder/disorder, with similar SANS results in both cases. With increasing temperature, the micellar aggregation number decreases, and the core radius is roughly maintained by the increased solvent swelling of the core. The critical micelle temperature is experimentally described by an abrupt decrease in the size, aggregation number, and volume fraction of micelles, which is approximately 20-30 C higher than the TODT. Rheological measurements, however, revealed a distinct plateau in elastic modulus just above the temperature of cylinder/disorder. The structure is attributed to the micellar congestions due to the slow break-up of cylindrical domains into an equilibrium distribution of micelles. An isothermal frequency sweep in this regime indicated a very long relaxation time and the transient response significantly depends on solvent selectivity. Possible origins of the remarkable solvent selectivity dependence are also discussed.

**Q1 82 Crystallization studies of polyethylene -poly(ethylene glycol) graft copolymers*** P.R. MARK, G.E. HOVEY, N.S. MURTHY, K. BREITENKAMP, M. KADE, T. EMERICK, *University of Massachusetts, Amherst* Structure and crystallization behavior of three copolymers obtained by grafting poly (ethylene glycol) (PEG) chains to polyethylene (PE) main chain was investigated by variable temperature x-ray diffraction and thermal

analysis. The results show that PEG side chains and PE main chains crystallize into separate domains. This is especially true when grafted chains are long (50 and 100 repeat units), in which the PEG domains are same as in PEG homopolymer both in structure and in melting behavior. In the copolymer with shorter chains (25 repeat units), the PEG crystals are not distinct and melting is broad. The PEG domains can be dissolved in water or ethanol without altering the mechanical integrity of the film. PE crystallites in both samples are similar to that in PE homopolymer. For instance, the thermal expansion of the basal cell plane (a- and b-axes) of the PE domains agrees well with that of PE homopolymer over the entire temperature range from ambient to melt. However, the chain-axis dimension PE-lattice in the copolymer is shorter by $\sim$ 0.05 Å and the basal dimensions are larger by $\sim$ 0.05 Å. The changes in these dimensions due to the changes in the length of the grafted PEG chains were investigated.

*This work was supported by an EPA grant X-83239001-0 to the New England Green Chemistry Consortium (NEGCC)

**Q1 83 Electroluminescence Emission of Fully Conjugated Heterocyclic Aromatic Rigid-rod Polymer Doped in itMulti-wall Carbon Nanotube** JEN WEI HUANG, SHIH JUNG BAI, *National Sun Yat-Sen University* Carbon nanotube and poly-*p*-phenylenebenzobisoxazole (PBO) contain fully conjugated rod-like backbone entailing excellent optoelectric properties and solvent resistance. Rigid-rod polymer PBO is only soluble in methanesulfonic acid or Lewis acid. itMulti-wall carbon nanotube (*M*WNT) was dissolved in a Lewis acid solution of PBO for dispersion of nanotube, and then spun for thin film. *M*WNT concentration in the films was from zero up to 5 wt. %. Compared to that of pure PBO film, composite films of *M*WNT doped PBO showed same UV-Vis absorption peaks which were enhanced with *M*WNT concentration but without overlapping electron orbitals to effect their energy gaps. All films were excited by He-Cd laser with excite wavelength of 325 nm for photoluminescence (PL) response. All PL spectra had maximum wavelength peak at 540 nm indicative of yellow-green light emission. For light emitting diodes, *M*WNT doped PBO would decrease threshold voltage for about 2 V. At 0.1 wt. % of *M*WNT, the composite device emission current was increased up to two orders of magnitude than the PBO diodes without *M*WNT. Further increase of *M*WNT caused a successive decrease in electroluminescence emission intensity attributed to a quench effect form aggregation of *M*WNTs.

**Q1 84 Layer Effects of Photovoltaic Heterojunction of Fully Conjugated Heterocyclic Aromatic Rigid-rod Polymer Poly-*p*-phenylenebenzobisoxazole** JEN WEI HUANG, SHIH JUNG BAI, *National Sun Yat-Sen University* Poly-*p*-phenylenebenzobisoxazole (PBO) contains fully conjugated rod like backbone entailing excellent optoelectronic properties and superior stabilities. Polystyrenesulfonate: poly(2,3−dihydrothieno−1,4−itdioxin) (PEDOT:PSS) is a hole transferring medium which could be spun in to a thin-film between indium-tin-oxide (ITO) and PBO to exhibit highly sensitive photovoltaic (PV) effect. PEDOT: PSS and PBO for medadonor-acceptor interlayer and made photoinduced charge transfer. Optimal absorption PV cell thickness for PBO was about 71nm. By using a layer of lithium fluoride (LiF) as an electron transferring layer, the most open circuit voltage (Voc) and short circuit current (Isc) were achieved at a LiF thickness of 1 nm. The Voc increased from 0.7 V to 0.9 V and the Isc increased one and half times.

**Q1 85 Induced Interaction between Polypyrrole and $SO_2$ via Molecular Sieve 13X** BOONCHOY SOONTORNWORAJIT, ANUVAT SIRIVAT, *PPC, Chulalongkorn University* Electrical conductivity sensitivity and interaction mechanisms between polypyrrole(Ppy)/molecular sieve 13X composites and $CO_2$, CO, and $SO_2$ were investigated. Polypyrrole was synthesized and composites were fabricated from dry mixing and dispersing zeolite particles into the Ppy matrix particles, and followed by compressing into a pellet form. Effects of zeolite concentration, cation type, and cation concentration were investigated. The electrical conductivity in air of Ppy doped with naphthalene-2-sulfonic acid($\beta$) sodium salt increased monotonically with the doping level. There were negligible negative electrical conductivity responses of Ppy and its composites when exposed to $CO_2$, and CO in contrast to definite positive responses towards $SO_2$ in which the interaction was irreversible. Undoped Ppy and doped Ppy composites at 10% v/v of zeolite13X content possessed the highest sensitivity to $SO_2$; beyond this volume fraction the sensitivity was reduced with increasing molecular sieve 13X content. The composites of unmodified 13X, with $Na^+$ fully present within its cavity, gave the greatest electrical conductivity sensitivity towards $SO_2$. The sensitivity of Ppy/13X composite to $SO_2$ diminished when the cation $Na^+$ was exchanged to other alkali cations in this decreasing order: $Cs^+$, $K^+$, and $Li^+$.

**Q1 86 Influence of Green Fluorescent Protein (GFP) Nanoparticles on the Optical and Mechanical Properties of Silk in Bio-Nanocomposites with Photonic Properties** SUREEPORN KOOMBHONGSE, RONALD EBY, *Dept. of Polymer Science, U. of Akron* SHARON JONES, MARK WALKER, RAJESH NAIK, *Air Force Research Laboratory, WPAFB, OH* KATHRYN WAHL, *The Naval Research Laboratory* We are examining the influence of Green Fluorescent Protein (GFP) nanoparticles on optical properties and mechanical properties of silk in bio-nanocomposites membranes. Liquid solutions of GFP have previously been shown to exhibit significant intrinsic two-photon absorption, coupled with fluorescent emission in the visible. The nonlinear absorption and emission of GFP have been shown to saturate at high pump intensities, and upconverted lasing of a GFP-doped polymer film has previously been demonstrated. The observed saturation intensity increases cubically with increasing GFP concentration, suggesting that better access to the intrinsic nonlinearity might be possible at higher concentrations than are possible in liquid solution. Silk and GFP solutions were mixed and cast at different concentration. The nonlinear optical properties of these membranes were examined by two-photon absorption measurements using near-infrared femtosecond pulses. Transmission and upconverted fluorescence of focused near-infrared pulses (780nm, 160fs pulsewidth) is being investigated.

**Q1 87 Fluctuations and Phase Transition-Like Phenomena of a Filled Elastomer Under Deformation** XIAORONG WANG, MINDAUGAS RACKAITIS, *Bridgestone CRT* Fluctuations, critical phenomena and phase transitions have drawn much attention for many years. But, no report anticipates that an elastomer containing fillers under gentle deformations will show similar effects. In this presentation, we show that a filled rubber system under about 2% strain may display feature fluctuations that could be associated with a transition from an elastic solid state to a dispersed fluid state and that is reminiscent of critical phenomena.

**Q1 88 Controlling the interaction between two rolling microcapsules on elastic substrates** ANNA BALAZS, ALEXANDER ALEXEEV, ROLF VERBERG, *Chemical Engineering Department, University of Pittsburgh, Pittsburgh, PA* We study the interaction between two rolling capsules, which model polymeric microcapsules or blood cells. Each capsule consists of an elastic shell that is filled with a viscous fluid. The capsules are driven by an imposed flow to roll along a compliant substrate. To model this multi-component system, we combine the lattice Boltzmann model for fluid dynamics and the lattice spring model for the micromechanics of elastic solids. This technique allows for a dynamic interaction between moving, elastic walls and the surrounding fluid. We determine how the mechanical properties of the substrate and the capsules, and the characteristics of the imposed flow, affect the dynamic behavior of two closely placed capsules. We find that the stiffness of the capsules and the substrate affects the relative motion of the capsules on the surface, i.e., by tuning the mechanical properties, the separation between the capsules can be increased or decreased as they move along the surface. The results provide guidelines for designing micro-reactors that utilize elastic capsules to transport reagents and carry out reactions.

**Q1 89 Tunable Nanoparticle Arrays by Immobilizing Nanoparticles on Polymer Single Crystal Surface*** BING LI, CHRISTOPHER LI, *The Department of Materials Science and Engineering, Drexel University* 2-Dimensional nanoparticle (NP) array has been extensively investigated and a number of techniques are available for fabricating this unique structure. One remaining technical challenge is controlling the inter-particle spacing, which could directly leads to numerous applications. We herein report a novel means to achieve tunable NP arrays by immobilizing AuNPs on polymer single crystal surface. The single crystals of thiol-terminated polyethylene oxide (PEO) were incubated in a monodisperse gold sol. Strong Au-S chemical bonds were formed between the AuNPs and the PEO single crystal surfaces. The inter-particle spacing was controlled by the crystallization temperatures, thus the thickness of the PEO single crystals, the incubation time, and the annealing temperatures after incubation. This research might lead to a novel method to fabricate NP arrays with controlled inter-particle distance from a few nanometers to $\sim$ 100 nm distances.

*This work is supported by NSF Career Award and 3M nontenured faculty grants

**Q1 90 Assessment of structure, dynamics, and stability of HPC microgel nanoparticles in good and poor solvents** KIRIL STRELETZKY, *Cleveland State University* JOHN McKENNA, *Cleveland State University* JERRY HILLIER, *Cleveland State University* RAMI MOHIEDDINE, *Case Western Reserve University* Microgel nanoparticles formed in aqueous solutions of neutral polymer hydroxypropylcellulose (HPC) is a promising drug carrier system due to their ability to solubilize hydrophobic drugs and to serve as vesicles for controlled drug delivery and release. Microgel was synthesized through self-association of amphiphilic HPC molecules at room temperature by lowering polymer phase-transition with salt addition and consequent cross-linking and dialysis. Dynamic Light Scattering and Optical Probe Diffusion techniques were used to study structure and dynamics of microgel of different polymer composition in good and poor solvents. We found the size distribution of microgel to be broad and multimodal in good solvents and narrow and unimodal in poor solvents, indicating shrinking of the nanoparticles. We present comparative analysis of microgel and HPC chain dynamics in good solvents and near good-poor solvent transition. The comparison with polymer transport properties gives important insights into the structure, dynamics, and, potentially, drug delivery capabilities of HPC microgel.

**Q1 91 Optical Effects on Laser Ablated Polymer Surfaces** R.D. PRABHU, R. GOVINTHASAMY, N.S. MURTHY, Laser ablation of poly (ethylene terephthalate) and polyimide films were investigated using Excimer-UV laser. SEM analyses indicate the presence of rings for a wide range of ablation parameters (fluence, frequency and number of pulses). It is proposed that the particles present in the plasma plume could cause the incident laser light to diffract, similar to the optical effects observed in the femtosecond laser ablation of solids. The polymer surface provides a perfect medium to register the optical signatures as seen in the SEM images. The fringe-spacings observed in the images are compared with the theoretical diffraction patterns and the height of the plasma particles above the surface is estimated using an optimization scheme. The results of the analysis are consistent with experimentally observed dynamics of the plasma plume. It is proposed that such optical effects could be a routine feature in the laser ablation of polymers. The significance of such artifacts for lithography is discussed.

**Q1 92 Lessons from Biology: How Patterns Control Adhesion** EDWIN CHAN, ALFRED CROSBY, TINA THOMAS, *University of Massachusetts* Polymer adhesion impacts applications from biomedical devices to semiconductor processing, yet our fundamental control of this property remains a challenge. Nature has shown us through numerous examples (e.g. gecko to lotus leaf) that a powerful strategy for tuning adhesion lies in the development of hierarchal structures at an interface. Although nature has demonstrated this solution, our understanding on using this approach effectively is relatively unexplored. In this work, we seek to understand the inter-relationship between material structure, patterns, and performance (i.e. adhesion) for soft, polymer materials. We present an overview of the importance of length scales in adhesion, our overall strategy, and results on the adhesion of soft elastomers to inorganic surfaces. Through these results, we explain critical scaling relationships that demonstrate the potential for using patterns to tune adhesion, while also illustrating the wide range of mechanisms through which patterns can interact with a polymer interface.

**Q1 93 Elastomer Friction: Understanding Schallamach Waves.** CHARLES RAND, ALFRED CROSBY, *University of Massachusetts, Department of Polymer Science and Engineering* From the dynamics of biomaterial interfaces to the interpretation of nanoscale characterization of polymer interfaces, the friction of soft polymer layers is critical to a wide range of advanced materials. In 1971, Schallamach discovered that friction of soft, elastomeric interfaces is often dominated by the onset and propagation of elastic instabilities in the form of surface waves[1]. Although significant contributions have been made, the fundamental relationship between the polymer structure and Schallamach waves has not been established. We present our results on the development and propagation of Schallamach waves at model, soft interfaces using a custom-built instrument. Our goal is to decouple the interfacial and bulk contributions to the onset and propagation of

these friction-dominating waves. Using interfaces of polydimethylsiloxane and fused silica, we observe critical transitions in the behavior of Schallamach waves and develop qualitative models to link these transitions to interfacial properties. (1)Schallamach, A.;Wear 1971,17, 301-312.

**Q1 94 On Fundamentals of Filler Reinforcement: an Investigation Using Polymeric Nanoparticles** XIAORONG WANG, *Bridgestone Americas, Center for Research & Technology* We investigate the filler reinforcing mechanisms and the interactions using polymer-grafted nanoparticles [1,2] of various brush lengths and densities in polymer matrices of various molecular weights. We find that the modulus enhancement and its nonlinearity vary and depend on the distance of the system approaching the critical state, and that simple laws of corresponding state could describe the phenomena. [1]. Chem. Phys, 2004, 16, 121.; ACS Proceedings: PMSE, March, 2006. [1]. USP6437050; 6689469; 6872785; 6875818; 6956084.

**Q1 95 AFM-TEM observations of effect of ''melt'' time on polytetrafluoroethylene morphology.*** J.P. KALISH, R.A. WILLIAMS, J. WANG, P.H. GEIL, *University of Illinois* T.-C. LONG, P. XU, *W. L. Gore & Assocs., Inc.* TEM observations of PTFE dispersion particles dispersed on glass and held at 350 [r]C or above for various times indicates that individual, $>$ 0.1 mm long molecules wander individually on the substrate and can, with time in the ''melt,'' aggregate and form either flat-on or on-edge, folded chain single crystals. If ''trapped'' by cooling before aggregation, on-edge, single molecule, single crystals can form. All on-edge crystals, both individually and as the shish of shish-kebabs, have a ''double-striation'' appearance, suggested to arise from nucleation of the Pt/C shadowing material, used for the TEM image, on the folds at the top edge of the crystals.[1] AFM observations have confirmed these suggestions and, furthermore, indicate the nascent, rod-like dispersion particles of a ''nano-emulsion,'' with a volume corresponding to a single molecule, have faceted ends. Combined with the TEM and ED observations that the molecular axis is parallel with the rod axis, not only must chain-folding occur during polymerization but the chain folds must be staggered on the end surfaces.

*This research was supported, in part, by the NSF Polymer Program. The TEM and AFM facilities used were supported, in part, by DOE through Grant DEFG02-91-ER45439.

[1]P. H. Geil, et al., Adv. Polym. Sci., 180, 89 (2005).

**Q1 96 Depth Profiling of $^{13}$C Labeled Polymers using Secondary Ion Mass Spectrometry** SHANE HARTON, FRED STEVIE, HARALD ADE, *NC State University* Deuterium labeling is known to change the thermodynamic properties of polymers and polymer blends (e.g. surface tension and bulk phase behavior). Anomalous segregation of dPS to an hPS:dPS/hPMMA interface has been recently observed, where the hPS:dPS blend is well within the single phase region of the phase diagram. Therefore, to probe various physical phenomena at polymer interfaces, such as chain mobility or reactive chain coupling, alternative labels must be established in order to provide a true tracer. It has been found that $^{13}$C labeling provides a true tracer for depth profiling of $^{13}$C-PS in $^{13}$C-PS:hPS and $^{13}$C-PS:hPS/hPMMA blends, with no observable segregation of $^{13}$C-PS to the $^{13}$C-PS:hPS surface or $^{13}$C-PS:hPS/hPMMA heterogeneous interface (Harton et al. Patent Pending). $^{13}$C-PS was synthesized with $\alpha$, $\beta$ $-$ $^{13}$C substituted styrene (33% v/v with 77% unlabeled styrene) using atom transfer radical polymerization with a low polydispersity ($M_w/M_n$ = 1.2). A magnetic sector instrument was used for this analysis to separate $^{13}$C from $^{12}$C$^1$H. This requires a mass resolution ($m/\Delta m$) of $\sim$ 3000, which cannot be achieved with a quadrupole (typical $m/\Delta m \sim$ 300) thereby eliminating its use for depth profiling of $^{13}$C labeled polymers. Mass spectra of labeled and unlabeled PS were also analyzed using time-of-flight (ToF) SIMS to demonstrate the possibility for detection of high molecular weight fragments as a function of depth.

**Q1 97 Solvent mediated assembly of Nanoparticles confined in Mesoporous Alumina*** KYLE ALVINE, DIEGO PONTONI, PETER PERSHAN, *Harvard University* OLEG SHPYRKO, *Center for Nanoscale Materials, ANL* DAVID COOKSON, *Australian Nuclear Science and Technology Organization* KYUSOON SHIN, THOMAS RUSSELL, *University of Massachusetts, Amherst* FRANCESCO STELLACCI, *Massachusetts Institute of Technology* OLEG GANG, *Center for Functional Nanomaterials, BNL* In-situ small angle x-ray scattering measurements of the solvent mediated assembly of 2 nm diameter Au-core colloidal nanoparticles inside mesoporous alumina are presented. The evolution of the self-assembly process was controlled reversibly via solvent condensed from vapor. Measurements of the absorption & desorption of solvent showed strong hysteresis upon thermal cycling. In addition, the capillary transition for the solvent in the nanoparticle-doped pores was shifted to greater under-saturation by a factor of four relative to the expected value for the same system sans nanoparticles. Analysis indicated that a cylindrical shell super-structure of the nanoparticles is maintained throughout the addition and removal of liquid solvent. Nanoparticle nearest-neighbor separation increased and the in-shell order decreased with the addition of solvent. The process was reversible with the removal of liquid. Isotropic clusters of nanoparticles were also observed to form temporarily during desorption of the liquid solvent and disappear upon complete removal of liquid.

*This work was supported in part by NSF Grant No. 03-03916

**Q1 98 APPLICATIONS POSTER SESSION**

**Q1 99 Beam propagation through a thermo-optic waveguide switch** CHANGBAO MA, EDWARD VAN KEUREN, *Georgetown University, Department of Physics* We present simulations and experiments of a thermo-optic waveguide switch using a novel 3-d wide angle beam propagation algorithm. The switch is based on a Y-branch directional coupler, with two microheaters embedded beneath both sides of the Y-branch. These two microheaters act to generate an inhomogeneous temperature profile, by which most of the energy of the light signal propagating in the waveguide will be shifted to one of the two branches. The oblique sections of the waveguides require that the second order terms in the beam propagation method be included in the simulation. Both the thermo-optic effects and beam propagation will be investigated to optimize the parameters of the device.

**Q1 100 Semiconductor lasers in optical communication band with very broadband tunability** GAGIK SHMAVONYAN, *State Engineering University of Armenia* Because the optical fiber has the low-loss window covering from below 1300 nm to above 1600 nm, devices used for optical communication are required to have the broadband characteristics. Several types of non-identical multiple quantum wells had been experimented. One has five 6 nm $In_{0.67}Ga_{0.33}As_{0.72}P_{0.28}$ quantum wells and two 15 nm $In_{0.53}Ga_{0.47}As$ quantum wells, bounded by 15 nm $In_{0.86}Ga_{0.14}As_{0.3}P_{0.7}$ quantum barrier. One type of the non-identical multiple quantum wells has been used to fabricate the semiconductor optical amplifiers for semiconductor lasers with broadband tunability. Inserting the semiconductor optical amplifier in an external-cavity configuration with a grating as the feedback, the external-cavity semiconductor laser is tunable from 1295 nm to 1570 nm, which covers almost the entire low-loss window of the optical fiber. Also, using reflected-type grating telescope configuration, we are able to simultaneously generate two wavelengths. The two lasing wavelengths are tunable from a few nm separation to 170 nm separation. Simultaneous generation of two wavelengths at 1344 nm and 1514 nm in optical communication band is demonstrated.

**Q1 101 Near Field Measurement of Broad Area Laser Diodes by Utilizing Near-Field Scanning Microscope** SOON IL JEONG, JOO IN LEE, *Korea Research Institute of Standards and Science* IL KI HAN, YOUNGCHAI YOO, KYOUNG CHAN KIM, JIN DONG SONG, WON JUN CHOI, WON JO CHO, JUNG IL LEE, *Korea Institute of Science and Technology* SI HYUNG CHO, *Potomac Optronics* MARIO DAGENAIS, *University of Maryland* NANOSURFACE GROUP TEAM, NANO DEVICE RESEARCH CENTER TEAM, POTOMAC OPTRONICS COLLABORATION, ELECTRICAL & COMPUTER ENGINEERING TEAM, It is well known that the filamentation in the broad area laser diodes (BALD) is closely related to the linewidth enhancement factor ($\alpha$-value). While normal $\alpha$ values in the multiple-quantum well (MQW) structure are 2$\sim$ 4, it is expected and calculated that $\alpha$ values in quantum dot (QD) are under 1. This means that the filamentation in the BALD with QD structure would be delayed until higher current level. In this study, we report the difference of near field between QD and QW BALDs by utilizing near-field scanning optical microscope (NSOM). $\alpha$ value in the QD BALD was measured to be around 0.6, while in the QW around 2. It was observed that the BALD with QD kept single mode beam under higher current level than the BALD with QW. This result shows another evidence that QD structure might be more adequate for high power laser diodes with single mode beam characteristics.

**Q1 102 Niobium Hot Electron Bolometer Development for Terahertz Detection*** MATTHEW REESE, *Yale. Univ.* DANIEL SANTAVICCA, *Yale Univ.* LUIGI FRUNZIO, *Yale Univ.* DANIEL PROBER, *Yale Univ.* We have developed both diffusion and phonon cooled Hot Electron Bolometers (HEBs) for detecting weak signals in the submillimeter or terahertz range. The device consists of a superconducting microbridge between two non-superconducting reservoirs. We use niobium as our superconductor and aluminum as our normal metal. The goal of the research is to produce very fast (100 MHz) direct detectors for spectroscopic use, and high bandwidth mixers. We will report the performance as both heterodyne and direct detectors. The microscopic properties of the devices, including the effects of the superconducting proximity effect have also been studied.

*Research Support by NSF-AST and NASA GSRP

**Q1 103 A Magneto-Electric Microwave Filter** A.S. TATARENKO, G. SRINIVASAN, *Oakland University* M.I. BICHURIN, *Novgorod State University, Russia* A new class of electric field-tunable ferrite-ferroelectric microwave band-pass filter is discussed. The electric field tunability is possible through magneto-electric (ME) interactions. The mechanical deformation due to piezoelectric effect in an electric field manifests as a magnetic field shift in the ferromagnetic resonance (FMR) for the ferrite. The filter was fabricated with an ME resonator consisting of bi-layers of 30-110 micron thick (111) yttrium iron garnet (YIG) films and lead zirconate titanate (PZT). The bilayer was positioned between input and output antenna in a microstripline structure. The device insertion loss was measured as a function of frequency f, bias magnetic field *H* (applied parallel to bilayer plane) and the electrical field *E* applied across PZT. The minimum insertion loss was 4-5 dB at 5-10 GHz. The off-resonance losses were about 20 dB. The E-field tunability was 120 MHz for E = 3 kV/cm for bilayers with 110 micron thick YIG. The ME microwave filters discussed here are miniature in size, would facilitate high-speed operation, and are compatibility with integrated circuit technology. – The work was supported by grants from ARO, ONR and NSF.

**Q1 104 A method for anhysteretic magnetization and magnetostriction measurement of a thin ferromagnetic films as a function of an applied isotropic stresses** PETER FINKEL, *Thomson/Rowan University* ED GARRITY, *Thomson* A new method of the stress dependant anhysteretic magnetization and magnetostriction measurements in a thin-film ferromagnetic materials is described. This method is based on conventional vibrating sample magnetometer system combined with the specially designed loading fixture providing sizable uniaxial stresses on thin film and wires. For determining uniaxial stresses in thin-film and wires anisotropic ferromagnetic samples contactless method was developed. Stresses are deduced from characteristic resonant frequency of the sample vibrating in the special fixture and verified using pulse propagation velocity monitoring. Vibration of the sample is measured remotely using a laser Doppler vibrometer. This contactless method has been demonstrated for membrane thickness down to 50 $\mu$m and stresses up to 1GPa. Estimated accuracy of this method is better than 0.2%. This method was applied to measure anhysteretic permeability and magnetization curve of Ni-Fe as a function of stress and temperature. This technique was also shown to be able also used to measure magnetostriction coefficient as a function of external magnetic field.

**Q1 105 Characterization of Binding Strengths of DNA on Various Indium Tin Oxide Conducting Substrates Using Surface Electrophoresis for Genomic Studies/Applications** MICHAEL DING, *Glen Cove High School* ELI HOORY, JONATHAN SOKOLOV, MIRIAM RAFAILOVICH, *Stony Brook University* STONY BROOK UNIVERSITY TEAM, We have analyzed DNA-surface interactions on solid surfaces using surface electrophoresis with λ Hind-III DNA. Laser scanning fluorescence microscopy on YOYO-labeled DNA was used to image molecules exiting deposited drops for different surfaces, buffer concentrations, DNA concentrations, and electric field

strengths. PET Indium Tin Oxide (ITO) and ITO coated glass were studied by varying TBE buffer concentrations from $10^{-2}$X to 3X, DNA concentrations from 5$\mu$g/ml to 50$\mu$g/ml and electric fields from 3 to 7 V/cm. We have obtained defined circular DNA droplets on these surfaces and observed DNA strands being pulled from the outer ring by the electric field. Various adsorption mechanisms and models of mobility will be discussed. Support from the NSF MRSEC program is gratefully acknowledged.

**Q1 106 Shift of Optical Absorbance with Pressure in Star Polymers** JOHN FERGUSON, *AF Research Laboratory, Materials and Manufacturing Directorate, WPAFB, OH 45433* BARRY LONG,* *Physics Dept., Juniata College, Huntingdon, PA 16652* The optical absorbance dependence on pressure is studied for star polymers dispersed (less than 1% wt./wt.) in either polymethylmethacrylate or polycarbonate. The star polymer is composed of a hyperbranched core and $\pi$-conjugated polymer arms. The optical absorbance red shifts with increasing pressure and is expected to be due to increase in the conjugation length. The sensitivity on pressure is greater with the star polymers than for a pure linear polymer of the conjugated arm. The proposed enhancement mechanism is a non-uniform distribution of strain in analogy with the impact toughening of a matrix material by multidimensional additives.

*Work performed under Wright State Univ. REU Program

**Q1 107 Novel biocompatible and biodegradable ultrathin films of poly (L-Lactic acid) by plasma polymerization** YI-HSIN CHANG, CHUN-CHIH CHANG, YING-CHU CHEN, A. C.-M. YANG, *Department of Materials Science and Engineering, National Tsing Hua University, Hsinchu, Taiwan* Y. C. LIU, *Department of Life Science, National Tsing Hua University, Hsinchu, Taiwan* Ultra-thin films ( $\leqslant$ 50 nm) of biodegradable poly (L-lactic acid) were prepared through efficient RF plasma synthesis. The surface morphology of deposited films was amorphous and molecularly uniform (Ra = 0.7 nm). The chemical compositions as determined from FTIR and NMR demonstrated extraordinarily high retention of ester groups with a small fraction of chain cross-linking that could be controlled by process parameters. The chemical routes of the polymerization were described and discussed. This versatile thin film coating technique is very useful for surface engineering of general biomedical devices and implants for improved biocompatibility. In addition, PLLA polymerized in the liquid phase by plasma was also explored and will be presented. This work is supported by National Science Council of Taiwan.

**Q1 108 Terawatt picosecond $CO_2$ laser** DANIIL STOLYAROV, IGOR POGORELSKY, IGOR PAVLISHIN, MARCUS BABZIEN, KARL KUSCHE, *Brookhaven National Lab* V. PLATONENKO, *Moscow University* VITALY YAKIMENKO, *Brookhaven National Lab* We present the design of a powerful $CO_2$ laser that generates short 3 ps pulses with energy exceeding 10 J/pulse. The output of a conventional 1 atm TEA oscillator undergoes pulse shortening via a semiconductor switching method in combination with nonlinear Kerr cell. Pressure broadening of $CO_2$rotational line in the 10 atm regenerative amplifier and the 9 atm final amplifier allows amplification of the short pulse up to several terawatts in peak power without pulse distortion. Present applications of the terawatt $CO_2$laser include various methods of laser acceleration of relativistic electron beams, generation of high-intensity X-rays via Thomson scattering, ion acceleration, etc.

**Q1 109 Synthesis and thermoelectric properties of $Na_xCoO_2$ single crystal*** QING JIE, YUFENG HU, QIANG LI, *Condensed Matter Physics and Materials Science Department, Brookhaven National Laboratory* $Na_xCoO_2$ has been known to be a potential thermoelectric material because of its large thermoelectric power and low resistivity. Recently, $Na_xCoO_2 \cdot yH_2O$ was discovered as a superconductor with a transition temperature $T_c$ of about 5K. Further understanding of the electron structure and properties of this material need larger samples of $Na_xCoO_2$single crystal. In our work, $Na_xCoO_2$ single crystals were grown by flux method. It was found that choosing an appropriate slow cooling temperature region can increase the size of the single crystals grown by this method. The size of the largest single crystal is about $5\times 4 \times 0.02mm^3$. The structure and thermoelectric properties of these crystals will be discussed.

*This work was supported by the U. S. Dept. of Energy, Office of Basic Energy Science, under contract No. DE-AC-02-98CH10886.

**Q1 110 Excitation of surface dipole and solenoidal modes on toroidal structures** MARK JACK, MARIO ENCINOSA, *Florida A&M University* The time-dependent Schrodinger equation inclusive of curvature effects is developed for a spinless electron constrained to motion on a toroidal surface and subjected to circularly and linearly polarized waves in the microwave regime. A seven-state basis set is employed with the goal of determining the character of the surface currents as the system is driven at a resonance frequency that selects for a solenoidal mode. Trajectory methods are used as a means of visualizing the character of the induced surface currents. Optical transitions into solenoidal modes of excitation can be observed.

**Q1 111 Magnetically Modulated Optical Nanoprobes: Live Cells and Bioassay Diagnostics** BRANDON H. McNAUGHTON, JEFFREY N. ANKER, RAOUL KOPELMAN, *University of Michigan, Applied Physics Program; University of Michigan, Chemistry* CALEB J. BEHREND TEAM, KAREN KEHBEIN TEAM, XIAOJING WANG TEAM, Fluorescent techniques are frequently used for chemical analysis in biological samples because fluorescent dyes produce strong signals that can be easily read with conventional photodetectors, spectrometers, and cameras. Magnetic techniques are used for chemical analysis and measurements of physical viscosity/elasticity because strong magnetic forces and torques are easily applied to magnetic particles without shielding or interference from biological samples. Combining fluorescence detection with magnetic manipulation of metal hemisphere coated ''Magnetically Modulated Optical Nanoprobes'' (MagMOONs) provides the best features of both techniques. We describe fabrication of uniform magnetic half-coated particles and MagMOON applications for immunoassays, intracellular chemical sensing, and passive or active viscosity measurements on a single particle and ensemble level that is based, in part, on a newly discovered effect: critical slipping of rotationally driven nanoparticles.

**Q1 112 Phonon engineering of electronic transport in hybrid nanotubes** ALEXANDER A. BALANDIN, VLADIMIR A. FONOBEROV, *Nano-Device Laboratory (http://ndl.ee.ucr.edu), Dept. of Electrical Engineering, University of California, River-*

*side, CA 92521* Recently, a number of biological nanoscale objects, including tobacco mosaic viruses (TMV), have been employed as templates for assembly of inorganic nanostructures. This approach can potentially lead to a new method of fabrication of nanoelectronic circuits beyond conventional CMOS. Here we theoretically demonstrate that in addition to their role as nanotemplates [1], the elastically soft TMVs can improve electron transport in the nanotubes grown on them [2]. In the simulated hybrid nanostructures, which consist of silicon or silica nanotubes on TMVs, the confined acoustic phonons are found to be redistributed between the nanotube shell and the acoustically soft virus enclosure. As a result, the low-temperature electron mobility in the hybrid TMV-silicon nanotube can increase up to a factor of four compared to that of an empty silicon nanotube [2]. Our estimates also indicate an enhancement of the low-temperature thermal conductivity in the TMV-silicon nanotube, which can lead to improvements in heat removal from the hybrid nanostructure-based circuits. The authors acknowledge the support of MARCO and its Functional Engineered Nano Architectonics (FENA) Focus Center. [1] W.L. Liu, K. Alim, A.A. Balandin et al., Appl. Phys. Lett. 86, 253108 (2005); [2] V.A. Fonoberov and A.A. Balandin, Nano Lett. 5, 1920 (2005).

**Q1 113 Nanoscale Silicon Particles in Sandwich Structures Fabricated on Silica Wafers: HRTEM and EDX Techniques as Imaging Tools** PAVAN SINGARAJU, KRISTINA E. LIPINSKA-KALITA, *Department of Electrical and Computer Engineering, University of Nevada Las Vegas* THOMAS HARTMANN, LONGZHOU MA, *Harry Reid Center for Environmental Studies, University of Nevada Las Vegas* BISWAJIT DAS, *Department of Electrical and Computer Engineering, University of Nevada Las Vegas* The use of silicon in optical applications is limited by its small and indirect band gap. However, recent observations of photoluminescence in porous Si and in Si ultra fine particles suggest that Si nanoclusters may become a promising material for optical applications. The nanometric Si clusters have a band gap enlarged into the visible range and quantum confinement effect is believed to be the mechanism for light emission. The ability to control the size and structure of nanoparticles would allow the fabrication of structures with desired electrical and optoelectronic properties for device applications. Nanosized Si particles with controlled diameter were fabricated on silica substrate wafers using an specially designed ultra-high vacuum nanocluster deposition apparatus. We present the structural characterization and composition studies of the fabricated nanostructures using high resolution transmission electron microcopy (HRTEM), x-ray diffraction (XRD) and energy dispersive x-ray (EDX).

**Q1 114 Hydrogen uptake in single-walled carbon nanotubes synthesized by the hydrogen arc plasma jet method.** L.A. MORENO-RUIZ, J. ORTIZ-LOPEZ, *Escuela Superior de Fisica y Matematicas, Mexico* A. DE ITA DE LA TORRE, J.S. ARELLANO-PERAZA, G. FLORES-DÍAZ, *UAM-Azcapotzalco, Mexico* Carbon nanotubes were synthesized by a modified electric arc discharge method under hydrogen atmosphere using a catalytic mixture of powders with composition C/Ni/Co/Fe/FeS. The samples were characterized with transmission and scanning electron microscopy, Raman spectroscopy and thermo-gravimetric analysis. Unpurified samples contain 20 wt% of carbon nanotubes, 2 wt% of other forms of carbon and 78 wt% of catalytic metals. Adsorption/desorption of hydrogen in unpurified samples at atmospheric pressure measured with gravimetric methods was of the order of 2 wt%. Samples for these measurements were prepared with a three-step treatment: (i) oxidation in air for 30 min at 500 °C, (ii) ball- milling for 1 hr, and (iii) second oxidation in air for 30 min at 500 °C. This treatment was applied to eliminate other forms of carbon as well as to shorten the tubes and open their caps. Hydrogen desorption was also measured in degassed samples (400 °C for 20 min in vacuum) which adsorbed $H_2$ while cooling to room temperature. Desorption in degassed/hydrogenated samples is a two-step process which we attribute to distinct desorption characteristics of nanotubes and of residual oxidized metal catalysts.

**Q1 115 Theoretical investigation of catalysed MgH2** PETER LARSSON, C. MOYSES ARAUJO, *Condensed Matter Theory Group, Physics Department, Uppsala University, Box 530, 751 21, Uppsala, Sweden* J. ANDREAS LARSSON, *Tyndall National Institute, Lee Maltings, Prospect Row, Cork, Ireland* PURU JENA, *Department of Physics, Virginia Commonwealth University, Richmond, Virginia 23284-2000* RAJEEV AHUJA, *Condensed Matter Theory Group, Physics Department, Uppsala University, Box 530, 751 21, Uppsala, Sweden* MgH2 has attracted much attention for being a good hydrogen storage material due to its light weight, low manufacturing cost and high storage capacity (7.6 wt%). But its slow absorption/desorption kinetics and high dissociation temperature (nearly 300[r]C) limit its practical applications for hydrogen storage. To overcome this, much effort has been paid mainly by making nanocrystalline Mg and/or by adding alloying elements. In this work, we provide a theoretical investigation of the electronic and structural properties of pure and M-doped MgH2 (with M=Sc, Ti, V, Fe, Ni, Al). We have made calculations for both the crystalline state and 1.0 nm particles. The self-consistent total energy calculations are performed within density functional theory using the VASP package for crystals and TURBOMOLE package for clusters. One aim of this study is to see if the alloying elements can weaken the Mg-H bonds, resulting in improved thermodynamics and faster kinetics. Another one is to understand the differences in the thermodynamics of clusters and crystals.

**Q1 116 Fabrication and Structural Studies of Nanostructured Alumina Templates Using X-Ray Diffraction and EDX Techniques** KRISTINA E. LIPINSKA-KALITA, PAVAN SINGARAJU, BISWAJIT DAS, *Department of Electrical and Computer Engineering, University of Nevada Las Vegas* We have previously developed a thin film template based nanostructure fabrication technique that is applicable for the development of high performance photonic devices. The template is created by the anodization of thin film aluminum deposited on an arbitrary substrate and contains nanoscale pores inside which a nanoscale material could be synthesized. An alumina template is characterized as a nonstoichiometric, amorphous film that is optically transparent over a wide spectral range and is also electrically insulating, which makes it a perfect embedding material for nanoscale devices. We investigated the formation of thin film alumina templates on various substrates, under different fabrication conditions. The final template structure was found to depend on the structure of the starting aluminum film (free standing or deposited on another substrate). We show that pre-anodization annealing of the substrate can dramatically alter the stoichiometry as well as the microstructure of the final template, changing it from amorphous to nanocrystalline.

**Q1 117 The adsorption and photo-degradation of oxalic acid at the $TiO_2$ surface.** CECILIA MENDIVE, *Universitaet Hannover, Germany* MIGUEL BLESA, *CNEA, Argentina* DETLEF BAHNEMANN, *Universitaet Hannover, Germany* Oxalic acid is the simplest model compound to study the heterogeneous photocatalytic oxidation of pollutants on $TiO_2$ containing more than one carboxylate group. We have carried out a study of a system of an oxalic acid solution in contact with a thin film of $TiO_2$ particles employing ATR - FTIR in combination with quantum chemical calculations. Thus, possible adsorption structures have been identified and molecular dynamic simulations have been used to compare their predictions with the experimental data. It was found that the adsorption of oxalic acid on $TiO_2$ in the dark can be explained in terms of two surface complexation modes for the anatase phase and only one surface complexation mode for the rutile phase. We have found that under illumination one of the complexes on the anatase phase preferably undergoes photo-degradation. At the same time water molecules are desorbed from the $TiO_2$ surface by a thermal mechanism induced by the absorption of photons. Both processes favor the adsorption of more molecules of oxalic acid at the $TiO_2$ surface which is thus enriched in the second complexation mode. A similar mechanism was found to occur on the rutile phase. The only complexation mode appears not to be photosensitive but the $TiO_2$ surface is enriched in oxalic acid under illumination due to the replacement of photo-desorbed water molecules.

**Q1 118 Infrared photodetector based on modulation-doped quantum-dot structures*** NIZAMI VAGIDOV, *University at Buffalo* ANDREI SERGEEV, *University at Buffalo* VLADIMIR MITIN, *University at Buffalo* We investigate a device model for the quantum-dot photodetector based on modulation-doped structures (for example, the modulation-doped AlGaAs/GaAS structure with InAs quantum dots). At room temperatures, the electron momentum relaxation is determined by electron- phonon scattering. The electron mean free path is small and the photoelectron capture is conditioned by electron diffusion in the potential relief created by modulation doping. Modeling with diffusion-limited capture is used to evaluate the photodetector performance. The results show that the modulation-doped structures provide longer lifetimes of photoelectrons, which in turn improves the photoconductive gain and sensitivity.

*Supported by NYSTAR

**Q1 119 Nanoscale Metal-molecule contacts** ARTUR ERBE, SIMON VERLEGER, BERND BRIECHLE, *FB Physik, Universitaet Konstanz, Germany* Studies of the influence of the metallic contacts to the electronic transport through single or a few molecules are reported. In order to separate these influences from intrinsic molecular properties we use a number of different, versatile contacting methods. The tested molecules vary from nominally insulating molecules to molecules with conjugated charge systems. It is important that the coupling of the molecules to the electrodes is mechanically and electronically stable throughout the experiment. As a first step two different structures allowing for the change of the mechanical coupling will be analysed to find an optimal configuration. On the one hand a mechanically controllable break-junction (MCB) technique will be studied, on the other a shadow evaporation technique based on a silicon structure will be tested. Transport through the molecules can be investigated at different temperatures. First results indicate that the interplay between the metallic electrodes and the molecules depends strongly on the coupling of the electrodes to the molecules and on the packing of the molecules on the metallic substrates.

**Q1 120 All Electronic Charge Carrier Transit Time Mobility Measurements and Data Analysis in Pentacene Organic Field Effect Transistors** LAWRENCE DUNN, *University of Texas at Austin and IMRE, Singapore* DEBARSHI BASU, LIANG WANG, ANANTH DODABALAPUR, *University of Texas at Austin* In organic field-effect transistors (OFETs), the most common method of estimating mobility is to extract it from the transfer characteristics (*e.g.*, $I_d$-$V_{ds}$ and $I_d$-$V_{dg}$ curves). Time-of-flight measurements via optical excitation of charge carriers in the organic material are also used, but this technique measures the mobility of carriers perpendicular to their motion in the OFET geometry. Additionally, in some polycrystalline organic semiconductors, the optically excited time-of-flight measurements are rendered difficult due to charge trapping. We present an all-electronic time of flight method for measuring the in-plane mobility of charge carriers using an applied voltage pulse to the source of the OFET with a rise time of $<$ 60 ns. The gate of the OFET was grounded and the drain was connected to ground across a small load resistor. The transit time of the charge carriers from the source to the drain was measured by recording the voltage drop across the load resistor using a high-speed oscilloscope. The fabrication of the OFET, extraction of the charge carrier transit time from recorded data and effect of the displacement current over varying temperature and voltage step magnitudes will be discussed.

**Q1 121 Temperature dependent spectroscopy of poly[bis-(2-ethyl) hexylfluorene]/ (9,9-di- *n* -octylfluorene) copolymers*** HYEUNSEOK CHEUN, *University of Wisconsin* MICHAEL WINOKUR, *University of Wisconsin* BENJAMIN NEHLS, *University of Wuppertal* FRANK GALBRECHT, *University of Wuppertal* ULRICH SCHERF, *University of Wuppertal* A series of random polyfluorene (PF8) copolymers comprised of linear di-*n*-octyl (F8) and branched bis(2-ethylhexyl) (F2/6) units has been synthesized and characterized by temperature dependent steady-state absorption and emission spectroscopy. The F2/6 polymer is already well known for forming conformationally disordered five fold helices while the F8 polyfluorene adopts a number of distinct near-planar type conformational isomers. One of these conformational sequences is an unusual low energy absorption and emission band known as the $\beta$ phase. In these copolymers the PF chains must temporize between differing interchain packing motifs, pentagonal and planar type structures, and different main chain morphologies. Increasing the content of F2/6 monomers strongly affects the formation of the $\beta$ phase conformer, enhances the extent of conformational disorder (and the effective electron-phonon coupling strengths) and also alters the bulk structural phase behavior. There are only weak correlations between the overall phase behavior and the observed spectroscopy at temperatures below 100 °C.

*Support through NSF grant DMR-0350383 (M.J.W., H.C) is gratefully acknowledged

**Q1 122 Vapor deposited organic thin films with large third order nonlinearities for integrated nonlinear optics** BWEH ESEMBESON, JOSHUA C. MAY, IVAN BIAGGIO, *Department of Physics and Center for Optical Technologies, Lehigh University* TSUYOSHI MICHINOBU, FRANÇOIS DIEDERICH, *Laboratorium für Organische Chemie, ETH-Hönggerberg* We used vapor deposition in high vacuum to fabricate homogenous organic thin films for third-order nonlinear optics. We used small molecules that have a high third order polarizability, are robust, and can be sublimated without decomposition. The most important example is 1,1,2-tricyano-2-[(4-dimethylaminophenyl)ethynyl]ethene (TDMEE), which has a itspecific third order polarizability one order of magnitude larger than other highly nonlinear molecules. It is a member of a family of donor-substituted cyanoethynylethene molecules that has recently been found to have polarizabilities that approach Kuzyk's fundamental limit.[1] The organic thin films have a high, flat transmission above 1000 nm, a high two-photon absorption near 1200 nm, and an essentially real third order polarizability at 1.5 $\mu$m that is three orders of magnitude larger than fused silica.

[1]J. C. May et al, Opt. Lett. 30, 3057 (2005)

## Q1 123 GENERAL THEORY (THEORETICAL METHODS) POSTER SESSION

**Q1 124 The Relativity of the Photon Mass** SERGEJ REISSIG, *EFBR* In the standard model of the electromagnetic radiation, a photon is mass-less. In [1] it was showed that the puzzling question – whether a photon does or does not have a zero mass – can be however answered. According to the new viewpoint, photons can exist in two states: 1) photons have energy and collide neither with a medium nor with surfaces; 2) photons collide with a medium or a surface. In the first case (1), photons possess latent or potential energy and are invisible. In the second case (2), they are visible Wirkungsquantums according to the Planck's quantum theory. The energy of a photon could in case (1) be determined by Planck's equation $E_P^1 = hf$ and in case (2) by Einstein's formula $E_P^2 = mc^2$. By a collision (Wirkung) between a photon and a medium or surface, an energy transformation takes place: the mass-less and invisible light particle (phantom) with latent energy, is converted into a visible photon, which now possesses an impulse mass and energy. For the case that the photons ''bomb'' a surface, which moves with a velocity $v$ into the same direction as the photons, a new equation for the photon mass has been derived: $m_P = 2.2102186 \cdot 10^{-42} \cdot \lambda^{-1} \cdot [(1 - v/c)/c)(1 + v/c) \times (1 + v/c)]^{0.5}$(kg) 1. Über die Relativität der Masse und Energie des Lichtquanten, S. Reißig, 2005, http://www.efbr.org in /Publikationen.

**Q1 125 Correlation Energy of A Model Problem** MAURICIO CAMPUZANO, VASSILIOS FESSATIDIS, *Fordham University* JAY D. MANCINI, *Kingsborough College of CUNY* SAMUEL P. BOWEN, *Chicago State University* The search for new analytic methods of calculating details of the energy spectrum of strongly interacting systems has long been the vocation of both theoretical chemists and physicists. In particular, the accurate calculation of both the ground-state and correlation energies are important in settling issues relating to the exact nature of the ground-state and low-lying excited states. Furthermore there exist a number of physically relevant systems that cannot be treated by perturbation theory or in which other approximation schemes yield completely erroneous results. Exact diagonalization studies are well known to suffer from size effects, while the neglection of correlations in fluctuations in mean-field theories, although calculationally tractable, leave much to be desired. Here we wish to apply a recently developed Generalized Moments Expansion (GMX) [1] to the problem of $N$ coupled one dimensional harmonic oscillators given by the Hamiltonian: $H = \frac{1}{2}\Sigma_{j=1}^{N}(-d^2/dx_j^2 + \omega^2 x_j^2) + g^2\Sigma_{ij}^{N} x_{ij}$. Comparisons are then made with other methods such as a Lanczos tridiagonalization scheme as well as a Canonical Sequence Method approach. [1] V. Fessatidis, J.D. Mancini, R. Murawski and S.P. Bowen, Phys. Lett. A.

**Q1 126 Zero-Point Energy of the Pullen-Edmonds Hamiltonian** JAY D. MANCINI, *Kingsborough College of CUNY* VASSILIOS FESSATIDIS, MAURICIO CAMPUZANO, *Fordham University* SAMUEL P. BOWEN, *Chicago State University* Here we wish to apply the newly developed Generalized Moments Expansion (GMX) to the well-known potential

$$U = 1/2\,(x^2 + y^2) + \alpha x^2 y^2,$$

which is used to model such molecular systems as formamide and rm$C_2O_3$. Our motivation is to investigate the numerical accuracy as well as the viability of the GMX for evaluating ground-state energies of quantum Hamiltonian systems. The zero-point energy of this potential is calculated and results are compared to an analogous Lanczos (tridiagonal) matrix truncation as well as to a Canonical Sequence Method approach.

**Q1 127 Ground-State Energy of A Two-Level System with Phonon Coupling** WILLIAM J. MASSANO, *SUNY Maritime* VASSILIOS FESSATIDIS, *Fordham University* JAY D. MANCINI, *Kingsborough College of CUNY* SAMUEL P. BOWEN, *Chicago State University* The coupling of a two-level system to a quantized boson mode has been the focus of many researchers for a number of years. Applications to exciton motion, molecular polaron formation, chaos in quantum systems as well as a number of other effects in condensed matter physics have also been studied. Here we investigate the interaction of a single bosonic mode with a two-level fermionic system given by the Hamiltonian

$$H = -\delta_0\sigma_x + \sum_k \hbar\omega_k a_k^\dagger + \sum_k g_k(a_k^\dagger + a_k)\sigma_z.$$

This quantum system is used as a testing ground for a newly developed Generalized Moments Expansion, GMX($m$,$n$), of which the well-known Connected Moments Expansion (CMX) and Alternate Moments Expansion (AMX) are special cases: rmCMX= rmGMX(1,1), rmAMX=GMX(1,2). The convergence and viability of this scheme is discussed and comparisons are made with other methods.

**Q1 128 Locating Regions of Complex Zeros of the Mittag-Leffler Function $E_{\alpha,\beta}(z)$ for $2 < \alpha \leq 3$** JOHN W. HANNEKEN, TRENTON R. ENSLEY, STEPHAN T. SPENCER, B. N. NARAHARI ACHAR, *University of Memphis* The Mittag-Leffler function $E_{\alpha,\beta}(z)$, which is a generalization of the exponential function, arises frequently in the solutions of differential and integral equa-

tions of fractional order. Moreover, the zeros of $E_{\alpha,\beta}(z)$ for some values of $\alpha$ and $\beta$ are the eigenvalues of fractional differential operators. Consequently, knowledge of the zeros and their distribution is of fundamental importance. This work focuses on the distribution of zeros in the region where the Mittag-Leffler function possesses an infinite number of real zeros and a finite number of complex zeros and is restricted to the range $2 < \alpha \leq 3$ and $\beta \leq 14$.

**Q1 129 Dynamics of a Pair of Coupled Fractional Oscillators** NARAHARI ACHAR, TANYA PROZNY, JOHN HANNEKEN, *University of Memphis* The integral equations of motion of a pair of coupled fractional oscillators are obtained by generalizing the equations of motion of a pair of coupled harmonic oscillators to integrals of fractional order. The Greens function dynamic response to sinusoidal forcing is given in terms of Mittag-Leffler functions. A direct and transparent derivation of the results of Ryabov and Puzenko obtained by a tedious perturbation method is presented.

**Q1 130 A Time Dependent Approach for Computing N-N Phase Shifts and Cross Sections** BRIAN DAVIS, DAVID WEEKS, *Air Force Institute of Technology* Scattering matrix elements for n-n, n-p, and p-p collisions are computed using a new time dependent wave packet technique. Using this approach, reactant and product channel packets are prepared in the asymptotic limit on the N-N potential energy surfaces. For these calculations we are using the Argonne v18 potential package (1). The channel packets are propagated in time using the split operator method together with a unitary transformation that diagonalizes the tensor potential. Scattering matrix elements are computed from the Fourier transform of the correlation function between the evolving channel packets. Phase shifts and cross sections are computed from the scattering matrix elements. (1) R.B.Wiringa, V.G.J. Stoks, and R.Schiavilla, Phys Rev C **51** (1995) 38

**Q1 131 Tunneling Density of States for 2D Fermi Liquid*** GODFREY GUMBS, *Hunter College of CUNY* EUGENE KOGAN, *Bar-Ilan University, Israel* We calculate the Green's function for an interacting two-dimensional electron liquid whose strength of interaction is characterized by the electron density parameter $r_s$. The screened electron-electron interaction is expressed in terms of a frequency and wave vector-dependent dielectric function $\varepsilon(q,\omega)$. If this screening is neglected, the tunneling density of states (DOS) is strongly modified due to electron-electron interaction. In particular, in this case, the DOS has a dip near the Fermi energy whose width increases with $r_s$. By treating $\varepsilon(q,\omega)$ in the hydrodynamical approximation, we investigate the way in which the tunneling DOS is modified at various electron densities, due to screened interaction. Preliminary results show considerable modification of the tunneling DOS at large $r_s$ for both a noninteracting and unscreened electron system. When there is screening, the dip becomes less pronounced but survives.

*Supported by Fulbright Foundation

**Q1 132 On the quantum master equation with nonhermitian operators** CHUN-FENG HUANG, *National Measurement Laboratoy, Center for Measurement Standards, Industrial Technology Research Institue* K.-N. HUANG, *Institute of Atomic and Molecular Sciences, Academia Sinica* A quantum master equation is derived for fermions by considering a relaxation term in addition to the mean-field Hamiltonian. [C. F. Huang and K.-N. Huang, Chinese J. Phys. **42**, 221 (2004); Ralph Gebauer and Roberto Car, Phys. Rev. B **70**, 125324 (2004).] The relaxation term is symmetric with respect to particles and holes, and its loss and gain factors can be obtained by incorporating nonhermitian parts to the Hamiltonian for the decays of particles and holes, respectively. Such an equation reduces to the Markoff master equation of the Lindblad form when the electrons or holes are of the low-density distribution. On the other hand, the derived equation reduces to the quasiclassical master equation in an incoherent limit. Both the loss and gain factors induce the decoherence. From Cauchy's inequality, we can see that the decoherence is important to keep both the density matrices for particles and holes as positive operators. The positivity of the density matrix for holes, in fact, indicates the validity of Pauli exclusion principle under the derived master equation. To further investigate the decoherence, we compare the master equation for fermion to that for bosons. The gain factor of the latter equation does not induce the decoherence, which is reasonable because bosons do not need to follow the Pauli exclusion principle.

**Q1 133 The Induced Coherent Interaction of Localized Spins via Thermal Bosonic Environment.** DENIS TOLKUNOV, DMITRY SOLENOV, VLADIMIR PRIVMAN, *Clarkson University* We obtain the indirect coherent interaction between two spins induced by the bath of bosonic modes, and demonstrate that this interaction can create entanglement. We utilize a perturbative approach to obtain a quantum evolution equation for the two-spin dynamics. The induced interaction is calculated exactly. The exact solution is then used to identify the time scales for which the spins remain entangled.

**Q1 134 Pair State Analysis of the Hubbard Hamiltonian in One-Dimension** W. B. HODGE, N. A. W. HOLZWARTH, W. C. KERR, *Wake Forest University* Using two-electron states as the basis, we have analyzed the one-dimensional Hubbard Hamiltonian (HH) with periodic boundary conditions for many-electron systems. The N-electron energy eigenvalues are simply the sum of the pair energies (eigenvalues of the two-particle reduced HH) weighted by two-particle density matrix elements. We are investigating the possibility that this approach will lead to a useful approximation scheme. For many weakly correlated systems, the pair-energy sum can be truncated and still the ground state energy can be obtained with reasonable accuracy. For example, in the case of six sites at half-filling (with U/t = 1) we need only include 12 of the 45 triplet pair states and 6 of the 21 singlet pair states, and still the ground state energy can be found with only 6% error. A comparison between the exact and approximate results for this system and several others are presented.

**Q1 135 P3/2 state in New Dirac Equation** DAVID MAKER, In this talk I explain the very interesting properties of the itmost probable excited state of a itnew type of Dirac equation and singularity when applied to a itsingle type of charge 'e'. Notably this first excited state psi*psi P3/2 (state lobes) shape is a trifolium, itthree lobed. Thus for each lobe there is a (1/3)e average charge given the charge 'e' spends on average 1/3 of the time in each lobe. Thus combinations of lobes have average charge, **e/3**, 2e/3 (FRACTIONAL CHARGE) or e. The lobes itcan't leave (ASSYMPTOTIC FREEDOM) or move so are NONRELATIVISTIC. The singularity of this Dirac equation results in containment at

about.6 Fermi, the TOTAL CHARGE is still '**e**'(explaining away the need for COLOR), etc. Most importantly the Frobenius series solution to this new Dirac equation also gives accurate hadron eigenvalues. You quickly see that you are getting here all the properties of quarks (identified here as individual lobes) obtained in a very simple way from the movement of a single unit charge 'e' using this new Dirac equation. There appears no simpler way to explain all these many quark properties.

**Q1 136 Some Interesting Symmetries of the Gravitational Stress Energy Tensor.** JOSEPH D. RUDMIN, *James Madison University* Some thoughts are presented on a few symmetries found in the Gravitational Stress Energy Tensor, with implications for black holes, fermion masses, and unification theories.

**Q1 137 ''Hidden Kinetic Energy'' and ''Mass-Electric'' Principle** PHILIP CHU, *Avery Dennison* A hypothesis is proposed which suggests another fundamental energy equation of Special Relativity. Another relativistic variance is described which gives self-consistent definition of Lagrange Function for both classical and relativistic dynamics. This hypothesis leads to a new ''Hidden Kinetic Energy'' concept as well as a new ''Mass-Electric'' Principle.

**Q1 138 Acceleration of Markov Chain Monte Carlo Simulations through Sequential Updating** RUICHAO REN, GERASSIMOS ORKOULAS, *University of California, Los Angeles* Strict detailed balance is not necessary for Markov chain Monte Carlo simulations to converge to the correct equilibrium distribution. In this work, we propose a new algorithm that only satisfies the weaker balance condition. The new algorithm is based on sequential updating moves with a small fraction of randomness to eliminate possible oscillatory effects. We prove analytically that the new algorithm identifies the correct equilibrium distribution. In addition, based on the properties of the diagonal elements of the underlying transition matrices, we demonstrate that the new algorithm converges faster than the Metropolis algorithm with strict detailed balance. We illustrate the efficiency of the new algorithm on the two- dimensional Ising model. The sequential update algorithm also compares well with multispin-based Monte Carlo techniques. The new method, however, is very general and can be readily extended to off-lattice continuum systems in various ensembles (canonical and grand canonical) with minor modifications. Simulation results on hard-spheres, square-well, and Lennard- Jones fluids indicate that the new method is more efficient in reducing autocorrelation times than conventional Metropolis- type of algorithms in canonical and grand canonical ensembles. Regarding off-lattice continuum fluids, autocorrelation time reduction is more substantial at higher densities due to the sequential nature of the Monte Carlo moves.

**Q1 139 Competing instabilities in correlated electronic systems in the FLEX framework** IRINA BARIAKHTAR, *Boston College* ALEXANDER NAZARENKO, *Sonic Software* JAN R. ENGELBRECHT, *Boston College* We consider the Hubbard model in the regime of strong correlations on bipartite and frustrated lattices. While it is well established that on a bipartite lattice at half filling the leading instability is in the SDW channel, upon varying the lattice symmetry and the electron concentration, competing instability channels emerge. We study possible channels such as pair, magnetic and charge correlations that can be either commensurate or incommensurate. We use the fluctuation-exchange approximation to investigate the development of, and competition between, different kinds of incipient instabilities in these particle-particle and particle-hole channels.

**Q1 140 Geometries of small cadmium selenide clusters*** MOHAN VARANASI, MICHAEL LISOWSKI, RONALD COSBY, *Ball State University* The sizes, shapes, relaxed atomic positions, eigenvalues, and total energies are calculated for selected ultrasmall CdSe clusters using SIESTA, a software package for electronic structure calculations and molecular dynamics simulations of molecules and solids. The properties of these bare clusters with small numbers of constituent atoms are studied using density functional theory (DFT) for energy calculations and the conjugate gradient approximation method in relaxing the structure to find the lowest energy configurations. The itab-initio norm-conserving pseudopotentials, the exchange-correlation approximation, and parameters used in the computations are discussed. We describe ancillary software for calculating initial atomic coordinates, testing pseudopotential transferability, and conveniently generating input data files.

*Supported by The Indiana 21st Century Research and Technology Fund.

**Q1 141 The wavefunction topography in the regime of Fano interference*** A. M. SATANIN, *Institute for Physics of Microstructures, Nizhny Novgorod, Russia* Y. S. JOE, R. M. COSBY, *Ball State University, Muncie, IN* In a point contact the wavefunctions belong to the continuum and the imaging of quantum states is based on measurements of the local density of states or the conductance. An attractive quantum dot in the 2D-waveguide can produce a Fano resonance in the conductance. We present here analytical calculations of conductance variation with the short range attractive potential for modeling the probe experiments in the regime of the Fano interference. It was shown that the wavefunction variation in the waveguide may be expressed through the Green's function of an unperturbed system if the characteristic size of the probing potential is less than the Fermi wavelength. We have found that in general the variation of the conductance depends on the phase interference of different waveguide modes. At the same time in the Fano regime in the conductance variation, there are dominant terms proportional to a resonant wavefunction. It was shown that this property suggests the possibility of extracting the wavefunction related to the Fano resonance.

*Supported by The Indiana 21st Century Research and Technology Fund and the Russian Basic Research Foundation, Grant No. 05-02-16762.

**Q1 142 A Numerical Investigation of the Non-Linear Interaction Forces in Tapping Mode Atomic Force Microscopy** NASTARAN HASHEMI, MARK PAUL, *Virginia Tech* There is an important need to measure the topography of soft materials including many of biological importance. Such soft and fragile materials can easily be damaged by the use of conventional nanoscale materials characterization instrumentation. Tapping mode atomic force microscopy routinely measures the topography of materials

with atomic resolution. For soft materials this is limited by the nonlinear contact forces imposed upon the sample by the oscillating cantilever tip. A fundamental understanding of these forces could lead to techniques capable of minimizing the possibly destructive tip-sample interactions. A physical model of the contact interactions is constructed and numerical simulations of the cantilever dynamics are presented to explore these possibilities.

**Q1 143 Analytical solutions of the Poisson-Boltzmann equation: biological applications** ANDREW FENLEY, *Virginia Tech (Physics Dept.)* JOHN GORDON, ALEXEY ONUFRIEV, *Virginia Tech (Computer Science Dept.)* Electrostatic interactions are a key factor for determining many properties of bio-molecules. The ability to compute the electrostatic potential generated by a molecule is often essential in understanding the mechanism behind its biological function such as catalytic activity, ligand binding, and macromolecular association. We propose an approximate analytical solution to the (linearized) Poisson-Boltzmann (PB) equation that is suitable for computing electrostatic potential around realistic biomolecules. The approximation is tested against the numerical solutions of the PB equation on a test set of 600 representative structures including proteins, DNA, and macromolecular complexes. The approach allows one to generate, with the power of a desktop PC, electrostatic potential maps of virtually any molecule of interest, from single proteins to large protein complexes such as viral capsids. The new approach is orders of magnitude less computationally intense than its numerical counterpart, yet is almost equal in accuracy. When studying very large molecular systems, our method is a practical and inexpensive way of computing bio- molecular potential at atomic resolution. We demonstrate the usefullnes of the new approach by exploring the details of electrostatic potentials generated by two of such systems: the nucleosome core particle (25,000 atoms) and tobacco ring spot virus (500,000 atoms). Biologically relevant insights are generated.

**Q1 144 Semi-Meissner state and neither type-I nor type-II superconductivity in multicomponent systems*** EGOR BABAEV, *Cornell University* MARTIN SPEIGHT, *Leeds University* Traditionally, superconductors are categorized as type-I or type-II. Type-I superconductors support only Meissner and normal states, while type-II superconductors form magnetic vortices in sufficiently strong applied magnetic fields. Recently there has been much interest in superconducting systems with several species of condensates, in fields ranging from Condensed Matter to High Energy Physics. Here we show that the type-I/type-II classification is insufficient for such multicomponent superconductors. We obtain solutions representing thermodynamically stable vortices with properties falling outside the usual type-I/type-II dichotomy, in that they have the following features: (i) Pippard electrodynamics, (ii) interaction potential with long-range attractive and short-range repulsive parts, (iii) for an n-quantum vortex, a non-monotonic ratio E(n)/n where E(n) is the energy per unit length, (iv) energetic preference for non-axisymmetric vortex states, ''vortex molecules.'' Consequently, these superconductors exhibit an emerging first order transition into a ''semi-Meissner'' state, an inhomogeneous state comprising a mixture of domains of two-component Meissner state and vortex clusters. We also discuss a counterpart of this state which may occur in type-I/type-II superconducting bilayers.

*supported by STINT and Swedish Research Council, National Science Foundation and Norwegian Research Council

## Q1 145 GENERAL POSTER SESSION

**Q1 146 The St.- Petersburg State University Experiment that discovered the Photon Acceleration Effect** KONSTANTIN GRIDNEV, RUSSELL MOON, VICTOR VASILIEV, Using the principles of the Vortex Theory, it was theorized that when a photon encounters an electromagnetic field, both the velocity and the frequency of the photon will change. To prove this revolutionary idea an experiment was devised using a laser interferometer and two electromagnets. The electromagnets were arranged so that when the beam splitter divided the initial beam of laser light into two secondary beams; one of the two secondary beams passed back and forth between the two magnets. With the DC current to the electromagnets turned off, the two beams formed an interference pattern on the target screen. When the current to the electromagnets was suddenly turned on, the pattern fluctuated wildly until the two beams again reached a quiescent state creating a stable pattern on the screen; when the current to the electromagnets was suddenly turned off, again the pattern fluctuated wildly until it reached a quiescent state forming the initial stable pattern on the screen. It was determined that this new effect was a phenomenon created by the changing frequency of the laser light whose velocity is increasing as it passes between the expanding electromagnetic field of the magnets. Because it is a new phenomenon in science revealing that the speed of light is not a constant but indeed can be varied, it possesses great historical significance. It is called the Photon Acceleration Effect.

**Q1 147 The Neutral Pentaquark** RUSSELL MOON, *Consultant* FABIAN CALVO, *Consultant* VICTOR VASILIEV, *Prof., Dr.* Using the principles of the Vortex Theory, it was discovered that when the gamma ray strikes a nucleon, the positively charged pentaquark [and the $K^-$ meson] had to be created by the collision with neutron. This discovery further reveals that if the gamma ray strikes a proton it can create a Neutral Pentaquark [and a $D^+$ meson]. The neutral pentaquark will consist of an up, up, down, down, and an anti-charm quark, while the $D^+$ meson will consist of a charm and an anti-down quark. The neutral pentaquark will later decay into a neutron and $D^0$meson. Because the vortex theory also reveals that the strong force couples a proton to a neutron, the neutron that was coupled to the proton in the nucleus will also be found amid the debris particles. References: 1. R.G. Moon, V.V. Vasiliev, Book of abstracts NUCLEUS-2003, October 7-10, Moscow, St.-Petersburg, Russia, p.251. 2. R.G. Moon, V.V. Vasiliev, Book of abstracts NUCLEUS-2004, June 22-25, Belgorod, Russia, p.259. 3. R.G. Moon, V.V. Vasiliev, Frontiers in the Physics of Nucleus, June 28-July 1, 2005, St-Petersburg, Russia, p. 34.7

## Q1 148 HIGH PRESSURE PHYSICS POSTER SESSION

**Q1 149 Partial Phonon Densities of States at the Fe-Sites in several Fe-Sn Intermetallic Compounds under Pressure*** HUBERTUS GIEFERS, *HiPSEC, Department of Physics, University of Nevada Las Vegas, Las Vegas, NV 89154-4002* MICHAEL PRAVICA, *HiPSEC, Department of Physics, University of Nevada Las Vegas, Las Vegas, NV 89154-4002* MICHAEL HU, *HPCAT and Carnegie Institute of Washington, Argonne, IL 60439* MALCOLM NICOL, *HiPSEC, Department of Physics, University of Nevada Las Vegas, Las Vegas NV 89154-4002* We studied the nuclear resonant inelastic x-ray scattering (NRIXS) of Fe-57 in several Fe-Sn intermetallic compounds up to 30 GPa. The samples ($FeSn_2$, FeSn, $Fe_5Sn_3$, and $Fe_3Sn$) were prepared in the HiPSEC laboratory with 95% enriched Fe-57 and 93% enriched Sn-119. NRIXS spectra were collected at HPCAT beamline 16-ID-D at the Advanced Photon Source. High-pressure experiments were conducted using a Paderborn-type DAC [1]. The pressure dependence of the partial phonon DOS spectra will be discussed in terms of elastic and thermodynamic parameters, such as the Lamb-Mössbauer factor, mean force constant, free energy, and Grüneisen parameters, using results from recent x-ray powder diffraction experiments of the Fe-Sn intermetallics under pressure. [1] H. Giefers et al., High Pressure Research 22 (2002) 501. [2] H. Giefers et al., J. Alloys Compd. accepted.

*Supported by DOE FC08-1NV14049. HPCAT is operated by UNLV, CIW, LLNL, CDAC, and U Hawaii. DOE W-31-109-Eng-38 supports the APS.

**Q1 150 High-Pressure Synchrotron RadiationX-Ray Diffraction and Vibrational Spectroscopic Studies of 3,3,7,7-tetrakis(difluoramino)octahydro-1,5-dinitro-1,5-diazocine (HNFX)*** CEDRIC GOBIN, JERRALIE ORWIG, MALCOLM NICOL, *High Pressure Science and Engineering Center, Department of Physics, University of Nevada Las Vegas, Las Vegas, NV 89154-4002, USA.* HNFX, 3,3,7,7-tetrakis(difluoramino)octahydro-1,5-dinitro-1,5-diazocine, belongs to a new class of compounds predicted to be potentially superior explosives or solid propellant oxidizers, the itgem-bis(difluoramino)-substituted heterocyclic nitramines [1,2]. HNFX has been studied in diamond anvil cell up to 30 GPa by synchrotron radiation x-ray diffraction, Raman and infrared spectroscopy at ambient temperature. The pressure-induced alterations in the profiles of the peaks, including their positions, widths and intensities are presented. No phase transition was observed on this range of pressure. The bulk modulus and its pressure derivative were estimated by the third-order Birch-Murnaghan isothermal equation of state up to 6.6 GPa. To the best of our knowledge, this work presents the first high-pressure investigations of HNFX and more generally of a itgem-bis(difluoramino)-substituted heterocyclic nitramine. [1] R. S. Miller; Chemistry of Energetic Materials; Ed. G. A. Olah and D. R. Squire; Chapt 4; p77; (**1996**). [2] R. D. Chapman, R. D.Gilardi, M. F. Welker, C. B. Kreutzberger; J. Org. Chem.; 64; p960; (**1999**).

*Supported by ARO W911NF-05-1-0266

**Q1 151 Structure phases of $MgSiO_3$ in Earth's lower Mantle: ab initio calculations** MOHAMMED SAHNOUN, PATRIC OULEVEY, *Department of Chemistry, University of Fribourg, CH-1700 Fribourg, Switzerland* BERNARD GROBETY, *Department of Mineralogy, University of Fribourg, CH-1700 Fribourg, Switzerland* CLAUDE DAUL, *Department of Chemistry, University of Fribourg, CH-1700 Fribourg, Switzerland* The Earth's mantle is divided into five layers with four major phase transitions at 410, 520, 660 and ~ 2600-km depths, due to a structural and chemical changes of its main constituent minerals. $MgSiO_3$ is believed to be a predominant mineral, at least in the upper part of the lower mantle. $MgSiO_3$ has a structural sequence from corundum-type ilmenite to $CaIrO_3$-type structure (Cmcm symmetry). First-principles calculations have been performed within the full-potential linearised augmented plane-wave method (FP-LAPW). We calculated equilibrium lattice parameters at different pressures up to 150 GPa. Four crystal structures relevant to $MgSiO_3$ were considered and they can grouped in two pairs of distinct types: **(a)** corundum-like and $Rh_2O_3$(II) structure-like, and **(b)** perovskite and $CaIrO_3$ structure-like. To investigate the structural phase transitions in $MgSiO_3$, we calculated the enthalpy (E+PV) of the four-structures as a function of pressure from 0 to 150 GPa. The intersection of the curves indicates which structure is more stable and gives the transition pressure.

**Q1 152 High-pressure X-ray diffraction study of the giant dielectric constant material $CaCu_3Ti_4O_{12}$: evidence of stiff grain surface** YANZHANG MA, *Department of Mechanical Engineering, Texas Tech University, Lubbock, TX 79409* JIANJUN LIU, *Department of Physics University of Nebraska at Omaha, Omaha, Nebraska 68182-0266* CHUNXIAO GAO, *National Laboratory of Superhard Materials, Jilin University, Changchun, China 130012* ALLEN D. WHITE, *Department of Mechanical Engineering, Texas Tech University, Lubbock, TX 79409* W. N. MEI, *Department of Physics University of Nebraska at Omaha, Omaha, Nebraska 68182-0266* JAHAN RASTY, *Department of Mechanical Engineering, Texas Tech University, Lubbock, TX 79409* We measured the high-pressure X-ray diffraction of the giant dielectric constant material $CaCu_3Ti_4O_{12}$ (CCTO) under both hydrostatic and uniaxial compressions. We found that the cubic structure of CCTO is stable up to 57 GPa. Nevertheless we observed CCTO has unusual compression behaviors under hydrostatic pressure. Specifically, the volume reduction is less than that under uniaxial compression below 25 GPa, above it the volume reduction starts to approach and finally reach the same value as that under the uniaxial compression at about 30 GPa. We explained these remarkable phenomena by using the model that the samples are composed of grains that have shells stiffer than the cores.

**Q1 153 Dynamic Ellipsometry Under Extreme Conditions*** JEFFREY H. NGUYEN, JEREMY R. PATTERSON, NEIL C. HOLMES, *Lawrence Livermore National Laboratory* Accurate temperature measurements at high temperatures and pressures require knowledge of emissivities at similar conditions. Presently, many temperature measurements at extreme conditions assume a constant ambient-condition emissivity. Development of a miniaturized ellipsometer has made it possible to measure optical properties, and thus emissivities, of materials under extreme shock conditions. We will present here past development and future directions of the miniaturized ellipsometer for use in high pressure-high temperature experiments. We will also discuss applications of

the technique including phase transitions under dynamic compression, observed changes in the complex dielectric constants of various solids and water. Since emissivity can be determined from the complex dielectric constants, we expect emissivity to change upon phase transition. We will present here results on various solid-solid, solid-liquid and liquid-solid phase transitions. In particular, we will focus on the change in emissivity at the $(\alpha, \epsilon)$ phase boundary in Fe and its implications for the Fe phase diagram.

*Work performed under the auspices of the U.S. DOE at the University of California/Lawrence Livermore National Laboratory under contract W-7405-ENG-48.

**Q1 154 Ab Initio Studies of $MgSiO_3$ Post-Perovskite*** FEIWU ZHANG,[†] ARTEM OGANOV,[‡] *ETH Zurich* Recent discovery of a post-perovsike phase of $MgSiO_3$ was considered as a new era in the studies of the Earth's deepest mantle. This discovery provides some explanations for many puzzling problems of the Earth's D'' layer (pressures $\sim$ 120-136 GPa, temperature $\sim$ 2000-4000 K), such as the large seismic anisotropy, heterogeneity, variable depth, strong shear wave velocity discontinuity at the top, and anticorrelation between shear and bulk sound velocities. High pressures and temperatures existing in planetary interiors dramatically alter the structure and properties of materials, but are difficult to reproduce in the laboratory. Present-day quantum-mechanical simulations often give accuracy sufficient for geophysical or planetological purposes. The key roles of the $MgSiO_3$ post-perovsike phase transition will be addressed by further theoretical studies, including elasticity and anelasticity, electrical conductivity, radiative conductivity, energetics of stacking faults, effects of impurities on stability and properties of post-perovskite.

*Acknowledge access to supercomputers at CSCS (Manno) and the HP Superdome of ETH Zurich. Funding by ETH Zurich
[†]http://olivine.ethz.ch/ feiwu
[‡]http://olivine.ethz.ch/ artem

## Q1 155 QUANTUM FLUIDS AND SOLIDS POSTER SESSION

**Q1 156 Supersolid $^4$He Likely Has Nearly Isotropic Superflow*** WAYNE M. SASLOW, *Texas A&M University* SHIVAKUMAR JOLAD, *Penn State University* We extend previous calculations of the zero temperature superfluid fraction $f_s$ (SFF) *vs* localization, from the fcc lattice to the experimentally realized (for solid $^4$He) hcp and bcc lattices. The superfluid velocity is assumed to be a one-body function, and dependent only on the local density, taken to be a sum over sites of gaussians of width $\sigma$. Localization is defined as $\sigma/d$, with $d$ the nearest-neighbor distance. As expected, for fcc and bcc lattices the superfluid density tensor is proportional to the unit tensor. To numerical accuracy of three-places (but no more), the hcp superfluid density tensor is proportional to the unit tensor. This implies that a larger spread in data on $f_s$, if measured on pure crystals, is unlikely to be due to crystal orientation. In addition, to three decimal places (but no more) the curves of $f_s$ *vs* $\sigma/d$ are the same for both the hcp and fcc cases. An expected value for the localization gives an $f_s$ in reasonable agreement with experiment. The bcc lattice has a similar curve of $f_s$ *vs* $\sigma/d$, but is generally smaller because the lattice is more dilute.

*Supported in part by DOE Grant No. DE-FG03-96ER45598.

**Q1 157 2D Imaging of Anti-relaxation Coating Quality Using Regionally Specific Hyperfine Polarization*** K. ZHAO, Z. WU, *Department of Physics, Rutgers University, Newark, NJ 07102* We show that the hyperfine polarization in the vicinity ($\sim 10^{-5}$ cm) of cell surfaces can be used as a novel way to quantify and map the regional surface property inside optical pumping cells. In silicone-coated cells our method allows us to image the regional quality of the coatings, revealing for the first time the existence of areas that have strikingly different qualities.

*Support from ONR is acknowledged.

## Q1 158 ATOMIC, MOLECULAR & OPTICAL (AMO) PHYSICS POSTER SESSION

**Q1 159 Improved Guillemin-Zener wave function useful in molecular and chemical physics.** ODIL YUSUPOV, Classical Guillemin-Zener[1] wave function for primary diatomic molecular system – molecular hydrogen ion have shown high accuracy and quality of exponential functions basis. We want to submit improved compact wave function useful in study quantum mechanic. Compact electronic wave function for ground state of molecular hydrogen ion is $\Psi$ = N*(**exp(-a1***$\xi$)**+c*exp(-a2***$\xi$))*( **cosh(-b1***$\eta$)**+d*cosh(-b2***$\eta$)) where N - normalization factor, $\xi$ and $\eta$ are spheroidal coordinates of electron, a1,a2,b1,b2 – nonlinear variational parameters, c and d - linear variational parameters. By optimization of energy functional we found optimal values of this parameters for any internuclear distance R. For example, at R=2 a.u.: a1= 1.4345, a2= 1.9753, b1= 0.5399, b2= 1.3001, c= -0.332876, d= 0.592279. Electronic energy of molecular hydrogen ion with this 4-term wave function equals -1.10263418 a. u. and very close to the ''exact'' value – 1.10263422 a.u. The comparison was shown that our improved wave function equivalent to about 25- term standard mathematical expansion in spheroidal coordinates. This function can be used in educational physics as well as for molecular theory, chemical physics, theory of few particle coulomb systems, etc.
V.Guillemin, C.Zener. Proc. Natl.Acad. Sci. U.S., 15, 314, (1929)
T.K.Rebane and O.N.Yusupov. Opt. and spectr. 72, 6, 1289 (1992)

**Q1 160 Breathing modes and stability of trapped two-component ultracold atoms*** CHOU-CHUN HUANG, WEN-CHIN WU, *National Taiwan Normal University* The breathing modes and stability of trapped two-component ultracold atoms are studied using a variational method. We consider a boson-boson, a boson-fermion, and a fermion-fermion mixture in a 3D isotropic harmonic trap and in a 1D optical lattice. When the two compo-

nents are miscible, the corresponding in-phase and out-of-phase breathing mode frequencies are calculated against the value of the inter-component interaction. The stability of the two-component system is shown to have strong correlation with the behaviors of breathing modes.

*Supported by the National Science Council of Taiwan.

**Q1 161 Semiclassical time-independent description of rapidly oscillating fields on a lattice in the Kapitza approximation.** JEAN-PIERRE GALLINAR, *Depto. de Fisica, Universidad Simon Bolivar, Aptdo. 89000, Caracas 1080A, Venezuela* We investigate a semiclassical dynamics driven by a high-frequency ($\omega$) field, plus a static arbitrary potential on a one-dimensional tight-binding lattice. We find -in the spirit of the Kapitza pendulum- an effective, time-independent potential $V_{eff}(x)$ that describes the average motion to order $\omega^{-2}$. This effective potential depends on the static external potential $V(x)$, on the lattice constant ''$a$'' and on the applied high-frequency field $f(x,t)$. One obtains that

$$V_{eff}(x)/m = a^2/2\, V^2(x) - a^2 E V(x) + a^4 \int dx (V(x) - E)^2\, \partial/\partial x \left[ \sum_{n=1}^{\infty} f_n^2(x)/\omega^2 n^2 \right].$$

Where ''$m$'' and ''$E$'' are, respectively, the effective mass and unperturbed energy of the particle's average motion, and $f_n(x)$ is the n-th Fourier component of the driving field. Where appropriate, our results should be suitable for the description of semiclassical electronic motion in a crystal lattice and/or atomic motion in an optical one.

**Q1 162 Role of Broken Gauge Symmetry in Transport Phenomena Involving Neutral and Charged Particles in Finite Lattices** SCOTT CHUBB, *Remote Sensing Division, Naval Research Laboratory* As opposed to the conventional, approximate theory of electrical conduction in solids, which is based on energy band, quasi-particle states in infinite lattices, a rigorous theory exists that can be used to explain transport phenomena, in finite lattices, at reduced temperature, through the effects of a broken gauge symmetry: The loss of translational invariance with respect to Galilean transformations that maintain particle-particle separation. Implications of this result in areas related to the transport of hydrogen (H) and its isotopes in nano-crystalline structures of palladium (Pd) and of neutral, coherent atomic waves in finite, optical lattices are presented. These include: 1. The prediction of a novel variant of a known, phenomenon, Zener/Electronic Breakdown in insulators, in which ions in nano-scale palladium-deuteride (PdD) crystals (as opposed to electrons in insulating crystals) that initially, effectively, are confined to particular regions of space, begin to move, spread-out, and conduct charge after they are subjected to an applied, external (constant) electric field for a sufficiently long period of time; and 2. A rigorous treatment of scattering at low temperatures that can be used to identify critical time- and length- scales for problems related to the transport of neutral atomic matter waves in finite, optical lattices, in the presence of gravitational fields.

**Q1 163 Quantum-degenerate Bose-Fermi mixtures on one-dimensional optical lattices** PINAKI SENGUPTA, *University of Southern California* LEONID P. PRYADKO, *University of California, Riverside* Using a quantum Monte Carlo method, mean field theory, and a strong-coupling expansion, we map out the ground state phase diagram of a mixture of ultracold bosons and spin-polarized fermions in a one-dimensional optical lattice. The properties of the uniform phases and their stability toward phase separation into pure boson and pure fermion phases are studied in detail over a wide range of chemical potentials for boson-boson and boson-fermion interactions ranging from weak to strong coupling limits. The nature of different phases is characterized by computing the charge stiffness, bosonic superfluid stiffness, and density-density correlation functions.

**Q1 164 Computer Simulations of Quantum Computational Operations Performed on the Vibrational Energy Levels of Small Molecules** DANIEL WEIDINGER, *University of Illinois* MARTIN GRUEBELE,* *University of Illinois* The vibrational energy levels of a molecule can be regarded as a register for quantum information. An applied electric field (provided by a shaped laser pulse) will transform the state vector of the molecule in a manner that can be regarded as a quantum computational operation. Optimization algorithms have been developed and computer simulations have been run to determine the optimum laser pulses to act as specific operators. Simulations of 1-, 2-, 3-, and 4-qubit gates have been run using 2-, 4-, 8-, and 16-level tracts of vibrational energy levels, respectively. Simulations have been generated to model a realistic experiment using available technology. In the case of thiophosgene ($SCCl_2$), vibrational levels on the ground electronic state may be coupled via one or several energy levels on an excited electronic state. The coupling is provided by a single femtosecond laser pulse, which is shaped according to parameters consistent with available pulse shapers. Within these parameters, pulses have been simulated that perform gates such as the CNOT (4 levels) and Hadamard (2 levels) with fidelities over 95 %. The limiting factors for efficacy of the shaped pulse in performing the gate—such as the number of ground state vibrational levels involved—have been explored.

*Principal Investigator

**Q1 165 Autler-Townes splitting in a sodium molecular-ladder scheme*** CHIN-CHUN TSAI, RAY-YUAN CHANG, *Deparment of Physics, National Cheng-Kung University, Tainan, 70101, Taiwan* THOU-JEN WHANG, CHUEN-PING CHENG, *Department of Chemistry, National Cheng-Kung University, Tainan 70101, Taiwan* We report results from studies of the Autler-Townes (AT) splitting observed in sodium dimer using optical-optical double resonance spectroscopy. In our experiment, a single line $Ar^+$ laser at 4727 Å pumps the thermally populated ground state level $X\,^1\Sigma_g^+(v'' = 1, J'' = 37)$ of $Na_2$ to the intermediate $B\,^1\Pi_u(v' = 9, J' = 38)$ level. Then, a single mode cw Ti:sappher or dye laser couples to the higher Rydberg states. The signals are detected by monitoring the UV fluorescence from the triplet *gerade* states back to the $a\,^3\Sigma_u^+$ state via collision energy transfer. Unlike all the other intermediate levels pumped by different $Ar^+$ laser lines, this strong transition populated the $B\,^1\Pi_u(v' = 9, J' = 38)$ level leads to an AT splitting on all the levels observed in the higher Rydberg states, for example, 3, 5, 6, $7\,^1\Pi_g$ states and 3, 5, $6\,^1\Delta_g$, states.

*We greatly acknowledge the support of the National Science Council, Taiwan.

**Q1 166 Sensitive detection of lead monofluoride** CHRIS MCRAVEN, *Homer L Dodge Department of Physics and Astronomy, The University of Oklahoma* SIVAKUMAR POOPALSINGAM, *Homer L Dodge Department of Physics and Astronomy, The University of Oklahoma* NEIL SHAFER-RAY, *Homer L Dodge Department of Physics and Astronomy, The University of*

*Oklahoma* The ground-state of lead monofluoride maybe uniquely sensitive to an electron electric dipole moment. Here we report on a radical-beam source of PbF and sensitive resonance-enhanced-multiphoton ionization detection of the molecule.

**Q1 167 Simple Analytic Theory of Cold Atom Feshbach Resonance Scattering** PAUL JULIENNE, *NIST* BO GAO, *U. of Toledo* Magnetically tunable Feshbach resonances have been used very successfully in cold atomic gases to study a variety of condensed matter phenomena. We describe a simple analytic theory, in excellent agreement with full quantum scattering calculations, for the near-threshold resonant scattering 2-body T-matrix for magnetically tunable Feshbach resonances in ultracold atomic collisions. The theory is based on the analytic properties of the exact solutions to the Schrodinger equation for the van der Waals potential, and is characterized by 5 parameters: the scattering length, van der Waals coefficient, and reduced mass of the background entrance channel, the coupling width of the resonance, and the difference in magnetic moments between the separated atoms and the resonance level. The resonance scattering phase shift is completely characterized by two functions, an energy-dependent width and an energy-dependent shift, which are analytic functions of the background van der Waals potential. The theory permits a simple classification of resonances as open- or closed-channel dominated, and gives insight into the nature of atom pairing in scattering states. The excellent quality of the theory is illustrated by calculations of above-threshold scattering for the fermionic isotopes K-40, and Li-6 and for bosonic Rb-85.

**Q1 168 Role of the van der Waals interaction in atom-diatom reaction dynamics at low temperatures*** PHILIPPE F. WECK, NADUVALATH BALAKRISHNAN, *University of Nevada Las Vegas, Las Vegas, NV 89154* JOAO BRANDAO, CARLA ROSA, WENLI WANG, *Universidade do Algarve, 8005-139 Faro, Portugal* Quantum-mechanical scattering calculations are reported for the $O(^3P) + H_2$ collision at energies close to the reaction threshold with emphasis on the sensitivity of the reaction dynamics to the van der Waals interaction. The dynamics has been investigated using the lowest $^3A''$ GLDP potential energy surface developed by Rogers et al. [J. Phys. Chem. A **104**, 2308 (2000)] and its recent BMS1 and BMS2 extensions by Brandão et al. [J. Chem. Phys. **121**, 8861 (2004)] which explicitly include the van der Waals interaction. Quasiclassical trajectory calculations on all three potential energy surfaces are also reported to explore the validity of this method near the reaction threshold and to assess the importance of quantum effects at low temperatures.

*This work was supported by NSF grant PHYS-0245019, DOE grant DE-FG36-05GO85028, the Research Corporation, and the FCT under the POCTI/CTA/41252/2001 Research Project, cofinanced by the European Community Fund, FEDER.

**Q1 169 Liouville-Space Descriptions for Intense-Field Coherent Electromagnetic Interactions*** VERNE JACOBS, *Naval Research Laboratory* Liouville-space (reduced-density-operator) descriptions are developed for coherent electromagnetic interactions of quantized electronic systems, taking into account environmental decoherence and relaxation phenomena. Applications of interest include many-electron atomic systems and semiconductor nanostructures. Time-domain (equation-of-motion) and frequency-domain (resolvent-operator) formulations are developed in a unified manner. In a preliminary semiclassical perturbative treatment of the electromagnetic interaction, compact Liouville-space operator expressions are derived for the linear and the general (nth order) non-linear electromagnetic-response tensors. Intense-field electromagnetic interactions are treated by an alternative reduced-density-operator approach based on the Liouville-space Floquet-Fourier representation.

*Work supported by the Office of Naval Research, the Defense Advanced Research Projects Agency, and the Department of Energy.

**Q1 170 High Intensity Ultrashort Pulse Interactions with Dielectric Filters** SARAH DUNNING, CARL M. LIEBIG, W.M. DENNIS, *University of Georgia* Modern ultrafast laser systems are capable of generating optical pulses of sufficient intensity to induce nonlinear effects in several of the materials used in thin-film dielectric optical filters. Such effects degrade the performance of these devices at high intensities. In this paper we describe computer simulations used to investigate the interaction of high intensity ultrashort laser pulses with three dielectric filters: a quarter- wave dielectric stack, a rugate filter, and an idealized rugate filter, with a continuously varying refractive index. Using the finite-difference time-domain (FDTD) technique, we simulated the reflection of optical pulses (with pulse widths in the range 5–100 fs and peak intensities up to $\sim$ 10 TW/cm$^2$) from all three devices. The simulated low intensity reflective properties were found to be in excellent agreement with calculations using the characteristic matrix method. For high intensity pulses a decrease of the filter reflectance and a distortion of the reflected pulse was observed.

**Q1 171 Study of ultrafast nonlinear pulse shaping effect of strained saturable Bragg reflector (SSBR) with coherent quantum control technique** CHAO-KUEI LEE, CHIA-CHEN HSU, *IEO, NSYSU* In this work, a strained saturable Bragg reflector (SSBR) for passive mode-locking of Ti:sapphire lasers was investigated by pulse shaping technique. Incident pulses of several wavelengths and with zero, positive, or negative chirp were employed. A Kramers-Kronig relation like behavior of pulse shaping factor in the strained quantum well was observed. The phenomenon is attributed to anomalous dispersion and higher order nonlinearity.

**Q1 172 Nearly Perfect Squeezing of the Signal mode in Parametric Oscillation with Coherent and Squeezed pumping*** DANIEL ERENSO, *Middle Tennessee State University* A degenerate parametric oscillator operating above threshold is studied when the cavity is injected by a squeezed vacuum field at the second harmonic frequency. We presented a different method of finding the Wigner function for the intracavity modes. We use the solution of the quantum Langevin equation for the signal and pump modes to construct the steady-state Wigner function for the joint pump-signal mode. Then, the one-mode Wigner functions for the signal and pump modes are derived and the corresponding phase space is studied. These functions are used to determine the quantum fluctuations in the intracavity signal and pump mode field quadratures. The results have shown that nearly perfect suppression of quantum noise can be achieved in both the signal and pump modes. We have also studied the spectrum of the squeezing for cavity output signal mode; our result reveals nearly perfect squeezing can be achieved by controlling the relative cavity damping rates between the signal and pump modes. The second-order

intensity correlation for zero time delay also studied for each mode and it is found that intracavity photons are always bunched, independent of the relative phase of the squeezed vacuum field with respect to the driving coherent field.

*This work was supported in part by the Geier fund from the Tennessee Board of Regents

**Q1 173 Time-dependent phenomena of electron-electron and electron-hole pairs confined in quantum dots** TETSURO SATAKE, MASAKAZU MURAGUCHI, KYOZABURO TAKEDA, *Waseda University* We report time-dependent (TD) phenomena of electron-electron (ee) and electron-hole (eh) pairs confined in 2D quantum dots (QDs). We solved TD Schrodinger equation numerically, under the assumption of the Hartree-type wave function with the singlet spin state for both pairs of ee and eh. The individual (e's and h's) QD orbitals are expanded by the basis of the real spatial mesh. We further combined Poisson's equation to determine the pair's coulomb interaction in QDs. The stationary ground states are first obtained by the scf-calculation. In accordance with the QD size, both of ee and eh pairs are characterized by confined, intermediate and free states, and the difference among them is more distinctive in ee pairs than in eh pairs. The coulomb repulsion calculated by Poisson equation extends the confined region, because of its logarithmic distance-dependence due to 2D QD. The TD change in the coulomb interaction induces the non-resonative oscillations among the individual eigen-states. The projection of the calculated pair's wave function into the QD single electron stationary states reveals that the resulting frequency is determined with the competition between the coulomb interaction and the size of QDs.

## Q1 174 PHYSICS EDUCATION POSTER SESSION



**Q1 175 Physical activities to enhance an understanding of acceleration** S.A. LEE, *University of Toledo* On the basis of their everyday experiences, students have developed an understanding of many of the concepts of mechanics by the time they take their first physics course. However, an accurate understanding of acceleration remains elusive. Many students have difficulties distinguishing between velocity and acceleration. In this report, a set of physical activities to highlight the differences between acceleration and velocity are described. These activities involve running and walking on sand (such as an outdoor volleyball court).

**Q1 176 Motion Sensors in Introductory Physics Laboratory and beyond.** PONN MAHESWARANATHAN, *Winthrop University* Motion sensors are commonly used to collect data in a typical computer-based introductory physics laboratory. It is part of the group of sensors that comes with an initial purchase of an interface. It is an important piece of equipment for the first year physics curriculum. It is used in position, velocity, and acceleration experiments as well as in momentum conservation, impulse-momentum theorem, and simple harmonic motion. In this paper its use will be expanded to few more experiments and lecture demonstrations pointing out its limitations and some of the pitfalls. A review of the websites that deal with motion sensors and computer assisted experiments will also be presented. In addition, their use in alarm and automation systems and surveillance technology will be introduced as an extrapolation to real world applications.

**Q1 177 Using the Open Source Physics Library to Teach Statistical and Thermal Physics*** HARVEY GOULD, HUI WANG, *Clark University* JAN TOBOCHNIK, NICHOLAS TUNG, *Kalamazoo College* Statistical and thermal physics is becoming an increasingly important part of the undergraduate and graduate curriculum due in part to the the availability of inexpensive and powerful computational resources and the importance of statistical concepts in much of current research in physics and related areas. We will show examples of curriculum materials for teaching topics in statistical and thermal physics with a focus on Java programs written using the Open Source Physics library. Examples of simulations will be demonstrated.

*Supported in part by NSF DUE-0442481 and DUE-0127363.

**Q1 178 Propagation of a pulse trough a Lorentz dispersive thin film using the Finite Difference Time Domain** JESUS MANZANARES-MARTINEZ, ADRIAN NAVARRO-BADILLA, RAUL ARCHULETA-GARCIA, *Universidad de Sonora* We consider the evolution of the main signal in a Lorentz dispersive thin film. The signal is a Gaussian-sine modulated pulse that is excited outside the thin film. We illustrate the change of the group velocity as the pulse changes its central frequency and we discuss the conditions to have a superluminal behavior. The results obtained are illustrated with animated graphics that obtained with our implementation of the Finite Difference Time Domain.

**Q1 179 Including Nanoscale Investigations in a General Introductory Physics Course*** KURT VANDERVOORT, STEPHANIE BARKER, RAUL TORRICO, *Physics Department, California State Polytechnic University, Pomona, CA 91768* Modules were developed to introduce atomic force microscope (AFM) applications into a general introductory physics course. The goal was to elucidate fundamental concepts in optics at the nanoscale that would complement existing investigations at the macroscale, and to expose students to advanced instrumentation at an early level. The nanoscale investigations were inserted where necessary and were used to help define and delineate the various topics in optics. In a lab on lenses, students first use the AFM to view smooth glass and rough glass at the microscopic level, illustrating the range of applicability of geometrical optics. In a physical optics lab, students measure patterns from diffraction gratings and then view the grating at the microscopic level, revealing groove spacings and a new feature, the blaze angle. Further investigation yields from the blaze angle a way to separate the effects of the single slit diffraction envelope from the multiple slit interference pattern. Another lab investigates the height of the bumps on a CD surface and exposes students to a direct application of destructive interference. These and other examples will be presented.

*Funding was provided by the National Science Foundation Nanotechnology Undergraduate Education program, award # 0406533.

**Q1 180 Deposition and Solidification of PPV Precursor*** EDWARD BURDETTE, *Grove City College* HANS HALLEN, *North Carolina State University* Future high performance polymer films will be comprised of molecules oriented in the plane of the substrate. As a first step, a mixture of poly(p-xylene tetrahy-

drothiophenium chloride) in methanol was spun onto a sapphire substrate. These samples were fabricated over a range of spin-coating times, methanol solution concentrations, and number of drops of solution. Analysis with an ellipsometer revealed that layer thickness is independent of spinning period and applied solution volume, and decreases as the parts per volume of methanol increases. Furthermore, the samples were exposed to various wavelengths of UV-visible radiation to determine the optimal wavelength for driving these precursor molecules into a solid thin film, insoluble in methanol. Light from a mercury arc-lamp with a wavelength of 365 nm was found to solidify the precursor within five minutes of exposure most effectively.

*Research sponsored by the National Science Foundation Research Experiences for Undergraduates Program in the Department of Physics, grant number DMR-0353719

**Q1 181 Complex Permittivity of Powder Metal Compacts by Cavity Perturbation Technique*** CHRIS LYNCH,[†] EARNIE JOHNSON, JUNKUN MA, NICHOLAS MISKOVSKY, GARY WEISEL, BROCK WEISS, DARIN ZIMMERMAN,[‡] *The Pennsylvania State University, Altoona College* We present measurements of the complex permittivity of powder metal compacts using microwave cavity perturbation techniques. Using a 2.45GHz, $TM_{010}$ microwave cavity operating in conjunction with a vector network analyzer, we have systematically measured the real ($\varepsilon$') and imaginary ($\varepsilon$'') parts of the effective complex permittivity of pure, powder metal, cylindrical samples (0.25in by 0.25in). By placing these in the electric-field antinode, the dielectric properties at microwave frequencies are obtained by comparison with the expected change in the cavity Q by perturbation theory. We have studied the effect of varying particle size and green density as means to understand the absorption and heating of powdered metals in microwave fields. We acknowledge the additional work of undergraduates Kelly Martin and Charles Smith, who assisted in the setup of experimental apparatus, sample preparation, and data acquisition.

*This work is supported by grants from the National Science Foundation (DMR-RUI 0406584) and The Pennsylvania State University
[†]Lead undergraduate researcher
[‡]Principal investigator

**Q1 182 Microwave Heating and Pre-sintering of Copper Powder Metal Compacts in Separated Electric and Magnetic Fields*** KELLY MARTIN,[†] EARNIE JOHNSON, JUNKUN MA, NICHOLAS MISKOVSKY, GARY WEISEL, BROCK WEISS, DARIN ZIMMERMAN,[‡] *The Pennsylvania State University, Altoona College* We present results of microwave heating and pre-sintering of pure copper metal powder compacts. Using a 2.45GHz, WR284 microwave system operating in TE102 single mode resonance, we have systematically studied the microwave heating and pre-sintering behavior of various copper powder metal compacts as a function of particle size and green density. Cylindrical samples (0.25in by 0.25in) were positioned in either the magnetic– or electric–field antinode, allowing the study of the separate effects of the two fields. The results show significant differences in heating rates and sample microstructure (SEM) even when average sample temperatures are below half the melting point of bulk copper. Numerical simulations of the absorption and heating have been developed to check the consistency of the experimental results. We acknowledge the additional work of undergraduate students John Diehl, John Rea, Charles Smith, and Devin Spratt, who assisted in the setup of experimental apparatus, sample preparation, and data acquisition.

*The work is supported by grants from the National Science Foundation (DMR-RUI 0406584) and The Pennsylvania State University
[†]Lead undergraduate researcher
[‡]Principal investigator

**Q1 183 Expected Properties and Experimental Signals of Bose-Einstein Condensates** MONA ALI, *Wellesley College, Wellesley, Massachusetts 02481* COURTNEY LANNERT, *Wellesley College, Wellesley, Massachusetts 02481* We have studied the expected response of Bose Einstein Condensed (BEC) atoms subject to various experimental probes. In the first part of this project, we modeled BEC atoms passing through a double slit and predicted the interference patterns that are expected to form on the screen. We contrast these interference patterns with those from thermal atoms and compare the patterns from condensed atoms with varying levels of inter-atomic interactions. This gives an experimental signature of the presence of BEC in the system as well as the strength of interactions. The second part of our project considers the response of BEC atoms trapped in an optical lattice, subject to an external oscillatory magnetic field. This system is modeled as having two discrete hyperfine energy states and we find the expected transitions between these states for the BEC atoms. The transitions are found to be similar to the Rabi oscillations observed with non-BEC atoms, subject to the same probe, with some notable differences.

**Q1 184 Variational Wavefunction Monte Carlo on Two-Dimensional Lattices** XINXIN DU, *Wellesley College, Wellesley, Massachusetts 02481* COURTNEY LANNERT, *Wellesley College, Wellesley, Massachusetts 02481* We apply numerical methods to the study of many-electron systems, in particular the cuprates, by using variational wavefunction Monte Carlo methods to search for the groundstate wavefunction. We investigate some of the current proposed models and wavefunctions for these compounds, in particular, the t-J model and the t-J model with ring-exchange on two- dimensional square lattices. We compute the energy of the Spin Density Wave (SDW) groundstate wavefunctions for the half- filled Heisenberg antiferromagnetic using the computing algorithm outlined by Gros. This verifies the agreement of the results with the current literature on the Heisenberg model. With the addition of the ring-exchange terms, we compare the energies of the Resonating Valence Bond state, the Gutzwiller state, the superconducting state, and the SDW state. This allows us to study the relationship between the non-magnetic and antiferromagnetic phases of the system at half- filling. The introduction of holes on the lattice allows us to simulate the relationship between the superconducting and the insulating phases of the magnet.

**Q1 185 A Fluorescence Spectroscopic Study of Cytochromes P450 1A2 and 3A4.** GLENN MARSCH, *Grove City College* F.P. GUENGERICH, *Vanderbilt University* JOSHUA INKS, *Grove City College* Fluorescence spectroscopy was used to study cytochromes P450 1A2 and 3A4. Spectra of P450s were acquired in the presence and absence of acrylamide quencher. In both P450s, quenching revealed three distinguishable species of amino acid fluorescence, with maxima at 297, 323, and 345 nm. The 345 nm

tryptophan fluorescence was quenched by low levels of acrylamide; the 297 nm tyrosine fluorescence was resistant to quenching. The 323 nm fluorescence was observed at intermediate concentrations of quencher. Stern-Volmer plots of P450 quenching were non-linear, but were well-fitted to a superposition of linear plots for each fluorophore species. The effect of P450 1A2 binding on pyrene fluorescence was also examined. Upon binding to P450 1A2, the intensity of the 383 nm pyrene vibronic band was decreased relative to the intensities of the 372 and 393 nm bands. Fluorescence quenching of pyrene and other ligands upon binding to P450s will be used to evaluate distances between ligands and the P450 heme moiety by fluorescence resonance energy transfer. Fluorescence quantum yields of ligands, overlap integrals, and Förster distances of many ligand-heme donor-acceptor pairs were calculated. Steady-state spectra and time-resolved data of bound ligand will be used to calculate substrate-heme distances in the P450 enzymes.

**Q1 186 Ferroelectric switching of KDP ($KH_2PO_4$) and doped KDP:Cr simultaneously studied by the epr and Mertz methods*** FRANCISCO RODRIGUEZ PEREZ, JUAN FRAGOSO, PAUL HARRIS, MARISELA APARICIO, KENNETH ULIBARRI, MONICA MARCIAL-ARMENTA, TIMOTHY USHER, *California State University San Bernardino* Preliminary experimental results on ferroelectric switching in KDP will be presented. Additionally, a modified closed cycle cryogenic system for epr will be presented. Our goal is to reconcile differences in (epr) spectroscopy and the Mertz method on the simple ferroelectric, KDP/$KH_2PO_4$. A closed cycle cryogenic system, capable of reaching temperatures well below the Curie point of KDP (123K) was modified to accommodate the two measurements. The epr measurements probe the bulk of the KDP and favors slow ferroelectric domain switching while the Mertz method probes the surface and favors fast switching. A compromise in switching time between epr and Mertz is necessary. Preliminary results show the expected splitting in the epr lines near 1.45 kG. The Mertz data show switching currents consistent with the nucleation and domain growth model. The switching times are on the order of 20 microseconds for temperatures of approximately 100K. In addition to doped KDP we plan to investigate irradiated KDP and DKDP.

*NASA Grant No. 0051-0078 DOD Control No. ISP02-EUG15 NSF DMR-0116744



## Q1 187 QUANTUM INFORMATION, CONCEPTS, AND COMPUTATION POSTER SESSION

**Q1 188 Quantum amplification in the presence of decoherence** JAE-SEUNG LEE, ANATOLY KHITRIN, *Department of Chemistry, Kent State University, Kent, Ohio, 44242-0001* A one-dimensional Ising chain irradiated by weak resonant transverse field is a simple analytically solvable model of quantum amplification [Phys. Rev. A **71**, 062338 (2005)]. Operation of any practical device would be affected by decoherence. Here we present the results of the effect of decoherence on amplification dynamics. The dynamics of a 100-spin chain perturbed by random phase kicks of individual spins has been studied numerically. Time evolution of the total polarization is monitored for different strengths of decoherence. It is shown that decoherence decreases the maximum coefficient of amplification in this model. In the limit of strong decoherence, quantum dynamics resembles classical diffusion.

**Q1 189 Quantum manipulation and simulation using Josephson junction arrays** XINGXIANG ZHOU, ARI MIZEL, *The Pennsylvania State University* We discuss the prospect of using quantum properties of large scale Josephson junction arrays for quantum manipulation and simulation. We study the collective vibrational quantum modes of a Josephson junction array and show that they provide a natural and practical method for realizing a high quality cavity for superconducting qubit based QED. We further demonstrate that by using Josephson junction arrays we can simulate a family of problems concerning spinless electron-phonon and electron-electron interactions. These protocols require no or few controls over the Josephson junction array and are thus relatively easy to realize given currently available technology.

**Q1 190 Abstract Withdrawn**

**Q1 191 Effect of correlated noise on a fault-tolerant quantum error correction protocol*** JAMES CLEMENS, *Miami University* JULIO GEA-BANACLOCHE, *University of Arkansas* We consider the effect of correlated noise in the context of a fault-tolerant quantum error correction protocol. The noise is represented by a set of classical fluctuating fields with partial spatial and temporal correlations. We explicitly account for the propagation of errors in the implementation of quantum circuits for ancilla verification and syndrome extraction. Errors arising from single-bit and two-bit gates are considered separately. The performance of the error correction protocol is characterized by means of the probability for an uncorrected error to occur calculated from numerical simulations of the error propagation. For single-bit gates we find that in the limit of strong correlations the crash probability is enhanced be an order of magnitude. For two-bit gates we find that the effect of correlated noise can be minimized by choosing an appropriate sequence of operations which takes advantage of the correlations.

*We gratefully acknowledge support from the US Army Research Office

**Q1 192 Modeling fluid dynamics on type II quantum computers** JAMES SCOVILLE, DAVID WEEKS, *Air Force Institute of Technology* JEFFREY YEPEZ, *Air Force Research Laboratory* A quantum algorithm is presented for modeling the time evolution of density and flow fields governed by classical equations, such as the diffusion equation, the nonlinear Burgers equation, and the damped wave equation. The algorithm is intended to run on a type-II quantum computer, a parallel quantum computer consisting of a lattice of small type I quantum computers undergoing unitary evolution and interacting via information interchanges represented by an orthogonal matrices. Information is effectively transferred between adjacent quantum computers over classical communications channels because of controlled state demolition following local quantum mechanical qubit-qubit interactions within each quantum computer. The type-II quantum algorithm presented in this paper describes a methodology for generating quantum logic operations as a generalization of classical operations associated

with finite-point group symmetries. The quantum mechanical evolution of multiple qubits within each node is described. Presented is a proof that the parallel quantum system obeys a finite-difference quantum Boltzman equation at the mesoscopic scale, leading in turn to various classical linear and nonlinear effective field theories at the macroscopic scale depending on the details of the local qubit-qubit interactions.

**Q1 193 Optimization of a quantum teleportation protocol based on collective spontaneous emission** JAMES CLEMENS, *Miami University* Recently a quantum teleportation protocol has been proposed by Chen, *et al.* in *New Journal of Physics* **7**, 172 (2005) which is based on the collective spontaneous emission of a photon from a pair of atoms. If one can successfully distinguish between the superradiant and subradiant emission channels then one can teleport the state of the second atom onto a cavity field mode with which the first atom has previously interacted. One can employ temporal resolution, spatial resolution, or both in combination, of the emitted photon in order to distinguish superradiant from subradiant emission on the basis of a single detected photon. The overall success probability of the teleportation protocol is calculated under all three detection strategies and is optimized with respect to the spacing of the two atoms.

**Q1 194 Measuring the parity of an *N*-qubit state** B. ZENG, *Department of Physics, Massachusetts Institute of Technology, Cambridge, MA 02139, USA* D.L. ZHOU, L. YOU, *School of Physics, Georgia Institute of Technology, Atlanta, Georgia 30332, USA* We present a scheme for a projective measurement of the parity operator $P_z = \Pi_{i=1}^{N} \sigma_z^{(i)}$ of *N*-qubits. Our protocol uses a single ancillary qubit, or a probe qubit, and involves manipulations of the total spin of the *N* qubits without requiring individual addressing. We illustrate our protocol in terms of an experimental implementation with atomic ions in a two-zone linear Paul trap, and further discuss its extensions to several more general cases.

**Q1 195 A Variation of the Classic Double-Slit Experiment in Quantum Mechanics** DOUGLAS SNYDER, The classic double-slit experiment in quantum mechanics was adapted previously to show that a distinct type of physical interaction between an atom with the double-slit screen through which it passes is not necessary to obtain which-way information concerning the atom. This adaptation relied on entanglement between: 1) an atom's emitting a photon in one of two micromaser cavities as the atom passes through the cavity system and 2) the atom's subsequent passage through the fixed double-slit screen. If the development of this entanglement is interrupted in a suitable fashion, it appears one can obtain complete interference as if there were no micromaser cavity system or laser through which the atom traveled on its way to the double-slit screen. It appears one can alter the development of an atomic distribution through an action that does not involve direct physical interaction with atoms that become part of the distribution. Distinct atomic distributions can be created that can convey binary information, apparently without the velocity limitation of the special theory.

**Q1 196 Circular Polarization and Quantum Spin: A Unified Real-Space Picture of Photons and Electrons** ALAN M. KADIN, *Princeton Junction, NJ 08550* It is generally believed that no simple real-space semiclassical picture can consistently explain both a quantum wave and its spin. However, it is shown here [1] that a rotating vector field carrying angular momentum leads directly to the Einstein-de Broglie relations ($E = h\nu$ and $p = h/\lambda$, the heart of quantum mechanics), assuming only quantization of spin and Lorentz invariance of the phase angle. For electromagnetism, such a circularly polarized wave packet defines the photon. A very similar picture of a massive rotating vector field maps onto a complex wavefunction obeying the time-dependent Schrödinger equation for a particle such as the electron, with $m > 0$ and $v < < c$. This real vector field rotates about the spin axis at $mc^2/h \sim 10^{20}$ Hz. This suggests a unified picture whereby all fundamental quantum particles consist of such coherent wave packets of rotating spin fields, with composite particles deriving their quantum properties from the coherent rotations of their fundamental constituents. This represents a consistent interpretation of quantum mechanics, an alternative to the conventional statistical or Copenhagen interpretation. [1] A.M. Kadin, http://arxiv.org/abs/quant-ph/0508064

**Q1 197 Paradox in Wave-Particle Duality for Non-Perturbative Measurements** ERNST KNOESEL, *Rowan University* EDUARDO FLORES, KEITH F. McDONALD, SHARIAR S. AFSHAR, In a modified double-slit experiment we determined the complementary wave and particle aspect of light in the low flux regime beyond the limitations set by Bohr's Principle of Complementarity (BPC). We inferred the presence of sharp interference fringes, while we maintain, with very high probability, the information about the particular pinhole through which each individual photon had passed. This paradoxical result poses interesting questions on the validity of BPC in cases, which employ non-perturbative measurement techniques that evade Heisenberg's uncertainty principle and/or quantum entanglement.

**Q1 198 Interconvertibility of single-rail optical qubits*** BARRY SANDERS,† *Institute for Quantum Information Science, University of Calgary* DOMINIC BERRY, *The University of Queensland* A. I. LVOVSKY, *Institute for Quantum Information Science, University of Calgary* We show how to convert between partially coherent superpositions of a single photon with the vacuum using linear optics and postselection based on homodyne measurements. We introduce a generalized quantum efficiency for such states and show that any conversion that decreases this quantity is possible. We also prove that our scheme is optimal by showing that no linear optical scheme with generalized conditional measurements, and with one single-rail qubit input can improve the generalized efficiency.

*Supported by iCORE, NSERC, and ARC
†Also: Centre for Quantum Computer Technology, Macquarie University, Sydney

**Q1 199 Magnetic Nanoparticles itin-vivo Detection of Transplant Rejection** E.R. FLYNN, *Senior Scientific* H.C. BRYANT,* *University of New Mexico* R.S. LARSON, *UNM* D.A. SERGATSKOV,† *UNM* Superparamagnetic nanoparticles are being used to develop methodology for the itin-vivo detection and imaging of immune system attacks on transplanted organs. The signature for impending rejection of a transplant is enhanced presence of T-cells. Magnetic nanoparticles coated with specific antibodies (CD-2 and CD-3) will target and attach to these T-cells. Approximately $3 \cdot 10^5$ nanoparticles can attach to each cell. When a pulsed external magnetic field is applied to the decorated cells for a fraction of a second, magnetic moments of the nanoparticles

aligned with the field. After the pulse is switched off, the net magnetic moment decays over several seconds by the Nèel mechanism. The resulting magnetic remanence field (typically $10^{-11}$ T) is measured using a multi-channel SQUID array. We present the data from live T-cells placed in realistic kidney phantom. The detection sensitivity was $\sim 2 \cdot 10^3$ T-cells - a small fraction of the number actually invading the rejected transplant. The 7-channel SQUID array allows us to image the cell clusters with a few millimeters resolution.

*also at Senior Scientific
†also at Senior Scientific

## Q1 200 POST-DEADLINE POSTER SESSION

**Q1 201 The silicon di-vacancy investigated with density functional theory** RYAN WIXOM, ALAN WRIGHT, *Sandia National Laboratories* As part of a larger effort to quantitatively model the behavior of point defects in silicon, we have investigated the silicon di-vacancy using density functional theory with three different exchange-correlation functionals and super-cells containing as many as 1000 atoms. The literature on this defect contains two proposed atomic structures and disagreement on the relative stability of the configurations. Our study indicates that the determination of the ground state configuration is dependant on the particular choice for exchange and correlation. We will report on the atomic and electronic structures of this defect as well as formation.

**Q1 202 The Effect of Nanoparticles on Selective Gas Permeability of Thin Film Membranes Using Supercritical Fluid** A. HO, R. ROSENFELD, *Hebrew Academy of the Five Towns & Rochway* J. JEROME, *Stony Brook University* Y.-S. SEO, T. KOGA, M. BRONNER, J. SOKOLOV, *Stony Brook University* M. RAFAILOVICH, *Stony Brook University* The addition of inorganic nanoparticles to polymer thin films can be highly beneficial to their lubrication, strength, and UV resistance. Since nanoparticles are rigid, they do not conform to the molecular order of the film, producing nano-scale voids. Consequently, the introduction of nanoparticles into polymer films alters their porosity and this phenomenon may be exploited to engineer selectively permeable membranes. Porosity can also be introduced by swelling the films in supercritical fluids and then rapidly removing the solvent by decreasing the pressure which converts the solvent to the gas state. In order to test this hypothesis, solutions were made of nanoparticles, clay or gold, with polystyrene or poly (methyl methacrylate) polymer to observe the change in porosity and to analyze its dependence on polymer structure and on polymer nanoparticles interactions. Samples were exposed to $ScCO_2$ at two different temperatures and pressures of 36[r]C, 1200psi and 50[r]C, 1450psi. We then measured the permeability of $O_2$ and $CO_2$ gas. We found that exposure to supercritical $CO_2$ greatly increased the permeability to both O2 and CO2 gas. The degree of change in permeability in the nano-composite film depended on the particle aspect ratio and intensity in the matrix.

**Q1 203 Accurate Determination of Pyridine – Poly (Amidoamine) Dendrimer Absolute Binding Constants with the OPLS-AA Force Field and Direct Integration of Radial Distribution Functions** YONG PENG, GEORGE KAMINSKI, OPLS-AA force field and direct integration of intermolecular radial distribution functions (RDF) were employed to calculate absolute binding constants of pyridine molecules to $NH_2$ and amide group hydrogen atoms in 0th and 1st generation poly (amidoamine) dendrimers in chloroform. The average errors in the absolute and relative association constants, as predicted with the calculations, are 14.1% and 10.8%, respectively, which translate into ca. 0.08 kcal/mol and 0.06 kcal/mol errors in the absolute and relative binding free energies. We believe that this level of accuracy proves the applicability of the OPLS-AA, force field, in combination with the direct RDF integration, to reproducing and predicting absolute intermolecular association constants of low magnitudes (ca. 0.2 – 2.0 range).

**Q1 204 Cell-fibril interaction in peptide based Hydrogels relative to hydrogel stiffness** HASSNA RAMAY, JOEL SCHNEIDER, DARRIN POCHAN, *University of Delaware* Peptide hydrogels are potentially ideal scaffolds for tissue repair and regeneration due to their ability to mimic natural extra cellular matrix. The 20 amino acid peptide MAX1 has been shown to fold and self-assemble into a rigid hydrogel based on environmental cues such as pH, salt, and temperature. The hydrogel is composed of network of short fibrils that are 3nm wide and up to several hundred nm long. In addition, slight design variations in the arms of the MAX1 sequence allow for tunability of the self-assembly/hydrogelation kinetics. In turn, by controlling hydrogel self-assembly kinetics, one dictates the ultimate stiffness of the resultant network. The cell-material interaction in normal and pathological conditions is investigated by 2D and 3D cell culture. As shown by optical and laser scanning confocal microscopy, cells are viable for 3 weeks and grow in clonogenic spheroids. Characterization of the proliferation, differentiation and constitutive expression of various osteoblastic markers is performed relative to hydrogel stiffness using spectrophotometeric methods. The well-defined, fibrillar nanostructure of the hydrogel directs the attachment and growth of osteoblast cells and dictates the mineralization of hydroxyapatite in a manner similar to bone. This study will enable control over the interaction of cellular systems with the peptide hydrogel for biomedical applications.

**Q1 205 Electronic structure calculations of the CePt3Si.** ARMANDO REYES-SERRATO, DONALD HOMERO GALVAN, *Centro de Ciencias de la Materia Condensada UNAM, Ensenada BC, Mexico* In a recent paper, Bauer et al. [1] synthesized CePt3Si, a heavy fermion material with both transitions magnetic and superconducting, without inversion center in the crystal structure. This compound is very interesting from many points of view. In the present work, we report the analysis of the electronic structure of the CePt3Si in normal state. The calculation was performed with the program package WIEN2k, which use density functional theory (DFT) based on the full-potential linearized augmented plane-wave (LAPW) plus local orbital (lo) method [2]. We report band structure, total and partial densities of states, 3D density of charge and Fermi surface. We analyze the possible implications of our results in the superconductivity of this material. [1] Phys. Rev. Letter **92**, 027003 (2004). [2] http://www.wien2k.at

**Q1 206 On the origin of the peak effect in the classical superconductor $Nb_3Sn$: the role of critical fluctuations** NICOLAS MUSOLINO, ROLF LORTZ, ALAIN JUNOD, *Department of Condensed Matter Physics, University of Geneva, 24 quai E. Ansermet, CH-1211 Geneva 4, Switzerland* NAOKI TOYOTA, *Physics Department, Graduate School of Science, Tohoku University, 980-8571 Sendai, Japan* We found a sharp pronounced peak effect in the magnetization and the isothermal magnetocaloric effect of a single crystal of the classical superconductor $Nb_3Sn$. The construction of a new type of isothermal calorimeter allowed us to study the underlying thermodynamics with an extremely high resolution. A small lambda-type anomaly could be resolved superimposed on the specific heat jump at $T_c$. It follows scaling laws as expected for the presence of critical fluctuations. We interpret this feature as the first clear observation of the regime of critical fluctuations in a classical superconductor. Simultaneous measurements of the specific heat and the isothermal magnetocaloric effect reveal that the peak effect occurs at the onset of fluctuations below the $H_{c2}$ line. No indications of a thermodynamic transition as the origin of the peak effect could be found. Our investigation favours thus rather a scenario in which a vortex lattice looses its topological order more continously due to the increasing strength of thermal fluctuations upon approaching the $H_{c2}$ line.

**Q1 207 Measurement of Local Reactive and Resistive Photoresponse of a Superconducting Microwave Device*** STEVEN M. ANLAGE, *CSR, Physics Dept., University of Maryland, USA* ALEXANDER P. ZHURAVEL, *Inst. for Low Temperature Physics, NASU, Kharkov, Ukraine* ALEXEY V. USTINOV, *Physics Institute III, University of Erlangen-Nuremberg, Germany* Despite the voluminous work on the nature of nonlinear effects in high-temperature superconductors (HTS), the causes are not completely clear and remain under debate. The Laser Scanning Microscope (LSM) is a spatially-resolved method that can simultaneously measure optical and high frequency properties of HTS devices. Earlier results showed high resolution images of non-uniform microwave current distributions near the edge of a patterned transmission line structure [A. P. Zhuravel, A. V. Ustinov, K. S. Harshavardhan, and S. M. Anlage, Appl. Phys. Lett. **81**, 4979 (2002)]. We have developed a new operational mode in which the microscope separately images the resistive and inductive components of the bolometric photoresponse. The two images show interesting and dramatic differences, leading to new insights about linear and nonlinear properties of HTS microwave devices.

*Work supported by NSF/GOALI DMR-0201261, a NASU program on nano-structures, materials and technologies, and a DFG Grant Vortex matter in mesoscopic superconductors

**Q1 208 $^{11}B$ NMR Measurements of $TbB_4$** MOOHEE LEE, B.J. MEAN, K.H. KANG, J.H. KIM, I.N. HYUN, *Konkuk University, Seoul 143-701 Korea* B.K. CHO, *GIST, Gwangjoo 500-712, Korea* $^{11}B$ pulsed NMR measurements have been performed to investigate local electronic structure and 4f spin dynamics for $TbB_4$ single crystals. $^{11}B$ NMR spectrum shows a broad peak due to the 4f local moment. $^{11}B$ NMR shift and linewidth are huge and strongly temperature-dependent. In addition, both are proportional to magnetic susceptibility, indicating that the hyperfine field at the boron site originates from the 4f spins of Tb. The shift and the spin- lattice relaxation rate show high anisotropy for field parallel and perpendicular to the c-axis. Anisotropy of the shift and the relaxation rates are analyzed with the results of magnetization to understand the microscopic details of anisotropic spin dynamics.

**Q1 209 $^{27}Al$ NMR Measurements of $YMn_4Al_8$** MOOHEE LEE, *Konkuk University, Seoul 143-701, Korea* K. H. KANG, B. J. MEAN, J. H. KIM, I. N. HYUN, *Konkuk University, Seoul 143-701 Korea* B. K. CHO, *GIST, Gwangjoo 500-712, Korea* We have performed $^{27}Al$ nuclear magnetic resonance (NMR) measurements on the single crystals of $YMn_4Al_3$. $^{27}Al$ NMR spectrum, Knight shift, spin-lattice and transverse relaxation rates, $1/T_1$ and $1/T_2$, were measured down to 4 K at 8 T. Experimental results of the Knight shift and the nuclear spin lattice relaxation rate as well as magneto-resistance and susceptibility are analyzed and discussed in conjunction with the pseudogap behavior in the spin excitation spectrum.

**Q1 210 On a partial differential equation for determining the free energy of ternary mixtures from light scattering data** GEORGE THURSTON, CARL LUTZER, *Dept Mathematics, Rochester Institute of Technology* DAVID ROSS, *Kaiser Permanente* With use of an approximation appropriate for liquid mixtures, we formulate a well- established relation for light scattering from ternary mixtures as a second-order nonlinear partial differential equation, which relates the inverse Hessian of the intensive free energy to the efficiency of light scattered near the forward direction. We examine the mathematical conditions under which light scattering data can be a suitable input for solving this equation, thereby to determine the free energy in a nearly model-independent fashion. We find that within the thermodynamically stable and metastable regions of the phase diagram, composition curves that are nearly perpendicular to the gradient of the dielectric constant are also not what are termed characteristic for the light scattering partial differential equation. This criterion, in turn, implies that free energy solutions in the neighborhood of a such a composition curve can be self-consistently constructed by combining a known free energy gradient along the curve with light scattering data in the surrounding region. These considerations suggest that an experimental method comprising light scattering in the ternary composition triangle, combined with other means of finding the needed boundary conditions along a suitable curve, should in principle be capable of determining ternary mixture free energies without adopting specific free energy models in advance.

**Q1 211 Abstract Withdrawn**

**Q1 212 Direct microscopic observations of fluctuations near critical point** ANA OPRISAN, JOHN HEGSETH, *University of New Orleans* A series of experiments were performed on in orbit to study boiling, phase separation and fluctuations taking place in pure fluids (SF6) near critical point. A specially designed apparatus (ALICE 2) allowed a precise control of fluid's temperature. Local density fluctuations were observed by illuminating a cylindrical cell filled with the pure fluid near its liquid-gas critical point using a microscope and a video recorder. The apparatus was placed in orbit where there is no gravitational limitation in the size of the fluctuations. Using image processing techniques, we were able to estimate properties of the fluid from the recorded images showing fluctuations of the transmitted and scattered light. We found that the histogram of the image can be fitted by a Gaussian and by determining its width we were able to estimate these properties. We also estimated the wave number corresponding to the maximum of the radial average of the power spectrum and the corresponding characteristic length of the fluctuations.

**Q1 213 Quantum Phase Transitions and Entanglement in the Detuned Dicke Model** RU-FEN LIU, *Phys. Depart., National Cheng Kung Univ.* CHIA-CHU CHEN, *Phys. Depart., National Cheng Kung Univ.* The quantum phase transition of mono-mode Dicke models with two atoms is discussed and analytical results are presented. For arbitrary detuning, the exact spectrum and the concurrence of entanglement are calculated for the two-atom system. It is shown that sequential quantum phase transitions occur in this system. Evidences have been found to support that quantum phase transition and concurrence are uncorrelated in this particular model. Furthermore, the results of quantum phase transition with extra mode are also discussed.

**Q1 214 Disorder and size effects in Kondo lattice nanoparticles** YANG-YUAN CHEN, P. H. HUANG, M. N. OU, *Institute of Physics, Academia Sinica, Taipei, Taiwan 115 ROC* J. M. LAWRENCE, *Department of Physics and Astronomy, University of California, Irvine, CA92717 USA* C.H. BOOTH, *Chemical Sciences Division, Lawrence Berkeley National Laboratory, Berkeley, CA 94720-8175 USA* The evolution of Kondo interactions and magnetic order with size variation was revealed by the specific heat and magnetic susceptibility in a series of $CePt_2$ Kondo lattice nanoparticles with various sizes. In addition to the magnetic order suppression with size reduction, two regimes of size dependence of Kondo temperature $T_K$ was observed. As size d decreases from the bulk down to 22 nm firstly $T_K$ slightly decreases from 4.6 K to 3.7 K, as d further decreases, inversely $T_K$ increases up to 100 K for size d=3.8 nm. It is confirmed that the size-induced lattice disorders are responsible for the result for $d \geqslant 22$ nm, while the rapid increase of $T_K$ for d =3.8 nm is attributed to the lattice contraction and quantum size effects.

**Q1 215 Potential use of combining the diffusion equation with the free Shrödinger equation to improve the Optical Coherence Tomography image analysis*** DELIA CABRERA FERNANDEZ, HARRY M. SALINAS, *Bascom Palmer Eye Institute, Miami, FL* GABOR SOMFAI, *Semmelweis University, Dept. of Ophthalmology, Hungary* CARMEN A. PULIAFITO, *Bascom Palmer Eye Institute, Miami, FL* OPHTHALMIC IMAGING GROUP, BASCOM PALMER EYE INSTITUTE TEAM, DEPT OF OPHTHALMOLOGY, SEMMELWEIS UNIVERSITY COLLABORATION, Optical coherence tomography (OCT) is a rapidly emerging medical imaging technology. In ophthalmology, OCT is a powerful tool because it enables visualization of the cross sectional structure of the retina and anterior eye with higher resolutions than any other non-invasive imaging modality. Furthermore, OCT image information can be quantitatively analyzed, enabling objective assessment of features such as macular edema and diabetes retinopathy. We present specific improvements in the quantitative analysis of the OCT system, by combining the diffusion equation with the free Shrödinger equation. In such formulation, important features of the image can be extracted by extending the analysis from the real axis to the complex domain. Experimental results indicate that our proposed novel approach has good performance in speckle noise removal, enhancement and segmentation of the various cellular layers of the retina using the OCT system.

*This study is supported by a NIH R01 EY008684-10S1

**Q1 216 Simulation of $Xe_nAr_m$ Cluster Formation in a Molecular Beam: Comparison with Photoelectron Spectroscopy** FRANCOIS G. AMAR, THOMAS J. PRESTON, *Department of Chemistry, University of Maine, Orono, ME 04469-5706* We perform direct MD simulations of the formation of mixed $Xe_nAr_m$ clusters ($500 < n+m < 3000$) in a supersonic beam as a function of initial beam conditions. We then model the $4d_{5/2}$ (Xe) and $2p_{3/2}$ (Ar) core hole photoelectron spectra of these clusters and compare them to the experimental spectra of Tchaplyguine itet al[1]. The predicted spectra are calculated as the sum of final state energy shifts of the ionized atoms (within the cluster) relative to the isolated gas phase ion using a self-consistent polarization formalism. We use the results of our earlier calculations on pure argon and xenon clusters [2] to determine the appropriate inelastic mean free path value for the signal electrons leaving the mixed clusters. These results allow us to gain a refined understanding of the size, stoichiometry, and core/shell structure of these mixed clusters. [1] M. Tchaplyguine, itet al, Phys. Rev A **69**, 031201 (2004); [2] F. Amar, itet al, JCP **122**, 244717 (2005).

**Q1 217 Helium Nanodroplets: spectroscopy and density-functional calculations** ROMAN SCHMIED, KEVIN K. LEHMANN, *Dept. of Chemistry, University of Virginia* Helium nanodroplet spectroscopy has shown to be an excellent tool for studying superfluid helium in nano-scale geometries. Experimental signatures of superfluidity are the free rotation of many molecules in helium nanodroplets, and the droplet phonon spectra observed in electronic transitions of molecular dopants. We present new results and interpretations from a study of helium nanodroplets using time- dependent density-functional theory and its normal-mode analysis.

**Q1 218 Chaotic Dynamics of a Harmonic Oscillator Interacting Linearly with a Free Particle*** ALEXANDER SILVIUS, *University of Missouri - Rolla* STEPHAN DE BIÈVRE, *Université des Sciences et Technologies de Lille* PAUL PARRIS, *University of Missouri - Rolla* We study the closed Hamiltonian dynamics of a free particle moving on a ring, over one section of which it interacts linearly with a single harmonic oscillator. On the basis of numerical and analytical evidence, we conjecture that at small positive energies the phase space of our model is completely chaotic except for a single region of complete integrability with a smooth sharp boundary showing no KAM-type structures of any kind. This results in the cleanest mixed phase space structure possible, in which motions in the integrable region and in the chaotic region are clearly separated and independent of one another. For certain system parameters, this mixed phase space structure can be tuned to make either of the two components disappear, leaving a completely integrable or completely chaotic phase space. For other values of the system parameters, additional structures appear, such as KAM-like elliptic islands, and one parameter families of parabolic periodic orbits embedded in the chaotic sea. The latter are analogous to bouncing ball orbits seen in the stadium billiard. The analytical part of our study proceeds from a geometric description of the dynamics, and shows it to be equivalent to a linked twist map on the union of two intersecting disks.

*This work supported by NSF grants DMR-0097210 and INT-0336343.

**Q1 219 Dielectric fluctuations and the origins of non-contact friction** SEPPE KUEHN, ROGER F. LORING, JOHN A. MAROHN, *Department of Chemistry and Chemical Biology, Cornell University, Ithaca, NY 14853* Dielectric fluctuations underlie a wide variety of physical phenomena, from ion mobility in electrolyte solutions and decoherence in quantum systems, to dynamics in glass-forming materials and conformational changes in proteins. Here we show that dielectric fluctuations also lead to non-contact friction. A detailed understanding of non-contact friction is essential to micromechanical systems and the continued success of high sensitivity scanned probe microcopies such as magnetic resonance force microscopy. We study non-contact friction by using high sensitivity, custom fabricated, single crystal silicon cantilevers to measure energy losses over poly(methyl methacrylate), poly(vinyl acetate), and polystyrene thin films. We present a new theoretical analysis, relating non-contact friction to the dielectric response of the film, which is consistent with our experimental observations. We believe this constitutes the first direct, mechanical detection of friction due to dielectric fluctuations, and establishes a new route to the measurement of these fluctuations at the nanoscale.

**Q1 220 Conductance Behavior of Molecularly Linked Gold Nanoparticle Films Near the Metal-Insulator Transition** JEFFREY DUNFORD, YOSHINORI SUGANUMA, AL-AMIN DHIRANI, BRYAN STATT, *University of Toronto* Self-assembled molecularly-linked metal nanoparticle films exhibit interesting electronic behavior that can range from insulating to metallic. In particular, the electronic behavior of 1,4-butanedithiol-linked gold nanoparticle films can be tuned by varying film thickness. We have investigated the temperature (T) dependence of the differential conductance (g) of 1,4-butane dithiol linked Au nanoparticle films. On the insulating side of the transition, the conductance behaves as $g = g_0 \exp[-(T_0/T)^{[**raise**]0.7ex1[**lower**]0.7ex2}]$. Qualitatively, this is consistent with an Efros- Shklovskii ''variable range hopping'' model based on a competition between Coulombic and intercluster tunnelling processes. However, we find that hopping distances are too large (62 nm to 720 nm at 100 K) to be consistent with tunneling between clusters, and tend to scale with cluster size. We propose a modified ''quasilocalized hopping'' model based on competition between single-electron cluster charging and intracluster electron backscattering to explain this temperature dependence.

**Q1 221 Spin relaxation in a GaAs quantum dot embedded inside a suspended phonon cavity*** YING-YEN LIAO, *Department of Electrophysics, National Chiao-Tung University, Hsinchu 300, Taiwan* YUEH-NAN CHEN, *Department of Electrophysics, National Chiao-Tung University, Hsinchu 300, Taiwan* DER-SAN CHUU, *Department of Electrophysics, National Chiao-Tung University, Hsinchu 300, Taiwan* TOBIAS BRANDES, *School of Physics and Astronomy, The University of Manchester P.O. Box 88, Manchester, M60 1QD, U.K.* The phonon-induced spin relaxation in a two-dimensional quantum dot embedded inside a semiconductor slab is investigated theoretically. An enhanced relaxation rate is found due to the phonon van Hove singularities. Oppositely, a vanishing deformation potential may also result in a suppression of the spin relaxation rate. For larger quantum dots, the interplay between the spin orbit interaction and Zeeman levels causes the suppression of the relaxation at several points. Furthermore, a crossover from confined to bulk-like systems is obtained by varying the width of the slab.

*This work is supported partially by the National Science Council, Taiwan under the grant numbers NSC 94-2112-M-009-019, NSC 94-2120-M-009-002 and NSC 94-2112-M-009-024.

**Q1 222 Optical properties of semiconductor nanocrystals in the tight-binding (TB) approximation** ANDREW SHABAEV, EUGENE TSIPER, ALEXANDER EFROS, DIMITRIS PAPACONSTANTOPOULOS, *Naval Research Laboratory and George Mason University* Tight-binding (TB) approach is very attractive for computing electronic properties of semiconductor nanocrystals since it can handle large numbers of atoms, and since nanocrystals of arbitrary shape can be studied. TB approach provides realistic boundary conditions at the surface, which are often defined with uncertainty in the effective mass approximation. This is especially important in small nanocrystals, where a large fraction of atoms belongs to the surface. For example, in a 1000-atom Si nanocrystal about 2/3 of all atoms have less than four nearest neighbors. Successful TB approaches, such as NRL-TB method, exist to compute electronic structure of various bulk materials. We use NRL-TB to compute electronic transitions in nanocrystals of arbitrary shape. It appears, that a given TB parameterization that yields adequate electronic structure is incomplete in terms of predicting oscillator strengths of the transitions, in contrast to a common belief. Such TB parameterization must be augmented with additional quantities that contribute to the transition dipole matrix elements between localized orbitals. We thus resolve the existing controversy, despite the arguments that these extra contributions are problematic and should not be incorporated into TB. We also discuss practical ways to calculate the extra quantities, which are not supplied by the conventional TB parameterizations.

**Q1 223 Impurity mode techniques applied to photonic crystal slabs** ARTHUR MCGURN, *Western Michigan University* A theoretical treatment is given of the modes of a photonic crystal slab containing an impurity. The photonic crystal slab is formed by embedding an hexagonal lattice array of dielectric cylinders in a background slab of uniform dielectric medium. This creates a free standing slab with a periodic patterning. The solution of Maxwell's equations for the modes of the slab are given as an expansion in the waveguide and radiative modes of a uniform slab of dielectric medium. The density of modes in frequency space is presented for the photonic crystal slab in the absence of an impurity. The impurity modes for a single site impurity introduced into the center of the photonic crystal patterning are computed using Green's function methods. Bound state impurities and in band resonances are studied and used to explain recent experimental results on photonic crystal light sources.

**Q1 224 Fabrication of nanoscale magnet-tipped cantilevers for magnetic resonance force microscopy** STEVEN A. HICKMAN, *Department of Chemistry and Chemical Biology, Cornell University* SEAN R. GARNER, *Department of Physics, Cornell University* LEE E. HARRELL, *Department of Physics, United States Military Academy* SEPPE KUEHN, JOHN A. MAROHN, *Department of Chemistry and Chemical Biology, Cornell University* Magnetic resonance force microscopy(MRFM) is a promising new technique for acquiring magnetic resonance images of a single molecule; to date we have demonstrated a sensitivity of approximately 10,000 proton spins. In MRFM the force exerted on the

cantilever, per spin, is proportional to the field gradient from the cantilever's magnetic tip. To increase the force requires shrinking the magnet size. Achieving the attonewton force sensitivity necessary to image single spins requires mitigating surface induced dissipation. We choose to meet both of these conditions by creating nanoscale magnets extending from the tips of silicon cantilevers. We will present a 50-nm wide overhanging cobalt magnet fabricated by a process involving electron beam lithography and anisotropic KOH etching. This process can be integrated into a fabrication protocol for ultrasensitive silicon cantilevers. With these cantilevers we expect a sensitivity of better than 1000 protons.

**Q1 225 Electrically Controlled Bandgap in a Chiral Material** JUAN REYES CERVANTES, AKHLESH LAKHTAKIA, *Instituto de Física UNAM* The propagation of light along the axis of nonhomogeneity of a structurally chiral medium (SCM) under the influence of a low– frequency (dc) electric field aligned along the same axis is investigated. The Pockels effect is assumed to occur, and the SCM is taken to possess locally a $\bar{4}2m$ point group symmetry. The frequency–domain Maxwell curl equations are cast in a $4\times 4$ matrix representation, and the Oseen transformation is invoked. The band structure is analyzed, as are also the eigenvectors as well as the transfer matrix. Finally, the reflection and transmission of a plane wave due to a SCM of finite thickness is considered. The low–frequency electric field is shown to control the bandgap.

**Q1 226 Organic Solar Cell with Carbon Nanotubes as Anode*** ROSS ULBRICHT, XIAOMEI JIANG, KANZAN INOUE, KAMIL MIELCZARECK, CARLOS MEDINA, SERGEY LEE, ANVAR ZAKHIDOV, Organic, polymer based solar cells present a low cost more versatile alternative to the current inorganic silicon based solar cells. In this research, carbon nanotubes have been used to replace the conventional anode used, indium tin oxide. Carbon nanotubes exhibit electronic, optical and mechanical properties desirable for polymeric based organic solar cells. In this study, an oriented muliwall carbon nanotube sheet is used as the hole collecting electrode with RR-P3HT as the donor material and PCBM as the acceptor material. An open circuit voltage of 0.57V, a short circuit current of 5.53mA/cm2, a fill factor of 0.37, and an efficiency of 1.16% has been obtained. Performance dependence on incident light intensity and spectral studies along with other various investigations are presented.

*The authors thank the Air Force Office of Scientific Research for the financial support of this work

**Q1 227 Theorems Determining Reciprocal and Nonreciprocal Properties of Negative Refractive Bi-Crystal Heterostructures** CLIFFORD KROWNE, *Naval Research Laboratory* One of the most interesting questions in regard to the negative refractive bicrystal heterostructure is what multi-terminal electronic characteristics it may possess. The heterostructure possesses a symmetry breaking operation creating asymmetric fields associated with the SO(2) rotation group [1]. Two terminal behavior may be addressed by examining generalized theorems for complex anisotropic media [2]. Applying the anisotropic reaction theorem to subregions of the heterostructure, and then to the composite structure, we find that passive nonreciprocity [3] is not possible while active nonreciprocity is possible as mentioned in [4]. Possible device applications include beam steering, and isolation devices requiring direction sensing control. Simulations show what happens to the asymmetry when making the heterostructure macroscopically using LINbO3 crystals versus using nanostructure technology which would work with ferroelectric films deposited by MBE. A fabrication effort used to build the structure, with metal patterning to test a derivative property of the asymmetry, namely terminal reciprocity/nonreciprocity, will be discussed too [5]. [1] C. M. Krowne, PRL 93, 053902, 30 July 2004. [2] C. M. Krowne, IEEE Trans. Ant. Propag. 32, 1224 Nov. 1984, [3] C. M. Krowne, IEEE Trans. MTT 53, 1345, 2005, [4] C. M. Krowne, arXiv.org/abs/cond-mat/0408369, 17 Aug. 2004. [5] Private commun. S. W. Kirchoefer, J. A. Bellotti, and J. M. Pond, 2005.

**Q1 228 Energetic Material Simulations Framework** WILLIAM MATTSON, BETSY RICE, *US Army Research Laboratory* We have created a computational framework for the easy implementation of the modeling needs of the advanced energetic materials (AEM) community, with rapid turnaround. The framework constructs simulations described in eXtensible Markup Language (XML) from a set of components in shared object libraries. The complete set of standard molecular simulation components can be combined in any fashion creating typical simulations and providing unanticipated functionality. The framework includes multimillion atom molecular dynamics in a several thermodynamic ensembles, including the recently developed uniaxial Hugoniostat method. This constrains the system to states that correspond to points on the shock Hugoniot curve. It also includes ab initio crystal prediction capability. This procedure predicts the crystal structure and density of a solid using only the molecular structure of a single molecule. This predictive capability is considered crucial to the design and development process of AEM, since one of the fundamental properties required for the initial screening of a candidate energetic material is its crystalline density.

**Q1 229 The radiation equilibrium is classical** V. GURUPRASAD, *Inspired Research, NY* By definition, standing wave modes cannot interact among themselves, plus non-zero temperature means real walls must vibrate. Modal interaction by Doppler shifts at the walls is thus an unavoidable premise in cavity equilibrium, but it also suffices to yield Planck's law itclassically, as follows. $\lambda/2$-intervals of the modes are immutable energy-bearing entities under these thermalizing interactions, like molecules in the kinetic theory, as Doppler shifts preserve phase and amplitude, thus only compressing or dilating the $\lambda/2$-intervals in time. The premise is really a conceptual aid, as energy immutability is guaranteed by definition: $E(\lambda/2) = \int_0^{\lambda/2} |a\sin(2\pi x/\lambda)|^2\, dx = \int_0^{\pi} a^2 \sin^2\theta\, d\theta$, independent of $\lambda$. Therefore, Boltzmann equipartition must be applied to these intervals, instead of to full modes as in Rayleigh-Jeans theory, and it dictates a common mean energy $u$, not $u \neq k_B T/2$ – modes are mere Fourier components, not full particulate entities. The intervals yield $E = h\nu$ with $h \equiv u$ as the number of such intervals in a mode is proportional to its frequency. Mode closure sets under the thermalizing interactions form Planck's harmonic oscillators – as the intervals are immutable, interacting modes can only differ by whole number of intervals, hence must be harmonically related, and itreplace each other by exchanging intervals. The energy expectation at any $\lambda$ is then an average over any such mode closure set, yielding Planck's law itwithout assumptions and itwithout breaking from classical physics. The result identifies $h \equiv u$ as the analogue of $k_B$ for the frequency domain.

**Q1 230 Experimental one-way quantum computation using linear optics** PHILIP WALTHER, *Institute of Experimental Physics, University of Vienna, Boltzmanngasse 5, 1090 Vienna, Austria* KEVIN RESCH, *University of Queensland, Physics Department, AUS* TERRY RUDOLPH, *QOLS, Blackett Laboratory, Imperial College London, London SW7 2BW, UK* EMMANUEL SCHENCK, *Institute of Experimental Physics, University of Vienna, Boltzmanngasse 5, 1090 Vienna, Austria* HARALD WEINFURTER, *Department of Physics, Ludwig Maximilians University, D-80799 Munich, Germany* VLATKO VEDRAL, *The School of Physics and Astronomy, University of Leeds, Leeds LS2 9JT, UK* MARKUS ASPELMEYER, ANTON ZEILINGER, *Institute of Experimental Physics, University of Vienna, Boltzmanngasse 5, 1090 Vienna, Austria* Standard quantum computation is based on a universal set of unitary quantum logic gates which process qubits. In contrast to the standard quantum model, Raussendorf and Briegel proposed the one-way quantum computer, based on a highly-entangled cluster state, which is entirely different. We have experimentally realized four-qubit cluster states encoded into the polarization state of four photons. We fully characterize the quantum state by implementing the first experimental four-qubit quantum state tomography. Using this cluster state we demonstrate the feasibility of one-way quantum computing through a universal set of one- and two-qubit operations. Finally, our implementation of Grover's search algorithm demonstrates that one-way quantum computation is ideally suited for such tasks.

**Q1 231 Direct current bias effect on the magnetoresistance of submicron spin-valve ellipses*** CHIEN-TU CHAO, S.G. LAI, JONG-CHING WU, LANCE HORNG, *National Changhua University of Education* TE-HO WU, *National Yun-lin University of Science & Technology* S. YOSHIMURA, M. TSUNODA, M. TAKAHASHI, *Tohoku University* TAIWAN SPIN RESEARCH CENTER TEAM, Submicron spin-valve devices with nonmagnetic I/V leads have been successfully fabricated using E-beam lithography in conjunction with an ion beam etching. The layer structures are SiO2/Ta(5nm)/ NiFe(2nm)/ MnIr(10nm)/ CoFe(2nm)/Cu(2.5nm)/CoFe(2nm)/NiFe(3nm)/Cu(1nm)/ Ta-O(3nm) prepared by DC sputtering. Low field ac MR measurements were carried out with an external magnetic field applied parallel to the biasing/current direction. A significant shift on minor loop, with respect to that of the non-patterned film, is associated with an antiferromagnetic coupling resulted from the pinned layer's stray field after patterning. In addition, a direct current bias was superimposed to the low field ac for the studies of joule heating and possible spin transfer torque effect. In comparison to the MR measured at various ambient temperatures Joule heating effect was identified from the resistance background change. Extra features were developed during the magnetization reversal that may be associated with spin torque effect. Details of the MR minor loops regarding to the magnetization evolution and the switching mechanism will be presented.

*Work is supported by the Ministry of Economic affairs of Taiwan.

**Q1 232 Interface Mott Transition and Colossal Electroresistance** TAKASHI OKA, *CERC, National Institute of Advanced Industrial Science and Technology (AIST)* NAOTO NAGAOSA, *University of Tokyo* Colossal electroresistance – devices with huge nonlinear $I - V$ with hysteresis – found in strongly correlated materials is now receiving wide interest as a candidate of a novel non-volatile memory. In order to design such devices, it is important to understand how phase transition takes place at the interface between SCES and an electrode. We propose a simple theoretical scheme to calculate the electronic state at such interfaces. A density matrix renormalization group (DMRG) calculation of a 1D tight binding model is performed, where we find that the Mott transition takes place, and by altering the external bias, we can change the transport property drastically from insulating to Ohmic (metallic). Next, we propose a mechanism of colossal electroresistance based on first order metal-insulator transition. In this mechanism, the switching between on and off states is realized by a hysteresis loop of bias voltage crossing the phase coexistence regime near the transition. (cond-mat/0509050, to appear in Phys. Rev. Lett.)

**Q1 233 Magnetic field effects in double-walled carbon nanotubes** ANDREA LATGE, *Universidade Federal Fluminense* DANIEL GRIMM, *Leibiniz Institute of Dresden* MAURO FERREIRA, *Trinity College - Dublin* Double-wall carbon nanotubes (DWCNs) are coaxial two-tube systems which are now considered very important from their mechanical and electronic properties. They may be achieved, for instance, by peapod-derived methods or synthetized by pulsed arc dicharge processes. The distance between both cilinders are quite the same of the one found between carbon planes in graphite structures, and the correspondent intertube electronic interactions (van der Waals energies) are also much inferior than the electronic correlation within each single tube. Here we present a theoretical discussion of electronic and transport properties of a particular family of DWCNs named commensurate structures of the armchair (n,n)@(2n,2n) and zigzag (n,o)@(2n,0) types. Emphasis is given on the role played by the geometrical aspects of the tubes and the relative atomic positions on the local density of states and conductance of the systems. We investigate the origin of the conductance suppression and the possibility of founding Aharonov-Bohm effects in the double walled carbon when applying a magnetic field along the axial direction. The field is theoretically described by following the Peierls approximation into the hopping energies and by adding a Zeeman energy in the diagonal term of the tight-binding Hamiltonian. This should be interesting not only for the basic understanding of DWCNs but also to allow a characterization upon their responses under external fields.

**Q1 234 Simple, Rapid Chirality Characterization of Single Walled Carbon Nanotubes** PHILLIP WILLIAMS, *National Institute of Aerospace* MIN NAMKUNG, *NASA Goddard Space Flight Center* CANDIS MAYWEATHER, JOSLYN PERKINS, *Spelman College* BUZZ WINCHESKI, *NASA Langley Research Center* CHEOL PARK, *National Institute of Aerospace* JUOCK NAMKUNG, *Naval Air Warfare Center* Raman scattering and optical absorption spectroscopy are used for the chirality characterization of single wall carbon nanotubes (SWNTs) dispersed in various solvent systems. Radial breathing mode (RBM) Raman peaks for semiconducting and metallic SWNTs are identified by directly comparing the Raman spectra with the Kataura plot. The SWNT diameters are then calculated from these resonant peak positions. Next, a list of (n, m) pairs, yielding the SWNT diameters within a few percent of that obtained from each resonant peak position, is established. The interband transition energies for the list of SWNT (n, m) pairs are calculated based on the tight binding energy expression for each list of the (n, m) pairs, and the pairs yielding the closest values to the corresponding experimental optical absorption peaks are selected. The results reveal the most

probable chiralities for the semiconducting nanotubes and for the metallic nanotubes present in a batch of SWNTs. Directly incorporating the Raman scattering data into the optical absorption spectra, the present method is considered the simplest practical technique currently available.

**Q1 235 Reentrant Disordering of Colloidal Molecular Crystals on 2D Periodic Substrates** MICHAEL MIKULIS, *Department of Physics, University of California, Davis* CYNTHIA REICHHARDT, CHARLES REICHHARDT, *Center for Nonlinear Studies and Theoretical Divison, Los Alamos National Laboratory* RICHARD SCALETTAR, GERGELY ZIMANYI, *Department of Physics, University of California, Davis* We study colloidal ordering and disordering on two-dimensional periodic substrates where the number of colloids per substrate minima is two or three. The colloids form dimer or trimer states with orientational ordering, referred to as colloidal molecular crystals. At a fixed temperature such that, in the absence of a substrate, the colloids are in a triangular floating solid state, upon increasing the substrate strength we find a transition to an ordered colloidal molecular crystal state, followed by a transition to a disordered state where the colloids still form dimers or trimers but the orientational order is lost. These results are in agreement with recent experiments.

**Q1 236 Behavior of $(Pb_{0.9}Ba_{0.05}Sr_{0.05})(Zr_{1-x}Ti_x)O_3$ solid solutions in the vicinity of morphotropic boundary** V. SOBOLEV, *Physics Department, South Dakota School of Mines and Technology, Rapid City, SD 57701* V. ISHCHUK, *Institute for Single Crystals of National Academy of Sciences of Ukraine, Kharkov, 61001, Ukraine* V. BAUMER, *Institute for Single Crystals of National Academy of Sciences of Ukraine, Kharkov, 61001, Ukraine* T. TEPLITSKAYA, *Institute for Single Crystals of National Academy of Sciences of Ukraine, Kharkov, 61001, Ukraine* $(Pb_{0.9}Ba_{0.05}Sr_{0.05})(Zr_{1-x}Ti_x)O_3$ series of solid solutions possess rather narrow width of the morphotropic region that does not exceed 5% (determined by X-ray diffraction studies). Using a modified ceramic technique, we obtained samples with a grain size of the order of 20-25 $\mu$m. We performed detailed investigations of piezoelectric and dielectric properties of these samples. It is shown that the temperature interval of the diffuse phase transition depends on the position of the given solid solution in the ''Ti concentration – Temperature'' phase diagram. The maximum interval is observed in the middle of the morphotropic region. There exists a temperature interval of the order of several decades of degrees above the Curie point where piezoelectric resonance can be observed. The width of this temperature interval reduces considerably when solid solution composition moves from morphotropic region.

**Q1 237 Electroabsorption of wide bandgap semiconductors GaN and ZnO: the theory and experiments** XIYAO ZHANG, *Department of Physics, North Carolina State University* ANDREW OBERHOFER, JOHN MUTH, *Department of Electrical and Computer Engineering, North Carolina State University* SEMICONDUCTOR PHOTONICS RESEARCH TEAM, Dow and Redfield developed a theoretical model in 1970's to describe the change of the broadening of exciton absorption peak and the tilting of band edge in semiconductor under an electrical field. In this work, we apply this generic model to different kinds of wide bandgap semiconductors, such as GaN and ZnO. The exciton electroabsorption problem can be treated non-perturbatively in the center-of-mass coordinate as one electron in a Coulomb potential and an electrical field. The corresponding three-dimensional Schrdinger equation was solved for the electron-hole envelope wavefunction at the origin and the density of states per unit energy by introducing parabolic coordinates. Elliot formula was then used to calculate the actual optical electroabsorption coefficient. Thermal broadening of the exciton absorption peak was considered by convoluting a Guassian function, whose line width is related to the temperature. Experimental temperature dependent absorption data of GaN and ZnO were measured from 77K to 300K. The electroabsorption spectra of GaN in an optical modulator structure have also been examined. These experiment results were used to verify the theoretical model of electroabsorption of wide bandgap semiconductors.

**Q1 238 Satellite bands in the rotational spectrum of doped helium clusters** TATJANA SKRBIC, SAVERIO MORONI, STEFANO BARONI, *INFM-DEMOCRITOS and SISSA, Trieste, Italy* Recent measurements of infrared spectra of Carbon dioxide molecules embedded in Helium droplets reveal a weak satellite band (SB) accompanying a sharp R(0) rovibrational line. By reanalyzing previous quantum Monte Carlo calculations of the rotational dynamics of various dopant molecules in Helium clusters, we find indeed evidence for rotational excitations with energies and spectral weights close to the measured values of the SB. We present new simulations, in which specifically devised imaginary-time correlation functions are introduced for an explicit theoretical characterization of individual excitations, as well as for enhanced computational efficiency in the calculation of weak spectral features. The proposed assigment of the SB to a coupled rotational state of the molecule and a ring of Helium atoms is discussed.

**Q1 239 Surface Studies of Enhanced Metal/Carbene Contacts** MARCUS LAY, *University of Georgia* GEORGE FLYNN, COLIN NUCKOLLS, GEORGE TULEVSKI, MIKE STEIGERWALD, MARK HYBERTSEN, *Columbia University* Scanning tunneling microscopy and spectroscopy (STM and STS) have proven invaluable in understanding and manipulating the physical and electronic properties of molecular-scale systems. Such systems show great promise in current and future electronic applications. Indeed, self-assembled monolayers (SAMs) composed of alkanethiols have been extensively explored as a possible route to formation of metal-organic semiconductor contacts. While S is effective in this function, it behaves more as a capacitor than a conductor at the metal-adsorbate interface. This presentation will focus on investigations of the formation of metal-carbene complexes. For molecular electronics applications, conjugated metal-carbenes are expected to exhibit significantly greater conductance in transistor applications than corresponding thiols. A particular emphasis of this presentation is the structural and electronic information yielded by ultra-high vacuum (UHV) STM/STS studies of the formation of a Ru-carbene from diazoalkane precursors. Early

theoretical predictions and UHV-STS indicate a strong coupling of the HOMO for bromophenyl diazomethane to the Ru d-band.

**Q1 240 Abstract Withdrawn**

**Q1 241 Single Photon Transport In One-Dimensional Circuit Quantum Electrodynamics Systems** JUNG-TSUNG SHEN, SHANHUI FAN, *Stanford University* Interesting transport properties of a single microwave photon emerge when a superconducting quantum bit in a cavity is coupled to a one-dimensional waveguide. Here we adopt a real-space model Hamiltonian to give a unified approach which accounts for the recent experimental results, and make new predictions on the properties of single photon transport, such as general Fano lineshape, symmetric vacuum Rabi splitting for leaky cavity at resonance, and one-photon switching capability. We further exploit the large tunability of the qubits to show that further interesting one-photon transport properties can emerge in multiple-qubit system, especially when the transition frequencies are dynamically controlled. In particular, having two qubits coupled to the waveguide gives rise to a transmission lineshape for electromagnetic wave that is analogous to the electromagneically induced transparency (EIT) in atomic system. Furthermore, by cascading these double-qubit structure together to form an array, and by dynamically tuning the transition frequency of the qubits, we show that a single photon pulse can be stopped, stored, and time-reversed in the system, leading to highly nontrivial information processing capabilities on chip. Moreover, with properly designed array, two photons can be stopped and stored in the system at the same time. Finally, the unit cell of the array can be designed to be of deep sub-wavelength scale, thereby realizes the miniaturization of the circuit.

**Q1 242 Electric Characterization of $FeSi_2$ Nanowires by Conductive-AFM** SHENGDE LIANG, *Arizona State University* Since continuing miniaturization of silicon electronics encounters the limits of lithography, silicide nanowires are proposed to act as both devices and the wires that access them in bottom-up fabrication scheme. Iron silicides nanowires can be metallic, magnetic and semiconducting depending on different phases it takes, which make it promising for nanodevices design. Here we characterized Schottky Barrier Height (SBH) of iron silicide nanowires on n-type silicon, which is not uniform ranging from 0.35 to 0.8eV with diamond coated tips. To measure electric transport properties within a single nanowire, we deposited a gold pad to partially cover one nanowire, and use diamond coated tip as another terminal. Nanowires with dimension of 5nm high by 10nm wide by several micrometer long have resistance about 20k ohm at room temperature, this is about 4 times larger than bulk iron silicide resistivity. We tried different metals coated tips and tips with different force constants. Diamond coated tips are most wear-resistant, but have highest contact resistance, which is estimated to be 20k ohm. Other metal coated tips, such as PtIr, PtCr coated tips, have lower contact resistance, less than 1k ohm, but these tips apex are easily scanned off. Suitable contact force were also calibrated to be around 200nN, too strong force will damage nanowire and tip coating layer, while too weak contact lead to high contact resistance.

**Q1 243 Novel commensurability effects in superconducting films with antidot arrays*** GOLIBJON BERDIYOROV, *Department of Physics, University of Antwerp, Belgium* MILORAD MILOSEVIC, *Department of Physics, University of Antwerp, Belgium* FRANCOIS PEETERS, *Department of Physics, University of Antwerp, Belgium* CONDENSED MATTER THEORY GROUP TEAM, Vortex pinning by arrays of microholes is already a well established tool for enhancing the critical current in superconducting films. The pronounced peaks in $j_c(H)$ characteristics at so-called matching fields are generally attributed to the collective locking of vortices to the pinning sites. However, the issues of symmetry and composition of the resulting vortex lattice are often oversimplified. We investigated in detail the vortex configurations in superconducting films with regular antidot-arrays within the non-linear Ginzburg-Landau theory, where demagnetization effects and overlapping vortex cores are fully taken into account (contrary to the London approach). In addition to the well-known matching phenomena, we predict: (i) the nucleation of giant-vortex states at interstitial sites; (ii) the combination of giant- and multi-vortices at rational matching fields; and (iii) for particular interstitial vorticity, the symmetry imposed creation of vortex-antivortex configurations.

*This work was supported by the Flemish Science Foundation (FWO-Vl), the Belgian Science Policy, the JSPS/ESF-NES program, and the ESF-AQDJJ network.

**Q1 244 Threefold onset of vortex loops in superconductors with a magnetic core*** MAURO DORIA, *Instituto de Fisica, Universidade Federal do Rio de Janeiro, Brazil.* MILORAD MILOSEVIC, *Department of Physics, University of Antwerp, Belgium* ANTONIO ROMAGUERA, *Instituto de Fisica, Universidade Federal do Rio de Janeiro, Brazil.* FRANCOIS PEETERS, *Department of Physics, University of Antwerp, Belgium.* Superconductivity and magnetism are known to coexist inside several compounds, such as $RuSr_2LnCu_2O$ and $ErNi_2B_2C$. Recently, artificially nano-engineered superconductors with magnetic inclusions have been realized experimentally. In mesoscopic samples, where the ratio volume to area is small, the vortex patterns vary according to the sample symmetry. On the other hand, magnetic inclusions give rise to vortex loops inside the superconductor. To capture these aspects, we consider theoretically a sub-micron superconductor (e.g. sphere) with a static magnetic moment in its center in order to observe these confined vortex states. The 3D Ginzburg-Landau theory is applied and solved in the finite difference scheme, from which we obtain the very complex 3D vortex configurations. For large samples, when the influence of the boundary diminishes, we found that vortex loops always nucleate in threes. The final superconducting state is characterized by the number of created vortex loops and the number of vortex-antivortex pairs that spring to the surface.

*This work was supported by the CNPq, Insto do Milenio Nanosciencias, the Flemish Science Foundation (FWO-Vl), and IUAP Belgium.

**Q1 245 The coexistence of type-I and type-II superconductivity in mesoscopic single crystals** MILORAD MILOSEVIC, *1* FRANCOIS PEETERS, *1* ANDREAS RYDH, *2,3* MICHAEL ZACH, *2* RUOBING XIE, *2* ZHILI XIAO, *2* DANIEL ROSENMANN, *2* ULRICH WELP, *2* WAI-KWONG KWOK, *2* GEORGE CRABTREE, *2* SIMON BENDING, *4* 1 DEPARTMENT OF PHYSICS, UNIVERSITY OF ANTWERP, BELGIUM. TEAM, 2 MATERIALS SCIENCE DIVISION, ARGONNE NATIONAL LABORATORY, USA. TEAM, 3 DEPARTMENT OF PHYSICS, STOCKHOLM UNIVERSITY, SWEDEN. TEAM, 4 DEPARTMENT OF PHYSICS, UNIVERSITY OF BATH, UK. TEAM, We show that the well established criteria for type-I to type-II transitions in bulk materials do not apply to mesoscopic superconductors, as the dual point depends both on the material properties and on temperature. In electrochemically formed triangular Pb single crystals, we even found the coexistence of both types of superconductivity – while retaining Meissner behavior with increasing magnetic field all the way through the superheated phase, the sample can still capture vortices in the metastable regime. When the field is swept back, in realistic type-I structures with intrinsic pinning, the vortices can survive in the sample even when the field changes polarity, contrary to conventional behavior. All findings are substantiated by state-of-the-art 3D Ginzburg-Landau simulations and $\mu$-Hall probe measurements.

**Q1 246 An Accurate Computation of the de Haas-van Alphen frequencies and effective masses of $NbSe_2$** CHRISTOPHER HOWELLS, MICHELLE JOHANNES, IGOR MAZIN, *Naval Research Laboratory* $NbSe_2$ is a layered superconducting material with a co-existing nearly commensurate CDW. Since both the CDW and superconducting transitions are related to a Fermi Surface instability, an accurate calculation of the Fermi Surface is essential for a microscopic understanding of the physical behavior of this compound. Here we demonstrate a novel computational method for calculating the dHvA frequencies and electron effective masses of $NbSe_2$. Our computational approach employs a FLAPW calculation of the $NbSe_2$ Fermi Surfaces using 40000 k-points. We extract the extremal cross sections (located in the Gamma-K-M and A-L-H planes) into a bitmap and then compute the dHvA frequencies from the number of pixels in the cross sections averaged over an extended Brilluoin zone. The effective masses are calculated by repeating this method with the Fermi energy shifted by 0.002 Ry. Our method satisfies Luttinger's theorem to within 0.1% - a full order of magnitude more accurate than previously published calculations. We use this accuracy to predict the dHvA frequencies and effective masses of $NbSe_2$ under pressure.

**Q1 247 Bipolar surface conduction of $BaTiO_3$ in ultrahigh vacuum corresponding to electron and hole accumulation** YUKIO WATANABE, YOSUKE URAKAMI, MIZUKI YAMATO, *Kyushu University* The surface of the ferroelectric is unique due to the spontaneous polarization. One of such properties is a self-field effect [1,2]. We have reported the self-field effect of $BaTiO_3$ [2,3], which does not seem to be accepted, probably due to the suspicions about the formation of the oxygen vacancies or water absorption at the surface in ultrahigh vacuum. Here, oxygen vacancies in $BaTiO_3$ facilitate *n*-type conduction. In this talk, we present the enhancement of both *n*- and *p*-type surface conduction in $10^{-10}$ –$10^{-11}$ torr. We observed this in both top-seed-solvent-growth (TSSG) and KF-flux grown samples that are nominally pure and transparent. Furthermore, we confirmed the evident reduction of surface conductance above Curie temperature, where it agreed with the conduction without a carrier surface layer. The significant reduction of the conduction by the exposition of the surface to the low vacuum indicates that the conduction occurs really at the very thin layer at the surface. Other several experiments verify the existence of the surface carrier layer by the ferroelectric self-field (depolarization field) effect. [1] Appl. Phys. Lett.66, 1770(1995), Phys. Rev. B57, 789(1998), [2]it Phys. Rev. Lett. 86, 332(2001), [3] Focus http://focus.aps.org/story/v7/st1

**Q1 248 Directional sliding of histone octamers caused by DNA bending** PENG-YE WANG, WEI LI, SHUO-XING DOU, PING XIE, *Laboratory of Soft Matter Physics, Institute of Physics, Chinese Academy of Sciences, Beijing 100080, China* Chromatin-remodeling complexes such as SWI/SNF and RSC of yeast can perturb the structure of nucleosomes in an ATP-dependent manner. Experimental results prove that this chromatin remodeling process involves DNA bending. We simulate the effect of DNA bending, caused by chromatin-remodeling complexes, on directional sliding of histone octamers by Brownian dynamics simulation. The simulation results show that, after a DNA loop being generated at the side of a nucleosome, the histone octamer slides towards this DNA loop until the loop disappears. The DNA loop size is an important factor affecting the process of directional sliding of the histone octamer. A model for directional sliding of histone octamers induced by chromatin-remodeling complexes is suggested. (This research was supported by National Natural Science Foundation of China, and the Innovation Project of the Chinese Academy of Sciences.) (Email: pywang@aphy.iphy.ac.cn)

**Q1 249 Oscillations of Cantilevers** J.D. TAYLOR, GAYATRI KESKAR, JAY GAILLARD, RAZVAN CIOCAN, MALCOLM SKOVE, APPARAO RAO, *Clemson University* Resonance vibration of micro and nano sized cantilevers can be used to measure elastic constants and mass, detect absorbed material, and form part of mechanically resonant filters in electronic devices. We have measured the harmonic content of cantilevers driven by electrostatic forces containing two harmonically related terms, as well as nonlinear terms and parametric terms. The results are compared to numerical simulations of the forces between the cantilever and the counter electrode and the resulting motion of the cantilever.

**Q1 250 Electrical Switching and Rectification in Carbon Nanotube Y_Junctions** JAY GAILLARD, K. YANG, *Clemson University* C. DARAIO, P. BANDARU, S. DIN, *UCSD* M.J. SKOVE, APPARAO PAO, *Clemson University* Recently, we have shown evidence for a dramatic electrical switching behavior in a Y-junction carbon-nanotube morphology [1]. The mutual interaction of the electron currents in the three branches of the Y-junction is shown to be the basis for a potentially new logic device. The Y-junction nanotubes that were prepared using our thermal CVD process [2] typically show the presence of a catalyst particle at the junction. The observed modulation of the current from an on- to an off state could be mediated by defects and the topology of the junction, or due to the presence of catalyst particle at the junction. We will compare the switching characteristics observed in a Y-junction nanotube that does not contain the catalyst particle to those reported in Ref. 1 with a view to elucidating the switching mechanism in branched nanotubes. (1) P. Bandaru et al., Nature Materials, vol. 4(9), 663-666, (2005) (2) N. Gothard, et al., Nanoletters 4, 213-217 (2004)

**Q1 251 Combined HRTEM and Auger spectroscopy evidence for the existence of grain boundary premelting in nickel-doped tungsten** JIAN LUO,* *SMSE and COMSET, Clemson University* VIVEK K. GUPTA, DANGHYOK YOON,† *SMSE, Clemson University* HARRY M. MEYER III, *HTML, Oak Ridge National Laboratory* A combined high resolution transmission electron microscopy (HRTEM) and Auger spectroscopy study has revealed the formation of 0.6 nanometer thick, nickel-enriched, ''liquid-like'' grain boundary (GB) films in Ni-doped W specimens at 95C below the bulk eutectic temperature where the bulk liquid phase is no longer stable [Appl. Phys. Lett. 87, 231902 (2005)]. The stabilization of subeutectic liquid-like grain boundary cores in this model two-component metallic alloy is phenomenologically analogous to the long-sought phenomenon of grain boundary premelting. Despite various macroscopic indications of GB structural transitions, this result, to our knowledge, is the first direct evidence for the existence of such disordered nanostructures at metallic GBs. This observation offers a new explanation to the long-standing mysterious solid-state activated sintering mechanism, where accelerated sintering is attributed to the enhanced diffusion in liquid-like GB layers. This discovery also provides insights to resolve several long-standing controversies, e.g., the mechanisms of Ni-induced abnormal grain growth and GB embrittlement.

*E-mail: jianluo@clemson.edu
†Present address: SMSE, Yeungnam University, Korea

**Q1 252 Enhanced near-field optical moiré effect.** ZHAOWEI LIU, STEPHANE DURANT, HYESOG LEE, YI XIONG, YURI PIKUS, CHENG SUN, XIANG ZHANG, We demonstrated an enhanced near-field optical Moiré effect by inserting a silver slab between two subwavelength gratings. The evanescent fields can be greatly enhanced by the surface plasmon excitation supported by the silver slab, which leads to a remarkable contrast improvement in the Moiré fringes. The crucial role of surface plasmon excitation was elucidated by numerical simulation. Experimental enhanced near-field optical Moiré effect, which agreed very well with the simulation, was also presented. This new effect can be used to extend the conventional Moiré techniques into usage of subwavelength gratings.

**Q1 253 Electroformation of Phospholipid Vesicles Monitored by Quartz Crystal Microbalance and Optical Microscopy** VADOUD HASSANZADEH NIRI, JAMES FORREST, *University of Waterloo* Quartz Crystal Microbalance with dissipation monitoring (QCM-D) and Optical Microscope were used in combination to investigate the electroformation of giant vesicles from 1,2-Dimyristoyl-sn-Glycero-3-Phosphocholine (DMPC). The gold-coated quartz crystal coated by lipid film and the ITO-coated glass slide were used as electrodes for electroformation. Immediately upon voltage application (1V, 10Hz) between the two electrodes increases in the frequency and decreases in the dissipation were observed indicating the loss of lipid from the QCM surface. Concurrently, we observed vesicles on the QCM electrode surface. By fitting the frequency shift (delta F), and dissipation change (delta D), to a viscoelastic model, we were able to find the time evolution of the lipid film thickness. By counting the vesicles in the active QCM area, and comparing it to the thickness of lost lipid, we are able to provide an upper bound for the average vesicle thickness.

**Q1 254 Hidden Variables and Placebo Effects** SHANTILAL GORADIA, God's response to prayers and placebo leads to a question. How does He respond deterministically? He may be controlling at least one of the two variables of the uncertainty principle by extending His invisible soul to each body particle locally. Amazingly, many Vedic verses support this answer. One describes the size of the soul as arithmetically matching the size of the nucleons as if a particle is a soul. One gives a name meaning particle soul (anu-atma), consistent with particle's indeterministic behavior like that of (soulful) birds flying in any directions irrespective of the direction of throw. One describes souls as eternal consistent with the conservation of baryon number. One links the souls to the omnipresent (param- atma) like Einstein Rosen bridges link particles to normal spacetime. One claims eternal coexistence of matter and soul as is inflationary universe in physics/0210040 V2. The implicit scientific consistency of such verses makes the relationship of particle source of consciousness to the omnipresent Supreme analogous to the relationship of quantum source of gravitons in my gr-qc/0507130 to normal spacetime This frees us from the postulation of quantum wormholes and quantum foam. Dr. Hooft's view in ''Does God play dice,'' Physicsword, Dec 2005 seems consistent with my progressive conference presentations in Russia, Europe, India, and USA (Hindu University) in 2004/05. I see implications for nanoscience.

**Q1 255 Electrically Tunable Chiral Materials for Spatial Light Modulators** SHIN-YING LU, LIANG-CHY CHIEN, *Chemical Physics Interdisciplinary Program and Liquid Crystal Institute, Kent State University* An electrically tunable chiral material is being used to develop a spatial light modulator in which the spectral wavelength is controlled by an electric field. We prepared a cholesteric liquid crystal cell by using a nematic host doped with chiral dopants. Upon applying an ac electric field parallel to the helical axis, different textures can be obtained. In addition to obtaining transitions among cholesteric textures by amplitude modulation, in this work we develop a scheme of switching the cholesteric liquid crystal among different textures and the reflected wavelength. We also analyzed the issue of the frequency and amplitude dependent behavior of cholesteric texture. With the combination of the amplitude and frequency modulation, reflected light with different wavelength is observed. This device can be operated in various spectrum regions as an optical filter. Furthermore, the device has good potential in display applications

**Q1 256 Polariton spectrum dependence on concentration of admixture layers in imperfect Si-superlattice.** VLADIMIR RUMYANTSEV, STANISLAV FEDOROV, ESFIR SHTAERMAN, *A.A.Galkin Physics Technical Institute of NASU* Advances in technology allowing growth of ultrathin crystalline films and periodic structures with controlled characteristics by molecular beam epitaxy has led to an increasing interest for study of excitations in perfect crystalline lattice. Investigation of disorder effects in imperfect superlattice allowing modeling the crystal properties is still of a great interest. We consider a model of superlattice as a macroscopically homogeneous system with randomly included admixture layers. The virtual crystal approach which is the method to describe quasi-particle excitations in disorder media is used. Polariton spectrum of imperfect superlattice (which is one-dimensional Si-crystal with two elements-layers in the cell) is obtained. Peculiarities of the dependence of band gap width on admixture layers concentration have been studied for different polariton branch. The results are the evidence of substantial polariton spectrum reconstruction caused by presence of defect layers.

**Q1 257 Low Background and Close Proximity Sensors of Atmospheric Gamma Radiation Following Lightning** M. GREENFIELD, M. ISHIGAKI, N. ITO, A. IWATA, K. KUBO, *Intn'l Christian U* K. KOMURA, *Kanzawa U* P. RUSCHER, W. COTTRILL, *Fla St. U.* G. AUSTIN, D. KROFCHECK, M. PEACE, P. BARKER, *Auckland U.* Atmospheric $\gamma$ radiation following lightning, 10-80% more than normal background, in excess of radon progeny attached to precipitation, which decays with a half-life of about 50 min, has been observed in Japan and at the Lightning Research Lab in Starke, Florida. This excess $\gamma$ radiation may be from the decay of radioactive ejectiles from nuclear reactions initiated by protons or photons resulting from the high potential gradients during thunderstorms. The most likely candidates for 10-100 min $\gamma$ activity resulting from reactions on atmospheric elements are $^{39}$Cl or $^{38}$Cl and/or annihilation $\gamma$ rays from positron emitters. Using a high resolution Ge detector the 1.267 MeV peak from $^{39}$Cl and excesses of the 511 MeV annihilation peak, as well as anomalous increases in the ratio of $^{214}$Bi to $^{214}$Pb (radon progeny), have been observed following thunderstorms but all with poor signal to noise ratios. Delayed activity in condensates from 10 liters of rain water with extremely low background at the underground LLRL in Ogoya, Japan is underway and activity in shielded detectors from nearby triggered lightning at the Lightning Research Lab is being planned in order to improve statistics and signal to noise ratios.

**Q1 258 NMR Studies of Water and Methanol Transport in Highly Sulfonated Membranes for Fuel Cells.*** EUGENE MANANGA, JAY JAYAKODY, AMEESH KHALFAN, STEVE GREENBAUM, *Hunter College of CUNY* THUY DONG, ZONGWU BAI, ROBERT MANTZ, *Wright Patterson Air Force Base* Pulse gradient spin echo NMR was used to characterize the diffusion of water in highly sulfonated polyarylenethioethersulfone (SPTES) polymers. The proton NMR spectra as well as the diffusion rates were determined as a function of temperature. Comparison of electrical conductivity and diffusion activation energies indicate that $H^+$ and water transport are closely correlated. Several of the membranes were selected for further study for possible applications in direct methanol fuel cells. Both water and methanol diffusion coefficients were determined for membranes equilibrated in 2M aqueous methanol solutions. Water mobility is correlated with proton conductivity whereas methanol mobility is associated with undesirable crossover effects. The membranes based on SPTES polymers present a superior water/methanol diffusion ratio to that of the widely studied NAFION membrane. Finally, the effect of hydrostatic pressure up to 2.5 kbar on diffusion has been determined. Using pressure as the thermodynamic variable allows one to compute activation volumes for molecular transport. The results obtained for SPTES materials are similar to those of other sulfonated polymers, in that the activation volume is observed to decrease with increasing water content of the membrane.

*Acknowledgement: MBRS-RISE/NIH

**Q1 259 Effect of $\gamma$-radiation on CdTe/CdS solar cells*** SOBIR MURATOV, *Senior teacher* Heterostructures on the base of CdTe/CdS is widely used in modern photovoltaics. It is well known that during preparation of the CdTe/CdS heterostructures and annealing solid solutions $CdTe_{1-x}S_x$ are formed due to diffusion of Te atoms into CdS and S atoms into CdTe. This work present a study of the effect of $\gamma$-radiation on CdTe/CdS solar cells. The heterostructures are prepared on 1cm$^2$ molybdenum substrate. It is found that output parameters of the cells change non-monotonicaly upon monotonic increase of the intensity of the $\gamma$-radiation. At lower intensities, short-circuit current increases and open-circuit voltage decrease, while at higher intensities short-circuit current decrease and open-circuit voltage increase with increasing the intensity of $\gamma$-radiation. It is found that the radiation-induced increase of the short-circuit current is much faster than decrease of the open-circuit voltage. As result, efficiency slightly increases with increasing the radiation intensity at low intensities and decreases at higher intensities. The reason of the non-monotonic change of the output parameters is related to generation of the radiation defects, which increases the compensation degree of the base layer. This suggestion is tested by measuring the specific resistance as a function of the $\gamma$-radiation intensity. It is found that the specific resistance also changes non-monotonically upon monotonic increase of the $\gamma$-radiation intensity, thus confirming the above suggestion.

*Institute granr number 20-04

**Q1 260 Spooky Phenomena in Two-Photon Coherent Atomic Absorption** MING-CHIANG LI, *Liceimer* Physical processes on two-photon coherent atomic absorption of multiple laser beams were discussed more than twenty five years ago. These processes can be divided into two distinct groups. In the first group, laser beams are from a single source[1,2], and in the second group laser beams are from two different sources[3]. Several experiments in the first group were carried out and have led to the 2005 Nobel Prize in physics. The second group is more interesting. Atoms are in random motion and two photons are from different sources. Classically, it is impossible for atoms to transit coherently in the absorption process, but quantum mechanically, such a transition is possible and that is one of the spooky phenomena in quantum mechanic. To assure the coherent transition, each photon as absorbed by the atom must have two possible paths of choices. If one photon has the choice and other one is not, then the atomic transitions cannot be coherent. The present talk will review various spooky phenomena associated with two-photon coherent atomic absorption, and will clarify some theoretical misunderstandings regarding these interesting transitions.

M. C. Li, Nuovo Cimento **39B** (1977) 165. M. C. Li, Phys. Rev. A **16** (1977) 2480. M. C. Li, Phys. Rev. A **22** (1980) 1323.

**Q1 261 Modulation of Luttinger liquid exponents in multi-walled carbon nanotubes** J. GONZALEZ, E. PERFETTO, *Instituto de Estructura de la Materia (CSIC), Madrid, Spain* S. BELLUCCI, P. ONORATO, *Laboratori Nazionali di Frascati (INFN), Frascati, Italy* We develop a theoretical framework that applies to the intermediate regime between the Coulomb blockade and the Luttinger liquid behavior in multi-walled carbon nanotubes [1]. We show that, in the crossover regime, the tunneling conductance follows a power-law behavior as a function of the temperature, with an exponent that oscillates with the gate voltage as observed in the experiments. We also evaluate the effects of a transverse magnetic field on the transport properties of the multi-walled nanotubes. For fields of the order of 4 T, we already find important changes in the band structure of the outer shells. We then predict the appearance of sensible modulations in the exponent of the conductance for higher magnetic fields, as the different subbands are shifted towards the formation of flat Landau levels. [1] S. Bellucci, J. Gonzalez and P. Onorato, Phys. Rev. Lett. 95, 186403 (2005).

**Q1 262 Superconductivity of multi-walled carbon nanotubes** E. PERFETTO, J. GONZALEZ, *Instituto de Estructura de la Materia (CSIC), Madrid, Spain* ≠wcounterbean We investigate the superconductivity of multi-walled carbon nanotubes, paying attention to the balance between the Coulomb interaction and the effective *e-e* interaction mediated by phonon-exchange. Our main aim is to confront the recent observation of sharp transitions in the resistance of multi-walled nanotubes, in situations where most part of the shells are electrically active [1]. For this purpose we will adapt the mechanism already shown for the superconductivity of nanotube ropes, where the electrostatic coupling among a large number of nanotubes leads to a drastic reduction of the Coulomb interaction [2]. We will consider in particular the interaction and Cooper-pair tunneling among a large number of shells in the multi-walled nanotubes, drawing a connection between the superconductivity of these structures and the more conventional one in the intercalated compounds of graphite.
I. Takesue *et al.*, to appear in Phys. Rev. Lett. J. González, Phys. Rev. Lett. **88**, 076403 (2002); J. V. Alvarez and J. González, Phys. Rev. Lett. **91**, 076401 (2003).

**Q1 263 Structural changes in $Bi_2Te_3$ under pressure.*** MATHEW JACOBSEN, RAVHI KUMAR, ANDREW CORNELIUS, *HiPSEC and Dep.Physics, University of Nevada Las Vegas* PETER LIERMANN, *HPCAT, Argonne National Laboratory* $Bi_2Te_3$ based compounds continue to receive intense research activities due to the enhanced figure of merit observed in the super lattice structure with $Sb_2Te_3$ [1]. Synthesis of different chemical compositions with varying particle sizes and doping has gained importance subsequently. The thermo electric properties of the new compositions strongly depend on the structure and P-T phase diagram of the parent compound $Bi_2Te_3$. In order to understand the structural properties of $Bi_2Te_3$ in detail, we have performed pressure studies up to 30GPa using insitu angle dispersive and energy dispersive x-ray diffraction techniques using a diamond anvil cell with different pressure media. $Bi_2Te_3$ is found to undergo pressure induced structural transition around 7.8 GPa to a new high pressure phase from the ambient rhombohedral phase. This transition is found to be completely reversible with a large hysteresis observed during downloading. The details of the high pressure phase and the pressure medium dependence of the transition will be discussed further. [1]. Venkatasubramanian et al., Nature, **413**, 597 (2001)

*Financial support from DOE is acknowledged.

**Q1 264 EPR, Biology, and Consciousness** SHANTILAL GORADIA, *Gravity Research Institute, Inc.* It seems that Darwin, in his concluding remark (1859, p490) ruled out the possibility of cosmic connection to evolution based on the fixed law of gravity, known then. More recent Diracs Large Number Hypothesis as described in http://www.arXiv.org/pdf/physics/0210040 v1 raises a possibility that the universal constant of gravity is decreasing and all coupling constants are increasing with time, so reported by some observations. Deeper investigation of the connection between evolution and the variation of the universal constant of gravity seems worthwhile to see if it impacts the passage of time in a stronger (gravitational according to the spirit of the above archive) field and affects the aging process, and explains locality and causality in random evolutionary mutations. If there is no physical locality and causality consistent with the special theory of relativity, there must be some spiritual locality and causality at superluminal speeds to explain the implicit hidden variables. Then there is a question of how to test spiritual locality and causality. Psychic effects and dream signals look promising, if they exist and can be tested with space age technology. This is neither about religion nor about Einsteins orthodoxy in light of the spirit of EPR. This is about frontiers of science of the new millennium: biology, and consciousness.

**Q1 265 Ion Size Effect in Glow Peak Temperature in Binary Mixed Crystals Doped with Divalente Europium*** RICARDO RODRIGUEZ-MIJANGOS, RAUL PEREZ-SALAS, *Universidad de Sonora* Thermoluminiscence measurements at room temperature of ''beta'' irradiated divalent Europium doped binary mixed alkali halides with KCl and KBr components at several concentrations x in molar fraction. The experiments have been carried out to identify the effect of composition of glow peaks. A typical glow peak has been distinguished for each composition. A linear dependence of its temperature on the composition x has been found. This is associated with the size change of ions Cl and Br. Initial comparative cathodoluminiscent measurement was carried out irradiating a single sample with electrons in an electron microscopy using a 30 KV voltage. With the present results is speculated the behavior of the mixed binary crystals with components KCl and RbCl, doped with divalent Europium.

*We are grateful for support by CONACYT under proyect 2002-C02-40497 and Direction de Investigacion y Posgrado UNISON under Project ''Catodoluminiscencia por MET.''

**Q1 266 Applications of the Microchannel Plate in Accelerator Mass Spectrometry** MISGANAW GETANEH, *University of Tennessee at Martin* KEN GRABOWSKI, DAVID KNIES, CATALINA CETINA, GRAHAM HUBLER, SCOTT TUMEY, *Naval Research Laboratory* A microchannel plate (MCP) detector with active area of 10 x 2 $cm^2$ is used as a position detector for mass spectrometry applications. The MCP detects electrons scattered by an MeV ion beam as it goes through a thin Carbon foil which is placed at a $45^o$ angle with respect to the beam. The scattered electrons' transverse motion is constrained by application of uniform electric and magnetic fields parallel to the axis of the MCP. The amplified charge is deposited on a double-delay line anode. Differential timing and charge partitioning are used to determine the horizontal and vertical positions of the ion in a plane normal to the MCP axis.

**Q1 267 Evaporation Driven Microdroplet Pattern Formation in Surfactant X-77.*** K.C. CHAN, SCOTT PIERCE, *Albany State University* HEPING ZHU, *OARDC/USDA* ALBANY STATE UNIVERSITY COLLABORATION, ATRU/OARDC, USDA COLLABORATION, The evaporation of sessile solution droplets of size 300-1000 $\mu$m on two different types of surface have been investigated using digital video microscopy. It is found that when the surfactant X-77 droplet is left to evaporate on a glass surface, the droplet evaporates without reducing its diameter while the fluid within the droplet flows from the center to the pinned edge causing it to swell. The final thin solution film eventually breaks away from the edge and shrink toward the center; simultaneously the edge coalesces into smaller droplets, forming islands on once the perimeter of the droplet. When the same experiment is repeated on hydrophobic surface, the droplet is found to shrink while its edge swells then forms islands. Depending on the con-

centration of X-77, ring or even a smooth round patch in the center instead of islands are formed. Solution concentration between 0.5-10 % were used for the experiments. The dynamic transition from islands to ring to round drop again will be presented.

*Support by a grant from NIH

**Q1 268 Investigations of Wafer Scale Etching with Xenon Difluoride** K.N. CHEN, N. HOIVIK, C.Y. (BLAKE) LIN, A. YOUNG, M. IEONG, G. SHAHIDI, *IBM T. J. Watson Research Center, Yorktown Heights, NY 10598, USA* A good and uniform bulk silicon wafer etching method can be applied to the wafer thinning process in MEMS and 3D applications. In this study, the use of a Xenon Difluoride (XeF2) gas-phase etching system, operating at room temperature, has been investigated for bulk silicon wafer thinning. We investigated the Si-wafer surface morphology and profile following each XeF2 etching process cycle. Theoretical results are used to compare with the experimental results as well. A clean wafer surface by proper surface treatments is significant to achieve a uniform surface profile and morphology for XeF2 etching. A proper design of etching cycle with nitrogen ambient during etching is necessary to achieve the fastest and uniform silicon etching rate. The silicon etching rate is reported as a function of etching pressure, nitrogen pressure, and etching duration.

**Q1 269 E/T-scaling of the spin fluctuations in the Zn-Mg-Ho magnetic quasicrystal*** TAKU J. SATO, *ISSP-NSL, University of Tokyo* AN PANG TSAI, *IMRAM Tohoku University* We report inelastic neutron-scattering results on the icosahedral Zn-Mg-RE (RE: rare-earth) magnetic quasicrystals. In the Zn-Mg-RE quasicrystals, slowing down of spin dynamics starts at considerably high temperatures (about 50 K) with developing antiferromagnetic correlations, nevertheless, the spins stay paramagnetic until low-temperature freezing transitions ($T_f$ = 1.95 K for RE = Ho), indicative of strong frustration effect. Neutron inelastic scattering further reveals that for RE = Ho, the scattering function $S(Q,\hbar\omega)$ is almost temperature independent for $\hbar\omega > 0$ in a wide temperature range up to 200 K. Corresponding dynamic susceptibility for $\hbar\omega < 1.5$ meV is scaled as $\mathrm{Im}\chi(\hbar\omega,T)T^{1/3} \propto (\hbar\omega/T)^{-1/3}Z(\hbar\omega/T)$, where $Z(\hbar\omega,T) = \tanh(\alpha\hbar\omega/T)$ is the scaling function. This $\hbar\omega/T$ (or $E/T$) scaling is identical to those frequently observed in systems near a quantum critical point, such as $UCu_4Pd$. In view of the frustration-reduced low freezing temperature of the Zn-Mg-Ho quasicrystal, the $E/T$-scaling may also be indicative of the quantum criticality in this magnetic quasicrystal.

*This work is supported by SORST-JST and MEXT.

**Q1 270 Perpendicular Hot Electron Transport in the Spin Valve Photo-Diode** BIQIN HUANG, IAN APPELBAUM, *Electrical and Computer Engineering Department, University of Delaware, Newark, Delaware, 19716* The spin valve photo diode (SVPD) provides a new way to explore perpendicular hot electron transport in ferromagnetic multilayers using photoexcitation and internal photoemission. Since electrons are excited everywhere in the metallic multilayer, structure geometry is vital to optimize the magnetocurrent (MC). Initial theoretical models indicate that the MC should increase by increasing the thickness of a capping layer at the surface, but experiments demonstrate a nonmonotonic dependence resulting in an optimum capping layer thickness to maximize MC. The inconsistency between experiment and this theoretical model is also discussed, leading to a new proposal for hot electron transport in the SVPD.

**Q1 271 Wafer Bow Effect on Copper Wafer Bonding** KUAN-NENG CHEN, *Microsystems Technology Laboratories, Massachusetts Institute of Technology, Cambridge, MA 02139* RAFAEL REIF, A good bonding quality of bonded interconnects is the key factor to achieve successful three-dimensional (3D) integration applications. Prior to copper interconnect bonding in real 3D devices, fundamental researches about copper blanket film bonding should be studied. Since two wafers with large wafer bows may be difficult to contact during bonding, the bonding quality may be affected. In this study, wafer bows of different silicon wafers coated with copper and tantalum films were measured at different temperatures to simulate the wafer bow evaluation during bonding. We further investigated the bonding qualities of bonded wafers with different wafer bows after bonded at different temperatures. Dicing tests were performed to analyze the qualities of copper bonded wafers. Based on the results, a criterion of wafer bows for good copper bonding quality is suggested.

**Q1 272 Toward a model for pattern formation in thin film polymer blends** NIGEL CLARKE, *University of Durham* We outline a dynamic theory for simultaneous phase separation and dewetting in thin film polymer blends with free surfaces. Although an understanding of the processes of both dewetting and phase separation is well advanced, the coupling between the two has received little attention theoretically. We consider the coupling between surface driven instabilities and compositional instabilities in a thin film on a flat solid substrate with a free upper surface. We utilise a simple model, in which only fluctuations of composition within the plane parallel to the substrate are allowed, and neglect the possibility of fluctuations normal to the substrate. Such a model yields quantitative relationships for the stability in terms of the height of the film and the various thermodynamic parameters. From a dynamic viewpoint, the attraction of such a model is that it permits an analytical description of the early dynamic stages of an instability. Reduction of the problem from 3D to 2D is important when undertaking numerical studies on films that are nanometers thick, in which the typical lengthscales of dewetting and phase separation in the plane of the film are of the order of microns. As an example, the consequences of phase separation within a system which has already undergone considerable dewetting is highlighted by comparing with the process of phase separation when no dewetting occurs. With simultaneous dewetting, the phase separation becomes retarded and the co-continuous nature of the phases are absent.

**Q1 273 Nonequilibrium theory of polymer stretching based on the Master Equation*** HANKÉ FELIX, *Dalhousie University, Halifax, NS, Canada* HANS JÜRGEN KREUZER, *Dalhousie University, Halifax, NS, Canada* Single polymer pulling experiments such as protein unfolding measurements and dynamic force spectroscopy are increasingly done at high loading rates where equilibrium statistical mechanics is no longer applicable. I will present a theory that takes into account non-equilibrium effects using a Master Equation [PRE v. 72, 031805 (2005)]. If the molecular length is used as a stochastic variable, the transition probabilities have a simple analytic form. This theory predicts signifi-

cant differences between experimental designs using controlled end-to-end positions and those that utilize a force-control mechanism. The most prominent non-equilibrium effect is a loading rate-dependent hysteresis in the force-extension curve. Molecular relaxation close to and far from equilibrium will also be discussed in the frame-work of the Master Equation theory.

*This work was supported in part by the Office of Naval Research and the National Science and Engineering Council of Canada. F.H. wishes to acknowledge financial support from the Killam Trusts.

**Q1 274 Mechanical and Tribological Properties of Amorphous Carbon Films** J. DAVID SCHALL, GUANGTU GAO, KEVIN VAN WORKUM, JUDITH A. HARRISON, *United States Naval Academy, Department of Chemistry* Incorporation of silicon into hydrogenated amorphous carbon films has been shown to reduce film stress, make the friction coefficient less sensitive to moisture, and increase thermal stability while maintaining high hardness, low wear, and small friction coefficient. Molecular dynamics simulations utilizing the reactive empirical bond-order potential (REBO) have been used to examine the temperature dependence of the material and tribological properties of hydrogenated amorphous carbon films containing silicon. The REBO potential is one of the few potential energy functions capable of modeling chemical reactions likely to accompany sliding. Existing models for the C-Si-H potential are based on the original REBO potential developed by Brenner in 1990. These models do not calculate elastic modulus accurately. A new parameterization for the inclusion of Si into the second generation REBO potential has been developed. Calculations of elastic modulus from the second generation Brenner potential are in much better agreement with experimental values. Initial studies have shown that the inclusion of Si in amorphous carbon films increases the amount of $sp^3$ bonding in the film while decreasing the graphitic $sp^2$ content, making the films more diamond-like.

**Q1 275 Neutron Diffraction study of Ru doping in $Pr_{0.5}Ca_{0.5}Mn_{1-x}Ru_xO_3$ ($x \leq 0.10$)** KANNADKA RAMESHA, ANNA LOBET-MEGIAS, THOMAS PROFFEN, *Los Alamos National Laboratory* LUJAN NEUTRON SCATTERING CENTER TEAM, Small amount of Ru substitution ( $< 10$ %) for Mn in charge-ordered manganites destroys charge-ordering (CO) and induces ferromagnetic metallic state. To probe the dramatic role played by Ru in preventing the CO state, we have carried out neutron diffraction studies of Pr0.5Ca0.5Mn1-xRuxO3 compounds ($x = 0.0$, 0.05 and 0.10) in the temperature range 300-10 K. Evolution of lattice parameters with temperature points out that lattice distortion which accompanies charge ordering disappears on Ru doping. Also Ru doping alters the $MnO_6$ octahedron shape from 4-long/2-short type to 2-long/4-short type that suppresses the antiferromagnetic ordering and hence induces ferromagnetism through double exchange interactions. The local structure of $x = 0$, 0.05 and 0.10 compositions were analyzed using Pair Distribution Function (PDF) at 295 K and 15 K.

**Q1 276 Pressure induced structural changes in AgPb18SbTe20*** RAVHI KUMAR, *HiPSEC and Department of Physics, University of Nevada Las Vegas, Las Vegas, Nevada* ANDREW CORNELIUS, MATHEW JACOBSEN, MALCOLM NICOL, *HiPSEC and Dep.Physics, University of Nevada Las Vegas, Las Vegas, Nevada* SEIJI YONEDA, *Kanagawa University, Yokohama, Japan* The cubic chalcogenide AgPbmSbTe2+m type compounds are an important class of thermoelectric materials for which figures of merit as high as 2.2 at 800 K have been reported recently [1]. The structures of these compounds have been investigated under pressures up to 30 GPa using a diamond-anvil cell and an imaging plate with synchrotron radiation at HPCAT. Various runs were performed with different pressure media such as 4:1 methanol-ethanol and silicone fluid. The results show pressure induced structural transitions in AgPb18SbTe20. The NaCl-type cubic phase transforms to an orthorhombic phase at 6.4 GPa and then to a CsCl-type cubic structure at 14 GPa. The high pressure CsCl-type phase is stable up to 30 GPa. The ambient structure is recovered on releasing the pressure from the cell. The results will be presented in detail. [1]. K.F. Hsu etal., Science, 303, 818 (2004)

*Supported by NNSA cooperative agreement DE-FC08-01NV14049.

**Q1 277 Metal-insulator transition in Hubbard-like models with random hopping** MATTHEW FOSTER, *University of California, Santa Barbara* ANDREAS LUDWIG, *University of California, Santa Barbara* We study the combined effects of random hopping disorder and short-ranged interparticle interactions in half-filled Hubbard-like models of spinless and spinful fermions in $D \geq 2$ dimensions. In a given realization, the hopping disorder is chosen to break time-reversal invariance, but to preserve the special ''nesting'' symmetry responsible for the charge density wave instability of the clean, non-interacting Fermi surface. For spinless fermions, the hopping disorder may arise from the application of a random orbital magnetic field to the otherwise *clean* Hubbard-like model. For the case of spin 1/2 fermions, in addition, the spin SU(2) rotational symmetry is assumed to be broken completely, e.g. by a homogeneous spin-orbit coupling. Using a perturbative renormalization group approach [1], we identify a new, disorder-driven metal-insulator transition in $D = 2 + \epsilon$ dimensions, stabilized by the presence of the interactions. Without the ''nesting'' symmetry, these systems would be in the unitary symmetry class ''with magnetic impurities,'' where interaction effects are irrelevant [1]. [1] For a review, see e.g. D. Belitz and T. R. Kirkpatrick, Rev. Mod. Phys. 66, 261 (1994).

**Q1 278 Carrier mobility as a function of InGaAs quantum well to quantum wire transition on GaAs (311)A** WILLIAM BLACK, VASYL KUNETS, BAOLAI LIANG, YURIY MAZUR, ZHIMING WANG, JOHN SHULTZ, GREG SALAMO, *University of Arkansas* Molecular beam epitaxy is used to study self-assembly of $In_{0.4}Ga_{0.6}As$ quantum wires on GaAs (311)A. Using an InGaAs layer embedded in an AlGaAs/GaAs heterostructure, the correlation between surface morphology, photoluminescence, and electrical transport is investigated. In particular, we will present data and discuss carrier mobility as a function of InGaAs deposition and the resulting surface morphology. As the thickness of the InGaAs layer is increased, a compressive strain field develops, which is relieved at a critical thickness in the form of faceted quantum wires. Paralleling this dramatic change in morphology, the conductivity of the sample is observed to change as measured using Hall bar structures oriented both parallel and perpendicular to the quantum wires. A large anisotropy in conductivity is found to be directly correlated to changes in surface morphology and photoluminescence measurements. The surface morphology was revealed using atomic force measurements on an InGaAs capping layer that reproduced the quantum well or quantum wires embedded in the AlGaAs/GaAs heterostructure.

**Q1 279 Synthesis and Electrical Characterization of Polymer based SiC Nanofibers** SAIMA KHAN, AURANGZEB KHAN, MARTIN KORDESCH, *Department of Physics and Astronomy and CMSS program, Ohio University* Silicon carbide nanofibers have been synthesized from a precursor solution of Polyethyleneoxide (PEO) using the electrospinning technique. The morphology of the fibers was investigated using the scanning electron microscope (SEM) and Transmission electron microscope (TEM). The electrospun fibers were annealed at various high temperatures and their electrical conductivity was measured using the four point probe method. The effect of the annealing temperature on the electrical conductivity of the fibers was investigated.

**Q1 280 Highly Sensitive Micro-Hall Magnetometers Using InSb Quantum Wells** SAPTHARISHI EASWARAN, VASYL KUNETS, DOREL GUZUN, YURIY MAZUR, *University of Arkansas* MIKE SANTOS, SHEENA MURPHY, *University of Oklahoma* GREGORY SALAMO, *University of Arkansas* DEPARTMENT OF PHYSICS: UNIVERSITY OF ARKANSAS COLLABORATION, DEPARTMENT OF PHYSICS AND ASTRONOMY: UNIVERSITY OF OKLAHOMA COLLABORATION, Delta doping in the barrier of $InSb/Al_{0.12}In_{0.88}Sb$ heterostructures grown by molecular beam epitaxy are studied as micro-Hall sensors. By varying the doping level and the delta position in the barrier, full control of the two dimensional electron gas confined in InSb quantum well is achieved. For example, we demonstrate control of device parameters such as the absolute magnetic sensitivity, noise level, and device detection limit of a micro-Hall sensor. The $200\mu$m x $35\mu$m device demonstrates a detection limit of 25 nT and 11 nT at 300 K and 80 K, respectively. These limits were measured at the operating frequency of 10 kHz where 1/f noise is negligible. In addition, if spatial resolution is not needed pT detectivity can be achieved using larger sensors on the order of $1mm^2$. The devices discussed here show a low thermal drift that is less than $2\%/^oK$ and attractive signal linearity up to 0.1 T for either polarity of the magnetic field at room temperature.

**Q1 281 Optical Properties of Hydrogenated Silicon Nanoclusters: First principles study*** SEUNG MI LEE, *Korea Research Institute of Standards and Science (KRISS)* HANCHUL KIM, KYUNG JOONG KIM, DAE WON MOON, Silicon nanoclusters have significant interest due to their potential application to optoelectronic devices in visible range. Using first principles approach, we investigate the electronic and optical properties of hydrogenated silicon nanoclusters. The highest occupied molecular orbital (HOMO) – lowest unoccupied molecular orbital (LUMO) gap dependence on the cluster size show the same trend by using any exchange-correlation functionals. However, a reasonable agreement to experimental absorption spectra peak values cannot be achieved from conventional LDA or GGA functional-based calculations. Using B3LYP hybrid functional within time-dependent density functional theory, we obtain excitonic energies in quantitatively good agreement to experimental data. The passivant effect on HOMO-LUMO gap and excitonic energies will be also presented.

*Computing facility support by KISTI under the 7th strategic supercomputing applications support program

**Q1 282 Spiral structure of a frustrated spinel $CdCr_2O_4$ studied by polarized neutron techniques** M. MATSUDA, *Japan Atomic Energy Agency (JAEA)* A. OOSAWA, *JAEA* M. TAKEDA, *JAEA* M. NAKAMURA, *JAEA* E. LELIEVRE-BERNA, *ILL* K. KAKURAI, *JAEA* J.-H. CHUNG, *NIST* S.-H. LEE, *Univ. of Virginia* H. UEDA, *Univ. of Tokyo* H. TAKAGI, *RIKEN* $CdCr_2O_4$ has the spinel structure, in which geometrical frustration exists between the $Cr^{3+}$ moments located at the corners of the tetrahedron. This compound shows a transition to a spiral magnetic structure with a characteristic wave vector of $Q = (0,\delta,1)$ ($\delta \sim 0.09$) at 7.8 K, which is accompanied by a tetragonal structural distortion with the $c$ axis elongated. [1] We first performed a 1D polarized neutron analysis and determined that the $Cr^{3+}$ moments has a planer anisotropy in the $ac$ plane. Finally, spherical neutron polarimetry experiments were performed using a CRYOPAD on TAS-1 at JRR-3. It is found that the spiral structure is elliptical with the spin component $\sim$ 24% elongated along the $c$ axis. [1] J.-H. Chung *et al.*, Phys. Rev. Lett. 95, 247204 (2005).

**Q1 283 Abstract Withdrawn**

**Q1 284 Classical Nuclear Motion in Quantum Transport** CLAUDIO VERDOZZI, GIANLUCA STEFANUCCI, CARL-OLOF ALMBLADH, *Solid State Theory, Lund University-Sweden* An *ab initio* quantum-classical mixed scheme for the time evolution of electrode-device-electrode systems is introduced to study nuclear dynamics in quantum transport. Two model systems are discussed to illustrate the method. Our results provide the first example of current-induced molecular desorption as obtained from a full time-dependent approach, and suggest the use of AC biases as a way to tailor electromigration.

**Q1 285 Production of Cold NO Molecules** JASON ALEXANDER, BRYAN BICHSEL,*MICHAEL MORRISON, NEIL SHAFER-RAY, ERIC ABRAHAM, *University of Oklahoma* Although the success of laser cooling and trapping has had a major impact on atomic physics, the requirements of simple internal structure have limited its use to a few atomic species. A modified Stark guide can be used as a source for cold polar molecules by filtering the cold fraction from a thermal source. We present experimental results for the enhancement of the lowest ro-vibrational states from an effusive source of nitric oxide by the Stark guide capturing those particles with the lowest transverse velocities. By inserting a sphere in our straight guide, we block line-of-sight trajectories between the source and the output of the guide. We have implemented the principle of velocity selection, only those molecules with sufficiently low energies to reflect from the guide will make it to the output. Using a field-stabilized Rydberg time of flight technique we measure the output speed distributions from this filtered source to be between 7-20 K, depending on strength of guide field.

*Presently Oklahoma Pan Handle State University

**Q1 286 THz Differential Radar for Detection of Weak Molecular Absorption Lines in Bio-Aerosol** HAMID JAVADI, *JPL, CA* ELLIOTT BROWN COLLABORATION,*ELAYNE BROWN COLLABORATION,† THz frequency range (300-3000 GHz) promises unique capabilities and advantages for detection of trace gases and biological aerosols immersed in the atmosphere. Tech-

niques used for microwave atmospheric remote sensing can be used within the atmospheric transmission windows to carry out standoff detection of biological markers in real time. THz spectroscopy has been used as an important new tool in investigations of atmospheric molecular gases and a wide range of airborne biological materials. We have embarked upon development of field deployable THz differential radar. Bio-aerosols are the most difficult analytes to face due to their heterogeneity in size, toxicity, and bio/chemical composition. JPL has demonstrated monolithic solid-state THz sources with impressive output power. The sources are enabled by W-band power amplifiers and planar Schottky diode multipliers. These, together with room temperature detectors (based on the same technology), allow one to make a compact and robust transmitter/receiver with sufficient sensitivity and frequency agility to carry out detailed investigation of various molecular vapors and bio-aerosols at standard temperature and pressure. Current status of the THz differential radar technology development effort along with future trends will be presented.

*UCSB, CA
†Physical Domains LLC., CA

**Q1 287 Metal–Insulator Transition in the Flux-Flow Resistivity of Optimally Doped $YBa_2Cu_3O_{6+x}$** BENJAMIN MORGAN, *University of Cambridge* DAVID BROUN, *Simon Fraser University* RUIXING LIANG, DOUGLAS BONN, WALTER HARDY, *University of British Columbia* JOHN WALDRAM, *University of Cambridge* We have made high resolution microwave measurements of the flux-flow resistivity of optimally doped $YBa_2Cu_3O_{6+x}$ in the mixed state at temperatures down to 1.2 K. We find that the effective resistivity of the vortex cores exhibits a metal–insulator transition, with a minimum at 13 K and a logarithmically growing form below 5 K, as has been seen in the low-temperature DC resistivity of under-doped cuprates in which superconductivity has been globally suppressed. Our work is the first report of a metal–insulator transition in optimally doped $YBa_2Cu_3O_{6+x}$, and the first to be seen in a system in which superconductivity has not been globally suppressed. The transition is seen in samples of the highest quality and in magnetic fields as low as 1 T.

**Q1 288 Glassy Dynamics in the Adaptive Immune Response Prevents Autoimmune Disease** JUN SUN, MICHAEL DEEM, *Rice University* The immune system normally protects the human host against death by infection. However, when an immune response is mistakenly directed at self antigens, autoimmune disease can occur. We describe a model of protein evolution to simulate the dynamics of the adaptive immune response to antigens. Computer simulations of the dynamics of antibody evolution show that different evolutionary mechanisms, namely gene segment swapping and point mutation, lead to different evolved antibody binding affinities. Although a combination of gene segment swapping and point mutation can yield a greater affinity to a specific antigen than point mutation alone, the antibodies so evolved are highly cross-reactive and would cause autoimmune disease, and this is not the chosen dynamics of the immune system. We suggest that in the immune system a balance has evolved between binding affinity and specificity in the mechanism for searching the amino acid sequence space of antibodies. Our model predicts that chronic infection may lead to autoimmune disease as well due to cross-reactivity and suggests a broad distribution for the time of onset of autoimmune disease due to chronic exposure. The slow search of antibody sequence space by point mutation leads to the broad of distribution times.

**Q1 289 Attractions Between Like-Charged Walls Via Local Molecular Field Theory*** JOCELYN M. RODGERS, CHARANBIR KAUR,† YNG-GWEI CHEN,‡ JOHN D. WEEKS, *University of Maryland, College Park* A simple model used to explore the interaction between like-charged macroions as mediated by intervening counterions is treated with local molecular field theory (LMF). LMF has recently been extended to general Coulombic systems by splitting the Coulomb potential $1/r$ into a short-ranged core that can be explicitly simulated and a long-ranged portion treated using a mean field approach; the potential separation is determined by a physically-relevant spacing parameter $\sigma$. Here we show that LMF can treat the two-wall model system surprisingly well using an analytical Poisson-Boltzmann type technique. Also, combining self-consistent solution of LMF with simulation of the short-ranged core particles using the minimum image convention yields even more accurate results without using costly and complex Lekner or Ewald sums.

*Thanks to NSF grant and NDSEG fellowship
†Now at University of Texas
‡Now at NIH

**Q1 290 Coverage and Temperature Dependence of Bond Character of Thiophene on Ge(100)** S.M. JEON, S.J. JUNG, *Dept. of Chem. and School of Mol. Sci. (BK21)* H.-D. KIM, *Beamline Research Div., Pohang Accelerator Lab (PAL)* D.K. LIM, *BK21* H. LEE, *PAL* S. KIM, *BK21* KAIST COLLABORATION, PAL COLLABORATION, We studied the adsorption and decomposition of thiophene (C4H4S) on Ge(100) using high-resolution core-level photoemission spectroscopy (HRPES) and scanning tunnelling microscopy (STM). Ge 3d, S 2p, and C 1s core level spectra show the existence of three different adsorption geometries, which are assigned to a weakly bound state, a chemisorbed bonding state ([4+2] cycloaddition reaction product), and a decomposed bonding state (desulfurization reaction product). Furthermore, we found that the ratio of the components induced by three adsorption geometries changes depending on the molecular coverage and the annealing temperature. Under 0.25 ML, the kinetically favorable weakly bound state is initially formed. As the molecular coverage is increased (over 0.25 ML), thermodynamically stable [4+2] cycloaddition reaction products are additionally produced. In addition, the temperature dependent behaviors show that the weakly bound state desorbs followed by the [4+2] cycloaddition reaction product as the molecular thiophene or may decompose to form metallocyclic compounds (C4H4Ge2) and sulfide (Ge2S). We elucidate systematically the change of the bonding states of adsorbed thiophene on Ge(100) according to the amounts of thiophene molecules and annealing temperature. Moreover, we performed density functional theory (DFT) calculations to observe the energetics of three bonding states of thiophene on Ge (100) system.

**Q1 291 Lattice Distortion Driven by Spin-Lattice Coupling** CHENGLONG JIA, JUNG HOON HAN, *Sungkyunkwan University* We analyzed lattice-coupled antiferromagnetic spin models on a variety of frustrated lattices. Inspired by the picture of a hexagonal spin cluster proposed for the paramagnetic $ZnCrO_4$ (S. H. Lee et al., Nature(2002).), we considered hexagon contraction in the *pyrochlore* lattice. Hexagon distortions give rise to mutually orthogonal arrangements of spins for nearby hexagons, and has an energy gain of $-alpha^2/2$ per spin, where $\alpha$ is the spin-lattice interaction strength. However, due to the local rotational symmetry of the $\langle S_i \cdot S_j \rangle$, mean-field theory predicts a lack of lattice

displacement in the *triangular* and *kagomé*lattices. In contrast to the valence-bond-solid(VBS) state of the Affleck-Kennedy-Lieb-Tesaki type, we argue that a type of VBS order (partial VBS, PVBS) with only four of the six bonds of the triangular lattice being filled by singlets can be stabilized through spin-lattice interactions and lead to lattice deformations as in the compound $YMnO_3$ (Seongsoo Lee et al., PRB(2005)). The ground state is derived as the direct product of states, one of which represents the conventional long-range ordered spins, and the other given by the $\sqrt{3} \times \sqrt{3}$ modulation of the valence bond amplitudes, $|GS\rangle = |LRO\rangle \otimes |PVBS\rangle$. The excitation spectrum for the modulated valence bond state is worked out within the single- mode approximation. The spectrum offers a new collective mode, which is distinct from the spin wave excitations of the magnetically ordered ground state, and in principle, observable by neutron scattering.

**Q1 292 Photonic digitizing by laser crossing in thin-film semiconductors** CHINTHAKA LIYANAGE,*ARTUR ERLACHER, BRUNO ULLRICH, *Bowling Green State University* NATALIA DUSHKINA, *Millersville University* During the last two years, we developed a straightforward laser modulation concept, which has the potential to be employed in similar ways as microelectromechanical systems (MEMS). The concept is realized by crossing two laser lines in a semiconducting thin-film on glass, i.e., by switching one of the beams, one achieves a clearly resolved (up to 30%) modulation of the other beam. In case of thin-film GaAs response times in the picosecond range are possible. We investigated the transmission mode of the modulation switch and demonstrated that the GaAs/glass interface exhibits a more effective switch as the GaAs film itself. The experiments have been carried out at room temperature with moderate laser powers on the order of 10 mW. We studied also the influence of polarization on the modulation characteristics in transmission and reflection using birefringent CdS samples. We observed that polarization variations of the green laser varies the modulation amplitude of the red transmitted and reflected ray, paving the way for polarization sensitive all-optical cross connects (OXCs) operating in the THz regime.

*presenter

**Q1 293 Electronic properties of carbon tori in external fields*** F. L. SHYU, *Department of Physics, Chinese Military Academy, Kaohsiung, Taiwan* C. C. TSAI, C. W. CHIU, M. F. LIN, *Department of Physics, National Cheng Kung University, Tainan, Taiwan* Electronic states of achiral carbon tori in electric and magnetic fields are studied by the tight-binding model with the curvature effect. Electronic properties, such as electronic states, energy gaps, and density of states, are very sensitive to the changes in the direction and the magnitude of the external fields. The electric field can widen the $\pi$-electron energy width; furthermore, there are more low- and extreme-energy states. Energy gaps are drastically modulated by **E.** The complete modulation of energy gap ($E_g \neq 0$ to $E_g = 0$) happens more frequently when **E** deviates from the symmetric axis, or its magnitude is sufficiently large. The electric field could change the state degeneracy. Moreover, the modulation of electronic states is enhanced by the magnetic field.

*NSC 93-2112-M-145-001; NSC 93-2112-M-006-002

**Q1 294 Electronic properties of multilayered nanographite ribbons in an electric field.** YUAN-CHENG HUANG, *Center for General Education, Kao Yuan University, Kaohsiung 821, Taiwan, Department of Physics, National Cheng Kung University, Tainan 701, Taiwan,* The low-energy electronic properties of the AB-stacked multilayered nanographite ribbons in an electric field are studied through the tight-binding model. They are strongly dependent on the geometric structures (the interlayer interactions, the ribbon edges, the ribbon width, and the ribbon number) and the field strength. The interlayer interactions significantly affect energy dispersions, energy gap ($E_g$), density of states (DOS), and free carriers. DOS exhibits many special structures, including plateau, discontinuities, and divergent peaks. The electric field leads to the shift of the Fermi level ($E_F$), the production of the new edge state, the change of the band gap, the alternation of the subband spacing, and the semiconductor-metal transitions. In gapless zigzag ribbons, the electric field not only lifts the degeneracy of flat bands at $E_F$ but also induces an energy gap. $E_g$ is dependent on the ribbon width and the field strength. The semiconductor-metal transitions occur in both armchair ribbons and zigzag ribbons in the increase of the electric field. The above-mentioned effects due to electric field is completely reflected in the features of DOS such as the generation of special structures, the shift of peak position, the change of peak height, and the alternation of band gap.

**Q1 295 Possible observations of microwave influences on quantum states and transition rates** ROBERT POTTER, *Coe College* SIMON BERKOVICH, *George Washington U.* A realistic interpretation of quantum phenomena leads to a conclusion that there might be a hidden mechanism guiding the transition of quantum objects. Thus, manipulations of such a mechanism may affect the regular pathways of quantum phenomena. A recently formulated hypothesis suggests that quantum phenomena on the mesoscopic scale can be influenced by microwave radiation of order 10[1]1 Hz. This frequency seems to present a watershed between observable quantum effects and classical physics. Electromagnetic activities at higher frequency exhibit characteristic quantum mechanical behavior whereas at lower frequency they present typical Maxwell waves. In the range of 10[1]1 Hz both kinds of electromagnetic activities coexist: millimeter microwaves and far-infrared quanta. The destruction of long-range quantum order in superconductors at about 10[1]1 Hz is interpreted in terms of energy gap influences. The same effect could be also responsible for a small but importunate impact of the 10[1]1 Hz radiation on biological objects. In this work, we propose to investigate the possible impacts of this radiation on quantum phenomena. This includes the study of the decay rate changes of certain nuclei when exposed to microwave radiation and electron tunneling between superconductors. The suspected mechanism could be recognized experimentally as it would imply a clear threshold effect at some point around the 10[1]1 Hz frequency.

**Q1 296 Structural and chemical changes in ultra-high-molecular-weight polyethylene due to gamma radiation-induced crosslinking and annealing in air.** ANN VIANO, KARYN SPENCE,*MATTHEW SHANKS, M. ANDREW SCOTT, RICHARD REDFEARN, CARL CARLSON, TERESE HOLM,† *Rhodes College* ASIT RAY, *Christian Brother's University* Ultra-High-Molecular-Weight-Polyethylene (UHMWPE) is used to fabricate one of the articulating surfaces used in many total joint replacements. Various sterilization and annealing methods affect the mechanical wear properties in ways still unknown at the microscopic and molecular levels. We have investigated crosslinking induced by gamma irradiation and annealing time (both done in air). TEM was used to probe the organization of crystalline lamellae in the polymer. Pyrolysis interfaced with GC-MS was

used to quantify the extent of crosslinking by identifying peaks that correlate with crosslinking structures along its backbone. Changes in lamellar stacking and the extent of the crosslinking suggest two types of crosslinking occuring in the material. Lamellar mobility is enhanced during the transitions from one type of bonding to the other, and this appears to optimize near eight hours of annealing time. Results from decomposition experiments and percent crystallinity measuresments provide further support for this postulated theory.

*currently at Washington University
†currently at The University of Arizona

**Q1 297 Antiferromagnetism in Superconducting Tl2223 well below Tc*** T. IMAM, B. LAUNSPACH, V. CHIKHANI, M. SILVEIRA, *San Jose State University* L. ROBLEDO, *CSU Long Beach* J. LEE, *Uo Illinois Urbana* C. BOEKEMA, *San Jose State University* We examine transverse field (TF; 5 kOe) Tl2223 muon-spin-rotation (muSR) data to search for antiferromagnetism (AF) near and in the vortex cores. [1] The vortex frequency signals are fitted by Gaussian and Lorentzian curves. For T $<$ 0.4Tc, Lorentzians fit much better, indicating AF. Since this is especially true for the high-field side, AF appears to exist near and in the vortex cores. [1] Zero field (ZF) muSR data of flux trapping in Tl2223 recorded at 10 K are also studied. We examine signals arising from the initial vortex core, critical field, and remnants of the initial mixed state at five kOe. Three signals at 1.5 MHz, 9-10 MHz (0.7 kOe; Bc1)and 24-25 MHz (1.8 kOe; a 2D-3D transition) are observed. The 110-Oe flux arises from magnetism initially present in the vortex state [1] before the flux trapping. Its ZF fit values are consistent with the AF-vortex TF-fit parameters. Both TF and ZF-muSR evidence suggests AF exists in the Tl2223 superconductor, supporting theories that predict a magnetic origin for cuprate superconductivity. [1] J. Lee et al, J Applied Physics 95 (2004) 6906; Virtual J Applications of Superconductivity, June 2004 V6 Issue 11; www.jyi.org/volumes/volume10/issue6/articles/prudchenko.html

*Research supported by REU-NSF and WiSE@SJSU.

**Q1 298 Interacting electrons in quantum-critical crossover regime in quantum dots*** IGOR ROZHKOV, GANPATHY MURTHY, *University of Kentucky, Department of Physics and Astronomy* We present numerical study of the statistics of ground state $S_z$ in the crossover in which spin-orbit scattering is tuned in 2D quantum dots [1]. The spin-orbit interaction introduces new symmetry limits of the single-particle Hamiltonian [2]. With the help of universal Hamiltonian for this case [1] we have created a framework for calculation of spin statistics in disordered quantum dots in the large Thouless number limit. In addition we have analyzed the spin excitation spectrum in the quantum critical regime dominated by collective critical fluctuations [3].
Y. Alhassid and T. Rupp, Phys. Rev. Lett. 91, 056801 (2003). I.L. Aleiner and V.I. Fal'ko, Phys. Rev. Lett. 87, 256801 (2001). G. Murthy, Phys. Rev. B 70, 153304 (2004).

**Q1 299 Eriksen model: neural network dynamics analysis and simulations** YUAN LIU, *Department of Physics, Princeton University* PHILIP HOLMES, *Mechanical and Aerospace Engineering and Program in Applied and Computational Mathematics, Princeton University* We analyze a connectionist neural network model of the two-alternative forced choice Eriksen task, in which subjects must correctly identify a central stimulus and disregard flankers that may or may not be compatible with it. We have analyzed a linearized version of the connectionist model for the Eriksen two-alternative forced-choice task. We show that, provided solutions remain within the central domain of the logistic function in which it may be approximated by a linear function that matches its slope g at the bias point b, analytical solutions of a decoupled, linearized model modulated by a pre-determined attention signal provide reasonable estimates of critical times at which evidence in favor of the correct and incorrect alternatives cross over for incompatible trials. We then derive estimates of accuracy as a function of response time by interrogating a drift-diffusion (DD) process with variable drift rate, fitted to outputs from the perception layer of the fully nonlinear model. We compare our results with numerical simulations of the full nonlinear model and discuss the possibility to use information theory to optimize our network model.

**Q1 300 Generation of Soft Shockwaves by High-Speed Non-Rigid Liquid Spray*** SEONG-KYUN CHEONG, *Argonne National Laboratory* KYOUNG-SU IM, CHRISTOPHER POWELL, XIN LIU, JIN WANG, MING-CHIA LAI, *Wayne State University* FUEL SPRAY TEAM TEAM, High-pressure, high-speed sprays are an essential technology in many applications, including fuel injection systems, thermal and plasma spray coating, and liquid-jet machining. Those liquid jets, often optically opaque due to the highly dense liquid droplets surrounding the sprays, can travel at supersonic speeds and generate shockwaves. It has been believed that the shock wave can be sustained through only continuous compression with dissipative and irreversible process. However, the characteristic of the shockwaves generated by the liquid jet is different from those generated by supersonic rigid objects. Unlike those created by supersonic rigid object, the soft shock wave reveals the reversible compression process followed by the decompression process behind of the shock wave front. We employed the time-resolved x-radiograph using synchrotron source to uncover ''soft'' nature of the shockwaves quantitatively, which is in good agreement with independent theoretical analysis using the computational simulation of fluid dynamics.

*This work and the use of the APS are supported by the U. S. Department of Energy under Contract No. W-31-109-Eng-38 and by the Department of Energy Office of FreedomCAR and Vehicle Technology.

**Q1 301 Shock Wave Effects on Polymer Morphology*** E. BALIZER, J. FEDDERLY, G. LEE, *Naval Surface Warfare Center Carderock Division* W. MOCK, JR., W. HOLT, *Naval Surface Warfare Center Dahlgren Division* A gas gun has been used to launch steel ogival-nosed projectiles at a selected impact velocity into steel plates with polyurea, polyurethane and polyethylene coatings. Experiments were performed for two polymer thicknesses, and with the coating cast or loosely held onto the steel plate. Recovered polyurea, polyurethane and polyethylene coatings were characterized by small angle x-ray scattering (SAX) to determine the plastic strain at the constrained metal/polymer interface and the free boundary polymer interface. The difference in plastic strain as found by SAX in polyurea shows both flow orientation and possible fibril morphology compared to only flow orientation in polyurethane and polyethylene. The relative amounts of resulting void damage at the free surface due to reflected rarefaction waves are also described.

*Research supported by ONR 331.

**Q1 302 Molecular Dynamics simulations of perpendicular tetracosane films*** MICHAEL ROTH, *University of Northern Iowa* CARLOS WEXLER, *University of Missouri - Columbia* We present the results of Molecular Dynamics computer simulations of perpendicular tetracosane ($C_{24}H_{50}$) films adsorbed onto a bilayer of tetracosane on graphite in the temperature range [100K, 500K]. Various structural and thermodynamic quantities are utilized to characterize the system's temperature evolution. The system goes from the low – temperature solid phase supporting a perpendicular third layer to the collapse of the perpendicular film near $T = 300$K to a dense, coalesced patch at high temperature.

*The authors gratefully acknowledge partial support of this work through Petroleum Research Fund grant PRF43277-B5

**Q1 303 Deterministic simulations of endohedral noble gas release from fullerene clusters*** M.K. BALASUBRAMANYA, *Texas A&M University - Corpus Christi* MICHAEL ROTH, *University of Northern Iowa* PHILIP TILTON, *Texas A&M University - Corpus Christi* BRYCE SUCHY, *University of Northern Iowa* Molecular Dynamics computer simulations are conducted on small ($N = 5$) endohedral $X@C_{60}$ clusters, where X = He, Ne, Ar, Kr and Xe. The cluster dissociates at a temperature between $T =$ 1150K and 1200K. As temperature is raised further, endohedral atoms begin leaving the cluster near $T = 4000$K. In the temperature range [4000K, 5000K] escape constants and half lives are calculated for release of the various gases. Helium exits much more quickly than any other noble gas examined, and larger species tend to exit more slowly not only because of their larger collision diameter but also because they stabilize the fullerene cage. Comparisons with and contrasts to experiment are mentioned.

*This work has been supported in part by an NSF MRI grant under the Division of Computer and Network Systems (# 0321218), and by a UNI Summer 2004 Fellowship for B.S.

**Q1 304 Systematic Study of magnetic Field Effects in Amorphous Solids at Ultra Low Temperatures.** LIDIYA POLUKHINA, SEUNGHWA RYU, DOUGLAS OSHEROFF, PHYSICS DEPARTMENT, STANFORD UNIVERSITY TEAM, The dielectric response of some amorphous solids below 100 mK is known to be sensitive to applied magnetic field. While a theoretical explanation for this phenomenon has been proposed, a systematic experimental study of different glasses in a broad parameter range is advised. We investigate and compare the behaviour of Suprasil, BK7, Aluminum-Barium-Silicate, Corning and Durane samples in the temperature range from 2 mK to 200 mK in presence of the magnetic field up to 30 milliTesla. In addition, we hope to find an amorphous solid whose dielectric constant shows no magnetic field dependence, making it suitable for thermometry in applied magnetic fields.

**Q1 305 Atomic Stability as Result of Electrodynamic Stability Condition** JX ZHENG-JOHANSSON, *IOFPR, SWE* P-I JOHANSSON, *Uppsala Univ, SWE* According to [1] an electron $e^-$ is formed of an oscillatory massless charge $-e$ in general also traveling at velocity $v$, and the resulting electromagnetic waves of angular frequency $\omega^j$, $j = \dagger$ and $\ddagger$ for generated in $+v$ and $-v$ directions. The wave energy $\hbar\sqrt{\omega^{\dagger}\omega^{\ddagger}}$ equals the charge oscillation energy $\varepsilon_q$ (with the $v = 0$ portion) endowed at the charge's creation; $\varepsilon_q/c^2$ gives the electron mass $m_e$, $c$ the wave speed. For an atomic orbiting electron, the charge's $v$ motion is along a circular (or projected-elliptic) orbit $\ell$ of radius $r$; so are its waves. (a) The waves meet in each loop with the charge, are absorbed a portion by it and reemitted, repeatedly, and thereby retained to it; the vacuum, having no lower energy levels for the charge to decay to except in a pair annihilation, is essentially a non-dissipative medium. (b) The two waves, being Doppler-differentiated for the moving source, meet each other over the loops and superpose into a beat, or de Broglie phase wave $\Psi$. $\Psi = Ce^{i(k_d\ell - \omega T)}$ is a maximum if $2\pi r_n = n\lambda_{dn}$, $n$ integer, $\lambda_d = 2\pi/k_d = (c/v)\lambda$ the de Broglie wavelength and $\lambda = 2\pi c/\omega$, and accordingly yields a stable state. The corresponding overall eigen solutions are exactly equivalent with the QM results. The classical electrodynamic stability conditions (a)-(b) entail the stability of the atomic system. [1] JX Zheng-Johansson & P-I Johansson, *Unification of Classical, Quantum and Relativistic Mechanics and the Four Forces*, Fwd Prof R Lundin, Nova Science, NY, 2005; see also B40.00003, this meeting.

**Q1 306 Domain wall soliton in a trapped spin-1 atomic Bose-Einstein condensate*** WENXIAN ZHANG, *Ames Laboratory, Iowa State University, Ames, Iowa 50011, USA* L. YOU, *School of Physics, Georgia Institute of Technology, Atlanta, Georgia 30332, USA* Solitons are interesting phenomenon in nonlinear systems, including atomic Bose-Einstein condensates. We investigate numerically a soliton state of a ferromagnetically interacting spin-1 condensate confined in a cigar shaped harmonic trap. The dynamics of this soliton, described by the coupled Gross- Pitaevskii equations within the mean field theory frame, is stable and intimately related to the recently observed domain structures in spin-1 condensate and similar to the domain wall soliton in two-component condensates. We present a rotating reference frame in which the local spin dynamics of the soliton becomes time independent.

*Supported by NSF.

**Q1 307 Near-wall turbulence structure in Poiseuille-Couette flow*** DIMITRIOS PAPAVASSILIOU, NICHOLAS SPENCER, *The University of Oklahoma* COMPUTATIONAL TRANSPORT PROCESSES TEAM, Given recent reports that ultra-hydrophobic surfaces generate slip at the wall in laminar flows, the question arises whether turbulence drag reduction can be achieved over such surfaces. If so, how is the near-wall turbulence structure affected? This work focuses on the effects that a specified wall velocity (or wall slip) can have on the turbulence field. Direct numerical simulations of a Poiseuille-Couette flow channel were used. Computations were completed for Re=5200 (based on centerline mean velocity and channel width). The runs included the cases where one wall moved with 0, 1, 2 and 4 plus velocity units in the flow direction relative to the opposite channel wall. The mean velocity maximum shifted towards the moving wall as the wall velocity increased, as well as the point at which the Reynolds stress crossed zero. The turbulence intensity was lower close to the moving wall side. The velocity correlation coefficients showed that near-wall structures became shorter. The paper will discuss the implications on slip-induced drag reduction.

*Office of Naval Research, Grant N00014-03-1-0684

**Q1 308 A methodology to separate single cells and single mitochondria to determine the location of heteroplasmy in mito-**

**chondrial DNA** JOSEPH REINER, *Physics Laboratory, NIST, Gaithersburg* RANI KISHORE, *NIST* THOMAS ALBANETTI, SARAH PEERY, ASHLEY KNIPE, AMANDA SHEETS, NICHOLAS BOIRE, KOREN DECKMAN, *Gettysburg College* BARBARA LEVIN, *CSTL-NIST* KRISTIAN HELMERSON, *NIST* A mixture of mutated and wild type mitochondrial DNA is referred to as a heteroplasmic population. Mitochondrial DNA heteroplasmies have been studied at the multi-cell level with some being linked to chronic symptoms of mitochondria-based diseases. However, the mechanism producing heteroplasmy is undetermined. One question is whether mitochondrial DNA heteroplasmies are present within single mitochondria. To address this issue we developed a protocol to isolate a single mitochondria from single human leukocyte cells. The cells from an HL-60 cell culture were labeled with Mitotracker Green FM and showed to contain a heteroplasmy at the cellular level (PCR and sequencing showed a 50/50 C/T heteroplasmy at nucleotide position 12071). In order to study heteroplasmy at the single mitochondria level a pulsed UV laser was used to lyse an individual cell. Mitochondria escaped from the cell and optical tweezers were used to transfer single mitochondria into a micropipette tip. Preliminary results suggest that single mitochondria also contain the heteroplasmy.

**Q1 309 Carrier Diffusion Model for Electrical Conductivity Response of Bi3TiNbO9 to Ambient Humidity*** RICARDO E. AVILA, *DMN, CCHEN, Cas. 188-D, Santiago, Chile* ALICIA CASTRO, *ICMM, CSIC, Madrid, Espaa* DANIEL SERAFINI, HCTOR ULLOA, *Depto. de Fsica, USACH, Santiago, Chile* The electrical properties of the metastable phase of $Bi_3TiNbO_9$ isomorphic to $\delta$-$Bi_2O_3$, in ceramic pellet form have been established. Pellets are formed by mechanochemical activation (1 to 48 h in an SPEX 8000 automatic mill), and uniaxial pressing, leading to the metastable phase in the 310 to 490 [r]C, as the activation time increases. Correspondingly, the stable Aurivillius phase forms in the 500 to 600 [r]C range. The current through pellets with $\sim$ 10 nm thick sputtered Pt electrodes increase by factors between 10 an 2000 in a transient from dry air to dew point of 10 [r]C at room temperature. The response time (10% to 90% of the current rise) is in the 15 to 30 s range, and it does not deteriorate under saline ambient, nor does it depend on the dry carrier gas (air, Ar, $N_2$, $O_2$, or 0.1% $H_2$ / He). A bulk carrier diffusion model achieves a close qualitative fit to the current response to bias and humidity cycling.

*Supported by Fondecyt Grant 1040213

**Q1 310 Influence of Gas Heating and Vibrational Kinetics on the Ionization Dynamics of Preformed Air Plasma Channels** HAROLD LADOUCEUR, ANDREW BARONAVSKI, *Naval Research Laboratory* TZVETELINA PETROVA*, *Naval Research Laboratory, NRC* An extensive self-consistent air-plasma model based upon the Boltzmann equation for the electron energy distribution function, coupled with a heavy particle kinetics was developed to study electric discharges in a preexisting air plasma column [1]. Incorporated in the model are the steady-state balance equations for various nitrogen and oxygen species in ground and excited states, as well as atomic and molecular ions. The influence of the gas temperature is accounted for by reduction of the neutral density, collisional processes such as recombination, dissociation, V-V and V-T reactions [2], and by reactions involving electronically excited states of $O_2$. The model was applied to study the influence of the gas temperature and vibrational kinetics on the breakdown processes in a preformed air plasma channel. Numerical calculations predict that electrical breakdown occurs at relatively low electric field. The calculated self-consistent breakdown electric field is $\sim$ 10 kV/cm for gas temperature of 300 K, while at temperature of 600 K it drops to $\sim$ 5.7 kV/cm, in excellent agreement with the experimentally determined breakdown electric field [1]. * NRC-NRL Postdoc [1] Tz.B. Petrova, H.D. Ladouceur, and A.P. Baronavski, 58th Gaseous Electronics Conference, 2005; San Jose, California, FM.00062 [2] J. Loureiro and C.M. Ferreira, J. Phys. D: Appl. Phys **19** (1986) 17-35

**Q1 311 Defend Science: The Attack on Scientific Thinking and What Must Be Done** JASON CURTIS, *UC Berkeley / Defend Science Project* ''In the United States today science, as science, is under attack as never before (Defend Science, defendscience-.org).'' Beyond, and underlying, the many particular attacks and outrages in different spheres and policy areas is the question of the scientific method and whether it is going to be upheld and applied, or whether – even in the realm of science itself – that method is going to be replaced by something antagonistically opposed to the scientific method. These attacks are increasingly coming from powerful forces, in and out of the Bush administration, with an extreme right-wing political agenda, a Biblical-literalist ideological agenda, and theocratic aspirations for society. Individual scientists may be atheists, agnostics, or may hold various religious beliefs, but if religious and theistic elements are forced into the definition of science, then the scientific process is undermined and science cannot really be practiced. We can and must develop a society wide battle, initiated by scientists, but involving ever growing masses of people to defend science and scientific thinking. Scientists from various fields must be mobilized to issue a public call to millions with this urgent message as the beginning of this effort. I will discuss the necessity, possibility, and some initial efforts toward developing this kind of societal movement in defense of science.

**Q1 312 Tod-Down Physics** MICHAEL SCHILLACI, *University of South Carolina* Over the past 7 years I have worked to develop two, two-semester course sequences in Theoretical and Computational Physics appropriate for undergraduate education in Physics. Covering material traditionally handled in Classical Mechanics and Electricity and Magnetism, the Theoretical Physics sequence stresses mathematical rigor, physical insight and a project- based paradigm, covering topics such as Landing on the Moon, Realistic Tidal Models, and The Solar Sail. A two- volume text (recently adopted by Mercer University) has been developed for the Computational Physics sequence and introduces students to the essentials of Maple, LaTeX and JAVA as well as web-page (HTML, JavaScript) publishing. While the bulk of the first semester is devoted to software use and algorithm development (i.e., numerical integration) wrote homework is supplemented by ''group quiz and project activities. In the second semester laboratory experiments such as the Toothpick Toss, The Not-So-Simple Harmonic Oscillator and the Chaotic Diode are performed and then computational simulations are developed using various tools (i.e., JAVA, Visual Basic, Matlab).

**Q1 313 Delayed Ionization Studies of Metal-Carbon Clusters*** KEVIN DAVIS, SAMUEL PEPPERNICK, A. CASTLEMAN, JR., *The Pennsylvania State University* Clusters of molecules, restricted to the nanometer size regime, display reduced size phenomena associated with the effects of quantum confinement. One

such occurrence, termed delayed ionization, is a fascinating phenomenon that has been observed in various metal, fullerene and metal-carbon cluster systems. Generally, favorable candidates to display delayed ionization characteristics are clusters containing a significant number of vibrational modes. Furthermore, the magnitude of the cluster's ionization potential must be in competition with its binding energy, whereby dissociation is impeded compared to ionization. The mechanism most commonly used to explain the delayed emission of electrons is termed thermionic emission. In order to interrogate this effect, delayed ionization studies are performed on early transition metal-carbon cluster systems. These clusters are produced in a laser induced plasma reactor cluster source coupled to a nanosecond ultraviolet photoionization laser, and are detected via the microchannel plates of a reflectron time-of-flight mass spectrometer. In this work, interesting delayed ionization characteristics of metal-carbon clusters will be presented in an effort to provide a better understanding of the relaxation processes that occur within clusters.

*Financial support by the USAFOSR, Grant No. F-49620-01-1-0380, is gratefully acknowledged.

**Q1 314 Probing minimal scattering events in enhanced backscattering of light using low-coherence induced dephasing** YOUNG KIM, PRABHAKAR PRADHAN, MIN KIM, HARIHARAN SUBRAMANIAN, YANG LIU, VADIM BACKMAN, *Northwestern University* We report the first experimental evidence that the minimum number of scattering events in enhanced backscattering (EBS, also known as coherent backscattering) of light is double scattering in discrete random media, which has been hypothesized since the first observation of EBS of light. We exploit low spatial coherence illumination to dephase time-reversed partial waves outside its finite coherence area, which virtually creates a controllable coherence volume and isolates the minimal number of scattering events from higher order scattering in EBS. In addition, EBS under low spatial coherence illumination possesses unique advantageous features compared to conventional EBS: (i) The spatial coherence length of illumination can be made to be the shortest length scale (except particle sizes) in weakly scattering media such as biological tissue. (ii) A large number of the independent coherence areas provide statistical information about the optical properties of random media in a single measurement, without configuration or ensemble averaging. (iii) LEBS allows varying the spatial coherence length of illumination to control the dephasing rate externally and LEBS does not require complicated sample preparations. Thus, these characteristics of LEBS will facilitate investigations of EBS in weakly scattering random media including biological tissue.

**Q1 315 Femtosecond time-resolved optical studies of collective modes in $La_{1-x}Ca_xMnO_3$** YUHANG REN, *Physics & Astronomy, Hunter College of the City University of New York* DAIMIAN WANG, MARIANO TRIGO, *Physics, The University of Michigan* VENIMADHAV ADYAM, QI LI, *Physics, The Pennsylvania State University* ROBERTO MERLIN, *Physics, The University of Michigan* We report on time-resolved ultrafast optical measurements on a $La_{1-x}Ca_xMnO_3$ (LCMO) single crystal ($x = 0.3$) and thin film ($x = 0.33$). The differential reflectivity shows coherent GHz oscillations due to the excitation of longitudinal acoustic (LA) phonons. The wavelength dependence of the period of such oscillations allows us to determine the sound velocity and elastic constant. Above $T_C$, the measured GHz sound velocity is more than 40% larger than the sound velocity in the MHz range as determined by ultrasound measurements. The data is explained by a possible existence of polaron liquid state. Also the differential polarization shows coherent magnons in LCMO. We determine the magnetic anisotropy and spin stiffness constants from the magnetic-field dependence of the frequency of the spin waves.

**Q1 316 Quartz Crystal Microbalance Measurements of Protein Deposition onto Cross-linked polyHEMA Hydrogel** JONATHAN TEICHROEB, JAMES FORREST, *University of Waterloo* LYNDON JONES, The adsorption of various concentrations of several opthalmologically relevant proteins was measured using Quartz Crystal Microbalance (QCM). Hen egg white lysozyme HEWL, bovine serum albumin BSA, and lactoferrin were measured both individually and in various combinations as they adsorbed onto cross-linked polyHEMA substrate. Results are discussed in terms of the concentration and time dependence of total adhered protein, as well as the amount of desorbable protein. Variations seen during competitive adsorption are also presented.

**Q1 317 Magnegtic Phase Diagram and Specific Heat of the Quasi-Two-Dimensional S=1/2 Antiferromagnet $Cs_2CuBr_4$** TODD E. SHERLINE, YASUMASA TAKANO, *University of Florida* $Cs_2CuBr_4$ is an excellent laboratory model for the S=1/2 Heisenberg antiferromagnet on a triangular lattice, with a small anisotropy. In a magnetic field, the most distinguishing feature of this antiferromagnet is a magnetization plateau, which occurs at 1/3 of the saturation magnetization. Previous specific heat and magnetocaloric effect measurements in DC fields of up to 20T have been used to determine the magnetic phase diagram in this regime. However, the nature of the phase diagram is unclear in higher fields. Further specific heat and magnetocaloric effect measurements have been made in DC fields up to 32T, the results of which will be presented in order to elucidate the nature of the phase diagram above the magnetization plateau.

**Q1 318 Experiments with Ultra-cold Atoms in an Optical Lattice with Dynamically Variable Lattice Constant** JOHN HUCKANS, IAN SPIELMAN, BRUNO LABURTHE TOLRA, *Institut Galile - Universit Paris 13* J.V. PORTO, W.D. PHILLIPS, LASER COOLING AND TRAPPING TEAM, We have implemented a one-dimensional optical lattice whose periodicity may be dynamically varied with ultra-cold atoms in-situ. We have measured atom heating rates in the lattice as a function of lattice periodicity ramp velocities and profiles. We superimpose another one-dimensional lattice with fixed periodicity and measure atom diffraction as a function of the ratio of the two competing periodicities. Finally, we report interesting near field atomic diffraction results for extremely large periodicity lattices.

**Q1 319 Effect of the anisotropy factor of scattering and the finite spatial coherence length of light source on enhanced backscattering** P. PRADHAN, YOUNG KIM, HARIHARAN SUBRAMANIAN, YANG LIU, VADIM BACKMAN, *Northwestern University, Evanston, IL 60208* Enhanced backscattering (EBS) of light (also known as coherent backscattering) is a constructive self-interference effect in the backscattered direction due to the photons traveling along time-reversed paths in a disordered medium. EBS can be used for characterization of disordered media and recently been used in cancer detection. Conventional EBS is determined by the scattering transport mean free path of the me-

dium. However, the properties of EBS become more complex and richer in case of anisotropy of scattering (anisotropy factor g$>$ 0) and finite spatial coherence length (Lsc) of a light source. We report our experimental and numerical studies of the effects of g and Lsc on EBS. We demonstrate for the first time that the profile of the EBS peak varies non-monotonically with mean free path length ls, and is a double valued function of ls for a range of values of Lsc and g. Hence, the value of g can be extracted from the EBS profile, which may provide important and previously unattainable information about biological tissue in situ.

**Q1 320 Modeling Low-Coherence Enhanced Backscattering (LEBS) using Photon random walk model of Light Scattering** HARIHARAN SUBRAMANIAN, PRABHAKAR PRADHAN, YOUNG KIM, YANG LIU, VADIM BACKMAN, *Northwestern University, Evanston, IL - 60208* Enhanced backscattering (EBS) peak from a biological media with transport mean free path length ($l_s^*$) $>>$ wavelength $\lambda$, is extremely small ( $\sim 0.001^0$) making the experimental observation of such narrow peaks to be difficult. Hence, we developed a low coherence enhanced backscattering (LEBS) technique by combining the EBS measurements with low spatial coherence (LSC) illumination and low temporal coherence detection. LSC behaves as a spatial filter preventing longer path lengths and collects photons undergoing low orders of scattering. The experimental angular width of these LEBS peaks ( $\sim 0.3^0$) are more than 100 times the width of the peak predicted by conventional diffusion theory. Here we present a photon random walk model of LEBS cones to further our understanding on the unprecedented broadening of the LEBS peaks. In general, the exit angles of the scattered photons are not considered while modeling EBS peaks in diffusion regime. We show that these photon exit angles are sensitive to the low orders of scattering, which plays a significant role in modeling LEBS peaks when the spatial coherence length of the light source is much smaller than $l_s^*$. Our results show that the model is in good agreement with experimental data obtained at different low spatial coherence illumination.

**Q1 321 Highly Ordered Arrays of Silicon Nanostructures Fabricated by Reactive Ion Etching and Atomic Fluorine Etching** MARK CURTIS, PRESTON LARSON, KEVIN HOBBS, MARK KEIL, MATTHEW JOHNSON, HOMER L. DODGE DEPARTMENT OF PHYSICS AND ASTRONOMY, UNIVERSITY OF OKLAHOMA, NORMAN, OK 73019 TEAM, High density arrays of conical nanostructures have been fabricated in silicon using a combination of anodic aluminum oxide (AAO) templating and dry etching techniques. Optically, such structures appear black, indicating strong optical absorption. Such structures have applications associated with field emitters and photo-voltaic cells. Silicon directly exposed to an atomic fluorine beam yields an array of sharp silicon spikes. Using the AAO template as a mask with the fluorine beam or reactive ion etcher (RIE) results in highly ordered arrays of nanostructures. In particular, the RIE samples have conical silicon nanostructures, approximately 150 nm in height. These nano-cones are arranged in a honeycomb pattern with a center-to-center spacing of approximately 100 nm and exhibit a high degree of ordering over micron by micron areas. Characterization of these nanostructures was carried out by scanning electron microscopy and various optical techniques.

**Q1 322 Synthesis and Mechanical and Electrical Properties of Carbon Nanotubes Grown at Low Temperatures by Thermal Chemical Vapor Deposition** YUNYU WANG, LI SHI, *Department of Mechanical Engineering, University of Texas at Austin* ZHEN YAO, *Department of Physics, University of Texas at Austin* PAUL HO, *Department of Mechanical Engineering, University of Texas at Austin* Carbon nanotubes (CNTs) have shown great potentials in versatile applications such as electron sources, heat interface materials and drug delivery vehicles due to their unique aspect ratio, thermal conductivity, and biocompatibility. CNTs have also attracted wide interests in applications for the next generation microelectronics, including interconnects, mainly due to its high current carrying capacity, *i.e.* $> 10^9$ A/cm$^2$. However, CNTs have been commonly synthesized under high temperatures, e.g. $>$ 1000 $^o$C for laser ablation and arc discharge and 600-900 $^o$C for chemical vapor deposition (CVD), which is not compatible with the $<$ 450 $^o$C requirement for microelectronic technology, and makes it difficult to integrate CNTs into integrated circuit chips. In this study, we present a controlled growth of CNTs at 450 $^o$C using a simple thermal CVD method. It has been shown that a combination of catalyst choice and preheating precursors is critical for the formation of CNTs at low temperatures. As-grown CNTs have been characterized using scanning electron microscopy, where vertically aligned dense short nanotubes films with lengths of $\sim$ 400 nm have been observed. For applications in microelectronics, mechanical and electrical properties of short CNT films are tested and the results will be discussed.

**Q1 323 Magneto-Transport Studies of Molecular Beam Epitaxial Grown Osmium Silicides*** RYAN COTTIER, WEI ZHAO, FATIMA AMIR, KHALID HOSSAIN, *University of North Texas* NOUREDDINE ANIBOU, WOLFGANG DONNER, *University of Houston* TERRY GOLDING, *University of North Texas* UNIVERSITY OF NORTH TEXAS COLLABORATION, UNIVERSITY OF HOUSTON COLLABORATION, Semiconducting transition metal silicides present a possible solution to on-chip integration of optical and electronic Si-based circuitry. Two phases of osmium silicide ($OsSi_2$ and $Os_2Si_3$) are predicted to have promising optical characteristics but require additional development to fully determine their feasibility for high-quality devices. This study has been motivated by reports that $OsSi_2$ has a bandgap between 1.4–1.8eV [1, 2] and $Os_2Si_3$ may have a direct bandgap of 0.95 eV [3] or 2.3 eV [1]. In this paper we will present temperature dependent ($20 < T < 300$ K) magneto Hall measurements of molecular beam epitaxial grown osmium silicide thin films. Os and Si were coevaporated onto Si(100) substrates at varying growth rates and temperatures. XRD was performed in order to identify the silicide phases present. We will discuss our results in relation to the known phase diagrams and our growth parameters. [1] L. Schellenberg et al., J. Less-Common Met. **144**, 341 (1988). [2] K. Mason and G. Müller-Vogt, J. Appl. Phys. **63**, 34 (1983). [3] A. B. Filonov et al., Phys. Rev. B **60**(24), 16494 (1999).

*Work supported by Office of Naval Research under Dr. C. Wood, Contract No. N00014-03-1-0820, and by the Advanced Technology Program of the State of Texas.

**Q1 324 Electron transport studies of superconducting Pb single-electron tunneling transistors** KANG LUO, ZHEN YAO, *Department of Physics, The University of Texas at Austin, Austin, TX 78712* We investigate the electronic transport properties of superconducting Pb single-electron tunneling transistors created by electromigration of Pb nanowires. In the superconducting state,

the conductance is suppressed by a combination of the Coulomb blockade effect and the absence of density of states within the superconducting gap. The tunneling spectroscopy at 2 K shows a strong even-odd parity effect which is smeared out at 4.2 K. Upon application of a magnetic field, the superconducting state is suppressed and single-electron tunneling behavior for normal metallic nanoparticles is recovered. We will present a theoretical model and compare it with our experimental data.

**Q1 325 Session M's Speakers Promote Evolution and Deny Creation Without Reference to My Widely Published Evidence of Earth's Rapid Creation and Without Reference to My Recent Discoveries Disproving the Big Bang: Congress Should Investigate Why They Did This** ROBERT GENTRY, I have long and widely described the primordial polonium radiohalos that exist in Earth's foundation rocks all over the world in the world's leading scientific journals. The short half-lves of the relevant polonoium isotopes – 3 min for Po- 218 – requires almost instantaneous creation of the host rocks, generally the hard crystalline rocks such as granites, showing that these rocks were the product of creation, not a long slow process of evolution. My publications can be found at www.halos.com. and have been accessible to the worldwide scientific community for over two decades without being refuted. More recently I have discovered fatal flaws in the big bang theory and also a New Cosmic Model that explains eight of the major predictions of the big bang (see CERN Preprint, Ext-2003-021, and CERN Preprint, Ext-2003-022. Additional disproof is available at www.orionfdn.org, which are papers that were submitted to and received arXiv numbers, but were promptly censored from being released, and continue to be suppresed by P Ginsparg and Cornell University. This is a practice borrowed from a totalitarian state and the Congress needs to investigate why supression of evidence of creation continues. There is no excuse for Session M's speakers not to acknowledge this evidence for the Genesis six- day creation of Earth and the visible heavens.

**Q1 326 Mesoscopic light transport properties of a single biological cell: Early detection of cancer** PRABHAKAR PRADHAN, YANG LIU, YOUNG KIM, XU LI, RAMESH K. WALI, HEMANT K. ROY, VADIM BACKMAN, *Northwestern University, Evanston, IL 60208* The progression of carcinogenesis involves morphological changes in the internal structure of a biological cell. These changes are reflected in the fluctuations of refractive index within the cell at scales ranging from a few nanometers to microns. We demonstrate that these fluctuations of refractive index can be measured by our newly developed technique – partial wave spectroscopic microscopy, and can be quantified using the mesoscopic transport theory of light. Our experimental and numerical results show that the statistics of the light reflection coefficient, the statistics of the localization length and the statistics of the refractive index fluctuation agree well with the mesoscopic light transport theory. Furthermore, our results show that we can detect the progress of carcinogenesis in a single biological cell earlier than any existing technique. We conclude that biological cells are nature made interesting disordered mesoscopic systems, and the changes in the statistics of fluctuations of refractive index in a single cell are highly diagnostic for noninvasive early detection of cancer using mesoscopic theory.

**Q1 327 Hydrogenation of Semiconductors Using an Ultra-Violet Light Source*** T.D. GOLDING, *University of North Texas/ Amethyst Research* R. HELLMER, *Amethyst Research* J. H. DINAN, *U.S. Army RDECOM CERDEC NVESD* R. J. COTTIER, *U. of North Texas* L. WANG, *Evans Analytical Group* W. ZHAO, *U. of North Texas* F. AMIR, *U. of North Texas* J. HOUSE, *U. of North Texas* Hydrogenation (also referred to as passivation) of semiconductors using a plasma discharge is routine. However, the process can cause unwanted modification of the surface, and requires contact masking if control of the lateral dosage is required. We will present results of a new technique for the hydrogenation of semiconductors based on the use of an ultra-violet (UV) light. While our studies have been conducted primarily on HgCdTe, we have similar results for the hydrogenation of GaAs and InP. Using the technique of secondary ion mass spectroscopy (SIMS) we have found that D is readily incorporated into semiconductors when the surface of the semiconductor is simultaneously exposed to a hydrogen (deuterium) gas and UV light. No D is observed to be present (to within the SIMS resolution) if the sample is treated under similar conditions without the UV light present. Early studies of the temperature dependence on the D concentration verses depth indicate that the process is diffusion driven. These results strongly suggest that the UV photons are dissociating adsorbed D molecules to atomic D on the semiconductor surface. In addition to our experimental results details of theoretical modeling to account for this phenomenon will be presented.

*Work supported by the US Army and National Science Foundation

**Q1 328 Magnetic Force Microscopy of Superconducting Vortices in Ordered Arrays of Artificial Pinning Centers** JOEL KEAY, PRESTON R. LARSON, KEVIN L. HOBBS, MATTHEW B. JOHNSON, *University of Oklahoma* OPHIR M. AUSLAENDER, KATHRYN A. MOLER, *Stanford University* Ordered arrays of artificial pinning centers were fabricated in Nb thin films using anodic aluminum oxide (AAO) as a template. The nanohole arrays show only a small decrease in the superconducting transition temperature, $T_c \simeq 7.1$ K, from comparable, unprocessed Nb thin films. These artificial pinning arrays have a triangular lattice parameter of 105 nm and antidot diameters of about 50 nm. Anomalous features at the first, second and third matching fields (matching field = 2170 Oe) were observed in the magnetization half-loops of these arrays at 5 K. Magnetic Force Microscopy (MFM) was used to image the nanohole arrays above and below $T_c$. The images clearly show the nanohole lattice. Individual vortices have also been imaged and their movement within the lattice is being investigated. Preliminary measurements of the depinning force of individual vortices at low fields will be presented. This work was supported by NSF grant nos. DMR-0080054 and NSF-0132534.

**Q1 329 Interference patterns in field emission images of Multi-Walled Carbon Nanotubes** GEORGIANNA MARTIN, P.R. SCHWOEBEL, *University of New Mexico* Carbon nanotubes are of interest due to their unusual chemical and electrical characteristics and have thus been suggested for use in a wide variety of applications including field emission cathodes. However, there are indications that their emission characteristics, like those of most field emitters, are sensitive to their vacuum environment. Interference patterns in the field emission images of nanotubes have been observed by others and associated with coherent electron emis-

sion. Here we report the observation of interference patterns with either a central node or anti-node which appear to be associated with phase shifts introduced by surface adsorbates. This work is supported by the NSF under grant number ECS-0245682.

**Q1 330 Search for a ferromagnetic quantum criticality in $YbIn1_{1-x}Rh_xCu_4$** Y. TOKIWA, F. RONNING, V. FRITSCH, R. MOVSHOVICH, J.D. THOMPSON, J.L. SARRAO, *Los Alamos National Laboratory, Los Alamos, New Mexico 87545, USA* The geometrically frustrated system $YbIn_{1-x}Rh_xCu_4$ is investigated in order to search for a quantum criticality associated with ferromagnetic correlations. The undoped $YbInCu_4$ undergoes a first-order isostructural valance transition at 42K. The valance transition is suppressed with Rh substitution of $x\sim 0.3$ and ferromagnetic correlations grow with increasing Rh content as can be seen from the increasing Weiss temperature in magnetic susceptibility. We report low temperature specific heat measurements down to 50mK on $YbIn_{1-x}Rh_xCu_4$with x around suspected critical concentration $x\sim 0.6$ and discuss the relation between the ferromagnetic correlations and non-Fermi liquid behavior.

**Q1 331 Atomic-resolution Spectroscopic Imaging Scanning Tunneling Microscopy of Triple Layer Cuprate: $Bi_2Sr_2Ca_2Cu_3O_{10+\delta}$** JHINHWAN LEE, S. ILLANI, JINHO LEE, J. W. ALLDREDGE, *Cornell University* C. T. LIN, B. KEIMER, *Max-Planck Institut* J. C. DAVIS, *Cornell University* We present preliminary high spatial resolution scanning tunneling spectroscopy (STS) study of triple layer cuprate $Bi_2Sr_2Ca_2Cu_3O_{10+\delta}$. The sample is near optimally doped, with $T_c = 110$ K. The local density of states (LDOS) map shows (1) strongly heterogeneous gap distributions, (2) significantly increased average superconducting gap, (3) equivalent energy-dispersive quasiparticle interference patterns and (4) stronger and sharper coherence peaks compared to double layer cuprate $Bi_2Sr_2CaCu_2O_{8+\delta}$ of similar doping. We also have preliminary observations of the disordered bosonic mode energy distribution qualitatively similar to those of $Bi_2Sr_2CaCu_2O_{8+\delta}$.

**Q1 332 Amphiphilic diblock copolymers with adhesive properties: structure and swelling with water** PASCALE FABRE, *CRPP-CNRS 115 av. Dr. Schweitzer F-33600 Pessac* SYLWIA POIVET,* FRÉDÉRIC NALLET, KAI SCHIERHOLZ,† GINU ABRAHAM, *CRPP-CNRS* ERIC PAPON, YVES GNANOU, *LCPO, 16 av. Pey-Berland, F-33607 Pessac cedex, France* RAYMOND OBER, *Laboratoire de physique des fluides organisés, UMR CNRS-Collège de France, 11 place Marcelin Berthelot, F-75231 Paris cedex 05, France* OLIVIER GUERRET, NOUREDDINE EL-BOUNIA, *ARKELA-GRL, B.P. 34, F-64170 Lacq, France* We study asymmetric block copolymers with the simple diblock AB architecture, in the case where the longer block A is both hydrophobic and ''soft,'' whereas the shorter block B is hydrophilic and ''hard.'' Materials with such a particular combination of physico-chemical and mechanical properties have distinctive advantages, in particular for designing water-compatible adhesive materials. The phase-diagram is established, combining NMR and SAXS characterizations of the materials. The swelling with water is monitored through gravimetry and ''time-resolved'' SAXS. Indications of maintained adhesive properties in a wet environment are given.

*present address: Bostik, rue Bailly, F-60170 Ribécourt, Dreslincourt, France

†present address: Nanoledge, av. de l'Europe, F-34830 Clapiers, France

**Q1 333 Ionisation Potentials of Metal Carbide Clusters** VIKTORAS DRYZA, *Department of Chemistry, The University of Adelaide, South Australia 5005, Australia* M. ADDICOAT, JASON GASCOOKE, MARK BUNTINE, GREGORY METHA Photo-Ionisation Efficiency (PIE) experiments have been performed on gas phase niobium and tantalum carbide clusters to determine their ionisation potentials (IPs). For TanCm ($n=3$–4, $m=0$–4) clusters an oscillatory behaviour is observed such that clusters with an odd number of carbon atoms have higher IPs and clusters with an even number of carbons have lower IPs. Excellent agreement is found with relative IPs calculated using density functional theory for the lowest energy structures, which are consistent with the development of a $2\times2\times2$ face-centred nanocrystal. For the niobium carbide clusters we observe the species $Nb_4C_5$ and $Nb_4C_6$. Initial calculations suggest that these clusters contain carbon-carbon bonding. Interestingly, the stoichiometry for $Nb_4C_6$ is half that of a metcar, $M_8C_{12}$. Preliminary data will also be shown on bimetallic-carbide clusters.



**SESSION R1: CYTOSKELETAL DYNAMICS AND MECHANICS**
**Wednesday Afternoon, 15 March 2006; Ballroom IV, Baltimore Convention Center at 14:30**
**Gerard Wong, University of Illinois, presiding**

**14:30**
**R1 1 Structural organization and dynamics of the cytoskeletal network.***
TATYANA SVITKINA, *Department of Biology, University of Pennsylvania, Philadelphia, PA*

Actin cytoskeleton is the major player in mechanisms driving multiple forms of cell motility. Actin filaments cooperating with numerous actin-binding proteins are able to form distinct types of higher order structures: networks and bundles, which are designed for carrying out various functions. One of important actin functions is generation of pushing force for protrusion of a leading edge of motile cells. Lamellipodia and filopodia are the two major protrusive organelles utilized by different cells for leading edge protrusion. Even though both are driven by actin polymerization, lamellipodia and filopodia have strikingly different structural design and use different sets of actin-binding proteins. Lamellipodia, which are broad, flat protrusions are filled with a branched network of actin filaments, which propagates through cycles of dendritic nucleation, elongation, capping, and depolymerization of actin filaments. Filopodia, which are thin cellular processes, contain a tight bundle of parallel actin filaments, which elongates at the tip and depolymerizes from the rear.

Although basic models for the leading edge protrusion have been formulated, many questions remain about the molecular design of the protrusive machinery and specific roles of individual molecules. Our approach is to analyze molecular architecture of actin cytoskeleton during protrusion and correlate these data with live cell behavior. Recent progress in understanding the molecular mechanisms of actin-based protrusion will be presented.

*Supported by NIH R01 GM070898.

**15:06**
**R1 2 Active Polar Gels: A Paradigm for Cytoskeletal Dynamics.**
FRANK JULICHER, *Max Planck Institut für Physik Komplexer Systeme, Nöthnitzer Str. 38, 01187 Dresden, Germany*

The cytoskeleton of eucaryotic cells is an intrinsically dynamic network of rod-like filaments. Active processes on the molecular scale such as the action of motor proteins and the polymerization and depolymerization of filaments drive active dynamic behaviors while consuming chemical energy in the form of a fuel. Such emergent dynamics is regulated by the cell and is important for many cellular processes such as cell locomotion and cell division. From a general point of view the cytoskeleton represents an active gel-like material with interesting material properties. We present a general theory of active viscoelastic materials made of polar filaments which is motivated by the the cytoskeleton. The continuous consumption of a fuel generates a non- equilibrium state characterized by the generation of flows and stresses. Our theory can be applied to experiments in which cytoskeletal patterns are set in motion by active processes such as those which are at work in cells. It can also capture generic aspects of the flows and stress profiles which occur during cell locomotion.

**15:42**
**R1 3 Elasticity, adhesion and actin based propulsion.***
AJAY GOPINATHAN,† *University of California Santa Barbara*

When a cells crawls, its shape re-organizes via polymerization and depolymerization of actin filaments. The growing ends of the filaments are oriented towards the outside of the cell, and their polymerization pushes the cell membrane forwards. The same mechanism comes into play when the bacterial pathogen Listeria monocytogenes infects a cell. The bacterium hijacks the host cell's actin machinery to create an actin network (the actin comet tail) that propels the bacterium through cells and into neighboring cells. We propose a mechanism for how polymerization gives rise to motility that incorporates the effects of inhomogeneous polymerization. We treat the actin comet tail as an elastic continuum tethered to the rear of the bacterium. The interplay of polymerization and tethering gives rise to inhomogeneous stresses calculated with a finite element analysis. We quantitatively reproduce many distinctive features of actin propulsion that have been observed experimentally, including stepped motion, hopping, tail shape and the propulsion of flat surfaces.

*This work was supported by NSF-DMR-0503347 and NSF-CHE-0096492.
†In collaboration with Andrea J. Liu.

**16:18**
**R1 4 Fluorescent Speckle Microrheology.**
MARGARET GARDEL, *The Scripps Research Institute*

The actin cortex is the dense shell of actin filaments between the cell membrane and the cytoplasm maintaining and regulating cell shape. It is one of the principal determinants of cell mechanical properties, whose spatiotemporal modulations play a central role in processes that involve architectural dynamics of a cell, such as cell migration, division and morphogenesis. However, the exact mechanism of cortical actin elasticity regulation itin vivo is still unresolved. We present a high-resolution and molecularly specific assay of itin vivo cortical actin elasticity, fluorescent speckle microrheology. Speckles originate when fluorescent actin is randomly incorporated into the network along with abundant endogeneous non-fluorescent actin, leading to high spatial variations of the local fluorophore density; high-density areas appear as diffraction-limited spots (speckles) upon high-resolution imaging. Speckles act as fiduciary marks of the network and can be used to directly image strain fluctuations, in contrast to classical microrheology techniques using imbedded probes. When tracking positional fluctuations of actin speckles in cells without convective network flow with subpixel precision, we find that the displacements of neighboring speckles are spatially correlated. Their correlation function decays as 1/r with interspeckle distance r, which is consistent with theoretical predictions for strain field decay in a 3D continuous viscoelastic medium. On the basis of these results, we use the amplitude of the correlation function to measure viscoelastic properties of the actin network. Due to high intracellular speckle densities and their homogeneous distribution throughout the cell, this approach yields much higher spatial resolution than other microrheology techniques, which is validated using itin vitro actin networks. Thus, this assay allows us to map intracellular actin cortex elasticity with micron resolution, and to relate intracellular heterogeneities of elasticity to heterogeneities in other dynamic cellular parameters.

**16:54**
**R1 5 Nonlinear Elasticity in Biological Gels.**
CORNELIS STORM, *University of Leiden*

The mechanical properties of soft biological tissues are essential to their physiologic function and cannot easily be duplicated by synthetic materials. Unlike simple polymer gels, many biological materials including blood vessels, mesentery tissue, lung parenchyma, cornea and blood clots, stiffen as they are deformed, or strained. Stiffening under deformation allows tissues to be compliant at small strains and strengthen at larger deformations that could threaten tissue integrity. The molecular structures and design principles responsible for this non-linear elasticity are unknown. I will outline a molecular theory that accounts for strain-stiffening in a range of molecularly distinct gels formed from cytoskeletal and extracellular proteins and reveals universal stress-strain relations at low to intermediate strains. The input to this theory is the force-extension curve for individual semi- flexible filaments and the assumptions that networks composed of them are isotropic and that their elastic response is affine. The theory shows that systems of filamentous proteins arranged in an open crosslinked meshwork invariably stiffen at low strains without requiring a specific architecture or multiple elements with different intrinsic stiffness.

## SESSION R2: FRACTIONAL QUANTUM HALL SYSTEMS
**Wednesday Afternoon, 15 March 2006; Ballroom III, Baltimore Convention Center at 14:30**
**Horst Stormer, Columbia University, presiding**

**14:30**
**R2 1 New physics in the second Landau Level.**
GABOR CSATHY, *Princeton University*

Clean two-dimensional electron systems subjected to perpendicular magnetic fields have a long history of revealing exotic ground states. A large number of these states are only possible in the presence of electron-electron interactions. Two notable examples of such collective ground states are the fractional quantum Hall liquids of the first two Landau levels and the electronic solids called the stripe and bubble phases forming beyond the first Landau level. These two classes of phases are simultaneously present and hence compete in the second Landau level. This talk will highlight our latest results on the evolution of the states of the second Landau level as the magnetic field is tilted away from the direction perpendicular to the sample. The challenging task of cooling to millidegree temperatures and in-situ tilting in this low temperature environment is achieved with a hydraulically driven rotator equipped with sintered Silver heat exchangers mounted onto the nuclear demagnetization stage of a dilution refrigerator. We found that the bubble states are rapidly destroyed with tilt and argue that such a behavior is consistent with the formation of an electronic solid. Furthermore, the well developed $\nu = 2+1/5$ and $2+4/5$ liquids are found to be driven insulating while the $2+1/3$ and $2+2/3$ states survive to the largest tilt angles accessible. The simplest interpretation of the rapid evolution of these states is that bubble phases melt into a classical Hall gas and the $\nu = 2+1/5$ and $2+4/5$ liquids solidify with tilt. Our data suggest that spin interaction plays an important role in the formation of these phases. In particular, we surmise that the bubble phases are not fully spin-polarized but most likely have a substantial antiferromagnetic order. These bubble phases could be first examples of antiferromagnetically ordered solids in a single layer two-dimensional electron system. This work was done in collaboration with J.S. Xia, C.L. Vicente, E.D. Adams, N.S. Sullivan, D.C. Tsui, H.L. Stormer, L.N. Pfeiffer, and K.W. West.

**15:06**
**R2 2 How free are composite fermions? An inelastic light scattering perpective.**
YANN GALLAIS, *Dept. of Physics and Dept. of Appl. Phys. & Appl. Math, Columbia University, New York*

The presentation is focused on the study of spin excitations in the regime of the Fractional Quantum Hall Effect (FQHE) to probe composite fermion interactions. The spin excitations are observed by inelastic light scattering methods. The composite fermion picture is appealing because the FQHE of strongly interacting electrons in 2D becomes the Integer Quantum Hall Effect of nearly-free composite fermions. Recent inelastic light scattering experiments show that the study of spin excitations of composite fermion quasiparticles offers unique venues to address the question: how free are composite fermions? Our experiments are conducted in the filling factor range $2/7<\nu<2/5$. We measured low energy spin-flip excitations of composite fermions in which orientation of spin and composite fermion Landau level quantum number change simultaneously. The filling factor dependence of the spin-flip excitation intensity displays a striking non-monotonic behavior as the occupation of composite fermion Landau levels are changed. This occurs when the filling factor moves above and below $\nu = 1/3$. We find remarkable behaviors that are attributed to the strong impact of residual

composite fermion interactions. The breakdown of the non-interacting composite fermion picture seen in our experiments seems to manifest quasiparticle condensations that in magneto-transport experiments are interpreted as the FQHE of composite fermions. *The work was done in collaboration with Jun Yan, T.H. Kirschenmann, C.F. Hirjibehedin, I. Dujovne, A. Pinczuk, B.S. Dennis, L.N. Pfeiffer and K.W. West.

**15:42**
**R2 3 Exotic Excitations of Composite Fermions.**
MICHAEL PETERSON, *University of California Santa Cruz*

The low-energy physics of the fractional quantum Hall effect (FQHE) is marked by the emergence of weakly correlated quasiparticles called composite fermions that are qualitatively distinct from the original strongly correlated electrons. A composite fermion (CF) is an electron bound to an even number of quantum mechanical vortices of the many-body wave function where the number of vortices characterizing the CF is called its flavor. Inelastic light scattering has played a crucial role in understanding the different types of excitations in the FQHE regime. While the lowest energy neutral excitations are accurately described as single CF particle-hole pairs, other types of interesting higher energy excitations are possible. We describe two such excitations. (i) Composite fermion flavor changing excitations (Peterson and Jain, PRL 93, 046402(2004), Wojs and Quinn, Philos. Mag. B 80, 1405(2000)): The lowest energy excitations are such that the flavor of the excited CF remains constant. We show that, in addition, there is a new class of excitations where the excited CF loses some of its vortices, i.e., it changes its flavor. Further, we suggest that these flavor changing excitations are relevant to the experimental observation of Hirjibehedin *et al. (PRL, 91, 186802(2003)) of co-existing excitation modes of differently flavored CFs in the filling factor range* $1/3 > \nu \geqslant 1/5$. (ii) Electronlike CF excitations (Jain and Peterson, PRL 94, 186808(2005)): We show that the electron is not irretrievably lost in the FQHE regime. In particular, we find that the electron (hole) couples to a complex high energy bound state of CF quasiparticles (holes). Experimental consequences of this complex bound state will be discussed.

**16:18**
**R2 4 A proposal for measuring fractional charge and statistics in fractional quantum Hall states through noise experiments.**
EUN-AH KIM, *Stanford Institute for Theoretical Physics*

Quasiparticles of fractional quantum Hall (FQH) fluids are predicted to be finite energy vortices carrying fractional charge and fractional statistics. These properties reflect the non-trivial topological order which characterizes each FQH state as a distinct phase. However, strong evidence for fractional statistics has remained an open experimental challenge. We propose a three-terminal ''T-junction'' as an experimental setup for directly detecting fractional charge and statistics of fractional quantum Hall quasiparticles via cross current noise measurements. Through a careful non-equilibrium calculation of the quantum noise in the T-junction setup for FQH Jain states, we showed that the cross current correlation (noise) can be written in a simple form with all the statistics dependence captured in a factor of $\cos\theta$ in one of two contributions, where the statistical angle $\theta$ is defined by the phase gained by a two quasiparticle wave function upon exchange. By analyzing these two contributions for different parameter ranges that are experimentally relevant, we demonstrated that the noise at finite temperature reveals signatures of generalized exclusion principles, fractional exchange statistics and fractional charge. We also predicted that the vortices of Laughlin states exhibit a ''bunching'' effect, while higher states in the Jain sequences exhibit an ''anti-bunching'' effect.

**16:54**
**R2 5 Phonon Absorption Experiments on Composite Fermions.**
FRITZ SCHULZE-WISCHELER, *Institut für Festkörperphysik, Universität Hannover, Appelstraß e 2, 30167 Hannover, Germany*

We present a time-resolved phonon absorption technique as an efficient tool to investigate the properties of the fractional quantum Hall effect (FQHE). We interpret our data within the Composite Fermion (CF) picture of the FQHE, were the CF quasiparticles are constructed by attaching two magnetic flux quanta $\phi_0$ to each electron. As a result, the CFs at filling factor $\nu$ and electron density $n$ experience only an reduced magnetic field $B^* = B - 2\phi_0 n$, so that they behave in $B^*$ in analogy to electrons in the magnetic field $B$ and form Landau levels of CFs with effective filling factor $p = \nu/1 - 2\nu$ in particular. In a first set of experiments, we measure phonon excitation gaps in the FQH regime for various filling factors and find that the measured gaps can be well described in the framework of Landau-level transitions of CFs involving no spin flip [1]. We are able to deduce the CF mass $m^*(10T) = 0{,}5m_0$ from these transitions. We apply the same model to energy gaps which we deduce from transport experiments. These gaps are transitions from one level to another reduced by disorder. Here, spin flip are allowed. From results near the crossing of two levels, we were able to deduce the g-factor of CFs [2]. A second set of phonon absorption experiments focuses on the specific heat $C$ of the 2DES at various filling factors $\nu$ [3]. Here, we find an exponential dependence $C \propto (1/T)^2 exp(-\Delta/T)$ on

temperature $T$ if the 2DES is in a state with an energy gap $\Delta$. At $\nu = 1/2$, where the external magnetic field is fully cancelled by the gauge field, we find a linear temperature dependence as expected for a Fermi sea of CFs.

[1]F. Schulze-Wischeler, F. Hohls, U. Zeitler, D. Reuter, A. D. Wieck, and R. J. Haug, Phys. Rev. Lett. **93**, 026801 (2004).

[2]F. Schulze-Wischeler, E. Mariani, F. Hohls, and R. J. Haug, Phys. Rev. Lett. **92**, 156401 (2004).

[3]F. Schulze-Wischeler *et al.*, to be published in 2006.

## SESSION R3: LATERAL SPIN TRANSPORT
**Wednesday Afternoon, 15 March 2006; Ballroom I, Baltimore Convention Center at 14:30**
**Chia-Ling Chien, Johns Hopkins University, presiding**

**14:30**
**R3 1 Spin injection, diffusion and detection in lateral spin valves.**
YI JI, *Materials Science Division and Center for Nanoscale Materials, Argonne National Lab*

Metallic heterostructures involving ferromagnetic metals (FM) and non-magnetic metals (NM) offer very rich spintronic phenomena, such as giant magnetoresistance and spin-transfer torque. Recently, new interests have been found in heterostructures that feature lateral variation of materials. The motivation originates from the possibility of lateral integration of future spintronic devices and the advantage of extra degrees of freedom in controlling spin accumulation offered by lateral structures. In this work, we demonstrate non- local spin injection and detection in lateral spin valves. A lateral spin valve consists of a NM nanowire connected with two FM electrodes, one as the spin injector and the other as the spin detector. The measurement configurations are arranged in such a way that the current injection circuit and voltage detection circuit are separated, and so are the charge current and the spin current. A pure spin current without charge flow can be obtained in lateral spin valves, and the detected spin signal exhibits very large percentage change. The spin accumulation in lateral spin valves strongly depends on the spin diffusion length of the NM and the injection polarization of FM/NM interface, both of which can be determined by measuring a series of spin valves with different injector detector separations. We have determined the spin diffusion lengths and injection polarizations for Py/Au/Py and Co/Cu/Co lateral spin valves, fabricated by different techniques. The differences of these quantities in two systems will be discussed. This work is done in collaboration with Axel Hoffmann, Sam Jiang, John Pearson, and Sam Bader, and supported by U.S. DOE Office of Basic Energy Science-Materials Science under contract No. W-31- 109-ENG-38.

**15:06**
**R3 2 Dynamics of lateral magnetoelectronic thin-film nanostructures.**
GERRIT BAUER, *TU Delft*

Hybrid nanostructures made from ferromagnetic and normal metals come in two main flavors: perpendicular multilayer nanopillars and lateral thin film devices. Current-induced magnetization dynamics have until now mainly been studied in perpendicular structures. However, lateral devices have several advantages compared to perpendicular ones, such as relative ease to study multi-terminal configurations and to directly observe the magnetic order parameter. In this talk I will discuss the magnetization dynamics of lateral thin-film structures in the framework of magnetoelectronic circuit theory. The research has been done in collaboration with Xuhui Wang, Yaroslav Tserkovnyak, Arne Brataas, Bart van Wees, Axel Hoffmann, and Teruo Ono.

**15:42**
**R3 3 Spin-polarized tunneling and spin diffusion in sub-micron lateral spin-transistors.***
SERGIO O. VALENZUELA, *Physics Department, Harvard University, Cambridge MA 02138, USA*

Much effort has been devoted to understand how the electron spin is transferred through interfaces and to identify the fundamental processes that suppress the spin polarization. Spin- transistors with the Johnson and Silsbees geometry are a unique tool to study these phenomena. In these devices, a spin- polarized current is injected into a non-magnetic metal using a tunnel junction in combination with a ferromagnet (FM), which acts as a spin source. The polarized current results in non- equilibrium spin populations in the non-magnetic metal, which are detected as voltages using a second FM. Fabricated aluminum- based devices with spin transresistances as high as 2 Ohm allow us to study spin-flip scattering mechanisms and spin-polarized tunneling. The tunneling polarization at zero bias is compared with the one estimated with the Meservey and Tedrow technique in the same sample. In addition, as the spin-transistor measurements can be extended to finite voltages and high temperatures, new valuable information is obtained on the character and polarization

of the electrons that tunnel out of or into the ferromagnetic source. Surprisingly, the polarization is found to be strongly bias-dependent and asymmetric around zero bias. The origin of these phenomena is analyzed.

*In collaboration with D.J. Monsma, M. Tinkham, C.M. Marcus and V. Narayanamurti.

**16:18**
**R3 4 Spin-torque effects due to pure spin currents in lateral geometries.**
YOSHICHIKA OTANI, *ISSP University of Tokyo*

Spin injection into the ferromagnetic materials induces a spin torque due to the spin angular momentum transfer between the conduction electron spin and the localized magnetic moment. The magnetization reversal of a nano-scale ferromagnet thereby takes place when the spin polarized current is injected into it. This has been demonstrated using metallic nanopillar devices consisting of magnetic multilayered systems with the spin polarized current flowing perpendicular to the plane. The spin torque mentioned above is known to be proportional to the spin current density. Therefore not the charge current causing the Joule heat but the spin current is essential to realize efficient magnetization reversal due to the spin torque. Thus non-local spin injection technique is employed to realize such a reversal. Here we discuss our resent results on the magnetization reversal due to non-local spin injection into a nano-scale ferromagnetic particle in a lateral ferromagnetic/nonmagnetic hybrid device [1].

[1] T. Kimura and Y. Otani cond-mat/0508559 submitted to PRL.

## SESSION R4: IONIC, DIPOLAR AND H-BONDING POLYMERS
**Wednesday Afternoon, 15 March 2006; 308, Baltimore Convention Center at 14:30**
**Sanat Kumar, Rensselaer Polytechnic Institute, presiding**

**14:30**
**R4 1 Solvent-induced changes in the structure and rheology of polyelectrolyte solutions.**
VICTOR BREEDVELD, *Georgia Institute of Technology*

By integrating microfluidics and particle tracking microrheology, we have constructed a dialysis cell for microrheology, which provides unique opportunities for studying the dynamics of microstructural changes induced by changes in solvent composition. Such experiments are virtually impossible with mechanical rheometers. The concept and design of the microdialysis cell will be discussed, and data will be presented on the structural and rheological response of polyelectrolyte solutions to changes in ionic strength. Sulphonated polystyrene is a water-soluble polymer and its molecular conformation in solution strongly depends on ionic strength of the solution. It will be shown that quantitative measurements of transient solution viscosity during solvent exchange can be performed with the new dialysis cell. Experiments were also performed on amphiphilic block copolypeptide (BCP) hydrogels, which self-assemble into fibrillar structures due to a subtle balance between attractive and repulsive intermolecular forces. Electrostatic repulsion between the hydrophilic L-lysine blocks plays a key role. Therefore, changes in ionic strength have a significant effect on the self-assembled local structure and mechanical properties of the BCP gels, as was previously observed in rheometer experiments. Microrheology in the dialysis cell provided a much more complete picture, revealing the occurrence of microscopic phase separation upon the addition of salt. For example, in a K160L40 lysine-leucine block copolypeptide, the motion of tracer particles in the hydrogel is homogeneous in DI water. After the addition of salt, microrheology reveals the co-existence of populations of freely moving and immobilized particles. The changes in local microstructure were found to be reversible when the ionic strength of the solution was lowered again. Data will be presented on the dynamics of the morphological and rheological changes of various block copolypeptide hydrogels.



**15:06**
**R4 2 Theoretical Modeling of Hydrogen Bonded and Metal-Ligand Associating Polymers.***
ELENA DORMIDONTOVA, *Department of Macromolecular Science and Engineering, Case Western Reserve University, Cleveland, Ohio 44106; E-mail:eed@case.edu*

Applying analytical modeling in combination with Monte Carlo simulations we have studied the association behavior and properties of two types of supramolecular polymers employing 1) hydrogen bonded and 2) metal-ligand associative motifs. In the first case association between the hydrogen bonded arrays results in numerous donor-acceptor interactions between the complementary end groups of linear oligomers leading primarily to formation of linear chains or rings. Similar architectures of self-assembled polymers can also be obtained by reversible 1:2 complex formation between metal ions (such as Zn(+2), Cd(+2), Co (+2), etc.) and ligands of end-functionalized oligomers. In this case the association is strongly influenced by metal- ligand ratio. We analyze the chain-ring equilibrium and study the influence of the strength

and type of association, rigidity of the complex and solution composition on the degree of association and the average molecular weight of the supramolecular polymers. For metal ions (such as La(+3), Nd(+3), Eu(+3), etc) capable of 1:3 complex formation with the ligands, self-assembly results in reversible polymers of more complex architecture, in particular a reversible network (in the percolation limit). Since the coordination sites of the metal possess unequal reactivity (having different energies of association with the first, second and third ligand) and due to the cooperativity of binding, network formation is influenced by different factors such as metal/ligand ratio, oligomer length and concentration. Predictions of an analytical model based on the equilibrium among different associating species and classical percolation theory compare favorably with simulation results for gel fraction and average molecular weight. Simulation results and theoretical predictions will be compared with available experimental data.

*This work was supported by the NSF Career Award CHE-0348302.

**15:42**
**R4 3 Soultion assembly of charged block copolymers and block copolypeptides.***
DARRIN POCHAN, *University of Delaware*

By considering peptidic or charged, synthetic polymers in the materials self-assembly design process, one can take advantage of inherently biomolecular attributes; intramolecular folding events, secondary structure stabilized by hydrogen bonding, and electrostatic interactions; in addition to more traditional self-assembling molecular attributes such as amphiphilicty, to define hierarchical material structure and consequent properties. The solution assembly behavior of two charged block copolymers will be discussed. First, diblock copolypeptides consisting of a hydrophilic, charged block and a hydrophobic block were designed to self-assemble due to their amphiphilic nature. The defined helical secondary structure of the leucine hydrophobic block forces these molecules to form a membraneous local nanostructure. However, diverse materials, ranging from rigid hydrogel, vesicle suspension, or hexagonal single crystal, can be formed depending on assembly pathway. Second, synthetic triblock copolymers with charged corona blocks can be assembled in dilute solution with multivalent organic counterions to produce complex micelle structures such as toroids and discs. Nanostructure can be tuned with different concentrations or molecular volumes of organic counterion. Transmission electron microscopy, small-angle neutron scattering, multiphoton confocal microscopy, dynamic light scattering, and atomic force microscopy results will be discussed.

*This work supported by the Division of Materials Research and Chemical Transport Systems of the NSF.

**16:18**
**R4 4 Water Solubility of Polymers with Salt: The Hofmeister Series.**
PAUL CREMER, *Texas A&M University*

We have designed temperature gradient microfluidic devices that allow high throughput, low sample volume assays to be performed on the folding of thermoresponsive polymers and proteins. These macromolecular systems are insoluble at high temperatures, but become hydrated and unfold as the temperature is decreased in a process analogous to the cold denaturation of proteins. Our assays enable highly precise measurements to be made rapidly of the physical behavior of the polymers. The device is specifically used to obtain data on poly (N-isopropylacrylamide) and alpha-elastin at multiple concentrations in the presence of a variety of ions. The results indicate that the folding process follows the Hofmeister series. This series, which dates back to 1888, is a rank ordering of anions and cations based upon their ability to salt-out or salt-in proteins. It had been historically believed that ions affect macromolecule solubility indirectly through their interactions with bulk water. This idea has been largely disproved by a variety of characterization techniques over the last decade. A new theory to explain the mechanism of the Hofmeister effect, however, still needs to be developed. Microfluidic assays in combination with vibrational sum frequency spectroscopy allowed us to develop a model based solely on the direct interaction of the ions with a macromolecule and its first hydration shell. In fact, the protein folding properties can be related to a few simple factors: an ion's hydration entropy, its effect on the surface tension of an aqueous interface, and its ability to interact directly with binding sights on a protein.

**16:54**
**R4 5 Polyelectrolyte effects in polymers for lithography.**
VIVEK PRABHU, *Polymers Division, National Institute of Standards and Technology*

The transformation of a solid-like film into a solution upon exposure to a miscible solvent is a complex process involving sluggish kinetic pathways associated with the slow transport of the liquid into the film and the evolution of the thermodynamic driving forces during the course of the dissolution process. In complex materials such as polymers, this process occurs in stages from the transformation of the glassy or crystalline film into a swollen state, followed at longer times by the final dissolution of the film. Dissolving polyelectrolyte films exhibit additional complexities in their dissolution dynamics over uncharged polymer films. Interfacial charge density, the dielectric constant of the medium, ionic strength and valence influence the phase behavior of charged polymers thus affecting their dissolution behavior. The dissolution mechanism can be tailored for different applications, for instance the microelectronics industry utilizes the selective dissolution of one component enabling lithographic pattern formation. We present neutron reflectivity and quartz crystal

microbalance results to address polyelectrolyte effects in thin films such as the counterion distribution, quasi-equilibrium swelling and kinetics. V.M. Prabhu, R.L. Jones, E.K. Lin, W-L Wu. ''Polyelectrolyte effects in model photoresist developer solutions.'' J. Vac. Sci. and Tech.B, 21, 1403 (2003). V.M. Prabhu, B.D. Vogt, W-L. Wu, J. Douglas, E. Lin, S. Satija, D. Goldfarb, and H. Ito. ''Direct measurement of the counterion distribution within swollen polyelectrolyte films'' Langmuir Letter, 21, 6647 (2005).

## SESSION R5: PATHS FROM ACADEMICS TO EMPLOYMENT

**Wednesday Afternoon, 15 March 2006; 309, Baltimore Convention Center at 14:30**
**John L. Orrell, Pacific Northwest National Laboratory, presiding**

**14:30**
**R5 1 AIP Statistics on Physics Employment Trends.**
ROMAN CZUJKO, *American Institute of Physics*

This talk provides a statistical overview of the employment trends for physicists. The work done by physics bachelors, masters, and PhDs is qualitatively different. This talk will describe the career paths commonly pursued by recent physics graduates at each degree level and will illustrate how these trends have changed over time. It will discuss the indicators that point to both the strengths and weaknesses of the current job market for physicists. The paper will include a discussion of recent reports that claim that American students are avoiding science and engineering. It will conclude with a discussion of the pro's and con's of recent calls for dramatic increases in U.S. degree production in the sciences.

**15:06**
**R5 2 Industry Job Hunting for PhDs.**
BERNARD SILBERNAGEL, *ExxonMobil Research & Engineering Co.*

The industrial environment presents opportunities and challenges that are significantly different from those in academia. The research problems encountered are often complex and the solutions are generally sought by teams of researchers with a variety of skills from different disciplines. An important criterion for a new researcher in industry is that they be able to represent their area of competency on such a team. In most instances, hiring decisions are based on a reasonable compatibility of the candidate's skills and the needs of the research area, but the supposition is that the individual will evolve with time and with changing assignments. Important attributes for the candidate are solid technical strength in their area of expertise, good ''peripheral vision'' of science and technology in proximate and more remote areas, and a willingness to adapt to changes in the direction of the project. In contrast to academia, there are a variety of career paths for the industrial scientist, including a long-term participation in research and development, migration into the more practical aspects of the business (such as problem-solving or technical liaison) or management. Initially, it will probably not be apparent which of these paths is the most desirable and, in fact, a person may be involved with more than one during the course of their career. Each of these paths, or a combination of them, can be extremely satisfying and rewarding.

**15:42**
**R5 3 Government Positions for Physicists.**
DAVID SEILER, *National Institute of Standards and Technology*

There are a number of government agencies that employ physicists in a wide variety of jobs – from student internships to post docs to full time staff positions. You can do real, creative, fore-front physics or pursue a wide range of leadership positions. The possibilities are almost unlimited and so is the impact your work can have on the government, academia, and industry. So how do you go about finding a government job? What qualities or abilities are deemed valuable? What are the advantages and disadvantages to working in the government? I will bring some personal experiences and observations from working in the government (one year as a rotator at the National Science Foundation in the Division of Materials Research and almost 18 years at the National Institute of Standards and Technology, both as a Group Leader and a Division Chief) to bear on these questions and more. Prior to my government career I was a physics professor pursuing research and teaching in academia.

**16:18**
**R5 4 Aiming for Professorship at a Research University.***
CHRISTOPHER J. STANTON, *University of Florida*

In this talk, I will discuss and provide guidance on how to prepare and approach applying for an academic faculty position at a research oriented university as a first time professor. First I will discuss what is expected of a beginning faculty member at a research university. Next I will cover what you should be doing as a postdoc to enhance the chances of a finding a research position at a university. Finally I will go over all aspects of the job search process. Topics that will be discussed include: 1) preparing your CV, research and teaching statements, and cover letter, 2) getting letters of recommendation, 3) preparing for the interview, 4) the ''Job Talk,'' 5) following up the interview, 6) negotiating the start-up package, and finally 7) accepting or rejecting an offer. Throughout the talk, I will try to emphasize what the ''search committee'' as well as the department is looking for in a successful candidate and some pitfalls to avoid in the process.

*Supported by NSF through grant DMR-0325474.

**16:54**
**R5 5 Teaching and Research at Undergraduate Institutions.**
SHILA GARG, *The College of Wooster*

My own career path has been non-traditional and I ended up at a primarily undergraduate institution by pure accident. However, teaching at a small college has been extremely rewarding to me, since I get to know and interact with my students, have an opportunity to work with them one-on-one and promote their intellectual growth and sense of social responsibility. One of the growing trends at undergraduate institutions in the past decade has been the crucial role of undergraduate research as part of the teaching process and the training of future scientists. There are several liberal arts institutions that expect research-active Faculty who can mentor undergraduate research activities. Often faculty members at these institutions consider their roles as teacher-scholars with no boundary between these two primary activities. A researcher who is in touch with the developments in his/her own field and contributes to new knowledge in the field is likely to be a more exciting teacher in the classroom and share the excitement of discovery with the students. At undergraduate institutions, there is generally very good support available for faculty development projects in both teaching and research. Often, there is a generous research leave program as well. For those who like advising and mentoring undergraduates and a teaching and learning centered paradigm, I will recommend a career at an undergraduate institution. In my presentation, I will talk about how one can prepare for such a career.

## SESSION R6: U. S. WOMEN IN PHYSICS: AN INTERNATIONAL PERSPECTIVE
**Wednesday Afternoon, 15 March 2006; 310, Baltimore Convention Center at 14:30**
**Kimberly Budil, Lawrence Livermore National Laboratory, presiding**



**14:30**
**R6 1 An International Perspective on Women in Physics.**
ARIEL MICHELMAN-RIBEIRO, *BU / NIH*

The 1$^{st}$ International Union of Pure and Applied Physics (IUPAP) Conference on Women in Physics, held in 2002 in Paris, France, highlighted a number of issues facing women physicists around the world. A second conference was held in May 2005 in Rio de Janeiro, Brazil, with the goal of examining the progress made since the last conference and also to provide an opportunity for the delegates to present their research, both physics research and gender-related research, and to make contacts for future collaborations. The conference was attended by 145 delegates from 42 countries, including a very diverse delegation of 22 women and men from the U.S. The conference was organized by the Working Group on Women in Physics of IUPAP, which is charged with making recommendations to IUPAP on how to attract, retain, and increase the participation of women in physics at all levels. The conference included a round table discussion on ''Research Funding and Women in Physics,'' several plenary talks, a poster session on women in physics in each country, a poster session on research by individual delegates, and discussion groups on six topics including attracting girls into physics, launching a successful career, getting women into leadership, improving the institutional climate, learning from regional differences, and balancing family and career. Conference proceedings have been published that include research abstracts, summaries from the discussion groups, articles on the plenary talks, and papers from each country on the status of women in physics in their country (proceedings can be found at http://proceedings.aip.org/proceedings/confproceed/795.jsp). This talk will discuss the U. S. delegation and their country paper on the situation for women in physics in the U.S. as well as highlights from the information presented by the delegates from other nations. The outcomes of the 2002 conference will be described briefly and then the signs of progress noted in 2005 will be summarized.

**15:06**
**R6 2 What Works for Women in Undergraduate Physics? Learning from Different Institutions.***
BARBARA L. WHITTEN, *Colorado College*

The participation of women in physics has increased in recent years, but the percentage of women receiving bachelor's degrees in physics is still less than half that in mathematics or chemistry. The undergraduate years have been identified as the biggest ''leak.'' With a team of women physicists, I have been studying undergraduate physics departments to learn what makes some departments female-friendly. An informal and supportive department culture is the most important factor we have identified. There are many elements that make up a female-friendly culture, and different kinds of institutions—small colleges, universities, women's colleges, and HBCUs—all have important ideas to contribute. I will discuss what these different institutions have to tell us about recruiting and retaining women in the undergraduate physics major.

*Supported by NSF grants #HRD-0120450 and #HRD-0332874.

**15:42**
**R6 3 Women Physicists of Color Achieving at the Intersection of Race and Gender.**
K. RENEE HORTON, *University of Alabama*

As minority women physicists, we stand at the intersection of race and gender. We are physicists to be sure, but we are also women of Native, African and Hispanic descent. We are colleagues, mothers, sisters, and wives, as are our white counterparts, but our experiences cannot be distilled to only gender or race. As Prudence Carter and Scott Page remind us, women of color emerge from the interaction between race and gender.[1] This distinction is important since most researchers who study American women's participation in science focus exclusively on the participation of white American women. Of those who acknowledge the existence of non-white women, most do so by disclaiming the exclusion of women of color because the numbers are so small or the experiences are different from white American women. There are some important differences however. While American women are 15 percent of all scientists and engineers, black American women are 60 percent of all black scientists and engineers. Yet less than 3 black women and 3 Hispanic women earn PhDs each year, out of about 1100. As Rachel Ivie and Kim Nies Ray point out, ''Minority women especially represent a great, untapped resource that could be drawn on to increase the size of the scientific workforce in the U.S.''[2] Donna Nelson's study of diversity in science and engineering faculties further finds that there are no female black or Native American full professors.[3] In physics, there are no black women professors and no Native American women professors at all. Despite such a bleak picture, there is hope. Of the 18 departments that award at least 40 percent of bachelor's degrees to women, 7 are Historically Black Colleges and Universities. Black women are earning degrees from HBCUs at rates above equity, and many singles and firsts at predominantly white institutions continue to persevere despite the obstacles.

[1]Prudence Carter. 2005. Intersectional Matters and Meanings: Ethnicity, Gender, and Resistance to ''Acting White.'' Annual Meeting of the American Educational Research Association. Montreal: AERA; Scott Page. 2004. The Logic of Diversity. Private Communication. Rachel Ivie and Kim Nies Ray. 2005. Women in Physics and Astronomy, 2005. AIP Publication R-430.02. College Park, MD: American Institute of Physics.
[2]munication. Rachel Ivie and Kim Nies Ray. 2005. Women in Physics and Astronomy, 2005. AIP Publication R-430.02. College Park, MD: American Institute of Physics.
[3]Donna J. Nelson. 2005. A National Analysis of Diversity in Science and Engineering Faculties at Research Universities. Norman, OK: University of Oklahoma.

**16:18**
**R6 4 Effects of Informal and Formal Support Groups on Retaining Women and Minorities in U. S. Physics.**
MIA ONG, *TERC*

This abstract was not received electronically.

**16:54**
**R6 5 Interacting in the Smog Factors that Shape Faculty Attitudes and Beliefs about Race and Inclusion.**
APRIEL K. HODARI, *The CNA Corporation*

Many faculty members realize that we must interact productively with diverse colleagues and students, and we must find ways to benefit from the talents of all members of our intellectual community. Put simply, we must aim for the ceiling rather than the floor. This means that we approach our work informed that engaging diversity in our classrooms will increase our success and the success of itall our students. But in physics, it is often difficult to measure and address diversity issues because doing so is not perceived as central to our discipline. To address this apparent disconnection, we present some ideas on race [1] and inclusion [2] within the context of the physics instruction. Specifically, we speak to how university faculty might use inclusive pedagogy in physics education research and curriculum. Our goal here is to open a frank dialogue and present concrete avenues to explore as you create activities that serve your classroom best. Tatum, Beverly Daniel. (2004). Changing demographics and challenges of the future. itDraft Proceedings of the National

Science Board Workshop on Broadening the Participation in Science and Engineering Research and Education. Arlington, VA: National Science Board; Tatum, Beverly Daniel. (1997). Why are All the Black Kids Sitting Together in the Cafeteria? And Other Conversations about Race. New York: Basic Books.

Bonilla-Silva, Eduardo. (2003). Racism without Racists: Color-blind Racism and the Persistence of Racial Inequality in the United States. Lanham, MD: Rowan & Littlefield; Thiederman, Sondra. (2003). Making Diversity Work: 7 Steps for Defeating Bias in the Workplace. Chicago: Dearborn Trade Publishing.

**SESSION R7: THE EXPERIMENTAL AND THEORETICAL FOUNDATIONS OF EVOLUTION**
**Wednesday Afternoon, 15 March 2006; 307, Baltimore Convention Center at 14:30**
**Herbert Levine, University of California, San Diego, presiding**

**14:30**
**R7 1 Evolutionary ecology of E. coli metapopulations in patchy landscapes.***
JUAN KEYMER, *Princeton University*

Spatial ecology and metapopulation biology are essential features of natural populations. Extinction of local populations, the colonization of new suitable habitat patches (metapopulation dynamics) as well as the creation and destruction of local habitats (patch dynamics) are basic components of the evolutionary process shaping life-history strategies. As Darwin liked to put it ''the zoology of archipelagoes.'' The role of spatial structure have been shown to be important for both, persistence and coexistence. However, the spatial ecology of microbial metapopulations have rarely been observed nor exploited technologically. We use nano and micro fabrication technology to build a spatially explicit (dynamic) landscape of habitat patches (the metapopulation chip) and a (UV) laser-based disturbance regime (patch dynamics). By building upon the theory of metapopulations in dynamic landscapes, we build fitness landscapes by linking patch dynamics to fluorescent patterns coming from molecular markers in the cell culture. We use landscape ecology and metapopulation biology to generate selective forces that can be used for evolutionary design of microorganisms.

*Thanks to Peter Galajda & Robert Austin.

**15:06**
**R7 2 Life has Evolved to Evolve.***
MICHAEL DEEM, *Rice University*

Concomitant with the evolution of biological diversity must have been the evolution of mechanisms that facilitate evolution, due to the essentially infinite complexity of protein sequence space. We describe how evolvability can be an object of Darwinian selection, emphasizing the collective nature of the process. Rapid or dramatic environmental change leads to selection for greater evolvability. The selective pressure for large scale genetic moves, such as DNA exchange, becomes increasingly strong as the environmental conditions become more uncertain. These results demonstrate that evolvability is a selectable trait and allow for the explanation of a large body of experimental results. Many observations within evolutionary biology, heretofore considered evolutionary happenstance or accidents, are explained by selection for evolvability. As specific examaples, we discuss evolution within the immune system and evolution of drug resistant microrganisims.

*DARPA #HR00110510057.

**15:42**
**R7 3 Can Evolution Be Understood Quantitatively?***
DANIEL S. FISHER, *Harvard University*

Although the underlying laws and mechanisms of biological evolution have been known for a long time, little is understood about the time scales of evolutionary processes. This talk will focus on quantitative questions about evolutionary dynamics and on the potential for progress on intermediate time-scale issues via combinations of microbial experiments and theory. A recent experiment on one of these will be presented. Some basic questions about long time-scale processes will also be raised, and potential roles of abstract models in sharpening these and advancing understanding addressed briefly.

*Supported in part by NSF via DMR0229243.

**16:18**
**R7 4**
RICHARD LENSKI, *Michigan State University*

This abstract was not received electronically.

**16:54**
**R7 5 Genome Evolution in the 21st Century.**
JAMES SHAPIRO, *University of Chicago*

Assume no previous theories about genetics and evolution. What conclusions would we draw from molecular data (e.g. genome sequences)? We start from basic principles of cellular information processing: cells behave cognitively using signal transduction networks; signal transduction involves weak noncovalent interactions; allosteric properties of biomolecules; multivalent storage of information in DNA sequences and nucleoprotein complexes; inertness of naked DNA. Genome informatics thus requires formation of nucleoprotein complexes. Complex formation requires generic repeated signals in the DNA; repetition also permits cooperativity to stabilize weak interactions. DNA is a functional structural component of nucleoprotein complexes, not a passive data tape. Specificity in DNA nucleoprotein complex formation involves combining multiple generic signals and/or sequence recognition by small RNAs. Novel combinations of generic signals and coding sequences arise in genomes by iteration and rearrangement. Cells possess natural genetic engineering functions that actively restructure DNA molecules. These internal DNA remodeling functions act cognitively in response to internal and external inputs. They operate non-randomly with respect to (1) the types of new structures produced and (2) the regions of the genome modified. Whole genome sequence data increasingly documents the historical role of natural genetic engineering in evolutionary changes. Basic principles of cellular molecular biology and DNA function lead to a complex interactive systems view of genome organization. This view incorporates different DNA components found in sequenced genomes. Regulated cellular natural genetic engineering functions permit genomes to serve as Read-Write information storage systems, not just Read-Only memories subject to accidental change. These 21st Century conclusions are most compatible with a systems engineering view of the evolutionary process.

**SESSION R8: MONOLAYERS, MEMBRANES & MICROEMULSIONS**
**Wednesday Afternoon, 15 March 2006**
**314, Baltimore Convention Center at 14:30**
**Mark Bowick, Syracuse University, presiding**



**14:30**
**R8 1 Theory of Myelin Coiling** JUNG-REN HUANG, THOMAS WITTEN, *University of Chicago* We propose a new model to explain coiling of myelins composed of fluid bilayers. This model allows the bilayer cylinders of a myelin to be non-coaxial and the bilayer lateral tension to vary from bilayer to bilayer. Our calculations suggest that a myelin would bend or coil to lower its free energy when the bilayer lateral tension is sufficiently large. The proposed coiling mechanism is in a sense similar to the classical Euler buckling of a thin elastic rod subject to axial compression. The analysis of a simple two-bilayer case shows that a bilayer lateral tension of about 1 dyne/cm can easily induce coiling of myelins of typical lipid bilayers. This model signifies the importance of bilayer lateral tension in determining the morphology of myelinic structures.

**14:42**
**R8 2 Curvature condensation and twinning in an indented elastic shell** MOUMITA DAS, ASHKAN VAZIRI, *Harvard University* ARSHAD KUDROLLI, *Clark University* L. MAHADEVAN, *Harvard University* We study the formation of a localized geometrical defect and its evolution in an elastic shell using a combination of experiment and numerical simulation. We find that as a symmetric localized indentation on a semi-cylindrical shell increases, there is a transition from a global mode of deformation to a localized one which leads to the condensation of curvature along a parabolic crease along the line of symmetry. Further indentation leads to a twinning phenomena wherein the crease bifurcates into two defects that move apart on either side of the line of symmetry. We present a simple theory to explain the main features of the experiments and numerical simulations.

**14:54**
**R8 3 Anomalous persistence of a pinch in a pipe** L. MAHADEVAN, A. VAZIRI, M. DAS, *Harvard University* The response of low-dimensional solid objects combines geometry and physics in unusual ways, exemplified in structures of great utility such as a tubular shell that is ubiquitous in nature and technology. Here we provide a particularly surprising consequence of this confluence of geometry and physics in tubular structures: the anomalously large persistence of a localized pinch in an elastic pipe whose effect decays very slowly as an oscillatory exponential with a persistence length that scales as $R^{3/2}/t^{1/2}$, diverging as the thickness of the tube vanishes. The result is more a consequence of geometry than material properties, and is thus equally applicable to carbon nanotubes and cytoskeletal microtubules as it is to aircraft fuselages and geological plates, with a number of consequences, some of which we consider.

**15:06**
**R8 4 Crystalline order on the paraboloid** LUCA GIOMI, MARK BOWICK, *Syracuse University* We describe an experimental and theoretical investigation of crystalline order on a two-dimensional paraboloid. In contrast to the sphere, the paraboloid exhibits both variable Gaussian curvature and a boundary. Both these features must be treated for a thorough theoretical understanding. A macroscopic model of a parabolic crystal can be obtained in the laboratory by assembling a single layer of soap bubbles on the surface of a rotating liquid, thus extending the classic work of Bragg and Nye on planar arrays of soap bubbles.

**15:18**

**R8 5 Elastic Stiffness of Grain Boundary Scars and Dislocation Dynamics** HOMIN SHIN, MARK BOWICK, *Syracuse University* We analytically calculate the stiffness of finite-length grain boundaries (scars) on a spherical crystal within the continuum elasticity theory. The scar is composed of an isolated disclination with $+1$ topological charge together with a finite number of dislocations. We determine the elastic free energy of a single finite-grain boundary scar by considering interacting defects, such as Disclination-Disclination (D-D), Disclination-dislocation (D-d), and dislocation-dislocation (d-d). The harmonic potential binding dislocations to the scar is obtained by determining the free energy of a single dislocation perturbed away from its equilibrium position. The elastic spring constants so obtained are compared to experimental data on dislocation dynamics [1]. We conclude with some comments on interstitial dynamics. [1] Lipowsky, P., Bowick, M. J., Meinke, J. H., Nelson, D. R. and Bausch, A. R., Nature Mater. 4, 407-411 (2005).

**15:30**

**R8 6 Membrane Nano-Structures: The Three Tether Junction** OLIVER RUEBENACKER, *University of Connecticut* GREG HUBER, *University of Connecticut* Tethers are robust cylindrical nanostructures of lipid bilayer membranes, including biomembranes. They can be easily produced in experiments and can be found in and on cells. Tethers are useful for probing the mechanical properties of membranes, because the radius of a tether is small enough to make the bending stiffness of the membrane relevant. In an experiment, a glass bead was attached to a tether and pulled with a laser tweezer leading to the formation of a three tether junction. I will present a theory explaining the observed force-displacement relationship and simulation results of the shape of the three tether junction.

**15:42**

**R8 7 Toward a multi-scale simulation of lipid bilayer systems** TAISUKE SUGII, SHU TAKAGI, YOICHIRO MATSUMOTO, *The University of Tokyo* In numerical simulations of lipid bilayer systems, it has become important to treat the membrane molecules (e.g., lipids, proteins, and drug molecules) explicitly for designing medical drugs and for developing drug delivery systems. However, it is difficult to apply straightforwardly a microscopic simulation technique such as the molecular dynamics method to the large-scale bilayer systems, because the length and the time scales of these systems are very large compared to the scales of the molecules. The authors take two approaches for this problem. First, we use the dissipative particle dynamics method and the coarse grained molecular dynamics method in addition to the standard molecular dynamics method. The results are compared with the molecular-dynamics results and experimental data. Secondly we use a molecular dynamics and continuum hybrid simulation method. In this method, the region near the membrane is computed by an atomistic-simulation method and the solvent region is computed by a continuum-simulation method. (In our study, the coarse grained molecular dynamics was used for the atomistic region.) The validity and availability of this later approach will be discussed.

**15:54**

**R8 8 Influence of the size of interacting domains on the diffusion of nano-particles** FLORIAN RÜCKERL, CARSTEN SELLE, JOSEF KÄS, Single particle tracking (SPT) is widely used for investigating the diffusion of proteins in cell membranes. However, short lifetime and the blinking of fluorescent tracers make it difficult to obtain sufficient data on the interactions with the inhomogeneities of the membrane. Langmuir lipid monolayers provide control over obstacle size and the corresponding interaction energy since their condensed domains within liquid phases exhibit a net dipole moment. The diffusion of a stable, negatively charged latex bead in the coexisting liquid phase, with a dipole moment anti parallel to the one of the domain, was observed by SPT. The interaction energy was obtained by Boltzmann statistics of the tracking data. The electric field of the monolayer domains varies with domain size. Its distance dependence can principally change from $E \sim 1/r^3$ for a single dipole to $E \sim 1/r$ for large domains ($R > 10m$). The influence of this change on the particle diffusion was investigated by Monte Carlo simulations. The analysis shows that the particles are stronger trapped at the domain border of smaller domains and that a change from two to one dimensional diffusion occurs. Recently, we also started analogous experiments using red blood cells and vesicles as biomembrane mimics.

**16:06**

**R8 9 Control of domain formation and budding in multicomponent bilayer membranes** KURT A. SMITH, ANNA C. BALAZS, *University of Pittsburgh* Phase separation in fluid bilayer membranes, of lipids or block copolymers, can lead to a budding transition when line tension between the two phases comes to dominate the bending rigidity of the membrane. This leads to a nearly spherical bud connected to the membrane by a small neck. We examine the role of molecular architecture and composition on this shape transformation. Specifically we consider the inclusion of twin-tail amphiphiles which lower the free energy of the system by segregating to the interface between the two phases. Such additives can be used to lower the surface tension, thus controlling the critical size at which buds form. In addition they stabilize the neck when budding does occur, by acting essentially as stitches, thereby increasing the energy needed to detach the bud from the membrane. Using dissipative particle dynamics we are able to simulate the dynamics of large mebrane patches over relevant time scales.

**16:18**

**R8 10 Ordering by collapse: Two-dimensional crystallization of hydrophobic dimers by folding Langmuir monolayers*** DAVID VAKNIN, *Ames Laboratory, Iowa State Univerisity* WEI BU, *Ames Laboratory, Iowa State Univerisity* ALEX TRAVESSET, *Ames Laboratory, Iowa State Univerisity* Synchrotron X-ray studies of arachidic-acid monolayers compressed to the collapse region, beyond their densely packed molecular area, reveal that the resulting structures are stable and exhibit a surprising degree of order. Different structures, depending on whether the monolayer is spread on pure water or on $CaCl_2$ solutions, are identified. On pure water the collapsed monolayer forms a stable crystalline trilayer, with acyl-chain packing practically identical to the 3D crystal structure of fatty acids. For monolayers spread on $Ca^{2+}$ solutions, the collapse regime consists of an inverted bilayer with the hydrophobic tails in contact with the water surface and the calcium ions bridging the polar heads. The inverted bilayer structure possesses a well ordered crystalline slab of calcium-oxalate-monohydrate

intercalated between two acyl-chains. We discuss the implications of our findings to recent reports on dewetting of water near hydrophobic surfaces, on the formation of super-lattice structures by ions beneath a monolayer, and the relevance to certain biological processes.

*The MUCAT sector at the APS, through Ames Laboratory, and the use of the APS are supported by U.S. DOE, Basic Energy Sciences under Contracts Nos. W-7405-Eng-82 and W-31-109-Eng-38, respectively.

**16:30**

**R8 11 Mechanical Properties of an Actin Filament Network Monolayer*** ROBERT WALDER, MICHAEL DENNIN, *U. C. Irvine Department of Physics and Astronomy* ALEX LEVINE, *UCLA Department of Chemistry and Biochemistry* Actin filament networks present a model system to study the mechanical properties of semi-rigid polymer networks. Because they are a network, the filaments can display behavior that deviates from continuum elasticity theory on sufficiently short length scales, resulting in interesting nonlinear response of the system to applied stresses and strains. We have developed a Couette (concentric cylinders) style apparatus to study monolayers of actin confined to the air-water interface. This talk will present results characterizing the response of the monolayer to continuous and step-wise strains. We will report on measurements of the viscosity of the actin network, as a macroscopic characterization, and on tracking of particles embedded in the network. The particle tracking is used to probe local displacements of the network in response to applied strain. We will report on tests of the predicted transition between affine and non-affine displacements as a function of cross-linking density.

*supported by NSF grant DMR-0354113

**16:42**

**R8 12 Shape Selection in Self-Assembled Chiral Membranes: New Mechanism Based on the Flexoelectric Effect** ZHAO LU, ROBIN SELINGER, JONATHAN SELINGER, *Liquid Crystal Institute, Kent State University* Many biological materials self-assemble into chiral microstructures such as cylindrical tubules and helical ribbons. A chiral elastic theory proposed by Selinger et al., based on the elastic properties and chirality of amphiphilic lipid molecules, has been successful in explaining the formation of tubules and helical ribbons. Recently, an experiment has shown that achiral lipid molecules can also form chiral microstructures. This challenges the previous theory based on molecular chirality. Toward understanding this problem, we develop a new model for membrane shape selection based on the flexoelectric effect. We investigate this model through both analytical calculations and dissipative particle dynamic simulations on tethered membranes.

**16:54**

**R8 13 Bile Salt Mediated Growth of Reverse Wormlike Micelles in Nonpolar Liquids** SHIH-HUANG TUNG, YI-EN HUANG, SRINIVASA RAGHAVAN, *Department of Chemical and Biomolecular Engineering, University of Maryland, College Park, MD 20742* We report the growth of reverse wormlike micelles induced by the addition of a bile salt in trace amounts to solutions of the phospholipid, lecithin in nonpolar organic solvents. Previous recipes for reverse wormlike micelles have usually required the addition of water to induce reverse micellar growth; here, we show that bile salts, due to their unique ''facially amphiphilic'' structure, can play a role analogous to water and promote the longitudinal aggregation of lecithin molecules into reverse micellar chains. The formation of transient entangled networks of these reverse micelles transforms low-viscosity lecithin organosols into strongly viscoelastic fluids. The zeroshear viscosity increases by more than five orders of magnitude, and it is the molar ratio of bile salt to lecithin that controls this viscosity enhancement. The growth of reverse wormlike micelles is also confirmed by small-angle neutron scattering (SANS) experiments on these fluids.

**17:06**

**R8 14 Mesoscopic simulations of binary mixtures and microemulsions using a stochastic, particle-based algorithm** ERKAN TUZEL, *School of Physics and Astronomy, University of Minnesota* GUOAI PAN, THOMAS IHLE, DANIEL KROLL, *Department of Physics, North Dakota State University* Particle-based simulation techniques provide an attractive alternative to traditional methods for the coarse-grained modeling of a fluctuating solvent. A particularly appealing algorithm introduced by Malevanets and Kapral[1], called Stochastic Rotation Dynamics, describes a fluid with an ideal gas equation of state. The algorithm has been successfully applied to study polymers, colloids, and vesicles in shear flow. Recently, this algorithm has been generalized to model fluids with non-ideal equations of state[2]. We will discuss how this can be used to study binary mixtures with a miscibility gap. Results for the demixing such as the phase diagram and measurements of interface fluctuations and the surface tension of a droplet will be shown. By tuning the ratio of surface tension and viscosity both damped and overdamped capillary waves were obtained.The coarsening of domains during spinodal decomposition is also investigated. In order to describe microemulsions, the model is further extended to include surfactant molecules. Preliminary results for the onset of emulsification will be presented. [1] A. Malevanets, R. Kapral, J. Chem. Phys. 110, 8605 (1999). [2] T. Ihle, E. Tuzel, D. M. Kroll, cond-mat/0509631; cond-mat/0511312.

**17:18**

**R8 15 On the bouncing of rigid spheres on thin polymer films** LAURENT COURBIN, ANTONIN MARCHAND, ASHKAN VAZIRI, HOWARD A. STONE, *Division of Engineering and Applied Sciences, Harvard University* We report on a study of the rebound of stainless steel spheres on thin polymer films. After the sphere is dropped it bounces off the plastic sheet and the evolution in time of the subsequent rebounds are recorded. Experiments are performed varying the sphere radius, the impact velocity, and the film tension. The variations of the contact time, the amplitude of deformation of the film, and the loss of energy of the sphere after impact, as reported via a coefficient of restitution, lead to a number of scaling relations. These results are interpreted in terms of linear and nonlinear theories of the elasticity of membranes.

**SESSION R9: IMAGING, SIGNAL DETECTION AND PROCESSING**
**Wednesday Afternoon, 15 March 2006**
**301, Baltimore Convention Center at 14:30**
**Karen Waldrip, Sandia National Laboratories, presiding**

**14:30**
**R9 1 A single pixel camera based on compressed sensing** KEVIN KELLY, *Electrical Engineering Dept., Rice University* DHARMPAL TAKHAR, JASON LASKA, MIKE WAKIN, MARCO DUARTE, BRIAN VAN OSDOL, DROR BARON, RICHARD BARANIUK, Digital micromirror devices have proven to be a commercially viable MEMs technology for the video/projector display market. Inspired by the success of this technology, we have combined a microcontrolled mirror with a single optical sensor so that it additionally acquire images, rather than merely adapt current camera technology to serve as an optical sensor. In this project, we have developed a practical image/video camera based on this concept and realized it through the use of itcompressed sensing. Our design has additional desirable properties including scalable output bit stream, variable image resolutions and video frame rates. We will also discuss the generalization of itcompressed sensing as a way of image formation for other single detector systems.

**14:42**
**R9 2 Low temperature confocal microscopy with a 4 K closed-cycle cryostat** ANGELIKA KUENG, CHRISTOPH BOEDEFELD, CHRISTIAN SCHULHAUSER, *Attocube System AG* MATTHIAS BUEHLER, JENS HOEHNE, *VeriCold Technologies GmbH* Low temperature confocal microscopy is a technique of major interest with regard to research fields ranging from material and surface science to single molecule spectroscopy. Common setups involve the use of expensive liquid helium and suffer from the lack of coarse positioning units at cryogenic temperatures. We present for the first time a highly flexible confocal microscope combined with a 4 K closed-cycle cryostat. This complete system solution enables plug-and-play high resolution confocal microscopy at low temperatures without the need of liquid helium. The low-vibration pulse tube based cryostat has been specially adapted for very low vibrations as required for applications in combination with scanning probe microscopy. The developed confocal microscope is thermally compensated guaranteeing ultra-high stability at low temperature providing at the same time very high optical resolution as will be shown in various examples. Furthermore, nanopositioning units based on the slip-stick principle allow coarse positioning over centimeters. The system allows operation at extreme conditions as high magnetic fields and high vacuum.

**14:54**
**R9 3 4Pi Spectral Self-interference Fluorescence Microscopy*** MEHMET DOGAN, *Department of Physics, Boston University* ANNA K. SWAN, *Department of ECE, Boston University* M. SELIM UNLU, *Department of ECE, Boston University* BENNETT B. GOLDBERG, *Department of Physics, Boston University* 4Pi fluorescence confocal microscopy [1] improves axial resolution, and Spectral Self-Interference Fluorescence Microscopy (SSFM) [2] provides sub-nanometer localization of fluorescent emitters in biological structures. Here we report on the construction and evaluation of a 4Pi fluorescence confocal microscope and discuss the efforts to combine the high resolution 4Pi technique with SSFM. In the 4Pi microscope, the back focal planes of two opposing high numerical aperture objectives are filled with coherent laser illumination and counter propagating spherical wave fronts form constructive interference at the common focus of two objectives, resulting in an improvement of the axial point spread function (PSF). We characterized the 3-D PSF of the microscope using fluorescent polystyrene beads and fluorescent monolayers. We measured a factor of 3 improvement of the axial PSF compared to a confocal microscope. [1] S. W. Hell et al. J. Opt. Soc.Am. A Vol. 9, No. 12, pp. 2159 (1992) [2] A. K. Swan et al. IEEE JSTQE Vol. 9, No. 2, pp. 294 (2003)

*Supported by NSF DBI 0138425 and NIH 5R01 EB00 756-03

**15:06**
**R9 4 Enhancing Diffraction-Limited Images Using the Properties of the Point Spread Function** ALEXANDER SMALL, *Laboratory of Integrative and Medical Biophysics, National Institute of Child Health and Human Development, NIH* ILKO ILEV, *Office of Science and Engineering Laboratories, FDA* AMIR GANDJBAKHCHE, *Laboratory of Integrative and Medical Biophysics, National Institute of Child Health and Human Development, NIH* We propose a simple method for enhancing diffraction-limited microscope images, enhancing the resolution by at least a factor of two. In its simplest implementation, our algorithm is ideally suited for enhancing images obtained with near-field illumination, such as scanning probe microscopy of cells. We exploit the fact that the finite width of the point spread function introduces correlations between pixels in an image. Our method is much simpler than other methods for beating the diffraction limit, requiring no specialized equipment beyond the microscopes commonly found in biology laboratories, and only a single computational step to yield significant enhancements. We have theoretically analyzed the performance of our algorithm by generating images with point objects, and convolving those images with the point spread function (PSF) of a diffraction- limited lens. After enhancing the resulting images, we find that our method reduces the width of the PSF by a factor of two, and also yields a much steeper profile, enhancing contrast. Even when objects are too close to be resolved distinctly, our method enhances the aspect ratio of the resulting diffraction blur, clearly pointing to the existence of structure.

**15:18**
**R9 5 Feasibility of using Backscattered Mueller Matrix Images for Bioaerosol Detection** CHANGHUI LI,* GEORGE W. KATTAWAR,† *Texas A&M University* It has been shown that by looking at the backscattered radiance from an object illuminated by a laser beam one could effectively distinguish different morphologies from one another. However, if one wants to obtain all the information possible from elastic scattering either from a single particle or an ensemble of particles then one must use the Mueller matrix which contains all the polarization and radiance information available. In this talk, we will show that if we take advantage of the polarization information of the object, many more images related to the overall morphology as well as the internal structure of the object can be obtained. We will present images of the complete Mueller matrix to show the sensitivity of its sixteen components to both external and internal particle prop-

erties. We will also show that by using only one or two elements of this matrix one might be able to distinguish bioaerosols such as anthrax from more benign aerosols. We also show that the back-scattering Mueller images contain more information than the forward scattering ones.

*PhD student in Physics Department
†Professor in Physics Department

**15:30**

**R9 6 The Role of Hyperspectral Imaging in the Visualization of Obliterated Writings** HINA AYUB, *Oak Ridge Institute for Science & Education- FBI Laboratory Research Division* DIANE WILLIAMS, *FBI Laboratory Research Division* The forensic questioned document community has encountered difficulty visualizing obliterated writing using conventional methods. Cases have been reported in which pencil obliterated by ink, and ink obliterated by ink, cannot be discerned visually. Conventional methods for visualization of obliterated writings do not adequately visualize writing when obliteration is made with the same color ink, or when graphite pencil writings are obliterated by ink. We report the use of hyperspectral imaging to successfully view obliterated writings in which a ''true black'' ink obliterated graphite as well as graphite/graphite and ink/ink obliterations. Hyperspectral imaging (HSI) is a novel optical technique in which hundreds of narrow contiguous bands, over a large range of wavelengths, can be viewed to yield a complete spectral profile at each pixel in the image. HSI has evolved as the product of conventional two-dimensional imaging and spectroscopy. The resultant image of HSI is a three-dimensional data cube, with the pixels constrained to a single plane, and the complete reflectance spectra seen along the orthogonal axis. We used three types of hyperspectral imaging systems, which provided a wavelength range spanning approximately 300-1700 nm, to visualize the obliterated writing samples. Additionally, we will present data obtained from the use of thermal imaging to successfully view obliterated writings.

**15:42**

**R9 7 Femto-second real-time single-shot digitizer** JASON CHOU, OZDAL BOYRAZ, BAHRAM JALALI, *Electrical Engineering Department, University of California, Los Angeles* We demonstrate a single-shot digitizer with a record 10 Tera Sample-per-Second sampling rate, an order of magnitude improvement over prior state-of-the-art. The feat is accomplished by using a photonic time stretch preprocessor which slows down the electrical waveform by a factor of 250 before it is captured by an electronic digitizer. To achieve this performance, distributed Raman optical amplification was realized in the dispersive medium that performs the time dilation. Experimentally, a 90 GHz electrical signal is digitized in real time at 100 femto-second intervals. To the best of our knowledge, this is the first femto-second real-time digitizer.

**15:54**

**R9 8 A photopyroelectric sensor for the high-resolution thermophysical characterization of liquid mixtures.** ANNA MATVIENKO, ANDREAS MANDELIS, *Center for Advanced Diffusion-Wave Technologies, University of Toronto* A common principle of photothermal techniques is the study of thermal wave propagation in a sample following heating by an intensity modulated laser beam. In this study, we applied the photopyroelectric thermal-wave cavity technique with the common-mode-rejection demodulation scheme to the measurements of thermal diffusivity of water-alcohol mixtures at low concentrations. The high sensitivity of the photothermal signal to the thermal diffusivity of samples relies on the exponential decay character of the thermal-wave field at a given modulation frequency. The common-mode-rejection demodulation scheme involves the launching of two unequal duration pulses over one modulation period. In this case, the lock-in amplifier output represents the difference between the response waves produced by each one of two pulses. This differential technique shows resolution at the level of 0.2% v/v of alcohol in water, the highest ever reported using thermophysical techniques. In terms of future applications the proposed system can eventually be implemented into a self-contained in-situ liquid pollution monitor.

**16:06**

**R9 9 Johnson Noise Thermometry in the range 505 K to 933 K** WESTON TEW, JOHN LABENSKI,*SAE WOO NAM, SAMUEL BENZ, PAUL DRESSELHAUS, *NIST, Boulder CO* JOHN MARTINIS, *UC Santa Barbara* The International Temperature Scale of 1990 (ITS-90) is an artifact-based temperature scale, $T_{90}$, designed to approximate thermodynamic temperature $T$. The thermodynamic errors of the ITS-90, characterized as the value of $T - T_{90}$, only recently have been quantified by primary thermodynamic methods. Johnson Noise Thermometry (JNT) is a primary method which can be applied over wide temperature ranges, and NIST is currently using JNT to determine $T - T_{90}$ in the range 505 K to 933 K, overlapping both acoustic gas-based and radiation-based thermometry. Advances in digital electronics have now made the computationally intensive processing required for JNT viable using noise voltage correlation in the frequency domain. We have also optimized the design of the 5-wire JNT temperature probes to minimize electromagnetic interference and transmission line effects. Statistical uncertainties under 50 $\mu$K/K are achievable using relatively modest bandwidths of $\sim$ 100 kHz. The NIST JNT system will provide critical data for $T - T_{90}$ linking together the highly accurate acoustic gas-based data at lower temperatures with the higher-temperature radiation-based data, forming the basis for a new International Temperature Scale with greatly improved thermodynamic accuracy.

*NIST, Gaithersburg, MD

**16:18**

**R9 10 Using Temperature-Dependent Phenomena at Oxide Surfaces for Species Recognition in Chemical Sensing.** STEVE SEMANCIK, DOUGLAS MEIER, JON EVJU, KURT BENKSTEIN, ZVI BOGER, CHIP MONTGOMERY, *Chemical Science and Technology Laboratory, NIST* Nanostructured films of $SnO_2$ and $TiO_2$ have been deposited on elements in MEMS arrays to fabricate solid state conductometric gas microsensors. The multilevel platforms within an array, called microhotplates, are individually addressable for localized temperature control and measurement of sensing film electrical conductance. Temperature variations of the microhotplates are employed in thermally-activated CVD oxide film growth, and for rapid temperature-programmed operation of the microsensors. Analytical information on environmental gas phase composition is produced temporally as purposeful thermal fluctuations provide energetic and kinetic control of surface reaction and adsorption/desorption

phenomena. Resulting modulations of oxide adsorbate populations cause changing charge transfer behavior and measurable conductance responses. Rich data streams from different sensing films in the arrays have been analyzed by Artificial Neural Networks (ANN) to successfully recognize low concentration species in mixed gases. We illustrate capabilities of the approach and technology in the homeland security area, where dangerous chemicals (TICs, CWSs and CWAs) have been detected at 10-100 ppb levels in interference-spiked air backgrounds.

**16:30**

**R9 11 2D Thermal Imaging of the Surfaces of Optoelectronic Devices by Thermoreflectance Microscopy** M. FARZANEH, D. LÜERßEN, *Mount Holyoke College, Massachusetts Institute of Technology* P. MAYER, R. J. RAM, *Massachusetts Institute of Technology* JANICE A. HUDGINGS, *Mount Holyoke College* For the last 40 years, thermoreflectance has been used to experimentally validate bandstructure calculations for semiconductor and metallic materials. The recent development of high resolution thermoreflectance microscopy as a noninvasive, 2D thermal imaging technique, based on measuring the variations of the surface reflectivity with temperature opens new avenues of probing the nanoscale properties of materials and devices. Recently, we have demonstrated that by utilizing stochastic resonance a thermal resolution of 10mK can be achieved, which exceeds the quantization limit of the camera by two orders of magnitude. Here, we report the use of thermoreflectance to characterize a photonic integrated circuit comprised of cascaded semiconductor optical amplifiers. Optical cooling of the biased amplifiers by 0.5K is observed which demonstrates the high spatial and thermal resolution achievable with stochastic resonance enhanced thermoreflectance microscopy.

**16:42**

**R9 12 Suppression of Non-Resonant Background in Broadband Coherent Anti-Stokes Raman Scattering Microscopy with Interferometry*** TAK KEE, MARCUS CICERONE, *National Institute of Standards and Technology* We demonstrate an interferometric technique for suppressing non-resonant background in broadband coherent anti-Stokes Raman scattering (CARS) microscopy. CARS microscopy has become an important biological imaging tool due to its non-invasiveness, and high spatial resolution. Our previous work on developing broadband CARS microscopy has improved the chemical specificity significantly by increasing the spectral coverage to $> 2500\ \mathrm{cm}^{-1}$ [T.W. Kee, M.T. Cicerone, Opt. Lett. **29**, 2701 (2004)]. Although CARS microscopy provides high sensitivity in the C-H stretch region of the vibrational spectrum, the signals in the Raman fingerprint region suffer from low signal-to-background ratio because of the presence of a non-resonant background due to the electronic response of the sample. Suppressing the non-resonant background signal is crucial in order to develop CARS microscopy into a powerful technique to image biochemical reactions in cells. In our approach, a broadband CARS signal with high spectral resolution interferes with another broadband CARS signal with lower spectral resolution. Fourier transform of the interferometric measurements allow the extraction of the imaginary part of the signal, which is free of the non-resonant background.

*NIST Polymers Division & NIH R21 EB002468-01

**16:54**

**R9 13 Digital ultrasonic pulse-echo overlap system and algorithm for unambiguous determination of pulse transit time** CRISTIAN PANTEA, DWIGHT RICKEL, ALBERT MIGLIORI, *Los Alamos National Laboratory, Materials Science and Technology (MST)-National High Magnetic Field Laboratory (NHMFL), Los Alamos, New Mexico 87545* JIANZHONG ZHANG, YUSHENG ZHAO, *Los Alamos National Laboratory, Los Alamos Neutron Scattering Center (LANSCE)-12, Los Alamos, New Mexico 87545* SAMI EL-KHATIB, *Physics Department, New Mexico State University, Las Cruces, New Mexico 88003* ROBERT LEISURE, *Colorado State University, Department of Physics, Fort Collins, Colorado 80523* BAOSHENG LI, *Mineral Physics Institute, State University of New York (SUNY) at Stony Brook, Stony Brook, New York 11794* We report an evolution of an all-digital ultrasonic pulse technique for measurements of elastic constants of solids. An unambiguous analytical procedure is described for determining the correct time delay of echoes without any need for actual echo overlap. We also provide a simple procedure for making corrections for transducer-bond-induced phase shifts. The precision of a measurement made with this system at ambient temperature exceeds one part in $10^7$ without the use of mixers, gates, time delays, and other complications normally associated with such measurements.

**17:06**

**R9 14 Application of the finite element method to resonant ultrasound spectroscopy data analysis.*** A. SUSLOV, I. DIXON, S. HEADLEY, E. DEYLE, *NHMFL, Tallahassee, FL* A. MIGLIORI, *LANL, Los-Alamos, NM.* Commercially available finite-element software is used to determine elastic moduli from experimental data acquired by resonant ultrasound spectroscopy (RUS) on an arbitrarily-shaped sample. The sample geometry must be provided in coordinate form, as well as the crystallographic symmetry and the crystallographic orientation relative to the coordinates. The algorithm has been tested on published resonance measurements obtained on rectangular parallelepipeds and cylinders of cubic, tetragonal, hexagonal and monoclinic symmetries. The results agree within expected numerical precision to the elastic constants found by other computational methods. The algorithm is much slower than the one normally implemented explicitly for RUS analysis but, for difficult-to-prepare or fragile samples such as a layered specimen prepared from several materials, moduli can be obtained without polishing or otherwise damaging the sample. Details of the model generation, meshing and optimization approach will be discussed.

*The research is supported by IHRP-NHMFL, NSF, DOE and State of Florida

**17:18**

**R9 15 Source distance information and frequency shifts by chirp decomposition** V. GURUPRASAD, *Inspired Research, NY* Innovative frequency shifts directly revealing the source distance of received signals are obtainable from phase spectra as follows. The phase expression for a travelling wave, $\phi = -\omega(t - r/c)$, implies increasing static phase differences $\delta\phi(r) = r\,\delta\omega/c$ between adjacent frequencies in the radiated waves. The static differences are useless for information transport and hard to measure, hence were hitherto generally ignored. Scanning the spectrum transforms them to Doppler-like shifts revealing the distance, given by the partial derivative $\delta\omega(r) = \partial\phi/\partial t|_{r,t} = \dot{\omega}r/c$, where $\dot{\omega}$ is the scanning rate, provided the signal has

nonzero bandwidth. By controlling $\dot{\omega}$, any source can now be instantly ranged or isolated, allowing separations down to 10 m at 100 m range for 10 MHz voice modulated carrier – without CDMA or power control, as described at IEEE WCNC 2005. The mechanism is also realizable by simple chirp transform, and has been verified by simulation and with acoustic signals. EM field tests are now being arranged. The results and other aspects of general physics interest will be discussed.

**SESSION R10: FOCUS SESSION: SURFACES AND INTERFACES IN ELECTRONIC MATERIALS I**
**Wednesday Afternoon, 15 March 2006; 302, Baltimore Convention Center at 14:30**
**Eric Borguet, Temple University, presiding**

*Invited Papers*

**14:30**
**R10 1 Broad-Band Sum-Frequency Generation Spectroscopy at Platinum/Solution Interfaces.***
ANDRZEJ WIECKOWSKI, *University of Illinois at Urbana-Champaign*

Vibrational Broad-Band Sum-Frequency Generation Spectroscopy (BB-SFG) is the second-generation SFG method for studying surfaces, including wet electrochemical interfaces. BB-SFG measurements, which are based upon the second-order nonlinear optical process are inherently interface specific (as is SFG) but add sensitivity and control to SFG. The electrochemical cell used for the reported measurements has an ideal configuration where the thickness of the supporting electrolyte (25 $\mu$m) is controlled by a spacer, allowing for rapid spectral acquisitions (5 $s^{-1}$) synchronized with the potential sweep at 5 mV $s^{-1}$). In the talk, simultaneous electrochemical and BB-SFG measurements will be reported for adsorption/oxidation of carbon monoxide on polycrystalline and well-ordered Pt(hkl) electrodes with both CO-free and CO-saturated electrolytes. The emphasis will be on the combination between thin layer electrochemistry (TLE) and vibrational electrode surface analysis, and on dynamics of Pt/solution interfaces probed by the CO molecule adsorption and oxidation.

*In collaboration with Guo-Qiang Lu, Alexei Lagoutchev, and Dana Dlott, University of Illinois at Urbana-Champaign.

*Contributed Papers*

**15:06 sche**
**R10 2 Charge inversion at ultra-low electrolyte concentrations*** DUNCAN J. McGILLIVRAY, MATHIAS LÖSCHE, *Dept of Physics, Carnegie Mellon University & CNBT, NIST Center for Neutron Research* JENS PITTLER, *Dept of Physics, University of Leipzig, Germany* WEI BU, ALEX TRAVESSET, DAVID VAKNIN, *Ames Lab & Dept of Physics & Astronomy, Iowa State University* Synchrotron x-ray reflectivity studies of the anionic phospholipid DMPA in monolayers spread on very dilute solutions of $LaCl_3$ reveal strong adsorption of the cations at nanomolar and micromolar concentrations, and a sharp transition in cation concentration at the interface as a function of ionic strength. Using anomalous X-ray reflection we determine the number of $La^{3+}$ ions per $DMPA^-$ (surface charge density, $\sigma \approx e^-/40$ Å$^2$) over four orders of magnitude in bulk ion concentration. We find that at concentrations in the range 10–300 nM $La^{3+}$ forms a Stern layer with $\approx$ 1 $La^{3+}$/ 3 $DMPA^-$, thus neutralizing the lipid surfaces charge. At a critical bulk concentration, $C_t \approx$ 500 nM, the surface concentration of $La^{3+}$ increases steeply, up to a saturation level with $\approx$ 1 $La^{3+}$/ DMPA. The strong condensation of $La^{3+}$ above $C_t$ implies that the charge at the interface is reversed. We provide theoretical arguments that the charge reversal is facilitated by 1) strong correlations between the phosphate groups and $La^{3+}$ ions and 2) hydrogen bonding of hydroxyl groups, effectively forming the complex $La^{3+}PO_4^{2-}OH^-$.

*Supported by DOE W-7405-Eng-82 & W-31-109-Eng-38; NSF-CTS-0304062; NSF-DMR-0426597; NIH 1R01 RR14812

**15:18**
**R10 3 Modeling Electrocatalysis – Electro-oxidation of Pt(111)** TIMO JACOB, MATTHIAS SCHEFFLER, *Fritz-Haber Institute, Faradayweg 4-6, D-14195 Berlin, Germany* Electrochemical reactions (such as in fuel cells) usually occur under conditions of finite temperature, pressure, and electrode potential, implying a very involved situation, possibly leading to novel surface materials. Especially the presence of an electrode potential, which results in the formation of an electric double-layer, affects the composition and structure of the electrode/electrolyte-interface. Towards a more realistic treatment of electrocatalysis we developed an appropriate theory in which the electrode of the interface is assumed to be in contact with a *bulk-electrode* reservoir (at chemical potential $\mu_{el}$) while the electrolyte is in contact with a *bulk-electrolyte* reservoir. Although we are in the process of simulating the entire electric-double layer self-consistently, the present approach already allows us to estimate the limites of the expected effects. As a first application we studied the electro-oxidation of Pt(111) by calculating the $p/T/\phi$-phase diagram. The obtained behavior, that positive electrode potentials stabilize higher oxygen coverages, is in qualitative agreement with cyclic-voltammetry experiments.

**15:30**
**R10 4 Electrochemical oxidation in solid oxide fuel cells – Where does it occur and how?** ROBERT WALKER, *Department of Chemistry and Biochemistry, University of Maryland* MICHAEL POMFRET, *Department of Chemistry and Biochemistry, University of Maryland* Electrochemical processes in solid-oxide fuel cells (SOFCs) are thought to occur at a ''triple phase boundary'' (TPB) – that junction between a conducting anode, a solid oxide electrolyte and the gas phase fuel mixture. A quanti-

tative, physical description of this boundary, however, remains elusive given difficulties associated with probing molecular species present in SOFCs under realistic operating conditions of high temperatures and reducing atmospheres. Recently, we have constructed an SOFC that has optical access to the anode assembly allowing us to probe with Raman spectroscopy the chemical intermediates present on anode and electrolyte surfaces as carbon containing fuels are electrochemically oxidized. Results show that chemistry occurs on both the anode and electrolyte surfaces as well as in the vicinity of the purported TPB. The reduced electrolyte surface is both catalytically active and, over micron distances, electrically conductive. The Ni anode shows strong evidence of adsorbed carboxylate intermediates. This talk will address mechanisms of electrochemical oxidation in SOFCs using direct and indirect experimental probes as well as the consequence of our findings for models of a well defined triple phase boundary.

*Invited Papers*

**15:42**
**R10 5 Epitaxial Electrodeposition of Chiral Metal Oxide Films.**
JAY SWITZER, *University of Missouri-Rolla*

Chirality is ubiquitous in Nature. One enantiomer of a molecule is often physiologically active, while the other enantiomer may be either inactive or toxic. Chiral surfaces offer the possibility of developing heterogeneous enantiospecific catalysts that can more readily be separated from the products and reused. Chiral surfaces might also serve as electrochemical sensors for chiral molecules- perhaps even implantable chiral sensors that could be used to monitor drug levels in the body. Our trick to produce chiral surfaces is to electrodeposit low symmetry metal oxide films with chiral orientations on achiral substrates (see, Nature **425**, 490, 2003). The relationship between three-dimensional and two-dimensional chirality will be discussed. Chiral surfaces lack mirror or glide plane symmetry. It is possible to produce chiral surfaces of materials which do not crystallize in chiral space groups. We have deposited chiral orientations of achiral CuO onto single-crystal Au and Cu using both tartaric acid and the amino acids alanine and valine to control the handedness of the electrodeposited films. We will present results on the chiral recognition of molecules such as tartaric or malic acid and L-dopa on the chiral electrodeposited CuO. Initial work on the electrochemical biomineralization of chiral nanostructures of calcite will also be discussed.

*Contributed Papers*

**16:18**
**R10 6 Ab initio structure and energetics of ice Ih - implications for wetting*** PETER J. FEIBELMAN, *Sandia National Laboratories* The lattice energy of ice Ih is found to equal 0.68 eV/$H_2O$, in a VASP-based, GGA/PW91 optimization of a 96-molecule cell, with zero dipole moment in every hexagonal layer.[1] This result agrees closely with Hamann's value, obtained for a small, proton-ordered, and thus polarized unit cell.[2] Slight inhomogeneous broadening of the O-H stretch peak is estimated, based on the computed O-O distance distribution. Implications regarding wetting-layer formation will be discussed.

*Supported by the DOE Office of Basic Energy Sciences. Sandia is operated by the Lockheed Martin Co. for USDOEs National Nuclear Security Administration under Contract DE-AC04-94AL85000.

[1]J. A. Hayward, J. R. Reimers, J. Chem. Phys. **106**, 1518(1997).
[2]D. R. Hamann, private communication. See, P. J. Feibelman, Science **295**, 99(2002), Ref. 19.

**16:30**
**R10 7 How Water Meets a Hydrophobic Surface – Reluctantly and with Fluctuations** ADELE POYNOR, LIANG HONG, STEVE GRANICK, *University of Illinois at Urbana-Champaign* The details of how water meets a hydrophobic surface are still hotly debated. Here we use two independent methods, ellipsometry in the time-resolved phase-modulated mode, and surface plasmon resonance, to investigate the view that thermodynamics causes a nanometer-sized low-density layer to form adjacent to the hydrophobic solid. Strong evidence in favor of the hypothesis is found. This zone of depleted density shows large fluctuations even within the spatial (over a beam size of 10 $\mu$m) and temporal (with a time constant of 30 ms) averaging inherent in ellipsometry measurement. Statistical analysis of these noise spectra reveal a remarkable scaling with the area over which the measurements are averaged.

**16:42**
**R10 8 Diffusion, adsorption and incorporation of antifreeze glycoprotein molecules at the ice/water interface** HIROYUKI NAKAYA, SALVADOR ZEPEDA, YUKIHIRO UDA, SHUICHIRO MATSUMOTO, *Hokkaido University* ETSURO YOKOYAMA, *Computer Center, Gakushuin University* YOSHINORI FURUKAWA, *Hokkaido University* Antifreeze glycoproteins(AFGP) are known to inhibit ice crystal growth by adsorbing to the interface. But, there is no direct observation of the distribution of AFGP molecules around the interface of the growing ice crystal. In order to observe the growing ice/water interface, one-directional growth experiments of ice crystal growth were carried out in AFGP solution. AFGPs were labeled with fluorescent markers to see the distribution of AFGP molecules. We obtained video image of the distribution of AFGP molecules near the growing ice/water interface by using fluorescent microscopy. Incorporation and accumulation of AFGP molecules at the interface were clearly observed, and strongly depend on the growth rate of the ice crystal. We also observed the diffusion field of AFGP molecules from the ice interface and calculated diffusion and segregation coefficients. We found that AFGP molecules strongly adsorb to the growing ice crystal interface, and incorporate between grain boundaries, but found little evidence for incorporation into the crystal lattice. This is contrary to previous paradigms for AFGP function.

**16:54**
**R10 9 Self-oscillatory ice crystal growth in antifreeze protein (AFP) and glycoprotein (AFGP) solutions** SALVADOR ZEPEDA, HIROYUKI NAKAYA, YUKIHIRO UDA, *Hokkaido University* ETSURO YOKOYAMA, *Gakushuin University* YOSHINORI FURUKAWA, *Hokkaido University* AFPs and AFGPs allow many organisms including fish, plants and insects to survive sub-freezing environments. They occur in a wide range of compositions and structure, but to some extent they all accomplish the same functions: they suppress the freezing temperature, inhibit recrystallization, and modify ice crystal growth. A complete description of the AFGP/AFP surface mechanism as well as other ice surface phenomenon has eluded scientists primarily due to a lack of direct surface studies. We study ice crystal growth in AFGP and AFP solutions with phase contrast microscopy during free solution growth under various conditions including microgravity. Free-solution growth experiments show an anisotropic self-oscillatory growth mode of the steps and interface near the freezing temperature and enhancement of the growth rates in the c-axis. These results contradict the previous ''tight-binding'' mechanism thought to be responsible for antifreeze function. To study the effects of temperature driven convective flows on the interface kinetics, microgravity experiments were performed in a jet airplane during a parabolic flight path. Step propagation on the basal plane slows down considerably when entering the microgravity condition and reaches a critical condition just below 0.2g.

**17:06**
**R10 10 Simulation study of water/silicon oxide interface** CHRISTIAN LORENZ, SUSAN REMPE, MARK STEVENS, GARY GREST, *Sandia National Laboratories* MESFIN TSIGE, *Southern Illinois University* The interaction of water with solid surfaces plays a crucial role in many phenomena. The water-silica interface is one of the typical systems encountered in technological and natural materials. Numerous technological applications of silica were found to rely on its specific surface properties. Large scale quantum mechanics (QM) and classical molecular dynamics (MD) simulations are used to study the molecular configurations and wetting properties of water at the interface of different silicon oxide surfaces. In order to understand how the surface coverage of silanols (-SiOH) affects the wetting behavior of the silica surfaces, both crystalline ((001) $\alpha$-quartz (coverage 9.6 $nm^{-2}$) and (100) $\beta$-cristobalite (7.8 $nm^{-2}$)) and amorphous silica (5.0 $nm^{-2}$) substrates have been studied. The binding energy of the water, the number of water molecules hydrogen-bonded to the surface and the configuration of the hydrogen-bonded water molecules are determined as a function of silanol coverage from QM simulations. The number of water molecules within a monolayer and the orientation of the water molecules within the monolayer and in the bulk are determined from MD simulations. Results from two classical force fields are compared to one another and to the relevant quantities from the QM simulations. Sandia is a multiprogram laboratory operated by Sandia Corporation, a Lockheed Martin Company, for the United States Department of Energy's National Nuclear Security Administration under contract DE-AC04-94AL85000.

**17:18**
**R10 11 Hydrogen etching and graphitization of 4H- and 6H-SiC** XUEBIN LI, ZHIMIN SONG, TIANBO LI, CLAIRE BERGER, PHILLIP FIRST, WALTER DE HEER, *Georgia Institute of Technology* Hydrogen etching and graphitization on the surfaces of 4H/6H-SiC with different off-axis angles were studied at temperatures ranging from 1300-1600$^0$C. Above 1500$^0$C, the scratches caused by polishing on the surfaces of SiC were effectively removed by the reaction with hydrogen. AFM images showed various topographies on the surfaces of 4H/6H SiC after hydrogen treatment, related to wafer type (4H or 6H), polar faces (Si- face or C-face), off-axis angles, and inherent substrate defects. Flat thin graphite films were grown by the thermal decomposition of SiC at high temperature on both C- and Si- faces of SiC in a vacuum furnace. Surface graphitization of 4H/6H SiC previously flattened by hydrogen etching was analyzed in UHV by LEED and AES, and in ambient air by AFM. Mobility of graphite films grown on the C-face of 4H-SiC ranges from 1000 to 10,000 $cm^2$/Vs. Magnetotransport of the graphite film shows 2D gas behavior, accompanying with SdH oscillations and Hall plateaus.



## SESSION R11: FOCUS SESSION: AEROSOLS, CLUSTERS, DROPLETS: PHYSICS AND CHEMISTRY OF NANOOBJECTS III: MOLECULAR CLUSTERS

**Wednesday Afternoon, 15 March 2006; 303, Baltimore Convention Center at 14:30**
**David Nesbit, University of Colorado, presiding**

***Invited Papers***

**14:30**
**R11 1 Unraveling proton accommodation in water with cluster spectroscopy.**
MARK JOHNSON, *Yale University*

We describe how argon-nanomatrix spectroscopy, implemented with broadly tunable solid state infrared laser sources, allows us to establish how water networks flex and distort to accommodate elementary aqueous species like protons and electrons. We will focus on the hydrated proton, as this charge defect accounts for charge conduction in many biological processes that occur in a hydrophobic environment. By freezing the water clusters to their minimum energy structures, sharp, characteristic bands are recovered very low in energy that reveal how the local solvent arrangement dictates the spatial extent of the excess charge delocalization.

*Contributed Papers*

**15:06**

**R11 2 Excess Electrons in Water Clusters** YING LI, *School of Physics, Georgia Institute of Technology* ROBERT BARNETT, *School of Physics, Georgia Institute of Technology* UZI LANDMAN, *School of Physics, Georgia Institute of Technology* Excess electrons in water systems are always a research topic of interest. In this talk, we will discuss the behavior and formation of the excess electrons in water cluster using DFT ab-initio simulations with a combination of quantum mechanics and molecular mechanics. System size is chosen so that the excess electrons will form a bound state rather than a surface state. Measurements will be performed to test the stability of the electron structure.

**15:18**

**R11 3 Surface-trapped excess electrons on ice** FRANCESCA BALETTO, MAL-SOON LEE,*SANDRO SCAMDOLO, *The Abdus Salam ICTP and INFM-CNR Democritos, Trieste (Italy)* Local surface trapping of excess electrons has recently been observed in large water clusters and at the ice/vacuum interface. The existence of stable surface-bound states for the excess electron may have important implications in atmospheric chemistry, electrochemistry, and radiation physics. By means of first-principles molecular dynamics we find that excess electrons induce a structural reconstruction of the ice surface on a time scale of a fraction of a picosecond [Baletto et al., PRL 95, 176801 (2005)]. Preliminary results on small neutral water clusters indicate that fast (on a picoseconds scale) structural changes occur already at the lowest atmospheric temperatures, suggesting that addition of excess electrons may lead to even more substantial structural rearrangements than those found for the ice surface.

*also at Dept. of Physics, Centre for Modelling and Simulation, Univ. of Pune, India

**15:30**

**R11 4 Hole-filling spectroscopy of the ittrans-formanilide-$H_2O$ and tryptamine-$H_2O$ complexes: Solvent shuttling and solvent loss*** TIMOTHY ZWIER, JASPER CLARKSON, *Dept. of Chemistry, Purdue University* Studies of molecular clusters formed and cooled in a supersonic expansion offer unique opportunities to study novel types of dynamical processes under well-defined conditions. This talk will highlight recent studies in our laboratory at Purdue involving water-containing complexes with ittrans-formanilide (TFA) and tryptamine (TRA). In TFA-$H_2O$, stimulated emission pumping is used to initiate a unique type of reaction in which a single water molecule is shuttled between remote hydrogen-bonding sites on the same solute molecule. The energy barrier to isomerization is measured for shuttling the molecule in either direction. In TRA-$H_2O$ and TRA($ND_2$)-$D_2O$, infrared excitation is used to dissociate the water molecule from a flexible molecule with well-defined starting geometry. Isomer-specific product quantum yields of the TRA monomer product will be reported as a function of the XH or XD oscillator excited. The interplay between water loss and conformational isomerization of the flexible TRA molecule will be discussed.

*Supported by NSF CHE0242818

**15:42**

**R11 5 Anharmonic Vibrational Spectra of Hydrogen Bonded Clusters*** SOTIRIS S. XANTHEAS, *Chemical Sciences Division, Pacific Northwest National Laboratory, 906 Battelle Boulevard, PO Box 999, MS K1-83, Richland, WA 99352* We report anharmonic vibrational spectra for a variety of hydrogen bonded clusters such as $(H_2O)_n$ and $(HF)_n$, $n$=1-5. We investigate the convergence of the hydrogen bonded frequencies with basis set and level of electron correlation and compare with the available experimental data. For this purpose we employ the correlation-consistent basis sets up to quintuple zeta (5z) quality and compute the spectra at the second order Møller-Plesset (MP2) and Coupled Cluster plus Single and Double with perturbative estimate of Triple excitations [CCSD(T)]. The correlation between the calculated elongations in the hydrogen bonding stretches and the corresponding computed/observed vibrational frequencies suggest an extension of Badger's rule for these hydrogen bonded systems.

*Battelle operates the Pacific Northwest National Laboratory for the US Department of Energy

**15:54**

**R11 6 Probing the Stepwise Solvation of the Sulfate Dianion: Gas Phase Infrared Spectroscopy of $SO_4^{2-} \cdot (H_2O)_n$ Clusters (n=3-24)** KNUT R. ASMIS, GERARD MEIJER, *Fritz-Haber-Institut der Max-Planck-Gesellschaft, Faradayweg 4-6, D-14195 Berlin, Germany.* GABRIELE SANTAMBROGIO, MATHIAS BRUEMMER, LUDGER WOESTE, *Institut fuer Experimentalphysik, Freie Universitaet Berlin, Arnimallee 14, D-14195 Berlin, Germany.* JIA ZHOU, DAVE T. MOORE, DANIEL M. NEUMARK, *Department of Chemistry, University of California and Chemical Sciences Division, Lawrence Berkeley National Laboratory, Berkeley, CA 94720, USA.* Hydrated sulfate dianions are of paramount importance in diverse branches of science. However, a microscopic, molecular level understanding of the nature of the solute-solvent interaction as well as the composition of the solvation shell has not yet been achieved. Here we report the first gas phase infrared spectra of multiple charged anions in general, namely of mass-selected $SO_4^{2-} \cdot (H_2O)_n$ dianions ($n$=3-24) employing the infrared multiple photon dissociation technique in combination with radiation from the free electron laser FELIX. The infrared spectra (550-1800 $cm^{-1}$) were measured in the region of the stretching and bending modes of the sulfate core as well as characteristic intra- and intermolecular water modes, allowing an unprecedented, atomic level insight into structure of the complex as well as the nature and strength of the underlying hydrogen bonding interaction.

**16:06**

**R11 7 Effective polarizabilities of water clusters** RAMIRO MORO, ROMAN RABINOVITCH, CHUNLEI XIA, VITALY KRESIN, *University of Southern California* We report the measurement of electrical polarizabilities of water clusters [$(H_2O)_n$, n=3-18] by deflection of a supersonic beam in an inhomogeneous field. In all the clusters studied, the deflections are only towards higher fields, indicating a polarizability-like behavior. The highest polarizability per one water molecule is seen in the trimer ($7.9 \pm 0.3$ Å$^3$) and it quickly decreases for larger clusters to about 4 Å$^3$ per molecule for n=6-18. These values are large and could be explained by the addition of two parts: an intrinsic electronic polarizability plus a contribution from a permanent dipole moment responding with a Langevin-like behavior. With a cluster temperature of $\sim$ 200 K, estimated from the evaporative ensemble picture, the permanent dipole moments are $\sim$ 1-2 Debye per cluster.

**16:18**

**R11 8 Experimental Evidence for Internal Structure in Aqueous – Organic Nanodroplets*** GERALD WILEMSKI, *University of Missouri-Rolla* BARBARA E. WYSLOUZIL, *The Ohio State University and Worcester Polytechnic Institute* REINHARD STREY, *University of Cologne, Germany* CHRISTOPHER H. HEATH, *Worcester Polytechnic Institute* UTA DIEREGSWEILER, *Worcester Polytechnic Institute* The spatial distribution of species within an aerosol droplet influences how it interacts with its environment. Despite the ubiquity of multicomponent nanodroplets in natural and technological aerosols, there are no published measurements of their internal structure. In a recent paper [Wyslouzil, et. al., Phys. Chem. Chem. Phys. **8**, xxx, (2006)], we report the first experimental results for structure in aqueous organic nanodroplets based on small angle neutron scattering by high number density aerosols. For $H_2O$ – n-butanol droplets, fitting of the diffraction patterns confirms the picture of an aqueous core containing $\sim$ 3 mol% alcohol covered by a shell of densely packed alcohol molecules.

*This work was supported by grants from the National Science Foundation, the Engineering Physics Program of DOE-BES, the Deutsche Forshungs Gesellshaft and NATO.

**16:30**

**R11 9 Imaging predissociation dynamics and energy flow pathways in vibrationally excited acetylene-HCl dimers** GUOSHENG LI, JESSICA PARR, IGOR FEDOROV, HANNA REISLER, *University of Southern California* We report photofragment imaging studies of the predissociation of acetylene-HCl dimers. The dimer is vibrationally excited by laser irradiation either in the CH asymmetric stretch mode of the acetylene subunit or in the HCl subunit. Photofragment ion images of HCl in specific rotational states are obtained from which kinetic energy release patterns are analyzed. The predissociation behavior in the two cases is different. CH stretch excitation is followed by IVR in acetylene and results in an acetylene fragment with one quantum of CC stretch excitation (in agreement with results of Roger Miller and coworkers) and a statistical rotational energy distribution. HCl excitation results in acetylene fragments with one or two quanta of bending excitation with no clear preference for a specific mode. In both cases HCl rotations are nonstatistical. The different predissociation outcomes reflect the different energy flow pathways followed in each case. Research supported by the US National Science Foundation.

**16:42**

**R11 10 Monte Carlo simulations of Phase Changes in Lennard-Jones nanoclusters.** SILVINA GATICA,* *Department of Physics and Astronomy, Howard University* XIAO DONG, ESTELA BLAISTEN-BAROJAS, *School of Computational Sciences, George Mason University* Monte Carlo simulations of Lennard-Jones clusters of less than 100 atoms are performed to explore the possible phase changes. The simulation is made at constant pressure and temperature. In the Monte Carlo the volume of the cluster is evaluated during the calculation in terms of the mean quadratic radius, and the reduced temperature is kept below 0.4 to avoid the evaporation of the cluster. We obtain a PV diagram and calculate the energy per particle, the radial distribution function, the coordination number and displacement function, to look for signatures of the presence of a solid-liquid-like phase change. The equilibrium structure and number of layers in the cluster at each pressure and temperature are also computed. We compare our findings with predictions of other authors.

*and School of Computational Sciences, George Mason University

**16:54**

**R11 11 Infrared spectroscopy of metal-solvent clusters: $Li(NH_3)_n$ and $Li(MeNH_2)_n$** ANDREW ELLIS, TOM SALTER, COREY EVANS, VICTOR MIKHAILOV, *University of Leicester* Mass-selected infrared spectra of the uncharged metal-solvent clusters $Li(NH_3)_n$ and $Li(MeNH_2)_n$ in the N-H stretching region have been recorded using two techniques, photodepletion spectroscopy and two-colour (IR+UV) REMPI. Infrared REMPI is the most suitable for the smaller clusters, since the energy input into the cluster by the IR photon is insufficient to cause dissociation. Our latest findings for this technique will be presented alongside computational predictions of the cluster spectra. For the larger clusters, injection of an IR photon in the N-H stretching region causes rapid dissociation and offers the opportunity to record mass-selected IR spectra by photodepletion spectroscopy. IR photodepletion spectra of $Li(NH_3)_n$ near 3 $\mu$m recorded for $n = 4$-7 show vibrational structure that points to completion of the first solvation shell at $n = 4$, with additional ammonia molecules entering a second shell in which the solvent molecules are more weakly bound to the cluster. Photodepletion spectra have also been recorded for other clusters, including $Li(MeNH_2)_n$, and the latest findings for these species will be described.

**17:06**

**R11 12 Rings, Towers and Cages in $Zn_nO_n$ Clusters** ARTHUR REBER, SHIV KHANNA, *Department of Physics, Virginia Commonwealth University, Richmond Va. 23284* JAGTAR HUNJAN, MARCELA BELTRAN, *Instituto de Investigaciones en Materiales, Universidad Nacional Autonoma de Mexico* It is shown that the transition from an elementary ZnO molecule to compact bulk wurtzite ZnO proceeds via hollow rings, towers, and cages. First principles electronic structure calculations within a gradient corrected density functional framework have been carried out to investigate the progression of geometries and electronic properties of $Zn_nO_n$ (n=2-12,15,16,21) clusters. It is shown that $Zn_nO_n$ (n=2, 3, 4, 5, 6, 7) clusters are all single, highly stable rings and that $Zn_3O_3$ is particularly stable. Starting at $Zn_8O_8$, these elementary rings begin to assemble into column structures that begin to distort at n=10. The ground states of $Zn_{12}O_{12}$, and $Zn_{16}O_{16}$ are single cages while the structure of $Zn_{11}O_{11}$, $Zn_{15}O_{15}$ and $Zn_{21}O_{21}$ can be described as barrels. The $Zn_{12}O_{12}$ cage has a high dissociation energy and a large highest occupied molecular orbital (HOMO)-lowest unoccupied molecular orbital (LUMO) gap of 2.51 eV making it a potential candidate for cluster assemblies.

**17:18**

**R11 13 On the Aluminum Cluster Superatoms acting as Halogens and Alkaline-earth Metals** DENNIS E. BERGERON, PATRICK J. ROACH, A. WELFORD CASTLEMAN, *Department of Chemistry and Physics, The Penn State University, College Park PA, 16802* NAICHE O. JONES, J. ULISES REVELES, SHIV KHANNA, *Department of Physics, Virginia Commonwealth University, Richmond VA, 23284* It is shown that a new class of super-polyhalides can be formed by combining the $Al_{13}$ super-halogen with the conventional halogen, I. Experimental reactivity studies demonstrate that the new super-polyhalides, $Al_{13}I_x^-$, exhibit pronounced stability for even numbers of I atoms.

Theoretical investigations probing the geometry and the electronic structure reveal that the enhanced stability is associated with pairs of I atoms occupying the on-top sites around the $Al_{13}^-$ core. We also demonstrate another series, $Al_{14}I_x^-$, that exhibits stability for odd numbers of I atoms. It is shown that this series can be described as consisting of an $Al_{14}I_3^-$ core upon which the I atoms occupy on-top locations around the Al atoms. The potential synthetic utility of superatom chemistry built upon these motifs will be addressed.

**17:30**

**R11 14 Induced super-halogen behavior of metal moieties in halogen-doped metal clusters** FEDOR NAUMKIN, *Faculty of Science, UOIT, Oshawa ON L1H 7K4, Canada* HOBART LEUNG, Recent studies of the $Al_{13}I^-$ cluster ion have shown negative charge localization on the aluminum core and associated this with its super-halogen character resulting from a high electron affinity EA of $Al_{13}$ (exceeding that of the I atom). The present work reports results of ab initio calculations for a similar halogen-doped metal cluster, $M_{13}X^-$. The charge is found to be localized on the $M_{13}$ core as well, even though its EA is lower than that of X. Other properties such as structure and stability for different spin-states are also investigated and compared with those for the neutral counterparts. Comparison to the corresponding smaller metal-halide species is made as well. The charge localization on the metal moieties is concluded to be associated not only with the relative EA values. An alternative, physically transparent interpretation is given, which explains the observed charge distributions on electrostatic basis. The super-halogen behavior of the metal moieties is linked to the presence of the halogen atom in the systems.

**SESSION R12: DYNAMICS AT SILICON SURFACES**
**Wednesday Afternoon, 15 March 2006**
**304, Baltimore Convention Center at 14:30**
**Paul G. Evans, University of Wisconsin-Madison, presiding**

**14:30**

**R12 1 Electron Phonon Interaction at the Si(111)−7 × 7 Surface** I. BARKE, FAN ZHENG, A. KONICEK, R. HATCH, F.J. HIMPSEL, *Dept. of Physics, University of Wisconsin Madison, 1150 University Ave, Madison, WI 53706* In recent years, it has become possible to study the electron-phonon interaction of metals by high resolution photoelectron spectroscopy. However, virtually no such experimental information is available for the case of semiconductors. It is shown that electron-phonon interaction at the Si(111)−7 × 7 surface provides a natural explanation for the unusual band dispersion of the metallic surface states. While local density theory predicts a hole-like dispersion for the adatom bands that cross the Fermi level $E_F$, photoemission finds an electron-like band with a break in the slope at 0.1 eV below $E_F$. Such behavior follows naturally from electron phonon interaction with the surface phonon mode at $\hbar\omega = 70$ meV that dominates electron energy loss spectra. It has been assigned to adatom vibrations by molecular dynamics calculations. Two independent determinations of the electron-phonon coupling parameter from the band dispersion and the temperature dependent phonon broadening yield very similar coupling parameters around $\lambda = 1.1$.

**14:42**

**R12 2 Ultrafast Electron Dynamics of Silicon Surface States: Second-Harmonic Hole Burning Spectroscopy on Si(111)7x7*** JOHN A. MCGUIRE, *University of California, Berkeley* MARKUS B. RASCHKE, *Max-Born-Institut fur Nichtlineare Optik und Kurzzeitspectroscopie D-12489 Berlin, Germany* Y.R. SHEN, *University of California, Berkeley* We used second harmonic generation (SHG) as an all-optical, surface-specific probe of spectral hole-burning to measure the ultrafast dynamics of electronic excitations into the adatomU1 band of the Si(111)7x7 surface. The time-delayed SHG obtained with tunable ~ 100 fs probe pulses was measured in response to the excitation of a ~ 100 fs pump pulse at 1.54 eV. The transient holes induced by the pump corresponded to a homogeneous dephasing time as short as 15 fs. Carrier-carrier scattering was responsible for the linear dependence of the dephasing rate on pump fluence. The hole-burning spectra also reveal a strong coupling between the localized dangling-bond states and the surface phonon mode at 570 $cm^{-1}$ associated with the adatoms. The technique can be extended to measurement of electron dynamics at any interface between two centrosymmetric media accessible to light.

*The work was supported by DOE.

**14:54**

**R12 3 Silicon surface evolution at high temperature in UHV** VALERIAN IGNATESCU, JACK BLAKELY, *Cornell University* The step distribution, associated with the miscut of a Si wafer can be modified by controlled step flow. There are many studies of step-flow dynamics during sublimation or deposition at high temperature. In our group, atomically flat, step-free surfaces were previously obtained over areas of up to 50 by 50 microns by annealing Si samples in UHV. The surface of a normal crystal wafer does not usually show a step-terrace structure. Instead, a Czochralski Si wafer, mirror polished by chemical-mechanical polishing, has an rms roughness of 1-2 nm. A sizable thermal budget has to be used to remove this initial roughness or that induced by reactive ion etching. We report here results of the evolution of step distributions over a range of temperatures. By inducing a temperature gradient on our Si samples we were able to study the stages that occur as the surface transforms towards an atomically flat one. The samples were later reannealed to see the morphological changes that occurred on previously examined regions. We have also investigated the processes of trench formation near the walls of etched craters and of ridge development around the edges of mesas structures.

**15:06**

**R12 4 Interacting dimer rows on Si(001): Reconstructed Si(001)*** ARIEF BUDIMAN, *University of Calgary* A continuum model involving elastic interactions of dimer rows on a two-dimensional surface is presented. It produces a logarithmic stress-domain interaction energy from the obtained partition function. Using dimer rows as the building blocks of a reconstructed surface thus generalizes Alerhand and Marchenko models of the stress-domain interaction on terraces, which have been previously used to predict step- height transition on reconstructed Si(001). The double-layer step phase is determined to be more stable that the single-layer step phase for typical temperatures and miscut angles. A mixed phase region in the temperature-versus-miscut-angle phase diagram is found.

*NSERC

**15:18**

**R12 5 Gold on silicon: Can theory and experiments for Si(111)-(5x2)-Au be reconciled?** STEVEN ERWIN, *Naval Research Laboratory* CHRISTOPH SEIFERT, *Universität Duisburg-Essen, Duisburg, Germany* Since its discovery 30 years ago, the 5x2 reconstruction of Si(111) induced by 2/5 monolayer of Au has been widely studied for its unusual one-dimensional electronic properties. Despite quite detailed and consistent data from a variety of surface science techniques, there is still no structural model consistent with the constraints inferred from those data. Here we combine density-functional theory (DFT) and scanning tunneling microscopy (STM) data to systematically develop and investigate new candidate structural models. The underlying 5x2 parent reconstruction is decorated by Si adatoms, whose density is at most one adatom per two 5x2 unit cells, and at equilibrium is half of this limit. We consider first the adatom-free parent reconstruction. Starting from simple principles of dangling bonds and surface stress relief, we construct a well-defined set of chemically plausible models that can be exhaustively generated by combinatorics. Several recently proposed models for Si(111)-(5x2)-Au are examples from this set. We then consider the role of the Si adatoms. We find that their role is two-fold: to passivate dangling bonds and to dope the parent band structure. Using the complete model, detailed predictions for STM imagery and surface band structure compare favorably with experiment.

**15:30**

**R12 6 Au-Induced Reconstructions on the Si(111) Surface*** F.-K. MEN, A.-L. CHIN, *Department of Physics, National Chung Cheng University, Chia-Yi 621, Taiwan, ROC* By depositing Au onto a Si(111)-(7× 7) surface at elevated temperatures, the existence of (5× 2), ($\sqrt{3} \times \sqrt{3}$), and (6× 6) reconstructions have long been studied as a function of Au coverage. The corresponding structures however are yet to be satisfactorily determined. By using scanning tunneling microscopy (STM), we have investigated these Au-induced surface structures at LN2 temperature. With STM image quality exceeding currently published results, we are able to identify fine details in those reconstructions, which may shed new light on constructing structural models.

*Work supported by NSC, Taiwan, ROC.

**15:42**

**R12 7 Ab Initio Studies of Indium Diffusion on the Si(111)-7x7/Ge(111)-5x5 Surface*** D. PSIACHOS, *Dept. of Physics, Queen's University* M. J. STOTT, *Dept. of Physics, Queen's University* The mechanisms for the self-assembly of ordered arrays of indium magic clusters on the Si(111)-7x7/Ge(111)-5x5 surface have been investigated theoretically using ab initio total energy simulations. Plane wave density functional methods have enabled us to obtain the potential energy surface for one indium atom adsorbed on the Ge(111)-5x5 surface. Using these ab initio-derived energies as input, a classical molecular dynamics simulation has yielded values for the temperature-dependent, trajectory-dependent, microscopic self-diffusion coefficients of an indium atom on the Ge(111)-5x5 surface. For comparison, we also have calculated the diffusion coefficient obtained through fully ab initio molecular dynamics where we have used the non-self-consistent Harris Functional due to computational cost. Also, as a third approach, the harmonic approximation of the transition state theory has been applied and is assessed in light of the two molecular dynamics simulations. The single-atom results show promise for providing useful information on how the magic clusters on semiconductor surfaces may be formed.

*Support by the NSERC of Canada is acknowledged.

**15:54**

**R12 8 Evolution of Si Surface Morphology under Oxygen Etching*** ALISON BASKI, *Virginia Commonwealth University* MARY WILLIS, *Virginia Commonwealth University* JONATHAN DICKINSON, *Georgetown College* We have studied the surface morphologies produced after oxygen etching of the following Si surfaces: (001), (111), (113), (5 5 12), and (112). Atomic force microscopy data show the evolution of the surface morphology as a function of dosage (50 to 400 Langmuirs) for sample temperatures from 700 to 900 [r]C and a pressure of $3x10^{-7}$ Torr. We have found that certain orientations are relatively stable against extended etching, whereas others are unstable and produce faceted morphologies. The (001), (111), and (113) surface orientations are stable and produce morphologies composed of terraces with islands caused by etching around oxide-induced pinning sites. As expected, the island density decreases as temperature increases, yielding an effective activation energy of 2 to 4 eV. High-index surfaces such as (5 5 12) and (112), however, are unstable against extended etching and produce faceted sawtooth morphologies. These sawtooths are aligned along the [110] direction and are primarily composed of the more stable (111) and (113) planes. Further studies are in progress to determine if steady-state morphologies exist at dosages above 1000 Langmuirs.

*This work was supported by NSF.

**16:06**

**R12 9 Dissociation pathways and multiple adsorption configurations of ammonia on Si(001)*** HANCHUL KIM, *Korea Research Institute of Standards and Science* OPTI NAGUAN CHUNG, SUKMIN CHUNG, *Pohang University of Science and Technology* JA-YONG KOO, *Korea Research Institute of Standards and Science* The adsorption of ammonia ($NH_3$) molecules on the Si(001) surface has been investigated by combining the scanning tunneling microscopy (STM) and the ab initio pseudopotential calculations. An $NH_3$ molecule had been known to spontaneously dissociate into $NH_2$ and H and form the so-called on-dimer configuration (OD). In OD, $NH_2$ and H bond with two Si atoms of one Si dimer. However, our study shows that there exist two distinct configurations of $NH_3$/Si(001). One is the existing model of OD, which is found to be the lowest energy state. The other is identified to be an inter-dimer configuration (ID), where $NH_2$ and H adsorb at two Si atoms at the same side of two adjacent dimers along the dimer row. The simulated STM images of OD and ID are in good agreement with experimental observations, proving the existence of two distinct adsorption configurations of $NH_3$/Si(001).

*This work was supported by the KISTI under 'The sixth Strategic Supercomputing Support Program.

**16:18**

**R12 10 Desorption of Hydrogen from Si(111) by Resonant Excitation of the Si-H Vibrational Stretch Mode*** ZHIHENG LIU, *University of Minnesota* LEONARD FELDMAN, *Vanderbilt University* NORMAN TOLK, *Vanderbilt University* ZHENYU ZHANG, *Oak Ridge National Laboratory* PHILIP COHEN, *University of Minnesota* We report first measurements of non-thermal, non-electronic resonant photodesorption of hydrogen from a Si(111) surface using tunable infrared radiation. The wavelength

dependence of the desorption yield Shows a peak at 0.26 eV, the energy of the Si-H vibrational stretch mode. The corresponding excitation cross section is determined to be $2.3 \times 10^{-18}$ cm$^2$. The desorption yield is quadratic in the infrared intensity and quartic in the electric field along the Si-H bond direction. We postulate that two neighboring hydrogen adatoms, once simultaneously excited in their vibrational stretch mode, can desorb associatively at room temperature.

*This work is funded by DARPA/SPAWAR grant N66001-04-1-8924, DOE grant ER45781 and NSFgrant DMR-0306239.

**16:30**

**R12 11 Empirical modeling of STM imaging and tunneling spectroscopy of adsorbates on the Si(111)7x7 surface.*** WEIMING LIU, *Department of Physics, University of Lethbridge, Lethbridge, Alberta, T1K 3M4, Canada* STEVEN A. HORN, *Department of Physics, University of Lethbridge, Lethbridge, Alberta, T1K 3M4, Canada* POUYA MARAGHECHI, *Department of Physics, University of Lethbridge, Lethbridge, Alberta, T1K 3M4, Canada* S.N. PATITSAS, *Department of Physics, University of Lethbridge, Lethbridge, Alberta, T1K 3M4, Canada* To accurately simulate experimentally measured STM results have developed an atomic orbital model for the top layer atoms of the Si(111)7x7 surface. Adatom, restatom and corner hole dangling bonds are represented by sp$^3$ hybrids of hydrogen-like orbitals adjusted to have the correct work function and including tip-induced electric field effects. Peak energies, widths and other DOS information, were extracted from known experimental data and theoretical calculations.[1] Restatom and adatom charge transfer was included. Back-bonding orbitals for adatoms, restatoms and dimers were also used. Bulk DOS data was used for deeper bonding orbitals. The Tersoff-Hamann approach is used calculate the tunneling current.[2] We will present numerically calculated topographic images as well as spectra and compare to experiments. [1]Brommer et al, Surf. Sci. **314**, 57 (1994). [2]Tersoff and Hamann, Phys. Rev. B, **31**, 805 (1985).

*The authors acknowledge the National Sciences and Engineering Research Council of Canada (NSERC) for their support of this work.

**16:42**

**R12 12 Chemical fingerprinting at the atomic level with scanning tunneling spectroscopy** KOJI S. NAKAYAMA, *Department of Materials Science and Engineering, UIUC, and IMR, Tohoku University* TOMOKO SUGANO, *Department of Materials Science and Engineering, UIUC* KENJI OHMORI, *Frederick Seitz Materials Research Laboratory, UIUC* A.W. SIGNOR, J.H. WEAVER, *Department of Materials Science and Engineering, UIUC* Atomic-scale chemical analysis has been a long-standing goal of materials characterization. It requires the ability to interrogate individual atoms and to recognize their distinguishing signatures. Scanning tunneling spectroscopy based on scanning tunneling microscopy makes it possible to map the local electronic density of states for clean surfaces and for those with adsorbates at 80 K. We have developed a protocol that allows us to obtain the spectral fingerprints of halogen atoms on Si(001), and we use those fingerprints to distinguish between adatom species for surfaces with Cl and Br mixed adsorbates. The key to the process is the energy distribution of the antibonding states that depend on the halogen species. The protocol developed here, with its emphasis on the distribution and distinction of energy states, should be applicable to other systems, and should yield new insights regarding chemical identification.

**16:54**

**R12 13 Spin echo resolved grazing incidence neutron scattering** GIAN FELCHER, SUZANNE TE VELTHUIS, PETER FALUS, *Argonne National Laboratory, Argonne IL 60439* ALEXEI VOROBIEV, JANOS MAJOR, HELMUT DOSCH, *Max Planck Institut für Metallforschung, D70569 Stuttgart Germany* Conventionally the spin-echo technique is used to encode energy transfer in neutron inelastic scattering experiments. However, spin-echo may encode the neutron momentum transfer, allowing the probing of large length scale structures without the need of a tight neutron beam collimation and resulting intensity loss. This concept has recently been successfully utilized for small angle scattering experiments in transmission geometry as well as scattering in the grazing incidence geometry at a reflectometer (EVA, Institut Laue-Langevin, Grenoble) equipped with neutron resonance spin echo circuits as well as appropriate neutron spin rotators. The tests included the measurement in transmission geometry of suspensions of polystyrene balls (1500 Å radius) as well as anodized aluminum oxide 2D gratings, as well as the measurement in reflection geometry of the characteristic lengths of assemblies of polystyrene droplets dewetted from a silicon surface. The results are guiding the design of an instrument for the Spallation Neutron Source capable of studying the structure and working of biological membranes.

**17:06**

**R12 14 Epitaxial growth and structure of the high-k dielectric $Pr_2O_3$ on Si(001) and Si(111)** JORG ZEGENHAGEN, LAURE LIBRALESSO, TIEN-LIN LEE, *ESRF, France* Keeping the capacitance of CMOS devices constant while shrinking further the gate dimensions requires intolerably thin $SiO_2$ layers for next generation devices. Thus, replacing $SiO_2$with a material with larger static permittivity k and matching properties is at present a very urgent task. Among others, the sesquioxide $Pr_2O_3$ is discussed as a possible candidate material. We deposited ultra thin films of $Pr_2O_3$by e-beam evaporation on atomically clean (001) and (111) surfaces. We studied the growth from the very early stages using low energy electron diffraction, scanning tunneling microscopy, Auger electron spectroscopy, grazing incidence X-ray diffraction, X-ray reflectivity and X-ray photoelectron spectroscopy. On Si(111), $Pr_2O_3$ grows pseudomorphically in the hexagonal phase. On Si(001) surface, a 0.6 nm thick layer of cubic $Pr_2O_3$ grows followed by the formation of a silicate layer on top. Growth under 10−8 mbar O2 atmosphere is needed in order to prevent Pr−silicide formation.

**SESSION R13: FOCUS SESSION: ULTRAFAST AND ULTRAHIGH FIELD CHEMISTRY III: ULTRAFAST PROCESSES**
**Wednesday Afternoon, 15 March 2006; 305, Baltimore Convention Center at 14:30**
**Yaron Silberberg, Weizmann Institute, presiding**

*Invited Papers*

**14:30**
**R13 1 Attosecond electron wave packets.***
KENNETH SCHAFER, *Department of Physics and Astronomy, Louisiana State University, Baton Rouge, LA 70803-4001*

Attosecond electron wave packets are created when a train of extreme ultraviolet attosecond pulses is used to ionize an atom or molecule via one photon absorption. These novel wave packets differ in several useful ways from the temporally confined electron wave packets that are made via tunnel ionization. They can, for instance, be tailored for different applications by controlling the light field that generates the attosecond pulse train. In this talk we will describe how attosecond electron wave packets can be used to study the one photon ionization process via interferometry, and their application in the study and control of strong field processes in such as harmonic generation and above threshold ionization.

*Research supported by National Science Foundation Grant No. PHY-0401625.

*Contributed Papers*

**15:06**
**R13 2 Probing ultrafast electronic motions in atoms with the attosecond pump-probe** LEE COLLINS, SUXING HU, *Los Alamos National Laboratory* BARRY SCHNEIDER, *National Science Foundation* Through full-dimensional numerical simulations with using our recently-developed efficient and accurate parallel solver for the time-dependent Schrödinger equation, we have demonstrated that an attosecond pulse can effectively *probe* the extremely fast motion of an electronic wave packet in atoms. Pumped by a broadband femtosecond UV pulse, one electron of ground-state Helium can be launched into a superposition of low-lying excited states, thus forming a wavepacket that begins to orbit the atomic core. A time-delayed attosecond EUV pulse (probe) then ionizes the atom causing three-body breakup. Measuring either the energy sharing of the ionized electrons or the total ionization probability as a function of the time delay displays the internal motion of the excited electron. Our simulation has shown that an ultrashort Kepler period of 2 $fs$ can be followed for several cylces. This opens the prospect of a wealth of similar pump-probe experiments to examine *electronic motion.*

*Invited Papers*

**15:18**
**R13 3 Tomographic Imaging of Molecular Orbitals Using Femtosecond Lasers.**
DAVID VILLENEUVE, *National Research Council of Canada*

I will show how we can experimentally reconstruct a single-electron orbital wave function from a simple molecule, dinitrogen. We use a seemingly unlikely technique, high harmonic generation (HHG). HHG occurs when a gas is irradiated with an intense femtosecond laser pulse. The atoms or molecules are tunnel-ionized by the laser field, and then are driven back to the parent ion within the same optical cycle. Some of these electrons recombine with the parent, and release their kinetic energy as xuv photons. The resulting spectrum covers the photon range of 10–100 eV. The radiation results from a transition from a continuum electron wave function, described as a plane wave, and the orbital from which the electron was removed, the HOMO. Thus the experiment is a measure of the transition dipole matrix elements between the single-electron orbital and a set of plane waves. By rotating the molecule in the gas phase using a second laser pulse, we can map out the matrix elements for different projections of the molecule. This data can then be inverted using a tomographic algorithm to yield an image of the orbital wave function. We will show the recovered $3\sigma_g$ orbital of $N_2$. Beyond the single active electron approximation, there are other transitions that are allowed between the HOMO and inner orbitals. This is due to the indistinguishability of the electrons. Including these exchange terms gives even better agreement between theory and experiment. Because this measurement is made with a 25 fsec laser pulse, it is now possible to perform pump-probe experiments to observe dynamic changes in the electronic structure of molecules. It may even be possible to observe *electronic* wave packet motion within an atom with attosecond resolution.

**15:54**
**R13 4 Coherent excitation and control of surface phonons.**
YOSHIYASU MATSUMOTO, *Institute for Molecular Science*

The excitation and control of nuclear wavepackets using tailored laser pulses have attracted a lot of interest recently and being realized mainly in gas-phase molecules. In contrast, there have been little studies on the coherent excitation and

control for adsorbates particularly on metal surfaces. This is because dephasing is substantially rapid on metal surfaces due to efficient couplings between adsorbates and metals. Recently, we have demonstrated the time-domain observation of nuclear wavepacket dynamics of monolayer adsorbate by femtosecond time-resolved second harmonic generation (TRSHG). When metal surfaces covered with alkali metal atoms are irradiated by ultrafast laser pulses, coherent surface phonon modes are excited. The formation and dissipation processes of coherent surface phonons are probed by time-resolved second harmonic generation. SHG signal intensities are enhanced by alkali atoms adsorption by various resonant transitions in the adsorbate-substrate system. However, not all resonant electronic transitions lead to the generation of coherent stretching vibrations of alkali atoms. The measurements of TRSHG traces as a function of the excitation photon energy at a fixed alkali coverage indicate that resonant transitions between adsorbate-induced surface states is responsible for the coherent vibrational motions. By carefully examining the Cs coverage dependence of the TRSHG waveform, we found that TR-SHG traces show beating structures. This indicates that the oscillatory TR-SHG traces are contributed by at least two kinds of coherent surface phonon modes: the Cs-Pt stretching mode (2.3 THz) and the Rayleigh phonon mode (2.6 or 2.9 THz, depending on the Cs coverage). We used fs pulse trains with the repetition frequencies of 2.0 - 2.9 THz that are synthesized by using a spatial-light modulator as an excitation source for the coherent phonons. By tuning the pulse train frequency, we succeed in the selective excitation of a coherent phonon mode.

***Contributed Papers***

**16:30**

**R13 5 Femtosecond microscopy of surface plasmon propagation on a silver film.*** ATSUSHI KUBO, *Department of Physics and Astronomy University of Pittsburgh, PRESTO JST* NIKO PONTIUS, *BESSY mbH* HRVOJE PETEK, *Department of Physics and Astronomy University of Pittsburgh* By using interferometric time-resolved photoelectron emission microscopy (ITR-PEEM), we investigate the dynamics of surface plasmon polariton (SPP) propagation with 0.33-fs per frame time and 40-nm spatial resolution. 10-fs phase-locked pump-probe pulse pairs with 400-nm center wavelength irradiate a silver film at 65 degree angle from the surface normal to launch a SPP wave from a line defect in the film. We image the propagation of the SPP wave through its interference with the external light field. The interference periodically modulates the total amplitude of the polarization field in silver, and thereby the two-photon photoemission current from the surface. Two-dimensional microscopic maps of the photoemission intensity at pump-probe delay $\tau_d$ are recorded by the PEEM. Sequential PEEM images taken with a delay increment step of 0.33-fs record the dynamics of SPP wave packet propagation and dissipation as a movement of the oscillatory interference pattern. The progression speed and the attenuation of the oscillatory pattern are reproduced by a simulation with the known dispersion of the complex SPP wave vector. The SPP imaging experiments demonstrate the possibility of coherent control of plasmon field in metallic nanostructures.

*This research was supported by the NSF Grant CHE-0507147.

**16:42**

**R13 6 Adaptive Control of the Spatial Position of White Light Filaments in an Aqueous Solution** ROBERT LEVIS, *Temple University* GEORGE HECK, *Temple University* JOSEPH SLOSS, *Temple University* White light filamentation produced from intense laser beams represents a method to produce highly nonlinear energy deposition both spatially and temporally in the gas, liquid, or solid phase. We have demonstrated control over the spatial coordinates (position and extent) of white light filaments (supercontinuum generation) in an aqueous solution using shaped ultrafast, strong field laser pulses. These are the first experiments to achieve control of filament position through the manipulation of the spectral phase of an ultra-fast (50 fs) 800nm excitation laser pulse. A closed feedback loop employing a spatial light modulator and a genetic algorithm was used to manipulate the spectral phase of the pulses to achieve a specified filament position and length.

**16:54**

**R13 7 Relaxation dynamics of dissolved molecule probed by a phase locked pulse pair:$Br_2$ in Ar*** MIZUHO FUSHITANI, HEIDE IBRAHIM, MARKUS GUEHR, NIKOLAUS SCHWENTNER, *Freie Universitaet Berlin* A phase locked pulse pair-(PLPP) is a strong tool to investigate the electronic coherence of molecules. Recently, we have shown that the PLPP experiment is also applicable to dissolved molecules[1]. Here, we apply this method to the $Br_2$/Ar system and investigate relaxation dynamics in the electronically excited *B* state of $Br_2$. We observed not only laser induced fluorescence(LIF) from the *B* state but also LIF from the *A* and *A'* states which are energetically lower than the *B* state. Tuning the relative phase between PLPPs provides the various LIF ratio among those states, indicating relaxation channels which can be coherently controlled. The PLPP results will be compared with those obtained by frequency resolved excitations which give the LIF ratio resulting from all possible relaxation. [1] M. Fushitani, et al. PCCP 7 (2005) 3143.

*This work is financially supported by the Deutsche Forschungsgemeinschaft via the Sfb 450.

**17:06**

**R13 8 Interfaces of methanol:water mixtures with an OTS-coated substrate probed by sum-frequency vibrational spectroscopy*** WEITAO LIU, LUNING ZHANG, Y. R. SHEN, *Physics Department, University of California at Berkeley* Aqueous solutions of short chain alcohols are important reagents in organic chemistry, and their physical and chemical properties at hydrophobic interfaces play key roles in many applications. To study their interfacial structures at the molecular level, we applied sum-frequency vibrational spectroscopy (SFVS) to the interfaces of methanol-water mixtures with an octyltrichlorosilane (OTS)-covered silica as model systems. From the methanol CH3 symmetric stretching mode, we deduced the interfacial coverage and orientation of methanol molecules vs. its molar concentration, and studied the hydrogen-bonding property of methanol with neighboring molecules. It appeared that methanol molecules adsorbed at the interfaces with the same average orientation at all concentra-

tions. From the dangling-OH stretching mode of water molecules, we observed the correlation between the methanol surface number density and the water free OH bonds. Ab initio calculations were used to help investigate the interfacial structures of hydrogen-bonded species.

*This work was supported by the NSF Science and Technology Center of Advanced Materials for Purification of Water with Systems (Water CAMPWS; CTS-0120978). WTL was supported by DOE.

**17:18**

**R13 9 Vibrational Relaxation of Anions in Nonaqueous Reverse Micelles** GERALD SANDO, JEFFREY OWRUTSKY, *Chemistry Division, US Naval Research Laboratory* Static and ultrafast infrared spectroscopy have been used to measure vibrational frequencies and vibrational energy relaxation (VER) times for high frequency bands of small ions in nonaqueous reverse micelles (RMs). Formamide RMs are stable with anionic (AOT) and nonionic surfactants. In AOT RMs, the vibrational frequencies of azide ($N_3^-$) are blue shifted, while the VER times are slower. Bulk behavior is approached as the RM size increases. The frequency-rate correlation is opposite of what is seen in bulk solvents and aqueous RMs. The effects are small in nonionic RMs because azide near surfactant headgroups resembles that in formamide, as shown by results in TGE, a model of the polar portion of the surfactant. The dynamics for $Fe(CN)_5NO^{2-}$ depend on the probe frequency because of the inhomogeneous distribution of solvation sites throughout the poorly defined interface. Ionic liquid containing reverse micelles are formed with nonionic surfactants. The VER rates of the ionic liquid anions are faster than in the bulk ionic liquids, but slower than in TGE, consistent with a mixed solvation environment of ionic liquid and surfactant.

**17:30**

**R13 10 Molecular quantum computation by using ultrashort intense laser pulses under the influence of non-Markovian dissipation** YUKIYOSHI OHTSUKI, *Tohoku University & JST-CREST* We numerically study molecular quantum computation by combining an ensemble of molecular states and shaped ultrashort intense laser pulses through a case study of Grover's quantum search algorithm, in which qubits are implemented in the vibrational states of I2. In the simulation, the Grover iteration is divided into two basis operations, the so-called oracle and the inversion about mean operation, which are realized by laser pulses designed by an optimal control method within the density matrix formalism. These pulses perform Grover iteration with high accuracy although the lack of extreme precision leads to a slight reduction in the population associated with the solution to the search problem. The accuracy of the Grover iteration is shown to be improved by the normalization with respect to the ''qubit population.'' The relaxation effects on the accuracy of the computation are systematically examined by using the non-Markovian master equation with phenomenological relaxation parameters. The gate pulses are designed under the influence of non-Markovian dissipation, in which the pulse design equation is solved by a newly proposed iteration algorithm.



**SESSION R16: THERMOELECTRICS**
**Wednesday Afternoon, 15 March 2006**
**312, Baltimore Convention Center at 14:30**
**Joseph P. Heremans, Ohio State University, presiding**

**14:30**

**R16 1 Fabrication and Characterization of Bi2Te3 Nanoparticles for Thermoelectric Applications** YI MA, BED POUDEL, WENZHONG WANG, DEZHI WANG, ZHIFENG REN, *Boston College, MA* Q. HAO, H. LEE, GANG CHEN, *Massachusetts Institute of Technology* Bi2Te3 nanoparticles with diameters of 10-30 nm have been successfully synthesized via a hydrothermal method. The as-prepared nanoparticles were characterized by X-ray diffractometer (XRD, Cu Kalpha, Bruker AXS), field emission scanning electron microscope (SEM, JEOL-6340F) and transmission electron microscope (TEM/HRTEM, JEOL-2010F) equipped with an energy-disperse X-ray spectrometer (EDS). The densification of Bi2Te3 nanopowders was conducted in two ways: plasma pressure compaction (P2C) and hot pressing. The density of the as-pressed pellet sample was about 98-99 % of theoretical density (7.7 g/cm3). The Seebeck coefficient, electrical and thermal conductivities were further investigated.

**14:42**

**R16 2 Characterization and thermoelectric properties of Si-Ge nanocomposite*** DEZHI WANG, WENZHONG WANG, SHUO CHEN, JIANYU HUANG, ZHIFENG REN, *Boston College, Dept. of Physics* HOHYUN LEE, GANG CHEN, *MIT, Dept. of mechanical Engineering* MING TANG, M. S. DRESSELHAUS, *MIT, Dept. of Electrical Engineering* PAWAN GOGNA, JEAN-PIERRE FLEURIAL, *Jet Propulsion Laboratory* BRADLEY KLOTZ, *Dynamic Science, Inc.* Low dimension is one of the most promising directions to search for high-ZT thermoelectric materials. It has been predicted by theory and proved by experiments that structures such as quantum well and superlattice can increase ZT by several times vs the corresponding bulk materials. However, it is very difficult to manufacture those low dimensional structures in large scale for bulk applications. To realize those principles, we have designed and synthesized successfully a new structure so called Si-Ge nanocomposite—nano Silicon particles in SiGe alloy matrix. The Si-Ge nanocomposite was made of nano silicon and germanium particles by a unique hot-press procedure. The samples are being characterized by TEM, SEM, XRD and thermoelectric property measurements. The results will be reported in detail.

*NASA

**14:54**

**R16 3 Prospects for nanoscale thermoelectric Bi(1-x)Sb(x) alloys** JOSEPH P. HEREMANS, *The Ohio State University, Department of Mechanical Engineering and Department of Physics* Bi(1-x)Sb(x) alloys are the materials with the highest thermoelectric figure of merit at cryogenic temperatures around 100 K. Recently, Thonhauser et al. (Appl. Phys. Lett. **85** 588 2004) calculated that heavily-doped pure Bi could be an excellent thermoelectric material at 300 K. Bi doped *p*-type with 1% Sn to a hole concentration of about $15x10^{21}cm^{-3}$ and a Fermi level 250 meV below that of the pure semimetal could reach itZT=1.44. Unfortunately, no *p*-type doping has been achieved experimentally in semimetallic Bi at room temperature, not only because of the solubility limit of Sn in Bi, but mostly because the band structure is very temperature-dependent, and the energy overlap between

conduction and valence band is much larger at 300 K than at 4 K. Two new approaches are suggested here. Firstly, one can attempt to use the model in dilute Bi(1-x)Sb(x) alloys. Secondly, one should be able to increase the power factor by adding nanoprecipitates to a Bi or Bi(1-x)Sb(x) alloy matrix, following a precipitation anneal similar to that used on PbTe:Pb by Heremans et al. (J. Appl. Phys. **98** 063703 2005). Model calculations, and the result of some preliminary experiments, will be given.

**15:06**

**R16 4 Quantum Confinement and Surface State Effects in the Thermopower of Bismuth Nanowires.** T.E. HUBER, *Howard University* A. NIKOLAEVA, *Academy of Sciences. Moldova* D. GITSU, *Academy of Sciences. Moldova* L. KONOPKO, *Academy of Sciences. Moldova* M.J. GRAF, *Boston College* Because of the increased density of states arising from one-dimensional confinement, it is anticipated that bismuth quantum wires will exhibit superior thermoelectric properties. Recently, angle-resolved photoemission spectroscopy (ARPES) studies have shown that Bi supports surface states that have not been considered in current models of quantum confinement. Studies of the Fermi surface, employing the Shubnikov-de Haas (SdH) method, in arrays of 30- to 80-nm bismuth nanowires partially corroborates ARPES findings. We have studied the thermopower of arrays of 50-nm Te- and Sn-doped Bi nanowires and we discuss these experimental results in terms of a Bi nanowire conduction model based on ARPES and SdH results.

**15:18**

**R16 5 The Order Disorder phase transition in $Zn_4Sb_3$** S. BHATTACHARYA, R.P. HERMANN, V. KEPPENS, *Department of Materials Science and Engineering, The University of Tennessee, Knoxville, TN* J. SNYDER, *Jet Propulsion Laboratory, California Institute of Technology, Pasadena, CA* T.M. TRITT, *Department of Physics, Clemson University, Clemson, SC* $Zn_4Sb_3$ has been widely investigated not only for its promise as a thermoelectric material, [1] but also for the unique transport properties it exhibits. $Zn_4Sb_3$ undergoes two distinct phase transitions (i) from $\alpha$ to $\beta$-phase at $T_C \approx$ 250 K and (ii) from $\beta$ to $\gamma$-phase at $T_C \approx$ 765 K. [2] We have performed electronic and thermal transport measurements exploring the structural phase transition at $T \approx$ 250 K from the ordered $\alpha$, to the disordered $\beta$ phase. The well-known $\alpha$ to $\beta$ phase transition manifests itself in anomalies in the resistivity, thermopower and specific heat measurements at $T \approx$ 250 K as well as a change in slope in the thermal conductivity, leading to a reduction in thermal conductivity as $Zn_4Sb_3$ changes phase from the ordered to the disordered state. Moreover, measurements of the elastic properties using resonant ultrasound spectroscopy (RUS) reveal dramatic changes at the order-disorder transition. [1] Snyder et al., Nature Materials **3**, 458-463, (2004) [2] Vuillard, G. et al., C.R. Seances, Acad. Sci., Ser. C: Sci. Chim. **263**, 1018-1021, (1966)

**15:30**

**R16 6 Presence of $\alpha$ phase domains in the phonon-glass thermoelectric $\beta$-$Zn_4Sb_3$ from atomic pair distribution function (PDF) analysis** H. J. KIM, E. S. BOZIN, S. J. L. BILLINGE, *Department of Physics and Astronomy, Michigan State University, East Lansing, MI 48824* S. HAILE, *Materials Science, California Institute of Technology, Pasadena, CA 91125* G. J. SNYDER, *Jet Propulsion Laboratory, 4800 Oak Grove Drive, Pasadena, CA 91109* The promisingly high ZT of $\beta$-$Zn_4Sb_3$ between 450 K and 670 K is known to be due to its exceptionally low thermal conductivity. The discovery of significant Zn interstitial disorder in $\beta$-$Zn_4Sb_3$ provides foundation for better understanding of the origin of the glass-like thermal conductivity[1]. Furthermore, it has been reported that Zn interstitial atoms become ordered in $\alpha$-phase[2]. We report on the local structural study of $\beta$-$Zn_4Sb_3$ using PDF technique, which has been successfully applied to solve the structures of crystallographically challenged materials[3,4]. Prominent diffuse scattering is found both in neutron and x-ray data. The PDF analysis suggests that the average $\beta$-structure consists of locally $\alpha$-structure like domains where Zn interstitial atoms are ordered. This provides an important local structural insight into not well understood $\alpha$ to $\beta$ order-disorder phase transition in $Zn_4Sb_3$ at 260 K. [1] G. J. Snyder et al. Nat. Mater. **3**, 458 (2004) [2] J. Nylén et al. J. Am. Chem. Soc. **126**, 16306 (2004) [3] T. Egami and S. J. L. Billinge, Underneath the Bragg peaks, Pergamon Press, Elsevier, Oxford, England, 2003 [4] S. J. L. Billinge and M. G. Kanatzidis, Chem. Commun., 749 (2004)

**15:42**

**R16 7 Theoretical study of thermal properties of Si clathrates*** XIAOLI TANG, JIANJUN DONG, *Physics Department, Auburn University* Pristine silicon clathrate ($Si_{136}$) is an ''expanded volume'' allotrope of Si that is metastably available at ambient conditions, and it exhibits a significant decrease in lattice thermal conductivity. We have theoretical studied vibrational, thermodynamic, and transport properties of $Si_{136}$ and compared its results with those of the ground state diamond-structured Si. The equilibrium temperature-pressure phase boundary between the two phases occurs in the negative pressure regime. Despite obvious differences in the energetics and lattice vibrational modes for the two polymorphic forms of Si, our calculations indicate that their heat capacities are quite similar. We further predict that $Si_{136}$ has a region of negative thermal expansion below T=140K. Our itab initio prediction shows that thermal expansion in the guest-free $Si_{136}$ clathrate is significantly smaller than the previously reported data of guest encapsulated clathrates. In contrast to similar thermal properties in the two phases, our calculations of lattice thermal conductivities reveal some dramatically different features in the phases. We will discuss the origin of the predicted ''oscillation'' in the current-current correlation functions.

*This work is supported by NSF (EPS0447675 and HRD0317741)

**15:54**

**R16 8 Optical and thermoelectric properties of Tl-filled $CoSb_3$ skutterudites from first-principles*** IN GEE KIM, *Northwestern University* ARTHUR J. FREEMAN, Filled skutterudite antimonides have attracted much interest as a new class of thermoelectric materials.[1] We have determined the electronic structures, optical and thermoelectric propertes of Tl-filled skutterudite $CoSb_3$ by using the highly precise full-potential linearized augmented plane wave (FLAPW) method[2] within the Perdew-Burke-Ernzerhof (PBE)[3] form of the generalized gradient approximation (GGA) to density functional theory. In contrast to the small-gap semiconducting $CoSb_3$, Tl-filled $CoSb_3$ is calculated to be metallic with Tl-*sp* bands stongly hybridized with all the other elements over the entire energy region. The thermoelectric

properties, e.g. the Seebeck coefficient, are evaluated and discussed in terms of the diagonal terms of the optical matrix elements.

*DARPA Grant B529527

[1]B.C. Sales, D. Mandrus, and R. K. Williams, Science **272**, 1325 (1996).
[2]Wimmer, Weinert, Krakauer, Freeman, Phys. Rev. B **24**, 864 (1981).
[3]Perdew, Burke, Ernzerhof, Phys. Rev. Lett. **77**, 3865 (1996).

**16:06**

**R16 9 Low-temperature Thermodynamic Properties of Eu-filled Skutterudites** Y. LUAN, S. BHATTACHARYA, V. KEPPENS, *Department of Materials Science and Engineering,The University of Tennessee, Knoxville, TN 37996* D. MANDRUS, B.C. SALES, *Condensed Matter Sciences Division, Oak Ridge National Laboratory, Oak Ridge, TN 37831* THE UNIVERSITY OF TENNESSEE COLLABORATION, OAK RIDGE NATIONAL LABORATORY COLLABORATION, It is well known that the presence of a ?rattling? atom in filled skutterudite antimonides leads to glasslike thermal properties, complemented by an unusual thermodynamic behavior that indicates the presence of low-energy vibrational modes in addition to the normal acoustic phonons. The current work focuses on a study of $EuFe_4Sb_{12}$, which combines ''rattling'' with magnetic ordering below $T_c = 90$ K. The elastic moduli have been measured as a function of temperature and magnetic field, using resonant ultrasound spectroscopy (RUS). The temperature-dependence of the elastic response is dominated by two phase transitions: the well-known magnetic ordering at 90 K, as well as a second transition at 40 K. In addition, specific heat measurements have been carried out for the same compound. Together these measurements provide us with an extensive set of data, probing the complex thermodynamic behavior of this material.

**16:18**

**R16 10 Effects of Substitution and Grain Size on the High Temperature Thermoelectric Properties of MNiSn Phases.** SLADE CULP, *University of Virginia* S. JOSEPH POON, *University of Virginia* TERRY M. TRITT, *Clemson University* NICOLETA HICKMAN, *Clemson University* BRAD EDWARDS, *Clemson University* UNIVERSITY OF VIRGINIA COLLABORATION, CLEMSON UNIVERSITY COLLABORATION, The merit of n-type Sb doped MNiSn (M=Ti, Zr, Hf) half-Heusler phase, as a promising material for use in high temperature power generation, is exhibited by large thermopower, and small, semimetallic, resistivity values. It has been observed that the level of Sb doping on the Sn site plays a fundamental role in the determining the temperature at which the material will achieve maximum thermoelectric efficiency. Meanwhile, the high thermal conductivity found in ternary MNiSn, can be reduced via mass fluctuations and strain field effects induced through substitution at the M and Ni sites. In addition, the effects of grain size modification, through supplemental synthesis techniques, on the lattice thermal conductivity will be discussed. The combination of substitutions and grain size modification in the ternary half-Heusler system results in a complex thermoelectric material with a figure of merit on the order of ZT=1.

**16:30**

**R16 11 Promising thermoelectric properties in some p-type half-Heuslers** MENG ZHU, S.J. POON, *Dept. of Physics, University of Virginia* V. PONNAMBALAM, T.M. TRITT, *Dept. of Physics and Astronomy, Clemson University* N-type half-Heuslers are well-known due to their potential thermoelectric properties, however, our study shows that p-type half-Heusler alloys can be prepared with promising values. A series of $Hf_xZr_{1-x}Co_yPt_{1-y}Sn_zSb_{1-z}$ samples have been synthesized, and thermoelectric properties have been measured. Our results show that the thermopower (S) increases and resistivity decreases in a good amount. In addition to the high power factors, thermal conductivity ($\kappa$) kept low values, which indicate that we can get promising value by optimizing the combination of elements.

**16:42**

**R16 12 Thermoelectric properties of some p-type half-Heusler alloys*** V. PONNAMBALAM, T.M. TRITT, *Dept. of Physics and Astronomy, Clemson University* MENG ZHU, S.J. POON, *Dept. of Physics, University of Virginia* We have synthesized a series of multi-component p-type half Heusler alloys by simultaneously substituting suitable elements at different crystallographic sites. Both electrical and thermal transport properties of these alloys are studied up to 1000K to evaluate their thermoelectric potential. At 300K, typical thermopower(S) and resistivity($\rho$) values are around $\sim$ 80 $\mu$V/K and $\sim$ 1m$\Omega$-cm respectively. Due to heavy substitution/doping, ($\rho$)-T behavior is similar to that of a degenerate semiconductor and the resistivity increases with increasing T with $\rho$ values in the range of few m$\Omega$-cm at 1000K. Thermopower also increases with increasing T and reaches a maximum of hundreds of $\mu$V/K at 1000K. Room temperature thermal conductivity ($\kappa$) values are about $\sim$ 4.5 W/m-K and these $\kappa$ values are low compared to those of ternary half-Heusler alloys. In well- optimized compositions, these values could improve even further.

*Funding: DOE # DE-FG02-04ER-46139 and SC EPSCoR / Clemson University Cost Share.

**16:54**

**R16 13 Growth, structural, and transport properties of epitaxial $NaxCoO_2$ thin films** ZHIGANG MA, A. VENIMADHAV, D.A. TENNE, QI LI, A. SOUKIASSIAN, X.X. XI, D.G. SCHLOM, R. ARROYAVE, Z.K. LIU, MINHYEA LEE, *Pennsylvania State University* N.P. ONG, *Princeton University* H.P. SUN, XIAOQING PAN, *University of Michigan* Layered cobaltate $NaxCoO_2$ has attracted much attention recently due to its superconductivity and exceptionally high thermoelectric power. Here we report structural, electrical, and thermopower properties of epitaxial and topotaxial $Na_xCoO_2$ thin films on (0001) sapphire substrate. Topotaxial $Na_xCoO_2$ films were prepared by converting an epitaxial $Co_3O_4$ film to $Na_xCoO_2$by annealing in Na vapor and epitaxial $Na_xCoO_2$films were obtained by pulsed laser deposition. Structural analysis showed the films are *c*-axis oriented. For topotaxial films, annealing in different Na vapor pressures resulted in films with different Na concentrations, which showed distinct transport properties. For directly deposited epitaxial films by pulsed laser deposition, deposition parameters are found to control the Na concentration and hence the film properties. The largest thermoelectric power of the samples made by different methods is found to be similar in the range of 70-100 $\mu$V/K at room temperature.

**17:06**

**R16 14 On the Thermoelectric Properties of Layered Cobaltates*** QIANG LI, *Brookhaven National Laboratory* A study on the thermoelectric properties of layered cobaltates is presented, based on the dynamic mean field theory for strongly correlated electron systems. Electron correlation results in a crossover from coherent quasi-particle excitation at low temperature to incoherent excitation at high temperatures in cobaltates. With an extremely narrow quasi-particle bandwidth ($h\omega_c \sim$ 50 meV), the thermal destruction of Fermi-liquid occurs at the moderate crossover temperature $T_M$ ( $\sim$ 200 K), and suggests a new scaling for thermoelectric power $S$ of cobaltates ($S \sim$ kT/ith$\omega_c \sim T/T_M$) at low temperatures. At high temperatures, the dominating incoherent excitation leads to a weak temperature dependent $S$, and electric resistivity $\rho$ approaches the Mott-limit $ha/e^2 \sim$ a few m$\Omega \cdot$ cm for cobaltates, where $a$ is a lattice constant.

*The work was supported by the U. S. Dept. of Energy, Office of Basic Energy Science, under contract No. DE-AC-02-98CH10886.

**17:18**

**R16 15 Microstructure and Growth Mechanism of $Ca_3Co_4O_9$ Thin Films on Si and Glass Substrates*** YUFENG HU, *Condensed Matter Physics and Materials Science Department, Brookhaven National Laboratory* ELI SUTTER, *Center for Functional Nanomaterials, Brookhaven National Laboratory* WEIDONG SI, QIANG LI, *Condensed Matter Physics and Materials Science Department, Brookhaven National Laboratory* It has been discovered recently that cobaltates have very large thermoelectric power, which shows that cobaltates hold great promise to be potential integrated heating spreading solution, such as thermal management of microprocessors. Among the cobaltates, $Ca_3Co_4O_9$ is exhibiting best thermoelectric properties. We have successfully grown highly c-axis orientated $Ca_3Co_4O_9$ thin films using Pulsed Laser Deposition (PLD) technique on amorphous substrates, such as glass. High-resolution electron microscopy (HREM), electron energy-loss spectroscopy (EELS) and dispersive x-ray spectrometry (EDS) have been used to study the chemical composition and microstructure of the films. The detailed microstructure and growth mechanism of $Ca_3Co_4O_9$ thin films will be discussed.

*This work was supported by the U. S. Dept. of Energy, Office of Basic Energy Science, under contract No. DE-AC-02-98CH10886.

**SESSION R17: FOCUS SESSION: SEMICONDUCTORS FOR THZ AND IR II**
**Wednesday Afternoon, 15 March 2006**
**313, Baltimore Convention Center at 14:30**
**A. G. U. Perera, Georgia State University, presiding**

*Contributed Papers*

**14:30**

**R17 1 Dependence of the groundstate interband optical transition in InAs-GaSb superlattices on the width of the GaSb layers** PATRICK FOLKES, J. LITTLE, S. SVENSSON, K. OLVER, *Army Research Laboratory, Adelphi Maryland* A. AMTOUT, S. KRISHNA, *Center for High Technology Materials, University of New Mexico, Albuquerque New Mexico* We have investigated the optical characteristics of a set of InAs-GaSb superlattice structures (SLS) which have InAs layers with a fixed width of 25 Å and GaSb layers whose width varies from stucture to structure over the range 25 Å to 100 Å. Photoluminescence measurements were carried out over the range 10K – 100K on the SLS. Using photodiodes fabricated from the SLS, measurements of the photocurrent-excitation energy spectrum and the time-resolved photoconductivity were carried out at 78K. The observed dependence of the relative oscillator strength of the SLS band-edge transition on the GaSb layer width will be compared with theory[1]. The effect of defects on the the optical and transport properties of the SLS and the dependence of this effect on the GaSb layer width will be discussed.

**14:42**

**R17 2 Comparison of terahertz emission from N-face and In-face indium nitride thin films** GRACE CHERN, *Army Reseach Laboratory* ERIC READINGER, *Army Reseach Laboratory* HONGEN SHEN, *Army Reseach Laboratory* MICHAEL WRABACK, *Army Reseach Laboratory* CHAD GALLINAT, *University of California, Santa Barbara* GREGOR KOBLMUELLER, *University of California, Santa Barbara* JAMES SPECK, *University of California, Santa Barbara* Narrow band gap semiconductors are attractive as emitters of terahertz radiation when optically excited with femtosecond laser pulses. We present a comparison of THz emission from N-face and In-face indium nitride (InN) thin films. The InN samples are optically pumped with a 160 fs laser pulse at 800nm. The subsequent THz radiation is detected by ultrafast electro-optic sampling using a 2mm thick ZnTe crystal. The measured In-face InN films have a Hall mobility of 838 $cm^2$/Vs and 2098 $cm^2$/Vs, and the measured N-face InN samples have a Hall mobility of 645 $cm^2$/Vs and 1460 $cm^2$/Vs. For both polarities, we show an increase in THz power from InN with higher mobilities. However, THz radiation from the In-face InN sample with a Hall mobility of 2098 $cm^2$/Vs is lower in power than from the N-face InN film with a lower Hall mobility of 1460 $cm^2$/Vs. We attribute the lower THz power from In-face InN samples to lower crystalline quality of the In-face material, as determined by x-ray, TEM and photoluminescence measurements. The ratio of the defect density and the PL intensity between the In-face and N-face materials is approximately 3 and 10, respectively.

**14:54**

**R17 3 Electro-Optical characterization of W-structured type-II superlattice photodetectors** J.G. TISCHLER, E.H. AIFER, I. VURGAFTMAN, J.R. MEYER, *Naval Research Laboratory* C.L. CANEDY, E.M. JACKSON, *SFA Inc.* Antimonide based superlattices (SLs) have shown promise as the next generation material system for very long wave infrared focal plane arrays. In particular, we investigated n-i-p diodes with ''W-structured'' type-II SLs, consisting of repetitions of AlGaInSb/InAs/InGaSb/InAs/AlGaInSb layers such that the bulk conduction band-edges of each period forms a ''W'' pattern. The performance of such photodiodes (PDs) depends on a combination of optical and transport properties, such as the absorption coefficient and

minority carrier diffusion length. In order to optimize such devices, it is necessary to measure these properties independently. Using a combination of techniques such as transmission and photoluminescence (PL) spectroscopies, and black-body responsivity measurements, we have systematically studied and optimized our PDs. We have found that the most sensitive parameter that limits the PD performance is the carrier lifetime, making PL measurements the most sensitive characterization technique. We report PDs with up to 100% charge collection efficiency and up to 35% external quantum efficiency.

*Invited Papers*

**15:06**

**R17 4 Recent development of terahertz wave sensing and imaging science, technology, and applications.**
X.-C. ZHANG, *Center for Terahertz Research, Rensselaer Polytechnic Institute, Troy, NY 12180 USA*

Recent advances in THz science and technology make it one of the most promising research areas in the 21st century for sensing and imaging, as well as in other interdisciplinary fields. We believe new T-ray capabilities will impact a range of interdisciplinary fields and industrial companies, including: communications, imaging, medical diagnosis, health monitoring, environmental control, and chemical and biological identification. While microwave and X-ray imaging modalities produce density pictures, T-ray imaging provides spectroscopic information within the THz frequency range. The unique rotational and vibrational responses of materials within the THz range provide information that is generally absent in optical, X-ray and NMR images. A THz wave can easily penetrate and inspect the insides of most dielectric materials, which are opaque to visible light and low contrast to X-rays, making T-rays a useful complementary imaging source in this context. Recent developments of THz wave technologies allow us to coherently control a THz wave (phase, amplitude, and directionality). I present its impacts the physics understanding and industrial applications. Examples of imaging a long distance target ( $>$ 100 meters), large scale industrial samples ( $>$ m2), or a small scale semiconductor device (a few nanometer) will be presented.

*Contributed Papers*

**15:42**

**R17 5 Self-assembled ErAs nanoislands for enhanced terahertz detection.** JOHN O'HARA, ROHIT PRASANKUMAR, *Los Alamos National Laboratory* JOSH ZIDE, ART GOSSARD, *University of California-Santa Barbara* ANTOINETTE TAYLOR, RICHARD AVERITT, *Los Alamos National Laboratory* Traditionally, THz detectors based on photoconductive (PC) antennas have utilized low-temperature grown GaAs (LT-GaAs) and radiation-damaged silicon-on-sapphire (RD-SOS) due to their fast carrier trapping times. However, the development of self-assembled ErAs nanoislands embedded in a GaAs matrix offers a particularly useful alternative for THz PC devices based on the ability to independently tune photo-excited carrier lifetimes, trap density, and dark resistance. In this work, we demonstrate enhanced THz detection using self-assembled ErAs:GaAs nanoisland structures. Three nearly identical THz PC antenna detectors are fabricated; one each on the LT-GaAs, RD-SOS, and ErAs:GaAs substrates. Their performance in a typical THz time-domain spectroscopy system is compared in terms of optical efficiency, bandwidth, and saturation behavior. Carrier lifetimes in all three substrates are also compared via pump-probe techniques.

**15:54**

**R17 6 Type II superlattice infrared focal plane arrays: Optical, electrical, and mid-wave infrared imaging characterization.** JOHN LITTLE, STEFAN SVENSSON, ARNIE GOLDBERG, STEVE KENNERLY, KIM OLVER, *Army Research Laboratory, Adelphi, MD 20783* TRIRAT HONGSMATIP, MICHAEL WINN, PARVEZ UPPAL, *BAE Systems, Nashua, NH 03060* We have studied the infrared optical and temperature dependent electrical properties of 320 x 256 arrays of GaSb/InAs type II superlattice infrared photodiodes. Good agreement between single-pixel and focal plane array measurements of the photon-to-electron/hole conversion efficiency was obtained, and the infrared absorption coefficient extracted from these measurements was found to be comparable to that of HgCdTe with the same bandgap as the type II superlattice. Temperature and voltage dependent dark current measurements and the voltage dependent photocurrent generated by a 300 K background scene were described well using a semi-empirical model of the photodiode. We will show high-quality images obtained from the mid-infrared focal plane array operating at 78 K.

**16:06**

**R17 7 Pulsed THz-emission and carrier concentrations in InN** RICARDO ASCAZUBI, INGRID WILKE, *Rensselaer Polytechnic Institute* WILLIAM SCHAFF, *Cornell University* InN grown on sapphire substrates with GaN or AlN buffer layers exhibits a variety of unique electronic properties for the development of brighter photo-conducting THz-radiation sources. Since InN is a narrow band gap semiconductor it is also an attractive candidate for compact and lightweight THz-spectroscopy and imaging systems based on femtosecond fiber laser operating at 1.55$\mu$m wavelength. The important properties of InN with regard to strong THz-emission are low probability of intervalley scattering and strong intrinsic electric fields near the surface. The electric fields at the InN surface are caused by a strong intrinsic electron surface accumulation. We report on THz-emission of n-type InN with carrier concentrations ranging from $10^{17}$cm$^{-3}$ to $10^{20}$cm$^{-3}$. We observe a strongly increasing THz-emission with decreasing carrier concentrations. Based on charge neutrality the dependence of THz-emission on carrier concentrations is explained by assuming an underpopulated region behind the surface accumulation layer, across which the surface field interacts with photo-injected carriers generating THz-transients. The surface state density calculated within this model agrees well data obtained by high resolution electron energy loss spectroscopy data.

**16:18**
**R17 8 A New All-Optical Imaging Scheme based on QWIP technology** DEBING ZENG, GANG CHEN, RAINER MARTINI, *Dept. of Physics and Engr. Physics, Stevens Institute of Technology* Infrared imaging applications have gained increasing interest over the recent decades due to favorable light propagation, night imaging as well as chemical sensing applications. However, the scalability of the existing techniques towards high resolution in the multi-megapixel range is one of the major challenges in today's IR imaging technologies. Here we present an alternative solution using an all-optical wavelength conversion scheme. QWIP has been successfully proven their potential in IR imaging applications. Yet the fundamental conversion process from IR light to electric current has been one of the major restrictions in such system. To overcome this problem we propose the use of an all-optical conversion scheme, which utilizes an interband resonant optical NIR beam to probe the electrical population of the QW structure. In this methodology the incident MIR radiation changes the occupation of the QWs, which in turn influences the NIR transmission. Hence the irradiated MIR images can be probed by spatially resolved measurement of the NIR transmission, as has been demonstrated by Nada et al. for all-optical switching purposes. In this talk we present an implementation scheme of the all-optical QWIP readout technique together with theoretical calculations of the sensitivity of the proposed device and its temperature dependence. First experimental results will be presented also. The Authors thankfully acknowledge financial support by US Army, Picatinny Arsenal.

**16:30**
**R17 9 A THz Microcavity with a Phononic Cavity Polariton** HADLEY LAWLER, *Naval Research Laboratory* SANJIV SHRESTA, *NIST* GAVIN BRENNEN, *NIST* Polaritons were originally considered within the context of the dielectric response of bulk systems, and its relation to the dispersion of fundamental solid-state excitations, such as excitons and optical phonons. More recently, excitonic cavity polaritons have been theoretically described and observed. These excitonic cavity polaritons represent a tunable Rabi coupling between a condensed matter excitation within a microstructure and a cavity-resonant electromagnetic mode. Like excitons, optical phonons possess well-characterized cross-sections with the electromagnetic field, but at lower energies and larger length and time scales. We present theory relevant to a phononic cavity polariton, discuss the prospects for the observation of such a system, and detail our progress toward the prediction of the Rabi coupling's variation with tunable parameters. While susceptibility-type measurements are a possible route for the detection of such a system, we emphasize the possibility of measuring the Rabi oscillation directly in the time domain using ultrafast lasers.

**16:42**
**R17 10 Interplay between plasmon and current due to terahertz radiation** DANHONG HUANG, *USAF Research Lab (VSSS)* CASEY RHODES, *The Johns Hopkins University* PAUL ALSING, DAVE CARDIMONA, *USAF Research Lab (VSSS)* A unique structure composed of a half-space of air and a semi- infinite n-doped bulk GaAs covered by a heavily-n-doped InAs conducting interface sheet is proposed to explore the physics behind the interplay between a transverse sheet current, evanescent modes, and a longitudinal field in the bulk. The presence of the 3D and 2D plasma waves and the sheet current enables the longitudinal and transverse electromagnetic oscillations to couple in directions both perpendicular and parallel to the conducting sheet. We derive a spatially-nonlocal dynamic theory in order to determine the effects of the longitudinal 3D plasma-wave excitation, transverse sheet current and 2D plasma waves, and evanescent modes on the enhancement of a transmitted near-E-field with an electromagnetic wave incident on our proposed structure. For p-polarized incident field, we find one sharp dip and a broad peak in the transmitted near-E-field due to absorption by the longitudinal 3D plasma wave and its coupling to the transverse sheet current.

**16:54**
**R17 11 Submicron Material Characterization Using Terahertz Scanning Near-Field Microscopy** HOU-TONG CHEN, ANTOINETTE TAYLOR, RICHARD AVERITT, *Los Alamos National Lab* FEDERICO BUERSGENS, ROLAND KERSTING, *University of Munich* The recent development of the apertureless terahertz scanning near-field optical microscope (THz-SNOM) allows for submicron spatial resolution [1] and enables a broad variety of novel applications in material characterization. The basic mechanism is that a metallic probe allows for mapping of the THz permittivity of a surface. In this contribution, we report on measurements of microscopic scale charge carrier distributions and dielectric contrast with sub-micrometer resolution in various material systems and structures using THz-SNOM. We have identified a novel imaging mechanism in terms of a configurational resonance [2], which contrasts the widely accepted scattering model at visible and near-infrared frequencies. [1] H.-T. Chen, et al., Appl. Phys. Lett. **83**, 3009 (2003). [2] H.-T. Chen, et al., Phys. Rev. Lett. **93**, 267401 (2004).



## SESSION R18: FOCUS SESSION: CARBON NANOTUBES: TRANSPORT II
**Wednesday Afternoon, 15 March 2006; 315, Baltimore Convention Center at 14:30**
**Brian LeRoy, TU Delft, presiding**

***Invited Papers***

**14:30**
**R18 1 Quantum Dephasing and Decoherence in Carbon Nanotubes: Role of Electron-Phonon coupling.** STEPHAN ROCHE, *CEA*

In this talk, the role of electron-phonon coupling on quantum transport is addressed in clean and disordered carbon nanotubes. Defects and impurities are modelled by static disorder, whereas dynamic disorder is driven by the time-dependent vibrations of carbon atoms, that impact on the electronic overlap matrix coupling. On the basis of the Kubo framework in the coherent regime, the conductance scaling properties in the weak localization regime are explored, and from the incorporation of the superimposed effect of acoustic phonon modes phonon, the energy-dependent coherence

length and coherence times will be derived, following a phenomenological perspective. Additionally, the strong disturbance of the electronic structure due to optic modes is analyzed, and shown to strongly alter the conductance scaling behaviour of both metallic and semiconducting otherwise clean nanotubes. Consequences for the high-bias regime of nanotubes-based field effect transistors and limitations of semi-classical focus will be discussed.

*Contributed Papers*

**15:06**

**R18 2 Combined electrical transport and STM of carbon nanotubes** B.J. LEROY, I. HELLER, V.K. PAHILWANI, C. DEKKER, S.G. LEMAY, *Kavli Institute of Nanoscience, Delft University of Technology* We have performed simultaneous electrical transport and scanning tunneling spectroscopy measurements on suspended carbon nanotubes. By combining these two measurement techniques we are able to probe the electronic states involved in transport through the nanotube. The spectroscopy shows peaks due to Coulomb blockade, which split and change energy as a function of the source-drain voltage across the nanotube. These peaks track the Fermi level of the source and drain electrodes. Unexpectedly, the strength of the peaks also depends on position along the tube.

**15:18**

**R18 3 Role of electronic excitations in ion collisions with carbon nanostructures.*** DAVID TOMANEK, *Michigan State University* YOSHIYUKI MIYAMOTO, *NEC Corporation* ARKADY KRASHENINNIKOV, *Helsinki University of Technology* We study the effect of electronic excitations during collisions of protons with $sp^2$ bonded carbon nanostructures by performing molecular dynamics simulations. To obtain microscopic insight into the collision process in real time, we combine time-dependent density functional calculations for electrons with molecular dynamics simulations for ions, and compare the results to molecular dynamics simulations in the electronic ground state. The simulations for protons colliding with carbon nanotubes and graphite are performed in the interesting range of impact energies of tens to hundreds of eV, corresponding to ion velocities covering a broad range around the Fermi velocity of the target, $v_F = 8 \times 10^5$ m/s. In agreement with the binary collision approximation, we find only negligible deviations from Born-Oppenheimer dynamics for projectile velocities well below the Fermi velocity. Our results establish validity limits for the Born-Oppenheimer approximation, and also the threshold energy for sputtering of carbon nanotubes and graphite.

*Supported by NSF NSEC grant EEC-425826.

**15:30**

**R18 4 Electrical conducting and breakdown behaviors of multiwall carbon nanotubes under different contact modes** SHUO CHEN, J.Y. HUANG, S.H. JO, Z.Q. WANG, D.X. HAN, *Boston College* G. CHEN, M. DRESSELHAUS, *MIT* Z.F. REN, *Boston College* We have carried out electrical transport property studies of individual multiwall carbon nanotubes while viewing the structural changes in-situ inside a high resolution transmission electron microscope. Two types of contact have been tested: end-contact with all layers contacted with the electrodes, and side-contact with only the outmost layer contacted with the electrodes. We found that in some cases electrical breakdown takes place in the innermost layer under both contact modes with a simultaneous current drop, which indicates that under high bias voltage, each layer carries a current even there is no direct contact with the electrodes. Eexperimental evidence shows that the temperature can reach around 3000 °C during breakdown, so the inter-layer conducting could be induced by strong electric field or by thermal excitation.

**15:42**

**R18 5 Distinct properties of single-wall carbon nanotubes with sidewall chemical functionalization** JIANPING LU, HYOUNGKI PARK, *Univ. of North Carolina at Chapel Hill* JIJUN ZHAO, *Washington State University* itAb initio calculations reveal distinct electronic properties associated with side wall functionalization of SWNTs. The metallic tubes are found to be more reactive than the semiconducting ones. The hybridization between the addend and the tube induces unique impurity states near the Fermi level. For semiconducting tubes the state is localized near the functionalized site with a characteristic length of 15 Å. In contrast, the impurity state is extended and acts as a strong scattering centre in metallic tubes. This effect greatly hinders the ballistic transport of electrons along the metallic nanotubes. The characteristic dependence of the electronic states and the conductance on functional molecules provides possible pathways for chemical sensor applications and the band structure engineering.

**15:54**

**R18 6 Effects of sidewall functionalization on the conducting properties of SWNTs** HYOUNGKI PARK, *Univ. of North Carolina at Chapel Hill* JIJUN ZHAO, *Washington State University* JIANPING LU, *Univ. of North Carolina at Chapel Hill* We investigated the conducting properties of sidewall functionalized SWNTs with a finite addend concentration. Robust differences are found between monovalent and divalent addends. For monovalent addition a small number of addends can significant disrupt the ballistic conductance of nanotubes near the Fermi level. As the addend concentration increases the conductance rapidly decreases and approaches zero at addends to C ratio around 25%. In contrast, divalent addends have only weak effects on the conducting properties and the nanotube quantum conductance remains above 1 even for addend concentration as large as 25%. These differences can be attributed to the formation of impurity state near the Fermi level for monovalent addition, while divalent addends create impurity states far away from the Fermi level.

**16:06**

**R18 7 Theory of scanned-gate microscopy of carbon nanotubes and nanowires** MATTHEW ZHANG, MISHA FOGLER, *UCSD* We model theoretically a scanned-gate microscopy experiment where a Coulomb-blockaded metallic carbon nanotube (nanowire) is probed by an AFM tip. The tip modifies the charge of the nanotube via an electrostatic coupling. The amount of induced charge can have a complicated dependence on the position and the voltage of the tip in a realistic experimental situation where several screening gates and nearby stray charges may be present, which may obscure the interpretation of the results. We demonstrate that such difficulties can be significantly reduced in the geometry where a nearby backgate screens the electrostatic interactions making them short-range. We show that it is then possible to calculate and simply distinguish among different con-

tributions to the induced charge. Combining the above electrostatic modelling with many-body bosonization methods we demonstrate that the presence of the tip causes an oscillatory shift in the Coulomb blockade peak positions. We show that the amplitude and the phase of this shift can be used to study the spin-charge separation and Luttinger-liquid effects in one-dimensional wires.

**16:18**

**R18 8 Re-entrant semiconducting behavior of zigzag carbon nanotubes on substitutional doping by oxygen dimers** SEUNG-HOON JHI, *Department of Physics, POSTECH* The electronic structures of carbon nanotubes doped with oxygen dimers are studied using the *ab initio* pseudopotential density functional method. The fundamental energy gap of zigzag semiconducting nanotubes exhibits a strong dependence on both the concentration and configuration of oxygen dimer defects that substitute for carbon atoms in the tubes and on the tube chiral index. For a certain type of zigzag nanotube when doped with oxygen dimers, the energy gap is closed and the tube becomes semimetallic. At higher oxygen-dimer concentrations the gap reopens, and the tube exhibits semiconducting behavior again. The change of the band gap of the zigzag tube is understood in terms of their response to the strains caused by the dimer substitutional doping.

**16:30**

**R18 9 Modulated conduction in single-walled carbon nanotubes using covalently bound chromophore functionalities** JASON SIMMONS, *Department of Physics* TYLER MARK, *Department of Chemical Engineering* GUANGDE CHEN, *Department of Chemistry* VICTORIA CAMPBELL, PADMA GOPALAN, *Department of Materials Science & Engineering* MARK ERIKSSON, *Department of Physics, University of Wisconsin - Madison* Carbon nanotube hybrid materials are widely studied in order to leverage the exceptional thermal and electronic properties for a number of applications. We demonstrate an optically active nanotube-hybrid material by covalently functionalizing single-walled nanotubes with an azo-based chromophore. Upon UV illumination, the conjugated chromophore functionality undergoes a cis-trans isomerization, breaking the conjugation and modulating the conductance of individual functionalized nanotubes. Though there is most likely no direct charge transfer between the chromophore and the nanotube, the isomerization results in a charge redistribution near the nanotube, modifying the local electrostatic environment and causing the change in conductance. Further, the conductance change is reversible; indicating that the chromophore functionalized nanotubes can be used as reversible photo-switches.

**16:42**

**R18 10 Electron Transport in Carbon Nanotubes with Superconducting Contacts** ALEXANDER MAKAROVSKI, GLEB FINKELSTEIN, *Duke University, Department of Physics* We report on our measurements of electron conductance in single-walled carbon nanotubes contacted by superconducting leads. We study the proximity effect induced by the superconducting contacts at temperatures below the transition temperature of the leads. Excess differential conductance (way above the ballistic limit of $4e^2/h$ for a single-wall nanotube with normal contacts) and subgap Andreev reflection peaks are observed.

**16:54**

**R18 11 Superconductivity in entirely end-bonded multi-walled carbon nanotubes** JUNJI HARUYAMA, IZUMI TAKESUE, NAOKI KOBAYASHI, *Aoyama Gakuin University* SHOHEI CHIASHI, SHIGEO MARUYAMA, *Tokyo University* TOSHIKI SUGAI, HISANORI SHINOHARA, *Nagoya University* One-dimensional (1D) systems face some obstructions that may prevent the emergence of superconductivity(SC), e.g., 1.a Tomonaga-Luttinger liquid (TLL), 2.Peierls transition, and 3.Low density of states due to VHSs. A carbon nanotube (CN) is one of the best candidates for investigating a possibility of 1D SC and its interplay with such obstructions. Only two groups have experimentally reported SC in ropes of single-walled CNs (SWNTs) and very thin SWNTs [1] to date. In addition, those interplay with 1D phenomena have never been clarified. Some theoretical papers also predicted strong correlation between TLL states and SC for SWNT ropes and importance of electron-phonon interaction for thin SWNTs [2]. Here, we report that entirely end-bonded multi-walled CNs (MWNTs) can show SC with the $T_c$ as high as 12K [3] (about 50-times larger than $T_c$ in former of [1]). We find that emergence of this SC and its interplay with TLL states are highly sensitive to junction structures of Au electrode/MWNTs. Only MWNTs with optimal numbers of electrically activated shells realized by the entire end-bonding can allow the SC due to intershell effects. 1. M. Kociak, et al., PRL 86, 2416 (2001); Z. K. Tang, et al., Science 292, 2462 (2001), 2. J.Gonzalez, PRL 88, 076403 (2002); R.Barnett, et al., PRB 71, 035429 (2005), 3. J.Haruyama et al., PRL Accepted

**17:06**

**R18 12 Zero-bias anomaly and possible superconductivity in single-walled carbon nanotubes** JIAN ZHANG, ALEXANDER TSELEV, YANFEI YANG, KYLE HATTON, PAOLA BARBARA, *Department of Physics, Georgetown University, Washington, DC 20057* SERHII SHAFRANIUK, *Physics and Astronomy Department, Northwestern University, Evanston IL 60208* We report measurements of field-effect transistors made of isolated single-walled carbon nanotubes contacted by superconducting electrodes. For large negative gate voltage, we find a dip in the low-bias differential resistance. Surprisingly, this dip persists well above the superconducting transition temperature of the electrodes, indicating that it is not caused by superconducting proximity effect from the electrodes. This conclusion is supported by measurements on carbon nanotubes contacted by normal electrodes showing similar features. One possible explanation is superconductivity in the nanotubes.

**17:18**

**R18 13 Shell filling and excited states in a fully tunable double quantum dot on a carbon nanotube** SAMI SAPMAZ, CAROLA MEYER, PIOTR BELICZYNSKI, PABLO JARILLO-HERRERO, LEO KOUWENHOVEN, *Kavli Institute of Nanoscience Delft* We have realized fully controllable and tunable nanotube quantum dots defined with electrostatic top-gates. Using three electrostatic top-gates we have made a NT double dot. Clear honeycomb patterns are observed in the charge stability diagram as a function of two independent side-gates. Furthermore, for the first time we have observed discrete excitations at finite bias. The origin of these excitations is discussed. The central top-gate is used to control the coupling between the two NT dots. Controlling electron interactions in a molecular system is important for many applications such as for example quantum computation.

**SESSION R19: FOCUS SESSION: SPIN HALL EFFECT AND SPIN TRANSPORT**
**Wednesday Afternoon, 15 March 2006; 316, Baltimore Convention Center at 14:30**
**Allan MacDonald, University of Texas, presiding**

*Invited Papers*

**14:30**
**R19 1 Theory of Spin Hall Effect in GaAs.**
HANS-ANDREAS ENGEL, *Harvard University*

In the spin Hall effect, an electric current in a system with spin-orbit coupling induces a transverse spin current which leads to non-equilibrium spin accumulation near sample boundaries. Generating and manipulating non-equilibrium spin magnetization by electric fields is one of the most desirable goals of semiconductor spintronics, because electric fields have potentialities for accessing individual spins at nanometer scales. In this talk, I review the different spin-orbit coupling mechanisms in direct gap semiconductors and the implications of these mechanisms for the spin Hall effect. In particular, we recently developed a theory that accounts for spin-orbit coupling at charged impurities. This coupling leads to itextrinsic spin currents that contain skew scattering and side jump contribution [1]. Applying our theory to bulk n-GaAs, without any free parameters, we find spin currents that are in reasonable agreement with recent experiments by Kato et al. [2]. Also, such contributions are important for p-doped GaAs. Furthermore, we analyzed the effect of itintrinsic spin-orbit coupling in the presence of anisotropic impurity scattering, and found that, somewhat surprisingly, an electrical field can lead to a bulk magnetization component itperpendicular to both the spin-orbit field and an external magnetic field. These works have been done in collaboration with B.I. Halperin, E.I. Rashba, and A.A. Burkov. [1] H.-A. Engel, B.I. Halperin, and E.I. Rashba, Phys. Rev.Lett. **95**, 166605 (2005). [2] Y.K. Kato, R.C. Myers, A.C. Gossard, and D.D. Awschalom, Science **306**, 1910 (2004).

*Contributed Papers*

**15:06**
**R19 2 Spin Hall Current Induced Edge-Spin Accumulation in Two-Dimensional Electron and Hole Systems** KENTARO NOMURA, *Department of Physics, University of Texas at Austin* JAIRO SINOVA, NIKOLAI SINITSYN, TOMAS JUNGWIRTH, JOERG WUNDERLICH, BERND KAETSNER, ALLAN MACDONALD, In spintronic devices, spin densities have traditionally been generated by external magnetic fields, circularly polarized light sources, or by spin injection from ferromagnets. Recently there has been considerable interest in a new strategy in which edge spin densities are generated electrically via the spin Hall effect. We have performed numerical studies on spin transport in two-dimensional systems with various spin-orbit interactions including both intrinsic and extrinsic effects. We find that the spin Hall current strongly depends on the character of the spin-orbit interactions. We address the relation between bulk spin currents and edge spin accumulations, and compare our results with recent experimental observations. K. Nomura, J. Sinova, N. A. Sinitsyn, A. H. MacDonald, Phys. Rev. B 72 165316 (2005). K. Nomura, J. Wunderlich, J. Sinova, B. Kaetsner, A. H. MacDonald, T. Jungwirth, to appear in Phys. Rev. B 72. J. Wunderlich, B. Kaetsner, J. Sinova, T. Jungwirth, Phys. Rev. Lett. 94, 047204 (2005).

**15:18**
**R19 3 Spin Hall effect in p-type semiconductors in magnetic fields** MEHDI ZAREA, SERGIO ULLOA, *Ohio University* We calculate the spin Hall conductivity driven by Rashba spin-orbit interaction in *p*-type two-dimensional semiconductors in the presence of a perpendicular magnetic field. For a highly confined quantum well the eigenstates and eigenvalues of the system, described by a *k*-cubic Rashba term for heavy holes, can be described by Landau spinor states, as in the *k*-linear case [1]. The contribution of the interband transitions to the Kubo-Greenwood formula gives the density-dependent *conventional* spin Hall conductivity, which approaches its universal value $\sigma^{z}_{xy} = 9e/8\pi$ for weak spin-orbit coupling and low Fermi energies, in agreement with previous work. However, two intraband contribution terms cancel this effect, resulting in *zero* conventional spin Hall conductivity. Adding the torque dipole contribution to the definition of spin current, we also study the *effective* spin conductivity. This is shown to be proportional to the total magnetization plus surface terms which exactly cancel it for small spin-orbit coupling. The fact that both effective and conventional spin Hall conductivities vanish is unexpected, especially as one expects the intraband transitions to evolve into vertex corrections for low magnetic fields. Supported by NSF-NIRT. [1] M. Zarea and S. E. Ulloa Phys. Rev. B 72, 085342 (2005).

**15:30**
**R19 4 Non-linear charge and spin Hall effect caused by insulating or charged disks in a two dimensional electron gas** DAVID SCHMELTZER, HSUAN-YEH CHANG, *City College of New York* We show that a time depend electric field in the presence of static vortices caused by insulating regions induces a non-linear time average Hall effect without breaking time reversal symmetry. A time dependent electric field will induce a time dependent Lorentz force in the presence of static vortices of size *D* giving rise to a Hall voltage in a two dimensional electronic gas. The origin of the vortices are insulating regions which cause the electronic wave function to vanish. This theory can explain the recent experiment in a two dimensional GaAs/AlGaAs dot with insulating disks. In this experiment, a driving microwave field in the y-direction has been applied and a DC voltage has been measured in the x-direction. When the insulating disks are replaced by charged disks, we suggest that the Aharonov-Casher effect will induce a spin-Hall effect.

**15:42**

**R19 5 The Helical Liquid and the Edge of Quantum Spin Hall Systems** CONGJUN WU, *Kavli Institute for Theoretical Physics, UCSB* B. ANDREI BERNEVIG, SHOU-CHENG ZHANG, *Physics Department, Stanford University* The edge states of the recently proposed quantum spin Hall systems constitute a new symmetry class of one-dimensional liquids dubbed the ''helical liquid,'' where the spin orientation is determined by the direction of electron motion. We prove a no-go theorem which states that a helical liquid with an odd number of components cannot be constructed in a purely 1D lattice system. In a helical liquid with an odd number of components, a uniform gap in the ground state can only appear when the time-reversal (TR) symmetry is spontaneously broken by interactions. On the other hand, a correlated two-particle backscattering term by an impurity can become relevant while keeping the TR invariance. We further study the Kondo effect in such a liquid which exhibits new features in the structure of the screening cloud.

**15:54**

**R19 6 ''Spin-orbit'' susceptibility in the quantum spin Hall systems** SHUICHI MURAKAMI, *Department of Applied Physics, University of Tokyo* There are two classes of insulators showing the spin Hall effect. One is a spin Hall insulator such as PbTe while the other is a quantum spin Hall system. They are distinguished by an absence or presence of edge states. To study such insulators showing the spin Hall effect, we construct a spin analog of the Středa formula. We use the conserved spin current as proposed by Zhang et al.[cond-mat/0503505], thereby the resulting Středa formula becomes quite simple (i.e. without any $\dot{\mathbf{s}}$ terms). As a result, the spin Hall conductivity for band insulators is proportional to a ''spin-orbit'' susceptibility, representing a response of the orbital magnetization to the Zeeman field (or equivalently a response of the spin magnetiation to the orbital magnetic field). We apply the result to real systems such as $Bi_{1-x}Sb_x$, because in insulating $Bi_{1-x}Sb_x$ the diamagnetic susceptibility is largely enhanced due to the spin-orbit coupling.

**16:06**

**R19 7 Stability of the quantum spin Hall effect with disorder and interactions** CENKE XU, JOEL MOORE, *University of California Berkeley* The stability to interactions and disorder of the quantum spin Hall effect (QSHE) proposed for time-reversal-invariant 2D systems is discussed. The QSHE requires an energy gap in the bulk and gapless edge modes that conduct spin-up and spin-down excitations in opposite directions. When the number of Kramers pairs of edge modes is odd, certain one-particle scattering processes are forbidden due to a topological $Z_2$ index. However, two particle scattering processes can localize the edge modes and destroy the QSHE: the region of stability for both classes of models (even or odd number of Kramers pairs) is obtained explicitly. For a single Kramers pair the QSHE is stable to weak interactions and disorder, while for two Kramers pairs it is not; however, the two-pair case can be stabilized by *either* finite attractive or repulsive interactions. We also discuss a mechanism to generate 1D localized states in magnetic semiconductors. These states are localized by the domain wall between two opposite ferromagnetic orderings. The total number of these localized states can be expressed in terms of a real space topological number. The existence of these localized states can result in a quantum spin Hall effect as well as a quantum charge Hall effect.

**16:18**

**R19 8 Mesoscopic Spin Hall effect** PHILIPPE JACQUOD, *University of Arizona* INANC ADAGIDELI, *University of British Columbia* We focus on the mesoscopic spin Hall effect in ballistic microstructures. Using an extension of Landauer-Buttiker formalism, we calculate the average and variance of spin Hall conductance using the semiclassical approximation as well as Random Matrix theory. We compare these calculations to numerical simulations. We show in particular that the diagonal contribution corresponding to the classical (spin)conductance vanishes. However, interference corrections lead to a finite spin-Hall conductance. This conductance depends crucially on whether the system is regular or chaotic.

**16:30**

**R19 9 The pseudospin degree of freedom and dynamics in degenerate bands** QIAN NIU, *The University of Texas at Austin, Austin, TX 78712* DIMITRIE CULCER, *Advanced Photon Source, Argonne National Laboratory, Argonne, IL 60439 and Department of Physics, Northern Illinois University, De Kalb, IL 60115* Carriers in degenerate bands possess an additional degree of freedom, which may be regarded as a pseudospin. In a wave- packet picture, along with the center of mass motion in crystal momentum and real space, one must also take into account the probability amplitudes, which characterize the inter-band dynamics. The additional degree of freedom introduces nontrivial non-Abelian corrections to the carrier dynamics. These corrections include non-Abelian Berry curvature terms and a non-Abelian correction to the group velocity. For the four- band Luttinger model we will demonstrate that, under the action of an electric field, coherent wave-packet evolution leads to separation of up and down spins, discussing the role of the pseudospin in this process. We find that the helicity in the four band model can be expressed in terms of the pseudospin and is not conserved in an electric field. In addition, we will discuss the role of the pseudospin in determining the Landau levels in the Luttinger Hamiltonian by semiclassical quantization.

**16:42**

**R19 10 Transport Equations and Spin-Charge Propagating Mode in a Two Dimensional Hole Gas with Spin-Orbit Coupling** TAYLOR HUGHES, ANDREI BERNEVIG, *Stanford University* YAROSLAW BAZALIY, *IBM Almaden Research Center* SHOU-CHENG ZHANG, *Stanford University* We find that the spin-charge motion in a strongly confined two-dimensional hole gas (2DHG) supports a propagating mode with cubic dispersion apart from the diffusive mode due to momentum scattering. Propagating modes seem to be a generic property of systems with spin-orbit coupling. Through a rigorous Keldysh approach, we obtain the transport equations for any system with spin-orbit coupling that can be represented using spin- 1/2 matrices. We specialize to the 2DHG and analyze the behavior of the hole spin relaxation time, diffusion coefficients, and spin-charge coupled motion. We also confirm the value of the spin Hall conductivity in the ballistic regime and discuss the viability of the propagating mode.

**16:54**

**R19 11 Spin-orbit coupling and Zeeman splitting of holes in GaAs nanostructures grown in [113] direction** TAISUKE MINAGAWA, YULI LYANDA-GELLER, *Department of Physics, Purdue University* We have calculated the anisotropic spectrum, g-factor and spin- orbit interactions for hole carriers in GaAs quantum wells grown in direction [113], and quantum wires and

quantum dots confined to such quantum wells. We have developed a simple analytical approach for calculations of spectra of holes confined to nanostructures within the Luttinger Hamiltonian scheme, which allows us to compute the wave functions and energies without invoking admixtures of ''light'' and ''heavy'' holes perturbatively. We have identified the dominant spin-orbit interaction terms and discuss their effects on dynamics of holes in external magnetic and electric fields. We have also calculated spin relaxation and dephasing times for 2D holes quantized along [113] direction.

**17:06**

**R19 12 Spin-orbit induced spin precession in 2D hole systems** DIMITRIE CULCER, *Advanced Photon Source, Argonne National Laboratory, Argonne, IL 60439 and Department of Physics, Northern Illinois University, De Kalb, IL 60115* CHRISTIAN LECHNER, *Institut fuer Theoretische Physik, Universitaet Regensburg, D-93040 Regensburg, Germany* ROLAND WINKLER, *Advanced Photon Source, Argonne National Laboratory, Argonne, IL 60439 and Department of Physics, Northern Illinois University, De Kalb, IL 60115* It is well known that two-dimensional hole systems are characterized by an effective spin 3/2. Recently it was shown that the spin density matrix for such spin-3/2 systems can be decomposed into a sequence of multipoles which has important contributions from higher-order multipoles beyond the ones known for electron systems [1]. We will show that these multipoles can precess even in the absence of a magnetic field if strong spin-orbit interactions are present. Particularly simple and enlightening expressions for the spin polarization and higher order multipoles emerge in certain geometries. We will discuss an experimental setup in which this precession can be observed and investigate promising spintronics applications. [1] R. Winkler, Phys. Rev. B 70, 125301 (2004)

**17:18**

**R19 13 A Luttinger Hamiltonian is not enough** M.C. CHANG, C.P. CHUU, Q. NIU, *University of Texas at Austin* In the study of spintronics, it is important to understand carrier transport in multiple energy bands, such as in the conduction or valence bands in semiconductors. Such bands are often described by effective Luttinger Hamiltonians, derived from k.p perturbation and symmetry considerations. A closely related case is the Pauli Hamiltonian, which suppose to give an effective description for the upper Dirac bands in the non-relativistic limits. Here we show that such an effective Hamiltonian alone is not really sufficient. Various Berry phase type corrections must be supplemented to give proper description of electron charge and spin dynamics.



**SESSION R20: FOCUS SESSION: MULTIFERROICS III: PEROVSKITES**
**Wednesday Afternoon, 15 March 2006**
**317, Baltimore Convention Center at 14:30**
**Craig Fennie, Rutgers University, presiding**

**14:30**

**R20 1 Multiferroicity of $BiMnO_3$ reexamined from first principles.** TATSUYA SHISHIDOU, TAMIO OGUCHI, *ADSM, Hiroshima University* $BiMnO_3$ is believed to show both ferromagnetic and ferroelectric orders. In contrast to its robustly confirmed ferromagnetism, only one experimental group has succeeded in observing ferroelectric hysteresis loop[1]. Another group has reported small magnetocapacitance effect around the ferromagnetic Curie temperature[2]. Using first-principles scalar-relativistic full-potential linear augmented plane wave (FLAPW) method and adopting the experimental lattice data, we have given several significant insights on physical properties of $BiMnO_3$ [3]. Further extended results will be shown in this talk. With including spin-orbit interaction, possible directional coupling between the polarization and magnetization will be discussed together with magnetocrystalline anisotropy. Results of structual optimization based on the first-principles atomic forces will be presented to verify its ferroelectricity. Possible doping effect will also be explored. [1] A. Moreira dos Santos *et al.*, Solid State Commun. **122** 49 (2002). [2] T. Kimura *et al.*, Phys. Rev. B **67** 180401(R) (2003). [3] T. Shishidou, N. Mikamo, Y. Uratani, F. Ishii, and T. Oguchi, J. Phys.: Condens. Matter **16** S5677 (2004).

**14:42**

**R20 2 Orbital order, ferromagnetism, and ferroelectricity of $BiMnO_3$ and related compounds** CHANHO YANG, TAEYEONG KOO, YOON HEE JEONG, *Dept of Physics, POSTECH* Multiferroic materials, where ferroelectricity and magnetism coexist, have been actively studied. This class of materials would offer a large application potential for new devices taking advantage of two coupled degrees of freedom based on local off-centered distortion and electron spin. Although most often the magnetic state in coexistence with ferroelectricity is antiferromagnetic, $BiMnO_3$ is an interesting exception with the simultaneous existence of ferromagnetism and ferroelectricity. However, the transition temperatures are in great disparity with $T_{FE} = 770$ K and $T_{FM} = 105$ K, and consequently its ME coupling is not large. In this talk, we will report on three aspects of $BiMnO_3$: (1) Long range ordering of 3d-orbital of $Mn^{3+}$ ions and its influence to the ferromagnetism and ferroelectricity (2) How to create a system to induce a large inter- property coupling by modifying $BiMnO_3$ (3) How to obtain a material with a large inter-coupling at room temperature

**14:54**

**R20 3 Magnetic Ferroelectrics Bi,Pb-3*d* Transition Metal Perovskites** MASAKI AZUMA, KAZUHIDE TAKATA, TAKASHI SAITO, YUICHI SHIMAKAWA, MIKIO TAKANO, *Inst. Chem. Res., Kyoto Univ.* SEIJI NIITAKA, *Mag. Res. Lab., RIKEN* ALEXEI BELIK, *ICYS, NIMS* SHINTARO ISHIWATA, *Dept. Appl. Phys., Waseda Univ.* Magnetic ferroelectrics attract much attention because of the possible application for the memory device and the fascinating coupling between magnetic and dielectric properties. A classical way to obtain a magnetic ferroelectric is to locate $Bi^{3+}$ or $Pb^{2+}$ ions and a magnetic transition metal ion on A and B sites of perovskite structure. The $6s^2$ lone pair and the strong covalent character of Bi(Pb)-O bonds stabilize a noncentrosymmetric distorted structure. For example, $BiFeO_3$ and $BiMnO_3$ are established antiferromagnetic and ferromagnetic ferroelectrics, respectively. We have studied structure, magnetic and electric properties of $BiMO_3$ with $M$=Cr, Co and Ni and $PbVO_3$ stabilized by high-pressure synthesis. $BiCrO_3$ is an antiferromagnetic ferroelectric with $BiMnO_3$ type structure. $BiCoO_3$ and $PbVO_3$ are found to have tetragonal $PbTiO_3$ type structures with expected polarizations of $\sim 100 \mu C/cm^2$. $BiNiO_3$crystallizes in a triclinic structure

where disproportionation into $Bi^{3+}$ and $Bi^{5+}$ takes place. We have also succeeded in preparing a designed ferromagnetic ferroelectric double provskite $Bi_2NiMnO_6$. In this compound, NaCl type ordering of $Ni^{2+}$ ($e_g^1$) and $Mn^{4+}$ ($t_{2g}^3$) leads to ferromagnetism with $T_C$=140 K.

**15:06**

**R20 4 Dielectric, magnetic, magneto-optical and nonlinear optical properties of ferroelectric ferromagnetic semiconductor $BiMnO_3$ from first-principles calculations** GUANG-YU GUO,* HAI-QING LIN, *Department of Physics, Chinese University of Hong Kong, Shatin, Hong Kong* $BiMnO_3$ is a biferroic (ferroelectric and ferromagnetic) semiconductor, and hence a member of the family of multiferroic materials. In order to gain a full understanding of its interesting properties such as biferroic behavior, we have calculated from first-principles the electronic structure, exchange coupling, linear and non-linear optical susceptibilities as well as magneto-optical Kerr rotation of $BiMnO_3$. The calculations are based on density functional theory with generalized gradient approximation plus on-site Coulomb correlation (GGA+U). The all-electron full potential linearized augmented plane wave (FLAPW), frozen core full potential projector augmented wave (PAW), and also all-electron tight-binding linear muffin-tin orbital methods (TB-LMTO) are used. In this contribution, we will present and analyze the obtained exchange coupling parameters, magneto-optical Kerr rotation spectra, dielectric constants and second-harmonic generation coefficients.

*On sabbatical leave from Department of Physics, National Taiwan University, Taipei, Taiwan

**15:18**

**R20 5 Properties and superlattice for multiferroics $BiMnO_3$.*** C.Q. JIN, Z.H. CHI, H. YANG, R.C. YU, S.M. FENG, F. Y. LI, *Institute of Physics, Chinese Academy of Sciences* Single-phase multiferroics $BiMnO_3$ceramic was synthesized via high-pressure high-temperature technique. Microstructure modification accompanied by emergence of superlattice due to electron-beam irradiation was observed wherein by means of ED and HRTEM. Magnetic evaluation manifesting a unique ferromagnetic phase transition at 103 K has corroborated our speculation that as-prepared BiMnO3 ceramic is free of polymorphism at room temperature. Furthermore, magnetization versus temperature ($M - T$) characterization combined with itin situ variable temperature powder X-ray diffraction (XRD) and dielectric constant versus temperature ($\varepsilon$-T) spectrum scanning confirmed that as-prepared $BiMnO_3$ specimen exhibits simultaneous occurrence of ferromagnetism and ferroelectricity below its ferromagnetic Curie temperature ($T_M$)of 103 K.

*This work was supported by NSF and Ministry of Science and Technology of China through the research projects.

**15:30**

**R20 6 Structural Investigations of Bi-containing, multiferroic thin films using Second Harmonic Generation** ERNST KNOESEL, S.E. LOFLAND, K.F. McDONALD, C.J. MEETING, *Rowan University* M. MURAKAMI, M. ARANOVA, I. TAKEUCHI, *University of Maryland* The intensity and polarisation of the bulk second harmonic generation (SHG) from thin films depends critically on the second-order susceptibility tensor, which in turn is strongly influenced by the crystal structure of the film. Multiferroic $BiMO_3$ (M=Fe,Cr) thin films were grown epitaxially as thin films on varies substrates with changing orientations. We have found a substantial bulk SHG signal from of these materials and performed comparative magnetic field and temperature dependent studies. The implication with respect to crystal structure, magnetic phase transitions and multiferroic properties are discussed.

**15:42**

**R20 7 Multiphase Formation In Bi based Multiferroic Thin Films: Structural Change And Strain Relaxation*** SUNG HWAN LIM, MAKOTO MURAKAMI, SHIGEHIRO FUJINO, MANFRED WUTTIG, ICHIRO TAKEUCHI, LOURDES G. SALAMANCA-RIBA, *University of Maryland, College Park* WENDY LYNN SARNEY, *Army Research Laboratories, Adelphi, Maryland* Bi based multiferroic epitaxial thin films like, Bi-Fe-O and Bi-Mn-O were grown on $SrTiO_3$(001) substrates by pulsed laser deposition under various oxygen partial pressures (0.1 – 20 mTorr) and thickness (35 – 500 nm). The structural properties of impurity phases in these systems were characterized by transmission electron microscopy, x-ray diffraction, and energy dispersive x-ray spectroscopy. In the Bi-Fe-O system growth at oxygen partial pressures lower than 5 mTorr gives rise to the formation of the canted antiferromagnetic phase, $\alpha$-$Fe_2O_3$ with a columnar structure in a matrix of $BiFeO_3$. Simultaneously, ferromagnetic phase, $\gamma$-$Fe_2O_3$ precipitates with plate-like structure in the $\alpha$-$Fe_2O_3$ matrix. Similarly, $Mn_3O_4$ impurity phase forms in the Bi-Mn-O system when the films are grown at low oxygen partial pressure. In Bi-Fe-O film, the friction of $\gamma$-$Fe_2O_3$ enhances the magnetic properties of the film, while $\alpha$-$Fe_2O_3$ reduces the compressive stress in $BiFeO_3$ due to its smaller volume compared to that of $BiFeO_3$. We also report structural and magnetic properties of $BiCrO_3$ thin film, a new multiferroic material.

*This work was supported by NSF MRSEC under account No. DMR-00-0520471

**15:54**

**R20 8 Dichroism and order parameter coupling in $BiFeO_3$ Films** MIKEL BARRY, T. ZHAO, F. ZAVALICHE, M.P. CRUZ, Y.H. CHU, R. RAMESH, *University of California, Berkeley* A. SCHOLL, A. DORAN, *Advanced Light Source, Lawrence Berkeley National Laboratory* $BiFeO_3$ is an attractive material because it is a possible multiferroic and lead-free replacement for ferroelectric memory cells and piezoelectric sensors and actuators. We are probing the possibility of coupling between ferroelectricity and antiferromagnetism in epitaxial thin films of this system. X-ray linear dichroism based PEEM images were obtained using a high spatial resolution photoelectron emission microscope (PEEM). This combination of XLD and PEEM provides high spatial resolution along with elemental and chemical specificity and surface sensitivity. A Piezoforce microscope (PFM) was used to switch the ferroelectric state in micron-sized regions of the film, which were subsequently probed using temperature dependent PEEM measurements. Temperature dependent structural measurements were carried out to probe the changes in the ferroelectric order parameter with temperature. We observe a strong change in XLD as the temperature is raised to and beyond the Neel temperature. We will present the results of our approaches to decouple the XLD responses that arise from purely the structural distortion (i.e., due to ferroelectricity) and that arising from the antiferromagnetic state, as well as the results of the coupling experiments. This work is supported by an LBL-LDRD program and by the ONR under a MURI program.

**16:06**

**R20 9 Systematic investigation of multiferroic properties of $(Bi_{1-x}Sm_x)FeO_3$ and $(Bi_{1-x}La_x)FeO_3$ thin films using composition spreads** MAKOTO MURAKAMI, *University of Maryland* V. NAGARAJAN, *University of New South Wales* A. VARTHARAJAN, *University of New South Wales* S. FUJINO, *University of Maryland* M. WUTTIG, *University of Maryland* I. TAKEUCHI, *University of Maryland* $BiFeO_3$ and its room temperature multiferroic properties have attracted much attention. However, it is generally believed that its magnetic and ferroelectric properties have not been unambiguously established. There have been some reports of A-site substituted $BiFeO_3$ aimed at improving its properties. In this study, we report on synthesis and multiferroic properties of La and Sm modified $BiFeO_3$ thin films. In particular, in order to systematically study these systems, we fabricated composition spread thin films of $(Bi_{1-x}Sm_x)FeO_3$ and $(Bi_{1-x}La_x)FeO_3$ ($x=0\sim 1$) on $SrTiO_3$ and $LaAlO_3$ substrates using combinatorial pulsed laser deposition. Several structural transitions were found in the middle of the spreads in both systems using x-ray microdiffraction. In $(Bi_{1-x}La_x)FeO_3$, the structure was found to change from rhombohedral to paramagnetic phase at about 20% of $BiFeO_3$. Ferroelectric properties and magnetic properties of the spreads were mapped using piezoforce microscopy and scanning SQUID microscopy. We report on the effect of the structural transitions on their multiferroic properties. This work was supported by NSF MRSEC DMR 0520471 and ONR.

**16:18**

**R20 10 Scanning probe imaging of coexistent ferroelectricity and ferromagnetism in thin films of room temperature multiferroics.** V.R. PALKAR, S.C. PURANDARE, J. JOHN, S. GOHIL, S. BHATTACHARYA, *Tata Institute of Fundamental Research, Mumbai-5, India* DEPARTMENT OF CONDENSED MATTER PHYSICS AND MATERIALS SCIENCE COLLABORATION, Scanning probe imaging methods, both piezoresponse and magnetic force types, are used to study domain patterns in thin films of room temperature multiferroics. The results demonstrate coexistence of the two order parameters in microscopic scale and rules out macroscopic phase separation. Furthermore, a tapping mode technique is shown to yield information of both order parameters allowing simultaneous observation of both types of domain structures. Prospects of imaging possible coupling between the two order parameters, as seen in bulk measurements, will be discussed.

**16:30**

**R20 11 The Nanostructure Formation and Growth Evolution of Ferroelectric/Ferromagnetic $BiFeO_3$-$CoFe_2O_4$ Thin Films*** SHENG YU YOUNG, LOURDES G. SALAMANCA-RIBA, *Materials Science and Engineering Department, University of Maryland, College Park* HAIMEI ZHENG, *Materials Science and Engineering Department, University of California Berkeley* We have investigated the mechanism of the self-assembly of $BiFeO_3$-$CoFe_2O_4$ (BFO-CFO) ferroelectric/ferromagnetic thin film nanostructures using high-resolution transmission electron microscopy. We discuss the formation of the CFO columnar structure during the deposition process. The BFO-CFO thin films were deposited on $SrTiO_3$ (001) single crystal substrates using pulsed laser deposition at a substrate temperature of 700 $^oC$ and deposition rate of around 5nm/min. In the early stages of growth, CFO domains form with dome like island shape and are covered by a BFO layer. After approximately 10 mins of continuous deposition, the nanocomposite rearranges and diffusion dominates to form a self-assembly of faceted CFO columns that extend to the surface of the film. These columns show pyramidal-like faceted shape and are embedded in the BFO matrix. A few atomic layers of BFO lie at the interface between the CFO columnar structures and the substrate. This layer helps relax the misfit strain between CFO and STO. The magnetic properties of the nanocomposite samples will also be presented.

*Supported by NSF MRSEC DMR 0520471

**16:42**

**R20 12 Electrical and Magnetic Properties of $Pb(Zr,Ti)O_3/CoFe_2O_4$ Composite Thin Films** NORA ORTEGA, S. MAJUMDER, P. BHATTACHARYA, R.S. KATIYAR, *University of Puerto Rico* P. DUTTA, M.S. SEEHRA, A. MANIVANNAN, *West Virginia University* Composite thin films made of ferroelectric and ferromagnetic materials are the potential candidates for sensors, data storage, and transducers due to possible manipulation of magnetic properties by electric field and vice versa. In this work, we have fabricated $Pb(Zr,Ti)O_3-CoFe_2O_4$ (PZT-CFO) multilayer thin films using pulsed laser deposition on $Pt/TiO_2/SiO_2/Si$ substrates at 400 °C and post annealed at 650°C using rapid thermal annealing (RTA) process. The X-ray diffraction studies revealed the growth of the perovskite PZT and the spinel CFO in two separated phases in the composite films. The dielectric constant ($\varepsilon_r$) of PZT-CFO multilayer showed strong frequency dispersion with an order of magnitude decrease in the frequency range of 1kHz to 1MHz. Similar decrease in $\varepsilon_r$ was also observed with decrease of temperature from 300 to 150 K. The remanent polarization ($P_r$) of the film (23 $\mu C/cm^2$) was also reduced to 1 $\mu C/cm^2$with decrease in the temperature (at 100 K). The magnetic measurements in the composite thin films showed the saturation magnetization ($M_s$) to be 9 emu/cm$^3$ at room temperature that increased to 38 emu/cm$^3$ at 5 K.

**16:54**

**R20 13 Quantum Monte Carlo calculations of $BiScO_3$ ferroelectric well-depths*** HENDRA KWEE, *College of William and Mary* HENRY KRAKAUER, *College of William and Mary* SHIWEI ZHANG, *College of William and Mary* The perovskite (1-x) $BiScO_3$-x $PbTiO_3$ alloy has been reported as having a large piezoelectric properties.[1] Density functional theory (DFT) using local density approximation (LDA) predicts an extraordinarily large ferroelectric well depths (about 1.2 eV) of the end point compound $BiScO_3$.[2] We perform quantum Monte Carlo calculations on $BiScO_3$ to calculate these well depths. In our QMC method,[3] the two-body terms coming from electron-electron interactions are decoupled using a Hubbard- Stratonovich transformation. The ground state is obtained from projection of an initial trial wave function by random walks in Slater determinant space. To control the sign/phase problem, a trial Slater determinant is used, which in our calculations is taken directly from the DFT calculations. We find in the QMC calculation large finite-size effects in the primitive cell, on the order of a few eV. We study these finite-size effects and explore several schemes to reduce them.

*Supported by ONR, DOE/CMSN, ORNL Natl. Cent. Comput. Sci., CPD

[1]R.E. Eitel, *et al.*, *Jpn. J. Appl. Phys.*, Part 1 **40**,5999 (2001); R.E. Eitel, *et al.*, ibid. **41**, 1 (2002)
[2]J. Íñiquez, D. Vanderbilt, L. Bellaiche, Phys. Rev B **67**, 224107 (2003)
[3]S. Zhang, H. Krakauer, Phys. Rev. Lett **90**, 136401 (2003)

**17:06**
**R20 14 Magnetic and structural properties of $CeO_2$ nanoparticles*** PRASANTA DUTTA, SUSMITA PAL, MOHINDAR SEEHRA, *West Virginia University* G. TURPIN, R. ERNST, *University of Utah* CONSORTIUM COLLABORATION, Nanoparticles of cerium oxide, $CeO_2$, have potential applications in catalysis, fuel cells, microelectronics etc [1]. In this work, we have investigated the magnetic and structural properties of 10%$CeO_2$ supported on $SiO_2$ aerogel with a BET surface area $\approx$ 700 $m^2$/g. X-ray diffraction (XRD) studies show cubic $CeO_2$ as the dominant phase with particle size $\approx$ 3 nm. Temperature variation (2K – 350K) of the magnetic susceptibility $\chi$ shows Curie-type variation with the Curie constant C = 5.9 $\times$ $10^{-5}$ emu K/g Oe. In electron magnetic resonance (EMR) studies from 5 K to 300 K at 9.28 GHz, an EMR line at g $\approx$ 2.1 with linewidth $\Delta$H $\approx$ 100 Oe is observed for T $<$ 40 K. Since $Ce^{4+}$ in $CeO_2$ is diamagnetic, we tentatively suggest that the observed Curie variation of $\chi$ and the EMR line [2] are due to paramagnetic $Ce^{3+}$ present in oxygen-lean $CeO_2$ nanoparticles. From the magnitude of C, the concentration of $Ce^{3+}$ is estimated to be $\approx$ 3 %. Further studies are in progress. [1]. S. Sathyamurthy et al, Nanotechnol. 16, 1960 (2005). [2]. D. Schaniel et al, Phys. Rev. B 70, 144410 (2004).

*Supported by a grant from the U.S Department of Energy.

## SESSION R21: FOCUS SESSION: BIOLOGICAL HYDRODYNAMICS
**Wednesday Afternoon, 15 March 2006; 318, Baltimore Convention Center at 14:30**
**Ray Goldstein, University of Arizona, presiding**

*Invited Papers*

**14:30**
**R21 1 Large-scale pattern formation in active particles suspensions: From interacting microtubules to swimming bacteria.***
IGOR ARANSON, *Argonne National Laboratory*

We consider two biological systems of active particles exhibiting large-scale collective behavior: microtubules interacting with molecular motors and hydrodynamically entrained swimming bacteria. Starting from a generic stochastic microscopic model of inelastically colliding polar rods with an anisotropic interaction kernel, we derive set of equations for the local rods concentration and orientation. Above certain critical density of rods the model exhibits orientational instability and onset of large-scale coherence. For the microtubules and molecular motors system we demonstrate that the orientational instability leads to the formation of vortices and asters seen in recent experiments. Similar approach is applied to colonies of swimming bacteria itBacillus subtilis confined in thin fluid film. The model is formulated in term of two-dimensional equations for local density and orientation of bacteria coupled to the low Reynolds number Navier-Stokes equation for the fluid flow velocity. The collective swimming of bacteria is represented by additional source term in the Navier-Stokes equation. We demonstrate that this system exhibits formation of dynamic large-scale patterns with the typical scale determined by the density of bacteria.

*This research was supported by US DOE, contract #W-31-109-ENG-38.

*Contributed Papers*

**15:06**
**R21 2 Elastic swimming I: Optimization** ERIC LAUGA, TONY YU, ANETTE HOSOI, *MIT* We consider the problem of swimming at low Reynolds number by oscillating an elastic filament in a viscous liquid, as investigated by Wiggins and Goldstein (1998, Phys Rev Lett). In this first part of the study, we characterize the optimal forcing conditions of the swimming strategy and its optimal geometrical characteristics.

**15:18**
**R21 3 Elastic swimming II: Experiments** TONY YU, ERIC LAUGA, ANETTE HOSOI, *MIT* We consider the problem of swimming at low Reynolds number by oscillating an elastic filament in a viscous liquid, as investigated by Wiggins and Goldstein (1998, Phys Rev Lett). In this second part of the study, we present results of a series of experiments characterizing the performance of the propulsive mechanism.

**15:30**
**R21 4 Stress-induced reversal of flagellar propulsion: an ingredient of quorum polarity of *Bacillus subtilis****
L. CISNEROS, C. DOMBROWSKI, R.E. GOLDSTEIN, J.O. KESSLER, *University of Arizona* Recent experiment have shown large-scale dynamic coherence in suspensions of the bacterium *B. subtilis*, characterized by quorum polarity – the collective parallel swimming of cells. To probe mechanisms leading to quorum polarity, we study the response of individual *B. subtilis* cells to steric stress brought on by swimming into a micron-sized spatial constriction. Careful visualization shows that cells can fully reverse their swimming direction at spatial constrictions without turning the cell body. This property, termed ''flippancy,'' is quantified by measurements of the inward and outward swimming velocities, accelerations and decelerations, and docking times. The asymptotic inward and outward swimming speeds far from the constriction show near perfect correlation, implying that the propelling flagella flip, and that ''forwards'' and ''backwards'' are dynamically indistinguishable, as with *E. coli*. Implications for the collective dynamics are discussed.

*Supported in party by NSF Grant PHY-0551742

**15:42**

**R21 5 Effects of nonlinear membrane elasticity on capsule recovery*** ANDRES GONZALEZ-MANCERA, CHARLES EGGLETON, *UMBC* The recovery of a capsule from an initially deformed shape is considered. The problem is solved numerically for a capsule made of an incompressible liquid surrounded by a thin elastic membrane using the Boundary Integral Method. Elastic membranes with different constitutive models providing a wide range of behaviors at large deformations (strain-hardening, strain-softening and linear elastic) were considered. The results suggest that the recovery process is dominated by the isotropic dilatation modulus. The recovery process from small deformations was seen to be nearly independent of the membrane constitutive model. Recovery from large deformations was highly dependent on the constitutive model and the initial geometry of the capsule. Analysis of the recovery from large deformations demonstrated that the process is modulated by the tangential component of the elastic traction, $\backslash F_t$, acting on the membrane. This component of the traction was seen to either favor or oppose the recovery depending on the constitutive equation used to model the elastic membrane. The differences in the recovery process can be used to identify the best model for a particular capsule based on features observed during the recovery process.

*supported by NIH/NIAID RO1AIO63366

**15:54**

**R21 6 Balancing energy input and viscous dissipation in the Zooming BioNematic*** J.O. KESSLER, *U. Arizona* R.E. GOLDSTEIN, *University of Arizona* R. CORTEZ, *Tulane U.* Beyond a concentration threshold, populations of the swimming bacteria *Bacillus subtilis* form a phase (the Zooming BioNematic=ZBN) comprising intermittent domains of co-aligned cells all swimming in the same direction. Collectively generated hydrodynamic forces between bacteria, the cells' ability to flip flagella, thereby changing swimming polarity, and their tendency to swim upstream into a collectively generated current are fundamental interactions leading to the ZBN. But how does the ZBN generate dynamic patterns, similar to ones at $Re \gg 1$? The energy put into the fluid by the swimming organisms overwhelms viscous damping, as demonstrated by a new dimensionless ratio $Bs$, analogous to $Re$ but replacing the numerator by a measure of bacterial energy input. The magnitude of $Bs$ is estimated via the Navier-Stokes equations, considering individual bacteria at moderate concentration, and entire domains at high. $Bs$ is proportional to the bacterial concentration, and in both of those regimes, $Bs \gg 1$. Remarkably, unlike the Reynolds number, $Bs$ is independent of viscosity.

*Supported in part by NSF grants PHY-05541742 and DEB-0075296

**16:06**

**R21 7 Multicellularity and the Functional Interdependence of Motility and Molecular Transport*** C. SOLARI, S. GANGULY, J.O. KESSLER, R. MICHOD, R.E. GOLDSTEIN, *U. of Arizona* Benefits, costs and requirements accompany the transition from motile totipotent unicellular organisms to multicellular organisms having cells specialized into reproductive (germ) and vegetative (sterile soma) functions such as motility. In flagellated colonial organisms such as the volvocalean green algae, organized beating by the somatic cells' flagella yields propulsion important in phototaxis and chemotaxis. It has not been generally appreciated that for the larger colonies, flagellar stirring of boundary layers and remote transport are fundamental for maintaining a sufficient rate of metabolite turnover, one not attainable by diffusive transport alone. We describe experiments that quantify the role of advective dynamics in enhancing productivity in germ-soma differentiated colonies. First, experiments with suspended deflagellated colonies of *Volvox carteri* show that forced advection improves productivity. Second, Particle Imaging Velocimetry of fluid motion around colonies reveals flow fields with very large characteristic velocities $U$ extending to length scales comparable to the colony radius $R$. For a typical metabolite diffusion constant $D$, the Peclet number $Pe = 2UR/D \gg 1$, indicative of the dominance of advection over diffusion, with striking augmentation at the cell division stage.

*Supported in part by NSF grants DEB-0075296 and PHY-0551742

**16:18**

**R21 8 Flagella-Driven Flows Circumvent Diffusive Bottlenecks that Inhibit Metabolite Exchange*** MARTIN SHORT, CRISTIAN SOLARI, SUJOY GANGULY, JOHN KESSLER, RAYMOND GOLDSTEIN, *University of Arizona* THOMAS POWERS, *Brown University* The evolution of single cells to large and multicellular organisms requires matching the organisms' needs to the rate of exchange of metabolites with the environment. This logistic problem can be a severe constraint on development. For organisms with a body plan that approximates a spherical shell, such as colonies of the volvocine green algae, the required current of metabolites grows quadratically with colony radius whereas the rate at which diffusion can exchange metabolites grows only linearly with radius. Hence, there is a bottleneck radius beyond which the diffusive current cannot keep up with metabolic demands. Using *Volvox carteri* as a model organism, we examine experimentally and theoretically the role that advection of fluid by surface-mounted flagella plays in enhancing nutrient uptake. We show that fluid flow driven by the coordinated beating of flagella produces a convective boundary layer in the concentration of a diffusing solute which in turn renders the metabolite exchange rate quadratic in the colony radius. This enhanced transport circumvents the diffusive bottleneck, allowing increase in size and thus evolutionary transitions to multicellularity in the Volvocales.

*Supported by NSF Grants DEB-0075296, PHY-0551742 and CMS-0093658

**16:30**

**R21 9 Measurement of Flow Patterns and Dispersion in the Human Airways*** FRANK E. FRESCONI, AJAY K. PRASAD, *Department of Mechanical Engineering, University of Delaware* A detailed knowledge of the flow and dispersion within the human respiratory tract is desirable for numerous reasons. Both risk assessments of exposure to toxic particles in the environment and the design of medical delivery systems targeting both lung-specific conditions (asthma, cystic fibrosis, and chronic obstructive pulmonary disease (COPD)) and system-wide ailments (diabetes, cancer, hormone replacement) would profit from such an understanding. The present work features experimental efforts aimed at elucidating the fluid mechanics of the lung. Particle image velocimetry (PIV) and laser induced fluorescence (LIF) measurements of oscillatory flows were undertaken in anatomically accurate models

(single and multi-generational) of the conductive region of the lung. PIV results captured primary and secondary velocity fields. LIF was used to determine the amount of convective dispersion across an individual generation of the lung.

*Sponsored by Philip Morris USA Inc. and Philip Morris International

**16:42**
**R21 10 On small insect flight – A two-dimensional study** PAULO FERREIRA DE SOUSA, *New Mexico State University* Small insect flight is characterized by very small Reynolds numbers and relatively simple wing motions. In this study, a two-dimensional approximation of small insect flight is calculated with a newly developed high-order immersed boundary incompressible Navier-Stokes flow solver. The simulated motion of the model wing is a simplification of the flight of Drosophila melanogaster, and was done in line with previous experimental and numerical simulations available in the literature. Calculations were carried out until a time-periodic steady-state was achieved. Changes in lift generation and vortex dynamics are studied for Reynolds numbers spanning two orders of magnitude, in order to accurately find the critical Re number above which flapping flight is possible. Above the critical Reynolds number, vortices are alternately shed during translation. Below the critical Reynolds number, vortices are formed but not shed during translation, creating two attached and almost identical vortices. This transition is significant because, below it, an important mechanism of lift generation no longer applies, effectively indicating a lower bound for insect flight to occur.

**16:54**
**R21 11 Wake characteristics of a model ornithopter** ALFREDO JUAREZ, *New Mexico State University* JACOB HARLOW, *New Mexico State University* JAMES ALLEN, *New Mexico State University* PAULO FERREIRA DE SOUSA, This paper details unsteady wake measurements from a model Ornithopther flying in a wind tunnel at representative flight conditions. Testing over a range of Strouhal number, 0.1-0.3, shows that the unsteady wake is composed of coherent vortical structures that resemble vortex rings. A single ring is formed in the wake of each wing during one wing beat. Momentum balance from velocity field measurements are reconciled with unsteady lift and drag measurements from a drag balance.

**17:06**
**R21 12 Vertical hovering of a symmetric flapping model** MAKOTO IIMA, TATSUO YANAGITA, *Hokkaido University* We study the motion of a model equipped with flapping wings under the influence of gravity (external force). This model moves in a two-dimensional fluid according to the hydrodynamic force generated by vortices separated from its wings. As a result of the interaction between the vortices and the wings, the model moves steadily in a direction against the gravity. Moreover, hovering, i.e., a steady flight staying in a particular position, can be achieved here by the effective use of vortex structures enhancing the hydrodynamic force that supports the model against gravity. The system exhibits a transition from the state with hovering to a state where hovering is impossible, as the model parameters are changed.

## SESSION R22: FOCUS SESSION: BIOMAGNETISM AND EXCHANGE BIASED THIN FILMS
**Wednesday Afternoon, 15 March 2006; 319, Baltimore Convention Center at 14:30**
**David Lederman, West Virginia University, presiding**



***Invited Papers***

**14:30**
**R22 1 Magnetic Viruses: Utilizing Self-Assembly for Biomedical Applications.***
AXEL HOFFMANN,† *Materials Science Division, Argonne National Laboratory*

Magnetic nanoparticles coated with biochemical surfactants have emerged recently as an important component for enabling many biological and medical applications. We implemented a biotemplating approach to create such magnetic nanoparticles by utilizing native protein capsid shells derived in high yield from the T7 bacteriophage virus.[1] The magnetic nanoparticles are grown via bio-mineralization reactions inside of hollowed-out capsids that retain their original chemical recognition properties. The resultant ''magnetic viruses'' are uniform in geometry, physical properties, and biochemical functionality. This makes these viruses ideally suited for many biomedical applications among which we investigated specifically a novel sensing scheme for target recognition based on Brownian relaxation.[2] For this scheme we use the *ac*-susceptibility of the functionalized magnetic nanoparticles suspended in liquid. Upon binding the target of interest to the particles, their Brownian relaxation time is modified, which is readily detected by a change of the frequency dependence of the magnetic susceptibility. This scheme has several advantages; (i) it requires only one binding event for sensing; (ii) there is a useful signal both in the absence and presence of the target; (iii) the signal contains information

about the size of the target besides the biochemical affinity; and (iv) since the binding modifies the magnetic susceptibility of the magnetic particles there is no need for removing unbound labels.

*Financial support was through DARPA (8C67400-110) and the U.S. DOE BES-MS under Contract no. W-31-109-ENG-38.
†With S.-H. Chung, K. Guslienko, S. D. Bader, C. Liu, Q. Jin, A. Sutton, F. Yan, B. K. Kay, L. Makowski, and L. Chen.

[1]C. Liu, S.-H. Chung, Q. Jin, A. Sutton, F. Yan, B. K. Kay, S. D. Bader, L. Makowski, and L. Chen, J. Magn. Magn. Mater, in press.
[2]S.H. Chung, A. Hoffmann, S. D. Bader, C. Liu, B. Kay, L. Makowski, and L. Chen, Appl. Phys. Lett. **85**, 2971 (2004); S. H. Chung, A. Hoffmann, K. Guslienko, S. D. Bader, C. Liu, B. Kay, L. Makowski, and L. Chen, J. Appl. Phys. **97**, 10R101 (2005).

***Contributed Papers***

**15:06**
**R22 2 Atomic model for the exchange bias in Fe/FePt(110) alloy** CHANYONG HWANG, W. KIM, *Korea Research Institute of Standards and Science* J.S. PARK, Y.P. LEE, *Department of Physics and q-Psi, Hanyang University* S.C. HONG, *Department of Physics, Ulsan University* Fe overlayers on top of Pt(110) surface have been studied using STM and SMOKE. Based on our atom-resolved STM data, we have shown the atomic model for the growth of this system. One of the interesting system is the one grown at elevated temperature. In this case, Fe-Pt surface alloy is formed on top of Pt(110) surface. This surface alloy still maintains the lattice constant of Pt substrate and reveals to be an antiferromagnet. In addition to the field cooling upon additional Fe layers, our first principles calculation clear shows the antiferromagnetic order. For the unified picture of the exchange bias phenomena, we need an atomically resolved antiferromagnetic surface and we will present the possible mechanism of this exchange bias in our system.

**15:18**
**R22 3 Competing Mechanisms in Asymmetric Magnetization Reversal in Exchange Biased Bilayers*** OLEG PETRACIC,† ZHI-PAN LI, IVAN K. SCHULLER, *Physics department, University of California, San Diego, La Jolla* A systematic micromagnetic simulation is performed to investigate the asymmetric magnetization reversal in exchange bias bilayers. When the unidirectional anisotropy is comparable with the uniaxial anisotropy of the ferromagnet, we found that the descending branch is dominated by rotation while the ascending one is dominated by domain wall motion. When the unidirectional anisotropy is large enough, the magnetization reversal occurs through FM incomplete domain walls parallel to the interface. This results in a larger transverse component in the ascending branch, opposite to the previous mechanism. These two mechanisms coexist and compete for intermediate unidirectional anisotropies and lead to very delicate situations in particular when a magnetic field misalignment and interfacial inhomogeneity are involved. The results are able to explain some of the confusion in the present study of the asymmetric reversal mechanisms.

*Work support by US-DOE, Cal(IT)2, and Alexander-von-Humboldt Foundation.
†Presently at Department of Physics, Imperial College London

**15:30**
**R22 4 Magnetization Precession in Interlayer Exchange-Coupled Thin Films*** STEVEN MICHALSKI, JIAN ZHOU, RALPH SKOMSKI, NIKOLAY POLUSHKIN, ROGER KIRBY, *Department of Physics and Astronomy and Center for Materials Research and Analysis, University of Nebraska-Lincoln, 68588-0111, Lincoln, NE* We have studied the static and fast dynamic magnetic properties of exchange-coupled magnetic layers using both magneto-optical measurements and conventional magnetometry. The samples studied include [Co/Pt] multilayers with perpendicular magnetic anisotropy (PMA) coupled via a variable thickness intervening Cu (Pt) layer to a Co (Sm-Co) layer with in-plane magnetic anisotropy. Such systems should exhibit a wide variety of magnetic configurations, permitting control of magnetic properties through control of exchange strength and PMA. The hysteresis loops show direct evidence of ferromagnetic exchange coupling. We report here the results of magnetization precession measurements using a femtosecond laser in a pump-probe experiment with direct optical excitation. For the samples studied so far, we observe only one precession frequency for a given applied magnetic field, rather than the expected two, but the frequency varies with the thickness of the coupling layer as expected. Our results are interpreted in terms of an LLG model which includes PMA and variable exchange coupling.

*Work supported by NSF-MRSEC, W. M. Keck Foundation and CMRA

**15:42**
**R22 5 Exchange coupling in multilayers with perpendicular magnetic anisotropy** JIAN ZHOU, RALPH SKOMSKI, STEVEN MICHALSKI, ROGER KIRBY, DAVID SELLMYER, *Department of Physics and Astronomy and CMRA, University of Nebraska, Lincoln, NE 68588* Recently much attention has been paid to the interlayer exchange coupling (IEC) through nonmagnetic layers, for especially certain applications. In this work we investigate the interlayer exchange coupling through Cu or Pt spacer layers between two magnetic phases with perpendicular or in-plane anisotropy. $(Pt5Å/Co3Å)_3$ layers with perpendicular magnetic anisotropy (PMA) are exchange-coupled to an in-plane anisotropic Sm-Co 30Å layer through a Pt spacer. The competing anisotropies and IEC in the system yield a spin-reorientation transition behavior with a varying Pt thickness. We also have studied $(Pt5Å/Co3Å)_3$ layers which are exchange-coupled to $(Co3Å/Pt5Å)_3$ through a Cu spacer. Transition from single phase hysteresis to two-phase behavior indicates a reducing IEC between the PMA layers with increasing Cu thickness. Both model calculations and micromagnetic simulations show that interlayer exchange

coupling is essential in calculating the hysteresis, and indicate how the interlayer coupling can be tuned by changing the spacer thickness. *This research is supported by DOE, NSF-MRSEC, the W. M. Keck Foundation, and CMRA.

**15:54**

**R22 6 Spin Dynamics in Exchange Biased Co/FeMn Bilayers*** JEFFREY PARKER, MUN CHAN, MELISSA HAUGEN, BRUCE BOLON, CHRIS LEIGHTON, PAUL CROWELL, *University of Minnesota* We report a study of the spin dynamics in exchange biased Co/FeMn bilayers using time resolved Kerr microscopy (TKRM) with sub-nanosecond resolution. Samples were prepared via UHV dc magnetron sputter deposition onto a $Si/SiO_x$ substrate at room temperature in an applied field of 300 Oe. Deposition of a 30nm Cu buffer layer allowed for (111) textured growth of the subsequent Co/FeMn layers. In all samples the Co thickness was held constant at 6nm, while the FeMn thickness, t, was varied between 0 and 20nm. In accordance with previous work we found a room temperature critical thickness of the FeMn layer of approximately 3.5nm and a broad peak in the coercivity at this thickness. For low FeMn thickness a noticable asymmetry occurs in the magnetization hysteresis loops only for temperatures below the blocking temperature. TRKM is used to probe the dynamic response of the magnetization to fast magnetic field pulses. The different reversal mechanisms on either side of the hysteresis loop were probed by both the static and dynamic magnetization of the films as a function of temperature (between 40 and 450 K), and applied field.

*Research supported by the NSF MRSEC program under DMR-0212032

**16:06**

**R22 7 Exchange Bias in $Fe_xNi_{1-x}F_2$/Co Bilayers*** MIYEON CHEON, ZHONGYUAN LIU, DAVID LEDERMAN, *Multifunctional Materials Laboratory, Dept of Physics, West Virginia University* $FeF_2$ is an ideal antiferromagnet with a tetragonal rutile crystal structure and a strong uniaxial magnetic anisotropy along the *c*-axis ([001] direction). $NiF_2$ also shares the rutile crystal structure with similar lattice parameters, but its magnetic anisotropy causes spins to be in the $a - b$ plane, resulting in a weak ferromagnetism due to a small tilting of the antiferromagnetic sublattices. Because several theories predict that exchange bias should be a strong function of the magnetic anisotropy in the antiferromagnet, the $Fe_xNi_{1-x}F_2$/Co bilayer system provides a framework whereby this can be studied experimentally. We have grown several single-crystalline $Fe_xNi_{1-x}F_2$50 nm thick films on $MgF_2$ (110) substrates via molecular beam epitaxy with *x* varying between 0 and 1.0. We will report on the exchange bias as a function of Fe concentration in the alloy.

*Supported by NSF grant DMR-0400578.

**16:18**

**R22 8 Dynamics of Spontaneous Magnetization Reversal in Exchange Biased Bilayers*** ZHI-PAN LI, CASEY W. MILLER, IGOR V. ROSHCHIN, IVAN K. SCHULLER, *Physics Department, UC San Diego, La Jolla, CA 92093* We observe a temperature-driven magnetization reversal of a ferromagnet (FM= Ni, Co) magnetization under a constant magnetic field, when it is exchange biased by an antiferromagnet (AF=$FeF_2$). We attribute this phenomenon to the competition of the AF interfacial coupling and the FM Zeeman energy. This striking behavior allows us to investigate the AF dynamics through the FM reversal behavior. We found that the magnitude of FM reversal for a given cooling field strongly depends on the cooling speed, and the wait time around the Néel temperature. This shows the magnetic viscosity of the AF around its phase transition temperature. Moreover, by thermal cycling, the FM exhibits successive spontaneous reversal. This thermal training effect further points to high energy barriers resulting in slow dynamic processes of the system.

*Work supported by US-DOE and Cal(IT)2.

**16:30**

**R22 9 Exchange bias measurements of epitaxial magnetic oxide exchange bias bilayers.** XIANGLIN KE, LAND BELENKY, CHANG-BEOM EOM, MARK RZCHOWSKI, *University of Wisconsin-Madison* NIRT TEAM, It has been shown in epitaxial bilayers that antiferromagnetic exchange coupling exists at atomically abrupt interfaces between ferromagnetic oxides $La_{0.67}Sr_{0.33}MnO_3$ and $SrRuO_3$ [1,2]. We have grown the bilayers on (001) $SrTiO_3$ substrates by pulsed laser deposition with atomic layer control. By analyzing the in-plane magnetization loops of the LSMO layer, and the total magnetization of the (frozen) SRO layer, we determine the exchange field of the bilayer and the domain structure of the $SrRuO_3$ biasing layer as a function of cooling field. This data shows evidence for domain walls both parallel and perpendicular to the interface. We support this conclusion with a simple energy minimization including contributions from the interfacial exchange, dipole interaction with the cooling field, domain wall energies, and magnetostatic energy. We also pattern the samples with e-beam and x-ray lithography techniques. Size effect on coercivities of both LSMO and SRO electrodes and exchange bias in the bilayers will be discussed. [1] X. Ke, M. S. Rzchowski, L.J. Belenky, C. B. Eom, Appl. Phys. Lett, **84**, 5458 (2004). [2] X. Ke, L.J. Belenky, C. B. Eom, M. S. Rzchowski, J. Appl. Phys. **97**, 10K115 (2005).

**16:42**

**R22 10 Quantitative Depth Profiling of Interfacial Moments in Paramagnetic CoO in Py/CoO bilayer.** SUJOY ROY, X. LIU, S.K. SINHA, B.J. TAYLOR, M.B. MAPLE, Y. TANG, JUNG-IL HONG, A.E. BERKOWITZ, *University of California-San Diego* T. LEO, D.J. SMITH, *Arizona State University, Tempe* S. PARK, M.R. FITZSIMMONS, *Los Alamos National Lab* C. SANCHEZ-HANKE, C.-C KAO, *NSLS, Brookhaven National Lab* We have employed soft x-ray resonant magnetic reflectometry to determine the depth dependence of the net ferromagnetic moment in a Permalloy/CoO bilayer itabove the Néel point of the antiferromagnetic CoO at 300K. itQuantitative element specific depth dependent charge and magnetization density profiles have been determined by analyzing the specular reflectivity data at the $L_3$ edges of Co and Ni using resonant magnetic scattering theory in the Distorted Wave Born Approximation. We have found that a thin interfacial layer with charge density different from either the Permalloy (Py) or CoO forms at the Py/CoO interface. This layer is magnetic even at room temperature and has a itdifferent temperature dependence of magnetization compared to Py. We have put the depth profile of magnetization in an itabsolute scale by combining the results of reflectivity measurements and SQUID magnetometry. Work of SKS and MBM supported by DOE.

**16:54**

**R22 11 Effects of coupling on domain structure of [Pt(6Å)/Co(4Å)]$_3$/NiO($t_{NiO}$)/[Co(4Å)/Pt(6Å)]$_3$ multilayers with oscilla-**

**tory coupling*** ANDREW BARUTH, S.H. LIOU, S. ADENWALLA, *Department of Physics and Astronomy and Center for Materials Research and Analysis, University of Nebraska, Lincoln, NE 68588* D.J. KEAVNEY, *Advanced Photon Source, Argonne National Laboratory, Argonne, IL 60439* Multilayered structures of Pt(6Å)/Co(4Å)$]_3$/NiO($t_{NiO}$)/[Co(4Å)/Pt(6 Å)$]_3$ show oscillatory exchange coupling between the two Co/Pt layers [1]. One possible mechanism for the exchange coupling may be via the propagation of canted NiO spins at the interface, an effect that can reproduce the oscillatory coupling [2] and that has been seen using X-ray Magnetic Circular Dichroism [3]. Domain images on virgin samples taken with XMCD-PEEM and MFM reveal a direct correlation between domain size and absolute coupling strength. The coupling strength was varied by changing both NiO and Pt thicknesses. MFM images show that the coupling in both FM and AFM coupled samples occurs domain by domain. FM domains form within the AFM domain wall due to a slight relative shift of the domains in the upper and lower multilayers. These FM regions contain visible stripes corresponding to opposite net magnetizations in the domain wall. [1] Phys. Rev. Lett. 91, 037207 (2003) [2] Phys. Rev. Lett. 92, 219703 (2004) [3] Phys. Rev. B 70, 224423 (2004)

*Funded by NSF MRSEC #9806308

**17:06**

**R22 12 Fabrication and characterization of lateral all-magnetic superlattices*** NIKOLAY POLUSHKIN, STEVEN MICHALSKI, LANPING YUE, ROGER KIRBY, *Department of Physics and Astronomy, University of Nebraska-Lincoln, 68588-0111, Lincoln, NE* FAST MAGNETIZATION DYNAMICS LABORATORY TEAM, Conventionally, patterned magnetic elements produced by lithographic methods are surrounded by nonmagnetic spacers. We describe a technique for itdirect laser fabrication of 1D and 2D superlattices composed of two different magnetic materials with itvariable properties. The approach is based on the phase transformations induced locally by interfering laser beams in thin alloyed layers of transition metals (Fe-V, Fe-Cr, Co-Pt). Using magnetic force microscopy and methods of magnetometry, we demonstrate that the structures patterned even in the submicron regime possess significant contrast in the magnetizations, with sharp interfaces between the constituents. We have used time-resolved magneto-optical Kerr effect measurements to further characterize the magnetic properties of these samples. These data allow us to obtain the magnetizations and gyromagnetic ratios of the constituents. Possible application to microwave nanophotonics of such all-magnetic superlattices with ittunable magnonic band gaps is briefly discussed.

*Work supported by NSF-MRSEC and W.M. Keck Foundation

**17:18**

**R22 13 Ferromagnetism of CoAl(100) induced by oxidation at 300 K** VOLKER ROSE, *Center for Nanoscale Materials (CNM), Argonne National Laboratory* KLAUS BRUEGGEMANN, RUDOLF DAVID, HARALD IBACH, *Institute for Surfaces and Interfaces (ISG 3), Research Center Juelich, Germany* In situ magneto-optical Kerr effect measurements were performed to investigate the magnetic behavior of CoAl(100) upon oxidation at room temperature. As an ideal $Co_{50}Al_{50}$ crystal is known to be paramagnetic at room temperature, our studies show a transformation into a ferromagnetic phase during increasing exposure to $O_2$. Oxidation of CoAl(100) at 300 K leads to the growth of an amorphous $Al_2O_3$ film [1], causing a Co excess at the metal/oxide interface that is sufficient to provide ferromagnetism. Annealing of the oxidized sample brings about a drastic increase of the coercive field, generated by diffusion of Al into the Co film. But, after annealing at 550 K, the ferromagnetism vanishes completely. [1] V. Rose, V. Podgurski, I. Costina, R. Franchy, Surf. Sci 541 (2003) 128.

## SESSION R23: FOCUS SESSION: THEORY AND SIMULATION FOR INFORMATION STORAGE APPLICATIONS

**Wednesday Afternoon, 15 March 2006; 320, Baltimore Convention Center at 14:30**
**Andreas Berger, Hitachi Global Storage Technologies, presiding**



***Invited Papers***

**14:30**

**R23 1 Nanomagnetic Simulations of Recording Media.***
THOMAS SCHREFL, *University of Sheffield*

The optimization of ultra-high density recording systems requires the joint simulation of the recording head, the data layer and the soft underlayer. This talk presents micromagnetic simulations of recording processes in perpendicular and patterned media. The numerical technique for the multiscale simulation combines the finite element method with an accelerated boundary method. The use of hierarchical matrices and FFT methods significantly speeds up the computation time for the magnetostatic interactions between the head and the data layer. In addition to dynamic magnetization processes, energy barriers of recording media are calculated using a nudged elastic band method. The rise time of the write field was found to depend significantly on vortex motion in the pole tip of the head. The shortest field rise time was obtained for intermediate values of the Gilbert damping constant. Under the influence of the write field, magnetization reversal in composite perpendicular media occurs by the nucleation and expansion of reversed domains. However, thermally activated switching in composite media shows reversal by quasi-uniform rotation. Therefore it is possible to keep a high energy barrier while reducing the switching field in composite media, where a soft magnetic layer is exchange coupled to the hard magnetic layer. The energy barrier of composite media was calculated as a function of the applied

field. The results show that the extrapolation of barriers measured at high fields underestimates the zero-field energy barrier. The calculated energy barrier of an island of a patterned media is smaller than the anisotropy constant times the island volume. This result shows that thermally activated magnetization reversal in patterned islands is non-uniform. The energy barrier of a square island with a size of only 20 nm was found to be 17% lower than the barrier expected for uniform rotation.

*Work supported by the Austrian Science Fund (Y132-N02).

***Contributed Papers***

**15:06**

**R23 2 Magnetization Dynamics in Ultrahigh-Density Magnetic Recording*** R. SKOMSKI, J. ZHOU, D. J. SELLMYER, *Department of Physics and Astronomy and Center for Materials Research and Analysis, University of Nebraska, Lincoln, NE* Thermally activated magnetization reversal is a key consideration in the development of magnetic recording materials with ultrahigh densities. We consider the onset of magnetization reversal (nucleation) and describe the magnetization by a Langevin model, where the magnetization dynamics is realized by random thermal forces. The exchange, anisotropy, and Zeeman energies are expanded into powers of a small perpendicular magnetization component, and the dynamics reduces to a time-dependent superposition of normal modes. In the Stoner-Wohlfarth (SW) model, the approach reproduces the Arrhenius-Néel-Brown law $\tau = \tau_o \exp(E_a \backslash k_B T)$ with an approximate energy barrier $E_a$ and a particle-size dependent constant $\tau_o$. The same is true for the micromagnetic approach, where the local micromagnetic parameters such as $K_1(\mathbf{r}) = < K_1(\mathbf{r})>$ give rise to nonuniform magnetization modes in inhomogeneous and interacting particles. However, both the coercivity $H_c$ and the energy barrier $E_a$ are smaller than the SW predictions. A further reduction of $H_c$ and $E_a$ is obtained by taking into account local anisotropy fluctuations of the type $< K_1(\mathbf{r})^2 > - K_1(\mathbf{r})^2$. This reduction corresponds to fluctuating energy barriers, and establishes a particle-shape and materials-dependent upper limit to energy barriers in very small particles.

*This research is supported by NSF MRSEC, DOE, INSIC, and CMRA.

**15:18**

**R23 3 Experimental determination of switching field distributions in perpendicular and patterned recording media** ANDREAS BERGER, *Hitachi Global Storage Technologies* BYRON LENGSFIELD, YOSHIHIRO IKEDA, OLAV HELLWIG, ERIC FULLERTON, We have developed and applied a magnetometry method for the measurement of intrinsic switching field distributions in magnetic recording media [1]. The method is based upon a comparison between the major loop and a set of recoil loops, which start at a certain distance $\Delta M$ away from saturation. Hereby, we measure the applied field difference $\Delta H$ between the recoil loops and the major loop at identical M-values. By simultaneously analyzing complete $\Delta H(M, \Delta M)$-data sets, we gain a refined measure of the entire switching field distribution $D(H_S)$. We studied the reliability of this method by means of micromagnetic modeling and find it to be robust and precise in reproducing the input parameters. In particular, the method is rather insensitive to inter-granular exchange coupling up to a certain threshold value. Also, a self-consistency check of the methodology was developed. An existing polar-MOKE setup was adapted to allow for $\Delta H(M, \Delta M)$-data acquisition, which enables a non-destructive sample characterization that is also compatible with the disk shape of recording media. Measurements on perpendicular and patterned recording media were made and results were compared to recording performance tests. [1] A. Berger, B. Lengsfield, Y. Ikeda, Y. H. Xu, and E. E. Fullerton, IEEE Trans. MAG **41**, 3178 (2005)

**15:30**

**R23 4 Simulations Of Nanomagnet Clusters With Perpendicular Uniaxial Anisotropy For Multilevel Data Storage** QIJUN XIAO, *Umass, Amherst, Physics Dept.* ROBERT KROTKOV, *Umass, Amherst, Physics Dept.* MARK TUOMINEN, *Umass, Amherst, Physics Dept.* UMASS, AMHERST, PHYSICS DEPT. TEAM, Digital data storage technology generally relies on a binary storage paradigm. In this work we explore a different scheme that exploits the stepwise, itmultilevel total magnetization of a small cluster of interacting nanomagnets. The magnetization of a cluster can be resolved more easily than that of a single nanomagnet, due to the larger lateral size. Micromagnetic simulations, based on the Landau-Lifshitz-Gilbert (LLG) equation with parameters representative of $Co_3Pt$, reveal that magnetostatic interactions within a cluster produce a rich multilevel magnetic response, each level providing a stable remanent magnetization state. This work describes simulations used to investigate a multilevel data storage unit based on a hexagonal cluster of interacting uniaxial single domain nanomagnets. The accessibility and stability of the discrete magnetization states are studied. The switching properties of the nanomagnet clusters can be tuned by modifying the geometry, providing the ability to engineer desirable magnetic properties.

**15:42**

**R23 5 Magnetic properties of nanosized systems, discrete and continuum approaches*** PATRICIO VARGAS, DAVID LAROZE, *Universidad Santa Maria* In this work we present results obtained with a scaled Monte Carlo technique in two systems: The first one is the system proposed at the NIST web page and known as the $\mu$MAg Standard Problem No 3. There, the system is a perfect cube made of a magnetic material, with uniaxial anisotropy and the problem is to find the critical edge length at which the magnetic vortex structure and the most uniform arrangement of magnetization (the so-called flower state) are of equal energy. The second system is a study of the reversion process in an ideally soft magnetic nanowire of cylindrical shape, (diameter of 60nm and 1$\mu$m length) at room temperature. By calculating magnetic energies, using continuum and exact methods, in a simple one dimensional discrete system, we show that the

usual scaling technique used in some micromagnetic models breaks down at the nanometer scale.

*Authors acknowledge support from Fondecyt grant No.1040354, Millennium Science Initiative grant No. P02-054F

**15:54**

**R23 6 Micromagnetism in the ultrathin limit** DANILO PESCIA, OLIVER PORTMANN, MATTHIAS BUESS, ALESSANDRO VINDIGNI, ANDREAS VATERLAUS, *Laboratory for Solid State Physics, ETH Zurich* CHRISTIAN HORST BACK, *Institut für Experimentelle und Angewandte Physik, Universität Regensburg,* We derive some results concerning the static and dynamic micromagnetic behavior of magnetic elements in the ultrathin limit. In this limit, a most remarkable, shape-independent, logarithmic correction of the magnetostatic energy appears, produced by the long-range character of the dipolar interaction. Apparently unrelated phenomena such as the pinning of the precessional motion at some of the boundaries of a thin magnetic element, the non-pinning at other boundaries and a multi-to-single-domain transition in ultrathin elements with perpendicular magnetization have a common origin: the logarithmic correction.

**16:06**

**R23 7 Magnetic properties of coupled Gd/Pd/Ni thin films** ILIR ZOTO, GARY MANKEY, *MINT Center, Department of Physics, University of Alabama* Transition metal-rare earth bilayers might allow magnetizations higher than that available from transition metal if the strong exchange interactions of the transition metal layer could be used to raise the Curie temperature of an adjacent, high moment rare earth layer. Literature suggested for a ferromagnetic interaction in the Ni-Gd bulk alloys and an increased moment at room temperature when Gd layer is deposited onto thin Co and permalloy films. Recently, we found that Ni/Gd bilayers couple antiferromagnetically at the interface. Adding a spacer layer could change the coupling behaviour. Here, a study of a Gd(15nm)/Pd(tnm)/Ni(10nm) trilayer is presented with t varying from 0.5 to 2.5nm. The hysteresis loops were measured with VSM in the temperature range 5-250K. A Stoner-Wolfarth model simulates the hysteresis loops through the minimization of the energy of the following expression:

$$E = -M_1 H t_1 \cos(\theta_1) - M_2 H t_2 \cos(\theta_2) + K_1 t_1 \sin^2(\theta_1) + K_2 t_2 \sin^2(\theta_2) + J_1 \cos(\theta_1 - \theta_2) + J_2 \cos^2(\theta_1 - \theta_2)$$

where $J_1$ and $J_2$ are the bilinear and biquadratic coupling constants. The simulated loops are in good agreement with the experimental results and confirm the antiferromagnetic coupling of Ni and Gd layers for $t < 2.5$nm and the disappearance of the coupling for $t > 2.5$nm.

**16:18**

**R23 8 Influence of the antiferromagnet spin structure on exchange bias.** R. MORALES,*ZHI-PAN LI, *Physics Department, University of California San Diego, La Jolla, CA, USA* J. M. ALAMEDA, *Departamento de Física, Universidad de Oviedo, Oviedo, Spain* IVAN K. SCHULLER, *Physics Department, University of California San Diego, La Jolla, CA, USA* The exchange bias phenomenon (EB) is known by a shift of the hysteresis loop along the magnetic field axis ($H_{EB}$). In ferromagnet/antiferromagnet (FM/AF) thin films EB originates from the exchange interaction between FM and AF spins at the interface. Therefore, some theoretical models consider the EB as a purely interfacial phenomenon, but some experimental results are incompatible with these models. In this work we investigate the influence of an internal AF spin structure on EB. FM1/AF/FM2 trilayers have been prepared with disimilar FM1 and FM2 coercivities, so the sample can be cooled down below the AF Néel temperature with parallel or antiparallel FM magnetizations. It has been observed that $H_{EB}$ changes drastically from the parallel to the antiparallel cooling configuration for AF thicknesses $t_{AF} < 200$nm while it hardly varies for $t_{AF} > 300$nm. This result demonstrates that the internal spin structure of the AF is a key point to the understanding of EB. Work supported by US-DOE and European Marie-Curie-OIF.

*Also: Departamento de Física, Universidad de Oviedo, Oviedo, Spain

**16:30**

**R23 9 First-principles study on the magnetic and structural properties of Fe-Co alloys*** DANGXIN WU, PING LIU, QIMING ZHANG, *The University of Texas at Arlington* RUQIAN WU, *University of California, Irvine* $Fe_xCo_{1-x}$ alloys with different compositions are investigated using first-principles methods, FLAPW and PAW, based on density functional theory. The structural geometries of the alloys were optimized at a given composition by PAW method implemented in VASP. The initial structures were fcc and hcp for Co-rich systems, and bcc for Fe-rich systems. The formation energies were then calculated and the stability of the alloys was studied. For those systems with lower symmetries and favorable formation energies, the magnetic properties, such as the saturated magnetization and the magnetocrystalline anisotropy, were carefully studied using the FLAPW method.

*This work is supported by ONR.

**16:42**

**R23 10 Magnetic depth profile of $La_{0.7}Ca_{0.3}MnO_3$/$YBa_2Cu_3O_{7-\delta}$ trilayers** S.G.E. TE VELTHUIS, A. HOFFMANN, *Argonne National Laboratory, Argonne, IL* V. PEÑA, D. ARIAS, C. LEON, J.L. MARTINEZ, J. SANTAMARIA, *Universidad Complutense de Madrid, Spain* M.R. FITZSIMMONS, B.J. KIRBY, *Los Alamos National Laboratory, Los Alamos, NM* M. VARELA, *Oak Ridge National Laboratory, Oak Ridge, TN* Recent experiments showed magnetoresistance in excess of 1000% in epitaxial tri- layers containing highly spin polarized $La_{0.7}Ca_{0.3}MnO_3$ (LCMO) manganite and high Tc superconducting $YBa_2Cu_3O_{7-\delta}$ [1]. This large magnetoresistance originates from spin imbalance due to the injection of spin polarized carriers. In a series of trilayers, with varying LCMO layer thickness, polarized neutron reflectometry has determined the detailed magnetization depth profile. For trilayers exhibiting a strong magnetoresistance, differences in the magnetization profiles of the two LCMO layers is observed, providing a mechanism for antiferromagnetic alignment during the magnetization reversal process. Obtained details of the magnetization at the interfaces lead to a better understanding of these variations. [1] V. Peña *et al.*, Phys. Rev. Lett **94** (2005) 057002.

**SESSION R24: BLOCK COPOLYMER APPLICATIONS**
**Wednesday Afternoon, 15 March 2006**
**321, Baltimore Convention Center at 14:30**
**Ting Xu, National Institute of Standards and Technology, presiding**

**14:30**
**R24 1 Catalysts from Block Copolymers** DAVID DURKEE, *Univ. of California-Berkeley* NITASH BALSARA, *Univ. of California-Berkeley* ALEXIS BELL, *Univ. of California-Berkeley* Homogeneous catalysts are widely used to catalyze chemical reactions in the liquid phase; however, the separation of the reactants and products from such a catalyst can be difficult and often limits their use in practice. For this reason there has been considerable interest in the heterogenization of homogeneous catalysts. The use of polymers for this purpose has been particularly attractive because of the availability of a wide range of polymeric structures and methods for catalyst incorporation. Our novel approach for heterogenizing homogeneous catalysts that involves the use of microphase separated block copolymers. Block copolymers are synthesized from a crosslinkable monomer that forms a supporting gel upon crosslinking, an organometallic monomer that is catalytically active, and a depolymerizable block that can be removed to form mass transfer pathways, or pores. When placed in a solvent, the polymer gel swells to facilitate transport of the reactants to the active centers and the transport of products from these centers. This is functionally similar to the synthesis of mesoporous siliceous materials created by an amphiphilic, structure-directing agent. However, in this system, placement of the catalyst site is also controlled by self-assembly.

**14:42**
**R24 2 Thermally Crosslinkable Diblock Copolymer Templates** JULIE LEISTON-BELANGER, THOMAS RUSSELL, *University of Massachusetts- Amherst* ERIC DROCKENMULLER, *IBM Almaden Research Center* CRAIG HAWKER, *University of California- Santa Barbara* The ability to create robust nanoporous templates using polymeric thin films is important for such applications as nanofabrication and selective filtration. Thermally crosslinkable diblock copolymers based on benzocylcobutene chemistry were synthesized that could be used to this end. Poly[(styrene-stat-benzocyclobutene)-b-(D,L-lactic acid)] (PSBCB-b-PLA) was made using living free radical and ring-opening polymerization techniques. This diblock copolymer was shown to microphase separate into a cylindrical morphology that could be stabilized by heating. The minor PLA component was then removed using base to create a nanoporous crosslinked template that was 30 nm thick, with pores about 14 nm in diameter. These nanoporous templates resisted pore collapse when subjected to harsh thermal and solvent conditions. Since the base degradation of PLA produces hydroxyl groups along the pore walls, the ability to access these groups, in conjuction with the thermal and solvent resistance, opens a wide range of organic reaction possibilities.

**14:54**
**R24 3 Ordered Hexagonal Arrays of Holes with 40 nm Period by Shear Alignment of Diblock Copolymer Bilayers** JOSE VEDRINE, DOUGLAS ADAMSON, RICHARD REGISTER, *Princeton University* THOMAS PICKTHORN, *Oxford University* PAUL CHAIKIN, *New York University* An ordered hexagonal array of holes was fabricated by shear-aligning a molten bilayer film of a sphere-forming diblock copolymer in a nitrogen atmosphere. The block copolymer consisted of a polystyrene (PS) matrix and polyisoprene (PI) spheres, and was spin-coated onto a Si substrate prior to shearing. The top layer of microdomains in the bilayer was removed via a nonselective fluorine-based reactive ion etch (RIE). The PI spheres in the remaining bottom layer were then degraded with ozone to produce a PS mask with an ordered array of voids. The voids were transferred into the Si substrate by RIE, producing a dense array of holes approximately 20 nm wide and spaced 40 nm apart. This bilayer shearing procedure allows for the production of hole arrays with excellent long-range orientational order and few grain boundaries, which are unachievable by shearing a single-layer film. In addition, Au was evaporated onto the array, yielding a film of Au with regular perforations having a 40 nm period.

**15:06**
**R24 4 Reversible Nanostructures Assembled from Amphiphilic Block Copolymers** CHEN XU, XUEFENG FU, MICHAEL FRYD, BRADFORD WAYLAND, KAREN WINEY, RUSSELL COMPOSTO, *University of Pennsylvania* We present a novel route to assemble perpendicular cylinders by converting an asymmetric diblock copolymer from poly(styrene-b-tert butyl acrylate) (PS-b-PtBA) to poly(styrene-b-acrylic acid) (PS-b-PAA) using an auto-catalytic reaction. Upon exposing films of PS-b-PAA to water, PAA cylinders constrained by the continuous, glassy PS phase protrude 10 nm above the surface and swell laterally to form mushroom caps, rendering the entire surface hydrophilic. The swelling dynamics of the PAA mushrooms is captured by a two-stage mechanism, where domain growth is controlled by super case II diffusion of water into PAA followed by the slow relaxation of the PAA chains. Upon partial drying in air, the mushroom collapses as stretched hydrophilic chains relax, which results in nanometer depression in the center of each cap. The nanostructures revert to their initial dimensions and area fractions upon complete drying, demonstrating reversibility of swelling. This finding provides a new route to fabricate stimuli-responsive materials for sensors, microactuators, and microfluidic devices.

**15:18**
**R24 5 Patterned mesoporous media via 3-D replication in supercritical Carbon dioxide.** SIVAKUMAR NAGARAJAN, THOMAS RUSSELL, JAMES WATKINS, *University of Massachusetts, Amherst* JOAN BOSWORTH, PETER BUSCH, DETLEF SMILGIES, CHRISTOPHER OBER, *Cornell University* Mesoporous metal oxide films having cylindrical channels oriented normal to the surface have generated intense interest due to their potential use as sensors, catalysts and detection devices. Further, the ability to pattern these mesostructured films makes it versatile to generate mesoporous materials with precisely controlled geometries and morphologies. Here we describe a novel route to mesoporous silica films with perpendicular nanochannels prepared by the 3-D replication of block copolymer templates in supercritical carbon dioxide. Templates comprised of poly(alpha-methyl styrene) cylinders oriented normal in the matrix of poly (hydroxy styrene) having trace amounts of acid catalyst was in-

fused with solutions of silica precursor in sc $CO_2$ to selectively deposit silica within the matrix. Calcination yielded the porous silica arrays. The phase selective deposition was enabled by segregation of acid catalyst into hydrophilic matrix. Substitution of acid catalyst with photo sensitive acid generators facilitates to pattern the mesoporous films, which could potentially have applications in microfluidic devices and low-dielectric constant layers for microelectronic devices.

**15:30**

**R24 6 Ordered Nanostructured Carbon Generated from Pyrolyzed Polymer Precursors inside Anodic Aluminum Oxide Template** JIUN-TAI CHEN, KYUSOON SHIN, JULIE LEISTON-BELANGER, MINGFU ZHANG, THOMAS RUSSELL, *Polymer Science and Engineering Department, University of Massachusetts Amherst* Various carbon structures were generated by using polystyrene-block-polyacrylonitrile (PS-b-PAN) as carbon precursors in the nanopores of anodic aluminum oxide (AAO) membranes. PS-b-PAN block copolymers were drawn into nanopores of AAO by capillary force. By using different annealing temperatures, block copolymer nanotubes or nanorods can be generated. The morphologies of PS-b-PAN inside the nanopores were induced by structural frustration and interfacial interactions and were investigated by transmission electron microscopy. After stabilization and pyrolysis of the carbon precursors, the morphologies were retained and various carbon structures can be obtained. The carbon structures were found to be amorphous by Raman spectroscopy and x-ray diffraction.

**15:42**

**R24 7 Soft molding to align cylindrical nanodomains of block copolymers*** HIDEAKI YOKOYAMA, LEI LI, *AIST* Block copolymers are a class of materials that self-assemble into ordered periodic nanostructures. However, we often find that such spontaneous self-assembly ends up with disappointing randomly oriented polygrain structures, which limit the application of the nanodomains. Soft molding is a unique technique to transfer topological pattern with a soft mold, which permits a conformal contact with surfaces. A soft mold with a periodic topological pattern is embossed on the block copolymer thin films. The soft molding not only replicates the topological pattern to the block copolymer thin films but also induces microscopic flow in block copolymer thin films and controls the orientation of cylindrical domains. We fabricated a single layer of $3 \times 10^5$ parallel cylindrical nanodomains over an area of 1 cm $\times$ 1 cm.

*The New Energy and Industrial Technology Development Organization (NEDO)

**15:54**

**R24 8 Nanopatterning of Viruses and Proteins Using Microphase Separated Block Copolymers** ARTHUR CRESCE, *University of Maryland, Dept. of Materials Science and Engineering* ANGELA LEWANDOWSKI, WILLIAM BENTLEY, PETER KOFINAS, *University of Maryland, Dept. of Chemical and Biomolecular Engineering* Diblock copolymers containing nickel ions have been prepared that are capable of selectively adsorbing histidine-tagged green fluorescent protein (hisGFP), and also binding tobacco mosaic virus (TMV). A block copolymer of norbornene and norbornene dicarboxylic acid was synthesized using ring-opening metathesis polymerization. A 400/50 block ratio achieved a spherical microphase-separated morphology with roughly 20 nm diameter dicarboxylic acid spheres. The spherical phase was exposed to nickel ions in solution, templating the formation of nickel nanoparticles. This process gave a nickel-loaded diblock copolymer film whose surface was used to chelate his-GFP. Fluorescence spectroscopy and TEM confirmed the presence of the protein on the polymer surface. A sulfonated triblock copolymer was loaded with nickel ions using a similar solution-doping procedure. The morphology of this copolymer was lamellar, and its sulfonated block was loaded with nickel ions. TEM studies revealed the presence of the virus on the surface of the copolymer and showed that the bond between the TMV and the polymer surface can withstand severe detergent washes.

**16:06**

**R24 9 Surface Directed Assembly of Viral Monolayers** S. WARGACKI, R. NAIK, D. PHILLIPS, *Air Force Research Laboratory* M. FRANCIS, *University of California, Berkley* V. WARD, *University of Otago* E. THOMAS, *Massachusetts Institute of Technology* R.A. VAIA, *Air Force Research Laboratory* The facile two-dimensional fabrication of micron-scale patterns of ordered-nanoscale structures on flexible substrates has numerous broad implications, including sacrificial templates for further assembly, deposition or material removal. Previous examinations of block-copolymer assembly on micron-scale patterns with topological and/or chemical relief have demonstrated the ability to not only dictate the larger superstructure of the surface but also to impact the local nano-scale self-assembly and defect stability via confinement. These processes are examined with respect to the surface directed assembly of colloidal particles, specifically rod-like Tobacco Mosaic Virus (TMV) and iscohoderhal viruses it-Wiseana Iridovirus (WIV) and MS2. The unique surface chemistry and shapes provide a complement to traditional colloidal building-blocks. Initially, high throughput processing by convective self assembly (CSA) with orthogonal temperature gradients is combined with chemical modification of Silicon surfaces via soft-lithography to determine the key processing parameters for monolayer assembly. The impact of the viral shape (rod v. iscohodra) as well as the critical range of enthalpic interactions between the virus and substrate that control in-plane order and pattern formation will be discussed.

**16:18**

**R24 10 Guided Molecular Self-Assembly of Block Copolymer and Nanoparticles** SHAN ZOU, *Department of Chemistry, University of Toronto* GILBERT WALKER, *Department of Chemistry, University of Toronto* Block copolymers form a variety of ordered structures on nanometer length scales, allowing them to serve as an ordered matrix for nanoparticles which add functionality to the composite. The result is an ordered array of nanoparticles with potential applications including magnetic storage media, photonic crystals, or high-surface-area catalysts. Here we demonstrate the molecular self-assembly of diblock copolymers and cadmium selenide based nanoparticles. In thin films, nanoparticles assemble into one of the ordered pattern domains formed by the diblock copolymers on Si substrates. Ideas for directing the individual particles to different locations normal to the surface will be discussed.

**16:30**

**R24 11 Effect of Casting Solvent on the Morphology of Block Copolymer / Maghemite Nanoparticle Mixtures** KOOKHEON CHAR, MOON JEONG PARK, *Seoul National University* We investigate the effect of casting solvent on the morphology of block copolymer / magnetic nanoparticle (NP) mixtures. Monodisperse maghemite NPs with surfaces modified with oleic acids

have been synthesized and PS-b-PI, PS-b-PB, PS-b-PEO, and PS-b-P4VP, diblock copolymers showing cylindrical morphology were used as structure-directing matrices for the NPs. Four different solvents, hexane, toluene, THF, and CHCl3 were used to prepare film specimens by static casting and the interaction between mesophase-forming copolymers and nanoparticles, which can be tuned by casting solvent, leads to remarkably different hybrid morphology. With casting with good solvent for both blocks, with the increase in NP concentration, domains of NP aggregates were observed while the NPs were selectively incorporated into the minor domains of block copolymer under selective solvent condition. The interplay between magnetic NPs and block copolymers was also tested with different size of magnetic NPs and also with different molecular weight of block copolymers. In order to characterize the structural change of block copolymers associated with different NP loadings small- angle x-ray scattering was performed and the structural information is in good agreement with transmission electron microscopy images and differential scanning calorimetry results.

**16:42**
**R24 12 2-D Hierarchical Structure of Block Copolymer / Bionanoparticle Complexes** DONGSEOK SHIN, *University of Massachusetts, Amherst* THOMAS RUSSELL, *University of Massachusetts, Amherst* The morphology of complexes made of poly(styrene-b-N-methyl-4- vinylpyridinium iodide) (PS-P4VPMeI) and horse spleen ferritin was investigated. A polymer film was casted on a substrate then was immersed in a protein solution to allow for protein adsorption. After rinsing the sample with deionized water and drying, the specimen was placed in a mixed vapor of benzene and water. This solvent annealing technique has allowed us to get the final morphology of the complex at ambient condition. At low loading of ferritin, the morphology of the block copolymer was conserved and the ferritin was localized at the microdomains of the minor component (P4VPMeI). As the loading of ferritin increased, the microdomains containing ferritin particles grew in size and elongated in shape. Eventually, the micordomains occupied by ferritin were connected and formed closed loops at high loading of ferritin. However, in the area enclosed with the loops, the morphology of the block copolymer itself was maintained. As a result, we were able to get a hierarchical structure by incorporating bio-nanoparticles into block copolymer thin films.

**16:54**
**R24 13 Effect of Interacting Nanoparticles on the Ordered Morphology of Block Copolymer / Nanoparticle Mixtures** MOON JEONG PARK, YU JIN KANG, KOOKHEON CHAR, *Seoul National University* We investigate the effect of hard additives, i.e., magnetic nanoparticles (NPs), on the ordered morphology of block copolymers by varying NP concentration. In order to characterize the structural change of block copolymer associated with different NP loadings, small-angle x-ray scattering and transmission electron microscopy were performed. Monodisperse maghemite NPs with surfaces modified with oleic acids have been synthesized and PS-b-PI diblock copolymers showing cylindrical morphology were used as structure-directing matrices for the NPs. With the increase in NP concentration, domains of NP aggregates were observed. It is surprising to note that regular lattice-like aggregates with maghemite NPs induce an intriguing morphological transformation from the hexagonal cylinders to the body-centered cubic spheres via undulated cylinders of block copolymers, which does not show such order-order transition without NPs. The interplay between magnetic NPs and block copolymers was also tested with different size of magnetic NPs and also with different molecular weight of PS-b-PIs. We also demonstrate the preferred orientation of anisotropic microdomains of PS-b-PI, which is known to be difficult to orient by applying electric or magnetic field. This result could add more flexibility in structural control and orientation of block templates opening up new applications in the future.

**17:06**
**R24 14 Magnetic Properties of Ni Nanoparticles Dispersed in Polystyrene-Isoprene-Polystyrene Triblockcopolymers** MIRCEA CHIPARA, *Indiana University* YOU QIANG, *University of Idaho* LINFENG GUO, *Indiana University* AMINIAN HOSSEIN, *Umicore* JEFFREY M. ZALESKI, *Indiana University* SY-HWANG LIOU, *University of Nebraska* Polymer based magnetic nanocomposites were obtained by dispersing Ni nanoparticles within polystyrene-isoprene-polystyrene block copolymers. High power sonication (500 W) was used to obtain an uniform dispersion of magnetic nanoparticles. The dependence of the magnetic properties of these nancomposite materials as a function of Ni concentration (from 0 % Ni to about 25 % Ni) and temperature (in the range 100 K to 500 K) was analyzed. The agglomeration of Ni nanoparticles above the glass transition of the hard phase was observed. The process is irreversible. The agglomeration of nanoparticles is triggered by the fast decrease of diffusion coefficients above the glass transition temperature of the hard phase. Such large changes of magnetic properties triggered by the elastic properties of the matrix were not yet been reported. Ferromagnetic resonance data on Ni based composites in the temperature range 100 to 500 K confirmed the agglomeration of Ni nanoparticles and supported the irreversible character of this modification. Additional magnetic data were obtained by SQUID, VSM, and AFM (with magnetic tips).

**17:18**
**R24 15 Penetrant Diffusion in a SEBS Triblock Copolymer by Pulse Field Gradient NMR** ALAN JONES, *Clark University* MARCUS GIOTTO, ALANA CANFIELD, GUOXING LIN, *Clark University* Solid triblock copolymers can serve as the basis for membranes in such applications as separations and fuel cells. Diffusion of a low molecular weight penetrant in such a membrane is strongly affected by the morphology. The effect of the morphology on the translational motion of the penetrant can be directly assessed by pulse field gradient NMR measurements. The rotational and translational motion of 2,2,4-trimethylpentane (TMP) in a SEBS triblock will be characterized by NMR. TMP is primarily soluble in the rubbery EB phase of the SEBS triblock so that this phase then acts as the conductive component of the membrane.

**SESSION R25: ADHESION AND VISCOELASTICITY IN POLYMER THIN FILMS**
**Wednesday Afternoon, 15 March 2006**
**322, Baltimore Convention Center at 14:30**
**Karen Winey, University of Pennsylvania, presiding**

**14:30**
**R25 1 QCM Studies of Polymer Gel Spreading in Liquid Environments** FRANK NUNALEE, BRUCE LEE, PHILLIP MESSERSMITH, KENNETH SHULL, *Northwestern University* Adhesion of polymer gels to substrates is a complicated phenomenon, particularly if the system is submerged in a liquid. Establishment

of mechanical contact hinges upon the details of the gel's surface structure. In many cases, the polymeric component of the gel is shielded by a segregated solvent layer. These issues have important implications for those interested in soft, adhesive materials for biological applications. In this investigation, we utilize the surface sensitivity of the quartz crystal microbalance (QCM) to study the spreading behavior of polymeric liquids and gels on a rigid surface while submerged in a liquid medium. While the QCM has been used extensively to study adsorption by exploiting its sensitivity to material properties in the direction normal to the crystal's electrodes, few studies have utilized the QCM's ability to sense changes in loading in the plane of the electrodes. We propose equations to describe the predicted response of the QCM to a generalized viscoelastic material spreading at the QCM surface at the expense of the surrounding liquid medium. Several experimental examples are given in order to support the validity of the proposed equations, including situations where the spreading material is a Newtonian liquid, a polymer solution, or a polymer gel.

**14:42**

**R25 2 Frictional properties of hydrophobic nanopatches in different solvents.** MATTEO CASTRONOVO, *University of Trieste, Trieste, Italy* ROBERT HUDEJ, *Synchrotron Trieste, Trieste, Italy; International School for Advanced Studies (ISAS), Trieste, Italy* DENIS SCAINI, MARTINA DELL'ANGELA, *Synchrotron Trieste, Trieste, Italy; Department of Physics, University of Trieste, Trieste, Italy* LOREDANA CASALIS, *Synchrotron Trieste, Trieste, Italy* GIACINTO SCOLES, *Synchrotron Trieste, Trieste, Italy; International School for Advanced Studies (ISAS), Trieste, Italy; Princeton University, Princeton, NJ* Controlling friction at the micro- and nano-scale is of crucial importance, especially in applications as micromachines. In order to develop new ways of controlling friction, it is extremely important to understand how friction depends on the atomic structure of the interface. Using nanografting, an AFM-assisted lithographic technique, we correlated frictional properties of alkanethiols with hydrophobic termination (CH3) and of alkenethiols with hydrophilic termination (OH) on the same surface in water and in 2-butanol, using the same tip. In 2-butanol friction on C11OH is higher than on the C18 patch since OH groups on the SiO2 AFM tip surface interact more strongly with OH groups on C11OH than with CH3 groups on C18. In water, due to the strong interactions between the OH groups, the solvent molecules form an ordered layer on OH terminated SAM, which can be penetrated by the AFM tip only at relatively high applied forces.

**14:54**

**R25 3 Viscoelastic behavior of PDMS thin films with POSS nanofillers** WEN YIN, JIANJUN DENG, JOHN R. HOTTLE, HYONG-JUN KIM, ALAN R. ESKER, *Department of Chemistry (0212), Virginia Tech, Blacksburg, VA, 24061* Blends of amphiphilic poly(dimethylsiloxane) (PDMS) and a model polyhedral oligomeric silsesquioxane (POSS) nanofiller, trisilanolisobutyl-POSS, have been studied via the Wilhelm plate technique and surface light scattering (SLS). The surface pressure – surface concentration isotherms indicate that as the weight percentage of POSS increases in the blend systems, the collapse pressure of PDMS. SLS results reveal that increasing film's POSS content increases the dilational modulus of the PDMS thin films. This system is ideal for studying how nanofillers affect the viscoelastic behavior of polymer thin films at an attractive surface.

**15:06**

**R25 4 Modified Side-Chain Liquid Crystalline Polymer Thin Films as Low Adhesion Surfaces** HARIS RETSOS, *E.S.P.C.I., PARIS, Lab PPMD* DAEWON LEE, *School of Chem & Bio. Engr., Seoul National University, Seoul, Korea* COSTANTINO CRETON, *E.S.P.C.I., PARIS, Lab PPMD* KOOKHEON CHAR, *School of Chem. & Biol. Engr., Seoul National University, Seoul, Korea* The adhesive properties of side-chain liquid crystalline block copolymer thin films against soft acrylic pressure-sensitive-adhesive layers have been investigated with the probe method. Since the structure of the thin films varies from crystalline to liquid crystalline or to fully isotropic state as a function of temperature, we investigated the effect of annealing temperature of the interface on the adhesive properties. All the layers displayed very low adhesion at room temperature but above the crystalline to LC transition temperature, this low adhesion property disappears, presumably due to the reorganization of interfacial structure. To avoid this reconstruction, the 14C alkyl side-chains were modified by the incorporation of $SO_2$ groups that experience the dipole-dipole interactions and provide remarkable temperature stability to the crystalline phases. We further investigated the influence of the position and the kind of polar group in the side-chains on the structural and adhesion properties of those block-copolymers.

**15:18**

**R25 5 Polydispersity Effects on Polymer-Polymer Welding.** ANNA BARNETTE, RICHARD WOOL, IAN McANINCH, *Dept Chemical Engineering, Univ Delaware* During polymer-polymer welding, it is generally accepted that molecular weight distribution $\phi$(M) and its polydispersity (PD) affects the weld strength and required welding times. However, current welding models do not adequately address the role of PD coupled with interdiffusion Reptation dynamics, entanglement connectivity and relations between the fractal interface structure and strength, which would allow the optimal selection of the molecular weight distribution $\phi$(M). A computer simulation was developed to predict the microscopic effects of PD on welding and the results are compared with experiments on model blends of monodisperse polystyrenes (PS). The validity of the model was tested using Double Cantilever Beam PS samples that were first wetted below, and then welded for various times t, above the glass transition temperature. Wedge cleavage fracture testing determined that the weld strength $G_{1c}$ reached the maximum strength G* at an interfacial penetration contour length of 240 kDa corresponding to M* = 8 $M_c$. The simulations and experiments for monodisperse interfaces yielded $G_{1c}(t) = G^*[t/\tau]^{1/2}$where the welding time behaved as $\tau \sim$ M, and $\tau$ was less than the Reptation time $T_r \sim M^3$. For polydisperse samples, the time exponent of $.5ex1\mathrm{ker}n - .1em/\mathrm{ker}n - .15em.25ex2$ decreased empirically with increasing PDI and the welding times were related to various moments of $\phi$(M) and increased with increasing PDI until a PDI of approximately 12 was reached. The welding times for strength development are much shorter than the welding times for maximum fatigue resistance.

**15:30**

**R25 6 Lubrication by glycoprotein brushes.** BRUNO ZAPPONE, *UCSB* MARINA RUTHS, *UMass Lowell* GEORGE W. GREENE, *UCSB* JACOB ISRAELACHVILI, *UCSB* Grafted polyelectrolyte brushes show excellent lubricating properties under water and have been proposed as a model to study boundary lubrication in biological system. Lubricin, a glycoprotein of the synovial fluid, is considered the major boundary lubricant of ar-

ticular joints. Using the Surface Force Apparatus, we have measured normal and friction forces between model surfaces (negatively charged mica, positively charged poly-lysine and aminothiol, hydrophobic alkanethiol) bearing adsorbed layers of lubricin. Lubricin layers acts like a versatile anti-adhesive, adsorbing on all the surfaces considered and creating a repulsion similar to the force between end-grafted polymer brushes. Analogies with polymer brushes also appear from bridging experiment, where proteins molecules are end-adsorbed on two opposing surfaces at the same time. Lubricin 'brushes' show good lubricating ability at low applied pressures ($P < 0.5$MPa), especially on negatively charged surfaces like mica. At higher load, the adsorbed layers wears and fails lubricating the surfaces, while still protecting the underlying substrate from wearing. Lubricin might thus be a first example of biological polyelectrolytes providing 'brush-like' lubrication and wear-protection.

**15:42**

**R25 7 Understanding Polymer Adhesion: Calculations of Adsorption of Organic Molecules onto Si and $SiO_2$ Surfaces** KAREN JOHNSTON, RISTO NIEMINEN, *Helsinki University of Technology* The adhesion of polymer films onto metal and oxide materials is important for many industrial and technological applications. It is therefore essential to understand the underlying structure and bonding of the polymer and the surface. The aim of this research is to seek methods to improve polymer adhesion by using a multiscale approach. The first step involves the use of density functional calculations to understand the atomic-scale structure and bonding of polymers on surfaces. I will present first-principles results for the adsorption of benzene and related molecules on Si and $SiO_2$ surfaces. I will then discuss how this information will be incorporated into larger scale methods, such as Kinetic Monte Carlo or coarse-graining techniques. This research is supported by a grant from the Finnish Technology Development Agency (TEKES).

**15:54**

**R25 8 Differential pressure experiment to probe adhesive interactions in thin films** ANNY FLORY, DAVID BRASS, KENNETH SHULL, *Department of Materials Science and Engineering, Northwestern University* In our laboratory we have developed a highly sensitive experiment which allows the measurement of very weak adhesive interactions between interfaces joined together by specific bonds. In the experiment, we place a membrane across a glass tube and use a syringe pump to apply a pressure difference across the membrane. The membrane is then inflated into contact with a glass substrate or the quartz disk of a quartz crystal resonator that is functionalized as desired and is immersed in an aqueous environment. A Langmuir layer is placed at the interface between air and water providing the modification of the surface chemistry of the membrane. The asymmetric Laplace equation is used to derive the energy release rate (G) from the experimental results. The advantage of this method is that specific and weak adhesive interactions as the ones encountered in biological systems can be accessed but also that the approach can be extended to measurement of very strong adhesive interactions such as those in synthetic gels. In this discussion, the validity of the method will be presented through results obtained on adhesive interactions between various model systems.

**16:06**

**R25 9 Capillary wave dynamics on viscoelastic polymer thin-films: Monolayers and bilayers** MARK HENLE, ALEX LEVINE, *Department of Chemistry and Biochemistry, University of California, Los Angeles* We investigate the capillary wave dynamics of supported polymeric thin-films both at the free surface and at the buried polymer/polymer interface in a bilayer system. Recent XPCS experiments (J. Lal, private communication) on such systems suggest that the decay rate of the coupled capillary waves at the free surface and at the buried interface are remarkably independent of the in-plane wavevector. In order to understand this phenomenon, we present the results of continuum hydrodynamic calculations of the capillary wave dynamics on supported monolayers and bilayers of both Newtonian and viscoelastic fluids. We find that the experimentally observed wavevector dependence of the capillary-wave decay rate can be accounted for by treating one or both of the polymers as a viscoelastic fluid with a single stress-relaxation time. We also investigate the effect of a finite slip length at either the polymer/polymer interface or the polymer/substrate interface.

**16:18**

**R25 10 Molecular recoiling forces in ultra-thin films of long entangled polymer chains** ARNOLD CHANG-MOU YANG, TONY MING-HSUN YANG, SEN-YEN HOU, YU-LUN CHANG, *Department of Material Science and Engineering, National Tsing Hua University, Hsinchu, Taiwan* Molecular recoiling force stemmed from non-equilibrium chain conformation was found to play a very important role in the dewetting stability of polymer thin films. Correct measurements and inclusion of this molecular force into thermodynamic consideration are crucial for analyzing dewetting phenomena and nanoscale polymer chain physics. This force was measured using a simple method based on contour relaxation at the incipient dewetting holes. The recoiling stress was found to increase dramatically with molecular weight and decreasing film thickness. The corresponding forces were calculated to be in the range from 9.0 to 28.2 mN/m, too large to be neglected when compared to the dispersive forces ( $\sim$ 10 mN/m) commonly operative in thin polymer films. This work is supported by Air Force (AFOSR-04-4074) and National Science Council of Taiwan.

**16:30**

**R25 11 The Effect of Nanobubbles on Microcantilever Bending** SANGMIN JEON, *Pohang University* RAMYA DESIKAN, *University of Tennessee* FANG TIAN, THOMAS THUNDAT, *Oak Ridge National Laboratory* Nanomechanical cantilevers are very small and extremely sensitive force and mass sensors. Here, we report on the impact of the vertical component of surface energy on microcantilevers when nanobubbles form on their surfaces. Young's equation, which is commonly used to determine the contact angle of liquid drops on a solid surface, ignores the vertical component of the surface energy. Despite this force being extremely small and its effect on the solid can be ignored, it plays a significant role for flexible surfaces such as microcantilevers. A gold-coated silicon microcantilever and a dodecanethiol coated silicon microcantilever were used to detect real-time formation of nanobubbles on their surfaces when exposed to air-rich water. As air nanobubbles form on the surfaces of the cantilever, the cantilever undergoes bending and we relate this to the vertical compo-

nent of surface energy in Young's equation. This implies that the vertical component of the surface tension should be considered for flexible solid surfaces, and the formation of nanobubbles should be avoided when cantilevers are used as sensors to avoid artifacts.

**16:42**
**R25 12 Measuring local viscoelastic properties of complex materials with atomic force microscopy** PAULA WOOD-ADAMS, WENSHENG XU, *Concordia University* Tapping mode atomic force microscopy is a technique to measure the topography and properties of surfaces involving a micro-cantilever with a tip at one end that is excited into an oscillation near its resonance frequency. The cantilever-tip assembly is positioned vertically such that the tip touches the surface at the bottom of its down-stroke and then scanned over the surface. The oscillation of the cantilever is affected by the topography of the surface, the local surface properties and the feed back controller which maintains the amplitude of the oscillation at a fixed set point value. The vertical movements needed to maintain constant oscillation amplitude are used to draw the topography image and the phase lag of the oscillation relative to the excitation force is used to draw the phase image. The phase lag is sensitive to local mechanical properties under certain experimental conditions and we have found that by using silicon as an internal standard reference surface we can unambiguously relate the phase lag to local viscolastic properties of a polymeric material. We have built a model describing this relation, validated the model with experimental data and finally inverted it such that it can be used to determine local properties. This allows us to measure high frequency local viscoelastic properties on length scales as small as several nanometers. This technique works well for relatively compliant polymer surfaces with a shear modulus less than about 1 GPa. Funding Provided by the Taiho Kogyo Tribology Research Foundation.

**16:54**
**R25 13 The kinetics of the reaction of telechelics at a soft interface by neutron reflectivity** J. KEVIN RICE, HELEN JI, MARK DADMUN, JIMMY MAYS, *University of Tennessee* The aim of this study is to gain a fundamental understanding of the kinetics of the in- situ formation of blocky copolymer molecules at a soft, immiscible polymer interface by the reaction of telechelic polymers across that interface. The resultant interfacial morphology that is formed from this reaction is also studied. Specular neutron reflectivity measurements were made after various annealing times on bilayer PS/PMMA samples, each of which contains dPS telechelics in one layer and monochelic PMMA in the other. Three reactive chain-end pairs were studied: epoxy-amine, epoxy-carboxylic acid, and amine-anhydride. After sufficient annealing of each system, an interfacial layer forms between the PS and PMMA that contains triblock copolymer formed by the reaction of the telechelics and the reactive PMMA chains. The thickness of this interfacial modifier layer, as well as the roughness between the matrix layers, increases with annealing time. Several molecular weights of the telechelics were studied and results relating the time evolution of the blocky copolymer volume fraction at the interface to interfacial excess, as well as interfacial coverage and reaction rate constants will be discussed.

## SESSION R26: FOCUS SESSION: COUNTERION DYNAMICS IN CHARGED BIOPOLYMER SYSTEMS
**Wednesday Afternoon, 15 March 2006; 323, Baltimore Convention Center at 14:30**
**Alex Travesset, Ames Laboratory, presiding**

*Invited Papers*



**14:30**
**R26 1 Counterion liquids between biological polyelectrolytes.**
GERARD WONG, *University of Illinois at Urbana-Champaign*

Electrostatic interactions between charged surfaces in water are dominated by counterion behavior. For example, repulsion between like-charged objects are due to the osmotic pressure of compressed counterions, and attraction between oppositely-charged objects are due to the entropy gain of counterion release. In systems with strong electrostatic interactions, mean field theories break down and counterion correlations and dynamics become important. To explain counterintuitive phenomena such as like-charge attraction between polyelectrolytes, exotic models such as counterion Wigner lattices were proposed, but no experimental comparisons at sufficient spatial resolution exist. Using inelastic x-ray scattering, the spatiotemporal correlations of counterions that mediate binding between charged polymers have been measured in aqueous solution down to molecular length-scales. We find that these ions are hierarchically organized into a dense, strongly correlated liquid that exhibits an acoustic-like phonon mode. The excitation spectra at high wave-vector Q reveal unexpected dynamics due to ions interacting with their ''cages'' of nearest neighbors. The measured speed of sound and collective relaxation rates in this liquid agree well with simple model calculations.

*Contributed Papers*

**15:06**
**R26 2 Bjerrum Pairing Correlations at Charged Interfaces*** ALEX TRAVESSET, DAVID VAKNIN, *Iowa State University and Ames Lab* Electrostatic correlations play a fundamental role in aqueous solutions. In this letter, we identify transverse and lateral correlations as two mutually exclusive regimes. We show that the transverse regime leads to binding by generalization of the Bjerrum pair formation theory and point out that this purely electrostatic correlation becomes dominant for strongly charged interfaces. We compare our theoretical predictions with different experiments on charged membranes and Langmuir monolayers and find good agreements. We contrast our approach with existing theories in the strong coupling limit and on charged modulated interfaces and discuss different scenarios leading to charge reversal and equal-charge attraction by macro-ions.

*funded by NSF grant DMR-0426597 and DOE under contract W-7405-ENG-82

*Invited Papers*

**15:18**
**R26 3 Charged Polymers in Electric Fields.**
ROLAND NETZ, *Technical University Munich*

Charged polymers in solution are considered under the action of external electric fields. An electric field acts simultaneously on charged groups of the polyelectrolyte and on mobile counterions. As a result, charges are displaced and a dipole moment is produced, which leads to stretching and orientation of the polymer parallel to the external field. On the the other hand, hydrodynamic effects favor a perpendicular orientation of stiff polymers with respect to the external field, which is related to the phenomenon of anomalous birefringence. By performing hydrodynamic simulations, the relation between the electrophoretic mobility and the non-equilibrium perturbation of the polymer structure is investigated which results from a competition between electro-friction effects when counterions glide along the polymer backbone and coupling between hydrodynamic and elastic forces. Friction effects are more pronounced when polymers are confined, for example when they move through pores or when they adsorbed at surfaces.

*Contributed Papers*

**15:54**
**R26 4 Migration of DNA on electrically inhomogeneous surfaces** ERIC PETERSEN, *Harvard College* BINGQUAN LI, VLADIMIR SAMUILOV, XIAOHUA FANG, JONATHAN SOKOLOV, MIRIAM RAFAILOVICH, *Dept. of Materials Science and Engineering, Stony Brook University* Surface electrophoresis of kilo-bp DNA on electrically inhomogeneous surfaces was studied. The surfaces were produced by stamping micropatterns of gold strips onto silicon wafers using the Whitesides microcontact printing technique. Simulations of the field distribution on the surface revealed regions of very high field strength localized at the Au/Si interface. As a result, both electrophoretic and dielectrophoretic forces contribute to the movement of DNA on the surface. The mobility of DNA across the patterned surface was measured via laser induced fluorescence detection with an electric field oriented normal to the strips in the plane of the surface. The interaction of DNA with the surface was imaged with a confocal microscope in laser scanning mode with a CCD camera. Results indicate the measured mobility of DNA on a chemically micropatterned surface depends on the period size of the gold striped pattern relative to the contour length of the DNA molecule and the persistence length of the chain relative to the size of the electric field disturbance at the Au/Si interface. Consequentially, surface separation of DNA of different size and flexibility is possible.

**16:06**
**R26 5 Evidence for High Conductivity in the Pili of Geobacter sulfurreducens: ''Nano-wires'' in a Prokaryotic Electron Transport Chain?*** KEVIN D. MCCARTHY, *Dept. of Physics and Dept. of Microbiology, UMass* GEMMA REGUERA, TEENA MEHTA, JULIE S. NICOLL, *Dept. of Microbiology, UMass* XINYU WANG, *Dept. of Phyics, UMass* MARK T. TUOMINEN,[†] DEREK R. LOVLEY, *Dept. of Microbiology and The Geobacter Project, UMass* We discuss results of Conducting-Probe Atomic Force Microscopy (CP-AFM) applied to the nanoscopic filamentary pili of the prokaryote Geobacter sulfurreducens. (G. Reguera, et al., Nature **435**, 1038, 2005) The apparently high cross-axis conductivity of this bacterial membrane protein complex, along with evidence of its necessity for respiratory reduction of insoluble Fe(III) deposits in nature, points to the possibility of a novel role for the pili protein complex in the electron transport chain of a prokaryote: as a kind of ''nano-wire'' for conduction of electrons to Fe(III) oxides. CP-AFM and itin vivo genetic engineering experiments supporting the ''nano-wire'' hypothesis are presented.

*This work was supported by DOE cooperative agreement DE-FC02-02ER63446 and NSF grant DMR-0306951
[†]Dept. of Physics and MassNanoTech, UMass

**16:18**
**R26 6 Dynamical Transition of the Protein Observed in Terahertz Dielectric Response** JING-YIN CHEN, JOSEPH KNAB, ANDREA MARKELZ, *Physics Department, University at Buffalo, SUNY, Buffalo, NY 14260* Temperature dependent measurements (10 K – 296 K) were made of the terahertz dielectric response of oxidized and reduced cytochrome C (CytC) buffer solutions using THz time domain spectroscopy (THzTDS) (0.12-2.0 THz). The imaginary part of the index ($\kappa$) for both ferri and ferro CytC solutions increases linearly with temperature at low temperatures and then strongly increases near 200 K with a plateau at 250 K. The change of $\kappa$ for ferroCytC between 200 K and 250 K is nearly half that of ferriCytC. The result is consistent with

Mossbauer measurements; however THzTDS measures motions in the significantly shorter time range, 0.5 – 8 ps. These are the first measurements of the transition in the THz range and put constraints on allowed mechanisms. The agreement with polarizability insensitive Mossbauer supports that the dramatic increase in the THz dielectric response with oxidation we reported for CytC films (Phys Rev E 72, 040901 (2005)) results mainly from a large increase in the low frequency vibrational density of states. Work was supported by NSF Career PHY-0349256, and NSF IGERT DGE0114330.

**16:30**

**R26 7 Terahertz dielectric response dependence on protein melting and hydration** YUNFEN HE, J.R. KNAB, *Physics, University at Buffalo, SUNY* B. SHAH, *Chem. Eng., Rutgers University* A.G. MARKELZ, *Physics, University at Buffalo, SUNY* Hydration is critical for protein structure stability and flexibility. The hydration dynamics of denatured proteins necessarily plays a significant role in protein folding/unfolding and aggregation. We previously reported the observation of a transition in the THz dielectric response for native state hen egg white lysozyme (HEWL) with hydration. As hydration increases the response slowly increases until at 0.25h (gm water/gm protein) the absorbance and index sharply increase. The frequency range is associated with structural vibrational modes and the hydration level coincides with the filling of the first solvation shell. We present recent THz hydration dependence results as a function of denaturing. The THz absorption coefficient is nearly independent of denaturation while the index of refraction significantly decreases compared to native state and has a stronger frequency dependence with a peak appearing near 0.5 THz. Most significantly the hydration transition at 0.25h is still present for the denatured samples, suggesting the net itbound water content is nearly identical to the native state.

**16:42**

**R26 8 Inorganic Surface and Structure Adhesion of Amino Acids and Peptides** LARUE DUNKLEBERGER, ROBERT WILLETT, LOREN PFEIFFER, *Bell Laboratories, Lucent Technologies* Interactions at the interface of biological molecules and inorganic materials are an open question in materials science; understanding these hybrid interfaces at the molecular level can have extensive basic and practical implications. In an extensive set of measurements we have systematically examined the adhesion of amino acids to a series of inorganic surfaces used in semiconductor devices. Peptides comprised of each of the twenty amino acids were exposed in solution to surfaces including metals, insulators, and semiconductors. Significant differential adhesion to the various surfaces is observed over the complement of amino acids, with adhesion determined largely by the amino acid side-chain charge. Mapping of adhesion findings for the amino acids versus materials in multiple solutions has been accomplished, in addition to examination of concentration and pH dependence. These results provide an empirical basis for building peptide to inorganic surface structures. In this vein, we have designed inorganic nano-structures using molecular beam epitaxy that are shown to selectively bind to prescribed primary peptide sequences. The inorganic structures fabricated here are shown to be able to discriminate between peptides with differences of only two to four amino acids. This surprising specific differential adhesion in both open surfaces to varied amino acids and in nanoscale structures to peptides is examined for the physical processes at play.

**16:54**

**R26 9 Interactions between the HIV-TAT transduction domain and cell membranes** ABHIJIT MISHRA, *University of Illinois, Department of Materials Science and Engineering* GERARD WONG, *University of Illinois, Department of Materials Science and Engineering, Department of Physics, Department of Bioengineering* Biologically active molecules such as proteins and oligonucleotides can be transduced into cells with high efficiency when covalently linked to a Protein Transduction Domain (PTD), such as the TAT domain in the HIV virus. All PTDs have a high content of basic amino acids resulting in a net positive charge. Electrostatic interactions between cationic PTDs and the negatively charged phospholipids that constitute the plasma membrane are likely to be responsible for peptide uptake, but no detailed structural studies exist. We compare membrane structures induced by the cationic TAT domain and those induced by other cationic polypeptides as a function of membrane composition using synchrotron x-ray scattering, and examine possible mechanisms of the anomalous transduction.

**17:06**

**R26 10 Temperature Effects on Threshold Counterion Concentration to Induce Aggregation of fd Virus** QI WEN, JAY TANG, *Brown University* We seek to determine the mechanism of like-charge attraction by measuring the temperature dependence of critical divalent counterion concentration ($C_c$) for the aggregation of fd viruses. We find that an increase in temperature leads to a decrease in the dielectric constant ($\varepsilon$) of the solvent, thus causing $C_c$ to decrease. At a constant $\varepsilon$, $C_c$ is found to increase as temperature increases. The effect of $T$ and $\varepsilon$ on $C_c$ is combined to that of one parameter: Bjerrum length ($l_B$). $C_c$ decreases exponentially as $l_B$ increases. The exponential decay of $C_c$ suggests that entropic effect of counterions plays an important role at the onset of bundle formation.

**17:18**

**R26 11 Ion Distribution around DNA: Can Transitions Be Observed?** KURT ANDRESEN, LISA KWOK, XIANGYUN QIU, HYE YOON PARK, JESSICA LAMB, LOIS POLLACK, *Cornell University* The spatial distribution of counterions that reduce or neutralize the charge of biopolymers is fundamentally important in determining how these polymers interact with each other and with their surroundings (i.e. with charged surfaces). We will discuss recent anomalous small-angle x-ray scattering (ASAXS) experiments that quantify the distribution of ions around DNA strands in solution. This counterion atmosphere has been studied as a function of a variety of experimental conditions, including those known to lead to structural transitions of the biopolymer.

**SESSION R27: MANY-BODY/STRONGLY CORRELATED**
**Wednesday Afternoon, 15 March 2006**
**324, Baltimore Convention Center at 14:30**
**Gerardo Ortiz, Los Alamos National Laboratory, presiding**

**14:30**

**R27 1 Density Matrix Renormalization Group algorithm on intersecting chains** HAIHUI GUO, STEVEN WHITE, *University of California, Irvine* Systems of intersecting chains are interesting both from a fundamental viewpoint and because of their potential use in nanoscale devices. Here, we will introduce a new density

matrix renormalization group algorithm to perform calculations on intersecting chains systems. The new DMRG algorithm greatly reduces the number of states kept per block to roughly $\sqrt{m}$ compared with the alternative ''non-local'' approach. We present results on 3-chain Heisenberg $S = 1$ system with two geometries, one with a single site in the center of junction, the other with three sites in the center of junction.

**14:42**

**R27 2 Finite-temperature density matrix renormalization using an enlarged Hilbert space** ADRIAN E. FEIGUIN, *Microsoft Research* STEVEN R. WHITE, *University of California, Irvine* We apply a generalization of the time-dependent DMRG to study finite temperature properties of several quantum spin chains, including the frustrated $J_1 - J_2$ model. We discuss several practical issues with the method, including use of quantum numbers and finite size effects. We compare with transfer-matrix DMRG, finding that both methods produce excellent results.

**14:54**

**R27 3 DMRG meets NRG*** ANDREAS WEICHSELBAUM, *Arnold Sommerfeld Center (LMU), Munich, Germany* FRANK VERSTRAETE, *Institute for Quantum Information, Caltech, Pasadena, US* ULRICH SCHOLLWÖCK, *Institut für Theoretische Physik C, RWTH-Aachen, Germany* J. IGNACIO CIRAC, *Max-Planck-Institut für Quantenoptik, Garching, Germany* JAN VON DELFT, *Arnold Sommerfeld Center (LMU), Munich, Germany* We present a unified framework of renormalization group methods, including Wilson's numerical renormalization group (NRG) and White's density-matrix renormalization group (DMRG), within the language of matrix product states. This allows to improve over Wilson's NRG for quantum impurity models by a variational method optimal in this framework. We illustrate it for the single-impurity Anderson model; moreover we use a variational method for evaluating Green's functions. The proposed method is more flexible in its description of off-resonance spectral properties, opening the way to time-dependent, out-of-equilibrium impurity problems. It also substantially improves computational efficiency for one-channel impurity problems, suggesting *linear* scaling of complexity for *n*-channel problems.

*Supported by DFG.

**15:06**

**R27 4 Strong Coupling Polaron in 2D in Terms of the Bethe-Salpter Equation** RUSSELL SELVA, YURIY MALOZOVSKY, *Southeastern Louisiana University* We consider the formation of polaron in two dimensions in terms of the Bethe-Salpeter equation. We develop the perturbation diagram approach to the electron-phonon interaction problem and show that the series of the ladder diagrams lead to the well-known Bethe-Salpeter equation. We evaluate the self-energy of the polaron. We show that even in the case of the weak electron-phonon interaction there at least one bound state exists for the polaron in two dimensions. We consider the formation of the polaron for the interaction of an electron both with acoustic and optical phonons. We have found the existence of the strong coupling polaron in both cases.

**15:18**

**R27 5 Collective fields in the functional RG for fermions: Vacuum expectation values and spontaneous symmetry breaking** FLORIAN SCHUETZ, PETER KOPIETZ, *Institut fuer Theoretische Physik, Universitaet Frankfurt, Max-von-Laue Strasse 1, 60438 Frankfurt* We discuss partial bosonization of interacting electron systems by a Hubbard-Stratonovich transformation and derive the functional renormalization group equations for the one-line-irreducible vertices of the resulting coupled field theory containing fermionic and collective bosonic fields. We analyze different choices of the cutoff in either the fermionic or the bosonic propagator. Recently,we have shown that for the Tomonaga-Luttinger model a purely bosonic cutoff can be combined with Ward identities to solve a whole hierarchy of flow equations and to reproduce the exact solution for the single particle Green's function known from bosonization [1]. Here, we generalize our approach to include the possibility that some bosonic components of the field have a finite vacuum expectation value. The system of flow equations is then modified and supplemented by a flow equation for the vacuum expectation value of the field. For bosonic fields describing fluctuations in the zero-sound channel, the vacuum expectation value of the zero mode is closely related to the fermionic density, which can be exploited to calculate the compressibility. By using a cutoff in the free bosonic propagator, the renormalization group flow can be set up to systematically yield corrections to the self-consistent Hartree approximation. [1] F. Schuetz, L. Bartosch, and P. Kopietz, Phys. Rev. B 72, 035105 (2005)

**15:30**

**R27 6 Ab initio Anderson impurity approach to x-ray absorption spectra of transition metal complexes*** DANIEL L. COX, *Department of Physics, University of California, Davis, CA 95616* ARND HUBSCH, *Max-Planck-Insitut für Physik komplexer Systeme, Nöthnitzer Str. 38, 01187 Dresden, Germany* MONTIAGO X. LABUTE, *Theoretical Biology and Biophysics, Los Alamos National Laboratory, Los Alamos, NM 87545* We present a generic Anderson impurity approach to transition metal molecules that allows to study correlation effects beyond the usual electronic structure calculations. Here, first principle density functional theory calculations (using SIESTA) are employed to determine the parameter of the model Anderson impurity Hamiltonian. We use the Lanczos algorithm to diagonalize the model Hamiltonian within a restricted set of basis states that is built up in the spirit of of the Gunnarsson Schönhammer trial wave function for heavy fermion compounds. The presented approach is applied to the K-edge x-ray absorption spectra of the valence tautomer molecule $Co(3,5\text{-}DTBSQ)_2(phen)$.

*Research supported by the US Department of Energy, Division of Materials Research, Office of Basic Energy Science, and by DFG grant HU 993/1-1.

**15:42**

**R27 7 Anomalous tunneling of bound pairs in crystal lattices** PAVEL KORNILOVITCH, *Hewlett-Packard Company* VLADIMIR BULATOV, A novel non-perturbative method of solving scattering problems for bound pairs on a lattice is developed. Two different break- ups of the Hamiltonian are employed to calculate the full Green operator and the wave function of the scattered pair. The calculation converges exponentially in the number of basis states used to represent the non-translationinvariant part of the Green operator. The method is general and applicable to a variety of scattering and tunneling problems. As the first application, the problem of pair tunneling through a weak link on a one-dimensional lattice is solved. It is found that at the momentum values close to $\pi$ the pair tunnels

much easier than one particle, with the transmission coefficient approaching unity. This anomalously high transmission is a consequence of the existence of a two-body resonant state localized at the weak link. [V.L. Bulatov and P.E. Kornilovitch, Europhys. Lett. **73**, 352 (2005).]

**15:54**

**R27 8 Non-Markovian dynamics on one-dimensional quantum lattices** MICHAEL ZWOLAK,* *California Institute of Technology* Recently ideas from Quantum Information have sparked a number of advances in the simulation of interacting quantum lattice systems. Vidal first proposed a method, dubbed the Time Evolving Block Decimation (TEBD) algorithm, to simulate real-time dynamics of pure states on one-dimensional lattices. [1] Subsequently this method was extended to the simulation of mixed states, including real-time dynamics governed by a Markovian master equation and construction of thermal states. [2] These methods scale linearly in the system size, enabling relatively large lattices to be studied. We present a more general extension of the TEBD algorithm which allows one to simulate non-Markovian master equations within the Born approximation. This method scales quadratically with the system size. We demonstrate the method with examples of spins and fermions. We also discuss applications to systems driven out of equilibrium by external reservoirs. [1] G. Vidal, Phys. Rev. Lett. 91, 147902 (2003); 93, 040502 (2004). [2] M. Zwolak, G. Vidal, Phys. Rev. Lett. 93, 207205 (2004).

*Institute for Quantum Information

**16:06**

**R27 9 Exotic excitations with fractional charges on frustrated lattices** ERICH RUNGE, *Technische Universität Ilmenau* FRANK POLLMANN, PETER FULDE, *Max-Planck-Institut für Physik komplexer Systeme* Geometrical frustration of lattices can lead to a macroscopic degeneracy in the classical limit and thus to many interesting physical effects. In spin systems these are e.g. translational invariant spin liquid ground states and deconfined spinons. In contrast to magnetic properties, one began only recently to explore the charge degrees of freedom on frustrated lattices. For the systematic study of charge degrees of freedom, we consider a model of spinless Fermions with nearest-neighbor hopping $t$ and Coulomb repulsion $V$. Quantum fluctuations reduce the classical ($t = 0$) macroscopic degeneracy. For the strongly correlated limit $V \gg |t|$, it has been predicted that an added electron can decay into two mobile quasi-particles, leading to fractional charges of $e/2$ in 2D and 3D systems. For a deeper understanding of these charge degrees of freedom we calculated numerically the properties of static and dynamic charges on the 2D checkerboard lattice. We find evidence for a weak confinement between two fractional charges leading to excitations with very large spatial extend. Furthermore, we argue that the fractional charges are probably deconfined on the 3D pyrochlore lattice.

**16:18**

**R27 10 Making an analogy between a multi-chain interaction in Charge Density Wave transport and the use of wave functionals to form S-S' pairs.** ANDREW BECKWITH, First, we show through a numerical simulation that the massive Schwinger model used to formulate solutions to CDW transport in itself is insufficient for transport of soliton-antisoliton (S-S') pairs through a pinning gap model of CDW transport. We show that a model Hamiltonian with Peierls condensation energy used to couple adjacent chains (or transverse wave vectors) permits formation of S-S' pairs which could be used to transport CDW through a potential barrier.Previously, we have argued that there are analogies between this construction and the false vacuum hypothesis used for showing a necessary and sufficient condition for formation of CDW S-S' pairs in wavefunctionals. Here we note that this can be established via either use of the Bogomil'nyi inequality or an experimental artifact which is due to use of the false vacuum hypothesis to obtain a proportional 'distance' between the S-S' charge centers.

**16:30**

**R27 11 Localized component method for few-body scattering and bound state calculations*** VLADIMIR ROUDNEV, *Kansas State University* A modification of Faddeev equations which admits a very effective computational scheme is proposed. The method allows to perform precise calculations of bound states and scattering in few-body systems. For the systems having loosely bound subsystems the method can reduce the computation time by an order of magnitude. We illustrate the method by calculating bound states and scattering of three atoms with a simple model interaction. We also report results for systems of noble gas atoms with realistic interactions.

*This work was partially supported by the Chemical Sciences, Geosciences, and Biosciences Division, Office of Basic Energy Sciences, Office of Science, U.S. Department of Energy.

**16:42**

**R27 12 Equilibrium technique applied to strongly correlated electron transport in steady-state nonequilibrium*** JONG HAN, *State University of New York at Buffalo* We present a quantum algorithm of nonequilibrium steady-state transport within the equilibrium formalism. Current-carrying nonequilibrium ensemble is constructed by the Boltzmann factor $\exp[-\beta(\hat{H} - \hat{Y})]$ using the bias operator $\hat{Y}$ which imposes the boundary condition of different chemical potentials in source-drain reservoirs of electronic device. In the limit of non-interacting quantum dot systems, the mapping of a nonequilibrium to an effective equilibrium system can be explicitly shown to reproduce the Landauer-Büttiker formula. The equilibrium formulation is successfully applied to the strongly correlated transport of the Kondo regime, with the anomalous Kondo peak at small voltage bias and incoherent inelastic transport at high bias. This demonstrates that the numerical tools developed in equilibrium theory, such as quantum Monte Carlo, exact diagonalization, or renormalization group methods, can be applied in nonequilibrium and complement the existing theories based on nonequilibrium Greens function technique.

*Supported by NSF DMR-0426836

**16:54**

**R27 13 Cluster Impurity Solver for LDA+DMFT Calculations** QUAN YIN, SERGEY SAVRASOV, *University of California, Davis* CA 95616 TEAM, We report the electronic structure calculations of strongly correlated systems such as Mott Insulators, using the LDA+DMFT method. LDA+DMFT is a combination of the Density Functional Theory and the Dynamical Mean Field Theory featuring both the one-electron approximation and the many-body treatment for electrons, which is suitable for any ratio of coulomb repulsion over band width, and all computations are self-consistent. In the process of solving the Anderson Impurity Model for DMFT, several solvers with different accuracy were used and their results are compared. This presentation will focus on our most recently developed cluster solver and its applications.

**17:06**
**R27 14 Many-body Co-tunneling in Coupled Quantum Dots** CAROLYN YOUNG, *McGill University* MICHAEL HILKE, *McGill University* We developed a new formalism which allows us to study co-tunneling events in coupled quantum dot structures. By generalizing the non-equilibrium Green's function (NEGF) method for the case of N-particle Green's functions, we are able to calculate the many-body self-energy associated with semi-infinite leads. This formalism can be used to calculate the co-tunneling contribution to the differential conductance of various structures, such as parallel- and serial-coupled quantum dots, as well as Aharonov-Bohm interference devices.

**SESSION R28: FOCUS SESSION: BIOLOGICAL NETWORKS: STRUCTURE, DYNAMICS AND FUNCTION**
**Wednesday Afternoon, 15 March 2006; 325, Baltimore Convention Center at 14:30**
**Chao Tang, University of California, San Francisco, presiding**

***Invited Papers***

**14:30**
**R28 1 Unraveling Biological Design Principles Using Engineering Methods: The Heat Shock Response as a Case Study.**
HANA EL-SAMAD, *Biochemistry and Biophysics, QB3, UC San Francisco*

The bacterial heat shock response refers to the mechanism by which bacteria react to a sudden increase in the ambient temperature. The consequences of such an unmediated temperature increase at the cellular level is the unfolding, misfolding, or aggregation of cell proteins, which threatens the life of the cell. To combat such effects, cells have evolved an intricate set of feedback and feedforward mechanisms. In this talk, we present a mathematical model that describes the core functionality of these mechanisms. We illustrate how such a model provides valuable insight, explaining dynamic phenomena exhibited by wild type and mutant heat shock responses, corroborating experimental data and guiding novel biological experiments. Furthermore, we demonstrate, through the careful control analysis of the model, several design principles that appear to have shaped the feedback structure of the heat shock system. Specifically, we itemize the roles of the various feedback strategies and demonstrate their necessity in achieving performance objectives such as efficiency, robustness, stability, good transient response, and noise rejection in the presence of limited cellular energies and materials. Examined from this perspective, the heat shock model can be decomposed, both conceptually and mathematically, into functional modules. These modules possess the characteristics of more familiar modular structures: sensors, actuators and controllers present in a typical technological control system. We finally point to various theoretical research challenges inspired by the heat shock response system, and discuss the crucial relevance of these challenges in the modeling and analysis of many classes of systems that are likely to arise in the study of gene regulatory networks.

***Contributed Papers***

**15:06**
**R28 2 Network growth models and genetic regulatory networks*** JOSHUA SOCOLAR, DAVID FOSTER, *Duke University, Durham, NC* STUART KAUFFMAN, *Institute for Biocomplexity and Informatics, University of Calgary* We study a class of growth algorithms for directed graphs that are candidate models for the evolution of genetic regulatory networks. The algorithms involve partial duplication of nodes and their links, together with innovation of new links, allowing for the possibility that input and output links from a newly created node may have different probabilities of survival. We find some counterintuitive trends as parameters are varied, including the broadening of indegree distribution when the probability for retaining input links is decreased. We also find that both the scaling of transcription factors with genome size and the measured degree distributions for genes in yeast can be reproduced by the growth algorithm if and only if a special seed is used to initiate the process.

*Supported by NSF Grant No. PHY-0417372.

**15:18**
**R28 3 Bistability of the naturally induced lactose utilization system of Escherichia coli** JELENA STAJIC, MICHAEL WALL, *Los Alamos National Laboratory* In the absence of the preferred sugar glucose, lactose utilization machinery in the bacterium E. coli is activated. The genetic circuit responsible for this response, lac operon, has been observed to exhibit bistability when induced by an artificial inducer, TMG. Here we investigate conditions under which bistability might be observed in response to lactose. The aim of our study is to establish whether the natural system exhibits bistability, as is often assumed despite the lack of experimental support.

**15:30**
**R28 4 Origins of sloppiness in biological models.** JOSHUA WATERFALL, FERGAL CASEY, RYAN GUTENKUNST, *Cornell University* KEVIN BROWN, *Harvard University* CHRISTOPHER MYERS, JAMES SETHNA, *Cornell University* Models of biological networks such as those involved in signal transduction, development, and the cell cycle routinely contain dozens of parameters. Even if high quality data on the dynamics of every form of every chemical species were available for such networks, some parameter combinations would be orders of magnitude more constrained than other combinations – a feature we term sloppiness. In order to understand this shared, possibly universal, behavior we turn to mathematically well-defined classes of models – multiple linear regression, sums of polynomials and sums of exponentials. The origins of sloppiness turn out to have nothing to do with how much data is available or how many parameters a model has, but are instead the scale of description at which a model is constructed

and how the parameters of the model map to the data. Thus describing a cloud of points by a plane, the core of linear regression, is not sloppy while describing complex biological networks by the biochemical reactions, just as fitting sums of exponentials or polynomials, is unavoidably sloppy.

**15:42**
**R28 5 Function Constrains Topology.** CHAO TANG, *University of California at San Francisco* WENZHE MA, QI OUYANG, *Center for Theoretical Biology, Peking University* In the biological world, intimate relations between function and form are well established on the macroscopic and the microscopic scales. However, on the ''mesoscopic'' scales, to what extend the function of a system and the organization of its parts are related? In this talk, I will present a case study of the segmentation polarity gene network in Drosophila. The function of this network is to stabilize the segmentation pattern of gene expression during the development. We found that although there are numerous networks which can perform the function, the requirement for the function to be robust severely constrains the network's topology. The network selected by nature is among the most robust topological classes. Furthermore, I will show that the knowledge of viable topologies can be used to help identify ''missing'' links in the network.

**15:54**
**R28 6 Stability tuned: An analysis of a gene network with counteracting feedback loops*** MURAT ACAR, ATTILA BECSKEI, ALEXANDER VAN OUDENAARDEN, *MIT* On induction of cell differentiation, distinct cell phenotypes are encoded by complex genetic networks. Here we explore the key parameters that determine the stability of cellular memory by using the yeast galactose-signalling network as a model system. This network contains multiple nested feedback loops. Of the two positive feedback loops, only the loop mediated by the signal transducer Gal3p is able to generate two stable expression states with a persistent memory of previous galactose consumption states. A negative feedback through the inhibitor Gal80p reduces the strength of the core positive feedback. Despite this, a constitutive increase in the Gal80p concentration tunes the system from having destabilized memory to having persistent memory. A model reveals that fluctuations are trapped more efficiently at higher Gal80p concentrations. Indeed, the rate at which single cells randomly switch back and forth between expression states was reduced. These observations provide a quantitative understanding of the stability and reversibility of cellular differentiation states. (For more information: Nature 435, 228-232 (2005)).

*Financial Support: (M.A.) MIT Presidential Fellowship endowed by Praecis Pharmaceuticals, Inc.; (A.B.) Long Term Fellowship of the Human Frontiers Science Program; (A.v.O.) NSF-CAREER and a NIH grant.

**16:06**
**R28 7 Parameters of the proteome evolution from the distribution of sequence identities of paralogous proteins** KOON-KIU YAN, *Stony Brook University* JACOB AXELSEN, *Compexity Lab, Niels Bohr Institute, Denmark* SERGEI MASLOV, *Brookhaven National Laboratory* The evolution of the full repertoire of proteins encoded in a given genome is driven by gene duplications, deletions and modifications of amino-acid sequences of already existing proteins. The information about relative rates and other intrinsic parameters of these three basic processes is contained in the distribution of sequence identities of pairs of paralogous proteins. We introduced a simple mathematical framework that allows one to extract some of this hidden information. It was then applied to the proteome-wide set of paralogous proteins in H. pylori, E. coli, S. cerevisiae, C. elegans, D. melanogaster and H. sapiens. We estimated the stationary per-gene deletion and duplication rates, the distribution of amino-acid substitution rate of these organisms. The validity of our mathematical framework was further confirmed by numerical simulations of a simple evolutionary model of a fixed-size proteome.



***Invited Papers***

**16:18**
**R28 8 Differentiation at the single cell level: Slow, noisy, and out of control.**
GUROL SUEL, *California Institute of Technology*

Transient differentiation allows genetically identical cells to generate dynamical phenotypic diversity in a homogeneous environment. In Bacillus subtilis, competence is a transient state associated with the capability for DNA uptake from the environment. Individual genes and proteins underlying differentiation into the competent state have been elucidated, but it is unclear how these genes interact dynamically in individual cells to control both entry into competence and return to vegetative growth. Here we show that transient differentiation can be understood in terms of excitable behavior of the underlying genetic circuit. Using quantitative fluorescence time-lapse microscopy, we directly observed the activities of multiple circuit components simultaneously in individual cells. We analyzed the resulting data in terms of a mathematical model. A core module containing positive and negative feedback loops controls both entry into, and exit from, the competent state. Reengineering the competence network to bypass the negative feedback loop specifically blocks exit from competence converting the excitable system into a bistable one. These results show that a simple genetic circuit combines stochastic and deterministic elements to support transient differentiation through excitability.

*Contributed Papers*

**16:54**
**R28 9 The Structure of Parasites in Food Webs** CHRISTOPHER WARREN, MERCEDES PASCUAL, *University of Michigan* KEVIN LAFFERTY, ARMAND KURIS, *University of California, Santa Barbara* Using the recent food web data, we investigate how parasites are connected to the rest of the web and see how they differ from random connection. To model these differences in a simple static model, we explore several approaches to extending the highly successful niche model to include parasites.

**17:06**
**R28 10 Quantitative study of gene regulation mediated by small RNA** EREL LEVINE, THOMAS KUHLMAN, *Center for Theoretical Biological Physics, UCSD* ZHONGGE ZHANG, *Division of Biological Sciences, UCSD* TERENCE HWA, *Center for Theoretical Biological Physics, UCSD* The role of small regulatory RNAs (sRNA) in controlling many pathways in bacteria has been highlighted in recent years. Small RNAs have been found in regulating the response of E. Coli to various stress conditions, frequently by destabilizing the mRNA molecules of their target. Here we describe quantitatively the unique properties of this mode of regulation. We characterize - both theoretically and experimentally - the expression of a sRNA-regulated reporter, under different regulatory signals and genetic backgrounds. Our analysis predicts the existence of two regimes of gene expression, separated by a sharp transition: When the transcription rate of the sRNA exceeds that of its targets, we expect very low level of protein synthesis, with fluctuations strongly suppressed. However, when the sRNA transcription rate becomes lower than that of its target, a proportional fraction of target transcripts are expected to be stable, leading to protein expression. In the context of stress response, our results suggest a ''stress-relief'' mechanism, where gradual response is evoked only once a ''tolerance threshold'' is exceeded. We also characterized an intriguing coupling effect between the mRNA levels of different genes, arising from their shared regulatory sRNA. Such coupling may be used by the cell to create a hierarchy of responses to changes in regulatory signals.

**17:18**
**R28 11 Quantitative Dissection of a Bacterial Promoter: Cooperativity, Sensitivity, and Combinatorial Control*** THOMAS KUHLMAN, *Center for Theoretical Biophysics, UCSD* ZHONGGE ZHANG, MILTON SAIER, *Division of Biological Sciences, UCSD* TERENCE HWA, *Center for Theoretical Biophysics, UCSD* E. coli's lac promoter offers a possibility of confronting system-level properties of transcriptional regulation with the known biochemistry of the molecular constituents and their mutual interactions. We repeated a previous study [Setty et al, PNAS 100: 7702-7 (2003)] by removing several extraneous factors which modulated expression of the itlac promoter. Through characterization of the promoter activity for key mutants and using thermodynamic modeling, we account for the control of the lac promoter in terms of known interactions. We reveal how the sensitive response to inducers arises from the accumulation of several weakly cooperative interactions, and depict how the activator CRP plays a dual role as the enhancer and sensitizer of repression by assisting LacI-mediated DNA looping.

*Supported by DOE grant DE-FG02-03-ER63691 and NIH grant GM70915; TK and TH additionally acknowledge support through the NSF PFC-sponsored Center for Theoretical Biophysics (Grants No. PHY-0216576 and PHY-0225630)

**SESSION R29: BIOMOLECULAR STRUCTURE AND FUNCTION**
**Wednesday Afternoon, 15 March 2006**
**326, Baltimore Convention Center at 14:30**
**Sonya Bahar, University of Missouri, St. Louis, presiding**

**14:30**
**R29 1 The Impact of Cholesterol on Lateral Organization in a Three-Species Non-Equilibrium Model of a Biomembrane** ANDREW P. PARADIS, SUSAN R. McKAY, SAMUEL T. HESS, *Department of Physics and Astronomy, University of Maine, Orono, Maine 04469-5709* Experimentally, cholesterol strongly influences many biological functions in cells. This study examines the mechanisms by which cholesterol affects membrane organization using a simple non-equilibrium model with exo- and endocytosis events. Three species, representing cholesterol, saturated and unsaturated lipids, move and interact on a two dimensional triangular lattice, simulated using a Metropolis algorithm. Interaction energies among the three species are adjustable, as are the rate and size of simulated endo- and exocytosis events. These events keep the system substantially out of equilibrium and yield a striped pattern comparable to those seen experimentally [1]. [1] Baumgart T, Hess ST, and Webb WW. Nature. 2003 Oct 23;425(6960):821-4.

**14:42**
**R29 2 Lipid Bilayers and Titanium: Controlling Surface Adsorption** LINDA S. HIRST, *MARTECH, Dept. of Physics, Florida State University* EMILY PARKER, NOEL C. MacDONALD, *Dept of Mechnical & Environmental Engineering, University of California, Santa Barbara* CYRUS R. SAFINYA, *Materials Dept. University of California, Santa Barbara* Used extensively for implants, titanium is relatively inert in the body, and considered a biocompatible metal. We have investigated the interactions of cationic lipid mixtures with a highly polished bulk $TiO_2$ surface and report the observation of an interesting cationic lipid tubule phase stabilized in 2D on the $TiO_2$ surface. This phase is distinct from the bulk tubule phase observed in some mixtures as the tubules form a network with small mesh size and appear to be more flexible. Cationic lipid vesicles were formed under various salt conditions and deposited on the $TiO_2$ surface via vesicle absorption, then observed with fluorescence microscopy. In certain mixtures, bulk tubule phases were observed. When deposited on glass the bulk tubule phase became unstable and bilayers gradually formed on the glass surface. However, deposition of the same cationic mixtures on $TiO_2$ resulted in the formation of a 2D network of lipid tubules on the surface. The network, although pinned to the surface remained fluid in nature, as confirmed by FRAP experiments. The tubules appear to be only weakly attracted to the $TiO_2$ and this may explain their stability on the surface.

**14:54**

**R29 3 Growth and Morphology of Solid-like Domains in Binary Giant Lipid Vesicles** PAUL BEALES, *University of Edinburgh* VERNITA GORDON, ZHIJUN ZHAO, STEFAN EGELHAAF, WILSON POON, *University of Edinburgh* Giant lipid vesicles are important, optically-resolvable, model systems for studying physical phenomena in biomembranes and have important applications as technological containers in the engineering of novel soft materials. Giant vesicles containing two different lipid components are well-mixed in the fluid phase; as the temperature is lowered phase separation occurs between fluid and solid-like phases. We observe this phase separation using confocal fluorescence microscopy. The varied domain morphologies have previously been assumed to result from interplay between line tension and the elastic properties of the bilayer. However, we find that the domain morphology can be understood from the structure of the solid-like phase: the molecular scale lipid organization determines the mesoscopic domain shape analogous to how unit cell symmetries determine the shape of three-dimensional crystals. We also show that the domains grow by a non-equilibrium mechanism that is well-know to occur in alloys. Slow diffusion in the solid-like phase results in a compositional gradient within these domains.

**15:06**

**R29 4 Laser Tweezer Deformation of Giant Unilamellar Vesicles** CORY POOLE, *University of Maryland* JOZSEF MESZAROS, KUMAR SENTHIL, WOLFGANG LOSERT, *University of Maryland* In an aqueous solution phospholipid bilayers self-assemble to form a closed surface which is called a vesicle. Vesicles have been studied extensively due to their relevance as a model for biomembranes as well as their practical uses for chemical containment and transport. We use a holographic optical tweezer array to study the mechanical response of giant unilamellar vesicles to applied stresses. By producing vesicles with encapsulated silica microspheres we use the tweezers to indirectly manipulate vesicled. Two or more spheres are used to stretch the vesicle membrane and subsequently the vesicle relaxes back to an equilibrium shape. These deformations are imaged at millisecond temporal resolution with spatial resolution on the order of 20 nm, and characteristic time and length scales of the relaxation are calculated. Further we are able to directly deform the membrane by pulling on the fluid utilizing an index of refraction mismatch between the inside and outside of the vesicle. We image the vesicle and extract the vesicle shape. Fourier analysis is used to track the vesicle as it returns to equilibrium after being stretched. We compare these deformations to preliminary data on deformations due to polymerization induced on both the inside and outside of vesicles.

**15:18**

**R29 5 Nanoscale characterization of solid-supported phospholipid multilayer films*** WILFRED NGWA, ANDREW GAO, TANIA CUBANO, KEZHENG CHEN, ALOK SAHGAL, WEILI LUO, *Department of Physics, University of Central Florida* Using atomic force microscopy (AFM) and the auxiliary molecular force probe (MFP) technique, we have studied the structure and nanomechanical response to nano-indentation of multilayered films of dioleoylphosphatidylcholine (DOPC) films prepared by solution spreading, spin-coating and capillary methods. Estimates for the Young's modulus for the different methods are found to be similar for sufficiently thick films. Our results demonstrate that previously reported estimates for the Young's modulus of adsorbed vesicles and lipid bilayers (membranes) by scanning probe techniques are ostensibly affected by the coupling of the substrate. Failure and self-healing of multilamellar lipid membranes is discussed.

*This work is partially supported by NSF NIRT 0103587.

**15:30**

**R29 6 A quasi-elastic neutron scattering study of the stabilization of freeze-dried cholesterol-containing DPPC liposomes by trehalose** V. GARCIA SAKAI, *NIST Center for Neutron Research* M. DOXASTAKIS, A.S. REDDY, J. DE PABLO, *Dept. Chem. Eng. University of Wisconsin* J.K. MARANAS, *Dept. Chem. Eng., Penn State University* The dissacharide trehalose has been employed extensively as a dehydroprotectant for stabilizing phospholipidic membranes, as a result of its ability to lower the gel-to-fluid phase transition temperature [Tm] of phospholipids. Upon rehydration of the membrane in the presence of trehalose, the transition is prevented and cell leakage is avoided. We use quasi-elastic neutron scattering [QENS] on selective deuterated samples to probe the dynamics of both the heads and tails of freeze-dried liposomes in the presence and absence of trehalose. The dynamics of the lipid tails are responsible for the melting transition, which is significantly lowered in the presence of the sugar. The mobility of the head-group is directly associated with the mobility of the sugar. In the current work, we add cholesterol to the liposomes. Cholesterol, abundant in mammalian cell membranes and embedded in the bilayer structure due to its hydrophobic nature, is added to the liposomes. QENS measurements on the stabilization by trehalose on cholesterol-containing liposomes are presented. At temperatures lower than Tm the mobility of the tails is greatly reduced by cholesterol, but the addition of trehalose has little effect dynamics. At temperatures above the transition though, the mobility of the tails is only slightly reduced, but the addition of trehalose leads to a large decrease in dynamics.

**15:42**

**R29 7 A Density Functional Theory Study of the Non-local Correlations between Nucleic Acid Base Pairs** VALENTINO R. COOPER, TIMO THONHAUSER, DAVID C. LANGRETH, *Rutgers University* The interactions of nucleic acid bases are fundamentally important in determining the behavior and structure of biologically important molecules such as DNA and RNA. However, the stacking of nucleic acid bases in a strand of genetic material involves significant van der Waals forces, which are often inaccurately represented or too expensive to compute in many modern theoretical methods. In this paper, we use Density Functional Theory (DFT) with a non-local van der Waals correlation functional[1] to study the stacking interactions of nucleic acid base pairs. This method correctly and seamlessly accounts for the long-range interactions present among isolated fragments through a density-density interaction formula. Since this technique is implemented within DFT it has the advantage of being able to draw on the speed, efficiency and accuracy of this *ab initio* method.

[1]M. Dion, H. Rydberg, E. Schröder, D. C. Langreth and B. I. Lundqvist, Phys. Rev. Lett. **92**, 24601-1 (2004).

**15:54**

**R29 8 Low Temperature Orbital Paramagnetism in B-DNA** MICHAEL J. HARRISON, *Michigan State University* A planar model of B-DNA has been developed that exhibits orbital paramagnetic properties at zero temperature. The paramagnetism is nonlinear in applied field and has a maximum several times the

magnitude of diamagnetism per particle in a 2DEG. The model depends on the assumption that approximately 1% of the pi-stack electrons in B-DNA are suffiffiently delocalized and have wave functions that permit them to move coherently parallel to the helix axis, and extend several diameters perpendicular to its axis. The theoretical results closely represent recent experimental data [1]. 1. S. Nakamae, et. al., Phys. Rev. 94, 248102-1 (2005)

**16:06**

**R29 9 Kinetic Modelling of Transcription Elongation** DAIBHID O'MAOILEIDIGH, *Rutgers University* VASISHT TADIGOTLA, *Rutgers University* ANIRVAN SENGUPTA, *Rutgers University* VITALY EPSHTEIN, *New York University Medical Center* RICHARD EBRIGHT, *Rutgers University* EVGENY NUDLER, *New York University Medical Center* ANDREI RUCKENSTEIN, *Rutgers University* Transcription is the first step in gene expression and it is at this stage that most of genetic regulation occurs. The enzyme RNA polymerase (RNAP) walks along DNA creating an RNA transcript at a highly non-uniform rate. We discuss how many non-intuitive features of the system may be experimentally and physically motivated and present first a model, which agrees qualitatively with a host of experimental evidence. We also examine intrinsic pauses where it is thought that the RNAP will move backwards along the DNA template without changing the length of the RNA transcript. We describe a simplified kinetic scheme for the recovery of intrinsic pauses with the same degree of predictive power as our thermodynamic model (presented separately). The separation of timescales between the movement of the RNAP and global changes in the RNA secondary structure is seen to be crucial for the function of RNAP. This is essentially a model of a Brownian ratchet where RNAP executes a 1D random walk in a sequence dependent potential over a range determined by the co-transcriptional RNA fold for each transcript length

**16:18**

**R29 10 Understanding spontaneous sharp bending of DNA** CHONGLI YUAN, ELIZABETH RHOADES, LYNDEN ARCHER, *Cornell University* Gene expression often requires the interplay of two distant genetic regions and thus sharp bending of DNA is essential for gene functioning. Contrary to the conventional thinking that the bending of DNA strand below its persistent length was essentially facilitated by DNA binding proteins, Widom's group recently demonstrated, using cyclization assay, that such kind of sharp bending can be spontaneously formed (Mol. Cell, 2004, 355). Two models were referred in the original work to explain this ''enhanced'' flexibility of short DNA strand, namely, the melted single- and double-bubble models. To elucidate the detailed mechanism behind the DNA sharp bending, DNA molecules containing single- and double-melted bubbles was synthesized by introducing non Watson-Crick base pairs to the DNA backbone. Time resolved fluorescence energy transfer was used as the major tool to evaluate the bending stiffness of afore mentioned short DNA strand. The effect of bubble size, number and position on the DNA stiffness was independently evaluated. The energetic penalty of forming the locally melted structure was determined using other individual experiments. These results not only clarify the physical origin of the previously observed cyclizability of short DNA strand but also help to interpret the cyclization data of DNA molecules of wider size ranges.

**16:30**

**R29 11 The role of stacking interactions in the folding dynamics of DNA hairpins** MARTA SALES-PARDO, *Northwestern University* JON WIDOM, *Northwestern University* LUIS AMARAL, *Northwestern University* To gain a deeper insight into cellular processes such as transcription and translation, one needs to uncover the mechanisms controlling the configurational changes of nucleic acids. As a step toward this aim, we present here a novel mesoscopic-level computational model that provides a *new window* into nucleic acid dynamics. We validate the model by studying DNA hairpins, single-stranded molecules with two complementary segments (''stems'') linked by a non-complementary ''loop.'' Our model reproduces experimental observations and enables us to monitor the configurational dynamics of hairpins, providing clear evidence of a ''zipping'' process in the closing toward the native configuration. In addition, our model allows us to demonstrate that there is a preferred zipping pathway for folding which is both the most frequent and the fastest way for the hairpin to fold. Most importantly, our model allows us to tune the importance of the different interactions in the nucleotides and uncover the role of stacking interactions as the driving force in the zipping dynamics.

**16:42**

**R29 12 Thermodynamic Model of Transcription Elongation** VASISHT TADIGOTLA, *Rutgers University* DAIBHID O'MAOILEIDIGH, *Rutgers University* ANIRVAN SENGUPTA, *Rutgers University* VITALY EPSHTEIN, *New York University Medical Center* RICHARD EBRIGHT, *Rutgers University* EVGENY NUDLER, *New York University Medical Center* ANDREI RUCKENSTEIN, *Rutgers University* We present a statistical mechanics approach to the prediction of backtracked pauses in prokaryotic transcription elongation derived from structural models of the transcription elongation complex (TEC). Our algorithm is based on the thermodynamic stability of TEC along the DNA template calculated from the sequence dependent free-energy of DNA-DNA, DNA-RNA and RNA-RNA base pairing associated with (a) the translocation and size fluctuations of the transcription bubble; (b) the changes in the DNA-RNA hybrid; and (c) the changes in the RNA folding free-energy. The calculations involve no adjustable parameters apart from a cutoff used to discriminate paused from non-paused complexes. When applied to 100 experimental pauses in transcription elongation by E. coli RNA polymerase on ten DNA templates the approach produces highly statistically significant results. Transcription elongation is an inherently kinetic process and a simplified kinetic model with the same predictive power is presented separately.

**16:54**

**R29 13 The role of telomere dynamics in aging and cancer** KRASTAN BLAGOEV, EDWIN GOODWIN, *Los Alamos National Laboratory* Telomere length changes are far more dynamic than previously thought. In addition to a gradual loss of $\sim$ 100 base pairs per telomere in each cell division, losses as well as gains may occur within a single cell cycle. We are investigating how telomere exchange, extension, and deletion affect the proliferative potential of telomerase-negative somatic cells. Experimental techniques are being devised to detect dynamic telomere processes and quantify both the frequency and length changes of each. In parallel, a ''dynamic telomere model'' is being used that incorporates telomere dynamics to study how the telomere size distribution evolves with time. This is an essential step towards understanding the role that telomere dynamics play in the normal

aging of tissues and organisms. The model casts light on relationships not otherwise easily explained by a deterministic ''mitotic clock,'' or to what extent the shortest initial telomere determines the onset of senescence. We also expect to identify biomarkers that will correlate with aging better than average telomere length and to shed light on the transition to unlimited growth found in telomerase-negative tumor cells having the ALT (alternative lengthening of telomeres) phenotype, and to evaluate strategies to suppress the growth of these tumors.

**17:06**

**R29 14 Optical Investigation of the Phases of Liquid Crystals of Nanoscale Duplex DNA** GIULIANO ZANCHETTA, *U. of Milano, Italy* MICHI NAKATA, *U. of Colorado* TOMMASO BELLINI, *U. of Milano, Italy* NOEL CLARK, *U. of Colorado* Polymeric DNA chains are known to exhibit chiral nematic and hexagonal columnar LC phases. Recently we found that even very short duplex DNA oligomers 6-basepairs (bp) to 20-bp in length also form nematic and columnar phases depending on the concentration of DNA. To investigate the structure of those phases, we used depolarized transmission light microscopy (DTLM) to probe texture and measure birefringence, and optical interferometry to measure DNA concentration. These observations show a chiral nematic and two distinct columnar phases in the short oligomer duplexes. We will discuss the structure of these phases and present data correlating their occurance with solution conditions and with the detailed base pair configuration and the ends of the oligomers, showing that, for example, unpaired bases at the ends of the oligomers tend to suppress the LC phases. Work supported by NSF MRSEC Grant DMR 0213918 and NSF Grant 0072989.

**SESSION R30: POLYMER NANOCOMPOSITES**
**Wednesday Afternoon, 15 March 2006**
**327, Baltimore Convention Center at 14:30**
**Alamgir Karim, National Institute of Standards and Technology, presiding**



**14:30**

**R30 1 Bridging, Steric Stabilization, Aggregation and Phase Separation in Polymer Nanocomposites** JUSTIN B. HOOPER, KENNETH S. SCHWEIZER, *University of Illinois* The polymer reference interaction site model theory is employed to study the potential of mean force (PMF) between nano-sized spherical particles in a dense polymer melt. A simple monomer-filler attractive potential is used to probe the competition between packing entropy and interfacial enthalpic effects. As interfacial cohesion increases the nanoparticle organization varies from contact depletion aggregation, to well dispersed sterically stabilized behavior corresponding to a thermodynamically stable polymer coating, to tightly bridged particles. Near linear scaling of the PMF with particle/monomer size asymmetry ratio is found, and the spatial range of the interfacial attraction is crucial in determining particle organization. Spinodal demixing calculations suggest two types of phase separated states and a miscibility window. The latter is rapidly destroyed as particle size and/or interfacial attraction strength increase. The presence of bound polymer layers in miscible nanocomposites is predicted to result in microphase separation like features in the collective polymer structure factor.

**14:42**

**R30 2 Glass transition behavior of polystyrene/silica nanocomposites.*** YUPING XIE, SUDEEPTO SEN, SANAT KUMAR, *Rensselaer Polytechnic Institute* AMITABH BANSAL, *GE* GE COLLABORATION, The change in thermomechanical properties of nano-filled polymers is of considerable scientific and technological interest. The interaction between the nanofillers and the matrix polymer controls the nanocomposite properties. We will present the results from recent and ongoing DSC experiments on polystyrene/silica nanocomposites. Polystyrene of different molecular weights (and from different sources) and silica nanoparticles 10-15 nm in diameter (both as received from Nissan and surface modified by grafted or physisorbed polystyrene) are being used to process the nanocomposites. We are studying trends in the glass transition behavior by changing the matrix molecular weights and the silica weight fractions. Recent data indicate that the glass transition temperature can both decrease and increase depending on the polymer-nanofiller combination as well as the thermal treatment of the nanocomposites prior to the DSC runs.

*Thanks to NSF for support.

**14:54**

**R30 3 Molecular model for the rheology of polymer nanocomposites** CATALIN PICU, ALIREZA SARVESTANI, *Rensselaer Polytechnic Institute* In this work we develop a molecular model for the rheology of entangled monodisperse homopolymers filled with nanoparticles at low filling volume fraction. This research is the continuation of our ongoing effort towards establishing a connection between the macroscopic time-dependent behavior of polymer nanocomposites and their molecular structure. The model is developed based on insight gained from molecular simulations, regarding the structure and dynamics of polymeric chains confined between nanoparticles. These simulations provide physically relevant parameters for the rheological model. The model accounts for reptation, chain stretch and contour length fluctuations. It also accounts for the short-range energetic interactions between polymers and fillers. Its predictions are compared with experimental data. The rheological model is implemented in a FEM package to simulate nanocomposite processing.

**15:06**

**R30 4 Comparison of the Glass Transition Temperature (Tg)-Confinement Effect in Real and Model Polymer Nanocomposites.** JOHN M. TORKELSON, PERLA RITTIGSTEIN, LINDA J. BROADBELT, RODNEY D. PRIESTLEY, *Northwestern University, Evanston, IL 60208* Addition of nanoparticles to polymers leads to enhancement of Tg when attractive interactions (e.g., hydrogen bonding) are present at the nanoparticle-polymer interface. Nanoparticle concentration and dispersion play major roles in determining the Tg enhancement. Unfortunately, characterization of dispersion by transmission electron microscopy is difficult and tedious. Here we show by determination of the Tg-confinement effect in ''model'' polymer-silica nanocomposites (NCs), i.e., a polymer film of known thickness with two silica substrates supporting both sides of the film, that it is possible to characterize the effect of interparticle spacing on Tg and the approximate interparticle spacing in real polymer-silica NCs. Studies of model poly(2-vinyl pyridine) (P2VP)-silica NCs with 200-900 nm interlayer spacing reveal that a significant Tg enhancement is observed at a 500-nm interlayer spacing and that the Tg enhancement exceeds 20 K at a 200-nm interlayer spacing. Studies of model poly(methyl methacrylate) (PMMA)-silica NCs exhibit lesser Tg changes at

smaller interlayer spacing. By comparison of Tg enhancements in real and model NCs, a 5 K Tg enhancement in a 0.4 vol% silica-PMMA NC relates to a 100-130 nm interparticle spacing while a 10 K Tg enhancement in a 4 vol% silica-P2VP NC relates to a 300 nm interparticle spacing.

**15:18**

**R30 5 Polymer-Nanoparticle Interfacial Interactions in Polymer Nanocomposites: Confinement Effects on Glass Transition Temperature and Suppression of Physical Aging.** PERLA RITTIGSTEIN, JOHN M. TORKELSON, *Northwestern University, Evanston, IL 60208-3120* Confinement effects on glass transition temperature (Tg) and physical aging are measured via fluorescence in polystyrene (PS), poly(methyl methacrylate) (PMMA) and poly(2-vinyl pyridine) (P2VP) nanocomposites (NCs) containing 10-15 nm diam. silica nanospheres or 47 nm diam. alumina nanospheres. At 0.1-10 vol% nanofiller, Tgs can be enhanced or depressed relative to neat, bulk Tg or invariant with nanofiller content. For alumina NCs, Tg increases relative to bulk Tg by as much as 16 K in P2VP, decreases by as much as 5 K in PMMA, and is invariant in PS. These results are explained by wetted P2VP-nanofiller interfaces with attractive interactions, non-wetted PMMA-nanofiller interfaces, and wetted PS-nanofiller interfaces lacking attractive interactions, respectively. The presence of wetted or non-wetted interfaces is controlled by choice of solvent; silica/PMMA NCs exhibit Tg enhancements or reductions relative to bulk Tg when films are made from methyl ethyl ketone or acetic acid solutions, respectively. A factor of 10 reduction of physical aging rate relative to that of neat P2VP is shown in a 4 vol% alumina/P2VP NC. Hence, a strategy for achieving non-equilibrium, glassy polymer systems that are nearly stable to physical aging is to incorporate well-dispersed nanoparticles possessing attractive interfacial interactions with the polymer.

**15:30**

**R30 6 Relaxation and Glass Transition in Confined and Filled Polymers.** VLADIMIR DOLIDZE, EDWIN ARROYO, MANUEL RIVERA, FOUAD ALIEV, *University of Puerto Rico* We report the results of the investigations of the influence of confinement and filling of polymers with nanosize aerosil particles on the glass transition and dynamics of the $\alpha$- and the $\beta$-relaxation processes in poly(octylmethacrylate) (POMA) by dielectric spectroscopy dynamic light scattering and differential scanning calorimetry. The polymer was synthesized directly in pores of the porous glass matrix with interconnected and randomly oriented pores with an average pore size of 100 nm by free radical polymerization of the monomer. Both the $\alpha$- and the $\beta$- processes were observed in confined polymer. We found that confinement is resulted in the reduction of the glass transition temperature $T_g$ of the polymer. This change in $T_g$ was mainly due to the existence of a developed pore wall-polymer interface and difference in the dynamic behavior of polymer in the surface layers compared to that in the bulk. The random structure of the host media was less important. Variations of size of filling particles and their concentration are helpful in understanding of relaxation properties at polymer – solid interface as well as a role of surface interactions in glass transition.

**15:42**

**R30 7 Directed Assembly of Nanoparticle Arrays using Block Copolymer Templates** HUIMAN KANG, *Department of Chemical and Biological Engineering and Center for Nanotechnology, University of Wisconsin, Madison 53706, USA*. ANDREW N. MANGHAM, *Department of Chemistry, University of Wisconsin, Madison 53706, USA*. MARK P. STOYKOVICH, *Department of Chemical and Biological Engineering and Center for Nanotechnology, University of Wisconsin, Madison 53706, USA*. ROBERT J. HAMERS, *Department of Chemistry, University of Wisconsin, Madison 53706, USA*. PAUL F. NEALEY, *Department of Chemical and Biological Engineering and Center for Nanotechnology, University of Wisconsin, Madison 53706, USA*. CdSe nanoparticles, functionalized with tetradecyl phosphonic acid (TDPA), were synthesized so as to preferentially segregate into the polystyrene (PS) domains of polystyrene-itblock-poly(methyl methacrylate) (PS-*b*-PMMA). Nanocomposites, composed with ternary blends (PS-*b*-PMMA/PS/PMMA) and CdSe, could be directed to assemble into defect-free and registered periodic and non-regular structures on chemically patterned substrates. The location of nanoparticles in the PS differs depending on the blend composition and the commensurability between the chemical surface pattern and the bulk lamellar period of the composite and can be interpreted in terms of the interplay between the phase behavior of the composite systems and surface and interfacial interactions. CdSe nanoparticle arrays, replicating the block copolymer patterns, were obtained by removing the polymer using $O_2$ plasma.

**15:54**

**R30 8 Surface segregation of silver nanoparticles in the in-situ synthesized Ag/PMMA nanocomposites.** RANJAN D. DESHMUKH, RUSSELL J. COMPOSTO, *Materials Science and Engineering, University of Pennsylvania* Silver nanoparticles were synthesized in-situ, by thermal decomposition of (1,1,1,5,5,5 Hexafluoroacetylacetonato)silver(I), Ag(hfac), precursor at 185 $^{o}$C, in thin films of Poly(methyl methacryalate), PMMA. Rutherford backscattering spectrometry, RBS, was used to observe and quantify the silver distribution along the thickness of the sample. Strong surface segregation of nanoparticles to the polymer surface and substrate was observed in PMMA thin films by RBS and also confirmed by cross-sectional transmission electron microscopy (TEM). Surface segregation mechanism has been attributed to simultaneous thermal decomposition and diffusion of precursor to polymer surface and substrate. It has been shown that the particles present near the surface could be initially exposed and then are eventually covered by the polymer leading to particle sinking as observed by TEM. Atomic force microscopy (AFM) showed bigger nanoparticles and wider size distribution on increasing the nanoparticle loading from 5 to 20-wt %. UV/Visible spectroscopy on PMMA/Ag nanocomposite films showed plasmon resonance peaked at 422 nm due to the presence of silver nanoparticles.

**16:06**

**R30 9 Selective Metallization of Well Aligned PS-*b*-P2VP Block Copolymers in Thin Films and in Confined Geometries** JAMES D. SIEVERT, JAMES J. WATKINS, THOMAS P. RUSSELL, *University of Massachusetts - Amherst* Well aligned, microphase-separated structures of styrene-2-vinylpyridine block copolymers are being used as templates for macromolecule-metal nanocomposites. These composites are either prepared as thin films or confined in nanoporous aluminum oxide membranes. Under optimal conditions, templates are prepared as thin films or confined nanorods and metallized without disturbing the ordered structure. We have developed a procedure that deposits metal within the polymer using supercritical carbon dioxide-soluble metal precursors. The use of supercritical carbon dioxide allows

for selective metallization of the polymer at or below the glass transition, without disrupting the morphology. In addition, similar procedures have been investigated using metal salts and acids. Using these techniques, metals and metal-sulfides including silver, gold, platinum and zinc sulfide have been selectively deposited.

**16:18**

**R30 10 Static and Dynamic Neutron Scattering Studies of Polystyrene-Silica Nanocomposites.*** SUDEEPTO SEN, YUPING XIE, SANAT KUMAR, *Rensselaer Polytechnic Institute* DEREK HO, VICTORIA GARCIA-SAKAI, *National Institute of Standards and Technology* RPI/NIST COLLABORATION, Studies of polymer chain conformation and dynamics in the presence of nanofillers are critical in the context of the mechanical properties of polymer nanocomposites. We will present the results from recent and ongoing SANS experiments on polystyrene-silica nanocomposites containing polystyrene matrices of different molecular weights and silica nanofillers (10 – 15 nm in diameter) over a range of weight fractions. Preliminary neutron backscattering fixed-window scans of these nanocomposites indicate a similarity between the dynamics of the nanocomposites and thin polystyrene films in the sub-glass region. These results and results from ongoing backscattering experiments will also be discussed.

*NSF-NSEC

**16:30**

**R30 11 Structure and properties of poly(methyl methacrylate) (PMMA)-fullerene ($C_{60}$) nanocomposites** JAMIE KROPKA, *Department of Chemical Engineering, The University of Texas at Austin* PETER GREEN, *Department of Material Science and Engineering, Applied Physics, Macromolecular Science and Engineering, University of Michigan* We examined the rheological and dynamical mechanical (DMA) properties of PMMA-$C_{60}$ nanocomposite materials with relatively low concentrations of $C_{60}$, 0.1-5wt%. Decreases of the glass transition temperature ($T_g$), $\sim 7\ ^oC$, were observed in samples with 0.5 and 1 wt% $C_{60}$. The decreases in $T_g$ are connected to decreases of the longest relaxation time measured for the system. The plateau modulus of the composites was enhanced relative to the homopolymer but did not increase monotonically with $C_{60}$ concentration. The relative changes of the relaxation time, the plateau modulus and $T_g$ cannot be explained by the Doi-Edwards model and appear to be connected to the distribution of the nanoparticles, as determined by electron microscopy.

**16:42**

**R30 12 Self-Corralling of nanorods under electric fields.** SURESH GUPTA, QINGLING ZHANG, TODD EMRICK, THOMAS RUSSELL, *Polymer Science and Engineering department, University of Massachusetts, Amherst* Orienting semiconductor nanorods normal to a surface is highly desirable for applications including photovoltaic, spintronics, etc. We have achieved this using solutions of mixture of alkane-covered CdSe nanorods with PMMA by solvent evaporation under an electric field. The electric field aligns the nanorods parallel to the field lines whereas incompatibility between the PMMA and alkane ligands causes a phase separation that tends to segregate the nanorods. This phase separation generates line tension that further compacts the packing of nanorods. Furthermore the nanorods are being synthesized that are covered with photoactive polymer such as poly (3-hexyl thiophene). This may lead to enhancement in efficiency of organic-inorganic heterojunction photovoltaic devices.

**16:54**

**R30 13 Theoretical and Experimental Studies of New Polymer-Metal High-Dielectric Constant Nanocomposites** VALERIY GINZBURG, MICHAEL ELWELL, KYLE MYERS, ROBERT CIESLINSKI, SARAH MALOWINSKI,*MARK BERNIUS, *The Dow Chemical Company* High-dielectric-constant (high-K) gate materials are important for the needs of electronics industry. Most polymers have dielectric constant in the range $2 < K < 5$; thus to create materials with $K > 10$ it is necessary to combine polymers with ceramic or metal nanoparticles. Several formulations based on functionalized Au-nanoparticles ($R \sim 5$ - 10 nm) and PMMA matrix polymer are prepared. Nanocomposite films are subsequently cast from solution. We study the morphology of those nanocomposites using theoretical (Self-Consistent Mean-Field Theory [SCMFT]) and experimental (Transmission Electron Microscopy [TEM]) techniques. Good qualitative agreement between theory and experiment is found. The study validates the utility of SCMFT as screening tool for the preparation of stable (or at least metastable) polymer/nanoparticle mixtures.

*Present address: Instron Corp., Norwood MA

**17:06**

**R30 14 Epoxy-silica composites for micro-electronic applications: effect of filler** HYUKSOO LEE, *Samsung Electro-mechanics Co.* MYEONGHO HONG, CHOONKEUN LEE, ILSANG MAENG, JAECHOON CHO, SANGMOON LEE, JEONGBOK KWAK, SEUNGHYUN RA, The epoxy composites filled with silica fillers having various amounts and sizes were prepared and a detailed study of the structure-property relationships of the resulting composites is reported. Scanning electron microscopy (SEM), thermomechanical analyzer (TMA), rheological behavior, and stress-strain analysis were used to evaluate the epoxy-silica composite morphology and physical properties. The stiffness and thermal expansion were improved with increasing filler amount. Whereas, the ductility decreased significantly as the filler content increased. Scanning electron micrographs of fractured composites revealed that the dispersion of the filler in the matrix is highly dependent on the size and amount of fillers and has a strong effect on the mechanical, thermal, and rheological properties of the composites. The processibility of the composites for micro-electronic applications such as printed circuit board (PCB), is briefly discussed.

**17:18**

**R30 15 Quantum dots tailored with water soluble conjugated polymer** JUN XU, *Materials Science and Engineering Department, Iowa State University* JOSEPH SHINAR, *Physics and Astronomy Department, Iowa State University* ZHIQUN LIN, *Materials Science and Engineering Department, Iowa State University* Placing the conjugated polymer (CP) in direct contact with the quantum dot (QD) offers advantages over cases where QD aggregation dominates. Such quantum dot- conjugated polymer nanocomposite (QD-CP) possesses a well-defined interface, thereby significantly promoting the charge or energy transfer between these two components. Here we demonstrate an approach to graft water soluble, negatively charged conjugated polymer, MPS-PPV from CdSe QD surfaces. The conjugation length of the MPS-PPV is adjustable by varying the ratio of co-solvents used. The photophysical properties of the nanocomposites in nanoscopic confined geometries are studied.

**SESSION R31: PROPERTIES OF CARBON NANOTUBES**
**Wednesday Afternoon, 15 March 2006**
**328, Baltimore Convention Center at 14:30**
**Nicola Marzari, Massachusetts Institute of Technology, presiding**

**14:30**
**R31 1 Neon adsorption on single walled carbon nanohorns*** V. KRUNGLEVICIUTE, K. LASK, A. D. MIGONE, *Southern Illinois University* B. BULLER, T. BEATTIE, U. VENKATESWARAN, *Oakland University* We present results for Ne adsorbed on single walled carbon nanohorns (SWNHs) purchased from NanoCraft, Inc. The as-received SWNHs were characterized with Raman spectroscopy. The spectra show two peaks attributable to the D and G-bands, with the G-band exhibiting a shoulder in contrast to a single Lorentzian peak reported in the literature. A portion of the SWNHs was sonicated in methanol for twenty minutes and heated under vacuum at 60oC for 12 hours (this treatment was followed to produce ''nanohorn- paper''). Full adsorption isotherms were measured on this sample between 22 and 31 K, and low coverage isotherms were measured between 40 and 49 K. Neon measurements were also performed at 31 K on a sample of SWNHs that was not subjected to the methanol treatment, for comparison. We found no difference between the results obtained on these two sets of samples. We will also present isotherm data on SWNHs that were heated to 520 K under vacuum.

*This work was supported by the NSF through grant DMR-0089713 (ADM) and DMR-0104176 (UV).

**14:42**
**R31 2 Carbon nanotube − metal cluster bond strengths: implications for catalytic growth.** PETER LARSSON, *Condensed Matter Theory Group, Physics Department, Uppsala University, Box 530, SE-751 21, Uppsala, Sweden* FENG DING, *Rice University, ME & MS Department, Houston, TX 77005* J. ANDREAS LARSSON, *Tyndall National Institute, Lee Maltings, Prospect Row, Cork, Ireland* ARNE ROSEN, *Physics Department, Goteborg University, SE-412 96, Goteborg, Sweden* RAJEEV AHUJA, *Condensed Matter Theory Group, Physics Department, Uppsala University, Box 530, SE-751 21, Uppsala, Sweden* KIM BOLTON, *Physics Department, Goteborg University, SE-412 96, Goteborg, Sweden* Catalysts play a crucial role in the production of carbon nanotubes (CNTs). Although a lot of experimental effort has been devoted to finding metals and alloys to optimize CNT growth, the importance of the CNT-metal interactions at the microscopic level are not well understood. Previous simulations based on analytic force fields indicate that a critical role of the catalyst particle is to maintain an open end of the growing CNT, and that sufficiently strong CNT-metal bond strengths are required for this criterion to be met. Here we report CNT-metal bond strengths obtained from density functional theory for a variety of metal clusters. In agreement with the simulations, these calculations reveal that CNT interactions with metals used for production (e.g., Fe and Ni) are stronger than for other metals (e.g. Au). These bond strengths are also compared to the C-C bond energies that form when a cap forms at the end of the growing CNT.

**14:54**
**R31 3 Uncatalyzed Etching of Single Walled Carbon Nanotubes on Surfaces** SEAN PHEASANT, VALERIE MOORE, ROBERT HAUGE, RICHARD SMALLEY, *Rice University* Aside from burning, the only way single walled carbon nanotubes (SWNTs) have been etched is with the use of a catalyst nanoparticle at high temperatures in an oxidative or reducing atmosphere. The catalyst is a particle close in size to the diameter of the nanotube, and is usually composed of iron, molybdenum, nickel or cobalt, or a combination of these metals. The catalyst operates at the ends of the SWNTs, where it dissociates molecules from the atmosphere on its surface, and combines them with carbon atoms from the tube to form a gas. It has been found that SWNTs can be oxidatively etched with CO2 at a high temperature (900°C) in the absence of catalyst particles. The reverse of the Boudard reaction occurs at high temperatures to produce two molecules of CO from a molecule of CO2 and a C atom. When the ends of the tubes are closed, no etching is observed, indicating that only the open ends of the tubes can be attacked by CO2 and not the sidewalls. Experiments were done on both SiO2 and highly oriented pyrolytic graphite (HOPG). Results suggest the tubes etch faster on HOPG than they do on the oxide surface.

**15:06**
**R31 4 Defects in carbon nanotubes** RODRIGO G. AMORIM, ANTÔNIO J. R. DA SILVA, A. FAZZIO, *Instituto de Física, Universidade de São Paulo* ALEX ANTONELLI, *Instituto de Física ''Gleb Wataghin,'' UNICAMP* It is a consensus that defects can alter in a significant way the mechanical properties of carbon nanotubes. We here will investigate, using ab initio total energy density functional theory calculations, some defects and their properties, such as: 1) an interstitial carbon atom right besides a vacancy that can connect tubes in bundles or in multiwall nanotubes; 2) two vacancies that can connect tubes in bundles; 3) a variety of configurations for two vacancies in one nanotube, and how their energies vary with separation. In particular, we will compare the formation energies of the 5-8-5 and 555-777 two-vacancy defects as a function of nanotube diameter.

**15:18**
**R31 5 Electroabsorption of Single-Walled Carbon Nanotubes*** W. JOSHUA KENNEDY, Z. VALY VARDENY, *University of Utah* We have measured the electric field modulated absorption (EA) of single-walled carbon nanotubes (SWNT) isolated in a poly-vinyl alcohol matrix (PVA). The derivative-like structure of the EA indicates that the low energy absorption bands are excitonic in origin. We report the voltage, temperature, and polarization dependence of the EA spectrum. Additionally, the sensitivity of the EA spectrum to the energy levels of the SWNT allows us to use EA spectroscopy to observe shifts in the absorption bands of our sampleS induced by various external fields that are difficult to resolve using CW techniques. Several examples will be discussed.

*Supported in part by the DOE

**15:30**
**R31 6 Phases of Ethane Adsorbed on Purified HiPco Single Walled CarbonNanotubes.** DINESH RAWAT, ALDO MIGONE, *Department of Physics, Southern Illinois University* We have measured adsorption isotherms of ethane on purified HiPco SWNTs for coverages in the first layer. We wanted to investigate the existence of different phases for ethane as a function of coverage on this substrate, and to compare the results to those on planar graphite. We measured isotherms at 103, 110,150,

160, and 165K. We used the low-coverage isotherm data to obtain an estimate for the binding energy of ethane on the SWNTs; we found a value of 363 meV for this quantity. This binding energy value is 1.81 times greater than the corresponding one for this quantity on planar graphite. We have also determined the coverage dependence of isosteric heat of adsorption for ethane using the results for isotherms obtained at above-mentioned temperatures. This work was supported through a grant from NSF, DMR#0089713, and by the Materials Technology Center of SIUC.

**15:42**

**R31 7 Single Electron Effects in a Carbon Nanotube Electromechanical Oscillator** AREND VAN DER ZANDE, *LASSP Cornell University* RENA ZIEVE, *Department of Physics, UC Davis* VERA SAZONOVA, PAUL MCEUEN, *LASSP Cornell University* We have fabricated suspended, doubly clamped, carbon nanotube (NT) transistors to investigate the low temperature coupling between mechanical vibration of the NT and single electron effects. At low temperatures of 0.3K to 4.2K, the NT behaves as a quantum dot. The NT quantum dot displays Coulomb oscillations in the conductance by sweeping a gate voltage. Mechanical vibrations are induced in the NT by applying a high frequency AC voltage relative to the gate [1]. The nonlinear conductance of the Coulomb oscillations can be used as a mixer to detect the NT's own motion. We find that the mechanical resonances of the NT are influenced by the Coulomb oscillations. We observe a dip in the resonance frequency and a dip in the quality factor as the gate voltage is swept through a Coulomb oscillation. We attribute these dips to the forces on the NT from the hopping of single electrons on and off the NT as it moves with respect to the gate. [1] V. Sazonova, Y. Yaish, H. Ustunel, D. Roundy, T.A. Arias, and P.L. McEuen, Nature 431, 284-287 (2004)

**15:54**

**R31 8 Anharmonic effects in carbon nanotubes: from thermal expansion to phonon lifetimes** N. BONINI, N. MOUNET, N. MARZARI, *Department of Materials Science and Engineering, MIT, Cambridge, MA, USA* M. LAZZERI, F. MAURI, *Institut de Minéralogie et Physique des Milieux Condensés, Paris, France* We study anharmonic effects in carbon nanotubes using a combination of density-functional theory and density-functional perturbation theory. In particular, we investigate thermal expansion and phonon lifetimes, which are key quantities that govern mechanical and transport properties in these systems. The thermal expansion coefficients are calculated from a minimization of the vibrational free energy in the quasi-harmonic approximation. Our results show that carbon nanotubes contract both in the axial and radial directions at low and room temperature and expand at higher temperatures. The role of different phonon modes in the thermal contraction is discussed together with their Grüneisen parameters. Anharmonic phonon lifetimes are evaluated from the cubic terms in the interatomic potential, using density-functional perturbation theory and the $2n+1$ theorem. Finally, we discuss the possibility of estimating anharmonic effects using downfolding from graphene.

**16:06**

**R31 9 Raman Spectroscopy of Carbon Nanotubes under Axial Strain** RAJAY KUMAR, *University of Southern California* HAO ZHOU, *University of Southern California* STEPHEN CRONIN, *University of Southern California* We measure the Resonance Raman spectra of individual carbon nanotubes under axial strain. A combination of atomic force microscopy (AFM) and lithography is used to produce strains in nanotubes ranging from 0.1% to 5%. The vibrational and electronic energies of the nanotubes are found to be very sensitive to strain. The D, G and G' band Raman modes are observed to downshift with strain indicating elongation, and hence weakening, of the carbon-carbon bonds. The intensities of the Raman modes are also observed to change as a function of strain, indicating a strain-induced shifting of the electronic subbands. A tight-binding model is presented to explain the changes observed in the Raman intensity in accordance with the Resonance Raman equation.

**16:18**

**R31 10 Synthesis and Raman characterization of Nitrogen doped single walled carbon nanotubes.** ADALBERTO ZAMUDIO, ANA-LAURA ELIAS, *IPICYT, Mexico* FEDERICO VILLALPANDO-PAEZ, *MIT, USA* JULIO A. RODRIGUEZ-MANZO, EDUARDO CRUZ-SILVA, HUMBERTO TERRONES, *IPICYT, Mexico* TAKUYA HAYASHI, Y.A. KIM, HIROYUKI MURAMATSU, MORINOBU ENDO, *Shinshu University, Japan* MILDRED S. DRESSELHAUS, GENE DRESSELHAUS, *MIT, USA* MAURICIO TERRONES, *IPICYT, Mexico* We report the production of macroscopic amounts of long strands consisting of SWNT doped with nitrogen, using a CVD approach. We performed series of experiments varying the concentration of the nitrogen precursor in the solution, from 0.01% to 26 % by weight. The materials were characterized using scanning electron microscopy (SEM), transmission electron microscopy (TEM), high resolution TEM, and Raman Spectroscopy. We will describe the changes in the Raman spectra caused by the nitrogen content using of different laser lines. First principle calculations on the electronic and vibrational properties of the doped SWNTs with N will also be presented.

**16:30**

**R31 11 Raman spectra and thermal stability analysis of 0.4 nm freestanding single-walled carbon nanotubes** JIAN TING YE, ZI KANG TANG, *Department of Physics and Institute of Nano Science and Technology, Hong Kong University of Science and Technology* SEMICONDUCTOR CLUSTER TEAM, Thermal stability of ultra-small 0.4 nm single-walled carbon nanotubes is studied by means of Raman scattering measurement under vacuum. The 0.4 nm SWNTs are very stable when they are confined inside the channels of the AFI crystal. When these SWNTs are extracted from the channels into free space, however, they become thermally unstable because of the strong curvature effect. All three structures of the 0.4 nm-sized SWNTs are destroyed between 730 to 790 K, a temperature range much lower than that of large-sized SWNTs. The (5,0) tube is only destroyed after temperature reaches 790 K and seems slightly stabler than the other two structures: the (3,3) and (4,2) tubes.

**16:42**

**R31 12 Effect of Magnetic Field in Carbon Nanotubes** YURIY MALOZOVSKY, ANDREW KINCHEN, *Southeastern Louisiana University* We study the effect of magnetic field in the armchair carbon nanotubes (CNT). We model the carbon nanotube as a tubule with electrons confined to the surface of the tubule by an attractive delta-function potential. We derived the dynamic pair interaction potential between two electrons in the tubule in the presence of magnetic field. Dispersion of plasma modes at differ-

ent values of angular momentum, and single-particle excitations in the presence of the magnetic field are derived as well. The self-energy part due to the interaction of an electron with plasma modes in magnetic field is also discussed.

**16:54**

**R31 13 Low-energy dark discharge growth of ultra-thin aligned carbon nanofibers for field emitter and optical antenna arrays*** YANG WANG, *Boston College* K. KEMPA, *Boston College* Z. F. REN, *Boston College* DEPT. OF PHYS., BOSTON COLLEGE TEAM, We show experimentally the applicability of using a dc low-energy dark discharge state to grow aligned carbon nanofibers with diameters of less than 10 nm and directly on polyimide and transparent conducting oxides without buffer layers. The average discharge current density used can be 2-3 orders of magnitude lower than that in a typical plasma-enhanced chemical vapor deposition (PECVD), so that the plasma heating and etching effects are greatly alleviated, leading to lower growth temperatures and higher substrate compatibility. The nanofibers grown by dark discharges exhibit similar optical antenna effects to those grown by PECVD methods, and their diameter and density can be reduced to achieve good field emission properties.

*Financial supports from US Army Natick Soldier Center and National Science Foundation are acknowledged.

**17:06**

**R31 14 Electronic and transport properties of carbon-based atomic chain structures** R. TUGRUL SENGER, ENGIN DURGUN, *Bilkent University* SEFA DAG, *Oak Ridge National Laboratory* SEFAATTIN TONGAY, *University of Florida* SALIM CIRACI, *Bilkent University* Our first-principles calculations show that monatomic chains of carbon have high cohesive energy and axial strength, and are stable even at high temperatures. Pure carbon chains are metallic, and periodic compounds of carbon with transition- metals exhibit half-metallic properties where the electronic spins are fully polarized at the Fermi level. Finite-length carbon atomic chains capped with single transition metal atoms constitute the ultimately small spin-valve systems with high magnetoresistive ratios. In all these structures the electronic, magnetic and transport properties show interesting variations depending on the number of carbon atoms being odd or even. [1] S. Tongay, R.T. Senger, S. Dag, and S. Ciraci, Phys. Rev. Lett. **93**, 136404 (2004). [2] R. T. Senger, S. Tongay, S. Dag, E. Durgun, and S. Ciraci, Phys. Rev. B **71**, 235406 (2005). [3] S. Dag, S. Tongay, T. Yildirim, E. Durgun, R. T. Senger, C. Y. Fong, and S. Ciraci, Phys. Rev. B **72**, 155444 (2005).

**SESSION R32: FOCUS SESSION: COMPUTATIONAL NANOSCIENCE V**
**Wednesday Afternoon, 15 March 2006**
**329, Baltimore Convention Center at 14:30**
**Wenchang Lu, North Carolina State University, presiding**

**14:30**

**R32 1 Multi-scale Modeling of Thermal-Electromechanical Response of Piezoelectric Thin Film** LIMING XIONG, *The George Washington University* JAMES LEE, *The George Washington University* YOUPING CHEN, *The George Washington University* YAJIE LEI, This study aims at understanding and improving the properties of the piezoelectric thin films through numerical simulation. On the basis of first principle calculation, empirical inter-atomic potential is obtained by fitting to the lattice parameters, energy surface and phonon dispersion relation. Both traditional MD simulation and a new atomistic multi-scale field theory are employed to simulate the material behavior of piezoelectric thin films under thermal, electrical and mechanical loading. Results are well agreed with each other between MD simulation and the newly developed field theory. Meanwhile, it is found out that the newly developed field theory is more efficient in studying nonequilibrium phenomenon, high temperature and high pressure working conditions for thin films. Size effects, thermal conductivity, failure process and material behavior in harsh environments for the thin films are investigated, which provide us with scientific information for the design and optimization of industrial application.

**14:42**

**R32 2 Multi-scale Simulations of $SiO_2$ Systems I: Classical and Hybrid Simulations*** CHAO CAO, YAO HE, HAI-PING CHENG, *University of Florida* Classical MD simulations show that bulk and nano-wire silica glass exhibit completely different stress-strain curves. A typical bulk sample breaks almost instantaneously while a nano-wire sample usually breaks ''gradually.'' A further simulation on nano-wire sample surrounded by water molecule shows that the stress-strain curve is not affected very much by the presence of water molecules. However, from previous quantum calculations (by Du et. al), one would believe that the water molecules do affect the fracture of silica a lot. Therefore, multi-scale simulations on a simple model $SiO_2$ chain are performed and compared with classical simulations on the same system to investigate mechanisms underlying the inconsistency. The multi-scale simulation is also compared with a full quantum calculation in our second talk.

*NSF/ITR grant number: DMR-0325553

**14:54**

**R32 3 Multiscale Simulation of SiO2 II: Quantum Simulations*** YAO HE, CHAO CAO, HAI-PING CHENG, *University of Florida* To investigate effects of external stress and the influence of water molecules on the energetic stability of low dimension silica systems, we have performed ab initio molecular-dynamics simulations as well as hybrid classical/quantum simulations of SiO2 chains. These silica chains are formed by edge-sharing two-rings. We present strain dependent interactions of silica-water systems at room temperature. Our investigations provide qualitative and quantitative descriptions of the reaction processes. We have also compared these ab initio results with results obtained from our multiscale simulations method, in which the quantum region is embedded in a classical region.

*NSF/ITR grant number: DMR-0325553

*Invited Papers*

**15:06**
**R32 4 Dissipation of Mechanical Energy in Carbon Nanotube-based Mechanical Devices.**
PAUL TANGNEY, *The Molecular Foundry, Lawrence Berkeley National Laboratory*

The creation of functional mechanical devices at the nanoscale is a major goal of nanoscience, and multiwalled carbon nanotubes (MWCNT) are promising materials for constructing such devices. The large disparity between the strengths of intralayer and interlayer interactions in MWCNTS allows for smooth relative motion of concentric tubes. Some simple mechanical elements such as linear and rotational bearings have already been constructed from MWCNTs by exploiting this feature [1]. However, little is known about the dominant mechanisms for dissipation of mechanical energy at the nano scale, and devices based on MWCNTs are both technologically important and useful as test systems for theoretical investigations. In this talk, atomistic simulations of some simple MWCNT-based mechanical systems will be presented. It is shown that reducing the dimensions of a device can have a strong impact on phononic friction. The small masses of nanotubes relative to the forces between them means that relative velocities can be comparable to and larger than atomic thermal velocities. In this regime, theories based on a quasi-adiabatic response of atoms to the relative motion of nanotubes fail and simulations reveal a strong and complex velocity dependence of friction [2]. Large edge to surface ratios mean that edges can play an important role in energy dissipation and for concentric nanotubes of length 10s of nm, the ends of the nanotubes have been shown to dominate sliding friction [2]. These and other important features of friction in nanotube-based devices will be discussed and illustrated with the results of molecular dynamics simulations. This work was supported by the NSF Grant No. DMR04-39768 and U.S. DOE Contract No. DE-AC03-76SF00098. [1] J. Cumings and A. Zettl, Science 289, 602 (2000); A. M. Fennimore et al., Nature 424, 408 (2003). [2] P. Tangney, S. G. Louie, and M. L. Cohen, Phys. Rev. Lett. 93,065503 (2004); P. Tangney, M. L. Cohen, and S. G. Louie, to be published.

*Contributed Papers*

**15:42**
**R32 5 Elastic properties of SiC nanoscopic wires** MAXIM MAKEEV, *NASA Ames Research Center, MS 229-1, Moffett Field, CA 94035* MADHU MENON, *Department of Physics and Astronomy, University of Kentucky, Lexington, KY 40506* DEEPAK SRIVASTAVA, *NASA Ames Research Center, MS 229-1, Moffett Field, CA 94035* Mechanical properties of crystalline and amorphous SiC nanowires have been investigated using molecular dynamics simulations with the Tersoff bond-order interatomic potential. The crystalline and a-SiC nanowires of different diameters were studied under tension/compression, torsion, and bending. The bending and torsion rigidities are found to be strongly dependent on the wire size. This is unlike the Young's modulus computed from uniaxial loading curves. Atomistic relaxations effects near the thresholds of structural stability are investigated for the four employed load types. The mechanical properties of crystalline SiC nanowires are compared with a-SiC wires of the same radii.

**15:54**
**R32 6 Simulation Studies of Mechanical Properties of Novel Silica Nano-structures** KRISHNA MURALIDHARAN, JOAN TORRAS COSTA, SAMUEL B. TRICKEY, *University of Florida* QTP NANOROD TEAM, Advances in nanotechnology and the importance of silica as a technological material continue to stimulate computational study of the properties of possible novel silica nanostructures. Thus we have done classical molecular dynamics (MD) and multi-scale quantum mechanical (QM/MD) simulation studies of the mechanical properties of single-wall and multi-wall silica nano-rods of varying dimensions. Such nano-rods have been predicted by Mallik et al. to be unusually strong in tensile failure. Here we compare failure mechanisms of such nano-rods under tension, compression, and bending. The concurrent multi-scale QM/MD studies use the general PUPIL system (Torras et al.). In this case, PUPIL provides automated interoperation of the MNDO Transfer Hamiltonian QM code (Taylor et al.) and a locally written MD code. Embedding of the QM-forces domain is via the scheme of Mallik et al. Work supported by NSF ITR award DMR-0325553.

**16:06**
**R32 7 On The Nonlinear Mechanics of Carbon Nanocones Using The Consistent Atomic-scale Finite Element Method** ARASH MAHDAVI, *Penn State, Department of Mechanical and Nuclear Engineering* ERIC MOCKENSTURM, *Penn Sate, Department of Mechanical and Nuclear Engineering* In the present work, a new multiscale modeling technique called the Consistent Atomic-scale Finite Element (CAFÉ) method is introduced. Unlike traditional approaches for linking the atomic structure to its equivalent continuum, this method directly connects the atomic degrees of freedom to a reduced set of finite element degrees of freedom without passing through an intermediate homogenized continuum. As a result, there is no need to introduce stress and strain measures at the atomic level. The Tersoff-Brenner interatomic potential is used to calculate the consistent tangent stiffness matrix of the structure. In this finite element formulation, all local and non-local interactions between carbon atoms are taken into account using overlapping finite elements. In addition, a consistent hierarchical finite element modeling technique is developed for adaptively coarsening and refining the mesh over different parts of the model. This process is consistent with the underlying atomic structure and, by refining the mesh, molecular dynamic results will be recovered. In contrast with most other multiscale methods, there is no need to introduce artificial boundaries for coupling atomistic and continuum regions. The applicability of the method is shown with several examples of deformation of carbon nanocones subjected to different loads and boundary conditions.

**16:18**
**R32 8 Nanocrystalline Domain Formation as a Strain Relaxation Mechanism in Ultra-Thin Metallic Films** M. RAUF GUNGOR, DIMITRIOS MAROUDAS, *University of Massachusetts, Amherst* In this presentation, we report results for the atomistic mechanisms of strain relaxation over a wide range of applied biaxial tensile strain (up to 17%) in free standing Cu thin films based

on isothermal-isostrain molecular-dynamics simulations. After an elastic response at low strain ( $<$ 2%), plastic deformation occurs through ductile void growth accompanied by emission of screw dislocations from the void surface, as well as emission of threading dislocation loops from the film's surface. At strain levels below 8%, expansion of the plastic zone around the void during void growth is the major strain relaxation mechanism. At higher levels of applied strain ( $>$ 8%), a practically uniform distribution of dislocations is generated in the metallic thin film, which mediates the transformation of the initially single-crystalline film structure to a nanocrystalline one. Furthermore, void growth is inhibited as the dislocations emitted from the void surface are pinned by the simultaneously generated network of defects in the nanocrystalline material.

**16:30**

**R32 9 New and exotic self-organized patterns for modulated nanoscale systems** ELIANA ASCIUTTO, CHRISTOPHER ROLAND, CELESTE SAGUI, *North Carolina State University* The self-organized domain patterns of modulated systems are characteristic of a wide variety of chemical and physical systems, and are the result of competing interactions. From a technological point of view, there is considerable interest in these domain patterns, as they form suitable templates for the fabrication of nanostructures. We have analyzed the domains and instabilities that form in modulated systems, and show that a large variety of new and exotic patterns – based on long-lived metastable or glassy states – may be formed as a compromise between the required equilibrium modulation period and the strain present in the system. The strain results from topologically constrained trajectories in phase space, the effectively preclude the equilibrium configuration.

**16:42**

**R32 10 Studies of elastic and plastic deformation of nanostructured materials: A continuum approach** MIKKO HAATAJA, *Princeton University* PETER STEFANOVIC, *McMaster University* NIKOLAS PROVATAS, *McMaster University* Nanostructured materials can have physical and mechanical properties that are strikingly different from their corresponding bulk counterparts. Consequently, unraveling the physical mechanisms that give rise to their behavior at the atomic scale is essential in order to exploit and harness their unique properties. From a theoretical perspective, capturing dynamic phenomena across very long time scales with direct atomistic simulation methods (e.g., Molecular Dynamics [MD]) becomes a very challenging task due to inherent time scale limitations. Here we present a continuum field theory approach for modeling both elastic and plastic deformations, free surfaces, and multiple crystal orientations in systems with both hexagonal and cubic symmetry in two spatial dimensions. The model is based on a free energy for the local, temporally coarse-grained atomic density, which is minimized by spatially periodic structures. Hence, it incorporates, by construction, both elastic phenomena as well as defects in the form of, e.g., vacancies, dislocations, and grain boundaries. Furthermore, its dynamics is constructed such that it incorporates both diffusive and elastic relaxation phenomena. By introducing a variable elastic time scale, we are able to maintain mechanical equilibrium while simulating microstructural evolution on time scales well beyond those accessible by conventional atomistic MD simulation methods.

**16:54**

**R32 11 Van der Waals forces between nanoclusters: importance of many-body effects** HYE-YOUNG KIM, JORGE SOFO, *Physics Department, The Pennsylvania State University, University Park, PA* DARRELL VELEGOL, *Chemical Engineering Department, The Pennsylvania State University, University Park, PA* MILTON COLE, *Physics Department, The Pennsylvania State University, University Park, PA* AMAND LUCAS, *Physics Department, University of Namur, Begium* Van der Waals (VDW) interactions between nanoclusters have been calculated using a self-consistent, coupled dipole method. The method accounts for all multi-body (MB) effects and can be used to calculate dispersion interaction energies between nanoclusters of arbitrary shape. Comparison is made between the exact potential energy, V, and the values obtained with two alternative methods: $V^{(2)}$, a sum of two-body interactions, and $V^{(2)} + V^{(3)}$, the sum of 2-body and 3-body interactions. For some clusters and orientations, $V^{(2)}$ is close to the exact result. In other situations, MB effects can be large. For all cases considered here, the 3-body term alone does itnot accurately represent the MB contributions to V. MB contributions are especially important for shape-anisotropic clusters.

**17:06**

**R32 12 Average speeds and durations of pulsed plane waves transmitted through chiral sculptured thin films** JOSEPH GEDDES, AKHLESH LAKHTAKIA, *Penn State University* We computed, with a finite-difference algorithm, the durations and average speeds of pulsed, ultrashort, optical plane waves transmitted through chiral sculptured thin films (STFs). Chiral STFs are assemblages of parallel nanohelixes affixed to a substrate; the helixes possess diameters of 10–300 nm, lengths of micrometers, and pitches that can be engineered during the fabrication via physical vapor deposition. We modeled the chiral STFs as continuously nonhomogeneous, anisotropic dielectric materials which are either linear or exhibit a Kerr-type nonlinearity. We computed the equivalent, root mean square, and correlation durations of the transmitted pulses and found that these quantities tend to increase with decreasing carrier wavelength, though there is an exception to this trend when the linear film exhibits the circular Bragg phenomenon. Increasing nonlinearity also tends to increase the durations of transmitted pulses. We computed the average peak speed, center-of-energy speed, and correlation speed of the pulsed plane wave and found that these speeds tend overall to increase with carrier wavelength but decrease with increased nonlinearity. Our results will have application in the design of optical pulse shaping devices.

**17:18**

**R32 13 Approximate Approach to Multi-Dimensional Tunneling in Solids** MARIO ANCONA, *Naval Research Laboratory* For reasons of tractability elastic tunneling within or from solids is typically treated with one-dimensional or quasi-one-dimensional approximations. In this presentation methods for analyzing multi-dimensional solid-state tunneling that maintain physical fidelity yet remain computationally efficient are discussed. After a brief review of the microscopic EBK approach, the discussion focuses on a macroscopic form of quantum transport theory whose equations are most easily understood via analogies with gas dynamics and electron optics. Various analytical implications of the theory are derived and numerical illustrations are provided.

**SESSION R33: FOCUS SESSION: FRICTION, FRACTURE AND DEFORMATION IV**
**Wednesday Afternoon, 15 March 2006; 336, Baltimore Convention Center at 14:30**
**Stefan Koehler, Emory University, presiding**

*Invited Papers*

**14:30**
**R33 1 Scanning Probe Applications to the Adhesive, Tribological and Rheological Properties of Materials.**
JACK E. HOUSTON, *Sandia National Laboratories*

Scanning probes are finding expanding application to the local analysis of a broad range of materials properties. I will discuss studies of adhesion, tribology and rheology applied to a range of materials using Interfacial Force Microscopy (IFM), a scanning force-probe technique distinguished by its use of a quantitative and mechanically stable force-feedback sensor. This unique sensor enables the force to be recorded as two interfaces approach, make contact, deform and separate making possible an accurate evaluation of the development of the adhesive bond and its failure. Thus, the nature of the adhesive bond, e.g., van der Waals, electrostatic, covalent, etc., can be established and the total adhesive energy measured quantitatively. Lateral forces can also be measured enabling direct observation of the interfacial friction force as a function of the normal force. These advantages will be illustrated with examples involving: (1) the interaction of a tip and substrate functionalized with self-assembled monolayer films having various combinations of chemically distinct end groups, as well as the interaction involving polymer surfaces, (2) the viscous properties of adventitious water adsorbed on various tip and substrate materials and (3) a quantitative, local rheological analysis of an extreme example of a viscoelastic material. These examples clearly demonstrate the intimate relationship between interfacial bond strength and the mechanical properties of the contact in determining overall adhesive strength. In addition, they dramatically demonstrate the weak correlation between the maximum adhesive force upon contact separation (the so called ''pull-off force'') and the quantitative work of adhesion. The assumptions required to make this correlation strong are seldom valid in ''real'' contact situations. Sandia is a multi-program laboratory operated by Sandia Corporation, a Lockheed Martin Company, for the U.S. Department of Energy's National Nuclear Security Administration under Contract DE-AC04-94AL85000.

*Contributed Papers*

**15:06**
**R33 2 Sub-micron void structure during spallation fracture*** JAMES BELAK, JOHN KINNEY, MUKUL KUMAR, *Lawrence Livermore National Laboratory* J. ILAVSKY, *Advanced Photon Source* LYLE LEVINE, *National Institute of Standards and Technology* Samples of single and poly-crystal aluminum were shocked to incipient spallation fracture and recovered on the LLNL light gas gun. Previously, we analyzed the void structure in these samples using 3D x-ray tomography. Here, we extend this analysis to sub-micron length scales using ultra-small-angle scattering (USAXS and USANS). The USANS data overlaps in length-scale with the tomography data. The data displays novel power law scaling and a Guinier region suggesting a mean size for sub-micron voids of 60nm. These results will be compared to direct numerical simulation using molecular dynamics.

*Work performed under the auspices of the U.S. DOE by University of California, LLNL under Contract W-7405-Eng-48, at APS under Contract No. W-31-109-ENG-38.

**15:18**
**R33 3 Dislocation Compression and Recovery Mechanisms in Shock-Recovered Al Single Crystals from White Beam Diffraction*** R. BARABASH, G. ICE, *ORNL* J. BELAK, M. KUMAR, *LLNL* J. ILLLAVSKY, *APS* A spatially resolved diffraction method with a sub-micron beam is applied to characterize both the dislocation structure and strain gradients in shock-recovered samples of Al (123) single crystal. Complementary OIM and SEM analysis were performed. The microbeam-Laue diffraction reveals several distinct zones located at different depths under the shock front. Pronounced streaking of Laue images are observed in the zones close to the front and back surface, consistent with a single slip mode. The portion of geometrically necessary dislocations reduces with depth while the portion of statistically stored dislocations increases. The Al sample was shocked to incipient spallation fracture and the Laue diffraction in the region of void formation shows a peculiarly complicated shape. To get a better understanding of the reasons for such a complex shape, 3D depth resolved measurements were performed. These measurements showed that in the central region alternating local lattice rotation takes place. This is due to the inhomogeneous plastic deformation surrounding each void. The density and organization of dislocations is presented as a function of depth under the shock front as well as comparison to SEM on the same samples. *This work was performed by DOE, at LLNL under Contract W-7405-Eng-48, at ORNL under the Contract DE-AC05-00OR22725 and at APS under Contract No. W-31-109-ENG-38.

**15:30**
**R33 4 Multiscale Simulations of High-Temperature Fracture in Silicon** NOAM BERNSTEIN, *Naval Research Lab* We simulate the effects of temperature on the dynamic fracture process in silicon. We use a dynamically coupled method that combines tight-binding at the crack tip with empirical potentials far from the tip in a molecular dynamics (MD) simulation.[1] This method has been shown to give brittle fracture at low temperatures, in agreement with experiment.[1] Here we present simulations of fracture at high temperatures, about 1000 K. These simulations are carried out in a strip geometry, and are relatively long and well equilibrated. There is no evidence that the velocity gap closes at these temperatures, at least not on the MD time scale. Fluctuations manifest themselves in the spontaneous nucleation of defects at

the crack tip. We discuss the nature and evolution of the defects, and their possible relation to the sharp brittle-to-ductile transition observed in silicon. [1] N. Bernstein and D. Hess, MRS Proc. vol. 653 (2001); – Phys. Rev. Lett. vol. 91 (2003).

**15:42**
**R33 5 Fracture scaling in columnar cornstarch** LUCAS GOEHRING, STEPHEN MORRIS, *University of Toronto* We have studied fracture spacing in desiccated cornstarch slurries, which exhibit columnar jointing. This fracture process creates long hexagonal pillars, and is famous for causing spectacular geologic features such as the Giants Causeway. The columnar pattern is formed as a planar network of cracks pass through a cooling or drying body. Even in simple 2D shrinkage fracture experiments it can be difficult to explain the spacing between cracks, however, in this case it is generally believed that the crack spacing depends on the average crack advance rate. Using computerized feedback, we controlled the desiccation rate of starch slurries. Continuous measurements of sample mass were converted into estimates of crack position and crack advance rate. After drying, direct measurements of crack spacing were made throughout the sample by cutting up the colonnade. With a constant crack advance rate, the jointing selects a particular scale after a transient coarsening. The selected scale does not uniquely depend on the final crack advance rate, but rather shows a type of memory inherited from its transient initiation. We present our investigations into this scaling, and how it depends on the fracture advance rate.

**15:54**
**R33 6 Reversible Rupture of a Two-Dimensional Alkane Crystal*** SHISHIR PRASAD, ALI DHINOJWALA, *The University of Akron* We present the first study of the rupture of a surface frozen monolayer of alkane (nonadecane) by oscillating an air bubble in its disordered melt. The two-dimensional (2D) crystal breaks abruptly at the start of every expansion and contraction cycle and recovers rapidly back to its original structure in a fraction of a second. This is unlike our experience of watching glass sheets or solids break due to the fast recovery times after the rupture of 2D crystals. The strength of this 2D crystal is determined by the presence of defects or grain boundaries and it is a strong function of temperature and rate of change in (surface) area. These results have important consequences in understanding the role of defect-mediated mechanical properties in crystals, colloids, glasses, granular materials, and fluids in confined geometries.

*Financial Support of NSF-DMR 0512156 and PRF

**16:06**
**R33 7 Spontaneous curvature cancellation in forced thin sheets** TAO LIANG, THOMAS WITTEN, *Department of Physics, University of Chicago* We report numerically observed spontaneous vanishing of mean curvature on a developable cone made by pushing a thin elastic sheet into a circular rim [1]. The mean curvature is seen to drop by nearly two orders of magnitude in a narrow zone near this rim, independent of thickness of the sheet, the supporting radius and the amount of deflection. Several variants of developable cone are studied to examine the necessary conditions that lead to the vanishing of mean curvature. It is found that the presence of appropriate amount of radial stress is necessary. The d-cone geometry somehow produces the right amount of radial stress to induce just enough radial curvature to cancel the conical azimuthal curvature. In addition, the circular symmetry of supporting rim plays an important role. When the supporting ring is elliptical, the radial curvature overcompensates the azimuthal curvature near the minor axis and undercompensates near the major axis. Our numerical finding is verified by a crude experiment using reflective plastic sheets. We expect this finding to have broad importance in describing the general geometrical properties of forced crumpling of thin sheets. [1] Cerda et al, Nature 401, 46 (1999)

**16:18**
**R33 8 Elasticity and gravity competing in a 2D system** P. MELLADO, *Johns Hopkins University* A. CONCHA, *Johns Hopkins University* We propose a minimal model for studying the consequences of the competition between elasticity and gravity on a surface. The model describes a cylindrically symmetric membrane composed of an elastic substrate and a stiff crust that experience a gravitational field directed radially inward. Under certain conditions an instability that breaks the initial symmetry can appear. When a stretching energy for the crust is introduced and an appropriate geometrical constraint on the system is imposed, an exotic periodic pattern forms. We provide an analytical solution to the model and show that while the stretching energy is responsible for the periodic pattern, faults in the stiff crust emerge generically when elasticity and gravity are competing. Possible implications in geology are discussed.

**16:30**
**R33 9 Development of First and Second Generation Fractures** MARTIN FERER, *National Energy Technology Laboratory and West Virginia University* DUANE SMITH, *U. S. Department of Energy, National Energy Technology Laboratory* In fractured reservoirs, one often finds a first generation of nearly parallel fractures and a second generation of fractures approximately perpendicular to the first-generation fractures. We have developed a simple blocks and springs model to study how the first generation fractures affect the development of the second generation. In the model, a layer of squares is connected to a substrate by spring-like shear forces, and each square is connected to its neighbors by intra-layer spring-like shear and tensile forces, of randomly chosen strengths. First the substrate gradually expands in the x direction generating stresses on the layer, which cause the failure of some of the intra-layer springs. Stopping this expansion at a maximum value X, we have the first generation of fractures. Then the substrate gradually expands in the y direction to a maximum value, Y, producing the second generation of fractures. During these expansions, we determine the length distribution of the first and the second generation fractures. Comparing the two distributions shows how the first-generation fractures affect the development of the second-generation fractures. After expansion has stopped, we determine the size (number of broken bonds) of each fracture, the maximum linear extent of each fracture, and the distributions of each.

**16:42**
**R33 10 Growing Fractures Using Iterated Conformal Maps.** H.G.E. HENTSCHEL, *Emory University* We will describe how iterated conformal mapping techniques can be used to grow fractures computationally and investigate their geometric characteristics as well as stress distributions. We will describe the similarities and differences between Mode I, II, and III fracturing patterns. Iterated conformal mapping techniques allows an efficient and accurate solution of the Lame equations without resorting to lattice models and for calculating the fracture roughness exponent.

**SESSION R34: TURBULENCE**
**Wednesday Afternoon, 15 March 2006**
**337, Baltimore Convention Center at 14:30**
**Walter Goldburg, University of Pittsburg, presiding**

**14:30**
**R34 1 Measurements of the Multifractal Dimension of Lagrangian Turbulence*** NICHOLAS OUELLETTE, HAITAO XU, *Cornell University* EBERHARD BODENSCHATZ, *Cornell University and Max Planck Institute for Dynamics and Self-Organization* We report experimental measurements of the Lagrangian multifractal dimension spectrum in an intensely turbulent laboratory water flow by the optical tracking of tracer particles. These measurements are compared with three model dimension spectra. The Legendre transform of the measured spectrum is compared with measurements of the scaling exponents of the Lagrangian structure functions, and excellent agreement between the two measurements is found.

*This work was supported by the NSF and by the Max Planck Society.

**14:42**
**R34 2 Multifractal particle distribution in compressible turbulence on a free surface.*** WALTER GOLDBURG, MAHESH BANDI, *Department of Physics and Astronomy, University of Pittsburgh* JOHN CRESSMAN, *Krasnow Institute, George Mason University* The distribution of particles in compressible turbulence on a free surface is inhomogeneous. The floaters flee regions of fluid up-wellings and cluster into ridge-like structures near fluid down-wellings. The concentration of floaters is measured on the surface of a large tank of turbulently stirred water. The multifractal structure of the clusters is reflected in the moments of particle concentration. The results are compared with recent work of Bec et al. [J. Bec, K. Gawedzki and P. Horvai, Phys. Rev. Lett., 92, 224501 (2004)] conducted on synthetic velocity fields that follow the compressible Kraichnan model.

*This work is supported by the NSF under Grant No. DMR-0201805.

**14:54**
**R34 3 Velocity and Scalar intermittency in restricted Euler dynamics** YI LI, CHARLES MENEVEAU, *Johns Hopkins University* A long standing problem in turbulence is to predict the intermittency from Navier-Stokes equation. Recently, by adopting a Lagrangian point of view and using the restricted Euler dynamics, we derived a simple nonlinear dynamical system, called advected delta-vee system, for the time evolution of longitudinal and transverse velocity increments, from which we showed that the non-Gaussian tails in turbulence originate from the inherent self-amplification of longitudinal velocity increments, and cross amplification of transverse velocity increments. Here, after reviewing previous results, the analysis is generalized to the increments of a passive scalar. A simple nonlinear equation is derived for the time evolution of scalar increments. The equation is coupled to the advected delta-vee system through the squeezing effect of the longitudinal velocity increment. Numerical integration of the equations starting from Gaussian initial conditions shows rapid development of non-Gaussian tails in the PDF of scalar increments, suggesting the system captures important trends in the original Navier-Stokes and scalar transport dynamics.

**15:06**
**R34 4 How Gaussian is the Velocity Gradient Tensor at Large Scales in Hydrodynamic Turbulence?** LAURENT CHEVILLARD, YI LI, CHARLES MENEVEAU, *The Johns Hopkins University, Baltimore, MD.* Fully developed turbulent flows exhibit a continuous range of exited scales, from the finest (dissipative range) towards the integral scale where energy is injected. Many theoretical approaches use the assumption that at large scales the fluctuations display Gaussian statistics. This has also been repeatedly confirmed based on measurements of longitudinal velocity increments in the Eulerian framework and temporal velocity increments in the Lagrangian framework. When the separation is comparable to integral scales of the flow, the PDFs of these velocity increments display Gaussian statistics, in contrast to the elongated tails and non-Gaussian statistics at smaller scales. Motivated by recent insights gained from Restricted Euler dynamics, we examine the statistics of the full velocity gradient tensor and several of its invariants relevant to the transfer of energy from large to small scales. Using Direct Numerical Simulations, we study the coarse-grained and band-pass Eulerian velocity gradient tensor. Among other features, we show that even at the integral length scale, the gradient statistics deviate from Gaussianity.

**15:18**
**R34 5 Quantum Fluid Mechanical Theory of Turbulence** DAVID DROSDOFF, ALLAN WIDOM, *Northeastern University* YOGENDRA SRIVASTAVA, *Northeastern University, INFN, University of Perugia* Turbulence has been called the last great unsolved problem of classical physics. The difficulty of solving the turbulence problem classically (even with the help of recent large scale computer simulations) may be that the problem is not classical. Turbulence will here be described as due to the non-commuting nature of the components of the Landau quantum fluid velocity field. The formation of fractal dimensional regions of quantum vortex strings in fully developed turbulence will be discussed along with the implied Kolmogorov scaling functions.

**15:30**
**R34 6 Counter-gradient transport in the atmospheric boundary layer** CHERYL KLIPP, *US Army Research Laboratory* Counter-gradient transport in turbulent flows, also called negative viscosity, has been theorized and observed over the past century at a variety of spatial scales. More than one mechanism may be responsible for the process of transferring momentum from slower moving fluid to faster moving fluid depending on the scale of the flow and other flow properties. Horizontal divergence is presented as a possible mechanism for counter-gradient momentum transport observed in the atmospheric boundary layer.

**15:42**
**R34 7 LES Simulations of Pulsed Gas Jets.** JONATHAN ANDERS, *Purdue University* VINICIO MAGI, *Purdue University* JOHN ABRAHAM, *Purdue University* The study of pulsed jets is motivated by their applications which include increasing mixing, enhancing heat transfer, and controlling flow separation and vortex structures. This work investigates the interaction between gas jet pulses in the near-field using large eddy simulation (LES). LES employing the constant coefficient Smagorinsky model is compared to Reynolds-averaged Navier-Stokes (RANS) simulations with a two-equation k-$\varepsilon$ model. RANS predictions indicate faster penetration of subsequent jet pulses caused by the mean flow field from the first pulse, and do not show enhanced mixing due to residual turbulence. LES of the jet near-field includes development

of the head vortex ring and transition to turbulence in the jet. LES of the pulsed gas jet predicts interaction of the head vortex with residual turbulence from an earlier pulse. The dominant effect of the mean flow field and the accelerated penetration seen in RANS predictions are not evident in the LES results.

**15:54**

**R34 8 Vortical structures in a flume** R. GURKA, *Dept. of Mech. and Mat. Engr., Univ. of Western Ontario* A. LIBERZON, *Inst. of Hydromechanics and Water Resources Mgmt., ETH Zurich, Switzerland* G. HETSRONI, *Faculty of Mech. Engr., Technion, Israel* We report the results of statistical spatial characterization of coherent structures in turbulent boundary layer in a flume. The characterization approach is based on the proper orthogonal decomposition (POD) of vorticity, elucidating large-scale coherent patterns in a turbulent boundary layer. The method was successfully applied to the two- and three-dimensional experimental data extracted from particle image velocimetry (PIV), and multi-plane stereoscopic PIV (XPIV) respectively, and the three-dimensional data from direct numerical simulation (DNS) in a channel flow. The large-scale structure was obtained by using linear combination of POD eigenmodes of vorticity. POD allows for methodological analysis of the properties of the educed structure in the different measurement planes (orthogonal in the case of 2D PIV and parallel in the case of XPIV) and in the different cross-sections of the DNS data. Based on the statistical approach we suggest a conceptual model of large-scale coherent structures in a turbulent boundary layer flow that incorporates the experimental and the numerical results. The proposed conceptual model is a spiral vortical structure attached to the wall and expanding in both the spanwise and the wall-normal directions. Its shape resembles a funnel structure and a 'double-cone eddy' concept. The relationship of the model to the structures in the near wall region is presented.

**16:06**

**R34 9 Single-point Velocity Statistics** YONGGUN JUN, X.L. WU, *University of Pittsburgh* The single-point (SP) velocity statistics is investigated in forced and decaying two-dimensional turbulence in a flowing soap film. It is shown that the probability distributin functions (PDF) in both cases deviate from a Gaussian distribution, which is normally anticipated in turbulent fluid flows. In the forced turbulence case, the tail of the SP velcoty PDF decays faster than Gaussian and can be correlated with the forcing statistics on small sclaes. In the decaying turbulence case, the SP velocity PDF evolves from a sub-Gaussion to a super- Gaussian behavior as a function of decaying time. In all times, however, the locally averaged vorticity distribution remains approximately Gaussian. While our forcing data may be explained by the instanton model put forward by Falkovich et al., the decaying turbulence data remain unexplained by theory.

**16:18**

**R34 10 Coherent Structures in Decaying Two-Dimensional Turbulence** MICHAEL RIVERA, *Los Alamos National Laboratory* MICHAEL TWARDOS, ROBERT ECKE, We revisit the matter of coherent structures, such as vortices, and their role in decaying two-dimensional turbulence. These experiments take place in an electromagnetically forced stratified layer within a square container with no slip boundaries and a linear dissipation with the container bottom. Results relating the energy and enstrophy of the bulk flow with the number and strength of coherent vortices are compared with earlier numerical and experimental work.

**16:30**

**R34 11 Multiscale Distribution of Energy Transfer in Two Dimensional Turbulence** MICHAEL TWARDOS, MICHAEL RIVERA, ROBERT ECKE, In two dimensional turbulence, the mechanisms responsible for energy transfer to larger scales are not well understood. We present results from an experimental system consisting of a square meter of electromagnetically driven thin salt water layer that is used to investigate this inverse energy cascade. A filter technique applied to high resolution velocity fields is used to understand scale to scale energy transfer. An extension of this technique determines the contribution of energy transfer across a given length scale from smaller scales. Expanding the subgrid coupling terms allows for some speculation of the energy transfer mechanisms.

**16:42**

**R34 12 Statistical Properties of 2 Dimensional Turbulence in a Finite Box** COLM CONNAUGHTON, *Center for Nonlinear Studies, Los Alamos National Laboratory* MISHA CHERTKOV, *Theoretical Division, Los Alamos National Laboratory* VLADIMIR LEBEDEV, *Landau Institute for Theoretical Physics* IGOR KOLOKOLOV, *Landau Institute for Theoretical Physics* In the standard statistical theory of two dimensional hydrodynamics forced at some intermiediate scale, two cascades are produced. Energy flows to large scales, producing Kolmogorov's $k^{-5/3}$ spectrum at small $k$ and enstrophy flows to small scales to produce Kraichnan's $k^{-3}$ spectrum at large $k$. If we consider turbulence in a finite box in the absence of large scale dissipation, the inverse cascade eventually reaches the size of the box and the cascade is blocked. This leads to accumulation of energy in the largest modes, a process which can be qualitatively thought of as a non-equilibrium condensation process. The ''condensate'' in this case is a coherent, large scale vortex dipole. We investigate how the system passes through a series of distinct regimes, leading to the emergence of this large scale structure. We show how it affects the scaling properties of two-dimensional turbulence and explain how the presence of very strong vortices leads to an apparent modification of the small scale statistical properties of the inverse cascade.

**16:54**

**R34 13 Direct Numerical Simulations of Turbulent Flow in a Wavy Channel** LUO WANG, KOSTAS HOUSIADAS, ANTONY BERIS, *University of Delaware* A spectrally preconditioned biconjugate gradient algorithm (Bi-CGSTAB) has been developed that enabled us to perform high accuracy (spectral) efficient Direct Numerical Simulations (DNS) of Newtonian turbulent flow in an undulating channel geometry. The DNS of have been performed in a channel geometry involving a single sinusoidal solid wavy wall with amplitude/half width ratio of 0.1 and a wave length of 2. Two different friction Reynolds numbers have been investigated, $Re_\tau$=160 and 220 corresponding to mean Reynolds numbers (based on the channel half width) 1800 and 2480, respectively. The computational domain used was 10x2x5 along the streamwise, shearwise and spanwise direction respectively, with spectral resolutions ranging from 160x257x64 to 320x385x128. The nu-

merical results compare well against Hudson's measurements (Hudson, Ph.D. Thesis, UIUC 1993). In addition, the DNS results allowed us to investigate in detail various turbulence statistics and the vorticity structure and its influence from the wall undulation.

**17:06**

**R34 14 Non-Boussinesq effects on heat transport in turbulent Rayleigh-Bénard convection of gases*** DENIS FUNFSCHILLING, *UCSB* GUENTER AHLERS, *UCSB* In turbulent Rayleigh-Bénard convection large temperature differences often are used in order to reach very high Rayleigh numbers. This can lead to a breakdown of the Boussinesq approximation which assumes temperature-independent fluid properties. We presents quantitative measurements of non-Boussinesq (NB) effects on the heat transport obtained by using Ethane gas at a mean temperature of 40°C and pressures up to 40 bars. At the largest temperature differences of about 40°C, where the top of the sample approached the vapor-liquid saturation curve, the Nusselt number was **increased** above the Boussinesq value by several percent. This contrasts with NB effects in liquids[1] where the heat transport is reduced below the Boussinesq value.

*Supported by DOE Grant DE-FG02-03ER46080

[1]G. Ahlers, E. Brown, D. Funfschilling, S. Grossmann, and D. Lohse, J. Fluid Mech., submitted.

**17:18**

**R34 15 Lattice Boltzmann studies of drag reduction in turbulent channel flow with polymers.** ALEXANDER KARPIKOV, *Yale University* S.A. ORSZAG, K.R. SREENIVASAN, Massive drag reduction in turbulent flow by dilute addition of polymers has long been a challenging problem in fluid dynamics. In order to study this problem here we use the Lattice Boltzmann method (LBM) to simulate turbulent channel flow. A polymer model, which is macroscopically equivalent to the FENE-P model, is included in LBM to represent polymers. Drag reduction with polymers was observed in the simulations. Although such drag reduction has been demonstrated in laboratory experiments, the mechanisms are not yet clear. In order to understand these results we investigated the role of dilute polymers on Kelvin-Helmholtz instability in the much simpler turbulent mixing layer. Our simulations of the mixing layer show that polymers produce a stabilizing effect and suppress momentum transport due to fluctuating velocity components. The simulations of these two systems together provide a clearer picture of the interaction between polymers and coherent structures in the near-wall region of the turbulent flow and shed light on the mechanism of drag reduction. The addition of polymers primarily modifies turbulent bursts in channel flow, and this phenomenon has several features in common with the effect of polymers on Kelvin-Helmholtz instability in the mixing layer.

## SESSION R36: FOCUS SESSION: OPTICAL AND X-RAY PROPERTIES OF NANOSTRUCTURES

**Wednesday Afternoon, 15 March 2006; 339, Baltimore Convention Center at 14:30**
**John Rehr, University of Washington, presiding**



***Invited Papers***

**14:30**

**R36 1 Time-Dependent Density Functional Calculations for Optical Excitations in Nanoscale Materials.*** IGOR VASILIEV, *New Mexico State University*

Optical properties play a crucial role in our understanding of the electronic structure of nanoscale materials. Despite significant progress in the development of computational methodologies, first principles calculations for optical excitations in nanomaterials remain extremely difficult. While the ground-state electronic structure formalism is relatively well established, calculations for excited states present major challenges to theoretical methods traditionally employed by condensed matter physics and quantum chemistry. This talk focuses on recent advances in a computational technique based on time-dependent density functional theory (TDDFT). Within the TDDFT method, electronic transition energies and oscillator strengths are obtained in the framework of linear response theory by solving a frequency-dependent equation for the dynamic polarizability. The linear-response TDDFT formalism is applied to compute the excitation energies and absorption spectra for a variety of nanoscale systems, including molecules, atomic clusters, semiconductor quantum dots, functionalized carbon nanotubes, and nanotube-polymer composites. The TDDFT approach is compared to other first principles computational methods for excited states and discussed in terms of accuracy, efficiency, and computational cost.

*Supported by the National Science Foundation under Grant No. DMR-0505270, Petroleum Research Fund under Grant No. PRF-43409-G10 and the Air Force Office of Scientific Research under Award No. FA-9550-05-1-0234.

***Contributed Papers***

**15:06**

**R36 2 Quantum Monte Carlo Calculations of Excitations in Hydrogenated Germanium Clusters** JORDAN VINCENT, *Physics Dept. at UIUC* JEONGNIM KIM, *NCSA/MCC at UIUC* RICHARD MARTIN, *Physics Dept. at UIUC* Quantum Monte Carlo (QMC) calculations are presented for energies of ground and excited states of Ge atom and hydrogen passivated closed-shell molecules and clusters: GeH4, Ge2H6, Ge5H12, Ge10H16 and Ge29H36. We compare the results for excitations with previous QMC and time-dependant Density Functional Theory (TDDFT) done for the corresponding Silicon clusters [1,2]; in particular; we find that preliminary results for lowest excitation enregy of Ge29H36 5.08[29]eV is lower than the gap 5.4eV reported for Si[2]. Core-valence partitioning for Ge is implemented by replacing the core-states with a Hartree-Fock pseudopotential plus a Core Polarization Potential (CPP)[3]. Core-valence correlation

treated by the CPP is shown to be essential for accurate atomic energies and significant for the molecules, but smaller in the clusters. [1] Porter et. al., PRB 64, 035320 (2001). [2] Williamson et. al., PRL 89, 196803 (2002). [3] Shirley and Martin, PRB 47, 15413 (1993)

**15:18**

**R36 3 Ab initio X-Ray Absorption Fine Structure Cumulants*** F. VILA, J.J. REHR, *University of Washington* H.H. ROSSNER, H.J. KRAPPE, *Hahn-Meitner-Institut* Theoretical calculations of vibrational effects in x-ray absorption spectra typically employ semi-phenomenological models, e.g. empirical force constants or correlated Debye or Einstein models. Instead we introduce an efficient and generally applicable ab initio approach based on electronic structure calculations of the dynamical matrix together with the Lanczos recursion algorithm [1] and relations between the cumulants. The approach yields 1) the thermal expansion coefficients (first cumulant of the vibrational distribution function); 2) correlated Debye-Waller factors (second cumulants) and 3) anharmonic contributions (third cumulants). Results are presented for crystalline (Cu, Au, Ge, GaAs) and molecular ($GeCl_4$, $C_6H_6$) systems. Our results for the Debye-Waller factors agree well with experiment. [1]H.J. Krappe and H.H. Rossner, Phys. Rev. B**70**, 104102 (2004).

*Supported by DOE Grant DE-FG02-04ER1599 (FV) and DE-FG02-97ER45623 (JJR) and facilitated by the DOE CMSN.

**15:30**

**R36 4 Real Space Multiple-Scattering Calculations of Optical Properties*** M.P. PRANGE, J.J. REHR, A.L. ANKUDINOV, *U. of Washington* J.A. SOININEN, *U. of Helsinki* We present a method for *ab initio* calculations of the dielectric function which is applicable for periodic and non-periodic materials alike. Our approach is a generalization to finite momentum transfer of that implemented in the real space multiple-scattering code FEFF8 and is the real-space analog of the KKR method. The approach includes self-consistent potentials, an energy dependent self-energy and screened core-hole effects. The method yields the dynamic structure factor $S(\vec{q},\omega)$ over a broad spectrum from the optical to x-ray energies, and in the long-wavelength limit, yields various optical constants. Results for several materials are presented and compared with experiment.

*Supported by DOE Grant DE-FG02-97ER45623 and facilitated by the DOE CMSN.

**15:42**

**R36 5 Ab initio Quasiparticle Self-Energies and X-ray spectra*** J. KAS, M. PRANGE, A. SORINI, J.J. REHR, *U. of Washington* Present calculations of inelastic losses in x-ray spectra typically employ semi-empirical or highly simplified models, such as the plasmon-pole self-energy, which are only semi-quantitative for near edge spectra. Here we present an efficient *ab initio* approach applicable to general materials, starting from a real-space multiple-scattering calculation of the dielectric function,[1] which is fit to a multiple-pole model with of order $10^2$ poles. This yields multiple-pole GW self-energies, and hence related quantities such as inelastic mean free paths (IMFP). The approach leads to improved amplitudes and phases for core-level x-ray spectra up to photo-electron energies of order $10^3$ eV. Results for the IMFP are found to be in good agreement with experiment and with other approaches.[2,3]

*Supported by DOE Grant DE-FG02-97ER45623 (JJR and MP), NIST Grant 70 NAMB 2H003 (AS), NIH NCRR BTP grant RR-01209 (AS), and facilitated by the DOE Computational Materials Science Network (CMSN).

[1]M. P. Prange, J. J. Rehr, A. L. Ankudinov and J. A. Soininen, APS March Meeting 2006 (unpublished).
[2]E. L. Shirley, J. A. Soininen and J.J. Rehr, APS March Meeting 2006 (unpublished).
[3]C. J. Powell and A. Jablonsky, J. Phys. Chem. Ref. Data **28**, 19 (1999).

**15:54**

**R36 6 Isolating symmetry components of the Mg and Al DOS using momentum-transfer dependent Inelastic X-ray Scattering** TIM FISTER, *Physics Department University of Washington, Seattle WA* GERALD SEIDLER, JOHN REHR, ALEKSI SOININEN, *University of Helsinki* JULIE CROSS, ALBERT MACRANDER, *Advanced Photon Source, Argonne National Labs* We have used the non-resonant inelastic x-ray scattering (NRIXS) from core electrons to measure the dynamic structure factor of the Mg and Al L-edges for momentum transfers ($q$) ranging from 0.8 10.1$Å^{-1}$. Changing $q$ alters the measured energy loss spectrum by allowing new, dipole-forbidden transitions to different symmetry final states. Here, we highlight the connection between dynamic structure factor and the projected components of the density of states (ldos) using a modified version of FEFF that incorporates multipole transitions. In addition to itab initio theoretical agreement with the observed $q$-dependence, we present preliminary efforts toward obtaining an experimentally-derived ldos.

**16:06**

**R36 7 Metal-metal nanolayered structures for generation of hard x-ray radiation** PETER SHKOLNIKOV, *ECE Department, SUNY at Stony Brook* ALEXANDER KAPLAN, ALEXANDER POKROVSKY, *ECE Department, Johns Hopkins University* Our new research effort is aimed at developing a new X-ray source for medical applications, using low-energy electrons. Generation of intense narrow-band X-ray transition radiation (TR) by few-MeV electrons traversing solid multilayer structures, initially proposed for by us $\sim$ 1 keV photons, changes dramatically at energies of interest to medicine, 30-50 keV, because of significant changes in dielectric constants. In particular, the choice of the materials for the multilayer target proposed by us for soft X- ray generation, is no longer applicable. In particular, our original approach was based on choosing a layer of a high-Z material as a ''radiator'' with a chosen $K$-shell transition, and the layer of low-Z material as a neutral ''spacer.'' However, in the 30-50 keV range, TR spectra with such pairs show a spectral $dip$, not a peak,at the chosen $K$-shell. Our new theoretical investigations have shown that the optimal spacer now, as a rule, should have higher Z than the radiator. One example of such combination is Mo/Ag; we predict that its X-ray TR spectrum contains a strong, 1% wide peak at the K-edge of Mo, $\sim$ 20 KeV. We present our recent theoretical results of the subject, as well as our experimental results for the Mo/Ag target.

**16:18**

**R36 8 Optical conductivity of granular metals** YEN LEE LOH, *Purdue University* VIKRAM TRIPATHI, *Cambridge University, UK* Arrays of metallic grains, which can be fabricated in a number of ways, exhibit interesting behavior in many properties due to the interplay between tunneling and Coulomb blockade effects. One such property is the AC conductivity, which can be measured using optical reflectivity techniques. We present here a calculation of the AC conductivity of a regular granular array. For this purpose we have found it necessary to generalize the Ambegaokar-Eckern-Schön (AES) model to include polarization fluctuations as well as charge fluctuations. In contrast to the DC conductivity, which is determined by inter-grain charge transfer and obeys an Arrhenius law at low temperature, we show that the AC conductivity is dominated by a resonance peak for intra-grain polarization oscillations, which has a power-law tail at low frequencies. Although the resonance frequency agrees with the classical prediction, the resonance width depends on quantum mechanical tunneling and Coulomb blockade parameters, in addition to intra-grain impurity scattering. This additional damping is due to inelastic cotunneling of polarization fluctuations to neighbouring grains.

**16:30**

**R36 9 Probing by transport the single-particle energy spectrum up to high energy of one quantum dot with the ground state of an adjacent weakly coupled quantum dot to examine the behavior of magnetic-field induced two- and three-level crossings** DAVID AUSTING, *National Research Council of Canada* GOULIN YU, JAMES GUPTA, MAREK KORKUSINSKI, GEOFFREY AERS, NATIONAL RESEARCH COUNCIL OF CANADA TEAM, We investigate high bias single electron resonant tunneling through sub-micron gated AlGaAs/InGaAs/AlGaAs/InGaAs/AlGaAs triple barrier structures for which the tunnel coupling energy between the two quantum dots is very weak ( $< 0.1$meV). The two quantum dot ''disks'' in the vertical diatomic artificial molecule located in the circular device mesa can be almost circular or elliptically deformed. In either case, assuming the lateral confining potential to be strictly parabolic, one would expect the single-particle states of one quantum dot to evolve with magnetic field in a very distinct and recognizable way, and that all energy level crossings are real crossings. We find, however, particularly for two quantum dots with an elliptical deformation ratio of about 4/3, numerous anti-crossings (levels split by up to about 1meV in energy) as well as crossings when two or three levels meet in the spectrum. We show the measured spectrum, attempt to classify the crossing and anti-crossing behavior, and offer possible explanations for this intriguing behavior.

**16:42**

**R36 10 Anomalous electronic transport features in a lateral quantum dot array sample** WEI PAN, R.G. DUNN, J.L. RENO, J.A. SIMMONS, *Sandia National Laboratories* D. LI, S.R.J. BRUECK, *CHTM, University of New Mexico* We will present in this talk experimental results obtained in a lateral quantum dot array sample, with a pitch size of $\sim$ 350 nm and a designed dot size of $\sim$ 150nm. The starting material is a high quality quantum well with the two-dimensional electron gas buried 200 nm below the surface. The quantum dot array is defined by a Ti/Au metal grid, which was fabricated using the interferometric lithograph and lift-off techniques. Around zero magnetic field, a pronounced positive magnetoresistance is observed, which can be explained by the semi-classical model of magnetic breakdown. The so-called commensurability oscillations together with the usual Shubnikov-de Hass oscillations are also observed. Surprisingly, in a pure DC measurement of longitudinal resistance, an anomalous resistance spike is clearly seen. The magnetic field position of this resistance spike depends on the amplitude of applied DC bias ($V_{ds}$) between source and drain, and shows roughly a $1/V_{ds}$ dependence. Sandia is a multiprogram laboratory operated by Sandia Corporation, a Lockheed Martin Company, for the United States Department of Energy's National Nuclear Security Administration under contract DE-AC04-94AL85000.

**16:54**

**R36 11 Polarization and orientation effects on energy transfer in semiconductor nanocrystals.*** AMEENAH N. AL-AHMADI, SERGIO E. ULLOA, *Ohio University* We study the effect of the orientation factor on coherent energy transfer from a donor to an acceptor quantum dot. We calculate the polarization of the acceptor dot as a function of incident light polarization in resonance with different donor levels. We demonstrate that the measurement of the acceptor polarization can be used to obtain information on the relative orientation between the donor-acceptor pair. We use the density matrix to study the dynamics of the luminescence polarization of the QDs in the Lindblad approximation [1]. We use a realistic model of the exciton levels and the oriented dipole transition of each level to predict the importance of the orientation factor on the energy transfer in semiconductor nanocrystals. We consider the band edge fine structure of the exciton in the QDs based on an effective mass description with eight exciton levels [2]. Our results show strong dependence of the polarization of the acceptor dot on the relative orientation between the donor-acceptor pair and the specific donor state under excitation. [1] A.N. Al-Ahmadi and S.E. Ulloa, Phys. Rev. B 70, 201302(R) (2004). [2] Al.L. Efros and M. Rosen, Ann. Rev. Mater. Sci. 30, 475 (2000).

*Supported by the Indiana 21st Century Research and Technology Fund.

**17:06**

**R36 12 Energy relaxation and phonon bottleneck in semiconductor quantum dots** SERGUEI GOUPALOV, *Los Alamos National Lab* We show explicitly that the so-called phonon bottleneck in energy relaxation in semiconductor quantum dots arises as a limiting case of a more general model originally due to Huang and Rhys [S.V.Goupalov, Phys. Rev. B **72**, 073301 (2005)]. Therefore, the restrictions on the energy relaxation imposed by the phonon bottleneck are much less fundamental than it is commonly believed. We calculate temperature dependence of the non-radiative multiphonon transition rate within the properly corrected Huang-Rhys model and discuss other models where the phonon bottleneck is circumvented in connection with recent experiments on epitaxial and colloidal quantum dots.

**17:18**

**R36 13 Spectroscopic studies of $Fe_3O_4$ nanocrystals** LAYRA REZA, *Physics Department, University of Texas at El Paso* FELICIA MANCIU, *Physics Department, University of Texas at El Paso* YUDHISTHIRA SAHOO, *Institute for Lasers, Photonics and Biophotonics, State University of New York at Buffalo* We have used IR spectroscopy to study the temperature dependence of optically active phonon modes of $Fe_3O_4$ nanocrystals, to obtain information about the possible Verwey transition, which is usually manifested in bulk material. The samples were synthesized by

colloidal chemistry. The crystallinity and sizes were examined by transmission electron microscopy (TEM) and X-ray diffraction. The TEM pictures show an average size of 6-8 nm for $Fe_3O_4$ nanocrystals. Samples for the IR studies were prepared in the form of pellets, by embedding them in a polycrystalline CsI matrix. The temperature dependence ($10K < T < 300K$) IR transmission results exhibit a frequency increase upon decreasing the temperature for the infrared-active phonons around 360 $cm^{-1}$ and 574 $cm^{-1}$, but without notable anomalies around the critical temperature (120K) as compared to those previously observed in a single $Fe_3O_4$ crystal. The appearance of a fine structure at low temperatures could account for the lifting of the degeneracy of the phonon modes. This splitting is associated with the degree of the distortion of the symmetry of the system.

**SESSION R37: FOCUS SESSION: NANOSCALE CONDUCTANCE THEORY I**
**Wednesday Afternoon, 15 March 2006; 340, Baltimore Convention Center at 14:30**
**Mark Hybertsen, Columbia University, presiding**

*Invited Papers*

**14:30**
**R37 1 Conductance Through Single Organometallic Molecules.***
HAROLD U. BARANGER, *Duke University*

We have undertaken ab initio calculations of the conductance and I-V curve of a variety of single molecules bridging two metallic leads. The method adopted is a non-equilibrium Green function (NEGF) approach to transport combined with density functional theory (DFT) calculations for the electronic structure. A principal motivation comes from experiments in the U. Maryland group [1]: they showed that a molecule containing a ferrocene moiety conducts nearly perfectly, in striking contrast to the severely impaired conduction through all fully conjugated but non-metallic molecules. Our calculations show that, indeed, there is a transmission resonance at the Fermi energy of the leads connected to the iron atom in the molecule. However, the comparison of theory and experiment also points to significant weaknesses caused by approximations in the standard NEGF+DFT approach. Thus, on a much simpler system—a H atomic chain—we carry out much improved calculations involving exact exchange, hybrid functionals, and the optimized effective potential method. These provide a cautionary illustration of the kind and magnitude of errors in the standard approach. Finally, emboldened by our success with the ferrocene-containing molecule, we turn to developing a true molecular spintronics based on cobaltocene moieties (spin 1/2). A simple molecule with a single cobaltocene provides a spin filter; we demonstrate a spintronic switch and spin valve using a dicobaltocene molecule [2]. [1] S.A. Getty, et al. (groups of M.S. Fuhrer, and L.R. Sita), PRB 71, 241401(R) (2005). [2] R.Liu, S.-H. Ke, H.U. Baranger, and W. Yang, Nano Lett. 5, 1959 (2005).

*Work done in collaboration with Rui Liu, San-Huang Ke, and Weitao Yang, and supported by the NSF (DMR-0506953).

*Contributed Papers*

**15:06**
**R37 2 Negative differential resistance (NDR) of ferrocenyl-alkanethiolate on the Au (111) surface** SHUCHUN WANG, *NC State U.* WENCHANG LU, QINGZHONG ZHAO, JERRY BERNHOLC, With the rapidly growing interest in the development of molecular electronics, the resonant tunneling diode (RTD) becomes an attractive molecular device goal due to its utility in switching logic and simplicity in integration. Molecular systems displaying Negative Differential Resistance (NDR) and resonant tunneling show great potential as RTDs. In a recent experiment, self-assembled monolayers (SAMs) of ferrocenyl-alkanethiolate on gold show clear molecular NDR, but its mechanism has not been identified. We report first-principles studies of electronic transport in such SAMs by the non-equilibrium Green functions method. The calculated I-V characteristics show strong NDR at both positive and negative biases, which are in good agreement with the experimental results. We find that the ferrocene group acts like a quantum dot and that the resonant coupling between its HOMO and the gold leads is responsible for the NDR features. Such molecules could lead to novel RTDs in nanoscale molecular devices.

**15:18**
**R37 3 Exploring the lead dependence of single-molecule conductance from first principles: The case of $H_2$ molecular junctions** K.H. KHOO, *Dept of Physics, UC Berkeley* J.B. NEATON, *The Molecular Foundry, LBNL* STEVEN G. LOUIE, *Dept of Physics, UC Berkeley, The Molecular Foundry, LBNL* Although the transport properties of several single-molecule junctions have now been reported, only a few studies have systematically examined the sensitivity of the junction conductance to the choice of metallic contacts. Recent break-junction experiments have revealed significantly lower conductance for $H_2$ molecular junctions when Pt leads were replaced with Pd,[1,2] suggesting a dramatic difference in electronic coupling between the molecule and lead. In this work, we examine this coupling directly by computing the conductance of $H_2$ with several different metallic contacts using an itab-initio scattering state approach[3] based on density functional theory. We find that by substituting Pt with Pd leads, the low-bias electron transport crossesover from a ballistic to an off-resonance tunneling regime, leading to a conductance smaller than unity in agreement with experiments. The extent to which substituting different leads may be used to tune the transport properties of this and other simple single-molecule junctions will be discussed. This work was supported by the NSF Grant No. DMR04-

39768 and U.S. DOE Contract No. DE-AC03-76SF00098. [1] R.H.M. Smitit et al., Nature (London) **419**, 906 (2002). [2] Sz. Csonkait et al., Phys. Rev. Lett. **93**, 016802 (2004). [3] H.J. Choi, M.L. Cohen and Steven G. Louie, to be published.

**15:30**

**R37 4 Electronic level alignment at metal-molecule interfaces from first principles*** JEFFREY B. NEATON, *The Molecular Foundry, LBNL* MARK S. HYBERTSEN, *Department of Applied Physics and Applied Mathematics and Center for Transport in Molecular Nanostructures, Columbia University* STEVEN G. LOUIE, *The Molecular Foundry, LBNL and Department of Physics, UC-Berkeley* Electronic transport through nanoscale molecular junctions critically depends on the energetic alignment of frontier molecular states with the contact Fermi levels. In this work, a first-principles Greens function approach is used to explore how frontier molecular energy levels are modified at metal-molecule interfaces. The electronic structure of a model interface, benzene on graphite (0001), is computed using the GW approximation for the electron self-energy operator. Upon adsorption on the surface, the benzene HOMO-LUMO gap is predicted to be 7.2 eV, substantially reduced from its calculated gas-phase value of 10.5 eV, and slightly smaller than its computed solid-phase gap of 7.5 eV. This decrease is attributed to the change in the electronic correlation energy of the frontier states in different environments. Comparison with a classical image interaction provides a quantitative measure of the contribution of the molecule-substrate coupling to the gap narrowing of the molecule.

*This work is supported by DOE contract DE-AC03-76SF00098; by NSF awards DMR04-39768 and CHE-0117752; and by NYSTAR. Computational resources are provided by NERSC.

**15:42**

**R37 5 Is a molecule a quantum wire or a quantum dot?** BHASKARAN MURALIDHARAN, *School of Electrical and Computer Engineering, Purdue University, West Lafayette, IN 47907* AVIK W. GHOSH, *Dept. of Electrical and Computer Engineering, University of Virginia, Charlottesvile, VA 22904* SUPRIYO DATTA, *School of Electrical and Computer Enginnering, Purdue University, West Lafayette, IN 47907* We address an important issue regarding the appropriate transport regime for molecular conduction. A typical transport calculation employs the Non Equilibrium Green's function (NEGF) transport scheme coupled with an appropriate self consistent field (SCF) method. This implies that the molecule is treated as a ''quantum wire,'' usually applicable when contact couplings are much larger than other energy scales involved. However, there exists a whole class of experimental data whose qualitative features depart significantly from the ones usually explained using the above approach. We show that these features can be naturally addressed by adopting a Coulomb Blockade (CB) approach used in ''quantum dot'' transport. This involves description of the molecule in its many-body space. Our analysis in the many-body space of a prototypical molecule explains the non-trivial features commonly observed in low temperature molecular conduction experiments. Hence, we point out the inadequacy of SCF approaches towards a concrete description of molecular conduction which should involve both quantum chemistry and transport in the many-body space of the molecule.

**15:54**

**R37 6 Constrained LDA ab-initio calculation of screening of charging energy in C60** JAY SAU, JEFFREY NEATON, K.H. KHOO, *Department of Physics UC Berkeley* HYOUNG CHOI, *Department of Physics, Yonsei University* STEVEN LOUIE, MARVIN COHEN, *Department of Physics UC Berkeley* Recent measurements and theoretical calculations of the electronic properties of C60 on metal substrates have shown that the electron-electron repulsion parameter U, which determines the coulomb blockade transport properties, is strongly screened in the presence of a metal susbtrate. Since standard Density Functional Theory calculations treat this charging energy in a mean field sense, it ignores the discreteness of the charge on the C60 that is critical to coulomb blockade. To account for the effect of the screened U in transport experiments we calculate the charging energy of C60 in a few environments using a constrained LDA approach and explore the implications for coulomb blockade transport phenomena. This work was supported by National Science Foundation Grant No. DMR04-39768 and by the Director, Office of Science, Office of Basic Energy Sciences, Division of Material Sciences and Engineering, U. S Department of Energy under Contract No. DE-AC03-76SF00098. Computational resources have been provided by DOE at the National Energy Research Scientific Computing Center(NERSC)

**16:06**

**R37 7 Physical manifestation of the Kohn-Sham energy gap in tunneling currents** XIAOGUANG ZHANG, *Oak Ridge National Laboratory* ZHONG-YI LU, *Institute of Theoretical Physics, Chinese Academy of Science* SOKRATES S. PANTELIDES, *Department of Physics and Astronomy, Vanderbilt University* Density-functional theory in the Kohn-Sham (KS) approximation yields accurate ground-state properties of molecules and solids. The KS energy gap, however, is much smaller than the gap obtained from experiments that entail electronic excitations. Here we point out that the zero-bias differential resistance of metal-insulator-metal structures is a ground state property and demonstrate that the KS gap, which is a feature of the ground-state KS Hamiltonian, acts as the effective tunnel barrier. The theory is validated by three sets of available data for the resistance of $SiO_2$ films as a function of film thickness.

**16:18**

**R37 8 Semiconductor/Molecule Transport Junctions: An Analytic Form For The Self-Energies** VLADIMIRO MUJICA, *Research Professor* MARK RATNER, *Professor* We have derived an approximate analytic expression for the spectral density of a simple model of a semiconductor/molecule junction. The semiconductor is considered as a tight-binding one-dimensional chain with periodic boundary conditions, and either bond or site-energy, alternation to mimic a two-band system. Using the simplest representation for an atomic or molecular site we obtain a spectral density whose main physical and mathematical features are independent of the alternation pattern. In this contribution, we show applications of our model to the description a variety of junctions where the relative position of the energy levels involved is changed.

**16:30**

**R37 9 Ab initio study of inleastic transport in molecular electronic devices** NIKOLAI SERGUEEV, *University of Texas at Austin* ALEX DEMKOV, *University of Texas at Austin* One of the most important issues of conduction at nano-scale concerns the effects of atomic vibration. Interaction between electrons and vibrational excitations in nanoelectronic devices has become the problem to solve in order to advance the research field of nanoelectronic theory. Understanding these effects is crucial for predicting device performance. In this talk, we present a method based on Density Functional Theory and Nonequilibrium Green's functions formalism for the calculation of tunneling current and conductance in molecular electronic devices in the presence of electron-phonon interaction. Using self-consistent Born approximation, we can determine the phonon self-energy, the electron Green's function, the electronic density matrix and the electronic Hamiltonian within equal footing of our formalism. As an example, we present numerical results obtained for several molecular electronic devices and show that only few molecular vibrational excitations seem to have an effect on the inelastic tunneling.

**16:42**

**R37 10 Microscopic Current Flow Patterns in Nanoscale Quantum Point Contacts** NA SAI, NEIL BUSHONG, *University of California, San Diego* RYAN HATCHER, *Vanderbilt University* MASSIMILIANO DI VENTRA, *University of California, San Diego* Transport in nanoscale conductors has been studied extensively mainly using the stationary scattering approach. However, the dynamical nature of transport, and in particular, the flow patterns of the microscopic current through a nanoscale junction, have remained poorly understood. We apply a novel time-dependent transport approach [1], which combines closed and finite geometries with time-dependent density functional theory,to study current flow patterns in nanoscale quantum point contacts [2]. The results of both atomistic and jellium calculations show that surface charges form dynamically at the junction-electrode interfaces in both abrupt and adiabatic junctions. The curr ent exhibits some characteristics of a classical hydrodynamic liquid but also displays unique patterns arising from the interaction with the surface charges. We also investigate the effect of the flow velocity, charge density, and lattice structures on the electron dynamics. If time permits we also discuss the effects of the viscosity of the electron liquid [3]. Work supported by DOE (DE-FG02-05ER46204). [1] M. Di Ventra and T.N. Todorov, J. Phys. Cond. Matt. 16, 8025 (2004). [2] N. Bushong, N. Sai and, M. Di Ventra, Nano Lett. (in press). [3] N. Sai, M. Zwolak, G. Vignale, and M. Di Ventra, Phys. Rev. Lett. 94, 186810 (2005 ).

**16:54**

**R37 11 Electron transport in molecular devices** SIMONE PICCININ, *Princeton Univeristy - Department of Chemistry* RALPH GEBAUER, *ICTP - Trieste (Italy)* ROBERTO CAR, *Princeton University - Department of Chemistry* We present an application of a recently proposed quantum-kinetic scheme for non equilibrium transport properties in nanoscale systems, based on a Liouville-master equation for the reduced density operator and combined with a Density Functional Theory description of the electronic structure [1,2]. The systems studied are the well known benzene-dithiol sandwiched between two gold electrodes and the gold quantum point contact. The results we obtain are in general agreement with previous theoretical works and with recent experimental measurements. We analyze the spatial distribution of the current density and the effect of geometrical distortions on the transport properties.

## SESSION R38: SUPERCONDUCTIVITY—OPTICAL SPECTROSCOPY OF CUPRATES: IR HALL EFFECT

**Wednesday Afternoon, 15 March 2006**
**341, Baltimore Convention Center at 14:30**
**John Cerne, University at Buffalo, SUNY, presiding**

**14:30**

**R38 1 Strong correlation effects in the IR Hall Effect in the cuprates: an overview*** H.D. DREW, *University of Maryland* The Hall Effect at infrared frequencies provides a sensitive probe of strong interaction effects in strongly correlated metals. Experimental results show that the strong interaction effects inter the Hall conductivity and the optical conductivity differently in the cuprates [1,2,3]. For hole doping the Hall angle at mid IR frequencies is nearly simple Drude but with a scattering rate that is nearly frequency dependent in contrast to the optical conductivity [1]. The Hall frequency is in good agreement with ARPES results at optimal doping but increases rapidly for underdoped samples in contrast to expectations from ARPES [1,2]. The electron doped cuprates show evidence for density wave gap excitations and are non Drude-like even outside the density wave regime of doping and temperature [3]. A recent theoretical analysis based on the exchange of magnetic excitations that includes vertex corrections in the conductivity appears to account for many of these observations [4]. [1] DC Schmadel, et al., cond-mat/0510793. [2] L Shi, et al., cond-mat/0510794. [3] A Zimmers, et al., cond-mat/0510085. [4] H Kontani, cond-mat/0507664.

*NSF supported

**14:42**

**R38 2 Significant Role of Current Vertex Correction in Optical Conductivity of Strongly Correlated Systems.** SEIICHIRO ONARI, HIROSHI KONTANI, *Nagoya University, Japan* Based on the microscopic Fermi liquid theory, we study DC and AC transport phenomena in strongly correlated systems. We take the current vertex correction (CVC), which is called the backflow in the phenomenological Fermi liquid theory, into account correctly to satisfy the conservation laws. In the vicinity of the antiferromagnetic (AF) quantum critical point (QCP), various transport coefficients show striking deviations from the Fermi liquid-type temperature dependences due to the CVC. Moreover, we find that the frequency dependence of the CVC gives rise to striking deviations of the optical conductivities from the conventional extended-Drude-type functions, when systems is close to the AF-QCP. We explain the important effect of the CVC on the temperature- and frequency-dependences of $\sigma(\omega)$ and $\sigma_{xy}(\omega)$ in strongly correlated systems.

**14:54**

**R38 3 Theory of Optical Conductivity and Hall Conductivity in High-Tc Superconductors** HIROSHI KONTANI, *Nagoya University, Japan* We study AC conductivities in high-Tc cuprates, which offer us significant information to determine the true ground states. We take the current vertex correction (CVC) into account correctly to satisfy the conservation laws in terms of the fluctuation-exchange (FLEX) approximation. The significant role of the CVC on the optical Hall conductivity, $\sigma_{xy}(\omega)$, is confirmed in the presence of strong antiferromagnetic (AF) fluctuations. This fact leads to the failure of the relaxation time approximation (RTA). As a result, experimental highly unusual behaviors, (i) prominent $\omega$ and temperature dependences of the optical Hall conductivity and the optical Hall coefficient, $R_H(\omega)$, and (ii) a simple Drude form of the optical Hall angle, $\theta_H(\omega)$, for a wide range of $\omega$, are satisfactorily reproduced. In conclusion, both DC and AC transport phenomena in (slightly under-doped) high-Tc cuprates can be explained comprehensively in terms of a nearly AF Fermi liquid, without assuming an exotic ground state.

**15:06**

**R38 4 The mid-infrared Hall effect in optimally-doped $Bi_2Sr_2CaCu_2O_{8+\delta}$*** DON SCHMADEL, *Department of Physics, University of Maryland, College Park, Maryland 20742 USA* GENDA GU, *Department of Physics, Brookhaven National Laboratory, Upton, New York 11973 USA* H.D. DREW, *Department of Physics, University of Maryland, College Park, Maryland 20742 USA* Heterodyne polarometry is used to measure the frequency dependence in the mid IR from 900 to 1100 cm$^-$1 and temperature dependence from 35 to 330 K of the normal state Hall transport in single crystal, optimally doped $Bi_2Sr_2CaCu_2O_{8+\delta}$. The results show a simple Drude behavior in the Hall conductivity $\sigma_{xy}$ which stands in contrast to the more complex, extended Drude behavior for the longitudinal conductivity $\sigma_{xx}$. The mid IR Hall scattering rate $\gamma_{xy}$ increases linearly with temperature and has a small, positive, projected intercept at $T = 0$. The longitudinal scatter rate, in contrast, is much larger and exhibits very little temperature dependnece. The Hall frequency indicates a carrier mass which is 6.7 times the band mass and which decrease slighly with increasing frequency. These disparate behaviors are consistent with calculations based on the fluctuation-exchange interaction using current vertex corrections (H Kontani, cond-mat/0507664).

*This research was partially supported by the NSF under Grant No. DMR-0303112.

**15:18**

**R38 5 Infrared Hall effect in underdoped and optimally doped $La_{2-x}Sr_xCuO_4$*** LINGYUN SHI, D. SCHMADEL, H.D. DREW, *University of Maryland, College Park, MD 20742* I. TSUKADA, Y. ANDO, *Materials Science Research Laboratory, CRIEPI, Tokyo, Japan* We report a study of magneto-optical properties in the mid-infrared region of a series of $La_{2-x}Sr_xCuO_4$ samples with hole doping level ranging from severely underdoped ($x = 0.03$) to optimally doped ($x = 0.15$). The Faraday rotation and circular dichroism are measured in a magnetic field of 8 Tesla and in a temperature range between 30K and 300K. The doping and temperature dependence of infrared Hall angle is found to be consistent with a simple Drude model. A significant increase of Hall frequency is observed when the hole doping level is reduced from optimal doping, which is consistent with a drastic reduction of the volume of Fermi surface in the underdoped sample. These results are similar to results of an earlier study of underdoped YBa2Cu3O6+x [L. B. Rigal, et al., Phys. Rev. Lett. 93,137002 (2004)]. Both experiments will be compared with theoretical models of the IR Hall effect.

*The support of NSF grant DMR-0303112 is acknowledged

**15:30**

**R38 6 Far IR Hall Angle Measurements on Single Crystal $Bi_2Sr_2CaCu_20_{8+x}$.*** GREGORY JENKINS, D.C. SCHMADEL, H.D. DREW, *Physics Department, University of Maryland, College Park, MD 20742* GENDA GU, *Department of Physics, Brookhaven National Laboratory, Upton, NY 11973* The far-infrared complex Hall angle was studied in thin optimally doped single crystal $Bi_2Sr_2CaCu_20_{8+x}$ as a continuous function of temperature from 25 to 300 K and at a discrete set of frequencies in the range of 25 cm$^{-1}$ to 175 cm$^{-1}$ using a heterodyne technique. The real part of the inverse Hall angle obeys a temperature power law, $T^n$, where n = 1.65 which is consistent with the dc-value. For the three frequencies below 90 cm$^{-1}$, the Hall frequency is a constant in temperature and frequency to within 20% from $T_C$ up to room temperature. The Hall mass of 2.5 $m_e$ in reasonable agreement with the values found in far IR optical measurements 3.0 $m_e$, ARPES dispersion results along the $(\pi, \pi)$ nodal direction (2.9 $m_e$), and mid IR Hall measurements (2.8 $m_e$) where $m_e$ is the bare electron mass. These results will be compared with theoretical predictions.

*The support of NSF through grant DMR-0303112 is acknowledged.

**15:42**

**R38 7 Infrared Hall Effect in the electron-doped high $T_c$ cuprate $Pr_{2-x}Ce_xCuO_4$** A. ZIMMERS, *Center for Superconductivity Research, Department of Physics, University of Maryland, College Park, Maryland 20742, USA* L. SHI, D. C. SCHMADEL, *Department of Physics, University of Maryland, College Park, Maryland 20742, USA* W. M. FISHER, R. L. GREENE, *Center for Superconductivity Research, Department of Physics, University of Maryland, College Park, Maryland 20742, USA.* H. D. DREW, *Department of Physics, University of Maryland, College Park, Maryland 20742, USA* We have performed infrared Hall measurements ($\sigma_{xy}$) as a function of temperature, frequency (950-1100 cm$^{-1}$) and wide doping range of $Pr_{2-x}Ce_xCuO_4$. Previous measurements have shown that electron-doped materials present clear evidence for a gap in the $\sigma_{xx}$ spectrum [1] and the DC Hall effect [2] for samples below both a critical doping of $x_c \sim 0.17$, a characteristic temperature $T_W$ and an energy $\omega_W$. Our results lend further support to a density wave state in underdoped PCCO. However, these results demonstrate that $\sigma_{xy}$ exhibits strong deviations from the extended Drude model in contrast to its success for $\sigma_{xx}$ in overdoped $Pr_{2-x}Ce_xCuO_4$ and in hole-doped cuprates. The work at University of Maryland was supported by NSF grants DMR-0352735 and DMR-0303112. [1] A. Zimmers *et al.*, Europhys. Lett., **70** (2), 225 (2005). [2] Y. Dagan *et al.*, Phy. Rev. Lett. **92**, 167001 (2004).

**15:54**

**R38 8 Extended frequency dependence of the infrared Hall Effect in electron-doped high $T_c$ cuprate $Pr_{2-x}Ce_xCuO_4$** M. HOUSEKNECHT, G. ACBAS, M.-H. YANG, J. CERNE, *Physics Dept., Univ. at Buffalo, SUNY, Buffalo, NY* A. ZIMMERS, L. SHI, D.C. SCHMADEL, R.L. GREENE, H.D. DREW, *Physics Dept., Univ. of Maryland, College Park, MD* Although the infrared longitudinal conductivity $\sigma_{xx}$ in $Pr_{2-x}Ce_xCuO_4$ can be modeled using a Drude model which includes density wave (DW) excitations at low temperatures and low doping concentrations (Zimmers, PRB 2004), the infrared Hall conductivity $\sigma_{xy}$ exhibits behavior (Zimmers, cond-mat/0510085) that is not consistent with this model even outside of the DW phase. By measuring the rotation and ellipticity of the polarization of transmitted light through a sample in magnetic fields up to 7 T, the infrared Faraday angle is determined in the 115 to 366 meV (930-3000 $cm^{-1}$) energy range. The Faraday angle is closely related to the Hall angle and $\sigma_{xy}$, which provide a sensitive test of the many-body interactions that could lead to deviations from Drude behavior. Three samples with doping levels of $x = 0.12$, 0.15 and 0.18 are probed at temperatures ranging from 50 K to 300 K. Non-Drude behavior is observed in the Faraday angle, which also changes sign as a function of frequency and temperature from electron-like to hole-like as expected from the hole-like underlying Fermi surface. Supported by the Research Corporation Cottrell Scholar Award (UB), NSF CAREER Award (UB), NSF DMR-0352735 (UMCP) and NSF DMR-0303112 (UMCP).

**16:06**

**R38 9 Raman scattering study of low energy charge dynamics in the normal state of $Pr_{2-x}Ce_xCuO_{4-\delta}$** G. BLUMBERG, B. S. DENNIS, *Bell Labs, Lucent Technologies* M. M. QAZILBASH, R. L. GREENE, *Center for Superconductivity Research, University of Maryland, College Park* Some of the normal state properties of the electron-doped (n-doped) superconducting cuprates $R_{2-x}Ce_xCuO_{4-\delta}$(R = La, Pr, Nd, Sm) are different from those of the hole-doped (p-doped) cuprates. In the n-doped cuprates at optimal doping (x = 0.15) the dc resistivity is a quadratic function of temperature whereas in the p-doped cuprates it is linear in temperature. The charge carriers in p-doped cuprates are holes whereas in the n-doped cuprates both electronlike and holelike carriers exist near optimal doping; the electronlike carriers reside near ( $\pm \pi$/a, $\pm \pi$/4a) and ( $\pm \pi$/4a, $\pm \pi$/a) regions and the holelike carriers reside near ( $\pm \pi$/2a, $\pm \pi$/2a) regions of the Brillouin Zone. We have performed temperature and doping dependent Raman scattering study in the normal state of the n-doped superconducting cuprate $Pr_{2-x}Ce_xCuO_{4-\delta}$. Using polarized light we have isolated the low energy dynamics of the electronlike and holelike carriers. We compare Raman data in the $B_{1g}$ and $B_{2g}$ channels to dc resistivity and discuss the implications.

**16:18**

**R38 10 Theory of Low-Temperature Hall Effect in Electron-Doped Cuprates*** JIE LIN, *Columbia University* ANDREW MILLIS, *Columbia University* A mean field calculation of the $T \rightarrow 0$ limit of the Hall conductance of electron-doped cuprates such as $Pr_{2-x}Ce_xCuO_{4+\delta}$ is presented. The data are found to be qualitatively consistent with the reconstruction of the Fermi surface expected upon density wave ordering. The magnitude of the density wave gap is found to be large. The Hall resistance exhibits a nonanalyticity at the quantum critical point for density wave ordering, but the amplitude of the anomaly is found to be unobservably small. The quantum critical contribution to $R_H(B)$ is determined. Quantitative discrepancies between calculation and data remain, suggesting that the experimental doping is not identical to the *Ce* concentration *x*.

*This work was supported by NSF-DMR-0431350

**16:30**

**R38 11 Infrared Hall effect measurement of correlated metal $Na_{0.75}CoO_2$*** E.J. CHOI, *Department of Physics, Univ. of Seoul, 130-743, Korea* A. ZIMMERS, *Department of Physics and Center of Superconductor Research, University of Maryland, College Park, MD 20742* L. SHI, A. SOUSHKOV, H.D. DREW, J.H. CHO, *Department of Physics, Pusan National University, Pusan, Korea* $Na_xCoO_2$ has a layered Co-O plane where Co ions form a triangular bonding block in contrast with the square Cu moments of HTSC Cu-O plane. With varying x, the compound exhibits rich phases like superconductivity (x=0.3, $H_2O$ intercalted), charge-ordering (x=0.5) and Curie-Weiss metal (x$\sim$ 0.7). $Na_xCoO_2$ thin film (x=0.75) was grown on $SrTiO_3$ substrate using PLD method. Resistivity and dc-Hall effect show same temperature dependence as those of single crystal. We studied ac Hall effect by measuring the complex Faraday rotation $\theta_F$ at infrared frequency (1100 $cm^{-1}$) for 30K$>$ T$<$ 300K and in magnetic fields up to 8 Tesla. As T decreases, real part of $\theta_F$ shows a slop change where dRe($\theta_F$)/dT from negative to positive sign at T=100K. At the same T, Im($\theta_F$)shows a dispersive structure. This anomaly comes from $\sigma_xy$ while $\sigma_xx$ is monotonic with T. Possible origin of the unusual infrared Hall conductivity sigma$_xy$ is considered in terms of spin density wave, Na-ordering, and electronic Kagome lattice.

*Work supported by KRF2005-C00137, CSCMR and NSF

**16:42**

**R38 12 Magneto-optical studies of high-$T_c$ cuprates in 33 Tesla** S.V. DORDEVIC, *The University of Akron* A. GOZAR, I. BOZOVIC, C.C. HOMES, G.D. GU, W. SI, *Brookhaven National Lab* Y.J. WANG, *National High Magnetic Field Laboratory* We will report results of our magneto-optical studies of high- $T_c$ cuprates in high magnetic field. An optimally doped LSCO thin film with thickness of 78 nm and $T_c$ = 41 K was studied in transmission geometry with magnetic field of 33 Tesla. The measurements have been performed in the mid-IR part of the spectrum, and at temperatures both below and above Tc. In addition, several other cuprates families, such as YBCO, Bi2212, LBCO and NCCO, have been studied in reflection geometry, with magnetic field of 18 Tesla applied perpendicular to $CuO_2$ planes. In all studied samples we find extreme insensitivity of optical properties to external magnetic field. The results will be discussed in the context of existing theoretical models.

**16:54**

**R38 13 c-axis magneto optics and vortex dynamics of underdoped YBCO** A.D. LAFORGE, K.S. BURCH, *University of California, San Diego* W.J. PADILLA, *Los Alamos National Laboratory* KOUJI SEGAWA, YOICHI ANDO, *Central Research Institute of Electric Power Industry, Japan* D.N. BASOV, *University of California, San Diego* c-axis reflectance measurements have been carried out on high quality single crystals of $YBa_2Cu_3O_x$ at two dopings, x = 6.65 and x = 6.75, with magnetic fields oriented both parallel and perpendicular to the $CuO_2$ plane. Fields applied parallel to the plane induced several interesting effects at temperatures below the superconducting transition, in-

cluding a strong suppression of superfluid density and the appearance of a new mode at frequencies below the Josephson plasma resonance (JPR). This mode is field-dependent both in magnitude and position, shifting to higher energies with increasing field. Here it is analyzed within several models of vortex dynamics, including that of Tachiki, Koyama, and Takahashi. Application of fields perpendicular to the plane creates a shift in the JPR frequency, as predicted by the TKT model.

**SESSION R39: SUPERCONDUCTIVITY—SODIUM COBALTATE**
**Wednesday Afternoon, 15 March 2006**
**342, Baltimore Convention Center at 14:30**
**Igor Mazin, Naval Research Laboratory, presiding**

**14:30**
**R39 1 Charge-fluctuation excitations in $Na_{1/3}CoO_2 \cdot yH_2O$*** O.D. RESTREPO(1), A.G. EGUILUZ(1), *University of Tennessee and CMSD,ORNL (2)* K.-W. LEE, J. KUNES, W.E. PICKETT(3), *University of California, Davis* We report a theoretical study of the electron-hole excitation spectrum of the hydrated superconductor $Na_{1/3}CoO_2 \cdot yH_2O$. We use a paramagnetic LDA ground state as our starting point, and calculate the dynamical density-response function using time- dependent density-functional theory. Our results are compared with calculations for the parent compound $Na_{1/3}CoO_2$ and with recent electron-energy loss spectroscopy (EELS) experiments reported by H. X. Yang et al. (PRB 72, 075106 (2005)). Interestingly, the dielectric function obtained from our ab-initio calculations differ appreciably, in the key spectral region, from the one extracted from the experimental loss function by H. X. Yang et al. In fact, our dielectric function shows better qualitative correspondence with the loss data; this finding highlights the relevance of ab-initio calculations for the study of the experimental manifestation of the electronic structure. The physics of the prominent peaks in the loss spectra is discussed; we identify signatures of the underlying electronic structure in the hydrated compounds. *DOE-CMSN PCSCS collaboration. (1) Supported by NSF ITR-DMR 0219332 (2) Managed by UT-Battelle for the U.S. DOE under contract DE- AC05-00OR22725. (3) Supported by DOE Grant DE-FG03-01ER45876

**14:42**
**R39 2 Charge and Spin Ordering in Insulator $Na_{0.5}CoO_2$: Effects of Correlation and Symmetry** KWAN-WOO LEE, WARREN PICKETT, *University of California, Davis* The discovery by Takada and coworkers of superconductivity in $Na_{0.3}CoO_2 \bullet 1.3 H_2O$ near 5K has led to extensive studies of the rich variation of properties in the $Na_xCoO_2$ system ($0.2 \leqslant x \leqslant 1$), which has a triangular lattice of Co sites and a layered structure. In addition, specifically at $x=0.5$, the system has been observed to undergo a charge disproportionation ($2Co^{3.5+} \rightarrow Co^{3+} + Co^{4+}$) and metal-insulator transition at 50 K, while the rest of the phase diagram is metallic. We will present results of studies of charge disproportionation and charge- and spin-ordering in insulating in $Na_{0.5}CoO_2$, applying ab initio band theory including correlations due to intra-atomic repulsion. Various ordering patterns (zigzag and two striped) for four-Co supercells are analyzed before focusing on the observed ''out-of-phase stripe'' pattern of antiferromagnetic $Co^{4+}$ spins along charge-ordered stripes. This pattern relieves frustration and shows distinct analogies with the cuprate layers: a bipartite lattice of antialigned spins, with axes at 90° angles. Substantial distinctions with cuprates are also discussed, including the tiny gap of a new variant of ''charge transfer'' type within the Co 3*d* system. [1] K. Takada et al., Nature **422**, 53 (2003). [2] M. L. Foo et al., Phys. Rev. Lett. **92**,247001 (2004). [3] K.-W. Lee, J. Kunes, P. Novak, and W. E. Pickett, Phys. Rev. Lett. **94**, 026403 (2005). [4] K.-W. Lee and W. E. Pickett, cond-mat/0510555.

**14:54**
**R39 3 Ab Initio Study on Na Ordering and its Relation to the Electronic/Magnetic Properties of P2-NaCoO2 Thermoelectrics** YING SHIRLEY MENG, *Massachusetts Institute of Technology* ANTON VAN DER VEN, *University of Michigan* MARIA CHAN, *M.I.T.* GERBRAND CEDER, *M.I.T.* The unusual electronic properties of NaxCoO2 make it a material of considerable interest. The system displays an unusual combination of high Seebeck coefficient and low metallic resistance. NaxCoO2 is also an interesting material on which to test our fundamental knowledge of mixed valence transition metals. NaxCoO2 is a mixed valence system with a fraction of x Co4+ and (1- x) Co3+ ions. Because of the high mobility of Na and large vacancy concentration, Na-vacancy ordering is likely in NaxCoO2. This ordering breaks the symmetry on the Co sublattice and may assist in charge ordering of Co3+ and Co4+. Mixed Co3+/Co4+ systems tend to display rich physics as they are often close to spin transitions and metal insulator transitions. In this study, we use both standard Density Functional Theory (DFT) in the Generalized Gradient Approximation (GGA) as well as GGA+U calculations to investigate the possible Na-vacancy and charge-ordered structure of P2-NaxCoO2 throughout the sodium composition range. We have identified new ground state structures at Na concentrations 0.11, 0.75 and 0.80. We have also found a strong coupling between the Na-vacancy ordering and Co3+/Co4+ charge ordering in the system. Such knowledge is crucial for understanding the thermoelectric properties of this material and similar mixed valence oxides.

**15:06**
**R39 4 Electron Correlation and Fermi Surface Topology of $Na_xCoO_2$** SEN ZHOU, *Boston College* MENG GAO, *Boston College* HONG DING, *Boston College* PATRICK LEE, *Massachusetts Institute of Technology* ZIQIANG WANG, *Boston College* The electronic structure of $Na_xCoO_2$ revealed by recent photoemission experiments shows important deviations from band theory predictions. The six small Fermi surface pockets predicted by LDA calculations have not been observed as the associated $e_g'$ band fails to cross the Fermi level for a wide range of sodium doping concentration $x$. In addition, significant bandwidth renormalizations of the $t_{2g}$ complex have been observed. We show that these discrepancies are due to strong electronic correlations by studying the multi-orbital Hubbard model in the Hartree-Fock and strong-coupling Gutzwiller approximation. The quasiparticle dispersion and the Fermi surface topology obtained in the presence of strong local Coulomb repulsion are in good agreement with experiments.

**15:18**

**R39 5 Systematic doping evolution of quasiparticle mode and Fermi surface topology in $NaxCoO_2$** DONG QIAN, *Department of Physics, Princeton University* A.V. FEDOROV, ZAHID HUSSAIN, *Advanced Light Source, Lawrence Berkeley National Laboratory* R.J. CAVA, *Department of Chemistry, Princeton University* N.L. WANG, *Beijing National Laboratory for Condensed Matter Physics, Institute of Physics, Chinese Academy of Sciences* M.Z. HASAN, *Department of Physics, Princeton University* We have carried out a detailed and systematic state-of-the-art photoemission study of $NaxCoO_2$ over a wide range of doping. The Fermi velocity is found to be weakly anisotropic and small leading to a strongly suppressed quasiparticle bandwidth as a universal behavior in all dopings. No surface state or Ruthanate-type reconstruction is observed. Systematic studies show that the 2-D Fermi-surface area evolves according to the Na doping count only below x=0.5. The measured Fermi surface topology near superconducting Na doping kinematically allows for commensurate fluctuations (charge or lattice) as potential competing instabilities. The temperature evolution of quasiparticles will be discussed in addition.

**15:30**

**R39 6 Correlation Effects and Magnetism in $Na_xCoO_2$** MENG GAO, SEN ZHOU, HONG DING, ZIQIANG WANG, *Boston College* Correlation effects are known to be important for the electronic structure and the Fermi surface topology of $Na_xCoO_2$ [ref to prl of Zhou et al.]. Here we study magnetic properties of $Na_xCoO_2$ based on the multi-orbital Hubbard model for the cobalt $t_{2g}$ electrons in weak and strong coupling limits using Hartree-Fock and Gutzwiller approximations. Both commensurate and incommensurate magnetic order is considered. We present the phase diagram in the parameter space of local Coulomb repulsion and Hunds rule coupling for different sodium doping concentrations. The interplay between the correlation effects and Fermi surface nesting on the magnetic properties will be discussed.

**15:42**

**R39 7 Thermal Expansion Measurements of the Antiferromagnetic Transition in $Na_xCoO_2$ Single Crystals (x=0.75 and 0.80)*** C. A. M. DOS SANTOS, *Departamento de Engenharia de Materiais - FAENQUIL and Montana State University* J. J. NEUMEIER, R. K. BOLLINGER, *Montana State University* Y.-K. YU, *NIH National Center for Biotechnology Information* R. JIN, D. MANDRUS, *Oak Ridge National Laboratory* Thermal expansion, heat capacity and magnetic susceptibility measurements of $Na_xCoO_2$ (x=0.75 and 0.80) single crystals are reported. The results show second-order antiferromagnetic transition near $T_N = 22$ K. The high-resolution thermal expansion measurements, performed with a fused quartz dilatometer cell in both basal plane and c-axis directions, reveal strong anisotropy that is attributed to the hexagonal structure. Above and below $T_N$, the thermal expansion coefficients and specific heat measurements exhibit λ-like peaks which are similar to those reported for other antiferromagnetic compounds. Analysis of the critical behavior for both samples will be discussed.

*Research supported by the Brazilian agency CAPES (Grant 0466/05-0) and NSF (DMR 0504769).

**15:54**

**R39 8 Specific-heat study for the coupling between two superconducting order parameters in $Na_xMn_zCo_{1-z}O_2yH_2O$.** C.P. SUN, *Dept. of Physics, Natl. Sun Yat Sen University, Taiwan* J. -Y. LIN, *Inst. of Physics, Natl. Chiao Tung University, Taiwan* C.L. HUANG, *Dept. of Physics, Natl. Sun Yat Sen University, Taiwan* C.-J. LIU, J.S. WANG, *Natl. Changhua University of Education, Taiwan* H.D. YANG, *Dept. of Physics, Natl. Sun Yat Sen University, Taiwan* The substitution of Mn doping into the Co site, has been confirmed by the Mn *L*-edge XANES and EXAFS spectra, is performed by the specific-heat measurement with and without magnetic field. Due to the possible coexistence of isotropic and nodal-line gap, the two superconducting order parameters should exhibit different $T_c$ suppression rate by the doping impurity. Without field, two anomalies are seen below $T_c$, $\sim$ 4 K determined from magnetization, may be caused by different superconducting contributions due to the impurity effect and then merge into one under higher magnetic field ( $\sim$ 1T). Schottky effect needs to be taken into account in the normal state.

**16:06**

**R39 9 Transport Properties and X-ray Absorption Spectroscopy in Layered Cobaltate $Na_xCoO_2$ thin films** W. J. CHANG, *Department of Electrophysics, National Chiao Tung University* J. Y. JUANG, J.-Y. LIN, *Institute of Physics, National Chiao Tung University* C. M. LEE, C.-M. HUANG, J. M. CHEN, C.-H. HSU, $Na_xCoO_2$ ($x \sim 0.7$) thin films ( $\sim$ 200 nm) were fabricated on sapphire (0001) substrates via lateral diffusion of sodium into $Co_3O_4$ (111) epitaxial films. From the results of x-ray diffraction and in-plane resistivity it$\rho_{ab}$, the single phase and the metallic behaviors of these $Na_xCoO_2$ films were identified, and consisting with the results of single crystals [1] and Ohta's films [2]. The anomalous Hall effect and the magnetoresistance were also measured in $Na_xCoO_2$ thin films. In addition, the O 1*s* x-ray absorption spectra of thin films show different anisotropy to those of single crystals. The electronic structures of $Na_xCoO_2$ single crystals and thin films will be discussed to investigate the splitting of $e_g$ and $t_{2g}$ states in Co 3*d* bands of $Na_xCoO_2$ thin films. *This work was supported by the National Science Council of Taiwan, under Grant Nos. NSC-94-2112-M-009-006. [1] Maw Lin Foo et al., Phys. Rev. Lett. **92**, 247001 (2004). [2] Hiromichi Ohta et al., Crystal Growth & Design **5**, 25 (2005).

**16:18**

**R39 10 Variational Monte Carlo study of pairing symmetries of Na0.3CoO2.1.3H2O*** RUI FAN, YONG-QIANG WANG, HAI-QING LIN, *Institute of Theoretical Physics and Physics Department, The Chinese University of Hong Kong, Hong Kong, China* To investigate possible pairing symmetries of Na0.3CoO2.1.3H2O, we study the single band extended Hubbard model on triangular lattice with variational Monte Carlo method. For the on site s-wave, the extended s-wave, the d-wave, the f-wave and the extended-f wave parings, we use the corresponding BCS type mean field wave functions with Jastrow factors as our trial wave functions. We found that in a suitable parameters region, the extended f-wave pairing is stabilized by the nearest-neighbor Coulomb interaction V. In order to further investigate the true ground state of this system we use the constrained path Monte Carlo (CPMC) method to calculate different correlation function in the ground state.

*This work is supported by RGC Projects CUHK

**16:30**

**R39 11 Band Structures, Fermi Surface Topology and Superconductivity in $Na_xCoO_2 \cdot yH_2O$: Effects of the trigonal $CoO_6$ distortion** MASAHITO MOCHIZUKI, MASAO OGATA, *Department of Physics, University of Tokyo* In the recently discovered Co-oxide superconductor $Na_xCoO_2 \cdot yH_2O$, the edge-shared $CoO_6$ octahedra are trigonally contracted along the *c*-axis in the $CoO_2$-plane. We study how this $CoO_6$ distortion affects the magnetic properties and superconductivity in this compound by analyzing the multiorbital Hubbard model using the fluctuation-exchange approximation. It is shown that through generating the trigonal crystal field, the distortion pushes the Co $e_g'$ bands up and consequently gives rise to the hole-pocket Fermi surfaces, which have been predicted in the band calculations. As the distortion increases, the hole pockets are enlarged and the ferromagnetic fluctuation as well as the pairing instability increases, which is in good agreement with recent NQR results.

**16:42**

**R39 12 Photoemission study on core levels of NaxCoO2** JIHUA MA, *Department of Physics, Boston College, Chestnut Hill, MA 02467* HONGBO YANG, *Condensed Matter Physics & Material Science Department, Brookhavan National Laboratory, Upton, NY 11973* ZHIHUI PAN, *Department of Physics, Boston College, Chestnut Hill, MA 02467* A.V. FEDOROV, *Advanced Light Source, Lawrence Berkeley National Laboratory, Berkeley, CA 94720* R. JIN, B.C. SALES, D. MANDRUS, *Condensed Matter Science Division, Oak Ridge National Laboratory, Oak Ridge, TN 37831* HONG DING, *Department of Physics, Boston College, Chestnut Hill, MA 02467* A Comprehensive study on Na 2p and Co 3p core levels of NaxCoO2 is carried out by photoemission. A surface component of Na 2p core level is found. By comparing the surface state and bulk state at different emission angles, different photon energies and different doping levels, we not only extract the electron escape length in this system, but also discover other interesting features.

**16:54**

**R39 13 Determination of $t_{2g}$ Complex in $Na_xCoO_2$ by Angle-Resolved Photoemission Spectroscopy** HONGBO YANG, *Brookhaven National Laboratory* JIHUA MA, ZHIHUI PAN, *Boston College* ALEXEI FEDOROV, *Lawrence Berkeley National Laboratory* JONGYIN JIN, BRIAN SALES, DAVID MANDRUS, *Oak Ridge National Laboratory* ZIQIANG WANG, HONG DING, *Boston College* A systematic investigation on $t_{2g}$ complex in $Na_xCoO_2$ is carried by ARPES. By taking advantage of the matrix element effect, we recover and trace the dispersion of all three $t_{2g}$ bands for different Na concentration ($x = 0.3 \sim 0.7$). The dispersion ''kink'' we observed before is found to be cause by the hybridization between $a_{1g}$ and $e_g'$ bands. This band hybridization forms a narrow band near the Fermi level, which causes a large mass renormalization. The width of the non- hybridized bands is about half of the one predicted by LDA calculations, which is possibly due to the correlation effect.

**17:06**

**R39 14 Possible coexistence of *s*-wave and unconventional pairing in hydrated $Na_xCoO_2$: a new insight from impurity effects*** JIUNN-YUAN LIN, Y.-J. CHEN, *Institute of Physics, National Chiao Tung University, Hsinchu 300, Taiwan* C.-J. LIU, J.-S. WANG, *Department of Physics, National Changhua University of Education, Changhua 50007, Taiwan* C. P. SUN, H. D. YANG, *Department of Physics, National Sun Yat Sen University, Kaohsiung 804, Taiwan* S. W. HUANG, *Department of Electrophysics, National Chiao Tung University, Hsinchu 300, Taiwan* J. M. CHEN, J. M. LEE, J. F. LEE, D. G. LIU, *National Synchrotron Radiation Research Center, Hsinchu 300, Taiwan* Impurity effects on $T_c$ were known to provide indispensable information in many novel superconductors. To shed light on the symmetry of the superconducting order parameter in hydrated $Na_xCoO_2$, the Mn doping effects have been studied. X-ray absorption spectroscopy reveals that the doped Mn impurities occupy the Co sites and have a valance close to 4+. Impurity scattering by Mn is in the unitary limit that, however, does not lead to strong $T_c$ suppression. This absence of the strong impurity effects on $T_c$ is not consistent with the simple picture of a sign-changing order parameter. For reconciliation among all existing experiments, the model of coexistence of *s*-wave and unconventional pairing is proposed.

*This work was support by the National Science Council of Taiwan, under grants: NSC 94-2112-M-009-006, 94-2112-M-018-001, and 94-2112-M-110-010.

**17:18**

**R39 15 Effect of heavy water intercalation in sodium cobaltate.** CINZIA METALLO, *University of Tennessee* TAKESHI EGAMI, *University of Tennessee, Oak Ridge National Laboratory* THOMAS PROFFEN, *Los Alamos National Laboratory* DAVID MANDRUS, *Oak Ridge National Laboratory* BRIAN SALES, *Oak Ridge National Laboratory* RONGYING JIN, *Oak Ridge National Laboratory* Superconductivity in the hydrated compound $Na_xCoO_2yH_2O$ (x=0.35, y=1.3) is directly related to water intercalation. Nevertheless, so far, no clear explanation of the effect of water on the superconducting mechanism has been given. Here we present our study on deuterated sodium cobaltate $Na_xCoO_2yD_2O$ (x=0.35, y=1.4) at two different temperatures, T=15K, 100K. Neutron diffraction data were analyzed using the PDF technique. The PDF of $Na_xCoO_2yD_2O$ was compared with the PDF of heavy water. The diffraction spectra at both temperatures show a weak D-D correlation, and a pronounced D-O correlation. The weakened D-D correlations imply that the dynamics of the hydrogen bond is modified. This increases the dielectric response, and may enhance the electron-phonon coupling. Our results suggest a modification of the geometry of the heavy water molecules inserted in Na $_xCoO_2$, and subsequently a possible active role of water in setting the superconducting state.

**SESSION R40: FOCUS SESSION: PATHWAYS TO PRACTICAL QUANTUM COMPUTING II**
**Wednesday Afternoon, 15 March 2006; 343, Baltimore Convention Center at 14:30**
**Juan Pablo Paz, Los Alamos National Laboratory, presiding**

*Invited Papers*

**14:30**
RAYMOND LAFLAMME, *Department of Physics, University of Waterloo*

This abstract was not received electronically.

*Contributed Papers*

**15:06**
**R40 2 Generating Spin Echoes in Dipolar Solids with $\pi$-Pulses: More is Different** DALE LI, *Yale University Department of Physics* YANQUN DONG, *Yale University Department of Physics* RONA RAMOS, *Yale University Department of Physics* ANATOLY DEMENTYEV, *Yale University Department of Physics* SEAN BARRETT, *Yale University Department of Physics* NMR spin echo measurements of $^{13}C$ in $C_{60}$, $^{89}Y$ in $Y_2O_3$, and $^{29}Si$ in Silicon are shown to defy conventional expectations when more than one $\pi$-pulse is used. Multiple $\pi$-pulse echo trains may either freeze-out or accelerate the dipolar decay of the signal, depending upon $\pi$-pulse phase, which suggests a connection to quantum dynamical decoupling and the formation of quantum Zeno subspaces. Exact quantum calculations (without a spin bath) reveal an intrinsic cause for these coherent phenomena: the dipolar coupling has a many-body effect during any real, finite pulse.

**15:18**
**R40 3 From Large to Small Spin Systems: Exploring Many-body Effects in NMR** YANQUN DONG, *Department of Physics, Yale University* DALE LI, *Department of Physics, Yale University* RONA RAMOS, *Department of Physics, Yale University* SEAN BARRETT, *Department of Physics, Yale University* NMR multi-pulse spin echo measurements on different nuclei and different samples show a dramatic Pulse Sequence Sensitivity (PSS): the multiple pi-pulse echo trains may either freeze out or accelerate the dipolar decay of the signal depending upon pi pulse phase. Finite-pulse spin simulations on small spin systems (7 spins) also show a tiny PSS. We propose that the dramatic PSS in experiments may be due to many-body effects during the finite pi pulses. If this is the case, the PSS should be less in small spin systems. This idea can be tested by performing spin echo experiments on small spin systems. The liquid crystal 5CB has a nematic phase, which enables the molecules to act like isolated spins systems in NMR. Since each molecule has 19 $^1H$ spins, this is an attractive system for our test. I will present experimental results on 5CB, and discuss their implication on our model.

**15:30**
**R40 4 Observation of Anomolously Long-Lived Spin Echoes in a Dense Dipolar Spin System** RONA RAMOS, YANQUN DONG, DALE LI, SEAN BARRETT, *Yale University, Department of Physics* Continuing the investigation of anomolously long-lived spin echoes found in multipulse $^{29}Si$ NMR experiments, similar proton NMR experiments were performed on adamantane ($C_{10}H_{16}$, a molecular solid that tumbles about its fcc lattice sites). In contrast to the dilute dipolar silicon samples from previous experiments [A.E. Dementyev, D. Li, K. MacLean, S.E. Barrett, Phys. Rev. B 68, 153302 (2003).], adamantane presents a densely populated, strongly coupled proton spin system in which to probe the basis of this puzzle. Despite these changes, this phenomenon, which defies conventional NMR theory, still remains. This talk will discuss the results of these experiments and its impact on our current understanding of this behavior.

**15:42**
**R40 5 Numerical modeling of the central spin problem using the spin coherent states P-representation** V.V. DOBROVITSKI, *Ames Laboratory and Iowa State University, Ames IA 50011* K.A. AL-HASSANIEH, E. DAGOTTO, *Oak Ridge National Laboratory, Oak Ridge TN, and University of Tennessee, Knoxville TN 37831* B.N. HARMON, *Ames Laboratory and Iowa State University, Ames IA 50011* We analyze decoherence of a central spin coupled to a spin bath (the central spin problem). Theoretical understanding of this process is important for many experiments, such as the recent study of decoherence of the electron spin by the nuclear spins in a quantum dot. To investigate the important non-perturbative decoherence regimes, we developed an efficient mean-field-based method for modeling the spin-bath decoherence. The method is based on the P-representation for the central spin density matrix, which is very useful in quantum optics, but has not been widely applied to quantum many-spin systems. In contrast with the standard time-dependent mean field theory, our method gives excellent agreement with the exact solution. We demonstrate performance of the method for longitudinal and transversal relaxation at different external fields. In particular, by modeling the quantum systems with up to 16000 bath spins, we make controlled predictions for the slow long-time decoherence of the central spin. We thank L. Glazman, M. Lukin, A. Polkovnikov, and J. Taylor for helpful discussions. This work was supported by NSA, ARDA, ARO, and NSF.

**15:54**
**R40 6 The sensitive electrical detection of spin coherence with pulsed electrically detected magnetic resonance** CHRISTOPH BOEHME, *University of Utah, Physics Department, 115 S 1400 E Suite 201, Salt Lake City, Utah 84112-0830, USA* KLAUS LIPS, *Hahn-Meitner-Institut Berlin, Abteilung Siliziumphotovoltaik, 12489 Berlin, Germany* We present a pulsed electrically detected magnetic resonance experiment which allows the very sensitive observation of the coherent evolution of localized electron spins in semiconductors. The experiment takes advantage of spin selection rules of electronic transport transitions which exist for tunneling through localized states of a 20 nm thick disordered silicon buffer layer between a crystalline silicon wafer and an 80 nm thick ZnO surface layer. When coherent spin states of defect pairs are prepared by means of pulsed electron spin resonance, the singlet

content (= the projection of density matrix onto the singlet state) of these states is directly proportional to the additional charge which is transmitted by the interface. Experimental data and the sensitivity limits of this spin measurement technique will be presented. The applicability of this for the readout of silicon based spin quantum information concepts is discussed.

**16:06**

**R40 7 Polarization Requirements for Ensemble Implementations of Quantum Algorithms with a Single Bit Output** BRANDON ANDERSON, *University of Texas at Dallas* DAVID COLLINS, *Bucknell University* We compare the failure probabilities of ensemble implementations of quantum algorithms which use pseudo-pure initial states, quantified by their polarization, to those of competing classical probabilistic algorithms. Specifically we consider a class algorithms which require only one bit to output the solution to problems. For large ensemble sizes, we present a general scheme to determine a critical polarization beneath which the quantum algorithm fails with greater probability than its classical competitor. We apply this to the Deutsch-Jozsa algorithm to determine the critical polarization.

**16:18**

**R40 8 Optimizing quantum gate fidelities using energy-optimal control*** SONIA SCHIRMER, *Univ. of Cambridge* Optimal control theory offers a promising framework for optimizing essential tasks in quantum computing from quantum state preparation to the implementation of quantum gates. It is applicable to a wide variety of systems from atoms and ions to quantum dots, different control mechanisms from all-optical to all-electronic, and allows implementation constraints and dissipation to be accommodated. Most existing approaches focus on the exact implementation of (unitary) quantum gates in a particular model and aim to optimize gate operation times subject to certain assumptions such as arbitrarily fast local operations, weak (inter-qubit) coupling and decoherence, etc. We consider a different paradigm for optimal control focussing on optimizing the overall gate fidelity for a desired gate and fixed gate operation time subject to physical and experimental contraints (including dissipative effects), which may be more appropriate for some systems such as electronically-controlled systems with non-weak, always-on inter-qubit coupling. We discuss the basic framework and illustrate the results using calculations for model systems.

*This work was supported by the Cambridge MIT Institute.

**16:30**

**R40 9 Exact solution of qubit decoherence models by a transfer matrix method.** DIU NGHIEM, *UW-Madison* ROBERT JOYNT, *UW-Madison* QUANTUM COMPUTING UW-MADISON TEAM, A new method for the solution of the behavior of an enesemble of qubits in a random time-dependent external field was found. In this method the forward evolution in time is governed by a transfer matrix whose eigenvalues determine the various decoherence times. The method provides an exact solution in cases where the noise is piecewise constant in time. It can apply to a realistic model of decoherence of electron spins in semiconductors as well. Results are obtained for the non-perturbative regimes of the models, and we see a transition from weak relaxation to overdamped behavior as a function of noise anisotropy.

**16:42**

**R40 10 Quantum kinetics of dynamical decoupling** LEONID P. PRYADKO, *University of California, Riverside* PINAKI SENGUPTA, *University of Southern California* In an ideal world, coherent control could be made perfect by running infinitely fast sequences of infinitely short pulses. In practice, in each system there are obvious spectral limitations. There is also a large-time limit set by decoherence due to environment coupling. Altogether, this makes pulse shape and sequence design an extremely complicated optimization problem. A systematic way to approach this problem is to consider a cumulant expansion of the evolution operator, treating the strong control fields exactly. The cumulants give the expansion of the effective Hamiltonian in powers of the system Hamiltonian. The locality of the cumulant expansion ensures that the classification by sequence order remains meaningful even for large systems. The corresponding calculation can be done efficiently by constructing a time-dependent perturbation theory expansion on small clusters [1]. Intuitively, refocusing should also remain effective in the presence of low-frequency environment, as long as the parameters of the system Hamiltonian are varying slowly compared to the refocusing period $\tau$. A systematic study of this effect will be presented, based on the Floquet analysis of the non-Markovian quantum kinetic (master) equation for the open multi-qubit system in the presence of continuous refocusing fields exact up to 2nd order in the cumulant expansion [2]. [1] P. Sengupta and L. P. Pryadko, Phys. Rev. Lett. **95**, 037202 (2005). [2] L. P. Pryadko and P. Sengupta, quant-ph/0510001 (2005).

**16:54**

**R40 11 Enhanced Convergence and Robust Performance of Randomized Dynamical Decoupling** LEA SANTOS, LORENZA VIOLA, *Dartmouth College* Dynamical decoupling methods consist of repetitive sequences of control operations, whose net effect is to coherently modify the natural target dynamics to a desired one. In addition to standard deterministic schemes, randomized decoupling strategies have been recently introduced. Here, we exhibit clear evidence of the benefits of randomization in reducing the effects of undesirable couplings. For control systems which are either time-varying or require decoupling cycles involving a large number of operations, we find that simple randomized protocols offer superior convergence and stability as compared to high-level deterministic designs, including combinatorial and concatenated methods. We also show how significant improvements may be achieved for long interaction times by combining deterministic and stochastic features into new hybrid decoupling schemes.

**17:06**

**R40 12 Resurrection of Schrödinger Cat** JAE-SEUNG LEE, ANATOLY KHITRIN, *Department of Chemistry, Kent State University, Kent, Ohio 44242-0001* The most striking difference between quantum and classical systems is the ability of quantum objects to be in a superposition state. A system in a superposition of macroscopically distinct states (italive and itdead states of the ''Schrödinger cat'') would demonstrate highly unusual behavior. Cat states are the central elements in recent proposals on high-precision spectroscopy, amplified quantum detection and measurement. Quantum decoherence is the major obstacle in building practical devices which could revolutionize high-precision measurements or information processing. Here we experimentally demonstrate that quantum state of a system can be recovered after the state is destroyed by uncontrollable natural decoherence. The physical system used in this experiment is a cluster of seven

dipolar-coupled nuclear spins of single-labeled $^{13}$C-benzene oriented in liquid crystal. After decoherence of the cat state, superposition of states with all spins up (alive) and all spins down (dead), information stored in a single ancillary spin ($^{13}$C) is used to bring the protons subsystem into the italive state, while the excess entropy produced by decoherence is transferred to the ancillary spin.

**17:18**

**R40 13 Statistical performance of ensemble quantum computers in search algorithms** DAVID COLLINS, TOMASZ KOTT, *Physics and Astronomy Department, Bucknell University* We consider the statistical performance of ensemble quantum computers applied to search algorithms. In particular we consider algorithms implemented on pseudo pure initial states and determine the initial polarization required so that the quantum algorithm outperforms classical probabilistic competitors in terms of failure probabilities.

**SESSION R41: FOCUS SESSION: DIELECTRIC, FERROELECTRIC, AND PIEZOELECTRIC OXIDES IV**
**Wednesday Afternoon, 15 March 2006**
**344, Baltimore Convention Center at 14:30**
**Maitri Warusawithana, Penn State University, presiding**

***Contributed Papers***

**14:30**

**R41 1 High-quality Thin Single-Crystal Y2O3 films Grown on Si (111)** C.-W. NIEH, W.-C. LEE, Z.-K. YANG, Y.-J. LEE, PEN CHENG, T.-D. LIN, M. HONG, *Dept. Mat. Sci. Eng., Natl Tsing Hua U, Taiwan* J. KWO, *Dept. of Phys., Natl Tsing Hua U, Hsinchu, Taiwan* C.-H. HSU, *Natl Synchrotron Rad. Res. Ctr, Taiwan* High-quality nano thick ( $\sim$ 3nm) single-crystal Y2O3 films have been MBE-grown epitaxially on Si (111) despite a 2% lattice mismatch. Studies carried out by x-ray diffraction, x-ray reflectivity, and cross-sectional HRTEM show the excellent structural properties. In-situ RHEED was used to monitor the growth quality, showing a sharp pattern of a (4x4) reconstruction. The strong oscillations of x-ray reflectivity and Pendellosung fringes surrounding the Y2O3 diffraction peaks point out that the film surfaces and the oxide/Si interfaces are atomically sharp and uniform. A record small FWHM of 0.01 degree in rocking scans was observed at Y2O3 (444), indicating the excellent quality of the nano films. The films are well aligned with the substrate with an orientation relationship of Si (111) // Y2O3 (111), and an in-plane expitaxy of Si [-110]// Y2O3 [-101]. In the thickness range of microelectronics applications, the nano Y2O3 layers have achieved a degree of perfection rarely observed in heterostructures of oxide/semiconductor.

**14:42**

**R41 2 Comparison of the Surface Structures of SrTiO3 (100) and BaTiO3 (100).** D. LI, *University of Pennsylvania* M. NIKIFOROV, DAWN BONNELL, While much research has been focused towards understanding the atomic structures on SrTiO3 surfaces, controversy still remains over the origin of the reconstructions. This talk will provide a rational description of the driving forces for previously observed and newly observed reconstructions on the (100) surface and compare these to analogous structures that occur on BaTiO3 (100). The degree to which the potential for ferroelectric ordering influences surface reconstruction will be discussed.

**14:54**

**R41 3 Coverage and bonding of thin, buried epitaxial $SrTiO_3$ on Si(100)** LENA FITTING, *Applied and Engineering Physics, Cornell University* VENUGOPALAN VAITHYANATHAN, *Department of Material Science and Engineering, Pennsylvania State University* MELANIE JONES, *Applied and Engineering Physics, Cornell University* DARRELL G. SCHLOM, *Department of Material Science and Engineering, Pennsylvania State University* DAVID A. MULLER, *Applied and Engineering Physics, Cornell University* $SrTiO_3$ can be used as a buffer layer for the growth of perovskite oxide heterostructures, opening up possibilities for the incorporation of novel materials into existing Si-based technology. While these layers have been studied during growth, a serious question for such thin layers is if their structure remains unaltered after they have been overgrown. Here, we present results of thin $SrTiO_3$ films grown on Si(100). Scanning transmission electron microscopy (STEM) of the buried structures shows the formation of islands and a non-uniform coverage of the first few monolayers after capping with a-Si. The island size increases if the $SrTiO_3$ film is grown on a $SrSi_x$ seed. An important question that arises is the existence of oxygen vacancies at the interface between the oxide and the substrate. Oxygen deficiency leads to a doping of the empty Ti 3d band in bulk $SrTiO_3$ with electrons, thereby inducing a metallic phase as the Ti formal valence changes from 4+ to 3+. Using electron energy loss spectroscopy in a STEM the Ti valence across the interface is probed on the atomic scale.

**15:06**

**R41 4 Structure of $SrTiO_3$ thin films grown on Si*** C. STEPHEN HELLBERG, *Naval Research Lab* KRISTOPHER ANDERSEN, *Naval Research Lab* Although $SrTiO_3$ films on Si have been extensively studied, the structure of the interface is not yet known. We present first-principles density-functional calculations of the energetics of the numerous proposed structures for the interface. We find that the energetically favored structure is one that has not been previously considered. The structure is consistent with x-ray and TEM probes of the interface. We discuss the implications of the interface for device applications.

*This work was supported by DARPA QuIST (DAAD-19-01-1-0650).

**15:18**

**R41 5 Band offsets of $SrTiO_3$ thin films grown on Si*** KRISTOPHER ANDERSEN, C. STEPHEN HELLBERG, *Naval Research Laboratory* $SrTiO_3$ is a promising material to replace $SiO_2$ as the gate dielectric in metal-oxide-semiconductor field-effect transistors (MOS-FETs). The advantage of $SrTiO_3$ is its large dielectric constant: an order of magnitude greater than other promising oxides. However, the negligible conduction band offset found experimentally for heterostructures of $SrTiO_3$ (001) grown on Si (001) limits the usefulness of $SrTiO_3$ in devices because of leakage current. Here we present first-principles calculations on $Si/SrTiO_3$ heterostructures and investigate ways to modify the band offsets. Experimentally motivated structures are considered,

and the effects of dopants and defects on the electronic structure are quantified.

*This work was supported by DARPA QuIST (DAAD-19-01-1-0650).

**15:30**

**R41 6 COBRA Studies of Ultrathin Ferroelectric Oxide Films*** CODRIN CIONCA, *Applied Physics, University of Michigan* D.P. KUMAH, *Applied Physics, University of Michigan* C-B EOM, *Materials Science and Engineering, University of Wisconsin-Madison* D-M KIM, *Materials Science and Engineering, University of Wisconsin-Madison* Y. YACOBY, *Racah Institute of Physics, Hebrew University, Jerusalem, Israel* D.A. WALKO, *Advanced Photon Source, Argonne National Laboratory* R. CLARKE, *Applied Physics, University of Michigan* We used Coherent Bragg Rod Analysis (COBRA) and x-ray synchrotron radiation to investigate the structure of epitaxial thin films of $PbTiO_3$ deposited by sputtering on $SrTiO_3$ substrates. The measurements were performed under different electric field conditions, including the presence of conducting electrodes. The data analysis reveals details of the atomic displacements in different layers and shows subtle variations as a function of distance from the interface. The effects of symmetry breaking at the substrate-film interface are discussed.

*Use of the Advanced Photon Source was supported by the U. S. Department of Energy, Office of Science, Office of Basic Energy Sciences, under Contract No. W-31-109-Eng-38 and Grant No. DE-FG02-03ER46023.

***Invited Papers***

**15:42**

**R41 7 Ferroelectricity in Ultrathin Perovskite Films.*** STEPHEN STREIFFER, *Argonne National Laboratory*

The ferroelectric phase transition in ultrathin perovskite films is exquisitely sensitive to strain and to compensation of depolarizing fields arising from divergences in polarization at interfaces. However, in most experiments there is significant uncertainty in the degree of compensation by internal or external space charge (even for electroded thin films), or by the formation of domain structures that minimize depolarization energy. This in turn affects interpretation of size effects in thin films, as depolarization contributions are film thickness dependent. Here we will describe our work utilizing in-situ synchrotron x-ray scattering to study the phase transition and equilibrium 180[r] domain structure in fully coherent, epitaxial $PbTiO_3$ thin films deposited onto $SrTiO_3$ and $SrRuO_3/SrTiO_3$ substrates by metalorganic chemical vapor deposition. We will show that we can control the degree of top interface compensation by controlling the gas environment in our deposition and analysis system, and monitor this via details of the 180[r] stripe domain pattern that forms for $PbTiO_3$ on insulating $SrTiO_3$. Furthermore, we will demonstrate that compensation can be accomplished at the ferroelectric film surface by adsorption of molecular or ionic species, in contrast to electronic mechanisms that occur in the presence of a conducting electrode. Exploitation of this for novel devices or templating techniques may be possible, both through chemical control of polarity and through polarization control of ionic adsorption.

*This work was performed in collaboration with the ANL MSD In-Situ Studies Team and the A. Rappe group (U. Penn).



***Contributed Papers***

**16:18**

**R41 8 Interface effect to the nanoscale ferroelectricity** CHUN-GANG DUAN, *Department of Physics and Astronomy, University of Nebraska, Lincoln, Nebraska, 68588* RENAT F. SABIRIANOV, WAI-NING MEI, *Department of Physics, University of Nebraska, Omaha, Nebraska 68182* SITARAM S. JASWAL, EVGENY Y. TSYMBAL, *Department of Physics and Astronomy, University of Nebraska, Lincoln, Nebraska 68588* Recent experimental results demonstrate that in thin films ferroelectricity persists down to film thickness of a few unit cells. This finding opens an avenue for novel electronic devices based on ultrathin ferroelectrics, but also raises questions about factors controlling ferroelectricity and the nature of the ferroelectric state at the nanoscale. Here we report a first-principles study of $KNbO_3$ ferroelectric thin films placed between two metal electrodes, either $SrRuO_3$ or Pt. We show that the bonding at the ferroelectric-metal interface imposes severe constraints on the displacement of atoms, destroying the bulk tetragonal soft mode in thin ferroelectric films. This does not, however, quench local polarization. The critical thickness for the net polarization of the $KNbO_3$ film we found are about 1 nm for Pt and 1.8 nm for $SrRuO_3$ electrodes.

**16:30**

**R41 9 Ferroelectric properties of nm-scale barium and lead titanate films** Y. -H. TANG, M. -H. TSAI, *National Sun Yat-Sen University, Kaohsiung 80424 Taiwan* The first-principles calculations of the total energies of nm-scale barium titanate ($BaTiO_3$) and lead titanate ($PbTiO_3$) films with respect to the off-center Ti ion displacement, $d_{Ti}$, have been carried out to understand ferroelectric properties of these films. Since the driving force of ferroelectricity is the attractive total dipole-dipole interactions associated with the collective off-center displacements of the transition metal ions in the octahedrons [1], the ferroelectric properties of nm-scale films is expected to be different from those of thick films because of the drastic reduction of the number of available dipoles. Thus, it is interesting to know whether the nm-scale films retain ferroelectricity. The calculated total energies as a function of $d_{Ti}$ along the (110) direction show a potential well at about 0.17 and 0.15Å for $BaTiO_3$ and $PbTiO_3$, respectively. By symmetry, the potential well is the same for $-d_{Ti}$. The existence of double potential wells is a characteristic of ferroelectricity. Thus, the total energy result shows that nm-scale $BaTiO_3$ and $PbTiO_3$ films retain ferroelectricity and resultant dipoles are parallel with the films. [1] M. –H. Tsai**, Y. –H. Tang**, and S. K. Dey, J. Phys.: Condens. Matter **15**, 7901 (2003).

**16:42**
**R41 10 Effects of surface layer composition in stabilizing thin film ferroelectrics** ALEXIE KOLPAK, *University of Pennsylvania* ANDREW RAPPE, *University of Pennsylvania* Using first-principles density functional theory calculations, we explore the ramifications of chemically altering the properties of the metal/ferroelectric interfaces in thin film ferroelectric capacitors. We show that a 3 unit-cell-thick $BaTiO_3$ film with $SrRuO_3$ electrodes has a stable, bulk-like polarization when the surface BaO layers are replaced with PbO, in contrast to the unmodified $SrRuO_3/BaTiO_3$ film which only begins to support a small polarization at 8-unit cell thickness. At the other extreme, BaO surface layers completely suppress polarization in $PbTiO_3$ films even with Pt electrodes, which have been shown to stabilize a large bulk-like polarization in unaltered one unit-cell-thick $PbTiO_3$ films. Our results show that in addition to screening by the metal electrodes, the atomic structure and the work functions of the ferroelectric surface layers play key roles in determining stability. Furthermore, our work suggests that particular properties can be achieved in ferroelectric thin films through a combination of chemical surface modification and judicious choice of ferroelectric and electrode materials.

**16:54**
**R41 11 Visable-Deep UV Dielectric Functions and Electronic Band Structure of Lead Zirconate Titanate Thin Films** HO-SUN LEE, T.D. KANG, *Kyung Hee Univ.* Y.S. KANG, S.-J. CHO, H. MORKOC, *Virginia Commonwealth Univ.* J. LI, S.-H. WEI, *NREL* P.G. SNYDER, *Univ. of Nebraska, Lincoln* We measure pseudodielectric functions in the visible-deep ultraviolet spectral range of $Pb(Zr_xTi_{1-x})O_3$ (x=0.2, 0.56, 0.82) (PZT), $Pb_{0.98}Nb_{0.04}(Zr_{0.2}Ti_{0.8})_{0.96}O_3$, $Pb_{0.91}La_{0.09}(Zr_{0.65}Ti_{0.35})_{0.98}O_3$, and $Pb_{0.85}La_{0.15}Ti_{0.96}O_3$ films. Using a parametric optical constant model, we estimate the dielectric functions ($\varepsilon$) of the perovskite oxide thin films. Taking the second derivative of the fitted layer dielectric functions and using the standard critical point model, we determine the parameters of the critical points. In the second derivative spectra, the lowest band gap energy peak near 4 eV is fitted as a double peak for annealed PZTs due to perovskite phase. As-grown PZTs have mainly pyrochlore phase and the lowest band gap peak is fitted as a single peak. We also examine the effect of dopants La and Nb, which substitute at Pb and Zr (Ti) sites, respectively. We found three band gaps $E_a$ ( $\sim$ 3.9eV),$E_b$ ( $\sim$ 4.5 eV) and $E_c$ ( $\sim$ 6.5eV) in the order of increasing energy. The E a and Eb band gap energies were not sensitive to Zr composition. We discuss the change of critical point (CP) parameters for PZTs in comparison to the band structure calculations based on local−density−approximation. The near−constancy of the lowest band gap energy independent of Zr composition is consistent with the band calculations.

**17:06**
**R41 12 Electrostatics of superlattices by first principles** XIFAN WU, OSWALDO DIÉGUEZ, KARIN RABE, DAVID VANDERBILT, *Rutgers University* A complete theory of epitaxial perovskite superlattices requires an understanding of both epitaxial strain effects and of electrostatic boundary conditions. Here, focusing on the latter issue, we have carried out first-principles calculations of the nonlinear dielectric properties of short-period $BaTiO_3/SrTiO_3$ and $PbTiO_3/SrTiO_3$ superlattices having the in-plane lattice constant of $SrTiO_3$. In particular, we have mapped the energy $E$ vs. polarization $P$ for these superlattices, and for the parent bulk materials, by extending the $E(P)$ mapping algorithm of Diéguez and Vanderbilt to handle strain relaxation in the $c$-direction. We then test whether the superlattice results can be understood quantitatively in terms of the $E(P)$ information for the bulk materials and similar information on the interfaces. We reformulate the theory in terms of the electric displacement field $D$ (since this is uniform throughout the superlattice) and the corresponding internal energy $U(D)$, and investigate how to model $U(D)$ in terms of ab-initio derived bulk and interface information. We stress that once the $U(D)$ is obtained for a given superlattice, all the electrostatic properties, both linear and non-linear, can be predicted.

**17:18**
**R41 13 Epitaxial strain effects from first principles** CLAUDE EDERER, NICOLA SPALDIN, *Materials Department, University of California, Santa Barbara* Epitaxial strain can substantially enhance the spontaneous polarizations and Curie temperatures of ferroelectric thin films compared to the corresponding bulk materials. In this work we use first principles calculations to calculate the effect of epitaxial strain on the spontaneous polarization of the ferroelectrics $BaTiO_3$, $PbTiO_3$, and $LiNbO_3$, and the multiferroic material $BiFeO_3$. We show that the epitaxial strain dependence of the polarization varies considerably for the different systems, and in some cases is in fact very small. We discuss possible reasons for this different behavior, and show that the effect of epitaxial strain can easily be understood in terms of the piezoelectric and elastic constants of the unstrained materials. Our results provide a computational tool for the quantitative prediction of strain behavior in ferroelectric thin films.



**SESSION R42: FOCUS SESSION: PLASTICITY AND PHASE TRANSITIONS**
**Wednesday Afternoon, 15 March 2006; 345, Baltimore Convention Center at 14:30**
**Ricky Chau, Lawrence Livermore National Laboratory, presiding**

***Invited Papers***

**14:30**
**R42 1 Multiphase Equations of State for Materials with Solid-Solid and Solid-Liquid Phase Transitions.** CHRISTOPHER ROBINSON, *AWE plc*

Many materials undergo a solid-solid phase transition where the crystal structure changes with a change in pressure or temperature. In addition materials melt, which is another phase transition. Across a phase boundary there are discontinuities in density and internal energy (latent heat). Although the volume change is small, even a small volume change may cause significant effects. For example under shock loading a phase transition may cause the shock to split into two distinct shocks. The equation of state (EoS) of a material with a phase transition may be modelled by determining the EoS

for each individual phase separately. The phase that exists at any pressure and temperature is the phase with the lowest Gibb's free energy. Then the phase boundaries between phases are the loci of points in the pressure/temperature plane where two phases have the same Gibb's free energy. Along a phase boundary the EoS may be determined by assuming that the material consists of a mixture of two phases. Then the EoS in the mixed-phase region is completely determined by the EoS of the single phases. It can be shown that the bulk sound speed always falls when passing from a single-phase region into a mixed-phase region. Therefore, under isentropic compression through a phase boundary a shock will form. When implementing the EoS into hydrocodes an iterative method may be used to determine the solution to the equations: An initial guess is made of which phases exist at the required specific volume and internal energy and then the pressure, temperature and mass fractions are calculated. If the chosen phases have the lowest Gibb's free energy the solution has been found, otherwise another guess of the stable phases is made, and the iteration is repeated.

*Contributed Papers*

**15:06**

**R42 2 First-principles study of high-pressure phase transitions in $Si_3N_4$*** BIN XU, JIANJUN DONG, *Physics Department, Auburn University* HAROLD STOKES, *Brigham Young University* DORIAN HATCH, *Brigham Young University* We have performed a systematic theoretical study of phase transitions in $Si_3N_4$ at high-pressure. We calculated the Gibbs free energies of the ground state $\beta$ phase and the high-pressure $\gamma$ phase at various temperatures and pressures based on the first- principles density functional theory and the statistical quasi-harmonic theory. The thermal equations of state and the Clapeyron slope of the $\beta$-to- $\gamma$ transition at high-pressure are determined and compared with available experimental data. In addition to the recently discovered high- pressure $\gamma$-phase, we predict a new high-pressure phase of hexagonal symmetry. This new high-pressure phase is likely to exist metastably at the high pressure itand room temperature, and it is associated with a non Å-point soft phonon distortion. The structural and elastic properties and the stability condition of this predicted metastable high-pressure phase will be discussed.

*This work is supported by DOE (DE-FG02-03ER46060).

**15:18**

**R42 3 Pressure-induced B1-to-B2 phase transition in $AgSbSe_2$*** EUNJA KIM, RAVHI KUMAR, ANDREW CORNELIUS, MALCOLM NICOL, *Department of Physics and High Pressure Science and Engineering Center, University of Nevada, Las Vegas, NV 89154* We have investigated the pressure-induced B1-to-B2 phase transitions in $AgSbSe_2$. High pressure x-ray diffraction experiments clearly show that the process starts at 20 GPa and completes at 55 GPa. Our density-functional calculations are in good agreement with the experiment and confirm the B1 to B2 transition which is similar to $AgSbTe_2$. The possible intermediate structure for B1-to-B2 transition in $AgSbSe_2$ occurring at 21-54 GPa is under investigation. Its similarity and difference to $AgSbTe_2$ will be discussed in this study.

*The UNLV High Pressure Science and Engineering Center was supported by the U.S. Department of Energy, National Nuclear Security Administration, under Cooperative Agreement DE-FC08-01NV14049.

**15:30**

**R42 4 High Pressure-Induced Phase Transition In $\beta$-$Ga_2O_3$: in situ Synchrotron X-Ray Diffraction Studies up to 70 Gpa*** KRISTINA E. LIPINSKA-KALITA, *Center for Nanoscale Device Research, Dept. of Electrical and Computer Eng. University of Nevada Las Vegas* PATRICIA E. KALITA, *High Pressure Science and Engineering Center, Dept. of Physics, University of Nevada Las Vegas* RUSSELL J. HEMLEY, *Geophysical Lab. Carnegie Institution of Washington, Washington DC* CEDRIC L. GOBIN, *High Pressure Science and Engineering Center, Dept. of Physics, University of Nevada Las Vegas* A renewed interest in $\beta$-$Ga_2O_3$ has arisen since it has potential applications in optoelectronic devices. We performed itin situ synchrotron radiation x-ray diffraction studies in a diamond anvil cell on $\beta$-$Ga_2O_3$ on compression up to 70 GPa and on successive decompression. The pressure-evolution of x-ray diffraction patterns was consistent with a low-to-high density phase transition. A thermodynamically stable it$\beta$-$Ga_20_3$ phase was converted into the it$\alpha$-$Ga_20_3$ phase, which is unstable at ambient conditions. The effect of hydrostatic and non-hydrostatic compression conditions on the evolution of the phase transition was also investigated in compression and decompression cycles. This work is the first report of high-pressure investigations of $Ga_2O_3$ on compression up to 70 GPa.

*Use of the HPCAT facility was supported by DOE-BES, DOE-NNSA (CDAC), NSF, DODTACOM, and the W.M. Keck Foundation. We acknowledge the support from the U.S. DoE Cooperative Agreement No. FC08-01NV14049 with the University of Nevada Las Vegas.

**15:42**

**R42 5 X-ray diffraction study of elemental thulium to 86 GPa*** MICHAEL PRAVICA, EDWARD ROMANO, ZACHARY QUINE, *University of Nevada, Las Vegas* WALTER PRAVICA, *Wilbur Wright College* We have studied the structures and equation of state of elemental thulium up to 86 GPa in a diamond anvil cell using angular-dispersive x-ray powder diffraction methods at the Advanced Photon Source. This is part of a study of phase transitions in the lanthanide-series metals using cyclohexane as a quasi-hydrostatic medium. We present evidence of a series of phase transitions that appear to follow the anticipated hcp $\rightarrow$ Sm-type $\rightarrow$ dhcp $\rightarrow$ distorted fcc sequence of transitions and show the equation of state derived from the x-ray fit data.

*Supported by DOE Cooperative Agreement No. DE-FC08-01NV14049. Use of HPCAT is supported by DOE-BES, DOE-NNSSA (CDAC), NSF, DOD-TACOM, and the W.M. Keck Foundation.

**15:54**

**R42 6 Fermi surface nesting and pre-martensitic softening in V-Nb system under high pressure*** ALEXANDER LANDA, JOHN KLEPEIS, PER SODERLIND, BABAK SADIGH, *Lawrence Livermore Nationa Laboratory, Livermore, CA 94550* IVAN NAUMOV, *University of Arkansas, Fayetteville, AR 72701* OLEG VELIKOKHATNYI, *Carnegie Mellon University, Pittsburgh, PA 15213* LEVENTE VITOS, ANDREI RUBAN, *Royal Institute of Technology, SE-10044, Stockholm* First-principles total energy calculation based on the exact muffin-tin orbital and full potential linear muffin-tin orbital methods were used to calculate

the equation of state and shear elastic constants of bcc V, Nb, and the $V_{95}Nb_{05}$ disordered alloy as a function of pressure up to 6 Mbar. We found a mechanical instability in $C_{44}$ and a corresponding softening in $C'$ at pressures $\sim$ 2 Mbar for V. Both shear elastic constants show softening at pressures $\sim$ 0.5 Mbar for Nb. Substitution of 5 at. % of V with Nb removes the instability of V with respect to trigonal distortions in the vicinity of 2 Mbar pressure, but still leaves the softening of $C_{44}$ in this pressure region. We argue that the pressure induced softening in the shear elastic constants of V and Nb can be attributed simultaneously to three different electronic structure peculiarities, namely to the Fermi Surface nesting, electronic topological transition, and the band Jahn-Teller effect.

*This work was performed under the auspices of the U.S. Department of Energy by the University of California, Lawrence Livermore National Laboratory under Contract W-7405-ENG-48.

**16:06**

**R42 7 Pressure-Induced Antifluorite-to-Anticotunnite Phase Transition in Lithium Oxide** AMY LAZICKI, *University of California at Davis, Lawrence Livermore National Laboratory* CHOONG-SHIK YOO, *Lawrence Livermore National Laboratory* WILLIAM EVANS, *Lawrence Livermore National Laboratory* WARREN PICKETT, *University of California, Davis* RICHARD SCALETTAR, *University of California, Davis* Using synchrotron angle-dispersive x-ray diffraction (ADXD) and Raman spectroscopy on samples of $Li_2O$ pressurized in a diamond anvil cell, we observed a reversible phase change from the cubic antifluorite ($\alpha$, Fm3m) to orthorhombic anticotunnite ($\beta$, Pnma) phase at 50( $\pm$ 5) GPa at ambient temperature. This transition is accompanied by a moderate volume collapse of 5.4 ( $\pm$ 0.8)% and large hysteresis upon pressure reversal ($P_{down}$ at $\sim$ 25 GPa). Contrary to a recent study, our data suggest that the high-pressure $\beta$-phase ($B_o$ = 188 $\pm$ 12 GPa) is substantially stiffer than the low-pressure $\alpha$-phase ($B_o$ = 90$\pm$ 1 GPa). A relatively strong and pressure-dependent preferred orientation in $\beta$-$Li_2O$, resulting in changes diffraction intensities, is observed. The present result is in accordance with the systematic behavior of antifluorite-to-anticotunnite phase transitions occurring in the alkali-metal sulfides. This work has been supported by LLNL, University of California, under the auspices of the U.S. DOE under Contract No. W-7405- ENG-48 and by the Stockpile Stewardship Academic Alliances Program under grant DOE DE-FG03-03NA00071, and by the NSF(ITR 031339) at UCD.

**16:18**

**R42 8 Novel Features in the Mixed-Valence State of TmTe at High Pressure: A Resonant Inelastic X-ray Scattering Study** IGNACE JARRIGE, YONG CAI, HIROFUMI ISHII, NOZOMU HIRAOKA, CHIEN-TE CHEN, *National Synchrotron Radiation Research Center, Taiwan* JEAN-PASCAL RUEFF, *Synchrotron Soleil, France* SEAN SHIEH, *National Cheng Kung University, Taiwan* CHING-PAO WANG, *National Cheng Kung University, Taiwan* TAKESHI MATSUMURA, *Tohoku University, Japan* Using resonant inelastic x-ray scattering, the mixed-valence state of TmTe under pressure is accurately determined up to 10.6 GPa. A remarkable interplay between electronic, magnetic and structural properties in TmTe under pressure is inferred throughout the considered pressure range. A nearly linear correlation is found between the pressure dependences of the valence and the volume in the metallic regime of TmTe. In the framework of the RKKY theory, the pressure dependence of the valence is found to explain both the steady decrease of the ferromagnetic state with increasing pressure in the 2-6 GPa range and the formation of the antiferromagnetic state above 6 GPa.

**16:30**

**R42 9 Elastic Stability Analysis of the Structural Response of Cubic Crystals to Hydrostatic Loading** HADRIAN DJOHARI, *Department of Chemical Engineering, University of Massachusetts, Amherst, MA 01003-3110* FREDERICK MILSTEIN, *Departments of Materials and Mechanical Engineering, University of California, Santa Barbara, CA 93106* DIMITRIOS MAROUDAS, *Department of Chemical Engineering, University of Massachusetts, Amherst, MA 01003-3110* We report results of systematic elastic stability analyses in metallic crystals based on isobaric molecular-dynamics simulations that capture the mechanical, geometric, and kinetic aspects of instabilities induced under hydrostatic loading. Our analysis emphasizes bifurcations in the crystal structural response as the applied load is varied and atomic pattern formation characteristics beyond the instability onset. Results are presented for various cases of structural evolution under hydrostatic loading for model crystals that have a cubic lattice structure at equilibrium, including crystals with structural heterogeneities such as internal nanovoids and free surfaces. The corresponding structural responses range from inhomogeneous structural transitions to fracture through decohesion and voiding. The observed instabilities are thermally activated and associated with vanishing or diminishing combinations of elastic moduli.

***Invited Papers***

**16:42**

**R42 10 Dynamic Strength of Metals at High Pressure and Strain Rate.** THOMAS LORENZ, *Lawrence Livermore National Laboratory*

A new approach to materials science at very high pressures and strain rates has been developed on the Omega laser, using a ramped plasma piston drive. A laser drives an ablative shock through a solid plastic reservoir where it unloads at the rear free surface, expands across a vacuum gap, and stagnates on the metal sample under study. This produces a gently increasing ram pressure, compressing the sample nearly isentropically. The peak pressure on the sample, diagnosed with VISAR measurements, can be varied by adjusting the laser energy and pulse length, gap size, and reservoir density, and obeys a simple scaling relation.[1] This has been demonstrated at OMEGA at pressures to 200 GPa in Al foils. In an important application, using in-flight x-ray radiography, the material strength of solid-state samples at high pressure can be inferred by measuring the reductions in the growth rates (stabilization) of Rayleigh-Taylor (RT) unstable interfaces. RT instability measurements of solid of Al-6061-T6 [2] and vanadium, at pressures of 20-100 GPa, and strain rates of $10^6$ to $10^8$ $s^{-1}$, show clear material strength effects. Modelling results for two constitutive strength models – Steinberg-Guinan and Preston-Tonks-Wallace, show enhanced dynamic strength that may be correlated with a high-strain-rate,

phono-drag mechanism. Data, modeling details and future prospects for this project using the National Ignition Facility laser, will be presented. [1] J. Edwards et al., Phys. Rev. Lett., **92**, 075002 (2004). [2] K. T. Lorenz et al., Phys. Plasmas **12**, 056309 (2005). This work was performed under the auspices of the U.S. Department of Energy by the University of California, Lawrence Livermore National Laboratory under Contract W-7405-Eng-48.

*Contributed Papers*

**17:18**
**R42 11 Atomistic simulations of quasi-static and shockwave loading of HMX crystals** THOMAS SEWELL, EUGENIO JARAMILLO, *Los Alamos National Laboratory* ALEJANDRO STRACHAN, *Purdue University* We have recently undertaken non-equilibrium molecular dynamics studies to aid our understanding of dynamical processes in the high explosive HMX, in particular the inelastic, anisotropic response of crystalline HMX subjected to quasi-static and shock loading. The same force field used by Sewell and co-workers in preceding simulations of HMX equilibrium properties is employed for the present research. The overarching goal of this work is to provide information that can serve as a foundation in basic science for the formulation of improved mesoscale constitutive models for the constituent materials in selected energetic formulations. The medium-term scientific challenge that stands as a prerequisite to this larger objective is to carefully identify, characterize, and quantify the dominant mechanisms of localization and dissipation in such materials, under a variety of prescribed quasi-static and dynamic loading scenarios. The focus of the present talk will be the shock response of structurally perfect, but properly thermalized, $\alpha$-HMX crystal shocked in the (100) direction, with specific discussion of results for loading below the hugoniot elastic limit, in the two-wave elastic-plastic region, and for overdriven shocks.

**SESSION R43: ONE DIMENSIONAL BOSE GASES**
**Wednesday Afternoon, 15 March 2006**
**346, Baltimore Convention Center at 14:30**
**A.B. Kuklov, The College of Staten Island, CUNY, presiding**



**14:30**
**R43 1 Interference between fluctuating condensates** EHUD ALTMAN, *Weizmann Institute* ANATOLI POLKOVNIKOV, *Boston University* EUGENE DEMLER, *Harvard University* Two independent Bose condensates that are released from their traps and let to overlap produce a sharp interference pattern. How does this picture change if each condensate lacks true long range order? As an example we consider the interference between a pair of one dimensional interacting Bose liquids at low temperature. We show that the average fringe contrast scales as a universal function of the system size that depends only on the Luttinger parameter. Moreover the full distribution of the fringe contrast changes with interaction strength and lends information on high order correlation functions. We also demonstrate that the interference between two-dimensional condensates at finite temperature can be used as a direct probe of the Kosterlitz-Thouless transition.

**14:42**
**R43 2 Bose-Einstein Condensation in low dimensionality*** KWANGSIK NHO, D.P. LANDAU, *Center for Simulational Physics, University of Georgia* Using path integral Monte Carlo simulation methods[1], we have studied properties of Bose-Einstein Condensates harmonically trapped in low dimemsion. Each boson has a hard-sphere potential whose core radius equals its corresponding scattering length. We have tightly confined the motion of trapped particles in one or more direction by increasing the trap anisotropy in order to simulate lower dimensional atomic gases. We have investigated the effect of both the temperature and the dimemsionality on the energetics and structural properties such as the total energy, the density profile, and the superfluid fraction. Our results show that the physics of low dimensional bosonic systems is very different from that of their three dimensional counterparts[2]. The superfluid fraction for a quasi-2D boson gas decreases faster than that for both a quasi-1D system[3] and a true 3D system with increasing temperature. The superfluid fraction decreases gradually as the two-body interaction strength increases although it shows no noticable dependence for both a quasi-1D system and a true 3D system. [1] K. Nho and D. P. Landau, Phys. Rev. A. **70**, 53614 (2004). [2] N. D. Mermin and H. Wagner, Phys. Rev. Lett. **22**, 1133 (1966); P. C. Hohenberg, Phys. Rev. **158**, 383 (1967). [3] K. Nho and D. Blume, Phys. Rev. Lett. **95**, 193601 (2005).

*Research supported by NASA.

**14:54**
**R43 3 Path-Integral quantum Monte Carlo study of Bose-Einstein condensates under attractive interactions*** HONG MA, TAO PANG, *University of Nevada, Las Vegas* A hard-core one-dimensional boson ring under attractive interactions is studied by using the path-integral quantum Monte Carlo method at low temperature. Condesate fraction, total energy, and angular pair correlation functions are obtained as a function of the interaction strength. Our simulation predicts a possible quantum phase transition from a uniform condensation state to a symmetry-broken cluster as the attractive interaction increases. The dependence of such a phase transition on temperature, hard-core size, and total number of particles in the system will be discussed.

*supported by DOE

**15:06**
**R43 4 One Dimensional Gas of Bosons with Feshbach Resonant Interactions*** VICTOR GURARIE, *University of Colorado* We present a study of a gas of bosons confined in one dimension with Feshbach resonant interactions, at zero temperature. Unlike the gas of one dimensional bosons with non-resonant interactions, which is known to be equivalent to a system of interacting spinless fermions and can be described using the Luttinger liquid formalism, the resonant gas possesses novel features. Depending on its parameters, the gas can be in one of several regimes. In the most interesting of them, it is equivalent to a Luttinger liquid at low density only. At higher density its excitation spectrum develops a

minimum, similar to the roton minimum in helium, at momenta where the excitations are in resonance with the Fermi sea. As the density of the gas is increased further, the minimum dips below the Fermi energy, thus making the ground state unstable. At this point the standard ground state gets replaced by a more complicated one, where not only the states with momentum below the Fermi points, but also the ones with momentum close to that minimum, get filled, and the excitation spectrum develops several branches.

*This work is supported by the NSF grant DMR-0449521

**15:18**

**R43 5 QMC study of the 1D boson Hubbard model with a superlattice potential** VALY ROUSSEAU, MARCOS RIGOL, *University of California, Davis* FRÉDÉRIC HÉBERT, *Institut Non Linéaire de Nice* DANIEL AROVAS, *University of California, San Diego* GEORGE BATROUNI, *Institut Non Linéaire de Nice* RICHARD SCALETTAR, *University of California, Davis* We use QMC simulations to explore the phase diagram of the Bose-Hubbard model with an additional superlattice potential. We first analyse the hard-core limit where an exact analytic treatment is possible, and then use QMC to solve the soft-core case and find the insulator/superfluid phase diagram as a function of potential strength and filling. These results are relevant to the behavior of cold atoms in optical superlattices which are beginning to be achieved experimentally.

**15:30**

**R43 6 Quantum coherence of Hard Core Bosons and Fermions in one dimensional quasi-periodic potentials: superfluid, Mott and glassy phases** ANA MARIA REY, *ITAMP, Harvard-Smithsonian Center of Astrophysics, Cambridge, MA, 02138.* INDUBALA I SATIJA, *Dept. of Physics, George Mason University, Fairfax, VA, 22030* CHARLES W CLARK, *NIST, Gaithersburg MD, 20899* We use Hanbury- Brown-Twiss interferometry (HBTI) to characterize and contrast the different quantum phases exhibited by hard core bosons (HCBs) and ideal fermions confined in a one-dimensional quasi-periodic potential. In addition to the Bose-glass, superfluid and Mott insulator phases characteristic of interacting disordered bosons, we show the quasi-periodic potential induces a cascade of Mott-like band insulator transitions triggered by the fermion-type statistics of HCBs. A comparative study of the fermion model shows that except for a sign difference, HCB and fermion interferometric patterns coincide in the localized phases. In the extended phase, however, fermions behave quite differently; their correlation functions reflect some of the multifractal properties characteristic of the metal-insulator transition. When plotted as a function of the filling factor, their quasi-momentum distribution displays an Arnold tongue-like structure and the HBTI peak intensity follows a step-like pattern which resembles a devil's staircase at the onset of the localization transition.

**15:42**

**R43 7 Bose/Anderson glass and re-entrant superfluidity in strongly correlated bosons in a disordered optical lattice** TOMMASO ROSCILDE, IGNACIO CIRAC, *Max-Planck-Institut fuer Quantenoptik - Germany* We investigate the one-dimensional Bose-Hubbard model in presence of a random bimodal on-site chemical potential, modeling strongly correlated bosons in an optical lattice in presence of a second species of bosons randomly frozen in the minima of the optical potential [U. Gavish and Y. Castin, Phys. Rev. Lett. 95, 020401 (2005)]. Making use of quantum Monte Carlo simulations, we investigate both the strongly and the weakly interacting regime. In the strongly interacting case, superfluidity is found to be robust against disorder, due to effective screening of the disorder potential. Close to commensurate filling disorder is seen to promote superfluidity vs. Mott insulating behavior, leading to re-entrant superfluid order. Moreover the presence of disorder introduces a disordered Anderson-glass phase for small interparticle repulsion and a Bose-glass phase for large repulsion, separated by the superfluid phase. Clear signature of these phases are observed on realistic sizes ( $\sim$ 60 lattice sites) making the above scenario amenable to experimental realization.

**15:54**

**R43 8 Bogoliubov Excitations and Superfluidity in a Kronig-Penney Potential*** IPPEI DANSHITA, *National Institute of Standards and Technology, Gaithersburg, MD 20899, USA* SUSUMU KURIHARA, *Department of Physics, Waseda University, Ohkubo, Shinjuku-ku, Tokyo 169-8555, Japan* SHUNJI TSUCHIYA, *Dipartimento di Fisica, Universita di Trento, and Istituto Nationale per la Fisica della Materia, I-38050 Povo, Italy* We study the elementary excitations of Bose-Einstein condensates in a Kronig-Penney potential. We solve the Bogoliubov equations analytically and obtain the band structure of the excitation spectrum. We show that the excitation spectrum is phononlike at low energies. It is found that the anomalous tunneling of low-energy excitations is crucial to the phonon dispersion, which is directly connected to the superfluidity of the condensate.

*I.D. is supported by a Grant-in-Aid from JSPS.

**16:06**

**R43 9 Atomic Josephson Vortex*** VITALIY KAUROV, ANATOLY KUKLOV, *CSI, CUNY* We show that atomic Josephson vortices [1] in a quasi-1D atomic junction can be controllably manipulated by imposing a tunneling bias current created by a difference of chemical potentials on the atomic BEC waveguides forming the junction. This effect, which has its origin in the Berry phase structure of a vortex, turns out to be very robust in the whole range of the parameters where such vortices can exist [2]. Acceleration of the vortex up to a certain threshold speed, determined by the strength of the Josephson coupling, results in the phase slip causing switching of the vorticity. This effect is directly related to the interconversion [1], when slow variation of the coupling can cause transformation of the vortex into the dark soliton and vice verse. We also propose that a Josephson vortex can be created by the phase imprinting technique and can be identified by a specific ittangential feature in the interference picture produced by expanding clouds released from the waveguides [2]. [1] V. M. Kaurov, A. B. Kuklov, Phys. Rev. A 71, 11601(R) (2005). [2] V. M. Kaurov, A. B. Kuklov cond-mat/0508342

*This work is supported by the NSF grant PHY-0426814 and PSC-CUNY grant 665560036.

**SESSION R44: EXPERIMENTAL STUDIES OF 115 MATERIALS**
**Wednesday Afternoon, 15 March 2006**
**347, Baltimore Convention Center at 14:30**
**J. Sarrao, Los Alamos National Laboratory, presiding**

**14:30**

**R44 1 Hidden magnetism and quantum criticality in the heavy fermion superconductor $CeRhIn_5$*** J.D. THOMPSON, T. PARK, F. RONNING, *Los Alamos National Laboratory* H.Q. YUAN, M.B. SALAMON, *University of Illinois* R. MOVSHOVICH, J.L. SARRAO, *Los Alamos National Laboratory* We report the dependence on pressure and magnetic field of the specific heat and electrical resistivity of the pressure-tuned heavy-fermion superconductor $CeRhIn_5$. Above a critical pressure, where long-range antiferromagnetic order (AFM) abruptly disappears, application of a field brings back magnetism inside the superconducting state. As a function of pressure at low temperatures, the set of fields required to induce magnetism defines a line of quantum-phase transitions that separates a phase of coexisting AFM and SC from a purely unconventional superconducting phase. This quantum-transition line and the upper critical field boundary, above which superconductivity is suppressed, merge at a quantum tetracritical point where another quantum-phase boundary separates magnetically ordered and disordered normal phases. The quasiparticle mass diverges as this normal-state quantum boundary is approached, and crossing it produces a change in the Fermi-surface volume [1]. [1] H. Shishido et al., J. Phys. Soc. Jpn. **74**, 1103 (2005).

*Work at Los Alamos was performed under the auspices of the US DOE/Office of Science

**14:42**

**R44 2 NMR Studies of $CeCoIn_5$ below 1K** N. CURRO, B.-L. YOUNG, R. URBANO, R. MOVSHOVICH, J. SARRAO, *Los Alamos National Laboratory* We present new NMR data in the normal and superconducting states of $CeCoIn_5$ below 1K and in fields up to 12T. The temperature dependence of the Knight shift anomalies exhibited by the Co and the two In sites is field dependent in the normal state, and may be related to the presence of a field-tuned quantum critical point. The spectra and relaxation rates exhibit dramatic changes in the superconducting and Fulde-Ferrell-Larkin- Ovchinnikov states.

**14:54**

**R44 3 Hall Effect under pressure in CeCoIn5*** S. SINGH, *MPI for Chemical Physics of Solids, 01187 Dresden, Germany* C. CAPAN, *Dept. of Physics and Astronomy, LSU, Baton Rouge, Louisiana 70803, USA* S. WIRTH, M. NICKLAS, A. GLADUN, *MPI for Chemical Physics of Solids, 01187 Dresden, Germany* H. LEE, Z. FISK, *Dept. of Physics, UC Davis, California 95616, USA* J. F. DITUSA, *Dept. of Physics and Astronomy, LSU, Baton Rouge, Louisiana 70803, USA* F. STEGLICH, *MPI for Chemical Physics of Solids, 01187 Dresden, Germany* Important deviations from Landau Fermi Liquid theory are observed in many rare-earth compounds known as heavy fermion compounds. These anomalies can be ascribed to the presence of a quantum critical point (QCP) separating two different ground states in the phase diagram of these compounds. A quantum phase transition is a continuous ground state transformation driven by quantum fluctuations. In this context, CeCoIn5, a recently discovered heavy fermion superconductor, has been at the focus of intensive investigations. In this material, thermodynamic and transport properties point to a field-tuned QCP, whose origin remains elusive. At ambient pressure, this QCP is close to the superconducting upper critical field, and a Sn-doping study has failed to separate the two. We present new results on Hall Effect under pressure in a single crystal CeCoIn5 and discuss the origin of the QCP and its evolution with pressure.

*HL is supported by NSF DMR 0533560 and JFD by NSF DMR0406140

**15:06**

**R44 4 Far-Infrared Properties of $CeCoIn_5$*** G.V. SUDHAKAR RAO, S. OCADLIK, F.S. RAZAVI, M. REEDYK, *Brock University* C. PETROVIC, *Brookhaven National Laboratory* Measurements of the optical response of far-infrared radiation on single crystals of heavy fermion superconductor $CeCoIn_5$ have been made at various temperatures from 0.5 K to 2.5 K using a step-and- integrate Martin-Puplett type polarizing interferometer. An energy gap-like structure reminiscent of that observed in antiferromagnetic Cr was observed below 12 $cm^{-1}$ in the superconducting state. The size of this gap feature reduces with the increase of temperature to the normal state. This observation suggests the possibility of the role of magnetic excitations in pairing the electrons in the superconducting state.

*Work at Brock University was supported by Natural Sciences and Engineering Research Council (NSERC) of Canada.

**15:18**

**R44 5 Is quantum criticality relevant to upper critical field ($H_{c2}$) scaling in the heavy-fermion compound $CeRhIn_5$?*** TUSON PARK, JOHN L. SARRAO, JOE D. THOMPSON, *Los Alamos National Laboratory* We report disparate forms of upper critical field ($H_{c2}$) scaling below and above a critical pressure $P_{c1}$, where long- range antiferromagnetic order (AFM) abruptly disappears in the pressure-tuned heavy-fermion superconductor $CeRhIn_5$. For $P > P_{c1}$, $h_{c2} = H_{c2}/H_{c2}(T = 0\ \mathrm{K})$ shows normal two- fluid type scaling with $t = T/T_c$, i.e., $h_{c2} = (1 - t^2)(1 - at^2)$, where $T_c$ is superconducting transition temperature at zero field and a is a fitting parameter. In this regime, the Maki parameter $\alpha$, a measure of Pauli limiting effects, is large, suggesting that an inhomogeneous superconducting state (FFLO) may be observable. For $P < P_{c1}$, in stark contrast, $h_{c2}$ linearly increases with decreasing $t$ down to $t = 0.1$ and the specific heat discontinuity $\Delta C/C_N$ at $T_c$ is much smaller than the BCS value (=1.43). These observations manifest the interplay between superconductivity and antiferromagnetic fluctuations that exist in the vicinity of $P_{c1}$.

*Work at Los Alamos was performed under the auspices of the U.S. Department of Energy.

**15:30**

**R44 6 $\mu$SR measurement of the superconducting penetration depth in aged $PuCoGa_5$** R. H. HEFFNER, K. OHISHI, W. HIGEMOTO, T. ITO, *Japan Atomic Energy Agency* G. D. MORRIS, *TRIUMF, Canada* M. J. FLUSS, *LLNL, USA* D. E. MACLAUGLIN, L. SHU, *U. C. Riverside, USA* E. D. BAUER, J. L. SARRAO, *LANL, USA* The superconductor $PuCoGa_5$ possesses a relatively high critical temperature ($T_c$ = 18.5 K), a moderate mass enhancement (Sommerfeld coefficient $\cong$ 80 mJ/mol-$K^2$) and exhibits behavior consistent with spin-fluctuation-induced d-wave superconductivity [1]. It is also radioactive, with its dominant ra-

dioisotope $^{239}$Pu having a half-life of 2.4 x $10^4$ yrs. We report $\mu$SR measurements of the temperature and field dependence of the magnetic field penetration depth $\lambda$(T,H) in a 400 day-old sample of $PuCoGa_5$ ($T_c$ = 15 K), and compare these results to data obtained on the same sample approximately one year earlier. In 600 Oe applied field both measurements show a linear low-temperature behavior for $\lambda(T) - \lambda(0) = bT$ for $T/T_c < 0.5$ with the same coefficient b. The magnitude of $\lambda$(0) in the aged sample has increased by a factor of about 1.8. The results are discussed in terms of the effects of radiation damage on the postulated d-wave superconducting order parameter. [1] J. L. Sarrao et al., Nature 420, 297 (2002); N. J. Curro et al., Nature 434, 622 (2005).

**15:42**

**R44 7 NMR investigation of Sn-doped $CeRhIn_5$** R. R. URBANO, N. J. CURRO, E. D. BAUER, D. MIXSON, J. L. SARRAO, J. D. THOMPSON, We have studied the local environment of the In(1) sites in the paramagnetic (PM) and antiferromagnetic (AFM) states of the heavy fermion compound $CeRhIn_{5-x}Sn_x$ ($0.0 \leq x \leq 0.4$) using Nuclear Magnetic Resonance (NMR) and Nuclear Quadrupole Resonance (NQR) measurements. The AFM state can be continuously suppressed by Sn doping such that the Neel temperature $T_N$ goes to zero at $x_c \cong 0.4$. $^{115}$In NQR data in the PM state reveal that the suppression of $T_N$ as a function of $x$ is accompanied by a frequency shift and a broadening of the line. We also report spin-lattice relaxation rate $T_1^{-1}$ as a function of $x$ and $T$.

**15:54**

**R44 8 In-plane Torque Measurement on $CeCoIn_5$ Single Crystals*** T. HU, H. XIAO, C. C. ALMASAN, *Kent State University* T. A. SAYLES, M. B. MAPLE, *University of California, San Diego* We report in-plane torque measurements on single crystals of the heavy fermion superconductor $CeCoIn_5$ performed in the normal state at 1.9, 3, 6, and 10 K, as a function of angle and applied magnetic field. The measurements at constant angle were done in sweeping the magnetic field up to 14 T. The measured torque has a reversible and an irreversible component, with the former larger than the latter. The reversible component can be expressed as $\tau_{rev}(\theta) = \tau_2 sin2\theta + \tau_4 sin4\theta$ ($\theta$ is the angle between the applied field and the a-axis of the crystal), which is typical of systems with long range magnetic order. However, it has been reported that the heavy fermion superconductor $CeCoIn_5$ has no long range magnetic order, but only short range antiferromagntic fluctuations. The temperature and magnetic field dependence of the coefficients $\tau_2$ and $\tau_4$ will be discussed. The torque vs field curves at fixed angles show De-Hass Van-Alphen effect at temperatures as high as 10 K. The possible reasons behind this will also be discussed.

*This research was supported by the National Science Foundation unver Grant No. DMR-0406471 at KSU and the US Department of Energy under Grant No. DE-FG03-86ER-45230 at UCSD

**16:06**

**R44 9 NMR Study of the Possible FFLO State in $CeCoIn_5$** V. F. MITROVIĆ, *Brown University, Providence, RI* M. HORVATIĆ, C. BERTHIER, *GHMFL, Grenoble, France* G. KNEBEL, G. LAPERTOT, J. FLOUQUET, *SPSMS, CEA, Grenoble, France* We report nuclear magnetic resonance (NMR) measurements of the heavy-fermion superconductor $CeCoIn_5$ in the vicinity of the superconducting critical field $H_{C2}$ for a magnetic field applied perpendicular to the $c$ axis. A possible inhomogeneous superconducting state, Fulde-Ferrel-Larkin- Ovchinnikov (FFLO), is stabilized in this part of the phase diagram. In 11 T applied magnetic field, we observe clear signatures of the two phase transitions. We show that a higher temperature transition is clearly associated with the transition to the homogeneous superconducting state. The low temperature phase cannot be characterized by a simple FFLO state, viewed as a stack of static, and spatially well separated, superconducting and normal regions. Alternative explanations of the nature of the low temperature phase are discussed.

**16:18**

**R44 10 Angular Dependent Torque Measurements on $CeCoIn_5$ Single Crystals*** H. XIAO, T. HU, C. C. ALMASAN, *Kent State University* T. A. SAYLES, M. B. MAPLE, *University of California, San Diego* Angular dependent torque measurements were performed on single crystals of $CeCoIn_5$ heavy fermion superconductor ($T_{c0}$ = 2.3 K) in the temperature $T$ range 1.9 K $\leq T \leq$ 20 K and magnetic fields $H$ up to 14 T. Large paramagnetic effect is found in the normal state due to magnetic moment of the magnetic ion $Ce^{3+}$. Torque measurements in the mixed state were also performed. The torque curves show sharp hysteresis peaks at $\theta = 90^o$ ($\theta$ is the angle between $H$ and the $c$ − axis of the crystal), a result of intrinsic pinning of vortices. The anisotropy $\gamma \equiv \sqrt{m_c/m_a}$ in the mixed state was determined from the reversible part of the vortex contribution to the torque signal using Kogan's model [Phys. Rev. B **38**, 7049 (1988)]. The anisotropy $\gamma$ decreases with increasing magnetic field and temperature. The fact that $\gamma$ is not a constant points towards a multiband scenario in this heavy fermion material.

*This research was supported by the National Science Foundation under Grant No. DMR-0406471 at KSU and the US Department of Energy under Grant No. DE-FG03-86ER-45230 at UCSD.

**16:30**

**R44 11 Penetration Depth Studies of Tin Doped $CeCoIn_5$** DANIEL VANDERVELDE, *University of Illinois Urbana-Champaign* H.Q. YUAN, *University of Illinois Urbana-Champaign* M.B. SALAMON, *University of Illinois Urbana-Champaign* E.D. BAUER, *LANL* N. HUR, *LANL* F. RONNING, *LANL* M.J. GRAF, *LANL* J.D. THOMPSON, *LANL* J.L. SARRAO, *LANL* R. MOVSHOVICH, *LANL* The heavy fermion superconductor $CeCoIn_5$ has attracted much attention recently. Its high $T_C$ ( $\sim$ 2.3K), nearby antiferromagnetic phases, and evidence of line nodes in the superconducting gap indicative of a d-wave order parameter have made it an interesting topic of study. Here we present measurements of the AC magnetic field penetration depth ($\Delta\lambda$(T)) undertaken on the same material, but with an impurity doping of Sn ($CeCoIn_{5-X}Sn_X$) at three concentrations x=0.03, x=0.06, and x=0.09. Our findings support the assertion that $CeCoIn_5$ is a nonlocal, d-wave superconductor, but that as impurity concentration is increased, scattering quickly becomes the dominant mechanism. All data was modeled as a quadratic, scattering-dominated temperature dependence that crosses over to a linear regime reminiscent of the pure sample at a temperature $^1$T*. The observed value of T* increases with the concentration of impurities as is predicted in the impurity model by Hirschfield and Goldenfeld ($T^* \sim \sqrt{n_i}$). [1] This dependence on the concentration of a nonmagnetic impurity adds further confirmation of the d-wave nature of the superconducting state. [1] P.J. Hirschfield and N. Goldenfeld, Phys Rev. B **48**, 4219 (1993)

**16:42**

**R44 12 Gap structure of heavy-fermion superconductor CeIrIn5 from heat transport** HAMIDEH SHAKERIPOUR, *Physique Department, Université de Sherbrooke* S.Y. LI, N. DOIRON-LEYRAUD, LOUIS TAILLEFER, C. PETROVIC, *Brookhaven National Laboratory* We present measurements of the in-plane and out-plane thermal conductivity of heavy-fermion superconductor CeIrIn5 down to temperatures approaching Tc/10, throughout the vortex state. We use the observed anisotropy in residual linear term and response to a magnetic field to shed light on the nodal structure of the superconducting gap. We compare our results to existing theoretical calculations and discuss the possibility of multi-band superconductivity, observed recently in the related material CeCoIn5 [1]. [1] M.A. Tanatar et al., Phys. Rev. Lett. 95, 067002 (2005).

**16:54**

**R44 13 Non-local Magnetic Field-tuned Quantum Criticality in Cubic $CeIn_{3-x}Sn_x$ ($x = 0.25$)** NEIL HARRISON, ALEJANDRO SILHANEK, MARCELO JAIME, VICTOR FANELLI, CRISTIAN BATISTA, *Los Alamos National Laboratory* TAKAO EBIHARA, KOJI TEZUKA, *Shizuoka University* We show that antiferromagnetism in lightly Sn-doped $CeIn_3$ terminates at a critical field $\mu_0 H_c = 38 \pm 1$ T. Electrical transport, specific heat and magnetization measurements reveal that $m^*$ does not diverge, suggesting that cubic $CeIn_3$ is representative of a critical spin-density wave (SDW) scenario, unlike the local quantum critical points observed in lower-symmetry systems such as $CeCu_{6-x}Au_x$ and $YbRh_2Si_{2-x}Ge_x$. The existence of a maximum in $m^a st$ at a lower field $\mu_0 H_x = 30 \pm 1$ T may be interpreted as a field-induced crossover from local moment to SDW behavior as the magnitude of the antiferromagnetic order parameter falls below the Fermi bandwidth.

**17:06**

**R44 14 Correlation induced phase transition in fcc Pu** SHAOPING CHEN, *Los Alamos National Laboratory* The density functional theory calculations (GGA+U) of fcc Pu indicate that as the Hubbard on-site Coulomb repulsion U increases the fcc Pu system goes through a sharp phase transition. Accompanying this transition are sharp drops of the bulk moduli, and large values and even negative values of pressure derivatives of the bulk moduli. Some evidence of these effects were consistent with current experimental observations.

**17:18**

**R44 15 Phonon mechanisms for structural phase transitions in Pu** AVADH SAXENA, TURAB LOOKMAN, R.C. ALBERS, *Los Alamos National Laboratory* CONDENSED MATTER THEORY TEAM, As a function of temeprature, pressure and alloying (Ga or Al) plutonium undergoes a series of structural transitions. Based on crystallography and symmetry we identify possible phonon mechanisms for various phase transitions. Coupling of shuffle modes corresponding to the specific phonons (primary order parameter) to the relevant strain tensor components (secondary order parameter) we develop Ginzburg-Landau free energies for some of the important structural transitions such as $\delta \rightarrow \alpha$ (FCC to simple monoclinic), $\delta \rightarrow \beta$ (FCC to side centered monoclinic) and $\beta \rightarrow \alpha$ (side centered monoclinic to simple monoclinic). We use these free energies to explore certain parts of the Pu phase diagram and relate to experimental structural and thermodynamic data such as specific heat and thermal expansion for the cases available. We also enumerate the orientational relationships between parent and product phases in these transitions.

**SESSION R45: STRONG CORRELATION IN METALS: MOTT TRANSITION**
**Wednesday Afternoon, 15 March 2006**
**348, Baltimore Convention Center at 14:30**
**Sergej Savrasov, University of California, Davis, presiding**

**14:30**

**R45 1 The metal-insulator transition in vanadium dioxide explored by optical methods** M.M. QAZILBASH, K.S. BURCH, D.N. BASOV, *University of California - San Diego* B.G. CHAE, H.T. KIM, *Basic Research Lab, ETRI, Daejeon, Korea* The nature of the metal-insulator transition (MIT) in vanadium dioxide ($VO_2$) remains a matter of debate. At the center of the debate is the relative importance of electron-electron correlations to the MIT. We study the MIT with spectroscopic ellipsometry on $VO_2$ films grown on sapphire substrates, and determine the optical constants in the insulating and metallic states from 50 meV to 5.5 eV. The changes in the optical constants with temperature in the metallic state have been tracked from 360 K up to 500 K. The redistribution of spectral weight in the real part of the optical conductivity as a result of the MIT will be discussed with emphasis on the changes to the interband transitions. This work has been supported by Department of Energy Grant No.DE-FG03-00ER45799.

**14:42**

**R45 2 First-order metal-insulator transition not accompanied by the structural phase transition observed in $VO_2$-based devices** HYUN-TAK KIM, BYUNG-GYU CHAE, BONG-JUN KIM, YONG-WOOK LEE, SUN-JIN YUN, KWANG-YONG KANG, *ETRI in Korea* An abrupt first-order metal-insulator transition (MIT) is observed during the application of a switching pulse voltage to $VO_2$-based two-terminal devices. When the abrupt MIT occurs, the structural phase transition (SPT) is investigated by a micro- Raman spectroscopy and a micro-XRD. The result shows that the MIT is not accompanied with the structural phase transition (SPT); the abrupt MIT is prior to the SPT. Moreover, any switching pulse over a threshold voltage of 7.1 V for the MIT enabled the device material to transform efficiently from an insulator to a metal. The measured delay time from the source switching pulse to an induced MIT pulse is an order of 20 nsec which is much less than a delay time of about one msec deduced by thermal model. This indicates that the first-order MIT does not occur due to thermal. We think this MIT is the Mott transition. (New J. Phys. 6 (1994) 52 (www.njp.org), Appl. Phys. Lett. 86 (2005) 242101, Physica B 369 (2005. December) xxxx)

**14:54**

**R45 3 Terahertz spectroscopy of the metal insulator transition in vanadium dioxide** DAVID HILTON, *Los Alamos National Laboratory* ROHIT PRASANKUMAR, *Los Alamos National Laboratory* ANDREA CAVALLERI, *Oxford University* SYLVAIN FOURMAUX, *Universite du Quebec* JEAN-CLAUDE KIEFFER, *Universite du Quebec* ANTOINETTE TAYLOR, *Los Alamos National Laboratory* RICHARD AVERITT, *Los Alamos National Laboratory* We employ terahertz spectroscopy to study the metal-insulator phase transition in vanadium dioxide ($VO_2$). We measure the terahertz frequency conductivity in the metallic phase that has a real conductivity of 1000 $\Omega^{-1}cm^{-1}$ and a negligible imaginary conductivity. The observed conductivity dynamics are consistent with a photoinduced transition in spatially inhomogeneous regions of the film, followed by a thermally driven transition to the maximum conductivity.

**15:06**

**R45 4 The role of dimers in the metal-insulator transitions in $VO_2$ and $Ti_2O_3$** T.C. KOETHE, J. GEGNER, Z. HU, C. SCHÜßLER-LANGEHEINE, H. ROTH, T. LORENZ, *II. Physikalisches Institut, Universität zu Köln, Germany* F. VENTURINI, N.B. BROOKES, *ESRF, Grenoble, France* W. REICHELT, *Institut für Anorganische Chemie, TU Dresden, Germany* L.H. TJENG, *II. Physikalisches Institut, Universität zu Köln, Germany* The nature of the metal-insulator-transition (MIT) in $VO_2$ has been subject of debate for a long time. Recently the scenario of an orbital assisted MIT has been proposed on the basis of the dramatic change of the orbital occupation as observed by soft-X-ray absorption spectroscopy measurements.[1] We present the results of our bulk sensitive photoemission study on the MIT in $VO_2$ using high quality single crystals. We observe a huge transfer of spectral weight across the MIT, supporting recent LDA+DMFT cluster calculations.[2] To investigate the possible role of dimers herein, we also studied the insulating phase of $Ti_2O_3$. Here we clearly observe a double peak structure which can be taken as a characteristic for the presence of dimers.

[1]M.W. Haverkort *et al.*, PRL **95**, 196404 (2005).
[2]S. Biermann *et al.*, PRL **94**, 026404 (2005).

**15:18**

**R45 5 Orbital-assisted metal-insulator transition in $VO_2$** M.W. HAVERKORT, *II. Physikalisches Institut, Universität zu Köln, Germany* Z. HU, *II. Physikalisches Institut, Universität zu Köln, Germany* A. TANAKA, *Department of Quantum Matter, ADSM, Hiroshima University, Japan* W. REICHELT, *Institut für Anorganische Chemie, Technische Universität Dresden, Germany* S. V. STRELTSOV, *Institute of Metal Physics, Ekaterinburg, Russia* M. A. KOROTIN, *Institute of Metal Physics, Ekaterinburg, Russia* V. I. ANISIMOV, *Institute of Metal Physics, Ekaterinburg, Russia* H. H. HSIEH, *Chung Cheng Institute of Technology, Taoyuan, Taiwan* H.-J. LIN, *National Synchrotron Radiation Research Center, Hsinchu, Taiwan* C. T. CHEN, *National Synchrotron Radiation Research Center, Hsinchu, Taiwan* D. I. KHOMSKII, *II. Physikalisches Institut, Universität zu Köln, Germany* L. H. TJENG, *II. Physikalisches Institut, Universität zu Köln, Germany* We found direct experimental evidence for an orbital switching in the V 3*d* states across the metal-insulator transition in $VO_2$. We have used soft-x-ray absorption spectroscopy at the V $L_{2,3}$ edges as a sensitive local probe, and have determined quantitatively the orbital polarizations. These results strongly suggest that, in going from the metallic to the insulating state, the orbital occupation changes in a manner that charge fluctuations and effective band widths are reduced, that the system becomes more 1-dimensional and more susceptible to a Peierls-like transition, and that the required massive orbital switching can only be made if the system is close to a Mott insulating regime.

**15:30**

**R45 6 X-ray Absorption Fine Structure Study of the Metal-Insulator Transition in Cr Doped $V_2O_3$*** A.I. FRENKEL, *Yeshiva University* D. PEASE, J. BUDNICK, P. SHANTHAKUMAR, T. HUANG, *University of Connecticut* N. ABITBOL, *Yeshiva University* P. METCALF, *Purdue University* We have applied the polarized x-ray absorption fine structure (XAFS) spectroscopy to study the series of $(V_{1-x}Cr_x)_2O_3$ where x ranges from 0 to 0.052. At room temperature, the metal-insulator transition (MIT) between paramagnetic metal 1 (PM-1) and paramagnetic insulator (PI) phases occurs as $x$ exceeds 0.01. At elevated temperatures, the second PM phase (PM 2) sets in the metallic samples ($x < 0.01$). We have obtained V K-edge and Cr K-edge spectra for the samples in the PM1, PM2 and PI phases at different concentrations (from 0.00365 to 0.0052) and temperatures (from 300 K to 673 K). V K-edge X-ray absorption near-edge structure (XANES) data show systematic changes across varies phase boundaries, both temperature and dopant-driven. Polarized Cr K-edge and V K-edge XANES and extended XAFS (EXAFS) data demonstrate, for the first time, that Cr enters the $V_2O_3$ lattice substitutionally, at all concentrations. Contrary to the Cr K-edge, the changes in the V K-edge XANES across the metal-insulator transition are strongly anisotropic. X-ray diffraction (XRD) and temperature dependent XANES and EXAFS results of Cr and V data will be discussed in terms of the possible percolative nature of the MIT in this system.

*DOE Grant No. DE-FG02-05ER36184

**15:42**

**R45 7 Nonequilibrium dynamical mean-field theory near the Mott transition** VOLODYMYR TURKOWSKI, JAMES FREERICKS, *Physics Department, Georgetown University, Washington, D.C. 20057* VELJKO ZLATIC, *Institute of Physics, Bijenicka c.46, P.O.B. 304, HR-10001, Zagreb, Croatia* We exactly calculate the non-equilibrium properties of the Falicov-Kimball model in an external electric field by using a recently developed non-equilibrium dynamical mean-field theory formalism [1,2]. In particular, we analyze the time-dependence of the electrical current in cases with different values of the on-site Coulomb interaction, when the system is in the metallic and in the insulating phases. The most interesting properties take place when the interaction energy is close to the metal-insulator transition value. The dynamics of the Bloch oscillations of the electrical current and the long time steady state nonlinear response are analyzed in detail. [1] J.K.Freericks, V.M.Turkowski, V. Zlatic, To be published in ''Proceedings of the 2005 Users Group Conference, IEEE Computer Society.''; cond-mat/0511061; [2] V.M. Turkowski, J.K. Freericks, Submitted to Phys. Rev. B; cond-mat/0511063.

**15:54**

**R45 8 Symmetry of Photoexcited States in Two-Dimensional Mott Insulators** TAKAMI TOHYAMA, *Institute for Materials Research, Tohoku University* The charge gap in Mott insulators is a consequence of strong electron correlation represented by large on-site Coulomb interaction. The correlation induces novel phenomena in terms of the interplay of charge and spin degrees of freedom. In this study, we examine symmetry of photoexcited

states with two photoinduced carriers in two-dimensional Mott insulators by applying the numerically exact diagonalization method to finite- size clusters of a half-filled Hubbard model in the strong- coupling limit [1]. The symmetry of minimum-energy bound state is found to be *s*-wave, which is different from a $d_{x^2-y^2}$ wave of a two-hole pair in doped Mott insulators. We demonstrate that the difference is originated from an exchange of fermions due to the motion of a doubly occupied site. Correspondingly large-shift Raman scattering across the Mott gap exhibits a minimum-energy excitation in the $A_1$ (*s*-wave) channel. We discuss implications of the results for the Raman scattering and other optical experiments. [1] T. Tohyama, cond-mat/0508519.

**16:06**

**R45 9 GW+DMFT Electronic Structure Calculations in Mott Insulators: Application to NiO** NIKOLAY ZEIN, *RRC ''Kurchatov Institute'' Moscow* SERGEY SAVRASOV, *University California, Davis* GABRIEL KOTLIAR, *University of Rutgers, NJ* We discuss the nature of Mott insulator ground state in transition metal oxides using newly developed GW+DMFT approach[1], which permits to join advantages of model (Hubbard-like) and density functional (LDA) calculations. The gap in LDA calculated antiferromagnetic state is usually much smaller than in experiment. Pure GW calculations increase the gap[2],but also cannot reproduce the paramagnetic insulating state. In GW +DMFT approach, without any fitting parameters, we calculate electronic structures of both antiferromagnetic and paramagnetic insulating states. We discuss relative position of d-metal and p-oxygen states,problems of renormalization of both electronic states near Fermi level and effective interaction at small energies, changes in static interaction under development of the gap in the paramagnetic state, effect of nearly filled bands on the value of self-energy correlation contribution. [1] N.E.Zein, S.Savrasov, G.Kotliar cond-mat/0511064 [2] S.V.Faleev, M.van Schilfgaarde, T.Kotani Phys.Rev.Lett. 93, 126406(2004)

**16:18**

**R45 10 Dynamical Mean Field Study of the Mott Transition on the Triangular Lattice Employing the Quantum Monte Carlo Technique** KARAN ARYANPOUR, RICHARD T. SCALETTAR, WARREN E. PICKETT, *Department of Physics, UC DAVIS* ALEXANDRU MACRIDIN, MARK JARRELL, *Department of Physics, Uinversity of Cincinnati* We present results on the Mott transition on the triangular lattice with nearest neighbor hopping employing the Dynamical Mean Field Theory (DMFT) and the Quantum Monte Carlo (QMC). DMFT and QMC can yield the critical value of electron-electron interaction U as a function of temperature T for the metal-insulator transition. By using the Maximum Entropy (MaxEnt) method, we calculate the Density of States (DOS) for a variety of U and T values. The formation of an Abrikosov-Suhl resonance peak in the intermediate coupling regime and a Mott gap in the strong coupling regime is observed. In addition, we discuss the behavior of the magnetic moment as a function of U and T.

**16:30**

**R45 11 First principles many-body approach to electron gas** PING SUN, *Rutgers University* GABRIEL KOTLIAR, *Rutgers University* We describe a first principles approach of constructing low energy, effective lattice model for the electron gas in a continuum of 2 and 3 spatial dimensions. The effects of the higher energy, unoccupied states are taken into account through virtue particle-hole excitations which screen the effective interactions at low energies. Using this effective model we obtain the correct order of magnitudes of the average inter- electron distance ($R_s$) at which the metal-insulator transition happens in 2d and 3d.

**16:42**

**R45 12 Effects of interorbital hopping on orbital fluctuations and metal-insulator transitions.** YUN SONG, *Department of Physics, Trent University* LIANG-JIAN ZOU, *Insititute of Solide State Physics, Chinese Academy of Sciences* We study the effects of inter-orbital hopping on orbital fluctuations and Mott-Hubbard metal-insulator transition (MIT) in the two-orbital Hubbard model within the extended linearized dynamical mean-field theory. By mapping the model onto an effective model with different bandwidths through the canonical transformation, we find that at half filling, the increases of the inter-orbital Coulomb interaction U′ and the Hund's coupling *J* drive the MIT, and the critical $J_c$ for MIT increases with the lift of the inter-orbital hopping integral $t_{ab}$. Meanwhile at quarter filling and in the strong correlation regime, the system without $t_{ab}$ exhibits MIT with the decreasing of *J*, and favors the orbital liquid ground state. However, the system transits from metal to insulator with the increasing of $t_{ab}$, accompanied with the rising of the orbital order parameter. These results show the important role of the inter-orbital hopping in the orbital fluctuation and orbital ordering.

## SESSION R46: ELECTRONIC AND OPTICAL PROPERTIES OF SEMICONDUCTORS: FIRST PRINCIPALS

**Wednesday Afternoon, 15 March 2006**
**349, Baltimore Convention Center at 14:30**
**Hai Ping Cheng, University of Florida, presiding**

**14:30**

**R46 1 Sequential Oxidation of Gallium Oxide Clusters—A First-Principles Study** S. GOWTHAM, *Michigan Technological University* AURORA COSTALES, *Universidad de Oviedo, Spain* RAVINDRA PANDEY, *Michigan Technological University, USA* The structural and electronic properties of gallium oxide lusters ($Ga_3O_n$; $n = 4 - 8$) are studied under the framework of density functional theory, with respect to sequential oxidation. The focus is on changes induced by the addition or removal of an electron from the neutral species as well as similarities/differences between aluminum oxide clusters of the same size. Lowest energy isomers in case of neutral clusters were found in doublet electronic state, and except for $Ga_3O_4^-$, $Ga_3O_4^+$, and $Ga_3O_5^-$, all ionized clusters were found in triplet electronic state. We observed that both addition and removal of an electron from the neutral cluster leads to significant changes in the structure of the lowest energy isomer, apart from altering the sequence of other low-lying geometries. Structural resemblance to corresponding alumina clusters is limited to a few cases while we predict new results for others. Binding energy remains almost constant throughout the oxidation process, with values for ionized systems bracketing the neutral ones. All clusters considered in this study are found to be stable against fragmentation via O and $O_2$ channels. Analysis of vibrational fre-

quencies confirms the tendency of $Ga_3O_6^+$ , $Ga_3O_7$ and $Ga_3O_8$ to form O-O bonds. HOMO-LUMO gap values show an oscillatory trend while calculated values of electron affinity and ionization potential are in good agreement with the corresponding values for alumina clusters.

**14:42**

**R46 2 Density Functional Band Gaps of AlAs** HUA JIN, GUANGLIN ZHAO, DIOLA BAGAYOKO, *Southern University and A&M College* We present results of ab-initio, self-consistent calculations of electronic properties of AlAs in the zinc-blende structure. Our non-relativistic calculations employed the generalized gradient approximation (GGA) of density functional potential and Bagayoko, Zhao and Williams (BZW) implementation of the linear combination of atomic orbitals (LCAO) formalism. Our calculated indirect band gaps at the X gand L points are 2.15 eV and 2.38 eV, respectively, in excellent agreement with experimental values. The calculated direct gap at $\Gamma$ is 25% smaller than the experimental one. This discrepancy may be due to experimental difficulties in the determination of this gap and it is also possibly due to the fact that it is not the fundamental one and hence may not be described by a ground state calculation. We also present calculated total and partial density of states and the electron effective mass at the bottom of the conduction band at the $\Gamma$gpoint. This work was funded in part by the Department of the Navy, Office of Naval Research (ONR, Grant No. N00014-05-1-0009), NASA (Award Nos. NCC 2-1344 and NAG 5-10253), and by the National Science Foundation (Award No. HRD 0000272). The authors are indebted to Dr. S. Hasan for his excellent technical support with the computing facilities.

**14:54**

**R46 3 The band gap of InN and ScN: A quasiparticle energy study based on exact-exchange density-functional theory** PATRICK RINKE, MATTHIAS SCHEFFLER, *Fritz-Haber-Institut der Max-Planck-Gesellschaft, Berlin - Germany* ABDALLAH QTEISH, *Yarmouk University, Irbid - Jordan* JÖRG NEUGEBAUER, *MPI für Eisenforschung, Düsseldorf - Germany* The group-IIIA nitride InN and the group-IIIB nitride ScN have recently received increased attention in the field of opto-electronics and optical coatings. Due to the difficulty of growing clean samples, however, the size of their band gap has not been well established, yet. We have recently shown, that quasiparticle energy calculations in the $G_0W_0$ approximation based on density-functional theory (DFT) calculations in the exact-exchange (EXX) approach yield band gaps in very good agreement with experiment for GaN and II-VI compounds [1]. For wurtzite InN our approach predicts a gap of 0.7 eV, suggesting an intrinsic value at the lower end of the experimentally observed range [2]. For ScN there exists a longstanding controversy if the material is a semimetal or semiconductor, which has only very recently been resolved in favor of the latter. Our calculations for rocksalt ScN predict an indirect band gap of 0.9 eV in good agreement with recent experimental findings [3]. [1] P. Rinke *et al.*, New J. Phys. **7**, 126 (2005) [2] W. Walukiewicz *et al.*, J. Crystal Growth **269**, 119 (2004) [3] A. A. Al-Brithen *et al.*, Phys. Rev. B **70**, 045303 (2004)

**15:06**

**R46 4 Calculated, Optical Proprieties of Wurtzite InN** DIOLA BAGAYOKO, HUA JIN, GUANGLIN ZHAO, *Southern University and A&M College* PHYSICS DEPARTMENT TEAM, We report the results of ab-initio calculations of the dielectric function of wurtzite indium nitride (w-InN). These optical properties are derived from ab-initio energy bands obtained with a local density function approximation (LDA) potential in the Bagayoko, Zhao, and Williams (BZW) implementation of the linear combination of atomic orbital (LCAO) formalism. We practically reproduced the measured, dielectric function (Superlattices and Microstructures 36, 591-597, 2004) at energies up to 6 eV. This agreement is not limited to major peaks; it also includes the fine structures of the shoulders. Indubitably, these findings vindicate density functional theory, in general, and the local density approximation (LDA), in particular, for the correct description of properties of semiconductors – provided the basis-set and variational effect, inherently associated with most calculations, is avoided with the first-principle BZW approach. This work was funded in part by the Department of the Navy, Office of Naval Research (ONR, Grant Nos. N00014-05-1-0009 and N00014-4-1-0587), NASA (Award Nos. NCC 2-1344, NAG 5-10253, and NNG 05G146G), and the National Science Foundation (Award No. HRD 0503362).

**15:18**

**R46 5 Predictions of Electronic and Optical Properties of Cubic InN** LASHOUNDA FRANKLIN, HUA JIN, G. L. ZHAO, DIOLA BAGAYOKO, *Southern University and A&M College* We present theoretical predictions of electronic, optical, and related properties of cubic indium nitride (c-InN). We utilized a local density functional approximation (LDA) potential and the linear combination of atomic orbitals (LCAO) in our ab-initio, self-consistent calculations that implemented the Bagayoko, Zhao, and Williams (BZW) method. The predicted band gap is 0.65 eV at a theoretical, equilibrium lattice constant of 5.017 Å. We discuss other predictions for the structural and optical properties of c-InN, including the bulk modulus, electron effective masses, and the calculated dielectric function. This work was funded in part by the Department of the Navy, Office of Naval Research (ONR, Grant Nos. N00014-05-1-0009 and N00014-4-1-0587), NASA (Award Nos. NCC 2-1344, NAG 5-10253, and NNG 05G146G), and the National Science Foundation (Award No. HRD 0503362).

**15:30**

**R46 6 Band offsets of semiconductor heterostructures : dependence on density functionals*** AMITA WADEHRA, RICHARD G. HENNIG, JOHN W. WILKINS, *Department of Physics, Ohio State University, Columbus, OH 43210* GUSTAVO E. SCUSERIA, *Department of Chemistry, Rice University, Houston, TX 77005* There is an increasing interest in In-based heterostructures for HEMT. Predictions of band offsets could speed up the development process of these devices. We assess various exchange-correlation potentials including hybrid functionals such as HSE[1] to analyze electronic properties and structural energetics of such systems. We calculate the band gaps and band offsets of InAs heterostructures such as InAs/InAlAs and InAs/InAsP. We also show a comparison of the structural energies for interfaces and site substitutions obtained by using different functionals. An accurate estimation of these properties is crucial for their application in the manufacture and performance of novel semiconductor devices.

*Supported by NSF (DMR-0313468) and DOE (DE-FG02-99ER45795). Computational resources provided by OSC

[1]J. Heyd, J.E. Peralta, G.E. Scuseria and R.L. Martin, *J. Chem. Phys.* **123**, 174101 (2005).

**15:42**

**R46 7 All-Electron *GW* Approximation in the Augmented-Plane-Wave Basis-Set Limit*** CHRISTOPH FRIEDRICH, ARNO SCHINDLMAYR, STEFAN BLÜGEL, *Forschungszentrum Jülich, Germany* TAKAO KOTANI, *Arizona State University, Tempe, USA* The *GW* approximation for the electronic self-energy is known to yield quasiparticle band structures in very good agreement with experiment, but almost all codes so far rely on the pseudopotential approach, which restricts the range of materials that can be treated efficiently. In addition, the adequacy of the pseudopotential approximation for quasiparticle calculations has recently come under debate. We have developed an alternative implementation within the full-potential linearized augmented-plane-wave (FLAPW) method. As possible errors resulting from the linearization of the basis set are frequently overlooked, we here investigate the influence on the *GW* self-energy correction. A systematic improvement is achieved by including additional local orbitals defined as second and higher energy derivatives of solutions to the radial scalar-relativistic Dirac equation, which constitute a natural extension of the FLAPW basis set. Within this approach we can systematically reduce the linearization error and reach the exact augmented-plane-wave basis-set limit. While the electronic self-energy and the quasiparticle energies benefit from the better description of the unoccupied states, the resulting band gaps remain relatively unaffected.

*We acknowledge financial support from the Deutsche Forschungsgemeinschaft through the Priority Program 1145.

**15:54**

**R46 8 Electronic transport in dilute GaAs:N** GEOFFREY STENUIT, STEPHEN FAHY, *Tyndall National Institute, Cork, Ireland* Plane-wave pseudopotential-based DFT (density functional theory) are used to determine the electronic properties (band structure, effective mass and energy gap) of dilute GaAs:N with substitutional nitrogen concentration $x = 1 - 3\%$.Calculations are performed using LDA (local density approximation) for the exchange-correlation functional and applied to large supercells (more than 64 atoms) to achieve the dilute limit. Scattering cross-section, as well as the mobility are derived from the nitrogen concentration dependence of the band gap in GaAsN. The effects of an $N_2$ split interstitial substitution on the electronic properties are also discussed. Finally, the presence of a localized nitrogen state in such material is also studied within this ab initio framework.

**16:06**

**R46 9 Electronic band structure, crystal structure and phonons of $ZnSiN_2$*** TULA R. PAUDEL, WALTER R. L. LAMBRECHT, *Case Western Reserve Univ* $ZnSiN_2$ is an interesting alternative to GaN. Its crystal structure is derived from the wurtzite structure of GaN by a particular ordered subsitution of the Ga atoms by Zn and Si in such as way that each N is coordinated with two Si and two Zn atoms. Electronic structure calculations were performed with two different approaches, the plane-wave ultrasoft pseudopotential approach and the full-potential linearized muffin-tin orbital method both using the local density approaximation (LDA). The structure was fully optimized. The relaxation consists primarily of the N atom finding its optimum position inside its nearest neighbor tetrahedron by making a shorter Si-N and longer Zn-N bond. An indirect LDA band gap of about 3.4 eV is obtained. Thus a gap larger than for GaN is expected. Calculations of the phonons at the center of the Brillouin zone are in progress using the linear response approach. A comparison with ZnGeN2, which was studied earlier, [W. R. L. Lambrecht et al. Phys Rev. B 72, 155202 (2005)] will be presented.

*Supported by AFOSR

**16:18**

**R46 10 Electronic and magnetic properties of Cu-doped ZnO** ANDREIA LUISA DA ROSA, LUNMEI HUANG, RAJEEV AHUJA, *Uppsala University, Dept. of Physics, Box 530, SE-75121, Uppsala, Sweden* Diluted magnetic semiconductors have attracted attention in the past years, since they open the possibility for new devices with integrated magnetic, electronic and optical functionality. Among possible candidates ZnO is especially attractive, since it is a wide band gap material and is also piezoelectric. On the other hand, Cu and its oxides are non-magnetic, so magnetism coming from Cu clusters or precipitates can be ruled out. Although some experimental results confirm room temperature ferromagnetism in Cu-doped ZnO, other works have reported its absence. In this work we use first-principles calculations to study Cu-doped ZnO for various Cu concentrations. The total energy differences were computed for parallel and antiparallel arrangements of the Cu spins to determine whether Cu-doped ZnO has a ferromagnetic or anti-ferromagnetic ground state. We found that Cu-doped ZnO has a ferromagnetic ground state for all calculated concentrations. We also found that the exchange coupling between the Cu atoms is short ranged. We suggest that the strong hybridization between the Cu-3*d* and O-2*p* states is responsible for mediating the ferromagnetic interaction between the Cu atoms.

**16:30**

**R46 11 Computational band-gap engineering in wide-gap MgO-ZnO alloys** R. MATT LEONE, GUS L. W. HART, *Dept. Physics & Astronomy, Northern Arizona University* Wide-gap semiconducting materials are extending critical applications in high temperature/power electronics and optoelectronics such as with the continued advancement of blue to ultraviolet LEDs and lasers. MgO-ZnO alloys have been increasingly investigated due to their UV luminescence from 150-400 nm, 3.3-7.8 eV. We have developed a first-principles model Hamiltonian that predicts band gaps of cubic MgO-ZnO alloys for any superlattice type or atomic configuration. First-principles band gap energies were used as input to construct an Ising-like cluster expansion, and the cluster types used were determined using a novel genetic algorithm. The itdesign of specific wide-gap MgO-ZnO alloy superlattices for desired target band gaps is now possible with this resultant model Hamiltonian.

**16:42**

**R46 12 Electronic Structure and Vibrational spectra of $C_2B_{10}$ Based Clusters and Films*** L. L. BOYER, KYUNGWHA PARK, M. R. PEDERSON, *Naval Research Laboratory* W. N. MEI, X. C. ZENG, S. BULUSU, ELLEN DAY, SHIREEN ADENWALLA, *University of Nebraska* SEAMUS CURRAN, JAMES DEWALD, *New Mexico State University* Semiconducting boron carbide films can be used to detect neutrons and convert energy of associated nuclear reactions directly into electrical current. Such films were prepared by removing hydrogen from the

three polytypes of $C_2B_{10}H_{12}$ (carborane) deposited on various surfaces. Results from Raman scattering measurements on these films will be presented and compared with results of calculations for clusters. The electronic structure, total energy and vibrational properties of carborane molecules and $C_2B_{10}$ clusters calculated using density functional theory are reported. Computed vibrational spectra for carborane molecules are found to be in close agreement with previously published measured spectra taken on carborane solids. Eleven vibrationally stable $C_2B_{10}$ clusters have been identified and their relative energies, HOMO-LUMO gaps and vibrational properties will be discussed. Good agreement with the experimental Raman spectra is achieved from theoretical spectra computed using a Boltzmann distribution of the six lowest energy free-clusters.

*Supported by the Office of Naval Research

**16:54**
**R46 13 Electron Distributions in Hexagonal Selenium and Tellurium and Monoclinic Selenium with Dilute Impurities and Associated Nuclear Quadrupole Interactions*.** N.B. MAHARJAN, D.D. PAUDYAL, D.R. MISHRA, S. BYAHUT, M.M. ARYAL, *Tribhuvan University, Kirtipur, Kathmandu, Nepal* HWA-SUCK CHO, *Yeung-Nam University, Taegu, S. Korea* R.H. SCHEICHER, *Michigan Technological University, Houghton* LEE CHOW, *University of Central Florida, Orlando* JUNHO JEONG, T.P. DAS**, *State University of New York at Albany* The electron structures of Selenium chains and rings with Te impurities in hexagonal and monoclinic structures respectively and Se impurities in Te chains in hexagonal lattice have been studied using Hartree-Fock cluster model including many-body effects, including lattice relaxation effects. The calculated electronic wave-functions are utilized to obtain $^{77}$Se and $^{125}$Te nuclear quadrupole coupling constants $e^2qQ$ and asymmetry parameters $\eta$ and compared with available experimental data from Mossbauer and perturbed angular correlation measurements. From our results, the expected nature of nuclear quadrupole interactions associated with Sb impurities will be discussed. *Supported by NSF US-Nepal Program and UGC Nepal **Also at UCF, Orlando

## SESSION S48: FED BUSINESS MEETING & RECEPTION
**Wednesday Evening, 15 March 2006; Grand Ballroom Salon III, Marriott Waterfront Hotel at 17:30**

**17:30**
**S48 1 FED Business Meeting & Reception**

## SESSION S49: DCOMP BUSINESS MEETING
**Wednesday Evening, 15 March 2006; Dover C, Marriott Waterfront Hotel at 18:30**

**18:30**
**S49 1 DCOMP Business Meeting**

## SESSION T7: PHYSICS, CHEMISTRY AND BIOLOGY OF THE HYDROPHOBIC EFFECT
**Wednesday Evening, 15 March 2006; 307, Baltimore Convention Center at 17:45**
**Chao Tang, University of California, San Francisco, presiding**

**17:45**
**T7 1 The Hydrophobic Effect ab initio.**
JE-LUEN LI, *Princeton University*

We employ fully quantum-mechanical molecular-dynamics simulations to evaluate the force between two methanes dissolved in water, as a model for hydrophobic association. A stable configuration is found near the methane-methane contact separation, while a shallow second potential minimum occurs for the solvent-separated configuration. The strength and shape of the potential of mean force are in conflict with earlier classical-force-field simulations but agree well with a simple hydrophobic burial model which is based on solubility experiments. Examination of solvent dynamics reveals stable water cages at several specific methane-methane separations.

**18:21**
**T7 2 Hydrophobic Effects as Seen in Lattice Models.**
BENJAMIN WIDOM, *Cornell University*

A class of lattice models incorporating the thermodynamic mechanism of hydrophobicity is defined and its properties derived. The models are equivalent to Ising models in a field. The solvent-mediated part of the potential of mean force between a pair of hydrophobic solute molecules is obtained from the pair correlation function of the underlying one-component lattice gas. The models yield a testable relation between the strength of the hydrophobic attraction between

solute molecules and the free energy of solvation of a single one. The properties of the models are obtainable analytically in Bethe-Guggenheim approximation. The local energy density in the solvent is obtained as a function of the distance from an inserted solute. As a consistency check, this energy density, when summed over the lattice, is found to satisfy the required thermodynamic relation between the total energy change due to the solute molecule and the temperature dependence of the solubility.

**18:57**
**T7 3 Hydrophobicity at small and large length scales.**
DAVID CHANDLER, *University of California, Berkeley*

This lecture is about the statistics of density fluctuations for liquids at thermodynamic states close to liquid-vapor coexistence. Theoretical and simulation results on the length scale dependence of this statistics will be described and used to explain hydrophobic solvation, hydrophobic forces of assembly and kinetics of hydrophobic collapse. Several issues concerning so-called ''drying'' near extended hydrophobic surfaces will be addressed, and biophysical implications will be discussed.

**19:33**
**T7 4 Modeling water, hydrophobic interactions, and polymer collapse.**
THOMAS TRUSKETT, *The University of Texas at Austin*

Small and large nonpolar solutes exhibit qualitatively different hydration thermodynamics. The former are naturally accommodated into bulk water via equilibrium density fluctuations, while the latter require the formation of a macroscopic solute-water interface. Although there has been significant progress on the theory of lengthscale-dependent hydration, there are still many open questions concerning how various thermodynamic parameters (e.g., pressure, additive concentration, and pH) impact the crossover between small and large solute behavior. Similarly, there is confusion over whether hydration of small, intermediate, or large lengthscales dominate in various biological self-assembly processes. In this talk, I discuss recent theoretical progress on understanding how solution conditions affect the crossover between small and large solute hydration phenomena and how simulation/theory of the collapse of hydrophobic polymers can provide new insights into the relevance of hydrophobic interactions at different lengthscales.

## SESSION T50: PERSPECTIVES ON OUR ENERGY FUTURE
**Wednesday Evening, 15 March 2006; Grand Salon V, Marriott Waterfront Hotel at 19:30**



**19:30**
**T50 1 TBD.**
STEVEN KOONIN, *Chief Scientist for BP*

This abstract was not submitted electronically.

**20:06**
**T50 2 Physics, Physicists, and Our Energy Future.**
PATRICIA DEHMER, *Office of Basic Energy Sciences, U.S. Department of Energy*

Abundant energy is intimately linked with global stability, economic prosperity, and quality of life. However, even with aggressive conservation and energy efficiency measures, the projected increase of the Earth's population accompanied by rapid technology development and economic growth is projected to double the demand for energy by mid century and more than triple the demand by the end of the century. The reserves of fossil fuels that currently account for 85% of U.S. energy will fall far short of demand over the long term, and their use is associated with environmental contaminants ranging from greenhouse gases and toxic gases to particulates. Our energy challenges cannot be met by incremental improvements to existing technologies. Transformational changes and disruptive technologies will be required to provide clean, reliable, economic solutions. As in the past, many of these changes will likely come from fundamental research in the physical sciences. How we approach the problem as a Nation and how we respond as a community of scientists will determine our success.

**SESSION U1: SPIN LIQUIDS AND SUPERCONDUCTIVITY NEAR THE MOTT TRANSITION**
**Thursday Morning, 16 March 2006; Ballroom IV, Baltimore Convention Center at 8:00**
**Dunghai Lee, University of California, Berkeley, presiding**

**8:00**
**U1 1 Spin Liquid States in the Hubbard Model: Implications for Organics.***
PATRICK LEE, *Department of Physics, MIT*

We formulate a U(1) gauge theory of the Hubbard model in the slave-rotor representation. From this formalism it is argued that spin liquid phases may exist near the Mott transition in the Hubbard model on triangular and honeycomb lattices at half filling. The organic compound $\kappa$-(BEDT-TTF)$_2$Cu$_2$(CN)$_3$ is a good candidate for the spin liquid state on a triangular lattice. We predict a highly unusual temperature dependence for the thermal conductivity of this material.

*Sung-Sik Lee and P.A. Lee, Phys. Rev. Lett. **95**, 036403.

**8:36**
**U1 2 Spin liquid and superconductivity in two-dimensional organic charge transfer salts.**
JOERG SCHMALIAN, *Iowa State University*

We introduce and analyze a variational wave function for quasi two-dimensional organic salts containing strong local and nonlocal correlation effects. We find an unconventional superconducting ground state for intermediate charge carrier interaction, sandwiched between a conventional metal at weak coupling and a spin liquid at larger coupling. Most remarkably, the excitation spectrum is dramatically renormalized and is found to be the driving force for the formation of the unusual superconducting state.

**9:12**
**U1 3 Anomalous superconductivity near the Mott transition.**
ANDRE-MARIE TREMBLAY,* *Universite de Sherbrooke*

High-temperature superconductivity appears near an antiferromagnetic Mott insulating phase and a normal phase with a pseudogap. It was suggested early on by Anderson that the strong-coupling limit of the Hubbard model should contain the main physics. It is only recently that we have begun to have access to sufficiently accurate algorithms and powerful enough computers to begin to extract the main features of the phase diagram of high-temperature superconductors from the Hubbard model in a nearly quantitative manner. In this talk, the zero temperature phase diagram of the two-dimensional Hubbard model is discussed based on several ''quantum cluster'' approaches, mainly Variational Cluster Perturbation Theory [1] and Cellular Dynamical Mean Field Theory [2], that shall be introduced. The overall ground state phase diagram of the high-temperature superconductors as well as the asymmetric one-particle excitation spectra for both hole- and electron-doping are reproduced. The d-wave order parameter is found to assume a dome shape as a function of doping and to scale like the magnetic exchange coupling J for U comparable to the bandwidth. We stress the features of superconductivity that are non-BCS like due to the proximity to the Mott insulator. In stark contrast with BCS theory, the superconducting gap can decrease monotonically at the same time as the d-wave order parameter increases away from half-filling. Also, d-wave superconductivity is driven by a lowering of kinetic energy instead of potential energy, in conformity with experiments on cuprates. The pseudogap [3-5] and results of other approaches will also be briefly touched upon. [1] David Sénéchal, P.-L. Lavertu, M.-A. Marois, and A.- M.S. Tremblay, Phys. Rev. Lett. **94**, 156404 (2005). [2] S. S. Kancharla, M. Civelli, M. Capone, B. Kyung, D. Senechal, G. Kotliar, A.-M.S. Tremblay, cond-mat/0508205. [3] B. Kyung, S.S. Kancharla, D. Sénéchal, A.-M.S. Tremblay, M. Civelli, and G. Kotliar cond-mat/0502565 [4] B. Kyung, V. Hankevych, A.-M. Daré et A.-M.S. Tremblay, Phys. Rev. Lett. **93**, 147004 (2004). [5] A.-M.S. Tremblay, B. Kyung and David Sénéchal, cond-mat/0511334.

*Supported by: NSERC, CFI, FQRNT, Canada Research Chair program and Canadian Institute of Advanced Research.

**9:48**
**U1 4 The origin of the pseudogap in the high Tc superconductors.**
HERB A. MOOK, *Center for Neutron Scattering and the Condensed Matter Sciences Division, Oak Ridge National Laboratory*

The origin of the pseudogap is one of the most important questions in high Tc superconductors. The idea of circulating currents as being responsible for the pseudogap will be considered and various current paths through the Cu-O plane examined in the light of recent neutron scattering experiments.

**10:24**
**U1 5 Polarized Neutron Diffraction to discover symmetry breaking in pseudogap region of Y(123)-Cuprate.**
PHIIPPE BOURGES, *Laboratoire Léon Brilllouin, CEA-Saclay*

One of the leading issues in high-$T_C$ superconductors is the origin of the pseudogap phase in underdoped cuprates. Using polarized elastic neutron diffraction, we identify a novel magnetic order in the $YBa_2Cu_3O_{6+x}$ system*. The observed magnetic order preserves translational symmetry as proposed for orbital moments in the circulating current theory of the pseudogap state (see C.M. Varma, at http://fr.arxiv.org/abs/cond-mat/0507214). To date, it is the first direct evidence of an hidden order parameter characterizing the pseudogap phase in high-$T_C$ cuprates. * B. Fauqué, Y. Sidis, V. Hinkov, S. Pailhès, C.T. Lin, X. Chaud and P. Bourges, at http://fr.arxiv.org/abs/cond- mat/0509210.

## SESSION U2: QUANTUM MAGNETS IN HIGH MAGNETIC FIELDS
**Thursday Morning, 16 March 2006; Ballroom III, Baltimore Convention Center at 8:00**
**Igor Zaliznyak, Brookhaven National Laboratory, presiding**

**8:00**
**U2 1 Spinons, Solitons, and Breathers in Quasi-One-Dimensional Magnets.***
COLLIN BROHOLM, *Johns Hopkins University*

By scattering neutrons from coordination polymer magnets, we contrast the effects of a uniform and a staggered magnetic field on the quantum critical state of a spin-1/2 chain. In a partially magnetized state of copper pyrazine dinitrate (CuPzN) we find bounded spectral continua indicating that neutrons scatter from spin-1/2 quasi-particle pairs [1]. The complex boundaries including an incommensurate soft spot result from a field induced shift in the Fermi points for these quasi-particles. The measurements indicate that the magnetized state of CuPzN remains quantum critical. Copper benzoate [2] and $CuCl_2$2(dimethylsulfoxide) (CDC) [3] differ from CuPzN in that there are two spins per unit cell along the spin chain. Rather than continuous spectra, we find resolution limited gapped excitations when these materials are subject to high fields. So with two spins per unit cell, an applied field can drive the spin-1/2 chain away from criticality. The explanation for this effect was provided by Affleck and Oshikawa. The alternating coordination environment induces a transverse staggered field and spinon binding. The quantum sine-Gordon model is the relevant low energy field theory and it predicts soliton and breather excitations at specific energies and wave vectors that we compare to the experiments. We shall also compare a complete measurement of the dynamic spin correlation function for CDC in a field to exact diagonalization results for a spin-1/2 chain with a staggered and uniform magnetic field [4]. [1] M. B. Stone, D. H. Reich, C. Broholm, K. Lefmann, C. Rischel, C. P. Landee, and M. M. Turnbull, Phys. Rev. Lett. **91**, 037205 (2003). [2] M. Kenzelmann, Y. Chien, C. Broholm, D. H. Reich, and Y. Qiu, Phys. Rev. Lett. **93**, 017204 (2004). [3] D. C. Dender, P. R. Hammar, Daniel H. Reich, C. Broholm, and G. Aeppli, Phys. Rev. Lett. **79**, 1750 (1997). [4] M. Kenzelmann, C. D. Batista, Y. Chen, C. Broholm, D. H. Reich, S. Park, and Y. Qiu, Phys. Rev. B **71**, 094411 (2005).

*Supported by DMR-0306940.

**8:36**
**U2 2 Ordering and Excitations in the Field-Induced Magnetic Phase of $Cs_3Cr_2Br_9$.**
BEATRICE GRENIER, *CEA-Grenoble*

$Cs_3Cr_2Br_9$ is an interesting example of interacting spin-dimer system. As in other isotropic antiferromagnets such as Haldane or alternating chains and ladders, the ground state in zero field is a total spin singlet separated from the excited triplet by an energy gap. In a magnetic field $H$, a phase transition occurs at a critical field $H_{c1}$, where the gap to the lowest component of the Zeeman-split triplet closes. Above $H_{c1}$, field-induced magnetic order (FIMO) for spin components perpendicular to $H$ is induced by inter-dimer or inter-chain couplings. The FIMO transition may be considered as a Bose-Einstein Condensation. $Cs_3Cr_2Br_9$ differs from other dimer systems currently studied (*e.g.* PHCC, $TlCuCl_3$) in two main ways: each $Cr^{3+}$ ion of the dimer has spin 3/2 rather than 1/2 for Cu-based systems and the arrangement of the dimers is hexagonal. This gives rise to anisotropy and frustration in a 3D lattice, respectively. The possibility of studying the magnetic ordering and the spin dynamics in a FIMO with sufficient detail to bring out features of frustration and anisotropy motivated the present neutron scattering study in $Cs_3Cr_2Br_9$.* Two field orientations have been exploited, perpendicular and parallel to the easy axis **c** (direction of the dimers). First, I present the diffraction study: the FIMO displays large hysteresis incommensurability, showing the importance of frustration. The impact of anisotropy is seen in the magnetic structure, whose nature strongly depends on the field direction. Second, I focus on spin dynamics: it

quantifies the presence of anisotropy and shows its crucial role on the energy gap at $H_{c1}$, which is measurably open or not, depending on whether $H$ is perpendicular or parallel to **c**. Third, an explanation is proposed for the large value of the gap at higher field: it involves the mixing of higher order states (itextended-FIMO), reflected by the absence of magnetization plateaus. Comparison with the sister $Cs_3Cr_2Cl_9$ compound provides a test of this hypothesis. *B. Grenier et al., Phys. Rev. Lett. **92**, 177202 (2004).

**9:12**
**U2 3 Quantum phase transitions in integer spin chains.**
ANDREY ZHELUDEV, *Oak Ridge National Laboratory*

High field inelastic neutron scattering experiments on the $S=1$ bond-alternating 1D antiferromagnet NTENP, the anisotropic $S = 1$-chain Haldane-gap compound NDMAP and the isotropic ''composite'' Haldane spin chain IPA-$CuCl_3$ [T. Masuda *et al.*, cond-mat/0506382] reveal key differences in the spin dynamics of these distinct types of quantum spin liquids. In modest applied fields the spectra of NDMAP [A. Zheludev *et al.*, Phys. Rev. Lett. **88**, 077206 (2002)] and IPA-$CuCl_3$ feature three sharp stable gap excitations. In contrast, in NTENP the highest mode is anomalously weak at $H = 0$ and rapidly broadens and vanishes when the field is turned on. Above the critical field of 1D Bose condensation of magnons and long-range ordering NDMAP retains a triplet of massive long-lived excitations [A. Zheludev *et al.*, Phys. Rev. B **68**, 134438 (2003)]. In IPA-$CuCl_3$ only two sharp gap excitations persist, with possibly an additional gapless mode. In NTENP only one sharp excitation branch is observed in this regime [Hagiwara *et al.*, Phys. Rev. Lett. **94**, 177202 (2005)], but there is new evidence of low-lying excitation continua. Work at ORNL was carried out under DOE Contract No. DE-AC05-00OR22725.

**9:48**
**U2 4 High-field ESR and thermodynamic studies of uniform and bond-alternating $S=1$ spin chains.**
MASAYUKI HAGIWARA

Recently, field-induced phenomena in quantum spin systems have attracted considerable interest. Gapped one-dimensional (1D) spin systems with a spin value $S=1$ subject to an external magnetic field strong enough to close the gap ($H_c$) are driven into a new phase. Spin excitations in this field-induced phase have been studied by experiments on a uniform S=1 antiferromagnetic spin chain $Ni(C_5H_{14}N_2)_2N_3(PF_6)$, alias NDMAP and a bond-alternating one $Ni(C_9H_{24}N_4)NO_2(ClO_4)$, alias NTENP. We performed high-field and multi-frequency ESR experiments at 1.5 K on these compounds and observed gapped excitations above $H_c$. Two or three excitation modes were observed depending on the field direction in NDMAP and only one excitation in NTENP. These results are consistent with those obtained by inelastic neutron scattering experiments in a magnetic field. Both compounds exhibit the long-range order (LRO) at a magnetic field above $H_c$ and a low temperature. Observed gapped excitations are very different from those expected from a conventional spin-wave theory in the LRO state. For NDMAP, observed branches satisfactorily agree with those analyzed by a phenomenological field theory. The difference of observed gapped excitations between NDMAP and NTENP can be explained by an interaction with a low-lying two magnon continuum at $q=\pi$ that is present in a bond-alternating chain but absent in a uniform one. When an antiferromagnetic spin chain with $S=1$ has an XY or Heisenberg symmetry, the phase above $H_c$ is critical and its low-energy physics is described by a Tomonaga-Luttinger liquid (TLL), which is characterized by a gapless $k$-linear energy dispersion with an incommensurate $k_0$ and a spin correlation having an algebraic decay. NTENP has nearly an XY symmetry and a linear temperature($T$) dependence of the specific heat ($C_{mag}$) was observed for the magnetic field parallel to the chain above $H_c$ in a temperature region above that of the LRO state. The ratio $C_{mag}/T$ increases as the magnetic field approaches $H_c$ from above and is in good agreement with the prediction of the $c=1$ conformal field theory, providing a conclusive evidence for a TLL in a gapped quasi-1D antiferromagnet.

**10:24**
**U2 5 Anisotropic Haldane-gap chains in a magnetic field.**
FABIAN ESSLER, *University of Oxford, UK*

We consider quasi one dimensional spin-1 Heisenberg chains with crystal field anisotropy in a uniform magnetic field. We determine the dynamical structure factor in various limits and obtain a fairly complete qualitative picture of how it changes with the applied field. In particular, we discuss how the width of the higher energy single magnon modes depends on the field. We consider the effects of a weak interchain coupling. We discuss the relevance of our results for neutron scattering experiments on the quasi-1D Haldane-gap compound NDMAP.

**SESSION U3: NANOMECHANICAL ARCHITECTURE OF STRAINED THIN FILMS**
**Thursday Morning, 16 March 2006; Ballroom I, Baltimore Convention Center at 8:00**
**Max Lagally, University of Wisconsin-Madison, presiding**

**8:00**
**U3 1 Precise semiconductor nanotubes and nanocorrugated quantum systems: concept, fabrication and properties.**
VICTOR PRINZ, *Institute of Semiconductor Physics, Siberian Branch of Russian Academy of Sciences*

Physics and technology of several new classes of nanostructures, namely, variously shaped semiconductor, metal, dielectric and hybrid nanoshells, are overviewed. Previously, we discoved that ultrathin epitaxial heterofilms (down to two monolayers in thickness in the case of InGaAs/GaAs) can be controllably released from substrates and rolled up under the action of internal stresses into various cylindrical micro- and nanotubes, scrolls, rings, helices, etc. [1]. In this way, nanotubes with minimum diameter of 2-nm can be obtained. The fabricated nanoshells offer much promise as building blocks for nanoelectronic and nanomechanic devices, their fabrication technology being fully compatible with the well-established integrated-circuit technology [2]. Experimental and theoretical results concerning the quantum processes in the fabricated micro - and nanoshells are reported, including ballistic and tunnel transport in bent waveguides, magnetotransport, bending-induced formation of deep quantum wells and quantum dots molecules [3]. New results on the formation of spatially periodic nanostructures, nanocorrugated systems, shells with 1-nm minimum radius of curvature, building blocks for nanodevices and new nanocomposite materials are described. The present report outlines the cornerstone stages in the development of this fabrication technology for semiconductor and metal nanoobjects, including: directional rolling of films, super-critical drying of nanoshells, passivation of electron states in them, etc. Benefits offered by the new approach in the creation of 3D ordered nanoobject arrays, as well as challenges met in the development of the original nano- and molecular technology are discussed.

V.Ya. Prinz et al., Physica E 6, 828 (2000).
V.Ya. Prinz, Physica E 23 260; 24, 54 (2004).
V. M. Osadchii and V. Ya. Prinz, Phys. Rev. B 72, 033313 (2005).

**8:36**
**U3 2 Nanomechanical Architecture of Strained Bi-layer Thin Films: From Design Principles to Fabrication.**
FENG LIU, *University of Utah*

Controlled and consistent fabrication of different classes and shapes of nanostructures (as opposed to simply stochastic self-assembly) will be a requirement if nanotechnology expects to achieve its promised impact on society. We illustrate by both theory and computation the design principles of an emerging nanofabrication approach based on the itnanomechanical architecture of strained bi-layer thin films, which are further confirmed by experiments through fabrication of a variety of nanostructures, including nanotubes, nanorings, nanodrills, and nanocoils. This approach demonstrates the possibility of fabricating nanostructures with an unprecedented level of control over their size, geometry, and uniformity, based on ita priori designs. It possesses also an unparallel level of versatility for making nanostructures with combinations of different materials. By combined multi-scale modeling and simulations from first-principles calculation, to molecular dynamics simulation, and to continuum mechanics modeling, we demonstrate how mechanical bending of nanoscale thin films differs from that of macroscopic thin films. For example, we show that surface stress will even play a more dominant role than misfit strain in bending a film that is down a few monolayers thick. *This work is supported by DOE and NSF.

**9:12**
**U3 3 Nonochannel networks, light emission and waveguidung of micro- and nanotubes, and ultra-compact coils.**
OLIVER G. SCHMIDT, *Max-Planck-Institut fuer Festkoerperforschung, Heisenbergstr. 1, D-70569 Stuttgart, Germany*

Quite generally, thin solid films can be partially released from a substrate surface by selective underetching and form into various 3D micro- and nano-objects [1-3]. Here, we show that such released layers form into complex nanochannel networks, which can be fluid-filled and emptied within fractions of a second. Furthermore, we demonstrate that single material layers roll-up into micro- and nanotubes. In particular, we show that all-Si tubes can be fabricated. Quantum emitters such as InAs/GaAs quantum dot heterostructures are integrated into the wall of rolled-up microtubes, and we study the emission and the waveguiding properties of such ''quantum dots in a tube'' [4]. Finally, metal/semiconductor bilayers are rolled up into microtubes. This technique opens the way to realize and integrate ultra-compact coils, transformers and capacitors on a single chip [5]. I am grateful to my collaborators Y. Mei, R. Songmuang, C. Mendach, C. Deneke, D. Thurmer, F. Cavallo, and A. Rastelli (all Max-Planck-Institut fuer Festkoerperforschung Stuttgart, Germany). [1] O. G. Schmidt and K. Eberl, Nature 410, 168 (2001). [2] O. G. Schmidt et al., Advanced Materials 13, 756 (2001). [3] V. Ya. Prinz et al., Physica E 6, 828 (2000). [4] S. Mendach et al., Appl. Phys. Lett. (submitted). [5] O. G. Schmidt et al., IEEE J. Selected Topics Quantum Electronics 8, 1025 (2002).

**9:48**
**U3 4 Fabrication and Applications of Tubular Semiconductor Membranes.***
ROBERT BLICK, *University of Wisconsin-Madison*

We present transport measurements on curved semiconductor membranes. The aim is to investigate geometric potentials in low dimensional electron systems. We have conducted first studies on topography dependant electron transport in complete tubes, using built in strain between lattice mismatched semiconductors. We will discuss the processing details in SiGe and InGaAs strained layers. Initial studies reveal two regimes of electron transport which are probed by a varying perpendicular magnetic field. At low magnetic field, we see an increase in electron scattering along curved regions due to an increase in electron scattering. At high magnetic field, we find a linear increase in resistance of the curved region as compared to planar regions. Finally, we will give an outlook into possible applications in nano-electromechanical systems.

*Support through the National Science Foundation is acknowledged (MRSEC/IRG1).

**SESSION U4: LITHOGRAPHY**
**Thursday Morning, 16 March 2006; 308, Baltimore Convention Center at 8:00**
**Vivek Prabhu, National Institute of Standards and Technology, Polymers Division, presiding**

**8:00**
**U4 1 Step and Flash Imprint Lithography.***
GRANT WILLSON, *The University of Texas*

Step and Flash Imprint Lithography has been recognized as a potentially low cost, high resolution patterning technique. Most of the published development work has been directed toward tool design and processing techniques. This work will be reviewed. There remains a tremendous opportunity and need to develop new materials for specific SFIL applications. An overview of relevant materials-related development work for SFIL lithographic applications will be presented. Material requirements for SFIL patterning for the sub-50 nm integrated circuit regime are discussed along with proposed new imprint applications, such as imprintable dielectrics that are targeted for use as on chip insulation layers.

*DARPA and The Semiconductor Research Corporation

**8:36**
**U4 2 Will optical lithography live forever?**
RALPH DAMMEL, *AZ Electronic Materials*

This abstract was not received electronically.

**9:12**
**U4 3 Directed assembly of block copolymer containing materials on chemically nanopatterned substrates: A platform for two and three-dimensional nanofabrication.**
PAUL NEALEY, *University of Wisconsin*

Directed assembly often refers to fabrication strategies that involve the organization of one or more materials on substrates through specific interactions with patterned activated regions. Based on engineered interfacial interactions between lithographically-defined chemically nanopatterned substrates and block copolymer thin films, the domain structure of the films can be directed to assembly into defect free periodic and non-regular structures over large areas, with each structure registered with the underlying substrate. Advantages of integrating self-assembling materials into the lithographic process, particularly for the fabrication of nanoelectronic devices, include sub 1 nm control over feature dimensions, reduced line edge roughness, and the opportunity to scale the approach to pattern at dimensions of 10 nm and below. Exciting opportunities exist to extend the use of self-assembling materials in conjunction with two-dimensionally (2D) patterned activate surfaces for the fabrication complex three-dimensional (3D) materials. Arrays of functional nanoparticles, for example, can be directed to assemble using block copolymer/particle nanocomposites or in a hierarchical process using chemically functional polymers followed by in situ particle synthesis. 3D bicontinuous morphologies in which the two phases of the assembly are readily addressable, a geometrically complex structure, can be created using materials that normally form lamellae and directing them to assemble on chemically patterned surfaces consisting of square arrays of spots. The principal concept of this work is that high value added 3D structures can be created from simple 2D templates, retaining the lithographic properties of perfection and registration for applications where input and output connections to the structures are required.

**9:48**
**U4 4 Probing the 3-Dimensional Structure of Nanomanufactured Materials using CD-SAXS.**
RONALD JONES, *NIST Polymers Division*

The realization of routine nanofabrication will demand new measurement platforms capable of probing the size, shape, internal morphology, and chemical uniformity of structures ranging from nanometers to 100's of nanometers in size. Traditional microscopies such as scanning electron microscopy and atomic force microscopy are often limited to exposed surfaces and are challenged to probe internal morphologies and structures with complex 3-dimensional shapes. We have developed a platform for non-destructive characterization of repeating nanostructures or nanostructured materials applicable to a wide range of sizes (5 to 500 nm) and materials (polymers, ceramics, and metals). Critical Dimension Small Angle X-ray Scattering (CD-SAXS) utilizes a relatively high energy, collimated x-ray beam to probe the dimensions, shape, and homogeneity of nanostructures fabricated on substrates such as silicon or quartz with sub-nm precision. CD-SAXS is capable of non-destructive measurements in real time during fabrication, providing insight into a wide range of fabrication methods. We demonstrate the wide ranging capabilities of CD-SAXS using recent data from structures created with photolithography, nanoimprint, and self-assembly. Patterns are characterized in terms of their average width, height, sidewall angle, and chemical uniformity. In addition, the distribution in orientation is quantified for self-organized systems, providing insights into the factors controlling defects. Finally, the technique is demonstrated for complex systems involving pattern directed self-assembly, such as in nanoimprinted block copolymers. In these systems, confinement between a mold and substrate prevent conventional imaging during fabrication. Real time data are used to elucidate the evolution of nanometer scale structures within 100 nm scale cavities.

**10:24**
**U4 5 Characterization of Materials for Nanoscale Lithography.**
WILLIAM HINSBERG, *IBM Almaden Research Center, San Jose CA*

Current state-of-the-art semiconductor devices are fabricated at dimensions below 100 nm and industry planning anticipates that devices at the 20 nm scale will be in production a decade from now. The sizes of the component molecules of typical polymeric photoresists are of this same magnitude, and due to this convergence of scales and intrinsic materials limitations, the formation of high fidelity relief images at these dimensions will be a significant challenge. We summarize here the materials issues that must be addressed to enable the practical application of nanoscale photolithography, and describe instrumentation and methods we have developed that allow their suitability for such use to be assessed by characterizing basic materials properties.

## SESSION U5: LOW TEMPERATURE PHYSICS, A HISTORICAL PERSPECTIVE
**Thursday Morning, 16 March 2006; 309, Baltimore Convention Center at 8:00**
**George O. Zimmerman, Boston University, presiding**

**8:00**
**U5 1 Low Temperature Physics at Yale in the late 30's through the early 50's.**
ROBERT WHEELER, *Yale University, Dept. of Applied Physics*

The low temperature program at Yale was initiated by C. T. Lane (1904-1991) in the fall of 1937 when he was appointed to the teaching staff as an instructor in the department of Physics. Following his doctorate from McGill in 1929 he investigated the magnetic susceptibilities of ''soft'' metals supported by the National Research Council of Canada, the Commissioners of the 1851 Exhibition and a Sterling Fellowship at Yale. Arranged by Louis McKeehan, with $5000 from the new George Sheffield research fund, he started the construction of a Kapitza type helium liquefier. The machine was largely completed in the fall of 1939, yet liquid helium was not made until early December 1940 due to the need for extensive on line purification of the gas. Returning in 1945 from war research, Lane and Henry A. Fairbank (Ph.D 1944) continued the metals work along with new thrusts into Second Sound, properties of helium$^3$ impurities in liquid helium and starting in the 50's on rotating He II. In 1933 both Lane and Onsager were awarded Sterling Fellowships, which initiated a stimulating experimental-theoretical exchange continuing until they both retired. The best-known example was the rediscovery at Yale of the de Haas–van Alphen effect, previously observed only in bismuth, in zinc; where upon Onsager and his students provided new insights into our understanding of the Fermi surface of metals. With the development of new instrumentation one observed vast changes in experimental style during this period. The evolution of the production of liquid helium from Lane's device though the Collins machine to the commodity business of today now makes experiments of huge size and importance possible.

**8:36**
**U5 2 Rotating Superfluids.**
RUSSELL DONNELLY, *University of Oregon*

Rotation of a fluid, particularly studying phenomena affected by Coriolis forces, plays a significant role in nearly all branches of fluid dynamics. Quantum fluids are no exception, as evidenced by remarkable devices such as ''Rota'' in Helsinki. This talk concerns the early days of rotating superfluids, starting long before superfluid helium-3 appeared on the scene. I will attempt to describe some of the early experiments, how the apparatus was designed, and what the experiments revealed. There has been so much activity in this area, I will discuss mostly experiments in my own fields of interest. Time will not permit an exhaustive review of this fascinating subject.

**9:12**
**U5 3 Fritz London's Legacy at Duke University.**
HORST MEYER, *Duke University*

When $^3$He became available in small quantities after WWII Fritz London, Professor at Duke University since 1939, became very interested in its properties in the liquid and solid phases, as contrasted with those of $^4$He. His influence and that of his colleague Walter Gordy led to the appointment of William Fairbank in 1952, who was able to verify experimentally the prediction on the Fermi degeneracy of liquid $^3$He below 1K, a few weeks before London's death in 1954. With his students and associates, Fairbank carried out a number of important experiments which became classics, several of which will be described. At Duke he also started planning other experiments inspired by London's predictions. After W. Fairbank's departure for Stanford in 1959, further research on liquid and solid $^3$He and $^3$He-$^4$He mixtures was carried out by his successors at Duke University and some of the results in the sixties will be briefly described.

**9:48**
**U5 4 Liquid Helium 3 and Solid Helium at Yale and Beyond.**
D.M. LEE, *Laboratory of Atomic and Solid State Physics, Cornell University*

Many of the foundations of low temperature physics in the latter half of the twentieth century were built at Yale University under the leadership of Professor Cecil T. Lane who came to Yale in 1932 and Henry A. Fairbank who obtained his Ph.D. at Yale in 1944 under Lane's guidance. This discussion will mainly treat the contributions of Henry Fairbank and his students during the period between 1954 and 1963, when Henry Fairbank left Yale to become chairman of the Physics Dept. at Duke University. Following World War II small amounts of helium three became available to low temperature experimenters. Henry Fairbanks graduate students were provided with the opportunity to investigate second sound in dilute and later concentrated mixtures of helium three in superfluid helium four. These measurements showed strong effects of the phase separation in helium 3-helium 4 mixtures previously discovered in the laboratory of William Fairbank (a student of Lane and a brother of Henry Fairbank). As more helium three became available, studies of pure helium three were performed, including measurements of the thermal conductivity, the density and the specific heat. Early evidence for the melting curve minimum was found. The main emphasis in this work was to search for Fermi liquid behavior. Much of the later work in this area was performed by the group of John Wheatley at the University of Illinois. In studies of solid helium four at Yale, a surprising observation was made. Hitherto it had been thought that hcp was the stable phase throughout the low temperature part of the phase diagram. It was found via ultrasound experiments that a small silver of bcc solid existed at the lowest pressures. While this author was a graduate student at Yale, Henry Fairbank pointed out to him the possibility of cooling helium three via adiabatic compression from the liquid into the solid phase. (Pomeranchuk Cooling). A brief discussion is given of the use of this technique in the discovery of superfluid helium 3 by Osheroff, Richardson and the author at Cornell.

**10:24**
**U5 5 Panel Discussion.**

**Panelists:**
Gerhard L. Salinger, National Science Foundation
John D. Reppy, Cornell University
Robert H. Romer, Amherst College
George B. Yntema, General Electric (retired)

**SESSION U6: STRONG ELECTRONIC CORRELATION IN SOLIDS: APPLICATIONS OF THE LDA+U METHOD**
**Thursday Morning, 16 March 2006; 310, Baltimore Convention Center at 8:00**
**Nicola Spaldin, University of California, Santa Barbara, presiding**

**8:00**
**U6 1 LDA+U Based Studies of Electronic, Vibrational and Spectroscopic Properties of Solids.***
STEVEN G. LOUIE, *University of California at Berkeley and Lawrence Berkeley National Laboratory*

The LDA+U method is a physically motivated approach that attempts to incorporate the effects of important orbital-specific local Coulomb interactions in strongly correlated electron systems while retaining the simplicity of local density approximation (LDA) calculations for real materials. In this talk, we discuss several applications of this method within the ab initio pseudopotential planewave framework. For transition metal oxides, the appropriate inclusion of the effects of onsite Coulomb U significantly alters their electronic structure leading to better agreement with experiment for quantities such as the nature of the electronic state, structural parameters, magnetic moments, phonon frequencies, etc. We have also studied the effects of doping on the electronic, magnetic, and structural properties of $NaxCoO_2$. Undoped $CoO_2$ is a metal with a high density of states at the Fermi level within LSDA, but a charge transfer insulator within LSDA+U. It is found that, due to a strong interaction between the doped electrons and the other Co d electrons, the calculated electronic structure is sensitively depended on the doping level. Finally, we discuss the use of LDA+U results as a starting mean-field solution for calculation of the electron self energy and quasiparticle excitations within the GW approximation.

*This work was done in collaboration with P.-H. Zhang and M. L. Cohen and supported by the NSF under Grant No. DMR04-39768 and the U.S. DOE under Contract No. DE-AC03-76SF00098.

**8:36**
**U6 2 LDA+*U* applied to oxide and nitride wide-band-gap semiconductors.***
ANDERSON JANOTTI, *University of California, Santa Barbara*

Nitride and oxide semiconductors have important technological applications, but the theoretical understanding of their properties is hampered by the shortcomings of density functional theory (DFT) in the local density approximation (LDA). In particular, DFT-LDA underestimates the binding energy of the semicore *d* states, leading to poor descriptions of quantities such as band offsets and deformation potentials. In this work we calculate the electronic and structural properties of wurtzite MgO, ZnO, and CdO, and discuss their similarities and dissimilarities with the corresponding nitrides AlN, GaN, and InN. We treat the semicore *d* states of Zn, Cd, Ga, and In explicitly as valence states in a pseudopotential framework, and improve the description of electron-electron interactions in these narrow bands by including an on-site Coulomb interaction through the LDA+*U* method. We propose a novel approach to calculate the parameter *U*, based on first-principles calculations for atoms. The approach is general and could be extended to other semiconductors and insulators where semicore *d* states play a fundamental role in the description of electronic and structural properties. The LDA+*U* approach systematically improves the LDA band gap by indirectly acting on both the valence-band maximum and conduction-band minimum. We investigate the effects of the on-site Coulomb interaction on lattice parameters, band structure, absolute deformation potentials, and band lineups. Finally we discuss how results based on LDA and LDA+*U* can be used to calculate defect transition levels and formation energies that can be directly compared with experiment.

*In collaboration with Chris G. Van de Walle. This work was supported in part by the Palo Alto Research Center and by AFOSR.

**9:12**
**U6 3 First-principles calculations of electronic structure and spectra of strongly correlated systems: the LDA+U method.**
ALEXANDER LICHTENSTEIN, *University of Hamburg*

Realistic approach to the electronic structure of complex materials which contains correlated d- or f- electrons will be discussed. The density functional theory within the local spin density approximation have been highly successful for electronic structure calculations and zero temperature magnetic properties of non-correlated systems. We investigate some failures of the LDA-scheme for the charge, spin and orbital ordering in transition metal compounds. General formulation of the LDA+U method which takes into account local Coulomb correlations for the d-shell of transition metals ions in the crystal within the mean-field approximation will be presented. The LDA+U scheme describe well the antiferromagnetic Mott insulators, rare-earth and actinide systems. Electronic structure, spin and orbital moments and lattice distortions of transition-metal compounds are investigated in the framework of rotationally invariant LDA+U method. Starting from conventional LDA+U scheme the different ways to go beyond the mean-field approximation which includes in effects of the spin- and charge-fluctuations will be analyzed. Dynamical mean field theory (DMFT) in combination with the first-principle LDA scheme (LDA+DMFT) is a good starting point for calculation of the quasi-particle spectrum for metallic transition metal systems. Recent progress in analysis of the metal-insulator transition for complex transition metal oxides and calculations of the spectral function for itinerant magnetic systems will be discussed.

**9:48**
**U6 4 Disproportionation, Metal-Insulator Transition, and Critical Interaction Strength in $Na_{1/2}CoO_2$.***
JAN KUNES, *University of California Davis*

Spontaneous breaking of symmetry is one of the key concepts of solid state physics related to phase transitions. Charge/spin density wave, or charge/spin ordering if the propagation vector is commensurate, are notorious examples of broken symmetry. The charge disproportionation in $Na_{0.5}CoO_2$ is the main theme of the present work. The results of LDA+U calculations will be presented, exhibiting a charge disproportionation transition at $U \approx 3$eV. $Na_xCoO_2$ attracted considerable attention mainly due to superconductivity of its hydrated form $Na_{0.3}CoO_2.1.3H_2O$ [1]. Besides the superconductivity $Na_xCoO_2$ exhibits several intriguing properties throughout its phase diagram, such crossover from Pauli-like to Curie-Weiss susceptibility at $x=0.5$, spin-density wave around $x=0.7$ or several phase transitions for $x=0.5$ including metal-insulator transition, charge ordering and magnetic ordering [2]. The $Na_xCoO_2$ lattice consists of triangular $CoO_2$ layers separated by Na layer. The mobility of Na ions and fractional occupation of Na sublattice provides an additional complication. Using LDA+U functional within FPLO [3] bandstructure method we have performed series of supercell calculations allowing for breaking of the symmetry between different Co sites. We have found that for large enough, but physically realistic, values of the on-site Coulomb interaction U the Co sublattice disproportionates into sites with formal valencies $Co^{4+}$ and $Co^{3+}$. We have found that at the same time a gap opens in the excitation spectrum. Details of the bandstructure across the transition as well as the driving forces of the transition in the LDA+U mean field picture will be discussed. [1] K. Takada *et al.*, Nature (London) **422**, 53 (2003). [2] M. L. Foo *et al.*, Phys. Rev. Lett. **92**, 247001 (2004). [3] K. Koepernik and H. Eschrig, Phys. Rev. B **59**, 1743 (1999).

*In collaboration with Kwan-Woo Lee and Warren E. Pickett.

**10:24**
**U6 5 A consistent, linear-response approach to LDA+U.**
MATTEO COCOCCIONI, *Department of Materials Science and Engineerig, MIT*

Hubbard U-correction to LDA or GGA has proven very effective in describing several strongly-correlated systems for which these approximations to DFT otherwise fail. Constrained DFT or semiempirical approaches have been often used to compute the Hubbard U. I introduce here an alternative scheme to evaluate the effective electronic interaction in a fully consistent way. This approach is based on the linear response of the system under consideration to a potential shift acting on the localized orbitals of the correlated sites. Using the occupations of these orbitals as the relevant electronic degrees of freedom we compute the on-site electronic coupling as the difference between the inverse of the bare and of the fully-interacting response matrices. The U computed in this way thus corresponds to the effective, atomically-averaged kernel of the Hartree-exchange-correlation interaction, in agreement with the second quantization expression of the ''+U'' energy functional. In this way the strength of the ''+U'' correction is evaluated from the same DFT scheme we aim to correct so that LDA+U becomes a consistent non-parametric method, with no need for semiempirical evaluations of the effective coupling. With this approach we successfully studied the structural, electronic, chemical and electrochemical properties of several transition-metal compounds. Examples will include minerals in the Earth's interior[1], cathode materials for next-generation lithium batteries[2] and metal-organic complexes [3]. [1] M. Cococcioni and S. de Gironcoli, PRB (2005). [2] F. Zhou, M. Cococcioni, A. C. Marianetti, D. Morgan and G. Ceder, PRB (2004). [3] H. J. Kulik, M. Cococcioni, D. Scherlis and N. Marzari, submitted to PRL.

## SESSION U7: NANOSCALE PATTERN GENERATION AND LITHOGRAPHY
**Thursday Morning, 16 March 2006; 307, Baltimore Convention Center at 8:00**
**Ya-Hong Xie, University of California, Los Angeles, presiding**

**8:00**
**U7 1**
SCOTT HECTOR, *International Sematech*

This abstract was not received electronically.

**8:36**
**U7 2 Maskless Electron-beam and Optical Lithography.**
HENRY I. SMITH, *Dept. Electrical Engineering and Computer Science, Massachusetts Institute of Technology*

Mask-based lithography is ideal for high-volume manufacturing because it enables enormous data transfer rates. In manufacturing, the high cost of masks and lithography tools can be amortized over large numbers of products. However, for low-volume manufacturing, research and the exploration of novel applications of lithography, maskless lithography systems have significant cost and convenience advantages. Scanning-electron-beam lithography (SEBL) systems are widely used in research and some low-volume manufacturing. They suffer from well known problems of pattern-placement accuracy, slow writing speed and, in some cases, substrate damage. Strategies for circumventing these

problems will be described. A maskless optical-lithography system, called zone-plate-array lithography (ZPAL), has recently been demonstrated that achieves high throughput by the parallel operation of 1000 diffractive-optical lenses [www.lumarray.com]. The performance of ZPAL will be described and compared to SEBL. Also, novel nonlinear strategies for pushing the resolution of ZPAL to feature sizes comparable to those achieved by SEBL will be described.

**9:12**
**U7 3 Ion Beam Patterning at the Nanometer Scale.**
JOHN BAGLIN, *IBM Almaden Research Center*

Due to the absence of diffraction limitations, the extensive available process parameter space, and the prospects for one-shot imposition of a projection-reduced master mask pattern, ion beam patterning appears to offer a viable path to large-scale manufacturing of devices and systems based on nanoscale features, while offering robustness, flexibility, high quality of image definition and high throughput. We will review a variety of process variables, and the strategies by which they can be optimized for a specific application, in terms of resolution of the smallest features, minimal proximity effects, minimal edge effects, minimal statistical noise, high dimensional stability and pattern registration, and minimal effects on underlying layers. We use SRIM and other simulations of ion interactions to model the effects of ion species, energy, fluence and beam current density, and their impact on the choice of mask structure and type of photoresist where appropriate. We consider the application of the ions to pattern photoresist layers, or to locally modify the topography of polymer films, or to locally activate surfaces for selective adsorption. We also consider options for in-situ growth of 3D nanoscale features. Direct modification of the interfaces of thin film structures, and local ballistic disordering will also be discussed. Experimental demonstrations of low energy ion beam patterning with $<$ 40 nm resolution will include contact mask patterning of thin films of various polymers, and patterning of high-anisotropy magnetic multilayers for high storage density disk drive applications.

**9:48**
**U7 4 Atomic Image Projection Electron Beam Lithography.***
KI-BUM KIM, *Seoul National University*

While we are approaching to the nanotechnology era, as was proposed by Richard Feynman in 1959, our main concern still lies in how one can controllably manufacture and utilize nanometer scale features. The top-down approaches, most notably, lithography based techniques still have the problem of throughput although it has been successfully demonstrate to make features with the size less than 10 nm. The bottom-up approaches, either utilizing chemical vapor deposition process to make carbon nanotube or wet-chemical process to make size controllable quantum dots and rods, still have the limitation of extending it to many different types of materials and also delivering them on a wafer size substrate to make nanodevices. In this talk, we will propose a novel electron beam lithography technique to make nanometer scale features. The novelty of this process lies in the fact that one can utilize the crystalline lattice image commonly observed by the high resolution transmission electron microscopy as an ultimate mask to generate nanometer scale patterns. Using this technique, we demonstrate that down to 45 nm pitch size can be resolved on hydrogen silsesquioxine (HSQ) e-beam resist material. The patterns are formed on Si substarte with the dot size of about 30 nm and the line size of about 25 nm. This technique can be extend to define less than 10 nm size features only if the suitable resist is developed.

*This work was supported by the Tera-Level Nano Devices, one of the Frontier programs supported by the Ministry of Science and Technology of Korea.

**10:24**
**U7 5 Diblock Copolymers for Nanoscale Patterning.**
THOMAS RUSSELL,* *University of Massachusetts at Amherst*

As the size scale of device features becomes increasingly smaller, conventional lithographic processes become increasingly more difficult and expensive, especially at a minimum feature size of less than 50 nm. Consequently, to achieve higher density circuits, storage devices or displays, it is evident that alternative routes need to be developed to circumvent both cost and manufacturing issues. An ideal process would be compatible with existing technological processes/ manufacturing techniques and these strategies, together with novel materials, could allow significant advances to be made in meeting both short-term and long-term demands for higher density and faster devices. The self-assembly of block copolymers (BCP), two polymer chains covalently linked together at one end, provides a robust solution to these challenges. As thin films, immiscible BCP self-assemble into a range of highly-ordered morphologies where with size scale of the features is limited to the size of the polymers chains and are, therefore, nanoscopic in size. While self-assembly alone is sufficient for a number of applications in fabricating advanced microelectronics, directed self-orienting self-assembly processes are also required to produce complex devices with the required density and addressability of elements to meet future demands. By combining tailored self-assembly processes, a bottom-up approach, with microfabrication processes, a top-down approach, the ever-present thirst of the consumer for faster, better and cheaper devices can be met in very simple, yet robust, ways.

*Craig Hawker, hawker@mrl.ucsb.edu, University of California at Santa Barbara.

**SESSION U8: GRANULAR MATERIALS**
**Thursday Morning, 16 March 2006**
**314, Baltimore Convention Center at 8:00**
**Wolfgang Losert, University of Maryland, presiding**

**8:00**
**U8 1 Statistical and dynamical properties of a vibrated granular polymer** ARSHAD KUDROLLI, MICAH VEILLEUX, *Physics Dept., Clark University* MEHRAN KARDAR, *Physics Dept., MIT* We investigate the structure and dynamics of granular polymers on a vibrated bed to test the applicability of models of self-avoiding random walks. The granular polymer is composed of a chain of hollow 3 mm steel beads connected by flexible links, and moves on a 30 cm diameter flat circular bed which is roughened by gluing a layer of 1 mm steel beads in order to give the chain random kicks in the vertical and horizontal directions. High speed digital imaging is used to track the position of the particles to a fraction of the bead diameter using a centroid technique. Using the identified bead positions, we analyze the motion of the center of mass over a time interval $\Delta t$, and its standard deviation as a function of chain length $L$. The standard deviation is consistent with a scaling of $\sqrt{\Delta t/L}$. The chain end-to-end distance scales as $L^{\nu}$, with $\nu \approx 3/4$ as for self-avoiding walks. The evolution of the scattering functions and the effect of the size of the container on the observed scaling will be also discussed.

**8:12**
**U8 2 Power Spectra of Force Fluctuations in Granular Materials Under Shear** ERIC CORWIN, HEINRICH JAEGER, SIDNEY NAGEL, *The James Franck Institute and Department of Physics, The University of Chicago* We measure the time-varying forces at the bottom surface of a granular system sheared at the top. The shear is applied by rotating a roughened piston while maintaining a constant, uniaxial compressive force. We report on the force autocorrelation and the corresponding power spectrum $S$ of the variation of force on individual grains at the bottom surface. These forces are obtained from video tracking of imprints in a pressure-sensitive birefringent layer across the bottom surface. Averaging over concentric annuli we find power-law behavior $S \sim 1/f^{\alpha}$ over several orders of magnitude in each annulus. The power law exponents $\alpha$ appear to be correlated with the in-plane shear strain rate. In our system friction with the stationary side walls introduces a radial gradient in the shear rate, which is maximum at the outer edge and zero at the center. The corresponding power law exponents suggest strict $1/f$ noise ($\alpha = 1$) at the outer, shearing edge and an increasing index as one approaches the center and the shear rate vanishes.

**8:24**
**U8 3 Self-diffusion of particles in gas-driven granular layers with periodic flow modulation*** CARLOS ORELLANA, *Departamento de Fisica, Universidad de Chile, Santiago, Chile* IGOR ARANSON, WAI KWOK, *Argonne National Laboratory* SERGIO RICA, *Departamento de Fisica, Universidad de Chile, Santiago, Chile* We study particles self-diffusion in gas-driven granular layers by high-speed fluorescent video-microscopy. We show that periodic flow modulation results in an enhancement of the particle's diffusion. The diffusion enhancement, which in turn is an indication of more efficient fluidization of the granular layer, is associated with the onset of disordered sub-harmonic patterns. Our measurements provide a sensitive characterization method of the fluidization properties of particulate/gas systems.

*This research was supported by US DOE, contract #W-31-109-ENG-38.

**8:36**
**U8 4 Free cooling of the one-dimensional wet granular gas** VASILY ZABURDAEV, MARTIN BRINKMANN, STEPHAN HERMINGHAUS, *Max Planck Institute for Dynamics and Self-Organization* In the present work we consider a one-dimensional gas of hard balls covered with a thin liquid film. A liquid bridge, formed at each collision, is responsible for the hysteretic and dissipative interaction. Each rupture of a liquid bridge requires a fixed amount of energy, and thus determines a threshold of relative velocities below which the two colliding particles form a bounded state loosing their relative kinetic energy. We aim to study the cluster formation process in the free cooling system. Macroscopic laws of energy dissipation and cluster growth are studied in this model on the basis of numerical simulations supported by a scaling-like system of equations. We show that the sticky gas regime is an attracting asymptotic limit of the wet granular gas and does not dependent on the liquid bridges strength. The next neighbor velocities correlations play the key role in the establishing of this regime.

**8:48**
**U8 5 A Theory of Stochastic Plasticity in Dense Granular Flow** KEN KAMRIN, MARTIN BAZANT, *MIT* There have been many attempts to derive continuum models for dense granular flow, but a general theory is still lacking, which can describe different flow conditions, such as gravity-driven silo drainage and forced shear cells. Here, we start with Mohr-Coulomb plasticity for quasi-2d granular materials to calculate stresses and slip planes, but we propose a simple ''stochastic flow rule'' to replace the principle of co-axiality in classical plasticity. This formulation takes into account two crucial features of granular materials – discreteness and randomness at the scale of a continuum element – via diffusing ''spots'' which cause chain-like cooperative particle displacements, as in recent simulations of silo drainage. We postulate that spots perform random walks along slip lines, biased by body forces (gravity) and local fluidization (switch from static to dynamic friction). Stochastic plasticity allows a natural description of dense granular flows in silos and shear cells within a single theory, rooted in classical mechanics.

**9:00**
**U8 6 The Solitary Wave Collision Problem in Granular Alignments*** EDGAR AVALOS, *SUNY-Buffalo* SURAJIT SEN, *SUNY-Buffalo* JAN PFANNES, *Univ of Wuerzburg* T.R. KRISHNA MOHAN, *SUNY-Buffalo* Any impulse travels as a solitary wave in an alignment of spherical elastic grains where the system grains are barely in contact. These solitary waves are about 7 grain diameters wide. Their speeds depend upon the maximum displacement amplitudes associated with these waves. We focus on the dynamical problem associated with the collision of two identical and opposite propagating solitary waves. Interface and grain center collisions reveal markedly different dynamics. Solitary wave collisions lead to the destruction of the original waves and the subsequent creation of new smaller waves along with ''baby'' or secondary solitary waves. In the absence of dissipation,

these granular systems point towards the existence of a generalized equilibrium phase that involves Maxwellian distribution of velocities with no depedence on initial conditions but one that violates the equipartition theorem.

*Supported in part by NSF, ARO

**9:12**

**U8 7 Toward Zero Surface Tension Limit: Granular Fingering Instability in a Radial Hele-Shaw Cell** XIANG CHENG, LEI XU, AARON PATTERSON, HEINRICH JAEGER, SIDNEY NAGEL, *The James Franck Institute and Department of Physics, The University of Chicago* Because of the absence of cohesive forces between grains, dry granular material can, in many respects, be thought of as a fluid with zero surface tension. In the zero surface-tension limit, viscous fingering is known to possess singular behavior. We have studied the viscous fingering instability in such a granular ''fluid.'' In our experiment, we use a conventional radial Hele-Shaw cell consisting of two parallel glass plates separated by a gap. Gas with controlled pressures is blown through a hole at the center of one glass plate and displaces the surrounding dry granular material. We have systematically studied the fingering pattern as a function of gas pressure, gap thickness, and grain size. Two stages are observed during pattern growth. In the first stage, we find fluid-like fingering. However, as opposed to normal fluids, the pattern is more ramified at low pressure. In the second stage, we find several new behaviors in the system such as merging and pinching off of fingers and the existence of satellite bubbles.

**9:24**

**U8 8 Force fluctuations in collisional and frictional granular flows** EMILY GARDEL, EFROSYNI SEITARIDOU, ELLEN KEENE, NALINI EASWAR, *Smith College, Northampton, MA*. NARAYANAN MENON, *University of Massachusetts, Amherst, MA*. We make measurements of the force delivered to the wall in 2D and 3D flow geometries to explore the difference between collisional and frictional flows, and between flow geometries with and without velocity gradients in the flow direction. The distribution of force fluctuations has an exponential tail at large force in collisional flows, but falls off slower than an exponential in frictional flows. We do not see a clear signature in the force distribution of the approach to jamming and therefore the connection to force distributions in quasistatic flows remains to be understood. However, the temporal characteristics of the force fluctuations do show the approach to jamming. As reported earlier, the distribution of collision times tends to a power law in collisional flows. Similarly, the power spectrum of forces in frictional flows develops power-law behaviour at low frequencies as jamming is approached. Supported by NSF DMR 0305396 and NSF MRSEC DMR 0213695

**9:36**

**U8 9 Thermal collapse of a granular gas under gravity*** LEV S. TSIMRING, *University of California at San Diego* DMITRI VOLFSON, *University of California at San Diego* BARUCH MEERSON, *Hebrew University of Jerusalem* Free cooling of a gas of inelastically colliding hard spheres is a central paradigm of the kinetic theory of granular gases. At zero gravity the temperature of a freely cooling homogeneous granular gas follows a power law in time. How does gravity affect the cooling? We consider a semi-infinite layer of granular gas bounded from below by an elastic wall. An initially isothermal dilute granular gas is prepared in the state of hydrostatic equilibrium with barometric density distribution. We combine molecular dynamics simulations, a numerical solution of granular hydrodynamic equations and an analytic theory to show that the cooling gas undergoes thermal collapse: it condenses on the bottom of the container and cools down to zero temperature in a finite time $t_c$ as $T \sim (t_c - t)^2$. The cooling scenraio is determined by the interplay between the collisional energy loss and heat conduction, while the collapse time $t_c$ is much longer than the typical free fall time of the grains if the inelasticity of the particle collisions is small. The hydrodynamic description is found to be in excellent agreement with molecular dynamics simulations until very close to $t_c$.

*Support of the U.S. Department of Energy (Grant DE-FG02-04ER46135) and Israel Science Foundation is gratefully acknowledged

**9:48**

**U8 10 Two particle contact lifetime distribution in gravity driven granular flow*** ROBERT BREWSTER, *UCLA* LEONARDO SILBERT, *University of Chicago* GARY GREST, *Sandia National Laboratories* ALEX LEVINE, *UCLA* The distribution of two particle contact life times for gravity driven granular flow down an inclined plane are determined from large-scale, three-dimensional discrete element simulations. Results are presented for both cohesive and non-cohesive particles for Hertzian and Hookean contact forces. The distribution of lifetimes is analyzed as a function of height from the surface for different strength $k_n$ of the normal force, coefficient of restitution $e_n$ and coefficient of friction $\mu$. In addition a generalized form of the Bagnold constitutive relation in which the shear stress depends on a sum of terms that are linear and quadratic in the shear rate is proposed for cohesive granular flows. The linear term represents a new mode of momentum transport made possible through the long lived contacts in the network while the quadratic term represents the usual Bagnold contribution from short time scale collisions. For non-cohesive grains, the strength of the linear term disappears as strength of the normal interaction $k_n$ increased.

*Sandia is a multiprogram laboratory operated by Sandia Corporation, a Lockheed Martin Company, for the United States Department of Energy's National Nuclear Security Administration under Contract No. DE-AC04-94AL85000.

**10:00**

**U8 11 Particle collisions in a granular gas*** HONG-QIANG WANG, KLEBERT FEITOSA, NARAYANAN MENON, *University of Massachusetts* We report a study of particle collisions in a 2D granular system vibrated in a vertical plane. We have previously studied this experimental system in a variety of contexts. With improved image analysis algorithms, we are able to locate particles with enough precision to allow detailed tracking of the collision process, when the particles are close to each other. This allows us to better study the role of the vertical walls in the collision process and to place a limit on the dissipation by mechanisms other than inelastic collisions. We report the distribution of collision parameters and comment on violations of molecular chaos resulting from the inelasticity of the system.

*We acknowledge support from NSF-DMR 0305396

**10:12**

**U8 12 Boltzmann's itstosszahlansatz generalized for granular contact forces** PHILIP METZGER, *NASA, John F. Kennedy Space Center* Is there a valid way to generalize Boltzmann's itstosszahlansatz (molecular chaos), the assumption that colliding molecules are not statistically correlated before the collision takes place, to the case of granular contact forces in a static packing? In thermal statistical mechanics the assumption produces a transport equation that obtains the density of single particle states and the Maxwell Boltzmann distribution. The problem in generalizing this to granular contact forces is that we must maintain the spatial symmetries of granular packing ensembles, which is not trivial. The essential trick is to sum the density of states over all particle exchanges, which destroys multi particle state information but maintains the distribution of single particle states. This summation transforms the equations into a generalized form of boson statistics. I will show that, in the summation, the first shell approximation of the fabric is transformed into the properly symmetric version of Boltzmann's itstosszahlansatz. This produces a transport equation that obtains the density of single particle states and hence the distribution of granular contact forces. Granular simulation data will also be presented to validate the theory.

**10:24**

**U8 13 Dynamical Heterogeneity close to the Jamming Transition in a Sheared Granular Material** OLIVIER DAUCHOT, *CEA/SPEC* GUILLAUME MARTY, *City College of New York* GIULIO BIROLI, *CEA/SPhT* The dynamics of a bi-dimensional dense granular packing under cyclic shear is experimentally investigated close to the jamming transition. Measurement of multipoint correlation functions are produced. The self-intermediate scattering function, displaying slower than exponential relaxation, suggests dynamic heterogeneity. Further analysis of four point correlation functions reveal that the grain relaxations are strongly correlated and spatially heterogeneous, especially at the time scale of the collective rearrangements. Finally, a dynamical correlation length is extracted from spatio-temporal pattern of mobility. Our experimental results open the way to a systematic study of dynamic correlation functions in granular materials.

**10:36**

**U8 14 The Decorated Tapered Chain as a Granular Shock Absorber*** ROBERT DONEY, *US Army Research Lab - APG* SURAJIT SEN, *SUNY-Buffalo* DORIAN DICOCCO, *SUNY-Buffalo* A 1*D* alignment of progressively shrinking spherical grains (a tapered chain) turns out to be an excellent impulse absorber with rich nonlinear dynamical behavior. Here we discuss a tapered chain with interstitial grains between every sphere of the original tapered chain and demonstrate analytically (using the hard sphere approximation), numerically and experimentally that the shock absorption ability of the ''decorated'' system is far superior to that of the system without the interstitial grains.

*Supported by ARO

**10:48**

**U8 15 Shock Absorption by Small, Scalable, Tapered Granular Chains*** JAN PFANNES, *University of Wuerzburg* ADAM SOKOLOW, *Duke University* ROBERT DONEY, *US Army Research Lab - APG* MASAMI NAKAGAWA, *Colorado School of Mines* JUAN AGUI, *NASA-Glenn Research Center* SURAJIT SEN, *SUNY-Buffalo* Making shock proof layers is an outstanding challenge. Elastic spheres are known to repel softer than springs when gently squeezed but develop strong repulsion upon compression and the forces between adjacent spheres lead to itballistic-like energy transfer between them. Here we demonstrate for the first time that a itsmall alignment of progressively shrinking spheres of a strong, light-mass material, placed horizontally in an appropriate casing, can absorb$\sim$ 80% ($\sim$ 90%) of the incident force (energy) pulse. The system can be scaled down in size. Effects of varying the size, radius shrinkage and restitutive losses are shown via computed ''dynamical phase diagrams.''

*Supported by ARO, NSF.

## SESSION U9: SCANNING PROBE MICROSCOPY
**Thursday Morning, 16 March 2006**
**301, Baltimore Convention Center at 8:00**
**Karen Waldrip, Sandia National Laboratories, presiding**

**8:00**

**U9 1 An itin-situ Study of Martensitic Transformation in Shape Memory Alloys using PEEM** GANG XIONG, T. DROUBAY, A. JOLY, W. HESS, *Pacific Northwest National Laboratory, Richland, WA 99352, USA* M. CAI, S. LANGFORD, J. DICKINSON, *Physics Department, Washington State University, Pullman, WA 99164 USA* M. WU, Q. HE, W. HUANG, *School of Mechanical Production Engineering, Nanyang Technological University, 50 Nanyang Ave., Singapore* The thermally-induced martensitic transformation in a polycrystalline CuZnAl and NiTi thin film shape memory alloy (SMA) was probed using photoemission electron microscopy (PEEM). Ultra-violet photoelectron spectroscopy (UPS) measurements indicate that the apparent surface work function changes reversibly during transformation, presumably due to the contrasting electronic structures of the martensitic and austenitic phases. itIn situ PEEM images provide information on the spatial distribution of these phases and the microstructural evolution during transformation. The evolution of the photoemission intensities obtained from PEEM images during transformation can provide quantitative information on fractional percentages of austenite and martensite phases as the transformation proceeds. PEEM offers considerable potential for improving our understanding of martensitic transformations in shape memory alloys in real time.

**8:12**

**U9 2 Investigation of ferroelectric materials with scanning microwave microscope*** JEWOOK PARK, JONGHOON CHO, SANGYUN LEE, KOOKRIN CHAR, *Seoul National University* By using scanning microwave microscope (SMM), we investigated dielectric properties of ferroelectric materials in high frequency regime (1.5GHz). Our SMM had the capability to measure a complex dielectric constant of the samples from the shift of resonant frequency (fr) and Q value of the probing resonator. In order to obtain non-linear dielectric constants of the ferroelectric samples, we applied oscillating electric field perpendicular to the sample and measured the $1^{st}$ order derivative of the resonant frequency of the resonator (dfr/dE) with respect to the applied field. In this way we could image the ferroelectric domain and the do-

main boundary structure of the triglycine sulfate single crystal using the dfr/dE and the fr signal, respectively. Moreover we observed the ferroelectric responses from the tunable dielectric $Ba_{0.6}Sr_{0.4}TiO_3$ thin film under the additional DC voltage bias to the film.

*This work is partially supported by the Korea Science and Engineering Foundation (KOSEF) through the Center for Strongly Correlated Materials Research (CSCMR).

**8:24**

**U9 3 Plasmon-based Enhanced NSOM Spectroscopy.** A.T. CHANG, C.L. NEHL, F. TAM, N.J. HALAS, J.H. HAFNER, K.F. KELLY, *Rice University* Surface enhanced Raman spectroscopy is a well established technique for enhancing the Raman signal of a particular sample, allowing for spectroscopy of far lower quantities of the molecule of interest than other procedures allow. This enhancement is mainly caused by the enhancement of the incident electric field by exciting the plasmon resonance of the surface. By attaching metal nanoparticles on an NSOM probe, we demonstrate that the plasmon-based enhancement can come from the probe itself instead of the surface, resulting in a powerful tool for the chemical analysis at the nanometer scale.

**8:36**

**U9 4 Dielectrophoretic Force Microscopy** AL HILTON, BRIAN LYNCH, GARTH SIMPSON, *Purdue University Dept. of Chemistry* Dielectrophoretic force microscopy, a novel scanning probe microscopy technique in which a tip-sample dielectrophoretic force is incorporated into the feedback mechanism of a standard atomic force microscope, is shown to allow for the facile noncontact imaging of the dieelctric properties of systems in aqueous media. By tuning the ac frequency, dielectric spectroscopy can be performed at solid/liquid interfaces with high spatial resolution. In studies of cells, the frequency-dependent dielectrophoretic force is sensitive to biologically relevant electrical properties, including local membrane capacitance and ion mobility. Additionally, the presence of a dielectrophoretic force reduces the mechanical tip-sample contact forces that frequently hinder microscopy studies of soft, deformable systems. Consequently, dielectrophoretic force microscopy is well suited for itin situ scanning probe microscopy studies of biological systems.

**8:48**

**U9 5 Spectral density of fluctuations for a driven, nonlinear micromechanical oscillator at kinetic phase transition** COREY STAMBAUGH, *University of Florida* HO BUN CHAN, *University of Florida* We measure the spectral densities of fluctuations of an underdamped nonlinear micromechanical torsional oscillator. By applying a sufficiently large periodic driving force, two stable dynamical states occur within a particular range of drive frequency. White noise is injected into the driving force allowing the system to overcome the activation barrier and to switch between the two states. While the system predominately resides in one of the two states for most excitation frequencies, a narrow range of frequencies exist where the population levels are approximately equal and the system is at a 'kinetic phase transition' that bears resemblance to the phase transition of thermal equilibrium systems. By examining the power spectral densities of the measured oscillation amplitude, the fluctuation characteristics of the system can be studied. At the 'kinetic phase transition' a supernarrow peak, centered at the excitation frequency, arises as a result of noise-induced transitions between the two dynamic states. Smaller, secondary peaks associated with fluctuations about the two attractors are also examined. Its dependence on noise and excitation frequency is shown to be distinct from that of the supernarrow peak.

**9:00**

**U9 6 Nonlinear coupling of nano mechanical resonators to Josephson quantum circuits** XINGXIANG ZHOU, ARI MIZEL, *The Pennsylvania State University* We study a technique to couple the position operator of a nano mechanical resonator to a SQUID device by modulating its magnetic flux bias. By tuning the magnetic field properly, either linear or quadratic couplings can be realized, with a discretely adjustable coupling strength. This allowes us to realize nonlinear dynamics on the nano mechanical resonator by coupling it to a Josephson quantum circuits. As an example we show how squeezing of the nano mechanical resonator can be realized with this technique. We also propose a simple method to measure the uncertainty in the position of the nano mechanical resonator without quantum state tomography.

**9:12**

**U9 7 Nanomanipulation with dynamic AFM** IVAN STICH, PETER DIESKA, *Slovak University of Technology* RUBEN PEREZ, *Universidad Autonoma de Madrid* Nanomanipulation [1] is one of the most important current issues in dynamic AFM (DAFM). Following the first vertical manipulation on Si(111)-(7x7) [1] a lateral manipulation was documented by interchange manipulation of Sn and Ge adatoms on the Ge(111)- c(2x8) surface [2]. However, the atomistic details and nature of these processes remain unclear. In order to shed light on these experiments we have performed DFT simulations on two model systems: (1) anionic antisite defect on the InP(110) surface [3], and (2) the Sn-covered Ge(111)-c(2x8) surface. In (1) the P defect atom moves vertically in a double well potential with two minima, which opens the possibility to vertically manipulate the defect atom from one minimum into the other. We will addresses issues such as whether the experiments can be performed in both attractive and repulsive interaction regimes and whether the basic atomistic mechanism is related to lowering of the barriers by the presence of the tip, or by a purely mechanical effect where the atom is pushed over a barrier. In (2) we will show how presence of the tip can affect the charge transfer processes between the different dangling bonds and hence induce atomic manipulation. [1] N. Oyabu et al., Phys. Rev. Lett. 90, 176102 (2003) [2] Y. Sugimoto et al., Nature Mater. 4, 156 (2005); N. Oyabu et al., Nanotechnology 16, S112 (2005). [3] P. Dieska, I. Stich, R. Perez, Phys. Rev. Lett. 95 126103 (2005)

**9:24**

**U9 8 Assembly of Nanoparticle-Attached AFM Tips for Nano-Optical Applications*** TAEKYEONG KIM, SUNG MYUNG, NARAE CHO, SEUNGHUN HONG, *School of Physics, Seoul National University, Seoul, Korea* The well-defined geometry and chemical properties of the end of atomic force microscopy tips are critical components for various tip-enhanced nano-optical applications such as nanoscale Raman and FRET imaging. However, conventional AFM tip fabrication method often results in a large variation of tip shapes and chemical properties. Recent nanotechnology allows us to synthesize 'nanoparticles' (e.g. Au, Ag, CdSe, etc). We developed a method to mass-produce 'AFM tips with well-defined geometry and chemical properties' by assembling a single nanoparticle at the end of the tip via self-assembly strategy.

In this way, only the end part of the tip is functionalized with organic molecules which attract nanoparticles in the solution. When the functionalized tip is placed in the nanoparticle solution, nanoparticles are selectively assembled only onto the end of the tip. We assembled a nanoparticle (e.g. 50nm diameter Au nanoparticle) at the end of the tip and demonstrated AFM imaging using these tips. Our method allows us to assemble nanoparticles at the end of the tip, and it can be scaled up for large scale assembly.

*Supported by the Ministry of Scince and Technology through the National Research Laboratory(NRL)

**9:36**

**U9 9 Investigation of Electrical Behaviors of Nanostructures through Scanning-Probe Microscopy** BEVERLY CLARK III, HANS HALLEN, *NC State University NSOM Lab* A scanning-probe microscope with two electrically-isolated electrodes fabricated on one probe is used to locally investigate electrical behavior of nanostructures. The split-tip probe, which we have recently developed, is optimized for light coupling into a particular region of a nanostructure while non-contact measurements are simultaneously made between the two electrodes. The capacitance is influenced by the presence of a conducting region on the surface beneath the electrodes. The capacitance coupled or scanning conductivity mode allows rapid characterization of large numbers of molecules so that molecules of interest can be identified for further study. Finite element models aid in the quantification and understanding of the data.

**9:48**

**U9 10 Scanning Tunneling Potentiometry for Nanoscale Transport Studies** MICHAEL ROZLER, M.R. BEASLEY, *Stanford University* We have developed a scanning tunneling potentiometry (STP) system for study of electrical transport on nanometer length scales. A novel biasing scheme is used to achieve electrochemical potential resolution at the theoretical limits of this measurement - the thermal noise of the tunnel junction. We apply this technique to several materials in order to explore the capabilities of the instrument. These include thin films of Au, the ''bad metal'' $SrRuO_3$ and amorphous indium oxide. Homogeneity of transport in these systems is discussed. Work supported initially by the AFOSR and currently by the NSF.

**10:00**

**U9 11 Alpha Control - A New Concept in SPM Control** P. SPIZIG, D. SANCHEN, G. VOLSWINKLER, W. IBACH, J. KOENEN, *WITec GmbH, www.WITec.de* Controlling modern Scanning Probe Microscopes demands highly sophisticated electronics. While flexibility and powerful computing power is of great importance in facilitating the variety of measurement modes, extremely low noise is also a necessity. Accordingly, modern SPM Controller designs are based on digital electronics to overcome the drawbacks of analog designs. While todays SPM controllers are based on DSPs or Microprocessors and often still incorporate analog parts, we are now introducing a completely new approach: Using a Field Programmable Gate Array (FPGA) to implement the digital control tasks allows unrivalled data processing speed by computing all tasks in parallel within a single chip. Time consuming task switching between data acquisition, digital filtering, scanning and the computing of feedback signals can be completely avoided. Together with a star topology to avoid any bus limitations in accessing the variety of ADCs and DACs, this design guarantees for the first time an entirely deterministic timing capability in the nanosecond regime for all tasks. This becomes especially useful for any external experiments which must be synchronized with the scan or for high speed scans that require not only closed loop control of the scanner, but also dynamic correction of the scan movement. Delicate samples additionally benefit from extremely high sample rates, allowing highly resolved signals and low noise levels.

**10:12**

**U9 12 Theory of Q-Controlled Dynamic Force Microscopy in Liquids** HENDRIK HOLSCHER, UDO D. SCHWARZ, *Dep. Mech. Eng., Yale University* The so-called Q-control method allows the active modification of the effective cantilever damping in dynamic force microscopy (DFM) by increasing or decreasing the Q-value of the cantilever. This feature has been used in recent years in numerous experimental studies to improve the apparent imaging capabilities of DFM in liquids. However, it is striking that an in-depth analytic description that would allow a rigorous theoretical explanation of the various features of Q-controlled dynamic force microscopy (QC-DFM) is still missing. Here, we present an analysis of QC-DFM based on the analytical solution of the equation of motion considering a model tip-sample interaction force. Explicit formulas allowing for the calculation of relevant parameters such as amplitude, surface deformation, and maximum forces during an individual oscillation cycle are given. It is found that higher effective Q-factors assist in reducing the maximum tip-sample forces. This helps suppressing unwanted deformations of the sample surface, leading to the reported enhanced image quality. Finally, the results are discussed in relation to the situation in air.

**10:24**

**U9 13 Simulation of contact and non-contact AFM images of H-terminated Si(100) surface with a CH3 impurity** AKIRA MASAGO, SATOSHI WATANABE, *Department of Materials Engineering, The University of Tokyo* KATSUNORI TAGAMI, MASARU TSUKADA, *Department of Nanoscience and Nanoengineering, Waseda University* Using a density-functional-based tight-binding method, we have investigated whether atomic force microscope (AFM) images with atomic resolution can be obtained for hydrogen-terminated silicon (100) 1x1 surface including a methyl. We have simulated contact mode images of this surface using a silicon tip with and without a hydrogen atom at the apex. For the silicon tip without hydrogen at the apex, we obtained good images with anisotropic spots reflecting the symmetry of a methyl for large tip-sample distance. For the silicon tip with hydrogen at the apex, we found that better images with atomic resolution, showing internal hydrogen and carbon atoms of a methyl, are expected if the forces can be measured precisely. We have also examined non-contact mode images. Although a force line profile of non-contact mode is smoother than one of contact mode, their difference is not so large.

**SESSION U10: FOCUS SESSION: SURFACES AND INTERFACES IN ELECTRONIC MATERIALS II**
**Thursday Morning, 16 March 2006; 302, Baltimore Convention Center at 8:00**
**Marcus Lay, University of Georgia, presiding**

***Invited Papers***

**8:00**
**U10 1 Nanoscale Patterning of Electrochemically Deposited Metallic Features on Si, Ge, InP and GaAs Surfaces.***
JILLIAN BURIAK, *Dept. of Chemistry, University of Alberta and the National Institute for Nanotechnology, National Research Council, Edmonton, Canada*

Nanostructured materials continue to be the focus of intense research due to their promise of innumerable practical applications as well as advancing the fundamental understanding of these intriguing materials. In particular, the need for metallic features of increasingly smaller size regimes has imposed stringent demands upon chemists to produce a variety of highly functional materials with reduced dimensions.While much effort has been expended towards the synthesis of nanoscale structures, one of the most challenging aspects for the nanoscale materials community is the question of how to 'wire in' these functional elements with the real world. In this talk, we will describe recent work towards the synthesis and nanoscale patterning of metallic structures on semiconductor surfaces such as silicon, germanium, gallium arsenide and indium phosphide. Through simple and efficient galvanic displacement reactions on these interfaces, complex metal nanostructures form spontaneously, and can be patterning via self-assembling soft block copolymer materials. The self-assembled materials direct transport of reagents to the semiconductor so that the reaction takes place in a spatially defined manner, with precise control over the quantity of reagent delivered. Even mixtures of reagents can be ''sorted out'' by these interfaces to produce nanoscale ( $\sim$ 10 nm) domains of different chemical functionalities, simultaneously. We will describe these and related approaches towards precise patterning of semiconductor surfaces, entirely via wet-chemical processes that are compatible with existing fabrication strategies.

*In collaboration with Masato Aizawa, Department of Chemistry, University of Alberta and the National Institute for Nanotechnology, National Research Council.

***Contributed Papers***

**8:36**
**U10 2 Scanning Tunneling Microscopy Study of Molecular Structure: Controlled Monolayer Formation on Graphite at the Liquid-solid Interface** C. SU, *Dept of Molecular Science and Engineering, National Taipei Univ. of Tech.* K. KANNAPPAN, V. NORA CHIN, L. AVILA-BRONT, S. JAYARAMAN, N.J. TURRO, *Dept of Chem, Columbia Univ* G.W. FLYNN, *Dept of Chem and Columbia Center for Integrated Science and Engineering, Columbia Univ* The self-assembly of heptadecanoic acid **1** and racemic 2-bromoheptadecanoic acid **2** mixtures on the basal plane of a graphite surface has been studied using scanning tunneling microscopy at the liquid-solid interface. The domain structure varies as a function of the ratio of coadsorbed molecules. At lower concentration of acid **2**, heptadecanoic acid controls the surface structure by forming a template with fixed lamellar axis-molecular axis angle and domains with alternating R- and S-enantiomer molecular rows. Increasing the concentration of acid **2** leads to the segregation of chiral domains. The inter-correlation between heptadecanoic acid and 2-bromoheptadecanoic acid determines the 2D chiral configuration in the mixed monolayer. A model based on energetically favorable molecular conformations is proposed and will be discussed.

**8:48**
**U10 3 Static and Dynamic Aspects of Surfactant Surface Aggregates studied by AFM** HANNES SCHNIEPP, DUDLEY SAVILLE, ILHAN AKSAY, *Department of Chemical Engineering, Princeton University* Using AFM, we show that surfactants form micellar aggregates of varying morphology, depending on the surface structure. While all previous studies were limited to atomically flat substrates, we achieve imaging the micelles on rough gold. By gradually annealing these surfaces, we show the influence of roughness on the aggregate structures. For crystalline gold (111), aligned, hemi-cylindrical micelles that recognize the symmetry axes of the gold lattice are found. With increasing roughness, the degree of organization of the aggregates decreases. We also show that the micellar pattern on HOPG and gold(111) surfaces changes with time and responds to perturbations in a self-healing way. Our results suggest that this organization happens at the molecular scale. Theoretical analysis for HOPG, however, show that the micelle orientation cannot be explained on the molecular level, but the anisotropic van der Waals interaction between micelles and HOPG has to be considered as well [1]. [1] Saville, D. A.; Chun, J.; Li, J.-L.; Schniepp, H. C.; Car, R.; Aksay, I. A., accepted by Physical Review Letters.

**9:00**
**U10 4 Accelerated Molecular Dynamics Simulation of Alkane Desorption** KELLY McLAUGHLIN, KRISTEN FICHTHORN, *Pennsylvania State University* Thermal desorption has been the focus of much surface science research. Studies of alkanes on graphite[1] and gold[2] have shown prefactors that are constant with alkane chain length but vary by over six orders of magnitude. Other studies on magnesium oxide[3] and gold[4] show a prefactor that increases with increasing chain length. We have developed an all-atom model to study alkane desorption from graphite. Transition state theory is used to obtain rate constants from the simulation. Accelerated MD is used to extend the desorption simulation to experimentally relevant temperatures. Our results show a prefactor that increases with increasing chain length. We predict that it will become constant as internal conformational changes occur significantly. We examine the effect of desorption environment

through varying the alkane surface coverage. 1. K.R. Paserba and A.J. Gellman, J. Chem. Phys.**115**, 6737 (2001). 2. S.M. Wetterer et al., J. Phys. Chem. **102**, 9266 (1998). 3. S.L. Tait et al., J. Chem. Phys. **122**, 164707 (2005). 4. K.A. Fichthorn and R.A. Miron, Phys. Rev. Lett.**89**, 196103 (2002).

**9:12**

**U10 5 Atomic force microscopy and fluorescence correlation spectroscopy studies of interfacial fluids.** S. PATIL, G. MATEI, C. GRABOWSKI, P. HOFFMANN, A. MUKHOPADHYAY, *Department of Physics, Wayne State University* We have studied the dynamic structure of thin ( $\sim$ few nm) liquid films of a nearly spherical, nonpolar molecule tetrakis(2-ethylhexoxy)silane by using a combination of atomic force microscopy (AFM) and fluorescence correlation spectroscopy (FCS). Ultra-sensitive interferometer-based AFM was used to determine the stiffness (force gradient) and the damping coefficient of the liquid film. The experiments show oscillations in the damping coefficient with a period of $\sim$ 1 nm, which is consistent with the molecular dimension as well as previous x-ray reflectivity measurements. However, it fails to detect any stiffness oscillation, indicating that molecules are layered weakly near the solid-liquid interface. Additionally, we performed FCS experiments for direct determination of the molecular dynamics within the liquid film. From the fluctuation autocorrelation curve, we measure the translational diffusion of the probe molecule. The autocorrelation function cannot be fitted with a single diffusion coefficient indicating that the dynamics may vary in different layers.

***Invited Papers***

**9:24**

**U10 6 A Single Molecule View of Bi-stilbene Photoisomerization Using Scanning Tunneling Microscopy.***
JUEN-KAI WANG, *National Taiwan University*

The advent of scanning tunnelling microscopy (STM) has permitted a detailed atomic view of organic molecules adsorbed on solid surfaces. With the use of the STM, we present an unprecedented direct single-molecule perspective on the cis-trans photoisomerization of stilbene molecules within ordered-monolayers physisorbed on the Ag/Ge(111) surface. The STM view of the molecular structure transformation upon irradiation provides a direct evidence for the generally accepted one-bond-flip mechanism proposed for the photoisomerization process. We also find that the surface environment produces a profound effect on the reaction mechanism. The reaction is observed to proceed mainly through pairs of co-isomerizing molecules situated at domain boundaries. To explain these observations, we propose a mechanism whereby excitation migrates to the domain boundary and the reaction occurs through a biexciton reaction pathway.

*In collaboration with Chih-Song Tsai, Rex T. Skodje and Jiing-Chyuan Lin, Institute of Atomic and Molecular Sciences, Academia Sinica, Taipei, Taiwan.

***Contributed Papers***

**10:00**

**U10 7 A combined theoretical and experimental study on the structure of Methylthiolates on the Au(111) surface** RICCARDO MAZZARELLO, R. ROUSSEAU, *SISSA and ICTP, Trieste, Italy* S. SCANDOLO, *ICTP, Trieste, Italy* A. VERDINI, A. COSSARO, *TASC-INFM, Trieste, Italy* L. CASALIS, *Sincrotrone, Trieste, Italy* L. FLOREANO, A. MORGANTE, *TASC-INFM, Trieste, Italy* M. F. DANISMAN, *Princeton University, USA* G. SCOLES, *SISSA, Trieste, Italy and Princeton University, USA* Self-assembled monolayers (SAMs) of sulphur containing organic molecules on gold have received enormous attention due to the central role these interfaces play in molecular electronic devices, biosensors, surface coatings and nanolithography. Despite their interest the atomic structure of Methylthiolates on Au(111) surfaces, the simplest SAM in this class, is not fully understood. Here we address this problem with a combined theoretical and experimental study. We show that an asymmetric bridge (quasi on-top) site fits both the X-Ray and Photoelectron Diffraction data better than either the symmetric bridge site or on-top site. To understand this phenomenon we have performed molecular dynamics simulations employing density functional theory within the generalized gradient approximation. We show that at high temperatures the presence of vacancies and gold adatoms tends to favour the quasi on-top site, in spite of the fact that the symmetric bridge site is the lowest energy site at $T = 0$.

**10:12**

**U10 8 Spectroscopic STM study of the binding configuration of benzene molecules on the Si(111)7x7 surface*** STEVEN A. HORN, *Department of Physics, University of Lethbridge, Lethbridge, Alberta, T1K 3M4, Canada* WEIMING LIU, *Department of Physics, University of Lethbridge, Lethbridge, Alberta, T1K 3M4, Canada* S.N. PATITSAS, *Department of Physics, University of Lethbridge, Lethbridge, Alberta, T1K 3M4, Canada* We have used a home-built UHV STM to study the bonding configuration of benzene molecules chemisorbed onto clean silicon. Our compact STM head is based on the symmetrical, Besocke design. In our design, thermal drift is eliminated to first order, by using the correct combination of materials with known thermal expansion coefficients.[1] This STM head is also capable of being positioned inside of a liquid helium cryostat currently under construction in our lab. Our long-term goal is to use spectroscopic dI/dV imaging to focus on spatial variations of the LDOS and gain valuable information not generally available in topographic imaging.[2] In particular we will present room-temperature results on the role of restatoms in the binding of benzene molecules to adjacent adatoms. Results on the spatial position and direction of C-C double bonds will also be presented. 1) Stipe et al, Rev. Sci. Instr. **70**, 137 (1999). 2) Hamers et al, Phys.Rev.Lett. **56**, 1972 (1986).

*The authors acknowledge the National Sciences and Engineering Research Council of Canada (NSERC) for their support of this work.

**10:24**

**U10 9 STM study of adsorption and dissociation of trichloroethylene molecules on the Si(111)7x7 surface.*** POUYA MARAGHECHI, *Department of Physics, University of Lethbridge, Lethbridge, Alberta, T1K 3M4, Canada* STEVEN A. HORN, *Department of Physics, University of Lethbridge, Lethbridge, Alberta, T1K 3M4, Canada* WEIMING LIU, *Department of Physics, University of Lethbridge, Lethbridge, Alberta, T1K 3M4, Canada* S.N. PATITSAS, *Department of Physics, University of Lethbridge, Lethbridge, Alberta, T1K 3M4, Canada* We have performed, for the first time, STM studies of the adsorption of trichloroethylene (TCE) on clean silicon. The results were taken with a home-built UHV STM operating at room temperature. Our STM is capable of obtaining both topographic as well spectroscopic images. One of the products of the dissociation has been determined to be single chlorine atoms bound to Si adatoms as evidenced by topographic imaging and tip induced diffusion.[1] The other product of the dissociation is believed to be a vinyl group attached to an adatom as proposed in a study using EELS and TDS.[2] Results on the binding site preference (ex. corner vs. middle adatoms) for the Cl and vinyl group will also be presented as well as conclusions about the diffusion of Cl on Si. 1) Nakamura et al, Surf. Sci. **487**, 127 (2001). 2) He et al, Surf. Sci. **583**, 179 (2005).

*The authors acknowledge the National Sciences and Engineering Research Council of Canada (NSERC) for their support of this work.

**10:36**

**U10 10 Decompositional, incommensurate growth of Ferrocene molecules on a Au(111) surface** KAI-FELIX BRAUN, VIOLETA IANCU, SAW HLA, *Ohio University* OHIO UNIVERSITY TEAM, We have investigated in depth the first layer growth of ferrocene molecules on a Au(111) surface with a low temperature scanning tunneling microscope. Ferrocene molecules adsorb dissociatively and form a two layer structure after being decomposed into fragments. The toplayer unit cell is composed of two tilted cyclopentadienyl rings, while the first layer consists of the remaining fragments. Surprisingly a fourfold symmetry is observed for the top layer while the first layer displays threefold symmetry elements. It is this symmetry mismatch which induces an incommensurability between these layers in all except one surface direction. The top layer is weakly bonded allowing for an antiferromagnetic ordering as shown by density functional theory calculations.

## SESSION U11: FOCUS SESSION: AEROSOLS, CLUSTERS, DROPLETS: PHYSICS AND CHEMISTRY OF NANOOBJECTS IV: METAL CLUSTERS I

**Thursday Morning, 16 March 2006; 303, Baltimore Convention Center at 8:00**
**Knut Asmis, Fritz Haber Institute, Berlin, presiding**

***Invited Papers***

**8:00**

**U11 1 Infrared Spectroscopy of Metal Ion Complexes: Models for Metal Ligand Interactions and Solvation.** MICHAEL DUNCAN, *University of Georgia*

Weakly bound complexes of the form $M^+$-$L_x$ (M=Fe, Ni, Co, etc.; L=$CO_2$, $C_2H_2$, $H_2O$, benzene, $N_2$) are prepared in supersonic molecular beams by laser vaporization in a pulsed-nozzle cluster source. These species are mass analyzed and size-selected in a reflectron time-of-flight mass spectrometer. Clusters are photodissociated at infrared wavelengths with a Nd:YAG pumped infrared optical parametric oscillator/amplifier (OPO/OPA) laser or with a tunable infrared free-electron laser. $M^+$-$(CO_2)_x$ complexes absorb near the free $CO_2$ asymmetric stretch near 2349 $cm^{-1}$ but with an interesting size dependent variation in the resonances. Small clusters have blue-shifted resonances, while larger complexes have additional bands due to surface $CO_2$ molecules not attached to the metal. $M^+(C_2H_2)_n$ complexes absorb near the C-H stretches in acetylene, but resonances in metal complexes are red-shifted with repect to the isolated molecule. $Ni^+$ and $Co^+$ complexes with acetylene undergo intracluster cyclization reactions to form cyclobutadiene. Transition metal water complexes are studied in the O-H stretch region, and partial rotational structure can be measured. $M^+$(benzene) and $M^+(benzene)_2$ ions (M=V, Ti, Al) represent half-sandwich and sandwich species, whose spectra are measured near the free benzene modes. These new IR spectra and their assignments will be discussed as well as other new IR spectra for similar complexes.

***Contributed Papers***

**8:36**

**U11 2 Adaptive Tempering Monte Carlo Optimization of Calcium Clusters.*** X. DONG, E. BLAISTEN-BAROJAS, *School of Computational Sciences, George Mason University, Fairfax, VA 22030* The global minimum energy structures of calcium clusters with 15 to 34 atoms were obtained by the Adaptive Tempering Monte Carlo (ATMC) method. The cluster binding energy was obtained within a tight binding approach with parameters reported in previous work[1]. The ATMC optimization process is fast and drives the system across configuration space very effectively reaching the global minimum within a small number of tempering events. The structure of six cluster sizes 15, 16, 18, 21, 23 and 25 corresponding to the global minimum has not been reported in the literature for any other metals. Three clusters $Ca_{15}$, $Ca_{21}$ and $Ca_{23}$ are relatively more stable than the others in this size range. Melting of these clusters are further studied with the weighted histogram analysis method and the free energy profile is predicted. The melting transition is monitored with a novel structural order parameter that reflects the mobility of surface atoms, their bonding order and bonding directionality. [1] X. Dong, G. M. Wang, E. Blaisten-Barojas, Phys. Rev. B 70, 205409 (2004).

*Acknowledgment for computing time Teragrid grant TG-PHY050023T.

**8:48**
**U11 3 Structures and ligand binding energies of size seleceted gold and silver clusters: Approach to the bulk** MICHAEL T. BOWERS, MANUEL MANARD, PAUL KEMPER, *University of California, Santa Barbara* Gold and silver clusters are formed by laser ablation, mass selected, and either reacted with ethene or subjected to ion mobility measurement. Structures are assigned by two methods. In the first sequential ligand binding energies are measured and correlated with possible structures. In the second experimental cross sections are correlated with cross sections from model structures. Both anionic and cationic clusters are measured in the size range 3 to 13. For the anions calculated and experimental detachment energies are also used as structural diagnostics. The various data are compared with bulk values and approach to the bulk assessed.

**9:00**
**U11 4 A comparison of the electronic structure and optical plasmons in $Cs_x$ clusters, $Cs_x$ shells and $C_{60}$ coated with a $Cs_x$ shell*** ARNE ROSEN, JENS EKENGREN, JOHAN SJOEHOLM, MATS ANDERSSON, DANIEL OESTLING, *Department of Physics, Goteborg University, SE-412 96, Goteborg, Sweden* DAVID TOMANEK, *Department of Physics and Astronomy, Michigan State University, East Lansing, Michigan 48824-2230, USA* We present calculations of the electronic structure and collective excitations in Cs clusters, Cs shells and $C_{60}$ coated with a shell of Cs atoms. The ground state properties of these systems are described using the Local Density Approximation and the electronic excitations by the Random Phase Approximation. The jellium shell approximation underlying our calculations correctly predicts the magic numbers. The optical excitation spectra in Cs clusters and Cs coated $C_{60}$ are found to be in agreement with available experimental data.

*Project funded by Swedish Research Council, Swedish Foundation for Strategic Research, NSF NIRT grants DMR-0103587, ECS-0506309, NSF-NSEC EEC-425826

**9:12**
**U11 5 Signatures of Random Matrix Theory in the Discrete Energy Spectra of Shaped Disordered Metallic Clusters** LAURA ADAMS, BRIAN LANG, ALLEN GOLDMAN, *University of Minnesota* It has been predicted that the distribution of the discrete energy levels of disordered metallic clusters should follow random matrix theory. It has been possible to study distributions of energy levels for different shaped metallic clusters using a low temperature scanning tunneling microscope. Depending on the degree of ''shape'' disorder, the statistics either follow Wigner-Dyson statistics, a mixed state, or Poisson-like statistics for the distribution of energy levels. We will present a summary of results on Pb clusters grown by a buffer layered assisted growth technique and in addition show how it is possible to use scanning tunneling spectroscopy to image a quantity proportional to the square of the amplitude of the eigenfunctions for quantum confined systems. These images resemble images acquired in microwave cavity experiments for classically chaotic and nonchaotic systems. This work was supported by the Department of Energy under grant DE-FG02-02ER46004.

***Invited Papers***

**9:24**
**U11 6 Real Time Observation and Control of Cluster Chemistry.**
LUDGER WOESTE, *Freie Universitat Berlin*

This abstract was not received electronically.

***Contributed Papers***

**10:00**
**U11 7 Structure in Binary Nanodroplets** HONG XIA NING, GERALD WILEMSKI, *University of Missouri-Rolla* Recent SANS measurements of core-shell structure in binary nanodroplets ( $\sim$ 9 nm) have stimulated our research on the structure of droplets of this size. [Wyslouzil, et. al., Phys. Chem. Chem. Phys. **8**, xxx (2006)] By structure, we mean the spatial distribution of chemical species within the droplet. Based on recent work by Cordeiro and Pakula [J. Phys. Chem. **109**, 4152 (2005)], we developed an efficient Lattice Monte Carlo (LMC) method to simulate binary droplets containing 5000 to 10000 particles. Simulations of nanodroplets of various compositions were made to study phenomena such as species segregation and phase separation. Depending on the relative strengths of the intermolecular interactions, various interesting structures were found. Droplets may be fairly well-mixed, strongly segregated core-shell structures, or even highly segregated nonspherical shapes resembling partially disassembled Russian dolls. We explored the temperature dependence of the droplet structures and observed that the reversible change between the core-shell and Russian doll structures could be viewed as a wetting—dewetting transition. The transition temperature was determined for a specific system.

**10:12**
**U11 8 Source for a Temperature-Controlled Metal Cluster Beam** WEI JIANG, FORREST PAYNE, LOUIS BLOOMFIELD, *University of Virginia* Metal clusters can be produced easily by laser vaporization of a sample into an inert cooling gas. We have used a pulsed Nd:YAG laser to evaporate cobalt from a rotating rod into a 20cm-long narrow pipe filled with helium gas, injected by a pulsed gas valve. The outgoing part of the pipe (15cm long) is attached to a helium refrigerator and an electrical heater, which allow us to control the pipe's temperature over the range from 60K to room temperature. If the gas-cluster mixture stays in the pipe long enough before supersonic expansion, it reaches thermal equilibrium with the pipe.

**10:24**
**U11 9 Modeling the Melting of Free and Supported Metal Clusters*** KIM BOLTON, *Physics Department, Goteborg University, SE-412 96, Goteborg, Sweden; School of Engineering, University College of Boras, SE-501 90, Boras, Sweden* FENG DING, *MEMS Department, Rice University, MS 321, Houston, TX 77005* HAIMING DUAN, ARNE ROSEN, *Physics Department, Goteborg University, SE-412 96, Goteborg, Sweden* AVETIK R.

HARUTYUNYAN, TOSHIO TOKUNE, *Honda Research Institute USA Inc., 1381 Kinnear Road, Columbus, OH 43212* STEFANO CURTAROLO, *Department of MEMS, Duke University, Durham, NC 27708* The growth rate and mechanism of one-dimensional structures, such as carbon nanotubes and zinc-oxide nanorods, is expected to be significantly affected by the phase of catalytic metal particle. It is therefore important to understand the structure and dynamics of these particles in their solid and liquid phases, and to know how their melting points depend on cluster size and substrate adhesion. Results from molecular dynamics studies on the structural and dynamic changes during melting of free and supported iron clusters, ranging from 150 to 10 000 atoms, will be presented. We will also present a method to determine effective diameters of supported metal clusters, so that the melting point dependence on cluster size can be predicted in a physically meaningful way by the same analytic model used for free clusters.

*Project funded by Honda Research Institute USA Inc., Swedish Research Council and the Swedish Foundation for Strategic Research

**10:36**

**U11 10 Geometric and electronic structure of mixed metal-semiconductor clusters from global optimization.** FRANK HAGELBERG, JIANHUA WU, *Jackson State University* In addition to pure metal and semiconductor clusters, hybrid species that contain both types of constituents occur at the metal-semiconductor interface. Thus, clusters of the form Cu(x)Si(y) were detected by mass spectrometry [1]. In this contribution, the geometric and energetic features of Me(m)Si(7-m) (Me=Cu and Li) clusters are discussed. The choice of these systems is motivated by the structural similarity of the pure Si(7), Li(7), and Cu(7) systems which all stabilize in D(5h) symmetry. On the other hand, Li and Cu, representing the alkali group (IA) and the noble metal group (IB) of the periodic system, are expected to display strongly differing behavior when integrated into a Si(n) cluster, resulting in different ground state geometries for the cases Me = Li and Me = Cu. Addressing this problem by means of geometry optimization requires, in view of the large number of possible atomic permutations for Me(m)Si(7-m) with $0 < m < 7$, the use of a global search algorithm. Equilibrium geometries are obtained by simulated annealing within the Nose' thermostat frame. It is observed that Cu(m)Si(7-m) clusters with $m < 6$ tend towards ground state geometries derived from the D(5h) prototype. For Li(m)Si(7-m), the Li(m) subsystem is found to adsorb on the framework of the Si(7-m) dianion. [1] J.J. Scherer, J.B. Pau, C.P. Collier, A. O'Keefe, and R.J. Saykally, J. Chem. Phys. 103, 9187 (1995).

**10:48**

**U11 11 Unbiased search of minimal energy nanocluster structures*** JOSÉ ROGAN, *Universidad de Chile* GRISELDA GARCÍA, *Universidad Católica de Chile* CLAUDIA LOYOLA, WALTER ORELLANA, *Universidad de Chile* RICARDO RAMÍREZ, MIGUEL KIWI, *Universidad Católica de Chile* A new strategy to find global minima is applied to the structure of metallic clusters. It consists in implementing a conformational space annealing (CSA) unbiased search in combination with many body phenomenological potential techniques to create a data bank of putative minima. Next, the clusters in this data bank are examined by first principle methods to obtain the minimum energy cluster. The scheme is successfully applied to magic number 13 atom clusters of rhodium, palladium and silver. Global minimum energy cluster structures not previously reported are found through our procedure.

*Supported by FONDECYT, Chile, under grants 1030957 (MK and JR), 1040356 (RR) and #1050197 (WO), and MECESUP (GG). WO supported by the Millennium Nucleus P02-004-F.

## SESSION U12: FOCUS SESSION: ELECTROCHEMICAL AND RELATED GROWTH
**Thursday Morning, 16 March 2006; 304, Baltimore Convention Center at 8:00**
**Shirley Chiang, University of California, Davis, presiding**

***Invited Papers***

**8:00**

**U12 1 Physical Origin of Long-Range-Order in Lateral Development of Crystallites: A New Lateral Growth Mode.***
MU WANG, *Department of Physics, Nanjing University, Nanjing 210093, China*

The basic picture of heteroepitaxial growth can be summarized as formation of islands on a foreign substrate first, followed by horizontal expansion of the islands on the substrate. Previously little attention has been paid to how the interfacial tensions affect the horizontal expansion of a crystalline island over the substrate, which has recently been found to affect the physical property of thin film significantly. For example, tilting of crystallographic orientation has frequently been observed in epitaxial layers, and our understanding of such effect is very limited. Recently Wang and his colleagues studied lateral growth of $NH_4Cl$ crystallite on a foreign substrate mediated by successive nucleation. With state-of-the-art structural and morphological characterization methods, they observed that the crystallographic orientation is consecutively rotated, leading to periodic structures on the surface of crystallite aggregate. They demonstrated that this unusual effect is related to the asymmetric surface/interface tensions in the early stage of nucleation, and should be enlightening for a class of thin film growth where nucleation plays a dominate role. Mu Wang, D.-W. Li, D.-J. Shu, P. Bennema, et al., Phys. Rev. Lett., **94**, 125505 (2005). D. W. Li, Mu Wang, P. Liu, et al., J. Phys. Chem. **B107**, 96-101, 2003. X. Y. Liu, Mu Wang, D. W. Li, et al., J. Cryst. Growth **208**, 687-695 (2000). Mu Wang, X.Y. Liu, C. Strom, et al., Phys. Rev. Lett. **80**, 3089 (1998).

*Project supported by MST and NSF of China.

*Contributed Papers*

**8:36**

**U12 2 Steering induced growth anisotropy as a probe for long range interaction** FRITS RABBERING, TEUN WARNAAR, HERBERT WORMEESTER, BENE POELSEMA, *Solid State Physics, MESA+ Institute for Nanotechnology, University of Twente, Enschede, The Netherlands* Grazing incidence homoepitaxy of 0.5 ML on Cu(001) leads to anisotropic structures as determined with high-resolution LEED. This is the result of attractive forces between the surface and the incoming particle. The trajectory of an incoming particle changes so dramatically that a large deposition flux enhancement on protruding structures results [1]. Trajectory calculations based on an attractive Lennard-Jones potential were combined with a kMC simulation that treats the surface diffusions processes in order to investigate the evolution of the observed anisotropy. Modifications of this potential at short range distances only slightly influence the anisotropy, while modifications at long range has a significant influence on the anisotropy as observed during sub-monolayer growth. This enables to probe the long range interaction. The experimental feasibility of the detailed probing will be discussed. [1] S. van Dijken, L.C. Jorritsma and B. Poelsema, Phys. Rev. Lett. 82 4038 (1999)

**8:48**

**U12 3 Analysis of Chemical Reactions between Radical Growth Precursors Adsorbed on Plasma-Deposited Silicon Thin-Film Surfaces** TAMAS BAKOS, MAYUR VALIPA, DIMITRIOS MAROUDAS, *University of Massachusetts, Amherst* The dominant precursor in the plasma deposition of hydrogenated amorphous silicon (a-Si:H) thin films is the $SiH_3$ radical. In this presentation, we report results of first-principles density functional theory calculations on the crystalline Si(001)-(2× 1):H surface and molecular-dynamics simulations on a-Si:H surfaces for the interactions between $SiH_3$ radicals adsorbed on Si thin-film surfaces. The analysis reveals that two $SiH_3$ radicals may either form disilane ($Si_2H_6$) that desorbs from the surface or undergo a disproportionation reaction producing an $SiH_2$ radical that is incorporated in the film and a silane molecule that is released in the gas phase. The corresponding activation barriers depend on the local atomic coordination of the surface Si atoms; $Si_2H_6$ formation is barrierless if both radicals are bonded to overcoordinated surface Si atoms and exhibits barriers in excess of 1 eV for two chemisorbed $SiH_3$ radicals.

**9:00**

**U12 4 Controlling the periodicity of the Si(112)nx1-Ga surface via tuning of the chemical potential** E.J. MOON, *University of Tennessee, Knoxville, USA* P.C. SNIJDERS, *Kavli Institute of Nanoscience, Delft, The Netherlands* S. ROGGE, *Kavli Institute of Nanoscience, Delft, The Netherlands* H.H. WEITERING, *University of Tennessee, Knoxville, and Oak Ridge National Laboratory* We show that the chemical potential, an important parameter in the initial stages of (hetero-) epitaxial semiconductor growth, can be tuned for the Ga atoms on the Si(112)nx1-Ga surface. As a result the periodicity of the surface can be controlled in the range of n=5 to n=6. STM shows that meandering vacancy lines determine the local size of the unit cell. Large scale statistics of the unit cell size extracted from STM images show that the average periodicity n is not an integer, but lies somewhere in between 5 and 6. These findings are confirmed by a careful analysis of new LEED data, which show a range of periodicities in between 5x1 and 6x1 depending on the surface preparation conditions. The extracted periodicities are consistent with periodicities extracted from Fourier Transform STM images. Thus, changes of the chemical potential of the Ga atoms on the surface can be easily monitored in situe by extracting the average surface periodicity from LEED images.

**9:12**

**U12 5 Nanolithographic Write, Read and Erase via Reversible Nanotemplated Nanostructure Electrodeposition on Alkanethiol Modified Au(111) in an Aqueous Solution*** KYOUNGJA SEO, ERIC BORGUET, *Temple University* A Write, Read and Erase nanolithographic method, combining in-situ electrodeposition of metal nanostructures with atomic force microscopy (AFM) nanoshaving of a 1-hexadecanethiol (HDT) self-assembled monolayer (SAM) on Au(111) in an aqueous solution, is reported. The AFM tip defines the local positioning of nanotemplates via the irreversible removal HDT molecules. Nanotemplates with lateral dimensions as narrow as 25 nm are created. The electroactive nanotemplates determine the size, shape and position of the metal nanostructures. The potential applied to the substrate controls the amount of metal deposited and the kinetics of deposition. Metal nanostructures can be reversibly and repeatedly electrodeposited and stripped out of the nanotemplates by applying appropriate potentials.

*This work was supported by the NSF (CHE 0456965). K.S. acknowledges the support of the Post-doctoral Fellowship Program of the Korea Science & Engineering Foundation (KOSEF)

**9:24**

**U12 6 Growth of Electrodeposited Ag Nanowires in Anionic Surfactant Nanotemplates on Au(111)*** ERIC BORGUET, *Temple University* KYOUNGJA SEO, *Temple University* TAO YE, *Pennsylvania State University* Ordered molecular systems should provide templates of molecular dimensions as demonstrated by the growth of silver nanostructures in the potential induced nanotemplates of SDS (sodium dodecyl sulfate). Electrochemical STM (Scanning Tunneling Microscopy) results suggest that SDS molecules form hemicylinders on the Au(111) surface in 0.1M $HClO_4$ solution. The hydrophilic sulfate groups self-assemble to face to the aqueous interface while the hydrophobic backbone adopts a tail to tail configuration. The SDS hemicylinders structures are stable over the potential range of -0.1 $V_{SCE}$ to 0.4 $V_{SCE}$. Silver electrodeposition takes place near the hydrophilic sulfate head, and leads to the formation of nanowires that grow in the same direction as the SDS hemicylinders. Ag nanowires are typically less than 2 nm wide.

*This work was supported by the NSF (NER DMI 0508508)

**9:36**

**U12 7 A New Phase of the Au(111) Surface in Electrolyte Revealed by STM and Asymmetric Potential Pulse Perturbation.*** YUFAN HE, ERIC BORGUET, Asymmetric potential pulse perturbations were combined with STM to separately the $(22\times \sqrt{3}) \leftrightarrow (1\times 1)$ phase transition from the dynamics of the dynamics of nanoscale island growth and dissolution at Au(111)/ 0.1M $HClO_4$ interfaces. In the course of these experiments a new surface phase, characterized by a gas of highly mobile Au adatoms on the surface, the absence of islands and a paucity of reconstruction stripes, was observed. This phase coexists with a low density of reconstructed stripes in ''holes.'' This new phase is an inter-

mediate state and can only be observed over a potential range range from 0.3 $V_{SCE}$ to 0.45$V_{SCE}$, after a potential pulse lifting the reconstruction. In addition, and contrary to previous reports, the (1× 1) ◇ (22× $\sqrt{3}$) reconstruction process can be fast.

*CHE 0456965

**9:48**

**U12 8 Observation of surface layering in a nonmetallic liquid** HAIDING MO, GUENNADI EVMENENKO, SUMIT KEWALRAMANI, KYUNGIL KIM, PULAK DUTTA, *Dept. of Physics & Astronomy, Northwestern University* STEVEN EHRLICH, *Brookhaven National Laboratory* Non-monotonic density profiles (layers) have previously been observed at the free surfaces of many metallic liquids, but not in isotropic dielectric liquids. Whether the presence of an electron gas is necessary for surface layering has been the subject of debate. Until recently, MD simulations have suggested that layering at free liquid interface may be a generic phenomenon and is not limited to the metallic liquids[1]. The theories predict that if normal liquids can be cooled down to temperatures low enough, layering structure should be observed experimentally. However, this is difficult for most molecular liquids because these liquids freeze well above the temperature necessary for observing the layering structure. By studying the surface structure of liquid TEHOS (tetrakis(2-ethylhexoxy)silane), which combines relatively low freezing point and high boiling point compared to that of most molecular liquids, we have observed the evidence of layering at the free interface of liquid TEHOS using x-ray reflectivity. When cooled to $T/T_c \approx 0.25$ (well above the bulk freezing point, Tc is the critical temperature of TEHOS), the surface roughness drops sharply and density oscillations appear near the surface. Lateral ordering of the surface layers is liquid-like, just as at liquid metal surfaces. 1. E. Chacón and P. Tarazona, Phys. Rev. Lett. **91** 166103-1 (2003)

**10:00**

**U12 9 Chemical Electrode Modification for Charge Injection in Organic Thin Film Transistors*** ELBA GOMAR-NADAL, DANIEL HINES, ANDREW TUNNELL, *Department of Physics, University of Maryland, College Park, MD 20742* WINSTON YAN, *T. Jefferson High School* ELLEN WILLIAMS, *Department of Physics, University of Maryland, College Park, MD 20742* The nature of the interface between an organic material and an inorganic electrode (metal or semiconductor) is critical to the performance of organic electronic and optoelectronic devises. To improve the electrical contact between gold electrodes and pentacene thin film transistors prepared by nanotransfer printing [1], the effect of coating the gold electrodes with self-assembled monolayers (SAMs) of organic molecules with electro-withdrawing groups is being explored. The first experiments have been done with commercially-available molecules and oligo(phenylene ethylene) derivatives have been synthesized for further investigation. The transport and noise characteristics of pentacene TFTs fabricated using the different coating groups will be presented. [1] D.R. Hines et al, Appl. Phys. Lett. 86, 163101 (2005).

*Supported by LPS and the UMD-NSF-MRSEC

**10:12**

**U12 10 Effects of Stress and Void-Void Interactions on Current-Driven Void Surface Evolution in Metallic Thin Films** JAESEOL CHO, M. RAUF GUNGOR, DIMITRIOS MAROUDAS, *University of Massachusetts, Amherst* We report results of electromigration- and stress-induced migration and morphological evolution of voids in metallic thin films based on self-consistent numerical simulations. The analysis reveals the complex nature of void-void interactions and their implications for the evolution of metallic thin-film electrical resistance, providing interpretation for experimental measurements in interconnect lines. Interestingly, for two voids migrating in the same direction under certain conditions, we find that a smaller void does not always approach and coalesce with a larger one, while a larger void may approach and coalesce with a smaller one. In addition, we find that under certain electromechanical conditions, biaxially applied mechanical stress can cause substantial retardation of void motion, as measured by the constant speed of electromigration-induced translation of morphologically stable voids. This effect suggests the possibility for complete inhibition of current-driven void motion under stress.

**10:24**

**U12 11 Characterization and Control of Microstructure in Combinatorially Prepared Aluminum-Silicon Thin Film Nanocomposites** DAAD HADDAD, *School of Materials Engineering, Purdue University, West Lafayette, IN 47907* CHARLES OLK, MICHAEL LUKITSCH, *Materials and Processes Laboratory, General Motors Research and Development Center, Warren, MI 48090* In this presentation, we describe the application of thin film combinatorial methods to systematically control the microstructure of $Al_xSi_{(1-x)}$ alloys through variations in composition and growth temperature. Libraries of compositionally graded films have been sputter deposited onto silicon substrates. The microstructure was investigated using x-ray diffraction while atomic force microscopy techniques were employed to obtain surface morphology and phase distribution. We will also report the results of the mechanical properties we have investigated on these films.

**10:36**

**U12 12 Mechanical Properties of Electrophoretically-Deposited CdSe Nanocrystal Films** SHENGGUO JIA, SARBAJIT BANERJEE, DONGYUN LEE, WEI WANG, JOZE BEVK, JEFFREY KYSAR, IRVING HERMAN, MATERIALS RESEARCH SCIENCE AND ENGINEERING CENTER, COLUMBIA UNIVERSITY, NEW YORK, NY TEAM, Approaches to measuring and then minimizing the strain in electrophoretically deposited CdSe nanocrystal films are investigated. The films are seen to fracture above a critical thickness which vaies with nanocrystal size. Cracking and delamination have been studied by SEM and AFM and are attributed to the high strain energy in the film. Raman microprobe scattering and EDX mapping show the strain distribution in the nanocrystal films. The Young's modulus measured by nanoindentation is in good agreement with the parameters obtained from Raman scattering. The deposition conditions have been varied to minimize this strain, which is thought to be due to the evaporation of residual hexane solvent after electrophoretic deposition. In situ observations confirm this assumption about the origin of film strain. Thermogravimetric analysis and differential scanning calorimetry measurements provide the chemical composition of CdSe nanocrystals. The CdSe nanocrystal films become mechanically stronger and more resistant to chemical dissolution after being treated by different cross-linker molecules. This work was supported primarily by the MRSEC Program of the National Science Foundation under Award No. DMR-0213574 and by the NYSTAR.

**10:48**
**U12 13 Characterization of electromigration in semiconductor device interconnects using microscopic techniques** NARAHARA DINGARI, DAVID HESKETT, *University of Rhode Island* Electromigration is an important failure mechanism which affects the functionality and lifetime of integrated circuits. The addition of relatively small amounts of copper has been previously shown to improve device interconnect lifetimes. Through the use of Scanning Electron Microscope (SEM) with Energy Dispersive Spectroscopic (EDS) capabilities we have measured the copper concentration as a function of position along an interconnect after several accelerated stress time periods. We observe a migration of copper atoms from the cathode to the anode side of the interconnect as a function of stressing time. In some cases, a pileup of copper near the middle of the interconnect indicates a blocking of copper diffusion and creates a site for interconnect failure. Metal pileup (hillocks) and depletion (voids) are observed by Atomic Force Microscopy (AFM). We also observe a correlation between relative reflectance using optical microscopy and roughness (observed by AFM) of an interconnect line.

**SESSION U16: NANOTECHNOLOGY: APPLICATIONS AND MEASUREMENTS**
**Thursday Morning, 16 March 2006**
**312, Baltimore Convention Center at 8:00**
**S. Sridhar, Northeastern University, presiding**

**8:00**
**U16 1 Development of Carbon Nanotube Based Isotropic X-ray Source for Cone-Beam Tomography Imaging** ZEJIAN LIU, YUEH LEE, GUANG YANG, JIAN ZHANG, JIANPING LU, OTTO ZHOU, *University of North Carolina at Chapel Hill* We have developed a carbon nanotube based microfocus X-ray source with an isotropic focal spot. Two focusing electrodes were implemented in the design with one electrode harnessing the divergence of field-emitted electrons from gate and the other focusing electrons onto the anode. Isotropic X-ray focal spot was achieved by utilizing an elliptical cathode that forms elliptical electron probe on the anode after electrostatic focusing. Based on the design method, an x-ray source with an isotropic focal spot of 65 $\mu$m in diameter was experimentally demonstrated in X-ray projection images. This type of X-ray source sees wide applications in cone-beam tomography imaging studies.

**8:12**
**U16 2 Stationary scanning x-ray source based on carbon nanotube field emitters** GUANG YANG, JIAN ZHANG, *Department of Physics and Astronomy, University of North Carolina, Chapel Hill, NC 27599* YUAN CHENG, BO GAO, QI QIU, *Xintek, Inc. P.O. Box 13788, 7020 Kit Creek Rd., Research Triangle Park, NC 27709* YUEH LEE, JIANPING LU, OTTO ZHOU, *Department of Physics and Astronomy, University of North Carolina, Chapel Hill, NC 27599* Carbon nanotube is an ideal field emitter thanks to its large aspect ratio and small diameter. Based on its field emission property, we have developed a stationary scanning x-ray source, which can generate a scanning x-ray beam to image an object from multiple projection angles without mechanical motion. The key component of the device is a gated carbon nanotube field emission cathode with an array of electron emitting pixels that are individually addressable via a metal-oxide-semiconductor field effect transistor-based electronic circuit. The characteristics of this x-ray source are measured and its imaging capability is demonstrated. The device can potentially lead to a fast data acquisition rate for laminography and tomosynthesis.

**8:24**
**U16 3 A New Thermionic Cathode Using Oxide Coated Carbon Nanotubes*** CHRISTOPHER DAY, FENG JIN, YAN LIU, SCOTT LITTLE, *Ball State University* We have demonstrated a new type of thermionic cathode utilizing carbon nanotubes that exhibited superior electron emission properties. A field enhancement factor as high as 2000 was observed and thermionic electron emission current at least an order of magnitude higher than the emission from a conventional oxide cathode was obtained. This cathode combines the low work function of the oxide coating with a high field enhancement factor introduced by carbon nanotubes and we have demonstrated that it can be used as a highly efficient electron source. The cathode was fabricated by sputter deposition of a thin film of oxide materials on aligned carbon nanotubes, which were grown on a tungsten substrate with plasma enhanced chemical vapor deposition.

*This work is supported by the Department of Energy.

**8:36**
**U16 4 Selective Adsorption and Alignment Phenomena of ZnO Nanorods on Molecular-Patterned Substrates for Large-Scale Integrated Device Fabrication*** JUWAN KANG, SUNG MYUNG, SEUNGHUN HONG, *School of Physics Seoul National University* DONGJIN OH, GYUTAE KIM, *Korea University* ZnO nanorods have been utilized for various device applications such as field effect transistor, UV sensor, etc. However, a major stumbling block holding back their practical applications is a lack of mass-production method of such devices. Since ZnO nanorods are first synthesized in solution, one has to pick up and assemble individual nanorods onto substrate for device fabrication, which is not an easy task. We studied the selective assembly and alignment phenomena of ZnO nanorods on molecule-patterned solid substrates. When the molecule-patterned substrate is placed in the solution of ZnO, ZnO nanorods are selectively adsorbed onto negatively charged surface region. Furthermore, we found the adsorbed nanorods slide on the substrate resulting in aligned nanorod structures. This presentation will discuss the systematic study of ZnO nanorod assembly process on patterned substrates and applications of this method for large-scale assembly of ZnO nanorod-based integrated devices.

*Supported by the Ministry of Science and Technology through the NRL program and NSI-NCRC of Korea Science and Engineering Foundation.

**8:48**
**U16 5 Atom selective force measurement with STM** APARNA DESHPANDE, *Ohio University* VIOLETA IANCU, *Ohio University* SAW-WAI HLA, *Ohio University* Scanning tunneling microscope (STM) manipulation and spectroscopy is used to determine the strength of interactions necessary to manipulate individual silver and bromine atoms on a Ag(111) surface at 4.6 K. In order to distinguish between the two types of atoms, we use local atom extraction procedures: bromine atoms are extracted from individual molecules of cobalt porphyrin (5,10,15,20-Tetrakis-(4-bromophenyl)-porphyrin-Co(II)), which are deposited prior to this

experiment, by selectively breaking the C-Br bonds with the STM tip. The individual silver atoms are extracted from the native Ag(111) surface by a controlled tip-crash procedure. Then, we laterally manipulate these two atoms using the same STM-tip along the close packed rows of the Ag(111) surface. The tip-height signals during manipulation are recorded as a function of the tip-atom distance, which include the force information necessary to move a halogen atom, bromine, and a metallic atom, silver, on this surface. This work is financially supported by US-DOE grant, DE-FG02-02ER46012.

**9:00**

**U16 6 Nanofabrication Based on Nanoporous Membranes** ZHEN WU, *Northeastern University* L. TIAN, *Texas Tech University* C. RICHTER, *Northeastern University* D NAGESHA, *Northeastern University* S. SRIDHAR, *Northeastern University* L. MENON, *Northeastern University* We describe nanofabrication methods to produce nanopore array templates in aluminum oxide and titanium dixode films. The method is based on anodization of thin films of aluminum and titanium under itdc conditions in an acid. We also describe non-lithographic means of transferring the pore pattern from such nanoporous membranes onto a generic substrate. This is based on reactive ion etching through the nanoporous template grown directly on the substrate. In our demonstration, a thin alumina template consisting of a hexagonal array of pores $\sim$ 50nm in diameter is first deposited on the substrate. The pores reach within 10-20 nm of aluminum, which is protected by an alumina barrier layer. By controlling reactive ion etching conditions, we demonstrate highly anisotropic etching through the aluminum layer, barrier alumina layer and into the substrate. The 50nm pore layer is thus directly transferred to create nanoporous and nanopillar arrays of a variety of materials such as Al, Si, GaN, GaAs, etc. Such nanoporous, nanopillar arrays will be useful in a variety of applications involving biosensors, optoelectronic and spintronic devices.

**9:12**

**U16 7 Resonant Operation of Nanoelectromechanical Systems in a Viscous Fluid** DEVREZ KARABACAK, KAMIL L. EKINCI, *Dept. of Aerospace and Mechanical Eng., Boston University* Up to date, most work on nanoelectromechanical systems (NEMS) has been done in high vacuum. Yet, many applications may require fluidic NEMS operation. Here, we present measurements of the quality ($Q$) factor and resonance frequency in nanomechanical doubly-clamped beam resonators as a function of surrounding gas pressure — from high vacuum to atmospheric conditions. Atmospheric $Q$s obtained are $\sim 10^2$. The experimental results also suggest that viscous effects become less severe in high frequency devices.

**9:24**

**U16 8 Experimental Measurement of Elastic Contact Diameter** CHARLES YING, *NIST* Manipulation of nano-objects, as well as further development of the MEMS technology, needs an understanding and control of surface forces, including friction and adhesion forces, which depend on contact area in the nanoscale. Meaningful measurements of surface forces and correct interpretation of the force data require knowledge of contact area. Due to experimental difficulties of contact area measurements, a common practice today in surface force research using atomic force microscopy (AFM) is to compute the contact area using the contact mechanics theories. In this talk, I will present a method of experimental determination of contact diameter, or contact width, between a diamond tip and a flat silicon surface. The experiments used diamond tips with their surface geometry determined by AFM imaging. The measured elastic contact widths for diamond tips with a spherical shape, under controlled magnitudes of force in the surface normal direction, agree with the Hertzian contact mechanism. The technique has also been used successfully to obtain contact widths for non-spherical tip geometry.

**9:36**

**U16 9 Preparation of different protected bimetallic nanoelectrodes with 30nm gapwidth and access window** STEPHAN KRONHOLZ, SILVIA KARTHÄUSER, RAINER WASER, *Center of Nanoelectronic Systems for Information Technology Research Center Jülich GmbH, 52425 Jülich, Germany* Reproducible fabrication of 30 nm metallic nanogaps on silicon chips and their electrochemical characterization are presented. The fabrication of the chip is a combination of an optical lithography step and two electron-beam (e-beam) steps. An optimized adhesion layer/metal layer combination (Ti/Pt/Au) and an adopted two layer e-beam resist are used. Specifically the chip has been covered with different protection layers, except of an access window located on top of the nanogaps, calibration electrodes and contact pads, respectively (Fig.1). After characterising the gaps and of the protection layer by cyclical voltammetry in 0.1 M $H_2SO_4$ aqueous electrolyte, the deposition of Cu onto the nanogaps will be presented. Fig.1: Different Nanoelectrode Structures with access window on top covered by $SiO_2/Si_3N_4/SiO_2$ used as protection layer.

**9:48**

**U16 10 Nanoscale metal thermometry using a radiofrequency single electron transistor** LOREN SWENSON, *University of California, Santa Barbara* DAVID WOOD, ANDREW CLELAND, We report on the development of single electron transistors for thermometric readout of nanoscale normal metal volumes. Due to the weak electron-phonon interaction at low temperatures, the electron gas in a normal metal can be heated to a temperature significantly greater than that of the surrounding lattice. Below 100 mK, the electron-phonon coupling time is on the order of microseconds to milliseconds, making direct measurements of the electron temperature's time dependence possible. Achieving sensitive and high frequency readout of this system is of critical importance for applications in nanocalorimetry and nanobolometry. We will describe the use of a radiofrequency single electron transistor to time-resolve the temperature of the electron gas in a submicron scale normal metal volume.

**10:00**

**U16 11 Electrothermal Tuning of Nanomechanical Resonators** MICHAEL MANOLIDIS, *Columbia University* SEONG CHAN JUN, X.M. HENRY HUANG, J. HONE, A highly effective electrothermal tuning method has been demonstrated for Al-SiC nanomechanical resonators. Doubly clamped beam devices are actuated and read out using a magnetomotive technique under moderate vacuum. DC current applied to a beam heats the structure and shifts the resonance frequency downward. Frequency shifts of 10 percent are easily achievable, and the thermal time constant of these structures is in the $\mu$s range. The initial frequency and frequency tunability are studied for beams of varying Al thickness, and the device performance can be accurately modeled using simple mechanical and thermal models. Because of the different mechanical properties of SiC and Al, both the initial frequency and the frequency tunability can be modified by varying

the Al layer thickness. This approach has the potential to become an important tool for effective frequency tuning in deployable SiC-based NEMS devices and systems for applications that would benefit from SiC as the structural material.

**10:12**
**U16 12 Resonant absorption in micrometer and nanometer absorbing particles*** ESHEL FARAGGI, BERNARD GERSTMAN, *Physics Department, Florida International University, Miami, Florida 33199* Resonance effects can occur in laser absorption by micrometer and nanometer sized particles when a train of pulses is used. The pressure generated by the train of pulses may be significantly different than the pressure generated by a single pulse with the same total energy. For pulsed lasers with a gap duration between pulses that is an integer multiple of the characteristic oscillation time of the absorber, constructive interference occurs and the pressure generated inside the absorber is approximately the same as that generated by a single laser pulse. For pulsed lasers with a gap duration between pulses that is not an integer multiple of the characteristic oscillation time, destructive interference occurs and the pressure is significantly decreased. We present numerical computations comparing this effect in two model systems: 1 micrometer melanosome and a 100 nm gold absorber. The resonance effects have implications for both damage thresholds and therapeutic applications of laser radiation.

*The authors would like to thank the Air Force Office of Scientific Research for funding through Grant F49620-03-1-0221.

**10:24**
**U16 13 Optical Trapping and Integration of Semiconductor Nanowire Assemblies in Water** ALEKSANDRA RADENOVIC, ELIANE TREPAGNIER, HARI SHROFF, JAN LIPHARDT, *UC Berkeley, Department of Physics* PETER PAUZAUSKIE, PEIDONG YANG, *UC Berkeley, Department of Chemistry* JAN LIPHARDT TEAM, PEIDONG YANG TEAM, The use of nanowires in scientific, biomedical, and microelectronic applications is greatly restricted due to a lack of methods to assemble nanowires into complex heterostructures with high spatial and angular precision. Here we show that an infrared single-beam optical trap can be used to individually trap, transfer, and assemble high-aspect-ratio semiconductor nanowires into arbitrary structures in a fluid environment. Nanowires with diameters as small as 20 nm and aspect ratios of above 100 can be trapped and transported in three dimensions, enabling the construction of nanowire architectures which may function as active photonic devices. Moreover, nanowire structures can now be assembled in physiological environments, offering novel forms of chemical, mechanical, and optical stimulation of living cells.

**10:36**
**U16 14 Low temperature internal friction peak in Boron doped nanocrystalline diamond** THOMAS METCALF, BRIAN HOUSTON, JAMES BUTLER, *Naval Research Laboratory* TATYANA FEYGELSON, *GeoCenters, Inc.* Recent measurements of the low-temperature internal friction ($Q^{-1}$) of nanocrystalline diamond films have revealed that these films have a broad but distinct internal friction peak at approximately 2K. In contrast to the off-peak baseline low-temperature $Q^{-1}$ of these films, which show no measureable variation over a factor of 4 span in amplitude, the $Q^{-1}$ at the peak decreases by as much as 60% when the measurement amplitude is increased by a factor of 4. The similarity of this peak with a low-temperature peak previously observed in boron-doped silicon led to the possibility that the peak is the result of boron contamination of the diamond films. To further investigate this, diamond films with varying degrees boron doping were grown and measured between room temperature and 400 mK. The films are typically 0.5 $\mu$m thick and are grown on silicon double paddle oscillator substrates, which have an extremely low internal friction background and enable highly sensitive measurements of the mechanical properties of thin films. Preliminary results show an upwards shift in temperature of the peak with increasing boron levels.

**10:48**
**U16 15 Microwave Dielectric Resonance and Negative Permittivity Behavior in $Al_2O_3$-CuO-Cu Nanocomposites*** JEFFREY CALAME, JACOB BATTAT, *Naval Research Laboratory, Washington DC 20375* The frequency-dependent microwave (0.1-18 GHz) complex permittivity of nanocomposites based on the $Al_2O_3$/CuO/Cu system is investigated. The composites are formed by solution infusion of copper precursors into a porous $Al_2O_3$ matrix, followed by thermal decomposition to copper oxides and localized formation of $CuAl_2O_4$ spinels, and finally partial reduction by $H_2$ firing. The final material has a complicated microstructure and exhibits strong amplitude, relatively narrowband dielectric resonance in the microwave regime at intermediate concentrations ( $\sim$ 15-18% by volume) of Cu. The resonances are superficially similar in structure to plasmon and Reststrahlen resonances typically seen in conductors at far-infrared to optical frequencies, but occurring at much lower frequencies in the composites. This is in contrast to the usual broadband induced-polarization dielectric relaxations observed in standard composites. Large concentrations of copper cause negative permittivity behavior below 6 GHz. Permittivity data, SEM micrographs, and possible explanations will be presented.

*Work supported by the Office of Naval Research

## SESSION U17: PHYSICS AND IMAGING IN MEDICINE
**Thursday Morning, 16 March 2006; 313, Baltimore Convention Center at 8:00**
**Steven Avery, University of Pennsylvania, presiding**

**8:00**
**U17 1 Careers in Medical Physics and the American Association of Physicists in Medicine.**
HOWARD AMOLS, *American Association of Physicists in Medicine*

The American Association of Physicists in Medicine (AAPM), a member society of the AIP is the largest professional society of medical physicists in the world with nearly 5700 members. Members operate in medical centers, university and community hospitals, research laboratories, industry, and private practice. Medical physics specialties include radiation

therapy physics, medical diagnostic and imaging physics, nuclear medicine physics, and medical radiation safety. The majority of AAPM members is based in hospital departments of radiation oncology or radiology and provide technical support for patient diagnosis and treatment in a clinical environment. Job functions include support of clinical care, calibration and quality assurance of medical devices such as linear accelerators for cancer therapy, CT, PET, MRI, and other diagnostic imaging devices, research, and teaching. Pathways into a career in medical physics require an advanced degree in medical physics, physics, engineering, or closely related field, plus clinical training in one or more medical physics specialties (radiation therapy physics, imaging physics, or radiation safety). Most clinically based medical physicists also obtain certification from the American Board of Radiology, and some states require licensure as well.

**8:36**
**U17 2 International Standardization of the Clinical Dosimetry of Beta Radiation Brachytherapy Sources: Progress of an ISO Standard.**
CHRISTOPHER SOARES, *National Institute of Standards and Technology*

In 2004 a new work item proposal (NWIP) was accepted by the International Organization for Standardization (ISO) Technical Committee 85 (TC85 – Nuclear Energy), Subcommittee 2 (Radiation Protection) for the development of a standard for the clinical dosimetry of beta radiation sources used for brachytherapy. To develop this standard, a new Working Group (WG 22 - Ionizing Radiation Dosimetry and Protocols in Medical Applications) was formed. The standard is based on the work of an ad-hoc working group initiated by the Dosimetry task group of the Deutsches Insitiut für Normung (DIN). Initially the work was geared mainly towards the needs of intravascular brachytherapy, but with the decline of this application, more focus has been placed on the challenges of accurate dosimetry for the concave eye plaques used to treat ocular melanoma. Guidance is given for dosimetry formalisms, reference data to be used, calibrations, measurement methods, modeling, uncertainty determinations, treatment planning and reporting, and clinical quality control. The document is currently undergoing review by the ISO member bodies for acceptance as a Committee Draft (CD) with publication of the final standard expected by 2007. There are opportunities for other ISO standards for medical dosimetry within the framework of WG22.

**9:12**
**U17 3 Scientific Programs and Funding Opportunities at the National Institute of Biomedical Imaging and Bioengineering.**
RICHARD BAIRD, *NIBIB, NIH*

The mission of the National Institute of Biomedical Imaging and Bioengineering (NIBIB) is to improve human health by promoting the development and translation of emerging technologies in biomedical imaging and bioengineering. To this end, NIBIB supports a coordinated agenda of research programs in advanced imaging technologies and engineering methods that enable fundamental biomedical discoveries across a broad spectrum of biological processes, disorders, and diseases and have significant potential for direct medical application. These research programs dramatically advance the Nation's healthcare by improving the detection, management and, ultimately, the prevention of disease. The research promoted and supported by NIBIB also is strongly synergistic with other NIH Institutes and Centers as well as across government agencies. This presentation will provide an overview of the scientific programs and funding opportunities supported by NIBIB, highlighting those that are of particular important to the field of medical physics.

**9:48**
**U17 4 Medical Physics Graduate Program At An HBCU.**
PAUL GUEYE, *Hampton University*

The Physics Department at Hampton University houses the first Medical Physics graduate program at a minority institution, and the first in the state of Virginia. Jointly established with the Eastern Virginia Medical School, the program requires students to take standard physics courses in addition to medical physics classes and clinical rotations performed at local hospitals. The associated medical physics research primarily focuses on detectors development for absolute 3D dose distribution measurements (with accuracy better than $\pm$ 100 microns), characterization of the uniformity or non-uniformity of Brachytherapy sources, and extraction of the 2D and 3D in-vivo dose maps for real time dose monitoring. Recent novel fundamental studies on the energy dependence of cancer cells to address, among others, mono-energetic Brachytherapy source treatments, reaction mechanisms associated with cancer cell destruction, and cancer genome identification have been launched. Each of the research conducted is strongly coupled to dedicated Geant4 Monte Carlo simulations. After presenting this unique medical physics program, we will review results obtained from its research group.

**SESSION U18: FOCUS SESSION: CARBON NANOTUBES: TRANSPORT III**
**Thursday Morning, 16 March 2006; 315, Baltimore Convention Center at 8:00**
**Angel Rubio, DIPC San Sebastian, presiding**

*Invited Papers*

**8:00**
**U18 1 Electron Phonon Coupling Effects in Nanotubes.**
ANDREA C. FERRARI,* *University of Cambridge*

Electron-phonon coupling (EPC) is a key physical parameter in nanotubes. Here we discuss its effects on phonon dispersions, Raman spectra and electron transport. The main EPC effect on the phonon dispersions is the presence of Kohn anomalies. These are distinct features of the phonon dispersion in metallic systems, associated to the presence of a Fermi surface [1]. Graphite has two Kohn anomalies for the Gamma-$E_{2g}$ and K-$A'_1$ optical modes [2]. Their strength is proportional to the EPC square [2]. Kohn anomalies are enhanced in metallic nanotubes due to their reduced dimensionality, but absent in semiconducting nanotubes [2,3]. At 0 K all metallic nanotubes are not stable and undergo a Peierls distortion. We show that the Peierls distortion temperature decreases exponentially with the tube diameter [3]. For nanotubes generally used in experiments, with diameters larger than 0.8 nm, we find that this temperature is smaller than $10^{-8}$ K [3]. We then show that EPC is the major source of broadening for the Raman G and $G^-$ peaks in graphite and metallic nanotubes [3]. The EPC explains the difference in the Raman spectra of metallic and semiconducting nanotubes and their dependence on tube diameter [3]. We dismiss the common assignment of the $G^-$ peak in metallic nanotubes to a Fano resonance between phonons and plasmons. We assign the $G^+$ and $G^-$ peaks to TO (circumferential) and LO (axial) modes, the opposite of what often done. We then present five independent approaches to directly measure the optical phonons EPC in graphite and nanotubes from their phonon dispersions and Raman spectra. This allows us to quantify the EPC effects on high field electron transport in nanotubes. High field measurements show that electron scattering by optical phonons breaks the ballistic behavior. From our EPCs we derive a simple formula for the electron mean free path for optical phonon scattering in high-field transport [4]. The comparison with the scattering lengths fitted from experimental I-V curves shows that hot phonons are created during high-bias transport [4]. Their effective temperature is thousands K and sets the ultimate limit of ballistic transport [4].

[1]W. Kohn, Phys. Rev. Lett. **2**, 393 (1959).

[2]S. Piscanec et al., Phys. Rev. Lett. **93**, 185503 (2004).

[3]M. Lazzeri et al., cond-mat/0508700; S. Piscanec et al., Phys. Rev. B submitted (2005).

[4]M. Lazzeri et al., Phys. Rev. Lett. **95**, 236802 (2005).

*This work done in collaboration with M. Lazzeri, F. Mauri (Institut de Mineralogie et Physique des Milieux Condenses, Paris, France) and S. Piscanec (University of Cambridge).

*Contributed Papers*

**8:36**
**U18 2 Self-Heating and Non-Equilibrium Optical Phonons in Suspended Carbon Nanotubes** DAVID MANN, ERIC POP, JIEN CAO, HONGJIE DAI, *Stanford University* Understanding of current-limited transport in single-walled carbon nanotubes (SWNTs) is vital to many potential nanotube applications. In this talk I will discuss the high bias electrical transport characteristics of well-contacted suspended SWNTs in various environments. Negative differential conductance at low bias (below 0.4V) appears as a result of extreme self-heating and the formation of non-equilibrium optical phonons. Various gas and molecular solid environments lead to the reduction or elimination of the non-equilibrium phenomenon. Finally I will discuss the ways in which we can use the data to directly and indirectly measure the nanotube's intrinsic properties and temperature.

**8:48**
**U18 3 Direct measurements of electron-phonon coupling of radial breathing modes in carbon nanotubes and their chirality dependence** Y. YIN, A. WALSH, B.B. GOLDBERG, *Physics Department, Boston University* S.B. CRONIN, *Electrical Engineering Department, University of Southern California* M. TINKHAM, *Department of Physics, Harvard University* A.N. VAMIVAKAS, M.S. ÜNLÜ, A.K. SWAN, *Electrical and Computer Engineering, Boston University* A method for direct measurement of electron-phonon coupling matrix elements, $M_{e-ph}$, is proposed and demonstrated experimentally by correlating resonant Raman excitation profiles of the first and second harmonics of the radial breathing mode. $M_{e-ph}$ values are quantitatively determined for individual carbon nanotubes (CNT) excited in small ropes suspended in air. The results show that the matrix elements satisfy S. V. Goupalov and coworkers empirical tight binding theory calculation[1] with quantitative values that show a smaller electron-phonon coupling than reported from ab initio calculations[2] for isolated carbon nanotubes. We find that resonant excitation profile broadening $\eta$ for CNTs in small ropes show a correlation with chiral angles that appears to be unchanged from isolated carbon nanotubes. 1. S. V. Goupalov, Satishkumar B. C., and S. K. Doorn, Pre- print (2005). 2. M. Machon, S. Reich, H. Telg et al., Phys. Rev. B 71 (3) (2005).

**9:00**

**U18 4 Nonequilibrium phonon occupation in carbon nanotube quantum dots*** LUTFE SIDDIQUI, *School of Electrical and Computer Engineering, Purdue University, West Lafayette, IN 47907* AVIK GHOSH, *Department of Electrical and Computer Engineering, University of Virginia, Charlottesville, VA 22903* SUPRIYO DATTA, *School of Electrical and Computer Engineering, Purdue University, West Lafayette, IN 47907* We present a formalism for electron transport through a coulomb blockaded quantum dot strongly coupled with vibrations and weakly with leads and the thermal environment. By calculating the joint electron-phonon probability distribution, we show that recently observed anomalous conductivity through single-walled carbon nanotube (SWCNT) quantum dots arises from 'hot' phonons that are generated by the current at a faster rate than their extraction rate by the surrounding. We explain semi-quantitative details of the experiment and predict a nontrivial temperature dependence of the phonon population arising from a subtle interplay between phonon emission and absorption rates at specific bias voltage values.

*DURINT, DARPA-ONR and NCN

**9:12**

**U18 5 Phonon scattering in Carbon Nanotube Field Effect Transistors – an NEGF Treatment.*** SIYURANGA KOSWATTA, SAYED HASAN, MARK LUNDSTROM, *Electrical and Computer Engineering, Purdue University* M.P. ANANTRAM, *NASA Ames Research Center* DMITRI NIKONOV, *Intel Corp.* We examine the influence of phonon scattering on DC current transport in carbon nanotube field-effect transistors using the non-equilibrium Green's function (NEGF) formalism. Both optical and acoustic phonon modes are considered, and electron-phonon interaction is modeled through a scattering self-energy. Intra-valley scattering due to longitudinal optical (LO) and radial breathing mode (RBM) phonons is examined. Zone-boundary phonon eigenmodes that mediate inter-valley scattering are found to be a mixture of fundamental polarizations such as LO/TA and to couple strongest to the electrons. The effect of phonon scattering on the current vs. voltage characteristic of a filed-effect transistor is found to have distinct gate voltage (Vg) dependence. High-energy optical phonons can significantly degrade the ON-current (large Vg) while their effect is negligible in the OFF-state (low Vg). On the other hand, low-energy phonons (acoustic and RBM) can considerably affect the current transport for all gate biases. Their influence is enhanced at low Vg due to the one-dimensional density of states.

*This work is supported by the grant NASA INAC NCC 2-1363

**9:24**

**U18 6 Transport properties of suspended carbon nanotubes** HENK POSTMA, *Caltech* HSIN-YING CHIU, MARC BOCKRATH, The study of suspended doubly clamped carbon nanotubes allows for the observation of many novel phenomena due to the intimate coupling of the mechanical and electrical degree of freedom, e.g. high frequency quantum limited displacement sensing, phonon adsorption and emission spectroscopy and quantized frequency tuning. We use a high frequency mixing technique originally develloped by Sazonova et al. to monitor the high frequency properties of suspended carbon nanotubes. Our setup allows for measurements from DC up to 4 GHz from room temperature down to 300 mK.

**9:36**

**U18 7 Electrical Switching in Metallic Carbon Nanotubes*** HYOUNG JOON CHOI, *Institute of Physics and Applied Physics, Yonsei University, Seoul, Korea* YOUNG-WOO SON, *Department of Physics, University of California at Berkeley and Materials Sciences Division, LBNL* JISOON IHM, *School of Physics, Seoul National University, Seoul, Korea* MARVIN L. COHEN, STEVEN G. LOUIE, *Department of Physics, University of California at Berkeley and Materials Sciences Division, LBNL* We present first-principles calculations of quantum transport which show that the resistance of metallic carbon nanotubes can be changed dramatically with homogeneous transverse electric fields if the nanotubes have impurities or defects. The change of the resistance is predicted to range over more than two orders of magnitude with experimentally attainable electric fields. This novel property has its origin that backscattering of conduction electrons by impurities or defects in the nanotubes is strongly dependent on the strength and/or direction of the applied electric fields. We expect that this property will open a path to new device applications of metallic carbon nanotubes. Ref.) Young-Woo Son *et al.*, Phys. Rev. Lett. **95**, 216602 (2005).

*This work was supported by NSF Grant No. DMR04-39768, DOE Contract No. DE-AC03-76SF00098, and SRC(CNNC) of MOST/KOSEF. Computational resources have been provided by the KISTI, NSF at the NPACI, and DOE at the NERSC.

**9:48**

**U18 8 High Temperature Conductivity and Reactivity of Carbon Nanotube Electronic Circuits*** A. KANE, PHILIP G. COLLINS, *University of California at Irvine* At sufficiently high temperatures, carbon nanotubes (CNTs) begin to react with their immediate environment. For example, adsorbates first desorb, then the carbon may react with connective electrodes, and ultimately Stone-Wales defects become mobile and can be annealed. These reactions are conventionally studied by thermogravimetric analysis (TGA), but they can also profoundly effect the conductance of the nanotubes. We have measured the four probe impedance and transimpedance of individual metallic and semiconducting nanotube devices from room temperature to 1200 K in ultra-high vacuum. When the nanotubes are initially heated from room temperature, the conductance increases as adsorbates are desorbed. On subsequent heating, the device resistance is linearly dependant on temperature over the range 300 to 900 K. Above 900 K the temperature dependence becomes more complex as chemical reactions change the nanotube and as optical phonon modes become thermally populated. This electronic characterization agrees with and complements TGA of bulk, purified CNTs.

*NSF grant DMR-0239842

**10:00**

**U18 9 On Current Carrying Capacity of Single Wall Semiconducting Carbon Nanotubes** YIJIAN OUYANG, YOUNGKI YOON, JING GUO, *Department of Electrical and Computer Engineering, University of Florida* The current carrying capacity of single wall semiconducting carbon nanotubes (CNTs) in the presence of phonon scattering and band-to-band tunneling is studied by self-consistently solving Poisson and Schrödinger equation using the non-equilibrium Green's function formalism. We show that the current delivery capacity of semiconducting CNTs strongly depends on the bias regime and is drastically different from metallic CNTs. A long metallic single wall CNT carries a saturation current of $\sim 25\mu$A due to optical phonon (OP) scatter-

ing. In contrast, a semiconducting CNT can deliver a current well above 25$\mu$A in ambipolar transport regime even when the channel length is much longer than the OP scattering mean free path (mfp). When the channel length is short (comparable to the OP scattering mfp), a semiconducting CNT biased in unipolar transport regime can deliver a current larger than 25$\mu$A. Biasing the CNT in ambipolar transport regime, however, further doubles the current. The different current carrying capacity in the ambipolar transport regime is due to nearly uncoupled dissipative transport through both the lowest conduction and valence subbands in the channel.

**10:12**

**U18 10 A comparison of measured electron-phonon and electron-photon coupling strengths in isolated and small ropes of single wall carbon nanotubes** B.B. GOLDBERG, Y. YIN, A. WALSH, *Physics Department, Boston University* S.B. CRONIN, *Electrical Engineering Department, University of Southern California* M. TINKHAM, *Department of Physics, Harvard University* A.N. VAMIVAKAS, M.S. ÜNLÜ, A.K. SWAN, *Electrical and Computer Engineering, Boston University* Resonant Raman scattering excitation profiles and photoluminescence (PL) are measured for isolated carbon nanotubes (CNT) and small ropes suspended in air. Most of the measured CNTs do not exhibit PL and are believed to be in small ropes. The radial breathing mode electron-phonon coupling, $M_{e-ph}$, are measured, and values for the isolated CNT are in good quantitative agreement with ab initio calculations. The matrix elements $M_{e-ph}$ and electron-photon coupling, $M_{e-op}$, for a CNT in a small rope are 1.7 times and 1.4-2.7 times weaker than in an isolated CNT. The reduced e-phonon coupling in small ropes is correlated with a smaller RRSE broadening $\eta$, compared to the value (45meV) obtained from an isolated CNT. Despite the reduced values of $M_{e-ph}$ and $\eta$, $M_{e-ph}$ in small ropes still display the same chiral dependence predicted for isolated CNTs.

**10:24**

**U18 11 Anharmonic decay of the Radial Breathing Mode in Suspended Single-walled Nanotubes** RAHUL RAO, *Dept. of Physics and Astronomy, Clemson University* JOSE MENENDEZ, *Dept. of Physics and Astronomy, Arizona State University* APPA-RAO RAO, *Dept. of Physics and Astronomy, Clemson University* The growth of isolated single-walled nanotubes (SWNTs) suspended over trenches in Si substrates makes it possible to study the Raman lineshapes of individual tubes. High-resolution room temperature resonant micro-Raman spectra from a number of suspended SWNTs exhibit very narrow radial breathing modes (RBMs), with full-width at half maximum (FWHM) values ranging from 1.3-2.5 $cm^{-1}$. These values are much smaller than previously reported in the literature. The observed FWHM is itnot a smooth function of the tube's radius. We note that the two-phonon density of states (2DOS) for the anharmonic decay of the RBM phonon shows many singularities whose energies depend both on the tube's radius itand chirality. Therefore, tubes with very similar RBM frequencies, and similar radii, could have different linewidths because of a different 2DOS. The observed linewidths increase with increasing incident laser power, as expected if the origin of the linewidth is anharmonic. We analyze the RBM linewidth in terms of down-conversion and up-conversion third-order anharmonic contributions. A comparison of the temperature dependence of both FWHM and peak frequency suggest that up-conversion processes are important, as found previously for low-frequency optical phonons in semiconductors.

**10:36**

**U18 12 Phonon anomalies in the resonance Raman spectra of graphite and single-wall carbon nanotubes** GEORGII G. SAMSONIDZE, HYUNGBIN SON, *Department of Electrical Engineering and Computer Science, MIT, Cambridge, MA* SHIN GRACE CHOU, *Department of Chemistry, MIT, Cambridge, MA* GENE DRESSELHAUS, *Francis Bitter Magnet Laboratory, MIT, Cambridge, MA* MILDRED S. DRESSELHAUS, *Department of Electrical Engineering and Computer Science and Department of Physics, MIT, Cambridge, MA* RIICHIRO SAITO, JIE JIANG, *Department of Physics, Tohoku University and CREST JST, Japan* EDUARDO B. BARROS, ANTONIO G. SOUZA FILHO, *Departamento de Fisica, Universidade Federal do Ceara, Fortaleza, CE, Brazil* Phonon dispersion relations for a graphene sheet and single-wall carbon nanotubes (SWNTs) are calculated within the extended tight-binding model that has recently been shown to accurately predict the optical transition energies in small-diameter SWNTs. Anomalies in the dispersion relations are found at certain high- symmetry points of the reciprocal lattice and these anomalies are attributed to the strong electron-phonon coupling. These anomalies are very sensitive to changes to electron and lattice temperatures, electron doping, mechanical stress, SWNT diameter, and SWNT metallicity. Resonance Raman measurements of doping and strain induced shifts of the phonon frequencies in SWNTs are in qualitative agreement with the present calculations. The MIT authors acknowledge support under NSF Grant DMR 04-05538.

**10:48**

**U18 13 Phonon stiffening in semiconducting single-walled carbon nanotubes under n-type doping** ELENA R. MARGINE, PAUL LAMMERT, VINCENT H. CRESPI, *The Pennsylvania State University* The doping dependence of the high-frequency Raman-active modes in single-walled semiconducting carbon nanotubes is studied by density functional theory. We find that the $A_{1g}$ longitudinal mode in $(3*n + 1,0)$ zigzag tubes shows a small anomalous upshift, followed by a large downshift under electron doping. This doping-induced stiffening of the $A_{1g}$ mode is related to the large anharmonicity of the mode. Connections are made to recent experiments in the group of P. C. Eklund.

## SESSION U19: FOCUS SESSION: SEMICONDUCTOR SPIN NANOSTRUCTURES FOR QUANTUM COMPUTING

**Thursday Morning, 16 March 2006**
**316, Baltimore Convention Center at 8:00**
**Jay Kikkawa, University of Pennsylvania, presiding**

***Contributed Papers***

**8:00**

**U19 1 Electron spin decoherence by interacting nuclear spins in quantum dot I: Quantum theory** WANG YAO, *Department of Physics, University of California, San Diego* R.-B. LIU, *Department of Physics, University of California, San Diego and Department of Physics, The Chinese University of Hong Kong* LU J. SHAM, *Department of Physics, University of California, San Diego* We present a quantum theory to the electron spin decoherence by a nuclear pair-correlation method for the electron-nuclear spin dynamics under a strong magnetic field and low temperature. The theory incorporates the electron nuclear hyperfine interaction, the

intrinsic nuclear interactions, and the nuclear coupling mediated by the hyperfine interaction with the electron in question. Results for both single electron spin free-induction decay (FID) and ensemble electron spin echo will be discussed. Single spin FID is affected by both the intrinsic and the hyperfine-mediated nuclear interactions, with the dominance determined by the dot size and external field. The spin echo eliminates the hyperfine-mediated decoherence but only reduces the decoherence by the intrinsic nuclear interactions. Thus, the decoherence times for FID and spin echo are significantly different. Electron spin decoherence is explained in terms of the quantum entanglement with the pair-flip excitations in the nuclear spin environment. This work was supported by NSF DMR- 0403465, NSA/ARO, and DARPA/AFOSR.

**8:12**

**U19 2 Electron spin decoherence by interacting nuclear spins in quantum dot II: Coherent control** REN-BAO LIU, *Department of Physics, University of California, San Diego, California and Department of Physics, The Chinese University of Hong Kong, Hong Kong* WANG YAO, LU J. SHAM, *Department of Physics, University of California, San Diego, California* Due to the hyperfine interaction, the nuclear spins in a quantum dot, driven by nuclear spin pair-wise flip-flops, evolve in different pathways in the Hilbert space for different electron spin states, resulting in the electron-nuclei entanglement and hence the electron spin decoherence. When the electron spin is flipped by a pulse, the nuclear spin states for different electron spin states swap their pathways, and could intersect in the Hilbert space, which disentangles the electron and the nuclei and hence restores the electron spin coherence. The coherence restoration by disentanglement and the conventional spin echo in ensemble dynamics are fundamentally different and generally occur at different time. Pulse sequences can be applied to force the disentanglement to coincide with the spin echo, making the coherence recovery observable in ensemble dynamics. This work was supported by NSF DMR-0403465, NSA/ARO, and DARPA/AFOSR.

**8:24**

**U19 3 Analytical Solution of Electron Spin Decoherence Through Hyperfine Interaction in a Quantum Dot** CHANGXUE DENG, XUEDONG HU, *State University of New York at Buffalo* We analytically solve the *Non-Markovian* single electron spin dynamics due to hyperfine interaction with surrounding nuclei in a quantum dot. We use the equation-of-motion method assisted with a large field expansion, and find that virtual nuclear spin flip-flops mediated by the electron contribute significantly to a complete decoherence of transverse electron spin correlation function. Our results show that a 90% nuclear polarization can enhance the electron spin $T_2$ time by almost two orders of magnitude. In the long time limit, the electron spin correlation function has a non-exponential $1/t^2$ decay in the presence of both polarized and unpolarized nuclei.

**8:36**

**U19 4 Quantum dot dynamical Quantum dot dynamical nuclear spin polarization in the** C.W. LAI, P. MALETINSKY, A. BADOLATO, A. IMAMOGLU, *ETH Zurich* Hyperfine interaction in quantum dots (QD) is qualitatively different than in atoms: coupling of a single electron spin to the otherwise well isolated QD nuclear spins plays a key role in spin-based solid-state quantum information processing. Dynamical nuclear spin polarization (DNSP) is observed by resonant optical pumping of single self-assembled QDs in gated structures that allow deterministic charging with a single excess electron or hole. In the absence of external magnetic fields, the optically polarized electron spin induces an effective inhomogeneous magnetic (Knight) field which determines the direction along which the mesoscopic ensemble of nuclear spins could polarize and enables nuclear spin cooling by surpassing depolarization induced by nuclear dipolar interactions. Due to the effective magnetic (Overhauser) field induced by the polarized nuclei, photoluminescence of these charged trion transitions exhibit spin splitting $\approx 15\mu eV$ which can be determined by high-spectral-resolution ( $< 1\mu eV$) spectroscopy based on a scanning Fabry-Perot interferometer. Our experiments constitute a first step towards a quantum measurement of the Overhauser field, which is in turn predicted to suppress electron spin decoherence in QDs.

**8:48**

**U19 5 Dynamical nuclear spin polarization in a double quantum dot*** GUY RAMON, CHANGXUE DENG, XUEDONG HU, *Department of Physics, University of Buffalo, SUNY* The hyperfine interaction between an electron spin confined in a semiconductor quantum dot and the nuclear spins in the surrounding lattice has been identified as one of the main sources for decoherence in low temperature GaAs quantum dots. Recent experiments in gated double dot systems [1] have attempted to utilize the degeneracy point between the two-electron singlet and polarized triplet states to polarize the nuclear spins, thereby reducing their decoherence effects on the electron spins. Here we analyze the dynamics of the system of two electrons and a nuclear spin bath subject to the hyperfine interaction. We consider the effective spin Hamiltonian for the two-electron system, and represent the nuclear spins in the basis of their collective states. The nuclear polarization rates are evaluated for various initial conditions of the nuclear spin system, and optimal conditions for efficient polarization are discussed. [1] J. R. Petta, A. C. Johnson, J. M. Taylor, E. A. Laird, A. Yacoby, M. D. Lukin, C. M. Marcus, M. P. Hanson, A. C. Gossard, Science 309, 2180 (2005).

*Supported by NSA/LPS and ARO

**9:00**

**U19 6 Coherent Control of Entangled Spin Pairs in a CdMnTe Quantum Well.** PAUL JACOBS, ROBERTO MERLIN, *University of Michigan* JACEK FURDYNA, *University of Notre Dame* We used ultrafast light pulses to control the spin state of electrons bound to donors in a CdMnTe quantum well. Previously, we reported on the observation of up to three harmonics of the bound electron spin flip transition indicating that at least three bound electron sites were entangled (J.M. Bao, A.V. Bragas, J.K. Furdyna, R. Merlin, Phys. Rev. B 71 045314 (2005)). Using a pulse shaper, we are now able to suppress all coherent oscillations, but the signal of the first spin flip overtone. Therefore, only entangled electron pairs remain oscillating; all non-entangled donor bound electrons have been restored to their ground state. The quantum state of the remaining entangled electron spins is closely related to the Bell state. This technique holds promise for quantum computing applications.

*Invited Papers*

**9:12**
**U19 7 Electron-spin quantum computation: Three- and four-body interactions and other implementation challenges.***
ARI MIZEL, *Pennsylvania State University*

Several leading quantum computer proposals are based upon electron spins. While these designs do potentially satisfy the DiVincenzo criteria, subtle implementation challenges have been uncovered that need to be addressed if these designs are to be realized successfully. In this talk, we start by pointing out that, when several spins are engaged mutually in pairwise interactions, a change can arise in those interactions. In the case of three spins, the quantitative strengths of the interactions can change. For four or more spins, qualitatively new terms can arise in the Hamiltonian, including four-body interactions. Other implementation challenges are also considered, including the difficulty of performing strong projective measurements on solid state qubits (weak measurements are generally more natural to implement but their behavior is more subtle). These issues will need to be handled in quantum computer realizations, either as a source of error to be overcome or as new physics to be exploited.

*Supported by the Packard Foundation and NSF NIRT program grant DMR-0103068.

*Contributed Papers*

**9:48**
**U19 8 Transport of Quantum Information Using Spin Wires*** VANITA SRINIVASA, *University of Pittsburgh* JEREMY LEVY, *University of Pittsburgh* C. STEPHEN HELLBERG, *Naval Research Laboratory* COSMQC TEAM, One-dimensional antiferromagnetically coupled spin systems have properties that make them useful as conduits for quantum information (PRL **90**, 047901 (2003)). Here we investigate possible mechanisms for using engineered spin chains as ''spin wires'' that can faithfully transport qubits. An analysis of the spin chains is carried out through numerical diagonalization of the effective spin Hamiltonian. We find that dimerized chains with a defect can support a highly localized qubit. We also demonstrate how it may be possible to propagate these kinks rapidly through a large system, thus providing a mechanism for producing''flying'' spin qubits in the solid state.

*This work was supported by DARPA QuIST (DAAD−19−01−1−0650).

**10:00**
**U19 9 GHz Optical Spin Transceiver*** PATRICK IRVIN, PETRU FODOR, JEREMY LEVY, *University of Pittsburgh* COSMQC TEAM, The ability to measure spin coherence in semiconductor nanostructures is important for determining the feasibility of spin-based quantum computing architectures. Quantum dots are often referred to as 'solid-state atoms' because of their sharp absorption and emission lines that resemble those of single atoms. Electron spins localized on these quantum dots may be useful for storing quantum information, but their small optical cross section makes detection challenging. In order to take advantage of resonant enhancement of spin detection using the magneto-optical Kerr effect, we have developed a GHz Optical Spin Transceiver (GHOST) which uses a cw optical probe to measure Kerr signals in the time domain with 5 GHz bandwidth. Initial results will be presented for a test sample consisting of n-doped GaAs.

*This work was supported by DARPA QuIST through ARO contract number DAAD-19-01-1-0650.

**10:12**
**U19 10 Photocurrent spectroscopy of self−assembled quantum dots.*** PETRU FODOR, JEREMY LEVY, *University of Pittsburgh* GILBERTO MEDEIROS-RIBEIRO, *Laboratorio Nacional de Luz Sincrotron* COSMQC TEAM, Quantum dots systems had been envisioned as possible candidates for building the hardware of quantum computers. They provide the necessary localization of electrons on length scales comparable to the electron Fermi wavelength and also exhibit distinct discrete energy spectra due to quantum confinement. Nevertheless, the characterization of optical and coherence properties of single quantum dots, especially at wavelengths larger than 1100 nm, is challenging due to the small SNR in these systems and the lack of high quantum efficiency detectors at these wavelengths. To circumvent these challenges, we use photocurrent measurements as a probe of the absorption spectra of quantum dots systems embedded in Schottky diode structures. The use of spectrally narrow laser sources allows the exciton absorption spectra of single quantum dots to be characterized as a function of temperature and magnetic field.

*This work was supported by DARPA QuIST through ARO contract number DAAD-19-01-1-0650.

**10:24**
**U19 11 Spin dynamics in coupled core/shell quantum dots*** J. BEREZOVSKY, M. OUYANG, F. MEIER, D. D. AWSCHALOM, *Center for Spintronics and Quantum Computation, University of California, Santa Barbara, CA 93106* D. BATTAGLIA, X. PENG, *Department of Chemistry and Biochemistry, University of Arkansas, Fayetteville, AR 72701* Colloidal nanoparticles provide a flexible system for studying individual quantum-confined electrons and holes. By layering different semiconducting materials in a single nanoparticle, we can create a low bandgap (CdSe) core and surrounding shell, separated by a high bandgap (ZnS) barrier. We have studied spin dynamics in such colloidal heterostructures using two-color time-resolved Faraday rotation (TRFR). By tuning the excitation energy, electron spins can be initialized into different states either in the core or the shell of the nanoparticle. The resulting spin dynamics show a g-factor (spin splitting) that depends on the size of the core or the shell. This g-factor dependence, as well as the spectroscopic dependence of the Faraday

effect, allow electron spins in the core or the shell to be addressed independently.

*This work was supported by DARPA, NSF, and ONR.

**10:36**
**U19 12 Spin Manipulation in lateral quantum dots under time-dependent confinement.*** JAMIE WALLS, ERIC HELLER, *Harvard University* Single spin manipulations are a critical component to potential realizations of spintronic devices and quantum computers in lateral quantum dots. In this work, we demonstrate a new method for creating spin excitations in lateral quantum dots which uses the interplay between the spin-orbit interaction and a time-dependent lateral confining potential. For an asymmetric dot in the presence of an in-plane magnetic field, the spin quantization axis can be tilted away from the applied magnetic field due to the Rashba spin-orbit coupling, with the degree of tilting depending parametrically upon the confinement potential. By making small modulations to the confinement potential at a frequency given roughly by the Zeeman splitting, efficient spin excitations can be performed. We have performed theoretical and numerical calculations which demonstrate that Rabi frequencies on the order of tens of megahertz can be achieved for experimentally accessible parameters. Extensions to spin excitations in multi-electron quantum dots will also be presented.

*This work was supported at Harvard University by the Nanoscale Science and Engineering Center (NSF Grant No. PHY-0117795) and by NSF Grant No. CHE-0073544.

**10:48**
**U19 13 Effect of photon-assisted tunneling through the leads on spin current polarization in ac-driven quantum dot molecules*** ERNESTO COTA, *Universidad Nacional Autonoma de Mexico* RAFAEL SANCHEZ, RAMON AGUADO, GLORIA PLATERO, *Instituto de Ciencia de Materiales de Madrid-CSIC* A new scheme for realizing spin pumping and spin filtering has been recently proposed using an ac-driven double quantum dot in the Coulomb blockade regime. Using a master equation approach for the density matrix, it was shown[1] that the spin polarization of the current through the system can be controlled by tuning the parameters (amplitude and frequency) of the ac-field. In the present work we extend our previous model to include photon-assisted tunneling through the contact barriers. This introduces new features in the current due to absorption and emission processes affecting the spin polarization of the current. We discuss these new features, their dependence on the ac-field parameters and the effects on the robustness of the proposed device as a spin pump and spin filter. In particular, we find that the spin filtering property depends strongly on the intensity of the applied ac field. The effect of photoassisted cotunneling on the spin current polarization will also be discussed. [1]E.Cota, R. Aguado and G. Platero, Phys. Rev. Lett. **94**, 107202 (2005)

*Work supported by Programa de Cooperacion Bilateral CSIC-CONACYT, DGAPA-UNAM-IN114403, EU Grant No. HPRN-CT-2000-00144, Ministerio de Ciencia y Tecnologia of Spain Grant No. MAT2002-20465

## SESSION U20: FOCUS SESSION: METAL-INSULATOR TRANSITION AND ELECTRON PHONON COUPLING IN PEROVSKITES

**Thursday Morning, 16 March 2006**
**317, Baltimore Convention Center at 8:00**
**Michael Hayward, University of Oxford, presiding**

***Contributed Papers***

**8:00**
**U20 1 'CMR' Manganites: Strongly or Weakly Correlated?*** ANDREW MILLIS, SATOSHI OKAMOTO, A newly developed ''semiclassical impurity solver'' [1] is used to perform dynamical mean field calculations of the kinetic energy, optical conductivity and magnetic transition temperature of the two-orbital double-exchange model for colossal magnetoresistance manganites, including the full Kanamori ($U - U' - J$) interactions for the $e_g$ multiplet as well as the $e_g - t_{2g}$ Hunds coupling $J_H$. The effective correlation strength is shown to be weak in the ferromagnetic ground state, while in the high temperature paramagnetic state the multiplet interactions block many of the possible final states, leading to an effectively strongly correlated situation characterized by a large effective $J_H$. [1] S. Okamoto et. al., Phys. Rev. **B71** 235113 (2005).

*NSF DMR 0431350

**8:12**
**U20 2 Resistivity peak in the one-band double-exchange model with cooperative phonons** CENGIZ SEN, *National High Magnetic Field Laboratory and Department of Physics, Florida State University, Tallahassee, FL* GONZALO ALVAREZ, HORACIO ALIAGA, *Oak Ridge National Laboratory, Oak Ridge, TN* ELBIO DAGOTTO, *Oak Ridge National Laboratory, Oak Ridge, TN and Department of Physics, University of Tennessee, Knoxville, TN* We present the results of Monte Carlo simulations of a single-band double-exchange model with cooperative phonons, both with and without quenched disorder, at a carrier density $n=0.3$. Both in two and three dimensions, the simulations reveal a peak in the resistivity at $T_{\mathrm{Curie}}$, in agreement with previous studies by other groups. The peak gets destroyed upon the application of an external field, resulting in a large magnetoresistance. The results are in good agreement with experiments involving CMR manganites. Studies at other densities are also presented, and an intuitive picture for the presence of the resistivity peak is discussed.

**8:24**
**U20 3 Exchange Striction and Heat Conduction in $Ca_{1-y}Sr_yMnO_3$ ($0 \leq y \leq 0.5$)*** JOSHUA COHN, *University of Miami* CORNELIU CHIORESCU, *University of Miami* JOHN NEUMEIER, *Montana State University* $CaMnO_3$, a G-type antiferromagnet with orthorhombic structure, exhibits a substantial enhancement of its thermal conductivity[a,b] ($\kappa$) for $T < T_N = 125$ K associated with exchange striction, the spin-phonon interactions for which are not well understood. One possibility[a] is that this enhancement results from a suppression, in the ordered state, of phonon scattering from bond disorder induced by magnetic fluctuations in the paramagnetic state. The homovalent substitution of Sr for Ca in the $Ca_{1-y}Sr_yMnO_3$ compounds increases the Mn-O-Mn bond angle without changing the crystal structure, and $T_N$ rises[c] to $\sim$ 165 K for $y = 0.5$. We present measurements demonstrating that the enhancement of $\kappa$ is gradually suppressed

as $y$ increases, disappearing for $y \simeq 0.5$. The implication of these results for the origin of the enhancement will be discussed. [a] J.-S. Zhou and J. B. Goodenough, Phys. Rev. B **66**, 052401 (2002). [b] J. L. Cohn and J. J. Neumeier, Phys. Rev. B **66**, 100404(R) (2002). [c] O. Chmaissem *et al.*, Phys. Rev. B **64**, 134412 (2001).

*This material is based upon work supported by the National Science Foundation under grants DMR-0072276 (Univ. Miami) and DMR-9982834 (Montana State Univ.).

**8:36**

**U20 4 Strong current dependence of resistivity in $CaMnO_3$*** CORNELIU CHIORESCU, *University of Miami* JOHN NEUMEIER, *Montana State University* JOSHUA COHN, *University of Miami* The perovskite manganite $CaMnO_3$ (CMO) has a G-type antiferromagnetic ground state with Néel temperature $T_N = 125$K. Prior transport measurements in the magnetic and paramagnetic phases[a] establish that CMO is a $n$-type semiconductor with $n \sim 10^{18} - 10^{19}\text{cm}^{-3}$ (from native defects like oxygen vacancies) and modestly heavy (large- polaron) mass, $m^* \sim 10m_0$. Here we report transport measurements on single crystal and polycrystalline CMO which reveal a strong current dependence of the resistivity ($\rho$) at low temperatures where $\rho > 10^6\Omega$cm and impurity-band conduction predominates. For example, at 30 K, $\rho$ decreases by an order of magnitude for small current densities ($J < 100\mu\text{A/cm}^2$), indicating that the effect is not associated with Joule heating. The possible role of spin-polarized hopping in this phenomenon will be discussed. [a] J. L. Cohn, C. Chiorescu, and J. J. Neumeier, Phys. Rev. B **72**, 024422 (2005).

*This material is based upon work supported by the National Science Foundation under grants DMR-0072276 (Univ. Miami) and DMR-9982834 (Montana State Univ.).

**8:48**

**U20 5 On the nature of the pressure-induced insulator-to-metal transition in $LaMnO_3$** ATSUSHI YAMASAKI, *Max-Planck-Institut für Festkörperforschung* MARTIN FELDBACHER, *Max-Planck-Institut für Festkörperforschung and Department of Physics and Astronomy, Rutgers University* OLE K. ANDERSEN, KARSTEN HELD, *Max-Planck-Institut für Festkörperforschung* Since the discovery of colossal magnetoresistance, manganites have been intensively studied. We focus on the pressure induced insulator-to-metal (IM) transition which was found experimentally [1] in the undoped parent compound $LaMnO_3$ with configuration $t_{2g}^3 e_g^1$. This transition occurs at room temperature (above $T_N = 140$ K) and at a hydrostatic pressure of 32 GPa where the Jahn-Teller distortion appears to be completely suppressed [1]. The IM transition thus seems to be a bandwidth-driven Mott-Hubbard transition of the $e_g$ electrons. We employ the local density approximation combined with static and dynamical mean-field theories (LDA+$U$ and LDA+DMFT) and conclude that the IM transition observed at 32 GPa in paramagnetic $LaMnO_3$ at room temperature is *not* a Mott transition, but is caused by the overlap of the majority-spin $e_g$ bands, orbitally polarized by the Coulomb repulsion. Crucial are also the bandwidth reduction of $\sim 0.6$ and 2/3 arising from, respectively, the gap generated by the crystal-field splitting and the random, spatially uncorrelated direction of the $t_{2g}$ spin at room temperature. [1] I. Loa *et al.*, Phys. Rev. Lett. **87**, 125501 (2001).

**9:00**

**U20 6 Double-exchange driven metal-insulating transition in Mn-doped CuO** ALESSIO FILIPPETTI, VINCENZO FIORENTINI, *SLACS and Physics Dept., University of Cagliari, Italy* Doping antiferromagnetic CuO with Mn causes a uncommon metal-insulating transition where the low-temperature ($T < T_c = 80$ K) phase is ferromagnetic, with a large but metallic-like resistivity, while the high-temperature phase is paramagnetic and insulating, but with a resistivity typical of Mott insulators in the hopping conducting regime. Applying a first-principles, self-interaction corrected local spin density approach, we are able to understand and rationalize this puzzling behavior: each doping Mn in CuO acts as a single donor, inducing a double-exchange driven metallic regime and a Mn-Mn ferromagnetic allignement. Nicely, here double-exchange can also work at rather low Mn concentrations since carriers can freely flow within the CuO (x,y) planes and only need the Mn assistance to move through the c axis. In the antiferromagnetic phase the system is insulating, but a polaron hopping conductivity through a few meV-wide Coulomb gap is envisaged. This scenario depicts the intriguing possibility of designing double-exchange driven ferromagnetic cuprates.

***Invited Papers***

**9:12**

**U20 7 Computational Studies of Magnetoresistance in Double-Exchange-Based Models for Manganites.*** GONZALO ALVAREZ, *Computer Science and Mathematics Division, Oak Ridge National Laboratory*

Double-exchange-based models for manganites are studied using Monte Carlo techniques, with both exact-diagonalization and polynomial-expansion of the fermionic sector. One and two- orbital models are investigated, with and without phonons. We focus our analysis on the study of the resistance (R) vs. temperature (T) using the Landauer formalism. Highlights of investigations by our group and others are: (1) R vs. T curves, parametric with magnetic fields, that closely resemble experimental data for the case of one orbital and considering cooperative phonons; and (2) an insulator to bad metal transition induced by quenched disorder for the two-orbital model. In spite of these positive results, we remark that this is just the beginning of a frontal attack to the manganite problem using realistic models and efficient algorithms that scale linearly with the lattice volume. Future directions and open problems will also be discussed.

*Research performed at the Oak Ridge National Laboratory, managed by UT-Battelle, LLC, for the U.S. Department of Energy under Contract DE-AC05-00OR22725.

*Contributed Papers*

**9:48**

**U20 8 Neutron Scattering Study of Electron- Phonon Coupling in $La_{1/3}Sr_{2/3}FeO_{3-\sigma}$ Perovskite** J. MA, J.-Q. YAN, S. CHANG, R. J. MCQUEENEY, *Ames Lab., Dept. of Phys. and Astro., Iowa State U., Ames, IA 50011* F. TROUW, M. HEHLEN, *Los Alamos National Laboratory, Los Alamos, NM 87545* $La_{1/3}Sr_{2/3}FeO_{3-\delta}$ compounds are reported to have an unusual magneto-structural transition at low temperatures. Below $\sim 210K$, it is proposed that charge disproportionation occurs according to $2Fe^{4+} => Fe^{3+}+Fe^{5+}$, thereby creating different valence on the iron sites. The different iron valences order along the body diagonal $[111]_c$, resulting in a change in crystal structure from rhombohedral to orthorhombic and antiferromagnetic ordering. Inelastic neutron scattering was used to determine the effect of simultaneous charge and magnetic ordering on the phonon and spin wave excitations. We find that the high frequency oxygen phonons ( $\sim$ 80 meV) soften above the transition by several meV. Spin wave excitations appear below the transition with a characteristic energy of 50 meV at the Brillouin zone boundary. The result and relationship between the charge ordering and the electron-phonon interaction are discussed.

**10:00**

**U20 9 Magnetic polarons in a one-dimensional antiferromagnetic chain** I. GONZALEZ, *Oak Ridge National Lab., USA* J. CASTRO, D. BALDOMIR, *Universidade de Santiago de Compostela, Spain* A.O. SBOYCHAKOV, A.L. RAKHMANOV, K.I. KUGEL, *Institute for Theoretical and Applied Electrodynamics, Russia* We present several results concerning magnetic polarons in a double-exchange system. We use a simplified model consisting on an antiferromagnetic (AF) chain doped with donor impurities. First, we study the ''back-effect'' in the AF background of a conduction electron bound to its donor impurity. We show that a region with extended spin distortions appear in the AF structure, similar to a domain wall and stabilizing the magnetic polaron. Second, we discuss the effect of these distortions in a system doped with a finite density of donor impurities. We show that from a critical density a non-trivial energy dependence on conduction electrons density appears, which can be interpreted as an attractive interaction between magnetic polarons. Third, we analyze temperature evolution of such a system of magnetic polarons. We show that they remain stable up to rather high temperatures, larger than the Néel temperature of the undoped chain. Our results may be relevant to understand the physics of low-doped manganites.

**10:12**

**U20 10 Zener Polarons Ordering Variants Induced by A-Site Ordering in Half-Doped Manganites** AZIZ DAOUD-ALADINE, *ISIS Department, Rutherford Appleton Laboratories, Chilton, Didcot, Oxfordshire OX11 0QX, UK* CRISTIAN PERCA TEAM, LOREYNNE PINSARD-GAUDART TEAM, JUAN RODRIGUEZ-CARVAJAL TEAM, Zener Polaron (ZP) ordering [1] provides a still polemic [2] and elusive interpretation of the charge ordering (CO) phenomenon in A site disordered half doped $(A_{1/2}Ca_{1/2})$ $MnO_3$, which is classically pictured by the Good-enough model (GM) of $Mn^{3+}$ and $Mn^{4+}$ CO [3,4]. ZP ordering considers instead the ordering of pre-formed ferromagnetic Mn pairs sharing an charge and keeping Mn in a $Mn^{+3.5}$ valence state. The recently synthesized A site cation ordered $ABaMn_2O_6$ were shown to not present the generic magnetic CE state found of $(A_{1/2}Ca_{1/2})MnO_3$ [5]. We present our magnetic structure determination of $YBaMn_2O_6$: the non- collinear magnetic order obtained unexpectedly reveals ferromagnetic plaquettes of four Mn attributable to larger 4-Mn ZPs, whose presence additionally fits very well the effective paramagnetic moments inferred from susceptibility measurements. The results unambiguously reveal the possible existence of ZP ordering variant in charge ordered manganites. [1] A. Daoud-Aladine et al., Phys. Rev. Lett. 89, 097205 (2002) [2] S. Grenier et al., Phys. Rev. B 69, 134419 (2004) [3] J. B. Goodenough, Phys. Rev. 100, 564 (1955) [4] P.G. Radaelli et al., Phys. Rev. B, 55, 3015 (1997) [5] T. Arima et al., Phys. Rev. B 66, 140408 (2002)

**10:24**

**U20 11 Evolution of the local Jahn-Teller distortion across the phase diagram of $La_{1-x}Ca_xMnO_3$ ($0 \leq x \leq 0.5$)** EMIL BOZIN, GIANLUCA PAGLIA, ADAM DECONINCK, SIMON BILLINGE, *Dept. of Physics and Astronomy, Michigan State University* MAREK SCHMIDT, PAOLO RADAELLI, *ISIS, Rutherford Appleton Laboratory* JOHN MITCHELL, *Material Science Division, Argonne National Laboratory* THOMAS PROFFEN, *LANSCE, Los Alamos National Laboratory* We report on the most comprehensive study to date of the *local* Jahn-Teller (JT) distortion across the phase diagram of the colossal magnetoresistive (CMR) $La_{1-x}Ca_xMnO_3$ ($0 \leq x \leq 0.5$). The local structure has been measured, using the neutron powder diffraction based atomic pair distribution function (PDF) approach, over the wide temperature and Ca-doping range. These results are compared to the conventional crystallographic results obtained by Rietveld analysis. The results will be compared with both homogeneous and inhomogeneous models of the electronic structure. The magnitude of the *local* JT distortion is quantified over the entire phase diagram. In agreement with earlier work, we see the local JT distortion disappear in the metallic phase. However, in contrast with some earlier studies, we show that in the insulating phases the magnitude of the JT distortion decreases with increasing doping, becoming constant at higher doping. This new result should be incorporated in theoretical models of CMR manganites.

**10:36**

**U20 12 Structural and Transport Study of $La_{0.9}MnO_3$ Under Pressure.** ZHIQIANG CHEN, TREVOR TYSON, *Department of Physics, New Jersey Institute of Technology, Newark, New Jersey 07102* ZHONG ZHONG, *National Synchrotron Light Source, Brookhaven National Laboratory* The detailed transport and structural properties of the self-doped system $La_{0.9}MnO_3$ have been studied under hydrostatic pressures extending to 6GPa and 11GPa, respectively. Like the doped manganite systems previously studied by our group, in the La deficiency (x=0.9) system a maximum shift of the peak resistivity is obtained at around 3.4GPa. A crossover from metallic to insulating behavior is observed above this optimum pressure. The x-ray diffraction study results show that the self-doped system is compatible with a single phase of monoclinic space group up to 11 GPa. The detailed changes in the lattice parameters, volume, bond distances and bond angles have been obtained. Comparisons with pressure dependent measurements on the doped manganites will be made. This work was supported by NSF DMR-0209243 and DMR-0512196.

**10:48**

**U20 13 A quantum phase transition in the monoxides of the first transition series** FRANCISCO RIVADULLA, *Dpto. Química-Física, Universidad de Santiago de Compostela* JOAQUÍN FERNÁNDEZ-ROSSIER, *Dpto. Física Aplicada, Universidad de Alicante* MAR GARCÍA-HERNÁNDEZ, *ICMM, CSIC, Madrid, Spain* JOSÉ RIVAS, *Dpto. Física Aplicada, Universidad de Santiago de Compostela* JOHN GOODENOUGH, *TMI, University of Texas at Austin, Austin TX, USA* The monoxides of the 3d metals (MO; M= Ti to Ni) provide an isostructural series (cubic, Fm $\bar{3}$m) in which to study the transition from metallic paramagnetism (TiO) to insulating antiferromagnetism (MnO, FeO, CoO, NiO). But the transition is not smooth, and while CrO has eluded synthesis over the years, the intrinsic properties of VO are under discussion. Here we present strong experimental and computational evidence that VO is a strongly correlated metal with Non-Fermi Liquid low temperature thermodynamics, a pseudogap in the density of states and an unusually strong spin-lattice coupling. All these properties are interpreted as signatures of the proximity to a magnetic quantum phase transition. Interestingly, TiOx displays a superconducting transition with a dome-shape dependence of the superconducting critical temperature with doping in x ($0.8 < x < 1.2$). The analogies with the phase diagram of the High Tc cuprates and their structural and electronic simplicity makes 3d monoxides ideal candidates to make progress in the understanding of correlated electron systems.

**SESSION U21: LIQUID CRYSTALS I**
**Thursday Morning, 16 March 2006**
**318, Baltimore Convention Center at 8:00**
**P. Palffy-Muhoray, Kent State University, presiding**

**8:00**

**U21 1 Aggregation in Two Dye Systems That Form Chromonic Liquid Crystals*** PETER J. COLLINGS,[†] VIVA R. HOROWITZ,[‡] MICHELLE R. TOMASIK, *Department of Physics & Astronomy, Swarthmore College, Swarthmore, PA 19081* X-ray scattering and various optical techniques are utilized to study the aggregation process and aggregate structure for two water-soluble dyes that form chromonic liquid crystal phases. The x-ray measurements indicate that the molecules stack in columns with a cross-section approximately equal to the area of a single molecule. The optical measurements point to an aggregation process that occurs at all concentrations, with the distribution of aggregate size shifting to larger and larger aggregates as the concentration is increased. A simple theory based on the law of mass action and an isodesmic aggregation process is in excellent agreement with the experimental data, yielding a value for the ''bond energy'' between the molecules in an aggregate.

*Partially supported by ACS-PRF Grant No. 41057-UPS
[†]Additional Affiliation: Department of Physics & Astronomy, University of Pennsylvania, Philadelphia, PA 19104
[‡]Present Address: Department of Physics, University of California, Santa Barbara, CA 93106

**8:12**

**U21 2 Orientational order of an ideal rodlike nematic: Rewriting the theory of nematic liquid crystals?** EDWARD SAMULSKI, LOUIS MADSEN, THEO DINGEMANS, *University of North Carolina - Department of Chemistry* Order in rodlike nematic liquid crystals (LCs) represents a rich field described by myriad theories and studied using various analytical methods. We have made deuterium (D) NMR observations on the labeled paraquinquephenyl LC, which closely approximates a rigid rod. To investigate this high-melting nematic (range 390 - 427 deg. C), we have fabricated a high-efficiency oven on an NMR probehead using fumed silica tiles and utilizing only ambient air cooling. Observations on p-quinquephenyl clearly and drastically deviate from the Maier-Saupe theory and all other molecular theories of nematics, thus indicating the necessity for more a complete theory (e.g., including microscopic director fluctuations) to describe nematic order. We measure the complete order tensor for this LC using combinations of quadrupole and dipolar NMR coupling constants and different D label positions. We will discuss progress on refinements to nematic order theory, relations to NMR measurements, and fits using the phenomenological Landau-deGennes theory.

**8:24**

**U21 3 Interlayer interactions in ferroelectric liquid crystals*** MEHDI HAMANEH, PHILIP TAYLOR, *Case Western Reserve University* We have recently drawn attention to a physical mechanism that can lead to an aligning interaction between distant layers in a ferroelectric smectic-C* liquid crystal. This effect arises because the amplitude of thermal fluctuations in layer shape is sensitive to correlations in *c*-director orientation in layers that are not nearest neighbors. This makes the entropy of the system dependent on the relative alignment of the *c*-director in all the smectic layers. In earlier treatments of this problem, a mean-field approximation was made in order to obtain an order-of-magnitude estimate of the strength of the interlayer interaction. While this was sufficient to demonstrate the significance of the mechanism, it led to an overestimate of the overall strength of the interaction because it included a self-energy term related to the anisotropy of a single layer. We have now remedied this shortcoming by evaluating in more detail the interlayer interaction due to layer shape fluctuations. We find that the rate at which the interaction decays as a function of interlayer distance does not follow any simple power-law form, but depends on a number of material parameters.

*Research supported by PRF/ACS

**8:36**

**U21 4 The B4 phase: layer curvature driven by frustrated intralayer packing** L.E. HOUGH, *LCMRC, Physics Dept., CU Boulder* D. KRUERKE, *Institute of Inorganic and Analytical Chemistry, TU of Berlin* C.D. JONES, *LCMRC, Physics Dept., CU Boulder* H.T. JUNG, J. ZASADZINSKI, *Dept. of Chemical Engineering, UCSB* G. HEPPKE, *Institute of Inorganic and Analytical Chemistry, TU of Berlin* J. RABE, W. STOCKER, *Institute for Physics, Humboldt U. Berlin* E. KORBLOVA, D. WALBA, *LCMRC, Dept of Chemistry and Biochemistry, CU Boulder* N.A. CLARK, *LCMRC, Physics Dept., CU Boulder* We combine freeze fracture transmission electron microscopy, atomic force microscopy, and x-ray diffraction to show that the B4 phase is a smectic phase with highly curved layers (mean radius $\sim$ 4 layer spacings). The layer structure of the phase is a TGB-like phase made up of parallel arrays of multiple burgers vector screw dislocations (grain boundaries) giving 45 degree rotations across the grain bound-

aries. Models of the layer structure are based on periodic arrays of grain boundaries, each described by Scherk's first surface, and yield key features of the observed structures. This layered structure is dominated by saddle splay and we propose that the energy cost of defects required to make such a structure is offset by an energy gain of the layer curvature. We show that analysis of the wide angle x-ray diffraction of this phase indicates that layer curvature relieves the intralayer frustration produced by the packing of bent-core molecules. This work is supported by a NSF GRF and by NSF MRSEC Grant DMR0213918.

**8:48**

**U21 5 Polarization-Enhanced Interaction between Islands on Freely-Suspended Smectic C* Liquid Crystal Films*** APICHART PATTANAPORKRATANA, *Department of Physics and Liquid Crystal Materials Research Center, University of Colorado, Boulder, CO 80309, U.S.A* CHEOL S. PARK TEAM, JOSEPH MACLENNAN TEAM, NOEL A. CLARK TEAM, Smectic liquid crystals can be made to form freely suspended films, two-dimensional systems locally quantized in thickness by an integral number of smectic layers, on which islands, circular regions of greater thickness than the surrounding film area, can be generated. In smectic C films, each such island is accompanied by a topological defect pair, an $s = +1$ topological defect inside and an $s = -1$ defect nearby on the background film. The distortions of the in-plane orientational order of the smectic C director field result in elastic interactions between the islands, with a short-range repulsion and a long-range dipolar attraction governing their stability and leading to their organization in chain-like structures with an equilibrium island separation. We have directly measured the repulsive and attractive forces between smectic C* islands using multiple optical traps and have compared the results quantitatively with theory. We find that the interactions between islands are much smaller in the racemic smectic C case than in the chiral smectic C*, an effect we attribute to long- range coulombic forces arising from polarization charges.

*This work was supported by NASA Grant NAG-NNC04GA50G and NSF MRSEC Grant No. DMR 0213918.

**9:00**

**U21 6 Riverbottom texture: Patterns of compressional stress in an SSFLC cell** CHRISTOPHER D. JONES, DAVID A. COLEMAN, NOEL A. CLARK, *Liquid Crystal Materials Research Center and Department of Physics, University of Colorado, Boulder, CO 80309 USA* MICHAEL D. WAND, *Diplaytech, Inc., Longmont, CO 80503 USA* We have been studying the texture of remnant compressional stress in a bookshelf aligned SmA phase of the Displaytech mixture MDW8068. MDW8068 exhibits isotropic - nematic - SmA - SmC phases, and throughout the range of the SmA phase the layers show significant expansion on cooling. This layer expansion causes layer compression, which is relieved by dislocation formation and surface depinning events throughout the cell. The resulting SmA has essentially perfect alignment, but with a pattern of remnant stress that can be visualized near the SmA - SmC transition because of the divergent tilt susceptibility and resulting compression-induced tilt near the SmA - SmC transition. Low dislocation density areas are the areas of greatest layer compression, implying that the edge dislocations relieve the compressive stress. Temperature cycling shows the texture is set near the N - SmA transition, though x-ray diffraction data shows that the layer expansion occurs through the entire range of the SmA. X-ray diffraction from oriented samples has been done which shows that the texture is a result of competition between smectic ordering and surface pinning. Work supported by ED GAAN Fellowships P200A030179 and P200A000839, and NSF MRSEC Grant DMR-0213918.

**9:12**

**U21 7 Random Lasing in Multidomain Cholesteric Liquid Crystals** MICHELE MOREIRA, MINGXIA GU, OLEG LAVRENTOVICH, BAHMAN TAHERI, PETER PALFFY-MUHORAY, *Liquid Crystal Institute, KSU* A conventional laser consists of a pumped amplifying medium and an optical cavity to provide feedback for light amplification. In disordered materials, light can be trapped by multiple scattering processes and, if a gain medium is added, random lasing can occur. This random laser source does not require a regular cavity, but instead depends on multiple scattering in a random medium. Random lasers have attracted considerable attention recently because of their low cost and ease of construction. We present recent results of our random lasing experiments in dye-doped multidomain cholesteric liquid crystals, with submicron pitch, where the highly reflective cholesteric domains are the scattering elements. We discuss the underlying physics, compare the performance of these systems with others, consider the effects of temperature on the emission spectrum, and suggest possible applications.

**9:24**

**U21 8 Wavelength Hopping in Cholesteric Liquid Crystal Lasers** MICHELE MOREIRA, CHRISTOPHER BAILEY, WENYI CAO, BAHMAN TAHERI, PETER PALFFY-MUHORAY, *Liquid Crystal Institute, KSU* Due to their birefringence and periodic structure, cholesteric liquid crystals (CLCs) in the helical cholesteric phase are one-dimensional photonic band gap materials. Gain enhancement and distributed feedback effects give rise to low threshold mirrorless lasing at the band edges. Since the wavelength at the band edge is proportional to the cholesteric pitch, which is a smooth function of temperature, one would expect the lasing wavelength to vary smoothly with temperature. Observations show, however, that the lasing wavelength does not depend smoothly on temperature, but instead exhibits periodic jumps between regions of smooth monotonic behavior. We have determined the reflection band dynamics, observed multiple lasing peaks at the hopping wavelength, and see evidence of hysteresis on measuring the reflection band and lasing peaks at different heating rates. We compare our observations with theoretical models, and propose an explanation for the observed dynamics.

**9:36**

**U21 9 Poisson-bracket formulation of the dynamics of polar liquid crystals*** WILLIAM KUNG, M. CRISTINA MARCHETTI, *Syracuse University* KARL SAUNDERS, *California Polytechnic State University* We develop the dynamical theory of polar liquid crystals with local $C_{\infty v}$-symmetry using the general Poisson-bracket formalism. We obtain dynamical equations for the slow macroscopic fields that govern the dynamics in both the polarized and the isotropic phases. Starting from a microscopic definition of an alignment vector proportional to the polarization, we obtain Poisson bracket relations for the director field. The hydrodynamic equations differ from those of nematic liquid crystals ($D_{\infty h}$) in that they contain terms violating the $\mathbf{n} \rightarrow -\mathbf{n}$ symmetry. We find that the $\mathcal{Z}_2$-odd terms induce a general splay instability of a uniform polarized state in a range of parameters.

*Work supported by NSF grants DMR- 0305407 and DMR-0219292.

**9:48**

**U21 10 Finite Element Elastodynamics Studies of Shape Evolution in Liquid Crystal Elastomers*** ROBIN SELINGER, BADEL MBANGA, JONATHAN SELINGER, *Kent State University* Liquid crystal elastomers change shape under heating/cooling, applied fields, or optical illumination, with induced strains up to 400%. We present a novel finite element elastodynamics technique to model dynamics of shape change in these materials, with explicit coupling between nematic order and elastic strain. Without added dissipation, the elastodynamics algorithm conserves the sum of kinetic and potential energy to one part in $10^6$, even for large strains and rotations. In initial studies, we model shape evolution during a transition from the isotropic phase to nematic and back again, and model the induced curvature of an elastomer strip under local optical illumination. This method allows modeling of complex geometries and dynamic perturbations, and can serve as a bridge between fundamental soft condensed matter theory and engineering design.

*Acknowledgment is made to the Donors of the ACS-PRF for support of this work.

**10:00**

**U21 11 Temperature Dependence of Acousto-Optic Effect in a Nematic Liquid Crystal Cell** STEVEN SUNDBECK, ANTHONY MALANOSKI, BRIAN WESLOWSKI, DEVANAND SHENOY, *United States Naval Research Laboratory* JONATHAN SELINGER, *Kent State University* The acousto-optic effect occurs in a nematic liquid crystal cell when an incident ultrasonic wave causes a rotation of the director. This effect is observable as a change in the optical transmission through a cell, and has been exploited as a means of nondestructive imaging. The sensitivity and speed of this rearrangement are dependent on the viscosity of the liquid crystal material. Because of this, the effect is sensitive to the temperature. In this work we investigate quantitatively how the acousto-optic response is affected by the temperature of the liquid crystal cell. We present the results of studies of changes to the acoustic sensitivity of the cells and changes of their dynamic responses to the introduction of the ultrasonic wave.

**10:12**

**U21 12 Elliptic Phases: A Study of the Nonlinear Elasticity of Twist** CHRISTIAN SANTANGELO, RANDALL KAMIEN, *University of Pennsylvania* The twist-grain boundary phase in smectic-A liquid crystals, constructed from rotating walls of parallel screw dislocations, is a prime example of a stable, ordered configuration of defects. In smectics, nonlinearities in the strains strongly affect the energetics and interactions between defects, thus complicating their analysis. By exploiting the properties of Jacobi elliptic functions, we construct a triply-periodic surface locally composed of screw dislocations, called Schnerk's surface, which has the structure of a series of ninety degree twist-grain boundaries. This is a candidate structure for the recently observed large-angle twist-grain boundary phases. Because of the analytic tractability of our construction, we compute that the grain boundaries interact exponentially at long distances through both the compression and bending energies, and that there is a preferred grain boundary spacing.

**10:24**

**U21 13 Calorimetric study of aligned liquid crystal + aerosil*** F. CRUCEANU, G. S. IANNACCHIONE, *Worcester Polytechnic Institute* D. LIANG, R. L. LEHENY, *Johns Hopkins University* A high-resolution ac-calorimetric study was performed on magnetically aligned colloidal dispersions of 8CB and aerosil spanning the weakly first-order itI-itN and second order itN-SmitA phase transitions. Stable aligned samples were prepared by repeated cycling between the isotropic and nematic phase in the presence of a 2 T magnetic field. Zero-field measurements were carried out on six aligned conjugate density samples ranging from 0.03 to 0.15 g $cm^{-3}$ (mass of aerosil per volume of liquid crystal). For comparison, two unaligned samples from the same batch (0.05 and 0.13 g $cm^{-3}$) were also studied. The unaligned samples reproduce very closely previous studies on this system. The magnetically aligned samples, exhibits lower transition temperatures for the same aerosil density sample and a shift to higher aerosil density of the non-monotonic $T_c$ evolution. The clear differences between aligned and unaligned sample indicate the ''memory'' of the magnetic field even after heating deep into the isotropic phase. The origin of this ''memory'' remains unexplained.

*Supported by NSF award DMR-0092786

**10:36**

**U21 14 Disordering Effects in Smectic − Aerosil Gels*** VISHAL PANDYA, DANIELE FINOTELLO, *Kent State University* We studied quenched disorder effects on the 12CB liquid crystal upon dispersion of silica nano particles (type A-300): hydrophilic silica spheres of diameter 7nm and surface area S = 300 $m^2g^{-1}$, with hydroxyl groups covering the surface. The LC-aerosil dispersions form a gel if aerosil density exceeds the percolation threshold. For low densities of aerosil dispersions and in cooling the sample, the LC director in the void volume is parallel and follows the external NMR field; a well defined and stable LC configuration forms. When a complete silica network forms and the sample orientation in the field is changed, a few silica links are broken by the field, re-aligning only a few Sm layers; the aerosil locks in the LC configuration which follows a $P_2$ ($Cos\Theta$) dependence. In contrast, if the dispersion is cooled from isotropic phase outside the field, the spectra in the Sm phase is a powder pattern. The field anneals the aerosil-induced random disorder up to a certain density beyond which, disordering effects dominate; for aerosil densities greater than $\rho_S \approx$ 0.055 g/$cm^3$ spectral patterns are consistent with an isotropic distribution of smectic domains. The quenching of the 12CB Sm-A phase at $\rho_S \approx$ 0.055 g/$cm^3$, is one order of magnitude less than that in 8CB [1]. The aerosil induced disorder, quantified by the percent of LC molecules in a powder pattern, depends linearly on the density. [1] T. Jin and D. Finotello, Phys. Rev. E 69, 041704 (2004); Phys. Rev Lett. 86, 818 (2001). *Supported by NSF-INT 03-06851, OBR B-7844 and B-7845.

**10:48**

**U21 15 The Effect of Aerosil Network on Smectic A-Reentrant Nematic Liquid Crystal** MEHMET RAMAZANOGLU, SIMON LAROCHELLE, *U. Toronto* ROBERT J. BIRGENEAU, *U. Toronto and U.C. Berkeley* We report on a high resolution x-ray scattering study of aerosil dispersion effects on nematic-smectic A and smectic A-reentrant nematic phase transitions in 6OCB (hexyloxycyanobiphenyl) and 8OCB (octyloxycyanobiphenyl) liquid crystal mixtures. Dispersed aerosil particles introduce quenched randomness to the liquid crystal phases, which destroys the long range smectic order [1]. The experiment was conducted on mix-

tures with different 6OCB:8OCB concentrations and aerosil densities. The parabolic smectic A phase boundary is found to be slightly distorted in the presence of the aerosil network, with shifted transition and median ($T_M$) temperatures. Above $T_M$, the order parameter, susceptibility and parallel correlation lengths for the thermal and random parts of the structure factor show behaviors similar to those observed in non-reentrant nematic-smectic A second order phase transitions [2]. At $T_M$, where the order parameter has its maximum value, the scattering peaks are only defined by the random part of the structure factor. The smectic order parameter decreases with a further decrease in temperature, while the susceptibility and thermal correlation length increasingly show nematic-like behavior. Finally, at the lowest temperature, the mixtures are found in the reentrant nematic phase. [1] P.S. Clegg et. al. PRE 67,021703 (2003) [2] S. Larochelle et. al. in preparation

**SESSION U22: FOCUS SESSION: MAGNETIC TUNNELING I**
**Thursday Morning, 16 March 2006; 319, Baltimore Convention Center at 8:00**
**Jonathan Sun, IBM, presiding**

***Invited Papers***

**8:00**
**U22 1 Tunneling spin polarization in planar tunnel junctions: measurements using NbN superconducting electrodes and evidence for Kondo-assisted tunneling.**
HYUNSOO YANG, *IBM Almaden Research Center*

The fundamental origin of tunneling magnetoresistance in magnetic tunnel junctions (MTJs) is the spin-polarized tunneling current, which can be measured directly using superconducting tunneling spectroscopy (STS). The STS technique was first developed by Meservey and Tedrow using aluminum superconducting electrodes. Al has been widely used because of its low spin orbit scattering. However, measurements must be made at low temperatures ( $<$ 0.4 K) because of the low superconducting transition temperature of Al. Here, we demonstrate that superconducting electrodes formed from NbN can be used to measure tunneling spin polarization (TSP) at higher temperatures up to $\sim$ 1.2K. The tunneling magnetoresistance and polarization of the tunneling current in MTJs is highly sensitive to the detailed structure of the tunneling barrier. Using MgO tunnel barriers we find TSP values as high as 90% at 0.25K. The TMR is, however, depressed by insertion of ultra thin layers of both non-magnetic and magnetic metals in the middle of the MgO barrier. For ultra-thin, discontinuous magnetic layers of CoFe, we find evidence of Kondo assisted tunneling, from increased conductance at low temperatures ( $<$ 50K) and bias voltage ( $<$ 20 mV). Over the same temperature and bias voltage regimes the tunneling magnetoresistance is strongly depressed. We present other evidence of Kondo resonance including the logarithmic temperature dependence of the zero bias conductance peak. We infer the Kondo temperature from both the spectra width of this conductance peak as well as the temperature dependence of the TMR depression. The Kondo temperature is sensitive to the thickness of the inserted CoFe layer and decreases with increased CoFe thickness.

*Performed in collaboration with S-H. Yang, C. Kaiser, and S. Parkin.

***Contributed Papers***

**8:36**
**U22 2 High sensitivity of tunneling spin polarization to chemical bonding of transition metal ferromagnetic alloys at interface with insulating barrier** SEE-HUN YANG, HYUNSOO YANG, CHRISTIAN KAISER, STUART PARKIN, *IBM Almaden Research Center* IBM ALMADEN RESEARCH CENTER TEAM, We report that the tunneling spin polarization (TSP) is found to be strongly influenced by the amount of oxygen used in the deposition of the tunnel barrier itself that chemical bonding at the interface between $Al_2O_3$ and ferromagnetic Co and Co-Pt alloys. For reactive sputter (RS) deposition of alumina using an argon-oxygen gas mixture with a low concentration of oxygen ( $\sim$ 0.1 mTorr), much lower TSP values are found than when the alumina barrier is formed by post-plasma oxidation (PO) with $\sim$ 100mTorr oxygen of Al layers. X-ray absorption spectroscopy (XAS) has been used to characterize the chemical bonding at the Co or Co-Pt/$Al_2O_3$ interface. These studies show that Co-O bonds are much more formed for the barrier fromed by PO of Al than for that formed by RS deposition. We attribute the changes in TSP to changes in the relative tunneling probabilities from Co and Pt which are strongly influenced by oxygen bond formation.[1] [1]C. Kaiser, S. van Dijken, S.-H. Yang, H. Yang, and S. S. P. Parkin, Phys. Rev. Lett. 94, 247203 (2005).

**8:48**
**U22 3 Anomalous magnetic behaviors in $AlO_x/Co_{84}Fe_{16}$ Tunneling Magnetoresistance (TMR) systems induced by the interfacial oxidations** K.-J. RHO, *POSTECH* K.-J. KIM, *PLS* J.-Y. KIM, *PLS* J.-H. PARK, *POSTECH/PLS* J.-S. LEE, *POSTECH* K.-B. LEE, *POSTECH* S. J. JOO, *KIST* K. RHIE, *Korea University* Due to the practical application of the magnetic tunnel junction as magnetic memory cells and sensors, tunneling magnetoresistance (TMR) in the magnetic tunnel junction (MTJ) has been very actively studied, and extensive effort has been exerted in order to improve the physical properties of MTJs. As a result, it is well recognized that the performance of the MTJs strongly depends on the environment at the interface between the magnetic layer and the insulating oxide layer. In spite of such critical importance, the interface environment and its effects on the magnetic behaviors have not been well understood yet. Here we present

anomalous magnetic behaviors observed in $AlO_x/Co_{84}Fe_{16}$ magnetic tunnel junction structures prepared in various oxidation processes. We examined the magnetic behaviors using the magneto-optical Kerr effect (MOKE) measurements in vacuum. The system turns out to exhibit a strong temperature dependence of the magnetic coersive field, and the behavior consistently varies with the oxidation process. The interface environments and the origin of the anomalous behaviors will be also discussed based on x-ray reflectivity and diffraction results.

**9:00**

**U22 4 Tunneling magnetoresistance in MgO-based magnetic tunneling junction with (001) oriented FeCo electrode fabricated by sputtering deposition.*** TAKAHIRO MORIYAMA, WEIGANG WANG, JOHN Q. XIAO, *Department of Physics and Astronomy, University of Delaware* MgO-based Magnetic Tunneling Junction (MTJ) is now one of the most promising structures for spintronics applications due to its very large Tunneling Magnetoresistance (TMR). However, the high TMR is generally achieved only after the annealing at high temperature that promotes the crystallization of MgO. We fabricated FeCo/MgO/FeCo MTJs on both oriented and non-oriented buffer layers by DC and RF sputtering depositions at room temperature. MgO barrier layer was formed by reactive sputtering method following a very thin Mg deposition. Without annealing, 70% TMR ratio was observed for MTJ with oriented buffer layers, whereas 40% TMR ratio was observed with non-oriented buffer layers. This indicates that an oriented buffer layer can enhance the TMR ratio even without high temperature annealing. We also studied the dependence of TMR on the Mg layer thickness, MgO barrier thickness, and annealing conditions.

*This work has been supported by NSF DMR Grant No.0405-136

**9:12**

**U22 5 Effect of interface states on spin-dependent tunneling in Fe/MgO/Fe tunnel junctions** KIRILL BELASHCHENKO, JULIAN VELEV, EVGENY TSYMBAL, *University of Nebraska-Lincoln* The electronic structure and spin-dependent tunneling in epitaxial Fe/MgO/Fe(001) tunnel junctions are studied using first-principles calculations.[1] For small MgO barrier thickness the minority-spin resonant bands at the two interfaces make a significant contribution to the tunneling conductance for the antiparallel magnetization, whereas these bands are, in practice, mismatched by disorder and/or small applied bias for the parallel magnetization. This explains the experimentally observed decrease in tunneling magnetoresistance (TMR) for thin MgO barriers. We predict that a monolayer of Ag epitaxially deposited at the interface between Fe and MgO suppresses tunneling through the interface band and may thus be used to enhance the TMR for thin barriers. [1] K. D. Belashchenko, J. Velev, and E. Y. Tsymbal, Phys. Rev. B **72**, 140404(R) (2005).

**9:24**

**U22 6 The atomic and electronic structure of the FeCoB/MgO interface** J.D. BURTON, S.S. JASWAL, E.Y. TSYMBAL, *University of Nebraska Lincoln* O.N. MRYASOV, O.G. HEINONEN, *Seagate Technology* Magnetic tunnel junctions (MTJs) have recently aroused much interest due to their potential applications as random access memories and magnetic field sensors. MTJs consist of a thin insulating layer separating two ferromagnetic electrodes. Very recently FeCoB/MgO/FeCoB MTJs have shown promising results. Upon annealing, the amorphous FeCoB electrodes crystallize in a bcc structure epitaxial to the MgO(001) surface. Many groups have observed a significant increase in TMR ratios (higher than 300% at room temperature [1]) after annealing. It is clear that the crystallization of the electrodes plays an important role in this increase. It is not clear, however, what happens to B after annealing and what role it plays in enhancing TMR. We present results of first-principles total energy calculations that suggest that it is energetically favorable for B to reside at the crystalline FeCoB/MgO interface rather than remain in the bulk of the FeCoB electrode. We also find that the presence of B at the interface significantly weakens bonding between the FeCoB electrode and the MgO barrier. We are investigating the presence of resonant states[2] at the FeCoB/MgO interface and will discuss the effects of interfacial B on them. [1] J. Hayakawa et al., 2005 MMM Conference. [2] Belashchenko et al., Phys. Rev. B **72**, R140404 (2005).

**9:36**

**U22 7 Structural and magnetic properties of Fe/MgO/Ge(100) heterostructures and Fe/MgO/Fe(100) magnetic tunnel junctions** YUEH-FENG CHIANG, KYLE PI, YAN LI, ROLAND KAWAKAMI, *University of California Riverside* MgO is one of the most attractive materials for spintronic devices due to a novel spin filtering effect that dramatically increases spin polarization. We utilize molecule beam epitaxy (MBE) to synthesize ferromagnet (FM)/MgO/semiconductor heterostructures for efficient spin injection and detection in Si, Ge and GaAs lateral devices and MgO-based magnetic tunnel junctions (MTJs) for MRAM applications. Initial studies have focused on optimizing the growth of Fe/MgO/Ge(100) heterostructures and Fe/MgO/Fe MTJs and investigating their magnetic properties. Results indicate high-quality layer-by-layer growth with roughness at the atomic scale. itIn situ reflection high energy electron diffraction (RHEED) is utilized for investigating surface roughness during growth. We observe streaky RHEED patterns and intensity oscillations for the homoepitaxial growth of Ge on Ge(100) at 370$^o$C, which indicates an atomically flat Ge buffer layer. Epitaxial MgO layers grown on top of the Ge buffer at room temperature also showed streaky RHEED patterns and atomic force microscopy (AFM) images revealed the rms roughness to be 0.2 nm ( $\sim$ 1 atomic layer) for a 3 nm thick MgO film. High remanance and small coercive field have been observed in epitaxial Fe (5nm)/MgO(3nm)/Ge(100) heterostructures via magneto-optic Kerr effect (MOKE) illustrating good magnetic properties.

**9:48**

**U22 8 XPS studies of MgO based magnetic tunnel junction structures** JOHN READ, *Cornell University* PHIL MATHER, *Cornell* EILEEN TAN, *TDSI, Singapore* ROBERT BUHRMAN, *Cornell* The very high tunneling magnetoresistance (TMR) obtained in MgO magnetic tunnel junctions (MTJ)[(1,2)] motivates the investigation of the electronic properties of the MgO barrier layer and the study of the ferromagnetic metal - MgO interface chemistry. Such large TMR values are predicted by theory due to the high degree of order apparent in the barrier and electrode materials. However, as grown ultra-thin MgO films generally contain defects that can influence electron transport properties through the creation of low energy states within the bulk MgO band-gap. We will report the results of x-ray photoelectron spectroscopy (XPS) studies of (001) textured ultra-thin MgO layers that are prepared by RF magnetron sputtering and electron beam evaporation on ordered ferromagnetic electrodes and in ordered MTJ structures with and without post growth vacuum annealing. XPS spectra for both MgO deposition techniques clearly indicate a surface oxygen

species that is likely bound by defects in the oxide[3] in half-formed junctions and improvements in MgO quality after counter electrode deposition. We will discuss our results regarding the chemical properties of the oxide and its interfaces directed towards possibly providing guidance to engineer improved MgO MTJ devices. [1] S.S.P. Parkin et. al., Nature Materials, **3**, 862 (2004). [2] S. Yuasa et. al., Nature Materials, **3**, 868 (2004). [3] E. Tan et. al., Phys. Rev. B., **71**, 161401 (2005).

**10:00**

**U22 9 Interlayer Exchange Coupling in Fe|MgO|Fe Magnetic Tunnel Junctions** T. KATAYAMA, S. YUASA, *National Institute of Advanced Industrial Science and Technology (AIST)* JULIAN VELEV, S. JASWAL, E. TSYMBAL, *University of Nebraska - Lincoln* Fully epitaxial Fe|MgO|Fe(001) films with wedge-shaped MgO layer were prepared on single-crystal MgO(001) substrates using MBE technique [1]. Structure of the films is Fe-free-layer(15, 20, 30 nm)/MgO(0.3-1.8 nm)/Fe-pinned-layer(10 nm)/Ir-Mn. The interlayer exchange coupling (IEC) energy was obtained at room temperature from a unidirectional shift of the Kerr hysteresis loop. The IEC was found to be antiferromagnetic for small MgO thickness but changed sign at 8.5Å. In order to explain this behavior we performed itab-initio calculations of IEC in Fe|MgO|Fe(001) MTJs with and without oxygen vacancies in MgO. Our results show that without O vacancies the IEC is ferromagnetic and decays exponentially with MgO thickness. However, in the presence of O vacancies the IEC is antiferromagnetic for thin barriers and changes sign with increasing barrier thickness. This behavior is consistent with our experimental observations and is explained by the resonance contribution to the IEC due to localized defect states [2]. [1] S. Yuasa itet al., Nature Mater. **3**, 868 (2004). [2] M. Y. Zhuravlev et al., Phys. Rev. Lett. **94**, 026806 (2005).

**10:12**

**U22 10 Inelastic electron tunneling spectroscopy of $MgO_xF_y$ barriers** JUN HYUNG KWON, TESU KIM, JINO LEE, KOOKRIN CHAR, *Center for Strongly Correlated Materials Research, School of Physics, Seoul National University, Seoul, Republic of Korea* Recent development in TMR junction with MgO barrier attracts a great deal of attention. It is reported that the junctions with MgO barrier exhibit higher TMR with lower RA value. Combined with the spin-transfer switching that has been demonstrated, the future MRAM architecture will to incorporate the MgO barrier TMR junctions. The device parameters for MRAM will require the RA value of about 100 $\Omega - \mu m^2$, corresponding to about 1 nm thick MgO barrier layer. In order to understand the electrical properties of MgO barrier, we have fabricated Mg/MgO/Mg tunneling junctions as the function of oxidation time of the Mg metal layer. These Mg/MgO/Mg cross-strip junctions are deposited using stencil masks without a vacuum break, and the size of junction area is about 130 $\mu$m by 160 $\mu$m. When measuring $d^2I/dV^2$-V, namely the inelastic tunneling spectroscopy, we observed the peaks correponding to MgO bonds, indicating that the MgO barrier is a stable and good insulator. Using the IETS measurement technique, we will present the interface properties between the ferromagnetic electrode and the MgO barrier layer. Moreover, we will report on our $MgO_xF_y$ tunnel barrier made by our fluorine-doping method.

**10:24**

**U22 11 Spin torque and spin current in magnetic tunnel junctions*** MAIRBEK CHSHIEV, WILLIAM H. BUTLER, *Center for Materials for Information Technology, The University of Alabama, Tuscaloosa, AL* ALAN KALITSOV, NICK KIOUSSIS, *Department of Physics, California State University, Northridge, CA* In recent years, current-induced spin torque [1] has attracted strong interest both because it may advance our understanding of fundamental physics and because it may have useful applications. We present a study of non-equilibrium spin currents and the corresponding spin torques in magnetic tunnel junctions with non-collinear moments. Calculations are based on the Keldysh formalism in which the non-equilibrium Green functions are calculated within a tight-binding model using the technique of Caroli et al. [2]. The properties of spin torque and spin currents are studied as a function of applied bias, barrier thickness and lattice structure type. In addition, the exchange coupling between ferromagnetic layers in magnetic tunnel junctions is investigated via its relation to the current induced spin torque. [1] J. C. Slonczewski, J. Magn. Magn. Mat. 159, L1 (1996); L. Berger, Phys. Rev. B 54, 9353 (1996); E. Myers, D. Ralph, J. Katine, R. Louie, R. Buhrman, Science, 285, 867 (1999). [2] C. Caroli, R. Combescot, P. Nozieres, D. Saint-James, J. Phys. C: Solid St. Phys., 4, 916 (1971).

*This work was supported by MRSEC NSF-DMR 0213985 and INSIC EHDR Program

**10:36**

**U22 12 Shot noise in Cr-doped and undoped $Co/Al_2O_3/Py$ magnetic tunnel junctions*** FARKHAD ALIEV, RUBEN GUERRERO, *Departamento de Física de la Materia Condensada, C-III, Universidad Autónoma de Madrid, Cantoblanco, 28049, Madrid, Spain* PATRICK LE CLAIR,† JAGADEESH MOODERA, *Massachusetts Institute of Technology, Massachusetts 02139, USA* We have found that shot noise in Co(80Å) /$Al_2O_3$(14Å)/Py(100Å) magnetic tunnel junctions (MTJs) is reduced with respect to Poisonian value. The Fano factor, obtained at frequencies ($100 < f < 1000$Hz), temperatures ($T < 10$K) and biases (below 150 meV) where the shot noise dominates, varies between $F \approx 0.8$ and 0.65, indicating correlated electron tunnelling. Doping of the insulating barrier with Cr inclusions suppresses the conductivity and tunnelling magnetoresistance, and restores the Fano factor to a value corresponding to uncorrelated transport ($F \approx 1$). These results indicate an enhanced cross-correlation between electrons due to trapping or spin-flip assisted tunnelling in the undopped MTJs, and a possible Coulomb blockade in the Cr doped MTJs.

*Supported by Spanish MEC (MAT2003-02600)

†Also: Department of Physics and Astronomy and MINT, University of Alabama, Tuscaloosa, Al 35487, USA

**SESSION U23: FRUSTRATION IN 2D**
**Thursday Morning, 16 March 2006**
**320, Baltimore Convention Center at 8:00**
**Bruce Gaulin, McMaster University, presiding**

**8:00**

**U23 1 Spin Frustration, Magnetic Susceptibility and Excitations in Spatially Anisotropic Triangular-Lattice Antiferromagnets*** RAJIV SINGH, *University of California at Davis* WEIHONG ZHENG, *University of New South Wales, Sydney, Australia* JOHN FJAERESTAD, ROSS McKENZIE, *University of Queensland, Brisbane, Australia* RADU COLDEA, *University of Bristol, UK* We calculate the temperature dependent

magnetic susceptibility and excitation spectra for the spatially anisotropic triangular- lattice Heisenberg model. We show that suitably scaled plots of magnetic susceptibility provide a direct measure of frustration in the system and allow one to infer the exchange parameters from the susceptibility data. We find that the organic material $\kappa - (BEDT - TTF)_2Cu_2(CN)_3$ is very well described by the isotropic triangular lattice model. We also find that the excitation spectra of the model shows various anomalies in the Neel and Spiral phases.

*Supported in Part by NSF-DMR-0240918

**8:12**

**U23 2 Anomalous renormalization of excitation spectra of the triangular-lattice antiferromagnet*** JOHN FJAERESTAD, *University of Queensland* WEIHONG ZHENG, *University of New South Wales* RAJIV SINGH, *University of California, Davis* ROSS McKENZIE, *University of Queensland* RADU COLDEA, *University of Oxford* We use series expansions to calculate the excitation spectra of the spin-1/2 triangular-lattice Heisenberg antiferromagnet above the 3-sublattice ordered phase. We find that the spectra are renormalized downwards with respect to linear spin-wave theory. This is in sharp contrast to the square-lattice antiferromagnet, where the spectral frequencies are renormalized upwards due to quantum fluctuations. The triangular-lattice spectra show sharp downward renormalization at special wavevectors, which (a) can be interpreted as evidence of high-energy spinons and (b) provides an explanation for rapid loss of antiferromagnetic correlations with temperature, consistent with earlier high-temperature series expansion studies.

*We thank the Australian Research Council, NSF, UK Engineering and Physical Sciences Research Council for financial support; Australian Partnership for Advanced Computing, Australian Centre for Advanced Computing and Communications for computing resources

**8:24**

**U23 3 Pairing of doped holes in the Shastry-Sutherland lattice** JUN LIU, JOERG SCHMALIAN, *Iowa State University* NANDINI TRIVEDI, *Ohio State University* We investigate the magnetic and pairing correlations in a hole doped Shastry-Sutherland lattice. We use a variational wave function that reproduces the valence bond ground state of the un-doped material, relevant to $SrCu_2(BO_3)_2$. For finite doping we study the disappearance of the valence bond crystal and the emergence of pairing of doped holes.

**8:36**

**U23 4 In Gap Excitations and Triplet Lifetime Broadening in the Dilute Singlet Ground State System $SrCu_{2-x}Mg_x(BO_3)_2$** S. HARAVIFARD, S.R. DUNSIGER, B.D. GAULIN, H.A. DABKOWSKA, *McMaster University* M.T.F. TELLING, *ISIS Pulsed Neutron Facility* S. EL SHAWISH, J. BONCA, *J. Stefan Institute* We have carried out high resolution time-of-flight neutron scattering measurements on a new high quality single crystal of $SrCu_{2-x}Mg_x(BO_3)_2$ with $x = 0.1$. These studies revealed the presence of new excitations within the singlet-triplet gap of this quasi-two dimensional, dilute, singlet ground state system. These new excitations showed little or no shift in energy with increasing applied magnetic field. In addition, we observe substantial broadening of the three triplet excitations in the dilute single crystal, as compared with pure $SrCu_2(BO_3)_2$.[1] The triplet excitations in doped $SrCu_{2-x}Mg_x(BO_3)_2$ therefore possess finite lifetimes at low temperatures in the range that can be measured with cold neutron spectroscopy. We have also calculated the dynamical spin structure factor using the zero temperature Lanczos method, and solving a Shastry-Sutherland model at zero and finite doping for different strengths of external magnetic field. This theory reproduces all the qualitative features observed in the experiments on $SrCu_{2-x}Mg_x(BO_3)_2$.

[1] B.D. Gaulin itet al., Phys. Rev. Lett., **93**, 267202, 2004.

**8:48**

**U23 5 Infrared studies of a quantum magnet $SrCu_2(BO_3)_2$** T. RÕÕM, D. HÜVONEN, U. NAGEL, *Natl. Inst. of Chem. Phys. & Biophysics, Akadeemia tee 23, EE12618 Tallinn, Estonia* S.V. DORDEVIC, C.C. HOMES, *Brookhaven National Laboratory* A. GOZAR, G. BLUMBERG, *Bell Laboratories* N. DRICHKO, M.M. DRESSEL, *Universitat Stuttgart* H. KAGEYAMA, *Kyoto University* We will report results of our infrared studies of $SrCu_2(BO_3)_2$, a two-dimensional spin system with a disordered ground state even at very low temperatures, and a spin gap of about 24 $cm^{-1}$ (3 meV). This material has recently attracted attention because of a possibility that doping may lead to a superconductivity mediated by antiferromagnetic fluctuations, possibly similar to high-$T_c$ cuprates. Using polarized light we have probed both crystallographic directions over a broad range of frequencies (from about 30 $cm^{-1}$ to 20,000 $cm^{-1}$) and temperatures (from 4.2 K to 300 K). The results reveal significant differences between the ab-plane and c-axis directions. We will discuss these findings in relation with the resonance effects observed in inelastic light scattering experiments from collective magnetic excitations.

**9:00**

**U23 6 Magnetization plateaus for $Cs_2CuBr_4$** SHIN MIYAHARA, KIYOSHI OGINO, MASAHIRO SHIMIZU, NOBUO FURUKAWA, *Aoyama Gakuin University* $Cs_2CuBr_4$ is a new two-dimensional spin-1/2 system, where 1/3- and 2/3-plateaus have been observed in external magnetic fields. The magnetic behaviors of the material are well explained by a two-dimensional antiferromagnetic Heisenberg model on a distorted triangular lattice. In the model, there are two types of interactions $J_1$ and $J_2$, where $J_1$ chains are coupled with inter chain interactions $J_2$. Using an exact diagonalization method, we investigated magnetic properties, especially magnetization curve. In the magnetization, 1/3-plateau appears for $0.7 .3ex < / \sim J_2/J_1 .3ex < / \sim 1.3$. At the plateau, three-fold degenerate ground state, up-up-down structure, is realized. Our results indicate that the material has a more frustrated character $J_2/J_1 \approx 0.7$ than what has been expected from a classical theory $J_2/J_1 = 0.47$. The magnetic properties at 2/3-plateau will also be discussed.

**9:12**

**U23 7 Dynamical properties of the anisotropic triangular quantum antiferromagnet with Dzyaloshinskii-Moriya interaction** RASTKO SKNEPNEK, DENIS DALIDOVICH, JOHN BERLINSKY, JUNHUA ZHANG, CATHERINE KALLIN, *Department of Physics and Astronomy, McMaster University, Hamilton, Ontario, Canada L8S 4M1* We present a detailed study of the anisotropic triangular quantum antiferromagent with Dzyaloshinskii-Moriya (DM) interaction building on earlier work by Veillette, James and Essler [Phys. Rev. B, **72**, 134429 (2005)]. The DM interaction generates an easy-plane anisotropy and opens a gap in the spin-wave spectrum at the incommensurate ordering wave vector $\vec{Q}$. Our calculation utilizes the Holstein-Primakoff representation of spins and goes beyond linear spin wave theory by taking into account magnon-magnon interactions in a $1/S$ ex-

pansion. We calculate renormalized dispersion relations for the magnons to order 1/$S$ for different values of the DM interaction and pay particular attention to the interesting case of zero DM interaction. The dynamical structure factor is calculated to order 1/$S$. It is found that, compared to linear spin wave theory, a significant fraction of the scattering intensity is shifted to higher energies. We compare our findings with the recent neutron scattering data measured on the frustrated quantum antiferromagnet $Cs_2CuCl_4$, [R. Coldea, *et. al.*, Phys. Rev. B, **68**, 134424, (2003)].

**9:24**

**U23 8 Spiral magnetic order on an anisotropic triangular lattice in the presence of Dzyaloshinskii-Moriya interaction** DENIS DALIDOVICH, RASTKO SKNEPNEK, A. JOHN BERLINSKY, JUNHUA ZHANG, CATHERINE KALLIN, *Department of Physics and Astronomy, McMaster University, Hamilton, Ontario, Canada L8S 4M1* We consider the ground state energy, magnetization and the energy spectrum of the two-dimensional antiferromagnets on the triangular lattice in the presence of anisotropy in the exchange couplings, and Dzyaloshinskii-Moriya (DM) interaction $D$. $J$ and $J'$ are meant to be the couplings along the chain direction and zigzag bonds respectively. Assuming that in the wide range of those parameters the system has the spiral Neel ordering, we consider the role of quantum fluctuations within the framework of a standard 1/$S$ expansion. We show that DM interaction considerably suppresses fluctuations and seems to play an important role in stabilizing the spiral Neel ordering in this frustrated system. We discuss our theoretical results within the context of the recent experimental measurements in the frustrated quantum magnet $Cs_2CuCl_4$, [R. Coldea, et. al., Phys. Rev. B, **68**, 134424, (2003)], and the recent theoretical structure factor calculations by M. Y. Veillette, et. al., Phys. Rev. B **72**, 134429 (2005)

**9:36**

**U23 9 A quasi-1d approach to the triangular antiferromagnet $Cs_2CuCl_4$** LEON BALENTS, *Physics Department, UCSB* OLEG STARYKH, *Physics Department, University of Utah* We discuss the low-temperature properties of a spin-1/2 triangular Heisenberg antiferromagnet in a field, including the effects of Dyaloshinskii-Moriya interactions, as believed appropriate to $Cs_2CuCl_4$.[1] Our treatment is based upon a view of the problem as a system of weakly-coupled spin chains. Analytic results are obtained through a combination of renormalization group, chain mean-field, and bosonization methods. Using various exactly-known properties of the individual Heisenberg chains, we calculate numerous physical properties, including various phase boundaries in longitudinal and transverse fields. We compare our results to published experimental data.

[1]R. Coldea et al., Phys. Rev. Lett. 88, 137203 (2002).

**9:48**

**U23 10 Simultaneous breaking of lattice symmetry and spin frustration in triangular lattice antiferromagnet $CuFeO_2$** Y. REN, *XFD/XOR, Argonne National Laboratory* F. YE, *Center for Neutron Scattering, Oak Ridge National Laboratory* Q. HUANG, *NIST Center for Neutron Research, NIST* J.A. FERNANDEZ-BACA, *Center for Neutron Scattering, Oak Ridge National Laboratory & Dept of Physics and Astronomy, Univ. of Tennessee* PENGCHENG DAI, *Dept of Physics and Astronomy, Univ. of Tennessee & Center for Neutron Scattering, Oak Ridge National Laboratory* J.W. LYNN, *NIST Center for Neutron Research, NIST* T. KIMURA, *Los Alamos National Laboratory* We use high resolution synchrotron X-ray and neutron diffraction to study the geometrically frustrated triangular lattice antiferromagnet (TLA) $CuFeO_2$. We show that the occurrence of the two magnetic transitions, at 14 K and 11 K, respectively is accompanied simultaneously by a second-and first- order structural phase transitions from a hexagonal structure to a monoclinic form. This is the first observation of two successive spin-driven structural transitions directly coupled with incommensurate and commensurate magnetic orderings in frustrated TLA systems. This work is supported by the U. S. NSF DMR-0453804 and DOE Nos. DE-FG02-05ER46202 and DE-AC05-00OR22725 with UT/Battelle LLC. Use of the Advanced Photon Source was supported by the U. S. Department of Energy, Office of Science, Office of Basic Energy Sciences, under Contract No. W-31-109-Eng-38.

**10:00**

**U23 11 Neutron scattering studies on Kagome bilayers − Spin fluctuations in a broad dynamic range** H. MUTKA, *Institut Laue Langevin, Grenoble, France* C. PAYEN, *Institut des Materiaux Jean Rouxel, Nantes, France* G. EHLERS, J.R. STEWART, *Institut Laue Langevin, Grenoble, France* A. MELLERGARD, *Studsvik Neutron Research Laboratory, Nyköping, Sweden* The kagome bilayer compounds Ba2Sn2ZnCr7xGa10-7xO22 and SrCr9xGa12-9xO19 are localized spin (S=3/2) systems with strong antiferromagnetic exchange (J/k $\approx$ 50 K) that show no long-range order down to mK temperatures. This remarkable behaviour originates from the geometrical frustration. We have examined these systems using polarized neutron diffraction, inelastic neutron scattering (INS) and neutron spin-echo (NSE) spectroscopy for characterizing the magnetic correlations in a very broad energy range. INS data reveals the dynamic nature of the broad diffuse scattering that characterises the quasi-elastic magnetic response above the spin freezing. New aspects on the freezing phenomenon and the ground state properties are revealed using NSE.

**10:12**

**U23 12 Hall constant on triangular lattice ladder systems** JAN HAERTER, MICHAEL PETERSON, SRIRAM SHASTRY, *University of California at Santa Cruz* To make the transition from a one-dimensional to a planar system one can connect $n$ 1D-chains to yield $n$-leg ladders. For square lattices, this approach has already led to quite interesting and unexpected results (Dagotto et al, Prelovšek et al). In this work, frustration is introduced through triangular geometry, achieved by adding additional bonds to the square lattice ladders. We study the response of such $t$-$J$ ladders to an applied magnetic field and investigate the Hall constant $R_H$ as function of temperature, interaction strength, doping, and frequency. These systems complement toroidal or spherical systems since these allow the limit $\partial/\partial B$ to be taken more accurately which leaves the geometric frustration fully preserved. We investigate the crossover from a degenerate Fermi system to a high T regime where $R_H$ grows indefinitely ($R_H \propto T$) with temperature.

**10:24**

**U23 13 Position-Space Renormalization-Group Treatment of the Triangular Ising Antiferromagnet with Quenched Disorder** MICHAEL E. MIHALCO, SUSAN R. McKAY, *University of Maine* We apply the Niemeijer-van Leeuwen cluster approximation [1] to frustrated Ising models on a triangular lattice. The homogeneous Ising antiferromagnet is fully frustrated and shows no ordered phase. Frustration can be relieved via the addition of

quenched randomness through either dilution or the introduction of ferromagnetic bonds. The result is a rich phase diagram with different types of ordering depending upon the details of the quenched disorder [2]. Using a binning procedure to retain the full distribution of interactions under rescaling [3], we are able to calculate the phase diagram of this system, with each phase having its own characteristic attractor. This model system provides a two-dimensional example of the impacts of tunable frustration on short- and long-range order. 1. T. Niemeijer and J.M.J. van Leeuwen, Phys. Rev. Lett. **31**, 1411 (1973); Physica (Utr.) **71**, 17 (1974). 2. G. S. Grest and E.G. Gabl, Phys. Rev. Lett. **43**, 1183 (1979); H. Kaya and A.N. Berker, Phys. Rev. E **62**, 1469 (2000); M. Robinson, M.S. Thesis, University of Maine (2003). 3. E. Hartford and S. McKay, J. Appl. Phys. **70**, 6068 (1991); E. Hartford, Ph.D. Thesis, University of Maine (1994); A. Falicov, A.N. Berker, and S.R. McKay, Phys. Rev. B **51**, 8266 (1995).

**SESSION U24: LIQUID-CRYSTALLINE POLYMERS**
**Thursday Morning, 16 March 2006**
**321, Baltimore Convention Center at 8:00**
**Matteo Pasquali, Rice University, presiding**

**8:00**
**U24 1 Patterns and Defects in Nematic Elastomers*** FANGFU YE, *University of Pennsylvania* TOM LUBENSKY, *University of Pennsylvania* Nematic elastomers are materials that combine the orientational properties of nematic liquid crystals with the elastic properties of rubber. Ideal nematic elastomers, formed via a spontaneous symmetry breaking transition from the isotropic rubber state, exhibit soft elasticity in which one of the five elastic moduli of a uniaxial elastic medium vanishes. Monodomain samples crosslinked under imposed strain exhibit semi-soft elasticity in which that elastic modulus is small but nonzero. Applying linear stability analysis to the semi-soft elastic energy, we investigate two phenomena observed in experiments on nematic elastomers: (1) the formation, in experiments by Bob Meyer at Brandeis, of periodic modulations of the nematic director and elastic displacement (stripes) in cells subjected to a normal electric field in which the direction of stripe normals is at an oblique angle to the original nematic director and (2) the formation of +1 disclination defects at the surface of nanotube gel films [Islam, M. F., Nobili, M., Ye, Fangfu, Lubensky, T. C. and Yodh, A. G., Phys. Rev. Lett. **95**, 148301/1-4 (2005)].

*Supported in part by NSF DMR under Grant No. 04-04670

**8:12**
**U24 2 In situ synchrotron studies of structure development during injection molding of liquid crystalline polymers** STANLEY RENDON, WESLEY BURGHARDT, *Northwestern University* As in all polymer materials, the effect of polymer processing on the underlying molecular structure has a profound effect on the properties of liquid crystalline polymer products. While in situ scattering techniques have proven powerful for studying complex polymer structure during comparatively simple shearing or channel flows, their application to processing flows has largely been limited to in situ x-ray scattering/diffraction studies of structure development during fiber spinning. Here we report a new experiment in which a lab-scale injection molding machine has been modified to allow real-time, in situ measurements of molecular orientation development and subsequent crystallization during injection molding. The experiment requires high x-ray energy to reduce absorption in the aluminum mold wall, and high flux and a fast area detectors to achieve the necessary resolution to track time-dependent changes in fluid structure during mold filling. Hence it is ideally suited to the capabilites of the Advanced Photon Source. We report measurements injection molding of a commercial liquid crystalline copolyester (Vectra A) as a function of position in the mold and various process variables.

**8:24**
**U24 3 Liquid crystalline pattern formation in drying droplets of biopolymers*** IVAN SMALYUKH, *University of Illinois at Urbana-Champaign and Kent State University* OLENA ZRIBI, *University of Illinois at Urbana-Champaign* JOHN BUTLER, *University of Illinois at Urbana-Champaign* OLEG LAVRENTOVICH, *Kent State University* GERARD WONG, *University of Illinois at Urbana-Champaign* When a droplet of DNA in water dries out, a ring-like deposit is observed along the perimeter, similar to the stains in spilled drops of coffee. However, the dried ring of DNA is a self-similar birefringent pattern composed of extended molecules. We examine dynamics of the pattern formation at the droplet's rim. This gives us an insight into the underlining physics. During the major part of drying process the contact line is pinned so that DNA molecules are brought to the perimeter and extended by the radial capillary flow. Lyotropic nematic phase is formed in which highly concentrated DNA aligns along the triple line to minimize elastic energy. When the contact angle becomes small, the contact line starts to retract and the radial dilative stress causes buckling distortions at the rim which then propagate deep into the elastic liquid-crystalline medium and give rise to the pattern.

*We acknowledge support of the Institute for Complex and Adaptive Matter

**8:36**
**U24 4 Orientational dynamics of dipolar or magnetized rigid nematic liquid crystal polymers and suspensions in imposed flow and external fields** QI WANG, In this talk, I will present a scheme for computing the exact solution of the Smoluchowski equation under imposed flow and electric or magnetic external fields for rigid nematic liquid crystal polymers. This includes a suite of mathematical theorems that reveal the intrinsic relationship among the lower order moments of the pdf and the flow as well as the external field. Then, a simple mathematical transformation links the problem to some target model problems for which the solutions can be readily obtained using the existing numerical tools. The orientational dynamics is then studied from the exact solutions of the Smoluchowski equation.

**8:48**
**U24 5 Spacer length controlled lamello-columnar to oblique-columnar mesophase transition in liquid crystalline DNA - discotic cationic lipid complexes** LEI ZHU, LI CUI, JIANJUN MIAO, *Polymer Program, Institute of Material Science and Department of Chemical Engineering, University of Connecticut, Storrs, Connecticut 06269-3136* A series of asymmetric triphenylene imidazolium salts with different spacer lengths (C5, C8, and C11) were synthesized and their ionic complexes with double-strand DNA were prepared in aqueous solution. The molecular composition of the complexes was determined by FTIR analysis. The liquid crystalline morphology was characterized by polarized

light microscopy, X-ray diffraction (XRD), and transmission electron microscope. 2D XRD results indicated an oblique columnar phase for the complex with a short spacer length of C5, while lamello-columnar phases for those with longer spacer lengths (C8 and C11). Thin film circular dichroism results showed the disappearing of any helical conformation in the DNA in all the complexes. Instead, the complexation between single-strand RNA and discotic cationic lipids did not show columnar morphology; therefore, the columnar liquid crystalline morphology in the DNA-discotic cationic lipid complexes was attributed to the DNA double-strand chain rigidity.

**9:00**

**U24 6 Binary phase diagrams of liquid crystal/polymer systems exhibiting crystal, smectic, and nematic transitions*** P. DAYAL, R. MATKAR, *University of Akron* V. GINZBURG, *Dow Chemicals* T. KYU, *University of Akron* Current theories describing the phase diagrams of nematic-nematic mixtures and polymer-nematic liquid crystal mixtures are based on the combination of classical Flory-Huggins (FH) theory of isotropic mixing and the Maier-Saupe (MS) free energy of nematic ordering. This combined FH-MS theory was extended by Kyu and Chiu to polymer-smectic-A systems by incorporating McMillan free energy of the nematic-smectic-A transition. We have developed a generalized model for an LC system undergoing crystallization, extending the Maier-Saupe-McMillan theory in conjunction with the Landau-Brazowiskii model of weak first order phase transition such as solidification. The generalized FH-extended MSM free energy is then minimized with respect to all order parameters and the phase diagram is constructed by balancing the chemical potentials of corresponding phases. This form of the free energy could be valuable in the time evolution studies of phase transitions in polymer/liquid crystal mixtures.

*Supported by NSF-DMR 05-14942

**9:12**

**U24 7 Interfacial Characteristics of Semi Fluorinated Polymeric and Polymeric Liquid Crystalline Surfaces** GANG CHENG, BRYAN SPRAUL, DENNIS SMITH, DVORA PERAHIA, *Clemson University* The interfacial interactions of semi fluorinated perfluorocyclobutane (PFCB) liquid crystalline, and semi crystalline polymers have been investigated. The interfacial characteristics are critical in any of their applications in which a well define stable interface is required from LCD technology to waveguides and lithography. The inherent segregation between fluorine rich and hydrogen rich segments results in induced liquid crystallinity within the polymers themselves, even though these groups are small. The segregation to the interfaces controls the capability of the surface energy of the system. In addition of interfacial tension measurements, we used their alignment of small LC molecules using of 4, 4'-octylcycanobiphenyl (8CB) as a model system to further explore their interfacial characteristics. The correlation between surface energies, dynamics of the interface and their effects of the orientation of small LC will be discussed.

**9:24**

**U24 8 The Origin of Supra-Molecular Columnar Structures from Symmetrically Tapered Bisamides** KWANG-UN JEONG, HONG SHEN, MATTEW J. GRAHAM, HUABING WANG, MINGMING GUO, FRANK W. HARRIS, STEPHEN Z. D. CHENG, MAURICE MORTON INSTITUTE AND DEPARTMENT OF POLYMER SCIENCE, THE UNIVERSITY OF AKRON TEAM, A series of symmetrically tapered 1,4-bis[3,4,5-tris(alkan-1-yloxy)benzamido] benzene bisamides (CnPhBA) were synthesized to study the effect of alkyl chain length on supramolecular structures. Phase transitions were studied with DSC, PLM, WAXD, IR, SAED, solid-state $^{13}C$ NMR and computer simulations. All of the CnPhBAs formed a highly-ordered oblique columnar ($\Phi_{OK}$) phase and a low-ordered oblique columnar ($\Phi_{OB}$) phase. The two main driving forces to form these supramolecular structures were identified: One is the *H*-bond between N-H and C=O groups, and the other is the micro-phase separation of the bisamide cores and the alkyl chains. With increasing alkyl length, the isotropization temperature decreased, while the alkyl chain disordering temperature increased. The 2D lattice structures perpendicular to the columnar axis also increasingly deviated from the pseudo-hexagonal packing with increasing alkyl length. However, the alkyl length did not have a significant influence on the packing along the columnar axis.

**9:36**

**U24 9 Crystallization, the gel point and DQ NMR in PDMS networks** MOSHE GOTTLIEB, YOAV HAYOUN, INBAL PREKER, RACHEL YERUSHALMI-ROZEN, *Chemical Engineering Department and Stadler Minerva Center for Mesoscopic Macromolecular Engineering, Ben-Gurion University, Beer Sheva, 84105 ISRAEL* KAY SAALWAECHTER, *Institut fur Makromolekulare Chemie, Universitaet Freiburg, 79104 Freiburg, GERMANY* In the framework of classical models, the presence of constraints that reduce the mobility of the chains should lead to a reduction in the crystallization rate of polymer melts and result in a lower degree of crystallinity at a given cooling rate. An increasing number of experimental observations which seem to contradict the basic premises of the classical picture have been reported in the last couple of years. In particular, recent experiments findings suggest that in some cases crystallization from a crosslinked melt is more efficient than that from the non crosslinked analogue. In this work we report on a detailed study carried out in order to examine the relation between crystallization and the crosslinked network parameters. The effect of precursor molecular weight, crosslinker functionality and degree of crosslinking were examined. The thermal characteristics of the system were obtained by DSC. These were complemented by DQ NMR (dynamic order parameter) and rheological measurements. The use of DQ NMR as means to determine the gel point is also discussed.

**9:48**

**U24 10 Phase Separation of Model Segmented Poly(Carbonate Urethanes)** REBECA HERNANDEZ, ELENA HUNG, JAMES RUNT, *Department of Materials Science and Engineering, Penn State University* The present paper focuses on the phase separated morphology and segment demixing of model poly(carbonate urethanes) [PCU] with hard segment contents ranging from 30 – 65% and soft segments composed of 1,6 poly(hexamethylene carbonate) [MW = 1K]. Hard segments were formed from 4,4'-methylenediphenyl diisocyanate and 1,4 butanediol. This family of materials represents a recent approach in the development of polyurethanes with improved long-term biostability, and is under clinical investigation in a number of biomedical devices. Only a single glass transition temperature was observed for each copolymer, increasing in temperature with increasing hard segment content. However, loss spectra from dynamic mechanical analysis showed clear evidence of two mixed phases. The results of small-angle X-ray scattering and tapping mode AFM experiments were

consistent with these observations and will be discussed. Finally, these results will be compared with initial findings on phase separation in another family of polyurethane copolymers of current interest as blood-contact materials in biomedical devices having mixed poly(dimethylsiloxane) – poly(hexamethyleneoxide) soft segments.

**10:00**
**U24 11 How Does Rubber Crystallizes Upon Application of Strain*** MINDAUGAS RACKAITIS, XIAORONG WANG, *Bridgestone CRT* Strain induced crystallization of natural and synthetic rubbers is one of the most interesting phenomena in the field of rubber science and technology. Most of the research in the field was done using X-ray diffraction techniques. However up to this day there are no reports of direct observation of strain induced crystallization of rubber. This presentation reports first atomic force micrographs of high cis polybutadiene rubber surface at various strains. The crystallization of the rubber was confirmed by X-ray diffraction and crystallite orientation is discussed.

*We are thankful to Dr. Jan Genzer and his collegues for NEXAFS and IR experiments

**10:12**
**U24 12 Melt-processable high acrylonitrile copolymers** SHAWN R. HUTCHINSON, *Institute of Textile Technology* JUAN HINESTROZA, *Cornell University* BHUPENDER S. GUPTA, DAVID R. BUCHANAN, ALAN E. TONELLI, *North Carolina State University* High acrylonitrile homo- and copolymers (PAN) are unique because of chemical, ultraviolet, and corrosion resistances. Historically, because of the atypical processing and thermal behavior of solution-processable PAN, consensus regarding the actual microstructure and paracrystalline order was elusive – it has been described as 'two-dimensional liquid crystalline-like structure with many defects.' New, sequence-structured copolymers rendered PAN for the first time melt-processable before degradation and are providing new insight into the solid state conformation. Solution $^{13}C$ nuclear magnetic resonance was used to compare the new and historical comonomer sequence lengths. Optimal processing conditions were obtained using capillary rheometry as a function of dwell time and melt temperature. A filament extrusion investigation was conducted and wide angle x-ray diffraction, differential scanning calorimetry thermograms and mechanical properties of the filaments were used to characterize the nonequilibrium melt transitions and paracrystal morphology as a function of processing parameters.

**SESSION U25: FOCUS SESSION: OLIGOACENE SEMICONDUCTORS**
**Thursday Morning, 16 March 2006**
**322, Baltimore Convention Center at 8:00**
**John Rogers, University of Illinois, presiding**

**8:00**
**U25 1 Preparation and properties of substituted acenes for organic electronics: pentacene through heptacene** JOHN ANTHONY, *Univ. of Kentucky, Dept. of Chemistry* Acenes (such as pentacene and tetracene) and functionalized acenes (such as rubrene) have demonstrated remarkable electronic properties in thin film devices and in single crystals. Our research effort is directed toward the synthesis of new classes of acene-based compounds that are stable, soluble, and that can be used to probe the relationships between solid-state order and electronic properties. Careful consideration of the relationship between molecular substituent and crystal packing has led to the development of new, soluble materials with thin-film properties comparable to their unfunctionalized counterparts. Functionalization of the central ring of pentacene can lead to a change in solid-state order from the classic herringbone arrangement to the less-common face-to-face interactions, while functionalization of the outermost rings of pentacene leads to subtle variations in the herringbone arrangement. Similar approaches can be taken with heteroacenes, again leading to solid-state interactions that favor strong interactions between the aromatic pi-clouds. Furthermore, the added stability gained through functionalization has allowed for the first time the preparation and study of derivatives of higher acenes such as hexacene and heptacene. The detailed study of the optical and electronic properties of a variety of functionalized acenes has led to the development of new materials for use in photovolatics, light-emitting diodes and thin-film transistors. We are grateful to the Office of Naval Research for support of this research.

**8:12**
**U25 2 Conducting AFM and 2D GIXD Studies on Pentacene Thin Films** HOICHANG YANG, CHANG Y. RYU, *Rensselaer Polytechnic Institute* TAE JOO SHIN, *Brookhaven National Laboratory* KILWON CHO, *POSTECH, Korea* MANG-MANG LING, ZHENAN BAO, *Stanford University* 2D GIXD, TM-, and C-AFM analyses of pentacene films support the idea that the morphology of ultrathin layers plays a crucial role in determining mobility in OTFT. While 60-nm-thick pentacene films exhibited similar terrace-like multilayer structure with the long axis of pentacene perpendicularly oriented as determined from TM-AFM and 2D GIXD, its charge mobility in an OTFT was quite different, depending on the types of hydrophobic SAM surface treatment. This difference is related to the morphological difference of the first pentacene layer ''buried'' under the terrace-like multilayers. We found that the faceted islands on HMDS showed larger current flow than the dendritic islands on OTS using C- AFM. This trend in C-AFM current images correlated well with the charge carrier mobility measured in OTFTs. Such faceted morphology represents single crystal-like pentacene islands, which have fewer internal crystal defects and higher current flow than the dendritic islands.

**8:24**
**U25 3 Hall Effect Measurements in Organic Single-Crystal FETs** VITALY PODZOROV, *Rutgers University* ETIENNE MENARD, JOHN ROGERS, MICHAEL GERSHENSON, RUTGERS UNIVERSITY TEAM, UNIVERSITY OF ILLINOIS AT URBANA CHAMPAIGN TEAM, We have observed classical Hall effect in the single-crystal rubrene OFETs [1]. The mobility determined from the Hall measurements (mu_H) represents intrinsic, i.e. trap independent mobility of the charge carriers. At high temperatures, Hall mobility coincides with the longitudinal mobility determined from the standard FET measurements. In the investigated temperature range T = 170-300 K, mu_H monotonically increases with decreasing T, while the longitudinal mobility first increases at high T (intrinsic regime) and then decreases at low T (non-intrinsic regime), consistent with the previous observations [2, 3]. In the intrinsic regime, the density of mobile field-induced charge carriers extracted from the Hall measurements, n_H, coincides with the density n calculated using the gate-

channel capacitance, and becomes smaller than n in the trap-dominated regime. The Hall data strongly support a band-like nature of the charge carrier transport in this system. 1. Podzorov, et al., Phys. Rev. Lett. 95, 226601 (2005); 2. V. C. Sundar, et al., Science 303, 1644 (2004); 3. V. Podzorov, et al., Phys. Rev. Lett. 93, 086602 (2004);

**8:36**

**U25 4 Hall effect in organic single-crystal field-effect transistors** J. TAKEYA, KOICHI YAMADA, *CRIEPI* K. TSUKAGOSHI, Y. AOYAGI, *RIKEN* T. TAKENOBU, Y. IWASA, *IMR, Tohoku University* Hall effect is detected in organic field-effect transistors at room temperature, using appropriately shaped rubrene ($C_{42}H_{28}$) single crystals. It turned out that inverse Hall coefficient, having a positive sign, is close to the amount of electric-field induced charge upon the hole accumulation. The observation of the normal Hall effect means that the accumulated surface charge is well extended in space over molecules, so that the external magnetic field can provide a transverse electromotive force. The result is consistent with band-like transport of the surface carriers rather than consecutive hopping processes occurring in response to the source-drain voltage in the organic transistors.

**8:48**

**U25 5 Control of Channel Conductivity of Rubrene Single Crystal Field Effect Transistors.** CHRISTIAN KLOC, MAGNUS WIKBERG, WOO-YOUNG SO, DAVE V. LANG, THEO SIEGRIST, ARTHUR P. RAMIREZ, *Bell Laboratories, Lucent Technologies* Carrier mobility higher than 1 $cm^2$/Vs has been measured in numerous organic single crystal FETs, making them interesting for microelectronic applications. The understanding why some organic pi-electron systems show high mobility and others, very similar molecules, show much lower mobility is crucial for design of efficient and robust organic semiconductor devices. It seems that transistor properties measured on FETs are extrinsic properties limited by technology used for transistor fabrication. However, to evaluate the applicability of organic semiconductors, intrinsic properties need to be assessed. We have carried out a program to purify and grow low defect density single crystals and fabricate FETs on their surfaces. Using graphite as electrodes and parylene as an insulator we measured maximal mobility in rubrene of 13 $cm^2$/Vs and significant anisotropy of transport properties. To control the transistor properties, we chemically modify the channel area and measured the conductivity of transistor channels before covering it with dielectrics and gate electrode. We found that the channel area of rubrene is very sensitive on reduction and oxidation and that the transistor properties may be modified by performing chemical reactions on the crystal surfaces before finishing transistor structure.

**9:00**

**U25 6 Thermal Expansion and Molecular Motion in Rubrene and Tetracene*** THEO SIEGRIST, CHRISTIAN KLOC, MAGNUS WIKBERG, *Bell Laboratories* SIMON HAAS, *ETH Zuerich* The closely related molecules rubrene (tetra-phenyl-tetracene) and tetracene are model systems for organic semiconductor materials. Very high carrier mobilities have been observed in rubrene crystals. Single crystals of rubrene and tetracene, produced by vapor phase growth at elevated temperatures, show clear differences in their quality. The thermal expansion/contraction coefficients for crystals of the two molecules have been measured using X-ray diffraction. The triclinic symmetry of tetracene crystals is reflected in the strongly anisotropic thermal expansion observed. In the case of rubrene, relatively small thermal expansion coefficients are found. Libration/translation values obtained using the rigid molecule model will be presented for both systems.

*supported in part by the U. S. Department of Energy's Nanoscale Science, Engineering, and Technology (NSET) program under Contract No. 04SCPE389

**9:12**

**U25 7 A Systematic Study of Metal Contacts on Single Crystalline Rubrene*** WOO-YOUNG SO, *Columbia University* A. MIKE SERGENT, *Bell Labs* CHRISTIAN KLOC, *Bell Labs* ARTHUR RAMIREZ, *Bell Labs, Columbia University* The performance of semiconductor devices is critically dependent on the metal- semiconductor heterojunction. In organics, despite the technological importance of such interfaces, little is known about the fundamental mechanisms that govern their performance in real devices. We have studied a series of metal contacts on rubrene single crystals and find systematic dependence of the transport barrier on the metal workfunction. These data provide insight into surface states that strongly influence the contact resistance. In the process of the study of metal-rubrene heterojunctions, we have realized an efficient single-crystal rubrene diode employing a hole-blocking metal contact.

*Supported in part by DOE under grant 04SCPE389.

**9:24**

**U25 8 Negative Thermal Expansion in Pentacene** S. HAAS, *ETH Zurich* T. SIEGRIST, *Bell Labs, Murray Hill, NJ* P. PATTISON, *EPF Lausanne, Switzerland* B. BATLOGG, *ETH Zurich, Switzerland* The molecules in organic semiconductors, such as the oligoacenes, are held together by weak van-der-Waals (v-d-W) forces. As a result, one observes low dissociation temperatures, and large thermal expansion coefficients. Surprisingly, we have found a negative expansion coefficient in particular crystal directions. We have performed a complete X-ray structure analysis of pentacene and tetracene single crystals in a temperature range from 100–380 K. The anisotropic thermal parameters are analyzed in terms of librations and translations of the rigid molecules. Interestingly, we find upon increasing temperature a near-zero thermal expansion along *a* in tetracene, and a distinct contraction in pentacene. Upon close inspection of the full expansivity tensor and the thermal parameters we find a consistent explanation assuming that the v-d-W forces tend to minimize the relative shift along the long axis of adjacent molecules. This is further supported by the observation of an unusually large thermal expansion perpendicular to the layers, and the indications in our data of a distinctly anharmonic potential for the sliding motion along the long axis. These v-d-W forces leading to negative thermal expansion are expected to be larger in longer molecules and also to be the driving force behind the well known polymorphism of pentacene.

**9:36**

**U25 9 Charge transport in single-crystals of pentacene studied with temperature dependent THz time-domain spectroscopy.** H.A. VAN LAARHOVEN, *Eindhoven, University of technology.* M. KOEBERG, E. HENDRY, M. BONN, *AMOLF, Amsterdam* C.F.J. FLIPSE, *Eindhoven, University of Technology* We study the charge dynamics and transport mechanisms in single crystals of pentacene by investigating the frequency dependent complex conductivity using THz time-domain spectroscopy. Such measurements on this material show generation of THz radiation from the

sample as well as ultra-fast charge decay. Our measurements have been corrected for these effects, giving us the ability to see the true frequency dependent behaviour of the conductivity. Two different pump energies were used (266 and 400 nm) in the experiments. In the low temperature regime the mobile charges give a different response when being photo-excited at different wavelength. This disparity in charge transfer will be discussed and compared to theoretical models.

**9:48**

**U25 10 Optical emission and vibrational modes of uniform pentacene monolayers*** RUI HE, *Columbia Univ* NANCY TASSI, GRACIELA BLANCHET, *Dupont, Central Research and Development* ARON PINCZUK, *Columbia Univ, Bell Labs* Pentacene monolayers are probed by photoluminescence and resonant Raman spectroscopies below 10K. Monolayers grown on polymeric substrate of poly-alpha-methyl-styrene (PAMS) exhibit high uniformity within micron size clusters. These films show sharp exciton luminescence bands, and the energy of the exciton optical emission displays a red-shift as the average film thickness increases. The large resonance enhancements of Raman scattering intensities enable the measurements of low-lying (40- 200cm-1) optical lattice vibrations from these monolayers. These experiments demonstrate that luminescence and resonant Raman scattering from single pentacene monolayers are venues for probing 2D properties, studies of interface effects, and thin film characterization. *Supported primarily by the Nanoscale Science and Engineering Initiative of the National Science Foundation under NSF Award No. CHE-0117752 and by the New York State Office of Science, Technology, and Academic Research (NYSTAR), and by a research grant of the W. M. Keck Foundation.

**10:00**

**U25 11 Sensitivity of 1/f Noise to Chemical Constituents in Pentacene Thin Film Transistors*** W. X. YAN, *Thomas Jefferson High School for Science and Technology, Alexandria, VA 22312* E. GOMAR-NADAL, MASA ISHIGAMI, M. S. FUHRER, E. D. WILLIAMS, *Department of Physics, University of Maryland, College Park, MD 20742* This study systematically investigates the sensitivity threshold of 1/f noise for use as a device diagnostic tool, with pentacene thin-film transistors (TFTs) as a model. When pentacene in TFTs was mixed with an incremental series of the oxidative impurity 6,13-pentacenequinone (PQ), 1/f noise power rose proportionate to increasing impurities with a preliminary sensitivity threshold of $\geqslant$ 0.6 % PQ, coupled with a decreasing hole mobility. The result and further theoretical interpretation can supplement current quality assessments and help better understand the innate deficiencies in organic electronics, thus potentially improving their quality.

*Materials Research Science and Engineering Center, University of Maryland, College Park

**10:12**

**U25 12 Interface and Contact Formation in Pentacene Monolayer Transistors** BYOUNG-NAM PARK, SOONJOO SEO, FAN ZHENG, FRANZ HIMPSEL, PAUL EVANS, *University of Wisconsin-Madison* Understanding charge transport in the accumulation layer of organic field effect transistors is crucial to improving their performance. Our in-situ electrical measurements during the deposition of pentacene onto a bottom-contact transistor structure with a silicon dioxide gate dielectric allowed us to study the formation of a transistor channel at the single-molecular-layer scale. At pentacene coverages near a percolation threshold the monolayer-high islands come into contact and current begins to flow through the channel. Using pauses in the deposition we have extracted transistor characteristic parameters with well-defined submonolayer island structures. Van der Pauw sheet resistance measurements show that the small field effect mobilities of monolayer transistors are associated with the formation of contacts rather than with the mobility of carriers within the semiconductor layer. Both near edge x-ray absorption fine structure measurements and atomic force microscopy show that the morphology and crystal structure of the pentacene layers changed as the total amount deposited onto the sample increased through the few-monolayer regime.

**10:24**

**U25 13 Growth and structure of pentacene thin films** BOQUAN LI, *Uniersity of Illinois at Urbana-Champaign, Department of Materials Science and Engineering* During the last few years, there has been an explosion of interests in exploring organic thin-films of small conjugated molecules, like pentacene ($C_{22}H_{14}$), as active semiconductor devices. The full potential of organic thin-film semiconductor devices for applications will not be realized until the growth of highly ordered organic thin films can be optimized and well controlled. Thin films of pentacene are known to crystallize in different polymorphs, which have layered structures characterized by their different interlayer spacings, d(001). How to grow highly ordered single phase molecular thin films remains a challenging subject. Motivated by this, we have investigated the growth of pentacene thin films on hydrogen-terminated Si (111) and clean Si (111) surfaces in an effort to gain a comprehensive understanding of the molecule-substrate interactions and explore strategies to suppress the formation of polymorphism and therefore to grow highly ordered pentacene thin films. Electron diffraction is used to investigate the in-plane molecular structure. The crystallographic results are correlated with growth. The detailed structural analysis results will be presented.

**10:36**

**U25 14 Electron and hole transport in organic single crystals*** J. PFLAUM, A.K. TRIPATHI, S. MEYER, *Dept. of Physics, University of Stuttgart, 70550 Stuttgart, Germany* Transport measurements reported in literature often classify the semiconducting behavior in organic thin films and single crystals to be whether p-type or n-type. Moreover, the majority of polyaromatic hydrocarbons such as pentacene in combination with technically relevant contact materials such as Au are found to preferentially show hole conductivity. In this presentation, we will discuss these key aspects of the charge carrier transport in case of highly-ordered organic crystals, the latter grown by diferent methods from previously purified material. By time-of-flight spectroscopy it will be demonstrated for various compounds that the chemical purity rather than the growth conditions determine the resulting semiconducting behavior. E.g. anthracene single crystals grown by sublimation provide as good electron as hole mobilities of about 1 $cm^2$/Vs if the material is purified by zone- refinement. For crystals made of sublimation purified anthracene, no electron transport could be detected. Finally, comparing various structural motifs we will discuss possible concepts of molecular design enabling stability against photo- oxidation and allowing for the formation of highly-ordered thin films.

*Financial support by DFG (project PF385/2-3).

**10:48**

**U25 15 Oxygen and water defect formation processes in pentacene.** LEONIDAS TSETSERIS, SOKRATES PANTELIDES, *Department of Physics and Astronomy, Vanderbilt University* Organic thin-film devices have emerged as promising candidates for novel electronic applications. Unlike traditional solid-state devices, the weak intermolecular non-covalent bonding of organic thin films leads to flexibility and possible pattern formation. The same mechanism, however, is responsible for the appearance of a variety of defects that may interfere with film growth and are potentially detrimental to the desired transport properties. Here we use first-principles calculations to study defect formation processes in the prototypical system of pentacene. In particular, we report on defect configurations of oxygen and water molecules in bulk pentacene and ultra-thin films on Si-based substrates. The results show that several stable configurations of such defects exist. Their presence has a direct bearing on growth processes and transport properties through strong covalent bonding and induced molecular distortions in their vicinity. This work was supported in part by DOE Grant DEFG0203ER46096.

**SESSION U26: FOCUS SESSION: CYTOSKELETAL DYNAMICS**
**Thursday Morning, 16 March 2006**
**323, Baltimore Convention Center at 8:00**
**Christina Marchetti, Syracuse University, presiding**

***Contributed Papers***

**8:00**

**U26 1 Isotropic, nematic and polarized states in active motor-filament solutions*** APHRODITE AHMADI, M. CRISTINA MARCHETTI, *Physics Department, Syracuse University, Syracuse, NY 13244* TANNIEMOLA B. LIVERPOOL, *Department of Applied Mathematics, University of Leeds, Leeds LS2 9JT, UK* We characterize the phase diagram of interacting polar biofilaments and motor proteins in terms of experimentally accessible parameters. The active filament solution is described by a set of hydrodynamic equations. These in turn are obtained by coarse-graining the Smoluchowski equation for rods coupled by active crosslinkers that mediate the exchange of forces among the filaments. We find that motor activity and the polarity of motor clusters play a key role in the formation of homogeneous isotropic, nematic and polarized states. We also investigate the stability of such homogeneous states against spatially varying fluctuations in the hydrodynamic fields. Motor-induced bundling can destabilize each homogeneous state at high filament and motor density, albeit via different mechanisms (diffusive versus oscillatory). Our analysis suggests that spatially inhomogeneous oscillatory structures, such as vortices, can be formed in the polarized state.

*This work was supported by the National Science Foundation through grants No. DMR-0219292 and DMR-0305407.

**8:12**

**U26 2 Rheology of active polymer solutions** M. CRISTINA MARCHETTI, *Syracuse University* TANNIEMOLA B. LIVERPOOL, *Leeds University, UK* In vitro solutions of biopolymers and associated motor proteins have been used to probe cytoskeletal dynamics under controlled conditions. Experiments have shown that motor-induced filament sliding competes with the slow Brownian polymer dynamics, driving the organization of the polymer network into complex patterns and altering its rheological and mechanical properties. Starting from a semi-microscopic model of the motor-mediated interaction among filaments, we have obtained continuum equations for the coarse-grained fields (filament and motor densities, polarization, alignment tensor) describing the response of the active solution to an externally imposed flow. After deriving an expression for the active contribution to the stress tensor, we have evaluated the linear viscoelastic response of a dilute solution to a shear stress. In the isotropic state motor activity strongly enhances the viscoelasticity of the system, especially near the transition to an orientationally ordered state. Activity also increases the high-frequency shear modulus of the solution. – MCM was support by the National Science Foundation, grants DMR-0305407 and DMR-0219292. TBL acknowledges the support of the Royal Society.

**8:24**

**U26 3 Thermally Controlling the Polymeric Cytoskeleton in Living Cells** CHAO-MIN CHENG, PHILIP LEDUC, *Department of Mechanical Engineering, Carnegie Mellon University* Cell structure is controlled to a large degree by the cytoskeleton, which is an intracellular polymer network. This cytoskeleton is critical as it strongly influences many cellular functions such as motility, organelle transport, mechanotransduction and mitosis. In our studies, we controlled the thermal environment of living cells and after applying an increase in temperature of only 5 $^{o}$C, we observed a change in the polymer network as the actin filaments depolymerized. Interestingly, when we then lowered the temperature, the actin repolymerized indicating a reversible phase that is controlled by the thermal environment. We characterized the presence of F-actin and G-actin for these phases through analyzing the intensity from immunofluorescent studies for these proteins. The F-actin concentration decreased when increasing the temperature from the initial state and then increased when decreasing the temperature. Although the cell is known to be affected by heat shock responses, this is not a function of just the polymers as they do not exhibit these polymerization characteristics when we probed them as single filaments in vitro. These studies suggest that the cell has distinct phases or patterns while maintaining a reversible equilibrium due to the thermal environment for these networked polymers.

**8:36**

**U26 4 How to detect single cancer cell?** NADINE PERNODET, *SUNY* JESSICA FIELDS, *Princeton* LENNY SLUTSKY, *Duke* TAYLOR BERNHEIM, KAUSTABH GHOSH, SHOUREN GE, MIRIAM RAFAILOVICH, *SUNY* Cell mechanics is now considered as a critical parameter closely related to cell functions. Moreover, we know that cytoplasm of cancer cells compared to normal cells is disorganized; therefore this should be directly translated to their mechanical properties. Here we show that we are able to distinguish cancer cells from normal cells in a cell mixture through their mechanical properties. Advantage of our method is that we measure single cell mechanical response where any cells, cancer or normal, are attached on a surface in situ. When imaged in the

mixture of cells, through usual microscopic imaging, cancer and normal cells did not show obvious differences and could not be identified with certitude unless using specific biochemical markers. In a mixture of cancer and normal cells, mechanical measurements were done randomly on six different cells. The relative modulus gave a bimodal distribution. These moduli were compared to the known modulus obtained from normal or cancer cell and assigned to each group of cells very precisely. This method, which is directly related to the intrinsic cytoskeleton cell mechanical properties, is a sensitive and reliable tool to detect cancer cells from a culture or a tissue at a single cell level.

**8:48**
**U26 5 The Effects of Chronological Age on the Cellular Mechanics of Human Dermal Fibroblasts** Z. PAN, V. HUNG, S. KAMBHAMPATI, S.R. GE, M. RAFAILOVICH, *Mat Sci & Eng Dept,SUNY Stony Brook* K. GHOSH, R. CLARK, *BME Dept, SUNY Stony Brook* Y.J. LIU, T. NAKAMURA, *Mech Eng Dept, SUNY Stony Brook* X.Z. SHU, G. PRESTWICH, *Med Chem Dept, Univ. Utah* It is often observed that older people display diminished wound healing abilities. Understanding of this phenomenon is important for many in vivo applications of tissue engineering. In this study, the cell mechanics of dermal fibroblasts from 25, 40 and 84 years old female subjects were compared. These cells were cultured on functionalized hyaluronic acid hydrogel substrates which emulated physiological conditions in dermal tissue. The deformation of the substrate caused by cellular traction forces was detected by tracing the displacement of fluorescent beads embedded in the substrate using Digital Image Speckle Correlation. Then cellular traction forces were quantitatively determined by Finite Element Method in a linear elastic model with a high spatial resolution. These results were correlated with auxiliary measurements of substrate modulus, cell modulus and migration. We found that with increasing age, the magnitude of the cellular traction forces diminished. Similarly, the ability of the cells to adapt to changes in the mechanical properties of their environment and migrate was also impaired. The interrelationship between these factors and wound healing will be discussed. This work is supported by NSF-MRSEC program.

**9:00**
**U26 6 Interplay between crosslinkers and dynamic molecular motor-induced instabilities in the moderation of biopolymer organization** DAVID SMITH, *University of Leipzig, Institute for Soft Matter Physics* DAVID HUMPHREY, *Center for Nonlinear Dynamics, University of Texas at Austin* FALKO ZIEBERT, WALTER ZIMMERMANN, *Physikalisches Institut, Universität Bayreuth* JOSEF KÄS, *University of Leipzig, Institute for Soft Matter Physics* Structure and function of biological cells rely on the highly-dynamic self-organization of protein filaments to an intracellular cytoskeleton responsive to mechanical and chemical stimuli. While dissolving these complex cellular structures through Brownian motion is inherently slow (tens of minutes), changes in the activity of the molecular motor myosin II cause rapid order-disorder transitions within 1-2 minutes in reconstituted cytoskeletal actin networks. When motor-induced filament sliding decreases, actin network structure rapidly and reversibly self-organizes into various assemblies triggered by a nonlinear instability. Modulation of static crosslinker concentrations allow for a wide phase space of order ranging from nematics to compact asters & dense packing of motor-filament clusters. The observed isothermal transitions between disorder and self-organization illustrate that molecular motors can substantially contribute to dynamic cellular organization.

***Invited Papers***

**9:12**
**U26 7 The mechanics of cell protrusion.***
GAUDENZ DANUSER, *The Scripps Research Institute*

The protrusion of the cell edge is the first step in a cycle of molecular processes that drive cell movements during development, immune responses, wound healing and many other physiological functions. It is also the earliest pathological event observed during metastasis of cancer. Textbook models associate protrusion with the assembly of an actin polymer network subadjacent to the cell plasma membrane. However, for this process to be transformed into edge advancement, polymerization-induced forces need to be balanced by adhesion complexes that link the actin network to the extracellular domain. Also, the effectiveness of network assembly in mediating forward movement of the cell edge depends on how contraction forces pull the network in the cell front retrogradly towards the cell center. Thus, what is observed in a microscope as cell protrusion reflects the kinematic output of at least three space- and time-modulated mechanisms of force generation. The coordination of these machineries is thought to be regulated by a complex network of mechano-chemical signals. Our goal is to establish the contributions of each those mechanisms and their control by reconstructing the spatiotemporal distribution of intracellular forces via inverse dynamics and molecular intervention with the relevant signalling pathways. To this end, we have developed quantitative Fluorescent Speckle Microscopy (qFSM) which provides high-resolution spatiotemporal measurements of actin network deformation and material properties in migrating cells. In addition, qFSM delivers maps of cytoskeleton assembly and disassembly, so that we can infer the plasticity of the material in situ. Together, this data allows us to deduce intracellular force distributions from the constitutive laws of strain and stress in the actin polymer network. Using this approach we discovered that unperturbed cells protrude in a dynamic steady state where periodic patterns of network assembly, adhesion formation, and cytoskeleton transport are tightly connected to protrusion waves. We exploited the sub-cellular heterogeneity of these patterns to identify the causality and timing between dynamic events in the actin network, leading towards a first integral view of the mechano-chemical process interaction in the protrusion machinery.

*NIH R01 GM67230, U54 RR22230.

*Contributed Papers*

**9:48**

**U26 8 Tensile Force Generation by Actin-Myosin Networks** ANDERS CARLSSON, *Washington University in St. Louis* Tensile force generation by the actin-myosin system is a crucial factor in many cellular processes, including the function of the contractile ring in cytokinesis. Calculations of such tensile forces have often been based on specific one-dimensional models of the structure based on parallel overlapping filaments, sometimes in sarcomere-like structures. However, the detailed arrangement of the actin filaments is not known in general, and it is likely to be disordered. For this reason we have developed a general theory of force generation by myosin in actin networks, based on treating the myosin motors as external forces in a viscoelastic medium. The analysis is based on two ingredients: the strain field of a force dipole in a homogeneous medium, and a correction for the inhomogeneity of the actin network. We obtain a simple expression for the tensile stress induced by the myosin motors in terms of the density of motors and the average actin filament length. This formula is used to relate the force that can be generated by a contractile ring to the actin network structure.

**10:00**

**U26 9 Simulation of Actin-Polymerization Near Moving Surface*** KUN-CHUN LEE, *University of Pennsylvania* ANDREA LIU, *University of Pennsylvania* An important component of the cellular cytoskeleton is F-actin, a biopolymer whose self-assembly is key to the process of cell crawling. The polymerization and branching of F-actin near the cell membrane is known to drive cell crawling, but the precise mechanism by which these processes lead to the generation of a mechanical force is still controversial. We have constructed a Brownian dynamics simulation of F-actin polymerizing near a surface, which includes all known important processes, including polymerization, depolymerization, branching, severing and capping. Using this model, we study the dynamics of the moving surface in conjunction with the morphology of the resulting actin network.

*This work is supported by NSF-CHE-0096492.

**10:12**

**U26 10 The Fysics of Filopodia (or The Physics of Philopodia)** JEN SCHWARZ, *Syracuse University* AJAY GOPINATHAN, *UCSB* KUN-CHUN LEE, *University of Pennsylvania* ANDREA LIU, *University of Pennsylvania* LOUISE YANG, *Cambridge University* Cell motility is driven by the dynamic reorganization of the cellular cytoskeleton which is composed of actin. Monomeric actin assembles into filaments that grow, shrink, branch and bundle. Branching generates new filaments that form a mesh-like structure that protrudes outward allowing the cell to move somewhere. But how does it know where to move? It has been proposed that filopodia serve as scouts for the cell. Filopodia are bundles of actin filaments that extend out ahead of the rest of the cell to probe its upcoming environment. Recent in vitro experiments [Vignjevic *et al.*, J. Cell Bio. **160**, 951 (2003)] determine the minimal ingredients required for such a process. We model these experiments analytically and via Monte Carlo simulations to estimate the typical bundle size and length. We also estimate the size of the mesh-like structure from which the filopodia emerge and explain the observed nonmonotonicity of this size as a function of capping protein concentration, which inhibits filament growth.

**10:24**

**U26 11 Lipid-Protein Nanotubes with Open or Closed Ends, Microtubules Bundles and Inverted Tubulin Nanotubes*** URI RAVIV, DANIEL J. NEEDLEMAN, MIGUEL A. OJEDA-LOPEZ, YOULI LI, HERB P. MILLER, LESLIE WILSON, CYRUS R. SAFINYA, *University of California, Santa Barbara* We describe synchrotron x-ray diffraction, electron microscopy, and optical imaging data of the self-assembly of microtubules (MTs) with various cationic agents. We established the conditions under which cationic liposomes can coat MTs and form lipid-protein nanotubes (LPNs). The LPNs exhibit a rather remarkable architecture with the cylindrical lipid bilayer sandwiched between a MT and outer tubulin oligomers forming rings or spirals. By controlling the cationic lipid/tubulin stoichiometry it is possible to switch between two states of nanotubes with either open ends or closed ends with lipid caps, a process which forms the basis for controlled chemical and drug encapsulation and release (Raviv et al, PNAS, 2005). Multivalent (3+,4+ and 5+) cations can form three dimensional MT bundles that in some cases become tubulin based inverted nanotubules. Divalent cations form two dimensional MT necklaces (Needleman et al, PNAS, 2004).

*This work was supported by the NIH GM-59288, the NSF DMR 0503347 and CTS 0404444. SSRL is supported by the U.S. DOE. U.R. received fellowships HFSP and EMBO.

**10:36**

**U26 12 The mechanics of cell crawling over a flat surface** BALDOMERO ALONSO-LATORRE, JAVIER RODRIGUEZ-RODRIGUEZ, ALBERTO ALISEDA, RUDOLF MEILI, RICHARD FIRTEL, JUAN LASHERAS, *UC San Diego* The chemotaxis of different strains of the amoeba itDictyostelium Dicoideum when exposed to a wide range of concentrations and gradients of chemoattractant has been studied experimentally. First, the time evolution of the velocity as well as the shape of the cell have been measured from microscopy images for a large number of individuals. Secondly, the force that the amoebas exert over the substrate in order to propel themselves has also been measured. Some insights into the physical mechanism by which cells crawl over the surface are obtained by comparing the time evolution of those magnitudes for the different strains under study.

**10:48**

**U26 13 Micromechanical Properties of Endothelial Cell Cytoskeleton** MERON MENGISTU, LINDA LOWE-KRENTZ, H. DANIEL OU-YANG, *Lehigh University* DEPARTMENT OF BIOLOGICAL SCIENCES, LEHIGH UNIVERSITY COLLABORATION, PHYSICS DEPARTMENT, LEHIGH UNIVERSITY COLLABORATION, Atherosclerotic plaques occur in regions of arterial curvature, where there is blood re-circulation and physiologically low shear stress conditions. This phenotype may be related to flow-induced shear stress on the monolayer of endothelial cells that make up the endothelium. When endothelial cells in static culture are exposed to laminar flow, they respond by rearranging their cytoskeleton, and aligning their actin filaments in the direction of flow. The changes in cytoskeletal structures induced by flow are different from region to region of the same cell. We employ the optical tweezers technique to obtain very local mechanical properties of endothelial cell cytoskeleton. We used endocytosed polystyrene beads, as well as intrinsic granular structures, as probes for our measurements. Endothelial cells were also

treated with Cytochalasin B and Nocadozole, which are drugs that de-polymerize actin filaments and microtubules respectively, to measure the visco-elastic moduli, and obtain the contribution of each cytoskeletal structure in the cells' micro-mechanical properties.

**SESSION U27: COMPUTATIONAL METHODS: MONTE CARLO/MOLECULAR DYNAMICS I**
**Thursday Morning, 16 March 2006**
**324, Baltimore Convention Center at 8:00**
**Andrew Williamsom, Lawrence Livermore National Laboratory, presiding**

**8:00**
**U27 1 Density-Matrix Based Fixed-Node and Fixed-Phase Approximation for Quantum Monte Carlo*** JOHN SHUMWAY, *Dept. of Physics and Astronomy, Arizona State University* We have generalized the fixed-node and fixed-phase approximations to use density matrices. For a given trial density matrix, we generate a quantum Monte Carlo algrithm that minimizes the free energy, subject to the nodal or phase restriction. This method has enabled us to perform efficient fermion path-integral simulations at all temperatures. In the T=0 limit the algorithm simulates two copies of the system that do not interact, but which are entangled through the nodal constraint. We illustrate the advantages of this density matrix formalism in applications to semiconductor nanostructures and small molecules. We are currently investigating the use of the Kubo formula and other linear response theories within the fixed-node approximation. (For simulation codes, preprints, and other information, see http://phy.asu.edu/shumway.)

*Work supported by NSF Grant DMR 0239819.

**8:12**
**U27 2 Worm algorithm for continuous-space Path Integral Monte Carlo simulations** MASSIMO BONINSEGNI, *University of Alberta* NIKOLAY PROKOF'EV, BORIS SVISTUNOV, *University of Massachusetts* We present a new approach to Path Integral Monte Carlo (PIMC) simulations based on the ''worm'' algorithm, originally developed for lattice models,[1] and recently extended to continuous-space many-body systems.[2] The scheme allows for efficient computation of thermodynamic properties, including winding numbers and off-diagonal correlations, for systems of much greater size than that accessible to conventional PIMC. We present results for the superfluid transition of Helium-four in two and three dimensions. Using systems comprising several thousand particles, a very accurate determination of the superfluid transition temperature is feasible.

[1]N. V. Prokof'ev, B. V. Svistunov, and I. S. Tupitsyn, Phys. Lett. **238**, 253 (1998)
[2]M. Boninsegni, N. Prokof'ev and B. Svistunov, cond-mat/0510214

**8:24**
**U27 3 Green's function analysis of path integral Monte Carlo molecular simulations*** DAEJIN SHIN, *Arizona State University* JOHN SHUMWAY, *Arizona State University* We demonstrate the direct determination of molecular properties from path integral Monte Carlo simulations. By sampling Matsubura Green's functions, we have calculated several linear response properties of the hydrogen molecule ($H_2$) directly from quantum Monte Carlo. We show that the vibration frequency of $H_2$ as calculated directly from the phonon temperature Green's function is in very good agreement with the calculated Born-Oppenheimer potential energy surface. We have also obtained the polarizability from the polarization correlation function, and we are looking at Raman spectra. For the high-accuracy simulations needed in chemical physics, we have developed new, fast and accurate techniques for the tabulation of Coulomb density matrices. This work motivates future path integral Monte Carlo simulations on larger molecules and could also be immediately useful in simulations of hydrogen storage materials.

*Work supported by NSF Grant DMR-0239819

**8:36**
**U27 4 Energy Optimization of Many-Body Wave Functions: Application to Silicon Interstitial Defects*** W. D. PARKER, K. P. DRIVER, R. G. HENNIG, J. W. WILKINS, *the Ohio State University* C. J. UMRIGAR, *Cornell University* Energy minimization [1], as opposed to the standard variance minimization [2], of the Jastrow factor results not only in lower variational Monte Carlo (VMC) energies but also in lower diffusion Monte Carlo (DMC) energies for systems that employ a nonlocal pseudopotential. We apply this approach to solids: single-interstitials in silicon. Allowing the Jastrow for the defect atom(s) to differ from that for bulk atoms lowers the VMC energy but not the DMC energy, indicating the pseudopotential locality error is small. DMC energies from 8 and 64 atom cells (plus interstitial) computed with energy-optimized trial wave functions estimate a 0.2 eV finite-size error in the formation energy. Cubic spline and Lagrange polynomial representations of orbitals have comparable efficiency in memory usage, run time and accuracy. [1] C. J. Umrigar and C. Filippi, Phys. Rev. Lett. 94, 150201 (2005). [2] C. J. Umrigar, K. G. Wilson and J. W. Wilkins, Phys. Rev. Lett. 60, 1719 (1988).

*Supported by DOE(DE-FG02-99ER45795), Ohio Supercomputing Center, NERSC, NSF(EAR-0530301,DMR-0205328) and Sandia National Laboratories

**8:48**
**U27 5 Study of Atoms and Molecules with Auxiliary-Field Quantum Monte Carlo*** WIRAWAN PURWANTO, MALLIGA SUEWATTANA,[†] HENRY KRAKAUER, SHIWEI ZHANG, ERIC J. WALTER, *College of William and Mary, VA* We study the ground-state properties of second-row atoms and molecules using the phaseless auxiliary-field quantum Monte Carlo (AF QMC) method.[1] This method projects the many-body ground state from a trial wave function by means of random walks in the Slater-determinant space. We use a single Slater-determinant trial wave function obtained from density-functional theory (DFT) or Hartree-Fock (HF) calculations. The calculations were done with a plane-wave basis and supercells with periodic boundary condition. We investigate the finite-size effects and the accuracy of pseudopotentials within DFT, HF, and AF QMC frameworks. Pseudopotentials generated from both LDA (OPIUM[2]) and HF[3] are em-

ployed. We find that the many-body QMC calculations show a greater sensitivity to the accuracy of the pseudopotentials. With reliable pseudopotentials, the ionization potentials and dissociation energies obtained using AF QMC are in excellent agreement with the experimental results.

*Supported by DOE CMSN. Computing was done in CPD and NCSA.
†Currently at Oak Ridge National Lab, TN

[1]S. Zhang and H. Krakauer, Phys. Rev. Lett. **90**, 136401 (2003)
[2]tthttp://opium.sourceforge.net
[3]I. Ovcharenko, A. Aspuru-Guzik, and W. A. Lester, J. Chem. Phys. **114**, 7790 (2001)

**9:00**
**U27 6 Auxiliary field quantum Monte Carlo study of transition metal and post-d group atoms and molecules*** HENRY KRAKAUER, *College of William and Mary* WISSAM A. ALSAIDI, *College of William and Mary* SHIWEI ZHANG, *College of William and Mary* We applied the phaseless auxiliary field quantum Monte Carlo [1] to the study of several transition metal and post-d atoms and molecules. The transition metal study includes both all-electron and pseudopotential calculations, while the post-d group elements are studied using the consistent correlated basis which employs a small core relativistic pseudopotential [2]. The obtained electron affinities, dissociation energies, and equilibrium geometries compare favorably with experiment and with coupled cluster results. [1] S. Zhang and H. Krakauer, Phys. Rev. Lett. **90**, 136401 (2003). [2] Kirk A. Peterson, J. Chem. Phys. **119**, 11099 (2003); Kirk A. Peterson et al., J. Chem. Phys. **119**, 11113 (2003)

*upported by ONR and DOE/CMSN

**9:12**
**U27 7 Accuracy of the pseudopotential and fixed-node approximations for $C_2$, $Si_2$ and defects in crystalline Si*** RICHARD G. HENNIG, *Department of Physics, Ohio State University* CYRUS J. UMRIGAR, JULIEN TOULOUSE, *Cornell Theory Center, Cornell University* JOHN W. WILKINS, *Department of Physics, Ohio State University* Quantum Monte Carlo calculates binding energies and atomic structures for molecules and defect energies in solids. Accurate QMC calculations require the control of the pseudopotential and the fixed-node approximation. The calculated binding energies and bond lengths for the Si and C dimer and the energies of defects in crystalline Si test the accuracy of a range of pseudopotentials and optimized trial-wave functions. For the Si dimer and defects in crystalline Si different pseudopotentials provide similar results. The results for the Si dimer are comparable with experiments with HF pseudopotentials being most accurate. While a single determinant wave functions is sufficient for the Si dimer, the C dimer requires an optimized multideterminant trial-wave function to achieve experimental accuracy.

*Supported by NSF (DMR-0205328, EAR-0530301) and DOE (DE-FG02-99ER45795). Computational resources provided by NERSC, NCSA and OSC.

**9:24**
**U27 8 Structure of fermion nodes and nodal cells for QMC wave functions*** LUBOS MITAS, *North Carolina State University* We study nodes of fermionic ground state wave functions. For $2D$ and higher we analytically prove that spin-polarized, noninteracting fermions in a harmonic well have two nodal cells for arbitrary system size. The result extends to other noninteracting/mean-field models such as fermions on a sphere, in a periodic box or in Hartree-Fock atomic states. Spin-unpolarized noninteracting states have multiple nodal cells, however, interactions and many-body correlations generally relax the multiple cells to the minimal number of two. This is again analytically proved, with some restrictions, for general interactions in $2D$ and higher-dimensional harmonic fermions of arbitrary size using the Bardeen-Cooper-Schrieffer variational wave function. We discuss implications and limits of the proofs for more complicated systems. The results offer an elegant and unifying framework for several previously conjectured or numerically investigated ideas and open exciting perspectives for studies of many-body effects which are beyond the usual fixed-node quantum Monte Carlo limits.

*Supported by NSF DMR and EAR grants.

**9:36**
**U27 9 Multi-pfaffian pairing wave functions for quantum Monte Carlo** MICHAL BAJDICH, LUBOS MITAS, *CHIPS, Department of Physics, North Carolina State University, Raleigh, NC 27695* KEVIN E. SCHMIDT, *Department of Physics, Arizona State University, Tempe, AZ 85287* We investigate the limits of accuracy of trial wave function for quantum Monte Carlo based on pfaffian functional form with singlet and triplet pairing. Using a set of first row atoms and molecules we find that this wave function provides very consistent and systematic behaviour in recovering the correlation energies on the level of 95%. In order to get beyond this limit we have explored the possibilities of multi-pfaffian pairing wave functions. We show that small number of pfaffians recovers another large fraction of the missing correlation energy comparable to the larger-scale configuration iteraction wave functions. The trade-offs between the size of the underlying optimization problem and amounts correlation energy recovered will be discussed.

**9:48**
**U27 10 Backflow transformations in inhomogeneous systems** PABLO LOPEZ RIOS, ANDREA MA, NEIL D. DRUMMOND, RICHARD J. NEEDS, *TCM Group, University of Cambridge* The quality of trial wave-functions, and of their nodal surface in particular, determines the accuracy of the results obtained within the Fixed-Node Diffusion Monte Carlo (DMC) method. Backflow transformations have been proven capable of improving the nodal surface of Slater-Jastrow (SJ) wave-functions in homogeneous systems. In this work we will present the extension of backflow to inhomogeneous systems, along with DMC results for atoms, molecules and solids which show the improved accuracy of this form of trial wave-function. We will also discuss the advantages of using electron-by-electron algorithms to enhance the computational efficiency of QMC with backflow wave-functions.

**10:00**
**U27 11 The equation of state of diamond from quantum Monte Carlo calculations** RYO MAEZONO,* *National Institute for Materials Science, Japan.* ANDREA MA, *TCM, Cavendish Laboratory, University of Cambrigde, U.K.* MIKE D. TOWLER, *TCM, Cavendish Laboratory, University of Cambrigde, U.K.* NEIL D. DRUMMOND, *TCM, Cavendish Laboratory, University of Cambrigde, U.K.* RICHARD J. NEEDS, *TCM, Cavendish Laboratory, University of Cambrigde, U.K.* We describe variational and diffusion quantum Monte Carlo (VMC and DMC) calculations that have been performed to evaluate the elastic properties of diamond up to pressures of about 500 GPa. We have used a smooth, norm-

conserving, Hartree-Fock carbon pseudopotential in our work. Our trial wave functions were of Slater-Jastrow form, containing orbitals generated in plane-wave DFT-GGA calculations, which were re-expanded in a blip-function basis set. We propose a new scheme for determining the cutoff lengths that occur in our Jastrow factor. Using a 512-electron simulation cell, and fitting a Vinet equation of state to our energy-volume data, we have calculated the equilibrium lattice constant (A, in Angstrom), bulk modulus (B, in GPa), and pressure derivative of the bulk modulus (B') to be (A,B,B')=(3.547, 4.83, 3.43) within VMC and (3.563, 4.52, 3.61) within DMC, as compared with the experimental values of (A,B,B')=(3.567, 4.4-4.5, 3.0-4.0).

*PREST, JST, Japan

**10:12**
**U27 12 Improved estimators for quantum Monte Carlo calculation of spherically averaged intracule densities*** JULIEN TOULOUSE, *Cornell University* ROLAND ASSARAF, *Universite Pierre et Marie Curie* CYRUS UMRIGAR, *Cornell University* System-averaged pair densities or ''intracule densities'' are important for qualitative and quantitative descriptions of electron correlation [1] In quantum Monte Carlo (QMC) simulations, spherically averaged intracule densities are usually calculated by means of the traditional histogram technique (i.e., by counting the number of times two electrons are found at a certain distance) that is very noisy at short electron-electron distances. We will show how previously-used improved estimators for the on-top pair density [2,3] can be generalized to the case of non-vanishing electron-electron distances, as an application of the ''zero-variance'' procedure [4]. The obtained estimators lead to noise several orders of magnitude smaller than the histogram technique, allowing unprecedented fast and accurate calculations of intracule densities in QMC. Illustrative calculations on simple atomic systems will be given. [1] J. M. Mercero, E. Valderrama and J. M. Ugalde, in ''NATO-ASI Series in Metal-Ligand Interaction in Molecular-, Nano-, Micro, and Macro-systems in Complex Environments,'' Ed.: N. Russo, D. R. Salahub and M. Witko, Kluwer Academic Publishers, Dordrecht (2003). [2] P. Langfelder, S. M. Rothstein and J. Vrbik, J. Chem. Phys. **107**, 8525 (1997). [3] A. Sarsa, F. J. Gálvez and E. Buendía, J. Chem. Phys. **109**, 7075 (1998). [4] R. Assaraf and M. Caffarel, Phys. Rev. Lett. **83**, 4682 (1999).

*Supported by NSF (DMR-0205328)

**10:24**
**U27 13 Accurate energy differences with Quantum Monte Carlo** SIMONE CHIESA, DAVID CEPERLEY, JEONGNIM KIM, RICHARD MARTIN, *UIUC* Computation of accurate energy differences is of primary importance in the study of transformations as those occurring in solid to solid phase transitions or chemical reactions. In stochastic quantum simulations this can be done efficiently, employing correlated sampling techniques whereby fluctuations cancel with each other leading to results with a much smaller statistical error. Although correlated sampling is very effective for variational Monte Carlo such is not the case for diffusion Monte Carlo where branching and different nodal structures force the introduction of uncontrolled approximations. Here we describe the use of reptation Monte Carlo as a method that maintains a single path for both systems and leads to energies which are exact within the fixed node approximation. We show how to combine umbrella sampling with coordinate transformations to give a simple and efficient algorithm to compute small energy differences. Application to dissociation reaction paths and weakly bound systems are presented.

## SESSION U28: FOCUS SESSION: BIOLOGICAL HYDRODYNAMICS II
**Thursday Morning, 16 March 2006; 325, Baltimore Convention Center at 8:00**
**Steve Quake, Stanford University, presiding**

***Invited Papers***

**8:00**
**U28 1 Fluidic control over cell proliferation and chemotaxis.**
ALEX GROISMAN, *University of California San Diego*

Microscopic flows are almost always stable and laminar that allows precise control of chemical environment in microchannels. We describe design and operation of several microfluidic devices, in which various types of environments are created for different experimental assays with live cells. In a microfluidic chemostat, colonies of non-adherent bacterial and yeast cells are trapped in micro-chambers with walls permeable for chemicals. Fast chemical exchange between the chambers and nearby flow-through channels creates essentially chemostatic medium conditions in the chambers and leads to exponential growth of the colonies up to very high cell densities. Another microfluidic device allows creation of linear concentration profiles of a pheromone ($\alpha$-factor) across channels with non-adherent yeast cells, without exposure of the cells to flow or other mechanical perturbation. The concentration profile remains stable for hours enabling studies of chemotropic response of the cells to the pheromone gradient. A third type of the microfluidic devices is used to study chemotaxis of human neutrophils exposed to gradients of a chemoattractant (fMLP). The devices generate concentration profiles of various shapes, with adjustable steepness and mean concentration. The ''gradient'' of the chemoattractant can be imposed and reversed within less than a second, allowing repeated quantitative experiments.

*Contributed Papers*

**8:36**
**U28 2 The Conformation of Clathrin Triskelia in Solution**
MATTHEW L. FERGUSON, *Department of Physics, University of Maryland College Park MD* KONDURY PRASAD, *Department of Biochemstry, University of Texas Health Science Center, San Antonio TX* DAN L. SACKETT, HACENE BOUKARI, *Laboratory of Integrative and Medical Biophysics, NICHD, National Institutes of Health, Bethesda MD* EILEEN M. LAFER, *Department of Biochemstry, University of Texas Health Science Center, San Antonio TX* RALPH NOSSAL, *Laboratory of Integrative and Medical Biophysics, NICHD, National Institutes of Health, Bethesda MD* A principal component in the protein coat of certain post-golgi and endocytic vesicles is clathrin, a three-legged heteropolymer (known as a triskelion) that assembles into polyhedral cages principally made up of pentagonal and hexagonal faces. In vitro, this assembly depends on the pH, with cages forming more readily at low pH and less readily at high pH. We have developed procedures, based on static and dynamic light scattering, to determine the radius of gyration, $R_g$, and hydrodynamic radius, $R_H$, of isolated triskelia, under conditions where cage assembly occurs. Calculations based on rigid molecular bead models of a clathrin triskelion show that the measured values can be accounted for by bending of the legs and a puckering at the vertex. We also show that the values of $R_g$ and $R_H$ measured for clathrin triskelia in solution are qualitatively consistent with the conformation of clathrin in a ''$D_6$ barrel'' cage assembly measured by cryoEM tomography.

**8:48**
**U28 3 A macromolecular model for the endothelial surface layer** JAMES HARDEN, *Department of Physics, University of Ottawa* DARINA DANOVA-OKPETU, *Department of Physics, Vrije Universiteit* GARY GREST, *Sandia National Labs* The endothelial surface layer (ESL) is a micron-scale macromolecular lining of the luminal side of blood vessels composed of proteoglycans, glycoproteins, polysaccharides and associated plasma proteins all in dynamic equilibrium. It has numerous physiological roles including the regulation of blood flow and microvascular permeability, and active participation in mechanotransduction and stress regulation, coagulation, cell adhesion, and inflammatory response. The dynamic structure and the mechanical properties of the ESL are crucial for many of its physiological properties. We present a topological model for the ESL composed of three basic macromolecular elements: branched proteoglycans, linear polysaccharide chains, and small plasma proteins. The model was studied using non-equilibrium molecular dynamics simulations and compared with scaling theories for associating tethered polymers. We discuss the observed dynamical and mechanical properties of the ESL captured by this model, and the possible physical insight it provides into the physiological behavior of the ESL.

**9:00**
**U28 4 Simulation of metachronal wave in a model of pulmonary cilia*** SORIN MITRAN, *UNC* A simulation of the formation of metachronal waves in carpets of pulmonary cilia is presented. The cilia move in a two-layer fluid model. The fluid layer adjacent to the cilia base is purely viscous while the tips of the cilia move through a viscoelastic fluid. An overlapping fixed-moving grid formulation is employed to capture the effect of the cilia on the surrounding fluid. The 9+2 internal microtubule structure of an individual cilium is modeled using large-deflection, curved, finite-element beams. Realistic models of the forces exerted by dynein molecules are extracted from measurements of observed cilia shapes. The possibility of formation of metachronal waves under different assumptions of boundary conditions is investigated and shown to be dependent on the surrounding geometry.

*Work performed under the auspices of the UNC ''Virtual Lung'' Project

*Invited Papers*

**9:12**
**U28 5 On the Evolution of Voltage Gated Ion Channels.**
MICHAEL BRENNER, *Harvard University*

This talk summarizes some ideas, calculations and data analysis/collection surrounding the structure and evolution of ion channels, in particular voltage gated sodium channels. The great advantage of ion channels is that they are individual proteins whose function has long been known and is readily inferred through voltage measurements. Their evolution can be tracked through the growing data base of sequences. Kinetic data is readily available, showing important differences between nearly identical channels. I will discuss our efforts to collate available functional data on voltage gated sodium channels into an ''ion channel property space''. We then use this dataset to infer underlying kinetic models, and to create evolutionary trees based on the function of the channels. Finally, I will discuss our endeavors to how ion channels evolved to be the way they are: Examples of questions we would like to answer include: to what extent do design principles dictate the details of the kinetic schemes of ion channels, such as (a) the symmetry of the sodium and potassium channels (or lack thereof), as reflected in their kinetic schemes; (b) the coupling of sodium channel kinetics to potassium channel kinetics; or (c) activation/inactivation of the channels themselves.

*Contributed Papers*

**9:48**
**U28 6 Optimization of Anguilliform Swimming** STEFAN KERN, PETROS KOUMOUTSAKOS, *ETH Zurich* Anguilliform swimming is investigated by 3D computer simulations coupling the dynamics of an undulating eel-like body with the surrounding viscous fluid flow. The body is self-propelled and, in contrast to previous computational studies of swimming, the motion pattern is not prescribed a priori but obtained by an evolutionary optimization procedure. Two different objective functions are used to characterize swimming efficiency and maximum swimming velocity with limited input power. The found optimal motion patterns represent two distinct swimming modes corresponding to migration, and burst swimming, respectively. The results support the hypothesis from observations of real animals that eels can modify their motion pattern generating wakes that reflect their propulsive mode. Unsteady drag and thrust production of the swimming body are thoroughly analyzed by recording the instantaneous fluid forces acting on partitions of the body surface.

**10:00**
**U28 7 Flow measurement in an in-vitro model of a single human alveolus*** SUDHAKER CHHABRA, AJAY PRASAD, *Department of Mechanical Engineering, University of Delaware, Newark, DE 19716* The alveolus is the smallest and most important unit in the acinar region of the human lung. It is responsible for gas exchange between the lungs and the blood. A complete knowledge of the airflow pattern in the acinar region is necessary to predict the transport and deposition of inhaled aerosol particles. Such knowledge will benefit the pharmaceutical community in its effort to deliver therapeutic aerosols for lung-specific as well as system-wide ailments. In addition, it can also help to assess the health effects of the toxic aerosols in the environment. We have constructed an in-vitro model of a single spherical alveolus on a circular tube. The alveolus is capable of expanding and contracting in phase with the oscillatory flow through the tube. Realistic breathing conditions are reproduced by matching Reynolds and Womersley numbers. Experimental methods such as particle imaging velocimetry and laser induced fluorescence are used to study the resulting flow patterns. In particular, recirculating flow within the alveolus, and the fluid exchange between the alveolar duct and the alveolus are important for better understanding the flow in the acinar region.

*Sponsored by Philip Morris USA Inc. and Philip Morris International

**10:12**
**U28 8 Transport and collective dynamics in suspensions of swimming particles** MICHAEL GRAHAM, JUAN HERNANDEZ, *Univ. of Wisconsin-Madison* Direct simulations of large populations of hydrodynamically interacting swimming particles at low Reynolds number are performed. Hydrodynamic coupling between the swimmers leads to large-scale coherent vortex motions in the flow that are consistent with experimental observations. At low concentrations, swimmers propelled from behind (like spermatazoa) strongly migrate toward solid surfaces in agreement with simple theoretical considerations; at higher concentrations this localization is disrupted by the large-scale coherent motions. Correspondingly, at large concentrations the swimmers move with velocities several times larger than they could achieve in isolation.

**10:24**
**U28 9 Computational Modeling of Microfluidic Rapid-Mixing Device Used in Infrared Micro-Spectroscopy** MARK DICKINS, *University of Texas at Austin* JARMILA GUIJARRO, AIHUA XIE, *Oklahoma State University* Microfluidic rapid-mixing device is employed to chemically trigger biological functions of proteins for time-resolved Fourier transform Infrared (FTIR) micro-spectroscopic study. There are two criteria for the optimal design of such devices: (i) minimizing the mixing time (thus better time-resolution) and (ii) minimizing the consumption of protein samples. Computational modeling has been performed on the Poiseuille and diffusional flow patterns. Due to the low-Reynolds number of microfluidic flow in study, finite-difference methods for the Navier-Stokes and advection-diffusion equations are employed in our computational modeling. The viscosity of the fluids is related to the pressure gradient required to achieve maximum velocity according to Pouisulle flow. Several mixing channels are modeled in order to determine the optimal dimensions for our microchip according to the design criteria. We will report our computational modeling results and their relevance to the optimal design of rapid-mixing devices used in time-resolved infrared micro-spectroscopy.

## SESSION U29: FOCUS SESSION: NONEQUILIBRIUM FLUCTUATION IN BIOMOLECULES AND ARTIFICIAL NANODEVICES

**Thursday Morning, 16 March 2006**
**326, Baltimore Convention Center at 8:00**
**Ioan Kosztin, University of Missouri, Columbia, presiding**

*Contributed Papers*

**8:00**
**U29 1 DNA's Liaison with RNA Polymerase Physical Consequences of a Twisted Relationship** IGOR KULIC, PHIL NELSON, *University of Pennsylvania* RNA polymerase is the molecular motor that performs the fundamental process of transcription. Besides being the key- protagonist of gene regulation it is one of the most powerful nano-mechanical force generators known inside the cell. The fact that polymerase strictly tracks only one of DNA's strands together with DNA's helical geometry induces a force-to-torque transmission, with several important biological consequences like the ''twin supercoil domain'' effect and remote torsional interaction of genes. In the first part of the talk we theoretically explore the mechanisms of non-equilibrium transport of twist generated by a moving polymerase. We show that these equations are intrinsically non-linear in the crowded cellular environment and lead to peculiar effects like self-confinement of torsional strain by generation of alternative DNA structures like cruciforms. We demonstrate how the asymmetric conformational properties of DNA lead to a ''torsional diode'' effect, i.e. a rectification of polymerase-generated twist currents of different signs. In the second part we explore the possibility of exploiting the polymerase as a powerful workhorse for nanomechanical devices. We propose simple and easy to assemble arrangements of DNA templates interconnected by strand-hybridization that when tran-

scribed by the polymerase linearly contract by tenfold. We show that the typical forces generated by such ''DNA stress fibers'' are in the piconewton range. We discuss their kinetics of contraction and relaxation and draw parallels to natural muscle fiber design.

**8:12**
**U29 2 Enhanced Fano factor in a molecular transistor coupled to phonons and Luttinger-liquid leads** SO TAKEI, YONG BAEK KIM,* *University of Toronto* ADITI MITRA,† *Columbia University* We study how the electron-phonon coupling *and* intralead electron interaction affect the transport properties of a molecular quantum dot coupled to leads. We consider the effects on the steady state current and DC noise for both equilibrated and unequilibrated on-dot phonons. The density matrix formalism is applied in the high temperature approximation and the resulting semi-classical rate equation is numerically solved for various strengths of electron-electron interactions in the leads and electron-phonon coupling. We have found that the Fano factor, which measures the noise to current ratio, is enhanced as the intralead electron interaction is increased, while both the current and its noise are smeared out and suppressed due to the interaction. Interestingly, the Fano factor exhibits super-poissonian behaviour as the electron-phonon coupling becomes greater than order one.

*Also affiliated with School of Physics, Korea Institute for Advanced Study
†Now a postdoctoral fellow at University of Toronto

***Invited Papers***

**8:24**
**U29 3 Least dissipation principle for single molecule dynamics.**
R. DEAN ASTUMIAN, *The University of Maine*

This abstract was not received electronically.

***Contributed Papers***

**9:00**
**U29 4 Multi-scale dynamics and relaxation of a tethered membrane in a solvent by Monte Carlo simulations*** RAS PANDEY, *University of Southern Mississippi* KELLY ANDERSON, *The Procter & Gamble Company* BARRY FARMER, *Air Force Research Laboratory* A tethered membrane modeled by a flexible sheet dissipates entropy as it wrinkles and crumples. Nodes of a coarse grained membrane are connected via multiple pathways for dynamical modes to propagate. We consider a sheet with nodes connected by fluctuating bonds on a cubic lattice. The empty lattice sites constitute an effective solvent medium via node-solvent interaction. Each node execute its stochastic motion with the Metropolis algorithm subject to bond fluctuations, excluded volume constraints, and interaction energy. Dynamics and conformation of the sheet are examined at a low and a high temperature with attractive and repulsive node-node interactions for the contrast in an attractive solvent medium. Variations of the mean square displacement of the center node of the sheet and that of its center of mass with the time steps are examined in detail which show different power-law motion from short to long time regimes. Relaxation of the gyration radius and scaling of its asymptotic value with the molecular weight are examined.

*We acknowledge supports from the Materials and Manufacturing Directorate of the Air Force Research Laboratory.

**9:12**
**U29 5 Ion distribution inside a nanopore in the presence of a polyelectrolyte** LEI GUO, ERIK LUIJTEN, *University of Illinois at Urbana-Champaign* Experimental studies of the translocation of DNA through nanopores rely on measurements of the ionic current. In order to understand the behavior of this current, we employ molecular dynamics simulations to study the ion distribution within a nanopore in the presence of a polyelectrolyte. We characterize the ion distribution in terms of radial density profiles around the polyelectrolyte. Several factors affecting the ion distribution are studied, including the role of chain flexibility, salt concentration, nanopore size and its polarizability. Our study also provides information on the dynamics of the ions inside the pore. The combination of static and dynamic information is used to explain experimental observations.

**9:24**
**U29 6 Measuring the direction of coupling between biological oscillators*** JORGE BREA, *Department of Physics and Astronomy, University of Missouri Saint Louis* ALEXANDER NEIMAN, *Department of Physics and Astronomy, Ohio University* DAVID RUSSELL, *Department of Biological Sciences, Ohio University* The electroreceptor system of the paddle fish comprises two self-sustained noisy oscillators: one oscillator resides in the sensory epithelium and is coupled through excitatory synapse with another oscillator residing in the afferent neuron terminal. We test recently developed algorithms for estimating the directionality of their coupling from experimental recordings of spontaneous and stimulated activity. These experimental bivariate time series are structurally different: while the signal from the epithelial oscillations is represented by a continuous stochastic process, the neuron oscillations are represented by a stochastic point process. We show that the tested algorithms detect reliably directionality of coupling both in experimental and simulated data and can be used for physiologically relevant short segments of data.

*Supported by NIH (DC-04922) and NSF (INT-0233264)

*Invited Papers*

**9:36**
**U29 7 Applications of the ratchet effect at nano- and mesoscopic scales.***
BOLDIZSAR JANKO,† *University of Notre Dame*

I will discuss the application the ratchet effect in superconducting vortex dynamics and interacting colloidal systems. We have shown theoretically how in superconductors patterned on sub-micron or nanometer scale with various pinning potentials a DC vortex transport and vortex manipulation can be achieved with an external AC drive. I will discuss several applications of the vortex ratchet effect as well as a series of experiments aimed at the detection and investigation of the vortex ratchet transport. For colloidal systems, we have recently shown that a rich variety of dynamic phases can be realized for mono- and bidisperse mixtures of interacting colloids under the influence of a symmetric flashing periodic substrate. With the addition of dc or ac drives, phase locking, jamming, and new types of ratchet effects occur. In some regimes we find that the addition of a non-ratcheting species increases the velocity of the ratcheting particles. We show that these effects occur due to the collective interactions of the colloids.

*Work supported by NSF-NIRT Grant No. DMR02-10519 and by the Alfred P. Sloan Foundation.
†Work done in collaboration with A.-L. Barabasi, I. Derenyi, M. B. Hastings, C.S. Lee, A. Libal, F. Nori, C. Reichhardt, C. Olson-Reichhardt.

*Contributed Papers*

**10:12**
**U29 8 On-Chip Integration of Cell-Free Gene Expression** AMNON BUXBOIM, *Department of Materials and Interfaces, Weizmann Institute of Science, Rehovot, Israel* MARGHERITA MORPURGO, *Department of Biological Chemistry, Weizmann Institute of Science, Rehovot, Israel* MAYA BAR-DAGAN, *Department of Materials and Interfaces, Weizmann Institute of Science, Rehovot, Israel* VERONICA FRYDMAN, *Chemical Research Support, Weizmann Institute of Science, Rehovot, Israel* DAVID ZBAIDA, *Department of Materials and Interfaces, Weizmann Institute of Science, Rehovot, Israel* ROY BAR-ZIV, *Department of Materials and Interfaces, Weizmann Institute of Science, Rehovot, Israel* We present a synthetic approach for the study of gene networks itin vitro which is complementary to traditional itin vivo methodologies. We have developed a technology for submicron integration of functional genes and on-chip protein synthesis using a cell-free transcription/translation system. The interaction between genes is facilitated by diffusion of on-chip gene expression products from 'source' genes towards 'acceptor' genes. Our technology is simple and inexpensive and can serve as an improved platform for a wide variety of protein and DNA biochip applications.

**10:24**
**U29 9 ''Burnt Bridge'' Mechanism of Molecular Motor Motion** TIBOR ANTAL, PAUL KRAPIVSKY, *Boston University* Motivated by a biased diffusion of molecular motors with the bias dependent on the state of the substrate, we investigate a random walk on a one-dimensional lattice that contains weak links (called ''bridges'') which are affected by the walker. Namely, a bridge is destroyed with probability $p$ when the walker crosses it; the walker is not allowed to cross it again and this leads to a directed motion. The velocity of the walker is determined analytically for equidistant bridges. The special case of $p = 1$ is more tractable — both the velocity and the diffusion constant are calculated for uncorrelated locations of bridges, including periodic and random distributions.

**SESSION U30: FOCUS SESSION: MECHANICAL PROPERTIES: DEFORMATION, RUPTURE AND FAILURE**
**Thursday Morning, 16 March 2006; 327, Baltimore Convention Center at 8:00**
**Teri Hermel-Davidock, Dow Chemical Company, presiding**

*Invited Papers*

**8:00**
**U30 1 Shock Wave Theory for Rupture of Rubber.**
MICHAEL MARDER, *The University of Texas at Austin*

The rupture of rubber differs from conventional fracture. It is supersonic, and the speed is determined by strain levels ahead of the tip rather than total strain energy as for ordinary cracks. Dissipation plays a very important role in allowing the propagation of ruptures, and the back edges of ruptures must toughen as they contract, or the rupture is unstable. In this talk I will review the experimental evidence for these claims. I will present several levels of theoretical description of the phenomenon: first, a numerical procedure called mesoscopic particle modeling, which is capable of incorporating large extensions, dynamics, and bond rupture; second, a simple continuum model that can be solved analytically, and which reproduces several features of elementary shock physics; and third, an analytically solvable discrete model that

accurately reproduces numerical and experimental results, and explains the scaling laws that underly this new failure mode. Rupture speeds compare well with experiments, although opening angles of the rupture are not captured especially well. Some additional interesting topics that may be encountered along the way include the question of how to model sound dissipation in disordered solids, and a numerical instability that is suggestive of the phenomenon of strain crystallization.

*Contributed Papers*

**8:36**

**U30 2 Tuning the Adhesion of Soft Elastomers with Topographic Patterns** ALFRED CROSBY, EDWIN CHAN, *University of Massachusetts* Nature (e.g. gecko and jumping spider) utilizes surface patterns to control adhesion. The primary mechanism of adhesion for these systems can be sufficiently described by linear elastic fracture mechanics theory and material-defined length scales. Based upon these natural inspirations, similar mechanisms can be used to control the adhesion of elastic polymers. For viscoelastic polymers, patterns tune adhesion through additional mechanisms that have not been previously observed. Here, we illustrate the effects of topographic patterns in tuning the adhesion for soft, elastic or viscoelastic, elastomers. Contact adhesion tests based on Johnson, Kendall and Roberts (JKR) theory are used to characterize the adhesion of patterned poly(dimethyl siloxane) as well as poly(n-butyl acrylate) elastomers. We demonstrate that patterns can be utilized to control the adhesion of these polymers by: 1) controlling the balance of initiation and propagation for local separation process, 2) controlling the local crack velocity to alter the global viscoelastic response, and 3) altering the local separation mode through modification of a polymer layer's lateral confinement.

**8:48**

**U30 3 Finite Element Calculations Using a New Constitutive Model for the Chemical Aging of Rubber** JOANNE BUDZIEN, DAVID LO, JOHN G. CURRO, *Sandia National Laboratories* DANA ROTTACH, *University of New Mexico* We have developed a constitutive model for rubber networks undergoing simultaneous crosslinking and scission reactions. This model is a modification of the independent network hypothesis that includes the coupling between strain history and chemical reactions. This coupling occurs because formation of networks in the strained state is greatly affected by the networks that were already present. Even when early networks scission, the overall material response shows some memory of the initial networks (i.e., some later stage networks act as earlier stage networks). We account for this effect using stress transfer functions. The model has been tested on microscopic molecular dynamics simulations. We will present results using this constitutive model in finite element calculations showing the large effect that the coupling of strain history and chemical reaction has.

**9:00**

**U30 4 Effect of chain bridging on mechanical properties of lamellae-forming block copolymers** ALHAD PHATAK, LISA LIM, CLETIS REAVES, FRANK BATES, *Department of Chemical Engineering and Materials Science, University of Minnesota* We report studies on solid-state mechanical properties of lamellae-forming block copolymers composed of poly(cyclohexylethylene) (C) and poly(ethylene) (E). Specifically, we have investigated the effect of bridging conformations in the semicrystalline E block. We studied CEC, ECEC, and ECECE architectures and found that tensile properties of C/E block copolymers are extremely sensitive to the fraction of ''soft'' E chains tethered between glassy C domains. While the CEC polymer has a strain-to-failure of $\sim$ 300%, the ECEC and ECECE polymers fail at $\sim$ 1% strain. By employing ECEC/CEC and ECECE/CEC blends, we have come up with a molecular parameter that describes a sharp brittle-to-ductile transition and captures the tensile properties of a broad range of C/E block copolymer architectures having equal sized E blocks. In another set of experiments, increasing the ''middle-to-loose'' E block length ratio was found to toughen the ECECE block copolymers. We propose that these effects are related to a critical concentration of bridged E chains that governs the failure mechanisms in glassy-semicrystalline block copolymers.

**9:12**

**U30 5 Probing the Contact and Sliding of Elastomer/Polymer Interfaces*** BETUL YURDUMAKAN, *The University of Akron* KUMAR NANJUNDIAH, ALI DHINOJWALA, In this study, we have designed a novel approach to couple interface sensitive infrared-visible sum frequency generation (SFG) spectroscopy with adhesion and friction experiments. This provides a direct probe of the interfacial structure in terms of orientation and density of molecules during contact and sliding which is important in understanding the molecular origin of adhesion and friction. Here, we show that the friction forces between poly(dimethyl siloxane) (PDMS) lens and glassy poly(styrene) (PS) are $\approx$ 4 times higher than PDMS sliding on surfaces of crystalline alkyl side chain comb polymers. This cannot be explained by the differences in adhesion energy or hysteresis. The in-situ SFG measurements indicate local interdigitation during contact, which is evident from the decrease in the number of oriented phenyl groups at the interface. The local penetration is unexpected at room temperature ($T_R$) that is much below the $T_g$ of PS. For comparison, we have also studied poly(n-butyl methacrylate) and poly(n-propyl methacrylate) having $T_g$ above and below $T_R$, respectively. Both of these polymers show similar adhesion and friction forces as PS. The SFG results indicate that local changes in interfacial structure affect friction, regardless of the bulk $T_g$. These results also show that the adhesion energy and hysteresis are not sufficient to predict friction, which makes the characterization of the molecular structure during contact and sliding essential.

*Financial Support from NSF (DMR-0512156)

**9:24**

**U30 6 Mesoscopic Random Lattice Models of Rupture in Rubber*** DAVID REYNOLDS, MICHAEL MARDER, *The University of Texas at Austin* In an earlier work, Marder illustrated how rupture in rubber differs from conventional fracture. Dissipation and toughening of the back edges of ruptures are critical for the propagation of stable ruptures. In this earlier work, mesoscopic models were arrived at by approximating the Mooney-Rivlin theory of rubber by a finite difference scheme on a triangular lattice. From this perspective, qualitatively the lattice sites are considered to be crosslinkers and the bonds are polymers. We extend this work by considering the crosslinkers to be randomly distributed throughout the material rather than being ordered. For both random and ordered lattices, without rupture, there are many

different ways to construct free energy functionals that reproduce the continuum theory. However, not all of the constructions are numerically stable. We explore the physical consequences of the disorder and the physical interpretations of the observed numerical instabilities.

*This work was supported in part by The Institute for Computational Engineering and Sciences.

**9:36**

**U30 7 Annealing History Dependence of Young's Modulus in Thin Polymer Films Using an Axi-symmetric Peel Test Apparatus** ADAM N. RAEGEN, KARI DALNOKI-VERESS, *Physics and Astronomy, McMaster University* We present a study of chain relaxation in thin spincast films above the glass transition temperature. We employ a novel axi-symmetric peel test, which uses the deformation of a thin spincast polymer film brought into contact with a flat substrate. The use of a thin membrane minimises uncertainty in the contact radius while the use of spincast films provides very smooth surfaces by means of a very simple method. The experimental profile of the deformed membrane shows good agreement with the expected logarithmic profile. While this agreement allows measurement of the Young's modulus and solid-solid work of adhesion in thin films, this study will focus on the dependence of the Young's modulus on the annealing history in thin films. The thermal history dependence shows that for short annealing times Young's modulus is larger than expected, suggesting that the chains are oriented during spincasting. For longer times, Young's modulus reaches literature values.

**9:48**

**U30 8 Contributions to the Adhesion of Glassy Polymers from Radical Recombination and Segmental Interpenetration at Elevated Temperatures** MURAT GUVENDIREN, MICHELLE LEFEBVRE, CHRISTINE DETTMER, SONBINH NGUYEN, KENNETH SHULL, *Northwestern University* We study two examples of adhesive interactions between glassy polymers that occur when the polymers are heated to elevated temperatures. First set is the adhesion between thin films of poly(phenylene oxide) (PPO). The samples are brought into contact at an elevated temperature and cooled to room temperature prior to measuring the fracture energy by using the contact mechanics approach based on JKR (Johnson, Kendall and Roberts) theory. Very little adhesion is observed at temperatures below about 130°C, which enables us to perform a second set of experiments, where adhesion is due to radical recombination across the interface. Polystyrene (PS) is synthesized by anionic polymerization, and terminated by an end-capped nitroxide radical group. Nitroxide mediated polymerization is used to attach a poly (tert-butyl acrylate) (tBA) block to the PS chains. These block copolymers are added to the PPO films that are brought into contact with one another. Nitroxide radicals become uncapped at elevated temperatures, with subsequent radical recombination providing another potential mechanism for the formation of bonds across the interface.

**10:00**

**U30 9 Adhesion and Spatial Distribution of Water in the Presence of Moisture: Surface Chemistry Affects.** CHRISOPHER WHITE, BRYAN VOGT, EMMETT OBRIEN, WEN-LI WU, *NIST* Many polymer adhesive bonds experience a complete loss of adhesion above a critical threshold relative humidity value. The adhesion loss from water exposure does not generally correlate with moisture solubility of the polymer; instead the surface layer of the polymer appears to be the controlling factor in the adhesion. Here, the adhesion and spatial distribution of water of a series of PMMA-Al adhesive samples in the presence of moisture is measured with neutron reflectivity, while the adhesive strength of the joint is measured using the shaft-loaded blister test. The role of changing surface chemistry was examined to determine their effect on this interfacial moisture content. The loss of adhesive strength upon exposure to moisture correlates directly with the interfacial water content. Surface modification methods that decrease the interfacial water content are used to tune the adhesive strength in moist environments. Minimization of the interfacial water concentration does not however result in the best adhesion in moist environments as interplay between the dry adhesion and water content exists.

**10:12**

**U30 10 Quantifying Ballistic Armor Performance: A Minimally Invasive Approach** GALE HOLMES, JAEHYUN KIM, WILLIAM BLAIR, WALTER McDONOUGH, CHAD SNYDER, *National Institute of Standards and Technology* Theoretical and non-dimensional analyses suggest a critical link between the performance of ballistic resistant armor and the fundamental mechanical properties of the polymeric materials that comprise them. Therefore, a test methodology that quantifies these properties without compromising an armored vest that is exposed to the industry standard V-50 ballistic performance test is needed. Currently, there is considerable speculation about the impact that competing degradation mechanisms (e.g., mechanical, humidity, ultraviolet) may have on ballistic resistant armor. We report on the use of a new test methodology that quantifies the mechanical properties of ballistic fibers and how each proposed degradation mechanism may impact a vest's ballistic performance.

**10:24**

**U30 11 Measurement of the Viscoelastic Bulk Modulus*** YAN MENG, SINDEE SIMON, *Texas Tech University* A new piston-cylinder type pressurizable dilatometer has been developed to measure the time-dependent bulk modulus of viscoelastic materials. The PVT behavior and the glass transition temperature of a polystyrene have been measured as a function of pressure. Preliminary measurements of the time-dependent bulk modulus have also been made. The isothermal bulk modulus is important because its magnitude is directly related to isotropic residual stress development in curing thermoset-reinforced composites; in addition, by comparing the bulk and shear responses, proposed differences in the molecular origins can be explored.

*Funding from NSF DMR 0308762 is gratefully acknowledged.

**10:36**

**U30 12 Influence of Physical Aging on the Mechanical Properties of a Random Polypropylene-Polyethylene Copolymer** SAMUEL AMANUEL, *Materials Science and Engineering* XIAOFENG CHEN, *Chemical and Biological Engineering* RAHMI OZISIK, SANFORD S. STERNSTEIN, *Materials Science and Engineering, Rensselaer Polytechnic Institute* Spontaneous aging of a random polypropylene-polyethylene copolymer was studied at 50 $^{o}$C above its glass transition temperature using differential scanning calorimetry, wide (WAXS) and small (SAXS) angle X-ray scattering, and dynamic mechanical relaxometry. Both the melting temperature and melting enthalpy of the copolymer increased with physical aging time at room temperature suggesting increased crystallinity. WAXS measurements also indicated an increase in crystallinity along with coexistence of $\gamma$ and $\alpha$ forms for highly aged samples. Dynamic mechanical measure-

ments showed that the shear storage modulus increased uniformly at all frequencies of measurement from 0.1 Hz to 20 Hz. Furthermore a direct correlation was observed between the storage modulus and the melting enthalpy of the copolymer. Conversely, the change in shear loss modulus was frequency dependent, with larger changes at 20 Hz than at 0.1 Hz. This suggests that there are changes in the relaxation time spectra with aging. The aging process will be explored in more detail using both the SAXS and stress relaxation data.

**10:48**

**U30 13 Fracture versus cavitation in probe-tack geometry: theory and experiments** PASCALE FABRE, *CRPP-CNRS 115 av. Dr. Schweitzer F-33600 Pessac* JÉRÉMIE TEISSEIRE, FRÉDÉRIC NALLET, CYPRIEN GAY, *CRPP-CNRS* We perform traction experiments on viscous liquids highly confined between parallel plates, a geometry known as the probe-tack test in the adhesion community. Direct observation during the experiment coupled to force measurement shows the existence of several mechanisms for releasing the stress. Bubble nucleation and instantaneous growth had been observed in a previous work. Upon increasing further the traction velocity or the viscosity, the bubble growth is progressively delayed. At even higher velocities, fractures at the interface between the plate and the liquid are observed before the bubbles have grown to their full size. We present a theoretical model that describes these regimes, using a Maxwell fluid as a model for the actual fluid. We present the resulting phase diagram for the different force peak regimes. It remarkably accounts for the data. Our results show that in addition to cavitation, interfacial fractures, commonly thought to be characteristic of soft viscoelastic solids like adhesives are already encountered in *liquid* materials.

**SESSION U31: NANOTUBES, EXPERIMENT**
**Thursday Morning, 16 March 2006**
**328, Baltimore Convention Center at 8:00**
**Chris Kendziora, Naval Research Laboratory, presiding**

**8:00**

**U31 1 Controlled Dielectrophoretic Positioning of Carbon Nanotubes** SARBAJIT BANERJEE, BRIAN WHITE, LIMIN HUANG, STEPHEN O'BRIEN, IRVING HERMAN, *Nanoscale Science and Engineering Center, Columbia University, New York, NY* Single-walled carbon nanotubes have been dielectrophoretically aligned between micropatterned electrodes. Use of a limiting resistor enables control over the number of carbon nanotubes deposited in the electrode gap. Further, the electric field between micropatterned electrodes can be perturbed by arrays of metal nanostructures. Simulating electric fields in the presence of metal objects allows us to design electrodes with arrays of metal dots for the precise positioning of nanotubes. Complex network structures can be fabricated using carefully placed metal nanostructures and also by varying the electrode geometry. Crossed-junction nanotube structures have been controllably fabricated by optimization of the electrode geometry, applied electric field, and load resistor. The dielectrophoretically aligned nanotube structures work as functional field-effect transistors. Several approaches to improving the contact resistances will be discussed. The work is supported by the NSEC program of the National Science Foundation under NSF Award Number CHE-0117752 and by NYSTAR.

**8:12**

**U31 2 Tuning the electrical and mechanical properties of carbon nanotubes interfaced with silicon surfaces using the UHV-STM** PETER ALBRECHT, JOSEPH LYDING, *University of Illinois at Urbana-Champaign* Nanoscale patterning of the Si(100)-2x1:H surface with the UHV-STM [1] is used to selectively modify the Si substrate acting as a semiconducting support for isolated single-walled carbon nanotubes (SWNTs) deposited via dry contact transfer (DCT) [2]. By desorbing H at the SWNT-Si interface, we can mechanically stabilize SWNTs that initially were only weakly coupled to the Si surface and thus highly sensitive to STM tip induced perturbations. Moreover, on the degenerately doped n-type H-Si(100) surface, the presence of negatively charged Si dangling ponds patterned in close proximity to a semiconducting SWNT decreases the magnitude of the substrate voltage required for the onset of filled states conduction through the SWNT. Our results suggest new opportunities for engineering – on the sub-nm scale – both the mechanical and electronic properties of SWNTs integrated with semiconductor platforms. [1] J.W. Lyding et al., APL 64, 2010 (1994). [2] P.M. Albrecht and J.W. Lyding, APL 83, 5029 (2003).

**8:24**

**U31 3 Effect of doping on electro-optical properties of thin carbon nanotube membranes** MATTHEW GARRETT, *University of Tennessee* ILIA IVANOV, BIN ZHAO, ALEX PURETZKY, DAVID GEOHEGAN, *Oak Ridge National Laboratory* Nanotube membranes can prove to be a practical alternative to the current transparent conductors, such as ITO, that are in touch screen displays and photovoltaic devices. ITO with a transmittance of 80% in the visible spectrum has a resistance of 10ohms/square. Similar transmittance could be obtained only with very thin membranes with nanotube loadings below the percolation threshold and would have very high resistance. Doping of membranes changes transmittance at the S11 and S22 transitions of semiconducting nanotubes, but does not change the transmission in the visible spectrum, while decreasing the resistance. Membranes of different thicknesses have been produced and characterized. Post-production doping of the membranes has been achieved and the change in resistance and in transmission spectrum has been examined. We will discuss effect of donor and acceptor dopants on the conductivity and transmittance of the nanotube membranes.

**8:36**

**U31 4 Environmental Manipulation of the Electronic Structure of Suspended Carbon Nanotubes** A.G. WALSH, Y. YIN, *Physics Dept, BU* A.N. VAMIVAKAS, *ECE Dept, BU* S.B. CRONIN, M. TINKHAM, *Physics Dept, Harvard* M.S. UNLU, *ECE Dept, BU* B.B. GOLDBERG, *Physics Dept, BU* A.K. SWAN, *ECE Dept, BU* We use tunable resonant Raman spectroscopy to study the effect of changing the dielectric environment on the electronic structure of single wall carbon nanotubes (CNTs) suspended over trenches. The 1D nature of CNTs is responsible for weak intrinsic screening and large Coulomb interactions are anticipated. Two-photon absorption experiments have determined the presence of excitons with large binding energies [1,2]. Therefore, modulation of the surrounding dielectric constant signifi-

cantly alters the strength of the Coulomb interactions and leads to changes in the exciton binding energy and band-gap renormalization which should be evident in the resulting spectra.[3] Until recently, CNTs were primarily studied in bulk, in suspensions, or coated in surfactants. We measure resonance excitation profiles (REPs) from individual suspended CNTs where the intensity of the Raman peak is plotted vs. excitation energy. We vary the humidity and monitor the shift of the REP peak of the radial breathing mode and the G-Band. We thereby directly measure the relative shift of the renormalized band-edge and exciton binding energy as a function of dielectric constant. [1] Wang, Science, 308, 838 (2005). [2] Maultzsch, arXiv, 0505150 (2005). [3] Perebeinos, PRL, 92, 257402 (2004).

**8:48**

**U31 5 Capacitance measurements of individual carbon nanotubes** LUKE A. K. DONEV, SHAHAL ILANI, PAUL L. McEUEN, *Laboratory of Atomic and Solid-State Physics, Cornell University* We present measurements of the capacitance of individual single walled carbon nanotubes. The nanotubes were grown from ethylene at 700°C using evaporated iron nanoclusters as the catalyst. Electrical contacts and local top gates were patterned using optical lithography and liftoff. The top gate consists of a thin oxide film ( $\sim$ 15 nm, different oxides have been used) covering the nanotube with metal on top. The capacitance was measured between the nanotube and the top gate using a commercially available capacitance bridge. We also measure the transport through the tube and correlate the transport and capacitance measurements. For semiconducting tubes, we measure the difference in capacitance between the conducting state and the state where the charge carriers in the tube are depleted. The measured capacitance per unit length of the nanotube is in reasonable agreement with the geometric capacitance of a metal wire embedded in oxide near a conducting plane.

**9:00**

**U31 6 Electrical Characterization of Y-junction Carbon Nanotubes of Fish-bone Structure*** Y. SUN, J. I. OH, S. CHEN, D. Z. WANG, K. KEMPA, Z. F. REN, *Boston College* W. Z. LI, *Florida International University* M. J. NAUGHTON, *Boston College* Y-junction carbon nanotubes (YCNTs) of fish-bone structure, synthesized by the pyrolysis of methane over cobalt supported on magnesium oxide [1], have been characterized by means of electrical transport measurements. We report both 2- and 4-probe I-V characteristics of YCNTs down to $T = 3$ K and up to $B = 8$ T. At 3 K, we found that change in magnetoresistance was about 0.5 % at 8 T, perhaps due to piezoeffect of YCNTs. Also, we report the piezoresistivity of YCNTs directly obtained by an itin situ STM incorporated into TEM. This piezoresistivity appeared to be substantially bigger than that of straight fish-bone CNTs. In addition, we fabricated some FET-shaped samples with YCNTs whose all 3 branches were contacted by Ti/Au electrodes. We found that there is no rectifying behavior in the fish-bone junctions unlike in similar YCNTs reported in [2]. [1] W. Z. Li, J. G. Wen, Z. F. Ren, Appl. Phys. Lett. **79**, 1879 (2001). [2] P. R. Bandaru, C. Daraio, S. Jin, A. M. Rao, Nature Mats. **4**, 663 (2005).

*This work was supported by the National Science Foundation Grant NIRT-0210533.

**9:12**

**U31 7 Resonant Raman spectroscopy analysis of single wall carbon nanotubes treated with high density plasma of different gases.*** DAVID MAST, CHAMINDA JAYASINGHE, ZHANDOS UTEGULOV,† *University of Cincinnati* Single wall carbon nanotubes (SWNTs) have been plasma treated with different gases (Ar, $O_2$ and Ar and $H_2$ gases mixtures) using an inductively coupled RF plasma system (IC-RFP). The gas pressure was varied from 50mtorr to 315mtorr at 50W plasma power. Microscopic plasma parameters including ion density ($n_i$) and electron temperature ($T_e$) (thermal energy of electrons) were been determined using a double Langmiur probe in the plasma. Treated SWNTs was been characterized using resonance Raman spectroscopy at 515nm and 633nm laser excitation. It was observed that there was a considerable increase of the D to G-band ratio of treated SWNTs with increasing gas pressures and also that the Breit-Wigner-Fano band ($G_{BWF}$) to $G^+$-band ratio was been considerably increased. Further, at 515nm laser excitation the frequency up-shift of the G-band for Ar &(5%) $H_2$ (gas mixture) plasma treated SWNTs was higher at all pressures than those of other gases.

*Thanks to Dr. John Maguire, AFRL/MLBP Wright-Patterson AFB for the use of the Raman Spectrometer.

†present address NIST, Boulder, CO.

**9:24**

**U31 8 Measurements of 1/f Noise in Carbon Nanotube Devices*** MASA ISHIGAMI, *Department of Physics, University of Maryland, College Park, Maryland 20742* W. X. YAN, *Thomas Jefferson High School for Science and Technology, Alexandria VA 22312* J.H. CHEN, M. S. FUHRER, E. D. WILLIAMS, *Department of Physics, University of Maryland, College Park, Maryland 20742* We have measured the low frequency noise of field effect transistors made from individual single-walled carbon nanotubes in an ultra high vacuum environment. We will compare Hooges constants measured in oxygen, argon, air, and ultra high vacuum, and propose a possible solution for reducing noise in nanotube devices. Furthermore, the utility of noise amplitude in carbon nanotube devices for chemical specific sensing will be discussed.

*Materials Research Science and Engineering Center at University of Maryland, College Park and Director of Central Intelligence Postdoctoral Fellowship Program

**9:36**

**U31 9 Temperature dependence of mean free length of electrons in single walled carbon nanotubes** MENINDER PUREWAL, *Columbia University, Department of Applied Physics and Applied Mathematics* ANIRUDDH RAVI, BYUNG HEE HONG, JOSHUA SMALL, *Columbia University, Department of Physics* BHUPESH CHANDRA, JAMES HONE, *Columbia University, Department of Mechanical Engineering* PHILIP KIM, *Columbia University, Department of Physics* We have measured how single walled carbon nanotube resistance scales with channel length. Multiple two-terminal devices of varying source-drain separation are fabricated on isolated ultra-long ( $>$ 1 mm) SWNTs grown by chemical vapor deposition. Pd electrodes provide low resistance contacts to the SWNTs. The resistance of SWNT devices are investigated in length scales ranging from 100 nm to 200 $\mu$m, from which the 1-dimensional resistivity is extracted. The temperature dependence of the electron mean free path obtained from the resistivity values indicate that in the majority of metallic SWNT devices the electron transport is ballistic up to $\sim$ 500 nm at room temperature and $\sim$ 10 $\mu$m at 1.6K.

**9:48**

**U31 10 Field Enhanced Thermionic Electron Emission from Oxide Coated Carbon Nanotubes*** CHRISTOPHER DAY, FENG JIN, YAN LIU, SCOTT LITTLE, *Ball State University* We have created a novel nanostructure by coating carbon nanotubes with a thin functional oxide layer. The structure was fabricated by sputter deposition of a thin film of oxide materials on aligned carbon nanotubes, which were grown on a tungsten substrate with plasma enhanced chemical vapor deposition. This structure combines the low work function of the oxide coating with a high field enhancement factor introduced by carbon nanotubes and we have demonstrated that it can be used as a highly efficient electron source. A field enhancement factor as high as 2000 was observed and thermionic electron emission current at least an order of magnitude higher than the emission from a conventional oxide cathode was obtained.

*This work is sponsored by the Department of Energy.

**10:00**

**U31 11 Low-temperature conductive tip scanning measurements of single walled carbon nanotubes.** MATTHEW PRIOR, ALEXANDER MAKAROVSKI, ALEXEI ZHUKOV, GLEB FINKELSTEIN, *Department of Physics, Duke University* We have built a low-temperature atomic force microscope (AFM) that fits inside a 38 mm bore cryostat. The scanning probe is attached to a quartz tuning fork, and a frequency shift is used as the feedback signal. By using a conductive tip we can locally tunnel into single walled carbon nanotubes grown on a non-conducting (SiO2) substrate. The nanotubes are contacted by a metal grid ''electrode'' evaporated on top of the sample. The tip is used as a second, movable contact. We measure the nanotube conduction as a function of the tip position and the gate voltage.

**10:12**

**U31 12 Local Density of States in Nanoscale Systems Measured by Electrostatic Force Microscopy*** CRISTIAN STAII, *Materials Science and Engineering, Drexel University* DOUGLAS R. STRACHAN, *Physics and Astronomy, University of Pennsylvania* DAWN A. BONNELL, *Materials Science and Engineering, University of Pennsylvania* ALAN T. JOHNSON, *Physics and Astronomy, University of Pennsylvania* JONATHAN E. SPANIER, *Materials Science and Engineering, Drexel University* DREXEL TEAM, PENN TEAM, We use Electrostatic Force Microscopy (EFM) to measure the local density of states (LDOS) in carbon nanotubes and semiconducting nanowires. A voltage biased EFM cantilever, driven at its resonant frequency is used to perturb the local charge density in these systems. The recorded change in the oscillation phase is proportional to the LDOS of the sample. We monitor the phase change as a function of both the tip voltage and cantilever oscillation amplitude for a fixed cantilever position above the sample. We also show that this is a general electrostatic method that can be used to measure the band gap and LDOS of both conducting and insulating nanoscale systems with no need for electrical contacts.

*Work supported by NSF-NSEC at Drexel University and University of Pennsylvania

**10:24**

**U31 13 Nanotorsional Actuator Devices Built on Individual Singlewall Carbon Nanotubes*** A. R. HALL, M. R. FALVO, *Curriculum in Applied and Materials Sciences, University of North Carolina at Chapel Hill, 27599* R. SUPERFINE, *Department of Physics and Astronomy, University of North Carolina at Chapel Hill, 27599* S. WASHBURN, *Department of Physics and Astronomy and Curriculum in Applied and Materials Sciences, University of North Carolina at Chapel Hill, 27599* Nanoelectromechnical devices have been fabricated comprising an individual singlewall carbon nanotube as a torsional spring for a fully suspended, lithographed metal platform. The torsional properties of the structure were measured through electrostatic deflections. We discuss the mechanical properties of the oscillator and the electrical response of the nanotube during deflections.

*Supported through NASA GSRP fellowship

## SESSION U33: DYNAMICS AND SYSTEMS FAR FROM EQUILIBRIUM

**Thursday Morning, 16 March 2006**
**336, Baltimore Convention Center at 8:00**
**Harvey Gould, Clark University, presiding**

**8:00**

**U33 1 Critical behavior and Griffiths effects in the disordered contact process** THOMAS VOJTA, MARK DICKISON, *Department of Physics, University of Missouri-Rolla* We study the nonequilibrium phase transition in the one-dimensional contact process with quenched spatial disorder by means of large-scale Monte-Carlo simulations for times up to $10^9$ and system sizes up to $10^7$ sites. In agreement with recent predictions of an infinite-randomness fixed point, our simulations demonstrate activated (exponential) dynamical scaling at the critical point. The critical behavior turns out to be universal, even for weak disorder. However, the approach to this asymptotic behavior is extremely slow, with crossover times of the order of $10^4$ or larger. In the Griffiths region between the clean and the dirty critical points, we find power-law dynamical behavior with continuously varying exponents. We discuss the generality of our findings and relate them to a broader theory of rare region effects at phase transitions with quenched disorder.

**8:12**

**U33 2 Monte Carlo Studies of Phase Separation in Compressible 2-dim Ising Models** S.J. MITCHELL, D.P. LANDAU, *Center for Simulational Physics, University of Georgia* Using high resolution Monte Carlo simulations, we study time-dependent domain growth in compressible 2-dim ferromagnetic ($s = 1/2$) Ising models with continuous spin positions and spin-exchange moves [1]. Spins interact with slightly modified Lennard-Jones potentials, and we consider a model with no lattice mismatch and one with 4% mismatch. For comparison, we repeat calculations for the rigid Ising model [2]. For all models, large systems ($512^2$) and long times ($10^6$ MCS) are examined over multiple runs, and the growth exponent is measured in the asymptotic scaling regime. For the rigid model and the compressible model with no lattice mismatch, the growth exponent is consistent with the theoretically expected value of 1/3 [1] for Model B type growth. However, we find that

non-zero lattice mismatch has a significant and unexpected effect on the growth behavior. Supported by the NSF. [1] D.P. Landau and K. Binder, *A Guide to Monte Carlo Simulations in Statistical Physics*, second ed. (Cambridge University Press, New York, 2005). [2] J. Amar, F. Sullivan, and R.D. Mountain, Phys. Rev. B 37, 196 (1988).

**8:24**

**U33 3 Rate of Entropy Extraction in Compressible Turbulence.*** MAHESH BANDI, WALTER GOLDBURG, *Department of Physics and Astronomy, University of Pittsburgh* JOHN CRESSMAN, *Krasnow Institute, George Mason University* The rate of change of entropy is measured for a system of particles floating on the surface of a fluid maintained in a turbulent steady state. This rate of entropy $\dot{S}$ equals the time integral of the two point temporal velocity divergence correlation function with a negative prefactor. The measurements satisfactorily agree with the sum of Lyapunov exponents (Kolmogorov-Sinai entropy rate) measured from previous simulations, as expected of dynamical systems that are very chaotic (Sinai-Ruelle-Bowen statistics).

*This work is supported by the NSF (Grant No. DMR-0201805).

**8:36**

**U33 4 Non-constant nucleation rate in a system in apparent metastable equilibrium** HUI WANG, HARVEY GOULD, *Clark University* KIPTON BARROS, AARON SCHWEIGER, BILL KLEIN, *Boston University* The distribution of nucleation times for the two-dimensional Ising model with nearest-neighbor and with long-range interactions is simulated using the Metropolis algorithm. The distribution is exponential at long times as would be expected if the nucleation rate is a constant, but is suppressed at earlier times even after the mean magnetization is apparently in metastable equilibrium. We explain this discrepancy by investigating the relaxation behavior of the clusters whose size is comparable to the nucleating droplet.

**8:48**

**U33 5 4:1 Resonance phenomena in the forced Belousov-Zhabotinsky chemical reaction** BRADLEY MARTS, *Duke University Physics* ANNA LIN, *Duke University Physics and Center for Nonlinear and Complex Systems* The oscillatory Belousov-Zhabotinsky (BZ) reaction has been successfully used to study generic aspects of resonance in spatially extended systems parametrically forced with pulses of light. Experiments have reproduced Arnol'd tongues and pattern forming behavior predicted by reaction diffusion models and amplitude equations. We use the BZ reaction to experimentally demonstrate a transition in the 4:1 resonance regime from patterns of $\pi/2$ fronts to patterns of $\pi$ fronts. The transition matches the theoretical predictions. Above a certain driving strength, traveling $\pi/2$ fronts become unstable and a new stable pattern of stationary $\pi$ fronts emerges.

**9:00**

**U33 6 Mode locking in quasiperiodic structures** THOMAS CREIGHTON, *Syracuse University* A. ALAN MIDDLETON, *Syracuse University* AC driven extended systems, such as charge density waves or arrays of Josephson junctions, exhibit mode locking or giant Shapiro steps. This mode locking is seen experimentally as plateaus in a generalized velocity or current as a function of drive parameter. In conventional mode locking, the frequency of the response is a rational multiple of the frequency of the AC drive. For a model, we use a sandpile automaton model with local nonlinear update rules. When random quenched disorder is present in the automaton, a Devil's staircase with mode locking at all rational numbers has been previously seen. We investigate the use of quasiperiodic structures in place of the disordered structures. We find the novel phenomena of mode locking where the currents are a quasiperiodic multiple of the drive frequency. These quasiperiodic steps turn out to be stable to thermal fluctuations. Application of this model to Josephson junction arrays and structured colloidal systems will be presented.

**9:12**

**U33 7 Periodic time dependent problems in nonequilibrium quantum statistical mechanics** SELMAN HERSHFIELD, *Univ. of Florida* The usual Kadanoff-Baym or Keldysh formulation of nonequilibrium quantum statistical mechanics can be reformulated for steady state problems in terms of a nonequilibrium density matrix of the form $\exp(-(H-Y)/k_BT)$, where $H$ is the hamiltonian and $Y$ contains the information about how the system is driven out of equilibrium.* This approach has now been used to solve exactly solvable models as well as in approximate techniques. Here we show that for a periodic time dependent hamiltonian there is a similar formulation in terms of a nonequilibrium density matrix, where the density matrix acts in one higher dimension than in the original problem. Thus, a time dependent nonequilibrum problem is mapped onto a time independent nonequilibrium problem in one higher dimension. This is true for interacting as well as noninteracting problems. The approach is illustrated by applying it to some exactly solvable time dependent nonequilibrium problems such as tunneling through a resonant level where the level and/or the voltage applied are time dependent. * S. Hershfield, PRL **70**, 2134 (1993).

**9:24**

**U33 8 On Rolling Loaded Dice*** GARY WHITE, When an unfair die is tossed, what are the factors that determine the side upon which it lands? Sir Hermann Bondi (see European Journal of Physics 14, pp. 136-140) asked a related theoretical question in 1993 with the intention of determining the theoretical probability of a coin landing on its edge. He notes that the center of mass, the coefficients of restitution and friction, and the radius of gyration all play a role, perhaps. A simple model assumes that the probability of landing on a particular side is proportional to the solid angle subtended from the center of mass, but this model predicts too few base landings for tall cylinders, and too many rolling landings for squatty cylinders. Here we propose a thermodynamic modification of this model which qualitatively improves the match between experiment and theory by introducing an effective ''temperature'' parameter. We apply the model to several different geometrical shapes where the landing odds are not even, including right circular cylinders, rectangular prisms, hemispheres and semicylinders. We obtain, perhaps unreasonably, somewhat promising results.

*The author would like to thank the Society of Physics Students, including dozens of local chapters and hundreds of students, for their participation in and support of this project.

**9:36**

**U33 9 Broad spectrum period adding chaos in a transistor circuit.** THOMAS CARROLL, *Naval Research Lab* Period adding chaos, in which a driven system makes transitions such as period 2-chaos-period 3-chaos-period 4, is well known. In most cases, however, the frequency of the chaotic signal is close to the frequencies of the periodic signals. I have done expriments with a

simple circuit in which the chaos has a very broad power spectrum, covering 6 orders of magnitude. I have confirmed this broad band feature in numerical simulations of the circuit. These experiments have technological implications, because they show that a narrow band high frequency signal could produce broad band interference in even simple circuits.

**9:48**

**U33 10 Solving the Problem of Excessive Time Delay in Attractor Reconstruction** LOUIS PECORA, JON NICHOLS, THOMAS CARROLL, *Naval Research Laboratory* LINDA MONIZ, *US Geological Survey* We recently showed that the seemingly separate problems of finding a proper time delay and then finding a proper embedding dimension for attractor reconstruction are really the same problem which can be solved with a mathematical statistic faithful to the Takens reconstruction theorem. This approach also deals well with disparate time scales in data, and optimally choosing time series to use from a multivariate data set. However, the problem of when a time delay is too long for a chaotic time series remains. We introduce a new statistic that resolves this issue. The statistic is based on the mathematical observation that long time delays will result in data points that do not adequately populate the dynamical system's manifold. We present results with models and data that show we can predict when we have used excessively long time delays in attractor reconstruction.

**10:00**

**U33 11 Stochastic Loewner evolution driven by Lévy processes** ILIA RUSHKIN, *University of Chicago* PANAGIOTIS OIKONOMOU, *University of Chicago* LEO KADANOFF, *University of Chicago* ILYA GRUZBERG, *University of Chicago* Standard stochastic Loewner evolution (SLE) is driven by a continuous Brownian motion, which then produces a continuous fractal trace. If jumps are added to the driving function, the trace branches. We consider a generalized SLE driven by a superposition of a Brownian motion and a stable Lévy process. The situation is defined by the usual SLE parameter, $\kappa$, as well as $\alpha$ which defines the shape of the stable Lévy distribution. The resulting behavior is characterized by two descriptors: $p$, the probability that the trace self- intersects, and $\tilde{p}$, the probability that it will approach arbitrarily close to doing so. These descriptors are shown to change qualitatively and singularly at critical values of $\kappa$ and $\alpha$. These transitions occur as $\kappa$ passes through four (a well-known result) and as $\alpha$ passes through one (a new result). Numerical simulations are then used to explore the associated touching and near-touching events.

**10:12**

**U33 12 Positional Order and Diffusion Processes in Particle Systems** HIROSHI WATANABE, *Department of Complex, Systems Science, Graduate School of Information Science, Nagoya University* YUKAWA SATOSHI, NOBUYASU ITO, *Department of Applied Physics, School of Engineering, The University of Tokyo* In particle systems, a relation between the positional order parameter $\Psi$ and the mean square displacement $M$ is derived to be $\Psi \sim \exp(-vK^2M/2d)$ with a reciprocal vector $vK$ and the dimension of the system $d$. On the basis of the equiation, the behavior of $\Psi$ is found to be $\Psi \sim \exp(-vK^2Dt)$ when the system involves normal diffusion with a diffusion constant $D$. While the behavior in two-dimensional solid is predicted to be $M \sim \ln t$, numerical simulations shows a linear diffusion $M \sim t$. This can be explained by a swapping diffusion process which allows particles to diffuse without destroying the positional order.

**10:24**

**U33 13 Brownian dynamics of colloids in tilted periodic potential*** WEIQIANG MU, *Northwestern University* GANG WANG, *Indiana University, Purdue University Fort Wayne* GABRIEL SPALDING, *Illinois Wesleyan University* JOHN KETTERSON, *Northwestern University* We have studied the Brownian movements of micron-sized colloidal spheres in the presence of a periodic potential and the potential associated with gravity (which together form a so-called tilted-washboard potential). The optical potential is generated by the interference of two argon laser beams that are tightly focused through a common objective lens to form an in-plane standing wave in the vicinity of a substrate surface. As the intensity of standing wave is increased, the escape time of a particle trapped in a given potential well to the next lower one increases super-exponentially. More generally we have measured the time dependence of the probability density distribution of a colloidal particle as a function of the amplitude of the standing wave. The experimental data have been compared with a simulation based on the numerical integration of the Smoluchowski equation in the presence of the optical and gravitational potentials.

*Work supported by the National Science Foundation under Grant 03-29957

## SESSION U35: NANOWIRES
**Thursday Morning, 16 March 2006**
**338, Baltimore Convention Center at 8:00**
**Hyun Park, Naval Research Laboratory, presiding**

**8:00**

**U35 1 Dielectrophoretic assembly of reversible and irreversible metal nanowire networks and vertically-aligned arrays** STERGIOS J. PAPADAKIS, *Johns Hopkins University Applied Physics Laboratory* ZHIYONG GU, *Johns Hopkins University Department of Chemical and Biomolecular Engineering* DAVID H. GRACIAS, *Johns Hopkins University Departments of Chemistry and Chemical and Biomolecular Engineering* We demonstrate dielectrophoretic control of metallic nanowires in liquid suspensions. By varying parameters including the magnitude and frequency of the applied electric field, the liquid suspending the nanotubes, the nanowire metal, and the flow conditions, we can generate sparse or dense networks, multiply branching or predominately end-to-end networks, and vertically aligned nanowires standing on top of metal electrodes. The networks can be made reversibly or irreversibly. These results demonstrate the applicability of dielectrophoresis in aligning and positioning nanowires, either in the plane of the substrate or perpendicular to it, thereby suggesting a simple and versatile strategy for fabricating a range of integrated devices composed of nanowires. For example, sparse end-to-end networks are promising for individual electronic devices, dense branching networks take advantage of the large surface-to-volume ratio of nanowires for use as sensors, vertically-aligned arrays of nanowires may be used as vertical interconnects in damascene integration of microelectronic devices or in controlling the flow of fluid or light in microfluidic or nanophotonic devices, etc.

**8:12**

**U35 2 The Dielectrophoretically Guided Growth of Submicron, Near Single Crystal Indium Wires*** BRET FLANDERS, *Oklahoma State University* ISHAN TALUKDAR, *Oklahoma State university* BIROL OZTURK, *Oklahoma State University* TETSUYA MISHIMA, *University of Oklahoma* Dielectrophoresis was used to direct the growth of crystalline indium wires between lithographic electrodes immersed in solutions of indium acetate. Determination of the conditions that suppress side branching on these structures has enabled the fabrication of arbitrarily long needle-shaped wires with diameters between 367nm and 556nm. Electron diffraction studies indicate that these wires are crystalline indium, that the unbranched wire segments are single-crystal domains, and that the predominant growth-direction is near $\langle 110 \rangle$. This outcome constitutes a critical step towards the use of simply prepared aqueous mixtures as a convenient means of controlling the composition of submicron, crystalline wires.

*Supported by the National Science Foundation and Oklahoma EPSCoR.

**8:24**

**U35 3 Growth Characteristics of Dielectrophoretically Fabricated Single Crystal Wires*** ISHAN TALUKDAR, *Department of Physics, Oklahoma State University, Stillwater, Oklahoma, 74078* BIROL OZTURK, *Department of Physics, Oklahoma State University, Stillwater, Oklahoma, 74078* BRET FLANDERS, *Department of Physics, Oklahoma State University, Stillwater, Oklahoma, 74078* We investigate the mechanism underlying the dielectrophoretically guided growth of single-crystal metallic wires in aqueous solutions of metal-salts. The weak dependence of the mass deposition rate on the growth velocity suggests that the growth mechanism is consistent with microscopic solvability theory. We have also observed interesting dependencies of the growth velocities and the radii of these wires on the frequency of the dielectrophoretic voltage, and will report on our progress towards understanding these phenomena. The dependence of the wire's radius on the frequency is of potential technological interest in that it provides a sensitive means of controlling the submicron wire diameter.

*Supported by the National Science Foundation and Oklahoma EPSCoR.

**8:36**

**U35 4 Self-assembly of $Eu_2O_3$ nanoneedles and nanocrystals** JAMES DICKERSON, *Dept. of Physics and Astronomy, Vanderbilt University* SAMEER MAHAJAN, *Interdisciplinary Program in Materials Science, Vanderbilt University* MARCELA REDIGOLO, *Dept. of Physics and Astronomy, Vanderbilt University* DMITRY KOKTYSH, *Department of Chemistry, Vanderbilt University* Growth of anisotropic nanostructures starting from isotropic nanostructures is observed in $Eu_2O_3$ system. Anisotropic structures, like nanoneedles and nanospindles, are grown from the concentrated solution of $Eu_2O_3$ nanocrystals. This process involved the stepwise thermal growth of nanocrystals into ordered, high aspect ratio, one dimensional nanoneedles and the subsequent assembly of said nanoneedles into larger, oriented bundles (nanospindles). The $Eu_2O_3$ nanocrystals were synthesized following a room temperature, colloidal chemistry procedure, adapted from the synthesis of G. Wakefield et al.[1] We present the results of this self-assembly phenomenon using 4-nm $Eu_2O_3$ nanocrystals. High resolution transmission electron microscopy was employed to characterize the approximate shape, size distribution, and crystallinity of the nanostructures. Absorption and photoluminescence measurements were performed to investigate what effect the size and shape of materials has on optical properties. 1. G. Wakefield, H. A. Keron, P. J. Dobson, and J. L. Hutchison, J. of Coll. Interf. Sci. **215**, 179, 1999.

**8:48**

**U35 5 Three-dimensional nanoscale composition mapping of semiconductor nanowires.*** LINCOLN LAUHON, DANIEL PEREA, JONATHAN ALLEN, STEVEN MAY, BRUCE WESSELS, DAVID SEIDMAN, *Northwestern University* The composition of a single InAs nanowire was mapped in three dimensions with single-atom sensitivity and sub-nanometer resolution using local-electrode atom probe (LEAP) tomography. Arrays of epitaxial InAs nanowires were grown by chemical vapor deposition on GaAs substrates. Nanowires with diameters of 10-20 nm were analyzed over lengths of hundreds of nanometers. Three-dimensional reconstructions of the atoms in the nanowire showed hexagonal faceting, indicating that the LEAP analysis accurately reproduces the cross-section and shape of the nanowires. The Au catalyst particle sitting atop a nanowire was also analyzed; tomographic slices across the nanowire diameter, when displayed in 0.5 nm increments along the growth axis, revealed an extremely abrupt catalyst-nanowire interface that is also very flat. Despite the abruptness of the catalyst-nanowire interface, individual gold atoms were detected within the nanowire at a concentration of 100 ppm. These results indicate that LEAP microscopy can be used to (1) image buried nanowire interfaces in three dimensions and (2) analyze the concentration and distribution of dopant and impurity atoms in nanowires.

*Support from ONR and NSF is gratefully acknowledged.

**9:00**

**U35 6 Ligand Functionality to Control Morphology, Solubility, and Assembly Behavior of CdSe Nanorods** WEI WANG, SHENGGUO JIA, SARBAJIT BANERJEE, MICHAEL STEIGERWALD, IRVING HERMAN, *Columbia University* MATERIALS RESEARCH SCIENCE AND ENGINEERING CENTER, COLUMBIA UNIVERSITY TEAM, By varying the length of the carbon chain of the ligand, while keeping other reaction parameters the same, CdSe nanorods with different diameters and lengths, branched nanorods, and even nano-arrows have been synthesized. Since all the ligands used are phosphonic acids with the same binding group, the length of the carbon chain of the ligand can dramatically change the size and morphology of the nanocrystals. Thermogravimetric analysis (TGA) and differential scanning calorimetry (DSC) have been used to investigate the chemical composition of the nanorods. CdSe nanorod thin films have been made in hexane by electrophoretic deposition. The number and length of the ligands can dramatically change solubility, electrophoretic mobility of the nanorods, and quality of the nanorod film. We shall discuss mechanisms for ligand control of the nanocrystal structure. This work is supported by the MRSEC program of the National Science Foundation under Award No. DMR-0213574 and by the New York State Office of Science, Technology, and Academic Research (NYSTAR).

**9:12**

**U35 7 Twinning Superlattices in Semiconducting Nanowires** QIHUA XIONG, *Department of Physics, The Pennsylvania State University, University Park, PA 16802 USA* J. WANG, *Materials Research Institute, The Pennsylvania State Unviersity* PETER EKLUND, *Department of Physics, The Pennsylvania State University* We report the first observation of quasi-periodic twinning superlattices (TSLs) in semiconducting nanowires. The periodicity of the superlattice appears to be controlled by $\Delta T = T_m - T$, i.e., the degree of undercooling of the liquid phase in contact with the solid phase during VLS growth, where $T_m$ is the melting point of the solid phase. We present results from two III-V systems (GaP, InP) in which the superlattice is generated by the periodic 180[r] flipping of the $< 112 >$ direction relative to the $< 111 >$ growth direction of the nanowire. We suspect that our observations mean that a TSL structure can be grown in many compound semiconducting nanowire systems. Control of the superlattice period should allow significant design possibilities for thermoelectric, electronic and electro-optic applications. This work was supported, in part, by NSF-NIRT DMR-0304178

**9:24**

**U35 8 First Principles Studies of the Structural and Opto-Electronic Properties of Silicon Nanowires*** TRINH VO, *LLNL* ANDREW WILLIAMSON, *LLNL* GIULIA GALLI, *UC Davis and LLNL* We report the results of first principles studies of the structural, electronic, and optical properties of hydrogen-passivated silicon nanowires with [001], [011], and [111] growth directions and diameters ranging from 1 to 3 nm. We show that the growth direction, diameter, and surface structure all have a significant effect on the structural stability, electronic band gap, band structure, and band edge effective masses of the nanowires. The band gap is found to decrease with increasing diameter and to be further reduced by surface reconstruction. The band gap is direct for [001] and [011] NWs with diameters smaller than 3nm and [111] NWs with diameters smaller than 2nm. While the electron and hole effective masses are found to depend on NW size for [001] and [111] NWs, they are almost independent of size for [011] NWs. Finally, we use FEFF calculations to predict the EXAFS spectra produced by the relaxed atomic structure of the NWs and show that these spectra can serve as a tool for detection of surface reconstructions of the NWs.

*This work was performed under the auspices of the U.S. Dept. of Energy at the University of California/Lawrence Livermore National Laboratory under contract no. W-7405-Eng-48.

**9:36**

**U35 9 Ab initio investigation into the stability and electronic properties of GaN-nanowires** D.J. CARTER, *The University of Sydney, Australia* J.D. GALE, *Curtin University of Technology, Australia* B. DELLEY, *Paul Scherrer Institut, Switzerland* C. STAMPFL, *The University of Sydney, Australia* Recent reports of successful fabrication of high quality gallium nanostructures such as quantum dots, nanocrystallites and nanowires, e.g. [1], open the door to their possible role as important nanoscale building blocks for future optoelectronic, high-temperature/power and spintronic device applications. In the present work we perform itab initio calculations, using the DMol$^3$ [2] and SIESTA [3] codes, for wurtzite GaN nanowires. We have examined nanowires in the [0001], $[10\bar{1}0]$, and $[11\bar{2}0]$ directions, and investigated the stability, electronic and atomic structures as a function of nanowire radius. We found that only nanowires in the [0001] direction are stable, and that wires in the other directions can be stabilised by saturating dangling bonds with hydrogen. We have also investigated the properties of key point defects and dopants. [1] J. C. Johnson, et al. Nature Materials **1**, 106 (2002). [2] B. Delley, J. Chem. Phys. **92**, 508 (1990); ibid **113**, 7756 (2000). [3] J.M. Soler, et al. J. Phys.: Condens. Matter. **14**, 2745 (2002).

**9:48**

**U35 10 Au wetting of GaAs(111) studied on the atomic scale** EMELIE HILNER, ANDERS MIKKELSEN, JESSICA ERIKSSON, EDVIN LUNDGREN, *Lund University, Sweden* HONGSUK YI, PETER KRATZER, *FHI-MPG, Berlin, Germany* Because of the potential importance of semiconductor nanowires in future devices, a full understanding of their growth mechanism is desired. Au is commonly used to catalyze III-V nanowire growth, however the exact role of the Au in the growth process of the resulting wire is not known. This makes atomic scale studies of the Au/GaAs interface system well motivated. Here we report on the interaction of thin Au films and Au aerosol nanoparticles with the GaAs(111)B surface on the atomic scale using STM, LEED,LEEM, PEEM and ab-initio DFT calculations. We show that after deposition of Au either as a thin film or as aerosol nanoparticles and subsequent annealing to 450-600°C, a well ordered ($\sqrt{3}$x $\sqrt{3}$)R30° structure is formed. A structural model with a Au atom on every third threefold hollow hcp site of the Ga lattice is proposed based on theoretical calculations and experimental data.

## SESSION U36: FOCUS SESSION: OPTICAL PROPERTIES OF NANO-DOTS, HOLES, AND WIRES

**Thursday Morning, 16 March 2006**
**339, Baltimore Convention Center at 8:00**
**Connie Li, Naval Research Laboratory, presiding**

**8:00**

**U36 1 Geometrical scale invariance of the enhanced transmission spectra of subwavelength hole arrays*** SINAN SELCUK, KWANGJE WOO, DAVID B. TANNER, ARTHUR F. HEBARD, *Department of Physics, University of Florida* There is at present a lack of consensus on the relative strength of contributions from surface plasmon polaritons (SPPs) and composite diffracted evanescent waves (CDEWs) to the mechanism responsible for enhanced transmission through subwavelength hole arrays. For regular square hole arrays with small open area fraction $d^2/a^2$ ($a$ = lattice constant and $d^2$ = square hole area), both theories predict that the wavelength $\lambda = \lambda_m$ at which maximum transmission occurs scales linearly with $a$. The two interpretations diverge however when the open area fraction increases and the distance between two adjacent hole edges decreases. We test these ideas by comparing transmission spectra of sets of arrays where each set has a fixed open area fraction but is scaled to different sizes by changing $a$. We find in our preliminary data that for a factor of 10 change in $a$, from 1 $\mu$m to 10 $\mu$m, the transmission peaks, when plotted as a function of $\lambda/a$, collapse onto the same scaling curve. This collapse is independent of hole size $d$ and is in good agreement with SPP theory when the wavelength-dependent refractive indices of the substrates (quartz and ZnSe) are taken into account.

*Supported by Raytheon

**8:12**

**U36 2 Polarization and hole-shape dependence of the transmission of sub-wavelength hole arrays*** KWANGJE WOO, SINAN SELCUK, ARTHUR F. HEBARD, DAVID B. TANNER, *Department of Physics, University of Florida* We have measured the infrared and visible transmission of arrays of holes in silver films, to study the effects of hole shape and hole spacing as a function of the polarization of the light. The anomalous transmission enhancement of sub-wavelength hole arrays in metal films has been attributed to surface plasmon polaritons (SPPs) but this picture is not enough to explain the dependence of hole shape on the transmission due to the long wavelength approximation. We have measured the transmission of arrays of square holes, rectangular holes, and slits in a silver film. We studied the effect of different hole shapes on the enhanced transmission as a function of the polarization angle of the light and found a strong dependence on the hole shape and the polarization angle. In addition, transmission spectra of an array of square holes on a rectangular grid will be presented.

*This work was supported by Raytheon.

**8:24**

**U36 3 Tunneling, dipole interactions and coherent Rabi oscillations in quantum dot molecules.*** JUAN E. ROLON, JOSE M. VILLAS-BOAS, SERGIO E. ULLOA, *Ohio University* Quantum dot molecules (QDMs) - coupled quantum dot systems - have proved to be a promising optoelectronic circuit element for future implementation of quantum computation at the nanoscale. Here we investigate theoretically the coherent manipulation between exciton states in a single QDM. In particular, we study Rabi oscillations induced via strong laser pumping and their dependence on the interdot quantum coupling strength, including particle interdot tunneling and Coulomb interactions. The dynamics of the system is extracted by solving a quantum master equation using a multilevel density matrix that considers direct and indirect excitons in a rotating wave approximation. Possible decoherence mechanisms, such as coupling to wetting layer states and nonradiative recombination, are incorporated into the master equation using a Lindblad formulation. Careful control of the interdot coupling strength, laser detuning, and intensity, results in different population level dynamics. These are found to be critical for the entanglement between exciton states and the ultimate realization of Bell states for potential quantum information processing.

*Supported by Indiana 21st Century Fund

**8:36**

**U36 4 Microscopic Models of Hybrid Nanocrystal Superstructures: photonic properties** ALEXANDER O. GOVOROV, *Department of Physics and Astronomy, Ohio University* GARNETT W. BRYANT, *NIST, Atomic Physics Division* WEI ZHANG, TIMUR SKEINI, *Department of Physics and Astronomy, Ohio University* JAEBEOM LEE, NICHOLAS A. KOTOV, *University of Michigan* We investigate the optical properties of hybrid superstructures composed of metal and semiconductor nanoparticles (NPs), and bio-linkers/polymers. Our study is inspired by recent experiments on bio-conjugated semiconductor-metal NP complexes and their potential applications as sensors. Metal NPs can quench semiconductor NP photoluminescence (PL). However, a plasmon enhancement can be achieved by organizing many Au NPs into a spherical or cylindrical shell around a CdTe NP. We compute electromagnetic fields induced in NP superstructures using a multipole expansion approach to describe the optical response of these complexes. Enhancement of CdTe emission can result from plasmon mediated enhancement of the excitation (Ag structures) or enhancement of the emission process (Au structures). The resultant optical response comes from a complex interplay of this enhancement and quenching and determines the potential applications of these superstructures.

**8:48**

**U36 5 Spectroscopy of Charged Quantum Dot Molecules** E.A. STINAFF, M. SCHEIBNER, A.S. BRACKER, I.V. PONOMAREV, M.E. WARE, M.F. DOTY, T.L. REINECKE, D. GAMMON, *Naval Research Laboratory* V.L. KORENEV, *A.F. Ioffe Physical Technical Institute* Spins of single charges in quantum dots are attractive for many quantum information and spintronic proposals. Scalable quantum information applications require the ability to entangle and operate on multiple spins in coupled quantum dots (CQDs). To further the understanding of these systems, we present detailed spectroscopic studies of InAs CQDs with control of the discrete electron or hole charging of the system. The optical spectrum reveals a pattern of energy anticrossings and crossings in the photoluminescence as a function of applied electric field. These features can be understood as a superposition of charge and spin configurations of the two dots and represent clear signatures of quantum mechanical coupling. The molecular resonance leading to these anticrossings is achieved at different electric fields for the optically excited (trion) states and the ground (hole) states allowing for the possibility of using the excited states for optically induced coupling of the qubits.

**9:00**

**U36 6 Multi-Excitonic Quantum Dot Molecules** M. SCHEIBNER, E.A. STINAFF, M.F. DOTY, M.E. WARE, A.S. BRACKER, D. GAMMON, I.V. PONOMAREV, T.L. REINECKE, *Naval Research Laboratory, Washington DC 20375 USA* V.L. KORENEV, *A.F. Ioffe Physical Technical Institute, St. Petersburg 194021 Russia* With the ability to create coupled pairs of quantum dots, the next step towards the realization of semiconductor based quantum information processing devices can be taken. However, so far little knowledge has been gained on these artificial molecules. Our photoluminescence experiments on single InAs/GaAs quantum dot molecules provide the systematics of coupled quantum dots by delineating the spectroscopic features of several key charge configurations in such quantum systems, including X, $X^+$,$X^{2+}$, XX, $XX^+$(with X being the neutral exciton). We extract general rules which determine the formation of molecular states of coupled quantum dots. These include the fact that quantum dot molecules provide the possibility to realize various spin configurations and to switch the electron hole exchange interaction on and off by shifting charges inside the molecule. This knowledge will be valuable in developing implementations for quantum information processing.

**9:12**

**U36 7 Spin interactions in InAs quantum dots** M.F. DOTY, M.E. WARE, E.A. STINAFF, M. SCHEIBNER, A.S. BRACKER, D. GAMMON, I.V. PONOMAREV, T.L. REINECKE, *Naval Research Laboratory* V.L. KORENEV, *A.F. Ioffe Physical Technical Institute* Fine structure splittings in optical spectra of self-assembled InAs quantum dots (QDs) generally arise from spin interactions between particles confined in the dots. We present experimental studies of the fine structure that arises from multiple charges confined in a single dot [1] or in molecular orbitals of coupled pairs of dots. To probe the underlying spin interactions we

inject particles with a known spin orientation (by using polarized light to perform photoluminescence excitation spectroscopy experiments) or use a magnetic field to orient and/or mix the spin states. We develop a model of the spin interactions that aids in the development of quantum information processing applications based on controllable interactions between spins confined to QDs. [1] Polarized Fine Structure in the Photoluminescence Excitation Spectrum of a Negatively Charged Quantum Dot, Phys. Rev. Lett. 95, 177403 (2005)

**9:24**

**U36 8 Theory of Charged Quantum Dot Molecules** I.V. PONOMAREV, M. SCHEIBNER, E.A. STINAFF, A.S. BRACKER, M.F. DOTY, M.E. WARE, D. GAMMON, T.L. REINECKE, *Naval Research Laboratory, Washington DC* V.L. KORENEV, *A.F. Ioffe Physical Technical Institute, St. Petersburg, Russia* Recent optical spectroscopy of excitonic molecules in coupled quantum dots (CQDs) tuned by electric field reveal a richer diversity in spectral line patterns than in their single quantum dot counterparts. We developed a theoretical model that allows us to classify energies and intensities of various PL transitions. In this approach the electric field induced resonance tunneling of the electron and hole states occurs at different biases due to the inherent asymmetry of CQDs. The truncated many-body basis configurations for each molecule are constructed from antisymmetrized products of single-particle states, where the electron occupies only one ground state level in single QD and the hole can occupy two lowest levels of CQD system. The Coulomb interaction between particles is treated with perturbation theory. As a result the observed PL spectral lines can be described with a small number of parameters. The theoretical predictions account well for recent experiments.

**9:36**

**U36 9 Ultrafast dynamics of surface plasmon polaritons in subwavelength nanohole array on metallic film*** A.S. KIRAKOSYAN, T.V. SHAHBAZYAN, *Jackson State University* M. TONG, Z.V. VARDENY, *University of Utah* The ultrafast dynamics of surface plasmon polaritons (SPP) photogenerated on the surfaces of an Al film perforated with 2D subwavelength hole array ( $\sim$ 300 nm lattice constant) was studied by the pump-probe correlation spectroscopy. Following an instantaneous rise at the onset of the impinging pulse, the transient differential transmission exhibits a fast rise with characteristic time constant of $\sim$ 300 fs reaching a plateau at $\sim$ 2 ps, followed by a slower decay with characteristic time of $\sim$ 40 ps. The observed dynamics can be explained by a fast energy transfer in the Al film from the electron gas to the lattice, with subsequent cooling of the Al film by heat transfer to the glass substrate. The fast dynamics is accompanied by a blue shift of the SPP band due to the increase in the Al lattice temperature. The obtained fast lattice temperature rise is caused by the strong electron-phonon interaction in Al, which makes the electron-lattice energy transfer rate comparable to the rate of nonequilibrium electrons thermalization via electron-electron interactions. A theoretical model based on the Boltzmann equation for nonequilibrium electron gas interacting with quasi-equilibrium phonons was developed, and is in good agreement with the data.

*Supported in part by ARO and NSF

**9:48**

**U36 10 Internal and external polarization memory loss in single quantum dots** Q.Q. WANG, A. MULLER, *University of Texas at Austin* M.T. CHENG, H.J. ZHOU, *Wuhan University, P.R. China* P. BIANUCCI, C.K. SHIH, *The University of Texas at Austin* Exciton spin relaxation counts among the most basic features of quantum dot (QD) ground-state dynamics and is intimately connected to the ubiquitous fine-structure doublet anisotropy. Numerous resonant measurements on QD ensembles support a spin relaxation frozen on the exciton lifetime, in agreement with theoretical expectations. Recent investigations, however, question this breakdown based on strictly non-resonant experiments on single QDs, pointing to possible variations among QDs. By using non-linear resonant control of single QDs we examine spin relaxation under different environments and excitation conditions. Data from dots with different dipole moments reveals two distinctive channels for polarization memory loss: (i) an external pathway due to carrier escape and capture to and from the wetting layer that is responsible for memory loss increasing with intensity; and (ii) an internal loss channel, independent of external excitation, due to intrinsic spin relaxation. The values obtained for the latter rule out a universal freezing of exciton spin relaxation in self-assembled QDs.

**10:00**

**U36 11 Polarized Mid-Infrared Surface Emission from InAs Quantum Dots** D. WASSERMAN, S.A. LYON, C. GMACHL, *Princeton University* E.A. SHANER, *Sandia National Laboratories* Polarized mid-infrared surface electroluminescence from self-assembled InAs quantum dots has been observed at 77K. A graded AlGaAs injector is used to inject electrons into excited states in the quantum dot layer. A superlattice electron filter prevents direct electron tunneling out of the quantum dot excited states, increasing the probability of optical transitions to lower energy dot states. Two mid-infrared peaks are seen in the electrically pumped surface emission spectra of the device, one at 100meV, the other at 170meV. The emission peaks are orthogonally polarized within the growth plane, indicating photon emission from intersublevel electron transitions within anisotropically shaped quantums dots. This work suggests the feasibility of using quantum dot mid-infrared emission to study both the morphology of, and intersublevel transitions within, self-assembled quantum dots.

**10:12**

**U36 12 Optical properties of semiconductor-metal nanocrystal molecules: Exciton-plasmon interactions** WEI ZHANG, ALEXANDER O. GOVOROV, *Department of Physics and Astronomy, Ohio University* GARNETT W. BRYANT, *NIST, Atomic Physics Division* Motivated by recent experiments on bio-conjugated semiconductor-metal hybrid nanocrystal superstructures, we develop a theory to describe a system composed of a semiconductor quantum dot (QD) and a metal nanoparticle (NP) in the presence of external electric fields. The interaction between exciton (in QD) and plasmon (in NP) leads to interesting optical properties. We explore both the linear regime (for weak external field) and the non-linear regime (for strong external field). The interference between the external field and the induced internal field results in strong enhancement of energy absorption (compared with the energy absorption of QD in the absence of a metal NP) and also leads to an asymmetric peak and valley in the total energy absorp-

tion (Fano-like shape). We also consider Rayleigh scattering which also reveals this type of behavior. Our theory is useful for understanding present experimental results and can give guidance for future experiments, which may have important applications.

**10:24**
**U36 13 The Optical Properties of Aluminum Oxide Templated Nanostructures** MAHNAZ EL-KOUEDI, BRANDY BROGLIN, JERRY HEATH, J. TRES BRAZELL, *Department of Chemistry, UNC-Charlotte* The optical properties of aluminum oxide templated nanostructures has been investigated with the specific goal of using the associated structures for enhanced transmission of light, and Surface Enhanced Raman Spectroscopy (SERS). We will present fabrication and characterization data for three different nanostructures based on the synthesis of anodic aluminum oxide (AAO) templates. These structures include self-assembled metal coated masks with sub-wavelength apertures for the enhanced transmission of light, striped Au/Ag nanowire arrays and nano-textured aluminum surfaces for SERS studies. Characterization using electron and atomic force microscopies, as well as absorbance, reflectance and Raman spectroscopy will be presented.

**10:36**
**U36 14 First-Principles Optical Cross-Sections of Ultrathin ZnO Nanowires** SHELLY ELIZONDO, JOHN MINTMIRE, *Oklahoma State University, Department of Physics* One-dimensional nanostructures such as inorganic nanowires and nanotubes represent potential materials for key components of future electronic, optoelectronic, and nanoelectromechanical systems. They will also serve as important model systems to demonstrate quantum-size effects in nanostructured materials. We examine the electronic and optical properties of ZnO nanowires with different geometrical configurations within a first-principles, all-electron self-consistent local density functional (LDF) approach. Orientations along different growth directions are taken into account, with the preferred $\pm$ [0001] direction as the primary focus. The ultrathin nanowires considered here range in diameter from approximately 0.50 nm to 3 nm. We discuss trends in electronic properties and resulting optical properties as a function of nanowire axis orientation and diameter. This work was supported by the US Office of Naval Research, the DoD HPCMO CHSSI program through the Naval Research Laboratory, and the NSF IGERT program.

**SESSION U37: FOCUS SESSION: NANOWIRE AND NANODOT QUANTUM DEVICES**
**Thursday Morning, 16 March 2006**
**340, Baltimore Convention Center at 8:00**
**Alexey Bezryadin, University of Illinois, Urbana-Champaign, presiding**

***Contributed Papers***

**8:00**
**U37 1 Quantum Coherence and Time Dependent Conductance Fluctuations in Dilute Magnetic Semiconductors** SUNGBAE LEE, AARON TRIONFI, *Dept. of Physics and Astronomy, Rice University* TIMO SCHALLENBERG, HIRO MUNEKATA, *Imaging Science and Engineering Lab., Tokyo Institute of Technology* DOUG NATELSON, *Dept. of Physics and Astronomy, Rice University* Low temperature electrical properties of ferromagnetic nanowires are influenced by the interplay between disorder, quantum coherence, and magnetic correlations. Quantum coherence corrections to the conductance are of particular interest, and can be difficult to characterize experimentally. Time dependent universal conductance fluctuation (TD-UCF) at low temperatures provides a means of assessing these effects. Samples were fabricated by standard electron beam lithography and ion etching technique using $In_{1-x}Mn_xAs$ quantum well samples grown by off-equilibrium molecular beam epitaxy. Initial measurements of temperature and field-dependent TD-UCF in these devices are presented and compared with permalloy nanowire data.

**8:12**
**U37 2 Microwave-enhanced decoherance in one-dimensional metal wires** JIAN WEI, SERGEI PEREVERZEV, MICHAEL GERSHENSON, *Rutgers University* We report the effect of monochromatic microwave (MW) radiation on the weak localization corrections to the conductivity of quasi-one-dimensional silver wires. Due to the improved electron cooling in the wires, the MW-induced dephasing was observed without a concomitant overheating of electrons over wide ranges of the MW power $P_{MW}$ and frequency $f$. The observed dependences of the conductivity and MW-induced dephasing rate on $P_{MW}$ and $f$ are in agreement with the theory by Altshuler, Aronov, and Khmelnitsky.[1] Our results suggest that the saturation of dephasing time, often observed at $T \leqslant 0.1$ K, may be caused by an insufficient screening of the sample from the external microwave noise.

[1]B.L. Altshuler, A.G. Aronov, and D.E. Khmelnitsky, Sol. State Communi. **39**, 619 (1981).

**8:24**
**U37 3 Toward Single-Walled Nanotube Aharonov-Bohm interferometers** JINSEONG HEO, *Caltech* MARC BOCKRATH, *Caltech* Single-walled carbon nanotubes (SWNTs), which have micron-scale phase coherent lengths at low temperatures, are grown so that they cross themselves, producing a loop that may act as an Aharonov-Bohm interferometer. In order to determine electron pathways at the junction, we performed scanned gate microscopy (SGM) using an Atomic Force Microscopy(AFM) tip as a local gate. If a SGM signal is observed when the tip is over any particular segment it indicates current flow in that segment. Surprisingly, one semiconducting tube showed that most electrons tunnel into the other segment at the junction without flowing through the loop. For other samples, however, current flow was observed in the loop. Taken together, this suggests the possibility of controlling tunneling probabilities at the junction. Moreover, for metallic or small bandgap nanotubes, we reproducibly observe an unusual conductance peak near zero gate voltage, obtaining nearly identical behavior from devices made from the same 100 micron long nanotube. The results and interpretations of our ongoing experiments will be discussed.

*Invited Papers*

**8:36**
**U37 4 Quantum Transport of Semiconductor Nanowires Coupled to Superconductors.***
YONG-JOO DOH, *Harvard University*

We report the electronic transport properties of the first superconducting transistors based on semiconductor nanowires [Y.-J. Doh et al., Science 309, 272 (2005)]. These nanoscale superconductor-semiconductor devices enable the fabrication of new nanoscale superconducting electronic circuits and at the same time provide new opportunities for the study of fundamental quantum transport phenomena. Indium arsenide (InAs) semiconductor nanowires individually contacted by two aluminum-based superconductor electrodes yield surprisingly low contact resistances. Below 1 kelvin, the high transparency of the contact gives rise to proximity-induced supercondcutivity and a resistance-free current (supercurrent) can flow through the nanowire from one superconducting contact to another. The supercurrent can be switched on and off by a gate voltage acting on the electron density in the nanowire. A variation in gate voltage induces universal fluctuations in the normal-state conductance, which are clearly correlated to critical current fluctuations. The alternating-current Josephson effect gives rise to Shapiro steps in the voltage- current characteristic under microwave irradiation. For indium phosphide (InP) nanowire devices, however, Coulomb blockade effect dominates the electrical transport, which can be modeled as a quantum dot weakly coupled to superconductors. As a result of BCS (Bardeen-Cooper-Schriffer) singularity of density of states, a negative differential conductance is observed in the superconducting state. By applying high magnetic field, Zeeman splitting is observed and g-factor of InP nanowire is estimated to be 1.5.

*This work is a result of collaboration between Kavli Institute of Nanoscience Delft and Philips Research Laboratories in the Netherlands and Laboratorio Nazionale TASC-INFM in Italy.

*Contributed Papers*

**9:12**
**U37 5 Four-probe measurements of individual metallic and superconducting nanowires** SHENG-YONG XU,* *DMP* MINGLIANG TIAN, *DMP* NITESH KUMAR, *DMP* MOSES H. W. CHAN, *DMP* CHAN GROUP TEAM, We have performed 4-probe measurements for a number of individual Au, Ag, Sn and Zn nanowires. The resistivity of these nanowires is always larger than their bulk values, and varies with the crystallinity of the nanowires. Single crystalline Sn nanowires have a resistivity similar to that of bulk Sn, while polycrystalline Au nanowires shows a resistivity twenty to thirty times higher than that of bulk Au. For Sn nanowires with diameter from 280 nm to 70 nm, the superconducting transition temperature $T_c$ remains the same as, or slightly lower than the $T_c$ of bulk Sn, 3.7 K. The critical current density of these Sn nanowires is measured to be in the order of 105 A/cm2 at low temperature. The critical fields of the nanowires, as expected, are much higher than that of Sn films. A finite resistance, which increases with increasing excitation current, is observed in all the samples. The origins of this finite resistance will be discussed. We have also obtained evidence that the four metallic leads assembled on each single nanowire may have remarkable effects on the transport properties of the nanowire.

*presenting author

**9:24**
**U37 6 Modifying Mesoscopic 1/f Noise Via Surface Chemistry.** A. TRIONFI, *Rice University Dept. of Physics and Astronomy* J.W. CISZEK, J.M. TOUR, *Rice University Dept. of Chemistry* D. NATELSON, *Rice University Dept. of Physics and Astronomy* Attempts to extrinsically control the 1/f noise related to Universal Conductance Fluctuation Theory in quasi-one dimensional Au wires were made using self-assembled monolayer (SAM) molecules. Measurements before and after the deposition of the SAM molecule comparing the noise power amplitude and the phase coherence of the devices via the weak localization magnetoresistance and noise power amplitude versus magnetic field were performed. The resulting data were used to determine if the 1/f noise is approaching the so-called saturated limit as the system is lowered from 14 to 2 K. The results may also shed light on the microscopic details of the two level systems responsible for time-dependent conductance fluctuations in normal metals. Preliminary results will be reported.

**9:36**
**U37 7 Coulomb Blockade Imaging of Few-Electron Quantum Dots in a Magnetic Field*** P. FALLAHI, R. WESTERVELT, M. STOPA, *Harvard University* M. HANSON, A.C. GOSSARD, *U.C. Santa Barbara* One-electron quantum dots are important candidates for quantum information processing. We have developed a technique to image electrons inside a quantum dot in the Coulomb blockade regime, using a scanning probe microscope (SPM) at liquid He temperatures (1). We have used this technique to image the last electron in the dot in a strong perpendicular magnetic field.dots are formed in a two-dimensional electron gas in a GaAs/AlGaAs heterostructure by surface gates. Images are obtained by recording the dot conductance while scanning the SPM tip above the dot. SPM Images show a ring of increased conductance about the center of the dot, corresponding to a Coulomb blockade peak in the dot conductance.observe changes in the shape and the size of the conductance rings with magnetic field. This is due to a combination of energy shifts and orbital changes of the electrons in the quantum dot. (1) P. Fallahi et al, Nano Letters 5, 223 (2005)

*This work was supported at Harvard University by DARPA DAAD19-01-1-0659 and by the NSEC, NSF PHY-01-17795, and at UCSB by IQCD NSF Science and Technology Center.

**9:48**
**U37 8 Kondo and Superconducting Proximity Effect in Semiconductor Nanostructures** ANDY VIDAN, MICHAEL STOPA, ROBERT WESTERVELT, *Harvard University* MICAH HANSON, A.C. GOSSARD, *UC Santa Barbara* JIE XIANG, CHARLES M. LIEBER, *Harvard University* We have fabricated a unique device containing three quantum dots in a GaAs/AlGaAs heterostructure containing a two-dimensional electron gas using

lithographically patterned gates and an etched trench in the center of the ring. By only energizing certain gates, this device allows us to study electron transport through a single dot, a double dot, or a triple dot ring. We can determine the absolute number of electrons in a quantum dot using a nearby charge sensor and find that we are able to tune a single dot to the one and two electron regime. We find several sharp peaks in the differential conductance, occurring at both zero and finite source-drain bias, for the one and two electron quantum dot. At zero source-drain bias, the temperature and magnetic field dependence of the conductance is consistent with a standard Kondo resonance. We attribute the peaks at finite-bias to a Kondo effect through excited states of the quantum dot. We also present recent observations of supercurrents in Gels: 1D nanowire heterostructures.

**10:00**

**U37 9 Transition to Scarred States Probed by a Single Electron Spectrometer** ROBERT E. PARROTT, *Harvard University* DOMINIK M. ZUMBUHL, *Massachusetts Institute Of Technology* ERIC J. HELLER, CHARLES M. MARCUS, *Harvard University* MICAH P. HANSON, ARTHUR C. GOSSARD, *University of California, Santa Barbara* We examine the use of a novel mesoscopic spectrometer to image electron dynamics in a large, open lateral quantum dot in a perpendicular magnetic field $B_z$. The spectrometer is comprised of a small single-electron quantum dot weakly coupled to the large dot via a tunnel junction; the current through the dots is measured at finite bias. By varying the energy level of the small dot, the local density of states, $g(r_o,E)$ is measured at the tunnel junction. An unexpected interference effect persists at energies 1 meV below $E_F$. Using semiclassical and quantum approaches, we show these interference bands in $(E,B_z)$ are due to a dominant, diamond-shaped periodic orbit in the large dot. As $B_z$ is varied, the orbit changes to unstable: the dominant state becomes a scar. This transition is marked by an abrupt change in the area of the orbit, and hence in the spacing $\Delta B_z$ of the bands. In a billiard model of the system, this coincides with a pitchfork bifurcation of the orbit. The existence of the bands depends strongly on whether the orbit has appreciable magnitude at the tunnel junction, belying the local nature of the measurement. In this way the tunnel junction, coupled to the small dot, acts like a fixed STM tip embedded in the 2DEG.

**10:12**

**U37 10 Magneto-transport studies in mesoscopic InAs 2DEG devices*** ERNESTO MARINERO, THOMAS BOONE, LIESL FOLKS, BRUCE GURNEY, JORDAN KATINE, SERGIO NICOLETTI, *Hitachi San Jose Research Center* We report on magneto-transport studies in lithographically patterned InAs 2DEG devices. Electron transport between adjacent current injection and extraction channels was studied as a function of temperature and magnetic field. The mean free path in the quantum well at RT and 5 K in our devices is approximately 280 nm and 980 nm respectively. The spacing between the current tabs in our devices range from 1000 nm to 300 nm and typical tab widths range from 300 nm to 100 nm. Low temperature measurements reveal contributions of ballistic transport in our devices; fluctuations in magneto-resistance are observed at distinct values of the perpendicularly applied magnetic field. Said fluctuations will be discussed in the context of ballistic electron focusing trajectories and possible contributions from the quantum Hall effect.

*We gratefully acknowledge collaborative efforts with Mark Field, Gerry Sullivan, and Robert Brar from Rockwell Scientific Co, who grew the InAs 2DEG structures.

**10:24**

**U37 11 Asymmetry of Nonlinear Transport and Electron Interactions in Quantum Dots** D. M. ZUMBÜHL, *MIT and Harvard University* C. M. MARCUS, *Harvard University* M. P. HANSON, *UCSB* A. C. GOSSARD, *UCSB* The magnetic field symmetry of conductance beyond the linear source-drain bias regime in open chaotic GaAs quantum dots is experimentally investigated using gate-controlled shape distortion to gather ensemble statistics. We measure a conductance component $g_{B-}$ antisymmetric in perpendicular magnetic field $B$ which is of the form $\tilde{g} = \alpha VB$ for source-drain bias voltages $V$ smaller than the quantum dot level spacing $\Delta$ and for $B$ smaller than a flux quantum through the device area. Interestingly, according to recent theories, $\tilde{g}$ of this form vanishes in absence of electron interactions and $\alpha$ is proportional to the electron interaction strength. $g_{B-}$ shows mesoscopic fluctuations with shape gate and with $B$ and $V$ on a scale of the flux quantum through the dot area and quantum dot level spacing $\Delta$, respectively. As anticipated by theories, the average coefficient $\alpha$ measured over an ensemble of dot shapes vanishes. The standard deviation of $\alpha$ is used to characterize the strength of electron interactions. We discuss the dependence of the typical $\alpha$ on the number of modes in the quantum-point-contact leads, compare our experiment with theories and discuss related issues of electron equilibration, decoherence and thermal smearing in the quantum dot. This work was partially supported by DARPA QuIST, ARO/ARDA and by the NSEC program of the NSF.

**10:36**

**U37 12 Two Electron Singlet Triplet Spectroscopy** IULIANA RADU, D.M. ZUMBÜHL, C.R. DILLARD, G. GRANGER, M.A. KASTNER, *MIT* M.P. HANSON, A.C. GOSSARD, *UCSB* We present measurements of few electron quantum dots formed by lateral depletion of a GaAs/AlGaAs 2D electron gas by surface gates. The two electron regime, on which we focus here, is characterized by singlet and triplet states which are relevant for quantum computation proposals. These two states are revealed in electronic transport through the dot in various ways: sequential tunneling, inelastic cotunneling as well as by an additional mode of transport we ascribe to sequential tunneling activated by inelastic cotunneling. These various signatures provide independent ways to measure the singlet-triplet energy splitting J over large ranges of gate voltages. We present the temperature, magnetic field and tunnel-coupling dependence of these transport features, which are in good agreement with recent theory. Further, we observe signatures of spin-blockade that becomes visible for source-drain voltages exceeding the triplet energy. This work was partially supported by the ARO (W911NF-05-1-0062), by the NSEC program of the NSF (PHY-0117795) and by NSF (DMR-0353209).

**10:48**

**U37 13 Superpoissonian noise with positive current correlations** YUANZHEN CHEN, RICHARD WEBB, *USC Nanocenter, University of South Carolina* We report shot noise cross correlation measurements in a beam splitter configuration. We fabricated our devices in a two dimensional electron gas in a GaAs/AlGaAs heterostructure using a splitting gate technology. Electrons tunneling across tunnel barriers are incident on a beam splitter and are scattered into two different channels. Shot noise cross correlation between the two electrical currents is measured as a function of both the transmission coefficient of the beam splitter and the Fano factor of the tunnel barriers. Due to the Fermi statistics of electrons, such a measurement usually yields a negative correlation.

However, in some barriers under certain circumstances, a positive correlation has also been observed. A correspondence between the Fano factor of the tunnel barriers and the cross correlation has been established. For example, positive cross correlation is always associated with barriers exhibiting superpoissonian shot noise (with a Fano factor greater than one). Studies on the frequency dependence of shot noise suggest that the observed positive cross correlation can be related to the dynamics of localized states in the tunnel barriers.

**SESSION U38: 1-D SUPERCONDUCTORS AND ORGANICS**
**Thursday Morning, 16 March 2006**
**341, Baltimore Convention Center at 8:00**
**Andrei Lebed, University of Arizona, presiding**

**8:00**
**U38 1 High-Tc superconductivity in entirely end-bonded carbon nanotubes** JUNJI HARUYAMA, IZUMI TAKESUE, NAOKI KOBAYASHI, *Aoyama Gakuin University* SHOHEI CHIASHI, SHIGEO MARUYAMA, *Tokyo University* TOSHIKI SUGAI, HISANORI SHINOHARA, *Nagoya University* One-dimensional (1D) systems face some obstructions that may prevent the emergence of superconductivity(SC), e.g., a Tomonaga-Luttinger liquid (TLL) and Peierls transition. A carbon nanotube (CN) is one of the best candidates for investigating a possibility of 1D SC and its interplay with such obstructions. Only two groups have experimentally reported SC in ropes of single-walled CNs (SWNTs) and very thin SWNTs [1] to date. In addition, those interplay with 1D phenomena have never been clarified. Some theoretical papers also predicted strong correlation between TLL states and SC for SWNT ropes and importance of electron-phonon interaction for thin SWNTs [2]. Here, we report that entirely end-bonded multi-walled CNs (MWNTs) can show SC with the $T_c$ as high as 12K [3] (about 50-times larger than $T_c$ in former of [1]). We find that emergence of this SC and its interplay with TLL states are highly sensitive to junction structures of Au electrode/MWNTs. Only MWNTs with optimal numbers of electrically activated shells realized by the entire end-bonding can allow the SC due to intershell effects. Refs. 1. M. Kociak, et al., PRL 86, 2416 (2001); Z. K. Tang, et al., Science 292, 2462 (2001). 2. J. Gonzalez, PRL 88, 076403 (2002); R. Barnett, et al., PRB 71, 035429 (2005). 3. J. Haruyama et al., PRL Accepted

**8:12**
**U38 2 Superconductivity of granular Bi nanowires fabricated by electrochemical deposition at ambient condition** MINGLIANG TIAN, JINGUO WANG, TIANHENG HAN, YOJI KOBAYASHI, NITESH KUMAR, SHENGYONG XU, YING LIU, THOMAS MALLOUK, MOSES CHAN, *Penn State University, University Park, PA 16802* Rhombohedral bulk Bi is a semimetal which is not superconducting down to low temperatures under ambient pressure. Amorphous Bi films and bulk Bi subjected to high pressure can be superconducting. We report here the observation of superconductivity of Bi nanowires (the diameter ranges from 40 to 100 nm) fabricated by electrochemical deposition at room temperature under atmospheric pressure. The superconducting transition temperature Tc, depending on the sample morphology, can be either of 3.7 K, 7.2 K or 8.3 K, which correspond exactly to the Tc's reported for the three high pressure Bi phases (II, III and V). However, structural studies showed that these superconducting Bi nanowires showed granular morphology consisting of rhombohedral Bi particles oriented along the [001] direction. Because the superconducting Bi wires did not show any detectable diamagnetic signature, the observed superconductivity might be related to the interfacial structures of the granular wires. Further studies are in progress. This work is supported by it the Center for Nanoscale Science (Penn State MRSEC) funded by NSF under grant DMR-0213623.

**8:24**
**U38 3 Enhancing superconductivity: Magnetic impurities and their quenching by magnetic fields** TZU-CHIEH WEI, DAVID PEKKER, ANDREY ROGACHEV, ALEXEY BEZRYADIN, PAUL M. GOLDBART, *University of Illinois at Urbana-Champaign* Magnetic fields and magnetic impurities are each known to suppress superconductivity. However, it has recently been found theoretically that in superconducting films with magnetic impurities the critical temperature can be raised by applying a magnetic field ($H$) [1]. Here, we extend the Eilenberger-Usadel formalism and use it to investigate this interplay of magnetic fields and magnetic impurities. Hence, we are able to compute the critical current ($J_c$) of a thin superconducting wire, in addition to its critical temperature ($T_c$). We find three regimes of wire parameters. In one, both $T_c$ and $J_c$ simply decrease with $H$; in a second, both $T_c$ and $J_c$ first rise and then fall with $H$; and in a third, $T_c$ simply decreases with $H$ but, at sufficiently low temperatures, $J_c$ first rises and then falls [2]. Our results are consistent with recent experiments on thin superconducting wires [3]. [1] M. Kharitonov and M. Feigel'man JETP Lett. **82**, 473 (2005). [2] T.-C. Wei et al. cond-mat/0510476. [3] A. Rogachev et al. (manuscript in preparation).

**8:36**
**U38 4 Anomalous behavior of the critical current in superconducting MoGe nanowires exposed to high magnetic fields.** A. ROGACHEV, T.-C. WEI, D. PEKKER, A.T. BOLLINGER, P.M. GOLDBART, A. BEZRYADIN, *University of Illinois at Urbana-Champaign* At low temperatures the critical current of superconducting MoGe nanowires with diameters 6-10 nm shows an unusual initial growth with increasing magnetic field, and reaches a maximum at the field 3-5 T. The non-monotonic behavior is present both in parallel and perpendicular field orientations and disappears at high temperatures. We suggest that the effect is caused by magnetic impurities, which suppress superfluid density in the nanowire at low fields but, due to partial polarization in the applied magnetic field, become less efficient pair-breakers in high fields. We compare our data with the microscopic theory that considers this competition of the reduced depairing by localized spins and the increasing depairing by the orbital effects [1]. The theory reproduces all experiential observations and suggests that magnetic impurities reside on a surface of a wire. [1] T.-C. Wei, D. Pekker, A. Rogachev, A. Bezryadin, and P.M. Goldbart, cond-mat/0510476.

**8:48**

**U38 5 Confined Vortices in $NbSe_2$ Nanowires** ABRAM FALK, *Department of Physics, Harvard University* MANDAR DESHMUKH, AMY PRIETO,* ANDREA JONES, *Department of Chemistry, Harvard University* HONGKUN PARK, *Department of Chemistry, Department of Physics, Harvard University* Superconducting $NbSe_2$ nanowires have been studied with electrical transport. The cross-sectional dimensions are smaller than the London penetration depth, and signatures of confined magnetic vortices have been observed. The critical current shows non-monotonic behavior as the external magnetic field is increased, including periodic features corresponding to matching fields. In the vicinity of the critical current, we observe several peaks in the differential resistance as a function of bias current, consistent with the plastic flow of vortices. These observations are discussed in the context of theoretical London model studies and experiments in thin-film superconductors and bulk $NbSe_2$.

*Present address: Department of Chemistry, Colorado State University

**9:00**

**U38 6 Growth Mechanism of $EuBa_2Cu_3O_{7-\delta}$ Whiskers and Their superconducting properties for Intrinsic Josephson Junction Applications*** A.T.M. NAZMUL ISLAM, T. KAWAE, Y. TACHIKI, S. WATAUCHI, Y. TAKANO, T. HATANO, T. YAMASHITA, I. TANAKA, We have grown Eu-123 single-crystal whiskers by annealing of precursor pellets containing Ca and Te. Microstructural and compositional analysis was performed on the longitudinal cross-section and the area of origin of a whisker to elucidated some aspects of the growth mechanism from bulk precursor. Sub-micron sized junctions fabricated by focus ion-beam etching on Eu-123 whiskers showed clear multi-branch with hysteresis structure in the I-V curve, which suggest excellent crystalline quality both of as-grown and high pressure annealed whiskers. We have also doped Er and Tm having a smaller ionic radius in single crystalline whiskers of (Eu,R)-123 (R= Er, Tm) and observed that Eu-rich whiskers, which require higher temperature to be grown, are more susceptible to oxygen deficiencies and structural instabilities. Our results shows that the carrier doping can be systematically controlled from highly underdoped to slightly overdoped range by suitable choice of average ionic radius of rare-earth elements in as-grown whiskers. The critical current density $J_c$ of a Eu-123 whisker ($T_c$=45K) was estimated to be $1.43 \times 10^5$ A/cm$^2$ at 4.2K, twice as much as observed for Y-123 having a similar $T_c$ .

*This work is partially supported by Marubun Research Promotion Foundation, Japan

**9:12**

**U38 7 Evidence for Current-Driven Phase Slip Lines in Submicron High-$T_c$ Superconducting Wires*** P. MORALES, J.Y.T. WEI, *Department of Physics, University of Toronto* We present superconducting current-voltage characteristics of submicron $YBa_2Cu_3O_{7-\delta}$ wires. The submicron-wide wires were fabricated using a chemical-free technique based on selective epitaxial growth. Pulsed current-biased and voltage-biased measurements were made between 4.2 K and $T_c$ and as a function of an applied magnetic field. The current-voltage characteristics exhibit distinctive behaviour suggesting that the current-driven or voltage-driven transition of our submicron high-$T_c$ wires into the resistive state is through the formation of phase slip lines.

*Work supported by NSERC, CFI/OIT, MMO/EMK, and Canadian Institute for Advanced Research.

**9:24**

**U38 8 Quantum phase slips in the presence of finite-range disorder** LEONID P. PRYADKO, *University of California, Riverside* SERGEI KHLEBNIKOV, *Purdue University* To study the effect of disorder on quantum phase slips (QPS) in superconducting nanowires, we consider the plasmon-only model where disorder can be incorporated into a first-principles instanton calculation. We consider weak but general finite-range disorder and compute the formfactor in the QPS rate associated with momentum transfer. We find that the system maps onto dissipative quantum mechanics, with the dissipative coefficient controlled by the wave (plasmon) impedance $Z$ of the wire and with a superconductor-insulator transition at $Z_c = 6.5$ kOhm. The usual Ohmic resistivity of the wire at the transition point is non-universal. Its value depends on both the strength and the correlation length of disorder, and in the considered regime is much smaller than the normal-state resistivity. We argue that the system will remain in the same universality class after resistive effects at the QPS core are taken into account.

**9:36**

**U38 9 Magnetization controlled superconductivity in a Pb film on a perpendicular array of ferromagnetic Co nanowires*** ZUXIN YE, DAYA RATHNAYAKA, WENHAO WU, HAIDONG LIU, HONG ZHANG, DONALD NAUGLE, IGOR LYUKSYUTOV, JOSEPH ROSS JR., *Texas A&M University* We report the studies of superconductivity in a Pb film on a perpendicular array of ferromagnetic Co nanowires. We first evaporate a Pb film of 300nm in thickness on a 60$\mu$m-thick porous $Al_2O_3$ membrane as the cathode for electroplating. Cobalt nanowires 100nm in diameter were electrochemically deposited in the pores starting from the Pb film. Scanning electron microscopy images showed uniform distribution of cobalt nanowires. The magnetization of the individual Co nanowires should be oriented perpendicular to the Pb film due to the high aspect ratio of the Co nanowires. We have observed significant difference in the superconducting behavior of the Pb film between zero-field cooled experiments and field-cooled experiments. In field-cooled experiments, the samples are cooled from room temperature to 20 K in fields of 1-5 T applied along the direction of the Co nanowires. This field aligns the magnetization of the Co nanowires, and as a result, enhances the superconducting transition temperature by 1.5-2.0 K in comparison to zero-field cooled experiments in which case the magnetization of the nanowires is not aligned. These experimental data support recent theory by I. F. Lyuksyutov et al. [PRL **81**, 2344(1998)].

*Supported by NSF Grant No. DMR-0551813.

**9:48**

**U38 10 Current carrying edges in unconventional superconductors** RAHUL ROY, *University of Illinois at Urbana Champaign* While the bulk of a p or d wave superconductor does not carry any current, a current can run along the edges of a sample even in the absence of a magnetic field, unlike the case of a s wave superconductor. Such a current is often quantized and is independent of the magnitude of the gap. However, the existence of such a current violates Bloch's theorem. Here, we examine, by computation and analytic calculation, the question of the edge current in p and d wave superconductors in various geometries and the connection with the Bloch argument. The computation of the edge current also allows us to shed some light on the angular momentum paradox in the A phase of Helium 3.

**10:00**
**U38 11 The coherence conundrum in BEDT-TTF superconductors; how does interlayer transport die as temperature rises?*** JOHN SINGLETON, *Natl. High Magnetic Field Lab* PAUL GODDARD, ARZHANG ARDAVAN, *Oxford University Physics* STAN TOZER, ROSS MCDONALD, *Natl. High Magnetic Field Lab* JOHN SCHLUETER, *ANL* Recent attention has focused on ''bad metals,'' systems which appear to be Fermi liquids at low temperatures ($T$), but whose conductivity falls below the minimum metallic limit as $T$ rises. A key question concerns the coherence of the electron orbitals, and whether, as suggested by Anderson and others, it is destroyed by thermal fluctuations as $T$ rises. To address this, we have studied magnetic-field-orientation-dependent transport in the organic superconductor $(BEDT\text{-}TTF)_2Cu(NCS)_2$ at temperatures of up to 45 K in magnetic fields of up to 45 T. This material was chosen because its Fermi surface (FS) is well characterized by experiment. We find that the angle-dependent magnetoresistance oscillations (AMROs) due to orbits on the quasi-one-dimensional (Q1D) and Q2D FS sections are suppressed by rising $T$, with a $T$ dependence suggesting phonon scattering. The coherence peak in the resistivity seen in exactly in-plane fields, and other signatures of a 3D FS, remain to values of $T$ that exceed the proposed Anderson criterion for incoherent transport by a factor of order 80! The implications of these data for currently-held ideas about bandstructure will be discussed.

*Work supported by DOE, NSF, the State of Florida and EPSRC (UK)

**10:12**
**U38 12 Interplane penetration depth in $\kappa$-$(ET)_2Cu[N(CN)_2]Br$*** RUSSELL GIANNETTA, *University of Illinois at Urbana-Champaign, Urbana, IL 61801* Z. SHI, T.A. OLHEISER, A. MCCORMICK, D.D. LAWRIE, *Loomis Laboratory of Physics, U. of Illinois at Urbana-Champaign, Urbana, IL 61801* R. PROZOROV, *Ames Laboratory and Department of Physics and Astronomy, Iowa State University, Ames, Iowa 50011* J.A. SCHLUETER, A.M. KINI, U. GEISER, *Material Sciences Division, Argonne National Laboratory, Argonne, IL 60439* We report measurements of the interplane penetration depth $\lambda_\perp(T)$ in the organic superconductor $\kappa - (ET)2Cu[N(CN)2]Br$ ($TC = 11.9$ K). At low temperatures, the superfluid density $\rho\perp = [\lambda\perp(0)/\lambda\perp(T)]2 \propto 1-ATN$ with $N = 1.3 -- 1.5$, close to the exponent measured for the in−plane superfluid density. This result adds support to a d−wave picture, but with transport between planes more coherent than is observed in similarly anisotropic copper oxide superconductors.

*Work at UIUC supported by NSF DMR 05−03882. Work at Argonne National Lab supported by DOE contract # W−31−109−ENG−38.

**10:24**
**U38 13 London penetration depth in fully deuterated $\kappa$-$(ET)_2Cu[N(CN)_2]Br$*** T.A. OLHEISER, R.W. GIANNETTA, D.D. LAWRIE, *Loomis Laboratory of Physics, University of Illinois at Urbana-Champaign, Urbana, IL 61801* R. PROZOROV, *Ames Laboratory of Physics and Department of Physics and Astronomy, Iowa State University, Ames, Iowa 50011* J.A. SCHLUETER, A.M. KINI, U. GEISER, *Materials Science Division, Argonne National Laboratory, Argonne, IL 60439* We report measurements of the London penetration depth, $\lambda$, for different magnetic field and crystal orientations in fully deuterated $\kappa$ $(ET)_2Cu[N(CN)_2]Br$, an organic superconductor with $T_C = 11.9$ K. $\lambda$ increases dramatically with deuteration and develops a strong magnetic field dependence. The superfluid density exhibits a power law temperature dependence indicative of a nodal order parameter. We discuss possible connections to nanoscale antiferromagnetic domains.

*Work at UIUC supported by NSF DMR 05-03882. Work at Argonne National Lab supported by DOE contract # W-31-109-ENG-38.

**10:36**
**U38 14 Pauli limiting in the superconductor $\kappa$-$(ET)_2Cu(NCS)_2$ under pressure** KYUIL CHO, BRAUNEN SMITH, CHRIS REA, MIKE VIOTTI, CHARLES AGOSTA, *Clark University* JOHN SCHLUETER, *Argonne National Laboratory* We have strong evidence that the organic superconductor $\kappa$-$(ET)_2Cu(NCS)_2$ is Pauli limited when it is compressed with a small ($< 2$ kbar) amount of pressure. A superconductor is considered Pauli limited when the magnetic energy, $\mu_b H$, overcomes the binding energy of the Cooper pairs to destroy superconductivity. In most situations superconductivity is destroyed by the formation of vortices. At ambient pressure, $\kappa$-$(ET)_2Cu(NCS)_2$ shows some behavior that is reminiscent of a Fulde Ferrell Larkin Ovchinnikov state, although no direct evidence of a transition into this state has been measured. Through a series of penetration depth measurements using a tunnel diode oscillator under pressure, we can show the evolution of the ambient pressure state to the clearly Pauli limited state at 1.75 kbar. We will also discuss the design of our new plastic, gas charged pressure cell that has allowed us to make these measurements in dc and pulsed magnetic fields. We acknowledge support from the DOE #ER46214 and the NSF #DMR- SGER-0331272.

## SESSION U39: SUPERCONDUCTING PROXIMITY EFFECT-S/N AND S/F
**Thursday Morning, 16 March 2006**
**342, Baltimore Convention Center at 8:00**
**James Eckstein, University of Illinois, Urbana-Champaign, presiding**

***Contributed Papers***

**8:00**
**U39 1 Proximity effect and Josephson current in clean strong/weak/strong superconducting tri-layers** FRANK MARSIGLIO, LUCIAN COVACI, *University of Alberta* Recent measurements of the Josephson critical current through LSCO/under-doped LSCO/LSCO thin films showed an unusually large proximity effect. Using the Bogoliubov-de Gennes (BdG) equations for a tight binding Hamiltonian we describe the proximity effect in weak links between a superconductor with critical temperature $T_c$ and one with critical temperature $T_c'$, where $T_c > T_c'$. The weak link (N') is considered to be a superconductor above it's critical temperature and the superconducting regions can have either s-wave or d-wave symmetry. We observe that the proximity effect is enhanced due to the presence of superconducting correlations in the weak link. The dc Josephson current is also calculated, and we

observe a non-zero value for temperatures greater than $T_c'$ for sizes of the weak links that are greater than the conventional coherence length. This effect alone is unable to explain the experimental results, instead, we also consider pockets of superconductivity in the weak link.

**8:12**
**U39 2 Superconducting Proximity Effect in Semiconductor Films - Experiment** SOREN FLEXNER, MICHAEL VISSERS, PAUL WELANDER, KEVIN INDERHEES, JIM ECKSTEIN, *University of Illinois at Urbana-Champaign* Interface transparency and device topology together determine the information regarding the superconducting proximity effect that can be obtained from transport measurements. We have introduced a new three terminal device design and use junctions formed entirely in-situ between niobium(S) and a thin heavily doped InGaAs epitaxial layer(N). The junction design allows us to separately extract the junction conductance and the sheet resistance of the InGaAs from the two terminal and three terminal voltage readings at low bias currents. We see evidence for both fluctuating and phase-stiff superconductivity (SC) in the normal material. At temperatures below, but close to Tc of the niobium, SC fluctuations cause the spreading resistance, Rs, on the normal side of the junction to drop. At lower temperatures, phase-stiff SC emerges in the InGaAs, effectively stealing volume from the normal region. This makes Rs appear to increase as the SC order sets in. The specific junction conductance, Gc, rises to values much greater than the normal value. We propose this is caused by the N-S boundary moving into the semiconductor.

**8:24**
**U39 3 Superconducting Proximity Effect in Semiconductor Films - Device Theory** MICHAEL VISSERS, SOREN FLEXNER, PAUL WELANDER, KEVIN INDERHEES, JIM ECKSTEIN, *University of Illinois at Urbana-Champaign* A new three terminal device architecture is introduced and analyzed for studying the superconducting proximity effect. It consists of a narrow superconducting injector line that injects current into a thin normal film. The current is extracted from one side of the injector line by a superconducting drain electrode that is many normal state coherence lengths ''downstream'' of the injector. A third voltage tap is provided on the other or ''upstream'' side of the injector. We present a theory showing how measurements made in various voltage sensing configurations can be combined to provide enough information to extract the two dimensional sheet resistance of the normal metal under the superconductor, as well as the specific contact conductance between the superconducting and normal parts of the device. This theory has been used to characterize the proximity effect in thin heavily doped InGaAs layers. A transition from fluctuating to phase stiff pair correlations in the normal layer has been observed at temperatures below Tc of the superconductor.

***Invited Papers***

**8:36**
**U39 4 Coexistence of, and Competition between, Magnetism and Superconductivity.***
MATTHIAS ESCHRIG, *Institut fuer Theoretische Festkoerperphysik, University of Kalrsruhe, 76128 Karlsruhe, Germany*

Magnetism and superconductivity are competitive types of order in correlated electron systems. However, when a magnetic material is brought in contact with a superconducting material to build a junction, a coexistence region exists near the boundary that can modify the properties of the heterostructure in a qualitative way. In the case of a ferromagnet in contact with a singlet superconductor, the importance of triplet pairing correlations in the interface region recently became the focus of research. Such triplet correlations have unusual properties. They are typically odd in frequency for the case of a diffusive material. For clean materials in addition a triplet component even in frequency but odd in momentum is present. We have predicted that such triplet correlations can lead to an unusual indirect Josephson effect in a superconductor/half-metal/superconductor structure. In the case of a long half-metal such a Josephson effect is solely due to equal-pair triplet superconducting correlations. The triplet supercurrent is converted into a singlet current in the interface regions of the structure. Although theoretically predicted, a direct experimental verification of the presence of triplet correlations in ferromagnet/superconductor hybrid structures is difficult. In addition to the above effect we propose to use the torque on a ferromagnet/superconductor/ferromagnet trilayer in an external magnetic field as a probe of the presence of triplet correlations in the superconducting phase.

*This work has been supported by the the Deutsche Forschungsgemeinschaft within the Center for Functional Nanostructures.

***Contributed Papers***

**9:12**
**U39 5 Magnetization-dependent $T_c$ shift in F/S/F trilayers with strong ferromagnets** ION C. MORARU, WILLIAM P. PRATT, NORMAN O. BIRGE, *Michigan State University* Hybrid systems combining ferromagnetic (F) and superconducting (S) metals in contact exhibit a wide range of fascinating behaviors. Several experimental groups have used weak ferromagnetic alloys in F/S experiments to enhance the penetration of Cooper pairs into the ferromagnet. In an F/S/F trilayer structure, a difference in the critical temperature $T_c$, based on the mutual orientation of the outer ferromagnets, has been reported [1] in CuNi/Nb/CuNi. Systems with strong ferromagnets, on the other hand, present new challenges, due to the very different density of states and Fermi velocity for the two different spin bands. Using the strong ferromagnets Ni and NiFe (Permalloy) in F/S/F exchange-biased spin valves [2], we observe that the $T_c$ for the parallel (P) orientation is lower than that of the anti-parallel (AP) case, i.e. $T_c$ (P) $<$ $T_c$ (AP). These results are consistent with theoretical expectations, but opposite to recent experimental work from another group

where an inverse spin switch has been reported in a NiFe/Nb/NiFe structure [3]. [1] J. Y. Gu et al, Phys. Rev. Lett. 89, 267001 (2002). [2] I. C. Moraru et al., submitted for publication (2005). [3] A. Yu. Rusanov et al., cond-mat/0509156 (2005).

**9:24**

**U39 6 Tunneling Studies of Superconductor/Strong Ferromagnet Bilayers** PAUL SANGIORGIO, *Stanford University* SERGE REYMOND, *Université de Lausanne* MALCOLM BEASLEY, *Stanford University* TESU KIM, JUNHYUNG KWON, KOOKRIN CHAR, *Seoul National University* Thin-film heterostructures composed of superconductors and ferromagnets have recently received much interest, as they provide a unique opportunity to study the proximity effect between superconductivity and magnetism. We report systematic tunneling density of states (DOS) measurements on superconductor (Nb) /strong ferromagnet (CoFe, Ni) bilayers made with high quality aluminum-oxide planar tunnel junctions as a function of ferromagnetic thickness, $d_F$. In CoFe, we find that as $d_F$ increases, the superconducting DOS exhibits a scaling behavior in which the deviations from the normal-state conductance have a universal shape, which decreases exponentially in amplitude. The decay length, $d_1$, is approximately 0.4 nm. We do not see oscillations in the DOS as a function of $d_F$, as one would expect from predictions based on the Usadel equations using reasonable parameters, although an oscillation in $T_c(d_F)$ has been seen in the same materials. Measurements on Nb/Ni bilayers will also be presented. This work is supported by AFOSR, DOE, and KOSEF through CSCMR.

**9:36**

**U39 7 Interplay between superconductivity and ferromagnetism in tunneling*** MARTIN GRONSLETH, JACOB LINDER, ASLE SUDBO, *Norwegian University of Science and Technology (NTNU), N-7491 Trondheim, Norway.* We study tunneling currents in a model consisting of ferromagnetic spin-triplet superconductors with magnetization in an arbitrary direction separated by a thin insulating layer. A novel effect is found with both ferromagnetic and superconducting phases entering in the expressions for the single- and two-particle tunneling currents in both spin and charge sector. This interplay between ferromagnetism and superconductivity is present when unconventional Cooper pairs with parallell spin pairing are allowed to form.

*Work supported by the NANOMAT Program, Research Council of Norway

**9:48**

**U39 8 Tunneling in Dilute Al-Mn Alloys: Observation of Resonant Scattering and Implications for High-Temperature Superconductors*** STEVEN RUGGIERO, *University of Notre Dame* GERALD ARNOLD, *University of Notre Dame* JOSEPH BYCHOWSKI, *University of Notre Dame* ANTHONY WILLIAMS, *University of Notre Dame* NAN SUN, *University of Notre Dame* ANNA CLARK, *Ball Aerospace & Technologies Corp.* NATHAN MILLER, *National Institute of Standards and Technology* JOEL ULLOM, *National Institute of Standards and Technology* We report on the observation of superconducting energy gap suppression by resonant scattering. Tunneling measurements of dilute Al-Mn alloys demonstrate the absence of density-of-states smearing that accompanies pair breaking and verify the detailed predictions of the Kaiser resonant scattering theory. These materials represent model systems for quasi-particle scattering and interference phenomena in the high- temperature superconductors.

*S.T.R. acknowledges support from the Department of Energy through grant DEFG02-88ER45373 and the DARPA SpinS program. A. M. C., N. A. M., and J. N. U. acknowledge the support of the NASA APRA program and the NIST Office of Microelectronics Programs.

**10:00**

**U39 9 Andreev reflection spectroscopy of the heavy-fermion superconductor $CeCoIn_5$ along different crystallographic orientations** WAN KYU PARK, LAURA GREENE, *University of Illinois at Urbana-Champaign* JOHN SARRAO, JOE THOMPSON, *Los Alamos National Laboratory* We have performed Andreev reflection spectroscopy on single crystals of the heavy-fermion superconductor $CeCoIn_5$. Conductance spectra obtained along both (001) and (110) crystallographic orientations exhibit similar features including asymmetry in the background conductance, the magnitude of zero-bias conductance enhancement (12 - 13%) and the energy scale for the conductance enhancement ( $\sim$ 1 meV). Analysis of the (001) junction data taken at the lowest temperature (400 mK) using an extended Blonder-Tinkham-Klapwijk model gives $2\Delta/k_BT_c = 4.64$ [1,2]. The failure to account for the full temperature dependence of the data sets requires further theoretical investigations to account for the magnitude of the Andreev signal, including the possibility of two-fluid behavior. Features in the (110) data may provide the first spectroscopic evidence for $d_{x2-y2}$ superconducting order parameter symmetry [2,3]. [1] W. K. Park et al., Phys. Rev. B **72**, 052509 (2005). [2] W. K. Park et al., cond-mat/0507353. [3] W. K. Park and L. H. Greene, cond-mat/0507489. This work was supported by the U.S. DoE Award No. DEFG02-91ER45439 through the FSMRL and the Center for Microanalysis of Materials at UIUC.

**10:12**

**U39 10 Elastic Cotunnelling and Crossed Andreev Reflection in Normal-Superconductor Nanostructures*** PAUL CADDEN-ZIMANSKY, ZHIGANG JIANG, VENKAT CHANDRASEKHAR, *Department of Physics and Astronomy, Northwestern University* Transport experiments were made on normal-superconductor-normal systems where the separation of the normal elements is less than a superconducting coherence length. For this geometry two coherent, nonlocal effects have been predicted. In elastic cotunnelling electrons from one normal element can tunnel to the other through a virtual state in the superconducting gap. In crossed Andreev reflection one electron from each spatially separated normal element join to enter the superconductor as a Cooper pair. We present evidence of these nonlocal effects and show that their spatial dependence agrees with theory.

*Supported by NSF-DMR-0201530.

**10:24**

**U39 11 Anomalous Proximity Effect in Nb/Al/CoFe Trilayers** KOOKRIN CHAR, JUN HYUNG KWON, JINHO KIM, KYUNGMOON KIM, *Center for Strongly Correlated Materials Research, School of Physics, Seoul National University, Seoul, Republic of Korea* HYEONJIN DOH, HAN-YONG CHOI, *Department of Physics, Sung Kyun Kwan University, Suwon, Republic of Korea* We have fabricated Nb/Al/CoFe(Ni, $Cu_{40}Ni_{60}$) trilayers to study the interaction between superconductivity and ferromagnetism. Increasing the thickness of Al in S/N/F trilayer, we observed that Tc values of S/N/F trilayers increase sharply close to the Tc of S/N bilayer until the Al thickness reaches 3 nm. As Al thickness increases from 3 nm to 180 nm, Tc value of S/N/F

decreases again, following those of the S/N data. In order to fit the Tc data of Nb/Al/CoFe trilayers as a function of Al thickness in a conventional Usadel formalism, we had to use a large $\gamma_b^F (= R_b A/\rho_f \xi_f)$ value of about 4, which seems unphysically large. In order to examine the role of Al/CoFe interface, we fabricated Nb/Cu(2 nm)/Al(2 nm)/CoFe and Nb/Au(2 nm)/Al(2 nm)/CoFe and compared them with Nb/Al(4 nm)/CoFe. The Tc of the double N layer system showed lower value than the Tc of the single Al layer system, although the three systems shared the same Al/CoFe interfaces. Our data suggests the large $\gamma_b^F$ value in a conventional Usadel picture is not sufficient and rather indicates towards the unique role of Al instead of the Al/CoFe interface. We will discuss other possibilities such as the triplet superconductivity in order to explain our experimental findings.

**10:36**
**U39 12 The Role of Inelastic Scattering in Intermediate Spin Polarized Normal Metal/Superconductor Point Contacts** CHARLES W. SMITH, *University of Maine, Orono, ME* PAUL J. DOLAN, JR., *Northeastern Illinois University, Chicago, IL* Charge transport in ferromagnetic normal metal/superconductor point contacts is constrained by both the limited minority spin population, which reduces the probability of the Andreev reflection process, and by quasiparticle finite-lifetime effects, i.e., inelastic scattering, which influences the probability of ordinary electron transport. For the case of intermediate polarization $0.30 \leqslant P \leqslant 0.60$, where $0 \leqslant P \leqslant 1.0$, these processes can play equally important roles. We present results for normalized conductance at zero bias, as a function of temperature, and for conductance as a function of voltage, at $P = 0.40$, parametrically, for the entire range of inelastic scattering. Experimental results for point contacts will be presented.

**10:48**
**U39 13 Magnetically Induced Superconductor-Metal-Insulator Transition in Thin Tantalum Films** CARLOS VICENTE, YONGGUANG QIN, JONGSOO YOON, *University of Virginia* Homogeneously disordered superconducting thin tantalum films are found to exhibit a metallic behavior in the limit of zero temperature when the superconductivity is suppressed by weak magnetic fields. The metallic behavior is characterized by an apparent saturation of sample resistance to a finite value, which can be order of magnitude smaller than the normal state resistance. This implies that the metallic state exists as a separate phase rather than a point in phase diagram. Such a metallic behavior is in strong contrast to the traditional belief that the electronic state of a 2D superconducting film can either be superconducting or insulating. We present details of transport characteristics in the magnetically induced metallic and insulating phase. We also discuss the influence of disorder, represented by normal conducting sheet resistance, on the metallic behavior and the superconductor-metal-insulator phase transition.

**11:00**
**U39 14 Magnetic Field-Induced Metallic Behavior in Superconducting Tantalum Films** YONGGUANG QIN, CARLOS VICENTE, JONGSOO YOON, *University of Virginia* We present the results of electronic transport measurements on superconducting thin tantalum films. The films are grown by dc sputtering on Si substrates. No sign of crystalline ordering is found from X- ray diffraction studies, particularly for films with thickness less than $\sim$ 5nm, indicating that the structure of the films is amorphous. The superconducting transition temperatures are found to continuously decrease with decreasing film thickness, which is characteristic of homogeneously disordered superconducting films. At zero magnetic field, a direct superconductor-insulator transition is observed at a critical thickness $\sim$ 3 nm. At this thickness the normal conducting sheet resistance is close to the quantum resistance, $h/4e^2$. When the superconductivity is suppressed by applying magnetic fields, however, the system exhibits an unexpected metallic behavior in the limit of zero temperature. The metallic behavior is characterized by a drop in resistance followed by an apparent saturation to a finite value as the temperature is reduced. We observe qualitatively different nonlinear voltage-current characteristics across the ''superconductor- metal'' boundary, and also the ''metal-insulator'' boundary.

## SESSION U40: FOCUS SESSION: PATHWAYS TO PRACTICAL QUANTUM COMPUTING III
**Thursday Morning, 16 March 2006; 343, Baltimore Convention Center at 8:00**
**Fernando M. Cucchietti, Los Alamos National Laboratory, presiding**

***Invited Papers***

**8:00**
**U40 1 Ion traps and cold atoms for quantum computers.**
IGNACIO CIRAC,* *Max-Planck Institute for Quantum Optics*

Atoms can be used to store and manipulate quantum information. In particular, their internal state can be considered to form a register, and they can also be manipulated using laser light. In the case of trapped ions, the Coulomb force gives the required interaction to perform two-qubit gates. For neutral atoms, cold collisions can be used for that purpose. During the last years there has been an extraordinary experimental progress with those systems, and it is now possible to perform simple quantum information tasks with them. In this talk I will review several proposals for implementing quantum computers and quantum simulators using trapped ions and neutral atoms in optical lattices, and I will report on the latest experimental advances. Then, I will consider two particular aspects of those systems: (i) the possibility of simulating spin and bosonic systems with trapped ions; (ii) the possibility of performing quantum computations with neutral atoms without addressing them and in the presence of defects.

*Other authors (with same affiliation): Diego Porras, Karl Vollbrecht, and Enrique Solano.

*Contributed Papers*

**8:36**
**U40 2 Ion trap quantum computing with transverse phonon modes** SHI-LIANG ZHU, CHRIS MONROE, LUMING DUAN, *Department of Physics, Michigan University* We propose a scheme to use the transverse modes to implement conditional phase gates on two trapped ions immersed in a large linear crystal of ions, without the sideband addressing. Comparing with the conventional approach using the longitudinal modes, with the cost that the laser power is slightly stronger, the proposed gate operation can be well inside Lamb-Dicke region and the gate infidelity due to the fluctuation of the effective Rabi frequency as well as the fundamental limits of the cooling procedure are approximately two orders smaller.

**8:48**
**U40 3 Robust quantum memory using magnetic-field-independent atomic qubits*** C. LANGER, R. OZERI, J. D. JOST, B. DEMARCO,† A. BEN-KISH,‡ B. BLAKESTAD, J. BRITTON, J. CHIAVERINI, D. B. HUME, W. M. ITANO, D. LEIBFRIED, R. REICHLE, T. ROSENBAND, P. SCHMIDT, D. J. WINELAND, Scalable quantum information processing requires physical systems capable of reliably storing coherent superpositions for times over which quantum error correction can be implemented. We experimentally demonstrate a robust quantum memory using a magnetic-field-independent hyperfine transition in $^9Be^+$ atomic ion qubits at a field B = 0.01194 T. Qubit superpositions are created and analyzed with two-photon stimulated-Raman transitions. We observe the single physical qubit memory coherence time to be greater than 10 seconds, an improvement of approximately five orders of magnitude from previous experiments. The probability of memory error for this qubit during the measurement period (the longest timescale in our system) is approximately $1.4 \times 10^{-5}$ which is below fault-tolerance threshold for common quantum error correcting codes.

*supported by DTO/NSA and NIST
†present address: University of Illinois, Urbana
‡present address: Technion, Haifa, Israel

**9:00**
**U40 4 Quantum logic in Group-II neutral atoms via nuclear-exchange interactions** DAVID HAYES, *University of New Mexico* IVAN DEUTSCH, PAUL JULIENNE, *NIST* The spin exchange-interaction generates an entangling quantum-logic gate, the square-root of SWAP, at the heart protocols employing single electron quantum dots. This is typically accompanied by strong Coulomb interactions and commensurate decoherence due to strong coupling of charge degrees of freedom to the noisy environment. We propose a protocol utilizing a itnuclear-exchange interaction that occurs through ultracold collisions of identical spin $.5ex1kern - .1em/kern - .15em.25ex2$ Group-II neutral atoms. A natural advantage is gained by storing the quantum information in nuclear spin states with long coherence times. Unlike NMR protocols based on weak magnetic dipole-dipole interaction, the nuclear exchange interaction stems from strong s-wave scattering of electrons. Nuclear exchange is ensured by the Fermi symmetry of the overall wave function. We have studied this protocol in the context of $^{171}Yb$ atoms trapped in far-off resonance optical dipole traps. Using quantum control analysis, high-fidelity operation is possible through controlled collisions in dynamically varied double-well trapping potentials.

**9:12**
**U40 5 Quantum state reconstruction via continuous measurement** ANDREW SILBERFARB, IVAN DEUTSCH, *University of New Mexico* GREG SMITH, POUL JESSEN, *University of Arizona, Tucson* We present a new protocol for quantum state reconstruction based on weak continuous measurement of an ensemble average. This procedure applies the techniques of quantum control theory and quantum measurement theory to achieve a more efficient reconstruction than those performed using standard projective measurement techniques. This efficiency allows reconstruction of a quantum state using an single emsemble with minimal quantum backaction, setting the stage for state-based feedback control. An experimental demonstration of the technique will be presented in the context of reconstruction of the spin state of the F=3 hyperfine ground-state manifold of Cs-133 using continuous polarization spectroscopy.

**9:24**
**U40 6 Quantum state control of atoms in microscopic optical traps*** MARK SAFFMAN, DENIZ YAVUZ, MARIE DELANEY, *University of Wisconsin* PASAD KULATUNGA, *Hobart and William Smith Colleges* TODD JOHNSON, ERICH URBAN, THOMAS HENAGE, NICHOLAS PROITE, THAD WALKER, *University of Wisconsin* We present recent progress in loading and manipulation of neutral atoms in microscopic optical traps. Single Rb atoms are loaded into far off resonant optical traps from a background vapor of cold atoms. Tightly focused optical beams are used to perform two-photon stimulated Raman rotations between hyperfine qubit states. We demonstrate qubit rotations at a rate of 1.4 MHz, 1 ms coherence time, and individual site addressing with crosstalk at the level of $10^{-3}$. These results are a significant step towards quantum computing using optically trapped neutral atoms. We discuss work in progress aimed at observing strong, angle independent dipole-dipole interactions for fast two-qubit gates using microwave dressing of Rydberg states. We demonstrate two-photon coherent excitation of Rydberg levels by a $5s_{1/2} - 5p_{3/2} - nd_{5/2}$ sequence. The possibility of dipole-dipole interactions without angular zeroes will be important for gates, as well as for coupling to mesoscopic qubits to enable transmission of quantum states.

*This work is funded by the NSF and the Army Research Office.

**9:36**
**U40 7 Stochastic One-Way Quantum Computing with Ultracold Atoms in Optical Lattices** MICHAEL C. GARRETT, *University of Calgary* DAVID L. FEDER, *University of Calgary* The one-way model of quantum computation has the advantage over conventional approaches of allowing all entanglement to be prepared in a single initial step prior to any logical operations, generating the so-called cluster state. One of the most promising experimental approaches to the formation of such a highly entangled resource employs a gas of ultracold atoms confined in an optical lattice. Starting with a Mott insulator state of pseudospin-1/2 bosons at unit filling, an Ising-type interaction can be induced by allowing weak nearest-neighbor tunneling, resulting in the formation of a cluster state. An alternate approach is to prepare each spin state in its own sublattice, and induce collisional phase shifts by varying the laser polarizations. In either case, however, there is a systematic phase error which is likely to arise, resulting in the formation of imperfect cluster states. We will present various approaches to one-way quantum computation using imperfect cluster states, and show that the algorithms are necessarily stochastic if the error syndrome is not known.

**9:48**

**U40 8 Generalized Coherent States via Markovian Decoherence** SERGIO BOIXO, *University of New Mexico, Albuquerque* LORENZA VIOLA, *Dartmouth College* GERARDO ORTIZ, HOWARD BARNUM, *Los Alamos National Laboratory* Coherent states were introduced in the early days of quantum physics as 'quasiclassical' quantum states of an isolated quantum system. The decoherence program defines 'quasiclassical' (or 'pointer') states as states which are most stable in the presence of a coupling with the environment. Pointer states may be identified through the extremization of a 'predictability' functional on the Hilbert space. It has been known for some time that for the harmonic oscillator both concepts coincide under very generic conditions. Coherent states have been extended in the 70s to generalized coherent states. Recently, this approach has served as the basis to define generalized entanglement and conditions for quantum complexity. Here, we investigate the stability of generalized coherent states under Markovian open-system dynamics. In particular, we identify conditions under which generalized coherent states emerge as pointer states for systems described by algebras more general that the standard oscillator algebra. We present a streamlined method to find pointer states in the weak-coupling approximation, and discuss conditions for this approximation to be valid. We find that generalized coherent states and pointer states coincide under more restrictive conditions than the canonical, harmonic-oscillator coherent states. Finally, we address the connection of generalized coherent states to noiseless subspaces and subsystems.

**10:00**

**U40 9 Generation of Werner states via collective decay of coherently driven atoms** KISHOR KAPALE, *Jet Propulsion Laboratory, California Institute of Technology* GIRISH AGARWAL, *Department of Physics, Oklahoma State University* We demonstrate deterministic generation of Werner states as a steady state of the collective decay dynamics of a pair of neutral atom coupled to a leaky cavity and strong coherent drive. We also show how the scheme can be extended to generate $2N$-particle analogue of the bipartite Werner states.

**10:12**

**U40 10 Two-Qubit Quantum Computing using Pulsed ESR of $N@C_{60}$** GAVIN MORLEY, *NHMFL* JOHAN VAN TOL, *NHMFL* JINYING ZHANG, *Materials Department, Oxford University* KYRIAKOS PORFYRAKIS, *Materials Department, Oxford University* ARZHANG ARDAVAN, *Clarendon Lab, Oxford University* ANDREW BRIGGS, *Materials Department, Oxford University* $N@C_{60}$ is a fullerene molecule containing an atom of nitrogen. The low-temperature decoherence time, $T_2$, can be increased to 215 $\mu$s, which is attractive for quantum information processing applications. The electronic and nuclear spins of the nitrogen atom are good quantum numbers in a strong magnetic field, coupled by the hyperfine interaction. Pulsed ENDOR (electron nuclear double resonance) can be used to initialize, manipulate and measure this two-qubit system. We used dynamic nuclear polarization (DNP) to prepare an initial state in which the nuclear and electronic spins were aligned with the applied field.

**10:24**

**U40 11 Optimal control of logical operations in the presence of decoherence: A two-spin model** MATTHEW GRACE, CONSTANTIN BRIF, HERSCHEL RABITZ, *Department of Chemistry, Princeton University, Princeton, NJ 08544* IAN WALMSLEY, *Department of Physics, University of Oxford, Oxford OX1 3PU, UK* ROBERT KOSUT, *SC Solutions, Inc., 1261 Oakmead Parkway, Sunnyvale, CA 94085* DANIEL LIDAR, *Chemistry and Electrical Engineering Departments, University of Southern California, Los Angeles, CA 90089* We study the feasibility of optimal control of logical operations in a simple model system composed of two interacting spins. In our model, one spin serves as a qubit and its evolution is controlled by a time-dependent external field. The other (uncontrolled) spin serves as an effective environment, coupling to which is a source of decoherence. The aim of control is to generate a target unitary operation for the qubit in the presence of the environmentally-induced decoherence. Given a target unitary operation $G$ for the system, the fidelity of the actual transformation achieved is maximized with respect to the electric field $\epsilon(t)$ using two techniques, optimal control theory (OCT) and ''pre-design'' methods, which are well-developed in the field of nuclear magnetic resonance. The primary goal of this work is to illustrate the importance of OCT in designing logical operations, especially in the presence of environmental coupling, and the inadequacy of pre-designed gates in such situations.

**10:36**

**U40 12 Rapid State-Reduction of Quantum Systems Using Feedback Control*** JOSHUA COMBES, *Griffith University* KURT JACOBS, *Louisiana State University* Many potential applications of quantum devices, particularly in information processing, require quantum systems to be prepared in pure states. Due to environmental noise quantum systems often exist naturally in mixed states, and as a result a process of cooling or measurement must be used to purify them. In this work we consider the use of measurement for this purpose. The speed with which a measurement can purify, or reduce, the state of a quantum system is determined by the interaction between the system and measuring device, and places a limit on the speed of state-preparation. Here we consider using feedback control during the measurement to increase the rate of state-reduction. It was shown in [1] that for a single qubit this rate could be increased by a factor of 2. Here we show that for higher dimensional systems feedback control can provide a much larger speed-up. In particular, we show that for a measurement of an observable with $N$ equally spaced eigenvalues, there exists a feedback algorithm which will increase the rate of state-reduction by a factor proportional to $N$. References: 1. K. Jacobs, Phys. Rev. A **67**, 030301(R) (2003). 2. J. Combes and K. Jacobs, Phys. Rev. Lett. (in press).

*We acknowledge support from the Australian Research Council and the State of Queensland

**10:48**

**U40 13 Quantum Zeno stabilization in weak continuous measurement of two qubits** RUSKO RUSKOV, *Penn State University* ALEXANDER N. KOROTKOV, *University of California, Riverside* ARI MIZEL, *Penn State University* We have studied quantum coherent oscillations of two qubits under continuous measurement by a symmetrically coupled mesoscopic detector. The analysis is based on a Bayesian formalism that is applicable to individual quantum systems. Measurement continuously collapses the two-qubit system to one of the sub-spaces of the Bell basis. For a detector with linear response this corresponds to measurement of

the total spin of the qubits. In the other extreme of purely quadratic response the operator $\sigma_y^1\sigma_y^2 + \sigma_z^1\sigma_z^2$ is measured. In both cases, collapse naturally leads to spontaneous entanglement which can be identified by measurement of the power spectrum and/or the average current of the detector. Asymmetry between the two qubits results in evolution between the different measurement subspaces. However, when the qubits are even weakly coupled to the detector, a kind of quantum Zeno effect cancels the gradual evolution and replaces it with rare, abrupt switching events. We obtain the asymptotic switching rates for these events and confirm them with numerical simulations. We show how such switching affects the observable power spectrum on different time scales.

**SESSION U41: DIELECTRICS: RESPONSE PROPERTIES**
**Thursday Morning, 16 March 2006**
**344, Baltimore Convention Center at 8:00**
**Serge M. Nakhmanson, Rutgers University, presiding**

**8:00**
**U41 1 Enhanced performance in nanotemplated dielectric structures** YUN PENG, K. KEMPA, M.J. NAUGHTON, *Boston College* The dielectric properties of nanoscale metallic inclusions in insulating media are anticipated to be significantly enhanced (1,2). We have prepared such nanocomposites via electrochemical deposition of metal (gold) in polycarbonate template membranes. We have characterized the properties of these via frequency-dependent capacitance measurements, and compare our results with a theory of enhanced $\varepsilon$ ($\omega$) at the nanoscale (2). - 1. J.Xu and C.P.Wong, Proceedings of the Ninth International Symposium on Advanced Packaging Materials: Process, Properties and Interfaces, Atlanta, GA, 24 March 2004 (IEEE, New York, 2004,) p.158 - 2. T. Kempa, D. Carnahan et al., Dielectric media based on isolated metallic nanostructures, J.Appl.Phys, 98, 34310 (2005)

**8:12**
**U41 2 Low temperature specific heat and Brillioun scattering in nano-oscillator arrays** DOUGLAS PHOTIADIS, JOSEPH BUCARO, XIAO LIU, *US Naval Research Laboratory* We consider a large, free-standing array of coupled, planar oscillators each several hundred nanometers on a side fabricated from a single layer of dielectric. In particular, we predict the low temperature heat capacity and Brillouin scattered cross section based upon a numerical calculation of the density of states (DOS) for this nano-structured array. The DOS, which is interesting in its own right, is found to have an average value nearly independent of frequency and a number of gaps of varying depths. The predictions suggest that it should be possible to use low temperature measurements of Brillouin cross section and/or the specific heat to observe the quantum statistics obeyed by various rigid body modes of the array, some of which involve the center of mass motion of a large number of atoms. As such, these measurements would result in a considerable extension of the domain in which quantum mechanics has been tested.

**8:24**
**U41 3 Determining the quantum phase coherence time of a NEMS resonator** EMILY PRITCHETT, *University of Georgia* MICHAEL GELLER COLLABORATION, Recently steps have been made toward characterizing macroscopic quantum behavior in nanoelectromechanical devices (NEMS), particularly resonators with large frequencies and high Q factors. While the quantum phase coherence time as well as energy relaxation time of NEMS resonators are believed to be long, this cannot be tested directly using standard techniques. Using formalism typically found in quantum computation, we propose a procedure for directly measuring both phase coherence and energy relaxation times of NEMs resonators by coupling them to anharmonic Josephson junction devices. We hope that using this proposed method experiments will verify current models of decoherence in harmonic oscillator systems.

**8:36**
**U41 4 Tunable Electronic Energy Transfer in Layered Inorganic Solids Codoped with $Tb^{3+}$ and $Eu^{3+}$** CHRISTIE LAROCHELLE, *Franklin & Marshall College* $Ln[M(CN)_2]_3$ systems (Ln=trivalent rare earth, M=Au,Ag) have a layered structure consisting of alternating layers of the $M(CN)_2^-$ ions and $Ln^{3+}$ ions. Our past studies of tunable energy transfer have focused on transfer from $Au(CN)_2^-$ or $Ag(CN)_2^-$ donor ions to a variety of rare earth ions, including $Tb^{3+}$ and $Eu^{3+}$. Most recently, we have characterized systems with mixed metal donors, such as $La[Ag_{.5}Au_{.5}(CN)_2]_3$, $La[Ag_{.75}Au_{.25}(CN)_2]_3$, and $La[Ag_{.9}Au_{.1}(CN)_2]_3$. We have found that these systems exhibit ''tunability'' of emission energy due to the variation of the donor emission associated with varying the Ag/Au ratio. Tunability also occurs with changing temperature and excitation wavelength. Also, the steady-state luminescence spectra of these compounds reveals that they are strongly luminescent at room temperature, in contrast to the corresponding $La[Ag(CN)_2]_3$ and $La[Au(CN)_2]_3$ pure metal systems. Results will be presented from a new series of samples incorporating both $Tb^{3+}$ and $Eu^{3+}$ as acceptors. The tunability of the donor's emission wavelength allows for changes in the spectral overlap with each of the two donors. Preliminary results show variation in the rare earth (acceptor) emission with changing temperature and excitation wavelength, indicating the possibility of tuning the energy transfer off of one acceptor and onto the other.

**8:48**
**U41 5 EPR and ENDOR of two axial $Fe^{3+}$ centers in stoichiometric lithium tantalate** VALENTIN GRACHEV, GALINA MALOVICHKO, ROBERT PETERSEN, *Physics Department, Montana State University* CHRISTOFF BAEUMAN, *Department of Physics, University of Osnabrück, D-49069, Osnabrück, Germany* The determination of structures of centers in oxide crystals created by impurity ions, including those of transition metals and rare- earth elements, is one of the most important tasks in defect study. The iron ions play a key-role in the photovoltaic and photorefractive effects, holographic records and many other physical properties of lithium tantalate. The axial $Fe^{3+}$ center, Fe1 with the crystal field parameter $b_2^0 \approx 0.313$ 1/cm is well studied in congruent lithium tantalate crystals. Using the EPR we have discovered and investigated a new axial $Fe^{3+}$ center, Fe2 in stoichiometric samples prepared by vapor transport equilibrium treatment. The crystal field parameter of the Fe2 center $b_2^0 \approx 0.205$ 1/cm is significantly smaller than for Fe1. The ENDOR measurements have shown that hyperfine interactions of the $Fe^{3+}$ electrons with

the surrounding Li nuclei for Fe2 are stronger than for Fe1. Therefore, the conclusion was made that in the case of Fe2 center the iron ion substitutes for Ta and has Li nuclei in the nearest neighborhood, whereas in the case of Fe1 it substitutes for Li, has Ta nuclei as nearest neighbors and Li nuclei in the second shell only.

**9:00**

**U41 6 Near infrared emission properties of Nd doped Potassium Lead Halides** JESSICA FREEMAN, EI NYEIN, UWE HOMMERICH, *Hampton University* SUDHIR TRIVEDI, *Brimrose Corporation of America* JOHN ZAVADA, *US Army Research Office* The incorporation of rare earth (RE) ions into host materials with low maximum phonon energies provides opportunities for improved RE infrared emission properties. In this work, we evaluated the IR emission from Nd doped potassium lead halides, namely Nd: $KPb_2Cl_5$ and Nd: $KPb_2Br_5$, for possible applications in IR lasers and optical communications. Both halides are nearly non-hygroscopic and have low maximum phonon energies, which reduces non-radiative decay rates through multi-phonon relaxations. Following optical excitation at 800nm, near IR emission bands were observed from the $^4F_{5/2}$ and $^4F_{3/2}$ excited states of $Nd^{3+}$. The $^4F_{5/2}$ level was strongly quenched through non-radiative processes in Nd: $KPb_2Cl_5$. On the contrary, for Nd: $KPb_2Br_5$ the $^4F_{5/2}$ was highly radiative with an emission efficiency of $\sim$ 50%. More detailed results of the material synthesis, purification, steady-state and time-resolved emission spectroscopy will be presented at the conference.

**9:12**

**U41 7 Non-resonant Inelastic X-Ray Scattering and Energy-Resolved Wannier Function Investigation of Local Excitations in Transition Metal Monoxides NiO and CoO** B.C. LARSON, J.Z. TISCHLER, *ORNL* WEI KU, *BNL and SUNY, Stoney Brook* CHII-CHENG LEE, *Tamkang Univ. Taiwan* OSCAR RESTREPO, *Univ. TN, Knoxville* A.G. EGUILUZ, *Univ. TN, Knoxville and ORNL* P. ZSCHACK, *FS-MRL UIUC* K.D. FINKELSTEIN, *CHESS, Cornell Univ.* Non-resonant inelastic x-ray scattering (NIXS) and energy- resolved Wannier function analysis have been used to probe the strongly correlated electronic structure of NiO and CoO. NIXS measurements of the dynamical structure factor s(q,w) as a function of momentum transfer q and frequency w have shown that dipole-forbidden, d-d excitations appear within the optical gap for large wavevectors ($q > 2/A$), become the dominant structure in the loss spectra for $q > 3/A$, and reach a maximum at $q \sim 7/A$. In contrast to the loss-spectra observed in resonant-probe studies of NiO and CoO, non-resonant spectra show only two excitations that are highly anisotropic - strongest in the [111] direction and weakest (or missing) in the [001] direction. Energy-resolved Wannier function analyses of vertex matrix elements within LDA+U demonstrate that the anisotropy provides a sensitive measure of electronic symmetry-breaking in these atomic-like d-d excitations as a result of point-group symmetry selection rules.

**9:24**

**U41 8 Self-consistent linear density response within the LDA+U method: Application to transition-metal oxides*** A. G. EGUILUZ(1), O. D. RESTREPO(1), *University of Tennessee and CMSD, ORNL (2)* J. KUNES, W. E. PICKETT (3), *University of California, Davis* We formulate a scheme to calculate self-consistently the dynamical linear density-response function based on correlated LDA+U theory. The orbital dependent $V_U$ term in the Kohn- Sham potential, leads to an additional self-consistent condition in the density fluctuations. The end result is a density response function which includes electron-hole interactions (that is, it goes beyond the random-phase approximation). We assess the performance of our scheme by calculating the electron-hole excitation spectrum of prototype transition metal oxides for arbitrary momentum transfers. *DOE-CMSN PCSCS collaboration. (1) Supported by NSF ITR-DMR 0219332. (2) Managed by UT-Battelle for the U.S. DOE under contract DE- AC05-00OR22725. (3) Supported by DOE Grant DE-FG03-01ER45876

**9:36**

**U41 9 Determining the Critical Dose Threshold of Electron-Induced Electron Yield for Minimally Charged Highly Insulating Materials** RYAN HOFFMANN, J.R. DENNISON, JONATHAN ABBOTT, *Utah State University* When incident energetic electrons interact with a material, they excite electrons within the material to escape energies. The electron emission is quantified as the ratio of emitted electrons to incident particle flux, termed electron yield. Measuring the electron yield of insulators is difficult due to dynamic surface charge accumulation which directly affects landing energies and the potential barrier that emitted electrons must overcome. Our recent measurements of highly insulating materials have demonstrated significant changes in total yield curves and yield decay curves for very small electron doses equivalent to a trapped charge density of $< 10^{10}$ electrons /$cm^3$. The Chung-Everhart theory provides a basic model for the behavior of the electron emission spectra which we relate to yield decay curves as charge is allowed to accumulate. Yield measurements as a function of dose for polyimide (Kapton$^{TM}$) and microcrystalline $SiO_2$ will be presented. We use our data and model to address the question of whether there is a minimal dose threshold at which the accumulated charge no longer affects the yield.

**9:48**

**U41 10 Comparison of Methods for Determining Crossover Energies in Insulators** JONATHAN ABBOTT, RYAN HOFFMANN, J.R. DENNISON,* SARAH BARTON, *Brigham Young University* When a material is irradiated with energetic particles electrons can be emitted from the material. For electron-induced emission, the number of electrons that leave a particular material depends on the incident energy of the electrons, among other things. There are two critical energies where the ratio of emitted electrons to incident electrons crosses unity, called crossover energies. Measurements of the absolute total yield, secondary electron emission spectra, and sample and detector currents are used for a variety of methods to determine first and second crossover energies of both conductors and insulators. Precision is discussed for the following methods: i) Total Yield Curve, ii) Backscattered-to-Secondary Yield Ratio, iii) Mirror Potential, iv) Emission Spectral Shift, and v) Sample Null Current. Also, theoretical models for the Emission Spectral shift and Sample Null Current methods will be discussed. This work was funded by the NASA Space Environments and Effects Program, a Willard L. Eccles Undergraduate Research Fellowship, and a USU Undergraduate Research and Creative Opportunities award.

*Utah State University

**10:00**

**U41 11 Piezoelectric Coupling in Non-piezoelectric Materials due to Nonlocal Size Effects at the Nanoscale: Fundamental Solutions, Embedded Inclusions and Piezoelectric Composites without Electromechanical Constituents** PRADEEP SHARMA, *University of Houston* In a piezoelectric material an applied ituniform strain can induce an electric polarization (or vice-versa). Crystallographic considerations restrict this technologically im-

portant property to non-centrosymmetric systems. It has been shown both mathematically and physically, that a itnon-uniform strain can potentially break the inversion symmetry and induce polarization in non-piezoelectric materials. The coupling between strain gradients and polarization; and strain and polarization gradients, is investigated in this work. Based on a field theoretic framework accounting for this phenomena, we (i) develop the fundamental solutions (Green's functions) for the governing equations (ii) solve the general embedded inclusion problem with explicit results for the spherical and cylindrical inclusion shape and, (iii) Illustrate using the simple example of a bilaminate how an apparently piezoelectric composite may be created without using constituent piezoelectric materials.

**10:12**

**U41 12 Ionic-Mode Contributions to the Refractive Index of Glasses*** CARRIE E. BLACK, E. SHILES, *University of Vermont* D. Y. SMITH, *University of Vermont and Argonne National Laboratory* The refractive index of materials transparent in the visible is commonly much smaller in the infrared than at shorter wavelengths because low-frequency ionic polarization lags the **E** field of higher-frequency light. This is often described by an IR Sellmeier term in empirical index fits. However, this separation of ionic and electronic contributions is not unique. A unique separation is given by Taylor expansion of the K-K relations in the region of transparency that yields a Laurent series in photon energy squared as the IR contribution. The coefficients are odd moments of the IR extinction coefficient. We studied this for vitreous silica and Corning ULE glass (92.5 % $SiO_2$ + 7.5% $TiO_2$). While the oscillator strength of the IR modes is four orders of magnitude less than that of the electronic transitions, the IR contribution to the index is comparable to the electronic contribution in the IR. In our examples, IR terms are sufficiently negative to bring the total index well below unity (but greater than zero) between 7 to 9 $\mu$m.

*Work supported by the U. S. Department of Energy.

**10:24**

**U41 13 Enhanced fluorescence in rare earth doped sol-gel glasses containing $Al^{3+}$*** GREGORY ARMSTRONG, ANN SILVERSMITH, *Hamilton College* DANIEL BOYE, *Davidson College* Sol-gel synthesis is a low temperature method for preparing rare earth (RE) doped glass. Aluminum is often used as a co-dopant because it increases fluorescence yield from RE's. There is a tendency for RE ions to form clusters in the sol-gel preparation, facilitating inter-ion interactions and fluorescence quenching from cross relaxation. It is generally believed that Al prevents clustering of RE ions, but recent work questions this long-established role of Al. We report on spectroscopic investigations of energy transfer in Tb- and Eu- doped glasses that probe the effect of Al co-doping. Pulsed laser excitation of $^5D_3$ fluorescence is used to measure Tb-Tb cross-relaxation rates. In materials containing Al, cross-relaxation occurs in concentrations much lower than 0.1%Tb, indicating that RE clustering persists in glasses with Al. Line narrowing experiments in dilute Eu glasses confirm that ions remain clustered in co-doped samples. Our results point toward a model of aluminum rich regions in the glass that attract and confine RE ions. Reduced association with $OH^-$ in the confined regions causes RE fluorescence enhancement.

*AS and DB acknowledge support from the American Chemical Society Petroleum Research Fund

**10:36**

**U41 14 Site-specific modification of oxide nanoclusters: Towards atomic-scale surface structuring*** KENNETH M. BECK, MATTHIAS HENYK, CHONGMIN WANG, WAYNE P. HESS, *Pacific Northwest National Laboratory* PAOLO E. TREVISANUTTO, PETER V. SUSHKO, ALEXANDER L. SHLUGER, *University College London* Atomic emission from MgO and CaO nanostructures is induced using laser light tuned to excite specific surface sites at energies well below the excitation threshold of the bulk material. Using selective 4.66 eV laser excitation of nanocrystalline thin films and nanocube metal oxide samples we have recorded a unique pattern of hyperthermal atomic desorption. Not only neutral O-atoms, but neutral Mg-atoms, with hyper-thermal kinetic energies in the range of 0.1–0.4 eV are readily observed. Our itab initio calculations suggest that metal atom emission is induced predominantly by electron trapping at surface 3-coordinated metal sites followed by electronic excitation at these sites- an 'electron plus an exciton' mechanism. The proposed elementary mechanism involves both sequential excitation and localization of excitons as well as electrons and holes at 3-coodinated surface sites. This mechanism differs from all previously suggested mechanisms for desorption induced by electronic transitions. This desorption process serves as an example of atomic scale modification of a nanostructured metal oxide using laser light tuned to excite specific surface sites at energies well below the excitation threshold of the bulk material.

*Department of Energy, Office of Basic Energy Sciences.

**10:48**

**U41 15 Optical Spectroscopy of Low-k Dielectric Films*** JOANNA ATKIN, DAOHUA SONG, SRIKANTH IYER, *Columbia University* NILS HOIVIK, ROBERT R. ROSENBERG, THOMAS M. SHAW, *IBM T. J. Watson Research Center, Yorktown Heights, NY 10598* ROBERT B. LAIBOWITZ, TONY F. HEINZ, *Columbia University, New York, NY 10027* Low-k dielectric materials based on porous carbon-doped oxides are widely used in the microelectronics industry. Despite their importance, relatively little is known about their spectroscopic properties. In this paper we report results of two classes of optical spectroscopy measurements, absorption spectroscopy and photocurrent spectroscopy. Optical absorption spectroscopy has been performed on various thin-film low-k materials. These measurements show the presence of strong optical absorption in the ultraviolet and yield the effective band gap of the medium. Photocurrent spectroscopy has been performed on films of low-k material deposited on both Si and metallic substrates using a transparent counter-electrode. A well-defined spectral dependence of the photocurrent efficiency is observed. The data provide information on the band offsets of the low-k materials, parameters that play a crucial role in models of electrical conduction.

*Supported by the Semiconductor Research Corporation

**SESSION U42: FOCUS SESSION: SIMULATIONS OF MATTER AT EXTREME CONDITIONS II**
**Thursday Morning, 16 March 2006; 345, Baltimore Convention Center at 8:00**
**Sandro Scandolo, ICTP, Trieste, presiding**

*Invited Papers*

**8:00**
**U42 1 Condensed Matter and its Orderings: The Pressure Variable.***
NEIL ASHCROFT, *Cornell University*

Advances in experimental high pressure condensed matter physics have led to near order-of-magnitude static isothermal compressions (high densities are also realizable in dynamic compressions). In sufficiently light systems the new realms of density have associated zero-point effects, which are substantial. Also generally anticipated are significant changes in electronic structure (band widths not always increasing with density, however) and effective state dependent interparticle potentials. Propitious use of the pressure variable can elucidate the many-body problem in incisive ways through new orderings including structural, magnetic and especially superconducting. Significant challenges to theory include the appearance at higher densities of exceedingly complex structures in systems hitherto regarded as ''simple''. Invasion of the valence electron domain by core space appears to impel an interesting clash of length scales. Not unrelated to the rise of quantum effects is the possibility (and even observation) of depression of melting points in low mass systems. Hydrogen, a tenacious insulator (but now a decreasingly reluctant alkali) remains a candidate for significant superconductivity in a metallic state, one which may also be manifested as a quantum liquid. In combination with other light elements further orderings are also predicted, but at pressures less than anticipated for pure hydrogen itself. For the future, this area of experimental investigation appears to be ideally matched to advanced electronic structure and simulation techniques.

*Work supported by the National Science Foundation.

*Contributed Papers*

**8:36**
**U42 2 The Nature of the Hydrogen Plasma Phase Transition** KRIS DELANEY, DAVID CEPERLEY, *University of Illinois at Urbana-Champaign* CARLO PIERLEONI, *Università del L'Aquila, Italy* We present details of a study of pure hydrogen fluid at high pressure. Using the Coupled Electron-Ion Monte Carlo (CEIMC) method [1,2], a quantum Monte Carlo scheme capable of accurately simulating systems at low temperature, we study the nature of the plasma phase transition (PPT): the mechanism by which a molecular to non-molecular transformation occurs under increasing pressure. We find no evidence for a first-order PPT. The CEIMC method centers on exploring the nuclear configuration space (classically or with quantum path integrals) using a modified Metropolis algorithm. Configurational energy differences are computed within the Born-Oppenheimer (BO) approximation using accurate ground-state quantum Monte Carlo techniques. 1. D. Ceperley, M. Dewing and C. Pierleoni, in Bridging Time Scales: Molecular Simulations for the Next Decade, eds. P. Nielaba *et al*, Springer-Verlag, pgs. 473-500 (2002). 2. C. Pierleoni, D. M. Ceperley and M. Holzmann, Phys. Rev. Lett. **93**, 146402 (2004)

**8:48**
**U42 3 Developments in the path integral Monte Carlo method for simulating fluids under extreme conditions** KENNETH ESLER, *University of Illinois at Urbana-Champaign* DAVID CEPERLEY, *University of Illinois at Urbana-Champaign* We summarize a number of improvements we have developed for the quantum simulation of fluids under extreme conditions with path integral Monte Carlo (PIMC). PIMC provides way to combine fully-correlated quantum effects with thermal fluctuations in a natural formalism by sampling the many-body thermal density matrix. These developments include the construction of accurate pseudohamiltonians and their incorporation into PIMC, computation of high-accuracy pair density matrices, improved optimization of the long/short-range breakup, a fast embedded band-structure calculation for the fermion nodal restriction, Brillouin-zone integration through twist-averaged boundary conditions, and coupled PIMC/Langevin dynamics. We present preliminary results for the simulation of sodium near its liquid/vapor critical point.

**9:00**
**U42 4 Vibron Dynamics of Hydrogen at High Pressures and Temperatures** KARL JOHNSON, *University of Pittsburgh* JOSEPH FELDMAN, *Center for Computational Materials Science, Naval Research Laboratory, and School of Computational Sciences, George Mason University* RUSSELL HEMLEY, *Geophysical Laboratory, Carnegie Institution of Washington* There is currently great interest in the behavior of molecular hydrogen at high pressures and temperatures. The van Kranendonk theory of vibrons in solid hydrogen has been used previously to provide a description of the Raman response as a function of pressure and para-ortho concentrations at low temperature. Here we apply the same model to very different environments, namely to the solid at high P-T conditions, and, with less justification, to the dense fluid. The effect of temperature is presumed to be to renormalize the hopping parameter. Within our model of the vibrons and approximate harmonic lattice dynamics, a $1/R^6$ dependence of the hopping parameter on intermolecular distance, $R$, gets averaged over fluctuations in the interatomic distance, and the average increases with temperature. Preliminary results using configurations obtained from hybrid path integral molecular dynamics calculations with empirical potentials suggest that there is very little change in the Raman peak upon melting at high pressure, in agreement with previous high P-T measurements.

**9:12**

**U42 5 A systematic search method for finding new high-pressure phases of polymeric nitrogen** SERGEY DUDIY, FEDERICO ZAHARIEV, JAMES HOOPER, *Department of Chemistry, University of Ottawa, Ottawa, Ontario, K1N 6N5, Canada* FAN ZHANG, *Defense Research and Development Canada - Suffield, PO Box 4000, Medicine Hat, Alberta, T1A 8K6, Canada* TOM WOO, *Department of Chemistry, University of Ottawa* A recent discovery of single-bonded polymeric form of nitrogen in diamond anvil cell high pressure experiments [Nature Mat. **3**, 558 (2004)] opens a new promising direction in the development of high energy density materials. Besides the cubic gauche phase of polynitrogen stabilized in experiment, other yet unidentified metastable phases could emerge under certain experimental conditions. We present a systematic search method for finding metastable phases of single bonded nitrogen based on a set of Peierls distortions of a given reference structure. Using the most basic reference structure, a simple cubic unit cell, our approach not only reproduces all the single-bonded nitrogen phases reported so far, but also reveals many new metastable structures with promising properties. The equations of state of the structures calculated at the first-principles level are studied over a broad range of pressures up to 300 GPa. The stability of the structures is analyzed using directly calculated phonon spectra. This approach can be extended using more complex reference structures and relaxing the constraint of a pure single bonded phase.

**9:24**

**U42 6 Complexity and Pressure Induced Fermi Surface Deformation in Lithium** AITOR BERGARA, ALVARO RODRIGUEZ-PRIETO, *University of the Basque Country (UPV/EHU) and Donostia International Physics Center (DIPC)* V.M. SILKIN, *Donostia International Physics Center (DIPC)* UPV/EHU AND DIPC TEAM, Recently reported structural complexity and high temperature superconducting transition in lithium under pressure has increased the interest in light alkalis, otherwise considered as simple and well known systems under normal conditions. In this work we present an analysis of the pressure induced Fermi surface deformation in lithium and its relation to the observed complexity. According to our calculations, the Fermi surface becomes increasingly anisotropic with pressure and at around 8 GPa it contacts the Brillouin zone boundary, which preludes the bcc to fcc phase transition. Furthermore, at around 30 GPa, besides the increasing necks in the Fermi surface along the fcc ΓL direction, it develops an extended and well defined nesting in the ΓW direction, which enhances the electronic response for the nesting momentum and induces an strong phonon softening along the ΓK. The increasing electron-phonon coupling associated to this softening, besides preluding the transition to complex structures, also provides a better understanding of the observed superconducting transition in lithium at around the same pressure range.

**9:36**

**U42 7 Prediction of a superionic phase of hydrogen fluoride (HF) at high temperature and pressure*** LAURENCE FRIED, NIR GOLDMAN, *Lawrence Livermore National Laboratory* We report first principles simulations of hydrogen fluoride. Ab initio molecular dynamics simulations of HF were conducted at densities of 1.8 – 4.0 g/cc along the 900 K isotherm. At experimentally observable conditions, we find a transition to a superionic phase, in which the fluorine ions exhibit a stable lattice and the hydrogen ions exhibit rapid diffusion. This phase is similar to the recently reported superionic phase in water, in that there is a symmetrization of the hydrogen bond, and we observe a transient partially covalent network at pressures greater than 66 GPa. In addition, we describe a mechanism for hydrogen diffusion through the fluorine sub- lattice. Our results provide evidence that superionic solids are prevalent in solids that manifest low temperature symmetric hydrogen bonding. The pressures needed to induce superionic diffusion in HF are significantly lower than what is required for other known superionic hydrides, and thus will permit much more extensive experimental studies of this exotic phase.

*This work was performed under the auspices of the U.S. Department of Energy by University of California, Lawrence Livermore National Laboratory under Contract W-7405-Eng-48.

**9:48**

**U42 8 High-pressure and high-temperature phases of nitrous oxide*** BRENDAN OSBERG, STANIMIR A. BONEV, *Department of Physics, Dalhousie University, Canada* The phase diagram of nitrous oxide ($N_2O$) is investigated up to 50 GPa and 1000 K using first principles theory. The calculated stability and properties of numerous crystalline structures are compared with experimental results. We identify the structure of phase II of $N_2O$. On the basis of its stability with respect to orthorhombic deformations, an explanation for measured Raman spectra is provided. Similarly to $CO_2$ [1], crystalline structures with bent molecules are found to be extremely unfavorable energetically. [1] Bonev et al., Phys. Rev. Lett. 91, 065501 (2003).

*Work supported by the NSERC of Canada.

**10:00**

**U42 9 Mechanical strength and coordination defects in compressed silica glass** YUNFENG LIANG, *International School for Advanced Studies (SISSA) and INFM-CNR Democritos National Simulation Center, Trieste (Italy)* CAETANO R. MIRANDA, SANDRO SCANDOLO, *The Abdus Salam International Centre for Theoretical Physics (ICTP) and INFM-CNR Democritos National Simulation Center, Trieste (Italy)* Contrary to ordinary solids, which are normally known to harden by compression, the mechanical strength of compressed $SiO_2$ glass shows a minimum around 10 GPa. Around this pressure, the compression of silica glass undergoes a change from purely elastic to plastic, leading to the recovery of a densified amorphous polymorph. The compressibility of silica glass is also anomalous, with a maximum at about 2-4 GPa. Despite the large pressure difference between the onset of the two anomalies, microscopic theories have traditionally attempted to explain both anomalies with the pressure induced appearance of coordination defects. Such models are seriously questioned however by the lack of evidence for coordination defects below 10 GPa, in Raman and NMR experiments. Here we show, using an improved interatomic potential for $SiO_2$, that a correct description of the pressure-induced appearance of five-fold coordination defects in silica glass is crucial to address the above phenomenology and to obtain a theoretical model consistent with experiments.

**10:12**

**U42 10 USPEX - Predicting crystal structures of new phases** COLIN W. GLASS, ARTEM R. OGANOV, *Lab. of Crystallography, ETH Zuerich* We have developed an very efficient and reliable method for crystal structure prediction [1], merging an evolutionary algorithm, based on local optimization and spatial heredity, with itab initio total-energy calculations. This method allows one to predict the most stable crystal structure and a large

number of robust metastable structures for a given compound at any $P - T$ condition, without requiring experimental input. The success rate is extremely high – USPEX succeeded in all of the 25 tests performed so far, including ionic, covalent, metallic, and molecular structures with up to 20 atoms per unit cell. Using this methodology we have succeeded in predicting hitherto unknown structures [2]. Implementation of the algorithm, several applications and physical reasons for its success will be discussed. [1] Glass C.W, Oganov A.R., Hansen N. (2005). USPEX: a universal structure prediction algorithm. In prep. [2] Oganov A.R., Glass C.W., Ono S. (2005). High-pressure phases of $CaCO_3$: crystal structure prediction and experiment. Earth Planet. Sci. Lett, in press.

**SESSION U43: FOCUS SESSION: NOVEL PHASES IN LOW DIMENSIONAL QUANTUM GASES**
**Thursday Morning, 16 March 2006**
**346, Baltimore Convention Center at 8:00**
**M. Olshanii, University of Southern California, presiding**

***Contributed Papers***

**8:00**
**U43 1 Low-Dimensional Fermi Gases** HENNING MORITZ, *ETH Zurich* KENNETH GÜENTER, THILO STÖFERLE, MICHAEL KÖHL, TILMAN ESSLINGER, Optical lattices are a powerful tool to create novel many-body quantum systems with ultracold atoms. They allow to study the role of interactions in the system in reduced dimensions. We have observed two-particle bound states of atoms confined in a one-dimensional matter waveguide. These bound states exist irrespective of the sign of the scattering length, contrary to the situation in free space. The strongly interacting one- dimensional Fermi gas which we create in an optical lattice represents a realization of a tunable Luttinger liquid. In a spin-polarized Fermi gas interacting via a p-wave Feshbach resonance the strong confinement allows us to restrict the asymptotic scattering states. When aligning the spins along (or perpendicular to) the axis of motion in a 1D gas, scattering into channels with the angular momentum projection of $|m| = 1$ (or $m = 0$) can be completely suppressed.

**8:12**
**U43 2 Empirical manifestations of integrability in cold quantum gases** MAXIM OLSHANII, VANJA DUNJKO, *USC* VLADIMIR YUROVSKY, *U Tel-Aviv* MARCOS RIGOL, *UC Davis* Integrable quantum many-body systems traditionally belong to the domain of mathematical physics, with little or no connection to experiments. However, the experiments on confined quantum-degenerate gases has recently yielded faithful realizations of a number of integrable systems, thus making them phenomenologicalily relevant. We show that the presence of few-body conserved quantities in a quantum system leads to dramatic, initial-state-dependent discrepancy between the state of the system after relaxation and the predictions of thermodynamics. Using the newly introduced concept of constrained thermal equilibrium we study quantitatively the effects of the memory of the initial conditions. As objects of study we choose bosons in one-dimensional optical lattices in the deep Mott regime and spin-0 Bose gases confined to waveguides, both of which have been experimentally realized already. We suggest momentum distribution and chemical composition as the simplest experimental observables sensitive to the effects of integrability. Overall, we argue that the kinetic and thermodynamic properties of integrable quantum gases are so different from the usual, that they well-qualify for a new state of quantum matter.

**8:24**
**U43 3 Noise and counting statistics in one-dimensional insulators** AUSTEN LAMACRAFT, *All Souls College, Oxford* We discuss the correlation properties of current carrying states of one-dimensional insulators, which could be realized by applying an impulse to atoms loaded onto an optical lattice. While the equilibrium noise has a gapped spectrum, the quantum uncertainty encoded in the amplitudes for the Zener process gives a zero frequency contribution out of equilibrium. We derive a general expression for the generating function of the full counting statistics and find that the particle transport obeys binomial statistics. Finally, we discuss the extent to which the technique employed in a recent experiment (Phys. Rev. Lett. 95, 090404 (2005)) can be considered an ideal measurement of counting statistics.

***Invited Papers***

**8:36**
**U43 4 Dynamics of reduced dimension Bose gases in optical lattices.**
J. V. PORTO, *National Institute of Standards and Technology*

We use deep optical lattices to tightly confine cold atoms in reduced dimensions. By applying shallower optical lattices in the weakly confined direction, we realize well-characterized one- and two- dimensional Bose-atom lattice gases. Transport dynamics is studied by observing motion of the atom cloud through the lattice. For a 1D quantum degenerate Bose gas, we report the observation of strongly damped dipole oscillations in a combined harmonic and optical lattice potential. Damping is significant for very shallow axial lattices (0.25 photon recoil energies), and increases dramatically with increasing lattice depth, such that the gas becomes nearly immobile for times an order of magnitude longer than the single-particle tunneling time. Surprisingly, we see no broadening of the atomic quasimomentum distribution after damped motion.

*Contributed Papers*

**9:12**
**U43 5 The superfluid-Mott insulator transition in 2D** I. B. SPIELMAN, J. HUCKANS, J. STRABLEY, M. ANDERLINI, J. KRUSE, J. V. PORTO, W. D. PHILLIPS, *NIST* Ultra-cold atoms in optical lattices have been exploited to study the Mott-insulator transition in 1, 2, and 3 dimensions; here focus on the 2D Mott-insulator transition. Initially Bose-condensed rubidium atoms are loaded into a 3D optical lattice with an average occupancy of one atom per-site. By making one lattice much deeper in one direction than the remaining two, we construct an ensemble of 2D lattice systems. These 2D systems exhibit a superfluid-insulator transition as the lattice depth is increased. In this talk I present new measurements that show that even when the conventional signature of long-range order (namely diffraction) disappears, the system is not a perfect insulator – partially responding to an impulsive force.

**9:24**
**U43 6 Crystalline phases of bosons in rotating traps: Tonks-Girardeau gas on a ring.*** IGOR ROMANOVSKY, *Georgia Inst. of Technology* CONSTANTINE YANNOULEAS, *Georgia Inst. of Technology* UZI LANDMAN, *Georgia Inst. of Technology* We analyze the systems of strongly repelling bosons in two-dimensional harmonic and ring-shaped traps as a function of the rotational frequency of the trap for neutral atoms (and of an applied magnetic field for charged bosons). Our two-step approach consists of breaking the rotational symmetry at the Hartree-Fock level and of subsequent symmetry restoration via projection techniques,[1] thus taking into account correlations beyond the Gross-Pitaevskii (GP) solution. The bosons localize and form crystalline patterns both for a repulsive contact potential and a Coulomb interaction, as revealed via conditional probability distribution (CPD) analysis. This behavior of the bosons in the ring-shaped traps in the strong repulsion limit is similar to the behavior of fermions and is a manifestation of the fermionization phenomenon. We present calculations for the ground state energies as a function of the rotational frequency (or the strength of the magnetic field) and as a function of the repulsion strength.

*Supported by the US D.O.E. (FG05-86ER-45234)

[1]Phys. Rev. Lett.**93**, 230405 (2004)

**9:36**
**U43 7 Ordering and Entropy Production Across Qauntum Phase Transitions** ROBERT CHERNG, *Harvard University* LEONID LEVITOV, *MIT* We consider the transverse field Ising spin chain swept through a quantum critical point from the disordered to the ordered phase (and vice versa) and present exact results on the ordering and entropy production. Prepared in the ground state of the initial Hamiltonian, the system evolves to a state characterized by a non-equilibrium distribution of excitations of the final Hamiltonian. We show that the evolved system, while described by a pure many-body state, possesses finite entropy if considered ''locally.'' The notion of local entropy is defined by coarse-graining in momentum space, and is linked to the properties of the system of Kibble-Zureck domain walls. Exact results obtained for the spin correlation functions are presented and used to elucidate the relationship with the Kibble-Zureck theory of critical dynamics. Possible manifestations in ultracold atoms trapped in optical lattices will be discussed.

*Invited Papers*

**9:48**
**U43 8 Spin 1/2 fermions on spin-dependent optical lattices.***
ANDREW HO, *School of Physics and Astronomy, Birmingham University*

We study the phase diagram of one-dimensional two-component (i.e. pseudo-''spin''-1/2) ultracold atomic Fermi gas. The two atom species can have different hopping or mass. A very rich phase diagram for equal densities of the species is found, containing Mott insulators with various quasi-long-range-order, superfluids and perhaps phase separation. We also discuss coupling such 1D systems together and the experimental signatures of the phases. In particular, we compute the ''spin''-structure factor at small momentum, which should reveal a ''spin'' gap.

*Supported by EPSRC(UK) and Leverhulme Trust (UK).

*Contributed Papers*

**10:24**
**U43 9 Quartetting and pairing instabilities in one dimensional spin 3/2 fermionic systems** CONGJUN WU, *Kavli Institute for Theoretical Physics, UCSB* Novel competing orders are found in spin 3/2 cold atomic systems in one-dimensional optical traps and lattices. In particular, the quartetting phase, a four-fermion counterpart of Cooper pairing, exists in a large portion of the phase diagram. The transition between the quartetting and singlet Cooper pairing phases is controlled by an Ising symmetry breaking in one of the spin channels. The singlet Cooper pairing phase also survives in the purely repulsive interaction regime. In addition, various charge and bond ordered phases are identified at commensurate fillings in lattice systems.

**10:36**
**U43 10 Spinfull bosons in an optical lattice** SARA BERGKVIST, *KTH, Stockholm, Sweden* IAN McCULLOCH, *RWTH, Aachen, Germany* ANDERS ROSENGREN, *KTH, Stockholm, Sweden* We have studied the phase diagram of spinfull bosons in a one-dimensional optical lattice, using DMRG. Correlation functions and the dimerization are calculated. We also present results for energy gap to excited states and magnetization energies. We confirm the expected phase diagram with a dimerized phase in the insulating regions with an odd density and on-site singlets in the other insulating systems.

**SESSION U44: MODELS OF STRONGLY CORRELATED ELECTRONS**
**Thursday Morning, 16 March 2006**
**347, Baltimore Convention Center at 8:00**
**S.-W. Tsai, University of California, Riverside, presiding**

**8:00**
**U44 1 First-principles calculations of magnetic transition temperatures** XIANGANG WAN, *University of California, Davis* SERGEY SAVRASOV, *University of California, Davis* We introduce a method to evaluate magnetic transition temperatures of strongly correlated systems. It is based on a combination of dynamical mean field theory, the local density functional theory, and employs ''magnetic force theorem'' for evaluating exchange constants. The method automatically predicts at a given temperature whether the system is ordered or disordered magnetically. We illustrate the approach on several systems, and discuss its accuracy in comparison with the experiment. The effect of electron-electron correlations on these predictions will be discussed.

**8:12**
**U44 2 Electron-phonon-coupling-driven pairing symmetry transition in a ladder** KA-MING TAM, ANTONIO H. CASTRO NETO, *Boston University* SHAN-WEN TSAI, *University of California, Riverside* DAVID K. CAMPBELL, *Boston University* We address the effects of electron-phonon coupling in the electron-electron interacting ladder using the recently developed functional renormalization group method, in which the full retardation effects can be taken into account impartially[1]. We study the doped Holstein-Hubbard ladder as a typical example and show that there is a transition between s-wave and d-wave pairing as a function of electron-phonon coupling and doping level. This contrasts with recent results from a two-step renormalization group, which suggest that the electron-phonon coupling only contributes in a subdominant fashion and that the spin-gapped pairing phase always has d-wave symmetry, unchanged from the doped Hubbard ladder without electron-phonon interaction[2].

[1]S.-W. Tsai, A.H. Castro Neto, R. Shankar, D.K. Campbell, Phys. Rev. B 72, 054531 (2005)
[2]Alexander Seidel, Hsiu-Hau Lin, Dung-Hai Lee, Phys. Rev. B 71, 220501 (2005)

**8:24**
**U44 3 Dynamical Mean Field Study of the Extended Hubbard Model** ANDREW BALDWIN, *University of California, in Davis* ALEXANDRU MACRIDIN, MARK JARRELL, *University of Cincinnati* RICHARD SCALETTAR, *University of California, in Davis* The competition between on-site $U$ and intersite $V$ repulsion in the extended Hubbard model drives ground state phase transitions between spin density wave (sdw) and charge density wave (cdw) phases. While it was originally thought that in one dimension the sdw-cdw transition was first order at strong coupling and second order at weak coupling, it is now known that for small $U$ and $V$ a bond ordered wave phase intervenes. Here we present studies of the extended Hubbard model using the dynamical cluster approximation. We study the influence of $V$ on the CDW and SDW transition temperatures, $T_c$ and $T_N$. We find $T_N$ is almost unmodified in the sdw region, even if $J = 4t^2/(U - V)$ is strongly modified. We also study the effect of V on the pairing interaction and the pseudogap.

**8:36**
**U44 4 Exact transformation for spin-charge separation of spin half fermions** STELLAN ÖSTLUND, *Göteborgs Universitet* MATS GRANATH, We demonstrate an exact local transformation which maps a purely Fermionic manybody system to a system of spinfull Bosons and spinless Fermions, demonstrating a possible path to a non-Fermi liquid state. We apply this to the half-filled Hubbard model and show how the transformation maps the ordinary spin half Fermionic degrees of freedom exactly and without introducing Hilbert space constraints to a charge-like ''quasicharge'' fermion and a spin-like ''quasispin'' Boson while preserving all the symmetries of the model. We present approximate solutions with localized charge which emerge naturally from the Hubbard model in this form. Our results strongly suggest that charge tends to remain localized for large values of the Hubbard U. The results suggest that checkerboard patterns are natural patterns that result for the strongly interacting Hubbard model away from half filling.

**8:48**
**U44 5 Dynamical Cluster Approximation Study of Ferromagnetism in the Periodic Anderson Model** MUHAMMAD AZIZ MAJIDI, *University of Cincinnati* MARK JARRELL, *University of Cincinnati* JUANA MORENO, *University of North Dakota* SUMITH DOLUWEERA, *University of Cincinnati* The ferromagnetic phase in the strong coupling limit of the Periodic Anderson Model (PAM) is not fully understood. Previous studies using the Dynamical Mean Field Approximation (DMFA) (Tahvildar-Zadeh *et al.* (PRB **55**, R3332 (1997)) pointed to the importance of a ferromagnetic mechanism other than RKKY at conduction-band fillings near a quarter. This mechanism is related to the formation of a charge-density wave of the conduction electrons. However, it is questionable whether or not this effect persists when non-local correlations are incorporated into the theory. We try to answer this question by performing parametric studies on the phase diagram, the RKKY coupling, and the charge and spin susceptibilities for a three-dimensional system using the Dynamical Cluster Approximation (DCA).

**9:00**
**U44 6 Phase Diagrams of Hubbard Models with Small Unit Cells** WEI-FENG TSAI, *Department of Physics and Astronomy, UCLA* STEVEN A. KIVELSON, *Department of Physics and Astronomy, UCLA, and Department of Physics, Stanford University* We present a controlled approach to the low temperature phase diagram of highly inhomogeneous Hubbard models in the limit of small coupling, $t'$, between clusters. We apply this to the dimerized and checkerboard models with any strength of $U$. The dimerized model is found to behave like a doped semiconductor, with a Fermi-liquid groundstate with parameters (*e.g.* the effective mass) which are smooth, and unspectacular functions of $U$. By contrast, the checkerboard model has a Fermi liquid phase at large $U > U_c = 4.67$, a d-wave superconducting state with a full gap for $U_c > U > 0$, and a narrow strip of an intermediate d-wave superconducting phase with gapless ''nodal'' quasiparticles for $|U - U_c| < \mathcal{O}(t')$.

**9:12**

**U44 7 Effects of interplay between electron-electron and electron-phonon interactions in two-dimensional systems** FILIPPOS KLIRONOMOS, SHAN-WEN TSAI, *Physics Department, University of California, Riverside* We study the two-dimensional Hubbard model in the presence of electron-phonon interaction which is integrated into an effective electron-electron coupling producing a retardation effect [S.-W. Tsai *et al* Phys. Rev. B **72**, 054531 (2005)]. We work in the context of the functional renormalization group method [R. Shankar, Rev. Mod. Phys. **66**, 129 (1994)] to one loop accuracy, where self-energy corrections are included, and investigate the effect that isotropic and anisotropic phonons have near van Hove band fillings. This approach conveniently takes into consideration the effect of phonons at every step of the renormalization group method. We focus on the two-patch and many-patch schemes, where the Fermi surface is subdivided into two or multiple patches that label the electrons involved in each interaction process and produce a phase diagram for the different instabilities associated with the Hubbard model. We also depart from half-filling and investigate various specific cases of momentum transfer as well.

**9:24**

**U44 8 Nearest-Neighbor Repulsion and Competing Charge and Spin Order in the Extended Hubbard Model.** DAVOUDI BAHMAN, A.-M.S. TREMBLAY,* *Universite de Sherbrooke* We generalize the Two-Particle Self-Consistent (TPSC) approach to study the extended Hubbard model where the nearest-neighbor interaction $V$ is present in addition to the local interaction $U$. Our results are in good agreement with available Quantum Monte-Carlo results over the whole range of density $n$ up to intermediate coupling. As a function of $U, V$ and $n$ we observe different kinds of charge and spin orders, like commensurate/incommensurate charge and spin density wave, phase separation, and ferromagnetic order. For attractive $V$ superconductivity could exist in the regions where the other types of charge and spin orders do not dominate. B. Davoudi and A.-M.S. Tremblay, cond-mat/0509707

*Supported by: NSERC, FQRNT, Canada Research Chair program and Canadian Institute of Advanced Research

**9:36**

**U44 9 Quantum Monte Carlo Study of the Triangular Hubbard Model** CHRISTOPHER VARNEY, RICHARD SCALETTAR, *University of California, Davis* MARK JARRELL, ALEXANDRU MACRIDIN, *University of Cincinnati* We study the Hubbard model on a triangular lattice using Determinant Quantum Monte Carlo and the Dynamic Cluster Approximation. We compare the spin, charge and pairing response functions obtained with the two methods as a function of spatial lattice and cluster size, and also compute the one particle spectrum. We examine the possibility of charge ordering at one third filling driven by the avoidance of magnetic frustration.

**9:48**

**U44 10 Theory of Cu K-edge Resonant Inelastic X-ray Scattering in Cuprates.** KENJI TSUTSUI, TAKAMI TOHYAMA, SADAMICHI MAEKAWA, *IMR, Tohoku Univ., Sendai 980-8577, Japan* Resonant inelastic x-ray scattering (RIXS) has received much attention as a powerful technique to investigate elementary excitations in strongly correlated electron systems. In particular, the momentum-dependent spectra of Cu K-edge RIXS in high-Tc cuprates have been obtained by several experimental groups. The knowledge of these excitations across the gap as well as single-particle excitations is of importance for understanding the electronic properties in cuprates. We demonstrate theoretically momentum dependences of the RIXS in insulating and doped cuprates. The RIXS spectra are calculated by using the exact diagonalization techniques on small clusters in two-dimensional Hubbard models with 1s-core bands. In the insulating case, we find the anisotropic momentum dependence in the RIXS spectrum. The dependence is explained by the particle-hole excitations in which the antiferromagnetic correlation of the ground state plays a crucial role. Upon hole-doping, the spectrum from the lower Hubbard band to the upper Hubbard band becomes broad and less momentum dependent. This is in contrast to the case of electron-doping, where the momentum dependence of the spectrum in the undoped system remains, except that along the $< 1,0 >$ direction. The difference in the spectra between hole- and electron-doped systems follows the carrier-dependence of short-range AF spin correlations.

**10:00**

**U44 11 Fermi Surface of the Half Heusler Compounds $Ce_{1-x}La_xBiPt$** A. D. BIANCHI, J. WOSNITZA, *HLD, FZR, P.O. Box 51 01 19, D-01314 Dresden, Germany* N. KOZLOVA, D. ECKERT, L. SCHULTZ, I. OPHALE, S. ELGAZZAR, M. RICHTER, *IFW Dresden, D-01171 Dresden, Germany* J. HAGEL, M. DOERR, *IFP, TU Dresden, D-01062 Dresden,Germany* G. GOLL, H. V. LÖHNEYSEN, *Physikalisches Institut, Universität Karlsruhe, D-76128 Karlsruhe, Germany* G. ZWICKNAGL, *Institut für Mathematische Physik, Technische Universität Braunschweig, D-38106 Braunschweig, Germany* T. YOSHINO, T. TAKABATAKE, *Department of Quantum Matter, ADSM, Hiroshima University, Higashi-Hiroshima 739-8530, Japan* We report on the Fermi surface in the correlated half-Heusler compound $Ce_{1-x}La_xBiPt$. In CeBiPt we find a field-induced change of the electronic band structure as discovered by electrical-transport measurements in pulsed magnetic fields. For magnetic fields above $\sim$ 25 T, the charge-carrier concentration determined from Hall-effect measurements increases nearly 30%, whereas the Shubnikov–de Haas (SdH) signal disappears at the same field. In the non-4$f$ compound LaBiPt the Fermi surface remains unaffected, suggesting that these features are intimately related to the Ce 4$f$ electrons. Electronic band-structure calculations point to a 4$f$-polarization-induced change of the Fermi-surface topology. In order to test this hypothesis, we have measured the (SdH) signal in a $Ce_{0.95}La_{0.05}BiPt$ sample with a low La concentration.

**10:12**

**U44 12 Charge Physics of the Falicov-Kimball Model** PHILIP BRYDON, MIKLOS GULACSI, *Australian National University, Canberra, Australia* The charge-ordered phases of the one-dimensional Falicov-Kimball model are examined using a non-perturbative representation of the itinerant electrons. An effective model allows us to understand the competition between phase separation and long-range order. We construct a ground-state phase diagram for partial band-filling. The addition of an on-site hybridization potential is found to significantly alter the form of the phase diagram, with the appearance of mixed-valence phenomena.

**10:24**

**U44 13 Application of LDA+DMFT to systems near volume collapse transition** KRISTJAN HAULE, The physical origin of the volume collapse transition in Cerium and related materials will be addressed. Using recently developed self-consistent LDA +DMFT method, we will show that the Kondo Volume collapse model, involving both the f and spd electrons, describes the optical data better than a Mott transition picture. We predict the full temperature dependence of the optical spectra and find the development of a hybridization pseudogap in the vicinity of the collapse transition.

**10:36**

**U44 14 Functional renormalization group analysis of the one-dimensional half-filled Holstein-Hubbard model** SHAN-WEN TSAI, *University of California, Riverside* KA-MING TAM, DAVID K. CAMPBELL, ANTONIO H. CASTRO NETO, *Boston University* The one-dimensional half-filled Holstein-Hubbard model (HHM) is studied by the newly developed electron-phonon coupled functional renormalization group (ep-FRG) [1]. The ep-FRG enables us to study the electron-phonon coupled system in an unbiased manner by taking account of the scatterings at different energy scales and momenta systematically. Previous studies of the half-filled HHM showed that there is a direct transition between the charge-gapped spin-density wave (SDW) phase and the spin-charge-gapped charge-density wave (CDW) phase. Recently, it has been proposed that there is an intermediate spin-gapped metallic phase with dominant superconducting (SC) pairing correlation between SDW phase and CDW phase [2]. Our ep-FRG results show that the dominant correlation in this intermediate phase is not SC pairing. [1] S.-W. Tsai, A. H. Castro Neto, R. Shankar, and D. K. Campbell, Phys. Rev. B 72, 054531 (2005). [2] R. T. Clay and R. P. Hardikar, Phys. Rev. Lett. 95, 096401 (2005).

**10:48**

**U44 15 Antiferromagnetism and hot spots in CeIn3*** PAVEL GRIGORIEV, LEV GOR'KOV, *NHMFL, FSU* Enormous mass enhancement at ''hot spots'' on the Fermi surface (FS) of the antiferromagnetic $CeIn_3$ has been reported at strong magnetic field near its antiferromagnetic quantum critical point [T. Ebihara et al., Phys. Rev. Lett. 93, 246401 (2004)]. The effect was ascribed to anomalous spin fluctuations at these spots owing to peculiar strong many-body interactions. The ''hot spots'' lie at the positions on FS same as in non-magnetic $LaIn_3$ where the narrow necks are protruded, thus, hinting on their possible relation. Assuming that in paramagnetic phase $CeIn_3$ has similar spectrum, we study the influence of the antiferromagnetic ordering (AFM) on the energy spectrum of $CeIn_3$ and show that its FS undergoes a topological change at the onset of AFM. The necks at the ''hot spots'' are truncated by the AFM, thus restoring the almost spherical d-part of the FS of $CeIn_3$. Applied field suppresses the AFM and restores the necks on the FS (so-called 2.5-order phase transition) leading to logarithmic divergence of the dHvA effective mass when the electron trajectory passes near or through the restored necks. This effect fully explains the observed dHvA mass enhancement in the ''hot spots'' in the frameworks of one-particle approximation and leads to the predictions concerning the spin-dependence of the effective electron mass.

*The work was supported by NSF Cooperative agreement No. DMR-0084173 and (PG) by DOE Grant DE-FG03-03NA00066

**SESSION U45: STRUCTURAL, SURFACE AND OTHER PHASE TRANSITIONS**
**Thursday Morning, 16 March 2006**
**348, Baltimore Convention Center at 8:00**
**P. Riseborough, Temple University, presiding**

**8:00**

**U45 1 Effect of external strain on the order-disorder phase transition of the Si(001) surface** MASANORI YATA, *National Research Institute for Materials Science* The Si(001) surface exhibits the phase transition from c(4× 2) to the (2× 1) structure at about 200 K[1, 2]. This is an order-disorder phase transition with respect to the buckling of the dimmer: the c(4× 2) structure results from an antiferromagnetic ordering of the buckled-dimmer and the (2× 1) structure is attributed to the time average of the flip-flop motion of the buckled-dimers. Externally applied tensile strain along the $< 110>$ direction on the Si(001) surface is found to induce the flip-flop motion of the buckled dimmer below the critical temperature. This motion occurs cooperatively to form the disordered domain of the (2× 1) structure. Then the shape of the ordered domain as well as the size change with the strain. These results can be interpreted by the spontaneous shape instability originated from the strain relaxation energy. References [1] J. Ihm, D.H. Lee, J.D. Joannopoulos and J.J. Xiong, Phys. Rev. Lett. **51**, 1872(1983). [2] T. Tabata, T. Aruga and Y. Murata, Surf. Sci. **179**, L63(1987).

**8:12**

**U45 2 Faceting and defaceting phase transitions of Pd/W(111)** YU-WEN LIAO, *Natl. Taiwan Univ., Taiwan and Inst. of Atomic and Molecular Sciences, Taiwan* L.H. CHEN, K.C. KAO, *Natl. Central Univ., Taiwan* MINN-TSONG LIN, *Natl. Taiwan Univ., Taiwan and Inst. of Atomic and Molecular Sciences, Taiwan* CHENG-HSUN NIEN, *Natl. Central Univ., Taiwan* KER-JAR SONG, *Inst. of Atomic and Molecular Sciences, Taiwan* We have studied the faceting and the defaceting phase transitions of the Pd/W(111) surface. Our studies show that for creating the largest facets, the best annealing temperature is right below the defaceting transition temperature, confirming the prediction by Oleksy (Surf. Sci. 549 (2004) 246). As we vary the programmed heating/cooling rate from 1/8 to 8 K/s, the paths of faceting transitions show normal retardation effect and shift to lower temperatures as the cooling rate increased. Surprisingly, the paths of defaceting transitions show negligible dependence on the heating rate. Detailed studies of this peculiarity lead us to propose that the defaceting transition is initiated at places subject to loss of too much Pd due to thermal desorption. As such loss can more readily be replenished at places near any one of the Pd 3-d islands, we propose that the rate independent path of defaceting transition is the consequence of a temperature dependent balance between the loss and the supply of Pd. Such balance should depend on the density of the Pd islands. Indeed, we find the paths of defaceting transition can be shifted to lower temperature by reducing the density of the Pd 3-d islands.

**8:24**

**U45 3 Ultrafast lattice dynamics of FeRh*** D.A. WALKO, E.C. LANDAHL, JIN WANG, *Argonne National Laboratory* J.-U. THIELE, E.E. FULLERTON, *Hitachi Global Storage Technologies* FeRh undergoes magnetic and structural phase transitions at $\sim$ 100° C where a transition from antiferromagnetic to ferromagnetic orders occurs upon heating. Commensurate with this magnetic transition is a $\sim$ 1% expansion in the lattice parameter. Recent optical measurements have shown that the magnetic transition can be quite fast, i.e., on the picosecond or sub-picosecond time scales [1,2]. We have used ultrafast x-ray diffraction techniques at the Advanced Photon Source to probe the speed of the corresponding structural transition. An epitaxial FeRh thin film on a MgO(001) substrate was driven through the phase transition by ultrafast laser excitation, and the response of the lattice was directly observed via picosecond-time-resolved x-ray diffraction. The temporal evolution of the FeRh lattice is reported as a function of laser fluence. [1] J.-U. Thiele et al., Appl. Phys. Lett. 85, 2857 (2004). [2] G. Ju et al., Phys. Rev. Lett. 93, 192301 (2004).

*Use of the Advanced Photon Source was supported by the U. S. Department of Energy, Office of Science, Office of Basic Energy Sciences, under Contract No. W-31-109-Eng-38.

**8:36**

**U45 4 Phase stability and Jahn-Teller distortion in doped lithiated manganese oxides: A LSDA+U study** RAJENDRA PRASAD, NITYA NATH SHUKLA, *Indian Institute of Technology, Kanpur* ROY BENEDEK, *Argonne National Laboratory* We discuss how the rhombohedral phase of lithiated manganese oxide can be stabilized by doping with various impurities. Our study is based on LSDA+U calculations as implemented in the VASP code. We have considered rhombohedral and monoclinic phases using a supercell of 16 atoms. Our results are based on total energy calculations for 25% dopant concentration and pure lithiated manganese oxide. Several dopants such as Co, Fe, Ni, Mg and Zn are considered. We find that oxidation state of the dopant plays an important role in suppressing the Jahn-Teller distortion. Divalent impurities are found to be most effective. The effect of including U in the calculation is discussed.

**8:48**

**U45 5 Crystal Fields and the $\gamma \rightarrow \alpha$ transition in Ce** SUKALPA BASU, PETER RISEBOROUGH, *Temple University* In the $\gamma \rightarrow \alpha$ transition of Cerium, the material undergoes an isostructural change at which the volume changes by 15% and the magnetic character changes. Recently, the transition has been described in terms of a balance between the free energy of the magnetic moments and the characteristic energy scale of the $\alpha$ phase. The field-temperature dependence of the phase diagram has been predicted, and was confirmed by experiment. Inelastic neutron scattering experiments on the $\gamma$-phase of Ce have shown indications of crystal field splittings, and similar experiments have determined the energy scale of the $\alpha$ phase. We shall examine the effects of the crystalline field splittings within the framework of NCA calculations on the single-impurity Anderson model, and examine their consequence for the phase diagram.

**9:00**

**U45 6 Bifurcation Techniques for Structural Phase Transitions** RYAN S. ELLIOTT, *University of Minnesota* JOHN A. SHAW, NICOLAS TRIANTAFYLLIDIS, *University of Michigan* A new technique for studying structural phase transitions in crystals has been developed which uses bifurcation theory to investigate a material's free energy landscape. In this method a material's behavior is numerically interrogated by beginning with its high temperature structure and mapping out the equilibrium branch corresponding to the distortions of the crystal structure that occur due to changes in parameters such as temperature or stress. The investigation of this equilibrium branch is continued into unstable regions of the material's free energy landscape, i.e., regions which are physically unobservable. In these unstable regions the equilibrium branch bifurcates, or splits, and leads to other stable regions corresponding to different crystal structure branches (phases), thus revealing the links and interactions between the various phases of the material. Often, unexpected stable phases are identified in this way. It is common to encounter non-generic bifurcation points, where a single equilibrium branch splits into many (instead of two) new equilibrium branches. In these complex situations, the current bifurcation method is guaranteed to systematically identify all of the new branches. To illustrate the method, an atomistic model for shape memory alloys is investigated and a commonly observed hysteretic transformation is identified between a cubic $B2$ (austenite) structure and an orthorhombic $B19$ (martensite) structure.

**9:12**

**U45 7 Imaging the evolution of a glassy magnetic transition in a disordered ferromagnetic manganite*** WEIDA WU, CASEY ISRAEL, ALEX DE LOZANNE, *Dept. of Physics, UT Austin* NAMJUNG HUR, *Los Alamos National Lab, Cond. Matt. and Thermal Physics* SOONYONG PARK, S.-W. CHEONG, *Dept. of Physics & Astronomy, Rutgers* An intriguing glass-like transition in (La,Pr,Ca)$MnO_3$ is, for the first time, imaged using a variable-temperature magnetic force microscope. Images showing the temperature and magnetic- field evolution of the local magnetic structure illustrate the microscopic origin of the bifurcation of magnetic susceptibility, which is a ubiquitous phenomenon in heavily-disordered ferromagnets, and traditionally considered as a signature of a ''cluster glass transition.'' The observed avalanche-type behavior reveals the collective nature of the glassy transition in the manganites, where ferromagnetic and antiferromagnetic phases are intricately mixed.

*This work is supported by NSF DMR-0308575

**9:24**

**U45 8 Quantum Relaxation in a Proton Glass** C. ANCONA-TORRES, Y. FENG, T. F. ROSENBAUM, S. R. NAGEL, *University of Chicago* E. COURTENS, *Universit Montpellier II* D. PRICE, *University of Orleans* G. REITER, *University of Houston* $Rb_{1-x}(NH_4)_xH_2PO_4$ is a dipolar structural glass with spatial frustration from the mixture of ferroelectric RDP and antiferroelectric ADP. We measure the ac dielectric susceptibility of RADP:72 and RADP:35 over 7 decades of frequency for $0.3 < T < 300$ K. The relaxation is quantitatively similar for both concentrations at low temperatures, pointing to a local mechanism. We correlate the dielectric susceptibility with the potential energy landscape derived from neutron Compton scattering experiments and solve for

the tunneling parameters of the protons, finding correlated rearrangements of the hydrogen network. By analogy with vortex tunneling in high-Tc superconductors, we relate the logarithmic decay of the polarization to the quantum mechanical action.

**9:36 t Hannover, Germmany**

**U45 9 Switching between one and two dimensions: Pb induced chain structures on Si(557)** CHRISTOPH TEGENKAMP, ZIAD KALLASY, HERBERT PFNÜR, *Institute for Solid State Physics, Universität Hannover, Germmany* The conductivity of epitaxially grown Pb-structures on Si(557) has been measured. Different characteristic transport mechanisms have been found: For coverages above the percolation limit(0.6ML) up to 3ML the electronic transport in the annealed Pb-films is activated. Furthermore, the uniaxial symmetry of the Si(557) surface is reflected directly in a higher conductance in the parallel direction compared to the direction perpendicular to the steps. For coverages higher than 3ML a metallic behavior is found for both directions, i.e. the conductance decreases with increasing temperature. In contrast, already one ML, but annealed to 640K, leads to the formation of atomic wires, as seen by STM, with an extremely high and quasi one-dimensional surface state conductance along the wire direction. At a critical temperature of $T_c = 78$K, the system switches from low to high conductance anisotropy, with a metal-insulator transition in the direction perpendicular to the chain structure, while in the direction along the chains conductance with a (1/T + const.) temperature dependence was found. STM has shown further, that the 1D/2D transition is associated with an order-disorder phase transition of a 10-fold superperiodicity along the Pb chains.

**9:48**

**U45 10 Spontaneous polarization in one-dimensional Pb(Zr-Ti)$O_3$ nanowires*** IVAN NAUMOV, HUAXIANG FU, *Department of Physics, University of Arkansas* Formation of spontaneous polarization in one-dimensional structures is the key phenomenon that reveals collective behaviors in systems of reduced dimension, but has remained unsolved for decades. Here we report *ab initio* studies on finite-temperature structural properties of infinite-length nanowires of $Pb(Zr_{0.5}Ti_{0.5})O_3$ solid solution. Whereas existing studies have ruled out the possibility of phase transition in 1D chains, our atomistic simulations demonstrate an unambiguous otherwise. We show that phase transitions in 1D wires occur on a remarkable macroscopic length scale, but not necessarily on an infinite length scale as assumed in the general theories of 1D phase transition. Such phase transitions are characterized by large longitudinal $d_{33}$, $\chi_{33}$ responses and a large $c/a$ strain. The long rang ordering in PZT nanowires is explained by use of depolarizing effects associated with finite thickness of wires. Our results suggest no fundamental constraint that limits the use of ferroelectric nanowires and nanotubes arising from the absence of spontaneous ordering.

*This work was supported by the Office of Naval Research and the Army

**10:00**

**U45 11 Computational investigation of wetting and prewetting phase behavior*** JEFFREY ERRINGTON, *Dept. of Chemical and Biological Engineering, University at Buffalo* Fluids in the presence of one or more surfaces exhibit a rich variety of phase transitions that are absent in bulk fluids. Even the simplest of systems display a broad range of phase behavior. In this presentation, we describe our recent efforts aimed towards obtaining a better understanding of surface phase behavior through the use of molecular simulation. The first part of the presentation will be used to provide an overview of transition-matrix based Monte Carlo algorithms that enable one to efficiently locate and characterize phase transitions. Results will then be presented that describe how the wetting behavior of a model substrate-fluid system evolves with temperature and the relative strength of the substrate-fluid interaction. Simulation results will be compared with density functional theory calculations. Finally, we will describe a series of calculations that enable us to estimate the boundary tension along the prewetting saturation line. This quantity is related to the line tension associated with the formation of liquid droplets on a solid substrate. The magnitude of this tension has been the subject of debate recently, with experimental values spanning several orders of magnitude.

*This material is based upon work supported by the National Science Foundation under Grant No. CTS-0238772.

**10:12**

**U45 12 Magnetic properties of weak itinerant ferromagnetic Ni-V alloys*** SARA UBAID-KASSIS, ALMUT SCHROEDER, *Kent State University* Magnetization measurements of a serie of Ni-V alloys at high magnetic fields and low temperatures will be presented. Characteristic exponents observed in the low field susceptibility and spontaneous magnetization can be extracted and traced upon dilution. Especially the changes around a critical V-concentration of 1/9 will be discussed probing and comparing the validity of itinerant models and significance of spin fluctuations and magnetic cluster contributions.

*Work supported by NSF DMR 0306766

**10:24**

**U45 13 Scaling Behavior of Classical Wave Transport in Mesoscopic Media at the Localization Transition** SAI-KIT CHEUNG, ZHAO-QING ZHANG, The propagation of classical wave in disordered media at the Anderson localization transition is studied. Our results show that the scaling behavior of wave transport depends on the sample's geometry. It is found that the averaged static diffusion constant $D(L)$ scales like $\ln L/L$ in cubes or slabs, and the corresponding transmission follows $\langle T(L)\rangle \propto \ln L/L^2$. This is in contrast to the scaling behavior of $D(L) \propto 1/L$ and $\langle T(L)\rangle \propto 1/L^2$ obtained previously for electrons or spherical samples. For wave dynamics, we solve the Bethe-Salpeter equation in a disordered slab with the recurrent scattering incorporated in a self-consistent manner. All of the static and dynamic transport quantities studied are found to follow the new scaling behavior of $D(L)$.

**10:36**

**U45 14 Optical Near-Field Based Nanoscale Rapid Melting and Crystallization of Amorphous Silicon Thin Films** DAVID HWANG, ANANT CHIMMALGI, COSTAS GRIGOROPOULOS, *Univ. of California Berkeley* Nanostructuring of thin films is gaining widespread importance owing to ever-increasing applications in a variety of fields. The current study details nanosecond laser-based rapid melting and crystallization of thin amorphous silicon (a-Si) films at the nanoscale. Two different near-field processing schemes were employed. In the first scheme, local field enhancement in the near-field of a SPM probe tip irradiated with nanosecond laser pulses was utilized. As a second approach, the laser beam was spatially confined by a cantilevered near field scanning microscope tip (NSOM) fiber tip. Details of various modification regimes produced as a result of the rapid a-Si melting

and crystallization transformations that critically depend on the input laser fluence are presented. At one extreme corresponding to relatively high laser fluence, ablated area surrounded by a narrow melt region was observed. At the other extreme, where the incident laser energy density is much lower, single nanostructures with a lateral dimension of $\sim$ 90 nm were defined. The ability to induce nucleation and produce single semiconductor nanostructures in a controlled fashion may be crucial in the field of nano-opto-electronics.

**10:48**

**U45 15 Explosive Crystallization of Amorphous Semiconductor Films in the Presence of Melting** ALEXANDER GOLOVIN, *Northwestern University* COSTAS GRIGOROPOULOS, MATTHEW ROGERS, SEUNG HWAN KO, *University of California Berkeley* BERNARD MATKOWSKY, *Northwestern University* Explosive crystallization (EC) of thin amorphous solid films of germanium is investigated theoretically and experimentally. EC regime characterized by a propagating melting layer between the amorphous and the crystalline phases is considered. Laser-induced, linear EC fronts, uniformly propagating over large distances are achieved in films with various thicknesses deposited on quartz substrate. Depending on the front speed, the film thickness and the substrate temperature, different types of morphology of the resulting crystal phase are observed: columnar, scalloped and mixed. A theory of EC in the presence of melting is developed. The EC front propagation speed is calculated as a function of the substrate temperature and the film thickness; it is found to be in a good agreement with experiments. Linear stability analysis of a uniformly propagating planar EC front is performed. It is shown that for the parameter values where the columnar crystalline structure was observed the front is unstable with respect to a fingering instability similar to the Mullins-Sekerka instability of a solidification front in an undercooled melt. Nonlinear evolution of this instability is simulated numerically and is shown to exhibit a structure similar to the columnar one.

## SESSION U46: OPTICAL PROPERTIES OF SEMICONDUCTORS: EXCITONS AND PHONONS

**Thursday Morning, 16 March 2006**
**349, Baltimore Convention Center at 8:00**
**David Reitze, University of Florida, presiding**

**8:00**

**U46 1 Laser induced trapping of excitons in coupled quantum wells** A.T. HAMMACK, M. GRISWOLD, L.V. BUTOV, *University of California, San Diego* A.L. IVANOV, L.E. SMALLWOOD, *Cardiff University* A.C. GOSSARD, *University of California, Santa Barbara* Optical trapping and manipulation of neutral particles plays a major role in single particle studies in physics, chemistry, and biology [1]. An exciting recent outgrowth of the technique has been the experimental implementation of atom Bose- Einstein Condensation [2,3]. In this contribution, we report proposal and demonstration of laser induced trapping for a new system - a cold gas of excitons in coupled quantum wells. We report trapping a cold gas of excitons in laser induced traps and on the formation of a highly degenerate Bose gas of excitons in the trap. [1] A. Ashkin, *IEEE Journal on Selected Items in Quantum Electronics* **6**, 841 (2000). [2] E. A. Cornell, C. E. Wieman, *Rev. Mod. Phys.* **74**, 875 (2002). [3] W. Ketterle, *Rev. Mod. Phys.* **74**, 1131 (2002).

**8:12**

**U46 2 Spontaneous First-order Optical Coherence in Cold Exciton Gases in Coupled Quantum Wells** SEN YANG, A.T. HAMMACK, L.V. BUTOV, *Department of Physics, University of California, San Diego* A.C. GOSSARD, *Materials Department, University of California, Santa Barbara* A Mach-Zehnder interferometer with spatial and spectral resolution was used to probe spontaneous coherence in cold exciton gases, which are implemented experimentally in the ring of indirect excitons in coupled quantum wells[1]. A strong enhancement of spontaneous first-order optical coherence was observed at low temperatures below a few Kelvin where the thermal de Broglie wavelength becomes comparable to the interparticle separation and the exciton gas becomes nonclassical. The onset of spontaneous first-order optical coherence was found to be correlated with macroscopic spatial ordering in the exciton system. [1] L.V. Butov, A.C. Gossard, D.S. Chemla, *Nature* **418**, 751 (2002).

**8:24**

**U46 3 Theory of coherent population trapping and electromagnetically induced transparency in quantum wells and dots** ZACHARY DUTTON, *Naval Research Lab* Recently, there has been important experimental progress in quantum coherent phenomena in quantum-wells and dots, opening up possibilities for observations of quantum optical effects previously observed in atomic systems. In particular, coherent population trapping (CPT), electromagnetically-induced transparency (EIT), and slow light can occur in systems with sufficiently long ground state coherence, optically connected to an excited level, forming a Lambda-like system. We find that a quantum well or ensemble of dots, in Voigt geometry and illuminated by a bi-chromatic circularly polarized laser, can exhibit CPT and EIT. In this scheme, the electron spin provides the long lived ground states and a trion excitation acts as the excited level. By including optical and g-factor inhomogenous broadening, dephasing due to nuclear hyperfine interaction, and coupling to the both trion excitations, we derive a compact set of criteria for observations of these effects. We compare with experiments to date and discuss future prospects.

**8:36**

**U46 4 Stimulated Emission of Terahertz Radiation from Internal ExcitonTransitions in $Cu_2O$*** B.A. SCHMID, R. HUBER, Y.R. SHEN, R.A. KAINDL, D.S. CHEMLA, *Department of Physics, UC Berkeley, and Materials Sciences Division, Lawrence Berkeley National Laboratory* Excitons are among the most fundamental optical excitation modes in semiconductors. Resonant infrared pulses have been used to sensitively probe absorptive transitions between hydrogen-like bound pair states [1,2]. We report the first observation of the reverse quantum process: stimulated emission of electromagnetic radiation from intra-excitonic transitions [3]. Broadband terahertz pulses monitor the far-infrared electromagnetic response of $Cu_2O$ after ultrafast resonant photogeneration of 3*p* excitons. Stimulated emission from the 3*p* to the energetically lower 2*s* bound level occurs at a photon energy of 6.6 meV, with a cross section of $\sim 10^{-14}$ cm$^2$. Simultaneous excitation of both exciton levels, in turn, drives quantum beats which lead to efficient terahertz emission sharply peaked at the difference

frequency. Our results demonstrate a new fundamental process of THz quantum optics and highlight analogies and differences between excitonic and atomic systems. [1] R. A. Kaindl et al., Nature **423**, 734 (2003). [2] M. Kubouchi et al., Phys. Rev. Lett. **94**, 016403 (2005). [3] R. Huber et al., Phys. Rev. Lett., to appear.

*Supported by the U.S. Department of Energy under Contract No. DE-AC02-05CH11231.

**8:48**

**U46 5 Ultrafast Raman Studies of Electron Transient Transport in InN Thick Film Grown on GaN** KONG-THON TSEN, D.K. FERRY, *Arizona State University* HAI LU, WILLIAM J. SCHAFF, *Cornell University* GaN, AlN, InN and their alloys have long been considered as very promising materials for device applications. Semiconductor alloys such as $In_xGa_{1-x}N$ have been successfully used in the fabrication of blue-green light emitting diodes and laser diodes. Recently, growth of high quality InN as well as $In_xGa_{1-x}N$ have been demonstrated. In Particular, progress in the manufacturing of very high quality, single-crystal InN thin films has opened up a new challenging research avenue in the III-nitride semiconductors. InN together with its alloys of GaN and AlN enable the operation of light emitting diodes and diode lasers ranging in spectral wavelength from infrared all the way down to deep ultraviolet. It has also been predicted that InN has the lowest electron effective mass among all the III-nitride semiconductors. As a result, very high electron mobility and very large saturation velocity are expected. In this paper, we report experimental results of electron transient transport on InN thick film grown on GaN. Electron drift velocity as large as $7.5x10^7 cm/\text{sec}$ has been found when the sample is excited by an ultrafast laser pulse with pulse width about 600 femtoseconds. Our findings demonstrate that InN has great potential for use in the ultrafast electronic devices.

**9:00**

**U46 6 Exciton-mediated one phonon resonant Raman scattering from 1-dimensional systems** A. N. VAMIVAKAS, *Department of ECE, Boston University* A. G. WALSH, *Department of Physics, Boston University* Y. YIN, *Department of Physics, Boston University* M. S. UNLU, *Department of ECE, Boston University* B. B. GOLDBERG, *Department of Physics, Boston University* A. K. SWAN, *Department of ECE, Boston University* The Kramer's-Heisenberg approach is well developed for the theory of one phonon resonant Raman scattering (OPRRS) based on both intermediate states of free electrons and correlated electron-hole pairs in 3, 2 and 0-dimensional (D) systems. But to our knowledge, a theory of OPRRS incorporating excitonic effects has not yet been developed for quantum confined 1D system. In this talk we present a generic expression for the resonant Raman scattering cross section from a 1D system explicitly accounting for excitonic effects. We show how the theory is useful for analyzing the Raman resonance excitation profile lineshapes for of a variety of 1D systems. We apply this formalism to simple model systems to the similarities and differences between the free electron and correlated electron-hole 1D theory and also compare with the 3D excitonic theory.

**9:12**

**U46 7 Wurtzite Effects on Spin Splitting of GaN*** WAN-TSANG WANG, M.H. GAU, IKAI LO, S.F. TSAY, J.K. TSAI, K.L. HSIEH, J.C. CHIANG, *Department of Physisc, Center for Nanoscience and Nanotechnology, National Sun Yat-Sen University, Kaohsiung, Taiwan, Republic of China* We report the theoretical study of the wurtzite effects on spin-splitting of GaN within a third-neighbor Linear Combination of Atomic Orbitals (LCAO) model. For wurtzite structure, there are two intrinsic wurtzite effects which are band-folding effect and structure inversion asymmetry. The band-folding effect generates two conduction bands ($\Delta_{C1}$and $\Delta_{C3}$), in which the *p*-wave probability and, consequently, the spin-splitting energy have abrupt changes when $k_z$ increases toward the anti-crossing zone. The wurtzite effects, in addition to Rashba and Dresselhaus effect, give significant contributions to the large spin-splitting in GaN/AlN quantum wells.

*Research supported by National Science Council, Core Facilities Laboratory in Kaohsiung-Pintung area, Taiwan (ROC).

**9:24**

**U46 8 Ab initio calculations of excitons in wurtzite-type semiconductors.** NIELS E. CHRISTENSEN, *University of Aarhus. DK-8000 Aarhus.* ROBERT LASKOWSKI, *Technical University of Vienna, A-1060 Vienna* The optical absorption spectra are calculated with inclusion of electron-hole correlations for GaN, ZnO, and AlN, all in the wurtzite structure. Quasi-particle states are approximated by local-density-functional calculations with gaps corrected by a scissors operator, and the final spectra are obtained by solving the Bethe-Salpeter Equation. The results for ZnO depend sensitively on the energetic positions of the Zn-3d states. These are corrected by means of LDA+U. The excitons originating from the valence-band maximum are labeled A, B, and C, but their symmetry type, and thus dependence on the polarization of the light, are related to the specific values of the spin-orbit and crystal field splittings, SOC and CFS. The SOC is positive in GaN and AlN, negative in ZnO. The CFS is positive in GaN and ZnO, but negative in AlN. The sensitivity of the excitonic states to structural parameters is discussed, and in one case, AlN, we examine the validity of Elliott's model, the effective hydrogen-atom model.

**9:36**

**U46 9 Pump-Probe studies of Carrier Dynamics in bulk ZnO and ZnO epilayers and Nanorods*** X. WANG, Y.D. JHO, D.H. REITZE, C. COOK, G.D. SANDERS, C.J. STANTON, *Department of Physics, University of Florida* X. WEI, *National High Magnetic Field Laboratory* J.K YOO, G.-C. YI, *Department of Materials Science and Engineering, Pohang University of Science and Technology* ZnO-based devices are potentially useful as short wavelength emitters and in spintronics applications, yet little is known about the ultrafast relaxation properties of ZnO. We have performed time-resolved differential reflectivity (TRDR) measurements of bulk ZnO, ZnO epilayers and nanorods as a function of temperature and excitation wavelength. Bi-exponential decays of the A and B exciton states are observed with fast ( $\sim$ ps scale) and slower ( $\sim$ 50-100 ps scale) components, which depend strongly on excitation wavelength. We find that decay times can be correlated with relaxation channels in the band structure. In addition to their bi-exponential nature, the relaxation times we observe on ZnO epilayers and nanorods are shorter than high quality bulk ZnO, indicating a higher density of defects and impurity states in these samples.

*Supported by the NSF through grant DMR-0325499 and by the NHMFL through an IHRP grant.

**9:48**

**U46 10 Rate Equation Model for Carrier and Exciton Dynamics in ZnO*** C. J. COOK, G. D. SANDERS, C. J. STANTON, X. WANG, Y. D. JHO, D. H. REITZE, *University of Florida* There has been a renewed interest in ZnO materials for possible applications to short wavelength optical devices including blue lasers owing to its wide band-gap (3.37) and large exciton binding energy (approx. 60 meV). Recently, there have been several experimentalstudies of the dynamics of photoexcited carriers in bulk ZnO as well as epitaxial films and nanorods. In this talk, we report on theoretical calculations of the exciton and photoexcited carrier dynamics based on a multi-state, coupled rate equation model. We compare our theoretical results with recent tunable time resolved reflectivity measurements performed at the National High Magnetic Field Laboratory that study the relaxation dynamics when pumping and probing near the A and B excitons. In addition to solving the coupled rate equations, we also discuss the role of diffusion as well as phase space filling (non-linear rate equations) on the experimental results.

*Supported by NSF DMR-0325474 and the NHMFL In-house Reasearch Program.

**10:00**

**U46 11 Direct Observation of the Strength of Plasmon-Longitudinal Optical Phonon Interaction in n-type GaAs** HAKAN ALTAN, XUYING XIN, DAVID MATTEN, ROBERT ALFANO, *City College of New York* The screening of longitudinal optical phonons by plasmons is investigated by time-resolved visible pump-mid infrared probe transmission measurements in a series of light to highly doped n-type GaAs wafers. The reduced relaxation of photogenerated carriers is strongly correlated to the coupling between longitudinal optical phonons and background plasmons as suggested by the variation of the phonon strength over the doping range. Our results show that at low photogeneration ( $< 10^{16}cm^{-3}$) the critical doping density at which the strength of the coupling between LO phonons and plasmons decreases significantly is on the order of $N_c \sim 1x10^{18}cm^{-3}$. The lack of LO phonons that participate in relaxation of carriers due to the hybridization of the longitudinal modes above this doping level, can either result in adverse effects in the spectrum of diode lasers and semiconductor electronic devices or enhance photonic device performance due to longer minority carrier recombination times.

**10:12**

**U46 12 THz radiation from coherent acoustic phonon waves in strained GaN-based heterostructures** YOUNG-DAHL JHO,* *Univ. of Florida* JIN-YOUNG SOHN, *Seoul Nat'l Univ.* GARY D. SANDERS, CHRISTOPHER J. STANTON, *Univ. of Florida* EUNSOON OH, *Chungnam Nat'l Univ.* DAI-SIK KIM, *Seoul Nat'l Univ.* We present experimental results and discuss the generation mechanism of newly found THz radiation in GaN/InGaN based light emitting diode (LED) structures. These structures show strong coherent acoustic phonon oscillations under ultra-short optical excitation and we discuss the role these coherent phonons play in the generation of the THz signal. To better understand the role of piezoelectricity on the generation of the acoustic phonons and THz radiation, an external field was applied to compensate the built-in piezoelectric field. The coherent oscillatory behavior of the differential reflectivity spectra was reduced and finally become independent of the increasing applied voltage. However, with reverse bias, the THz emission from these structures was found to increase with increasing reverse voltage and excitation energy, slightly distinct from the trend of the photocurrent. The frequency of the THz emission is related to the transit time of the acoustic phonons between the AlGaN layers. The bias and wavelength dependence of the THz generation suggests that wavefunctions of confined carriers at the AlGaN/GaN and AlGaN/InGaN interfaces, are modulated by a temporally-changing potential shape associated with the piezoelectric field of the lattice and are responsible for the THz radiation.

*also at Seoul Nat'l Univ.

**10:24**

**U46 13 Theory of carrier dynamics and coherent phonons in piezoelectric semiconductor heterostructures*** GARY SANDERS, CHRIS STANTON, *University of Florida* We model generation and propagation of coherent acoustic phonons in time resolved reflectivity experiments on InGaN/GaN multi quantum wells embedded in a pin diode structure. Carriers are created in the InGaN wells by ultrafast pumping below the GaN band gap. The electronic states in the multiquantum well structure are obtained in an effective mass model and the generation and subsequent relaxation of photogenerated carriers in the well are treated in a Boltzmann equation formalism. Coherent acoustic phonons are generated in the quantum well via a strong piezoelectric electron-phonon interaction with photogenerated carriers. These propagate into the structure at the LA sound speed modifying the optical properties and giving rise to an oscillatory differential reflectivity signal. We also study the THz radiation emitted by the photoexcited carriers and phonons. In addition to studying the multiquantum well structure, we also study chirped superlattices were the well widths increase with distance and investigate the possibility of selectively exciting carriers in a given well to coherently control the response.

*Supported by NSF DMR-0325474

**10:36**

**U46 14 Studies of Coherent Acoustic Phonons in CdMnTe Single Crystals** D. WANG, S. WU, R. SOBOLEWSKI, *University of Rochester, Rochester, NY 14627* A. MYCIELSKI, *Polish Academy of Sciences, PL-02668 Warszawa, Poland* We have demonstrated generation and detection of coherent acoustic phonons (CAPs) in $Cd_{0.91}Mn_{0.09}Te$ (CdMnTe) single crystals using a femtosecond pump-probe spectroscopy technique. The Thomsen model based on propagation of a strain pulse in a crystalline lattice accounted very well the observed dependences of the frequency and the dephasing time of our CAP oscillations on the optical probe beam wave-vector. The CAP oscillation frequency was found to be dispersionless with the speed of sound equal to 3579 m/s. The comparison studies, performed using the pump beam with the photon energy well above the CdMnTe energy gap and the sub-gap probe beam demonstrated that in our crystals the measured dephasing time of CAP oscillations was limited by the absorption depth of the probe light rather than the intrinsic decay time of the coherent phonons. The latter value was estimated to be at least in the nanosecond range. Optically-induced electronic stress was determined to be the main generation mechanism of CAPs in CdMnTe.

**10:48**
**U46 15 Dynamical interfacial-electric-field-induced electro-optics in multilayer semiconductors** Y.D. GLINKA, J.K. MILLER, N.H. TOLK, *Vanderbilt University* X. LIU, Y. SASAKI, J.K. FURDYNA, *University of Notre Dame* Multilayer semiconductors with the thickness of layers of a few tens of nanometers are common materials for designing novel multifunctional electronic and opto-electronic devices. Once the materials are subjected to ultrafast laser light, the dynamical interfacial electric fields between adjacent layers is created as a result of charge separation at the interfaces within the carrier thermalization process. This dynamical electric field affects the ultrafast optical properties of the materials additionally to that of the bleaching effect (phase space filling-Pauli blocking). We report the first application of pump−probe technique allowing the interfacial-field-induced both electro-optical refractive-index change and the second harmonic generation to be monitored simultaneously. The pump-probe spectroscopy of GaAs/GaSb/InAs multilayers reveals predominantly the electro-optical nature. The interfacial fields contribute to the variety of electro-optical effects allowing the temporal and spatial resolution in carrier dynamics to be reached by monitoring responses resulted from different order nonlinear polarizations. The absorption bleaching is a secondary effect appearing with much smaller magnitude.

## SESSION V1: QUANTUM HALL EDGES
**Thursday Morning, 16 March 2006; Ballroom IV, Baltimore Convention Center at 11:15**
**Woowon Kang, University of Chicago, presiding**

**11:15**
**V1 1 Bending the quantum Hall effect: Novel metallic and insulating states in one dimension.***
MATTHEW GRAYSON, *Walter Schottky Institut, Tech. Univ. Muenchen*

One-dimensional conductors are the wires that will connect the circuits of tomorrow's nanoworld, so it is important to characterize their possible conducting phases. We study a novel one-dimensional wire state which arises at the corner of two quantum Hall systems joined at a 90 degree angle, and observe one-dimensional metallic and insulating states. Such non-planar confinement structures are unconventional for the quantum Hall effect and reveal the striking observation of a macroscopic one- dimensional state whose conductance increases with decreasing temperature. This single system can map out generic properties of disordered one-dimensional conductors since the metallic, critical, or insulating character is tunable with an external parameter, the magnetic field.

*In collaboration with L. Steinke, D. Schuh, M. Bichler, L. Hoeppel, J. Smet, K. Klitzing, D. K. Maude, and G. Abstreiter.

**11:51**
**V1 2 Coupled Luttinger Liquid State in Quantum Hall Line Junction.***
INSEOK YANG, *University of Chicago, and Korea Research Institute of Standards and Science*

We report on tunneling spectroscopy of quantum Hall tunnel junctions that juxtaposes two counterpropagating edge states across a high quality tunnel barrier. As the only current-carrying excitation of quantum Hall effect, edge states possess a unique ability to form robust one-dimensional electronic state along the perimeter of two-dimensional electron system. In our tunnel junctions, produced by cleaved edge overgrowth, the two edge states are laterally separated by an in-plane semiconductor barrier on the order of magnetic length and interact strongly over a junction that is $\sim 100\mu m$ long. Due to the quality of the tunnel barrier and the ballistic property of the edge states, inter-edge electron-electron interaction effects become predominant and disorder plays a negligible role to the leading order. Tunneling strongly mix the single particle states from two chiral one-dimensional systems, and the inter- edge correlation transforms the two counterpropagating edge states into a system of coupled, non- chiral Luttinger liquid whose Luttinger liquid properties are continuously tuned by magnetic field through the filling factor $\nu$ of the bulk quantum Hall state. The tunneling density of states of this many-body state possesses a power- law dependence on energy with an exponent $\alpha$, that is inversely proportional to the bulk filling factor, $\alpha \sim 1/\nu$. Inter-edge correlation also manifests in a series of quantum critical points between successive strong and weak tunneling regimes that are reminiscent of the plateau-transitions in quantum Hall effect. Tunneling spectroscopy consequently provides a direct probe of the quantum order underlying within these highly correlated one-dimensional states.

*This work was done in collaboration with P. Jiang, W. Kang (University of Chicago), L. Pfeiffer, K.W. Baldwin, and K.W. West (Lucent Technologies). The work at the University of Chicago was supported by NSF DMR-0203579.

**12:27**
**V1 3 Universality of the Edge-Tunneling Exponent of Fractional Quantum Hall Liquids.***
EDWARD REZAYI, *Physics Department CSU-Los Angeles*

Fractional quantum Hall states are characterized by their topological order. For example, the edge physics is uniquely determined by the bulk and gives a non-Ohmic relation $I \propto V^{\alpha}$ for tunneling into the edge, where the exponent $\alpha$ is a universal constant. In the simplest case of filling factors $\nu = n/(np + 1)$, ($n$ and $p$ are integers $> 0$, $p$ even) the

exponent is $p + 1$. However, experiments show substantial deviations. In a microscopic model of fractional quantum Hall liquids, we calculate the edge Greens function by exact diagonalization and obtain the exponent $\alpha$. We consider the 1/3 and 2/3 states with the Coulomb interaction and a variety of edge confining potentials. We find that the form of the confinement, such as sharpness of the edge and/or the strength of the confining potential which could lead to edge reconstruction, may cause deviations from universality in the edge-tunneling I-V exponent. We study two types of edge potentials: a sharp edge induced by a cut-off of angular momentum beyond $m_{max}$) and one induced by a uniform neutralizing background charge (a distance $d$ from the 2-d layer). Without the background charge, the exponent retains its universal value for soft edges (large $m_{max}$) but is non-universal for hard edges. In the presence of background charge and strong confinement (small $d$), the exponent is universal even for hard edges; for weak confinement and hard edges there is a deviation from the universal value while for soft edges there are finite-size corrections to $\alpha$, consistent with the edge reconstruction scenario. The relation of these results to experiments will be discussed.

*Supported by DOE.

**13:03**
**V1 4 Particle-hole symmetry and Luttinger liquids in a quantum Hall circuit.***
STEFANO RODDARO, *NEST-INFM CNR and Scuola Normale Superiore*

I shall present recent experimental results on edge-state transport through quantum point contacts in the quantum Hall (QH) regime. Finite-bias backscattering measurements between edge channels at filling factor $\nu = 1$ will be presented at different temperatures. Transport through the constriction displays a non-linear Luttinger-like behavior even in the integer QH regime in contrast with the linear tunneling predicted for integer edge states [1,2]. Both zero-bias enhancement and suppression of the inter-edge tunneling will be shown in a controllable way as a function of gate bias [2,3,4]. The observed evolution is connected to the local charge depletion in the constriction region and offers new insight into the link between QH charge-conjugation and Luttinger liquid description of edge channels [2]. I shall discuss the relevance of these experimental results in the context of the dynamics of the highly-correlated edge channels in the fractional QH regime [5]. Finally I shall demonstrate how charge-conjugation can be exploited in the design of new QH circuits where the transport properties of the hole component of a partially filled Landau level can be directly addressed. [1] X.-G. Wen, Phys. Rev. Lett. **62**, 2206 (1990); P. Fendley *et al.* Phys. Rev. Lett. **74**, 3005 (1995). [2] S. Roddaro, V. Pellegrini, F. Beltram, L. N. Pfeiffer, K. W. West, Phys. Rev. Lett. **95**, 156804 (2005). [3] S. Roddaro, V. Pellegrini, F. Beltram, G. Biasiol, L. Sorba., Phys. Rev. Lett. **93**, 046801 (2004). [4] S. Roddaro, V. Pellegrini, F. Beltram, G. Biasiol, L. Sorba, R. Raimondi, G. Vignale, Phys. Rev. Lett. **90**, 046805 (2003). [5] A. M. Chang, Rev. Mod. Phys. **75**, 1449 (2003).

*Work done in collaboration with V. Pellegrini, F. Beltram, L. N. Pfeiffer, K. W. West.

**13:39**
**V1 5 Edge State Tunneling in Split Hall Bar Models.**
EMILIANO PAPA

Edge states of Quantum Hall systems offer a rich ground for testing theoretical predictions on the properties of 1D strongly interacting fermionic systems. More importantly they are considered clean realizations the Luttinger Liquid description. In the past two years we [1,2,3,4] have examined a number of models that attempt to describe coupled edge density waves in the quantum Hall regime in various different geometries and to confront the large number of experimental observations that are at odds with the models that have been thought to apply in the past. Work that is currently in progress attempts to explain experimental results of the Pisa experimental group in which tunneling through a constriction between incompressible quantum Hall edge states is tuned from relevance to irrelevance by adjusting a gate voltage. This property is explained in terms of an interplay of the change in the connectivity of multi-mode edge magnetosplasmon and the role played by the metallic gates on the structure of the edge state, as well as the interactions between the edges. I will talk also for unresolved questions that have appeared in recent experiments in quantum Hall systems divided by thin cleaved-edge-overgrowth barriers. An important difficulty that arises in interpreting transport properties of QH line junction systems is the uncertainty about the strength and sometimes even the sign of these interactions, which can be difficult to estimate because of subtleties in understanding their relationship to underlying Coulombic interactions, because of edge reconstruction or because of the role played by the nearby metallic gates. We propose theoretical ideas and experimental measurements to obtain the required information. [1] E. Papa and A. H. MacDonald, Phys. Rev. Lett. 93, 126801 (2004). [2] E. Papa and A. H. MacDonald, Phys. Rev. B 72, 045324 (2005). [3] W.-C. Lee, N. A. Sinitsyn, E. Papa, and A. H. MacDonald, Phys. Rev. B 72, 121304 (2005). [4] E. Papa, and T. Stroh, in preparation.

**SESSION V2: EXCITONS IN SINGLE-WALLED CARBON NANOTUBES**
**Thursday Morning, 16 March 2006; Ballroom III, Baltimore Convention Center at 11:15**
**Sumitendra Mazumdar, University of Arizona, presiding**

**11:15**
**V2 1 Photoexcitation dynamics in SWCNT from sub-10 fs to ms.**
GUGLIELMO LANZANI, *Politecnico di Milano*

Photophisics in Single Walled Carbon Nanotubes, SWCNT-PEG, prepared by HiPco embedded PMMA is investigated with cw and pulse photo-excitation. Using ultra-short pulses in the visible and near infrared, with time duration of 7 fs and 20 fs respectively, pump-probe spectroscopy is carried out in SWCNT-PEG films in air at room temperature. Photo-bleaching recovery and photoinduced absorption build-up, upon excitation into the second absorption band, are time resolved providing a time constant of 40 plus/minus 5 fs. This is associated to exciton relaxation within semiconducting NTs, due to Fano-type resonances between localized excitonic levels and the underlying continuum density. Pumping in different regions of the absorption spectrum and probing a broad range of wavelengths, gives a complete description of the phenomenon. After relaxation, the decay of the equilibrated exciton occurs with a broad distribution of time constants, which is consistent with the inhomogeneous broadening of the sample. When using the shortest pulses (sub-10 fs) coherent phonons are clearly detected in the transmission difference traces. A radial breathing mode (RBM) at 250 wavenumber is observed, with dephasing of 1.2 ps. Anharmonic coupling between the RBM mode and the G-mode is detected for the first time in the time domain. Using cw excitation at 2.3 and 1.3 eV we observed photorefractivity in SWCNT-PEG samples, kept in vacuum at low temperature, in close analogy with conjugated polymers. Charges, which are photogenerated in the films, can separate giving rise to local electric fields which in turn induce Stark shift of the excitonic resonance.

**11:51**
**V2 2 Ultrafast and CW Optical Probes of Photoexcitations in Semiconducting Carbon Nanotubes.***
CHUAN-XIANG SHENG, *Department of Physics, University of Utah, Salt Lake City, Utah 84112*

Ultrafast dynamics of photoexcitations in semiconducting single walled carbon nanotubes (S-NT) in the form of films and $D_2O$ solutions, have been investigated using low intensity high repetition rate femtosecond laser system based on Ti-sapphire optical parametric oscillator in the spectral range from 0.13 to 1.05 eV. Various transient photoinduced bleaching (PB) and photoinduced absorption (PA) bands were observed, which also show pronounced polarization memory. The PA spectrum does not show Drude free carrier absorption, but instead is composed of two PA bands below the PB of the lowest S-NT absorption band. Also the PB spectrum exactly follows the cw photoluminescence (PL) emission spectrum. We therefore conclude that the primary photoexcitations in S-NT are itexcitons polarized along the NTs. We thus conjecture that the S-NT absorption bands are excitonic in origin; this conclusion is also supported by electroabsorption measurements that show quadratic Stark shift of the absorption bands. In addition, we found that the PL emission is also polarized; from the average PL polarization degree and ps transient polarization memory decay we estimate the PL lifetime in isolated S-NTs in solution to be of the order of 500 ps. Non-radiative decay processes dominate this relatively long PL lifetime. From the PL lifetime and the minute PL quantum efficiency we estimate the radiative PL lifetime in S-NTs to be $\sim$ $\mu$sec. This shows that the lowest lying exciton in S-NTs has small oscillator strength, and is in fact dark. The similarity of the PA spectrum in S-NTs and $\pi$-conjugated polymers indicates that quasi-1D excitons dominate the photophysics in both organic semiconducting materials. From this and the photon energy of the PA band we estimate the binding energy of the lowest exciton in S-NTs with diameters $\geqslant$ 1 nm to be $\sim$ 0.4 eV; in good agreement with two-photon absorption spectroscopy. Supported in part by the DOE.

*In collaboration with R. Baughman, A. Dalton, A. Gambetta, J. Kennedy, and Z. V. Vardeny.

**12:27**
**V2 3 Photophysics of single-walled carbon nanotubes: similarity with $\pi$-conjugated polymer.***
HONGBO ZHAO, *University of Arizona*

Coulomb electron-electron (e-e) interactions among the $\pi$-electrons have a strong effect on the energy spectra of semiconducting single-walled carbon nanotubes (S-SWCNTs), because of their quasi-one-dimensionality. The primary photoexcitations in S-SWCNTs as a consequence of e-e interactions are excitons, as opposed to free electrons and holes. There already exists a vast literature on excitons in $\pi$-conjugated polymers, the other class of carbon-based quasi-one-dimensional semiconductors. In order to seek guidance from this knowledge base, we have performed theoretical calculations of the excited state electronic structures, linear absorptions and excited state absorptions for ten different S-SWCNTs with a wide range in diameters,[1] within the same correlated $\pi$-electron model that has previously been applied to $\pi$-conjugated polymers. We found remarkable similarities in the excitonic energy spectra and nonlinear optical properties of S-SWCNTs on the one hand, and $\pi$-conjugated polymers on the other. The ''essential states'' model[2] of third-order optical nonlinearity, previously developed for $\pi$-conjugated polymers, applies also to S-SWCNTs (with minor

modifications for chiral S-SWCNTs which lack center of inversion). Our theory is able to explain semiquantitatively the results of nonlinear spectroscopic measurements on both S-SWCNTs and $\pi$-conjugated polymers. For wide S-SWCNTs with diameters ranging from 0.8–1.0 nm, we calculate exciton binding energies of 0.3–0.4 eV, in strong agreement with the values predicted from the experiments. We also remark on the occurrence of dark excitons below the optical excitons in the S-SWCNTs,[3] and the consequence thereof on the photoluminescence of these materials.

*In collaboration with S. Mazumdar and Z. Wang; Supported by NSF-DMR-0406604.

[1]H. Zhao *et al.*, cond-mat/0506097; J. W. Kennedy *et al.*, cond-mat/0505071.
[2]S. N. Dixit, D. Guo, and S. Mazumdar, Phys. Rev. B **43**, R6781 (1991).
[3]H. Zhao and S. Mazumdar, Phys. Rev. Lett. **93**, 157402 (2004).

**13:03**
**V2 4 Dephasing and weak localization in an interacting 1D system.***
ALEXANDER MIRLIN, *Forschungszentrum Karlsruhe*

We study the transport properties of interacting electrons in a disordered quantum wire (e.g. carbon nanotube) within the framework of the Luttinger liquid model. The conductivity at finite temperature is nonzero only because of inelastic electron-electron (e-e) scattering. We demonstrate that the notion of weak localization (WL) is applicable to the strongly correlated one-dimensional electron system and calculate the WL correction to the conductivity at not too low temperatures. The relevant dephasing rate is governed, for spinless electrons, by the interplay of e-e interaction and disorder. This WL dephasing rate is parametrically different from the dephasing rate of Aharonov-Bohm oscillations in a ring. Our approach, combining bosonization with fermionic treatment of the problem, provides a framework for systematically studying the mesoscopic phenomena in strongly correlated 1D electron systems. In the end, the fate of dephasing at lower temperatures (in the strong-localization regime) is briefly discussed.

*In collaboration with I.V. Gornyi and D.G. Polyakov.

**13:39**
**V2 5 Tuning photo-carrier lifetimes by the atomic structure and environment of single-walled carbon nanotubes.**
STEPHANIE REICH, *Department of Materials Science and Engineering, Massachusetts Institute of Technology*

Carrier relaxation in single-walled carbon nanotubes depends on their chirality, the tube's atomic structure. Excitons decay by interacting with phonons in most tubes, but a fast electron-electron channel becomes available in a subset of tubes. Carrier relaxation at the band gap depends on the tube's environment, with an order of magnitude difference between isolated (10-100 ps) and bundled tubes (1 ps). In this talk we discuss carrier relaxation in carbon nanotubes after photoexcitation. Our results explain the varying luminescence intensity in nanotubes and why nanotube bundles do not emit light. We estimate nanotube abundances from luminescence and discuss our concepts in view of non-linear optical devices made from single-walled carbon nanotubes.

## SESSION V3: NONEQUILIBRIUM NANO-OSCILLATORS
**Thursday Morning, 16 March 2006; Ballroom I, Baltimore Convention Center at 11:15**
**B. Golding, Michigan State University, presiding**

**11:15**
**V3 1 Noise in nonlinear nanomechanical resonators.**
ANDREW CLELAND, *UC Santa Barbara*

Noise limits the sensitivity of linear sensors, in a manner that is well understood, but also limits nonlinear systems in a less trivial way. Nonlinear nanomechanical resonators present interesting possibilities for the sensitive detection of forces and masses, but the noise limitations have not been explored much to date. Here we report on noise effects on nonlinear resonators operated in regimes where they have either one or two stable attractors. We have made quantitative measurements of the nonlinear response of a radiofrequency mechanical resonator with very high quality factor, measuring the noise-free transitions between the two attractors, and find good agreement with theory. We measure the transition rate response to controlled levels of white noise, and extract the basin activation energy. This allows us to obtain precise values for the relevant frequencies and the cubic nonlinearity in the Duffing oscillator, with applications to parametric sensing, in particular mass sensing.

[1]J.S. Aldridge and A.N. Cleland, ''Noise-enabled precision measurements of a Duffing nanomechanical resonator,'' Phys. Rev. Lett. 94, 156403 (2005).

[2]A.N. Cleland, ''Thermomechanical noise limits on parametric sensing with nanomechanical resonators,'' New J. Phys. 7, 235 (2005).

**11:51**
**V3 2 Noise activated switching in a driven, nonlinear micromechanical torsional oscillator.**
HO BUN CHAN, *University of Florida*

We study noise induced switching in an underdamped micromechanical torsional oscillator driven into the nonlinear regime, a system that is far from equilibrium. Within a certain range of driving frequencies, the oscillator possesses two stable dynamical states with different oscillation amplitudes. We induce the oscillator to escape from one dynamical state into the other by introducing noise in the excitation. Close to the birfucation point, the activation energy for switching is expected to display system-independent scaling. By measuring the rate of random transitions at different noise intensities, we deduce the activation energy as a function of frequency detuning and measure a critical exponent that is in good agreement with theoretical predictions. While the oscillator predominately resides in one of the two states for most excitation frequencies, a narrow range of frequencies exist where the occupations of the two states are approximately equal. At these frequencies, the oscillator undergoes 'kinetic phase transition' that resembles phase transition of thermal equilibrium systems. We observe a supernarrow peak in the power spectral densities of fluctuations in the measured oscillation amplitude. This peak is centered at the driving frequency and arises as a result of noise-induced transitions between the two dynamic states.

**12:27**
**V3 3 Multiphoton antiresonance and quantum activation in driven oscillators.***
MARK DYKMAN, *Michigan State University*

Resonantly modulated oscillators are predicted to display quantum effects, which have no analog in two-level systems. One of them is antiresonance of the coherent nonlinear response: the amplitude of forced vibrations of the oscillator displays a sharp minimum or maximum when the modulation frequency passes adiabatically through multiphoton resonance. The other is escape from metastable states of forced vibrations via quantum diffusion over quasienergy levels. The escape is studied for the cases of resonant and parametric modulation of the oscillator. In both cases, even for zero temperature, the rate of diffusion over quasienergy states is faster than the rate of interstate dynamical tunneling given that the latter is smaller than the relaxation rate. The effective activation energy of escape is a sharp function of temperature in the quantum regime. It displays a power-law dependence on the distance to the bifurcation value of the modulation amplitude or frequency. We show the fragility of the distribution over quasienergy for $T = 0$, when the system has detailed balance: it strongly differs from the distribution for $T \to 0$ and from the distribution in the presence of dephasing even where the dephasing rate is small.

[1]M. I. Dykman and M. V. Fistul, Phys. Rev. B **71**, 140508 (R) (2005).

[2]M. I. Dykman, Multiphoton antiresonance and quantum activation in driven systems, quant-ph/0507261.

*The research was supported in part by the NSF ITR-0085922 and by the Institute for Quantum Sciences at Michigan State University.

**13:03**
**V3 4 Metastable states in an RF-driven Josephson oscillator.**
RAJAMANI VIJAYARAGHAVAN, *Yale University*

A superconducting tunnel (Josephson) junction can be viewed as a non-linear, non-dissipative inductor and can be used to construct an oscillator by shunting it with a capacitor. Under certain driving conditions, the non-linear oscillator can adopt one of two possible modes of oscillation with different amplitude and phase. I will present experimental results which characterize these metastable states, and the transitions between them in the thermal and quantum regime. The dynamical switching between the metastable states can be used to make sensitive detectors. I will present data demonstrating the successful implementation of such a detector (Josephson Bifurcation Amplifier) to measure superconducting quantum bits. Other implementations of such non-linear oscillators using superconducting transmission line resonators will also be discussed.

**13:39**
**V3 5 Quantum nano-electromechanics: non-equilibrium cooling and strong feedback effects.**
AASHISH CLERK, *Dept. of Physics, McGill University*

A nano-electromechanical system consists of a micron-scale mechanical resonator coupled to a mesoscopic electronic conductor (e.g. a single-electron transistor, an atomic quantum point contact, etc.). The dissipative quantum mechanics of these systems are particularly interesting. How do the tunneling excitations in the conductor heat and damp the oscillator? To what extent do they act as an effective thermal bath? I will review recent theoretical work which demonstrates how a generic out-of-equilibrium mesoscopic conductor can act as an effective thermal bath. I will also

discuss the interesting case where this bath is formed by out-of-equilibrium, incoherently-tunneling Cooper pairs. This is system is remarkable in that significant cooling of the oscillator is possible, as well as a negative-damping instability which leads to a regime of strong-feedback between the oscillator and the Cooper pairs. Both these effects are analogous to ponderomotive effects occurring in a driven optical Fabry-Perot cavity having a moveable mirror; in our case, tunneling Cooper pairs play the role of the cavity photons.

[1]A. Clerk, Phys. Rev. B, 70, 245306, 2004.

[2]A. Clerk and S. Bennett, New J. Phys. 7 238, 2005.

**SESSION V4: DYNAMICS AND NON-EQUILIBRIUM PHENOMENA IN OPTICAL LATTICES**
**Thursday Morning, 16 March 2006; 308, Baltimore Convention Center at 11:15**
**Eugene Demler, Harvard University, presiding**

**11:15**
**V4 1 Phase coherence, visibility, and the signatures of superfluid-Mott and metal-Mott insulator transitions on optical lattices.**
GEORGE BATROUNI, *Institut Non-Linéaire de Nice, University of Nice*

Experiments are revealing, with increasing precision, details of the Mott insulating (MI) and superfluid (SF) phases of atomic condensates confined on optical lattices. Recently, details of the transition between the MI and the SF phases, as the lattice potential is changed, were examined by studying the visibility and phase coherence of the condensate. Reproducible kinks were observed in the visibility as the lattice potential was made deeper and the system moved into the MI phase. These kinks were interpreted as being due to the formation of the Mott region. We shall first review briefly the properties of the various phases of this system and how it makes the transition from SF to MI. Then we present a detailed Quantum Monte Carlo study of the visibility and other physical quantities as Mott domains begin to form. We show that as the lattice potential gets deeper and Mott domains become well established, the evolution of the system stalls: the density profile stops evolving for a substantial range of values of the lattice potential. As a consequence, the evolution of several other quantities also stalls and the visibility kink is produced. We offer an explanation of this behavior. We then extend our study to the formation of Mott domains in fermionic atoms on confined one-dimensional optical lattices. We find a new property of the metal–Mott insulator transition in a trap. The sum of kinetic and interaction energies exhibits minima when Mott domains appear in the system. In addition, we examine the derivatives of the kinetic and interaction energies, and of their sum, which display clear signatures of the Mott transition. We discuss the relevance of these findings to time of flight experiments that could allow the detection of the metal–Mott-insulator transition in confined fermions on optical lattices.

**11:51**
**V4 2 Superfluid-Insulator Transition in a Moving System of Interacting Bosons.**
ANATOLI POLKOVNIKOV, *Boston University*

Cold atomic systems with their high tunability and nearly perfect isolation from environment give an exciting possibility to address non-equilibrium problems, where both quantumand dynamic effects are important. In this talk I describe a moving system of interacting bosons in a periodic optical lattice potential and generalize the conventional superfluid-Mott insulator transition to this highly non-equilibrium situation. I will discuss implications of our results to recent and future experiments.

**12:27**
**V4 3 Non-equilibrium one-dimensional Bose gases.***
DAVID WEISS, *Penn State*

I will describe the preparation and time evolution of arrays of trapped one-dimensional Bose gases with highly non-equilibrium momentum distributions. We observe negligible thermalization, in both the strong and intermediate coupling regimes, even after each atom has undergone thousands of collisions. These experiments can be understood as quantum mechanical versions of Newton's cradle, with hundreds of particles simply exchanging specific momentum values. The absence of thermalization demonstrates nearly integrable dynamics, which is a theoretical rarity and an experimental first for many-body systems with many degrees of freedom. By allowing tunnelling among the tubes, we can continuously change the collisions from one-dimensional to three-dimensional. We have thus been able to study the onset of thermalization in a many-body system.

*This work was supported by the N.S.F., and performed in collaboration with Toshiya Kinoshita and Trevor Wenger.

**13:03**
**V4 4 Equilibrium and nonequilibrium properties of Tonks-Girardeau gases confined on optical lattices.***
MARCOS RIGOL, *University of California, Davis*

In this talk we discuss recent exact results for the in and out of equilibrium properties of Tonks-Girardeau (TG) bosons confined on one-dimensional lattices. The TG gas, introduced theoretically more than 40 years ago, has been recently realized in experiments with ultracold quantum gases loaded on optical lattices. We show that universal quasi-long range correlations are present in the ground state of trapped TG gases. These correlations account for the existence of quasi-condensates whose occupation scales proportionally to the square root of the number of particles in the trap. We find that when such systems are allowed to expand, by turning off the confining potential, their momentum distribution function rapidly approaches the one of noninteracting fermions. Remarkably, no loss in coherence is observed in the system as reflected by a large occupation of the quasi-condensates. We also study the expansion of TG gases starting their evolution from a pure Mott insulating state with one particle per lattice site. In this case quasi-long range correlations develop dynamically, and lead to the formation of traveling quasicondensates with a momentum determined by the underlying lattice. This effect could be used to create atom lasers with full control of the wavelength. Finally, we analyze the dipolar oscillations of TG gases in the combination harmonic trap - optical lattice. We show that damping is always present, and produces dramatic effects in the momentum distribution of the bosons. These effects are similar to the ones that would create a finite temperature in the system. In the presence of Mott insulating domains, the dipolar oscillations of the TG gas are overdamped and the center of mass barely moves from its initial displaced position.

*This work was supported by NSF-DMR-0312261, NSF-DMR-0240918, and SFB 382.

**13:39**
**V4 5 One-dimensional spin-polarized fermions.**
ANNA MINGUZZI, *Laboratoire de Physique et Modelisation des Mileux Condenses, C.N.R.S., B.P. 166, 38042 Grenoble, France*

The fermionic Tonks-Girardeau (FTG)gas is a spin-aligned one-dimensional Fermi gas with infinitely strong attractive zero-range odd-wave interactions. This model describes experiments on ultracold atomic gases subjected to tight quasi-1D waveguides and close to a Feshbach resonance. I will report on the recent investigations of the FTG gas under different trapping conditions (harmonic and ring traps) and in the presence of disorder. In particular I will discuss the pairing properties of this gas, the possibility of metastable current flows and the response to rotation. Finally, for a gas initially under harmonic confinement I will show that during an expansion the momentum distribution undergoes a ''dynamical bosonization,'' i.e., approaches the one of an ideal Bose gas, without violating the Pauli exclusion principle.

## SESSION V5: SURFACES AND INTERFACES OF CORRELATED OXIDES
**Thursday Morning, 16 March 2006; 309, Baltimore Convention Center at 11:15**
**James Eckstein, University of Illinois, presiding**

**11:15**
**V5 1 Magnetic Oxide Superlattices.***
MASASHI KAWASAKI, *IMR Tohoku University and CERC-AIST*

Atomically regulated interfaces and superlattices composed of oxides are very interesting research arena for physics and possible applications. By selecting magnetic oxides as one of the components, one can study basic phenomena of spin polarized electrons at the interfaces [1]. Also, one can realized ?multiferroics? at the interface because magnetization and electric dipole due to interface charge imbalance can coexist. We demonstrated that non-linear Kerr effect [2] can be a tool of detecting interface magnetism in ?tricolor superlattices? composed of asymmetric A-B-C-A-B-C- sequence with A, B, and C being component oxides [3]. This technique was successfully applied to detect, design and enhance interface magnetism in a single heterointerface [4]. We now extend the artificially built-in multiferroic superlattices to other sequences, which include DNA superlattices (D: donor, N: neutral, and A: acceptor) and Ratchet superlattices (asymmetric doping profile). We also demonstrate realization of interface ferromagnetism at pn junctions made of two Mott insulators and tuning the magnitude through the channels of orbital and charge degrees of freedom. [1] M. Izumi et al., J. Phys. Soc. Jpn., 71, 2621 (2002); Phys. Rev. B 64, 064429 (2001). [2] Y. Ogawa et al., Phys. Rev. Lett. 90, 217403 (2003). [3] H. Yamada et al., Appl. Phys. Lett., 80, 622 (2002). [4] H. Yamada et al., Science, 305, 646 (2004).

*This work has been performed under the collaboration with H. Yamada, T. Lottermoser, J. Matsuno, H. Okamoto, T. Arima, and Y. Tokura.

**11:51**
**V5 2 Electrostatic Modulation of the Charge Density of Correlated Oxides.***
CHARLES AHN, *Yale University*

A commonly occurring feature of correlated complex oxides is the sensitivity of their physical properties to changes in the carrier concentration. Modification of the carrier concentration is typically accomplished through chemical doping, which can introduce chemical and structural disorder into the system. Here, we discuss electric field effect experiments on colossal magnetoresistive manganites, showing the possibility of inducing large, reversible changes in the magnetic properties through electrostatic modulation of the carrier concentration. We compare electrostatic doping with chemical doping, showing that differences in transport properties arise because of structural distortions that occur during chemical substitution.

*In collaboration with X. Hong, A. Posadas, J.-B. Yau, Y. Bason, and L. Klein.

**12:27**
**V5 3 Ferromagnet / superconductor oxide superlattices.**
JACOBO SANTAMARIA, *GFMC, Departamento de Fisica Aplicada, Universidad Complutense de Madrid, 28040 Madrid*

The growth of heterostructures combining oxide materials is a new strategy to design novel artificial multifunctional materials with interesting behaviors ruled by the interface. With the (re)discovery of colossal magnetoresistance (CMR) materials, there has been renewed interest in heterostructures involving oxide superconductors and CMR ferromagnets where ferromagnetism (F) and superconductivity (S) compete within nanometric distances from the interface. In F/S/F structures involving oxides, interfaces are especially complex and various factors like interface disorder and roughness, epitaxial strain, polarity mismatch etc., are responsible for depressed magnetic and superconducting properties at the interface over nanometer length scales. In this talk I will focus in F/S/F structures made of $YBa_2Cu_3O_7$ (YBCO) and $La_{0.7}Ca_{0.3}MnO_3$ (LCMO). The high degree of spin polarization of the LCMO conduction band, together with the d-wave superconductivity of the YBCO make this F/S system an adequate candidate for the search of novel spin dependent effects in transport. We show that superconductivity at the interface is depressed by various factors like charge transfer, spin injection or ferromagnetic superconducting proximity effect. I will present experiments to examine the characteristic distances of the various mechanisms of superconductivity depression. In particular, I will discuss that the critical temperature of the superconductor depends on the relative orientation of the magnetization of the F layers, giving rise to a new giant magnetoresistance effect which might be of interest for spintronic applications. Work done in collaboration with V. Peña,[1] Z. Sefrioui,[1] J. Garcia-Barriocanal,[1] C. Visani,[1] D. Arias,[1] C. Leon,[1] N. Nemes,[2] M. Garcia Hernandez,[2] S. G. E. te Velthuis,[3] A. Hoffmann,[3] M. Varela,[4] S. J. Pennycook,[4]. Work supported by MCYT MAT 2005-06024, CAM GR- MAT-0771/2004, UCM PR3/04-12399 Work at Argonne supported by the Department of Energy, Basic Energy Sciences, Contract No.W-31-109-ENG-38. [1]GFMC, Departamento de Física Aplicada III, Universidad Complutense de Madrid, 28040 Madrid, Spain [2]Instituto de Ciencia de Materiales de Madrid (ICMM-CSIC). 28049 Cantoblanco. Madrid. [3]Materials Science Division, Argonne National Laboratory, Argonne, Illinois 60439, USA. [4]Condensed Matter Sciences Division, Oak Ridge National Laboratory, Oak Ridge, Tennessee 37831-6031, USA.

**13:03**
**V5 4 (Giant) Proximity Effects in high-$T_c$ superlattices.**
IVAN BOZOVIC, *Brookhaven National Laboratory*

Molecular beam epitaxy enables one to synthesize HTS thin films with rms surface roughness in the range 0.2-0.5 nm, much less than the unit cell height (1-2 nm).[1] One can also make atomically smooth multilayers and superlattices in which HTS or spacer layers can be just one unit cell thick if so desired. A detailed study of transport properties of such heterostructures has already revealed some unexpected findings.[2] In junctions where the barrier is made out of underdoped cuprate with a reduced critical temperature $T_c$, we observe the Giant Proximity Effect: supercurrent runs through very thick barrier layers even at temperature well above $T_c$ (contrary to what is expected from the standard theory). Atomic smoothness of films and multilayers, excellent device uniformity, and reversible modulation of barrier properties by oxygen intake provided solid evidence against experimental artifacts such as pinholes and micro-shorts. Hence, the effect is real and intrinsic, and it defies the conventional explanation. Interpretation and significance of our experimental results will be discussed in the context of theoretical concepts such as the pseudogap, midgap states, electronic inhomogeneity, preformed pairs, and possibly resonant pair tunneling. The work at BNL is done in collaboration with G. Logvenov, V. Butko, A. Gozar, and A. Bollinger. [1] I. Bozovic et al., Phys. Rev. Lett. **89**, 107001 (2002); P. Abbamonte et al., Science **297**, 581 (2002). [2] I. Bozovic et al., Nature **421**, 873 (2003); Phys. Rev. Lett. **93**, 157002 (2004).

**13:39**
**V5 5 Surprising Properties of Interfaces in the Cuprate Superconductors.***
JOCHEN MANNHART, *Augsburg University*

Interfaces in the cuprate superconductors, in particular the grain boundaries, play a decisive role for the realization of large scale applications of these materials, such as superconducting power cables. The approach followed worldwide to optimize the boundaries for superconducting cables consists in aligning all grains in the cables to less than 10[r], which presents an enormous effort. From the viewpoint of a solid state physicist, the grain boundaries in the cuprates are interfaces at which two oxides with highly correlated electron systems meet. If described as linear defects in the $CuO_2$-planes, can the properties of the boundaries be understood and new approaches for their optimization be identified? To address these questions, we have performed experiments to study the properties of these interfaces below and above the superconducting transition temperature. We find for the superconducting as well as for the normal state startling phenomena which challenge our understanding of the underlying physics.

*This work was performed together with C.W. Schneider, T. Kopp, B. Kuru, A. Kampf, A.A. Aligia, and J.R. Kirtley, and was supported by the BMBF (13N6918), the DFG (SFB484) and the ESF (THIOX).

## SESSION V7: NOISE IN BIOLOGICAL SYSTEMS
**Thursday Morning, 16 March 2006; 307, Baltimore Convention Center at 11:15**
**Alex van Oudenaarden, Massachusetts Institute of Technology, presiding**

**11:15**
**V7 1 Fluctuation-adaptation relation in bacterial chemotaxis.**
PHILIPPE CLUZEL, *University of Chicago*

I will present experiments and computer simulations demonstrating, at the single cell level, that the expression of key chemotaxis proteins is fine-tuned to values that maximize fluctuations and the chemotactic response.

**11:51**
**V7 2 Noise effects in bacterial motor switch.**
YUHAI TU

The clockwise (CW) or counter clockwise (CCW) spinning of bacterial flagellar motors is controlled by the concentration of a phosphorylated protein CheY-P. In this talk, we represent the stochastic switching behavior of a bacterial flagellar motor by a dynamical two-state (CW and CCW) model, with the energy levels of the two states fluctuating in time according to the variation of the CheY-P concentration in the cell. We show that with a generic normal distribution and a modest amplitude for CheY-P concentration fluctuations, the dynamical two-state model is capable of generating a power-law distribution (as opposed to an exponential Poisson-like distribution) for the durations of the CCW states, in agreement with recent experimental observations of Korobkova et al. [Nature 428, 574 (2004)]. In addition, we show that the power spectrum for the flagellar motor switching time series is not determined solely by the power-law duration distribution, but also by the temporal correlation between the duration times of different CCW intervals. We point out the intrinsic connection between anomalously large fluctuations of the motor output and the overall high gain of the bacterial chemotaxis system. Suggestions for experimental verification of the dynamical two-state model will also be discussed.

**12:27**
**V7 3 Noise limitations on E. Coli cell division accuracy.**
HERBERT LEVINE, *University of California, San Diego*

Accurate cell division in E. Coli requires the Min family of proteins. Remarkable, MinD and MinE exhibit spatial oscillations, resulting in a minimum of MinD near the center of the cell. This minimum is thought to be the signal for assembly of the cell division machinery. Although deterministic models reproduce many observed features, a stochastic treatment is needed to test the extent to which finite particle number noise limits the accuracy of this determination. This talk describes a stochastic dynamics based simulation of this system; our results are then compared to the measured cell division accuracy.

**13:03**
**V7 4 Physical Limits to Biochemical Signaling.***
SIMA SETAYESHGAR, *Department of Physics, Indiana University*

Many crucial biological processes operate with surprisingly small numbers of molecules, where the impact of noise associated with these small numbers is potentially significant. Over twenty–five years ago, Berg and Purcell [1] showed that bacterial chemotaxis, where a single celled organism must respond to small changes in concentration of chemicals outside the cell, is limited directly by molecule counting noise, and that aspects of the bacteria's behavioral and computational strategies must be chosen to minimize the effects of this noise. We revisit and generalize their arguments to estimate the physical limits to biochemical signaling, where a ligand interacts with its receptor or cluster of receptors within the cell, and argue that recent experiments are consistent with performance approaching these limits [2]. [1] H. C. Berg and E. M. Purcell, *Biophysical Journal* **20**, 193 (1977). [2] W. Bialek and S. Setayeshgar, *Proc. Natl. Acad. Sci.* **102**, 10040 (2005).

*This work is in collaboration with Prof. William Bialek at Princeton University.

**13:39**
**V7 5 Gene expression noise and robustness of signaling in bacterial chemotaxis.***
VICTOR SOURJIK, *ZMBH, University of Heidelberg*

Stochastic variations in protein levels are one of the major sources of noise affecting biological networks. Since networks involved in gene regulation and signal transduction must have a defined input-output relation, they can be expected to have undergone evolution for inherent robustness against such perturbations. Chemotaxis of a model bacterium itEscherichia coli – a mechanism that allows motile cells to follow chemical gradients in the environment – has one of the most thoroughly studied signaling networks in biology. Combining theoretical and experimental analysis, we investigated robustness of this network to intercellular variations in expression levels of chemotaxis proteins, or gene expression noise. The single-cell levels of different chemotaxis proteins showed strong co-variation, which implies that stochastic variations in transcriptional control are the main source of the noise. We demonstrated that the pathway is indeed robust to such kind of perturbations by testing the effect of concerted overexpression of all chemotaxis proteins on the pathway output. Using computer simulations and theoretical analysis, we determined the network design features responsible for robustness and showed that the experimentally established network in itEscherichia coli has the smallest topology that is sufficiently robust to allow a majority of the individuals in a population to maintain a correct pathway output.

*In collaboration with Markus Kollmann, Institut für Physik, Universität Freiburg.

## SESSION V8: FOCUS SESSION: SIMULATIONS USING PARTICLES
**Thursday Morning, 16 March 2006; 314, Baltimore Convention Center at 11:15**
**Lorena Barba, University of Bristol, presiding**

***Invited Papers***

**11:15**
**V8 1 Nanoscale flows on open chemical channels.**
JOEL KOPLIK, *City College of New York*

We investigate the nano-scale flows of low-volatility liquids along ''chemical channels'': patterns of completely-wetting solid embedded in a planar substrate, and sandwiched between less wetting solid regions. In the case of a long, straight wetting stripe, we use molecular dynamics simulations as basic computational tool, comparing the results to a simple long-wavelength approximation and a full stability analysis based on the Stokes equations. The different approaches are qualitatively consistent, and we find that while thin liquid ridges are stable both statically and during flow, a (linear) pearling instability develops if the thickness of the ridge exceeds half of the width of the channel. In the flowing case periodic bulges propagate along the channel and subsequently merge due to nonlinear effects. However, the ridge does not break up even in the unstable case, and the qualitative behavior is unchanged when the fluid can spill over onto a partially wetting exterior solid region. For more complicated patterns involving the splitting or merger of wetting stripes, we again find that liquid flows continuously along the wetting region despite the pearling instability. In this case, intriguing switching dynamics is found for moving pearls at junctions.

**11:51**
**V8 2 Immersed boundaries and particles.**
GEORGES-HENRI COTTET, *Universite Joseph Fourier*

This talk will present ongoing works in our group dealing with particle simulation of complex flows. We will show some non conventional particle methods to simulate incompressible elasticity and fluid-structure interactions. We will also show how particle methods in these fields, as well as for more conventional advection dominated physics, can lead to new ideas for Eulerian schemes.

***Contributed Papers***

**12:27**
**V8 3 Particle Methods in Numerical Cosmology** HUGH COUCHMAN, *McMaster University* Particle methods play a central role in numerical simulations of cosmic structure. These methods are particularly important for simulations of two-component universes that include both baryonic and ''dark matter.'' Particles are used to model both the collisionless dark matter—using a classical inverse square law gravitational attraction—and, with Smoothed Particle Hydrodynamics (SPH), the baryonic component. Although Eulerian methods are also now widely used to model cosmological hydrodynamics, SPH exhibits many useful and important properties for cosmology: it is robust and simple to code, meshes well with the necessary particle representation of the collisionless dark matter and is able to model large density contrasts and irregular geometries easily and reliably. These methods have been used to model purely collisionless cosmic fluids with up to $10^{10}$ particles and to model both baryonic and dark matter universes with approximately $10^{8.5}$ particles.

**12:39**
**V8 4 Fast Parallel Particle Methods: Angstroms to Gigaparsecs** MICHAEL WARREN, *Los Alamos National Laboratory* Fast multipole methods have become an ubiquitous tool for the simulation of physical systems with long-range interactions. Since their introduction they have been applied to a vast range of problems. Our own parallel hashed oct-tree code (HOT) has been applied to a number of physical systems with long-range interactions, including gravitational and smoothed particle hydrodynamic interactions in astrophysical systems, fluid flows with vortex-particle methods, electromagnetic scattering and aerodynamics. Several these simulations were recognized with Gordon Bell prizes for significant achievement in parallel processing. We will discuss some recent work which used a series of 1-billion particle dark matter simulations to accurately determine the mass function of galaxy halos. These simulations required over $4 \times 10^{18}$ floating point operations (4 exaflops). Another focus of our current research is extending the HOT framework to biological systems, with the goal of simulating systems using over ten times as many atoms as the current state-of-the-art. This requires addressing several issues with current multipole algorithms, such as spatially-correlated errors and the ability to handle disparate time scales efficiently.

**12:51**
**V8 5 Efficient particle simulations based on combining the Vortex-In-Cell and the Parallel Fast Multipole methods** GREGOIRE WINCKELMANS, ROGER COCLE, GOERIC DAENINCK, *Universite catholique de Louvain (UCL)* FRANCOIS THIRIFAY, *CENAERO and UCL* Particle methods are quality methods for simulating unsteady, convection dominated, flows, as they have negligible dissipation and dispersion. The vortex particle method is used for incompressible flows; also for buoyancy-driven flows by adding the temperature. The method can also be used for combustion, by using variable volume particles with vorticity, velocity divergence, temperature and species mass fractions. Quality particle methods also require interpolation/redistribution schemes. We here consider the Vortex-In-Cell (VIC) approach, where all operations, except convection, are done using a grid: Poisson solver, stretching, diffusion, etc. The vorticity field is also maintained divergence free by projection when required (which also requires solving a Poisson equation). In our implementation, we use the Fast Multipole method to obtain the boundary condition for solving the Poisson equation: this allows for a grid that tightly contains the particles. The method is also parallelized: the Parallel Fast Multipole (PFM) code provides the proper boundary condition on each subdomain, without iteration. Illustrative results will be presented in DNS and LES (also using multiscale models): vortex rings, wake vortices (also with ground effects), combustion.

**13:03**
**V8 6 A Particle/Panel Method for Vortex Sheet Roll-Up** ROBERT KRASNY, *University of Michigan* Vortex sheets are commonly used in fluid dynamics to model thin shear layers in slightly viscous flow. Some of the first Lagrangian particle simulations in fluid dynamics used the point vortex approximation to study vortex sheet roll-up. We will review the early fundamental contributions on this topic by Rosenhead, Birkhoff, and Moore, and then discuss more recent developments. In particular, a method is described for computing vortex sheet roll-up in 3D flow in which the sheet surface is represented by a set of quadrilateral panels with Lagrangian particles at the vertices. The particles are advected by a regularized Biot-Savart integral and the induced velocity is evaluated by a particle-cluster treecode. The panels are adaptively subdivided to maintain resolution as the sheet deforms. The method is applied to simulate the collision of two vortex rings. The results shed light on the dynamics of vortex filaments in fully 3D flow.

**13:15**
**V8 7 Particle dynamics-based hybrid simulation of vibrated gas-fluidized beds of cohesive fine powders** SUNG JOON MOON, YANNIS KEVREKIDIS, SANKARAN SUNDARESAN, *Princeton University* We use three-dimensional molecular dynamics simulations of macroscopic particles, coupled with volume-averaged gas phase hydrodynamics, to study vertically vibrated gas-fluidized beds of fine, cohesive powders. The interstitial gas flow is restricted to be effectively one-dimensional (1D) in the beds of narrow cross-sectional areas we consider. This model captures the spontaneous development of 1D traveling voidage waves, which corresponds to bubble formation in real fluidized beds. We use this model to probe the manner in which vibration and gas flow combine to influence the dynamics of cohesive particles. We find that as the gas flow rate increases, cyclic pressure pulsation produced by vibration becomes more and more significant than direct impact, and in a fully fluidized bed this pulsation is virtually the only relevant mechanism. We demon-

strate that vibration assists fluidization by creating large tensile stresses during transient periods, which helps break up the cohesive assembly into agglomerates. We also study spontaneous demixing in beds of a mixture of particles of different densities, so-called the ''phase separation,'' using an equation-free multiscale approach.

**13:27**

**V8 8 Dissipative Particle Dynamics Simulations of Two-Phase Flows** ANUPAM TIWARI, JOHN ABRAHAM, *School of Mechanical Engineering, Purdue University* Dissipative particle dynamics (DPD) is a coarse-grained particle method that includes thermal fluctuations. A mean-field theory based model is developed for two-phase flows. Surface tension arises in the model due to terms that account for long-range attractive forces. The model is validated through static simulations carried out to reproduce the Laplace law relationship, and dynamic simulations of liquid cylinder and drop oscillations. It is shown that in both cases analytical and computed results agree within 8%. We will also present results from simulations of capillary waves and Rayleigh-Taylor instability. In the case of capillary waves, comparisons will be shown with analytical results, and in the case of Rayleigh-Taylor instability, comparisons will be shown with analytical and other computed results. As an application of the model, results from simulations of thermally induced jet breakup will also be presented.

**13:39**

**V8 9 Polymer chain simulations in microchannels with Dissipative Particle Dynamics** VASILEIOS SYMEONIDIS, *MIT / Brown University* GEORGE KARNIADAKIS, *Brown University* BRUCE CASWELL, *Brown University* In this work we employ Dissipative Particle Dynamics (scdpd) for simulations of dilute polymer solutions using bead-spring representations. We present comparison of two time-marching schemes: the popular velocity-Verlet and Lowe's scheme. Schmidt number effects are investigated for a series of cases, including $\lambda$-scdna molecules under shear (using the Marko-Siggia wormlike chain spring law) and Poiseuille flow in microchannels. Effects on the polymer depletion layer, power-law profiles and apparent viscosities are presented as a function of the number of beads per polymer chain.

**13:51**

**V8 10 High order viscous vortex methods with deforming elliptical Gaussians** LOUIS ROSSI, *University of Delaware* RODRIGO PLATTE, *Arizona State University* Vortex methods are numerical schemes for approximating solutions to the Navier-Stokes equations using a linear combination of moving basis functions to approximate the vorticity field of a fluid. Typically, the basis function velocity is determined through a Biot-Savart integral applied at the basis function centroid. Since vortex methods are naturally adaptive, they are advantageous in flows dominated by localized regions of vorticity such as jets, wakes and boundary layers. A semi-discrete convergence formulation leads to a new viscous vortex method based on deforming elliptical Gaussian basis functions that achieves fourth order spatial convergence. One odd thing about the new method is that basis functions do not move with the physical flow velocity at the basis function centroid as is usually specified in vortex methods. Rather, high order accuracy is obtained when one adds a consistently small flow field curvature correction. We will present two distinct approaches to the evaluation of the Biot-Savart integral for elliptical Gaussian basis functions. Non-trivial flow field calculations will demonstrate the efficacy of the method for both convection-diffusion problems and Navier-Stokes flows in 2D.

**14:03**

**V8 11 Accelerating Atomistic Molecular Dynamics Simulation in Entropic Systems** XIN ZHOU, *Los Alamos National Laboratory* The time scale of the traditional atomistic molecular dynamics simulations is too short to study wide slow dynamics of complex systems. Hyperdynamics method developed by A. F. Voter in studying of solids can not use directly in entropic systems such as fluids, biopolymers etc. By applying suitable order parameters with the symmetry of the studied systems and the characteristics of short trajectory, we build the condition of extending the hyperdynamics into fluids and algorithms. We test our results in a few modeling systems and expect the methods is used generally in simulating atomistically slow dynamics of complex fluids and biopolymers.

**SESSION V9: MAGNETIC FORCE MICROSCOPIES**
**Thursday Morning, 16 March 2006**
**301, Baltimore Convention Center at 11:15**
**Albert Macrander, Argonne National Laboratory, presiding**

**11:15**

**V9 1 Localized Spectroscopy using a Magnetic Resonance Force Microscope.** GIORGIO MORESI, QIONG LIN, *ETHZ* SCHAHRAZEDE MOUAZIZ, *EPFL* ANDREAS HUNKELER, CHRISTIAN DEGEN, URBAN MEIER, *ETHZ* JUERGER BRUGGER, *EPFL* BEAT MEIER, *ETHZ* LABORATORY OF PHYSICAL CHEMISTRY, ETHZ, CH-8093 ZUERICH TEAM, LABORATORY OF MICROSYSTEMS, EPFL, CH-1015 LAUSANNE TEAM, The Magnetic Resonance Force Microscope (MRFM) constitutes a promising next-generation magnetic resonance detection device at room temperature. A MRFM observes nuclear (or electron) spin magnetization as a force, which occurs when a paramagnetic sample is polarized in inhomogeneous static magnetic field (10E5 T/m) and a high frequency drives the cantilever on-resonance by a cyclic adiabatic modulation, which make able to measure T1 rho. In this contribution, we combine the MRFM with spin-echo spectroscopy to add spectral resolution to NMR signals of micro-scale objects at room temperature. First experimental spectra recorded with the amplitude detection technique from a sample of barium chlorate monohydrate and ammonium sulfate single crystals mounted on a non commercial cantilever show resolution of $2\mu$m and a sensitivity of 10E13 spins. The new microscope, which uses the frequency detection down to m-Hz resolution and the annealed non-commercials cantilevers, which have Q factor up to 250000 at room temperature, improve the sensitivity to 10E9 spins. This new setup and a new measurement technique should make able to measure T1.

**11:27**

**V9 2 High Sensitivity Magnetic Resonance Force Microscopy** P. BANERJEE, Y. CHE, K.C. FONG, T. MEWES,* V. BHALLAMUDI, YU OBUKHOV, D.V. PELEKHOV, P.C. HAMMEL, *Ohio State University* We report high sensitivity detection of electron spin resonance from E′ centers in fused silica using the Magnetic Resonance Force Microscope. Operating at low temperatures and with high magnetic field gradients in the 2–3 G/nm range, we easily observe magnetic resonance signals from less than 1000 $\mu_B$, and signal averaging enables detection of less than 100 $\mu_B$ with a spin sensitivity of 10 $\mu_B$. While $T_1$ at low temperatures is approximately 5 sec, the lifetime of the magnetization under conditions of periodic adiabatic reversal is considerably shorter and is observed to be of order 100 ms. We will discuss design features necessary to operate the microscope at millikelvin temperatures.

*now at University of Alabama

**11:39**

**V9 3 Using High Coercivity Magnet Particle for High Sensitivity Magnetic Resonance Force Microscopy** K.C. FONG, I.H. LEE, P. BANERJEE, Y. CHE, YU. OBUKHOV, D.V. PELEKHOV, P.C. HAMMEL, *Physics Department, Ohio State University* We report on the application of a 40 micron diameter, high coercivity NdFeB magnetic particle for high sensitivity electron spin resonance detection using Magnetic Resonance Force Microscopy. The relatively large NdFeB magnetic particle allows us to obtain large field gradients at relatively large tip-sample separations which can reduce surface induced noise. Force signals due to two different spin manipulation protocols in high field gradient will be presented. Model of the forces generated by these excitation schemes provide insight, into the various spin manipulation techniques and the impact of magnetic particle size on high sensitivity spin detection.

**11:51**

**V9 4 Experiments in Nuclear Magnetic Resonance Microscopy** YONG LEE, WEI LU, J.-H. CHOI, *Korea Research Institute of Standard and Science* H.J. CHIA, U.M. MIRSAIDOV, S. GUCHHAIT, A.D. CAMBOU, R. CARDENAS, K. PARK, J.T. MARKERT, *University of Texas at Austin* We report our group's effort in the construction of an 8-T, $^3$He cryostat based nuclear magnetic resonance force microscope (NMRFM). The probe has two independent 3-D of piezoelectric x-y-z positioners for precise positioning of a fiber optic interferometer and a sample/gradient-producing magnet with respect to a micro-cantilever. The piezoelectric positioners have a very uniform controllable step size with virtually no backlash. A novel RF tuning circuit board design is implemented which allows us to simply swap out one RF component board with another for experiments involving different nuclear species. We successfully fabricated and are characterizing $50\mu m \times 50\mu m \times 0.2\mu m$ double torsional oscillators. We have also been characterizing ultrasoft cantilevers whose spring constant is on the order of $10^{-4}$ N/m. We also report NMRFM data for ammonium dihydrogen phosphate(ADP) at room temperature using our 1.2-T system. Observed features include the correct shift of the NMR peak with carrier frequency, increases in signal amplitude with both RF field strength and frequency modulation amplitude, and signal oscillation (spin nutation) as a function of tipping RF pulse length. Experiments in progress on $NH_4MgF_3$ (at 1.2 T) and $MgB_2$ (at 8.1 T) will also be briefly reviewed. Robert A. Welch Foundation grant No.F-1191 and the National Science Foundation grant No. DMR-0210383.

**12:03**

**V9 5 Three-dimensional Imaging using Magnetic Resonance Force Microscopy** I. H. LEE, *The Ohio State University* K.C. FONG, *The Ohio State University* YU. OBUKHOV, *The Ohio State University* D.V. PELEKHOV, *The Ohio State University* P.C. HAMMEL, *The Ohio State University* We describe techniques for obtaining 3D spin density images using Magnetic Resonance Force Microscopy. The apparatus, specifically designed to test imaging techniques, operates in vacuum at room temperature. We record the spatial dependence of the force generated by the Electron Spin Resonance signal from a DPPH particle mounted on the cantilever as it is scanned over a spherical NdFeB particle used as a high gradient probe magnet. Details of apparatus design, experimental data, challenges and approaches to 3D MRFM image deconvolution will be presented.

**12:15**

**V9 6 Development of a Room Temperature High Sensitivity Magnetoelectric Scanning Microscope*** JASON HATTRICK-SIMPERS, LIYANG DAI, ICHIRO TAKEUCHI, MANFRED WUTTIG, *Department of Materials Science and Engineering, University of Maryland* In recent years the interest in magnetoelectric (ME) materials has increased dramatically, since they promise to have a number of unique functionalities and capabilities including ultrahigh magnetic field sensitivity. To date there has been little work done to actually use them in applications. We have constructed a high sensitivity room temperature scanning magnetic field microscope using a ME composite device made of a metglass/xyz(PVDF)/metglass sandwitch structured laminate. The smallest ME composite device used was 1 mm x 2 mm x 200 microns. The ME coefficient and the peak voltage of a typical device are 50 mV/Gcm and 3 mV at an AC modulation field of 10 Gauss. Scans of a conducting ring carrying an AC current, with the sensor DC biased at 100 Gauss, will be shown for various ring dimensions and AC currents. Through the variation of AC current we have shown that the sensitivity of the microscope to the z-axis component of AC field is better than $10^{-9}$ T. We will discuss the relationship between the ME device dimensions and the spatial resolution of the microscope.

*This work was supported by NSF DMR-0520471

**12:27**

**V9 7 Feature doubling in MFM imaging** ZHIFENG DENG, *Department of Physics, Stanford University, Stanford CA 94305, USA* ERHAN YENILMEZ, HONGJIE DAI, KATHRYN MOLER, Recently, magnetic material coated nanotube tips have been used for high resolution magnetic force microscopy. It is convenient to control the total thickness of a metal-coated nanotube by change the nominal deposition thickness. The thinner the coating is, the less magnetic material attaches to the nanotube. With cobalt coated nanotube tip eleven nanometers in diameter, we measure twenty-five nanometer features clearly. We also observe feature doubling with cobalt coated carbon nanotube tips in an experimental hard drive sample, indicating paramagnetic behavior for the smallest tips.

**12:39**

**V9 8 Progress of Magnetic Force Microscope for detecting spin-polarized electrons in non-magnetic materials** V.P. BHALLAMUDI, *The Ohio State University* Y. JUNG, *The Ohio State University* D.V. PELEKHOV, *The Ohio State University* YU OBUKHOV, *The Ohio State University* P.C. HAMMEL, *The Ohio State University* T. MEWES, *University of Alabama* While optical methods for detection of spin-polarized currents and spin accumulation in non-magnetic materials have proved quite successful, their applicability is limited to certain class of materials. Magnetic force microscopy (MFM) offers a more widely applicable alternative. We report here on the progress towards building such a high sensitivity low temperature-MFM spin detector. It employs optical interferometry for displacement detection. Issues related to techniques for detection and various challenges are discussed. Sample images demonstrating the high force sensitivity of the microscope are also presented.

**12:51**

**V9 9 Focused ion beam deposition of $Co_{71}Cr_{17}Pt_{12}$ and $Ni_{80}Fe_{20}$ on tips for magnetic force microscopy*** ALFRED LEE, CHANGBAE HYUN, ALEX DE LOZANNE, *Department of Physics, University of Texas at Austin, Austin, TX 78712* We demonstrate that a focused ion beam can deposit magnetic coatings on cantilevers used for atomic force microscopy, thereby producing a sensor for magnetic force microscopy. This technique is highly versatile, allowing the convenient deposition of complex or expensive materials, such as $Co_{71}Cr_{17}Pt_{12}$. A second material chosen for this demonstration was permalloy ($Ni_{80}Fe_{20}$). We show magnetic images acquired with these cantilevers to illustrate their excellent properties and the differences between coatings. In principle, multilayer coatings could be easily made with this technique.

*This work is supported by NSF DMR-0308575.

**13:03**

**V9 10 High-resolution scanning hall probe microscopy*** CLIFFORD HICKS, LAN LUAN, J. HENDRIK BLUHM, KATHRYN MOLER, *Geballe Laboratory for Advanced Materials, Stanford University* JANICE GUIKEMA, *Laboratory of Atomic and Solid State Physics, Cornell University* ELI ZELDOV, HADAS SHTRIKMAN, *Department of Condensed Matter Physics, Weizmann Institute of Science* Scanning hall sensors can be used to directly image magnetic fields at surfaces. They offer high resolution, high sensitivity, operability over a broad temperature range, and linearity. We have fabricated hall sensors on GaAs / $Al_{0.35}Ga_{0.65}As$ and GaAs / $Al_{0.3}Ga_{0.7}As$ heterostructures containing 2D electron gases 40, 39 and 140nm beneath the surface. The sensitive areas of our probes range from microns to 85nm on a side. We report on the field sensitivities of probes of various sizes and their spatial resolution in a scanning configuration.

*supported by the NSC Center for Probing the Nanoscale

**13:15**

**V9 11 Scanning Hall Probe Microscopy (SHPM) using Quartz Crystal AFM Feedback** MUNIR DEDE, KORAY URKMEN, AHMET ORAL, *Bilkent* IAN FARRER, DAVID RITCHIE, *Cambridge* Scanning Hall Probe Microscopy (SHPM) [1] is a quantitative and non-invasive technique for imaging localized surface magnetic field fluctuations such as ferromagnetic domains with high spatial and magnetic field resolution of $\sim$ 50nm & $7mG/Hz^{-1/2}$ at room temperature. In the SHPM technique, Scanning Tunneling Microscope (STM) [1] or Atomic Force Microscope (AFM) [2] feedback is usually used for bringing the Hall sensor into close proximity of the sample. In the latter, the Hall probe has to be integrated with an AFM cantilever in a complicated microfabrication process. In this work, we have eliminated the difficult cantilever-Hall probe integration process; a Hall sensor is simply glued at the end of 32,768Hz Quartz tuning fork, as force sensor. The sensor assembly is set to oscillate with a PLL. SHPM electronics is modified to detect AFM topography and the frequency shift, along with the magnetic field image. The resonant frequency of the sensor drops to $\sim$ 5 kHz due to mass of the Hall sensor. Hard Disk, NdFeB Magnet, Garnet samples are imaged with the Quartz Crystal AFM feedback and the performance is found to be comparable with the SHPM using STM feedback. Quartz Crystal AFM feedback offers a very simple sensor fabrication and operation in SHPM. This method eliminates the necessity of conducting samples for SHPM. [1] A. Oral et al. Appl. Phys. Lett., 69, 1324 (1996) [2] A.J. Brook et al. Appl. Phys. Lett. 82, 3538 (2003)

**13:27**

**V9 12 Approach to Dipolar Field Microscopy** CARLOS MERILES, WEI DONG, PHILLIP STALLWORTH, *CUNY - City College of New York* Nuclear Magnetic Resonance (NMR) is arguably one of the most powerful techniques available today to characterize diverse systems. However, the low sensitivity of the standard detection method constrains the applicability of this technique to samples having effective dimensions not less than a few microns. Here, we propose a novel scheme and device for the indirect detection of the nuclear spin signal at a submicroscopic scale. This approach – for which the name Dipolar Field Microscopy (DFM) is suggested – is based on the manipulation of the long-range nuclear dipolar interaction created between the sample and a semiconductor tip located close to its surface. After a preparation interval, the local magnetization of the sample is used to modulate the nuclear magnetization in the semiconductor tip, which, in turn is determined by an optical inspection. Based on results previously reported, it is shown that, in principle, images and/or localized high-resolution spectra of the sample can be retrieved with spatial resolution proportional to the size of the tip. These calculations are accompanied by recent proof-of-principle experimental results in a model system.

**13:39**

**V9 13 Force-gradient detection of electron spin resonance** NEIL JENKINS, JOHN MAROHN, *Cornell University* Electron spin resonance of single unpaired electron spins in fused silica has recently been demonstrated [Rugar, *et al*, *Nature* **430** 329 (2004)]. The techniques employed rely on being able to coherently modulate electron spin magnetization for many hundreds of milliseconds, and are thus not well suited for observing unpaired electrons in spin-labeled biomolecules, for example, where the relevant spin relaxation times will be orders of magnitude shorter. In this presentation, we will discuss force gradient methods for detecting and imaging electron spin resonance that are more generally applicable. In our methods, applied rf is used to cyclically saturate electron spin magnetization at twice the cantilever frequency. A theory for the effect will be presented and data from sample-on-cantilever experiments performed at cryogenic temperatures will compare conventional force-detected MRFM to the signal from the force gradient experiment.

**SESSION V10: FOCUS SESSION: SURFACES AND INTERFACES IN ELECTRONIC MATERIALS III**
**Thursday Morning, 16 March 2006; 302, Baltimore Convention Center at 11:15**
**Yuh-Lin Wang, IAMS Taiwan, presiding**

*Invited Papers*

**11:15**
**V10 1 Formation Processes and (Photo-)electrochemical Properties of Organic Monolayers on Hydrogen Terminated Si(111).**
KOHEI UOSAKI, *Hokkaido University*

Construction of molecular layers on solid surfaces is one of the most important subjects not only for fundamental science but also for a wide range of applications. The most studied mono-molecular layer system is self-assembled monolayers (SAMs) of alkanethiols on various metals especially on gold and SAMs with a wide variety of functionalities have been constructed. It may be more important, however, to construct ordered molecular layers with various functionalities on a semiconductor surface, Si in particular, as far as technological applications are concerned because of possible applications for molecular and biomolecular devices in conjunction with the advanced silicon technology. Here we followed the thermal and photochemical organic monolayer formation process of by ATR-IR, ellipsometry, and sum frequency generation spectroscopy, and constructed and investigated electrochemical and photoelectrochemical properties of the organic monolayers with electron transfer function, i.e., viologen moiety, on hydrogen-terminated Si(111) surface. Furthermore, effect of platinum nanoparticles deposited on the surface on hydrogen evolution reaction was also investigated [1]. Photo-switching property was also introduced by incorporating a diarylethene moiety. [1] T. Masuda, K. Uosaki, Chem. Lett. **33**, 788 (2004).

*Contributed Papers*

**11:51**
**V10 2 New SiOH complexes and proton release mechanism in silica as a source of Si/$SiO_2$ interface-trap build up** I.G. BATYREV, S.T. PANTELIDES, *Department of Physics and Astronomy, Vanderbilt University* M.P. RODGERS, D.M. FLEETWOOD, R.D. SCHRIMPF, *Electrical Engineering and Computer Science Department, Vanderbilt University* Water molecules in $SiO_2$ have been studied extensively in the context of reliability of electronic devices. Here we report results of new density-functional first-principles calculations and experimental data that demonstrate a key role of $H_2O$ molecules in the long-term degradation of MOSFETs by increases in interface-trap densities. A new low energy complex formed by $H_2O$ has been identified. The complex consists of two SiOH groups located on neighboring rings. The energy of the complex is 0.3 eV lower than that for the free interstitial water molecule in the ring of $\sim$ 0.7 nm. The two silanol groups have different local topology, which results in different ability of the SiOH elements to capture holes and release protons under X-irradiation. The release of $H^+$ has a barrier of the reaction $\sim$ 0.45 eV and is accompanied by creation of a peroxy-type structure inside network ring. The released protons can diffuse or drift (driven by electric fields) to the interface, where they depassivate dangling bonds by forming $H_2$ molecules. We will present experimental data on the radiation response of devices that have been in storage for 20 years. The results are consistent with the theoretical picture, when water molecules are responsible for a substantial increase of interface-trap densities over time.

**12:03**
**V10 3 Scanning tunnelling spectroscopy of single molecule on a semiconductor surface** BORISLAV NAYDENOV, PETER RYAN, *Trinity College Dublin* LUCILE TEAGUE, *NIST* JOHN BOLAND, *Trinity College Dublin* Scanning tunnelling spectroscopy was performed on 1,3-cyclohexadiene molecules on Si(100) surface at 5K. Degenerated N-type semiconductor and platinum covered tungsten tips were used. For the first time a vibrational spectrum of chemisorbed molecule on semiconductor surface was obtained. The probe induced perturbations of the molecule electronic density of states and its vibrational properties were also investigated. Transition from tunnelling to contact regime between the probe and the molecule was successfully monitored.

**12:15**
**V10 4 X-ray Photoelectron Spectroscopy of Buried Electronic Layers and Interfaces** JASON J. BLACKSTOCK, CARRIE L. DONLEY, *Quantum Science Research, HP Labs* WILLIAM F. STICKLE, *HP Labs Corvallis* DUNCAN R. STEWART, DOUGLAS OHLBERG, R. STANLEY WILLIAMS, *Quantum Science Research, HP Labs* Miniaturization of integrated circuits requires ever more detailed nanoscale physical and chemical characterization to engineer successful devices, as critical device layers are now only nanometers thick and frequently buried within complex material stacks. Nonetheless, correlating electronic device behavior with internal chemical structure remains essential for producing reliable devices. We present a new method for accessing the internal chemical structure of critical nanoscale layers in electronic device stacks via x-ray photoelectron spectroscopy (XPS). The method is based on engineering a weakened interface between two critical layers, then cleaving the stacks at this interface in a UHV environment and using XPS to characterize the layers and interfaces adjacent the cleave-plane. We present data from Pt/Pt-oxide/organic-monolayer/metal device stacks which show useful electrical switching behavior. This method reveals unexpected changes to the metastable Pt-oxide occur during stack fabrication. These changes to the buried nanoscale Pt-oxide layer are also shown to be inaccessible with conventional ion-milling or sputtering techniques that destroy the evidence of these subtle changes.

*Invited Papers*

**12:27**
**V10 5 Quantum Size Effects in Nanostructures.**
CHING-MING WEI, *Institute of Atomic and Molecular Sciences, Academia Sinica, Taipei, TAIWAN 106*

Quantum size effects in metal thin films and metallic clusters are studied using first-principles density functional theory. For metal thin films, Pb(111), Pb(100), Al(110), and Al(111) films up to 30 monolayers are calculated. Significant oscillatory quantum size effects are found on surface energy, work function, and surface relaxations. These oscillations are correlated with the thickness dependence of the energies of confined electrons, which can be properly modelled by an energy-dependent phase shift of the electronic wave function upon reflection at the interface. It is found that a quantitative description of these quantum size effects requires full consideration of the crystal band structure. For metallic clusters, the highly symmetric particles of sizes up 4 nm ($Al_{923}$, $Pb_{923}$, and $Au_{309}$) in the icosahedral (ico), decahedral, and cubotohedral (fcc) structures are calculated. We propose a simple scheme to compare their relative stability and to identify the quantum size effect. In addition, the famous Mackay (fcc-to-ico) transition for metallic clusters is investigated by itab-initio elastic-band method. The transition path can in general be described by an angular variable **its**. The barriers of the Mackay transition for large Al, Pb, and Au clusters are found to be smaller than the thermal energy at room temperature. Finally CO oxidation on metallic clusters will be presented. A catalytic reaction path for CO oxidation on $Au_{55}$, $Ag_{55}$, and $Au_{25}Ag_{30}$ ico clusters is found with activation energies of less than 0.5 eV. The reaction consists of a peroxolike transition intermediate involving the OOCO configuration. A crucial factor to determine the reaction rate on these clusters is identified as the co-adsorption energy of CO and $O_2$ on these clusters.

*Contributed Papers*

**13:03**
**V10 6 Direct visualization of metal ions in supramolecules.**
M.S. ALAM, V. DREMOV, P. MÜLLER, *Physikalisches Institut III, Universität Erlangen, Germany* R. ALSFASSER, *Institut für Anorganische Chemie, Universität Freiburg, Germany* U. KORTZ, *School of Engineering and Sciences, International University Bremen, Germany* M. RUBEN, *INT, FZ Karlsruhe, Germany* L.K. THOMPSON, *Dept. of Chemistry, Memorial University, St. Johns, NL, Canada* J.M. LEHN, *ISIS, Université Louis Pasteur, Strasbourg, France* We performed high resolution scanning-tunneling microscopy with simultaneous current-voltage characteristics (STS) measurements on single molecules deposited on graphite surfaces. We present our recent results on Co [2× 2], Mn [3× 3] grid-type molecules, $Cu_{20}$ wheel-shaped polyoxoanions, as well as on Cu coordination polymers. In our STS measurements we found a rather large signal at the positions of the metal centers in the molecules i.e. the location of the individual metal ions in their organic matrix is directly addressable by STS even if these ions are covered by the organic ligands.

**13:15**
**V10 7 Surface-enhanced Raman scattering of wurtzite-type GaN(0001) and ZnO(0001):** CHIH-YI LIU, MYKHAYLO M. DVOYNENKO, TSU-SHIN CHAN, JUEN-KAI WANG, YUH-LIN WANG, INSTITUTE OF ATOMIC AND MOLECULAR SCIENCES, ACADEMIA SINICA, TAIPEI, TAIWAN, REPUBLIC OF CHINA COLLABORATION, CENTER FOR CONDENSED MATTER SCIENCES, NATIONAL TAIWAN UNIVERSITY, TAIPEI, TAIWAN, REPUBLIC OF CHINA COLLABORATION, DEPARTMENT OF PHYSICS, NATIONAL TAIWAN UNIVERSITY, TAIPEI, TAIWAN, REPUBLIC OF CHINA COLLABORATION, We first-time report surface-enhanced Raman scattering (SERS) of Ag-deposited wurtzite-type GaN(0001) epitaxial film and ZnO(0001) substrate. On non-deposited region, two Raman-active modes, $A_1$(LO) and $E_2$(high), were observed in backscattering geometry, which is consistent with the Raman selection rule on wurtzite structure. In contrast, on the Ag-deposited region of both samples, only $A_1$(LO) mode (734 $cm^{-1}$ for GaN and 572 $cm^{-1}$ for ZnO) exhibits clear Raman enhancement. We propose that the macroscopic polarization field accompanied by LO-phonons is responsible for this anomalous Raman enhancement. The study of SERS effect on ionic crystals thus provides a simple test to investigate the mechanism beside electromagnetic effect in enhanced Raman scattering.

**13:27**
**V10 8 Organic Field Effect Transistor Interfaces Probed In-situ during operation by Sum Frequency Generation**
HONGKE YE, ASHRAF ABU-AKEEL, *Department of Chemical and Biomolecular Engineering* JIA HUANG, HOWARD KATZ, *Department of Materials Science and Engineering* DAVID H. GRACIAS, *Department of Chemical and Biomolecular Engineering, Johns Hopkins University, Baltimore, Maryland 21218* In order to gain a molecular level understanding of the electrical conduction in thin film organic semiconductors, we have integrated an electrical probe station with an SFG spectroscopy system. Thin film transistors consisting of organic semiconductors 5,5'-bis(4-hexylphenyl)-2,2'-bithiophene (6PTTP6) and pentacene, were fabricated on silicon substrates with top contacts. SFG spectra show strong correlations with the electrical characteristics measured. In particular, the SFG spectra of the interfaces changed with increasing gate voltage (Vg). For both 6pttp6 and pentacene the nonresonant SFG background correlated with the increase in conductivity (slope of the IV curve after turn on) measured of the semiconductor layer with increasing Vg. For 6pttp6 we observed that the dependency of the methylene peak intensity on gate voltage correlated well with the dependence of the saturation current on gate voltage. These results point to the fact that charging of molecules and the field effects in OFETs can be probed in-situ using SFG and electrical testing, and we can gain a molecular level understanding of OFET interfaces from the results.

**SESSION V11: FOCUS SESSION: AEROSOLS, CLUSTERS, DROPLETS: PHYSICS AND CHEMISTRY OF NANOOBJECTS V: METAL CLUSTERS II**
**Thursday Morning, 16 March 2006; 303, Baltimore Convention Center at 11:15**
**Michael Duncan, University of Georgia, presiding**

*Invited Papers*

**11:15**
**V11 1 Structure Determination of Noble Metal Clusters by Trapped Ion Electron Diffraction.**
DETLEF SCHOOSS, *Institute for Nanotechnology, Forschungszentrum Karlsruhe*

The structures of noble metal cluster ions have been studied by the recently developed technique of trapped ion electron diffraction (TIED)[1]. In brief, cluster ions are generated by a magnetron sputter source and injected into a cooled (95 K) quadrupole ion trap. After mass selection and thermalization, the trapped ions are irradiated with a 40 keV electron beam. The resulting diffraction pattern is integrated with a CCD detector. The assignment of the structural motif is done via a comparison of the experimental and simulated scattering function, calculated from density functional theory structure calculations. The structures of mass selected silver cluster cations $Ag_{19}^+$, $Ag_{38}^+$, $Ag_{55}^+$, $Ag_{59}^+$, $Ag_{75}^+$ and $Ag_{79}^+$ have been investigated.[2] The resulting experimental data are best described by structures based on the icosahedral motif, while closed packed structures could be ruled out. Additionally, we present a comparison of the structures of $Cu_{20}^{+/-}$, $Ag_{20}^{+/-}$ and $Au_{20}^{+/-}$. Our findings show unambiguously that the structure of $Au_{20}^-$ is predominantly given by a tetrahedron in agreement with the results of L.S. Wang et al.[3] In contrast, structures of $Ag_{20}^-$ and $Cu_{20}^-$ based on the icosahedral motif agree best with the experimental data. Small structural differences between the charge states are observed. The possibilities and limitations of the TIED method are discussed. [1] M. Maier-Borst, D. B. Cameron, M. Rokni, and J. H. Parks, Physical Review A **59** (5), R3162 (1999); S. Krückeberg, D. Schooss, M. Maier-Borst, and J. H. Parks, Physical Review Letters **85** (21), 4494 (2000). [2] D. Schooss, M.N. Blom, B. v. Issendorff, J. H. Parks, and M.M. Kappes, Nano Letters **5** (10), 1972 (2005). [3] J. Li, X. Li, H. J. Zhai, and L. S. Wang, Science **299**, 864 (2003).

*Contributed Papers*

**11:51**
**V11 2 Electric deflection studies of rhodium clusters*** MARK KNICKELBEIN, *Argonne National Laboratory* MARTIN BEYER, *Technische Universität Berlin* The electric susceptibilities of rhodium clusters ($Rh_n$, n=5-32) have been studied via a DC molecular beam deflection technique. It is observed that all clusters are high-field seekers, indicating that the induced dipole moments are larger than any small permanent dipole moments that may be present. The per atom polarizabilities determined from the beam deflections exceed the classical value. $Rh_7$ and $Rh_{10}$ exhibit per- atom polarizabilities that are both anomalously large and temperature dependent. Peak broadening is most pronounced for $Rh_7$, indicating the presence of a small permanent dipole moment. It is proposed that the anomalous polarizabilities exhibited by $Rh_7$ and $Rh_{10}$ are a consequence of their being dynamic Jahn-Teller molecules.

*This work is supported by the US Department of Energy, Office of Basic Energy Sciences, Division of Chemical Sciences, under Contract W-31-109-ENG-38 and by the CREST program of the Japan Science and Technology Agency (JST).

**12:03**
**V11 3 On the Possibility of Multiple Valence Superatoms** SHIV KHANNA, J. ULISES REVELES, *Department of Physics, Virginia Commonwealth University, Richmond Va. 23284* A. WELFORD CASTLEMAN JR., DENNIS BERGERON, PATRICK ROACH, *Department of Chemistry and Physics, The Penn State University, University Park, PA 16802* It was recently demonstrated that an $Al_{13}$ cluster behaves like a halogen atom while an $Al_{14}$ cluster has properties analogous to an alkaline earth atom in gas phase clusters containing aluminum and iodine atoms. These observations, together with findings that $Al_{13}^-$ is inert like a rare gas atom, have reinforced the idea that chosen clusters can exhibit chemical behaviors reminiscent of atoms in the periodic table, offering the exciting prospect of a new dimension of the periodic table formed by cluster elements, called the superatoms. As the properties of the clusters can be controlled by size and composition, the superatoms offer the potential to create unique compounds with tailored properties. In this paper, we provide evidence of a new class of superatoms that exhibit multiple valences, like some of the atoms in the periodic table, and hence have the potential to form stable compounds when combined with diverse atoms.

**12:15**
**V11 4 Geometrical and electronic properties of sodium, copper, and silver clusters: A comparative study*** MINGLI YANG, KOBLAR A. JACKSON, *Department of Physics, Central Michigan University, Mt. Pleasant, MI 48859* JULIUS JELLINEK, *Chemistry Division, Argonne National Laboratory, Argonne, IL 60439* The structures of sodium, copper, and silver clusters with up to 20 atoms are investigated using density functional theory computations. Utilizing an extensive unbiased search procedure, we first find a large number of low-energy isomers of Cu clusters. The structures of these isomers are then reoptimized for Na and Ag clusters. We find a strong propensity to form similar conformations for clusters of these three elements. In most cases their energetically preferred forms have the same packing. As the cluster size increases, it changes from planar (less than 7 atoms) to layered (7 to 16 atoms) and eventually to compact (17 to 20 atoms). The similarities and differences between the clusters of the three elements will also be characterized in terms of their

electronic properties such as ionization potential, HOMO-LUMO gap, dipole moment, and polarizability.

*This work was supported by DOE Grant No. DE-FG02-03ER15489 (KAJ and MY) and by the Office of Basic Energy Sciences, Division of Chemical Sciences, Geosciences, and Biosciences, U. S. Department of Energy under Contract No. W-31-109-Eng-38 (JJ).

**12:27**

**V11 5 Self-Similar Size Distribution of Atom Clusters in Cooling Vapors** YONG W. KIM, HEDOK LEE, PAUL BELONY, JR., *Lehigh University* Aluminum atom clusters of nanometer dimensions grow out of dense vapors. We have both measured and modeled their formation process by first creating dense atomic vapors as remnants of a 3-D laser-produced plasma plume from a solid aluminum target. By real-time diagnosis, we have fully characterized the plume into more than 140,000 vapor cells. [Kim, Lee, Rev. Sci. Instr. **75**, 3953 (2004)] Clustering of atoms in each cell has been followed during the cooling of the vapors by numerical simulation of atom-atom and atom-cluster collisions. The distribution of clusters by size evolves as the vapor cools, and is sensitively dependent on the initial atom density in each plasma cell. When the population and cluster size are rescaled as fractions of their respective maximal values, the distribution functions all collapse into a single functional form regardless of the time in the evolution or the initial value of the vapor density. The maximal population decreases while the maximal size grows over time. The cluster size distribution for the plasma plume is found by summing the distributions from all plasma cells. Independently, the clusters are captured onto electron microscope grids and size analyzed by means of transmission electron microscopy. The computed result is in excellent agreement with the measured histogram of clusters by size. The agreement is absolute, indicating the Brownian motion nature of cluster-cluster interaction.

***Invited Papers***

**12:39**

**V11 6 On Metal to Insulator Transitions in Bivalent Metal Clusters.***

ORI CHESHNOVSKY, *School of Chemistry, Tel Aviv University, 69978 Tel Aviv Israel*

We discuss the issue of metal to insulator transitions in bivalent metal clusters, in view of our new photoelectron spectroscopy (PES) studies on $Zn_n^-$ clusters in the size range of n=3-117. We show that zinc clusters exhibit a distinct transition in their electronic structure characteristics as a function of their size. At small sizes up to $n=18$ the clusters follow the Bloch-Wilson picture of the development of a metal from closed-shell atoms, exhibiting a gradual decrease of the gap between the fully occupied *s* band and the empty *p* band. For large sizes ($n \geq 32$) the band overlap allows the valence electrons to fully delocalize. This leads to an almost perfect free-electron density of states, as is demonstrated by discussing the spectra in the light of standard free-electron models and by comparison to the results obtained on sodium clusters. These results will be compared with the PES of $Hg_n^-$ and $Mg_n^-$ clusters.

*In collaboration with Bernd von Issendorf, Department of Physics, Universitat Freiburg, D-79104, Germany.

***Contributed Papers***

**13:15**

**V11 7 Quantized Ferromagnetic Moments of Free Cobalt Clusters** XIAOSHAN XU, SHUANGYE YIN, ANTHONY LIANG, WALTER DE HEER, The magnetic moments $\mu$(N) of free $Co_N$($20 <= N <= 200$) clusters has been measured in a cryogenic molecular beam. Besides the ground states with $\mu(N)/N \sim 2\ \mu B$, an electronic state has been found in all clusters studied. The magnetic moments $\mu^*(N)/N$ of this state is approximately 1/2 $\mu$(N)/N. Ionization potential of Co clusters at each of the two states are determined from photo-ionization efficiency measurements. The ionization potentials for the excited states are systematically lower than that for ground states by about 100meV for small clusters, and merge for larger clusters ($N > 100$). This suggests that molecular magnetism of small clusters evolves to itinerant (band) ferromagnetism in the bulk ($\mu(N)/N \sim 1.7\ \mu B$) when the energy gap between these two states vanishes.

**13:27**

**V11 8 Magnetism in Gold Nano-clusters*** R.J. MAGYAR, V. MUJICA, *INEST Group, Philip Morris USA Postgraduate Research Program and NIST* C. GONZALEZ, *NIST* M. MARQUEZ, *Philip Morris USA Research Center* Intrinsic magnetism in thiolated and unthiolated gold nano-clusters is explored from a first-principles perspective. The computed electronic structures elucidate the relevant mechanism whereby these nano-clusters develop a permanent magnetic moment. Polarized ground states are favorable due to surface paramagnetism, and bare clusters are expected to be magnetic for $Au_{38}$ and larger. How the thiolates effect the magnetic moment is also considered.

*This research has been conducted by the INEST (Interdisciplinary Network of Emerging Science) group, Philip Morris USA Postgraduate Research Program

**13:39**

**V11 9 Anomalous magnetic enhancement by doping Mn in Co clusters** SHUANGYE YIN, *Georgia Institute of Technology* RAMIRO MORO, XIAOSHAN XU, WALTER DE HEER, Magnetic moments of $Co_NMn_M$ and $Co_NV_M$ clusters (with Mn and V concentration less than 30%) are measured using Stern-Gerlach deflection method in molecular beams. Their average moments per atom as a function of impurity concentrations are studied and compared with bulk. Both $Co_NMn_M$ and $Co_NV_M$ clusters have higher average moments than their bulk counterpart due to reduced sizes. The average moments for $Co_NMn_M$ clusters are found to increase with Mn concentration, opposite to that of CoMn bulk. The enhancement effect is found to be independent of cluster size and composition. Meanwhile, $Co_NV_M$ clusters show reduction of average moments with V doping, consistent with what are expected in CoV bulk. The results are discussed within the virtual bound states model.

**13:51**

**V11 10 Analysis of the response of atomic clusters to static electric fields in terms of position-dependent polarizabilities*** KOBLAR A. JACKSON, MINGLI YANG, *Department of Physics, Central Michigan University, Mt. Pleasant, MI 48859* JULIUS JELLINEK, *Chemistry Division, Argonne National Laboratory, Argonne, IL 60439* To explore in detail the response of atomic clusters to external electric fields, we have developed a method to compute position-dependent polarizabilities (PDP's). The essence of the method is to partition the overall cluster dipole into local, atom-centered contributions. The local moments are naturally decomposed further into charge-transfer and dipole components. This decomposition furnishes added insight into the response behavior of the clusters. By tracking the changes in the local moments with an external field, we arrive at the PDP's. In this talk we will present the details of the method and will compare and contrast different approaches to computing the local moments. We will also discuss results for $Na_n$, $Si_n$ and $Ar_n$ as a function of cluster size. These results show strong qualitative similarities in the response of $Na_n$ and $Si_n$ clusters, including clear evidence for metallic screening of the cluster interiors.

*This work was supported by DOE Grant No. DE-FG02-03ER15489 (KAJ and MY) and by the Office of Basic Energy Sciences, Division of Chemical Sciences, Geosciences, and Biosciences, U. S. Department of Energy under Contract No. W-31-109-Eng-38 (JJ).

**SESSION V12: FOCUS SESSION: WETTING AND HARD-SOFT INTERFACES**
**Thursday Morning, 16 March 2006**
**304, Baltimore Convention Center at 11:15**
**E. Kaxiras, Harvard University, presiding**

***Contributed Papers***

**11:15**

**V12 1 Water Enhanced Catalysis of CO Oxidation on Free and Supported Gold Nanoclusters** ANGELO BONGIORNO, UZI LANDMAN, *Georgia Institute of Technology* The enhancement by water molecules of the catalytic activity of gas-phase and supported gold nanoclusters toward CO oxidation is investigated with first-principles calculations. Coadsorption of water and oxygen molecules leads to formation of a complex well-bound to the gold cluster, even on a defect-free MgO(100) support. Formation of the complex involves partial proton-sharing between the adsorbates, that in certain configurations results in proton transfer leading to the appearance of a hydroperoxyl-like complex. The O-O bond is activated, leading to a weakened peroxo or superoxo-like state, and consequently the reaction with carbon oxide to form carbon dioxide occurs with a small activation barrier of about 0.5 eV. A complete catalytic cycle of the water-enhanced CO oxidation is discussed.

**11:27**

**V12 2 Tuning the diamond surface from hydrophobic to superhydrophilic by submonolayer surface modification*** SHENG MENG, *Physics, University of Texas at Austin and Physics, Harvard University* ZHENYU ZHANG, *Condensed Matter Sciences Division, Oak Ridge National Lab* EFTHIMIOS KAXIRAS, *Physics, Harvard University* The extreme limits of wettability, superhydrophilic and superhydrophobic behavior, are useful in industrial applications such as anti-fogging and self-cleaning. Superhydrophilic behavior is highly desirable in biomedical applications, protecting biomolecules from damage in their interaction with biomaterials. While substantial progress has been made in designing superhydrophobic materials, relatively little effort has been devoted to the development of superhydrophilic materials, particularly biocompatible ones. Here we show, using first-principles calculations, that the water affinity of an initially highly hydrophobic H-passivated diamond (111) surface can be drastically altered with introducing a fraction of a monolayer of alkali metals. In particular, terminating the diamond surface with F and replacing 1/3ML F by Na, or introducing one third monolayer of Li and methylating half of the remaining surface sites, produces stable surfaces with superhydrophilic behavior which are perfect candidates for biomedical applications.

*Funded by US NSF and DOE.

**11:39**

**V12 3 Infrared Studies of Water Adsorption on Acetic Acid thin films** MICHEL MALICK THIAM, MARYAM EBRAHIMI, KAM TONG LEUNG, *WATLABs, Department of Chemistry, University of Waterloo, 200 University Ave. W., Waterloo, Ontario, N2L 3G1, Canada* WATLABS TEAM, Infrared reflection-absorption spectroscopy is used to investigate $H_2O$ ice deposited onto non-crystalline (dimers [1]) and polycrystalline (infinite chains [1]) acetic acid films. The condensed water film grown at $\sim$ 135 K on these different substrates can be characterized as amorphous dense ice. The $H_2O$ molecules are shown to interact mainly with the carbonyl and the carboxyl oxygens, forming hydrogen bonds. Upon water adsorption on the non-crystalline acetic acid film, saturation of the change induced in the intensity of the C=O and C-O peaks occurs at an average $H_2O$ exposure of $\sim$ 2.52 L. The amount of H-bonding involving C=O or C-O (of acetic acid) and OH (of water) on the polycrystalline film has been reduced considerably compared to the situation on the non-annealed one, but saturation of the carbonyl oxygen even for a water exposure of 9 L has not been observed while the carboxyl oxygen saturates at $\sim$ 2.76 L. Thermal evolution studies for the ice film on non-crystalline and polycrystalline acetic acid films show that water co-evaporates with acetic acid likely as a water-acetic acid complex in the temperature range of 140-155 K, which continues until the entire ice film has been exhausted at 160 K. [1]: Q. Gao and K. T. Leung, J. Phys. Chem. B 109, (2005) 13263.

*Invited Papers*

**11:51**
**V12 4 Ab-initio simulations of H2O interaction with b-SiC surfaces.**
GIANCARLO CICERO, *Politecnico of Turin*

We report on the interaction of gas phase water molecules with polar and non polar stoichiometric surfaces of cubic silicon carbide, a leading candidate semiconductor for bio-compatible devices. Finite temperature ab-initio molecular dynamics shows that the specific geometric arrangement of atoms on the outermost surface layer is responsible for water orientation and coordination and thus plays a major role in determining the surface reactivity. In particular, irrespective of coverage, water spontaneously dissociates on both polar [1] Si-terminated (001) and non-polar [2] (110) surfaces, while the C-terminated1 (001) surface is non-reactive and hydrophobic. Based on our results, we propose that STM images and photoemission experiments may detect specific changes induced by water on both the structural and electronic properties of SiC surfaces. We completed our investigation by studying a realistic solid/liquid interface [3] for the case of Si-SiC(001), after full hydroxylation takes place. We observed the formation of a thin (3/AA) interfacial layer, which presents a higher density than bulk water. The liquid does not uniformly wet the surface, rather molecules preferably bind along directions parallel to the Si dimer rows. Our calculations also predict that at 1 nm, the structural and electronic properties of liquid water are weakly affected by one-dimensional confinement between hydrophilic, solid substrates. [1] G. Cicero, A. Catellani and G. Galli Phys Rev. Lett. 93 (2004), 0161102; G. Cicero, A. Catellani and G. Galli J. Phys. Chem. B 108 (2004), 16518. [2] A. Catellani, G. Cicero and G. Galli J. Chem. Phys., in press. [3] G. Cicero, J. Grossman, A. Catellani and G. Galli J. Am. Chem. Soc. 127 (2005), 6830.

*Contributed Papers*

**12:27**
**V12 5 Physics of solid and liquid alkali halide surfaces near the melting point** TATYANA ZYKOVA-TIMAN, DAVIDE CERESOLI, UGO TARTAGLINO, *SISSA, INFM, Democritos, via Beirut 2-4* ERIO TOSATTI, *SISSA, Democritos, ICTP, P.O. Box 586, I-34014 Trieste, Italy* NaCl (and other alkali halide) crystal surfaces have the peculiar property of repelling their own melt. As a result they let themselves be wetted only partially by their own liquid at the melting point $T_M$. We recently investigated the physical reasons for this unusual behavior. We found them through theory and molecular dynamics simulation to stem from the conspiracy of three factors. First, the solid NaCl(100) surface is exceptionally anharmonic,but also exceptionally stable. It can in fact survive even well above the melting point, for unlike most other surfaces it does not spontaneously melt. Second, the solid-liquid interface is very costly, due to a 27% density difference between solid and liquid. Third, the surface tension of liquid NaCl is relatively high. This last feature is due to an unexpected entropy deficit, that can in turn be traced to incipient molecular charge order in the outermost regions of the molten salt surface[1,2]. [1] T. Zykova-Timan, D. Ceresoli, U. Tartaglino, E. Tosatti, Phys. Rev. Lett. 94, 176105 (2005) [2] T. Zykova-Timan, D. Ceresoli, U. Tartaglino, E. Tosatti, J. Chem. Phys. 123, 164701 (2005)

**12:39**
**V12 6 Nanoscale Observation of Alkane Dewetting*** MENGJUN BAI, KLAUS KNORR, MATTHEW SIMPSON, SVEN TROGISCH, HASKELL TAUB, *U. Mo.-Columbia* ULRICH VOLKMANN, *P. U. Católica Chile* FLEMMING HANSEN, *Tech. U. Denmark* To investigate the structure, morphology, and wetting of both solid and liquid films of an intermediate-length alkane, we have conducted Atomic Force Microscopy measurements in the noncontact mode on dotriacontane ($n$-$C_{32}H_{66}$ or C32) films deposited from a heptane solution onto $SiO_2$-coated Si(100) wafers. At low coverages after annealing, the C32 film consists at room temperature of isolated bulk particles situated above one to two layers of molecules oriented with their long axis parallel to the surface. For such samples, we find a narrow temperature range close to the bulk C32 melting point $T_b$ in which a monolayer with C32 molecules oriented perpendicular to surface is stable. This perpendicular monolayer phase undergoes a dewetting transition to a three-dimensional (3D) fluid phase on heating to just above $T_b$ and to a 3D crystalline phase on cooling to a few degrees below $T_b$. We summarize our results in terms of an equilibrium phase diagram that provides a useful framework for interpreting the unusual spreading and receding behavior that we observe for the perpendicular monolayer phase.

*Supported by Grant Nos. NSF DMR-0411748, DOE W-7405-Eng-82 and W-31-109-Eng-38, and FONDECYT 1010548 and 7010548.

**12:51**
**V12 7 Energetics of benzene and phenol adsorption on a $TiO_2$(110) surface** S. DAG, J. ZHOU, S. KALININ, S. OVERBURY, D. MULLINS, A. BADDORF, V. MEUNIER, *Oak Ridge National Laboratory* Using large-scale density functional theory calculations, we have studied the structural and electronic properties of benzene and phenol adsorbed on a $TiO_2$ (110) surface. We found that at low coverage, a benzene molecule impinging to the $TiO_2$ surface is most likely to be adsorbed flat on the surface 3.3 Å above the Ti row, such that the $C_{2[]'}$ symmetry axis of the molecule is oriented along the top Ti row, between consecutive bridging oxygen rows. Because of the high repulsive energy between benzene and bridging oxygens, benzene molecules diffuse in quasi one-dimensional channels along a Ti row. At high coverage, benzene molecules organize in a chain-like fashion with two of their C-C bonds being oriented alternatively parallel and perpendicular to a Ti row. The interaction of phenol molecules on the same surface has also been studied. In this case, the adsorption is much stronger and involves interaction between multiple phenol molecules and bridging oxygen rows. Results of our calculations are in excellent agreement with experimental STM data.

**13:03**
**V12 8 Adsorption and reaction of benzene and phenol with Pd nanoparticles supported on $TiO_2$(110)*** J. ZHOU, S. V. KALININ, S. DAG, V. MEUNIER, S. H. OVERBURY, D. R. MULLINS, A. P. BADDORF, *Oak Ridge National Laboratory* Adsorption and reaction of benzene and phenol molecules on a $TiO_2$(110)(1× 1) surface and with titania-supported Pd particles were

studied under ultrahigh vacuum conditions using scanning tunneling microscopy (STM) and temperature programmed desorption (TPD). At 300 K, benzene could not be imaged with STM due to its high mobility. At 20 K, images show benzene in ordered rows on top of substrate Ti. Adsorption of phenol differs due to the presence of the OH functional group. At 300 K, adsorption of phenoxy adjacent to surface defects is indicated in STM images. Low temperature studies indicate that phenol adsorbs on the titania surface with a different configuration than benzene, with tunneling spanning two Ti rows. No obvious modifications to benzene or phenol adsorption were observed adjacent to Pd particles by STM, however catalytic effects were explored by TPD. Our results are in excellent agreement with calculations obtained using first-principles density functional theory.

*Research was sponsored by the Laboratory Directed Research and Development Program of ORNL, managed by UT-Battelle, LLC for the US DOE under Contract DE-AC05-00OR22725.

**13:15**

**V12 9 LEEM study of the growth of 6,13-pentacenequinone thin films** JERZY SADOWSKI, ABDULLAH AL-MAHBOOB, TSUGUKI NISHIHARA, YASUNORI FUJIKAWA, TOSHIO SAKURAI, *Institute for Materials Research, Tohoku University, Sendai, Japan* The morphology and dynamics of the growth of 6,13-pentacenequinone (PnQ – $C_{22}H_{12}O_2$) films on Si(111)-7x7 surface have been investigated itin-situ by the low-energy electron microscopy (LEEM), in order to evaluate the possibility of using PnQ molecules as an organic dopant in pentacene (Pn) films. The results of the experiments show that the nucleation and growth mechanisms dramatically differ between Pn and PnQ films, respectively. At the initial stage of the PnQ growth, after the saturation of the Si dangling bonds by the formation of a disordered wetting layer, the amorphous islands (type-I) having compact shapes were formed. After they have reached a critical size (few hundreds to several thousands nanometers, depending on the molecular flux), a second stage nucleation of the crystalline, highly anisotropic, needle-shaped islands (type-II) occurred. A gradual rotation of the in-plane (**ab**) unit cell along the type-II islands have been observed, with the direction of the 2D 'chirality' dependent on the direction of the **c** axis of the PnQ crystal lattice and associated with selective mass incorporation at the side of the island having edge parallel to long diagonal (direction of minimum strain and a favorable direction of a kink formation) of the **ab** unit cell.

**13:27**

**V12 10 Growth of divalent metal carbonates at soft organic templates.** SUMIT KEWALRAMANI, GEOFFREY DOMMETT, KYUNGIL KIM, GUENNADI EVMENENKO, HAIDING MO, PULAK DUTTA, *Northwestern University* PULAK DUTTA, DEPARTMENT OF PHYSICS AND ASTRONOMY, NORTHWESTERN UNIVERSITY TEAM, Soft template mediated inorganic mineral nucleation and growth proceeds via specific interactions between the ordered organic lattice headgroups and inorganic constituents at the organic-inorganic interface. We are studying the growth of divalent metal carbonates of R-3 (167) space group from supersaturated solutions under fatty acid, alcohol and glutamic acid rich poypeptide monolayers via in-situ grazing incidence X-ray diffraction and scanning electron microscopy. Previous studies[1] show that the presence of $Cd^{2+}$, $Mn^{2+}$, $Mg^{2+}$, even in small quantities produce highly ordered fatty acid monolayer phases and result in the formation of ionic inorganic superlattices under them. For $Ba^{2+}$, $Ca^{2+}$ and $Co^{2+}$ the extent of organic monolayer order is lower and no ionic lattice is observed. We now find that the orientation and morphology of bulk crystals grown from supersaturated solutions is strongly correlated to the order induced in organic monolayers by dilute subphases. Headgroup- ion interactions in the dilute phase can thus serve as a better guideline for choosing the monolayer for face specific nucleation as opposed to the proposed[2] geometric and stereochemical match mechanism. 1.Kmetko et al. J. Phys. Chem. B 105, 10818 (2001). 2. Mann et al. Science, 261, 1286 (1993).

**13:39**

**V12 11 Structural characterization and molecular dynamics within low-coverage films of *p*-terphenyl adsorbed onto graphite** EDWARD KINTZEL, KENNETH HERWIG, *Oak Ridge National Laboratory* Neutron scattering experiments have been carried out on low-coverage films of *p*-terphenyl molecules physisorbed onto the surface of graphite. The molecular arrangement within these films has been determined as a function of temperature and coverage. Analysis of the diffraction data reveals two-dimensional film structures where the molecules prefer a parallel orientation relative to the underlying substrate. Further examination provides evidence for an order-disorder phase transition within a monolayer film, temperature-dependent structural evolution within bilayer films, and structural variations based on film coverage. Initial dynamics results indicate a structural phase change in the temperature range 275-325 K. Below this temperature range, the scattering is consistent with phenyl ring reorientations around the long molecular axis. At elevated temperatures, the quasielastic signal is stronger and consistent with translational motion in combination with the phenyl ring reorientations.

**13:51**

**V12 12 Comparative STM study of azobenzene derivatives on bare and insulator coated metal surfaces** NIV LEVY, MATTHEW J. COMSTOCK, JONGWEON CHO, ARMEN KIRAKOSIAN, CARINE EDDER, JEAN M. J. FRECHET, FRANK LAUTERWASSER, JESSICA HARVEY, DIRK TRAUNER, M. F. CROMMIE, *Dept. of Physics, Dept. of Chemistry, UC Berkeley; Mat. Sci. Div, Lawrence Berkeley Natl. Lab* Photoactive molecules, such as azobenzene and its derivatives, have great potential for nanoscale opto-mechanical applications. However, one of the main difficulties in optical actuation of singe molecules at a surface is decoupling them from the electronic states of the substrate. One technique to accomplish this is to coat the substrate with a thin insulating layer, while another is to functionalize the molecule with ''spacer legs'' to lift it off the surface. We have conducted a comparative study of adsorption and self-assembly behavior of bare azobenzene, functionalized bis-tert-butyl-azobenzene, and functionalized tetra-tert-butyl-azobenzene molecules on bare and insulator coated metal surfaces using a variable temperature UHV STM. We observe a variety of temperature dependent molecular configurations, from which we infer the degree of molecule/surface decoupling due to surface modification and molecular functionalization.

**14:03**

**V12 13 Unoccupied electronic states at the interface of alkanethiol SAMs on Au(111)** MATTHIAS MUNTWILER, CHAD LINDSTROM, XIAOYANG ZHU, *University of Minnesota, Minneapolis* Alkanethiol self-assembled monolayers (SAMs) on Au(111) are model systems for metal-molecule contacts in molecular electronics. Using time-resolved two-photon photoemission (TR- 2PPE) we probe the unoccupied electronic structure of the alkanethiolate/Au interface. Two distinct peaks appear in

the spectra: The first, non-dispersive peak is attributed to the antibonding $\sigma^\star$ orbital of the Au-S chemisorption bond, and the second, dispersive peak to a laterally delocalized interfacial resonance induced by the image potential at the metal surface. Both peaks show lifetimes shorter than 30 fs. For the $\sigma^\star$ resonance such a short lifetime is expected due to the wavefunction overlap with the metal, whereas for the second resonance it is an effect of scattering at S atoms inside the molecular layer. In fact, the insensitivity of the energy level, dispersion, and lifetime to layer thickness suggests that the electron wavefunction is concentrated inside the dielectric layer close to the metal-molecule interface – in contrast to physisorbed alkanes where it is pushed out of the layer.

**SESSION V16: NANOTECHNOLOGY: BIOLOGICAL AND POLYMER**
**Thursday Morning, 16 March 2006**
**312, Baltimore Convention Center at 11:15**
**Robert Austin, Princeton University, presiding**

**11:15**
**V16 1 Microfluidic device for bacterial genome extraction and analysis** PETER GALAJDA, ROBERT RIEHN, YAN-MEI WANG, JUAN KEYMER, *Department of Physics, Princeton University* IDO GOLDING, EDWARD C. COX, *Department of Molecular Biology, Princeton University* ROBERT H. AUSTIN, *Department of Physics, Princeton University* Although single molecule DNA manipulation and analysis techniques are emerging, methods for whole genome extraction from single cells, genomic length DNA handling and analytics is still to be developed. Here we present a microfabricated device to address some of these needs. This microfluidic chip is suitable for culturing bacteria and subsequently retrieve their genetic content. As a next step, the extracted DNA can be introduced in a nanostructured segment of the chip for precise handling, stretching and analysis. We hope that similar microdevices can be useful in studying genetic aspects of the cell lifecycle in a variety of organisms.

**11:27**
**V16 2 Virus-Mimetic DNA Encapsulation Using Novel ABC Triblock Copolymers** RAHUL SHARMA, YOU-YEON WON, *School of Chemical Engineering, Purdue University, West Lafayette, IN-47907* To address the challenge of developing a safe and effective delivery system currently faced in gene therapy technologies, our research explores a novel approach for improving DNA encapsulation and delivery using a novel three-component block copolymer which by design has the self-assembling properties tailored for virus-like encapsulation of DNA. Our approach utilizes an ABC triblock copolymer composed of (A) ithydrophilic poly(ethylene oxide) (PEO), (B) ithydrophobic poly(n-butyl acrylate) (PnBA) and (C) itcationic poly(ethyleneimine) (PEI). With such an ABC sequence of blocks, the C block primarily interacts with the negatively charged phosphates on DNA, and the viral capsid-like morphology of the nanometers-thick membrane can be derived from the A and B blocks at the outer surface of collapsed DNA. In this presentation, we will discuss our recent experiments that establish a proof of concept and processing strategies for achieving the desired virus-mimetic DNA-encapsulating morphology composed of a compact DNA core covered with a layer of protective coating created by the ABC triblock copolymer.

**11:39**
**V16 3 Electron Binding Energies in DNA Modified Surfaces: Theory and Experiment** JAMES SULLIVAN, *Virginia Commonwealth University* DMITRI PETROVYKH, *University of Maryland-College Park, Naval Research Lab* GEORGE SCHATZ, *Northwestern University* LLOYD WHITMAN, *Naval Research Lab* X-ray photoelectron spectroscopy is emerging as a powerful method for characterizing DNA on surfaces [1]. The relative positions of core electron binding energies (CBEs) suggest likely binding geometries and strength of chemical bonds, and the peak areas provide a quantitative measure of the coverage. Although CBEs for simple molecules can often be readily assigned to specific adsorption sites and bonding configurations based on historical data, such interpretation for CBEs of DNA is not generally possible. We are using density functional theory to determine the geometric and electronic configuration of DNA nucleobases, nucleosides, and nucleotides. We find the theoretical XPS spectra for isolated nucleic components are surprisingly similar to experimental spectra measured on DNA films, suggesting that—although the films are adsorbed on the surface—the underlying electronic structure of the nucleobases is ''free-like.'' 1. D. Y. Petrovykh, et al., J. Am. Chem. Soc. 125, 5219 (2003); D. Y. Petrovykh, et al., Langmuir 20, 429 (2004).

**11:51**
**V16 4 Sequencing by Hybridization with Noisy Inputs** RICHARD YEH, Sequencing by hybridization (SBH) is a proposed method for obtaining the base-by-base sequence of an unknown nucleic acid molecule in two steps: hybridization of fragments of the unknown DNA molecule to known subsequences, and reconstruction of the entire unknown sequence from the hybridization spectrum. Work in computer science has produced algorithms for the reconstruction process approaching information-theoretic bounds, but most treatments have ignored the effect of physical hybridization noise. I have been working on this problem by modeling the effect of noisy inputs on SBH algorithms and by calculating bounds on their reconstruction fidelity. This talk will give the progress of this effort.

**12:03**
**V16 5 Surface Electrophoresis of DNA on Microporous Materials** ELI HOORY, *Stony Brook University* ANDREW DUBITSKY, JOHN FRENNA, *Pall Corporation* MICHAEL DING, *Glen Cove High School* JONATHAN SOKOLOV, MIRIAM RAFAILOVICH, *Stony Brook University* PALL CORPORATION COLLABORATION, STONY BROOK UNIVERSITY TEAM, Separation of single strand DNA molecules on solid surfaces can potentially be used for genomic research and diagnostic applications. Feasibility of DNA electrophoresis on solid surfaces has been demonstrated using insulating and semi-conducting substrates. Microporous membranes can offer advantages in separation because of the variety of surface-DNA interactions and surface morphologies. Droplets of Lambda Hind III DNA were applied to surfaces containing 0.2 to 2ng DNA. Results showed that variations in the electric field and Tris Borate EDTA buffer concentration both affected efficiency of separation. Significant differences in separation were found between different membrane types, including polyethersulfone and polyvinylidene fluoride.

Better separation was obtained on low binding, small pore size membranes which could retain the DNA molecules on the surface. Further work includes sputter coating and other surface modifications of best candidate membranes to optimize efficiency of separation.

**12:15**

**V16 6 Design of Mao Tensegrity Triangles – Successful Prediction of Stable DNA Nanostructures.*** WILLIAM B. SHERMAN,† *Department of Chemistry, New York University* JENS KOPATSCH, *Department of Chemistry, New York University* PAMELA E. CONSTANTINOU, *Department of Chemistry, New York University* NADRIAN C. SEEMAN, *Department of Chemistry, New York University* One of the most promising motifs for crystal formation is the tensegrity triangle first developed by Mao and co-workers. This structure consists of three duplex domains ''woven'' across each other. Because the three edges of the triangle are not coplanar, it can serve as a fundamentally three-dimensional motif. This nonplanarity, however, makes the design of tensegrity triangles more complicated than most of the other DNA motifs built to date. We present a geometry-based method for estimating the strain associated with various tensegrity triangle edge lengths. Experiments confirm that the predicted low-strain structures form stably, while structures with strain larger than about 5% tend to form multimers easily.

*This research supported by NIGMS, ONR, NSF and Nanoscience Technologies, Inc.

†Now at the Center for Functional Nanomaterials, Brookhaven National Laboratory

**12:27**

**V16 7 Co-electrospinning of bacteria and viruses** WAEL SALALHA, *Faculty of Mechanical Enginnering* JONATHAN KUHN, *Faculty of Biology* SHMUEL CHERVINSKY, EYAL ZUSSMAN, *Faculty of Mechanical Enginnering, Technion* Co-electrospinning provides a novel and highly versatile approach towards composite fibers with diameters ranging from a few hundred nm down to 30 nm with embedded elements. In the present work, co-electrospinning of poly(vinyl alcohol) (PVA) and viruses (T7, T4, λ) or bacteria (Escherichia coli, Staphylococcus albus) was carried out. These preparations should have applications for tissue engineering, gene therapy, phage therapy and biosensing. The average diameter of the co-spun nanofibers was about 300 nm. We found that the encapsulated viruses and bacteria manage to survive the electrospinning process, its pressure buildup in the core of the fiber and the electrostatic field in the co-electrospinning process. Approximately 10% of the Escherichia coli and 20% of Staphylococcus italbus cells are viable after spinning. Approximately 5% of the bacterial viruses were also viable after the electrospinning. It should be noted that the encapsulated cells and viruses remain stable for two months without a further decrease in number. These results demonstrate the potential of the co-electrospinning process for the encapsulation and immobilization of bio-objects and the possibility of adapting them to technical applications (e.g., bio-chips).

**12:39**

**V16 8 The Design of Potent Liposome-Based Inhibitors of Anthrax Toxin** PRAKASH RAI, CHAKRADHAR PADALA, VINCENT POON, ARUNDHATI SARAPH, SALEEM BASHA, SANDESH KATE, KEVIN TAO, JEREMY MOGRIDGE, RAVI KANE, Several biological processes involve the recognition of a specific pattern of binding sites on a target surface. Theoreticians have predicted that endowing synthetic biomimetic structures with statistical pattern matching capabilities may impact the development of sensors and separation processes. We demonstrated for the first time that statistical pattern matching significantly enhances the potency of a polyvalent therapeutic – an anthrax toxin inhibitor. We functionalized liposomes with an inhibitory peptide at different densities and observed a transition in potency at an inter-peptide separation that matches the distance between ligand-binding sites on the heptameric subunit of anthrax toxin. Pattern-matched polyvalent liposomes neutralized anthrax toxin itin vitro at concentrations four orders of magnitude lower than the corresponding monovalent peptide. We also showed that polyvalent liposome-based inhibitors can neutralize a microbial toxin itin vivo. Statistical pattern matching represents a facile strategy to enhance the potency of therapeutics targeting toxins or pathogens. Our results also illuminate other fundamental aspects of polyvalent recognition –specifically we found that the efficiency of polyvalent inhibition is influenced by the competition between the rates of ligand dissociation and diffusion.

**12:51**

**V16 9 Submicrometer Hall sensors for detection of magnetic nanoparticles in biomolecular sensing*** GORAN MIHAJLOVIC, P. XIONG, S. VON MOLNAR, *MARTECH and Dept. of Physics, Florida State Univ.* K. OHTANI, H. OHNO, *Research Inst. of Electrical Communication, Tohoku Univ.* M. FIELD, G.J. SULLIVAN, *Rockwell Scientific Company LLC* Significant progress has been made in the recent years in synthesis and biomolecular functionalization of magnetic nanoparticles. These magnetic bio-nanolabels can be utilized as protein or gene markers in biomolecular sensing assays, in contrast to the much larger micron sized magnetic beads that are usually limited to cell labeling. However, the low magnetic moments of individual nanoparticles ($10^4$-$10^5$it$\mu_B$) render their sensitive detection still a challenging task. In order to address this issue we are developing miniaturized Hall sensors from InAs/AlSb quantum well semiconductor heterostructures with active Hall cross areas down to 300 nm $\times$ 300 nm. Our preliminary characterization measurements performed at room temperature show functional devices with magnetic field resolution $< 100\ \mu\mathrm{T}/\sqrt{\mathrm{Hz}}$ at frequencies above 100 Hz, yielding a moment sensitivity $\sim\ 10^5\ \mu_B$. In addition to the progress in improving the moment sensitivity of the submicrometer Hall detectors, we will also present efforts in device integration with on-chip microcoils for the generation of local magnetic excitation fields. Results on nanoparticle detection will also be presented.

*This work has been supported by NSF NIRT Grant ECS-0210332.

**13:03**

**V16 10 Novel glucose biosensor based on organic thin-film transistors.** MARIA NIKOLOU, SEIICHI TAKAMATSU, DANIEL MACAYA, GEORGE MALLIARAS, *Department of Materials Science and Engineering Cornell University, Ithaca, NY*

GRACIELA BLANCHET, *Dupont, Central Research, Wilmington, DE* We report on a novel design of an organic thin-film transistor which utilizes a double channel transistor configuration. This electrochemical sensor-transistor is based on conducting polymers and operates at low voltages. The sensor response is measured as the drain-source current of one channel while a potential is applied on the other channel. The behavior of the transistor can be understood in terms of an electrochemical mechanism which is proven to depend on the ionic concentration of the electrolyte. The possible applications of these devices in biological sensing are explored as the advantages of their use are many, e.g. high sensitivity and selectivity, and low manufacturing cost. We present results from devices exploiting different conducting polymers, e.g. PEDOT:PSS, PANI, on a variety of substrates, e.g. glass, plastic, and demonstrate the capability of this type of device to sense glucose in a neutral pH buffer solution by a mechanism involving sensing of hydrogen peroxide. These devices can also be used effectively in the detection of other biological analytes.

**13:15**

**V16 11 Application of hydroxyapatite thin film as a biosensor*** HIROAKI NISHIKAWA, *B.O.S.T., Kinki Univ., CREST-JST, Wakayama PRef. C.R.E.A.T.E. of the JST* DAICHI OKUMURA, *B.O.S.T., Kinki Univ., CREST-JST* MASANOBU KUSUNOKI, SHIGEKI HONTSU, *B.O.S.T., Kinki Univ., CREST-JST, Wakayama PRef. C.R.E.A.T.E. of the JST* Hydroxyapatite (HAp) surface has an excellent ability of adsorption for functional biomolecules such as protein, DNA and so on. The surface electronic state of the HAp is affected by the adsorption of biomolecules. Thus, the electric properties of the surface such as resistivity and capacitance will vary. Because the property is effective for a receptor and transducer of biomolecule, we have investigated the application of the HAp as a suitable material for a biosensor. In this study, thin film of the sodium-doped HAp (Na-HAp) is prepared. The sodium doping is to decrease the resistivity of the HAp because the stoichiometric HAp is a good insulator. When bovine serum albumin of 1 ml was dropped to a Na-HAp thin film in a 100 ml pure water, the sample shows the drastic change of the AC resistance (at 120 kHz). This result shows that the Na-HAp will be one of the most effective materials for the biosensor applications.

*This study was supported by a grant from the Wakayama Prefecture Collaboration of Regional Entities for the Advancement of Technological Excellence of the JST.

**13:27**

**V16 12 Directed Diblock Copolymer Self-Assembly Using Engineered Topologies To Drive Defect Motion.** RICARDO RUIZ, CHARLES BLACK, ROBERT SANDSTROM, *IBM T.J. Watson Research Ctr.* Self-organizing materials hold great promise for delineating the critical nanometer-scale elements of future integrated circuits. While self assembly provides a pathway to defining sub-lithographic dimensions, its Achilles heel lies in minimizing defects. Unlike lithographic processes, self assembly involves optimization of thermodynamic free energy, which can require prohibitively long equilibration times and may never reach pattern perfection. We have begun to address this intrinsic limitation by engineering surfaces to influence the assembly process. In this way we eliminate defects in the critical device areas, while driving unavoidable imperfections to predefined, non-crucial regions. We discuss this approach within the context of lamellar-phase poly(styrene-b-methylmethacrylate) diblock copolymer films, which possess excellent material characteristics for use as lithographic templates. Understanding the dynamics of pattern formation in these materials is crucial to optimizing their performance. We use correlation length measurements of lamellar diblock copolymer domains to extract information about mechanisms of defect annihilation. We also quantify the quality of these self-assembled materials within a framework of resist performance metrics, including resist profile, line-edge roughness, and etch characteristics.

**13:39**

**V16 13 Conformational molecular architecture in alkylthiolate monolayer using atomic force microscopy electrostatic nanolithography** OLGA MAYEVSKA, SERGEI LYUKSYUTOV, *The University of Akron, OH* PAVEL PARAMONOV, *Georgia Tech University, GA* KAZUO UMEMURA, *Musashi Intitute of Technology, Tokyo, Japan* SHANE JUHL, RICHARD VAIA, *AF Research Laboratory, WPAFB OH* We propose a simple approach to form 50-nm raised structures based on conformational changes of organomercaptan molecules assembled in monolayer on surface of gold. Manipulation of amphifunctional molecules may be performed using a strong electric field ($10^8$-$10^{10}$ $Vm^{-1}$) induced by an atomic force microscope (AFM) tip. Such a field leads to rearrangement of alkylthiolates assembled on Au (111) resulting in nano-patterning of raised nanostructure (1.5-9 nm high, 20-50 nm wide) arrays on a second-time scale by manipulating the tip above the monolayer. It is suspected, that as a result of the oxidative cleavage initiated by a weak bias of the tip, the S-end of the chain carrying a sulfenium cation is attracted to the tip forming a bilayer, and the higher-layer structures in monolayer. Stabilization of the multiple-layered structures is accomplished via mutual attraction and entanglement of the hydrocarbon chains.

**13:51**

**V16 14 Neutron Reflectometry Measurements of the Depth Profile of Water in a Fuel Cell Membrane.** JOSEPH DURA, CHARLES MAJKRZAK, SUSHIL SATIJA, NORMAN BERK, *Center for Neutron Research, NIST, Gaithersburg, MD 20899* JON OWEJAN, THOMAS TRABOLD, *General Motors Corporation, Fuel Cell Activities, Honeoye Falls, NY 14472* Specular neutron reflectometry (NR) measurements have been performed on a prototypical polymer electrolyte membrane (PEM) for fuel cell application, e.g., Nafion. The samples were formed by spin coating onto a variety of substrates, and annealing in vacuum. The measurements are designed to reveal the water distribution across the thickness of the membrane material, as a function of relative humidity and for the case in which the film is in contact with a liquid water reservoir. Data from several samples indicates how the water profile for a given humidity changes with annealing temperature of the polymer film. Finally, we consider the application of phase-sensitive methods to eliminate potential ambiguity in the scattering length density profile of the membrane obtained from NR.

**SESSION V17: MEDICAL PHYSICS PANEL DISCUSSION**
**Thursday Morning, 16 March 2006**
**313, Baltimore Convention Center at 11:15**
**Paul Gueye, Hampton College, presiding**

**11:15**
**V17 1 Medical Physics Panel Discussion** PAUL GUÈYE, STEVEN AVERY, *NSBP* RICHARD BAIRD, *NIH/NIBIB* CHRISTOPHER SOARES, *NIST* HOWARD AMOLS, *AAPM* PRABHAKAR TRIPURANENI, *ASTRO* STAN MAJEWSKI, DREW WEISENBERGER, *Jefferson Lab* The panel discussion will explore opportunities and vistas in medical physics research and practice, medical imaging, teaching medical physics to undergraduates, and medical physics curricula as a recruiting tool for physics departments. Panel members consist of representatives from NSBP (Paul Guèye and Steven Avery), NIH/NIBIB (Richard Baird), NIST (Christopher Soares), AAPM (Howard Amols), ASTRO (Prabhakar Tripuraneni), and Jefferson Lab (Stan Majewski and Drew Weisenberger). Medical Physicists are part of Departments of Radiation Oncology at hospitals and medical centers. The field of medical physics includes radiation therapy physics, medical diagnostic and imaging physics, nuclear medicine physics, and medical radiation safety. It also ranges from basic researcher (at college institutions, industries, and laboratories) to applications in clinical environments.

**SESSION V18: FOCUS SESSION: CARBON NANOTUBES: TRANSPORT IV**
**Thursday Morning, 16 March 2006; 315, Baltimore Convention Center at 11:15**
**Michael Fuhrer, University of Maryland, presiding**

***Invited Papers***

**11:15**
**V18 1 2D Carbon Nanotube Network: A New Material for Electronics.**
GEORGE GRUNER, *University of California Los Angeles*

This talk will focus on the electronic properties of two dimensional carbon nanotube networks, and on their application potential. Percolation issues, together with the frequency, and temperature dependent activity will be discussed. The network can be tuned from having semiconducting to metallic like behavior, and doping with electron withdrawing and donating species leads to networks with tailor-made electronic properties. The network is also highly transparent in the visible spectral range, this attribute – together with simple room temperature fab processes – opens up application opportunities in the area of electronics, opto-electronics, photovoltaics and sensors. Recent results on solar cells, OLEDs and smart windows will be reviewed. Field effect transistors that incorporate nanotube network conducting channels, together with complex functional devices that incorporate networks and functional molecules will also be discussed. Finally a comparison will be made with conventional and emerging materials that compete area of disposable, flexible and printable electronics.

***Contributed Papers***

**11:51**
**V18 2 Understanding 1/f noise in carbon nanotube devices** YU-MING LIN, JOERG APPENZELLER, *IBM T. J. Watson Research Center* JOACHIM KNOCH, *Forschungszentrum Juelich* ZHIHONG CHEN, PHAEDON AVOURIS, *IBM T. J. Watson Research Center* Nanotubes and nanowires provide an ideal platform to study the electronic behavior of low-dimensional systems. Although a great deal has been learned about the electronic properties of nanotubes and nanowires, little is known about their noise characteristics. We have characterized the 1/f noise behavior of nano-devices consisting of individual single-walled semiconducting carbon nanotubes. Two types of carbon nanotube field-effect transistors (CNFETs) are fabricated and investigated in order to distinguish between the impacts of the contact and bulk channel on the noise. The first type of CNFET is a back-gated device where the conductance is entirely modulated by the Schottky barriers (SBs) at the nanotube/metal interfaces, while the second type of CNFET incorporates an additional gate electrode so that the device switching can be achieved through the bulk channel of the nanotube. We have also fabricated SB-CNFETs with very different channel lengths using a itsingle nanotube in order to elucidate the impact of scattering on 1/*f* noise. The results indicate that that 1/*f* noise in a 1D system with quasi-ballistic transport behavior provides a measure of the total number of transport carriers in the channel. Morover, the intrinsic 1/*f* noise amplitude of individual single-walled carbon nanotube is, in fact, not larger than that of most bulk materials.

**12:03**
**V18 3 Time-Dependent Transport in Carbon Nanotube Transistors*** YUPENG CHEN, *University of Central Florida* JING GUO, *University of Florida* THOMAS WU, *University of Central Florida* Recently, very high frequency properties of carbon nanotube field-effect transistors (FETs) are attracting extensive research interests due to their high mobility and near ballistic transport [1 – 4]. To explore the performance limit of CNTFETs for very high frequency applications, it is important to understand time-dependent transport in CNTFETs. Self-consistent, quasi-static quantum simulations have been applied to assess the high-frequency performance [4]. However, the validity of quasi-static approximation needs to be examined. In addition, a full-time dependent simulation is necessary to examine some very important characteristics, such as frequency-dependent conductance. Our

study on AC characteristics of CNTFETs is based on solving a full time-dependent quantum transport equation for CNTFETs using the finite difference time domain (FDTD) method for the first time. The dependence of small signal transconductance and gate capacitance on the frequency of the applied bias is examined. The intrinsic cut-off frequency, a device metric important for radio-frequency (RF) applications, and the intrinsic switching time, a metric important for digital switch applications, are computed using the full time-dependent simulations. The validity of the widely used quasi-static approximation is examined.

*Contact email: tomwu@mail.ucf.edu

**12:15**

**V18 4 Carbon Nanotube Low Power Integrated Circuit.** ZHIHONG CHEN, JOERG APPENZELLER, YU-MING LIN, *IBM T.J. Watson Research Center* JENNIFER SIPPEL-OAKLEY, ANDREW G. RINZLER, *University of Florida, Physics Department* JINYAO TANG, *Columbia University, Department of Chemistry* SHALOM J. WIND, *Columbia University, Department of Applied Physics and Applied Mathematics* PAUL M. SOLOMON, PHAEDON AVOURIS, *IBM T.J. Watson Research Center* Identifying a material that can outperform silicon in terms of device density, power consumption and performance is one of the main goals of today's nano-electronics effort. Carbon nanotubes are considered to offer the greatest potential in this context. So far, the emphasis has been on fabricating and characterizing individual nanotube devices. A critical next step is the construction of integrated circuits. Complementary metal-oxide semiconductor (CMOS) technology is the dominant approach for microprocessors, memories, and many other applications, in particular due to its small power consumption. Here, we demonstrate the first CMOS-type, high performance, multiple components logic circuit based on a single carbon nanotube molecule.

**12:27**

**V18 5 Electron Transport in Carbon Nanotube Devices with Several Narrow Top-Gates** JOSEPH SULPIZIO, CHARIS QUAY, *Department of Physics, Stanford University* ZVONIMIR BANDIC, *Hitachi San Jose Research Center, Hitachi Global Storage Technologies* DAVID GOLDHABER-GORDON, *Department of Physics, Stanford University* Carbon nanotubes provide an excellent system for studying one-dimensional (1D) electron systems, known as Luttinger liquids. We report on the nanofabrication of carbon nanotube devices with several narrow top-gates, and provide initial electron transport measurements. Using the top-gates to induce tunable tunnel barriers within the nanotubes, we aim to probe electron-electron interactions by measuring transport across the devices. Fine control over the properties of such devices should enable the further study of other interesting quantum properties of 1D systems (e.g. spin-charge separation).

**12:39**

**V18 6 Probing Chemical Potentials in Solution with Carbon Nanotube Transistors** LISA LARRIMORE, *Laboratory of Atomic and Solid State Physics, Cornell University* SUDDHASATTWA NAD, *Department of Chemistry and Chemical Biology, Cornell University* XINJIAN ZHOU, *Laboratory of Atomic and Solid State Physics, Cornell University* HÉCTOR ABRUÑA, *Department of Chemistry and Chemical Biology, Cornell University* PAUL McEUEN, *Laboratory of Atomic and Solid State Physics, Cornell University* We have used single-walled carbon nanotube transistors to sense redox-active transition metal complexes in a conducting liquid environment. The molecules shift the gate voltage dependence of the nanotube conductance. This shift depends logarithmically on the ratio of oxidized to reduced molecules, which is changed and measured using traditional electrochemical methods. We attribute this signal primarily to the changing electrostatic potential of the solution as set by the water-gate wire, and not to a local interaction between the molecules and the nanotube.

**12:51**

**V18 7 Conductance switching in carbon nanotube transistors induced by electrochemical reactions** JAAN MANNIK, BRETT R. GOLDSMITH, ALEXANDER A. KANE, PHILIP G. COLLINS, *Department of Physics and Astronomy, University of California Irvine, Irvine, CA 92697-4576* Carbon nanotube transistors provide a promising architecture for studying biomolecular dynamics at the single molecule level. To achieve this goal, single bioactive molecules must be integrated into the circuits in a controllable and reliable way. While techniques can be borrowed from bulk chemical functionalization, we focus on the controlled production of a single, chemically-functional site on the sidewall of an operational nanotube transistor circuit. Our approach allows real-time, in situ monitoring of electrical signals from the transistor in order to discern reaction events. Using an electrochemical cell biased under oxidizing or reducing conditions, we have observed sharp, reversible conductance switching events consistent with single-site reactions. The reactions have well-defined electrochemical thresholds, which provides an electronic means to control their production. The dynamics of the switching events, including the rates and degree of reversibility, changes in different electrolyte solutions. This work is partly supported by NSF grant EF-0404057.

**13:03**

**V18 8 Integration of Carbon Nanotubes with III-V(110) Surfaces** LAURA RUPPALT, JOSEPH LYDING, *University of Illinois at Urbana-Champaign* We have used scanning tunneling microscopy (STM) to investigate the unique electronic and physical properties of individual isolated carbon nanotubes dispersed onto semiconducting III-V substrates in an ultrahigh vacuum (UHV) environment. Pristine III-V(110) surfaces were obtained through in situ cleavage, with single-walled carbon nanotubes (SWNTs) subsequently deposited via an UHV-compatible Dry Contact Transfer process[1]. Room temperature STM imagery confirms the intact transfer of individual tubes to the surface, while STM-enabled nanomanipulation suggests a substrate-induced stabilization of isolated SWNTs aligned along the (1bar 1 0) crystallographic direction, in registration with the substrate sublattice rows. Additionally, current image tunneling spectroscopy (CITS) maps of these SWNT/III-V(110) systems yield correlated topographic and electronic information with subnanometer resolution that provide evidence of the sensitivity of local nanotube electronic character to both inherent features of the nanotube as well as to proximal features of the underlying support substrate. [1]P.M. Albrecht and J.W. Lyding, APL 83, 5029 (2003).

**13:15**

**V18 9 Graphene Nanostructures, Fabrication, Physics and Devices.** LI LU, *Beijing National Laboratory for Condensed Matter Physics, and the Institute of Physics, Chinese Academy of Sci-*

*ences, Beijing 100080, China.* S. P. LIU, L. W. LIU, F. ZHOU, H. F. YANG, H. LI, Z. JIN, A. Z. JIN, J. MIAO, W. J. KONG, J. H. FANG, C. Z. GU, Y. X. WENG, Q. K. XUE, *Beijing National Laboratory for Condensed Matter Physics, and the Institute of Physics, Chinese Academy of Sciences, Beijing 100080, China.* S. WANG, L.-M. PENG, *Department of Electronics, Peking University, Beijing 100871, China.* B. JIANG, Q. S. ZHENG, *Department of Engineering Mechanics, Tsinghua University, Beijing 100084, China.* We propose to construct nanoelectronic circuits by directly tailoring graphite, and demonstrate the feasibility of this idea by fabricating specially designed multi-terminal graphene patterns down to a minimum strip width of 50 nm. Electron tunneling measurement confirms the formation of quasi-one-dimensional subbands due to the effect of quantum size confinement. This new approach would in the future provide an efficient way of producing numerous layers of identical graphene nanoelectronic circuits.

**13:27**

**V18 10 Electrical Transport in Carbon Nanotubes with Chirality Changes** B. CHANDRA, Y. WU, H. HAN, M. HUANG, L. HUANG, S. O'BRIEN, T.F. HEINZ, J. HONE, *Columbia University* We present electrical transport measurements of individual single-wall carbon nanotubes in which the chiral indices (n,m) are not fixed along the nanotube length. The nanotube structures are first probed by Rayleigh scattering spectroscopy, after which the tube is transferred to a substrate by a mechanical transfer process. Electrical leads are then fabricated by e-beam lithography. The transport behavior is measured in various sections of the tube to probe the behavior of the molecular junctions.

**V18 11 Miniature Organic Transistors with Carbon Nanotubes as Quasi-One-Dimensional Electrodes.** PENGFEI QI, ALI JAVEY, MARCO ROLANDI, QIAN WANG, ERHAN YENILMEZ, HONGJIE DAI, *Stanford University* As the dimensions of electronic devices approach those of molecules, the size, geometry and chemical composition of the contact electrodes play increasingly dominant roles in device functions. It is shown here that single-walled carbon nanotubes (SWNT) can be used as quasi one-dimensional (1D) electrodes to construct organic field effect transistors (FET) with molecular scale width (about 2 nm) and channel length (1 to 3 nm). An important feature owing to the quasi 1D electrode geometry is the favorable gate electrostatics that allows for efficient switching of ultra-short organic channels. This affords room temperature conductance modulation by orders of magnitude for organic transistors that are only several-molecules in length, with switching characteristics superior to similar devices with lithographically patterned metal electrodes. With nanotubes, covalent carbon-carbon bonds could be utilized to form contacts to molecular materials. The unique geometrical, physical and chemical properties of carbon nanotube electrodes may lead to various interesting molecular devices.

**V18 12 Microwave Conductivity of Single Wall Carbon Nanotube Arrays** C. HIGHSTRETE, MARK LEE, E.A. SHANER, F.E. JONES, A.A. TALIN, D.B. ROBINSON, P.M. DENTINGER, *Sandia National Laboratories* We have developed a coplanar waveguide (CPW) platform compatible with both broadband (0.01 to 50 GHz) microwave scattering parameter measurements and directed assembly of carbon nanotubes (CNTs) and semiconductor nanowires. Utilizing AC dielectrophoresis and lithographic masking techniques, single-wall CNTs prepared with single-stranded DNA as a surfactant were assembled in localized parallel arrays between CPW signal and ground electrodes. This places the CNTs parallel to the electric field in the propagating region where coupling to the CNT conductivity alters the impedance of the CPW. The conductivity of the CNT arrays is deduced from scattering parameter measurements before and after assembly of the CNTs. Preliminary measurements show that at least some types of CNT material have a small but definite high-frequency loss that increases with frequency. Sandia is a multi-program laboratory operated by Sandia Corporation, a Lockheed Martin Company, for the United States Department of Energy's National Nuclear Security Administration under contract DE-AC04-94AL85000.

**14:03**

**V18 13 Computer Simulations for a Novel Topological Defect on Carbon Nanotube** TAKAZUMI KAWAI, *Fundamental and Environmental Research Lab., NEC Corp.* SUSUMU OKADA, *Inst. of Physics and Center for Computational Sciences, Univ. of Tsukuba* KEI KUWABARA, KOTA DAIGOKU, KYOKO NAKADA, *Dept. of Chemistry and Biological Science, Aoyama Gakuin Univ.* YOSHIYUKI MIYAMOTO, *Fundamental and Environmental Research Lab., NEC Corp.* Topological defects in carbon nanotubes do not just causes a nuisance to the nanotube devices, but they sometimes provide new and interesting properties to them. Since the defect physics of nanotube is just in the early stage of research, it is very important to verify the stability and electronic properties of such defects theoretically prior to experiments. Here, we performed TBMD simulations for defect formations by $C_2$ molecule irradiation. Although $C_2$ molecule often bounce back even with a high kinetic energy of $\sim$ 20 eV, it irradiates several famous defects such as mono-vacancy, di- vacancy, and also Stone-Wales defect. In similar simulations, we also found a novel defect structure, where $C_2$ molecule is incorporated into $sp^2$ network of nanotube. Thermal stability of the nanotubes with the defects is similar to that of intact ones. Interestingly, DFT-LSDA calculations showed that nanotubes with a line of the novel topological defects are found to cause a magnetic ordering, where the polarized electron spins are localized around the defect and ferromagnetically aligned along the tube axis. This work was in part performed under the management of Nano Carbon Technology project supported by NEDO.

**SESSION V19: THE CHANGING DYNAMICS OF INDUSTRIAL RESEARCH AS A CONSEQUENCE OF GLOBAL TRENDS (CO-SPONSORED BY APS AND AIP CORPORATE ASSOCIATES)**
**Thursday Morning, 16 March 2006; 316, Baltimore Convention Center at 11:15**
**Mark Bernius, Dow Chemical Company, presiding**

**11:15**
**V19 1 General Motors' R&D: Managing Innovation Globally.**
ALAN TAUB, *Executive Director of R&D, General Motors Corporation*

The rapid pace of technology development and the globalization of the automobile industry are major forces driving General Motors to devise new ways to innovate faster and more efficiently. In response, GM has developed a global R&D network that has transformed GM's research and development organization from a U.S.-based enterprise to one that is over 30 percent leveraged with collaboration in 16 countries. This talk will focus on the challenges faced as well as the lessons learned and best practices developed in building this network.

**11:51**
**V19 2 Not only Texas is flat.**
HANS STORK, *Chief Technology Officer, Texas Instruments*

The internet communication infrastructure has been one of the main factors creating a ''flat'' world, a level playing field for innovation and the value of intellectual contributions. Furthermore, it has enabled a 24×7 frame of mind for development as well as manufacturing. Today it is therefore no longer optional but in fact a necessity to leverage skills and resources around the world, from research through production.

**12:27**
**V19 3 Micron R&D: Global Scope and Nano-Scale in N-Dimensions.**
MARK DURCAN, *CTO & VP Research and Development, Micron Technology*

The Globalization of world markets and the globally dispersed manufacturing that supports them, drives complexity in managing today's leading edge R&D organizations beyond that historically experienced. The dimensions involve not only location, but time, economics, government relations, complex supply and customer chains, and Intellectual Property strategy. Each must be contemplated and optimized in light of the nature of worldwide 24 hour a day competition.

**13:03**
**V19 4 Leap Ahead: Global R&D at Intel.**
ABEL WEINRIB, *VP and Director Corporate Technology Group, Intel Corporation*

Intel does research, development, and manufacturing for our products across the globe for a worldwide market. Get a glimpse into Intel's latest global R&D efforts driving future processor and platform architecture innovations; how these innovations could address existing user needs and enable new possibilities for emerging markets; and the challenges to managing an international research organization.

**13:39**
**V19 5 Sustaining Breakthrough Research in a Changing Global Environment.**
THOMAS FEIST, *Manager, Thin Films Lab, GE Global Research*

As companies face ever-increasing economic and competitive pressures, the imperative to deliver real, sustained growth through innovation is clear. Corporations need to develop and maintain a research and development portfolio that recognizes this reality. This talk examines how General Electric's Global Research Center is implementing a technology portfolio that balances long- and shorter-term RD across four global facilities. Examples from medical imaging and energy business segments will be used to illustrate strategies for delivering growth through sustained investment in technology.

**SESSION V20: FOCUS SESSION: SEMICONDUCTOR SPIN DYNAMICS: OPTICS**
**Thursday Morning, 16 March 2006**
**317, Baltimore Convention Center at 11:15**
**Dimitri Basov, University of California, San Diego, presiding**

*Contributed Papers*

**11:15**
**V20 1 Unusual Nuclear Spin Alignment in GaAs** JAMES McGUIRE, *NIST* TOM SILVA, *NIST* Time-resolved Faraday rotation experiments are used to measure nuclear spin polarization in GaAs due to hyperfine coupling with pumped electron spins. Both bulk and epilayer samples are examined. We find unusual dependence of the induced nuclear field on the cw pump power, the cw pump helicity, and the external magnetic field. Our results are compared with existing theories and experiments of the coupling of the electron and nuclear spin systems.

**11:27**
**V20 2 $^{69}$Ga Knight shift in semi-insulating GaAs observed by optically polarized NMR** KANNAN RAMASWAMY, *Washington University in St.Louis* STACY MUI, *Washington University in St.Louis* SOPHIA HAYES, *Washington University in St.Louis* Optical orientation in semiconductors continues to capture the attention of many researchers all over the world[1,2]. This is especially due to the emergence of a new area called ''spintronics'' where it is proposed that the spin of the electrons instead of its charge will be manipulated to create various devices. We report $^{69}$Ga optically polarized NMR investigations in semi-insulating GaAs at 6K. In our investigations, we have observed $^{69}$Ga Knight shifts for photon energies above and below the band gap. This observation is important in understanding the mechanism of NMR signal enhancement in semiconductors by polarized light. Our investigations also indicate that nuclear spin-diffusion plays a role in the NMR signal intensity for illumination times of the order of 100s and above. Furthermore, an estimate of $\sim$ 0.067 has been obtained for the average electron spin polarization which is 26% of the maximum achievable polarization in bulk GaAs. The cause for the reduction is under investigation. 1. Meier and B. P. Zakharchenya, Modern Problems in Condensed Matter Sciences, Vol 8, F. (1984) 2. D.D.Awschalom, D.Loss and N.Samarth, Semiconductor Spintronics and Quantum Computation, (2002)

**11:39**
**V20 3 Electrically induced changes to optical nuclear polarizations in bulk GaAs*** PATRICK COLES, ANANT PARAVASTU, JEFFREY REIMER, *University of California, Berkeley* The semiconductor crystal contains a spin refrigeration system, which turns on in the presence of near-band-gap laser light. Simultaneous application of a DC electric field to bulk, semi-insulating GaAs was observed to significantly alter the nuclear polarization process. At certain photon energies, the nuclear polarization inverted. Changes to nuclear polarization occurred upon the onset of nonlinear photoconductivity. Polarization in this regime could originate from electron spins that are perturbed first by the light and subsequently by relaxation with their (hot) momentum reservoir, while rapid spin-exchange equilibrates the electron spin reservoirs. The results suggest that a pathway towards localized optical and electric field control of nuclear spin may exist within bulk semiconductors.

*Supported by National Science Foundation

*Invited Papers*

**11:51**
**V20 4 Bias-dependent spin lifetimes in quantum wells.**
KIMBERLEY HALL, *Dalhousie University*

The prospect of novel high-performance spin-based semiconductor technologies has lead to new research in spintronics, in which the fields of electronics, photonics, and magnetics merge with the promise of applications in ultra-low-power logic architectures, non-volatile reprogrammable gate arrays, and optoelectronic technologies. Innovation in these areas requires the development of efficient methods for spin manipulation in semiconductor materials. Spintronic device architectures that do not require external magnetic fields or magnetic contacts are especially attractive as they would provide seamless integration with the materials and processing techniques of existing semiconductor devices, while avoiding undesirable stray magnetic fields that may hinder device performance. InAs is an excellent candidate for non-magnetic spintronic device applications due to its strong spin-orbit effects, which lead to gate-controllable pseudomagnetic fields in excess of 1 Tesla [1]. We report the demonstration of room temperature gate control over the electron spin dynamics using the Rashba effect in a (110) InAs/AlSb two-dimensional electron gas. Using the large pseudomagnetic fields in this system, we demonstrate spin manipulation on a picosecond time scale with a low threshold voltage.[1] Our findings are promising for the prospect of nonmagnetic low-power, high-speed spintronics.[2] This research is supported by DARPA MDA972-01-C-0002, DARPA/ARO DAAD19-01-1-0490, NSF ECS 03-22021, and NSERC. [1] K.C. Hall et al., Appl. Phys. Lett. 86, 202114 (2005). [2] K.C. Hall et al., Appl. Phys. Lett. 83, 2937 (2003).

*Contributed Papers*

**12:27**

**V20 5 Electron dephasing and decoherence of neutral donor bound electrons in GaAs** KAI-MEI FU, *Stanford University* SUSAN CLARK, *Stanford University* CHARLES SANTORI, *Hewlett-Packard Laboratories* BINGYANG ZHANG, *Stanford University* COLIN STANLEY, *University of Glasgow* M.C. HOLLAND, *University of Glasgow* YOSHIHISA YAMAMOTO, *Stanford University* Strong oscillator strengths, small inhomogeneous broadenings of the optical transitions, and semiconductor device integration possibilities make the GaAs donor-bound exciton (D0X) system an attractive candidate for electromagnetically induced transparency based applications. However, the recent observation of coherent population trapping in the GaAs D0X system indicates a fast (1-2 ns) dephasing rate of the bound- electron spin states which severely limits the achievable transparency. Theoretical and experimental research in other groups indicate the fast dephasing is due to the random nuclear spin environment in the GaAs lattice. We perform measurements of the electron Zeeman Raman transition linewidth which confirm the 1-2 ns dephasing rate. Using this technique, we study the effect of doping density and magnetic field on the Raman linewidth. Both variables can theoretically affect the inhomogeneous broadening due to the nuclear spin environment. If the inhomogeneous broadening can be decreased, spin-echo techniques should be possible to further increase the spin dephasing time to the homogeneous microsecond regime.

**12:39**

**V20 6 Temperature and doping dependence of spin-flip times in n-GaAs** JOHN COLTON, LEE WIENKES, MICHAEL HEEB, *University of Wisconsin-La Crosse* Previously-reported time resolved photoluminescence experiments [1] in lightly-doped n-GaAs have been extended to provide additional measurements of $T_1$ spin-flip times as a function of temperature and of doping density. The samples studied were MBE-grown 1 micron thick layers of doping densities from 3E14 $cm^{-3}$ to 3E15 $cm^{-3}$. The technique was to use a pump pulse to inject spin polarized electrons and a probe pulse to read out the polarization at some later time; spin flips caused the polarization to decrease exponentially with pump-probe delay. Some measured $T_1$ spin-flip times (at low temperature, at low doping densities) were even longer than the previously-reported 1 microsecond value. Work supported by NSF, ACS/PRF, and Research Corporation. [1] J.S. Colton et al., Phys Rev B 69, 121307(R) (2004).

**12:51**

**V20 7 Long-lived precession of spin gratings in *n*-doped GaAs** SAM CARTER, ZHIGANG CHEN, STEVEN CUNDIFF, *JILA and National Institute of Standards and Technology* Transient grating experiments have been performed in lightly *n*-doped GaAs to measure population and spin dynamics. In the presence of a magnetic field perpendicular to the optical axis (Voigt geometry), the spin grating precesses, leading to a diffracted probe signal that oscillates at twice the precession frequency. In contrast to previous experiments in undoped [1] and heavily doped [2] samples, the spin gratings last up to $\sim$ 1 ns at low temperatures, much longer than the lifetime of the photo-excited carriers. These results indicate that a spin grating is formed in the itinerant electrons, which decays due to spin relaxation and diffusion. By measuring changes in the grating decay rate with the grating period, the spin and population diffusion rates have been determined. Attempts to generate a spin grating without generating photo-excited carriers using Raman excitation will also be discussed. [1] A. R. Cameron, P. Riblet, and A. Miller, Phys. Rev. Lett. **76**, 4793 (1996). [2] C. P. Weber, N. Gedik, J. E. Moore, J. Orenstein, J. Stephens, and D. D. Awschalom, Nature **437**, 1330 (2005).

**13:03**

**V20 8 Spin dynamics in a GaAs quantum well with optically controlled charge density: localization vs. delocalization** ZHIGANG CHEN, SAM CARTER, RUDOLF BRATSCHITSCH, STEVEN CUNDIFF, *JILA, University of Colorado and National Institute of Standards and Technology, Boulder, CO 80309-0440, USA* PHIL DAWSON, *School of Physics and Astronomy, Sackville St Building, University of Manchester, Manchester, M60 1QD, England* We have studied electron spin dynamics in a mixed type I/type II quantum well (QW) structure, which consists of narrow and wide GaAs QWs separated by AlAs barriers. The electron (hole) densities in the wide (narrow) QW can be varied continuously over a wide range by low power photoexcitation at an energy above the narrow QW bandgap. We have performed time-resolved Kerr rotation measurements in the Voigt geometry to probe the electron spin dynamics in the wide QW. We measure two *g*-factors for electron spin precession, which we ascribe to the localized and delocalized electrons in the wide QW. Photoexcited holes, localized by the well-width fluctuations in the narrow QW, bind and localize the electrons in the wide QW. A study of the spectral dependence shows strong inhomogeneity of the localized electron *g*-factor, while the delocalized electrons have a constant *g*-factor. With increasing carrier density, the precession amplitude of the delocalized (localized) electrons increases (decreases) until only the delocalized electron precession can be observed at high density.

**13:15**

**V20 9 Coupling single bright spins with channels of intermediate dark spins in diamond*** FELIX M. MENDOZA, RONALD HANSON, RYAN J. EPSTEIN, DAVID D. AWSCHALOM, *Center for Spintronics and Quantum Computation, University of California, Santa Barbara, CA 93106* The nitrogen-vacancy (N-V) center in diamond has garnered interest as a room-temperature solid-state system not only for exploring electronic and nuclear spin phenomena but also as a candidate for spin-based quantum information processing. Recent experiments reveal the coupling of a single bright electron spin of an N-V center to small numbers of dark electron spins of nitrogen defects in its immediate vicinity, not otherwise detected in luminescence[1]. We explore the possibility of utilizing this magnetic dipole coupling between bright and dark spins to couple two spatially separated single N-V center spins by means of intermediate dark nitrogen spins. The angle-resolved magneto-photoluminescence microscopy technique is extended to simultaneously detect a pair of single N-V centers a few microns apart.

*This work was supported by AFOSR, DARPA/MARCO, DARPA/CNID and ARO.

[1]R.J. Epstein, F.M. Mendoza, Y.K. Kato and D.D. Awschalom, Nature Physics **1**, 94 (2005)

**13:27**

**V20 10 Anisotropic Interactions of a Single Spin and Dark-Spin Spectroscopy in Diamond*** R.J. EPSTEIN, F.M. MENDOZA, Y.K. KATO, D.D. AWSCHALOM, *Center for Spintronics and Quantum Computation, University of California, Santa*

*Barbara, CA 93106* Anisotropic spin interactions of single nitrogen-vacancy color centers in diamond are investigated at room temperature using angle-resolved magneto-photoluminescence microscopy.[1] Negative peaks in the photoluminescence intensity are observed as a function of both magnetic field magnitude and angle, and are modeled by coherent spin precession and anisotropic relaxation at spin-level anti-crossings. In addition, precise field alignment reveals the resonant magnetic dipolar coupling to nearby dark nitrogen spins, otherwise undetected by photoluminescence. The results present an avenue for transferring spin information between bright spins through the intermediate dark spins.

*Work supported by AFOSR, DARPA/MARCO and ARO.

[1]R. J. Epstein *et al.*, Nature Physics **1**, 94 (2005); cond-mat/ 0507706.

**13:39**

**V20 11 External strain engineering of the optical response of (Al,Ga)As/GaAs microdisk lasers** X. LI, M. H. MIKKELSEN, S. GHOSH, D. D. AWSCHALOM, N. SAMARTH, *Materials Research Institute, Penn State University and Center for Spintronics and Quantum Computation, University of California-Santa Barbara* Recent studies show that semiconductor microcavities provide unexpected ways of controlling electron spin coherence via light-matter interactions in confined geometries [S. Ghosh et al., cond-mat/ 0509500], suggesting new routes towards spin-based quantum information processing. Here, we use optical spectroscopy to study the effects of external strain on lattice-matched (Al,Ga)As/GaAs microdisk lasers. We demonstrate that the encapsulation of such lasers with $SiN_x$ allows systematic strain engineering of steady state optical characteristics, where measurements of spontaneous emission show that GaAs quantum wells in the active region of the microdisks experience strain from both the $SiN_x$ and the free standing disk shape, and measurements of stimulated emission show that the laser threshold decreases with the magnitude of net compressive strain. Further, we also explore related modifications in the electron spin coherence time. Work supported by DARPA/QUIST and NSF.

**13:51**

**V20 12 Polarized luminescence in silicon** FREDERIC ROUX, GEORGES LAMPEL, YVES LASSAILLY, JACQUES PERETTI,* Although silicon is a widely used semiconductor in the microelectronic industry, few studies habe been performed so far about its spin-transport properties. Creating and manipulating both spin and charge of electrons in silicon could be very promising in the research of convenient spintronic devices. One way to create and detect spin orientation of the conduction electrons is to perform a photoluminescence experiment under optical pumping conditions. We will present here a stationary photoluminescence experiment. Silicon samples of various doping concentrations, at nitrogen or room temperature, are optically pumped by a Ti:saphir laser. In silicon, the spin relaxation time is much shorter than the carrier life-time, thus yielding to a weak polarization of the recombination radiation. Polarization spectra under either modulated excitation or modulated reception have shown spectral regions where the degree of polarization of the luminescence can be as high as 5 percents. The possibility of a depolarization effect by a transverse magnetic field will be discussed (Hanle effect).

*Laboratoire de Physique de la matiere condensee, UMR 7643-CNRS, Ecole Polytechnique, 91128 Palaiseau Cedex, France

**14:03**

**V20 13 An Interferometric Approach to Time Resolved Faraday Rotation Measurements** J.M. LAFORGE, *University of Victoria* G.M. STEEVES, *University of Victoria* Time Resolved Faraday Rotation (TRFR) is an optical pump-probe technique used to detect electron spin precession about an external magnetic field in semiconductors. In TRFR a net electron magnetic moment can induce small rotations in the polarization of the probe beam, which are detected through a polarizing cube beam splitter and two balanced photodiodes. We present a new approach that divides the probe beam into two orthogonally polarized arms of a free-space Mach-Zender interferometer where one arm contains the sample being studied. Recombination of the probe beams optically amplifies the Faraday Rotation (FR) signal. There are two benefits to this approach; traditional samples can be probed at lower intensities while maintaining signal quality, and weak FR signals, such as those found in the spintronic studies of quantum dot materials, can be optically amplified before detection. Vibrational isolation and thermal stability are important operational factors since the optical gain can be affected by optical path length difference between the two arms of the interferometer.

## SESSION V21: LIQUID CRYSTALS II: NANO & BIO

**Thursday Morning, 16 March 2006**
**318 Baltimore Convention Center at 11:15**
**P. A. Heiney, University of Pennsylvania, presiding**

***Contributed Papers***

**11:15**

**V21 1 A Phenomenological Model of the Effect of Magnetic Nanoparticles and Their Surface Coating on Smectic - A Liquid Crystal Order** LUZ J. MARTINEZ-MIRANDA, *University of Maryland, College Park, MD* LYNN K. KURIHARA, *Naval Research Laboratory, Washington, DC* KEVIN McCARTHEY, *University of Maryland, College Park, MD* JASON HARRY, *Xavier University, New Orleans, LA* ALEXIS NOEL, *Morgan State University, Baltimore, MD* We studied the interaction of a smectic-A liquid crystal with magnetic nanoparticles. The behavior of smectic-A liquid crystals with magnetic particles has not been very well characterized., especially where it concerns the effect of the particles' surface coating. The effect of this termination compound on the effect the nanoparticles have on liquid crystals, smectic or nematic, has not been systematically or consistently characterized. The surface coating is needed to ensure that the particles and the smectic liquid crystals do not phase separate. The surface coating in a nanoparticle is used in biological applications to identify a particular cell. We have found out that depending on the surface coating the interaction of the nanoparticles with the liquid crystal varies. This variation is related with how the surface coating aligns the liquid crystal and how it contributes to the concentration of the nanoparticles in the liquid crystal-nanoparticle mixture. This work was partially supported by NSF grant No. NSF-DMR-0080008.

**11:27**

**V21 2 Carbon nanotube liquid crystal composites*** REZA DODGE, SHIN-WOONG KANG, SATYENDRA KUMAR, *Department of Physics, Kent State University, Kent, Ohio 44242* CHEOL PARK, MIA SIOCHI, *National Institute of Aerospace, Hampton, VA 23666, Advanced Materials and Processing Branch, NASA Langley Research Center, Hampton, VA 23681* The miscibility of carbon nanotubes (CNTs) in thermotropic liquid crystals is extremely low, yet they can have marked influence on the properties of their host medium. We mixed very small amounts of multi-walled CNTs in a number of cyanobiphenyl mesogens and measured the dielectric and electro-optical properties, and studied the optical textures of the composites. The homeotropic samples show a unique texture, under polarizing microscope, which indicates that the nanotubes behave as line singularities with the strength of +1. The distorted alignment around these singularities covers a limited range, which is comparable with the sample thickness. The results of experiments on composites with various concentrations of CNT will be presented.

*Supported by NASA Langley Research Center through grant # NNL04AA14A.

**11:39**

**V21 3 Organization of Magnetic Nanowires via Elastic Forces in a Periodic Multi-Domain Nematic Liquid Crystal*** CLAYTON LAPOINTE, DANIEL REICH, ROBERT LEHENY, *Johns Hopkins University* An anisotropic particle suspended in a thermotropic nematic liquid crystal imposes an elastic energy cost on the nematic that depends on the orientation of the particle relative to the nematic director. In a nematic with a spatially varying director field, such a particle can hence experience translational forces that depend on its orientation. We report experiments in which we exploit these forces to organize ferromagnetic Ni nanowires suspended in the nematic 4-pentyl-4-cyanobiphenyl (5CB). Using lithographic techniques to pattern the nematic anchoring conditions on substrates, we generate periodic multi-domain nematic environments for the wires. With their orientation controlled by a small external magnetic field, the wires sediment to preferred domains to minimize elastic energy.

*Johns Hopkins University

**11:51**

**V21 4 Liquid Crystal Alignment Induced by a Magnetic Field and the Associated Surface Memory Effect*** RUI GUO, QINGBING WANG, SATYENDRA KUMAR, *Department of Physics, Kent State University, Kent, Ohio 44242* YURI REZNIKOV, *Institute of Physics of National Academy of Science, Prospect Nauki 46, Kyiv 252022, Ukraine* Nematic liquid crystals, 4, 4'-n-pentylcyanobiphenyl (5CB) and a commercial mixture, *E*7, have been found to align in thin cells prepared by cooling from the isotropic phase in the presence of a strong magnetic field parallel to the ITO coated glass substrates. The field induced alignment is very stable and possesses surface memory effect [1]. Surprisingly, the azimuthal anchoring energy is as high as $10^{-3}$erg/cm$^2$ and comparable to that obtained for rubbed polymer alignment layers. The surface memory effect is thermally stable and cannot be erased even after holding the cell more than 40K above the clearing point for up to two hours.We believe that the magnetic field directed rearrangement of the LC molecules adsorbed [2] at the substrate is responsible for the observed behavior. [1] N.A. Clark, Phys. Rev. Lett. **55**, 292 (1985). [2] Y. Shi, B. Cull, and S. Kumar, Phys. Rev. Lett. **71**, 2773 (1993).

*Supported by the National Science Foundation grant DMI-04-23619.

**12:03**

**V21 5 The Study of the Fluorescent Spectrum of Cd-Se Quantum Dots in Liquid Crystal Cell*** YU-SUNG LIN, *Department of Physics, National Sun Yat-sen University, Kaohsiung, 804, Taiwan* WEN-CHI HUNG, WOOD-HI CHENG, *Institute of Electro-Optical Engineering, National Sun Yat- sen University, Kaohsiung, 804, Taiwan* I-MIN JIANG, *Department of Physics, National Sun Yat-sen University, Kaohsiung, 804, Taiwan* MING-SHAN TSAI, *Department of Applied Physics, National Chiayi University, Chiayi, 600, Taiwan* We report the analysis of the fluorescent spectrum of Cd-Se quantum dots in liquid crystal matrices. The cell is filled with the commercial liquid crystal (E7) in homogeneous alignment. We can vary the director field orientation of liquid crystals by applying electrical fields. With a light source of a xenon lamp to excite the Cd-Se quantum dots, the effect on the fluorescent spectrum due to liquid crystal environment is then explored. The shift of fluorescent spectrum affected by the concentration of Cd-Se quantum dots is also discussed in the report. Then the Cd-Se quantum dots are excited by use of a monochromatic Nd-YAG laser, which is a polarized light source. We explore the effects of polarization on fluorescent spectrum of Cd-Se quantum dots also.

*National Science Council of Taiwan, R.O.C. NSC94-2112-M-110-013

**12:15**

**V21 6 Transmissive Fabry-Perot Spectrum of Liquid Crystal Device for measuring the Surface Plasmon Effect of Silver nano-Particle*** WEN-CHI HUNG, *Inst. of Electro-Optical Engr., Natl. Sun Yat-sen Univ.,Taiwan* YU-SUNG LIN, *Dept. of Physics, Natl. Sun Yat-sen Univ., Taiwan* MING-SHAN TSAI, *Dept. of Applied Physics, Natl. Chiayi Univ., Taiwan* I-MIN JIANG, *Dept. of Physics, Natl. Sun Yat-sen Univ., Taiwan* WOOD-HI CHENG, *Inst. of Electro-Optical Engr., Natl. Sun Yat-sen Univ.,Taiwan* A Fabry-Perot scheme for measuring the surface plasmon effect of Ag nano-particles has been presented. As an optical spectrum ananlyzer, the resolution of the Fabry-Perot etalon.is determined by the morphology of reflectors and resonated cavity of the etalon. Ag nano-particles of size 50 nm are deposited on the surfaces of two reflectors. The cavity is filled with liquid crystals which are homogeneous alignment. Because the surface plasmon effect (SPE) of metal nano particles is sensitive to the polarization of incident light (P-wave or S-wave), we apply various polarization lights to explore the spectra of Fabry-Perot etalon filled with liquid crystal to study the SPE of metal nano-particles. In the transmissive spectra, we find the wavelength shift at the peak (603 nm) is about 8 nm when the probed light is changed from P-wave to S-wave. Comparing the measurements of the etalon without filled with the liquid crystal; we discuss the correlation of the wavelength shift and SPE of Ag nano-particles in the liquid crystal etalon device.

*National Science Council of Taiwan, R.O.C. NSC94-2112-M-110-013

**12:27**

**V21 7 Investigating mixtures of rotor molecules and liquid crystals by dielectric spectroscopy and optical microscopy** DEBRA KRAUSE, CHARLES T. ROGERS, *Dept. of Physics, University of Colorado, Boulder* JOSE E. NUNEZ, MIGUEL GARCIA-GARIBAY, *Dept. of Chemistry and Biochemistry, University of California, Los Angeles* Rotor molecules are fundamental in nanotechnology. These molecules are synthesized with one part of the molecule designed to freely rotate while other parts are attached to a surface or within a crystalline super-structure. One class of rotor molecules have fluorobenzene rotors surrounded by bulky triphenyl groups. Studies of these electric dipole rotors in a crystalline state have shown that steric interactions between neighboring molecules can result in large energy barriers (up to 21 kcal/mol) that inhibit motion of the rotor. In an effort to free the rotor but maintain degrees of order in position and orientation, we mix these molecules with liquid crystals, particularly those based on benzylidene-(4-phenylazo-phenyl)-amine. The rotor molecules can dissolve in these liquid crystals into solutions of up to 20 percent by mass. To characterize the environment of the rotor, we study the mixtures using dielectric spectroscopy and optical microscopy.

**12:39**

**V21 8 Flexible plastic cells fabricated using phase separation of liquid crystal from its mixture in a prepolymer*** QINGBING WANG, RUI GUO, SATYENDRA KUMAR, *Department of Physics, Kent State University, OH 44240* During phase separation of liquid crystal (LC) from its mixture in a prepolymer, in a cell, the prepolymer accumulates near the spacers. After the phase separation is complete, UV irradiation is used to crosslink the polymer thereby fixing the position of the spacers and bonding them to the substrates. We employ this method to create polymer-embedded spacers to improve cell gap uniformity for LC displays using plastic substrates. Spacers remain adhered to their initial positions thus preventing them from movement or aggregation during temporary cell deformation. Scanning electron microscopy was employed to evaluate the internal polymer morphologies formed under different polymerization conditions. Electro-optical performances and the flexibility of plastic LC cells were determined and the details will be presented.

*Supported by a grant from Samsung Electronics Corporation

**12:51**

**V21 9 Adding Mono- and Multivalent Ions to Lyotropic Chromonic Liquid Crystals** LUANA TORTORA, HEUNG-SHIK PARK, KELLY ANTION, CHRIS WOOLWERTON, DANIELE FINOTELLO, OLEG LAVRENTOVICH, *Kent State University* Lyotropic Chromonic Liquid Crystals (LCLCs) are a distinct class of liquid crystals formed in aqueous solutions by molecules with rigid polyaromatic cores and ionic groups at the periphery [1-4]. The phase diagrams of these materials should depend on entropic factors (as in the Onsager model) and electrostatic interactions. Using optical polarizing microscopy, we studied the effects of mono- and multivalent ions on the phase diagrams of Blue 27 [3] and Sunset Yellow [2]. The monovalent ions change the temperatures of phase transitions, as described in [4], while the effect of multivalent ions is more dramatic and, in addition to the changed temperatures of phase transitions by tens of degrees, it often involves condensation of LCLC aggregates into domains with birefringence much higher than that in a normal nematic phase. Work supported by OBR B-7844. [1] J. Lydon, Current Opin. Colloid & Interface Sci. **3**, 458 (1998);**8**, 480-489 (2004); [2] V. R. Horowitz, L. A. Janowitz, A. L. Modic, P. J. Heiney, and P. J. Collings, 2005, Phys. Rew. E **72**, 041710; [3] Yu. A. Nastishin, H. Liu, T. Schneider, T., V. Nazarenko, R. Vasyuta, S. V. Shiyanovskii, and O. D. Lavrentovich, 2005, Phys. Rev. E **72**, 041711; [4] A.F. Kostko, B. H. Cipriano, O. A. Pinchuk, L. Ziserman, M. A. Anisimov, D. Danino, and S. R. Raghavan, J. Phys. Chem. B **109**, 19126-19133 (2005)

**13:03**

**V21 10 Building Shape Surfactants: Creating rod-coil complexes using genetically engineered viruses** PHIL HUANG, SETH FRADEN, *Brandeis University* Complex self-assembled structures (micelles, lamellar phases) are often found in dispersions of amphiphilic molecules like surfactants. We genetically engineered M13 bacteriophage, a long filamentous particle that forms liquid crystalline phases, and coupled a 15 base pair oligonucleotide to one end of the virus. A plasmid DNA fragment was then ligated to the oligonucleotide to form a rod-coil particle. Based on the above complex conjugate, we are attempting to create supramolecular liquid crystalline structures.

**13:15**

**V21 11 Stretching the limits of membrane charge density using Dendrimer Lipids - New Highly Transfecting Hexagonal Phases for Gene Delivery** KAI EWERT, ALEXANDRA ZIDOVSKA, HEATHER M. EVANS, CYRUS R. SAFINYA, *Materials, Physics, and Molecular, Cellular and Developmental Biology Departments, UCSB, Santa Barbara, CA 93106* Newly designed multivalent lipids ranging in head group charge from 4+ to 16+ have been synthesized and investigated as DNA delivery vectors. These dendritic lipids (DLs) allow a controlled study of the relationship between membrane charge density ($\sigma$) and transfection efficiency (TE). An earlier report from our group described that TE of different cationic lipids of charge 1+ to 5+ follows a common, bell shaped curve as a function of membrane charge density [1]. To further probe this universal behavior, the dendritic lipids with higher valence were designed in order to reach higher values of $\sigma$. Structural studies using x-ray diffraction reveal new phases, where cylindrical micelles of DLs form a hexagonal lattice which holds together a continuous DNA network, described as $H_I^C$ [2]. The new hexagonal phase is highly transfecting in the regime where the TE of lamellar complexes follows a decrease in the bell curve. Small angle x-ray scattering studies have revealed a rich phase diagram of micelles made from DL/DOPC mixtures. Funding provided by NIH GM-59288 and NSF DMR-0503347. [1] A. Ahmad et al., itJ. Gene Med., 2005, V7:739-748. [2] K. Ewert et al., itJ. Am. Chem. Soc., (submitted).

**13:27**

**V21 12 Hollow Rectangular Columnar Structure in Dendritic Supramolecular Assemblies*** MIHAI PETERCA, PAUL HEINEY, *Dept. of Physics, Univ. of Pennsylvania* MARC ILIES, ANDRES DULCEY, SAMI NUMMELIN, VIRGIL PERCEC, *Dept. of Chemistry, Univ. of Pennsylvania* Hollow columnar phases have recently attracted interest for their potential applications as channel mimics in membrane transport, as photonic band gap materials, and for selective encapsulation. The first dendritic structures that self-assemble into hollow rectangular phases have been synthesized and a method for their structural analysis by x- ray diffraction experiments has been developed. The structural analysis method developed allows the calculation of the pore separation,

shape and size, creating new opportunities for separation processes of symmetric or asymmetric compounds.

*Supported by the MRSEC program of the National Science Foundation under award # DMR05-20020.

**13:39**

**V21 13 X-Ray Determination of the Structure and Phases of Liquid Crystals of Nanoscale Duplex DNA** MICHI NAKATA, *U. of Colorado* GIULIANO ZANCHETTA, *U. of Milano (IT)* CHRISTOPHER JONES, *U. of Colorado* BRANDON CHAPMAN, *Brookhaven National Lab.* RONALD PINDAK, *Brookhaven National Lab.* TOMMASO BELLINI, *U. of Milano* NOEL CLARK, *U. of Colorado* Polymeric DNA chains are known to exhibit chiral nematic and hexagonal columnar LC phases. Recently we found that even very short duplex B-DNA oligomers 6-basepairs (bp) to 16-bp in length also form nematic and columnar phases depending on the concentration of DNA. To investigate the structure of those phases, we used micro-beam x-ray diffraction (10 micron spot size), enabling the study of single LC domains. In the columnar phases of 8bp, 12bp and 16bp all shows reflection spots corresponding to 20/*AA* which almost the same length scale of the width of DNA double helix. By selecting a proper orientation of the domains the diffraction pattern shows a hexagonal packing of columns of spacing which does not depend on the length of the basepair. On the other hand, there is no clear diffraction in the chiral nematic phase, which indicates that there is no significant highly ordered molecular aggregation. Those data indicate that short oligomers stack end- to end to form flexible rod-shaped DNA aggregates can then form LC phases. Work supported by NSF MRSEC Grant DMR 0213918 and NSF Grant 0072989.

**13:51**

**V21 14 Probing the mechanical unzipping of DNA** NIKOS K. VOULGARAKIS, ALAN R. BISHOP, KIM O. RASMUSSEN, *Theoretical Division and Center for Nonlinear Studies, Los Alamos National Laboratory, Los Alamos, New Mexico 87545, USA* Recent advances in single-molecule force spectroscopy have made a systematic study of local melting in DNA possible. This provide new insight into important biological processes as replication and transcription. In this work, we present an extensive study of the micromechanical unzipping of DNA in the framework of the Peyrard-Bishop-Dauxois (PBD) model. The force required to separate the doubled strand is derived through analysis of the force-extension curve, while an estimation of the nucleation bubble size of the unzipping process is obtained by the distribution of the rapture force. Our findings are in very good agreement with existing experimental results; for example the force-temperature phase diagram obtained by the PBD model agrees excellently with recent constant-force experimental measurements of the lambda-phage DNA. Fundamental differences between the in vivo and vitro DNA unzipping, as predicted by the PBD model, are also discussed.

**14:03**

**V21 15 Asymmetrical binding of cationic peptides onto an oppositely-charged lipid-bilayer membrane: area expansion and membrane rupture*** SATTAR TAHERI-ARAGHI, BAE-YEUN HA, *Department of Physics, University of Waterloo, Ontario N2L 3G1, Canada* We study asymmetrical binding of cationic peptides onto a negatively charged lipid-bilayer membrane. The peptide not only interacts electrostatically with anionic lipids, rearranging their spatial distributions, but it can also insert hydrophobically into the membrane, expanding the area of its binding layer (i.e., the outer layer). We examine how peptide charges and peptide insertion (thus area expansion) are intertwined. Our results illustrate why high valences are required for selective toxicity of antimicrobial peptides, (i.e., they selectively rupture bacterial membranes while leaving host cells intact).

*This work was supported by the Natural Sciences and Engineering Research Council of Canada

**SESSION V22: FOCUS SESSION: MAGNETIC TUNNELING II**
**Thursday Morning, 16 March 2006**
**319, Baltimore Convention Center at 11:15**
**Alex Panchula, Grandis Inc., presiding**

**11:15**

**V22 1 From ballistic transport to tunneling in electromigrated ferromagnetic breakjunctions** KIRILL BOLOTIN, F. KUEMMETH, A.N. PASUPATHY, D.C. RALPH, *Cornell University* We fabricate ferromagnetic constrictions whose cross section can be reduced gradually from $100 \times 30$ nm$^2$ to the atomic scale and eventually to the tunneling regime by means of electromigration. The contacts are attached to non-magnetic substrates and are measured at 4.2 K, so they are much more mechanically stable than previous room-temperature studies. We measure magnetoresistances (MR) $< 3\%$ for contacts $< 400\ \Omega$, consistent with previous experiments. As the contact diameter is reduced in the range $400\ \Omega$ - $25\ k\Omega$, we observe reproducible non-monotonic changes in the MR. We find first a minimum in the MR and sometimes a change in sign to small negative values, and then a strongly increasing positive MR as the contact approaches the atomic scale ($\sim 25\ k\Omega$). For near-atomic-sized constrictions the maximum MR is 80%. Measurements as a function of the direction of applied magnetic field allow us to separate the contribution of anisotropic magnetoresistance from the MR due to a domain wall. In the tunneling regime the MR fluctuates over a wide range, $-10\%$ to 85%, even for small changes in the atomic structure in a single device.

**11:27**

**V22 2 Magnetoresistance in oxidized Ni nanocontacts** D. JACOB, *Universidad de Alicante* J. FERNANDEZ-ROSSIER, J. J. PALACIOS, Whether or not ferromagnetic nanocontacts display large magnetoresistance (MR) is still a matter of debate [1,2]. From the theory side it has been shown[3] that MR in pure Ni nanocontacts is certainly not large in good agreement with recent experiments [2]. Here we explore the effect of oxygen atoms in the electronic structure and transport of nickel nanocontacts. Since bulk nickel oxide is an insulating antiferromagnets, nano-oxidized nickel is an interesting system on its own. Here we present ab-initio quantum transport calculations of Ni nanocontacts in the presence of oxygen adsorbates in the contact region. We show that the presence of a single oxygen atom leads to strongly spin-polarized transport for parallel alignment of electrodes magnetizations while for antiparallel alignment the conduction is strongly

suppressed resulting in large MR. (1) H. D. Chopra, Nature Materials 4, 832 (2005) (2) K. I. Bolotin et al., cond-mat/0510410; W. F. Egelhoff et al., J. Appl. Phys. 95, 7554 (2004) (3) D. Jacob et al., Phys. Rev. B 71, 220403(R) (2005)

**11:39**

**V22 3 Bias dependent oscillations in spin polarized tunneling*** CASEY MILLER,† *Physics Dept., Univ. Calif. San Diego* JOHAN AKERMAN, *Dept. of Materials Physics, Royal Institute of Technology, Electrum 229, 164 40 Kista, Sweden* ZHI-PAN LI, *Physics Dept., Univ. Calif. San Diego* IVAN K. SCHULLER, *Physics Dept., Univ. Calif. San Diego, 9500 Gilman Dr., La Jolla CA 92093* We investigated the bias dependence of spin polarized tunnelling in (pinned)CoFeB/ MgO/(free)CoFeB and (pinned)CoFeB/ MgO/(free)NiFe tunnel junctions as a function of temperature and applied field angle. The differential magnetoresistance (MR) exhibits oscillations about zero MR when the free layer of the asymmetric devices is above +0.7 V; no oscillations were observed for negative bias. Oscillations were not observed for any bias in the symmetric devices. The zero-crossing voltages were independent of temperature and relative magnetization angle between the two ferromagnetic layers. A model using spin-split free electron energy bands in the ferromagnets and a trapezoidal tunnel barrier demonstrates qualitative agreement with the experimental data.

*Supported by US Department of Energy. In collaboration with Freescale Semiconductor.
†cmiller@physics.ucsd.edu

**11:51**

**V22 4 Negative spin polarization in Co|$SrTiO_3$|Co magnetic tunnel junctions**[1] J. VELEV, K. BELASHCHENKO, *University of Nebraska - Lincoln* D. STEWART, *Cornell University* M. VAN SCHILFGAARDE, *Arizona State University* S. JASWAL, E. TSYMBAL, *University of Nebraska - Lincoln* We perform an itab-initio study of spin-polarized tunneling in epitaxial Coit |$SrTiO_3$|Co magnetic tunnel junctions with bcc Co(001) electrodes. We predict a large tunneling magnetoresistance in these junctions, originating from a mismatch in the majority- and minority-spin bands both in bulk bcc Co and at the Co|$SrTiO_3$ interface. The intricate complex band structure of $SrTiO_3$ enables effcient tunneling of the minority *d*-electrons which causes the spin polarization of the Co|$SrTiO_3$ interface to be negative in agreement with experimental data[2]. Our results indicate that epitaxial Co|$SrTiO_3$|Co MTJs with bcc Co(001) electrodes is a viable alternative for device applications. [1] J. Velev et al., Phys. Rev. Lett. **95**, 216601(2005). [2] J. M. De Teresa et al., Phys. Rev. Lett. **82**, 4288 (1999); J. M. De Teresa, et al., Science **286**, 507 (1999).

**12:03**

**V22 5 Probing spin-dependent tunneling and transmission below the Fermi level with a p-type magnetic tunnel transistor.** B.G. PARK, T. BANERJEE, B.C. MIN, J.C. LODDER, R. JANSEN, *MESA + Institute for Nanotechnology, University of Twente, The Netherlands* A magnetic tunnel transistor (MTT) can be used to probe spin-polarized tunneling involving states away from the Fermi level, as well as spin-dependent transmission of nonequilibrium carriers in a ferromagnet. Here we have used a p-type MTT, in which the magnetocurrent (MC) is determined by the tunnel spin polarization of the states below the Fermi level, and the spin-dependent scattering of hot holes in the magnetic base. For p-type MTT's with the structure p-Si/Au/Co/$Al_2O_3$/NiFe and large Co base thickness (8nm) and/or large emitter bias, the MC has the usual positive sign. Thus, the transmission of holes in the majority spin band of Co is larger than that of minority spin holes. Surprisingly, for smaller Co thickness and bias near the collection threshold (0.3 eV), the MC reverses sign and becomes negative. This unusual result shows that the Co interfaces preferentially transmit carriers of minority spin. With help of specifically designed MTT's and ab-initio calculations we discuss possible contributions of spin-dependent transmission across Au/Co interfaces in the base, and of a negative tunneling spin-polarization of the Co/$Al_2O_3$ interface for states below the Fermi level.

**12:15**

**V22 6 Spin-polarized tunneling time for non-centrosymmetric photonic barriers with out-of-plane magnetization.*** ION BITA, EDWIN THOMAS, *Dept. of Materials Sci & Eng, Massachusetts Institute of Technology* Tunneling barriers that lack space-inversion and time-reversal symmetries along the tunneling axis are found to display fundamentally different tunneling dynamics properties than normally expected. In a model 1D photonic crystal barrier, we show that the two symmetry constraints lead to indirect photonic band gaps which contain eigenmodes that are complex, with nonzero and frequency dispersive real components of their wavevectors. These nonpropagating modes are circularly polarized, and appear as complex conjugate pairs for opposite decay directions. We show that the Hartman effect does not apply, and that the tunneling phase time becomes dependent on barrier length, with, remarkably, the sign of the group delay changing with spin. The tunneling phase time for finite barriers of varying widths is found to agree with the group-like velocity, $1/v_g$ = dRe $\{k_{gap}\}/d\omega$, of the gap eigenmodes of the photonic crystal. The implications of these results for the case of spin-polarized electronic tunneling in noncentrosymmetric barriers (e.g. GaAs-like semiconductors, or chiral carbon nanotubes) with magnetization along the tunneling axis will be discussed.

*Acknowledge support from NSF DMR 02-13282, NSF DMR-0308133.

**12:27**

**V22 7 Spin-Polarized Electron Transport through Nanometer-Scale Al Grains** LIYUAN ZHANG, *School of Physics, Georgia Tech* We had investigated the spin-polarized electron tunnelling through ensembles of nanometer scale Al grains embedded between two Co-reservoirs at 4.2K, and observed tunnelling-magnetoresistance (TMR) and the Hanle effect. The Spin-coherence time ($T2$), measured from the Hanle effect, is around nanoseconds. Fast dephasing is attributed to electron spin-precession in the local fringing fields. Dephasing does not destroy TMR, in contrast to spin-relaxation. itTMR is strongly asymmetric with bias voltage, which we explain by spin-relaxation.

**12:39**

**V22 8 Electron-magnon coupling and non-linear tunneling transport in magnetic nanoparticles** LUKASZ MICHALAK, *Kalmar/Lund University, Sweden* CARLO M. CANALI, *Kalmar University, Sweden* VINCENZO G. BENZA, *Universita' dell'Insubria, Como, Italy* We present a theory of single-electron tunneling transport through a ferromagnetic nanoparticle in which particle-hole excitations are coupled to spin collective modes. The model employed to describe the interaction between quasiparticles and collective excitations captures the salient features of a recent microscopic study. Our analysis of nonlinear quantum transport in the regime of weak coupling to the external electrodes is based on a rate-equation formalism for the nonequilibrium occupation prob-

ability of the nanoparticle many- body states. For strong electron-boson coupling, we find that the tunneling conductance as a function of bias voltage is characterized by a large and dense set of resonances. Their magnetic field dependence in the large-field regime is linear, with slopes of the same sign. Both features are in agreement with recent tunneling experiments.

**12:51**

**V22 9 Point Contact Spin Spectroscopy of Ferromagnetic Fe3Si epitaxial Films** Y.H. CHIU, *Dept. of Phys., National Tsing Hua Univ.* T.W. CHIANG, *Dept. of Phys., National Taiwan Univ.* S.Y. HUANG, S.F. LEE, *Inst. of Phys., Academia Sinica* J. KWO, *Dept. of Phys., National Tsing Hua Univ.* We report transport study of ferromagnetic $Fe_3Si$ epitaxial films using point contact Andreev reflection technique. $Fe_3Si$ is a ferromagnetic metal with a high Curie temperature of 840K and nearly lattice-matched to GaAs. The Heusler-like structure makes it a good candidate of half metals for spintronics. The observed spectra of Nb and NbTi/$Fe_3Si$ point contacts using a Nb or NbTi etched tip are often broad, along with the presence of sharp dips at the superconducting Fermi energy possibly attributed to the proximity effect occurring at the interface of the contact. Using a modified Blonder-Tinkham-Klapwijk theory, the data analysis gave a spin polarization ranging from 27% to 47% under various contact conditions. The best-fit gave P= 41%, Z= 0.05, =1.49 meV at 2K. Since the thickness of our $Fe_3Si$ samples are often small, current distribution effects in the probed layer are specially considered by varying the sample thickness.

**13:03**

**V22 10 Magneto−Optical Ellipsometry on $Ni_2MnIn$ and NiMnIn Heusler Alloys** GERD NEUBER, JAN SCHOLTYSSEK, MARTA BASTJAN, *University of Hamburg* RALF RAUER, *Chalmers University of Technology* ULRICH MERKT, MICHAEL RÜBHAUSEN, GUIDO MEIER, *University of Hamburg* We use generalized magneto-optical ellipsometry [1,2] for measurements of the complete dielectric tensor of $Ni_2MnIn$ [3] and NiMnIn Heusler alloys in the energy range from 1.6 eV to 5.5 eV and in the temperature range from 50 K to 450 K. Generalized magneto-optical ellipsometry allows the investigation of spin-polarized states and to understand the coupling between spin and charge degrees of freedom. We show differences in the metallic behavior of the semi-Heusler alloy NiMnIn and the full-Heusler alloy $Ni_2MnIn$ related to the half-metallic ferromagnetism of the latter one. The polycrystalline $Ni_2MnIn$ and NiMnIn films were co-evaporated from two independent sources of Ni and MnIn on a Si(100) substrate under UHV conditions. The $Ni_2MnIn$ alloy exhibits the ordered $L2_1$ crystalline structure and the NiMnIn alloy has a $C1_b$ structure. [1] A. Berger and M. Pufall, Appl. Phys. Lett. **71**, 965 (1997). [2] R. Rauer, G. Neuber, J. Kunze, J. Bäckström, and M. Rübhausen, Rev. Sci. Instr. **76**, 023910 (2005). [3] S. von Oehsen, J.M. Scholtyssek, C. Pels, G. Neuber, R. Rauer, M. Rübhausen, and G. Meier et al., JMMM **290**, 1371 (2005).

**13:15**

**V22 11 Electronic and structural properties of TBrPP-Fe-Cl molecular self-assembly** GAYANI PERERA, VIOLETA IANCU, SAW-WAI HLA, *Nanoscale & Quantum Phenomena Institute, and Department of Physics and Astronomy, Ohio University, Athens, Ohio, 45701, USA* Self-assembled molecular (SAM) layers of TBrPP-Fe-Cl [5, 10, 15, 20 –Tetrakis -(4-bromophenyl)-Porphyrin-iron-chloride] are formed on a Cu(111) surface. The electronic and structural properties of these SAM layers are investigated by using scanning tunneling microscopy (STM) imaging and tunneling spectroscopy at 4.6 K. The STM images reveal three distinct molecular conformations inside the SAM layers. Local tunneling spectroscopy data are acquired on individual molecules with different conformations. These spectroscopic investigations provide the conformation dependent HOMO-LUMO orbital alignments of the molecules. Further more, the conductance tunneling spectroscopy measured in a small voltage range near the surface. Fermi level show a Kondo resonance originated by interactions between the spin of iron atom inside the molecule, and the surface state free electrons of Cu(111). This work is supported by a US-DOE grant, DE-FG02-02ER46012, and a NSF-NIRT grant, DMR-0304314.

**13:27**

**V22 12 Single molecule Kondo switch** VIOLETA IANCU, APARNA DESHPANDE, SAW-WAI HLA, *Nanoscale & Quantum Phenomena Institute, and Department of Physics and Astronomy, Ohio University, Athens, Ohio, 45701, USA* We present manipulation of Kondo resonance originated from the interaction between the spin of a Co atom inside a TBrPP-Co molecule and free electrons from a copper surface by switching the conformation of isolated single molecules with a scanning tunneling microscope (STM) tip. The STM studies of isolated TBrPP-Co molecules [5, 10, 15, 20 –Tetrakis -(4-bromophenyl)-porphyrin-Co] deposited on a Cu(111) are performed at 4.6K in an ultra-high-vacuum environment. The molecules anchor on Cu(111) with two molecular conformations, planar and saddle. In the saddle conformation, the metal atom is lifted away from the surface as compared to the planar. We are able to switch from a saddle conformation of TBrPP-Co to a planar conformation by applying +2.2V voltage pulses from the STM-tip, thereby varying the vertical distance of Co atom from the Cu(111) surface. This conformational switching increases molecule-substrate interaction resulting in an enhanced spin-electron coupling and changes the associated Kondo temperature from 130K to 170K. This work is supported by a US-DOE grant, DE-FG02-02ER46012, and a NSF-NIRT grant, DMR-0304314.

**SESSION V23: SPIN WAVES**
**Thursday Morning, 16 March 2006**
**320, Baltimore Convention Center at 11:15**
**James J. Rhyne, Los Alamos National Laboratory, presiding**

**11:15**

**V23 1 Spin-wave interactions in quantum antiferromagnets** NILS HASSELMANN, PETER KOPIETZ, *Institut für Theoretische Physik, Universität Frankfurt, Germany* We study spin-wave interactions in quantum antiferromagnets in terms of Hermitian field operators representing staggered and ferromagnetic transverse spin fluctuations. In this parameterization, the two-body interaction vertex between staggered spin fluctuations vanishes at long wavelengths. We derive a new effective action for the staggered fluctuations and show that the quantum critical point separating the renormalized classical from the quantum disordered regime in $D > 1$ dimensions is characterized by an anomalous dimension of the field operator $\eta = D - 1$. We further use this

technique to derive the effective long-wavelength Euclidean action for the antiferromagnetic spin-waves of ordered antiferromagnets subject to a magnetic field. We point out, that the magnetic field dependence of the spin-wave dispersion predicted by the usual $O(3)$ nonlinear sigma model disagrees with spin-wave theory. We argue that the nonlinear sigma-model does not take into account all relevant spin-wave interactions and derive a modified effective action for the spin-waves which contains an additional quartic interaction. At zero temperature the corresponding vertex is relevant in the renormalization group sense below three dimensions.

**11:27**

**V23 2 Spin dynamics of a Half-Metallic Ferromagnet*** RAUL CHURA, KEVIN BEDELL, *Boston College* We determine the dispersion relations, and therefore, the collective modes of a model for a half-metallic ferromagnet by using two approaches: the particle-hole propagator method and the kinetic equation method. We formulate the latter by using the theory of spin polarized Fermi liquids. In both cases we express the results in terms of Landau interaction parameters and make the corresponding comparisons. We also calculate the velocities of propagation of the modes and study the spin stiffness. We discuss the results in the context of the currently available experimental data.

*Work supported in part by grant DOE DEF G0297ER45636

**11:39**

**V23 3 Evolution of Spin-Wave Excitations in Ferromagnetic Metallic Manganites** J. ZHANG, H. SHA, *Florida Intl. Univ.* F. YE, J. FERNANDEZ-BACA, *ORNL* P. DAI, *Univ. of Tenn. and ORNL* J. LYNN, *NIST* H. KAWANO-FURUKAWA, *Ochanomizu Univ., Japan* Y. TOMIOKA, *CERC, Japan* Y. TOKURA, *Univ. of Tokyo and CERC, Japan* The deviation of spin dynamics from the Double-Exchange mechanism in the ferromagnetic metallic manganites is an important yet unsettled issue in the understanding of the close coupling behavior between charge, lattice, orbital, and spin degrees of freedom in these doped ''colossal'' magnetoresistive materials. We have used neutron scattering to systematically study the spin-wave excitations of three ferromagnetic metallic $A_{1-x}A'_xMnO_3$ manganites (where $A$ and $A'$ are rare- and alkaline-earth ions respectively). By combining with previous work, we elucidate the systematics of the spin-spin interaction and interactions between spin and other degrees of freedom as a function of carrier concentration $x$, on-site disorder, and strength of the lattice distortion. The long wavelength spin dynamics show only a very weak dependence across the series, while the Curie temperatures vary substantially. The ratio of the fourth to the first neighbor exchange ($J_4 = J_1$) that controls the zone boundary magnon softening changes systematically with $x$, but does not depend on the other parameters. None of the prevailing models can account for these behaviors. The work was supported by NSF-DMR0453804, NSF-DMR0346826, DE-FG02-05ER46202 and DOE DE-FG02-04ER46125. ORNL is managed by UT-Battelle, LLC, for the U.S. DOE under contract DE-AC05-00OR22725.

**11:51**

**V23 4 Coherent spin waves in epitaxial Fe films on GaAs (001)** HAIBIN ZHAO, DIYAR TALBAYEV, GUNTER LUEPKE, *College of William and Mary* AUBREY HANBICKI, CONNIE LI, BEREND JONKER, *Naval Research Laboratory* Recently, coherent spin waves have been investigated in ferromagnetic thin film using optical pump-probe technique by exploiting the temperature dependence of the magnetic anisotropy. Here, we report on low-order spin wave modes in the dipole-exchange regime in Fe films epitaxially grown on GaAs (001). Three precession modes with zero in-plane wave-vector are observed by applying an external magnetic field along the in-plane hard axis. The lowest frequency mode can be well described by the uniform magnetization precession. The cubic magnetocrystalline anisotropy constant $K_1/M_s$ and effective demagnetization field $4\pi M_s$ are determined to be 270 Oe and 17.5 KOe, respectively. The modes with higher frequencies correspond to the first- and second-order spin waves. An effective exchange stiffness constant of $0.8\times10^{-6}$ erg/cm is obtained from the calculation assuming the single sine- or cosine- type standing spin waves with free spins at both interfaces. The exchange constant is smaller than the values obtained from high order spin wave modes in ferromagnetic resonance experiments and neutron scattering. The difference may result from pinning effects, which modifies the location of the surface antinodes of the standing spin waves thereby changing their effective wavelength.

**12:03**

**V23 5 Evolution of Cr's charge and spin density waves under GPa pressures** YEJUN FENG, R. JARAMILLO, T.F. ROSENBAUM, *JFI, U. Chicago* O.G. SHPYRKO, E.D. ISAACS, *CNM, Argonne* G. SRAJER, J. LANG, Z. ISLAM, *APS, Argonne* M.S. SOMAYAZULU, H.-K. MAO, *Geophys. Lab, CIW* V.B. PRAKAPENKA, *GSECARS, Argonne* We trace the development of Cr's charge density wave (intensity $10^{-4}\times$ Bragg peak) and spin density wave (intensity $10^{-8}\times$ Bragg peak) at GPa pressures at the Advanced Photon Source. Using a diamond anvil cell combined with a newly developed chemical filtering technique, we find a previously unknown incommensurate to commensurate transition at 2 GPa. We analyze the incommensurate Q-vector and intensity changes at the approach to the transition. At much higher pressures ( $>$ 7 GPa), Cr's antiferromagnetism is completely suppressed and the evolution of the line shape at the approach to the quantum critical point directly reveals the role played by quantum fluctuations.

**12:15**

**V23 6 Spin wave in quasi-equilibrium spin systems*** HARI DAHAL, KEVIN BEDELL, *Boston College* Using the Landau Fermi liquid theory we can study a quasi- equilibrium spin system at T=0K to determine the dispersion relations of possible collective modes. By quasi-equilibrium spin system we refer to a spin system which has finite magnetization in the absence of an external magnetic field. Such a system has been realized in liquid helium and in spintronic materials using different methods; one of those is the optical pumping. We have predicted the existence of gapless spin wave modes in such a system. We compare the dispersion relations of different modes of the quasi- equilibrium system with those of a paramagnetic system, in the presence of a magnetic field, and a ferromagnetic system. Using the relaxation time approximation for the collision integral we study the effect of temperature on the dispersion relation of the modes. We will also present the behavior of the dynamical structure function as a function of frequency and discuss the contribution of different modes to the sum rules.

*Supported in part by grant #DOE/DEFG0297ER45636

**12:27**

**V23 7 Valence values of the cations in selenospinel $Cu(Cr,Ti)_2Se_4$*** HAN-JIN NOH, S.-W. HAN, S.-J. OH, *Center for Strongly Correlated Materials Research, Seoul National University, Seoul, Korea* J.-S. KANG, S. S. LEE, G. KIM, *Dep. of Phys. The Catholic University of Korea, Puchon, Korea* J.-Y. KIM, H.-G. LEE, *Pohang Accelerator Laboratory, Pohang, Korea* S. YEO, S.-W. CHEONG, *Dep. of Phys. & Astro. Rutgers University, NJ* A long-standing issue about the Cu valency in selenospinel $CuCr_2Se_4$ was investigated by soft x-ray absorption spectroscopy (XAS) and magnetic circular dichroism (XMCD). Using the sensitivity of XAS and XMCD to the valence value of transition metal ion and its local symmetry, we checked the valence value of each cation in selenospinel $CuCr_xTi_{2-x}Se_4$ ($x$ = 1.0, 1.1, 1.5, and 2.0) and obtained spectroscopic evidence that a small amount of the Cu cation changes the valency from Cu(I) to Cu(II) as the Cr concentration increases from 1.0 to 2.0. Dependence of the Cu(II) concentration and the mean field magnetic exchange energy on the Cr concentration suggests the Cu *d*-hole plays a crucial role in the intriguing magnetic/electrical properties of $CuCr_2Se_4$.

*This work was supported by the KOSEF through the CSCMR at Seoul National University.

**12:39**

**V23 8 The optical and acoustic magnetic excitations in optimum-doped superconductor $YBa_2Cu_3O_{6.95}$ ($T_c$ = 93$K$)*** HYUNGJE WOO, *The University of Tennessee* PENGCHENG DAI, *The University of Tennessee / ORNL* STEPHEN HAYDEN, *University of Bristol UK* HERB MOOK, *ORNL* TOBY PERRING, *ISIS Facility,Rutherford Appleton Laboratory UK* THOMAS DAHM, *Institut fur Theoretische Physik Germany* DOUGLAS SCALAPINO, *UCSB* FATIH DOGAN, *University of Missouri-Rolla* We use high-resolution inelastic neutron scattering to map out the full spin excitations spectra in $YBa_2Cu_3O_{6.95}$ ($T_c$ = 93$K$), probably the most studied high-transition temperature superconductor. In the bi-layer materials where there are two magnetic ions per unit cell, magnetic excitations have two distinct symmetries: odd (or acoustic) and even (or optical) channels. We show that magnetic excitations in the acoustic channel of $YBa_2Cu_3O_{6.95}$ are remarkably similar to that of $YBa_2Cu_3O_{6.6}$ [1] and $La_{1.88}Ba_{0.12}CuO_4$ [2]. That is, they have the universal hourglass shape with incommensurate spin fluctuations below the commensurate resonance. In the optical channel, we discovered incommensurate magnetic excitations in superconducting state. We establish the both the acoustic and optical magnetic excitations spectra of $YBa_2Cu_3O_{6.95}$ in absolute units and compare the results with underdoped $YBa_2Cu_3O_{6.6}$ and single layer families of cuprate superconductors. [1] S. M. Hayden et al. Nature 429, 531 (2004);[2] J. M. Tranquada et al. Nature 429, 534 (2004).

*Grants: NSF-DMR0453804 and DOE DE-FG02-05ER46202

**12:51**

**V23 9 Spin excitations and phonons in $La_{1.5}Sr_{0.5}CoO_4$** ANDREI SAVICI, IGOR ZALIZNYAK, *Brookhaven National Laboratory* Inelastic neutron scattering measurements were performed in $La_{1.5}Sr_{0.5}CoO_4$. At room temperature, the excitation spectrum is dominated by phonons. At low temperatures we see a mix of lattice vibrations and spin modes. By subtracting phonon contributions we are able to identify purely magnetic modes. A resonance mode was found at energies around 25-27meV, the nature of which is under investigation.

**13:03**

**V23 10 Ferromagnetic Relaxation by Magnon Induced Currents** ARKAJYOTI MISRA, RANDALL VICTORA, *University of Minnesota* A theory for calculating spin wave relaxation times based on the magnon-electron interaction is developed. In a conducting ferromagnet the interaction between the conduction electrons and the magnons is important. The magnetic field generated by the spin wave is time dependent and therefore it creates an electric field in the system. In a metallic system, the fields drive the conduction electrons. These magnon induced currents help dissipate the energy of the system by Joule heating. Our study incorporates a thin film geometry and explores relaxation time for a wide range of magnon wave vectors spanning both the magnetostatic and exchange regimes. The relaxation time is calculated directly from the ratio of the energy density of the system and the power loss by magnon induced currents. We propose a wave vector dependent damping constant which approaches values as high as 0.2 for high conductivity metals such as permalloy, showing the large magnitude of the effect. The theory compares reasonably well with spin wave resonance experiments for lower modes. We propose the following picture of ferromagnetic relaxation in switching experiments. The initial rapid approach of magnetization direction to equilibrium is enabled by magnon-magnon scattering that converts the energy into the higher spin wave modes. These modes then decay at a slower pace via the magnon-electron interaction investigated in this work or by the trditionally invoked mechanisms in less pure, lower conductivity films.

**13:15**

**V23 11 On the possibility of electrical detection of spin echoes in a ferromagnetic thin film** MARK FILIPKOWSKI, EDWIN HACH, *Booz Allen Hamilton* We show, via a straightforward calculation, that it is feasible to detect nuclear spin echoes in a ferromagnetic thin film by electrical means. The detection scheme is based on the deflection of the electronic magnetization when the nuclear magnetization reforms during an echo. This deflection is observed as a time-dependent magnetoresistive signal.

**13:27**

**V23 12 Quantum vs. Thermal Annealing of Magnetic Domain Walls in Elemental Chromium** OLEG G. SHPYRKO, ERIC D. ISAACS, *Center for Nanoscale Materials, Argonne National Laboratory, Argonne, IL* JONATHAN M. LOGAN, YEJUN FENG, RAFAEL JARAMILLO, THOMAS F. ROSENBAUM, *James Franck Institute and Department of Physics, University of Chicago, Chicago, IL* PAUL ZSCHACK, *Frederick Seitz Materials Research Laboratory, University of Illinois at Urbana-Champaign, Urbana-Champaign, IL* GABRIEL AEPPLI, *London Centre for Nanotechnology and Dpt of Physics and Astronomy, University College London, London, UK* MICHAEL SPRUNG, ALEC R. SANDY, *Advanced Photon Source, Argonne National Laboratory, Argonne, IL* Dynamics of magnetic domain walls separating regions with different orientations of the spin (charge) density wave has been studied with x-ray photon correlated spectroscopy (XPCS) in bulk Cr samples. Measurements were carried out at temperatures ranging from 298K to 4K. Upon cooling down to 4K thermal exploration of energetic landscape is replaced by quantum tunneling between discrete low-energy configurations of domain walls. Direct comparison of coherent speckle pattern fluctuations for Bragg reflection and charge density wave satellite peak provides information about magnetic superlattice dynamics, deconvolved from the motion of underlying atomic lattice or beam components.

**SESSION V24: CHARGED AND ION-CONTAINING POLYMERS: PROPERTIES**
**Thursday Morning, 16 March 2006**
**321, Baltimore Convention Center at 11:15**
**Alexei Sokolov, University of Akron, presiding**

**11:15**
**V24 1 Morphology Diagrams for Polyelectrolytic Diblock Copolymers** RAJEEV KUMAR, MURUGAPPAN MUTHUKUMAR, *University of Massachusetts Amherst* We have calculated morphology diagrams for polyelectrolytic diblock copolymers in melts and highly concentrated solutions. Using the random phase approximation and self-consistent field theory, stability limits of the standard morphologies (lamellae, cylinders and spheres) have been considered both in weak and strong segregation limits. Effects of Coulomb interaction strength, degree of ionization, Debye screening length, block length, chain length, and the chi parameter on the periods of these morphologies will be discussed. Also, the crossover behavior in the whole range of segregation will be presented. Charging a polymer block with electrical charges leads to many unexpected behaviors, which will be discussed in the context of previous theories and experiments.

**11:27**
**V24 2 Synthesis, Solution Phase Behavior, and Properties of Ionic/Nonionic Block Copolymers** MEHUL VORA, FRANK BATES, *Department of Chemical Engineering and Materials Science, University of Minnesota* The study of amphiphilic block copolymers in aqueous solutions has shown rich phase behavior and interesting solution properties. The aim of the current work is to develop an amphiphilic diblock copolymer system containing an ionic block in order to better understand how ionicity affects the phase behavior and solution properties. Relatively monodisperse PEP-*b*-PMAA (poly(ethylene propylene)-*b*-methacrylic acid) copolymer was prepared from anionically synthesized poly(isoprene-*b*-ittert-butyl methacrylate). The rheological behavior of aqueous solutions of PEP-*b*-PMAA in the presence of different counterions was studied. The choice of counterion has a strong influence on the final solution properties. Cryo-TEM and SAXS experiments are used to determine the morphology of the copolymers in these solutions, while rheological experiments revealed the role of diblock composition, counterion type and concentration, and overall polymer loading on the viscometric properties.

**11:39**
**V24 3 Morphological Origin of Thermomechanical Behavior in Semicrystalline Ethylene/Methacrylic Acid Ionomers** KATSUYUKI WAKABAYASHI, RICHARD A. REGISTER, *Department of Chemical Engineering, Princeton University* Two peculiar and intriguing phenomena in ethylene/methacrylic acid (E/MAA) ionomers are an initial sharp increase in stiffness with neutralization and an inverse dependence of Youngs modulus on crystallinity. We have identified how the polyethylene crystallites, amorphous polymer segments, and ionic aggregates combine to produce these unusual effects. At temperatures just below the melting point of the primary crystallites, the ionomers can be satisfactorily described as two-phase composites of crystallites and ionically-crosslinked rubber, but at room temperature, the modulus is much greater. We trace this effect to a synergy between the ionic aggregates and secondary crystallites, which together form percolated rigid pathways through the amorphous phase at room temperature, generating a far higher modulus than one would anticipate from the modest crystallinity and ion content. When the secondary crystallites melt and/or the segments in the regions of restricted mobility surrounding the aggregates devitrify, these paths break down and the simple two-phase composite description is recovered.

**11:51**
**V24 4 Influence of Chain Flexibility on the Self-Assembly of Nanoscale Ionic Aggregates in Ionomers.** NICHOLAS BENETATOS, KAREN WINEY, *Department of Materials Science and Engineering, University of Pennsylvania, Philadelphia, PA 19104* Rigorously establishing the fundamental physics that govern the morphology of ionomers is essential to continuing the development of this versatile class of materials. To explore how chain flexibility impacts the nanoscale self assembly of ionic aggregates, we have investigated the morphology of Cu neutralized poly(styrene-itran-methacrylic acid) (SMAA) and poly(3-methylstyrene-itran-methacrylic acid) (3Me-SMAA) ionomers with small angle X-ray scattering (SAXS) and real space imaging via scanning transmission electron microscopy (STEM). The copolymer 3Me-SMAA is slightly less flexible on local length scales as evidenced by a shift in the position of the ''polymerization'' SAXS peak ($q \sim 6\ nm^{-1}$) to lower q compared to that of SMAA ($q \sim 7\ nm^{-1}$). A commensurate shift toward lower q in the position of the ionomer SAXS peak was observed for Cu-3Me-SMAA. Interpreting these SAXS data with a multi-functional model, including that of Yarusso and Cooper, suggests a homogeneous collection of spherical ionic aggregates with diameters of 1.0 nm and 1.2 nm in Cu-SMAA and Cu-3Me-SMAA, respectively. From STEM imaging, the ionic aggregates in both Cu-SMAA and Cu-3Me-SMAA are indeed spherical with a uniform, dense spatial distribution and average diameters of 1.2 + 0.3 nm and 1.4 + 0.3 nm, respectively, showing slightly larger size as local chain flexibility decreases.

**12:03**
**V24 5 The Effect of Counterions on the Blend Miscibility of Polystyrene with Sulfonated Polystyrene Ionomers** NANCY C. ZHOU, *Department of Chemical and Biomolecular Engineering, University of Pennsylvania* WESLEY R. BURGHARDT, *Department of Chemical and Biological Engineering, Northwestern University* RUSSELL J. COMPOSTO, KAREN I. WINEY, *Department of Materials Science and Engineering, University of Pennsylvania* Our previous study probed the miscibility of polystyrene (PS) and sulfonated polystyrene (P(S-SS$x$)) of differing sulfonation levels ($x$) and found a narrow window of miscibility. Specifically, the PS:P(S-SS$x$) blend system becomes completely immiscible at unexpectedly low sulfonation level, x = 2.7 mol%. Here we extend the study of blend miscibility of PS with P(S-$SS_{0.007}$) to include materials neutralized with sodium, barium and zinc cations. These ionomer blends exhibit an upper critical solution temperature (UCST) behavior with an increase in critical temperature as compared to the blend with unneutralized P(S-$SS_{0.007}$). Forward recoil spectrometry (FRES) results indicate that $Zn^{++}$ and $Ba^{++}$ neutralized ionomers are less miscible than $Na^{+}$ when fully neutralized, while the blend miscibility for $Na^{+}$ and $Zn^{++}$ neutralized ionomers behave similarly when partially neutralized. Rheological studies are underway to compliment the blend miscibility studies. These miscibility information gained from PS/P(S-SS$x$) ionomers blends will serve as a foundation for future ionomer morphology studies.

**12:15**

**V24 6 Viscosity of Aqueous Polyelectrolyte Solutions with Oppositely Charged Surfactant** MATTHEW EGGERT, RALPH COLBY, *Penn State University* The viscosity of polyelectrolyte solutions with oppositely charged surfactants is measured for a series of anionic polyelectrolytes of variable hydrophobicity (alternating copolymers of sodium maleate with hydrocarbon comonomers) in the presence of cationic trimethyl ammonium bromides with various alkyl tail lengths. These results are compared with a simple model that modifies the scaling theory for unentangled semidilute polyelectrolyte solutions to account for the addition of oppositely charged surfactant. The surfactant lowers the viscosity of these solutions through two means. The polyelectrolyte binds to the surface of the surfactant micelle, reducing the effective chain length of the polymer. The binding also causes counterions of the polyelectrolyte and the surfactant to be released into solution, acting as a salt that screens the repulsion between charges of the polyelectrolyte, causing the chains to have smaller size. The fraction of effectively charged monomers (*i.e.*, free counterions) on the polyelectrolyte is measured via an ion-selective electrode, meaning the simple model has no adjustable parameters. Additional electrodes are used to measure the amount of free surfactant in solution in order to estimate the amount of surfactant associated with each polyelectrolyte chain.

**12:27**

**V24 7 Simulations of Volume Phase Transitions in Polyelectrolyte Networks Upon Counterion Exchange** DE-WEI YIN, *Dept of Chemical and Biological Engineering, Univ of Wisconsin-Madison* JUAN J. DE PABLO, *Dept of Chemical and Biological Engineering, Univ of Wisconsin-Madison* Polyelectrolyte networks are known to undergo discontinuous volume phase transitions, the onset of which may be caused by a number of factors. We have shown through molecular dynamics simulations that the interplay between the counterion excluded-volume entropy and the electrostatic energy—factors not explicitly considered in the classical Flory–Tanaka model—appears to have an important role in driving the phase transitions [Yin, Yan, and de Pablo, J. Chem. Phys. 123(17):174909, (2005)]. In our current work, we examine how the exchange of monovalent and divalent counterions induces discontinuous phase transitions in polyelectrolyte networks. It is revealed that divalent counterions condense preferentially over monovalent counterions onto the polyelectrolyte network backbone, thereby screening the charges on the backbone, and thus the different counterion species contribute differently to the osmotic pressure and hence to the free energy of the system. We present our findings as they relate to experiments performed near physiological conditions.

**12:39**

**V24 8 Electrophoretically Assessing Polyelectrolyte Effective Charge** ALEXEY POPOV, DAVID HOAGLAND, *Polymer Science & Engineering, University of Massachusetts, Amherst, MA* Capillary electrophoresis revealed how polyelectrolyte effective charge density varies with backbone charge spacing and solvent dielectric constant. The study focused on ionenes, polyelectrolytes that possess regularly spaced quaternary ammonium groups in the backbone. Complete ionization of functional units and good solvency in water and mixtures of water with methanol or acetonitrile enabled measurements of ionene effective charge density as solvent dielectric constant continuously varied. Ionenes with aliphatic and oxyethylene spacers in the backbone were examined. As expected, effective charge density rose linearly with fixed charge density to a critical value, above which effective charge was nearly constant. Deviating from expectation, the onset of condensation did not occur at a critical fixed charge density predicted by Manning theory. Instead, condensation initiated at the constant critical Bjerrum length. The same onset condition was found for quaternized poly(vinyl pyridine). These results suggest a new type of condensation, one driven by ion-pairing. In support of the ion-pairing hypothesis, the onset of condensation correlates with counterion size.

**12:51**

**V24 9 SAXS Determination of the Correlation Length of Semidilute Polyelectrolyte Solutions** SHICHEN DOU, RALPH H. COLBY, *Materials Science and Engineering, Pennsylvania State University* In semidilute solutions, polyelectrolyte chains have a random walk conformation of correlation blobs. The size of those space filling correlation blobs can be measured using Small Angle X-ray Scattering from the wavevector at which there is a peak. In this study we randomly quaternized monodisperse poly(2-vinyl pyridine) (P2VP) and neutralized to make polyelectrolytes with either chloride or iodide counterions. We study a random copolymer for which 60% of the charges are neutralized, at 25 $^{o}$C in three solvents: (1) Ethylene glycol (EG) is a good solvent for P2VP, with dielectric constant $\varepsilon = 37$ making the Bjerrum length 15 Å and dielectric spectroscopy measures the fraction of monomers bearing an effective charge $f = 0.17$ for $Cl^-$ and $f = 0.07$ for $I^-$ counterions. (2) Water is a poor solvent for P2VP, with $\varepsilon = 78$ making the Bjerrum length 7.1 Å and $f = 0.25$ for $I^-$ counterions. (3) N-methyl formamide (NMF) is a good solvent for P2VP, with $\varepsilon = 182$ making the Bjerrum length 3.1 Å and $f = 0.60$ for $I^-$ counterions (meaning that all counterions are free in NMF). We find that the correlation length of these polyelectrolyte solutions obeys the power law concentration dependence expected by scaling theory, and the correlation length decreases at a given concentration as the solvent is made more polar, because the polyelectrolyte chain has a larger effective charge.

**13:03**

**V24 10 Phase behavior of semidilute polyelectrolyte mixtures of F-actin and DNA** JOHN BUTLER, *Department of Materials Science, Univeristy of Illinois at Urbana Champaign* OLENA V. ZRIBI, *Department of Physics, University of Illinois at Urbana Champaign* GERARD C. L. WONG, *Department of Materials Science and Engineering, Department of Physics, Department of Bioengineering, University of Illinois at Urbana Champaign* RAMIN GOLASTANIAN, *Isaac Newton Institute for Mathematical Sciences, Cambridge, UK, Institute for Advanced Studies in Basic Sciences, Zanjan, Iran* We investigate the phase behavior of semidilute mixtures of polyelectrolyte DNA coils and F-actin rods. F-actin has a persistence length of $\sim$ 10 microns and a linear charge density of $-$1e/0.25nm. DNA has a persistence length of $\sim$ 50nm and a linear charge density of –1e/0.17nm. Confocal and polarized microscopy data show that actin-DNA phase separates into ribbon-like birefringent domains of nematic F-actin and a disordered mesh of DNA coils. Synchrotron Small Angle X-ray Scattering (SAXS) show that DNA compresses F-actin into an ultradense dense nematic phase. The spacing between nematic F-actin domains shows a power-law dependence on DNA concentration which is independent of the contour lenth of either DNA or F-actin.

**13:15**
**V24 11 Counterion correlations in charged macromolecular systems** ARBEN JUSUFI, YU MEI, MATTHIAS BALLAUFF, *Physical Chemistry I, University of Bayreuth, 95440 Bayreuth, Germany* We perfomed Molecular Dynamics simulations of a charged macroion surrounded by counterions. Various scattering contributions result from correlations between counterions, macroion, and between both of them. Experimentally, these scattering contributions can be measured by anomalous small-angle X-ray scattering (ASAXS) experiments. As a result the cross-correlation between the rigid macroion and counterions yields always a meanfield expression for the counterion density distribution even if the counterions exhibit correlated fluctuations. In contrast, in star-like polyelectrolytes, representing a fluctuating macroion, meanfield approximations are valid only if the functionality is sufficiently high. A systematic investigation of the strength of correlated fluctuations and their effect in scattering intensities is demonstrated for these systems. Furthermore, we demonstrate a collapse transition for spherical polyelectroylte brushes (SPB) by adding trivalent counterions. The collapse of the SPB is observed by simulations and experiments.

**13:27**
**V24 12 Chiral Symmetry Breaking and Elastic Response of Frustrated Polyelectrolyte Bundles** GREGORY GRASON, *Department of Physics and Astronomy, University of California, Los Angeles* ROBIJN BRUINSMA, *Department of Physics and Astronomy, University of California, Los Angeles* We present a model for hexagonal aggregates of charged, cylindrical macromolecules (DNA, microtubules, F-actin, *etc.*) in the presence of multivalent counterions at low temperature. Using the Wigner crystal picture of the neutralizing charge condensed onto the rod-like macromolecules, we establish a one-to-one mapping between the statistical mechanics of the charged bundle system and those governing the $T = 0$ properties of a two-dimensional, frustrated Josephson junction array. We find that the superconducting phase of the *quantum* system corresponds to the low-temperature phase of our *classical* bundle system, where the condensed counterions are ordered in three dimensions, while the insulating phase corresponds to the phase where one-dimensional phonon fluctuations destroy long-range order of the condensed charge. Remarkably, the mapping makes the prediction that the transition to the charge-ordered state should be accompanied by a spontaneous breaking of chiral symmetry (even in the absence of any molecular chirality). Finally, we exploit the well-studied critical properties of the electromagnetic response of the two-dimensional *quantum* system to deduce the elastic response of the *classical* charged-rod bundle system.

**13:39**
**V24 13 Studies of Glassy Dynamics in Ionomer melts** MONOJOY GOSWAMI, SANAT KUMAR, *Rensselaer Polytechnic Institute* ANIKET BHATTACHARYA, *University of Central Florida* In this work we investigate one of the challenging problems, the dynamics of ionomer aggregates using Molecular Dynamics simulations. Experimental results show that the glass transition temperature ($T_g$), diffusion and relaxation mechanisms can be influenced dramatically by ion-incorporation or by changing temperature of the system e.g., increase in ion content raises the $T_g$. In this work we show the dynamical behavior of ionomer melts as it goes from liquid to glass/gel state. In the context of ionomers, we investigated the analogy between reversible gelation and the glass transition, and show that many of the beneficial properties of ionomers and difficulties in understanding them can be understood in this framework.

## SESSION V25: POLYMER COMPOSITES - NANOTUBES AND NANOCLAYS
**Thursday Morning, 16 March 2006; 322, Baltimore Convention Center at 11:15**
**Rick Beyer, Army Research Laboratory, presiding**

***Invited Papers***

**11:15**
**V25 1 Synthetic Gecko Foot-hairs from Multiwalled Carbon Nanotubes.***
ALI DHINOJWALA, *The University of Akron*

The mechanism that allows a gecko lizard to climb any vertical surface and hang from a ceiling with one toe has attracted considerable interest and awe for over two millennia. Recent studies have discovered that the gecko's ability to defy gravity comes from its remarkable feet and toes. Each five-toed foot is covered with microscopic elastic hairs called setae. The ends of these hairs split into spatulas which come in contact with the surface and induce enough intermolecular [van der Waals (VdW)] forces to hold them in place. Similarly, the same VdW forces act between our two hands when they are held together, but in this case, they do not stick to each other. The reason is that the roughness of our hands prevents them from coming close to each other at separations relevant for VdW forces. On the other hand, based on the gecko's foot anatomy, if our hands were made up of tiny elastic structures that were able to deform or bend at different length scales in accordance with the contact surface and correct for the roughness, then perhaps our hands could also adhere to the surfaces we touch. In my talk, I will present the recent advances we have made in fabricating polymer surfaces with multiwalled carbon nanotube hairs with strong nanometer-level adhesion forces that are 200 times higher than those observed for Gecko foot-hairs. This fabrication process allows the flexibility to create structures that are found in nature on the Gecko's foot and offer excellent potential for applications as dry adhesives for space, microelectronics and MEMS devices. This work was done in collaboration with Betul Yurdumakan, Nachiket Raravikar and Pulickel Ajayan.

*Financial Support from NSF-DMR 0512156.

*Contributed Papers*

**11:51**

**V25 2 Flow Kills Conductivity of Single Wall Carbon Nanotubes (SWNT) Composites** SANJIV BHATT, *Entegris Inc., Chaska, MN* CHRISTOPHER MACOSKO, *Department of Chemical Engineering and Materials Science, University of Minnesota* Most composites of polymer and single wall carbon nanotubes (SWNT) reported in the literature are made by solvent casting or simple compression molding. Commercial utility of these composites requires use of precision injection molding. We have observed a unique behavior wherein the SWNT composites made by injection molding or by extrusion are insulators but upon heating become electrically conductive. This behavior appears to be the result of a relaxation phenomenon in the SWNT composite. During flow into an injection mold or through an extrusion die the well-dispersed SWNT in the polymer matrix tend to align such that they are not in contact with each other and are farther than the minimum required distance, 5 nm (1), to achieve electrical percolation through electron hopping. Upon heating the SWNT relax and either touch each other or are at a distance less than or equal to 5 nm from each other to create a percolating. [1] Du, F., Scogna, R, C., Zhou, W., Brand, Stijn, Fischer, J. E., and Winey, K. I., Macromolecules 2004, 37, 9048-9055.

**12:03**

**V25 3 Fabrication and Characterization of Polyamide Nanocomposites Using Functionalized Nanotubes.** KAREN I. WINEY, M. MONIRUZZAMAN, *University of Pennsylvania* J. CHATTOPADHYAY, W.E. BILLUPS, *Rice University* We have prepared nylon 6,10 nanocomposites with functionalized single wall nanotubes (fSWNT) using an interfacial polycondensation method previously developed in our lab. The specific functional groups (CH2)nCOCl on the sidewall of the nanotubes were designed to permit covalent bonding to the nylon matrix while fabricating the nanocomposite. Using a binary mixture of dichlorobenzene/water solvent system, we have been able to prepare nylon 6,10 and nylon 6,10 / fSWNT nanocomposites with a yield of 80%. The composites were characterized using FTIR and Raman spectroscopies, optical and scanning electron microscopies, differential scanning calorimetry, and thermogravimetric analysis. The composites show good dispersion of nanotubes at the micron and submicron levels. Improved protocols have been developed to reduce the degradation of the composites at elevated temperatures. The nylon 6,10 / fSWNT nanocomposites were spun into fibers using melt fiber spinning at 240C and the mechanical properties of the fibers were studied as a function of nanotube loading.

**12:15**

**V25 4 Electrical, Mechanical, and Morphological Characterization of Carbon Nanotube filled Polymeric Nanofibers** RUSSELL GORGA[1], LAURA CLARKE[2], SETH McCULLEN[1], SATYAJEET OJHA[1], WESLEY ROBERTS[2], *N.C. State University* This work focuses on the inclusion of conductive nanotubes into polymeric matrices with the end goal of creating conductive nanocomposites. This investigation has been carried out by uniform dispersion of multi-walled carbon nanotubes in aqueous solutions of polyvinyl alcohol (PVA) and polyethylene oxide (PEO), which are inherently nonconductive polymers. To fabricate these structures we are using the electrospinning process encompassing an array of collection methods including parallel bars and a static plate. Carbon nanotubes are known to have excellent electrical conductivity and mechanical properties. This investigation shows that the inclusion of carbon nanotubes increases the electronic conduction in these polymers and enhances the mechanical properties of the composites. Dispersion of these nanotubes is the key factor in this process; gum Arabic and surfactants have been utilized for the dispersion of these nanotubes. Conductivity measurements have been carried out by two point probe method and by performing sensitive current and conductance measurements with a femtoammeter. Further morphological characterization has been performed using scanning electron microscopy (SEM) and transmission electron microscopy (TEM). [1] Department of Textile Engineering, Chemistry, and Science [2] Department of Physics

**12:27**

**V25 5 Thermomechanical Properties of Polystyrene-MWNT Nanocomposites.*** ANUPA GEORGE, SUDEEPTO SEN, YUPING XIE, SCHADLER LINDA, SANAT KUMAR, *Rensselaer Polytechnic Institute* In this work we have studied the thermomechanical properties of polystyrene nanocomposites-MWNTs (Multi-walled carbon nanotubes) concentration. A number of different combinations of the matrix and the filler concentrations are being analyzed to study the effect on glass transition temperature using differential scanning calorimetry and a dynamic mechanical analyzer. FE-SEM (Field Emission Scanning Electron Microscope) is being used to study the dispersion and interaction of nanotubes in the matrix. We show that the thermomechanical properties of these materials are very similar to composites with SWNT, thus suggesting that the tube stiffness may not play an important role in this context.

*NSF-NSEC

**12:39**

**V25 6 Carbon Nanotube Composites from Modified Plant Oils** IAN McANINCH, RICHARD WOOL, *Dept Chemical Engineering, University of Delaware* Carbon nanotubes (CNTs) with their impressive mechanical properties are ideal reinforcement material. Acrylated epoxidized soy oil (AESO) has been previously shown to have favorable interactions with carbon nanotubes. CNTs mixed into AESO, both with and without styrene as a co-monomer, using mechanical shear mixing showed dispersion only on the micron level, resulting in modest mechanical property improvements. Greater improvements were seen, especially in the rubbery modulus, when the resin's viscosity was kept high, either through a reduction of the styrene content, or by curing at a lower temperature. CNTs were also dispersed via sonication in methyl methacrylate. The resulting dispersion was then mixed with AESO. The resulting composites showed better CNT dispersion, with no micron-sized aggregates, as verified using SEM and optical microscopy. The mechanical properties also showed greater improvement.

**12:51**

**V25 7 Carbon Fibers from Chicken Feather Keratin** MELISSA E. MILLER, RICHARD WOOL, *Dept Chemical Engineering, University of Delaware* As the availability of synthetic and fossil-fuel based resources is becoming limited, bio-based materials offer an environmentally friendly alternative. Chicken feathers remain a huge agricultural waste. The feathers are comprised of approximately 97% keratin, but are currently used only to enrich animal feed. However, this usage is becoming a problem with the spread of diseases such as Bovine Spongiform Encephalopathy, commonly called ''Mad Cow Disease.'' The hollow, microcrystalline, oriented keratin feather fibers offer a novel, low cost ap-

proach to producing carbon fibers through controlled pyrolysis. Carbonized feather fibers (CFF) were prepared by first heating to 225 $^{o}$C (below the melting point)in $N_2$ for 26 hours to crosslink and stabilize the fiber structure; then carbonization occurred by increasing the temperature to 450 $^{o}$C for two more hours. The resulting CFF were hollow, stiff and strong and had an affine 80% weight loss, which is near the theoretical value for the C-content of keratin. Initial studies showed that a composite with the CFF and an epoxidized soybean oil (AESO) gave an improved fiber modulus $E_{CFF}$ of order 13.5–66.1 GPa. With continued research, the goals are to increase the stiffness of the feathers to 100 GPa, while increasing the strength in the range of 5-10 GPa.

**13:03**

**V25 8 Enhanced Dispersion in Polymer Nanocomposites by Optimized Hydrogen Bonding** MARK DADMUN, ASIF RASHEED, *University of Tennessee* PHILLIP BRITT, DAVID GEOHEGAN, ILIA IVANOV, *Oak Ridge National Laboratory* HAN GI CHAE, SATISH KUMAR, *Georgia Tech* The dispersion of the minor phase in a multi-component polymer system can readily lead to nonlinear enhancement of material properties. In any multi-component polymer system, including polymer nanocomposites, understanding and control of the dispersion of the nanofiller in the polymer matrix is critical to rationally design and create a ituseful new material. This presentation will discuss the work in our group to optimize the specific interactions between components of polymer nanocomposites. We will discuss results that indicate that the optimization of intermolecular interaction between components provides a controllable mechanism to improve the dispersion of nanoscale fillers in a polymer matrix and that the improved dispersion correlates directly to improved thermal, mechanical, and electrical properties.

**13:15**

**V25 9 Supercritical $CO_2$ Processing: A Novel Method for Producing Highly Dispersed Clay-Polymer Nanocomposites** STEVEN HORSCH, ESIN GULARI, RANGARAMANUJAM KANNAN, *Wayne State University* The key challenges in producing high performance nanocomposites are separation of the layered filler into individual platelets, preservation of large aspect ratios and promotion of polymer-filler interactions. By exploiting the ability of $scCO_2$ to diffuse into the layered filler and solvate/swell polymers we have been able to disperse the nanoclay and facilitate polymer-clay interactions even with $Na^+$ montmorillonite. Nanocomposites are prepared by processing the pristine nanoclay and compounding it with an appropriate polymer or processing clay/polymer simultaneously. SEM and WAXD results show significant clay layer separation and preservation of platelet aspect ratios. A high degree of dispersion is also observed in TEM images of these nanocomposites. The facilitation of polymer-clay interactions during the $scCO_2$ process results in higher glass transition temperatures and improved dynamic moduli for these systems. For example, a 5wt% 93A/PS nanocomposite has a 10 degree increase in $T_g$ and G' becomes nearly independent of frequency at low shear rates where it demonstrates an order of magnitude increase.

**13:27**

**V25 10 Evidence of re-entrant behavior in polymer-nanoclay systems** HOSEEIN BAGHDADI, SURITA BHATIA, *University of Massachusetts Amherst* Polymer-clay systems are of interest in a variety of applications, including nanocomposites, personal care products, and oil field products. Rheology and dynamic light scattering capture re-entrant behavior of laponite-polymer systems. Neat laponite at basic pH and concentrations of 2 weight percent or greater forms a viscoelastic isotropic solid due to electrostatic repulsions. This phase appears to be a colloidal glass of laponite particles. We show that that addition of low molecular weight poly(ethylene oxide) (PEO) melts the glass due to a depletion force. The depletion force speeds up dynamics in the system resulting in a low viscosity solution. A re-entrant viscoelastic solid is formed with the addition of high molecular weight PEO due to the polymer chains bridging between laponite particles. In addition we present non-linear rheological behavior below and above the transition. As expected the transition from a low to high viscosity solution scales with size of the polymer mean square end-to-end distance and gap between laponite particles.

**13:39**

**V25 11 Organoclay Networking in Polypropylene-Clay Nanocomposites** JAMES OBERHAUSER, MARK TREECE, *University of Virginia* We report on networking of organoclays and its influence on the rheology of polypropylene-clay nanocomposites. Samples are blended using either a twin screw extruder (TSE) or a single screw extruder with itin situ addition of supercritical $CO_2$ ($SCCO_2$). Blends contain proportional amounts (3:1) of maleic anhydride functionalized PP and organically modified montmorillonite (Cloisite® 15A, Southern Clay Products) at several clay loadings in a base PP resin (MFI 12 g/10 min at 230°C). Small-amplitude oscillatory shear (SAOS) and steady shear flow were utilized to probe clay morphology with varying annealing time. In SAOS experiments repeated over several hours, the terminal behavior of the TSE samples became increasingly solid-like; in steady shear, the magnitude of the viscosity overshoot increased with annealing time. The single-screw/$SCCO_2$ materials at the same clay loadings differed little rheologically from the neat resin. Finally, network formation kinetics accelerated with increasing temperature, and sufficiently large deformations irreversibly weakened the network structure.

**13:51**

**V25 12 Morphology and Gas Barrier of Polystyrene-Clay Nanocomposites** SERGEI NAZARENKO, *School of Polymers and High Performance Materials, University of Southern Mississippi* SYED QUTUBUDDIN, *Department of Chemical Engineering, Case Western Reserve University* Gas barrier of polymer clay nano-composites are often found to be substantially smaller than expected, especially in the case of exfoliated polymer clay nanocomposites where the improvement of gas barrier should be especially noticeable. This fact remains a subject of great controversy and calls for fundamental understanding. Model intercalated and exfoliated polystyrene/montmorillonite (MMT) systems were prepared by in-situ polymerization method, and their oxygen barrier was examined as a function of NaMMT content and related to nano-composite morphology studied by TEM. It was shown that apparent exfoliation of mineral layers, as confirmed by WAXS, not necessary was associated with their homogeneous dispersion. Agglomerates containing 3-6 practically parallel exfoliated layers were observed instead, and this morphology was responsible for poor gas barrier. In contrast, intercalated polymer clay nanocomposites exhibited an interesting phenomenon of layer staircase sliding leading to gas barrier properties better than expected. Gas barrier in both cases was successfully modeled by applying the Nielsen model which was modified to take into account layer agglomeration.

**14:03**

**V25 13 Rheology of Supercritical $CO_2$ dispersed Polymer/Clay Nanocomposites** RANGARAMANUJAM KANNAN, STEVEN HORSCH, GANAPATHY SUBRAMANIUM, ESIN GULARI, *Wayne State University* Effective dispersion of the fillers in a polymer matrix has been a key challenge in the field of nanocomposites. Supercritical carbon dioxide ($scCO_2$) appears, PS/clay, The nanocomposites are characterized using WAXD, SEM, TEM, Rheology and DSC. The high degree of dispersion achieved through sc-$CO_2$ appears to result in an order of magnitude increase in the rheological properties of PS, associated with an increase in the $T_g$ of around 13°C, at 10% clay loading. These moduli improvements are significant better than those obtained with conventional, chemically-modified intercalated clay nanocomposites. The degree of enhancement in the properties appears to be strongly dependant on the polymer-clay interactions, and how it is promoted by the supercritical fluid. In the case of PDMS nanocomposites, where the clay-polymer interactions were weak, the modulus increase at low frequencies (for sc-$CO_2$ processed system) was only a factor of 2. In the case of PVME- I30P clay nanocomposites, the modulus increase was substantial even at moderate loadings and dispersions, perhaps to be hydrogen-bonding interactions. The clay and the polymer orientation and interactions in these nanocomposites are also being probed using rheo-optical FTIR spectroscopy.

**SESSION V26: CELLULAR BIOMECHANICS**
**Thursday Morning, 16 March 2006**
**323, Baltimore Convention Center at 11:15**
**Dapne Manoussaki, Vanderbilt University, presiding**

**11:15**

**V26 1 Difference in cellular mechanics of cancer and normal cervical cells as seen with the AFM** IGOR SOKOLOV, SWAMINATHAN IYER, VENKATESH SUBBA-RAO, CRAIG WOODWORTH, *Clarkson University* Oncogenically transformed cells differ from their normal counter parts in many aspects, including organization and the amount of cytoskeleton. Consequently it is natural to expect to see the difference in cellular mechanics. Here we will present the study of such differences by using atomic force microscopy (AFM) in-vitro. So far the present research is the first study of mechanics of cervical cells, and the third comparative study of differences between mechanics of cancer and normal cells down with the help of AFM. Using a micron size silica ball as the AFM probe, we presumably do not overstress the cell surface as it can be in the case of the sharp AFM tip, and consequently, we may use the classical Hertz model. In contrast to the reported previously studies (bladder and fibroblast cells), we found that oncogenically transformed cervical cells are more rigid than the normal cells. The reason for such difference will be discussed. To demonstrate the complexity of the problem, we study cell mechanics in detail. The Young's modulus of rigidity clearly shows two separate regions of rigidity depending on the depth of the probe penetration. There may be two alternative explanations of the difference in rigidity of this top layer: it is either the cell membrane layer or detected long-range (presumably steric) forces due to the molecular ''brush'' of glycocalyx molecules. Experiments and modal calculations will be presented to choose between these two possibilities.

**11:27**

**V26 2 The Penetration of Titanium Dioxide Nanoparticles: From Dermal Fibroblasts to Skin Tissue** LAUREN SIPZNER, JAIMIE STETTIN, *Yeshivah University High School* ZHI PAN, XIAOHUA FANG, WILSON LEE, *Materials Sci. & Engr. Dept, SUNY at Stony Brook* NADINE PERNODET, MIRIAM RAFAILOVICH, *Program in Chemical and Molecular Engineering, SUNY at Stony Brook* $TiO_2$ particles are widely used in industry; however concerns are arising about their penetration into cells and tissue. In this study, we cultured dermal fibroblasts together with different commercial formulations of $TiO_2$ nanoparticles and observed the morphology,traction forces, proliferation, and migration of the cells as a function of nanoparticles dispersion and concentration. The location of the particles within the cell was studied with TEM. We found significant penetration after 30 minutes. In all cases damage to cell structure and function was observed. Actin fibril formation was disturbed, proliferation was severely hindered, and cell motility was impaired. The effects were more pronounced in fibroblasts from older subjects. These effects were attributed to both dimensionality, as well as UV photocatalysis of the particles. The implications for tissues will be discussed. This work is supported by NSF-MRSEC program.

**11:39**

**V26 3 Curvature-induced microphase separation and lipid polar localization in cell membranes - II*** KERWYN HUANG, *Princeton University* RANJAN MUKHOPADHYAY, *Clark University* NED WINGREEN, *Princeton University* In part II of this talk, we discuss how domain sizes in microphase-separated membranes are determined by the physical properties of lipids such as intrinsic curvature in our minimal model for membrane energetics. We then make contact between our model and experiments on the localization of the bacterial phospholipid cardiolipin. We demonstrate that the slight difference in curvature between the poles and midcell region of a micron-sized bacterium is enough to stably localize cardiolipin clusters to the poles, suggesting that cardiolipin clusters could be a target for polarly-localized proteins. We also show that the cardiolipin domain sizes are not sensitive to changes in the membrane composition. Finally, we propose experiments to test our model using inducible expression of cardiolipin in the bacterium *Bacillus subtilis*.

*This work is supported in part by NIH grant number 1K25 GM075000.

**11:51**

**V26 4 Curvature-induced microphase separation and lipid polar localization in cell membranes - I** RANJAN MUKHOPADHYAY, *Clark University* KERWYN HUANG, NED WINGREEN, *Princeton University* Recent research has revealed the prevalence of lipid domains and heterogeneities in biological cell membranes: examples include lipid rafts found in the outer leaflet of eukaryotic plasma membranes and polar localization of the phospholipid, cardiolipin, in bacteria. One of the mysteries has been why domains obsereved in biological cell membranes, such as lipid rafts which are believed to be 10-100 nanometers in size, appear to be much smaller than micron-sized domains observed in model multicomponent lipid vesicles. In this talk we will develop

a minimal model for membrane energetics that accounts for the coupling of the bilayer to an elastic substrate such as the actin cortex or cell wall, and will demonstrate how this coupling can lead to microphase separation and formation of stable lipid domains.

**12:03**

**V26 5 Using Optical Tweezers to Study Cell Mechanics during Airway Reopening*** HUSEYIN YALCIN, *Mechanical Eng., Lehigh University* JING WANG, *Physics Dept., Lehigh University* SAMIR GHADIALI, *Mechanical Eng., Lehigh University* H. DANIEL OU-YANG, *Physics Dept., Lehigh University* Patients suffering from the acute respiratory distress syndrome (ARDS) must be mechanically ventilated in order to survive. However, these ventilation protocols may generate injurious hydrodynamic stresses especially during low tidal volume (VT) ventilation when the flow of micron-sized air bubbles displace the surrounding liquid. In-vitro studies in our lab revealed that microbubble flows can severally damage lung epithelial cells (EC). The degree of injury was elevated for sub-confluent monolayers in small channel heights. Under these conditions, the micromechanics of individual EC may influence the degree of cellular injury. To investigate the role of cell mechanics, we used an oscillating Optical Tweezers (OT) technique to measure the intrinsic mechanical properties of EC before and after the flow of microbubbles. Knowledge of how the EC's micromechanical properties influence cell viability may lead to the development of novel treatment therapies that enhance the EC's ability to withstand injurious hydrodynamic stresses during ventilation treatment.

*Supported by the Parker B. Francis Foundation and the NSF.

**12:15**

**V26 6 Probing subcellular force transduction with magnetic soft actuator arrays*** ALEXANDRE ANGUELOUCH, STUART KIRSCHNER, DANIEL REICH, *Johns Hopkins University* NATHAN SNIADECKI, CHRISTOPHER CHEN, *University of Pennsylvania* Microfabricated poly(dimethylsulfoxide) PDMS post arrays provide a method for mapping the distribution of contractile forces produced by adherent cells grown on the tips of the posts through optical tracking of the posts deflections (1). We describe a new technique whereby large local mechanical stimuli can be applied to such cells via magnetic torques applied to anisotropic magnetic nanowires embedded in selected posts. These magnetic post arrays thus serve both as actuators and detectors of cellular contractile response. Experiments characterizing the performance of these post arrays will be presented along with results on global changes in cell contractility induced by magnetic forces applied to a single post under a cell. (1) J. Tan *et al.* PNAS **100**, 1484 (2003).

*Work supported by the David and Lucile Packard Foundation Grant #2001-17715

**12:27**

**V26 7 Establishing threshold toxicity for introducing magnetic nanoparticles into HeLa and HEK 293 cells*** KEZHENG CHEN, WEILI LUO, *Department of Physics, University of Central Florida* PAPPACHAN KOLATTUKUTY, *Bernard College of Biomedical Sciences, University of Central Florida* UNIVERSITY OF CENTRAL FLORIDA TEAM, Although iron oxide nanoparticles have been suggested as candidate in diverse applications such as drug delivery agents, contrast agents of magnetic resonance imaging, cancer treatment through hyperthermia, etc., the upper limit for safe dosage beyond which the toxicity sets in has never been studied. In this work we report quantitative studies on the percentage change in the number of cell as a function of concentration of magnetic nanoparticles. The incubation is at 37°C and lasted for 24 hours. We found that there is a critical value of particle volume fraction, above which appreciable number of cell death occurs. This critical value was found to differ in two different cell lines indicating that HEK cells are more robust against the magnetic nanoparticles.

*This work is partially supported by NSF NIRT 0103587.

**12:39**

**V26 8 Modeling cell – extracellular matrix mechanical interactions during in vitro network formation** DAPHNE MANOUSSAKI, *Vanderbilt University* During the formation of vascular networks in vitro, endothelial cells exert traction forces onto the extracellular matrix (ECM), changing both the density and the orientation distribution of ECM fibers. ECM strain, in turn, affects cell migration. We study the effect of mechanical cell-ECM interactions on cell migration and cell distribution assuming a continuum description for the cells and the ECM. The theory assumes that the ECM is a viscoelastic material which deforms under cellular traction, and that resulting ECM strain influences cell movement. Numerical simulations predict that under certain mechanical conditions, cell traction can reorganize the cells and associated ECM into a network that compares well with the vascular networks that arise in vitro. I discuss the potential role of cell mechanical forces and ECM mechanical behavior on cell migration, and compare results with in vitro studies.

**12:51**

**V26 9 Axon growth and dynamics in 3D collagen gels*** RYAN MCALLISTER, WILL ROSOFF, JEFFREY URBACH, *Georgetown University* Living cells exhibit importantly different morphology and behavior in 3D hydrogels than on 2D substrates, but there have been very few studies of the dynamics of axons growing in 3D environments. To compare shape and outgrowth behavior of neuronal cells in 2- and 3D, we have developed a live-cell imaging apparatus using a spinning-disk confocal microscope. We compare growth cone cytoskeletal dynamics in fluorescently transfected neuronal cell-lines growing on a coated glass coverslip with those growing in a collagen matrix. We will describe some of the experimental challenges and our results (movies) to date.

*Work done in collaboration with Herb Geller's lab at NIH and Josef Kas' lab at U. Leipzig.

**13:03**

**V26 10 Investigating the glycocalyx using atomic force microscopy** REBECCA BOREN, ADAM RAFI, JESSICA FARRELL, ANTONIO PERAMO, W. GARRETT MATTHEWS, *Dept. of Physics, University of South Florida* The extracellular surfaces of the peripheral vascular system are coated with an outer filamentous layer of proteoglycan (PG) molecules, forming a brush-like structure known as the glycocalyx. The mechanical properties of PGs have become of increased interest due to their roles in a variety of interactions, including the adhesion of metastatic cells and their use as flow sensors. The goal of this project is to investigate the mechanical properties of the glycocalyx as a function of differing environmental conditions (i.e. pH, various ion concentrations, etc). We use as an experimental model of the glycocalyx an end-tethered brush of PGs oriented so that the protein backbone is upright, emulating their itin vivo formation. We have developed

a technique for patterning PG onto substrates allowing the exposure of the PG layer to different biologically relevant solvents. Resulting brush height changes will be measured using atomic force microscopy. The compression and extension of these PG molecules also will be measured and used to explain the imaged structures and the behaviors relevant to their biological function.

**13:15**
**V26 11 Local structure in diatom biosilica probed by synchrotron x-ray diffraction** MICHAEL DIBICCARI, *Hauppauge High School* SEO-YOUNG KWAK, *Brookhaven National Laboratory* GEOFFREY HIND, *Brookhaven National Laboratory* ELAINE DIMASI, *Brookhaven National Laboratory* Diatoms are single-celled algae that form intricate outer shells, or frustrules, composed of biosilica. They have attracted attention in the context of nanotechnology, since the submicron architectures are genetically determined and thus potentially could be reproduced synthetically, by using organic additives that mimic the proteins responsible for controlling biological silicification. We have compared the local atomic structure of diatom biosilica to that of inorganic silica with synchrotron x-ray diffraction, analyzed as the Pair Distribution Function (PDF). Specimens of Thalassiosira weissflogii (Tw) were cleaned of organic matter using either hydrogen peroxide, commercial bleach, or sodium dodecyl sulfate treatments. Low resolution PDF measurements ($q_{\max} \approx 13.6$ Å$^{-1}$) were made of wet and dry Tw, pure silica microspheres, and diatomaceous earth containing 15% mineral impurities. All samples have similar PDFs, demonstrating that local structure in diatoms and synthetic silica are equivalent, and that the PDF method is insensitive to biological impurites.

**13:27**
**V26 12 Bundle Buckling and Nesting Model of Striated Pattern Formation in Microtubule Solutions*** YONGXING GUO, YIFENG LIU, JAMES VALLES, JAY TANG, *Department of Physics, Brown University* Microtubules that are aligned by magnetic field or flow during the initial stages of polymerization form bundles in high concentration tubulin solutions. These bundles thicken and elongate with time and buckle in coordination with their neighbors into a wave shape. These nested and buckled bundles produce a macroscopically striped pattern of birefringence. We propose a mechanism for the buckling and present a normal mode stability analysis of a simplified model of it. The results show that the characteristic wavelength and critical buckling force are determined by the properties of the bundles and their neighboring elastic network, which is formed by unaligned and relatively short Microtubules.

*NASA NNA04CC57G

**SESSION V27: COMPUTATIONAL METHODS: MONTE CARLO/MOLECULAR DYNAMICS II**
**Thursday Morning, 16 March 2006**
**324, Baltimore Convention Center at 11:15**
**Lee Collins, Los Alamos National Laboratory, presiding**

**11:15**
**V27 1 Parallel kinetic Monte Carlo simulations of island-coarsening in two dimensions*** F. SHI, Y. SHIM, J. G. AMAR, *University of Toledo* The evaporation-driven coarsening of 2D islands is studied using a simple bond-counting model along with a recently developed semi-rigorous parallel algorithm for kinetic Monte Carlo (KMC) simulation. Using our parallel algorithm we have been able to simulate both larger system sizes and longer time scales than could be studied using serial KMC simulations. After deposition of less than a half monolayer on a substrate, the flux is stopped and the subsequent time evolution of the average island size and island size distributions were studied for different initial coverages. As expected, the average island size grows as $t^{1/2}$ at intermediate time and approaches the asymptotic $t^{2/3}$ behavior at very late time. Scaled island-size distributions in both regimes are obtained and compared with the predictions of mean-field theory. The efficiency of our parallel KMC simulations is also discussed.

*Supported by NSF DMR-0219328 and CCF-0428826

**11:27**
**V27 2 Energy optimization of quantum Monte Carlo wave functions*** C.J. UMRIGAR, J. TOULOUSE, *Cornell University* In recent years many methods have been proposed for energy optimizing quantum Monte Carlo wave functions. Of these, the three highly efficient methods are: 1) The generalized eigenvalue method of Nightingale and Melik-Alaverdian, which was proposed by them for linear parameters only but extended by us to nonlinear parameters. 2) The effective fluctuation potential (EFP) method of Fahy, Filippi and coworkers, and the recent perturbative EFP of Schautz, Scemama and Filippi. We show that the latter can be more simply derived as first-order perturbation theory in a nonorthogonal basis. 3) The modified Newton method of Umrigar and Filippi and of Sorella. We show that the three methods are related to each other and point out that a control parameter can be employed in each of them to make them totally stable. We use these methods to optimize all the parameters in the Jastrow and the determinantal parts of the wave function and point out that different issues arise in optimizing the Jastrow and the determinantal parameters. By systematically increasing the number of determinants we find that seemingly similar systems, such as $C_2$ and $Si_2$ have vastly different fixed-node errors for single-determinant wave functions.

*We thank Claudia Filippi, John Lawson, Peter Nightingale and Andreas Savin for valuable discussions. Supported by NSF.

**11:39**
**V27 3 Monte Carlo Modeling of Luminescent Solar Concentrators** ALEX MOONEY, PAUL FONTECCHIO, BRUCE WITTMERSHAUS, *School of Science, Pennsylvania State University: Erie, The Behrend College* Luminescent Solar Concentrators (LSCs) offer an inexpensive alternative for solar power generation. A LSC is a flat, translucent plate that absorbs sunlight through embedded, highly fluorescent molecules. The emitted light is concentrated via total internal reflection at the edges of the LSC, where photovoltaic cells covert it into electricity. We've developed a Monte Carlo model that predicts the properties of LSCs by tracing individual light rays. The user controls the plate's geometry and spectral properties, along with the spectral profile of the excitation source. The user can include a specular or diffuse reflective background under the LSC. We've demonstrated the ability to predict the output of a LSC as a function of its optical density. Reabsorption distorts the profile of fluorescence as light propagates through a LSC, and the program can accurately reproduce the effect. The goal is to use the model as a predictive tool for improving the design of LSCs.

**11:51**

**V27 4 Efficiency of rejection free Monte Carlo methods** HIROSHI WATANABE, *Department of Complex, Systems Science, Graduate School of Information Science, Nagoya University* YUKAWA SATOSHI, *Department of Applied Physics, School of Engineering, The University of Tokyo* MARK A. NOVOTNY, *Department of Physics & Astronomy, ERC Center for Computational Sciences, Mississippi State University* NOBUYASU ITO, *Department of Applied Physics, School of Engineering, The University of Tokyo* We construct asymptotic arguments for the waiting time, the number of trials to achieve one update in Monte Carlo (MC) methods. We find that the waiting time is proportional to $e^{\beta}$ in the Ising, $\sqrt{\beta}$ in the classical XY, and $\beta$ in the classical Heisenberg spin systems with inverse temperature $\beta$, regardless of the dimension. The behavior in hard particle systems is also obtained, and found to be proportional to $(\rho c - \rho)^{-d}$ with the closest packing density $\rho c$, density $\rho$, and dimension $d$ of the systems. The waiting time determines the efficiency of rejection-free Monte Carlo (RFMC) methods, as well as the inefficiency of the standard MC. Our arguments are general, and applicable to any RFMC implementation of any model studied using kinetic Monte Carlo.

**12:03**

**V27 5 Improved sampling of computationally expensive potentials** MARK DEWING, We wish to evaluate statistical properties of systems using potentials that are accurate but computationally expensive, such as those obtained from Density Functional Theory or Quantum Monte Carlo. Using a cheap, approximate potential that is sufficiently close to the potential of interest, sample points can be generated that allow efficient evaluation of properties of the accurate potential.

**12:15**

**V27 6 Optimally efficient coarse-grained Monte Carlo simulation of rare transition events** BABAK SADIGH, TOMAS OPPELSTRUP, *Lawrence Livermore National Laboratory* WEI CAI, *Dept of Mechanical Engineering, Stanford University* MAURICE DE KONING, MALVIN KALOS, VASILY BUOLATOV, *Lawrence Livermore National Laboratory* We use the idea of coarse graining the multidimensional free energy landscape and present a new Monte Carlo scheme that allows for the exact calculation of the rate of rare transition events within the coarse-grained space defined by a few collective coordinates. This approach is based on a variational algorithm for determining an optimal importance function by which the absolute probability of sampling successful transition events is significantly enhanced, while the relative probabilities of any pair of successful events are preserved.

**12:27**

**V27 7 Optimized parallel tempering simulations of proteins** SIMON TREBST, *Microsoft, Project Q, and Kavli Institute for Theoretical Physics, Santa Barbara, CA 93106* MATTHIAS TROYER, *Theoretische Physik, ETH Zurich, CH-8093 Zurich, Switzerland* ULRICH HANSMANN, *John-von-Neumann Institute for Computing, Forschungszentrum Julich, D-52425 Julich, Germany* We introduce an adaptive algorithm that systematically improves the efficiency of parallel tempering or replica exchange methods in the numerical simulation of small proteins. Feedback iterations allow us to identify an optimal set of temperatures/replicas which are found to concentrate at the bottlenecks of the simulations. A measure of convergence for the equilibration of the parallel tempering algorithm is discussed. We test our algorithm by simulating the 36-residue villin headpiece sub-domain HP-36 where we find a lowest-energy configuration with a root-mean-square-deviation of less than 4 Å to the experimentally determined structure.

**12:39**

**V27 8 Hybrid DFT/Thomas-Fermi simulations and applications to biological systems** MIROSLAV HODAK, *North Carolina State University, Raleigh* WENCHANG LU, JERRY BERNHOLC, We have developped a hybrid simulation method suitable for performing calculations on biological systems. Within this method, Density Functional Theory (DFT) is used for the chemically active region and some solvent molecules, while the rest of the solvent molecules are treated with a variant of Thomas-Fermi (TF) theory, which uses the generalized gradient approximation (GGA) kinetic energy functional. These TF solvent molecules are assumed to be rigid and have frozen electron densities, which allows for their efficient treatment. Both Kleinman-Bylander and ultrasoft types of pseudopotentials are implemented within our method. We find it efficient to first equilibriate bio-molecules in solvent environment using classical molecular dynamics. After the initial equilibriation we use the hybrid method to study chemical reactions involving the bio-molecule. Initial applications to transition metal ions-protein complexes in solution will be discussed.

**12:51**

**V27 9 Environment Dependent Dynamic Charge Interatomic Potential for Silica** LEX KEMPER, KRISHNA MURALIDHARAN, YINGXIA WAN, HAI-PING CHENG, *University of Florida* We present a new interatomic potential to model the various silica polymorphs. Our formulation is loosely based on the embedded atom method (EAM), and accounts for explicit charge variations of atoms as a function of the local chemical environment of atoms. The parameters for the potential are derived from density functional (DFT) calculations. Some preliminary results will be discussed. Work supported by NSF ITR award DMR-0325553.

**13:03**

**V27 10 Universal Dynamic Exponent at the Liquid-Gas Transition from Molecular Dynamics** SUBHRANIL DE, AN CHEN, ELDRED CHIMOWITZ, YONATHAN SHAPIR, The liquid-gas system is expected to exhibit distinct dynamic behavior in the fluid's critical region (Model H). In this work we present molecular dynamics simulations of a Lennard-Jones fluid model starting from specially designed, near-equilibrium, initial conditions. By following the fluid's relaxation towards equilibrium, we calculate the requisite transport coefficients in the fluid's critical region. The results yield the scaling behavior of the thermal diffusion coefficient $D_T \sim \xi^{-1.023 \pm 0.018}$ ($\xi$ is the correlation length) and a non-conventional divergent heat conductivity, all of which are in accord with mode-coupling and renormalization group predictions, as well as some experimental data.

**13:15**

**V27 11 Global and local properties used as analyses tools for molecular-dynamics simulations*** MARTINA E. BACHLECHNER, *West Virginia University, Physics Department* JONAS T. ANDERSON,[†] DENG CAO, ROBERT H. LEONARD, ELI T. OWENS, JARROD E. SCHIFFBAUER, *West Virginia University, Physics Department* MELISSA R. BURKY,[‡] *Chemistry Department, Davis & Elkins College, Elkins, West Virginia 26241* SAMUEL C. DUCATMAN, ERIC J. GUFFEY,[§] *University High School, Morgantown, West Virginia 26505* FERNANDO SERRANO RAMOS, *Department of Computer Science, Metropolitan University, San Juan, Puerto Rico 00928* Molecular dynamics simulations have been used to study mechanical failure in realistic interface materials. Averaging over the individual atoms' contributions yields local and global information including displacements, bond angles, strains, stress tensor components, and pair distribution functions. A combined analysis of global and local properties facilitates detailed insight in the mechanisms of failure, which will eventually guide on how to prevent failure of interfaces.

*Supported in parts by NASA.
[†]NSF (Virtual Environments REU at WVU)
[‡]Undergraduate Research Experience (SURE) Program funded by WV EPSCoR
[§]NASA Independent Verification and Validation Facility Science and Engineering Apprenticeship Program

**13:27**

**V27 12 Molecular Dynamics Simulations of Nanoscratching of 3C-SiC*** ALICE NOREYAN, J.G. AMAR, *University of Toledo* We have carried out molecular dynamics simulations of nanoindentation followed by nanoscratching on the Si terminated (001) surface of 3C-SiC. In particular, we have investigated the dependence of the friction coefficient, scratch hardness and wear on indentation-scratching depth, scratching velocity, scratching direction, indenter size and indenter shape. In general, the scratch hardness decreases with increasing scratching speed, while it increases with increasing indentation depth. In addition, the scratch hardness and the nanoscale chip formation mechanisms depend on the scratching direction. We also find that scratching leads to amorphization of the material along the scratching trajectory. The size of the amorphization region increases with an increase in scratching velocity, which causes the decrease in scratch hardness and friction coefficient for higher scratching velocities.

*Supported by NSF DMR-0219328 and CCF-0428826

**13:39**

**V27 13 Charge density wave and phonon softening in the Holstein model: A Quantum Monte Carlo study** PRABUDDHA CHAKRABORTY, *University of California, Davis* ALEXANDRU MACRIDIN, *University of Cincinnati* RICHARD SCALETTAR, *University of California, Davis* WARREN PICKETT, *University of California, Davis* RAJIV SINGH, *University of California, Davis* We present a Quantum Monte Carlo study of electron-phonon dynamics in the two dimensional Holstein model on a square lattice. We concentrate here on the softening of the phonon modes as the coupling between the electrons and the phonons is varied. Information about the instability of the electronic system toward the formation of a charge-density wave is also extracted from the phonon correlation functions. We also extract information about the phonon spectral densities using the Maximum Entropy method. Results are presented for various values of the wave-vectors in the two dimensional lattice. An intriguing softening of the phonon frequency at vanishing wave-vector is presented. We also present the effect of anharmonicity on the dynamics of the Holstein model.

## SESSION V28: RHEOLOGY OF BIOPOLYMER SOLUTIONS

**Thursday Morning, 16 March 2006**
**325, Baltimore Convention Center at 11:15**
**Daniel Savin, University of Vermont, presiding**

**11:15**

**V28 1 Massively-parallel fluorescence correlation spectroscopy using a spinning disk confocal microscope** DANIEL R. SISAN, RICH AREVALO, CAT GRAVES, RYAN McALLISTER, JEFFREY S. URBACH, *Dept. of Physics, Georgetown University* We describe an extension of fluorescence correlation spectroscopy (FCS) using a spinning disk confocal microscope. This approach can spatially map diffusion coefficients or flow velocities at up to $\sim 10^5$ independent locations simultaneously. Complex media—e.g., a tumor, cell nucleus, or extracellular matrix—are spatially-heterogeneous, making this spatially-resolved technique an ideal tool to understand hindered diffusion. There have been a number of recent extensions to FCS based on laser scanning microscopy. Spinning disk confocal microscopy, however, can be much faster at high resolution—potentially up to 1000 Hz at full resolution for the fastest available cameras—and without temporal delays between pixels. We show how to correct for a pixel size effect not encountered with standard or scanning FCS, and we introduce a method to correct for photobleaching. Finally, we apply this technique to microspheres diffusing in Type I collagen, which show non-trivial spatially varying diffusion caused by hydrodynamic and steric interactions with the collagen matrix.

**11:27**

**V28 2 Diffractive Imaging of Single Biomolecules** NATHAN SCHMIDT, ROBERT CORIDAN, *University of Illinois, Dept. of Physics* JOHN BUTLER, THOMAS ANGELINI, JIAN-MIN ZUO, GERARD WONG, *University of Illinois, Dept. of Physics, Dept. of Materials Science and Engineering* The resolution of Electron Microscopy (EM) images is limited by instrumentation lens aberration. Moreover, many biomolecules and supramolecular complexes are too soft and too large to be crystallized, and crystalline diffraction provides only aggregate structural properties. Coherent nanobeam electron diffraction in principle allows for diffraction-limited resolution analysis of single biomolecules. Image recovery can be achieved using oversampling and iterative phase retrieval to solve the phase problem. We will discuss the use of coherent electron diffraction and its potential to improve TEM image resolution of biomolecular systems. Preliminary diffraction data obtained from cryogenically prepared biomolecules will be presented.

**11:39**

**V28 3 Mechanical Properties of Actin Networks near the Polymerization Transition*** ANDREW POMERANCE, *University of Maryland* ERIN RERICHA, *University of Maryland* WOLFGANG LOSERT, *University of Maryland* Here we present studies of the mechanical properties of actin networks close to the polymerization transition. In the presence of divalent ions, the critical concentration (CC) for polymerization of actin decreases by two orders of magnitude. By studying concentrated actin samples (3 mg/mL) with and without added ions, we compare the behavior near and far above the CC for a sample with very similar concentrations of filamentous actin. To study the response to large forces we use holographic laser tweezers to pull microspheres through an actin network. We found that in samples far above the CC the microspheres strongly resist pulling, and have a well-defined relaxation time. Near the CC, the microspheres are easily pulled through the actin networks, and the relaxation is far more variable, which indicates that the actin filaments may be more dynamic and breakable.

*Work supported by NIH grant R21-EB-00328501.

**11:51**

**V28 4 Rheological Investigation of Protein Interactions in Synovial Fluid** REBECCA KLOSSNER, *North Carolina State University* WENDY KRAUSE, *North Carolina State University* RALPH COLBY, *Pennsylvania State University* Hyaluronic acid and the plasma proteins, albumin and $\gamma$-globulins, are the most abundant macromolecules in synovial fluid, the fluid that lubricates our freely moving (synovial) joints. In previous studies, bovine synovial fluid, a synovial fluid model and albumin in phosphate buffered saline (PBS) were observed to be rheopectic—viscosity increases over time under constant shear. Rheopexy is indicative of structure building in solution. To further investigate the contribution of albumin to the observed rheopexy, rheological experiments were conducted on bovine serum albumin (BSA) in PBS at concentrations comparable to those found in the synovial joints. Our data suggests that the plasma proteins aggregate together under these low shear conditions further entangling the hyaluronic acid chains, which results in an increase in the apparent viscosity of the synovial fluid over time. The nature of the proposed aggregation was probed by varying the salt concentration and pH in order to partially denature the protein and interrupt any hydrogen bonding. Additionally, similar rheological experiments were carried out using methylated albumin in order to observe the role of the disulfide bridges in the protein aggregation.

**12:03**

**V28 5 Influence of Anti-inflammatory Drugs on the Rheological Properties of Synovial Fluid and Its Components** WENDY E. KRAUSE, *North Carolina State University* REBECCA R. KLOSSNER, *North Carolina State University* JING LIANG, *North Carolina State University* RALPH H. COLBY, *The Pennsylvania State University* The polyelectrolyte hyaluronic acid (HA, hyaluronan), its interactions with anti-inflammatory drugs and other biopolymers, and its role in synovial fluid are being studied. We are investigating the rheological properties of sodium hyaluronate (NaHA) solutions and an experimental model of synovial fluid (comprised of NaHA, and the plasma proteins albumin and $\gamma$-globulins). Steady shear measurements on bovine synovial fluid, the synovial fluid model, and plasma protein solutions indicate that the fluids are rheopectic (stress increases with time under steady shear). In addition, the influence of anti-inflammatory agents on these solutions is being explored. Initial results indicate that D-penicillamine and hydroxychloroquine (HCQ) affect the rheology of the synovial fluid model and its components. While HCQ has no effect on the viscosity of NaHA solutions, it inhibits/suppresses the observed rheopexy of the synovial fluid model and plasma protein solutions. In contrast, D-penicillamine has a complex, time dependent effect on the viscosity of NaHA solutions,—reducing the zero shear rate viscosity of a 3 mg/mL NaHA (in phosphate buffered saline) by ca. 40% after 44 days. The potential implications of these results will be discussed.

**12:15**

**V28 6 Micromechanics of the pericellular matrix** J. E. CURTIS, H. BOEHM, C. H. J. SCHMITZ, J. P. SPATZ, *University of Heidelberg, Institute of Physical Chemistry and Max Planck Institute for Metals Research, Dept. of New Materials and Biosystems* In recent years, much attention has been directed towards the properties and activities of the cell surface. In particular, the coupling of the membrane to the underlying protein polymer network called the actin cortex plays an important role in many events. The other side of the cell surface is less studied, although it too has a bound polymer network comprised of gigantic cross-linked polysaccharides (sugars). Called the pericellular matrix (PCM), it is associated with many cells including fibroblasts, chondrocytes, endothelial and smooth muscle cells. Its thickness can vary from 10's of nanometers to 10 microns and it is associated with adhesion dependent events like migration and mitosis. Biologists often hypothesize that its viscoelastic properties are responsible for the modulation of cell adhesion activities. To investigate this proposal, we measure the PCM's viscoelasticity using microrheology and probe the sharpness of its edge and its mesh size. The elastic modulus of the PCM under different condition is determined, and we characterize the long, elastic cables that can be pulled from the PCM. These results are compared with an externally reconstituted model PCM on the cell surface.

**12:27**

**V28 7 Microrheology of active actin networks** TRAVIS H. LARSEN, *University of Delaware* ERIC M. FURST, *University of Delaware* To provide insight into the viscoelastic response of non-equilibrium, entangled semi-flexible polymeric networks, we study the model system of F-actin networks in the presence of active fragments of skeletal myosin. To characterize the microrheological response of this system, polystyrene microspheres of $1\mu$m in diameter are suspended into the three-dimensional, entangled F-actin network and diffusing wave spectroscopy is used to measure the mean-squared displacement of the particles on timescales from 100ns to 10ms. Particle motion is a result of both random thermal forces and the dissipation of actin filament fluctuations caused by the interactions of the suspended motor proteins with the network. Upon addition of myosin, we observe an increase in the MSD of the tracer particles and a shift in the scaling–dependence with respect to lag time from $t^{3/4}$ to $t^x$, where $3/4 < x < 1$. This shift indicates that the random, parallel ''tugs'' on the filaments by the motor proteins cause the filaments to develop an apparent decreased persistence length at length scales longer than the crossover length. Finally, we demonstrate that the addition of the cross-linking protein, $\alpha$-actinin, suppresses this ''active'' scaling behavior, while maintaining elevated probe particle diffusivity relative to the control.

**12:39**

**V28 8 Filamin cross-linkers as rheology regulators in biopolymer networks** BRIAN DIDONNA, *University of Minnesota* ALEX LEVINE, *University of California, Los Angeles* We report on the nonlinear mechanical properties of a statistically homogeneous, isotropic semiflexible network cross-linked by polymers containing numerous small unfolding domains. This model captures the main mechanical features of F-actin networks cross-linked by filamin proteins, which contain twenty-four such Ig-domains that may unfold under applied strain. We show that under sufficiently high strain the network spontaneously organizes itself so that an appreciable fraction of the filamin cross-linkers are at the threshold of domain unfolding. We discuss via a simple model the cause of this network organization. We also discuss how observation of this critical state validates a mechanism proposed by Crocker *et al.* to explain the weak power law dependence of the measured strain modulus as observed in intracellular microrheology experiments.

**12:51**

**V28 9 Microrheology of Microtubules ''Networks''** NAAMA GAL, CRAIG MANDATO, MARIA KILFOIL, Microtubules are the largest of the three protein biopolymers comprising the cytoskeleton, the other two being intermediate filaments and filamentous actin. While the mechanical properties of actin networks have been studied extensively, less is known about the mechanical properties of microtubules at high concentrations in the cytosol. Microtubules are involved in many of the cell functions, such as cell division and cargo transport within the cell. We use passive microrheology, extracting a viscoelastic modulus of the network based on the thermal motion of micron sized beads, to measure the elasticity of microtubules under various conditions in vitro. Our results show that the bead motion varies from highly confined to free, indicating the heterogeneous, structure of the network. We study the mechanical properties and the spatial heterogeneity and structure of these microtubule ''networks'' as a function of tubulin monomer concentration, ratio of microtubule associated protein to tubulin monomer concentration, and DMSO or nucleating factor concentration.

**13:03**

**V28 10 Anisotropic dynamic response of stiff biopolymers** OSKAR HALLATSCHEK, *Department of Physics, Harvard* BENEDIKT OBERMAYER, *Institut of Theoretical Physics, University of Leipzig* ERWIN FREY, *Department of Physics und CeNS, Ludwig-Maximilians-University Munich* KLAUS KROY, *Institute of Theoretical Physics, University of Leipzig* We have analyzed the dynamic response of stiff polymers under different force protocols, such as the sudden onset/release of a longitudinal or transverse point forces. In these non-equilibrium situations, an ordinary small gradient expansion fails to describe the Brownian motion of stiff polymers in the limit of short times due to the neglect of tension dynamics. We present an improved (multiple scale) perturbation theory unravelling the underlying nonlinear phenomenon that renders the short time dynamics quite complex. The polymers response exhibits asymptotic power law behaviour with distinct dynamic exponents that depend on the experimental scenario and the time regime.

**13:15**

**V28 11 Biopolymers in Aqueous Medium: Solvent Forces Explored through Atomistic Dynamics Simulations and Continuum Modeling of Solvent Effects** SERGIO A. HASSAN, *CMM/DCB/CIT/NIH/U.S.DHHS* Molecular interactions in solution are modulated by the bulk liquid and by the solvent-induced forces (SIF) originating in the structure of the liquid surrounding the solutes. Because of the difficulty in representing these effects, purely empirical solvation models are commonly used in simulations. Here, a semi-empirical continuum model is presented based on the theory of polar/polarizable liquids, which allows for a derivation of the electrostatic component of the potential. The effects of SIF are still introduced empirically to reproduce interaction energies in amino acids dimers (AAD). The limitations of the model are discussed based on its performance to reproduce structural, dynamic, and thermodynamic properties of peptides and proteins. To reduce the level of empiricism, the molecular origins of the SIF are investigated through dynamics simulations in explicit solvent. The solvent forces on AAD in pure water and NaCl solutions are studied. The reorganization of water and ions due to dimer dissociation is analyzed based on spatial density profiles. The solvent forms a network of high-density peaks consistent with extensive H-bonded water clusters. Long-range structural order develops in the space separating the monomers and contributes to the intermolecular SIF. The ions disrupt this network leading to either a stabilization or destabilization of the dimers. The relevance of these results to quantify SIF in complex solutes en route to a parameter-free continuum model is discussed.

**13:27**

**V28 12 Random energy model for heteropolymer sequence design: the role of solvation** LONGHUA HU, ALEXANDER GROSBERG, *Department of Physics, University of Minnesota* We study the role of surface of the globule and the role of interactions with the solvent for the process of sequence design for heteropolymers. We follow the method developed in recent work (P.Geissler et al, Phys. Rev. E, **70**, 021802, 2004) in which solvation of random sequence heteropolymer was addressed using properly generalized random energy model (REM). By comparing the freezing transition in random and designed sequence heteropolymers, we discuss the effects of design. We discuss phase diagram of the system in the traditional variables of actual temperature versus design temperature. Based on our results we are able to show under which conditions solvation effects improve the quality of sequence design. Finally we discuss sequence space entropy and study how many sequences are available for design at a certain design condition.

**13:39**

**V28 13 Recovery and Stiffening -Transition of Hydrogels Formed Via Peptide Self-Assembly** BULENT OZBAS, KARTHIKAN RAJAGOPAL, JOEL P. SCHNEIDER, DARRIN J. POCHAN, *Materials Sci Eng and Chemistry and Biochemistry, Univ. of Delaware* In this work we present the local nano- and overall network structure, and resultant viscoelastic properties, of hydrogels that are formed via $\beta$-hairpin peptide self-assembly that is triggered either by increasing the solution pH, temperature or ionic strength. These physiological stimuli induce the random-coil to $\beta$ -sheet intramolecular folding event that, in turn, causes intermoleculer self-assembly. The peptide molecules are locally amphiphilic with two linear strands flanking a central tetrapeptide turn sequence. SANS and TEM studies reveal that the peptide molecules self-assemble into semiflexible, fibrillar structures with monodisperse width that is dictated by the strand length of the molecule. Rheological measurements demonstrate that the hydrogels behave as soft-solid materials with tunable rigidity. Hydrogels

recover their initial viscoelastic properties after cessation of high magnitude of strain due to the physically crosslinked network structure and strong inter-fibrillar interactions. These interactions can be turned off by either condensing anions or covalently attaching PEG chains on the lysine-decorated fibrillar surfaces. In addition, stiffening transitions are observed when the hydrogels are cooled due to the hydrogen bonding capability of boric acid/borate ion with lysine residues.

**13:51**

**V28 14 Nanoscale structure and dynamics of colloid-semiflexible polymer solutions** JI YEON HUH, ERIC M. FURST, *University of Delaware* Interactions and structure in colloid-polymer solutions control the phase behavior, viscoelasticity, stability, and vitrification, which play significant roles in many industrial applications. Filled semiflexible networks demonstrate distinctive rheological properties due to their large persistence length. They are important in many biological and surfactant systems, and display additional complexity because of the alignment and isotropic-nematic transition. In this work, we report diffusing wave spectroscopy studies of the dynamics of colloidal particles suspended in F-actin solutions in time scales $10^{-6} < t < 10^{-2}$s, and in the concentration of 14.7$\mu$M. Monodisperse polystyrene spheres are coated using bovin serum albumin to reduce filament adsorption. By adjusting the actin filament length with the capping protein gelsolin, we observe the entanglement transition from dilute to semi-dilute regimes. Our data shows quantitative agreement with the theory of semiflexible polymer solutions in the dilute limit[1]. However, we find discrepancies in the entangled limit which may indicate the difference between local and bulk properties. Using a shell model for the local viscoelastic response[2], we find that the response is consistent with a depletion-like structure surrounding the embedded colloidal particles[3]. [1]Shankar et al., itJ. Rheol. 46, 1111 (2002) [2]A. Levine and T. Lubensky, itPhys. Rev. E 63, 041510 (2001) [3]Y. L. Chen and K. S. Schweizer, itJ. Phys. Chem. B 108, 6687 (2004)

**14:03**

**V28 15 Relaxation Behavior of Acrylic Triblock Copolymer Gels** MICHELLE SEITZ, KENNETH SHULL, WESLEY BURGHARDT, *Northwestern University* When dissolved in alcohol, poly(methyl methacrylate)-poly(n-butyl actylate)-poly(methyl methacrylate) triblock copolymers form physical gels by the aggregation of the PMMA blocks into sperhical domains. Shear rheometry was used to study the relaxation behavior of gels formed in 2-ethylhexanol with different block lengths and polymer concentrations. Master curves were used to determine relaxation times at different temperatures. The relaxation time given by zero shear viscosity divided by the plateau modulus were in good agreement with the low frequency limit for a system with a single relaxation time. By increasing the PMMA block length from 9k to 25k or increasing polymer concentration from 5 to 30 vol. percent, the relaxation time increases by five orders of magnitude at a given temperature. The effect of block length and concentration on the aggregation number of the PMMA domains was determined by small angle X-ray scattering. Relaxation behavior is of practical importance because these gels are used for thermoreversible gelcasting of ceramics.

## SESSION V29: NONLINEAR PHENOMENA & PATTERN FORMATION IN BIOLOGY

**Thursday Morning, 16 March 2006**
**326, Baltimore Convention Center at 11:15**
**Igor Aronson, Argonne National Laboratory, presiding**

**11:15**

**V29 1 Thermally activated escape rate for a Brownian particle in a double-well potential for all values of the dissipation** WILLIAM COFFEY, *Department of Electronic and Electrical Engineering, Trinity College, Dublin 2, Ireland* YURI KALMYKOV, *MEPS, Université de Perpignan, 52 Avenue Paul Alduy, 66860 Perpignan Cedex, France* SERGEY TITOV, *Institute of Radio Engineering and Electronics of the Russian Academy of Sciences, Fryazino, Moscow Region, 141190, Russian Federation* The translational Brownian motion in a (2-4) double-well potential is considered. The escape rate, the position correlation function and correlation time, and the generalized susceptibility are evaluated from the solution of the underlying Langevin equation by using the matrix continued fraction method. The escape rate and the correlation time are compared with the Kramers theory of the escape rate of a Brownian particle from a potential well as extended by Mel'nikov and Meshkov [J. Chem. Phys. **85**, 1018 (1986)]. It is shown that in the low temperature limit, the universal Mel'nikov and Meshkov expression for the escape rate provides a good estimate of both escape rate and inverse position correlation time for all values of the dissipation including the very low damping (VLD), very high damping (VHD), and turnover regimes. Moreover, for low barriers, where the Mel'nikov and Meshkov method is not applicable, analytic equations for the correlation time in the VLD and VHD limits are derived.

**11:27**

**V29 2 The spectra of spiral wave breakup** DWIGHT BARKLEY, *University of Warwick* PAUL WHEELER, *University of Warwick* It has been known for many years that spiral waves in excitable reaction-diffusion systems can break up into a state of spatio-temporal chaos. The breakup may occur near the spiral tip (core breakup) or far from the tip (far-field breakup). Past analyses of these phenomena have been almost exclusively based on the study of 1D wave trains. This talk focuses on the computation of linear stability spectra and nonlinear simulations of spiral waves on large 2D disks. Through such computations we determine point eigenvalues associated with both types of breakup and show that these are near to, but not in, the absolute spectra. Hence spiral breakup occurs before the crossing of the absolute spectrum, contrary to prediction. Both types of breakup appear to be simply due to subcritical Hopf bifurcations.

**11:39**

**V29 3 Pattern Formation without Patterning Proteins in Cyanobacteria** JUN ALLARD, ANDREW RUTENBERG, *Department of Physics and Atmospheric Science, Dalhousie University, Halifax, Canada* Filaments of cyanobacteria respond to nitrogen starvation by differentiating one cell in ten into a heterocyst, which is devoted to fixing atmospheric nitrogen. This is an example of self-organized pattern formation. We present a dynamical model explaining the initial selection of heterocysts in mutated cyanobacteria that are effectively without normal patterning pro-

teins. Our simulations of this model produce distributions of heterocyst spacings that are consistent with experimental data, and lead to new qualitative predictions on the mechanisms of pattern formation in filamentous cyanobacteria. We discuss possible experimental tests of our results.

**11:51**

**V29 4 Experimental studies of large-scale collective swimming in dense suspensions of bacteria*** ANDREY SOKOLOV, *Illinois Institute of Technology/Argonne National Laboratory* IGOR ARANSON, *Argonne National Laboratory* RAYMOND GOLDSTEIN, JOHN KESSLER, *University of Arizona* We conducted experimental investigation of large-scale collective swimming in dense suspensions of itBacillus subtilis. This microorganism is flagellated, rod-shaped objects, 5-10 microns long and capable of swimming up to 20 microns/second. The hydrodynamic and chemical interactions between individual cells results in remarkably rich collective behavior; self-concentration due to gradients of dissolved oxygen or pH level; phase transitions and self-organization in confined geometries. The self-organization often takes the form of coherent structures with typical sizes that are many times larger than those of the individual bacteria. The studies were performed in thin liquid film with controlled thickness. We explored experimentally the dependence of the scales of large-scale flow structures on the concentration of cells. The experimental results are compared with the predictions of continuum mathematical model of this phenomenon.

*This research was supported by US DOE, contract #W-31-109-ENG-38

**12:03**

**V29 5 Fiber optical measurements of electrical activity in canine ventricular preparations** AMGAD SQUIRES, GISA E. LUTHER, MICHAEL ENYEART, ROBERT F. GILMOUR, EBERHARD BODENSCHATZ, STEFAN LUTHER, *Department of Biomedical Sciences, Cornell University, NY, and Max Planck Institute for Dynamics and Self-Organization, Goettingen, Germany* Ventricular fibrillation (VF) is a cardiac arrhythmia that kills over 300,000 people every year in the US alone, yet efforts at finding a cure have been stymied by our incomplete information about patterns of electrical activity in the whole heart. As an excitable medium, the heart is a pattern forming system; but only a very limited subset of patterns is compatible with life. In particular, spiral waves have been associated with both tachycardia and VF, but their origin and spatial and temporal dynamics is not fully understood. We propose a novel measurement technique that combines optical mapping of the epicardial surface with data from intramural fiber optical probe arrays. The data obtained from the fiber optical probes is sparse in space but dense in time. The data processing is based on sequential data assimilation using an ensemble Kalman filter. The ensemble Kalman filter provides a numerically efficient (sub-) optimum state space estimate based on the available spatial and temporal observations. The feasibility of the method is demonstrated with numerical data and arterially perfused canine heart preparations.

**12:15**

**V29 6 Motion artifact removal in the optical mapping of cardiac tissue** GISA E. LUTHER, AMGAD SQUIRES, MICHAEL W. ENYEART, ROBERT F. GILMOUR, EBERHARD BODENSCHATZ, STEFAN LUTHER, *Department of Biomedical Sciences, Cornell University, NY, and Max Planck Institute for Dynamics and Self-Organization, Goettingen, Germany* Optical mapping provides measurements of the transmembrane potential in cardiac tissue with high spatial and temporal resolution using voltage senitive dye. However, the contractile motion of cardiac tissue causes substantial artifacts in optical recordings. On the other hand, mechanical or pharmacological inhibition of motion is known to promote ischemia or alter the electrophysiological properties of the tissue and therefore limits the application of the optical mapping technique. Motion artifacts arise due to two dominant mechanisms: (a) Relative motion of the tissue with respect to the optical imaging system or the fiber optical probe. (b) Change of the optical properties of the tissue and of the dye associated with the variation of the tissues mean density. We present a novel model based algorithm, which accounts for both mechanisms. It combines a Lukas-Kanade feature tracking with two-wavelength ratiometric imaging. The robustness and accuracy of this approach is validated using numerical and experimental data. Our approach allows to rephrase the contamination of the signal with motion artifacts as a nonlinear mixing process. De-mixing the signal opens the perspective of retrieving information on both the transmembrane potential and contractile force.

**12:27**

**V29 7 Compact Dynamical Equations for Brain Activity** JONG WON KIM, PETER A. ROBINSON, *School of Physics, University of Sydney, Australia. Brain Dynamics Center, Westmead Hospital and University of Sydney, Australia* A continuum model of brain dynamics has recently been developed to reproduce and unify many features of electroencephalographic (EEG) signals. We further investigate the model and propose a new, more compact, model based on a single delay differential equation which captures the essential features, such as rapid corticocortical feedbacks and delayed feedbacks from extra cortical pathways. Experimentally observed frequency spectra of EEGs, including resonances, are reproduced in relevant regions of parameter space. In the nonlinear regime, onsets of seizures, which often show limit cycles, are explained by the instabilities of resonances at the boundary of a stability zone in the parameter space. This compact model also shows several other points of agreement with previous models and experiments, and thus provides a theoretical basis for analyzing complex brain activities, especially when they exhibit low-dimensional dynamics.

**12:39**

**V29 8 Pattern recognition through collective behaviour in neural networks** JAN R. ENGELBRECHT, *Boston College* We investigate how collective order in networks of integrate-and-fire neurons can lead to computation. Specifically we show that patterns in static and dynamic sensory stimuli can be recognized through the development of synchrony in a simple neural network with a hierarchy of layers. The recognition events ultimately trigger activity in 'grandmother' neurons in the last layer.

**12:51**

**V29 9 Modeling of Protein Subcellular Localization in Bacteria** XIAOHUA XU, RAHUL KULKARNI, Specific subcellular localization of proteins is a vital component of important bacterial processes: e.g. the Min proteins which regulate cell division in *E. coli* and Spo0J-Soj system which is critical for sporulation in *B. subtilis*. We examine how the processes of diffusion and membrane attachment contribute to protein subcellular localization for the above systems. We use previous experimental results to suggest minimal models for these processes. For the minimal models,

we derive analytic expressions which provide insight into the processes that determine protein subcellular localization. Finally, we present the results of numerical simulations for the systems studied and make connections to the observed experiemental phenomenology.

**13:03**

**V29 10 Quantitative measures for mitotic spindle pattern formation structures** STUART SCHAFFNER, *Northeastern U.* JORGE JOSE, *SUNY at Buffalo, Northeastern U.* Recently introduced biophysical models successfully reproduce the basic spindle patterns found in in-vitro meiotic experiments. Numerical simulations of the model show the detailed behavior of microtubules and positive and negative walking molecular motors as they interact to form spindle patterns. Previous results were mostly qualitative in nature, but we are now developing quantitative measures to characterize the formation of spindle structures. In particular, minus-directed crosslinking motors bind microtubules together in pairs. This pairwise binding can be represented by a graph where the vertices are microtubules and the edges are crosslinking motors. Highly interconnected components of this graph correspond to bundles of motion-correlated microtubules. Numerical simulations show that these bundles are a prominent feature of spindle pole assembly. Using general ideas of random graph theory, we can measure deviations from random connectivity. We also calculate an approximation of the strain energy induced by contact forces between the microtubules and make estimates that could be tested experimentally.

**13:15**

**V29 11 Stability and Perturbation Analysis on a Model of Cell Chemotaxis** COLIN McCANN, *University of Maryland* RON SKUPSKY, *National Institutes of Health* WOLFGANG LOSERT, *University of Maryland* RALPH NOSSAL, *National Institutes of Health* Many eukaryotic cells respond with directional movement to spatial and/or temporal gradients of small molecules that bind to cell surface receptors. The computational model of a chemotaxing cell developed in [1], which models cells such as neutrophils or Dictyostelium discoideum, is investigated with regard to stability and response to perturbations. A formal stability analysis finds that, when placed in an initial linear gradient, the model is most sensitive to perturbations at a 60-90 degree offset from the direction of the initial gradient. The model also responds most quickly and strongly to external point sources placed in that direction. These responses hold for all four of the model variants developed in [1]. This suggests that the observed 'zigzag' behavior of real cell movement in a gradient may be influenced by the nature of the biochemical reactions that control a cell's chemotactic response. This research was funded in by the National Institutes of Health (NIH) and the National Institute of Standards and Technology (NIST). [1] Skupsky, R., W. Losert, and R.J. Nossal. 2005. ''Distinguishing modes of eukaryotic gradient sensing.'' Biophys. J. 89:2806–2823

**13:27**

**V29 12 Raman Correlation Spectroscopy*** EDWARD VAN KEUREN, *Georgetown University, Department of Physics* MAKI NISHIDA, *Georgetown University, Department of Physics* We have developed a simple method for measurement of diffusion coefficients of specific components in complex mixtures of suspended particles in a liquid. The method, a variation of photon correlation spectroscopy (PCS), uses temporal fluctuations of Raman scattered light to characterize the particle Brownian motion. This is possible due to the key fact that Raman scattering is a coherent process, which is necessary for meaningful photon autocorrelation functions to be obtained. The time autocorrelation functions of Raman emission lines will yield information similar to that obtained by PCS. However, since the scattering at a particular wavelength is usually specific to only one type of molecule, only the diffusion coefficient of the particles containing that chemical species will be measured. We demonstrate this method with several multicomponent nanoparticle dispersions.

*This material is based upon work supported by the National Science Foundation under Grant No. DMR 0348955

**13:39**

**V29 13 A New Paradigm for Nanoparticle Biosensing: Magnetically Driven Critical Phase Slipping** BRANDON H McNAUGHTON, RAOUL KOPELMAN, *University of Michigan, Applied Physics Program; University of Michigan, Chemistry* Could a single opto-magnetic micro or nanoparticle be used as a noninvasive nanobiosensor? In this work, we imitated microorganism or bacteria sensing by binding a micron sized sphere to a larger rotating magnetic particle. The magnetic particle exhibits a nonlinear rotational behavior that marks a crossover from phase-locking to phase slipping with a remote rotating magnetic field. This critical transition is very sensitive to volume and shape changes, allowing for the detection of an attaching particle or biomolecule. Further miniaturization, combined with the remote sensing ability of this probe, could allow for measurements of viruses or biomolecules like DNA or proteins in a variety of environments, including closed biological systems.

**13:51**

**V29 14 Sum frequency generation microscopy for imaging chirality*** NA JI, *Department of Physics, University of California, Berkeley* KAI ZHANG, HAW YANG, *Department of Chemistry, University of California, Berkeley* YUEN-RON SHEN, *Department of Physics, University of California, Berkeley* Optically active sum frequency generation microscopy was demonstrated for the first time. Using films of solution of chiral 1,1'-bi-naphthol molecules with microstructures, we showed that sum frequency generation microscopy can image molecular chirality with three-dimensional sectioning capability and sub-micron spatial resolution. Because the image contrast originates from the intrinsic chirality of the system, no staining is required. Our microscopy scheme also allows the simultaneous detection of two-photon fluorescence. As a result, optically active sum frequency generation microscopy can be potentially very useful for live cell imaging. Preliminary results of applying this technique to DNA conformation study will also be described.

*This work was supported by DOE and NSF.

**14:03**

**V29 15 Upconversion-Detected Ultrafast Two-Dimensional Infrared Spectroscopy*** KEVIN KUBARYCH, *University of Michigan* MANUEL JOFFRE, *Laboratoire d'Optique et Biosciences Ecole Polytechnique* Two-dimensional infrared (2DIR) spectroscopy provides direct access to ultrafast molecular dynamics by measuring time- and structure-dependent couplings between vibrational transitions. Biological molecules, such as proteins, have rich vibrational spectra that relate to key structural elements including secondary structure ($\alpha$-helix, $\beta$-sheet), hydrogen bonding and protonation state. The ability to reliably measure 2DIR spectra in biological molecules represents a major step towards an

atomic-level picture of biochemical dynamics. A key limitation of ultrafast IR spectroscopy has been the measurement of the spectrum in a grating-based spectrometer due to HgCdTe detectors limited to linear arrays of 128 or fewer pixels. We have circumvented this problem by converting the coherently generated four-wave mixing 2DIR signal into the visible spectrum, and recording it using a 1340x100 pixel silicon CCD camera. The IR signal is mixed in a MgO:$LiNbO_3$ crystal with a chirped, $< 10\ \mu$J, 0.5 ns, 800 nm pulse. Signal detection is sufficient to measure single-shot dispersed vibrational echo spectra, as well as heterodyne detected 2DIR in $Mn_2(CO)_{10}$. The IR emission temporally overlaps only a narrow frequency range of the chirped near-IR pulse resulting in negligible spectral broadening.

*We acknowledge support from the Human Frontier Science Program

**SESSION V30: FOCUS SESSION: MECHANICAL PROPERTIES: MICROSCALE DEFORMATION AND FAILURE**
**Thursday Morning, 16 March 2006; 327, Baltimore Convention Center at 11:15**
**Gale Holmes, National Institute of Standards and Technology, presiding**

***Invited Papers***

**11:15**
**V30 1 Fundamental Fracture Behavior of Polymer Nanocomposites.**
HUNG-JUE SUE, *Texas AM University*

This abstract was not received electronically.

***Contributed Papers***

**11:51**
**V30 2 Adhesion at Entangled Polymer Interfaces: A Unified Approach.** RICHARD WOOL, *Univeristy of Delaware* A unified theory of fracture of polymer interfaces was developed which was based on the Rigidity Percolation model of fracture [R.P. Wool, J.Polym.Sci. Part A: Polym Phys., 43,168(2005)]. The polymer fractured critically when the normalized entanglement density p, approached the percolation threshold $p_c$. The fracture energy was found to be $G_{1c} \sim [p\text{-}p_c]$. When applied to interfaces of width X, containing an areal density $\Sigma$ of chains, each contributing L chain entanglements, the percolation term $p \sim \Sigma L/X$ and the percolation threshold was related to $\Sigma_c$, $L_c$, or $X_c$. For welding of A/A symmetric interfaces, $p = \Sigma L/X$, and $p_c \approx L_c/M \approx 0$, such that when $\Sigma/X \sim 1/M$ for randomly distributed chain ends, $p \sim L \sim (t/M)^{1/2}$, $G/G^* = (t/\tau^*)^{1/2}$, where the weld time $\tau^* \sim M$. When the chain ends are segregated to the surface, $\Sigma$ is constant with time and $G/G^* = [t/\tau^*]^{1/4}$. For sub-$T_g$ welding, there exists a surface mobile layer (due to the critical Lindemann Atom fraction) of depth $X \sim 1/\Delta T^{\nu}$ such that $G \sim \Delta T^{-2\nu}$, where the critical exponent $\nu = 0.8$. For incompatible A/B interfaces of Helfand width d, normalized width $w = d/R_{ge}$, and entanglement density $N_{ent} \sim d/L_e$, $p \sim d$ such that, $G_{1c} \sim [d\text{-}d_c]$, $G_{1c} \sim [w\text{-}1]$, and $G \sim [N_{ent}\text{-}N_c]$. For incompatible A/B interfaces reinforced by an areal density $\Sigma$ of compatibilizer chains, L and X are constant, $p \sim \Sigma$, $p_c \sim \Sigma_c$, such that $G_{1c} \sim [\Sigma - \Sigma_c]$, which is in excellent agreement with experimental data.

**12:03**
**V30 3 Effect of entanglement density on mechanical properties of glassy polymers*** ROBERT HOY, *Johns Hopkins University* MARK ROBBINS, *Johns Hopkins University* The mechanical properties of model glassy polymers are studied using computer simulations. Using primitive path analysis, we relate the macroscopic stress-strain behavior of polymer glasses to the microscopic evolution of the underlying entanglement network. The network plays little role in phenomena such as the initial yield and strain softening, but dominates the mechanical response at larger strains. Comparison of results for systems with a wide range of entanglement densities allows study of the onset of network- dominated behavior. The density of entanglements is varied by changing the bending stiffness and diluting with shorter chains.

*This work was supported in part by the National Science Foundation Grants No. DMR-0454947 and PHY99-07949

**12:15**
**V30 4 Entanglement Effects in Plastic Deformation of Filled Linear Polymer Glasses*** CAMERON ABRAMS, *Dept. Chemical and Biological Engineering, Drexel University* DAVID RICHARDSON, *Dept. Computer Science, Drexel University* We have performed coarse-grained molecular dynamics simulations of linear polymer glasses with low weight fractions of stiff rodlike particles. This is relevant to understanding the molecular-scale origins of toughness in nanotube-filled polymer composites. Linear polymer glasses are tougher than classical brittle glasses because chains are force to slide along each other under tensile load to undo entanglements. We focus here on the role of (a) the concentration and (b) orientational distibution of the rod-like inclusion particles on the entanglement network. We observed a substantial (10%) increase in the amount of work required to deform a particular glass plastically to a given strain (2.0) when equal weight fractions of rods were oriented randomly vs. parallel to the pulling axis. Using the method of primitive path analysis [Everaers, et al., Science 303:823 (2004)], we identify entanglements and particle-particle bridging interactions which are operative for a given pulling direction in a simulated tensile test in order to predict this enhancement from chain conformations in the initial unstrained sample. We apply this method to many samples with different weight fractions of rods, rod orientations, and rod-polymer interaction strengths.

*US Office of Naval Research Young Investigator Program (N00014-03-1-0655)

**12:27**

**V30 5 Nanoparticles alignment, exclusion and entrapment during failure of Glassy Polymer Nanocomposite** JONG-YOUNG LEE, QINGLING ZHANG, TODD EMRICK, ALFRED CROSBY, *University of Massachusetts* Crazing is a polymer deformation process during which dense arrays of nanoscale fibrils grow prior to the propagation of a crack. In the presence of nanoscale inorganic fillers, the mechanisms of craze formation and propagation are altered significantly. We use a model material of polystyrene blended with surface modified CdSe nanoparticles to investigate the interaction between polymer molecules and nanoparticles during the process of crazing. We demonstrate that nanoparticles in the presence of a craze undergo three stages of rearrangement: 1) Alignment along the precraze (fluid-like region), 2) Expulsion from nanoscale craze fibrils, and 3) Assembly into clusters trapped between craze fibrils. These results not only provide direct evidence for the physical mechanisms that control the mechanical properties of polymer nanocomposites, but they give fundamental insight into the behavior of polymers and nanoparticles in the presence of a directed field, which will impact a wide array of advanced material applications.

**12:39**

**V30 6 Crazing in Glassy Polymer Nanocomposites** JONG-YOUNG LEE, QINGLING ZHANG, TODD EMRICK, ALFRED CROSBY, *University of Massachusetts* Crazing is a polymer deformation process in which dense arrays of nanoscale fibrils grow prior to the propagation of a crack. Here, we discuss experimental results on the impact of two nanostructured materials on the crazing process: 1) ordered glassy block copolymers and 2) homopolymer/nanoparticle composites. We not only find that an ordered lamellar microstructure leads a lower craze growth rate compared with polystyrene homopolymer, but also nanoscale, surface terraces significantly decrease the failure strain of these advanced materials. For homopolymer/nanoparticle composites, we discover significant alterations in the crazing process. Specifically, nanoparticles in the presence of a craze undergo three stages of rearrangement: 1) Alignment along the precraze (fluid-like region), 2) Expulsion from nanoscale craze fibrils, and 3) Assembly into clusters trapped between craze fibrils. Although nanoparticles have no effect on the initiation strain, fibril breakdown strain, and craze growth rate, the composite failure strain can be increased significantly by nearly 100% compared to neat homopolymer films. These results provide direct evidence for the physical mechanisms that control the mechanical properties of polymer nanocomposites.

**12:51**

**V30 7 Tensile Modulus Measurements of Carbon Nanotube Incorporated Electrospun Polymer Fibers** YAVUZ OZTURK, JAEMIN KIM, KWANWOO SHIN, *Dep.of Mat.Sci.and Eng., Gwangju Ins.of Sci.and Tech., Gwangju 500-712, Korea.* Electrospinning has become a popular method for producing continuous polymer fibers with diameters in sub-micron scale. By this technique uniaxially aligned fibers can also be obtained, by using two separate parallel strips as conductive collectors. Uniaxial alignment of polymer fibers gives us the chance to well-characterize their structural properties via tensile modulus measurements. Here we report a simple and new technique for tensile testing of polymer fibers which employs a computerized spring-balance/step-motor setup. The key point in our technique is the production of fibers directly on the tensile tester by using two vertical strips as collectors. By this way, even fibers of very brittle nature can be tested without handling them. Calculation of total cross-sectional areas - which is crucial for determining stress values - was done by using scanning electron and optical microscope images for each sample. In this study we have investigated mechanical properties of Polystyrene (PS), Polymethylmethacrylate (PMMA) and PS/PMMA blend fibers; as well as Carbon Nanotube (CNT) incorporated PS, PMMA and PS/PMMA blend fibers. It is expected that the extraordinary mechanical properties of CNTs can be transferred into polymer matrix, by their incorporation into confined space within electrospun fibers. Here we analyzed the influence of CNT on polymer fibers as function of CNT amounts.

**13:03**

**V30 8 Rate-dependent Mechanical Deformation Behavior of POSS-filled and Plasticized Poly(vinyl chloride).** SHARON SOONG, ROBERT COHEN, MARY BOYCE, *Massachusetts Institute of Technology* In different temperatures or strain-rate regimes, the rate sensitivities of polymers change as various primary and secondary molecular mobility mechanisms are accessed. Incorporating nanoparticles into the polymer matrix can potentially alter the molecular level structure and offers an opportunity to tailor the rate-dependent mechanical deformation behavior of the polymer. In this study, methacryl-POSS (C56H88O28Si8) and dioctyl phthalate (DOP) were incorporated into poly(vinyl chloride) (PVC) through melt blending. Dynamic Mechanical Analysis revealed that the incorporation of POSS in PVC plasticizes PVC and reduces both the alpha and beta transition temperatures. As for the PVC/DOP blends, while the alpha-transition temperatures were reduced, beta-motions vanishes with high DOP contents. The rate dependent yield behavior is characterized in compression testing. Zwick Mechine is used for low to moderate strain rate (0.0001 to 0.1/s) and Split Hopkinson Bar is used for high strain rate (500 to 2000/s). It was found that PVC with POSS shows a delay in yield strength rate-sensitivity transition. For PVC with higher DOP contents which show restricted beta-motions, the rate-sensitivity transition in yield stress faded away. Constitutive model used was able to predict the rate-sensitivity transitions in the compression yield behavior of PVC compounds.

**13:15**

**V30 9 Tensile Properties and Hysteresis Behavior of Graft Copolymers with Complex Molecular Architecture** R. WEIDISCH, *Institute of Materials Science and Technology, Friedrich-Schiller-University Jena, Loebdergraben 32, D-07743 Jena, Germany* U. STAUDINGER, *Leibniz-Institute of Polymer Research Dresden, Germany* Y. ZHU, S.P. GIDO, *Polymer Science and Engineering Dept., University of Massachusetts, Amherst, USA* D. UHRIG, J.W. MAYS, *Chemical Sciences Division and Center for Nanophase Materials Sciences, Oak Ridge National Laboratory, Oak Ridge,TN 37831, USA* N. HADJICHRISTIDIS, H. IATROU, *Department of Chemistry, University of Athens, Greece* PS-PI multigraft copolymers with tri- tetra- and hexafunctional polystyrene branch points have been studied to investigate the influence of molecular architecture on tensile properties and hysteresis behaviour. It was found that mechanical properties are mainly controlled by functionality of the graft copolymers and the number of branch points per molecule. Tetrafunctional multigraft copolymers show surprising high strain at break values up to 1550%. With increasing number of branch points strain at break and tensile strength increase, where a linear dependence of mechanical properties on the number of branch points is obvious. Hysteresis ex-

periments have proved excellent elasticity of tetra and hexafunctional multigrafts far exceeding that of commercial elastomers like Styroflex. A tetrafunctional multigraft copolymer can be deformed till 1400% showing a residual strain of only 40% demonstrating super elastic property profile.

**13:27**

**V30 10 Structure and Tensile mechanical properties of poly-(ester urethane) materials.** MARILYN HAWLEY, ROBERT HOULTON, PHILIP RAE, E. BRUCE ORLER, DEBRA WROBLESKI, *Los Alamos National Laboratory* Scanning probe microscopy (SPM) techniques, primarily phase imaging, and Stress/Strain Tensile Measurements were used to study the properties of model poly (ester urethane) and 23% Estanetrademark compression molded samples. SPM was used to characterize the surface microstructure and the corresponding distribution of hard and soft segments within these samples. The model samples contained a range of nitroplasticizer (NP) content from 0 to 15%. SPM phase imaging yielded maps of variations in local mechanical properties at the nanometer scale. Tensile stress/strain measurements were carried out at 0.1 mm/min. Sequential tensile stress/strain measurements to increasing strains, sequential tensile stress/strain measurements to the sample strain, and at different temperatures allow us to understand the deformation mechanism in this complex material. Significant elastic behavior was seen below the glass transition.

**13:39**

**V30 11 Identification of key deformation mechanisms of polyethylene materials via in-situ x-ray scattering** THERESA HERMEL-DAVIDOCK, WILLEM DEGROOT, MEHMET DEMIRORS, BRIAN LANDES, RAJEN PATEL, TRACY PELTIER, *Dow Chemical Company* Changes in the microstructure of ethylene based copolymers can be used to modify and enhance their mechanical performance. In this study, the effects of comonomer content, molecular weight, and molecular weight distribution on the mechanical performance of select polyethylene polymers were examined. Two key performance parameters for commercial polymer materials, especially in the area of blown film applications, are tear resistance and puncture resistance. However, polyethylene films exhibiting very different Dart and Elmendorf tear values cannot be differentiated by standard tensile test methods even though they exhibit very similar morphology. Alternative methods to link morphology and mechanical response need to be found. Wide-angle and small-angle x-ray scattering was collected during in-situ tensile testing to understand how compositional and structural differences affect the mechanical response of semicrystalline polyethylene polymers. Microstructural changes observed during the in-situ deformation process are correlated to Elmendorf tear and Dart impact performance for both intrinsic and blown film samples.

**13:51**

**V30 12 Microindentation Studies in Polymers at Very Low Crystallinities** FRANCISCO BALTA-CALLEJA, ARACELI FLORES, *IEM, CSIC, Madrid, Spain* MACROMOL. PHYS. TEAM, Indentation with a sharp indenter, involving a deformation on a micron and submicron scale is known to be a convenient method to measure the mechanical properties of polymers [1-2]. The aim of the present talk is to offer an overview on recent advances concerning the microindentation hardness, H, of a series of very low crystallinity (below 7 percent) polyethylene materials relating to nanostructure. The H values for the ethylene-octene copolymers are found to be notably smaller than those of linear and commercial short-chain branched polyethylene. The microhardness of an ethylene based material having a nearly zero crystallinity value has been measured for the first time. Results are discussed on the basis of the surface free energy, dimensions of the nanocrystals and the energy required for plastic deformation. In these low crystallinity materials the deformation modes involve bond rotation of the molecules within the amorphous phase, and elastic compression, bending and slippage of the nanocrystals. According to these deformation mechanisms, which are mainly modulated by the viscosity of the amorphous phase, the average dimensions of the nanocrystals after deformation remain practically unaffected. [1] A. Flores, F.J. Balta Calleja, T. Asano, J. Appl. Phys. 90, 6006 (2001). [2] A. Flores, V.B.F. Mathot, G.H. Michler, R. Adhikari, F.J. Balta Calleja, Polymer (in press).

**14:03**

**V30 13 Effect of crystalline organization on toughness.*** LAURENT CORTE, *Matiere Molle et Chimie, ESPCI-CNRS* LUDWIK LEIBLER, *Matiere Molle et Chimie, ESPCI-CNRS* Impact resistance of semi-crystalline polymers can be greatly improved by the incorporation of rubber or inorganic particles. We report that the crystalline organization of the polymer matrix is a key-parameter for toughening. Cutting test bars into injected plates of toughened polyamide allows to study the impact behaviour of a same sample volume under various impact directions. When impact is applied perpendicularly to the injection direction, these systems exhibit a ductile behaviour while they become dramatically brittle when impact is parallel to it. More generally, the impact properties of these toughened systems depend strongly on thermo-mechanical history and processing conditions. We show by X-ray and TEM observations that this behaviour is to be correlated to the crystalline organization and propose a theoretical model that links toughness and crystalline organization.

*Financial support by Arkema, ESPCI and CNRS is gratefully acknowledged.

**SESSION V31: NANOTUBES: TRANSPORT**
**Thursday Morning, 16 March 2006**
**328, Baltimore Convention Center at 11:15**
**Laxmidhar Senapati, Naval Research Laboratory, presiding**

**11:15**

**V31 1 Ab initio charge transport through N-doped carbon nanotubes: microscopic understanding of carbon nanotube sensors** FREDERICO D. NOVAES, MARIANA ROSSI, ANTÔNIO J. R. DA SILVA, A. FAZZIO, *Instituto de Física, Universidade de Säo Paulo* We calculate, using an ab initio non-equilibrium Green's function formalism, the conductance of metallic carbon nanotubes with pyridine-like defects. We show that there is a decrease of the conductance at the Fermi energy due to these defects, which is caused by nitrogen related levels within an energy window of 1.5 eV below the Fermi energy. We then investigate how exposure to NH3 can affect the conductance. At the pyridine- like structure the NH3 dissociated into NH2 and H, with both molecules binding to nitrogen atoms. This configuration leads to an increase of the conductance, and cannot, therefore,

explain the increase of resistance that has been experimentally observed. We then investigate other configurations, and suggest that a possible cause of the resistance increase is adsorption of atomic or molecular species at the wall of pristine nanotubes.

**11:27**

**V31 2 A Semi-Empirical Approach to Bandstructure, Chemistry and Transport: Extended Hückel Theory applied to Carbon Nantotubes and Silicon*** DIEGO KIENLE, *Purdue University* JORGE CERDA, *Instituto de Ciencia de Materiales de Madrid* KIRK BEVAN, *Purdue University* GENGCHIAU LIANG, *Purdue University* LUTFE SIDDIQUI, *Purdue University* AVIK GHOSH, *University of Virginia* M.P. ANANTRAM, *NASA Ames Research Center* We apply semi-empirical Extended Hückel Theory (EHT) to calculate electronic structure and zero bias density-of states and transmission for two technologially important materials: carbon nantotubes and silicon. We demonstrate that the EHT-parameters optimized for bulk-silicon and 2D-graphene are transferable to describe qualitatively and quantitatively the electronic structure of structural deformed systems such as small diameter CNTs and relaxed silicon surfaces for different orientations. Finally, we show that the non-orthogonal EHT-approach can handle electronic structure and bonding chemistry simultaneously considering a carbon-monoxide-CNT heterostructure as example for a molecule sensor. To study transport through large nanoscale devices along with attached molecules a semi-empirical approach such as EHT might offer a good compromise between computational expensive DFT-methods and effective mass models which do not capture molecular features.

*DURINT

**11:39**

**V31 3 Ab initio Bandbending and Schottky Barriers of a Carbon Nanotube and Boron Nitride Device** KHORGOLKHUU ODBADRAKH, PAWEL POMORSKI, CHRISTOPHER ROLAND, *North Carolina State University* The quantum transport characteristics of two semiconducting nanotubes (i.e., single-wall (8,0) carbon and boron nitride nanotubes) coupled to metallic leads (i.e., Al (100)) was investigated with a combined nonequilibrium Greens function/density functional theory formalism. The resulting transmission depends very muchon the size of the nanotubes: very short tubes are characterized by metallic current-voltage behavior because of transmission via evanescent modes, while longer tubes are dominated by bandbending and Schottky barrier phenomena. An analysis of the latter phenomena as a function of nanotube characteristics, charge transfer, and gate voltage will be presented.

**11:51**

**V31 4 Effect of Strain and Defects on Transport Properties of Carbon Nanotubes** YAO HE, *University of Florida* CHUN ZHANG, *Georgia Technology Institute* CHAO CAO, HAI-PING CHENG, *University of Florida* Strain dependence of electronic transport properties of carbon nanotubes has been studied using first-principles calculations. We have found that the quantum conductance decreases monotonically with increasing strain, due to the strain-dependent contribution of molecular orbitals. Transport properties are also affected by the presence of defects. Our results have demonstrated that the electronic transport properties of a nano-scale device are closely related to the nature of the band structure of the metallic lead and the details of chemical bonding in the scattering region. DOE/BES under grant FG02-02ER45995 is acknowledged.

**12:03**

**V31 5 Dependence of transport through carbon nanotubes on local Coulomb potential.** ALEXEY ZHUKOV, *Duke University, Physics Department* ALEXANDER MAKAROVSKI, MATTHEW PRIOR, GLEB FINKELSTEIN, ELECTRONIC NANOSTRUCTURES GROUP TEAM, With home made atomic force microscope we perform scanned probed imaging of single-walled carbon nanotube devices at 4.2 K. We also observe changing of the heights and positions of the conductivity peaks in Coulomb Blockade regime with displacement of the AFM conductive tip. Influence of the Coulomb potential of the AFM tip on single-electron charge states in carbon nanotube is discussed.

**12:15**

**V31 6 Origin of hysteresis in gate-modulated transport in single-wall carbon nanotubes** SWASTIK KAR, ARAVIND VIJAYARAGHAVAN, *Department of Materials Science and Engineering, Rensselaer Polytechnic Institute, Troy New York* SAIKAT TALAPATRA, *Rensselaer Nanotechnology Center, Rensselaer Polytechnic Institute, Troy New York* CATERINA SOLDANO, SAROJ K. NAYAK, *Department of Physics, Applied Physics and Astronomy, Rensselaer Polytechnic Institute, Troy New York* OMKARAM NALAMASU, PULICKEL M. AJAYAN, *Department of Materials Science and Engineering, Rensselaer Polytechnic Institute, Troy New York* Transfer characteristics of gate-modulated transport in single-wall carbon nanotubes show significant hysteresis. This hysteresis is usually attributed to a screening of the gate voltage due to mobile charges/ions in the presence of a trapping/de-trapping mechanism within the gate architecture. From a temperature dependence of the hysteresis behavior, we suggest an alternate mechanism, where the screening charges are injected from the nanotube itself into the surrounding dielectric. Any trapping/de-trapping mechanism does not appear to play a significant role, and the experimental results can be understood in terms of a capacitive charging of the surrounding dielectric.

**12:27**

**V31 7 Electrical transport properties of selective area CVD grown single wall carbon nanotube devices*** ZHIXIAN ZHOU, RONGYING JIN, GYULA ERES, DAVID MANDRUS, *Oak Ridge National Laboratory* Individual single wall carbon nanotube (SWNT) devices were constructed by the direct assembly of an individual SWNT on two opposing Au electrons using an acetylene based low temperature selective area Chemical Vapor Deposition (CVD) method. Standard electron beam lithography and subsequent electron-gun assisted metal deposition were used to fabricate both the electrodes and catalyst islands. Electrical transport properties of the SWNT circuits were measured by applying a gate voltage to the Si substrate at various temperatures down to 0.3 K. Both semiconducting and metallic individual SWNTs were found bridging the Au electrodes with relatively small contact resistances. The semiconducting SWNTs exhibit a significant electrical field effect at room temperature with the conductance modulation approaching 5 orders of magnitude. High bias measurements on both suspended and substrate-supported metallic SWNTs reveal strikingly different phenomena. The details of the electrical transport results will be discussed.

*Oak Ridge National Laboratory is managed by UT-Battelle, LLC, for the U.S. Department of Energy under contract DE-AC05-00OR22725.

**12:39**

**V31 8 Electron transport in as-grown suspended semiconducting carbon nanotubes** VIKRAM DESHPANDE, MARC BOCKRATH, *Applied Physics, CalTech* Recently it was reported [1] that as-grown suspended single-walled carbon nanotubes (SWNTs) contacted with Pt or Mo leads afford devices that are devoid of perturbations due to substrate interaction and relatively defect-free. Previously, low-resistance contacts to semiconducting SWNTs have been obtained with Au [2], since the work-function of Au aligns with the valence band of the SWNTs creating ohmic contacts in the p-type region. We present fabrication of as-grown SWNTs with Au contacts, to fully exploit this behavior. We discuss electron transport in semiconducting devices obtained as above, with the aim of understanding the role of electron interactions in transport. Metallic SWNTs are known to exhibit Luttinger liquid behavior as is evident in the power-law dependence of conductance and density of states in a tunneling experiment [3]. We explore Luttinger liquid behavior in devices obtained using our fabrication technique. We will present latest experiments and inferences. [1] Cao et al, Nature Materials (2005) [2] Yaish et al, PRL (2004) [3] Bockrath et al, Nature (1999)

**12:51**

**V31 9 The effect of purification on electron transport properties of single-wall carbon nanotubes** HISASHI KAJIURA, MASASHI SHIRAISHI, MASAFUMI ATA, *Sony* ANIL NANDYALA, ULAS COSKUN, ALEXEY BEZRYADIN, *University of Illinois* The effect of purification on room temperature electronic transport properties of laser-produced single-wall carbon nanotubes (SWNTs) was studied by submerging the nanotubes into liquid mercury. As-produced SWNTs were purified using H2O2, HCl, and NaOH solutions and heated at 923K at 0.01Pa for 1 h. Purified SWNTs having clean surface wall showed weak dependence of the electrical resistance on the length of the nanotube segment connecting electrodes. This provides evidence of quasi-ballistic electron transport in SWNTs. The estimated electronic mean free path of the purified SWNTs reached a few microns, which is longer than that of as-produced tubes. The electronic mean free path in purified SWNTs is consistent with the calculation based on the electron scattering by acoustic phonons. [H. Kajiura et al. Appl Phys Lett 86, 2005, 122106.]

**13:03**

**V31 10 Probing the transport property of each individual wall within a multiwall carbon nanotube** X. YAN, J.Y. HUANG, S. CHEN, Z. WANG, *Department of Physics, Boston College, Chestnut Hill, MA 02467* G. CHEN, *Department of Mechanical Engineering, MIT, Cambridge, MA 02139* M.S. DRESSELHAUS, *Department of Physics, Electrical Engineering and Computer Science, MIT, Cambridge, MA 02139* Z.F. REN, *Department of Physics, Boston College, Chestnut Hill, MA 02467* We report the atomic-scale imaging with concurrent transport measurements of the breakdownof individual multiwall carbon nanotubes inside a transmission electron microscope equipped with a piezo manipulator [1]. We found unexpectedly three distinct breakdown sequences; namely, from the outermost wall inward, from the innermost wall outward, and alternatively between the innermost and the outermost walls. Remarkably, a significant amount of current drop was observed when an innermost wall is broken, proving unambiguously that every wall is conducting. Moreover, the breakdown of each wall in any sequence initiates in the middle of the nanotube, not at the contact, proving that the transport is not ballistic. [1] J.Y. Huangetal, Phys. Rev. Lett. 94, 236802 (2005).

**13:15**

**V31 11 Electronic transport in single-walled nanotubes of known chiral indices** R. CALDWELL, *Columbia University* F. WANG, Y. WU, M. HUANG, L. HUANG, S. O'BRIEN, T.F. HEINZ, J. HONE, By measuring the Rayleigh scattering spectra of individual single-walled carbon nanotubes, we are able to measure the optical transition energies and therefore deduce the chiral indices (n,m). Using a simple mechanical transfer process, we can transfer the optically characterized tubes to a substrate. Following fabrication of metallic leads using e-beam lithography, the electrical transport properties of these tubes can be probed. We will present data on semiconducting, chiral metal and armchair metal SWNTs.

**13:27**

**V31 12 Hopping Conduction in Individual Template-Produced Multiwalled Carbon Nanotubes** D. P. WANG, B. R. PERKINS, A. J. YIN, D. E. FELDMAN, A. ZASLVASKY, J. M. XU, *Department of Physics and Division of Engineering, Brown University* We report electrical transport measurements of individual multiwalled carbon nanotubes grown catalytically in a nonporous anodic aluminum oxide template by thermal chemical vapor deposition of acetylene. The conductance shows an $\exp[-(T_0/T)^{1/2}]$ dependence on temperature $T$ and $\exp[-\xi_0/\xi]$ dependence on the applied electric field $\xi$ in the high field regime, suggesting that hopping conduction between the grains is the dominant transportation mechanism. As the nanotubes are granular and highly defective, annealing has been used to change the granularity. Similar $T$- and $\xi$- dependence of conductance is observed for annealed nanotubes with different granularity-related coefficients $T_0$and $\xi_0$. Small magnetoresistance is observed for both types of nanotubes. Comparison with theory is presented and the $T_0$and $\xi_0$ coefficients are used to extract the characteristic conducting grain size.

**13:39**

**V31 13 Thermal effects in non-linear electronic transport in metallic carbon nanotubes*** MARCELO KURODA, *Beckman Institute and Dept. of Physics, University of Illinois at Urbana-Champaign* JEAN-PIERRE LEBURTON, *Beckman Institute and Dept. of Electrical and Computer Engineering, University of Illinois at Urbana-Champaign* Recent experiments have shown that metallic carbon nanotubes exhibit different *IV* characteristics depending on whether or not they lie on a substrate. These interesting features range from current saturation to negative differential resistance at high bias. In this talk, we present a model based on the solution of the Boltzmann transport equation that accounts for the interplay between thermal and electronic transport in the metallic system. Our results reproduce the experimental observations and emphasize the role of heat dissipation in the nanotube nonlinear characteristics.

*This work is supported by the Beckman Institute and the National Computation Network under NSF grant # EEC-0228390

**13:51**

**V31 14 Thermal Transport in MWNT sheet.** ALI ALIEV, MEI ZHANG, SHAOLI FANG, SERGEY LEE, ANVAR ZAKHIDOV, RAY BAUGHMAN, *Nanotech Institute, University of Texas at Dallas, Richardson, TX 75083* We present the comparative study of the anisotropic thermal conductivity and the thermal diffusivity of aligned multiwalled carbon nanotube sheet using two methods: laser flash and 3 omega methods. The highly aligned transparent nanotube sheets are drawn from a sidewall of a mul-

tiwalled carbon nanotube (MWNT) forest that was synthesized by chemical vapor deposition. The sectional analysis by AFM tip shows that suspended sheet consists on average one layer of 10 nm MWNT. Increase of the sheet density by stacking the layer to layer decreases the thermal conductivity and thermal diffusivity due to phonon-phonon interaction. High thermal conductivity and thermal diffusivity of studied specimens combined with extremely high surface area suggests a variety of application of MWNT sheets.

**14:03**
**V31 15 Nanotube-Metal Junctions: 2- and 3- Terminal Electrical Transport*** SAN-HUANG KE, WEITAO YANG, HAROLD U. BARANGER, *Duke University* We address the quality of electrical contact between carbon nanotubes and metallic electrodes by performing first-principles calculations for the electron transmission through ideal 2- and 3-terminal junctions, thus revealing the physical limit of tube-metal conduction. The structural model constructed involves surrounding the tube by the metal atoms of the electrode as in most experiments; we consider metallic (5,5) and n-doped semiconducting (10,0) tubes surrounded by Au or Pd. In the case of metallic tubes, the contact conductance is shown to approach the ideal $4e^2/h$ in the limit of large contact area. For three-terminals, the division of flux among the different transmission channels depends strongly on the metal material. A Pd electrode has nearly perfect tube-electrode transmission and therefore turns off the straight transport along the tube. The carrier injection is found to occur only at the edge of the contact region. Our results are in good agreement with some recent experimental reports and clarify a fundamental discrepancy between theory and experiment.

*Supported by the NSF (DMR-0103003 and DMR-0506953).

## SESSION V33: FOCUS SESSION: SOCIAL NETWORKS
**Thursday Morning, 16 March 2006; 336, Baltimore Convention Center at 11:15**
**Alessandro Vespignani, Indiana University, presiding**

***Invited Papers***

**11:15**
**V33 1 Social Balance on Networks: The Dynamics of Friendship and Hatred.***
SIDNEY REDNER, *Boston University*

We study the evolution of social networks that contain both friendly and unfriendly pairwise links between individual nodes. The network is endowed with dynamics in which the sense of a link in an imbalanced triad—a triangular loop with 1 or 3 unfriendly links—is reversed to make the triad balanced. Thus an imbalanced triad is analogous to a frustrated plaquette in a random magnet, while a balanced triad fulfills the adage: ''a friend of my friend is my friend; an enemy of my friend is my enemy; a friend of my enemy is my enemy; an enemy of my enemy is my friend.'' With this frustration-reducing dynamics, an infinite network undergoes a dynamic phase transition from a steady state to ''paradise''—all links are friendly—as the propensity for friendly links to be created in an update event passes through 1/2. On the other hand, a finite network always falls into a socially-balanced absorbing state where no imbalanced triads remain. A prominent example of the achievement of social balance is the evolution of pacts and treaties between various European countries during the late 1800's and early 1900's. Here social balance gave rise to the two major alliances that comprised the protagonists of World War I.

*Co-authors: T. Antal and P. L. Krapivsky.

***Contributed Papers***

**11:51**
**V33 2 Lamb-lion Problem on Networks and Its Applications** SUNGMIN LEE, SOON-HYUNG YOOK, YUP KIM, *Department of Physics, Kyung Hee University* We numerically study the dynamic properties of diffusing lamb captured by diffusing lion on the complex networks. We find that the survival probability $S(t)$ of a lamb decays exponentially on the complex networks including scale-free networks whose degree distribution follows $P(k) \sim k^{-\gamma}$. We also find that the average life time $< T >$ depends on the size of the underlying networks, $N$, and it satisfies the relation $< T > \sim N^{\alpha}$ for $\gamma > 3$. However, for small values of $\gamma$ ($< 3$) we find that $< T >$ does not follow the power-law. Finally, we investigate the topological property of the node at which the lion captures the lamb by measuring the degree of the node. We also discuss some possible applications of our findings.

**12:03**
**V33 3 Preferential attachment in the growth of social networks: the case of Wikipedia** GUIDO CALDARELLI, *CNR-INFM Istituto dei Sistemi Complessi, and Dipartimento Fisica, Università di Roma ''La Sapienza,'' Piazzale Aldo Moro 2, Rome Italy* ANDREA CAPOCCI, *Centro Studi e Ricerche Enrico Fermi, Rome Italy* VITO SERVEDIO, *Dipartimento di Fisica, Università ''La Sapienza'' Piazzale Aldo Moro 5 00185 Rome, Italy* LUCIANA BURIOL, DEBORA DONATO, *Dipartimento di Informatica e Sistemistica, Università ''La Sapienza''* STEFANO LEONARDI, *Dipartimento di Informatica e Sistemistica, Universita' ''La Sapienza'' via Salaria 113 00198 Rome Italy* CNR-INFM TEAM, CENTRO FERMI TEAM, DIP. DI INF. E SIST. TEAM, Here we present experimental data and a model in order to describe the evolution of a socio-technological system. The case of study presented is that of the online free encyclopedia Wikipedia, for which we have the complete series of pages addition during time. The varioius entries and the hyperlinks between them can be described as a graph. We find scale-invariant behaviour in the

distribution of the degree and a topology similar to that of the World Wide Web. By using the information on dynamics we are able to model and reproduce the features of this system. We also find that regardless the fact that any user has the possibility of global reshape, still Wikipedia has a growth described by local rules as that of the preferential attachment.

**12:15**

**V33 4 Social inertia in collaboration networks** JOSE J. RAMASCO, *Emory University* STEVEN A. MORRIS, *Oklahoma State University* This work is a study of the properties of collaboration networks employing the formalism of weighted graphs to represent their one-mode projection. The weight of the edges is directly the number of times that a partnership has been repeated. This representation allows us to define the concept of *social inertia* that measures thetendency of authors to keep on collaborating with previouspartners. We use a collection of empirical datasets to analyze several aspects of the social inertia: 1) its probability distribution, 2) its correlation with other properties, and 3) the correlations of the inertia between neighbors in the network. We also contrast these empirical results with the predictions of a recently proposed theoretical model for the growth of collaboration networks.

**12:27**

**V33 5 Efficiently achieving consensus in scientific collaboration networks** R. DEAN MALMGREN, SAM SEAVER, ROGER GUIMERA, DANIEL DIERMEIER, JULIO OTTINO, LUIS AMARAL, *Northwestern University* Recent work by Guimerá et al. [1] indicates that successful collaborative networks are developed from a balance of new and old blood. To first approximation, the efficiency of these collaborative networks to reach consensus on a problem depends on (i) the difficulty of the problem and (ii) the fraction of time each individual spends working on his own versus interacting with his peers. We mimic problem difficulty by the likelihood that an individual obtains the correct answer, and we model social interactions by the majority rule, which is efficient even in the presence of noise [2]. We then study the asynchronous dynamics of small-world [3] and collaborative networks [1] to quantify the efficiency of empirical collaborative networks to achieve consensus. Finally, we examine how altering the balance of new and old blood affects the efficiency of collaborative networks to reach consensus. [1] R. Guimerá, B. Uzzi, J. Spiro, and L. A. N. Amaral. *Science* **308**, 697–702 (2005). [2] A. A. Moreira, A. Mathur, D. Diermeier, and L. A. N. Amaral. *PNAS* **101**(33), 12085–12090 (2004). [3] D. J. Watts and S. H. Strogatz. *Nature* **393**, 440–442 (1998).

**12:39**

**V33 6 A Network Analysis of Committees in the United States House of Representatives** MASON PORTER, *Caltech* Network theory provides a powerful tool for the representation and analysis of complex systems of interacting agents. Here we investigate the networks of committee and subcommittee assignments in the United States House of Representatives from the 101st–108th Congresses, with committees connected according to ''interlocks'' or common membership. We examine the House's community structure using several algorithms and reveal strong links between different committees as well as the intrinsic hierarchical structure within the House as a whole. We show additionally that structural changes, including a tighter community structure, resulted from the 1994 elections, in which the Republican party earned majority status in the House for the first time in more than forty years. In this work, we combine our network theory approach with analysis of roll call votes using singular value decomposition and successfully uncover political and organizational correlations between committees in the House without the need to incorporate other political information. This is joint work with A.J. Friend, Peter Mucha, Mark Newman, and Casey Warmbrand.

**12:51**

**V33 7 DIMES – New Results from Wide-area Internet Topology Mapping** SHLOMO HAVLIN, SHAI CARMI, *The Physics Department, Bar-Ilan University, Israel* ERAN SHIR, YUVAL SHAVITT, *Department of Electrical Engineering, Tel Aviv University, Israel* SCOTT KIRKPARTRICK, *School of Computer Science and Engineering, The Hebrew University of Jerusalem, Israel* DIMES is a distributed agent-based Internet mapping effort which at present has attracted thousands of volunteers running clients world-wide. Despite the ''law of diminishing returns'' seen when when adding agents in past mapping attempts, we find that significant amounts of new information can be found in the long tails of our measurement process. We use the k-pruning method to decompose the network into nodes with distinct roles. The analysis suggests a new picture of the AS-level Internet structure, which distinguishes a relatively large, redundantly connected core of nearly 100 ASes and two components that flow data in and out from this core. One component is fractally interconnected through peer links; the second makes direct connections to the core only. We plan to use this picture as a framework for measuring and extrapolating changes in the Internet's physical structure. Our analysis may also be relevant for estimating the function of nodes in the ''scale free'' graphs extracted from other naturally-occurring processes.

**13:03**

**V33 8 Modeling search-dominated Web growth** SANTO FORTUNATO, ALESSANDRO FLAMMINI, FILIPPO MENCZER, ALESSANDRO VESPIGNANI, *School of Informatics, Indiana University* Our present understanding of the Web growth, beyond the large number of existing models, is very much based on the paradigm of preferential attachment, that reflects a surf-dominated Web. In fact nowadays most of the traffic on the Web goes through and is driven by search engines. This profoundly affects the dynamics behind Web growth, potentially leading to a monopolistic scenario where few nodes attract a large share of traffic and links. We propose a minimalistic model to describe the evolution of the Web based on the interaction between users and search engines. The model reproduces several characterizing properties of the topology and traffic on the Web, and explains apparently counterintuitive empirical evidences. S. Fortunato, A. Flammini, F. Menczer and A. Vespignani, School of Informatics, Indiana University ''The egalitarian effect of search engines,'' http://arxiv.org/abs/cs.CY/0511005

**13:15**

**V33 9 Evidence of accelerated growth by edge copying and unfairness in the evolution of the AS level of the Internet*** BRUNO GONÇALVES, *Emory University* JOSE MENDES, *Universidade de Aveiro* It is well known that the Internet on the Autonomous System level is in constant evolution and growth. In this paper we show that for the freely available data for the period between Nov, 97 to March, 01 is compatible with a edge-copying model with a probability $p = 0.58$. We also demonstrate that the

Internet is intrinsically unfair since the nodes with higher connectivities remain the same throughout its history.

*JFFM was partially supported by project POCTI/FAT/46241/2002, POCTI/MAT/46176/2002 and NATO grant PST.CLG.979688 (2003).

**13:27**

**V33 10 Vulnerability of complex networks: Effect of traffic and geography** MARC BARTHELEMY, *Indiana University and CEA* LUCA DALL'ASTA, ALAIN BARRAT, *LPT-Universite Paris-Sud* ALESSANDRO VESPIGNANI, *Indiana University* Real-world networks present different levels of complexity: the topology, the weights and the spatial properties are often nontrivial and very different from simple random assumptions. In order to understand the vulnerability to malicious attacks of such networks one has therefore to consider not only topological quantities but also weights and space. We will present results on the paradigmatic example of the airport network which is a weighted heterogeneous network with complex traffic and spatial structures. We define different measures of damage and show that different attack strategies lead to different conclusions about the vulnerability of the network. In particular, we show that strategies need to be adapted depending on the type of damage and on the geographical region considered.

**13:39**

**V33 11 Network theory model of the United States Patent citation network*** JAN TOBOCHNIK, PETER ERDI, *Kalamazoo College* KATHERINE STRANDBURG, *DePaul University College of Law* GABOR CSARDI, LASZLO ZALANYI, *Department of Biophysics, KFKI Research Institute* We report results of a network theory approach to the study of the United States patent system. We model the patent citation network as a discrete time, discrete space stochastic dynamic system. From data on more than two million patents and their citations, we extract an attractiveness function, $A(k,l)$, which determines the likelihood that a patent will be cited. A(k,l) is approximately separable into a product of a function $A_k(k)$ and a function $A_l(l)$, where $k$ is the number of citations already received (in-degree) and $l$ is the age measured in patent number units. $A_l(l)$ displays a peak at low $l$ and a long power law tail, suggesting that some patented technologies have very long-term effects. $A_k(k)$ exhibits super-linear preferential attachment. The preferential attachment exponent has been increasing since 1991, suggesting that patent citations are increasingly concentrated on a relatively small number of patents. The overall average probability that a new patent will be cited by a given patent has increased slightly during the same period.

*Funded in part by the NSF and the Hungarian Academy of Sciences

**13:51**

**V33 12 The social cost of partisanship** SAM SEAVER, ROBERT MALMGREN, ANDRE MOREIRA, DANIEL DIERMEIER, LUIS AMARAL, *Northwestern University* Implementing policies that bring an overall social benefit can be quite difficult due to the myriad of ways in which different individuals and groups may be impacted, and the variety of targets, beliefs and agendas the policy-makers themselves may have. Examples include the implementation of measures with the objective of reducing carbon dioxide emissions and the implementation of guidelines for conducting stem cell research. Here, we use an agent-based modeling approach to investigate the effects of conservatism and partisanship on the efficiency with which large populations reach consensus on the ''correct'' decision. Remarkably, we find that conservative agents do not destroy the groups' ability to reach consensus. In fact, conservatives enable the system to maintain high efficiency, even in the presence of large levels of noise. In contrast, we find that even a small number of partisans results in low efficiency, especially for large levels of noise. We conclude that while conservatism improves social outcomes, partisanship can have significant social costs.

## SESSION V35: PHOTONIC CRYSTALS

**Thursday Morning, 16 March 2006**
**338, Baltimore Convention Center at 11:15**
**Xiaomei Jiang, University of Texas at Dallas, presiding**

**11:15**

**V35 1 A Dynamical Effective Medium Theory for Metamaterials** YING WU, JENSEN LI, ZHAO-QING ZHANG, C.T. CHAN, *Department of Physics,The Hong Kong University of Science and Technology* We present a new dynamical effective medium theory in the framework of two-parameter coherent potential approximation. While conventional homogenization theories will fail near resonances, our theory gives simultaneously accurate effective permittivity and permeability near resonant frequencies. The theory can also describe the absorption. Our assertions are supported by the band structure and transmission calculations of periodic composites in both two and three dimensions.

**11:27**

**V35 2 The gap structures and wave functions of two-dimensional quasicrystals for classical waves.** YUN LAI, ZHAO-QING ZHANG, *Department of Physics, The Hong Kong University of Science and Technology, Hong Kong* CHI-HOU CHAN, *Department of Electronic Engineering, City University of Hong Kong, Hong Kong* LEUNG TSANG, *Department of Electrical Engineering, University of Washington, US* By using the sparse-matrix canonical-grid (SMCG) method, we have performed large-scale multiple scattering calculations to study the gap structures and wave functions of two-dimensional quasicrystals for classical waves. As sample size is increased, we find self-similar-like evolution in the gap structures. We also find the self-similar state and large-size localized states. All these findings arise from the quasiperiodic long-range order. A self-similar state at band edge is identified in a large sample containing 33919 scatterers. A coherent picture is presented to describe the relationship between the self-similar-like evolution of gap structures and the formation of self-similar states.

**11:39**

**V35 3 Electromagnetic wave propagation in media whose permittivity varies periodically in time*** JUAN CARLOS CERVANTES, PETER HALEVI, We have developed a general theory for propagation of plane electromagnetic waves in a medium with permittivity that is varying periodically in time. The Bloch-Floquet theorem dictates that these are a superposition of harmonic modes whose frequencies differ by $2\pi/T$, where $T$ is the period of $\varepsilon(t)$. For arbitrary periodicity, the dispersion relation $\omega(t)$ for the ''Bloch frequency'' is given in terms of the roots of an infinite determinant whose elements depend on the Fourier coefficients of $\varepsilon(t)$. For small variation of $\varepsilon(t)$ around an average

$\varepsilon_0$, $\omega(t)$ is characterized by regions of the wave vector $k$ that are forbidden for propagation. These are centered at it$\omega$ and $k$ values that are, respectively, integer multiples of $\pi/T$ and of $\pi\varepsilon_0^{1/2}/cT$. The widths of the gaps are proportional to the corresponding Fourier coefficients of $\varepsilon(t)$. In the special case of square-periodic variation of $\varepsilon(t)$, there is no need to recur to a perturbational calculation, because the dispersion relation can be derived analytically, with no approximations. Again, we find wave vectors gaps whose edges are located at the frequencies $\omega$=0,$\pi$/T,2$\pi$/T.

*This work has been supported by CONACyT Grant No. 41195-F

**11:51**

**V35 4 Achieving a Photonic Band-Edge Near Visible Wavelengths by Copper Coating on 3D Tungsten Photonic-lattices.** DEXIAN YE, SHAWN-YU LIN, JAMES BUR, TOH-MING LU, *Rensselaer Polytechnic Institute* The fabrication of all-metal three-dimensional (3D) photonic lattices (PLs) is a subject that has raised great interest due to their potential in energy applications [1]. However, there are very few metals are suitable for the architecture of 3D PLs with a photonic band-edge near visible wavelengths. 3D tungsten (W) photonic lattice in ''wood-pile'' architecture has been successfully fabricated [1]. But the intrinsic limitation of W prevents the photonic band-edge to go beyond 2 $\mu$m. We show that by material engineering this limitation can be overcome. We coated a very thin layer of copper (Cu) conformally onto the W PLs and modified their optical properties. The Cu thin films were coated on the PLs by electroless deposition. This thin Cu film ( $\sim$ 70 nm) has dramatic effects on the photonic band-gap behavior of the W PLs. After the coating of Cu, the photonic lattice has a much larger photonic band-gap. The band-edge of the photonic lattice is shifted from $\lambda \sim 2\mu$m to $\lambda \sim$ 750nm. Our experimental data agree with the predictions by finite difference time domain calculations. This method provides a new route for tailoring photonic properties and it should work for 3D PLs constructed from other materials. [1] J. G. Fleming, S.Y. Lin, I. El-Kady, R. Biswas and K. M. Ho, Nature **417**, 52-55 (2002).

**12:03**

**V35 5 From Photonic Crystals to Photonic Metamaterials. I*** PETER HALEVI, FELIPE PEREZ-RODRIGUEZ, *INAOE* We present a very general mean-field theory for a photonic crystal (dielectric or metallo-dielectric) with arbitrary (3D) Bravais lattice and arbitrary inclusions within the unit cell. The material properties are characterized by a generalized conductivity at every point in the unit cell. Averaging over many unit cells for very small Bloch wave vectors, we derive the macroscopic response for the metamaterial. This, in general, turns out to be the bianisotropic response, specified in terms of permittivity and permeability tensors and, also, ''crossed'' D/H and B/E tensors. These four tensors are derived in terms of the content of the unit cell. However, in case of inversion symmetry these ''crossed'' tensors vanish. Moreover, for cubic symmetry the system becomes isotropic, described by scalar, frequency-dependent, permittivity and permeability.The response is essentially local, although, spatial dispersion can also be accounted for. Our mean-field theory is valid for optical photonic bands, as well as acoustic bands.

*The authors acknoledge their CONACYT projects 41195-F and 46425-F.

**12:15**

**V35 6 From Photonic Crystals to Photonic Metamaterials. II*** FELIPE PEREZ-RODRIGUEZ, PETER HALEVI, *INAOE* We have applied the mean-field theory (I) described in the preceding abstract to metallo-dielectric photonic crystals with cubic symmetry and for different forms of the metallic inclusions. In particular, we have calculated analytically the effective permittivity and permeability for periodic composites with ''cages'' of thin metallic wires or ''3D crosses'' and for arrays of small metallic or dielectric spheres in vacuum. We compare our results for the permittivity of such systems with former theories and find agreement as far as the real part is concerned. Our results for the imaginary part of the permittivity differ from other works and those for the permeability are new. In fact, the extinction coefficient that we derive for small metallic spheres is three orders of magnitude greater than the prediction of the Maxwell-Garnett theory. We are in the process of applying our theory to other interesting metallo-dielectric systems.

*The authors acknowledge their CONACYT projects 41195-F and 46425-F.

**12:27**

**V35 7 Quantum Hall effect analogs in photonic crystals: semiclassical treatment of ''chiral'' (unidirectional) edge modes*** SRINIVAS RAGHU, F.D.M. HALDANE, *Princeton University* Previously, we have shown that ''photonic crystals'' (periodic metamaterials that transmit electromagnetic waves) made of nonreciprocal media (Faraday effect) can theoretically possess channels that allow light to propagate in one direction only. These channels are the direct photonic analog of the ''chiral edge states'' of electronic systems exhibiting a quantum Hall effect. Here, we construct exactly soluble models of photonic systems having these properties. The models considered here correspond to photonic systems with smoothly varying domain walls across which the Faraday coupling changes. The spectrum of bound states of this model contains bi-directionally propagating modes localized to the interface, and ''zero modes,'' in which light remains localized to the interface and propagates only in a forward direction perpendicular to it. In the semiclassical treatment of this model, we show that the quantization condition for the bound states has an additional contribution from a Z2 Berry phase factor picked up by the modes as they encircle points of degeneracy.

*Supported by NSF MRSEC DMR-0213706 at Princeton Center for Complex Materials

**12:39**

**V35 8 Influence of disorder on the band structure of a photonic crystal** ILYA PONOMAREV, T.L. REINECKE, *Naval Research Laboratory, Washington DC* M. BAYER, *Experimentelle Physik 2, Universitaet Dortmund, Germany* A. FORCHEL, *Technische Physik, Universitaet Wuerzburg, Germany* We investigate both theoretically and experimentally the influence of disorder on the optical mode spectra of chains of coupled micropillar cavities (photonic dot resonators - PDR). These quasi one-dimensional structures were fabricated by lateral patterning of planar Bragg microcavities. Maxwell equations were solved by finite elements methods. The disorder is introduced by systematic variation of the cavity sizes. For periodic chains without disorder (equal PDRs) angle-resolved photoluminescence shows well-pronounced photonic band gaps. We show that even small disorder drastically modi-

fies the properties of the optical modes and their spectra. Instead of set of propagating energy bands with Bloch states, impurity bands with Anderson-like localized states appear. The dependences of the energy bands and their intensities on cavities sizes are investigated and explained.

**12:51**

**V35 9 Photonic band-gaps in two dimensional semiconductor-dielctric composite structures** GERARDO MARTINEZ, MANVIR KUSHWAHA, *Institute of Physics, University of Puebla, Mexico* This paper reports the multiple band-gaps in the two-dimensional semiconductor-dielectric photonic crystals of several compositions: semiconductor (dielectric) cylinders in the dielectric (semiconductor) background. We consider both square lattice and triangular lattice arrangements and compute extensive band structures using a plane-wave method within the framework of an efficient standard eigenvalue problem for both E- and H-polarizations. The whole range of filling fractions has been explored to claim the existence of the lowest (the so-called acoustic band gap) and multiple higher-frequency band gaps within the first thirty to forty bands for various compositions. The completeness of the existing band gaps is substantiated by computing the band structures via detailed scanning of the principal symmetry directions covering periphery as well as the interior of the irreducible part of the first Brillouin zone and through the computation of the density of states. In general, the composition made up of doped semiconducting cylinders in the insulating background is found to be the optimum case for both geometries. Such semiconductor-dielectric photonic crystals which are shown to possess huge lowest band gaps below a threshold frequency (the plasma frequency) have an advantage over the dielectric photonic crystals in the emerging technology based on the photonic crystals.

**13:03**

**V35 10 Fabrication of Highly Reflecting $Si/SiO_2$ Bragg Mirrors Using Transferred Nanomembranes*** WEINA PENG, FRANK S. FLACK, MICHELLE M. ROBERTS, PAULA E. COLAVITA, DONALD E. SAVAGE, ROBERT J. HAMERS, MAX G. LAGALLY, MARK A. ERIKSSON, *University of Wisconsin Madison* A long term goal of electronics and photonics is the integration of both on the same materials platform and substrate. Silicon and silicon- dioxide are an excellent photonic materials pair, due to the superior properties of the oxide-silicon interface, and due to the large index-of- refraction contrast in this materials pair. We present a novel method to fabricate $Si/SiO_2$ mirrors based on transfer of freely released silicon nanomembranes and subsequent thermal oxidation. The surface roughness of the transferred membranes is examined using atomic force microscopy. RMS roughnesses as small as 0.25nm are achieved. The reflectivity is also measured for our transferred membranes, and an increase in reflection is easily observed as the number of stacked membranes is increased. The experimental reflectivity data match theoretical calculations within 10%. We discuss the possibility of aligning many membranes to make complicated photonic structures.

*Supported by DOE and AFOSR

**13:15**

**V35 11 Tuning of the Optical Response of a $Si/SiO_2$ Superlattice at the Wavelength of 1.54$\mu$m** E. GALINDO, P. HALEVI, *INAOE, Apdo. Post. 51, Puebla, Pue.72000, México* ADAN S. SANCHEZ, *INAOE and INTEL, Guadalajara, Mexico* We have studied a one-dimensional photonic crystal of alternating layers of silicon and silicon oxide (and, also, air), fixing the wavelength at 1.54$\mu$m, of great importance for communications in the near infrared. We assume strong doping of the Si layers, the density of free electrons reaching values up to $3\times10^{20}cm^3$. Using a realistic plasma model that takes into account electrons, holes, and the corresponding attenuation, our calculations lead to the conclusion that the reflectance and transmittance can depend very strongly on the carrier density. With a careful choice of parameters, a change in the reflectance from 0 to 90% can be attained in the vicinity of a photonic band edge, with only a moderate change in the impurity concentration.

**13:27**

**V35 12 Improved Photonic Bandgap Structures via Symmetry Breaking** DAVID MACKIE, *Army Research Laboratory* We have previously reported on our efforts to develop a semiconductor based photonic bandgap nano-membrane device with 3D MEMS features which is designed to reconfigure the photonic crystal structure into different types of waveguide devices such as switches, modulators, delay lines, etc.[1] As design and fabrication interact there is tension between what one would like to make and what one can actually make. We have found that in many cases, by breaking some of the symmetry, it is possible to shift gaps around and to introduce new gaps. We discuss various examples of this. As an example with especially good performance, we discuss the case of rotated square holes in a square lattice. 1. ''Design and Fabrication of a Reconfigurable Photonic Bandgap Waveguide Device with MEMS Features,'' Weimin Zhou, Monica Taysing-Lara, Gerard Dang, Lorna Harrison, David Mackie, Matthew Ervin, and Peter Newman, presented at CLEO 2004.

**13:39**

**V35 13 Wannier Function Expansion of Localized States in Photonic Crystals** J. D. ALBRECHT, *Air Force Research Laboratory* P. SOTIRELIS, *High Performance Technologies, Inc., The Advanced Computational Analysis Directorate, Wright-Patterson Air Force Base, OH* We present a theoretical treatment of localized electromagnetic modes in infinite photonic crystals. Our basis states are local vector Wannier functions calculated from the unperturbed crystal eigenstates. Analogous to the calculation of localized electronic states by expansion in terms of electronic orbitals, this Wannier basis is used to expand photonic crystal defect states. The localized nature of the basis states is critical so that the basis can be truncated after a small number of neighbor lattice sites in the vicinity of the defect. We present results that verify the eigenmodes of the crystal and examine defect modes. An analysis is done to determine the convergence of the mode as a function of the number of basis states included in the computation. This formalism equally treats localized states that are bound in a photonic band gap and states resonant with the propagating photon states of the infinite crystal. The present method has certain advantages with regard to computational complexity, spatial resolution, and the efficient accommodation of non-spherical geometric features.

**13:51**

**V35 14 Tangent formulation for the band structure of one-dimensional N-period layered photonic crystals** FRANK SZMULOWICZ,* *Air Force Research Laboratory* At symmetry points of the Brillouin zone, the two-layer Kronig-Penney (KP) problem has even and odd parity solutions that are expressible with tangents and cotangents. Similar solutions are derived here

for an arbitrary number of layers. Namely, the eigenvalue-eigenvector problem for the energy spectra and wave functions of arbitrary, one-dimensional, N-period layered systems is formulated in terms of tangents only. The resulting equations are compact, algorithmically simple, numerically stable, and physically appealing. The derived secular equation is Hermitian and only of order N× N, i.e., half the size of the KP secular equation. The eigenfrequency condition has physically attractive geometric representation in terms of N-sided figures such as triangles and tetrahedrons for N=3. The analytic power of the formalism is demonstrated by diagonalizing the secular equation for N=3, finding a factored form of the KP equation, and deriving analytic eigenfrequency conditions and analytic wave functions for the three layer problem. The analyticity of the formalism should aid the band gap engineering of the band structure and wave functions of multilayer structures. The numerical ease of implementation is demonstrated by calculating the eigenfrequencies and wave functions for a three-layer photonic crystal.

*Also University of Dayton Research Institute

**14:03**

**V35 15 Temperature tuning of two-dimensional photonic crystals in the presence of phonons and a plasma of electrons and holes** JESUS MANZANARES-MARTINEZ, FELIPE RAMOS-MENDIETA, *Universidad de Sonora* PETER HALEVI, *Instituto Nacional de Astrofisica, Opticay Electronica* We have theoretically studied the electromagnetic transmittance in finite samples of InSb-based two-dimensional photonic crystals. Due to the temperature dependence of the intrinsic carrier concentration in the semiconductor, our square arrays of parallel InSb cylinders in air give rise to tunable transmission spectra. As the temperature increases from 200 to 290 K, we find that the midgap frequencies move up in frequency while the widths of the gaps diminish, in agreement with the bulk band structure. We find that absorption affects considerably the transmittance intensity. In order to achieve significant tuning of the transmission, appropriate structural parameters and spectral regions are proposed. We have also studied transmission of light through two-dimensional photonic crystals of finite width, with the radii of the cylinders in the middle row altered in comparison to the host cylinders.

## SESSION V36: FOCUS SESSION: OPTICAL PROPERTIES OF CARBON NANOTUBES AND C60

**Thursday Morning, 16 March 2006; 339\ Baltimore Convention Center at 11:15**
**Eric Shirley, National Institute of Standards and Technology, presiding**

***Invited Papers***

**11:15**

**V36 1 Spectroscopy of Optical Excitations in Carbon Nanotubes.**
YINGZHONG MA, *University of California, Berkeley and Physical Biosciences Division, Lawrence Berkeley National Laboratory*

Understanding the optical spectra and electronic excited state dynamics of carbon naotubes is important both for fundamental research and a wide variety of potential applications. In this presentation, we will report the results of a systematic study on semiconducting single-walled carbon nanotubes (SWNTs) obtained by utilizing complementary femtosecond spectroscopic techniques, including fluorescence up-conversion, frequency-resolved transient absorption, and three-pulse photon echo peakshift (3PEPS) spectroscopy. Our efforts have focused on optically selective detection of the spectra and dynamics associated with structurally distinct semiconducting SWNT species. Using individual nanotube enriched micelle-dispersed SWNT preparations, in combination with resonant excitation and detection, has enabled us to independently access selected species, such as the (8,3), (6,5), (7,5), (11,0), (7,6) and (9,5) nanotubes. We will discuss the following topics: (1) the excitonic nature of the elementary excitation and its unambiguous identification from direct determination of the exciton binding energy for a selected semiconducting nanotube, the (8,3) tube; (2) the spectroscopic and dynamical signatures of exciton-exciton annihilation and its predominant role in governing ultrafast excited state relaxation; (3) the annihilation-concomitant exciton dissociation and the spectroscopic and dynamic features of the resulting electron-hole continuum; (4) timescales characterizing the ultrafast thermalization processes. In addition, we will demonstrate the power of 3PEPS spectroscopy to elucidate the spectral properties and dynamics of SWNTs. This work was supported by the NSF.

***Contributed Papers***

**11:51**

**V36 2 Real time approach for non-linear optical response of nano-scale systems*** Y. TAKIMOTO, F. VILA, J.J. REHR, *U. of Washington* We present a real-time, time-dependent density-functional approach for the calculation of the frequency-dependent linear and non-linear optical response, which is based on the approach of Tsolakidis et al.[1] Tensor components of linear polarizabilities and first order hyper-polarizabilities are extracted by fitting net time dependent polarizations with different electric field strengths. The method is computationally efficient and can be applied to large, molecular and nano-scale systems. Results are presented for $C_{60}$ and for a number of ''push-pull'' molecules. Our results for the static limit are in good agreement with other density-functional calculations.

*Supported by NSF Grant DMR-0120967 (Y.T. and F.V) and DOE Grant DE-FG02-97ER45623 (JJR) and facilitated by the DOE CMSN

[1]A. Tsolakidis, D. Sanchez-Portal and R.M. Martin, Phys. Rev. B **66**, 235416 (2002).

**12:03**

**V36 3 First-Principles study of the optical properties of BN nanotubes and h-BN** CHEOL HWAN PARK, CATALIN SPATARU, STEVEN LOUIE, *UC Berkeley and Lawrence Berkeley National Laboratory* We present first-principles calculations of the effects of quasiparticle self-energy and electron-hole interaction on the optical properties of single-walled BN nanotubes (both zigzag and armchair tubes) and bulk h-BN. Excitonic effects are shown to be even more important in BN nanotubes than in carbon nanotubes, giving rise to excitons with binding energy larger than 2 eV for the zigzag (8,0) BN nanotubes. Moreover, unlike the carbon nanotubes, theory predicts that these exciton states are comprised of coherent supposition of transitions from several different subband pairs, giving rise to novel behaviors. Our calculatioins are in quantitative agreement with available experimental data. We also compare the optical properties of single-walled BN nanotubes with those of bulk h-BN. This work was supported by the NSF under Grant No. DMR04-39768, and the U.S. DOE under Contract No. DE-AC03-76SF00098. Computer time was provided by NERSC and NPACI.

**12:15**

**V36 4 *Ab initio* Studies of Potassium Adsorption on Graphite and Carbon Nanotubes*** ALEJANDRO LUGO-SOLIS, IGOR VASILIEV, *New Mexico State University* We present an *ab initio* study of a single potassium atom adsorption on the surface of graphite and single walled carbon nanotubes using density functional theory within the pseudopotential approximation. Our study is, in part, inspired by inconsistent results reported for this system in the existing literature. The potassium adsorption energy on graphite obtained in different calculations ranges from approximately 0.4 eV to 1.75 eV. Our calculations demonstrate that the reported disagreements can be explained by electrostatic interactions rather than complex quantum factors. We illustrate this with a simple model based on a classical electrostatic interaction between the potassium atom and the graphite surface. Adsorption energies predicted by the electrostatic model are in good agreement with our *ab initio* calculations. In contrast, we find that the adsorption energies of potassium on carbon nanotubes are directly related to the nanotube geometry and chirality and cannot be described in terms of a simple classical model.

*Supported by the National Science Foundation under Grant No. DMR-0505270, Petroleum Research Fund under Grant No. PRF-43409-G10 and the Air Force Office of Scientific Research under Award No. FA-9550-05-1-0234.

**12:27**

**V36 5 Bound excitons and optical absorption spectra of (10,10) metallic single-walled carbon nanotubes*** JACK DESLIPPE, *University of California at Berkeley* CATALIN SPATARU, STEVEN LOUIE, *University of California at Berkeley and Lawrence Berkeley National Laboratory* Motivated by recent theoretical prediction of bound excitons [1] in small diameter metallic single-walled carbon nanotubes, we study the optical spectra of the larger diameter (10,10) metallic tube. We use an interacting-particle Greens function approach which includes calculations of the quasiparticle excitation spectrum (within the GW approximation for the electron self energy) and the electron-hole excitation spectrum (within the Bethe-Salpeter formalism). We show that the (10,10) tube has important excitonic effects despite being a metal, due to the quasi-one dimensional nature of the carbon nanotubes. A bound exciton with binding energy of 60 meV is found, and the location of the excitonic peak in the optical spectrum is at 1.8 eV. [1] C. D. Spataru, S. Ismail-Beigi, L. X. Benedict, and S. G. Louie, Phys. Rev. Lett. 92, 077402 (2004).

*This work was supported by the NSF under Grant No. DMR04-39768, and the U.S. DOE under Contract No. DE-AC03-76SF00098. Computer time was provided by NERSC and NPACI.

**12:39**

**V36 6 Photocurrent Generation in Bent Nanostructures*** YURIY PERSHIN, CARLO PIERMAROCCHI, *Michigan State University* We study theoretically the effect of circularly-polarized electro-magnetic radiation on electrons confined in quantum rings and in bent ballistic quantum wires. The radiation couples to clockwise- or counterclockwise-propagating charge excitations in regions of the system with non-zero curvature, depending on the light polarization. This provides a transfer of the angular momentum from the radiation to the electrons. Response of the electron system to the external radiation displays a resonant behavior and can be measured through a current-induced magnetic field in quantum rings or using a standard current measurement technique in quantum wires.

*Supported in part by NSF DMR-0312491.

**12:51**

**V36 7 Ultrafast Carrier Relaxation Measurements of SWCNT-Doped Polymer Thin Films*** ELAINE LALANNE, BRENITRA MOSLEY, ANTHONY JOHNSON, *Center for Advanced Studies in Photonics Research (CASPR), University of Maryland Baltimore County* The primary application of interest of single-walled carbon nanotube (SWCNT) -doped polymer thin films is to serve as a replacement of gold active regions on integrated optic surface enhanced biosensors and as potential transparent conducting polymers. In addition, the ultrafast nonlinear optical switching properties are of particular interest. We report femtosecond time-resolved measurements on SWCNT -doped polymer thin films. These films were made by spin-coating the monomer-SWCNTs suspension onto glass substrates and UV curing to initiate polymerization. The SWCNTs are predominately semiconducting. The thin film contains $\sim$ 0.4 wt % of SWCNTs, with an average thickness of 7 $\mu$m. Non-degenerate pump-probe transmission experiments were performed using $\lambda_{pump}$ at 400 nm and white light continuum as the probe beam generated by a mode-locked Ti:Sapphire laser ($\tau_p$=160 fs, rep. rate 250 kHz). Preliminary results indicated two lifetimes: the fast decay of 1.4 ps and a longer relaxation time of 18 ps. Experiments are underway to study the carrier dynamics and determine the magnitude of the nonlinearity.

*The samples were prepared using facilities at LLNL. This work was partially supported by grant from NSF (DMR-0120967)

**13:03**

**V36 8 Carbon nanotube field effect transistors under high magnetic fields** GEORGY FEDOROV, DMITRY SMIRNOV, *Natl. High Magnetic Field Lab, Florida State Univ.* ALEXANDER TSELEV, YANFEI YANG, *Dept. of Physics, Georgetown Univ.* NIKOLAY KALUGIN, *Dept. of Physics, Texas A&M Univ.* Magnetic field, when applied parallel to the CNT axis, alters the energy gap in the CNT electron spectrum with a period corresponding to one quantum of magnetic flux through the cross-

section of the CNT. With available magnetic fields ($10^1$T by the order of magnitude), gap oscillations can be observed only in multi-wall CNTs with diameters larger than approx 5 nm, where effects of band structure variation are smeared out by defects and by quantum interference effects. As follows from [1], it is possible to separate effects of disorder from those of the band structure modification by studying magnetotransport in small diameter CNTs while controllably changing the position of the Fermi level of the CNT by electrostatic doping, i.e. by applying a gate voltage in the field effect transistor configuration. We have studied several samples of individual CTNs contacted by palladium electrodes placed on an oxidized heavily doped silicon substrate that served as a back-gate. We find that magnetoresistance of a CNT strongly depends on the Fermi level position with respect to the nanotube's charge neutrality point (CNP). Details and the analysis of our experimental data will be presented. [1] S. Roche, R. Saito, Phys. Rev. Lett. 87, 246803 (2001)

**SESSION V38: SUPERCONDUCTIVITY—THERMODYNAMICS AND STRUCTURE**
**Thursday Morning, 16 March 2006**
**341, Baltimore Convention Center at 11:15**
**Jeff Tallon, Industrial Research Limited, presiding**

**11:15**

**V38 1 Specific heat studies of heavy ion irradiated YBCO*** RUOBING XIE, A. RYDH,† U. WELP, W. K. KWOK, M. ESKILDSEN, *Department of Physics, University of Notre Dame, Notre Dame, IN 46556* L. PAULIUS, *Department of Physics, Western Michigan University, Kalamazoo, MI 49008* We present a systematic study of the effect of heavy ion irradiation induced columnar defects on the vortex phase diagram in single-crystal $YB_2Cu_3O_7$using ac-specific heat measurements. In pristine, naturally untwinned crystals the transition between the vortex liquid and vortex lattice states in intermediate fields is of first order as evidenced by a sharp peak in the specific heat. On our sample we observed the first order transition between the lower critical point near 0.35T and the upper critical point near 6T. The pristine sample was cleaved into several pieces of typical size $70\times100\times9$ $\mu$m, which were irradiated along the c axis with 1.1 GeV Pb ions at different dose matching fields ranging from 0.1 T to 0.35 T. Specific heat measurements pertaining to the transformation of the first order transition to higher order with increasing disorder as exemplified by the shift in the lower critical point will be addressed.

*This work was supported by the U.S. Department of Energy BES-Materials Science and Division of Nuclear Physics (ATLAS) under grant no. W-31-109-ENG-38.

†present address: Stockholm University, Albanova, SE-10691, Sweden

**11:27**

**V38 2 Low temperature specific heat study on $Pr_{0.88}LaCe_{0.12}CuO_{4-\delta}$** SHILIANG LI, SONGXUE CHI, PENGCHENG DAI,* *Department of Physics and Astronomy, The University of Tennessee, Knoxville, Tennessee 37996-1200, USA* HAIHU WEN, *National Laboratory for Superconductivity, Institute of Physics & Center for Condensed Matter Physics, Beijing 100080, China* By annealing the electron-doped $Pr_{0.88}LaCe_{0.12}CuO_{4-\delta}$ (PLCCO) in vacuum at different temperatures, we have successfully obtained several superconducting PLCCO samples with different $T_c$. The specific heat of all the samples show a $1/T^2$ behavior below 1K. Above 1K, the low field specific heat can be fitted by $\gamma(H)T + \beta T^3$, where the $\gamma(H)$ is the Sommerfeld coefficient. We present magnetic field dependent data of $\gamma(H)$ for several samples of PLCCO and discuss the evolution of $\gamma(H)$ as PLCCO is tuned from an antiferromagnetically ordered insulator to a Tc=25 K superconductor.

*also Condensed Matter Sciences Division and Center for Neutron Scattering, Oak Ridge National Laboratory, Oak Ridge, Tennessee 37831, USA

**11:39**

**V38 3 Anisotropic properties of unconventional superconductors in a magnetic field: testing the nodal stucture** ANTON VORONTSOV, ILYA VEKHTER, *Lousiana State University* We present a calculation of electronic specific heat and heat conductivity in a vortex state of quasi-two dimensional d-wave superconductors. We employ quasiclassical theory and use the Brand-Pesch-Tewordt approximation to model the superconducting state at moderate to high magnetic fields. Within this framework we investigate the dependence of heat capacity and heat conductivity on the angle of rotation of magnetic field with respect to the nodal directions. We find that the fourfold anisotropy due to nodal structure in both quantities changes sign in the temperature-field plane. This result helps resolve the apparent disagreement about the gap symmetry reached from the specific heat and the thermal conductivity measurements in $CeCoIn_5$. We comment on the physics behind the difference between our results and those obtained in the Doppler shift approximation.

**11:51**

**V38 4 Comparative analysis of specific heat of $YNi_2B_2C$ using nodal and two-gap models** HUNG DUEN YANG, CHIEN LUNG HUANG, *Department of Physics, National Sun Yat-Sen University, Kaohsiung 804, Taiwan* JIUNN YUAN LIN, *Institutre of Physics, National Chiao-Tung University, Hsinchu 300, Taiwan* CHIA PIN SUN, *Department of Physics, National Sun Yat-Sen University, Kaohsiung 804, Taiwan* TING KUO LEE, *Institute of Physics, Academia Sinica, Nankang 11592, Taiwan* SUNG IK LEE, *National Creative Research Initiative Center for Superconductivity and Department of Physics, Pohang University of Science and Technology, Pohang, 794* The magnetic field dependence of low temperature specific heat in$YNi_2B_2C$ was measured and analyzed using various pairing order parameters. At zero magnetic field, the two-gap model which has been successfully applied to $MgB_2$and the point-node model, appear to describe the superconducting gap function of YNi2B2C better than other models based on the isotropic s−wave, the d−wave line nodes, or the s+g wave. The two energy gaps, $\Delta$ L=2.67 meV and $\Delta$ S=1.19 meV are obtained. The observed nonlinear field dependence of electronic specific heat coefficient, $\gamma$ (H)∼ H0.47, is quantitatively close to $\gamma$ (H)∼ H0.5expected for nodal superconductivity or can be qualitatively explained using two−gap scenario. Furthermore, the positive curvature in Hc2(T) near Tc is qualitatively similar to that in the other two−gap superconductor MgB2.

**12:03**

**V38 5 Probing the anisotropic phonon attenuation in superconducting lead.*** T.L. HEAD, J.P. WOLFE, *University of Illinois Urbana-Champaign* Phonon imaging of single crystals of superconducting Pb have uncovered a strong attenuation of phonons in (111) planes. Early data by Wolfe and Short[1] raised the possibility of a spin-density-wave ground state as proposed by Overhauser and Daemen.[2] This interpretation depends on the frequencies of the ballistic phonons, which previously were determined by a Planckian heater source and isotope scattering. We have designed and fabricated a low-pass filter in an attempt to select phonon energies below a characteristic activation energy, in order to clarify the source of the attenuation lines. We present new phonon-imaging data under various conditions and discuss the possible interpretations. [1]Physica B 316-317 (2002) 107-109 [2] Phys. Rev. B 39, 6431 (1989)

*Supported By the Department of Energy MRL grant DEFG02-96ER45439

**12:15**

**V38 6 Hard X-ray Structural Studies of $HgBa_2CuO_{4+\delta}$** GUILLAUME CHABOT-COUTURE, *Applied Physics Department, Stanford University* JASON N. HANCOCK, *Stanford Synchroton Radiation Laboratory, Stanford University* LI LU, *Applied Physics Department, Stanford University* ZAHIRUL ISLAM, *Advanced Photon Source, Argonne National Lab* MARTIN GREVEN, *Stanford University* Recent high-energy x-ray diffuse scattering work on the compounds YBCO and BSCCO shows that these high-$T_c$ superconductors are typically intrinsically inhomogeneous [1-3]. These inhomogeneities are short-range-ordered lattice modulations driven by oxygen dopants, and they appear to have an important role in the electronic, transport, and spectroscopic properties of these systems. $HgBa_2CuO_{4+\delta}$ (Hg1201) has a simple structure and the highest $T_c$ (at optimal doping) among all single-layer compounds. It is thus a perfect candidate system to address the issue of charge modulations. Here we present evidence for short-range incommensurate displacement modulations and discus our results in the context of similar findings in other compounds.

[1] Z. Islam et al., PRL 93, 157008 (2004).
[2] J. Strempfer et al., PRL 93, 157007 (2004).
[3] J. P. Castellan et al., http://arXiv.org/abs/cond-mat/0507505.

**12:27**

**V38 7 Structure at low temperature of oxygen isotope exchanged $La_{1.8875}Sr_{0.1125}CuO_4$*** A. R. MOODENBAUGH, D. E. COX, T. VOGT, B. NOHEDA, *Brookhaven National Lab.* M. K. CRAWFORD, E. M. McCARRON, W. E. FARNETH, *Dupont* The crystal structures at low temperatures of oxygen isotope-exchanged pairs of $La_{1.8875}Sr_{0.1125}CuO_4$ were examined using high resolution synchrotron powder x-ray diffraction at NSLS X7A. This study was designed to examine the possibility that small structural differences might contribute to the observed superconducting isotope effects. The x-ray diffraction regions about the orthorhombic (200),(020) peaks of $^{16}O$ and $^{18}O$ isotope-exchanged pairs were studied in detail. There is no significant difference in orthorhombic lattice parameters at any temperature. A minority ( $\sim$ 10%) tetragonal (LTT) phase is also necessary to adequately account for the observed intensities at low temperatures. The fraction of LTT phase does not differ perceptibly with oxygen isotope exchange. We conclude, based on direct measurement of crystal structure at low temperatures, that the observed differences in superconductivity of oxygen isotope exchanged pairs are likely intrinsic effects.

*Research Supported by the U.S. Dept. of Energy Contract DE-AC02-98CH10886.

**12:39**

**V38 8 Preliminary Inelastic Neutron Scattering Results for the Magnetic Excitations in the Model Superconductor $HgBa_2CuO_{4+\delta}$*** G. YU, X. ZHAO, Y. C. CHO, G. CHABOT-COUTURE, E. M. MOTOYAMA, *Department of Applied Physics, Physics, and Stanford Synchrotron Radiation Laboratory, Stanford University, Stanford, CA 94305, USA* P. BOURGES, *Laboratoire Leon Brillouin, CEA-Saclay, 91191 Gif-sur-Yvette, Cedex, France* M. GREVEN, *Department of Applied Physics and Stanford Synchrotron Radiation Laboratory, Stanford University, Stanford, CA 94305, USA* $HgBa_2CuO_{4+\delta}$ has a simple crystal structure and possess the highest $T_c$ (97 K at optimal doping) among all the single-layer cuprates. In a significant breakthrough, we were able to grow large $HgBa_2CuO_{4+\delta}$ single crystals, enabling us to perform the first inelastic magnetic neutron scattering experiments on this model superconductor. We performed energy scans at $(\pi, \pi)$ and momentum scans at fixed energy at 10 K and above Tc. Our preliminary results include the observation of a 52 meV feature at $(\pi, \pi)$ that resembles the ''resonance'' found in other cuprates.

*The authors gratefully acknowledge support from NSF and DOE.

**12:51**

**V38 9 Stability Constraints and Local Criteria for the Bounds on $T_c$ of Conventional Superconductors*** JONATHAN E. MOUSSA, MARVIN L. COHEN, *University of California at Berkeley and Lawrence Berkeley National Laboratory* In the regime of weak electron-phonon coupling, the scale of and bounds on $T_c$ are set by the real phonon frequencies of a material. In the strong coupling limit of Eliashberg theory, the phonon frequencies no longer limit the transition temperature because $T_c$ can grow without bound as $\sim \sqrt{\lambda}\,\omega_{ph}$, where $\lambda$ is the electron-phonon coupling parameter. However, structural stability of the system puts bounds on $T_c$ even in the strongly coupled regime due to the softening of phonons. In this case, $T_c$ is also bounded by an averaged unrenormalized phonon frequency defined for a non-metallic precursor material. Additional features of this model will also be discussed.

*This work was supported by NSF Grant No. DMR04-39768 and by the Director, Office of Science, Office of Basic Energy Sciences, Division of Materials Sciences and Engineering, U.S. Department of Energy under Contract No. DE-AC03-76SF00098.

**13:03**

**V38 10 Anisotropic Superconducting Phase Diagram of $C_6Ca$*** ULRICH WELP, R. XIE, D. ROSENMANN, A. RYDH,† H. CLAUS, G. KARAPETROV, W. K. KWOK, *Materials Science Division, Argonne National Laboratory, Argonne, IL 60439* We present a study of the anisotropic superconducting phase diagram of the new carbon intercalation superconductor $C_6Ca$ employing magnetization and specific heat measurements. The intercalation of Ca into flakes of natural graphite takes place through vapor transport at temperatures near 500°C. The resulting crystals dis-

play an onset of superconductivity at 11.3 K and a transition width of about 1 K as seen in heat capacity and low-field magnetization measurements. A clear step in the heat capacity confirms the bulk nature of the superconducting state. Roughly 1/3 to 1/2 of the sample volume is superconducting as evidenced by the reduced step height of the heat capacity. From measurements of the upper critical field, $H_{c2}$, we determined an in-plane coherence length of $\xi_{ab} \approx$ 36 nm. The angular dependence of $H_{c2}$ is well described within the model of effective mass anisotropy yielding an anisotropy parameter of $\Gamma \approx$ 3.5 to 4.

*This work was supported by the U.S. Department of Energy under grant no. W-31-109-ENG-38

†present address: Stockholm University, Albanova, SE-10691, Sweden

**13:15**

**V38 11 Upper critical field $H_{c2}$ in $PrOs_4Sb_{12}$*** DAVID PARKER, *USC Dept. of Physics* KAZUMI MAKI, *USC Dept. of Physics* HYEKYUNG WON, *Hallym Univ. Dept. of Physics* We study the upper critical field of the A and B phases in the triplet superconductor $PrOs_4Sb_{12}$ within the p+h-wave superconductivity proposed recently for this material. The present result is compared with $H_{c2}$(t) and H*(t), the boundary between the A and B phase in $PrOs_4Sb_{12}$, reported earlier and with more recent data of $H_{c2}(t)$ for the single phase crystal. We find $H_{c2}$(t)'s for both the two phase crystal and the single phase crystal are described by the model for the A phase. From this fitting one can deduce the Fermi velocity as $v = 2.5 \times 10^6$ cm/s. On the other hand $H_{c2}$(t) for the B phase is found to be somewhat smaller than H*(t), which is rather puzzling.

*The authors gratefully acknowledge the hospitality and support of the Max-Planck Institute for the Physics of Complex Systems, Dresden.

**13:27**

**V38 12 Superconductivity and magnetism in small attractive and repulsive Hubbard clusters** ARMEN KOCHARIAN, *California State University* GAYANATH FERNANDO, KALUM PALANDAGE, *University of Connecticut* JAMES DAVENPORT, *Brookhaven National Laboratory* The existing mapping between the ground state properties of $U > 0$ and $U < 0$ Hubbard models are extended to finite temperatures, arbitrary magnetic field and electron doping or chemical potential for small two and four sites clusters. The microscopic origin of charge-spin separation effect and pseudogap formation are studied in response thermodynamics for spin and charge susceptibilities, using exact analytical diagonalization technique and grand canonical ensemble method. In the limiting case of non-interacting particles there are no temperature or magnetically driven driven spin-charge separation. The obtained knowledge we use to compare the thermodynamic phase diagrams of $U > 0$ and $U < 0$ clusters in a multidimensional parameter space of temperature, magnetic field and chemical potential. Magnetism and superconductivity are often thought to be incomparable with one another, however, we found many identical features for $U > 0$ and $U < 0$ at various range of doping level in the specific heat, spin and charge pseudogaps, Mott-Hubbard and antiferromagnetic crossovers, when these physical characteristics are monitored as a function of chemical potential or doping level. The developed bottom up approach for small clusters displays important intrinsic characteristics of high $T_c$ superconductors.

**13:39**

**V38 13 Spin-triplet pairing in noncentrosymmetric superconductors: $Li_2Pd_3B$ and $Li_2Pt_3B$** H.Q. YUAN, M.B. SALAMON, D. VANDERVELDE, *Department of Physics, University of Illinois at Urbana and Champaign* D.F. AGTERBERG, *Department of Physics, U. Wisconsin-Milwaukee* N. HAYASHI, M. SIGRIST, *Theoretische Phyik, ETHZ* P. BADICA, *Institute for Materials Research, Tohoku University* K. TOGANO, *NIMS, Japan* Superconductors lacking inversion symmetry exhibit qualitatively distinct properties from those with an inversion center. In this presentation, we report strong evidence for triplet superconductivity caused solely by the absence of parity symmetry in two closely related cubic compounds $Li_2Pd_3B$ and $Li_2Pt_3B$. Broken inversion symmetry admits antisymmetric spin-orbit coupling, admixing spin-singlet and spin-triplet pairing even with s-wave orbital symmetry. The triplet contribution is weak in $Li_2Pd_3B$, a BCS-like superconductor with an anisotropic gap. With increased spin- orbit coupling the spin-triplet component dominates in $Li_2Pt_3B$, producing line nodes in the energy gap. Results are supported by the quantitative agreement between experimental penetration depth data and theory. Our findings demonstrate that unconventional superconducting properties can originate from a conventional phonon pairing mechanism rather than requiring purely electronic coupling mechanisms as usually considered.

**13:51**

**V38 14 Low Temperature Normal State Specific Heat properties of $La_{2-x}Sr_xCuO_4$ using High Magnetic Fields** SCOTT RIGGS, GREG BOEBINGER, JON BETTS, FEDOR BALAKIREV, ALBERT MIGLORI, MARCELO JAIME, *Florida State University* A number of models for high Tc cuprates suggest that the anomalous electronic properties of HTS are governed by the existence of a quantum critical point (QCP). According to this scenario, the superconductivity arises from the competition between two states and the resulting fluctuation-mediated pairing. In heavy fermions, non-Fermi liquid behavior has often been observed near a QCP: eg near-linear power-law resistivity and a divergence in the Sommerfeld coefficient in the zero temperature limit. By using extremely high magnetic fields we suppress superconductivity and reveal the normal state in the zero temperature limit. The specific heat is measured using the relaxation technique on several different dopings of LSCO. The electronic specific heat is isolated by subtracting the phonon specific heat measured on LCO, the parent insulating compound. One overdoped single crystal studied (LSCO with a nominal Srx=0.22) was cut from the same crystal that displays a linear electrical resistivity between room temperature and $\sim$ 5K, when the superconductivity is suppressed with a 45T magnetic field applied along the *c*-axis.

**SESSION V39: FOCUS SESSION: SUPERCONDUCTIVITY-THEORY AND COMPUTATION III**
**Thursday Morning, 16 March 2006**
**342, Baltimore Convention Center at 11:15**
**Alex Gurevich, University of Wisconsin-Madison, presiding**

**11:15**

**V39 1 Non-Fermi liquid and pairing in electron-doped cuprates*** ANDREY CHUBUKOV, *University of Wisconsin* PAVEL KROTKOV, *University of Maryland* In electron-doped cuprates near optimal doping we show that in the normal state the fermionic self-energy has a non-Fermi liquid form leading to pe-

culiar frequency dependencies of the conductivity and the Raman response. We solve the pairing problem and demonstrate that $T_c$ is determined by the curvature of the Fermi surface, and the pairing gap $\Delta(\mathbf{k},\omega)$ is strongly non-monotonic along the Fermi surface. The normal state frequency dependencies, the value of $T_c \sim 10K$ and the **k**-dependence of the gap agree with the experiment.

*Supported by NSF DMR 0240238.

**11:27**
**V39 2 Antiferromagnetic superconducting state in the electron-doped cuprates?** TANMOY DAS, ROBERT S. MARKIEWICZ, ARUN BANSIL, *Northeastern University* Recent angle-resolved photoemission (ARPES) studies of the electron-doped cuprate $Nd_{2-x}Ce_xCuO_4$ (NCCO)[1] have been interpreted in terms of a uniform antiferromagnetic (AF) metal, with doping into the upper magnetic band and gap collapse close to optimal doping[2]. An open question is whether the system remains uniform in the simultaneous presence of AF and (d-wave) superconducting (SC) order. Here, we explore the properties of a *uniform* AF-SC model for NCCO, to ascertain to what extent we can explain anomalous features, such as the nonmonotonic angle dependence of the superconducting gap[3]. Work supported by the USDOE. [1] N.P. Armitage, *et al.,* PRL **87**, 147003 (2002). [2] C. Kusko, *et al.,* PRB**66**, 140513 (2002); A.-M.S. Tremblay, *et al.,* cond-mat/0511334. [3] H. Matsui, *et al.,* PRL **95**, 017003 (2005).

**11:39**
**V39 3 Spin response in high-$T_c$ superconductors at higher energies** BABAK SERADJEH, IGOR HERBUT, *Simon Fraser University* We discuss our recent results on the spin sector of the theory of underdoped cuprates as fluctating d-wave superconductors (I. Herbut, PRL 94, 237001 (2005)). We improve on an earlier computation of spin response (I. Herbut and D. Lee, PRB 68, 104518 (2003)) by including the effects of non-relativistic terms in the dispersion of nodal quasipartciles and thus by going beyond the low-energy approximation employed in the earlier work. We find that non-relativistic effects tend to reduce the spin gap at $(\pi,\pi)$. This could be relevant for recent neutron scattering measurements.

**11:51**
**V39 4 Screening in anisotropic superfluids and the superfluid density in underdoped cuprates** MATTHEW CASE, IGOR HERBUT, *Simon Fraser University* The effects of quantum and classical phase fluctuations on the superfluid density of underdoped cuprates can be modeled by an anisotropic system of Coulomb interacting bosons. In such a system, the collective excitations screen the Coulomb interaction whose effective strength, together with the strength of the anisotropy, determines the temperature dependence of the superfluid density. We will argue that the underdoped cuprates are in the short-ranged, weakly interacting regime characterized by an approximately linear superfluid density.

**12:03**
**V39 5 Impurity effects in metals and superconductors** KURT SCHARNBERG, SIMON SCHEFFLER, CARSTEN RIECK, In the theoretical analyses of impurity effects in superconductors the assumption is usually made that all quantities are slowly varying functions of energy except for the Green functions, whose energy dependence is integrated out. The energy-integrated normals state Green function for the NFE model is $-i$ and the divergent real part is omitted. The argument of any other momentum dependent quantity is replaced by the Fermi momentum. When defects modelled by scattering potentials of finite range, which lead to scattering in infinitely many angular momentum channels, are treated within this so-called Fermi Surface Restricted Approximation, unacceptable results for the selfenergies, the pair breaking parameters and others follow in the strong scattering limit. It has been found necessary to consider the principal value integral involving the real part of the Green function in the *T*-matrix equation. In this way, the range of the potential is re-introduced as an essential parameter and resonant scattering in different $\ell$-channels can occur for moderately large potentials, while $\delta$-function potentials, even when there strength is infinite, do not scatter at all. This generalized theory of impurity effects will be applied to calculations of the local density of states near an impurity and, using the selfconsistent *T*-matrix approximation for an ensemble of impurities, to calculations of spectral functions.

**12:15**
**V39 6 Type-IV Superconductivity Phenomenon: Cooper Pairs with Broken Parity and Spin-Rotational Symmetries in D- and S-wave Singlet Superconductors** ANDREI LEBED, *Dept. of Physics, University of Arizona* Paramagnetic effects are shown to result in the appearance of a triplet component of order parameter in vortex phases of d- and s-wave singlet superconductors in the absence of impurities. This component, which breaks both parity and spin-rotational symmetries of Cooper pairs, is expected to be of the order of unity in a number of modern superconductors such as high-Tc, organic, $MgB_2$, and some others. A generic phase diagram of such type-IV superconductors [1], which are singlet ones at H=0 and in the Meissner phase and characterized by singlet-triplet mixed Copper pairs, $\Delta_s + i\Delta_t$, in a vortex phase, is suggested. [1] A.G. Lebed, Physical Review Letters, accepted (2006).

**12:27**
**V39 7 Superfluid density and competing orders in *d*-wave superconductors** SERGEI SHARAPOV, *Department of Physics and Astronomy, McMaster University* JULES CARBOTTE, We derive expressions for the superfluid density $\rho_s$ in the low-temperature limit $T \to 0$ in *d*-wave superconductors, taking into account the presence of competing orders such as spin-density waves, *is*-pairing, etc. Recent experimental data for the thermal conductivity and for elastic neutron scattering in $La_{2-x}Sr_xCuO_4$ suggest there are magnetic field induced anomalies that can be interpreted in terms of competing orders. We consider the implications of these results for the superfluid density and show in the case of competing spin-density wave order the usual Volovik-like $\sqrt{H}$ depletion of $\rho_s(H)$ is replaced by a slower dependence of $\rho_s$ on the applied magnetic field *H*. We show that it is crucial to include the competing order parameter in the self-consistent equation for the impurity scattering rate.

**12:39**
**V39 8 Index theorem and quantum order of d-wave superconductors in the vortex state*** OSKAR VAFEK, *Stanford University* ASHOT MELIKYAN, *University of Florida* It is argued that the ground state of the lattice d-wave superconductor in the lattice of singly quantized $hc/2e$ vortices can posses quantum order. This is due to simultaneous crystallization of both the superflow and the fluxes of the $Z_2$ gauge field, the second of which has no classical analog. In the presence of particle hole symmetry we prove an

index theorem which puts a lower bound on the number of zero energy modes. This bound is equal to 4 times the number of lattice sites coinciding with the centers of inversion within the magnetic unit cell. Generic cases are constructed in which this bound exceeds the number of zero modes of an equivalent lattice of doubly quantized vortices (as well as singly quantized vortices without Z2), despite identical classical symmetries. The spectrum around the zero modes is doubly degenerate and Dirac-like, with velocities that become universal functions of $\Delta/t$ in the limit of low magnetic field. For small, but finite strength of particle-hole symmetry breaking, the gapped state can be characterized by a topological quantum number, related to spin Hall conductivity, which differs in the case of $hc/2e$ and $hc/e$ vortex lattice.

*cond-mat/0509258

**12:51**

**V39 9 Electronic Density of States of a Superconductor with a Spatially Varying Gap and Phase Fluctuations: A Monte Carlo Simulation*** DANIEL VALDEZ-BALDERAS, DAVID STROUD, *Department of Physics, The Ohio State University* Recent experiments have shown that the superconducting energy gap in some high-$T_c$ superconductors is spatially inhomogeneous. Motivated by these experiments, and using exact diagonalization of a model d-wave Hamiltonian (T. Eckl et al. PRB 66 140510), combined with Monte Carlo simulations of a Ginzburg-Landau free energy functional, we have calculated the electronic density of states $n(E)$ of a model high-$T_c$ superconductor with an inhomogeneous gap. The free energy functional incorporates both phase and amplitude fluctuations together with quenched disorder. It leads to a superconducting transition temperature $T_c$ well below the pseudogap temperature $T_{c0}$, and has a spatially varying gap at very low $T$, both consistent with experiments in underdoped Bi2212. Our calculated $n(E)$ shows coherence peaks for $T < T_c$, which disappear for $T > T_c$. We will also present calculated results for both the global and local $n(E)$ as a function of temperature and disorder.

*Work supported by NSF DMR04-13395

**13:03**

**V39 10 Raising Bi-O bands above the Fermi energy level of hole-doped $Bi_2Sr_2CaCu_2O_{8+\delta}$ and other cuprate superconductors** HSIN LIN, S. SAHRAKORPI, R.S. MARKIEWICZ, A. BANSIL, *Northeastern University* The Fermi surface (FS) of $Bi_2Sr_2CaCu_2O_8$ (Bi2212) predicted by band theory displays Bi-related pockets around the $(\pi,0)$ point, which have never been observed experimentally. We show that when the effects of hole doping by substituting Pb for Bi or by adding excess O in Bi2212 are included, the Bi-O bands are lifted above the Fermi energy ($E_F$) and the resulting first-principles FS is in remarkable accord with measurements. With decreasing hole-doping the Bi-O bands drop below the $E_F$ and the system self-dopes below a critical hole concentration. Computations on other Bi- as well as Tl- and Hg-based compounds indicate that lifting of the cation-derived band with hole doping is a general property of the electronic structures of the cuprates. Work supported by the USDOE.

**13:15**

**V39 11 Evolution of Mid-gap States and Residual 3-Dimensionality in Cuprates*** S. SAHRAKORPI, *Northeastern University* M. LINDROOS, *Tampere University of Technology* R. MARKIEWICZ, *Northeastern University* A. BANSIL, *Northeastern University* We have carried out extensive first principles doping-dependent computations of angle-resolved photoemission (ARPES) intensities in $Bi_2Sr_2CaCu_2O_8$ (Bi2212) and $La_{2-x}Sr_xCuO_4$ (LSCO) over a wide range of binding energies.[1,2,3] Intercell hopping and the associated 3-dimensionality, which is usually neglected in discussing cuprate physics, is shown to play a key role in shaping the ARPES spectra. Despite the obvious importance of strong coupling effects (e.g. the presence of a lower Hubbard band coexisting with mid-gap states in the doped insulator), a number of salient features of the experimental ARPES spectra of LSCO are captured to a surprising extent when $k_z$-dispersion is properly included in the analysis. 1. S. Sahrakorpi, et al., Phys. Rev. Lett. 95, 157601 (2005). 2. A. Bansil, et al., Phys. Rev. B 71, 012503 (2005). 3. A. Bansil, et al., New Journal of Physics 7, 140 (2005); http://www.iop.org/EJ/abstract/1367-2630/7/1/140.

*Work supported by U.S. D.O.E.

**13:27**

**V39 12 Dirac-Bogoliubov-de Gennes quasiparticles in the mixed state of lattice d-wave superconductors*** ASHOT MELIKYAN, *University of Florida* ZLATKO TESANOVIC, *Johns Hopkins University* In the mixed state of cuprate superconductors the low energy quasiparticles can be effectively described as Dirac fermions moving in the field of singular scalar and vector potentials. Although the effective linearized Hamiltonian operator formally does not depend on the structure of vortex cores, singular nature of the perturbation requires imposing additional boundary conditions at vortex locations. Each vortex is described by a parameter $\theta$ that effectively represents all effects beyond linearization. We identify the parameters $\theta$ of the solutions found earlier, analyze the relation between fully self-consistent formulation of the problem and the linearized model, and construct the low-field scaling form of the quasiparticle spectra incorporating the parameters $\theta$ explicitly and generalizing the conventional Simon-Lee scaling. We present a detailed numerical study of the lattice $d$-wave superconductor model and examine its low energy, low magnetic field behavior. The low energy limit is faithfully represented by Dirac-like fermions which are either truly massless, massless at the linearized level or massive, depending on the commensuration of magnetic length and lattice spacing.

*Supported in part by NSF grants DMR-0094981 and DMR-0531159. A.M. was supported by the Inst. of Fundamental Theory, Florida

**13:39**

**V39 13 Phase Fluctuations in Strongly Coupled d-Wave Superconductors** MATTHIAS MAYR, *UT/Knoxville and Oak Ridge National Laboratory* GONZALO ALVAREZ, *Oak Ridge National Laboratory* CENGIZ SEN, *FSU/NHMFL* ELBIO DAGOTTO, *UT/Knoxville and Oak Ridge National Laboratory* We present a numerically exact solution for the BCS Hamiltonian at any temperature, including the degrees of freedom associated with classical phase, as well as amplitude fluctuations via a Monte Carlo integration. This allows for an investigation over the whole range of couplings: from weak attraction, as in the well-known BCS limit, to the mainly unexplored strong-coupling regime of

pronounced phase fluctuations. In the latter, two characteristic temperatures T* and $T_c$, associated with short- and long-range ordering, respectively, can be identified in a mean-field-motivated Hamiltonian. T* at the same time corresponds to the opening of a gap in the excitation spectrum. In addition to introducing a novel procedure to study strongly coupled *d*-wave superconductors, our results indicate that classical phase fluctuations are not sufficient to explain the pseudogap features of high-temperature superconductors.

**13:51**

**V39 14 Excitonic pairing between nodal fermions** WILLIAM SHIVELY, DMITRI KHVESHCHENKO, *Dept. Physics & Astronomy, University of North Carolina at Chapel Hill* We discuss excitonic pairing in nodal fermion systems, characterized by a vanishing quasiparticle density of states at the point-like Fermi surface and a concomitant lack of screening for long-range interactions. We solve the gap equation and obtain the free energy and critical values of the interaction strength for a variety of algebraically interactions and power-law densities of states. On the basis of this insight, we analyze possible phase transitions in this interesting class of non-fermi-liquid systems.

**14:03**

**V39 15 Nodal Quasiparticles at a Nematic Quantum Critical Point** PAUL ORETO, EUN-AH KIM, STEVEN KIVELSON, *Department of Physics, Stanford University* EDUARDO FRADKIN, *Department of Physics, University of Illinois at Urbana-Champaign* The nodal quasiparticles in the high-Tc superconductors are robust consequences of the d-wave symmetry. Under most circumstances, the properties of these Dirac-like particles are generally simple, since most interactions involving them are ''irrelevant.'' However, they are strongly scattered by the symmetry breaking fluctuations near an electronic nematic quantum critical point. In the quantum critical regime, an anomalous damping and enhancement of the dispersion anisotropy of the quasi-particles results. Possible relevance of this to the so-called ''Fermi arc'' seen in the underdoped cuprates is discussed.

**SESSION V40: FOCUS SESSION: LINEAR OPTICS QUANTUM COMPUTATION**
**Thursday Morning, 16 March 2006**
**343, Baltimore Convention Center at 11:15**
**Jonathan Dowling, Louisiana State University, presiding**

***Contributed Papers***

**11:15**

**V40 1 High-fidelity linear optical quantum computing with polarization encoding** FEDERICO SPEDALIERI, *Jet Propulsion Laboratory* HWANG LEE, *Lousiana State University* JONATHAN DOWLING, *Louisiana State University* We show that the KLM scheme [Knill, Laflamme and Milburn, Nature **409**, 46] can be implemented using polarization encoding, thus reducing the number of path modes required by half. One of the main advantages of this new implementation is that it naturally incorporates a loss detection mechanism that makes the probability of a gate introducing a non-detected error, when non-ideal detectors are considered, dependent only on the detector dark-count rate and independent of its efficiency. Since very low dark-count rate detectors are currently available, a high-fidelity gate (probability of error of order $10^{-6}$ conditional on the gate being successful) can be implemented using polarization encoding. The detector efficiency determines the overall success probability of the gate but does not affect its fidelity. This can be applied to the efficient construction of optical cluster states with very high fidelity for quantum computing.

**11:27**

**V40 2 Single Photon Source Using Chiral Nematic Liquid Crystal** GANESH SELVARAJ, *Louisiana State University* ANAND JHA, *University of Rochester* PAVEL LOUGOVSKI, MARIAN FLORESCU, *Louisiana State University* ROBERT BOYD, *University of Rochester* JONATHAN DOWLING, *Louisiana State University* With the development of Linear Optics Quantum Computing, a demand for a good single photon source has increased. Here we describe how a cholesteric liquid crystal can be used as a photonic band-gap material to design a single-photon source. We have a dipole embedded in a liquid crystal for which we find the spontaneous emission rate. We calculate the band structureof the cholesteric liquid crystal using the eigenfuncton expansion method and ultimately compute the density of modes. We also determine the field of the dipole embedded inside the cholesteric liquid crystal using the Green's function method from which we determine the spontaneous emmission rate.

**11:39**

**V40 3 How to construct a Universal Linear Optical State Generator?** PAVEL LOUGOVSKI, HWANG LEE, JONATHAN DOWLING, *Louisiana State University* We consider all optical realization of a universal quantum state generator utilizing projective photon measurements to create an effective non-linearity. Specifically we are interested in finding a set of unitary optical devices required in order to generate a given quantum state for a given input and a projective measurement. We illustrate the formalism for a case of multi-photon path entangled states (N00N states). We conjecture an existence of necessary criteria connecting a size of a N00N state to a number of input modes of a generator.

*Invited Papers*

**11:51**
**V40 4 Towards one-way quantum computation with realistic devices.**
TERRY RUDOLPH, *Imperial College London*

The one-way model seems particularly suited to certain proposed architectures for quantum computation, particularly those involving non-deterministic quantum gates. This talk will focus on strategies for dealing with faulty devices in the one-way model, particularly within the framework of linear optical quantum computation, although the results have more general significance. Special mention will made of strategies for dealing with faulty single photon sources and detectors, which are the primary experimental challenge for many proposed implementations of optical quantum computation.

*Contributed Papers*

**12:27**
**V40 5 Single-photon sources for linear optics quantum computation** TODD PITTMAN, BRYAN JACOBS, JAMES FRANSON, *Johns Hopkins Univ. Applied Physics Laboratory* JOHNS HOPKINS UNIV. APPLIED PHYSICS LABORATORY TEAM, Although single-photon sources have recently been realized in a number of physical systems, only of few of them have experimentally demonstrated the types of properties required for linear optics quantum computing. In this talk, we review these requirements, and discuss the technical and fundamental challenges in meeting them. We will focus on a periodic source in which single-photons heralded from parametric down-conversion pairs are trapped and released from a storage loop.

**12:39**
**V40 6 Optical Switches for Quantum Information Processing** BRYAN JACOBS, *Johns Hopkins University* TODD PITTMAN, JAMES FRANSON, *Johns Hopkins University* Many of the basic components required for optical quantum computing and quantum communications have recently been demonstrated, including: single photon sources, quantum memories, logic operations, and photon number resolving detectors. Although the results of these proof-of-concept demonstrations are encouraging, errors in the current devices limit the range of applications to relatively small quantum circuits. The majority of the errors in the current devices originates from photon loss and decoherence in the switching elements. The single-photon nature of the signal, when coupled with quantum coherence requirements, limits the feasibility of using standard telecom switches in these applications. Here we discuss our recent work toward the development of optical switches specifically designed to accommodate the characteristics of photonic qubits.

**12:51**
**V40 7 Entangled Photon Holes*** JAMES FRANSON, *Johns Hopkins University* The probabilistic failure events of linear optics logic gates can be suppressed using the quantum Zeno effect enforced by strong two-photon absorption [1]. This would allow deterministic logic operations as a possible alternative to the use of cluster states. We have recently shown, however, that the rate of two-photon absorption can be substantially reduced by the generation of entangled photon holes that are analogous to the holes of semiconductor theory [2]. This reduction in the two-photon absorption rate is inconsistent with classical or semiclassical theory, and the entangled photon holes can violate Bell's inequality as well. As a practical matter, these difficulties can be avoided if the photons travel in opposite directions, in which case the entangled photon holes propagate away from each. The theory of entangled photon holes and their implications for the design of Zeno gates will be discussed.
[1] J.D. Franson, B.C. Jacobs, and T.B. Pittman, Phys. Rev. A **70**, 062302 (2004).
[2] J.D. Franson, submitted to Phys. Rev. Lett. (quant-ph/0510175).

*This work was supported by DTO and ARO.

**13:03**
**V40 8 Creating single time-bin entangled photon pairs** CHRISTOPH SIMON, *University of Grenoble (France)* JEAN-PHILIPPE POIZAT, *University of Grenoble* When a single emitter is excited by two phase-coherent pulses with a time delay, each of the pulses can lead to the emission of a photon pair, thus creating a ''time-bin entangled'' state. Double pair emission can be avoided by initially preparing the emitter in a metastable state. We show how photons from separate emissions can be made indistinguishable, permitting their use for multi-photon interference. Possible realizations with single atoms or ions and with quantum dots are discussed. The method might also allow the direct creation of $n$-photon entangled states (n$>$ 2).

**13:15**
**V40 9 Towards a Quantum Memory for Photons in Erbium Doped Materials** SARA HASTINGS-SIMON, *University of Geneva* MATTHIAS STAUDT, BARBARA KRAUS, WOLFGANG TITTEL, MIKAEL AFZELIUS, NICOLAS GISIN, *University of Geneva* IGNACIO CIRAC, *Max Planck Institute for Quantum Optics* MATTIAS NILSSON, STEFAN KROLL, *Lund Institute of Technology* Quantum memories for single photons could play an important role in quantum communication and optical quantum computing. We present a proposal for the efficient storage and recall of photonic time-bin qubits, based on reversible absorption in a controllably broadened homogeneous absorption line. We report on the first experimental steps towards the realization of this quantum memory protocol. In particular, we have measured the homogenous lifetime of the relevant optical transition in erbium doped optical fibers and erbium doped lithium niobate waveguides by spectral hole burning and photon echo. We have also observed the controlled reversible broadening of spectral holes and spectral hole line shifts due to the Stark effect.

**13:27**
**V40 10 Design of an on demand single photon source using a metal-insulator-semiconductor capacitor structure** B.H. HU, C.H. YANG, *Department of Electrical and Computer Engineering, University of Maryland at College Park* M.J. YANG, *Naval Research Laboratory* We propose an on-demand single photon source for unconditionally secure quantum cryptography. Similar to a typical metal-insulator-semicondoctor capacitor structure, the

main component in the semiconductor is a p-doped quantum well, and the cylindrical gate under consideration is only nanometers in diameter. This MIS system can be biased to inversion, and, due to the small gate area, there are only a few electrons residing in a quantum dot at the onset of inversion. Considering the strong size quantization and large Coulomb energy, the number of electrons can be precisely controlled by the gate voltage. After holding just one electron in the inversion layer, the capacitor is quickly biased back to the flat band condition and the subsequent radiative recombination across the bandgap results in single photon emission. Using GaAs/AlAs as the model system, we present a numerical simulation of three-dimensional band bending and merits of this single photon source.

**13:39**

**V40 11 Superconducting Bolometric Photon Detectors Using Epitaxial Niobium Thin Films** KEVIN M. INDERHEES, PAUL B. WELANDER, SEONGSHIK OH,* JAMES N. ECKSTEIN, *Department of Physics, Frederick Seitz Materials Research Laboratory, University of Illinois at Urbana-Champaign, Urbana, Illinois 61801* Efficient single photon detection is a key part of optical qubit systems. We have made and tested superconducting bolometric photon detectors constructed from high quality epitaxial single crystal niobium films that are very flat. The devices operate at 4.2K and consist of narrow links which are current biased close to their critical current value. Absorption of a photon drives a portion of the device into the normal state, generating an observable voltage signal. The sensitivity is maximized when the link is biased near the critical current. The time averaged output voltage is linearly dependent on the optical power that illuminates the link. In order to optimize detector characteristics, we have studied the effects of changing the film thickness, the device geometry, and adding a protective cap.

*now at National Institute of Standards and Technology, Boulder, CO

**13:51**

**V40 12 Quantum dots as a source of entangled photon pairs.** MARK STEVENSON, ROBERT YOUNG, *Toshiba Research Europe Limited* PAOLA ATKINSON, KEN COOPER, DAVID RITCHIE, *Cavendish Laboratory, University of Cambridge* ANDREW SHIELDS, *Toshiba Research Europe Limited* Quantum dots are considered an attractive system for applications in quantum communication and quantum logic, confirmed by experimental demonstrations of quantum dot based single photon emission devices. Another key quantum optics resource is the on-demand generation of entangled photon pairs, for which the radiative decay of the biexciton state in a quantum dot has been proposed. The realization of such a device has been prevented due to polarization splitting of the exciton fine structure, caused by anisotropies of various structural parameters of the dot. We present the results of recent experiments that manage the splitting in quantum dots, in order to allow entangled photon emission. We demonstrate that dots with splitting within the homogeneous linewidth can be realized by carefully controlling the thickness of the dot layer. Furthermore, we show that the splitting can be reduced to zero by the application of an in-plane magnetic field. Polarization dependent correlation measurements on these dots will be presented that show characteristic features of entanglement, such as polarization correlation for all linear detection bases, and circular polarization anti-correlation. Our results indicate that for the first time, we have observed triggered entangled photon pair emission from a quantum dot.

## SESSION V41: FOCUS SESSION: DIELECTRIC, FERROELECTRIC, AND PIEZOELECTRIC OXIDES V

**Thursday Morning, 16 March 2006**
**344, Baltimore Convention Center at 11:15**
**Eric Cockayne, National Institute of Standards and Technology, presiding**

***Contributed Papers***

**11:15**

**V41 1 First principles theory of metal-oxide interfaces: the Schottky-Mott theory revisited** MATIAS NUNEZ, MARCO BUONGIORNO NARDELLI, *North Carolina State University* Using calculations from first principles, we discuss the interplay between structure and functionality at metal-insulator interfaces using the paradigmatic example of the junctions between various metals (Ag, Pd,Pt,Ni,Cu,Al) and binary crystalline oxides (BaO-,CaO and SrO). Our results demonstrate that it is possible to tune the Schottky barrier height in a very broad range of values just manipulating the metal at the interface and elucidate the role of the relative overlap in the density of states of the different components in determining the band alignment. We will also show how we can apply this concepts to interfaces between metals and ferroelectric oxides where the interface structure and charge transfer affect the spontaneous polarization of the ferroelectric.

**11:27**

**V41 2 Strains observed in 180° domain walls in $LiNbO_3$ with Laue topography** TERRENCE JACH, *NIST* SUNGWON KIM, *Penn State University* STEPHEN DURBIN, *Purdue University* VENKATRAMAN GOPALAN, *Penn State University* A comparison of the strains associated with domains in congruent $LiNbO_3$,previously observed with Bragg x-ray topography and currently with Laue x-ray topography, reveals some surprising differences. The Laue geometry allows imaging through the entire crystal. Using monochromatic collimated synchrotron radiation and a magnifying x-ray camera, we are able to image domains and the strains created by electric field poling, as well the additional strain created by the application of electric fields in real time. The unusual strain patterns can be taken into account with higher order terms in the ferroelectric Ginzberg-Landau theory. Electric fields below the coercive field applied along the c-axis produce Pendellösung stripes due to complex strains that are precursors to 180° domain wall switching. The strains observed with field off and field on in the Laue topographs differ significantly from the surface strains observed previously with Bragg topography.

**11:39**

**V41 3 Predicting polarization enhancement in multicomponent ferroelectric superlattices** SERGE NAKHMANSON, *Rutgers University* KARIN RABE, DAVID VANDERBILT, We use ab initio calculations as an input to develop a one-dimensional chain model of the local polarization in epitaxial short-period $CaTiO_3/SrTiO_3/BaTiO_3$ superlattices grown on a $SrTiO_3$ substrate. The model is then combined with a genetic algorithm optimization technique to predict the arrangement of individual $CaTiO_3$, $SrTiO_3$ and $BaTiO_3$ layers in a superlattice that would simultaneously have the highest possible polarization and a low in-plane lattice constant mismatch with the substrate. This modelling procedure can be applied to a wide range of layered perovskite-oxide nanostructures providing guidance for experimental development of nanoelectromechanical devices with substantially improved polar properties.

*Invited Papers*

**11:51**
**V41 4 Self-Poling in Strained Asymmetric Superlattices.***
MAITRI WARUSAWITHANA,† *Department of Physics, University of Illinois at Urbana-Champaign*

We have constructed strained dielectric superlattices consisting of three different perovskite titanate phases - $BaTiO_3$, $SrTiO_3$ and $CaTiO_3$ using ozone assisted atomic layer by layer molecular beam epitaxy, where the stacking architecture of the different phases controls the symmetry of the superlattice. To investigate the effect of structural symmetry (or the lack of symmetry) on the dielectric properties of such superlattices, avoiding effects due to asymmetric electrode interfaces, capacitor devices were constructed with symmetric, lattice-matched, conducting oxide electrodes. I will show that the stacking architecture modifies the dielectric and ferroelectric properties of the constituents leading to new electronic properties uncharacteristic of naturally occurring phases. Superlattices with broken inversion symmetry are self poled and generate a second order susceptibility, $\chi^{(2)}$, as a result of the built-in asymmetric strain fields. The resulting polarization direction and the sign of $\chi^{(2)}$ are fixed by the symmetry of the superlattice. Sensitive pyrocurrent measurements indicate an increasing polarization as the temperature is lowered while below a temperature, $T_x$, an onset of a hysteretic response is observed. I will discuss an unusual ferro-like phase with two unequal polarization states which emerges below $T_x$ where the P-E loops are displaced not only along the E-field-axis by an effective polarizing field, but also along the P-axis by an offset polarization.

*This work was done in collaboration with James Eckstein, Michael Weissman, Hao Chen, Jian-Min Zuo and Eugene Colla and was supported by the US Department of Energy.
†Present address - Department of Materials Science and Engineering, Penn State University.

*Contributed Papers*

**12:27**
**V41 5 X-ray catastrophe focusing with ferroelectrics** STEPHEN DURBIN, *Purdue University* TERRENCE JACH, *NIST* SUNGWON KIM, *Penn State University* VENKATRAMAN GOPALAN, *Penn State University* Familiar ripple patterns reflected from water waves and the characteristic cusp of light seen in the bottom of a coffee cup are examples of catastrophe optics, where focusing occurs without need for highly engineered optical elements; catastrophe theory provides the mathematical tools needed to describe the stability and topology of the caustics that produce these effects. We have discovered catastrophe focusing in the diffraction of hard x-rays from crystalline wafers of ferroelectric lithium niobate, by diffracting monochromated synchrotron undulator radiation from surface planes while applying a voltage across the thin crystal. The presence of anti-phase ferroelectric domains causes a rippling of the surface that produces focusing at an x-ray CCD camera a half meter away. The catastrophe focusing pattern can be uniquely controlled by the applied voltage. These results suggest possible applications of catastrophe optics to x-ray microfocusing, and to the use of voltage-controlled patterned ferroelectrics as a new concept in x-ray optical devices.

**12:39**
**V41 6 The Effect of Grain Boundary Charge on Ferroelectric Transitions in Nanograin $BaTiO_3$** I-WEI CHEN, XIAOHUI WANG, YUDI WANG, *Department of Materials Science and Engineering, University of Pennsylvania, Philadelphia, PA19104-6272, USA* We have recently reported dense polycrystalline $BaTiO_3$ that has sub-100 nm grains. As grain size decreases, the electrical field due to grain boundary charge extends to an increasingly larger fraction of the grain giving rise to a size effect that is fundamentally different from those previously considered in the literature. Using Ginsberg Landau theory we have modeled this effect on ferroelectric transition, polarization/phase distribution and dielectric/piezoelectric responses, and compared it with the experimental results of $BaTiO_3$ (XRD, TEM, and $\varepsilon(T)$). Such nanograin ferroelectric ceramics, currently available at sub-10 nm grain size, are of considerable interest for the next-generation microelectronic component applications. A related grain boundary effect on phase transition has also been reported in coarse grain and bicrystal $SrTiO_3$.

**12:51**
**V41 7 Epitaxial Growth of $BaTiO_3/SrTiO_3$ and $BaO/SrTiO_3$ Superlattices for Phonon Confinement*** A. SOUKIASSIAN, *Materials Research Institute, The Pennsylvania State University* N.D. LANZILLOTTI KIMURA, A. BRUCHHAUSEN, A. FAINSTEIN, *Centro Atómico Bariloche & Instituto Balseiro, C.N.E.A., Argentina* A. CROSS, A. CANTARERO, *Materials Science Inst., University of Valencia, Spain* H.P. SUN, X.P. PAN, *Dept. of Materials Science and Engineering, University of Michigan* W. TIAN, D.A. TENNE, X.X. XI, D.G. SCHLOM, *Materials Research Inst., The Pennsylvania State University* We discuss the design and material parameters of $BaTiO_3/SrTiO_3$ and $BaO/SrTiO_3$ heterostructures relevant for novel phonon devices, including mirrors, filters, and cavities for coherent phonon generation and control. The advantages of using these ferroelectric superlattices include that they have an enormous stop band compared to the GaAs/AlAs superlattices previously reported for this application and that there can be greatly amplified light-sound interaction in these ferroelectric materials. We have grown $BaTiO_3/SrTiO_3$ and $BaO/SrTiO_3$ superlattices on $TiO_2$-terminated $SrTiO_3$ substrates by reactive MBE. Structural characterization by XRD and TEM revealed that the samples studied are of high quality with nearly atomically abrupt interfaces. We have observed folded acoustic phonons at the expected frequencies using UV Raman spectroscopy.

*This work is supported by NSF and DOE.

**13:03**
**V41 8 Site-Selective Studies of Er-doped $SiO_2$/SRO layers** ZACKERY FLEISCHMAN, VOLKMAR DIEROLF, *Physics, Lehigh University* YANLI ZHANG, MARVIN WHITE, *ECE, Lehigh University* Er-doped $SiO_2$ has attracted much attention as a possible pathway to realizing Si-based optoelectronic devices. Of particular interest is how the presence of silicon nanocrystals af-

fects the Er emission in this host material. In samples containing nanocrystals, there are three possible environments for the Er defect to occupy: within, near, and far from the nanocrystal silicon; each environment having the possibility for clustered and nonclustered Er. We present site-selective photoluminescence results obtained from samples with and without nanocrystals to analyze the spectral differences between these two types of samples. We can spectrally identify the different Er environments by directly comparing the results from the two types of samples. We observed Er clustering sites which become dominant as the activation anneal temperature increases. This Er clustering site emission is decreased in the samples containing nanocrystals, indicating that the excess silicon inhibits the formation of clusters. Despite our good site-selectivity, we were unable to find any special spectral signature of nanocrystal-related Er suggesting that their local environment is similar to that of isolated Er ions in $SiO_2$.

**13:15**

**V41 9 First principles theory of the local dielectric permittivity: Application to surfaces and interfaces** NING SHI, RAMPI RAMPRASAD, *Department of Materials Science and Engineering, Institute of Materials Science, University of Connecticut, 97 N. Eagleville Road, Storrs, CT 06269* A new computationally efficient method has been developed within the framework of density functional theory to aid in the study of the dielectric properties of multi-component systems, with explicit treatment of surface and interface effects. The local polarization and permittivity functions, induced due to a finite external electric field, are introduced to describe variation of the dielectric response over length scales of the order of interatomic distances. Specifically, we have determined the position dependent dielectric permittivity profiles for Si-$SiO_2$ and $SiO_2$ -polymer systems. We find that at regions close to surfaces and interfaces, the dielectric permittivity is enhanced compared to the corresponding bulk values, while in interior regions it approaches the corresponding bulk values. The calculated optical and static dielectric constant values of these systems are in excellent agreement with experimental results, and other more involved computational treatments.

**13:27**

**V41 10 Surface Micromachined Ferroelectric MEMS Devices: Correlating Device Performance with Film Microstructure*** JENNIFER RUGLOVSKY, MATTHEW DICKEN, KENNETH DIEST, MOHAMED EL-NAGGAR, SHARLOTTE BOLYARD, DAVID GOODWIN, GURUSWAMI RAVICHANDRAN, KAUSHIK BHATTACHARYA, HARRY ATWATER, *California Institute of Technology* The realization of free-standing ferroelectric thin film devices compatible with CMOS processing is a priority in achieving sophisticated MEMs systems. To release an active film from a silicon substrate with a back-etch technique requires the removal of hundreds of microns of the substrate as well as a suitable and robust mask for the device layer. A more flexible and process compatible technique is surface micromachining. We present work utilizing a $XeF_2$ etch process for surface micromachining silicon with a resistant patterned oxide layer to create free-standing ferroelectric MEMs structures. With surface patterning, we are able to realize both bridge and cantilever geometries. Lead titanate thin films grown by MOCVD for the active layer will be discussed. The devices have been synthesized in three different thin film microstructures: 1) poorly oriented, 2) fiber textured, and 3) biaxially textured. The realization of such a continuum of microstructures allows the switching mechanism to be better resolved and for the correlation between macroscopic device performance and microscopic properties to be more fully understood.

*Supported by ARO-MURI:DAAD 19-01-1-0517

**13:39**

**V41 11 Interaction between ferroelectric nanodots: a first-principles-based study** S. PROSANDEEV,* I. PONOMAREVA, I. NAUMOV, I. KORNEV, L. BELLAICHE, UNIVERSITY OF ARKANSAS TEAM, We have performed Monte-Carlo simulations within a first- principles-based effective Hamiltonian approach to investigate the consequences (if any) of the interaction between nanodots made of lead titanium zirconate. We found that two dots under open circuit electrical boundary conditions weakly interact with each other, implying that they both adopt a vortex structure for their dipoles that is very similar to the one occurring in a single isolated dot. The situation is dramatically different if the first dot is polarized (e.g., by being under an external field) while the second dot is still under open circuit condition. In that case, the dots interact stronger, with this interaction causing the development of a relatively small spontaneous polarization in the second dot and, more importantly, being able to influence the direction of the toroid moment in this second dot – which is of technological importance. We further show how this last interaction, and its consequences, depend on the geometry and shape of the two dots, and reveal that all the striking features can be well understood within a multipole expansion of the field produced by the lattice polarization vortex in the free dot. This work is supported by DOE grant DE- FG02-05ER46188, by ONR grants N00014-01-1-0365, N00014-04-1- 0413 and N00014-01-1-0600, and by NSF grants DMR-0404335 and DMR-9983678.

*also Rostov State University

**13:51**

**V41 12 *Ab-initio* theory of nanoscale capacitors at finite bias** MASSIMILIANO STENGEL, *Materials Department, University of California, Santa Barbara* NICOLA SPALDIN, We present a novel technique for calculating the properties of an electric field applied to a periodic heterostructure with alternating metallic and insulating layers. This scheme allows us to investigate fully from first- principles the microscopic properties of a thin-film capacitor at finite bias potential. We demonstrate how the capacitance and local permittivity profiles can be readily obtained by performing calculations for the Ag(100)/MgO(100) and $SrTiO_3$(100)/$SrRuO_3$(100) systems. Applications range from the emerging field of electronic devices based on ferroelectric materials, to the *ab-initio* simulation of electrochemical cells.

**14:03**

**V41 13 Electrophoresis of Ferroelectric Nanoparticles** XIYA LIU, DRAGOMIR DAVIDOVIC, SCHOOL OF PHYSICS, GEORGIA TECH TEAM, We have studied the electrophoresis of ferroelectric nanoparticles(Ba1-xSrxTiO3). We used de-ionized (DI) water as solvent and an optical microscope to observe the motion of suspended ferroelectric nanoparticles driven by AC electric fields. The immediate start and stop of motion were noticed when the driving electric field was turned on and off, which was similar to dielectricphoresis. Higher voltage generated higher speed as expected. In some instances, the dielectric constant $\varepsilon$ of ferroelectric materials can increase greatly, which makes it pos-

sible that a low driving voltage (no larger than 10V) could induce a relatively high speed. At room temperature, we studied the frequency dependence of the motion speed. By comparing a serial of captured motion movies, we found that higher speeds were corresponding to lower frequencies of driving AC electric field. Further, we use well defined electrodes made by electron-beam lithography and high-vacuum deposition, which may regulate the electric field distribution. Consequently, we can characterize the electric force applied on those nanoparticles.

**SESSION V42: HISTORY AND PHYSICS OUTREACH**
**Thursday Morning, 16 March 2006**
**345, Baltimore Convention Center at 11:15**
**Bill Evenson, Utah Valley State College, presiding**

**11:15**
**V42 1 Brotherly Advice: Letters from Hugo to Paul Ehrenfest in his Final Years** PAUL HALPERN, *University of the Sciences in Philadelphia* At the start of the 1930s, theoretician Paul Ehrenfest spent much of his time traveling through America and Europe while engaged in a steady stream of lectures. This traveling phase coincided with a frantic and intense period of negative self-examination, financial difficulty, and various other personal concerns that would ultimately lead to his 1933 suicide. Throughout these final years, he kept up a steady correspondence with his brother Hugo, a physician based in Saint Louis. Ten years older than Paul, Hugo freely doled out frank psychological advice about subjects ranging from the proper treatment of children to the dangers of self-pity. Through a look at some of the letters exchanged between the two brothers, this talk will examine the role Hugo played during the dark final years of Paul Ehrenfest's life.

**11:39**
**V42 2 E. U. Condon: Science, Religion, and Scientific Responsibility** MICHAEL DAY, *Lebanon Valley College* In the spring of 1947, Walter Michels, a long-time friend and professor of physics at Bryn Mawr College, introduced Condon to Quakerism. In December of that year, Condon was accepted into membership in the Religious Society of Friends. The main purpose of this talk is to consider Condon's views on science and religion that he began setting forth in 1948. Further, Condon's views, which emphasize the ''harmony of science and religion,'' are compared and contrasted with the views of I. I. Rabi and Arthur Compton on science and religion. The talk concludes with a discussion of Condon's views on the responsibilities of scientists. In certain ways, Condon's views on science, religion, and scientific responsibility represent a philosophical minimalism with respect to their commitments.

**12:03**
**V42 3 Particles and Waves in Classical Dynamics** RONALD MICKENS, Two central concepts in classical dynamics involve the notions of ''particles'' and ''waves.'' However, their definitions must take into consideration two aspects related to how they may be characterized: 1) physical properties and 2) their mathematical formulation within particular dynamic theories. An issue of particular importance is that these concepts are abstractions of physical phenomena and may not correspond to any actual physical system component. We first examine the concepts of ''particles'' and ''waves'' from the perspective of how they have been defined in textbooks, scientific dictionaries, handbooks, research monograms, etc. From these readings and their analysis, we formulate definitions based on how these concepts are represented in the general framework of classical dynamics. Our tentative conclusion is that this procedure allows particle and waves systems to be unambiguously defined.

**12:27**
**V42 4 CUNY Doctoral Students Expand Access to Advanced Placement Physics in Urban High Schools** PAULA FEKETE, AMISH KHALFAN, *Hunter College, CUNY* VICTOR STROZAK, *Center for Advanced Study in Education, The Graduate Center, CUNY* The CUNY GK-12 Fellows Program addresses the need to increase the participation of low-income and underrepresented minority students in high-school-level Advanced Placement (AP) courses in mathematics and sciences, particularly in urban schools. The project provides a unique opportunity for doctoral science and math students to work with AP teachers and students in public high schools in the Bronx, NY. The project has demonstrated that doctoral science students can be a valuable resource to both teachers and students and that their presence in the classroom can greatly enhance instruction at this level. Participation in the program also enhances the fellows' communication and teaching skills and deepens their awareness of issues in urban science and math education. We present the results of our work in Advanced Placement Physics during the project's first three years.

**12:39**
**V42 5 High School Visitation Program in New York City for Materials Science and Engineering Outreach** SIU-WAI CHAN, IRVING HERMAN, JUSTINE HERRERA, *Columbia University* MRSEC TEAM, We report on a school science outreach program that we have carried out since 1999 under the National Science Foundation funded Materials Research Science and Engineering Center (MRSEC) at Columbia University. Under this program, we have made 34 visits to twenty New York City public high schools and middle schools and have reached over three thousand students. The demographic of the schools are around 81% historically underrepresented minorities (37% African Americans and 44% Hispanic Americans) and around 55% female. This report shows how a similar program can be set up in an urban area, which can directly address the vital shortage of youths going into science, engineering and mathematics (SEM) careers. Logistics and experiences of running the program are described. Lessons learned and certain important issues of the program are addressed for an easy adaptation in a new city.

**12:51**
**V42 6 Using nanotechnology to illustrate concepts at the secondary school level** M.S. RZCHOWSKI, S.J. RUTHERFORD, C.M. FOLKMAN, C.B. EOM, *University of Wisconsin-Madison* E. MONTALVO, J. STARTEK, E. SEDA, *SESO, Mayaguez, Puerto-Rico* Although nanotechnology is beginning to permeate many aspects of modern society, most people have only a limited awareness of these advances. Here we describe a program in which nanotechnology is used as a vehicle to communicate basic ideas of nanoscale phenomena and materials at the secondary school level. Secondary school teachers from the SESO K-12 school in Mayaguez Puerto Rico participated in a summer nanotechnology workshop at the University of Wisconsin-Madison, where they learned basic aspects of nanotechnology through tuto-

rials and laboratory participation, and developed teaching modules and lesson plans. These materials were incorporated into the curriculum at SESO. We discuss the organization and evaluation of the workshop at UW-Madison, and the implementation and evaluation of the nanotechnology modules at SESO.

**13:03**

**V42 7 Let physics substantiate music and music enhance physics—give principle to the other disciplines.** HUI-YIING CHANG, *Texas State University* A conventional practice in K-12 education is to synchronize the arts and the sciences. Physics, traditionally been considered the mother of the sciences, and music, the mother of the arts, are interdependent and help to establishing a complete understanding of the other disciplines. Intense musical expression is attained when progression aims towards infinity. Motions are made in curves across time, imitating physical phenomena. The meaning of each element is enhanced according to the relative duration and dynamics of its context. Complete musical expression considers the three dimensions of space-length, breadth and height- and the three dimensions of time- past, present and future when balancing the instrumental parts and developing the structural elements. Overall, equilibrium is sought for like gravitational forces as expressed in equations. In learning processes, sensing precedes reasoning. Music attunes one to sensitive reactions towards the environment while physics substantiates the concepts by imposing a hierarchical order, the highest form of which is elegantly beautiful and most effectively expressed in music.

**13:15**

**V42 8 The Art Speed of Light** JAN WOJCIK, The Roman poet Horace predicted correctly his phrase aere perennius, would last ''longer than bronze'' because the Ode he wrote travels to the eye at nearly the speed of light regardless of the rate of the decay of the paper it's written on. John Keats's 19th century Ode predicted correctly the youthful figures he saw on a bronze age Grecian Urn moved in ''slow time'' aging little from the time of painting to the time of his viewing in the British museum-and to ours today of the same urn. The youthful images of the Keystone Kops have aged slower than their twins– their mortal actors. Discoveries about light's speed occurred synchronously with the engineering of telegraph and radio transmissions in the 19th century-which allowed anyone an experience of what Physics had discovered. Einstein's privotal papers appeared in the same year as the first feature film shot and transmitted at the speed of light regardless of the aging of the film stock. Experiencing the light-like speed of art in Keat's ode, Cubism, Bob and Ray's radio, the Keystone Kops provides an aesthetic, visceral understanding of Einstein's Twin's Paradox about the dilation of time.

**13:27**

**V42 9 Online Muon Capture and Decay Experiment*** MEGAN ALEXANDER, DANIEL MINER, WOJTEK SKULSKI, FRANK WOLFS, *Department of Physics and Astronomy, University of Rochester, Rochester NY, 14627* With the aid of the internet, the classic muon lifetime experiment has been made globally accessible. Our muon detector consists of a 2000 $cm^3$ plastic scintillator and 2″ phototube. The muon signals trigger a digital signal processor, which samples the waveform every 25 ns during an 8 microsecond period following the trigger. Signals characteristic of muons that stop and decay in the detector contain two pulses: one from the muon itself, and one from the decay products. The muon lifetime is obtained from the time difference between these pulses. The digitized data are sent to the host computer via a USB link, and fed to a website (http://wolfspc.pas.rochester.edu/muon). The website provides access to the muon waveforms, a lifetime histogram, and energy spectra. Raw data are available for download and can be imported and processed by programs such as Excel or MATLAB. The site allows the user to watch the incoming data in real time, carry out data analysis of a fraction or all of the data collected since November 2005, and explore the underlying particle physics concepts.

*Work funded by a grant from the APS for the World Year of Physics 2005 and a grant from the National Science Foundation under Grant No. PHY-024283.

## SESSION V43: ATOMIC/MOLECULAR STRUCTURE AND AMO PROCESSES ON SURFACES AND IN CONDENSED MATTER

**Thursday Morning, 16 March 2006**
**346, Baltimore Convention Center at 11:15**
**M. Safronova, University of Delaware, presiding**

**11:15**

**V43 1 Oscillating Mechanical Electron Cloud Due to Nuclear Vibration** STEWART BREKKE, *Northeastern Illinois University (former grad student)* The nucleus is vibrating rapidly thereby creating a mechanical sphere of charge as the electrons vibrate due to the moving electric field. The mechanical sphere of charge reconciles the Bohr concept of a circular orbit with Schrodinger's idea of an electon cloud in which the electron is a DeBroglie wave surrounding the nucleus. If the electron is vibrating rapidly in itself as well as due to the vibrating electric field of the nucleus we also have an electon cloud. The resulting mechanical electron cloud is a combination of the two vibrational components. Effectively, there is a vibrating sphere of electronic charge surrounding the nucleus. If r, the distance to the electron from the center of the nucleus minus the Amplitude of nuclear vibration, Acos2($\pi$)ft, then a spherical shell of charge S = 4 ($\pi$)(r - Acos2($\pi$)ft)$^2$ is created.

**11:27**

**V43 2 Hydrogen Molecule in the Frame of the Three-Body Santilli-Shillady Model** RAUL PEREZ-ENRIQUEZ, *Departamento de Fisica, Universidad de Sonora* J. MARIN, R. RIERA, *Departamento de Investigación en Física, Universidad de Sonora* We analyze the charge distribution structure of a Hydrogen molecule under the Restricted Three-body Santilli-Shillady Model. Using the stable isoelectronium model, a particle with $M = 2\,m_e$ and $q = -2\,e$, we found a compatible ground state of $H_2$ which overcomes the problems of that developed by Aringazin and Kucherenko. Our model makes use of energies and bond lengths of the ground state of Hydrogen as calculated by Kolos and Wolniewicz in 1968, and assumes that the isoelectronium is restricted to move over a confined region of space around the nuclei. This compatible ground state can be obtained following the Ley-Koo solution to Schrödinger equation for Hydrogen molecular ion confined by a spheroidal box and we think it could be used for a better understanding of phenomena associated with correlated electrons in molecular bonds as it is observed in double photoionization and neutron scattering experiments. The self consistency of our results comes right from the correlation between

the protons bond length, $R$, and the size of the spheroidal box, $a = 1/2\,\xi_0 \cdot R$.

**11:39**

**V43 3 Explicitly Correlated Wavefunctions for Few-Body Problems*** FRANK E. HARRIS, *Quantum Theory Project, U. of Florida and Dept. of Physics, U. of Utah* Explicitly correlated wavefunctions enable far more compact, yet accurate descriptions of few-body systems than are possible using basis functions built from orbital products. The most efficient functions of this type contain all the interparticle distances as exponentials. Progress in evaluating the matrix elements for such a basis is reviewed for three and four-body systems, with particular attention to the difficult analytical problems posed by the four-body system and the challenges associated with highly singular integrals in the three-body system (which arise in the computation of relativistic effects). An alternative basis is provided by Gaussians in all the interparticle distances; recent contributions toward systematizing the use of such functions are also reported. Application of the exponential basis to the He isoelectronic series is described; the results differ from those reported by others in that their quality does not decrease with increasing nuclear charge $Z$. This feature permits an improved characterization of the coefficients in the $1/Z$ expansion. Also disscused is the cancellation of divergences in the combinations of individually divergent integrals arising in the treatment of relativistic effects in the He system.

*Supported by U.S. National Science Foundation Grant PHY-0303412

**11:51**

**V43 4 Lattice Regularized Diffusion Monte Carlo Simulations of Iron Dimer** MICHELE CASULA, *Department of Physics, University of Illinois at Urbana-Champaign, 1110 W. Green Street, Urbana, Illinois 61801, USA* LEONARDO GUIDONI, *Università degli Studi di Roma ''La Sapienza,'' Physics Department,* SANDRO SORELLA, *International School for Advanced Studies (SISSA), Via Beirut 2-4, 34014 Trieste, Italy* Transition metal compounds play a crucial role in various fields, ranging from biomolecular reactions to magnetic solid state properties. On the other hand, the strong dynamic correlation present in the unfilled d-shell makes the predictions of the density functional theory unreliable and requires the use of post-Hartree-Fock methods, limited however to small systems. The Lattice Regularized Diffusion Monte Carlo (LRDMC) method, recently introduced [M. Casula, C. Filippi, and S. Sorella, Phys. Rev. Lett. 95, 100201 (2005)], seems to be an effective alternative, since it can provide accurate results with a favorable size scaling. One of the main advantages of this framework is the possibility to include non-local potentials in a consistent variational scheme, substantially improving both the accuracy and the computational stability upon previous non-variational diffusion Monte Carlo approaches. Here, we apply the LRDMC framework to the iron dimer, by using a fully optimized Jastrow geminal wave function as guiding state. Despite its simplicity, its neutral and anionic ground states are controversial, and we try to clarify their symmetry by comparing our LRDMC results with experimental spectroscopic data.

**12:03**

**V43 5 Regionally specific hyperfine polarization of Rb atoms at micron/submicron distance from the Pyrex glass surfaces in optical pumping cells*** K. ZHAO, Z. WU, *Department of Physics, Rutgers University, Newark, NJ 07102* We made *regionally specific* measurement of the hyperfine polarization of Rb atoms in the vicinity ( $\sim 10^{-5}$ cm) of coated and uncoated Pyrex glass surfaces in optical pumping cells. This is in contrast to the previous hyperfine polarization studies, where the quantity measured is the bulk hyperfine polarization, which depends on surface interactions *averaged over the entire cell surfaces*. We probe the hyperfine polarization of the Rb atoms in the vicinity of cell surfaces using the evanescent wave of a weak laser beam. We find that the polarization in the vicinity of uncoated surfaces is significantly lower than that in the bulk. The polarization decreases rapidly with decreasing distance from the surface. By contrast, the polarization in the vicinity of a silicone coated Pyrex glass surface is independent of the distance from the cell surface and is equal to the bulk polarization. Regionally specific measurement of the hyperfine polarization as a function of the penetration depth of the evanescent wave allows us to deduce the hyperfine polarization, its normal gradient and normal gradient coefficient at the cell surface. We present the values of these quantities for three representative uncoated cells.

*Support from ONR is acknowledged

**12:15**

**V43 6 Q-factor spoiling of a fused silica microsphere** PABLO BIANUCCI, JOHN ROBERTSON, ANDREAS MULLER, C. K. SHIH, *The University of Texas at Austin* When a planar transparent surface if brought close to a microsphere resonator, the induced leakage will result in a decrease of the Q-factor of the resonant modes. We present a systematic study of the Q-factor spoiling on a fused silica microsphere using a tapered optical fiber as a waveguide and a cleaved fiber as a planar surface. The Q-spoiling is measured as function of the distance between the microsphere and the cleaved fiber. Different modes show quite different deterioration rate for the Q-value as a function of sphere-fiber distance. This Q-decay rate is directly related to the evanescent nature of the cavity modes.

**12:27**

**V43 7 Radiation Patterns of Electric Dipoles Close to a Plane Interface*** LAN LUAN, PAUL SIEVERT, JOHN KETTERSON, *Northwestern University* The radiation pattern of an electric dipole is modified when located in the vicinity of a dielectric or metal interface. We have investigated this phenomenon through numerical simulations and direct measurements. Our simulations are based on the Sommerfeld integral formalism. The effects of the dipole position and orientation, the dielectric constants of the media, and the observation position on the radiation pattern for TE and TM modes were studied. On the experimental side, we used fluorescent molecules to simulate the electric dipoles. The angular distribution of the fluorescence emission was recorded. Both our simulations and the experiments showed that the dipole radiation pattern is strongly modified from the free space form. Our results are potentially important for optical signal collection associated with spectroscopic studies of molecules bound to a surface.

*Work supported by the National Science Foundation under Grant 03-29957, and the NSF-supported Northwestern Materials Research Center under Grant DMR 00-76097.

**12:39**

**V43 8 Quadrupole $nd \rightarrow nl$ resonances in valence ns-photoelectron angular distributions from half-filled shell atoms.*** VALERIY DOLMATOV, *University of North Alabama* Nondipole photoelectron angular distributions from atoms have

become an itad hoc topic of intensive research in recent years. To date, such distributions have largely remained unstudied, with a few exceptions, in open-shell atoms in view of difficulties in handling such atoms. Therefore, we have unfolded a theoretical program focusing on studies of nondipole photoelectron angular distributions from open-shell atoms. In the present work, we choose the Mn($3d^5 4s^2$, $^6$S) atom as a case study owing to its relative ''simplicity'' because its open $3d^5$ subshell is only half-filled. We explore features of nondipole angular asymmetries for valence 4s-photoelectrons in a region of $3d \rightarrow nl(l = 0,2,4)$ quadrupole resonances. A removal of a 4s electron leaves the Mn atom either in a $3d^5 4s,(^7S)$ or $3d^5 4s,(^5S)$ final state. It is found that, due to demonstrated exclusive for a half-filled shell atom electron correlation effects, resonance enhancements of 4s nondipole angular asymmetry parameters depend markedly on final state terms of the atom, both in their magnitudes and shapes, with one of them overshooting the other by almost an order of magnitude at the resonance maximum, and with both of them far overshooting the dipole approximation value of 2. A ''spin-polarized'' RPAE has been employed in this study.

*The NSF financial support PHY-0456480 is acknowledged.

**12:51**

**V43 9 Cooperative Emission from Semiconductor Quantum Wells in High Magnetic Fields*** D. H. REITZE, Y. D. JHO, X. WANG, *Physics Dept., University of Florida* J. KONO, *Dept. of Electrical and Computer Engineering, Rice University* A. A. BELYANIN, V. V. KOCHAROVSKY, *Physics Department, Texas A&M University* G. SOLOMON, *Solid State Laboratories, Stanford University* X. WEI, *NHMFL* Stochastically oriented, spectrally-peaked emissions is generated in $In_{0.2}Ga_{0.8}As/GaAs$ multiple quantum wells (QW). Using intense 150 fs, 775 nm pulses for excitation, we investigate the spatial and temporal characteristics of the emission in dense magneto-plasmas in high magnetic fields (30 T) and at carrier densities approaching $10^{13}$ cm$^{-2}$. Above a threshold intensity and magnetic field, the emission from Landau levels exhibit anomalous narrow features appearing asymmetrically on the high-energy side of the peaks. An examination of the spot size dependence of emission strength relative to the coherence length, temperature dependence of threshold magnetic field, and differential transmission spectra suggest that the inter-LL emission arises from the spontaneous polarization of the dense magneto-plasma.

*Supported by the NSF through grant DMR-0325499 and by the NHMFL through an IHRP grant.

**13:03**

**V43 10 Dielectric Modification of the Casimir force between a gold sphere and a silicon surface** FENG CHEN, UMAR MOHIDEEN, *Department of Physics, University of California, Riverside, CA 92521* The Casimir force (retarded van der Waals force) can become very large at micron and nano distance scales and can affect the performance and fabrication of microelectromechanical (MEMS) and nanoelectromechanical systems (NEMS). Here we demonstrate that it is possible to modify the Casimir force in the microelectromechanical systems, through alteration of the dielectric properties of the silicon boundary. This will open new opportunities for the application of the Casimir force in MEMS and NEMS. This experiment also helps improve our understanding of the Casimir force between dielectric surfaces.

**13:15**

**V43 11 Analysis of van der Waals Interaction Energies from Quantum Chemistry: Aromatic Clusters and Rare Gas Dimers** STEPHEN GARRISON,* *National Institute of Standards and Technology, NIST Center for Theoretical and Computational Nanosciences* INEZ GONZALEZ, *University of Akron, Department of Chemistry* CARLOS GONZALEZ, *National Institute of Standards and Technology, NIST Center for Theoretical and Computational Nanosciences* MANUEL MARQUEZ, *Philip Morris USA Research Center* EDWARD LIM, *University of Akron, Department of Chemistry* The weak van der Waals (vdW) interactions in aromatic clusters and rare gas systems are studied using ab initio quantum chemistry and the Hartree-Fock Dispersion (HFD) method. The results, extrapolated to the complete basis set limit and along with comparisons to experiment, are used to understand and explain a fortuitous cancellation of errors in the benzene interaction calculations. Additionally, interesting results are found for the all-electron calculations for argon.

*I am also with the Interdisciplinary Network of Emerging Science and Technologies (INEST) Group

**13:27**

**V43 12 Energy Distribution of Cluster Assemble with Isomers** SONGBAI YE, LOUIS BLOOMFIELD, BLOOMFIELD LAB TEAM, The internal energy of cluster assemble without isomers will be a single-peak distribution in thermal equilibrium. However, if it has several isomers and each isomer has different state density distribution, the internal energy distribution will be structured in certain circumstance. By destroying the equilibrium of isomer populations and observing the building-up of the new equilibrium, we can gain information of the internal energy of the cluster assemble. We can also study the change of the internal energy of the cluster assemble by selectively burning some isomers before we proceed the deplete-probe method. This presentation is based upon work supported by the National Science Foundation under Grant No. DMR-0405203.

## SESSION V44: KONDO PHYSICS AND LUTTINGER LIQUIDS

**Thursday Morning, 16 March 2006**
**347, Baltimore Convention Center at 11:15**
**K. Ingersent, University of Florida, presiding**

**11:15**

**V44 1 Quantum Phase Transition in an Anisotropic Kondo Lattice** M.T. GLOSSOP, K. INGERSENT, *U. Florida* The Kondo lattice model (KLM), which captures the competition between Kondo screening of localized moments by conduction electrons and their ordering due to the RKKY interaction, is of interest in the context of non-Fermi-liquid behavior in quantum critical heavy-fermions. An important issue concerns the possibility of a local quantum critical point (QCP) — where Kondo screening is itself critical at the magnetic ordering transition — recently invoked [1] to explain anomalous properties of, e.g., $CeCu_{5.9}Au_{0.1}$. We study the anisotropic KLM using the extended dynamical mean-field theory (EDMFT), which maps the KLM onto a self-consistent Bose-Fermi Kondo model (BFKM). Whether a local QCP arises as a self-consistent EDMFT solution of the KLM is a

contentious issue that we seek to resolve. Separate studies [2,3], both employing Quantum Monte Carlo (QMC) to solve the BFKM, have reached opposite conclusions, but limitations of QMC at low temperatures $T$ obscures the picture at $T = 0$. We address this matter, providing reliable $T = 0$ solutions using our extension of [4] Wilson's numerical renormalization group method to solve the BFKM. We present results for both paramagnetic and antiferromagnetic phases, shedding light on the nature of the QPT. Supported by NSF Grant DMR-0312939. [1] Q. Si, S. Rabello, K. Ingersent, and J. L. Smith, Nature **413**, 804 (2001). [2] J-X Zhu, D. R. Grempel and Q. Si, Phys. Rev. Lett. 91, 156404 (2003). [3] P. Sun and G. Kotliar, Phys. Rev. Lett. 91, 037209 (2003). [4] M. T. Glossop and K. Ingersent, Phys. Rev. Lett. 95, 067202 (2005).

**11:27**

**V44 2 Zero temperature phase diagram of the periodic Anderson model** LORENZO DE LEO, *Rutgers University* MARCELLO CIVELLI, *Rutgers University* GABRIEL KOTLIAR, *Rutgers University* We study the phase diagram of the periodic Anderson model using a cluster extension of DMFT to take into account non-local effects generated by the RKKY exchange. We employ exact diagonalization in order to access the zero temperature regime which was previously unexplored. In particular we focus our attention away from half filling where the competition between the localization of the heavy electrons and their magnetic ordering could result in a quantum critical point with unusual properties. We also consider the effect of a direct hopping between the *f*-electrons in order to understand if an indipendent tuning of the RKKY interaction influences the character of the transition.

**11:39**

**V44 3 Non-Fermi-liquid phase in a frustrated Kondo trimer*** KEVIN INGERSENT, DOHYUNG SEO, *U. of Florida* ANDREAS LUDWIG, *U. of California, Santa Barbara* IAN AFFLECK, *U. of British Columbia* The Kondo model for three antiferromagnetically coupled half-integer spins exhibits a non-Fermi-liquid phase that is stable against magnetic fields and against particle-hole symmetry breaking [1,2]. This phase has been argued [3] to describe the low-energy physics of equilateral Cr trimers on Au (111) surfaces [4]. It also has potential realizations in quantum-dot devices of triangular symmetry. We report properties of this phase obtained using the boundary conformal field-theory (CFT) technique, including characteristic signatures in the conductance, and apply CFT and renormalization-group methods to examine the phase's behavior under various perturbations. [1] B. C. Paul and K. Ingersent, cond-mat/9607190. [2] K. Ingersent, A. W. W. Ludwig, and I. Affleck, cond-mat/0505303 (Phys. Rev. Lett., in press). [3] B. Lazarovits et al., Phys. Rev. Lett. 95, 077202 (2005). [4] T. Jamneala, V. Madhavan, and M. F. Crommie, Phys. Rev. Lett. 87, 256804 (2001).

*Supported by NSF, NSERC, and the Canadian Institute for Advanced Research

**11:51**

**V44 4 Egxact ground states for the periodic Anderson model at half filling in two dimensions** ZSOLT GULACSI,* *University of Debrecen, Department of Theoretical Physics, Hungary* Recently, starting from a procedure based on the decomposition of the Hamiltonian in positive semidefinite operators, exact ground states have been deduced for the periodic Anderson model at finite value of the interaction at 1/4 and 3/4 filling even in three dimensions (PRL 91,186401,(2003); PRB 72,075130, (2005)), the method being so powerfull that its application for disordered systems, at the same values of the filling, and two dimensions, is also possible (PRB 69, 054204, (2004)). Herewith we extend the procedure such to be applicable at half filling as well, in the presence of finite on-site Hubbard interaction acting at the level of the correlated band. The extensions lead to a method which uses extended operators, (e.g. linear combinations of the starting fermionic operators acting along the whole system), and also sublattice operators, in constructing the ground state wave functions. The ground states describing conducting spin-singlet states, are presented in two dimensions.

*Research supported by Grant OTKA-T037212 of the Hungarian Scientific Research Fund and Alexander von Humboldt Foundation

**12:03**

**V44 5 Dynamic Magnetic Response of Heavy Fermion Semimetals** PETER RISEBOROUGH, *Temple University* We have calculated the dynamical magnetic response of a model of a heavy fermion semimetal, which is characterized by a narrow gap in the f density of states and a low conduction electron density of states at the Fermi energy. The model is used to fit optical absorbtion measurements on $CeRu_4Sb_{12}$ performed by Dordevic *et al.*, Phys. Rev. Lett. **86**, 684 (2001). The temperature dependence of the dissipative part of the magnetic response is compared with the experimentally determined inelastic neutron scattering cross-section of $CeRu_4Sb_{12}$ measured by Adroja *et al.* Phys. Rev. B **68**, 099426 (2003).

**12:15**

**V44 6 Magnetic Quantum Phase Transitions of a Kondo Lattice Model with Ising Anisotropy** JIAN-XIN ZHU, *Theoretical Division, Los Alamos National Laboratory, Los Alamos, New Mexico 87545, USA* STEFAN KIRCHNER, QIMIAO SI, *Department of Physics & Astronomy, Rice University, Houston, Texas 77005-1892, USA* DANIEL R. GREMPEL, *CEA-Saclay/DRECAM/SPCSI, 91191 Gif-sur-Yvette, France* RALF BULLA, *Theoretische Physik III, Elektronische Korrelationen und Magnetismus, Universitaet Augsburg, 86135 Augsburg, Germany* We study the Kondo Lattice model with Ising anisotropy, within an extended dynamical mean field theory (EDMFT) in the presence or absence of antiferromagnetic ordering. The EDMFT equations are studied using both the Quantum Monte Carlo (QMC) and Numerical Renormalization Group (NRG) methods. We discuss the overall magnetic phase diagram by studying the evolution, as a function of the ratio of the RKKY interaction and bare Kondo scale, of the local spin susceptibility, magnetic order parameter, and the effective Curie constant of a nominally paramagnetic solution with a finite moment. We show that, within the numerical accuracy, the quantum magnetic transition is second order. The local quantum critical aspect of the transition is also discussed.

**12:27**

**V44 7 Coherence in the two-impurity Kondo problem** LIJUN ZHU, C.M. VARMA, *University of California, Riverside* We use the Wilson's renormalization group method to investigate the splitting of the even and odd Kondo resonances in the problem of two interacting Kondo impurities which presages the band-width or the coherence scale in the heavy-Fermion lattice. A finite splitting requires both potential scattering V which lifts particle-hole degeneracy and a difference between the exchange in the even and the odd parity channels(Je-Jo)[1]. We also investigate the elimi-

nation of the quantum critical point in the two-impurity Kondo problem[2] due to loss of particle-hole symmetry. [1] I. Affleck and A. W. W. Ludwig, Phys. Rev. Lett. 68, 1046(1992). [2] B. A. Jones, C. M. Varma, and J. W. Wilkins, Phys. Rev. Lett. 61, 125(1988).

**12:39**

**V44 8 Large temperature renormalization of anomalous Luttinger exponent in $Li_{0.9}Mo_6O_{17}$*** FENG WANG, S.-K. MO, J.W. ALLEN, J.V. ALVAREZ, *U. of Michigan* G.-H. GWEON, *Lawrence Berkeley National Lab* J. HE, *U. of Tennessee* R. JIN, R. MANDRUS, *Oak Ridge National Lab* H. HÖCHST, *SRC, U. of Wisconsin* $Li_{0.9}Mo_6O_{17}$ is unique as a quasi-1 dimensional metal for which both photoemission spectroscopy (PES) [1] and tunneling [2] find Luttinger liquid (LL) power law behaviors in spectra near the Fermi energy $E_F$, albeit with differing values of the anomalous exponent $\alpha$, $\approx$ 0.9 at temperature 300K and $\approx$ 0.6 below 50K, respectively. New T-dependent PES spectra from T = 300K down to 15K can be well fit by finite-T LL theory, with $\alpha$ varying continuously from $\approx$ 0.9 to $\approx$ 0.6, showing consistency of PES and tunneling. We find that its incommensurate Fermi wavevector would preclude such a large renormalization of $\alpha$ with T for $Li_{0.9}Mo_6O_{17}$ were it not for interband dynamics and residual interaction scattering that can occur only because there are two (nearly degenerate) bands crossing $E_F$. We also discuss implications of the theory for further experiments. [1] G.-H. Gweon et al, Phys. Rev. B **68**, 195117 (2003). [2] J. Hager et al, Phys. Rev. Lett. **95**, 186402 (2005).

*Supported at U. Mich. by the U.S. NSF Grant(DMR-03-02825)

**12:51**

**V44 9 Finite temperature ac conductivity of disordered Luttinger liquids** ANDREAS GLATZ, *Materials Science Division, Argonne National Laboratory, Argonne, Illinois 60439, USA* BERND ROSENOW, *Physics Department, Harvard University, Cambridge, Massachusetts 02138, USA* THOMAS NATTERMANN, *Institut fuer theoretische Physik, Universitaet zu Koeln, 50937 Koeln, Germany* Due to the strong effect of interactions in one spatial dimension, elementary charge excitations of a Luttinger liquid are plasmons. Backscattering of electrons from a random impurity potential creates single particle excitations, which strongly interact with these plasmons. In this way, backscattering from the impurity potential is modified by interactions and acquires a strong energy dependence first described in [1]. Based on a finite temperature renormalization group (RG) calculation [2], we determine the ac conductivity and include both the renormalization of the impurity strength and of the charge dynamics. The latter was neglected in [1], where the conductivity was calculated using the effective impurity strength obtained from the RG. We discuss the full frequency and temperature dependence of the conductivity and compare our results with those of [1]. [1] T. Giamarchi and H.J. Schulz, Phys. Rev. B 37, 325 (1988). [2] A. Glatz and T. Nattermann, Phys. Rev. Lett. 88, 256401 (2002).

**13:03**

**V44 10 Dynamics of Strongly Correlated 1D Fermi Gases** RAZVAN TEODORESCU, *Columbia University* Dynamics of special collective modes in cold, degenerate Fermi gases are investigated through bosonization. The study applies to a variety of 1D or quasi-1D systems of fermions, including opticaly trapped cold gases and nanowires.

**13:15**

**V44 11 Tunneling, charge spreading, and the infrared catastrophe in conductors** KELLY PATTON, MICHAEL GELLER, *The University of Georgia* In many strongly correlated and low-dimensional electron systems the tunneling density of states (DOS) is suppressed near the Fermi energy; for example, the Luttinger-liquid characterization of one-dimensional conductors predicts that the DOS vanishes as a power law. Here we establish a connection between these DOS anomalies and the infrared catastrophe. The infrared catastrophe can occur during a tunneling event in systems where the relaxation of the newly introduced charge is inhibited by low dimensionality or other localizing effects. This catastrophe is known to be responsible for the x-ray edge spectra of metals, the Anderson orthogonality catastrophe, and the Kondo effect. By expressing the exact Green's function as a functional average of non-interacting Green's functions over of all space and time dependent potentials, we can appropriately treat the potentials responsible for the infrared catastrophe. The resulting interacting Green's function is the product of the noninteracting Green's function and $e^{-S}$, where $S$ is interpreted as a classical electrostatic action of a charge density spreading in time. These results give justification to other previously introduced phenomenological charge spreading theories. We apply this formalism to the Tomonaga-Luttinger, Calogero-Sutherland and other models.

**13:27**

**V44 12 Boundary Green's Function for Spin-incoherent Interacting Electrons in One Dimension** PAATA KAKASHVILI, *Chalmers University of Technology* HENRIK JOHANNESSON, *Göteborg University* Recently the spin-incoherent regime of 1D strongly interacting, very low density electrons has attracted a lot of interest[1,2]. For sufficiently low densities the potential energy dominates the kinetic energy, driving the system towards a Wigner crystal and leading to an exponentially small spin exchange energy. One can then easily reach the spin-incoherent regime where the exchange energy is much less than the temperature. The physics of the spin-incoherent regime has been addressed using Bethe's Ansatz and a bosonized path integral approach, revealing that the spin incoherence dramatically influences the correlations of charge excitations. We have generalized the description to account for the presence of a boundary. By calculating the exact Green's function we find that the charge sector exponent is highly sensitive to the boundary, strongly modifying the tunneling of electrons close to it. Our approach also allows for a detailed description of the crossover between boundary and bulk regimes. 1. V.V. Cheianov and M.B. Zvonarev, PRL 92, 176401 (2004) 2. G.A. Fiete and L. Balents, PRL 93, 226401 (2004)

**13:39**

**V44 13 Phonon Effects on Spin-Charge Separation in One Dimension*** CHANG-QIN WU, WEN-QIANG NING, HUI ZHAO, *Department of Physics, Fudan University, Shanghai 200433, China* HAI-QING LIN, *Department of Physics and Institute of Theoretical Physics, The Chinese University of Hong Kong, Shatin, Hong Kong, China* Phonon effects on spin-charge separation in one dimension are investigated through the calculation of one-electron spectral functions in terms of the recently developed cluster perturbation theory together with an optimized phonon approach. It is found that the retardation effect due to the finiteness of phonon frequency suppresses the spin-charge separation and eventually makes it invisible in the spectral function. A signature of electrons pairing in weak interaction regimes was found to be consistent with the existence of a metallic phase proposed recently

by Clay and Hardikar [Phys. Rev. Lett. **95**, 096401 (2005)]. By a comparison between our result and the experimental data of TTF-TCNQ, it is observed that electron-phonon interaction must be taken into account even in the strongly correlated system.

*This work was partially supported by National Natural Science Foundation of China and CUHK 401504.

**13:51**

**V44 14 Dynamic Properties of 1-D Ising Chain in a Random Transverse Field*** XUN JIA, SUDIP CHAKRAVARTY, *Department of Physics, University of California at Los Angeles* We considered a one dimensional spin-1/2 Ising chain in a random transverse magnetic field. Dynamic structure factor $S(k,\omega)$ at $T = 0$ is numerically computed by mapping to Jordon-Weigner fermions. Two types of distributions of magnetic fields are introduced into our model. With rectangular distribution, single branch of dispersion relation is observed, and disorder tends to broaden the dispersion peak and close the excitation gap. With a binary distribution, a non-dispersing branch at almost zero energy is recovered. This is reminiscent of neutron scattering measurement in $LiHoF_4$, although this is a three-dimensional system with long-range dipolar coupling between the electronic spins, which are in turn coupled to the nuclear spins through the hyperfine interactions. The implications of this similarity will be discussed.

*This work was supported by the NSF under grant: DMR-0411931

**14:03**

**V44 15 Stripe Glass from Competing Short and Long Range Interactions** GERGELY ZIMANYI, CHRIS PIKE, RICHARD SCALETTAR, *Physics Department, UC Davis* We investigate a film of dipoles oriented perpendicular to the film. The system's behavior is related to inhomogeneous non-Fermi liquid states, recently studied by Kivelson and Spivak and by Schmalian and Wolynes. The competition of short range ferromagnetic and long range antiferromagnetic interactions causes the formation of stripes. The system has an ordered stripe-crystal phase. However, this phase is avoided unless an extremely slow annealing protocol is utilized. Without any quenched disorder during normal annealing protocols the frustrated competing interactions self-generate a stripe-glass state. The stripe glass exhibits aging, manifesting itself in waiting-time dependent correlations. A scaling analysis of the aging is presented. The long time behavior shows stretched exponential behavior, the relaxation time surprisingly exhibiting a simple activated form. Dynamical inhomogeneities are identified, both frozen domains and instantaneous crystallites.

## SESSION V45: SPIN STRUCTURE AND PHASE TRANSITIONS: THEORY

**Thursday Morning, 16 March 2006**
**348, Baltimore Convention Center at 11:15**
**Donald J. Priour, Jr., University of Maryland, presiding**

**11:15**

**V45 1 Disorder and ferromagnetism in a graphene sheet** NUNO M.R. PERES, *Universidade do Minho, Portugal* FRANCISCO GUINEA, *Instituto de Ciencia de Materiales de Madrid. CSIC* ANTONIO H.C. NETO, *Boston University* We study the presence of ferromagnetism in the phase diagram of the two-dimensional honeycomb lattice close to half-filling (graphene) as a function of the strength of the Coulomb interaction and doping. We show that exchange interactions between Dirac fermions can stabilize a ferromagnetic phase at low doping when the coupling is sufficiently large. In clean systems the zero temperature phase diagram shows both first order and second order transition lines and two distinct ferromagnetic phases: one phase with only one type of carriers (either electrons or holes) and another with two types of carriers (electrons and holes). Using the coherent potential approximation we argue that disorder further stabilizes the ferromagnetic phase.

**11:27**

**V45 2 The exchange instability in a graphene bilayer** JOHAN NILSSON, ANTONIO CASTRO NETO, *Boston University* NUNO PERES, *Univ. Minho* FRANCISCO GUINEA, *ICMM* We study the problem of the formation of electron-hole pockets in a graphene bilayer (two layers of graphite). By means of a variational calculation in a simple model we show that pockets can be formed due to the combined effects of the Coulomb interaction and a coherent nearest neighbor hopping within the planes and between the layers. The variational calculation shows that the non-interacting ground-state is unstable and that a small net ferromagnetism can be obtained. Upon doping the system away from half filling the instability goes away above a critical value of the doping. We also discuss how modifications to the model such as the inclusion of screening and disorder will affect the instability.

**11:39**

**V45 3 Spin Liquid States on the Triangular Lattice: A Projective Symmetry Group Analysis of Schwinger Boson States** FA WANG, ASHVIN VISHWANATH, *UC Berkeley* Recent numerical and experimental results on quantum spin systems on the triangular lattice have revealed several unusual phenomena. Motivated by these developments, we apply the Projective Symmetry Group Analysis, previously used to classify spin liquid states obtained within a fermionic spin representation, to Schwinger bosons mean field states on the triangular lattice. We find several distinct $Z_2$ spin liquid states, but restricting attention to states with non-vanishing nearest neighbor amplitudes we find only two candidates. The first (zero-flux state) is the well known state introduced by Sachdev, which on condensation of spinons leads to the 120 degree ordered state. The other solution which we call the Pi-flux state has not previously been discussed. It is found to be stable against order up to a much larger value of the quantum parameter than the zero-flux state, which makes it an attractive candidate spin liquid state. When spinon condensation does occur, the ordering wavevector is at the Brillouin zone edge centers, different from the 120 degree state. While the zero-flux state is more stable with just nearest neighbor exchange, we find that the introduction of either next-neighbor antiferromagnetic exchange or four spin ring exchange tends to favor the Pi-flux state.

**11:51**

**V45 4 Spin current and spiral spinons in the Heisenberg spin chain*** YUPENG WANG,[†] *Institute of Physics, Chinese Academy of Sciences* The twisted boundary magnetic field effects on the one dimensional antiferromagnetic spin chains with spin half and spin one are studied via the density matrix renormalization group method. A spin voltage controlled by the twisted boundary fields as well as the spin current are observed for the spin half chain. The

correlation functions reveal the spiral nature of spin structure for both ground state and the spinon excitations for the spin half case. For the spin one chain, a kink is generated in the ground state and the midgap state is induced by small boundary fields.

*Supported by NSFC
†Presenter

**12:03**
**V45 5 Partial order in MnSi?** JOHN HOPKINSON, HAE-YOUNG KEE, *University of Toronto* Motivated by a recent neutron scattering study of MnSi, we study the ferromagnetic Heisenberg model with Dzyaloshinskii-Moriya interactions on the 3D corner-shared triangle lattice, the magnetic sublattice of MnSi. For classical spins we find evidence of a partially ordered state: degenerate states form a sphere with a fixed radius in momentum space. Further, for a metallic system, we propose an assignment of the Moriya vectors following an RKKY derivation of Fert and Levy. We calculate the structure factor within the mean field approximation and test this result against classical monte carlo calculations. We discuss the connection of our results to phenomenological Landau-Ginzburg treatments of the Dzyaloshinskii-Moriya coupling on this lattice.

**12:15**
**V45 6 No dominance of RKKY interaction in 4f-magnets** GERMAN SAMOLYUK, VLADIMIR ANTROPOV, *Ames Laboratory* It is a common belief that in the rare earth materials the dominating exchange mechanism is the magnetic coupling between localized 4fmoments mediated by nearly free conduction electrons resulting in so-called indirect coupling or RKKY interaction. In addition, several experimental proofs have been published in the past. We reanalyzed the validity of this statement from a point of view of realistic atomic and solid state electronic structure. The experimental proofs have been reanalyzed as well. In general, we found that no theoretical validation of RKKY dominance in 4f-magnets exist and all experimental evidences cannot rule out other mechanisms. We claim that the direct interatomic exchange between conduction electrons must be always taken into account.

**12:27**
**V45 7 New classification of magnets** VLADIMIR ANTROPOV, *Condensed Matter Theory, Ames Laboratory, Ames, IA, 50011* Standard methods classify magnets using their magnetic long range order at T=0 (ferromagnets, antiferromagnets and so on). Some classifications can be created inside those groups as well. In addition, there is a very attractive and widely used qualitative localized-itinerant picture, which, however, does not have any real criteria behind. I would like to introduce a rather universal and possible quantitative classification using the idea of magnetic short range order, which we recently found theoretically and which has been for years observed experimentally in many materials.

**12:39**
**V45 8 Exact Diagonalization Study of the Quantum Antiferromagnet $Cs_2CuCl_4$*** OOKIE MA, J. B. MARSTON, V. F. MITROVIĆ, M.-A. VACHON, *Brown University* We exactly diagonalize a model of the quantum antiferromagnet $Cs_2CuCl_4$. The quasi two-dimensional material is one of only two strong candidate systems that may exhibit a spin-liquid phase[1]. To compare with NMR experiments we calculate the total magnetization for clusters of up to 24 sites as a function of temperature and the applied magnetic field. The spin-1/2 degrees of freedom reside on an anisotropic triangular lattice; in addition to the usual nearest-neighbor Heisenberg exchange, interactions of the Dzyaloshinskii-Moriya type must also be included[2]. We investigate the potential importance of additional higher-order terms[3].

*Supported in part by NSF DMR-0213818.

[1]R. Coldea, D. A. Tennant, A. M. Tsvelik and Z. Tylczynski, Phys. Rev. Lett. **86**, 1335 (2001).
[2]K. Kodama, S. Miyahara, M. Takigawa, M. Horvatic, C. Berthier, F. Mila, H. Kageyama and Y. Ueda, J. Phys.: Condens. Matter **17** L61 (2005).
[3]T. Yildirim, A. B. Harris, Amnon Aharony and O. Entin-Wohlman, Phys. Rev. B **52**, 10239 (1995).

**12:51**
**V45 9 An ab initio study of the giant magnetocaloric effect in MnAs*** HYEJUNG KIM, YIA-CHUNG CHANG, SAHRAOUI CHAIEB, *University of Illinois at Urbana-Champaign* MnAs is one of the materials which show a giant magnetocaloric effect. Electronic and magnetic properties of MnAs in NiAs structure and hypothetical zinc-blende structure are studied using a full potential linear augmented-Slater-type-orbital (LASTO) method within the local spin density approximation. Total energies and magnetic moments as a function of volume as well as band structures are in agreement with previous calculations employing different methods such as full potential linearized augmented plane wave method and a plane-wave pseudopotential implementation. Exchange coupling parameters are determined with a frozen magnon approach. Using the exchange coupling parameters obtained, a mean-field theory is applied to calculate the quantities of interest such as the magnetic entropy and free energy as a function of temperature and the critical temperature, to evaluate the giant magnetocaloric effect in MnAs.

*supported by Research Board, University of Illinois at Urbana-Champaign

**13:03**
**V45 10 Spatially Anisotropic d=3 Ising, XY Magnetic and Percolation Systems: Exact Renormalization-Group Solutions of Hierarchical Models** AYKUT ERBAŞ, *Koç U. and ITU* ASLI TUNCER, *ITU* BURCU YÜCESOY, *ITU* A. NIHAT BERKER, *Koç U. and MIT* Hierarchical lattices that constitute spatially anisotropic systems are introduced. These lattices provide exact solutions for hierarchical models and, simultaneously, approximate solutions for uniaxially or fully anisotropic $d = 3$ physical models. The global phase diagrams, with $d = 2$ and $d = 1$ to $d = 3$ crossovers, are obtained for Ising, XY magnetic models and percolation systems, including crossovers from algebraic order to true long-range order.[1] Our approach has been applied to spatially anisotropic $d = 3$ tJ models of electronic conduction.[2] 1. A. Erbaş, A. Tuncer, B. Yücesoy, and A.N. Berker, Phys. Rev. E **72**, 026129 (2005). 2. M. Hinczewski and A.N. Berker, cond-mat/0504741.

**13:15**
**V45 11 Simulation of magnetization configurations with constricting magnetization boundary conditions in 2 and 3-D soft-hard magnetic structures*** JONG HAN, HEMACHANDER SUBRAMANIAN, *State University of New York at Buffalo* A soft magnet embedded with hard-magnetic spheres/cylinders magnetized to constrict the soft magnets magnetization creates a system

with multiple minima and related hysterisis effects. Due to many distinct magnetic structures in the soft-magnetic region at fixed magnetization on hard-magnets, frustration develops even in simple hard-magnetic arrays coupled via ferromagnetic exchange interaction. This presentation reports the simulation of such systems. We observed multiple minimum energy configurations and transitions between them in an externally applied magnetic field and/or change in hard magnets magnetization. Hysteresis effects due to the above changes are observed. Electron transport through these systems can generate interesting magneto-resistance effects.

*Supported by NSF DMR-0426836

**13:27**

**V45 12 Topological transition in a two-dimensional model of liquid crystal** ANA ISABEL FARIÑAS-SANCHEZ, RICARDO PAREDES V, BERTRAND BERCHE, Simulations of nematic-isotropic transition of liquid crystals in two dimensions are performed using an O(2) vector model characterized by nonlinear nearest neighbor spin interaction governed by the fourth Legendre polynomial $P_4$. The system is studied through standard finite-size scaling and conformal rescaling of density profiles of correlation functions. A topological transition between a paramagnetic phase at high temperature and a critical phase at low temperature is observed. The low temperature limit is discussed in the spin wave approximation and confirms the numerical results.

**SESSION V46: DEFECTS AND IMPURITIES IN SI/GE**
**Thursday Morning, 16 March 2006**
**349, Baltimore Convention Center at 11:15**
**Torgny Gustafsson, Rutgers University, presiding**

**11:15**

**V46 1 Pathway connecting the four-interstitial ground state and chain in silicon** YAOJUN DU, *Wake Forest University* THOMAS LENOSKY, *879 Meadowview Dr, Columbus OH 43224* STEFAN GOEDECKER, *University of Basel* RICHARD HENNIG, JOHN WILKINS, *The Ohio State University* Dimer searches, minima hopping and nudged elastic band (NEB) calculations try to identify the lowest pathway connecting the two important silicon four-interstitial structures: $I_4$-chain and ground state. First, 400 tight-binding dimer searches reveal several local minima. However, the minima have high DFT formation energies and no pathway connecting chain and ground state is found. Second, we fit a classical modified embedded atom method potential to a database of interstitial clusters. Minima hopping using this potential finds several structures with DFT energies between chain and ground state but no pathway connecting them. Finally, we construct a pathway between chain and ground state with small displacements. The NEB energy barrier with DFT from chain to ground state is 0.6 eV. This indicates that during annealings the $I_4$-chain decays into the nearly immobile ground state, implying that chain structures predominate only for longer chains.

**11:27**

**V46 2 Recombination rate annealing following transient neutron irradiation*** HAROLD HJALMARSON, PETER SCHULTZ, NORMAND MODINE, *Sandia National Laboratories* Neutron irradiation of bipolar transistors generates defects by displacing silicon atoms. For each displacement collision, a pair of defects is created, the interstitial atom and the vacancy left behind. These defects reduce transistor gain by increasing the recombination rate of electrons and holes thereby increasing the base current of these devices. After the radiation ceases, these defects undergo reactions that produce composite defects that are less effective at carrier recombination. In this presentation, we discuss simulations of the temporal evolution of these defects and the carrier recombination rate. We find that the initial carrier recombination rate is dominated by recombination at interstitials in p-type silicon and vacancies in n-type silicon. For p-type silicon, the short-time annealing is controlled by athermal diffusion of interstitials, and this diffusion rate, which is governed by carrier recombination at the interstitial, can be controlled by injection of minority carrier electrons. Our results will be compared with experimental data.

*Sandia is a multiprogram laboratory operated by Sandia Corporation, a Lockheed Martin company, for the United States Department of Energy under contract DE-AC04-94AL85000.

**11:39**

**V46 3 Theory of the Cyclotron Resonance in Si and Ge** SHIGEJI FUJITA, ROBERT SIMION, ROHIT SINGH, *University at Buffalo, SUNY* SEIICHI WATANABE, *Hokkaido University* A quantum theory is developed for the cyclotron resonance (CR) in silicon(Si) and germanium(Ge). The angular dependent CR peaks for heavy ''holes'' are analyzed, using the Dresselhaus-Kip- Kittel (DKK) formula: $\omega = (\omega_t^2 cos^2\theta + \omega_t\omega_l sin^2\theta)$, $\omega_t \equiv eB/m_t$, $\omega_l \equiv eB/m_l$.Their Fermi surfaces for Si(Ge) are spheroids oriented along $\langle 100 \rangle$ axes with the transverse mass $m_t = 0.46(0.29)m$ and the longitudinal mass $m_l = 1.03(0.78)m$.The fluted energy surfaces represented by the quartic dispersion relations used by DKK were avoided.The CR should be observed only, when a substantial number of conduction electrons with a quadratic dispersion relation resonate at a single frequency.

**11:51**

**V46 4 Stability of strained monohydride H:Si(105) and H:Ge(105) surfaces** CRISTIAN V. CIOBANU, *Colorado School of Mines* RYAN M. BRIGGS, *Colorado School of Mines* We report atomic scale studies of the effect of applied strain and hydrogen environment on the reconstructions of the (105) Si and Ge surfaces. Surface energy calculations for monohydride-terminated (001) and (105) reconstructions reveal that the recently established single-height rebonded model is unstable not only with respect to (001), but also in comparison to other monohydride (105) structures. This finding persists for both Si and Ge, for applied biaxial strains from -4% to 4%, and for nearly the entire relevant domain of the chemical potential of hydrogen, thus providing a thermodynamics perspective on the recently observed H-induced destabilization of the Ge(105) surface.

**12:03**

**V46 5 Using Si(100) - 2 x 1:H as a Platform for Patterned Silicon Growth** MATTHEW M. SZTELLE, *Department of Electrical and Computer Engineering and Beckman Institute for Advanced Science and Technology, University of Illinois, Urbana,*

*Illinois* SCOTT W. SCHMUCKER, *Department of Electrical and Computer Engineering and Beckman Institute for Advanced Science and Technology, University of Illinois, Urbana, Illinois* JOSEPH W. LYDING, *Department of Electrical and Computer Engineering and Beckman Institute for Advanced Science and Technology, University of Illinois, Urbana, Illinois* An ultra-high vacuum scanning tunneling microscope (UHV-STM) is used to create patterns at the atomic level by desorbing hydrogen atoms from the Si(100) – 2 x 1:H surface thereby creating a clean silicon template for selective area chemical vapor deposition (CVD). Disilane ($Si_2H_6$) gas, when introduced, repassivates the clean silicon pattern with an inert mix of hydride and silicon-hydride species. Subsequent layers can be grown through repeated patterning allowing controlled silicon growth at the nanometer scale. Amorphous silicon growth has been demonstrated at room temperature with nanometer scale control over feature sizes. Results will also be presented on our attempts to grow single crystal silicon features by performing these experiments at elevated temperatures to promote silicon surface diffusion.

**12:15**

**V46 6 Hole mobility in SiGe alloys from first principles.** SIAN JOYCE, FELIPE MURPHY-ARMANDO, *Tyndall National Institute, Lee Maltings, Prospect Row, Cork, Ireland* STEPHEN FAHY, *Tyndall National Institute and Dept. of Physics University College Cork, Ireland* First principles density functional theory is used to calculate the mobility of holes in $Si_{1-x}Ge_x$ alloys as a function of alloy composition. The alloy host is modelled within the virtual crystal approximation (VCA) using supercell techniques. The scattering matrix for carrier scattering in the presence of a Ge or Si substitutional atom in the VCA lattice is determined from the resultant energy splitting in the valence bands. The effect of the spin-orbit interaction is included in these calculations. The mobility is obtained from the scattering rate using the Boltzmann transport equation in the relaxation time approximation.

**12:27**

**V46 7 First-principles calculation of phonon scattering of n-type carriers in SiGe alloys** FELIPE MURPHY ARMANDO, STEPHEN FAHY, *Tyndall National Institute, University College Cork* We calculate the scattering matrix due to phonons in a $Si_{1-x}Ge_x$ random substitutional alloy using first principles density functional theory. The electron-phonon matrix elements are obtained from linear response theory in supercells containing up to 128 atoms. We calculate the n-type carrier mobility from the scattering rates of phonon and alloy scattering using the Boltzmann transport equation. Results are compared to experiments.

**12:39**

**V46 8 MEIS study of As and Sb implantation in Si(001) with excess vacancy concentration and SIMOX.** MATEUS DALPONTE, HENRI BOUDINOV, *UFRGS, Brazil* LYUDMILA GONCHAROVA, ERIC GARFUNKEL, TORGNY GUSTAFSSON, *Rutgers University, USA* We have studied the behavior of dopants (As and Sb) in Separation-by-IMplanted-OXygen (SIMOX) and in vacancy-rich layers in bulk Si(100). The vacancy layers were created by 240 keV $O_2^+$ or $N_2^+$ ion implantation at 400°C with a dose of $2.5x10^{16}$ $cm^{-2}$. Each of the O or N pre-implanted samples was then implanted at 20 keV at room temperature with only one of the dopants to a dose of $5x10^{14}cm^{-2}$. The samples were then annealed either using Rapid Thermal Annealing (RTA) or Furnace Annealing (FA) and characterized using Medium Energy Ion Scattering (MEIS) in both channeling and random directions. Bulk Si samples without O or N pre-implantation were also prepared for reference. The results showed marked differences in dopant diffusion between all of the samples, for instance, faster diffusion of As in the N pre-implanted compared to the O pre-implanted ones. Also, diffusion is faster for Sb in SIMOX than in Si without N or O pre-implantation. Another observed effect was that both dopants presented stronger Transient Enhanced Diffusion (TED) in the N pre-implanted samples. These differences might be associated with the structure of the vacancies (large clusters in SIMOX and point defects in the O or N pre-implanted samples) as well as with chemical effects of O or N in the pre-implanted samples.

**12:51**

**V46 9 DFT calculations of formation energy and properties of Frenkel pairs in Si** MATTHEW J. BECK, S. T. PANTELIDES, *Department of Physics and Astronomy, Vanderbilt University, Nashville, TN* The formation of vacancy-interstitial pairs (Frenkel pairs) underlies many materials processes, including the production of defects by irradiation or ion implantation. Here we present the results of density functional calculations of the formation and properties of Frenkel pairs in Silicon for various pair configurations. The detailed relaxations and overall stability of these pairs against recombination, even at large separations, are strongly dependent on the transfer of charge among the vacancy and interstitial states in the Si band gap, and are highly sensitive to the interstitial configuration. The results are discussed with respect to their implications for models of radiation-induced defect damage and related processes. This work was supported in part by AFOSR grant FA9550-05-1-0306.

**13:03**

**V46 10 Effect of Hydrogen on the Migration Processes of Dislocations in Silicon** NORIHISA OYAMA, TAKAHISA OHNO, *NIMS* It was reported that the dislocation glide mobility in Si is enhanced by irradiation with H plasma. In this work, we perform the first-principles total-energy calculations, and investigate the effect of H on the migration processes of dislocations in Si. We found that the most stable site in the dislocation core is not located at the bond center (BC) site but at the back-bond (BB) site. By interacting with a H atom, the formation energy of a kink becomes negative, and the dislocation is spontaneously bent. As a result, the activation energy of dislocation motion decreases by 1.1eV. The migration processes of the kinks are discussed in the presentation. This study was supported by RSS21 project and Grant-in-Aid for Scientific Research (No.17064017) of MEXT of the Japanese government. The calculations in this work were carried out partly using the Numerical Materials Simulator in National Institute for Materials Science (NIMS), and partly using the NEC-SX5 at Cybermedia Center, Osaka University.

**13:15**

**V46 11 Self-trapping-enhanced carrier recombination at light-induced boron-oxygen complexes in silicon** SHENGBAI ZHANG, MAO-HUA DU, HOWARD BRANZ, RICHARD CRANDALL, *National Renewable Energy Laboratory* First-principles study of the $BO_2$ complex in B-doped Czochralski silicon reveals a self-trapping-enhanced carrier recombination mechanism that contrasts with the standard fixed-level Shockley-Read-Hall model for recombination. An $O_2$ dimer distant from the boron causes only a slow carrier recombination, which is, nevertheless, enough to drive the $O_2$ diffusion under light to form the $BO_2$ complex. We find that the $BO_2$ and $O_2$ produce nearly identical

defect levels in the bandgap. Despite that, recombination at the $BO_2$ is substantially faster than that at the $O_2$, because the charge state of the latter inhibits a key step in the recombination, namely, the capture of the hole. This work was supported by the U. S. Department of Energy, BES and EERE, under Contract No. DE-AC39-98-GO10337.

**13:27**

**V46 12 Energy gain by defect formation: a new tight binding annealed model for a-Si** JOSEPH FELDMAN, *Naval Research Laboratory and George Mason University* NOAM BERNSTEIN, *Naval Research Laboratory* MARCO FORNARI, *Central Michigan University* DIMITRIS PAPACONSTANTOPOULOS, *Naval Research Laboratory and George Mason University* We have obtained a new structure of a-Si by annealing with QM forces a Wooten CRN type 216 model. The annealing was done for 1.2 ns (1.2 million time steps) and the NRL tight binding method was employed. We obtain the total energy, electronic density of states, and force constants of the model. Whereas the starting model had no coordination defects several were present in the final model. As expected these defects were found to give rise to states in the gap as determined both by charge self-consistent TB calculations and DFT (pseudopotential) calculations, where the latter were performed on related ''relaxed'' models within DFT. The final model was of lower total energy than the starting model, both within the TB method and within the psedopotential method. The normal mode properties based on our force constant determination within TB will also be discussed.

**13:39**

**V46 13 Effect of e-h Pairs on the Stability of Bond-Center Hydrogen in Silicon** NAGESWARA RAO SUNKARANAM, *Department of Physics and Astronomy, Vanderbilt University* SRIRAM DIXIT, *Interdisciplinary Materials Science Program, Vanderbilt University* GUNTER LUPKE, *Department of Applied Science, College of William and Mary* NORMAN TOLK, *Department of Physics and Astronomy, Vanderbilt University* LEONARD FELDMAN, *Department of Physics and Astronomy & Interdisciplinary Materials Science Program, Vanderbilt University* Hydrogen injected into silicon at low temperature resides in the bond-centered site, $H^+$ [BC]. This is the most fundamental hydrogen related defect in many covalent semiconductors. Thermal annealing shows $H^+$ [BC] stability up to 150K, and correlates with Si vacancy migration. We report the first observation of the decay of $H^+$ [BC] due to e-h pairs induced by energetic ions. Thin single crystal silicon films containing $H^+$ [BC] ( $\sim 35\mu$m) were fabricated to permit subsequent transmission of energetic protons, creating high e-h pair concentrations and minimal displacement damage. In-situ infrared studies revealed a 90% reduction of $H^+$ [BC] sites after a 1.8 MeV proton dose of $50\mu C/cm^2$ at 80K. Recombination of e-h pairs at defect sites is known to cause vacancy diffusion providing another mechanism for loss of $H^+$ [BC]. Our results show the effect of e-h pairs on $H^+$ [BC] stability. We interpret this in terms of the e-h pair/vacancy interaction.

**SESSION V47: SPECTROSCOPY AND TRANSPORT IN 2D SEMICONDUCTORS**
**Thursday Morning, 16 March 2006**
**350, Baltimore Convention Center at 11:15**
**Emilio Mendez, SUNY at Stony Brook, presiding**

**11:15**

**V47 1 Magnetotunneling Spectroscopy in InGaAs Double-well Structures** Y. LIN, *National Tsing Hua University, Taiwan* A.K.M. NEWAZ, E.E. MENDEZ, *SUNY at Stony Brook* J. NITTA, *Tohoku University, Japan* We have used magnetotunneling spectroscopy to elucidate the mechanism of electron tunneling in double-well (DW) heterostructures whose current-voltage ($I - V$) characteristics are quite different from the $\delta$-function-like shapes expected from energy- and momentum-conservation laws. Our DW tunneling structure consisted of two $In_{0.53}Ga_{0.47}As$ wells 53 Å and 82 Å wide, confined by $In_{0.52}Al_{0.48}As$ barriers with thickness of 100 Å, 53 Å and 100 Å. Without magnetic field, at $T = 4.2$K the $I - V$ characteristics had several distinct regions, each one quasi- triangular in shape and corresponding to the alignment of states in adjacent wells. Under a field ($H \leq 14$T) parallel to the current, each region revealed strong features that shifted to higher voltages with increasing field and are related to Landau levels from states in individual wells. The field dependence of those features yielded, in addition to the band parameters, the zero-field energies of the states at representative voltages of the $I - V$ characteristics. In the physical picture that emerges from the analysis, electrons tunnel via the two wells as long as in each of them there are states below the emitter's Fermi energy, without any consideration to in-plane momentum (or Landau-level index) conservation. This conclusion is supported by remarkably similar results we have also obtained in GaAs-GaAlAs double- well structures.

**11:27**

**V47 2 Shot Noise in Coherently Coupled GaAs-AlGaAs Double-Well Resonant-Tunneling Diodes** A.K.M. NEWAZ, W. SONG, B. NIELSEN, E.E. MENDEZ, *SUNY at Stony Brook* R. HEY, H. KOSTIAL, H.T. GRAHN, *Paul Drude Institute, Berlin* We have found experimentally that, regarding shot-noise, there is no difference between coherent and sequential resonant tunneling, in contrast with calculations that predict that the suppression of noise in a coherent-tunneling process should be larger. Our measurements were done at 4.2 K in GaAs-AlGaAs Double-Well Resonant-Tunneling Diodes (DWRTD) grown by molecular beam epitaxy on $n^+$GaAs substrates. Each AlGaAs barrier at the two ends of each structure was 100 Å, while the central barriers were 60 Å (uncoupled DWRTD), 20 Å and 15 Å (coupled DWRTDs) thick, depending on the sample. In all cases, the two quantum wells between the barriers were 53 Å and 80 Å wide, each well having two confined quantum states. The current-voltage characteristics of the diodes exhibited current peaks associated with voltage-induced alignment of states in adjacent wells. In the coupled DWRTDs each peak split into two, as a result of symmetric and anti- symmetric wavefunctions being extended to both wells. Noise measurements revealed a shot noise power spectrum up to about 50% smaller than that of Poissonian noise $2eI$, regardless of whether the wells were coupled or uncoupled. Our results support those calculations in multiple-barrier structures that predict that the shot-noise reduction should be independent of whether the electronic transport is sequential or coherent.

**11:39**

**V47 3 Observation of a periodic structure in quantum rings using Scanning Gate Microscopy** F. MARTINS, B. HACKENS, T. OUISSE, J.F. MOTTE, M. STARK, H. SELLIER, J. CHEVRIER, S. HUANT, *CNRS, UJF, Grenoble, France* V. BAYOT, *CERMIN, UCL Belgium* S. BOLLAERT, X. WALLART, A. CAPPY, *IEMN, France* Recent advances in scanning gate microscopies (SGM) have made it possible to image electron flow in nanostructures, using the tip as a moving gate (M.A. Topinka et al., Science 289, 2323 (2000)). Our experiment focuses on quantum rings (QR), patterned from a two-dimensional electron gas (2DEG) buried close to the sample surface (25 nm). We can therefore reach a very small tip-sample distance, thereby improving the imaging resolution. Furthermore, the absence of metallic gates on the top of our sample allows to probe the electron flow directly inside the QR. The SGM images, obtained at 4.2 K, reveal striking periodic oscillations of the resistance along the QR circumference as the tip scans over the sample surface. These oscillations respect the radial symmetry of the QR, and their periodicity is much larger than the Fermi wavelength. We analyze the influence of the tip-induced perturbation on the 2DEG by changing the tip voltage (both in accumulation and depletion regimes) and the tip-sample distance.

**11:51**

**V47 4 Scanning gate microscopy on Aharonov-Bohm rings in a magnetic field: experiments and simulations** B. HACKENS, F. MARTINS, T. OUISSE, J.F. MOTTE, M. STARK, H. SELLIER, J. CHEVRIER, S. HUANT, *CNRS, UJF, Grenoble, France* V. BAYOT, *CERMIN, UCL Belgium* S. BOLLAERT, X. WALLART, A. CAPPY, *IEMN, France* We use low temperature scanning gate microscopy to study the electron dynamics inside Aharonov-Bohm (AB) rings in the phase-coherent regime. Our samples are prepared by etching from high-mobility two-dimensional electron systems 25 nm below the surface (B. Hackens et al., Phys. Rev. Lett. 94, 146802 (2005)). The bias applied on the AFM tip, as it is scanned over the AB ring, induces a local perturbation of the electric potential experienced by the electrons, thereby affecting the ring resistance. In particular, we observe in detail the effect of small variations of the perpendicular magnetic field in different regimes (up to B=6 T). As we plot these resistance variations as a function of the AFM tip position, we observe resistance modulations which have the spatial symmetry of the ring, and an amplitude equal to that of the AB oscillations. This strongly suggests that our resistance maps are closely linked to the periodic modulations of the electron probability density. Finally, we also performed simulations of the electron wavefunctions in AB rings, as well as of the electron transmission through the AB rings. Including the effect of the perturbating potential of the tip in such simulations, we get valuable informations which help to explain our experimental results.

**12:03**

**V47 5 Optical Imaging for the Determination of Minority Carrier Transport*** DAVID LUBER, *Naval Postgraduate School* FRANK BRADLEY, NANCY HAEGEL, A scanning electron microscope technique is used, in combination with an optical imaging system, to measure minority carrier diffusion length in a heavily doped GaAs double heterostructure. Both diffusion and drift of charge are imaged. A diffusion length of $\sim$ 3.2 - 4 $\mu$m is measured, corresponding to a minority carrier mobility of 950-1480 $cm^2/Vs$ in p-type material, doped $\sim$ 5 x $10^{18}$ $cm^{-3}$, in good agreement with theoretical predictions. Drift and diffusion behavior are also studied in more heavily doped regimes where plasmon scattering is expected to play a significant role. Measurements will be presented as a function of doping level, local electric field and sample temperature. We explore the limitations on determination of the diffusion length due to effects such as the finite nature of the excitation volume and photon recycling near the point of generation and compare approaches for extracting key material parameters. The technique offers a flexible approach to direct measurement of various transport properties and is applicable to a range of luminescent materials and multilayer devices. Examples from high resolution mapping of non-uniform electric field distributions will also be presented.

*This work has been supported by NSF Grants DMR-02033997 and DMR-0526330.

**12:15**

**V47 6 Transverse magnetic focusing and spin-dependent reflection experiments in InSb- and InAs-based heterostructures** HONG CHEN, J.J. HEREMANS, *Department of Physics, Virginia Tech* J.A. PETERS, J.T. BEARDSLEY, *Department of Physics and Astronomy, Ohio University* N. GOEL, S.J. CHUNG, M.B. SANTOS, *Department of Physics and Astronomy, University of Oklahoma* W. VAN ROY, G. BORGHS, *IMEC, Leuven, Belgium* We report on mesoscopic spin-dependent ballistic transport in InSb/InAlSb and InAs/AlGaSb heterostructures, characterized by strong spin-orbit interaction. Spin-orbit interaction in two-dimensional electron systems can lead to spin-splitting in semiclassical ballistic trajectories and in spin-dependent reflection of carriers. We experimentally demonstrate the spin reflection in open and closed ballistic geometries optimizing scattering off a lithographic barrier. Further, experimentally obtained transverse magnetic focusing spectra can be interpreted as demonstrating both spin-split ballistic transport and spin-dependent reflection for higher order peaks involving carrier reflection off the barrier. NSF DMR-0094055 (JJH), DMR-0080054, DMR-0209371 (MBS).

**12:27**

**V47 7 Effect of dc and ac excitations on the longitudinal resistance of a two-dimensional electron gas in highly doped GaAs quantum wells*** JINGQIAO ZHANG, ALEXEY BYKOV, SERGEY VITKALOV, *The City College of New York* A. K. KALAGIN, A. K. BAKAROV, *Institute of Semiconductor Physics, 630090 Novosibirsk, Russia* Linear AC (888 Hz) resistance of highly mobile two dimensional electrons in GaAs heavily doped quantum wells is studied at different magnitude of dc and ac (10 KHz to 20 GHz) excitations. In the DC excitation regime the differential resistance oscillates with the dc current and external magnetic field similar to that observed earlier in AlGaAs/GaAs heterostructures. At external ac excitations the resistance is also found to be oscillating with the magnetic field. However the form of the oscillations is considerably different from the dc case. We show that at frequency below 100 KHz the difference is result of a specific average of the dc differential resistance during the period of the external ac excitations.

*Work was supported by NSF: DMR 0349049, by DOE: DOE-FG02-84-ER45153 and RFBR: project No.04-02-16789

**12:39**

**V47 8 Thermodynamic and transport properties of two-dimensional GaAs systems near the apparent metal-insulator**

**transition** E.A. GALAKTIONOV, G.D. ALLISON, A.K. SAVCHENKO, S.S. SAFONOV, *University of Exeter, UK* M.M. FOGLER, *UCSD* M.Y. SIMMONS, D.A. RITCHIE, *Cavendish Lab, Cambridge, UK* An extensive study of the charge compressibility and resistance of two-dimensional electron and hole systems is reported. A total of five GaAs samples were examined, two 2DEGs and three 2DHGs. All samples have high mobilities but vary in spacer, doping, and other growth parameters. The inverse compressibility is found to have a negative minimum at a sample-dependent carrier concentration followed by an upturn to large positive values as the concentration decreases. This behavior is shown to agree quantitatively with the theory of nonlinear screening of the random impurity potential, for both types of carriers, despite a ten-fold difference in their $r_s$ parameters. The region of the apparent metal-insulator transition (MIT) where $\partial R/\partial T$ changes sign, and the position of the inverse compressibility minimum can differ by as much as 50%. Their relative positions vary with sample and cooldown. No thermodynamic anomalies at the apparent MIT are detected. In a range of $T$ where both the capacitance and the resistance of 2DHG samples were studied, the latter exhibits a scaling characteristic of the percolation transition. The corresponding percolation threshold is different from the MIT but agrees quantitatively with the percolation point deduced from the analysis of the compressibility.

**12:51**

**V47 9 Evidence for coherent transport in GaAs hole open quantum dots.** S. FANIEL, B. HACKENS, A. VLAD, C. GUSTIN, L. MOLDOVAN, S. MELINTE, V. BAYOT, *Cermin, Universite Catholique de Louvain, Louvain-la-Neuve, Belgium* M. SHAYEGAN, *Department of Electrical Engineering, Princeton University, Princeton, New Jersey 08544* We report magnetotransport measurements in GaAs hole open quantum dots. Our samples were fabricated from a *p*-type GaAs quantum well with a density of $2.2 \times 10^{15} m^{-2}$ and a mobility of $35 m^2$/Vs. Two different dots were patterned using e-beam lithography and wet etching. A top gate was added in order to control the dots openings and the hole density. The measurements were performed down to 30 mK with the magnetic field applied perpendicular to the plane of the two- dimensional system. We observed large, reproducible conductance fluctuations associated with the coherent transport of holes inside the dots at lowest temperatures which vanish above 500 mK. From the variance of these fluctuations and from the Random Matrix Theory, we extracted the hole dephasing time $\tau_\varphi$. The temperature dependence of the calculated $\tau_\varphi$ lies between a $T^{-1}$ and $T^{-2}$ behavior and exhibits a saturation at very low temperature which is similar with $\tau_\varphi$ measured in 2D electron systems[1].

[1]B. Hackens *et al.*, Phys. Rev. Lett. **94**, 146802 (2005)

**13:03**

**V47 10 Surface Gated Quantum Hall Effect in InAs Heterostructures** IAN GELFAND, *Harvard University* SAMI AMASHA, DOMINIK ZUMBUHL, MARC KASTNER, *Massachusetts Institute of Technology* CHRISTOPH KADOW,* ARTHUR GOSSARD, *University of California at Santa Barbara* NANOSCALE SCIENCE AND ENGINEERING CENTER COLLABORATION, We demonstrate low leakage surface gating of Indium Arsenide two dimensional electron gasses by observing a surface gated quantum Hall effect in an InAs-AlSb heterostructure. Gating is made possible by growing an aluminum oxide layer on top of the device. We find the depletion point can be changed by applying a large positive gate voltage, and we see hysteresis below depletion. Supported by ARO W911NF-05-1-0062, NSEC PHY-0117795, NSF DMR-0353209 and DMR-0213282.

*Currently at Infineon Technologies AG

**13:15**

**V47 11 Anisotropic thermopower and planar Nernst effect in Ga1-xMnxAs*** YONG PU, JING SHI, *Dept. of Physics, UC-Riverside* We have carried out the thermopower and magneto-thermopower measurements on three Ga1-xMnxAs (x=0.039, 0.049, and 0.059) samples above and below their Curie temperatures. Below the Curie temperature, we have observed magnetic field dependence in both parallel (longitudinal) and perpendicular (transverse) directions to the temperature gradient. The magnetic field dependence does not depend on the relative orientation between the temperature gradient and crystallographic direction of the GaAs. The transverse thermopower or the planar Nernst effect, shows abrupt jumps as the magnetization switches between the four-fold symmetry axes, which resembles the giant planar Hall effect found in similar materials. Although the longitudinal thermopower is not sensitive to the same switchings of the magnetization, it has a strong magnetic field dependence as the magnetization rotates. We have measured both effects vs. the magnetic field orientation with respect to the temperature gradient. Similar to the origin of the giant planar Hall effect, we attribute the longitudinal and transverse effects to the anistropic magneto-thermopower. We interpret the both effects in the context of the anisotropic transport.

*In collaboration with Ezekiel Johnston Halperin, Dept. of Physics, UC-Barbara; and David Awschalom, Dept. of Physics, UC-Barbara. Supported by ONR/DARPA and CNID.

**13:27**

**V47 12 Long-Lived Coherent Cyclotron Oscillations in a 2D Electron Gas** X. WANG, R. SRIVASTAVA, A. BARKAN, D. M. MITTLEMAN, J. KONO, *Department of Electrical and Computer Engineering, Rice University* J. L. RENO, *Sandia National Laboratories* DEPARTMENT OF ELECTRICAL AND COMPUTER ENGINEERING, RICE UNIVERSITY TEAM, SANDIA NATIONAL LABORATORIES COLLABORATION, We have used the technique of time-domain THz spectroscopy to study coherent charge dynamics in a high-mobility two-dimensional electron gas (2DEG) in quantizing magnetic fields. By analyzing the magnetic field dependence of the transmitted THz waveform, we successfully extracted the real and imaginary parts of the dynamic conductivity at various magnetic fields and temperatures for a GaAs/AlGaAs 2DEG with a 1.5 K mobility of $3.7 \times 10^6$ cm$^2$/Vs. We observed pronounced coherent cyclotron oscillations persisting more than 50 picoseconds and 20 periods. From the frequency and decay time of these oscillations, we can directly determine the cyclotron mass and phase coherence time. The basic phenomenon observed can be understood as the free induction decay of a coherent superposition between the lowest unfilled Landau level and the highest filled Landau level induced by the incident coherent THz pulse. Finally, we discuss the possibility of using this technique to overcome the saturation effect, which is

known to prevent the determination of true cyclotron resonance linewidths in high-mobility ( $> 10^5$ $cm^2/Vs$) 2DEG measured with conventional far-infrared techniques using CW and incoherent sources.

**13:39**
**V47 13 Modulation of two-dimensional electrons in Si/SiGe heterostructures using atomic-layer-deposited gate dielectric** T. M. LU, K. LAI, *Princeton University* P. D. YE, *Purdue Univeristy* W. PAN, *Sandia National Lab* D. C. TSUI, S. LYON, *Princeton University* M. MUHLBERGER, F. SCHAFFLER, *Univ. Linz* Field effect transistors (FETs) have been fabricated using Atomic-Layer-Deposited (ALD) $Al_2O_3$ as gate dielectric on the Si/SiGe heterostructures to modulate the density of the two-dimensional (2D) electrons in the strained silicon channel [1]. Magnetotransport measurements taken at 0.3K show that the 2D density (n) can be uniformly tuned by the gate voltage (VG) with virtually no leakage current and negligible gate hysteresis. The characteristic of modulation using ALD $Al_2O_3$ as gate dielectric is shown to be better than that using Pd Schottky barrier or the PECVD $SiO_2$ dielectric. We also performed a numerical simulation that solves the one-dimensional Poisson-Schrodinger equations self-consistently for different $V_G$s. The measured n vs. $V_G$ relation can be reproduced in our calculation by assuming a density of $0.6\times 10^{13} eV^{-1}cm^{-2}$ of the surface states. [1] K. Lai et al., Appl. Phys. Lett. 87, 142103 (2005)

**13:51**
**V47 14 Hysteresis and saturation of intersubband absorption by electrons on helium** DMITRI RYVKINE, *Michigan State University* MICHAEL LEA, *Royal Holloway, University of London, Egham, Surrey TW20 0EX, UK* MARK DYKMAN, *Michigan State University* We propose a mechanism, develop a theory, and provide experimental data that demonstrate hysteresis of resonant inter-subband absorption by a quasi two-dimensional electron system on the surface of helium. The electrons form a strongly correlated nondegenerate electron liquid. The absorption occurs at the frequency of the transition from the ground to the first excited state of motion normal to the helium surface. The lifetime of the excited state is extremely long, 0.1 $\mu$s at 0.3 K, leading to strong absorption nonlinearity even for low radiation intensity [1]. Besides absorption saturation, radiation-induced occupation of the excited subband causes a shift of the resonant transition frequency. We show that this shift leads to absorption hysteresis with varying radiation frequency or intensity. As a result of electron correlations, the in-plane motion in all subbands is described by the same electron temperature, which is found self-consistently. The results bear on quantum computing with electrons on helium, since they demonstrate resonant transitions responsible for a single-qubit operation; the hysteresis results from the same mechanism that leads to two-qubit operations. 1. E. Collin et al., Phys. Rev. Lett. 89, 245301 (2002)

## SESSION W1: ARPES IN HIGH TC SUPERCONDUCTORS
**Thursday Afternoon, 16 March 2006; Ballroom IV, Baltimore Convention Center at 14:30**
**Peter Johnson, Brookhaven National Laboratory, presiding**

**14:30**
**W1 1 Laser ARPES, the sudden approximation, and quasiparticle-like peaks in $Bi_2Sr_2CaCu_2O_{8+d}$.**
DAN DESSAU, *University of Colorado, Boulder*

A new low photon energy regime of angle resolved photoemission spectroscopy is accessed with lasers and used to study the superconductor $Bi_2Sr_2CaCu_2O_{8+d}$. The low energy increases bulk-sensitivity, reduces background, and improves resolution. Crucial aspects of the data such as the dispersion, superconducting gaps, and the bosonic coupling kink are found to be robust to a possible breakdown of the sudden approximation. We observe spectral peaks which are sharp on the scale of their binding energy - the clearest evidence yet for quasiparticles in the normal state. The very sharp spectral peaks and high statistics enables detailed investigations of the temperature and energy dependences of the lineshapes, giving critical insights into the nature of the scattering mechanisms in these materials. We thank collaborations with J. D. Koralek, J.F. Douglas, N.C. Plumb, Z. Sun, A.V. Fedorov, M. Murnane, H. Kapteyn, S. Cundiff, Y. Aiura, K. Oka, and H. Eisaki.

**15:06**
**W1 2 What is the ''glue'' for high temperature superconductivity?**
TONICA VALLA, *Brookhaven National Laboratory*

It has been 20 years since the high-temperature superconductivity (HTSC) was discovered in $La_{2-x}Ba_xCuO_4$, by Bednorz and Müller. Since then, many different HTSC compounds, all containing copper-oxide planes, were synthesized and HTSC became one of the most studied problems in science. However, the mechanism of HTSC still remains unknown. Recent advancements in Angle-Resolved Photoemission Spectroscopy (ARPES) have enabled a direct probing of effects of interactions between electrons and different bosonic excitations in a system, raising the expectations that a ''pairing boson'' responsible for HTSC could finally be identified. Here, we will present the study of single-particle excitations in two different cuprates: $Bi_2Sr_2CaCu_2O_{8+\delta}$, a high-temperature superconductor with $T_C = 91$ K and $La_{1.875}Ba_{0.125}CuO_4$, a system with suppressed superconductivity ($T_C \leqslant 2.5$ K) due to the spin/charge ordering. The extracted self-energies and single-particle gaps will be compared and possible coupling mechanisms will be discussed. This work was supported by the DOE under contract number DE- AC02-98CH10886.

**15:42**
**W1 3 Dispersion Anomalies and High Frequency Optical Conductivity in Cuprate Superconductors.***
ANDREY CHUBUKOV, *University of Wisconsin*

We argue that the shape of the dispersion along the nodal and antinodal directions in the cuprates can be understood as a consequence of the interaction of the electrons with collective spin excitations. In the normal state, the dispersion displays a crossover at an energy where the decay into spin fluctuations becomes relevant. In the superconducting state, the antinodal dispersion is strongly affected by the $(\pi,\pi)$ spin resonance and displays an S-shape whose magnitude scales with the resonance intensity. For nodal fermions, relevant spin excitations do not have resonance behavior, rather they are better characterized as a gapped continuum. As a consequence, the S-shape becomes a kink, and superconductivity does not affect the dispersion as strongly. We also analyzed recent infrared conductivity data in the normal state. We find that the high frequency behavior, which has been suggested as evidence for quantum critical scaling, is well described by the same interaction with overdamped collective modes. From explicit calculations, we find a frequency exponent for the modulus of the conductivity, and a phase angle, in good agreement with experiment.

*In collaboration with M. Norman (Argonne Natl Lab).

**16:18**
**W1 4 ARPES Investigation of Quasiparticle Renormalization in Cuprates.**
TANJA CUK, *Stanford University*

We investigated by Angle-Resolved-Photoemission-Spectroscopy the renormalization of the bands in Bi2212 as a function of doping, including underdoped ($T_c$ =85K), optimally doped ($T_c$ = 94K), andoverdoped($T_c$ = 65K) samples. We identified the sharp energy scale seen in the superconducting state with the $B_{1g}$ bond buckling mode, the out-of-phase vibrations of the in-plane oxygen. More recently, we compare doping dependent data to a theoretical calculation involving the identified modes, including both temperature and momentum dependence. This comparison brings insights to the doping induced spectral changes in the overdoped regime, in connection to some recent discussions. We will also present complimentary pressure dependent Raman scattering and X-Ray diffraction data showing how the $B_{1g}$ mode renormalizes with metallization of the insulating parent compound of Bi2212. The pressure variable allows a continuous assessment of the electron−phonon coupling lambda, based on both phonon frequency and lineshape, across the phase diagram. Finally, we discuss ways to test whether these mode couplings have a direct bearing on superconductivity.

**16:54**
**W1 5 ARPES Study of Nodal Quasiparticles Using Low-Energy Tunable Photons.**
AKIHIRO INO, *Graduate School of Science, Hiroshima University*

Low-energy quasiparticle excitations govern the thermodynamic properties of a superconductor both in the zero-field and vortex-mixed states. For a *d*-wave superconductor, nodal quasiparticles are crucial excitations starting from zero energy. So far, however, the nodal quasiparticle dynamics of high-Tc cuprates has been controversial. For example, it has been reported by an angle-resolved-photoemission (ARPES) experiment that the marginal-Fermi-liquid behavior persists into the superconducting state without appreciable change in the scattering rate, while microwave conductivity increases upon the superconducting transition. Here, we show a new ARPES result that solves the controversies with unprecedented momentum-resolution. Low-energy tunable photons have enabled us to resolve a small nodal bilayer splitting clearly, and to reveal the detailed temperature- and energy-dependence of the scattering rate, indicating the behaviors unique to the nodal quasiparticles. Due to the opening of the *d*-wave gap, the nodal scattering rate is remarkably suppressed, and shows a linear energy dependence. The difference in the energy-linear term between the bilayer-resolved scattering rates hints the nature of impurities involved. This work was done in collaboration with T. Yamasaki, T. Kamo, K. Yamazaki, H. Anzai, M. Arita, H. Namatame, M. Taniguchi, Grad. Sch. of Science and Hiroshima Synchrotron Radiation Center, Hiroshima Univ., A. Fujimori, Dept. of Complexity Science and Engineering, Univ. of Tokyo, Z.-X. Shen, Dept. of Physics, Applied Physics and SSRL, Stanford Univ., M. Ishikado, K. Fujita, and S. Uchida, Dept. of Physics, Univ. of Tokyo.

## SESSION W2: IMAGING CHARGE AND SPIN AND SEMICONDUCTORS
**Thursday Afternoon, 16 March 2006; Ballroom III, Baltimore Convention Center at 14:30**
**Robert Westervelt, Harvard University, presiding**

**14:30**
**W2 1 Imaging Transport Resonances in the Quantum Hall Effect.**
GARY STEELE, *MIT*

We image charge transport in the quantum Hall effect using a charge accumulation microscope. Scanning a charge sensitive tip just above the surface of a very high mobility AlGaAs/GaAs heterostructure, we measure the charging underneath the tip that results from applying an ac voltage to the 2D electron system (2DES). Applying a dc bias voltage

to the tip induces a highly resistive ring-shaped incompressible strip (IS) in the 2D electron system (2DES) that moves along with the tip. This IS acts as a barrier that prevents charging of the region under the tip. At certain tip positions, short-range disorder in the 2DES creates a quantum dot island inside the IS that enables breaching of the IS barrier by means of resonant tunneling through the island. The images that result show striking ring shapes that directly reflect the shape of the IS. Within the ring shaped features, we also observe striations that arise from Coulomb Blockade of the quantum dot island. Varying the magnetic field, the tunneling resistance of the IS varies significantly, and takes on drastically different values at different filling factors. Measuring this tunneling resistance provides a unique *microscopic* probe of energy gaps in the quantum Hall system. To better understand the origin of the transport resonances, we have completed a series of simulations that show that the native disorder from remote ionized donors can create islands in the IS. Comparing the simulations with the experimental images provides a direct view of the disorder potential of a very high mobility 2DES. The experiments and simulations reveal the potential importance of single-electron resonant tunneling to bulk transport in the quantum Hall effect.

**15:06**
**W2 2 Terahertz Imaging of cyclotron emission from quantum Hall conductors.**
SUSUMU KOMIYAMA, *Department of Basic Science, University of Tokyo*

Microscopy of extremely weak terahertz (THz) waves via photon-counting method is reported. A quantum-dot photon detector [1] is incorporated into a scanning terahertz microscope [2]. By using a quantum Hall detector [3] as well, measurements cover the intensity dynamic range more than five orders of magnitude. The minimum intensity reaches as lo as 10-21watt (one photon per one second). Applying the measurement system to the study of semiconductor quantum Hall (QH) devices, we image cyclotron radiation emitted by non-equilibrium electrons generated in QH electron systems. Owing to the unprecedented sensitivity, a variety of new features of electron kinetics are unveiled [4]. It is stressed that the present approach is in marked contrast to the THz- wave applications recently discussed extensively in a wide variety of fields including clinic, security, and environment. In the vast majority of those applications, room-temperature operation is implicit. The intensity of treated THz radiation is hence well beyond the level of 300K blackbody radiation (roughly 10[l]m-7 watts or 10 [1] 4 photons/s per square centimeter in a 1/10 relative bandwidth). From the scientific viewpoint, however, detecting extremely weak THz waves from an object without external illumination such as applied in the present work is of strong importance, because the microscopic kinetics of an object can be probed only in such a passive method. Besides semiconductor electric devices studied here, we will also discuss possible applications of the present method for molecular dynamics, microthermography, and cell activities. [1] S. Komiyama et al., Nature 403, 405 (2000). [2] K. Ikushimaetal, Rev. Sci. Instrum. 74, 4209 (2003). [3] Y. Kawanoetal, J. Appl. Phys. 89, 4037 (2001). [4] K. Ikushimaetal, Phys. Rev. Lett. 93, 146804 (2004).

**15:42**
**W2 3 Imaging coherent electron flow in a two-dimensional electron gas.***
BRIAN LEROY, *Kavli Institute of Nanoscience, Delft University of Technology*

Images of electron flow through a two-dimensional electron gas can be obtained at liquid He temperatures using scanning probe microscopy. Near a quantum point contact (QPC), the images show angular lobe patterns characteristic of the wavefunctions in the QPC. At distances greater than one micron from the QPC, narrow branches of electron flow are observed due to the cumulative effect of small angle scattering. All of the images are decorated by interference fringes spaced by half the Fermi wavelength demonstrating that the flow is coherent. To determine the origin of the interference fringes, an imaging interferometer is created by adding a circular reflecting gate. The strength and position of the interference fringes can then be controlled by the voltage on this reflecting gate. Using the interferometer, we show that the interference fringes are due to backscattering to the QPC. Both experiments and theory demonstrate that the interference signal is robust against thermal averaging.

*In collaboration with A.C. Bleszynski, K.E. Aidala, M.A. Topinka, R.M. Westervelt, A. Kalben, S.E.J. Shaw and E.J. Heller, Harvard University; K.D. Maranowski and A.C. Gossard University of California Santa Barbara.

**16:18**
**W2 4 Imaging Magnetic Focusing in a Two-Dimensional Electron Gas.***
KATHERINE AIDALA, *Harvard University*

Using a liquid-He cooled scanning probe microscope (SPM), we have directly imaged cyclotron orbits of electrons in a two-dimensional electron gas (2DEG) traveling between two side-by-side quantum point contacts (QPCs). The images show magnetic focusing when the spacing between the QPCs is an integer multiple of twice the cyclotron radius. An image is created by deflecting electrons away from their original trajectories using a capacitively coupled SPM tip, and recording the change in conductance as the tip is raster scanned above the surface. The cyclotron orbits are clearly visualized, as well as fringes that demonstrate the coherent nature of the flow. Classical and quantum simulations show

how electrons are deflected by the tip to produce the image. With an applied magnetic field, the simulated images of magnetic focusing agree very well with the measured images. The simulations also show the effect of small angle scattering due to the ionized donor atoms. Fully quantum simulations show that interference fringes can be produced. Imaging and understanding the motion of electrons in magnetic fields is useful for the development of devices for spintronics and quantum information processing.

*In collaboration with Robert E. Parrott, T. Kramer, M. Stopa, E.J. Heller, R.M. Westervelt, M.P. Hanson and A.C. Gossard. Supported in part by ARO grant W911NF-04-1-0343.

**16:54**
**W2 5 STM and AFM: Which is Better for Surface Structural Analysis? Non-contact AFM Studies on Ge/Si(105) Surface.**
YUKIO HASEGAWA, *Institute for Solid State Physics, The University of Tokyo*

Scanning tunneling microscopy (STM) has been utilized to determine surface atomic structure with its highly resolved images. Probing surface electronic states near the Fermi energy ($E_F$), STM images, however, do not necessarily represent the atomic structure of surfaces. It has been believed that atomic force microscopy (AFM) provides us surface topographic images without being disturbed by the electronic states. In order to prove the surpassing performance, we performed noncontact (nc) AFM on the Ge/Si(105) surface [1], which is a facet plane of the ''hut'' clusters formed on Ge-deposited Si(001) surface. It is found that STM images taken on the surface, either filled- or empty-state images, do not show all surface atoms because of the electronic effect; some surface atoms have dangling bond states below $E_F$ and other surface atoms have states above $E_F$ . [2]. In a nc-AFM image, on the other hand, all surface atoms having a dangling bond are observed [3], directly representing an atomic structure of the surface. Electronic information can also be obtained in AFM by using a Kelvin-probe method. From atomically resolved potential profile we obtained, charge transfer among the dangling bond states is directly demonstrated. These results clearly demonstrate that highly-resolved nc-AFM with a Kelvin-probe method is an ideal tool for analysis of atomic structures and electronic properties of surfaces. This work was done in collaboration with T. Eguchi, K. Akiyama, T. An, and M. Ono, ISSP, Univ. Tokyo and JST; Y. Fujikawa and T. Sakurai, IMR. Tohoku Univ. T. Hashimoto, AIST; Y. Morikawa, ISIR, Osaka Univ. K. Terakura, Hokkaido Univ., and M.G. Lagally, University of Wisconsin-Madison. [1] T. Eguchi et al., Phys. Rev. Lett. 93, 266102 (2004). [2] Y. Fujikawa et al., Phys. Rev. Lett. 88, 176101 (2002). [3] T. Eguchi and Y. Hasegawa, Phys. Rev. Lett. 89, 256105 (2002).

## SESSION W3: TOPOLOGICAL ASPECTS OF ELECTRON TRANSPORT IN SOLIDS
**Thursday Afternoon, 16 March 2006; Ballroom I, Baltimore Convention Center at 14:30**
**Shoucheng Zhang, Stanford University, presiding**

**14:30**
**W3 1 Berry Phase and Dissipationless Currents in Solids.**
NAOTO NAGAOSA, *The University of Tokyo*

It is now recognized that the electronic band structures in solids are characterized by nontrivial quantum topological nature associated with Berry phase. This situation is analogous to the quantum Hall system under the strong magnetic field, but occurs in almost every material even without the magnetic field. Anomalous Hall effect in ferromagnets is a representative example, where the anomalous velocity induced by Berry phase leads to the transverse motion of the electrons to the applied electric field. In paramagnetic materials, on the other hand, the Kramers degeneracy makes the Berry connection non-Abelian. The spin dependent anomalous velocity leads to the spin Hall effect in semiconductors such as GaAs. These charge and spin currents are distinct from the usual transport current since it is not due to the deviation from the equilibrium electron distribution in momentum space, but is driven by the anomalous velocity of all the occupied states in equilibrium. Therefore it is essentially dissipationless. However, in real situation, the disorder effect and contact to the leads introduces the dissipation. This aspect is discussed in detail using the Keldysh formalism for each problem. Ideas of anomalous Hall insulator and spin Hall insulator are also proposed to avoid this dissipation. Applications to optical phenomena are also discussed. This work has been done in collaboration with Z. Fang, S. Murakami, K. Ohgushi, M. Onoda, S. Onoda, K. Sawada, R. Shindou, N. Sugimoto, K. Terakura, and S.C. Zhang.

**15:06**
**W3 2 Fermi Liquid Berry Phase Theory of the Anomalous Hall Effect.***
F. D. M. HALDANE, *Princeton University*

Charged Fermi liquids with broken time-reversal symmetry have an intrinsic anomalous Hall effect that derives from the Berry phases accumulated by accelerated quasiparticles that move on the Fermi surface. The intrinsic Hall conductivity is given by a new fundamental geometric Fermi liquid formula that can be regarded as the derivative with respect to magnetic flux density of the Luttinger fomula relating the density of mobile charge carriers to the k-space volume enclosed by the Fermi surface. This formula can be derived by an integration-by-parts of the Karplus-Luttinger free-electron band-structure formula to yield a topological (QHE) part plus a geometrical part expressed completely at the Fermi surface, and which has a natural generalization to interacting Fermi liquid quasiparticles (QP's). The QP Berry phases are properties of the *eigenstates* of the (exact) single-particle Green's function at the Fermi surface, which is a Hermitian matrix with Bloch-state eigenvectors; the Berry phases derive from the variation on the Fermi surface of the spatially-periodic factor of the QP Bloch state that characterizes how the total QP amplitude is distributed among the different electronic orbitals in the unit cell. In the case of 3D ferromagnetic metals, the Berry phases derive from the interplay of exchange splitting with spin-orbit coupling (both must be present). Remarkably, the new formula also applies to Fermi-liquid analogs such as the 2D composite fermion (CF) fluid in the half-filled lowest Landau level: in this case, the QP is a bound electron+vortex composite and not a Bloch state. This QP structure varies on the CF Fermi surface in a way that exactly gives the expected result $\sigma^{xy} = e^2/2h$, unaffected by any Fermi surface anisotropy, thus explaining how a quantized value of $\sigma^{xy}$ persists even though the CF Fermi liquid is *not* an incompressible FQHE state. The geometric anomalous Hall effect formula suggests a more intrinsic geometric description of the Fermi surface, where the Fermi vector $\boldsymbol{k}_F(\mathbf{s})$ is only one of a number of properties that vary on a curved $(D-1)$-dimensional Fermi surface manifold parametrized by curvilinear coordinates $\mathbf{s}$; other properties include the Berry curvature field $\mathcal{F}(\mathbf{s})$, quasiparticle mean free path $\ell(\mathbf{s})$, etc. The new formula also naturally takes into account non-trivial (multiply-connected) Fermi surface topology and open orbits.

*Supported by NSF DMR-0213706.

**15:42**
**W3 3 The Quantum Spin Hall Effect.**
CHARLES KANE, *University of Pennsylvania*

We show that the intrinsic spin orbit interaction in a single plane of graphene converts the ideal two dimensional semi metallic groundstate of graphene into a quantum spin Hall (QSH) state [1]. This novel electronic phase shares many similarities with the quantum Hall effect. It has a bulk excitation gap, but supports the transport of spin and charge in gapless ''spin filtered'' edge states on the sample boundary. We show that the QSH phase is associated with a $Z_2$ topological invariant, which distinguishes it from an ordinary insulator [2]. The $Z_2$ classification, which is defined for any time reversal invariant Hamiltonian with a bulk excitation gap, is analogous to the Chern number classification of the quantum Hall effect. We argue that the QSH phase is topologically stable with respect to weak interactions and disorder. The QSH phase exhibits a finite (though not quantized) dissipationless spin Hall conductance even in the presence of weak disorder, providing a new direction for realizing dissipationless spin transport. [1] C.L. Kane and E.J. Mele, Phys. Rev. Lett. **95**, 226801 (2005). [2] C.L. Kane and E.J. Mele, Phys. Rev. Lett. **95**, 146802 (2005).

**16:18**
**W3 4 Spintronics, propagating mode, (quantum) spin transport, and new electron liquids.**
B. ANDREI BERNEVIG,* *Department of Physics, Stanford University, Stanford, CA 94305*

The field of spintronics deals with the physics of the electron-spin in semiconductors, metals, insulators and other materials. Among these, the systems which are characterized by strong spin-orbit coupling hold a special place and exhibit a plethora of new phenomena. In classical transport in semiconductors, a propagating spin-charge collective mode appears that is qualitatively different from the diffusive charge transport. The propagating spin-charge mode is the hallmark of spin-orbit coupled systems with a Fermi surface. The Boltzmann transport equations are qualitatively different from the diffusive normal behavior. Three dimensional bulk transport will be analyzed for the first time. In semiconductors without spin-orbit coupling, an orbital Hall effect (similar to the spin-Hall effect) is present in which electrons selectively occupy different orbitals depending on their direction of motion. In quantum transport, a spatially varying spin-orbit coupling is equivalent to a Landau level problem in which electrons of opposite spin feel opposite magnetic fields, thereby exhibiting a quantum Spin-Hall effect. Time-reversal symmetry is unbroken. In these spin Hall insulators, the quantum spin transport takes place through edge states that cross the bulk gap and the Fermi level. The electron liquid on the edges is a helical liquid, in which spin is correlated with chirality, and represents a new class of one-dimensional liquids different from the Luttinger spinless, spinful or chiral liquids. I will also briefly discuss the possibility of three-dimensional quantization in systems with spin-orbit coupling. New experiments are needed and proposed to verify these predictions.

*Collaborators: Taylor Hughes, Shoucheng Zhang.

**SESSION W4: CARBON NANOTUBE DISPERSIONS**
**Thursday Afternoon, 16 March 2006; 308, Baltimore Convention Center at 14:30**
**Ramanan Krishnamoorti, University of Houston, presiding**

**14:30**
**W4 1 From Networks to Nematics – Carbon Nanotubes as Soft Matter.**
ERIK K. HOBBIE, *NIST*

Carbon nanotubes represent just one example of an emerging paradigm in condensed matter physics and materials science: traditionally ''hard'' materials appearing in new ''soft'' applications and environments. In part, this trend being is being fueled by the desire to exploit solution and fluid-based approaches, such as self assembly and flow processing, in an effort to streamline the engineering and commercialization of new materials and applications. In this talk I will review our recent work on dispersing, aligning and manipulating carbon nanotubes in complex fluids and polymer melts. Due to the large aspect ratios and strong attractive interaction potentials intrinsic to such materials, a number of scientific and technical challenges become immediately apparent. In particular, I will focus on the subtle interplay of rheological influences, such as externally applied shear and elongation stresses, with the inherent ''stickiness'' of carbon nanotube suspensions and melts, where the latter typically favors the formation of disordered networks or ''gels'' over the more desirable liquid-crystalline order. For simple shear, the strength of the applied stress is found to be a critical factor in dictating carbon nanotube morphology, which varies from a quiescent network to macroscopic aggregates to a fully dispersed, flow-aligned (para)nematic state. Although we find remarkably low loading thresholds for elastic percolation, our results highlight a fundamental dilemma for the engineering of conducting carbon nanotube polymer composites; dispersion stability will often be achieved at the expense of electrical conductivity.

**15:06**
**W4 2 Single-walled carbon nanotubes in strong acids: controlling solubility and the liquid crystal phase.**
MATTEO PASQUALI, *Depts. of Chemical & Biomolecular Engineering and Chemistry, Carbon Nanotechnology Laboratory, Rice University*

Single Walled Nanotubes (SWNTs) have remarkable electrical, thermal, and mechanical properties. Neat, well-aligned SWNT fibers and sheets could be the ultimate building blocks of strong, ultra-light multifunctional materials for aerospace applications, and could yield electromechanical actuators and sensors with unprecedented performance. After the achievement of scalable production of SWNTs, the difficulty of processing pristine SWNTs by liquid-phase methods has been the single most important roadblock to manufacturing macroscopic materials composed solely of SWNTs. Here we show that SWNTs dissolve at high concentration in acids; the SWNTs are stabilized because acids protonate their sidewalls, balancing wall-wall van der Waals forces. Acid strength controls the phase behaviour. At low concentration, SWNTs in acids dissolve as individual tubes which behave as Brownian rods. At higher concentration, SWNTs form a highly unusual nematic liquid phase consisting of spaghetti-like self assembled supermolecular strands of mobile, solvated tubes in equilibrium with a dilute isotropic phase. At even higher concentration, the spaghetti strands self-assemble into a polydomain nematic liquid crystal, where the domains are entangled with each other. Under anhydrous condition, the liquid crystalline phase can be processed into continuous highly aligned fibers of pure SWNTs without the aid of surfactants or polymers. By using a new fluorescent staining technique, we measure the rotational diffusivity and persistence length of SWNTs suspended in water with the aid of surfactants, and show that SWNTs behave as Brownian rods.

**15:42**
**W4 3 Phase Behavior of Carbon Nanotube Suspensions.**
PHILIPPE POULIN, *Centre de Recherche Paul Pascal - CNRS*

We study the phase behavior of nanotube suspensions stabilized by surfactants or amphiphilic polymers. The control of the composition of the solutions allows the interaction potential between the nanotubes to be finely tuned. As a consequence, it is possible to quantitatively analyze important phenomena such as percolation or liquid crystalline phase transitions. In particular, we describe how the percolation of rod-like particles is quantitatively decreased in the presence of attractive interactions [1]. We show that rod-like particles respond much more strongly than spheres to attractive interactions; strengthening thereby the technological interest of carbon nanotubes to achieve low percolation thresholds for electrostatic dissipation or electromagnetic shielding. By contrast, carbon nanotubes which experience repulsive interactions can spontaneously order and form liquid crystalline solutions [2]. Aligning and packing nanotubes is a major challenge to obtain macroscopic materials with improved properties. We will briefly discuss at the end of the presentation,

our latest results concerning the fabrication of fibers aligned nanotubes [3]. In particular, we will present new treatments of these fibers which lead to unusual mechanical properties and shape memory effects with giant stress recovery [4].

[1] B. Vigolo, C. Coulon, M. Maugey, C. Zakri, P. Poulin, Science, 2005.

[2] S. Badaire, C. Zakri, M. Maugey, A. Derré, J. Barisci, G. Wallace, P. Poulin, Adv. Mat., 2005.

[3] P. Miaudet, M. Maugey, A. Derré, V. Pichot, P. Launois, P. Poulin, C. Zakri, Nanoletters, 2005.

[4] P. Miaudet, A. Derré, M. Maugey, C. Zakri, P. Poulin, in preparation.

**16:18**
**W4 4 Carbon Nanotube Suspensions: some underlying issues.***
ALAN WINDLE, *Department of Materials Science, University of Cambridge*

Entropy of mixing of rigid particles in a suspending medium is determined on a per-particle basis and thus, for a given weight fraction will decrease with increasing particle size. In the case of carbon nanotubes, the entropy contribution to mixing will thus be small compared with the interparticle forces which comprise the enthalpic energy contribution to any thermodynamic equilibrium. These forces will generally be short range with the exception of electrostatic forces in the cases that the particles carry a charge. The ability to form carbon nanotube suspensions depends on both the chemical affinity between the medium and the tubes and, it appears, the size of the medium molecules. Surface treatments of the nanotubes have been developed both using covalently attached functional groups and surfactants, and each strategy has been successfully applied to both multi and single wall CNTs. Because carbon nanotubes are long, thin, rigid and comparatively straight, they have been shown to self assemble into liquid crystalline phases showing all the attributes of conventional systems. The relationship between such CNT systems and the conventional Flory phase diagram will be described, as will the exploitation of these phase equilibria to fractionate nanotubes on the basis of mesogenicity. The use of liquid crystalline phases as a basis for the processing of carbon nanotubes into aligned assemblies such as fibres will also be outlined.

*In collaboration with Ian Kinlock and Shanju Zhang, Department of Materials Science, University of Cambridge.

**16:54**
**W4 5 Processes for Dispersing Single Wall Carbon Nanotubes in Polymers and How to Determine Their Spatial and Alignment Distributions.**
KAREN I. WINEY, *University of Pennsylvania*

We are currently designing and making polymer nanocomposites with single wall carbon nanotubes (SWNT) to obtain improved mechanical properties, electrical conductivity, flammability, and thermal conductivity. Our coagulation method is broadly applicable to nanocomposites using readily-soluble thermoplastics such as polystyrene and poly (methyl methacrylate). A variation of this method has been developed for nanotube/polymer composites based on high-density polyethylene. Nylon-based composites are prepared using our adaptation of an itin situ interfacial polymerization method. Epoxy-based SWNT composites are prepared using either shear mixing with multi-step thermal treatments or an infiltration method using a freestanding SWNT network. Recent studies have explored the use of solid-state shear pulverization to disperse SWNT. Rheology is employed to evaluate the spatial distribution of SWNT based on the onset of solid-like behavior associated with the formation of a SWNT network. Morphological tools including various microscopy methods, x-ray scattering and Raman imaging, are used to evaluate both dispersion and alignment. The resulting spatial and alignment distributions of SWNT depend on the composite fabrication method and any subsequent processing, such as melt fiber spinning to effectively align SWNT. Examples will be given detailing the importance of (1) SWNT dispersion on flammability and thermal conductivity and (2) SWNT alignment on electrical conductivity.

## SESSION W5: A CENTURY OF CRITICAL PHENOMENA
**Thursday Afternoon, 16 March 2006; 309, Baltimore Convention Center at 14:30**
**Pierre Hohenberg, New York University, presiding**

**14:30**
**W5 1 Supercritical Phase Separation from 1890 to the Present.**
JOHANNA LEVELT SENGERS, *NIST*

This abstract was not received electronically.

**15:06**
**W5 2 The Richard T. Cox Lecture: Liquid State as an Occasional Result of Competing Interactions.**
ALEXANDER VORONEL, *Tel-Aviv University*

Limits of the liquid state region of a pure substance is considered relative to the form of an interatomic potential curve. While the upper limit of the liquid state is determined by its liquid-vapor critical point, the lower one is linked to the freezing process. The liquid state region of fullerene is about zero since a size of its particles is close to an effective radius of their attraction force. Lindemann criterion of melting. The freezing point may be situated above the critical one. Metastable critical points. Generalization of the Lindemann criterion of melting for mixed crystals and a reduction of their freezing points. Properties of small clusters with structures different from the equili-brium crystalline symmetries. ''Melting'' of clusters and the Lindemann criterion. Supercooled liquids – inhomogenious (composite) states. Liquid-liquid transitions and polymorphism of liquids.

**15:42**
**W5 3 The Role of Experiment in Our Understanding of Critical Phenomena.**
GUENTER AHLERS, *University of California - Santa Barbara*

This abstract was not received electronically.

**16:18**
**W5 4 Some Fruits of Genius: Lars Onsager and the Ising Model.**
MICHAEL E. FISHER, *University of Maryland*

The story of the exact solution of the two-dimensional Ising model by Lars Onsager in the 1940's will be sketched and some of the striking developments following from it, especially for the behavior of fluctuating interfaces, will be recounted.

**16:54**
**W5 5 From Gibbs to Schramm: How the Concepts were Developed.**
LEO P. KADANOFF, *The James Franck Institute*

This abstract was not received electronically.

## SESSION W6: NEW APPLICATIONS OF SILICON IN PHOTONICS AND BIOMEDICINE
**Thursday Afternoon, 16 March 2006; 310, Baltimore Convention Center at 14:30**
**Sharon Weiss, Vanderbilt University, presiding**

**14:30**
**W6 1 TBD.**
SCOTT MANALIS

This abstract has not been submitted electronically.

**15:06**
**W6 2 Prospects of Mid Infrared Silicon Raman Laser.**
BAHRAM JALALI, *University of California Los Angeles*

Mid wave infrared (MWIR) lasers in the wavelength range of 2-5$\mu$m form an important tool for free space communications, bio-chemical detection and certain medical applications. Most organic chemicals and biological agents have unique signatures in the MWIR and can be detected using these lasers. The strong water absorption peak at 2.9$\mu$m renders such a laser attractive for surgery and dentistry. Solid state lasers comprising OPO-based nonlinear frequency converters and Raman lasers have been the popular choice for these applications. However, the low damage threshold, poor thermal conductivity and high cost limit the commercial availability of these sources. The recent demonstration of the first silicon Raman laser in 2004 combined with excellent transmission of silicon in the mid-IR suggests that silicon should be considered as a MWIR Raman crystal. In the near IR, where current silicon Raman lasers operate, free carriers that are generated by two photon absorption (TPA) create severe losses. TPA vanishes in the MWIR regime ($\lambda > 2.25$ $\mu$m), hence eliminating the main problem with silicon Raman lasers. This combined with (i) the unsurpassed quality of

commercial silicon crystals, (ii) the low cost and wide availability of the material, (iii) extremely high optical damage threshold of 1-4 GW/cm$^2$ (depending on the crystal resistivity), and (iv) excellent thermal conductivity renders silicon a very attractive Raman crystal. Moreover, integrated waveguide and resonator technologies can lead to device miniaturization. This talk discusses the MWIR silicon laser and its applications.

**15:42**
**W6 3**
MICHAL LIPSON, *Cornell University*

This abstract was not received electronically.

**16:18**
**W6 4 Nonlinear Optics in Silicon—Applications in Optical Communication Systems.**
THOMAS MURPHY, *University of Maryland*

Silicon photonics is quickly becoming an important and active research area, primarily because of the desire to leverage existing silicon fabrication technology and the potential for integration with conventional silicon electronic components. In this talk, I will discuss nonlinear optical effects in silicon, and ways in which they can be employed in optical telecommunication systems. The nonlinear effect that we have been exploring is two-photon absorption: a process in which two photons are simultaneously absorbed in a silicon photodiode to generate a single electron-hole pair. Unlike many other nonlinear processes, two-photon absorption does not require phase matching, and can occur over a very broad wavelength range with an ultrafast (fs) response time. In silicon, two-photon absorption can be observed at wavelengths from 1100 to 2200 nm, a range that spans the entire spectrum presently used in fiber telecommunications. For years, two-photon absorption was regarded as a deleterious effect in nonlinear optics, because it consumes the optical signal that was meant to produce a nonlinear phase shift. More recently, researchers have found ways to exploit two-photon absorption effects for optical signal processing. For example, if the electrical carriers produced by two-photon absorption are collected by an en external electrical bias circuit, the resulting photocurrent can be directly used in a number of nonlinear processing functions including optical autocorrelation, cross-correlation, quality monitoring, demultiplexing, optical sampling, and clock recovery. In this presentation, I will review the recent applications of two-photon absorption in communication systems, and describe ongoing research being conducted at the University of Maryland. In particular, we have found an explanation for the polarization dependence that is often observed in two-photon absorption, and we have developed a new way to overcome this dependence. As an example of how two-photon absorption can be used in a real communication system, we have demonstrated an 80 Gb/s optical clock recovery system based upon two-photon absorption in a silicon photodiode, and we deployed the system in a 1000 km fiber transmission experiment.

**16:54**
**W6 5**
YURII VLASOV, *IBM*

This abstract was not received electronically.

## SESSION W7: PHYSICS OF CELL ELASTICITY, INTERACTIONS AND TISSUE FORMATION
**Thursday Afternoon, 16 March 2006; 307, Baltimore Convention Center at 14:30**
**Philip Nelson, University of Pennsylvania, presiding**

**14:30**
**W7 1 Nucleation and growth of cell contacts.***
DANIEL RIVELINE, *Laboratoire de Spectrométrie Physique, UMR 5588, Grenoble*

Living cells develop adhesive contacts with their environments. We present experiments which are dedicated to measure geometric and density evolutions of these contacts in living cells. We focus on two contacts: focal contacts, formed between a cell and the extracellular matrix, and adherens junctions, assembled between neighbouring cells. Both include: (i) a transmembraneous protein dictating the given adhesive junction assembly, (ii) a specific protein complex with tens of different components, (iii) an actin cytoskeletal structure. Our experiments involve the observations of fluorescently labelled proteins of these contacts in living cells, local force application, force measurements, and optical development such as evanescent wave excitation. These adhesive cellular entities are usually described as a result of activation of signalling events. However cell adhesive contacts can be seen as discrete itparticles aggregates, which undergo nucleation and growth like in a first order phase transition. We will show that self-assembly processes are indeed imposing contacts

shapes and dynamics. Far from being two antagonistic ways of describing cells dynamics, signalling pathways and cell self-assembly complement each other to dictate contacts shapes. In addition, eventhough focal contacts and adherens junctions involve different proteins, we will show that they share common features such as mechanosensitivity. Via these contacts, cells behave as climbers seeking to probe the resistance of their environment in order to reinforce appropriately specific adhesive areas.

*Including PhD works of Julien Brevier and Hélène Delanoë-Ayari.

**15:06**
**W7 2 Integrin activation and cell adhesion by mechanical forces.**
ROBIJN BRUINSMA, *UCLA*

This abstract was not received electronically.

**15:42**
**W7 3 Cell morphologies depend on substrate rigidity.**
PAUL JANMEY, *University of Pennsylvania*

Extracellular matrices and intracellular cytoskeletons are composed mainly of open meshworks formed by semi-flexible polymers linked by accessory proteins in networks with specific geometries. The viscoelastic properties of such networks often differ strongly from those of flexible polymer gels and are characterized by relatively large elastic moduli for low volume fractions, increased rigidity at increasing strains, and in some cases, negative normal stresses when deformed in simple shear. Cell structure and function depend on the stiffness of the surfaces on which cells adhere as well as on the type of adhesion complex by which the cell binds its extracellular ligand. Most cell types, including fibroblasts and endothelial cells, switch from round to spread morphology as stiffness is increased between 1000 and 10,000 Pa. In contrast, other cells types such as neutrophils do not require rigid substrates in order to spread, and neurons extend processes better on soft (50 Pa) materials than on stiffer gels. Differences in rigidity sensing and response can be exploited to design soft matrices optimized for growth and differentiation of specific cell types.

**16:18**
**W7 4 Physics of adhesion and elasticity of biological cells.***
S.A. SAFRAN, *Dept. Materials and Interfaces, Weizmann Institute of Science, Rehovot, Israel 76100*

Forces exerted by adherent cells are important for many physiological processes such as wound healing and tissue formation. By pulling on their environment, cells sense rigidity gradients, boundaries and strains induced by the presence of other cells. Many cell types respond to these signals by actively adjusting the magnitude and direction of the adhesions that connect cells to surfaces or to each other. These adhesions are formed from membrane-bound integrin proteins and other cytoplasmic proteins that form condensed domains that grow in the direction of externally applied or internal, cytoskeletal forces. We present a model for the adsorption of adhesion proteins from the cell interior to the adhesion site and the resulting, force-sensitive anisotropic growth. The theory couples the mechanical forces to the non- linear adsorption dynamics and predicts the growth velocities of the back and front of the adhesion in qualitative agreement with experiment. The adhesion forces generated by a collection of cells in a tissue significantly alter the overall elastic response of the system. We model an ensemble of cells by an extension of the treatment of dielectric response of polar molecules to elastic interactions. By introducing the elastic analogy of the dielectric constant of the medium, we are able to predict the average cell polarization, their orientational order, and the effective material constants.

*Collaborations with A. Besser, I. Bischofs, B. Geiger, A. Nicolas, U. Schwarz, J. Spatz, A. Zemel are gratefully acknowledged.

**16:54**
**W7 5 Cell mechanics and human disease states.**
SUBRA SURESH, *MIT*

This presentation will provide summary of our very recent studies exploring the effects of biochemical factors, influenced by foreign organisms or itin vivo processes, on intracellular structural reorganization, single-cell mechanical response and motility of a population of cells in the context of two human diseases: malaria induced by Plasmodium falciparum merozoites that invade red blood cells, and gastrointestinal cancer metastasis involving epithelial cells. In both cases, particular attention will be devoted to systematic changes induced in specific molecular species in response to controlled alterations in disease state. The role of critical proteins in influencing the mechanical response of human red bloods during the intra-erythrocytic development of P. falciparum merozoites has also been assessed quantitatively using specific protein knock-out experiments by recourse to gene inactivation methods. Single-cell mechanical response characterization entails such tools as optical tweezers and mechanical plate stretchers whereas cell motility assays and cell-population biorheology characterization involves microfluidic channels. The experimental studies are accompanied by three-

dimensional computational simulations at the continuum and mesoscopic scales of cell deformation. An outcome of such combined experimental and computational biophysical studies is the realization of how chemical factors influence single-cell mechanical response, cytoadherence, the biorheology of a large population of cells through microchannels representative of in vivo conditions, and the onset and progression of disease states.

## SESSION W8: FOCUS SESSION: NONLINEAR ELECTROKINETICS

**Thursday Afternoon, 16 March 2006; 314, Baltimore Convention Center at 14:30**
**Martin Bazant, Massachusetts Institute of Technology, presiding**

*Invited Papers*

**14:30**
**W8 1 Electro-Convective and Non-Equilibrium Electro-Osmotic Instability of Electric Conduction from an Electrolyte Solution into a Charge Selective Solid.**
ISAAK RUBINSTEIN, *Blaustein Institutes for Desert Research, Ben-Gurion University of the Negev*

Electro-convection is reviewed as a mechanism of mixing in the diffusion layer of a strong electrolyte adjacent to a charge-selective solid, such as an ion exchange (electrodialysis) membrane or an electrode. Two types of electro-convection in strong electrolytes may be distinguished: bulk electro-convection, due to the action of the electric field upon the residual space charge of a quasi-electro-neutral bulk solution, and convection induced by electro-osmotic slip, due to electric forces acting in the thin electric double layer of either quasi-equilibrium or non-equilibrium type near the solid/liquid interface. According to recent studies, the latter appears to be the likely source of mixing in the diffusion layer, leading to 'over-limiting' conductance in electrodialysis. Electro-convection near a uniform charge selective solid/liquid interface sets on as a result of hydrodynamic instability of one-dimensional steady state electric conduction through such an interface. We discuss instabilities of this kind appearing in the full electro-convective and limiting non-equilibrium electro-osmotic formulations. The short- and long-wave aspects of these instabilities are discussed along with the wave-number selection principles and possible sources of low frequency excess electric noise experimentally observed in these systems.

*Contributed Papers*

**15:06**
**W8 2 Nonlinear Surface Transport in the Thin Double-Layer Limit** KEVIN CHU, *Princeton University* MARTIN BAZANT, *Massachusetts Institute of Technology* At high applied electric fields, ionic transport within the double layer plays a significant role in the overall response of electrokinetic systems. It is well-known that surface transport processes, including surface electromigration, surface diffusion and surface advection, may impact the strength of electrokinetic phenomena by affecting both the zeta-potential and the magnitude of the tangential electric field. Therefore, it is important to include these effects when formulating the effective boundary conditions for the equations that govern electrokinetic flow outside of the double layer. In this talk, we discuss the application of a general formulation of ''surface conservation laws'' for diffuse boundary layers to derive effective boundary conditions that capture the physics of electrokinetic surface transport. Previous analyses (e.g. Deryagin & Dukhin 1969) are only valid for weak applied fields and are based on a linearization of the concentration and potential about a reference solution, but our results are fully nonlinear and hold at large applied fields as long as the double layer is sufficiently thin. We compare our nonlinear surface transport theory with existing linear analogues and apply it to the canonical problem of induced-charge electro-osmosis around a metal sphere or cylinder in a strong DC field.

**15:18**
**W8 3 Experiments on Nonlinear Electrokinetic Pumps in Microfluidics*** JOHN PAUL URBANSKI, TODD THORSEN, *Department of Mechanical Engineering, MIT* JEREMY A. LEVITAN, MARTIN Z. BAZANT, *Department of Mathematics, MIT* Nonlinear electrokinetic pumps are attractive in the development of portable and flexible microfluidic analysis systems, since they operate without moving parts using low (battery powered) alternating potentials. Since the discovery of AC electro-osmosis (ACEO) in the late 1990s, there has been much work in designing and building two-dimensional, periodic micro-electrode geometries, which exploit broken symmetry to rectify AC forcing and produce steaming flow over a surface. Building on this work, we exploit more general principles of induced-charge electro-osmosis (ICEO) in three-dimensional electrode geometries to enhance pumping in microfluidic devices. Our fabrication efforts are guided by theoretical analysis and simulations using the standard low-voltage theory, which, in some cases, predict flow rates faster than existing planar ACEO pumps by an order of magnitude (for the same voltage and feature size). We test various microfabricated pump geometries in a microfluidic loop following the methodology of Studer et al (2004). We are also measuring the strong effect of solution chemistry (e.g. ion valence and concentration) on ICEO flow to guide further developments in the theory of nonlinear electrokinetics.

*Supported by the US Army through the Institute for Soldier Nanotechnologies.

**15:30**

**W8 4 Microfluidic pumps based on Induced Charge Electroosmosis and flow Field Effect Transistor phenomena*** GAURAV SONI, TODD SQUIRES, CARL MEINHART, *University of California Santa Barbara* We are developing AC electrokinetic micropumps to drive electrically conductive biological fluids in microchannels. These pumps work on the principles of Induced Charge Electroosmosis (ICEO) and flow Field Effect Transistor (flowFET) phenomena. AC (as well as DC) electric fields can induce electrical double layer on a polarizable surface and in turn, cause fluid motion by moving this layer. However, when the polarizable surface is electrically floating, symmetric vortices are observed on the surface. Symmetry of this flow leads to zero net pumping. In order to achieve pumping, we apply a second AC signal to the polarizable surface. When the magnitude of this second AC signal is different from the floating potential of the surface, unidirectional flow is observed i.e., pumping is achieved by modulating the induced zeta potential of the surface. Pumping caused by modulation of zeta potential is also known as flowFET phenomenon and has been shown to work with DC electric fields by other community members. We show a detailed study of flowFET with AC electric fields.

*Supported by an Army grant: 8-487859-25500.

**15:42**

**W8 5 Nonlinear studies of AC electrokinetic micropumps** HENRIK BRUUS, LAURITS H. OLESEN, *Technical University of Denmark* ARMAND AJDARI, *Ecole Superieure de Physique et de Chimie Industrielles* Recent experiments have demonstrated that AC electrokinetic micropumps permit integrable, local, and fast pumping (velocities $\sim$ mm/s) with low driving voltage of a few volts only. However, they also displayed many quantitative and qualitative discrepancies with existing theories. We therefore extend the latter theories to account for three experimentally relevant effects: ($i$) vertical confinement of the pumping channel, ($ii$) Faradaic currents from electrochemical reactions at the electrodes, and ($iii$) nonlinear surface capacitance of the Debye layer. We report here that these effects indeed affect the pump performance in a way that we can rationalize by physical arguments.

**15:54**

**W8 6 Electric field driven motion of flexible polyelectrolytes*** TAK SHING LO, *Levich Institute, City College of CUNY* BORIS KHUSID, *Dept. of Mechanical Engineering, NJIT* ANDREAS ACRIVOS, JOEL KOPLIK, *Levich Institute, City College of CUNY* Our work aims to study dielectrophoresis of biomolecules in micro/nano-fluidics using molecular dynamics (MD) simulations. Our model combines electrohydrodynamics with molecular theories for the macromolecule polarization caused by the distortion of the counterion cloud. Unlike most available MD studies of polyelectrolytes, solvent atoms are explicitly represented in our model, so that hydrodynamic interactions are included naturally with no ad hoc assumption. The polyelectrolyte is modeled as a negatively charged bead-spring chain. The charges interact through the Coulomb potential and other molecular interactions are included via Lennard-Jones potentials. We study the transport properties of flexible polyelectrolytes suspended in a solvent, with or without added salt, under the action of DC or AC electric fields. MD data provide the information needed to compute the dipole moments of the molecule and the surrounding double layer, which are required for understanding the dielectrophoretic behavior of these molecules in nanoscopic channels.

*This work was supported by NSF (CTS-0307099) and NSF/Sandia (NIRT/NER-0330703).

**16:06**

**W8 7 Anomalous ionic transport at nanometer-scale electrodes** DIEGO KRAPF, *Delft University of Technology* BERNADETTE QUINN, MENG-YUE WU, HENNY ZANDBERGEN, CEES DEKKER, SERGE LEMAY, We probe the transport of charged species in high ionic strength solutions on the scale of a few nanometers by monitoring electrochemical reactions at correspondingly sized electrodes. The electrical current through the nanoelectrode provides a direct measure of the flux of ions across the diffuse double layer. Because both the concentration gradient and the electric field are localized in the immediate vicinity of the nanoelectrode, this provides very local information. Furthermore, when the electrode dimensions are in the order of a few nanometers, very steep concentration gradients are achieved. To carry out these experiments, we have developed a method for fabricating nanoelectrodes with a well-defined size and geometry. A pore is first drilled in an insulating membrane with a focused electron beam and it is then filled with a noble metal yielding conically shaped, convex electrodes with radii as small as 2 nm. We observe pronounced non-linearities of ion flux versus concentration when transport is localized within a region smaller than 10 nm in size. We numerically calculate the predicted ion flux using the Stern-Poisson-Nernst-Planck formalism. We show that our observations cannot be explained using this widely applied mean-field description of ionic transport.

**16:18**

**W8 8 Nonlinear Electroosmosis and Biomolecule Electrokinetic Trapping Induced by Ion Selective Nanofluidic Channels** YING-CHIH WANG, *Dept. of Mech. Eng., MIT* JONGYOON HAN, *Bio. Eng. Division, Dept. of EECS, MIT* This paper describes a nanofluidic device that can concentrate dilute biomolecule by electrokinetic trapping mechanism. This device has nanofluidic channels with a depth down to 40 nm, therefore, having significant Debye layer overlap. Depending on the strength of the applied potential across the nanochannel, one can observe phenomena such as concentration polarization; charge depletion and nonlinear electrokinetic flow in the adjacent microfluidic channel using fluorescent microscopy. By manipulating the electric field, the device can generate an extended space charge region, maintained for several hours, within a microchannel as a mean to collect and trap biomolecules. Our studies demonstrate such device can achieve up to 10 million fold sample preconcentration within 30 minutes. Besides, if applied a higher potential, a much faster chaotic flow can be seen in the microchannel adjacent to nanochannels. This kind of nonlinear electrokinetic flow is often called the electroosmosis of the second kind or induced-charge electroosmosis in electrode and ion exchange membrane studies. The presented device can be used as either a preconcentrator or an injector to other separation and detection systems preferred its performance and integrabilty. Also, it is an ideal experimental platform for studying such nonlinear electrokinetic effects, by directly tracking molecules in situ.

**16:30**
**W8 9 Modeling of Selectively Permeale Vesicle Membrane in Electrolytes: An Energetic Variational Formulation** CHUN LIU, ROLF RYHAM, *Dept of Math, PSU* We introduce a self consistent coupled system to model the deformation of selectively permeable vesicle membranes in electrolytes via an energetic variational formulation. The equations governing a diffuse charge system and the evolution of the vesicle membrane are coupled with the momentum equations of the electrolyte through the Lorentz force along with the induced elastic forces due to the membrane bending energy. The force coupling and charge flux selectivity are consequences of the energetic balance and competition of kinetic, electric and membrane elastic bending energy. We will also present some numerical simulation results of the system.

**16:42**
**W8 10 Reversible Transitions on Electrically-Tunable Nanostructured Superhydrophobic Surfaces** TOM KRUPENKIN, J. ASHLEY TAYLOR, PAUL KOLODNER, MARC HODES, JOANNA AIZENBERG, *Bell Labs, Lucent Technologies* Recently demonstrated electrically tunable nanostructured superhydrophobic surfaces provide a promising new way of manipulating liquids at both micro and macro scales. Dynamic control over the interaction of liquids with the solid substrate is of great interest to many research areas ranging from biology and chemistry to physics and nanotechnology. In this work the reversibility of the electrically induced superhydrophobic – hydrophilic transition on nanostructured surfaces is addressed. Recently demonstrated approach based on momentarily induction of film boiling in a very thin layer of liquid adjacent to the solid-liquid interface is discussed. The dependence of the hydrophilic – superhydrophobic transition on the topography of the nanostructured layer, as well as on the energy and duration of the electrical pulse is investigated. Several emerging applications of these surfaces, including lab-on-a-chip, chemical microreactor, and on-chip power sources are discussed.

**16:54**
**W8 11 Nonlinear alternating current susceptibilities of rotating microparticles in electrorheological fluids*** KIN WAH YU, *Chinese University of Hong Kong* J.P. HUANG, W.J. TIAN, *Fudan University* A perturbation approach [1] has been employed to investigate the nonlinear alternating current (AC) responses of the rotating microparticles in electrorheological (ER) fluids under AC or direct current electric fields. The shear flow of ER fluids exerts a torque on the particles and leads to the rotational motion of the particles about their centers [2]. We show that the dynamic effects can play a significant role in the AC responses. Our results can be conveniently interpreted in the dielectric dispersion spectral representation [3], thus offering a convenient method to determine the relaxation time and the rotation velocity of the ER particles by measuring the nonlinear AC responses. [1] G. Q. Gu and K. W. Yu, Phys. Rev. B 46, 4502 (1992); K. W. Yu, P. M. Hui, and D. Stroud, Phys. Rev. B 47, 14150 (1993). [2] Jones T. K. Wan, K. W. Yu, and G. Q. Gu, Phys. Rev. E 62, 6846 (2000). [3] Jun Lei, Jones T. K. Wan, K. W. Yu, and Hong Sun, Phys. Rev. E 64, 012903 (2001).

*Work supported by RGC Earmarked Grant

**17:06**
**W8 12 Electrophoresis in bounded doamins** EHUD YARIV, *Technion* Electrophoretic motion is usually described by a linear model, based upon the smallness of the applied field relative to the equilibrium field in the screening Debye layer surrounding the particle. This model, in turn, leads to the Smoluchowski's slip condition and eventually results in mobility relations. The mobility concept is valid provided the external electric force is neglected — a procedure superficially supported by the net electric neutrality of the combined particle-layer system. In this talk, however, I will show that this force does not vanish in general. Accordingly, a consistent scheme is formulated for analyzing the nonlinear motion of a particle in an applied field. This motion is illustrated in two contexts: rotation of non-spherical particles, and drift of a spherical particle away from a planar wall. I will also describe an analogy to incompressible and inviscid fluid motion. This analogy enables for experimental verification of three-dimensional potential flow solutions.

**17:18**
**W8 13 How accurate is the Poisson-Boltzmann theory for monovalent ions near highly charged interfaces?*** WEI BU, ALEX TRAVESSET, DAVID VAKNIN, *Ames Laboratory, Iowa State University* Monovalent ion distributions next to highly charged interfaces were determined by synchrotron surface X-ray sensitive techniques. A lipid phosphate (dihexadecyl hydrogenphosphate) was spread as a monolayer at the air-water interface, containing CsI at various concentrations. Using anomalous reflectivity off and at the $L_3$ $Cs^+$ resonance, we provide, for the first time, spatial counterion distributions ($Cs^+$) next to the negatively charged interface over a wide range of ionic concentrations. We argue that at low salt concentrations and for pure water the enhanced concentration of hydroniums $H_3O^+$ at the interface leads to proton-transfer back to the phosphate group by a high contact-potential, whereas high salt concentrations lower the contact-potential resulting in proton- release and increased surface charge-density. The experimental ionic distributions are in excellent agreement with a renormalized-surface-charge Poisson-Boltzmann theory without fitting parameters or additional assumptions.

*The MUCAT sector at the APS and the use of the APS are supported by the U.S. DOE, Basic Energy Sciences through Ames Laboratory under Contracts No. W-7405-Eng-82, and No. W-31-109-Eng-38, respectively.

**SESSION W9: X-RAY, LIGHT, AND PARTICLE SCATTERING AND DIFFRACTION**
**Thursday Afternoon, 16 March 2006**
**301, Baltimore Convention Center at 14:30**
**Carolyn MacDonald, University at Albany, SUNY, presiding**

**14:30**
**W9 1 Strain maps with ppm resolution for single crystal wafers obtained from x-ray rocking curve maps** ALBERT MACRANDER, YUNCHENG ZHONG, JOSEF MAJ, YONG CHU, *Argonne National Laboratory* SZCZESNY KRASNICKI, *Carnegie Institute* A double crystal (+,−) x-ray technique has been used to obtain separate maps of strain and tilt across single crystal samples of high crystalline perfection. Rocking curves were ob-

tained for each pixel of a CCD detector and from these data angular shifts of the rocking curve center were mapped. By using data for two azimuthal rotations, that is, by combining data from two diffraction conditions separated by 180° rotation around the diffraction vector, we obtained separately the tilt and the strain. Data for diamonds has been obtained to demonstrate the technique in the case of a symmetric reflection[1]. Extensions of the method to asymmetric reflections in order to also extract strains parallel to the surface[2] will be discussed. Also a correction for wavelength dispersion in the case of different d-spacings for first and second crystals will be discussed. This work was supported by DOE Basic Energy Sciences-Materials Science, under contract No. W-31-109-ENG-38 and by NSF under contract No. EAR-0421020. [1] A.T. Macrander et al., Applied Physics Letters, 87, 194113 (2003). [2] V. Swaminathan and A.T. Macrander, ''Materials Aspects of GaAs and InP Based Structures,'' Prentice Hall, 1991, ISBN 0-13-346826-7.

**14:42**

**W9 2 Is Resonant X-ray Scattering Sensitive to the Electronic Structure of the CDW State?** J.-D. SU, *School of Applied and Engineering Physics, Cornell University, Ithaca, NY 14853* J.D. BROCK, *School of Applied and Engineering Physics, Cornell University, Ithaca, NY 14853* K.D. FINKELSTEIN, *Cornell High Energy Synchrotron Source, Ithaca, NY 14853* The strong ''white-line'' observed at the Ta $L_{III}$ x-ray absorption edge (9.881KeV) in 1*T*-$TaS_2$ indicates resonance with the 2p $\rightarrow$ 5d atomic transition. Theories of the charge density wave (CDW) state in $TaS_2$ highlight the special role played by the 5d states of the thirteen Ta atoms in each unit cell of the super-lattice in forming the reconstructed conduction bands of the CDW state. By measuring the resonant diffraction at the CDW satellites, we combine this additional periodicity with the resonant scattering to amplify and isolate the x-ray signal from the CDW. Then, by studying the behavior as the system goes through the incommensurate-commensurate transition, we probe the sensitivity of this resonant x-ray scattering technique to changes in the electronic structure near the Fermi surface.

**14:54**

**W9 3 Diffraction by Distorted Object – A Unified Description of Coherent X-ray Diffraction and Imaging.*** QUN SHEN, *Argonne National Laboratory* XIANGHUI XIAO, *Argonne National Laboratory* It is well-known that a diffracted or scattered wave by an object can be simply described by a Fourier transform of the electron density distribution of the object. This, in principle, is true only in the so-called far-field regime. In the near-field regime, evaluations of wave field amplitudes become more complicated and Fresnel diffraction and imaging effects have to be taken into account. In this paper, we present a unified diffraction theory that is valid in both far-field and near-field regime. Using the concept of a 'phase-chirped' distorted object, where Fresnel-zone construction is embedded on an original object, we show that the Fourier transform of this distorted object can be used to evaluate Fresnel coherent diffraction images or phase-contrast images from objects. This approach is valid continuously from the near-field to the far-field regimes. In addition, the distorted-object approach extends the applicability of Fourier-based iterative phasing algorithm that is already established for far-field diffraction into the near-field holographic regime where phase retrieval had been difficult in high-resolution structural imaging of noncrystalline specimens. Imaging in near-field also possesses the advantage that it can eliminate twin image ambiguity that may exist in far-field diffraction.

*Supported by the U. S. Department of Energy, Office of Science, Office of Basic Energy Sciences, under Contract No. W-31-109-Eng-38.

**15:06**

**W9 4 Recovering Ancient Inscriptions by X-ray Fluorescence Imaging** JUDSON POWERS, NORA DIMITROVA, *Cornell University* RONG HUANG, *Advanced Photon Source* DETLEF-M. SMILGIES, DON BILDERBACK, *Cornell High-Energy Synchrotron Source* KEVIN CLINTON, ROBERT THORNE, *Cornell University* For many ancient cultures including those of the Mediterranean, carved stone inscriptions provide our most detailed historical record. Over the ages the surfaces of many of these inscriptions have been eroded so that the original text can no longer be distinguished. A method that allowed at least partial recovery of this lost text would provide a major breakthrough for the study of these cultures. The scope of analytical techniques that can be applied to stone tablets is limited by their large size and weight. We have applied X-ray fluorescence imaging to study the text of ancient stone inscriptions [1]. This method allows the concentrations of trace elements, including those introduced during inscription and painting, to be measured and mapped. The images created in this way correspond exactly to the published text of the inscription, both when traces of letters are visible with the naked eye and when they are barely detectable. [1] J. Powers et al., Zeitschrift für Papyrologie und Epigraphik 152: 221-227 (2005).

**15:18**

**W9 5 Site specific valence band structure of $SrTiO_3$ determined with X-ray standing waves** JORG ZEGENHAGEN, SEBASTIAN THIESS, TIEN-LIN LEE, *ESRF, France* FRANCOIS BOTTIN, *CEA/DIF, France* Structure and chemical composition define the properties of materials, notably band structure and electronic characteristics of solids. Ab initio calculations deliver frequently reliably predictions, which are, however, difficult to verify, in particular in view of the direct relationship between atomic and electronic structure. Combining the x-ray standing wave (XSW) technique with X-ray photoelectron spectroscopy (XPS) is a unique tool in this sense. It is used here to identify unambiguously parts of the valence band of $SrTiO_3$, which can be assigned to Sr, Ti, or O-sites of the lattice. The XSW/XPS measurements were performed in UHV at the ID32 insertion device beamline at the ESRF using a (001) oriented, atomically clean $SrTiO_3$ crystal. Traversing the (111) and (112) Bragg reflections and recording the valence band for different standing wave positions within the lattice unit cell, the site specific contributions could directly be identified. Obtained experimental results are in very good agreement with theory, by utilizing as adjustable parameters the X-ray absorption cross sections of the valence electrons.

**15:30**

**W9 6 CMR Manganite Sensors for Total Energy Measurements of the Linear Coherent Light Source Pulsed X-ray Laser** RAJESWARI M. KOLAGANI,* G.J. YONG, D.E. COX, R. MUNDLE, A. DAVIDSON III, V.N. SMOLYANINOVA, E. TA-

LANOVA, D. SCHAEFER, *Towson University* S. FRIEDRICH, O. DRURY, Z. ALI, L. LI, L. OTT, *Lawrence Livermore National Labs* L. YONG, *Motorola Labs* TOWSON UNIVERSITY TEAM, LAWRENCE LIVERMORE NATIONAL LABORATORY TEAM, MOTOROLA LABS COLLABORATION, We are developing CMR manganite thin film bolometric sensors for total energy measurements of the Linear Coherent Light Source (LCLS) pulsed free electron x-ray laser (FEL). This application requires the sensor array to be fabricated on a low Z substrate capable of withstanding the pulse impact of 2 mJ in $\sim$ 200 femtoseconds, without the thermal expansion exceeding the yield strength, when the back side of the substrate is irradiated. Si is a potential candidate for meeting this requirement though its stability for long term exposure is a concern that needs to be tested. Optimal operating temperature of the sensor is estimated to be $\sim$ 100 K-200 K, based on finite element simulations of the temperature evolution in the sensor pixel. Our initial work has identified $Nd_{1-x}Sr_xMnO_3$ as the manganite material suitable for the LCLS sensor. We will present our materials development efforts towards LCLS sensor design as well as simulations of the sensor response.

*formerly M.Rajeswari

**15:42**

**W9 7 Verification and Application of a New Analysis Method for X-ray Diffraction Microscopy*** ROBERT SUTER, CHANGSHI XIAO, DANIEL HENNESSY, *Department of Physics, Carnegie Mellon Univeristy* ULRICH LIENERT, *Advanced Photon Source, Argonne National Laboratory* X-ray diffraction microscopy has been used to determine microstructure maps of bulk polycrystalline material. Data are collected at the Advanced Photon Source beamline 1-ID using line focused 50keV x-rays. Diffracted beams are imaged with a CCD camera and are tracked through space so that orientation, point-of-origin, and shape of individual grains are encoded. Analysis uses a computer simulation of the measurement and sample to generate calculated diffraction patterns; orientations of sample space area elements are adjusted to obtain a match to the data. We illustrate data and analysis using a thin silicon wafer sample. We then show images of several layers of an aluminum polycrystal. The ability to obtain such images in a non-destructive way opens the possibility of measurements of the response to external stimuli of ensembles of individual grains. Our analysis is amenable to inclusion of complex scattering rules such as will be needed to study defected materials.

*This work was supported primarily by the MRSEC program of the National Science Foundation under Award Number DMR-0520425. Use of the Advanced Photon Source is supported by the U. S. Department of Energy under Contract No. W-31-109-ENG-38.

**15:54**

**W9 8 Nanometer Focusing X-rays With Multiple Kinoform Lenses*** KENNETH EVANS-LUTTERODT, AARON STEIN, *Brookhaven National Laboratory* NATIONAL SYNCHROTRON LIGHT SOURCE TEAM, It has been suggested that for refractive optics operating at photon energies of order 10 keV, that the resolution is limited to the wavelength divided by the critical angle. Using a compound kinoform lens consisting of individually optimized kinoform lenses, we investigate the possibility of exceeding this limit. Single-dimensional, kinoform lens stacks in deep-etched silicon have been fabricated that in principle can exceed the critical angle limit. These optics have been tested and the results will be presented. Additionally we present calculations that show that the resolution of radially-symmetric kinoform lenses is limited only by x-ray wavelength.

*This abstract has been authored by Brookhaven Science Associates, LLC under Contract No. DE-AC02-98CH10886 with the U.S. Department of Energy.

**16:06**

**W9 9 Comparison of polycapillary and curved crystal optics for convergent beam powder x-ray diffraction*** AYHAN BINGOBALI, WEI ZHOU, CAROLYN MACDONALD, *University at Albany, SUNY* Comparisons were made of diffracted ring width, ring uniformity, system resolution and diffracted beam intensity for convergent beam powder diffraction using two different types of x-rays optics, doubly curved crystal optics[1] and polycapillary x-ray optics.[2,3] Measurements were made using very low power microfocus sources for small inorganic and organic standard samples. Detailed source and optics characterizations were performed to develop comparisons with theoretical calculations. Resolution and intensity were in good agreement with those obtained from simple geometrical calculations. [1]Z. W. Chen, N. Mail, F.Z. Wei, C. A. MacDonald, W. M. Gibson ''Total reflection x-ray fluorescence with low power sources coupled to doubly curved crystal optics,'' Spectrochimica. Acta. B, 60 (4), pp.471-8, 2005. [2]C.A. MacDonald and W.M. Gibson, ''Applications and Advances In Polycapillary Optics,'' X-ray Spectrometry, **32** (3), 2003, pp 258-268. [3]C.A. MacDonald, S.M. Owens, and W.M. Gibson, ''Polycapillary X-Ray Optics for Microdiffraction,'' Journal of Applied Crystallography, **32**, pp160-7, 1999.

*This work was supported by the Breast Cancer Research Program

**16:18**

**W9 10 Light diffraction from a metallic bigrating.*** RAUL GARCIA-LLAMAS, *Departamento de Investigacion en Fisica. Universidad de Sonora* MANUEL LEYVA-LUCERO, *Escuela de Ciencias Fisico-Matematicas. Universidad Autonoma de Sinaloa* JORGE GASPAR-ARMENTA, *Departamento de Investigacion en Fisica. Universidad de Sonora* The diffraction of $\pi$- and $\sigma$-polarized electromagnetic plane waves from metallic bigratings is studied theoretically. The reduced Rayleigh equations are solved using a perturbation approach. The diffracted amplitudes are calculated until second order on the surface height profile. Numerical results of the diffraction orders and Near-Field are obtained using both, two-dimensional sinusoidal and semicircular profiles.

*Consejo Nacional de Ciencia y Tecnología. Proyecto 47391

**16:30**

**W9 11 Electron structure factor: a unique quantity in probing material's properties.*** JIN-CHENG ZHENG, LIJUN WU, YIMEI ZHU, *Center For Functional Nanomaterials, Brookhaven National Laboratory, Upton, New York 11973* Electron diffraction is very sensitive to valence charge distribution compared with x-ray at small scattering angles due to the near cancellation of the scattering from the positively charged nucleus and the negatively charged electrons. Thus, small changes in electron density can lead to considerable variations in the scattering amplitude. The well known divergence at small scattering vector for Coulomb scattering leads to strong measurable scattered intensities. How-

ever, the advantage of the accurate measurement using quantitative electron diffraction has not been well appreciated. We propose here that the accurate measured electron structure factor can be a unique quantity in probing properties of materials. We demonstrate this by examining the sensitivity of electron structure factor to valence charge distribution, chemical composition variations, and charge / orbital orderings in many functional materials. We also show that the accurately measured low-order electron structure factors can be used to test first principles theories, especially to optimize exchange-correlation functionals.

*The authors acknowledge support from DOE

**16:42**

**W9 12 $^3$He neutron spin filters for polarized neutron scattering.** WANGCHUN CHEN, JULIE BORCHERS, YING CHEN, KEVIN O'DONOVAN, ROSS ERWIN, JEFFREY LYNN, CHARLES MAJKRZAK, SARAH MCKENNEY, THOMAS GENTILE, *NIST, Gaithersburg, Maryland* Polarized neutron scattering (PNS) is a powerful tool that probes the magnetic structures in a wide variety of magnetic materials. Polarized $^3$He gas, produced by optical pumping, can be used to polarize or analyze neutron beams because of the strong spin dependence of the neutron absorption cross section for $^3$He. Polarized $^3$He neutron spin filters (NSF) have been of great interest in PNS community due to recent significant improvement of their performance. Here I will discuss successful applications using $^3$He NSFs in polarized neutron reflectometry (PNR) and triple-axis spectrometry (TAS). In PNR, a $^3$He NSF in conjunction with a position-sensitive detector allows for efficient polarization analysis of off-specular scattering over a broad range of reciprocal space. In TAS, a $^3$He NSF in combination with a double focusing pyrolytic graphite monochromator provides greater versatility and higher intensity compared to a Heusler polarizer. Finally I will present the results from patterned magnetically-coupled thin films in PNR and our first ''proof-of-principle'' experiment in TAS, both of which were performed using $^3$He NSF(s) at the NIST Center for Neutron Research.

**16:54**

**W9 13 A low and hyperthemal energy UHV ion beamline for surface scattering spectroscopies** M.P. RAY, S.A. MOODY, C.E. SOSOLIK, *Clemson University Department of Physics and Astronomy* We are using a differentially pumped beamline to provide well- collimated, monoenergetic beams of noble gas and alkali-metal ions that range in energy from $<$ 10eV to 10keV. These ion beams are scattered from a surface (e.g. Cu(001)) to study charge transfer effects, energy loss, and the excitation of surface phonons and excitons. The ion beam is focused into a UHV scattering chamber that possesses capabilities for studying and characterizing samples using LEED, Auger spectroscopy, and a Kelvin probe for work function measurements. Recent additions to this setup include replacing diffusion pumps with turbo pumps as well as the addition of a fast entry load-lock sample exchange system. Our current research is focused on developing a source to produce an ion beam of $C_{60}$ as well as studying charge transfer and energy loss effects at the low and hyperthermal energy range. Also, we are investigating chemicurrents associated with Schottky diodes in this energy regime.

## SESSION W10: FOCUS SESSION: SURFACES AND INTERFACES IN ELECTRONIC MATERIALS IV

**Thursday Afternoon, 16 March 2006; 302, Baltimore Convention Center at 14:30**
**Shaowei Chen, University of California, Santa Cruz, presiding**

*Invited Papers*

**14:30**

**W10 1 Synthesizing Metal Nanowires that Detect Molecules.**
REGINALD M. PENNER, *Department of Chemistry, University of California, Irvine, CA 92697-2025 USA*

Noble metal nanowires have attributes including strength, ductility, and chemical stability, that make them attractive candidates for chemical sensing applications. However, in contrast to semiconductor nanowires, the conductivity of metal nanowires is not expected to be responsive to ''charge gating'' induced by the presence at the surface of the nanowire of bound ions. Consequently the properties of metal nanowires for chemical sensing have not been explored. We have developed a new method for preparing arrays of noble metal nanowires that involves the electrodeposition of metals (palladium, silver, platinum and gold) onto stepped graphite surfaces. Under the conditions employed for nanowire growth, metal is deposited selectively at step edges on the graphite surface leading to the formation of polycrystalline nanowires that are up to 1 mm in length and 30-500 nm in diameter. These nanowires adhere weakly to the graphite surface, and arrays of hundreds of wires may be transferred onto glass surfaces using a simple embedding process. These transferred nanowires can form the basis for chemical sensors in which the resistance of the nanowire array is modulated by molecules that chemisorb at the surfaces of these metals. Two examples involve palladium nanowires in the presence of hydrogen, and silver nanowires in the presence of amines. For both of these systems, the changes in resistance ($\Delta R/R_o$) can be 1000% or more, but the mechanism response for the resistance changes are completely different. What is the origin of these enormous and unexpected resistance changes? In this talk, we focus attention on this issue and we discuss the prospects for developing practical chemical sensors based on these novel mechanisms.

*Contributed Papers*

**15:06**
**W10 2 Novel Metallic Surface Arrays for SERS and Surface Forces Experiments** MARGO GRACA, JEFF TURNER, SUNG CHUL BAE, STEVE GRANICK, *Departments of Physics, Chemistry, and Materials Science and Engineering, University of Illinois at Urbana-Champaign* Nanofabrication techniques based on FIB (dual-beam focused ion beam lithography) and utilizing a novel solid masking scheme have produced extended arrays of coinage metal nanostructures on muscovite mica and semiconductor wafers. First, the FIB process is used to drill holes in the mask with various alternative shapes, from circles to squares to triangles. Their size is variable from $<$ 100nm to many microns, and their spacing and arrangement are also easily varied. These novel structures were used for two emerging applications. First, we demonstrate nanostructured ''forest'' patterns, arranged perpendicular to the solid, with a high aspect ratio in height to cross-section. Alternatively, these new structures were embedded into hollow spaces within the solid substrate, producing a physically flat yet itchemically rough surface capable of electronic field enhancement. We demonstrate the ability of these new structures to enhance a Raman (SERS) signal with applications to nanoplasmonics.

**15:18**
**W10 3 Scattering T-matrix theory for surface enhanced Raman scattering in clusters of nanoscale metal particles** KARAMJEET ARYA, Very large enhancements up to 14 orders of magnitude in the Raman cross-section from a molecule adsorbed on a single cluster of a few nanaoscale metal particles has been reported recently. The enhancement is believed mainly due to the enhanced electric field because of the excitation of the localized surface plasmon modes. We have developed a Green's function theory using scattering t-matrix approach in the wave-vector space to solve the Maxwell equations for the enhanced field near a metal particle cluster. The large enhancement in the field is due to the multiple scattering of the local modes of the individual metal particles that has been included exactly. We have considered clusters of different shape and size, for example, clusters of two, three, or four spherical particles forming a liner chain, a triangle or a square. Examples of clusters formed on the glass and metal plates are also discussed. We find the enhancement in the Raman cross section can reach up to 10 orders of magnitude for silver particle clusters and is in a broad frequency range. The results for gold particle clusters are also presented.

*Invited Papers*

**15:30**
**W10 4 Ordered Pore Arrays in Arrays in Alumina: Fabrication and Application Issues.***
ULRICH GOESELE, *Max Planck Institute of Microstructure Physics*

Ordered two-dimensional arrays of nanopores in alumina have become a popular model system in nanotechnology because of its ease of fabrication and versatility in terms of geometrical parameters and of using it as template for a variety of materials. The presentation will cover the original two-step approach by Masuda published in Science in 1995 for selfordered pore arrays without long range order as well as nanoimprint and interference lithography approaches for long range ordered pore arrays. Guided self-assembly will also be covered. Metal filling of the pores by electrochemical deposition methods for magnetic storage applications and wetting of the pores by polymers which allows the fabrication of complex tube structures will be discussed. A novel method to get segmented nanotubes consisting e.g. of various gold and nickel segments will be described. Finally, the potential of atomic layer deposition in combination with porous alumina will be touched upon.

*In collaboration with Woo Lee, Kornelius Nielsch, Mato Knez, Ran Ji, Martin Steinhart, Jinsub Choi, and Danilo Zschech, Max Planck Institute of Microstructure Physics.

*Contributed Papers*

**16:06**
**W10 5 Fabrication of and application of anodic alumina film with custom-designed nanochannel arrays** NAI-WEI LIU, *Institute of Atomic and Molecular Sciences, Academia Sinica, Taipei, Taiwan, Republic of China* ANINDYA DATTA, CHIH-YI LIU, CHENG-YI PENG, HUAI-HSIEN WANG, SHR-BIN WU, TSU-SHIN CHAN, CHEN-FENG HSU, JUEN-KAI WANG, YUH-LIN WANG, *National Taiwan University, Taipei, Taiwan, Republic of China* Among the strategies for growing one-dimensional straight nanostructure such as nanorods and nanowires, a viable approach is to grow the materials into templates with aligned nanochannels. Recently, porous anodic aluminum oxide (AAO) film has become an attractive template material for its self-aligned array of nanochannels. In this work, we have demonstrated, for the first time, a focused ion beam (FIB) direct-write lithographic method for selectively closing part of the channels of an ordered array on an AAO film creates a custom-designed nanochannels array. The initial ordered arrays are fabricated by FIB lithographic guiding techniques while the closure of the nanochannels within certain area is achieved by FIB bombardment of the AAO film. Besides, arrays of Ag-nanoparticles grown on anodic alumina nanochannels with precisely tunable gaps (5-25 nm) are exploited for surface-enhanced Raman spectroscopy. The enhancement becomes significant for gaps below 10 nm and turns dramatic when gaps reach an unprecedented value of 5 nm. The results are quantitatively consistent with theories based on collectively coupled surface plasmon.

**16:18**
**W10 6 Novel Solid State Fabrication Techniques*** T. L. MOORE, *Department of Physics, University of Maryland, College Park, MD 20742* D. R. HINES, *Laboratory for Physical Sciences, University of Maryland, College Park, MD 20742* E. GOMAR-NADAL, E. D. WILLIAMS, *Department of Physics, University of Maryland, College Park, MD 20742* We have electrochemically fabricated high dielectric coatings and nanowires in porous membranes. TEM images showed the nanowires to contain grains of

single crystallinity. I-V characteristics of dielectric coatings have been investigated to optimize resistivity for minimum thickness. We will report on transport properties of structures constructed using these novel components. The feasibility of incorporating these electrochemically prepared solid state structures in nanoimprinted pentacene thin-film transistors will be evaluated.

*Laboratory for Physical Sciences at University of Maryland, College Park, MD 20742

**16:30**

**W10 7 Confined self-organization of a lattice of surface magic-cluster and its structure determination** HSUAN-HAO CHANG, MING-YU LAI, YUH-LIN WANG, CHING-MING WEI, INSTITUTE OF ATOMIC AND MOLECULAR SCIENCES COLLABORATION, DEPARTMENT OF PHYSICS, NATIONAL TAIWAN UNIVERSITY COLLABORATION, The ability to create an ensemble of nanostructures with specific size, shape, and arrangement on particular positions in space is one of the most important issue in the exploration nanoscience and realization nanotechnology. We have been exploring methods to set an initial structure of a substrate surface, which provides desirable constrains to self-organization process and lead to the formation of arrays of nanostructures with identical size and structure. A two dimensional lattice of Ga surface-magic-clusters (SMC), i. e. clusters exhibiting enhanced stability at certain sizes on a particular surface, has created by using the Si(111)-7x7 surface as a confining template. The structure of the individual SMC is determined by a combination of STM, density-functional calculations, and dynamic low energy electron diffraction. The diffraction method is applicable because the SMCs have identical size/structure and form an ordered array with the exact translational symmetry. The unprecedented detailed structure information provided by the diffraction measurement is consistent with direct microscopic imaging and theoretical calculations.

**16:42**

**W10 8 Reversible adsorption of Au nanoparticles on $SiO_2$/Si: an in situ ATR-IR study*** D. ENDERS, *KIP, Heidelberg Univ.* T. NAGAO, *NIMS, Tsukuba, Japan* A. PUCCI, *KIP, Heidelberg Univ.* T. NAKAYAMA, *NIMS, Tsukuba, Japan* Adsorption and desorption of Au nanoparticles (AuNP) on the (aminopropyl)triethoxysilan (APTES) treated $SiO_2$/Si surface was monitored by itin situ attenuated total reflection (ATR) infrared spectroscopy in combination with a liquid flow cell. With increasing the AuNP coverage at the surface, the absorption by water vibration was increased due to surface enhanced infrared absorption (SEIRA). Repulsive electrostatic forces between the incoming AuNP and the already adsorbed AuNP layer lead to saturation at submonolayer coverage of the surface. We clarified that the adsorption process can be described very well by a diffusion limited first-order Langmuir-kinetics model. Furthermore, we show that the AuNPs desorb from the surface when they are exposed to the solution of aminoethanethiol (AET).

*This work has been suported by ICORP JST and Grants-in-Aid from JSPS

## SESSION W11: FOCUS SESSION: AEROSOLS, CLUSTERS, DROPLETS: PHYSICS AND CHEMISTRY OF NANOOBJECTS IV: NANOCATALYSIS, SUPPORTED CLUSTERS

**Thursday Afternoon, 16 March 2006; 303, Baltimore Convention Center at 14:30**
**Peter Lievens, Leuven University, Belgium, presiding**

*Invited Papers*

**14:30**

**W11 1 Chemical Functionalities in the non-scalable size-regime.**
UELI HEIZ, *Technische Universität München, Lehrstuhl für Physikalische Chemie I, Garching*

The reactivity and optical properties of nanoscale systems are mainly dominated by quantum-size effects that govern the electronic spectra of clusters, by the structural dynamical fluxionality of clusters, as well as by impurity-doping effects. In this talk these fundamental and unique cluster properties will be illustrated by specific examples obtained from molecular beam experiments in the gas phase and experiments on size-selected clusters on surfaces. Where possible, concepts for their understanding are given. Specifically, in the first part of the talk new results on the optical properties of small gold clusters on amorphous silica will be presented, where Cavity Ringdown Spectroscopy is used to measure optical transitions of clusters at surfaces with extremely high sensitivity. In the second part of the talk a new approach for obtaining thermodynamic properties of chemical reactions by using micromechanical devices is introduced and an overview of results on the catalysis of gold clusters is presented. By combining these experimental data with ab-initio calculations, a picture of the peculiar catalytic behavior of gold is now emerging.

*Contributed Papers*

**15:06**

**W11 2 Structure and Reactivity of $M_xS_y^+$ (M= Mo,W) Clusters with CO in the Gas Phase: an Experimental and DFT Study** MELISSA PATTERSON, JAMES LIGHTSTONE, *Stony Brook University* MICHAEL WHITE, *Stony Brook University / Brookhaven National Laboratory* We have recently constructed a cluster deposition apparatus which employs a magnetron sputtering source for generating gas-phase cation clusters of pure metals and metallic compounds. Of particular interest are clusters of the transition metal sulfides, $M_xS_y^+$ (M = Mo, W), which are known in their bulk form to be active catalysts for a wide range of heterogeneous reactions. The work reported here examines the gas-phase reactivity of small transition metal sulfide clusters as a first step towards investigations of model catalysts prepared by size-selected deposition. Specifically, we have used density functional theory (DFT) along with mass spectroscopy and gas-phase collision studies to examine the structure and stability of small sulfide clusters, $M_xS_y^+$ (x/y = 2/6, 3/7, 4/6, 5/7, 6/8, 7/10, 8/12). The

number of metal sites was probed through the formation of adducts with CO, which was introduced into a hexapole collision cell. Calculated binding energy curves for the addition of CO onto available metal sites were compared with experiment to give insight as to which geometry for the bare clusters fit best. Results will be presented for the calculated structures and stabilities of the prominent clusters as well as their adducts.

**15:18**

**W11 3 Oxidation of CO on various $Fe_2O_3$ surfaces: A Theoretical Study** ANIL KANDALAM, PURU JENA, SHIV KHANNA, BAPPA CHATTERJEE,* *Virginia Commonwealth University* B.V. REDDY, *Philip Morris USA* Recent experiments indicate that $Fe_2O_3$ nanoparticles can oxidize CO to $CO_2$ in the absence or presence of $O_2$. Depending on the size and experimental conditions, a $Fe_2O_3$ nanoparticle can have different faces that correspond to bulk surfaces of various orientations; which in turn can affect the catalytic activity of the nanoparticle. Hence, an understanding of the reaction pathways, transition barriers, and the feasibility of CO oxidation on bulk surfaces of different orientations are critical to optimize the selection of nanoparticles. Theoretical investigations of the oxidation of CO on various $Fe_2O_3$ surfaces using gradient corrected density functional approach has been carried out. BPW91 functional form and double numeric basis set (DNP), as implemented in Dmol3 code are employed here. Different $Fe_2O_3$ (corundum) faces/surfaces are modeled by a cluster where the edge atoms are saturated by H atoms to simulate the effect of the infinite surface. Results corresponding to the reaction of CO with (100) and oxygen terminated (0001) surfaces at various surface sites; oxidation of CO, both in the presence as well as absence of oxygen, will be presented and discussed.

*Deceased

**15:30**

**W11 4 Efficient Low-Temperature Oxidation of Carbon-Cluster Anions by $SO_2$** ANDREW LEAVITT, *University of West Georgia* RICHARD WYWRAS, WILLIAM WALLACE, *Georgia Institute of Technology* DANIEL SERRANO, *University of West Georgia* MELISSA ARREDONDO, *Georgia Institute of Technology* LOGAN LESLIE, FAROOQ KHAN, *University of West Georgia* ROBERT WHETTEN, *Georgia Institute of Technology* Carbon-cluster anions, $C_N^-$, are very reactive toward $SO_2$ (sticking probability of $0.012 \pm 0.005$ for $C_{27}^-$ at 25 $^o$C), in contrast to their inertness toward other common atmospheric gases and pollutants. In flow-reactor experiments at ambient temperature and near atmospheric pressure, primary adsorption of $SO_2$ by the carbon cluster anions, $N = 4 - 60$, yields $C_NSO_2^-$ or $C_{N-1}S^-$. The inferred elimination of neutral $CO_2$ is also detected as meta-stable decay in collision-induced dissociation. At higher temperatures, the reaction of $SO_2$ with nascent carbon clusters yields $C_{N-1}SO^-$ as well as undetected CO. Such carbon clusters are formed in sooting flames and may act as nuclei for the formation of primary soot particles, and serve as models for the local structural features of active soot particle sites for black-carbon soot. The facile generation of reactive carbon-sulfide and –sulfinate units may therefore have implications for understanding the health and environmental effects attributed to the coincidence of soot and $SO_2$.

***Invited Papers***

**15:42**

**W11 5 Oxidation of magnesia-supported Pd-clusters leads to the ultimate limit of epitaxy with a catalytic function.** MICHAEL MOSELER, *Fraunhofer Institute for Mechanics of Materials*

Oxide-supported transition metal clusters and nanoparticles have recently attracted significant attention due to their important role as components of model-catalysts, sensors, solar-cells and magnetic recording devices. For small clusters, functionality and structure are closely interrelated. However, knowledge of the structure of the bare cluster is insufficient since the interaction with the chemical environment might cause drastic structural changes. Here we show by ab initio simulations based on the density functional theory that the reaction with molecular oxygen transforms small, non-crystalline, magnesia-supported Pd-clusters to crystalline $Pd_xO_y$ nano-oxide clusters that are in epitaxy with the underlying support [1]. Restructuring of the Pd backbone is controlled by the electrostatic interaction with magnesia leading to a strong reduction of the $O_2$dissociation barrier. The supported $Pd_xO_y$ clusters are likely to serve as Mars-van-Krevelen oxygen reservoirs in catalytic oxidation reactions as observed previously for PdO overlayers and demonstrated here for the oxidation of CO molecules. [1] B. Huber, P. Koskinen, H. Häkkinen, M. Moseler, Nature Materials, advanced online publication 4 Dec. 2005.

***Contributed Papers***

**16:18**

**W11 6 Size effects on catalytic activity of supported metal clusters** TIANPIN WU, WILLIAM KADEN, SCOTT ANDERSON, *Chemistry/U of Utah* Size-selected cluster deposition is used to prepare and study model catalysts with size-selected gold and iridium clusters supported on single crystal oxide supports. Chemistry is found to be strongly size-dependent and a combination of ion scattering and xray photoemission is used to probe the origins of the effects.

**16:30**

**W11 7 The origin of catalytic activity of supported noble-metal nanoparticles** S.N. RASHKEEV, A.R. LUPINI, S. J. PENNYCOOK, S.T. PANTELIDES, *Oak Ridge National Laboratory* Supported Au nanoparticles $< 5$ nm show a sharp rise in the low-temperature catalytic oxidation of CO while the reverse occurs for Pt nanoparticles. Subsequent experimental and theoretical investigations focused on Au nanoparticles and reached conflicting conclusions, attributing the enhanced Au activity to particular nanoscale features such as perimeter sites and low-coordination atoms, or to a particular bilayer structures, independent of particle size. Here we report atomically-resolved Z-contrast images of on $TiO_2$-supported Au nanoparticles and theoretical results on an ensemble of rutile- and anatase- supported Au and Pt nanoparticles. We

show that high catalytic activity requires that (i) reaction barriers are small, (ii) reaction barriers are smaller than desorption energies of reacting molecules. As nanoparticle size is reduced, attached molecules induce reconstruction of Au clusters, resulting in looser Au-Au bonding and higher desorption energies and smaller reaction barriers for the attached molecules. Pt clusters get tighter by attached molecules, resulting in larger reaction barriers. The bilayer gold structures (M. S. Chen and D. W. Goodman, Science **306**, 252 (2004)) are extremely active because local reconstruction significantly reduces coordination of Au atoms. This work was supported in part by DOE Grant DE-FC02-01CH11085 and by DOE Division of Chemical Sciences under contract No. DE-AC05-00OR22725 with ORNL.

**16:42**

**W11 8 Supported Gold and Platinum Clusters: Stability under Vacuum and Hydrogen at Elevated Temperatures; Optical Properties*** STEFAN VAJDA, RANDALL WINANS, GREGORY BALLENTINE, ALEXANDRE BOUHELIER, JEFFREY ELAM, BYEONGDU LEE, MICHAEL PELLIN, SOENKE SEIFERT, GEORGE TIKHONOV, GARY WIEDERRECHT, *Argonne National Laboratory* The Achilles heal of supported clusters remains their low stability at elevated temperatures or when exposed to reactive gases. In this paper, the stability of $Au_n$ and $Pt_n$ clusters (n=6-10) supported on $SiO_2$, $Al_2O_3$ & $TiO_2$ films is addressed. The clusters were heated in vacuum and in $H_2$ atmosphere, their stability monitored by synchrotron grazing incidence small angle X-ray scattering. Pt clusters supported on $Al_2O_3$ did not undergo sintering in vacuum and when exposed to hydrogen during a lengthy heat treatment reaching 400°C; Au clusters on $SiO_2$ remained stable up to 350°C. These temperatures are considerably higher than those characteristic for the onset of the catalytic activity of these clusters. Results on heat-induced structural isomerization of clusters will be shown. Single-particle UV-VIS spectra of Au-particles obtained by dark-field microscopy will be presented as well.

*This work was supported by the U.S. Department of Energy, Office of Basic Energy Sciences, Division of Chemical Sciences, Geosciences, and Biosciences under contract number W-31-109-ENG-38

**16:54**

**W11 9 Clusters at Surfaces Studied with Low-Temperature STM and UPS*** T. IRAWAN, S. KRAUSE, M. BIELETZKI, H. HÖVEL, *Universität Dortmund, Experimentelle Physik I, 44221 Dortmund, Germany* C. YIN, B. V. ISSENDORFF, *Universität Freiburg, Fakultät für Physik, 79104 Freiburg, Germany* We study the electronic structure of cluster/surface systems and the nature of charge transfer processes between the cluster and the surface. STM/STS and UPS on size selected large clusters in contact with a surface will be combined with photoemission on the same clusters in the gas phase. For metal islands (Au, Pb) on different surfaces (HOPG, Au(111) and Pb(111)) we observed significant energetic shifts in UPS if the islands were decoupled from the surface by a thick rare gas layer and different materials for the substrate and the islands were used [1]. In addition we measure mass spectra of size selected Ag clusters with a cluster machine consisting of a magnetron sputter gas aggregation source, a differential pumping stage with a cryo pump and a high transmission infinite range mass selector. In current experiments we extend these studies to the deposition of mass selected clusters on rare gas layers and different substrate systems. For these samples low-temperature STM and UPS will be compared with photoemission on the same clusters in a free cluster beam. [1] T. Irawan, D. Boecker, F. Ghaleh, C. Yin, B. v. Issendorff and H. Hövel, Appl. Phys. A (published online Sept. 2005)

*Work supported by the DFG (SPP 1153, GK 726)

**17:06**

**W11 10 Size-Selected $Au_n$ and $Ag_n$ Nanoclusters on Rutlie $TiO_2$(110)-1x1 Surfaces Probed by UHV-STM.*** STEVE BURATTO, XIAO TONG, LAUREN BENZ, STEEVE CHRETIEN, PAUL KEMPER, HORIA METIU, MICHAEL BOWERS, *University of California, Santa Barbara* Catalysis of the oxidation of CO and small olefins by $Au_n$ and $Ag_n$ nanoclusters on oxide supports is known to be strongly dependent on the size of the cluster and its interaction with the oxide surface. In our group we have probed this size dependence by depositing size-selected clusters of $Ag_n^+$ and $Au_n^+$(n = 1-7) from the gas phase onto single crystal rutile $TiO_2$ (110) (1x1) surfaces at room temperature under soft-landing ( $<$ 2 eV/atom) conditions. We analyze the clusters on the surface using ultra-high vacuum scanning tunneling microscopy (UHV-STM) and compare the resulting structures with theory. In the case of $Au_n^+$, $Ag^+$and $Ag_2^+$ clusters deposited under soft-landing conditions we observe large, sintered clusters indicating high mobility for these species on the surface. For $Au_n^+$ ($n \geqslant 2$) and $Ag_n^+$ ($n \geqslant 3$) clusters deposited under soft-landing conditions, however, we observe a high density of intact clusters bound to the surface and no sintered clusters indicating that these species have very limited mobility on the surface. For the intact clusters we can also observe the binding site and geometry of the cluster in the STM image and compare these with structures calculated using density functional theory (DFT) as well as with structures observed in the gas phase.

*The work was supported by the AFOSR DURINT program.

**17:18**

**W11 11 Angle-resolved photoemission of Au clusters on graphite: quantized surface states on cluster facets*** H. HÖVEL, I. BARKE, *Universität Dortmund, Experimentelle Physik I, 44221 Dortmund, Germany* We present an experimental study for the electronic properties of metal clusters on surfaces. For the specific case of the confined Shockley surface state on the top (111) facets of gold clusters on graphite [1] we were able to detect the quantized electronic structure with two independent experimental techniques, scanning tunneling spectroscopy (STS) and ultraviolet photoelectron spectroscopy (UPS). Here we present new UPS data and their analysis which shows a quantitative agreement if we compare the density of states, extracted from the STS spectra by averaging over the cluster size distribution, with the UPS spectra using a deconvolution to compensate the dynamic final state effect [2] which leads to a systematic asymmetric broadening of all valance band UPS features [3]. [1] I. Barke, H. Hövel, Phys. Rev. Lett. 90, 166801 (2003). [2] H. Hövel, B. Grimm, M. Pollmann, B. Reihl, Phys. Rev. Lett. 81, 4608 (1998). [3] H. Hövel, I. Barke, Prog. Surf. Sci., submitted for publication.

*Work supported by the Deutsche Forschungsgemeinschaft

**SESSION W12: MOLECULES ON SURFACES**
**Thursday Afternoon, 16 March 2006**
**304, Baltimore Convention Center at 14:30**
**Michael Altman, Hong Kong University of Science and Technology, presiding**

**14:30**
**W12 1 Influence of interfacial structure on the charge transfer between adsorbed $C_{60}$ and Cu(111)** WOEI WU PAI, J.H. LIN, *Center for Condensed Matter Sciences, National Taiwan University, Taipei 106, Taiwan R.O.C.* A.D. ZHAO, X.Q. ZHANG, X.D. XIAO, *Department of Physics, Hong Kong University of Science and Technology, Clear Water Bay, Kowloon, Hong Kong* $C_{60}$ adsorption on metal surfaces typically incurs different amount of charge transfer from the substrate to the molecules. The charge transfer amount has never been found to approach that of optimally doped fulleride, e.g., $K_3C_{60}$, in which three electrons occupy the $C_{60}$ LUMO states. Here we demonstrate that $C_{60}$ adsorbed on Cu(111) render a nearly optimally doped fullerene film. The critical factor to produce such strong charge transfer is the identification of interfacial reconstruction in which a $C_{60}$ most probably resides in a monolayer pit consisting of seven removed Cu atoms. A direct comparison of low temperature (77 K, 4 K) STS on $C_{60}$ regions with and without interfacial reconstruction reveals drastic differences in charge transfer amount. Our STM/STS results are also consistent with a recent photoemission study [1] showing the optimal doping characteristic of the same system. This study thus demonstrates the importance of interfacial structure, which is often based on assumption, on prominent properties of molecular thin films. [1] C. M. Cheng, K. D. Tsuei, unpublished.

**14:42**
**W12 2 Coverage dependent supramolecular structures: 2D phases of $C_{60}$:ACA monolayers on Ag(111)*** BO XU, CHENGGANG TAO, ELLEN WILLIAMS, JANICE REUTT-ROBEY, *University of Maryland* The dependence of supramolecular structures on fractional molecular coverage in a 2-component adlayer has been investigated using scanning tunneling microscopy. A series of acridine-9-carboxylic acid (ACA) surface structures emerges sequentially when deposited on Ag(111) at room temperature. At low molecular coverage ($\theta < 0.4ML$), ACA forms a two-dimensional gas phase. Ordered ACA structures appear with increased coverage: firstly a chain structure composed of ACA molecules linked by O–H $\cdots$ N hydrogen bonds ($\theta > 0.4ML$), then a dimer structure composed of ACA dimers linked by carboxyl-carboxyl hydrogen bonds ($\theta \sim 1.0ML$). The structures of the $C_{60}$:ACA binary system depend on the coverage of pre-deposited ACA. When the initial ACA coverage is between 0.4 ML and 0.8 ML, subsequent $C_{60}$ deposition results in a hexagonal cooperative structure with $C_{60}$ period nearly three times as large as the normal $C_{60}$ 2-D packing of 1 nm, and exists in enantiopure domains. A $C_{60}$ quasi-chain structure is formed when the initial ACA coverage is above 0.8 ML. Parallel $C_{60}$ chains are separated in space by the ACA dimer structure. Chemically reasonable molecular packing model are presented based on the observed STM images.

*This work is supported by NSF under the MRSEC grant DMR0520471.

**14:54**
**W12 3 Step fluctuations on Ag(111) surfaces with $C_{60}$*** CHENGGANG TAO, TIM STASEVICH, TED EINSTEIN, ELLEN WILLIAMS, *Physics Department, University of Maryland, College Park* STM has been used to characterize fluctuation properties of segments of step edges partly covered by $C_{60}$ on Ag(111) at room temperature. The distribution of $C_{60}$ at step edges exhibits a step orientation dependence: low-symmetry step edges are more favorable for $C_{60}$ binding. The temporal correlation functions of step segments between $C_{60}$-covered step regions scale as a power law, with an average exponent of $0.23 \pm 0.02$, indicating that fluctuations of these ''confined'' steps are consistent with step-edge diffusion limited fluctuations. Parameters extracted from temporal correlation and autocorrelation analysis consistently indicate that close-packed steps have smaller fluctuation magnitude and higher step mobility than low-symmetry steps. The measured system sizes of step segments with different lengths show at most a weak step-length dependence. Fluctuation features thus yield the surprising conclusion that $C_{60}$ molecules are not acting as pinning points that constrain mass transport along the step edges.

*Supported by the UMD NSF-MRSEC

**15:06**
**W12 4 Self-intermixed patterns of perylene derivatives** MEIKE STOEHR, MARKUS WAHL, TOMAS SAMUELY, *University of Basel, Switzerland* THOMAS A. JUNG, LUTZ H. GADE, *University of Heidelberg, Germany* Self-assembled systems are in the focus of nanotechnology research because of their potential use in the ''bottom-up'' creation of functional supramolecular structures. Potential applications of such systems include several functional groups. Therefore, the intermixing of different molecular compounds will become a key issue. In our approach we made use of H-bonding to form well-ordered intermixed patterns of two different perylene derivatives - PTCDA and DPDI. In an UHV-setup thin films of DPDI and PTCDA were prepared by evaporation on Ag(111). The sample characterization was carried out with a homebuilt STM. For a ratio of 1:1 and a total coverage of about one monolayer, an ordered intermixed pattern was observed. Each PTCDA molecule is interacting via H-bonding with four neighbouring DPDI molecules and vice versa. Furthermore, different intermixed patterns were observed depending on the ratio of the molecules and on the total coverage.

**15:18**
**W12 5 Directed self-assembly of virus particles at nanoscale chemical templates** SUNG-WOOK CHUNG, CHIN LI CHEUNG, *Lawrence Livermore National Laboratory* ANJU CHATTERJI, TIANWEI LIN, JACK JOHNSON, *Scripps Research Institute* JIM DE YOREO, *Lawrence Livermore National Laboratory* Because viruses can be site-specifically engineered to present catalytic, electronic, and optical moieties, they are attractive as building blocks for hierarchical nanostructures. We report results using scanned probe nanolithography to direct virus organization into 1D and 2D patterns and itin situ AFM investigations of organization dynamics as pattern geometry, inter-viral potential, virus flux, and virus-pattern interaction are varied. Cowpea Mosaic Virus was modified to present surface sites with histidine (His) or cysteine (Cys) groups. Flat gold substrates were patterned with 10-100nm features of alkyl thiols terminated by Ni-NTA or meleimide groups to reversibly and irreversibly bind to the Hys and Cys groups, respectively. We show how assembly kinetics, degree of ordering and cluster-size distribution at these templates depend on the control parameters and present a physical picture of

virus assembly at templates that incorporates growth dynamics of small-molecule epitaxial systems and condensation dynamics of colloidal systems. This work was performed under the auspices of the U. S. Department of Energy by the University of California, Lawrence Livermore National Laboratory under Contract No. W-7405-Eng-48.

**15:30**

**W12 6 Enhanced Chemisorption of $Cu(hfac)_2$ on Parylene Surface by $N_2$ Plasma Treatment** S. PIMANPANG, P.-I WANG, D.-X. YE, J. S. JUNEJA, G.-C. WANG, T.-M. LU, *Dept. of Physics, Rensselaer Polytechnic Inst., Troy, NY 12180* The metallization of polymers has been intensively studied due to its wide industrial applications. We report a study of interfacial interaction of metalorganic $Cu(hfac)_2$ with the Parylene surface. Parylene is a low k dielectric polymer prepared by a chemical vapor deposition technique. The as-deposited Parylene surface is shown to be hydrophobic with a measured water droplet contact angle $\sim$ 72°. However, after the $N_2$ plasma treatment, the water droplet contact angle decreases to $\sim$ 40° due to the formation of oxygen and nitrogen functional groups on the surface, as observed by x-ray photoelectron spectroscopy (XPS). These functional groups improve $Cu(hfac)_2$ chemisorption on the plasma treated Parylene surface. Further studies by XPS show that chemisorption of $Cu(hfac)_2$ is self-limiting up to 20 sec of $Cu(hfac)_2$ precursor exposure time. The enhancement of chemisorption of metalorganic precursors on the polymer surface is an important step for chemical vapor deposition or atomic layer deposition of metal. [a]Supported by Thai govt. fellowship (SP) and SRC (JSJ).

**15:42**

**W12 7 Surface Dynamics in thin films of a small organic glass-former** STEPHEN SWALLEN, MARIE MAPES, KENNETH KEARNS, MARK EDIGER, *University of Wisconsin - Madison* SUSHIL SATIJA, *NIST* Enhanced dynamics of molecules near the free surface of thin supported films have been measured using neutron reflectivity. Thin films of the small molecule glass former tris-naphthylbenzene were vapor deposited with subnanometer initial surface roughness, allowing diffusion rates to be measured between isotopically labeled layers. Measured dynamics suggest a mobile surface layer of about 4 nm with a significant decrease in Tg. This can be compared with recent measurements in polymeric systems which find thick active layers and Tg shifts up to 30 K.

**15:54**

**W12 8 Topography and Wetting of Dotriacontane Films on Graphite Surfaces*** MATTHEW SIMPSON, MENGJUN BAI, KLAUS KNORR, HAIDING MO, HASKELL TAUB, *U. Mo.-Columbia* STEVEN EHRLICH, *Brookhaven Nat. Lab.* ULRICH VOLLKMANN, *P. U. Católica Chile* FLEMMING HANSEN, *Tech. U. Denmark* We have used Atomic Force Microscopy (AFM) in the noncontact mode and synchrotron x-ray diffraction to investigate the structure, morphology, and wetting of dotriacontane ($n$-$C_{32}H_{66}$ or C32) films deposited from a heptane solution onto highly-oriented pyrolytic graphite (HOPG). Consistent with previous neutron diffraction measurements,[1] the x-ray patterns indicate one to two layers immediately adjacent to the HOPG surface in which the molecules are oriented with their long axis parallel to the interface. Above these parallel layers, the AFM images show a partial layer of C32 molecules oriented with their long axis perpendicular to the surface. Upon heating above room temperature, we observe the area occupied by the perpendicular monolayer first to increase and then to decrease. Just above the bulk melting point, the perpendicular monolayer dewets the underlying parallel layers as we have found for C32 films adsorbed on a $SiO_2$substrate. [1]K. W. Herwig, B. Matthies, and H. Taub, Phys. Rev. Lett. **75**, 3154 (1995).

*Supported by Grant Nos. NSF DMR-0411748, DOE W-7405-Eng-82 and W-31-109-Eng-38, and FONDECYT 1010548 and 7010548.

**16:06**

**W12 9 Ellipsometric Measurements of Dotriacontane Films Adsorbed on Au(111) Surfaces*** P. SOZA, V. DEL CAMPO, E. CISTERNAS, M. PINO, U.G. VOLKMANN, H. TAUB, F.Y. HANSEN, We have conducted ellipsometric and stray light intensity measurements on dotriacontane ($n$-$C_{32}H_{66}$ or C32) films adsorbed on Au(111) substrates in air as a function of temperature in order to determine their optical thickness and surface roughness. The C32 films were deposited from a heptane ($n$-$C_7H_{16}$) solution onto the gold surface. Our large, atomically flat gold substrates were produced by the method reported by Hegner et al.[1] in which gold films grown on mica are glued onto Si(100) wafers. For films of 25 Å thickness, our ellipsometry measurements show a decrease of about 75% in the height of the monolayer substep compared to the same film adsorbed on $SiO_2$substrates.[2] This substep is believed to be contributed by a monolayer phase in which the molecules are oriented with their long axis perpendicular to the surface. The substep decrease may be interpreted as reduction in the number of molecules in this phase or possibly a tilting of the molecules. [1]M. Hegner et al., Surf. Sci. **291**, 39 (1993). [2]U.G. Volkmann et al., J. Chem. Phys. **116**, 2107 (2002).

*Supported by Grant Nos. DIPUC 2005/03P, CONICYT, and NSF DMR-0411748.

**16:18**

**W12 10 Comparison of Thickness and Morphology of Dotriacontane Films on $SiO_2$/Si Surfaces Vapor-deposited in High Vacuum with those Deposited from Solution*** E. CISTERNAS, P. SOZA, V. DEL CAMPO, E. RAMIREZ, U.G. VOLKMANN, *P. U. Católica Chile* H. TAUB, *U. Mo.-Columbia* F.Y. HANSEN, *Tech. U. Denmark* We have used Very High Resolution Ellipsometry (VHRE) and Atomic Force Microscopy in the noncontact mode to compare the thickness and morphology of dotriacontane ($n$-$C_{32}H_{66}$ or C32) films deposited by two different methods on Si(100) wafers coated with their native oxide. During deposition, the substrate temperature was held below the bulk melting point of C32. As monitored by VHRE, the film thickness of different samples was found to be in the range 20 Å to 400 Å. Films deposited by physical vapor deposition from a Knudsen cell in high vacuum are optically smooth and homogeneous, while deposition by dip-coating from a heptane solution also results in optically smooth but less homogeneous layers. Heating/cooling cycles were performed on these two sample types while conducting VHRE and stray light intensity measurements in order to compare the wetting behavior and surface roughness of C32 as a function of film thickness on both hydrophilic and hydrophobic $SiO_2$/Si surfaces.

*Supported by Grant Nos. DIPUC 2005/03P, CONICYT, and NSF DMR-0411748.

**16:30**

**W12 11 Controlling growth kinetics and morphology of crystal surfaces through biomolecular interactions** JIM DE YOREO, ROGER QIU, *Lawrence Livermore National Laboratory* SELIM ELHADJ, PATRICIA DOVE, *Virginia Tech* GERMAINE FU, DANIEL MORSE, *University of California at Santa Barbara* ALAN SALTER, ANDRZEJ WIERZBICKI, *University of South Alabama* The complex shapes and hierarchical designs of biomineralized nanostructures arise from biomolecular controls over crystallization. One prevailing view is that mineral-associated macromolecules are responsible for nucleating and stabilizing non-equilibrium polymorphs and morphologies through interactions at crystal surfaces. Here we report results of itin situ AFM and molecular modeling investigations of calcite growth in the presence of acidic amino acids, polypeptides, and proteins associated with biomineral formation. We show how the sterochemical relationship between modifier and crystal lattice lead to step-specific interactions and how those interactions account for the changes in kinetics and morphology. We analyze the results in terms of classic physical models of crystal growth and epitaxy and show that there are important deviations from those classic models that stem, in part, from the low kink density of steps on calcite. This work was performed under the auspices of the U.S. Department of Energy by the University of California, Lawrence Livermore National Laboratory under contract No. W-7405-Eng-48.

**16:42**

**W12 12 Mixing in a Solid Monolayer: $SF_6$ + $C_2F_6$ on Graphite*** G. B. HESS, *Univ. of Virginia* B. L. ELLIS, YIZE LI, We have studied mixing of $SF_6$ and $C_2F_6$ in a solid monolayer film on graphite by admitting one gas to the cell to a pressure between monolayer condensation and saturation, then slowly admitting the other gas. The total coverage is monitored by ellipsometry and the condition of the individual adsorbates is determined by infrared absorption spectra. In particular, shifts in absorption lines due to dynamic dipole coupling indicate the local environment of molecules of each species. At 75 and 80 K there is no detectable solubility of $C_2F_6$in a dense $SF_6$ monolayer, then a layer of nearly pure $C_2F_6$condenses on top. At 86 K there is limited solubility of $C_2F_6$ in dense $SF_6$, followed by appearance of a second $C_2F_6$–rich phase in the monolayer. At 90 K and above, $C_2F_6$ appears to replace $SF_6$ by continuous substitution; thus there appears to be a 2-D solid consolute critical point near 90 K. If $SF_6$ is added to a higher-temperature, low-density $C_2F_6$ layer, the $C_2F_6$ molecules are rapidly compressed from flat or tilted orientation to axes perpendicular to the substrate, then are continuously diluted.

*Supported by NSF grant DMR0305194

**16:54**

**W12 13 Energetic Study of the Flip-flop Motion of P(VDF-TrFE)*** XUEWEN WANG, LEI CAI, JIANDI ZHANG, *Florida International University* P. A. DOWBEN, *University of Nebraska-Lincoln* Ferroelectric copolymer P(VDF-TrFE) has attracted significant attention in material science and technology due to its excellent electromechanical properties and easy manipulation of the individual monomer or monomer clusters resulting in the change of the such properties. Theoretical aspect of the switching dynamics of P(VDF-TrFE) has been investigated by using the density function theory and compared with experimental results. Through calculation, we find a simple flipping of the individual monomer with lower energy that involves no change of the bond length and the bond angle of –C–C–, –C–H–, and –C–F–. These consist with the experimental results obtained with STM. We compare the STM image before and after the flipping of the monomers. Except the observation of the lattice shift at the boundary, we find no other structure distortion and no change in the inter- and intra- chain spacing.

*Work supported by NSF CHE0415421 and DMR-0346826

**17:06**

**W12 14 Exploiting Photo-induced Reactions in Polymeric Thin Films to Create Hierarchically Ordered, Defect-free Materials** RUI TRAVASSO, OLGA KUKSENOK, ANNA BALAZS, *University of Pittsburgh* Computer simulations reveal how photo-induced chemical reactions in polymeric thin films can be exploited to create long-range order in materials whose features range from the sub-micron to the nanoscale. The process is initiated by shining a spatially uniform light on a 2D photosensitive AB binary blend, which thereby undergoes both a reversible chemical reaction and phase separation. When a well-collimated, higher intensity light is rastered over the sample, the system forms defect-free, spatially periodic structures, which resemble the phases of microphase-separated diblock copolymers. We then add a non-reactive homopolymer C, which is immiscible with both A and B. This component localizes in regions that are irradiated with a higher intensity light and one can effectively write a pattern of C onto the AB film. Rastering over the ternary blend with the collimated light now leads to hierarchically ordered patterns of A, B and C. The findings point to a facile, non-intrusive process for manufacturing high quality polymeric devices in a low-cost, efficient manner.

## SESSION W16: SEMICONDUCTOR APPLICATIONS
**Thursday Afternoon, 16 March 2006**
**312, Baltimore Convention Center at 14:30**
**James Levine, Kodak, presiding**

**14:30**

**W16 1 Extraordinary Electrical Conductance in GaAs-In Hybrid Structures*** YUN WANG, K.A. WIELAND, S.A. SOLIN, *Washington University in St.Louis* Following the demonstration of extraordinary magnetoresistance (EMR)in semiconductor-metal hybrids[1], it has been realized that EMR is but one example of a general class of EXX phenomena that can be geometrically enhanced by the judicious choice of sample geometry. Two other EXX phenomena reported recently are extraordinary piezoconductance, EPC, and extraordinary Optoconductance, EOC. Here we address a fourth EXX phenomena, extraordinary electrical conductance, EEC. We develop a new design concept for an EEC sensor, which is a van der Pauw plate structure of Si-doped GaAs with a non-magnetic metallic shunt on top so that the external E field is perpendicular to the interface. EEC arises from the current redistribution between the shunt and GaAs when an external E field lowers the Schottky barrier at the interface. This allows more electrons to tunnel through and results in a larger conductance. We compare the response of a sample with a Schottky barrier to an unshunted sample and to a shunted sample with an Ohmic contact.

The conductance of each sample was measured as a function of temperature, bias current and external perturbing field. In addition, we will compare the EEC structure to the Schottky diode structure to illustrate the advantages of an EEC sensor for static charge imaging.

*Supported by NSF grant ECS-0329347 and WU CMI

[1]S.A. Solin et al., Science **289**,1530 (2000).

**14:42**

**W16 2 High-power mid-infrared interband cascade lasers** MIJIN KIM, CHUL SOO KIM, CHADWICK CANEDY, WILLIAM BEWLEY, JAMES LINDLE, IGOR VURGAFTMAN, JERRY MEYER, *Code 5613, Naval Research Laboratory, Washington DC 20375* We have grown and fabricated interband cascade lasers (ICLs) with ''W'' active regions. The ICL structures were etched into 140-$\mu$m-wide ridges, with 100-$\mu$m-wide metal strips deposited in the middle, and operated epitaxial-side-up. Initial devices displayed lasing thresholds as low as 12 A/cm$^2$ at 78 K, series resistance as low as 0.21 m$\Omega \cdot$ cm$^2$, and a voltage efficiency of 96%. Cavity length studies on a series of ICLs with 5, 10, and 15 stages determined that the internal losses at 78 K were 16, 27, and 37 cm$^{-1}$, respectively, while the internal efficiencies were $\approx$ 80% in all cases. Pulsed operating temperatures as high as 300 K were obtained, and a 5-stage device with 0.5 mm cavity length had a wallplug efficiency per facet of $\approx$ 20% without facet coatings. A 3-mm-long laser with high-reflection (95%) and antireflection (5%) coatings produced $>$ 1.1 W of cw output power at 78 K.

**14:54**

**W16 3 Single-Mode Distributed-Feedback ''W'' Diode and Interband Cascade Lasers in the Mid-Infrared** CHUL SOO KIM, MIJIN KIM, CHADWICK CANEDY, WILLIAM BEWLEY, JAMES LINDLE, IGOR VURGAFTMAN, JERRY MEYER, *Code 5613, Naval Research Laboratory, Washington DC 20375* To obtain spectrally pure output, we have fabricated narrow index–guided ridges with lateral distributed-feedback (DFB) line gratings on both ''W'' diode and interband cascade lasers. The ''W'' diode structure containing a GaSb *p*-SCH etch-stop layer was chemically etched into a 5 $\mu$m ridge and a first-order DFB grating constructed on both side walls of the ridge. For the interband cascade laser, a first-order top DFB grating was patterned on top of a chemically-etched ridge that was 15 $\mu$m wide. The low-loss DFB mode was roughly resonant with the gain peak at $T =$ 165 K for the ''W'' diode and at $T =$ 110 K for the interband cascade laser. The sidemode suppression ratios were definitely $>$ 20 dB for both devices, and all of the features above 30 dB appeared to result from instrument noise rather than actual parasitic modes. Just beyond the stop band on the long-wavelength side of the ''W'' diode DFB, a series of longitudinal modes became apparent at $>$ 30 dB suppression. For the narrow-ridge waveguide DFB devices, the temperature ranges over which single-mode lasing were successfully obtained were 140-162 K for the ''W'' diode, for which $\lambda = 3.195 \sim 3.202$ $\mu$m (0.29 nm/K), and 110-125 K for the interband cascade laser, for which $\lambda = 3.452 \sim 3.456$ $\mu$m (0.27 nm/K).

**15:06**

**W16 4 High Resolution 2D dopant profiling of FinFET structures and Silicon-based Devices using Scanning Probe Microscopies** A. KHAJETOORIANS, *UT at Austin Physics Dept.* X.D. WANG, *APRDL, Freescale Semiconductor* J. LI, *UT at Austin Physics Dept.* D. GARCIA-GUTIERREZ, *UT at Austin Dept. of Chem. Engr.* J. DENYSZYN, *UT at Austin: Texas Materials Inst.* H. CELIO, D. PHAM, A. DIEBOLD, *International SEMATECH* J. GOODENOUGH, *UT at Austin: Texas Materials Inst.* M. JOSE-YACAMAN, *UT at Austin Dept. of Chem. Engr.* C.K. SHIH, *UT at Austin Dept. of Physics* The ability to perform dopant/junction profiling with high spatial resolution is critical for development of future generation devices such as FinFET structures. Among various forms of scanning probe microscopy, scanning tunneling microscopy (STM) has demonstrated direct atomic imaging of dopant atoms on GaAs (110) surfaces. More recently, scanning thermoelectric microscopy (SThEM) (H.K. Lyeo et al itScience v.303 p816 (2004)) has been applied to profile GaAs $p - n$ junction with unprecedented spatial resolution. The key challenge to successfully apply these techniques to silicon-based devices is to prepare a surface that is both chemically and electronically passivated. Here we present our progress toward this goal. We present STM and SThEM studies on Si $p - n$ junction devices including FinFET structures. We also present in-depth profiling of fin structures using scanning capacitance (SCM) and conductive atomic force microscopy (C-AFM) (Khajetoorians itet al APL (submission)).

**15:18**

**W16 5 Photoelectron Multipliers Based On Avalanche Pn-I-Pn Structures** HILDA CERDEIRA, *Max Planck Institut fuer Physik komplexer Systeme, Noethnitzerstr. 38, D-01187 Dresden* KONSTANTYN LUKIN, *Institute for Radiophysics and Electronics, National Academy of Sciences of Ukraine, 12 Akademika Proskura St., Kharkov, 61085, Ukraine* PAVEL MAKSYMOV, *Institute for Radiophysics and Electronics, National Academy of Sciences of Ukraine, 12 Akademika Proskura St., Kharkov, 61085, Ukraine* We present a new optoelectronic device, which consists of a multilayered semiconductor structure, where the necessary conditions for the creation of photoelectrons are met, such that it will enable sequential avalanche multiplication of electrons and holes inside two depletion slabs created around the p-n junctions of a reverse biased pn-i-pn structure [1]. The mathematical model and computer simulations of this Semiconductor Photo-electron Multiplier (SPM) for different semiconductor materials are presented. Its performance is evaluated and later on compared with conventional devices. [1] K.A.Lukin, H.A.Cerdeira, A.A.Colavita, Current Oscillations in Avalanche Particle Detectors with pnipn-Structure. IEEE Transactions on Electron Devices. 43(3), 1996, 473-478.

**15:30**

**W16 6 Electron relaxation through multiphonon processes in a double quantum dot** VASILIOS STAVROU, *Dept. of Physics and Astronomy, University of Iowa, Iowa City, IA 52242-1479* XUEDONG HU, *Department of Physics, State University of New York at Buffalo, NY 14260-1500* We theoretically study the relaxation of the electron orbital states of a double quantum dot system due to two-phonon processes. In particular, we calculate how the relaxation rates depend on the separation distance between the quantum dots, the strength of quantum dot confinement, and the lattice temperature. Our results show interesting crossovers in the relative strength of different scattering channels as temperature is

varied. Furthermore, although at low temperatures two-phonon processes are much weaker compared to one-phonon processes in relaxing electron orbital states, at room temperature they are as important as one-phonon processes.

**15:42**

**W16 7 Dark current generation in a confined and depleted region of silicon** JAMES LAVINE, DANIEL MCGRATH, *Eastman Kodak Company* Dark current generation degrades the performance of silicon solid-state imagers. The present study examines whether a depleted region with defects supplies dark current to a photodiode when it is separated by a neutral region. Thermally-excited electron-hole pairs appear in the depleted region, which is confined by infinite potential barriers in two dimensions and a triangular potential well in the third. The triangular well has ground states of 0.036 and 0.058 eV for electric fields of 0.1 and 0.2 MV/cm, respectively. Lateral dimensions of 0.1 to 1.0 micrometers lead to high electron densities, which quench further dark current generation before excited states are occupied. As a result, the electrons must diffuse against the strong electric field and are unlikely to reach the photodiode. The same potential barrier accelerates the holes and creates electron-hole pairs by impact ionization. The electron would be generated near the top of the potential barrier. However, the probability that the hole acquires sufficient energy is 0.00001 for 0.2 MV/cm and 0.0028 for 0.3 MV/cm, based on J. S. Marsland in Solid-State Electronics 30, 125 (1987). If the defect is a gold atom at 55 C, this leads to 0.0056 and 1.6 electrons/s.

**15:54**

**W16 8 Measuring Ionization and Athermal Phonons: Detectors of the Cyrogenic Dark Matter Search*** KYLE SUNDQVIST, *University of California, Berkeley* FOR THE CDMS COLLABORATION, The Cryogenic Dark Matter Search (CDMS) is a search for weakly-interacting massive particles (WIMPS) in the halo of our galaxy. WIMPs are a favored solution to the dark matter problem in cosmology and particle physics. We will describe how CDMS measures simultaneously the number of charge carriers and the energy in athermal phonons created by particle interactions in Ge and Si crystals at a temperature of 50 mK. Together these distinct signals create a signature response for each event, allowing candidate WIMP interactions with nuclei to be discriminated from electromagnetic radioactive background which interacts with electrons. Combining this method with additional information contained in the athermal phonon signal shape, CDMS has achieved a sensitivity roughly ten times better than any other experiment in the world. These techniques introduce a number of unique challenges. Bias levels must remain at only a few volts, else the secondary phonons emitted by the drifted carriers dominate the original phonon signal. The neutralization of charge-trapping sites, even at concentrations of only $\sim 10^{10} cm^{-3}$, is of primary importance to the performance of charge collection. We present the methods of crystal neutralization, subsequent characterization, and representative phenomena encountered in practice.

*Funded by NSF and DOE

**16:06**

**W16 9 Resistive all boron carbide neutron detectors*** ELLEN DAY, MANUEL DIAZ, CAROLINA ILIE, SHIREEN ADENWALLA, *Mechanical Engr., Physics and Astronomy and CMRA, Univ. of Nebraska-Lincoln* Semiconducting boron carbide is a promising material for true solid-state neutron detection [1]. An all boron carbide (BC) layer was deposited on sapphire ($Al_2O_3$) with sputtered Chrome/Gold electrical contacts. Resistance vs. temperature measurements indicate a $T^{-3/2}$ dependence and a band gap of $\sim$ 0.17eV. X-ray diffraction measurements confirm the similarities in crystal structure of the films grown on $Al_2O_3$ and Si. Detection area ranged from $0.25mm^2$ to $1mm^2$ and the thickness of the films ranged from 280nm to 600nm. Neutron detection measurements show no sharp spectral peaks but a long high energy tail which increased in counts as the reactor power was increased, in agreement with both monte carlo simulations and simple model calculations [2]. The low thermal neutron capture cross section of Al and O ensures that the entire neutron signal observed is from the resistive boron carbide layer, thus demonstrating the fabrication of an all boron carbide neutron detector. We show plots as a function of reactor power and thickness. [1] B.W. Robertson, S. Adenwalla, A. Harken, et al., Appl. Phys. Lett. **80**, 3644 (2002). [2] C. Lundstedt, A. Harken, E. Day, B. W. Robertson, S. Adenwalla, submitted to NIM.

*Work is funded by the State of Nebraska, ONR [N00014-04-1-0605] and NASA.

**16:18**

**W16 10 What should neutron spectra from boron carbide devices look like?*** CARL LUNDSTEDT, ELLEN DAY, SHIREEN ADENWALLA, *Physics and Astronomy, Mechanical Engineering and CMRA, University of Nebraska-Lincoln, Lincoln, NE 68588* GEANT4 (Geometry ANd Tracking) monte carlo modeling was performed on boron based neutron detectors [1]. Two different detector geometries were used. Geometry 1 consisted of a boron carbide (BC) layer placed on a Silicon (Si) layer in a cylindrical design with thermal neutrons of energy 0.025eV incident on the BC face. Geometry 2 was a rudimentary calorimeter made by sandwiching a moderator material between two BC/Si layers. The energy deposition spectra for the BC/Si device of various BC layer thicknesses for geometry 1 are presented as well as the spectra for geometry 2. In geometry 2, by changing the moderator material and thickness, higher energy neutrons may be detected, due to thermaization of neutrons in the moderator material. We show results for incident neutrons ranging in energy from 0.025eV to 2.5MeV. [1] C. Lundstedt, A. Harken, E. Day, B. W. Robertson, S. Adenwalla, submitted to NIM.

*Work is funded by the State of Nebraska, ONR [N00014-04-1-0605] and NASA.

**16:30**

**W16 11 Neutron detection characteristics of semiconducting boron carbide*** ANDREW HARKEN, *Mechanical Engineering and CMRA, University of Nebraska-Lincoln, Lincoln, NE 68588* BRIAN ROBERTSON, *Mechanical Engineering and CMRA, University of Nebraska-Lincoln, Lincoln, NE 68588* The all boron carbide semiconducting neutron detector is sought because is could potentially yield the most useful and efficient of all thermal neutron detectors. We report on experiments to obtain data using alpha particle and neutron capture measurements. The results are analyzed in relation to our measurements of the dielectric properties and to initial charge transport considerations. The neutron capture results are compared with our modeling of the ideal neutron detector behavior calculated for an all boron carbide semiconductor device.

*Research supported by NSF, NASA, the Office of Naval Research and the State of Nebraska.

**16:42**
**W16 12 Alpha-Energy-Deposition-Profiling of Radioisotope $p-i-n$ Diodes for Power Generation** CORY CRESS, RYNE RAFFAELLE, *NanoPower Research Labs, R.I.T.* The high energy density and long half-life of certain alpha-emitting radioisotopes enables viable and long-lived power supplies to be fabricated on the micro-scale. A design incorporating an InGaP $p-i-n$ photovoltaic (PV) device that directly converts the kinetic energy of the alpha-particles into electricity represents both a scalable and efficient microsystem design. To better understand the relationship between the alpha-energy-deposition-profile (ADEP) and the maximum power conversion efficiency for this device structure, we have performed two systematic studies. In these studies, I-V characteristics for the InGaP PV device under alpha-flux are measured as a function of alpha source distance, and as function of aluminum film thickness (10 nm to 10 $\mu$m) which is deposited onto the surface of the PV device. Both techniques will alter the ADEP in relation to the active region of the PV device. These experimental results are compared to a theoretical model which utilizes Monte Carlo simulations and numerical calculations to determine the ADEP for the same device configuration. The understanding gained from this analysis has direct implications towards the fabrication of radioisotope microbatteries with structural characteristics that enable optimal power conversion efficiencies to be achieved.

**16:54**
**W16 13 Analysis of microwave-frequency field patterns in an externally-driven Single-Electron Transistor*** BRYAN HEMINGWAY, ANDREI KOGAN, *University of Cincinnati* We report a numerical study of electromagnetic field patterns that emerge in a Single-Electron Transistor (SET) device driven by a microwave-frequency signal. In an SET, an electronic droplet (quantum dot) containing a few electrons is connected to two macroscopic conductors via tunnel barriers, and DC current measurements are used to investigate the quantum properties of the lead-dot system. Our goal is to develop a method for a well-controlled excitation of few-electron devices with microwaves. Such capability is needed for investigating the intrinsic time scales of Kondo-correlated electrons, not accessible in static experiments. We study realistic model geometry of an SET defined lithographically on a semiconductor heterostructure such as GaAs/AlGaAs. We find that at frequencies $\sim$ 10 GHz and above, the microwave voltages across the sub-micron features of the SET can be drastically different from those applied to the large-scale pads and depend in a complex and sensitive way on the excitation frequency, thus presenting a challenge for dynamic transport experiments with SETs. We discuss possible strategies for resolving the problem.

*supported by UC startup funds

**17:06**
**W16 14 The effect of negative electron affinity emitter materials on space charge mitigation of vacuum thermionic energy conversion devices** JOSHUA SMITH, *North Carolina State University* GRIFF BILBRO, *North Carolina State University* ROBERT NEMANICH, *North Carolina State University* Vacuum thermionic energy conversion (TEC) devices provide a way to convert heat directly into electrical work. The negative space charge effect has been an effect that significantly degrades the performance of these devices, requiring small interelectrode spacings for reasonable performance. Recently, Nitrogen doped, Hydrogen terminated, ultra-nanocrystalline diamond films have been investigated as possible candidates for low operating temperature, low work function emitter materials. Furthermore, these materials exhibit a so-called negative electron affinity (NEA) where the vacuum level lies below the conduction band minimum of the material. As a result of this NEA property, the distribution of thermionically emitted electrons will have some nonzero minimum initial velocity. A model was developed to determine the effect that the NEA property of these types of emitters have on mitigation of the space charge effect. The model shows that a TEC with an NEA emitter material will have comparable performance with a non-NEA emitter TEC with a smaller gap. Thus, it is possible to use NEA emitters to relax the requirement of a small gap distance.

## SESSION W18: FOCUS SESSION: CARBON NANOTUBES: ELECTRONIC AND OPTICAL PROPERTIES III
**Thursday Afternoon, 16 March 2006; 315, Baltimore Convention Center at 14:30**
**Gordana Dukovic, Columbia University, presiding**

***Invited Papers***

**14:30**
**W18 1 Phonon sideband in optical spectra of C13 carbon nanotubes.**
SHIGEO MARUYAMA, *Dept. of Mech. Eng., The University of Tokyo*

Photoluminescence (PL) of single-walled carbon nanotubes (SWNTs) has been widely used for the measurement of chirality distribution of single-walled carbon nanotubes (SWNTs). However, there are unassigned peaks in the 2-D photoluminescence map plotted as a function of emission and excitation photon energy. In order to clarify the origin of these peaks, we have studied photoluminescence (PL) and resonant Raman scattering of single-walled carbon nanotubes (SWNTs) consisting of carbon-13 ($SW^{13}CNTs$) synthesized from a small amount of isotopically modified ethanol [1]. There was almost no change in the Raman spectra shape for $SW^{13}CNTs$ except for a downshift of the Raman shift frequency by the square-root of the mass ratio 12/13. By comparing photoluminescence excitation (PLE) spectra of $SW^{13}CNTs$ and normal SWNTs, the excitonic phonon sideband due to strong exciton-phonon interaction was clearly identified with the expected isotope shift [2]. The PLE line shape and energy difference from $E_{ii}$ are remarkably similar to the excitonic phonon sideband predicted by Perebeinos itet al. for (7, 5) and (6, 5) nanotubes. In addition to these phonon sideband features, we also found low-intensity 'pure electronic' features whose origin has never been elucidated. In order to examine these 'pure electronic' features, polarized PLE measurements on individually-dispersed SWNTs

aligned in a gelatin-based thin film. By comparing optical transitions of SWNTs for incident light parallel or perpendicularly polarized to the nanotube axis, we have attributed these features to excitation by perpendicularly polarized light to the nanotube axis. The measured absorption energies of perpendicularly polarized light are compared with cross-polarized version of the Kataura plot. [1] S. Maruyama and Y. Miyauchi, AIP Conf. Proc. 786, 2005, 100-105. [2] Y. Miyauchi and S. Maruyama, cond-mat/0508232.

*Contributed Papers*

**15:06**

**W18 2 Raman Studies of Exciton-Phonon Coupling in Single-Walled Carbon Nanotubes** STEPHEN DOORN, *Los Alamos National Lab* SERGUEI GOUPALOV, SATISHKUMAR CHIKKANNANAVAR, Significant chirality-dependent effects on nanotube Raman intensities have recently been observed whose origins lie in the chirality dependence of exciton-phonon coupling. We present resonance Raman excitation data that demonstrates this dependence in radial breathing mode (RBM) intensities for both E11 and E22 excitation. For E22 excitation, intensities for (n-m)mod 3 = -1 chiralities are significantly more intense than for (n-m)mod 3 = +1, with more complex behavior in E11 excitation. We discuss the results in terms of a new theoretical analysis of exciton-phonon coupling that accurately describes the observations with simple intuitive analytical expressions. Relative intensities can be easily predicted using a newly introduced parameter that is also able to explain a number of anomalies in the observations. We also present the first direct comparison of E11 vs. E22 intensities for a number of chiralities. This comparison yields the ratio of the decay rates for the excited and ground excitonic states serving as intermediate states in the Raman process under E22 and E11 excitations, respectively.

**15:18**

**W18 3 Resonance Raman Spectroscopy of 1.2< dt < 2.0 nm Diameter Single Wall Carbon Nanotubes in the E33S and E44S Optical Range*** PAULO A. T. ARAÚJO, *UFMG* S.K. DOORN, *Los Alamos National Lab* A.G. SOUZA FILHO, *UFC* J.JIANG, *Tohoku University* R. SAITO, *Tohoku University* S. MARUYAMA, *Tokyo University* M.A. PIMENTA, *UFMG* A. JORIO, *UFMG* This work uses Resonant Raman Spectroscopy with excitation laser energy from 1.26 to 2.98 eV to measure the E33S and E44Soptical transition energies, for single wall carbon nanotubes (SWNTs) with diameters in the range 1.2 < dt < 2.0 nm. We identify the families of (2n+m) = constant and analyse the radial breathing mode (RBM) frequencies, the E33S and E44S energies and intensities as a function of (n,m). The excitonic effects are weaker in the E33S and E44S , the energies being blue-shifted when compared with earlier predictions. We also study the relation between the RBM intensity and tube chirality, clearly showing that the RBM Raman spectrum is less intense for armchair tubes.

*BrazilianauthorsacknowledgeCNPq−Brazil

**15:30**

**W18 4 Raman spectroscopy and imaging of surface and suspended carbon nanotubes*** KATE KAMINSKA, *NRC, Ottawa* JACQUES LEFEBVRE, *NRC, Ottawa* D. GUY AUSTING, *NRC, Ottawa* JEFFERY BOND, *University of Ottawa* PAUL FINNIE, *NRC, Ottawa* Freely suspended single walled carbon nanotubes show enhanced photoluminescence and Raman signals compared with those from nanotubes on surfaces. We prepared suspended carbon nanotubes by chemical vapor deposition on lithographically patterned substrates. The nanotubes were of the order of 100 microns in length with suspended segments ranging from 1 to 20 microns. Individual nanotubes and bundles were characterized with both Raman spectroscopy and scanning electron microscopy. Raman signals from suspended and non-suspended segments of the same nanotube were detected with up to a tenfold signal enhancement observed for the suspended segments. The effect of suspension is clearly illustrated in spatially resolved confocal images of nanotubes extending over many microns.

*This work was supported by a grant from JST-CREST

**15:42**

**W18 5 Effects of collective excitations on the G-band and RBM modes in the Raman spectra of metallic unfilled and filled carbon nanotubes** SAURABH GAYEN, *Drexel University* SURJYO BEHERA, SHYAMALENDU BOSE, *Drexel University* The Raman spectra of a single-wall carbon nanotube (SWNT) consist of three types of modes; (i) the high frequency G-mode arising out of tangential oscillations of carbon atoms, (ii) D-mode due to the defects in the nanotube and (iii) the low frequency radial breathing mode (RBM) resulting out of radial oscillations of the carbon atoms. In this paper we theoretically investigate the effects of collective oscillations of electrons (plasmons) on the G and RBM modes in the Raman spectra of a filled and unfilled metallic SWNT. Inclusion of plasmon and the filling (rattler) atom produces four peaks in the Raman spectra in general. The positions and relative strengths of the Raman peaks [1] depend upon phonon frequencies of the nanotube and that of the filling atoms, the plasmon frequency, the strength of the electron-phonon interaction, strength of the interactions between the nanotube phonons and rattler phonon and radius of the nanotube [2]. Usually the intensity of the G-mode is higher than that of RBM. For heavier filling atoms the frequency of the rattler phonon is lower in value, which may broaden the peak to such an extent that it may disappear in the background spectrum altogether. 1.S.M. Bose et al., Physica B **351**, 129 (2004) 2. S.M. Bose, S.Gayen and S. Behera, Phys. Rev. B **72**, 153402 (2005).

**15:54**

**W18 6 Chirality dependence of Raman intensity of single wall cabon nanotubes*** RIICHIRO SAITO, JIE JIANG, KENTARO SATO, *Tohoku UNIV. and CREST JST* ADO JORIO, *UFMG* GEORGII SAMSONIDZE, GRACE CHOU, GENE DRESSELHAUS, MILDRED DRESSELHAUS, *MIT* We present calculated Raman intensity of radial breathing modes (RBM), and other first and second order Raman signals as a function of (n,m) with exciton wavefunctions. Because of strong k dependent electron-phonon and electron-photon matrix elements, the Raman intensity shows (2n+m) family pattern. Within the extended tight binding calculation, we make exciton Kataura-plot for RBM. The Raman intensity is enhanced by localized wavefunction of the bright exciton which decreases with increasing energy and diameter. We will further discuss disorder induced D-band Raman intensity with some experimental results.

*RS acknowledges MEXT Grant 16076201, MIT authors acknowledges NSF Grants DMR 04-05538

**16:06**

**W18 7 Carbon Nanotube Population Analysis from Raman and Photoluminescence Intensities*** ADO JORIO, *UFMG* C. FANTINI, *UFMG* P.A.T. ARAUJO, *UFMG* M.A. PIMENTA, *UFMG* D.A. HELLER, *UIUC* M.S. STRANO, *UIUC* M.S. DRESSELHAUS, *MIT* Y. OYAMA, *Tohoku Univ.* J. JIANG, *Tohoku Univ.* R. SAITO, *Tohoku Univ.* Large efforts are now being directed to developing synthesis or manipulation processes able to generate single-wall carbon nanotubes (SWNT) with well-defined geometric structure, i.e. $(n,m)$ indices. The $(n,m)$ population in a SWNT sample can be obtained from intensity analysis of photoluminescence excitation (PLE) and Resonance Raman spectroscopy (RRS) experiments, after the information is corrected to account for the $(n,m)$ dependence of the RRS and PLE efficiency. In the absence of standard single-wall carbon nanotube samples with well-known (n,m) population, we provide both a photoluminescence excitation (PLE) and resonance Raman scattering (RRS) analysis that together can be used to check the calculations for PLE and RRS efficiency. We show that available models describe well the chirality dependence of the intensity ratio, confirming the differences between type 1 and type 2 semiconducting tubes and the existence of a node in the radial breathing mode intensity for type 2 carbon nanotubes with chiral angles between 20° and 25°. The method is used to characterize SWNT samples grown by the CoMoCAT, HiPco and alcohol-CVD processes.

*Brazilian authors acknowleadge CNPq-Brazil

**16:18**

**W18 8 Optical studies of finite length effects in short DNA-wrapped carbon nanotubes** SHIN GRACE CHOU, *Chemistry, MIT* H. SON, *EECS, MIT* EDUARDO BARROS, *EECS/Physics, UFC, Brazil/MIT* GEORGII G. SAMSONIDZE, *EECS, MIT* MING ZHENG, *Experimental Station, Dupont Central Research and Development* RIICHIRO SAITO, *Department of Physics, Tohoku University and CREST JST, Japan* GENE DRESSELHAUS, *Francis Bitter Magnet Laboratory, MIT* MILDRED DRESSELHAUS, *EECS/Physics, MIT* In this study, a systematic resonance Raman study was carried out on samples of DNA-wrapped SWNTs with average lengths between 50 and 100nm using multiple laser excitation energies. The different Raman features have been studied in detail as a function of nanotube length and laser excitation energies. The ratio of the D-band to G-band intensities has been found to increase with decreasing average SWNT length and decreasing laser excitation energy. As the nanotubes becomes much shorter than 1/4 wavelength of light, distinct finite length effects are also observed in overtone and intermediate frequency modes between 400 and 1500cm$^{-1}$. The MIT authors acknowledge supports under the Dupont-MIT Alliance, and NSF Grant DMR 04-05538.

**16:30**

**W18 9 $(n, m)$-dependent environmental effect on photoluminescence of single-walled carbon nanotubes** YUTAKA OHNO, *Nagoya Univ., PRESTO/JST* SHINYA IWASAKI, *Nagoya Univ.* YOICHI MURAKAMI, *Univ. of Tokyo* SHIGERU KISHIMOTO, *Nagoya Univ.* SHIGERU MARUYAMA, *Univ. of Tokyo* TAKASHI MIZUTANI, *Nagoya Univ.* NAGOYA UNIV. COLLABORATION, PRESTO/JST COLLABORATION, UNIV. OF TOKYO COLLABORATION, The photoluminescence (PL) map was measured for 20 chiralities of single-walled carbon nanotubes (SWNTs) suspended in air, and the $E_{11}$ and $E_{22}$ were compared to the results reported for SDS-wrapped SWNTs [1]. The $E_{11}$ and $E_{22}$ are mostly blueshifted by a few tens of meV, except for $E_{22}$ of type-II near zigzag SWNTs which show a redshift. The energy shifts of $E_{11}$ and $E_{22}$ from those of SDS-wrapped SWNTs, $\Delta E_{11}$ and $\Delta E_{22}$, show clear dependence on the chirality, in particular on the chiral angle rather than the diameter. $E_{11}$ and $E_{22}$ show different dependences on the chiral angle between type-I and type-II SWNTs. In the case of type-I SWNTs, $\Delta E_{11}$ is lager for the larger chiral angle whereas $\Delta E_{22}$ is smaller for the larger chiral angle. In contrast, type-II SWNTs shows the opposite dependences. The difference between type-I and type-II disappears for the SWNTs with the chirality near armchair. The chiral angle dependence of environmental effect can be explained by difference in effective mass. [1] R. B. Weisman itet al. itNano Lett. **3** 1235(2003).

**16:42**

**W18 10 Raman Scattering from few-layer Graphene Films** A. GUPTA, *Dept. of Physics, The Pennsylvania State University* P. JOSHI, T. SRINIVAS, *Dept. of Electrical Engineering, The Pennsylvania State University* PETER EKLUND, *Department of Physics, The Pennsylvania State University, University Park, PA 16802 USA* Few layer-graphene sheet ($n$GL's) films, where n is the number of graphene layers, are new two-dimensional sp$^2$ carbon systems that have been shown to produce exciting Fractional Quantum Hall phenomena. We report here on the first Raman scattering (RS) results of $n$GLs. $n$GLs with lateral dimensions of $\sim$ 1-3 $\mu$m were prepared by chemical delamination of graphite flake or HOPG and then transferred from solution onto substrates (mica, pyrex,In/pyrex and Au/pyrex). RS spectra have been collected on $n$GL's with n=1, 2, 3 and compared with the graphite. Graphite exhibits two $E_{2g}$ interlayer modes at 42 cm$^{-1}$ and 1582 cm$^{-1}$. The Raman spectra of (n=1-3) $n$GLs were found to exhibit peaks at 1350 cm$^{-1}$ and 1620 cm$^{-1}$, i.e., near frequencies associated with high phonon density of states. The high frequency $E_{2g}$ band is found to split into two bands when the $n$GL is supported on metallic substrates (In,Au). In both these cases, we observe bands at 1583 cm$^{-1}$, $\sim$ 1592 cm$^{-1}$ rather than one band at 1581 cm$^{-1}$when the nGL is on insulating pyrex. The splitting of the interlayer band when on metallic substrates is identified with charge transfer between the nGL and the substrate. The phonon density of states scattering observed does not appear to be due to disorder in the basal plane.

**16:54**

**W18 11 Resonance Raman Study of Linear Carbon Chains Formed by the Heat Treatment of Double-Wall Carbon Nanotubes** C. FANTINI, *UFMG, Brazil* E. CRUZ, *IPICYT, Mexico* A. JORIO, *UFMG, Brazil* M. TERRONES, H. TERRONES, *IPICYT, Mexico* G. VAN LIER, J-C. CHARLIER, *Un. Cath. de Louvain, Belgium* M. S. DRESSELHAUS, *MIT, USA* R. SAITO, *Tohoku Un., Japan* Y. A. KIM, T. HAYASHI, M. MARAMATSU, M. ENDO, *Shinshu Un., Japan* M. A. PIMENTA, *UFMG, Brazil* The Raman spectra of carbon nanotubes exhibit weak features in the spectral range between 1600 and 2000 cm$^{-1}$ that are ascribed to a second-order Raman process. However, the observation of unusual and strong spectral features around 1850 cm$^{-1}$ have been reported recently in the Raman spectra of carbon nanotube systems, and have been ascribed to the vibration of one-dimensional chains of carbon atoms. We study the resonance behavior of the unusual Raman feature known as the coalescence-inducing mode (CIM), observed at $\sim$ 1850 cm$^{-1}$, in samples of double-wall carbon nanotubes annealed at high temperatures. Resonance Raman spectra taken with many different laser energies show that the intensity of the CIM band exhibits a maximum around 2.20 eV. By

comparing the experimental results with first principles calculations for the vibrational frequency and the energy gap, we propose that the CIM feature is associated with short carbon chains with an odd number of atoms, interconnecting the nanotube surfaces.

**17:06**

**W18 12 Raman Scattering Study of the Thermal Conversion of SWNTs into Graphitic NanoRibbons.** U.J. KIM, H.R. GUTIÉRREZ, PETER EKLUND, *Department of Physics, The Pennsylvania State University, University Park, PA 16802 USA* Thermal processing of purified bundled SWNTs in vacuum at high temperatures has been found to lead to a series of important structural transformations: SWNT coalescence (1400 [r]C-1600 [r]C), formation of MWNTs ( $\sim$ 1600-1800 [r]C) and the formation of a new filamentary allotrope, i.e., Graphitic Nanoribbons (GNRs). HRTEM indicates that GNRs are collapsed MWNTS. ARC and HiPCO SWNTs go through the first two transformations, but only ARC material transforms to GNRs. At the highest temperatures, the ARC material is almost completely transformed into GNRs. Here we present the results of Raman scattering experiments on these carbon filaments after high temperature heat treatment (HTT) for $\sim$ 6 hr. For coalesced SWNTs, the structural order in the tube walls is sufficient to observe new low frequency radial (R) Raman modes ( $\sim$ 100 $cm^{-1}$) identified with the diameter-doubled tubes. We can conclude that small diameter tubes (d$<$ 1.4 nm) are preferentially lost in the range HTT$\sim$ 1600-1800 [r]C. After HTT$\sim$ 1800 [r]C, the formation of MWNTs occurs via massive bond rearrangement of coalesced SWNTs, and this transformation is observed in Raman as a broadening of the high frequency bands and a loss of R-band intensity. A few isolated SWNTs with d $\sim$ 1.3-1.5 nm were found to survive HTT$\sim$ 2000 [r]C, but not HTT$\sim$ 2200 [r]C.

**17:18**

**W18 13 Coherent phonon oscillations from micelle-suspended single-walled carbon nanotubes** E. HAROZ, J. SHAVER, J. KONO, R. HAUGE, R. SMALLEY, *Rice Univerisity-USA* Y.S. LIM, *Rice University-USA, Konkuk University-Korea* K.J. LEE, J.H. KIM, *Chungnam National University-Korea* S. DOORN, *Los Alamos National Laboratory-USA* Time-domain oscillations were generated via degenerate pump- probe spectroscopy from individual single-walled carbon nanotubes (SWNTs) dispersed in aqueous media using ultrafast excitation pulses from a Ti:sapphire laser over the range of 710- 860 nm. Fast Fourier transform of such oscillations reveals the observation of coherent phonons (CP) corresponding to the radial breathing mode (RBMs) of 16 distinct (n,m) SWNTs. Comparison to Resonance Raman scattering (RRS) experiments indicates excellent agreement with observed RBMs, with significantly narrower linewidths seen for CP. Additionally, different RBM intensity behavior is observed within 2n+m families compared to RRS. Finally, we have directly observed two-peak maxima, separated by tens of meV, in the excitation profile for a given RBM. A possible origin of this two-peak structure is discussed. This technique represents a novel method for (n,m) characterization as well as electronic structure probing.

**SESSION W19: FOCUS SESSION: SEMICONDUCTOR SPIN TRANSPORT: NOISE/THEORY**
**Thursday Afternoon, 16 March 2006**
**316, Baltimore Convention Center at 14:30**
**Gerrit Bauer, TU Delft, presiding**

**14:30**

**W19 1 Shot noise and s-o coherent control of entangled and spin polarized electrons.** J. CARLOS EGUES, *University of Sao Paulo and University of Basel* GUIDO BURKARD, *University of Basel* DANIEL SARAGA, *University of Basel* JOHN SCHLIEMANN, *University of Regensburg and University of Basel* DANIEL LOSS, *University of Basel* We extend our previous work on shot noise for entangled and spin polarized electrons in a beam-splitter geometry with spin-orbit (s-o) interaction in the incoming leads. Besides accounting for both the Dresselhaus and the Rashba spin-orbit terms, we present general formulas for the shot noise of singlet and triplets states derived within the scattering approach. We determine the full scattering matrix of the system for the case of leads with two orbital channels coupled via a weak s-o interaction inducing channel anti-crossings. We show that this inter-band coupling gives rise to an additional modulation angle which allows for further coherent control of the electrons. We also derive explicit shot noise formulas for a variety of correlated pairs (e.g., Bell states) and lead spin polarizations. Interestingly, the singlet and each of the triplets defined along the quantization axis perpendicular to lead 1 and in the plane of the beam splitter display distinctive shot noise for injection energies near the channel anti-crossings – one can tell apart all the triplets through noise measurements. Finally, we find that backscattering within lead 1 reduces the visibility of the noise oscillations. This work was supported by NCCR Nanoscale Science, EU-Spintronics, CNPq, Swiss NSF, DARPA, ARO, and ONR (to appear in PRB).

**14:42**

**W19 2 Shot Noise of a Quantum Point Contact*** YIMING ZHANG, *Harvard University* LEONARDO DICARLO, *Harvard University* DOUGLAS McCLURE, *Harvard University* DAVID REILLY, *Harvard University* CHARLES MARCUS, *Harvard University* LOREN PFEIFFER, *Bell Laboratories* KEN WEST, *Bell Laboratories* We report detailed simultaneous measurements of shot noise and DC transport in a quantum point contact (QPC) as a function of source-drain bias, gate voltage and in-plane magnetic field. The magnetic field evolution of the 0.7 feature in both conductance and noise is clearly visible and is compared to a simple model, giving good quantitative agreement.

*We acknowledge NSF-NSEC and ARO/ARDA for partial support

**14:54**

**W19 3 Theory of spin noise spectroscopy of itinerant fermions** SIMON KOS, *University of Cambridge* ALEXANDER BALATSKY, *Los Alamos National Laboratory* SCOTT CROOKER, *Los Alamos National Laboratory* PETER LITTLEWOOD, *University of Cambridge* DWIGHT RICKEL, *Los Alamos National Laboratory* DARRYL SMITH, *Los Alamos National Laboratory* We study the noise of spin magnetization in a region within a system of fermions in different regimes of temperature (degenerate/non-degenerate) and disorder (ballistic/diffusive), with and without spin-flip processes included, and with no particle-particle interactions. We obtain a single spectral line, ana-

lyze the dependence of its width and spectral weight on the parameters of the system and the size of the region of interest, and discuss conditions for the maximal effect. We compare our results to the recent measurements of spin noise of alkali-gas vapor and of conduction electrons in a GaAs epilayer.

**15:06**
**W19 4 Spin-resolved shot noise in multichannel spin-orbit coupled quantum wires** RALITSA DRAGOMIROVA, BRANISLAV NIKOLIĆ, *University of Delaware* The characterization of spin-dependent transport via shot noise has recently attracted considerable attention in semiconductor spintronics. The key quantity that makes it possible to obtain the shot noise of both spin currents and spin-polarized charge currents is the correlation function between the spin-resolved charge currents. We extend the Landauer-Büttiker scattering formalism to obtain the spin-resolved shot noise for arbitrary polarization of the injected current and apply it to two-probe multichannel quantum wire with the Rashba spin-orbit interaction. We find that the Fano factor of the charge shot noise is non-zero even for ballistic transport and increases with the strength of the Rashba spin-orbit coupling due to enhancement of the backscattering at the lead-wire interface. In disordered quantum wires this effect enhances the Fano factor beyond the standard $F = 1/3$ shot noise suppression.

**15:18**
**W19 5 Valley-Kondo Effect in Transport Through a Silicon Quantum Dot** SHIUEYUAN SHIAU, *Department of Physics. UW, Madison* The Anderson model is applied to transport through a silicon quantum dot with infinite Coulomb interaction U with the valley degeneracy taken into account. At zero temperature, we study the conductance in the Kondo regime as a function of applied magnetic field, using the variational method developed by Gunnarsson and Schönhammer. The conductance peaks show a characteristic evolution due to the interplay of Zeeman splitting and valley splitting.

**15:30**
**W19 6 Time-dependent multiple scattering approach for a single finger-gate in a Rashba-type quantum channel.** LU-YAO WANG, *Department of Electrophysics, National Chiao-Tung University, Hsinchu 30010, Taiwan* C.S.TANG TEAM,* C.S. CHU TEAM,† We consider a Rashba-type quantum channel (RQC) consisting of one AC-biased finger-gates (FG) that orient perpendicularly and located above the RQC. Such an AC-biased FG gives rise to a local time-modulation in the Rashba coupling parameter, and generates a dc spin current (SC). A static potential is located inside or outside the FG in the RQC and the backscattering effect is studied. We use analytical time-dependent multiple scattering approach to treat the effect of the SC suppression due to a static potential in the RQC.

*Physics Division, National Center for Theoretical Science, P. O. Box 2-131, Hsinchu,30013,Taiwan
†Department of Electrophysics, National Chiao-Tung University, Hsinchu 30010, Taiwan

**15:42**
**W19 7 Spin-current detector by a periodic array of quantum dots with Rashba Hamiltonian** JUN-QIANG LU, X.-G. ZHANG, *Center for Nanophase Materials Sciences, and Computer Science and Mathematics Division, Oak Ridge National Laboratory, Oak Ridge, TN 37831* SOKRATES T. PANTELIDES, *Department of Physics and Astronomy, Vanderbilt University, Nashville, TN 37235 and Oak Ridge National Laboratory, Oak Ridge, TN 37831* Electron diffraction by a periodic array of quantum dots is studied using the Rashba Hamiltonian and a plane wave-based Green function method. A transverse charge current is found due to the asymmetric spatial diffraction of a spin-polarized electron injection. The spin-polarization of the forward electon current is maintained after passing through the array. Such an array can be used as a non-magnetic spin-current detector. Detailed results in terms of the parameters relevant to experimental design, such as the size of the quantum dots, strength of the spin-orbit coupling, are presented.

**15:54**
**W19 8 Effect of Coulomb interaction on the spin-galvanic mode in a two dimensional electron gas with Rashba spin-orbit interaction.** GERNOT GUNTHERODT, *Physikal. Institut IIA, RWTH Aachen, 52056 Aachen, Germany* YAROSLAW B. BAZALIY, STUART S. P. PARKIN, *IBM Almaden Research Center, 650 Harry Road, San Jose, CA 95120* B. V. BAZALIY, *Appl. Mathematics Inst., Natl. Academy of Science, Donetsk, Ukraine* Recently a new propagating mode of coupled charge and spin oscillations was predicted in a two dimensional electron gas with a sufficiently strong Rashba interaction. We show [cond-mat/0511534] that Coulomb interaction qualitatively modifies the spectrum and increases the characteristic wavelength of this mode by orders of magnitude, but does not suppress it. An absorption experiment that can conclusively detect the presence or absence of such a propagating mode is proposed.

**16:06**
**W19 9 Quantum coherence oscillations in InSb and InAs** J.A. PETERS, *Department of Physics, Ohio University* HONG CHEN, J.J. HEREMANS, *Department of Physics, Virginia Tech* N. GOEL, S.J. CHUNG, M.B. SANTOS, *Department of Physics and Astronomy, University of Oklahoma* W. VAN ROY, G. BORGHS, *IMEC, Leuven, Belgium* Quantum oscillation phenomena in parallel arrays of loops have been investigated in InSb/AlInSb and InAs/AlGaSb heterostructures, notable for their strong spin-orbit interaction. The arrays consist of parallel lines of hexagonal lattice cells, forming linear concatenations of loops. From the h/2e periodicity, the dominance of Altshuler-Aronov-Spivak (AAS) oscillations is deduced. Measurement of the temperature dependence of the oscillations enables the extraction of spin and phase coherence lengths in InSb and InAs. The spin coherence lengths show a weak drop with increasing temperature, akin to the mobility mean free path behavior, and consistent with a dominant Elliott-Yafet related spin relaxation mechanism in both heterostructures. The phase coherence lengths follow a power law without observed saturation at the lowest temperatures. NSF DMR-0094055 (JJH), DMR-0080054, DMR-0209371 (MBS).

**16:18**
**W19 10 Rashba spin-orbit and lateral local confinement effects in quasi-two-dimensional electronic systems** GABRIELE GIULIANI, STEFANO CHESI, *Purdue University* We consider the effects of lateral confinement on a two dimensional electron gas in the presence of different types of spin-orbit coupling as applied to the electrons and holes in *GaAs* heterostructures. Both the linear and cubic Rashba spin-orbit coupling mechanisms have been studied. We show that confinement leads to interesting spin polarization effects that can in principle be observed by transport measurements across a quantum point contact.

**16:30**
**W19 11 Response Functions and Collective Oscillations of a Two Dimensional Electron Gas in the Presence of Rashba Spin-Orbit Coupling** GEORGE SIMION, GABRIELE F. GIULIANI, *Physics Department, Purdue University* Various response functions and the spectrum of the collective excitations of a two dimensional electron liquid in the presence of Rashba type spin-orbit coupling have been studied within time dependent mean field formalism. Of particular interest are the results concerning the in-plane and out-of- plane spin susceptibility of the paramagnetic phase and the corresponding spin excitations. As an by product of this analysis we have derived an exact analytical expression for the static density response function which corrects formulas previously appeared in the literature. Approximate analytical expressions have also be derived for the low frequency, long wave length dependence of the same function.

**16:42**
**W19 12 Mean field phase diagram of a two dimensional electron liquid with Rashba spin-orbit** STEFANO CHESI, GABRIELE GIULIANI, *Purdue University* By a combination of analytic an numerical techniques we have mapped out the mean field phase diagram of a two dimensional electron liquid in the presence of Rashba or Dresselhaus spin-orbit. Although inhomogeneous solutions can be found that minimize the total energy, we have carried out a systematic study of the spatially homogeneous phases in the $(r_s, \alpha)$ diagram (with $r_s$ the density parameter and $\alpha$ the strength of the spin-orbit coupling). The scenario is intriguing for a number of broken symmetry states have been unraveled that can be characterized by suitable momentum space occupation numbers $n_{\mathbf{k}}$ and local spin quantization axes $\hat{s}_{\mathbf{k}}$. While at high densities the system is as expected paramagnetic, at lower densities (or larger $\alpha$ values) markedly different ferromagnetic phases exist with spontaneous polarization oriented perpendicular or parallel to the plane of motion that are characterized by non trivial spin textures in momentum space. Of particular interest is a phase transition between an isotropic paramagnetic state to an anisotropic ferromagnetic one that occurs in the large $\alpha$ limit. The relation between the various phase transitions and the differential instabilities signaled by the in plane and out of plane spin susceptibilities will be discussed.

**16:54**
**W19 13 Cubic Dresselhaus Spin Orbit Coupling in Small Quantum Dots*** JACOB J. KRICH, BERTRAND I. HALPERIN, *Harvard University* Due to the suppression of linear spin-orbit effects in small quantum dots in two-dimensional electron systems, the cubic Dresselhaus spin-orbit coupling can play a significant role in such phenomena as the variance of conductance through a dot. We characterize the different spin-orbit coupling terms by the strength of the anti-crossings they induce in the eigenstates of a closed quantum dot as an in-plane magnetic field is increased, and we perform numerical simulations in a chaotic billiard model to estimate the RMS anti-crossing energy. We investigate the conditions under which the cubic Dresselhaus effects may be measurable and significant for realizable dot configurations.

*This work has been supported in part by NSF grants PHY-01-17795 and DMR-02-33773 and the Fannie and John Hertz Foundation.

**17:06**
**W19 14 g-factor anisotropy in p-type GaAs/AlGaAs quantum point contacts** SUNANDA KODUVAYUR, LEONID ROKHINSON, *Purdue University* In this work we report the influence of lateral confinement on the effective Lande **g**-factor for holes in GaAs. For 2D hole gas grown along crystallographic direction other than the high symmetry [100] or [111], mixing of heavy and light hole subbands leads to anisotropic g-factor depending on the direction of the in-plane magnetic field.Further lateral confinement of the holes into 1D channel modifies g-factor depending on the strength and direction of the confining potential. We investigate **g**-factor in quantum point contacts (QPC) fabricated on 2D hole gas on $[\bar{3}11]$A GaAs by AFM lithography using the local anodic oxidation technique. Several QPCs are oriented along the major $[\bar{2}33]$ or $[\bar{1}10]$ axis. In-plane **B** is predominantly acting on the spin part of the Hamiltonian and the magnitude of the Zeeman splitting can be obtained from energy level spectroscopy combined with the critical fields at which half-integer steps in the conductance (in units of $2e^2/h$) appear. The **g**-factor is found to be strongly modified compared to the values reported for a 2D hole gas and has strong dependence on the quantized momentum normal to the current flow (number of filled energy levels in the point contact). Thus the g-factor can be modulated electrostatically, providing an extra degree of control of spintronic devices.

**17:18**
**W19 15 The effect of interactions on the geometrical structure of the Fermi surface in systems with spin-orbit interactions** VICTOR GALITSKI, *Physics Department, University of Virginia* The spectrum of many electronic systems contains band degeneracies, which can be thought of as monopoles in momentum space leading to a non-trivial topological structure of the Fermi surface. This structure is characterized by two quantities: curvature and metric, which, being gauge invariant, are in principle observable in experiment. In electronic systems with spin-orbit interactions, the Berry's curvature determines the so-called spin Hall conductivity, which may be related to observable spin accumulation near the edges. We consider Rashba, Dresselhaus, and Luttinger models and study the effect of interactions on the topology of the Fermi surface in these systems. We find that interactions renormalize the spin-orbit couplings but in certain cases do not change the Berry's phase structure. This suggests that the non-trivial geometry of the Fermi surface is a true Fermi liquid property.

## SESSION W20: FOCUS SESSION: MULTIFERROICS IV
**Thursday Afternoon, 16 March 2006**
**317, Baltimore Convention Center at 14:30**
**Sang-Wook Cheong, Rutgers University, presiding**

***Contributed Papers***

**14:30**
**W20 1 Electronic Mechanism for the Coexistence of Ferroelectricity and Ferromagnetism*** JAMES GUBERNATIS, CRISTIAN BATISTA, *Los Alamos National Laboratory* WEI-GUO YIN, *Brookhaven National Laboratory* We study the strong coupling limit of a two-band Hubbard Hamiltonian that also includes an inter-orbital on-site repulsive interaction $U_{ab}$. When the two

bands have opposite parity and are quarter filled, we prove that the ground state is simultaneously ferromagnetic and ferroelectric for infinite intra-orbital Coulomb interactions $U_{aa}$ and $U_{bb}$. We also show that this coexistence leads to a singular magnetoelectric effect.

*Work supported by the Department of Energy

**14:42**

**W20 2 ''Lorentz force'' acting on a ray of light in multiferroics** KEI SAWADA, NAOTO NAGAOSA, *CREST, Department of Applied Physics, the University of Tokyo* We theoretically propose that optical analogue of a Lorentz force acting on a ray of light is realized in multiferroic materials showing an optical magnetoelectric effect. The toroidal moment $\vec{T} = \Sigma_j \vec{r}_j \times \vec{S}_j$ plays a role of ''vector potential'' while its rotation corresponds to a ''magnetic field'' for photons. Hence the light is subject to the Lorentz force when propagating through the domain wall region of the ferromagnetic or ferroelectric order. Realistic estimate on the magnitude of this effect is given.

**14:54**

**W20 3 Enhanced optical magnetoelectric effect in a patterned polar ferrimagnet*** N. KIDA, *ERATO-JST* Y. KANEKO, *ERATO-JST* J.P. HE, *ERATO-JST* M. MATSUBARA, *CERC-AIST* H. SATO, *CERC-AIST* T. ARIMA, *ERATO-JST and Tohoku Univ.* H. AKOH, *CERC-AIST* Y. TOKURA, *ERATO-JST, CERC-AIST, and Univ. Tokyo* A simple method to dramatically enhance the optical magnetoelectric (ME) effect, i.e., nonreciprocal directional birefringence, is proposed and demonstrated for a polar ferrimagnet $GaFeO_3$ as a typical example. We patterned a simple grating with a pitch of 4 $\mu$m on a surface of $GaFeO_3$ crystal and used the diffracted light as a probe. Optical ME modulation signal for Bragg spot of the order $n = 1$ becomes gigantic in the photon energy 1–4 eV and reaches 1–2% of the bare diffracted light intensity in a magnetic field of 500 Oe. This is amplified by more than three orders of magnitude compared to that for the reflection of bulk $GaFeO_3$. Fabricating a photonic crystal will make it possible to lead a new route for the practical use of the optical ME effect.

*This work was in part supported by a Grant-In-Aid for Scientific Research from the Ministry of Education, Culture, Sports, Science and Technology (MEXT), Japan.

***Invited Papers***

**15:06**

**W20 4 Magnetoelectric effects in multiferroics.**

ALOIS LOIDL, *Center for Electronic Correlations and Magnetism, University of Augsburg*

Magneto-electric phenomena were investigated in two different multiferroic systems: The strong coupling of dielectric and magnetic properties and the simultaneous occurrence of long-range magnetic and ferroelectric order are discussed for rare earth manganites and sulfo spinels. A phase diagram of $Eu_{1-x}Y_xMnO_3$ is established, which recovers the main features of the well-known magneto-electric phase diagram for the pure rare earth manganites $RMnO_3$. Here a variety of magnetic and electric phases emerge with varying rare earth ions R. As function of temperature and external magnetic field, also Y doped $EuMnO_3$compounds undergo a sequence of different magnetic and polar phase transitions for varying effective ionic radii of the rare earth ions. Special attention is paid to the occurrence of fundamentally new hybrid spin-electromagnetic excitations, which we name electromagnons and are characterized as spin waves that can be excited by an ac electric field. These excitations are identified in $Eu_{1-x}Y_xMnO_3$with x = 0.2, in $GdMnO_3$, and in $TbMnO_3$. Specifically in $GdMnO_3$ the electromagnons can easily be suppressed by external magnetic fields and allow tuning the index of refraction by moderate fields. In the second part we discuss the simultaneous appearance of colossal magnetoresistance (CMR) and colossal magneto-capacitance (CMC) effects in chromium sulfo spinels. In $CdCr_2S_4$ ferromagnetism of localized Cr spins evolves at 85 K, while polar order is established below 130 K. The onset of ferroelectric order is neither accompanied by the occurrence of soft modes nor by structural changes which break the inversion symmetry of the high-temperature cubic phase. $HgCr_2S_4$ becomes ferroelectric close to 70 K while a complex antiferromagnetic order is found below 25 K. CMR and CMC effects are specifically strong in the mercury compound, as moderate magnetic fields of only 0.1 T induce ferromagnetism at much higher temperatures. We speculate that the occurrence of ferroelectricity in these multiferroic compounds is rather of electronic than of ionic origin.

***Contributed Papers***

**15:42**

**W20 5 A neutron scattering study on a ferrimagnetic magnetocapacitance system $Mn_3O_4$** JAE-HO CHUNG, *NIST Center for Neutron Research & University of Maryland* JUNG HWA KIM, SEUNG-HUN LEE, *University of Virginia* TAKURO KATSUFUJI, *Waseda University* The low-temperature phase of the tetragonal $Mn_3O_4$ has long been known as a ferrimagnet with the Yafet-Kittel structure. The long-range ferrimagnetic order first develops at 41.2 K, upon cooling, and a commensurate cell-doubling magnetic order occurs along the *b*-axis at 32.7 K. Recently magnetocapacitance behaviors were observed in $Mn_3O_4$. We present our high-resolution neutron scattering data to show that $Mn_3O_4$ undergoes an additional lattice distortion around 25 K. Peak broadening of selected reflections suggests that the crystal structure becomes pseudo-orthorhombic at low temperatures. Relation between the lattice distortion and magnetism will also be discussed.

**15:54**

**W20 6 Magnetodielectric consequences of phase separation in the colossal magnetoresistance manganite $Pr_{0.7}Ca_{0.3}MnO_3$** R.S. FREITAS, *Department of Physics and Materials Research Institute, Pennsylvania State Univeristy, University Park PA 16802* J.F. MITCHELL, *Materials Science Division, Argonne National Laboratory, Argonne IL 60439* P. SCHIFFER, *Department of Physics and Materials Research Institute, Pennsylvania State*

*Univeristy, University Park PA 16802* We have studied the low-frequency dielectric properties of the phase-separated manganite $Pr_{0.7}Ca_{0.3}MnO_3$ as a function of applied magnetic field in the low temperature phase-separated state. The dielectric constant is strongly field dependent and also depends on the magnetic field history of the sample. The dielectric behavior appears to be associated with the hopping of polaronic charge carriers, and we can derive the field dependent hopping energy barrier from the frequency dependence of the dielectric constant. This analysis allows us to associate the metal-insulator transition observed in this material with the field-induced suppression of the polaron activation energy. Reference: Phys. Rev. B **72**, 144429 (2005). Research was supported by the NSF and DOE.

**16:06**

**W20 7 Dielectric anomalies in $CoCr_2O_4$** G. LAWES, *Wayne State University* B. MELOT, K. PAGE, C. EDERER, *UCSB* M.A. HAYWARD, *Oxford* TH. PROFFEN, *LANL* R. SESHADRI, *UCSB* We investigate the magnetic,dielectric, and thermodynamic properties of $CoCr_2O_4$ polycrystalline samples. AC susceptibility and specific heat measurements show the existence of two distinct magnetic transitions in this material. Neutron scattering experiments confirm a ferrimagnetic ordering transition at $T_c = 95$ K and a transition to a spiral magnetic phase below $T_N$ 25 K. We observe a significant dielectric anomaly coincident with the onset to long-range spiral magnetic order, and a separate feature with significant thermal hysteresis above T=50 K. We associate this higher temperature dielectric anomaly with short-range spiral magnetic order, and discuss these results in the context of utilizing magnetodielectric couplings to capacitively probe short range magnetic structures.

**16:18**

**W20 8 Mossbauer Spectroscopy Investigation of Substituted Cobalt Ferrites ($CoM_xFe_{2-x}O_4$, where M = Mn or Cr, and x = 0.0-0.8)*** JOHN SNYDER, CHESTER LO, YEVGEN MELIKHOV, PAUL MATLAGE, *MSE Dept and CNDE, Iowa State Univ, Ames IA* KELLY KRIEBLE, *Physics Dept, Moravian College, Bethlehem PA* In order to enable applications of substituted cobalt ferrites for strain sensing, magnetostrictive actuating, and ''multiferroic'' composites, more basic knowledge is needed concerning how cation substitution affects the atomic level environments, distributions, and interactions of the cations. In this study, the local environments of the Fe atoms in two series of substituted cobalt ferrites ($CoM_xFe_{2-x}O_4$, where M = Mn or Cr, and x = 0.0-0.8) have been investigated using Mossbauer spectroscopy. Results of both series show two distinct six-line hyperfine patterns, indicating Fe in A (tetrahedral) and B (octahedral) sites. They can be identified by isomer shift and hyperfine distribution width. Both series show some similar behavior: with increasing substitution, magnetic hyperfine field decreases and hyperfine field distribution width increases for both A and B sites. B-site hyperfine fields and distribution widths are more affected than A. All of these effects are more pronounced for Cr-substitution than for Mn. Results are consistent with a model of Mn or Cr ions substituting into B-sites and displacing Co ions onto A sites. It would appear that Cr has an even stronger B-site preference than Mn, and displaces more of the Co to the A sites.

*Supported by NSF Grant No.DMR-0402716.

**16:30**

**W20 9 Preparation and properties of single phase $PbTi_{1-x}Mn_xO_3$ perovskites at high Mn concentrations.** STANISLAV STOUPIN, CARLO SEGRE, SOMA CHATTOPADHYAY, *Physics Division, Illinois Institute of Technology* Recent observation of multiferroic properties in the $PbTi_{0.5}Fe_{0.5}O_3$ perovskite material raises questions about the electronic and structural driving forces causing the coupling between ferroelectric and ferromagnetic properties. It is known that the Jahn-Teller distortion of oxygen octahedra due to d orbital occupancy inhibits formation of the ferroelectric double well potential in $ABO_3$ perovskites. Thus, the presence of a ferroelectric distortion in $d^n$ magnetic transition metal perovskite oxide is an unexpected result. We report observation of tetragonal structure (XRD) in a similar $PbTi_{1-x}Mn_xO_3$ system. The material is prepared using the sol-gel method with various Mn concentrations. In this study, we access a range of concentrations starting from a relatively high value of x=0.1 in order to introduce considerable amount of magnetic sites into the system. Reduction in the tetragonal ratio (c/a) is observed with increase in x as expected. Further characterization of the material involves magnetoelectric measurements and X-ray Absorption Spectroscopy. Preliminary results are discussed.

**16:42**

**W20 10 Colossal magnetocapacitance and scale-invariant dielectric response in mixed phase manganites** RYAN RAIRIGH, AMLAN BISWAS, ARTHUR HEBARD, *Dept. of Physics, University of Florida, Gainesville, FL 32611-8440* We are studying thin-film capacitors utilizing $(La_{0.5}Pr_{0.5})_{0.7}Ca_{0.3}MnO_3$ (LPCMO) as the base electrode, AlOx as the dielectric and Al as the counter-electrode. The LPCMO films exhibit itcolossal magnetoresistance (CMR). Likewise, the capacitance changes by three orders of magnitude in the region of the resistance drop. These itcolossal magnetocapacitance (CMC) effects are related to magnetic field induced changes in the relative extent of coexisting ferromagnetic metal and charge ordered insulating phases. The widths of the hysteresis loops, in capacitance and resistance, are about the same, but the center of the capacitance loop is shifted 20 K below the center of the resistance loop. When the LPCMO resistance is at a maximum (low capacitance) the electrode comprises filamentary conductors threading an insulating medium. In this region log-log Cole-Cole plots reveal an intrinsic dielectric response in which the data plotted as a function of frequency ($\omega$) collapse onto single straight lines, implying scale-invariance over a wide range of $\omega$, magnetic field and temperature.

**16:54**

**W20 11 Epitaxial thin films of novel multiferroic double perovskites.** A. VENIMADHAV, QI LI, *Department of Physics, Pennsylvania State University, PA16801* Recently multiferroic materials have attracted great interest. However, relatively a few pure multiferroic compounds are currently known. Here we show the exploration of design of multiferroic properties in double perovskites by combining the ferrolectrisity driven by the Bi lone pairs and selectively choosing the 3d transition metals following Goodenough-Kanamori's rules to bring in ferromagnetism. We present growth issues in stabilizing the single phase, epitaxial thin films of new double perovskite multiferroic systems such as $Bi_2NiMnO_6$, $Bi_2FeCrO_6$and $La_2NiMnO_6$by pulsed laser deposition. Targets of these compositions were synthesized by solid state method with 15% of excess Bi in the composition to compensate the volatility of Bi during the deposition. We also present the synthesis of $Bi_2FeCrO_6$by growing a superlattice structures from

individual targets of Bi $FeO_3$ and $BiCrO_3$. In the cubic double perovskites, cations show rock salt kind of ordering in the (111) direction and hence growing these films on STO (111) substrates has an advantage. We present the growth, structural and multiferroic properties in these double perovskite thin films.

**17:06**

**W20 12 First-principles exploration of multiferroic oxides with double-perovskite structure** TAMIO OGUCHI, TATSUYA SHISHIDOU, YOSHITAKA URATANI, *ADSM, Hiroshima University* Multiferroics have attracted much attention recently because of their novel properties. There are a few known as ferromagnetic and ferroelectric materials, particularly with perovskite-type crystal structure. Ferroelectrics should be insulating and likely ionic. Furthermore, it is widely recognized that covalent bonds between the cation and anion orbitals are crucial to realize atomic displacements to a noncentrosymmetric structure. As for magnetism, most of magnetic perovskite oxides usually have an antiferromagnetic order (mostly frustrating) due to a superexchange coupling. According to the Kanamori-Goodenough rule for the superexchange coupling, certain combinations of the transition-metals ions ($d^3$-$d^5$ and $d^3$-$d^8$ configurations) may possibly give a ferromagnetic coupling by the 180° superexchange mechanism. In this study, we explore possible co-existence of spontaneous electric polarization and ferromagnetic ordering from first principles, by focusing bismuth double-perovskite oxides $Bi_2BB'O_6$ ($B$,$B'$ = 3$d$ ions) as target materials. Ferromagnetic and ferrimagnetic solutions are obtained for cubic $Bi_2MnNiO_6$, $Bi_2CrFeO_6$ and $Bi_2CrCuO_6$ with nearly gapped electronic structure. Quite recently, $Bi_2MnNiO_6$ has been successfully synthesized by a high-pressure technique and revealed multiferroic properties. Possible multiferroic properties of $Bi_2MnNiO_6$ with the observed monoclinic structure are investigated in detail.

**17:18**

**W20 13 Magnetoelectric gyrator** DWIGHT VIEHLAND, JUNYI ZHAI, JIEFANG LI, *Virginia Tech* M.I. BICHURIN, *Novgorod State University, Russia* VIRGINIA TECH TEAM, NOVGOROD STATE UNIVERSITY TEAM, As well-known [1], an ideal gyrator would be an unusual device with respect to other network elements. It would have the unique properties of (i) antireciprocity, and (ii) being capable of acting like an impedance inverter. Here, for the first time, we report the design and study of such an ideal gyrator. Our ideal gyrator consists of a trilayer composite of Terfenol-D/PZT/Terfenol-D operated in a L-L mode at its electromechanical resonance (f≈ 80kHz). Measurements have shown that magnetoelectric (ME) susceptibility of our composite is comparable with its permeability and permittivity, and that the gyration coefficient achieves a value 0.9. In addition, we have observed a 180o phase-shift between an input current and an output voltage, or vice versa, and proved that our ME laminate behaves as an impedance inverter. We believe that our gyrator may enable resolutions to numerous important and complex network problems. [1] B.D.H. Tellegen, Phillips Research Reports 3, 81 (1948). The work was supported by grants from the Office of Naval Research.

**SESSION W21: LIQUID CRYSTALS III**
**Thursday Afternoon, 16 March 2006**
**318, Baltimore Convention Center at 14:30**
**P. Collings, Swarthmore College, presiding**

**14:30**

**W21 1 Dielectric Dispersion Effects in Liquid Crystals.*** OLEG LAVRENTOVICH, *Liquid Crystal Institute, Kent State University* YE YIN, MINGXIA GU, SERGIJ SHIYANOVSKII, As the switching speed in practical LC devices is pushed from the currently common 10 ms to sub-millisecond levels, it is important to take into account the effects associated with the finite rate with which the electric displacement changes in the external electric field. We discuss two important general consequences of the dielectric relaxation phenomenon: (1) Non-local time relationship between the electric displacement and the electric field [1]. In a quickly changing electric field, orientation of the liquid crystal depends not only on the instantaneous value of the electric field, but also on the previous values of the field and previous orientations of the material. (2) Dielectric heating. [1] Y. Yin, S.V. Shiyanovskii, A.B. Golovin, and O. D. Lavrentovich, itPhys. Rev. Lett. **95**, 087801 (2005) .

*Work partially supported by NSF DMR0315523

**14:42**

**W21 2 Using micro-focus synchrotron X-ray diffraction to probe textured liquid crystal samples*** RONALD PINDAK, BRANDON CHAPMAN, *Brookhaven National Lab* RUITING WANG, ISHTIAQUE SYED, GIOVANNI CARBONE, CHARLES ROSENBLATT, *Case Western Reserve Univ.* MICHI NAKATA, CHRISTOPHER JONES, NOEL CLARK, *Univ. of Colorado* SHIN-WOONG KANG, *Kent State Univ.* SATYENDRA KUMAR, *National Science Foundation* JULIE CROSS, *Argonne National Lab* 16 KeV X-rays from a bend magnet source at Sector 20 of the Advanced Photon Source were micro-focused by Kirkpatrick-Baez mirrors to a 14$\mu$m x 14$\mu$m cross-section and used in conjunction with an in-situ polarizing optical microscope to measure the diffraction from select areas in textured liquid crystal samples between thin glass plates. The technique will be described and its utility illustrated by three examples: (1) measuring the orientational deformation of smectic-A liquid crystal layers under the bend strain imposed by an AFM-scribed polymer alignment film, (2) mapping the concentration dependence of the liquid crystal phases exhibited by suspensions of short DNA oligomers of 6 to 16 base-pairs, and (3) selecting local monodomain regions from a globally unaligned conducting porphyrin-derivative sample for structural determination of its liquid crystal phases.

*supported in part by the U.S. Department of Energy under grant No. 04SCPE389

**14:54**

**W21 3 Impurity Induced Cross-over from Continuous to First-order Nematic-to-Smectic A Phase Transitions in a Liquid Crystal.** JAN THOEN, KATLEEN DENOLF, BERT VAN ROIE, CHRIST GLORIEUX, *Lab. Akoestiek en Thermische Fysica, Dept. Natuurkunde en Sterrenkunde, Katholieke Universiteit Leuven, Celestijnenlaan 200 D, B-3001 Leuven, Belgium* We used adiabatic scanning calorimetry (ASC) to study the impact of adding small amounts of cyclohexane on the N-SmA transition of the liquid crystal octylcyanobiphenyl (8CB). The transition re-

mains continuous upto a mole fraction of cyclohexane near 0.05, where at a tricritical point the transition becomes first- order with latent heats increasing with mole fraction of cyclohexane. Along the continuous part of the N-SmA transition line the effective specific heat capacity critical exponent increases from 0.31 for 8CB to 0.50 at the tricritical point. Ongoing experiments with other non-mesogenic impurities will also be reported.

**15:06**

**W21 4 Phase morphology of a disk-sphere dyad molecule.** LI CUI, JEFFREY COLLET, LEI ZHU, *Polymer Program, Institute of Materials Science and Department of Chemical Engineering, The University of Connecticut, Storrs, CT 06269-3136* A disk-sphere dyad molecule was synthesized by attaching a discotic triphenylene molecule to a spherical polyhedral oligomeric silsesquioxane (POSS) molecule via esterification reaction. The self-assembly behavior of the dyad molecule was studied by differential scanning calorimetry, polarized light microscopy, X-ray diffraction (XRD), and transmission electron microscope. Two-dimensional (2D) XRD results showed the dyad molecules self-assembled into a lamellar structure, which composed of a crystalline POSS layer and a discotic-nematic triphenylene double-layer. The POSS layer consisted four layers of ABCA-stacked spherical molecules. The liquid crystalline triphenylene molecules were parallel and staggered in the double-layer. Computer simulation of the XRD intensity confirmed the proposed structural model. Compared with that of the POSS crystal in bulk (melting point at ca 220 $^{o}$C), the melting temperature of POSS crystal was dramatically decreased to 67 $^{o}$C, possibly due to effects of the asymmetry molecular shape and plasticization of the discotic triphenylene moieties between POSS layers.

**15:18**

**W21 5 Excitation-Enhanced Optical Reorientation in Pure Liquid Crystalline Materials** THAI V. TRUONG, YUEN-RON SHEN, *Department of Physics, University of California, Berkeley* Electronic excitation with polarized light necessarily creates complementary orientational anisotropies from the excited and ground-state molecules. If the intermolecular interaction with the surrounding experienced by the excited-state molecules is different from that experienced by the ground-state molecules, a net excitation-induced orientational anisotropy will develop, enhancing the molecular reorientation provided directly by the optical field. This effect is analogous to that observed in dye-doped liquid crystals (LC) when dye molecules are excited. We report here the study of the effect in a pure isotropic LC medium. We use an optical pump-probe method to observe the excitation-induced reorientational dynamics. As the system relaxes back from picosecond pulse excitation, an increase in the orientational anisotropy of the ground-state molecules is observed, signifying the enhanced optical reorientation due to the state-dependent intermolecular interaction. The observed dynamics is well predicted by a mean-field model describing the intermolecular interaction between LC molecules. This work was supported by NSF

**15:30**

**W21 6 Effect of disorder on a nematic-smectic A phase transition*** SIMON LAROCHELLE, MEHMET RAMAZANOGLU, *Dept. of Physics, University of Toronto* ROBERT J. BIRGENEAU, *Dept. of Physics, University of Toronto and Dept. of Physics, University of California Berkeley* Using X-ray scattering, we studied the nematic to smectic A phase transition of the liquid crystal butyloxybenzilidene-octylaniline (4O.8) confined in an aerosil gel. The aerosil particles introduce quenched randomness in the system by providing pinning centers to the liquid crystal molecules. We find that the introduced disorder destroys the long range nature of the phase transition, and that the transition becomes similar to a transition in a finite-size system. Finite low temperature correlation lengths of the ordered moments are measured and the order parameter follows a power law behavior with respect to the reduced temperature in a limited temperature range. We also show evidence for a shift of the effective order parameter critical exponent $\beta$ with increasing disorder.

*Work supported by NSERC Canada and U. S. DOE

**15:42**

**W21 7 Observation of polarization current accompanying smectic A electroclinic reorientation** RENFAN SHAO, LIXING WANG, CHRISTOPHER D. JONES, DAVID A. COLEMAN, DUONG NGUYEN, MICHI NAKATA, JOSEPH E. MACLENNAN, *LCMRC and Univ of Colorado* PER RUDQUIST, *Chalmers Univ of Tech* DAVID M. WALBA, NOEL A. CLARK, *LCMRC and Univ of Colorado* We have been studying the liquid crystalline material W530, and report observations of polarization current of the field-induced molecular reorientation in the SmA phase. W530 exhibits the following phase diagram on cooling: isotropic – SmA – uncharacterized Sm'X' – metastable SmC – crystal. The temperature range of the SmA and SmX phases is $\sim$ 50[r]C, and x-ray diffraction (XRD) shows very little layer spacing change throughout the width of these two phases, while the SmC fractional layer compression is $\sim$ 5%. The SmX is nearly identical in appearance to the SmA phase under depolarized light microscopy (DPLM). However, when measuring polarization current while cooling from SmA to SmX, two polarization peaks appear throughout the range of the SmX phase. By adapting the Langevin model for deVries SmA, we are able to explain the two polarization peaks. Through a combination of DPLM cone angle and birefringence measurements, dielectric spectroscopy measurements, aligned sample and powder XRD experiments, and freely suspended film observations, we are able to show that the previously uncharacterized phase is a deVries SmA. Work supported by NSF MRSEC Grant DMR-0213918.

**15:54**

**W21 8 Defects in liquid crystal nematic shells** A. FERNANDEZ-NIEVES, A.S. UTADA, V. VITELLI, D.R. LINK, D.R. NELSON, D.A. WEITZ, *Harvard University* We generate water/liquid crystal (LC)/water double emulsions via recent micro-capillary fluidic devices [A. S. Utada, et.al. Science 308, 537 (2005)]. The resultant objects are stabilized against coalescence by using surfactants or adequate polymers; these also fix the boundary conditions for the director field n. We use 4-pentyl-4-cyanobiphenyl (5CB) and impose tangential boundary conditions at both water/LC interfaces by having polyvinyl alcohol (PVA) dispersed in the inner and outer water phases. We confirm recent predictions [D. R. Nelson, NanoLetters 2, 1125 (2002)] and find that four strength $s=+1/2$ defects are present; this is in contrast to the two $s=+1$ defect bipolar configuration observed for bulk spheres [A. Fernandez-Nieves, et.al. Phys. Rev. Lett. 92, 105503 (2004)]. However, these defects do not lie in the vertices of a tetrahedron but are pushed towards each other until certain equilibration distance is reached. In addition to the four defect shells, we observe shells with two $s=+1$ defects and even with three defects, a $s=+1$ and two $s=+1/2$. We argue these configurations arise from nematic bulk distortions that become important as the shell thickness increases. Finally, by adding a different surfactant, so-

dium dodecyl sulphate (SDS), to the outer phase, we can change the director boundary conditions at the outermost interface from parallel to homeotropic, to induce coalescing of the two pair of defects in the four defect shell configuration to yield two defect bipolar shells.

**16:06**

**W21 9 Water as a Wetting Agent for Liquid Crystal Films** ERGYS SUBASHI, RAFAEL GARCIA, *Worcester Polytechnic Institute* The dewetting of nCB liquid crystals from silicon wafer surfaces was first observed in 1999 [1] and has since grown into a subject of great fascination. The dewetting behavior occurs within a narrow coexistence region just below the nematic-to-isotropic phase transition temperature. When a wetted film is brought within this coexistence region, the film splits into two film thicknesses that are in apparent equilibrium with each other. A tentative but highly controversial explanation for this phase diagram has been proposed van Effenterre [2] in terms of mean field forces acting within the film. In our laboratory, we have undertaken a high-resolution measurement of the shape of this dewetting region for 5CB on silicon in search of evidence for the existence of fluctuation-induced forces that affect the thickness of these films. We have found, to our surprise, that ambient humidity affects the wetting behavior. Based on preliminary evidence taken thus far, water appears to act as a wetting agent that promotes the wetting of 5CB on silicon. We will present measurements showing how water affects the two-film thickness coexistence region. [1] F Vandenbrouck et al., Phys. Rev. Lett. 82, 2693 (1999). [2] D. Van Effenterre et al., Phys. Rev. Lett. 87, 125701 (2001).

**16:18**

**W21 10 Surface morphology of SiO deposited substrates and alignment of nematic LC*** LEELA JOSHI, SATYENDRA KUMAR, *Department of Physics, Kent State University, Kent, OH 44242* RICCARDO BARBERI, *Physics Department, University of Calabria, 87036 Rende (CS), Italy* Glass substrates with thin film of SiO are known to align nematic liquid crystals homogeneously for oblique deposition. X-ray reflectivity was employed to probe the surface morphology of approximately 150Å thick SiO films deposited at different landing angles. The interfacial roughness and morphological anisotropy was determined along the two orthogonal in-plane directions and the average electron density profile of the film calculated. The results show that the homogeneous and planar aligning films consists of SiO film with different roughness anisotropy and film thickness. The results will be discussed in light of previous reflectivity and AFM results on SiO [1] and other [2] surfaces. [1]. R. Barberi, Giocondo, G.V. Sayko, AK. Zvezdin, Phys. Lett. **A213**, 293 (1996). [2]. S. Kumar, J.-H. Kim, and Y. Shi, Phys. Rev. Lett. **94**, 077803 (2005).

*Supported by the National Science Foundation grant DMR-03-12792.

**16:30**

**W21 11 Crystal Nucleation behavior near gas-liquid spinodal line** LIMEI XU, *Boston University* GIANCARLO FRANZESE, *Universitat de Barcelona* SERGEY V. BULDYREV, *Yeshiva University* H. E. STANLEY, *Boston University* The complex problem of crystal nucleation is currently at stage. Using molecular dynamics simulations, we study the crystal nucleation behavior of colloids modeled by hard-core particles with narrow square well attractive potential. For this system the liquid gas critical point lies below the gas-crystal equilibrium line. We investigate how the nucleation rate depends on the pressure and density, in particular in the vicinity of the liquid-gas spinodal. We find that there is a correlation between nucleation rate and spinodal line. We interprete our results using classical nucleation theory.

**16:42**

**W21 12 Entropy driven formation of a chiral liquid crystalline phase of helical rods** ZVONIMIR DOGIC, *Rowland Institute at Harvard University* EDWARD BARRY, ZACH HENSEL, MICHAEL SHRIBAK, *Marine Biological Laboratory, Woods Hole* RUDOLF OLDENBOURG, *Marine Biological Laboratory, Woods Hole* We study the liquid crystalline phase behavior of a concentrated suspension of helical flagella isolated from Salmonella typhimurium. With increasing concentration, a suspension of helical flagella undergo an entropy driven first order phase transition to a liquid crystalline state having a novel chiral symmetry. Flagella are prepared with different polymorphic states, some of which have a pronounced helical character while others assume a rod-like shape. We show that the static phase behavior and dynamics of chiral helices are very different when compared to simpler achiral hard rods.

**16:54**

**W21 13 Dynamics of Director Fluctuations in Confined and Filled Liquid Crystals.** EDWIN ARROYO, SARMISTHA BASU, FOUAD ALIEV, *University of Puerto Rico* Dynamic light scattering was applied to study the influence of randomness as well of boundary conditions (planar-axial and homeotropic-radial) and layer thickness (at nanoscale) of 5CB and 8CB confined to random porous matrices, to cylindrical pores and filled with Aerosil particles (hydrophilic and hydrophobic) on phase transitions and relaxation of director orientational fluctuations. For confined 8CB in the nematic phase two well-defined relaxation processes were for confined liquid crystals. The first process is associated with bulk-like nematic director fluctuations. The second relaxation process (with relaxation time slower than the first one) is most likely due to the fluctuations in layers nearest the wall surface. We found that for homeotropic boundary conditions of confined liquid crystal, the pore wall-liquid crystal interactions influence on the properties of the surface layer is stronger than in the case of axial orientation, particularly, and the influence of boundary conditions on N-Sm-A phase transition in confined 8CB is stronger than on isotropic- nematic phase transition. The separation between the first and the second (slow) process is clearer for thinner layers and the amplitude of slow process is greater for thinner layers. This suggests that the slow process is surface related relaxation. This relaxation was observed in filled liquid crystals as well.

**17:06**

**W21 14 Micro-focus synhrotron X-ray diffraction study of novel mesomorphic porphyrin derivatives*** SHIN-WOONG KANG, LANFANG LI, QUAN LI, *Kent State University, Kent, OH 44242* MICHI NAKATA, *University of Colorado, Boulder, CO 80309* BRANDON CHAPMAN, RONALD PINDAK, *Brookhaven National Laboratory, Upton, NY 11973* SATYENDRA KUMAR, *National Science Foundation, 4201 Wilson Blvd., Arlington, VA 22230* The mesophase structures of three novel mesomorphic porphyrin derivatives were examined using polarized optical microscopy and microfocus synchrotron X-ray diffraction at various temperatures using a beam with a 14 $\mu$m$\times$ 14 $\mu$m cross-section at the bending magnet beamline of Sector 20 at the Advanced Photon Source. The x rays were diffracted from microscopic monodomains in thin glass cells while simultaneously

observing the optical textures. The results confirmed a hexagonal arrangement of discotic columns in the liquid crystalline phase. At a lower temperature, highly ordered plastic crystal phase was obtained. The results of the microdiffraction experiment and promising properties of these compounds as a carrier transporting material will be presented.

*Supported by the National Science Foundation grant DMR-0312793.

**17:18**
**W21 15 Stochastic Rotation Dynamics: generalizations and applications for non-ideal fluids, binary mixtures and colloids** THOMAS IHLE, *Department of Physics, North Dakota State University* ERKAN TUZEL, *School of Physics and Astronomy, University of Minnesota* DANIEL KROLL, *Department of Physics, North Dakota State University* A particle-based algorithm for the coarse-grained modeling of a fluctuating Solvent, namely Stochastic Rotation Dynamics (SRD), was recently introduced by Malevanets and Kapral[1]. This algorithm describes a fluid with an ideal gas equation of state and has been successfully applied to study polymers, colloids, and vesicles in flow. Here, we present generalizations of SRD for modeling fluids with non-trivial equations of state[2]. In particular, we show how to model a simple liquid with a non-ideal equation of state by incorporating excluded volume effects. We show the thermodynamic consistency of the model by independently measuring the pressure, density fluctuations and the speed of sound and compare with analytical results. This idea is extended to model binary mixtures with a miscibility gap; and the phase diagram of such a mixture will be presented. Furthermore, colloids are included in the SRD solvent and results for colloidal suspensions driven by external forces will be shown. [1] A. Malevanets, R. Kapral, J. Chem. Phys. 110, 8605 (1999). [2] T. Ihle, E. Tuzel, D. M. Kroll, cond-mat/0509631.

## SESSION W22: FOCUS SESSION: MAGNETIC NANOPARTICLES II
**Thursday Afternoon, 16 March 2006; 319, Baltimore Convention Center at 14:30**
**Dimitris Kechrakos, Institute for Materials Science, Greece, presiding**

***Invited Papers***

**14:30**
**W22 1 The Structure and Magnetic Properties of Nanoparticles and Their Arrays.**
JOSEPH DVORAK, *Montana State University*

The physics of magnetic nanoparticles and arrays is a very important topic of current research. Many questions remain. How does the structure of a single nanoparticle influence its magnetic properties? For instance, core/shell interactions can increase the coercivity and lead to exchange biasing, causing ferromagnetic rather than superparamagnetic behavior. At what thickness does the oxide shell begin to behave like an antiferromagnet? How do uncompensated surface spins affect the magnetic behavior? In addition, novel nanoparticle structures can lead to interesting physical behavior. In a bio-inspired approach, we are synthesizing ithighly monodisperse oxide nanoparticles inside of protein cages. For these systems, magnetocrystalline anisotropy plays an important role; the surface anisotropy term becomes large, reducing the total particle moment. However, we find that the encapsulating protein shell reduces the surface anisotropy and increases the particle moment. Furthermore, we have synthesized mixed phase gamma-$Fe_2O_3$/CoO nanoparticles with large exchange biasing. Further questions arise for nanoparticle arrays. Dipole interactions modify the collective magnetic behavior. What are the strength and orientation of these interactions, and how do they depend on particle size, spacing, itand array ordering. Recent experiments have shown the importance of array order in determining the collective magnetic properties. The physics of magnetic nanoparticles is rich and complex, and depends upon both the structure of the individual particles and their assemblies. By using synchrotron based magnetic circular dichroism, small angle X-ray scattering and neutron scattering, we have been able to quantify many aspects of both nanoparticle and array structures. A quantitative understanding of these structural relationships has led to a better understanding of their magnetic behavior.

***Contributed Papers***

**15:06**
**W22 2 Particle Size Control of Polyethylene Glycol Coated Fe Nanoparticles*** B. SRINIVASAN, M.J. BONDER, Y. ZHANG, D. GALLO, G.C. HADJIPANAYIS, *Department of Physics and Astronomy, University of Delaware, Newark, DE 19716* Recent interest in Fe nanoparticles with high magnetization is driven by their potential use in biomedical applications such as targeted drug delivery, MRI contrast enhancement and hyperthermia treatment of cancer. This study looks at the use of a polyethylene glycol (PEG) solution to mediate the particle size and therefore control the coercivity of the resulting nanoparticles. Iron nanoparticles were synthesized using an aqueous sodium borohydride reduction of ferrous chloride by a simultaneous introduction of reagents in a Y- junction. The resulting product was collected in a vessel containing a 15 mg/ml carboxyl terminated polyethylene glycol (cPEG) in ethyl alcohol solution located under the Y junction. By varying the length of tubing below the Y junction, the particle size was varied from 5-25 nm. X-ray diffraction data indicates the presence of either amorphous Fe-B or crystalline alpha Fe, depending on the molar ratio of reagents. Magnetic measurements indicate the particles are ferromagnetic with values of coercivity ranging from 200-500 Oe and a saturation magnetization in range of 70-110 emu/g. The XRD shows that the particles are not affected by the polymer coating.

*Work Supported by NSF- DMR PHYS312129

**15:18**

**W22 3 Using Single Nanoparticle Devices to Investigate Nanojunction GMR and TMR** J.J. KAVICH, R.H. KODAMA, *University of Illinois at Chicago, Chicago, IL 60607* J.W. FREELAND, *Advanced Photon Source, Argonne National Laboratory, Argonne, IL 60439* High-pressure sputtering / cluster-beam deposited single nanoparticle devices were fabricated to study giant magneto- resistance (GMR) and tunneling magneto-resistance (TMR) of nano- junctions. The junction used to investigate GMR was formed by the point contact of a nearly spherical $\sim$ 20 nm diameter ferromagnetic (FM) particle on a FM thin film deposited on a silicon substrate. The particles were covered with a thick $Al_2O_3$ dielectric layer. The tunneling device is identical, except for an additional $Al_2O_3$ tunnel barrier sandwiched between the FM particle and film. Using a focused ion beam (FIB), small apertures were milled in the dielectric layer to expose individual particles and metallic contacts were subsequently deposited. Other contacts were made directly to the underlying FM film creating a simple two- contact measurement geometry. Temperature dependent TMR and GMR are presented for isolated particles that are independent of proximity and ensemble effects. This work is supported by the ACS Petroleum Research Fund.

**15:30**

**W22 4 High Frequency Properties of Magnetodielectric Composites Consisting of Oriented Fe-based Flakes Embedded in a Polymeric Matrix*** MICHAEL GOLT, *University of Delaware* XIAOKAI ZHANG, *University of Delaware* THOMAS EKIERT, *University of Delaware* SHRIDHAR YARLAGADDA, *Center for Composite Materials* KARL UNRUH, *University of Delaware* JOHN XIAO, *University of Delaware* Magnetodielectric composites containing small ferromagnetic inclusions in a continuous dielectric matrix could be useful high frequency materials if relatively large and similar values of the permeability ($\mu$) and permittivity ($\varepsilon$) could be obtained. This potential, however, can not be fully achieved for spherical inclusions because their demagnetizing fields severely limit the effective permeability of the composite. Therefore, we have prepared and studied a series of magnetodielectric composites containing oriented Fe-based flakes. The flakes were produced by a mechanical deformation technique and were typically several 100 $\mu$m wide and several $\mu$m thick. These flakes were mixed with a styrene based liquid resin and aligned in an applied magnetic field prior to polymerizing the resin. X-ray diffraction and hysteresis loop measurements confirm a significant degree of alignment. Permeability and permittivity measurements indicate that values of $\mu$ and $\varepsilon$ in excess of 20 can be achieved in these samples with small losses when the loading fraction of the Fe flakes approaches 50%.

*This work has been supported by ARO DEPSCOR grant no. W911NF-04-1-0264

**15:42**

**W22 5 Fabrication of Ordered Mesoporous Silica with Encapsulated Iron Oxide Particles using Ferritin-Doped Block Copolymer Templates** D. HESS, J. WATKINS, *Univ. of Mass.* R. NAIK, *W-P AFB* Recently, two-dimensional arrays of iron oxide clusters were fabricated by dip-coating a silica substrate into an aqueous solution. Here we report the encapsulation of ferritin in 3D mesoporous silica structures by the replication of block copolymer templates in supercritical $CO_2$. In our approach, preparation of the highly ordered, doped template via spincasting and microphase separation and silica network formation occur in discreet steps. A solution of an amphiphilic PEO-PPO-PEO triblock copolymer (Pluronic) template, horse spleen ferritin and a low concentration of PTSA acid was prepared and spin-coated onto a Si wafer. Upon drying the block copolymer microphase separates resulting in partitioning of the acid catalyst and ferritin to the hydrophilic domain. The polymer template was then exposed to a solution of supercritical carbon dioxide and tetraethyl orthosilicate (TEOS) at 125 bar and 40$^o$C. Equilibrium limited $CO_2$ sorption in the block copolymer template resulted in modest dialation of the microphase segregated structure. Under these conditions, the precursor was readily infused into the copolymer and reacted within the hydrophilic domain containing the acid catalyst. The resultant film was calcined in air at 400$^o$C for 6 hours producing a well-ordered iron oxide-doped mesoporous silica film. TEM and XRD revealed crystalline iron oxide structures within the mesoporous silica supports. Magnetic properties were analyzed using a superconducting quantum intereference device (SQUID).

**15:54**

**W22 6 Synthesis of Barium hexaferrite nanoparticles for functional multilayers** S.L. MORROW, N.A. FREY, S. SRINATH, H. SRIKANTH, *Functional Materials Laboratory, Physics Department, University of South Florida,* Magnetic barium ferrite ($BaFe_{12}O_{19}$or BaM) nanoparticles were synthesized by a two system microemulsion process. X-ray diffraction of these nanoparticles confirmed the presence of a dominant hexagonal BaM phase. The magnetic characterization of the nanoparticles was performed using a Physical Properties Measurement System (PPMS). The M-H hysteresis of the BaM, at 5K and 300K, displays a saturation magnetization of $\sim$ 68 emu/g, 48 emu/g and large coercivities of $\sim$ 2300 Oe, 3100 Oe respectively, consistent with bulk BaM. The zero field cooled (ZFC) and field cooled (FC) curves illustrate that superparamagnetism was not present in the BaM below 300K. These particles will be used to prepare multilayers of ferroelectric and ferromagnetic films by depositing on a ferroelectric polymer (polyvinylidene fluoride) matrix using the Langmuir-Blodgett technique. The functional properties of these multilayers will be discussed. Work supported by NSF grant #CTS-0408933 and NSF Integrated Interdisciplinary Nanoscience REU DMR 0243997.

**16:06**

**W22 7 Theory of Brillouin Light Scattering from Ferromagnetic Nanospheres*** PING CHU, DOUGLAS MILLS, *University of California, Irvine* We develop the theory of Brillouin light scattering (BLS) from spin waves in ferromagnetic nanospheres, within a framework that incorporates the spatial variation of the optical fields within the sphere. Through use of our recent theory [1] of exchange dipole spin wave modes of the sphere, we develop a method which properly normalizes the eigenvectors. We then describe the BLS spectrum associated with the first few dipole/exchange spin wave modes with emphasis on their relative intensity. We also discuss the stokes/anti stokes ratio. [1] Rodrigo Arias, Ping Chu and D. L. Mills, Phys. Rev.B71, 224410 (2005).

*This research was supported by U. S. DOD Grant No.W911NF-04-1-0247.

**16:18**

**W22 8 Self Assembled $CoFe_2O_4$ Nanoparticles within Block Copolymer Films: Structural and Magnetic Properties** G.C. PAPAEFTHYMIOU, A.J. VIESCAS, *Villanova University, Villanova, PA* S.R. AHMED, P. KOFINAS, *University of Maryland, College Park, MD* Nanosize $CoFe_2O_4$ particles have been synthesized by self-assembly within diblock co-polymers, through a room-temperature templating strategy, amenable to large scale

fabrication. XRD, TEM, SQUID and Mossbauer studies are combined in order to explore the morphological, structural, micromagnetic and interfacial characteristics of this nanocomposite system. TEM micrographs indicate low polydispersity, with particle size of 9.6 nm diam. Low temperature Mossbauer studies predict average sub lattice saturation hyperfine magnetic fields H (A) =501 kOe and H [B] = 527 kOe, respectively, for the tetrahedral and octahedral iron coordination sites of the ferrite spinel structure. Superparamagnetic relaxation processes, analyzed within a cubic magnetic anisotropy model, give a magnetic anisotropy density K = $3.23x10^5 J/m^3$, while SQUID magnetometry predicts a saturation coercivity of 6.1 kOe. Deviations from bulk $CoFe_2O_4$ and unsupported $CoFe_2O_4$ nanoparticles are discussed in terms of finite-size effects and interfacial interactions.

**16:30**

**W22 9 Magnetization of iron clusters from first-principles calculations*** JAMES R. CHELIKOWSKY, *University of Texas* MURILO L. TIAGO, *University of Minnesota* SHEN LI, *Rutgers University* MANUEL M.G. ALEMANY, *Universidade de Santiago de Compostela, Spain* YUNKAI ZHOU, YOUSEF SAAD, *University of Minnesota* The magnetic moment of Fe clusters as function of number of atoms has been observed to show a slow decrease from the isolated atom value (4 Bohr magnetons) to its bulk value of 2.2 Bohr magnetons per atom. In addition, a series of peaks has been observed, for which the causes are not yet fully understood (see Billas, Chatelain, and de Heer, Science, 1994). We analyze the dependence of total magnetic moment, local magnetic moment, cohesive energy and other physical quantities in iron clusters $Fe_n$ ($1 < n < 250$), and compare these results with available experimental data. We use a real-space method, pseudopotentials and first-principles DFT to obtain the properties of the cluster in its ground state. Calculations are done using the PARSEC code ( www.ices.utexas.edu/parsec). We also discuss some of the recently developed capabilities of PARSEC.

*Supported by DOE under Grants DE-FG02-03ER25585/15491, NSF grant DMR-0551195 and NERSC

**16:42**

**W22 10 Chern-number spin Hamiltonians for magnetic nanoclusters by ab-initio methods** TOR OLOF STRANDBERG, *Kalmar/Lund University* HONGKI MIN, *University of Texas, Austin* CARLO M. CANALI, *Kalmar/Lund University* ALLAN H. MACDONALD, *University of Texas, Austin* Combining field-theory methods and ab-initio calculations, we construct an effective Hamiltonian with a single giant-spin degree of freedom, capable of describing the low-energy spin dynamics of ferromagnetic metal nanoclusters consisting of up to a few tens of atoms. In our procedure, the magnetic moment direction of the Kohn-sham SDFT wave-function is constrained by means of a penalty functional, allowing us to explore the entire parameter space of directions, and to extract the magnetic anisotropy energy and the Berry curvature functionals. The average of the Berry curvature over all magnetization directions is a Chern number, a topological invariant that can only take on values equal to multiples of half-integers, which represents the dimension of the Hilbert space of the effective spin system. The spin Hamiltonian is obtained by quantizing the classical anisotropy-energy functional, after a change of variables which yields a constant Berry curvature. We illustrate this procedure by explicitly constructing the Hamiltonian for dimers and trimers of Co and Cr, whose spin dynamics has been recently investigated experimentally by STM methods.

**16:54**

**W22 11 The coupling of magnetic and dielectric properties in magnetic nanoparticles** R. TACKETT, *Wayne State University* O. MASALA, *UCSB* B. ADHIKARY, R. NAIK, *Wayne State University* A.P. RAMIREZ, *Bell Labs* R. SESHADRI, *UCSB* G. LAWES, *Wayne State University* The low frequency dielectric properties of it$\gamma$-$Fe_2O_3$ and $MnFe_2O_4$ magnetic nanoparticles have been investigated. These samples showed frequency dependent dielectric anomalies near their respective magnetic blocking temperatures suggesting a coupling between the magnetic and dielectric properties of the systems. In addition, the samples exhibited considerable magnetocapacitance above the magnetic blocking temperature. The magnetic field induced change in the dielectric constant was shown to be proportional to the square of the magnetization, suggesting that the dielectric properties of these systems are strongly connected to the distribution of magnetic moments in the samples. The results will be discussed in the framework of a theory explaining how magnetodielectric effects can arise from magnetoresistance in a Maxwell-Wagner capacitance model.

**17:06**

**W22 12 A new magnetization-reversal strategy for Stoner particles** XIANGRONG WANG, ZHOUZHOU SUN, *The Hong Kong University of Science and Technology* A new strategy is proposed aimed at substantially reducing the minimal magnetization switching field for a Stoner particle. Unlike the normal method of applying a static magnetic field which must be larger than the magnetic anisotropy, a much weaker field, proportional to the damping constant in the weak damping regime, can be used to switch the magnetization from one state to another if the field is along the motion of the magnetization. The concept is to constantly supply energy to the particle from the time-dependent magnetic field to allow the particle to climb over the potential barrier between the initial and the target states.

**17:18**

**W22 13 Structural, Magnetic and Dynamical Properties of Dipolar Nanoparticles** PETER ENTEL, STEPHAN BUSCHMANN, ALFRED HUCHT, *Theoretische Physik, Universitt Duisburg-Essen, D-47048 Duisburg* We investigated the structural, magnetic and collective properties of dipolar nanoparticles. The dynamic of the systems is determined by differential equations for the translational and rotational degrees of freedom, which are studied using molecular dynamics. The interaction potential of the particles consists of both an anisotropic dipolar interaction and an isotropic hard-sphere potential. Dependent on the temperature and external magnetic field, the system is found to be in different states. These states can be characterized by their respective structural ordering, that is closely related to the magnetic and energetic properties of the assembly of particles. In the ground state the

particles arrange themselves in closed rings due to the anisotropic nature of the interaction. Besides this structure also the formation of metastable chains and network-like structures can be observed. Thermal excitations lead to a destabilization while the influence of an external magnetic field depends on its relative orientation with respect to the structures. In this work the phase diagrams in two and three dimensions of the various structures are determined as a function of temperature and external field.

**SESSION W23: FOCUS SESSION: MAG.THY IV / AB INITIO STUDIES**
**Thursday Afternoon, 16 March 2006; 320, Baltimore Convention Center at 14:30**
**Renat Sabiryanov, University of Nebraska, Omaha, presiding**

***Invited Papers***

**14:30**
**W23 1 Ab initio Study of Mirages and Magnetic Interactions in Quantum Corrals.**
VALERIY STEPANYUK, *Max-Planck Institute, Halle Germany*

We present the state of the art ab initio studies of mirages and magnetic interactions in quantum corrals. Our results demonstrate that quantum corrals could permit to manipulate the exchange interaction between magnetic adatoms on metal surfaces at large distances. We show that the spin-polarization of surface-state electrons can be projected to a remote location by quantum states of corrals. Our study gives a clear evidence that the 'spin-polarization transfer' takes place in a mirage experiment of Manoharan et al.,[2]. We find that the spin-polarization of surface-state electrons on transition metal surfaces[3] can be manipulated by quantum corrals. Our results reveal that an atomic motion in quantum corrals could be strongly affected by the quantum confinement of surface-state electrons. 1. V. S. Stepanyuk, L. Niebergall, W. Hergert, P. Bruno, Phys. Rev. Lett. 94, 187201 (2005). 2. H.C. Manoharan, C.P. Lutz, D.M. Eigler, Nature 403, 512 (2000). 3.L. Diekhöner, M.A. Schneider, A.N. Baranov, V.S. Stepanyuk, P. Bruno, K. Kern Phys. Rev. Lett. 90, 236801 (2003).

***Contributed Papers***

**15:06**
**W23 2 Noncollinear magnetism in antiferromagnetic manganese chalcogenides** KOHJI NAKAMURA, TORU AKIYAMA, TOMONORI ITO, *Mie University* A.J. FREEMAN*, *Northwestern University* Metastable zincblende compounds of transition-metal pnictides and chalcogenides have recently become the subject of much attention due to their unique properties exhibiting combinations of magnetism and semiconductivity. Here we investigate magnetism in the antiferromagnetic (AFM) transition-metal chalcogenides, namely MnSe and MnTe, by using the FLAPW method.[1] Assuming a collinear magnetic structure, we demonstrate that the AFM structure consisting of alternating Mn (001) spin-up and spin-down planes is favored over the ferromagnetic state, since the majority-spin *d*-bands are completely filled and so achieve the half-filling state that leads to the superexchange interaction. However, with FLAPW calculations that now treat full noncollinear magnetism,[2] we find that the lowest energy state is a noncollinear AFM structure — the so-called AFM type III structure — which relaxes frustration in the AFM Mn moment alignment on the fcc sublattice, a result that agrees with neutron experiments.[3] *Supported by NSF MRSEC through the NU MRC.

[1]Wimmer, *et al.*, PRB 24, 864(1981)
[2]Nakamura, *et al.*, PRB 65, 12402 (2002); 67, 14420 (2003)
[3]Samarth, *et al.*, PRB 44, R4701 (1991)

**15:18**
**W23 3 Embedded Clustering and Metastable Magnetism in Transition-Metal doped III-Nitrides*** CUI XIANGYUAN, *The University of Sydney* JULIA MEDVEDEVA, *University of Missouri-Rolla* ARTHUR J. FREEMAN, *Northwestern University* BERNARD DELLEY, *Paul-Scherrer-Institut* CATHERINE STAMPFL, *The University of Sydney* From extensive density-functional theory calculations [1] we find that Cr atoms in GaN prefer to form embedded clusters, occupying Ga sites [2]. Significantly, for larger than 2-Cr- atom clusters, states containing antiferromagnetic coupling with net spin in the range 0.06-1.47 $\mu_B$/Cr are favored. Similar behavior is found for Mn:GaN, and Cr:AlN and Mn:AlN. We show that various configurations may coexist leading to a strong dependence of the magnetic properties on the growth conditions. This elucidates many puzzling observations such as the 5 (20-30) times lower value of the measured magnetic moment on Cr (Mn) as compared to the theoretically predicted one for the isolated dopants. In addition to the expected ground high spin (HS) states for isolated Mn and Fe in GaN (4 $\mu_B$/Mn and 5 $\mu_B$/Fe), metastable low spin (LS) states (0 $\mu_B$/Mn and 1 $\mu_B$/Fe) are found. The transition between the HS and LS states corresponds to an intra-ionic electron transfer between the $t_2$ and $e$ orbitals, accompanied by a spin-flip process. [1] B. Delley, J. Jchem. Phys. **113**, 7756 (2000). [2] X.Y. Cui, *et al.*, Phys. Rev. Lett. Dec. 2005.

*Supported by the ARC and the NSF through the NU MRC

**15:30**
**W23 4 Optimized Effective Potential Method for Non-Collinear Magnetism** CLAUDIA AMBROSCH-DRAXL, SANGEETA SHARMA, JOHN K. DEWHURST, *University Graz* NICOLE HELBIG, STEFAN KURTH, EBERHARD K. U. GROSS, *Free University Berlin* SAM SHALLCROSS, *Linköping University* LARS NORDSTRÖM, *Uppsala University* A description of non-collinear magnetism in the framework of spin-density functional theory is presented for an exact exchange energy functional which depends explicitly on two-component spinor orbitals. The equations or the effective Kohn-Sham scalar potential and magnetic field are derived within the optimized effective potential framework. We have implemented this formalism within the full-potential linearized augmented planewave method, with an unconstrained magnetization density. Our calculations for Co and Fe

show that the overestimation of moments seen in previous work was an artifact of the decoupled equations used. We further demonstrate, with the example of a magnetically frustrated Cr monolayer, how intra-atomic non-collinearity may be underestimated by local functionals.

**15:42**

**W23 5 Spin susceptibility calculation based on the QP self-consistent GW method** TAKAO KOTANI, *ASU* MARK VAN SCHILFGAARDE, *ASU* Recently we have developed the quasiparticle self-consistent *GW* method (QPsc*GW*) based on the full-potential LMTO method. The method is designed to determine the best independent-particle picture. The most significant impact is that QPsc*GW* covers rather wide-range of materials, including semiconductor and transition metal oxides with acceptable accuracy [1,2]. In contrast to LDA+ $U$, QPsc*GW* can provide reasonable description of the $d$ band position relative to the $sp$ band without any free parameters. The $d$ band position critically affects the exchange coupling between magnetic ions. We are now developing the method to calculate the dynamic spin susceptibility based on the QPsc*GW* method. We will show results for elemental transition metals and zincblende(ZB)-type of materials including magnetic ions. We have found that the ferromagnetic phase of ZB-MnAs is stable, contrary to the LDA result. In addition, we will show analysis of the exchange-coupling between magnetic ions. [1] Mark van Schilfgaarde, Takao Kotani, and Sergey V. Faleev, cond-mat/0510408 [2] Sergey V. Faleev, Mark van Schilfgaarde, and Takao Kotani, PRL93, 126406 (2004)

**15:54**

**W23 6 A band theory for magnetic cuprates based on self-interaction free local density approximation** VINCENZO FIORENTINI, ALESSIO FILIPPETTI, *SLACS and Physics Dept., University of Cagliari* The pseudo-SIC approach is based on an approximate form of self-interaction corrected (SIC) Kohn-Sham Equations. We overview the functionalities of this method applied to cuprates, which are prototypes of difficult materials for standard local-spin density functional theories such as LSDA (or even GGA). Indeed, theories based on local exchange-correlation potentials fail to predict the correct spin-polarized ground-state solution expected for the low-magnetization state (S=1/2) of the Cu(I) ions, thus describing these systems as metallic and nonmagnetic. Here we present our results for a series of relevant cases, including CuO, $Cu_2O$, $CuGeO_3$, and $YBa_2Cu_3O_{6+x}$, showing that the pseudo-SIC is capable to correct the gross failures of LSDA, restoring the expected S=1/2 electronic ground state and an overall satisfying description of the chemistry and the electronic and magnetic properties of these systems. Furthermore, since the pseudo-SIC is designed to work for metals as well as for insulators we can approach the challenging task of studying by first-principles the insulating-metal transition in doped Mott insulators. We will consider the example of Mn-doped CuO, where Mn-doping induces a simultaneous insulating-to-metal and antiferromagnetic-to-ferromagnetic phase transition.

**16:06**

**W23 7 Interplay of Vacancy Defects and Magnetism in Carbon Structures** YIMING ZHANG, SAIKAT TALAPATRA, SWASTIK KAR, ROBERT VAJTAI, SAROJ NAYAK, PULICKEL AJAYAN, *Rensselaer Polytechnic Institute* Magnetic properties of diamond and graphite with vacancy defects have been studied using spin-polarized plane-wave basis density functional theory. Various scenarios of vacancy defects are investigated in these two allotropic configurations. The calculation shows that the vacancy defect concentration and nearby bonding structure is critical to determine the induced magnetism. The total magnetism start to decrease after vacancy accumulation reach the interacting configuration, in both diamond and graphite. We also shows that foreign species like nitrogen close to the vacancy is able to further enhance the magnetic moment in graphite.

**16:18**

**W23 8 The effect of disorder and short-range correlations on ferromagnetism in dilute magnetic semiconductors** B. MORITZ, *University North Dakota, University of Cincinnati* K. MIKELSONS, *University of Cincinnati, Oak Ridge National Lab* J. MORENO, *University of North Dakota* M. JARRELL, *University of Cincinnati* R. S. FISHMAN, *Oak Ridge National Lab* We use the Dynamical Cluster Approximation (DCA) and double exchange model, coupling spin one-half holes to magnetic impurities, to study the ferromagnetic transition in semiconductors doped with transition metal magnetic ions. Our approach includes the effect of local dynamics as well as short-range correlations between the magnetic impurities. We systematically incorporate the effect of disorder in the impurity positional configurations with a new algorithm, based on the DCA, specific to dilute systems. This new algorithm serves as a replacement for the Traveling Cluster Approximation and Coherent Potential Approximation. We focus on the appearance of the impurity band and the development of the magnetization for a range of coupling strengths and hole and impurity concentrations. In addition, we discuss the effect of impurity clustering on the hole mobility and the ferromagnetic transition temperature. We conclude that the successful design of spintronic nanostructures based on ferromagnetic semiconductors must include an understanding and careful analysis of disorder and spatial correlations.

**16:30**

**W23 9 Spatial correlations, spin-orbit coupling, and ferromagnetism in Ga(Mn)As** K. MIKELSONS, *University of Cincinnati, Oak Ridge National Lab* B. MORITZ, *University of North Dakota, University of Cincinnati* S. KANCHARLA, *Oak Ridge National Lab* J. MORENO, *University of North Dakota* R.S. FISHMAN, *Oak Ridge National Lab* M. JARRELL, *University of Cincinnati* The self-consistent Dynamical Cluster Approximation (DCA) is used to study the effect of strong spin-orbit coupling in models of GaMnAs. Both heavy and light carrier bands, degenerate at the $\Gamma$-point, are included using the spherical approximation. Local dynamics as well as short-range spatial correlations are studied using the DCA, adapted for impurity systems in the dilute limit. The critical temperature for ferromagnetism is obtained for different arrangements of magnetic impurities and a range of coupling strengths and carrier concentrations. These calculations clearly demonstrate the suppression of the ferromagnetic transition temperature when one accounts for spatial correlations between impurities and the reduction in saturation magnetization due to the strong spin-orbit coupling.

**16:42**

**W23 10 Structural, electronic and magnetic properties of Mn-doped GaAs(110) surface** ALESSANDRO STROPPA, MARIA PERESSI, *Dep. of Theoretical Physics, University of Trieste and DEMOCRITOS National Simulation Center, Trieste (Italy)* First principles total-energy pseudopotential calculations have been performed to investigate structural, electronic—including scanning tunneling microscopy (STM) images—and magnetic properties of

the (110) cross-sectional surface of Mn-doped GaAs. We have considered configurations with Mn in interstitial positions in the uppermost surface layers with Mn surrounded by As ($Int_{As}$) or Ga ($Int_{Ga}$) atoms. The presence of Mn on the GaAs(110) surface originates strong local distortion in the underlying crystal lattice, with variations of interatomic distances up to 8%. In both cases, $Int_{As}$ and $Int_{Ga}$, the surface electronic structure is half-metallic (or *nearly* half metallic) with details strongly dependent on the local Mn environment. The atoms surrounding the Mn impurity show an induced polarization resulting in a ferromagnetic Mn–As and antiferromagnetic Mn–Ga configuration respectively in the two cases. The simulation of the STM images show very different patterns of the impurity region in the two cases, suggesting that they could be easily discerned by STM analysis. We have also simulated STM images of Mn interstitials pairs on surface. The comparison of the simulated images with recent experimental cross-sectional STM images of Mn $\delta$-doped GaAs is discussed.

**16:54**
**W23 11 Structures and magnetic properties of Cr-doped GaN nanotubes** QIAN WANG, QIANG SUN, PURU JENA, *VCU* YOSHIYUKI KAWAZOE, *IMS, Japan* VCU TEAM, IMS JAPAN COLLABORATION, The electronic and magnetic properties of Cr-doped GaN nanotubes are investigated theoretically from first principles using the generalized gradient approximation (GGA) as well as LSDA+U method. We have shown that GaN single wall nanotube, which was generated from GaN wurtzite crystal undergoes large structural relaxation and resemble the structure of carbon (9,0) single wall nanotubes. In addition, it is stable at room temperature. Cr-doped GaN single wall and multiwall nanotubes are ferromagnetic with each Cr atom carrying a magnetic moment of about 2.67 it$\mu_B$. This ferromagnetic coupling is mediated by the neighboring N atoms which are weakly polarized and carry a magnetic moment of -0.18 it$\mu_B$. These results are not sensitive to the tube diameter, Cr concentration, and the level of correlation. Thus, Cr doped GaN nanotubes may be a robust system for applications in spintronics.

**17:06**
**W23 12 Ferromagnetism in Mn doped GaN Nanowires** QIANG SUN, QIAN WANG, PURU JENA, *VCU* Using density functional theory and generalized gradient approximation for exchange and correlation potential we show that the magnetic coupling of Mn atoms in the nanowires, unlike that in the thin film, is ferromagnetic in spite of the thickness of the wire and the contraction of the Mn-Mn and Mn-N bond distances. This ferromagnetic coupling, brought about due to the confinement of electrons in the radial direction and the curvature of the Mn-doped GaN nanowires' surface, is mediated by N as is evidenced from the overlap between Mn 3*d* and N 2*p* states. The Mn atoms prefer to occupy the nearest neighbor positions on the outer surface of the wire and carry a magnetic moment ranging from 0.56 to 3.5 it $\mu_B$/atom depending on the thickness of the wire. Calculations of the anisotropic energy show that the magnetic moment orients preferably along the $[10\bar{1}0]$ direction while the wire axis points along the [0001] direction. The flexibility of both controlling the magnetic coupling and the magnetic moment by choosing the dimensionality and the size of the wire may be useful in practical applications. The results are in agreement with the recent experimental data which show that Mn-doped GaN nanowire can be ferromagnetic without the presence of other defects.

**17:18**
**W23 13 First-principles calculation of Mn Atoms on the CuN/Cu(100) Surface*** CHIUNG-YUAN LIN, *IBM Almaden Research Center, San Jose, CA 95120-6099 and Stanford University Department of Applied Physics, Stanford, CA 94305-4090* BARBARA JONES, ANDREAS HEINRICH, *IBM Almaden Research Center, San Jose, CA 95120-6099* The electronic structure is calculated using GGA+U for one and two Mn atoms on a single CuN layer coated on the Cu(100) surface. This unique insulator-metal junction surface prevents the Mn spins from being screened by the conduction electrons and at the same time allows experimentalists to pass tunneling electrons through the Mn atoms to flip their spins. Our spin-density analysis shows that Mn atoms in such a surface preserve their atomic spins S=5/2. This result agrees with a recent STM measurement on such systems. Electron-density change and surface relaxation due to the Mn atoms are also analyzed.

*Partially supported by the Center for Probing the Nanoscale, An NSF Nanoscale Science and Engineering Center, http://www.stanford.edu/group/cpn/

## SESSION W24: FOCUS SESSION: LITHOGRAPHY
**Thursday Afternoon, 16 March 2006; 321, Baltimore Convention Center at 14:30**
**Ronald Jones, National Institute of Standards and Technology, presiding**

*Invited Papers*

**14:30**
**W24 1 Nanoimprint Lithography: Process Induced Stresses and Pattern Stability.** CHRISTOPHER SOLES, *NIST*

Nanoimprint lithography is emerging as an economical technique for fabricating polymeric nanostructures. Features as small as 10 nm in a hard master or mold can be faithfully replicated by imprinting this master into a polymer film. At elevated temperatures and pressures, the molten polymer fills the nanoscale cavities of the mold. When the film is cooled to the vitreous state and the mold removed, freestanding polymeric nanostructures remain. In this presentation we illustrate that the NIL process induces large degrees of residual stress into these structures. Upon heating imprinted nanostructures to just above the glass transition temperature of the polymer, a physical relaxation of the nanostructure

shape occurs. The features shrink in height and broaden in width with increased annealing time. However, this decay or slumping of the imprinted pattern is not driven by a simple viscous flow. High molecular mass polymer patterns slump faster than their low molecular mass analogs, contrary to the viscosity changes. Rather, the high viscosity resins generate greater shear stresses along the mold interfaces that lead to extensional flow of the polymer in the fill directions of the patterns. This traps residual stresses in the nanostructures when they are cooled into the glassy state. We quantify this slumping process using X-ray scattering and reflectivity techniques for a range of polymers and pattern sizes and explore potential relations with the glass transition of the polymer within the nanostructure.

**15:06**
**W24 2 Nanometer-scale control of the crystallization of oligomers and polymers.**
ALAIN M. JONAS, *Universite catholique de Louvain*

The ability to control the position and local orientation of organic crystals at the nanometer scale paves the way to the fabrication of hybrid nano-devices displaying better properties. Here, we present two ways to control the assembly of organic chain compounds into nanometric crystals of defined location or orientation. We first show how the location of crystals of model oligomers can be directed by chemical nano-templates [1]. The templates are obtained by combining electron-beam lithography with the deposition of self-assembled monolayers [2]. These surfaces can then be used to control a variety of assembly processes [3], such as the crystallization of model alkane-1-ol oligomers in solution. By using directing maps with the appropriate chemical inks, nano-squares, nano-corrals and nano-lines of organic crystals are rapidly and massively grown at pre-defined locations, at least down to 60 nm. At this scale, confinement effects mediated by van der Waals forces become prominent, providing a unique handle to design crystal growth. Then, we show how the nucleation and orientation of polymer crystals can be controlled by nano-imprint lithography [4]. The combination of confinement, and of preferential nucleation at the vertical walls of the nano-molds probably arising from partial chain orientation due to the polymer flow during embossing, results in local control over the 3D orientation of the crystals. We demonstrate that crystals may be guided through complex geometries, and investigate the case of systems where conflicting instructions are delivered to the crystallizing chains. References: [1] J. Plain et al., submitted. [2] A. Pallandre et al., Nano Letters 2004, 4, 365. [3] A. Pallandre et al., J. Am. Chem. Soc. 2005, 127, 4320; F.A. Denis et al., Small 2005, 1, 984; A. Pallandre et al., Adv. Mater., in press. [4] Zhijun Hu et al., Nano Letters 2005, 5, 1738.

***Contributed Papers***

**15:42**
**W24 3 UV Polarizer Fabricated by Diblock Copolymer Lithography** KOJI ASAKAWA, VINCENT PELLETIER, MINGSHAW WU, DOUGLAS H. ADAMSON, RICHARD A. REGISTER, PAUL M. CHAIKIN, *Princeton University* Transmission UV polarizers are desired for next-generation semiconductor device fabrication using ArF or $F_2$ excimer laser lithography. Controlling polarization is essential especially for high numerical aperture (NA) immersion lithography processes. The polarizer requirements are thickness less than 1 mm and low absorption of the light used for the exposure. A wire grid polarizer is ideal for this purpose but it requires wires with a pitch less than quarter of wavelength of the light. A cylinder-forming polystyrene-polyhexylmethacrylate diblock copolymer (PS-PHMA, 21-64 kg/mol) was used as a mask for fabrication because its cylinders macroscopically align by simple application of shear stress, and the PHMA domains etch faster than PS by reactive-ion etching (RIE), providing sufficient contrast for pattern transfer. The diblock was spin-coated on a UV transparent fused silica substrate and shear-aligned. The stripe pattern was transferred by RIE onto the substrate by a multilayer technique to enhance the pattern height, then a metal was deposited by evaporation. Finally, the remaining polymer was lifted off to complete the wire grid, having a 33nm pitch (16.5nm line and space). The UV light polarization characteristics of these grids will be presented.

**15:54**
**W24 4 Simple Analytic Model for Nanowire Array Polarizers** VINCENT PELLETIER, KOJI ASAKAWA, MINGSHAW WU, RICHARD REGISTER, PAUL CHAIKIN, *Princeton University* Cylinder-forming diblock copolymers can be used to pattern nanowire arrays on a transparent substrate to be used as a polarizer, as described by Koji Asakawa in a complementary talk at this meeting. With a 33nm period, these wire arrays can polarize UV radiation, which is of great interest in lithography, astronomy and other areas. One can gain an analytical understanding of such an array made of non-perfectly conducting material of finite thickness using a model with an appropriately averaged complex dielectric function in an infinite wavelength approximation. This analysis predicts that the grid can go from an E-polarizer to an H-polarizer as the wavelength decreases below a cross-over wavelength, and experimental data confirm this cross-over. The overall response of the polarizing grid depends primarily on the plasma frequency of the metal used and the volume fraction of the nanowires, as well as the grid thickness. A numerical approach is also used to confirm the analytical model and assess departure from infinite wavelength effects. For our array dimensions, the polarization is only slightly different from this approximation for wavelengths down to 150nm.

**16:06**
**W24 5 Robust Nanopatterns from Self-Assembly of a Diblock Copolymer and an Inorganic Precursor** HO-CHEOL KIM, LINNEA SUNDSTROM, LESLIE KRUPP, EUGENE DELENIA, CHARLES RETTNER, MARTHA SANCHEZ, MARK HART, YING ZHANG, *IBM Watson Research Center* Nanoscopic patterns from self-assembled block copolymer thin films have been recognized as a promising route to sub-lithographic patterns on substrates. Line patterns from lamellar phase of block copolymers are particularly attractive as they can be used as an etch mask for transferring patterns into substrates. A few organic block copolymers have been studied for generating line patterns by controlling the orientation of lamellar microdomains. The organic nature of the block copolymers, however, often gives poor thermal stability and etching contrast, which limits potential applications. Indeed robust nanostructures of sub-lithographic length scales are highly desirable to comply with common nanofabrica-

tion processes. Here we report a simple method to create robust nanoscopic line patterns on surfaces from self-assembly of mixtures of a diblock copolymer and an inorganic precursor. The organic diblock copolymer directs the structure of the inorganic precursor and can be removed by thermal treatment. By tuning the interfacial energy at two interfaces, normally oriented lamellar patterns of approximately 20nm half-pitch and 40nm thick were obtained. Results on transferring patterns to substrate will be reported as well.

**16:18**

**W24 6 Fabrication of inorganic photonic crystals from interference lithography** JUN HYUK MOON, SHU YANG, *Department of Materials Science and Engineering, University of Pennsylvania, Philadelphia, Pennsylvania 19104* We have fabricated 3D FCC-like microstructure using multi-beam interference pattern. This polymeric structure was used as a sacrificial template. Silica was deposited into the pores by alternating exposure to water and silicon tetrachloride vapors under atmospheric pressure and at room temperature. This inorganic structure can provide a platform for the deposition of high refractive index materials such as silicon, germanium, and titania. We investigate the photonic bandgap property of this structure as a function of refractive index as well as filling ratio. Using a two-parameter level-set approach, we find that the FCC-like structure has multiple complete photonic bandgaps at 2-3 and 7-8 bands, respectively, while the bandgap width is sensitive to the morphology of coated-structure. Our calculation results suggest that the complete-filled structure possessed a wider photonic bandgap between 2 and 3 bands than the incompletely-coated core-shell structure.

**16:30**

**W24 7 Effects on Low Voltage Electron Beam Lithography** MEHDI BOLORIZADEH, *EM Facility, University of Tennessee* DAVID C. JOY, *Oak Ridge National Laboratory* To examine the practical limits and problems of low voltage operation we have studied e-beam lithography in the low (few keV) to ultra-low ( $<$ 500eV) energy range, employing commonly used resists such as PMMA and compared the results to those from conventional high voltage processing. We have directly imaged, exposed and developed resist profiles as well as deposited metal after liftoff, using scanning electron microscopy, and compared to our advanced Monte Carlo simulations which incorporate elastic, inelastic, fast secondary electrons, and plasmon contributions. The results show that the exposed profiles and resolutions experimentally achieved at low energy can only be matched by simulations which include a significant FSE and plasmon contributions to the energy PSF. With an optimized resist thickness proximity effects are greatly reduced and process latitude is improved.

**16:42**

**W24 8 Hierarchical Organization of Nanoparticle Composites through Nano-Imprinting** AZAR ALIZADEH, CHRIS KEIMEL, KENNETH CONWAY, ANDREA PETERS, *GE Global Research, Niskayuna, NY 12309* Formation of highly ordered and morphologically controlled nanoparticle/polymeric assemblies is highly desirable in a variety of applications including optoelectronics, sensing, photonics and catalysis. Structure-guiding polymer matrices, such as block copolymers, have demonstrated to be an effective means for controlling the composite morphology as well as localizing particles in nanoscale domains. Yet, fabrication of polymer/nanoparticle composites with precise control over final morphology and particle location is still a major challenge. In this paper, we will show the use of nano-imprint lithography to pattern polystyrene/gold composites at different length scales (20 nm to 1micron). Imprint lithography (the technique of physically pressing and deforming a polymer layer for patterning purposes) is a low cost and high throughput alternative to conventional patterning. PS coated gold nanoparticles were synthesized following Brust's method and subsequently dispersed in PS matrices of varying molecular weights. Nano- imprinting was conducted under different temperature and pressure conditions. TEM, SEM, AFM and UV-Vis techniques were used to characterize these composites.

**16:54**

**W24 9 Mesoscale Simulation of the Lithography Process*** GRANT WILLSON, *The University of Texas* GERARD SCHMID, *Molecular Imprints, Inc Austin, Texas* JASON MEIRING, *The University of Texas* Process simulation is an important tool for the semiconductor industry. Optimization of the microlithography process is extremely expensive since exposure tools that cost in excess of 20 million dollars, which could be dedicated to manufacturing, must be used in the optimization experiments. There exist several commercial simulation packages that work efficiently and accurately all of which are based on parameterized continuum models. Continuing improvements in materials and equipment for microlithography have now provided the ability to print circuit elements with minimum dimensions approaching the size of the molecules that comprise the photoresist. As a result, stochastic and molecular scale effects such as line edge roughness have become an increasing concern and may limit continued progress in this industry. These effects can not be captured by continuum models. Hence, we have worked to develop a mesoscale simulation of the process. The simulator is based upon with discretization of the photoresist film into cells on a three dimensional lattice and a Monte Carlo approach. The entire process has now been simulated in this way. New models for reactive transport, polymer dissolution, etc. have been incorporated in this simulator. Progress will be reported.

*Semiconductor Research Corporation

**17:06**

**W24 10 New Directions in 3-D Multiphoton Lithography.** JOHN FOURKAS, CHRISTOPHER LAFRATTA, *University of Maryland* RICHARD FARRER, *Pine Manor College* LINJIE LI, *University of Maryland* MICHAEL NAUGHTON, *Boston College* Multiphoton absorption polymerization (MAP) is a promising technique for the lithographic fabrication of 3-D microdevices. However, this technique also has two major shortcomings that have so far precluded its use in the mass production of devices. First, MAP is an inherently serial technique, and structures must be created on a voxel-by-voxel basis. Second, the fabrication of many desirable 3-D devices requires incorporation of materials other than polymers. We will discuss our recent progress in attacking both of these problems. We have developed soft-lithographic techniques that allow for the creation of complex 3-D structures that can include closed loops based on master structures created using MAP. We have also developed a technique that allows for the selective deposition of materials that include metals, metal oxides, and biomolecules on desired regions of 3-D structures fabricated with MAP. We demonstrate the use of the latter technique in the creation of functional microinductors.

**17:18**
**W24 11 High efficient LEDs having columnar structure surface fabricated by block copolymer lithography** AKIRA FUJIMOTO, KOJI ASAKAWA, *Corporate Research and Development Center, Toshiba Corporation* Recently, the internal quantum efficiency of LEDs has improved, but the external efficiency remains low due to the high refractive index of semiconductors. To extract more light, a columnar structure with sub-micron period was fabricated on the LED surface by block copolymer lithography. Since the desired pattern is relatively larger than the block copolymer microdomains, a super-high molecular weight block copolymer was used. The polystyrene (PS) - polymethyl methacrylate (PMMA) diblock copolymer was used in this study since the PMMA has a much faster etch rate than the PS by reactive-ion etching (RIE). The PMMA was removed by RIE, and the gallium phosphide (GaP) substrate was etched by chlorine-based inductively coupled plasma RIE using the remaining PS dots as a mask. The optical extraction efficiency of the patterned substrates improved 2.6 times compared to unprocessed flat GaP substrates; the pillars' height was 450 nm, diameter was 100 nm, and pitch was 150 nm. We also prototyped a real LED and increased light emission volume 1.8 times compared with conventional LED at the same energy consumption.

**SESSION W25: GELS AND NETWORKS**
**Thursday Afternoon, 16 March 2006**
**322, Baltimore Convention Center at 14:30**
**Vijay Tirumala, National Institute of Standards and Technology, presiding**

**14:30**
**W25 1 Tunable and Reversible Swelling of a p(tBA)-*b*-p(HEMA-itco-DMAEMA) Block Copolymer** KYLE GUICE, YUEH-LIN LOO, *University of Texas at Austin* Hydroxyethyl methacrylate (HEMA) and dimethylaminoethyl methacrylate (DMAEMA) have been investigated as precursor materials for pH-responsive hydrogels. DMAEMA in these hydrogel systems allows for pH-tunability, as it is reversibly protonated below its pKa (7.5). In this work, we present the design of a nano-structured hydrogel diblock copolymer whose major block consists of a statistical copolymer of p(HEMA-itco-DMAEMA) (30.5 kg/mol) polymerized at the azeotropic composition (71 mol% HEMA), with a poly(tert-butyl acrylate), p(tBA), (12.1 kg/mol) minor block. The resulting diblock copolymer is narrow in molecular weight distribution (PDI = 1.24) and spontaneously self-assembles to form hexagonally-packed p(tBA) cylinders (R = 9.5 nm) within a p(HEMA-itco-DMAEMA) matrix in the solid state. When swollen in an aqueous medium, hydrophobic p(tBA) cylinders serve as physical cross-links. We monitor the extents of swelling by quantifying changes in the characteristic (10) spacing of the hexagonal lattice by SAXS. Swelling is tunable and reversible with changes in pH; we observe 35% and 21% swelling relative to the dry state at pH 5 and 8.5, respectively.

**14:42**
**W25 2 Highly Responsive Self-Assembled Gels from Triblock Copolymers in Liquid Crystal Solvent** NEAL SCRUGGS, *California Institute of Technology* RAFAEL VERDUZCO, *California Institute of Technology* JULIA KORNFIELD, *California Institute of Technology* Triblock copolymers having random coil endblocks and a side-group liquid crystalline polymer (SGLCP) midblock self-assemble in small-molecule liquid crystal (LC) solvent to form highly responsive gels. In these block copolymers, the LC solvent switches from being strongly selective toward the SGLCP block below its isotropic-nematic transition ($T < T_{NI}$) to being a good solvent for both blocks in the isotropic phase. In the nematic phase, the LC solvent is a poor solvent for the polystyrene (PS) endblocks, driving them to physically associate to form the network crosslinks. In the isotropic phase, at dilute polymer concentrations, the PS endblocks are solubilized to yield a solution of free polymer chains. Synergistic coupling between polymer and solvent results in a gel with novel properties; the orientational order of the nematic LC solvent imparts electo-optic and mechano-optic properties that are forbidden by symmetry in isotropic gels, and the polymer network provides memory via long-time relaxation processes that do not exist in the bulk LC. Gels can be aligned into a single-crystal monodomain by applied shear, electric fields, magnetic fields, or surface effects, and the alignment state is preserved by the network's elastic restoring force. Insights into the structure and dynamics of the gels are gained by rheometry, small-angle neutron scattering, and electro-optical switching experiments.

**14:54**
**W25 3 Nanoparticle-reinforced associative PLA-PEO-PLA hydrogels** SARVESH AGRAWAL, NAOMI SANABRIA-DELONG, SURITA BHATIA, GREGORY TEW, *University of Massachusetts Amherst* Hydrogels of poly(lactide)-poly (ethylene glycol)-poly (lactide) have potential applications in drug delivery and tissue engineering. Control over the structure and rheology of the gels is of fundamental importance for the use of this polymer in medical applications. We have performed a complete rheological and structural characterization of these hydrogels using dynamic mechanical rheology, SANS, and USAXS. These polymers form very stiff hydrogels and the structure and properties of these materials can be substantially modified by varying the crystallinity or degree of polymerization (DP) of the hydrophobic PLA block. We have also created reinforced hydrogels with enhanced mechanical properties by addition of laponite nanoparticles. Our recent studies show that the elasticity of the PLA-PEO-PLA hydrogels can be enhanced by orders of magnitude by addition of small amounts of laponite particles to the hydrogels. It is expected that the triblock copolymer micelles adsorb on the surface of the laponite particles to form additional junctions in the hydrogels leading to enhancement in their elasticity. We verify this hypothesis using DLS and SANS techniques.

**15:06**
**W25 4 Controlling the Self-Assembly of ABCBA Pentablock Copolymer Gels in Water Solution by the Hydrophobic Effect*** JOSHUA ANDERSON, ALEX TRAVESSET, *Iowa State University* We characterize the phases of a system of non-ionic pentablock copolymers with an ABCBA structure in water solution, where the A and C blocks are hydrophobic and the B blocks are hydrophilic. Coarse-grained simulations are performed using molecular dynamics with the solvent modeled implicitly, and the interaction potential includes a parameter that controls the quality

of the solvent. In a good solvent, spherical micelles form and assemble into a swollen gel. We examine the aggregation number, gyration radii, micelle superstructures and percolation at various concentrations for this phase. As the B blocks become less hydrophilic, which occurs for increasing temperature, the micelles move close to one another and expel water. There is a gradual phase transition from spherical micelles to cylindrical worm-like micelles. We model the further expelling of water by increasing the concentration of polymers in the simulation and find that a lamellar phase forms. We compare our simulations with experimental results on recently synthesized modified Pluronic systems.

*Work funded by the Department of Energy through the Ames Laboratory under contract W-7405-ENG-82.

**15:18**

**W25 5 PEO Hydrogels Prepared by End-linking with PAMAM Dendrimers** BURCU UNAL, RONALD C. HEDDEN, End-linking is a preferred synthetic technique for preparing polymer networks and gels for fundamental structure/property studies. End-functionalized telechelic linear polymers are joined to a multifunctional crosslinker to form a network in which the molar mass of the polymer chains between chemical crosslink points is known. Although end-linked elastomers prepared in bulk have been well-studied over the preceding decade, much remains to be learned about how the presence of a good solvent affects the equilibrium swelling and modulus of end-linked gels. We prepared well-defined hydrogels in a good solvent (water) by linking epoxide end-functionalized, linear poly(ethylene oxide) (PEO) to the amine endgroups of poly(amidoamine) (PAMAM) dendrimers of generations 0, 2, and 4. Dendrimers can serve as well-defined macromolecular crosslink junctions because they can have nearly monodisperse numbers of reactive endgroups. We have characterized how reaction conditions such as junction functionality, polymer concentration at preparation, ratio of crosslinker endgroups to precursor endgroups, and precursor molar mass affect gelation and equilibrium swelling. We will discuss the somewhat surprising observation of ''superabsorbent'' behavior in selected PAMAM-PEO gels.

**15:30**

**W25 6 Probe diffusion in polymer solutions and hydrogels using fluorescence correlation spectroscopy** ARIEL MICHELMAN-RIBEIRO, *NIH / Boston University* HACENE BOUKARI, *NIH* FERENC HORKAY, *NIH* RALPH NOSSAL, *NIH* We apply fluorescence correlation spectroscopy (FCS) to measure the diffusion of small fluorescent probes (TAMRA, Mw = 430 Da; dextran, Mw = 10 kDa) in poly(vinyl alcohol) (PVA) solutions and hydrogels. PVA is a linear, neutral, biocompatible polymer, whose hydrogels have many biotechnology applications, such as drug-delivery devices and tissue scaffolds. The FCS measurements indicate that the probe diffusion decreases when the polymer solution is cross-linked. Further, the more the polymer chains are cross-linked, the slower the particles diffuse. These results suggest that the cross-link density, which is often ignored in the analysis of probe diffusion data in gels, must be taken into account. Remarkably, we find that the apparent diffusion time and the elastic modulus of the gels show a linear correlation.

**15:42**

**W25 7 Large-strain deformation and fracture of tough hydrogels** REBECCA WEBBER, GUILLAUME MIQUELARD, COSTANTINO CRETON, *ESPCI* JIAN PING GONG, *Hokkaido University* Highly-swollen, chemically-crosslinked hydrogels generally behave in a very brittle manner, fracturing suddenly after a small amount of reversible deformation. Because of their importance as biomaterials, it is useful to control and augment the resistance to fracture of these materials. Tougher, stronger hydrogels are emerging, and it is important to understand the structural origins of strength in these relatively robust, highly-swollen, polymer systems. We have investigated the rheological, mechanical and fracture properties of tough hydrogels, using novel testing techniques and focusing on the high-strain compression and tension behavior. Results from large-strain and fracture experiments were correlated to the chemical structure of the hydrogels. Because we believe that the mechanical properties of these tough hydrogels are due to the presence of dissipative mechanisms at the molecular level, we have explored several methods of synthesis to create these materials.

**15:54**

**W25 8 Rheological behavior of Slide Ring Gels.** VIVEK SHARMA, JONG SEUNG PARK, JUNG O. PARK, *School of Polymer, Textile and Fiber Engineering* MOHAN SRINIVASARAO, *School of Polymer, Textile and Fiber Engineering and School of Chemistry and Biochemistry, Georgia Institute of Technology, Atlanta, GA* Slide ring gels were synthesized by chemically crosslinking, sparsely populated $\alpha$-cyclodextrin ($\alpha$-CD) present on the polyrotaxanes consisting of $\alpha$-CD and polyethylene glycol (PEG). [1] Unlike physically or chemically crosslinked gels, slide ring gels are topological gels where crosslinks can slide along the chain. [2] We investigate the rheological behavior of these gels swollen in water and compare their viscoelastic properties to those of physical and chemical gels. We also study the equilibrium swelling behavior of these gels. [1] Okumura and Ito, Adv. Mater. 2001, 13, 485 [2] C. Zhao et al, J. Phys. Cond. Mat. 2005, 17, S2841

**16:06**

**W25 9 Mechanical and swelling properties of PDMS interpenetrating polymer networks** CLAUDE COHEN, SEONG HYUN YOO, *Cornell University* Poly(dimethylsiloxane) (PDMS) interpenetrating networks (IPNs) of a large and a small molar mass PDMS were prepared. Six series of IPNs were obtained by first tetra-functionally end-linking long vinyl-terminated PDMS neat or in a 50 per cent solution with unreactive PDMS chains. These networks were then dried and swollen with short reactive telechelic PDMS that were subsequently end-linked. We found that the correlation between modulus (E) and equilibrium swelling (Q) in toluene of the PDMS IPNs obeys a scaling relation identical to that of normal uni-modal PDMS networks. The results of the toughness of the networks represented by the energy required to rupture them were analyzed in terms of a recent model by Okumura (Europhysics Letters 67(3), 470, 2004). A modified version of this model that assumes each component of the double network to be subjected to an equal stress gives a good representation of the data.

**16:18**

**W25 10 Generation of Oriented Buckling Patterns by Modulation of Local Elastic Moduli** EDWIN CHAN, ALFRED CROSBY, *University of Massachusetts* Wrinkling patterns based on elastic instabilities are interesting due to the spontaneous formation of relief structures that consists of a dominant periodicity. While a wide variety of soft materials has been utilized to generate surface buckling patterns, alignment of these structures has only been demonstrated previously through pre-defined topographic patterns. In this contribution, we introduce a new methodology to producing aligned, or patterned, surface wrinkles through the manipulation of the local stress distributions. We define the specific regions of local differences in the elastic moduli of a poly(dimethyl siloxane) (PDMS) elastomer by selective oxidation of the PDMS surface into a silicate thin film. Subsequent swelling with a photopolymerizable monomer provides the buckling stress necessary for the formation of aligned surface wrinkles. We show that geometric confinement of the oxidized regions coupled with an osmotic stress controls the formation and orientation of the wrinkling structures.

**16:30**

**W25 11 Melting Point Depression of Small Molecules in Crosslinked and Uncross-linked Polyisoprene: Deviations from Flory-Huggins Theory*** QIAN QIN, GREGORY MCKENNA, *Texas Tech University* Thermoporosimetry (TPY) is becoming increasingly used to study nano-scale heterogeneity in polymers. The starting point for TPY is the Gibbs-Thomson (GT) relation between melting point and inverse crystal size. In the case of polymers, the Flory-Huggins (FH) model predicts that there is a depression of melting point due to the mixing of the polymer and the solvent molecules, and this needs to be taken into account. The first step in analysis of heterogeneity size using TPY and the GT equation requires that there be quantitative agreement between FH and the melting points in the uncross-linked rubber. We find that both benzene and hexadecane exhibit excessive melting point depressions in uncross-linked polyisoprene. This may imply that the uncross-linked polymer is divided into 'nanoheterogeneities.' We further find that the heat of fusion decreases as polymer concentration increases for the benzene, but not for the hexadecane. To our knowledge this is the first systematic investigation of the validity of melting of small organics in un-cross-linked polymers using the FH expressions.

*Thanks to NSF under grant # DMR-0304640 for support of this project.

**16:42**

**W25 12 Elastic Fluctuations and Rubber Elasticity** XIANGJUN XING, *Syracuse University* PAUL GOLDBART, *University of Illinois* LEO RRADZIHOVSKY, *University of Colorado* A coarse-grained phenomenological model is constructed to describe both phonon fluctuations and elastic heterogeneities in rubbery materials. It is a nonlocal, spatially heterogeneous generalization of the classical model of rubber elasticity, and with a tunable repulsion interaction. This model can also be derived from the Vulcanization theory. The residual stress and the non-affine deformation field, as well as their correlations, are calculated perturbatively, to the leading order of quenched randomness. It is explicitly shown that the interplay between the repulsive interaction and quenched randomness induces non- affine deformation. The spatial correlations of the non- affine deformation field and residual stress exhibit power-law scaling, with no characteristic length scale. We also calculate the contributions to the elastic free energy from both thermal and quenched fluctuations for arbitrary deformation. We find that they naturally explain the universal features in the Mooney-Rivlin plot of the stress-strain curve for rubbery materials. The (disorder averaged) thermal fluctuation of monomers is shown to depend on deformation, and becomes anisotropic upon shear deformation, as long as the repulsive interaction is finite.

**16:54**

**W25 13 Developing a lattice spring model to simulate the behavior of polymer gels** VICTOR YASHIN, ANNA BALAZS, *Department of Chemical Engineering, University of Pittsburgh, Pittsburgh, PA* A basic feature of responsive polymer gels is an inherent coupling of multiple physicochemical processes with a finite deformation of the material. We have developed a new, computationally efficient approach - the gel lattice spring model (gLSM) - which allows us to model responsive gels that undergo relatively large deformations in 2D. We start by writing an equation for the energy of the deformed gel in terms of the invariants of the strain tensor. We introduce the representative, rectangular-shaped unit element of the system, obtain an approximation of the total gel energy as a function of the coordinates (nodes) of this element, and derive the equations for the forces acting on the nodes. In accordance with the two-fluid model of gel dynamics, we assume a purely relaxational dynamics by taking the velocity of a node to be proportional to the force acting on that site. Using this gLSM, we simulate the structural evolution of a swelling gel in 2D, and the propagation of the swelling-deswelling waves through a rectangular chemo-responsive gel undergoing the Belousov-Zhabotinsky reaction.

**17:06**

**W25 14 MD simulations of chemically reacting networks: analysis of permanent set** DANA ROTTACH, *University of New Mexico* JOHN CURRO, JOANNE BUDZIEN, GARY GREST, AIDAN THOMPSON, *Sandia National Laboratories* The Independent Network Model (INM) has proven to be a useful tool for understanding the development of permanent set in strained elastomers. Our previous work showed the applicability of the INM to our simulations of polymer systems crosslinking in strained states. This study looks at the INM applied to theoretical models incorporating entanglement effects, including Flory's constrained junction model and more recent tube models. The effect of entanglements has been treated as a separate network formed at gelation, with additional curing treated as traditional phantom contributions. Theoretical predictions are compared with large-scale molecular dynamics simulations.

**17:18**

**W25 15 A Gaussian Slip-Link Model for Polymer Single and Double Networks** JAY D. SCHIEBER, *Professor* MAHNAZ ESKANDARI, *Ph.D. student* HAMID ARASTOOPOUR, *Professor* In this study, we developed Schieber's slip-link model for lightly cross-linked polymers assuming the equilibration of deformed Gaussian chains. Our simulation consists of two steps: preparation and deformation. In the preparation step, cross-links and slip-links are assumed to be distributed randomly along the chain, but with independent statistical parameters: the average number of Kuhn steps between entanglements, $N_e$, and the average number of Kuhn steps between cross-links, $N_c$. In the second step, the cross-links and slip-links are deformed affinely, but since the chain can slide through the slip-links, its deformation is non-affine. The

stress tensor can be determined as a function of deformation using Brownian dynamics as a sort of Monte Carlo algorithm. The Mooney plot of our simulation result has good agreement with most experimental data for uniaxial elongation deformation for cross-linked NR, PDMS, and PBd. The model is used to predict values for the Mooney plot parameters ($C_1$ and $C_2$) as a function of $N_e$ and the $N_c/N_e$ ratio. The $C_2/C_1$ ratio is found to be strongly dependent on $N_c/N_e$, but weakly dependent on $N_e$. This observation provides a new way of predicting the cross-link density and separating it from the entanglement density and for systems of known $N_e$ and $N_c$, the model requires no adjustable parameters. We are also developing our model for double network polymers in order to demonstrate different applications for the model.

**SESSION W26: FOCUS SESSION: BIOLOGICAL PHOTOPHYSICS**
**Thursday Afternoon, 16 March 2006; 323, Baltimore Convention Center at 14:30**
**J. Timothy Sage, Northeastern University, presiding**

*Invited Papers*

**14:30**
**W26 1 Direct Observation of Thymine Dimer Repair in DNA by Photolyase.**
DONGPING ZHONG, *Ohio State University*

Departments of Physics, Chemistry, and Biochemistry, Programs of Biophysics, Chemical Physics, and Biochemistry, The Ohio State University, Columbus, 191 West Woodruff Avenue, OH 43210. Photolyase uses light energy to split ultraviolet-induced cyclobutane pyrimidine dimers in damaged DNA, but its molecular mechanism has never been directly revealed. We report here the direct mapping of catalytic processes through femtosecond synchronization of the enzymatic dynamics with the repair function. We observed direct electron transfer from the excited flavin cofactor to the dimer in 170 ps and back electron transfer from the repaired thymines in 560 ps. Both reactions are strongly modulated by active-site solvation to achieve maximum repair efficiency. These results show that the photocycle of DNA repair by photolyase is through a radical mechanism and completed on subnanosecond time scale at the dynamic active site with no net electron change in redox states of the flavin cofactor.

*Contributed Papers*

**15:06**
**W26 2 Near-infrared femtosecond laser assisted cell membrane permeabilization** CHENG PENG, ROBERT PALAZZO, INGRID WILKE, *Rensselaer Polytechnic Institute* The controlled delivery of membrane impermeable molecules into single living cells (micro-injection) is important for a variety of applications such genomics, proteomics or drug screening and testing. Recently, it has been demonstrated that opto-injection with tightly focused ( $\sim$ 300nm) femtosecond (fs) laser pulses at near-infrared (nir) wavelengths (700-1100nm) has the potential to create highly localized transient pores in single living cells with high cell survival rates and transfection efficiency. We have investigated the creation of transient pores in single living BAEC cells by focused fs nir laser pulses dependent on the incident laser intensity by dye uptake studies. Our experimental data agree very well with the experimentally and theoretically determined thresholds for laser-induced plasma formation and LIB. We observe that pore creation is observed for laser intensities of $4.0 \times 10^{12}$W/cm$^2$ and higher. For laser intensities above $3.3 \times 10^{13}$W/cm$^2$ BAEC cells are irreversibly destroyed. Within these two limits the pore size increases logarithmically with increasing laser intensity. This functional dependence is explained by considering the Gaussian intensity distribution across the laser focal spot. The physical understanding of the relationship between pore size and laser intensity allows the control of the number of molecules delivered into a cell per unit time through the control of the pore size.

*Invited Papers*

**15:18**
**W26 3**
VASAN VENUGOPALAN, *University of California Irvine*

This abstract was not received electronically.

*Contributed Papers*

**15:54**
**W26 4 DFT calculation of photo-induced charge transfer in organic molecule** MARK PEDERSON, *Naval Research Laboratory* TUNNA BARUAH, *University of Texas at El Paso* We propose a method for obtaining the charge transfer time for a chromophore-donor-acceptor system from density functional theory. Our calculations are done on a porphyrin-carotene-$C_{60}$ molecular triad. The geometry of the large molecular triad was optimized at the all-electron level using GGA. We are considering single electron excitations, the energies of which are obtained using a newly developed approach. The electronic dipolar transition probabilities are calculated from Einstein's A and B coefficients. However, in real systems the polarization effects play an important role in the transfer process since the charge separated

states can possess huge dipole moments. The stabilization of the large dipole state can be calculated from the classical dipole-dipole interaction and the polarizability of the surrounding medium. The stabilization of the dipole states is an important aspect which dominates the charge transfer process and therefore the rise time. The efficiency of the molecule as a solar energy converter will also be discussed.

**16:06**

**W26 5 Structural colours in blue-banded bee** JONES WAN,* LIXIIN DAI, JENSEN LI, KWOK-KWONG FUNG, CHE-TING CHAN, *Department of Physics, Hong Kong University of Science and Technology* Periodic, micro-textured biological materials are ubiquitous in nature. Electromagnetic waves at different frequencies are selectively reflected by such materials. This phenomenon is the origin of structural colours observed in variety of insects. In this work, we analyze the mechanisms that lead to the bluish-green colour of the blue-banded bee feathers. The reflection spectrum of the blue-banded bee feather was calculated by the transfer matrix method (TMM). The reflection peaks found are compatible within the experimental data. In addition to Bragg scattering, guided resonance has been observed in our theoretical calculation, which leads to a novel understanding of the structural colours in blue-banded bees.

*Also at: Department of Physics and Institute of Theoretical Physics, The Chinese University of Hong Kong

**16:18**

**W26 6 Wavelength-Dependent Conformational Changes of Collagen in Mid-IR Ablation** M. SHANE HUTSON, YAOWU XIAO, *Dept of Physics and Astronomy, Vanderbilt University and VIIBRE - Vanderbilt Institute for Integrative Biosystem Research and Education* MINGSHENG GUO, *Dept of Physics, Fisk University* Single pulses of the Mark-III free electron laser have been used to ablate porcine corneas at a fluence of 240 J/cm$^2$ and wavelengths of 2.77 and 6.45 $\mu$m. As previously characterized, the non-volatile ablation debris shows evidence of wavelength-dependent collagen fragmentation. We have measured micro-Raman spectra of the debris and the ablation crater to determine if any wavelength-dependent conformational changes have taken place. Comparison of the spectra from two different wavelengths shows that a 938 cm$^{-1}$ Raman band – assignable to the peptide C$_{C=O}$-C$_\alpha$ stretch of collagen – loses substantial intensity during 6.45-$\mu$m ablation, but not in 2.77-$\mu$m ablation. This intensity decrease may be associated with a reduction of collagen triple-helix structure. Other spectral techniques yield mixed results; signatures for the loss of triple-helix structure are evident in UV-CD and some aspects of $^{13}$C-NMR spectra, but not in FTIR spectra. Raman measurements on thermally-treated corneal slices display similar changes at high temperatures, suggesting that higher protein temperatures are reached during ablation at 6.45 $\mu$m when compared to 2.77 $\mu$m. These observations suggest that any pre-vaporization loss of protein structural integrity includes not only collagen fragmentation, but also a loss of collagen triple-helix structure.

**16:30**

**W26 7 Novel protection mechanisms against singlet oxygen formation by the Chl *a* molecule in the cytochrome $b_6f$ complex of oxygenic photosynthesis** SERGEI SAVIKHIN, *Department of Physics, Purdue University* HANYOUP KIM, NARANBAATAR DASHDORJ, *Department of Physics, Purdue University* HUAMIN ZHANG, JIUSHENG YAN, WILLIAM CRAMER, *Department of Biological Sciences, Purdue University* A Chl molecule is known to produce highly toxic singlet oxygen under light illumination as a result of energy transfer from its triplet excited state to oxygen. To prevent that, a carotenoid is typically positioned close to a Chl molecule ( $\sim$ 4 Å) in Chl containing proteins to ensure rapid triplet-triplet energy transfer from Chl to carotenoid. Surprisingly, the X-ray structures of the cytochrome $b_6f$ complex show that the $\beta$ -carotene is much too far from the only Chl *a* found in this complex to provide effective protection by the usual triplet-triplet energy transfer mechanism. Our optical femtosecond time resolved experiments on diluted samples as well as on the single crystals of the $b_6f$ complex suggest that the Chl *a* is protected by two novel mechanisms: (i) the yield of the Chl *a* triplet state formation is reduced through electron-transfer exchange with the nearby amino acid residues, and (ii) a long distance triplet energy transfer to carotenoid mediated by a third mobile molecule (NSF MCB- 0516939, NIH GM-38323).

**16:42**

**W26 8 Electrostatic Steering of Functional Dynamics in GFP** J. TIMOTHY SAGE, *Northeastern Univ.* GEORGI Y. GEORGIEV, *Assumption College* JASPER J. VAN THOR, *University of Oxford* Distinctive photodynamic properties of the green fluorescent protein (GFP) from the jellyfish *A. victoria* result from charge transfer processes involving the autocatalytically generated chromophore. We investigate structural changes in response to chromophore photoionization at cryogenic temperatures, using both X-ray crystallography and polarized infrared measurements on oriented single crystals. These measurements identify conformational changes of Gln 69, Cys 70, and an associated H-bonded cluster of internal water molecules in the chromophore environment. These structural changes take place at 100 K, far below the ''dynamical transition'' traditionally regarded as enabling functional protein motions. This contrasts with the prevailing view that the rigid interior of the GFP $\beta$-barrel sterically inhibits nonradiative processes. Instead, we propose that rapid rearrangements of the chromophore environment enhance the fluorescence quantum yield by stabilizing the abruptly altered charge distribution in the radiative state. We suggest that the conformational response to charge transfer influences two fundamental and useful spectroscopic properties of GFP—the large frequency separation between excitation and emission and the efficient fluorescence.

**16:54**

**W26 9 Terahertz Dielectric Response of Photoactive Yellow Protein (PYP): Influence of Conformational-Vibrational State during Photocycle and Hydration Effects** JOSEPH KNAB, JING-YIN CHEN, *Physics Department, University at Buffalo, Buffalo, NY 14260* WOUTER HOFF, *Department of Microbiology and Molecular Genetics, Oklahoma State University, Stillwater, OK 74078* ANDREA MARKELZ, *Physics Department, University at Buffalo, Buffalo, NY 14260* Protein conformational change alters flexibility and conformational-vibrational modes that occur on a picosecond or sub-picosecond time scale. Terahertz dielectric measurements are sensitive to protein flexibility as they directly probe the density of states of these vibrational modes. Using terahertz time-domain spectroscopy, we measured the dielectric response of PYP thin films as a function of resting and photointer-

mediate state. The absorbance increases smoothly as a function of frequency while the index of refraction exhibits no frequency dependence. A sharp transition in the dielectric response of the ground state is observed at 86% relative humidity (r.h.), corresponding to the point where the protein film has lost $\sim$ 50 water molecules relative to a 100% r.h. environment. Similar transitions observed for hen egg white lysozyme and cytochrome c correspond to the filling point of the first hydration shell.

**17:06**

**W26 10 Novel Photo-Protecticon Mechanisms in Chlorosomes from Green Sulfur Bacterium itChlorobium Tepidum** HANYOUP KIM, SERGEI SAVIKHIN, *Department of Physics, Purdue University, West Lafayette, IN 47907* HUI LI, JULIA MARESCA, DONALD BRYANT, *Department of Biochemistry and Molecular Biology, The Pennsylvania State University, University Park, PA 16802* Chlorosome is the largest known photosynthetic light-harvesting antenna complex that incorporates thousands of bacteriochlorophtylls (BChl) and carotenoids (Car) in a closely packed quasi-regular structure. BChl is known to produce highly toxic singlet oxygen as the result of energy transfer from their excited triplet states to oxygen molecules. It has been proposed that that the carotenoids in chlorosome serve both light harvesting and photo-protection functions, transferring light excitations to nearby BChl and simultaneously quenching excited triplet state of BChl. However, experiments indicate that photoprotective role of carotenoids in chlorosomes is not as extensive as expected—photo-degradation of carotenoid-free mutants occurs only twice faster than photo-degradation of native complexes. An additional non-conventional photoprotection mechanism must exist in chlorosomes. The possible nature of this mechanism is discussed based on optical kinetic measurements of BChl and Car excited states.

**17:18**

**W26 11 Hydration Dependence of Energy Relaxation Time for Cytochrome C** SHUJI YE, JING-YIN CHEN, JOSEPH R. KNAB, ANDREA MARKELZ, *Physics, University at Buffalo, SUNY* Hydration plays a critical role in protein dynamics. Here we consider the effects of hydration on energy relaxation for an electronically excited heme protein cytochrome c. We measure the hydration dependence of energy relaxation time of cytochrome C films after photoexcitation in the Soret regionusing two-color pump/probe time resolved transmission measurements. Thin films were prepared from cytochrome C/ Trizma buffer solutions and mounted in a hydration controlled cell. We used 400nm ( $\sim$ 3 mW) to pump the B band and 800 nm ( $\sim$ 1 mW) to probe the III band. The III band corresponds to the charge-transfer transition between heme $\pi$ and iron d orbital, and is assigned to the ground electronic state of the heme. Therefore this band can be used to probe the ground state population. Three separate dynamic components were observed: a very fast transient $\tau_1 \sim$ 200 fs; a several hundred femtosecond component ($\tau_2$); and a recovery of the ground state absorption($\tau_3$). We find $\tau_3$ apparently decreases with decreasing hydration while $\tau_1$ and $\tau_2$ are independent of hydration.

**SESSION W28: FOCUS SESSION: ORDERED OPTOELECTRONIC ORGANICS**
**Thursday Afternoon, 16 March 2006**
**325, Baltimore Convention Center at 14:30**
**Howard Katz, Johns Hopkins University, presiding**

**14:30**

**W28 1 The phase diagram of the organic charge transfer salts $(TMTTF)_2X$*** F. ZHANG, *UCLA* W. YU, B. ALAVI, A. BAUR, C. A. MERLIC, S. E. BROWN, We report on NMR spectroscopy and relaxation measurements probing the temperature/pressure phase diagram of the quasi-one-dimensional organic conductor $(TMTTF)_2SbF_6$. This material undergoes a charge ordering (CO) phase transition at $T = 156K$, and the ground state is antiferromagnetic (AF) at ambient pressure. Our experiments show that the AF ground state is supressed sharply by applying hydrostatic pressure and a new phase appears at higher pressure. At intermediate pressures, magnetic ordering is suppressed to temperatures below the minimum measured so far, $T = 2K$. The nature of the high pressure phase is not yet established; there are features consistent with both spin-Peierls (SP), and antiferromagnetic ordering. We discuss the possible role of counterion disorder in producing an inhomogenous system consistent with our observations, and the implications for a general phase diagram for the TMTTF/TMTSF family of organic conductors.

*NSF Grant No. DMR-0203806.

**14:42**

**W28 2 Intermolecular bonding in conjugated polymers: The effect on aggregate morphology.** JEREMY SCHMIT, *Brandeis University* ALEX LEVINE, *UCLA* Intermolecular interactions play an important role in the mechanical and optical properties of conjugated polymer films and solutions. However, the nature of such inter-polymer interactions is poorly understood. We present a calculation showing that in the tight-binding approximation, conjugated polymers that approach each other on the angstrom length scale will form weak, covalent-like bonds. These bonds then drive the formation of aggregate structures. The morphology of the aggregates formed by the polymers depends on the net binding strength of the interaction. At low bond strength, the polymers form loose aggregates, while strong bonds lead to the formation of tight bundles with an effective persistence length one order of magnitude greater than the free polymer.

**14:54**

**W28 3 Effects of polymer side chains on the self-assembling of conjugated polymer in thin film** YUNFEI JIANG, *Chemistry Department, Clemson University, Clemson, SC, 29634-0973* YI-QING WANG, *School of Chemistry and Biochemistry, Georgia Institute of Technology, Atlanta, GA 30332* UVW H. F. BUNZ, *School of Chemistry and Biochemistry, Georgia Institute of Technology, Atlanta, GA 30332* DVORA PERAHIA, *Chemistry Department, Clemson University, Clemson, SC, 29634* Conjugated polymers are inherently semi-conducting and optically active materials, with immense potential applications in organic electro-optical devices. The chemical structure of the polymer including the rigidity of the backbone and the nature of substituents affect their association as well as their electro-optical response. The following work reports the effects of different side chains on the structure and fluorescence of highly conjugated polymer, poly-(para phenyleneethynylene) (PPE). When substituted by long

polylactide side chains they self-assemble into wires with fingerprint-like arrangement, casting from chloroform solutions on oxidized silicon wafer. With increasing content of poor solvent, the dimension of the structures increased and then crystallized area appeared, as showed in AFM studies. The introducing of the long flexible polymer side chains has significantly reduced the stacking between rigid backbones. This in tern results in a frequency shift in their fluoresces response, indication changes in the electronic levels. Direct measurements of the electronic levels using ATM are currently in progress.

**15:06**

**W28 4 Chain morphologies in semi-crystalline polyfluorene: evidence from Raman scattering*** S. GUHA, C. VOLZ, M. ARIF, *Department of Physics, University of Missouri-Columbia MO* Organic semiconductors, such as short-chain oligomers and long- chain polymers, are now a core constituent in numerous organic and organic-inorganic hybrid technologies. Polyfluorenes (PF) have emerged as attractive alternatives to other polymers due to their strong blue emission and high charge carrier mobilities. Almost all PF derivatives utilize side-chain substitution that improves solution processing and confers new functionality. There are many ambiguities regarding structure- property relationships in various side-chain substituted PFs. Di-octyl substituted PF (PF8) is known for its mesomorphic behavior, multitude of crystalline phases, and several conformational isomers that depend on the torsional angle between monomer units. In particular, the $\beta$ phase that represents a more planar backbone conformation dominates the optical emission although it appears as a minority constituent. We present Raman scattering studies of PF8 as a function of thermal cycling, which establishes a connection between the conformational isomers and the side and main chain morphology. Density-functional calculations of the vibrational spectra of single chain oligomers in conjunction with the experimental results demonstrate the incompatibility of the $\beta$ phase with the overall $\alpha$ crystalline phase in PF8.

*This work was supported by NSF-ECS # 0523656 and the Univ. of Missouri Research Board

**15:18**

**W28 5 Structural Changes in Phthalocyanine Thin Films from Analyte Vapor Exposure*** THOMAS GREDIG, GE LIU, CORNELIU N. COLESNIUC, *Department of Physics, UC San Diego* FOREST I. BOHRER, ANDREW C. KUMMEL, *Department of Chemistry and Biochemistry, UC San Diego* IVAN K. SCHULLER, *Department of Physics, UC San Diego* Organic phthalocyanine thin films were fabricated with varied thicknesses and varied grain size structure. These films act as gas sensors as detected via conduction measurements due to analyte vapors. We have observed structural changes with high-resolution x-ray diffraction due to exposure to different analyte vapors. In thin films with small grains ( $\sim$ 30nm diameter), low-angle irreversible changes and high-angle reversible variations were observed. We associate the irreversible behavior with current drift observed in transport measurements. In contrast, reversible variations of the first Bragg peak of the phthalocyanine are compared to the sensing changes in conductivity from exposure to analyte vapors.

*Work supported by AFOSR-MURI.

**15:30**

**W28 6 Electronic Structure of Potassium-doped Magnesium Phthalocyanine measured using Soft X-ray Spectroscopies.** YUFENG ZHANG, SHANCAI WANG, LEYLA COLERK-EROL, TIMOTHY LEARMONTH, LUKASZ PLUKINSKI, KEVIN SMITH, *Boston University* JAMES DOWNES, *SCPS, Victoria Univeristy of Wellington* ANNE MATSUURA, *Air Force Office of Scientific Research* We report a synchrotron radiation-excited resonant soft x-ray emission spectroscopy (XES) study of the electronic structure of magnesium phthalocyanine (MgPc) doped with potassium. XES measures directly the element specific partial density of states (PDOS) in solids. The electronic structure near the Fermi level in organic systems can be accurately measured by using this non-ionizing spectroscopy. The MgPc films were grown itin-situ by using a custom designed ultra-high vacuum organic molecular beam deposition system, and transferred under vacuum to the spectrometer system. As with our earlier study of Cu-Pc and vanadium oxide phthalocyanine (VO-Pc), the K-doped MgPc films were discovered to be highly susceptible to synchrotron radiation beam damage. We successfully circumvented this effect by continuous translation of the films during measurement. We find that the measured C $2p$ PDOS for K-doped MgPc differs from that of pure MgPc, and will discuss the possible origins of these results. Supported in part by ACS Petroleum Research Fund, and by the NSF. Experiments were performed at the NSLS.

**15:42**

**W28 7 Polaron transport in triphenylene-based discotic liquid crystals** VOLODIMYR DUZHKO, *Department of Physics, Case Western Reserve University, OH 44106* ALEXANDER N. SEMYONOV, ROBERT J. TWIEG, *Department of Chemistry, Kent State University, OH 44242* KENNETH D. SINGER, *Department of Physics, Case Western Reserve University, OH 44106* We report on the investigation of charge carrier transport in the columnar phase of the triphenylene-based discotic liquid crystal, hexapentyloxytriphenylene, by the time-of-flight technique. The hole mobility was found to be temperature and electric field dependent with a maximum value of $2\times\ 10^{-3}$ cm$^2$/Vs. Its temperature dependence is described by a $T^{-n}$ power law, with an electric field dependent n varying from 2.5 to 4.5 corresponding to electric field values from $5\times\ 10^4$ V/cm to $5\times\ 10^3$ V/cm, respectively. The drift velocity of charge carriers is a linear function of the electric field for small fields below $5\times\ 10^4$V/cm and tends to saturation at strong fields. These results are interpreted in the framework of correlated polaron motion as described by the non-adiabatic low-temperature limit of Holstein's small polaron theory. The applicability of the Holstein polaron model to triphenylene-based materials showing thermally activated or temperature-independent carrier mobilities will be discussed.

**15:54**

**W28 8 Atomic Force Microscope-Based Surface Potential and Surface Photovoltage Studies of Porphyrin Nanorod Thin Films** TODD HOLDEN, *Brooklyn College of CUNY* WALTER SMITH, *Haverford College* A.D. SCHWAB, *Appalachian State University* J.C. DE PAULA, *Lewis and Clark College* We have performed atomic force microscope-based surface potential and surface photovoltage measurements on porphyrin grown as nanorods about 5 nm in diameter and 1 micron long. These nanorods have been shown to have peculiar photoconducting properties in that the photoconductivity grows under light illumination for up to 1 hour. In addition, when a current is flowed through the nanorods,

they become ''trained.'' That is after the light is turned off and the ends of the nanorod are short circuited together, a small current will flow opposite to the direction of the original photocurrent. The material exhibits nanoscale potential fluctuations as well as selective surface potential sensitivity to light. These offer some insight to the material's novel properties.

**16:06**

**W28 9 Holographic liquid crystal photonic materials stabilized with monoacrylate LC monomer.** AUGUSTINE URBAS, ERIC BECKEL, VINCENT TONDIGLIA, LALGUDI NATARAJAN, TIMOTHY BUNNING, *AFRL* Active structured optical materials such as dynamically tunable photonic crystals have potential technological applications in imaging and communications. Structured liquid crystal materials are especially promising for their observed high performance and wide range of dynamic response. In addition, they provide multiple routes of response, including electro-optic and photo-optic. Reverse mode holographic polymer dispersed liquid crystals (HPDLCs) are typically fabricated by multiple laser beam exposure of an LC photo-sensitive syrup containing diacrylate liquid crystal (LC) monomer. The function of the diacrylate monomer is to form the basis of a highly crosslinked network which stabilizes regions with high polymer content. The use of monoacrylate functional liquid crystals in this application has the potential of tuning the stabilizing effect of the polymer network by changing the crosslink density. This affects the switching time and the contrast between stabilized and unstabilized regions of the patterned structure. These parameters are particularly important to photo-switchable patterned photonic structures containing azobenzene derivatives. The effects on electro-optic and photo-optic properties of reverse mode HPDLCs containg of different monoacrlyate functional liquid crystal fractions in the stabilizing patterned polymer network will be presented.

**16:18**

**W28 10 Electrooptic Properties of Holographic Polymer-Stabilized Cholesteric Liquid Crystals** ERIC BECKEL, MELISSA INGRAM, *Air Force Research Laboratory* LALGUDI NATARAJAN, VINCENT TONDIGLIA, RICHARD SUTHERLAND, *Science Applications International Corporation* TIMOTHY BUNNING, *Air Force Research Laboratory* Cholesteric liquid crystals (CLCs) have attracted significant attention for uses in photonic and electrooptic devices, such as photonic crystals, light switches, and display applications. These materials selectively reflect circularly polarized light due to the existence of a macroscopic helical structure. Application of an electric field reorients the LC from a planar geometry to a homeotropic alignment, eliminating the reflection notch. This LC reorientation to the clear state is rapid with the application of an electric field. After the electric field is removed, the return to the cholesteric orientation is compounded by the long lifetime of a highly scattering focal conic state. To avoid this undesired prolonged focal conic lifetime, a small concentration of monomer can be polymerized, which acts as a memory for the rapid return into the cholesteric state. In this research, we examine the effect of holographically patterning the polymer stabilization. Reflection grating patterning is studied and varying bilayer spacings are examined. This research shows the possibility of minimal notch broadening, with no apparent chirp in the reflection notch. Additionally, we examine the possibility of incorporating a narrow notch Bragg reflection at a differing wavelength than the CLC broad reflection notch, within the same device.

**16:30**

**W28 11 High Refractive Index Poly(thiophene) for Organic 3-D Photonic Crystals with a Complete Photonic Band Gap*** MATTHEW J. GRAHAM, *The University of Akron* SHI JIN, *CUNY, Staten Island* FRANK W. HARRIS, *University of Akron* STEPHEN Z.D. CHENG, *The University of Akron* Photonic crystals (PC) with a complete 3-D photonic band gap (PBG) require materials with sufficient refractive index ($n$) contrast to be in specific 3-D periodic structures on the length scale of light. Currently, only inorganics have an adequate $n$ to open a complete 3-D PBG. Poly(thiophene) (PT), a sulfur containing conjugated polymer, is predicted to have a sufficient $n$, but this has not been realized. By optimizing the electropolymerization of PT including reaction rates, temperatures, additives, and reactant concentrations, high quality PT films with an adequately high $n$ can be synthesized. Using a density differential colloidal crystallization technique, which allows the crystallization process to approach thermodynamic equilibrium, high quality templates were produced. A nano-mechanical annealing technique was developed to enable the further perfection of the entropy driven structures. The next step is to combine these to fabricate an organic 3-D PC with a complete PBG.

*This work was supported by the Collaborative Center for Polymer Photonics and a NSF graduate fellowship

**16:42**

**W28 12 Thermopower of Pentacene Thin-film Transistors** DANIEL LENSKI, ALEXANDRA CURTIN, M.S. FUHRER, *University of Maryland* FUHRER NANOTECHNOLOGY GROUP TEAM, The mechanism of conduction in organic thin-film transistors remains poorly understood, though it is generally thought that conduction occurs via hopping in a disordered band tail. Thermopower in principle can give additional information about the density of states D(E), and the dependence of the mobility on D(E); such information can be used to discriminate between various conduction mechanisms. We report for the first time measurements of the thermopower of pentacene thin films on $SiO_2$/Si in a field-effect transistor configuration as a function of charge carrier density and temperature. This work was supported by the Laboratory for Physical Sciences.

**16:54**

**W28 13 In-Situ Measurements of Organic Electronic Devices Fabricated via Transfer Printing on Flexible Substrates** ANDREW TUNNELL, DANIEL R. HINES, VINCE W. BALLAROTTO, MIHAELA BREBAN, ELLEN D. WILLIAMS, *Laboratory for Physical Sciences and Department of Physics, University of Maryland, College Park, MD.* Transfer printing was used to fabricate high quality organic thin-film transistors (TFT) on flexible substrates. The model system of a pentacene (Pn) TFT with 600 nm thick poly(methyl methacrylate) dielectric layer and gold electrodes on a polyethylene terephthalate substrate has shown a mobility (adjusted for contact resistance) of 0.237 $cm^2$/Vs, on/off ratio of $10^5$ and threshold voltage of -7 V. To optimize the transfer printing parameters of the Pn semiconductor layer, mobility and contact resistance were studied as a function of printing temperature and pressure. The best TFT devices resulted from printing at 120 $^oC$ and 600 psi. A detailed study of the effect of transfer printing on the device properties was performed via in-situ measurements of drain current (ID) as a function of both

drain (VD) and gate (VG) voltages. Details of the in-situ measurements while transfer printing the Pn layer will be presented and discussed. *Work supported by the Laboratory for Physical Sciences, College Park, MD and ARDA.

**SESSION W29: BIOLOGICAL NETWORKS AND SYSTEM BIOLOGY**
**Thursday Afternoon, 16 March 2006**
**326, Baltimore Convention Center at 14:30**
**Alexander Neiman, Ohio University, presiding**

**14:30**
**W29 1 Self-Organization of Networks Via Synchrony-Dependent Plasticity** JACK WADDELL, MICHAL ZOCHOWSKI, *University of Michigan - Physics* We employ an adaptive parameter control technique based on a previously developed measure that detects phase/lag synchrony in the system to dynamically modify the structure of a network of non-identical, weakly coupled Rössler oscillators. Two processes are simulated: adaptation, under which the initially different properties (such as frequency) of the units converge, and aggregation, in which coupling between units is altered and clusters of interconnected elements are formed based on the temporal correlations. We show that adaptation speed depends on connectivity and topology, with more global connections resulting in greater temporal order and faster convergence of adaptation. We find that aggregation leads to unidirectional clusters, and that asymmetric aggregation (with differing rates for increasing or decreasing coupling strength) has an optimum ratio of rates to make denser clusters that maintain their selectivity. Combining adaptation and aggregation results in clusters of identical oscillators with bi-directional coupling. An optimum ratio of process rates results in stable coupling between the units. Change from this ratio may result in annihilation of the network for slow aggregation, or more numerous, denser, and more transient clusters for faster aggregation.

**14:42**
**W29 2 Phase reduction analysis of coupled neural oscillators: application to epileptic seizure dynamics** DAISUKE TAKESHITA, *University of Missouri at St. Louis* YASUOMI SATO, *J.W. Goethe-University* SONYA BAHAR, *University of Missouri at St. Louis* Epileptic seizures are generally held to be result from excess and synchronized neural activity. To investigate how seizures initiate, we develop a model of a neocortical network based on a model suggested by Wilson [1]. We simulate the effect of the potassium channel blocker 4-aminopyridine, which is often used in experiments to induce epileptic seizures, by decreasing the conductance of the potassium channels ($g_K$) in neurons in our model. We applied phase reduction to the Wilson model to study how $g_K$ in the model affects the stability of the phase difference. At a normal value of $g_K$, the stable phase difference is small, but the neurons are not exactly in phase. At low $g_K$, in-phase and out-of-phase firing patterns become simultaneously stable. We constructed a network of 20 by 20 neurons. By decreasing $g_K$to zero, a dramatic increase in the amplitude of mean field was observed. This is due to the fact that in-phase firing becomes stable at low $g_K$. The pattern was similar to local field potential in 4-aminopyridine induced seizures. Therefore, it was concluded that the neural activity in drug-induced seizure may be caused by a bifurcation in stable phase differences between neurons. [1] Wilson H.R., J. Theor. Biol. (1999) 200, 375-388 [2] Ermentrout, G.B. and Kopell, N., SIAM J. Math. Anal. (1984), 215-237

**14:54**
**W29 3 Effect of Delays and Network Topology in Spatiotemporal Pattern Formation** RHONDA DZAKPASU, MICHAL ZOCHOWSKI, *Department of Physics, Biophysics Research Division, University of Michigan* Synchronization between connected neurons is believed to play a role in the processing of information within the brain. This implies a temporal ordering in the discharge of their electrical signals but since the axons have a finite length over which a signal must traverse, information relating to a particular process and emanating from different neurons reaches a target neuron after a time delay. We investigate the effects of delays on the formation of temporally ordered states in a model network with SWN topology. We show that incorporation of two different types of delay, length independent and length dependent, lead to dramatically different properties of the network. In the first case, the formation of global random connections leads to an increase in temporal ordering, while in the second case locally ordered clusters are annihilated and form a disordered state.

**15:06**
**W29 4 Inhibitory Synaptic Coupling and Spatiotemporal Synchrony in a Neural Model** ROXANA CONTRERAS, *University of Missouri-Saint Louis* SONYA BAHAR, *University of Missouri-Saint Louis* We study the behavior of an array of neurons, connected by excitatory and inhibitory synapses, when the relative proportion of such connections is varied. The cells, described by the Huber-Braun model [1], exhibit different bursting states as parameters such as temperature and coupling strength are tuned. In a recent paper [2], stochastic phase synchronization was studied in this model, using gap-junction type connections. Here, we extend this work to more realistic synaptic connectivities, to investigate the connection between bursting and synchronization, which has been implicated in the triggering of pathological processes such as epilepsy, since synchronous firing in neuronal populations is viewed as a hallmark of seizures. We also present evidence suggesting that noise could be responsible for transitions between various types of field potential oscillations, reminiscent of the transitions between spike-and-wave firing and low voltage fast activity observed in the epileptic cortex. [1] H. A. Braun, M. T. Huber, M. Dewald, K. Schäfer, and K. Voigt. Computer simulations of neuronal signal transduction: the role of nonlinear dynamics and noise. Intl. J. Bifurcation and Chaos 8(5): 881-889, 1998. [2] S. Bahar. Burst-enhanced synchronization in an array of noisy coupled neurons. Fluctuation and Noise Letters 4(1):L87-L96, 2004.

**15:18**
**W29 5 Attentional modulation of stimulus competition in a large scale model of the visual pathway** CALIN BUIA, *University of North Carolina at Chapel Hill* PAUL TIESINGA, *University of North Carolina at Chapel Hill* Neurons in cortical area V4 are sensitive to shape and have large receptive fields. In a typical visual scene there are multiple objects in the V4 cell's receptive field, only a few of which may be behaviorally relevant. The visual system is capable of selecting relevant objects by increasing the neural response to them and reducing the response to non-relevant objects. Neuronal synchrony may play an important role in this

process. Using a large-scale network model of the visual pathway, we study the emergence of shape selectivity in V4, the competition between different objects for control of the firing rate of individual V4 neurons, the attentional modulation of this stimulus competition and the role of synchrony.

**15:30**

**W29 6 Specificity, promiscuity, and the structure of complex information processing networks** CHRISTOPHER MYERS, *Cornell University* Both the top-down designs of engineered systems and the bottom-up serendipities of biological evolution must negotiate tradeoffs between specificity and control: overly specific interactions between components can make systems brittle and unevolvable, while more generic interactions can require elaborate control in order to aggregate specificity from distributed pieces. Complex information processing systems reveal network organizations that navigate this landscape of constraints: regulatory and signaling networks in cells involve the coordination of molecular interactions that are surprisingly promiscuous, and object-oriented design in software systems emphasizes the polymorphic composition of objects of minimal necessary specificity [C.R. Myers, Phys Rev E 68, 046116 (2003)]. Models of information processing arising both in systems biology and engineered computation are explored to better understand how particular network organizations can coordinate the activity of promiscuous components to achieve robust and evolvable function.

**15:42**

**W29 7 Modeling of signal transduction in bacterial quorum-sensing** ANDREW FENLEY, *Virginia Tech* SUMAN BANIK, *Virginia Tech* RAHUL KULKARNI, *Virginia Tech* Several species of bacteria are able to coordinate gene regulation in response to population density, a process known as ''quorum-sensing.'' Quorum-sensing bacteria produce, secrete, and detect signal molecules called autoinducers. For several species of bacteria in the *Vibrio* genus, recent results have shown that the external autoinducer concentrations control the expression of regulatory small RNA(s) which are critical to the process of quorum-sensing. We present a theoretical analysis of the network which relates the rate of small RNA expression to the external autoinducer concentrations. We relate the results from our modeling to previous experimental observations and suggest new experiments based on testable predictions of the model.

**15:54**

**W29 8 Sloppiness is universal in systems biology: making predictions nonetheless** RYAN GUTENKUNST, *Physics, Cornell* FERGAL CASEY, *Applied Math, Cornell* JOSHUA WATERFALL, *Physics, Cornell* KEVIN BROWN, *Molecular and Cellular Biology, Harvard* CHRISTOPHER MYERS, *Theory Center, Cornell* JAMES SETHNA, *Physics, Cornell* Quantitative models of complex biological systems often possess dozens of unknown parameters. We argue that such systems are universally ''sloppy''; their behaviors are orders of magnitude more sensitive to moves in some directions in parameter space than others. To establish this, we survey models from the literature and show that their ''complete and perfect data'' Fisher Information Matrices possess eigenvalues typically spanning a range of more than $10^6$. Sloppiness implies that collectively fitting model parameters to even the best experimental data will tightly constrain only a few parameter combinations, perhaps suggesting the necessity of a difficult experimental program to measure each individual parameter. An example demonstrates, however, that a collective fit to a modest amount of real data may tightly constrain model behavior even though it only poorly constrains many parameter combinations. Low uncertainty predictions can thus be made without knowledge of precise values for individual parameters.

**16:06**

**W29 9 Inference and analysis of gene-regulatory networks in the bacterium B.subtilis** CLAIRE CHRISTENSEN, *Dept. of Physics, Penn State University* ANSHUMAN GUPTA, *Dept. Chem. E., Penn State University* REKA ALBERT, *Dept. of Physics, Penn State University* COSTAS MARANAS, *Dept. Chem. E., Penn State University* We present the methods and results of a two-stage modeling process that generates candidate gene-regulatory networks of the bacterium B.subtilis from experimentally obtained, yet mathematically underdetermined microchip array data. By employing a computational, linear correlative procedure to generate these networks, and by analyzing the networks from a graph theoretical perspective, we are able to verify the biological viability of our simulated networks, and we demonstrate that our networks' graph theoretical properties are remarkably similar to those of other, more well-studied biological systems. We test the robustness of the inference process first by introducing noise into the experimental data, and then by comparing the graph theoretical properties of the resulting perturbed networks to those of the original networks.

**16:18**

**W29 10 Sensitivity-based approach to optimal experimental design in a receptor trafficking and down regulation model** FERGAL CASEY, JOSHUA WATERFALL, RYAN GUTENKUNST, *Cornell University* KEVIN BROWN, *Harvard University* CHRISTOPHER MYERS, JAMES SETHNA, *Cornell University* We apply the ideas of optimal experimental design to systems biology models: minimizing a design criterion based on the average variance of predictions, we suggest new experiments that need to be performed to optimally test a given biological hypothesis. The estimated variance in predictions is derived from the sensitivities of protein and chemical species in the model to changes in reaction rates. The sensitivities also allow us to determine which interactions in the biological network dominate the system behavior. To test the design principles, we have developed a differential equation model incorporating the processes of endocytosis, recycling and degradation of activated epidermal growth factor (EGF) receptor in a mammalian cell line. Recent experimental work has discovered mutant proteins that cause receptor accumulation and a prolonged growth signal. Our model is optimized to fit this mutant experimental data and wild type data for a variety of experimental conditions. Of biological interest is the effect on surface and internalized receptor levels after the overexpression or inactivation of regulator proteins in the network: the optimal design method allows us to fine tune the conditions to best predict the behavior of these unknown components of the system.

**16:30**

**W29 11 Stochasticity in the Expression of LamB and its Affect on λ phage Infection** EMILY CHAPMAN, XIAO-LUN WU, *University of Pittsburgh* λ phage binds to itE. Coli's lamB protein and injects its DNA into the cell. The phage quickly replicates and after a latent period the bacteria bursts, emitting mature phages. We developed a mathematical model based on the known physical events that occur when a λ phage infects an itE.Coli cell. The results of these models predict that the bacteria and phage popu-

lations become extinct unless the parameters of the model are very finely tuned, which is untrue in the nature. The lamB protein is part of the maltose regulon and can be repressed to minimal levels when grown in the absence of inducer. Therefore, a cell that is not expressing any lamB protein at that moment is resistant against phage infection. We studied the dynamic relationship between λ phage and itE. Coli when the concentration of phage greatly outnumbers the concentration of bacteria. We study how the stochasticity of the expression of lamB affects the percentage of cells that the λ phage infects. We show that even in the case when the maltose regulon is fully induced a percentage of cells continue to persist against phage infection.

**16:42**

**W29 12 Control of lineage stability and its role in resolving cell fates** ARYEH WARMFLASH, *University of Chicago* AARON DINNER, *University of Chicago* We synthesize experimental data from recent studies to construct a computational model for the gene regulatory network that governs the development of immune cells and use it to explain several surprising results. At the heart of the model is a cross-antagonism between the macrophage-promoting factor Egr and the neutrophil-promoting factor Gfi. This module is capable of giving rise to both graded and bistable responses. Increasing the concentrations of these factors forces the system into the bistable regime in which cells can decide stochastically between fates. This bistable switch can be used to explain cell reprogramming experiments in which a gene associated with one cell fate is induced in progenitors of another. In one such experiment, C/EBP$\alpha$, a neutrophil promoting factor, was induced in B cell progenitors which then differentiated to macrophages. Our model shows that if C/EBP$\alpha$ is induced early, it can induce differentiation to a neutrophil. In B cell progenitors, however, the bistable switch is already in a macrophage promoting state. Thus, expression of C/EBP$\alpha$ cannot activate the neutrophil pathway, but it can repress the B cell pathway and promote macrophage differentiation.

**16:54**

**W29 13 Role of finite-size fragments in analysis of DNA replication** JOHN BECHHOEFER, HAIYANG ZHANG, *Dept. of Physics, Simon Fraser University* In higher organisms, DNA replicates simultaneously from many origins. Recent in- vitro experiments have yielded large amounts of data on the state of replication of DNA fragments. From measurements of the time dependence of the average size of replicated and non-replicated domains, one can estimate the rate of initiation of DNA replication origins, as well as the average rate at which DNA bases are copied. One problem in making such estimates is that, in the experiments, the DNA is broken up into small fragments, whose finite size can bias downwards the measured averages. Here, we present a systematic way of accounting for this bias by deriving theoretical relationships between the original domain-length distributions and fragment-domain length distributions. We also derive unbiased average-domain-length estimators that yield accurate results even in cases where the replicated (or non-replicated) domains are larger than the average DNA fragment. Then we apply these estimators to previously obtained experimental data to extract improved estimates of replication kinetics parameters.

**17:06**

**W29 14 Stochastic dynamics of macromolecular-assembly networks.** LEONOR SAIZ, *Memorial Sloan-Kettering Cancer Center* JOSE VILAR, *Memorial Sloan-Kettering Cancer Center* The formation and regulation of macromolecular complexes provides the backbone of most cellular processes, including gene regulation and signal transduction. The inherent complexity of assembling macromolecular structures makes current computational methods strongly limited for understanding how the physical interactions between cellular components give rise to systemic properties of cells. Here we present a stochastic approach to study the dynamics of networks formed by macromolecular complexes in terms of the molecular interactions of their components [1]. Exploiting key thermodynamic concepts, this approach makes it possible to both estimate reaction rates and incorporate the resulting assembly dynamics into the stochastic kinetics of cellular networks. As prototype systems, we consider the itlac operon and phage λ induction switches, which rely on the formation of DNA loops by proteins [2] and on the integration of these protein-DNA complexes into intracellular networks. This cross-scale approach offers an effective starting point to move forward from network diagrams, such as those of protein-protein and DNA-protein interaction networks, to the actual dynamics of cellular processes. [1] L. Saiz and J.M.G. Vilar, submitted (2005). [2] J.M.G. Vilar and L. Saiz, Current Opinion in Genetics & Development, 15, 136-144 (2005).

**17:18**

**W29 15 Selective advantage for sexual reproduction*** EMMANUEL TANNENBAUM, *Ben-Gurion University of the Negev* We develop a simplified model for sexual replication within the quasispecies formalism. We assume that the genomes of the replicating organisms are two-chromosomed and diploid, and that the fitness is determined by the number of chromosomes that are identical to a given master sequence. We also assume that there is a cost to sexual replication, given by a characteristic time $\tau_{seek}$ during which haploid cells seek out a mate with which to recombine. If the mating strategy is such that only viable haploids can mate, then when $\tau_{seek} = 0$, it is possible to show that sexual replication will always outcompete asexual replication. However, as $\tau_{seek}$ increases, sexual replication only becomes advantageous at progressively higher mutation rates. Once the time cost for sex reaches a critical threshold, the selective advantage for sexual replication disappears entirely. The results of this talk suggest that sexual replication is not advantageous in small populations per se, but rather in populations with low replication rates. In this regime, the cost for sex is sufficiently low that the selective advantage obtained through recombination leads to the dominance of the strategy. In fact, at a given replication rate and for a fixed environment volume, sexual replication is selected for in high populations because of the reduced time spent finding a reproductive partner.

*Israel Science Foundation

**SESSION W30: FOCUS SESSION: BIOPOLYMERS AT INTERFACES**
**Thursday Afternoon, 16 March 2006; 327, Baltimore Convention Center at 14:30**
**Darrin Pochan, University of Delaware, presiding**

*Invited Papers*

**14:30**
**W30 1 Studies in Biological-Materials Interfaces.***
CHRISTOPHER OBER, *Cornell University*

The control of the physicochemical properties of surfaces in contact with biological systems represents a fundamental issue in many applications ranging from coatings to biotechnology and microelectronics. In particular, advances in biotechnology depend on the ability to fashion materials with precise control of feature size and functionality. This presentation focuses on issues of specific and non-specific binding and strategies being developed to control both. Examples of specific binding that enable investigation of cell function will be presented. The broader issue of non-specific binding and how it relates to fouling release will also be discussed in terms of surface structure. Both polar and non-polar surfaces have been investigated and each type shows promise for release specific biological systems. The identification of a ''universal'' surface for release of all biological systems remains elusive.

*The author would like to thank his many collaborators, group members and financial support from the Office of Naval Research, the National Science Foundation and the Cornell Nanobiotechnology Center.

*Contributed Papers*

**15:06**
**W30 2 Universality Classes and Unusual Thermodynamics of Unbinding Transitions of Semi-flexible Polymers Confined to a Surface** LEONARDO GOLUBOVIC, *Physics Department, West Virginia University* LIANGHUI GAO, *Max Planck Institute for Colloids and Surfaces, Potsdam, Germany* We theoretically address unbinding of semi-flexible polymers from long line-like attractive potential wells of various forms. These transition phenomena are seen in recent experiments with DNA adsorbed on microstructured supported cationic lipid membranes, and they provide a new way to stretch single DNA molecules [Hochrein, Leierseder, Golubovic, and Raedler, 2005]. For simple attractive potential wells (''rectangular wells'') the transition is of the second order. Heat capacity divergence however has a non-standard from, $C\sim 1/[|Tc - T| \log(|Tc - T|)]$, marked by a logarithmic correction related to the fact that the probability to find the polymer within the well region vanishes as $\sim 1/\log(|Tc-T|)$ at the transition point. On the other hand, for attractive potential wells having a hard wall potential added on one side, the transition becomes a non-standard hybrid between the first and second order phase transitions: the probability to find the polymer within the well approaches a non-zero value as the transition is approached and then it discontinuously drops to zero (producing a latent heat consumption). However, interestingly, in addition to the latent heat consumption, an unusual heat capacity divergence (of the form $C\sim 1/|Tc - T|^{1/2}$) also occurs as the polymer unbinding point is approached.

**15:18**
**W30 3 Polymer confinement and bacterial gliding motility** JUNHWAN JEON, ANDREY DOBRYNIN, *Polymer Program, Institute of Materials Science, Department of Physics, University of Connecticut* Cyanobacteria and myxobacteria use slime secretion for gliding motility over surfaces. In cyanobacteria the slime is extruded from the nozzle-like pores of 14-16 nm outer diameter and approximately 7nm inner diameter located near the septa that separate the cells of a filament. The pores are inclined at an angle of 30-40 degrees relative to the cell axes, and are oppositely directed on both sides of the septum. Such pore orientation provides directionality for the slime secretion as well as cell motion. To understand the mechanism of gliding motion and its relation to slime polymerization, we have performed molecular dynamics simulations of a molecular nozzle with growing inside polymer chains. These simulations show that the compression of polymer chains inside the nozzle is a driving force for its propulsion. There is a linear relationship between the average nozzle velocity and the chain polymerization rate with a proportionality coefficient dependent on the geometric characteristics of the nozzle such as its length and friction coefficient. This minimal model of the molecular engine was used to explain the gliding motion of cyanobacteria and myxobacteria over surfaces.

**15:30**
**W30 4 Direct Observation of Biaxial Confinement of a Semi-flexible Filament in a Channel** M.C. CHOI, *Univ. of Calif. Santa Barbara* J.H.KIM, M.W.KIM, S.Y.KWON TEAM,*O.PELLETIER, Y.LI, P.A.PINCUS, C.R.SAFINYA TEAM,†C.D.SANTANGELO TEAM,‡Z.WEN TEAM,§ We have studied the biaxial confinement of a semi-flexible filament in a channel by in situ video fluorescence microscopy*. As the channel width decreases, F-actin undergoes a transition from a 2D random regime to a 1D biaxially confined regime, leading to an increased effective persistence length. A theoretical calculation shows that the tangent-tangent correlation function in the confined regime shows a minimum, then reaches to a constant at long distances, indicating that confinement induces long-range order in a semi-flexible filament. The location of the minimum of the experimental correlation function is consistent with our theoretical calculation. This work was supported by KISTEP I-03-064, KISTEP IMT-2000-B3-2, MOHW 0405-MN01-0604-0007, NSF DMR 00-80034, 05-03347, 02-03755, 01-29804, NSF CTS-0404444, ONR N00014-05-1-0540, and DOE W-7405-ENG-36. M.C.Choi acknowledges partial support from the Korea Research Foundation Grant KRF-2005-214-C00202. *M.C.Choi et al., Macromolecules, 38, 9882 (2005)

*KAIST, KRISS
†Univ. of Calif. Santa Barbara
‡Univ. of Pennsylvania
§Univ. of Chongqing, China

**15:42**

**W30 5 Conformation of Lysozymes Confined to nano Particles** YUYING WEI, R. KENNETH MARCUS, DVORA PERAHIA, *Chemistry Department Clemson University* Confinement of biomolecules while retaining their activity is a key to many applications. The main challenge lies in the fact that when protein molecules interact with other particles they often lose their tertiary structure, resulting in irreversible reduction of their biological activity. The interfacial interactions of including direct chemical interactions, morphological factors, as well as adsorption under shear and hydrodynamic characteristics of flow next to the interfaces are among the factors that control the configuration. Using lysozyme as a model protein, the effects of physical absorption as a function of the topography of the confining surface from flat to curve with controlled roughness will be discussed. Atomic Force Microscopy together with small angle neutron studies correlated with measurements of retaining the degree of helicity in the system, provide a new insight into the factors that affect the conformational changes in protein upon confinement. While the chemical nature of the surface is an important parameter the topography of the surface determine many characteristics from the amount of absorption to distribution as well as the desoption of the protein.

**15:54**

**W30 6 Interaction forces and surface morphology of microtubule-associated protein tau** KENNETH ROSENBERG, *University of California, Santa Barbara* JENNIFER ROSS, *University of Pennsylvania* ERIC FEINSTEIN, STUART FEINSTEIN, JACOB ISRAELACHVILI, *University of California, Santa Barbara* The microtubule-associated protein tau exists in six isoforms due to alternative mRNA splicing and is localized in the axons of neuronal cells. These isoforms differ by the inclusion of 3 or 4 microtubule-binding imperfect repeat regions (31 aa each) at the C-terminal end of the protein or by 0, 1, or 2 N-terminal end inserts (29 aa each). Using a surface forces apparatus (SFA), we have measured the interaction forces as a function of distance between two symmetric layers of tau protein (all six isoforms) adsorbed onto mica. By comparing the interaction forces between the different isoforms, it is clear that the tau protein forms a brush-like layer on the mica surface which swells upon increasing ionic strength. Additionally, we have looked at an asymmetric system with one surface of tau opposite bare mica. In the asymmetric system of tau and an opposing mica surface, there is a $> 10^2$ increase in the magnitude of this adhesive force suggesting that the tau-mica interaction is much more adhesive than the tau-tau interaction. These data clearly show that tau adsorbed onto mica acts as a spacer and due to the cross-bridging between the mica surfaces, provides a strong adhesion, as has been observed in vitro with microtubules.

**16:06**

**W30 7 Surface Plasmon Resonance Studies of Polysaccharide Self-Assembly on Cellulose** ABDULAZIZ KAYA, ALAN R. ESKER, *Virginia Tech Department of Chemistry (0212) Blacksburg, VA 24061* WOLFGANG G. GLASSER, *Virginia Tech Department of Wood Science and Forest Products (0323) Blacksburg, VA 24061* Wood is a multiphase material consisting of cellulose crystals embedded within a non-crystalline heteroepolysaccharide (hemicellulose) and lignin rich phase. The hierarchial arrangement of these three chief components in wood produces excellent properties like resistance to fracture and toughness. Through the study of polysaccharide self-assembly onto a model cellulose surface, further insight into the interactions between hemicelluloses and cellulose can be gained. In our study, we synthesized pullulan cinnamates with different degrees of substitution of cinnamoyl groups as a model for a hemicellulose with lignin-like moieties. Surface plasmon resonance measurements probe the self-assembly behavior of pullulan and pullulan cinnamate onto a cellulose coated gold surface. Our results suggest that pullulan does not adsorb onto the model cellulose surface, whereas pullulan cinnamate does. These preliminary results signify the important role that lignin-like substituents play on hemicellulose self-assembly onto cellulose surfaces.

**16:18**

**W30 8 Assembly artificial proteins and conjugated porphyrins for biomolecular materials*** TING XU, *University of Pennsylvania* JOE STRZALKA, SHIXIN YE, SOPHIA WU, JIAYU WANG, *University of Massachusetts, Amherst* THOMAS P. RUSSELL, MICHAEL THERIEN, *University of Pennsylvania* J. KENT BLASIE, *University of Pennsylvania* It is non-trivia to incorporate both the electron donor and acceptor in a controlled manner into amphiphilic 4-helix bundle peptides. Extended pi-electronsystems have been designed and tailored, with appropriate donors, acceptors and constituents, exhibit selected light-induced electron transport and/or proton translocation over large distances. We studied the binding between a series of conjugated porphyrins and the designed amphiphilic 4-helix bundles peptides at selected locations. Incorporation of the conjugated porphyrins into the 4-helix bundle did not interfere the protein secondary structure or the 4-helix bundle formation. The amphiphilic protein/cofactor complexes have good thermal stability.The artificial protein Langmuir monolayers, both the apo- and holo-form, can be oriented vectorially at the air/water interface upon compression. GID show a glass-like inter-bundle positional ordering in the monolayer plane. We will discuss the efforts on re-designing the artificial proteins to incorporate them into these nanoporous templates made from diblock copolymers.

*DOE, NSF-MRSEC, NIH

**16:30**

**W30 9 Structural Transitions of F-actin Polyelectrolyte Bundles in the Presence of Strongly Size-mismatched Cations** ROBERT CORIDAN, *Dept. of Physics, University of Illinois, Urbana-Champaign* LORI K. SANDERS, *Dept. of Materials Science and Engineering, University of Illinois, Urbana-Champaign* WUJING XIAN, *Dept. of Materials Science and Engineering, Dept of Bioengineering, University of Illinois, Urbana-Champaign* GERARD C. L. WONG, *Dept of Materials Science and Engineering, Dept. of Physics, Dept. of Bioengineering, University of Illinois, Urbana-Champaign* In the presence of multivalent cations, the polyelectrolyte F-actin exhibits the phenomenon of 'like-charge attraction'. Simple divalent ions cause F-actin to form close-packed bundles with an interstitial 1-D density wave of ions along the length of the bundle. Lysozyme, a nonavalent (+9) cationic globular protein (45Åx25Åx25Å) causes F-actin to form similar bundles, with a larger inter-actin distance and an incommensurate 1-D column of close-packed lysozyme along the three-fold tunnel within the bundle. Using genetically engineered lysozyme with different charges, we examine the competition of these cationic agents and their effect on F-actin bundle structure.

**16:42**

**W30 10 Defect Induced Morphologies of Biopolymer Bundles** AJAY GOPINATHAN, *Department of Phyics, University of California, Santa Barbara* MARK HENLE, *Department of Chemistry and Biochemistry, University of California, Los Angeles* URI RAVIV, *Materials Research Laboratory, University of California, Santa Barbara* DANIEL NEEDLEMAN, *Department of Systems Biology, Harvard University* Bundles of stiff biopolymers, such as actin and microtubules, form important structural elements in the cell, including filopodia, microvili, cilia and contractile rings. These structures perform specific functions that rely crucially on their mechanical properties, which in turn depend on the internal organization of the bundles. Recent experiments on microtubule bundle formation in the presence of multivalent counterions [D. J. Needleman, et. al, Proc. Natl. Acad. Sci., **101** 16099 (2004)] have observed that the bundles adopt static curved configurations whose wavelengths are several orders of magnitude less than their persistence length. In this talk, we show that these severe distortions can be explained by the presence of edge dislocation and twist defects, indicating that these defects could play a significant role itin vivo.

**16:54**

**W30 11 Polyamine Induced Bundling of F-actin** GLENNA Z. SOWA, *University of California, Los Angeles* DAVID S. CANNELL, *University of California, Santa Barbara* EMIL REISLER, *University of California, Los Angeles* ANDREA J. LIU, *University of Pennsylvania* To better understand the mechanism of F-actin bundle formation, we have measured the phase boundary between isotropic F-actin and F-actin bundles as a function of polyamine concentration. F-actin was incubated with spermine or spermidine overnight, and the samples were spun at low speeds to separate bundles from unbundled F-actin. The relative amounts of actin in the pellet and supernatant were determined via gel electrophoresis. With this approach, we have mapped the phase boundary between bundled F-actin and isotropic unbundled F-actin for two F-actin/polyamine linker systems. Surprisingly, the dependence of bundle formation on actin concentration is small to non-existent. At the actin concentrations we studied, actin tends to form bundles at or above a single linker concentration. In order to understand the interactions holding F-actin together in bundles, we used NMR to determine where the polyamines were with respect to the bundled and unbundled phases of actin. Surprisingly, the spermine and spermidine did not segregate with the bundled actin indicating that they do not bind to the actin strongly even though their addition to F-actin solutions induces bundle formation.

**17:06**

**W30 12 The fluctuating-rod limit of semiflexible biopolymers** ASHOK PRASAD, YUKOH HORI, JANÉ KONDEV, *Brandeis University Physics Department* We study the mechanical properties of semiflexible polymers, such as DNA and actin, in the ''fluctuating rod'' limit. This limit is attained when the contour length of the polymer is comparable to its persistence length, or when thermal fluctuations have been smoothed out by a large applied force. In this limit, we compute the exact average end-to-end distance and shape of the polymer for boundary conditions that correspond to different single molecule stretching experiments. We consider both the case of a force applied at one end of the polymer, when the tension is uniform along the chain, and the case of an applied field, when the tension increases linearly. For the latter case, we derive the force-extension relation valid for a wide range of electric field strengths, which may be used to extract the effective charge density of actin in solution. We also show that the experimental condition of axis-clamping by a laser tweezer gives rise to a measurable effect on its force-extension properties. This calculation underscores the importance of taking the entropic effects of the boundary conditions into account in single molecule experiments. This work is supported by NSF DMR-0403997. JK is a Cottrell Scholar of Research Corporation.

**17:18**

**W30 13 Statistical and Mechanical Properties of Semiflexible Polymers in an External Field** YA LIU, BULBUL CHAKRABORTY, *Martin Fisher School of Physics, Brandeis University* Semiflexible polymers such as the double-stranded DNA, are well described by the worm-like chain model originally proposed by Kratky and Porod (Rec. Trav. Chim. 68, 1106, (1949)). Recent work has focused on understanding statistical properties such as their end-to-end distribution function (J.Chem.Phys 121, 6064 (2004), PRE 71, 031803 (2005)) and their mechanical properties in response to a stretching force or the electric field (PRE 72, 041918 (2005)). The problem becomes very complicated unless the long-chain or rod-like-chain approximations for the persistence length are made. Self-avoidance effects are always neglected even for long chain in two dimensions and for confined polymers where these effects could become important. We make use of the Bond Fluctuation Algorithm (Macromolecules 21, 2819(1988)) to study the behavior of semiflexible polymers for all persistence lengths and investigate the relationship of their shape to the persistence length, the chain length and the external field. We will compare our results for the extension of a polymer under a constant stretching with analytical results in weak and strong force limit (PRE 72, 041918 (2005)). This work has been supported by NSF-DMR 0403997.

**SESSION W31: NANOTUBES: DEVICES**
**Thursday Afternoon, 16 March 2006**
**328, Baltimore Convention Center at 14:30**
**Kris Andersen, Naval Research Laboratory, presiding**

**14:30**

**W31 1 High On-Currents in Doped Schottky-Barrier Nanotube Transistors** YUNG-FU CHEN, MICHAEL FUHRER, *Department of Physics and Center for Superconductivity Research, University of Maryland, College Park, MD 20742-4111, USA* For many contact metals, the short channel single-walled carbon nanotube field-effect transistor (SWNT-FET) has been understood as a ballistic Schottky barrier-FET (SB-FET), in which high on- currents may be realized with thin gate dielectrics through narrowing of the SB by the gate field [1]. Recently Ohmic contacts to nanotubes have been achieved through the use of high work function metals; such devices show high on-currents and near-ideal subthreshold swings [2]. Here we demonstrate that SWNTs in ambient on $SiO_2$ are p-doped. Doped SB-SWNT- FETs exhibit high on-currents due to thinning of the SB by doping, but retain the poor subthreshold behavior of SB-FETs. Dopants in SWNT-FETs can be removed by applying up to 50 V drain bias in vacuum, corresponding to dissipated power of $>$ 1 mW. Undoped devices

exhibit much lower on-currents, and intrinsic, ambipolar behavior with symmetric SB. This work is supported by National Science Foundation under Grant No. 0102950. [1] S. Heinze, et al., Phys. Rev. Lett. 89, 106801 (2002). [2] A. Javey, et al., Nature 424, 654 (2003).

**14:42**

**W31 2 Temperature and Carrier-Density Dependence of 1/f Noise in Single-walled Carbon Nanotube Transistors** DAVID TOBIAS, MASA ISHIGAMI, C.J. LOBB, MICHAEL S. FUHRER, *Center for Superconductivity Research, Department of Physics, University of Maryland College Park, College Park, MD 20742* Field-effect transistors (FETs) have been fabricated from individual semiconducting single-walled carbon nanotubes (SWNTs) grown by chemical vapor deposition on $SiO_2$/Si substrates and contacted by metal (Cr/Au) electrodes. We have measured the low-frequency anomalous noise (1/f noise) in such SWNT-FETs as a function of temperature and charge carrier density. This material is based upon work supported by the National Science Foundation under Grant No. 0102950 and the Center for Superconductivity Research.

**14:54**

**W31 3 Optical switching of functionalized carbon nanotube transistors** JULIEN BORGHETTI, VINCENT DERYCKE, PASCALE CHENEVIER, ARIANNA FILORAMO, MARCELLO GOFFMAN, JEAN-PHILIPPE BOURGOIN, *LEM, CEA-Saclay SPEC, 91191 Gif-sur-Yvette, France* STEPHANE LENFANT, DOMINIQUE VUILLAUME, *IEMN, Avenue Poincaré, 59652 Villeneuve d'Ascq, France* Carbon Nanotube (CNT) transistors can emit or detect photons at wavelengths defined by the CNT chirality. To extend their capabilities in optoelectronics, it is important to be able to tune this wavelength independently of the CNT structure. A way to achieve such a goal is to chemically functionalize the CNT. In the present study, we demonstrate that drastic photo-induced modifications of the electrical characteristics of self-assembled CNT transistors functionalized by photoactive polymers can be achieved. We show that the polymer film acts as a wavelength dependent 'optical gate', which is much more efficient than a conventional electrostatic gate and can induce changes in conductance exceeding four orders of magnitude. The switching mechanism involves the creation and separation of photo-excited charges in the polymer, the spatial distribution and relaxation rates of which are studied taking advantage of the very high charge sensitivity of the CNT transistor.

**15:06**

**W31 4 Large Area Aligned Arrays of SWNTs for High Performance Thin Film Transistors.** COSKUN KOCABAS, *University of Illinois Urbana Champaign Department of Physics* SEONG JUN KANG, JOHN ROGERS, *University of Illinois Urbana Champaign Materials Science and Engineering* This talk will emphasize a convenient method for generating large scale, horizontally aligned arrays of pristine, single walled carbon nanotubes (SWNTs). The approach uses guided growth, by chemical vapor deposition (CVD), of SWNTs on Y-cut single crystal quartz substrates. Studies of the growth reveal important relationships between the density and alignment of these tubes, the CVD conditions and the morphology of the quartz. Electrodes and dielectrics patterned on top of these arrays yield thin film transistors (TFTs) that use the SWNTs as effective thin film semiconductors. Channel length scaling of device mobility, on current and off current provide insights into the transport characteristics. Combining the aligned arrays with random networks, which are grown simultaneously through the use of patterned catalysts, yields 'all-tube' based devices. The ability to build high performance devices of this type suggests significant promise for large scale aligned arrays of SWNT in electronics, sensors and other applications.

**15:18**

**W31 5 Field-Effect Transistors Assembled From Functionalized Carbon Nanotubes** CHRISTIAN KLINKE, JAMES HANNON, ALI AFZALI, PHAEDON AVOURIS, *IBM Research Division* We have fabricated field effect transistors from carbon nanotubes using a novel selective placement scheme. We use carbon nanotubes that are covalently bound to molecules containing hydroxamic acid functionality. The functionalized nanotubes bind strongly to basic metal oxide surfaces, but not to silicon dioxide. Upon annealing, the functionalization is removed, restoring the electronic properties of the nanotubes. The devices we have fabricated show high ON current (about 1 uA) and an ON/OFF ratio of more than 1e6.

**15:30**

**W31 6 Template-directed Self-assembly of Carbon Nanotube Field-Effect Transistors** STEPHEN MCGILL, SALEEM RAO, PRADEEP MANANDHAR, *Physics & MARTECH, Florida State University, Tallahassee, FL* SEUNGHUN HONG, *Physics & Nano-Systems Institute, Seoul National University, Seoul, South Korea* PENG XIONG, *Physics & MARTECH, Florida State University, Tallahassee, FL* We pattern self-assembled monolayers (SAMs) of organic molecules to control the interactions between carbon nanotubes and inorganic surfaces. Deposition of the SAMs forms a template that directs the placement and alignment of nanotubes on lithographically defined electrodes to create field-effect transistors (FETs). Our assembly process is highly scalable and we demonstrate parallel fabrication of five FETs on a single substrate. These FETs exhibit large ''on'' currents of $\sim 1\mu$A with ''on/off'' ratios as high as $10^6$. Furthermore, our devices exhibit novel functionality by operating hysteresis-free without passivation of the nanotube or electrode surfaces. These features may lead to enhanced performance for delicate sensing applications utilizing these devices. We discuss the electrical characteristics of these FETs and contrast them with other state-of-the-art devices and assembly strategies. This work has been supported by NSF NIRT grant ECS-0210332.

**15:42**

**W31 7 Gas Sensitivity of Carbon Nanotube Devices*** J. H. CHEN, MASA ISHIGAMI, M. S. FUHRER, E. D. WILLIAMS, *Department of Physics, University of Maryland, College Park, Maryland 20742* We have measured the gas sensitivity of field effect transistors made from individual single-walled carbon nanotubes in an ultra high vacuum environment. We exposed nanotube devices to varying partial pressures of oxygen and argon. We will compare the results to existing theoretical calculations for oxygen sensitivity of carbon nanotubes and discuss the ultimate gas sensitivity for these devices.

*Materials Research Science and Engineering Center at University of Maryland, College Park and Director of Central Intelligence Postdoctoral Fellowship Program

**15:54**

**W31 8 Single Walled Carbon Nanotube-based Aqueous Sensors** SARAH LASTELLA, ARAVIND VIJAYARAGHAVAN, SWASTIK KAR, PULICKEL M. AJAYAN, CHANG Y. RYU, *Rensselaer Polytechnic Institute* Single walled carbon nanotube (SWNT) field effect transistors (FETs) have been utilized as chemical specific sensors by incorporating a sensitizing agent into the nanotube sidewalls. Here we report the non-covalent sidewall functionalization of SWNT FETs through the adsorption of macro-organic molecules. The modified SWNT FETs recognize changes in pH and oxidation states through a change in current flow across the devices. These uniformly dispersed nanotubes, grown directly on the FET substrate prior to electrode deposition, enhance the available tube surface area for molecular adsorption, and thus enhance the signal sensitivity.

**16:06**

**W31 9 Atomic Nanotube Welders.** MORINOBU ENDO, HIROYUKI MURAMATSU, TAKUYA HAYASHI, YOONG-AHM KIM, *Shinshu University, Japan* GREGORY VAN LIER, JEAN-CHRISTOPHE CHARLIER, *Université Catholique de Louvain, Belgium* HUMBERTO TERRONES, *IPICYT, Mexico* MILDRED S. DRESSELHAUS, *MIT, USA* MAURICIO TERRONES, *IPICYT, Mexico* We demonstrate that the incorporation of boron between double walled carbon nanotubes (DWNTs) during thermal annealing results in covalent nanotube ''Y'' junctions, DWNT coalescence and the formation of flattened multi-walled carbon nanotubes (MWNTs). The processes occur via the merging of adjacent tubes which is triggered by B interstitial atoms. In order to demonstrate the unique welder properties of B in the process, we have carried out itAM1 molecular dynamics simulations at high temperatures and itab-initio calculations. We observe that B atom interstitials between DWNTs are responsible for the rapid establishment of covalent connections between neighboring tubes (polymerization). Once B is in the lattice, tube faceting (polygonization) starts to occur, and the electronic properties are expected to change dramatically.

**16:18**

**W31 10 Quantized conductance observed in reversible atomic contacts fabricated by template electroplating using an on-membrane anode*** ZUXIN YE, WENHAO WU, *Texas A&M University* We report a new template electroplating method for fabricating reversible atomic contacts between a long nanowire and a macroscopic contact pad. In comparison to a typical template method using a standing-alone anode, we directly evaporate the anode on one of the porous membrane surfaces. Single nanowires, upon emerging from the pores, make reversible atomic contacts with the on-membrane anode via a self-terminating mechanism. Quantized conductance steps have been observed in a controlled fashion during deposition and dissolution. This method can potentially be applied for the controlled fabrication and integration of nanowires, point contacts, and nanosized interconnects in template-based nanofabrication.

*Supported by NSF Grant No. DMR-0551813.

**16:30**

**W31 11 Structural and Transport Properties of Dielectrophoretically Assembled Interconnects*** BIROL OZTURK, *Department of Physics, Oklahoma State University, Stillwater, OK 74078* ISHAN TALUKDAR, *Department of Physics, Oklahoma State University, Stillwater, OK 74078* PREM THAPA, *Department of Physics, Oklahoma State University, Stillwater, OK 74078* CHARLES BLACKLEDGE, *Department of Physics, Oklahoma State University, Stillwater, OK 74078* DANIEL GRISCHKOWSKY, *School of Electrical and Computer Engineering, Oklahoma State University, Stillwater, OK 74078* BRET FLANDERS, *Department of Physics, Oklahoma State University, Stillwater, OK 74078* Dielectrophoresis was used to form $\sim$ 140nm diameter interconnects composed of gold nanorods between targeted points in a circuit. Cleanroom-based lithographic procedures were used to produce identical arrays of electrodes, improving the sample-to-sample reproducibility of the interconnect-conductances to $\sim$ 10%. Transmission electron microscopy and low temperature conductivity analyses indicate that the Coulomb Blockade associated with the individual nanorods is the primary conductance-limiting feature. To further improve the reproducibility of the structural and transport properties of dielectrophoretic interconnects, we investigate submicron wire formation in aqueous solutions of indium acetate. Our preliminary data show that single crystal wires with submicron diameters may be fabricated from such solutions.

*Supported by the National Science Foundation.

**16:42**

**W31 12 DNA-Functionalized Carbon Nanotubes for Chemical Sensing*** M. CHEN, C. STAII, S. KHAMIS, A.T. JOHNSON, J.E. FISCHER, *U. of Pennsylvania* A GELPERIN, *Monell Senses Center* We demonstrate nanoscale sensors based on single-stranded DNA (ss-DNA) as the chemical recognition site and single-walled carbon nanotube field effect transistors (swCN-FETs) as the electronic readout component. SwCN-FETs functionalized with ss-DNA respond to gaseous analytes that do not cause a detectable current change in bare swCN-FETs. The response differs in sign and magnitude depending on the type of analyte and the DNA base sequence. The sensors maintain a constant response through at least 50 air-analyte cycles, and have response and recovery times on the scale of seconds. Furthermore, ss-DNA is found to chemically gate swCN-FET. The analytes used are found to interact with both the nanotube and the substrate. This sensor is promising for electronic olfaction systems consist of coupled sensor arrays and an odor recognition algorithm. Applications range from homeland security to disease diagnosis.

*C. Staii et al. Nano Lett. 5, 1774 (2005). Support by the Laboratory for Research on the Structure of Matter (NSF DMR00-79909), and US Department of Energy, grant No. DE-FG02-98ER45701 (M.C.).

**16:54**

**W31 13 Electrical transport behavior of all - carbon nanotube - based three terminal junctions*** YUN-HI LEE, JE-MIN YOO, JONG-HEE LEE, *Department of Physics, Korea University, Seoul, Korea* NDPL TEAM, In this study, we propose a process for suspended itin situ lateral growth of all - carbon nanotube(CNT) based junction and report on the high current capacity of the CNT junction, especially, its current (I) response characteristics with and after UV. Furthermore, the analogy between current suppression and reversible switching of capacitor was studied by capacitance(C) spectroscopy. The designed diluted magnetic impurity doped oxide film was adopted as catalyst for the fabrication of all - CNT-based junction. 40 suspended junctions was tested and normally, one junction produced current of a few uA/1um at room temperature. The suspended CNT with the same electrode materials is expected to operate with ambipolarity. The nearly same low barrier height for the hole and electron conduc-

tion was estimated via I-T(K) measurements. Also, the surface of CNT was easily cleaned by low intensity UV treatment, resulting in a highly conductive channel that showed high current carrying behavior. Our result can be applied to develop a practical, accessible system for forming reproducible nanoelectronic junctions as well as to accelerate the realization of all low dimensional molecular devices.

*This work was supported by KRF(Pure Basic Research Group) Program and KOSEF(Nano Basic Technology Project).

**17:06 onardois**

**W31 14 Energy Conversion Efficiency in Nanotube Optoelectronics** FRANÇOIS LÉONARD, *Sandia National Laboratories* DEREK STEWART, *Cornell Nanoscale Facility* We present theoretical performance estimates of nanotube optoelectronic devices under bias. Current-voltage characteristics of illuminated nanotube *p-n* junctions are calculated using a self-consistent non-equilibrium Green's function approach. Energy conversion rates in the tens of percent range are predicted for incident photon energies near the band gap energy. In addition, the energy conversion rate increases as the diameter of the nanotube is reduced, even though the quantum efficiency shows little dependence on nanotube radius. These results indicate that the quantum efficiency is not a limiting factor for use of nanotubes in optoelectronics.

**17:18**

**W31 15 A Novel Nanotube-on-Insulator (NOI) Approach toward Single-Walled Carbon Nanotube Devices** CHONGWU ZHOU, XIAOLEI LIU, DAIHUA ZHANG, *University of Southern California* We present a novel nanotube-on-insulator (NOI) approach to produce high-yield nanotube devices based on aligned single-walled carbon nanotubes. First, we managed to grow aligned nanotube arrays with controlled density on crystalline, insulating sapphire substrates, which bear analogy to industry-adopted silicon-on-insulator substrates. Based on the nanotube arrays, we demonstrated registration-free fabrication of both top-gated and polymer-electrolyte-gated field-effect transistors with minimized parasitic capacitance. In addition, we have successfully developed a way to transfer these aligned nanotube arrays to flexible substrates. Our approach has great potential for high-density, large-scale integrated systems based on carbon nanotubes for both micro- and flexible electronics.

## SESSION W32: GLASSY AND AMORPHOUS SYSTEMS

**Thursday Afternoon, 16 March 2006**
**329, Baltimore Convention Center at 14:30**
**Michael Mehl, Naval Research Laboratory, presiding**

**14:30**

**W32 1 First-principles investigation of pressure-induced amorphization in zeolites** INMACULADA PERAL, JORGE INIGUEZ,* *ICMAB–CSIC* Crystalline zeolites can be transformed into amorphous structures by application of pressure, without ever forming a liquid. Upon release of the applied pressure, some zeolites transform back to their crystalline structure while others do not. Thus, zeolites are very interesting from the point of view of the theories trying to explain *reversible* amorphization by pressure [Cohen et al., JNCS 307-310, 602 (2002)]. On the other hand, recent studies of the amorphization process in zeolites have led to the identification of co-existing phases of the same composition but markedly different densities and degrees of disorder [Greaves et al., Nat. Mats. 2, 622 (2003)]. Further, it has been argued that upon application of pressure (or, equivalently, temperature) zeolites render a low-entropy, low-density, amorphous phase that could constitute a new type of glass, with physical properties that might differ considerably from those of *typical* glasses obtained by slow cooling from the melt. In this talk we will report a first-principles investigation of the structural changes induced by pressure in zeolites. More precisely, we will show results for three zeolites with the so-called LTA structure (Na-ZK4, Na-A, and an idealized $SiO_2$ system with the ZK4 structure). We will discuss the implications regarding the various amorphous phases experimentally found and the reversibility of the amorphization.

*Presenting author

**14:42**

**W32 2 Glass transition and viscosity of simple glasses and liquids*** TAKESHI EGAMI, *University of Tennessee* S. JOSEPH POON, *University of Virginia* VALENTIN LEVASHOV, *University of Tennessee* RACHEL AGA, JAMES MORRIS, *Oak Ridge National Laboratory* The theoretical understanding of liquids and glasses at an atomistic level lags well behind that of crystalline materials, even though they are important in many fields including biology and the medical sciences. We present a simple microscopic model for the glass transition based on topological fluctuations in the bonding network. The model makes predictions for important parameters of the glassy state, such as the glass transition temperature, $T_g$, and the liquid fragility coefficient, $m$, based on microscopic variables. Excellent agreement with a number of experimental observations from metallic glasses is demonstrated. A key to this success is to focus on the dependence on Poisson's ratio, following the work of Novikov and Sokolov,[1] that characterizes the interaction between local density and shear fluctuations. To our knowledge, this is the first model to predict $T_g$ and $m$ quantitatively from microscopic variables. It presents a simple conceptual framework that should provide the basis for a more general microscopic understanding of liquids and glasses, including molecular systems. 1. V. N. Novikov and A. P. Sokolov, Nature, **431**, 961-963 (2004).

*Supported by DOE-BES through DE-AC05-00OR-22725.

**14:54**

**W32 3 Temperature induced density anomaly in Te rich liquid Germanium Tellurides: p versus sp3 bonding?*** CHRISTOPHE BICHARA, *CNRS -CRMCN University Aix-Marseille, France* MARK JOHNSON, *Institut Laue Langevin, Grenoble, France* JEAN-YVES RATY, *University of Liege, Belgium* The density anomaly of liquid $Ge_{0.15}Te_{0.85}$ measured between 633K and 733K is investigated with ab initio Molecular Dynamics calculations at four temperatures and at the corresponding experimental densities. For box sizes ranging from 56 to 112 atoms, an 8 k-points sampling of the Brillouin zone is necessary to obtain reliable results. Contrary to other Ge chalcogenides, no sp3 hybridization of the Ge bonding is observed. As a consequence the negative thermal expansion of the liquid is not related to a tetra-

hedral bonding as in the case of water or silica. We show that it results from the symmetry recovery of the local environment of Ge atoms that is distorted at low temperature by a Peierls-like mechanism acting in the liquid state in the same way as in the parent solid phases.

*JYR acknowledges support by the FNRS, the FAME network of excellence and the NOMADE Region Wallonne contract. Part of this work was done under the auspices of the U.S. DOE at the University of California/LLNL.

**15:06**

**W32 4 Giant photocontraction effects in obliquely-deposited chalcogenide glass thin-films*** M. JIN, P. BOOLCHAND, *University of Cincinnati* T. RAJAGOPALAN, K.L. CHOPRA, *Indian Institute of Technology, New Delhi* $Ge_xSe_{1-x}$ thin-films at several obliqueness angles $\alpha$ (= 0, 20, 45, 60, 80) and compositions x ( = 0.15, 0.20, 0.23, 0.25 and 0.33) were vapor-deposited, and examined in Raman scattering and SEM measurements both in the pristine and illuminated state. The films, placed in an inert ambient, were exposed to Hg lamp radiation, and photo-contraction of the films established using a profilometer. Raman scattering of the pristine and exposed films were studied as a function of depth using a confocal microscope attachment. Our results show (i) Raman scattering of the normally deposited ($\alpha$ = 0) films in the pristine state are similar to those of corresponding bulk glasses, (ii) obliquely deposited films at x = 1/3 reveal Raman lineshapes that change qualitatively with $\alpha$, suggestive of nanoscale phase separation of the films, while those at x = 0.23 show Raman lineshapes that are largely independent of $\alpha$, (iii) the photocontraction effect maximizes in the $0.20 < x < 0.25$ range, confirming the earlier finding (ref1) (iv) light illumination partially undoes effects associated with nanoscale phase separation. Possible interpretation of these results in relation to origin of photocontraction effects will be presented. *Supported by NSF grant DMR 04-56472. 1.Bhanwar Singh, S. Rajagopalan, P. K. Bhat, D. K. Pandya and K. L. Chopra, Solid State Communications, Vol. 29, pp. 167-169 (1979)

**15:18**

**W32 5 Non-perturbative Renormalization Group Study of A Kinetically Constrained Model for Glasses** HAI QIAN, *The James Franck Institute and Department of Physics, The University of Chicago* We study a dynamic field theory, which is based on the dynamic heterogeneity, with the non-perturbative renormalization group (NRG) method. Dynamic heterogeneity has been observed both experimentally, and in numerical simulations. It may play an important role in the physics of glass transition. Dynamic heterogeneity means that the slow dynamics of glass formers is dominated by the spatial fluctuations. And the length scales of dynamically correlated regions increase when the system approaches the glass transition, together with the increase of time scale. This is similar to the conventional dynamic critical phenomena. People have derived a dynamical field theory for a kinetically constrained model based on the Fredrickson-Anderson (FA) model, which puts the dynamic heterogeneity at its core. Here we study this field theory with the NRG method. The NRG method is not restricted to small parameters, and thus can be applied to more general cases. The critical exponents are calculated, and the phase structure is given. Especially the 1D spatial dimension case, which is difficult for the usual perturbative calculation, is also studied. Other possible models are also mentioned.

**15:30**

**W32 6 Self-organization of glass networks in a model with equilibration*** MARC-ANDRÉ BRIÉRE, M.V. CHUBYNSKY, NORMAND MOUSSEAU, *Département de physique and RQMP, Université de Montréal* Recent experimental results suggest the existence of an intermediate phase in covalent glasses attributed to a self-organization of the glass network minimizing its internal stress. While a number of models have been proposed recently to explain this phenomenon, a full understanding of the network self-organization and the intermediate phase is lacking. We modify a previously studied model,[*] in which a network is grown in a way that keeps it stressless, by allowing continuous equilibration as the mean coordination is increased while still avoiding stress. In our model, an unusual intermediate phase appears, in which both rigid and floppy networks have a chance to occur, a result similar to that obtained by Barré *et al.* for less realistic Bethe lattices. We discuss various structural properties of the resulting self-organized networks, as well as some results for the entropy cost of self-organization. [*] M.F. Thorpe, D.J. Jacobs, M.V. Chubynsky, and J.C. Phillips, *J. Non-Cryst. Solids* **266-269**, 859 (2000)

*Supported by MESL (Québec), FQRNT (Québec), NSERC (Canada) and the Canada Research Chair program.

**15:42**

**W32 7 The Impact of Liquid Structure and Long Range Diffusion on Glass Formation and Nanoscale Devitrification*** K. F. KELTON, *Department of Physics, Washington University, St. Louis, MO 63130* Recently, synchrotron X-ray diffraction measurements of electrostatically levitated samples revealed a growing icosahedral order in many undercooled metallic liquids and alloys. In a TiZrNi liquid, this icosahedral order catalyzed the nucleation of a metastable icosahedral phase, instead of the stable C14 tetrahedral Laves phase, confirming a half-century-old hypothesis made by Frank that connects the crystal nucleation barrier with the local structure of the liquid. This is one example of a growing number of cases of multiple order parameter coupling in nucleation, which are not readily described within the framework of the commonly used classical theory of nucleation. The implications for glass formation, nanoscale devitrification and the role of microalloying of such coupled nucleation processes and of a new coupled flux kinetic model for nucleation are discussed.

*Partially supported by NSF under DMR 03-07410, NASA under NNM04AA016 and AFOSR under FA9550-05-1-0110

**15:54**

**W32 8 Thermally Activated Processes in Polymer Glasses** VIVEK PARIHAR, DAVID DROSDOFF, ALLAN WIDOM, *Northeastern University* YOGENDRA SRIVASTAVA, *Northeastern University & University of Perugia, INFN* A derivation is given for the Vogel-Fulcher-Tammann thermal activation law for the glassy state of a bulk polymer. Our microscopic considerations involve the entropy of closed polymer molecular chains (i.e. polymer closed strings). For thin film polymer glasses, one obtains open polymer strings in that the boundary surfaces serve as possible string endpoint locations. The Vogel-Fulcher-Tammann thermal activation law thereby holds true for bulk polymer glass but does not hold true in the ultra thin film limit of polymer glass.

**16:06**

**W32 9 Transient nucleation in a Zr-Ti-Cu-Ni-Al metallic glass*** Y. T. SHEN, K. F. KELTON, *Dept. of physics, Washington University, St. Louis* Upon annealing Zr-Ti-Cu-Ni-Al bulk metallic glasses (BMG) crystallize to a nano-quasicrystal/amorphous composite. To probe the nucleation processes that underlie this microstructure formation we have determined the nucleation rate as a function of temperature, employing the two-step annealing method commonly used in silicate glasses. Samples were first annealed at temperatures where the nucleation rates were high, but the growth rates were low to produce a population of nuclei. These were subsequently grown to an observable size for transmission electron microscopy study by annealing at a higher temperature where the nucleation rate is small. We present the first quantitative time-dependent nucleation data obtained for a metallic glass by this method. The data are analyzed in terms of the classical theory of nucleation and an extended kinetic model that includes the coupling between the interfacial attachment and long-range diffusion fluxes.

*Supported by National Science Foundation under grant DMR 03-07410

**16:18**

**W32 10 The role of Ti in the formation of Zr-Ti-Cu-Ni-Al glasses*** T.H. KIM, A.K. GANGOPADHYAY, L.Q. XING, G.W. LEE, Y.T. SHEN, K. F. KELTON, *Dept. of Physics, Washington U., St. Louis, MO* A.I. GOLDMAN, *Ames Laboratory USDOE and Iowa State U., Ames, IA* R.W. HYERS, *U. Mass, Amherst, MA* J.R. ROGERS, *NASA MSFC, Huntsville, AL* It has been widely reported that glass formation improves in $Zr_{62}Cu_{20}Ni_8Al_{10}$alloys when small amounts of Ti are substituted for Zr. Glasses containing greater than 3 at.% Ti crystallize to a metastable icosahedral phase, suggesting that Ti enhances icosahedral short range order (ISRO) in the liquid/glass, making crystallization more difficult during cooling. Based on itin-situ high-energy synchrotron diffraction studies of electrostatically levitated (ESL) supercooled liquids and rapidly quenched amorphous alloys, we demonstrate ISRO in all cases irrespective of the Ti concentration. Further, our ESL solidification studies show that Ti inhibits surface crystallization, but does not improve glass formation.

*The work at Washington University supported by the NSF under Grant No. DMR 03-07410 and by NASA under contract NNM04AA016.

**16:30**

**W32 11 High-Energy X-ray Diffraction Study of Liquid Structure of Zr-based Binary Alloys** AKITOSHI MIZUNO, SEIICHI MATSUMURA, MASAHITO WATANABE, *Gakushuin University* SHINJI KOHARA, MASAKI TAKATA, *Japan Synchrotron Radiation Research Institute* High-energy (E = 113 keV) synchrotron x-ray diffraction experiments were performed for metallic glass-forming Zr-Cu alloys in the liquid state at high temperatures. Accurate structure information of highly reactive melts has been obtained by applying conical nozzle levitation technique as a containerless method. The total structure factor extracted for the liquid $Zr_{50}Cu_{50}$ alloy near its melting temperature shows a particular shoulder at the high-$Q$ side on the second peak as well as the liquid $Zr_{70}Cu_{30}$ alloy. This feature of structure factor is similar to those of structure factors observed in deeply undercooled metallic liquids or metallic glasses, in which local icosahedral short range ordering was found to exist. With the use of reverse Monte Carlo simulation analysis, it was demonstrated that short-range ordered clusters exist even in the equilibrium liquid state of $Zr_{70}Cu_{30}$ alloy.

**16:42**

**W32 12 Elasticity and conductivity thresholds in solid electrolyte glasses*** D. NOVITA, P. BOOLCHAND, *University of Cincinnati* M. MALKI, F. FAYON, *CNRS-Orleans* M. MICOULAUT, *University of Paris VI* The solid electrolyte glass, AgI, possesses a low mean coordination number [1], and when alloyed in the base oxide glass, $AgPO_3$, steadily lowers the connectivity of the alloyed glass, (AgI)x(AgPO3)1-x, as reflected in reduction of glass transition temperatures $T_g(x)$. Non-reversing enthalpy associated with $T_g$s vanish in the $0.10 < x < 0.35$ range, the reversibility window, which we identify with the Intermediate elastic phase [2]. Glasses at $x < 0.10$ belong to the Stressed-Rigid while those at $x > 0.35$ to the Floppy elastic phase. Electrical conductivity, $\sigma(x)$, reveal a mild increase near $x = 0.10$ as glasses become unstressed, and a pronounced increase near $x = 0.35$, when glasses become floppy. The correlation between $\sigma(x)$ and the elastic phases opens a new paradigm in understanding electrical transport in glasses. Chains of $PO_4$ tetrahedra ( $Q^2$) present in the pristine oxide are steadily cut and eventually transformed into rings as networks become less connected with increasing x, as revealed by Raman and $P^{31}$ NMR measurements. [1] P. Boolchand and W.J.Bresser, Nature **410**, 1070 (2001). [2] S.Chakravarty, D.Georgiev, P.Boolchand & M.M.Micoulant, JPCM **17**, L1-L7 (2005).

*Supported by NSF grant DMR 04-56472.

**16:54**

**W32 13 Chemical alloying induced collapse of reversibility windows in ternary As-S-I glasses*** FEI WANG, *Department of EE, California Polytechnic State University* P. BOOLCHAND, *Department of ECECS, University of Cincinnati* Thermally reversing windows represent glass compositions across which glass transitions are thermally reversing in character. These windows have been observed in several chalcogenide glasses, and are identified[1] with self-organized phases of glassy networks. Upon alloying halogen (iodine) in base chalcogenide glasses (Ge-Se, Ge-S), the reversibility windows collapse[2] about the mean-field rigidity transition. We attempt to understand this behavior better. We have now synthesized ternary glass compositions of the type, $(AsI_3)_x(As_{0.30}S_{0.70})_{1-x}$ and $(AsI_3)_y\ (As_2S_3)_{1-y}$ over wide composition ranges of x and y, and have examined them systematically in Raman scattering and MDSC experiments. Along with earlier results[3] on binary $As_zS_{1-z}$ glasses, the present results permit mapping the reversibility window over the glass forming range of the present As-S-I ternary. The results show the window region to be of nearly triangular shape, with a base extending in the $0.20 < z < 0.27$ range and a vertex located near $y = 0.28$. A possible interpretation of the results will be presented. * Supported by NSF grant DMR-04 -56472 1. P.Boolchand et al.Phil. Mag 85,3823

(2005). 2. Y. Wang et al. Phys. Rev. Lett. 87, 18, 5503 (2001) 3. D.G. Georgiev, Ph.D. Thesis, Univ. of Cincinnati (2003) unpublished

**17:06**

**W32 14 Glass structure and electrical conductivity in $(As_2S_{3\ 1-x}\ (Ag_2S)_x$*** C. HOLBROOK, P. CHEN, D. NOVITA, P. BOOLCHAND, *University of Cincinnati* We have synthesized titled glasses in the $0 < x < 0.16$ range, and have examined them in modulated DSC experiments. The starting materials, $As_2S_3$ and $Ag_2S$ lumps, were reacted in evacuated fused quartz tubings, and glasses synthesized by water-quench of homogenized melts. Thermal measurements used a TA instruments model 2920 operated at 3[r]C/min scan rate and 1[r]C/100s modulation rate. Preliminary results reveal a single glass transition in the $0 < x < 0.05$ range, which steadily decrease from a value of 210[r]C at $x = 0$ to 182[r]C near $x = 0.05$. In contrast, bimodal glass transitions are observed at $x > 0.09$, with one $T_g(1)$ near 167[r]C and the second, $T_g(2)$ near 186[r]C, and with the endotherm associated with $T_g(1)$ steadily increasing with x. Non-reversing enthalpies associated with $T_g$s are found to steadily decrease in the $0 < x < 0.09$ range, to nearly vanish in the $0.10 < x < 0.12$ range and to increase thereafter ( $x > 0.12$).These findings suggest that glasses at low x ( $< 0.09$) are Stressed- rigid, those at $x > 0.12$ Floppy while those in between in the Intermediate phase[1]. The present results correlate well with earlier[2] electrical conductivity results in suggesting the possibility of an elastic origin to the conductivity thresholds in solid electrolyte glasses. 1. P. Boolchand, D.Georgiev and B. Goodman, J.Opto & Adm. Mater. 3, 703 (2001). 2. E.A. Kazakova and Z.U.Borisova, Fiz. Khim.Stekla **6**, 424(1980).

*Supported by NSF grant DMR 04-56472.

**17:18**

**W32 15 New glasses in the alumina-calcia-monazite ($LaPO_4$) system: structural evidence from NMR, Raman scattering and thermal properties*** ROBERT MARZKE, *Physics and Astronomy, Arizona State University, Tempe, AZ 85287-1504* SUSAN BOUCHER, *Chemistry and Biochemistry, Arizona State University, Tempe, AZ 85287-1604* JEREMY PIWOWARCZYK, *Physics and Astronomy, Arizona State University, Tempe, AZ 85287-1504* GEORGE WOLF, *Chemistry and Biochemistry, Arizona State University, Tempe, AZ 85287-1604* A new group of glasses has been synthesized from the well-known compounds $CaAl_2O_4$ and $(CaO)_{12}(Al_2O_3)_7$, melted together with monazite ($LaPO_4$) in compositions containing 2 to > 75% of the latter. Raman and $^{31}P$ NMR spectra in the solid state show that $PO_4$ groups do not share bridging oxygens, i.e. that the materials are orthophosphates. Thermal properties and $^{27}Al$ NMR in both liquid and solid states indicate the presence of a strong aluminate network, based upon $AlO_4$ tetrahedra sharing corners. P/Al TRAPDOR NMR measurements show that P and Al are in close proximity in the glasses, most likely sharing P-O-Al linkages. However, clear and unambiguous signatures of the aluminate network are still sought. Models for the structures of these glasses, drawn from experiment, will be presented.

*Supported by NSF DMR01 16361 and AFOSR F4962-03-1-0346

**SESSION W33: NONEQUILIBRIUM AND TEMPLATED ASSEMBLY**
**Thursday Afternoon, 16 March 2006**
**336, Baltimore Convention Center at 14:30**
**Srinivasa R Raghavan, University of Maryland, presiding**

**14:30**

**W33 1 Designing elastic sheets to self-assemble in a viscous environment** SILAS ALBEN, MICHAEL BRENNER, *Harvard University* A recent work by Boncheva et al. (Proc. Nat. Acad. Sci. 2005 102: 3924-3929) has raised some basic issues about designable self-assembly within the context of planar elastic sheets which fold into 3D structures under magnetic forces. While being agitated in water, millimeter-scale structures were shown to fold with varying success depending on the locations of magnets on the sheets. Our work considers how to design such structures, an understanding of which will be necessary when moving this process to the micron scale. Among the important parameters are the geometry of the flat sheet, the configurations of the magnets, and the ratios of magnetic to elastic forces. We consider this problem using a numerical model of an elastic sheet, and restrict to the simpler case of electrostatic forces in a quasi-static limit. We identify a simple algorithm for choosing configurations of electrostatic charges, and select ratios of charge strength to elastic energy using physical arguments. We then demonstrate our algorithm on dynamical foldings of a sphere and more general geometries, in the overdamped viscous regime. We also give an asymptotic formula for the elastic energy in the thin-plate limit.

**14:42**

**W33 2 Dynamic self-assembly of magnetic particles on the fluid interface: surface wave assisted effective magnetic exchange** ALEXEY SNEZHKO, IGOR ARANSON, WAI-KWONG KWOK, *Materials Science Division, Argonne National Laboratory, 9700 South Cass Avenue, Argonne, IL 60439* Novel dynamic self-assembled multi-segment magnetic structures (''snakes'') induced by a vertical alternating magnetic field in an ensemble of magnetic particles suspended on a liquid/air interface are reported. We demonstrate that these structures are directly related to surface waves in the liquid generated by the collective response of magnetic microparticles to the alternating magnetic field. The segments of magnetic ''snake'' exhibit long-range antiferromagnetic ordering mediated by the surface waves, while each segment is composed of ferromagnetically aligned chains of microparticles. To describe observed magnetic behavior of the generated structures we propose a simple phenomenological model where the effect of surface waves is replaced by an effective exchange interaction. In the framework of the proposed model the effective exchange constants corresponding to different regimes of magnetic driving were extracted from the experimental data.

**14:54**

**W33 3 Demonstration of shape selectivity in depletion-induced colloidal aggregation** STEPHANE BADAIRE, JOSEPH W. WOODY, CECILE COTTIN-BIZONNE, ABRAHAM D. STROOCK, *Dept of Chemical and Biomolecular Engineering - Cornell University* We have developed a set of monodisperse, non-spherical colloids using photolithography in order to elucidate fundamental questions related to the role of shape in defining colloidal phase behaviour and, eventually, to build new micro-

structured materials. Our goal is to use depletion and DLVO forces to induce specific and directional interactions during the aggregation process of these non-spherical colloids. We will first describe the development and basic characterization of these particles, including index of refraction, zeta potential, polydispersity, and surface roughness. We will then present an initial state diagram of depletion-induced structure, and provide mechanistic insight into the role of specific characteristics of the particles in defining this behaviour. We will finally discuss theoretical calculations of the expected interactions and the possibility of generalizing the results to other colloidal systems.

**15:06**

**W33 4 Pattern formation and liquid crystallinity in evaporating drops of gold nanorods.** KYOUNGWEON PARK, VIVEK SHARMA, *School of Polymer, Textile and Fiber Engineering* MOHAN SRINIVASARAO, *School of Polymer, Textile and Fiber Engineering and School of Chemistry and Biochemistry, Georgia Institute of Technology, Atlanta, GA* The drying drops of colloidal rods on glass provide a coffee ring type stain accompanied by formation of highly birefringent deposit, suggesting lyotropic liquid crystalline phase forms prior to deposit formation. Further, Liesegang ring like patterns which have concentric deposits, appear on drying, only under specific conditions, and in optical microscope show similar birefringent bands. Similar experiments done on carbon coated copper TEM grids and observed under TEM, show smectic and nematic-like phases as well as create vortex-like assembly of nanorods reminiscent of defect structures in liquid crystals, and are likewise explained in terms of lowest energy configuration of twist configuration. In the present, work we compliment the rich experimental observations, by proposing mechanisms that explain formation of concentric rings, as well as other complex patterns using both the existing framework based on coffee ring stain models and on basis the observed liquid crystalline phase behavior.

**15:18**

**W33 5 Molecular Detection with Self-Assembled Gold Nanoparticle Wires** J.B. HUTCHISON, *George Washington University* J.A. HOFFMANN, *George Washington University* J.W. SUN, *George Washington University* M.E. REEVES, *George Washington University* Recently, we have reported the creation of gold nanowires by evaporation-driven vertical colloidal deposition (VCD) of gold nanoparticles. Subsequently, we have noted systematic changes in conductivity associated with post-deposition annealing. Here we describe the change in room temperature conductivity of gold nanoparticle wires after exposure to thiol-derivatized molecules. A self-assembled gold nanoparticle wire is immersed into a solution of octadecanethiol (ODT) dissolved in ethanol. An ODT molecule comprises a sulfur atom and a short hydrocarbon chain. The sulfur atoms form metallic bonds with the conduction electrons on the surface of the gold nanoparticles, and the high surface to volume ratio of the wire allows us to see a marked jump in resistance. We have seen roughly a 10 percent increase in the resistance of previously annealed wires when immersed in 2 millimolar ODT solution. Further experiments include measurement of resistance as a function of thiol-concentration and as a function of wire preparation prior to immersion.

**15:30**

**W33 6 Orientational Order of Molecular Assemblies on Inorganic Crystals*** JAEHUN CHUN, *Department of Chemical Engineering, Princeton University* DUDLEY SAVILLE, *Department of Chemical Engineering, Princeton University* JE-LUEN LI, *Department of Chemistry, Princeton University* HANNES SCHNIEPP, *Department of Chemical Engineering, Princeton University* ROBERTO CAR, *Department of Chemistry, Princeton University* ILHAN AKSAY, *Department of Chemical Engineering, Princeton University* Surfactant micelles form oriented arrays on crystalline substrates such as HOPG (Highly Ordered Pyrolytic Graphite) although registration is unexpected since the template unit cell is small compared to the size of a rod-like micelle. In addition, with atomic force microscopy, we show that orientational ordering is a dynamic, multi-molecule process. Interaction energy calculations based on molecular simulations reveal that orientational energy differences on a molecular scale are too small to explain matters. However, treating the cooperative processes as a balance between van der Waals torque on a large, rod-like micellar assembly and Brownian motion shows that orientation is favored. Our study provides a physical insight on regulation of self-assembly structures at small length scale.

*The NASA University Research, Engineering, and Technology Institute on BioInspired Materials (BIMat) under Award No. NCC-1-02037 and the National Science Foundation (MRSEC program) through the Princeton Center for Complex Materials (DMR 0213706)

**15:42**

**W33 7 Vesicle-Templated Supramolecular Assembly of Alginate Nanogels** JENNIFER HONG, *National Institutes of Standards and Technology NIST/University of Maryland College Park* WYATT VREELAND, *NIST, Analytical Chemistry Division CSTL* SRINIVASA RAGHAVAN, *University of Maryland College Park. Department of Chemical & Biomolecular Engineering* LAURIE LOCASCIO, *NIST, Analytical Chemistry Division CSTL* MICHAEL GAITAN, *NIST, Semiconductor Electronics Division EEEL* In this work, large uni- and multilamellar dipalmitoyl phosphatidylcholine (DPPC) liposomes (800-900 nm in diameter) were used as templates for the formation of alginate gels. DPPC liposomes encapsulating sodium alginate were prepared in a 15 mM NaCl buffer solution by the solvent injection method, followed by several freeze/thaw cycles to achieve higher encapsulation efficiency and larger vesicle size. Purified liposomes were placed in a 10 mM CaCl2 buffer solution and permeabilized by heating and cooling over the phase transition temperature (Tm) of DPPC. The increased membrane permeability at the Tm allowed calcium ions from the surrounding buffer solution to traverse the membrane to the interior region and subsequently crosslink the encapsulated alginate. Removal of the lipid by detergent resulted in nanogels that were similar in size (800-900 nm in diameter) to the template liposome, as characterized by multi-angle and dynamic light scattering techniques. In the future these nanogels may be useful for single-molecule encapsulation or controlled release applications.

**15:54**

**W33 8 Self-Assembly of Two Dimensional Hard Rod Fluids in the Presence of Surface Barriers** DEREK A. TRIPLETT, KRISTEN A. FICHTHORN, *The Pennsylvania State University* Hard rods are interesting building blocks for assembly as they organize themselves into different phases depending on their aspect ratio and concentration. Much work has been done to develop an understanding of the various phases exhibited by bulk, hard-rod flu-

ids in two and three dimensions. For applications in nanoelectronics, it is desirable to be able to assemble nanowires into various structures conducive to nanocircuitry. In this work, we use Monte Carlo simulations to examine the phase behavior of two different systems involving two-dimensional, colloidal nanowires. In the first study, we probe the influence of regularly spaced surface barriers on the ordering of two-dimensional hard rods. By varying the spacing between the barriers and their size relative to the rods, we demonstrate that a number of interesting phases can be achieved, indicating that surface barriers can effectively tune the alignment of the rods. In a second study, we probe the hard-sphere templated assembly of colloidal nanowires. We demonstrate that a number of interesting and potentially beneficial phases occur as the rod length relative to the sphere diameter, rod aspect ratio, and concentration is varied.

**16:06**

**W33 9 Multipolar interaction model for microtubule self-assembly*** KYLE GUSTAFSON, *Univ. of MD, Dept. of Physics, IREAP* JUSTIN STAMBAUGH, *MIT Lincoln Lab.* WOLFGANG LOSERT, *Univ. of MD, Dept. of Physics, IPST and IREAP* Tubulin protein monomers (m = 50 kDa, d = 4-5 nm) are known to self-assemble into biologically significant structures called microtubules. Calculations for microtubule models using the full crystallographic structure of tubulin are prohibitive. As a substitute, we investigate a simpler multipolar interaction model of tubulin which can capture important features of microtubules. We present energy-minimization calculations showing that a four point-charge rectangular model reproduces the 0.93 nm staggering of observed microtubules. We then attempt to validate these static Coulomb calculations with molecular dynamics (MD) using NAMD (from the Theoretical and Computational Biophysics group at the University of Illinois). These simulations include electrostatic interactions, stiff bonded interactions, a Lennard-Jones potential and Langevin damping. The results of the MD simulations are strongly dependent on each of these influences. We find stable filaments of tubulin using the multipole model in MD simulations. When these filaments are combined into a realistic microtubule in MD, an energy minimum is found which supports a stable tube. The study encompasses fraying of tube ends, staggering angle, and ring stability for tubulin and microtubules based on our simple, four charge multipolar model.

*The primary author is supported by a Fannie and John Hertz Foundation Graduate Fellowship.

**16:18**

**W33 10 Thermoreversible Vesicle-to-Micelle Transitions in Surfactant-Salt Mixtures** AIMEE KETNER, TANNER DAVIES, SRINIVASA RAGHAVAN, *Department of Chemical and Biomolecular Engineering, University of Maryland, College Park, MD 20742* Mixtures of the cationic surfactant, CTAB and the organic compound, 5-methyl salicylic acid (5mS) spontaneously self-assemble into unilamellar vesicles at room temperature. Upon heating, these vesicles undergo a thermoreversible transition to wormlike micelles. This phase transition results in a 1000-fold increase in the solution viscosity with increasing temperature. Small-angle neutron scattering (SANS) measurements show that the phase transition from vesicles to micelles is a continuous one, with the vesicles and micelles co-existing over a range of temperatures. A mechanism for the above phase transition is proposed, based on the desorption of bound aromatic counterions from the vesicle as a function of temperature.

**16:30**

**W33 11 Self-assembly models for lipid mixtures** DIVYA SINGH, *Johns Hopkins University* LIONEL PORCAR, *NIST Center for Neutron Research* PAUL BUTLER, *NIST Center for Neutron Research* URSULA PEREZ-SALAS, *UC, Irvine* Solutions of mixed long and short (detergent-like) phospholipids referred to as ''bicelle'' mixtures in the literature, are known to form a variety of different morphologies based on their total lipid composition and temperature in a complex phase diagram. Some of these morphologies have been found to orient in a magnetic field, and consequently bicelle mixtures are widely used to study the structure of soluble as well as membrane embedded proteins using NMR. In this work, we report on the low temperature phase of the DMPC and DHPC bicelle mixture, where there is agreement on the discoid structures but where molecular packing models are still being contested. The most widely accepted packing arrangement, first proposed by Vold and Prosser had the lipids completely segregated in the disk: DHPC in the rim and DMPC in the disk. Using data from small angle neutron scattering (SANS) experiments, we show how radius of the planar domain of the disks is governed by the effective molar ratio $q_{eff}$ of lipids in aggregate and not the molar ratio $q(q = [\mathrm{DMPC}]/[\mathrm{DHPC}])$ as has been understood previously. We propose a new quantitative (packing) model and show that in this self assembly scheme, $q_{eff}$is the real determinant of disk sizes. Based on $q_{eff}$, a master equation can then scale the radii of disks from mixtures with varying $q$ and total lipid concentration.

**16:42**

**W33 12 End-to-End Adhesion of Short Duplex DNA Oligomers** TOMMASO BELLINI, *University of Milano, Italy* NOEL CLARK, *University of Colorado* The classic model for the formation of liquid crystal phases of rod shaped objects was presented by Onsager, who showed that hard rods of length L and diameter D form a nematic phase when volume fraction is $f > fc = 4D/L$. This criterion is obeyed reasonably well for rod-shaped nucleosomal [150 base pair (bp)] B-DNA duplexes (L = 50nm, D = 2nm). Recently we found, however, that very short duplex B-DNA oligomers, 6bp – 20bp (2 to 6nm) in length, form similar nematic and columnar LC phases, even though their L/D ratio is almost 1 and $f << fc$. We attribute these phases to intermolecular interaction which provides an end-to-end adhesion force between these short oligomers to form extended anisotropic ''living polymers.'' The theory of the formation of such anisotropic aggregates will be reviewed and applied to the DNA observations. Work supported by NSF MRSEC Grant DMR 0213918 and NSF Grant 0072989.

**16:54**

**W33 13 Modeling of fractal intermediates in the self-assembly of silicatein filaments*** MEREDITH MURR, *UCSB* GUNJAN THAKUR, *UCSB* IGOR MEZIC, *UCSB* DANIEL MORSE, *UCSB* Silicateins are proteins with catalytic, structure-directing activity that are responsible for silica biosynthesis in certain sponges, Self-assembly of the silicatein monomers and oligomers was previously shown experimentally (Murr and Morse 2005) to form fibrous structures through the formation of diffusion limited, fractally patterned aggregates on the path to filament formation. We present a diffusion-limited aggregation (DLA) based model that is capable of capturing the basic properties of this self-assembly process. The Silicatein oligomer is modeled with three sites of attachment. Rules of attachment are specified that allow for specific interaction between these sites when oligomers are in proximity. The process differs from a DLA process in the follow-

ing: 1) The process of aggregation is continued dynamically, i.e. the growing structures are spatially distributed and keep diffusing as they are growing 2) The molecules are oriented. Thus rotational diffusion is important. 3) The attachment can happen at more than 1 site and the strength of the active sites can be varied. We show that the self-assembled structures have a good level of similarity with the in-vitro experimental results. We quantify this by comparing the fractal dimension of the experimental data and the model output.

*Partially funded by the Institute for Collaborative Technologies, UCSB.

**17:06**

**W33 14 Structure of Porous Columns Self-assembled from Dendritic Dipeptides*** PAUL HEINEY, MIHAI PETERCA, VENKAT BALAGURUSAMY, *Physics Dept., Univ. of Pennsylvania* STEVEN HUDSON, *National Inst. of Standards and Technology* ANDRES DULCEY, VIRGIL PERCEC, *Dept. of Chemistry, Univ. of Pennsylvania* Synthetic pores are an important step in the development of biomimetic materials incorporating features such as trans-membrane channels, gene delivery, protein folding, and selective encapsulation. We have used small-angle xray scattering to study helical pores self-assembled from dendritic dipeptides. The main features of the supramolecular assembly are computed by least-squares fitting the parameters of a simplified structural model to the x-ray diffraction data. This work reports the supramolecular assembly temperature stability and conformational changes of the 3-dimensional packing as a function of dipeptide structure and stereochemistry. The results provide a methodology to design the synthetic pores in order to control the pore size and separation at the Å level, according to the desired function.

*Supported by the MRSEC program of the National Science Foundation under award DMR05-20020.

**17:18**

**W33 15 X-ray Study of the Electrical Double Layer at the Oil - Water Interface*** ALEKSEY TIKHONOV, *CARS-The University of Chicago* Our understanding of the structure of the insulator/electrolyte solution interface is of fundamental importance in describing electrochemical processes in systems involving membranes, absorbers, catalysts, surfactants, or surfaces of other dielectrics. Due to the specific interaction of the solvent with the insulator, a heterogeneous highly polarized region or an electrical double layer forms at the boundary between bulk phases. We studied the spatial structure of the transition region between n-hexane (insulator) and silica sol (electrolyte) solution by x-ray scattering. The structure factor of the interface and the angular dependence of the grazing incidence small-angle scattering can be explained by the interfacial model, which agrees with the theory of the electrical double layer, shows the separation of positive and negative charge, and consists of three layers, i.e., a thin layer of $Na^+$, a monolayer of nanocolloidal particles as the part of the diffuse layer, and a low-density layer sandwiched between them.

*Brookhaven National Laboratory is supported by U.S.D.O.E., Contract No. DEAC0298CH10886. X19C is partially supported through funding from the ChemMatCARS National Synchrotron Resource and the University of Chicago.

**SESSION W34: FLUID STRUCTURE & PROPERTIES**
**Thursday Afternoon, 16 March 2006**
**337, Baltimore Convention Center at 14:30**
**Steve Granick, University of Illinois, presiding**

**14:30**

**W34 1 Scaling fields and the nature of liquid-gas asymmetry in fluids** JINGTAO WANG, *University of Maryland* CLAUDIO CERDEIRIÑA, *Universidad de Vigo, Spain* MIKHAIL ANISIMOV, JAN SENGERS, *University of Maryland* Fisher and coworkers [Phys. Rev. Lett. **85**, 696 (2000); Phys. Rev. E **67**, 061506 (2003).] recently suggested that in fluids the two theoretical scaling fields, commonly known as ''ordering'' and ''thermal,'' are mixtures of three physical fields, namely, chemical potential, temperature, and pressure. We have examined experimental consequences of this formulation (''complete scaling'') with regard to the asymmetry of vapor-liquid coexistence in real fluids. By analyzing the coexisting curves of various fluids, we have shown that the vapor-liquid asymmetry originates from two different sources: one from mixing of chemical potential and pressure into the thermal field and another one from mixing of pressure into the ordering field. The first source is attributed to a correlation between entropy and density, whereas the second source is associated with the excluded volume. Real fluids can be mapped into the symmetric lattice-gas (Ising-like) model by a redefinition of the order parameter that can be now expressed through a combination of density, entropy, and molar volume. We have also demonstrated which molecular parameters of fluids control these two sources of vapor-liquid asymmetry.

**14:42**

**W34 2 NMR characterization of complex fluids by diffusion – relaxation distribution functions** MARTIN HURLIMANN, *Schlumberger - Doll Research* ALBINA MUTINA, *Kazan State University, Russia* Many natural fluids are complex mixtures of different types of molecules. As an example, the molecular composition of crude oils typically consists of molecules with a number of carbon atoms that range between one to over 100. In addition to the diverse size, the constituent molecules can be classified into different chemical classes, such as saturates, aromatics, resins and asphaltenes. It is well known that measurements of diffusion and NMR relaxation times can give information on molecular size. We demonstrate that two-dimensional diffusion – relaxation time distribution functions, f(D,T2), can provide a more unique fingerprint of complex fluids with information on both chain length distribution and chemical composition. The new approach is illustrated with results for different crude oils. The experiments were conducted at a Larmor frequency of 5 MHz and temperatures between 10 C and 58 C. The measurements show a strong correlation between the distributions of diffusion coefficients and relaxation times that are sample specific. The diffusion - relaxation correlation function provides information on the correlation between the rotational and the translational diffusion coefficients of each component of the fluid.

**14:54**

**W34 3 Structural Change of the Mixtures of Ionic Liquid and Water Studied by Infrared Absorption Spectroscopy** DOSEOK KIM, YOONNAM JEON, JAEHO SUNG, *Department of Physics and Interdisciplinary Program of Integrated Biotechnology,*

*Sogang University, Seoul 121-742 Korea* YUKIO OUCHI, *Department of Chemistry, Nagoya University, Chikusa-ku, Nagoya 464-8602 Japan* Infrared absorption spectra of the mixtures of ionic liquid and water (1-butyl-3-methylimidazolium tetrafluoroborate, $[BMIM]BF_4$) with varying concentrations were obtained by Attenuated Total Reflection (ATR) method. Investigation of the spectra in the OH-stretch vibration range indicated the structural change of the water with the change in the concentration. At very low concentration of water, two peaks around $3600cm^{-1}$ were assigned to the monomeric form of water molecules weakly hydrogen bonded to the $BF_4^-$ anions. With the increase in the water concentration, the broad feature at $\sim 3460cm^{-1}$ corresponding to the bulk water took over the above monomeric peaks, which gradually redshifted with the increased water concentration. In the range from 2800 to $3200cm^{-1}$ for the various CH-stretch vibration modes in the cation, the peaks in this ranged blueshifted with the increase in the water concentration. This blueshift was as much as $\sim 7cm^{-1}$ for the $CH_3$ vibration modes of butyl chain while it hardly changed for the modes for the CH attached to the imidazolium core, suggesting varying degree of interactions between the carbon-bonded hydrogen and the water molecules.

**15:06**

**W34 4 Weighted density functional theory for water** SAHAK PETROSYAN, DAVID ROUNDY, JEAN-FRANCOIS BRIERE, TOMÁS ARIAS, *Cornell University* We report a weighted density functional theory for water that correctly describes bulk properties of water as well as perturbations at large and small length scales. Calculation of the free energy of solvation for hard sphere solutes of different sizes verifies that this functional gives a simple description of the hydrophobic effects in water. Use of this functional within a joint-density functional theory framework allows a rigorous replacement of molecular water with a continuum in Kohn-Sham calculations of systems in equilibrium with a solution.

**15:18**

**W34 5 Small-angle neutron scattering study of pH dependence of the liquid structure factor of concentrated solutions of eye lens gamma-B crystallin** KENNETH DESMOND, GEORGE THURSTON, *Department of Physics, Rochester Institute of Technology* ANNA STRADNER, PETER SCHURTENBERGER, *Department of Physics, U. Fribourg* We are evaluating the pH dependence of the liquid structure of aqueous solutions of the eye lens protein, gammaB crystallin, near its critical point for liquid-liquid phase separation, to help evaluate the influence of protein charge on the phase separation. We have obtained small-angle neutron scattering data from gammaB crystallin solutions at pH 6.4, 7.1 and 7.4 in a 0.1 M sodium phosphate buffer, and at pH 4.5 in a 0.020M sodium acetate buffer, all in D2O. Protein concentrations ranged from 6 to 260 mg protein/ml solution and the scattering vector magnitude (q) ranged from 0.004 to 0.45 inverse Angstroms. At pH 6.4 to 7.4 liquid structure factors vs. concentration and temperature near the cloud point for liquid-liquid phase separation are well represented, in general, by the Baxter sticky sphere model. In contrast, at pH 4.5, concentrated gammaB shows a very different liquid structure indicating highly repulsive interprotein interactions, consistent with both high net protein charge and reduced screening.

**15:30**

**W34 6 Phase behavior and mixing-demixing transitions in binary liquid mixtures with spherical and non-spherical interactions*** ENRIQUE DIAZ-HERRERA, *Depto. de Fisica, UAM-I (MEXICO)* GUILLERMO RAMIREZ-SANTIAGO, *Instituto de Fisica, UNAM (MEXICO)* J. ANTONIO MORENO-RAZO, *Depto. de Fisica, UAM-I (MEXICO)* We have carried out extensive equilibrium molecular dynamics simulations to study the temperature versus density phase diagrams and the mixing-demixing transition line in fluid equimolar binary mixtures modeled by: (i) Lennard-Jones, (ii) Stock-Mayer, and (iii) Gay- Berne molecular interactions. These studies are performed as function of miscibility parameter, $\alpha = \epsilon_{AB}/\epsilon_{AA}$, where $\epsilon_{AA} = \epsilon_{BB}$ and $\epsilon_{AB}$ stand for the parameters related to the attractive part of the intermolecular interactions for similar and dissimilar particles, respectively. When the miscibility of the Lennard-Jones mixture varies in the range $0 < \alpha < 1$, a continuous critical line of consolute points $T_{cons}(\rho)$, appears. This line intersects the liquid-vapor coexistence curve at different positions depending on the values of $\alpha$, yielding mainly three different topologies for the phase diagrams. These results are in qualitative agreement to those found previously for square well and hard-core Yukawa binary mixtures. We also carry out a detailed study of the liquid-liquid interfacial and liquid-vapor surface tensions, as function of temperature and miscibility as well as its relationship to the topologies of the phase diagrams. Similar studies and analysis are also performed for Stock-Mayer and Gay-Berne binary mixtures.

*Supported by DGAPA-UNAM IN110103 & CONACYT 43596-F

**15:42**

**W34 7 Confined Fluids: the Time Variable in the Force-Distance Profile** JANET WONG, SUNG-CHUL BAE, STEVE GRANICK, *Department of Materials Science and Engineering, University of Illinois at Urbana-Champaign* Hitherto-overlooked time dependence is known to play a prominent role in determining the friction of confined fluids. In this study, for the first time we introduce the time variable into measuring force-distance profiles of several simple alkane fluids. The existence of near-surface layered structures in confined fluids is generally manifested as oscillatory forces in force-distance profiles obtained using surface forces apparatus (SFA) and atomic force miscroscopy (AFM) experiments. While it is generally agreed that the rate of the experiment should be slow enough to achieve a quasi-static state, it is less clear what the appropriate rate should be. In this study, while maintaining the experimental time scale uniformly slow enough to avoid trivial hydrodyanamically-induced surface deformations, we demonstrate time dependence in the measured force-distance profile. The role of time scale on the actual structure of the confined fluid will be discussed.

**15:54**

**W34 8 Spectroscopic Observation of Fluid Molecular Alignment in a Molecularly-Thin Confined Geometry** MINSU KIM, SHAN JIANG, SUNG CHUL BAE, STEVE GRANICK, *Department of Materials Science and Engineering, University of Illinois at Urbana-Champaign* For the first time, we present data of molecular alignment of a linear chain (1,3-dicyanopropane) under confinement. Confinement was produced between two mica surfaces within a surface forces apparatus (SFA) and measurements employed confocal Raman spectroscopy. We focused on the $CH_2$ symmetric stretch vibrations and CN triple bond stretch vibrations. A polar plot of Raman band intensity as a function of incident light polarization allows us to determine the orientation and order

parameter of alignment. It is confirmed that alignment can be achieved in molecularly-thin films. The decrease of alignment as the film thickness increases will be mentioned. Also, the effect of shear on molecular alignment will be discussed.

**16:06**
**W34 9 Active Microrheology of Dense Colloidal Suspensions** ALEXANDER MEYER, ERIC M. FURST, *Department of Chemical Engineering, University of Delaware* We investigate the active microrheology of a colloidal suspension using laser tweezers. The experimental system described here is composed of a hard sphere suspension of fluorescent, index-matched poly(methyl methacrylate) particles seeded with a low concentration of index-mismatched melamine probes. The probe particles are held in an optical trap and subjected to a uniform flow, enabling measurements of the suspension microrheology. Additionally, confocal microscopy is used to obtain non-equilibrium microstructural information. An anisotropic pair distribution function, with a dense region at the leading surface of the probe and a wake trailing it, is observed as the Péclet number increases to much greater than unity. This structural transition gives rise to a shear thinning regime in the measured microviscosity. The results are in qualitative agreement with recent simulation [I. C. Carpen and J. F. Brady, J. Rheol. 49, 1483-1502 (2005)], and demonstrate the non-linear microrheology of colloidal suspensions.

**16:18**
**W34 10 Nonlinear microrheology of wormlike micelle solutions using magnetic nanowire probes** NATHAN CAPPALLO, CLAYTON LAPOINTE, ROBERT L. LEHENY, DANIEL H. REICH, *Johns Hopkins University* Using ferromagnetic Ni nanowires we investigate the local mechanical properties of wormlike micelle solutions composed of equimolar concentrations of the surfactant cetylpyridinium chloride (CPCl) and sodium salicylate (NaSal). Rotating the nanowires with external magnetic fields, we access both linear and nonlinear regimes of the fluid's rheology. The linear viscosity at low rotation rates is strongly temperature dependent as expected from mechanical rheometry experiments. At high rotation rates the viscosity exhibits pronounced shear thinning that is independent of temperature. The onset of the nonlinear response is characterized by a hysteretic shear thickening that is strongly dependent on temperature, but has no counterpart in the macroscopic rheometry. Further, the nonlinear regime coincides with a transient, anisotropic shear-induced state in the fluid that generates a torque on the wire, causing it to tip out of the plane of rotation when the field is removed.

**16:30**
**W34 11 Myelin figures: an Elastic Instability?** LING-NAN ZOU, SIDNEY R. NAGEL, *The James Franck Institute, the University of Chicago* Myelin figures form when certain lamellar phase surfactants swell upon exposure to water. The formation of these myelins, which are tubular structures composed of multiple bilayers of surfactant, is puzzling because it represents the formation of a higher bending-energy configuration from a lower bending-energy initial state. We show that single myelins can be produced in isolation and require a driving force to form and grow; they retract into their parent structure when the driving is removed. We present a model, consistent with our experimental observations, where the formation of myelins is due to an elastic instability of the lamellar phase under internal stress. We propose an experiment to test of this model in comparison to other models, such as that of Huang et al.[1] [1]J.-R. Huang, L.-N. Zou, and T. A. Witten, Eur. Phys. J. E (2005). DOI: 10.1140/epje/e2005-00035-8.

**16:42**
**W34 12 Charge fluctuations and correlations in finite electrolytes** YOUNG C. KIM, *Laboratory of Chemical Physics, NIDDK, NIH, Bethesda, 20892* MICHAEL E. FISHER, *Institute for Physical Science and Technology, University of Maryland, College Park, 20742* Charge fluctuations, $\langle Q_\Lambda^2 \rangle$, for the 1:1 equisize hard-sphere electrolyte with the diameter $a$ are computed via grand canonical Monte Carlo simulations, where $Q_\Lambda$ is the total charge inside a subvolume $\Lambda$ contained in a simulation box of dimensions $L \times L \times L$ with periodic boundary conditions. The charge fluctuations increase like the surface area $|\partial\Lambda|$ as $\Lambda$ increases, even for small system sizes $L \leqslant 12a$. For slabs of dimensions $L \times L \times \lambda L$ with $0 < \lambda < 1$, the scaled charge fluctuations, $\langle Q_\Lambda^2 \rangle / |\partial\Lambda|$, approach the thermodynamic limits exponentially fast. The extrapolations to $L \to \infty$ then yield the Lebowitz length, $\xi_L(T,\rho)$, where densities $\rho \lesssim 3\rho_c$ and temperatures $T \gtrsim T_c$ have been studied. An exact asymptotic expression is obtained for $\langle Q_\Lambda^2 \rangle$. This enables one to compute the charge correlation length $\xi_Z(T,\rho)$ precisely. The results for $\xi_Z(T,\rho)$ agree with Debye-Hückel-type theories at low densities, but show deviations as the density increases. Charge oscillations at higher densities are also observed, as anticipated theoretically. [1] Y. C. Kim, E. Luijten, and M. E. Fisher, Phys. Rev. Lett. **95**, 145701 (2005).

**16:54**
**W34 13 Solid or Liquid ? – Kinetically induced solidification in a simple nanoconfined liquid*** PETER HOFFMANN, *Wayne State University* GEORGE MATEI, *Wayne State University* SHIVPRASAD PATIL, *Wayne State University* AHMET ORAL, *Bilkent University* For many years there has been a controversy regarding the supposed solidification of simple liquids when they are confined to a few nanometer film thickness. By using a novel, ultra-small amplitude Atomic Force Microscopy (AFM) technique, we have found that solidification in these systems seems to be due to a kinetic effect and does not occur in thermodynamic equilibrium. In particular, we studied OMCTS confined between a flat silicon surface and a silicon tip and found that at very low approach speeds ( < = 0.3 Å/sec) the confined fluid remains liquid-like with no change in mechanical relaxation time from the bulk, although ordering is observed in the stiffness and damping of the film. However, when approaching the tip slightly faster at or above 6 Å/sec, the liquid suddenly changes properties dramatically. In the ordered regime, damping is greatly reduced and the mechanical relaxation times show large peaks, indicating an elastic, solid-like response. This result suggests that the observed solidification is a non-equilibrium effect induced at very long time scales.

*Funding is acknowledged from NSF-MRI and NSF-CAREER

**17:06**
**W34 14 Investigation of Liquid Transport/Diffusion through a Nanopore Driven by a Constant Pressure/Chemical Potential**

**Difference.** CUNKUI HUANG, *University of Alberta* KUMAR NANDAKUMAR, *University of Alberta* PHILLIP CHOI, *University of Alberta* LARRY KOSTIUK, *University of Alberta* Fluid transport/diffusion through a nanopore in a membrane was investigated by using a novel molecular dynamics approach proposed in this study. The advantages of this method, relative to dual-control-volume grand-canonical molecular dynamics (DCV-GCMD), are that it eliminates disruptions to the system dynamics that normally created by inserting or deleting particles from control volumes, and that it functions well for dense systems as the number of particles in the studied system remain fixed. Using this method, we examined liquid argon transport/diffusion through a nanopore by performing non-equilibrium molecular dynamics (NEMD) simulations under different back-pressures/chemical potentials. The MD code was validated firstly by comparison with published experimental data, and NEMD results of the present method show that constant pressure/chemical potential difference across the membrane was readily achieved. The soundness of classical Navier-Stokes (NS) solutions for these nanochannel flows was also checked by direct comparison between the NS predictions and results from the proposed NEMD method. The density distributions along the nanopore for both methods were found to be significantly different, but the velocity profile had a similar pattern, although some difference between them exists.

**17:18**
**W34 15 Phase behavior in binary fluid mixtures with spherical and non-spherical interactions** ENRIQUE DIAZ-HERRERA, *Universidad Autonoma Metropolitana (Mexico)* GUILLERMO RAMIREZ-SANTIAGO, *Instituto de Fisica, UNAM (Mexico)* J. ANTONIO MORENO-RAZO, *Universidad Autonoma Metropolitana (Mexico)* We have carried out extensive MD simulations to study the T vs. $\rho$ phase diagram and the mix-demix transition in fluid binary mixtures with (1) Lennard-Jones, (2) Stock-Mayer and (3) Gay-Berne molecular interactions. This analysis is performed in terms of the miscibility parameter, $\alpha = \epsilon_{AB}/\epsilon_{AA}$, with $\epsilon_{AA} = \epsilon_{BB}$. When the miscibility of the mixture is in the range $0 < \alpha < 1$, a continuous critical line of consolute points appears. This line interscts the LV coexistence curve at different positions depending on the value of $\alpha$, yielding mainly three different topologies for the phase diagrams. We also carried out a detailed study of the interfacial properties as function of $T$ and $\alpha$.

**17:30**
**W34 16 Vectorial Loading of Processive Motor Proteins: Microtubule buckling experiment revisited** MICHAEL E. FISHER, *Institute for Physical Science and Technology, University of Maryland, College Park, MD 20742,* YOUNG C. KIM, *Laboratory of Chemical Physics, NIDDK, NIH, Bethesda, MD 20892* Experiments on the motor protein kinesin by Howard and coworkers (1996) observed the buckling of partially clamped microtubules caused by bound motors responding to the induced parallel, $F_x$, and perpendicular, $F_z$, load components. To analyze such results, we have applied simple mechanochemical models for vectorial loads $F = (F_x,F_y,F_z)$ by implementing a three-dimensional free-energy landscape formulation. An expression for the velocity, $V(F_x,F_z;[ATP])$, is obtained by fitting to the velocity and randomness data of Block and coworkers (2003) who imposed both resisting ($F_x < 0$) and assisting ($F_x > 0$) loads. While our results agree qualitatively with the buckling experiments, the analysis predicts that the velocity *decreases* under perpendicular loading ($F_z > 0$) contrary to the conclusion of Howard and coworkers. This suggests the possibility that the geometry of stressed microtubules might influence the mobility of kinesin motors.

[1] Y. C. Kim and M. E. Fisher, J. Phys.: Condens. Matter 17, S3821 (2005).

**SESSION W36: FOCUS SESSION: OPTICAL PROPERTIES OF NANOSTRUCTURES OF SI & GAAS**
**Thursday Afternoon, 16 March 2006; 339, Baltimore Convention Center at 14:30**
**Matt Doty, Naval Research Laboratory, presiding**

***Invited Papers***

**14:30**
**W36 1 Excitonic Effects and the Optical Properties of Silicon Nanowires.***
M.Y. CHOU, *Georgia Institute of Technology*

Semiconductor nanowires have potential applications in many fields such as optoelectronics, photovoltaic cells, and especially device miniaturization. The excited-state properties are of critical importance in the design of these functional devices. The low dimensionality and reduced size tend to strengthen the effective Coulomb interaction in these nanostructures. In this study, we focus on the correlated electron-hole states in semiconductor nanowires and the influence of this excitonic effect on the optical absorption spectra. First-principles calculations are performed for a hydrogen-passivated silicon nanowire of a diameter of 1.2 nm. Using plane waves and pseudopotentials, the quasiparticle states are calculated within the many-body perturbation theory with the so-called GW approximation. It is found that the fundamental gap depends on both the orientation and size of the wire, and that the gap increases as the diameter decreases in an inverse quadratic fashion [1]. The electron-hole interaction is then evaluated by the Bethe-Salpeter equation (BSE). The enhanced Coulomb interaction in this confined geometry not only gives rise to an unusually large exciton binding energy of more than 1 eV (compared to a value of 14.7 meV in silicon bulk), but also significantly modifies the relative strength of the absorption peaks. The characteristics of these exciton states will be discussed. [1] ''Quantum Confinement and Electronic Properties of Silicon Nanowires,'' X. Zhao, C. M. Wei, L. Yang, and M. Y. Chou, Phys. Rev. Lett. 92, 236805 (2004).

*In collaboration with Li Yang, Catalin D. Spataru, and Steven G. Louie.

*Contributed Papers*

**15:06**
**W36 2 Electronic structures and optical properties of silicon nanowires** JUN LI, *Northwestern University* ARTHUR FREEMAN, Recent optical spectroscopic[1] and theoretical/computational studies[2] challenge the previous consensus on the nature of the optical properties of Si nanowires (SiNW). Here, we present results of precise theoretical FLAPW[3] determinations of the electronic structures and optical properties of (001) and (111) one nm SiNW. The electronic states at the gaps demonstrate a strong orientation dependent parabolic character in the Brillouin zone and a clear entanglement in real space between 1D and 2D dimensions of the wire. The local symmetry imposed by quantum confinement quenches the transitions around the gap, yielding an optically inactive direct gap. The observed (001) photoluminescence is attributed to a transition rooted in an $Si_8$ ring. The optical structure in the experimental range is well reproduced by our first-principles calculations that include the screened exchange-LDA correction to the well-known failure of the LDA. Our predictions about the anisotropy and orientation dependent optical absorption are easily verified experimentally. Work supported by DARPA B529527//W-7405-Eng-48.

[1]Holmes, Johnston, Doty, and Korgel, Science 287, 1471 (2000)
[2]Zhao, Wei, Yang, and Chou, Phys. Rev. Lett. 92, 236805 (2004)
[3]Wimmer, Krakauer, Weinert, and Freeman, PRB 24, 864 (1981)

**15:18**
**W36 3 Comparison of the optical properties of bare and capped GaAs nanowires** L.M. SMITH, THANG B. HOANG, L.V. TITOVA, H.E. JACKSON, *Dept. of Phys., Univ. of Cincinnati, Cincinnati, OH 45221* J.M. YARRISON-RICE, *Dept. of Phys., Miami Univ., Oxford, OH 45056* YONG KIM, H.H. TAN, C. JAGADISH, *Australian National University, Australia* We study the optical properties of single bare GaAs nanowires and GaAs/AlGaAs core/shell nanowires fabricated by the VLS technique. SEM and AFM images show that the wires are uniform in length (3-4$\mu$m long) and needle-shaped. Low temperature photoluminescence measurements of individual nanowires indicate that the quantum efficiency of the core/shell nanowires is significantly larger compared to the uncapped nanowires. We believe that the reason for the low emission efficiency of the uncapped nanowires is the significant influence of the surface-related non-radiative trap states. We anticipate that time-resolved measurements will show a significant increase of the recombination lifetime in the core/shell nanowires compared to the uncapped nanowires due to the passivation of the surface-related states by the AlGaAs shell. We acknowledge the support of the NSF through grants 0071797, 0216374, and the Australian Research Council.

**15:30**
**W36 4 Linear optical absorption in silicon and GaAs nanocrystals*** MURILO L. TIAGO,† *University of Minnesota, Twin Cities* JAMES R. CHELIKOWSKY, *University of Texas at Austin* The linear optical spectrum of Si and GaAs nanocrystals containing up to 100 atoms is calculated and discussed. We use two first-principles theories: time-dependent density-functional theory in the local adiabatic approximation (TDLDA), and the many-body solution of the Bethe-Salpeter equation (BSE). Both theories predict a strong blue shift in the energy-resolved polarizability and in the absorption cross section, which is characteristic of confined systems in the nanoscale. When many-body effects are included, in the framework of the BSE, the low-energy range of the spectrum is modified in two ways: the energy of excitation lines increases by almost 1 eV, as a result of self-energy and screening corrections; and the oscillator strength of those lines is enhanced. In bulk semiconductors, many-body effects are known to produce exciton lines and enhanced absorption in the low-energy range of the spectrum. Although the size of the nanocrystals studied is much smaller than the radius of Wannier excitons, the enhancement in oscillator strength is suggested to have the same source as excitonic effects in bulk samples.

*Supported by DOE under Grants DE-FG02-03ER25585/15491, NSF Grant DMR-0551195 and NERSC
†currently at University of Texas

*Invited Papers*

**15:42**
**W36 5 Light from Silicon-Based Nanostructures.**
LUCA DAL NEGRO, *MIT & Boston University*

Si-nanocrystals (Si-nc) embedded in $SiO_2$ glass matrices shows undoubtedly efficient room temperature light emission under optical pumping and sizable optical gain and light amplification have been demonstrated [1]. However, the presence of an insulating $SiO_2$ matrix prevents the fabrication of reliable and efficient electrically-driven devices and the efficiency of light emission is severely curtailed by the slow radiative lifetime of Si-nc. An alternative possibility is offered by the nucleation of Si-nc in dielectric hosts with smaller band-gaps. In this talk we will show our results on light-emitting Si-rich silicon nitride films (SRN) and photonic structures obtained by Plasma Enhanced Chemical Vapor Deposition (PE-CVD) followed by low temperature (500-900°C) thermal annealing [2]. The optical properties of SRN films are studied by micro-Raman and photo luminescence spectroscopy and demonstrate the presence of small Si-clusters with nanosecond recombination time and negligible emission thermal quenching. The electrical transport properties of SRN films are also investigated and efficient charge injection at low bias voltages is demonstrated. Additionally, we show that SRN matrices are suitable for efficient energy sensitization of Er ions emitting at 1.54 $\mu$m. The light emission mechanism in SRN nanostructures is studied by DFT−LDA first principles calculations showing that, largely Stokes−shifted, nanosecond−fast and efficient light emission in PE−CVD deposited SRN samples originates from strongly localized excitons transitions at the surface of small Si−nc ($\sim$ 1−2 nm) embedded in Silicon nitride [3].

Additionally, we show that the presence of bridging nitrogen groups at the surface of small Si nanocrystals can explain the origin of the experimentally measured Stokes−shift and the nanosecond relaxation times [3].
L. Pavesi, L. Dal Negro, C. Mazzoleni, G. Franzo, F. Priolo ''Optical gain in Si nanocrystals'', Nature 408, 440, 23 November 2000.

L. Dal Negro, J.H. Yi, V. Nguyen, Y. Yi, J. Michel, L.C. Kimerling, ''Spectrally enhanced light emission from aperiodic photonic structures'', Appl. Phys. Lett., **86**, 261905, (2005).

L. Dal Negro, J. H. Yi, L. C. Kimerling, S. Hamel, A. Williamson, G. Galli, Light Emission from Silicon−rich Nitride Nanostructures, Appl. Phys. Lett., submitted 2005.

***Contributed Papers***

**16:18**
**W36 6 Optical characterizations of one-dimensional wetting layers in InGaAs/GaAs quantum dot chains** XIAOYONG WANG, CHIH-KANG SHIH, *Department of Physics, the University of Texas at Austin* ZHIMING WANG, GREGORY SALAMO, *Department of Physics, University of Arkansas* We report spectroscopic evidence for the formation of 1D wetting layers (WLs) during the Stransky-Krastanov (SK) growth of multi-layered InGaAs/GaAs quantum dot (QD) chains. The wire-like features of these 1D WLs were demonstrated by their 1D density of states as well as the anisotropic absorption and emission properties. Two groups of QD's were found sitting on these 1D and the traditional 2D WLs, respectively, with size-dependent polarization anisotropies of $\sim$ 6%-25% due to their elongated shapes. The previously-unexplored new SK growth mode of 1D WLs could be potentially tailored by varying the In content and barrier thickness to yield QD's and 1D WLs with expected energy level separations. This may lead to the efficient carrier transfer between QD's on top of the same 1D WL for quantum technology applications that require quantum information transfer between different nanostructures of controlled positioning.

**16:30**
**W36 7 Electronic and optical fine structure of GaAs nanocrystals: the role of d orbitals in a tight-binding approach** J.G. DIAZ, GARNETT W. BRYANT, *National Institute of Standards and Technology* Electronic structure and optical spectra of GaAs nanocrystals for a wide range of sizes are studied by using both $sp^3s^*$ and $sp^3s^*d^5$ nearest-neighbor tight-binding models. Our results show that the inclusion of $d$ orbitals into a minimal basis set is necessary for a proper description of the lowest electron states, especially in the strong confinement regime. For dot sizes below 2.5 nm, the ground electron state is primarily built of L-point bulk band-states, giving the nanocrystals indirect-gap character. Simpler $sp^3s^*$ models yield an incorrect description of electron states made from bulk band- states away from the Brillouin zone center. In contrast, $sp^3s^*d^5$ models are able to provide a consistent picture of the main optical features in agreement with experiments.

**16:42**
**W36 8 Neutral and charged excitons in single GaAs-based interface quantum dots** C.J. MEINING, V.R. WHITESIDE, B.D. McCOMBE, *University at Buffalo, The State University of New York, NY 14260* J.G. TISCHLER, A.S. BRACKER, D. GAMMON, *Naval Research Laboratory, Washington, D.C. 20375-5347* A.B. DZYUBENKO, *California State University at Bakersfield, CA 93311* M. BYSZEWSKI, M. POTEMSKI, *Grenoble High Magnetic Field Laboratory, France* We report circularly polarized photoluminescence (PL) in high magnetic fields ($<$ 28 T) and optically detected resonance (ODR) experiments of interface fluctuation quantum dots (IFQDs) in narrow GaAs/AlGaAs quantum wells (QWs) doped in the barriers with donors to allow creation of both neutral and negatively charged excitons. In the narrowest QW the diamagnetic shift of the trion is smaller than that of the neutral exciton. This is attributed to the larger spatial extent of the trion wavefunction in these ensembles of weakly confined QDs. Along with a careful study of the excitonic Zeeman splitting and complemented by a comparison of ensemble and single dot ODR measurements, this signature can be used to assign the narrow spectral lines observed in single dot PL studies as neutral and charged excitons. The PL of the trion is found to increase under resonant irradiation with far-infrared laser light, opposite to the behavior observed for wide QWs. Lateral carrier redistribution is believed to be the dominant mechanism that gives rise to the ODR signal in QWs with monolayer well width fluctuations. Work supported in part by NSF-DMR #0203560.

**16:54**
**W36 9 Nanostructured solar cells*** OZGUR YAVUZCETIN, CHEOL-SOO YANG, TOM RUSSELL, MARK TUOMINEN, *University of Massachusettts* In this work we investigate the use of nanofabrication technique to improve the overall efficiency of silicon solar cells. The efficiency and the durability of silicon solar cells largely depends on the quality of the anti-reflectivecoating. In this work, the change in the index of refraction on the surface of a substrate can be controlled by the amount of porosity, which is well known in effective medium theory. Also by changing the thickness of the porous layer, the medium can be fine tuned to a specific wavelength as an AR coating. We fabricate the nanoporous layer by using a self-assembled P(S-b-MMA) coating as a mask to etch into the silicon substrate using reactive ion etching. The use of different molecular weight diblock copolymer and different etching time allow us to tune the index of refraction. FT-IR and variable angle ellipsometry provide information about the transmission and reflection properties along with the index of refraction and the thickness of the coating. The investigation of the efficiencies are performed by comparing the I-V plots of conventional and nanostructured cells. Additional research is underway in order to apply this technology to other types of substrates.

*This work is supported by NSF grants DMR-0306951, DMI-0103024 and MRSEC.

**17:06**
**W36 10 Effects of high magnetic fields on the scattering rates of GaAs/AlGaAs and GaInAs/AlInAs quantum cascade lasers** A. WADE, G. FEDOROV, D. SMIRNOV, *National High Magnetic Field Laboratory* A. LEULIET, A. VASANELLI, C. SIRTORI, *Laboratoire Matériaux et Phénomènes Quantiques, Université, France* Using magneto-spectroscopy, we investigate the influence of a strong magnetic field on the intersubband scattering rates in MIR GaAs/AlGaAs and GaInAs/AlInAs quantum cascade

lasers (QCLs). In our experiments, we measured light-current, voltage-current and laser emission spectra as a function of magnetic field up to 40T with the magnetic field perpendicular to the 2DEG. We observed strong oscillations in the intensity and threshold current. From these, the magnetic field dependences of the intersubband lifetime of both structures were derived and compared to their calculated dependence of electron-LO phonon scattering rates.

**17:18**

**W36 11 Ultra-low threshold quantum dot microdisk laser** G.S. SOLOMON, *Ginzton and Solid-State Laboratories, Stanford University* Z.G. XIE, *Solid-State Laboratory, Stanford University* S. GOETZINGER, Y. YAMAMOTO, *Ginzton Laboratory, Stanford University* W. FANG, H. CAO, *Department of Physics and Astronomy, Northwestern University* Ultra-low threshold lasers have applications in low-power communications. These lasers are also of fundamental interest, where a full understanding of lasing based on a few discrete emitters is evolving. This is especially true in solid-state systems, for instance those with a quantum dot (QD) gain medium, where a typical spectrum of discrete emission lines observed at lower pump power is often highly modified under higher pump powers. Here we discuss a microcavity laser containing a dilute QD gain medium that has an ultra low, sub-microwatt CW lasing threshold. The structure is based on a high-quality factor microdisk cavity of GaAs with a low density of InAs-based QDs embedded in the microdisk. We estimate 250 QDs in the 1.8 $\mu$m diameter microdisk under investigation. Of these QDs approximately 60 are spatially located within the modal region of the disk, which extends inwards approximately 250 nm from the disk edge. Only a small portion of these QDs couple to the narrow cavity modes, which have a free spectral range of 45 nm and an initial linewidth of 0.06-0.07 nm. Linewidth narrowing and lifetime reduction with increasing pump are both observed. Despite the small number of QDs it is unlikely from our estimates the system lases from a single QD state.

## SESSION W37: NANOSCALE CONDUCTANCE THEORY II

**Thursday Afternoon, 16 March 2006**
**340, Baltimore Convention Center at 14:30**
**Harold Baranger, Duke University, presiding**

**14:30**

**W37 1 Variable-range cotunneling and non-Ohmic transport in a chain of one-dimensional quantum dots** MICHAEL M. FOGLER, *University of California San Diego* SERGEY V. MALININ, *Wayne State University* THOMAS NATTERMANN, *Universitat zu Koln* A 1D wire with a finite density of strong random impurities is modeled as a chain of weakly coupled quantum dots. The resistance of such a system is shown to exhibit a rich dependence on bias voltage $V$ and temperature $T$ due to the interplay of Coulomb blockade, Luttinger-liquid, and disorder effects. At low $T$ and $V$ electrons propagate through the wire by means of thermal activation and a multiple cotunneling. In this regime the resistance is limited by the ''breaks'': randomly occurring clusters of dots with a special length distribution pattern that inhibits the transport no matter how the activation and tunneling are combined. As $T$ or $V$ increases, the breaks become shorter and less resistive. The resistance can exhibit a (stretched) exponential and a quasi power-law dependence on $T$ and $V$ depending on the position at the $T$-$V$ diagram. Unlike the case of a single impurity the effect of $T$ and $eV$ is not symmetric. The Ohmic resistance of a macroscopic wire is always dictated by breaks not single impurities. Our results imply that the power-laws reported in several recent transport measurements of one-dimensional systems may reflect not only intrinsic Luttinger parameters but also impurity distribution statistics.

**14:42**

**W37 2 Pair tunneling through single molecules** JENS KOCH, *Institut für Theoretische Physik, Freie Universität Berlin, Arnimallee 14, 14195 Berlin, Germany* MIKHAIL E. RAIKH, *Department of Physics, University of Utah, Salt Lake City, UT 84112, USA* FELIX VON OPPEN, *Institut für Theoretische Physik, Freie Universität Berlin, Arnimallee 14, 14195 Berlin, Germany* By a polaronic energy shift, the effective charging energy of molecules can become negative, favoring ground states with even numbers of electrons. Here, we show that charge transport through such molecules near ground-state degeneracies is dominated by tunneling of electron pairs which coexists with (featureless) single-electron cotunneling. Due to the restricted phase space for pair tunneling, the current-voltage characteristics exhibits striking differences from the conventional Coulomb blockade. In asymmetric junctions, pair tunneling can be used for gate-controlled current rectification and switching. We find that pair tunneling also has interesting consequences for the shot noise.

**14:54**

**W37 3 Spin Related Effects in Transport Properties of ''Open'' Quantum Dots** YASHAR AHMADIAN, GIANLUIGI CATELANI,*IGOR ALEINER, *Columbia University* We study the interaction corrections to the transport coefficients in open quantum dots (i.e. dots connected to leads of large conductance $G \gg e^2/\pi\hbar$), via a quantum kinetic equation approach. The effects of all the channels of the universal (in the Random Matrix Theory sense) interaction Hamiltonian are accounted for at one loop approximation. For the electrical conductance we find that even though the magnitude of the triplet channel interaction is smaller than the charging energy, the differential conductance at small bias is greatly affected by this interaction. Furthermore, the application of a magnetic field can significantly change the conductance due to the Zeeman splitting, producing finite bias anomalies. For the thermal conductance we find that the Wiedemann-Franz law is violated by the interaction corrections, and we investigated the effect of magnetic field on the Lorentz ratio for contacts of finite reflection. The charge and triplet channel corrections to the electrical and thermal conductance vanish for reflectionless contacts. In the latter case the temperature and magnetic field dependence of the conductance is determined by the Maki-Thompson correction in the Cooper channel.

*Currently a postdoc at Cornell University

**15:06**

**W37 4 Numerical studies of the dynamics of interacting electrons confined in nanostructures** ROK ZITKO, *Jozef Stefan Institute, Ljubljana, Slovenia* JANEZ BONCA, ANTON RAMSAK, *FMF, University of Ljubljana, Slovenia* TOMAZ REJEC, *Ben-Gurion University, Beer Sheva, Israel* At low temperatures electrons have long phase-relaxation time. They tunnel coherently through nanostructures in a wave-like manner, which leads to vari-

ous interference effects. We presently have adequate knowledge about the transport phenomena that can be described using single-electron models. The transport in the presence of interactions is, however, still a subject of intensive research. More refined theoretical tools are required to tackle problems such as that of the transport through systems of coupled quantum dots in the Kondo regime. We present our studies using complementary methods: the quantum Monte Carlo, the variational method and the numerical renormalization group. We show the phase diagram of the triple quantum dot and explain the various regimes of enhanced conductance.

**15:18**

**W37 5 Non-equilibrium conductance of a three-terminal quantum dot in the Kondo regime: Perturbative Renormalization Group** NAYANA SHAH, ACHIM ROSCH, *University of Cologne* Motivated by recent experiments, we consider a single-electron transistor in the Kondo regime which is coupled to three leads in the presence of large bias voltages. Such a steady-state non-equilibrium system is to a large extent governed by a decoherence rate induced by the current through the dot. As the two-terminal conductance turns out to be rather insensitive to the decoherence rate, we study the conductance in a three-terminal device using perturbative renormalization group and calculate the characteristic splitting of the Kondo resonance. The interplay between potential biases and anisotropy in coupling to the three leads determines the decoherence rate and the conditions for strong coupling.

**15:30**

**W37 6 Dissipative quantum phase transition in a single electron transistor** ALFRED ZAWADOWSKI, LASZLO BORDA, GERGELY ZARAND, *Institute of Physics, TU Budapest* DAVID GOLDHABER-GORDON, *Stanford University* We study the transport properties of a single electron transistor (SET) with highly resistive gate electrodes, and show that the SET displays a quantum phase transition analogous to the famous dissipative phase transition studied by Leggett. At temperature $T = 0$, the charge on the central island of a conventional SET changes smoothly as a function of gate voltage, dueto quantum fluctuations. However, sufficiently-strong dissipation, $R_g > R_C$, can freeze out charge fluctuations on the island even at the degeneracy point, causing the charge on the island to change in sharp steps as a function of gate voltage. For $R_g < R_C$ the steps remain smeared out by quantum fluctuations. The Coulomb blockade peaks in conductance display anomalous scaling at intermediate temperatures.

**15:42**

**W37 7 The Interplay of Spin and Charge Channels in Zero Dimensional Systems*** MIKHAIL KISELEV, *Institute for Theoretical Physics, Universität Würzburg, Würzburg D-97074, Germany* YUVAL GEFEN, *Department of Condensed Matter Physics, The Weizmann Institute of Science, Rehovot 76100, Israel* We study the interplay of charge and spin (zero-mode) channels in quantum dots. The latter affects the former in the form of a distinct signature on the differential conductance. We also obtain both longitudinal and transverse spin susceptibilities. All these observables, underlain by spin fluctuations, become accentuated as one approaches the Stoner instability. The non-perturbative effects of zero-mode interaction are described in terms of the propagation of gauge bosons associated with charge (U(1)) and spin (SU(2)) fluctuations in the dot, while transverse spin fluctuations are analyzed perturbatively.

*We acknowledge support by SFB-410 grant and through the Heisenberg program of the DFG (MK), an ISF grant of the Israel Academy of Science, the EC HPRN-CT-2002-00302-RTN and the AvH Foundation (YG).

**15:54**

**W37 8 The 0.7 anomaly in quantum point contacts: a scattering approach*** CAIO LEWENKOPF, PAULO BONFIM, *Universidade do Estado do Rio de Janeiro, Brazil* The conductance steps observed in the electronic transport through quantum point contacts (QPCs) became a paradigm of the Landauer conductance formula. For this reason, the ubiquitous experimental observation of the 0.7 anomaly in the first conductance step of QPCs, that defied the single-particle scenario, raised a lot of attention. The most successful theoretical explanation of this transport feature is in terms of Kondo physics: It builds on an Anderson-like model, whose parameters, namely, the resonance position, its couplings to the reservoirs and the charging energy are adjusted to give meaningful results. Starting from a scattering approach, that uses the Feshbach projection formalism, we construct a single-particle basis that allows us to directly calculate the resonance position and its coupling to left and right reservoirs. We then include an electron-eletron interaction term and proceed as standard. This approach unveils a novel interpretation for the underlying physics of the 0.7 anomaly.

*CNPq and FAPERJ (Brazil)

**16:06**

**W37 9 Electron transport in the presence of a magnetic field and the absence of translational invariance** TOBIAS KRAMER, ROBERT E. PARROTT, ERIC J. HELLER, *Physics Department Harvard University* Recent experimental techniques in 2DEGs using scanning probe microscope tips allow one to spatially image electron flow directly (see also the talk by Kathy Aidala). These developments motivate theoretical consideration of (localized) magnetic edge states in position space. For the case of a parabolic confinement, a semi-analytic expression of the Green function is given. The underlying physics differs from a conventional edge-state model by the absence of translational invariance. It is also possible to derive a semiclassical interpretation of the current density, which provides additional physical insight into the nature of transport in position space. For additional information, see also http://people.deas.harvard.edu/~ tkramer

**16:18**

**W37 10 Divergent beams of nonlocally entangled electrons emitted from NS structures*** FERNANDO SOLS, *Universidad Complutense de Madrid* ELSA PRADA, *Universität Karlsruhe* We propose the use of normal and Andreev resonances in normal-superconducting structures to generate divergent beams of nonlocally entangled electrons. Resonant levels are tuned to selectively transmit electrons with specific values of the perpendicular energy, thus fixing the magnitude of the exit angle. When the normal metal is a ballistic two-dimensional electron gas, the proposed scheme guarantees arbitrarily large spatial separation of the entangled electron beams emitted from a finite interface. We perform a quantitative study of the linear and nonlinear transport properties of some suitable structures, taking into account the large mismatch in

effective masses and Fermi wavelengths. Numerical estimates confirm the feasibility of the proposed beam separation method.

*Work supported by MEC, No. BFM2001-0172 and FIS2004-05120, and the Ramon Areces Foundation.

**16:30**

**W37 11 Non-equilibrium Entanglement and Noise in Coupled Double Quantum Dots** RAMON AGUADO, *Instituto de Ciencia de Materiales, CSIC* NEILL LAMBERT, *University of Tokyo, Japan* TOBIAS BRANDES, *University of Manchester, UK* We study charge entanglement in two capacitively-coupled double quantum dots in thermal equilibrium and under stationary non-equilibrium transport conditions. In the transport regime, the entanglement exhibits a clear switching threshold and various limits due to suppression of tunneling by Quantum Zeno localisation or by an interaction induced energy gap. We also calculate quantum noise spectra and discuss current cross-correlations as an indicator of the entanglement in transport experiments.

**16:42**

**W37 12 Conductance Fano lineshapes for Kondo impurities on surfaces: A numerical renormalization group description.** NANCY SANDLER, LUIS DIAS DA SILVA, SERGIO ULLOA, *Department of Physics and Astronomy, Ohio University* Scanning tunneling microscopy (STM) measurements of Kondo impurities on metallic surfaces has been an active field in recent years. For a flat density-of-states (DoS) near the Fermi energy in the host metal, the low-bias STM conductance acquires the characteristic Fano lineshape, with width proportional to the Kondo temperature $T_K$. In this work, we study how this picture is modified when a itstructured DoS (non-flat) is considered. A variety of physical effects can introduce peak/dips in the DoS, including the presence of a second impurity, hybridization between surface and bulk conduction states, and a magnetic impurity embedded in a molecule. Using numerical renormalization group techniques, we calculate the low-temperature conductance for this system. The zero-bias dip in the Fano conductance is modified by the presence of resonances or anti-resonances in the DoS near $E_F$. In particular, for DoS with pseudogaps and impurities in the mixed-valence regime, zero-bias Fano-like dips appear *even when no Kondo state has developed*, but governed by energy scales much larger than $T_K$. We further show that measurements of the scattering phase could be used as an additional probe into the Kondo regime. Supported by NFS-NIRT.

**16:54**

**W37 13 Effects of the electron-phonon interaction on the electron transport in low-dimensional disordered semiconductor structures** ANDREI SERGEEV, *University at Buffalo* MICHAEL REIZER, *5614 Naiche Road, Columbus, OH 43213* VLADIMIR MITIN, *University at Buffalo* We investigate the effects of the interference between electron-phonon scattering and elastic electron scattering in heterostructures and nanotubes. Interference strongly enhances the effective electron-phonon coupling in semiconductor structures and strengthens the electron-phonon relaxation [1]. Employing the quantum transport equitation, we calculate the interference contribution to the electrical conductivity and phonon drag thermopower. Our results show that the interference term follows to the logT-law and dominates in the temperature dependence of the conductivity. Phonon drag is also enhanced due to disorder. [1] A. Sergeev et al., Phys. Rev. Lett., 94, 136602 (2005).

**17:06**

**W37 14 Mesoscopic and nanoscopic physics of molecular-scale electronics** YONGQIANG XUE, *SUNY-Albany* Going from the mesoscopic regime of quantum semiconductor device to nanoscopic molecular device, the dominant or first-order transport mechanism remains quantum mechanical coherent transport due to the small size. A large part of the theoretical efforts in nanoelectronics is thus to recast the accumulated knowledge about mesoscopic physics into forms that are suitable for evaluating quantum transport phenomena at the atomic-scale. On the other hand, electrical conduction is intrinsically a dynamical phenomenon. Since the different degrees of freedom (electronic, mechanical, phonon . . . ) in the nanostructures can be strongly coupled to each other and to their nano-environment, the measured electrical signal is often the result of complex dynamic coupling processes without requiring ensemble average. New theoretical principles and computational techniques may be needed to unravel the rich physics involved in molecular-scale transport. In this talk, we discuss our efforts in moving from mesoscopic theory to nanoscopic theory of molecular-scale electronics.

**17:18**

**W37 15 Phonon Broadening of Spectral Lines in Scanning Tunneling Spectroscopy** J. W. GADZUK, *Electron Physics Group, NIST, Gaithersburg, MD 20899-8412* The observation and interpretation of spectral lines associated with quasi-localized states in condensed matter systems has provided a rich source of information pertaining to the transient coupling of these states to their dynamic environment.[1] While polaron/Franck-Condon models in which a transient localized potential excites the ambient phonon system have formed the basis for phonon broadening in a wide variety of core level spectroscopies, Sunjic and Lucas have put forth an elegantly simple solution to the problem in terms of driven harmonic oscillators which easily incorporates the time scales for both the switching on and the decay of the localized potential.[2] In recent STS studies of thin NaCl films on Cu substrates, Repp et al. have observed Gaussian-broadened lines that are signatures of bound electrons at Cl vacancies (F-centers).[3] These resonance tunneling line shapes are here analyzed within the context of the SL model, properly accounting for lifetime effects due to both tip-to-vacancy and also vacancy-to-substrate tunneling, thus enabling determination of the actual electron-phonon interaction. [1]J.W.Gadzuk, PRB **44**, 13466 (1991). [2]M.Sunjic and A.A.Lucas, CPL **42**, 462 (1976). [3]J.Repp et al., PRL **95**, 225503 (2005).

## SESSION W38: FLUX PINNING AND CRITICAL CURRENTS

**Thursday Afternoon, 16 March 2006**
**341, Baltimore Convention Center at 14:30**
**Judy Wu, University of Kansas, presiding**

**14:30**

**W38 1 Theory for the Dependence on Thickness Shown by the Critical Current vs. Magnetic Field in Films of PLD-YBCO*** MARTIN P. MALEY, *Los Alamos National Laboratory* JOSE P. RODRIGUEZ, *California State University at Los Angeles* The theoretical consequences of the proposal that the vortex lattice induced by perpendicular magnetic field in films of PLD-YBCO is

in a thermodynamic Bose glass state are explored. Attention is focused on the high-field regime at the extreme type-II limit, in which case only a small fraction of the vortex lines are localized at the dislocations that thread the film along the c axis, and in which case the pinning of the vortex lattice is collective. The critical current density along the film is predicted to follow an inverse square-root power law as a function of external magnetic field in the collective-pinning regime. It gives a fair account of the critical current density at kG magnetic fields in films of PLD-YBCO that are microns thick, at liquid nitrogen temperature. It fails, however, for much thinner films at lower temperature. This failure is corrected by including the effect of point pins along the interstitial vortex lines that lie in between the correlated pins. They contribute an inverse dependence on film thickness to the critical current density in magnetic field oriented near the c axis.

*Supported in part by the Department of Energy.

**14:42**

**W38 2 The growth mechanism of pinning-effective nanostructures embedded in $YBa_2Cu_3O_{7-x}$ (YBCO) superconducting thin film** A. GAPUD, A. KHAN, M. PARANTHAMAN, *Univ. of South Alabama* D. CHRISTEN, *Oak Ridge Natl. Lab.* Following up on previous success in modifying the pulsed-laser-deposition (PLD) film processing to introduce self-assembled pinning defects in films of various high-temperature superconductors (HTSC), specifically the case of self-assembled columnar arrays of oxide nanodots in $YBa_2Cu_3O_{7-x}$ (YBCO) thin film [itSuperconductor Science and Technology **18**, 1533 (2005)] using a nanodot-doped YBCO target, a careful and systematic examination of the growth mechanism is yet to be conducted on this and similar systems. This study examines (1) how the oxide nanodots retain their character during the deposition and (2) how the nanodots both influence, and are influenced by, the local potential-energy landscape that promotes spontaneous assembly into coherent stacks. This is done by growing the film subject to slight variations in the processing parameters which may influence the nature of the heterogeneity of any given layer in the film. Particular attention is paid to the influence of varying laser-pulse frequency which determines the time duration by which the potential-energy landscape of a pulsed layer is consolidated in time for the next pulsed layer. The mechanism is also tested for a system in which the embedded nanostructures are made from a non-oxide material (gold). Results consist of microstructure (cross-sectional HRTEM, XRD, surface SEM), transport properties (critical temperature and critical current), and magnetic susceptibility.

**14:54**

**W38 3 Magnetic coupling between vortices in superconductors and adjacent magnetic layers** MASAKI SUENAGA, QIANG LI, QING JIE, *Brookhaven National Laboratory* We presented a study of magnetic coupling between vortices in superconductors and adjacent magnetic layers in two systems: superconductor/magnetic multilayers and HTS films on magnetic substrates. The flux motion in superconductor and the behavior of magnetic layer (or magnetic substrate) were captured by quantitative Magneto-optical imaging (MOI) technique with an external magnetic field applied perpendicular to the sample surface and varied along a whole hysterisis loop cycle. Bulk dc SQUID magnetization, ac loss, and direct transport measurements were performed to compliment the MOI studies. It was found that magnetic substrate has limited effect on transport properties of HTS films, although some enhancement of $J_c$ was observed near $T_c$ in the multilayers due to the magnetic coupling. However, magnetic substrate did result in significant reduction of the ac losses.

**15:06**

**W38 4 Time resolved magneto-optical imaging of ac currents in YBCO conductor.** ANDREA LUCARELLI, GUNTER LUEPKE, *Department of Applied Science, The College of William and Mary, Williamsburg, VA* TIMOTHY HAUGAN, GEORGE LEVIN, PAUL BARNES, *Power Generation Branch, Air Force Research Laboratory, Wright-Patterson AFB, OH* The use of $YBa_2Cu_3O_{7-\delta}$ (YBCO) in ac applications, whether with applied ac currents or alternating magnetic fields, is strictly related to the availability of long-length ac-tolerant YBCO coated conductor. These ac applications, such as fully superconducting generators and motors or transformers, may operate with ac currents in a range of frequencies from tens of Hz up to a thousand Hz. We present a newly developed time-resolved magneto-optical imaging (MOI) technique for studying high-temperature superconductors (HTS) with applied alternating currents (AC) in the frequency range 30 – 1000 Hz. The evolution of the magnetic flux density distribution in YBCO thin films and coated conductors is studied as a function of the phase of the applied AC current. Time- and spatially-resolved images of the magnetic flux profiles are presented for a detailed series of values of the phase. A quantitative analysis of the data allows us to calculate the current density profiles at different phases. We observe for the first time that the maxima of the AC current density is shifted from the edges further inside the sample which may be caused by the higher self-induced field in that region.

**15:18**

**W38 5 Scanning Hall probe microscopy of AC losses in YBCO coated conductors** RAFAEL DINNER, KATHRYN MOLER, M. R. BEASLEY, *Stanford University* D. MATTHEW FELDMANN, DAVID LARBALESTIER, *University of Wisconsin—Madison* Magnetic imaging of current-induced vortex movement in superconducting films yields detailed information about dissipation and the path of an applied current. In our cryogenic scanning Hall probe microscope, a micro-Hall probe is rastered near the sample surface with submicron resolution and centimeter scan range. Hall probe time traces taken at each point are assembled into movies of the flux penetration as a function of time over a cycle of AC sample current. We image coated conductors—films of the high-temperature superconductor YBCO grown on metal tapes which give rise to grain boundaries. We then isolate the effects of the boundaries by imaging YBCO grown on bicrystal substrates that induce a single boundary at various angles to the current path. Current density, electric field, and dissipation distributions are reconstucted from the images.

**15:30**

**W38 6 Twins, Their Microstructure and Correlation to Critical Current Densities in Superconducting Melt-Textured Grown Y-Ba-Cu-O** SIU-WAI CHAN, *Columbia University* LIN-FENG MEI, *Columbia University* APPLIED PHYSICS TEAM, Refinement of twin microstructure in melt-textured grown (MTG) Y-Ba-Cu-O (YBCO) is engineered by annealing at different temperatures. This isothermal method exploits the temperature dependence of twin-boundary-energy. The twin boundary energy is obtained by two independent methods: (1) twin spacing and (2) twin-tip shape. The twin boundary energy measurement is

accomplished with transmission electron microscopy. Refinement of twin spacing with increasing temperature is confirmed. Twin spacing decreases from 190 nm to 54 nm as the temperature increases from 450 to 680°C. Critical current measurements support that a sample with a higher density twin density often results in a higher pinning-force i.e. 3.4 x $10^8$ N/m$^3$ versa 1.2 x $10^8$ N/m$^3$.

**15:42**

**W38 7 Scanning Hall Probe Microscope and Imaging of Vortex Penetration into Nb** A. BOVE, *Purdue University, Phys. Dpt.* N. KUNDTZ, A. M. CHANG, *Duke University, Phys. Dpt.* V. GUSIATNIKOV, *Stanford Research Systems* ART LICHTENBERGER, *U. of Virginia, ECE.* We report on the construction of a scanning Hall probe microscope with 100 nm lateral resolution and a large scan range, which exceeds 40 $\mu$m at 4.2 K. The microscope is based on the beetle design and operates between room temperature and 1.5 K. The DSP-based control electronics achieves a high (100 kHz) sampling rate and a low noise. The system is capable of simultaneous tunneling and Hall signal acquisition. The Hall sensor for measuring local magnetic fields is fabricated on a GaAs heterostructure through standard EBL and wet etching. It has an active area of 300 nm x 300 nm and a sensistivity of 0.2 Ω/Gauss. We will present (1) a description of the microscope, and (2) progress on imaging the penetration of vortices and the growth of vortex dendritic patterns into thin Nb films[1] and grid arrays[2].

[1]Altshuler E. itet al., Rev. Mod. Phys.**76**, 471 (April 2004)
[2]Hallen H. D. itet al., Solid State Commumications **99** (9), 651-654 (SEP 1996)

**15:54**

**W38 8 Vortex Pinning in a $YBa_2Cu_3O_{7-\delta}$ Thin Film** OPHIR M. AUSLAENDER, NICHOLAS C. KOSHNICK, KATHRYN A. MOLER, *Stanford University* ROB A. HUGHES, JOHN S. PRESTON, *McMaster University* Vortices, and the nanoscale structures that pin them, are important both fundamentally and for the development of high temperature superconductor technologies. We use a home-built magnetic force microscope (MFM) to determine the depinning forces required to move individual vortices in a 200nm thick $YBa_2Cu_3O_{7-\delta}$ film. Our results indicate a wide distribution of depinning forces for different vortices. A comparison between distributions at various temperatures is underway, qualitatively showing a decrease of forces with increasing temperature.

**16:06**

**W38 9 Anomalous Slow Relaxation of the Magnetization in $Y_{1-x}Pr_xBa_2Cu_30_{7-\delta}$*** P. GYAWALI, V. SANDU,[†]C. C. ALMASAN, *Kent State University* B. J. TAYLOR, M. B. MAPLE, *University of California at San Diego* We have investigated the time $t$ evolution of the irreversible magnetization $M_{irr}$ in a series of single crystals of $Y_{1-x}Pr_xBa_2Cu_30_{7-\delta}$, $x = 0.13$ ($T_c = 82$ K), $x = 0.34$ (($T_c = 50$ K), and $x = 0.47$ (($T_c = 34$ K), all displaying a second peak in magnetization. In all cases, $M_{irr}(t)$ follows the well known law of relaxation, $M_{irr}(t) \propto [\mu k_B T/U_o ln(t/t_0)]^{-1/\mu}$. For fields/temperatures lower than the corresponding values of the second magnetization peak, $\mu$ is anomalously large, $2.5 \leqslant \mu \leqslant 4$, in contrast with theoretical predictions which gives a maximum value of 2.5, and with data reported for other cuprates. These large $\mu$ values in the vortex glass state, which give rise to a low relaxation rate, occur for all Pr doping and could be due to the presence of Pr ions. In contrast, at fields/temperatures above the second magnetization peak, $\mu$ decreases to values expected from theories of plastic vortex liquid and validated by most experimental reports.

*This research was supported by the NSF under Grant No DMR 0406471 at KSU and the USDOE under Grant No DE-FG03-86ER-45230 at UCSD

[†]Permanent address: National Institute of Materials Physics, Bucharest-Magurele, Romania

**16:18**

**W38 10 Effective Action for Vortex Dynamics in Clean d-wave Superconductors** PREDRAG NIKOLIC, SUBIR SACHDEV, *Harvard University* We describe influence of gapless nodal quasiparticles on vortex dynamics in clean two-dimensional d-wave superconductors. At zero temperature, the guasiparticles give rise to a finite renormalization of vortex mass, as well as a universal sub-Ohmic damping of vortex motion. Slow vortex motion is dissipated only at finite temperatures, or when some perturbation, such as disorder, creates a finite quasiparticle density of states at the gap nodes. These results are obtained by a non-perturbative derivation of the effective vortex action, where the quasiparticles are integrated out exactly in a continuum functional formalism. Fortunately, an uncontrolled perturbative analysis reaches the same conclusions, and all findings are reflected in a simple scaling argument where the gapless Dirac quasiparticles are regarded as a quantum-critical system. Our results appear to differ from those of the semiclassical theory, which obtains singular corrections to a vortex mass appearing in transport equations.

**16:30**

**W38 11 Flux pinning and Critical current density in $La_{2-x}Sr_xCuO_{4+d}$** HASHINI MOHOTTALA, B. O. WELLS, J. I. BUDNICK, W. A. HINES, *University of Connecticut* A. R. MOODENBAUGH, *BNL* F.C. CHOU, *MIT* UNIVERSITY OF CONNECTICUT TEAM, BNL COLLABORATION, MIT COLLABORATION, We have studied the magnetic characteristics of the critical states in a series of samples of the type $La_{2-x}Sr_xCuO_{4+d}$ that is doped with both Sr and excess O incorporated using electrochemistry. These samples spontaneously phase separate and show both a superconducting phase with $T_C$ near 40 K and a magnetic phase with $T_M$ near 40 K. Our previous studies established that the superconducting phase is similar to an optimally doped sample while the magnetic phase is consistent with the static spin density wave reported for x=1/8 Sr or Ba doped samples. Magnetization data at various temperatures showed large reversibility in all the samples. The critical current densities $J_C(0)$ values were at least an order of magnitude smaller than that of the reported values for $YBa_2Cu_3O_{7-d}$and $La_{2-x}Sr_xCuO_4$. At higher fields $J_C(H)$ was smaller indicating the existence of weak flux pinning in the system. Based on our magnetization data we conclude that the vortex lattice pinning is different from non-phase separated cuprates. This work was partially supported by the US-DOE through contract DE-FG02-00ER45801 and the Cottrell Scholar Program of the Research Corporation.

**16:42**

**W38 12 Magnetic Pinning in Nb and YBCO Thin Films by Co/Pt Multilayers with Perpendicular Magnetic Anisotropy** X.M. CHENG, L.Y. ZHU, C.L. CHIEN, *Johns Hopkins University* MARTA Z. CIEPLAK, Z. ADAMUS, A. ABAL'OSHEV, M. BERKOWSKI, *Inst. of Physics PAS, Warsaw, Poland* Magnetic pinning of vortices has the advantage over intrinsic pinning in that the superconducting critical current can be reversibly tuned by the magnetic field (H). Magnetic pinning by Co/Pt multilayers with perpendicular magnetic anisotropy has been studied in two ferromagnetic/superconducting bilayers of Nb and YBCO with different superconducting properties (e.g. penetration depth $\lambda$). Magnetic force microscopy reveals similar magnetization (M) reversal process in the two cases, both exhibiting a large density of narrow residual domains but with different domain width w at the final reversal stage. However, the magnetic pinning, revealed by the M-H loop shape in the superconducting state, is different. The Nb film exhibits an enhancement of M with the strongest effect during the final reversal stage, while the YBCO film shows a suppression of M in the vicinity of central M peak and an enhancement of M in large magnetic fields. These different behaviors are related to the different $\lambda$/w ratio in the two cases.

**16:54**

**W38 13 Flux penetration in a ferromagnetic/superconducting bilayer utilizing perpendicular magnetic anisotropy*** MARTA Z. CIEPLAK, Z. ADAMUS, A. ABAL'OSHEV, M. BERKOWSKI, *Inst. of Physics, PAS* M. KONCZYKOWSKI, *Ecole Polytechnique, Palaiseau, France* X. M. CHENG, L. Y. ZHU, C. L. CHIEN, *Johns Hopkins University* The Hall sensor array is a useful tool for measuring local magnetic fields. An array of miniature Hall sensors has been used to study the flux penetration in a ferromagnetic/superconducting (F/S) bilayer consisting of Nb as the S layer and Co/Pt multilayer with perpendicular magnetic anisotropy as the F layer, separated by an amorphous Si layer to avoid proximity effect. The F layer is first premagnetized to different magnetization reversal stages to obtain various magnetic domain patterns. The effect of these domain patterns on the flux behavior in the S layer is then studied at various temperatures in the superconducting state. We have observed that, in addition to the vortex pinning enhancement, some domain patterns strongly increase the first penetration field and induce large thermomagnetic instabilities (flux jumps), which are not detectable by magnetometry. We also discuss the profiles of the flux distribution across these F/S bilayers.

*Supported in part by the French-Polish Bilateral program Polonium.

**SESSION W39: SUPERCONDUCTIVITY-JOSEPHSON JUNCTIONS AND QUBITS**
**Thursday Afternoon, 16 March 2006**
**342, Baltimore Convention Center at 14:30**
**J. Robert Anderson, University of Maryland, presiding**

**14:30**

**W39 1 Finite size scaling analysis of the helicity modulus and the inverse dielectric constant in two capacitvely coupled Ultrasmall 2D Josephson Junction Arrays*** GUILLERMO RAMIREZ-SANTIAGO, *Instituto de Fisica, UNAM (MEXICO)* JORGE JOSE, *Dept. of Physics, University at Buffalo, State University of New York* We have carried out a finite size scaling analysis of the helicity modulus $\Upsilon_i$ and the inverse dielectric constant $\epsilon_i$, $(i = 1,2)$ of two capacitively coupled Josephson junction arrays with charging energy, $E_c$, and Josephson coupling energy, $E_J$. The arrays are coupled via the capacitance, $C_{\rm inter}$, at each site of the lattices. The parameter that measures the importance of quantum fluctuations in the i-th array is, $\alpha_i \equiv E_{c_i}/E_{J_i}$. We have considered the interplay between vortex and charge dominated individual array phases by means of extensive path integral Monte Carlo simulations. It has been found that this system develops a *reentrant transition* in $\Upsilon(T,\alpha)$, at low temperatures, when one of the arrays is in the semiclassical limit (i.e. $\alpha_1 = 0.5$) and the quantum array has $2.0 \leqslant \alpha_2 \leqslant 2.5$, for $C_{\rm inter} = 0.26087, 0.52174, 0.78261, 1.04348$ and $1.30435$. Similar behavior was obtained for larger values of $\alpha_2 = 4.0$ with $C_{\rm inter} = 1.04348$ and $1.30435$.

*Supported by DGAPA-UNAM IN110103 & CONACYT 43596-F

**14:42**

**W39 2 RF critical current of Josephson junction** VLADIMIR MANUCHARYAN, ETIENNE BOAKNIN, MICHAEL METCALFE, R. VIJAY, *Department of Applied Physics, Yale University* IRFAN SIDDIQI, *Department of Applied Physics, Yale University, Department of Physics, University of California, Berkeley* ANDREAS WALLRAFF, R.J. SCHOELKOPF, MICHEL DEVORET, *Department of Applied Physics, Yale University* The Josephson junction is the only radio-frequency electrical element which can be both non-dissipative and non-linear at low temperatures. While the stability of the junction dynamics in presence of a DC drive has been extensively studied, the microwave drive case is relatively poorly understood, at least experimentally. It is explored by driving an increasing AC current through a Josephson junction which is effectively biased by an AC voltage generator in series with a finite linear imbedding impedance $Z(\omega)$. For small signal amplitude, the junction behaves as a linear inductor. For higher signal amplitudes, we show that there exists a critical current $I_c^{RF}$ beyond which the dynamics of the junction changes qualitatively as a result of its non-linear characteristic. This AC critical current depends strongly on the biasing impedance. We provide a detailed stability diagram from experimental measurements and show that it obeys the simple theory of nonlinear resonance.

**14:54**

**W39 3 Parametric amplification with the Cavity Josephson Amplifier** ETIENNE BOAKNIN, R. VIJAY, MICHAEL METCALFE, VLADIMIR MANUCHARYAN, *Department of Applied Physics, Yale University* IRFAN SIDDIQI, *Department of Applied Physics, Yale University; Department of Physics, University of California, Berkeley* MICHEL DEVORET, *Department of Applied Physics, Yale University* Several types of amplifiers are approaching the quantum limit, namely, the SQUID, the RF-SET (radio-frequency single electron transistor) and the QCP (quantum point contact). We investigate a new amplifier which harnesses the nonlinearity of a Josephson junction for parametric amplification. It consists of a Josephson junction placed in a high-quality on-chip superconducting cavity, pumped by microwave radiation. The high level of control over the environment provides a system which is well described by the simplest nonlinear oscillator for-

malism with no adjustable parameters. such that theoretical predictions can be compared with experimental results. The planar geometry of the device can accommodate operation over a wide range of frequencies, opening the possibility of a quantum limited amplifier for practical use. We present preliminary results on the performance of the amplifier and discuss the possibility of observing quantum noise squeezing.

**15:06**

**W39 4 Josephson current through a molecular transistor in a dissipative environment** TOMAS NOVOTNY, ALESSANDRA ROSSINI, KARSTEN FLENSBERG, *Nano-Science Center, Univeristy of Copenhagen, Denmark* THEORY GROUP TEAM, We study the Josephson coupling between two superconductors through a single correlated molecular level, including Coulomb interaction on the level and coupling to a bosonic environment. All calculations are done to the lowest, i.e., the fourth, order in the tunneling coupling and we find a suppression of the supercurrent due to the combined effect of the Coulomb interaction and the coupling to environmental degrees of freedom. Both analytic and numerical results are presented.

**15:18**

**W39 5 Vortex doping into finite-sized superconducting Pb networks.*** TAKEKAZU ISHIDA, HIROSHI NODA, MASARU KATO, *Osaka Prefecture University, Sakai, Osaka 599-8531* OSAMU SATO, *Osaka Prefectural College of Technology, Neyagawa, Osaka 572-8572* MASAHIKO HAYASHI, HIROMICHI EBISAWA, *Graduate School of Information Sciences, Tohoku University, Sendai980-8579* KAZUO SATOH, TSUTOMU YOTSUYA, *Technology Research Institute of Osaka Prefecture, Izumi, Osaka 594-1157* Superconducting finite-sized Pb square networks with 2x2, 3x3, 5x5 and 10x10 square holes have been fabricated by electron beam lithography of photoresist layer and a lift-off process after depositing Pb film on the resist patterns. The application of magnetic field corresponds to the particle (vortex) doping into networks. Vortex image observations were carried out by a SQUID microscope to compare with the theoretical predictions. We found the exactly reversed pattern between the vortex doping x and the anitivortex doping x into the fully occupied network (x=1/4). The Ginzburg-Landau calculations show that there are several vortex configurations with almost equivalent free energy. The complete coincidence of the two patterns might be due to residual randomness caused in the fabrication processes.

*This work is partially supported by JST-CREST.

**15:30**

**W39 6 Nano-mechanical-resonator induced synchronization in Josephson junction arrays*** BRAD TREES, *Ohio Wesleyan University* STEFAN NATU, *Ohio Wesleyan University* DAVID STROUD, *The Ohio State University* We show that a serial array of N critical-current disordered, underdamped, Josephson junctions coupled piezoelectrically to a nanomechanical (NEM) oscillator results in phase locking (synchronization) of the junctions. We find a semi-classical solution to the coupled differential equations generated by Heisenberg operator equations, based on a Hamiltonian including the following effects: charging and Josephson energies of the junctions, junction dissipation, effect of a dc bias current, and an undamped simple harmonic oscillator representing the NEM. Synchronization of the array is signaled by a step in the current- voltage (I-V) curve. Stability analysis reveals that the phase-locked junctions are neutrally stable at the bottom and top of the step. We calculate an analytic expression for the location of the resonance step in the I-V curve. We also find it is possible to set a desired number $N_a \leqslant N$ of junctions on the resonance step, with $N_a - N$junctions in zero-voltage state.

*DS supported by Ohio Supercomputer Center and NSF grant DMR04-13395

**15:42**

**W39 7 Effect of Microwaves on the Current-Phase-Relation of diffusive SNS Junctions** M. FUCHSLE, J. BENTNER, P. TRANITZ, W. WEGSCHEIDER, C. STRUNK,* We investigate the current-phase-relation (CPR) of long diffusive superconductor - normal metal - superconductor (SNS) Josephson junctions under microwave irradiation. The samples consist of narrow Ag bridges with a length between 300 and 500 nm inserted into a Nb loop by shadow evaporation on top of a mesoscopic Hall cross. Our Hall-sensors are based on high mobility GaAs/AlGaAs- heterostructures. They directly detect the magnetic response of the loop to an external magnetic field, from which the full CPR can be reconstructed. The measurements are done in the high-temperature regime $E_{Th} < k_B T$, where $E_{Th}$ is the Thouless energy of the junctions and $\hbar\omega \approx E_{Th}$. We find that the CPR can be strongly affected by microwave radiation. A strong deviation of the CPR from the well-known sinusoidal $I(\Phi)$ relation is observed: depending on the applied frequency and amplitude, the supercurrent can be strongly suppressed for phase differences in the vicinity of $\phi = \pi$. At some frequencies, the sin($\Phi$) term in the CPR can be completely suppressed, resulting in a dominant second harmonic.

*presenting author

**15:54**

**W39 8 Generation of Microwave Single Photons and Homodyne Tomography on a Chip*** MATTEO MARIANTONI, *Walter-Meissner Institute, Bavarian Academy of Sciences* MARKUS STORCZ, FRANK WILHELM,† *Ludwig-Maximilians-Universitaet* WILLIAM OLIVER, *MIT Lincoln Laboratories* ANDREAS EMMERT, ACHIM MARX, RUDOLF GROSS, *Walter-Meissner Institute, Bavarian Academy of Sciences* HENNING CHRIST, ENRIQUE SOLANO, *Max-Planck Institute for Quantum Optics* We show that flux-based qubits can be coupled to superconductive resonators by means of a quantum-optical Raman excitation scheme and utilized for the deterministic generation of propagating microwave single photons. We introduce also a microwave quantum homodyning technique that enables the detection of single photons and other weak signals, and full state reconstruction via quantum tomography, realizing linear optics on a chip. These generation and detection protocols are building blocks for the advent of quantum information processing in the field of circuit QED (M. Mariantoni *et al.* cond-mat/0509737). We discuss further applications of these ideas to create multipartite nonclassical states of the electromagnetic field.

*supported by the Deutsche Forschungsgemeinschaft within SFB 631

†present address: University of Waterloo

**16:06**

**W39 9 Crossover from single electron counting to Cooper pair counting** TIM DUTY, JONAS BYLANDER, PER DELSING, *Microtechnolgy and Nanoscience, Chalmers University of Technology, Sweden* We present experimental studies of charge transport in a one-dimensional array of Josephson junctions using a single charge counting device based upon a radio-frequency single-electron transistor[1]. We observe a crossover from time-correlated tunneling of single electrons to Cooper pairs as a function of an applied magnetic field. At relatively high magnetic field, single electron transport dominates and the frequency is given by f=I/e. As the magnetic field is lowered the frequency gradually shifts to f=I/2e, indicating tunneling of Cooper pairs. [1]Jonas Bylander, Tim Duty and Per Delsing, Nature 434 (2005) 285.

**16:18**

**W39 10 1/f Noise in Josephson Junctions** MAGDALENA CONSTANTIN, CLARE C. YU, *Department of Physics and Astronomy, University of California, Irvine* A major obstacle to the realization of Josephson junction qubits is decoherence due to noise. Our goal is to understand the microscopic mechanisms which lead to the 1/f critical current noise spectrum at low temperatures. One possible source of critical current fluctuations is the presence of defects such as two level systems in the insulating junction barrier. We present a model of the critical current noise spectrum and compare it with recent experiments.

**16:30**

**W39 11 Decoherence in Josephson Vortex Quantum Bits** JU KIM, RAMESH DHUNGANA, *University of North Dakota* KEE-SU PARK, *Pohang University of Science and Technology* We investigated decoherence of a Josephson vortex quantum bit (qubit) in dissipative and noisy environment. As the Josephson vortex qubit is fabricated by using a long Josephson junction (LJJ), we use the perturbed sine-Gordon equation to describe the phase dynamics representing a two-state system and estimate the effects of quasiparticle dissipation and weakly fluctuating critical and bias currents on the relaxation time $T_1$ and on the dephasing time $T_\phi$. We show that the critical current fluctuation does not contribute to dephasing of the qubit in the lowest order approximation. Modeling the weak current variation from magnetic field fluctuations in the LJJ by using the Gaussian colored noise with long correlation time, we show that the time $T_2$ is limited by the low frequency current noise at very low temperatures. Also, we show that a ultra-long coherence time may be obtained from the Josephson vortex qubit by using experimentally accessible value of physical parameters.

**16:42**

**W39 12 Phase-space theory for nonlinear detectors of superconducting qubits** IOANA SERBAN, *Ludwig-Maximilians-Universitaet, Munich* FRANK WILHELM, *University of Waterloo, Waterloo, ON* Superconducting circuits are envisioned as quantum bits and demonstrate quantum-coherent features i.e. Rabi oscillations and Ramsey fringes. The detector (e.g. a superconducting quantum interference device, SQUID) can itself be described by a Hamiltonian and treated quantum-mechanically.This allows more insights into the measurement process. Several experimental groups have recently realized good detectors with strong coupling to the measured system, where nonlinear dynamics plays a significant role. Motivated by the recent experiment [1], we study a nonlinear detector where the qubit couples to the square amplitude of a driven oscillator, which can be used for dispersive detection. We use a complex-environment approach treating the qubit and the oscillator exactly, expressing their full Floquet-state master equations in phase space. We investigate the backaction of the environment on the measured qubit and explore the resolution of measurement. We discuss the possibility for using the squeezing capability of the nonlinear interaction for beating the standard quantum limit and emphasize the resulting role of non-Gaussian and non-Markovian effects in the backaction including significant non-exponential shape of the coherence decay. [1] A. Lupascu et al. PRL 93 177006 (2004)

**16:54**

**W39 13 Quasiparticle Poisoning in a Cooper Pair Box caused by a measuring SET*** CARLOS SANCHEZ, *Laboratory for Physical Sciences* BENJAMIN PALMER, *Laboratory for Physical Sciences* MARC MANHEIMER, *Laboratory for Physical Sciences* FRED WELLSTOOD, *University of Maryland* We have developed a model to calculate the average charge on a Cooper pair box in the presence of quasiparticle poisoning. The model uses a master equation approach to find the probabilities for the box to be in the even or odd state. The transition rates between the two states are calculated assuming a fixed number of non-equilibrium quasiparticles in the leads and island of the box. We fabricated Al/AlOx/Al devices with a Cooper pair box capacitively coupled to an SET and measured the charge on the box for SET bias currents ranging from about 1 pA to 1 nA. We find good agreement between the theory and measurements in the temperature range from 60 mK to 300 mK. For large SET bias the poisoning in the Cooper pair box increases and the charge staircase develops additional features. Our model is capable of qualitatively reproducing the features induced by the measuring SET.

*This work was supported by the National Security Agency

**17:06**

**W39 14 Cavity Josephson Bifurcation Amplifier: a microwave readout for a superconducting qubit** MICHAEL METCALFE, ETIENNE BOAKNIN, VLADIMIR MANUCHARYAN, *Department of Applied Physics, Yale University, New Haven, CT, 06511* SIMON FISSETTE, *Departement de Physique, Universite de Sherbrooke, Sherbrooke, Canada* IRFAN SIDDIQI, RAJAMANI VIJAYARAGHAVAN, CHAD RIGETTI, ANDREAS WALLRAFF, ROBERT SCHOELKOPF, MICHEL DEVORET, *Department of Applied Physics, Yale University, New Haven, CT, 06511* A Josephson junction, embedded in a microwave circuit that displays a resonance, and driven near the resonance frequency by a sinusoidal signal with adequate amplitude, can adopt one of two dynamical metastable states. The transition between the two states can be triggered by a small variation in the environment of the junction. This switching phenomenon naturally lends itself to the readout of a superconducting quantum bit. We are approaching the problem of mapping the two states of a qubit onto the two dynamical states of the Josephson junction by placing it in an on-chip coplanar waveguide superconducting cavity. We present the characterization of the cavity Josephson bifurcation amplifier (CJBA) and show that it follows theoretical predictions over a wide range of operating frequencies and bandwidth. This architecture provides a calculable RF environment which can be readily optimized. We also discuss a multi-resonator chip geometry that would implement the multiplexed readout of more than 10 qubits.

**17:18**
**W39 15 Quantum dynamics and leakage of the superconducting flux qubit** EZEQUIEL POZZO, *Centro Atomico Bariloche, Argentina* DANIEL DOMINGUEZ, *Centro Atomico Bariloche, Argentina* We study the quantum dynamics of the superconducting flux qubit of Mooij et al, which consists on a SQUID with 3 Josephson junctions. We simulate the corresponding time-dependent Schrodinger equation and also eigenfunctions and eigenvalues are computed. We calculate the dynamical evolution of the qubit device after a pulse in magnetic field is applied from the operational point at half flux quantum. The system is started in the lowest energy level and we calculate the leakage into the non-computational basis after the pulse is applied, computing the change in the average population of the two lowest energy levels. The leakage is analyzed for different pulse intensities. Two different regimes are found for weak and strong pulses. We discuss the relationship of the response to strong pulses with the quantum chaoticity of the spectrum of high energy levels outside the computational space.

**SESSION W40: QUANTUM COMMUNICATION, CRYPTOGRAPHY AND COMPUTATION**
**Thursday Afternoon, 16 March 2006**
**343, Baltimore Convention Center at 14:30**
**Steven H. Simon, Bell Labs, Lucent Technologies, presiding**

**14:30**
**W40 1 Quantum Communication via Frequency Upconversion*** AARON VANDEVENDER, PAUL KWIAT, *University of Illinois at Urbana-Champaign* We describe a method for efficiently and coherently converting photonic qubits from one frequency to another for quantum communication. The conversion is done using quasi-phase-matched up-conversion in a Periodically Poled Lithium Niobate (PPLN) crystal. We have observed 99%-efficient and 95%-coherent conversion which allows faithful conversion of ''flying'' qubits to ''stationary'' qubits for use in quantum communication. We have also used up-conversion to prepare photons in arbitrary superpositions of widely separated frequency states, enlarging the accessible Hilbert space for communication of quantum states. Finally, we have seen 56%-efficient detection of 1550-nm photons using up-conversion to the visible and silicon Avalanche Photodiodes (APD), which would enhance the performance of quantum communication protocols (e.g., BB84) based on infrared (IR) photons over what is achievable with conventional IR single-photon detectors.

*This work was supported by the MURI Center for Photonic Quantum Information Systems (ARO/DTO program DAAD19-03-1-0199)

**14:42**
**W40 2 Relativistic Quantum Cryptography** EVAN JEFFREY, PAUL KWIAT, *University of Illinois at Urbana-Champaign* We present results from a relativistic quantum cryptography system which uses photon storage to avoid bit sifting, in principle doubling the useful key rate. Bob stores the photon he receives from Alice in an optical delay line until she sends him the classical basis information, allowing him to measure every photon in the correct basis. Accounting for loss in our 489-ns storage cavity, we achieve a 66% increase in the BB84 key rate. The same system could be used for even greater gains in either the six-state protocol or cryptography using a larger Hilbert space. We show that the security of this protocol is equivalent to standard BB84: assuming the quantum and classical signals are space-like separated, no eavesdropper bound by special relativity can access both simultaneously.

**14:54**
**W40 3 Quantum Cryptography in Existing Telecommunications Infrastructure** DANIEL ROGERS,* JOSHUA BIENFANG, ALAN MINK, BARRY HERSHMAN, ANASTASE NAKASSIS, XIAO TANG, LIJUN MA, DAVID SU, CARL WILLIAMS, CHARLES CLARK, *National Institute of Standards and Technology* Quantum cryptography has shown the potential for ultra-secure communications. However, all systems demonstrated to date operate at speeds that make them impractical for performing continuous one-time-pad encryption of today's broadband communications. By adapting clock and data recovery techniques from modern telecommunications engineering practice, and by designing and implementing expeditious error correction and privacy amplification algorithms, we have demonstrated error-corrected and privacy-amplified key rates up to 1.0 Mbps over a free-space link with a 1.25 Gbps clock. Using new detectors with improved timing resolution, careful wavelength selection and an increased clock speed, we expect to quadruple the transmission rate over a 1.5 km free-space link. We have identified scalable solutions for delivering sustained one-time-pad encryption at 10 Mbps, thus making it possible to integrate quantum cryptography with first-generation Ethernet protocols.

*also with the University of Maryland Chemical Physics Program

**15:06**
**W40 4 Alternative Design for Quantum Cryptographic Entangling Probe** HOWARD BRANDT, *U.S. Army Research Laboratory* An alternative design is given for an optimized quantum cryptographic entangling probe for attacking the BB84 protocol of quantum key distribution [1], [2]. The initial state of the probe has a simpler analytical dependence on the set error rate to be induced by the probe than in the earlier design. The new device yields the same maximum information to the probe for a full range of induced error rates. As in the earlier design, the probe contains a single CNOT gate which produces the optimum entanglement between the BB84 signal states and the correlated probe states. [1] H. E. Brandt, Phys. Rev. A **71**, 042312 (2005). [2] H. E. Brandt, ''Design for a quantum cryptographic entangling probe,'' to appear in J. Mod. Optics (2005).

**15:18**
**W40 5 $\pi/3$ Phase-Shift Quantum Searching** LOV GROVER, *Bell Labs, Lucent Technologies* Quantum searching normally consists of an alternate sequence of selective inversion and diffusion operations. The algorithm has been extensively studied and is well understood. However, there was a surprising result that was discovered last year. According to this, if we change the selective inversions to $\pi/3$ phase shifts and adjust the sign of the phase shift in a prescribed manner, we obtain an algorithm that converges monotonically towards the solution [1]. This is in contrast to the well-known search algorithm that has an oscillatory character. This leads to a number of new and interesting applications. For example, if we consider a situation where the probability of getting a target state for a random item, is $1 - \epsilon$ (with $\epsilon$ unknown), then the probability of getting a target state after a single query in

the new algorithm, can be increased to $1 - \epsilon^3$, classically this can be increased to only $1 - \epsilon^2$. The performance of the new algorithm has recently been proved to be optimal. Another important application of this technique is in correction of systematic errors [2]. (1) L.K. Grover (2005), Fixed-point quantum search, Phys. Rev. Letters, Oct. 3, 2005. (2) B.W. Reichardt and L.K. Grover, Quantum error correction of systematic errors using a quantum search framework, Phys. Rev. A, Oct. 25, 2005

**15:30**

**W40 6 Relativistic Connection of Continuous and Discrete Quantum Walks** FREDERICK STRAUCH, *National Institute of Standards and Technology* Quantum algorithms, based on a quantum-mechanical generalization of random walks, have been shown to be very effective at solving local search problems. These quantum walks come in two very different forms (discrete and continuous-time) with surprisingly similar properties. An open problem has been to identify just what makes these two walks so similar. In this talk I present the analytical connection of these two walks, by way of an analogy with properties of the Dirac equation, including entanglement, zitterbewegung, and most importantly, relativistic wave-packet spreading.

**15:42**

**W40 7 Mixing and Decoherence in Continuous-Time Quantum Walks** LEONID FEDICHKIN, DMITRY SOLENOV, CHRISTINO TAMON, *Clarkson University* VLADIMIR PRIVMAN, *Clarkson University* We present analytical results showing that decoherence can be useful for speed-up of mixing in a continuous-time quantum walks on finite cycles. Our treatment of continuous-time quantum walks includes a continuous monitoring of all vertices that induces the decoherence process. We identify the dynamics of the probability distribution and observe how mixing times undergo the transition from quantum to classical behavior as our decoherence parameter grows from zero to infinity. Our results show that, for small rates of decoherence, the mixing time improves linearly with decoherence, whereas for large rates of decoherence, the mixing time deteriorates linearly towards the classical limit. In the intermediate region of decoherence rates, our numerical calculations confirm the existence of a unique optimal rate for which the mixing time is minimized.

**15:54**

**W40 8 Decoherence by Correlated Noise and Quantum Error Correction*** EDUARDO NOVAIS, HAROLD U. BARANGER, *Duke University* We study the decoherence of a quantum computer in an environment which is inherently non-Markovian and spatially correlated. We first derive the non-unitary time evolution of the computer and environment in the presence of a stabilizer error correction code. Our results demonstrate that effects of long-range correlation can be systematically reduced by suitable changes in the error correction codes. The new element that we discuss is that the periodic measurements in the QEC method separate the environmental modes into high and low frequencies. This natural ''new'' scale can then be used to better engineer quantum codes. As an example of this general discussion, we study decoherence in a quantum memory protected by Steane's three qubit code. The memory interacts with a bosonic enviroment through the spin-boson Hamiltonian. We calculate explicitly the long-range correlations in this case and demonstrate that a simple change in Steane's code reduces their effect.

*This work was supported in part by (1) the NSA and ARDA under ARO contract DAAD19-02-1-0079 and (2) the NSF Grant No. CCF-0523509.

**16:06**

**W40 9 Topological Quantum Computing with Only One Mobile Quasiparticle** STEVEN H. SIMON, *Lucent Technologies, Bell Labs* NICK BONESTEEL, *Dept Physics and NHMFL, Florida State University* MICHAEL FREEDMAN, *Microsoft Research* LAYLA HORMOZI, *Dept Physics and NHMFL, Florida State University* NADA PETROVIC, *UC Santa Barbara* In a topological quantum computer, universal quantum computation is performed by dragging quasiparticle excitations of certain two dimensional systems around each other to form braids of their world lines in 2+1 dimensional space-time. We show that any such quantum computation that can be done by braiding $n$ identical quasiparticles can also be done by moving a single quasiparticle around $n - 1$ other identical quasiparticles whose positions remain fixed. This result may greatly reduce the technological challenge of realizing topological quantum computation.

**16:18**

**W40 10 CNOT for Fibonacci anyons with only one mobile quasiparticle*** LAYLA HORMOZI, GEORGIOS ZIKOS, NICK BONESTEEL, *Dept. of Physics and NHMFL, Florida State University* STEVEN H. SIMON, *Bell Laboratories, Lucent Technologies* Certain two-dimensional systems with non-abelian quasiparticle excitations can be used for topological quantum computation (TQC). In TQC qubits are encoded using 3 or 4 quasiparticles and quantum gates are carried out by braiding quasiparticle world lines. We focus on the problem of finding explicit braiding patterns that yield a universal set of quantum gates, using Fibonacci anyons — quasiparticles which are thought to exist in an experimentally observed fractional quantum Hall state at filling fraction $\nu = 12/5$. In previous work[1] we have shown how to construct arbitrary controlled rotation gates (which together with single qubit gates provide a universal set of quantum gates) by moving a pair of quasiparticles from the control qubit around the quasiparticles in the target qubit while keeping the latter at fixed positions. In this talk we show how to take advantage of one of the structural properties of Fibonacci anyons (namely the fusion matrix) to construct a certain class of two-qubit gates (including CNOT) with only *one* mobile quasiparticle — therefore reducing the number of braiding operations by a factor of two.

*This work is supported by US DOE grant DE-FG02-97ER45639.

[1]N.E. Bonesteel, L. Hormozi, G. Zikos, and S. H. Simon, Phys. Rev. Lett. **95**, 140503 (2005).

**16:30**

**W40 11 Quantum Phase Transitions and Typical Case, Polynomial Time Solution of Randomly Generated NP-Complete Problems via Adiabatic Quantum Computation*** WILLIAM KAMINSKY, SETH LLOYD, *MIT* We argue theoretically that adiabatic quantum computation using only polynomial resources can solve almost all members of a nontrivial randomly generated set of NP-complete problem instances, namely the problem of finding the ground states of spin glasses on 3D cubic lattices having independent, identically Gaussian-distributed couplings. The argument uses the droplet model of quantum spin glasses, particu-

larly its prediction that the paramagnet-spin glass transition is unstable to even infinitesimal longitudinal fields. We then review the ongoing debate as to how well the droplet model describes 3D spin glasses and note that those inclined to view the intractability of NP-complete problems as a guiding physical intuition could take the results presented here as justifying greater suspicion toward the droplet model. Finally, due to this uncertainty as well as uncertainty in regard to the typical case classical complexity of this random NP-complete problem, we outline work using rigorous mean-field methods on a NP-complete problem whose typical-case classical complexity on random instances is better established, namely MAX CLIQUE on random graphs.

*This work is supported in part by ARDA and DoD under the AFOSR DURINT Program. WMK gratefully acknowledges fellowship support from the Fannie and John Hertz Foundation.

**16:42**

**W40 12 Adiabatic Quantum Computing in systems with constant inter-qubit couplings** VADIM SMELYANSKIY, *NASA Ames Research Center* SERGEI KNYSH, *Mission Critical Technologies* We propose an approach suitable for solving NP-complete problems via adiabatic quantum computation with an architecture based on a lattice of interacting spins (qubits) driven by locally adjustable magnetic fields. Interactions between qubits are assumed constant and instance-independent, programming is done only by changing local magnetic fields. Implementations using qubits coupled by magnetic-dipole, electric-dipole and exchange interactions are discussed.

**16:54**

**W40 13 Quantum Phase Transition and complexity of adiabatic quantum algorithm for Constraint Satisfaction problem** SERGEI KNYSH, *Mission Critical Technologies* VADIM SMELYANSKIY, *NASA Ames Research Center* We study the dynamics of adiabatic quantum computation (AQC) for solving the problem of satisfiability of randomly chosen clauses, each with 3 Boolean variables (3sat). We map this problem to that of a diluted long-range spin glass in traverse magnetic field and derive a self-consistent equation for the order parameter. We show the existence of the first-order quantum phase transition and investigate analytically and numerically the phase diagram on the plane: strength of the transverse field $\Gamma$ vs the ratio $\gamma$=M/N of a number of clauses M to a number of variables N. We show that the phase transition line approaches $\Gamma=0$ at the point of a classical replica symmetry breaking transition $\gamma_{RSB}$. We discuss the implications of the quantum phase transition for the complexity of the AQC for the 3sat.

**17:06**

**W40 14 Computation in Finitary Quantum Processes** KAROLINE WIESNER, *University of California, Davis* JAMES P. CRUTCHFIELD, *University of California, Davis* We introduce quantum finite-state generators as a first step toward a computational description of quantum dynamical processes. We developed their mathematical foundations, establishing probability conservation, reversibility, and consistency with quantum mechanical laws, and connect the class to the existing theory of finite-state recognizers and generators. These computational models allow for a quantitative description of quantum languages generated by quantum dynamical systems. Their descriptive power is explored via several example quantum dynamical systems.

**17:18**

**W40 15 Some Thoughts Regarding Practical Quantum Computing** DEBABRATA GHOSHAL, RICHARD GOMEZ, *George Mason University* MARCO LANZAGORTA, *US Naval Research Laboratory* JEFFREY UHLMANN, *University of Missouri - Columbia* Quantum computing has become an important area of research in computer science because of its potential to provide more efficient algorithmic solutions to certain problems than are possible with classical computing. The ability of performing parallel operations over an exponentially large computational space has proved to be the main advantage of the quantum computing model. In this regard, we are particularly interested in the potential applications of quantum computers to enhance real software systems of interest to the defense, industrial, scientific and financial communities. However, while much has been written in popular and scientific literature about the benefits of the quantum computational model, several of the problems associated to the practical implementation of real-life complex software systems in quantum computers are often ignored. In this presentation we will argue that practical quantum computation is not as straightforward as commonly advertised, even if the technological problems associated to the manufacturing and engineering of large-scale quantum registers were solved overnight. We will discuss some of the frequently overlooked difficulties that plague quantum computing in the areas of memories, I/O, addressing schemes, compilers, oracles, approximate information copying, logical debugging, error correction and fault-tolerant computing protocols.

## SESSION W41: COLD FUSION
**Thursday Afternoon, 16 March 2006**
**344, Baltimore Convention Center at 14:30**
**Scott Chubb, Naval Research Laboratory, presiding**

**14:30**

**W41 1 Cold Fusion A 17 Year Retrospective** MICHAEL C. H. McKUBRE, FRANCIS L. TANZELLA, *SRI International, Menlo Park, CA.* Seventeen years after the APS voted to refute the reality of Cold Fusion in Baltimore, it is appropriate to consider what has changed. Who was right? We will review the current state of knowledge from the perspective of what we know now compared to what we knew then. Discussion will be made of various avenues of research that have followed from the original Fleischmann-Pons proposal: some failed, some unresolved and some successful.

**14:42**

**W41 2 Recent Developments in Cold Fusion / Condensed Matter Nuclear Science** STEVEN B. KRIVIT, *New Energy Times, 11664 National Blvd., Suite 142, Los Angeles, CA 90064* Krivit is recognized internationally as an expert on the subject matter of cold fusion / condensed matter nuclear science. He is the editor of *New Energy Times*, the leading source of information for the field of cold fusion. He is the author of the 2005 book, *The Rebirth of Cold Fusion* and founder of New Energy Institute, an independent nonprofit public benefit corporation dedicated to accelerating the progress of new, sustainable and environmentally friendly energy sources.

**14:54**

**W41 3 Role of Finite Size in Triggering Excess Heat: Why Nanoscale PdD Crystals Turn on Faster** SCOTT CHUBB, *Research Systems Inc, 9822 Pebble Weigh Ct., Burke, VA 22015* Two persistent questions have been: 1. Why is a finite triggering time required after the near full-loading condition ($PdD_x$, $0.85 \approx < x \rightarrow 1$) before the ExcessH eat effect[1] is observed? 2. Is it possible to identify physical properties of the materials and/or crystals that are used that might be playing a role in the length of the interval of time associated with this phenomenon? In the talk, through a generalization[2] of conventional energy band theory, as it applies to infinitely−repeating, periodic lattices to situations involving finite lattices, I have been able to address both questions. In particular, the tunneling time depends on crystal size. Crystals with dimensions $\approx$ <6nm, which have tunneling times $\approx$microseconds, either cannot provide enough momentum to initiated+d$\rightarrow$ 4He reactions or conduct ion charge so rapidly that collisions occur. Crystals with dimensions $\approx$60 nm create heat and load rapidly ($\approx$3ms). But crystals with dimensions $> \approx$60 microns have tunneling times that are longer than a month.

[1]C.G. Beaudette, Excess Heat: Why Cold Fusion Research Prevailed. (Oak Grove Press, Bristol, ME, 2002)
[2]S.R. Chubb, ''Role of Broken Gauge Symmetry on Conduction of Charged and Neutral Particles in Finite Lattices,'' submitted to Proc. Roy. Soc. Series A (2005).

**15:06**

**W41 4 Resolving the Laughlin Paradox** TALBOT CHUBB, *Physicist Consultant, 5023 N. 38th St., Arlington, VA 22207* For paired Bloch electrons in a metal not subject to Pauli exclusion, the 2-electron Hamiltonian has the form $H = -\hbar^2/4m_e\Delta_{cm} + (2e)U_{lattice}(r_{cm},N_{cell}) + e^2/(N_{cell}r_{12}) - \hbar^2/3m_e\Delta_{12}$, where $r_{cm} = r_1 + r_2, r_{12} = r_1 - r_2$, and $r_1$ and $r_2$ are position vectors in configuration space, involving independent Bravais vectors $R_1$ and $R_2$, such that $R_1 - R_2 = R_{12}$ is an independent Bravais lattice vector, and $N_{cell}$ is the number of mutually shared potential wells over which the 2 electrons are coherently partitioned with entangled local density maxima. At large $N_{cell}$, the magnitude of term $3 <<$ the magnitude of term 1. When coordinate exchange symmetry is satisfied and energy minimized, term 3 cancels term 1 at $r_{12} = 0$, eliminating the singularity in the wave equation, thereby resolving Laughlin's paradox[1]

[1]R.B. Laughlin, ''A Different Universe,'' (Basic Books, Cambridge MA, 2005) pp. 84-85.

**15:18**

**W41 5 Dynamics of Non-linear Soft X-Ray Emission from a Plasma Discharge-Driven Hydride Target** GEORGE H. MILEY, YANG YANG, MICHAEL ROMER, MUNIMA HAQUE, IAN PERCEL, ANDREI LIPSON, *University of Illinois at Urbana-Champaign, Urbana, IL, 61801, USA* HEINZ HORA, *University of New S. Wales, Sydney, Australia* A high current discharge apparatus with a pulsed power supply has been constructed and successfully demonstrated an intense soft x-ray ($> 600$ eV) emission during bombardment by a 300 V deuterium plsma discharge. Emission is delayed until $\sim$ 1/2 ms into the msec voltage pulse[1]. Both electron and ion Bremsstrahlung have been ruled out as significant contibutions to the emission. A possible mechanism to explain this highly nonlinear x-ray emission is collective generation of soft x-ray quanta induced by a coherent D-diffusion process near the cathode's surface. This combined with continuous high current deuteron bombardment results in the penetration of recoil deuterons into the inner electron shell of the cathode material, generating x-ray emission.

[1]G, Miley, et al., Trans. ANS, Washington, DC (Nov. 2005)

**15:30**

**W41 6 Control of Tardive Thermal Power** MITCHELL SWARTZ, *JET Thermal Products, Wellesley, MA 02481* Previously, calorimetric improvements including thermal power analysis, dual ohmic controls, noise measurement and time-integration of multi-ring calorimetric systems with waveform reconstruction has led to the development of Phusor$^{TM}$ devices providing undeniable proof of excess heat in palladium heavy water (Pt/$D_2O$/Pd; 0.5 $cm^3$, peak excess power ratios of 2.30 $^{+/-}$ 0.84; 1). We now report improved control of tardive thermal power (TTP) which develops long after the termination of electric input power. From an engineering perspective, this is important because the effective excess power generated is further greatly increased (up to an additional $\sim$ 410% beyond that obtained without tardive thermal power operation); and because this improved means of operation can be coupled into over-unity motors and other work-producing systems. In addition, these systems have revealed further insight into the kinetics of the desired condensed matter reactions.

**15:42**

**W41 7 Progress in Excess of Power Experiments with Electrochemical Loading of Deuterium in Palladium** V. VIOLANTE, *ENEA Frascati Research Center Frascati (Italy)* M. BERTOLOTTI, E. CASTAGNA, C. SIBILIA, *University of Rome La Sapienza Dpt. Energetica Rome (Italy)* IRV DARDIK, *Energetics LLC, 7 Fieldview Lane, Califon, NJ 07830* S. LESIN, T. ZILOY, *Energetics, Ltd, Omer Industrial Park 84965, Israel* F. SARTO, *La Sapienza University, Via Scarpa, 14 00100 (Roma) Italy* F. TANZELLA, MICHAEL C. H. McKUBRE, *International 333 Ravenswood Ave, Menlo Park, CA 94025* A research activity has been carried out, during the last three years, in the field of triggering anomalous heat effects in palladium deuteride. An enhancement of the excess of power reproducibility in deuterated palladium was obtained by using HeNe laser irradiation during electrochemical loading. A preliminary correlation between excess of energy and helium-4 concentration increasing above the background was found. The continuation of the experimental program confirmed that laser triggering produces an interesting gain of reproducibility. An upgrade of the experimental set-up has been realized.

**15:54**

**W41 8 Cavitation Foil Damage** ROGER STRINGHAM, *Firstgate Energies, PO Box 1230 Kilauea, HI 96754, Phone: 808 828 2859* We have developed a much improved cavitation system for sonofusion, compared to our initial systems. The new system is a low mass 1.6 MHz unit that produces 40 watts of excess heat with an acoustic input power of 17 watts. The increase in frequency (to 1.6 MHz from 40 KHz) increases the heat, improves the performance, shows reproducible results, and indicates durability. The calorimetry is a simple in flow through system. The difference between output and input temperature ($T_{out}$ - $T_{in}$) at steady- state, times the flow gives the power (calories/s) output of the sonofusion reactor. The energy density of this system is of the order of commercial energy suppliers.

**16:06**

**W41 9 Isoperibolic Calorimetry Applied To The Pt/$D_2O$ Blank System** MARTIN FLEISCHMANN, *Fellow of the Royal Society, Bury Lodge, Duck Street, Tisbury Salisbury, Wilts, SP3 6LJ, U.K* MELVIN MILES, *Department of Chemistry, University of La Verne, La Verne, CA 91750* Doubts have often been expressed about the precision and accuracy of isoperibolic calorimeters where the heat transfer is controlled by radiation across the vacuum gap of the Dewar cells. Therefore, experiments were conducted on blank systems consisting of Pt cathodes polarized in 0.1 M LiOD/$D_2O$. Both the differential and intergral heat transfer coefficients were evaluated, and the latter based on backward integration of the data sets should be used for accurate evaluations of the experimental data. The heat transfer coefficients obtained are in agreement with values given by the product of the Stefan-Boltzmann coefficient and the radiant surface area. It is shown that the precision of this calorimetry is better than 99.99 percent while the accuracy is close to this figure. This high precision and accuracy allows the determination of the rate of enthalpy generation due to the reduction of oxygen electrogenerated in the cell. This rate was 0.0011 W for oxygen reduction whereas the input enthalpy to the cell was about 0.8 W for these experiments.

**16:18**

**W41 10 New Mechanism of Low Energy Nuclear Reactions Using Superlow** F.A. GAREEV, I.E. ZHIDKOVA, *Joint Institute for Nuclear Research, Dubna, Russia* We proposed a new mechanism of LENR (low energy nuclear reactions)[1]: cooperative processes in the whole system - nuclei+atoms+condensed matter can occur at smaller threshold than the corresponding ones assoiciated with free constituents. The cooperative processes can be induced and enhanced by (''superlow energy'') external fields. The excess heat is the emission of internal energy, and transmutations from LENR are the result of redistribution of the internal energy of the whole system. A review of possible stimulation mechanisms of LENR is presented. We have concluded that transmutation of nuclei at low energies and excess heat are possible in the framework of the known fundamental physical laws: The universal resonance synchronization principle[2], and, based on it, different enhancement mechanisms of reaction rates are responsible for these processes[3,4]. The excitation and ionization of atoms may play the role of a trigger for LENR.

[1]F.A. Gareev, I.E. Zhidkova, E-print arXiv Nucl-th/0511092 v1 30 Nov 2005.
[2]F.A. Gareev, In: FPB-98, Novosibirsk, June 1998, p.92; F.A.Gareev, G.F. Gareeva, in: Novosibirsk, July 2000, p.161.
[3]F.A. Gareev, I.E. Zhidkova and Yu.L. Ratis, Preprint JINR P4-2004-68, Dubna, 2004.
[4]F.A. Gareev, I.E. Zhidkova, E-print arXiv Nucl-th/0505021 9 May 2005

**16:30**

**W41 11 Comments on Summary of Condensed Matter Nuclear Science** XING Z. LI, BIN LIU, QING M. WEI, *Department of Physics, Tsinghua University, Beijing, 100084,China.* SHU X. ZHENG, DONG X. CAO, *Department of Engineering Physics, Tsinghua University, Beijing, 100084, China* Research involving investigations of the production of tritium in electrolytic cells was a topic that was recommended by the Energy Research Advisory Board(ERAB) report of the U. S. Department of Energy (DOE) in November, 1989. Fifteen years later, the evolution of related research has proven that this was an important recommendation. In the talk, a selective resonant tunneling model is used to attempt to explain the initial discoveries of tritium production. Deuterium flux might play a key role for solving the problem of reproducibility. A further investigation is suggested, based on this model.

**16:42**

**W41 12 Excess heat observed during electrolysis of deuterated phosphoric acid with palladium electrodes and a solid state electrolyte in deuterium gas** J.-P. BIBERIAN, *CRMCN, Faculte des Sciences de Luminy,163 Avenue de Luminy, 13288 Marseille cedex 9, France* G. LONCHAMPT, *CEA-Centre D'Etudes Nucleaire, Grenoble (retired); 31 Chemin Malanot, 38700 Corenc, France* We start with the hypothesis that the production of excess heat is occurring at the recombination $H+H\rightarrow H_2$ gas. If the pressure of hydrogen at the time of recombination is high enough, nuclear reactions can occur. In the case of hydrogen $H+H\rightarrow D+e^+$ and in the case of deuterium $D+D\rightarrow He^{-4}$. The high pressure can be obtained using Nernst's law, the potential between a hydrogen electrode and the cathode is given by $E=E_o+RTln(P/P_o)$. There are two sources for the potential: the electrochemical potential which is a characteristic of the metal in the presence of the metal ions, and on the other side,the overpotential for the formation of the hydrogen molecules. In this study we use palladium anodes and cathodes, but the cathode is covered with a thin film of a metal having either a low chemical potential or a high over-voltage for hydrogen formation. When deuterium molecules form at the surface of the electrode, very high pressures can be produced during a very short period of time during which possible nuclear reactions can happen. We show that excess heat is observed with clean palladium foils, and more excess heat is produced when the cathode is covered by a thin, metallic film, constructed using one of many possible metals.

**16:54**

**W41 13 Creating an International Scientific Society as an Act of Scientific Rebellion** WILLIAM COLLIS, *International Society of Condensed Matter Nuclear Science* When a new science is born, it is often necessary to unite dispersed groups of researchers all over the world. In this talk, I intend to describe the process of constituting and managing a new international scientific society covering such diverse issues as: 1.) Rationale; 2.) Initial feelers; 3.) Achieving consensus in the international community; 4.) Choice of jurisdicition; 5.) Corporate format; 6.) Establishing international pre-eminence in law; 7.) Reducing expenses; 8.) Tax minimization; 9.) Decision making; 10.) Democracy & transparency; 11.) Raising funds; 12.) Rewarding excellence; 13.) Online publishing; 14.) Organizing meetings. These issues will be covered with reference to the history of the International Society of Condensed Matter Nuclear Science, which will celebrate its second birthday in March 2006. It currently has nearly 200 members from 23 different countries.

**SESSION W42: FOCUS SESSION: SIMULATIONS OF MATTER AT EXTREME CONDITIONS III**
**Thursday Afternoon, 16 March 2006**
**345, Baltimore Convention Center at 14:30**
**Stephane Mazevet, Los Alamos National Laboratory, presiding**

*Contributed Papers*

**14:30**
**W42 1 Ab Initio Studies of High Pressure States of Crystalline Nitromethane.** FRANK ZERILLI, *Naval Surface Warfare Center* JOSEPH HOOPER, *Tulane University* MAIJA KUKLA, *National Science Foundation* We have calculated the mechanical compression curve for solid nitromethane with the ab-initio periodic structure code CRYSTAL using both Hartree-Fock and Density Functional Methods. In addition, calculations with both 6-21G and 6-31G** basis sets were performed and the effect of basis set superposition error was estimated using the counterpoise method. In each calculation the internal atomic coordinates and the crystal lattice parameters were relaxed at constant unit cell volume to the minimum energy configuration. The 6-31G** basis set was optimized by scaling the outer valence and polarization orbitals. It was found that Hartree-Fock calculations with a 6-21G basis set, uncorrected for basis set superposition error, gave the best agreement with experiment. These results may be due to the cancellation of basis set superposition error with dispersion force errors. While this result may be accidental, it appears that it extends to a number of other energetic organic molecular crystals, including beta HMX, PETN, and 1,1-diamino-2,2-dinitroethylene.

**14:42**
**W42 2 Atomistic Studies of Plastic Deformation and Dissipation in Crystalline HMX** EUGENIO JARAMILLO, THOMAS D. SEWELL, *Los Alamos National Laboratory* ALEJANDRO STRACHAN, *Purdue University* We are using large scale molecular dynamics simulations of crystalline octahydro-1,3,5,7-tetranitro-1,3,5,7-tetrazocine (HMX) to better understand the dominant fundamental mechanisms of inelastic deformation and other dissipative processes in anisotropic organic molecular crystals. A fully flexible force field (Smith, G. D. and Bharadwaj, R. K.; J. Phys. Chem. B 1999, 103, 3570) used in numerous preceding studies is used without modification in the present work. Our results, based on the results of simulations containing 25,000-250,000 molecules, indicate a large degree of directional anisotropy in response to compression, for both quasi-static and shock loading. Plastic deformation is observed for some loading directions whereas solid-solid phase transitions are observed for others. The emphasis of the present talk will be identifying and characterizing detailed molecular mechanisms and rate dependencies in those cases for which dislocation-induced plasticity occurs.

**14:54**
**W42 3 First-principles Study of Shock Compressed Carbon** NICHOLS ROMERO, WILLIAM MATTSON, BETSY RICE, *U.S. Army Research Laboratory* The phase diagram of carbon at high pressures and temperatures is of scientific interest to material science, geology and astrophysics. Major issues include the liquid-liquid phase transition, the melting curve of graphite and diamond, the nature of the liquid state and the nature of carbon in the interior of Uranus and Neptune. Strong shock waves generated by lasers, and even nuclear explosions have been used to study carbon at these extreme conditions. Because it is often difficult to replicate these shock-wave experiments, first-principles electronic structure calculations can play a prominent role in verifying, guiding, and interpreting these experiments. We report DFT results for the diamond Hugoniot.

**15:06**
**W42 4 Molecular dynamics simulation of shock compression of silicon** MIKHAIL LADANOV, *University of South Florida* IVAN OLEYNIK, *University of South Florida* SERGEY ZYBIN, *California Institute of Technology* MARK ELERT, *U.S. Naval Academy* CARTER WHITE, *Naval Research Laboratory* Shock compression of condensed matter is a fascinating scientific field that provides an excellent opportunity to probe the fundamental physics and chemistry of matter at extreme pressures and temperatures. In spite of substantial theoretical and experimental efforts, a full understanding of shock-induced elastic and plastic responses and polymorphic phase transitions is still far from complete. These phenomena often occur at the nanometer size and picosecond time scales, which makes molecular dynamics simulations an ideal tool for exploring nanoscale mechanisms of shock induced processes such as chemical reactions and phase transitions. We report the results of a molecular dynamics simulation of shock wave propagation in silicon in the [100], [110], and [111] directions obtained using a classical interatomic potential. Several regimes of materials response are classified as a function of shock wave intensity and crystalline orientation of shock wave propagation using calculated shock Hugoniot. The shock induced chemistry and shock wave splitting are discussed in relation to recent experimental results [1] that indicate an anomalous elastic response of the lattice at high compression ratios. [1] A. Loveridge-Smith, Phys. Rev. Let. **86**, 2349 (2001).

**15:18**
**W42 5 Molecular Dynamics Studies of Dynamical High-Pressure Phase Transitions in Rare-Gas Solids** EUGENE PECHENIK, *School of Physics and Astronomy, The Raymond and Beverly Sackler Faculty of Exact Sciences, Tel Aviv University, Tel Aviv 69978, Israel* GUY MAKOV, *Department of Physics, NRCN, P.O. Box 9001, Beer Sheva, Israel* The phase diagram of pair potential models of rare-gases was studied with respect to the effect of the choice of potential on the nature of the phase diagram. In particular the existence of a high-pressure bcc phase is shown to be potential sensitive. We show using molecular dynamics that the fcc-bcc phase transition cannot be reproduced with the Lennard-Jones (12-6) pair potential, though it is reproduced with the Buckingham pair potential. We propose a simple analytical technique, based on the Einstein theory of a harmonic solid, for predicting an fcc-bcc phase transition in a given system. Using the atomic volume and the pair potential as input, we were able to predict the transition temperature. These findings agree with an earlier work by A. B. Belonoshko et al., Phys. Rev. Lett. 87, 165505 (2001). Additionally, shock wave simulations of several model systems were conducted. The structure of shock wave in this model was examined as a function of shock strength and the existence of a dynamic phase transition was explored.

**15:30**
**W42 6 Interfacial instabilities and structure during high velocity sliding*** J.E. HAMMERBERG, T.C. GERMANN, B.L. HOLIAN, *Los Alamos National Laboratory* R. RAVELO, *University of Texas - El Paso* Interfacial sliding under high pressure loading at high velocities ($0 < v < 1$ km/s) results in a variety of mesosc ale phenomena at extreme strain rates. For ductile metal interfacial pairs, these include nano- and mesoscale dynami c strucutral transitions, local melting and amorphization, material mixing, and localization of plastic deformation. We illustrate these phenomena with large scale NonEquilibrium Molecular Dynamics (NEMD) simulations for Cu/Ag, Ta/Al, and Al/Al interfaces. These suggest universal behavior in sliding velocity for the frictional force and a scaling form for the frictional force vs. velocity at high velocities which will be discussed.

*This work supported by the Department of Energy under contract W-7405-ENG-36.

***Invited Papers***

**15:42**
**W42 7 Simulations of Rapid Solidification in Metals at High Pressure.***
FREDERICK H. STREITZ, *Lawrence Livermore National Laboratory*

Although computer simulation has played a central role in the study of nucleation and growth since the earliest molecular dynamics simulations almost 50 years ago, confusion surrounding the effect of finite size on such simulations have limited their applicability. Modeling molten tantalum in systems ranging from 64,000 to 131,072,000 atoms on the BlueGene/L computer, I will discuss the first atomistic simulations of solidification that demonstrate independence from finite size effects during the entire nucleation and growth process, up to the onset of coarsening. Using both our new results and historical data, we show that the observed maximal grain sizes for systems smaller than about 8,000,000 atoms are functions of the simulation size, following the predictions of finite size scaling theory. For larger simulations, a crossover from finite size scaling to more physical size-independent behavior is observed.

*This work was performed under the auspices of the U.S. Department of Energy by University of California Lawrence Livermore National Laboratory under contract No. W-7405-ENG-48.

***Contributed Papers***

**16:18**
**W42 8 Properties of molten sodium under pressure from first principles theory.*** JEAN-YVES RATY, *University of Liege, Belgium* ERIC SCHWEGLER, *Lawrence Livermore National Laboratory* STANIMIR BONEV, *Dalhousie University, Canada* Recent measurements of the melting curve of sodium [1] have found a sharp decline in the melting temperatures from 1000 to 300 K in the pressure range from 30 to 120 GPa. In this study, we investigate the stability and structural properties of solid and liquid sodium at high pressure and temperature using first principles molecular dynamics. The experimental melting curve is reproduced from 0 to 120 GPa. The local structure of the liquid is found to be strongly correlated to the multiple finite temperature crystalline phases of sodium. Based on a quantitative analysis of the structural and electronic properties of the solid and liquid phases, we propose an explanation for the unusual melting curve and a new perspective on the phase diagram of sodium. [1] Gregoryantz et al., Phys. Rev. Lett. 94, 185502 (2005).

*Work supported by the NSERC of Canada. J.Y.R. acknowledges support by the FNRS, the Nomade Region Wallonne contract and the FAME NoE. E.S. worked under the auspices of the U.S. Dept. of Energy at the University of California/LLNL.

**16:30**
**W42 9 Melting and phase stability of high-density beryllium** ANDREA TRAVE, ERIC SCHWEGLER, *Lawrence Livermore National Laboratory* FRANCOIS GYGI, GIULIA GALLI, *University of California, Davis and Lawrence Livermore National Laboratory* First-principles Molecular Dynamics calculations have been performed to determine the liquid vs. solid phase boundary for beryllium up to 250 GPa. Shock Hugoniot curves have been calculated for both solid and liquid beryllium in this range of pressures and temperatures to determine the shock melting onset conditions and pressure range of liquid-solid coexistence. The results of these simulations also provide insights on the problem of relative stability of various crystalline forms of beryllium at high temperature. This work was performed under the auspices of the US Department of Energy by the University of California at the LLNL under contract no W- 7405-Eng-48.

**16:42**
**W42 10 Ab initio simulation of intense short-pulse laser irradiation of metals and semi-conductors** VANINA RECOULES, *CEA/DIF - Departement de Physique Theorique et Appliquee* PIERRE-MATHIEU ANGLADE, *CECAM* JEAN CLÉROUIN, *CEA/DIF* GILLES ZÉRAH, *CEA/DIF* STEPHANE MAZEVET, *Los Alamos National Laboratory* The effect of intense ultra-laser irradiation on crystal stability is not completely elucidated. Ultrashort laser pulses heat electrons to a very high temperature and leave the lattice relatively cool since the heat capacity of electrons is much smaller than that of lattice. This non-equilibrium system can be described as two subequilibrium systems : the hot electrons and a cold lattice. We studied the effect of this intense electronic excitations on the interatomic forces and the possible melting of the underlying lattice for a semi-conductor (Si) and two metals (Al and Au). We used *ab initio* linear response to compute the phonon spectrum in the Density Functional Theory framework for several electronic temperatures ranging from 1 to 6 eV. We found that semi-conductors and metals behave in an opposite ways when increasing electronic temperature. Phonon instability appears in silicon at a electronic temperature of 1.5 *eV* inducing the melting of the lattice. Gold samples become more stable. The Debye tem-

perature was deduced from the phonon spectrum and using the Linderman criterion, we showed that gold undergoes a sharp increase of its melting temperature under intense laser irradiation. The same effect is observed for aluminium.

**16:54**

**W42 11 Nonequilibrium Dynamics of Ultracold Neutral Plasmas** THOMAS POHL, *ITAMP, Harvard-Smithsonian Center for Astrophysics, Cambridge* THOMAS PATTARD, *Max-Planck-Institute for the Physics of Complex Systems, Dresden, Germany* JAN-MICHAEL ROST, *Max-Planck-Institute for the Physics of Complex Systems, Dresden, Germany* In a number of recent experiments ultracold plasmas (UNPs) have been produced by photoionizing laser-cooled atomic ensembles [1]. Their very low initial kinetic energies suggest that they are created deeply in the strongly correlated regime. Moreover, UNPs are produced far from equilibrium, leading to a complex relaxation dynamics. We present a hybrid-molecular dynamics approach [2], to describe the long-time plasma evolution while fully taking into account the strongly correlated character of the ionic motion. We demonstrate that the method yields an accurate description of recent measurements [2,3] and allows to address problems beyond present experimental capabilities [3]. It turns out that under the conditions in UNPs the commonly applied Bogoliubov assumption about a hierarchy of relaxation timescale becomes invalid, resulting in an unusual relaxation dynamics connected with a wave-like temperature evolution and an ultimate relaxation to a non-equilibrium undercorrelated state. (1) Y.C. Chen et al., Phys. Rev. Lett. 93, 265003 (2004). (2) T. Pohl, T. Pattard and J.M. Rost, Phys. Rev. A 70, 033416 (2004). (3) T. Pohl, T. Pattard and J.M. Rost, Phys. Rev. Lett. 94, 205003 (2005); Phys. Rev. Lett. 92, 205003 (2004).

**17:06**

**W42 12 Shock-Induced Polarization in Distilled Water** YURI SKRYL, *Institute of Mathematics and Computer Science, University of Latvia, Latvia* ANNA BELAK, *Virginia Polytechnic Institute and State University, Blacksburg, VA* MAIJA KUKLJA, *National Science Foundation, DMR/MPS, Arlington, VA* This study is aimed at developing a theoretical model to describe shock-induced polarization in water. The model is based on the notion that polar water molecules tend to align in the shock front due to inertial and stress forces. Analytical formulas for calculation of the shock-induced polarization charge, potential generated by this charge, and accompanied polarization current produced by the shock wave are derived. A comparison with experimental curves for polarization currents suggests that two factors contribute into the measured polarization signal: change of the polarization charge once the wave front enters the sample and change of the sample capacity while the front is progressing across the sample. Good agreement with experimental data on polarization in distilled water leads us to believe that the results obtained bring about a better understanding of mechanisms of shock induced polarization in liquids containing polar molecules.

**17:18**

**W42 13 Quantum Dynamics of Energy Transfer under Shock Conditions*** R.C. MOWREY, *NRL* M.L. ELERT, *U. S. Naval Academy* C.T. WHITE, *NRL* Classical molecular dynamics (MD) simulations predict efficient energy transfer from translational to vibrational modes near shock fronts in molecular solids. The validity of the classical description of collisional energy transfer under shock conditions has not been tested for extended systems. In this research effort, quantum mechanical (QM) simulations are used to study energy transfer in a system consisting of three collinear diatomic molecules and a stationary wall. A fast-moving projectile diatom collides with its neighbor initiating a collision cascade. The multiplicity of collisions precludes ita priori prediction of the detailed collision dynamics. The time dependence of the six-degrees-of-freedom wave function is determined using QM time-dependent wave packet methods. Intra- and inter-molecular interactions are described using nearest-neighbor potentials. Probabilities for vibrational excitation and bond rearrangement are predicted as a function of the collision energy of the projectile for differing interaction potentials and atomic masses.

*Supported by ONR

## SESSION W43: FOCUS SESSION: COLD ATOMS IN OPTICAL LATTICES

**Thursday Afternoon, 16 March 2006**
**346, Baltimore Convention Center at 14:30**
**S. das Sarma, University of Maryland, presiding**

***Contributed Papers***

**14:30**

**W43 1 Macroscopic Quantum Tunneling and Entangled States in Bose-Einstein Condensates*** LINCOLN D. CARR, DIMITRI R. DOUNAS-FRAZER, ANN M. HERMUNDSTAD, *Physics Department, Colorado School of Mines* We use a multi-band Hubbard model to study beyond-mean-field effects in macroscopic quantum tunneling of excited states in Bose-Einstein condensates. Our goal is to determine straightforward observables such as the oscillation frequency of kink-like structures between two wells or the propagation speed of such structures on a lattice. As a preliminary step, we present some surprising new results for entangled states of N bosons in two wells.

*Partial support by the National Science Foundation is very much appreciated.

**14:42**

**W43 2 Disorder-induced enhancement of phase coherence in trapped bosons on optical lattices** PINAKI SENGUPTA, ADITYA RAGHAVAN, STEPHAN HAAS, *Univ. of Southern California* Using numerical methods, we have investigated the effects of disorder on a system of interacting bosons trapped in a one-dimensional optical lattice. Our results show that there is a unique effect at small to moderate strengths of disorder if there is a Mott plateau at the center of the trap in the ordered system - long range phase coherence actually *increases* as a result of disorder. The localization effects due to correlation and disorder compete against each other which results in a partial delocalization of the particles in the Mott region leading to increased coherence. Eventually, at large disorder strengths, the phase coherence decreases. In the absence of a Mott plateau at the center, this effect is absent and the phase coherence decreases for all disorder strenghts. Fur-

ther analysis of the uniform (no trap) system shows that the disordered states belong to the Bose glass phase.

**14:54**
**W43 3 Cold Atom Optical Lattices as Quantum Analog Simulators for Aperiodic One-Dimensional Localization Without Disorder** VITO SCAROLA, SANKAR DAS SARMA, *University of Maryland* Cold atom optical lattices allow for the study of quantum localization and mobility edges in a disorder-free environment. We predict the existence of an Anderson-like insulator with sharp mobility edges in a one-dimensional nearly-periodic optical lattice. We show that the mobility edge manifests itself as the early onset of pinning in center of mass dipole oscillations in the presence of a magnetic trap which should be observable in optical lattices. This work is supported by NSA-LPS and ARO-ARDA.

***Invited Papers***

**15:06**
**W43 4 Measuring correlation functions in interacting systems of cold atoms.***
EUGENE DEMLER, *Harvard University*

I will discuss two approaches to measuring correlation functions in experiments with cold atoms. The first approach is based on analyzing atom shot noise in the time of flight experiments. I will compare this approach to Hanburry-Brown-Twiss experiments and show that it can be used to probe novel quantum states of cold atoms including paired states of fermions and magnetically ordered states in optical lattices. The second approach relies on interference experiments between extended condensates. I will show that the interference pattern contains information about correlation functions within individual condensates and that the full distribution of the fringe contrast provides information about high order correlation functions. I will discuss possible applications of this method to study Luttinger liquid behavior in one dimensional systems and probe Kosterlitz-Thouless transition in two dimensional condensates.

*Work done in collaboration with E. Altman, M. Lukin, A. Polkovnikov.

***Contributed Papers***

**15:42**
**W43 5 Feshbach resonances in optical lattices** DENNIS DICKERSCHEID, *ITP Utrecht University* D. VAN OOSTEN COLLABORATION, H. T. C. STOOF COLLABORATION, In the last few years there has been much excitement in the field of ultracold atomic gases. In a large amount this is due to the use of so-called Feshbach resonances and, in addition, the use of an optical lattice for the atoms. Recently, the first steps have been made to experimentally combine these techniques, which can both be used to tune the interactions between the atoms. Motivated by these developments, we show that the physics of these systems is described by a generalized Hubbard model for which the microscopic parameters are determined by the details of the lattice and the experimentally known parameters of the Feshbach resonance in the absence of the optical lattice. As a particular application we also discuss the phasediagrams of a Bose gas and a Bose-Fermi mixture near a Feshbach resonance in an optical lattice.

**15:54**
**W43 6 Ramping Fermions in Optical Lattices across a Feshbach resonance** ANIELLO ESPOSITO, HELMUT G. KATZGRABER, MATTHIAS TROYER, *Theoretische Physik, ETH Zurich* We study the properties of ultracold Fermi gases in a three-dimensional optical lattice when crossing a Feshbach resonance. By using a zero-temperature formalism, we show that three-body processes are enhanced in a lattice system in comparison to the continuum case. This poses one possible explanation for the short molecule lifetimes found when decreasing the magnetic field across a Feshbach resonance. Effects of finite temperatures on the molecule formation rates are also discussed by computing the fraction of double-occupied sites. Our results show that current experiments are performed at temperatures considerably higher than expected: lower temperatures are required for fermionic systems to be used as quantum simulators. In addition, by relating the double occupancy of the lattice to the temperature, we provide a means for thermometry in fermionic lattice systems, previously not accessible experimentally. The effects of ramping a filled lowest band across a Feshbach resonance when increasing the magnetic field are also discussed: fermions are lifted into higher bands due to entanglement of Bloch states. Our results are in good agreement with recent experiments.

**16:06**
**W43 7 Competing phases in Bose-Fermi mixtures of ultracold atoms in optical lattices** LUDWIG MATHEY, *Harvard University* SHAN-WEN TSAI, *UC Riverside* ANTONIO CASTRO-NETO, *Boston University* We study mixtures of ultracold bosonic and fermionic atoms, confined to a two-dimensional lattice, with a numerical functional renormalization group (RG) method. The method is an extension of the RG approach to interacting fermions[1] which also takes into account couplings of the fermions to bosonic modes.[2] We obtain the phase diagram of the system for the limit of large bosonic phonon velocity in comparison to the Fermi velocity. The renormalization group method provides the value of the gaps of the various phases, as well as the subdominant orders and the short range fluctuations.

[1]R. Shankar, Rev. Mod. Phys. 66, 129 (1994).
[2]S.-W. Tsai, A. H. Castro Neto, R. Shankar, and D. K. Campbell, Phys. Rev. B 72, 054531 (2005).

**16:18**
**W43 8 Vidals simulation method applied to two coupled 1D lattices** JAMES WILLIAMS, IPPEI DANSHITA, CHARLES CLARK, *NIST-Gaithersburg* Recently, a method was developed employing matrix product states to simulate the quantum dynamics of a one dimensional lattice system using an adaptive time stepping technique [G. Vidal, Phys. Rev. Lett. 91, 147902 (1993); Phys. Rev. Lett. 93, 040502 (1994)]. We use this approach to

simulate the dynamics of bosons loaded into a double-well optical lattice geometry relevant to recent experiments at NIST [I. Spielman et al., Bull. Am. Phys. Soc. (2005)]. We study a pair of coupled 1D lattices, which can be mapped into a single 1D lattice with next-nearest neighbor interactions.

**16:30**

**W43 9 The speed of sound in a Bose-Einstein condensate in optical lattices** BIAO WU, ZHAOXIN LIANG, *Institute of Physics, Chinese Academy of Sciences, Beijing, China* XI DONG, *Department of Physics, Tsinghua University, Beijing, China* We have studied the speed of sound of a Bose-Einstein condensate in optical lattices both analytically and numerically. We find that in the one-dimensional case, the speed of sound falls monotonically with increasing lattice strength. However, the trends are different in two and three dimensional cases. In these two cases, when the interaction is strong, the speed of sound also decreases monotonically with increasing lattice strength. But when the interaction is weak, the sound speed first increases then decreases when the lattice strengh increases.

**16:42**

**W43 10 Instability of a superfluid Bose gas induced by a locked thermal gas in an optical lattice** SATORU KONABE, TETSURO NIKUNI, *Tokyo University of Science* We use a dissipative Gross-Petaevskii equation derived from the Bose-Hubbard Hamiltonian to study the effect of the thermal component on the stability of a current-carrying superfluid state of a Bose gas in an optical lattice potential. We explicitly show that the superfluid state becomes unstable at certain quasi-momentum of the condensate due to a thermal component which is locked by an optical lattice potential. It is shown that this instability coincides with the Landau instability derived from the GP equation.

**16:54**

**W43 11 Imaging of diverging correlations close to a quantum phase transition in optical lattices*** A.B. KUKLOV, *Department of Physics, College of Staten Island, CUNY, NY 10314* Q. NIU, *Department of Physics, University of Texas, Austin, TX 78712* I. CARUSOTTO, *BEC-CNR-INFM and Dipartimento di Fisica, Universita di Trento, I-38050 Povo, Italy* We suggest real space determination of diverging space-time correlations close to a quantum phase transition from Bose Mott insulator to superfluid in optical lattices. The method relies on interference of either the released cloud or the outcoupled atomic beam with some reference Bose-Einstein condensate. Upon approaching the transition from the Mott phase, the resulting interference pattern represents a set of uncorrelated domains, with a typical size determined by the correlation length $\xi$ as long as it is smaller than a system size $L$. Repetition of the measurements in a progression of $L$ for $\xi > L$ provides crucial information on the critical behavior in the context of the finite size scaling approach. The Hanbury Brown & Twiss type measurements allow extracting the average spatial correlator, which is insensitive to the expansion time and decaying on distances $\approx \xi$ (for $\xi < L$). The non- destructive scheme employing two outcoupling pulses separated by some time $\tau$ can probe both the spatial and time correlations.

*Authors acknowledge hospitality of the Aspen Center for Physics during the Summer 2005. This work is supported by the NSF grant PHY-0426814 and PSC-CUNY- grant 665560036

**17:06**

**W43 12 Attractive Bosons in Optical Lattices*** DANIEL GOLDBAUM, ERICH MUELLER, *Cornell University* We study the theory of attractive bosons in an optical lattice with a hard-core constraint, limiting on-site occupations to 0, 1, or 2 particles per site. Our goal is to investigate the Boson pairing phase transition. We describe how an off-resonant Raman photoassociation transition [C. Ryu, et. al. Cond-mat/0508201] may be used to generate this model. We explore the properties of this system through a mean-field theory that allows short-range correlations. We write a wavefunction that describes both atomic and molecular superfluid phases, and study properties of the system near the phase transition, including the structure of vortices.

*NSF PHY-0456261, Department of Education Fellowship, and Sloan Foundation

**17:18**

**W43 13 The repulsive interacting bosons in an one dimensional moving lattice ring** QI ZHOU, *Ohio State University* TIN-LUN HO, *Ohio State University* We investigate the properties of the ground state of the repulsive interacting bosons in an one dimensional moving lattice ring, and reveal that the superfluid density of the system is a periodic function of the velocity of the lattice. In the weakly interacting limit, the Umklapp process of the mutual scattering of bosons in the moving lattice provide the generation mechanism for the vortices. In the strongly interacting limit, the moving lattice can cause transitions between the Mott insulator and the different superfluid phases carrying vortex with different winding number.

## SESSION W45: SPIN STRUCTURE IN MAGNETIC MATERIALS

**Thursday Afternoon, 16 March 2006**
**348, Baltimore Convention Center at 14:30**
**Mike Fitzsimmons, Los Alamos National Laboratory, presiding**

**14:30**

**W45 1 Magnetism in the diluted induced moment system $(La,Pr)_6Ni_2Si_3$*** R. W. McCALLUM, Y. JANSSEN, K. W. DENNIS, P. C. CANFIELD, *Ames Laboratory, Iowa State University, Ames IA 50011* $Pr_6Ni_2Si_3$ crystallizes in a complex hexagonal structure with two distinct Pr sites with no point symmetry, thus the $2J+1=9$ ground state levels are CEF-split into singlets. Single-crystal magnetization and specific heat measurements suggest that this splitting is large compared to the ordering temperature. As CEF-induced singlets are nonmagnetic, any ordered magnetic moment is induced by magnetic interactions. $Pr_6Ni_2Si_3$ orders with a ferromagnetic component parallel to the c-axis at $\sim$ 40K, whereas $La_6Ni_2Si_3$ appears to be nonmagnetic. Upon substitution of Pr by La the ordering temperature decreases more rapidly than predicted by a rule of mixtures. For substitutions of more than 50% La, no ordering is observed above 5 K. For 50% La, both AC and DC magnetization measurements suggest superparamagnetic or spin glass type behavior. This behavior will be discussed in terms of clusters of Pr ions with size-dependent moment and anisotropy.

*Ames Laboratory is operated for the US Department of Energy by Iowa State University under contract number W-7405-ENG-82.

**14:42**

**W45 2 Ferromagnetism in $Ba_2NaOsO_6$** ANN ERICKSON, *Stanford University and Geballe Laboratory for Advanced Materials* GORDON MILLER, *Iowa State University and Ames Laboratory* SUMOHAN MISRA, *Iowa State University* ZACK SCHLESINGER, RAJ GUPTA, *University of California, Santa Cruz* IAN FISHER, *Stanford University and Geballe Laboratory for Advanced Materials* Due to the extended nature of 5d orbitals, magnetism in systems of 5d electrons is uncommon. Here we present results of structural, thermodynamic and optical reflectivity experiments on single crystals of the novel magnetic material $Ba_2NaOsO_6$. The material has a double perovskite structure, space group Fm-3m, with full occupancy of all sites. The osmium ions have a $7^+$ valence, corresponding to a $5d^1$ electron configuration. The effective moment at high temperatures is 1.10 $\mu_B$, somewhat less than the spin-only value due to spin-orbit coupling, with no apparent anisotropy. The Weiss temperatures are -11.0 and -12.4 $\pm$ 0.4 K for fields orinted along the [100] and [111] directions respectively. At 6.8 K a sharp anomaly in the heat capacity indicates the onset of long range magnetic order. The ordered state is characterized by a small ferromagnetic moment of just 0.2 $\mu_B$ per formula unit, with only a slight anisotropy, indicative of a helical magnetic structure. Infra red reflectivitity measurements confirm that the material is an insulator.

**14:54**

**W45 3 Magnetic properties of (R, R', R'',...)$Ni_2Ge_2$ solid solutions** S.A. LAW, S.L. BUD'KO, P.C. CANFIELD, *Ames Laboratory and Dept. of Physics and Astronomy, Iowa State University* Anisotropic magnetic properties of single crystals of (R, R', R,'' ...)$Ni_2Ge_2$ (R = rare earth) solid solutions will be presented. Whereas the magnetic ordering temperatures and the paramagnetic $\Theta$'s broadly follow de Gennes scaling there are some systematic deviations from this oversimplfied trend. In this talk we will examine these deviations and also discuss the apparent absence of a spin-glass state induced by random magnetic anisotropy for the most highly mixed samples.

**15:06**

**W45 4 Temperature dependence of magnetization of hcp Gd** A. CHERNYSHEV, V. PECHARSKY, K. GSCHNEIDNER, *Department of Materials Science and Engineering, Iowa State University and Ames Laboratory, Ames, IA, 50011* V. ANTROPOV, *Condensed Matter Physics, Ames Laboratory, Ames, IA, 50011* Careful magnetization measurements of high purity Gd single crystal have been performed. Our results confirm a strong deviation from the Bloch law for the magnetization at low temperatures, and we demonstrate that this effect is even stronger than had been previously measured on less pure Gd samples. We have analyzed the physical nature of this deviation qualitatively and quantitatively using known theoretical models and the newly obtained results. However, no fully satisfactory agreement between the new experimental data and existing theories has been reached.

**15:18**

**W45 5 Magnetic phase separation in electron-doped Bi1-xCaxMnO3 systems** YUHAI QIN, TREVOR A. TYSON, *New Jersey Institute of Technology* KENJI SHIMIZU, *Toyama University* The manganite system Bi1-xCaxMnO3 possesses intriguing properties in the low bismuth doping region. In this electron doped region ($0.6< x< 1$), a ferromagnetic (FM) moment of $\sim$ 1.2 Bohr magnetons per Mn site is found for $x\sim$ 0.875. The magnetic moment per Mn site maintains a value $\sim$ 1/3 the theoretical limit even in fields a high as 60 T. The physical origin of this high moment region is not well understood. Various models including canted ferromagnetism and ferromagnetic clusters hosted by an antiferromagnetic background have been proposed. In our previous work, we have conducted small-angle neutron scattering (SANS) on Bi0.125Ca0.875MnO3 polycrystalline samples as has revealed existence of FM clusters embedded in an AFM background. New 55Mn NMR results give more evidence supporting of this heterogeneous phase model: resonance signals from both AFM and FM phases were identified. More progress from multiple-temperature Bi-L3 edge XAFS measurements will be presented as well. This work is supported by NSF DMR-0209243 and NSF DMR-0512196.

**15:30**

**W45 6 Physical Properties of Single Crystal $EuIn_2P_2$ and $EuGa_2P_2$*** NEWELL JENSEN, SAMUEL MAQUILON, PETER KLAVINS, ZACHARY FISK, *UC Davis Physics* CATHIE CONDRON, JIONG JIANG, SUSAN KAUZLARICH, *UC Davis Chemistry* PHYSICS/CHEMISTRY UC DAVIS COLLABORATION, Single crystals of $EuIn_2P_2$ and $EuGa_2P_2$ have been grown by a metal flux method. The EuIn 2P2 material crystallizes in a new hexagonal structure type and orders magnetically at 24 K. The magnetic ordering is anisotropic suggesting a possible canted ferromagnetic magnetic structure. The temperature dependent resistivity data indicate semi−metallic behavior. Negative colossal magnetoresistance is observed at the ordering temperature. The gallium metal analogue, EuGa2P2, crystallizes in a related monoclinic structure and magnetically orders at a slightly higher temperature. Magnetization, resistivity and specific heat data are presented for both compounds.

*This work is partially supported by NSF DMR−0433560 and DMR−0120990

**15:42**

**W45 7 Structural and magnetic properties of single layered manganite Pr0.5Ca1.5MnO4*** SONGXUE CHI, *University of Tennessee, Knoxville* PENGCHENG DAI, *University of Tennessee, Knoxville* FENG YE, *Oak Ridge National Laboratory* JAIME FERNANDEZ-BACA, *Oak Ridge National Laboratory* ROLAND MATHIEU, *University of Tokyo* YOSHI TOKURA, *University of Tokyo* QINGZHEN HUANG, *NIST Center for Neutron Scattering* JEFFREY LYNN, *NIST Center for Neutron Scattering* High resolution neutron powder diffraction and elastic neutron scattering have been used to determine the lattice and magnetic structure of the single layer manganite Pr0.5Ca1.5MnO4. The system becomes charge/orbital ordered (CO-OO) near 300K and antiferromagnetically ordered with a Neel temperature ($T_N$) near 125K, which has CE-type (checkerboard like) structure in the Mn-O plane. At temperatures above $T_N$ but below $T_{CO-OO}$, we discovered an anomalous lattice response around 160K. We discuss the microscopic origin of this lattice distortion and its association with competing CO-OO and antiferromagnetic states.

*The work was supported by NSF-DMR0453804 and DOE DE-FG02-05ER46202. ORNL is managed by UT-Battelle, LLC, for the U.S. Dept. of Energy under contract DE-AC05-00OR22725. This work was also performed under the US-Japan Cooperative Program on Neutron Scatteri

**15:54**

**W45 8 Magnetic structure of the Kondo lattice compound $CeZn_{0.6}Sb_2$** Y. CHEN, J. W. LYNN, *NIST Center for Neutron Research and University of Maryland* H. LEE, P. KLAVINS, Z. FISK, *Dept. of Physics, University of California at Davis* S. NAKATSUJI, *Dept. of physics, Kyoto University* W. BAO, J. THOMPSON, T. PARK, *Los Alamos National Laboratory* R. MACALUSO, J. CHAN, *Louisiana State University* B. CARTER, *National High Magnetic Field Laboratory, Florida State University* The new Kondo lattice compound $CeZn_{0.6}Sb_2$ has a tetragonal structure with space group P4/nmm and shows ferromagnetic behavior below 2.5 K. The Curie-Weiss temperature is 22 K along the tetragonal *ab* plane, indicating ferromagnetic interactions in the plane. Along the *c* axis, however, the Curie-Weiss temperature is -145 K, suggesting antiferromagnetic exchange interaction in this direction [1]. We determined the magnetic structure of $CeZn_{0.6}Sb_2$ using single crystal neutron diffraction. $(h,0,l)$ and $(h, h,l)$ scattering planes were investigated. We found $CeZn_{0.6}Sb_2$ orders ferromagnetically at $T_C$=2.5 K. The magnetic structure is collinear with a low temperature ordered Ce moment of 1.3 (1) $\mu_B$ that lies in the *ab* plane. In addition, we measured the order parameter of the ferromagnetic transition. [1] Studies of the ferromagnetic Kondo lattice system of single crystal $CeZnSb_2$, H. Lee, S. Nakatsuji, Y. Chen, W. Bao, R. Macaluso, J. Chan, T. Park, B. Carter, P. Klavins, J. Thompson, Z. Fisk, BAPS, Session L41, 2005.

**16:06**

**W45 9 APRES Study of Spin Spiral States in $TlCo_2Se_2$*** HAEKYUNG JEONG, *Boston University* TONICA VALLA, *Brookhaven National Lab* ROLF BERGER, *Upssla University* PETER JOHNSON, *Brookhaven National Lab* KEVIN SMITH, *Boston University* The electronic structure of $TlCo_2Se_2$ has been measured using high resolution angle resolved photoemission spectroscopy (ARPES). $TlCo_2Se_2$ is thought to be a spin spiral system, but experimental evidence from the electronic structure supporting the spin spiral states has been lacking. The original indication of a spin spiral state came from neutron powder diffraction experiments, and was confirmed in a subsequent neutron diffraction study of single crystals. However, it was not possible to distinguish between the helical structure and the sine-modulated moments since the intensity of the magnetic pattern satellites from neutron diffraction was very low. We used high resolution ARPES to study the electronic structure of single crystals of $TlCo_2Se_2$ cleaved in ultra high vacuum. Our experimental results clearly show the existence of band crossings near the Fermi level that would support spin spiral states, and reveals the predicted quasi-two dimensional electronic structure. The Boston University program is supported in part by the Department of Energy under DE-FG02-98ER45680.

*ARPES Study of Spin Spiral States in TlCo2Se2

**16:18**

**W45 10 Magnetic Ordering in Copper Pyrazine Perchlorate, a S=1/2 2D Quantum Heisenberg Antiferromagnet** F. XIAO, C. P. LANDEE, M. M. TURNBULL, *Clark University, Worcester, MA 01610* M. NOVAK, S. SORIANO, *Universidade Federal do Rio de Janeiro, Rio de Janeiro, Brasil* Copper pyrazine perchlorate, $Cu(Pz)_2(ClO_4)_2$, consists of antiferromagnetic layers of $Cu^{2+}$ ions bridged by neutral pyrazine molecules. The exchange strength within the layers is $J/k_B$ = 17.5 K; excellent isolation between layers is provided by the bulky perchlorate ions. Specific heat studies and muon spin resonance measurements [1] show the ordering temperature to be 4.25 K, corresponding [2] to an interlayer/intralayer exchange ratio of 1 x $10^{-3}$. The specific heat data show no characteristic anomaly at $T_N$, only a broad contribution attributable to the short-range order within the layers. This result is consistent with recent theoretical predictions [3]. The excellent isolation results in the observation of field-induced XY-behavior in the magnetic susceptibility, as predicted elsewhere [4]. 1. J. Manson et al, unpublished results. 2. C. Yasuda et al, Phys. Rev. Lett. **94**, 217201 (2005). 3. P. Sengupta et al, Phys. Rev. B, **68**, 094423 (2003). 4. A. Cuccoli et al, Phys. Rev. B, **68**, 060402 (2003).

**16:30**

**W45 11 Magnetic field dependence of the order parameter in weakly ordered quasi-1D antiferromagnets** IGOR ZALIZNYAK, ANDREI SAVICI, *Brookhaven National Laboratory* BEATRICE GRENIER, LOUIS-PIERRE REGNAULT, SERGEI PETROV, We report neutron diffraction study of the antiferomagnetic order in two isostructural quasi-one-dimensional S=1 Heisenberg antiferromagnets, CsNiCl3 and RbNiCl3, in magnetic fields up to 15 T. These materials present model systems of Haldane spin chains with very similar in-chain exchange interaction, but coupled by the inter-chain exchange of different strengths. In both cases the inter-chain coupling is super-critical, so that the Haldane gap is suppressed and weak antiferromagnetic order appears below 4.84 K in CsNiCl3 and 11.1 K in RbNiCl3. In zero field the ordered magnetic moments in CsNiCl3 and RbNiCl3 are approximately 0.9 and 1.2 Bohr magnetons, respectively. We find that the antiferromagnetic order is enhanced by application of the magnetic field, as it is expected both for coupled Haldane chains and from the spin-wave theory arguments. However, we show that the spin-wave theory can not reproduce the observed behavior quantitatively.

**16:42**

**W45 12 Neutron Diffraction Study of A-site Size and Variance Effect on the Spin and Orbital Ordering in $RVO_3$ Perovskites** J.-Q. YAN, S. CHANG, J. ZARESTKY, O. GARLEA, R. MCQUEENEY, *Ames Laboratory, Neutron and X-ray Group, Ames, IA50011* A. LIOBET, *Los Alamos National Lab* Y. REN, *Argonne National Lab* J. FIERAMOSCA, *Argonne National Lab* $RVO_3$ members all exhibit an intriguing sequence of orbital and magnetic orderings below a Too and a $T_N$, respectively. Since only t-electrons are active in this system, they have been a prototype to study cooperative orbital ordering among the $\pi$-bonding t orbitals in the absence of $\sigma$-bonding e electrons and the relationship of this orbital order to long-range magnetic ordering. We have studied the A-site size and variance effect on the spin and orbital ordering in single phase (YLa)VO3 and (YLaLu)VO3 systems by magnetization, specific heat, thermal conductivity, and nenutron diffraction measurements. The results show that both A-site size and variance stabilize G-type magnetically, C-type orbitally ordered state before an electronic phase segregation takes place. The results will be presented with special emphasis on the neutron diffraction experiments for both single crystal and polycrystalline samples.

**16:54**

**W45 13 Soft X-ray absorption Spectroscopic Investigation on Electronic Evolutions in $SrFe_{1-x}Mo_xO_{3\pm\delta}$ ($0 \leq x \leq 1$)** B.-K. PARK, *POSTECH* J.-H. PARK, *POSTECH/PLS* J.-Y. KIM, *PLS* H.-J. LEE, J.H. SONG, Y.H. JEONG, *POSTECH* H.-J. LIN, C.T. CHEN, *NSRRC* A double perovskite $Sr_2FeMoO_6$, which an alternative mixture of $SrFeO_3$ and $SrMoO_3$, is a half-metallic ferrimagnet with a high critical temperature $T_C \sim$ 400K, although a

certain amount of anti-site disorder diminishes the half-metallicity in a real system. $SrFeO_3$ and $SrMoO_3$, which have the ionic states of $Fe^{4+}$ and $Mo^{4+}$, are known to be an antiferromagnetic insulator and a non- magnetic metal, respectively. However, as they forms the double perovskite, the ionic states primarily form $Fe^{3+}$ $(3d^5_\uparrow)$ and $Mo^{5+}$ $(4d^1_\downarrow)$, and then the Fe 3*d*-Mo4*d* hybridization makes a down spin band at the Fermi level. Hence the real ground state becomes a state with $Fe^{2+}$-$Fe^{3+}$ and $Mo^{5+}$-$Mo^{6+}$ mixed valences. It means that the valences of Fe and Mo can vary by two, i.e. from $Fe^{4+}$ to $Fe^{2+}$ and from $Mo^{4+}$ to $Mo^{6+}$ in $SrFe_{1-x}Mo_xO_{3\pm\delta}$ $(0 \leqslant x \leqslant 1)$, respectively. Here we presents the structural, electrical, and magnetic phase diagram and electronic evolutions in $SrFe_{1-x}Mo_xO_{3\pm\delta}$ $(0 \leqslant x \leqslant 1)$.

**17:06**

**W45 14 Electronic bandstructure of the NiMnSb(001) surface above and below the Fermi energy** JULIET CORREA, *Physikalisches Institut, Westfälische Wilhelms-Universität Münster* CHRISTIAN EIBL, GEORGI RANGELOV, JÜRGEN BRAUN, MARKUS DONATH, The predicted 100% spin polarization at the Fermi energy ($E_F$), together with the high Curie temperature (750K) of the half-Heusler alloy NiMnSb makes it interesting for technological applications. However, experimentally only 50% surface polarization has been observed. Knowledge of the electronic structure of NiMnSb is key to improving our understanding of this material. We report on surface bandstructure measurements for the (001) surface of single crystal NiMnSb. The experimental techniques used are angle resolved ultraviolet photoemission spectroscopy (ARUPS)and inverse photoemission spectroscopy (ARIPES) to probe the bandstructure both below and above $E_F$. ARUPS and ARIPES are used quasi-simultaneously in a multichamber UHV-system to ensure well defined and equal sample preparation conditions. We see both non-dispersive (ARIPES) and dispersive (ARUPS) structures in the spectra, which stem from d-like bulk states. With our normal emission UPS data, we resolve the conflict in the various contradictory reports in the literature about the position of spectral features for both polycrystal and single-crystal samples. Finally, through comparison with theoretical calculations we have identified a surface state candidate.

**17:18**

**W45 15 Contact-less measurements of Shubnikov-de Haas oscillations below Néel temperature in single crystals $SmAgSb_2$** M. D. VANNETTE, R. PROZOROV, S. L. BUD'KO, P. C. CANFIELD, B. N. HARMON, *Ames Laboratory and Department of Physics and Astronomy, Iowa State University, Ames, Iowa 50011* Oscillations of a skin depth with magnetic field were measured in single crystals $SmAgSb_2$ by using radio-frequency resonant technique. Comparison with directly measured de Haas – van Alphen and Shubnikov – de Haas oscillations revealed additional details in the frequency spectra, probably due to high sensitivity of the measurements $\Delta\rho_{min} \approx 20$ p$\Omega \cdot$ cm. The temperature evolution of the frequency spectra was obtained. The correlation of the observed oscillations with calculated Fermi surface and possible influence of antiferromagnetic ordering are discussed.

**SESSION W46: COMPOUND SEMICONDUCTOR DEFECTS AND DOPANTS**
**Thursday Afternoon, 16 March 2006**
**349, Baltimore Convention Center at 14:30**
**H. T. Johnson, University of Illinois, Champagne, presiding**

**14:30**

**W46 1 Silicon-interstitials-based Benchmarking of DFT Exchange-correlation Potentials*** K. P. DRIVER, W. D. PARKER, R. G. HENNIG, J. W. WILKINS, *Ohio State U.* C. J. UMRIGAR, *Cornell U.* R. MARTIN, E. BATISTA, B. UBERUAGA, *LANL* J. HEYD, G. SCUSERIA, *Rice U.* Diffusion Monte Carlo (DMC) benchmarks DFT functionals: LDA, GGA, and HSE [1]. Extensive DFT studies on single-, di-, and tri-interstitials [2] provide stable structures and converged energies. For single-interstitial formation energies, our DMC results confirm earlier work [3], with 1.5 and 1.0 eV underpredictions for LDA and GGA, respectively. We continue to observe this trend in most di- and tri-interstitials. Additionally, we find HSE reproduces DMC results for single-interstitals. Preliminary analysis indicates that large LDA and GGA discrepancies with DMC occur for highly distorted defect configurations. [1] J. Heyd *et al.*, J.Chem.Phys. **118**, 8207 (2003). [2] D. A. Richie *et al.*, Phys. Rev. Lett. **92**, 45501 (2004). [3] W. -K. Leung *et al.*, Phys. Rev. Lett. **83**, 2351 (1999).

*Supported by DOE(DE-FG02-99ER45795), NSF (EAR-0530301, DMR-0205328), and Sandia National Laboratory. Computation performed at OSC and NERSC.

**14:42**

**W46 2 Random doping and oxide roughness induced fluctuations in nanoscale semiconductor devices*** PETRU ANDREI, *Florida State University* Random doping and oxide roughness induced fluctuations in nanoscale semiconductor devices are analyzed by using self-consistent Poisson-Schrödinger computations. A very fast and robust technique based on linearization of the transport equations is presented for the computation of fluctuations of various parameters (such as threshold voltages, terminal currents, and cutoff frequencies) of the semiconductor device. This technique is computationally much more efficient than the traditional Monte-Carlo approach and yields information on the sensitivity of device parameters fluctuations to the locations of doping and oxide thickness fluctuations. Hence, it can be used in the design of fluctuation resistant structures of semiconductor devices. Sample simulation results obtained by using the linearization technique are reported for MOSFET devices with channel lengths under 25 nm and compared with results obtained by using the Monte-Carlo technique.

*This work is supported by the Army High Performance Computing Research Center under agreement number DAAD19-01-2-0014.

**14:54**

**W46 3 Thermodynamics of semiconductor doping and stoichiometry from first-principles methods*** STEPHAN LANY, ALEX ZUNGER, *National Renewable Energy Laboratory, Golden, CO 80401* The theoretical investigation of semiconductor doping involves assessment of opposing physical effects: While itextrinsic doping can shift the Fermi level in the desired direction, such shifts disturb the balance between itintrinsic defects (vacan-

cies, interstitials, etc.) leading to the creation of ''killer-defects'' and, in some materials, to considerable deviation from ideal stoichiometry. We have developed a self-consistent procedure which uses first- principles calculated formation enthalpies of impurities and intrinsic defects, to predict the correlation between doping, stoichiometry, and equilibrium carrier density. With this method, we explore the deviation from ideal stoichiometry and the electrical properties of the photovoltaic materials $CuInSe_2$ and $CuGaSe_2$, sampling the entire space of thermodynamical variables. We find a systematic correlation between stoichiometry and conductivity type, which in case of $CuInSe_2$ spans the whole range from *p*- to *n*-type. Application to the case of N-doping of ZnO, identifies the narrow window for growth conditions that lead to *p*-type doping by $N_O$ acceptors.

*Funded by DOE-EERE under contract no. DE-AC36-98GO10337 to NREL

**15:06**

**W46 4 Stoichiometry Driven Impurity Configurations in Compound Semiconductors*** G. CHEN, I. MIOTKOWSKI, S. RODRIGUEZ, A. K. RAMDAS, *Purdue University* Precise stoichiometry and departures therefrom in the composition of the tetrahedrally coordinated compound semiconductors allow impurity incorporation in more than one configuration. Ultra-high resolution infrared spectroscopy of CdTe:O at low temperatures reveals a unique pair of sharp lines, a non-degenerate $\nu_1 = 1096.78$ $cm^{-1}$ and a doubly degenerate $\nu_2 = 1108.35$ $cm^{-1}$ at 5 K, associated with the local vibrational modes of $O_{Te}$ in a $(O_{Te} - V_{Cd})$ complex in crystals grown with (CdTe + CdO + excess Te) or $(CdTe + TeO_2)$ which enhances the occurrence of Cd vacancy $(V_{Cd})$; in contrast, a single, triply degenerate sharp line at $\nu_0 = 349.79$ $cm^{-1}$ observed at 5 K occurs in CdTe grown with (CdTe + CdO + excess Cd) in which the appearance of $V_{Cd}$ is inhibited. In the former, oxygen, $O_{Te}$, is bonded to three nearest neighbor Cd's with a nearby $V_{Cd}$. The latter corresponds to $O_{Te}$ attached to all the four nearest neighbor Cd cations. With increasing temperature, $\nu_1$ and $\nu_2$ approach each other and behave as a single triply degenerate line at $\nu_0^*$ for temperature $T \geqslant T^* \sim 300$ K; the uniaxial $(C_{3v})$ symmetry of $(O_{Te} - V_{Cd})$ transforms to $T_d$ symmetry at T*, acquired due to an increasing rate of bond switching among the four possible $O_{Te} - V_{Cd}$ directions as T approaches T*.

*Work supported by NSF (DMR 0405082)

**15:18**

**W46 5 Ab initio studies of defects in CdTe and HgTe with symmetrized basis*** YIA-CHUNG CHANG, HYEJUNG KIM, *University of Illinois at Urbana-Champaign* We have performed ab initio pseudopotential calculations of the total energies and atomic realxations of neutral and charged Cd vacancies in CdTe and Hg vacancies in HgTe. Our method takes advantage of the high point symmetry of the system, which enables us to use large supercells containing up to 64 atoms per unit cell. Supercells of 8, 16, 32, 54, and 64 atoms are employed and spin-orbit interactions are included. Considering only symmetric relaxations of neighboring atoms in CdTe system of a 64-atom supercell, we find that first-neighbor atoms around a Cd vacancy move toward the vacancy with a 9% contraction in bond length and second-neighbor atoms move toward the vacancy with a 2.5% lowering contraction in inter-atomic distance. The relaxation lowers the total energy by about 0.2eV. Similarly in HgTe, the contractions are 7% and 1.5%, respectively for first-neighbor and second-neighbor atoms. Three defect levels (with symmetry$\Gamma_6$, $\Gamma_7$, and$\Gamma_8$) are found for both CdTe and HgTe systems and one of the levels is located in the band gap while two of them are buried under the valence band maximum. Separate calculations are carried out using a full potential linearized augmented Slater-type orbital (LASTO) method and give consistent results. Self-energy corrections due to many-body effect are also estimated with the GW approach.

*supported by ARO/MURI Contract DAAD19-01-1-0591

**15:30**

**W46 6 Dislocation filtering by buffer layer interfaces in $InSb/Al_xIn_{1-x}Sb$ heterostructures grown on GaAs (001) substrates*** MADHAVIE EDIRISOORIYA, TETSUYA MISHIMA, MICHAEL SANTOS, *University of Oklahoma* Recent efforts have been devoted to the development of InSb-based transport devices, including mesoscopic magnetoresistors and field-effect transistors, on GaAs (001) substrates. The small effective mass of electrons in InSb leads to a high mobility at room temperature. Remotely-doped InSb quantum wells offer the additional advantage of a conducting layer that is close to the surface. One key to maximizing the performance of such devices is the reduction of dislocation and micro-twin densities induced by the large lattice mismatch between $InSb/Al_xIn_{1-x}Sb$ and GaAs. We investigated the dislocation filtering effects of the interfaces formed between an $Al_yIn_{1-y}Sb$ interlayer and an $Al_xIn_{1-x}Sb$ matrix layer with $y > x$. Transmission electron microscopy analysis shows that the interlayer interfaces filter out threading dislocations. We improve this dislocation filtering by optimizing the interlayer thickness, the number of interlayers, and the growth conditions.

*This work was supported by the NSF under Grants DMR-0510056 and DMR-0520550.

**15:42**

**W46 7 Thermodynamic model for the structure of the 90 degree partial dislocation in diamond cubic semiconductors.*** S. P. BECKMAN, *The University of Texas at Austin* D. C. CHRZAN, *The University of California at Berkeley* Recent studies of the 90 degree partial dislocation in diamond cubic semiconductors indicate that the structure of the core is not homogeneous, but rather is a combination of reconstructions and low energy structural excitations, such as kinks and anti-phase defects. As a result, direct investigation of the macroscopic properties of dislocation core by itab initio methods is unfeasible. A model is presented that maps the complicated structure of a dislocation core onto a one-dimensional spin lattice. At each lattice site two spins are present, one to represent the reconstructed bonds, and the other kink structures. The model is sufficiently complex to allow expression of the essential nature of the structural excitations along a dislocation line. This Ising-like model can be investigated within a Monte Carlo framework.

*This work is supported by the Department of Energy, Office of Science, Basic Energy Sciences. Computational resources were provided by NERSC.

**15:54**

**W46 8 Strain relaxation and crystal quality in compositionally graded GaAsSb/GaAs metamorphic buffer layers*** BENNY PEREZ RODRIGUEZ, JOANNA MIRECKI MILLUNCHICK, *University of Michigan* We have compared linearly graded, step graded, and constant composition layers of GaAs(1-x)Sb(x)/GaAs grown by Molecular Beam Epitaxy to determine which grading

schemes result in the highest crystalline quality, while relaxing the lattice parameter most effectively. The incorporation rates used throughout the experiment for Ga and As were kept constant at 0.96 and 1.11 ML/s respectively. The Sb incorporation rate was varied from 0 to 0.63 ML/s to obtain a final composition of the topmost layers of x=0.5. The real-time stress evolution was obtained using an in situ multi-beam optical stress sensor. In our experiments, aggressive grading of the Sb flux results in decreased Sb incorporation at low x, a higher residual stress, and a bifurcation in the tilt of the sample. Less aggressive grading increases results in more uniform incorporation and lower residual stress, but the tilt remains. The tilt may be reduced by incorporating large steps in the grading, and completely eliminated when a constant composition layer of GaAs(0.5)Sb(0.5) is deposited directly on GaAs. The defect density of constant composition layers is somewhat higher than linearly graded layers with the same thickness and final composition. However, increasing the thickness of the layer reduces the defect density.

*This work is supported by the National Science Foundation DMR 0092602

**16:06**

**W46 9 Mutual Passivation of Donors and Isovalent Nitrogen in GaAs** JINGBO LI, PIERRE CARRIER, SU-HUAI WEI, *National Renewable Energy Laboratory* SHU-SHEN LI, JIAN-BAI XIA, *State Key Lab for Superlattices and Microstructures, Institute of Semiconductors, CAS* Using large supercell total energy and band structure calculations, we have studied the mutual passivation mechanism of isovalent N and shallow donors in GaAs. We find that all the donor impurities, $Si_{Ga}$, $Ge_{Ga}$, $S_{As}$, and $Se_{As}$, bind to N in GaAs:N, which has a large N-induced band gap reduction relative to GaAs. For group-IV impurity such as Si, the formation of the nearest-neighbor $Si_{Ga}$-$N_{As}$ defect complex creates a deep donor level below the conduction band minimum (CBM). The coupling between this defect level with the CBM pushes the CBM upwards, thus restoring the GaAs band gap; the lowering of the defect level relative to the isolated $Si_{Ga}$ shallow donor level is responsible for the increased electrical resistivity. Therefore, Si and N mutually passivate each other's electrical and optical activities in GaAs. For group-VI shallow donors such as S, the Coulomb binding between $S_{As}$ and $N_{As}$ does not form a direct bond and a deep level inside the gap; thus, no mutual passivation exists in the GaAs:(S+N) system. We also explained the difference between the mutal passivation of Si and N and the mutal passivation of H and N in GaAs. Our study provides a deep understanding of the mutual passivation mechanism and explained some of the recent puzzling experimental observations.

**16:18**

**W46 10 Effect of indium on the localized vibrational mode of nitrogen in $GaN_xAs_{1-x}$*** A. M. TEWELDEBERHAN, *Tyndall National Institute, Lee Maltings, Prospect Row, Cork, Ireland* STEPHEN FAHY, *Department of Physics, University College Cork, Ireland* The effect of the substitution of nearest-neighbor gallium atoms by indium (In-N-Ga, In-N-In) on the frequency of the localized vibrational mode of substitutional nitrogen in the dilute nitride, $GaN_xAs_{1-x}$, has been studied within first-principles density functional theory, using a supercell approach. The splitting of the highly localized triply-degenerate mode into singly- and doubly-degenerate modes is obtained and compared with available Raman and FTIR spectroscopy measurements. The results are in good agreement with the experimental values.

*Work supported by Science Foundation Ireland

**16:30**

**W46 11 Effects of edge and screw dislocations on optical properties of Wurtzite GaN** JEONG HO YOU, H.T. JOHNSON, *University of Illinois at Urbana-Champaign* The wide bandgap and high temperature stability of GaN makes it a desirable material for applications such as blue light-emitting diodes, blue lasers, and high-power transistors. Despite these advantages, the large lattice mismatch in most epitaxial GaN leads to a high density of dislocations, on the order of $10^9 cm^{-2}$ for edge dislocations and $10^8 cm^{-2}$ for screw dislocations in WZ GaN. Edge dislocations are electron acceptors and take on a negative charge. Open-core screw dislocations are essentially voids, or nanopipes, in the material. The presence of these defects, plus the strain field associated with each dislocation type, change the density of states and reduce the PL intensity in typical epitaxial GaN device layers. In the present work, the effects of edge and screw dislocations in WZ GaN have been studied computationally as a function of dislocation density. Spectral properties are determined by solving a 6x6 multiband kp Hamiltonian in three-dimensions using a real-space finite element method. Results compare favorably to available experimental data.

**16:42**

**W46 12 Vacancy induced localized states in graphene*** J.M.B. LOPES DOS SANTOS, VITOR M. PEREIRA, *CFP and Departamento de Física, Faculdade de Ciências, Universidade de Porto* F. GUINEA, *Instituto de Ciencia de Materiales de Madrid, CSIC, Cantoblanco E28049 Madrid, Spain* N.M.R. PERES, *Center of Physics and Departamento de Física, Universidade do Minho, P-4710-057, Braga, Portugal* A.H. CASTRO NETO, *Department of Physics, Boston University, 590 Commonwealth Avenue, Boston, MA 02215, USA* We show, analytically, that vacancies in an half-filled honeycomb lattice induce the formation of quasi-localized electronic states. If particle-hole symmetry is broken, these states become resonances close to the Fermi level. We also calculate numerically the electronic density of states for a finite density of vacancies, and discuss the issue of electronic localization in these systems. Our results have also relevance for the problem of disorder in d-wave superconductor.

*Acknowledgements: C. Mudry for discussions, the Quantum Condensed Matter Visitor's Program at Boston University; FCT, Portugal, grant SFRH/BD/4655/2001; NSF grant DMR-0343790; FCT and EU through POCTI (QCAIII).

**16:54**

**W46 13 Low temperature photoluminescence in the strongly disordered dilute nitride GaAsN.** IVANA BOSA, DERMOT McPEAKE, *Tyndall National Institute, University College Cork, Ireland* STEPHEN FAHY, *Tyndall National Institute and Department of Physics, University College Cork, Ireland* Photoluminescence (PL) due to the radiative recombination of excitons is used to study the structural disorder of alloys. We calculate the PL spectra at finite temperatures in the dilute nitride GaAsN. The shape of PL spectra is determined by the exciton occupation under steady-state optical excitation. Exciton energy levels and wave functions are calculated numerically in a supercell geometry with a strong random alloy potential acting on the electron. The distribution of electrons in states of the random potential is found by solving a kinetic equation, including phonon-assisted transitions between states and radiative recombination. Results are compared to the recent experiments.

**SESSION W47: QUANTUM TRANSPORT IN SEMICONDUCTORS: THEORY AND EXPERIMENT**
**Thursday Afternoon, 16 March 2006**
**350, Baltimore Convention Center at 14:30**
**Andrey Kiselev, North Carolina State University, presiding**

**14:30**
**W47 1 Wigner approach to quantum transport in graded semiconductors*** A.A. KISELEV, G.J. IAFRATE, *Dept. of Electrical and Computer Eng., North Carolina State Univ., Box 7911, Raleigh, NC 27695* Graded electron bandstructures have long being used to beneficially influence the performance and functionality of electronic devices. In this work, we have developed a consistent fully quantum description of electron transport in terms of the Wigner distribution function, making use of the symmetric and hermitian effective-mass-like single band Hamiltonian that can be unambiguously constructed for graded systems. The generalized Wigner equation includes contributions that, in the quasiclassical limit, can be interpreted as directly corresponding to the drift and diffusion terms, but, unlike the homogeneous materials, the velocity operator is coordinate dependent and the electron is subject to the influence of the k-dependent quasielectric fields originating from both the inhomogeneous potential profile and composition-dependent modulation of the quasiparticle inertia. The approach is useful for the analysis of a broad class of transport phenomena in graded systems, where quantum effects are important, but a full quantum treatment would be prohibitively costly.

*This work was supported by ONR.

**14:42**
**W47 2 Variational studies of quantum liquid crystal phases of 2DEG** EFSTRATIOS MANOUSAKIS, *MARTECH, Physics Department, FSU, Tallahassee, FL and University of Athens, Greece* QUOC DOAN, *MARTECH and Physics Department, FSU, Tallahassee, FL* The ground state of a nematic phase of the 2DEG at filling fraction $\nu = 1/2$ is studied. The pair distribution function and interaction energy are calculated for a wavefunction having the Jastrow form for the correlation part of $\Pi_{i<j}(z_i - z_j)^2$ and an elliptical Fermi surface. First, the Fermi hypernetted chain (FHNC) approximation was employed in which, as usual, the contribution of the elementary diagrams is neglected. Our HNC/FHNC results agree very well with earlier reported results for various cases studied by the same approximation. Second we used the Monte Carlo (MC) method using periodic boundary conditions for a square geometry including the contribution of the image charges. To test our correct implementation of the second method, we computed for the same square geometry the pair distribution function and the energies of $\nu = 1,1/3,1/5$ states and our results are in excellent agreement with earlier results in which the disk geometry was used. Our preliminary results indicate that there are important differences between FHNC and the MC. We find that in the FHNC calculation the nematic state is energetically favorable as compared to the isotropic state, while in the MC we find the contrary. Further work is necessary to study the role of the finite-size effects in MC, and more final results and conclusions will be presented at the meeting.

**14:54**
**W47 3 Photoconductivity in AC-driven modulated two dimensional electron gas*** MANUEL TORRES, *Instituto de Fisica, UNAM Mexico* ALEJANDRO KUNOLD, *Departamento de Ciencias Basicas, UAM Mexico* We study the photoconductivity of two-dimensional electron system in a perpendicular homogeneous magnetic field, under the influence of periodic modulation potential and microwave irradiation. The model includes the microwave and Landau contributions in a non-perturbative exact way, the periodic potential is treated perturbatively. The Landau-Floquet states provide a convenient base with respect to which the lattice potential becomes time-dependent, inducing transitions between the Landau-Floquet levels. Based on this formalism, we provide a Kubo-like formula that takes into account the oscillatory Floquet structure of the problem. The total resistivity exhibits strong oscillations, leading to negative resistance states as the electron mobility and the intensity of the microwave power increases. It is proposed that, depending on the geometry, negative conductance sates or negative resistance states may be observed in lateral superlattices fabricated in $GaAs/AlGaAs$ heterostructures.

*Supported by CONACyT and DGAPA-UNAM

**15:06**
**W47 4 Charge transfer between a superconductor and a hopping insulator*** YURI GALPERIN, *University of Oslo* VENIAMIN KOZUB, ALEXANDER ZYUZIN, *Ioffe Institute RAS, Russia* VALERII VINOKUR, *Argonne National Laboratory, USA* We develop a theory of the low-temperature charge transfer between a superconductor and a hopping insulator. We show that the charge transfer is governed by the coherent two-electron – Cooper pair conversion process, ittime reversal reflection, where electrons tunnel into superconductor from the localized states in the hopping insulator located near the interface, and calculate the corresponding interface resistance. This process is an analog to conventional Andreev show that the time reversal interface resistance is accessible experimentally, and that in mesoscopic structures it can exceed the bulk hopping resistance.

*The work was supported by the U. S. Department of Energy Office of Science through contract No. W-31-109-ENG-38.

**15:18**
**W47 5 Simulating the interaction of a scanning probe with the quantum Hall liquid** GARY STEELE, RAYMOND ASHOORI, NEMANJA SPASOJEVIC, *MIT* Motivated by recent experiments [1], we have developed a simulation of the interaction of a metallic scanning probe with a 2D electron system (2DES) in the quantum Hall regime. The simulation is based on an electrostatic relaxation method, modified to include the non-linear screening of the 2D electron system at high magnetic fields. Using 2D simulations with cylindrical symmetry that allow us to account for the exact shape of the tip, we predict the diameter and width of ring shaped incompressible strips (ISs) induced by DC tip biases. Extending these results to 3 dimensions, we incorporate the effect of the disorder on the shape of the IS, and predict the formation of quantum dot islands observed in [1]. Comparison of the simulation results with experimental data provides a direct and quantitative view of the disorder of a very high mobility 2DES. [1] G. A. Steele, R. C. Ashoori, L. N. Pfeiffer, and K. W. West, Phys. Rev. Lett. 95, 136804 (2005)

**15:30**

**W47 6 Quantum dynamics for a dissipative quantum harmonic oscillator as a model for a NEMS frequency control resonator*** ILKI KIM, GERALD J. IAFRATE, *Dept. of Electrical and Computer Eng., NC State Univ., Raleigh, NC 27695* For the simplest model of dissipation, that is, a linear oscillator coupled to an infinite number of degrees of freedom to form a dissipative bath, it is found that the Heisenberg equation of motion for the oscillator displacement takes the form of a Langevin equation with a memory dependent dissipation [Ford, Lewis, O'Connell; Phys. Rev. A 37, 004419 (1988)]. When Fourier analyzed, this leads to a complex susceptibility which gives rise to a generalized frequency dependent ''quality factor'' which relates to the dissipative environment. We explore the limits of resonator integrity, especially with regard to insights afforded by the dependence of quality factor and other observables on the microscopic connection between resonator material parameters and circuit performance.

*This work is supported by NSF.

**15:42**

**W47 7 Kohn localization in the quantum Hall regime** RAFFAELE RESTA, *University of Trieste, Italy* A two-dimensional electron fluid in the quantum Hall regime shows both quantized transverse conductivity and vanishing longitudinal conductivity: the latter property characterizes insulators. According to Kohn's theory of the insulating state, electron localization—defined in an appropriate sense—is the *cause* for the insulating behavior in any insulator. I show that a quantum Hall ''insulator'' is no exception; furthermore both quantization of the transverse conductivity and vanishing of the longitudinal one stem here from the same elegant formalism. Since 1999 onwards, the theory of the insulating state has been reformulated in term of a ''localization tensor'' which provides a measure of electron localization. This tensor is an intensive property, geometric in nature, having the dimensions of a squared length; it characterizes the ground wavefunction as a whole, *not* the individual states. It is finite in any insulator and divergent in any metal. A fluctuation-dissipation theorem relates this ground-state property to the system conductivity. So far, the theory has only addressed systems with time-reversal symmetry, in which case the localization tensor is real. I show that in absence of such symmetry the localization tensor is naturally endowed with an imaginary part, proportional to transverse dc conductivity, and quantized in two-dimensional systems. Therefore electron localization is the *common cause* for both vanishing of the dc conductivity and quantization of the transverse one in quantum Hall fluids.

**15:54**

**W47 8 The mass of the electron in Shubnikov-de Haas effect:Spin-charge locking** KESHAV SHRIVASTAVA, *University of Hyderabad* At low temperatures, the integration over the Fermi distribution leads to x/sinh x type expression which is called the Dingle's formula. The spin symmetry is found to modify this formula which determines the oscillation amplitude of resistivity as a function of magnetic field. The theory introduces the effective charge so that the cyclotron frequency gets fractionalized resulting into $m/\nu_{\pm}$. At a certain magnetic field 1.5m is found instead of m. The Shubnikov-de Haas effect uses quantization of Landau levels but not the flux quantization. Hence we find that there is a ''quantized S-dH effect'' which measures the $m/h^2$. We determine that when fractional values of the filling factor are taken into account, the mass of the electron, equal to the band mass is obtained. 1. K. N. Shrivastava, Phys. Lett. A113, 435(1986). 2. K. N. Shrivastava, Phys. Lett. A 326,469(2004). 3. K. N. Shrivastava, Introduction to quantum Hall effect, Nova Sci. Pub. N.Y. (2002).

**16:06**

**W47 9 Conductance reduction without shot noise in quantum wires** MARKUS KINDERMANN, PIET W. BROUWER, *Cornell University* Shot noise can only be avoided in conductors without backscattering of conduction electrons. Such conductors without backscattering and a twofold spin-degeneracy have a minimal (nonzero) conductance of $2\ e^2/h$ in the case of weak interactions. In recent experiments, however, also conductors with a reduced conductance of $1.4\ e^2/h$ have shown a clear tendency of noise suppression in zero magnetic field. It has been argued, that these experiments point to a lifted spin-degeneracy in these wires, spin-polarizing their conductance electrons. In this talk I will describe a model of an interacting quantum wire that is able to reproduce the transport behavior observed in these experiments qualitatively: that of the ''Coulomb Tonks gas'' of impenetrable electrons. It can be realized in ultra-thin wires, such as carbon nanotubes. We have studied transport through a finite-length Coulomb Tonks gas connected to bulk leads in various exactly solvable limits, both in and out of equilibrium. While we find a reduction of the conductance of such a wire to $e^2/h$ in all cases, the current in the wire does not exhibit any fluctuations at zero temperature. Most importantly, our model demonstrates that such noise suppression does not require a spin-polarization.

**16:18**

**W47 10 Low-temperature transport in high quality strained Ge channels in SiGe** BENJAMIN ROESSNER, *Laboratory for Solid State Physics, ETH Zurich, Zurich, Switzerland* HANS VON KAENEL, *Politecnico di Milano, Como, Italy* DANIEL CHRASTINA, *Politecnico di Milano, Como, Italy* GIOVANNI ISELLA, *Politecnico di Milano, Como, Italy* BERTRAM BATLOGG, *ETH Zurich, Zurich, Switzerland* Presently, the mobility of holes in strained germanium achieved so far exceeds 100000 $cm^2/Vs$ at a carrier density of $\sim 8*10^{11}cm^{-2}$. For lower carrier density, the highest reported mobilities are roughly proportional to the carrier density. Accessing the upper left corner in the density-mobility diagram remains a challenge. Background charges, inhomogeneous strain distribution and growth defects are the main difficulties of growing strained Ge channels. We have fabricated high quality Ge channels and measured the transport parameters at temperatures down to 0.4 K. We discuss the influence of growth problems on the mobility as a whole and how these mechanisms may influence the magnetic field dependence of the sheet resistance. We explore the effects of different doping geometries, in particular backside doping and symmetrical doping on electrical transport, including the effects of dopant segregation. Our quantitative analysis shows that local charged impurities dominate the scattering rate. It also shows the effect of too low substrate temperature, leading to point defects whose existence can be detected by a pure transport measurement.

**16:30**

**W47 11 Electronic transport properties of amorphous $Sb_2Te_3$ and $Ge_2Sb_2Te_5$ films** S.A. BAILY, *Space Vehicles Directorate, Air Force Research Laboratory, Kirtland AFB, NM 87117* DAVID EMIN, *Department of Physics and Astronomy, University of New Mexico, Albuquerque, NM 87131* The electrical conductivity, Seebeck coefficient, and Hall coefficient of amorphous $Sb_2Te_3$ and $Ge_2Sb_2Te_5$ films have been measured as functions of

temperature from room temperature down to as low as 200 K. The electrical conductivities manifest an Arrhenius behavior with a larger pre-exponential factor. In $Sb_2Te_3$ the energy characterizing the p-type Seebeck coefficient's temperature dependence, about 0.10 eV, is considerably smaller than the activation energy of the electrical conductivity, about 0.28 eV. In addition, the heat-of-transport constant of the Seebeck coefficient is much larger than that of conventional semiconductors. The Hall mobility is low (near 0.1 $cm^2$/V-sec at room temperature), anomalously signed (n-type), and increases with rising temperature with an activation energy of about 0.05 eV. These results are consistent with the charge carriers being hole-like small polarons that move by thermally assisted hopping. $Ge_2Sb_2Te_5$ also has low mobility (0.7 $cm^2$/V-sec) and a high conductivity activation energy (0.41 eV), but Seebeck data is indicative of multi-band transport.

**16:42**

**W47 12 Magnetic and transport properties of $Fe_{1-x}Co_xSb_2$** RONGWEI HU, *Physics Department Brown University Providence RI 02912 and Condensed Matter Physics Brookhaven National Laboratory, Upton NY 11973* CEDOMIR PETROVIC, *Condensed Matter Physics Brookhaven National Laboratory, Upton NY 11973* VESNA MITROVIC, *Physics Department Brown University Providence RI 02912* Anisotropic magnetic and electronic transport measurements were carried out on large single crystals of $Fe_{1-x}Co_xSb_2$, grown by self flux method, in the temperature range 1.8-350K for $0 \leqslant x \leqslant 1$. The diamagnetic semiconducting state of $FeSb_2$ evolved into metallic by substitution of Fe with Co for $x < 0.5$. With further doping there was a structural transformation from orthorhombic Pnnm structure of $FeSb_2$ to monoclinic P21/c structure of $CoSb_2$. Large magnetoresistance and anisotropy in electronic transport were observed.

**16:54**

**W47 13 Transport Properties of Ag Nanoparticles in Carbon Matrix Prepared with a Cluster Gun*** PENG LIU, YUNHE HUANG, MICHAEL BONDER, GEORGE HADJIPANAYIS, *Department of Physics and Astronomy, University of Delaware, Newark, DE 19716* DIONISIOS VLACHOS, SOUMITRA DESHMUKH, *Department of Chemical Engineering, University of Delaware, Newark, DE 19716* The use of ''cluster guns'' with in-situ processing capabilities has been found to be suitable for the fabrication of nanoparticles in a wide range of materials, avoiding external annealing and possible surface oxidation of the nanoparticles[1, 2]. In this study, we have used our cluster gun to fabricate Ag nanoparticles and embed them in a C matrix formed by conventional sputtering. With the increased amount of Ag, the transport properties of thin films show a gradual transition from a semiconductor-like behavior to a metallic one. At cryogenic temperatures, the magnetoresistance (MR) is generally negative at low fields and becomes positive at high fields. The field at which the MR changes sign increases with increased temperature. At higher temperatures (around 20 K), only negative MR is observed. For the samples with semiconductor-like behavior, the temperature dependence of resistance follows the relation $R = R_0\exp[(T_0/T)^{1/2}]$ in the temperature range from 5 to 50 K. We are investigating the origin of this behavior and those results will be reported.

*This work is supported by NSF DMR 0302544

**17:06**

**W47 14 Controlling the Inherent Magnetoresistance in thin InSb epilayers on GaAs (001)*** T. ZHANG, J.J. HARRIS, S.K. CLOWES, W.R. BRANDFORD, L.F. COHEN, *Imperial College* S.A. SOLIN, *Washington University in St.Louis* There is great advantage to controlling the magnetoresistance (MR) in high mobility semiconductors for a number of applications which require thin active surface layers. Previously we have produced n type thin epilayers of InSb with the highest reported mobility[1] and we have used these epilayers to explore novel geometries that enhance the high field MR.[2] Here we show that by virtue of the inherent inhomogeneity in the growth direction, thin InSb epilayers can be designed to have significant MR without external geometric manipulation. The observations can be explained using a transport model that describes the electrical properties of the layers including contributions from conduction and impurity bands.[3] We will explore using the model, the possibility of maximizing or minimizing the inherent MR in these layers and we show experimentally how to create thin high mobility layers where the inherent MR is significantly reduced or enhanced without compromising the layer mobility.[4]

*Supported by EPSRC EP/C511816/1, NSF ECS-0329347, WU CMI.

[1]T. Zhang et al. Appl. Phys Lett. **84**, 4463 (2004).
[2]W.R. Branford et al., Appl. Phys Lett. **86**, 202116 (2005).
[3]J.J. Harris et al., Semicond. Sci. Tech. **19**, 1406 (2004).
[4]T Zhang et al., Semicond. Sci. Tech., in press.

**17:18**

**W47 15 Magnetocapacitance of Semiconductors with Nonmagnetic and Magnetic Impurities** JEREMY NESBITT, ARTHUR HEBARD, *University of Florida* Positive magnetoresistance in semiconductors has been studied by previous investigators and found to have an exponential dependence on magnetic field in the regime of hopping conduction and a power law dependence at higher temperatures, due to band carriers. To our knowledge, little experimental study has been performed on the magnetocapacitance of semiconductors outside of the low temperature regime, where phenomena such as the quantum Hall effect have been studied. Here we report on the magnetocapacitance of lightly doped ($\rho > 1\ \Omega$-cm) n- and p-type silicon, using both Schottky and oxide barriers to form capacitor structures. The frequency-dependent negative magnetocapacitance can be as large as 30% at 50K and decreases to a few percent at room temperature. We attribute this effect to a field-induced localization of shallow donor impurity wavefunctions in directions transverse to the applied magnetic field. The effect can only be observed if the measurement frequency ( $\sim$ 1MHz) is comparable to or greater than the field-dependent transition rate between impurity sites. We will also contrast the differences in the magnetocapacitance effect for diluted magnetic semiconductors such as GaCrN and GaMnAs.

**SESSION Y1: ENGINEERING BIOMOLECULES AND CIRCUITS BY RATIONAL DESIGN AND GENETIC SELECTION**
**Friday Morning, 17 March 2006; Ballroom IV, Baltimore Convention Center at 8:00**
**Andrea Liu, University of Pennsylvania, presiding**

**8:00**
**Y1 1 Molecular Evolution of Gene Expression in E. coli.**
TERRY HWA, *University of California San Diego*

Understanding the evolution of gene regulation is an outstanding challenge to systems biology. Here we use molecular methods to study in detail the evolution of promoter sequences needed to express gene(s) essential to the growth of E. coli cells. We quantitatively characterize changes in the genotype and phenotype of the evolving population, and study how different challenges imposed by the environment affect the dynamics and the final outcome of the evolutionary process.

**8:36**
**Y1 2 Tinkering with Genetic Networks In Vivo.**
CALIN GUET, *The University of Chicago*

Synthetic genetic networks have recently emerged as an alternative experimental framework for studying cellular networks. Biological systems have evolved through a process of blind molecular tinkering. I will present an experimental genetic system which mimics this tinkering process. This system is composed of a few well characterized genetic elements: the promoters and genes of lambda cI, LacR and TetR. Using a combinatorial synthesis method we create libraries of simple genetic networks with various connectivities that function as logical gates. We observe how new computational functions arise through one-step changes in network connectivity. The connectivity-function map is found to be many-to-many even for these small networks.

**9:12**
**Y1 3 Directed Evolution of Bacterial Chemoreceptors.**
MARK GOULIAN, *University of Pennsylvania*

The methyl-accepting chemotaxis proteins are a family of receptors in bacteria that mediate chemotaxis to diverse signals. We have developed a simple method for selecting bacteria that swim towards target attractants, which makes it possible to isolate novel chemoreceptors. The procedure is based on establishing a diffusive gradient in semi-soft agar and does not require that the attractant be metabolized or degraded. We have applied this method to evolve the itE. coli aspartate receptor, Tar, to mediate chemotaxis to new attractants. We found that Tar is quite plastic and can be readily mutated to respond to diverse compounds. The overall change in specificity depended on the target attractant. In some cases the mutated receptors still showed significant sensitivity to aspartate, indicating that the receptors had a broadened specificity relative to wild-type Tar. In other cases, however, the Tar variants showed a dramatic decrease in their response to aspartate. This occurred in the absence of any counter-selection steps. For many of the receptors, the maximal sensitivity that was obtained could not be attributed solely to substitutions within the ligand binding pocket. The receptors that we have isolated, together with additional variants that may be obtained with our technique, provide new tools for exploring the molecular mechanisms of signal transduction by chemoreceptors. Our selection method will also be useful for constructing new receptors for the development of biosensors and for engineering bacteria for applications in biotechnology.

**9:48**
**Y1 4 Building a cellular oscillator from metabolic and cell signaling components.**
JAMES LIAO, *UCLA*

One of the key features of cellular oscillators is their interaction with metabolism and cellular physiology. To understand such interaction and to uncover operating principles behind these networks, we designed a synthetic gene-metabolic oscillator that links metabolism with gene regulation. The conceptual design was inspired by physical and mathematical insight, but constrained by biological and chemical realities. Biological implementation was built on detailed understanding of the physiology of the organism of interest. Non-linear dynamic analysis was used to guide the search of experimental conditions and evaluate different design. Interestingly, most of the predictions were experimentally verified, suggesting that the underlying mechanisms were properly captured by the conceptual and mathematical models.

**10:24**
**Y1 5 An artificial cell based on gene expression in vesicle.**
VINCENT NOIREAUX, *University of Minnesota*

A new experimental approach is presented to build an artificial cell using the translation machinery of a cell-free expression system as the hardware and a DNA synthetic program as the software. Cytoplasmic extracts, encapsulated in phospholipid vesicles, are used to assemble custom-made genetic circuits to develop the functions of a minimal cell. The objective is to understand how a DNA algorithm can be designed to build an operating system that has some of the properties of life. We show how a long-lived bioreactor is built to carry out in vitro transcription and translation in cell-sized vesicles. To develop the synthetic membrane into an active interface, a few amphipathic peptides and an insertion mechanism of integral membrane proteins have been tested. With vesicles composed of different phospholipids, the fusion protein alpha-hemolysin-eGFP can be expressed to reveal patterns on the membrane. Finally, specific degradation mechanisms are introduced to create a sink for the synthesized messengers and proteins. Perspectives and limitations of this approach will be discussed.

## SESSION Y2: ELECTROSTATIC LEVITATION AND HIGH ENERGY X-RAYS
**Friday Morning, 17 March 2006; Ballroom III, Baltimore Convention Center at 8:00**
**Kenneth F. Kelton, Washington University, presiding**

**8:00**
**Y2 1 Floating the Ball: Advances in the technology of electrostatic levitation.**
JAN ROGERS, *NASA/Marshall Space Flight Center*

Electrostatic Levitation (ESL) is an emerging technology. The MSFC ESL is a NASA facility that supports investigations of refractory solids and melts. The facility can be used to process a wide variety of materials including metals, alloys, ceramics, glasses and semiconductors. Containerless processing via ESL provides a high-purity environment for the study of high temperature materials and access to metastable states. Scientific topics investigated in the facility include nucleation, undercooling, metastable state formation and metallic glass formation. Additionally, the MSFC ESL provides data for the determination of phase diagrams, time-temperature-transition diagrams, viscosity, surface tension, density, heat capacity and creep resistance. In order to support a diverse research community, the MSFC ESL facility has developed a number of technical capabilities, including a portable system for in situ studies of structural transformations during processing at the high-energy X-ray beamline at the Advanced Photon Source of Argonne National Laboratory. The capabilities of the MSFC ESL facilities will be discussed and selected results of materials processing and characterization studies will be presented.

**8:36**
**Y2 2 New insights into the thermophysical properties of materials using electrostatic levitation.**
ROBERT HYERS, *University of Massachusetts*

Electrostatic Levitation (ESL) allows non-contact measurement of the thermophysical properties of materials in both the solid and liquid states, from over 3500C to deep in the undercooled liquid, for a wide range of materials including metals, ceramics, and semiconductors. The combination of ESL with synchrotron x-ray structural measurements allows unprecedented insight into the relation between structure and properties in reactive and undercooled materials. Of the many different thermophysical and thermomechanical properties that have been measured using levitation techniques, four will be discussed. The density of the sample is calculated from the shape of the free surface in video images and the known mass. The surface tension and viscosity are determined from the natural frequency and damping, respectively, of free surface oscillations. Creep is measured by observing the changes in free surface shape due to centrifugal acceleration in a rapidly rotating drop. Combined with the x-ray structure measurements, these mechanical measurements can reveal the development of texture and strain-induced phase transformations. Any of these measurements may be performed on the same sample, in the same environment, at the same time as the x-ray structural measurements, allowing direct observation of the effect of changes in the structure of the sample on the thermophysical properties.

**9:12**
**Y2 3 A Deeper View of Materials: Coupling electrostatic levitation and high energy x-ray diffraction.**
ALAN GOLDMAN, *Ames Laboratory, USDOE and Department of Physics and Astronomy, Iowa State University*

The ability to measure changes in the atomic scale structure, associated with novel thermophysical properties, will lead to tremendous advances in our understanding of the underlying physics of materials. This talk will focus on the integration of electrostatic levitation (ESL) techniques and high energy x-ray diffraction. The use of high energy x-rays

($E > 100$ keV) offers several distinct advantages over conventional x-ray methods. First and foremost, high energy x-rays are required for full penetration of the levitated samples, which are typically 2-3 millimeters in diameter. This ensures that the bulk, rather than near-surface, structures are sampled in the measurement. A second important benefit of high energy x-rays lies in the fact that diffraction patterns can be collected over a relatively wide momentum transfer range for a small range of angles. The relatively small range of scattering angles required for most measurements allows the use of area detectors for fast data acquisition while the sample is either held at a constant temperature or during continuous heating/cooling cycles. The latter method is particularly suitable for continuous studies of phase transformations as the sample is heated from room temperature to the liquidus temperature and above, or cooled from high temperatures. This is, perhaps, best illustrated by recent work on the atomic scale structure of deeply undercooled liquid metals and semiconductors, such as silicon, where time resolved (100ms/frame) data have shown that, in contrast to previous structural measurements and several theoretical treatments, there is no evidence for a liquid-liquid phase transition in the undercooled regime.

**9:48**
**Y2 4 X-ray photoelectron spectroscopy in the hard x-ray regime.***
CHARLES S. FADLEY, *UC Davis & LBNL*

Photoelectron spectroscopy is by now a very widely used tool for the study of atoms, molecules, solids, surfaces, and nanoscale structures. Until very recently, the exciting radiation has been limited to the energy range below about 2 keV. However, within the past few years, a few experimental projects have been initiated in which photon energies in the 5-15 keV range are employed. By matching the characteristics of undulator beamlines at third-generation synchrotron radiation sources to the optical properties of the electron spectrometer, it has proven possible to overcome the reduced photoelectric cross sections at such high energies and to study both core and valence electronic levels with resolutions down to ca. 50 meV [1]. Such hard x-ray photoelectron spectroscopy (HXPS or HAXPES) has the advantage of being more bulk sensitive, with electron inelastic attenuation lengths in the 50-150 Angstrom range. In this talk, I will discuss the advantages and disadvantages of this new direction, including highlights from recent work, as well as suggested future avenues for HXPS studies. [1] Nuclear Instruments and Methods A 547, 24 (2005), special issue dedicated to hard x-ray photoelectron spectroscopy, edited by J. Zegenhagen and C. Kunz.

*Work supported by the Director, Office of Science, Office of Basic Energy Sciences, Materials Science and Engineering Division, U.S. Department of Energy under Contract No. DE-AC03-76SF00098.

**10:24**
**Y2 5 Hard x-ray photoelectron spectroscopy and x-ray standing waves.**
TIEN-LIN LEE, *European Synchrotron Radiation Facility*

Using the brilliant undulator radiation available from the third generation synchrotron sources, hard x-ray photoelectron spectroscopy (HAXPES) has become an emerging field in the recent years. With the excitation energy used in HAXPES one can benefits from the large mean free path of fast electrons ( $\sim$ 5 nm for electrons of 6 keV kinetic energy) in probing the bulk electronic properties of materials. For high-resolution studies, photon energy bandwidth narrower than 100 meV is also readily achievable in the hard x-ray range with crystal monochromators. In addition, working with hard x-ray offers the possibility for combining photoelectron spectroscopy with x-ray standing wave (XSW) method. With the high spatial resolution from XSWs, this unique combination can provide site-specific, chemical and electronic information for studying surfaces, buried interfaces, thin films and bulk crystals. In this talk, I will briefly mention some HAXPES experiments detecting electrons up to 14.5 keV [1,2]. I will then sketch the principle of combining XSWs with HAXPES and present results from some recent applications using this combination: (1) chemical state-specific surface structure determination with core-level photoemission, (2) site-specific valence x-ray photoelectron spectroscopy and (3) XSW imaging with core-level photoemission. [1] S. Thiess, C. Kunz, B.C.C. Cowie, T.-L. Lee, M. Renier, and J. Zegenhagen. Solid State Communications 132, 589 (2004) [2] C. Kunz, S. Thiess, B.C.C. Cowie, T.-L. Lee, and J. Zegenhagen, Nuclear Instruments and Methods A 547, 73 (2005).

## SESSION Y4: HIGH TMR MGO TUNNELING AND SPIN MOMENTUM TRANSFER MATERIALS, PHYSICS, AND DEVICES

**Friday Morning, 17 March 2006; 308, Baltimore Convention Center at 8:00**
**Robert Buhrman, Cornell University, presiding**

**8:00**
**Y4 1 Giant tunneling magnetoresistance and tunneling spin polarization in magnetic tunnel junctions with MgO (100) tunnel barriers.**
STUART PARKIN, *IBM Almaden Research Center*

Recent advances in generating, manipulating and detecting spin-polarized electrons and electrical current make possible new classes of spin based sensor, memory and logic devices [1]. One key component of many such devices is the

magnetic tunneling junction (MTJ) - a sandwich of thin layers of metallic ferromagnetic electrodes separated by a tunneling barrier, typically an oxide material only a few atoms thick. The magnitude of the tunneling current passing through the barrier can be adjusted by varying the relative magnetic orientation of the adjacent ferromagnetic layers. As a result, MTJs can be used to sense the magnitude of magnetic fields or to store information. The electronic structure of the ferromagnet together with that of the insulator determines the spin polarization of the current through an MTJ – the ratio of 'up' to 'down' spin electrons. Using conventional amorphous alumina tunnel barriers tunneling spin polarization (TSP) values of up to $\sim$ 55% are found for conventional 3d ferromagnets, such as CoFe, but using highly textured crystalline MgO tunnel barriers TSP values of more than 90% can be achieved for otherwise the same ferromagnet [2]. Such TSP values rival those previously observed only with half-metallic ferromagnets. Corresponding giant values of tunneling magnetoresistance (TMR) are found, exceeding 350% at room temperature and nearly 600% at 3K. Perhaps surprisingly the MgO tunnel barrier can be quite rough: its thickness depends on the local crystalline texture of the barrier, which itself is influenced by structural defects in the underlayer. We show that the magnitude and the sign of the TMR is strongly influenced by defects in the tunnel barrier and by the detailed structure of the barrier/ferromagnet interfaces. The observation of Kondo-assisted tunneling phenomena will be discussed as well as the detailed dependence of TMR on chemical bonding at the interfaces [3]. [1].S.S.P. Parkin, X. Jiang, C. Kaiser, et al., Proc. IEEE 91, 661 (2003). [2] S. S. P. Parkin, C. Kaiser, A. Panchula, et al., Nature Mater. 3, 862 (2004). [3] C. Kaiser, S. van Dijken, S.-H. Yang, H. Yang and S.S.P. Parkin, Phys. Rev. Lett. 94, 247203 (2005).

**8:36**

**Y4 2 Giant TMR effect and spin momentum transfer in MgO-based magnetic tunnel junctions.***

SHINJI YUASA, *National Institute of Advanced Industrial Science and Technology (AIST)*

First-principle theories predicted an extremely high magnetoresistance (MR) ratio over 1000% in fully epitaxial Fe(001)/MgO(001)/Fe(001) MTJs [1]. This giant tunneling magnetoresistance (TMR) effect originates from a coherent spin-dependent tunneling of highly spin-polarized $\Delta_1$ electronic states. We have fabricated fully epitaxial $Fe_{1-x}Co_x$(001)/MgO(001)/Fe(001) MTJs [2,3] and CoFeB/MgO(001)/CoFeB MTJs [4] and achieved giant MR ratios above 200% at room temperature. A low resistance-area (itRA) product indispensable for magnetic sensor application has also been achieved in CoFeB/MgO(001)/CoFeB MTJs [5]. Because of the high spin polarization of tunneling electrons, the MgO-based MTJs have an advantage in spin transfer phenomena, too. Current-induced magnetization reversal due to spin transfer torque has been demonstrated using CoFeB/MgO(001)/CoFeB MTJs [6]. The MTJ was also found to act as a microwave detector [7]. When an ac current with a microwave frequency is applied to the MTJ, a dc offset voltage is generated. This phenomenon, named as spin-torque diode effect, originates from spin momentum transfer, ferromagnetic resonance and the giant TMR effect. The giant TMR effect and spin momentum transfer in MgO-based MTJs are the key for next-generation spintronic devices. References [1] W. H. Butler et al., Phys. Rev. B **63**, 054416 (2001). [2] S. Yuasa et al., Nature Mater. **3**, 868 (2004). [3] S. Yuasa et al., Appl. Phys. Lett. **87**, 222508 (2005). [4] D. D. Djayaprawira et al., Appl. Phys. Lett. **86**, 092502 (2005). [5] K. Tsunekawa et al., Appl. Phys. Lett. **87**, 072503 (2005). [6] H. Kubota et al., Jpn. J. Appl. Phys. **44**, L1237 (2005). [7] A. A. Tulapurkar et al., Nature **438**, 339 (2005).

*This study was supported by Japan Science and Technology Agency (JST).

**9:12**

**Y4 3 Spin torque, tunnel-current spin polarization and magnetoresistance in MgO magnetic tunnel junctions.**

GREGORY FUCHS, *Cornell University*

The ability of electron currents to transfer spin angular momentum, as well as charge, from one ferromagnetic electrode to another, and hence to exert a significant spin-torque on the electrodes, provides a powerful new tool for the study of spin transport in electronic structures, in addition to establishing new opportunities for future applications. The closely related issue of spin-dependent electron transport in magnetic tunnel junctions (MTJs) is of wide-spread interest, both fundamentally and because the importance this phenomena has for information storage. A critical aspect of MTJs is the bias dependence of the tunnel magnetoresistance (TMR), which in general, decreases as the voltage bias ($V$) increases. Currently, there is no consensus as to a microscopic model that accounts for this behavior. In this study, we employ the spin torque response of MTJs with ultra-thin MgO tunnel barrier layers to investigate the relationship between spin transfer and TMR under finite bias, and find that the spin torque per unit current exerted on the free layer decreases by $<$ 10% over a bias range where the TMR decreases by $>$ 40%. This behavior is inconsistent with a decrease in the tunnel polarization factors calculated with the Julliere formula extended to finite bias, and as predicted by free-electron tunneling models, or by surface-magnon emission models that substantially decrease the surface magnetization with increasing bias. We find, however, that magnetic-state-dependent tunneling decay lengths (effective masses) as theoretically predicted for MgO tunnel barriers, are consistent with our results. Since these results also have significant implications for spin-torque driven magnetic random access memory, we will consider these effects in addition to our work with MTJs having two polarizing magnetic layers in order to boost spin-torque as well as allow us to determine the extent of the considerable self-heating for MTJs under bias.

**9:48**

**Y4 4 Structure Engineering And Shape Optimization To Decrease Switching Current For Spin Transfer MRAM Application.**

YIMING HUAI, *Grandis, Inc.*

We present a systematic study of spin transfer switching in magnetic tunneling junctions (MTJs) to decrease the switching current density through material and structural engineering and MTJ element shape optimization. Data are presented for switching on MgO-based MTJs with high TMR of 170 % and low intrinsic switching current density $J_{c0} \leqslant 1\text{x}10^6$ A/cm$^2$. Micromagnetic modeling is used to study the spin transfer switching mechanism in nanosecond regime for elliptical shape of the MTJ element. The results suggest that the elliptical shape provides faster switching (lower switching current) and more reproducible switching than the conventional shapes optimized for magnetic field switched MRAM (Magnetic Random Access Memory).

**10:24**

**Y4 5 Thermal activation and switching dynamics in spin-torque-induced magnetic reversal in magnetic tunnel junctions with MgO barriers.**

JONATHAN SUN, *IBM T. J. Watson Research Center*

Spin-torque induced magnetic reversal has been unambiguously demonstrated in magnetic tunnel junctions with MgO barriers. During a quasi-static measurement, the reversal is dominated by events determined by spin-current amplified thermal activation, resulting in a measured average switching current below that of the zero-temperature dynamic threshold. Such sub-threshold switching current generally shows stronger and non-linear magnetic field dependence, following a shape determined by the magnetic field dependence of the thermal barrier height. Time-resolved measurements are usually required for adequately assessing the dynamic switching threshold current for fast (nano-second-level) deterministic switching, and for revealing the magnetic field dependence of the threshold current. The later would give direct experimental verification of the role a large easy-plane demagnetization field plays as it determines the value of the dynamic switching current threshold.

## SESSION Y5: NEW FUNCTIONALITIES IN GLASSES AND NANOMATERIALS

**Friday Morning, 17 March 2006; 309, Baltimore Convention Center at 8:00**
**Punit Boolchand, University of Cincinatti, presiding**

**8:00**

**Y5 1 Glasses and Ceramics as Templates for Generating Nanostructures and Novel Properties.**

DIPANKAR CHAKRAVORTY, *Indian Association for the Cultivation of Science*

Silica glasses containing substantial amounts of modifying oxides have considerable void spaces within their structure. These systems have therefore been exploited to generate different kinds of nanostructures e.g., nanoparticles,core-shell structures and nanowires. Similarly, ceramic structure like mica have well-defined crystal channels. The latter have been used to prepare nanowires or nanosheets. In this lecture the author will discuss some examples in which the above strategies of material synthesis have been applied. Copper core-copper oxide shell nanostructures with diameters $\sim$ 6 nm were grown within a gel-derived silicate glass containing copper ions[1]. Electrical conductivity of the nanocomposites was several orders of magnitude higher than that of the parent glass. An interfacial amorphous phase gave rise to this behaviour. Electrical conduction was ascribed to a small polaron hopping mechanism. Silver metal core–silver oxide shell structure with nanometer dimensions were generated in a silicate glass by first precipitating silver particles of $\sim$ 6nm diameter by an electrodeposition process and subsequently subjecting the material to an oxidation treatment[2]. Detailed analysis of the optical absorption spectra led to the conclusion that there is a metal non metal transition for particles having diameters less than $\sim$ 2.5 nm. Similar results were obtained in the case of copper core- copper oxide shell nanostructures grown within a silicate glass[3]. Core-shell structure of Fe-$Fe_3O_4$ system was also produced within a gel derived silica glass which exhibited a four order of magnitude change in electrical resistivity when the relative humidity was changed from 25%to 95% [4]. Silver and copper nanowires respectively were grown within a silicate glass by the application of an electric field. These nanowires were found to consist of arrays of metal nanoparticles. The latter gave rise to nano-junctions between large and small particles which behaved as metal–semiconductor junctions. A diode like voltage current characteristic was observed in these nanocomposites.[5] Silver nanowires were grown by electrodeposition within gel–derived silica glasses containing pores having diameters in the nanometre range. After suitable treatment to these nanowires these exhibited single electron tunnelling property[6]. Silver nanowires were grown within the channels of fluorophlogopite mica crystals precipitated within a suitably chosen glass composition. The nanocomposites exhibited giant dielectric permittivity ( $\sim 10^7$) which were explained on the basis of Gorkov-Eliashberg and Rice–Bernasconi model[7]. Na-4mica structure was used to grow CdS nanowire[8]. The former was also used to prepare films of $BaTiO_3$ with

a thickness of 1.2 nm. These films did not show any ferroelectric behaviour which was consistent with recent theoretical prediction[9]. [1] D.Das and D.Chakravorty, Appl. Phys. Lett. 76, 1273 (2000). [2] K.Chatterjee,S.Banerjee and D. Chakravorty, Phys. Rev. B66, 085421 (2002). [3] K.Chatterjee, D.Das and D.Chakravorty, J.Phys.D : Appl. Phys. 38 451 (2005) [4] B.N.Pal,S.Basuand D.Chakravorty, J. Appl. Phys. 97, 034311 (2005). [5] A.Dan,B.Satpati,P. V.Satyam and D.Chakravorty, J.Appl. Phys. 93, 4794 (2003). [6] S.Bhattacharyya,S.K.Saha and D.Chakravorty, Appl. Phys. Lett. 77, 3770 (2000). [7] P.K.Mukherjee and D.Chakravorty, J. Mater. Res. 17 3127 (2002). [8] P.K.Mukherjee and D.Chakravorty, J. Appl. Phys. 95, 3164 (2004). A.Dan,P.K.Mukherjee and D.Chakravorty, J. Mater. Chemistry 15, 1477 (2005).

**8:36**
**Y5 2 Local structure and dynamics of ferroelectric domain walls in perovskite oxides.**
VENKATARAN GOPALAN, *Pennsylvania State University*

This abstract was not received electronically.

**9:12**
**Y5 3 Novel polarization dependent photoinduced effects in glass.**
HIMANSHU JAIN, *Lehigh University*

For centuries oxide glasses have been used successfully in windows, thus indicating that they remain stable, unlike plastics, against exposure to sunlight. By comparison, the structure and properties of closely related chalcogenide glasses are easily altered by exposure to visible light of energy $\geqslant$ bandgap of the material. In general, such photoinduced changes may be classified into three categories depending on their stability: (a) permanent changes which cannot be recovered unless the sample is melted and prepared again, (b) metastable changes which can be reversed by heating the sample to the glass transition temperature, and (c) temporary changes which can be reversed simply by removing the light source, or exposing the specimen to another appropriate light subsequently. Among the numerous photoinduced phenomena, the photoinduced vector effects like anisotropic light transmission, mass transport, opto-mechanical effect, etc. are particularly fascinating as they depend on the direction of light polarization in spite of the isotropic glass structure. The transient 'vector' optical effects, which are produced by linearly polarized light and then erased by either unpolarized or circularly polarized light, are even more intriguing and novel. This paper will review the various observations of photoinduced vector effects. It will then focus on the origin of such effects, which we have sought by probing the changes in atomic and electronic structure under in situ laser irradiation.

**9:48**
**Y5 4 Polyamorphic transitions in network glasses and glass-forming liquids.**
JOHN KIEFFER, *University of Michigan*

Over the past two decades, we have witnessed increasing evidence for the occurrence of polyamorphism, i.e., the existence of more than one thermodynamically and structurally distinct non-crystalline state of a given substance. This concept is manifest predominantly through the transitions between different polyamorphic states, as we are still not able to unequivocally describe a given amorphous structure. However, if substantiated, the concept of polyamorphism should facilitate such a description, since it implies that polyamorphic states are uniquely defined and a distinctive structural character must exist for each state. We have observed polyamorphic transitions in a number of glass-forming systems, e.g., when probing their high-frequency visco-elastic response as a function of temperature,[1] or when compacting such systems at high pressures. We have carried out molecular dynamics simulations to reveal explanations for the phenomena observed in experiments.[2] In this presentation we discuss reversible and irreversible transitions in silica glass, their relation to the anomalous thermo-mechanical properties of this material, and the effects of permanent densification on structure and properties. We present an unusual transition in boron oxide glass, which is continuous upon compression and discontinuous upon decompression.[3] We show how the manifestations of polyamorphic transitions and their are related to structural transformations in the crystalline counterparts of these materials, and how this can even lead to the discovery of previously unknown metastable crystalline phases. [1] J. Kieffer, J.E. Masnik, O. Nickolayev, and J.D. Bass, Phys. Rev. B **58**, 694 (1998). [2] L. Huang, and J. Kieffer, Phys. Rev. B **69**, 224203 and 224204 (2004). [3] J.D. Nicholas, S.V. Sinogeikin, J. Kieffer, and J.D. Bass, Phys. Rev. Letters **92**, 215701 (2004).

**10:24**
**Y5 5 Nanoscale glass for photonic applications.**
ERIC MAZUR, *Harvard University*

This abstract was not received electronically.

**SESSION Y6: IS THE HUBBARD/T-J MODEL A HIGH TEMPERATURE SUPERCONDUCTOR?**
**Friday Morning, 17 March 2006; 310, Baltimore Convention Center at 8:00**
**Steven Kivelson, University of California, Los Angeles, presiding**

**8:00**
**Y6 1 High-$T_c$ and *t-J* model: passions and disappointments.**
LEONID P. PRYADKO, *University of California, Riverside*

I will discuss the high-temperature phase diagram of the two-dimensional *t-J* and related models. Among the many numerical and analytical techniques which have been used to search for superconductivity in these models, only a few provide unbiased results. Particularly, the high-temperature series constructed for a number of thermodynamical correlation functions indicate that in the accessible range of temperatures, $T \geqslant J/2$, the superconducting fluctuations are only pronounced in the unphysical regime, $J > t$, while they are strongly suppressed in the physical regime, $J < t$. Additionally, in the physical regime, the correlation length for superconducting fluctuations is small on the scale of the lattice constant. This is suggestive evidence that high-temperature superconductivity does not occur in the *t-J* model. I will analyze the validity of these results by looking at high-temperature series for the *t-J* model on small clusters and ladders, as well as for related bosonic models, whose finite-temperature phase diagram is relatively well understood from other numerical methods.

**8:36**
**Y6 2 Enhanced d-wave Superconducting Fluctuations in the 2D t-J model.***
WILLIAM PUTIKKA, *Ohio State University*

I have calculated high temperature series to 12th order in inverse temperature for singlet superconducting correlation functions of the 2D *t-J* model with *s*-, $d_{x^2-y^2}$ and $d_{xy}$-symmetry pairs. The strengths of the different symmetry correlations are measured using $\mathbf{q} = 0$ correlation lengths. I find that for $J/t = 0.4$ the correlation length for $d_{x^2-y^2}$ pairing grows strongly with decreasing temperature, developing a broad peak around doping $\delta = 0.25$ when the temperature is reduced to $T/J = 0.25$. The correlation lengths for *s* and $d_{xy}$ pairs remain small and do not display peaks as a function of doping. The temperature scale for growth in the $d_{x^2-y^2}$ correlation length agrees with the temperature scale where the temperature derivative of the momentum distribution function $dn_{\mathbf{k}}/dT$ and the gradient of the momentum distribution function $|\nabla_{\mathbf{k}} n_{\mathbf{k}}|$ develop peaks on the Brillouin zone diagonal. This indicates that the low energy excitations in the 2D *t-J* model are concentrated near the zone diagonal, as would be expected for superconducting order with $d_{x^2-y^2}$-symmetry pairs. I will also discuss differences between my calculation and previous calculations for superconducting correlations in the 2D *t-J* model.

*Supported by NSF DMR-0105659 and the Ohio Supercomputer Center.

**9:12**
**Y6 3 *d*-wave resonating valence bond states of ultracold fermionic atoms in optical lattices.**
MATTHIAS TROYER, *ETH Zurich*

In view of the apparently exponential complexity of fermionic simulations in two and more dimensions, we consider a controlled quantum simulation to probe the ground state properties of the two-dimensional Hubbard model. We present a controlled experimental setup to adiabatically construct superfluid *d*-wave resonating valence bond (RVB) states of fermionic atoms confined in a 2D optical lattice. The key idea is to start from a pure initial state which is adiabatically transformed to *d*-wave RVB states at ultralow temperatures of a few percent of the Fermi temperature. We discuss hole doping techniques and describe a simple experimental measurement to study *d*-wave pairing.The proposed experiment can be used to effectively probe ground state properties of the repulsive Hubbard model on (coupled) plaquettes, ladders and the 2D square lattice. The proposal is within the capabilities of current technology, and shows how an adiabatic quantum simulator could answer a question that cannot currently be reliably answered by classical computational methods. Reference: S. Trebst, U. Schollwöck, M. Troyer and P. Zoller, cond-mat/0506809.

**9:48**
**Y6 4 Superconducting correlations and thermodynamic properties in 2D square and triangular *t-J* model.***
MASAO OGATA, *Department of Physics, University of Tokyo*

Equal-time superconducting correlation functions of the two-dimensional *t-J* model on the square lattice are studied using high-temperature expansion method.[1] The sum of the pairing correlation, its spatial dependence and correlation length are obtained down to $T \simeq 0.2t$. By comparison of single-particle contributions in the correlation functions, we find effective attractive interactions between quasi-particles in $d_{x^2-y^2}$-wave channel. It is shown that *d*-wave correlation grows rapidly at low temperatures for the doping $0.1 < \delta < 0.5$. The temperature for this growth is roughly scaled by $J/2$. This is in sharp contrast to the Hubbard model in a weak or intermediate coupling region, where there are few numerical

evidences of superconductivity. We also study the possible *d*- and *f*-wave pairing in the triangular *t-J* model.[2] When $t > 0$ with hole doping, a rapid growth of effective *d*-wave paring interaction is found that indicates the resonating-valence-bond superconductivity. In contrast, when $t < 0$, where the ferromagnetic- and antiferromagnetic correlation compete, correlation lengths of the *f*-wave triplet paring tends to diverge around $\delta = 0.6$, although its effective interaction is small. This result is compared and discussed with the recently discovered superconductor, $Na_xCoO_2 \cdot yH_2O$, where Co atoms form a triangular lattice. Specific heat in low temperatures are also obtained in the high-temperature expansion method. We will discuss that the doping dependence of the specific heat coefficient, $\gamma$, agrees with experimental data.

[1] T. Koretsune and M. Ogata, J. Phys. Soc. Japan **74**, 1390 (2005). [2] T. Koretsune and M. Ogata, Phys. Rev. Lett. **89**, 116401 (2002), and Phys. Rev. B**72**, 134513 (2005).

*In collaboration with T. Koretsune.

**SESSION Y7: CHALLENGES AND ISSUES IN NANOWIRE NANODEVICES**
**Friday Morning, 17 March 2006; 307, Baltimore Convention Center at 8:00**
**Paul S. Weiss, Pennsylvania State University, presiding**

**8:00**
**Y7 1 Nanowires for High-Performance Integrated Macroelectronics.**
ROBIN FRIEDMAN, *Harvard University*

Extensive electrical and optical characterization has shown that single-crystal semiconductor nanowires display physical properties that match or exceed those of their bulk counterparts. In addition, our studies have shown that it is possible to manipulate and assemble high-performance devices using low-temperature liquid based processes. These high-performance semiconductor device properties and unconventional processing advantages possible with nanowires can be readily applied in the field of macroelectronics, where integrated devices are patterned over large noncrystalline and/or flexible substrates. The separation of high temperature nanowire synthesis from subsequent ambient temperature assembly allows for electronic devices of varied functionality to be fabricated on virtually any substrate. We have fabricated p-Si nanowire transistors on glass and plastic substrates that display parameters rivaling those of single crystal silicon and exceeding those of state-of-the-art amorphous silicon and organic transistors currently used for flexible electronics on plastic substrates today. With the improved reproducibility obtained through improvements in nanowire growth and the use of multi-nanowire transistors, we have been able to demonstrate integrated logic structures with gain up to megahertz frequencies. On-chip integration of nanowire-based inverters was accomplished in a fully parallel process, and has enabled the fabrication of inverters and ring oscillators with frequencies up to 200 MHz, the highest observed for circuits based on nanoscale materials.

**8:36**
**Y7 2 Property of individual conducting-polymer nanowires: conductance and FET devices.***
TOMIHIRO HASHIZUME, *Advanced Research Laboratory, Hitachi, Ltd., Hatoyama, Saitama 350-0395 Japan*

Electronic devices using organic molecules and nanowires have been intensively studied in dream of a smart life utilizing charming functions of organic materials, that are thin, light, flexible and yet inexpensive and safe for environment. A key step for measuring the property of organic nanowires and evaluating the performance of the nanowire devices is how to access them by appropriate nanoscopic methods. Scanning probe microscopy (SPM) based nanofabrication (SP nanofabrication) has been used to fabricate two- or four-probe fine electrodes and several kinds of nanowires made of conducting polymers have been evaluated by SPM and the fine electrodes made with Pt thin film fabricated on SiO2/doped Si or sapphire substrates [1,2]. We have tested conductivity of single poly (3,4-ethylenedioxythiophene) / poly (styrenesulfonate) (PEDOT/PSS) nanowires. After cutting each nanowires placed on the fine electrodes, the current was checked and we were able to confirm that the conductivity was derived from the PEDOT nanowires themselves. The temperature dependence of the conductivity was explained by the quasi one-dimensional variable range hopping (VRH) model. We also will discuss on the field-effect-transistor (FET) made of a single nanowire. In collaboration with: S. Heike, M. Fujimori, Y. Suwa (ARL), H. Ichihara, S. Samitsu, A. Inomata, T. Shimomura, K. Ito (Univ. Tokyo), K. Miki, T. Ohno (NIMS), H. Mizuseki (IMR), Y. Terada, H. Shigekawa (Univ. Tsukuba). [1] J. P. Hill, W. Jin, A. Kosaka, T. Fukushima, H. Ichihara, T. Shimomura, K. Ito, T. Hashizume, N. Ishii, and T. Aida, Science 304, 1481 (2004). [2] S. Samitsu, T. Shimomura, K. Ito, S. Heike, M. Fujimori, S. Heike, and T. Hashizume, Appl. Phys. Lett., 86, 233103 (2005).

*Supported by MEXT of the Japanese Government.

**9:12**

**Y7 3 Magnetic field asymmetry and high temperature magnetoresistance in single-walled carbon nanotubes.**

DAVID COBDEN, *Department of Physics, University of Washington*

The length scales and scattering processes in the one-dimensional electron system in single-walled carbon nanotubes remain only partially understood. Measuring the magnetoresistance, in both linear and nonlinear response, is a way to investigate these processes. In disordered nanotubes with ballistic paths much shorter than the length, we observe magnetoresistance in the metallic regime which at low temperatures resembles the universal fluctuations and weak localization seen in higher dimensional metals. A parabolic magnetoresistance persists at room temperature, indicating a significant role for phase coherence and/or interactions at high temperatures. While the linear resistance of a two-terminal sample must be an even function of magnetic field $B$ by Onsager's principle, the nonlinear resistance need not be. Importantly, the $B$-asymmetric nonlinear terms can in principle be used to infer the strength of electron-electron interactions in the sample [1]. We have therefore also measured in detail the lowest order $B$-asymmetric current contributions, with a focus on the $B$-linear term. This has apparently not been done before in any system. Consistent with general theory, at high temperatures the term is small and has a constant sign independent of Fermi energy. At low temperatures it grows and develops mesoscopic fluctuations. Although these result imply that interactions are involved in the transport, calculations specific to nanotubes are needed in order to extract interaction parameters. This work was done by the authors of Ref [2]. itReferences: [1] E.L. Ivchenko and B. Spivak, Phys. Rev. B 66, 155404 (2002); [2] Jiang Wei, Michael Shimogawa, Zenghui Wang, Iuliana Radu, Robert Dormaier, and David H. Cobden, Phys. Rev. Lett. (Dec. 2005) (cond-mat/0506275).

**9:48**

**Y7 4 Electrical Conductivity of Organic and Inorganic Nanowires Measured by Multi-probe Scanning Tunneling Microscopes.***

MASAKAZU AONO, *Nanomaterials Laboratory, National Institute for Materials Science (NIMS), Japan*

Since 1998 [1], the authors and co-workers have developed multi-probe scanning tunneling microscopes (MPSTMs), in which two, three or four probes are operated independently. All probes of the MPSTMs can observe STM images independently, but the main role of the multiple probes is to be used as nanoscale electrodes that can contact any points selected in an observed STM image. It is therefore possible to measure electrical conductivity at the nanoscale through the multiple probes. By using MPSTMs and related methods, we measured the electrical conductivity of organic and inorganic nanowires, i.e., single-wall carbon nanotubes (SWCNTs), erbium disilicide (ErSi2) metallic nanowires, and single polydiacetylene (PDA) molecular wires. For a SWCNT and an ErSi2 nanowire, ballistic conduction was observed at lengths less than about 500 and 20 nm, respectively, at room temperature. For a PDA molecular wire, polaron formation due to charge injection caused by applying a voltage to an STM tip placed close to the PDA molecular wire was observed, and when the voltage exceeded a critical value, the PDA molecular wire changed into a metallic state. [1] M. Aono, C.-S. Jiang, T. Nakayama, T. Okuda, S. Qiao, M. Sakurai, C. Thirstrup, Z.-H. Wu: Oyo Buturi (Applied Physics) 67, 1361 (1998) (in Japanese); A brief English abstract is available on INSPEC.

*Supported by JST and MEXT, Japan.

## SESSION Y8: GENERAL FLUID DYNAMICS

**Friday Morning, 17 March 2006; 314, Baltimore Convention Center at 8:00**
**John Labenski, National Institute of Standards and Technology, presiding**

***Invited Papers***

**8:00**

**Y8 1 DCOMP Award Lecture (Metropolis): A 3D Spectral Anelastic Hydrodynamic Code for Shearing, Stratified Flows.***

JOSEPH BARRANCO, *Harvard University*

We have developed a three-dimensional (3D) spectral hydrodynamic code to study vortex dynamics in rotating, shearing, stratified systems (eg, the atmosphere of gas giant planets, protoplanetary disks around newly forming protostars). The time-independent background state is stably stratified in the vertical direction and has a unidirectional linear shear flow aligned with one horizontal axis. Superposed on this background state is an unsteady, subsonic flow that is evolved with the Euler equations subject to the anelastic approximation to filter acoustic phenomena. A Fourier-Fourier basis in a set of quasi-Lagrangian coordinates that advect with the background shear is used for spectral expansions in the two horizontal directions. For the vertical direction, two different sets of basis functions have been implemented: (1) Cheby-

shev polynomials on a truncated, finite domain, and (2) rational Chebyshev functions on an infinite domain. Use of this latter set is equivalent to transforming the infinite domain to a finite one with a cotangent mapping, and using cosine and sine expansions in the mapped coordinate. The nonlinear advection terms are time integrated explicitly, whereas the Coriolis force, buoyancy terms, and pressure/enthalpy gradient are integrated semi- implicitly. We show that internal gravity waves can be damped by adding new terms to the Euler equations. The code exhibits excellent parallel performance with the Message Passing Interface (MPI). As a demonstration of the code, we simulate vortex dynamics in protoplanetary disks and the Kelvin-Helmholtz instability in the dusty midplanes of protoplanetary disks.

*In collaboration with Philip Marcus.

***Contributed Papers***

**8:36**
**Y8 2 Evaporating droplets** NOUSHINE SHAHIDZADEH-BONN, *Laboratoire des Materiaux et Structures du Genie Civil (LMSGC)* SALIMA RAFAI, *WZI/University of Amsterdam* AZA AZOUNI, *LMSGC* DANIEL BONN, *LPS/Ecole Normale Superieure* LMSGC TEAM, LPS/ENS TEAM, WZI/UVA COLLABORATION, In our everyday life we are constantly confronted with evaporating drops and the consequences of it. The seemingly simple problem of an evaporating droplet has attracted a great deal of attention over the past years. The problem is complicated due to the fact that the form of the droplet during the evaporation is a priori unknown, and due to the large number of effects that have to be taken into account (temperature, convection, Marangoni effects . . . ). We consider the very simple situation of the evaporation of a perfectly wetting liquid on a molecularly smooth surface. The radius R(t) of the droplet is followed in time until it reaches zero. If the evaporation is purely diffusive, a radius that decreases as the square root of time is expected; this is indeed found for organic liquids, but water has a different exponent. We show that the difference is likely to be due to the fact that water vapor is lighter than air, and the vapor of other liquids more dense. If we carefully confine the water so that the diffusive boundary layer may develop, we retrieve the square root of time behavior. On the other hand, if we force convection for an organic liquid, we retrieve the anomalous exponent for water.

**8:48**
**Y8 3 Effect of Viscoelasticity on Drop Deformation** NISHITH AGGARWAL, *University of Delaware* KAUSIK SARKAR, *University of Delaware* Deformation of a drop is numerically investigated when one or both of the drop and continuous phases is viscoelastic. A three-dimensional front-tracking finite difference method is used to simulate the deforming drop. The viscoelasticity is modeled using the Giesekus and Oldroyd−B constitutive relations. In a shear flow, a viscoelastic drops in a Newtonian matrix deforms less than a Newtonian drop. Specifically, bounded viscoelastic drop shapes are found for capillary numbers where a Newtonian drop would break up. Matrix viscoelasticity, however is observed to cause non-monotonic change in drop deformation with increasing viscoelasticity. The effects of inertia, interfacial tension, viscosity ratio and imposed flow periodicity (in oscillatory shear) will be presented. The detailed results about transient dynamics, viscous and viscoelastic stresses and the velocity fields inside and outside the drop will be discussed and explained.

**9:00**
**Y8 4 Pressure Driven Liquid-Vapor Phase Transitions** TIANSHI LU, ROMAN SAMULYAK, *Computational Science Center, Brookhaven National Laboratory* JAMES GLIMM, *Department of Applied Mathematics and Statistics, Stony Brook University* Liquid-vapor phase transitions driven by pressure waves have been studied analytically and numerically. The Stefan problem has been extended to incorporate the compressibility of the vapor phase. Both internal heat conduction and external heat deposition (such as from electrons in tokamak fusion reactors) have been considered. The steady state and the transient waves in the phase transitions have been investigated. A numerical scheme has been developed for the simulation of compressible two-phase flows with phase transitions in the frame of front tracking. Phase boundaries can be created dynamically in regions under critical conditions. The numerical method has been applied to the simulation of boiling and cavitating processes.

**9:12**
**Y8 5 Interaction between a free boundary and thermal convection in an annulus** JIN-QIANG ZHONG, *Physics Dept., NYU* JUN ZHANG, *Physics Dept. and Courant Inst., NYU* We report an experimental study in turbulent thermal convection that has a free upper surface. The geometry of the convective system is annular with aspect ratio (girth/height) 6.8 and with periodic boundary condition. Our experiment studies the interaction between the convective flow and a freely moving floating boundary that partially covers the open surface. The floating boundary position and the corresponding convective pattern are recorded at the same time and are correlated to reveal the dynamics of the coupled system. Our experiment aims to illustrate the intricate mechanism of continental drift that is driven by mantle convection.

**9:24**
**Y8 6 The Stochastic Dynamics of an Array of Atomic Force Microscope Cantilevers in a Viscous Fluid** MATTHEW CLARK, *Virginia Tech* MARK PAUL, *Virginia Tech* The hydrodynamic coupling between micron scale atomic force microscope cantilevers in a viscous fluid is studied. Using the fluctuation-dissipation theorem, the stochastic dynamics of the cantilevers are quantified from deterministic calculations. Numerical simulations of individual cantilevers immersed in fluid are used to verify the approach. A simple harmonic oscillator model is shown to be reasonable for the description of the dynamics of a single cantilever. The fluid induced correlations in an array of cantilevers are then explored and quantified. Absolute predictions of the cross-correlations in the equilibrium fluctuations of cantilever displacement are presented. This is used to yield limits of the force and time scales of operation for a correlation detection method using multiple atomic force microscope cantilevers.

**9:36**
**Y8 7 Co-rotating Batchelor vortex merging** PAULO FERREIRA DE SOUSA, *New Mexico State University* JOSE CARLOS FERNANDES PEREIRA, *Instituto Superior Tecnico* The dynamics of co-rotating vortex pairs without axial flow has been recently thoroughly studied through theoretical, experimental and numerical studies, which revealed different instabilities contribut-

ing to the decay of the vortices. In this paper the objective is to extend the analysis to the case of co-rotating vortices with axial flow at low Reynolds numbers. A high-order incompressible Navier-Stokes flow solver is used. The momentum equations are spatially discretized on a staggered mesh by finite differences and all derivatives are evaluated with 4th order compact finite difference schemes with RK-4 temporal discretization. The initial condition is a linear superposition of two co-rotating circular Batchelor vortices with q = 1. It is found that there is an initial evolution that resembles the evolution that single q = 1 vortices go through. Azimuthal disturbances grow and result in the appearance of large-scale helical sheets of vorticity. With the development of these instability waves, the axial velocity deficit is weakened. The redistribution of both angular and axial momentum between the core and the surroundings drives the vortex core to a more stable configuration, with a higher q value. After these processes, the evolution is somewhat similar to a pair of co-rotating Lamb-Oseen vortices. A three-dimensional instability develops, with a large band of unstable modes, with the most amplified mode corresponding scaling with the vortex initial separation distance.

**9:48**

**Y8 8 Magnetic Body Force Sustained Temperature Gradient*** JONATHAN FRAINE, WEILI LUO, *University of Central Florida* UNIVERSITY OF CENTRAL FLORIDA TEAM, The temperature gradient was established in a magnetic fluid by controlling the rate of cycling coolant. Measurements were done to monitor temperature gradient verses time before and after the cooling was stopped in both zero and applied magnetic field. We found that the magnetic field can sustain a larger temperature gradient. The theoretical calculation shows that the effect of field on the temperature gradient is attributed to the magnetic body force that depends on the gradient of the susceptibility.

*This work is partially supported by NSF NIRT 0103587.

**10:00**

**Y8 9 Shock Interaction with a Finite Thickness Two-Gas Interface** JOHN LABENSKI, *NIST* YONG KIM, *Lehigh University* A dual-driver shock tube was used to investigate the growth rate of a finite thickness two-gas interface after shock forcing. One driver was used to create an argon-refrigerant interface as the contact surface behind a weak shock wave. The other driver, at the opposite end of the driven section, generates a stronger shock of Mach 1.1 to 1.3 to force the interface back in front of the detector station. Two schlieren systems record the density fluctuations while light scattering detectors record the density of the refrigerant as a function of position over the interface during both it's initial passage and return. A pair of digital cameras take stereo images of the interface, as mapped out by the tracer particles under illumination by a Q-switched ruby laser. The amount of time that the interface is allowed to travel up the driven section determines the interaction time as a control. Comparisons made between the schlieren signals, light scattering detector outputs, and the images quantify the fingered characteristics of the interface and its growth due to shock forcing. The results show that the interface has a distribution of thicknesses and that the interaction with a shock further broadens the interface.

**10:12**

**Y8 10 Investigation of Oxygen Transfer Enhancement in Thermally Driven Cavities By Lattice Boltzmann Simulation.** HUIDAN YU, *CNLS, Los Alamos National Lab* JINSUO ZHANG, *D-5, Los Alamos National Lab* NING LI, *MST-10, Los Alamos National Lab* We investigate the enhancement of mass transfer in 2D thermally driven cavities using lattice Boltzmann equation (LBE) method. The computational technique integrates three coupled LBEs for solving velocity, temperature, and concentration fields simultaneously. Simulation is performed for oxygen transfer in lead/lead-bismuth eutectic with variations of temperature boundary, Schmidt number, and field aspect ratio to investigate the effects on enhancement of oxygen transfer. Interested characteristics include oxygen concentration, Sherwood number, and velocity profiles, etc. Our results clearly indicate that oxygen transfer is dominated by convection while diffusion also plays a role on it. Comparative studies demonstrate that side heating and top cooling device is more efficient to transfer oxygen than side heating and cooling device and oxygen transfers more rapidly in square cavity than in rectangular cavity. This work establishes a reliable thermal LBE model for thermally driven heat and mass transfer.

**10:24**

**Y8 11 Energy from Ocean Waves, River Currents, and Wind** SHYAMAL GUHA, *Texas Southern University* The Earth we live in is surrounded by fluids, which are in perpetual motion. The air in the atmosphere and water found in lakes, ocean, and rivers form our natural environment. Much of the fluid medium is in constant motion. The kinetic energy of this moving fluid is astronomical in magnitude. Over the years, I have considered methods of converting a fraction of the vast reserve of this kinetic energy into electro-mechanical energy. I have conceived a few schemes of such conversions. The fluids whose kinetic energy can be converted into electro-mechanical energy are the following: ocean waters, river currents and atmospheric air. In a book to be published in the spring of 2006, I have described different techniques of energy conversion. In the upcoming APS meeting, I plan to discuss some of these techniques.

**10:36**

**Y8 12 Motion of Rigid Bodies in Newtonian and non-Newtonian Fluids** ASHWIN VAIDYA, *Florida State University* The properties of non-Newtonian fluids, such as normal stress effects and non-constant viscosities are known to result in flow phenomenon which are dramatically different from those of Newtonian fluids. One such interesting difference in the behavior of these kinds of fluids is in their interaction with submerged rigid bodies. In this talk, we will focus on the problem of steady motions of symmetric rigid bodies as they freefall in Newtonian and viscoelastic fluids, modeled by the Navier Stokes, Power Law, Second order and the Generalized Second order fluid models. We will examine how variations in forces and torques in these two kinds of fluids can result in remarkably different phenomenon.

**10:48**

**Y8 13 Particle Dynamics in Low Reynolds Number Fluidized Beds** PHIL SEGRE, *Physics Dep., Emory Univ., Atlanta Ga.* JIM McCLYMER, *Physics Dep., Univ. of Maine, Orono ME* The sedimentation dynamics of extremely low polydispersity, $\sigma_a/a \sim 1.5\%$, non-Brownian, particles are studied in a liquid fluidized bed at low Reynolds number, $Re \ll 1$. When fluidized, the system reaches a steady state in which the local velocity fluctuations and

particle concentration are found to become highly stratified with height in the column. Results are presented for the degree of stratification with normalized bed height $H/a$. We find that taller beds are more stratified than shorter beds. However, recent computer simulations have not found any measurable stratification with height. We reconcile this apparent disagreement by showing that the stratification in experiments of comparably small systems such as those studied by simulation are indeed very small. We also develop a simple advection-diffusion model that connects the velocity fluctuations to the concentration gradients, and account for the observed bed stability.

**SESSION Y12: OXIDE SURFACE AND INTERFACES**
**Friday Morning, 17 March 2006**
**304, Baltimore Convention Center at 8:00**
**Jiandi Zhang, Florida International University, presiding**

**8:00**
**Y12 1 Capacitance Investigation of the Field-Induced Resistive Switching Interface** STEPHEN TSUI, NILANJAN DAS, YAQI WANG, YUYI XUE, *Texas Center for Superconductivity at the University of Houston* C.W. CHU, *Hong Kong University of Science and Technology; Texas Center for Superconductivity at the University of Houston; Lawrence Berkeley National Laboratory* We investigate the capacitance associated with the field-induced resistive switch formed at the interface between metal and perovskite oxide, in particular Ag deposited on $Pr_{0.7}Ca_{0.3}MnO_3$ thin film. The switch is dictated by the polarity of the applied voltage pulses, which drives the interface into either a nonvolatile high or low resistance state. Different models for this phenomenon have been proposed. We verify these models by examining the changes in the capacitance. The nature of the switching is therefore investigated through the measurement of the dielectric response with respect to frequency for both high and low resistance states. As a result, we can deduce information regarding the thickness of the switching interface, the density of the defects, and the distributions of the trap potentials. These parameters signal clear changes in both the defect density and the associated trapping potential. Lattice rearrangement, therefore, may play a major role in the switching.

**8:12**
**Y12 2 Strain Relaxation in Buried $SrRuO_3$ Thin Film under a Biaxial Compression: $CaZrO_3/SrRuO_3/SrTiO_3$ System** SOO GIL KIM, YUDI WANG, I-WEI CHEN, *Deparment of Materials Science and Engineering, University of Pennsylvania* We have observed a novel strain relaxation phenomenon in the buried thin film that develops during the deposition of an overcoat layer. In $SrRuO_3/SrTiO_3$ (100) system, the $SrRuO_3$ film is initially in biaxial compression, but the strain relaxation develops after a $CaZrO_3$ overcoat is deposited, manifested as misfit dislocations at the $CaZrO_3/SrRuO_3$ interface and a cross-hatch pattern of surface corrugation on the $CaZrO_3$ surface. This arises because $CaZrO_3$ (0.4012 nm) has a larger lattice parameter than those of $SrRuO_3$ (0.393 nm) and $SrTiO_3$ (0.3905 nm), thus contributing to the strain energy. By increasing point defect population in $CaZrO_3$ to accommodate the misfit strain, this phenomenon can be avoided and atomically flat thin film stacks obtained.

**8:24**
**Y12 3 Atomically Flat $SrRuO_3$ Conductive Thin Films on $SrTiO_3$ (001) by Pulsed Laser Deposition** YUDI WANG, SOO GIL KIM, I-WEI CHEN, *Department of Materials Science and Engineering, University of Pennsylvania, Philadelphia, PA19104-6272, USA* Atomically flat surfaces are important for thin film multilayers, superlattices, and heterostructures. For $SrRuO_3$ thin films grown on perovskite substrates, higher oxygen pressure is commonly used to achieve desired stoichiometry, crystallinity and conductivity, but it can also cause step bunching, pin holes and finger-like structures which destroy film/substrate coherency. We have found the finger-like structure is due to the slow 3-layer-nucleation process that occurs on the $TiO_2$ terminated $SrTiO_3$substrate, whereas step bunching is due to excessive step mobility. Using a transition layer on $SrTiO_3$ that establishes the SrO termination, and adjusting deposition parameters and step spacing that reduce step migration time, we have obtained atomically flat $SrRuO_3$ films free of the above morphological defects. These films show a large enhancement of electrical conductivity, making them suitable for various applications.

**8:36**
**Y12 4 Growth Transient Scaling During Pulsed Laser Deposition of SrTiO3*** J.Z. TISCHLER, B.C. LARSON, GYULA ERES, C.M. ROULEAU, *Oak Ridge National Laboratory* P. ZSCHACK, *UNICAT, Univ. of Ill* Time resolved surface x-ray diffraction studies of pulsed laser deposition show that laser-pulse growth-transients nearly scale with the time between pulses, for dwell times varying by a factor of 250 (0.2s to 50s). AFM measurements show that shorter dwell times produce smoother surfaces than longer dwell times, and that the improved growth for short dwell times correlates with small but systematic changes in the observed growth-transients as the dwell time was varied from 0.2s to 50s. These results imply that the transverse length scale of surface structures in layer-by-layer growth is determined by the annealing time between laser pulses as well as the amount of material deposited per pulse. The impact of dwell time on layer-by-growth of will be discussed.

*Sponsored by Div. of Mat. Sci., US DOE, DE-AC05-00OR22725 (UT-Battelle). Measurements from the Advanced Photon Source, UNICAT supported by UIUC, ORNL, State of Ill., NIST and UOP.

**8:48**
**Y12 5 Transport properties of $SrTiO_3$ / wide-gap insulator heterointerfaces** KESIUKE SHIBUYA, TSUYOSHI OHNISHI, TAKAYUKI UOZUMI, TAISUKE SATO, MIKK LIPPMAA, *University of Tokyo* HIDEOMI KOINUMA, *National Institute for Materials Science* A field-effect transistor is a sensitive probe for the investigation of interfacial electronic properties. We have demonstrated the importance of an epitaxial interface, using $SrTiO_3$ (100) single crystal field-effect transistors with amorphous and epitaxial $CaHfO_3$ layers as gate insulators. The devices with amorphous insulator layers showed n-type transistor operation with a field-effect mobility of 0.4 to 0.5 $cm^2$ / V s at room temperature. A large threshold voltage shift was observed at low temperatures and the transistor performance was temperature independent when that shift was taken into account. The device properties were greatly affected by the interface between amorphous insulator and $SrTiO_3$. To improve the quality of the channel layer-insulator interface, an ultra-thin epitaxial $CaHfO_3$ layer was grown on the $SrTiO_3$ substrate surface at high temperature, followed by room-temperature deposition of an amorphous insulator layer. The de-

vices with epitaxial interfaces exhibited a large improvement over the amorphous transistors. A field-effect mobility of around 2 $cm^2$ / V s was attained at room temperature and found to increase at low temperature, reaching 25 $cm^2$ / V s at 50 K. This result means that the carriers induced by the field effect behaved as would be expected for electron-doped $SrTiO_3$.

**9:00**

**Y12 6 Strain effects on the magnetic properties of epitaxial $SrRuO_3$ thin films** CHANGKUN XIE, JOSEPH BUDNICK, BARRETT WELLS, *Department of Physics, University of Connecticut, Storrs, CT 06269-3046* DEPARTMENT OF PHYSICS, UNIVERSITY OF CONNECTICUT, STORRS, CT 06269-3046 TEAM, We study the effects of lattice strain on the magnetic behavior of epitaxial $SrRuO_3$ thin films grown by pulsed laser deposition. Most films have been grown on $SrTiO_3$ and $KTaO_3$ substrates that provide compressive and tensile strain, respectively. The Curie temperature (Tc) is reduced compared to the corresponding bulk for compressively strained $SrRuO_3$ films. This is consistent with previous results. Tc is enhanced an almost equal amount for films under tension. The transition temperature shows a fairly large change between the films with different types of strain (compressive and tensile), but further variation of strain produces only small changes in Tc. The rise in Tc with tensile strain is unique as far as we know. We present the temperature-strain phase diagram of $SrRuO_3$ thin films and discuss possible mechanisms for the strain dependent changes in magnetic properties. This work is supported through NSF DMR-0239667. Some data was taken at the National Synchrotron Light Source, Brookhaven National Laboratory, which is supported by the U.S. Department of Energy, Division of Materials Sciences and Division of Chemical Sciences, under Contract No. DE-AC02-98CH10886.

**9:12**

**Y12 7 Structural Analysis of $La_x$ Mn $O_3$ Films** M.A. DELEON, T. TYSON, *New Jersey Institute of Technology, Applied Physics* C. DUBOURDIEU, *Laboratoire des Máteriaux et du Génie Physique UMR CNRS 5628, INPG, 38402 St.Martin d'Héres, France* J. BAI, *ORNL* J. KIRKLAND, *NRL* Local and long-range structure have been correlated with the magnetic and transport properties in $La_xMnO_3$ films (2000Å) with La:Mn content (x) ranging from 0.83 to 1.09. The local structure has been investigated by Mn K-edge X-Ray Absorption spectroscopy as a function of x. The long range structure has been evaluated by detailed measurements of the in-plane and out-of-plane lattice parameters via high-resolution synchrotron x-ray diffraction. The detailed local distortions of the $MnO_6$ octahedra are related to the low temperature magnetization. This research is supported by NSF DMR-0209243 and DMR-0512196.

**9:24**

**Y12 8 Effect of polarization on the surface reactivity of ferroelectric materials** JOHN GARRA, *University of Pennsylvania* DAWN BONNELL, *University of Pennsylvania* JOHN VOHS, *University of Pennsylvania* ANDREW RAPPE, *University of Pennsylvania* Temperature programmed desorption (TPD) has been used to study the effect of polarization on the surface reactivity of ferroelectric materials including single crystal lithium niobate (0001) and barium titanate (001). In the case of barium titanate, the polarization state of the crystal is controlled by electrical poling in UHV. Several suitable probe molecules have been identified including methanol, water, carbon dioxide, and pyridine. By comparing the desorption spectra of these molecules for the positive and negative surfaces of the crystal, one can determine the effect of polarization on the surface-adsorbate interaction.

**9:36**

**Y12 9 Structure of Hydrated $\alpha$-$Fe_2O_3$ (0001) and (1$\bar{1}$02)*** CYNTHIA LO, *National Institute of Standards and Technology, Chemical Science and Technology Laboratory* ANNE CHAKA, *National Institute of Standards and Technology, Chemical Science and Technology Laboratory* THOMAS TRAINOR, *University of Alaska Fairbanks, Department of Chemistry and Biochemistry* The structure and reactivity of $\alpha$-$Fe_2O_3$ depends on several factors, including the composition of the bulk material, crystallographic orientation, and local coordination of the surface atoms. As an example, the adsorption and dissociation of water on $\alpha$-$Fe_2O_3$ and other metal oxide surfaces is not well understood, since the oxide surface has largely been characterized under ultra-high vacuum or clean conditions. However, interactions at the solid-liquid and solid-solid interface play major roles in environmental processes, including contaminant sequestration, mobility, and bioavailability. In this work, we present density functional theory results on the structure of clean and hydrated $\alpha$-$Fe_2O_3$ (0001) and (1$\bar{1}$02), and show the changes in surface structure upon heterolytic water dissociation and water physisorption.

*National Science Foundation BES-0404400

**9:48**

**Y12 10 Dopant induced surface reconstruction in N-doped rutile $TiO_2$(110)** MATTHIAS BATZILL, *Tulane University* ERIE MORALES, ULRIKE DIEBOLD, Recently N-doping of $TiO_2$ has attracted some attention because it has been demonstrated to shift the photocatalytic activity of $TiO_2$ from the UV-region to the visible light. Here we examine the impact of N-doping on the electronic structure and surface morphology of single crystal $TiO_2$ surfaces.* Often it is assumed that bulk dopants have little influence on the surface properties. In the case of rutile $TiO_2$(110) it is, however, well established that intrinsic O-vacancies cause the surface to reconstruct to form a 1x2 superstructure. We find that N-doping reduces the formation energy of O-vacancies in $TiO_2$ and as a consequence destabilizes the surface to cause a 1x2 reconstruction. Similar surface effects may be expected for other bulk dopants that are know to induce oxygen vacancies in $TiO_2$. * M. Batzill, E.H. Morales, U. Diebold, Phys. Rev. Lett. accepted

**10:00**

**Y12 11 Electron-stimulated desorption ion angular distribution (ESDIAD) investigations of the rutile $TiO_2$(011)-(2x1) surface*** SERGEY SOLOVEV, *Rutgers State University* MATTHIAS BATZILL, ULRIKE DIEBOLD, *Tulane University* THEODORE MADEY, *Rutgers State University* A wide variety of potential applications have stimulated investigations of the atomic-scale properties of $TiO_2$surfaces. In a combined experimental and theoretical study it was shown recently that the rutile $TiO_2$(011)-(2x1) reconstruction is distinct from other $TiO_2$ surfaces: a model was proposed based on onefold coordinated (titanyl) oxygen atoms, giving rise to double-bonded Ti=O species at the surface [T. J. Beck et al., PRL 93 (2004) 036104]. These species may play a significant role in the enhanced photocatalytic activity of $TiO_2$(011). The present work is an attempt to provide a direct experimental test of the model. The ESDIAD method com-

bined with LEED is used to determine the orientation of Ti-O bonds relative to the (2x1) surface. The ESDIAD data for $O^+$ exhibit two beams along [100] azimuths, each tilted $>$ 20 degrees from the surface normal; the data provide supporting evidence for the proposed model. *supported in part by NSF

**10:12**

**Y12 12 Structure and energetics of step edges on anatase $TiO_2$(101)** XUE-QING GONG, *Princeton University* ANNABELLA SELLONI, *Princeton University* MATTHIAS BATZILL, *Tulane University* ULRIKE DIEBOLD, *Tulane University* PRINCETON UNIVERSITY COLLABORATION, TULANE UNIVERSITY COLLABORATION, Defects, such as step edges, are of paramount importance to the physical and chemical properties of metal and metal oxide surfaces. However, while steps on metal surfaces have been extensively investigated both experimentally and theoretically, much less is known about the structure and properties of steps on metal oxide surfaces. Recent STM work examined the step structure of the (101) surface of anatase $TiO_2$, which is the most stable and widely exposed surface of this interesting $TiO_2$ polymorph. Steps were found to exhibit a few preferred orientations, giving rise to islands with identical shape on the surface. Motivated by these observations, we have carried out extensive density functional theory calculations to determine the formation energies of steps along various orientations and with different structures. A procedure based on systematic calculations of related vicinal anatase $TiO_2$ surfaces has been used, which yields step edge energies with remarkable accuracy. The electronic structures of the stepped surfaces and adsorption of prototype molecules have been also investigated. The present results allow us to obtain a very detailed and complete understanding of the experimental observations.

**10:24**

**Y12 13 Atomic structure of a Ultrathin $TiO_2$ film on Mo(112) surface*** RUQIAN WU, *Department of Physics and Astronomy, UCI, CA* Materials with reduced dimensions attract much interest because their properties are often significantly different from the properties of bulk materials. Additionally, thin oxide films represent model systems well suited for studying structure reactivity relationships on oxides and oxide supported metal particles considered as models for heterogeneous catalysts. Recently, gold clusters on titania/Mo(112) surface are found to be high catalytic activity, attributing to the structural effects. Despite extensive experimental and theoretical studies the detailed atomic structure of $TiO_2$ films on Mo(112) substrate remain unknown. The geometrical and electronic structures of a ultrathin $TiO_2$ film expitaxially grown on a Mo(112) substrate have been determined by first principles density-functional theory calculations. The results show that the $TiO_2$ perfer to the $8\times 2$ surface structure on the Mo(112) surface, which is well agreement with the experiments.

*Work was supported by the DOE (grant No: DE-FG02-04ER15611) and ICTS, Chinese Academy of Science.

**10:36**

**Y12 14 Thin oxide films: analysis of finite-size effects** C. FREYSOLDT, P. RINKE, M. SCHEFFLER, *Fritz-Haber-Institut, Berlin, Germany* Oxide surfaces have attracted considerable interest over the last years. In order to employ surface science tools, oxides are often grown epitaxially on metals. Recent findings for $SiO_2$ on Mo(112) indicate that well-ordered films are only 2-3 atomic layers thick – less than previously thought[1,2]. But is the surface of the films characteristic for the surface of a bulk oxide? Not only the structure may differ from any known bulk structure, but also the metal might alter the electronic structure. Also, sizeable quantum effects are expected at these dimensions. We present DFT simulations for oxide films of various thicknesses for $SiO_2$, $Al_2O_3$, and $HfO_2$. In order to separate the thickness from the substrate dependence, free-standing films are considered. We find that the electronic structure at the DFT level becomes bulk-like for very few atomic layers. The case of silica is discussed in detail. The film structure on Mo(112) corresponds to the most stable quartz(0001) surface. The electronic structure is essentially bulk-like and independent of the film thickness. The presence of the substrate does not alter these findings. For the electronic response of the thin film, however, the quasiparticle picture predicts a thickness-dependent band gap due to the dielectric discontinuity at the interface. Likewise, the chemistry and stability of defects is expected to be influenced by the substrate.

[1]L. Giordano *et al.*, Surf. Sci. 584, 225 (2005).
[2]J. Weissenrieder *et al.*, Phys. Rev.Lett. 95, 076103 (2005).

**10:48**

**Y12 15 Surface and Interface Structures of Crystalline Oxides on Silicon (COS)** FRED WALKER, *Oak Ridge National Laboratory* MARCO BUONGIORNO-NARDELLI, *North Carolina State University* RODNEY McKEE, *Oak Ridge National Laboratory* The structure of the Sr-covered Si(001) surface (the precursor to COS heteroepitaxy) is a matter of on-going scientific debate with experiment and theory casting opposing views. Real space Z-contrast imaging shows that half of the silicon atoms on the (001) surface are absent, and this has presented us with the intriguing question – ''Where does the silicon go?'' A metallic surface termination of silicon was required in the layer-sequenced heteroepitaxy of COS. What has been common to all experimental realizations of the layer-sequenced COS structure, is the presence of hydrogen evolving from the metal sources during the film growth. We report here that this hydrogen has inadvertently played a pivotal role in defining the silicon termination and thus the evolution of the interface structure for COS. We will describe the thermodynamic basis for this hydrogen effect along with experimental and theoretical characterization of the structural details. Research sponsored jointly by the Division of Materials Sciences and Engineering, Office of Basic Energy Sciences, U.S. Department of Energy at Oak Ridge National Laboratory under contract DE-AC05-00OR22725 with UT-Battelle, LLC and at the University of Tennessee under contract DE-FG02-01ER45937. Calculations have been performed on CCS supercomputers at Oak Ridge National Laboratory.

## SESSION Y16: OPTICS AND OPTOELECTRONICS
**Friday Morning, 17 March 2006**
**312, Baltimore Convention Center at 8:00**
**Stuart A Solin, Washington University, presiding**

**8:00**

**Y16 1 Investigations of Carbon Nanotube Networks for use as Transparent Conductors** MARK TOPINKA, *Stanford University* Recently there has been increasing interest in the physics of conduction through carbon nanotube networks and the possibility of using carbon nanotube networks as transparent conducting lay-

ers for solar cells and other optoelectronic applications(1). Conductivities as high as 30 ohm/square with transparencies of about 80% have been reported(2). Here we present results of our work on understanding the underlying physics behind the real-world behavior of these systems and identifying the bottlenecks which are currently limiting their performance. We focus in particular on their possible use in solar cells as a low-cost alternative to more expensive transparent conductor technologies such as Indium Tin Oxide (ITO). We include numerical simulations of conduction through nanotube networks and scanning probe microscopy studies of transport through these systems. (1) L.Hu, D.S.Hecht, G.Gruner, NanoLetters **4**, 2513 (2) Z.Wu, et al, Science **305**, 1273

**8:12**

**Y16 2 Theoretical model of extraordinary optoconductance in GaAs-In hybrid structures*** A.M. GIRGIS, L.R. RAMMOHAN, *Worcester Polytechnic Institute* K.A. WIELAND, YUN WANG, S.A. SOLIN, *Washington University in St. Louis* We have recently demonstrated extraordinary optoconductance (EOC) of order 500% in GaAs-In metal semiconductor hybrid structures (MSHs).[1] This is the third example of a geometry driven ''EXX'' phenomenon, the first example of which was extraordinary magnetoresistance (EMR).[2] However, EOC is the first example of an EXX effect in which the bulk properties of the semiconductor and not the interfacial properties are modified by the external perturbation. Here we describe a Gaussian broadened point charge theoretical model which quantititavely accounts for the dependence of the optocondutance on the position of a focussed Ar laser beam. We also account quantitatively for the temperature dependence of the EOC. Our theoretical model incorporates the Dember effect[3] directly via the differential mobilities of the electrons and holes. Using these mobilities and a third variable corresponding to the net charge, a good fit to the positional dependence of the voltage is achieved. The strengths and limitations of this theory will be highlighted.

*Supported by WU CMI and NSF grant ECS-0329347

[1]K.A. Wieland et al., Applied Physics Letters, submitted.
[2]S.A. Solin et al., Science **289**, 1530 (2000).
[3]H. Dember, Phys. Z. **32**, 544 (1931).

**8:24**

**Y16 3 Extraordinary optoconductance in InSb-In hybrid structures*** K.A. WIELAND, YUN WANG, S.A. SOLIN, *Washington University in St. Louis* A.M. GIRGIS, L.R. RAMMOHAN, *Worcester Polytechnic Institute* Previously reported extraordinary optoconductance (EOC)[1] in degenerate Si-doped ($n \sim 1 \times 10^{18}$ cm$^{-3}$) GaAs-In metal-semiconductor hybrid structures (MSHs) is compared to new experimental results on intrinsic Te-doped ($n \sim 4 \times 10^{14}$cm$^{-3}$) InSb-In MSHs. Using a shunted van der Pauw plate, DC and AC voltage measurements of InSb MSHs were acquired. The sample was illuminated with a focused Ar ion laser and studied as a function of wavelength (457 $-$ 526nm), bias current ( $\pm$ 100mA), lateral position (transverse to the beam), and at 300K and 10K. Whereas the optimal room temperature position sensitivity in the case of GaAs is 137 mV/mm for 100mW of 488.0 nm illumination, the corresponding sensitivity of InSb is found to be 1.2 mV/mm for 10 mW of 514.5 nm illumination. The magnitude of the InSb result is surprisingly large given the relative values of band gaps, mobility, carrier concentration, and laser illumination.[2] The origin of this large position sensitive photovoltage will be discussed.

*Supported by WU CMI and NSF grant ECS-0329347

[1]K.A. Wieland itet al., Applied Physics Letters, submitted.
[2]O. Madelung, editor, Data in Science and Technology: Semiconductors - Group IV Elements and III-V Compounds (Springer, New York, 1991).

**8:36**

**Y16 4 All-Epitaxial Microcavity for Cavity-QED with Quantum Dots** ANDREAS MULLER, *University of Texas at Austin, Dept. of Physics* DINGYUAN LU, JAEMIN AHN, DEEPA GAZULA, SONIA QUADERY, SABINE FREISEM, DENNIS DEPPE, *University of Texas at Austin, Dept. of Electrical and Computer Engineering* CHIH-KANG SHIH, *University of Texas at Austin, Dept. of Physics* We report on the optical characterization of a novel type of optical microcavity that forms a fully-buried semiconductor heterostructure and offers numerous technological advantages such as chemical/mechanical stability, good thermal heat-sinking, and compatibility with electrical injection. Based on epitaxial re-growth over a lithographically-defined, quantum dot-containing mesa, this approach leads to self-alignment of single dots with the field anti-node while simultaneously providing quality factors exceeding 10,000 that support lasing with only a single quantum dot layer. Time-resolved measurements reveal the most basic cavity-QED effect in this structure, namely the Purcell spontaneous emission enhancement. A strong spectral and spatial dependence of this effect is observed using photoluminescence imaging, highlighting in particular the importance of the spatial overlap.

**8:48**

**Y16 5 Ultra-high-Q Microcavities for $D_2O$ Detection*** ANDREA ARMANI, DENIZ ARMANI, *California Institute of Technology* SEAN SPILLANE, *Hewlett-Packard Laboratories* KERRY VAHALA, *California Institute of Technology* Ultra high Q optical microcavities ($Q > 10^6$) provide a method for boosting detection sensitivity over conventional detection methods. In a recently published work, the difference between quality factors (Q) of microcavities immersed in $D_2O$ and $H_2O$ was measured and calculated. Due to the higher absorption of $H_2O$, resonators immersed in $H_2O$ have lower Q's than those immersed in $D_2O$. This difference in absorption can be exploited to use the resonator as a $D_2O$ detector. The effect on Q is most noticeable at 1300nm, where the Q in water is $10^6$ and the Q in $D_2O$ is $10^7$. At longer wavelengths, both $Q(D_2O)$ and $Q(H_2O)$ are further degraded, reducing the efficacy of detection, and at shorter wavelengths, $Q(D_2O)$ and $Q(H_2O)$ become similar, reducing the effect that the presence of $D_2O$ alone has on Q. By monitoring the quality factor,01 M concentration of $D_2O$ in water ($10^{17}$ molecules of $D_2O$) has been detected; however, the actual sensitivity limit is far better than this concentration value. Detection has also been demonstrated by cyclic introduction and flushing of $D_2O$, leading to cyclic degradation and improvement of the Q, thereby demonstrating reversible detection.

*The authors would like to thank the DARPA Center for OptoFluidics for support.

**9:00**

**Y16 6 Radiation-pressure-induced regenerative mechanical oscillations in optical microcavities** HOSSEIN ROKHSARI, MANI HOSSEIN-ZADEH, TOBIAS KIPPENBERG, TAL CARMON, KERRY VAHALA, *California Institute of Technology* VAHALA RESEARCH GROUP TEAM, A silica microcavity is shown to allow both circulation of long lived cavity photons as well as mechanical vibrations at characteristic radio frequencies. Radiation pressure or the force due to impact of photons can couple the mechanical modes of an optical cavity structure to its optical modes, leading to regenerative RF mechanical oscillations of the micro structure with only micro-Watts of optical threshold power. Embodied within a microscale, chip-based device, this mechanism can benefit both research into macroscale quantum mechanical phenomena and improve the understanding of the mechanism within the context of Laser interferometer gravitational-wave observatory (LIGO). This novel class of oscillators that acquire gain directly from CW optical fields may also find applications in all-optical photonic systems. Through a detailed study of the short-term stability of these optomechanical oscillators we demonstrate that thermo-mechanical noise also referred to as Brownian noise, is the dominant noise mechanism at room temperatures. Preliminary calculations show that lowering the temperature in a vacuum environment may enable the observation of quantum back action noise in microtoroidal resonators.

**9:12**

**Y16 7 Optimizing planar waveguide design for multi-wavelength and nonlinear quantum cascade lasers** SCOTT HOWARD, FATIMA TOOR, ANTHONY HOFFMAN, CLAIRE GMACHL, *Princeton University* DEBORAH SIVCO, *Lucent Technologies* High performance and novel multi-wavelength quantum cascade (QC) lasers present unique challenges in designing waveguides. We present a computational approach that uses the projected threshold current densities and mode overlaps to iteratively optimize the waveguide design. This program has been used to solve three specific problems by designing: (1) two dual wavelength QC laser structures (a 7.5 and 13.5 $\mu$m, and a 9.5 and 11.5 $\mu$m structure) with the goal of minimizing the threshold current of each pair of lasers simultaneously below the continuous wave threshold while maintaining an operating voltage less than 10 V; (2) a waveguide for high performance QC lasers with the goal of minimizing input electrical power at high operating temperatures; and (3) waveguides for nonlinear QC lasers designed for difference frequency generation with the goal of minimizing the threshold currents of the two integrated pump lasers, maximizing the overlap of the pump light with the monolithically-integrated nonlinear mixing region, and reducing the loss of the non-linear guided mode.

**9:24**

**Y16 8 Distributed Bragg reflectors on quantum cascade lasers fabricated by focused ion beam milling** AFUSAT DIRISU, CLAIRE GMACHL, *Princeton University* DEBORAH SIVCO, *Lucent Technologies* The use of Focused Ion Beam (FIB) milling to fabricate custom gratings on Quantum Cascade (QC) lasers for single mode operation is reported. Using the FIB, gratings that fit specific laser wavelength requirements can be fabricated after all other laser processing is completed. This has the advantage that the processed lasers can be fully characterized before milling to determine the laser gain spectrum and its alignment with the desired emission wavelength, hence allowing the proper choice of the grating parameters, such as period and strength to be tailored to the final device. We have been able to mill gratings onto QC laser ridges using the FIB method to significantly narrow the emission spectrum without compromising other properties, such as output power or threshold, of the working device. We fabricated distributed Bragg reflector gratings approximately 1.2 $\mu$m deep, 250 $\mu$m long, with square profile, and with a period of 1.2 $\mu$m; these were processed on top of 2.7-3 mm long QC laser ridges emitting at 7.7 $\mu$m. We observed single mode operation with a side mode suppression ratio of about 12dB.

**9:36**

**Y16 9 Light propagation in random colloidal films with varying coordination number** XIAOTAO PENG, ANTHONY DINSMORE, *University of Massachusetts, Amherst* We measure the propagation of light through a random film of strongly-scattering microspheres as a function of the mean number of contacts per particle (the coordination number, Z). Decreasing Z reduces the local average refractive index and enhances the optical contrast of each scattering sphere with the effective background. In our experiments, we mix two kinds of colloidal spheres and prepare a dried film with random structure. Latex spheres coated with a high-index ZnS and poly(methylmethacrylate) spheres are used, as well as $SnS_2$ core-shell spheres for the near infrared. The transport mean-free path is then extracted from measurements of coherent backscattering of light from the films; its value is sensitive to Z. The results may guide our understanding of the propagation of waves in random media in general and may lead to new photonic materials. This work is supported by the NSF-sponsored UMass MRSEC. A.D.D. is a Cottrell Scholar of the Research Corporation.

**9:48**

**Y16 10 Calculations of the Photonic Properties of Two Dimensional QuasiCrystals** WEINING MAN, ORION CRISAFULLI, PAUL STEINHARDT, *Princeton University* PAUL CHAIKIN, *New York University* PRINCETON UNIV. TEAM, NYU COLLABORATION, Quasicrystals have higher point group symmetry than ordinary crystals, and hence are good candidates for complete photonic bandgaps. Our model system consists of infinite long cylinder dielectric (or air) rods at each Penrose lattice point We took three different approaches in using periodic approximants for these calculations. Our first approach uses a rectangular section of a Penrose tiling of different sizes and at different positions. In the second set of calculations, we generate a series of periodic approximants of the Penrose lattice via an inflation method. Our third approach, a rational number approximation, has the fewest number of defects. The rational number approximant is the best since there are no modes localized along the defects and no artificial modes appear in the gap frequency region. In each case we increased the approximant size until the results converged. Our calculations on 2-D Penrose quasicrystals show very isotropic sizeable complete photonic bandgaps which can be identified with known Bragg scattering peaks. We predict the best Bragg scattering spot and optimize the cylinder size for the widest over all band gap for a given dielectric contrast. We also discuss experimental results on 3D icosahedral quasicrystals in the microwave regime and show that 3D icosahedral quasicrystals are better photonic bandgap candidates than crystalline structures.

**10:00**

**Y16 11 A Magnus Expansion Analysis of Frequency-Dependent Mueller Matrices** MICHAEL REIMER, DAVID YEVICK, *University of Waterloo* We have recently demonstrated that, for any physical system characterized by a non-singular, frequency dependent Jones matrix, the frequency evolution of the corresponding Mueller matrix is described by a differential equation whose general solution can be compactly formulated through the Magnus expansion [M. Reimer, D. Yevick, and D. Dumas, submitted to J. Opt. Soc. Am. A, Photon. Technol. Lett.]. [D. Yevick, T. Lu, W. Huang and W. Bardyszewski to be published in J. Opt. Soc. Am. A]. We subsequently applied our analytic results to optical compensators for communications networks and to the estimation of a system's frequency dependent Mueller matrix based on repeated measurements of the output state of polarization for randomly generated input polarization states [M. Reimer, D. Yevick and D. Dumas, submitted to Photon. Technol. Lett.]. We have also incorporated the Magnus expansion into a Clifford algebra description of polarization evolution. This procedure reformulates numerous physical transformations in a simple and transparent manner [M. Reimer and D. Yevick, submitted to Photon. Technol. Lett.].

**10:12**

**Y16 12 Nanoscale Motion Detection by Diffraction of Evanescent Waves** P. SCOTT CARNEY, *Dept. of Electrical and Computer Eng., University of Illinois at Urbana-Champaign* DEVREZ KARABACAK, *Dept. of Aerospace and Mechanical Eng., Boston University* STEPHEN B. IPPOLITO, M. SELIM UNLU, *Dept. of Electrical and Computer Eng., Boston University* KAMIL L. EKINCI, *Dept. of Aerospace and Mechanical Eng., Boston University* Conventional optical techniques such as Michelson interferometry and Fabry-Perot interferometry have been widely used for ultrasensitive motion detection in micro- and nanoscale mechanical devices. Here, we propose a novel motion detection scheme based upon the diffraction of evanescent waves. In this scheme, an evanescent field is formed within the vicinity of a moving device surface. The motion of the surface results in an enhanced scattering of the evanescent field into propagating states. This novel detection scheme appears to have several advantages over conventional techniques: it lowers the background optical signal; if implemented using a solid immersion lens, the effective spot size is reduced. We shall describe a possible implementation of a dark-field microscope for motion detection in a nanomechanical resonator and present numerical analyses.

**10:24**

**Y16 13 High Sensitivity Electro-Optic Field Sensors** ANTHONY GARZARELLA, DONG HO WU, TERENCE WIETING, SYED QADRI, *Naval Research Lab* RANDAL HINTON, *Temple University* The use of electro-optic (EO) crystals for electric field detection has recently gained considerable interest, due to their nonperturbative method of detecting both field amplitude and phase over a wide range of frequencies. One of the technical challenges facing this detection technique is to improve the detection sensitivity. Since the sensor responsivity is proportional to the EO coefficient of the crystal ($r_{33}$), utilizing materials with a large $r_{33}$ values, such as $Sr_{0.75}Ba_{0.25}Nb_2O_6$ (SBN-75), is the most straightforward approach. However, it was found that in spite of its large EO coefficient, sensors utilizing SBN-75 ($r_{33}^{expt} \sim 700$ pm/V) showed similar or weaker responsivities than sensors utilizing $LiNbO_3$ ($r_{33}^{expt} \sim 30$ pm/V). The detailed data indicate that the responsivity losses in SBN-75 are produced by optically-induced incoherence in the birefringence of the crystal. In this report, we measure this incoherence, and demonstrate its direct impact on the sensitivity and stability of the EO sensor.

**10:36**

**Y16 14 Characterization of triangular-structured two-dimensional photonic crystals designed for visible wavelengths.** JEFFREY CLARK, MICHAEL MARCINIAK, ROBERT NELSON, *Air Force Research Laboratory* JAMES LOTT, *Air Force Institute of Technology* The growing number of fabrication techniques of photonic crystals (PhC) is increasing the number of applications for these devices. This work focuses on the fabrication and characterization of triangular-structured, two-dimensional PhC designed for visible wavelengths. The fabrication processes studied for this PhC are focused ion beam, electron lithography, photolithography, and holographic photopolymerization/lithography. The fabrication techniques and materials used to create the PhC in part determine the characterization technique required to investigate the PBG. Techniques examined here include the coupling of a beam by means of a prism into a wave-guiding medium in which the PhC has been fabricated, and the guiding of a beam to a PhC through a cylindrical glass container filled with an index matching medium. Analyses of the transmission and reflectance properties of a PhC for various incident angles confirm the presence of a PBG. The design of the PhC was based on a program created to display gap maps for triangular structures. The PBG of the structure, designed from the gap maps, was modeled using another program created to display band diagrams for triangular structures. Finally, FDTD modeling and simulation results are compared to the experimental results.

**10:48**

**Y16 15 Dynamics of lasers coupled by nearest-neighbor interaction** ALEXANDRA LANDSMAN,* *Naval Research Laboratory* IRA SCHWARTZ, The dynamics of arrays of nonlinear oscillators with diffusive coupling are investigated. The types of coupling needed to achieve synchronization are explored. The effects of time-delayed coupling are also considered. The results have implications for the production of coherent radiation in lasers and with suitable modification of the equations may be extended to biological networks.

*NRC Postdoctoral Fellow

**SESSION Y18: FOCUS SESSION: CARBON NANOTUBES: ADSORPTION AND GAS SURFACE INTERACTIONS WITH CARBON NANOTUBES**
**Friday Morning, 17 March 2006**
**315, Baltimore Convention Center at 8:00**
**Aleksey Kolmogorov, Duke University, presiding**

**8:00**

**Y18 1 Adhesion of single functional groups to individual carbon nanotubes: electronic effects probed by itab-initio**

**calculations*** JEFFREY GROSSMAN, *University of California, Berkeley* GIANCARLO CICERO, *INFM, Torino Polytechnic* GIULIA GALLI, *University of California, Davis* The interfacial interaction of simple functional groups (-$NH_2$, -CN, -$CH_3$ -$CHOCH_2$) with single wall carbon nanotubes (SWCNT) was investigated using itab-initio calculations. Binding energies and attachment forces were computed using Density Functional Theory (DFT) in the local density approximation, and Quantum Monte Carlo calculations were employed to test DFT accuracy in describing weak interactions for the controversial case of an oxygen molecule. We find that computed energies and forces are very sensitive to small variations of the electronic charge on the nanotube. In particular, the presence of a solvent (polar or non-polar), and thus of a small charge transfer from or to the tube, may alter the relative strength of adhesion forces for different functional groups, as compared to vacuum.

*This material is based upon work supported by the National Science Foundation under Grant No. EEC-0425914.

**8:12**

**Y18 2 Tunable Nanoresonators Constructed from Telescoping Nanotubes** KENNETH JENSEN, *U.C. Berkeley* CAGLAR GIRIT, *U.C. Berkeley* WILLIAM MICKELSON, *U.C. Berkeley* ALEX ZETTL, *U.C. Berkeley* We have created a tunable mechanical nanoscale resonator with potential applications in precise mass, force, position, and frequency measurement. The device consists of a specially prepared multiwalled carbon nanotube (MWNT) suspended between a metal electrode and a mobile, piezo-controlled contact. By exploiting the unique telescoping ability of MWNTs, we controllably slide an inner nanotube core from its outer nanotube casing, effectively changing its length and tuning its flexural resonance frequency.

**8:24**

**Y18 3 Interlayer forces in telescoping nanotubes** ANDRAS KIS, KENNETH JENSEN, *University of California, Berkeley* SHAUL ALONI, *Materials Sciences Division, Lawrence Berkeley National Laboratory* WILLIAM MICKELSON, ALEX ZETTL, *University of California, Berkeley* The ability to fabricate low-friction surfaces and lubricants is one of the key requirements for the miniaturization of mechanical systems, especially on the nanoscale where friction and surface adhesion often dominate over gravity and even electrostatic attraction. In this context, multi-walled carbon nanotubes (MWNT) have been proposed as the ideal nanobearing because of their inert, ultra-smooth surfaces and the narrow separation between their neighboring shells that prevents the accumulation of contaminant particles between sliding parts. In analogy with graphite, the weak van der Waals interaction between nanotube shells could provide the equivalent of lubrication, allowing easy relative sliding of nanotube layers. We have externally induced telescoping motion in MWNTs while measuring the force acting between the two layers involved in this motion. The restoring van der Waals force is comparable with theoretically predicted values. Defects are found to modulate this force and can lead to jamming.

**8:36**

**Y18 4 Registry-dependent interlayer potential for graphitic systems** ALEKSEY KOLMOGOROV, *Duke University* VINCENT CRESPI, *Pennsylvania State University* Standard applications of density functional theory (the local density approximation (LDA) and the generalized gradient approximation (GGA)) without nonlocal corrections do not adequately describe the exfoliation energy of graphite. The GGA, in particular, does not show any binding at physically meaningful interlayer distances. However, the *variation* in the energy under interlayer shifts, defined predominantly by the overlap of $\pi$ orbitals, is nearly identical in the two approximations and appears to be much more sound than previously suspected. We combine these results with experimental information on the exfoliation energy to create an improved registry-dependent classical potential for the interlayer interaction in graphitic structures.

**8:48**

**Y18 5 Adsorption of simple aromatic molecules on single-wall carbon nanotubes** LILIA M. WOODS, *Univ of South Florida, Tampa FL* STEFAN C. BADESCU, *NRL, Washington DC* THOMAS L. REINECKE, *NRL, Washington DC* Understanding the adsorption of aromatic molecules on carbon nanotubes is important for nanotube functionalization. We perform ab-initio plane-wave calculations for the adsorption of benzene derivatives such as nitrobenzene, aniline and toluene, using pseudopotentials in the local density approximation. We find that the minimum energy configurations of the molecules are flat along the nanotube, in agreement with experiments on polar molecules [1], and that the dominant part of the binding is physisorbtion. The physisorbed benzene used for reference lies in a graphite-stacking configuration, whereas benzene derivatives have small deviations from this perfect alignment. The deviation from ideal $\pi - \pi$ stacking is a complex process that involves the hybridization between molecular and nanotube levels, a small charge redistribution, and in some cases the formation of narrow conduction bands in the energy gap of semiconductor nanotubes. We trace the differences between derivatives to the properties of the molecular fragments attached to the benzene ring. [1] Snow E.S. et al, Science 307 (5717), 1942 (2005)

**9:00**

**Y18 6 DNA-CNT Interaction - A Density Functional Approach** RALPH SCHEICHER, S. GOWTHAM, RAJEEV AHUJA, *Fysiska Institutionen, Uppsala Universitet, Sweden* RAVINDRA PANDEY, *Michigan Technological University, USA* Standing at the intersection of the biological regime and the nanomaterials world, DNA-coated carbon nanotubes (CNT) possess features which can make them attractive for a range of applications, e.g., as highly specific nanosensors [1], or as a method to efficiently separate CNTs according to their structure [2]. It is therefore certainly worthwhile to obtain a detailed understanding of the binding between the bases in DNA and the surface of CNTs, preferably from first principles. To this end, we have studied the interaction between single-stranded DNA and single-walled CNTs (SWCNTs) using density functional theory. More specifically, we were interested in assessing the differences in the interaction of the four different bases in DNA, and how important the underlying structure of the CNT is for the orientation of the bases relative to the tube axis. We will report our results on the binding energy, the charge density, and the respective distortion in the electronic structure of the constituents of this hybrid system, depending on the geometrical properties of the CNT and the relative positioning of the DNA. [1] C. Staii et al., Nano Letters **5**, 1774-1778 (2005) [2] M. Zheng et al., Science **302**, 1545-1548 (2003)

**9:12**

**Y18 7 Molecular hydrogen adsorption on the boron-doped graphene sheet in presence of magnesium and transition metal**

ZHAOHUI HUANG, VNICENT CRESPI, *Dept. of Physics, Penn State University* Adsorption of hydrogen molecules onto a boron-doped graphene sheet in the simultaneous presence of magnesium and a transition metal has been studied using density functional methods. This setup is inspired by magnesium dihydride. We obersve that there form bonds between metal and boron atoms, which suggest a potential way to prevent metal from aggregating. Macroscopic aggregation of metal atoms makes this structure useless to adsorb hydrogen. We present results for different combination of transition metal and magnesium, and compare the binding energy of hydrogen molecule adorbed onto those structures.

**9:24**

**Y18 8 Controlled Confinement and Release of Gases in Single-Walled Carbon Nanotube Bundles** CHRISTOPHER MATRANGA, BRADLEY BOCKRATH, *U. S. Dept. of Energy, National Energy Technology Laboratory* A simple procedure is described which locks small quantities of $SF_6$, $CO_2$, and $^{13}CO_2$ into opened single-walled carbon nanotube (SWNT) bundles and keeps the gas inside the SWNTs above the desorption temperature of these molecules. The confinement technique involves opening the SWNTs with ozonolysis at 300 K followed by vacuum annealing at 700 K. Gases are then cryogenically adsorbed into the opened SWNTs and a locked into the SWNT pores by functionalizing the sample with a low temperature ozone treatment. The low temperature ozone treatment functionalizes the entry ports into the SWNT pores which in turn create a physical barrier for gases trying to desorb through these functionalized ports. The samples are stable under vacuum for periods of at least 24 hours and the trapped gases can be released by vacuum heating to 700 K. Reduced quantities of the trapped gases remain in the SWNTs even after exposure to room air. Fourier Transform Infrared Spectroscopy is used to monitor the functionalities resulting from the ozone treatment and to detect the trapped gas species.

**9:36**

**Y18 9 Physisorption Kinetics in Carbon Nanotube Bundles** JARED BURDE, M. MERCEDES CALBI, *Southern Illinois Univesity, Carbondale* The possibility of adsorbing gases in the interstitial channels that lie between nanotubes in a bundle is still the subject of much discussion because experimental observations do not seem to confirm the existence of adsorbed gases on this site as it has been predicted by several theoretical studies (that assume infinitely long tubes). After exploring the potential energy surfaces near the ends of the tubes, we have recently shown how the presence of a high binding energy site right before the entrance of the channel slows down the adsorption rate of $H_2$ dramatically [1]. Using a Kinetic Monte Carlo scheme, we present here a comprehensive study of the adsorption kinetics in the channels modeling the transport of various gases through the ends of the bundle. In order to facilitate the comparison with adsorption experiments, the results are given in terms of the equilibration time as a function of coverage, for different temperatures. In addition, the effect of cluster formation at the end of the bundle is analyzed. [1] M. Mercedes Calbi and J. L. Riccardo, ''Energy barriers at the ends of carbon nanotube bundles: Effects on interstitial adsorption kinetics,'' Phys. Rev. Lett. **94**, 246103 1-4 (2005).

**9:48**

**Y18 10 Adsorption of TCNQ on the inside and outside surface of single-wall carbon nanohorn aggregates*** RYOTA YUGE, *NEC* MASAKO YUDASAKA, *NEC, SORST-JST* JIN MIYAWAKI, *SORST-JST* TOSHINARI ICHIHASHI, *NEC* HIDETO IMAI, *NEC* YOSHIMI KUBO, *NEC* SUMIO IIJIMA, *NEC, SORST-JST, Meijo University* Storage and release of various materials into/from single-wall carbon nanohorns (SWNH), a type of single-wall carbon nanotubes, have been studied well, thus SWNHs have become potentially useful in many fields. However, not much is known about the mechanism of adsorption on the walls of SWNHs, which we have investigated using Tetracyano-*p*-quinodimethane (TCNQ). SWNHs were pretreated with $O_2$ at $550^oC$ to open holes, followed by the treatment with $H_2$ at $1200^oC$ to remove functional groups (SWNHh). Thermogravimetric analysis revealed that the quantities of TCNQ inside and outside were estimated to be about 0.07 and 0.11 g per 1 g of SWNHh, respectively, which did not increase even for the TCNQ overdosing. Raman spectra of TCNQ adsorbed on SWNHh (TCNQ/SWNHh) showed red shifts of several vibration modes of TCNQ, while the C=C ring stretching (CCr) showed the large blue-shift. This indicates that the quinoid ring of TCNQ strongly interacted with graphene sheets of SWNHh. The blue-shift of CCr Raman-peak is not observed for the charge transfer complexes such ash TTF/TCNQ, Cu/TCNQ, and so on. We will discuss the reason for the large-blue shift of CCr peak of TCNQ adsorbed on SWNHs in the talk.

*Supported by Nano Carbon Technology Project in NEDO

**10:00**

**Y18 11 Investigation of Fluorinated and Hydrogenated Carbon Nanotubes by STM** DHARMPAL TAKHAR, Z. GU, A. A. PEERA, W. E. BILLUPS, J. L. MARGRAVE, K. F. KELLY, *Department of Electrical and Computer Engineering, Rice University, Houston, Texas* There is a great deal of interest in the functionalization, in particular fluorination, of carbon nanotubes for the purposes of solvation and subsequent chemical reaction. Towards this end, we report the investigation of fluorinated nanotubes by variable-temperature STM. The atomic-scale fluorine coverage on the fluorotubes with composition was observed as a function of annealing temperature. Upon heating of the fluorotubes, we observe the subsequent desorption of the fluorine initiated around $240\ ^oC$ and proceeding up to $650\ ^oC$. At higher temperatures, all the fluorine desorbs revealing a number of small defects. Further heating leads to cutting of the fluorotubes which is initiated at these defect locations. We compare these results to our recent investigation of dihydrogen functionalized carbon nanotubes.

**10:12**

**Y18 12 Fast Mass Transport through Sub-2nm Carbon Nanotubes*** JASON K. HOLT, *LLNL* HYUNG GYU PARK, *LLNL & UC Berkeley* YINMIN WANG, MICHAEL STADERMANN, ALEXANDER B. ARTYUKHIN, *LLNL* COSTAS P. GRIGOROPOULOS, *UC Berkeley* ALEKSANDR NOY, OLGICA BAKAJIN, *LLNL* We report gas and water flow measurements through microfabricated membranes with sub-2nm aligned carbon nanotubes as pores. The measured gas flow exceeds predictions of the Knudsen diffusion model by at least an order of magnitude. The measured water flow rate exceeds values calculated from continuum hydrodynamics models by two to three orders of magnitude and agrees with flow rates extrapolated from molecular dynamics simulations. The gas and water permeabilities

of these nanotube-based membranes are orders of magnitude higher than those of commercial polycarbonate membranes, despite having an order of magnitude smaller pore sizes. These properties should enable more energy-efficient nanoscale filtration, as well as fundamental studies of mass transport in confined environments.

*The authors acknowledge U.S. Department of Energy for the auspieces under Contract No. W-7405-Eng-48 with the funding from the LDRD program in Lawrence Livermore National Laboratory, University of California.

**10:24**

**Y18 13 STM Investigation of Functionalized Carbon Nanotube Self-Assembly on Gold** JUN ZHANG, *Rice University, Department of Electrical and Computer Engineering* LEI ZHANG, *Rice Univeresity, Department of Chemistry* VALERY KHABASHESKU, *Rice Univeresity, Department of Chemistry* ANDREW BARRON, *Rice Univeresity, Department of Chemistry* KEVIN KELLY, *Rice University, Department of Electrical and Computer Engineering* Self-assembly has proven a powerful technique for patterning and building devices at the nanometer level. Scanning tunneling microscopy (STM) is the ideal tool for probing the chemistry and physics of these types of nanostructures. Building upon on our previous carbon nanotube research, we have investigated thiol- and thiophene-functionalized nanotubes. The motivation is to use these functional groups as a means to self-assemble tubes on surfaces by exploiting the well-established Au-S chemistry. Thiol and thiophene substituted nanotubes were assembled on bare gold surfaces as well as inserted into hexanethiol self-assembled monolayers and imaged by STM. The thiol and thiophene functional groups work as anchors, strongly binding the SWNTs to the gold. Additionally, we have measured the size and spatial distribution of the functional groups along the nanotube sidewalls.

## SESSION Y19: FOCUS SESSION: NOVEL FERROMAGNETIC SEMICONDUCTORS I

**Friday Morning, 17 March 2006**
**316, Baltimore Convention Center at 8:00**
**Chris Palmstrom, University of Minnesota, presiding**

***Contributed Papers***

**8:00**

**Y19 1 Mn dopant distribution and magnetic ordering in Mn-doped Ge ferromagnetic semiconductor** AN-PING LI, K. VON BENTHEM, M.F. CHISHOLM, K. VARGA, J. SHEN, *Oak Ridge National Laboratory* N. RAO, S.K. DIXIT, L.C. FELDMAN, *Vanderbilt University* H.H. WEITERING, *The University of Tennessee* We report the spatial distribution of Mn dopant atoms in germanium, grown with molecular-beam epitaxy. Cross-sectional transmission electron microscopy shows the stripe-shaped nanostructures with 2 nm in diameter, which arise from the chemical phase separation of the Mn dopants. Electron energy loss spectroscopy and ion-channeling spectroscopy indicate that these nano-stripes have $\sim$ 5 times higher Mn concentration than in the dilute doped Ge host. Only about 20% of total Mn atoms are incorporated in Ge lattice sites. Ferromagnetism in the doped Ge is characterized by two different ordering temperatures. A critical temperature $T_C$* is obtained as ferromagnetic spin clusters form, and a second transition occurs at much lower temperature itTc at the onset of global ferromagnetic ordering. Both transition temperatures can be enhanced significantly by an appropriate post-annealing process. The Mn aggregated clusters provide seeds of magnetic spin clusters, these spin clusters expand in size with lowering temperature and percolate eventually to form infinite magnetic clusters at low temperature. [1] A. P. Li, et al., Appl. Phys. Lett. **86**, 152507 (2005). [2] A. P. Li, et al., Phys. Rev. B 72, 195205 (2005).

**8:12**

**Y19 2 Epitaxial Growth and Properties of Fe and Co Co-doped Ge (100) Magnetic Semiconductor Films** LIANG HE, BRIAN COLLINS, FRANK TSUI, *University of North Carolina* YUNCHENG ZHONG, STEFAN VOGT, YONG CHU, *Advanced Photon Source* Structural, magnetic and electronic properties of Fe and Co co-doped Ge (100) epitaxial films, grown by combinatorial molecular beam epitaxy techniques, have been studied systematically using diffraction, magnetometry, magnetotransport techniques. These experiments reveal that this epitaxial ternary system can be grown coherently on Ge (100) substrates for total doping concentrations of the transition metal dopants as high as 14 at. %, where high quality p-type magnetic semiconductor films have been synthesized with Curie temperature as high as 270 K. Above this concentration rough disordered growth occurs, which is characterized by a large number of stacking faults along the $< 111 >$ directions; no phase separation has been detected for doping concentrations as high as 20 at. %. The observed magnetotransport properties exhibit large anomalous Hall coefficients and large magnetoresistance (MR) with MR ratios $> 100$. They also indicate the presence of an acceptor level at $\sim$ 70 meV above the valence band with the resulting hole concentrations that can be controlled up to $10^{19}$ $cm^{-3}$by the doping concentrations. Ferromagnetic ordering, specifically the Curie temperature is shown to depend on the carrier concentration.

**8:24**

**Y19 3 Optimal doping control of magnetic semiconductors** CHANGGAN ZENG, ZHENYU ZHANG, KLAUS VAN BENTHEM, MATTHEW CHISHOLM, HANNO WEITERING, Dilute magnetic semiconductors (DMS) with high ferromagnetic ordering temperatures ($T_C$)have vast potential for advancing spin-based electronics or ''spintronics.'' To date, achieving high-$T_C$ DMS typically required doping levels of order 5%. Such high doping levels inevitably compromise the structural homogeneity and carrier mobility of the DMS. Here, we establish ''itsubsurfactant epitaxy'' as a novel kinetic pathway for synthesizing Mn-doped germanium with $T_C$ much higher than room temperature, at dramatically reduced doping levels. This is accomplished by optimal control of the diffusion kinetics of the dopant atoms near the growth front in two separate deposition steps. The first involves a submonolayer dose of Mn on Ge(100) at low temperature, which populates subsurface interstitial sites with Mn while suppressing lateral Mn diffusion and clustering. The second step involves epitaxial growth of Ge at elevated temperature, taking advantage of the strong floating ability of the interstitial Mn dopants towards the newly defined subsurface sites at the growth front. Most remarkably, the Mn dopants trapped inside the film are uniformly distributed at substitutional sites, and the resulting film exhibits ferromagnetism above 400 K at the nominal doping level of only 0.2%.

*Invited Papers*

**8:36**
**Y19 4 Room-temperature ferromagnetism in (Zn,Cr)Te.**
HIDEKAZU SAITO, *Nanoelectronics Research Institute, National Institute of Advanced Industrial Science and Technology*

Ferromagnetic diluted magnetic semiconductors (DMSs) are the key material to developing semiconductor spintronic devices. One of the most characteristics physical phenomena in DMS is a strong interaction between itsp-carriers and localized *d*-spins (itsp-*d* exchange interaction) [1]. Confirmation of this interaction is essential to prove a synthesis of real DMS, and can be done directly by the magneto-optical studies such as a magnetic circular dichroism (MCD) measurement [2]. Here, we report room-temperature (RT) ferromagnetism with the itsp-*d* exchange interaction in $Zn_{1-x}Cr_xTe$ (x=0.20) [3]. $Zn_{1-x}Cr_xTe$ films with $x \leqslant 0.20$ were grown on GaAs (001) substrates by a molecular beam epitaxy method. No sign of a secondary phase was detected in any films by the reflection high-energy electron and X-ray diffractions. MCD spectra were measured in a transmission mode. Magnetization ($M$) measurements were carried out using a SQUID. The $M - H$curves of $Zn_{1-x}Cr_xTe$ (x=0.20) showed a ferromagnetic behavior up to about RT. Curie temperature $T_C$ was estimated to be $300 \pm 10$ K by the Arrott plot analysis. A strong enhancement of the MCD signal at the optical transition energies of critical points of host ZnTe was observed in $Zn_{1-x}Cr_xTe$, indicating a strong itsp-*d* exchange interaction. The MCD spectra of $Zn_{1-x}Cr_xTe$ at any magnetic field could be superposed upon a single spectrum, indicating that the observed MCD signals come from a single material, that is, $Zn_{1-x}Cr_xTe$. The magnetic field dependence of MCD intensity showed the ferromagnetic feature, which coincides with the $M - H$ curves measured using a SQUID. Furthermore, the MCD data showed the same $T_C$ as that obtained from magnetization data. These results indicate that $Zn_{1-x}Cr_xTe$ (x=0.20) is an intrinsic DMS with RT ferromagnetism. References [1] J. K. Furdyna, J. Appl. Phys. **64**, R29 (1988). [2] K. Ando, in Magneto-Optics, Springer Series in Solid-State Science, edited by S. Sugano and N. Kojima (Springer, Berlin, 2000), Vol.128, p. 211. [3] H. Saito, V. Zayets, S. Yamagata, and K. Ando, Phys. Rev. Lett., **90** 207202 (2003).

*Contributed Papers*

**9:12**
**Y19 5 Room-Temperature Femtosecond Faraday Effect in Cd-MnTe Single Crystals** D. WANG, R. SOBOLEWSKI, *University of Rochester, Rochester, NY 14627* M. MIKULICS, *Technical University Carolo-Wilhelmina, D-38106 Braunschweig, and Research Center Juelich, D-52425 Juelich, Germany* A. MYCIELSKI, *Polish Academy of Sciences, PL-02668 Warszawa, Poland* We report the subpicosecond Faraday effect, measured in high quality $Cd_{1-x}Mn_xTe$ ($x = 0.12$ and $x = 0.09$) single crystals at room temperature. Using a femtosecond pump-probe technique, we were able to generate sub-picosecond current pulses by illuminating a free-standing LT-GaAs photoswitch, couple those pulses to the CdMnTe probe crystal using a coplanar transmission line, and, finally, optically sample the temporal evolution of the resulting magnetic transients with subpicosecond resolution and the excellent signal-to-noise ratio. The ultrafast (below 600 fs) Faraday rotation, responsible for the observed magneto-optical effect, has been attributed to the ultrafast spin dynamics of holes in our p-type CdMnTe crystals. The observed femtosecond Faraday effect can be the basis for a development of a magneto-optical sampling system for ultrafast, time-resolved characterization of current transients in novel electronic and spintronic devices.

**9:24**
**Y19 6 Spin-Polarization of a 2DEG in $Cd_{1-x}Mn_xTe$ Quantum Wells** C. AKU-LEH,*F. PEREZ, B. JUSSERAND, *INSP, UMR 7588, CNRS/Paris VI et VII, France* D. RICHARDS, *Dept. of Physics, King's College London, UK* G. KARCZEWSKI, *Polish Academy of Sciences, Warsaw, Poland* Low energy excitations of a spin-polarized electron gas embedded in $Cd_{1-x}Mn_xTe$ quantum wells are studied by magneto-resonant Raman scattering and magneto-photoluminescence at superfluid helium temperature in the Voigt geometry. From Raman, we measured the one electron spin flip energy as a function of the bare Zeeman splitting originating from exchange interaction between *s* electrons and localized Mn d electrons. The ratio between the spin flip energy and the bare Zeeman splitting shows a strong dependence on the electron density. From photoluminescence measurements, we extract the spin flip energy and the spin-polarization rate. Comparison of the measured spin flip energy with our theoretical model [1] shows that the Raman values are in better agreement with the theory. The photoluminescence lineshape, however, gives estimation of the spin-polarization rate that is in good agreement with our model. [1] F. Perez et al. ACTA Physics Polonica A, **106**, 311 (2004).

*King's College London, UK

**9:36**
**Y19 7 Theory of the spin EPR shift and application to $Pb_{1-x}Mn_xTe$** PRASANTA MISRA, *University of Houston* R.K. DAS, *Gopalpur College, India* GOURI TRIPATHI, *Berhampur University, India* We consider a system with a periodic potential, spin-orbit interaction, conduction electron-local moment interaction and an applied magnetic field. We derive a theory for the spin-contribution to the electron-paramagnetic resonance shift ($P_s$) by considering an effective equation of motion of the Green's function in a representation defined by the periodic part of the Bloch function. The spin-EPR shift is expressed as a function of the matrix elements of the momentum, Pauli spin-operators, and conduction electron-local moment interactions. We apply the theory to calculate $P_s$ at $Mn^{2+}$ ion in the diluted magnetic semiconductor $Pb_{1-x}Mn_xTe$, as a function of the carrier concentration. Contributions from band-edge interactions as well as from far bands are included and their relative strengths are analyzed. $P_s$ is found to be anisotropic arising mainly due to spin-orbit interactions. Our results of $P_s$ for two typical hole densities agree fairly well with the recent experimental results for p-$Pb_{1-x}Mn_xTe$.

**9:48**

**Y19 8 Density functional study of manganese doped bulk silicon*** BHAGAWAN SAHU, *Microelectronics Research Center, University of Texas at Austin, Austin, TX 78758* LEONARD KLEINMAN, *Department of Physics, University of Texas at Austin, Austin, TX 78712* SANJAY BANERJEE, *Microelectronics Research Center, University of Texas at Austin, Austin, TX 78758* Using a 250 atom Si supercell with two manganese impurities at the substitutional and tetrahedral interstitial positions, we find, using the density functional projector-augmented wave method, that the ferromagnetic arrangement of manganese atoms at the tetrahedral interstitial position is energetically more stable compared to that at the substitutional position. We find a half-metallic density of states (integer spin magnetic moment over the supercell) for both the interstitial and substitutional manganese. However, the total energy difference (or magnetic energy difference) between interstitial manganese in the ferro and anti-ferro spin-alignments are not large enough to conclude whether ferromagnetic or antiferro-magnetic stability is preferred in the pure Si samples doped with manganese.

*Texas Advanced Technology program and Welch Foundation

**10:00**

**Y19 9 Static and dynamic magnetic response in Mn-doped InP diluted magnetic semiconductor (DMS) nanoparticles** H. SRIKANTH, P. PODDAR, S. SRINATH, *Department of Physics, University of South Florida, Tampa, FL* Y. SAHOO, P.N. PRASAD, *IPLB, University at Buffalo, Buffalo, NY* Soft chemical synthesis of nanostructured diluted magnetic semiconductor (DMS) materials is promising for achieving single phase, ferromagnetic materials. We report the first observation of ferromagnetic ordering at 25K in Mn-doped InP nanoparticles of average size 3 nm. A hot colloidal method without any external surfactant was used to synthesize the nanoparticles. Structural and elemental characterizations established the occurrence of the zinc-blende phase of the DMS without any impurity phases. DC, AC and RF susceptibility measurements were done over a wide range in temperature and magnetic fields to probe the static and dynamic magnetic response. The samples showed a ferromagnetic transition at 25K and frozen spin state below 15K. Transverse susceptibility experiments done using a resonant radio-frequency method revealed a strong temperature-dependent effective anisotropy. Frequency dependence observed in the AC susceptibility was reminiscent of spin-glass characteristics.

## SESSION Y20: FOCUS SESSION: RUDDLESDEN-POPPER PHASE MANGANITES

**Friday Morning, 17 March 2006**
**317, Baltimore Convention Center at 8:00**
**Jeff Lynn, National Institute of Standards and Technology, presiding**

*Contributed Papers*

**8:00**

**Y20 1 Nodal quasiparticle in pseudogapped colossal magnetoresistive manganites** N. MANNELLA, W. L. YANG, X. J. ZHOU, K. TANAKA, H. ZHENG, J. F. MITCHELL, J. ZAANEN, T. P. DEVEREAUX, N. NAGAOSA, Z. HUSSAIN, Z. X. SHEN, In this talk, the result of a recent angle-resolved photoemission spectroscopy (ARPES) investigation which allowed elucidating the controversial nature of the ferromagnetic metallic groundstate in the prototypical colossal magnetoresistive manganite bilayer compound $La_{1.2}Sr_{1.8}Mn_2O_7$ will be discussed [1]. The distribution of spectral weight in momentum space exhibits a nodal–antinodal dichotomous character. Quasiparticle excitations have been detected for the first time along the nodal direction (i.e. diagonal), and they are found to determine the metallic transport properties of this compound. The weight of the quasiparticle peak diminishes rapidly while crossing over to the antinodal (i.e. parallel to the Mn–O bonds) parallel sections of the Fermi surface, with the spectra strongly resembling those found in heavily underdoped cuprates high temperature superconductors (HTSC) such as $Ca_{2-x}Na_xCuO_2Cl_2$ [2]. This dichotomy between the electronic excitations along the nodal and antinodal directions in momentum space was so far considered a characteristic unique feature of the copper oxide HTSC. These findings therefore cast doubt on the assumption that the pseudogap state in the cuprate HTSC and the nodal-antinodal dichotomy are hallmarks of the superconductivity state. [1] N. Mannella et al., Nature 438, 474 (2005) [2] K. M Shen et al., Science 307, 901 (2005).

**8:12**

**Y20 2 Near-Fermi electronic structure of $La_{2-2x}Sr_{1+2x}Mn_2O_7$ revealed by ARPES** Z. SUN, J. F. DOUGLAS, D. S. DESSAU, *University of Colorado, Boulder, CO 80309* Y. -D. CHUANG, A. V. FEDOROV, *Lawrence Berkeley National Lab, Berkeley, CA 94720* H. LIN, M. LINDROOS, S. SAHRAKORPI, R. S. MARKIEWICZ, A. BANSIL, *Northeastern University, Boston, MA 02115* H. ZHENG, J. F. MITCHELL, *Argonne National Laboratory, Argonne, IL 60439* T. KIMURA, Y. TOKURA, *University of Tokyo, Tokyo, Japan 113-8656* Angle-resolved photoemission experiments were performed on the bi-layer manganite $La_{2-2x}Sr_{1+2x}Mn_2O_7$ as a function of doping and temperature. High resolution and sensitivity allows us to observe the fine details including bi-layer splitting, dispersion kinks, electron-phonon coupling, and pseudogaps. We discuss new insights into the underlying physics of these compounds, as well as a comparison of some of these properties to what is observed in the cuprates.

**8:24**

**Y20 3 First-order metal-insulator transitions in manganites: Are they universal?*** KENNETH GRAY, QING'AN LI, STINE KLAUSEN, HONG ZHENG, STEPHAN ROSENKRANZ, RAY OSBORN, JOHN MITCHELL, *Argonne National Laboratory* Conductivity data for $La_{2-2x}Sr_{1+2x}Mn_2O_7$ ($x=0.6$) show a first-order transition from an orbital/charge-ordered insulator to a metal as the temperature falls below $\sim$ 160 K. The change in conductivity of $\sim$ 10000 is 100 times larger than that seen previously in any single-phase manganite in zero field. The metallic low-temperature state is similar to that found at $x=0.58$, but $x=0.58$ shows no evidence of orbital/charge order. This result, and further analysis, supports a conclusion that strongly coupled magnetic/conductive transitions are universally of first order.

*This research was supported by the U.S. Department of Energy, Office of Science, under Contract No. W-31-109-Eng-38.

*Invited Papers*

**8:36**
**Y20 4 Topotactic Reduction of Complex Manganese Oxides.**
MICHAEL HAYWARD, *University of Oxford*

Mixed-valent manganese (III/IV) perovskite and Ruddlesden-Popper oxides have received considerable attention due to the observation of strong coupling between spin, charge and lattice degrees of freedom in these materials. Little attention however has been focused on the analogous Mn (II/III) oxides due to the difficulty of their synthesis. The topotactic reduction of the Mn(III/IV) perovskites $La_{1-x}Sr_xMnO_3$ ($0.2 < x < 0.4$) results in the formation of the corresponding $La_{1-x}Sr_xMnO_{2.5}$ brownmillerite phases. The $x = 0.25$ and 0.2 phases adopt structures with an unusual ordered L-R-L-R alternation of twisted chains of Mn(II) tetrahedra which is accompanied by Mn(II)/(III) charge ordering within the remaining $MnO_6$ octahedral layers. In contrast the $x = 0.4$ phase adopts a structure in which the twisted chains of tetrahedra are disordered. Temperature dependant magnetization data collected from similarly reduced $n = 2$ Ruddlesden-Popper phases of composition $YSr_2Mn_2O_{7-x}$ ($0 < x < 1.5$) indicate strong antiferromagnetic coupling interactions in all samples. Long range magnetic order is suppressed by structural and/or charge disorder in all samples except $YSr_2Mn_2O_{5.5}$ which adopts a G-type antiferromagnetic ordering scheme.

*Contributed Papers*

**9:12**
**Y20 5 Tunneling evidence for weak localization in layered manganites*** DANIEL MAZUR, *Illinois Institute of Technology* KEN E. GRAY, *Argonne National Laboratory* JOHN F. ZASADZINSKI, *Illinois Institute of Technology* HONG ZHENG, JOHN MITCHELL, *Argonne National Laboratory* Our point contact tunneling experiments on $La_{1.28}Sr_{1.72}Mn_2O_7$ (bi-layered LSMO $x=0.36$) at low temperatures reveals a $\sqrt{V}$ low bias anomaly in the tunneling conductance. This anomally qualitatively matches the $\sqrt{E}$ predictions of the weak localization effect on the electronic DOS. The data could provide an important corroboration of the weak localization hypothesis, which was concluded previously from low-temperature conductivity and magnetoresistance data.

*Contributed by UofC under U.S. DoE contract no. W-31-109-ENG-38.

**9:24**
**Y20 6 Doping Dependence of Polaron Correlations in Bilayer Manganites*** RAYMOND OSBORN, STINE KLAUSEN, STEPHAN ROSENKRANZ, PETER CHUPAS, JOHN MITCHELL, *Materials Science Division, Argonne National Laboratory, Argonne, IL 60439* It is now well established that colossal magnetoresistance (CMR) in manganite compounds is strongly enhanced by competing interactions close to the magnetic phase transitions. In the paramagnetic phase of the bilayer manganites, diffuse x-ray scattering data has shown evidence of polaron correlations that grow with decreasing temperature and coexist with the critical magnetic fluctuations down to the ferromagnetic phase transition, before collapsing below $T_C$. These correlations, which have a length scale of about 20Å, are in the form of longitudinal Jahn-Teller stripes within the bilayers, characterized by an incommensurate wavevector. There have been proposals that these nanoscale correlations are evidence of an incipient charge density wave, whose wavevector corresponds to nesting features in the Fermi surface. We report new measurements of the doping dependence of these correlations that show that the wavevector increases from 0.26 at a hole doping of $x = 0.32$ to about 0.3 at $x = 0.46$, which is inconsistent with the anticipated change in the Fermi surface volume, and will discuss alternate models of the short-range order.

*This work was supported by the US Department of Energy, Office of Science, under contract no. W-31-109-ENG-38.

**9:36**
**Y20 7 Magneto-optical investigation of the field-induced transition in bilayer manganese oxide $(La_{0.4}Pr_{0.6})_{1.2}Sr_{1.8}Mn_2O_7$*** J. CAO, J.T. HARALDSEN, R.C. RAI, S. BROWN, J.L. MUSFELDT, *University of Tennessee* X. WEI, Y.J. WANG, *National High Magnetic Field Laboratory* M. APOSTU, R. SURYANARAYANAN, A. REVCOLEVSCHI, *Université Paris-Sud* We measured the magneto-optical response of PrLSMO in order to investigate the microscopic aspects of the magnetic field driven paramagnetic insulator to ferromagnetic metal transition. With applied magnetic field, optical weight transfers to lower energy and develops a clear signature of ferromagnetic domains. Mn-O stretching and bending modes soften through the phase transition as well, demonstrating precisely how the lattice is coupled to the transition. We also extract the H-T optical phase diagram and compare it with that from resistivity, magnetization, and magnetostriction to show that the lattice responds more slowly than charge and spin at low temperature. Color rendering allows visualization of the thermochromic and magnetochromic effect.

*This work is supported by the U. S. Department of Energy.

**9:48**
**Y20 8 Is CE-type orbital order the true ground state for $LaSr_2Mn_2O_7$?*** HELMUT CLAUS, QING'AN LI, HONG ZHENG, KENNETH GRAY, STINE KAUSEN, STEPHAN ROSENKRANZ, RAY OSBORN, JOHN MITCHELL, *Argonne National Laboratory* Previous scattering and conductivity data for $La_{2-2x}Sr_{1+2x}Mn_2O_7$ ($x=0.5$) indicate the CE phase, predicted by Goodenough 50 years ago, is only stable between $\sim$ 100 and 200 K and below $\sim$ 100 K an A-type antiferromagnet is the ground state. We present scattering, magnetization and transport evidence that the CE phase is the ground state, but only in a very narrow composition range, presumably at exactly $x=0.5$. The vitally important roles of crystal homogeneity and methodology of transport measurements will be demonstrated for this conclusion as well as for the field of layered manganites in general.

*This research was supported by the U.S. Department of Energy, Office of Science, under Contract No. W-31-109-Eng-38.

**10:00**

**Y20 9 Polarons and polaron correlations in 40% doped bilayer manganite.*** S. N. KLAUSEN, S. ROSENKRANZ, R. OSBORN, P. J. CHUPAS, J. F. MITCHELL, *Materials Science Division, Argonne National Laboratory, Argonne, IL 606439* Among the compounds exhibiting colossal magnetoresistance, the bilayer manganites, $La_{2-2x}Sr_{1+2x}Mn_2O_7$, where $x$ is the hole doping in the $MnO_2$ layers, are advantageous to study because the reduced dimensionality strongly enhances the spin and charge fluctuations. For the intermediate doping regime ($32\% \leqslant x \leqslant 42\%$), the magnetoresistance is strongly enhanced near the combined metal-insulator and ferromagnetic transition. Here, we report on our detailed x-ray scattering investigation of the diffuse scattering associated with lattice distortions around localized charges (polarons) as well as short-ranged polaron correlations present in the paramagnetic phase of the $x = 40\%$ doped compound, both collapsing at $T_C = 112$ K. We have studied in detail the temperature dependence to high temperatures ($T = 50$ K - 500 K) and are able to directly extract a polaron activation energy from the data.

*This work was supported by the US Department of Energy, Office of Science, under contract no. W-31-109-ENG-38.

**10:12**

**Y20 10 A Polaronic Picture of Bilayer Colossal Magnetoresistive Manganites in Angle Resolved Photoemission Spectroscopy** C. JOZWIAK, G.-H. GWEON, *Department of Physics, UC Berkeley* J. GRAFF, *Materials Science Division, LBNL* S.Y. ZHOU, *Department of Physics, UC Berkeley* H. ZHENG, J. F. MITCHELL, *Material Sciences Division, ANL* A. LANZARA, *Department of Physics, UC Berkeley and Material Sciences Division, LBNL* It is becoming generally recognized that the presence of a strong electron-lattice interaction, in the limit of polaronic coupling, is a common feature to transition metal oxides such as cuprate superconductors and colossal magnetoresistive manganites. Angle resolved photoemission spectroscopy (ARPES) is the ideal tool to address and gain insight on the polaronic nature of the electron-lattice interaction through a direct study of the ARPES single particle spectral function. Here we present a detailed momentum dependent study of the ARPES single particle spectral function in double layer manganites $La_{1.2}Sr_{1.8}Mn_2O_7$,and Bi2212 and LSCO cuprates. A direct comparison between the two classes of materials and the peculiar momentum dependence of the ARPES lineshapes, also known as nodal-antinodal dichotomy, will be discussed in terms of a polaronic picture.

**10:24**

**Y20 11 Order/Disorder Effects in Perovskite Manganites** B. DABROWSKI, *Argonne National Laboratory* S. KOLESNIK, *Dept. of Physics, Northern Illinois University* O. CHMAISSEM, *ANL* E.N. CASPI, *Nuclear Research Centre-Negev, Beer-Sheva, Israel* J. MAIS, *Dept. of Physics, Northern Illinois University* J.D. JORGENSEN, *ANL* Indirect magnetic interactions between transition metals in perovskites $ABO_3$ are commonly described in terms of superexchange and double-exchange interactions that depend on the bond angle B-O-B. By useing the tolerance factor parameterization procedure we have designed and obtained new substituted manganites with randomly-mixed and layer-ordered structures having identical chemical compositions. The order/disorder effects on magnetic properties have been investigated as a function of the bond angle disorder for both the A- and Mn-sites. By comparing ordered (containing planes of the $RO_2$ and $BaO_2$) and disordered ferromagnetic compounds $La_{1-x}Ba_{1+x}Mn_2O_6$, we have demonstrated that by decreasing local structural and charge disorder, an increase of $T_c$ of over 100 K can be achieved. Similar effects have been demonstrated for $Sr_2MnGaO_{6-d}$ where transitions from spin-glass seen for the disordered compound to antiferromagnetic behavior seen for the ordered material (containing planes of the $MnO_2$ and $GaO_{2-d}$), have been observed. Supported by NSF (DMR-0302617) and U.S. Department of Energy, BES – Materials Sciences (W-31-109-ENG-38)

## SESSION Y22: FOCUS SESSION: COUPLED THIN-FILM STRUCTURES FOR MAGNETIC RECORDING

**Friday Morning, 17 March 2006**
**319, Baltimore Convention Center at 8:00**
**Axel Hoffmann, Argonne National Laboratory, presiding**

**8:00**

**Y22 1 Interface magnetocrystalline anisotropy induced by charge transfer on Pd/Ni/Cu films** J.-S. LEE, *eSSC and Department of Physics, Pohang University of Science and Technology, Pohang 790-784, Korea* J.-Y. KIM, *Pohang Accelerator Laboratory, Pohang University of Science and Technology, Pohang 790-784, Korea* B.H. SEUNG, J.-H. PARK, K.-B. LEE, *eSSC and Department of Physics, Pohang University of Science and Technology, Pohang 790-784, Korea* POSTECH TEAM, PLS COLLABORATION, We investigated microscopic mechanisms of interface magnetocrystalline anisotropy in epitaxial Pd/Ni/Cu films using x-ray magnetic circular dichroism and x-ray absorption spectroscopy at Ni $L_{2;3}$ edge and Pd $M_{2;3}$ edge. We found that a considerably charge transfer (from $4d$ to $3d$) of Pd and Ni dominantly occurs near the interface of Pd/Ni. The interfacial charge transfer result is enhanced the orbital magnetic moment, and leads to the interface magnetocrystalline anisotropy induced by about 19.1%.

**8:12**

**Y22 2 Magnetic properties of $L1_0$ FePtCu:Au films for high-density perpendicular recording*** M.L. YAN, Y.F. XU, Y.C. SUI, R. SKOMSKI, D.J. SELLMYER, *University of Nebraska* We present fabrication methods for tunable magnetic properties of non-epitaxially grown, nanocomposite $L1_0$ FePtCu:Au films including a coupled FePt continuous gradient layer (CGL) for the application of high-density perpendicular recording media. The films are deposited with the structure FePt(x)/[FePtCuAu] on a thermally oxidized Si wafer and subsequently annealed. [FePtCuAu] is a nanocomposite layer (NL) with a fixed layer thickness, 12nm, and FePt(x) is the continuous gradient layer, with the thickness x varying from 0 to 10 nm, which is coupled to the NL. X-ray diffraction patterns show an enhanced degree of orientation for FePtCu:Au films with an increase of the CGL thickness. SQUID measurements show that magnetic properties of the films are tunable by changing the CGL layer thickness. When the CGL thickness is 10 nm, the magnetic properties of the film are $M_s \cong 600$ emu/cc, slope $\alpha$ ($= 4\pi d\mathrm{M}/d\mathrm{H}$) at the coercivity $\cong 1$ and $H_c \cong 6$ kOe. These results are discussed in terms of exchange-coupled layers with differing properties, and demonstrate the

possibility of fabricating FePt-based nanocomposite media with properties suitable for high-density perpendicular recording.

*Research supported by DOE, NSF-MRSEC, INSIC, NRI and CMRA

**8:24**

**Y22 3 Parallel and anti-parallel coupling of CoPt/Ru/CoFe trilayers investigated with magnetometry and ferromagnetic resonance** MICHAEL PECHAN, CHENGTAO YU, *Miami University, Oxford, OH* STEFAN MAAT, *Hitachi Global Storage Technologies, San Jose, CA* Due to their low resistivity ( $\sim$ 30 $\mu\Omega$-cm) and critical thickness $CoPt_x$ ($16 \leqslant x \leqslant 24$ at %) thin films are interesting pinning materials for current perpendicular to the plane (CPP) spin-valve sensors [1]. These properties help to minimize serial resistance and thus enhance the magnetoresistance. 4 nm thick CoPt films deposited on Cr were shown to exhibit coercivities up to 1.5 kOe. One requirement for using CoPt as a pinned layer in a CPP spin-valve is that anti-parallel (AP) coupling to a reference layer can be demonstrated to minimize magnetostatic coupling to the free layer to keep the free layer magnetically soft. Here we investigate the parallel (P) and AP coupling of $CoPt_{18}(50)/Ru(x)/CoFe_{16}(36)$ trilayers with $0 \leqslant x \leqslant 2.1$ nm with magnetometry and ferromagnetic resonance (FMR). We found the coupling to be oscillatory with peaks at x = 0.7 nm (AP) 1.4 nm (P) and 2.0 nm (AP), respectively. These peaks were also observed using 35 GHz FMR in saturation. From the FMR technique the coupling strengths were determined to be 1150 (AP), 250 (P) and 660 (AP) Oe respectively. Variable temperature magnetometry reveals the exchange, coercivity and saturation fields increase monotonically with decreasing temperature. Supported at Miami by U.S. Dept. of Energy [1] S. Maat et al. J. Appl. Phys. Dec. 1 issue (2005)

**8:36**

**Y22 4 X-ray reflectivity of ruthenium nano-oxide layer in a CoFe-Ru-CoFe trilayer system** SAEID ASGHARI ZADEH, MARK SUTTON, ZAVEN ALTONIAN, *Physics Department and Centre for the Physics of Materials, McGill University, 3600 University street, Montreal, Quebec* MING MAO, CHIH-LING LEE, *Veeco Instruments Fremont, Fremont, CA 94538* A grazing incidence X-ray reflectivity technique is used to determine electron density profile(EDP) as a function of depth in CoFe-Ru-CoFe and CoFe-Ru nano oxide layer(NOL)-CoFe trilayers. Four trilayers with ruthenium thicknesses of 8,8.5 and 9 Å and one with Ru8.5 NOL, prepared by a dc planetary sputtering system, were investigated. For all samples, EDP shows a central peak which is related to the Ru layer. Natural oxidation in all samples introduces a graded EDP of the top CoFe layer that decreases gradually to zero. The large surface resistivity of Ru8.5 Å NOL compared to Ru 8.5Å can be related to the remarkable difference between their EDP.

**8:48**

**Y22 5 Systematic Investigation of Exchange Coupled $Fe_xCo_{1-x}$/CoPt Magnetic Bilayers Using the High-Throughput Approach** H. OGUCHI, *Univ. of MD* M. YU, *Univ. of New Orleans* J. HATTRICK-SIMPERS, *Univ. of MD* A. ZAMBANO, I. TAKEUCHI, *Univ. of MD* S. LOFLAND, *Rowan Univ.* D. JOSELL, L.A. BENDERSKY, *NIST* J.P. LI, *Univ. of Texas at Arlington* Exchange-coupled magnetic nanocomposites are being pursued for future permanent magnets with high energy products. To gain better understanding of the exchange coupling behavior between the soft and hard magnetic layers, we are using the high-throughput approach. $Fe_xCo_{1-x}$/CoPt magnetic bilayers are grown on MgO(110) substrates using the combinatorial electron-beam deposition. CoPt hard magnetic layer is epitaxially grown at 600° C. The $Fe_xCo_{1-x}$ soft layer is deposited at 200° C. To study the effect of changing soft phase parameters on exchange coupling, we have fabricated libraries where in one direction the composition of the soft-phase is continuously changing from Fe to Co and the thickness of the soft layer is changing in the other direction. The magnetic hysteresis loop for each soft layer composition and the thickness is measured using a magneto-optical Kerr effect system. From systematically changing hysteresis loops, we calculate the exchange field ($H_{ex}$) as a function of anisotropy and magnetization of the soft phase. Observed dependence of $H_{ex}$ on soft phase parameters are directly compared against theoretical models of the exchange mechanism. ONR N00014-05-1-0497, NSF DMR -0520471.

**9:00**

**Y22 6 Molecular Beam Epitaxial Growth and Magnetic properties of Fe(001)/$Mn_3N_2$(010) Thin Films** RONG YANG, *Ohio University* ERDONG LU, *Ohio University* MUHAMMAD HAIDER, *Ohio University* ARTHUR SMITH, *Ohio University* DIANA LEITNER, *Oberlin College* YUMI IJIRI, *Oberlin College* Exchange bias systems have attracted considerable attention due to their importance to magnetic sensor technology. Considering that $T_{Neel}$ of $Mn_3N_2$ ($T_N$=652°C) is less than $T_{Curie}$ of Fe ($T_C$=770 °C), and also since Mn-Mn spacing of $Mn_3N_2$(010) ( $\simeq$ 2.86 angstrom) is closely matched to the Fe-Fe spacing of Fe(001)(2.87 angstrom), it is therefore of great interest to explore Fe epitaxy on Mn3N2(010). We have grown thin Fe films on $Mn_3N_2$(010)/MgO(001) using molecular beam epitaxy at 150°C, and then following by annealing at 450°C for 10 minutes. The growth is monitored by reflection high-energy electron diffraction, which shows c(2x2) reconstructed surface for the as-grown sample, and a change to (1x1) after annealing. Annealing leads to a smoothening of the film surface.The epitaxial orientation have been determined to be Fe [100] (001)// Mn3N2[101] (010)// MgO[110](001). Annealed samples are transferred to the in situ analysis chamber for scanning tunneling microscopy studies. Images show smooth terraces and atomic-height steps. Vibrating sample magnetometry measurements found in-plane anisotropy and hysteresis loop shifting after field cooling. The work is supported by NSF9983816 and 0304314.

***Invited Papers***

**9:12**

**Y22 7 Novel materials and media concepts for thermally assisted magnetic recording.**
JAN-ULRICH THIELE, *Hitachi Global Storage Technologies*

Magnetic media using materials with high uniaxial magneto-crystalline anisotropy, $K_U$, combined with a thermal assist to overcome thermal stability and write field limitations are widely seen as a potential extension of current magnetic recording technology. Here we present an overview of recent work on adapting the thermo-magnetic properties of FePt-based high-$K_U$ materials for the requirements of such a recording system. In [1] we recently proposed a novel media

structure consisting of two exchange coupled films, a high anisotropy film like, e.g., FePt, and a FeRh film. At close to equiatomic compositions FeRh is an antiferromagnet at low temperatures. Interestingly, upon heating beyond a critical temperature, $T_{AF-FM}$, FeRh becomes ferromagnetic for temperatures $T_{AF-FM} < T < T_C$. This opens interesting possibilities for media applications for thermally assisted recording: at a storage temperature, $T_S < T_{AF-FM}$, the magnetic information is stored in the high-$K_U$ FePt layer. For writing at increased temperature, $T_{AF-FM} < T_W < T_{C-FeRh}$, the FeRh becomes ferromagnetic, effectively lowering $K_U$ and increasing the total magnetic moment of the bilayer, thus lowering its coercivity via an exchange spring mechanism and helping magnetization reversal at temperatures well below $T_C$ of the FePt layer. A related area of great interest is the magnetization dynamics upon rapid heating and cooling of FeRh films using itfs-laser pump-probe techniques. First results indicate that the AF-FM transition can be driven on a timescale below 1 itps [2], yielding interesting insight into the interaction of the spin, electron and lattice subsystems. [1] J.-U. Thiele, S. Maat, E. E. Fullerton, Appl. Phys. Lett. **82** (2003) p2859-2861 [2] J.-U. Thiele, M. Buess, C. H. Back, Appl. Phys. Lett. **85** (2004) p2857-2859 and G. Ju et al., Phys. Rev. Lett. **93** (2004) 197403.

***Contributed Papers***

**9:48**

**Y22 8 Uncompensated Fe moments in positively exchange biased Ni/$FeF_2$ bilayers** ELKE ARENHOLZ, *LBNL* KAI LIU, *University of California, Davis, CA* ZHI-PAN LI, I.K. SCHULLER, *University of California San Diego, La Jolla, CA* The magnetization reversal of uncompensated Fe moments in exchange biased Ni/$FeF_2$ bilayers was determined using soft x-ray magnetic circular dichroism. Hysteresis loops resulting from Fe moments oriented parallel and perpendicular to the external field are almost identical to those of the ferromagnetic Ni layer. However, a small vertical loop shift indicates that some Fe moments are pinned antiparallel to small cooling fields leading to negative exchange bias but parallel to large cooling fields resulting in positive exchange bias. For intermediate cooling fields, loop bifurcation is observed. This is attributed to a coexistence of domains with uncompensated Fe moments pinned parallel and antiparallel to the cooling field. Furthermore, x-ray magnetic linear dichroism was employed to characterize the spin structure of the antiferromagnetically ordered $FeF_2$ but no indication for the formation of a parallel antiferromagnetic domain wall upon magnetization reversal in the ferromagnetic layer was found. The ALS at LBNL and work at UCSD are supported by DOE and work at UCD by ACS-PRF and Sloan Foundation.

**10:00**

**Y22 9 On the method of exchange bias measurement** ONDREJ HOVORKA (*), ANDREAS BERGER, *San Jose Research Center, Hitachi Global Storage Technologies, San Jose, CA 95120* GARY FRIEDMAN (*), *Electrical and Computer Engineering Department, Drexel University, Philadelphia, PA 19104* Exchange bias is the observation of a hysteresis loop shift in ferromagnetic-antiferromagnetic compound structures [1]. Recently, such a shift was also observed in all ferromagnetic bilayer systems [2]. Conventionally, exchange bias fields are measured by determining the average coercive field of a hysteresis loop (two-point method). However, hysteresis loops in exchange biased systems can also change in shape and even exhibit asymmetrical reversal [3], which can affect the estimate of the exchange bias field significantly. A different method for measuring the exchange bias based on obtaining the ''center of mass'' for exchange biased hysteresis loops is proposed and analyzed in this work. The method is validated by numerical simulation, using a realistic model system composed of soft and hard ferromagnetic layers coupled antiferromagnetically. Our calculations allow us to determine the laterally averaged bias field $< Hbias >$ created by the hard layer grains. We find that $< Hbias >$ is in excellent quantitative agreement with the proposed ''center of mass'' measurement, but not with the conventional two-point method. [1] A. Berkowitz, K. Takano, J. Magn. Magn. Mater. 200,552 (1999) [2] A. Berger et. al., Appl. Phys. Lett. 85, 1571 (2004) [3] S. G. E. te Velthuis et. al., J. Appl. Phys. 87, 5046 (2001)

**10:12**

**Y22 10 Magnetic anisotropy in $CrO_2$ and $CrO_2/Cr_2O_3$ bilayer thin films** N.A. FREY, S. SRINATH, H. SRIKANTH, *Physics Department, University of South Florida, Tampa, FL 33620, USA* G. MIAO, A. GUPTA, *MINT Center, University of Alabama, Tuscaloosa, AL,35487, USA* We have investigated the effective magnetic anisotropy in CVD-grown epitaxial $CrO_2$ films and $Cr_2O_3/CrO_2$ bilayers using a resonant RF transverse susceptibility (TS) technique. These materials are of interest due to their high spin polarization and the potential for exhibiting interesting magnetoelectric (ME) effects. In $CrO_2$, the measured values for the room temperature anisotropy constant for the films scaled with the film thickness and the data is influenced by magnetoelastic contributions at low temperature. TS in $CrO_2/Cr_2O_3$ bilayers revealed features associated with both the ferromagnetic and antiferromagnetic phases. In addition, a considerable broadening of the anisotropy fields and large $K_{eff}$ values were observed depending on the amount of $Cr_2O_3$. These anomalously large $K_{eff}$ values observed with $Cr_2O_3$ content cannot be accounted for by the variable thickness of $CrO_2$alone and is indicative of intimate coupling between the two phases that has a significant effect on the magnetic properties.

## SESSION Y23: SINGLE MOLECULE MAGNETS
**Friday Morning, 17 March 2006**
**320, Baltimore Convention Center at 8:00**
**Mark Pederson, Naval Research Laboratory, presiding**

**8:00**

**Y23 1 Pulsed-Radiation-Induced Magnetization Relaxation in Single-Molecule Magnets** M. BAL, J. R. FRIEDMAN, *Dept. of Physics, Amherst College* W. CHEN, *Physics Dept., Stony Brook University* M.T. TUOMINEN, *Dept. of Physics, Univeristy of Massachusetts at Amherst* S. SHAH, E.M. RUMBERGER, D.N. HENDRICKSON, *Dept. of Chemistry and Biochemistry, UC San Diego* N. AVRAHAM, Y. MYASOEDOV, H. SHTRIKMAN, E. ZELDOV, *Dept. of Condensed Matter Physics, The Weizmann Institute of Science* Millimeter-wave radiation induces large dips in the magnetization of a single crystal of the $Fe_8$ single-molecule magnet (SMM) when the radiation is on resonance with transitions

between energy levels. In our recent studies, we pulsed the radiation with the goal of determining $T_1$, the lifetime of the first excited state. We found that during a 0.2-ms pulse of intense radiation the spin system and the lattice are driven out of thermal equilibrium. Experiments at shorter time scales, carried out with the use of an inductive thin-film pick-up loop, revealed a surprisingly long relaxation time for magnetization on the order of $\sim 10$ $\mu$s. A poor signal-to-noise (S/N) ratio required averaging of $\sim 4 \times 10^5$ individual traces to obtain acceptable data. Incorporating a superconducting interference device (SQUID) as a low-noise voltmeter into our experimental setup improves the S/N ratio, allowing us to explore the origin of the observed long relaxation time. The results of these experiments on $Fe_8$ as well as other SMMs will be presented.

**8:12**

**Y23 2 Control of quantum magnetic deflagration in Mn12 acetate.** ALBERTO HERNANDEZ-MINGUEZ, JOAN MANEL HERNANDEZ, FERRAN MACIA, ANTONIO GARCIA-SANTIAGO, JAVIER TEJADA, *Universitat de Barcelona* PAULO SANTOS, *Paul Drude Institut* EXPERIMENTAL MAGNETISM TEAM, SEMICONDUCTOR SPECTROSCOPY COLLABORATION, Magnetic avalanches in Mn12-ac involve spin tunneling through an energy barrier which is controlled by the applied magnetic field. The reversal proceeds through the propagation of a narrow magnetic reversal front at constant velocity through the crystal [1]. In this contribution, we demonstrate that the ignition of the deflagration can be controlled in a deterministic way using surface acoustic waves (SAWs). For that purpose, the Mn12 crystal was mounted on the surface of a piezoelectric LiNbO3 substrate containing an interdigital transducer (IDT) for the excitation of SAWs. In the super-paramagnetic regime (above 3 K), the Mn12 magnetization shows pronounced changes when the IDT is excited at its resonant frequencies, thus proving that the crystals can be used as very sensitive acoustic detectors. At low temperatures (below 3 K), both the ignition rate and the velocity of the deflagration front present peaks for the values of the magnetic fields that bring the spin levels on both sides of the tunneling barrier into resonance, thus demonstrating the occurrence of both quantum magnetic ignition and quantum magnetic deflagration [2]. [1] Y. Suzuki et. al., Phys. Rev. Lett. 95, 147201 (2005). [2] A. Hernández-Mínguez et. al., Phys. Rev. Lett. 95, 217205 (2005).

**8:24**

**Y23 3 Pressure-dependence of the zero-field splittings for the $Fe_8$ single-molecule magnet** S. TAKAHASHI, E. THOMPSON, S. HILL, *Physics, University of Florida* S. W. TOZER, *NHMFL, Florida State University* A. G. HARTER, N. S. DALAL, *Chemistry and Biochemistry and NHMFL, Florida State Univerisity* We present a study of the pressure-dependent electron paramagnetic resonance (EPR) spectrum for the $Fe_8$ single-molecule magnet (SMM). The biaxial $[Fe_8O_2(OH)_{12}(tacn)_6]Br_8 \cdot 9H_2O$ ($Fe_8$) SMM has recently been studied extensively because its low-temperature magnetization dynamics are dominated by quantum tunneling of its spin $S = 10$ magnetic moment through a sizeable anisotropy barrier. To date, chemical methods have usually been employed in order to control the magnetic quantum tunneling (MQT) behavior of a SMM, e.g. by varying the magnetic ions in the molecular core, or the ligand/solvent environment. The advantage of this approach is that many different SMMs can be realized in this way, with widely varying MQT behavior. However, controllable variation of MQT is difficult. As an alternative approach for manipulation of the MQT, we have recently studied the effect of physical pressure on the $Fe_8$ SMM. In this presentation, we show the pressure dependence of the zero-field splittings of $Fe_8$, as studied by an angle and pressure-dependent high-frequency EPR technique.

**8:36**

**Y23 4 Alignment of $Mn_{12}$-acetate in Suspension*** D. SEO, W. TEIZER, *Department of Physics, Texas A&M University, College Station, TX 77843-4242* The magnetization of $Mn_{12}$-acetate single molecule magnets has been studied in an oriented $Mn_{12}$-acetate suspension that, unlike in prior work [1, 2], exceeds the solution saturation. We observe magnetic properties of the frozen suspension similar to large oriented single crystals, specifically several sharp steps in the low temperature hysteresis loop, indicating alignment. The surface morphology of a film made from this suspension, which was studied by atomic force microscopy, indicates micron-size crystals are likely the main source of the magnetization signal. The greater the external magnetic field during alignment, the sharper the steps in the low temperature hysteresis loops. Experimental data showed that $\sim$ 5000 Oe was sufficient to orient the micro crystals in the organic solvent to a degree comparable to a single crystal. [1] D. M. Seo et al., J. Mag. Magn. Mater. in press (2005), doi:10.1016/j.jmmm.2005.06.005 [2] K. Kim et al., Appl. Phys. Lett. **85,** 3872 (2004).

*We thank the NSF (DMR-0315476) and the Robert A. Welch Foundation (A-1585) for financial support.

**8:48**

**Y23 5 V, C, and N soft x-ray absorption and MCD of molecular magnet $V[TCNE]_{x\sim2}$ films*** JEFF KORTRIGHT, *LBNL* R. SHIMA EDELSTEIN, D.M. LINCOLN, J.W. YOO, A.J. EPSTEIN, *The Ohio State University* CVD films of $V[TCNE]_{x\sim2}$ are magnetic room temperature and of interest as prototypes in functional organic magnetic systems. In addition to potential technological interest, fundamental questions regarding the electronic structure and spin distribution in $V[TCNE]_{x\sim2}$ films remain, and motivate these measurements of x-ray absorption (XAS) and magnetic circular dichroism (MCD) spectra at the vanadium L, carbon K, and nitrogen K edges. XAS spectra reveal strong multiplet splitting at the V edge and strong $\pi^*$ features at the C and N edges. The registry of these features at different edges indicates a distinct molecular orbital structure involving all constituents. That this molecular orbital structure supports magnetism is indicated by vanadium MCD spectrum and by the loss of specific XAS and MCD features for oxidized samples. Results are interpreted in the context of prior neutron scattering [1] and EXAFS [2] studies, multiplet calculations of V XAS and MCD, and established C and N XAS features. [1] A. Zheludev, et al., J. Am. Chem. Soc. 116, 7243 (1994). [2] D. Haskel, et al., Phys. Rev. B 70, 054422 (2004).

*Measurements were made at the ALS and work was supported by DOE (DE-AC03-76SF00098, DE-FG02-86ER45271, and DE-FG02-01ER45931), NSF-DMR (0114098), and AFOSR (F49620-03-1-0175).

**9:00**

**Y23 6 Understanding the Gap in Polyoxovanadate Molecular-Based Magnets** A. BARBOUR, R.D. LUTTRELL, J. CHOI, J.L. MUSFELDT, *University of Tennessee* D. ZIPSE, N.S. DALAL, *Florida State University* D.W. BOUKHVALOV, *Russian Academy of Sciences Ural Division* V.V. DOBROVITSKI, *Ames Laboratory* M.I. KATSNELSON, *Radboud University* A.I. LICHTENSTEIN, *Universität Hamburg* B.N. HARMON, P. KÖGERLER, *Ames Laboratory* We report a joint experimental and theoretical investigation of the transport gap, optical properties, and electronic structure of two chemically similar, inhomogeneously mixed-valent polyoxavanadate molecule-based magnets. We attribute the substantial gap in $[NHEt_3]_4\ [V_8^{IV}V_4^{V}As_8O_{40}(H_2O))]\cdot H_2O$ to weak *p-d* hybridization and a large on-site Coulomb repulsion ($U = 5$ eV). The reduced gap in $[NHEt_3]_3\ [V_6^{IV}V_6^{V}As_8O_{40}(HCO_2)] \cdot 2H_2O$ is associated with a smaller value of $U$, at least from a molecular point of view, although the transport properties also reflect subtle organization of the molecular structure and the difference between direct and indirect intermolecular charge transfer. A detailed analysis of the vibrational response supports the important role of local molecular distortion and hydrogen bonding in the intramolecular and intermolecular charge transport in $[NHEt_3]_4\ [V_8^{IV}V_4^{V}As_8O_{40}(H_2O))]\cdot H_2O$. This work is supported by PRF and the U.S. Department of Energy.

**9:12**

**Y23 7 High-frequency Infrared Studies of Manganese-based Single-molecule Magnets*** JIUFENG TU, *The City College of New York* YOKO SUZUKI, S. McHUGH, D. GRAYBILL, M.P. SARACHIK, *CCNY* L. MIHALY, *SUNY-Stony Brook* G.L. CARR, *BNL* N.E. CHAKOV, G. CHRISTOU, *University of Florida* High-resolution far-infrared transmission studies of $Mn_{12}$ single crystals (both aligned crystal assemblies and randomly oriented samples) have been carried out as a function of temperature and magnetic field over a wide frequency region (7 - 100 $cm^{-1}$). Several absorption lines corresponding to different transitions within the S = 10 manifold can be observed as a function of temperature. Our previous low frequency studies have shown that the sum of absorption coefficients of these absorption lines does not seem to conserve as a function of temperature. The new high-frequency measurements indicate that the oscillator strength is recovered at higher frequencies with the appearance of new absorption bands. The origin and the frequency dependence of these new absorption bands will be discussed.

*Supported by NSF grant DMR-0451605, DOE-AC02-98CH10886, DMR-0103290 and CHE-0123603.

**9:24**

**Y23 8 Field-dependent magnetic parameters in $\{Ni_4Mo_{12}\}$: Magnetostriction at the molecular level?*** R. C. RAI, J. CAO, J. L. MUSFELDT, *University of Tennessee* X. WEI, *National High Magnetic Field Laboratory* J. SCHNACK, M. BRÜGER, *Universität Osnabrück* M. LUBAN, P. KÖGERLER, E. MOROSAN, R. FUCHS, *Ames Laboratory & Iowa State University* R. MODLER, *Johann Modler GmbH* H. NOJIRI, *Tohoku University* We present the optical and magneto-optical properties (0 - 32 T) of $Mo_{12}^{V}O_{30}(\mu_2\text{-}OH)_{10}H_2\{Ni^{II}(H_2O)_3\}_4$, a magnetic molecule with antiferromagnetically coupled tetrahedral $Ni^{II}$ in a diamagnetic molybdenum matrix. A magnetochromic effect, centered at $\sim$ 1.9 eV, is observed at 4.2 K, and it is attributed to a change in the Ni $d \rightarrow d$ on-site excitation. The low-temperature magnetization exhibits steps at irregular field intervals, a result that cannot be explained using a Heisenberg model even if it is augmented by magnetic anisotropy and biquadratic terms. Field-dependent exchange parameter, however, provides the best fit to magnetization, suggesting that the molecular structure (and thus the interactions between spins) may be changing with applied magnetic field. The magneto-optical response of $Mo_{12}^{V}O_{30}(\mu_2\text{-}OH)_{10}H_2\{Ni^{II}(H_2O)_3\}_4$ supports a small change in the $NiO_6$ coordination geometry and the associated electronic single-ion properties.

*This work is supported by the U.S. Department of Energy.

**9:36**

**Y23 9 Numerical Analysis of the EPR Spectrum of a $Ni_4$ Single-Molecule Magnet through Direct Diagonalization of the Four-Spin Hamiltonian** ANTHONY WILSON, *University of Florida, Department of Physics* STEVE HILL, *University of Florida, Department of Physics* EPR studies have established the Giant Spin (GS) Hamiltonian parameters, $D$, $B_4^0$ and $B_4^4$, for members of the $[Ni(hmp)(ROH)X]_4$ (R = Me, Et, etc., and X = Cl and Br) family of single-molecule magnets.[1] Four $S = 1$ $Ni^{II}$ ions, aligned on corners of a cubic core, couple ferromagnetically creating a spin $S = 4$ ground state. Experiments on an isostructural Ni/Zn alloy established single-ion $d_i$ and $e_i$ parameters, as well as the orientations of the local magnetic axes.[1] A numerical model utilizing matrix diagonalization has simulated EPR spectra for the coupled $S = 1$ $Ni^{II}$ ions using parameters from the Ni/Zn studies. Fourth order anisotropy parameters in the giant spin model arise from the isotropic Heisenberg coupling, $itJS_1 \cdot S_2$, and quadratic single-ion anisotropy in the four-spin Hamiltonian. Heisenberg coupling causes higher energy states to influence the $S = 4$ ground state addressed in the GS model. Matching the lowest nine energies of the four-spin model to those of the GS model allows direct spectroscopic determination of $J$. [1]E.-C. Yang et al., Inorg. Chem. **44**, 3827-3836 (2005).

**9:48**

**Y23 10 Magnetic Quantum Tunneling in a $Mn_{12}$ Single-Molecule Magnet Measured With High Frequency Electron Paramagnetic Resonance** JON LAWRENCE, SUNG-SU KIM, STEVE HILL, *University of Florida, Physics* MURALEE MURUGESU, *University of California at Berkeley, Chemistry* GEORGE CHRISTOU, *University of Florida, Chemistry* The low temperature spin dynamics of the single-molecule magnet $[Mn_{12}O_{12}(CH_3COOH)_{16}(H_2O)_4] \cdot 2CH_3COOH \cdot 4H_2O$, were studied using High Frequency Electron Paramagnetic Resonance (HFEPR) in order to demonstrate magnetic quantum tunneling between resonant spin projection states. We prepare the spins such that they populate only one side of the axial potential energy barrier and, using a magnetic field, we cause tunneling of the magnetic moment between resonant spin projection states. We then use HFEPR to monitor the populations on each side of the potential energy barrier. We show that, in addition to measuring the ensemble average of the relaxation, these HFEPR experiments demonstrate that one can separately monitor the relaxation from different parts of the inhomogeneous distribution of spin environments. This technique, therefore, provides an alternative method for performing hole-digging experiments for measuring spin relaxation dynamics.

**10:00**

**Y23 11 Acoustomagnetic pulse experiments in LiNbO3/Mn12 hybrids** JOAN MANEL HERNANDEZ, FERRAN MACIA, ALBERTO HERNANDEZ-MINGUEZ, ANTONIO GARCIA-SANTIAGO, JAVIER TEJADA, *Universitat de Barcelona* PAULO SANTOS, *Paul Drude Institut* EXPERIMENTAL MAGNETISM TEAM, SEMICONDUCTOR SPECTROSCOPY COLLABORATION, We report here that single crystals of molecular magnets like Mn12 and Fe8 mounted on the surface of piezoelectric LiNbO3 can be used as very sensitive detectors for surface acoustic waves (SAW). These SAWs are generated by sending microwave pulses in the time range between 1 $\mu$s and several tens of ms to an interdigital transducer mounted on the LiNbO3. Our experiments were carried at low temperatures and in the presence of external magnetic fields, and the analysis of the magnetization variations was done using an SQUID magnetometer with time resolution of 1 $\mu$s that allows us to study the quantum properties of these nanomagnets. The results obtained show that the variation of magnetization depends: 1) on the intensity and quality factor of the SAW at the different frequencies, 2) on whether the temperature of the experiment is above or below the magnetic blocking temperature of the molecular clusters. Furthermore, the heat released by the scattering of the coherent phonons forming the SAW contributes to the generation of the so-called magnetic avalanches. J.M. Hernandez et. al., App. Phys. Lett., (accepted).

**10:12**

**Y23 12 Magnetism in Metal Clusters** FORREST PAYNE, WEI JIANG, L.A. BLOOFIELD, *University of Virginia* We have measured the magnetic moments of clusters of Cobalt, Niobium, and Chromium, ranging in size from $<$ 20 to 200 atoms. Improvements to our cluster source have allowed us to produce smaller and colder ( $\sim$ 60K) clusters than we were able to study in previous work and to study each cluster size individually. We will present measured values for the magnetic moments of these clusters as functions of size, temperature, and applied field. We have also investigated superparamagnetic behaviors of these clusters, looking for deviations from that behavior. This presentation is based upon work supported by the National Science Foundation under Grant No. DMR-0405203.

**10:24**

**Y23 13 STM differential conductance of a pair of magnetic adatoms*** BRIAN LANE, KEVIN INGERSENT, *University of Florida Department of Physics* Competition between screening of local moments through the Kondo effect and magnetic ordering of those moments through direct or induced (RKKY) exchange interactions is a key feature of heavy-fermion systems and of metals containing dilute magnetic impurities. It should be possible to probe this competition in its purest form through scanning tunneling microscopy (STM) studies of pairs of magnetic adatoms on metallic surfaces. However, in order to interpret the STM differential conductance through a pair of nearby adatoms, it is necessary to understand the effects of Fano-like interference between different tunneling paths from the STM tip into the substrate. We report preliminary results of numerical renormalization-group calculations of the impurity spectral function and the differential tunneling conductance for the two-impurity Anderson model, and compare our results with those for the well-studied one-impurity case.

*Supported by NSF Grant DMR-0312939

**10:36**

**Y23 14 Electronic Structure of Magnetic Titanocene Dimer Molecules at a Metal Surface Measured by Scanning Tunneling Microscopy** XINGHUA LU, YAYU WANG, R. YAMACHIKA, A. WACHOWIAK, M. F. CROMMIE, *Department of Physics, University of California, Berkeley, and Materials Sciences Division, Lawrence Berkeley National Laboratory, Berkeley* L. BELTRAN, J. R. LONG, *Department of Chemistry, University of California, Berkeley* The titanocene dimer ($[Cp_2TiCl]_2$, where $Cp = C_5H_5$) is an interesting magnetic molecule because it incorporates two spin-1/2 Ti atoms in an antiferromagnetic configuration. We have used cryogenic scanning tunneling microscopy to study the local electronic properties of titanocene dimer molecules adsorbed onto metal surfaces. Ordered patterns of titanocene dimmers have been observed for submonolayer coverage on Au(111). Scanning tunneling spectroscopy of the molecules shows sharp features near the Fermi energy that may be magnetic in origin.

## SESSION Y24: POLYMER MELTS & SOLUTIONS: STRUCTURE & SOLUBILITY

**Friday Morning, 17 March 2006**
**321, Baltimore Convention Center at 8:00**
**Ferenc Horkay, National Institutes of Health, presiding**

**8:00**

**Y24 1 Why Good Solvents Are Seldom All That Good** S. T. MILNER, *ExxonMobil* M.-D. LACASSE, *ExxonMobil* W. W. GRAESSLEY, The strength of interactions between polymers and solvents is most commonly summarized in a chi parameter. Chi greater than 0.5 leads to phase separation, while a value of zero indicates an ''ideal'' solvent. In fact, chi values less than 0.25 are quite rare, even among so-called ''good solvents'' for a given polymer. Why should this be? The origin of energetic interactions between nonpolar polymers and solvents is primarily dispersive forces, which are proportional to the square of the difference in solubility parameter; hence it should be possible to choose polymer and solvent with matched solubility parameters to achieve an ideal solvent. We shall argue that there is also a generic entropic contribution to chi. One way of describing it is to say that polymer and solvent have a different propensity to explore free volume; when obliged to mix, there is an entropic penalty resulting from the necessary compromise in free volume per mer. One may also say that the solvent molecules induce a depletion attraction between chain segments, analogous to the attraction between colloidal particles induced by micellar solutions. This effect can be observed in simulations of hard-sphere chains in identical hard sphere solvent. There one finds that the radius of gyration of such chains in solvent are significantly smaller than in vacuum, though still scaling as self-avoiding walks. From this result, a chi value of about 0.3 may be inferred.

**8:12**

**Y24 2 Re-examination of the slow mode in semidilute solutions** CHI WU, *The Chinese University of Hong Kong* Dynamics of semidilute solutions has been well described by two different motions, respectively, related to the ''blobs'' and the reptation of an entire chain. In the past, dynamic LLS results revealed that besides the fast relaxation related to the ''blobs,'' there existed an addi-

tional slow relaxation. In the earlier time, such a slow mode was wrongly identified as the reptation. Later, this slow mode was attributed to possible problems in the sample preparation, such as dust particles or a concentration gradient. Whether this slow mode is real has remained a challenging problem since 80's. Recently, we found that it appears only when the solvent quality is less good. To avoid problems in the sample preparation, we, respectively, used the coil-to-globule transition of long polystyrene chains, the high-vacuum anionic polymerization of styrene in cyclohexane, and the living bulk polymerization of MMA to alternate the size of polymer chains (i.e., the overlap concentration) to induce an itin-situ dilute-semidilute transition. Our results confirm that this slow mode is real with no ambiguity. In theory, we can demonstrate that this slow mode appears whenever segments (monomers) in different ''blobs'' start to interact with each other and its characteristic relaxation time is related to the correlation length of these interacting ''blobs.''

**8:24**

**Y24 3 On Fluctuations in Polymer Systems: Field Theoretic Simulations** KIRILL KATSOV, *Materials Research Lab, UCSB* ERIN LENNON, *Chemical Engineering, UCSB* GLENN FREDRICKSON, *Materials Research Lab, UCSB* We use variety of approaches to sample equilibrium fluctuations in polymersystems within a field theoretic framework. Comparison of (complex) Langevin and (smart) Monte Carlo sampling techniques is presented with special attention paid to their efficient implementation. We apply these methods to study effect of fluctuations on phase behavior in diblock copolymer melts and correlations in semidilute polymer solutions.

**8:36**

**Y24 4 Molecular Dynamics Simulations of a Dendritic Polyelectrolyte with Flexible Spacers in Salt-free Solution** QI LIAO, YONG LIN, XIGAO JIN, CHARLES C. HAN, *PPCL, Joint Lab. of Polymer Science and Materials,Institute of Chemistry, Chinese Academy of Science, Beijing 100080, China* We present the results of molecular dynamics simulation of a dendritic polyelectrolyte in a dilute salt–free solution. The dendritic polyelectrolyte is modeled as an ensemble of bead spring regular-branched chain of charged Lernard-Jones particles with explicit counterions. The simulations were performed covering a wide range of molecular variables of the dendritic polyelectrolyte such as generation number, spacer length, and charge density. The relaxation time of dendrimer size, the conformation of spacers, the size depend of dendrimer on the generation and charge density are discussed and compared with a Flory-type theory. We determined the osmotic coefficients of the dilute dendritic polyelectrolyte solution, and compared with the prediction of cell model of charged sphere.

**8:48**

**Y24 5 Solution and Melt Rheology of Polypropylene Comb and Star Polymers** ARNAV GHOSH, RALPH H. COLBY, *Department of Materials Science and Engineering, Penn State University* JEFFREY M. ROSE, ANNA E. CHERIAN, GEOFFREY W. COATES, *Department of Chemistry, Cornell University* Syndiotactic polypropylene macromonomer arms have been prepared by coordination-insertion polymerization. These arms have been made into polypropylene star polymers by the homopolymerization of the syndiotactic arms with a living alkene polymerization catalyst. The macromonomer arms have also been randomly copolymerized with propylene using rac-dimethylsilyl(2-methyl-4-phenylindenyl) zirconium dichloride catalysts to make polypropylene combs. Consequently we have star polymers and a series of comb polymers with different backbone lengths that are all made from the same macromonomer arms. We compare linear viscoelastic data on star and comb polypropylene melts and solutions in squalane to predictions of the tube dilation model and the tube model without tube dilation. The ratio of comb terminal relaxation time to star terminal relaxation time eliminates the friction coefficient and allows determination of the extent of tube dilation the backbone experiences when it relaxes. The concentration dependence of the comb/star terminal relaxation time ratio can be described by either model, owing to adjustable parameters that are not known itapriori, so independent means to evaluate those parameters will be discussed.

**9:00**

**Y24 6 Watching nucleation and growth of chain disentanglement in large-amplitude oscillatory shear of entangled polymer solutions** P. TAPADIA, A. PHILIPS, SHI-QING WANG, *Department of Polymer Science, The University of Akron* Our recent stress-controlled measurements show that a sufficient yet moderate level of chain deformation due to shear can produce spatial topological rearrangement to free chains from mutual dynamic constraint [1]. The chain disentanglement seems to occur catastrophically, resulting in an inhomogeneously sheared sample during rate-controlled shear [2]. Thus, chain disentanglement is also expected to take place during large amplitude oscillatory shear (LAOS) at frequencies higher than the overall chain relaxation rate. We applied our particle-tracking velocimetric technique to probe the state of chain entanglement during LAOS. We found that the chain orientation produced by LAOS led to a new environment in which the initially well-entangled chains managed to disentangle inhomogeneously in space. A layer free of chain entanglement developed to take the load of the imposed strain. As a result of this nonlinearity, the rest of the sample avoided significant deformation and its chain entanglement remained intact. [1] Tapadia, P.; Wang, S. Q. Phys Rev. Lett, **91**, 198301 (2003); Tapadia, P.; Wang, S. Q. Macromolecules **37**, 9083 (2004). [2] Tapadia, P.; Wang, S. Q. Phys. Rev. Lett., in press (2005).

**9:12**

**Y24 7 Anomalous Sorption of Carbon Dioxide in Polymer Thin Films** XIAOCHU WANG, ISAAC SANCHEZ, *University of Texas* Unusual sorption has been reported in thin polymer films exposed to near-critical CO2. When the supercritical fluid approaches the critical point the film appears to thicken, but it is not clear whether the film swells or if there is adsorption on the film surface A combination of the gradient model of inhomogeneous systems and the lattice fluid model have been used to investigate this phenomenon. It is shown that gas surface adsorption on an attractive surface is proportional to the compressibility of the fluid. We have also investigated numerically the sorption of supercritical CO2 on PDMS and PIB, and supercritical 1,1-difluorethane on PS. By calculating the Gibbs adsorption and adsorption layer thickness of the supercritical fluids, we found in all cases that maximum adsorption occurred when the supercritical fluid was near its compressibility maximum.

**9:24**

**Y24 8 Gas Diffusion in Polyethylene Terepthalate By Molecular Dynamics*** SIMON BUTLER, DAVID ADOLF, *School of Physics & Astronomy, University of Leeds, Leeds, LS2 9JT, UK*

Molecular dynamics simulations of the diffusion of small penetrants through PET have been performed utilising the anisotropic united atom model [1] and a virtual liquid technique. [2] The accuracy and reliability of these two approaches has been assessed in terms of the improvement in equation of state behaviour and of diffusion co-efficients and solubilities. The effect of the diffusion of nitrogen, carbon dioxide, and oxygen on the local dynamics of PET have been investigated as a result. Attention has been focused on the dual mode effect [3] observed during mixed gas diffusion. [1] Molecular dynamics calculation of the equation of state of alkanes, J. Chem. Phys. 93, 6 (1990) [2] Kikuchi, Kuwajima, Fukada, Novel method to estimate the solubility of small molecules in cis-polyisoprene by molecular dynamics simulations, J. Chem. Phys, 115, 13 (2001) [3] Lewis, Duckett, Ward, Fairclough, Ryan, The barrier properties of polyethylene terephthalate to mixtures of oxygen, carbon dioxide and nitrogen, Polymer, 1631, 44 (2003)

*This work is funded by the European Physical Sciences Research Council

**9:36**

**Y24 9 Overcoming the difficulty in performing large step-strain experiments: A first reliable comparison with Doi-Edwards tube model** PAULA X. WANG, SHI-QING WANG, *Department of Polymer Science, The University of Akron* Large step shear has been a popular way to interrogate nonlinear viscoelastic responses of polymeric materials. In absence of any severe interfacial failure, the experimental data [1] were found to agree with the Doi-Edwards model of entangled chains. A separate set of experimental studies [2-4] produced strain-softening and showed disagreement with the D-E model. We have successfully prevented interfacial breakdown for the first time to show that the strain-softening is an interfacial artifact [5] and that the stress relaxation behavior of entangled melts and solutions can be reliably depicted experimentally and accounted for within the D-E model. [1] Osaki, K. et al Macromolecules **15**, 1068 (1982). [2] Osaki, K.; Kurata, M. Macromolecules **13**, 671 (1980). [3] Vrentas, C. M.; Graessley, W. W. J. Rheol.**26**, 359 (1982). [4] Osaki, K. Rheol. Acta **32**, 429 (1993). [5] Venerus, D. J. Rheol. **49**, 277 (2005).

**9:48**

**Y24 10 Simulations of the dynamics of polymer solutions in unidirectional flows*** BERK USTA, *University of Florida* JASON BUTLER, TONY LADD, We investigate migration and dispersion of polymer chains in unidirectional channel flows by numerical simulation. The algorithm combines the fluctuating lattice-Boltzmann equation with a bead-spring model of a flexible polymer. The method has been shown to be very efficient, capable of simulating polymers in excess of 1000 beads with Oseen level hydrodynamic interactions. The grid-based solution of the fluid equations makes it straightforward to incorporate complex confining boundaries, but here we examine flows in a narrow channel. We observe lateral migration of a single polymer chain in both shear and Poiseuille flows. The direction and extent of migration depend on the degree of confinement as well as the Peclet number, contrary to previous reports. Numerical results show that the longitudinal dispersion deviates from the Taylor dispersion theory at high Peclet numbers, resulting in smaller dispersion coefficients. We will discuss the underlying mechanisms for the reduced dispersion, and also the possibility of improved separation scenarios.

*This work was supported by the National Science Foundation (CTS-0505929)

**10:00**

**Y24 11 Heat Capacity of Liquid Poly(vinyl methyl ether) With and Without Water*** MAREK PYDA, *Department of Chemistry, The University of Technology, Rzeszow, 35959 Rzeszow, Poland* B. WUNDERLICH, *Dept. of Chemistry, The Univ. of Tenn., and Chemical Sciences Div., ORNL* K. VAN DURME, B. VAN MELE, *Dept. of Physical Chem. and Polymer Science, Vrije Universiteit, Belgium* The liquid heat capacities at constant pressure Cp, of amorphous poly(vinyl methyl ether), PVME, without and with water have been computed as the sum of vibrational, external, and conformational contributions. The vibrational contribution was calculated from the heat capacity arising from group and skeletal vibrations. The external contribution was estimated from experimental data of the thermal expansivity and compressibility in the liquid state. The conformational heat capacity was evaluated from a fit of experimental part to a one-dimensional Ising model for two discrete states, characterized by parameters linked to stiffness, cooperativity, and degeneracy. For the PVME-water system the additional changes in the conformational heat capacity arising from the interaction of the PVME chains with water. The experimental liquid Cp agrees with these calculations to better than 3%. The calculated liquid Cp was employed in the interpretation of the thermal analysis of the apparent Cp in the region of the melting, demixing, remixing, and crystallization within the PVME-water system.

*Supported by NSF, Polymers Program, DMR-0312233, and the Div. of Mat. Sci., BES, DOE at ORNL, managed by UT-Battelle, LLC, for the U.S. Department of Energy, under contract number DOE-AC05-00OR22725.

**10:12**

**Y24 12 Thermodynamically Constrained Inverse Monte Carlo Determination of Effective Pair Interactions** HENRY ASHBAUGH, *Tulane University* LU YANG, *Tulane* SHEKHAR GARDE, *RPI* SANAT KUMAR, *RPI* TULANE COLLABORATION, RPI COLLABORATION, Bridging length scales with molecular simulations requires the development of effective interactions in which degrees of freedom are integrated out to reduce computational expense. Such coarse graining strategies often lose critical thermodynamic information as molecular detail is washed out. Inverse Monte Carlo methods which focus on the reproduction of fluid structure, for example, typically have heats of vaporization and vapor pressures which are significantly greater than experiment. We propose a new method, Thermodynamically Constrained Inverse Monte Carlo (TCIMC), which systematically constrains empirical potential functions to reproduce known energetics and pressures while minimizing the difference between experimental and model pair correlations. We demonstrate the application of TCIMC to the recovery of model pair interactions for the Lennard Jones fluid. This method is subsequently extended to the development of united atom potentials for the alkanes from more complex all atom descriptions. The development of thermodynamically consistent coarse grained potentials for the modeling of polymers is discussed.

**10:24**
**Y24 13 Equivalence of particle and field representation of coarse-grained polymer models** KIRILL TITIEVSKY, KENNETH BEERS, *Massachusetts Institute of Technology* Particle-based and field theoretic coarse-grained models of heterogeneous polymer melts have been difficult to compare quantitatively because of the differences in state variables and simulation parameters. We reconcile the two approaches by noting that assumptions involved in discretizing a polymer field theory allow each molecule to be treated as several particles connected by spring bonds. In effect, these particles are the grid points on which the fields are discretized. The interaction potentials of the points, therefore, are obtained directly from the energy model (e.g. Flory) used in the field theory. The equilibrium phase behavior of a melt of such coarse-grained chains is calculated by stochastic dynamics or Monte Carlo simulations. Unlike field theory which becomes infeasible away from the mean field limit due to complex terms in the Hamiltonian, our simulations converge for realistic chain lengths because the potentials are smooth and real. Also, unlike in existing particle-based methods, all parameters in our model are explicitly related to experimentally measurable quantities. Our simulations of diblock copolymers, furthermore, are quantitatively consistent with experimental and field theoretic results.

**10:36**
**Y24 14 Coarse-graining and dynamics of complex macromolecular liquids: melts and blends** MARINA GUENZA, *University of Oregon* Processes of scientific interest in macromolecular liquids can involve more than ten orders of magnitude in space and time variables, impairing our ability of performing atomic-level simulations in the long-time regime. A way to overcome this problem is to resort to multiscale modeling procedures. Here the challenge is to have a formally rigorous, possible analytical, coarse-graining procedure that enables accurate transfer of information between different lengthscales of interest. Starting from the Ornstein-Zernike equation we derived (G.Yatsenko et al. PRL 93, 257803 (2004)) an analytical procedure to coarse-grain structure and dynamics of macromolecular liquids (homo- and diblockcopolymers) and their mixtures. Our procedure maps macromolecules into interacting soft-colloidal particles and provides the effective soft-core potentials input to mesoscale simulations of the coarse-grained systems. Because analytical, our procedure provides a universal formalism easily implemented to treat different systems of interest. Our procedure efficiently extends the range of length- and timescales accessible in simulations of macromolecular liquids. The soft-core mean-force potential enters the Langevin Equation for Cooperative Dynamics (M.Guenza PRL 88, 025901 (2002)), which predicts anomalous subdiffusive center-of-mass motion in excellent agreement with simulations and recent experimental data.

**10:48**
**Y24 15 Kac-Dirac propagators modeling crossover between entangled and unentangled conformations in polymer melts** YITZHAK SHNIDMAN, *College of Staten Island, City University of New York* We will discuss the advantages of using the Kac stochastic process on a lattice for modeling the statistics of chain conformations in polymers melts. Certain projections of the master equation governing such a process assume the form of the telegrapher's equation in the continuum limit, while other projections assume the form of Dirac's equation for free fermions that can also be recast as the Klein-Gordon equation. The statistics of ideal chain conformations and the onset of entanglement in a dense polymer melt will be related to the finite path statistics and the onset of quantum entanglement in a system of free fermions. A persistence length above the Kuhn length scale emerges naturally in the entangled regime without assuming a confining tube as in the Doi-Edwards theory. Kac-Dirac propagators may also provide a better description than Wiener-Schroedinger propagators for conformations of interacting chains across interfaces in inhomogeneous polymer fluids.

## SESSION Y25: CHARGED AND ION-CONTAINING POLYMERS: COMPUTATION
**Friday Morning, 17 March 2006**
**322, Baltimore Convention Center at 8:00**
**Cameron Abrams, Drexel University, presiding**

**8:00**
**Y25 1 A New Necklace Model** ANDREY DOBRYNIN, *University of Connecticut* MICHAEL RUBINSTEIN, *University of North Carolina* QI LIAO, *Institute of Chemistry, China* We have developed a necklace model of hydrophobic polyelectrolytes in which the necklace structure consisting of polymeric globules (beads) connected by extended sections of the chain (strings of monomers) appears as a result of the counterion condensation and is caused by the balance of the correlation-induced attraction of condensed counterions to charged monomers and electrostatic repulsion between uncompensated charges. The size of the beads increases with polymer concentration while their number per chain decreases. We predict coexistence of necklaces with different number of beads on a polymer backbone at any polymer concentration. To test this necklace model we performed molecular dynamics simulations of polyelectrolyte chains with degree of polymerization N varying from 25 to 373 and with fraction of charged monomers f=1/3, 1/2 and 1 in poor solvent conditions for polymer backbone. The observed concentration dependence of the bead size supports the assumption of the counterion condensation origin of the necklace structure. The overlap concentration is almost independent of the degree of polymerization for weakly charged chains (f=1/3). For strongly charged chains with f=1 the overlap concentration follows the normal N-dependence observed for polyelectrolyte solutions in q and good solvent regimes for polymer backbone. In semidilute solutions the correlation length of fully charged chains is inversely proportional to square root of polymer concentration.

**8:12**
**Y25 2 Electrostatic Complexation between Membrane and Colloid** JIAFANG WANG, *University of Massachusetts, Amherst* M. MUTHUKUMAR, *University of Massachusetts, Amherst* As a primary model of endocytosis, the electrostatic complexation between membrane and colloid is studied. Using a simple approximation, the membrane shape can be determined easily without solving the nonlinear differential shape equation, which facilitates the consideration of electrostatic effects. The phase diagram for the electrostatic complexes can be constructed in terms of the rescaled stretching tension, adhesion strength, and the screening length. By referring to the phase diagram, the possible phase transitions due to the variations of the electrostatic factors (including the charge density, and the screening length) are discussed.

**8:24**

**Y25 3 Molecular Dynamics Simulations of Multilayer Polyelectrolyte Films** PRITESH PATEL, *Macromolecular Science and Engineering, Case Western Reserve University* JUNHWAN JEON, *Polymer Program, Institute of Materials Science, University of Connecticut* PATRICK MATHER, *Macromolecular Science and Engineering, Case Western Reserve University* ANDREY DOBRYNIN, *Polymer Program, Institute of Materials Science and Department of Physics, University of Connecticut* We have performed molecular dynamics simulations of multilayer assembly of oppositely charged polyelectrolytes at charged surfaces. The multilayer build-up was achieved through sequential adsorption of charged polymers in a layer-by-layer fashion from dilute polyelectrolyte solutions. The strong electrostatic attraction between oppositely charged polyelectrolytes at each deposition step is a driving force behind the nanometer-scale multilayer growth. Our simulations have shown that a charge reversal after each deposition step is critical for steady multilayer growth and that there is a linear increase in amount of polymer adsorbed after the first few deposition steps. There is substantial intermixing between chains adsorbed during different deposition steps within multilayer film. Despite significant chain intermixing, however, there are almost perfect periodic oscillations in local composition of positively and negatively charged polymers in the adsorbed film. We show that the film thickness, polymer surface coverage exhibit strong correlation with the strength of electrostatic and short-range interactions.

**8:36**

**Y25 4 Langevin dynamics simulations of dsDNA translocation through synthetic nanopores** CHRISTOPHER FORREY, MURUGAPPAN MUTHUKUMAR, *University of Massachusetts, Amherst* We have modeled dsDNA using a coarse-grained bead-spring method to study its behavior as it is driven by a potential gradient through a nanoscopic pore located in a rigid membrane. Using the Poisson-Nernst-Plank formalism, we calculate traces of the ionic current corresponding to the translocation process and compare our findings with experimental results. In agreement with recent experiments, we find that the dsDNA frequently translocates in a folded configuration. We explore the role of chain length, potential difference and pore diameter on the frequency of translocation events, average residence time, electrophoretic mobility and percentage of unfolded events.

**8:48**

**Y25 5 Modeling Layer-by-Layer Assembly of Flexible Polyelectrolytes** QIANG WANG, *Department of Chemical and Biological Engineering, Colorado State University* Using a continuum self-consistent field theory, we have modelled the sequential process of layer-by-layer assembly of flexible polyelectrolytes on flat surfaces as a series of kinetically trapped states. Up to 60 depositions of oppositely charged polyelectrolytes are performed, each followed by a washing step. The multilayer has a three-zone structure. An exponential growth is found for the first several layers, followed by a linear growth for subsequent layers evolving towards a steady state. Each layer inverts the total charge of the multilayer film (including the bare substrate charge). While adjacent layers are highly interpenetrating, stratification can be seen for every four or more layers. We have also examined the effects of surface charge density, bulk salt concentration, and solvent quality on the thickness and internal structure of the multilayer. Our results agree with most experimental findings on polyelectrolyte layer-by-layer assembly.

**9:00**

**Y25 6 Simulations of comb polyelectrolytes** ZHAOYANG OU, M. MUTHUKUMAR, *University of Massachusetts, Amherst* Using Langevin dynamics, we have characterized the effects on backbone stretching by systematically varying grafting density, grafted-chain length, and backbone length. Chain persistence length, conformational asphericity, and counterion and monomer density profiles were determined. We have found that increasing grafting density leads to increases in both chain persistence length and overall asphericity. Increasing the length of side chains also creates a stiffer backbone, but overall asphericity is decreased. Simulation results will be compared with theory.

**9:12**

**Y25 7 Spanning the gap between strong and weak-coupling electrostatics for charged rods*** CHRISTIAN SANTANGELO, *University of Pennsylvania* I present a method to compute the distribution of counterions near a charged macromolecule at intermediate coupling. The procedure involves decomposing the Coulomb interaction into a separate short and long distance piece. The long distance piece is treated within mean-field theory and a strong-coupling expansion is performed for the long distance part. The theory recovers both the strong and weak coupling results in the appropriate limit for charged surfaces. Furthermore, it is accurate for describing the density at intermediate coupling. I derive from this a two-fluid model for a charged rod with discrete charges along its center axis, making contact with previous models of discretely-charged rods.

*NSF under Award No. DMR02-03755, Award No. DMR01-29804, and by the Materials Research Laboratory at UCSB under Award No. DMR00-80034

**9:24**

**Y25 8 Electrostatic attraction between cationic-anionic assemblies with surface compositional heterogeneities** YURY VELICHKO, MONICA OLVERA DE LA CRUZ, *Northwestern University* Biological assemblies of heterogenous cationic and anionic molecules with hydrophobic groups have important functional properties controlled by interdependencies of the architectures and the intermolecular interactions. The net incompatibility among chemically different charged components, which in water can be due to different degrees of hydrophobicity, promotes macroscopic segregation, while electrostatics promotes mixing of the charges into ionic crystal structure. This competition results in formation of surface charge domains. We analyze attractions among two cylindrical assemblies with surface charge heterogeneities. The compositional heterogeneities are correlated and strongly polarized in the presence of the second assembly. This leads to a strong attraction. The strength of the effective attraction is studied as a function of the distance for different values of the net incompatibility. We compare results of computer simulations and theory.

**9:36**

**Y25 9 Relevance of Solvent Characteristics on Ion-Binding and the Structure Formation of Neutral Polymers in Electrolyte Solutions** ILHEM FAIZA HAKEM, *Carnegie Mellon University* JYOTSANA LAL, *IPNS, Argonne National Laboratory* MICHAEL BOCKSTALLER, *Carnegie Mellon University* Polymers carrying functional groups constituted of heteroatoms are omnipresent in biology and polymer technology, for example in the development of solid state polymer electrolytes. When dissolved in polar solvents, these polymers can coordinate ions that result in an effective transformation of the neutral polymer into a

weakly charged polyelectrolyte as indicated by the characteristic changes in the polymers solution characteristics. In our contribution we discuss the implications of solvent characteristics – i.e. dielectric constant and hydrogen bonding capacity – and the ion-strength of the added electrolyte on the polymer-ion coordination as well as polymer solution characteristics. A mean-field model to predict the amount of ion-coordination is presented and validated for the particular case of poly(oxy ethylene)/salt solutions. The Random Phase Approximation (RPA) is applied to extract quantitative information about the coordination of ions to the polymer in solution from small-angle neutron scattering (SANS) data.

**9:48**

**Y25 10 Conformational Properties and Phase Behavior of Mixed Brushes between Charged and Neutral Polymers: SCF Modeling Using the Edwards Hamiltonian Approach** KEVIN WITTE, YOU-YEON WON, *Purdue University* We present a theoretical study of the single-chain statistics and two-dimensional (2-D) phase behavior of mixed brushes composed of charged and non-charged polymers. We extend the Edwards Hamiltonian formulation for the Green function to investigation of mixed brushes containing a polyelectrolyte species through the incorporation of the combined electrostatic effects as an additional external field which can be self-consistently computed by a corresponding Poisson-Boltzmann-like equation. The resultant SCF equations were numerically analyzed to achieve results that are exact within the assumption of mean field. The 2-D phase behavior of the mixed brushes (assuming that the brushes are laterally mobile) was examined using the conventional free energy of mixing analysis. The predictions on the effects of such control variables as the brush hydrophilicity/hydrophobicity, surface grafting density, charge content of the polyelectrolyte species, and ionic strength of the medium on the conformation properties and phase behavior of the mixed brushes will be discussed.

**10:00**

**Y25 11 Electrostatic Origin of Single-Stranded Genome Packing in Viruses** VLADIMIR BELYI, M. MUTHUKUMAR, *University of Massachusetts, Amherst* We develop an electrostatic model for single-stranded RNA/DNA viruses that bind their genome via highly basic semiflexible peptide arms. We show that genome-capsid binding is dominated by non-specific electrostatic interactions, rather than actual amino-acid content. Proposed model explains many universal features of the viral genome. Good agreement is found with wide range of qualified wild-type and mutant viruses.

**10:12**

**Y25 12 Regimes of Conformational Transitions of Diblock Polyampholytes** ZUOWEI WANG, MICHAEL RUBINSTEIN, *Department of Chemistry, University of North Carolina at Chapel Hill* Regimes of electrostatically-driven conformational transitions of diblock polyampholytes are investigated by scaling theory and molecular dynamics simulations. The coil-globule transition of a symmetric diblock polyampholyte is found to consist of three regimes identified with increasing interaction strength: (i) the folding regime where the electrostatic attraction causes the diblock chain to to fold through the overlap of the two blocks, while each block is slightly stretched by self-repulsion; (ii) the weak association regime which is the classical collapse of the chain into a globule dominated by the fluctuation-induced attractions between oppositely charged chain sections; (iii) the strong association regime that starts with direct binding of oppositely charged monomers (dipole formation), followed by a cascade of multipole formation leading to multiplets. The conformation of a charge-asymmetric diblock polyampholyte changes from extended polyelectrolyte structure, to tadpole-shape with a globular head and a polyelectrolyte tail, and then to polyelectrolyte structure with the variation of the ratio between the charges of the two blocks.

**10:24**

**Y25 13 Polyelectrolyte condensation by linear molecules of variable length: a grand-canonical Monte Carlo study** CAMILO GUAQUETA, ERIK LUIJTEN, *University of Illinois at Urbana-Champaign* The condensation of like-charged polyelectrolytes has been observed to occur under the addition of a variety of oppositely-charged species, such as multivalent counterions, charged globular proteins, and even short chain molecules with monovalent end groups. Inspired by the latter, we study via computer simulations a prototypical polyelectrolyte bundle where condensation is induced by dumbbell-like charged molecules of variable length. We present results from a systematic investigation into the effects of the concentration of bundling agent on the stability of the system. We also consider the effect of changing the length of the dumbbells, as well as the surface charge density of the polyelectrolytes. Recent work[1] has illustrated the important role of the osmotic pressure exerted by the excess solution. In order to take this effect directly into account, we perform simulations in the grand-canonical ensemble, which allows us to equilibrate the bundle with an excess solution of dumbbell molecules at fixed chemical potential.

[1]L. K. Sanders, C. Guáqueta *et al.*, Phys. Rev. Lett.**95**, 108302 (2005).

## SESSION Y26: FOCUS SESSION: PHYSICS OF PHYSIOLOGICAL SYSTEMS

**Friday Morning, 17 March 2006**
**323, Baltimore Convention Center at 8:00**
**Peter Jung, Ohio University, presiding**

***Contributed Papers***

**8:00**

**Y26 1 Electrical Wave Propagation in a Minimally Realistic Fiber Architecture Model of the Left Ventricle** XIANFENG SONG, SIMA SETAYESHGAR, *Department of Physics, Indiana University, Bloomington, IN* Experimental results indicate a nested, layered geometry for the fiber surfaces of the left ventricle, where fiber directions are approximately aligned in each surface and gradually rotate through the thickness of the ventricle. Numerical and analytical results have highlighted the importance of this rotating anisotropy and its possible destabilizing role on the dynamics of scroll waves in excitable media with application to the heart. Based on the work of Peskin[1] and Peskin and McQueen[2], we present a minimally realistic model of the left ventricle that adequately captures the geometry and anisotropic properties of the heart as a conducting medium while being easily parallelizable, and computationally more tractable than fully realistic anatomical models. Complementary to fully realistic and anatomically-based computational approaches, studies using such

a minimal model with the addition of successively realistic features, such as excitation-contraction coupling, should provide unique insight into the basic mechanisms of formation and obliteration of electrical wave instabilities. We describe our construction, implementation and validation of this model. [1] C. S. Peskin, Communications on Pure and Applied Mathematics **42**, 79 (1989). [2] C. S. Peskin and D. M. McQueen, in Case Studies in Mathematical Modeling: Ecology, Physiology, and Cell Biology, 309(1996)

**8:12**

**Y26 2 Scaling behavior and a Markov model for ventricular fibrillation generated by ectopic beats*** HAROLD HASTINGS, *Hofstra University* STEVEN EVANS, ALEX ZAHARAKIS, CHRISTIAN HILAIRE, Sudden cardiac death is a major cause of death in the industrialized world, responsible for 300,000 deaths per year in the US. Although the cardiac electrical system normally produces one ventricular activation in response to each stimulus from the sinus node, ''spontaneous'' activations, called premature ventricular contractions (PVCs), can arise in the ventricles themselves, and propagate through the ventricles. Although usually harmless in the absence of underlying disease, PVCs can generate broken wavefronts when they meet gradients of refractoriness generated by other beats. These broken wavefronts may generate spiral waves producing ventricular tachycardia and ultimately degenerate into ventricular fibrillation (VF), causing sudden cardiac death. When does a PVC lead to ventricular fibrillation? This is a stiff problem, involving time scales from milliseconds to many years. We overcome this problem by developing universal scaling properties and using these rules to drive a Markov process. We find two significant ''amplifiers'' and discuss consequences for variability of VF rates in human populations. We thank Elizabeth Cherry, Flavio Fenton, Anna Gelzer and James Glimm for helpful discussions.

*Partially supported by the NSF and NIH.

**8:24**

**Y26 3 Indeterminacy and Image Improvement in Snake Infrared ''Vision''*** J. LEO VAN HEMMEN, *Physik Department, TU Munich* Many snake species have infrared sense organs located on their head that can detect warm-blooded prey even in total darkness. The physical mechanism underlying this sense is that of a pinhole camera. The infrared image is projected onto a sensory 'pit membrane' of small size (of order $mm^2$). To get a neuronal response the energy flux per unit time has to exceed a minimum threshold; furthermore, the source of this energy, the prey, is moving at a finite speed so the pinhole substituting for a lens has to be rather large ( $\sim$ 1 mm). Accordingly the image is totally blurred. We have therefore done two things. First, we have determined the precise optical resolution that a snake can achieve for a given input. Second, in view of known, though still restricted, precision one may ask whether, and how, a snake can reconstruct the original image. The point is that the information needed to reconstruct the original temperature distribution in space is still available. We present an explicit mathematical model [1] allowing even high-quality reconstruction from the low-quality image on the pit membrane and indicate how a neuronal implementation might be realized. Ref: [1] A.B. Sichert, P. Friedel, and J.L. van Hemmen, TU Munich preprint (2005).

*Supported by BCCN Munich & DFG (HE 3252/1-4)

**8:36**

**Y26 4 Diffusion Weighted MRI and MRS to Differentiate Radiation Necrosis and Recurrent Disease in Gliomas** LARS EWELL, *Medical Physics* A difficulty encountered in the diagnosis of patients with gliomas is the differentiation between recurrent disease and Radiation Induced Necrosis (RIN). Both can appear as enhancing lesions on a typical T2 weighted MRI scan. Magnetic Resonance Spectroscopy (MRS) and Diffusion Weighted MRI (DWMRI) have the potential to be helpful regarding this differentiation. MRS has the ability to measure the concentration of brain metabolites, such as Choline, Creatin and N- Acetyl Aspartate, the ratios of which have been shown to discriminate between RIN and recurrent disease. DWMRI has been linked via a rise in the Apparent Diffusion Coefficient (ADC) to successful treatment of disease. Using both of these complimentary non-invasive imaging modalities, we intend to initiate an imaging protocol whereby we will study how best to combine metabolite ratios and ADC values to obtain the most useful information in the least amount of scan time. We will look for correlations over time between ADC values, and MRS, among different sized voxels.

**8:48**

**Y26 5 Modeling the statistics of elementary calcium release events*** GHANIM ULLAH, PETER JUNG, *Ohio University* Elementary $Ca^{2+}$ signals, such as '$Ca^{2+}$ puffs', which arise from the release of $Ca^{2+}$ from Endoplasmic Reticulum through small clusters of inositol 1,4,5-trisphosphate receptors, are the building blocks for intracellular $Ca^{2+}$ - signaling. The small number of release channels involved during a $Ca^{2+}$ puff renders the puffs stochastic with distributed amplitudes, durations and frequency, well characterized experimentally. We present a stochastic model that accurately describes simultaneously the statistical properties of the duration, amplitudes, frequencies, and spatial spread with a single set of parameters.

*NSF Grant No. (IOB-0345500)

**9:00**

**Y26 6 Calcium Signaling enhancement during oocyte maturation** PETER JUNG, *Department of Physics and Astronomy, Ohio university* GHANIM ULLAH, *Ohio University* KHALED MACHACA, *Department of Physiology and Biophysics, University of Arkansas for Medical Sciences* A Ca2+ signal with a special spatial and temporal characteristic universally removes cell-cycle arrest after fertilization of a mature egg cell. The Ca2+ signal is characterized by a fast rise of intracellular Ca2+ and a slow decay on the time scale of minutes. We use computational modeling of Ca2+ release on the microscale (Ca2+ puffs) and cell-scale in conjunction with experimental knowledge of the changes in the Ca2+ signaling apparatus during oocyte maturation and changing signaling patterns to explore the relationship between organization and sensitivity of IP3 receptors and SERCA pumps and the resulting signaling patterns. We hypothesize that potentiation of the IP3 receptors during oocyte maturation is the main cause for the differentiation in the signaling patterns.

*Invited Papers*

**9:12**
**Y26 7 Functional Complexity of Biological Networks.**
ESHEL BEN-JACOB, *Tel Aviv University*

It is now widely accepted that the complexity of the dynamical behavior of task-performing biological networks affords the latter adaptability to perform a wide variety of different tasks. Hence, understanding complexity is crucial for understanding the activity of biological systems. However, even in the context of simpler, man-made systems, complexity is still largely an intuitive blurry concept with no agreed-upon definition. In this lecture I will present new quantified observables of regularity and structural complexity that were first developed in the context of neural networks activity. I will then address the challenge of the complexity-function relationship via the introduction of a new quantified observable of functional complexity and will demonstrate that for neural networks this observable is connected with the capacity for information storage.

*Contributed Papers*

**9:48**
**Y26 8 A model for the volume regulatory mechanism of the Airway Surface Layer** MICHAEL LANG, MICHAEL RUBINSTEIN, *Department of Chemistry, University of North Carolina at Chapel Hill, N.C.* C. WILLIAM DAVIS, ROBERT TARRAN, *Department of Cell and Molecular Physiology, University of North Carolina at Chapel Hill, N.C.* RICHARD BOUCHER, *Department of Pulmonary and Critical Care Medicine, University of North Carolina at Chapel Hill, N.C.* VIRTUAL LUNG PROJECT COLLABORATION, The airway surface layer (ASL) of a lung consists of two parts: a mucus layer with thickness of about 30 $\mu$m in contact with air and a periciliary layer (PCL) of about 7 $\mu$m below. Mucus collects dust and bacteria and is swept to throat by beating cilia, while riding on top of PCL. It is important that the thickness of PCL is matched with the length of cilia in order to optimize clearance of mucus. Decrease of PCL thickness would finally lead to an occlusion of the respiratory system. Experiments show that the height of PCL stays constant after removing mucus. When modifying height or composition of this open PCL by removing fluid or adding isotonic solution leads to the same final height of PCL. Thus, there must be a regulatory mechanism, that controls height, i.e. ASL volume. Additional experiments show that mechanical stimulus of the cells like shear leads to an increase of ASL volume, thus, the cell is able to actively adjust this volume. Based on these observations a class of models is introduced that describes the experiments and a specific minimum model for the given problem is proposed.

**10:00**
**Y26 9 Development of dielectric biosensors for diagnostic applications** CHRISTOPHER BASSEY, *Western Kentucky University, Bowling Green, KY 42101* Dielectric biosensors utilize the intrinsic electrical properties (permittivity and conductivity) of materials to determine their dielectric characterization. Dielectric measurements, both in vivo and in vitro, provide information on the electrical properties of biomaterials (tissues and organs) as a function of frequency. This information can be used to determine the state of health of the subject since diseased and healthy tissues show significantly different dielectric characteristics. The dielectric properties of tissues depend largely on their water contents, hence dielectric data can provide information on the level of dehydration. In this work, the development of instrumentation and methods for determining dielectric properties of biomaterials is proposed. The principle of using dielectric data for diagnostic purposes is discussed.

**10:12**
**Y26 10 Analytical model of induced transmembrane potentials in cells and organelles** VIJAYANAND VAJRALA, *Department of Physics and Texas Center for Superconductivity, University of Houston* JAMES CLAYCOMB, *Department of Mathematics and Physics, Houston Baptist University* JOHN H. MILLER, JR., *Department of Physics and Texas Center for Superconductivity, University of Houston* Oscillatory electric fields cause morphological and functional changes in biological cells by perturbing the resting potentials across the cell and organelle membranes. Although much work has been reported on ac field induced transmembrane voltages in cells, this has mainly been limited to the plasma membrane. We have developed a three-membrane analytical model describing the plasma membrane surrounding inner and outer mitochondrial membranes. Frequency dependent induced plasma and mitochondrial membrane potentials are calculated with mobile interfacial charges on either side of the membranes. The dependence of the induced membrane potentials on the membrane conductivity and permittivity is also calculated. A finite element electromagnetic model is used to calculate the induced mitochondrial membrane potentials for arbitrary geometries with axial symmetry. Modeling results are compared to nonlinear harmonic response measurements of cells and isolated mitochondria exposed to ac electric fields.

**10:24**
**Y26 11 Phase locking in driven integrate-and-fire neuron models** CHRISTOPHER BEDELL, *Boston College* JAN R. ENGELBRECHT, *Boston College* We investigate phase locking between a particular non-linear oscillator and a periodic drive. The nonlinear equation we study is a reduced version of the celebrated Hodgkin-Huxley equations, which we couple to a cosine drive representing an EEG Rhythm. This model is motivated by the growing interest in the role of the exact timing of action potentials in neurons. For instance, electro-physiology experiments indicate that the phase differences between action potential times and large-scale oscillatory neuron activity (EEG rhythms) carry reliable information. We study various thresholds for phase locking and the delicate interplay between coherence and decoherence leading to chaos near these phase-locking thresholds.

**10:36**
**Y26 12 The Influence of Environment Geometry on Injury Outcome: I. Cervical Spine** SAAMI J. SHAIBANI, *Independent Modeling, Algorithms & Analytical Studies (IMAAS)* Previous studies with some 500 patients have indicated that the forces at particular injury sites of occupants in motor-vehicle accidents can-

not be simply related to parameters for the occupant or the impact.[1-2] Another factor that might play a role is assessed in this research, namely passenger compartment geometry, which in most low-severity insults involves the seating arrangement and the restraint system. Analysis of the former is achieved here by considering the heights, lengths and angles of the seat cushion and seat back. The separate effect of geometric environment on the potential for neck injury is then found from studying only those cases with isometric occupants in isokinetic impacts. Such stringent constraints require the matching of numerous data fields, thus reducing the number of suitable candidates quite significantly. However, enough cases remain from the large population available for a proper evaluation to be undertaken. 1. Effect of occupant and impact factors on forces within neck, Bull Am Phys Soc, 45, 1018 (2000). 2. within low back, Bull Am Phys Soc, 46, 1174 (2001).

**10:48**

**Y26 13 Flux Analysis of Hypoxia Response Network.** YIHAI YU, *Department of Physics, George Washington University* RAHUL SIMHA, *Department of Computer Science, George Washington University* FRANK TURANO, *Department of Biological Sciences, George Washington University* CHEN ZENG, *Department of Physics, George Washington University* The availability of cellular oxygen regulates many physiological processes. Oxygen deficiency, i.e., hypoxia, induces expression of a set of genes that are involved in angiogenesis and metabolism. Here we report a detailed flux analysis on a theoretical model on hypoxia response network proposed by Kohn et al. The network is decomposed into smaller underlying pathways which are amenable to direct analytical calculations and capture the essence of the original larger network as observed in numerical simulations. Our analysis elucidates a generic mechanism for the switch-like response of gene up-regulation to hypoxia.

## SESSION Y28: FOCUS SESSION: MAGNETIC AND DOPING EFFECTS IN COJUGATED ORGANICS

**Friday Morning, 17 March 2006**
**325, Baltimore Convention Center at 8:00**
**Maria Nikolou, Cornell University, presiding**

**8:00**

**Y28 1 Anomalous Magnetoresistance Phenomena in Organic Semiconductors*** JEREMY D. BERGESON, DEREK M. LINCOLN, RUTH SHIMA EDELSTEIN, VLADIMIR N. PRIGODIN, ARTHUR J. EPSTEIN, *The Ohio State University, Columbus, OH 43210-1117* We report magnetoresistance (MR) phenomena with temperature and bias dependence in organic semiconductor thin films with either nonmagnetic or magnetic contacts through high field reaching 9T. For nonmagnetic organic thin films such as $Alq_3$ we find a low field MR up to 15%. A similar magnetic field effect has been reported earlier[1] but, as noted, the mechanism remains unclear. We propose a model of the anomalous MR where charge transport is space-charge limited. The current is determined by the e-h recombination rate. The recombination rate is field dependent, analogous to the chemical yield for radical pairs[2]. Using an organic- based magnetic semiconductor[3], $V[TCNE]_x$, and Co as magnetic contacts, with a nonmagnetic organic semiconductor ($\alpha$-6T) leads to an order-of-magnitude broader zero-centered MR peak superimposed on a spin-valve effect. Possible origins of this broader MR will be discussed. 1. Francis, et al., New J. Phys. **6** 185 (2004); Frankevich, et al., Phys. Rev. B **53** 4498 (1996) 2. Steiner and Ulrich, Chem. Rev. **89** 51 (1989) 3. Pokhodnya, et al., Adv. Mater. **12** 410 (2000); Prigodin, et al., Adv. Mater. **14** 1230 (2002); Shima Edelstein, et al., Mater. Res. Soc. Symp. Proc. **871E** I7.3 (2005)

*Supported by AFOSR Grant No. F49620-03-1-0175 and DOE Grant Nos DE-FG02-86ER45271 and DE-FG02-01ER45931

**8:12**

**Y28 2 Preparation, Magnetism, and Applications of Thin Films of the Organic Semiconductor $V[TCNE]_{x\sim2}$** R. SHIMA EDELSTEIN, D.M. LINCOLN, J.-W. YOO, N.P. RAJU, J.D. BERGESON, A.J. EPSTEIN, *The Ohio State University, Columbus, OH, 43210* J.B. KORTRIGHT, *Lawrence Berkeley National Lab, Berkeley, CA, 94720* Different aspects of the room-temperature ($T_c > 350K$) molecular magnet vanadium tetracyanoethylene ($V[TCNE]_{x\sim2}$) remain only partially understood, including its intra- and inter-molecular bonding and spin distribution, degradation mechanisms, and mesoscopic magnetic and chemical order. Previous studies have shown that control of the local order, structure, spin, and chemical composition determines the magnetic state achieved and its charge transport and dynamic properties[1]. In this study, we focus on thin films ( $\sim$ 0.05-0.5 $\mu$m) prepared by CVD[2,3] (room temperature conductivity $10^{-4}$-$10^{-3}$S/cm). Soft x-ray absorption and Magnetic Circular Dichroism (MCD) spectra of the atomic edges are presented, together with XPS, SQUID magnetometry, and EPR spectroscopy. The knowledge gained enables successful demonstration of spin valve devices and photoinduced magnetism in this molecule-based magnetic semiconductor. 1. Pokhodnya, et al, PRB **63**, 174408 (2001) 2. Pokhodnya, et al, Adv. Mater. **12**, 410 (2000) 3. Shima, et al, MRS Proc. **871E**, I7.3 (2005) Supported by DOE grants #DE-FG02-86ER45271, DE-FG02- 01ER45931, DE-AC03-76SF00098, and AFOSR grant #F49620-03-1-0175. NSF-DMR grant #0114098 and Dr. Lisa Hommel are acknowledged for XPS studies.

**8:24**

**Y28 3 Magnetoresistance and Ferrimagnetic Resonance (FMR) on Thin Films of Organic-based Magnetic Semiconductor $V[TCNE]_{x\sim2}$ with $T_c$ above 350 K.*** N.P. RAJU, R. SHIMA EDELSTEIN, A.J. EPSTEIN, *The Ohio State University, Columbus, OH 43210* We present magnetoresistance and ferrimagnetic resonance (FMR) results on a CVD-prepared [1] thin films (about 0.5 micron thick) [2] of ferrimagnetic semiconductor $V(TCNE)_{x\sim2}$. The temperature dependence of resistance, and the magnetoresistance variation with magnetic field and temperature show similar to the trends reported earlier. [3] FMR spectra reported here show marked differences from the earlier studies on thicker samples (up to 2 microns). [4] Earlier reported FMR shows several sharp peaks compared to only two in the present study. We report temperature dependence of linewidth and integrated intensity for each of these two peaks. The earlier study suggested that the porosity of the sample as one of the possible origins for many peaks. It appears that absence of many sharp FMR peaks in the present sample may reflect less porosity of the thin film which is important for the development of spin-valve devices. 1. K.I. Pokhodnya et. al., Adv. Mater **12**, 410 (2000). 2. Shima et. al., MRS Proc. **871E**, I7.3 (2005) 3. N.P. Raju et. al., J. Applied

Physics **93**, 6799 (2003). 4. R. Plachy et. al., Phys. Rev. B **70**, 064411 (2004).

*Supported by DOE grants # DE-FG02-86ER45271, DE-FG02-01ER45931, and AFOSR grant # F49620-03-1-0175.

**8:36**

**Y28 4 Semiconducting Organic Thin Film Devices with Large Magnetoresistance** Y. SHENG, Ö. MERMER, *Dept. of Phys. & Astr., Univ. of Iowa* G. VEERARAGHAVAN, *Dept of Elec. & Comp. Engr., Univ. of Iowa* T.D. NGUYEN, *Dept. of Phys. & Astr., Univ. of Iowa* T.L. FRANCIS, *OMR Sensors Inc., Dubuque, Iowa* M. WOHLGENANNT, *Dept. of Phys. & Astr., Univ. of Iowa* A comprehensive study on a recently discovered, large magnetoresistance (MR) effect in sandwich devices comprised of nonmagnetic electrodes and organic thin films is performed. Devices were fabricated from pi-conjugated polymers and small molecular weight compounds in combination with different electrode materials, and characterized extensively at different voltages, temperatures, and at weak magnetic fields from DC up to 100 kHz in frequency. The MR effect shows only weak temperature dependence and is independent of the sign and direction of the magnetic field. The effect reaches up to 10% in a magnetic field of 10 mT at room temperature. To illustrate a potential application of the effect, we demonstrate a prototype organic LED (OLED) touchscreen using the MR effect. To the best of our knowledge, the discovered effect is not adequately described by any of the MR mechanisms known to date.

**8:48**

**Y28 5 Structure-property relationships of water-dispersible, conductive PANI-PAMPSA** JOUNG EUN YOO, KWANG SEOK LEE, JAMES NORMAN, *University of Texas at Austin* MATTHEW ESPE, *University of Akron* YUEH-LIN LOO, *University of Texas at Austin* Polyaniline (PANI) is an attractive candidate for organic and polymer electronics because of its high electrical conductivity when doped with molecular acids. Its utility as functional components in electrical devices, however, has been severely restricted by processing and patterning limitations because molecular acid-doped PANI does not dissolve in any common solvents. To overcome this barrier, we have investigated polyaniline that is template polymerized in the presence of a polymer acid, poly(2-acrylamino-2-methyl-1-propanesulfonic acid), PAMPSA. In addition to doping polyaniline, the sulfonic acid groups along the polymer acid chain render water- dispersability to PANI-PAMPSA. The doped polymer is therefore not only electrically conductive, it can be easily processed and patterned from an aqueous medium. Solid-State NMR indicates that template polymerization results in linear, defect-free polyaniline. Both X-ray diffraction and electron microscopy experiments on PANI-PAMPSA synthesized at varying PAMPSA molecular weights reveal that PANI-PAMPSA crystallinity increases with decreasing PAMPSA molecular weight. The conductivities of PANI-PAMPSA increase accordingly with crystallinity. These results are corroborated by UV-vis-NIR experiments where the polaron peaks become progressively broader and red-shifted with decreasing PAMPSA molecular weights.

**9:00**

**Y28 6 The Optical Conductivity and Dielectric Constant of Polyaniline Nanofiber-based Film** OLUDUROTIMI O. ADETUNJI, NAN-RONG CHIOU, ARTHUR J. EPSTEIN, *The Ohio State University, Columbus, OH 43210-1117* We report the optical properties of polyaniline/HCl nanofiber (PANN) films with interconnecting nanofibers of average diameter 100 nm. The room temperature dc conductivity is in the range of 2-4 S/cm in the insulating regime of the disorder induced metal- insulator (M-I) transition [1]. PANN films were probed by reflectance spectroscopy at room temperature over a broad energy range 2meV-6eV. The reflectance ( $< 4200 cm^{-1}$) increases monotonically as the frequency is lowered but has no indication of a plasma edge. Optical constants such as frequency dependent dielectric constant and frequency dependent conductivity have been derived via Kramers-Kronig (K-K) analysis of the reflectance data using appropriate extrapolations. The resulting optical conductivity extrapolated to near-zero frequency scales is in agreement with the measured dc conductivity of 2-4 S/cm [2]. A maximum of the frequency dependent conductivity is found at $\sim 2400 cm^{-1}$ while the K-K analysis shows no zero crossing of the dielectric constant between 40-50000$cm^{-1}$. We discuss these results in terms of roles of disorder and localization. This leads us to the conclusion that PANN films are on the insulating side of the disorder induced metal- insulator transition. [1]R.S. Kohlman, et al., PRL 77, 13 (1996) [2]N.-R. Chiou and A.J. Epstein, Adv. Mater. 17, 1679 (2005) Supported in part by NSF-IGERT Grant No DGE-0221678.

**9:12**

**Y28 7 Charge transport in conducting polymer nanofibers** NATALYA ZIMBOVSKAYA, *University of Puerto Rico - Humacao* Here, we present theoretical analysis of electron transport in polyaniline based (PANi) nanofibers assuming the metalic state of the material. To build up this theory we treat conducting polymers as a special kind of granular metals, and we apply the quantum theory of conduction in mesoscopic systems to describe the transport between metallic-like granules. Our results show that the concept of resonance electron tunneling as the predominating mechanism providing charge transport between the grains is supported with recent experiments on the electrical characterization of single PANi nanofibers. By contacting the proposed theory with the experimental data we estimate some important parameters characterizing the electron transport in these materials [1]. Using the Buttiker dephasing model within the scattering matrix formalism we analyze dephasing effects, and we show that these effects could be reduced enough to allow the structure of the electron transmission function to be exposed in the experiments on the electronic transport through fibers [2]. Also, we discuss the origin of rectifying features observed in current-voltage characteristics of fibers with varying cross-sectional areas. 1. N. A. Zimbovskaya, A. T. Johnson, Jr., and N. J. Pinto, Phys. Rev. B 72, 024213 (2005). 2. N. A. Zimbovskaya, J. Chem. Phys. 123, 114708 (2005).

**9:24**

**Y28 8 Effects of confinement on the transport properties of CSA doped polyaniline** RAUL PEREZ, NELIZA LEON, IDALIA RAMOS, NICHOLAS PINTO, *Department of Phys. and Electr., University of Puerto Rico - Humacao* PAWAN KAHOL, *Dept. of Physics, Astronomy and Materials Science, Missouri State University* Polyaniline doped with camphor sulfonic acid (CSA) and cast from *m*-cresol can exhibit metallic behavior depending on the conditions of preparation. Under standard methods

of preparation the transport properties of cast films generally lie on the insulating side of the metal-insulator transition. We have confined CSA doped PANi into the cylindrical pores of a dielectrically inert porous matrix and measured the temperature dependence of the resistance. The resistance of the confined polymer is seen to have a weaker dependence at low temperatures than that of the cast film. Further analysis of the results show that the charge transport of the confined polymer has moved into the metallic regime while that of the cast film lies in the insulating regime. Reduced barriers to charge transport that result from the suppression of microphase separation of the non-dopable forms of polyaniline due to extreme confinement in the porous matrix are believed to be responsible for this crossover.

**9:36**

**Y28 9 Gas sensing using the microwave conductivity of conducting polymer nanofiber thin films.** ALEXEY KOVALEV, LINTAO CAI, THERESA MAYER, *Pennsilvania State University, University Park, PA, 16802.* There are a variety of chemoresistive sensors based on conducting polymer thin films, and studies of conducting polymer nanofiber thin films and single nanofibers sensors are an active area of research because of their enhanced sensitivity. Traditional chemoresistive sensors monitor a change in DC resistance that arises when a low concentration of a chemical vapor is present. In this talk, we will discuss the use of conducting polymer nanofiber thin films as gas sensors that operate in the microwave frequency range. Polyaniline nanofiber films that were 1 - 10 $\mu$m thick were characterized measuring DC conductivity (four-point) and microwave conductivity in the range of 4 - 8 GHz. We found a direct correlation between changes in the DC and microwave conductivity during exposure to ammonia and hydrochloric acid at concentrations of 10 - 1000 ppm. These films show a significant response over this range of concentrations, thus opening the possibility of using conducting polymers thin films as remote wireless gas sensors.

**9:48**

**Y28 10 Anomalous transmission through a periodic subwavelength hole array in heavily doped conducting polymer films*** TATSUNOSUKE MATSUI, Z. VALY VARDENY, *Physics Department, University of Utah* AMIT AGRAWAL, AJAY NAHATA, *Department of Electrical and Computer Engineering, University of Utah* REGHU MENON, *Department of Physics, Indian Institute of Science* PHYSICS DEPARTMENT, UNIVERSITY OF UTAH COLLABORATION, DEPARTMENT OF ELECTRICAL AND COMPUTER ENGINEERING, UNIVERSITY OF UTAH COLLABORATION, DEPARTMENT OF PHYSICS, INDIAN INSTITUTE OF SCIENCE COLLABORATION, Since Ebbesen et al. reported the phenomenon of ''anomalous transmission'' through optically thick metallic films perforated with two-dimensional (2D) subwavelength hole array, numerous studies have been carried out to explore both fundamental issues and potential device applications. So far, studies on ''anomalous transmission'' were carried out using metals and semiconductors. We report here the observation of ''anomalous transmission'' in 2D hole array on films of another, more exotic class of conductors, namely heavily-doped organic conducting polymers. Specifically, the conductivity of conducting polymers can be controlled in situ by changing doping level using an electrochemical technique, so that we could tune the transmission characteristics by applied voltage. With this goal in mind we will report the ''anomalous transmission'' spectra of conducting polymer films at various doping levels. *supported in part by ARO.

**SESSION Y29: FOCUS SESSION: NOISE AND FLUCTUATION IN BIOLOGICAL SYSTEMS**
**Friday Morning, 17 March 2006**
**326, Baltimore Convention Center at 8:00**
**Peter Jung, Ohio University, presiding**

***Contributed Papers***

**8:00**

**Y29 1 How stability can lead to variability: An example from eukaryotic gene expression** GABOR BALAZSI, WILLIAM BLAKE, *Applied BioDynamics Laboratory, Boston University* FARREN ISAACS, *Genetics Department, Harvard Medical School* KEVIN MURPHY, JAMES J. COLLINS, *Applied BioDynamics Laboratory, Boston University* Eukaryotic genes have the potential for transcriptional reinitiation, resulting in repeated rounds of transcription from a scaffold of proteins assembled near the promoter region. We use stochastic simulations and mathematics to analyze the effect of the promoter-scaffold stability on gene expression noise for various steady-state levels of induction. In agreement with experimental observations, we find that decreasing transcription scaffold stability results in lower levels of noise at the protein level. We track the cause of this decrease through mRNA expression down to the level of an engineered GAL1 promoter.

**8:12**

**Y29 2 How stability can lead to variability: Induction timecourse of a eukaryotic gene** WILLIAM BLAKE, GABOR BALAZSI, *Applied BioDynamics Laboratory, Boston University* FARREN ISAACS, *Genetics Department, Harvard Medical School* KEVIN MURPHY, *Applied BioDynamics Laboratory, Boston University* YINA KUANG, DAVID R. WALT, *Department of Chemistry, Tufts University* JAMES J. COLLINS, *Applied BioDynamics Laboratory, Boston University* Using an engineered GAL1 promoter as a model, we study the effect of the promoter-scaffold stability on the mean and noise of gene expression during an induction timecourse. In agreement with experimental observations, we find that decreasing transcription scaffold stability results in slower buildup of protein product and lower levels of noise at the protein level. This is a consequence of ''transcriptional bursting,'' observed in the simulations as well as experiment, where optical fiber-based technology was used to monitor induction timecourses in individual cells.

**8:24**

**Y29 3 Origins of extrinsic variability in eukaryotic gene expression** DMITRI VOLFSON, JENNIFER MARCINIAK, *UC San Diego* WILLIAM J. BLAKE, *Boston University* NATALIE OSTROFF, LEV S. TSIMRING, JEFF HASTY, *UC San Diego* Variable gene expression within a clonal population of cells has been implicated in a number of important processes including mutation and evolution, determination of cell fates and the development of genetic disease. Recent studies have demonstrated that a significant component of expression variability arises from extrinsic factors thought to influence multiple genes in concert, yet the biological origins of this extrinsic variability have received little attention. Here we combine computational modeling with fluorescence data generated from multiple promoter-gene inserts in *Saccharomyces cerevisiae* to identify two major sources of extrinsic variability. One unavoidable source arising from the cou-

pling of gene expression with population dynamics leads to a ubiquitous noise floor in expression variability. A second source which is modeled as originating from a common upstream transcription factor exemplifies how regulatory networks can convert noise in upstream regulator expression into extrinsic noise at the output of a target gene. Our results highlight the importance of the interplay of gene regulatory networks with population heterogeneity for understanding the origins of cellular diversity.

*Invited Papers*

**8:36**
**Y29 4 Noisy cellular decision-making: from temporal to spatial choices.**
ALEXANDER VAN OUDENAARDEN, *Massachusetts Institute of Technology*

This abstract was not received electronically.

*Contributed Papers*

**9:12**
**Y29 5 Absolute Rate Theories of Epigenetic Stability** ALEKSANDRA M. WALCZAK, JOSE N. ONUCHIC, PETER G. WOLYNES, *Center for Theoretical Biological Physics, UCSD* Spontaneous switching events in most characterized genetic switches are rare, resulting in extremely stable epigenetic properties. We show how simple arguments lead to theories of the rate of such events much like the absolute rate theory of chemical reactions corrected by a transmission factor. Both the probability of the rare cellular states that allow epigenetic escape, and the transmission factor, depend on the rates of DNA binding and unbinding events and on the rates of protein synthesis and degradation. Different mechanisms of escape from the stable attractors occur in the nonadiabatic, weakly adiabatic and strictly adiabatic regimes, characterized by the relative values of those input rates.

**9:24**
**Y29 6 Noise and correlations in genes silenced by small RNA.** TERENCE HWA, EREL LEVINE, *Center for Theoretical Biological Physics, UCSD* Many small regulatory RNAs have been identified in prokaryotes and eukaryotes in recent years. In many cases, RNA regulation is found in critical pathways. These include stress response and quorum sensing pathways in bacteria, and cell differentiation and programmed cell death in eukaryotes. In many cases, regulation by small RNA is used in switching off a response program as long as it is not required, allowing for a fast switching on when necessary. Clearly, accidental execution of such a program may bare grave consequences on the cell, and should be avoided. Here we analyze a stochastic model for gene regulation by the most abundant class of small RNA in bacteria. This class of small RNAs acts by base pairing with target mRNAs, silencing its translation and actively promoting its degradation. Importantly, the small RNA molecule is not recycled. Our model suggests that genes silenced by sRNA exhibits smooth noise, as opposed to the bursty noise characteristic to genes repressed at the level of transcription, with coupling between intrinsic noise and global, extrinsic fluctuations. In addition, we investigate how noise propagates through the indirect coupling between different targets of the same sRNA. These features are discussed in the context of circuits exhibiting multi-stability, where protein bursts have strong implications on spontaneous switching.

**9:36**
**Y29 7 A model for codon position bias in RNA editing*** RALF BUNDSCHUH, TSUNGLIN LIU, *The Ohio State University* RNA editing can be crucial for the expression of genetic information via inserting, deleting, or substituting a few nucleotides at specific positions in an RNA sequence. Within coding regions in an RNA sequence, editing usually occurs with a certain bias in choosing the positions of the editing sites. In the mitochondrial genes of *Physarum polycephalum*, many more editing events have been observed at the third codon position than at the first and second, while in some plant mitochondria the second codon position dominates. Here we propose an evolutionary model that explains this bias as the basis of selection at the protein level. The model predicts a distribution of the three positions rather close to the experimental observation in *Physarum*. This suggests that the codon position bias in *Physarum* is mainly a consequence of selection at the protein level.

*This work has been supported by grant no. DMR-0404615 from the NSF.

**9:48**
**Y29 8 From Asymmetric Exclusion Processes to Protein Synthesis*** JIAJIA DONG, BEATE SCHMITTMANN, ROYCE K.P. ZIA, *Department of Physics, Virginia Tech* Protein production rates are clearly vital for all biological systems. Thus, there is considerable interest in understanding the origins of these rates, as well as in manipulating them, especially for physiological and pharmaceutical applications. Since some codons are ''fast'' and others ''slow,'' we propose to exploit these differences and modify the production rate for any specific protein by replacing codons in the associated mRNA by their synonymous counterparts. As an illustration, we study a simple model of protein production: the one-dimensional driven lattice gas, also known as the totally asymmetric simple exclusion process (TASEP). We investigate systematically the effects on the overall current (the protein production rate) of having one or two slow/fast sites (i.e., codons) in an otherwise homogeneous lattice. The currents show a nontrivial dependence on the location of a single ''defect'' as well as on the separation between two defects. We discuss the implications for more realistic models of protein production.

*Supported by NSF DMR-0414122

**10:00**
**Y29 9 Intrinsic Fluctuations, Robustness and Tunability in Signaling Cycles.** JOSEPH LEVINE, *Caltech* HAO YUAN KUEH, *Harvard Univ.* LEONID MIRNY, *MIT* Covalent modification cycles (e.g. phosphorylation) underlie most cellular

signaling. Low molecular copy number, arising from compartmental segregation and slow diffusion between compartments, potentially renders these cycles vulnerable to intrinsic chemical fluctuations. How can a cell operate reliably in the presence of this inherent stochasticity? How do changes in extrinsic parameters lead to variability of response? Can cells exploit these parameters to tune cycles to different ranges of stimuli? We study the dynamics of an isolated phosphorylation cycle. Our model shows that the cycle transmits information reliably if it is tuned to an optimal parameter range, in spite of intrinsic fluctuations and even for small input signal amplitudes. At the same time, the cycle is sensitive to changes in the concentration and activity of kinases and phosphatases. This sensitivity can lead to significant cell-to-cell response variability Our results show that signaling cycles possess a surprising combination of robustness and tunability. This combination makes them ubiquitous in eukaryotic signaling, optimizing signaling in the presence of fluctuations using their inherent flexibility. On the other hand, cycles tuned to suppress intrinsic fluctuations can be fragile to changes in the number and activity of kinases and phosphatases. Such trade-offs in robustness to fluctuations can influence the evolution of signaling cascades, making them the weakest links in cellular circuits.

*Invited Papers*

**10:12**
**Y29 10 The Nature of Memory Objects in the Brain.**
PIERRE-GILLES DE GENNES, *Physico-Chime Institut Curie*

Our minds keep a huge number of memories. We discuss here the number $M$ of neurons which must be implied in one primal memory object (the smell of a rose). We find that (in a storage area which is not genetically designed) spatial and connectivity requirements impose that $M$ be *very small* (of the order of 3). We then extend these considerations to associative memories (where the smell of a rose evokes the color of a rose).

*Contributed Papers*

**10:48**
**Y29 11 Resource allocation in neural networks for motor control** J. MILTON, *Claremont Colleges, USA* J. CUMMINS, *Claremont McKenna College, USA* J. GUNNOE, M. TOLLEFSON, *Scripps College, USA* J.L. CABRERA, *IVIC, Venezuela* T. OHIRA, *Sony Computer Science Lab, Japan* Multiplicative noise plays an important part of a non-predictive control mechanism for stick balancing at the fingertip. However, intentionally-directed movements are also used in stick balancing, particularly by beginners. The interplay between intentional and non-predictive control mechanisms for stick balancing was assessed using two dual task paradigms: the subject was asked to either move one of their legs rhythmically or to imagine moving their leg while balancing a stick (55.4 cm, 35 g) at their fingertip. Performance was measured by determining the stick survival function, i.e. the fraction of trials (total $\geqslant 25$) for which the stick remained balanced at time t as a function of t. Performance was increased by concurrent rhythmic leg movements (50% survival time shifted from 8-9s to 15s in a typical subject). Imagined movements resulted in a similar improvement (50% survival time of 20s for the above subject) suggesting that this enhancement is not simply related to mechanical vibrations of the fingertip induced by leg movement. These observations emphasize the importance of the development of mathematical models for neural control of skilled motor movements that take into resource allocation of limited resources, such as intention.

## SESSION Y30: FOCUS SESSION: BIOPOLYMERS I: PHASE TRANSITIONS
**Friday Morning, 17 March 2006; 327, Baltimore Convention Center at 8:00**
**Jose Onuchic, University of California, San Diego, presiding**

*Invited Papers*

**8:00**
**Y30 1 Temperature and Pressure effects on folding/unfolding of proteins.**
ANGEL GARCIA, *Department of Physics and Astronomy*

High hydrostatic pressures change the energy landscape of proteins, affecting the thermodynamics and kinetics of folding. Proteins denature at high hydrostatic pressures, implying that the unfolded proteins in aqueous solution have lower volume than the folded state. A model that explains pressure unfolding requires water to penetrate the protein interior and disrupt the protein hydrophobic core. I will explore the energetics of water penetration and the effect of pressure on hydrophobic interactions. I will also describe molecular simulations of the reversible folding/unfolding equilibrium as a function of density and temperature of solvated peptides that can form alpha helices (the AK peptide) and beta hairpins (the C terminal domain of protein G). I will characterize the structural, thermodynamic and hydration changes as a function of temperature and pressure. To study protein folding equilibrium thermodynamics we use an extension of the replica exchange molecular dynamics (REMD) method that allows for density and temperature Monte Carlo exchange moves.

**8:36**
**Y30 2 The energy landscape for folding and function.***
JOSE ONUCHIC, *Center for Theoretical Biological Physics, UCSD*

Globally the energy landscape of a folding protein resembles a partially rough funnel. The local roughness of the funnel reflects transient trapping of the protein configurations in local free energy minima. The kinetics of folding is best considered as a progressive organization of an ensemble of partially folded structures through which the protein passes through on its way to the folded structure. The folding mechanisms for several fast-folding proteins can be described using an energy landscape theory to set up the correspondence with simulations of protein minimalist models. Using these simulations together with analytical theory, we can learn about good (minimally frustrated) folding sequences and non-folding (frustrated) sequences. An important idea that emerges from this theory is that subtle features of the protein landscape can profoundly affect the apparent mechanism of folding. Experiments on the dependence of the folding/unfolding times, and the stability of these proteins to denaturant concentration and site-directed mutagenesis, and on the early events of folding allow to infer the global characteristics of the landscape. In addition to need to minimize energetic frustration, the topology of the native fold also plays a major role in the folding mechanism. Some folding motifs are easier to design than others suggesting the possibility that evolution not only selected sequences with sufficiently small energetic frustration but also selected more easily designable native structures. Several proteins (such as CI2 and SH3) have sufficiently reduced energetic frustration) that much of the heterogeneity observed in their transition state ensemble (TSE) is determined by topology. Topological effects go beyond the structure of the TSE. The overall structure of the on-route and off-route (traps) intermediates for the folding of more complex proteins is also influenced by topology. Utilizing this theoretical framework, simulations of minimalist models and computationally-expensive all-atom simulations, we are now obtaining a quantitative understanding of the folding problem, which allows for a direct comparison to a new generation of folding experiments. Connections between the folding landscape and protein function will also be discussed.

*Supported by the NSF.

***Contributed Papers***

**9:12**
**Y30 3 RNA folding inside a virus capsid and dimensional reduction.** ROUZBEH GHAFOURI, *Department of Physics, UCLA* ROBIJN BRUINSMA, *Department of Physics, UCLA* JOSEPH RUDNICK, *Department of Physics, UCLA* As RNA folds on itself, in certain conditions, it takes the form of a branched polymer. So the problem of RNA folding in a virus capsid is essentially the problem of a branched polymer in a confined environment. In this paper we attack the problem using the technique of dimensional reduction which relates a branched polymer with self interation in D dimension to a hardcore classical gas in (D-2) dimension. We look for phase transitions and intersting physical quantities such as pressure.

**9:24**
**Y30 4 On the Melting Transition of RNA** DAVID SCHWAB, *Deparment of Physics, UCLA* ROBIJN BRUINSMA, *Deparment of Physics, UCLA* The secondary structure of RNA can undergo a phase transition from a designed native state to a branched molten-globule. This melting transition is continuous, neglecting excluded volume. We study the effect of excluded volume interactions in good solvent on the melting transition. First, we calculate the effect of a constant external tension on the melting transition in the ideal polymer case and then, in the context of Flory theory, equate the tension with what would be generated by excluded volume. We find that, with excluded volume, the continuous melting transition is still second order but with a different exponent.

**9:36**
**Y30 5 Trapping and Condensing DNA at the Air/Water Interface** JAIME RUIZ-GARCIA, *Instituo de Fisica – UASLP* DNA is a highly charged polyelectrolite and as such it is considered to be completely soluble in pure water. Surprisingly, we found that DNA can be trapped at the air/water interface and does not go back into a pure water subphase. Once at the interface, DNA molecules condense to form different two-dimensional mesostructures such as foams, giant rings, disks and rods at low density. This condensation occurs without the presence of multivalent cationic ions, as it is required in bulk, for example in condensing DNA toroids. At high density, the molecules form a regular monomolecular network. At the interface, DNA is only partially immersed in water, which originates that the chains get only partially charged, but the charges are of the same sign. Therefore, this can be considered another case of like-charge attraction, similar to those found in colloids trapped between glass plates and at the air/water interface. However, the origin of the attractive part of the interaction potential is unknown. In addition, we found that DNA at the air/water interface can form 2D smectic-like domains tens of microns in size, which are interesting from a theoretical and application standpoints.

**9:48**
**Y30 6 Insight into the Helix-to-Coil Transition in DNA** BOUALEM HAMMOUDA, *National Institute of Standards and Technology* Dissolved DNA is known to undergo a helix-to-coil transition when temperature is increased. For a solution of 4% DNA in water, the transition temperature is around 94$^o$C. UV absorption spectroscopy was performed to characterize such a transition. The 260 nm absorption line is a good monitor of the un-stacking of the DNA amine bases. Small-Angle Neutron Scattering was also performed to investigate structural changes that accompany the transition. A characteristic DNA cross section correlation length was found to increase from 9A to 15A and the Porod exponent was found to decrease from close to 4 to around 2 across the transition. The average sugar-sugar inter-distance is larger in the open molecule coil phase. The helix phase is characterized by a cylindrical structure with well-defined interface whereas melted DNA macromolecules behave like Gaussian coils. Jump in the scattered (solvation) intensity was also observed across the transition. A hysteresis cycle was observed upon a sub-

sequent temperature decrease. Once DNA melts, it does not reform the helix phase easily. DNA solvation (interaction of DNA and solvent molecules) has also been investigated. When solvent mixtures (for example water/alcohol mixtures) are used, ideal solvent mixing is observed for the helix phase but a highly non-ideal mixing behavior is observed for the coil phase.

**10:00**

**Y30 7 Diffusion of Isolated DNA molecules: dependence on length and topology** RAE M. ROBERTSON, STEPHAN LAIB, DOUGLAS E. SMITH, *University of California at San Diego* Diffusion coefficients (D) for relaxed circular and linear DNA molecules ranging in length (L) from 5.9 to 287.1 kilobasepairs were measured by tracking the Brownian motion of single molecules. A topology independent scaling law, $D\sim L^{-0.58+/-0.016}$, was observed, in good agreement with the –0.588 exponent predicted by renormalization group theory. The measured ratio $D_{Circular}/D_{Linear}$ = 1.32+/-0.014 fell between predictions of 1.18 for Kirkwood hydrodynamic theory and 1.45 for renormalization group theory and agreed best with a value 1.31 predicted using the Zimm model and an expression for the radius of gyration proposed by Bensafi, Maschke, and Benmouna. Measurements on supercoiled DNA molecules were also made and qualitatively compared to theoretical predictions.

**10:12**

**Y30 8 Mobility of DNA on supported lipid bilayers** CHAKRADHAR PADALA, *Rensselaer Polytechnic Institute* RICHARD COLE, *Wadsworth Center* SANAT KUMAR, RAVI KANE, *Rensselaer Polytechnic Institute* Extensive theoretical ideas have been developed to understand the transport properties of transmembrane proteins in the lipid bilayer. However, of late, there has been a rising interest in understanding the transport properties of non-compact macromolecules strongly adsorbed ''on'' and not incorporated into lipid bilayers in light of the relevance for designing improved DNA separation strategies and for gene therapy. Previously, researchers like Radler itet al. have suggested that such strongly adsorbed polymers can be treated similar to a polymer in a two-dimensional fluid, but there exists no experimental proof to date. In order to test this hypothesis and also to gain a better understanding of polymer dynamics in two dimensions, we studied the lateral transport of a short, single stranded DNA oligonucleotide adsorbed on a supported cationic lipid bilayer. Fluorescence Recovery After Photobleaching (FRAP) analysis reveals that diffusivity of the adsorbed DNA quantitatively tracks that of the underlying lipid. These results, along with the comparison between our results for short, non-compact adsorbed biopolymers and those reported for globular proteins incorporated into the lipid bilayer will be discussed.

**10:24**

**Y30 9 Electrophoresis of DNA on a disordered two-dimensional substrate** CYNTHIA J. OLSON REICHHARDT, CHARLES REICHHARDT, *Theoretical Division and Center for Nonlinear Studies, Los Alamos National Laboratory* We propose a new method for electrophoretic separation of DNA in which adsorbed polymers are driven over a disordreed two-dimensional substrate which contains attractive sites for the polymers. Using simulations of a model for long polymer chains, we show that the mobility increases with polymer length, in contrast to gel electrophoresis techniques, and that separation can be achieved for a range of length scales. We demonstrate that the separation mechanism relies on excluded volume interactions between polymer segments.

**10:36**

**Y30 10 Kinetic Modeling of Designed Signaling DNA Aptamers** ISSEI NAKAMURA, RAZVAN NUTIU, JASMINE YU, YINGFU LI, AN-CHANG SHI, *McMaster University* Aptamers are recently developed molecular biosensors made of single functionalized DNA molecules. They can bind a protein target specifically or a complementary DNA sequence. The binding kinetics can be studied based on the principle of fluorescence quenching, which in turn provides an understanding of the binding mechanism and the conformational structure of DNA during the binding reaction. Despite many experimental studies, an understanding of the binding reaction is still lacking. In our study, we constructed kinetic models for the aptamer binding reaction, and showed that the theoretical models can be studied to describe experimental observations. Determined parameters for the rate constant for the reaction provided us with an understanding of the binding mechanism of aptamers. We will discuss the numerical solutions to them in comparison with the experiment and show how the binding reaction of aptamers occurs as time proceeds.

**10:48**

**Y30 11 AFM Imaging of Counterion-Induced Phase Transition of Biological Polyelectrolyte Network on a Photopolymer Containing Azo-Dye*** TAIJI IKAWA, OSAMU WATANABE, *Toyota CRDL, Inc., Japan* YOULI LI, CYRUS SAFINYA, *UC, Santa Barbara* We present a new method for direct imaging of protein assembly based on atomic force microscopy and a protein immobilization technique using a nonionic photopolymer containing azo-dye; the photopolymer was found to be capable of holding proteins in an aqueous solution by exposure to blue-wavelength light. As a model system, we examine the association of actin filament in the presence of divalentcation. We find the method clearly represents phase transitions of the filament network as a function of both cation concentration and filament length. Longer filaments (up to 10 $\mu$m) shows an isolated single filament phase (0 mM of $Mg^{2+}$) transforms to a web-like network phase (5-10 mM) and finally condenses into a close-packed bundled phase (20-80 mM). Meanwhile, shorter filaments (up to 200 nm) form a co-existing nematic-like raft phase at intermediate cation concentration (5-40 mM), coinciding with the previous result obtained by small-angle x-ray scattering study. From angular analysis, the longer filament is shown to prefer wider angular configuration, suggesting the interaction between filaments is dependent on their length such that longer filaments are more repulsive than shorter one.

*Supported, in part, by NSF-DMR0503347 and NSF-CTS-0404444.

**SESSION Y31: QUASICRYSTALS, ADSORPTION ON QUASICRYSTALS, POROUS AND RANDOM MATERIALS**
**Friday Morning, 17 March 2006**
**329, Baltimore Convention Center at 8:00**
**Stefano Curtarolo, Duke University, presiding**

**8:00**
**Y31 1 Magnetism in $Fe_4Al_{13}$ and related FeAl intermetallics** JI CHI, YANG LI, WEIPING GOU, V. GORUGANTI, K. D. D. RATHNAYAKA, JOSEPH H. ROSS, JR., *Department of Physics, Texas A&M University* We report the results of an experimental study of FeAl alloys, including $Fe_4Al_{13}$, $FeAl_2$ and $Fe_2Al_5$. By using NMR, dc magnetic susceptibility, and specific heat, we found that $Fe_4Al_{13}$ and $Fe_2Al_5$ are non-magnetic with some dilute magnetic moments, while $FeAl_2$ can be characterized as a concentrated local moment system. $Fe_4Al_{13}$ is a decagonal quasicrystal approximant with 102 atoms in its unit cell. The $^{27}$Al NMR spin-lattice relaxation indicates a very narrow pseudogap in the electronic density of states $[g(E)]$ in the vicinity of the Fermi energy. The observations could be fit assuming a parabolic variation of $g(E)$, consistent with observations in other quasicrystals and approximants. NMR lineshape measurements also agree with this analysis, and show that the system is dilute-magnetic, in strong contrast to the $FeAl_2$ ordered intermetallic. We use specific heat to analyze the dilute moment density. This work was supported by the Robert A. Welch Foundation, Grant No. A-1526, by the National Science Foundation (DMR-0103455), and by Texas A&M University through the Telecommunications and Informatics Task Force.

**8:12**
**Y31 2 3D octagonal quasicrystals fabricated by phase mask lithography** TAEYI CHOI, ION BITA, EDWIN THOMAS, *Massachusetts Institute of Technology* Quasicrystals were discovered in 1984 and have shown unusual physical and mechanical properties. Artificially patterned quasicrystalline structures have attracted a lot of attention due to their promise as photonic and phononic crystals. A challenge is to create 3D quasicrystalline patterns on the 100nm scale. Using phase mask lithography, we successfully fabricated in photopolymer films 3D quasicrystals having eight-fold rotation axes on a submicron length scale. Conformable phase masks of eight-fold rotation symmetry were first made with multiple interference lithography on a silicone substrate. Light at normal incidence to the phase mask generates a 3D distribution of intensity with quasicrystalline eight-fold symmetry. This intensity distribution is then transferred into a photosensitive material, SU8, generating 3D quasiperiodic structures that we further characterize both structurally and optically.

**8:24**
**Y31 3 Band Structure, Density Waves, and the Third Invariant*** DAVID RABSON, JOHN HUESMAN, *University of South Florida* There are three types of invariants in crystals. The first two, corresponding to electronic degeneracies, are well known, but the third is novel, realized in incommensurate crystals of non-minimal rank. Since the first two invariants have consequences in band structure, it is natural to look there for the third type as well. Rather than developing an atomic or tiling model with the third type of symmetry, we introduce a tight-binding approach based on a density-wave pattern, which is easy to generate from the Rokhsar-Wright-Mermin phase functions.

*Supported by the National Science Foundation through grant DMS-0204845

**8:36**
**Y31 4 Epitaxial orientations and temperature dependence of the 5- to 6-fold ordering transition** STEFANO CURTAROLO, WAHYU SETYAWAN, *Duke University* NICOLA FERRALIS, MILTON W. COLE, RENEE DIEHL, *Penn State University* The ordering of Xe films on an $Al_{73}Ni_{10}Co_{17}$ quasicrystalline surface is studied using grand canonical Monte Carlo simulations with an empirical adsorption potential based on Lennard-Jones interatomic potentials. At all temperatures studied (20-140K), there is a continuous 5- to 6-fold ordering transition in the monolayer [1]. The ordering transition shows interesting temperature-dependent phenomena [2]. At intermediate $T$ ($40K < T < 130K$), the transition occurs before the second layer forms. Moreover, this T-dependent transition shows a non-monotonic dependence on coverage, completing earliest at $T \sim 70K$. At low $T$ ($< 40K$), the transition does not complete, whereas at high $T$ ($> 130K$), the transition completes by the transfer of atoms from the second layer to the first layer. At all temperatures, after the transition completes, the orientations of the monolayer domains are along the 5-fold axes of the quasicrystal. The existence of pentagonal defects gives rise to domains that are rotated by n*60°/5 with n = 1, 2, 3, 4, or 5. The defect density increases with T, suggesting that entropy plays the major role in defect formation [2]. Research sponsored by NSF. [1] S. Curtarolo et al., Phys. Rev. Lett. **95**, 136104 (2005). [2] W. Setyawan, N. Ferralis, R. D. Diehl, M. W. Cole, and S. Curtarolo, *Xe films on a decagonal Al-Ni-Co quasicrystal surface*, (2005).

**8:48**
**Y31 5 Evolution of noble gas films on a decagonal Al-Ni-Co quasicrystal surface.** WAHYU SETYAWAN, *Duke University* NICOLA FERRALIS, RENEE D. DIEHL, MILTON W. COLE, *Penn State University* STEFANO CURTAROLO, *Duke University* The evolution of Ne, Ar, Kr, and Xe films on an $Al_{73}Ni_{10}Co_{17}$ quasicrystalline surface is studied using grand canonical Monte Carlo simulations with an empirical adsorption potential based on Lennard-Jones interatomic potentials. Layer by layer growth is observed for all the studied noble gases. The monolayer of Ar, Kr, and Xe grows abruptly, where as the monolayer of Ne grows gradually. The next layers of all gases grow step wise. At a comparable range of temperatures, the evolution of the monolayer density profiles shows a continuous commensurate 5-fold to incommensurate 6-fold ordering transition for all gases. However, the degree of completeness of the transition varies and shows an increase from Ne, Ar, Kr, to Xe. Research sponsored by NSF.

**9:00**
**Y31 6 Argon adsorption on a microporous metal organic framework, $Cu_3(BTC)_2(H_2O)_3$(Benzene-1,3,5-tricarboxylate)*** K. LASK, V. KRUNGLEVICIUTE, L. HEROUX, A. D. MIGONE, *Southern Illinois University* J.-Y. LEE, J. LI, *Rutgers University* We will present results for argon adsorbed on $Cu_3(BTC)_2(H_2O)_3$(Benzene-1,3,5-tricarboxylate) metal-organic frameworks. Full adsorption isotherms (up to saturation) were measured at four temperatures between 66 and 92 K. We

observe three distinct sub-steps in the data, indicating that there are at least three different types of binding sites available for argon. We have calculated isosteric heats of adsorption as a function of coverage for this system. We have also measured four isotherms at low coverage for temperatures between 112 and 143 K in order to determine the binding energy for argon on the strongest binding sites available on this microporous metal organic framework. Our results will be compared to previous experimental and computer simulations for this system.

*This work was supported by the NSF through grant DMR-0089713, by the Materials Technology Center from SIUC (ADM), and by the Petroleum Research Fund administrated by the ACS (PRF# 42614-AC3,10)(JL).

**9:12**

**Y31 7 Microstructure of a phase-separating liquid mixture confined in mesoporous Controlled Pore Glass – A study combining SANS, NSE and adsorption measurements*** GERNOT ROTHER, *Oak Ridge National Laboratory* SEBASTIAN SCHEMMEL, *TU Berlin* DIRK WOYWOD, *TU Berlin* MARTIN SCHOEN, *TU Berlin* GERHARD H. FINDENEGG, *TU Berlin* The physical properties of liquid mixtures with miscibility gap in pores of mesoscopic size are drastically altered from their bulk states, due to adsorption on the pore walls and confinement effects, and it is highly desirable to gain knowledge in the adsorption and separation processes, due to the widescale use of such media in chromatography and other applications [1]. In this work, three complementary techniques were used to address this issue, including both elastic (SANS) and inelastic (neutron- spin-echo) techniques, backed up by physical adsorption measurements of binary liquid mixtures with a miscibility gap [i.e. iso-butyric acid and heavy water] [2,3]. We found a shift in the phase separation temperature by $\sim$ 10 K towards the two-phase region and a drastical slowing down of the dynamics in the two-phase region. [1] K. Binder and E. Luijten, Phys. Reports 344, 179 (2001) [2] S. Schemmel et al., J. Chem. Phys. **122**, 244718 (2005) [3] T. Hellweg et al., Eur. Phys. J. E **12**, s01 (2003) 001

*This work was financed by the DFG through Sfb 448.

**9:24**

**Y31 8 Time dependent diffusion in a disordered medium with partially absorbing walls** JIANG QIANG, *Harvard University* PABITRA N. SEN, *Schlumberger-Doll Research* We present an analytical and numerical study of time dependent diffusion coefficient in systems with partially absorbing boundary condition. We obtain a perturbative expansion for time dependent propagator in terms of volume fraction $f$ of spheres in a dilute suspension of spheres. Exact single sphere $t$-operator for partially absorbing boundary condition is used to obtain a time-dependent diffusion coefficient $D(t)$ for a random distribution of spheres, accurate to the lowest order of volume fraction $f$. Short and long time limits of $D(t)$ are obtained and compared to the known exact results. We then present a significantly improved numerical method for dealing with random walk with partially absorbing boundary on curved surfaces. The method is applied to the dilute suspension of spheres to obtain $D(t)$ and compared with the analytical solution. Numerical simulation on a random closed packed (Finney pack) is used to study correlation between time-dependent relaxation and diffusion.

**9:36**

**Y31 9 Percolation and diffusion in two dimensional random media** BONG JUNE SUNG, ARUN YETHIRAJ, *Department of Chemistry, University of Wisconsin-Madison* The diffusion of hard disc fluids in two dimensional porous media (composed of immobile hard discs) is studied using discontinuous molecular dynamics (DMD) simulations and analyzed using a Voronoi tessellation procedure. A pore is defined as a circle tangential to three neighbor matrix discs with a pore center at a Voronoi vertex. If an edge of Voronoi diagram connecting two pores is too narrow for a fluid particle to move along, the edge is considered disconnected. This procedure maps the system onto a lattice model with diffusion possible in the bond percolation limit. The percolation threshold, $p_c$ of edges connecting pores is found to be 0.526, where p is the fraction of connected edges. $p_c$ is significantly different from $p_r = 2/3$ of random bond percolation theory where the edge connectivity of the same Voronoi diagram is determined randomly. This suggests that the edge connectivity is strongly correlated even for randomly distributed medium particles. DMD simulations show normal diffusion for $p > p_r$, confined dynamics for $p < p_c$, and anomalous diffusion for $p_c < p < p_r$.

**9:48**

**Y31 10 Well defined arrays of silica nanotubes for the study of processes at nanoscale: example of one-dimensional diffusion** YAROSLAV KIEVSKY, BRENT CAREY, DANIEL BEN-AVRAHAM, IGOR SOKOLOV, *Clarkson University, Potsdam, NY 13699* Using organic templating synthesis of inorganic precursor, silica, we synthesized well defined fibers of $\sim$ 2 microns in diameter and 5 microns in length. Structurally these fibers are parallel arrays of closely packed silica nanotubes (ASNT). BET, SAXS, SEM, TEM, and light scattering techniques were used to characterize these ASNT. Each nanotube is $\sim$ 3nm in diameter, and extends to the full length of the fiber, 5 microns. Thus, each array has about a quarter of a million of nanotubes in parallel. We expect these ASNT to be a popular system for the study of processes at nanoscale confined space. Signals from the processes that happen inside each silica nanotube will be amplified by the number of nanotubes, i.e., a few hundred thousand times for each fiber. High monodespersity of the fibers ( $\sim$ 10% standard deviation in the length distribution) allows for amplifying the signals even more. To demonstrate the proposed method, we study diffusion of a dye from a single silica nanotube. Due to the size of the dye molecule, one can treat this process as truly one-dimensional diffusion. Experimental data are compared with a diffusion model. Apart from just pure demonstration, these data show the potential of ASNT in the controlled drug release.

**10:00**

**Y31 11 A Two-dimensional Porphyrin-based Porous Network Featuring Communicating Cavities** A. KIEBELE, H. SPILLMANN, M. STOEHR, N. WINTJES, *University of Basel* T. JUNG, *Paul Scherrer Institute* D. BONIFAZI, F. CHENG, F. DIEDERICH, *ETH-Zurich* Metallo-porphyrins and their derivatives have been shown to be exceedingly useful building blocks for the construction of 3D supramolecular functional networks due to their excellent thermal and chemical stability and synthetic versatility. Nonetheless, no 2D analogon has been reported so far, although these could be interesting for various potential applications such as molecular sieves or chemical sensors. Herein we report on an unprecedented 2D porphyrin network featuring pores capable of hosting fullerenes following a bottom-up approach at a

single crystal silver surface. Surface- and porphyrin-driven long-range interactions between the $C_{60}$ guest molecules and porphyrin layer resulted in the formation of exceptionally large supramolecular hybrid chains and islands as evidenced by Scanning Tunneling Microscopy.

**10:12**
**Y31 12 Analysis of the Complex Dielectric Permittivity Behavior of Porous $Al_2O_3$-SiC Composites in the 1 MHz − 18GHz Frequency Range*** JACOB BATTAT, JEFFREY CALAME, *Naval Research Laboratory* The complex dielectric permittivity of electrically lossy, porous $Al_2O_3$-SiC composites was measured as a function of frequency over the range of 0.001-18 GHz (broadband). These composites were fabricated by an infusion method of incorporating SiC polymer precursor into porous alumina discs. Repeat polymer infusions and pyrolysis steps to $1000^oC$ were carried out, with some samples undergoing an additional air-fire prior to each subsequent step. Generally, it was found that for non-air-fired samples, moderate, controllable losses were attainable over a broad frequency range with $\log\varepsilon''$ being inversely proportional to $\log f$. By contrast, the dielectric loss attainable for air-fired samples was generally very low. For all samples, various aspects of the variation of permittivity components $\varepsilon'$ and $\varepsilon''$ with frequency were analyzed, with a view to determine the various factors contributing to dielectric response. In addition, the ramifications of this behavior on the properties of the material as a lossy composite were addressed.

*Supported by the U.S. Office of Naval Research

**10:24**
**Y31 13 Low field NMR study of the pre-asymptotic Stokes flow in porous rocks.** PHILIP SINGER, *Schlumberger-Doll-Research* GABRIELA LEU, EDMUND FORDHAM, PABITRA SEN, Dispersion in porous media is a powerful tool for probing the microgeometry of porous media and the topology of flow fields. Pulsed field gradient nuclear magnetic resonance (PFG-NMR) methods are emerging as very powerful techniques for measuring fluid propagation and dispersion. However, high magnetic field techniques have proven limited since the susceptibility contrast between fluid components and solid interfaces can give rise to strong internal field gradients which corrupt the measurement, and which cannot be easily corrected for. Here for the first time we present PFG-NMR data on a variety of rocks (Bentheimer and Berea sandstones, Portland carbonate) using an unusually low applied magnetic field (2 MHz for protons) to limit these internal field artifacts. We find remarkable differences with the high field data, and we quantify these differences as a function of the mean flow velocity and the interrogation time.

**10:36**
**Y31 14 Influence of Local Field Effects on the Radiative Properties of Nd:YAG Nanoparticles in a Liquid Suspension** KSENIA DOLGALEVA, ROBERT BOYD, *Institute of Optics, University of Rochester* Local field effects can significantly modify the optical properties of laser materials. Neodymium-doped yttrium-aluminum garnet (Nd:YAG) nanopowder with particle sizes on the order of 50 nm was suspended in different organic and inorganic liquids to produce Maxwell-Garnett-type composite materials. The fluorescence decay time of Nd:YAG nanocomposites was experimentally investigated as functions of the refractive index of the liquid, Nd:YAG filling fraction, and the pump-radiation wavelength. The results of these measurements were compared to the predictions of various theoretical models that include in influence of local field effects in nanocomposite materials.

**10:48**
**Y31 15 Thermodynamic studies of one and two dimensional Neon adsorbed on single walled carbon nanotube bundles*** SUBRAMANIAN RAMACHANDRAN, GREGORY DASH, OSCAR VILCHES, *University of Washington* In this study we report heat capacity measurements between 2 and 20 K for films of Neon adsorbed on single-walled closed end carbon nanotube bundles. The heat capacity of the adsorbed layer is measured from $1/60^{th}$ (2 scc) of a monolayer to $\sim$ 1.2 monolayer (155 scc). The heat capacity is used to identify if the phases are solid, liquid or gaseous. The heat capacity at a fixed coverage (less than 12 scc) as a function of temperature reveals some agreement with the values predicted from a 1D solid model by Kostov et.al **(**Phys. Rev. B **68,** 245403 (2003)**)** between 2 and 4 K. For coverage higher than 24 scc, the heat capacity at low temperature shows a clear $T^2$ dependence. The calculated 2D Debye Temperatures are in the range of 50-60K and are in good agreement with what has been measured by G.B. Huff and J. G. Dash **(**JLTP **24,** 1 / 2, 1976**)** for Neon adsorbed on Grafoil. The specific heat values are greater than 2 for temperatures greater than $\sim$ 14 K. There is no evidence of first order phase transition due to melting.

*NSF-DMR Grant 0245423 and the Bosack-Kruger Foundation

**SESSION Y33: STATISTICAL PHYSICS: DYNAMICS AND TRANSITIONS**
**Friday Morning, 17 March 2006**
**336, Baltimore Convention Center at 8:00**
**AlfredHubler, University of Illinois, presiding**

**8:00**
**Y33 1 Higher Order Phase Transitions and Tachyon Condensation** PRADEEP KUMAR, *University of Florida* AVADH SAXENA, *Los Alamos National Lab* AVINASH KHARE, *Institute of Physics, India* We discuss the similarities (and the differences) between the models which describe a $p$'th order phase transition (in the Ehrenfest sense) and that which describes tachyon condensation in string theory. Using the appropriate free energy for the two systems, we obtain exact domain wall solutions and study their stability for some cases. Extrapolating this analogy, we suggest that the tachyon condensation is analogous to the celebrated Kosterlitz-Thouless transition. It has been suggested that the superconducting transition in BKBO may be of order four. Similarly, the Ising ferromagnet on a Cayley tree and a model by Gross and Witten in particle physics are believed to be order three.

**8:12**
**Y33 2 Analysis of the long-range random field quantum antiferromagnetic Ising model : Some exact results*** JUN-ICHI INOUE, *Hokkaido University* ARNAB DAS, *SINP* BIKAS K. CHAKRABARTI, *SINP* With the realization in the mid last century, that the Neel state cannot be the ground state of a quantum Heisenberg anti-ferromagnet (AF), considerable effort has gone in

search of and in understanding the nature of the ground stateof such and similar quantum AF. Since early 1960s, quantum spin systems described by Ising model in a transverse tunneling field was investigated, particularly because of easy mapping of the quantum system to its equivalent classical system and some cases of exact solubility. However, there has, so far, been very few models with AF interactions. It is well-known, the transverse Ising model with long range interactions is solved exactly, even if the system has some special kind of quenched disorder, like in spin glasses. However, it is not so easy to consider the AF version of the model due to a lack of sub-lattice to capture the Neel ordering at low temperature. In this paper, we introduce and study a solvable quantum AF model. In our model system each spin is influenced by the infinite range AF interactions in a transverse field. We also consider the case under the random fields. By introducing two sub-groups of the spin system, we describe the system by means of the effective single spin Hamiltonian and solve it exactly.

*This work was supported by IKETANI SCIENCE AND TECHNOLOGY FOUNDATION no. 0174004

**8:24**

**Y33 3 Lattice dimers and the tilting transition*** ERCAN KAMBER, JANÉ KONDEV, *Martin A. Fisher School of Physics Brandeis University* We study the statistics of dimer coverings of the honeycomb lattice by Monte Carlo simulations. Dimer configurations are given by placing dimers on adjacent sites with the constraint that every site is covered by one and only one dimer. We implement the pocket algorithm [1], which is believed to be ergodic on the space of dimer coverings. The pocket algorithm enables global updates of dimer configurations without violating the packing constraint. Dimer configurations can be mapped to a height model [2], which associates a discrete interface with every dimer covering. If the dimers are aligned along one direction of the honeycomb lattice, the height interface will be tilted. We investigate the fluctuations of the associated height model, when the system undergoes a transition from an untilted rough interface to a tilted smooth interface. We impose a fixed tilt of the interface and measure fluctuations of the height. For a tilted surface the height fluctuations are anisotropic with a variance that increases logarithmically with system size. We compute the effective stiffness of the interface and find that it increases with increasing tilt. [1] W. Krauth, R. Moessner, Phys. Rev. B 67, 2003. [2] H.W.J. Blote, H.J. Hilhorst, J. Phys. A 15, 1982.

*This work is supported by NSF DMR-0403997. JK is a Cotrell Scholar of Research Corporation.

**8:36**

**Y33 4 A non-Hermitian analysis of strongly correlated quantum systems** YUICHI NAKAMURA, *Dept. of Phys., Univ. of Tokyo, Japan* NAOMICHI HATANO, *IIS. Univ. of Tokyo* We study a non-Hermitian generalization of strongly correlated quantum systems in which the transfer energy of electrons is asymmetric. Hatano and Nelson[1] applied this technique to non-interacting random electron systems. They related a non-Hermitian critical point to the inverse localization length of the Hermitian systems. We here conjecture that we can obtain in the same way the correlation length of Hermitian interacting non-random systems[2]. We show for the Hubbard model and the antiferromagnetic XXZ model in one dimension that the non-Hermitian critical point of the ground state, where the energy gap vanishes, is equal to the inverse correlation length. We also show that the conjecture is consistent with numerical results for $S=1/2$ frustrated quantum spin chains with the nearest- and next-nearest-neighbor interactions including the Majumdar-Ghosh model[3]. [1] N. Hatano and D. R. Nelson, PRL 77 (1996) 570; PRB 56 (1997) 8651. [2] Y. Nakamura and N. Hatano, Physica B, accepted. [3] C. K. Majumdar and D. K. Ghosh, J. Phys. C3 (1970) 911; J. Math. Phys. 10 (1969) 1388, 1399.

**8:48**

**Y33 5 Spectrum of superintegrable chiral Potts model and $L(sl_2)$ symmetry in associated XXZ-type spin chain** AKINORI NISHINO, *Institute of Industrial Science, The University of Tokyo* TETSUO DEGUCHI, *Department of Physics, Ochanomizu University* We study the correspondence between the Ising-like spectra of superintegrable N-state chiral Potts (SCP) model [1,2] and the energy degenerate subspaces of XXZ-type spin chain, called nilpotent Bazhanov-Stroganov (NBS) model [3], whose transfer matrix commutes with the SCP transfer matrix. We show that, if the number of sites is a multiple of N, the NBS model has a loop algebra $L(sl_2)$ symmetry in the subspace with $Z_N$-charge $Q=0$. Applying the approach [4] to the case, we obtain the dimension of $L(sl_2)$-degenerate subspaces through the calculation of Drinfeld polynomials. The Drinfeld polynomials are in fact identified with Baxter's polynomials [2] characterizing the SCP's Ising-like spectra, which shows that each subspace with the Ising-like spectra have the same dimension as the corresponding $L(sl_2)$-degenerate subspace of NBS model. [1] G. Albertini, B. M. McCoy, J. H. H. Perk and S. Tang, Nucl. Phys. B 314 (1989) 741. [2] R. J. Baxter, J. Statist. Phys. 57 (1989) 1. [3] V. V. Bazhanov and Yu. G. Stroganov, J. Statist. Phys. 59 (1990) 803. [4] T. Deguchi, cond-mat/0503564.

**9:00**

**Y33 6 Alignment of Rods and Partition of Integers, an Exact Solution** ELI BEN-NAIM, *Los Alamos National Laboratory* We study dynamical alignment of rods, a process in which rods become parallel by pairwise interactions, and also, wiggle in a diffusive manner. With strong diffusion, the system is disordered, but with weak diffusion, the system is ordered. We present an exact solution for the nonlinear and nonlocal kinetic theory of this alignment process, at the steady-state. The Fourier transform is expressed as a function of the order parameter, and generally, the Fourier modes decay exponentially with the wave number. The order parameter is found as a root of a closed equation. This solution involves iterated partitions of the integer numbers.

**9:12**

**Y33 7 Integrable Chiral Potts Model Alive and Well** JACQUES H.H. PERK, *Oklahoma State University* HELEN AU-YANG, *Oklahoma State University* About two decades have passed since the introduction of the integrable chiral Potts model, parametrized by a high-genus curve [1,2]. In spite of this mathematical complication, several exact results have been obtained since, culminating in Baxter's proof [3,4] of the conjecture for the order parameters. Here we shall discuss several other results. First we shall show how the model fits in the phase diagram of a more general non-integrable chiral Potts model and what we have learned about critical exponents and scaling behavior. Next, we shall mention some mathematical implications. Finally, we shall discuss our preliminary work on the pair correlation functions.
H. Au-Yang, B.M. McCoy, J.H.H. Perk, S. Tang and M.-L.Yan,

Phys. Lett. **123**, 219–223 (1987). R.J. Baxter, J.H.H. Perk and H. Au-Yang, Phys. Lett. **128**, 138–142 (1988). R.J. Baxter, J. Stat. Phys. **120**, 1–36, (2005). C. Day, Physics Today, **58** # 11, 19–21 (November 2005). H. Au-Yang and J.H.H. Perk, to be published.

**9:24**

**Y33 8 Statistics of work done by flow on a polymer** MICHAEL CHERTKOV, *LANL* We study polymer immersed in a flow and subjected to thermal fluctuations. Shear flow as well as chaotic flows are considered. Flow does work on the polymer while the polymer in its turn releases access of energy into heat. Statistics of work/heat production is analyzed in this non-equilibrium (off detailed balance) but steady problem theoretically and numerically. Analogs of fluctuation theorem and Jarzynski equality for annealed/quenched averaging procedures applied to the system are established. We also discuss possible generalization of this approach/study to more complex non-equilibrium problems, like turbulence. This is a joint work with A. Puliafito (INLN, Nice) and K. Turitsyn (Landau Inst., Moscow).

**9:36**

**Y33 9 On Harmonic Measure of Critical Curves** ILIA RUSHKIN, *University of Chicago* ELDAD BETTELHEIM, *University of Chicago* ILYA GRUZBERG, *University of Chicago* PAUL WIEGMANN, *University of Chicago* Fractal geometry of critical curves appearing in 2D critical systems is characterized by their harmonic measure. For systems described by conformal field theories with central charge $c \leqslant 1$ the scaling exponents of the harmonic measure have been computed by B. Duplantier [Phys. Rev. Lett. **84**, 1363 (2000)] by relating the problem to boundary two-dimensional gravity. We present a simple argument connecting the harmonic measure of critical curves to operators obtained by fusion of primary fields, and compute characteristics of the fractal geometry by means of regular methods of conformal field theory. The method is not limited to theories with $c \leqslant 1$.

**9:48**

**Y33 10 Methods of calculating Ruelle-Pollicott resonances** ELIZABETH KELLER, MARK SREDNICKI, *University of California, Santa Barbara* We develop a method to compute the Ruelle-Pollicott resonances for the classical perturbed cat map. Using sine and cosine basis states, we calculate the matrix elements of the Frobenius-Perron operator and find the eigenvalues of the resulting matrix. Because the matrix is sparse, we are able to reach sufficiently large matrix dimensions to obtain stable, convergent values for the Ruelle-Pollicott resonances.

**10:00**

**Y33 11 Phase Transition of a Dynamical System with a Bi-Directional, Instantaneous Coupling to a Virtual System** VADAS GINTAUTAS, ALFRED HUBLER, *University of Illinois at Urbana-Champaign* As worldwide computer resources increase in power and decrease in cost, real-time simulations of physical systems are becoming increasingly prevalent, from laboratory models to stock market projections and entire ''virtual worlds'' in computer games. Often, these systems are meticulously designed to match real-world systems as closely as possible. We study the limiting behavior of a virtual horizontally driven pendulum coupled to its real-world counterpart, where the interaction occurs on a time scale that is much shorter than the time scale of the dynamical system. We find that if the physical parameters of the virtual system match those of the real system within a certain tolerance, there is a qualitative change in the behavior of the two-pendulum system as the strength of the coupling is increased. Applications include a new method to measure the physical parameters of a real system and the use of resonance spectroscopy to refine a computer model. As virtual systems better approximate real ones, even very weak interactions may produce unexpected and dramatic behavior. The research is supported by the National Science Foundation Grant No. NSF PHY 01-40179, NSF DMS 03-25939 ITR, and NSF DGE 03-38215.

**10:12**

**Y33 12 Wave stability on one-dimensional non-linear lattices** CHIA-CHEN CHANG, *Department of Physics, The Pennsylvania State University* GERALD D. MAHAN, *Department of Physics, The Pennsylvania State University* We report the results of our stability analysis of exact travling wave solutions for two non-linear mono-atomic lattices in one dimension. One lattice has nearest-neighbor potential energy containg quadratic and quartic terms (Fermi-Pasta-Ulam model). The other lattice has potential energy which goes as $cosh(q)$, a generalization of the Toda lattice. These exact traveling wave solutions have wave lengths that are commensurate with the lattice constant. It is found that on the quadratic-quartic lattice, the traveling wave solutions are unstable. For the $cosh(q)$ lattice, on the other hand, the solutions are stable.

**10:24**

**Y33 13 Effective Masses of Vector Polarons** CHARLES FOELL, DENNIS CLOUGHERTY, *University of Vermont* We consider the vector polarons of a one-dimensional model of an electron in a doubly (or nearly) degenerate band that couples to two elastic distortions, as described previously by Clougherty and Foell [1]. A variational approach is used to analytically and numerically calculate effective masses of the three types of vector polarons. [1] D. P. Clougherty and C. A. Foell, Phys. Rev. B 70, 052301 (2004).

## SESSION Y37: FOCUS SESSION: PROBING NOVEL NANOSTRUCTURES

**Friday Morning, 17 March 2006**
**340, Baltimore Convention Center at 8:00**
**Daniel Ralph, Cornell University, presiding**

***Contributed Papers***

**8:00**

**Y37 1 Highly Ordered Graphene for Two Dimensional Electronics*** RUI FENG, J.R. HASS, E.H. CONRAD, X LI, C. BERGER, W.A. DE HEER, T. LI, P.N. FIRST, *School of Physics, Georgia Institute of Technology* C.A. JEFFREY, *Dept. of Physics and Astronomy, University of Missouri-Columbia* Many of the same electrical properties of carbon nanotubes can be realized by confining grapheme sheets to nano-dimensions. Scalability issues of nanotube devices can therefore be overcome by lithographic patterning of graphene films if thin well ordered graphene films can be grown. We have been able to grow ultrathin epitaxial graphite films that show remarkable 2D electron gas (2DEG) be-

havior by thermal decomposition of both Si-face and C-face 4H-SiC. Early studies of the structure of both surfaces of 4H-SiC showed that graphite grown on the C- face was rotationally disordered compared to the Si-face. For this reason the C-face graphite was ignored as a potential substrate for graphitic devices. However, our surface X-ray scattering measurements show that while the orientational order is reduced, the coherent film size of the C-face graphite is more than three time greater than the Si-face. Part of the reason is that the Si-face step density increases dramatically with graphitization while the C-face shows little change in step structure. These observations are consistent with the improved 2D conductivity measurement on the C-face graphite films.

*Research funding is supported by NSF-NIRT and Intel.

**8:12**
**Y37 2 2d electronic gas properties of epitaxial graphene** CLAIRE BERGER, *GATECH / CNRS* CECILE NAUD, *CNRS* ZHIMIN SONG, *GATECH* XUEBIN LI, *GATECH* WALT DE HEER, *GATECH* We present transport measurement on multilayered epitaxial graphene grown on SiC. The films, a few to a few dozen layers thick, can be lithographically patterned and show remarkable 2d electron gas properties. In high mobility samples (up to $10^4$ $cm^2/Vs$) perpendicular magnetoresistance measurements indicate micrometer long electronic phase coherence lengths at 4K, comparable to the sample size. Pronounced Shubnikov –de Haas oscillations are consistent with graphene-like electronic dispersion relation. A novel low temperature electronic phase transition was also observed. Most recent development of his ongoing research will be presented.

**8:24**
**Y37 3 STM studies of graphite microdevices** ELENA POLYAKOVA, *Chemistry Department, Columbia University* GEORGE FLYNN, *Chemistry Department, Columbia University* YUANBO ZHANG, *Physics Department, Columbia University* MINA FAZLOLLAHI, *Physics Department, Columbia University* PHILIP KIM, *Physics Department, Columbia University* A novel scanning tunneling microscope (STM) has been designed and built to study transport phenomena in mesoscopic conductive films, self-assembled monolayers, and nanostructures on insulating substrates under ambient conditions. In this work we present experimental STM studies of monocrystalline ultrathin graphite films including single graphite sheets (graphene) at the atomic scale. Electronic transport is possible only in the lateral direction for graphene. Graphite microscopic devices ( $\sim$ 10 $\mu$m) have been prepared by mechanical exfoliation followed by deposition of macroscopic gold electrodes over the graphite film and its surrounding insulator. Evolution of STM images during the transition from multilayer to single graphene sheets as well as the dependence of STM images on tunneling conditions near the Fermi energy will be discussed.

***Invited Papers***

**8:36**
**Y37 4 Low temperature scanning tunneling microscopy of metallic and organic nanostructures.***
STEFAN FÖLSCH, *Paul Drude Institute for Solid-State Electronics, 10117 Berlin, Germany*

Low temperature scanning tunneling microscopy (LT-STM) is capable of both characterizing and manipulating atomic-scale structures at surfaces. It thus provides a powerful experimental tool to gain fundamental insight into how electronic properties evolve when controlling size, geometry, and composition of nanometric model systems at the level of single atoms and molecules. The experiments discussed in this talk employ a Cu(111) surface onto which perfect nanostructures are assembled from native adatoms and organic molecules. Using single Cu adatoms as building blocks, we obtain zero-, one-, and two-dimensional quantum objects (corresponding to the discrete adatom, monatomic adatom chains, and compact adatom assemblies) with intriguing electronic properties. Depending on the structure shape and the number of incorporated atoms we observe the formation of characteristic quantum levels which merge into the sp-derived Shockley surface state in the limit of extended 2D islands; this state exists on many surfaces, such as Cu(111). Our results reveal the natural linkage between this traditional surface property, the quantum confinement in compact adatom structures, and the quasi-atomic state associated with the single adatom. In a second step, we study the interaction of pentacene ($C_{22}H_{14}$) with Cu adatom chains serving as model quantum wires. We find that STM-based manipulation is capable of connecting single molecules to the chain ends in a defined way, and that the molecule-chain interaction shifts the chain-localized quantum states to higher binding energies. The present system provides an instructive model case to study single organic molecules interacting with metallic nanostructures. The microscopic nature of such composite structures is of importance for any future molecular-based device realization since it determines the contact conductance between the molecular unit and its metal ''contact pad.''

*Support by the European Union RTN network project NANOSPECTRA (contract No. RTN2-2001-00311) is gratefully acknowledged

***Contributed Papers***

**9:12**
**Y37 5 Imaging Electron Flow in Two-Dimensional Electron Gases** M. P. JURA, M. A. TOPINKA, A. R. SCIAMBI, D. H. LO, D. GOLDHABER-GORDON, *Stanford University* We present images of electron flow from a quantum point contact (QPC) into a surrounding two-dimensional electron gas (2DEG). We resolve flow patterns associated with the one-dimensional modes responsible for quantized conductance through the QPC. The imaging technique relies on scanning a charged tip over the 2DEG and simultaneously measuring the conductance through the sample [1]. We show images of electron flow in different GaAs/AlGaAs heterostructures, and we discuss which features of 2DEGs can affect both application of this technique and the observed current flow paths. [1] M. A. Topinka et al., Nature 410, 183 (2001).

**9:24**

**Y37 6 Probing Single-Electron Charging and Dissipation of Au Nanocrystals with Electric Force Microscopy** J. ZHU, M. BRINK, P. L. McEUEN, *LASSP, Cornell University, Ithaca, NY 14853* We synthesize and link Au nanocrystals to carbon nanotube (CNT) field effect transistors through thiol and aromatic ring bifunctionalized molecules. AFM images taken at room temperature using tapping mode and at 77 K using force microscopy both show specific binding of Au nanocrystals onto the CNTs. At 77 K, the small size of the Au nanocrystals (d $\sim$ 12 nm) leads to quantum dot phenomena. A metalized AFM tip perturbs the electrostatic potential of the dot and brings electrons onto the dot one by one. The CNT serves as a charge transfer line and a reservoir. We study the force, frequency shift, and dissipation generated by this single-electron motion using AFM-based electric force microscopies. We observe Coulomb oscillations of the Au nanocrystal and derive its capacitances to the gates, i.e. the backgate, the AFM tip, and the anchoring CNT, through charge addition spectra. The total capacitance of the Au nanocrystals was found to be approximately 1.6 aF, corresponding to a charging energy of 100 meV. Most interestingly, we observe a typical power dissipation of $\sim$ 10 aW, extracted from the decrease of the quality factor Q of the AFM cantilever, for many charging events. We discuss the possible origins of the observed dissipation.

**9:36**

**Y37 7 Quantitative Investigation of Quantum Dots Using Frequency Shift Microscopy at Low Temperatures.** MARKUS BRINK, JUN ZHU, PAUL L. McEUEN, *LASSP, Cornell University, Ithaca, NY 14853* We use frequency shift microscopy (FSM), an AFM-based scanned probe technique, to study quantum dots formed in carbon nanotubes at 4K. FSM requires the quantum dot to be coupled to only one charge reservoir, allowing us to probe quantum dots in single-terminal geometries; furthermore, FSM requires only weak coupling between the quantum dot and the charge reservoir, permitting measurements in poorly conducting regimes that are inaccessible to transport measurements. Charging events of individual quantum dots are detected with single-electron sensitivity down to the few electron regime. We describe a general method to extract the charging energy of a quantum dot from frequency shift measurements. Coupled dots show avoided crossings in FSM charge addition spectra, from which we extract their mutual capacitance.

**9:48**

**Y37 8 Measurements of electron-in-a-box level spectra in chemically-synthesized metal nanoparticles** FERDINAND KUEMMETH, K.I. BOLOTIN, D.C. RALPH, *Laboratory of Atomic and Solid State Physics, Cornell University, Ithaca, NY 14853* We incorporate chemically-synthesized metal nanoparticles into a single electron transistor geometry such that tunneling spectroscopy can be used to measure the electron energy levels within a single nanoparticle at dilution refrigerator temperatures. This technique gives better control over the size and shape of the nanoparticle than previous studies of level spectra in metals. We use a monolayer of dithiols or propylamines as a self-assembled tunnel barrier on top of a back-gated pair of gold electrodes, separated by a nm-sized gap. Into the gap we trap gold nanospheres 5 to 15 nm in diameter from a citrate based colloid solution, with control provided by adjusting the pH. Previous experiments on gold nanoparticles found a wide range of g-factors for Zeeman splitting in an applied magnetic field, with some values inconsistent with expected orbital contributions. Our measurements clarify the relationship between g-factors and level spacing through systematic variation of the particle's size and composition.

**10:00**

**Y37 9 Single-electron transport through a $Mn_{12}$ (2-thiophenecarboxylate) single-molecule magnet** CHRISTOPHER M. RAMSEY, ENRIQUE DEL BARCO, EDUARDO MUCCIOLO, *Department of Physics, University of Central Florida, Orlando, FL* FIROZE HAQUE, SAIFUL KHONDAKER, MICHAEL LEUENBERGER, *Nanoscience Technology Center, University of Central Florida, Orlando, FL* ABHUDAYA MISHRA, GEORGE CHRISTOU, *Department of Chemistry, University of Florida, Gainesville, FL* We report single-electron transport measurements on $Mn_{12}$ based single-molecule magnet, which has been functionalized with 2-thiophenecarboxylate ligands that bind to gold. The self-assembly of these molecules was confirmed by scanning probe microscopy and XPS measurements. Because it is well known that the molecule's environment within the crystal can have a profound influence on the quantum properties of the system, it is important to study the quantum spin dynamics in individual isolated molecules. Single electron transistor devices have been prepared for this purpose by electron beam lithography and electromigration. The transport properties of a single, isolated $Mn_{12}$(2-thiophenecarboxylate) molecule were measured down to mK temperatures in a 3-D superconducting vector magnet with arbitrary field direction. The data are characteristic of a molecular single-electron transistor device where the SMM bridges the gap between two gold nanoelectrodes. Magnetic field and temperature dependence as well as theoretical aspects will be discussed.

**10:12**

**Y37 10 Local electronic structure of a quantum point contact observed with STM** KATSUMI NAGAOKA, SNIN YAGINUMA, TADAAKI NAGAO, TOMONOBU NAKAYAMA, *National Institute for Materials Science* A quantum point contact (QPC) is realized when a width of an electron conduction channel is comparable to the Fermi wavelength of electrons in a material. Since the first observation that QPCs show the conductance quantization in units of $G_0 = 2e^2/h$, QPCs have been mainly used in transport measurements. But the quantized states of confined electrons, which are the origin of the quantized conductance in the transport measurements, have not been observed directly so far. We report the direct observation of electronic structures of QPCs using an STM spectroscopy at 77K. The QPCs are formed across boundary gaps between a multi-domain Bi film on a Si(111)-$\beta\sqrt{3}$x$\sqrt{3}$-Bi substrate. Since the QPCs are formed in the direction parallel to the substrate, the direct observations of the atomic and the local electronic structures by using STM are possible. The electronic structure of the QPCs is neither sensitive to the external electric field induced by the STM tip nor to the length of the bridging part, and is well-explained by electronic confinement in a one-dimensional cylindrical potential well.

**10:24**

**Y37 11 Spectral diffusion in the tunneling spectra of ligand-stabilized undecagold clusters** THOMAS P. PEARL, *North Carolina State University* RACHEL K. SMITH, SANJINI U. NANAYAKKARA, PAUL S. WEISS, *The Pennsylvania State University* GERD H. WOEHRLE,*JAMES E. HUTCHISON, *University of Oregon* Electronic properties of isolated, solution-derived, and ligand-stabilized undecagold clusters ($Au_{11}L_{10}$) in both cryogenic (4 K, UHV) and ambient conditions were measured using scanning tunneling microscopy and spectroscopy. Clusters were immobilized on alkanethiolate self-assembled monolayer matrices with inserted dithiol tethers. At low temperature, $Au_{11}L_{10}$ clusters demonstrated Coulomb blockade, with zero-conductance gaps resulting from quantum size effects, and spectral hopping. While these clusters were immobilized for probing, we hypothesize that these assemblies may be dynamic and influence their charge transport significantly. Diffusion in the conductance resonances of the tunneling spectra of $Au_{11}L_{10}$ clusters is observed for a itsingle cluster, as well as across multiple clusters. The observed spectral diffusion is independent of tunneling conditions and varies significantly for spectra recorded with identical setpoint/tunneling junction conditions.

*Current address: Abbott Laboratories, Ludwigshafen, Germany

**10:36**

**Y37 12 Influence of Linker Molecules on Charge Transport through Self-Assembled Single-Nanoparticle Devices.** AL-AMIN DHIRANI, AMIR ZABET-KHOSOUSI, YOSHINORI SUGANUMA, KENNETH LOPATA, PAUL-EMILE TRUDEAU, *Department of Chemistry, University of Toronto* We investigate electrical characteristics of single-electron electrode/nanoisland/electrode devices formed by alkanedithiol assisted self-assembly. Contrary to predictions of the orthodox model for double tunnel junction devices, we find a significant ( $\sim$ five fold) discrepancy in single-electron charging energies determined by Coulomb blockade (CB) voltage thresholds in current-voltage measurements versus those determined by an Arrhenius analysis of conductance in the CB region. The energies do, however, scale with particle sizes, consistent with single-electron charging phenomena. We propose that the discrepancy is caused by a multi-barrier junction potential that leads to a voltage divider effect. Temperature and voltage dependent conductance measurements performed outside the blockade region are consistent with this picture. We simulated our data using a suitably modified orthodox model.

**10:48**

**Y37 13 Absence of Even-Odd Effect in Kondo Resonance in Single-Molecule Transistors** DONG-HUN CHAE, ZHEN YAO, *Department of Physics, The University of Texas at Austin, Austin, TX 78712* JEONG T. LEE, JONATHAN L. SESSLER, *Department of Chemistry and Biochemistry, The University of Texas at Austin, Austin, TX78712* We have observed the Kondo effect in single-electron transistors incorporating individual cyclo[*n*]pyrrole molecules. In contrast to the usual spin-1/2 Kondo effect, the zero-bias Kondo resonance in these devices appears for both even and odd number of electrons. We suggest a model in which instead of alternate spin filling, two successive electrons are added to the molecule with parallel spins due to strong exchange interaction within the molecule.

**SESSION Y38: SUPERCONDUCTIVITY—VORTEX LATTICES AND PINNING CENTER ARRAYS**
**Friday Morning, 17 March 2006**
**341, Baltimore Convention Center at 8:00**
**Ulrich Welp, Argonne National Laboratory, presiding**

**8:00**

**Y38 1 Vortex-lattices in quasiperiodic pinning potentials*** JAVIER E. VILLEGAS, MARIA I. MONTERO, CHANG-PENG LI, IVAN K. SCHULLER, *Physics Department, University of California-San Diego, 9500 Gilman Drive, La Jolla CA 92093-0319, USA* We have investigated vortex-lattice dynamics in superconducting Nb thin films with different types of quasiperiodic arrays of magnetic pinning centers. The mixed-state magnetoresistance show minima for particular applied fields, which reveal matching effects between the vortex-lattice and the quasiperiodic array. These minima are as sharp and well defined as those found with periodic pinning arrays. Moreover, a larger number of minima are observed for quasiperiodic arrays, which in some cases indicate a high ratio of vortices per pinning site. These results suggest that matching between the vortex-lattice and the array of magnetic dots takes place on a very local scale, indicating a short local correlation-length of the vortex-lattice.

*Work supported by US-NSF Grant DMR 03-53729. J.E.V. wants to acknowledge Spanish ''Ministerio de Educacion y Ciencia'' for a fellowship.

**8:12**

**Y38 2 Resistance anomaly in superconducting films containing disordered arrays of holes** Z.L. XIAO,*J. HUA, U. PATEL, D. ROSENMANN, U. WELP, W.K. KWOK, G.W. CRABTREE, *Argonne National Laboratory* Anomalous resistive peaks with values larger than the normal-state resistance has been observed in the resistance versus temperature and magnetic field curves of superconducting nanostructures of Al nanowires, nanoloops and nanodiscs. The excess resistance in these systems is believed to originate at the normal-superconducting ($N - S$) interface and induced by dynamic phase slip centers or by different critical temperatures ($Tc$) in the neighboring parts. Here we report on a new type of resistance anomaly which occurs only at high driving currents in disordered superconducting films. The samples were formed by sputtering niobium onto substrates containing arrays of irregularly distributed nanoscale holes. Resistance peaks appear as a function of temperature or magnetic field in the superconducting transition, with peak values up to 2% above the typical normal-state value. We attribute the observed resistance peak effect to dissipation-induced granularity which enhances contributions from the fluctuation-induced decrease of the quasiparticle density of states. The granularity of the superconducting film arises from inhomogeneous heat-transfer due to the size variation of the Nb sections between the nanoholes.

*Also at Northern Illinois University

**8:24**

**Y38 3 Origin of the resistance and critical current oscillations in superconducting films with hole arrays** U. PATEL,* *Argonne National Laboratory* Z.L. XIAO, J. HUA, T. XU, D. ROSENMANN, V. NOVOSAD, U. WELP, W.K. KWOK, G.W. CRABTREE, The resistance and critical current of a superconducting film containing a regular array of microscale or nanoscale holes are found to oscillate with magnetic field. These oscillations are

generally interpreted as commensurate pinning. On the other hand, oscillations of the critical temperature of such films with magnetic field due to the Little-Parks effect can also induce oscillations of the resistance and critical current. We present a new method to separate the contributions of commensurate pinning from the Little-Parks effect in superconducting niobium films containing triangular lattices of holes with diameter of tens of nanometers. Remarkably, we find the oscillations of the resistance and critical current with respect to field and temperature to originate purely from the Little-Parks effect. Details on sample preparation, morphological characterization and transport measurements of the critical temperature, the resistance and critical current will be reported.

*Also at Northern Illinois University

**8:36**

**Y38 4 Stochastic resonance in a periodic superconducting array** MAXIM MARCHEVSKY, MICHAEL DEFEO, *Syrcause University* VITALI METLUSHKO, *University of Illinois at Chicago* Magnetic fluxon dynamics was studied in superconducting Nb films patterned with a periodic array of holes. A sum of weak harmonic and Gaussian white noise magnetic fields is applied to the sample at $T \ll T_c$ and the local magnetic response is measured with a scanning Hall sensor. We find that the fluxon jump rate in the array exhibits locking with the half-period of the harmonic magnetic drive at a certain quotedblleft optimalquotedblright nonzero amplitude of the white noise. Peaks in the resident time distribution and formation of the quasi-periodic flux patterns is observed. We explain our observations with the phenomenon of array enhanced stochastic resonance earlier seen in various driven non-linear systems with dynamic threshold. Implications of our results for the fluxon-based superconducting devices will be discussed.

**8:48**

**Y38 5 Vortex Rectification in Thickness Modulated Films*** YAOHUA LIU, DANIEL H. REICH, *The Johns Hopkins University* CALEB D. BLISSETT, STUART B. FIELD, *Colorado State University* Rectification effects of Abrikosov vortices have been addressed theoretically in both one-dimensional (1D) and two-dimensional (2D) asymmetric potentials. However, experimentally, vortex ratchets have typically been realized in 2D arrays of asymmetric micropatterned features in superconducting films. Here we report vortex rectification in a smooth, 1D modulation potential fabricated by a novel method. Low- pinning granular Al films were deposited on sinusoidal glass gratings by angle evaporation to achieve an asymmetrical thickness modulation with a period $\sim 2\mu m$. The varying thickness yields a 1D periodic pinning potential for the vortices, which is confirmed experimentally by observation of matching field effects in magneto-transport measurements. A rectified longitudinal DC voltage is generated when the sample is driven by a zero-biased AC current at $T < T_C$, which implies a unidirectional mean motion of the vortices. Weak frequency dependence up to 10 KHz signifies that the system is in the adiabatic regime. The maximum rectified voltage decreases as the applied field increases, but is detectable far above the first matching field. In some cases, a sign reversal in the DC voltage is observed, implying that the preferred direction for vortex motion can change.

*Work Supported by NSF DMR-0308669

**9:00**

**Y38 6 Interacting particles ratchet effect: Experiments and theoretical simulations.*** JOSE L. VICENT, NURIA O. NUNEZ, *Departamento Fisica Materiales, Universidad Complutense, 28040 Madrid (Spain)* LUIS DINIS, JUAN M. R. PARRONDO, *Departamento Fisica Atomica, Molecular y Nuclear, Universidad Complutense, 28040 Madrid (Spain)* JOSE V. ANGUITA, *Instituto Microelectronica Madrid, CSIC, 28670 Madrid (Spain)* Ratchet effect occurs when out of equilibrium particles move on asymmetric potentials. The outcome is a net motion without the need of being driven by non-zero average forces or temperatures gradients. This effect spans in Nature for example from molecular motors to particles separation. Most of the theoretical models have dealt with non-interacting particles. From the experimental point of view superconducting vortices are a powerful tool to study ratchet effect on interacting particles. We will present the experimental behavior of vortex lattice motion on asymmetric pinning potentials, when the asymmetric potentials are modified and extensive simulations of a two-dimensional gas of vortices in an asymmetric substrate. We simulate the vortices as Langevin particles interacting by means of a repulsive potential. The defects in the substrate are simulated as potential wells for the Langevin particles. We will analyse the experimental data in comparison with the simulations when the shape and periodicity of the asymmetric potentials are varied.

*We thank Spanish Ministerio Educacion y Ciencia (NAN2004-09087)

**9:12**

**Y38 7 Direct experimental visualization of magnetic flux guidance in artificially patterned $YBa_2Cu_3O_{7-x}$ thin films.** V.V. YURCHENKO, *Department of Physics, University of Oslo, Norway* R. WOERDENWEBER, *Research Centre of Juelich, Germany* J.I. VESTGAARDEN, YU.M. GALPERIN, D.V. SHANTSEV, T.H. JOHANSEN, *Department of Physics, University of Oslo, Norway* Development of new 'fluxonic' devices, based on controlled motion of magnetic vortices, requires understanding of the principles of magnetic flux distribution and its dynamics in patterned superconductors. We investigated $YBa_2Cu_3O_{7-x}$ thin films equipped with various arrangements of antidots (holes of 1 $\mu$m radius) by means of real-time magneto-optical imaging. We demosntrate that 1D antidot arrays facilitate propagation of magnetic flux: each antidot concentrates the flux and tends to pass it on to the next antidot. Some flux from the antidot enters the superconductor creating a characteristic parabolic pattern. At high fields a whole line of antidots represents a cascade of parabolas with the centres in the holes. Flux 'channels' and 'reservoirs' were created in a superconducting strip by combining antidots of different size. We demonstrate that transfer of magnetic flux between two 'reservoirs' lying parallel to the edge of the strip can be realized without applying additional transverse currents. At alternating magnetic field dynamics of the flux can be localized inside the 'reservoirs'.

**9:24**

**Y38 8 Induced in-plane order in vortex liquid by regular holes array in $Bi_2Sr_2CaCu_2O_{8+y}$*** SHUUICHI OOI, TAKASHI MOCHIKU, SATOSHI ISHII, SHAN YU, KAZUTO HIRATA, *National Institute for Materials Science* SUPERCONDUCTING MATERIALS RESEARCH CENTER COLLABORATION, To study the influence of artificial hole defects on the vortex matter in high-$T_c$ superconductors, we have measured electrical transport properties in the vortex state of $Bi_2Sr_2CaCu_2O_{8+y}$ single-crystal

thin films which have holes configurations with different symmetries. In samples with triangular and square holes arrays, the flow resistance of pancake vortices exhibits dips at multiples of the matching fields, while it is absent in a random hole configuration. Such matching effect occurs even in a vortex liquid phase, suggesting that the periodicity in holes configuration induces in-plane order in liquid flow.

*This research is partially supported by the Ministry of Education, Science, Sports and Culture, Grant-in-Aid for Young Scientists (B), 17760017, 2005.

**9:36**

**Y38 9 Niobium superconducting networks and its anisotropy** J. HUA,*Z.L. XIAO, U. PATEL, T. XU, D. ROSENMANN, V. NOVOSAD, U. WELP, W.K. KWOK, G.W. CRABTREE, *Argonne National Laboratory* Novel properties such as an oscillating phase boundary in the magnetic field – temperature (H-T) diagram have been reported in superconducting films containing a regular hole array where the interhole separation is comparable to the superconducting coherence length – the superconducting networks. Aluminum is the most common material used in fabricating such superconducting networks due to its large coherence length. However, they require low $He^3$ refrigeration temperatures due to aluminum's low critical temperature of about 1 K. Here, we report on the fabrication of Nb superconducting networks with interhole separation down to tens of nanometers and critical temperatures up to 9K. In addition, we present results on angular dependence of the critical temperature and magnetoresistance of the superconducting networks.

*Also at Northern Illinois University

**9:48**

**Y38 10 Anisotropic model for plastic flow with pinning: 3D simulations** B. ELIZABETH RODRIGUEZ-MILLA, A. ALAN MIDDLETON, M. CRISTINA MARCHETTI, *Syracuse University* Switching and macroscopic hysteresis are seen in the driven transport of flux liquids (and in charge density waves). Such effects are ruled out for purely elastic models of flux array transport. Results are presented for a coarse-grained model of flux arrays which generically incorporates both elastic coupling and plastic viscous coupling. This anisotropic model, describing elastic channels interacting in a plastic fashion, has a complex phase diagram with many interesting features that have been found in exact mean-field calculations, including a tricritical point which separates the non-hysteretic region from the region where there is coexistence of stuck and moving states. Our most recent work examines this coarse-grained model in finite dimensions in detail, for distinct models of couplings between the elastic channels. Strong evidence for the existence of a tricritical point has been found. The shape of the phase diagram has a shape significantly different from the mean-field calculations. Results for the critical behavior in finite dimensions will be presented.

**10:00**

**Y38 11 Flux Quantization in Thick Mesoscopic Pb Superconductors.*** WAI-KWONG KWOK, ANDREAS RYDH,†RUOBING XIE, ULRICH WELP, MICHAEL ZACH, GEORGE CRABTREE, *Materials Science Division, Argonne National Laboratory* ZHILI XIAO, *Dept. of Physics, Northern Illinois University* SIMON BENDING, *School of Physics, University of Bath, U.K.* We present studies of novel vortex behavior on a thick triangular-shaped mesoscopic Pb crystal using ballistic micro-Hall probe magnetometry. The Pb single crystal with dimensions of 2 microns on each edge and 0.7 $\mu$m thick was placed on a 2DEG Hall sensor with a detection area of 1 $\mu m^2$ and the magnetization was studied as a function of applied magnetic field and temperature. The critical field was found to be $H_c = 78$ mT and $T_c = 7.20$ K, in good agreement with values of clean, bulk Pb. Above $T_x = 6.6$ K, we observe a stable Meissner state for increasing field and a remarkable quantized flux entry behavior with decreasing field. Below $T_x$, we observe quantized flux entry (removal) with increasing (decreasing) field. These behaviors indicate that thick mesoscopic Pb superconductors can be tuned with temperature to exhibit type I or type II superconducting behavior.

*This work was supported by the U.S. Department of Energy, BES, Materials Science under Contract No. W-31-109-ENG-38 at Argonne National Laboratory.

†present address: Stockholm University, Albanova, SE-10691, Sweden.

**10:12**

**Y38 12 SANS Study of Edge-Contaminated Vortex States in a $V_{21at\%}Ti$ Superconducting Alloy*** X.S. LING, N.D. DANIILIDIS, I.K. DIMITROV, *Brown University* In this talk, we report the first direct observation of edge-contaminated vortex matter using small angle neutron scattering (SANS). The vortex structures of Zero Field Cooled and Field Cooled states in a high-$\kappa$ superconducting alloy have been studied using SANS. In this sample FC states are partially ordered as shown by the coexistence of a diffuse scattering ring with two Bragg peaks. ZFC states are disordered at low fields and more disordered than FC states at all fields. For example, the ZFC vortex state at H=6 kOe gives a diffuse ring indicating an amorphous state. Upon further increasing the field, Bragg peaks emerge from the ring, indicating ordering. On increasing temperature from the disordered structure at 6 kOe, the ring gradually transforms into distinct peaks. The experiments were performed at the NIST Center For High Resolution Neutron Scattering (CHRNS).

*This work was supported by the National Science Foundation under Grant No. DMR-0406626.

**10:24**

**Y38 13 AC-Susceptibility and SANS Studies of the Vortex States in $V_{-21at.\%}Ti$*** I.K. DIMITROV, N.D. DANIILIDIS, V. MITROVIC, C. ELBAUM, *Brown University* J.W. LYNN, *NIST* Y. SHAPIRA, *Tufts University* X.S. LING, *Brown University* The vortex matter phase diagram of a binary alloy ($V_{-21at.\%}Ti$) has been mapped out using mutual-inductance ac susceptometry, and explored using small angle neutron scattering (SANS). In this sample, a peak effect (PE) appears at high fields, but disappears at low fields. The phase diagram shows a trend remarkably similar to that of a single-crystal itNb, despite the vast differences in their respective values of $\kappa$ and $H_{c2}$. SANS measurements of the vortex states in this sample shows the survival of quasi-long range order, suggesting the existence of a Bragg glass phase in this system. The SANS experiments were performed at the NIST Center For High Resolution Neutron Scattering (CHRNS).

*This work was supported by the National Science Foundation under Grant No. DMR-0406626.

**10:36**

**Y38 14 Vortex Fractionalization in a Josephson Ladder*** DAVID STROUD, IVAN TORNES, *Ohio State University* We show numerically that in a Josephson ladder with periodic boundary conditions and subject to a suitable transverse magnetic field, a vortex excitation can break up into two or more fractional excitations. If the ladder has N plaquettes, and N is divisible by an integer q, then in an applied field of 1/q flux quanta per plaquette, the ground state is a regular lattice of one fluxon every q plaquettes. When an additional fluxon is added, it spontaneously breaks up into q fractional fluxons, each carrying 1/q units of vorticity. The fractional fluxons are basically walls between different domains of the underlying 1/q lattice. The fractional fluxons are all depinned at the same applied current and move as a unit. For certain applied fields and ladder lengths, we show that there are isolated fractional fluxons. The fractional fluxons produce a time-averaged voltage related in a characteristic way to the ac voltage frequency.

*Supported by NSF DMR04-13395

## SESSION Y39: SUPERCONDUCTIVITY—MATERIALS AND PROCESSING

**Friday Morning, 17 March 2006**
**342, Baltimore Convention Center at 8:00**
**Doug Kirven, Sigma-K Corporation, presiding**

**8:00**

**Y39 1 Superconductivity in Yttrium Metal at 17 K*** JAMES J. HAMLIN, *Department of Physics, Washington University, St. Louis, MO* VLADIMIR G. TISSEN, *Institute of Solid State Physics, Chernogolovka, Russia* JAMES S. SCHILLING, *Department of Physics, Washington University, St. Louis, MO* Many of the known elemental superconductors only become superconducting if high pressure is applied. In 1970 J. Wittig [1] discovered superconductivity in yttrium metal at 1.2 K under 11 GPa pressure, $T_c$ increasing to 2.7 K at 16 GPa. Using a diamond-anvil cell with dense helium pressure medium, we have extended this pressure range to 89 GPa. We find that $T_c$ for yttrium metal reaches values as high as 17 K (ac susceptibility midpoint), one of the highest transition temperatures ever observed for an elemental superconductor. [1] J. Wittig, Phys. Rev. Lett. 24, 812 (1970).

*This research supported by NSF grant DMR-0404505.

**8:12**

**Y39 2 Synthesis and Characterization of Multilayer Bi(1.6)Pb(0.4)Sr(1.85)Ca(n)Cu(2n+1)O(x)** DERRICK McRAE, NATHANIEL ROBINSON, JAFAR AMIRZADEH, *Morris College, Sumter, SC* MING YIN, *Benedict College, Columbia, SC* TIMIR DATTA, *University of South Carolina, Columbia, SC* A modified solid-state reaction is used to synthesized muli-layer bismuth high Tc superconductor Bi(1.6)Pb(0.4)Sr(1.85)Ca(n)Cu(2n+1)O(x). The number of Ca layers ranged from n=2 to n=9. The resulting ceramic materials were investigated by electron microscopy (SEM) and EDAX. Samples were tested for superconducting transitions. Transport properties were characterized with four-probe method. Influence of synthesis on the temperature dependant behavior of electrical conductivity and superconductivity will be reported.

**8:24**

**Y39 3 Correlation of superconductivity with the apical oxygen ordering.*** C. Q. JIN, Q. Q. LIU, H. YANG, R.C. YU, X.M. QIN, L. X. YANG, Y. YU, F.Y. LI, *Institute of Physics, Chinese Academy of Sciences* We discuss the evolution of superconducting transition temperature (Tc) with the ordering state at the apical oxygen layer of a high temperature superconductor (HTS). This study became available in $Sr_2CuO_{3+\delta}$ superconductor with K2NiF4 structure showing so far rarely formed partially occupied apical oxygen which also acts as the dopant. With observation of a series of modulation structures at apical oxygen layer, we found a well-defined links between Tc (from 75 to 95 K) and modulated structures. We address that the distribution geometry of dopant such as the partially occupied apical oxygen here can be an additional route to reach further higher Tc.

*This work was supported by NSF and Ministry of Science and Technology of China through the research projects.

**8:36**

**Y39 4 Oxygen isotope effect in layered cuprate superconductors** XIAOJIA CHEN, VIKTOR V. STRUZHKIN, ZHIGANG WU, RUSSELL J. HEMLEY, HO-KWANG MAO, *Geophysical Laboratory, Carnegie Institution of Washington,Washington, DC 20015, USA* BING LIANG, *Center for Superconductivity Research, University of Maryland, College Park, MD 20742, USA* CLEMENS ULRICH, CHENGTIAN LIN, *Max-Planck-Institut für Festkörperforschung, D-70569 Stuttgart, Germany* HAI-QING LIN, *Department of Physics, The Chinese University of Hong Kong, Hong Kong, China* The isotope effect has generally been believed to be important in providing information about the high-temperature superconductivity. We report systematic studies of the oxygen isotope effect in nearly optimally doped $Bi_2Sr_2Ca_{n-1}Cu_nO_{2n+4+\delta}$ (n=1,2,3) single crystals. We find that $\alpha$ decreases monotonically with increasing the number of $CuO_2$ layers in this series, which is considered as a result of the interlayer coupling effect. Our results suggest that a *d*-wave BCS equation with a phonon cutoff is able to provide a self-consistent explanation for both the Tc and $\alpha$ behaviors of cuprates covering the parameters of doping, $CuO_2$ layer, and compound. The proposed theoretical model is also used to predict the pressure dependence of the oxygen isotope exponent in the optimally doped $YBa_2Cu_3O_{7-\delta}$ based on our measured Tc and Raman data. We find that $\alpha$ decreases with increasing pressure and becomes negative at some pressure. Such prediction is waiting for direct isotope measurements under high pressures.

**8:48**

**Y39 5 The effect of process gas pressure, target composition, Ar:$O_2$ ratio and substrate bias on the preparation of thin films of the superconductor $Bi_2Sr_2CaCu_2O_{8+\delta}$*** ROBERT J. SANDERSON, KEVIN C. HEWITT, *Dalhousie University* Thin films prepared by DC magnetron sputtering of single targets of the well known superconductor $Bi_2Sr_2CaCu_2O_{8+\delta}$ and an enriched target of composition $Bi_{2.2}Sr_2Ca_{1.1}Cu_2O_{8+\delta}$ were studied to determine the effect of deposition conditions on the resulting film. The targets were both sputtered at a power of 60 Watts for 83.3 minutes, at a base pressure of $(5\pm 1)\times10^{-7}$ Torr. Films were deposited onto

Al foil using a comprehensive range of deposition pressures (3.96 to 27.3 mTorr), Ar:$O_2$ gas ratios (1:1, 1:2, 1:3 and 2:1) and substrate biases (-5, -20, and -30 V). Elemental analysis using energy dispersive spectroscopy allows us to determine the effect of these variables on each individual element in the deposited film. The proportion of Bi increases linearly with increasing process gas pressure. Changing the Ar:$O_2$ ratio does not have a major effect on the composition, but it does slightly vary the Sr and Ca concentrations. Resputtering was present in the film which had a -5 V bias, the -30 V bias also showed a reduced elemental composition, while the -20 V bias produced the best composition. The results of this study show the fickle nature of depositing films from multi-element oxide targets, and the need to optimize conditions to produce the desired film.

*The financial support of the Natural Sciences and Engineering Research Council of Canada is gratefully acknowledged

**9:00**

**Y39 6 Large Single Crystal growth of Bi-2212 superconducting oxide** GENDA GU, GANGYONG XU, *Condensed Matter Physics and Materials Science, BNL, USA* JOHN TRANQUADA, *BNL* A floating zone method was used to study the effects of the growth velocity and starting composition of the feed rod on the crystal growth behaviour of Bi-2212 superconducting materials. It shows that a necessary condition for large single crystal growth is that the solid-liquid interface of a rod maintains a planar interface during crystal growth. The planar solid-liquid interface tends to break down into the cellular interface while increasing the velocity from 0.3 mm/h, or while deviating from the optimum starting composition of the feed rod $Bi_{2.1}Sr_{1.9}Ca_{1.0}Cu_{2.0}O_x$. The single crystals up to $100_*7_*3.8$ mm$^3$along the *a*-, the *b*- and the *c*-axis have been grown in a itΦ7mm rod with optimum growth conditions. The single crystals of up to 50*7*3.8 mm$^3$ have been picked up from the cut section of the as-grown rod. The neutron measurements show that the quality of the single crystals is good. The superconducting transition temperature $Tc_{onset}$ by SQUID is 91K for as-grown crystals.

**9:12**

**Y39 7 A Search for Novel Superconductors: A Study of the Lithium-Boron System** MICHAEL BLEIWEISS, *Naval Academy Preparatory School, Newport, RI* JAFAR AMIRZADEH, *Morris College, Sumter, SC* MING YIN, *Benedict College, Columbia, SC* DOUGLAS KIRVEN, *Sigma-K Corp, Durham, NC* ED SHARP, TIMIR DATTA, *University of South Carolina, Columbia, SC* A rapid solid-state reaction was used to synthesize a class of novel lithium-boron based ceramics. The resulting multiphase ceramic materials were investigated by XRD, electron microscopy (SEM) and EDAX. Efforts were taken to avoid contamination by magnesium diboride; $MgB_2$ was not detectable by XRD or EDAX. A number of the samples were electrically conducting and some were found to be superconducting in the 30-40 K range. Superconducting transitions were confirmed by SQUID magnetometry. Efforts are in progress to identify and isolate the superconducting phase. Influence of preparation on the electrical conductivity and superconductivity will be reported.

**9:24**

**Y39 8 A Novel Method to Detect Oxygen Vacancies in the Grain Boundaries of High-Tc Superconductors*** TAKAHIRO TOMITA, JAMES S. SCHILLING, *Department of Physics, Washington University, St. Louis, MO* LIHUA CHEN, BOYD W. VEAL, HELMUT CLAUS, *Materials Science Division, Argonne National Labs* A new diagnostic method is introduced (pressure-induced $J_c$ relaxation) which is capable of detecting oxygen vacancies in the grain boundaries of oxide superconductors. A series of bicrystalline rings of $YBa_2Cu_3O_x$ containing single [001]-tilt grain boundaries with mismatch angles from 0 to 31 degrees are studied. Even for samples with nearly optimal doping in the bulk, a significant oxygen deficiency in the grain boundary region is revealed. In addition, compressing the grain boundary region is found to lead to a considerable enhancement of the critical current density $J_c$.

*Research at Washington University supported by NSF grant DMR-0404505 and that at the Argonne National Labs by the U.S. Department of Energy, Basic Energy Sciences-Materials Sciences, under contract W-31-109-ENG-38.

**9:36**

**Y39 9 Crystal Growth and Electrical Transport Properties of Low Dimensional Nb-Se Superconducting Phases** CEDOMIR PETROVIC, *Condensed Matter Physics, Brookhaven National Laboratory, Upton NY 11973* RONGWEI HU, *Physics Department, Brown University, Providence RI 02912* VESNA MITROVIC, *Physics Department Brown University Providence RI 02912* Single crystals of $NbSe_2$ and $Nb_2Se_3$ have been grown by molten metallic flux technique. Powder x-ray diffraction confirms phase purity. Superconducting transitions have been observed for both materials. Electronic transport properties and comparison with samples made with conventional chemical vapor transport method will be discussed.

**9:48**

**Y39 10 Epitaxial thin films of the superconducting spinel oxide $LiTi_2O_4$** RAJESH CHOPDEKAR, *Applied Physics, Cornell University* YURI SUZUKI, *Materials Science, UC Berkeley* Lithium titanate is the only superconducting spinel oxide documented in literature. Related oxide spinels[1] such as the heavy fermion system $LiV_2O_4$ and charge-ordered $LiMn_2O_4$ indicate that electron correlations are strong in these systems. We have fabricated epitaxial films of $LiTi_2O_4$ on $MgAl_2O_4$ and MgO single crystalline substrates to explore such behavior in thin film form. Atomic force microscopy indicates $<$ 1nm RMS surface roughness, and 2- and 4-circle x-ray diffraction confirms film epitaxy. Films on $MgAl_2O_4$ have a critical temperature $T_c$ of up to 11.3K with a resistivity transition width of 0.25K, while films on MgO have lower $T_c$ with broader transitions. Magnetization vs. magnetic field of a zero-field cooled sample shows Meissner shielding consistent with Type II superconductors. Such films can be used in spin-polarization measurements of complex oxide half-metallic thin films, as well as fundamental studies of the effect of epitaxial strain, microstructure, and cation disorder/substitution on the superconducting properties of $LiTi_2O_4$. [1] M. Lauer et al, Phys Rev B 69, 075117 (2004).

**10:00**

**Y39 11 The annealing process and its relationship to superconductivity in the electron-doped superconductors** HYE JUNG KANG, *NIST, University of MD* PENGCHENG DAI, *University of Tennessee, ORNL* BRANTON CAMPBELL, *Brigham Young University* STEPHAN ROSENKRANZ, PETER CHUPUS, *ANL* SHILIANG LI, *University of Tennessee* Y. KURITA, SEIKI KOMIYA, YOICHI ANDO, *CRIEPI, Japan* Superconductivity in the high transition temperature superconductors can be achieved when the antiferromagnetic insulating parent compounds are doped with holes or electrons. The discovery of the electron-doped superconductors has obtained special attention because of the symmetry with doped charge carriers. The electron-doped superconductors can provide important clues in the mechanism of high temperature superconductivity by finding fundamental features seen in the hole-doped superconductors. Unlike hole-doped superconductors, the electron-doped compounds require the annealing process to achieve superconductivity. The role and effects of the annealing process on superconductivity have been one of the unresolved problems in the electron-doped superconductors. To investigate how the annealing process is associated to superconductivity, we performed X-ray measurement on an as-grown, an annealed superconducting, an oxygenated nonsuperconducting, and a reannealed Pr0.88LaCe0.12CuO4 samples.

**10:12**

**Y39 12 Pressure Dependence Transport Studies of the Possible Charge Kondo Effect in Tl-doped PbTe** YOSUKE KUROSAKI, JUN SHINAGAWA, *Dept. Physics and Astronomy, UCLA* YANA MATSUSHITA, *Dept. Materials Science and Engineering, Stanford Univ.* TED GEBALLE, IAN FISHER, *Dept. Applied Physics, Stanford Univ.* STUART BROWN, *Dept. Physics and Astronomy, UCLA* $Pb_{1-x}Tl_xTe$ is noteworthy for a high superconducting transition temperature relative to carrier concentration, as well as normal state properties consistent with a charge-Kondo effect. Recent experiments also demonstrate that the onset of an observable superconducting $T_c$ with Tl concentration at x$\sim$ 0.3% coincides with features characteristic of charge Kondo [1], including $d\rho/dT < 0$ at low temperatures and an unusual linear variation of the resistivity $\rho(T)=\rho_0+AT$ at higher temperatures. Together, these observations are consistent with an association between the two phenomena [2]. We report the effect of applied pressures up to P$\sim$ 1.5GPa on $\rho(T)$, $T_c$, and the Hall number $p_H \equiv R_H^{-1}$ for x= 0.3%, 0.8%, and 1.3%. $T_c$ is reduced sharply with pressure, $dT_c/dP$=400-500mK/GPa as the low temperature Kondo- like upturn in $\rho(T)$ is weakened. Also, $dA/dP < 0$ and $dp_H/dP > 0$. These observations are discussed in the context of the proposed charge-Kondo model for $Pb_{1-x}Tl_xTe$. [1] Y. Matsushita, H. Bluhm, T.H. Geballe and I.R. Fisher, Phys.Rev.Lett. 94, 157002(2005).[2] M. Dzero and J. Schmalian, Phys.Rev.Lett. 94, 157003 (2005). This work is supported by NSF frant DMR-0520552.

**10:24**

**Y39 13 Superconductivity and anomalous transport in PbTe:Tl** ELIHU ABRAHAMS, PIERS COLEMAN, *Rutgers University* MAXIM DZERO, JOERG SCHMALIAN, *Iowa State University/Ames Lab* We analyze the transport properties of Tl-doped PbTe. We show that upon doping, Tl has degenerate valence states 1+ and 3+. Quantum valence fluctuations lead to the superconductivity and a charge Kondo effect at low-temperatures and cause linear temperature dependence of resistivity at high temperatures.

**10:36**

**Y39 14 Superconducting Properties of Tl-Doped PbTe** Y. MATSUSHITA, P. A. WIANECKI, *Department of Materials Science and Engineering, Stanford University* T. H. GEBALLE, I. R. FISHER, *Department of Applied Physics, Stanford University* R. J. ORMENO, P. J. BAKER, C. E. GOUGH, *School of Physics and Astronomy, University of Birmingham* Tl-doped PbTe ($Pb_{1-x}Tl_xTe$) has a remarkably high $T_c$ given its relatively low carrier concentration and also exhibits unusual electronic properties [1–2]. For Tl concentrations $x$ beyond a critical value $x_c \sim 0.3\%$, it is observed to superconduct with $T_c$ rapidly increasing with $x$ up to a maximum doping of 1.5% and a maximum $T_c$ of 1.5 K. Here we present results of heat capacity, transport, and microwave conductivity experiments for single crystal samples. We extract estimates of superconducting parameters including $\Delta C/\gamma T_c$, $H_{c2}$, coherence length, and penetration depth. For the highest Tl concentrations, we find that the heat capacity anomaly and the temperature dependence of the superfluid density are consistent with BCS predictions and that the material is in the dirty limit. [1] Y. Matsushita, H. Bluhm, T. H. Geballe, and I. R. Fisher, Phys. Rev. Lett. **94**, 157002 (2005). [2] M. Dzero and J. Schmalian, Phys. Rev. Lett. **94**, 157003 (2005).

**SESSION Y40: SOLID STATE QUANTUM COMPUTING I**
**Friday Morning, 17 March 2006**
**343, Baltimore Convention Center at 8:00**
**John Martinis, University of California, Santa Barbara, presiding**

**8:00 ä**

**Y40 1 Landau-Zener interferometry in a Cooper pair box** MIKA SILLANPÄÄ, TEIJO LEHTINEN, ANTTI PAILA, *Low Temperature Laboratory, Helsinki University of Technology, Finland* YURIY MAKHLIN, *The Landau Institute of Theoretical Physics, Moscow, Russia* PERTTI HAKONEN, *Low Temperature Laboratory, Helsinki University of Technology, Finland* Quantum-mechanical systems having two crossing energy levels are ubiquitous in nature. The rate $v = d(E_1 - E_0)/dt$ at which such levels in a driven system approach each other determines the probability $P_{LZ}$ of a Landau-Zener (LZ) tunneling between them. The traditional treatment of the LZ process, however, ignores quantum-mechanical interference. Here we report an observation of phase-sensitive interference between consecutive LZ tunneling attempts in an artificial two-state system, a superconducting charge qubit. We interpret the experiment in terms of a multi-pass analog to the optical Mach- Zehnder interferometer: The beam splitting occurs by LZ tunneling at the charge degeneracy, while the arms of the Mach- Zehnder interferometer in energy space are represented by the ground and excited state. In accord with theory, we observe constructive interference when the Stokes phase $\phi_S$ picked up during the LZ interaction, and the dynamical phase of one drive period $\phi = \int(E_1 - E_0)dt$ satisfy the condition: $(\phi - 2\phi_S) = m \cdot 2\pi$. Our LZ interferometer can be used as a high-resolution detector for phase and charge owing to interferometric sensitivity- enhancement.

**8:12**

**Y40 2 Measuring the environmental impedance of the Cooper-pair box** BENJAMIN TUREK, JOHANNES MAJER, JOHN TEUFEL, *Yale University* AASHISH CLERK, *McGill University* STEVEN GIRVIN, ROBERT SCHOELKOPF, *Yale University* The Cooper-pair box qubit measured by the SET can have long decoherence times that are limited by the quantum noise of the environment. Qubits fabricated at Yale are designed with 50 ohm transmission lines that control this environmental impedance to very high frequencies. We use the AC Josephson effect of a hysteretic DC-Squid to measure the frequency dependence of this impedance. At frequencies where the real part of the environmental impedance is large, the AC Josephson effect causes the small-junction analogue of self-induced Shapiro steps in the IV curves of a DC Squid [T. Holst et al., PRL 73, 3455 (1994)]. We determine that the environmental impedance of our qubit is well behaved at frequencies less than 20 GHz.

**8:24**

**Y40 3 Anomalously low tunneling escape rates from the excited states of an inductively−isolated current−biased Josephson junction phase qubit*** R.M. LEWIS, T.A. PALOMAKI, HANHEE PAIK, S.K. DUTTA, A. PRZYBYSZ, B.K. COOPER, J.R. ANDERSON, A.J. DRAGT, C.J. LOBB, F.C. WELLSTOOD, *University of Maryland* We present measurements of an inductively-isolated current-biased Nb/AlOx/Nb Josephson junction quantum bit at 20 mK. Density matrix fits of Rabi oscillations in our system suggest that the tunneling rate ($\Gamma_1$) from the first excited state is an order of magnitude lower than expected from a single current-biased junction. Furthermore, measurements of the energy relaxation time, $T_1$, through both pulse/decay and thermal population[1] techniques only agree if $\Gamma_1$ is approximately an order of magnitude lower than our single junction model predicts. To test for low $\Gamma_1$, we use a fast-ramp technique ($\alpha = d(ln\Gamma)/dt > 1/T_1$) to directly measure $\Gamma_1$. We propose that an increase in the Josephson inductance of the qubit junction when in the excited state causes this effective reduction in $\Gamma_1$.

*Supported by NSF grant #EIA0323261, the NSA, and the Center for Superconductivity Research

[1]S. K. Dutta *et al.*, Phys. Rev. B **70** 140502(R) (2004).

**8:36**

**Y40 4 Variable coupling between the inductively isolated current-biased Josephson junction qubit and the current bias leads*** HANHEE PAIK, S. K. DUTTA, R. M. LEWIS, R. C. RAMOS, H. XU, T. A. PALOMAKI, B. K. COOPER, A. J. PRZYBYSZ, A. J. DRAGT, J. R. ANDERSON, C. J. LOBB, F. C. WELLSTOOD, *Center for superconductivity Research, Department of Physics, University of Maryland* We examined the behavior of inductively isolated Josephson junction qubits in which the coupling to the bias leads could be varied in situ. The variable coupling was achieved by using a second Josephson junction and an inductor that act as an inductive current divider. The coupling between the current bias leads and the qubit was varied by changing the current through the second junction, altering its Josephson inductance. We measured the tunneling escape rates of Al/Al$O_x$/Al and Nb/Al$O_x$/Nb junctions with continuous or pulsed microwave power, showing the allowed energy transitions and coherent Rabi oscillations. We found that $T_2$, $T_2^*$ and $T_1$ did not change significantly as the coupling to the current bias leads was varied.

*This work is supported by NSA, NSF and Center for Superconductivity Research at University of Maryland. NSF grant number EIA0323261.

**8:48**

**Y40 5 Analysis of Rabi Oscillations of a Josephson Phase Qubit*** S. K. DUTTA, H. XU, FREDERICK W. STRAUCH, PHILIP R. JOHNSON, R. C. RAMOS, HANHEE PAIK, T. A. PALOMAKI, R. M. LEWIS, J. R. ANDERSON, ALEX J. DRAGT, C. J. LOBB, F. C. WELLSTOOD, *Department of Physics, University of Maryland* We have experimentally studied asymmetric Nb/AlOx/Nb dc SQUID qubits at 25 mK. The two lowest metastable levels localized within a single well of the complex two-dimensional potential of the device can serve as qubit states, if they are not unduly perturbed by resonant coupling to higher states of the full potential. Rabi oscillations between the qubit states can be driven with a microwave bias current. State readout is performed by measuring the tunneling rate from all energy levels with non-zero occupation probability to the finite voltage state. To interpret the results of our Rabi oscillation measurements, we have used a multi-level density matrix simulation to extract the populations of the individual quantum states from this total rate. We can then calculate the visibility of the oscillations and determine the effects of the higher levels and multi-photon transitions.

*This work is supported by the NSA, NSF Grant EIA 0323261, and the Center for Superconductivity Research.

**9:00**

**Y40 6 Two Coupled Inductively-Isolated Josephson Junction Qubits*** TAUNO PALOMAKI, SUDEEP DUTTA, HANHEE PAIK, RUPERT LEWIS, ROBERTO RAMOS, HUIZHONG XU, BOB ANDERSON, CHRIS LOBB, FRED WELLSTOOD, *University of Maryland* We report experimental measurements on coherent quantum oscillations and entangled macroscopic quantum states in two capacitively-coupled inductively-isolated Nb/$Al_2O_3$/Nb Josephson qubits at 25mK. The interaction between the two qubits is controlled by tuning the energy level spacings of the junctions using the bias current and applied flux. We discuss transitions to various states of the coupled device, show Rabi oscillations, and analyze the spectroscopy of the system when the junctions are in and out of resonance with each other.

*This work is supported by the NSA, NSF Grant EIA 0323261, and the Center for Superconductivity Research.

**9:12**

**Y40 7 Flux Noise in an Inductively Isolated Josephson Junction Qubit*** B. K. COOPER, HANHEE PAIK, R. M. LEWIS, S. K. DUTTA, T. A. PALOMAKI, A. J. PRZYBYSZ, J. R. ANDERSON, ALEX J. DRAGT, C. J. LOBB, F. C. WELLSTOOD, *Department of Physics, University of Maryland* Martinis et al. [1] first proposed a technique for inductively isolating a Josephson junction qubit from the bias leads. It involves using one junction of a dc SQUID as a qubit, and the SQUID inductance and second junction of the SQUID as an inductance divider. This arrangement allows for isolation from current bias lines but potentially introduces greater sensitivity to flux noise. By introducing counter-wound inductors on the qubit arm of the SQUID, we can reduce spatially uniform flux noise. We compare experimental coherence

times for a $Nb/Al_2O_3/Nb$ qubit in such gradiometer designs to similar devices lacking the counterwound inductors. No significant difference is seen, suggesting that uniform flux noise is not the major source of decoherence in our system. [1] J. M. Martinis et al., PRL **89**, 117901

*This research is supported by NSF grant number EIA0323261, NSA and the Center for Superconductivity Research.

**9:24**

**Y40 8 Measurement of Microwave Resonators for Improved $T_1$ in Josephson Qubits** MATTHEW NEELEY, M. ANSMANN, R. BIALCZAK, N. KATZ, E. LUCERO, R. McDERMOTT, M. STEFFEN, E. WEIG, A. CLELAND, J. M. MARTINIS, *UC Santa Barbara* To realize a quantum computer with Josephson qubits, the energy relaxation time $T_1$ must be increased by an order of magnitude or more over current qubits. One of the dominant sources of energy decoherence is dielectric loss due to two-level defect states in the Josephson junction and in wiring cross-overs. Easily-fabricated microwave resonators provide a convenient way to measure the dielectric loss of candidate materials before incorporating them into qubits. We describe the measurement process and the results for several candidate dielectric materials. The loss tangents have been observed to vary with applied magnetic field. This variation is explained by a simple model of flux vortex trapping in the type I superconducting aluminum films of the resonators.

**9:36**

**Y40 9 High Q Dielectrics for Josephson Phase Qubits** E. M. WEIG, M. ANSMANN, R. BIALCZAK, N. KATZ, E. LUCERO, R. McDERMOTT, M. NEELEY, M. STEFFEN, J. M. MARTINIS, A. N. CLELAND, *California NanoSystems Institute & Department of Physics, UC Santa Barbara* Dielectric loss in the bulk insulating material surrounding a superconducting phase qubit has recently attracted attention as a major source of decoherence. Dissipation arises from the excitation of a bath of two-level defects that is unsaturated in the limit of low microwave power and low temperature. This gives rise to much lower intrinsic Q factors than expected from material characterization typically performed in the saturated higher power or temperature regime. The density of these two-level systems in the insulator can be distinctively reduced by carefully choosing and engineering the dielectric material. We have investigated LC resonators fabricated using various amorphous dielectrics ranging from silicon dioxide or silicon nitride to silicon hydride (a-Si:H). The intrinsic Q factors of the materials have been measured at microwave frequencies in the unsaturated regime. The data demonstrates that by proper choice of material the dielectric loss tangent can be dramatically reduced, thus allowing for long coherence time phase qubits.

**9:48**

**Y40 10 Fabrication and Testing of AlN Josephson Junction Qubits** RADOSLAW BIALCZAK, *University of California, Santa Barbara* MARKUS ANSMANN, NADAV KATZ, ERIK LUCERO, ROBERT McDERMOTT, MATTHEW NEELEY, MATTHIAS STEFFEN, EWA WEIG, ANDREW CLELAND, JOHN MARTINIS, Recently, it has been shown that a major source of decoherence in Josephson junction (JJ) qubits comes from coupling to two-level systems (TLS) in the dielectric materials used to construct these qubits. These TLS's result from defects in the dielectric material. In our previous work we have shown that the energy relaxation times of our JJ phase qubits improve 20-fold when we substitute SiO2 with SiN as the dielectric material used for cross-over wiring. This shows that nitride based dielectrics might be less prone to defects and suggests that the next logical step would be to replace the Al2O3 tunnel barrier dielectric of the JJ with AlN. We have used atomic nitrogen to successfully fabricate a JJ phase qubit with AlN as the JJ tunnel barrier material. Through spectroscopy measurements, we have found that qubits made with AlN as the tunnel barrier material have only slightly lower concentrations of defects compared with previously studied qubits made with Al2O3 grown by natural oxidation. Also, the measured T1 times for these AlN qubits were low ( $\sim$ 15ns). This agrees with theoretical predictions of Ioffe et al. which state that piezoelectric materials, such as AlN, might have other loss mechanisms due to phonon radiation.

**10:00**

**Y40 11 Evolution and decay of a superconducting Josephson junction qubit due to partial measurement** N. KATZ, M. ANSMANN, R. BIALCZEK, E. LUCERO, R. McDERMOTT, M. NEELEY, M. STEFFEN, E. WEIG, A. CLELAND, J. M. MARTINIS, *California NanoSystems Institute and Physics Dept., University of California, Santa Barbara* A. KOROTKOV, *Electrical Engineering Dept., University of California, Riverside* Superconducting Josephson phase qubits have been shown to be a promising candidate for scalable quantum computing. In many such quantum computing algorithms, partial measurement of the quantum state is used to project the system into a required subspace. We experimentally study the effect of a partial measurement on our Josephson phase qubit using state tomography and high fidelity measurement capabilities. We also explore related multi-photon effects which appear naturally in such a system during state preparation, evolution and measurement.

**10:12**

**Y40 12 Quantized Rabi oscillation observed in the superconducting flux qubit LC-harmonic oscillator system** K. SEMBA, J. JOHANSSON, S. SAITO, *NTT Basic Research Labs, NTT Corp. and CREST Japan Science and Technology Agency* T. MENO, *NTT Advanced Technology* H. NAKANO, *NTT Basic Research Labs, NTT Corp. and CREST JSTA* M. UEDA, *NTT Basic Research Labs, NTT Corp., CREST JSTA, Dept. of Physics, Tokyo Inst. of Tech.* H. TAKAYANAGI, *NTT Basic Research Labs, NTT Corp. and CREST JSTA* Superconducting circuit containing Josephson junctions is one of the promising candidates as a quantum bit (qubit) which is an essential building block for quantum computation. A flux qubit is represented by energetically lowest two collective states of macroscopic numbers of Cooper pairs which are linear combination of clockwise and counterclockwise persistent-current states. By replacing an atom with a flux qubit (artificial atom), and a high-Q cavity with an LC-circuit, quantum optics type experiments are possible on a superconductor chip. We have observed, for the first time, the vacuum Rabi oscillations in a superconducting flux qubit LC-oscillator coupled system [1]. We have also obtained evidence of level quantization of the LC circuit by observing the change in quantum oscillation frequency when the LC circuit was not initially in the vacuum state. Sharing a single superconducting LC-circuit with many flux qubits as a quantum information bus, spatially separated multiple qubits can be controlled by a set of microwave pulses. [1] J. Johansson et al., arXiv:cond-mat/0510457, http://www.brl.ntt.co.jp/group/shitsuryo-g/index.html

**10:24**

**Y40 13 Quantum Computing Architectural Design** JACOB WEST, GEOFFREY SIMMS, MARK GYURE, *HRL Laboratories, LLC. Malibu, CA* Large scale quantum computers will invariably require scalable architectures in addition to high fidelity gate operations. Quantum computing architectural design (QCAD) addresses the problems of actually implementing fault-tolerant algorithms given physical and architectural constraints beyond those of basic gate-level fidelity. Here we introduce a unified framework for QCAD that enables the scientist to study the impact of varying error correction schemes, architectural parameters including layout and scheduling, and physical operations native to a given architecture. Our software package, aptly named QCAD, provides compilation, manipulation/transformation, multi-paradigm simulation, and visualization tools. We demonstrate various features of the QCAD software package through several examples.

**10:36**

**Y40 14 Threshold calculation and optimization for measurementless quantum error correction** GEOFFREY SIMMS, MARK GYURE, JACOB WEST, *HRL Laboratories, LLC. Malibu, California* General-purpose quantum computing will rely on measurement as a primitive operation, but the operations of measurement and classical feed-forward are not necessary to perform certain useful computations, including quantum error correction. Measurementless quantum computation is appealing because it reduces the classical control system to an automaton, having no conditional operations. Measurementless, fault-tolerant quantum error correction (MFTQEC) of Calderbank-Shor-Steane (CSS) encoded logical qubits requires logical zero states to be prepared with high fidelity as an initial step, and this logical zero preparation has a threshold of its own, analogous to, but not identical to, the threshold of the entire error correction algorithm. In this talk, we present the results of mapping the MFTQEC algorithm onto a specific semiconductor-based qubit system using the Quantum Computing Architectural Design (QCAD) program, discussed in another talk in this session. The algorithm is translated from the set of ''design gates'' to the set of accessible ''physical gates,'' and the resulting quantum circuit is optimized to improve the threshold. Limited 2-dimensional connectivity is assumed, making this well suited to the ''enhancement mode'' quantum dot qubits described in other talks in this session.

**10:48**

**Y40 15 Shift register in a SQUID architecture with untunable couplings*** PREETHIKA GAGNEBIN, STEVEN SKINNER, *Department of Electrical and Computer Engineering, Wichita State University* ELIZABETH BEHRMAN, *Department of Physics, Wichita State University* JAMES STECK, *Department of Aerospace Engineering, Wichita State University* A scheme to implement a qubit shift register in a one-dimensional series of superconducting quantum interference devices (SQUIDs), using a sequence of pulsed biases, is described. Each SQUID is coupled to its neighbors through an untunable coupling parameter. The only variable parameter of the system is the bias on each SQUID, which is pulsed low during a shift operation. Our design requires only two bias control signals for any size of shift register, with an additional one on the output qubit to shift out the data. The shift register operation is realized by copying the state of one qubit onto another, in the direction of the shift, during the bias pulse. As the no-cloning theorem prohibits the cloning of an unknown arbitrary quantum state, this device works as a classical shift register or, in other words, a binary wire. We show here how to find the time duration of the bias pulse and the minimum value of the bias during the pulse given the fixed physical parameters of the system.

*Supported by NSF, ECS 0201995

## SESSION Y45: MAGNETIC PHASE TRANSITIONS

**Friday Morning, 17 March 2006**
**348, Baltimore Convention Center at 8:00**
**Julie Borchers, National Institute of Standards and Technology Center for Neutron Research, presiding**

**8:00**

**Y45 1 Discovery of remarkably high magnetic ordering temperatures in dilute rare earth intermetallic compounds** S. JIA, G.D. SAMOLYUK, NI NI, E-D. MUN, S.L. BUD'KO, P.C. CANFIELD, *Ames Laboratory and Dept. of Physics and Astronomy, Iowa State University* Dilute, rare earth intermetallic compounds are ordered structures in which the rare earth comprises less than 5% atomic of the compound, but still fully occupies a unique crystallographic site. When none of the other elements are moment bearing, it is generally anticipated that such a compound will have magnetic ordering temperatures near 10 K for the R = Gd member of the series and systematically lower temperatures for heavier R members. In this talk we will present a series of dilute rare earth intermetallic compounds that have ferromagnetic ordering temperatures that range from $T_C \sim 90$ K for R = Gd to $T_C \sim 5$ K for R = Tm. The origin of this high ordering temperature as well as systematic trends across the series will be discussed.

**8:12**

**Y45 2 The effects of pressure and chemical substitution on the transition temperature and groundstate of Gd-based dilute rare earth intermetallic compounds** P.C. CANFIELD, S. JIA, G.M. SAMOLYUK, S.L. BUD'KO, *Ames Laboratory and Dept. of Physics and Astronomy, Iowa State University* Dilute, rare earth intermetallic compounds are ordered structures in which the rare earth comprises less than 5% atomic of the compound, but still fully occupies a unique crystallographic site. We have investigated a family of Gd-based, ternary, dilute, rare earth intermetallic compounds in an attempt to understand the remarkably high ferromagnetic ordering found for some of the members ($T_C$ as high as 90 K). By studies of the thermodynamic and transport properties as a function of temperature, field and hydrostatic pressure and combining these results with band-structure calculations we have been able to determine that some of these compounds have an enhanced DOS at the Fermi level that may be correlated with the enhanced ordering temperatures.

**8:24**

**Y45 3 Paramagnetic Semiconductor to itinerant Ferromagnet in $Fe_{1-x}Co_xS_2$** SONG GUO, *Dept. of Physics and Astronomy, Louisiana State University* JOHN DITUSA, *Dept. of Physics and Astronomy, Louisiana State University* DAVID YOUNG, *Dept. of Physics and Astronomy, Louisiana State University* ROBIN MACALUSO, *Dept. of Chemistry, Louisiana State University* DANA BROWNE, *Dept. of Physics and Astronomy, Louisiana State University* NATHAN HENDERSON, *Dept. of Chemistry, Louisiana State University* JULIA CHAN, *Dept. of Chemistry, Louisiana State University* Carrier doping of ''fool's gold,'' the paramagnetic insulator $FeS_2$ by partial substitution of Co for Fe, results in an insulator-to-metal transition at $x \leqslant 0.001$. Magnetization and susceptibility measurements for samples with Co substitution beyond $x0.01$ reveal the emergence of a highly itinerant ferromagnet with no discontinuous changes with $x$, field, or temperature ($T$) suggesting either a continuous crossover or quantum phase transition to ferromagnetism. For $x \leqslant 0.01$ and low-$T$, the conductivity decreases with smaller $T$ and displays a positive magnetoconductance. Samples which order magnetically show similar magnetoconductance, but with a minimum in conductivity near $T_c$. We conclude that either Kondo or magnetic polaron effects are responsible for these low-$T$ anomalies. Specific heat measurements display extraordinarily large carrier masses that diverge logarithmically or with a small power law at low-$T$ close to the ferromagnetic critical concentration, similar to the behavior near quantum critical points.

**8:36**

**Y45 4 Ferromagnetic Transition in Heusler Alloys** ANKE HUSMANN, *Toshiba Research Europe Ltd* MARK C. HICKEY,* *University of Cambridge* MINHYEA LEE, *Princeton University* TOSHIBA RESEARCH EUROPE LTD COLLABORATION, UNIVERSITY OF CAMBRIDGE COLLABORATION, PRINCETON UNIVERSITY COLLABORATION, The transition from a magnetically disordered (paramagnetic) to a magnetically ordered (ferromagnetic) state at finite temperature in zero magnetic field has long been regarded as one of *the* text book examples for a second order phase transition. However, this mean field Weiss model leaves out some of the physics that can become crucial for itinerant magnets when approaching the transition temperature. $Co_2TiSn$ and $Co_2CrAl$ are two Heusler alloys with Curie temperatures just above room temperature. Theoretical band structure calculations, ours as well as by others, predict them to be close to half metals. Magnetisation data as a function of temperature and magnetic field show deviations from the mean field Weiss model which we argue are due to band structure properties.

*also Toshiba Research Europe Ltd

**8:48**

**Y45 5 Field and temperature dependence of the first order antiferromagnetic to ferromagnetic phase transition in FeRh thin films** STEFAN MAAT, JAN-ULRICH THIELE, ERIC E. FULLERTON, *Hitachi Global Storage Technologies* Chemically ordered FeRh exhibits a first order antiferromagnetic (AF) to a ferromagnetic (F) phase transition upon heating from room temperature to above a transition temperature of approximately 370 K. This transition is accompanied by a volume increase of $\sim$ 1%, a change in resistivity, and a large change in entropy. The phase transition occurs within a few ps allowing it to be used in thermal assisted recording. For example, it was recently proposed to use exchange coupled FeRh/FePt bilayers for thermally assisted magnetic recording media. Here we studied the thermodynamics of the transition in thin FeRh films epitaxially grown onto MgO and sapphire substrates. A shift to lower transition temperatures is observed in external magnetic fields and supercooling is easily observed by cycling either the temperature or the magnetic field. A temperature-field phase diagram was constructed revealing a linear -8 K/ Tesla temperature-field relationship. The observed field dependence of the shift in transition temperature is modeled with an Ising spin type model utilizing a mean field approach. The computational results are in excellent agreement with the experimental data.

**9:00**

**Y45 6 Vector-magnetometry determination of magnetization processes in $Pr_6Ni_2Si_3$ and $Nd_6Ni_2Si_3$*** Y. JANSSEN, K. W. DENNIS, R. PROZOROV, P. C. CANFIELD, R. W. McCALLUM, *Ames Laboratory, Iowa State University, Ames, IA 50011* Hexagonal $Pr_6Ni_2Si_3$ and $Nd_6Ni_2Si_3$ order magnetically at 40 and 85 K, repectively. At 5 K, the magnetic order of both compounds appears to have a ferromagnetic component parallel to the hexagonal c-axis, and an antiferromagnetic component perpendicular to it. In both compounds, at 5 K and in a magnetic field of $\sim$ 2-3 T, applied perpendicular to the c-axis, a magnetic transition occurs. Using a QD-MPMS equipped with a transverse pickup coil system, we have studied the behavior of the magnetization vector in single-crystal samples during this transition. In both cases, the magnetization vector becomes anomalously itlonger during the transition. This indicates the transition may be related to an antiferromagnetic component of the magnetic order, which is consistent with the magnetic order having both antiferro and ferromagnetic components.

*Ames Laboratory is operated for the US Department of Energy by Iowa State University under contract number W-7405-ENG-82.

**9:12**

**Y45 7 Observation of two distinct energy scales in the magnetization measurements of the anisotropic antiferromagnet TmAgGe** ANA LIMA, *NHMFL - LANL* PAUL GODDARD, *Clarendon Laboratory, Oxford University, Oxford, UK* JOHN SINGLETON, *NHMFL - LANL* EMILIA MOROSAN, SERGEY BUD'KO, PAUL CANFIELD, *Dept. of Phys. & Astronomy, ISU and Ames Laboratory* TmAgGe is an antiferromagnet ($T_N = 4.2$ K) that crystallizes in a variant of the hexagonal $Fe_2P$ structure (three Tm atoms per unit cell). We have studied the magnetization of the TmAgGe single crystals in fields $\mu_0 H$ of up to 65 T as a function of the field orientation and the temperature $T$. With **H** in the basal **ab**-plane, a number of metamagnetic transitions are observed for $\mu_0 H < 5$ T and $T < T_N$. However, when $\mathbf{H}||\mathbf{c}$, three steps in the magnetization occur between 30 and 35 T, persisting to $T \cong 60$ K. On tilting **H** away from **c,** both sets of features (high-field steps and low-field metamagnetism transitions) are seen, showing that they arise from two distinct mechanisms. The dependence of the high-field steps on $T$ and field orientation suggests that they are associated with crystalline electric field (CEF) level crossing; the CEF confines the moments to the **ab**-plane. By contrast, it is the rearrangement of the moments within the basal plane that gives to the low-field metamagnetic transitions. To the best of our knowledge, TmAgGe is the first intermetallic system in which these two energy scales (CEF and in-plane exchange) can be unambiguously distinguished in this way.

**9:24**

**Y45 8 Anomalous Magnetic Properties near the Spin-Flop Bicritical Point in $Mn_2AS_4$ ($A$ = Si and Ge)** KENYA OHGUSHI, YUTAKA UEDA, *ISSP, Univ. of Tokyo* The magnetic properties of the single crystalline $Mn_2AS_4$ ($A$ = Si and Ge) with an olivine structure, which are the uniaxially anisotropic antiferromagnets (the $b$-axis as an easy axis), were investigated. Near the Néel temperature, both compounds exhibit the contrastive magnetic responses along the $c$-axis, namely, the spontaneous weak ferromagnetism in $A$ = Si and the significant enhancement of the differential susceptibility (itdM/dH) under the small magnetic field in $A$ = Ge. When $A$ = Ge, we also observed the evolution of itdM/dH along the $a$-axis at low temperatures. We discuss these phenomena on the basis of the magnetic field-temperature ($H - T$) phase diagram with the spin-flop bicritical point ($H_{BP}$, $T_{BP}$). The role of the thermal or quantum fluctuation was stressed. (Ref.) K. Ohgushi and Y. Ueda, Phys. Rev. Lett. **95**, 217202 (2005)

**9:36**

**Y45 9 Composition dependent properties of mixed magnetic Fe/Ni dichloride dihydrate*** G.C. DEFOTIS, M.G. KIM, D.G. CHAN, Z.D. REED, A.T. HOPKINSON, Y. MATSUYAMA, *College of William and Mary* This mixed magnet is composed of two approximate 3D-Ising antiferromagnets ordering at 22.3 K (Fe component) and 7.3 K (Ni component). The pure substances also display metamagnetic transitions at low temperature near 39 kG (Fe) and 19 kG (Ni). Ferromagnetically coupled metal-dichloride-metal . . . chemical and structural chains occur in each component, with predominantly antiferromagnetic interchain interactions. Homogeneous mixtures have been obtained and examined by dc susceptibility and magnetization measurements over the entire composition range. Curie and Weiss constants are obtained from fits to high temperature data. In many mixtures two magnetic transitions at different temperatures are observed. In several mixtures marked nonlinearities in magnetization vs field appear, with signficant temperature dependence, and suggestive of metamagnetic transitions with associated hysteresis. Most interestingly, the inferred transition fields are lower than those of either component. The overall behavior can be compared with that in the previously studied and closely related Co/Ni mixed system. Some similarities appear, but also notable differences.

*Supported by NSF-SSC Grant No. DMR-0085662 and by an ACS-PRF grant.

**9:48**

**Y45 10 Hysteresis effect in $^{55}Mn$ NMR of $TbMn_2O_5$** SEUNG-HO BAEK, ANDREW HARTER, ARNEIL REYES, *National High Magnetic Field Lab* SANG-WOOK CHEONG, N. HUR, *Rutgers University* $^{55}Mn$ zero-field NMR has been performed on antiferromagnetic magnetoelectric multiferroic compound $TbMnO_5$ from 60 K to 1.8 K. The broad and complex spectrum is distributed between 240 MHz and 280 MHz implying a superposition of NMR lines arising from the several inequivalent Mn ions due to the amplitude-modulated spin structure. When external perturbing field up to 3 T is applied, a dramatic change in the first moment and the signal enhancement is observed which are hysteretic in nature. The behavior is attributed to antiferromagnetic domain walls which are coupled to ferroelectric domains similar to that observed in weakly ferromagnetic $\alpha$-$Fe_2O_3$. The nature of strong coupling of magnetic and electric ordering and its subsequent effect on its multiferroic behavior are discussed.

**10:00**

**Y45 11 Magnetic Field Induced Phases in the Quantum Antiferromagnet $Cs_2CuCl_4$ as revealed by NMR.** M.-A. VACHON, V.F. MITROVIC, O. MA, J.B. MARSTON, *Brown University* A.P. REYES, P. KUHNS, *NHMFL* R. COLDEA, *University of Bristol* We report nuclear magnetic resonance (NMR) measurements on the 2D frustrated quantum antiferromagnet $Cs_2CuCl_4$. $^{133}Cs$ spectra at temperatures down to 60 mK and in external magnetic field up to 15 T are presented. At the lowest temperature we observe multiple field induced quantum phase transitions in a magnetic field applied within the spin plane. The phases are distinguished by their local spin textures. The possible nature of these phases and their underlying spin structure are discussed. Furthermore, simulations of spectra are presented.

**10:12**

**Y45 12 Phase Transitions at the $Cr_{1-x}V_x$/W(110) System** OLEG KRUPIN, *Department of Physics, University of Oregon, Eugene, Oregon* ELI ROTENBERG, *Advanced Light Source, Lawrence Berkeley National Laboratory, Berkeley, California* STEVE KEVAN, *Department of Physics, University of Oregon, Eugene, Oregon* The rich phase diagram of thin films of chromium-vanadium ($Cr_{1-x}V_x$) alloys offers a unique possibility to study the phenomena associated with the spin-density wave (SDW) ground state and quantum phase transition (QPT). Using angular-resolved photoemission (ARP) we have studied the periodicity of SDW in the region of commensurate-incommensurate phase transition followed by quantum phase transition as a function of two non-thermal parameters: film thickness and vanadium concentration. That allows probing the interplay between spatial confinement and Fermi surface topology change resulting from modification of chromium electron structure by vanadium doping.

**10:24**

**Y45 13 The spin state transition in $LaCoO_3$; revising a revision** L. H. TJENG, M. W. HAVERKORT, Z. HU, T. BURNUS, C. ZOBEL, M. REUTHER, H. HARTMANN, T. LORENZ, *II. Physikalisches Institut, Universität zu Köln, Germany* J. C. CEZAR, N. B. BROOKES, *European Synchrotron Radiation Facility, Grenoble, France* A. TANAKA, *Department of Quantum Matter, ADSM, Hiroshima University, Japan* H. H. HSIEH, *Chung Cheng Institute of Technology, National Defense University, Taoyuan, Taiwan* H.-J. LIN, C. T. CHEN, *National Synchrotron Radiation Research Center, Hsinchu, Taiwan* Using soft x-ray absorption spectroscopy and magnetic circular dichroism at the Co-$L_{2,3}$ edge we demonstrate that the spin state transition in $LaCoO_3$ can be well described by a low-spin ground state and a high-spin first excited state which becomes populated at elevated temperatures. From the temperature dependence of the spectral lineshapes we find that $LaCoO_3$ at finite temperatures is an inhomogeneous mixed-spin-state system. Crucial is that the magnetic circular dichroism signal in the paramagnetic state carries a large orbital momentum. This directly shows that the currently accepted low-/intermediate-spin picture is at variance, and that instead the original low-/high-spin scenario is the better itansatz.

**10:36**

**Y45 14 Transport and Magnetic Properties of $Nd_2Ni_2Pb$ and NdNiPb** V. GORUGANTI, YANG LI, JOSEPH H. ROSS, JR., K.D.D. RATHNAYAKA, *Department of Physics, Texas A&M University* Y. ÖNER, *Deparment of Physics, Istanbul Technical University* We report magnetic, transport and thermodynamic measurements for $Nd_2Ni_2Pb$ and NdNiPb, members of recently-discovered $R$-Ni-Pb families of intermetallics. In $Nd_2Ni_2Pb$ a

λ-type specific heat jump was observed at 19 K corresponding to an antiferromagnetic transition. Magnetization measurements show this phase to have a canted structure, with a metamagnetic transition in $H = 3$ T at low temperatures. We have further explored the metamagnetic transition using field dependent specific heat, concluding that the metamagnetic phase is a fully aligned phase. The single antiferromagnetic phase stands in contrast to the more complex magnetic structures observed in the heavy-rare-earth members of this family. Nd is the lightest RE forming this type strucure. At high temperatures the magnetization obeys a Curie law and the magnetic moment agrees with the free ion moment of Nd. Resistivity measurements showed metallic behavior with a kink at 19 K. We performed similar measurements on NdNiPb and observed an antiferromagnetic transition at 4 K. Specific heat indicated rather different critical behavior, with magnetic fluctuations extending well above the transition. This work was supported by the Robert A. Welch Foundation (grant A-1526), the National Science Foundation (DMR-0103455), and by the Texas A&M University Telecommunications and Informatics Task Force.

**10:48**

**Y45 15 Magnetic Susceptibility Experiments on the Heavy Lanthanides Using Designer Diamond Anvils** DAMON JACKSON, VINCE MALBA, SAMUEL WEIR, *Lawrence Livermore National Laboratory* PAUL BAKER, YOGESH VOHRA, *University of Alabama, Birmingham* The high pressure magnetic properties of the heavy lanthanide elements Gd, Tb, Dy, Ho, Er, and Tm have been investigated by ac magnetic susceptibility using designer diamond anvils. It is found that the magnetic transition temperatures monotonically decrease with increasing pressure. In addition, the amplitudes of the magnetic transition signals decrease with increasing pressure, with the signals all eventually disappearing at pressures by 20 GPa. The transition temperatures, $T_{Crit}$ are all found to drop at a rate proportional to their de Gennes factor, and the values of $T_{Crit}/T_{Crit}(P = 0)$ vs $P/P_{Crit}$, where $P_{Crit}$ is the pressure where the magnetic transition disappears, all sit on a single phase diagram.

## SESSION Y46: BILAYERS, WIGNER CRYSTALS

**Friday Morning, 17 March 2006**
**349, Baltimore Convention Center at 8:00**
**Alan Dorsey, University of Florida, presiding**

**8:00**

**Y46 1 Coulomb frustrated phase separation in bilayer electronic systems** REZA JAMEI, STEVEN KIVELSON, *Stanford University* BORIS SPIVAK, *University of Washington* We have previously proven that in clean two dimensional electronic systems, long range Coulomb interactions convert what might otherwise have been a first order transition between a high density liquid and a low density insulating electron crystalline phase into a sequence of continuous phase transitions between various sorts of intermediate ''electronic microemulsion phases.'' Here, we consider the electronic micromemulsion phases in a bilayer system, with Coulomb interactions both within and between the layers. At mean-field level, we find infinite families of modulated phases, with a subtle interplay of the period and magnitude of the density oscillations in the two layers.

**8:12**

**Y46 2 Interlayer CF Pairing in a Symmetric $\nu_T = 1$ Quantum Hall Bilayer** GUNNAR MOLLER, *LPTMS Orsay/France* STEVEN H. SIMON, *Lucent Technologies* EDWARD REZAYI, *California State University Los Angeles* In bilayer quantum Hall systems at filling fractions near $\nu = \frac{1}{2} + \frac{1}{2}$, as the spacing $d$ between the layers is continuously decreased, intra-layer correlations must be replaced by inter-layer correlations, and the composite fermion (CF) Fermi seas at large $d$ must eventually be replaced by a composite boson (CB) condensate at small $d$. In recent work [1], trial wave functions were constructed that can describe how composite fermion-like intra-layer correlations can be continuously replaced by 111-like inter-layer correlations using a picture of two classes of quasi particles: composite bosons and composite fermions. Here, we present how to extend this approach both qualitatively and quantitatively, introducing a new way of writing the previously introduced wave functions, which allows for the introduction of composite fermion inter-layer positive p-wave pairing. These wave functions depend on a small number of variational parameters related to the momentum distribution of $(\mathbf{k},\uparrow; -\mathbf{k},\downarrow)$ CF pairs. Comparison of energies and correlation functions to results from exact diagonalizations for small systems shows close to perfect agreement, thus giving evidence for inter layer CF pairing in QH bilayer systems [2]. This work was supported by the DOE. [1] S. H. Simon, E. H. Rezayi, and M. V. Milovanovic, Phys.Rev.Lett. **91**, 046803 (2003). [2] G. Möller, S. H. Simon, to be published, G. Möller, S. H. Simon, E. H. Rezayi, to be published.

**8:24**

**Y46 3 Excitonic codensation in quantum Hall electron-hole bilayers** YOGESH JOGLEKAR, *IUPUI* ALEXANDER BALATSKY, *LANL* Bose-Einstein condensation of excitons in bilayers has been explored increasingly over the past decade. We present an effective theory of excitonic condensate phase in electron-hole systems in the quantum Hall regime and its derivation from a microscopic Hamiltonian using mean-field analysis. We present results for the critical layer separation $d$ as a function of electron-layer filling factor $\nu_e$, hole-layer filling factor $\nu_h$, and interlayer bias voltage $\Delta_v$. We extend our analysis to singlet and triplet excitons. We point out the salient differences between these systems and the (electron-electron) quantum Hall bilayers near total filling factor $\nu = 1$ which have been investigated experimentally in recent years.

**8:36**

**Y46 4 Development of the excitonic state of bilayer quantum Hall system at total filling one** DAIJIRO YOSHIOKA, *The University of Tokyo* NAOKAZU SHIBATA, *Tohoku University* Excitonic phase, namely Haplerin's $\Psi_{1,1,1}$ state, is realized in bilayer quantum Hall systems at $\nu = 1$ at small layer separation $d$ as evidenced by various experiments. This phase vanishes as $d$ is increased, and at large enough separation, composite-fermion Fermi-liquid states are realized in each layer. How the excitonic state develops into independent Fermi-liquid states has not been fully understood. We investigated this development by the density matrix renormalization group method (DMRG). We calculated the ground state wave function and energy gap for various values of $d$

for systems with up to 24 electrons. From the ground state wave function, two-particle distribution function $g(r)$ and excitonic correlation function have been calculated. The results indicate that the transition between the two limits is continuous. There is a smooth crossover of the ground state at around $d/l \simeq 1.6$ from the excitonic character at small $d/l$ to independent Fermi-liquid character at large $d/l$, where $l$ is the magnetic length.

**8:48**

**Y46 5 Spin-pseudospin textures in a strongly correlated bilayer quantum Hall system near $\nu = 1$** RENE COTE, JEROME BOURASSA, *Universite de Sherbrooke* BAHMAN ROOSTAEI, *University of Oklahoma* HERB A. FERTIG, *University of Indiana* KIERAN MULLEN, *University of Oklahoma* Recent experiments on strongly correlated bilayer quantum Hall systems [1,2] strongly suggest that contrary to the usual assumption, the electron spin degree of freedom is not completely frozen either in the quantum Hall or the compressibles states that occur near filling factor $\nu = 1$. These experiments imply that the quasiparticles near $\nu = 1$ could have both spin and pseudospin textures i.e. they could be CP3 skyrmions. Assuming that these skyrmions crystallize at very low temperature, we use a microscopic unrestricted Hartree-Fock calculation to compute the energy of these excitations as well as the number of flipped spins and pseudospins for various values of the separation between the well and of potential biais. We compare our results to previous calculations based on a field-theoretical description and discuss their relevance for the experiments of Refs. [1,2]. (1) I. B. Spielman, L. A. Tracy, J. P. Eisenstein, L. N. Pfeiffer, and K. W. West, Phys. Rev. Lett. 94, 76803 (2005). (2) N. Kumada, K. Muraki, K. Hashimoto, and Y. Hirayama, Phys. Rev. Lett. 94, 96802 (2005).

**9:00**

**Y46 6 Pseudospin Vortex-Antivortex States with Interwoven Spin Texture in Double Layer Quantum Hall Systems*** B. ROOSTAEI, *U. of Oklahoma* J. BOURASSA, *U. of Sherbrooke* H. FERTIG, *U. of Indiana* K. MULLEN, *U. of Oklahoma* R. COTE, *U. of Sherbrooke* Enhanced nuclear spin relaxation rates have been observed in recent experiments[1] on double layer quantum Hall systems near total filling factor $\nu_T = 1$. The effect is analogous to what happens in single layer systems, where a possible explanation lies in the development of a Skyrme crystal with low energy spin wave modes as the system is doped away from integer filling. Double layer systems are thought to support bimeron excitations, analogous to skyrmions but with layer indices playing the role of spin states. We demonstrate,within the Hartree-Fock approximation, that for low interlayer tunneling and large separations the bimerons reorganize into a vortex-antivortex lattice with an interwoven real spin texture. These states are most stable at large layer separation, where the introduction of the spin degree of freedom can relax an interlayer charge imbalance at the cores of the merons. The presence of the real spin texture produces a true spontaneously broken symmetry whose Goldstone modes can explain the enhancement of the nuclear spin relaxation. [1]I.B. Spielman et al., Phys. Rev. Lett. 94, 076803 (2005).

*NSF Grant No. DMR-0520220,NSF Grant No. DMR-0454699. B. Roostaei is thanking KITP, U. of California,Santa barbara where part of this work was performed.

**9:12**

**Y46 7 Correlated Jumps in Magnetotransport of Imbalanced Bilayer Two Dimensional Hole Systems** NATHANIEL C. BISHOP, *Princeton University* SHASHANK MISRA, *Princeton University* EMANUEL TUTUC, *IBM/ T.J. Watson Research Center* MANSOUR SHAYEGAN, *Princeton University* A pair of dilute two-dimensional hole layers can interact to produce correlated electronic states unique to the bilayer geometry. Here, we examine the nonequilibrium resistivity of one layer when the other layer is tuned to the $\nu = 1$ quantum Hall state. Previous studies have shown that the longitudinal resistivity of the detuned layer jumps with a slow ($\tau \approx 100s$) relaxation.[1] Surprisingly, we find that both the longitudinal and Hall resistivities of the detuned layer jump at the same time for contacts located hundreds of microns apart. This suggests either that the instabilities in charge distribution of the two layers occur over domains of macroscopic size, or that some novel quantum correlation manifests itself over similarly large length scales. [1] E. Tutuc *et al.*, PRB **68**, 201308 (2003).

**9:24**

**Y46 8 Time Dependent Magnetotransport of Imbalanced Bilayer Two Dimensional Hole Systems** SHASHANK MISRA, *Princeton University* NATHANIEL C. BISHOP, *Princeton University* EMANUEL TUTUC, *IBM/ T.J. Watson Research Center* MANSOUR SHAYEGAN, *Princeton University* The magnetotransport of a two dimensional hole layer in close proximity to a second layer tuned to the $\nu = 1$ quantum Hall state exhibits correlations novel to the bilayer geometry. Previous experiments have shown the resistivity of the detuned layer to be hysteretic when sweeping the magnetic field, and to exhibit jumps as a function of time when staying at a fixed field.[1] We find that allowing the system to relax in middle of taking a hysteresis loop results in the magnetoresistance following a curve in between the two branches of the hysteresis loop, a hallmark of a glassy system. We further find that the seemingly random resistance jumps occur at similar times in separate measurements, each performed upon resetting the bilayer state. Work performed with support from the NSF and DOE. [1] E. Tutuc *et al.*, PRB **68**, 201308 (2003).

**9:36**

**Y46 9 Electron Drag in Intermediate Magnetic Fields** SANGHUN AN, GOKUL GOPALAKRISHNAN, YUKO SHIROYANAGI, SARAH PARKS, DONGKYUN KO, THOMAS GRAMILA, *Ohio State University, Physics Dept.* LOREN PFEIFFER, KEN WEST, *Bell Labs, Lucent Technologies* We report measurements of electron drag on the bilayer two-dimensional electron gas (2DEG) in intermediate magnetic fields, for which anomalous temperature-dependence and field-dependence of the drag resistivity have been previously observed. In this regime, drag resistivity shows surprisingly little temperature dependence, as well as a highly unusual field dependence which varies roughly as the cube of magnetic field. To our knowledge, no theoretical works have predicted such behavior. We have continued investigation of drag in this regime, therefore, in an attempt to understand the source of this anomalous behavior. We report detailed measurements exploring the potential role of spin in the process via application of an in-plane magnetic field, as well as examination of possible correlation effects, and a careful study of the temperature dependence.

**9:48**

**Y46 10 Plasmon Enhanced Drag Measurements at Low Densities** YUKO SHIROYANAGI, GOKUL GOPALAKRISHNAN, SANGHUN AN, SARAH PARKS, THOMAS GRAMILA, *Ohio State University* LOREN PFEIFFER, KEN WEST, *Bell Labs, Lucent Technologies* The plasmons of the two-dimensional electron gas(2DEG) can provide valuable information about electronic many-body correlation effects, while electron drag provides a unique method to probe electron-electron scattering processes in a double layer 2DEG system. An enhancement of electron drag by plasmons was predicted[1] and subsequently observed[2,3]. Experimental studies of the strength of the plasmon enhancement as a function of relative density, however, revealed that the maximum enhancement occurred for mis-matched layer densities, in disagreement with theoretical expectation. It has been argued that this results from correlation effects, in particular the presence of multi-particle excitations. We report new measurements of plasmon enhanced drag, which examine lower overall electron densities than had been reported earlier. Since correlation effects are stronger for lower densities, these measurements provide a means to test the role of correlations in determining the dependence of plasmon enhanced drag on relative densities. [1] K.Flensberg and B.Y.K.Hu, PRL 73, 3572(1994). [2] N.P.R.Hill et.al. PRL 78, 2204(1997). [3] H.Noh, S.Zelakiwicz, X.G.Feng, and T.J.Gramila PRB 58, 12621(1998).

**10:00**

**Y46 11 A Physical Picture for the Negative Drag in High Landau Levels** ADY STERN, RAFI BISTRITZER, *Weizmann* Experimental investigation of the longitudinal drag resistivity, $\rho^D$, of a bi-layer subjected to a strong magnetic field in the regime of large filling factors found an anomalous behavior at low temperatures $T$: $\rho^D$ depends non monotonously on $T$ and becomes negative when the filling factors of the two layers differ by an odd number. A calculation of $\rho_D$ within the framework of the self consistent Born approximation was generally consistent with the experiment; nevertheless, it left the physical picture obscure. We employ the exact eigenstates method to unravel that picture. We find the oscillating sign of $\rho^D$ to originate from the effect of disorder on the relation between an adiabatic momentum transfer to an electron and the displacement of its position. For localized states a momentum transfer $\mathbf{q}$ implies a displacement of $ql_H^2$, with $l_H$ being the magnetic length. For extended states, the combined effect of a short range disorder and a rapidly oscillating wave function at high Landau levels results in an additional, potentially larger, displacement whose sign depends on the electron's energy.

**10:12**

**Y46 12 Pinned Bilayer Wigner Crystals with Pseudospin Magnetism** YONG CHEN, *Princeton University and National High Magnetic Field Lab* We study a model of itpinned bilayer Wigner crystals (WC) and focus on the effects of interlayer coherence (IC) on pinning. We consider both a pseudospin ferromagnetic WC (FMWC) with IC and a pseudospin antiferromagnetic WC (AFMWC) without IC. Our central finding is that a FMWC can be pinned more strongly due to the presence of IC. One specific mechanism is through the disorder induced interlayer tunneling, which effectively manifests as an extra pinning in a FMWC. We also construct a general ''effective disorder'' model and effective pinning Hamiltonian for the case of FMWC and AFMWC respectively. Under this framework, pinning in the presence of IC involves itinterlayer spatial correlation of disorder in addition to intralayer correlation, leading to itenhanced pinning in the FMWC. The pinning mode frequency ($\omega_{pk}$) of a FMWC is found to decease with the effective layer separation, whereas for an AFMWC the opposite behavior is expected. An abrupt drop of $\omega_{pk}$ is predicted at a transition from a FMWC to AFMWC. Possible effects of in-plane magnetic fields and finite temperatures are addressed. Finally we discuss some other possible ramifications of the FMWC as an electronic supersolid- like phase. [1] Yong P. Chen, cond-mat/0507124

**10:24**

**Y46 13 Effect of vertical confinement on pinning mode of electron solids** G. SAMBANDAMURTHY, *NHMFL and Princeton University* YONG P. CHEN, *Princeton University and NHMFL* LLOYD ENGEL, *NHMFL* D.C. TSUI, *Princeton University* L.N. PFEIFFER, K.W. WEST, *Bell Labs, Lucent Technologies* We present the results from a study of the electron solid regime that terminates the fractional quantum Hall series in very clean two-dimensional electron systems (2DES). The disorder-induced pinning mode of the electron solid appears as a resonance in the microwave conductivity spectrum. In the present study, we compare results from two quantum well samples that were grown in the same way, with the only difference being the well widths (15 and 65 nm), allowing us to observe the effect of vertical confinement of electrons on the pinning mode of electron solids. We find that the narrower well (15 nm width) has a resonance with peak frequency ($f_{pk}$) $\sim$ 6-8 GHz, whereas the wider well (65 nm width) has $f_{pk} \sim$ 100-200 MHz. Moreover, $f_{pk}$ vs. $B$ for the two samples show markedly different behaviors. Our results suggest that the disorder that dominates the pinning of electron solids is from the interface roughness associated with the quantum well.

**10:36**

**Y46 14 A Numerical Study of 1/4 filling in the N=2 Landau Level** BARRY FRIEDMAN, MOSES MARCHANTE, Recently, it has been proposed that anisotropic Wigner crystals of electrons, with 1 electron per lattice site, have in certain circumstances, lower energies then the 2 electron bubble state or isotropic Wigner crystals. Using direct diagonalization and the density matrix renormalization group (dmrg) we have re examined 1/4 filling in the N=2 Landau level. Preliminary results indicate that the ground state consists of the 2 electron bubble state. Implementation of the dmrg, for quantum Hall systems, will also be discussed.

**10:48**

**Y46 15 Remote sensing of the radiation induced zero-resistance state in the high mobility GaAs/AlGaAs system** RAMESH MANI, *Harvard University* The possibility of inducing novel zero-resistance states by photo-exciting a high mobility GaAs/AlGaAs device, with radiation from the microwave and Terahertz parts of the electromagnetic wave spectrum, has recently motivated a broad theoretical examination of the photoexcited steady states of the low dimensional electron system. Present theory suggests that radiation- induced resistance oscillations originate from a field dependent scattering at impurities and/or a steady state change in the electronic distribution function. In these theoretical scenarios, the amplitude of the magnetoresistance oscillations increases with the radiation intensity such that the resistivity/conductivity is able to take on negative values at the minima of the oscillatory magnetoresistivity (or magnetoconductivity) for sufficiently large radiation intensities. The negative resistivity/conductivity state is believed to give way, however, to a zero-resistance state as a result of domain formation, providing for

the experimentally observed phenomenon. Here, we report the results of experiments which sought to find signatures of the radiation-induced zero-resistance states in microwave transmission and reflection measurements of the high mobility 2DES. Remarkable changes are observed in the remotely observed photoresponse as a function of both the frequency and intensity. From the results, we deduce that the remote sensing of the radiation-induced zero-resistance state lies within the realm of possibility.

**SESSION Z1: STRONG INTERACTION EFFECTS IN SMALL CONDUCTORS**
**Friday Morning, 17 March 2006; Ballroom IV, Baltimore Convention Center at 11:15**
**Leon Balents, University of California, Santa Barbara, presiding**

**11:15**
**Z1 1 Controlling a Singlet-Triplet Spin Qubit.***
JASON PETTA, *Harvard University*

An attractive candidate for a solid-state quantum bit is based on semiconductor quantum dots, which allow controlled coupling of one or more electrons, using rapidly switchable voltages applied to electrostatic gates [1]. Due to tight confinement and the high degree of isolation from the environment, spin relaxation times in quantum dots can approach millisecond timescales [2]. In this talk I will describe how fast electrical control of the exchange interaction can be used to coherently manipulate two-electron spin states [3]. By separating a spin singlet state on-chip, we measure an ensemble averaged spin dephasing time $T_2^*$ of 10 ns, limited by the contact hyperfine interaction with the GaAs host nuclei. We develop quantum control techniques based on the exchange interaction to correct for hyperfine dephasing. Coherent spin state rotations are achieved, including spin SWAP. By using a spin-echo pulse sequence based on the exchange interaction we extend the spin coherence time, $T_2$ beyond 1.2 microseconds. The quantum control techniques demonstrated here are general and may be used to manipulate singlet-triplet spin qubits in carbon nanotubes, electrons on helium, and semiconducting nanowires.

In collaboration with A. C. Johnson, J. M. Taylor, E. A. Laird, A. Yacoby, M. D. Lukin, C. M. Marcus, M. P. Hanson, A. C. Gossard.

[1] J. R. Petta, A. C. Johnson, A. Yacoby, C. M. Marcus, A. C. Gossard, M. P. Hanson, Phys. Rev. B **72**, R161301 (2005).
[2] A. C. Johnson, J. R. Petta, J. M. Taylor, A. Yacoby, M. D. Lukin, C. M. Marcus, M. P. Hanson, A. C. Gossard, Nature **435**, 925 (2005).
[3] J. R. Petta, A. C. Johnson, J. M. Taylor, E. A. Laird, A. Yacoby, M. D. Lukin, C. M. Marcus, M. P. Hanson, A. C. Gossard, Science **309**, 2180 (2005).

*Partial support from DARPA-QUIST and ARO-STIC gratefully acknowledged.

**11:51**
**Z1 2 Conductance of a quantum wire at low electron density.**
KONSTANTIN MATVEEV, *Argonne National Laboratory*

We study the transport of electrons through a long quantum wire connecting two bulk leads. As the electron density in the wire is lowered, the Coulomb interactions lead to short-range crystalline ordering of electrons. In this Wigner crystal state the spins of electrons form an antiferromagnetic Heisenberg spin chain with exponentially small exchange coupling $J$. Inhomogeneity of the electron density due to the coupling of the wire to the leads results in violation of spin-charge separation in the device. As a result the spins affect the conductance of the wire. At zero temperature the low-energy spin excitations propagate freely through the wire, and its conductance remains $2e^2/h$. At finite temperature some of the spin excitations are reflected by the wire and contribute to its resistance. Since the energy of the elementary excitations in the spin chain (spinons) cannot exceed $\pi J/2$, the conductance of the wire acquires an exponentially small negative correction $\delta G \propto -\exp(-\pi J/2T)$ at low temperatures $T \ll J$. At higher temperatures, $T \gg J$, most of the spin excitations in the leads are reflected by the wire, and the conductance levels off at a new universal value $e^2/h$. This result is consistent with experimental observations of a mini-plateau of conductance at $e^2/h$ in quantum wires in the absence of magnetic field.

**12:27**
**Z1 3 Localization Transition in a Ballistic Quantum Wire.**
HADAR STEINBERG, *Weizmann Institute of Science*

We report measurements probing the many-body wave-function of localized states in one dimension. We utilize tunneling between two long, clean, parallel quantum wires in a GaAs/AlGaAs heterostructure, where one of the two wires is driven into the localized regime using a density tuning gate, and the other wire, still in the regime of extended electronic states, serves as a momentum spectrometer. Our measurements show that as the electron density is lowered to a critical value, the many-body state abruptly changes from an extended state with a well-defined momentum to a localized state with a

wide range of momentum components. The signature of the localized states appears as discrete tunneling features at resonant gate-voltages, corresponding to the depletion of single electrons from the localized region and showing Coulomb-blockade behavior. Typically 5 - 10 such features appear, where the one-electron state has a single-lobed momentum distribution, and the few-electron states have double-lobed distributions with peaks at the Fermi momenta.

**13:03**
**Z1 4 Spin incoherent effects in momentum resolved tunneling, transport, and Coulomb drag in Luttinger liquids.***
GREGORY FIETE, *Kavli Institute for Theoretical Physics, UC Santa Barbara*

In a one dimensional electron gas at low enough density the magnetic exchange energy $J$ between neighboring electrons is exponentially suppressed relative to the Fermi energy, $E_F$. At finite temperature $T$, the energy hierarchy $J << T << E_F$ can be reached, and we refer to this as the spin incoherent (SI) Luttinger liquid state. By using a model of a fluctuating Wigner solid, we theoretically explore the signatures of spin incoherence in the single particle Greens function[1], momentum resolved tunneling[2], transport[3], and Coulomb drag[4]. In the SI Greens function the spin modes of a Luttinger liquid (LL) are thermally washed out leaving only singular behavior from the charge modes. The charge modes are broadened in momentum space by an amount of order $k_F$ and the energy dependence of the tunneling density of states qualitatively changes from the low energy suppression of the LL regime to a possible low energy divergence in the SI regime. Such a state may be probed directly in momentum resolved tunneling between parallel quantum wires. Deep in the SI regime, the physics of transport and Coulomb drag can be mapped onto spinless electrons. Various crossovers in temperature and for finite systems connected to Fermi liquid leads are discussed. Both transport and Coulomb drag may exhibit interesting non-monotonic temperature dependence. [1] G. A. Fiete and L. Balents, Phys. Rev. Lett. 93, 226401 (2004). [2] G. A. Fiete, J. Qian, Y. Tserkovnyak, and B. I. Halperin, Phys. Rev. B 72, 045315 (2005). [3] G. A. Fiete, K. Le Hur, and L. Balents, Phys. Rev. B 72, 125416 (2005). [4] G. A. Fiete, K. Le Hur, and L. Balents, Submitted, cond-mat/0511715.

*I am grateful to B. I. Halperin for introducing me to this problem.

**13:39**
**Z1 5 Dephasing of mesoscopic interferences from Electron Fractionalization.***
KARYN LEHUR, *Université de Sherbrooke*

The understanding of dephasing processes (the physical causes of supressed interference effects) constitutes a topics of perpetual interest in mesoscopic systems. Phase-breaking mechanisms in ballistic systems of dimensionality less than two are presently not completely understood and therefore deserve intensive theoretical and experimental endeavors. In this talk, we investigate the dephasing of mesoscopic interferences by electron-electron interactions in a well-defined geometry composed of two tunnel-coupled wires embodied by a Luttinger liquid. We thoroughly demonstrate that interactions can produce a visible attenuation of Aharonov-Bohm oscillations [1]. Moreover, in our geometry, we firmly emphasize that the emerging dephasing time results from the electron factionalization phenomenon that is known to produce an electron life-time in 1/T with T being the temperature [2]. A dephasing time in 1/T has been reported in one-dimensional GaAs rings. [1] Karyn Le Hur, Phys. Rev. Lett. 95, 076801 (2005). [2] Karyn Le Hur, Phys. Rev. B 65, 233314 (2002).

*K. Le Hur acknowledges supports from CIAR, FQRNT, and NSERC.

## SESSION Z2: RESONANT INELASTIC X-RAY SCATTERING IN COMPLEX OXIDES
**Friday Morning, 17 March 2006; Ballroom III, Baltimore Convention Center at 11:15**
**Trevor Tyson, New Jersey Institute of Technology, presiding**

**11:15**
**Z2 1 Resonant Inelastic X-ray Scattering in Correlated Electron Systems.***
YOUNG-JUNE KIM, *University of Toronto*

Extremely bright photons generated at the new generation of synchrotron light sources have made a huge impact on various scientific disciplines ranging from biology to materials science. One of the exciting new developments is the use of x-rays in the field of solid-state spectroscopy. Inelastic x-ray scattering, analogous to the well-known inelastic neutron scattering, is a powerful tool for studying momentum-dependent electronic excitations and phonons. In particular, resonant inelastic x-ray scattering in the hard x-ray regime has been widely utilized to study the momentum dependence of various electronic excitations in strongly correlated electron systems. For example, by tuning the incident photon energy to the Cu K-edge, one can gain a large intensity enhancement as well as element specific knowledge of the electronic excitations in various copper oxide compounds. Most of the work to date has been focused on the charge-

transfer excitation between the bonding and antibonding molecular orbitals, the excitation across the Mott gap, and crystal field excitations between the d-orbitals. Recent improvements in instrumentation have allowed us to observe a new mode in the mid-infrared frequency region. We will discuss the momentum dependence of these excitations in prototypical cuprate superconductors, $La_{2-x}Sr_xCuO_4$, and also examine the evolution of such excitations as charge carriers are doped into the system.

*Work done in collaboration with D. S. Ellis, S. Wakimoto, R. J. Birgeneau (Univ of Toronto), J. P. Hill (Brookhaven Natl Lab), G. Blumberg (Lucent), S. Komiya, Y. Ando (CRIEPI, Japan), D. Casa, and T. Gog (Argonne Natl Lab).

**11:51**
**Z2 2 Intermediate-Energy Charge-Transfer Excitations in the Cuprate Superconductors and the Photon Energy Dependence of the RIXS process.***
JASON HANCOCK, *Stanford University*

We present a study of the charge-transfer excitations of the structurally simple high-Tc superconductor $HgBa_2CuO_4 + \delta$ and of the Mott insulator $La_2CuO_4$ using the burgeoning experimental technique of resonant inelastic X-ray scattering (RIXS). Our measurements address the 1-7 eV spectral range and place particular emphasis on the incident photon energy dependence of the cross section. Our results reveal clear evidence for a group of weakly-dispersing excitations[12]. Collectively, these results call for the use of a multi-band theoretical approach for the description of the charge dynamics of high-Tc cuprate superconductors in this intermediate-energy regime.

*We gratefully acknowledge support from NSF and DOE.

[1]L. Lu et al., Phys. Rev. Lett. **95**, 217003 (2005).
[2]J. N. Hancock et al., unpublished.

**12:27**
**Z2 3 Momentum Dependence of Charge Excitations in $YBa_2Cu_3O_{7-\delta}$ and $Nd_{2-x}Ce_xCuO_4$.**
KENJI ISHII, *SPring-8, Japan Atomic Energy Agency*

Resonant inelastic x-ray scattering (RIXS) studies at Cu *K*-edge on high-$T_c$ superconducting cuprates, $YBa_2Cu_3O_{7-\delta}$ and $Nd_{2-x}Ce_xCuO_4$ are presented. The superconductivity occurs in the vicinity of the Mott insulating state and it is important to clarify the nature of the Mott gap and its doping dependence. Because RIXS has an advantage that we can measure charge excitation in a wide energy-momentum space, it gives a unique opportunity to study the electronic structure of materials. We apply this technique to high-$T_c$ superconducting cuprates. In particular the electronic structure of strongly correlated metals is in the focus of our RIXS study. The experiments were performed at BL11XU of SPring-8, Japan, where a specially designed spectrometer for inelastic x-ray scattering is installed. In optimally doped $YBa_2Cu_3O_{7-\delta}$, anisotropic spectra are observed in the ab plane of a twin-free crystal. The Mott gap excitation from the one-dimensional CuO chain is enhanced at 2 eV near the zone boundary of the chain direction, while the excitation from the $CuO_2$ plane is broad at 1.5-4 eV and almost independent of momentum. Theoretical calculation based on the one-dimensional and two-dimensional Hubbard model reproduces the observed features in the RIXS spectra when smaller values of the on-site Coulomb energy of the chain than that of the plane are assumed. This means that the charge transfer gap of the chain is smaller than that of the plane. On the other hand, both interband excitation across the Mott gap and intraband excitation in the upper Hubbard band are observed in the electron-doped $Nd_{2-x}Ce_xCuO_4$. The intensity of the interband excitation is concentrated at $\sim$ 2 eV near the zone boundary while a dispersion relation with a momentum-dependent width emerges in the intraband excitation. The author would like to acknowledge to his collaborators, K. Tsutsui, Y. Endoh, T. Tohyama, K. Kuzushita, T. Inami, K. Ohwada, M. Hoesch, M. Tsubota, Y. Murakami, J. Mizuki, S. Maekawa, T. Masui, S. Tajima, and K. Yamada. The crystal growth of $YBa_2Cu_3O_{7-\delta}$ was supported by the New Energy and Industrial Technology Development Organization (NEDO) as the Collaborative Research and Development of Fundamental Technologies for Superconductivity Applications.

**13:03**
**Z2 4 Low-Energy Electronic Excitations in the Layered Cuprates Studied by Copper $L_3$ Resonant Inelastic X-Ray Scattering.***
GIACOMO GHIRINGHELLI, *Politecnico di Milano*

Resonant inelastic x-ray scattering (RIXS) can be effectively used to measure the energy and symmetry of neutral electronic excitations in solids. In the soft x-ray range it is particularly powerful for strongly correlated electron systems based on 3*d* transition metals, because at the $L_{2,3}$ edges it involves directly the 3*d* states. In those systems it can be considered as a chemically selective, bulk sensitive alternative to optical absorption and electron energy loss spectroscopy in the study of low energy electronic excitations. The reduced intensity and the instrumental energy resolution usually hinder the detection of very detailed spectral features, but the recent progress in the energy resolving power of our RIXS apparatus has opened new exciting possibilities in the 400-1000 eV range. We present spectra measured using the AXES spectrometer, installed at the beam line ID08 of the ESRF, France. The combined resolution ranges from 240 meV to 650 meV going from the Ti to the Cu $L_3$ edges. We have measured the itdd excitations in cuprates [1,2,3,4] and other

interesting systems where electronic correlation plays a central role [5]. In the specific case of cuprate superconductors, $L_3$ RIXS can be used to estimate the energy of the itxy, ityz, itzx and $z^2$ excited states. We report the examples of $La_2CuO_4$, $CaCuO_2$, Tl2212 and $Nd_{1.2}Ba_{1.8}Cu_3O_7$, where the different coordination and Cu-O distances result in a variety of itdd excitation spectra. [1] G. Ghiringhelli, N. B. Brookes, et al, Phys. Rev. Lett. **92**, 117406 (2004). [2] W.A. Little, G. Ghiringhelli, et al, unpublished. [3] M. Salluzzo, G. Ghiringhelli, et al, unpublished [4]. C. Aruta, P.G. Medaglia, G. Balestrino, G. Ghiringhelli, et al, unpublished. [5] G. Ghiringhelli, et al, J. Phys. Cond. Matter **17**, 5397 (2005).

*The essential contribution of all the authors of references [1-5] is acknowledged. Work done under the AXES contract.

**13:39**
**Z2 5 Asymmetric evolution of low-energy electron-hole pair modes and the Mott pseudogap in doped cuprates.***
YINWAN LI, *Princeton University & Argonne Lab*

A central issue in the universal Mott behavior in a variety of complex systems is to understand the nature of the electron-hole pair excitation modes. Using high resolution resonant x- ray scattering we resolve the momentum dependence of low-energy electron-hole pair modes in two major classes of doped copper oxides which reveals the momentum structure of the Mott pseudogap over the entire phase diagram including the superconducting states. The pair bandwidth and zone-boundary velocity renormalize on either sides of the phase diagram at different rates indicating strong doping asymmetries observed in the momentum resolved particle-hole collective channels for the first time. The measured asymmetry of modes is qualitatively consistent with Hubbard model.

*In collaboration with M.Z. Hasan, H. Eisaki and T. Sasagawa. This work is supported by U.S. DOE, NSF and Princeton Center for Complex Materials and partly carried out at the Advanced Photon Source.

**SESSION Z4: BIOPOLYMERS**
**Friday Morning, 17 March 2006; 308, Baltimore Convention Center at 11:15**
**Rangaramanujam Kannan, Wayne State University, presiding**

**11:15**
**Z4 1 Bonds that strengthen under force.**
VIOLA VOGEL, *Swiss Federal Institute of Technology, ETH*

While the adhesive strength of most receptor-ligand interactions is exponentially reduced if strained, some receptor-ligand complexes exist that strengthen under force which is the hallmark of catch bonds. Although the existence of catch bonds was theoretically predicted, the first experimental demonstrations of their existence were given only recently, i.e. for the bacterial adhesin FimH that is located at the tip of type I fimbriae of itE. coli and for p-selectin. In a major collaborative effort, we studied the structural origin by which the FimH-mannose bond is switched by force to a high binding state. Mutational studies were thereby combined with steered molecular dynamic simulations to decipher how force might affect protein conformation. Force-activation of FimH leads to a complex 'stick-and-roll' bacterial adhesion behavior in which itE. coli preferentially rolls over mannosylated surfaces at low shear but increasingly sticks firmly as the shear is increased. Interesting similarities are further seen if comparing the structural mechanisms by which liganded FimH and liganded integrins are switched to a high binding state. This comparison was made possible by docking fibronectin's $10^{th}$ type III module ($fnIII_{10}$) to $\alpha_V\beta_3$ integrin. $\alpha_V\beta_3$ can switch from the ''closed'' $\alpha_V\beta_3$ integrin headpiece to the ''open'' conformation by opening the hinge angle between the $\beta$A domain and the hybrid domain of the $\beta$-integrin. The ''open'' state has been implicated by many experimental laboratories to correspond to the activated state of integrins. W. E. Thomas, E. Trintchina, M. Forero, V. Vogel, E. Sokurenko, Bacterial adhesion to target cells enhanced by shear-force, Cell, 109 (2002) 913. W. E. Thomas, L. M. Nilsson, M. Forero, E. V. Sokurenko, V. Vogel, Shear-dependent 'stick-and-roll' adhesion of type 1 fimbriated itEscherichia coli, Molecular Microbiology 53 (2004) 1545. W. Thomas, M. Forero, O. Yakovenko, L. Nilsson, P. Vicini, E. Sokurenko, V. Vogel, Catch Bond Model Derived from Allostery Explains Force-Activated Bacterial Adhesion, Biophys. J, in press E. Puklin-Faucher, M. Gao, K. Schulten, V. Vogel, How the opening of the $\beta$A/hybrid domain hinge angle in the $\alpha_v\beta_3$ integrin headpiece is regulated by the liganded MIDAS conformation and by ligand-mediated mechanical force, submitted.

**11:51**
**Z4 2 Cellular Force, and Geometry Sensing (Over Time) Can Detect Matrix Rigidity: Local Modules Produce Global Signals.**
MICHAEL SHEETZ, *Columbia University*

The shape and behavior of mammalian cells is defined by an interplay between extracellular signals and the cellular responses. Although the chemical nature of the external signals is important, there is a growing realization that the physical aspects of the external environment are equally important. In particular, the stresses, rigidity and form of the external environment have major effects on cell behavior. Of particular importance is rigidity since cancerous cells can often grow on soft agar or in a fluid phase without force production. For most mammalian cells there are relatively few types of motility that are evident from quantitative analyses of rapidly spreading fibroblasts (Dubin-Thaler et al., Biophys. J. 86:1794-1806, 2004). One motile phase that we have studied extensively involves periodic contractions (24 s period) in local regions of the leading edge of the cell (Giannone et al., Cell, 116:431-443, 2004). The periodic signal is carried radially from the cell edge toward the center and is part of a general mechanism for rigidity-directed movement and pathfinding. Another motile phase involves the movement of individual collagen fibers in a hand-over-hand fashion (Meshel et al., Nature Cell Biol. 7:157-164, 2005) where the form of the fiber is being sensed. Rigidity and form sensing in these systems is dependent upon the cytoskeleton and force-dependent tyrosine phosphorylation through oncogenes (Sawada and Sheetz, J Cell Biol. 156:609-15, 2002; Tamada et al., Developmental Cell, 7:706-718, 2004). Recent studies indicate that the cell rigidity sensing occurs preferentially at the leading edges of moving cells and involves forces of 10-20 pN generated by displacements of 50-100 nm (Jiang et al., Biophys J. In Press). We will discuss how cells organize motility tools in motile phases (Döbereiner et al., Phys. Rev. Letters. 93:108105-1-4, 2004) in a dialogue with the environment to define cell morphology and behavior over time.

**12:27**
**Z4 3 Looking for steps of individual enzymes moving along DNA.**
THOMAS PERKINS, *JILA, NIST and CU-Boulder*

Understanding the molecular mechanism of any motor activity involves determining the elementary step size with which it moves. RecBCD is a processive, DNA-based motor with both helicase and nuclease activities. To directly measure RecBCD's putative step size of 4 base pairs (1.4 nm), several technical advances were incorporated in a new high-resolution optical trapping instrument capable of resolving 0.1 nm motion. First, mechanical drift was eliminated by developing a differential measurement system based upon improved laser beam-pointing stability and the introduction of a fiducial mark attached to a microscope coverslip (e.g., a stuck bead). To generalize this technique to measure subnanometer vertical motion, we intensity stabilized the detection laser and differentially amplified the vertical signal. We further enhanced this process by actively stabilizing the sample in 3D. In the presence of substantial thermal heating, 3D differential measurements with active stabilization achieved short term (1 s) stabilities of 0.13, 0.08 and 0.22 nm (RMS) in x, y, and z, respectively. Positional stability, as demonstrated by our differential subtraction, does not guarantee subnanometer resolution of an optically trapped bead itunder load. We therefore intensity stabilized our trapping laser to $\sim$ 0.1% at 100 Hz. Finally, our technique requires a DNA tether to be within a small distance (3 $\mu$m) of a fiducial mark. If the stuck bead is too close or directly along one of the primary axes of the stage motion, it interferes with the measurement. Since the location of stuck beads and DNA tethers is random, this leads to only a few stuck bead/DNA tether pairs that can be successfully used. To overcome these limitations, we developed a regular grid of nanoposts. We will present our progress on integrating these technological advances to measure individual steps of RecBCD.

**13:03**
**Z4 4 Thermodynamics and Structure of Polymerizing Actin.**
SANDRA GREER, *University of Maryland College Park*

The polymerization of the globular protein G-actin to form filamentary F-actin is an important cellular process, serving major functions in cell structure and cell motility. This transition from monomeric G-actin to polymeric F-actin can be initiated by the variation of thermodynamic variables such as temperature, pressure, and compositions of G-actin and salts. We use fluorescence spectroscopy to obtain the fraction of monomer converted to polymer, and model these data using a Flory-Huggins type of theory. We measure the size and shape of the actin species by small angle neutron scattering, and find an unexpected spherical shape for G-actin in salt buffer.

**13:39**
**Z4 5 Synthetic and Biopolymer Gels - Similarities and Difference.**
FERENC HORKAY

Ion exchange plays a central role in a variety of physiological processes, such as nerve excitation, muscle contraction and cell locomotion. Hydrogels can be used as model systems for identifying fundamental chemical and physical interactions that govern structure formation, phase transition, etc. in biopolymer systems. Polyelectrolyte gels are particularly well-suited to study ion-polymer interactions because their structure and physical-chemical properties (charge density, crosslink density, etc) can be carefully controlled. They are sensitive to different external stimuli such as temperature,

ionic composition and pH. Surprisingly few investigations have been made on polyelectrolyte gels in salt solutions containing both monovalent and multivalent cations. We have developed an experimental approach that combines small angle neutron scattering and osmotic swelling pressure measurements. The osmotic pressure exerted on a macroscopic scale is a consequence of changes occurring at a molecular level. The intensity of the neutron scattering signal, which provides structural information as a function of spatial resolution, is directly related to the osmotic pressure. We have found a striking similarity in the scattering and osmotic behavior of polyacrylic acid gels and DNA gels swollen in nearly physiological salt solutions. Addition of calcium ions to both systems causes a sudden volume change. This volume transition, which occurs when the majority of the sodium counterions are replaced by calcium ions, is reversible. Such reversibility implies that the calcium ions are not strongly bound by the polyanion, but are free to move along the polymer chain, which allows these ions to form temporary bridges between negative charges on adjacent chains. Mechanical measurements reveal that the elastic modulus is practically unchanged in the calcium-containing gels, i.e., ion bridging is qualitatively different from covalent crosslinks.

## SESSION Z7: SYNCHRONY AND COMPLEXITY IN BRAIN ACTIVITY AND FUNCTION

**Friday Morning, 17 March 2006; 307, Baltimore Convention Center at 11:15**
**Michael Zochowski, University of Michigan; Eshel Ben-Jacob, Tel Aviv University, presiding**

**11:15**
**Z7 1 Analysis of Direct Recordings from the Surface of the Human Brain.**
VERNON L. TOWLE, *University of Chicago*

Recording electrophysiologic signals directly from the cortex of patients with chronically implanted subdural electrodes provides an opportunity to map the functional organization of human cortex. In addition to using direct cortical stimulation, sensory evoked potentials, and electrocorticography (ECoG) can also be used. The analysis of ECoG power spectrums and inter-electrode lateral coherence patterns may be helpful in identifying important eloquent cortical areas and epileptogenic regions in cortical multifocal epilepsy. Analysis of interictal ECoG coherence can reveal pathological cortical areas that are functionally distinct from patent cortex. Subdural ECoGs have been analyzed from 50 medically refractive pediatric epileptic patients as part of their routine surgical work-up. Recording arrays were implanted over the frontal, parietal, occipital or temporal lobes for 4-10 days, depending on the patient's seizure semiology and imaging studies. Segments of interictal ECoG ranging in duration from 5 sec to 45 min were examined to identify areas of increased local coherence. Ictal records were examined to identify the stages and spread of the seizures. Immediately before a seizure began, lateral coherence values decreased, reorganized, and then increased during the late ictal and post-ictal periods. When computed over relatively long interictal periods (45 min) coherence patterns were found to be highly stable ($r = 0.97$, $p < .001$), and only changed gradually over days. On the other hand, when calculated over short periods of time (5 sec) coherence patterns were highly dynamic. Coherence patterns revealed a rich topography, with reduced coherence across sulci and major fissures. Areas that participate in receptive and expressive speech can be mapped through event-related potentials and analysis of task-specific changes in power spectrums. Information processing is associated with local increases in high frequency activity, with concomitant changes in coherence, suggestive of a transiently active language network. Our findings suggest that analysis of coherence patterns can supplement visual inspection of conventional records to help identify pathological regions of cortex. With further study, it is hoped that analysis of single channel dynamics, along with analysis of multichannel lateral coherence patterns, and the functional holographic technique may allow determination of the boundaries of epileptic foci based on brief interictal recordings, possibly obviating the current need for extended monitoring of seizures.

**11:51**
**Z7 2 Astrocytes, Synapses and Brain Function: A Computational Approach.***
SUHITA NADKARNI, *Center for Theoretical Biological Physics, University of California, San Diego*

Modulation of synaptic reliability is one of the leading mechanisms involved in long- term potentiation (LTP) and long-term depression (LTD) and therefore has implications in information processing in the brain. A recently discovered mechanism for modulating synaptic reliability critically involves recruitments of astrocytes - star- shaped cells that outnumber the neurons in most parts of the central nervous system. Astrocytes until recently were thought to be subordinate cells merely participating in supporting neuronal functions. New evidence, however, made available by advances in imaging technology has changed the way we envision the role of these cells in synaptic transmission and as modulator of neuronal excitability. We put forward a novel mathematical framework based on the biophysics of the bidirectional neuron-astrocyte interactions that quantitatively accounts for two distinct experimental manifestation of recruitment of astrocytes in synaptic transmission: a) transformation of a low fidelity synapse transforms into a high

fidelity synapse and b) enhanced postsynaptic spontaneous currents when astrocytes are activated. Such a framework is not only useful for modeling neuronal dynamics in a realistic environment but also provides a conceptual basis for interpreting experiments. Based on this modeling framework, we explore the role of astrocytes for neuronal network behavior such as synchrony and correlations and compare with experimental data from cultured networks.

*Supported by NSF, IBN-0078055.

**12:27**
**Z7 3 Neuronal Spatiotemporal Pattern Discrimination: The Dynamical Evolution of Seizures.**
STEVEN SCHIFF, *George Mason University*

We developed a modern numerical approach to the multivariate linear discrimination of Fisher from 1936 based upon singular value decomposition that is sufficiently stable to permit widespread application to spatiotemporal neuronal patterns. We demonstrate this approach on an old problem in neuroscience – whether seizures have distinct dynamical states as they evolve with time. A practical result was the first demonstration that human seizures have distinct initiation and termination dynamics, an important characterization as we seek to better understand how seizures start and stop. Such strategies are also useful in defining the onset of a seizure dynamically, and whether there is a dynamically distinct preseizure state. A proper orthogonal decomposition helps illustrate the changing coherent structures that underlie such activities. Our approach is broadly applicable to a wide variety of spatiotemporal dynamical data, from multichannel EEG or MEG, to sequentially acquired optical imaging data or fMRI.

**13:03**
**Z7 4 Measuring complexity and synchronization phenomena in the human epileptic brain.***
KLAUS LEHNERTZ, *Dept. of Epileptology, Neurophysics Group and Helmholtz-Institute for Radiation and Nuclear Physics, University of Bonn, Bonn, Germany*

The framework of the theory of nonlinear dynamics provides new concepts and powerful algorithms to study complicated dynamics such as the human electroencephalogram (EEG). Although different influencing factors render the use of nonlinear measures (such as measures for complexity, synchronization, or interdependencies) in a strict sense problematic, converging evidence from various investigations now indicates that nonlinear EEG analysis provides a means to reliably characterize different states of normal and pathological brain function and thus, promises to be important for clinical practice. This talk will focus on applications of nonlinear EEG analysis in epileptology. Epilepsy affects more than 50 million individuals worldwide - approximately 1 % of the world's population. The disease is characterized by a recurrent and sudden malfunction of the brain that is termed seizure. Epileptic seizures are the clinical manifestation of an excessive and hypersynchronous activity of neurons in the brain. It is assumed that seizure activity will be induced when a critical mass of neurons is progressively involved in closely time-linked high frequency discharging. Recent investigations of intracranially recorded EEG involving nonlinear time series analysis techniques indicate that this build up of a critical mass can indeed be tracked over time scales lasting minutes to hours. Future real-time analysis devices may enable both investigations of basic mechanisms leading to seizure initiation in humans and the development of adequate seizure warning and prevention strategies.

*Supported by the Deutsche Forschungsgemeinschaft.

**13:39**
**Z7 5 Detection of phase and lag synchrony as an adaptive measure of asymmetric neuronal interactions.**
MICHAL ZOCHOWSKI, *University of Michigan*

Asymmetric temporal interdependencies between individual neurons and their populations are though to underlie learning and memory formation and can provide information about direction of information transfer in neural systems. We have developed an adaptive measure that detects asymmetries in phase and lag synchrony between activities of individual neurons of synchronized networks. In the first part of the talk I will discuss the properties of the measure on network models of coupled non-linear oscillators and show progression of rapid transitions in temporal patterning in such networks as a function of their topology. In the second part of the talk I will present its application in analysis of normal and pathological neural activity: detection of evolving asymmetry in interactions of hippocampal neurons in freely behaving rats, and characterization of dynamical progression of synchronous seizure-like activity recorded from intact rat hippocampus.

**SESSION Z18: FOCUS SESSION: CARBON NANOTUBES: DOUBLE WALL NANOTUBES, SHEETS AND CHAINS**
**Friday Morning, 17 March 2006; 315, Baltimore Convention Center at 11:15**
**Feng Wang, University of California, Berkeley, presiding**

*Invited Papers*

**11:15**
**Z18 1 Tube-tube interaction and high curvature effects in double wall carbon nanotubes.***
HANS KUZMANY,† *Universitaet Wien, Austria*

Recent results will be reported on the consequences of the interaction between peapod grown inner shell carbon nanotubes and the corresponding outer shell tubes in double wall carbon nanotubes (DWCNTs). The results were obtained from resonance Raman experiments on natural and $^{13}C$ isotope substituted nanotubes, from time resolved NMR experiments and from calculations which include tube-tube interaction and high curvature effects of the inner tubes. The Raman analysis of the radial breathing mode of the inner tubes exhibits extremely narrow line widths which indicates unusual long phonon life times. It also confirms family behaviour of the tubes and the large number of observed lines is a consequence of pair spectrum response between inner shell and outer shell tube pairs. The response from the RBM is used to demonstrate reversible filling and release of the fullerenes from the tubes. Measurements of the longitudinal relaxation time $T_1$ in NMR experiments from $^{13}C$ substituted inner tubes reveal a Korringa behaviour for temperatures above 150 K. This indicates a metallic character of the inner tubes. Below 20 K the metallicity is lost and a gap of about 4 meV opens up. The properties of the inner tubes will be discussed in the frame of a inner shell-outer shell orbital hybridization and curvature enhanced electron-phonon interaction.

*Work supported by the Austrian Science Foundation, project 17345.
†Multiple authors: R. Pfeiffer[1], V. Popov[2], F. Simon[3], J. Kuerti[4], V. Zolyomi[4], P. Singer[5], H. Alloul[5], P. Wzietek[5]; [1]Univ. Wien, A; 2Univ. Sofia, BG; [3]Budapest Univ. of Technology, HU; [4]Eoetvoes Univ. of Budapest, HU; [5]Univ. Paris-Sud, F.

*Contributed Papers*

**11:51**
**Z18 2 Density Functional Calculations of the $^{13}C$ NMR Chemical Shifts in Single-Walled Carbon Nanotubes** JOCHEN AUTSCHBACH, *Department of Chemistry, State University of New York at Buffalo, Buffalo, NY 14260-3000* EVA ZUREK, *Max Planck Institut für Festkörperforschung, Stuttgart, Germany* Nuclear Magnetic Resonance (NMR) chemical shifts of single–walled carbon nanotubes were computed for capped finite–sized tube fragments and for infinite–length tubes. Molecular density functional calculations using atom–centered basis sets have been performed for the electronic structure and $^{13}C$ NMR chemical shifts of (5,0), (9,0) and (10,0) single-walled carbon nanotube (SWNT) fragments. For the (9,0) tube, a $C_{30}$-capped fragment appeared to be a more suitable model to represent an infinite tube then a fragment capped with hydrogens. Thus, the study of the finite (5,0) and (10,0) tubes were restricted to the systems capped with carbon hemispheres. The chemical shift for the (9,0) system [1] is in good agreement with experimental data that were recently obtained from a solution of functionalized nanotubes. Further, we have calculated the $^{13}C$ chemical shift for a number of infinite small-radius SWNTs using a plane–wave approach. Here, the effect of inter-tube interactions upon the chemical shift was also considered. The results will be compared with those obtained for the finite systems. We believe that our computations may be useful in determining new experimental methods which rely upon NMR to characterize a nanotube sample. [1] E. Zurek, J. Autschbach, J. Am. Chem. Soc.**126**, 13079 (2004).

**12:03**
**Z18 3 Comparative Raman spectroscopy study of Single-Wall and Double-Wall carbon nanotube systems doped with $H_2SO_4$** EDUARDO BARROS, ANTONIO G. SOUZA FILHO, *Universidade Federal do Ceara* YOONG-AHM KIM, HIROYUKI MURAMATSU, TAKUYA HAYASHI, MORINOBU ENDO, *Shinshu University* MILDRED DRESSELHAUS, *Massachusetts Institute of Technology* In this work, we performed Raman experiments on a mixture of Single-wall and Double-wall carbon nanotubes for different relative concentrations and using different laser energies. Two sets of samples were analyzed, one which was exposed to $H_2SO_4$ for 5*s* and one which is pristine. The $H_2SO_4$ is known to act as an acceptor for the electrons of graphitic materials. The effect of the hole doping on the vibrational and electronic properties of the double and single-wall carbon nanotubes is probed using Resonant Raman scattering with different excitation energies probing different nanotubes. The inner and outer walls of double-wall nanotubes can also be studied at the same time for selected excitation energies. A detailed analysis of the charge transfer in single wall and double wall nanotubes and its effects on the nanotube properties is obtained.

**12:15**
**Z18 4 Spectroscopy of Functionalized Double-Walled Carbon Nanotubes** J. SHAVER, *Rice University, Houston TX* J. KONO, F. LIANG, W.E. BILLUPS, R.H. HAUGE, *Rice University, Houston TX* E. FLAHAUT, *Universite Paul Sabatier, CIRIMAT/LCMIE, Toulouse France* Double walled nanotubes are of recent interest for spectroscopic study partly due to the protected nature of the inner tubes. Functionalization of single walled nanotubes has been used to increase solubility, though this comes at the expense of disrupting the electronic properties. We present spectroscopy of DWNTs functionalized with various organic and inorganic compounds. Photoluminescence, Raman, and coherent phonon oscillations are utilized to determine the effect of sidewall modification of outer tubes on the DWNT spectra.

**12:27**

**Z18 5 Defects in single and double wall carbon nanotubes*** JIAN-MIN ZUO, T.K. KIM, *Dept. Mat. Sci. Eng., University of Illinois, Urbana* We show that single and double wall carbon nanotubes grown by catalytic chemical vapor deposition can change its chirality and create junctions along the tube direction. These tubes often appear straight (perfect) in electron images. The change in structure is often subtle and only detectable by electron diffraction. The experimental evidence of defects, structure determination and consequence on tube transport properties will be presented and discussed.

*Support by DOE DEFG02-01ER45923

**12:39**

**Z18 6 Resonant Raman scattering in Br2-adsorbed double wall carbon nanotubes*** ANTONIO SOUZA FILHO, *Univ. Federal do Ceara - Frotaleza - Brazil* MORINOBU ENDO, HIROYUKI MURAMATSU, YOONG A. KIM, TAKUYA HAYASHI, *Shinshu University - Nagano - Japan* N. AKUZAWA, *Tokyo National College of Technology - Japan* RIICHIRO SAITO, *Tohoku University - Japan* MILDRED S. DRESSELHAUS, *MIT - USA* The vibrational and electronic properties of Br2-adsorbed double-wall carbon nanotubes (DWNTs) were investigated by resonance Raman scattering. We have found that Br2 molecules interact with the DWNTs and their intercalation characteristics are completely reversible upon thermal annealing. Upshifts in the Raman frequencies for the tangential modes and depression of their Raman intensities indicate that electrons are transferred from the nanotubes to the Br2 molecules. Metallic nanotubes are specially sensitive to the adsorption of Br2 molecules, even when they are the inner tubes of DWNTs. The vibrational spectra of the bromine dopant also provide information about the intercalation process.

*Acknowledgements: CNPq-Brazil and NSF-USA for funding this research

**12:51**

**Z18 7 Growth transition from single wall- to double walled-carbon nanotubes by using acetylene gas*** VIJAYA KAYASTHA, *Michigan Tech University* YOKE KHIN YAP, *Michigan Tech University* Based on a growth model that we have proposed for multiwalled carbon nanotubes (CNTs) [1, 2], we found that similar mechanism is applied for the growth of single wall- and double walled- CNTs by acetylene gas. This model combines disociative adsorption of acetylene molecules on Fe catalyst and the vapor-liquid-solid mechanism. Basically, the growth is the consequence of optimization of decomposition rate of acetylene molecules as referred to the diffusion rate and segregation rate of carbon into and from the catalyst. For the growth of single wall- and double walled- CNTs, catalytic film consists of layers of aluminum, iron, and molybdenum were used. We found that samples grown at $\sim$ 600-700 $^{o}$C contained more than 80% double walled CNTs with diameters in the range 3-5nm and length 15 $\mu$m. These CNTs are vertically aligned on substrates. As the temperature increased to 1000 $^{o}$C the growth of single wall CNTs are detected. [1]. Kayastha et al., APL 86, 253105 (2005), [2] Kayastha et al., APL 85, 3265 (2004).

*Y.K.Y acknowledges supports from the Michigan Tech Research Excellence Fund, Army Research Office (W911NF-04-1-0029) and CNMS at ORNL,

**13:03**

**Z18 8 Electronic structure of a linear carbon-atom chain inside single-walled carbon nanotubes*** ROMEO DE COSS, ALEJANDRO TAPIA, CESAR CAB, *Department of Applied Physics, CINVESTAV-Merida, Mexico* JORGE MEDINA, GABRIEL CANTO, *CCMC-UNAM, Ensenada, Mexico* CESAR ACOSTA, *FI-UADY, Yucatan, Mexico.* Recently has been reported a new type of one-dimensional carbon structures. Carbon nanowires formed by a linear carbon-atom chain inside an armchair (5,5) carbon nanotube has been observed using high-resolution transmission electron microscopy. In the present work we have studied the electronic structure of a linear carbon-atom chain inside the (5,5) and (8,0) single-walled carbon nanotubes (SWCN) using the Density Functional Theory. The calculations where performed with the pseudopotentials LCAO method (SIESTA code) and the Generalized Gradient Approximation (GGA) for the exchange-correlation potential. We have analyzed the band structure, the local density of states (LDOS), and the local orbital population. We find charge transfer from the nanotube to the linear chain in both systems chain@(5,5) and chain@(8,0). However, the electronic character of the chain and nanotube sub-systems in chain@SWCN is the same that in the corresponding isolated chain or SWCN systems.

*This research was supported by PRIORI-UADY under Grant No. FING-05-004 and CONACYT under Grants No. 43830-F and No. 44831-F.

**13:15**

**Z18 9 Optical Anisotropy of Aligned Single Wall Carbon Nanotubes** JEFFREY A. FAGAN, BARRY J. BAUER, IDAN MANDELBAUM, MATTHEW L. BECKER, ERIK K. HOBBIE, *NIST* The optical properties of single wall carbon nanotubes (SWCNTs) are of significant importance for a variety of applications, particularly for fractions containing well defined tube lengths and chiralities. In this work, stable suspensions of DNA wrapped SWCNTs were mechanically aligned by dispersing them in amorphous polymer films, and their intrinsic optical anisotropy measured through a combination of polarized light spectroscopy, polarized Raman spectroscopy, and small-angle neutron scattering (SANS). Conventional measures of nematic alignment in the stretched polymer films typically varied from 0.7 to 0.9. The quality of the nanotube dispersion within the centimeter scale polymer film samples was also directly investigated by means of atomic force and electron microscopy. We obtain the intrinsic optical anisotropy of the SWCNTs over a broad range of photon energies, with a number of well-resolved absorption peaks corresponding to specific SWCNT chiralities.

**13:27**

**Z18 10 Boron Nanotubes and Boron Sheets – New Perspectives for Nanotechnology** JENS KUNSTMANN, *Max Planck Institute for Solid State Research, Heisenbergstrasse 1, 70569 Stuttgart, Germany* ALEXANDER QUANDT, *Institut fuer Physik der Universitaet Greifswald, Domstrasse 10a, 17489 Greifswald, Germany* We report about a recent ab initio study of boron nanotubes (BNTs). The latter were first predicted by theory, and have recently been synthesized experimentally. To understand the basic properties of BNTs, we have derived a structure model for an extended boron sheet (i.e. a boron analogue of a single graphene sheet) as a possible structural precursor of boron nanotubes. This sheet has a puckered structure, high stiffness, and anisotropic bonding properties. Puckering turns out to be the key mechanism for stabilizing sp sigma bonds lying along the armchair direction

of the sheet. The BNTs have puckered surfaces as well, and their chiral angles are defined in a range from 0 to 90 degree. We show that all ideal boron nanotubes are metallic, irrespective of their radii and chiral angles, and discuss the possible existence of helical currents in chiral BNTs. Furthermore we show that strain energies of BNTs depend on their radii AND on their chiral angles. This unique property could be the basis of a new structure control mechanism in nanotechnology that permits to make nanotubes of a specified type, only. Zigzag nanotubes for example seem to have very little strain energy, if any. Therefore they should be highly susceptible to structural collapses, and might not exist at all.

**SESSION Z19: FOCUS SESSION: SPIN DYNAMICS IN QUANTUM DOTS**
**Friday Morning, 17 March 2006**
**316, Baltimore Convention Center at 11:15**
**Ari Mizel, Pennsylvania State University, presiding**

***Contributed Papers***

**11:15**
**Z19 1 Single electron Transport in diluted magnetic semiconductor quantum dots** J. FERNANDEZ-ROSSIER, *Universidad de Alicante* R. AGUADO, *Instituto de Ciencia de Materiales, CSIC* We consider a single electron transistor based upon a II-VI semiconductor quantum dot doped with a few Mn atoms.Our proposal is motivated by the recent fabrication and optical probing of single CdTe quantum dots doped with a single Mn [1]. The numerical diagonalization of the quantum dot Hamiltonian is possible in the case of small number of both carriers and Mn [2],[3],[4]. Our calculations [5] reveal that the magnetic ions behave like a quantum nanomagnet whose the total spin and magnetic anisotropy depend dramatically both on the number of carriers and their orbital nature. We show that single electron transport spectroscopy permits a complete characterization of electronic excitations of the dot. A protocol of gate voltage pulses that permits the preparation and detection of the quantum state of a single Mn spin is presented. (1) L. Besombes, et al. Phys. Rev. Lett. **93**, 207403 (2004) (2) J. Fernández-Rossier, PRB, Jan 2006 (3) A. O. Govorov, Phys. Rev. B**72** , 075359(2005). (4) F. Qu, P. Hawrylak, Phys. Rev. Lett. **95**, 217206 (2005) (5) J. Fernández-Rossier, R. Aguado, in prep.

**11:27**
**Z19 2 Optimizing g-factor tuning with electric fields in self-assembled InAs/GaAs quantum dots** JOSEPH PINGENOT, CRAIG E. PRYOR, MICHAEL E. FLATTÉ, *Dept. of Physics and Astronomy, The University of Iowa* Single-spin manipulation in quantum dots can be achieved without a time-dependent magnetic field by modulating the electron g tensor in the dots with an electric field. Using a recently-developed envelope-function formalism for quantum dot g factor calculations[1], we have studied the dependence of the electron g tensor tuning range on quantum dot size and shape. The electric field is applied in the growth direction of the dot, assumed to be along [001]. We find that larger percentage changes in the g factors along the principal axes can be achieved in taller dots (more extended along the growth direction) and also, surprisingly, in more elliptical dots. The [110] and $[1\bar{1}0]$ g factors change sign as a function of dot height and lateral extent. Tuning ranges are of the order of $\Delta$ g 0.02 for electric fields changing from 0 to $\pm$ 100 kV/cm. By choosing a dot with a g factor near 0 we identify dots whose g factors should change sign along one principal axis as a function of electric field. This should generate very rapid spin manipulation using g tensor modulation resonance[2]. This work supported by DARPA/ARO DAAD19-01-1-0490. [1] C. E. Pryor and M. E. Flatté, Phys. Rev. Lett. in press. [2] Y. Kato et al., Science **299**, 1201 (2003).

**11:39**
**Z19 3 Calculations of Landé g-factors in III-V nanowhisker quantum dots** A. DE, *Dept. of Physics and Astronomy, University of Iowa* C. E. PRYOR, *Dept. of Physics and Astronomy, University of Iowa* We present detailed numerical calculations of Landé g-factors in semiconductor nanowire based quantum dots. We consider 111 oriented InAs nanowires with InP double barriers forming the dot, for which transport properties have recently been investigated[1]. We find that compared to recent calculations of self-assembled InAs/GaAs quantum dots[2], typical nanowire dots have larger, and negative, g-factors. We attribute this to the nanowire dots being larger than self-assembled dots, resulting in less angular momentum quenching. For nanowire sizes typical of those that have been fabricated to date, we find $g \approx -3.1$. M. T. Björk et al., Nano Letters, **4**, 1621 (2004).2. C. E. Pryor, M. E. Flatte, Phys. Rev. Lett., in press, www.arxiv.org/abs/cond-mat/0410678

***Invited Papers***

**11:51**
**Z19 4 Control and manipulation of charge and spin in single and coupled quantum dots.**
GERHARD ABSTREITER

I will discuss measurements of the spin lifetime in self-assembled InGaAs dots in GaAs. The spin relaxation time ($T_1$) is found to be extremely long (e.g. $>$ 25ms at T=1K, B=4T) decreasing with magnetic field according roughly to a clear $B^{-4}$ power law [1]. Furthermore, $T_1$ is found to reduce linearly with lattice temperature and be very strongly sensitive to the motional quantisation (s-p shell splitting). Another topic is the the coherent quantum coupling of a vertically stacked pair of quantum dots. The interaction can be tuned in such quantum dot molecule devices using an applied voltage as external parameter [2]. At the resonance the electron component of the exciton wave function hybridizes, giving rise

to a quantum coupling energy in the excitonic spectrum. This work is supported financially by Deutsche Forschungsgemeinschaft via collaborative research center 631 and by German Federal Ministry of Research via NanoQuit. [1] M. Kroutvar, Y. Ducommun, D. Heiss, D. Schuh, M. Bichler, G. Abstreiter and J. J. Finley. Nature **432**, 81 (2004) [2] H. J. Krenner, E. C. Clark, A. Kress, D. Schuh, M. Bichler, G. Abstreiter and J.J. Finley. PRL **94**, 057402 (2005)

***Contributed Papers***

**12:27**

**Z19 5 Anisotropic phonon-assisted spin relaxation in elliptical quantum dots*** OLEG OLENDSKI, TIGRAN V. SHAHBAZYAN, *Jackson State University* We study theoretically phonon-assisted spin relaxation of an electron confined in elliptical quantum dot subjected to a tilted magnetic field. We show that in the presence of both Rashba and Dresselhaus spin-orbit terms the relaxation rate exhibits anisotropy with respect to the in-plane field orientation. This anisotropy originates from the interference, at non-zero tilt angle, between the two spin-orbit terms that couple adjacent spin-split energy levels. The variation of the relaxation rate for different azimuthal angles is determined by the quantum dot geometry and by the relative strengths of the Rashba and Dresselhaus coupling constants. The effect is strongest when adjacent spin-split levels are brought into resonance by tuning the total field magnitude and tilt angle. In this case, for certain values of tilt angle, the relaxation rate can be drastically reduced by varying the in-plane field orientation. Calculations were performed for InSb quantum dots.

*Supported by NSF grant DMR-0305557

**12:39**

**Z19 6 Spin Relaxation in Spherical CdS Quantum Dots** P. NAHALKOVA, *Charles University in Prague, Ke Karlovu 3, 121 16 Prague, Czech Republic and Universiteit Antwerpen, Universiteitsplein 1, B-2610 Antwerpen, Belgium* D. SPRINZL, P. NEMEC, P. MALY, *Charles University in Prague, Ke Karlovu 3, 121 16 Prague, Czech Republic* V. N. GLADILIN, J. T. DEVREESE, *Universiteit Antwerpen, Universiteitsplein 1, B-2610 Antwerpen, Belgium* We present results of the time-resolved spin-sensitive differential transmission experiments and the quantitative theoretical analysis of the spin relaxation mechanism in quasi-spherical CdS quantum dots (QD) in a glass matrix. The measured decay of the degree of circular polarization (DCP) on ns timescale can be explained well by intralevel exciton transitions with electron spin flip, driven by the electron-hole exchange interaction and assisted by two LO phonons. The predicted spin relaxation rates for different QD sizes and temperatures are in line with experimentally determined values. The developed theoretical model provides also a qualitative understanding of the observed behavior of DCP as a function of central energy of pump and probe pulses. This work was supported by the Ministry of Education of the Czech Republic in the framework of research plan MSM 0021620834 and the research centre LC510, as well as by the GOA BOF UA 2000, IUAP, FWO-V projects G.0274.01N, G.0435.03, WOG WO.035.04N (Belgium) and the European Commission SANDiE Network of Excellence, contract No. NMP4-CT-2004-500101.

**12:51**

**Z19 7 Theory of spin-orbit effects and spin relaxation in single and coupled quantum dots.*** PETER STANO, *University of Regensburg* JAROSLAV FABIAN, Spin-orbit effects and phonon-induced spin relaxation in laterally coupled quantum dots in the presence of magnetic field are investigated by exact numerical diagonalization. Both Bychkov-Rashba and Dresselhaus spin-orbit couplings are included. Several new phenomena are predicted. In particular, we shown that coherent tunneling between the dots depend on the spin, enabling a scheme for spin-to-charge conversion by spin separation in a *homogeneous* magnetic field. Furthermore, we show that spin relaxation is highly anisotropic, both in terms of the direction of the double-dot axis as well as the direction of the magnetic field. The anisotropy comes from spin-orbit coupling. Calculated spin relaxation rates of GaAs single dots agree with a recent experiment.

*work supported by US ONR

**13:03**

**Z19 8 Asymmetric electron-electron exchange in a single quantum dot** STEFAN C. BADESCU, *NRL, Washington DC* YULI B. LYANDA-GELLER, *Purdue Univ, West Lafayette IN* THOMAS L. REINECKE, *NRL, Washington DC* Recent photoluminescence experiments on negative trions in a self-assembled quantum dot [1] reveal a high dephasing rate inconsistent with the electron-hole exchange mechanism. We find, however, that this rate can be explained by the asymmetric electron-electron exchange due to electron spin-orbit coupling in the excited singlet and triplet states. The necessary and sufficient condition for the existence of asymmetric exchange is the lack of inversion symmetry in the plane transverse to the growth direction. We develop a model that describes the two relevant cases of this asymmetry: when the system has a single reflection plane along the growth axis, and when the system has no reflection plane along the growth axis. These asymmetries are characteristic for shapes of self-assembled quantum dots. We find typical values for the dephasing part of the asymmetric exchange that are $\sim 10^{-1}$ of the symmetric exchange. We also find that the asymmetric exchange is important for electron spin relaxation when the triplet states with non-zero projection of spin are brought into resonance with the singlet. [1] Ware M.E. et al – Phys. Rev. Lett. 95(17), 177403 (2005)

**13:15**

**Z19 9 Spin Dynamics in InAs Quantum Dots** JANICA WHITAKER, ALLAN BRACKER, DANIEL GAMMON, THOMAS KENNEDY, *Naval Research Laboratory* Spin coherence in InAs Self-Assemble Quantum Dots (SAQD's) could be useful for optical delay lines and quantum information technology. Very uniform dots and a very accurate measurement of dephasing processes are required to realize these possibilities. To this effect we report decoherence times in InAs SAQD. Here we describe measurements of spin dynamics from a 17 layered nominally undoped wafer of InAs SAQDs with a varying dot-size. We used Time Resolved Kerr Rotation (TRKR) for a wavelength resonant with the 3D InAs Stranski-Krastanow strain mediated quantum dots. Response is observed from 0 to 5 T that corresponds to a freely precessing spin with $g = 0.45$, a 1.2 ns lifetime at $B=0$ that decreases with B, and a sine-like phase. We attribute this spin to an electron from either the ground state of a negative trion or the excited state of a positive trion. The dots are dots unintentionally doped from background doping in the MBE chamber. Work supported in part by ONR, NSA/ARO, and DARPA/QUIST. JW is an NRC/NRL Postdoctoral Research Associate.

**13:27**

**Z19 10 Optical Control of Spin Coherence in Singly Charged Quantum Dots** A. SHABAEV,*AL. L. EFROS, *Naval Research Laboratory, Washington DC, USA* I. A. MERKULOV, *A. F. Ioffe Institute, RAS, St. Petersburg, Russia* A. GREILICH, R. OULTON, E. A. ZHUKOV, I. A. YUGOVA,†D. R. YAKOVLEV,‡M. BAYER, *Universität Dortmund, Dortmund, Germany* V. STAVARACHE, D. REUTER, A. WIECK, *Ruhr-Universität Bochum, Bochum, Germany* In singly charged dots, resonant light couples an electron in the ground state with a trion consisting of the electron and an excited electron-hole pair. We show that a polarized laser pulse, driving the electron/trion transition, coherently changes the spin state of the ground state electron. The controlled spin dynamics provide a mechanism for the optical orientation of an electron spin in a quantum dot. The theory is supported by experimental evidence of the electron spin coherence induced and controlled by optical pulses in (In,Ga)As/GaAs quantum dots.

*also at George Mason University, Fairfax VA, USA
†also at St. Petersburg State University, St. Petersburg, Russia
‡also at A. F. Ioffe Institute, RAS, St. Petersburg, Russia

**13:39**

**Z19 11 Dynamics of Coupled Qubits Interacting with an Off-Resonant Cavity*** OLIVER GYWAT, FLORIAN MEIER, DANIEL LOSS, DAVID D. AWSCHALOM, *Center for Spintronics and Quantum Computation, University of California, Santa Barbara, California 93106, USA* We study a model for a pair of qubits which interact with a single off-resonant cavity mode and, in addition, exhibit a direct inter-qubit coupling[1]. Possible realizations for such a system include coupled superconducting qubits in a line resonator as well as exciton states or electron spin states of quantum dots in a cavity. The emergent dynamical phenomena are strongly dependent on the relative energy scales of the inter-qubit coupling strength, the coupling strength between qubits and cavity mode, and the cavity mode detuning. We show that the cavity mode dispersion enables a measurement of the state of the coupled-qubit system in the perturbative regime. We discuss the effect of the direct inter-qubit interaction on a cavity-mediated two-qubit gate. Further, we show that for asymmetric coupling of the two qubits to the cavity, the direct inter-qubit coupling can be controlled optically via the ac Stark effect.

*We acknowledge support from DARPA SPINS, DARPA QUIST, CNID, ARO, ONR, NCCR Nanoscience, and the Swiss NSF.

[1]O. Gywat, F. Meier, D. Loss, and D. D. Awschalom, cond-mat/0511592

**13:51**

**Z19 12 Cavity Enhanced Faraday Rotation in Semiconductor Quantum Dots*** D.W. STEUERMAN, Y.Q. LI, J. BEREZOVSKY, D.S. SEFEROS, G.C. BAZAN, D.D. AWSCHALOM, *Center for Spintronics and Quantum Computation, University of California, Santa Barbara, CA 93106* The promise of quantum computation is helping fuel the development of single spin manipulation and measurement techniques. Photonic cavities provide an intriguing platform to increase the sensitivity of optical measurements, as well as the possibility to explore emergent light-matter interactions. The flexibility of a dielectric vertical cavity is exploited to study the spin dynamics within molecularly self-assembled CdSe quantum dots (QDs). Through the integration of QDs in microcavities, a twenty-fold enhancement of Faraday rotation is observed, which scales with the quality factor of the cavity. In this weak coupling regime, the amplified rotation is attributed to optically generated excited spins and multiple passes of the probe photons in the cavity. By applying this general planar cavity motif to Faraday rotation, dynamical measurements are accessible at extremely low powers on relatively small numbers of quantum confined states. In CdSe QDs, low power measurements reveal that contributions from both exciton and electron spin precession are largely dependent upon the power of excitation. This scheme is amenable to both soft and hard systems as a means to increase detection sensitivity.

*This work was supported by DARPA/CNID and the NSF.

**14:03**

**Z19 13 Optical manipulation of electron spin in quantum dot systems*** JOSE VILLAS-BOAS, SERGIO ULLOA, ALEXANDER GOVOROV, *Ohio University* Self-assembled quantum dots (QDs) are of particular interest for fundamental physics because of their similarity with atoms. Coupling two of such dots and addressing them with polarized laser light pulses is perhaps even more interesting. In this paper we use a multi-exciton density matrix formalism to model the spin dynamics of a system with single or double layers of QDs. Our model includes the anisotropic electron-hole exchange in the dots, the presence of wetting layer states, and interdot tunneling [1]. Our results show that it is possible to *switch* the spin polarization of a single self-assembled quantum dot under elliptically polarized light by increasing the laser intensity. In the nonlinear mechanism described here, intense elliptically polarized light creates an effective exchange channel between the exciton spin states through biexciton states, as we demonstrate by numerical and analytical methods. We further show that the effect persists in realistic ensembles of dots, and we propose alternative ways to detect it. We also extend our study to a double layer of quantum dots, where we find a competition between Rabi frequency and tunneling oscillations. [1] J. M. Villas-Boas, S. E. Ulloa, and A. O. Govorov, Phys. Rev. Lett. 94, 057404 (2005); Phys. Rev. B 69, 125342 (2004).

*Supported by the Indiana 21st Century Fund and BNNT at Ohio University.

## SESSION Z20: FOCUS SESSION: NOVEL FERROMAGNETIC SEMICONDUCTORS II
**Friday Morning, 17 March 2006**
**317, Baltimore Convention Center at 11:15**
**Jacek Furdyna, University of Notre Dame, presiding**

**11:15**

**Z20 1 Defect-induced Ferromagnetism in Insulators without Magnetic Ions: The Case of Cation Vacancy in CaO*** JORGE OSORIO-GUILLEN, S. LANY, S.V. BARABASH, ALEX ZUNGER, *National Renewable Energy Laboratory* We have investigated by means of first-principle supercell calculations the posibility of ferromagnetism being induced by cation vacancies in non-magnetic oxides in four steps: (*i*) A single neutral Ca vacancy $V_{Ca}^{0}$ is found to have a magnetic moment of 1.9 $\mu_B$ due to its electronic configuration: $(a_1^2\, t_{1+}^3\, e_+^2) t_{1-}^p\, e_-^q$ where, the $e_-$ state is partially occupied ($q \approx 0.5$), leading to a transfer of some hole density to the $t_{1-}$ valence band states ($p \approx 2.5$). (*ii*) The ferro-

magnetic interaction between two vacancies is found to extend only to four neighbors or less. (*iii*) To achieve magnetic percolation on a fcc lattice with such an interaction range one needs a minimum vacancy concentration of $1.8 \times 10^{21}$ $cm^{-3}$ (4.9 %). However, (*iv*) due to the high vacancy formation energy even under the most favorable growth conditions one can not obtain at equilibrium more than $10^{18}$ $cm^{-3}$ vacancies. Thus, a non-equilibrium vacancy-enhancement factor of $10^3$ is needed to achieve ferromagnetism in such systems. Comparison with other non-magnetic oxides will be also discussed.

*This work was funded by DARPA under NREL contract No. DE-AC36-99GO10337

**11:27**

**Z20 2 Ferromagnetism in Transparent ZnO:xCu Sputter Deposited Thin Films** CHANDRAN SUDAKAR, R. NAIK, *Wayne State University, Detroit* G. MOHAN RAO, *ISU, IISc, Bangalore, India* V.M. NAIK, *University of Michigan-Dearborn* K.V. RAO, *Tmfy-MSE, KTH, Stockholm, Sweden* Currently, detailed understanding on the intrinsic or extrinsic nature of the diluted magnetic oxides when doped with cations (magnetic or nonmagnetic) is an intricate issue. We report a systematic study of ferromagnetism (FM) above room temperature in transparent ZnO:xCu (x in at.%) films deposited by reactive magnetron sputtering. $Cu^{2+}$ ions are found to be in wurtzite structure for $x < 3$, whereas CuO phase is deciphered for $x > 3$, and located within the ZnO lattice with the associated stacking faults or at grain boundary regions. An anomalous large magnetic moment (**itM**) of $\approx 1.76 \pm 0.2$ $\mu_B$/Cu is observed for $x \approx 0.6$. **itM** decreases drastically ( $< < 0.4$ $\mu_B$/Cu) for $x > 1$ due to increased Cu-O-Cu anti-FM interactions. Micro-Raman spectral studies reveal plausible Cu-O clusters of few Å in ZnO lattice giving rise to anomalous high **itM** even at low concentrations ($x < 1$) in ZnO lattice. Detailed discussion will be presented on related results.

**11:39**

**Z20 3 Measurement of the spin polarization of the magnetic semiconductor EuS with zero-field and Zeeman-split Andreev reflection spectroscopy*** CONG REN, J. TRBOVIC, J.G. BRADEN, R.L. KALLAHER, J.S. PARKER, P. SCHLOTTMANN, S. VON MOLNAR, P. XIONG, DEPARTMENT OF PHYSICS/MARTECH, FLORIDA STATE UNIVERSITY TEAM, Measurements of the spin polarization (**itP**) of doped EuS using zero-field and Zeeman-split Andreev reflection spectroscopy (ARS) on EuS/Al planar junctions are reported. EuS films (100nm thick) of different conductivities were grown via UHV electron-beam deposition at various substrate temperatures. A thin (7nm) Al film was used as the counterelectrode. The zero-field ARS spectra can be fit straightforwardly, with itzero spectral broadening and expected gap values, to the spin-polarized BTK model. The fits consistently yield **itP** on the order of 80% regardless of the barrier strength. Moreover, we performed ARS in the presence of a Zeeman-splitting of the quasiparticle density of states in Al. The Zeeman-split ARS spectra are well described theoretically by combining the solution to the Maki-Fulde equations with the spin-polarized BTK analysis. The results have provided an independent verification of the validity of the zero-field ARS, and demonstrated the utility of field-split superconducting spectroscopy on Andreev junctions of arbitrary barrier strengths.

*This work was supported by DARPA SPINS program.

**11:51**

**Z20 4 Observation of the Temperature driven Insulator to Semiconductor (Ferromagnetic) Phase** HANGIL LEE, *Beamline Research Division, Pohang Accelerator Laboratory (PAL)* K.-J RHO, *Electron Spectroscopy Laboratory, Department of Physics, POSTECH* J.-Y KIM, *Beamline Research Division, Pohang Accelerator Laboratory (PAL)* J.-H PARK, *Electron Spectroscopy Laboratory, Department of Physics, POSTECH* PAL TEAM, POSTECH TEAM, We investigated the changes of magnetic properties (para to ferromagnetic) and phase transitions (insulator to semiconductor) in films of EuO grown on a MgO(100) single crystal as a function of temperature. In between 70 K, we found a clear phase transition and magnetic transition using the spin-summed and spin-resolved photoemission spectra, as well as the low energy electron diffraction. We will elucidate the temperature driven electronic and magnetic property in EuO on MgO(100) substrate.

**12:03**

**Z20 5 Critical behavior and spin polarization of a single crystal $Mn_5Ge_3$.** T.Y. CHEN, J. VALENTINE, C.L. CHIEN, *The Johns Hopkins University* C. PETROVIC, *Brookhaven National Laboratory* Despite difficulties of injecting spin into semiconductor using ferromagnetic metals, spin injection into semiconductor is essential for spintronics in order to take advantage of the silicon-based electronics. The intermetallic compound $Mn_5Ge_3$ is a promising candidate as a spin injector for semiconductor because of its relatively high Curie temperature and good lattice match with semiconductors. Recent theoretical calculations show that $Mn_5Ge_3$ has a spin polarization of as much as 70% in the purely diffusive region. In this work, we have determined the critical exponents of a single crystal $Mn_5Ge_3$ using magnetometry. The critical temperature has been determined to be $T_C = 283.68 \pm 0.02$ K from spontaneous magnetization with the critical exponents of $\beta = 0.358 \pm 0.005$ and $\gamma = 1.367 \pm 0.005$. The spin polarization of the crystal determined using point contact Andreev reflection (PCAR) is $54 \pm 2\%$, indicating that it is a good spin injector with a substantial spin polarization compared with ordinary ferromagnetic metals such as Fe, Co and Ni. Work supported by NSF grant No. DMR05-20491 and DMR04-03849.

**12:15**

**Z20 6 Epitaxial Ferromagnet on Ge(111) : $Mn_5Ge_3$** MICHAEL HOCHSTRASSER, DANILO PESCIA, *ETH Zurich* ROY WILLIS, *The Pennsylvania State University* IVANA VOBORNIK, GIANCARLO PANACCIONE, GIORGIO ROSSI, *TASC, INFM-CNR* Magnetic materials used for recording and reading information involve the use of the electron spin, while semiconducting devices normally take advantage of the electron charge. Recently, a big effort has been made in adding the spin degree of freedom to conventional semiconductors. A good potential candidate for spin injection in a silicon- compatible semiconductor are $Mn_5Ge_3$ thin films on Ge(111) [1]. To further gain information on the usefulness of possible spintronics applications of $Mn_5Ge_3$/Ge(111) multilayers angle resolved photoemission spectroscopy (ARPES) was employed to map the band dispersion of

$Mn_5Ge_3$ films on Ge(111) above and below the Curie temperature. Furthermore, we performed temperature dependent x-ray magnetic dichroism measurements of $Mn_5Ge_3$ films on Ge(111) to probe the magnetic properties of $Mn_5Ge_3$. [1] C. Zeng et al., Appl. Phys. Lett. **83**, 5002 (2003).

**12:27**

**Z20 7 Growth and magnetization dynamics of thin film tetradymite-type diluted magnetic semiconductors based on Sb2-xTMxTe3 (M = V, Cr)** ZHENHUA ZHOU, YI-JIUNN CHIEN, CTIRAD UHER, *Department of Physics, University of Michigan* Recently we reported on a new MBE-grown thin film ferromagnetic semiconductor based on Sb2-xVxTe3 with a Curie temperature of 177 K when x = 0.35 [1]. Ferromagnetism was confirmed by magnetization measurements and anomalous Hall effect. We have now extended our investigations to thin films of Sb2-xCrxTe3 and we observed ferromagnetism in this system through magnetic measurements. The Curie temperature increases with the increasing concentration of Cr. Ferromagnetic resonance (FMR) was detected in both Sb2-xVxTe3 and Sb2-xCrxTe3 thin films at low temperatures using an electron paramagnetic resonance (EPR) spectrometer. Optical ultrafast spin dynamics investigations in both Sb2-xVxTe3 and Sb2-xCrxTe3 thin films reveal the existence of spin waves in these diluted magnetic semiconductors. The spin wave parameters are obtained based on the FMR and optical methods. [1] Z. Zhou, Y.-J. Chien and C. Uher, Thin film ferromagnetic semiconductors Sb2-xVxTe3 with TC of 177 K, Applied Physics Letters, vol.87, 112503 (2005).

**12:39**

**Z20 8 A Study of Magnetoresistance of $Yb_{14-x}La_xMnSb_{11}$ : an Ordered Dilute Magnetic Semiconductor*** DAVID MANDRUS, RONGYING JIN, ZHIXIAN ZHOU, BRIAN SALES, *Oak Ridge National Laboratory* LUIS BALICAS COLLABORATION,† $Yb_{14-x}La_xMnSb_{11}$is an ordered dilute magnetic semiconductor, showing evidence for partial screening of the Mn magnetic moments and mass renormalization from 2 $m_e$ near room temperature to 20 $m_e$ at 5 K. We have measured both the transverse (I⊥ H) and longitudinal (I//H) magnetoresistance (MR) of $Yb_{14-x}La_xMnSb_{11}$(x=0, 0.7) single crystals above and below the ferromagnetic (FM) transition temperature $T_c$ = 53 K (x=0) and 39 K (x=0.7). While it is negative in a wide temperature range, the MR becomes positive below $T_c/2$ and increases with decreasing temperature. Strikingly, the positive MR increases linearly with applied field, showing no sign of saturation up to 32 tesla. Quantitative analysis and implications of the data will be reported.

*ORNL is managed by UT-Battelle, LLC, for the U.S. DOE under contract DE-AC05-00OR22725.
†National High Magnetic Field Lab

**12:51**

**Z20 9 Observation of a new magnetic anomaly in low field ac and dc magnetic measurements in $Yb_{14}MnSb_{11}$** S. SRINATH, P. PANKAJ, H. SRIKANTH, *Department of Physics, University of South Florida, Tampa FL 33620* B.C. SALES, D. MANDRUS, *Condensed Matter Sciences Division, Oak Ridge National Laboratory, Oak Ridge, TN 37831* $Yb_{14}MnSb_{11}$ is the first known example of a ferromagnetic Kondo lattice compound in the underscreened limit. Recent optical, Hall, magnetic, and thermodynamic measurements indicate that $Yb_{14}MnSb_{11}$ may be a rare example of an underscreened Kondo lattice. This heavily doped magnetic semiconductor is ferromagnetic below 52 ± 1 K. We report the first experimental observation of a new magnetic anomaly in this system at around 47 K, a few degrees below the Curie temperature. Systematic investigations of the AC and DC susceptibilities of $Yb_{14}MnSb_{11}$ single crystals reveal features associated with possible spin re-orientation at this temperature. This new anomaly is extremely sensitive to the applied field and is absent in DC magnetization measurements for fields above 50 Oe. The origin of this could be related to a change in magnetic anisotropy caused by the decoupling of energetically close FM and AFM sub-lattices.

**13:03**

**Z20 10 Transport and magnetic properties of rare-earth nitrides** JOE TRODAHL, SIMON GRANVILLE, BEN RUCK, FELIX BUDDE, *Victoria University of Wellington, Wellington, New Zealand* TONY BITTAR, GRANT WILLIAMS, *Industrial Research Ltd., Lower Hutt, New Zealand* There is controversy about the conducting character of the rare-earth nitrides, with reports existing from metallic to moderately wide band-gap semiconductors. In a programme intended to clarify that issue we have grown thin films of the rare-earth mononitrides GdN, SmN, DyN and ErN by ion assisted deposition (IAD). Their stoichiometry and nanocrystalline structure have been characterised by RBS, SIMS, XRD, TEM, and EXAFS. The as-prepared materials are very reactive in the atmosphere, but they are effectively passivated by capping layers of either $MgF_2$ or IAD GaN. Their magnetic properties have been studied from ambient temperature to 5 K and found to be in agreement with reported behaviour in the literature. The conductivity is typical of semiconductors, as regards both its magnitude and its temperature dependence.

## SESSION Z22: FOCUS SESSION: FEPT NANOPARTICLES FOR INFORMATION STORAGE

**Friday Morning, 17 March 2006; 319, Baltimore Convention Center at 11:15**
**Kai Liu, University of California, Davis, presiding**

*Invited Papers*

**11:15**

**Z22 1 Media for Extremely High-Density Recording.**
DIETER WELLER, *Seagate Recording Media Operation*

This abstract was not received electronically.

*Contributed Papers*

**11:51**

**Z22 2 Novel Chemical Synthesis of FePt and CoPt Magnetic Nanoclusters** YUCHENG SUI, YAO ZHAO, MINGLANG YAN, DAVID SELLMYER, *Department of Physics & CMRA, University of Nebraska* $L1_0$ ordered FePt and CoPt clusters are very promising candidates for ultrahigh magnetic recording media applications due to their large magnetocrystalline anisotropies and chemical stability. We report simple and highly efficient approaches for synthesizing FePt and CoPt nanoclusters by the pyrolysis of corresponding Fe, Co and Pt compounds in organic solvents. A mixture of Fe and Pt acetylacetonates was heated in trioctylamine, producing FePt clusters with average size about 4.2 nm and with a narrow size distribution. When the clusters with equal Fe and Pt atomic ratio were dispersed onto a silicon wafer and heated in forming gas, high- anisotropy magnetic FePt clusters with $L1_0$ chemical order were obtained. Coercivity values as high as 23 kOe were realized after annealing at 750$^o$C for 5 min. When the pyrolysis of Co and Pt acetylacetonates mixture was carried out in trioctylamine, CoPt clusters about 4 nm and narrow size distribution also were produced. The atomic ratio of CoPt clusters can be tuned by the addition of proper reducing agents. The chemical reaction mechanism, the phase transformation and the magnetic properties will be discussed. This research is supported by DOE, NSF-MRSEC, INSIC, NRI and CMRA.

**12:03**

**Z22 3 Size Effect on Chemical Ordering in Face-Centered Tetragonal FePt Nanoparticles*** DAREN LI, NARAYAN POUDYAL, VIKAS NANDWANA, J.PING LIU, *Department of Physics, University of Texas - Arlington* Monodisperse face-centered tetragonal (fct) FePt nanoparticles with high magnetocrystalline anisotropy have been obtained by means of the salt-matrix annealing technique. The as-synthesized face-centred cubic (fcc) FePt nanoparticles of different sizes were mixed with NaCl powder particles and the mixture was annealed at temperatures up to 750 $^o$C for several hours. X-ray diffraction (XRD) and transmission electronic microscopy (TEM) analyses showed that the annealed particles transfered to the fct structure without sintering and agglomeration. Magnetization measurements gave the coercivity of the nanoparticles increasing with the particle size. Extended annealing does not change the size dependence of the coercivity. Further XRD analysis revealed that the size dependence of the coercivity is related to the particle size dependance of long-range chemical ordering degree. The long-range order parameter S is 0.78, 0.92, 0.98 and 0.94 for the 4 nm, 6 nm, 8 nm and 15 nm particles, respetively. This trend is consistent with that of the coercivity measured from the nanoparticles. The relatively low ordering parameter of the 15 nm particles may be related to the polycrystalline morphology as shown by the high resolution TEM.

*Work supported by MURI, DARPA

**12:15**

**Z22 4 Chemically Synthesized FePt Binary Alloy Nanoparticles with Different Shapes*** L. COLAK, Y. HUANG, M.J. BONDER, G.C. HADJIPANAYIS, *Dept. of Physics and Astronomy, U of Delaware, Newark,DE,USA* D. WELLER, *Seagate Technology, Pittsburg, PA,USA* Chemically synthesized FePt nanoparticles are promising candidates for future high density magnetic recording media. In this work, FePt and $FePt_3$ binary alloy nanoparticles have been synthesized by thermal decomposition of iron pentacarbonyl ($Fe(CO)_5$) and reduction of platinum acetylacetonate (Pt $(acac)_2$) in the presence of oleic acid (OA) and oleyl amine (OY) surfactants at low refluxing temperatures. $FePt_3$ and FePt nanoparticles were obtained by varying the Fe:Pt molar ratio in the range of 1.4-1.7. With control of the heating rate to the refluxing temperature, nanoparticles with a size of $\sim$ 5 nm and with different shapes were obtained for both compositions. The particles showed very little agglomeration to an annealing temperature of 650$^o$C, as observed using X-Ray Diffraction (XRD) and Transmission Electron Microscopy (TEM). Magnetic measurements show that annealing at 700$^o$C partially transforms the FePt and $FePt_3$ nanoparticles from the disordered fcc phase to the ordered $L1_0$ and $L1_2$ phases, respectively. HRTEM and Mossbauer studies will be discussed in terms of the temperature and time dependent evolution of microstructure with annealing.

*Work supported by NSF DMR-0302544 and Seagate Technology

**12:27**

**Z22 5 Variability in the extent of ordering for individual FePt $L1_0$ nanoparticles** RUMYANA V. PETROVA, BO YAO, VU LAM, K.R. COFFEY, *University of Central Florida, Orlando, FL 32815 USA* R.R. VANFLEET, *Brigham Young University, Provo, Utah 84602, USA* $L1_0$ordered phase FePt nanoparticles are of interest as high-density magnetic recording media due to the large uniaxial magnetocrystalline anisotropy,$K_u$ observed in bulk and thin film samples. Similarly high itKu values have not yet been achieved for small ( $<$ 10nm) FePt nanoparticles. Mixtures of ordered and disordered nanoparticles are often observed and have been attributed to nucleation barriers for the ordering transformation in individual small nanoparticles. For FePt, $K_u$ is known to depend strongly on the extent of long-range chemical order. In this work we report on the variability of the extent of order amongst ordered $L1_0$ FePt particles. Well-isolated, small FePt nanoparticles were prepared from discontinuous FePt films, using ultra high vacuum dc magnetron sputtering. A Tecnai F30 analytical transmission electron microscope was used to characterize the FePt nanoparticles. Convergent beam electron diffraction patterns from individual nanoparticles were compared to multislice simulations to determine the extent of order of single nanoparticles.

**12:39**

**Z22 6 Direct Fabrication and Magnetic Characterization of Highly Ordered $L1_0$ FePt Nanoparticles** JIAO-MING QIU, JIAN-PING WANG, *MINT & Department of Electrical and Computer Engineering,University of Minnesota* Future advanced magnetic recording media require the grains to be small and uniform with sufficient anisotropy to sustain thermal fluctuation. $L1_0$ phase FePt nanoparticles fit these requirements but their fabrication turns out to be difficult. Conventional methods were reported to be able to make monodispersed FePt nanoparticles with disordered structure[1]. The inevitable phase transformation process is believed to be kinetically limited[2] and such issues as agglomeration and twinning are to be addressed. Here we report a novel technique that can fabricate monodispersed highly ordered FePt nanoparticles with no need for phase transformation process. In this technique, particle nucleation and growth processes happened in the gas phase and they were separated in space. Modified sputtering plasma made the ordering and particle growth processes proceed simultaneously. Uniform $L1_0$ FePt nanoparticles with room temperature coercivity of 8.25 kOe were achieved for particle randomly assembled film. HRTEM analysis shows that these particles have perfect octahedron shape with only {111} surfaces exposed. Ref: 1. Sun, S, et al, Science, 287, 1989, 2000 2. Ding, Y. et al, Appl. Phys. Lett. 87, 022508, 2005

**12:51**

**Z22 7 Effects of Annealing on the Magnetic and Structural Properties of FePt Nanoparticles by Chemical Synthesis*** HONGLI WANG, Y. HUANG, Y. ZHANG, G. HADJIPANAYIS, *Department of physics, University of Delaware, Newark, DE 19716, USA* D. WELLER, *Seagate Technology, Pittsburgh, PA 15203, USA* A. SIMOPOULOS, *IMS, NCSR ''DEMOKRITOS,'' Ag. Paraskevi, Athens 15310, Greece* In this paper, we have studied the effects of annealing atmospheres on the particle size, the degree of ordering, and the magnetic properties of FePt nanoparticles made by chemical synthesis. Measurements were made on particle assemblies with controlled dimension and thickness. Annealing was done under forming gas and vacuum atmospheres. Particles did not grow much after annealing at 550 $^{o}$C for 30 min under forming gas, resulting in an average particle size D $\approx$ 5 nm and a coercivity of 4 kOe. After annealing under vacuum using the same annealing temperature and time, the morphology of particles is similar to that of particles annealed under forming gas but with a coercivity less than 1 kOe. We believe that this large difference in coercivity is due to the fact that the forming gas not only assists the transformation from the chemically disordered fcc phase to the chemically ordered $L1_0$ phase but also makes the atomic composition of FePt nanoparticles more uniform. Mössbauer studies showed a higher percentage of $L1_0$phase in the sample annealed under forming gas than that under vacuum, which further confirms the hypothesis stated above.

*Work supported by NSF DMR 0302544 and Seagate

**13:03**

**Z22 8 Enhanced orbital magnetism in oxide free Fe50Pt50 nanoparticles probed by x-ray magnetic circular dichroism*** MICHAEL FARLE, *Universitaet Duisburg-Essen* X-ray absorption spectra at both the Fe and Pt L3,2 edges were measured on wet-chemically synthesized Fe50Pt50 particles with a mean diameter of 6.3 nm. The organic ligands and the oxide shell covering the particles in the as prepared state were removed by soft hydrogen plasma. After thermal treatment under hydrogen atmosphere of 5 Pa, the coercive field increased by a factor of 6. This indicates the formation of the chemically ordered L10 phase and is accompanied by an enhancement of the orbital magnetic moment at the Fe site by 275%. Changes in the frequency of oscillations in the extended x-ray absorption fine structure at the Pt L3,2 edges provide additional crystallographic evidence for the formation of the L10 phase.

*Supported by EU network ''SyntOrbMag'' and DFG, Sfb 445

**13:15**

**Z22 9 FePt-Si Nanoparticles With Perpendicular Anisotropy*** J. WAN, Y. ZHANG, Y. HUANG, M. BONDER, G.C. HADJIPANAYIS, *Department of Physics and Astronomy, University of Delaware, Newark DE 19711* C. NI, *Department of Materials Science and Engineering, University of Delaware, Newark DE 19711* D. WELLER, *Seagate Technology, Pittsburgh, PA 15203* FePt Nanoparticles are attractive for applications in magnetic recording media because of their high magnetocrystalline anisotropy. In this work, FePt-Si nanoparticles were fabricated by sputtering an FePt-Si target onto heated MgO substrates. The deposition temperature varied from 350$^{o}$ to 500$^{o}$C. The ratio of FePt to Si in the films was changed by varying the amount of Si in the target. XRD results show that the lattice parameters of L10 phase changed in the FePt-Si nanoparticles from 3.71 to 3.61 Å for the c parameter and from 3.85 to 3.87 Å for the a parameter. Higher amounts of Si led to a larger change in lattice parameters. The change of lattice parameters in FePt nanoparticles affected the magnetic properties as indicated by the decrease of the coercivity in the FePt-Si samples. TEM images show that the FePt/Si nanoparticles have a better size distribution than the FePt/C nanoparticles. Selected area electron diffraction patterns show that the FePt-Si nanoparticles deposited on MgO have a (001) texture due to the lattice matching between FePt and MgO. The FePt-Si nanoparticles have properties that can be tailored for applications in magnetic recording media.

*This work is supported by Seagate Technology.

**13:27**

**Z22 10 Magnetic force microscopy (MFM) study of FePt nanocrystals overcoated with silica*** ALEX DE LOZANNE, CHANGBAE HYUN, *Department of Physics, University of Texas at Austin, Austin, TX 78712* DOH C. LEE, BRIAN A. KORGEL, *Department of Chemical Engineering, University of Texas at Austin, Austin, TX 78712* Chemically-synthesized FePt nanocrystals must be annealed at $\sim$ 550C to induce the hard magnetic L10 phase. Sintering of nanocrystal films occurs at these temperatures, resulting in the loss of control over nanocrystal size and separation in the film. We have developed a silica overcoating strategy to prevent nanocrystal sintering. In this study, 6 nm diameter FePt nanocrystals were coated with 20 nm thick shells of silica using an inverse micelle process. Magnetization measurements of the annealed FePt@SiO2 nanocrystals indicate ferromagnetism at room temperature. The micromagnetic properties of thin films of these nanocrystals were studied using MFM.

*This work is supported by NSF DMR-0308575.

**13:39**

**Z22 11 Enhancement of $L1_0$Order in FePt Thin Films and X-ray Rapid Thermal Annealing (XRTA)*** ROSA ALEJANDRA LUKASZEW, JONATHAN SKUZA,† *University of Toledo* ERIC DUFRESNE, *Argonne National Laboratory* CODRIN CIONCA, *University of Michigan* ALFONSO CEBOLLADA, *IMM-Spain* CESAR CLAVERO, *IMM-Spain* CORA LIND, *University of Toledo* Highly ordered $L1_0$ FePt thin films and nanostructures are important for magneto-recording applications because this ordered phase exhibits very large magnetic anisotropy. One possibility to achieve high degree of chemical order in epitaxial, but somewhat chemically disordered films is to perform annealing treatments. One variation of such treatments is rapid thermal annealing (RTA). Here we describe an innovative application of x-ray undulator radiation to simultaneously perform RTA and probe structural changes that occur itduring annealing. In our studies, we have used XRTA to enhance chemical order in epitaxial (001) FePt thin films. We observed the enhancement of the itfcc-fct transition with 30 ms temporal resolution in Bragg geometry. The results demonstrate that undulator radiation offers unique possibilities for materials processing, particularly the ability to use the itsame beam for heating and probing.

*Project funded by NSF-DMR-0355171and ACS-PRF
†graduate student and presenter

**SESSION Z23: STRONGLY CORRELATED ELECTRONS II**
**Friday Morning, 17 March 2006**
**320, Baltimore Convention Center at 11:15**
**Patrick Morales, presiding**

**11:15**
**Z23 1 Yb- and Ce- based, dilute rare earth intermetallic compounds: Fully ordered compounds that approach the single Kondo-impurity limit** M.S. TORIKACHVILI, *Dept. of Physics, San Diego State University* S. JIA, *Ames Laboratory and Dept of Physics and Astronomy, Iowa State University* S.T. HANNAHS, *NHMFL-Florida State University, Tallahassee* NI NI, E-D. MUN, S.L. BUD'KO, P.C. CANFIELD, *Ames Laboratory and Dept of Physics and Astronomy, Iowa State University* Dilute, rare earth intermetallic compounds are ordered structures in which the rare earth comprises less than 5% atomic of the compound, but still fully occupies a unique crystallographic site. Whereas for local moment bearing R-members these series offer the possibility of studying the RKKY interaction for relatively large R R spacing, the R = Yb and Ce members offer a unique opportunity to study the Kondo lattice for concentrations that start to approach the single ion limit. In this talk we will present data on six Yb-based, and two Ce-based, dilute rare earth intermetallic compounds. Despite the rather different behavior of the analogous Gd-based members, the thermodynamic and transport properties of the Yb-based materials are rather similar. This new family of heavy Fermion materials promises to be a fruitful testing ground for current theories of correlated electron physics.

**11:27**
**Z23 2 The low temperature thermodynamic properties and Hall effect in YbAgGe close to the field-induced quantum** Y. TOKIWA, A. PIKUL, P. GEGENWART, F. STEGLICH, *Max-Planck Institute for Chemical Physics of Solids, Dresden* V.S. ZAPF, *NHMFL - Los Alamos* S.L. BUD'KO, P.C. CANFIELD, *Ames Laboratory and Department of Physics and Astronomy, Iowa State University* We present temperature and field dependent heat capacity and magnetization data ($T \geqslant 50$ mK, $H \leqslant 11.5$ T) as well as field dependent Hall effect data ($T \geqslant 50$ mK, $H \leqslant 18$ T) for YbAgGe, a heavy-fermion compound with a field induced quantum critical point. These data clearly indicate that the same electronic degrees of freedom are responsible for the features seen in both specific heat and magnetization data. In addition, they further refine the different boundaries suggested for the $H - T$ phase diagram of YbAgGe through previous, magneto-transport measurements, and allow for further understanding of different phases on the $H - T$ phase diagram, in particular, clearly disconnecting the field-induced quantum critical point in YbAgGe from any sort of saturation of the Yb moment in higher applied magnetic field.

**11:39**
**Z23 3 Study of low carrier density heavy fermion $Ce_3Au_3Sb_4$*** HAN-OH LEE, *Department of Physics, University of California, Davis* PETER KLAVINS, *Department of Physics, University of California, Davis, California, 95616* ZACHARY FISK, *Department of Physics, University of California, Davis, California, 95616* CATHIE CONDRON, *Department of Chemistry, University of California, Davis, California, 95616* A. D. CHRISTIANSON, *Department of Physics and Astronomy, University of California, Irvine, California, 92698-4575* J. M. LAWRENCE, *Department of Physics and Astronomy, University of California, Irvine, California, 92698-4575* J. S. GARDNER, *Physics Department, Brookhaven National Laboratory, Upton, New York, 11973-5000,NIST Center for Neutron Research, National Institute* $Ce_3Au_3Sb_4$ is a narrow gap semiconductor with a well localized $Ce^{3+}$ state. The specific heat measurements, however, show a Kondo impurity like behavior with a large increase of the specific heat coefficient at low temperature, suggesting a heavy fermionic character in this low carrier concentration system. Magnetic susceptibility, resistivity, and specific heat data will be shown for single crystal $Ce_3Au_3Sb_4$. The dilution study with La substituted on the Ce site will be also presented to further discuss the Kondo effect in this system.

*This work has been supported by NSF DMR-0433560

**11:51**
**Z23 4 Rare-earth nitrides: an LSDA+U study** PAUL LARSON, WALTER LAMBRECHT, *Case Western Reserve University* MARK VAN SCHILFGAARDE, *Arizona State University* The class of rare-earth (Ce-Lu) nitrides all form in the rocksalt crystal structure. One member in particular, GdN, has received considerable theoretical and experimental interest because it appears to be a bulk ferromagnetic semiconductor. The other members of this class of compounds have received much less attention. Electronic structure calculations for the entire series are presented here using a full-potential linear muffin-tin orbital (FP-LMTO) method within the LSDA+U approach. In this approach the localized orbitals have their Coulomb interactions treated in a screened Hartree-Fock mean field approximation while the remaining orbitals are treated in the standard local spin density approximation. $U$ terms were also added to the rare-earth 5$d$ states to correct for the underestimation of the band gap in LSDA. In a cubic field, the 4$f$ states split into triply degenerate $t_{1u}$ and $t_{2u}$ states and a singly degenerate $a_{2u}$ state. The large Hubbard $U$ is found to dominate crystal field splitting to determine the order of minority and majority spins. Avoiding partially filled states at the Fermi level is the dominant principle, yielding narrow gap semiconducting or semimetallic band structures. In a few cases, namely those which correspond to configurations deviating by 2 electrons from a completely empty, completely full, or half-full configuration, however, an $f$-band is forced to cross the Fermi level, possibly resulting in heavy-fermion metallic behavior.

**12:03**
**Z23 5 Electronic structure of CrN: a Mott insulator** ADITI HERWADKAR, WALTER R.L. LAMBRECHT, *Case Western Reserve* MARK VAN SCHILFGAARDE, *Arizona State University* It was recently reported by D. Gall et al. [J. Appl. Phys. 91, 5882, 2002] that CrN in the rocksalt structure has an optical band gap of about 0.7 eV, though in local spin density approximation, this materials is predicted to be metallic. We examine this possibility using the LSDA+U approach in the fully localized limit implemented in our full-potential muffin-tin orbital method. Slater integral $F^0 = U$ is screened such that the position of the occupied 3$d$ levels agrees well with the photoelectron spectra of CrN. We find that a band gap opens in the band structure. The actual value of the gap obviously depends on the choice of $U$. To understand the origin of the gap it is essential to study how the $d$ states split in cubic symmetry and what their filling is. Cr in forming CrN is

trivalent and hence has three $3d$ electrons. The Cr $e_g$, form antibonding states in the conduction band. Adding $U$ tends to push these empty states further up for both spins. The $t_{2g}$ on the other hand form weaker $\pi$ bonds with N $2p$, which in LSDA occur near the Fermi energy. Adding a Hubbard $U$ now shift the majority spin electrons by $-U/2$ and the minority spin ones by $U/2$ and remove them from the Fermi level. This works because the three fold degenerate majority spin state $t_{2g\uparrow}$ becomes completely filled while the minority $t_{2g\downarrow}$ becomes empty. The valence band maximum then has predominantly N$2p$ character, which makes CrN a charge transfer type Mott-insulator.

**12:15**

**Z23 6 Free Magnetic Moments in Disordered Metals*** EDUARDO R. MUCCIOLO, *University of Central Florida* STEFAN KETTEMANN, *Institut für Theoretische Physik, Universit at Hamburg, Germany, and Max-Planck Institute for Physics of Complex Systems, Dresden, Germany* The screening of magnetic moments in metals, the Kondo effect, is found to be quenched with a finite probability in the presence of nonmagnetic disorder. Numerical results for a disordered electron system show that the distribution of Kondo temperatures deviates strongly from the result expected from random matrix theory even in the diffusive regime. A pronounced second peak emerges for small Kondo temperatures, showing that the probability that magnetic moments remain unscreened at low temperatures increases with disorder. Analytical calculations, taking into account correlations between eigenfunction intensities yield a finite width for the distribution that survives the thermodynamic limit. Experimental consequences for the electron dephasing in disordered mesoscopic metals and the thermodynamic properties of heavy-fermion compounds are discussed.

*This research was supported by the German Research Council (DFG) and the EU TMR-network

**12:27**

**Z23 7 d-wave Kondo liquids** POUYAN GHAEMI MOHAMMADI, *Massachusetts Institute of Technology* T. SENTHIL, *Massachusetts Institute of Technology & Center for Condenced matter theory, Indian Institute of Science* Conventional heavy Fermi liquid phases of Kondo lattices involve the formation of a ''Kondo singlet'' between the local moments and the conduction electrons. This Kondo singlet is usually taken to be in an internal s-wave angular momentum state. Here we explore the possibility of Fermi liquid phases where the Kondo singlet has internal angular momentum that is d- wave. Such states are readily acessed in a slave boson mean field formulation, and are energetically favorable when the Kondo interaction is between a local moment and an electron at a nearest neighbor site. The properties of the d- wave Kondo lattice are studied. Effective mass and quasiparticle residue show large angle dependence on the Fermi surface. We suggest that such d-wave Kondo pairing may provide a useful route to thinking about correlated Fermi liquids with strong anisotropy along the Fermi surface.

**12:39**

**Z23 8 Randomly Depleted Kondo Lattices** RIBHU KAUL, *Duke U. and TKM Uni-Karlsruhe* MATTHIAS VOJTA, *TKM Uni-Karlsruhe* How is the ''heavy Fermi liquid'' of the Kondo lattice connected to the Kondo impurity ''local Fermi liquid'' as the concentration of f-moments is varied? We study the ensuing interplay of strong correlations and disorder within an $SU(N)$ model in a $N \to \infty$ limit. Although normal Fermi liquid behavior is well defined close to the two limits of Kondo-lattice and Kondo-impurity, we find that in between them there are strongly inhomogeneous phases with large fractions of quasi-free moments that result in a violation of the usual Fermi-liquid behavior. The full spatial dependence of the mean field solutions allows us to study the depletion driven evolution of inhomogeneities in local quantities like the local susceptibility and the local spectral function in detail. We describe the relevance of our results to recent experiments on $Ce_{1-x}La_xCoIn_5$.

**12:51**

**Z23 9 Multipole properties of one-dimensional *f*-electron systems** HIROAKI ONISHI, TAKASHI HOTTA, *Advanced Science Research Center, Japan Atomic Energy Agency* By exploiting a density matrix renormalization group method, we investigate the ground-state properties of a one-dimensional three-orbital Hubbard model on the basis of a *j-j* coupling scheme. Here we focus on the case where the *f*-electron number per site is one ($f^1$). When three orbitals are degenerate, we observe a peak at $q=0$ in $\Gamma_{3g}$ quadrupole correlation, indicating a ferro-orbital state. Namely, $f$ electron occupies an itinerant $\Gamma_8^b$ orbital to gain kinetic energy, while localized $\Gamma_8^a$ and $\Gamma_7$ orbitals are found to be almost empty. Furthermore, we find a peak at $q=\pi$ in $\Gamma_{4u}$ dipole correlation, suggesting an antiferromagnetic state. On the other hand, when we take account of the level splitting between $\Gamma_8$ and $\Gamma_7$ orbitals, due to the competition between itinerant and localized orbitals, we observe a characteristic change of $\Gamma_{3g}$ quadrupole correlation into an incommensurate structure in accordance with the change of the orbital structure. We will also discuss a key role of multipole degrees of freedom in $f^2$- and $f^3$-electron systems.

**13:03**

**Z23 10 Correlation Behavior in Nanoassembled Spin Lattices*** LAILA S. MATTOS, *Stanford University* G.A. FIETE, *UC Santa Barbara* B.A. JONES, C.P. LUTZ, D.M. EIGLER, *IBM Almaden* H.C. MANOHARAN, *Stanford University* The single-impurity Kondo problem, in which an isolated magnetic impurity in a nonmagnetic metallic host has its spin screened by that of the conduction electrons, has been extensively studied both theoretically and through bulk experiments. Only recently, however, have new methods allowed detailed experimental probing of single-impurity Kondo effect of individual magnetic atoms. When many magnetic impurities are present in a bulk conductor or on its surface, the interactions between them may engender novel collective effects. Using a scanning tunneling microscope (STM) we assembled and studied atomically precise periodic arrangements of (magnetic) Co atoms and (non-magnetic) CO molecules on the Cu(111) surface. We observe signs of spin correlation effects when the lattice row spacing for the Co lattices approached half of the Fermi wavelength for the Cu(111) surface electrons. Removing the central atom in each lattice and directly probing the energetics of the resulting hole provides a novel method to search for global spin correlations and investigate Kondo hole behavior in these systems.

*This work was supported by DoE, NSF, and ONR.

**13:15**

**Z23 11 Studies on Single Crystal CeCo3B2** LONG PHAM, *Department of Physics, University of California, Davis, California,*

*95616* VLADIMIR SIDOROV, *Vereshchagin Institute of High Pressure Physics, 142190 Troitsk, Russia* JASON LASHLEY, JOE THOMPSON, *Los Alamos National Laboratory, Los Alamos, New Mexico 87545* HANOH LEE, ZACH FISK, *Department of Physics, University of California, Davis, California, 95616* Magnetization, resisitivity, and specific heat measurements, under pressure, on weak ferromagnet CeCo3B2 are reported. This hexagonal structure with space group P6/mmm ($D^1_{6h}$), and one formula unit per unit cell, forms in the $CaCu_5$-type structure. At ambient pressure, dc and ac susceptibility displayed an ordering below a $T_{curie}$ of $\sim$ 210K, with the highly anisotropic ordering along the c axis, which is weakly suppressed with the application of pressure(- 4 K/GPa). Along the ordering axis, the saturation moment, taking into account the linear behavior at higher fields, reaches only $\sim 0.01\mu_B$ at 2K. This work was supported by NSF-DMR 0433560.

**13:27**
**Z23 12 Evolving Magnetism from self damage in $\alpha$ and $\delta$-Pu** SCOTT McCALL, *LLNL* MICHEAL FLUSS, BRANDON CHUNG, MICHEAL McELFRESH, DAMON JACKSON, As a consequence of the unusual nature of plutonium's electronic structure, point- and extended-defects are expected to, and do exhibit extraordinary properties. Low temperature magnetic susceptibility measurements on Pu and fcc-Pu(Ga) show that the magnetic susceptibility increases as a function of time, yet upon annealing the specimen returns to its initial magnetic susceptibility. This excess magnetic susceptibility (EMS) arises from the $\alpha$-decay and U recoil damage cascades which produce vacancy and interstitials as point and extended defects. The time dependence of the EMS leads to an estimate of the number of atoms influenced by each $\alpha$-decay, as well as a temperature dependence well described by a Curie-Weiss law. These results will be described in context of recent time dependent studies of the elastic modulus in delta Pu. Work performed under the auspices of the U.S. Department of Energy by Lawrence Livermore National Laboratory under Contract W-7405-Eng-48.

**13:39**
**Z23 13 Volume collapse of Cerium*** J.L. SMITH, J.C. LASHLEY, C.P. OPEIL, A.C. LAWSON, *Los Alamos National Laborataory* P.S. RISEBOROUGH, *Temple University* The gamma-to-alpha (low-density fcc to high-density fcc) transition in cerium alloys is measured as a function of magnetic field using specific heat, magnetization, and thermal expansion. The dependence of the transition on magnetic field is discussed within the context of the entropy of the 4f moments in the gamma phase.

*Work performed under the auspices of the US Dept. of Energy.

**13:51**
**Z23 14 Evidence for Kondo effect in Zn:Fe** ELISA BAGGIO-SAITOVITCH, PABLO MUNAYCO, J. LARREA, Y.T. XING, *Centro Brasileiro de Pesquisas Físicas, Brazil* H. MICKLITZ, *II.Physikalisches Institut, Germany* Zn films doped with $^{57}$Fe (atomic concentration c between 0.2 and 2.0 at %) have been prepared by the co-evaporation of the two metals onto a cooled substrate ($T_s$ = 80 K). *In- situ* electrical resistance measurements on these films show resistance minima at $T_K$ ($T_K$ = 10 K for c = 1.0 at %) which disappear in an external magnetic field $B_{ex}$ = 5 T and, therefore, are interpreted as Kondo minima. $^{57}$Fe Mö ssbauer effect studies on the films with c = 0.6 at % taken at T = 4.3 K and for various $B_{ex}$ values, reveal that the effective paramagnetic Fe moments, $\mu$, are $\mu < 0.1\ \mu_B$ for $B_{ex}$ = 3 T. For larger magnetic fields the magnitude of $\mu$ is increasing with increasing $B_{ex}$ [$\mu \sim 0.30(3)\ \mu_B$ for $B_{ex}$ = 7 T], as expected for a spin-compensated Kondo state.

**SESSION Z24: POLYMER MELTS & SOLUTIONS: RHEOLOGY & DYNAMICS**
**Friday Morning, 17 March 2006**
**321, Baltimore Convention Center at 11:15**
**Yonathan Thio, Georgia Tech, presiding**

**11:15**
**Z24 1 Predicting the Positions and Breadths of the Glass Transitions in Polymer-Diluent Mixtures** J.E.G. LIPSON, *Dartmouth College* S.T. MILNER, *ExxonMobil* When a plasticizer is added to a polymer the effect is to lower and broaden the glass transition of the polymer. Less frequently studied is the opposite range of the concentration scale, which presumably raises and broadens the diluent glass transition. In fact, although the default assumption is that this miscible combination will exhibit only one transition, we expect two transitions on theoretical grounds, one for the polymer and one for the diluent. Both should be visible at intermediate compositions unless the pure component glass temperatures are rather close. The development of our theory has been stimulated by the appearance of recent experimental data on polystyrene dibutylphthalate; the results presented in the talk will focus on its application to a series of polystyrene-diluent mixtures. Finally, the ability of our approach to predict both the transition temperatures and breadths, as well as the conditions under which two transitions may be observed, will be discussed.

**11:27**
**Z24 2 A Novel Technique to Measure Enthalpy Recovery for Polymer Glasses Subsequent to Temperature and Plasticizer Concentration Jumps.*** LAMECK BANDA, *Dept. of Chemical Engr., Texas Tech University* MATAZ ALCOUTLABI, *Dept. of Chemical Engr., University of Utah* GREGORY McKENNA, *Dept. of Chemical Engr., Texas Tech University* We report results of the enthalpy recovery of polymer glasses subsequent to temperature jumps and carbon dioxide pressure jumps in the isothermal mode. The results were performed on a novel system that was built in our laboratory. The system is a Setaram C80 calvet calorimeter that we modified to include pressure capabilities. The system also offers the advantage of large bore chambers that facilitate the use of large samples. Additionally, experiments of enthalpy recovery subsequent to plasticizer concentration histories in the isothermal mode are feasible. Enthalpy recovery results show qualitative similarities with volumetric measurements reported in our previous work. Particularly, the three signatures of structural recovery; intrinsic isopiestics, asymmetry and the memory effect are observed. Further, consistent with the volumetric observations, enthalpy recovery results also show that equilibration times for the polymer glass are longer when the glass transition is traversed

through a plasticizer jump than when traversed through a temperature jump.

*The authors would like to thank the National Science Foundation for supporting this work under grant numbers DMR-0070052 and DMR-0307084.

**11:39**

**Z24 3 Glass Transition Temperature of Polyetherimide: Relationship between Thin Films and Nanoporous Materials*** RAHMI OZISIK, TONG LIU, RICHARD W. SIEGEL, *Materials Science and Engineering Department, Rensselaer Nanotechnology Center; Rensselaer Polytechnic Institute* The glass transition temperature ($T_g$) of nanoporous polyetherimide (PEI) was investigated using differential scanning calorimetry. Nanosized pores were created by spin coating a solution of PEI and polycaprolactone-diol (PCLD) in their common solvent dichloromethane. The nanoporous structure was created by fast phase separation during spin coating and subsequent removal of PCLD with acetone. Atomic force microscopy, scanning electron microscopy and statistical methods were used to characterize the pore structure. The glass transition temperatures of both the thin PEI films and nanoporous PEI samples were lower than that of bulk PEI. The $T_g$ of nanoporous PEI was found to depend strongly on pore volume fraction. A Monte Carlo simulation was performed to investigate the relationship between thin films and nanoporous systems. The distribution of nearest neighbor distances (ith) were obtained from the Monte Carlo simulation, which was biased to create the pore size distribution obtained from experiments. Various moments of ith was calculated and used to compare the findings to thin film data.

*This work was supported by IBM and the Nanoscale Science and Engineering Initiative of the National Science Foundation under NSF award number DMR-0117792.

**11:51**

**Z24 4 Dynamics of Polyethylene, Studied by Monte-Carlo Simulations*** E. VON MEERWALL, H. LIN, W.L. MATTICE, *Univ. Akron* To compare with our diffusion (D) measurements in polyethylene (PE) melts and blends we have performed Monte-Carlo simulations on the second-nearest-neighbor diamond lattice, exploring static and dynamic properties of PE from C40 to C324 (molecular weights M from 584 to 4538) at 180 deg. C. The bridging method is based on beads combining neighboring moieties and now incorporates two-bead moves; it permits detailed reconstruction of the PE chain at any stage. It uses the short-range rotational isomeric state model and long-range intra- and interchain Lennard-Jones potentials as discretized. Reliable results depend on extended prior equilibration. In static properties, chain statistics is non-Gaussian for all but the longest chains, evidenced by an anomalous non-Rouse scaling of Rg with M; at low M chain-end effects become important. But the autocorrelation functions of the end-to-end vectors still adhere to Rouse and reptation theories for chains longer than C82. Above C100 the relaxation times scale with M in keeping with reptation theory. Center-of-mass D, converted from Monte-Carlo steps to time units according to D measured at a single M, is in excellent agreement with experiment at all M. D of five n-alkanes in M=33k PE extrapolated to trace concentration conforms to the pure Rouse 1/M prediction in the absence of chain-end free-volume enhancements, in good agreement with current experiment.

*Supported in part by NSF DMR 0098321 and DMR 0455117

**12:03**

**Z24 5 Molecular dynamics studies of slow relaxation phenomena in glassy polymeric systems.** SANAT KUMAR, SERGEI SHENOGIN, *Rensselaer Polytechnic Institute* ARUN YETHIRAJ, *University of Wisconsin, Madison* JACK F. DOUGLAS, *Polymer Division, NIST, Gaithersburg, MD.* Molecular dynamics simulations were used to study long-time structural relaxations in glass-forming polymeric systems. The model system was composed of identical hard spherical beads linked into the chains by the bonds. The minimum length of each bond was limited to 1.05 of the bead diameter to prohibit crystallization at higher densities and create completely amorphous structures. The packing volume fraction ranges from 0.45 to 0.62, with glass transition at volume fraction around 0.565. It was shown that for glassy structures the distribution of mean-squared displacements deviates from Fickian form, showing the presence of ''mobile'' particles with caged (hop-like) mechanism of mobility. As the result, dynamic heterogeneity emerges in glassy structures with two distinct distributions of ''mobile'' and ''immobile'' particles relative to the Brownian motion. Structural relaxation, shear viscosity and their relationship to particle mobility was studied for systems with different densities. These results provide the evidence that the excessive mobility of ''hopping'' particles is the reason of breakdown of Stokes-Einstein relationship in glassy systems.

**12:15**

**Z24 6 On the determination of primitive paths in entangled polymer melts and networks** MICHAEL LANG, MICHAEL RUBINSTEIN, *Department of Chemistry, University of North Carolina at Chapel Hill, N.C.* The primitive path of a polymer chain in a melt or a network can be understood as the center line for the minima of a constraining potential, which describes the essence of the entanglement interactions of neighboring chains with a given polymer. Thus, the conformation of the primitive path plays a key role for the determination of tube parameters or the shape of the tube potential. In recent years, different methods and models for the determination of the primitive paths in entangled polymer melts and networks have been proposed leading to different results for the primitive path. In this contribution, the differences of these models as well as their assumptions on systems, calculations, or simulations will be compared and discussed in order to determine the optimal method for finding a primitive path.

**12:27**

**Z24 7 Properties of Well-Defined Elastomeric Poly(alkylnorbornene)s and Their Hydrogenated Derivatives** RICHARD REGISTER, JOHN HATJOPOULOS, JOHN BISHOP, *Princeton University* Narrow-distribution homopolymers of various 5-n-alkylnorbornenes were synthesized by living ring-opening metathesis polymerization (ROMP), and subsequently hydrogenated to yield materials with the good thermooxidative stability of polyolefins. The unsubstituted hydrogenated polynorbornene is highly crystalline, with Tm = 140-150C, but all the substituted norbornenes (before and after hydrogenation) are amorphous. Hydrogenation reduces the glass transition temperature (Tg) modestly; polymers with butyl or longer substituents have Tg below ambient due to internal plasticization by the alkyl sidechains (Tg = -40C for hydrogenated polydecylnorbornene). The fractional decrease in Tg with increasing sidechain length is in good quantitative agreement with that for polyolefins, polymethacrylates, and poly(alkylstyrene)s, when the sidechain length is normalized by the number of backbone carbons per mer. The rubbery plateau moduli

for these hydrogenated products are typical for elastomers, and tunable through the length of the alkyl sidechain; lengthening the sidechain from butyl to decyl increases the entanglement molecular weight by nearly a factor of three. These materials show promise as the midblocks in ROMP thermoplastic elastomers with crystalline endblocks. [work supported by NSF Polymers Program, DMR-0505940]

**12:39**

**Z24 8 The viscoelastic properties of ultrathin polymer films as measured with a novel nanobubble inflation technique** PAUL OCONNELL, GREGORY MCKENNA, *Texas Tech University* Using a novel microbubble inflation technique developed within our laboratory, we are able to measure the absolute biaxial compliance of polymer films as thin as 13 nm. Experiments performed on both poly(vinyl acetate) (PVAc) and polystyrene (PS) films show that large reductions in the glass transition temperature at the nano-scale are non-universal, viz., the PVAc shows no reduction even for the thinnest films while the PS shows a significant reduction at a thickness below approximately 80nm. More surprisingly, the rubbery plateau region for both materials shows dramatic stiffening as the thickness is reduced (by up to 300 times), perhaps due to surface pinning of the entanglement network. The compliance increases as approximately the square of film thickness until the bulk values are achieved at a thickness of the order of 300nm.

**12:51**

**Z24 9 Viscoelastic Properties of Metathesis Synthesized Linear and Cyclic Macromolecules** JIAN WANG, GREGORY MCKENNA, *Texas Tech University* IRINA GORODETSKAYA, ROBERT GRUBBS, *California Institute of Technology* A novel method of synthesis[1] now permits the creation of closed, uncatenated rings in relatively large amounts ( $>$ 1g). The metathesis synthesis route results in samples with relatively low polydispersities of $<$ 2. Here we report on a series of experiments on poly(octenamer) and polyethylene rings made by hydrogenating the poly(octenamer). The samples are being characterized for molecular weight, radius of gyration and intrinsic viscosity to assure their ring-like nature. Then, using conventional methods of rheometry, we are obtaining the dynamic moduli and zero shear rate (zero frequency) viscosities of the materials and comparing them to their linear analogues. Results for polymers having molecular weights between $1x10^5$ and $5x10^5$ g/mol, which is between 80 and 400 entanglements per chain assuming the linear entanglement molecular weight, will be discussed. Finally, in spite of the relatively low polydispersity of these samples, additional work is ongoing to fractionate them in order to obtain narrow fractions ($M_w/M_n < 1.1$) in order that the plateau modulus and the steady state rubbery plateau modulus can be obtained. Initial work suggests that $G_N^0$ for the rings and for the linear chains is similar.
[1] Bielawki, C. W.; Benitez, D; Grubbs, R. H.; itScience **2002**, 297, 2041.

**13:03**

**Z24 10 Observation of high viscous stress of oriented polyolefin under uniaxial tensile** QIANG FU, BING NA, HAO ZOU, KE WANG, QIN ZHANG, *Department of Polymer Science & Materials, Sichuan University, State Key Laboratory of Polymer Materials Engineering, Chengdu, 610065, China* CHARLES C. HAN, *PPCL, Joint Lab. of Polymer Science and Materials, Institute of Chemistry, Chinese Academy of Science, Beijing 100080, China* In this work, by means of stress relaxation experiments, the viscous stress at various strains during tensile deformation of oriented polyolefin samples, including high density polyethylene (HDPE), linear low density polyethylene (LLDPE) and isotactic polypropylene (iPP), has been determined. The viscous stress in the oriented samples takes up to 50 -70% of the total stress, which is unusually high, compared with their isotropic counterparts. More over, the enhanced modulus of oriented polyolefin was found not mainly caused by the existence of shish-kebab structure, but mainly come from the contribution of viscous stress. The result is new and provides deep understanding of the origin of high modulus for oriented polymers.

**13:15**

**Z24 11 Probing the breakdown of chain entanglement in simple shear: The effect of molecular weight distribution** POUYAN BOUKANY, SHI-QING WANG, *Department of Polymer Science, University of Akron* Our latest particle-tracking velocimetric (PTV) observations indicate [1] that a shear rate gradient develops across the gap in cone-plate shear cell when a fairly polydisperse entangled polymer solution is subjected to a velocity-controlled shear. The co-existence of a continuous spectrum of shear rates in the different layers is inconsistent with any theoretical description of shear banding (where only two values of shear rate would coexist). Could the smooth shear rate gradient be an artifact of the cone-plate shear cell? The present study applies the PTV measurements for a linearly-displaced shear cell that is free of any stress gradient. By examining a highly monodisperse sample and comparing its behavior with that of the polydisperse sample, we aim to explore the origin of the shear rate gradient and find out whether shear banding occurs in the monodisperse sample instead of a gradient of shear rate. [1] Tapadia, P.; Wang, S. Q. Phys. Rev. Lett., in press (2005).

**13:27**

**Z24 12 Short-Range Helical Ordering of Isotactic Vinyl Polymers in the Liquid State*** JOHN G. CURRO, *Sandia National Laboratories* A. HABENSCHUSS, *Oak Ridge National Laboratory* GUSTAVO A. CARRI, *The University of Akron* Wide-angle x-ray scattering measurements on various vinyl polymer melts show that the main amorphous peak (at $k\sim 1.5\ A^{-1}$) in the structure factor initially broadens, and then forms a ''pre-peak'' that shifts to lower k as the size of the pendant group increases. To investigate this behavior we performed self-consistent PRISM calculations on isotactic polypropylene and polystyrene liquids. Good qualitative agreement was seen for the theoretical structure factors with scattering data. Analysis of the torsional angle distribution shows a significant amount of short-range helical content in the iPP and iPS melts. At $450^oK$ the average number of consecutive trans/gauche pairs along the chain backbone was significantly higher than for a random distribution of torsional angles. The theory indicates that the location of the pre-peak is a measure of the helix-helix correlation distance or helix ''thickness.''

*SNL is operated by Sandia Corporation, a Lockheed Martin Company for the U.S. DOE under Contract No. DE-AC04094AL85000. ORNL is operated by UT-Battelle, LLC, for the U.S. DOE under Contract DE-AC05-00OR22725.

**13:39**

**Z24 13 Concurrent Physical Aging and Polymer Degradation during Weathering of Coatings*** STUART CROLL, DILHAN FERNANDO, *North Dakota State University* A polyester-urethane coating system was subjected to ''accelerated'' weathering cycles under UV light, elevated temperature and moisture (in a Q-Sun 1000 chamber). Cross-link density values obtained from high temperature modulus data demonstrated chain scission with increased exposure. However, increasing Tg and tensile modulus with weathering require an additional explanation to chemical degradation. Physical aging was explored to explain the behavior. Regular and modulated DSC analysis of the coating clearly shows increasing enthalpy recovery with increased weathering of the coating. Enthalpy recovery rate in degraded polymer films was much larger than in films that had only undergone the thermal component of exposure. An effort was also made to characterize the concurrent physical-chemical aging effects by tracking the changes in the non-linearity of the molecular relaxation times and the distribution of molecular relaxation times of the weathered coating. Understanding the physical relaxation properties of polymers subjected to accelerated weathering may help in resolving differences between natural weathering and accelerated weathering cycles, and also may be used to refine models for lifetime prediction of coatings.

*Research funded by the Air Force Office of Scientific Research, FA9599-04-1-0368

**13:51**

**Z24 14 Statics and Dynamics in model Dendrimer Melts*** KOSTAS KARATASOS, *Aristotle University of Thessaloniki, Thessaloniki, Greece* Molecular Dynamics simulations were employed in order to explore the static and dynamic response of model AB2 dendrimer melts of generations 3 to 6. This study was performed in a temperature range covering the states of enhanced mobility, as well as the states where a significant dynamic slowdown led to the freezing-in of the dendrimer motion. Particular emphasis was given to the investigation of the effects of the dendritic geometry and the dendrimer size to local polymer dynamics associated with the glass transition phenomena.

*Part of this Research is supported by the Greek General Secretariat for Research and Technology (PENED 2003 Program). A computer time grant under the HPC-EUROPA project (RII3-CT-2003-506079), is gratefully acknowledged

## SESSION Z25: MOLECULAR DYNAMICS: THEORY AND SIMULATION

**Friday Morning, 17 March 2006**
**322, Baltimore Convention Center at 11:15**
**Eric Cochran, Iowa State University, presiding**

**11:15**

**Z25 1 Application of a Semi-Grand Canonical Monte Carlo (SGMC) Method for the Simulation of Non-Equilibrium Systems** FREDERICK BERNARDIN, GREGORY RUTLEDGE, *Massachusetts Institute of Technology* The use of the SGMC as a generalized descriptive tool for interpreting experimental data obtained from non-equilibrium systems will be summarized. The usefulness of the method will be demonstrated specifically by interpreting the orientation distribution functions (odf's) of polymer melts which have been uniaxially oriented. Using SGMC, we identify the thermodynamic variables that serve as chemical potentials in a polydisperse system of orientations, and then generate the ensemble of configurations that minimizes the free energy subject to the constraints set by the odf. In this demonstration, the axial symmetry leads to the use of Legendre polynomials as the basis set for the odf. We apply our approach to obtain molecular ensembles corresponding to different values of $P_2$ (the first non-zero Legendre term), which are obtainable through measurements by light scattering or birefringence. Comparisons will be made to a related method by Mavrantzas and Theodorou (Macromolecules, 31, 6310 1998).

**11:27**

**Z25 2 Multiscale modeling of polystyrene dynamics in different environments** ROLAND FALLER, QI SUN, FLORENCE PON, *UC Davis* Polystyrene is a very abundant and industrially important polymer. We are modeling its dynamical behavior on multiple length scales and different environments. We start with pure PS where we develop a mesoscale polystyrene model based on atomistic simulations. The non-bonded effective potential is optimized against the atomistic simulation until the radial distribution function generated from the mesoscale model is consistent with the atomistic simulation. The mesoscale model allows understanding the polymer dynamics of long chains in reasonable computer time. The dynamics of polystyrene melts are investigated at various chain lengths ranging from 15 to 240 monomers and the crossover to entangled dynamics is observed. As computer simulations cannot only address average properties of the system under study but also the distribution over any observable of interest we are study mixtures of polystyrene and polyisoprene by atomistic molecular dynamics and calculate correlation times for all segments in the system. We then identify fast and slow segments and can correlate the segment speed with the local neighborhood and obtain that fast segments have a surplus of the faster component in their neighborhood and vice versa. A coarse grained mixture model will be presented as well.

**11:39**

**Z25 3 Polymer dynamics within a harmonic confinement potential** JEREMY SCHMIT, JOSHUA MARTIN, BULBUL CHAKRABORTY, JANÉ KONDEV, *Brandeis University* We study the effects of confinement on the Rouse dynamics of polymers inspired by the question of chromosome confinement in the nucleus. We propose a simple model of a polymer diffusing within a three-dimensional harmonic potential. Within this model, the Rouse modes relax as independent particles within the harmonic potential so that the inverse relaxation times increase linearly with the confinement strength. This linear regime is also seen in simulations of phantom chains trapped within a hollow sphere. We also address the effect of self-avoidance using a self-consistent variational approximation to the propagator and compare the results to simulation.

**11:51**

**Z25 4 Monte Carlo simulations of polymer translocation through a nanopore*** TAPIO ALA-NISSILA, KAIFU LUO, ILKKA HUOPANIEMI, *Laboratory of Physics, Helsinki University of Technology, P.O. Box 1100, FIN-02015 HUT, Espoo, Finland* SEE-CHEN YING, *Department of Physics, Box 1843, Brown University, Providence, RI 02912-1843, U.S.A.* HELSINKI UNIVERSITY OF TECHNOLOGY TEAM, BROWN UNIVERSITY COLLABORATION, We investigate the problem of polymer translocation through a nanopore using the fluctuating bond model with single-segment Monte Carlo moves. For non-driven case we study the escape time $\tau_e$ required for a polymer, which is initially placed in the middle of the pore, to completely exit the pore on either end. We find $\tau_e \sim N^{1+2\nu}$, where $N$ is the chain length and $\nu$ is the Flory exponent. We also examine the interplay between the pore length $L$ and the radius of gyration $R_g$. For driven case we find a crossover scaling for the translocation time $\tau$ with $N$ from $\tau \sim N^{2\nu}$ for relatively short polymers to $\tau \sim N^{1+\nu}$ for longer chains. This crossover is due to the change of the translocation velocity v from $v \sim N^{-\nu}$ for relatively short chains to $v \sim N^{-1}$ for long polymers. The reason is that a high density of segments near the exit of the pore for long polymer slows down the translocation process due to slow relaxation of the chain.

*This work has been supported in part by a Center of Excellence grant from the Academy of Finland.

**12:03**

**Z25 5 Calculating probability distributions for knot sizes and locations** PETER VIRNAU, *MIT* YACOV KANTOR, *Tel Aviv University* MEHRAN KARDAR, *MIT* We generate three dimensional random walks and loops with Monte Carlo simulations, and analyze them using various operational definitions of knot sizes and locations. We find that the size of a knot follows a power-law distribution with an exponent of approximately -1.5. As a consequence, knots in open chains are on the average larger when they are located close to the center.

**12:15**

**Z25 6 The Role of Quenched Randomness in the Stereochemical Sequences of Atactic Vinyl Polymers** NUMAN WAHEED, WAYNE L. MATTICE, *Institute of Polymer Science, University of Akron* The influence of quenched randomness on the mean square unperturbed end-to-end distance, $\langle r^2 \rangle_0$, is assessed in polystyrene, using a rotational isomeric state (RIS) model based on virtual bonds between the centers of mass of the $C_6$ rings. This coarse-grained model is derived from a conventional RIS model expressed in terms of the C-C bonds in the main chain and contains bond lengths, angles, and torsions determined by the stereochemistry and conformations of the underlying tetrad. The zeroth approximation virtual bond model, which retains only the most probable conformation(s) of the six stereochemically unique tetrads, correctly finds $\langle r^2 \rangle_0 \sim n$ in the limit as $n \to \infty$ if the probability for a itmeso diad, $p_m$, is $0 < p_m < 1$, although the same zeroth approximation model yields $\langle r^2 \rangle_0 \sim n^2$ if $p_m$ is either 0 or 1. The values of $\langle r^2 \rangle_0$ at intermediate $p_m$ are surprisingly close to those obtained from a full, C-C bond based RIS model. This achievement of the zeroth approximation model demonstrates the important role of quenched randomness in determining the unperturbed dimensions of atactic chains. Excellent agreement with the $\langle r^2 \rangle_0$ from the full RIS model over the entire range of stereochemical composition, $0 \leqslant p_m \leqslant 1$, can be achieved in a first-approximation virtual bond model, which includes the next most probable conformations at each tetrad and refines slightly some of the conformations by minor adjustments in soft degrees of freedom.

**12:27**

**Z25 7 Effects of Confinement on Tethered Chains** JOHN MCCOY, TITUS ISPIRESCU, *New Mexico Tech* JOHN CURRO, *Sandia National Laboratories* Density Functional Theory (DFT) is used to analyze tethered Bead-Spring Chains. Previous work has demonstrated the ability of DFT to accurately predict both the density profiles of and colloidal force generated by such chains as compared to the results of computer simulation. In addition, the chains are found to display a collapse transition as a function of either surface coverage or temperature. In the current work, we explore the additional effect of confinement on the collapse transition, and the ability of simple scaling models to describe the behavior.

**12:39**

**Z25 8 Mixtures of Monomer and Dimer Square-well Fluids** JAMES PORTER, JANE LIPSON, *Dartmouth College* In previous work, we have used the continuum version of Born-Green-Yvon (BGY) theory, in conjunction with the square-well potential, to model structural and thermodynamic properties of alkanes and, in the case of one-component fluids, have also suggested mappings between the continuum and lattice versions of the theory. Having applied the lattice description to numerous mixtures, we are now interested in determining whether an analogous mapping is possible between the lattice and continuum descriptions when both are used to study mixtures. Towards this end, we present in this talk the first continuum BGY results for monomer/dimer square-well fluid mixtures. Thermodynamic and structural properties are compared with available simulation data, and the effect of changing both monomer diameters and square-well interaction strengths is examined.

**12:51**

**Z25 9 Field-Theoretic Models for Supramolecular Polymers** EDWARD FENG, *Miller Institute, UC Berkeley* WON BO LEE, *UC Santa Barbara* GLENN FREDRICKSON, *UC Santa Barbara* Supramolecular polymer systems consist of polymers with bonding groups that can form reversible inter-polymer linkages. These materials have great technological potential since one can use temperature to tune the material properties such as viscosity. Moreover, new methods in synthesizing bonding groups point the way to making supramolecular polymer systems that self-assemble into inhomogeneous phases. To understand these materials, we develop a field-theoretic model for a system in which an A and B homopolymer can reversibly bond to form a diblock copolymer. An energy of bonding governs the strength of this reversible bond. Using computational methods, we calculate a mean-field phase diagram for the symmetric case in which the A and B parts of the system consist of polymers of the same length and occupy the same volume. At low temperatures, we find either a lamellar phase or macrophase separation depending on the strength of the bonding reaction. We are collaborating with experimental groups interested in synthesizing and characterizing these systems.

**13:03**

**Z25 10 Hybrid Two-Chain Simulation and Integral Equation Theory: Application to Polyethylene Liquids** HUIMIN LI, *Dept. of Chemical Engr., Colorado School of Mines, Golden, CO 80401* DAVID T. WU, *Dept. of Chemical Engr. and Chemistry, Colorado School of Mines, Golden, CO 80401* JOHN G. CURRO, *Sandia National Laboratories, Albuquerque, NM 87185* JOHN D. McCOY, *Dept. of Materials Engr., New Mexico Technology, Socorro, NM 87801* We present results from a hybrid simulation and integral equation approach to the calculation of polymer melt properties. The simulation consists of explicit Monte Carlo (MC) sampling of two polymer molecules, where the effect of the surrounding chains is accounted for by an HNC solvation potential. The solvation potential is determined from the Polymer Reference Interaction Site Model (PRISM) as a functional of the pair correlation function from simulation. This hybrid two-chain MC-PRISM approach was carried out on liquids of polyethylene chains of 24 and 66 $CH_2$ units. The results are compared with MD simulation and self-consistent PRISM-PY theory under the same conditions, revealing that the two-chain calculation is close to MD, and able to overcome the defects of the PRISM-PY closure and predict more accurate structures of the liquid at both short and long range. The direct correlation function, for instance, has a tail at longer range which is consistent with MD simulation and avoids the short-range assumptions in PRISM-PY theory. As a result, the self-consistent two-chain MC-PRISM calculation predicts an isothermal compressibility closer to the MD results.

**13:15**

**Z25 11 Phase coherence in LDOT diblock copolymer films** KWANWOO SHIN, *Gwangju Institute of Science and Technology* JUNHAN CHO, *Dankook University* KWANGSOO CHO, *Kyungpook National University* JI HYUK KIM, *Gwangju Institute of Science and Technology* SUSHIL K. SATIJA, *National Institute of Standards and Technology* DU YEOL RYU, *Yonsei University* JIN KON KIM, *Pohang University of Science and Technology* Theoretical and experimental studies of the thin films of LDOT (lower disorder-order transition) diblock copolymers have been studied. The recently developed compressible Landau analysis has been applied to the copolymer films to interpret phase-coherent decaying profiles and other thermodynamic aspects of the LDOT films. Specific interactions and finite compressibility were considered in a unified way in this compressible Landau approach. The linearized and then nonlinear solutions of the minimized free energy functional under proper constraints were discussed. The neutron reflectivity and the surface topography measurements on the copolymer films were reported here to compare them with the theoretical analysis.

**13:27**

**Z25 12 Relation between cyclization of polymers with different initial conditions** CHUCK YEUNG, *School of Science, Penn State Erie, Erie, PA* BARRY FRIEDMAN, *Dept. of Physics, Sam Houston State Univ, Huntsville, TX* We study cyclization of polymer chains in which the reactive ends of the chains are initially in close proximity (ring initial conditions). We find a surprising general relation between cyclization with ring and equilibrium initial conditions, namely that $\Phi_{ring}(t) \propto d\Phi/dt_{eq}$ where $\Phi(t)$ is the survival fraction. We show that this proportionality is exact for a special type of non-generic ring initial conditions and use an approximate argument to motivate the proportionality for more general ring initial condition. Our analytic results are confirmed by Langevin simulations of Gaussian chains. Earlier work for very long Rouse chains with equilibrium initial conditions show that $d\Phi/dt_{eq} \sim t^{-1/4}$ for times less than the longest polymer relaxation time. Therefore our relation shows that $d\Phi/dt_{ring} \sim t^{-5/4}$ for a ring initial distribution under the same conditions.

## SESSION Z26: RADIATION THERAPY AND MEDICAL IMAGING TECHNIQUES

**Friday Morning, 17 March 2006**
**323, Baltimore Convention Center at 11:15**
**Paul Gueye, Hampton University, presiding**

**11:15**

**Z26 1 Monte Carlo study of interseed attenuation and tissue composition effect for clinical cases of prostate permanent implants.** JEAN-FRANCOIS CARRIER, *Hopital Notre-Dame du CHUM* LUC BEAULIEU, *CHUQ, Pavillon Hotel-Dieu de Quebec* Monte Carlo simulations were used to study the interseed attenuation and the effect of tissue composition on prostate implant dosimetry. Using computed tomography images of postimplant analysis, the precise anatomy of the patient was considered voxel by voxel. The physical density of each voxel was set according to the Hounsfield Unit and the specific elemental composition of each voxel was set depending on the radiation-oncologist organ contours and the local density. Mixes of different tissues were available: muscle, prostate tissue, rectum tissue, adipose tissue, bone and prostate calcification. Typically, more than 300 combinations of elemental composition and density were used for each patient. The Monte Carlo dosimetry results were compared to the clinically approved TG43-based calculations for 30 patients. The results show an interseed attenuation of about 4.5% for the $D_{90}$parameter (minimal dose received by 90% of the target volume). The effect of the tissue composition varies from one patient to the other. Globally, the difference between the TG43-based calculations and the Monte Carlo results can reach more than 10 Gy for the $D_{90}$ values. From a clinical perspective, the difference level can be non-negligible for the target volume and for the surrounding organs at risk.

**11:27**

**Z26 2 Effects Of The Inhomogeneity of Brachytherapy Sources In Cancer Treatments** NNENNA ONUMAH, *Hampton University* FOR CAMI COLLABORATION, Uniformity of radioactive sources is vital in delivering accurate doses in Brachytherapy. The International Atomic Energy Agency (IAEA) defines source uniformity as no more than a 20 % deviation from the average value of the dose along a transverse region. Brachytherapy induced cell damages occur at the microdosimetric levels, and as such, small deviations in dose delivered from different geometrical positions on the source can lead to huge deviations in proper treatment. A Geant4 simulation of a uniform source and a non-uniform source was simulated to check the validity of IAEA's proposed definition. A realistic source of non-uniformity, air bubbles of differing diameters (from 20 to 80 microns) were simulated and their uniformity checked against the model suggested by IAEA in two ways: (1) using the average obtained from the non-

uniform source (2) using that obtained from the uniform source. Significant deviations of up to 50% were observed. These results validate the need for the scintillating fiber based detector currently in development within our research group.

**11:39**

**Z26 3 Absolute Dose Distribution Measurements Of Beta Sources Using A Scintillating Fiber Based Detector** LAWRENCE TYNES, *Hampton University* FOR CAMI COLLABORATION, Brachytherapy using catheter based high dose rate $\beta$ sources has taken nowadays an important role in out-patient cancer treatments. At the present time, there is no detector system which can record accurate quantitative doses and spatial information for Brachytherapy sources. This is partly because of the short-range of the low energy beta emission of these sources (having typically an average energy of a few hundreds of keV), and the resolution limitation of existing extrapolation chambers and radiochromatic-dye films (currently the preferred method used). For the latter, transfer of data from one method to the other can lead to a loss of accuracy as high as 7%, well beyond the required 2% limits of current protocols. We have developed a scintillating fiber based beta detector prototype which will provide solution to this problem. It is composed of an array of 0.5 $mm^2$ and 1 $mm^2$ fibers optically coupled to photo-multiplier tubes for photon-to-current conversion. Preliminary results from high dose rate $^{90}Sr/^{90}Y$ and $^{32}Ru$ sources comparing film dosimetry, well chambers, and our scintillating fiber based detector will be presented.

**11:51**

**Z26 4 An Active Mammosite For Breast Brachytherapy** THOMAS CUDJOE, *Hampton University* FOR CAMI COLLABORATION, Brachytherapy is an advanced cancer treatment that uses radioactive sources inside or in close proximity to cancerous tumors, thus minimizing exposure to neighboring healthy cells. This radiation oncology treatment unlike many others is localized and precise. The latest involvement of the Brachytherapy research group of the medical physics program at Hampton University is in the development of a scintillator fiber based detector for the breast cancer specific Mammosite (balloon device) from Cytyc Inc. Radioactive sources are inserted into a small plastic catheter (shaft) and pushed at the end of the tube. At that location, a water filled balloon surrounds the source and allow uniform gamma emission into cancer tumors. There is presently no capability for this device to provide measurements of the location of the source, as well as the radiation emitted from the source. Recent data were acquired to evaluate the possibility of measuring the dose distribution during breast Brachytherapy cancer treatments with this device. A high activity $^{192}Ir$ radioactive source and a 0.5 and 1 $mm^2$ scintillating fibers were used. Results will be presented and discussed.

**12:03**

**Z26 5 Calibration Of An Active Mammosite Using A Low Activity Sr-90 Radioactive Source** JACQUELYN WINSTON, *Morgan State University* FOR CAMI COLLABORATION, The latest involvement of the Brachytherapy research group of the medical physics program at Hampton University is in the development of a scintillator fiber based detector for the breast cancer specific Mammosite (balloon device) from Cytyc Inc. Recent data were acquired at a local hospital to evaluate the possibility of measuring the dose distribution during breast Brachytherapy cancer treatments with this device. Since sub-millimeter accuracy in position is required, precision of the device relies on the accurate calibration of the scintillating fiber element. As part of a collaboration work, data were acquired for that purpose at Hampton University and subsequently analyzed at Morgan State University. An 8 mm diameter strontium-90 radioactive field source with a low activity of 25 $\mu$Ci was used along with a dedicated LabView data acquisition system. We will discuss the data collected and address some of the features of this novel system.

**12:15**

**Z26 6 Modelization For Electromagnetic Electron Scattering at Low Energies for Radiotherapy applications.*** VAHAGN NAZARYAN, *Hampton University, The College of William and Mary* PAUL GUEYE, *Hampton University* Since release of the GEANT4 particle simulation toolkit in 2003, there has been a growing interest in its applications to medical physics. The applicability of GEANT4 to radiotherapy has been a subject of several investigations in recent years, and it was found to be of great use. Its low-energy model allows for electromagnetic interaction simulations down to 250 eV. The electron physics data are obtained from the Lawrence Livermore National Laboratory's Evaluated Electron Data Library (EEDL). At very lower energies (below 10 MeV), some of the tabulated data in EEDL have big uncertainties (more than 50%), and rely on various extrapolations to energy regions where there is no experimental data. We have investigated the variations of these cross-section data to radiotherapy applications. Our study suggests a strong need for better theoretical models of electron interactions with matter at these energies, and the necessity of new and more reliable experimental data. The progress towards such theoretical model will be presented.

*This work was supported by the NSF under grant PHY-0400332

**12:27**

**Z26 7 Fully Complex Magnetoencephalography*** JONATHAN SIMON, YADONG WANG, *University of Maryland* Complex numbers appear naturally in biology whenever a system can be analyzed in the frequency domain, such as physiological data from magnetoencephalography (MEG). For example, the MEG steady state response to a modulated auditory stimulus generates a complex magnetic field measurement at each MEG channel, equal to the response's Fourier transform at the stimulus modulation frequency. The complex nature of these data sets, often not taken advantage of, is fully exploited here with new methods. Whole-head, complex magnetic data can be used to estimate complex neural current sources, and standard methods of source estimation naturally generalize for complex sources. We show that a general complex neural vector source, e.g. a current dipole, is described by its location, magnitude, and direction, but also by a phase and by an additional two-dimensional perpendicular component. We give natural interpretations of all the parameters for the complex equivalent-current dipole by linking them to the underlying neurophysiology. We demonstrate biologically generated complex magnetic fields, and their equivalent fully complex current sources, with both simulations and experimental data.

*Y.W. is supported by NIH R01 DC05660

**12:39**

**Z26 8 Multi-Active Catheters For Real Time Dose Distribution Measurements In Prostate Brachytherapy Treatments** CARLOS VELASCO, *Hampton University* FOR CAMI COLLABORATION, We have performed real time 3D dose distribution measurements of high dose rate brachytherapy sources. These data demonstrate the possibility of in-vivo dosimetry monitoring of the dose rate while treating patients with particle radiation therapy. The prototype used for these experiments is made out of 16 scintillating fibers, 30 cm long and with a 1 $mm^2$ transverse cross section. Each fiber was coupled to a 16 channel Hamamatsu photo-multiplier tube for photon to current conversion. Millimeter accuracy in position was attained with sub-seconds timing scale. No correction was done from Cherenkov radiation background. The (over)estimated systematic uncertainty is 10% and includes electronic and computer dead times, channel-to-channel efficiency, and signal attenuation. We will discuss the impact of such device to clinical prostate cancer treatments and treatment planning softwares.

**12:51**

**Z26 9 Speckle Patterns in Coherence Domain Biomedical Imaging** PING YU, *Department of Physics and Astronomy, University of Missouri-Columbia* We have shown previously that coherence domain biomedical imaging can be used for optically sectioning small tumors such as rat osteogenic sarcoma (bone tumors). Speckle patterns of such small tumors provided quantitative measures of the health, necrotic, and poisoned tissues. However, the origins of these speckle patterns are not clear. Although the nuclei, mitochondria and other organelles inside cells are responsible for the speckle under the illumination of low coherence light source, these patterns at the imaging plane are related to the photon pathways both inside and outside the tissue. We report systematic experiments and simulation of the speckle patterns from coherence domain imaging of small tumors. The image frames are acquired at different depths inside the tumor tissue and analyzed by using a turbid medium model. The results reveal that the speckle patterns are dominated by the scattering properties of the tissue, which is characterized by the mean free path of the photons, and the collection geometry of the backscattered light photons. This work was supported by a University of Missouri Research Board grant URB-04-072 and NIH grant P50-CA-103130.

**13:03**

**Z26 10 Clinical implementation of proton Monte Carlo dose calculation.*** HARALD PAGANETTI, *Massachusetts General Hospital* HONGYU JIANG, SHASHIDHAR KOLLIPARA, HANNE KOOY, Goal was the clinical implementation of Monte Carlo dose calculation for use in parallel to a commercial planning system. Treatment heads were modeled in detail. To describe the patient anatomy, Hounsfield Units were converted into materials with explicit element composition and density. We developed a method to dynamically assign the mass density to the materials during particle transport. Memory for CT voxels is assigned dynamically. A software link was created between the commercial planning system, the treatment machine control system and the Monte Carlo program. The prescribed range and modulation are automatically translated into the corresponding settings of the treatment head. For broad beam modulation treatment, the Monte Carlo code simulates apertures and compensators based on the milling machine files. Treatment information, like prescribed dose per field, size of the air gap, couch angle and gantry angle, is read from the departmental patient database. For absolute dosimetry, the dose delivered to the patient per monitor unit is calculated based on the simulation of the reading of a segmented transmission ionization chamber. Dose calculations are done on the CT grid resolution and have been performed for various treatment sites. Monte Carlo results can be imported into the planning system.

*Work supported by NIH PO1 CA 21239

**13:15**

**Z26 11 A Universal Scaling of Proton Energy Deposition in Biological Materials*** DAN FRY, WILFRED SEWCHAND, JOHN O'CONNELL, *Walter Reed Army Medical Center, Radiation Oncology, Washington, DC 20307* We have used GEANT 4.7.0 to simulate the dosimetric properties of various materials. Bragg curves for monoenergetic pencil beams with incident energies ranging from 70 MeV to 250 MeV have been characterized by the width (90%-10%) of distal and lateral edges, peak-to- entrance dose ratio, and FWHM. In all materials ionization by primary protons is the dominant energy loss channel. Energy loss by electrons and secondary protons is approximately an order of magnitude lower and dose from all other secondary particles is three orders of magnitude lower. We have found that a single scaling factor (material density) is most inadequate for fully defining the characteristics of the percent depth- dose distribution. However, the distal and lateral edge widths and FWHM can be universally scaled by scaling the proton beam energy by a material dependent factor. In addition, when the peak-to- entrance dose ratio is scaled by the stopping power ratio $S_w$ relative to water, energy deposition properties of all materials appear to behave alike. Our results suggest that knowledge of the incident proton energy and effective $Z$ of the target are sufficient to fully predict the depth-dose distribution irrespective of material type.

*This work was supported by the US Army Medical Research and Materiel Command under Contract Agreement No. DAMD 17-W81XWH-04-2-0022. Opinions and conclusions are those of the authors.

**13:27**

**Z26 12 Feasibility Study Of Kaon Therapy** SOLOMON SAHLE, *Hampton University* FOR CAMI COLLABORATION, Proton therapy is a new emerging radiation modality that supersedes electron machines for cancer treatments. The strength of these beams lies in their Bragg peak distribution that allows sparing healthy tissues while depositing the majority of the dose at the (targeted) tumor location. Although promising, there are still unresolved issues with this technique due to the impossibility of viewing the beam within a patient and the production of low energy neutrons at the end of the distribution. Simulation studies on the use of kaon beams were made using the Geant4 toolkit. The strangeness content of these particles permits to extract the spatial beam information in-vivo, as well as providing a similar Bragg distribution as protons. We will discuss the impact of such beams for hadron therapy in cancer treatments.

**13:39**

**Z26 13 Low Energy Experimental Elastic Cross Sections for Medical Physics Application** MICHAEL EPPS, *Hampton University* FOR CAMI COLLABORATION, Elastic cross sections for electron energies below 10 MeV are fundamental quantities needed in treatment planning systems used at hospitals and health facilities. To date, there is very little if not no data within that energy regime. In collaboration with the high current, high energy resolution continuous electron beam of the Department of Energy's Jefferson Lab accelerator, we have performed a first stage of dedicated experiments with energies of 100-150 keV to collect data for this type of reactions. The targets used were gold, copper and silver. A Mott scattering chamber was used to detect the outgoing electrons. We will present the first results of this program that aims at performing a wide range of measurements including the use of polarization data for spin studies.

**13:51**

**Z26 14 Wavelet assessment of cerebrospinal compensatory reserve and cerebrovascular pressure reactivity** M. LATKA, M. TURALSKA, *Wroclaw University of Technology* W. KOLODZIEJ, D. LATKA, *Opole Regional Medical Center* B. WEST, *Army Research Office* We employ complex continuous wavelet transforms to develop a consistent mathematical framework capable of quantifying both cerebrospinal compensatory reserve and cerebrovascular pressure–reactivity. The wavelet gain, defined as the frequency dependent ratio of time averaged wavelet coefficients of intracranial (ICP) and arterial blood pressure (ABP) fluctuations, characterizes the dampening of spontaneous arterial blood oscillations. This gain is introduced as a novel measure of cerebrospinal compensatory reserve. For a group of 10 patients who died as a result of head trauma (Glasgow Outcome Scale GOS =1) the average gain is 0.45 calculated at 0.05 Hz significantly exceeds that of 16 patients with favorable outcome (GOS=2): with gain of 0.24 with $p = 4 \times 10^{-5}$. We also study the dynamics of instantaneous phase difference between the fluctuations of the ABP and ICP time series. The time-averaged synchronization index, which depends upon frequency, yields the information about the stability of the phase difference and is used as a cerebrovascular pressure–reactivity index. The average phase difference for GOS=1 is close to zero in sharp contrast to the mean value of $30^o$ for patients with GOS=2. We hypothesize that in patients who died the impairment of cerebral autoregulation is followed by the break down of residual pressure reactivity.

**14:03**

**Z26 15 Convolution Product And Lyapunov Stability In Medical Imaging** LESLIE UPTON, *Hampton University* FOR CAMI COLLABORATION, Resolution is one of the most important aspects of any apparatus used in medical imaging. Several mathematical algorithms have been developed to best extract anatomical features and tumors within patients suffering from cancer diseases. Distortions of images are a result of blood flow, breathing, apparatus efficiency etc. This problem is also inherent to other disciplines in physics, like nuclear physics. Here, study of the electromagnetic nuclear structure relies in the extraction of the form factors from the nuclear medium (nucleus or nucleons). Data collected depend on a number of different variables. A new approach which consists of using the mathematical convolution product combined with the (entropy equivalent) Lyapunov stability was tested in this area of physics, since easier to implement. A deconvolution technique allowed isolating the individual dependencies of the differential cross section and extracting meson form factors of interest (pion and kaon). Preliminary results will be presented, as well as a discussion on the application of this technique to medical imaging.

## SESSION Z28: METHODS OF STATISTICAL PHYSICS, POPULATION DYNAMICS AND EPIDEMIOLOGY

**Friday Morning, 17 March 2006**
**325, Baltimore Convention Center at 11:15**
**Michelle Johannes, Naval Research Laboratory, presiding**

***Contributed Papers***

**11:15**

**Z28 1 Mathematical Modeling of the Dynamics of Salmonella Cerro Infection in a US Dairy Herd** PREM CHAPAGAIN, *Department of Population Medicine and Diagnostic Sciences, Cornell University, Ithaca, NY 14853, USA* JO ANN VAN KESSEL, JEFFREY KARNS, *Environmental Microbial Safety Laboratory, Agricultural Research Service, USDA, Beltsville, MD 20705, USA* DAVID WOLFGANG, *Animal Diagnostic Laboratory, Pennsylvania State University, PA 16802, USA* YNTE SCHUKKEN, YRJO GROHN, *Department of Population Medicine and Diagnostic Sciences, Cornell University, Ithaca, NY 14853, USA* Salmonellosis has been one of the major causes of human foodborne illness in the US. The high prevalence of infections makes transmission dynamics of Salmonella in a farm environment of interest both from animal and human health perspectives. Mathematical modeling approaches are increasingly being applied to understand the dynamics of various infectious diseases in dairy herds. Here, we describe the transmission dynamics of Salmonella infection in a dairy herd with a set of non-linear differential equations. Although the infection dynamics of different serotypes of Salmonella in cattle are likely to be different, we find that a relatively simple SIR-type model can describe the observed dynamics of the Salmonella enterica serotype Cerro infection in the herd.

**11:27**

**Z28 2 Desynchronization and spatial effects in multistrain diseases** LEAH SHAW, *Naval Research Lab* LORA BILLINGS, *Montclair University* IRA SCHWARTZ, *Naval Research Lab* Dengue fever, a multistrain disease, has four distinct co- existing serotypes (strains). The serotypes interact by antibody- dependent enhancement (ADE), in which infection with a single serotype is asymptomatic, but contact with a second serotype leads to serious illness accompanied by greater infectivity. We present a compartmental model for multiple serotypes with ADE, and consider autonomous, seasonally driven, and stochastic versions of the model. Spatial effects are included in a multipatch model. We observe desynchronization between outbreaks of the different serotypes, as well as desynchronization between spatially distinct regions.

**11:39**

**Z28 3 Improved Epidemic Path Predictability in Complex Networks*** MARKUS LOECHER, *APS* JIM KADTKE, *NSI* We apply recent results on random walkers to the analysis of idealized epidemic outbreaks in scale-free networks. By replacing the node degree with the *random walk centrality* we observe a refined hierarchical cascade leading to a greatly enhanced predictability for the order of infected nodes. We confirm our model results on data from real-world Internet maps at the autonomous system level. The present results are highly relevant for the advancement of dynamic and adaptive strategies that aim to mitigate network attacks.

*This work was supported by ARDA under Air Force Research Laboratory Contract No. F30602-03-C-0234.

***Invited Papers***

**11:51**

**Z28 4 The scaling laws of human travel—A message from George.**
DIRK BROCKMANN, *Max Planck Institute for Dynamics and Self-Organization*

In the light of increasing international trade, intensified human mobility and an imminent influenza A epidemic the knowledge of dynamical and statistical properties of human travel is of fundamental importance. Despite its crucial role, a quantitative assessment of these properties on geographical scales remains elusive and the assumption that humans disperse diffusively still prevails in models. I will report on a solid and quantitative assessment of human travelling statistics by analysing the circulation of bank notes in the United States. Based on a comprehensive dataset of over a million individual displacements we find that dispersal is anomalous in two ways. First, the distribution of travelling distances decays as a power law, indicating that trajectories of bank notes are reminiscent of scale free random walks known as Lévy flights. Secondly, the probability of remaining in a small, spatially confined region for a time $T$ is dominated by algebraic tails which attenuate the superdiffusive spread. We show that human travel can be described mathematically on many spatiotemporal scales by a two parameter continuous time random walk model to a surprising accuracy and conclude that human travel on geographical scales is an ambivalent effectively superdiffusive process.

***Contributed Papers***

**12:27**

**Z28 5 Prediction and predictability of global epidemics: the role of the airline transportation network** VITTORIA COLIZZA, *School of Informatics and Center for Biocomplexity - Indiana University, Bloomington IN, USA* ALAIN BARRAT, *Unite' Mixte de Recherche (UMR 8627) du CNRS, Universite' de Paris-Sud. ORSAY* MARC BARTHELEMY, ALESSANDRO VESPIGNANI, *School of Informatics and Center for Biocomplexity - Indiana University, Bloomington IN, USA* The systematic study of large-scale networks has unveiled the ubiquitous presence of connectivity patterns characterized by large scale heterogeneities and unbounded statistical fluctuations. These features affect dramatically the behavior of the diffusion processes occurring on networks, determining the ensuing statistical properties of their evolution pattern and dynamics. We present a stochastic computational framework for the forecast of global epidemics that considers the complete world-wide air travel infrastructure complemented with census population data. We address two basic issues in global epidemic modeling: i) We study the role of the large scale properties of the airline transportation network in determining the global diffusion pattern of emerging diseases; ii) We evaluate the reliability of forecasts and outbreak scenarios with respect to the intrinsic stochasticity of disease transmission and traffic flows. In order to address these issues we define a set of novel quantitative measures able to characterize the level of heterogeneity and predictability of the epidemic pattern. These measures may be used for the analysis of containment policies and epidemic risk assessment.

**12:39**

**Z28 6 Success of mutants in an evolutionary game in finite populations** TIBOR ANTAL, *Boston University* ISTVAN SCHEURING, *Eotvos University, Budapest, Hungary* A stochastic evolutionary dynamics of two strategies given by $2 \times 2$ matrix games is studied in finite populations. We focus on stochastic properties of fixation: how a strategy represented by a single individual wins over the entire population. The process is discussed in the framework of a random walk with site dependent hopping rates. The time of fixation is found to be identical for both strategies in any particular game. The asymptotic behavior of the fixation time and fixation probabilities in the large population size limit is also discussed. We show that fixation is fast when there is at least one pure evolutionary stable strategy (ESS) in the infinite population size limit, while fixation is slow when the ESS is the coexistence of the two strategies.

**12:51**

**Z28 7 Invasion of mutants in an evolutionary process on a graph.** VISHAL SOOD, TIBOR ANTAL, We study the Moran process (MP) on an undirected graph. The MP has been studied on the complete graph and lattices extensively. Remarkably the fixation probability of the mutants is the same for all undirected degree-regular graphs. However, this is not true for degree-heterogeneous graphs. Some graphs can enhance the fixation probabilities over the degree-regular graphs. We derive fixation probabilities for general graphs when the mutants have a small advantage over the resident population. For the general bias case, we derive exact results for the bipartite graphs and discuss the structure of graphs where such a result can be applicable.

**13:03**

**Z28 8 Seeing beyond invisible with noise: application to populational biology** DMITRY LUCHINSKY, *Mission Critical Technologies, Inc* VADIM SMELYANSKIY, *NASA Ames Research Center* The problem of determining dynamical models and trajectories that describe observed timeseries data (dynamical inference) allowing for the understanding, prediction and possibly control of complex systems in nature is of great interest in a variety of fields. Often, however, in multidimensional systems only part of the systems dynamical variables can be measured directly. The measure-

ments are usually corrupted by noise and the dynamics is complicated by interplay of nonlinearity and random perturbations. We solve the problem of dynamical inference in these general settings by applying a path-integral approach to fuctuational dynamics, and show that, given the measurements, the most probable system trajectory can be obtained from the solution of the certain auxiliary Hamiltonian problem in which measured data act effectively as a control force driving algorithm towards the most probable solution. We illustrate the efficiency of the approach by solving an intensively studied problem from the population dynamics of a predator-prey system where the prey populations may be observed while the number of predators is difficult or impossible to estimate. We apply our approach to recover both the unknown dynamics of predators and model parameters (including parameters that are traditionally very difficult to estimate) directly from real data measurements of the prey dynamics.

**13:15**

**Z28 9 Eigen model with general fitness functions and degradation rates*** CHIN-KUN HU, *Institute of Physics, Academia Sinica, Taipei* DAVID B. SAAKIAN, *Academia Sinica, Taipei and Yerevan Physics Institute, Armenia* We present an exact solution of Eigen's quasispecies model with a general degradation rate and fitness functions, including a square root decrease of fitness with increasing Hamming distance from the wild type. The found behavior of the model with a degradation rate is analogous to a viral quasi-species under attack by the immune system of the host. Our exact solutions also revise the known results of neutral networks in quasispecies theory. To explain the existence of mutants with large Hamming distances from the wild type, we propose three different modifications of the Eigen model: mutation landscape, multiple adjacent mutations, and frequency-dependent fitness in which the steady state solution shows a multi-center behavior.

*Supported by Grants NSC 94-2112-M 001-014, 94-2811-M001-014, and AS-92-TP-A09.

**13:27**

**Z28 10 Combining a total cell population growth and cell population dynamics in the presence of anti-cancer agents** MITRA SHOJANIA FEIZABADI, *Canisius College* A two-compartment Webb-Gyllenberg model describes the population dynamics of proliferating and quiescent cancer cells. Combination of the total cell growth curve and the two-compartment model yields an analytical solution for the behavior of proliferating subpopulation and the net transition rate between proliferating and quiescent cells as a function of time. This work presents a qualitative model for drug interaction with cancer cells in the Webb-Gyllenberg model. The drug is assumed to kill all cell types, each at a specific rate. Considering the total cell population growth in the presence of the drug, the behavior and the size of proliferating and quiescence subpopulations, as well as the related transition rates have been investigated.

## SESSION Z31: COMPLEXED STRUCTURED MATERIALS, GLASSES AND CLATHRATES
**Friday Morning, 17 March 2006**
**329, Baltimore Convention Center at 11:15**
**M. J. Mehl, Naval Research Laboratory, presiding**

**11:15**

**Z31 1 Electronic structure of interfaces between insulating $LaAlO_3$ and $SrTiO_3$ perovskite oxides*** MIN SIK PARK, S.H. RHIM, A.J. FREEMAN, *Northwestern University* Since heteroepitaxial structures of perovskite oxides are potent candidates for multifunctional devices, understanding their interface properties is very important for applications, because they often show completely different properties from bulk. Recently, interfaces between the wide-band gap insulators of $LaAlO_3$ and $SrTiO_3$, were found to be insulating when hole-doped, and conducting when electron-doped[1]. First-principles calculations with the highly precise full-potential linearized augmented plane wave (FLAPW) method[2] for the stoichiometric compounds on [001] superlattices composed of perovskite unit cells of $LaAlO_3$ and $SrTiO_3$, show metallicity in both the hole-doped $AlO_2$/SrO and electron-doped $LaO/TiO_2$ interfaces, even with inclusion of geometry relaxation. Only by considering oxygen vacancies is the experimental result of insulating behavior in the hole-doped $AlO_2$/SrO interface obtained.

*Supported by KRF Grant (KRF-2005-214-C00035) and NSF through the NU MRS Grant (DMR-0076097)

[1]A. Ohtommo and H. Y. Hwang, Nature **427**, 423 (2004)
[2]Wimmer, Krakauer, Weinert, Freeman, Phys.Rev.B, **24**, 864 (1981)

**11:27**

**Z31 2 Local atomic ordering in nanocrystalline $ZrO_2$ and $Zr_xCe_{1-x}O_2$ studied with the Atomic Pair Distribution Technique.*** MILEN GATESHKI, VALERI PETKOV, *Dept. of Physics, Central Michigan University* A number of $ZrO_2$ and $Zr_xCe_{1-x}O_2$ nanocrystalline samples have been prepared using different techniques, such as ball-milling ($ZrO_2$) and soft chemistry ($ZrO_2$ and $Zr_xCe_{1-x}O_2$). The atomic-scale structure of these samples has been studied using high-energy x-ray diffraction and the atomic pair distribution function technique. For the ball-milled materials, the studies show that the parent crystalline material, monoclinic $ZrO_2$, evolves into a nanocrystalline phase that is locally similar to monoclinic zirconia but shows a cubic-type ordering at nanometer-range distances. The atomic-scale structure of the $ZrO_2$ samples obtained by soft chemistry techniques varies depending on the preparation method and the degree of structural coherence. The studies reveal that all samples show Zr-O distances typical for monoclinic-like local atomic ordering, while the Zr-Zr distances depend on the morphology of the samples. For the $Zr_xCe_{1-x}O_2$ samples, interatomic distances typical for both monoclinic $ZrO_2$ and cubic $CeO_2$ are observed up to 5Å, while the longer interatomic distances are attributed solely to a cubic-type structure. The result underlines the importance of local structural disorder and the medium-range order in stabilizing the technologically important cubic zirconia at room temperature.

*The work was supported by the NSF through Grant No. DMR 0304391 (NIRT).

**11:39**

**Z31 3 Atomic PDF study of size and structure of CdSe nanoparticles** A. S. MASADEH, G. PAGLIA, E. S. BOZIN, S. J. L. BILLINGE, *Department of Physics and Astronomy, Michigan State University, East Lansing, Michigan 48824-1116* A. KARKAMKAR, M. G. KANATZIDIS, *Department of Chemistry, Michigan State University, East Lansing, Michigan 48824-1116.* The atomic pair distribution function (PDF) is used to address the size and structure of series of CdSe nanoparticles prepared by the method of distribution focusing [1]. Due to their limiting structure coherence conventional crystallographic methods, such as Rietveld can't be used to assess quantitative size or structural information. Total scattering techniques, such PDF have been successfully applied recently on some similar systems [2, 3]. The PDF includes both Bragg and diffuse scattering and provides quantitative information about the local structure of the materials at different length scales. We report on results of the PDF analysis of synchrotron x-ray diffraction on series of CdSe nanoparticles, data were collected using the rapid acquisition PDF (RA-PDF) technique [4]. [1] X. G. Peng, J. Wickham, A. P. Alivisatos, J. Am. Chem. Soc. **1998**, 120, 5343-5344 [2] B. Gilbert, F. Huang,H. Zhang, G. A. Waychunas, J. F. Banfield.Science, 305, 651–654 (2004). [3]R. B. Neder, V. I. Korsunskiy, J. Phys: Condens. Matter 17, 125–134 (2005) [4] P. J. Chupas, X. Qiu, J. C. Hanson, P. L. Lee, C. P. Grey and S. J. L. Billinge. J. Appl. Crystallogr. 36, 1342–1347 (2003).

**11:51**

**Z31 4 Interactions of $Ga_nAs_n$ Clusters with CGaAs Cages: Possible Nanostructures** A.S. HIRA, E. ALLISON, M.F. FERNANDEZ, J. SHIPMAN, E.R. VELARDE, *Northern New Mexico College* Extending our work on fullerene-alkali complexes[1], we now examine the interactions of small $Ga_nAs_n$ clusters (n = 1 thru 10) with mixed CGaAs cage clusters. First, we derive the physical and chemical properties of the GaAs clusters, including their binding energies, bondlengths, ionization potentials and charge distributions. The geometries of the small gallium arsenide clusters are based on full optimizations. Electron correlation effects are included for binding energies and optimal intermolecular bondlengths. Next we focus on the physical and chemical properties of 60-atom mixed CGaAs cages. The optimization of the cages is subject to symmetry constraints. The third phase of the investigation examines the interactions of the small GaAs clusters with the CGaAs cages. For these complexes various properties, including dissociation channels and dissociation energies, are tabulated. We also explore the implications of this research for the design of nanostructures. 1. Daniel Bulnes, Nichole Moya-Leyba, Erica Velarde and Ajit Hira, '' Theoretical Study of $Na_3C_{60}$ and $Na_4C_{60}$Clusters: Pathways to Nanoscale Contacts,'' Bull. Am. Phys. Soc. 50, 1475 (March 2005).

**12:03**

**Z31 5 Statistical Mechanics for Linking Length Scales in Complex Solids** YING HU, SOKRATES T. PANTELIDES, *Department of Physics and Astronomy, Vanderbilt University, Nashville, TN* Linking scales is usually pursued by computational means, either by passing information from calculations at one scale to another or by constructing a composite simulation with different features treated at different length scales. Here we report on a formulation that is based on the principles of statistical mechanics, applied to a complex solid. Two new concepts, 'lattice space' and 'atom space', are introduced. The deformed state of a crystal is described in terms of deformations of the lattice space and atom space. The distribution function is decomposed in a Born-Oppenheimer-like fashion into slow and fast components. Phonons are integrated out to give a driving force to the lattice deformation. Interplay between the two spaces leads to the formation of defects and such phenomena as elastic deformation, thermal expansion, creep, and dislocation motion. New distribution functions are constructed by adapting the method of local integrals of motion from the theory of liquids. Simulations can be implemented at different mesoscopic length scales, tracking fluxes of point defects, impurities, dislocations, etc.

**12:15**

**Z31 6 Study of structure and thermophysical properties of molten BaGe by using electrostatic levitation technique** AKIKO ISHIKURA, *Gakushuin University* TADAHIKO MASAKI, TAKEHIKO ISHIKAWA, *Japan Aerospace Exploration Agency* NORIYUKI KOIKE, *Chiba Institute of Technology* SHINJI KOHARA, *Japan Synchrotron Radiation Research Institute (SPring-8/JASRI)* AKITOSHI MIZUNO, MASAHITO WATANABE, *Gakushuin University* BaGe alloys with two compositions around their eutectic point form open framework structures called clathrate structure. However, the formation mechanism of clathrate structure has not yet been clarified due to lack of study and understanding of their liquid state structure and properties. Therefore, in order to clarify the formation mechanism of the clathrate structure, thermophysical properties (density, surface tension, and viscosity) of BaGe alloys melts around eutectic compositions were measured by using the electrostatic levitation (ESL) technique and also the structure of them was observed by using the high-energy X-ray diffraction method combined with the ESL. We found that from experimental results, the short range order based on the clathrate structure would exist even in the liquid state at the clathrate forming compositions.

**12:27**

**Z31 7 Localized probe of dielectric response of polymer free surface near the glass transition*** PHILIP CRIDER, NATHAN ISRAELOFF, *Northeastern University* Experimental study of length scales in glassy systems can give new insights into the glassy dynamics. Finite size effects are studied in a polymer (PVAc) utilizing UHV non-contact atomic force microscopy (NCAFM) methods. Localized dielectric susceptibility is probed using the electrostatic interaction of a metal-coated AFM tip with a thick polymer film on a metal substrate. The depth probed below the free surface of the polymer is as small as 10 nm. A lockin amplifier is utilized to measure response from the surface in the second harmonic to extract the Tan(delta) (C/C) response over frequencies of 0.1 - 100 Hz. Preliminary results for the smallest probed depths show an increase in the frequency of the alpha relaxation peak in Tan(delta) as compared with macroscopic measurements. Results for various probed depths will be discussed.

*This work was supported by NSF DMR 0205258, ACS PRF 38113-AC7, and NSF NSEC Award for Center for High-rate Nanomanufacturing EEC-0425826

**12:39**

**Z31 8 Spatio-temporal imaging of polarization fluctuations near the glass transition*** NATHAN ISRAELOFF, PHILIP CRIDER, HASSAN OUKRIS, *Northeastern University* Mesoscopic scale spatio-temporal fluctuations are mapped using novel non-contact atomic force microscopy (NCAFM)-based methods in polymer (PVAc) films near the glass transition. Utilizing the localized electrostatic interaction of a NCAFM conducting tip, we

measure polarization fluctuations within depths as small as 10nm. Applying a sinusoidal bias voltage between the AFM tip and sample results in a response in the AFM cantilever frequency that is offset by surface potential due to thermally induced local polarizations. The measured fluctuations agree quantitatively with predictions. Measurements of these spontaneous fluctuations along a single space-dimension as a function of time yield space-time maps of the dynamics. Spatial and temporal correlation functions were studied as a function of temperature. Results show the expected slowing of the dynamics with decreasing temperature, and hints of spatially varying dynamics. Space-time maps will be compared with recent model simulations which show foam-like space-time trajectories.

*This work was supported by NSF DMR 0205258, ACS PRF 38113-AC7, and NSF NSEC Award for Center for High-rate Nanomanufacturing EEC-0425826

**12:51**

**Z31 9 Raman scattering and modulated-DSC experiments on Potassium Germanate glasses*** N. WANG, D. NOVITA, P. BOOLCHAND, *University of Cincinnati* We have synthesized titled glasses in the $0 < x < 0.16$ range by traditional melt-quenching, and have examined them in Raman scattering and modulated-DSC (MDSC) experiments. Raman lineshapes observed in the present work are quite similar to those reported by Henderson and Wang [1]. Preliminary MDSC experiments reveal glass transition temperatures, $T_g(x)$, starting from a value of 570[r]C at $x = 0$, to decrease to 508[r]C near $x = 0.06$, and to increase thereafter almost linearly to 552[r]C as x increases to 0.15. On the other hand, the non-reversing enthalpy associated with $T_g$ provides evidence of a global minimum in the $0.08 < x < 0.10$ range, the reversibility window[2]. These results are consistent with glasses at $x < 0.08$ as Stressed-Rigid, those at $x > 0.10$ as Floppy, while those in the reversibility window as representing the Intermediate Phase[2]. The space filling nature of the Intermediate Phase is, independently, corroborated by trends in molar volumes which show a broad global minimum in the 9-11% range. Identification of the three elastic phases provides a physical basis to understand the origin of the Germanate anomaly, and the electrical conductivity threshold when glasses become mechanically floppy. *Supported by NSF grant DMR 04-56472. [1] G.S.Henderson and H.M.Wang, Eur. J. Mineral. 14, 733 (2002). [2] P.Boolchand, G.Lucovsky, J.C. Phillips and M.F.Thorpe, Phil. Mag 85,3823 (2005).

**13:03**

**Z31 10 Damped elastic relaxation seen in glassy colloidal suspensions*** ERIC R. WEEKS, DOUGLAS ANDERSON, *Physics Dept., Emory University* PIOTR HABDAS, *Physics Dept., St. Joseph's University* We study concentrated colloidal suspensions, a model system which has a glass transition when the particle concentration is high. We use an optical confocal microscope to view the motion of these colloidal particles in three dimensions. We add small magnetic particles to locally ''poke'' the colloidal samples. We find a yield force (below which the magnetic particles are unable to move through the sample), which grows as the glass transition is approached. When a force is applied below this yield force, the sample deforms elastically, but with relaxation seen after the force is removed. This relaxation seems to behave in a nonexponential fashion. We characterize this elastic response and relaxation and study how both change as the glass transition is approached.

*Work supported by NSF and NASA.

**13:15**

**Z31 11 Cohesion in clathrates I; covalencies and ionicity** KAZUO TSUMURAYA, *Meiji University* HARUKI EGUCHI, *Ishikawajima Harima Heavy Industry (IHI)* HIDEKAZU TOMONO, *Meiji University* We present the roles of endohedral atoms in the cohesion of group 14 clathrates I. Taking a view that the clathrate I consists of a sheaf of one-dimensional connections of $Na@Si_{24}$ cages interleaved in three perpendicular directions, we calculate the electronic structures with an itab initio method and find that 30% of the $3s^1$ charge of each endohedral sodium atom transfers to the frame and the remaining charge forms a bonding state between the endohedral atoms: the roles of cohesion is the covalent bonds between the endohedral atoms in the cages and between the frame atoms, together with the ionic bond between the host and the endohedral atoms.

**13:27**

**Z31 12 Stabilities of earlier row atoms in group 1 and 2 for encapsulation in silicon clathrates I** TOSHIHIKO OGURA, KAZUO TSUMURAYA, *Meiji University* Group 14 clathrates consisting of Si, Ge, or Sn atoms have been synthesized only when they contain some specific endohedral atoms. They are Na, K, Rb, or Cs atoms in group 1, Sr or Ba atoms in group 2, and Cl, Br, or I atoms in group 17.[K.A.Kovnir, et al. Russian Chem. Rev.73,923(2004).] No experiment has been reported on the encapsulation of the earlier row atoms than the atoms mentioned above. We predict the stability of the encapsulation of these atoms using ab initio methods. We evaluate the stability of the guest atom in double caged M2@Si42H36 cluster in the clathrate I, where M is group 1, 2, or 17 atom. The encapsulation of two lithium atoms into one cage and the other is vacant is more stable than the separate encapsulation of lithium atoms into each cage by 0.436eV. The Be2 is the same case and by 0.0859 eV. For sodium case, the separate encapsulation into each cage is more stable by 1.473eV. The strong dimer formation prevents the stabilization of the cage structure. We also evaluate the stabilities in the crystalline states.

**13:39**

**Z31 13 Electronic structures and displacements of endohedral sodium atoms in silicon clathrate II** HIROYUKI TAKENAKA, KAZUO TSUMURAYA, *Meiji University* Since group 14 clathrates encapsulate specific atoms in their cages, the atoms give rise to rattling motion in the cages leading to low thermal conductivity. The clathrate II consists of $Si_{28}$ and $Si_{20}$ cages and the $Si_{28}$ cage is the largest among the cages in the clathrates. We investigate the displacements and the charge densities between the endohedral sodium atoms in the clathrate II using ab initio methods. First we present the displacements of the guest sodium atoms in double caged $Na_2@Si_{50}H_{44}$ cluster, which is a piece of clathrate II being hydrogenated in order to terminate the dangling bonds. Although in a single $Si_{28}H_{28}$ cage the endohedral sodium atom is the most the most stable at the center of the cage, the sodium atoms in each of the double cage cluster displace about 0.06 nm away from each center of the cages to shorten the distance of the sodium atoms. The displacements are attributed to the formation of covalent bond between the sodium atoms and the ionic bonding between the sodium atoms and the cage silicon atoms. Secondly we present the bonding charge densities between the sodium atoms in the clathrate II.

**13:51**

**Z31 14 Stabilities of Al or Ga atoms for encapsulation in silicon clathrates I** HIDEKAZU TOMONO, KAZUO TSUMURAYA, *Meiji University* Clathrates are cagelike compounds and encapsulate endohedral atoms inside the cages of the host network. On the one hand, the clathrates with host atoms silicon, germanium, or tin have been synthesized only when group 1 alkali metal atoms or group 2 alkaline earth metal atoms coexist as electron donors or group 17 halogen atoms coexist as electron acceptors. On the other hand, the group 13 atoms such as Al, Ga, In atoms are substituted for the host frame atoms. There has been no explanation of the mechanism of the solution of these atoms into the frame or insoluble into the cages. We investigate this through calculating the enthalpies of solution of these atoms into silicon clathrate I by use of an itab initio method. We discuss the energies of solution of group 13 atoms into the cages with those into frame structure.

**14:03**

**Z31 15 Vacancy defect formation energies in Ba8@Ge46 clathrates** KATSUHITO SAKAI, KAZUO TSUMURAYA, *Meiji University* The clathrates I Ba8@Ge46 have been found experimentally to have vacancy defects in the framework and to form Ba8Ge43. This has been explained by the Zintl-Klemn empirical concept: the inclusion of the barium atoms leads to increase the valence electrons in the framework of the clathrates and the introduction of vacancy defects relaxes the hypervalence of the electrons. We clarify the process of the defect formation by analyzing the electric structure with the first-principle method. We calculate formation energy of a single vacancy in the clathrates in which we use Ceperley-Alder with LDA exchange correlation functional for the pseudopotential of barium atom.[J. Junquera et al. Phys.Rev.B 67,155327(2003)] The energies are 0.09eV for 6c, 0.39eV for 24k, and 0.74eV for 16i sites in the clathrate Ba8@Ge45, although 1.15eV for 6c, 1.31eV for 24k, and 1.70eV for 16i sites in the clathrate Ba8@Si45. The small energy of the 6c site is due to the small binding energy of Ge clathrate. We will present the reason why vacancy defects are introduced at the 6c sites.

## SESSION Z33: STATISTICAL AND NONLINEAR PHYSICS

**Friday Morning, 17 March 2006**
**336, Baltimore Convention Center at 11:15**
**Kurt Wiesenfeld, Georgia Institute of Technology, presiding**

**11:15**

**Z33 1 Synchronization of phase oscillators in large complex networks** JUAN RESTREPO, EDWARD OTT, *IREAP, University of Maryland* BRIAN HUNT, *IPST, University of Maryland* It has been shown in recent years that many real world networks have a complex structure (e.g., scale-free networks). The effect of a complex interaction network on the dyamics of coupled dynamical systems is, therefore, of interest. An important aspect of the dynamics is the synchronization of coupled oscillators. I will present a generalization of the classical Kuramoto model of all-to-all coupled oscillators to the case of a general topology of the network of interactions. We find that for a large class of networks, there is still a transition from incoherence to coherent behavior at a critical coupling strength that depends on the largest eigenvalue of the adjacency matrix of the network. I will discuss the application of our theory to study the effect of heterogeneity in the degree distribution and degree-degree correlations in the network. Finally, I will comment on generalizations to more realistic dynamical systems.

**11:27**

**Z33 2 Weak Dynamic Links for Synchronizing Oscillator Arrays.*** DENIS TSYGANKOV, *University of Maryland, IPST* KURT WIESENFELD, *Georgia Institute of Technology, CNS* A novel synchronization mechanism observed in a model of coupled fiber laser arrays is explained [1]. The arrays can operate in a highly coherent way if some elements are driven more strongly than others. The synchronized state of such an inhomogeneous array, although sub-optimal relative to a uniformly pumped array, is far more robust with respect to parameter mismatch among the individual elements. Similar dynamical behavior might be useful for synchronizing more general coupled oscillator systems when amplitude dynamics is crucial.

*1. D. Tsygankov and K. Wiesenfeld, Weak Link Synchronization, submitted.

**11:39**

**Z33 3 Competing Synchronization of Nonlinear Oscillators*** EPAMINONDAS ROSA, *Department of Physics, Illinois State University* Coupled nonlinear oscillators abound in nature and in man-made devices. Think for example of two neurons in the brain competing to get the attention of a third neuron, and eventually developing some sort of synchronization process. This is a common feature involving oscillators in general, and can be studied using numerical simulations and/or experimental setups. In this talk, results involving electronic circuits and plasma discharges will be presented showing interesting features related to the types of oscillators and to the types of couplings. In particular, for the case of two oscillators competing for synchronization with a third one, the target oscillator synchronizes alternately to one or the other of the competing oscillators. The time intervals of synchronous states vary in a random-like manner. Numerical and experimental results will be presented and the consistency between them will be discussed.

*The author acknowledges financial support from Research Corporation.

**11:51**

**Z33 4 Complexity, Parallel Computation and Statistical Physics** JONATHAN MACHTA, *University of Massachusetts Amherst* The intuition that a long history is required for the emergence of complexity in natural systems is formalized using the notion of *depth* (related to Bennett's *logical depth*). The depth of a system is defined in terms of the number of parallel computational steps needed to simulate it. Depth provides an objective, irreducible measure of history applicable to systems of the kind studied in statistical physics. The talk will review concepts of parallel computational complexity theory and then present results for the depth of several well-known model systems in non-equilibrium statistical physics. It is argued that physical complexity cannot occur in the absence of substantial depth and that depth is a useful proxy for physical complexity.

**12:03**

**Z33 5 Vortex-Phonon Interaction in the Kosterlitz-Thouless Theory** EVGENY KOZIK, NIKOLAY PROKOF'EV, BORIS SVISTUNOV, *University of Massachusetts Amherst* The ''canonical'' variables of the Kosterlitz-Thouless theory– fields $\Phi_0(\mathbf{r})$ and $\phi(\mathbf{r})$, generally believed to stand for vortices and phonons (or their XY equivalents, like spin waves, etc.) turn out to be neither vortices and phonons, nor, strictly speaking, *canonical* variables. The latter fact explains paradoxes of (i) absence of interaction between $\Phi_0$ and $\phi$, and (ii) non-physical contribution of small vortex pairs to long-range phase correlations. We resolve the paradoxes by explicitly relating $\Phi_0$ and $\phi$ to canonical vortex-pair and phonon variables.

**12:15**

**Z33 6 Sticky Random Walks** TORU OHIRA, *Sony Computer Science Laboratories, Japan* TADAAKI HOSAKA, *National Institute of Advanced Industrial Science and Technology, Japan* Entangled strings is something we commonly observe. For example, wires for electrical appliances or communication network cords sometimes require us to disentangle them. We describe here a concept of sticky random walks to gain some insight into this phenomenon. The strings are represented by the trajectory of a random walker. This random walker leaves sticks or marks at certain time intervals. Therefore, a string is represented by this trajectory with these marks on it. By sending out multiple sticky random walkers, we obtained multiple sticky strings. Furthermore, a string is considered as entangled with another when these marks overlap at the same site in space, and not when they are simply crossed. Thus, the string is considered more sticky when there are more marks on it. We tested a situation having multiple sticky strings in a bounded two-dimensional square grid by sending out sticky random walks in this space. We found that in certain situations, the optimal balance between stickiness and number of strings gives most entangled situation.

**12:27**

**Z33 7 Finite-Connectivity Spin-Glass Phase Diagrams and Low Density Parity Check Codes** GABRIELE MIGLIORINI, *Aston University* DAVID SAAD, *Aston University* We present phase diagrams of finite connectivity spin-glasses. We firstly compare the properties of the phase diagrams with the performance of low density parity check codes (LDPC) within the Replica Symmetric (RS) ansatz. We study the location of the dynamical and critical transition points within the one step Replica Symmetry Breaking theory (RSB), extending similar calculations that have been performed in the past for the Bethe spin-glass. The location of the dynamical transition line *does* change within the RSB theory, when comparing with the results obtained in the RS case. For LDPC decoding of messages transmitted over the binary erasure channel (BEC) we find, at zero temperature and rate $R = 1/4$ an RSB transition point located at $p_c \simeq 0.7450 \pm 0.0050$, to be compared with the corresponding Shannon bound $1 - R$. For the binary symmetric channel (BSC) we show that the low temperature reentrant dynamical transition boundary occurs at higher values of the channel noise when comparing with the RS case. Possible practical implications to improve the performance of the state-of-the-art error correcting codes are discussed.

**12:39**

**Z33 8 Novel Approach in Statistical Physics for Accurate Multiscale Materials Investigation** UDUZEI EDGAL, *North Carolina Agricultural and Technical State University* This paper discusses a novel scheme recently developed by the author [(i)Edgal, U. F., J. Chem. Phys. **94**, 8179, 1991; (ii)Edgal, U. F. and Huber, D. L., J. Phys. Chem. B, **108**, 13777, 2004; (iii)Edgal, U. F. and Huber, D. L., accepted for publication in the journal ''Physica A,'' 2005] for **accurately** determining the free energy of arbitrary equilibrium classical and quantum (material) systems at arbitrary densities, temperatures, and interaction potentials. Nearest neighbor probability density functions are formulated. The scheme allows us avert the ''sign'' problem usually encountered in Fermion calculations. Extension to mixed systems, as well as a novel ensemble, the ''Nearest Neighbor'' ensemble, used to effect the computational component of the novel approach are briefly discussed.

**12:51**

**Z33 9 Reversal of motion induced by mechanical coupling in Brownian motors** ERIN CRAIG, *University of Oregon* MARTIN ZUCKERMANN, *Simon Fraser University* HEINER LINKE, *University of Oregon* Many studies of Brownian ratchets have dealt with the asymmetric pumping of individual point-like particles. Here, we consider the transport of objects with internal structure in a flashing ratchet potential by investigating the overdamped behavior of a rod-like chain of evenly spaced point particles. In 1D, analytical arguments show that the current can reverse direction multiple times in response to changing the size of the chain or the temperature of the heat bath. However, if the rods are allowed to rotate freely in 3D, or if their length is much less than the spatial period of the ratchet potential, current reversal is no longer observed, and the qualitative behavior of single particle motion is recovered. All analytical predictions are confirmed by Brownian dynamics simulations. These results are relevant to the design of novel particle separation technology, and may provide the basis for simple, coarse-grained models of molecular motor transport that incorporate an object's size and internal degrees of freedom into the mechanism of transport.

**13:03**

**Z33 10 Optimal Resonance Forcing of Nonlinear Systems** GLENN FOSTER, ALFRED HUBLER, *Center for Complex Systems Research, Department of Physics, University of Illinois at Urbana-Champaign* We study the response of dynamical systems to additive forcing and find that, for a broad class of systems, the response is maximized by a pattern of forcing that mimics the time-reversed dynamics of the unforced system. Applying these results, we numerically construct families of optimal inputs and successfully perform spectroscopic system identification on our modeled systems.

**13:15**

**Z33 11 Quantum wave packets in hard-disk and hard-sphere billiards** ARSENI GOUSSEV, *University of Regensburg* J. ROBERT DORFMAN, *University of Maryland* Analysis of quantum dynamics in systems with classically chaotic analogs constitutes one of the main objectives for the field of *Quantum Chaos*. The quantum dynamics is known to be determined, to a large extent, by chaotic features of counterpart classical systems. We address time evolution of wave packets in open chaotic billiards, in which a quantum particle travels among a collection of fixed scatterers taken to be hard disks or hard spheres in two or three spatial

dimensions respectively. By studying the autocorrelation function for the wave packets we provide a detailed analysis of the phenomenon of wave packet partial reconstruction in the course of the time evolution, and discuss a close connection between the reconstruction dynamics and such important properties of the counterpart classical systems as the Lyapunov exponents, the Kolmogorov-Sinai and the topological entropies.

**13:27**

**Z33 12 Universal Impedance, Admittance and Scattering Fluctuations in Quantum-chaotic Systems.** SAMEER HEMMADY, XING ZHENG, THOMAS ANTONSEN, EDWARD OTT, STEVEN M. ANLAGE, *Univ. of MD-College Park, USA.* We experimentally investigate fluctuations in the eigenvalues of the impedance, admittance and scattering matrices of wave chaotic systems using a microwave analog of a quantum chaotic infinite square well potential. We consider a 2-D, time-reversal symmetric chaotic microwave resonator driven by two non-ideally coupled ports. The system-specific coupling effects are removed using the measured radiation impedance matrix ($\vec{Z}_{Rad}$) [1] of the two ports. A normalized impedance matrix ($\vec{z}$) is thus obtained, and the Probability Density Function (PDF) of its eigenvalues is predicted to be universal depending only on the cavity loss. We observe remarkable agreement between the statistical properties of $\vec{z}$ and $\vec{y} = \vec{z}^{-1}$ for all degrees of loss, which is in accordance with [1, 2] and Random Matrix Theory (RMT). We compare the joint PDF of the eigenphases of the normalized scattering matrix ($\vec{s}$) with that obtained from RMT for varying degrees of loss. We study the joint PDF of the eigenvalues of $\vec{s}\vec{s}^{\dagger}$ and find good agreement with [3]. [1] X. Zheng, itet al., – Electromagnetics (in press); condmat/0408317; S. Hemmady, *et al.*, Phys. Rev. Lett. **94**, 014102 (2005).[2] Y. V. Fyodorov, *et al.*, –condmat/0507016.[3] P. W. Brouwer and C. W. J Beenakker–PRB **55**, 4695 (1997). Work supported by DOD MURI AFOSR Grant F496200110374, DURIP Grants FA95500410295 and FA95500510240.

**13:39**

**Z33 13 Controlling transitions in a Duffing oscillator by sweeping the driving frequency.** OLEG KOGAN, *Caltech* BARUCH MEERSON, *Hebrew University of Jerusalem* We consider a high-$Q$ Duffing oscillator in a weakly non-linear regime with the driving frequency $\sigma$ varying in time between $\sigma_i$ and $\sigma_f$ at a characteristic rate $r$. We found that the frequency sweep can cause controlled transitions between two stable states of the system. Moreover, these transitions are accomplished via a transient that lingers for a long time around the third, unstable fixed point of saddle type. We propose a simple explanation for this phenomenon and find the transient life-time to scale as $-(\ln|r - r_c|)/\lambda_r$ where $r_c$ is the critical rate necessary to induce a transition and $\lambda_r$ is the repulsive eigenvalue of the saddle. The same type of phenomena is expected to hold for a large class of driven nonlinear oscillators which are describable by a two-basin model.

**13:51**

**Z33 14 Structure and Complexity in Rule Ensemble Cellular Automata** ALEXANDER WISSNER-GROSS, *Harvard University, Department of Physics* Individual elementary cellular automata (ECA) rules are attractive models for a range of non-equilibrium physical systems, but rule ensembles remain poorly understood. This paper presents the first known analysis of the equally weighted ensemble of all ECA rules. Ensemble dynamics reveal persistent, localized, non-interacting structures strongly correlated by velocity and reminiscent of solitons, instead of equilibration. Dispersion from a single initial site generates peaks traveling at low-denominator fractional velocities, some of which are not discernable in individual rules, implying collective excitation. Principal component analysis of the rule space shows the ECA are dense (with $\sim$ 111 eigenrules out of 128 ECA rules, up to symmetry), but can be transformed to a simple basis set that is quasi-linear in initial conditions. These results suggest that the ECA, often considered to be the simplest nontrivial set of ''short program'' models for self-assembly, might be approximated well by computationally simpler models. This work also shows, surprisingly, that structure can develop without favoring a single evolution rule.

**14:03**

**Z33 15 Universality away from Critical Points: Collapse of Observables in a Thermostatistical Model** CINTIA LAPILLI, PETER PFEIFER, CARLOS WEXLER, *Department of Physics and Astronomy, University of Missouri-Columbia, Columbia, Missouri 65211, USA* The $p$-state clock model in two dimensions is a discrete model exhibiting, for $p > 4$, a quasi-liquid phase in a region $T_1 < T < T_2$. We show that above a temperature $T_{\rm eu}$ the model exhibits *extended universality* in which, for $p > 4$ and all $T > T_{\rm eu}$, all thermal averages become identical to those of the continuous, planar rotor model ($p = \infty$). This *collapse of thermodynamic observables* amounts to an emergent symmetry, not present in the Hamiltonian. For $p \geqslant 8$, the collapse starts in the quasi-liquid phase and makes the transition at $T_2$ indistinguishable from the Berezinskii-Kosterlitz-Thouless (BKT) transition of the planar rotor. For $p \leqslant 6$, we find $T_{\rm eu} > T_2$, and the transition at $T_2$ is no longer BKT. The results include a detailed analysis of the critical properties at $T_1$ and $T_2$. Broader implications are discussed.

**SESSION Z37: FOCUS SESSION: NANOSCALE CONDUCTANCE THEORY III**
**Friday Morning, 17 March 2006**
**340, Baltimore Convention Center at 11:15**
**Jeffrey Neaton, Lawrence Berkeley National Laboratory, presiding**

**11:15**

**Z37 1 First-principles studies of the electronic structure of cyclopentene on Si(100)*** SU YING QUEK, *Division of Engineering and Applied Sciences, Harvard University* JEFFREY NEATON, *The Molecular Foundry, Materials Sciences Division, Lawrence Berkeley National Laboratory* MARK HYBERTSEN, *Department of Applied Physics and Center for Transport in Molecular Nanostructures* EFTHIMIOS KAXIRAS, *Department of Physics and Division of Engineering and Applied Sciences, Harvard University* STEVEN LOUIE, *Department of Physics, University of California, Berkeley & The Molecular Foundry, Materials Sciences Division,Lawrence Berkeley National Laboratory* Small organic molecules on silicon surfaces are promising candidates for active elements in nanoelectronic devices. The interplay between electronic states of the molecule and the silicon surface can change the molecular HOMO-LUMO gap, as well as result in interesting transport properties that depend sensitively on the alignment of molecular frontier orbitals with the silicon band

structure. In this work, we determine this alignment quantitatively using the GW method for cyclopentene on Si(100), a prototypical organic-molecule/silicon junction of interest in molecular electronics. We will discuss our results in the context of recent STM experiments that observed negative differential resistance in this system.

*This work is supported by NSF(DMR04-39768, CHE-0117752), DOE(DE-AC03-76SF00098), A-STAR & NYSTAR. Computer time was provided by NERSC, NPACI & IHPC.

**11:27**

**Z37 2 Hydrodynamical approach to transport in nanostructures** ROBERTO D'AGOSTA, MASSIMILIANO DI VENTRA, *Department of Physics, University of California - San Diego* The electrical resistance induced by the viscous properties of the electron liquid has been recently derived.[1] In addition, it is known that the geometric constriction experienced by electrons flowing in a nanostructure gives rise to a fast ''collisional'' process.[2] These facts allow us to derive Navier-Stokes-type of equations, and therefore describe the electron flow on a par with a viscous and compressible liquid. By using this hydrodynamical approach we study electron transport in nanoscale systems and derive the conditions for the transition from laminar to turbulent flow in quantum point contacts. We also discuss possible experimental tests of these predictions. [1] N. Sai, M. Zwolak, G. Vignale, and M. Di Ventra, Phys. Rev. Lett. **94**, 186810 (2005). [2] M. Di Ventra and T.N. Todorov, J. Phys. Cond. Matt. **16**, 8025 (2004); N. Bushong, N. Sai and, M. Di Ventra, Nano Lett. (in press). Work supported by the Department of Energy (DE-FG02-05ER46204)

**11:39**

**Z37 3 Source and sink approach to calculate transport properties of nanostructures** KALMAN VARGA, SOKRATES PANTELIDES, *Vanderbilt University* We have calculated the transport properties of single molecule and carbon nanotube devices using the the Source and Sink method. We have carefully tested the convergence of the current by enlarging the basis. The fully converged current-voltage characteristics presented in this paper can serve as benchmark for transport calculations. We also compare our results to those obtained by other approaches and analyze the source of disagreements.

**11:51**

**Z37 4 Theory of the Conductance of a Single Molecule Connected to Metallic Single Wall Carbon Nanotube Electrodes*** LEI ZHANG, YIING-REI CHEN, *Chemistry Dept., Columbia University* MARK S. HYBERTSEN, *Applied Physics and Applied Math Dept, Columbia University* Metallic single wall carbon nanotubes intuitively are expected to be ideal electrodes for making contact to small, conjugated organic molecules. In this work, the conductance of ideal junctions consisting of armchair nanotube electrodes connected by conjugated carbon chains is studied. A pi-electron tight binding model is used with a Greens function formulation of the electronic states in the junction and the conductance. Key factors that influence the conductance of these junctions include molecule length, electrode attachment topology, and even versus odd length. This study delimits the maximum conductance that can be ideally expected using metallic nanotube electrodes.

*This work is supported by the NSF under award numbers CHE-0117752 and DMR-0213574, the DOE under grant number DE-FG0290ER14162, and by NYSTAR

**12:03**

**Z37 5 Role of the evanescent states in the elastic quantum transport*** ARANTZAZU GARCIA-LEKUE, *Chemical Science Division, Lawrence Berkeley National Laboratory, Berkeley, California 94720, USA* LIN-WANG WANG, *Computational Research Division, Lawrence Berkeley National Laboratory, Berkeley, California 94720, USA* The role of evanescent states is always an issue in electronic transport, especially when the energy of the propagating electron is close to a band structure minimum. In this work, we investigate the effects of exact evanescent states on the calculation of the elastic quantum transport through a molecule connected by two quantum wires, based on the method presented in Ref. [1]. An exact treatment of evanescent (decaying) states involves the calculation of the complex band structure of the electrodes with imaginary parts of the k vectors. We have calculated the complex band structure under the plane-wave pseudopotential approach. The exact evanescent states are used in the transport calculations with auxiliary boundary condition as described in Ref. [1]. The results are exact numerical solutions of the scattering states under a plane-wave pseudopotential formalism. [1] L.W. Wang, Phys. Rev. B. **72**, 045417 (2005).

*This work was supported by U.S. Department of Energy under Contract No. DE-AC02-05CH11231 and used the resources of the National Energy Research Scientific Computing Center.

**12:15**

**Z37 6 First-principles investigation of electronic coupling effects between organic molecules and transition metal electrodes on conduction** GUNN KIM, MARCO BUONGIORNO NARDELLI, J. BERNHOLC, *North Carolina State University, Raleigh* We investigate electronic transport in long chain molecules sandwiched between metallic electrodes. The calculations are carried out using the non-equilibrium Green function method and a basis set of localized orbitals, which are optimized to minimize the DFT total energy of the system. The optimization is performed on a grid, using multigrid techniques to accelerate convergence. Our model systems consist of saturated hydrocarbon (alkane) chains having thiol (-SH) and amino ($-NO_2$) end groups attached to transition metal electrodes. We show that the current-voltage characteristics strongly depend on the coupling between the molecule and the metal electrodes.

**12:27**

**Z37 7 Effect of doping and molecular coverage on the I-V characteristics of organic molecules on silicon surfaces** WEN-CHANG LU, *N.C. State University* V. MEUNIER, *ORNL* S. WANG, Q. ZHAO, J. BERNHOLC, *N.C. State University* Quantum transport properties of organic molecules on the silicon (001) surface have been studied by ab initio non- equilibrium Green function calculations in a basis of optimal localized orbitals. Our calculated results provide a qualitative picture and quantitative understanding of the importance of self-consistent screening and broadening of quasi- molecular orbitals under a large bias. Negative Differential Resistance (NDR) is found to be a general feature of organic molecules on Si surfaces [1]. By comparing the I-V characteristics of a monolayer of cyclopentene molecules with that of a single molecule, we show that interactions between the molecules attenuate the NDR, as seen in experiments. We have also investigated the effects of proximal dopant atoms on the NDR in a large unit cell. [1]. W. Lu, V. Meunier, J. Bernholc, Phys. Rev. Lett. 95, 206805 (2005).

**12:39**

**Z37 8 Calculation of Single-Electron Transport Through Molecules** JINGBIN LI, NIKITA SIMONIAN, KONSTANTIN LIKHAREV, *Department of Physics and Astronomy, Stony Brook University* We have carried out numerical calculations of electron transport through OPE terminated with isocyanide groups. The electron spectra and orbitals are calculated using the NRLMOL DFT package (http://cst-www.nrl.navy.mil/~ nrlmol/). The wave functions are then used to calculate the transmission of the interface energy barriers, within the Bardeen approximation. If the transmission is high, we calculate the current using the standard methods of the theory of ballistic field effect transistors, while if it is sufficiently low, we use the general theory of single-electron tunneling in systems with discrete energy spectrum [1]. (In order to understand the best way of resolving the problems due to the intrinsic limitations of the DFT approach, initial calculations have been carried out for a simple model: a Na atom sandwiched between two Au electrodes.) Our results yield I-V curves with substantial negative differential resistance (NDR) of conducting branches, due to a new mechanism: the enhancement of one of the tunnel barriers of the system by the applied electric field. The work is supported in part by AFOSR and NSF. [1]. D. V. Averin, A. N. Korotkov, and K. K. Likharev, Phys. Rev. B, 44, 6199 (1991).

**12:51**

**Z37 9 Contact Effects on Transport Properties through Single Molecules — ab initio RTM/NEGF method study** KENJI HIROSE, *Fund.Res.Labs., NEC Corporation* NOBUHIKO KOBAYASHI, *NRI, National Institute of AIST* Recently much attention has been focused on the transport properties of single molecules sandwiched between electrodes, aiming at construction of ultimate functional devices with molecular electronics. Since the transfer of an electron through single molecules attached to electrodes is sensitivily affected by the atomic-scale contacts and also it is difficult at present to construct well-characterized nanostructures and to directly observe their atomic structures, theoretical approaches based on the ab inito calculations is indispensable to study the transport properties of molecular-scale devices. Using the ab initio RTM/NEGF method developed recently, we study the the transport properties through single molecules attached to electrodes. This method is based on the plane-wave basis sets and thus not dependent on the atomic positions, which enables us to treat accurate tails of wavefunctions in the tunneling regimes as well as those in the ballistic regimes on the same footing. We investigate especially atomic-scale contact effects on the I-V characteristics through single molecules, changing the distance to electrodes. We find strong non-linear behaviors appear in the I-V characteristics at some distances with and even without single molecules connected to electrodes. We clarify the relationship between electronic states of single molecules and the contact effect at the electrodes for the transport properties.

**13:03**

**Z37 10 All Electron Calculations of IV Characteristics For Molecular Junctions** JOHN LAWSON, CHARLES BAUSCHLICHER, *NASA Ames Research Center* We present current-voltage (I-V) characteristics computed using all-electron basis sets on the conducting molecule. We consider benzene dithiol with gold contacts as our model system. The all-electron results are very similar to previous results obtained using effective core potentials (ECP). A hybrid integration scheme is used that keeps the all-electron calculations cost competitive with the ECP calculations. By neglecting the coupling of states to the contacts below a fixed energy cutoff, the density matrix for the core electrons can be evaluated analytically. The full density matrix is formed by adding this core contribution to the valence part that is evaluated numerically. Expanding the definition of the core in the all-electron calculations significantly reduces the computational effort and, up to biases of about 2 V, the results are very similar to those obtained using more rigorous approaches. The convergence of the I-V curve and the transmission function with respect to basis set is discussed.

**13:15**

**Z37 11 Spin-polarized electron transport in a molecular wire: tuning the conductivity through conformational changes** L. SENAPATI, S.C. ERWIN, *Center for Computational Materials Science, Naval Research Lab, Washington DC* R. PATI, *Department of Physics, Michigan Technological University, Houghton MI* We investigate theoretically the electrical conductivity of a molecular wire consisting of three linked benzene molecules. By using magnetic electrodes the conductivity becomes spin-dependent, the degree of this dependence varying with the relative spin-alignment of the two electrodes. Of particular interest is how the the conductivity depends on the geometrical conformation of the benzene wire. Here we use density-functional theory and the Landauer-Büttiker method to calculate this dependence from first principles. We find that the current depends sensitively on the conformation, with a near-planar configuration of the three benzene rings giving significantly higher current (by ~ 30%) than the ground-state non-planar structure.

**13:27**

**Z37 12 Ab initio modeling of molecular spintronics** DEREK WALDRON, VLADIMIR TIMOCHEVSKI, *Dept. of Physics, McGill University* BRIAN LARADE, *QuantuModeling Inc.* HONG GUO, *Department of Physics, McGill University* We report on theoretical studies of spin polarized quantum transport through molecular scale magnetic tunnel junctions. Our theoretical formalism is based on carrying out density functional theory (DFT) analysis within the Keldysh nonequilibrium Green's function (NEGF) formalism. The NEGF-DFT technique allows one to calculate nonlinear quantum transport features from atomic point of view. We will report these features for systems such as Ni-bezenedithiol(BDT)-Ni molecular magnetic tunnel junction, conventional Fe-MgO-Fe device, and spin injection through Fe-GaAs interfaces, including all the microscopic material properties.

**13:39**

**Z37 13 Theory of electron-vibration coupling in the electron transport of molecular bridges** MASARU TSUKADA, *Waseda University* KUNIHIRO MITSUTAKE, *Canon Research Center, Canon Inc.* Electron transport through molecules connecting nano-electrodes is the key issue for molecular devices. The competition and coexistence of the coherent and dissipative transport are unresolved issue, in spite of its importance. In this work, this problem is investigated by a novel theoretical approach of an itab initio molecular orbital model with combining polaron effect. When carriers are injected into molecules from electrodes, the structure of the molecule changes, which leads the coupling term of the electron/hole and the molecular vibration. The model Hamiltonian for the thiophene oligomer is solved by a variational approach, and a mixed states of dressed polaron with molecular orbital states mediated by the phonon cloud is found. The former and latter are predominant for small or large transfer integral, respectively. The excited states can be calculated in the same framework as the

ground state. The overall carrier transport properties can be analyzed by solving the master equation with the transition rate estimated by the golden rule including the phonon degrees of freedom. In this theoretical approach, the coherent and dissipative electron transport through molecular bridges can be described in a uniform systematic way.

**13:51**

**Z37 14 Inter-strand coupling and base pairing sequences in DNA charge transport.*** EFTA YUDIARSAH, *Ohio University* SERGIO ULLOA, *Ohio University* The electronic transport properties of double-stranded DNA are studied using a tight-binding Hamiltonian. Transfer and scattering matrix methods for double strands are employed simultaneously in the calculation, guaranteeing numerical stability. Realistic on-site energies [1] and hopping constants are used in the model [2]. The role of inter-strand coupling is shown to be extremely important for random sequences typical of genetic DNA. In contrast, inter-strand coupling only changes slightly the charge transport properties for more periodic sequences. The effect of base-pairing across strands and details of the sequences were investigated. Our model shows that the resistance of DNA depends on the sequences and the ratio of the bases. This agrees with previous results by Roche [3]. The resistance is also shown to increase with the concentration of different bases in a homogenous strand, and we find that for certain sequences only short-range electronic transport is possible. [1] H. Sugiyama and I. Saito, J. Am. Chem. Soc. 118, 7063 (1996). [2] A. A. Voityuk, J. Jortner, M. Bixon, and N. Rosch, J. Chem. Phys. 114, 5614 (2001). [3] S. Roche, Phys. Rev. Lett. 91, 108101 (2003).

*Supported by NSF-NIRT.

**14:03**

**Z37 15 Rabi-assisted transport in diatomic molecules*** EDSON VERNEK, ENRIQUE V. ANDA, *Pontifícia Universidade Católica do Rio de Janeiro* SERGIO E. ULLOA, NANCY SANDLER, *Ohio University* Electronic transport through few atoms, molecules and quantum dots has captured much attention recently among physicists. The confinement of electrons going alongin these systems gives rise to strong Coulomb repulsion that produces a very rich phenomenology. Electrons also interact with phonons, which affect transport characteristics under resonant conditions. We have modeled electronic transport in a diatomic molecule by a system composed of two orbital sites coupled in parallel between two leads [1]. We studied the regime where both electron- electron and electron-phonon interactions are important and have shown dramatic effects on the conductance. Using Green's functions and equation of motion techniques we found new conducting channels in the presence of Coulomb interactions when the energy of phonons matches the energy difference between quasei-particle levels. We call this phenomenon Rabi-assisted tunneling. We now present a detailed study that includes the super-exchange interaction between the atoms in the molecules (indirectly coupled through the leads), which was not included in the previous work. We describe how the indirect coupling affects resonance conditions and the conductance of the system. [1] E. Vernek, et al., Phys. Rev. B (R) **72**, 121405 (2005). (Rapid comm.)

*Supported by NSF-IMC and CAPES-Brazil.

**SESSION Z38: HIGH TC CUPRATES: ARPES**
**Friday Morning, 17 March 2006**
**341, Baltimore Convention Center at 11:15**
**Thomas Deveraux, University of Waterloo, presiding**

**11:15**

**Z38 1 From Fermi Arcs to Nodal Metal: Scaling of the Pseudogap with Temperature and Doping** AMIT KANIGEL, *Univ. of Illinois at Chicago* M.R. NORAMN, *Materials Science Div., ANL* M. RANDERIA, *Dept. of Physics, Ohio State Univ.* U. CHATERJEE, *Dept. of Physics, Univ. of Illinois at Chicago* A. KAMINSKI, H.M. FRETWELL, *Ames Laboratory and Dept. of Physics and Astronomy, Iowa State Univ.* S. ROSENKRANZ, *Materials Science Div., ANL* M. SHI, *Dept. of Physics, Univ. of Illinois at Chicago* T. SATO, T. TAKAHASHI, *Dept. of Physics, Tohoku Univ., Japan* Z.Z. LI, H. RAFFY, *Laboratorie de Physique des Solides, Universite Paris-Sud, France* K. KADWAKI, *Inst. of Materials Science, Univ. of Tsukuba, Japan* J.C. CAMPUZANO, *Dept. of Physics, Univ. of Illinois at Chicago* The pseudogap phase in the cuprates is a most unusual state of matter[1–4]: it is a metal, but its Fermi surface is broken up into disconnected segments known as Fermi arcs[5]. Using angle resolved photoemission spectroscopy, we show that the anisotropy of the pseudogap in momentum space and the resulting arcs depend only on the ratio itT/T*(x), where itT*(x) is the temperature below which the pseudogap first develops at a given hole doping, itx. In particular, the arcs, which extend at itT* to the hot spots where the antiferromagnetic zone boundary crosses the Fermi surface, collapse linearly with itT/T* and extrapolate to zero extent as itT 0. This suggests that the itT = 0 state is a nodal liquid, a strange metallic state whose gapless excitations are located only at points in momentum space, just as for a itd-wave superconductor.

**11:27**

**Z38 2 Pseudogap and Superconducting Gap in $(La_{2-x}Sr_x)CuO_4$** X.J. ZHOU, *Stanford University and Lawrence Berkeley National Lab* T. YOSHIDA, *University of Tokyo* W.L. YANG, *Stanford University and LBNL* SEIKI KOMIYA, YOICHI ANDO, *Central Research Institute of Electric Power Industry, Japan* T. SASAGAWA, *University of Tokyo* F. ZHOU, W.X. TI, J.W. XIONG, Z.X. ZHAO, *Institute of Physics, Chinese Academy of Sciences* T. KAKESHITA, H. EISAKI, S. UCHIDA, *University of Tokyo* A. FUJIMORI, *University of Tokyo* Z. HUSSAIN, *Lawrence Berkeley National Lab* Z.-X. SHEN, *Stanford University* We have carried out high resolution angle-resolved photoemission measurements on $(La_{2-x}Sr_x)CuO_4$ (LSCO) over the entire doping range (x=0~ 0.3). We will present doping-dependence and momentum-dependence of the pseudogap and superconducting gap in the LSCO system.

**11:39**

**Z38 3 ARPES Study of Nodal Quasiparticles of $Bi_2Sr_{1.6}La_{0.4}CuO_{6+\delta}$ Using Low-Energy Excitation Photons** T. KAMO, K. YAMAZAKI, T. YAMASAKI, H. ANZAI, A. INO, M. ARITA, H. NAMATAME, M. TANIGUICHI, *Graduate School of Science and Hiroshima Synchrotron Radiation Center, Hiroshima University* A. FUJIMORI, *University of Tokyo* Z.-X. SHEN, *Stanford University* K. FUJITA, S. UCHIDA, *Department of Physics, University of Tokyo* Using low-energy synchrotron radiation ($h\nu$ = 7.75 eV) as excitation photons, the quasiparticle-momentum resolution has been dramatically improved ($\Delta k$

$\sim 0.01\text{Å}^{-1}$) in the angle-resolved photoemission (ARPES) study of single-layer high-$T_c$ cuprate $Bi_2Sr_{1.6}La_{0.4}CuO_{6+\delta}$ (Bi2201). We report the new experimental result on the nodal quasiparticle dispersion and scattering rate of optimally doped Bi2201 ($T_c = 33$ K) over an extended temperature range. Since only a single quasiparticle band is involved for the single-layer cuprate, the high-resolution quasiparticle images have provided us the direct information on fine quasiparticle structures. In comparison to the result on the bilayer cuprate Bi2212, we will discuss the character of the multiple excitation modes coupled with the electrons.

**11:51**

**Z38 4 Nodal Quasiparticle Life Time in High-Tc Cuprates** Z.H. PAN, H.B. YANG, P. RICHARD, J.H. MA, M. NEUPANE, Y.M. XU, A. SHEKHARAN, H. DING, G. GU, T. VALLA, P.D. JOHNSON, *Department of Physics, Boston College, MA* Angle-Resolved Photoemission Spectroscopy (ARPES) are used to study the temperature dependence of nodal quasiparticle life time of $Bi_2Sr_2CaCu_2O_8$ (Bi2212) with different doping levels. For optimally doped (OP) and overdoped (OD) samples, a sudden change is observed in the temperature dependence of the scattering rate at Tc, however this change is not obvious in the underdoped (UD) samples.

**12:03**

**Z38 5 A reexamination of the oxygen isotope effect in ARPES spectra of BSCCO** FRASER DOUGLAS, Z. SUN, D.S. DESSAU, *University of Colorado at Boulder* A.V. FEDOROV, *Advanced Light Source* H. EISAKI, *AIST* H. IWASAWA, *AIST* Y. AIURA, *AIST* T. MASUI, S. TAJIMA, *Osaka University* High resolution angle-resolved photoemission spectroscopy (ARPES) has been utilized to further explore the effects of oxygen isotope substitution in Bi2212 and Bi2201 high temperature superconductors. First presented as evidence for the importance of phonons in the nodal dispersion of 2212, the use of several synchrotron beamlines with many different photon energies suggests an alternate explanation for the observed effect.

**12:15**

**Z38 6 Selective Observation of Bilayer-Split Nodal Quasiparticles in $Bi_2Sr_2CaCu_2O_{8+\delta}$ by ARPES Using Low-Energy Tunable Photons** T. YAMASAKI, T. KAMO, H. ANZAI, A. INO, M. ARITA, H. NAMATAME, M. TANIGUCHI, *Graduate School of Science and Hiroshima Synchrotron Radiation Center, Hiroshima University* A. FUJIMORI, *Department of Complexity Science and Engineering, University of Tokyo* Z.-X. SHEN, *Department of Applied Physics and SSRL, Stanford University* M. ISHIKADO, S. UCHIDA, *Department of Physics, University of Tokyo* Doubling the $CuO_2$ layer is considered to enhance the transition temperature of cuprate superconductors. However, since a recent breakthrough in angle-resolved-photoemission spectroscopy (ARPES) using low-energy excitation photons, it has been controversial whether the nodal bilayer splitting is resolvable or not. We have performed the photon-energy-dependent ARPES study of bilayer cuprate $Bi_2Sr_2CaCu_2O_{8+\delta}$ using low-energy synchrotron radiation ($h\nu = 7$-8 eV). While the bonding and antibonding band are consistently resolved by a constant splitting width of $\Delta k \cong 0.008\text{A}^{-1}$, the spectral weight drastically transfers between them with changing photon energy. The tunable photons enabled us to control the bonding-to-antibonding ratio from 0% to 162%. We will discuss the nodal quasiparticle properties using this bilayer-selective probe.

**12:27**

**Z38 7 Impurity-effect on the electronic structure in $Bi_2Sr_2CaCu_2O_{8+\delta}$ studied by angle-resolved photoemission spectroscopy** KENSEI TERASHIMA, HIROAKI MATSUI, DAISUKE HASHIMOTO, TAKAFUMI SATO, TAKASHI TAKAHASHI, *Department of Physics, Tohoku University* HONG DING, *Department of Physics, Boston College* TAKASHI YAMAMOTO, KAZUO KADOWAKI, *Institute of Materials Science, University of Tsukuba* We studied the impurity effect on the electronic structure near the Fermi level in $Bi_2Sr_2CaCu_2O_{8+\delta}$ by high-resolution angle-resolved photoemission spectroscopy to clarify the origin of dispersion kink in high-$T_c$ superconductors. We found that the dispersion kink at the off-nodal region is significantly suppressed by Zn or Ni impurity while that at the node is less affected. The impurity-induced change of the self-energy and its temperature dependence show a good correspondence to those of the magnetic excitation of $Q = (\pi, \pi)$, suggesting that electrons are strongly coupled to the spin fluctuation at the antinodal region.

**12:39**

**Z38 8 Laser ARPES on the cuprate superconductor Bi2212** JAKE KORALEK, *University of Colorado and NIST* FRASER DOUGLAS, NICK PLUMB, *University of Colorado* ZHE SUN, *University of Colorado and the Advanced Light Source* MARGARET MURNANE, HENRY KAPTEYN, STEVE CUNDIFF, *University of Colorado and NIST* Y. AIURA, K. OKA, H. EISAKI, *AIST* DAN DESSAU, *University of Colorado and NIST* We use 6 eV photons from the fourth harmonic of a Ti:Sapphire laser to perform ARPES on the cuprate superconductor Bi2212. The very low photon energy improves momentum resolution and reduces extrinsic background, offering the clearest picture yet of the single electron spectral function. We will present detailed analysis of the temperature dependence of the nodal spectral lineshapes and compare the predictions of Fermi liquid theory and marginal Fermi liquid theory to what is seen in the data. We will also discuss recent laser ARPES results for overdoped and underdoped Bi2212.

**12:51**

**Z38 9 ARPES investigation of deeply underdoped BISCO 2212** K. TANAKA, W. S. LEE, D. H. LU, T. FUJII, A. FUJIMORI, Z. HUSSAIN, Z. X. SHEN, We present ARPES results from deeply underdoped BISCO 2212 with Tc ranging from 30 to 50 K. The improved sample quality with Y subsitution enables the detection of much sharper spectral features. We uncovered experimental evidence for two distinct energy gaps in these deeply underdoped samples. The theoretical implications of these findings will de discussed in conjunction with ARPES and RAMAN data.

**13:03**

**Z38 10 APRES study of the High temperature cuprates with high superconducting transition temperature ($T_c > 90$K)** WEI-SHENG LEE, WORAWAT MEEVASANA, DONGHUI LU, KYLE SHEN, GUICHUAN YU, XUDONG ZHAO, MARTIN GREVEN, ZHI-XUN SHEN, *Department of Physics and Stanford Synchrotron Radiation Laboratory, Stanford University, Stanford, California, US* WANLI YANG, *Advanced Light Source, Lawrence Berkeley Lab, Berkeley, California, US* AKIRA IYO, HIROSHI EISAKI, *AIST, Japan* The curprates with high superconducting transition temperature, nearly optimally doped $HgBa_2CuO_{4+\delta}$ system ( Hg1201, $T_c$=96K) and nearly optimally-doped $TlBa2Ca_2Cu_3\ O_{8+\delta}$ ( Tl1223, $T_c$=120K), were studied by the Angle Resolved Photoemission Spectroscopy (ARPES). These

materials provide us an opportunity to examine the universal properties of the cuprates and their material dependence trend. Although they are not easy to be cleaved, we managed to measure the band dispersions and the Fermi surfaces of these materials. Interestingly, in Hg1201 system, we found the existence of a quasi-particle peak along (0,0) to ($\pi$, $\pi$) direction (nodal direction); whereas no structure was observed near the zone boundary. Contrarily, in Tl1223 system, a well-defined peak in EDCs was observed near the zone boundary; whereas no peak was observed in the nodal region. A comparison to other most studied cuprates will also be presented.

**13:15**

**Z38 11 Doping dependence study by ARPES on four layered cuprate superconductor $Ba_2Ca_3Cu_4O_8(O_\delta F_{1-\delta})_2$** YULIN CHEN, AKIRA IYO, WANLI YANG, XINGJIANG ZHOU, DONGHUI LU, HIROSHI EISAKI, THOMAS DEVEREAUX, ZAHID HUSSAIN, ZHI-XUN SHEN, An interesting phenomenon in various families of cuprate superconductors is that with the increase of the number of $CuO_2$ layers (which are believed to be responsible for the superconducting phenomenon) within a unit cell of the crystal, the superconducting transition temperature ($T_c$) increases first with the layer number n when n$<$ =3, then decreases when n$>$ 3 and reaches the maximum at n=3. To understand this phenomenon, we investigate a four layered cuprate family $Ba_2Ca_3Cu_4O_8(O_\delta F_{1-\delta})_2$ by Angular Resolved Photoemission Spectroscopy (ARPES). We find that the electronic band structure of this four layered system exhibits clear difference from the previously studied cuprate superconductors with less layers where layers are doped uniformly when n$<$ =2. Our doing ($\delta$) dependence study reveals the band structure, Fermi surface and superconducting gap evolution, with insights on important microscopic process.

**13:27**

**Z38 12 Dimensional crossover in the electronic structure of $(Bi,Pb)_2(Sr,La)_2CuO_{6+\delta}$** T. KONDO, T. TAKEUCHI, *EcoTopia Science Institute, Nagoya Univ., Japan* H. YANG, H. DING, *Dept. of Physics, Boston College* A. KAMINSKI, *Dept. of Physics and Astronomy, Ames Lab.* J.C. CAMPUZANO, *Materials Sciences Division, Argonne National Lab.* The hole-concentration ($p$) dependence of the 3D energy- momentum ($\varepsilon - \boldsymbol{k}$) dispersion in Bi2201 was investigated by ARPES. We observe a significant $\varepsilon - k_z$ dispersion ( $\sim$ 10 meV wide) around ($\pi$,0) in a heavily overdoped sample ($T_c \leq$ 0.5 K). This $\varepsilon - k_z$ dispersion shrinks with decreasing $p$, and is not observed in lightly overdoped and optimally doped samples ($T_c$ = 21 K and 35 K, respectively) indicating a crossover from a 3D to 2D electronic structure.

**13:39**

**Z38 13 Universal spectral weight transfer in high temperature superconductors** JEFF GRAF, *Materials Sciences Division, Lawrence Berkeley Natl. Laboratory, Berkeley, CA 94720, USA* G.-H. GWEON, *Dept. of Physics, University of California Berkeley, CA 94720, USA* K. McELROY, *Materials Sciences Division, Lawrence Berkeley Natl. Laboratory, Berkeley, CA 94720, USA* S.Y. ZHOU, C. JOZWIAK, *Dept. of Physics, University of California Berkeley, CA 94720, USA* E. ROTENBERG, *Advanced Light Source, Lawrence Berkeley Natl. Laboratory, Berkeley, CA 94720, USA* A. BILL, *Dept. of Physics, University of California Berkeley, CA 94720, USA* T. SASAGAWA, *Dept. of Advanced Materials Science, University of Tokyo, Kashiwa, Chiba 277-8561, Japan* H. EISAKI, *AIST, 1-1-1 Central 2, Umezono, Tsukuba, Ibaraki, 305-8568, Japan* S. UCHIDA, *Dept. of Physics, University of Tokyo, Yayoi, 2-11-16 Bunkyoku, Tokyo 113-8656, Japan* H. TAKAGI, *Dept. of Advanced Materials Science, University of Tokyo, Kashiwa, Chiba 277-8561, Japan* D.-H. LEE, A. LANZARA, *Dept. of Physics, University of California Berkeley, CA 94720, USA* High resolution angle resolved photoemission spectroscopy (ARPES) studies of the electronic structure of several cuprate families, over the entire phase diagram, from undoped to highly overdoped regime are reported. A detailed study of the one-electron dynamics as a function of momentum, temperature and doping is presented. A universal spectral weight transfer is observed for all systems and discussed in terms of a strong interplay between the electron-lattice and electron-electron interaction in these materials.

**SESSION Z39: FOCUS SESSION: SUPERCONDUCTIVITY-THEORY AND COMPUTATIONS (MOSTLY PHONONS)**
**Friday Morning, 17 March 2006**
**342, Baltimore Convention Center at 11:15**
**Boldizsar Janko University of Notre Dame, presiding**

**11:15**

**Z39 1 Apical oxygen electron-phonon coupling and poor screening in the cuprates*** THOMAS DEVEREAUX, *University of Waterloo* A theory of the effect of screening in anisotropic planar materials on the electron-phonon coupling for phonon vibrations out of the plane is presented. Specifically it is shown that the poor ability of electrons to propagate along the c-axis has consequences on the screened electron-phonon interaction. A theory for the coupling of charge-transfer excitations to apical oxygen phonons in the cuprates is presented, and strong doping dependence of the magnitude and anisotropy of the electron-phonon coupling is demonstrated.

*Support by Office of Naval Research Grant N00014-05-1-0127

**11:27**

**Z39 2 Interaction of Zhang-Rice singlets with the buckling phonons in Cuprates** EHSAN KHATAMI, ALEXANDRU MACRIDIN, MARK JARRELL, *University of Cincinnati* THOMAS DEVEREAUX, *University of Waterloo* Starting from a fully interacting three-band model we derive an effective single-band Hamiltonian which describes the interaction of Zhang-Rice (ZR) singlets[1] with the buckling phonons. Our approach is based on exact diagonalization of small clusters which contain both Cu and O atoms[2]. We study the parametric dependence of the electron-phonon coupling. The coupling to the phonon mode with $B_{1g}$ symmetry is one order of magnitude stronger than the coupling to the $A_{1g}$ phonon mode and there is an anisotropy in the interaction. For the $B_{1g}$ phonon, the antinodes contribute to the interaction more than the nodes, in agreement with weak coupling approaches[3]. By increasing the O-O hopping, the coupling amplitude becomes smaller in antinodal points. We also find that a simpler model, which considers the modulation of the ZR hopping

by the corresponding bond phonons, captures the symmetry of the electron-phonon interaction. Reference: [1] F. C. Zhang and T. M. Rice, PRB **37**, 3759 (1988) [2] H. Eskes *et.al.*, Physica C **160**, 424 (1989) [3] T. P. Devereaux *et.al.*, PRL **93**, 117004 (2004)

**11:39**

**Z39 3 Anisotropic electron-phonon coupling in Bi2212 and Bi2223*** STEVEN JOHNSTON, *University of Waterloo* THOMAS DEVEREAUX, *University of Waterloo* In this talk we present calculations of self energy effects due to anisotropic electron-phonon coupling in the Bi-family of cuprates. The specific anisotropy of a number of phonon modes yields momentum-dependent signatures in the spectral function and renormalizations in the tunneling density of states both above and below Tc. The spectral functions are compared to angle-resolved photoemission and SIS break junction measurements and renormalizations at specific wavevectors and energies are in accordance with coupling primarily to the B1g phonon. Self-consistent treatment of the electron-phonon interaction is shown to display band renormalizations at energies well above that of the characteristic phonon energy.

*supported by Office of Naval Research N00014-05-1-0127

**11:51**

**Z39 4 Numerical study of the isotope effect of underdoped high-temperature superconductors** ANDREI MISHCHENKO, *CREST, JST* NAOTO NAGAOSA, *CREST, The University of Tokyo* RRC KURCHATOV INSTITUTE TEAM, CERC, AIST TEAM, ERATO-SSH TEAM, We present a numerical study of the isotope effect on the angle resolved photoemission spectra (ARPES) in the undoped cuprates. By the systematic-error-free Diagrammatic Monte Carlo method, the Lehman spectral function of a single hole in the $tt't'' - J$ model in the regime of intermediate and strong couplings to optical phonons is calculated for normal and isotope substituted systems. We found that the isotope effect is strongly energy-momentum dependent, and is anomalously enhanced in the intermediate coupling regime while it approaches to that of the localized hole model in the strong coupling regime. We predict the strengths of effect as well as the fine details of the ARPES lineshape change. Implications to the doped case are also discussed.

**12:03**

**Z39 5 Polaronic effect in lightly doped high-Tc cuprates** TORU SAKAI, *JAEA, SPring-8* DIDIER POILBLANC, *Laboratore de Physique Quantique, Universite Paul Sabatier* The effect of in-plane oxygen phonons is investigated by numerical exact diagonalizations of the t-J Holstein model.[1] The present study indicates that the breathing vibration mode gives rise to a polaronic effect which yields a broadening of the single hole quasiparticle spectrum and a shift from the chemical potential, as the one observed in angle-resolved photoemission spectroscopy.[2] [1] T. Sakai, D.Poilblanc and D.J.Scalapino, Phys. Rev. B 55 (1997) 8445. [2] K. M. Shen et al., Phys. Rev. Lett. 93 (2004) 267002.

**12:15**

**Z39 6 Transport and thermodynamic properties of cuprate superconductors: E(k) dispersion, pseudogap and isotope effects.** JAMES STOREY, *MacDiarmid Institute, Victoria University* JEFFERY TALLON, *MacDiarmid Institute, Industrial Research Ltd and Victoria University* GRANT WILLIAMS, SURESH NARAYANASWAMY, *MacDiarmid Institute, Industrial Research Ltd* We have calculated the thermoelectric power, susceptibility and entropy of Bi-2212 and Bi-2201 using the ARPES-derived energy dispersion, a model scattering rate and including a normal-state pseudogap. The doping and temperature dependence is found to closely mimic the experimentally measured data. We have used this approach to examine isotope effects and in particular note that the kink in the dispersion near $E_F$ (including its isotope effect) can be probed through the high temperature thermoelectric power.

**12:27**

**Z39 7 Renormalization Group Study of the Electron-phonon Interaction in High $T_c$ Cuprates** HENRY FU, *University of California, Berkeley* CARSTEN HONERKAMP, *Institute for Theoretical Physics, Universitat Wuerzburg* DUNG-HAI LEE, *University of California, Berkeley* We apply a numerical renormalization group scheme to study the phonon-mediated retarded interactions in the high $T_c$ cuprates. We find that three sets of phonon-mediated retarded quasiparticle scatterings grow under RG flow. These scatterings share the following common features: 1) the initial and final quasiparticle momenta are in the antinodal regions, and 2) the scattering amplitudes have a $x^2 - y^2$ symmetry. All three sets of retarded interactions are driven to strong coupling by the magnetic fluctuations around $(\pi, \pi)$. After growing strong, these retarded interactions can trigger density wave orders with d-wave symmetry. However, due to the d-wave form factor they will leave the nodal quasiparticle unaffected. We conclude that the main effect of electron-phonon coupling in the cuprates is to promote these density wave orders.

**12:39**

**Z39 8 Phonon renormalization reflecting dynamic charge inhomogeneity in copper-oxide superconductors** D. REZNIK, L. PINTSCHOVIUS, *Forschungszentrum Karlsruhe, Institut für Festkörperphysik, P.O.B. 3640, D-76021 Karlsruhe, Germany* M. ITO, S. IIKUBO, M. SATO, *Department of Physics, Division of Materials Science, Nagoya University, Furo-cho, Chikusa-ku, Nagoya 464-8602, Japan* H. GOKA, M. FUJUTA, K. YAMADA, *Institute for Material Research, Tohoku University, Katahira, Aoba-ku, Sendai, 980-8577, Japan.* G. GU, J. TRANQUADA, *Condensed Matter Physics and Materials Science Department, Brookhaven National Laboratory, Upton, New York 11973-5000, USA* Our inelastic neutron scattering measurements show that there is a strong anomaly in the Cu-O bond-stretching phonon in cup rate superconductors $La_{2-x}Sr_xCuO_4$ (x=0.07,0.15). This behavior also appears in superconducting $YBa_2Cu_3O_{6+x}$, however it is completely absent in undoped and overdoped LSCO. $InLa_{1.875}Ba_{0.125}CuO_4$ and $La_{1.48}Nd_{0.4}Sr_{0.12}LCuO_4$, compounds that exhibit spatially modulated charge and magnetic order, often called stripe order, the anomaly occurs at a wave vector corresponding to the charge order. The results suggest that this giant electron−phonon anomaly, which is absent in LDA calculations, is associated with charge inhomogeneity induced by strong electronic correlations. It follows that electron−phonon coupling may be important to understanding the superconductivity although its contribution to the mechanism is probably non−BCS−like.

**12:51**

**Z39 9 Is room-temperature superconductivity with phonons possible?** MANUEL DE LLANO, *Instituto de Investigaciones en Materiales, UNAM, Mexico City* By recognizing the vital importance of two-hole Cooper pairs in addition to the usual two-electron ones in a strongly-interacting many-electron system, the concept of Cooper pairing was re-examined with striking conclusions, namely gapped and linearly-dispersive resonances with a finite lifetime. Based on this, Bose-Einstein condensation (BEC) theory has been generalized to include not boson-boson interactions (also neglected in BCS theory) but rather boson-fermion interaction vertices reminiscent of the Froehlich electron-phonon interaction in metals. Instead of phonons, the bosons in the generalized BEC (GBEC) theory are now both particle and hole Cooper pairs. Each kind is responsible for half the condensation energy. The GBEC reduces to all the old known statistical theories as special cases—including the so-called ''BCS-Bose crossover'' picture which in turn generalizes BCS theory. With no adjustable parameters, the GBEC theory yields superconducting transition temperatures substantially higher than the BCS limitation of around 45K [including room-temperature superconductivity (RTSC)] without relying on non-phononic dynamics involving excitons, plasmons, magnons or otherwise purely-electronic mechanisms. The results are expected to shed light in the experimental search for RTSCs.

**13:03**

**Z39 10 Duality and normal modes in a Cooper pair Wigner crystal** TAMAR PEREG-BARNEA, *University of Texas* MARCEL FRANZ, *University of British Columbia* A duality transformation from a phase fluctuating d-wave superconductor to a condensed state of vortices shows that Cooper pairs may form a Wigner crystal once the phase fluctuations destroy the superconducting long range order [1]. The lattice constant and the basis of this crystal are consistent with the charge modulations seen by the STM experiments in strongly underdoped cuprates [2]. Based on this vortex-boson duality we suggest a theoretical picture to relate the charge modulations seen by STM and the mysterious increase in the thermal conductivity [3] recently observed in the underdoped non-superconducting state. This addition to the thermal conductivity has bosonic temperature dependence and is attributed within our picture to the vibrational modes of the pair Wigner crystal. We analyze the spectrum of these modes and find it qualitatively consistent with the experimental observations. 1. Z. Tesanovic, Phys. Rev. Lett. 93, 217004 (2004). 2. J. E. Hoffman et al., Science 295, 466 (2002). 3. L. Taillefer (unpublished).

**13:15**

**Z39 11 Cooper-Pair Molasses: Cooling a nanomechanical resonator with quantum backaction** A.K. NAIK, O. BUU, M.D. LAHAYE, K.C. SCHWAB, *Laboratory for Physical Science* A.D. ARMOUR, *School of Physics and Astronomy, University of Nottingham, Nottingham, United Kingdom* A.A. CLERK, *Department of Physics, McGill University, Montreal, QC Canada* M.P. BLENCOWE, *Department of Physics and Astronomy, Dartmouth College, Hanover, NH USA* We have measured the back-action of a superconducting single electron transistor using a radio frequency nanomechanical resonator. The backaction forces are a factor of 15 above the intensity required by the Heisenberg uncertainty principle: $\sqrt{S_x S_f} = 15\hbar/2$. This system has also shown a record position and force sensitivity of $0.4fm/\sqrt{Hz}$ and $0.5aN/\sqrt{Hz}$, and the closest approach to the quantum ground state of a mechanical system (N=25) (1). In addition, we have discovered a novel cooling mechanism, analogous to optical molasses, which is a result of resonant Josephson effects in the transistor (2,3). Using devices of similar design and performance, we are anticipating the observation of squeezed, superposition, and entangled states of a mechanical device. 1. M.LaHaye, O. Buu, B. Camarota, K. Schwab, Science 304, 74 (2004). 2. M. P. Blencowe, J. Imbers and A. D. Armour, xxx.lanl.gov/ cond-mat/0507645. 3. A. A. Clerk, S. Bennett, xxx.lanl.gov/ cond-mat/0507646.

**13:27**

**Z39 12 Real-Space Picture of the Cooper Pair** ALAN M. KADIN, *Princeton Junction, NJ 08550* The Cooper pair is generally analyzed in momentum space, but its real-space structure also follows directly from the BCS theory. From this viewpoint [1], a Cooper pair consists of a spherical quasi-atomic wavefunction of radius $\sim \pi\xi_0$ for both electrons, with radial nodes separated by $\pi/k_F$. An induced commensurate quasi-static charge modulation in the underlying lattice provides the interaction potential, similar to that in the simple BCS approximation, which leads to a bound state. This picture can be generalized for alternative pairing symmetries (p or d-wave) as well as alternative pairing mechanisms (excitonic or spin-based) and extended to disordered superconductors. While it does not derive essentially new physics, this real-space approach may provide a more heuristic picture for developing and understanding new phenomena in superconductivity. [1] A.M. Kadin, http://www.arxiv.org/abs/cond-mat/0510279

**13:39**

**Z39 13 Cooper pairs on a spherical surface*** JACQUES TEMPERE, VLADIMIR GLADILIN, *Universiteit Antwerpen* ISAAC SILVERA, *Harvard University* JOZEF DEVREESE, *Universiteit Antwerpen* Superconductivity has been widely studied for flat, two-dimensional electron systems, such as electrons in copper-oxide planes or electron films on helium. In this contribution, we investigate how Cooper pairing is affected by curvature. In particular we investigate the pairing correlations of a spherical, two-dimensional electron gas. This system is realized in for example multielectron bubbles, and in metallic nanoshells. For the case of multielectron bubbles, the pairing Hamiltonian can be solved exactly using Richardson's method. This reveals not only the structure of the ground state, but also the density of states of the excited states. We find that in the ground state, a redistribution of the electrons over the angular momentum levels occur, and that in the density of states a pseudogap appears. These results are put in the context of multielectron bubbles in helium, and compared to those for a flat 2D electron system.

*Financial support from FWO, BOF NOI UA, IUAP, DoE is acknowledged.

**13:51**

**Z39 14 Cooper Pair Wavefunction Approach to the AC Josephson Effect** YONG-JIHN KIM, *University of Puerto Rico - Mayaguez* Recently, we have proposed Cooper pair wavefunction approach to the DC Josephson effect, which shows the threshold resistance of SIS Josephson junctions (in the high tunneling resistance regime). In the $MgB_2$case, since the threshold resistance is so small for the big gap, $MgB_2$break junctions and SIS tunnel junctions display the Josephson supercurrent only for the small gap. We apply this approach to the AC Josephson effect. The amplitude of the oscillating supercurrent in the presence of the electric field is calculated, using the Cooper pair wavefunctions formed by the Airy functions. We also discuss the sign problem of the pair-quasi-particle interference term.

**SESSION Z40: SOLID STATE QUANTUM COMPUTING II**
**Friday Morning, 17 March 2006**
**343, Baltimore Convention Center at 11:15**
**Mark Gyure, HRL Laboratories, presiding**

**11:15**

**Z40 1 Double quantum dot coupled to a superconducting single-electron transistor for measurement of back action** MADHU THALAKULAM, *Rice University, Houston, TX 77005* JOEL STETTENHEIM, A. J. RIMBERG, *Dartmouth College, Hanover, NH 03755* L.N. PFEIFFER, K. W. WEST, *Bell Laboratories, Lucent Technologies Inc., Murray Hill, NJ 079745* The superconducting single electron transistor SET is a highly sensitive electrometer operating near the quantum limit. The back action current noise of the SET has been a topic of interest ever since the SET was proposed as a readout device for charge or spin based qubits [1]. We study the back-action noise of a superconducting SET by means of an electrostatically coupled double quantum dot (DQD) system. Inelastic current through the DQD is sensitive to the spectral density of voltage fluctuation in its electromagnetic environment [2,3]. By properly choosing the dot size and inter-dot tunnel barrier, one can cause inelastic processes to dominate the transport. A measurement of the inelastic current through the double dot system can then be used to calculate the spectral density of quantum noise associated with the RF-SET and hence its back-action. We have fabricated samples consisting of a DQD formed in a GaAs/AlGaAs heterostructure and strongly coupled to an Al/$AlO_x$/Al SET@. Recent results of measurements on such devices will be discussed. [1] M.H. Devoret and R.J. Schoelkopf, Nature, **406**, 1039(2000). [2]T. Fujisawa et al., Science, **282**, 932 (1998). [3]R. Aguado and L. P. Kouwenhoven, Phys. Rev. Lett., **84**, 1986(2000).

**11:27**

**Z40 2 Quantum Capacitance for Quantum Computation** C.M. WILSON, T. DUTY, F. PERSSON, M. SANDBERG, G. JOHANSSON, L. TORNBERG, J. BYLANDER, P. DELSING, *Chalmers University* We present measurements of superconducting quantum bit (qubit) circuits utilizing the quantum capacitance (QC) of a single cooper-pair box (SCB). The QC is essentially the curvature of the SCB energy bands near the charge degeneracy point, and has recently been measured by our group and others. The curvature arises from the avoided level crossing induced by the Josephson coupling of the SCB. The QC can be much larger than the geometric capacitance, and changes sign between the ground and excited states. We present a qubit with integrated readout that embeds a SCB in a resonant circuit and detects changes in the QC as changes in the phase of a reflected microwave signal. We have calculated that this readout method is strictly quantum limited independent of the quality factor (Q) of the the resonator. This allows great flexibility in the design and optimization of the readout. Calculations show that the method should be able to achieve single-shot discrimination of the qubit state under realistic experimental conditions. We also present preliminary measurements of coupled qubit circuits, with both fixed coupling and a variable coupling scheme based on the ground-state QC.

**11:39**

**Z40 3 Manipulation and readout of deep-submicron Nb-trilayer-based persistent-current qubits*** DAVID M. BERNS, SERGIO O. VALENZUELA, *MIT* WILLIAM D. OLIVER, *MIT Lincoln Laboratory* TERRY P. ORLANDO, *MIT* Lithographically patterned persistent-current (PC) qubits are promising candidates for realizing a large-scale quantum computer. While challenging to fabricate in a trilayer technology, deep-submicron Josephson junctions (JJs) are required to realize large qubit tunnel-couplings and allow improved immunity to dielectric-induced decoherence. Here, we present recent results on the measurement and characterization of PC qubits designed with deep-submicron JJs and fabricated with Nb-Al/AlOx-Nb trilayers.

*This work is supported in part by the AFOSR grant F49620-01-1-0457 under the DoD University Research Initiative on Nanotechnology (DURINT) Program and the AFOSR/NM grant FA 9550-04-1-0221.

**11:51**

**Z40 4 Macroscopic Quantum Coherence in a Multi-Level Nb Persistent-Current Qubit*** YANG YU, *MIT* W. D. OLIVER, *MIT Lincoln Laboratory* J. C. LEE, K.K. BERGGREN, L.S. LEVITOV, T.P. ORLANDO, *MIT* We drove a niobium persistent-current qubit with strong microwaves and observed single-, two-, and three-photon transitions between its macroscopic quantum states. A multi- level energy-band diagram was extracted by mapping the frequency of the induced transitions as a function of applied magnetic flux to the qubit, and the anti-crossing caused by the superposition between the third and fourth excited states were directly measured. The energy relaxation time T1 between two states connected by multi-photon transitions ranged from 30 to 100 ms. In addition, three-photon coherent temporal oscillations between the ground state and fourth excited state were observed with a decoherence time of approximately 50 ns.

*Supported by AFOSR Grant No. F49620-01-1-0457 and the DOD under the Air Force, Contract No. F19628-00-C-0002

**12:03**

**Z40 5 Electronic control and readout of qubit states in Si:Li-based quantum computing system** V.V. OSIPOV, V.N. SMELYANSKIY, *NASA Ames Research Center, Moffett Field, CA* A.G. PETUKHOV, *Physics Department, South Dakota School of Mines and Technology* In our previous work (V. N. Smelyanskiy *et al.* Phys. Rev. B **72**, 081304 (2005)) we predicted a gigantically long lifetime of the first excited state of an interstitial lithium donor in silicon. The nature of this effect roots in the anomalous level structure of the 1*s* Li manifold under external stress. Namely, the coupling between the lowest two states of the opposite parity is very weak and occurs via intervalley phonon transitions only. We proposed to use these states under the controlled ac and dc stress to process quantum information. In this work we consider some practical aspects of the proposed scheme such as formation of heavily doped semiconductor electrodes for electrical control of the qubit states and single-qubit readout by means of the resonant tunneling stimulated by polarized infrared radiation. We propose a proof-of-the principle experiment on photo-stimulated time-dependent resonant tunneling in a $\delta$-doped layer of Li donors in Si placed between two $n^+$ Si electrodes. The effect will be characterized by a high sensitivity of the signal to the polarization of photons and by long-term relaxation of the resonant tunneling photocurrent.

**12:15**

**Z40 6 Single electron tunneling in a controllable electromagnetic environment** Z. JI, *Rice University* W. XUE, A.J. RIMBERG, *Dartmouth College* L.N. PFEIFFER, K.W. WEST, *Bell Laboratories* Real-time counting of single electrons is the most fundamental means of measuring current [1]. Direct observation of single electron tunneling oscillations requires embedding a tunnel barrier in a high-impedance electromagnetic environment. Beginning with a two dimensional electron gas in a GaAs heterostructure we first etch a narrow mesa to serve as a conducting channel. We fabricate two staggered arrays of quantum point contacts (QPCs) across the mesa to serve as ballistic resistors controlled by tuning the QPC gate voltage. An additional QPC placed between the arrays serves as the tunnel barrier and a nearby radio-frequency single electron transistor (RF-SET) serves as an electrometer. We have fabricated several such samples. Typically the conductance G versus gate voltage of such an array of 10 QPCs shows plateau-like structures at fractions of the conductance quantum, $G_0 = 2e^2/h$. The first plateau, below which the conductance drops rapidly to zero, is the preferred working point corresponding to one open channel in each QPC. When the arrays are at their working points and the central barrier is formed, the samples show a large gap in their I-V characteristics corresponding to dynamical Coulomb blockade. Recent measurements of such samples will be presented, and the use of the RF-SET to directly observe single electron tunneling will be discussed. [1] J. Bylander, T. Duty and P. Delsing, Nature **434**, 361 (2005).

**12:27**

**Z40 7 Calculated tunneling rates for single electron charging events in Vertical ''Enhancement Mode'' quantum dot devices.** RICHARD ROSS, MARK GYURE, *HRL Laboratories, LLC* CHRIS ANDERSON, *Dep't of Mathematics, UCLA* We report on calculations of tunneling rates associated with single electron charging events in vertical ''enhancement mode'' quantum dot device structures. These devices consist of two vertically stacked quantum well layers. A pair of surface depletion gates define a Quantum Point Contact (QPC) and a single localized enhancement gate creates a quantum dot (QD) in the upper quantum well. Single electron charging events in this device occur via tunneling between the vertically separated QD and QPC states. Tunneling rates are computed using Fermi's Golden Rule based on numerical eigenstates derived from fully 3-dimensional self-consistent Poisson-Schroedinger calculations. The effects of coulomb interaction on the quantum dot states and hence tunneling rates will be considered. Additionally, a comparison of these numerical results with experimental estimates of tunneling rates derived from random telegraph signals will be presented.

**12:39**

**Z40 8 Observation of Sequential Single Electron Charging in Vertical ''Enhancement Mode'' Quantum Dot Devices*** EDWARD CROKE, GEOFFREY SIMMS, MARK GYURE, *HRL Laboratories, LLC* The vast majority of devices currently being explored for quantum information processing with semiconductor quantum dots rely on multiple surface gates operating in reverse bias (depletion mode) to constrict a buried 2D electron gas to the few electron regime. Although successful in demonstrating one and two qubit operations, they are unlikely to scale to large arrays that are needed to perform practical quantum information processing. In this talk, we present the first experimental results from a new type of ''enhancement mode'' device that requires only a single gate electrode operating in forward bias to create a few electron quantum dot. We observe random telegraph signals in several well defined regions of gate voltage, indicative of single electrons tunneling between states of the quantum dot and the readout channel. The absence of these signatures below a particular gate voltage suggests that these quantum dots are in the few electron regime and can be easily depleted to contain only one electron.

*This work was supported by the Defense Advanced Research Projects Agency and the Army Research Office under Contract Number DAAD19-01-C-0077.

**12:51**

**Z40 9 Analysis of Random Telegraph Signals from Vertical ''Enhancement Mode'' Qunatum Dot Devices** MARK GYURE, GEOFFREY SIMMS, RICHARD ROSS, EDWARD CROKE, *HRL Laboratories, LLC* Clear signatures of single electron tunneling in vertical ''enhancement mode'' semiconductor quantum dot devices have recently been observed. These devices hold great promise for future scalability of semiconductor-based quantum information processing because they require only a single gate electrode to create the quantum dot. In this talk, we present a detailed analysis of the random telegraph signals observed in these devices as various N to N+1 electron transitions are swept through by varying the gate voltage and magnetic field. This analysis allows us to extract a variety of information about the transitions and further supports our conclusion that electrons are tunneling between the gate-induced quantum dot and the readout channel below. Results of self-consistent Schrodinger-Poisson simulations of these devices are presented that also support this interpretation of the experimental results.

**13:03**

**Z40 10 MOSFET-like single electron transistor built in pure silicon** G.M. JONES, B.H. HU, C.H. YANG, *Department of Electrical and Computer Engineering, University of Maryland at College Park* M.J. YANG, *Naval Research Laboratory* Solid state implementations of qubits offer the advantage of being scalable, and, in particular, those based on semiconductors can be integrated by existing technologies. The two Zeeman states of an electron spin in a quantum dot (QD) provide a promising candidate for a qubit, and lateral quantum dots provide the best opportunity for scaling. Spins in lateral QDs in the GaAs/AlGaAs single electron transistors (SETs) have been intensively investigated. In contrast, Si provides a number of advantages, including long spin coherence time, large g-factor, and small spin-orbit coupling effect. However, isolation of a single electron in a Si QD has not yet been achieved. We will report a fabrication technique that utilizes the established MOSFET concept on highly resistive Si substrates in order to minimize the potential disorder resulting from impurities. In our approach, 2D (or 1D) electrons are induced by a top gate, which laterally overlaps with the ion-implanted source/drain, but vertically separated by SiO2. Several side gates buried in the SiO2 help define the tunneling barriers and control the number of electrons in the island. We will discuss the operating principle, computer simulation, and experimental results that confirm the validity of the design concept.

**13:15**

**Z40 11 Proposal to stabilize and detect half-quantum vortices in strontium ruthenate thin films: Non-Abelian braiding statistics of vortex matter in a $p_x + ip_y$ superconductor*** SUMANTA TEWARI, SANKAR DAS SARMA, *Condensed Matter Theory Center, Department of Physics, University of*

*Maryland, College Park, MD 20742* CHETAN NAYAK, *Microsoft Research, Project Q, Kohn Hall, University of California, Santa Barbara, CA 93108* We propose a simple way to stabilize half-quantum vortices in superconducting strontium ruthenate, assuming the order parameter is of chiral $p_x + ip_y$ symmetry, as is suggested by recent experiments. The method, first given by Salomaa and Volovik in the context of Helium-3, is very naturally suited for strontium ruthenate, which has a layered, quasi-two-dimensional, perovskite crystal structure. We propose possible experiments to detect their non-abelian braiding statistics. These experiments are of potential importance for topological quantum computation.

*Work supported by the ARO-ARDA

**13:27**

**Z40 12 Measurement errors for phase qubits*** QIN ZHANG, ABRAHAM KOFMAN, ALEXANDER KOROTKOV, *University of California, Riverside* We analyze error mechanisms in measurement of superconducting phase qubits, including measurement cross-talk for two coupled phase qubits and effect of nonadiabaticity during the measurement pulse. Each qubit is represented by a fictitious particle moving in an asymmetric double-well potential. A measurement, e.g., of the state $|10\rangle$ perturbs the second qubit which may result in a wrong measurement result $|11\rangle$. In the study of this cross-talk the first qubit is described classically, since it is highly excited, whereas the second qubit can be treated either classically or quantum- mechanically. We obtain conditions for minimizing the cross- talk. We also study the nonadiabatic errors for different shapes and durations of the measurement pulse and discuss optimal conditions for fast and reliable measurements.

*Supported by NSA/ARDA/ARO grant

**13:39**

**Z40 13 Entanglement distillation by adiabatic passage in coupled quantum dots*** JAROSLAV FABIAN, *University of Regensburg* ULRICH HOHENESTER, *University of Graz* Adiabatic passage of two correlated electrons in three coupled quantum dots is shown to provide a robust and controlled way of distilling, transporting and detecting spin entanglement, as well as of measuring the rate of spin disentanglement. Employing tunable interdot coupling the scheme creates, from an unentangled two-electron state, a superposition of spatially separated singlet and triplet states. A single measurement of a dot population (charge) collapses the wave function to either of these states, realizing entanglement to charge conversion. The scheme is robust, with the efficiency close to 100%, for a large range of realistic spectral parameters.

*Work supported by US ONR

**13:51**

**Z40 14 Detecting the squeezing and entanglement of nanomechanical modes: a practical scheme** L. TIAN, S. M. CARR, *National Institute of Standards and Technology, 100 Bureau Drive, Stop 8423, Gaithersburg, MD 20899* Nanomechanical systems are promising candidates for realizing the continuous variable protocols of quantum information processing. The detection of the squeezing and entanglement of nanomechanical modes is a crucial step towards such applications. Here, we show that by coupling a nanomechanical mode with another continuous variable mode – a superconducting phase variable, the squeezing and entanglement can be observed within current experimental techniques.

## SESSION Z45: MOSTLY SPINELS
**Friday Morning, 17 March 2006**
**348, Baltimore Convention Center at 11:15**
**S H Lee, University of Virginia, presiding**

**11:15**

**Z45 1 $Ba_2CoO_4$: Crystal Growth, Structure Refinement, and Physical Properties*** RONGYING JIN, *Oak Ridge National Laboratory* HAO SHA, *Florida International University* PETER KHALIFAH, *Oak Ridge National Laboratory and University of Massachusetts* RICHARD SYKORA, BRIAN SALES, DAVID MANDRUS, *Oak Ridge National Laboratory* JIANDI ZHANG, *Florida International University* Single crystalline $Ba_2CoO_4$ is grown for the first time using the floating-zone technique. Single-crystal refinement of X-ray diffraction data indicates that $Ba_2CoO_4$ has a monoclinic structure with $a = 5.9176(13)$ Å, $b = 7.6192(16)$ Å, $c = 10.3790(22)$ Å, and ß $= 91.734(4)^o$ at room temperature. Magnetic susceptibility, specific heat, and thermal conductivity show anomalies at $T_N = 25$ K, due to antiferromagnetic ordering. However, the magnitude of the Néel temperature $T_N$ is significantly lower than the Curie-Weiss temperature ($|\Theta| \sim 110$ K), suggesting either reduced-dimensional magnetic interactions and/or the existence of magnetic frustration. The latter may be induced by disorder evident from the variable-range-hopping behavior in electrical resistivity, non-zero T term in specific heat and $T^2$ dependence in thermal conductivity at low temperatures.

*ORNL is managed by UT-Battelle, LLC, for the U.S. DOE under contract DE-AC05-00OR22725. Work at FIU is supported by the U.S. DOE-FG02-05ER46125 and NSF DMR-0346826.

**11:27**

**Z45 2 Spin disordered state of the triangular lattice antiferromagnet $NiGa_2S_4$*** SATORU NAKATSUJI, YUSUKE NAMBU, HIROSHI TONOMURA, OSAMU SAKAI, *Department of Physics, Kyoto University, Kyoto 606-8502, Japan* SETH JONAS, COLLIN BROHOLM, *Department of Physics and Astronomy, Johns Hopkins University, Baltimore, MD 21218, USA* HIROKAZU TSUNETSUGU, *Yukawa Institute for Theoretical Physics, Kyoto University, Kyoto 606-8502, Japan* YIMING QIU, *NIST Center for Neutron Research, NIST, Gaithersburg, MD 20899, USA* YOSHITERU MAENO, *Department of Physics, Kyoto University, Kyoto 606-8502, Japan* We have recently found a spin disordered state in two dimensions in $NiGa_2S_4$, a bulk insulating antiferromagnet on a triangular lattice.Despite strong antiferromagnetic interactions of $\sim$ 80 K, no magnetic long-range order has been observed down to 0.35 K where we instead find nano-scale quasi-static correlation. The spin disordered state appears on cooling through highly degenerate states with an entropy plateau, and exhibits gapless linearly dispersive modes, suggesting

coherence beyond the two-spin correlation length. A possible ground state will be discussed.

*This work was supported in part by Grants-in-Aid for Scientific Research from JSPS.

**11:39**

**Z45 3 Incommensurate spin correlations in a spin-1 triangular lattice antiferromagnet** SETH JONAS, CHRIS STOCK, COLLIN BROHOLM, *Department of Physics and Astronomy, Johns Hopkins University, Baltimore, MD 21218, USA* SATORU NAKATSUJI, YUSUKE NAMBU, HIROSHI TONOMURA, OSAMU SAKAI, YOSHITERU MAENO, *Department of Physics, Kyoto University, Kyoto 606-8502, Japan* Spin correlations in the triangular lattice antiferromagnet NiGa2S4 were investigated as a function of temperature and magnetic field through neutron scattering. At T=1.5 K the in plane correlations are incommensurate with a wave vector $(\frac{1}{6} - \delta, \frac{1}{6} - \delta, 0)$ where $\delta = 0.00866$. The in-plane correlation length is 6.9(8) lattice spacings while inter-plane correlations cannot be detected beyond the second nearest plane. These correlations persist on a time scale that exceeds 0.3 ns. Application of an in-plane magnetic field of 10 Tesla only slightly reduces the inter-plane correlations with no appreciable effect on intra-plane correlations, while heating reduces the frozen moment, the in-plane correlation length, and the correlation time. We shall discuss what can be inferred about the spin Hamiltonian for NiGa2S4 as well as the spin-1 triangular lattice antiferromagnet from these data.

**11:51**

**Z45 4 Nonmagnetic impurity effects of the spin disordered state in $NiGa_2S_4$*** YUSUKE NAMBU, SATORU NAKATSUJI, YOSHITERU MAENO, *Department of Physics, Kyoto University* Nonmagnetic impurity effects of the spin disordered state in the triangular antiferromagnet $NiGa_2S_4$ [1] was studied through magnetic and thermal measurements for Zn substituted insulating materials $Ni_{1-x}Zn_xGa_2S_4$ $(0.0 \leqslant x \leqslant 0.3)$[2]. Only 1 % Zn substitution is enough to strongly suppress the coherence observed in the spin disordered state. However, suppression is not complete and the robust feature of the quadratic temperature dependent specific heat and its scaling behavior with the Weiss temperature indicate the existence of a coherent Nambu-Goldstone mode. Absence of either conventional magnetic long-range order or bulk spin freezing suggests a novel symmetry breaking of the ground state. [1] Satoru Nakatsuji, Yusuke Nambu, Hiroshi Tonomura, Osamu Sakai, Seth Jonas, Collin Broholm, Hirokazu Tsunetsugu, Yiming Qiu and Yoshiteru Maeno, Science **309**, 1697 (2005). [2] Yusuke Nambu, Satoru Nakatsuji and Yoshiteru Maeno, preprint.

*This work was supported in part by Grants-in-Aid for Scientific Research from JSPS

**12:03**

**Z45 5 Novel spin structures in Mn and Co chromite** THOMAS KAPLAN, *Michigan State University* The ferrimagnetic or conical spiral (FS), a variational approximation to the ground state of the classical Heisenberg model with competing AB and BB interactions in cubic spinels[1], is in qualitative to quantitative agreement with neutron diffraction (ND) results for $MnCr_2O_4$ and $CoCr_2O_4$. [2] This despite its local instability for the experimental parameter values.[1] It also was used to interpret related NMR studies.[3] Understanding recent ND experiments[4] on both materials again was generally based on the FS. However, these measurements, done on single crystals, and with highly improved resolution, uncovered a subtle but important modification of the FS: while the fundamental Bragg peaks (originating from the spin components along the cone axes) are typical, the satellite peaks (coming from the transverse or spiral components) are broadened.[4] Efforts to understand this based on the classical spin model will be discussed. 1. D. H. Lyons et al., Phys. Rev. **126**, 540 (1962). 2. J. Hastings et al., Phys. Rev. **126**, 556 (1962). N. Menyuk et al., J. de Physique **25**, 528 (1964). 3. A. J. Heeger et al., J. Phys. Chem Solids **29**, 1085 (1968); T. Tsuda et al., Solid State Comm. **9**, 2207 (1971). 4. K. Tomiyasu et al., Phys. Rev. B **70**, 214434 (2004).

**12:15**

**Z45 6 Competing phases in a frustrated magnet: a study with neutron scattering.*** DAVID HSIEH, *Princeton University* YINWAN LI, ZHIMING TAN, ROBERT CAVA, ZAHID HASAN, *Princeton University* YIMING QIU, JAE-HO CHUNG, JEFFREY LYNN, *NIST* Zero-field magnetic neutron diffraction on the pyrochlore magnet $ZnCr_2S_4$ reveals successive phase transitions from a paramagnet into a helical ($T_{N1} = 13$ K) then collinear ($T_{N2} = 8$ K) spin ordered state as the system is cooled. This occurs as the system crosses a critical line in $J_1$-$J_2$ space, where $J_1$ and $J_2$ are the first and second nearest neighbor exchange constants respectively. We report the magnetic field dependence of the dc susceptibility and neutron scattering of $ZnCr_2S_4$ in the form of a temperature-field phase diagram. We also study the low energy excitation spectrum of $ZnCr_2S_4$ which was found to be consistent with the $J_1$-$J_2$ model.

*This work is supported by NSF

**12:27**

**Z45 7 Quantum effects in a half-polarized pyrochlore antiferromagnet** DORON BERGMAN, RYUICHI SHINDOU, *Department of Physics, UC Santa Barbara* GREGORY FIETE, *Kavli Institute for Theoretical Physics, UC Santa* LEON BALENTS, *Department of Physics, UC Santa Barbara* We study quantum effects in a spin-3/2 antiferromagnet on the pyrochlore lattice in an external magnetic field, focusing on the vicinity of a plateau in the magnetization at half the saturation value, observed in $CdCr_2O_4$ and $HgCr_2O_4$. Our theory, based on quantum fluctuations, results in an effective quantum dimer model of the dynamics. We predict the existence of a symmetry-broken ground state on the plateau, even with only nearest-neighbor microscopic exchange. This symmetry broken state consists of a particular arrangement of spins polarized parallel and antiparallel to the field in a 3:1 ratio on each tetrahedron. It quadruples the lattice unit cell, and reduces the space group from $Fd\bar{3}m$ to $P4_332$. We also predict that for fields just above the plateau, the low temperature phase has transverse spin order, describable as a Bose-Einstein condensate of magnons. Other comparisons to and suggestions for experiments are discussed.

**12:39**

**Z45 8 Ordering in a frustrated pyrochlore antiferromagnet proximate to a spin liquid** GREGORY A. FIETE, *Kavli Institute for Theoretical Physics, UC Santa Barbara* DORON L. BERGMAN, LEON BALENTS, *Department of Physics, UC Santa Barbara* We perform a general study of spin ordering on the pyrochlore lattice with a 3:1 proportionality of two spin polarizations[1]. Equivalently, this describes valence bond solid conformations of a quantum dimer model on the diamond lattice. We determine the set of likely low temperature ordered phases, on

the assumption that the ordering is weak, i.e the system is close to a ''U(1)'' quantum spin liquid in which the 3:1 proportionality is maintained but the spins are strongly fluctuating. The nature of the 9 ordered states we find is determined by a ''projective symmetry'' analysis. All the phases exhibit translational and rotational symmetry breaking, with an enlarged unit cell containing 4 to 64 primitive cells of the underlying pyrochlore. The simplest of the 9 phases is the same ''R'' state found earlier in a theoretical study[2] of the ordering on the magnetization plateau in the $S = 3/2$ materials $CdCr_20_4$ and $HgCr_20_4$. We suggest that the spin/ dimer model proposed therein undergoes a direct transition from the spin liquid to the R state, and describe a field theory for the universal properties of this critical point, at zero and non-zero temperatures. [1] D. L. Bergman, G. A. Fiete, and L. Balents, cond-mat/0511176. [2] D. L. Bergman, R. Shindou, G. A. Fiete, and L. Balents, cond-mat/0510202.

**12:51**

**Z45 9 Nature of magnetic structure in a geometrically frustrated manganite spinel** KAZUYA KAMAZAWA, ZHE ZHANG, DESPINA LOUCA, *Dept. of Physics, University of Virginia* Unlike the pyrochlore geometrically frustrated magnets, several normal spinels such as $ZnCr_2O_4$ and $ZnV_2O_4$ undergo magnetic long-range order as well as cubic to tetragonal structural transitions at low temperatures. By comparison, $ZnMn_2O_4$, although tetragonal at room temperature, does not undergo a magnetic transition in spite of the rather large Curie-Weiss temperature of $\sim$ -800K indicative of strong antiferromagnetic fluctuations. The absence of an antiferromagnetic transition is surprising considering the nature of the $Mn^{3+}$ ion that is Jahn-Teller active and its effect on the ground state degeneracy. With the orbital degree of freedom active and a crystal anisotropy created by the Jahn-Teller octahedral distortions the system is tetragonally distorted just as in the vanadates where the V ion is orbitally active, but no magnetic transition is observed. Using neutron scattering we investigated how the magnetic structure changes as a function of temperature. We observed the presence of incommensurate magnetic peaks close to nuclear Bragg peaks that exhibit a first order phase transition. The FWHM of the magnetic peaks is much wider than that of nuclear peaks that indicates that the magnetic order is short range. Considering the 1-dimensional Boner-Fisher like behavior of the bulk susceptibility, it is proposed that the spin structure is helical and one-dimensional.

**13:03**

**Z45 10 Local structural disorder by chemical pressure in geometrically frustrated magnets, $Cd_{1-x}Zn_xV2O4$** ZHE ZHANG, DESPINA LOUCA, ALINA VISINOIU,*SEUNGH-HUN LEE, *University of Virginia* The orbital degree of freedom plays an important role in the physics of frustration in $Cd_xZn_{1-x}V2O4$ spinels. The magnetic and structural properties for $0 < =x < =1$ compounds were investigated using neutron scattering. While the end members, x = 0 and 1, are magnetically frustrated in the high temperature cubic phase, the frustration is relieved with the transformation to the tetragonal Néel state through a spin-orbital coupling mechanism. In the doped compounds, both macroscopic transitions are absent due to the local randomness induced by the difference in the chemical pressure imposed by Zn and Cd ions. This leads to the loss of cooperative orbital ordering and suppression of any long range antiferromagnetic coupling. However, from the local atomic structure it is deduced that in the mixed compounds the local environments around Zn and Cd ions correspond to ZnV2O4 and CdV2O4, respectively. Thus locally short-range orbital ordering is possible that explains why the magnetic exchange interactions remain largely unchanged with doping.

*formerly from the Unversity of Virginia

**13:15**

**Z45 11 Magnetic ordering in $EuNiO_3$ and $NdNiO_3$** JOCHEN LITTERST, *TU Braunschweig, Germany* ELISA BAGGIO-SAITOVITCH, ALEXANDER CAYTUERO, *CBPF, Rio de Janeiro, Brazil* MOHSEN ABDELMEGUID, HANS MICKLITZ, *University of Cologne, Germany* J.A. ALONSO, *CSIC, Madrid, Spain* We report Mössbauer and magnetization studies on $^{57}Fe$:$EuNiO_3$ and $^{57}Fe$:$NdNiO_3$ between 1.5 K and 300 K. Below $T_N \approx$ 190 K and 132 K for the Eu and the Nd compound, resp., the Mössbauer spectra reveal two magnetically inequivalent Ni (Fe) sites. Roughly 50% of the spectral area split into a sextet (A) with a well defined magnetic hyperfine field. The spectra A are due to the antiferromagnetically ordered Ni sublattices. The other 50% of the spectral area remain unsplit and only gradually broaden on decreasing temperature (spectra B). The observation of two kinds of magnetically inequivalent Ni(Fe) sites is both compatible with charge ordering or orbital ordering leaving 50% of Ni sites frustrated. Spectrum B is typical for a slowing down magnetic fluctuations. A best approach is yielded by a model allowing for stochastic jumps of the hyperfine field in random directions. Both compounds yield nearly identical fluctuation rates with a roughly linear temperature dependence indicating that the influence of the magnetic moment of the rare earth on Ni is negligible.

**13:27**

**Z45 12 Ultrasonic Study of Critical Behavior in the Magnetic Phase Diagram of $CsNiCl_3$*** G. QUIRION, X. HAN, M. L. PLUMER, *Department of Physics, Memorial University, St.-John's, NL, Canada* M. POIRIER, *Department of Physics, Sherbrooke University, Sherbrooke, Qc, Canada* It is now well established that many quasi-one-dimensional frustrated triangular antiferromagnets of the $ABX_3$ family exhibit exotic magnetic phase diagrams with new types of multicritical points [1]. Nevertheless, investigations into the nature of some phase boundaries remain controversial. While some theoretical and numerical studies suggest new chiral universality classes, others conclude these transitions are weakly first order [2]. Results are presented here of a systematic investigation of the critical behavior associated with the magnetic field - temperature phase diagram of $CsNiCl_3$ using high resolution ultrasonic measurements of the elastic constants, along with analysis based on a Landau-type model of magneto-elastic coupling [3]. In particularly, we will show how it is possible to obtain very reliable values for the critical exponents associated with the transitions to elliptical and the spin-flop ordered states. Exponent estimates very close to the multicritical point are also presented. [1] M.L. Plumer et al, in Magnetic Systems with Competing Interactions, Ed. H.T. Diep (World Scientific, Singapore, 1994). [2] A. Peles et al, Phys. Rev. B 69, 220408 (R) (2004). [3] G. Quirion, T. Taylor and M. Poirier, Phys. Rev. B 72, 094403 (2005).

*Supported by grants from NSERCand CFI

**SESSION Z46: 2D MULTI-VALLEY SYSTEMS: QHE EXPERIMENT**
**Friday Morning, 17 March 2006**
**349, Baltimore Convention Center at 11:15**
**Bruce Kane, University of Maryland, presiding**

**11:15**
**Z46 1 Observation of Inter-valley Gap Anomaly in Two Dimensional Electrons in Si** K. LAI, T.M. LU, D.C. TSUI, S.A. LYON, *Princeton University* W. PAN, *Sandia National Laboratories* M. MUHLBERGER, F. SCHAFFLER, *University of Linz* J. LIU, Y.H. XIE, *UCLA* We report a systematic study of the energy gaps at the odd-integer quantum Hall states $\nu=3$ and 5 under tilted magnetic (B) fields in the two-dimensional electron system (2DES) in $Si/Si_{1-x}Ge_x$ heterostructures [1]. Consistent with previous studies, we find that out of the coincidence region, the valley splitting is independent of the in-plane B-field. However, the $\nu=3$ valley gap appears to be highly asymmetric and differs significantly on different sides of the coincidence. Similar behaviors were observed in both high ($20m^2/Vs$) and low ($6m^2/Vs$) mobility samples. More surprisingly, instead of reducing to zero at coincidence, as expected in the independent-electron model, the inter-valley gaps at $\nu=3$ and 5 rise rapidly towards the coincidence angles. We will discuss our results in the framework of two known models, level coupling with random-matrix elements and quantum Hall ferromagnetism, and show that the anomaly is related to the strong couplings of the Landau levels close in energy in the coincidence region. [1] K. Lai *et al.*, cond-mat/0510599.

**11:27**
**Z46 2 Integer quantum Hall effect and valley splitting on a H-Si(111) surface** KEVIN ENG, ROBERT N. McFARLAND, BRUCE E. KANE, *Laboratory for Physical Sciences, University of Maryland at College Park* We have recently developed a high mobility two-dimensional electron system, where an electric field is applied through an encapsulated vacuum cavity and induces electrons on a clean and atomically flat hydrogen-passivated Si surface. Low temperature magneto-transport measurements ($0< B < 12T$) made on such an inversion layer has led us to the first observation of the integer quantum Hall effect on a Si(111) surface. With a mobility of $\sim$ 10,000 $cm^2/Vs$ at T=150 mK and $n_s=6.75 \times 10^{11}\ cm^{-2}$, we observed filling factors $\nu=6$, 4, 3, and 2. This is particularly interesting, because Si(111) is expected to have a six-fold valley degeneracy. Activation energy measurements within filling factors 6 and 2 coupled with analysis of Shubnikov-de Haas oscillations suggests that the six-fold valley degeneracy is broken asymmetrically into 2-fold and 4-fold at B=0. In addition, the observation of $\nu=3$ indicates that individual valleys are splitting at higher fields. We will discuss these results along with the possible origins of the breaking of the six-fold valley degeneracy at B=0.

**11:39**
**Z46 3 Valley Dynamics on H-Si(111) in Tilted Magnetic Fields** ROBERT N. McFARLAND, KEVIN ENG, BRUCE E. KANE, *Laboratory for Physical Sciences, University of Maryland, College Park* Because of the predicted sixfold valley degeneracy of the Si(111) surface and the numerous mechanisms that can lift this degeneracy, 2D electron transport on this surface displays complex and interesting behavior. To explore this behavior, we have performed low temperature ( $\sim$ 150 mK) tilted-field magneto-transport measurements ($0< B_{tot} < 12$ T) on H-passivated Si(111) surfaces encapsulated in a vacuum cavity. We find a strong dependence of the longitudinal magneto-resistance on the in-plane B field. At low fields ( $< 2$ T) this manifests as an amplification of the Shubnikov-de Hass amplitudes without a significant effect on the phase or frequency. At high fields ( $> 6$ T, $\nu < 6$) the valley degeneracy is lifted, and we observe energy gaps at $\nu=4$ and $\nu=3$ which are strongly affected by small in-plane fields. Since in neither case are the observed effects linear in total B field, the results are inconsistent with Zeeman-like effects. We present measurements of the activation energies for the gaps at $\nu=4$ and 3 as a function of tilt angle. Finally, we consider possible mechanisms for this field-dependent splitting and propose future experiments that may shed further light on the matter.

**11:51**
**Z46 4 The spin susceptibility in Si-MOSFETs.** MARIAPIA MARCHI, *Democritos-INFM and Universita' di Trieste* DE PALO STEFANIA, *Democritos-INFM* SAVERIO MORONI, *Democritos-INFM* GAETANO SENATORE, *Democritos-INFM and Universita' di Trieste* We have performed for the first time DMC simulations of a symmetric two-valley electron gas with variable spin polarization, both in the strictly 2D limit and with a thickness appropriate to Si-MOSFETs. We find that valley degeneracy substantially reduces the spin susceptibility enhancement $\alpha$, with respect to the conventional 2DEG. The farther reduction of $\alpha$, caused by thickness, brings our prediction in excellent agreement with the available experimental data on Si-MOSFETs[1] up to $r_s \approx 5$. The agreement extends to the full experimental range ($r_s \leqslant 8$) when weak disorder is kept into account within a response function formalism, generalizing to the two valley system the approach previously employed for the conventional 2DEG [2]. [1] See, e.g, S.V. Kravchenko and M.P.Sarachik, Rep. Prog. Phys. **67**, 1 (2004) and references therein. [2] S. De Palo et. al., Phys. Rev. Lett. **94**, 226405 (2005).

**12:03**
**Z46 5 Valley susceptibility of an interacting two-dimensional electron system.** YAKOV SHKOLNIKOV,*OKI GUNAWAN, KAMRAN VAKILI, TAYFUN GOKMEN, ETIENNE DE POORTERE,†MANSOUR SHAYEGAN, *Princeton University* In a wide AlAs quantum well grown on a (001) GaAs substrate, 2D electrons occupy two elliptical conduction band minima (valleys), whose major axes lie along the two in-plane $<100>$ directions. Strain-induced energy splitting between these valleys results in an inter-valley charge transfer and consequently in a change of the system's valley polarization. We parameterize this strain-induced change of the valley polarization using valley susceptibility $\chi_v$, in analogy to the spin-susceptibility traditionally used to characterize the magnetic field induced spin-polarization. We find that $\chi_v$ dramatically increases relative to its band value as the electron density is reduced, reflecting the dominant role of electron-electron interaction.

*Currently at Exponent Failure Analysis Associates
†Currently at Columbia University

**12:15**

**Z46 6 Selective occupation of conduction band valleys in AlAs quantum wells.** MEDINI PADMANABHAN, K. VAKILI, Y.P. SHKOLNIKOV, O. GUNAWAN, T. GOKMEN, E. TUTUC, E.P. DE POORTERE, M. SHAYEGAN, We report our progress in the controlled and selective occupation of various conduction band minima in AlAs quantum wells and the corresponding magnetotransport behaviors. AlAs has three conduction band minima, or valleys, located at the X-points of the Brillouin zone. By a suitable choice of well width and in-plane stress, these minima can be occupied by two-dimensional electrons singly or in various combinations. We review the factors that determine the valley occupation and show how we have used them to produce a variety of systems with different valley occupations. In particular, we will discuss two methods that we have successfully used: (a) using a piezoelectric material to impart uniaxial strain and, (b) using a material with a different thermal expansion coefficient than our samples to impart biaxial tensile strain.

**12:27**

**Z46 7 Landau level crossings in imbalanced, two-valley two-dimensional electron systems** KAMRAN VAKILI, TAYFUN GOKMEN, MEDINI PADMANABHAN, OKI GUNAWAN, YAKOV P. SHKOLNIKOV, EMANUEL TUTUC, MANSOUR SHAYEGAN, *Department of Electrical Engineering, Princeton University, Princeton, NJ 08544* We report results of magnetotransport measurements performed on two-dimensional electron systems in AlAs quantum wells with highly imbalanced valley occupation. We observe spikes in the diagonal resistance that signal the crossing of Landau levels originating from each of the occupied valleys. From the positions of these spikes and their dependence on tilt angle, we can extract the valley splitting as well as the ratios of the effective electron masses and g-factors for the two-valleys. We find that the mass ratio is unchanged from the band value and the g-factors are equal between the two valleys despite the high degree of density imbalance. We have also explored the interaction-induced finite gaps that persist at avoided crossings between Landau levels and discuss some of our results.

**12:39**

**Z46 8 Parallel magnetic field induced valley splitting** T. GOKMEN, O. GUNAWAN, K. VAKILI, E. P. DE POORTERE, M. SHAYEGAN, *Department of Electrical Engineering, Princeton University, Princeton, NJ 08544* In an 11nm-wide thick AlAs quantum well grown on a GaAs (001) substrate, the two-dimensional electrons occupy two in-plane conduction-band valleys. The Fermi contours for these two valleys are ellipses whose major axes are rotated by 90 degrees. The energy separation between these two valleys at zero magnetic field is normally controlled via the application of in-plane strain along the major axis of one of the valleys. In this talk, through a combination of experimental results and calculations, we demonstrate a novel method for tuning of the valley splitting. Namely, we show that the application of a magnetic field parallel to the major axis of one the ellipses leads to a lifting of the valley degeneracy. This is because the parallel field which, thanks to the finite thickness of the electron layer couples to the electrons' orbital motion modifies the effective masses of the two valleys (in the direction perpendicular to the field direction) by different amounts.

**12:51**

**Z46 9 Multiple Phases with the Same Quantized Hall Conductance in a Two-Subband System** XINCHANG ZHANG, DONALD RICHARD FAULHABER, HONGWEN JIANG, *UCLA* In a GaAs/AlGaAs two-dimensional electron system with two occupied subbands, the experimentally determined phase diagram exhibits rich topological features. Ring-like structures are observed at even integer filling factors. Even with the identical quantized Hall resistance values as those given rise by the ordinary integer quantum Hall effect due to the Landau level quantization; the activation energies of these states within the rings are much smaller. These ring structures cannot account for by the simple single particle picture. We argue that ferromagnetic quantum Hall states, due to the interaction of two energy levels with opposite spin and different subband indices, are responsible for these unusual structures.

**13:03**

**Z46 10 Anomalous magnetoresistance peaks: Evidence for Landau level spin-anticrossing in (110) GaAs two-dimensional hole systems*** M. GRAYSON, S. F. ROTH, Y. XIANG, F. FISCHER, M. BICHLER, D. SCHUH,† *Walter Schottky Institut, TU-Muenchen, 85748 Garching, Germany* R. WINKLER,‡ *Inst. fuer Festkoerperphysik, U. Hannover, 30167 Hannover, Germany* We report anomalous peaks in the longitudinal resistance of (110) GaAs two-dimensional hole systems (2DHS), which we associate with an anticrossing of spin split Landau levels. GaAs hole systems are of research interest due to their heavy mass and strong spin-orbit coupling. With modulated growth conditions, Si can be used as an acceptor for high mobility 2DHS on (110) wafers with mobilities up to $7 \times 10^5$ cm$^2$/Vs at a hole density of $1.2 \times 10^{11}$cm$^{-2}$. Resistance peaks within the $\nu = 1$ minimum of the quantum Hall effect are observed in various samples. We propose that these anomalous peaks arise from an anticrossing of Landau levels with magnetic field. The position of the anticrossing field is independent of top-gate voltage, but can be tuned by illumination. This behaviour is in agreement with self- consistent calculations of the valence band mixing, assuming an illumination dependent background charge in the substrate. Band calculations predict a spin-flip at the anticrossing, which might be exploited to test new spin based device concepts.

*cond-mat/0509288
†Currently at the Univ. Regensburg
‡Currently at Northern Illinois University

**13:15**

**Z46 11 Monitoring the Motion of Charge Carriers in the Integer Quantum Hall Bulk with a Single Electron Transistor** LEE FARINA, ÇAGLIYAN KURDAK, *Physics Department, University of Michigan, Ann Arbor, MI* MANSOUR SHAYEGAN, *Department of Electrical Engineering, Princeton University, Princeton, NJ* Using an Al/AlO$_x$/Al single electron transistor on top of an antidot etched into a GaAs/AlGaAs heterostructure containing a two-dimensional electron gas, we studied the quantum Hall system in the middle of the $\nu=2$ plateau. In this highly insulating regime, oscillations in single electron transistor resistance indicate that the charges in the system adjust slowly ( $\sim$ 1 hour) to changes in the back gate voltage or magnetic field. We find that after a small increase in magnetic field an excess of electrons leave the bulk. Moreover, the presence of the etched antidot under the SET creates a small but clear discrepancy between behavior after a change in magnetic field and change in back gate voltage indicating charging of the antidot after a change

in magnetic field. When the antidot is accounted for we find the expected ratio of 2 electrons/flux quanta at $\nu=2$. We also present the time dependence of the charge equilibration for 18 mK to 280 mK. Bulk conductivities in the range of $10^{-18}$-$10^{-18}$ /$\Omega$ are obtained from this measurement and compared to conductivies obtained from lock-in measurements at high temperatures (1-10 K).

**13:27**

**Z46 12 Frozen Charges, Persistent Eddy Currents, and Nearly Perfect Diamagnetism in Stacked Integer Quantum Hall Layers** CAGLIYAN KURDAK, *University of Michigan* LEE A. FARINA, *University of Michigan* Faraday's law of induction for an integer quantum Hall liquid dictates that after the application of a small additional magnetic field an integer number of electrons for each additional magnetic flux quanta must enter the 2DEG. Since the diagonal conductivity is close to zero, these charges are nearly frozen. The electric field associated with these charges leads to a persistent eddy current flowing in the bulk of the 2DEG. The magnetic field generated by the persistent eddy currents is much smaller than the additional magnetic field applied. However, the magnetic field generated by the persistent eddy currents can be greatly enhanced in closed stacked layers of integer quantum disks. In fact, we find that when the number of layers is much greater than inverse fine structure constant, these persistent eddy currents can perfectly screen the applied additional magnetic field at zero temperature.

**13:39**

**Z46 13 Spin and Valley Splitting of Two-Dimensional Electrons in Graphene in the High Magnetic Field Limit** YUANBO ZHANG, ZHIGANG JIANG, JOSHUA SMALL, *Department of Physics, Columbia University* MENINDER PUREWAL, *Department of Applied Physics, Columbia University* YAN-WEN TAN, MINA FAZLOLLAHI, JOEL CHUDOW, *Department of Physics, Columbia University* JOHN JASZCZAK, *Department of Physics, Michigan Technological University* HORST STORMER, PHILIP KIM, *Department of Physics, Columbia University* The quantum Hall effect in high quality graphene, a sinlge atomic layer of graphite, is studied in strong magnetic fields up to 45 Tesla. The splitting of Landau levels $n = 0$ and $\pm$ 1, caused by the lifting of the spin and valley degeneracies in strong magnetic fields, is observed at T $<$ 5 K. In particular, the quantum Hall state $\nu = \pm 4$ is found to arise from the spin splitting of Landau level n = $\pm$ 1. The effective Lande g-factor measured at this state is close to 2. The spin origin of $\nu = \pm 4$ is further confirmed in magnetotransport experiments performed in the presence of an in-plane magnetic field. While the exact origin of the valley degeneracy lifting is not yet clear, we propose several possibilities.

**13:51**

**Z46 14 Quantized conductance in an AlAs 2D electron system quantum point contact** M. SHAYEGAN, O. GUNAWAN, B. HABIB, E.P.D. POORTERE, *Princeton University* We report experimental results on a quantum point contact (QPC) device fabricated in a wide AlAs quantum well where the electrons occupy two conduction-band valleys with in-plane, elliptical Fermi contours. To probe the closely-spaced, one-dimensional, electric subbands (channels), we fabricated a QPC structure where the point contact is defined by a split-etched region covered by a global top gate. The conductance versus top gate bias trace shows a series of weak plateaus at every $2e^2/h$, consistent with the fact that the one-dimensional confinement and the anisotropy of the Fermi contours break the valley degeneracy for the QPC channels. Moreover, we observe a ''0.7 structure'' which is much better developed than the $2e^2/h$ plateaus, possibly reflecting the stronger electron-electron interaction in this system because of the larger electron effective mass.

**14:03**

**Z46 15 Nonlinearities in Strongly Coupled Lateral Quantum Hall Droplets** P. JIANG, C. CHIEN, I. YANG, W. KANG, *James Franck Institute and Department of Physics, University of Chicago* L.N. PFEIFFER, K.W. BALDWIN, K.W. WEST, *Bell Laboratories, Lucent Technologies* We report on conductance characteristics of a lateral quantum Hall line junction with an aperture in a thin tunnel barrier (width = 8.8 nm). Due to the small opening inside the barrier, the charge distribution in the junction resembles that around a narrow split gate. In the presence of a magnetic field, the edge states of the two- dimensional electron systems across these particular junctions are strongly coupled compared to those with pristine barriers. In the integer quantum Hall effect (IQHE) regime, a strong resonance in conductance is detected at zero bias, while it evolves into an anomalous suppression as the system enters the fractional quantum Hall effect (FQHE) regime. The dramatic suppression of the conductance in the FQHE regime is consistent with the presence of strong repulsive interaction in the lowest Landau levels, while the enhanced conductance in the IQHE regime supports the prediction of softened Coulomb interaction. The contrasting conductance behaviors in the IQHE and the FQHE regimes clearly distinguish the effects of electron-electron interaction in the inter-edge transport in these two regimes.

## C

## F

## G

## H

## M

## O

## P

## Q

## R

## S

## U

**V**

## W

## X

## Y

## Z

# NOTES

# NOTES

# NOTES

# NOTES

# NOTES

# NOTES

# NOTES

# NOTES

# NOTES

# NOTES

# NOTES

# NOTES

# NOTES

# The Baltimore Convention Center Overview

## Level 400

- 36,672 square foot ballroom.
- Divides into 4 sections.
- Ceiling height 28 feet.
- Prefunction space.

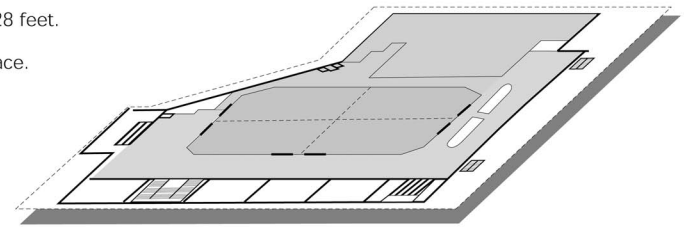

## Level 300

- 50 meeting rooms accommodate 85 to 1,600 people.
- Information kiosk.
- Prefunction space.

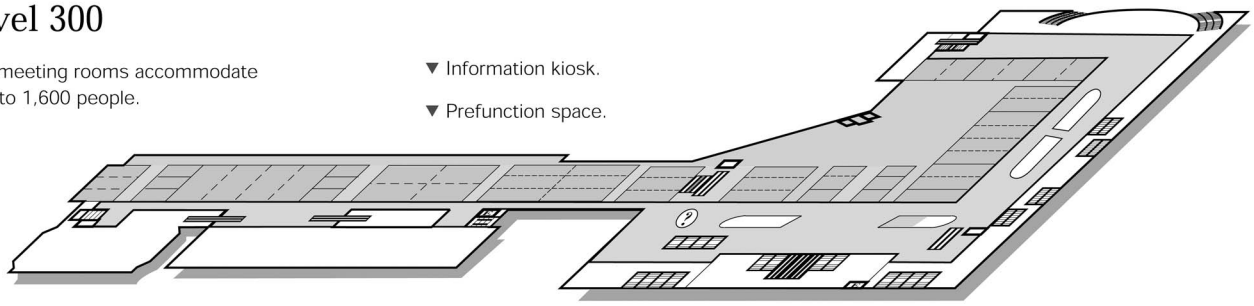

## Level 200

- Access to all areas of Convention Center.
- Convention Center Offices.
- Access to Skywalk, Inner Harbor and hotels.
- Information kiosk.

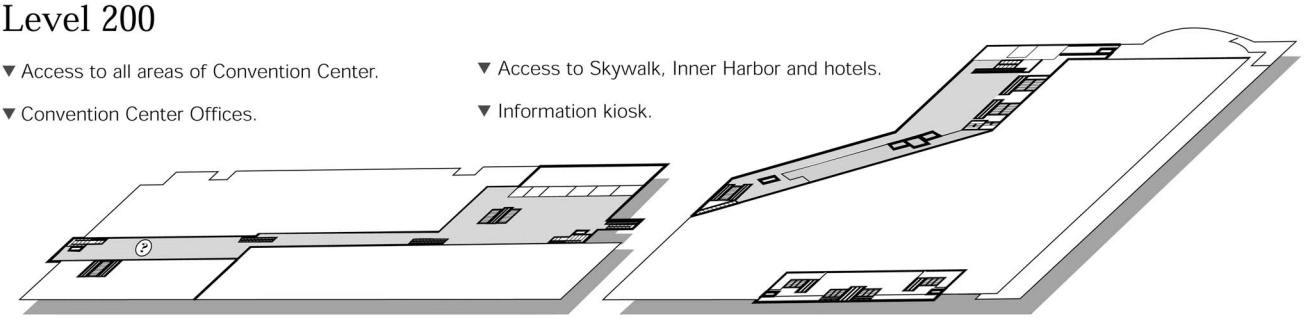

## Level 100

- 300,000 square feet of exhibit space.
- Divides into 7 separate halls.
- Ceiling height 30 feet at center.
- 32 covered loading docks.

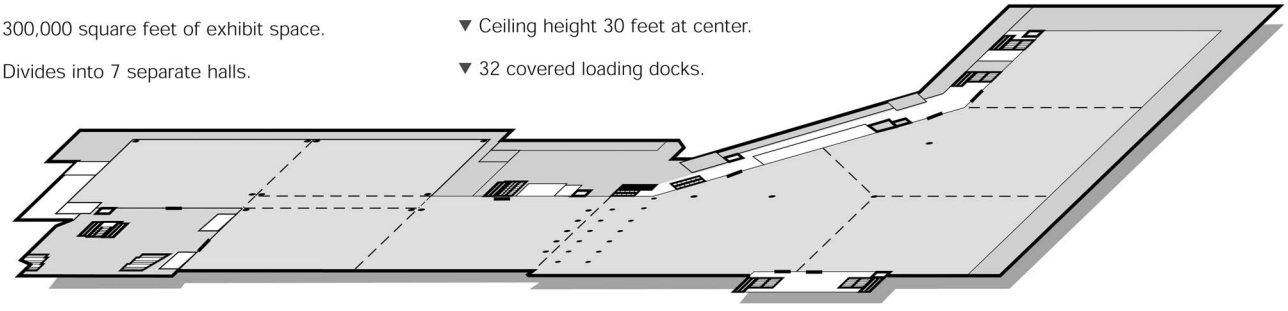

# The Baltimore Convention Center

## Level 100

- 300,000 square foot exhibit space divides into 7 sections.
- Ceiling height 30 feet at center.
- 120/208V and 277/480V electrical services at approximately 30-foot spacing on the floor.
- Cold water, sanitary drain, compressed air available.
- Direct drive-in access for vehicles through 15'x18' overhead doors.
- 32 covered loading docks.
- All halls have available public address system and telephone outlets.
- Complimentary show offices come with exhibition halls.
- VIP Suite available in Charles Lobby.
- The entire exhibition space is relatively column-free.

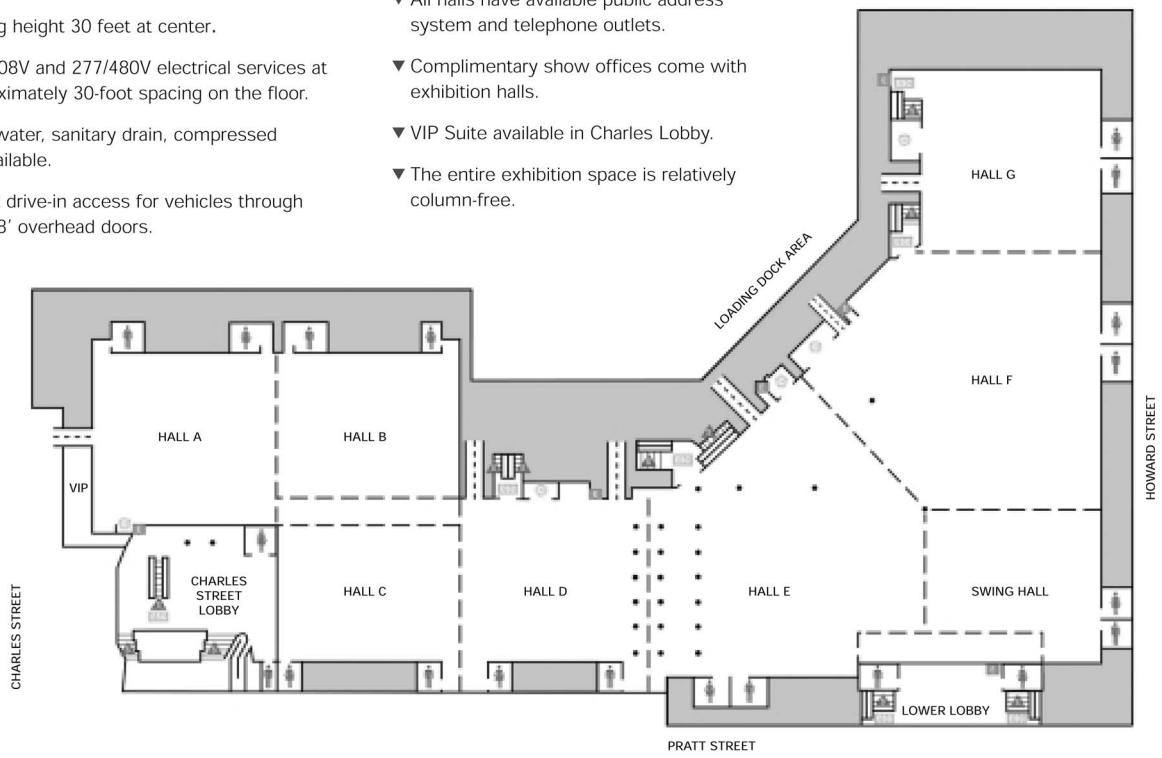


| key | concessions | elevator | escalator | stairs |
|---|---|---|---|---|

# The Baltimore Convention Center

## Level 200

- Includes Otterbein and Sharp Street Lobbies, Pratt Street Entrance and Convention Center Offices.
- Access to Skywalk, Inner Harbor, and hotels. Access to Baltimore's Light Rail System providing a direct route to BWI Airport. Walking distance to the MARC train system with service to Washington, D.C.
- Prefunction space.
- Visitor information kiosk.

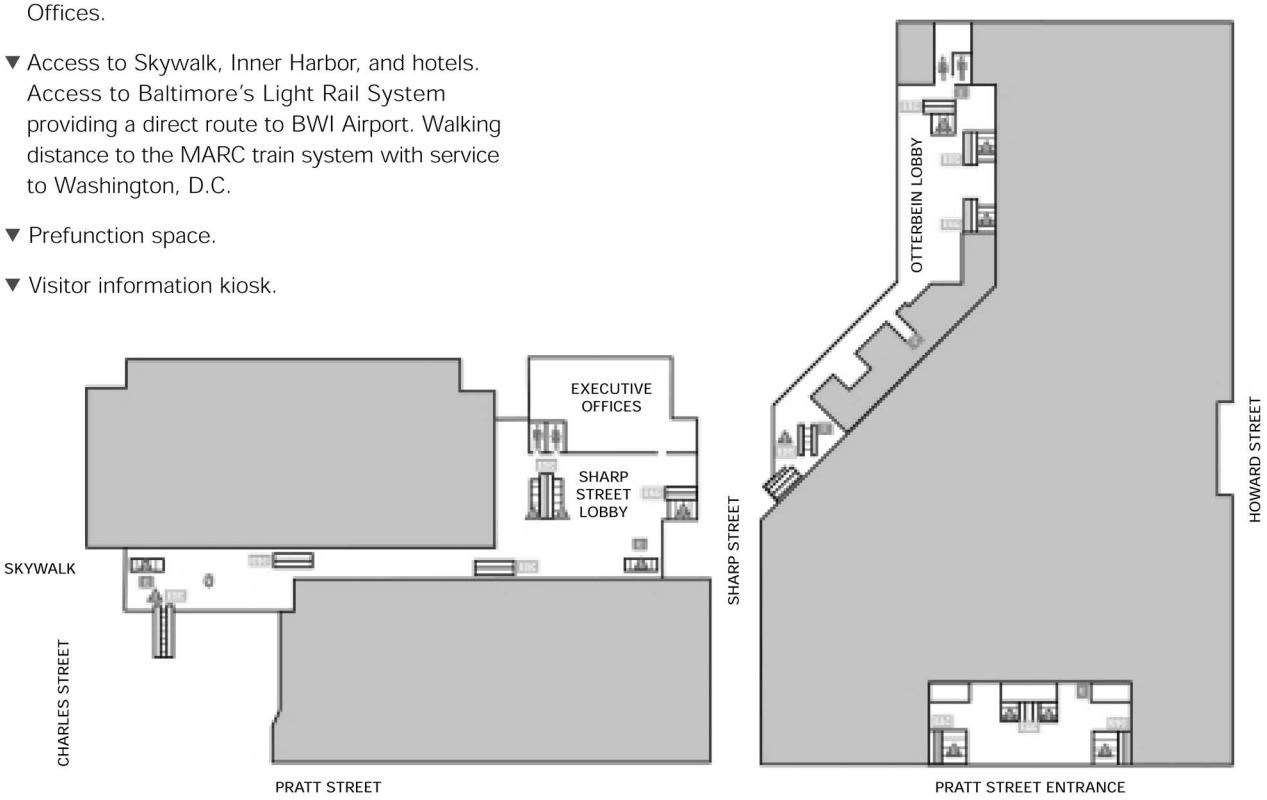


| key | restrooms – public restrooms are handicap accessible | handicap accessible restroom and assistant | drive in access | visitor kiosk |
|---|---|---|---|---|

# The Baltimore Convention Center

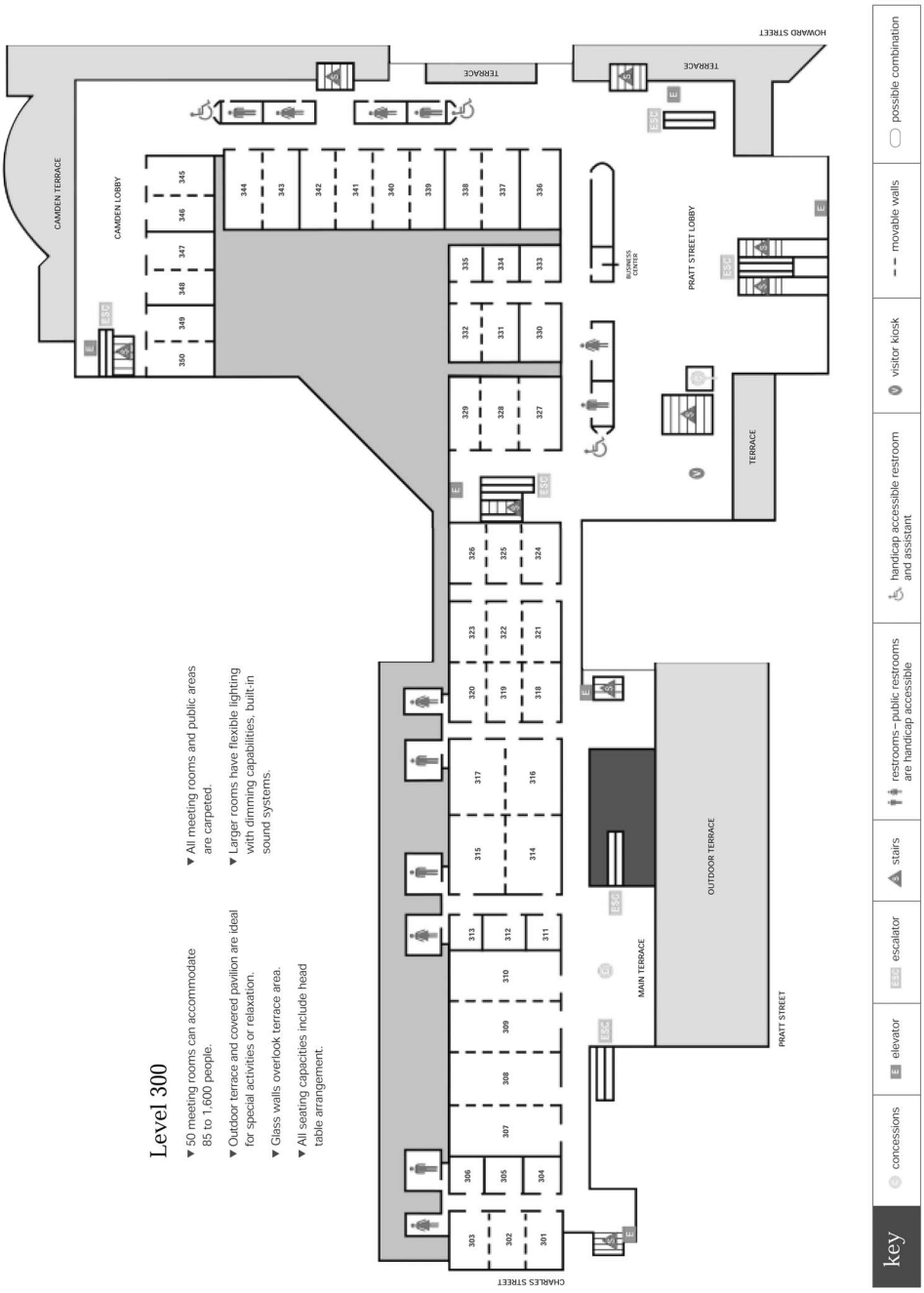

# The Baltimore Convention Center

## Level 400

- 36,672 square foot ballroom.
- Divisible into 4 sections.
- Ceiling height 28 feet.
- Complete kitchen/catering facilities.
- Built-in sound system.
- Fluorescent and incandescent lighting with dimmers.
- VIP Suites available.
- Ballroom foyer provides spacious prefunction space.

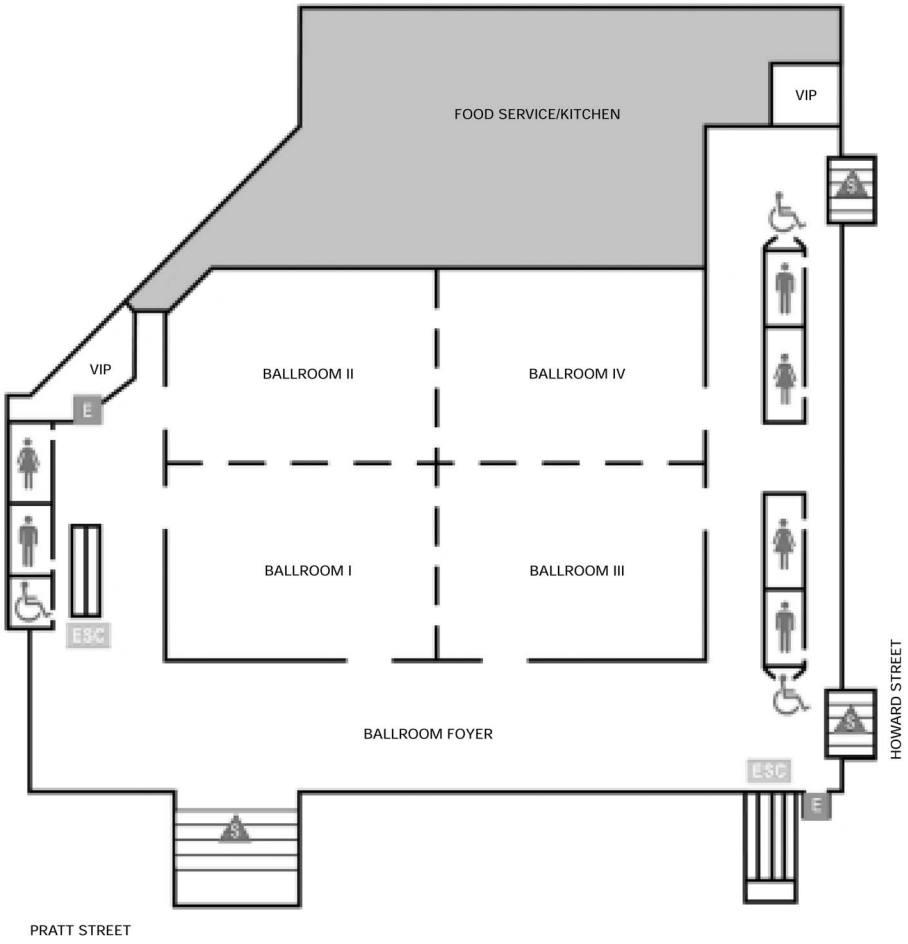


| key | | | | |
|---|---|---|---|---|
| | C concessions | E elevator | ESC escalator | stairs |
| | restrooms<br>public restrooms are handicap accessible | handicap accessible restroom & assistant | V visitor kiosk | |